SPRINGER
REFERENCE

Albert L. Baert
Editor

Encyclopedia of Diagnostic Imaging

Springer

Albert L. Baert (Ed.)

Encyclopedia of Diagnostic Imaging

Volume 1
A–K

With 1334 Figures and 141 Tables

Albert L. Baert (Ed.)

Encyclopedia of Diagnostic Imaging

Volume 2
L–Z

With 1334 Figures and 141 Tables

Editorial Board

Editor:
Albert L. Baert
Department of Radiology
University Hospital Gasthuisberg
Herestraat 49
B-3000 Leuven
Belgium

A C.I.P. Catalog record for this book is available from the Library of Congress

ISBN: 978-3-540-35278-5
This publication is available also as:
Electronic publication under ISBN 978-3-540-35280-8 and
Print and electronic bundle under ISBN 978-3-540-35860-2

Springer is part of Springer Science+Business Media

springer.com

Printed on acid-free paper SPIN: 11008750 2109 — 5 4 3 2 1 0

Preface

This compact "Encyclopedia of Diagnostic Imaging" is conceived as a two-volume printed work but will also be available online.

It aims to provide basic but up-to-date information on all aspects of the very large field of medical imaging.

The state of the art character of the encyclopedia is particularly evident in such topics as molecular imaging, magnetic resonance, and contrast media.

Around 4000 entries are arranged in alphabetical order with extensive cross-referencing between them. They have been written by internationally recognised leading experts in the field.

The encyclopedia should be used as a quick reference book. It can be recommended to medical specialists outside the discipline of radiology, to scientists involved in clinical medical research, but also to general radiologists, radiologists in training, students in medicine, radiographers and interested laypeople, particularly persons from industry and business dealing with medical imaging.

For the completion of this encyclopedia, I am very much indebted to Mr. Andrew Spencer from Springer Verlag who provided excellent technical support during the preparation of this work.

A.L. Baert
Editor

List of Contributors

Eric Achten
University of Ghent
Ghent
Belgium
rik.achten@ugent.be

Federica Agosta
Neuroimaging Research Unit, Department of Neurology
Scientific Institute and University Ospedale San Raffaele
Via Olgettina
Italy

Thomas Albrecht
Department of Radiology and Nuclear Medicine, Campus Benjamin Franklin
Charité - Universitätsmedizin Berlin
Berlin
Germany
thomas.albrecht@charite.de

K. Alfke
Neuroradiology
UK SH
Kiel
Germany
k.alfke@neurorad.uni-kiel.de

Cristina Gutiérrez Alonso
University Hospital Miguel Servet
Department of Radiology
Zaragoza
Spain

K. Anders
University of Erlangen-Nürnberg
Institute of Radiology, Gynaecological Radiology,
Erlangen
Germany

Suzanne E. Anderson
University Hospital of Bern
Inselspital
Bern
Switzerland
suzanne.anderson@bluewin.ch

Günther Antes
Department of Radiology, Klinikum Kempton-Oberallgäu
Kempton
Germany
gantes@gmx.de

Luis C. Apesteguía
Hospital Virgen del Cashino
Pamplona
Spain
luis.apesteguia.ciriza@cfnavarra.es

Remide Arkun
Department of Radiology
Ege University, School of Medicine
Izmir
Turkey
rarkun@yahoo.com

Fischmann Arne
Department of Diagnostic Radiology, University of Tübingen
Tübingen
Germany
arne.fischmann@med.uni-tuebingen.de

Rosemary Arthur
Department of Pediatric Radiology, Leeds General Infirmary
Clarendon Wing
Leeds
UK
r.arthur@ukonline.co.uk

Dewi Ashi
Department of Radiology, Faculty of Medicine
University of Indonesia
Cipto Mangunkusumo General Hospital
Salemba
Jakarta Pusat
Indonesia
j.blickman@rad.umcn.nl

Alessio Auci
Department of Diagnostic and Interventional Radiology
University of Pisa
Pisa
Italy
bartolozzi@do.med.unipi.it

Klaus K. Gast
Department of Radiology
Mainz University Hospital
Mainz
Germany
kgast@radiologie.klinik.uni-mainz.de

F. E. Avni
Department of Medical Imaging
University Clinics of Brussels, Erasme Hospital
Brussels
Belgium
favni@ulb.ac.be

W. H. Backes
Department of Radiology, University Hospital Maastricht
Maastricht
The Netherlands

Pinar Balci
Dokuz Eylül University School of Medicine
Department of Radiology
Izmir
Turkey
pinar.balci@den.edu.tr

Danielle Baleriaux
Clinique de Neuroradiologie, Hôpital Erasme
Université Libre de Bruxelles
Brussels
Belgium
dbaleri@ulb.ac.be

Roland Bares
University of Tuebingen
Tuebingen
Germany
bares@uni-tuebingen.de

Jörg Barkhausen
Department of Diagnostic and Interventional Radiology and Neuroradiology
University Hospital Essen
Essen
Germany
joerg.barkhausen@uni-essen.de

Jean-Philippe Barraud
Guerbet
Roissy
France
barraudj@guerbet-group.com

Sue Barter
Cambridge Breast Unit, Addenbrookes Hospital
Cambridge
UK
sue.barter@addenbrookes.nhs.uk

Carlo Bartolozzi
Department of Diagnostic and Interventional Radiology
University of Pisa
Italy

Valentina Battaglia
Diagnostic and Interventional Radiology
University of Pisa
Pisa
Italy

Jan S. Bauer
Institut für Röntgendiagnostik, Technical University Munich
Munich
Germany
jsb@roe.med.tum.de

Jan S. Bauer
Department of Radiology
San Francisco
USA

W. Bautz
University of Erlangen-Nürnberg
Institute of Radiology, Gynaecological Radiology
Erlangen
Germany

Cédric de Bazelaire
Service de Radiologie
Hôpital Saint-Louis
Paris
France

Massimo Bazzocchi
Department of Diagnostic and Interventional Radiology
University of Udine
Udine
Italy
massimo.bazzocchi@med.uniud.it

Harald Becher
Oxford University, John Radcliffe Hospital
Oxford
UK
harald.becher@orh.nhs.uk

Christoph R Becker
Ludwig-Maximilians-Universität
Munich
Germany
christoph.becker@med.uni-muenchen.de

Edwin J. R. van Beek
Department of Radiology, Carver College of Medicine, C-751 GH,
Iowa City
USA
edwin-vanbeek@uiowa.edu

G. L. Beets
Department of Radiology
University of Trieste
Trieste
Italy

R. G. H. Beets-Tan
Department of Surgery
University Hospital Maastricht
Maastricht
Netherlands

Manuel Belgrano
Department of Radiology
University of Trieste
Trieste
Italy

Marie-France Bellin
Department of Radiology, University Hospital Paul Brousse AP-HP
University Paris-Sud 11
Villejuif
France
marie-france.bellin@pbr.ap-hop-paris.fr

Michele Bertolotto
Department of Radiology
University of Trieste
Trieste
Italy
bertolot@univ.trieste.it

Jürgen Biederer
German Cancer Research Center
Heidelberg
Germany
j.biederer@dkfz.de

Alfredo Blandino
Department of Radiological Science, University of Messina
Messina
Italy
ablandino@unime.it

Johan G. Blickman
Department of Radiology
UMC St Radboud
Nijmegen
The Netherlands
j.blickman@rad.umcn.nl

Martin J. K. Blomley
Hammersmith and Charing Cross Hospital NHS Trust &
Imperial College
London
UK

Karin Bock
University of Marburg
Marburg
Germany
bock@med.uni-marburg.de

Andreas Bockisch
Klinik fur Nuklearmedizin, Universitaetsklinikum Essen
Essen
Germany

Carla Boetes
Department of Radiology, Faculty of Medicine
University of Indonesia, Cipto Mangunkusumo General
Hospital
Jakarta Pusat
Indonesia

Alexei Bogdanov
Departments of Radiology and Cell Biology
University of Massachusetts Medical School
Worcester
USA
alexei.bogdanov@umassmed.edu

Nicolae Bolog
Institute of Diagnostic Radiology
University Hospital
Zurich
Switzerland

Bruno Bonnemain
Villeparisis
France
bruno.bonnemain@wanadoo.fr

Piero Boraschi
2nd Department of Radiology
University Hospital of Pisa
Pisa
Italy
p.boraschi@do.med.unipi.it

Alexandra Borges
Instituto Português de oncologia Francisco Gentil
Centro Regional Oncológico de Lisboa
1093, Lisboa
Portugal
borgesalexandra@clix.pt

Ulrike Brehmer
Department of Diagnostic Imaging
University Children's Hospital
Zürich
Switzerland
ulrike.brehmer@kispi.unizh.ch

Christoph Bremer
Department of Clinical Radiology & Interdisciplinary
Center for Clinical Research (1ZKF), University of Muenster
Muenster
Germany
bremerc@uni-muenster.de

Jens Bremerich
Department of Radiology
University Hospital Basel
Basel
Switzerland
jens.bremerich@unibas.ch

Pauline Brice
Hôpital de jour d'Hématologie
Hôpital Saint-Louis
Paris
France

Elias N. Brountzos
Department of Radiology
Athens University
Medical School, Athans
Greece
ebrountz@cc.uoa.gr

Patrick A. Brouwer
Leids Universitair Centrum Leiden
The Netherlands
b.schenk@lumc.nl

Jean Michel Bruel
Service d'Imagerie Médicale Hôpital St. Éloi CHU de
Montpellier
Montpellier
France
jm-bruel@chu-montpellie.fr

Laurent Brunereau
Pôle d'imagerie médicale
CHU de Tours
France
brunereau@chu-tours.fr

J-N. Bruneton
Service d'Imagerie Médicale Diagnostique et
Interventionelle, Hopital de I'Archet
Nice
France

Orla Buckley
Department of Radiology
Tallaght Hospital
Dublin
Ireland

Carlos H. Buitrago-Tellez
University of Basel, Head Radiological Institute, Zofingen Hospital
Switzerland
carlos.buitrago@spitalzofingen.ch

Dorothy Bulas
Division of Diagnostic Imaging and Radiology, Children's National Medical Center, The George Washington University School of Medicine and Health Sciences
Washington DC
USA
dbulas@cnmc.org

William H. Bush, Jr.
Department of Radiology
University of Washington
Seattle
USA

Jose Caceres
Department of Radiology, HGU Vall d'Hebron, Universitat Autonoma
Barcelona
Spain
josecac@gmail.com

Filippo Cademartiri
Department of Radiology
Erasmus Medical Center
Rotterdam
The Netherlands

Carla Cappelli
Department of Diagnostic and Interventional Radiology
University of Pisa
Pisa
Italy
bartolozzi@do.med.unipi.it

Gabriele Caproni
Department of Diagnostic and Interventional Radiology
University of Pisa
Pisa
Italy

Davide Caramella
Department of Diagnostic and Interventional Radiology
University of Pisa
Pisa
Italy
caramella@do.med.unipi.it

Nicholas R. Carroll
Cambridge University Hospitals, NHS Foundation Trust
Cambridge
UK
nicholas.carroll@addenbrookes.nhs.uk

Federica Carrozzo
Department of Radiological Sciences
Policlinico Umberto I-University of Rome La Sapienza, Rome
Italy

M. Cassart
Department of Medical Imaging
University Clinics of Brussels, Erasme Hospital
Brussels
Belgium

Mauricio Castillo
Department of Radiology
University of North Carolina at Chapel Hill
Chapel Hill
USA

Stefano Cernic
Department of Radiology
University of Trieste
Trieste
Italy

Francesca Cerri
Diagnostic and Interventional Radiology
University of Pisa
Pisa
Italy

A. G. Chalmers
Consultant Radiologists
Leeds General Infirmary
Leeds
UK

Carmel T. Chan
Department of Radiology, Molecular Imaging Program at Stanford (MIPS) and Bio-X Program
Stanford University School of Medicine
Stanford
USA
carmelc@stanford.edu

Frederique Chapon
Department of Neuroradiology
Hopital Timone Adultes
France

Natalie Charnley
Wolfson Molecular Imaging Centre
The University of Manchester
Manchester
UK

J.-F. Chateil
Department of Pediatric Imaging
Hospital Pellegrin
Bordeaux
France

Simon R. Cherry
Department of Biomedical Engineering, Center for Molecular and Genomic Imaging
University of California—Davis
Davis
USA
srcherry@ucdavis.edu

P. Chevallier
Service d'Imagerie Médicale Diagnostique et Interventionelle, Hopital de l'Archet
Nice
France
bruneton.jn@chu-nice.fr

Chiara Franchini
W K 'Kling' Chong
Pediatric Neuroradiologist
Great Ormond Street Hospital for Children
London
UK
k.chong@ich.ucl.ac.uk

C. Chossegros
Department of Maxillofacial surgery
CHU La Timone
Marseille
France

Malik Chouli
Hôpital de Bicêtre
Paris
France

M.A. Chrestian
Department of Pathology
CHU La Timone
Marseille
France
guy.moulin@mail.ap-hm.fr

Stefano Cirillo
Institute for Cancer Research and Treatment
Turin
Italy
stefano.cirillo@ircc.it

Michel Claudon
Department of Radiology
Childrens Hospital, Nancy University Hospital
Nancy
France
m.claudon@chu-nancy.fr

Richard H. Cohan
University of Michigan
Michigan
USA

Aron Cohen
Department of Urology
University Hospital Zurich
Zurich
Switzerland
cohen@swissonline.ch

Xavier Combaz
Department of Neuroradiology
Hopital Timone Adultes
France

Giuseppe Como
Department of Diagnostic and Interventional Radiology
University of Udine
Udine
Italy

JM Correas
University of Paris V
Paris
France
jean-michel.correas@nck.ap-hop-paris.fr

David O. Cosgrove
Hammersmith and Charing Cross Hospital NHS Trust & Imperial College
London
UK

Maria Assunta Cova
Department of Radiology
University of Trieste
Trieste
Italy

Laura Crocetti
Department of Diagnostic and Interventional Radiology
University of Pisa
Pisa
Italy
l.crocetti@med.unipi.it

Heike E. Daldrup-Link
Department of Radiology, Pediatric Radiology section and Director, Contrast agent Research Group University of California in San Francisco
USA
daldrup@radiology.ucsf.edu

Kassa Darge
Department of Pediatric Radiology
Institute of Radiodiagnostic, Bavarian Julius-Maximilians-University Wuerzburg
Wuerzburg
Germany
darge@roentgen.uni-wuerzburg.de

Mark Davies
MRI Centre, Royal Orthopedic Hospital NHS Trust
Birmingham
UK
wendy.turner@roh.nhs.uk

Albert de Roos
Department of Radiology, C2-S
Leiden
The Netherlands
A.de_Roos@lumc.nl

Karel Deblaere
University of Ghent
Ghent
Belgium

E Dekeiser
Necker Hôpital, Service de Radiologie
Paris
France

Anna Dell'Acqua
Department of Radiology
Giannina Gaslini Hospital for Sick Children
Genova
Italy

Philippe Demaerel
Department of Radiology, University Hospitals
Leuven, Belgium
philippe.demaerel@uz.kuleuven.ac.be

Philippe Demaerel
Department of Radiology
University Hospital K.U.Leuven
Leuven
Belgium
philippe.demaerel@uz.kuleuven.ac.be

Dr Hubert John
John Räto
T. Strebel
Department of Urology
University Hospital Zurich
Zurich
Switzerland
raeto.strebel@usz.ch

Alban Denys
Centre Hospitalies Universitire Vandois Lausanne,
Lausanne
Switzerland
alban.denys@chuv.hospvd.ch

Lorenzo E. Derchi
Centre Hospitalies Universitire Vandois Lausanne,
Lausanne
Switzerland

Malone Dermot
University of Genova
Larva R. Benzi, 8, I-16122 Genova
Italy
d.malone@st-vincents.ie

Antonia Dimitrakopoulou-Strauss
Medical PET Group-Biological Imaging (E0601)
Clinical Cooperation Unit Nuclear Medicine, German
Cancer Research Center
Heidelberg
Germany
a.dimitrakopoulou-strauss@dkfz.de

H. Dittmann
University of Tuebingen
Tuebingen
Germany

Selcuk Dogan
Istanbul University
Department of Radiology
Istanbul
Turkey

Jiri Dolina
Department of Gastroenterology
University Hospital Brno
Brno
Czech Republic
jdolina@fnbrno.cz

Francescamaria Donati
2nd Department of Radiology
University Hospital of Pisa
Pisa
Italy

Veronica Donoghue
Radiology Department
Children's University Hospital
Dublin 1
Ireland
veronica.donoghue@cuh.ie

Valeria D'Ovidio
Department of Clinical Sciences, Gastroenteroly Unit,
Policlinico Umberto I
University of Rome "La Sapienza"
Italy

Antonios Drevelegas
Radiology Department
Aristoteles University of Thessaloniki
Thessaloniki
Greece
adrev@med.auth.gr

Volker Duda
University of Marburg
Marburg
Germany
duda@med.uni-marburg.de

Robert Eckersley
Imaging Sciences Department, Faculty of Medicine
Imperial College London
London
UK
r.eckersley@imperial.ac.uk

Michael Eisenhut
Abteilung Radiopharmazeutische Chemie Deutsches
Krebsforschungszentrum
Heidelberg
Germany

Olle Ekberg
Department of Clinical Sciences/Medical Radiology, Lund
University, Malmö University Hospital
Malmö
Sweden
olle.ekberg@med.lu.se

James H. Ellis
Department of Radiology
University of Michigan
Ann Arbor,
Michigan
USA
jimellis@umich.edu

Nevra Elmas
Ege Üniversitesì Tip Fakultesi
Izmin
Turkey
elmas@med.ege.edu.tr

S. M. E. Engelen
Department of Surgery
University Hospital Maastricht
Maastricht
Netherlands

Christoph Engelke
Department of Radiology, Klinikum rechts der Isar,
Technical University Munich,
Munich
Germany

Giovanni Carlo Ettorre
Istituto di Radiologia
Università degli Studi di Catania
Catania
Italy
g.ettorre@unict.it

F. Facon
Department of Otorhinolaryngology
CHU La Timone
Marseille
France

Kantarci Fatih
Istanbul University
Department of Radiology
Istanbul
Turkey

Rossella Fattori
Department of Radiology, Cardiovascular Unit
University Hospital S. Orsola
Bologna
Italy
ross@med.unibo.it

Katherine Ferrara
Department of Biomedical Engineering, Center for
Molecular and Genomic Imaging
University of California
Davis
USA

Pim J de Feyter
Department of Radiology
Erasmus Medical Center
Rotterdam
The Netherlands

Massimo Filippi
Neuroimaging Research Unit, Dept. of Neurology,
Scientific Institute and University of Ospedale
San Raffaele
Via Olgettina
Italy
filippi.massimo@hsr.it

Arne Fischmann
Department of Diagnostic Radiology
University of Tübingen
Tübingen
Germany
arne.fischmann@med.uni-tuebingen.de

Flavio Forrer
Department of Nuclear Medicine
Erasmus Medical Centre
Rotterdam
The Netherlands
fforrer@uhbs.ch

Rosemarie Forstner
Department of Radiology
Paracelsus Private Medical University
Salzburger Landeskliniken
Salzburg
Austria
r.forstner@salk.at

Richard Fotter
Department of Radiology
Division of Pediatric Radiology, Universiy Hospital Graz
Graz
Austria
richard.fotter@meduni-graz.at

Chiara Franchini
Department of Diagnostic and Interventional Radiology
University of Pisa
Pisa
Italy
lencioni@med.unipi.it

Alan H. Freeman
Consultant Radiologist Cambridge University Hospitals
NHS Trust
Cambridge
UK
alan.freeman@addenbrookes.nhs.uk

Jacques Frija
Service de Radiologie
Hôpital Saint-Louis
Paris
France

Jurgen J. Fütterer
Department of Radiology
University Medical Centre Nijmegen
6500HB Nijmegen
The Netherlands
j.futterer@rad.umcn.nl

Massimo Gallucci
Department of Neuroradiology
University of L'Aquila
Italy
massimo.gallucci@cc.univaq.it

Sanjiv Sam Gambhir
Department of Radiology, Molecular Imaging Program at
Stanford (MIPS) and Bio-X Program
Stanford University School of Medicine
Stanford
USA
sgambhir@stanford.edu

Viola Garbarino
Department of Radiological Sciences, Policlinico Umberto I
University of Rome "La Sapienza"
Rome
Italy

Roberto Martínez García
University Hospital Miguel Servet,
Department of Radiology
Zaragoza
Spain
lhros@wanadoo.es

Cristiana Gasparini
Department of Radiology
University of Trieste
Trieste
Italy

J. Y. Gauvrit
Neuroradiology Department Salengro Hospital
Lille
France
jygauvrit@gmail.com

Heinrich K. Geiss
Qualitätsmanagement-Hygiene-Konzern
Bad Neustadt/Saale
Germany
h.geiss.qm@rhoen-klinikum-ag.com

Lilli Geworski
Charité-Universitätsmedizin
Berlin
Germany
lilli.geworski@charite.de

Gino Ghigi
University of Bologna
Bologna
Italy
gghigi@alma.unibo.it

Jonathan Gillard
Cambridge University Hospitals Foundation Trust
Cambridge
UK
Jhg21@cam.ac.uk

Nadine J Girard
Department of Neuroradiology
Hopital Timone Adultes
France
nadine.girard@mail.ap-hm.fr

Christian Glaser
Institut für Klinische Radiologie der LMU München GH München
Germany
christian.glaser@med.uni-muenchen.de

Fergus V. Gleeson
Consultant Radiologist
Department of Radiology, Churchill Hospital, Headington
Oxford
UK
fergus.gleeson@radiology.oxford.ac.uk

Neslïhan Gültaşli
Clinique de Neuroradiologie, Hôpital Erasme
Université Libre de Bruxelles
Brussels
Belgium
ngultasli@yahoo.com

Claudio Granata
Department of Radiology
Giannina Gaslini Hospital for Sick Children
Genova
Italy

Francesca Granata
University of Messina
Messina
Italy
longomar@tin.it

Holger Greess
Department of Radiology
University Erlangen-Nürnberg
Erlangen
Germany

Christian Greis
Bracco ALTANA Pharma GmbH
Klinische Entwicklung Ultraschallkontrastmittel,
Konstanz
Germany
christian.greis@altanapharma.com

Philippe A. Grenier
Hôpital Pitié-Salpêtrière
Paris
France
philippe.grenier@psl.ap-hop-paris.fr

Nicolas Grenier
Service d'Imagerie Diagnostique et Thérapeutique de l'Adulte
Groupe Hospitalier Pellegrin
Bordeaux
France
nicolas.grenier@chu-bordeaux.fr

Norbert Gritzmann
KH Barmherzige Brüder Salzburg
Salzburg
Austria
norbert.gritzmann@bbsalz.at

Ludovico La Grutta
Department of Radiology
Erasmus Medical Center
Rotterdam
The Netherlands

F. Z. Gueddari
Service de Radiologie Centrale, CHN
Rabat
Morocco
fzgueddari@hotmail.com

Giuseppe Guglielmi
University of Foggia,
Foggia, Department of Radiology, Scientific Institute
Hospital San Giovanni Rotondo
Italy
guglielmi_g@hotmail.com

Alexander R. Guimaraes
Center for Molecular Imaging Research
Massachusetts General Hospital
Charlestown
USA
weissleder@helix.mgh.harvard.edu

G. L. Guit
Radiology Department
Kennemer Gasthuis
Haarlem
The Netherlands

Serap Gultekin
Section of Neuroradiology & MRI Center
Department of Radiology, Gazi University School of Medicine
Besevler, Ankara 06510
Turkey
sergultekin@yahoo.com

Patrick Haage
Department of Diagnostic and Interventional Radiology
HELIOS Klinikum Wuppertal, University Hospital Witten/Herdecke
Wuppertal
Germany
patrick.haage@helios-kliniken.de

Uwe Haberkorn
Radiologische Klinik und Poliklinik
Universitätsklinikum Heidelberg
Heidelberg
Germany
uwe.haberkorn@med.uni-heidelberg.de

Monia Hamami
Klinik fur Nuklearmedizin, Universitaetsklinikum Essen
Essen
Germany

David M. Hansell
Department of Radiology
Royal Brompton Hospital
London
UK
d.hansell@rbh.nthames.nhs.uk

K. M. Harris
Consultant Radiologists
Leeds General Infirmary
Leeds
UK

Robert P. Hartman
Department of Diagnostic Radiology
Mayo Clinic
Rochester MN
USA

Christopher J. Harvey
Hammersmith and Charing Cross Hospital NHS Trust & Imperial College
London
UK
charvey_99@yahoo.com

Peter Hauff
Research Laboratories
Bayer Schering Pharma
Berlin
Germany
peter.hauff@schering.de

Stijn W. T. P. J. Heijmink
Department of Radiology, Radboud University
Nijmegen Medical Centre
Geert Grooteplein 10
The Netherlands

G. Heinz-Peer
Department of Radiology
Medical University
Vienna
Austria
gertraud.heinz-peer@akhwien.at

Olivier Helenon
Neckert
Paris
France

Thomas Helmberger
Clinic of Radiology and Nuclear medicine
University Hospitals Schleswig-Holstein
Campus Luebeck
Germany
thomas.helmberger@uni-luebeck.de

K. G. Hering
Beratender Arzt für Diagnostische Radiologie
bei arbeits – und umweltbedingten Erkrankungen
Knappschaftskrankenhaus
Dortmund
Germany
k.g.hering@kk-dortmund.de

Klaus-Peter Hermann
Gesellschaft Wissenschaftliche Datenverarbeitung mbH
Göttingen
Germany
kherman@gwdg.de

Beatriz Izquierdo Hernández
University Hospital Miguel Servet,
Department of Radiology,
Zaragoza
Spain

Franc H. Hetzer
Clinic of Visceral and Transplant Surgery
University Hospital
Zurich
Switzerland

Claus Peter Heussel
Diagnostic and Interventional Radiology
Thoraxklinik Heidelberg
Heidelberg
Germany
heussel@thoraxklinik-heidelberg.de

Melanie Hiorns
Radiology Department, Great Ormond Street Hospital for Children
London
UK
HiornM@gosh.nhs.uk

O. Hélénon
Necker Hôpital, Service de Radiologie
Paris
France
olivier.helenon@nck.aphp.fr

Thilo Hoelscher
Department of Radiology
University of California
San Diego
USA
thoelscher@ucsd.edu

P. A. M. Hofman
Department of Radiology, University Hospital
Maastricht
The Netherlands
pho@rdia.azm.nl

Yvonne L. Hoogeveen
Department of Radiology, Faculty of Medicine
University of Indonesia, Cipto Mangunkusumo General Hospital
Jakarta Pusat
Indonesia

Benjamin Y. Huang
Department of Radiology
University of North Carolina at Chapel Hill
Chapel Hill
USA
bhuang@unch.unc.edu

T. A. Huisman
Johns Hopkins University
Baltimore
USA
thierry.huisman@kispi.unizh.ch

Robert W. Hurst
Radiology, Neurology, and Neurosurgery
University of Pennsylvania
Philadelphia
USA
robert.hurst@uphs.upenn.edu

Franco Iafrate
Director of Unit of CT and MR, University of Rome "La Sapienza"
Polo Pontino, I.C.O.T. Latina
Italy
francoiafrate@tin.it

Jean-Marc Idée
Guerbet Research Division
Aulnay-sous-Bois
France
jean-mar.idee@guerbet-group.com

Judy Illes
Stanford Center for Biomedical Ethics
Stanford University
Stanford
USA
illes@stanford.edu

F. Imani
Service de Radiologie Centrale, CHN
Rabat
Morocco

Ahi Sema Issever
Institut für Radiologie
Charité Campus Mitte
Berlin
Germany

Simon A Jackson
Imaging Directorate
Derriford Hospital
Plymouth
UK
simon.jackson@phnt.swest.nhs.uk

Jarl Å. Jakobsen
Department of Radiology
Rikshospitalet
Oslo
Norway

O. Jansen
Neuroradiology
UK SH
Kiel
Germany

Hohmann Joachim
Universitätsspital Basel
Institut für Radiologie
Basel
Switzerland
jhohmann@uhbs.ch

Francis Joffre
CHU
Toulouse
France
joffre.f@chu-toulouse.fr

Hubert John
Klinik Hirslanden
Zentrum für Urologie,
8008 Zurich
Switzerland
hubert.john@hirslanden.ch

Marion De Jong
Department of Nuclear Medicine
Erasmus Medical Centre
Rotterdam
The Netherlands

Nico de Jong
ErasmusMC
Rotterdam
The Netherlands
n.dejong@erasmnsc.nl

Hans-Ulrich Kauczor
Department of Radiology
German Cancer Research Center
Heidelberg
Germany
hu.kauczor@dkfz-heidelberg.de

Eric de Kerviler
Service de Radiologie
Hôpital Saint-Louis
Paris
France
eric.de-kerviler@sls.ap-hop-paris.fr

Eric de Kerviler

Bernard King
Department of Diagnostic Radiology
Mayo Clinic
Rochester MN
USA

Matthew P. Kirschen
Stanford Center for Biomedical Ethics
Stanford University
Stanford
USA

Patrick R. Knüsel
Institut für Radiologie
Kontonsspital Baden
Baden
Switzerland
patrick.knuesel@ksb.ch

Takahashi Koji
Department of Radiology, Asahikawa Medical college,
Asahikawa
Japan
taka1019@asahikawa_med.ac.jp

Elisa E. Konofagou
Department of Biomedical Engineering and Radiology
Columbia University
New York
USA
ek2191@columbia.edu

Franck Koskas
Department of Radiology
University Paris-Sud 11, Paul Brousse Hospital
Villejuif
France
franckkoskas@hotmail.com

S. I. Koukouraki
Department of Nuclear Medicine University, Iraklion
Crete
Greece
sophiak@her.forthnet.gr

Silvia Kovacs
Department of Radiology
University Hospital

Bodo Kress
Department of Neurology
University of Heidelberg Medical Section
Heidelberg
Germany

Christian R. Krestan
Department of Radiology
Medical University of Vienna, Vienna General Hospital
Vienna
Austria
christian.krestan@meduniwien.ac.at

Gabriel P. Krestin
Department of Radiology
Erasmus Medical Center
Rotterdam
The Netherlands

Martin Krix
Bracco ALTANA Pharma GmbH
Clinical Research
Konstanz
Germany
martin.krix@altanapharma.com

Gabriele A. Krombach
Department of Radiology
University Hospital
Aachen
Germany
krombach@rad.rwth-aachen.de

Gerrit Krupski-Berdien
Universitätsklinikum Hamburg-Eppendorf
Hamburg
Germany
krupski@uke.uni-hamburg.de

Sabrina Kösling
Martin-Luther-Universität Halle-Wittenberg Klinik für
Diagnostische Radiologie
Halle
Germany
sabrina.koesling@medizin.un-halle.de

Barbara Kötz
Wolfson Molecular Imaging Centre
The University of Manchester
Manchester
UK
pat.price@manchester.ac.uk

Rahel A. Kubik-Huch
Institute of Radiology, Kantonsspital Badan
Badan
Switzerland
Martin.Unterweger@ksb.ch

Rüdiger von Kummer
Universitätsklinikum Carl Gustav
Carns
Dresden
Germany
ruediger.vonkummer@uniklinikum-dresden.de

Pascal Lacombe
Department of Radiology Hôpital Ambroise Paré
Université Paris Ile-de-France Ouest
Boulogne-Billancourt
France

Andrea Laghi
Director of Unit of CT and MR, University of Rome "La Sapienza"
Polo Pontino, I.C.O.T. Latina
Italy
andrea.laghi@uniromal.it

M. J. Lahaye
Department of Surgery
University Hospital Maastricht
Maastricht
Netherlands

Thomas C. Lauenstein
Department of Radiology
The Emory Clinic
Atlanta
USA
tlauens@emory.edu

H. P. Ledermann
Department of Radiology
University Hospital Basel, Institute of Diagnostic Radiology
Basel
Switzerland
Ledermannhp@uhbs.ch

Michael Lell
Department of Radiology
University Erlangen-Nürnberg
Erlangen
Germany
michael.lell@idr.imed.uni-erlangen.de

Riccardo Lencioni
Department of Diagnostic and Interventional Radiology
University of Pisa
Pisa
Italy
lencioni@med.unipi.it

Adrian K. P. Lim
Hammersmith and Charing Cross Hospital NHS Trust &
Imperial College
London
UK

Nicola Limbucci
Department of Neuroradiology
University of L'Aquila
Italy

G. M. Lingg
Department of Radiology
Sana Rheumazentrum Rheinland Pfalz
Bad Kreuznach
Germany
dr.lingg@sana-rheumazentrum-rlp.de

Thomas M. Link
Department of Radiology
University of California
San Francisco
USA
tmlink@radiology.ucsf.edu

Karl Ludwig
Department of Diagnostic Radiology
Orthopedic University Hospital Heidelberg
Heidelberg
Germany
karl.ludwig@ok.uni-heidelberg.de

Pina Luis
Clínica Universitaria de Navarra,
Navarra
Spain
ljpina@unav.es

Clemens Löwik
Endocrinology Research Laboratory and Molecular Imaging
Leiden University Medical Center
The Netherlands
c.w.g.m.lowik@lumc.nl

Francesca Maccioni
Department of Radiological Sciences
Policlinico Umberto I-University of Rome La Sapienza,
Rome
Italy
francesca.maccioni@uniroma1.it

Frederik Maes
Universitaire Ziekenhuizen
Lenven
Belgium
Frederik.Maes@uz.kuleuven.ac.be

Dean D. T. Maglinte
Indiana University School of Medicine
Indianapolis
USA
dmaglint@iupui.edu

Brinder Mahon
Queen Elizabeth Hospital
Birmingham
UK

Patrizia Malagutti
Department of Radiology
Erasmus Medical Center
Rotterdam
The Netherlands

Geert Maleux
Department of Radiology
University Hospitals Leuven
Leuven
Belgium
geert.maleux@uz.kuleuven.ac.be

David Malfair
UCSF
San Francisco
USA
dmalfair@hotmail.com

Ada Mandic
Department of Radiology
University of Trieste
Trieste
Italy

Damien Mandry
Department of Radiology
Childrens Hospital, Nancy University Hospital
Nancy
France

Vassilios Maniatis
CT and MRI Department HYGEIA Hospital Eritherou stvrou 4, GR-15123, Maroussi
Athens
Greece
vmaniatis@hotmail.com

Giuliano Mariani
Department of Diagnostic and Interventional Radiology and of Nuclear Medicine
University of Pisa
Italy

Katharina Marten
Department of Radiology, Klinikum rechts der Isar,
Technical University Munich,
Munich
Germany
katharina.marten@roe.med.tu-muenchen.de

F. Martinelli
Radiodiagnostic Unit
University of Florence Careggi Hospital
Florence
Italy

Olivier Mathieu
Service de Radiologie
Hôpital Saint-Louis
Paris
France

C. Matos
Department of Medical Imaging
University Clinics of Brussels, Erasme Hospital
Brussels
Belgium

Julian Matthews
Wolfson Molecular Imaging Centre
The University of Manchester
Manchester
UK
Julian.matthews@manchester.ac.uk

Salvatore Mazzeo
Divisions of Diagnostic and Interventional Radiology
University of Pisa
Pisa
Italy

Silvio Mazziotti
Department of Radiological Sciences, University of Messina,
Messina
Italy
smazziotti@unime.it

Colm McMahon
Department of Radiology, St Vincent's University Hospital
Dublin
Ireland

W. Bob Meijboom
Department of Radiology
Erasmus Medical Center
Rotterdam
The Netherlands

Luis H. Ros Mendoza
University Hospital Miguel Servet
Department of Radiology
Zaragoza
Spain
lhros@wanadoo.es

Yves Menu
Hôpital de Bicêtre
Paris
France
laurence.rocher@bct.ap-hop-paris.fr

Samuel Merran
Neckert
Paris
France

Sven Michel
Radiology
Kantonsspital Baden,
5404 Baden
Switzerland
sven.michel@ksb.ch

Walter Mier
Abteilung Radiopharmazeutische Chemie Deutsches Krebsforschungszentrum
Heidelberg
Germany

Paola Milillo
Istituto di Radiologia
Università degli Studi di Catania
Catania
Italy

Fabio Minutoli
Department of Radiological Sciences University of Messina,
Messina
Italy
fminutoli@unime.it

Stefan Müller-Hülsbeck
Department of Radiology
University Hospital Schleswig-Holstein, Campus Kiel
Kiel
Germany
muehue@rad.uni-kiel.de

Nico R Mollet
Department of Radiology
Erasmus Medical Center
Rotterdam
The Netherlands

O Monnet
Department of Radiology
CHU La Timone
Marseille
France

Sandra Moore
NYU Medical Center
New York
USA
sandra.moore@nyumc.org

Sameh K. Morcos
Department of Diagnostic Imaging
Northern General Hospital, Sheffield Teaching Hospitals
NHS Trust
Sheffield
UK

Robert Morgan
St George's NHS Trust
London
UK
robert.morgan@stgeorges.nhs.uk

W. B. Morrison
Department of Radiology
Thomas Jefferson University Hospital
Philadelphia
USA

G. Moulin
Department of Radiology
CHU La Timone
Marseille
France

Takashi Nakamura
Department of Radiology and Cancer Biology
Nagasaki University School of Dentistry
Nagasaki
Japan
misa@nagasaki-u.ac.jp

L. Napolitano
Radiodiagnostic Unit
University of Florence Careggi Hospital
Florence
Italy
gianni.pellicano@unifi.it

Emanuele Neri
Diagnostic and Interventional Radiology
University of Pisa
Italy
neri@med.unipi.it

Tony Nicholson
Leeds Teaching Hospitals NHS Trust
Leeds
UK
Tony.Nicholson@leedsth.nhs.uk

Corinna E. E. Nierhoff
Department of Diagnostic Radiology
Orthopedic University Hospital Heidelberg
Heidelberg
Germany

R. J. Nijenhuis
Department of Radiology, University Hospital Maastricht
The Netherlands

Anders Nilsson
Department of Radiology, Ultrasound University, Uppsala
University Hospital
Uppsala
Sweden
anders.nilsson@akademiska.se

Vasilis Ntziachristos
Harvard Medical School
Harvard University HMS/MGH, Center for Molecular
Imaging Research
Charlestown
USA
vasilis@helix.mgh.harvard.edu

Silvia Obenauer
Department of Radiology
Georg-August-University of Goettingen
Goettingen
Germany
obenauerheuser@yahoo.de

Alan E. Oestreich
Cincinnati Children's Hospital Medical Center
Cincinnati, Ohio
USA
Alan.Oestreich@cchmc.org

Monica Olar
Pôle d'imagerie médicale
CHU de Tours
France

Robert Olszewski
Department of Cardiology
Military Medical Institute
Warsaw
Poland

Patrick Omoumi
Pôle d'imagerie médicale
CHU de Tours
France

Philippe Otal
CHU
Toulouse
France
otal.p@chu-toulouse.fr

R. H. Oyen
Department of Radiology
University Hospitals Gasthuisberg
Leuven
Belgium
raymond.oyen@uz.kuleuven.ac.be

Enver Ozer
Department of Otolaryngology, Head and Neck Surgery
University Medical Center, The Ohio State University
Columbus
USA

Bernard P. Paelinck
University Hospital Antwerp
Antwerp
Belgium
bernard.paelinck@ua.ac.be

Alessandro Palumbo
Department of Radiology
Erasmus Medical Center
Rotterdam
The Netherlands

Ignazio Pandolfo
Department of Radiological Science
University of Messina
Italy
ablandino@unime.it

Amalia Paonessa
Department of Neuroradiology
University of L'Aquila
Italy

J. Paris
Department of Otorhinolaryngology
CHU La Timone
Marseille
France

Sara Parlanti
Department of Radiological Sciences, Policlinico Umberto I
University of Rome "La Sapienza"
Italy

Zoltan Patay
Department of Radiological Sciences
St. Jude Children's Research Hospital
Memphis
USA
zoltan.patay@stjude.org

Anne Paterson
Royal Belfast Hospital for Sick Children
Belfast
UK
annie.paterson@royalhospitals.n-i.nhs.uk

Jacob Patijn
Pain Management and Research Centre, Department of Anaesthesiology
University Medical Centre Maastricht
Maastricht
The Netherlands
jpat@sane.azm.nl

Pietro Pavlica
Department of Radiology
Hospital M. Malpighi
Bologna
Italy

Pietro Pavlica
University of Genova
Largo R. Benzi, 8,
I-16122 Genova
Italy

Ronald Peeters
Department of Radiology
University Hospital

Jean-Pierre Pelage
Department of Radiology Hôpital Ambroise Paré
Université Paris Ile-de-France Ouest
Boulogne-Billancourt
France
jean-pierre.pelage@apr.ap-hop-paris.fr

G. Pellicanò
Radiodiagnostic Unit
University of Florence Careggi Hospital
Florence
Italy

Marzio Perri
Department of Diagnostic and Interventional Radiology
University of Pisa
Italy
lencioni@med.unipi.it

Darja Babnik Peskar
University Medical Center Ljubljana
Ljubljana
Slovenia

Wilco Peul
Medisch Centrum Haaglanden,
Netherlands
w.peul@mchaaglanden.nl

Catherine M. Phan
Hôpital de Bicêtre
Service de Radiologie BROCA
Le Kremlin-Bicêtre
France
catherine.phan@bct.aphp.fr

Frank Pilleul
Gastro-intestinal and Emergency Imaging Department,
Hôpital Universitaire Edouard Herriot,
Lyon
France
frank.pilleul@chu-lyon.fr

Luis Pina
Department of Radiology
Clínica Universitaria de Navarra
Navarra
Spain
ljpina@unav.es

Emmanuelle Pinès
Pharmacovigilance Department
Guerbet
Roissy CDG
France
emmanuelle.pines@guerbet-group.com

Brian W. Pogue
Thayer School of Engineering
Dartmouth College
Hanover
USA
brian.w.pogue@dartmouth.edu

Peter Pokieser
Medical University of Vienna, Medical Media Services,
Department of Radiology
Vienna
Austria

Panos K. Prassopoulos
Department of Radiology
University Hospital of Alexandronpolis, Medical School of Thace
Alexandronpolis
Greece
pprasopo@med.duth.gr

Pat Price
Wolfson Molecular Imaging Centre
The University of Manchester
Manchester
UK

Francesca Pugliese
Department of Radiology
Erasmus Medical Center
Rotterdam
The Netherlands

Nagmi R. Qureshi
Fellow in Thoracic Radiology
nagmiqureshi@doctors.org.uk

E. W. Radue
Department of Neuroradiology
University Hospital
Basel
Switzerland
eradue@uhbs.ch

Thomas Rand
Allgemeines Krankenhaus-Universitätskliniken
Vienna
Austria
thomas.rand@akhwien.at

Finn Rasmussen
Aarhus University Hospital
Aarhus
Denmark
frasm@as.aaa.dk

Margrit Reichel
Referenzzentrumsleiterin Mammographie-Screening
Wiesbaden
Germany
margrit.reichel@mammascreening-wiesbaden.de

Peter Reimer
Department of Radiology
Klinikum Karlsruhe, Academic Teaching Hospital of the University of Freiburg
Karlsruhe
Germany
peter.reimer@klinik.um-karlsruhe.com

Patrick Reinartz
Department of Nuclear Medicine, University Hospital Aachen,
Aachen
Germany
preinartz@arcor.de

Raphaelle Renard-Penna
Service de Radiologie
Hospital Pitiè Salpetrière, Assistance Publique des hospitaux de Paris Université
Pierre et Marie Curie
Paris,
France
raphaelle.renard-penna@psl.ap-hop-paris.fr

Shelley Renowden
Department of Neuroradiology
University of Bristol
Bristol
UK
shelley.renowden@north-bristol.swest.nhs.uk

M. Riccabona
Division of Pediatric Radiology
Medical University of Graz, University Hospital
Graz
Austria
michael.riccabona@meduni-graz.at

Ashley Roberts
University Hospital of Wales
Cardiff
UK
ashley.roberts@cardiffandvale.wales.nhs.uk

Maria A. Rocca
MRI Research Group
Scientific Institute Fondazione Don Gnocchi
Milan
Italy

Laurence Rocher
Hôpital de Bicêtre
Paris
France

Mathieu H. Rodallec
Department of Radiology Fondation Hôpital Saint-Joseph
Paris
France

Justus E. Roos
Department of Radiology
Stanford University Medical Center
Stanford
USA
justus.roos@stanford.edu

Rosemary Arthur
Department of Pediatric Radiology, Leeds General Infirmary
Clarendon Wing
Leeds
UK
r.arthur@ukonline.co.uk

Sandra J. Rosenbaum-Krumme
Klinik für Nuklearmedizin, Universitaetsklinikum
Essen
Germany

Andrea Rossi
Department of Pediatric Neuroradiology
G. Gaslini Children's Research Hospital
Genoa
Italy
andrearossi@ospedale-gaslini.ge.it

Catherine Roy
Department of Radiology B
University Hospital of Strasbourg, Hôpital Civil 1
Strasbourg
France
catherine.roy@chru-strasbourg.fr

Giuseppe Runza
Department of Radiology
Erasmus Medical Center
Rotterdam
The Netherlands

Mary Rutherford
Robert Steiner MR Unit Imaging Science Dept
MRC Clinical Sciences Centre Imperial College
Hammersmith Campus
London
UK
m.rutherford@imperial.ac.uk

Niloufar Sadeghi
Department of Radiology, Erasme Hospital,
Brussels
Belgium
nsadeghi@ulb.ac.be

Caroline Sage
Department of Radiology
University Hospital

M. A. Sahraian
Department of Neurology
Sina Hospital
Hassan abad Square
Tehran
Iran

Simonetta Salemi
Department of Diagnostic and Interventional Radiology
University of Pisa
Pisa
Italy

Kumaresan Sandrasegaran
Indiana University School of Medicine
Indianapolis
USA

Marek J. Sasiadek
Department of General Radiology, Interventional Radiology
and Neuroradiology, Wroclaw University
Wroclaw
Poland
mareks@rad.am.wroc.pl

Cornelia Schaefer-Prokop
AMC
Amsterdam
The Netherlands
c.m.schaefer@amc.uva.nl

Martina Scharitzer
Medical University of Vienna, Medical Media Services,
Department of Radiology
Vienna
Austria

Barry Schenk
Leids Universitair Centrum Leiden
Leiden
The Netherlands

A. M. De Schepper
Leiden University Medical Centre
Leiden
The Netherlands
arthurdeschepper@hotmail.com
A.M.de_Schepper@lumc.nl

M. Schäfers
Department of Nuclear Medicine
University of Münster
Münster
Germany
schafmi@uni-muenster.de

Marc Schmitter
Department of Prosthodontic, Department of Neurology
University of Heidelberg Medical Section
Heidelberg
Germany

U. Schnöckel
Department of Nuclear Medicine
University of Münster
Münster
Germany

Otmar Schober
Department of Nuclear Medicine, Coordinator Collaborative
Research Center
Molecular Cardiovascular Imaging (SFB 656-MoBil),
University Hospital Münster
Münster
Germany
schober.otmar@uni-muenster.de

Maria Schoder
Medizinische Universitat Wien
Vienna
Austria
maria.schoder@meduniwien.ac.at

C. Schorn
Department of Radiology
Sana Rheumazentrum Rheinland Pfalz
Bad Kreuznach
Germany

R. Schulz-Wendtland
University of Erlangen-Nürnberg, Institute of Radiology
Gynaecological Radiology
Erlangen
Germany
ruediger.schulz-wendtland@idr.imed.uni-erlangen.de

Daniel Scoffings
Cambridge University Hospitals Foundation Trust,
Cambridge
UK

Kurugoglu Sebuh
Istanbul University
Department of Radiology
Istanbul
Turkey

Ashley S. Shaw
Consultant Radiologist Cambridge University Hospitals
NHS Trust
Cambridge
UK

John Shirley
Imaging Directorate
Derriford Hospital
Plymouth
UK
john.shirley@phnt.swest.nhs.uk

Phil Shorvon
Central Middlessex hospital
London
UK
phils@intonet.co.uk

Francesca Siliquini
Department of Radiological Sciences, Policlinico Umberto I
University of Rome "La Sapienza"
Italy
francesca.maccioni@uniroma1.it

Akif Sirikci
Radiology Department
Gaziantep University, School of Medicine
Gaziantep
Turkey
sirikci@yahoo.com

Dominique Sirinelli
Pôle d'imagerie médicale
CHU de Tours
France

Marc Sirol
Department of Cardiology
Lariboisière Hospital
Paris
France
marc.sirol@mssm.edu

Eveline Smrtnik
University Medical Center Ljubljana
Ljubljana
Slovenia
darja.babnik@kclj.si

Sat Somers
Department of Radiology
McMaster University, West Hamilton
Ontario
Canada
somers@mcmaster.ca

Erich Sorantin
Department of Radiology, Division of
Pediatric Radiology
University Hospital Graz
Graz
Austria
erich.sorantin@meduni-graz.at

Gundula Staatz
Department of Radiology, Division of
Pediatric Radiology University of
Erlangen-Nürnberg
Erlangen
Germany
gu.stz.uni-erlangen@t-online.de

Fulvio Stacul
Department of Radiology
University of Trieste
Trieste
Italy
fulvio.stacul@aots.sanita.fvg.it

Lynne Steinbach
Department of Radiology
University of California
San Francisco
USA
lynne.steinbach@radiology.ucsf.edu

Giles Stevenson
McMaster University
Cowichan Hospital
Duncan
British Columbia
Canada
gilse@shaw.ca

M. P. M. Stokkel
Department of Nuclear Medicine
LUMC
Leiden
The Netherlands
m.p.m.stokkel@lumc.nl

Neil Stoodley
North Bristol NHS Trust
Bristol
UK
neil.stoodley@north-bristol.swest.nhs.uk

A. van Straten
Radiology Department
Kennemer Gasthuis
Haarlem
The Netherlands
straten@knmg.nl

Räto T. Strebel
Department of Urology
University Hospital Zurich
Zurich
Switzerland
raeto.strebel@usz.ch

Mª Eugenia Guillén Subirán
University Hospital Miguel Servet
Department of Radiology
Zaragoza
Spain

Misa Sumi
Department of Radiology and Cancer Biology
Nagasaki University School of Dentistry
Nagasaki
Japan
misa@nagasaki-u.ac.jp

Stefan Sunaert
Department of Radiology
University Hospital
Leuven
The Netherlands
Stefan.Sunaert@uz.kuleuven.ac.be

Nicola Sverzellati
Department of Clinical Sciences,
Section of Radiology
University of Parma
Italy
nicolasve@tiscali.it

Koji Takahashi
Department of Radiology
Asahikawa Medical College
Asahikawa
Japan
taka1019@asahikawa-med.ac.jp

E. Turgut Tali
Section of Neuroradiology & MRI Center
Department of Radiology, Gazi University School of Medicine
Besevler Ankara 06510
Turkey
turgut.tali@gazi.edu.tr

Patrice Taourel
Service d'Imagerie Médicale, Hôpital Lapeyronie
Montpellier
France
p-taourel@chu-montpellier.fr

I. Kaare Tesdal
Universitätsklinikum Mannheim
Institut für Radiologie und Nuklearmedizin Klinikum Friedrichshafen
Friedrichshafen
Germany
k.tesdal@klinikum-fn.de

Henrik S. Thomsen
Department of Diagnostic Radiology
Copenhagen University Hospital at Herlev
Herlev
Denmark
hentho01@heh.regionh.dk

Majda M. Thurnher
Universitätsklinik für Radiodiagnostik
Medizinische Universität Wien
Vienna
Austria
majda.thurnher@meduniwien.ac.at

Paolo Toma
Department of Radiology
Giannina Gaslini Hospital for Sick Children
Genova
Italy
paolotoma@ospedale-gaslini.ge.it

Bernd Tombach
Department of Clinical Radiology, University of Münster
Institut für Klinische Radiologie, Universitätsklinikum Münster
Münster
Germany
tombach@uni-muenster.de

William C Torreggiani
Department of Radiology
Tallaght Hospital
Dublin
Ireland
williammart@hotmail.com

Paolo Tortori-Donati
Department of Pediatric Neuroradiology
G. Gaslini Children's Research Hospital
Genoa
Italy

Thomas C. Treumann
Kantonspital Luzern
Luzern
Switzerland
thomas.treumann@ksl.ch

Elena Trincia
Department of Radiology
University of Trieste
Trieste
Italy
bertolot@univ.trieste.it

Francesca Turini
Diagnostic and Interventional Radiology
University of Pisa
Pisa
Italy

Michael Uder
Universitätklinikum Erlangen
Erlangen
Germany
michael.uder@idr.imed.uni-erlangen.de

Korman Ugur
Istanbul University
Department of Radiology
Istanbul
Turkey
ugurk9@istanbul.edu.tr

Volkmar Uhlendorf
ETH Zürich
Institut für Pharmazeutische
Wissenschaften
Zürich
Switzerland
volkmar.uhlendorf@pharma.ethz.ch

Martin Unterweger
Diagnostic Radiology
Cantonal Hospital Baden
Baden
Switzerland
Martin.Unterweger@ksb.ch

Paola Vagli
Department of Diagnostic and Interventional Radiology
University of Pisa
Italy

Vlastimil Valek
Department of Radiology
University Hospital Brno
Brno
Czech Republic
vlvalek@med.muni.cz

Els M. Vanherreweghe
Department of Radiology
Ghent University Hospital
Ghent
Belgium

Filip M. Vanhoenacker
Department of Radiology
University Hospital Antwerp
Belgium
Antwerp
filip.vanhoenacker@pandora.be

Annick Vieillefond
Neckert
Paris
France

Claudio Vignali
Department of Diagnostic and Interventional Radiology
University of Pisa,
Pisa
Italy

Geert M. Villeirs
Genitourinary Radiology
Ghent University Hospital
Ghent
Belgium
geert.villeirs@ugent.be

Carmela Visalli
Department of Radiologic Sciences, University of Messina
Messina
Italy
cvisalli@unime.it

Dierk Vorwerk
Klinikum Ingolstadt GmbH
Direktor des Institutes für diagnostische und interventionelle
Radiologie
Ingolstadt
Germany
dierk.vorwerk@klinikum-ingolstadt.de

Rolf Vosshenrich
Radiologen-Gemeinschaftspraxis MRT im Friederikenstift
Hannover
Germany
vosshenrich@t-online.de

Patrick Vroomen
University Medical Center Groningen
Groningen
Netherlands
c.a.j.vroomen@neuro.umcg.nl

Pieter Waer
Dept of Radiology
University Hospitals K.U. Leuven
Leuven
Belgium

M. Warmuth-Metz
Department of Neuroradiology University of Würzburg
Würzburg
Germany
warmuth@neuroradiologie.uni-wuerzburg.de

Judith A. W. Webb
Diagnostic Radiology Department
The London Clinic
St Bartholomew's Hospital
London
UK
jawwebb@btopenworld.com

Johannes Weber
Section of Neuroradiology
University of Freiburg Medical School
Freiburg
Germany
johannes.weber@uniklinik-freiburg.de

S. Weckbach
Institut für Klinische Radiologie der LMU München GH
München
Germany

R. E. Weijers
Department of Radiology
University Hospital Maastricht
Maastricht
The Netherlands
rwe@rdia.azm.nl

Dominik Weishaupt
Institute of Diagnostic Radiology
University Hospital
Zurich
Switzerland
dominik.weishaupt@usz.ch

Ralph Weissleder
Center for Molecular Imaging Research
Massachusetts General Hospital
Charlestown
USA

Jan T. Wilmink
Radiology Department University Hospital Maastricht
Maastricht
The Netherlands
jwil@rdia.azm.nl

Guido Wilms
Universitaire Ziekenhuizen Leuven
Leuven
Belgium
Guido.Wilms@uz.kuleuven.ac.be

Klaus Woertler
Department of Radiology, Klinikum rechts der Isar
Technical University Munich
Munich
Germany
woertler@roe.med.tum.de

A. Wuttge-hannig
Radiologie-Strahlentherapie-Nuklearmedizin
Munich
Germany
a.wuttge-hannig@gmx.de

Indra Yousry
Institute of Neurology
London
UK

Tarek A. Yousry
Institute of Neurology
London
UK
t.yousry@ion.ucl.ac.uk

Johannes Zacherl
Medical University of Vienna, Medical Media Services,
Department of Radiology
Vienna
Austria

Johannes Zenk
Department of Head and Neck Surgery
University Erlangen-Nürnberg
Erlangen
Germany

Marc Zins
Department of Radiology Fondation Hôpital Saint-Joseph
Paris,
France
mzins@hopital-saint-joseph.org

ABBI and Site-Select Devices, Breast

R. Schulz-Wendtland, K. Anders, W. Bautz
University of Erlangen-Nürnberg, Institute of Radiology, Gynaecological Radiology, Erlangen
ruediger.schulz-wendtland@idr.imed.uni-erlangen.de

Indications

An advanced breast biopsy instrumentation (ABBI)/site-select system may be used for stereotactically aimed biopsy in lesions smaller than 5 mm to avoid or to reduce sampling errors in the following settings:

- Histological assessment of suspicious lesions seen at mammography only (BI-RADS IV);
- Presurgical confirmation of malignancy in suspicious lesions seen at mammography only (RADS V);
- Histological assessment in the differential diagnosis of mastopathic changes versus ductal carcinoma *in situ* (DCIS) (suspicious calcifications; BI-RADS IV/V).

Contraindications

Severe coagulopathy as well as allergic reactions to local anesthetics constitute absolute contraindications to using the ABBI/site-select system.

Technology

Both the ABBI (advanced breast biopsy instrumentation; Firma Lorad) and the site-select system (Firma Ethicon Endo-Surgery, Breast Care) support digital stereotactic excisional biopsy. Computerized digital mammography (10 line pairs/mm, monitor matrix of 1024×1024 pixel) is used to guide stereotactic excision with oscillating knives to perform en-bloc resection of mammographic lesions (BI-RADS IV/V) with patients in prone position (biopsy tables provided by Lorad and Fischer).

For stereotactic excision, the patient's breast is positioned in a table opening, thereby being accessible from under the table. Following disinfection of the biopsy area, the stereotactic equipment is calibrated and the target area for the subsequent intervention and stereo views (±15°) is determined by means of orthogonal mammography. The breast tissue is fixed by the compression pads, and color marks are used to display positioning as well as localization and biopsy route on the patient's skin.

As a matter of principle, oncological as well as surgical considerations—transection route in planned subsequent segmental resection—should be taken into account in suspicious lesions (BI-RADS IV/V).

Biopsy is performed following local anesthesia and cutaneous incision. Biopsy needles can be chosen according to the size of the target lesion (diameter 5/10/15 or 20 mm). If the 20-mm rotational-scalpel cannula is used, conventional surgical hemostasis has to be applied, whereas when using smaller biopsy needles, local compression for about 30 min is sufficient.

The biopsy is performed after digital stereotactic localization of the equivocal lesion (BI-RADS IV/V) and placement of a t-lock needle. After additional infiltration with local anesthetics and enlargement of the stab incision, the biopsy cannula is slowly pushed forward according to the depth of the lesion. The oscillating knife is advanced 15 mm beyond the calculated location of the target, and subsequently the entire lesion is excised. With the help of an electrocoagulation wire, the tissue bloc is displaced *in situ*. Digital reevaluation views are used to document complete excision, and a Mikromark clip (Biopsis Medical) is placed in the resulting cavity to mark the biopsy area for follow-up studies. The biopsy material is thereafter marked with thread to facilitate the surgeon's and pathologist's orientations. For monitoring reasons, an X-ray of the biopsy tissue is also made (Fig. 1a–d).

The tissue is deep-frozen and then paraffin-cut microscopic work-up is performed (time needed: approximately 24 h) according to the "European Guidelines for Quality Assurance." Further proceedings are determined depending on the histological findings and the concordance or discrepancy between imaging findings and histology.

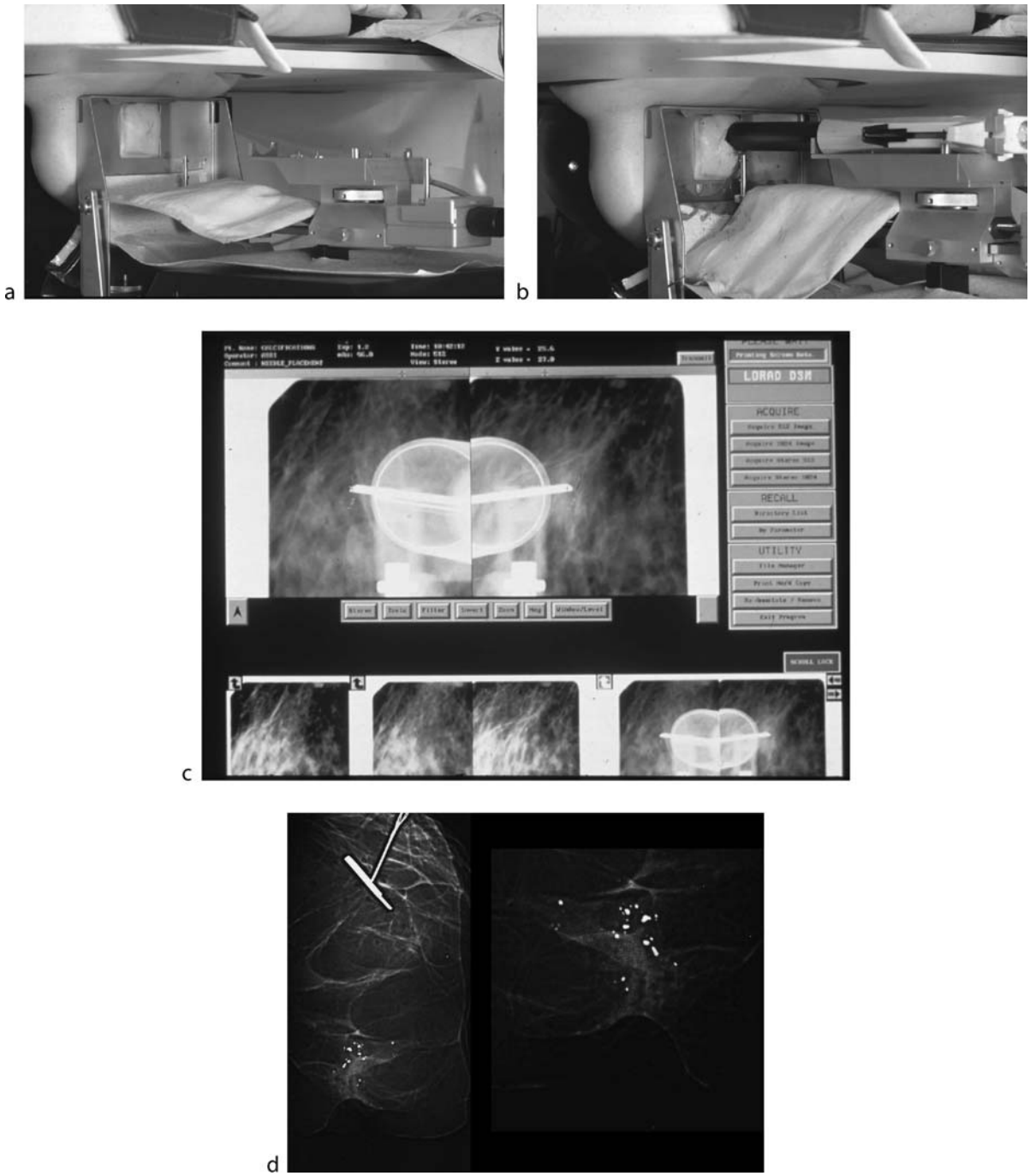

ABBI and Site-Select Devices, Breast. Figure 1 (a) Positioning and compression of the patient's breast in a table opening before digital stereotactic localization and excision biopsy. (b) After digital stereotactic localization, desinfection of the biopsy area, local anesthesia and cutaneous incision, the 20 mm cannula is placed. (c) Whole stereotactic/radiological procedure: Scout view, stereotactic localization (+/− 15 degree), placing of the 20 mm cannula at the microcalcifications and the t-lock needle. (d) Preparation radiogram with t-lock needle of the lesion of Fig. 1c: High grade DCIS.

As soon as the biopsy procedure is finished, the patient is put in supine position for thorough hemostasis using electrocoagulation and compression. The cutaneous defect is sutured with absorbable thread. In addition, to avoid secondary bleeding and hematoma, a compression bandage is provided.

In benign findings, follow-up mammography should be performed 6 and 12 months after biopsy; in case of progression of suspicious findings, surgical clarification is mandatory.

Results

The sensitivity and specificity as quoted in the current literature approach or even reach 100%.

Adverse Events

Minor pain, hemorrhage, or vasovagal reactions may occur.

- Pain may be minimized by profound local anesthesia; since the breast parenchyma itself is obviously less algesic than skin, thorough dermal anesthesia in particular should be of concern.
- Stab incisions usually entail minor bleeding; to avoid larger hematoma, broad compression is applied (30-min manual compression, compression bandage).
- Vasovagal reactions seem to occur more frequently if mammographic intervention is performed in seated rather than recumbent patients. Individual support and suitable premises may help to prevent these reactions.

Outlook

Stereotactic biopsy is approved and established for diagnostic purposes only. In the future, questions will arise about whether small carcinoma (<10 mm) or DCIS (<5 mm) may be treated by stereotactic excision with a biopsy cannula of up to 3 cm in diameter—hand in hand with the abandonment of axillary lymph node dissection in favor of sentinel node biopsy and mandatory postinterventional radiation in all cases of invasive cancer.

Prospective multicenter trials aimed at answering these questions are currently being planned.

Bibliography

1. American College of Radiology (ACR) (2004) (Hrsg) Breast Imaging—Reporting and Data System (BI-RADS™). Reston, Philadelphia
2. Duda VF, Schulz-Wendtland R (2004) (Hrsg) Mammadiagnostik. Springer-Verlag, Berlin, Heidelberg, New York
3. Fischer U (2003) (Hrsg) Mammographiebefund nach BI-RADS. Thieme-Verlag, Stuttgart
4. Heywang-Köbrunner SH, Schreer J (2003) (Hrsg) Bildgebende Mammadiagnostik. Thieme-Verlag, Stuttgart
5. Lanyi M (2003) (Hrsg) Brustkrankheiten im Mammogramm. Springer-Verlag, Berlin, Heidelberg, New York
6. Parker SH, Jobe WE (1993) (Hrsg) Percutaneous Breast Biopsy. Raven Press, New York
7. Sickles EA (2001) (Hrsg) Breast Imaging. Lippincott Williams & Wilkins, Baltimore
8. Tabar L, Tot T, Dean PB (2003) (Hrsg) Breast Cancer. Thieme-Verlag, Stuttgart

Abdominal Cramps

▶Acute Abdomen, Genital Causes

Abdominal Injury

▶Trauma Hepatobiliary

Abdominal Trauma

▶Trauma Hepatobiliary

Abdominal Wall Defects

▶Hernia, Abdominal and Inguinal

Aberrations of Normal Development and Involution (ANDI)

▶Fibrocystic Disease, Breast

ABPA

►Allergic Bronchopulmonary Aspergillosis

Abscess

Abscess is an accumulation of purulent material in tissues, organs or circumscribed spaces, often associated with signs of infection. Aseptic abscesses do occur.
►Oral Cavity, Inflammatory Diseases
►Pulmonary Infections

Abscess, Gallbladder

Purulent process involving the gallbladder walls and surrounding soft tissues occurring in the case of a perforating complication of ►acute cholecystitis. US features include an anechoic mass in the gallbladder wall, while significant changes in the surrounding tissue such as pericholecystic fluid collection and infiltration of the omentum or mesentery are well depicted by CT.
►Cholecystitis

Abscess, Hepatic

Davide Caramella, Chiara Franchini, Paola Vagli
Department of Diagnostic and Interventional Radiology, University of Pisa, Italy
caramella@do.med.unipi.it

Synonyms

Intrahepatic suppuration

Definition

Localized intrahepatic collection of pus due to infection.

Pathology and Histopathology

Hepatic abscesses can be classified on the basis of their etiology into ►pyogenic, ►amebic, and ►fungal abscesses.

Pyogenic Abscess

Pyogenic abscesses of the liver are relatively uncommon. The infectious agents can reach the hepatic parenchyma via different ways of diffusion. Ascending cholangitis and portal diffusion are the most frequent causes of pyogenic hepatic abscesses (1). Ascending cholangitis and subsequent abscess formation is due to extrahepatic biliary obstruction usually caused by choledocholithiasis, benign and malignant tumors, or postsurgical strictures. Biliary-enteric anastomoses (choledochoduodenostomy) are also associated with a high incidence of liver abscesses. In cases of portal diffusion, the infectious process originates in the abdomen and reaches the liver through the portal vein. Pylephlebitis and appendicitis are the most frequent causes. Other causes include diverticulitis and inflammatory diseases of the bowel. Abscesses derived from portal diffusion are usually single and more often localized in the right lobe, while those related to biliary mechanisms are typically multiple and localized in both lobes. More rarely, pyogenic abscesses may derive from arterial diffusion, in cases of systemic septicemia (e.g., bacterial endocarditis), or following intra-arterial procedures (e.g., intra-arterial therapies for hepatic tumors). Other possible ways of diffusion are the direct extension from adjacent organs (e.g., perforated ulcer, subphrenic abscess) and traumatic penetrating lesions, including iatrogenic lesions due to surgical interventions of the abdomen or percutaneous procedures (e.g., liver biopsy or percutaneous treatments for hepatic tumors). In a large number of patients the origin of the liver abscess remains unknown. However, the incidence is increased in patients with diabetes or metastatic cancer.

Most abscesses contain more than one organism and frequently are of biliary or enteric origin. Pyogenic abscesses are most commonly caused by *Clostridium* species and gram-negative bacteria, such as *Escherichia coli* and *Bacteroides* species.

At gross examination, pyogenic abscesses appear as solitary or multiple lesions ranging from a few millimeters to several centimeters in diameter. At histopathologic analysis, the abscess cavity is filled with purulent material, while the edges are composed of a chronic inflammatory infiltrate and fibrous tissue. The fibrotic edge is often 1 cm or more thick. Depending on the stage, suppuration, liquefaction with presence of debris, and fibrosis are found at microscopic analysis (2).

Amebic Abscess

Amebic abscess is the most common type of hepatic abscess worldwide and is endemic in many developing countries. It is the most frequent extraintestinal manifestation of *Entamoeba histolytica* infection. *Entamoeba histolytica* is a protozoan which exists in two forms: the cyst stage is the infective form, while the trophozoite stage causes invasive disease. Chronic carriers release cysts in their feces; these cysts are transmitted primarily by food and water contamination. The cyst's wall is broken as it passes through the small intestine; trophozoites are released and colonize the colonic mucosa. The protozoan may invade mesenteric venules and ascend the portal-venous system, thus reaching the liver.

The right hepatic lobe is more often affected than the left lobe.

The incidence of amebic liver abscess in patients with amebic colitis is about 4%. There is a significant male preponderance.

Histologic features of amebic liver abscesses include inflammatory reaction at the margins. The abscesses sometimes contain a chocolate-colored material, due to hemorrhage. Secondary bacterial infection may occur (2).

Fungal Abscess

Fungal abscesses are most often caused by *Candida albicans*, and they occur in immunocompromised individuals. They are a manifestation of disseminated fungal disease. Microabscesses often also involve the spleen and, occasionally, the kidney. Hepatic abscesses caused by *Cryptococcus* infection and *Aspergillus* species have also been reported. The typical histologic pattern of hepatic candidiasis is characterized by microabscesses, with fungi in the center of the lesion and a surrounding area of necrosis and polymorphonuclear infiltrate; in the healing stage there is a fibrotic evolution of the lesions (2).

Clinical Presentation

Clinical manifestations are related to the presence of sepsis and of space-occupying lesions in the liver (1).

Fever is the most common sign in patients with hepatic abscess and is usually associated with chills. Pain is a very common complaint and is most frequently located in the right upper quadrant. It may be associated with pleural pain and may radiate to the right shoulder or scapular area.

Anorexia, nausea, vomiting, weight loss, and mental confusion are also common symptoms. The most important finding at physical examination is right upper quadrant tenderness. Hepatomegaly, palpable liver mass, and jaundice are also common. Furthermore, diarrhea may be present in these patients at the time of diagnosis or within the previous few months, sometimes with bloody feces.

Occasionally, patients may present with pleural effusion, friction rub, or pulmonary consolidation. These manifestations are a sign of secondary pulmonary involvement by abscess rupture in the pleural cavity.

Signs of peritoneal irritation are present when the abscess ruptures in the peritoneum.

Pericardial friction rub can be audible when the abscess extends into the pericardium. This sign is associated with very high mortality.

Imaging

Pyogenic Abscess

Computed tomography (CT) and ultrasound (US) have a high sensitivity in detecting pyogenic abscesses.

A pyogenic abscess usually appears as a large focal lesion which can demonstrate a wide range of US and CT appearances, according to the stage of the infectious process.

At US, early-stage pyogenic abscesses usually present as round or oval lesions with a hypoechoic structure and ill-defined borders. Acute abscesses frequently appear as a cluster of small coalescent hypoechoic lesions. In the colliquative phase, the abscess becomes fluid: US shows a lesion containing a variable quantity of hyperechoic spots, corresponding to necrotic debris; the appearance may vary from anechoic to hyperechoic, depending on the degree of internal echoes. Increased posterior acoustic transmission and lateral acoustic shadows may be present. The demonstration of gas, when present, is indicative of infection by gas-producing agents. At US, gas causes hyperechoic linear echoes with reverberation artifacts. In the resolution phase, the lesion shows a progressive reduction in size and becomes hypo-hyperechoic (2, 3).

At CT, the demonstration of the "cluster sign" in the acute phase of abscess formation is suggestive of pyogenic abscess. This sign consists in the presence of a group of coalescent small hypodense lesions. In the subacute or colliquative phase, the pyogenic abscess appears as an irregular round or oval, hypodense area with well-defined margins; the density values are usually higher than those of simple cysts. Abscesses may be unilocular or have a complex structure with internal septa.

The presence of gas within the lesion, either air microbubbles or air-fluid levels, is easily recognizable at CT and represents a specific sign of pyogenic abscess (4) (Fig. 1).

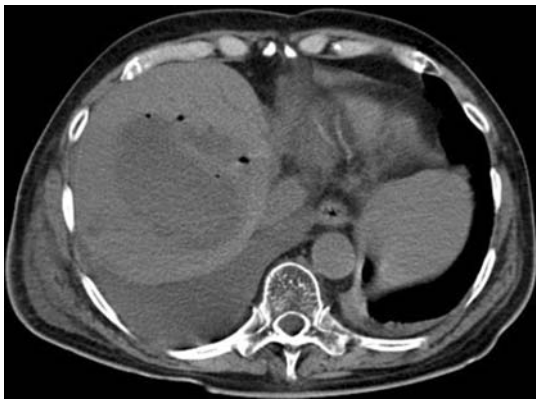

Abscess, Hepatic. Figure 1 Pyogenic hepatic abscess—Unenhanced CT. Unenhanced CT scan shows a large hypodense area involving hepatic parenchyma with gas–fluid levels. Right pleural effusion coexists.

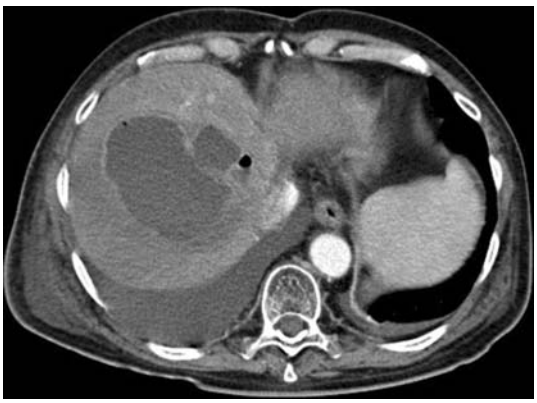

Abscess, Hepatic. Figure 2 Pyogenic hepatic abscess—Arterial phase. In the arterial phase a peripheral rim of enhancement is noted, while the central necrotic area fails to enhance.

Typically the lesion has a thick, irregular wall and presents a characteristic rim enhancement, while the central necrotic portion remains unenhanced (Fig. 2). A CT finding suggestive of abscess is the "double target" sign; it represents a hypodense lesion surrounded by an enhancing rim, corresponding to the wall, and an outer hypodense halo, due to perilesional edema (Fig. 3).

At magnetic resonance imaging (MR), pyogenic abscesses appear as areas of decreased signal intensity on T1-weighted images and increased signal intensity on T2-weighted images. Perilesional edema, characterized by subtly increased signal intensity, can be seen on

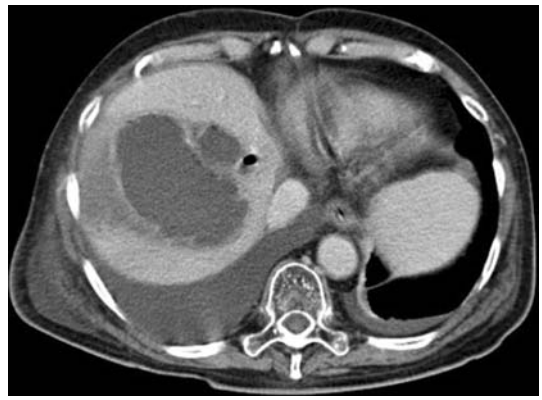

Abscess, Hepatic. Figure 3 Pyogenic hepatic abscess. In the portal-venous phase the rim enhancement is still present and a peripheral hypodense halo, corresponding to perilesional edema, is better appreciable.

T2-weighted images. The abscess cavity may have homogeneous or inhomogeneous signal intensity. After contrast material administration, the lesion shows marked peripheral enhancement.

Miliary pyogenic microabscesses are usually found in patients with generalized septicemia and may appear as multiple lesions scattered throughout the liver or as a cluster of small lesions which tend to coalesce. This coalescent, clustered pattern is suggestive of pyogenic infection and is thought to represent an early stage of the formation of a pyogenic macroabscess. At US, pyogenic microabscesses may be visualized as multiple, small (<2 cm) hypoechoic lesions with a miliary distribution. Such lesions may have a clear nodular aspect or appear as ill-defined areas. At CT, pyogenic microabscesses are better visualized after contrast material administration, appearing as multiple small, hypodense lesions. A slight rim enhancement and perilesional edema may sometimes be observed (2).

In a large number of patients abnormal findings are demonstrated at chest radiography. These findings are aspecific and may include elevated right hemidiaphragm, subdiaphragmatic air-fluid level, pleural effusion, and consolidation.

Amebic Abscess

Both US and CT are sensitive in the detection of amebic abscesses. At US, an amebic abscess usually appears as a large, well-defined, hypoechoic lesion, and contains low-level internal echoes. There are no significant wall echoes. The lesion is typically oval or round and is located near the liver capsule.

At CT, amebic abscesses do not show a specific and constant appearance. They usually appear as round or oval well-defined lesions with water-like attenuation values. The demonstration of a wall and a peripheral edema surrounding the abscess is a common finding. The wall may be hyperdense on unenhanced scans and always shows enhancement after administration of contrast material. The central abscess cavity may show multiple septa or fluid-debris levels and nodularity at the margins, while the presence of air bubbles and hemorrhage has been rarely reported (2, 3).

MR is a sensitive technique in detecting amebic abscesses, but the findings are not specific. Amebic abscesses have a homogeneous or inhomogeneous aspect with decreased signal intensity on T1-weighted images and increased signal intensity on T2-weighted images. Perilesional edema is often seen as a halo of even higher signal intensity on T2-weighted MR images. The central necrosis does not show any enhancement after contrast material administration, while the periphery strongly enhances, due to the presence of inflammatory tissue (4).

In cases of hepatic amebic abscess, extrahepatic extension is a relatively common event.

Chest or abdominal radiographs may show elevation of the right hemidiaphragm, subdiaphragmatic air-fluid level, pleural effusion, and consolidation.

Fungal Abscess

Hepatic fungal microabscesses in immunosuppressed patients have a miliary distribution and appear as multiple small, often subcentimetric, lesions scattered throughout the liver. They are usually associated with splenic involvement (2).

At US, four patterns of hepatosplenic candidiasis have been described. The US appearance of hepatic candidiasis in the initial phase is pathognomonic: the "wheel-within-a-wheel" sign consists in a central hypoechoic nidus of necrosis containing fungi surrounded by a hyperechoic zone represented by inflammatory cells, and an outer hypoechoic halo corresponding to fibrosis at pathologic analysis. The second pattern has a "bull's-eye" appearance, due to the presence of a central echogenic area surrounded by a hypoechoic rim. The third pattern is the most commonly encountered at US and consists of uniformly hypoechoic nodules; however, it is the least specific. After therapy the lesions tend to decrease in size and increase in echogenicity, leading to the fourth pattern, which consists of echogenic foci with variable degrees of posterior acoustic shadowing (2, 5).

At CT, fungal abscesses appear as multiple small, round lesions distributed in both lobes with low density both on unenhanced and enhanced scans, but better visualized after contrast material administration. Calcifications are often present. These microabscesses usually show central enhancement, although peripheral enhancement may occur (2, 4).

At MR, fungal abscesses show variable signal intensity. The untreated nodules are minimally hypointense on T1-weighted images before and after administration of contrast material and hyperintense on T2-weighted images. After treatment, lesions appear mildly hyperintense both on T1- and T2-weighted images and show contrast enhancement. A dark ring is usually seen around these lesions in all sequences (2).

Interventional Radiology

Pyogenic Abscess

The mortality rates of patients with pyogenic abscess and the need for surgery have been markedly reduced thanks to early diagnosis and imaging-guided percutaneous drainage. Usually, US is chosen to guide the positioning of the drainage, but CT may also be used (2). Diagnostic aspiration is usually followed by placement of a drainage catheter, which is removed when the abscess cavity collapses, as confirmed at imaging. Some authors reported percutaneous needle aspiration of pyogenic abscesses in association with antibiotic therapy as a valid alternative to prolonged catheter drainage (6).

Immunocompromised patients with multiple microabscesses are not candidates for either percutaneous or open surgical drainage and are best treated with high-dose antibiotics.

Amebic Abscess

Catheter drainage or percutaneous needle aspiration of amebic abscess is rarely necessary, because amebicidal therapy is generally highly effective (2).

Aspiration of an amebic abscess is indicated in case of high risk of imminent rupture (lesion greater than 5 cm) or if differentiation between amebic and pyogenic abscess is critical (no response to antibiotic therapy after few days). Aspiration may be performed under US or CT guidance.

Fungal Abscess

Imaging findings are not specific and are often overlapping with those of pyogenic and amebic abscesses, metastases, and lymphoma. Frequently, percutaneous needle biopsy is needed to achieve a definite diagnosis (4).

Diagnosis

Imaging alone cannot definitely differentiate a pyogenic from an amebic abscess or from malignant disease. The diagnosis derives from the combination of clinical, epidemiological, serological, and imaging data. In some cases, aspiration of abscess content may be required.

Clinical suspicion of a liver abscess mandates an investigation of the liver for evidence of a liver abscess by US or CT.

Serum antibodies to *Entamoeba* species are present in more than 90% of cases, but serologic findings may be negative in acute disease and may be positive if the patient had amebiasis in the past (2).

In patients with fungal microabscesses, imaging findings are not specific and percutaneous needle biopsy is often needed to achieve a definite diagnosis (4).

Bibliography

1. Mortele KJ, Ros PR (2001) Cystic focal liver lesions in the adult: differential CT and MR imaging features. Radiographics 21 (4):895–910
2. Mortele KJ, Segatto E, Ros PR (2004) The infected liver: radiologic-pathologic correlation. Radiographics 24(4):937–955
3. Ralls PW, Barnes PF, Radin DR et al (1987) Sonographic features of amebic and pyogenic liver abscesses: a blinded comparison. AJR Am J Roentgenol 149(3):499–501
4. Schneider G, Grazioli L, Saini S (2003) Imaging of benign focal liver lesions. In: Schneider G, Grazioli L, Saini S (eds) MRI of the liver, 105–170. Springer Verlag
5. Pastakia B, Shawker TH, Thaler M et al (1988) Hepatosplenic candidiasis: wheels within wheels. Radiology 166(2):417–421
6. Giorgio A, Tarantino L, Mariniello N et al (1995) Pyogenic liver abscesses: 13 years of experience in percutaneous needle aspiration with US guidance. Radiology 195(1):122–124

Abscess, Pancreatic

Pancreatic abscess is a circumscribed collection of pus, usually in proximity to the pancreas, containing little or no pancreatic necrosis, which arise as a consequence of acute pancreatitis or pancreatic trauma. Pancreatic abscesses occur later in the course of severe acute pancreatitis, often 4 weeks or more after onset. The distinction between pancreatic abscess and infected necrosis is critical because the mortality risk for infected necrosis is double than that for abscess. The presence of pus and positive culture for bacteria or fungi, but little or no pancreatic necrosis, differentiate a pancreatic abscess from infected necrosis.

▶Pancreatitis, Acute

Abscess, Prostate

Jurgen J. Fütterer
Department of Radiology, University Medical Centre Nijmegen, 6500HB Nijmegen, The Netherlands
j.futterer@rad.umcn.nl

Definition

Prostate abscess is a closed pocket containing pus within the prostate. It is an infrequent but well-described complication of (acute) prostatitis or it may occur independently.

Epidemiology

Prostatic abscess is uncommon and rarely diagnosed. There has been a great shift in its mortality rate and in the types of etiologic agents observed since the discovery and use of penicillin (1). The increased use of antibiotics and the falling incidence of urethral gonococcal infections, which were the most common infecting cause in the early reports of the disease (2), have also had an impact on the mortality rate. It is now diagnosed in only 0.2% of patients with urological symptoms and in 0.5–2.5% of patients hospitalized for prostatic symptoms.

Pathophysiology

The incidence of prostatic abscess is highest between the fifth and sixth decade of life and may be associated with benign prostatic hyperplasia, bladder neck obstruction, or urethral stricture. The etiology is hypothesized to be due to reflux of infected urine along prostatic ducts into the prostate. Gram-negative microorganisms, particularly *Escherichia coli* (3), cause more than 70% of cases of prostatic abscess.

Symptoms

The prostatic abscess is difficult to diagnose, because the symptoms at onset may mimic several diseases of the lower urinary tract. Presentation is similar to that of prostatitis. Prostatic abscess is an infrequent but well-described complication of acute bacterial prostatitis. It most often occurs in patients who are immunocompromised. Diabetes mellitus (4), prostatitis, and urethral instrumentation are predisposing factors for developing prostate abscess. A prostatic abscess should be suspected when a palpable fluctuant mass develops in the prostate.

Diagnostic Imaging Techniques of Prostate Abscess

Transrectal ultrasound—In prostate abscess the investigation of choice is transrectal ultrasonography (TRUS) (5). In abscesses in many cases an irregularly shaped area of hypoechogenic masses, with or without internal echoes, is found.

Computed tomography—With computed tomography (CT) (6), prostatic abscesses appear as a single or multilocular area of low attenuation (Fig. 1). Imaging studies, including ultrasonography and CT of the prostate, should only be performed in cases where laboratory analysis is equivocal or when no improvement is observed following medical therapy. Ruling out a prostatic abscess in patients with prostatitis is a strong indication to proceed to imaging studies. The primary imaging investigation of choice is TRUS of the prostate, which may be performed either by a urologist or radiologist, depending on the local availability of expertise.

Magnetic resonance imaging—On magnetic resonance (MR) imaging, prostatic abscess may appear as intermediate or high signal intensity on T2-weighted images (7). MR imaging should only be used for diagnosis in cases of potential bacteremic consequences, sometimes leading to septic shock, which may be encountered during a TRUS examination. Additionally, MR imaging has the ability to provide contrast enhancement without the potentially nephrotoxic effects of iodinated intravenous CT contrast material (8).

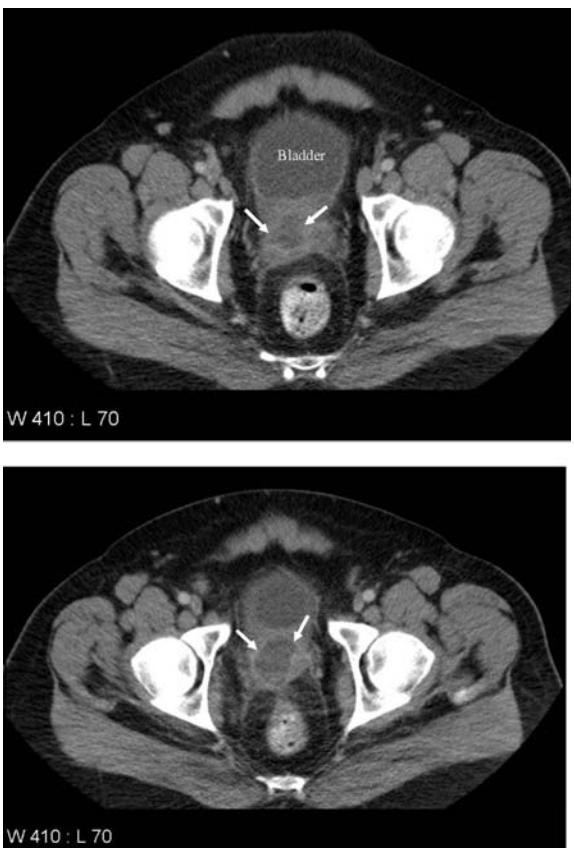

Abscess, Prostate. Figure 1 A contrast-enhanced CT scan of the pelvis shows abnormal enlargement of the prostate gland, multiloculated prostatic abscess (*arrows*) that involves the entire prostate. Additionally, there is a diffuse inflammatory stranding towards the rectum. (Images courtesy of Julia R. Fielding, MD,Associate Professor of Radiology, University of North Carolina at Chapel Hill, 101 Manning Drive, Chapel Hill, NC 27599).

Therapy

Antimicrobial treatment is the therapy of first choice in these patients (9). Medical management of prostate abscess is often not successful. Prostatic abscess is a potential indication for surgery. The treatment of choice is surgical intervention combined with the appropriate broad-spectrum antibiotic; however, the abscess may be drained transperineally under TRUS guidance. TRUS has an important value in diagnosis and treatment of prostatic abscess. TRUS-guided aspiration is an effective and minimally invasive treatment modality for prostatic abscess which causes no serious complications (10–12, 5). Transrectal or perineal aspiration of the abscess is preferred if symptoms do not improve after 1 week of medical therapy. Transurethral resection of the prostate and drainage of the cavity is another approach. However, this approach is less desirable because of the potential hematogenic spread of germs.

Bibliography

1. Weinberger M, Cytron S, Servadio C et al (1998) Prostatic abscess in the antibiotics era. Rev Infect Dis 10:239–249
2. Youngen R, Mahoney SA, Persky L (1967) Prostatic abscess. Surg Gynecol Obstet, vol 124, pp 1043
3. Roberts RO, Lieber NM, Bostwick DG et al (1997) A review of clinical and pathological prostatitis syndromes. Urology 49:809–821
4. Jacobsen JD, Kvist E (1993) Prostatic abscess: a review of literature and a presentation of 5 cases. Scand J Urol Nephrol 27:281–284
5. Barozzi L, Pavlica P, Menchi I et al (1998) Prostatic abscess: diagnosis and treatment. Am J Roentgenol, Mar 170:753–757
6. Davidson KC, Garlow WB, Brewer J (1986) Computerized tomography of prostatic and periurethral abscess: 2 case reports. J Urol 135:1257–1258
7. Papanicolaou N, Pfister RC, Stafford SA et al (1987) Prostatic abscess: Imaging with transrectal sonography and MR. Am J Roentgenol 149:981–982
8. Rich MW, Crecelius CA (1990) Incidence, risk factors, and clinical course of acute renal insufficiency after cardiac catheterization in patients 70 years of age or older. A prospective study. Arch Intern Med 150:1237–1242

9. Fowler JE Jr (2003) Antimicrobial therapy of prostatitis. Exper Rev Anti Infect Ther 1:275–282
10. Gogus C, Ozden E, Karaboga R, Yagci C (2004) The value of transrectal ultrasound guided needle aspiration in treatment of prostatic abscess. Eur J Radiol 52:94–98
11. Lim JW, Ko YT, Lee DH et al (2000) Treatment of prostatic abscess: value of transrectal ultrasonographically guided needle aspiration. J Ultrasound Med, Sep 19:609–617
12. Weinberger M, Pitlik SD, Rabinovitz M et al (1985) Per-rectal ultrasonography for diagnosis of and guide to drainage prostatic abscess. Lancet 5:772

Abscess, Renal

O Hélénon, JM Correas
Radiology Department, Necker Hospital,
Paris, France
olivier.helenon@nck.aphp.fr

Synonyms

Focal acute pyelonephritis with abscess formation; Intrarenal abscess; Renal corticomedullary abscess; Suppurative fluid collection

Definition

Renal abscess is defined as a parenchymal fluid-filled mass of infectious origin containing suppurative material and delineated by a pseudocapsule.

Pathology—Histopathology

Abscess formation results from ascending lobar bacterial infection or hematogeneous spread of bacteria from extrarenal primary source of infection (skin, teeth, heart valve) especially in patients known to be immunocompromised or in patients known to abuse IV drugs. At an early stage, before frank abscess formation, severe acute focal nephritis causes interstitial inflammation with polymorphonuclear leukocytes infiltration, tubule obstruction and vasoconstriction that lead to focal ischemia and liquefaction. Frank abscess formation is responsible for a cortiomedullary or cortical mass filled with fluid pus and delineated by a pseudocapsule due to compressed inflammatory neighboring renal parenchyma. Hematogeneous abscesses have no lobar distribution but are typically multiple and peripherally located within the renal cortex. The infectious process can extend to renal capsule and perinephric space that can lead to perinephric abscess formation.

Clinical Presentation

Acute abscess formation produces symptoms including fever, flank or abdominal pain and urinary tract symptoms. Associated nausea and vomiting also can be observed. Physical examination and laboratory data provide no specific characteristics different from signs of acute urinary infection. Predisposing factors are common such as a history of recurrent urinary infection, urinary tract obstruction, renal calculi or prior urinary tract instrumentation.

Imaging

Intravenous Urography

Intravenous Urography (IVU) is of poor value in the diagnosis of renal abscess. It can however demonstrate features of severe acute pyelonephritis including kidney enlargement, decrease contrast material opacity in the collecting system associated with focal areas of decreased nephrographic opacity. Urologic abnormalities that can be responsible for ascending bacterial infection such as obstruction or urinary tract malformation also can be demonstrated.

Ultrasonography

Ultrasonography (US) is a useful first step modality for screening abscess formation in a patient with severe acute pyelonephritis. The presence of an ill-defined fluid-filled renal mass with internal echos is suggestive of abscess formation (1) (Fig. 1). Contrast-enhanced US can help detect small abscesses including abscesses resulting from hematogenous infection of small size, located within the cortex and multiple in distribution. Advantages of the technique are that it can be performed at bed side and it uses US contrast medium without nephrotoxicity. As a matter of fact, it appears to be particularly useful for the assessment of acute parenchymal infection in renal

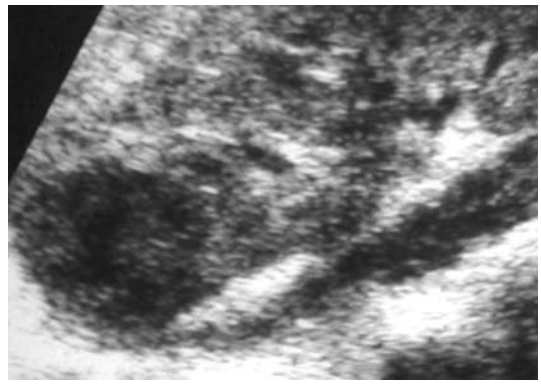

Abscess, Renal. Figure 1 Renal abscess. US shows a round-shaped hypoechoic mass of the upper pole of the right kidney.

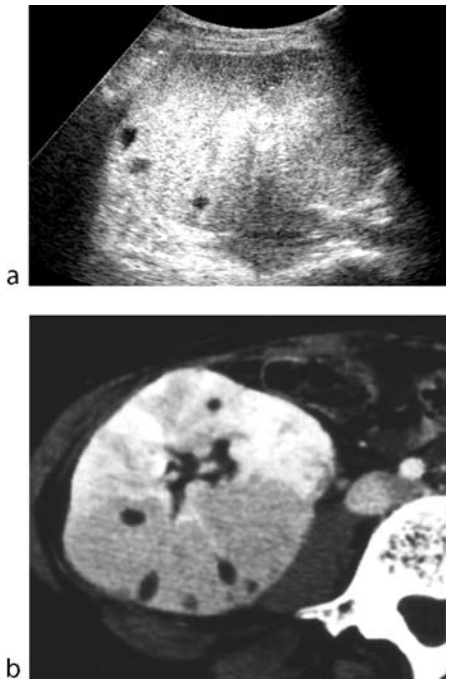

Abscess, Renal. Figure 2 Microabscess formation in a renal transplant with severe acute pyelonephritis. Post-contrast US (a) using non linear imaging sequence shows small round-shaped defects within the renal cortex related to early abscess formation. Contrast-enhanced CT (b) shows good correlation with typical acute focal pyelonephritis.

transplant which is usually associated with acute renal insufficiency (2) (Fig. 2).

Computed Tomography

Computed Tomography (CT) is the gold standard in diagnosing and evaluating renal and perinephric abscess formation. It typically shows a fluid-filled mass located within the parenchyma surrounded by an area of hypoattenuating cortex at nephrographic phase after contrast injection (Fig. 3). Such a so-called pseudocapsule results from inflammation of the renal parenchyma that precedes abscess formation. The presence of an ill-defined outer border help differentiate such periabscess pseudocapsule from the thick wall of complex cystic renal mass including infected cyst and calyceal diverticulum. Perinephric features of inflammation including fascial and septal thickening are usually associated to abscess formation. ►CT provides an accurate evaluation of the exact volume of the suppurative material and of its perinephric extent that can involve the subcapsular space, the perinephric fat and the neighboring muscles (1, 3, 4). Perinephric abscess formation also may result primarily

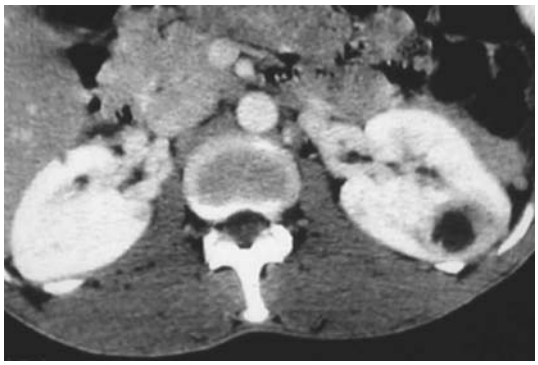

Abscess, Renal. Figure 3 Typical renal abscess of the left kidney. Contrast-enhanced CT (nephrographic phase) shows a fluid filled mass with a pseudocapsule.

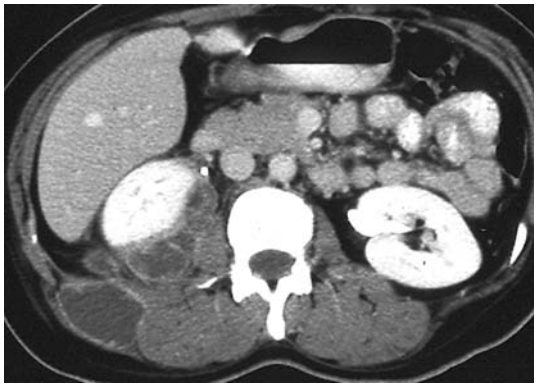

Abscess, Renal. Figure 4 Perinephric abscess. Contrast-enhanced CT shows abscess formation involving the perinephric space with extension to the posterior wall.

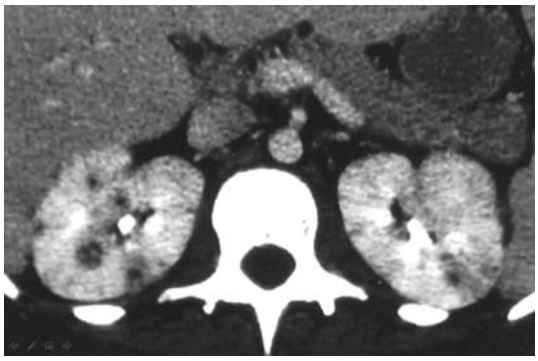

Abscess, Renal. Figure 5 Multiple renal microabscesses in a patient with drug abuse. Post-contrast CT shows multiple hypoattenuating round-shaped lesions within the renal cortex of both kidneys.

from hematogeneous infectious spread. The diagnosis relies on the demonstration of a fluid field perinephric mass with a thick wall that enhances after contrast injection (Fig. 4).

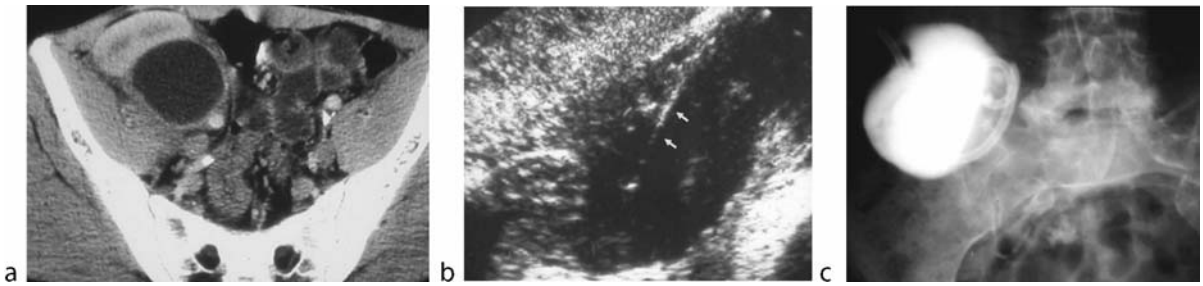

Abscess, Renal. Figure 6 Percutaneous drainage of a perinephric abscess after renal transplantation. (a) Contrast-enhanced CT. (b) Needle puncture (*arrows*) under US guidance. (c) Opacification of the abscess cavity after catheter placement.

Multiple and bilateral small rounded hypoattenuating cortical lesions suggest cortical abscesses of hematogeneous origin (Fig. 5).

Follow-up CT is needed to ensure resolution of the infectious process under treatment (antibiotics alone or associated with drainage). It can show total regression or scarring of the renal cortex (5, 6).

Magnetic Resonance Imaging

Magnetic Resonance Imaging (MRI) plays no role in the diagnosis and evaluation of renal abscesses. It may however provide similar information compared to CT. Therefore, it is a useful substitute in cases of contraindication to CT especially in renal transplant with renal insufficiency.

Nuclear Medicine

While renal scintigraphy (Tc-99m DMSA) is sensitive in detecting focal loss of tracer uptake that may correspond to focal liquefaction of the infected parenchyma, it does not distinguish between frank abscess and focal acute pyelonephritis.

Diagnosis

In most cases the diagnosis relies on CT in a patient with clinical findings suggestive of severe acute renal infection. CT is indicated at initial screening or after a first step US evaluation that usually shows suggestive findings. In cases of suspected hematogeneous renal or perinephric infection contrast-enhanced CT should be performed as a first step diagnostic modality since US is of poor sensitivity in the detection of small cortical abscesses and in the evaluation of perinephric abscess formation. Contrast-enhanced US or MRI using nonnephrotoxic contrast media should be performed in patients with renal insufficiency.

Percutaneous Drainage

Large renal or perinephric abscesses usually require precutaneous drainage in addition to medical therapy. Diagnostic aspiration or percutaneous drainage also should be considered in abscesses of smaller size with absence of clinical improvement after several days of antimicrobial therapy. Both procedures benefit from US or CT guidance (6, 7) (Fig. 6). Initial puncture of the abscess cavity using an 18-gauge needle is usually performed before drainage tube placement. The drainage catheter should be left until the patient recovers and becomes stable with minimal output from the drain. Follow-up CT also should demonstrate no residual suppurative material before catheter ablation.

Bibliography

1. Hoddick W, Jeffrey RB, Goldberg HI et al (1983) CT and sonography of severe renal and perirenal infections. Am J Roentgenol 140:517–520
2. Correas JM, Duval A, Morelon E et al (in press) Diagnosis of acute pyelonephritis in renal transplants using contrast-enhanced sonography: a quantitative approach. Ultrasound Med Biol
3. Lowe LH, Zagoria RJ, Baumgartner BR et al (1994) Role of imaging and intervention in complex infections of the urinary tract (1994). Am J Roentgenol 163:363–367
4. Soulen MC, Fishman EK, Goldman SM et al (1989) Bacterial renal infection: role of CT. Radiology 171:703–707
5. Dalla Palma L, Pozzi-Mucelli F, Ene V (1999) Medical treatment of renal and perirenal abscesses: CT evaluation. Clin Radiol 54:792–797
6. Hélénon O, Cornud F, Di Stefano D et al (1989) Percutaneous treatment of abscess of the kidney and retroperitoneum. J Radiol 70:541–548
7. Lang EK (1990) Renal, perirenal, and pararenal abscesses: percutaneous drainage. Radiology 174:109–113

Abscess Tubo-Ovarian

Forstner Rosemarie
Department of Radiology
Paracelsus Private Medical University
Salzburger Landeskliniken
Salzburg, Austria
r.forstner@salk.at

Synonyms

Inflammatory mass of ovaries and fallopian tubes

Definition

The vast majority of ▶tubo-ovarian abscesses (TOA) develop as a complication of ▶pelvic inflammatory disease (PID). They are reported to occur in a frequency of up to 1/3 of patients hospitalized for PID (1). TOA are typically encountered in women of reproductive age and result from longstanding or nonadequately treated ascending urogenital infection. Secondary TOA may arise by direct or lymphatic spread of infection after pelvic surgery, or as a complication of enteric inflammatory diseases, such as appendicitis, diverticulitis, and Crohn's disease, or rarely as complication of pelvic malignancy (1). TOA may manifest as a frank pelvic abscess formation or an inflammatory mass involving fallopian tubes and ovaries (2).

Pathology/Histopathology

A unilateral or bilateral abscess located in the adnexal region associated with ▶pyosalpinx is the hallmark at macroscopy. Extension of the abscess into the cul-de-sac is a common finding. The size of TOA varies between 5 and 10 cm in the majority of cases (3). The ovary may adhere to the pyosalpinx and become the lateral wall of the abscess (2). Intense surrounding inflammatory reaction of pelvic fat and parietal peritoneum results in adhesions of adjacent organs, particularly the uterus and large and small bowel loops. In hematogenously spread abscesses the external surface of the enlarged ovaries may be normal; the necrotic contents are demonstrated only within the ovary (2). Rarely, a chronic abscess may result in a solid tumor like mass, also defined as xanthogranulomatous oophoritis (2). Most TOA result from a mixed polymicrobial infection with a predominance of anaerobes (1). The cultures reveal typically *Neisseria gonorrhea*, *Chlamydia trachomatis*, *E. coli*, *Bacteroides fragilis*, and *Streptococcal* species (1). Unusual causes of TOA include pseudomonas, tuberculosis, and actinomycosis. The latter tends to form solid granulomatous adnexal lesions, and is associated with intrauterine device insertion (4). Leakage of a TOA leads to peritonitis or may produce metastatic abscesses.

Clinical Presentation

Clinical features of TOA are often nonspecific and do not differ from those of PID (1). Abdominal and often bilateral pelvic pain is the leading clinical manifestation, and is found in more than 90% of patients with TOA (1). Fever, leucocytosis, elevated c-reactive protein, vaginal discharge and bleeding, and urinary symptoms are less common findings. CA-125 levels may also be elevated (1). The majority of TOA develops in women between 20 and 40 years of age. In children TOA usually occur as a complication of appendicitis. TOA in postmenopausal women are rare, and tend to be associated with diabetes and increased morbidity and mortality.

Imaging

Conventional radiographs are not suited to diagnose TOA. However, they are useful to demonstrate obstructive complications, e.g., ileus. Combination of transabdominal and endovaginal Sonography is the first line imaging tool to assess PID. In approximately 25–33% of these patients findings of TOA are encountered (1). Normal fallopian tubes measure less than 4 mm in diameter. In case of pyosalpinx they become tortuous, dilated tubular structures with mural thickening (5). Due to infection they may contain internal echoes presenting pus or blood (5). Tubal wall thickening is nonspecific for pyosalpinx. It may also be associated with chronic interstitial salpingitis, endometriosis, ectopic pregnancy, and fallopian tube cancer. Other sonographic findings of TOA include a mass in the ovarian fossa or cul-de-sac, which varies depending on the consistency as homogenous hypoechogenic or more commonly as a mass of mixed echogenicity (3) (Fig. 1a). Irregular wall thickening, septations, fluid-debris levels are other findings encountered in abscesses. Color Doppler reveals hyperemia of the fallopian tube, ovary, and of adnexal fat (3). In many cases, however, ultrasonographic findings of TOA are not specific (3).

CT and MRI serve as noninvasive second line diagnostic modalities to assess TOA (Fig. 1b). They are usually performed complementary to sonography to (a) confirm the diagnosis of a TOA, (b) assess complications of TOA, and (c) for percutaneous abscess treatment.

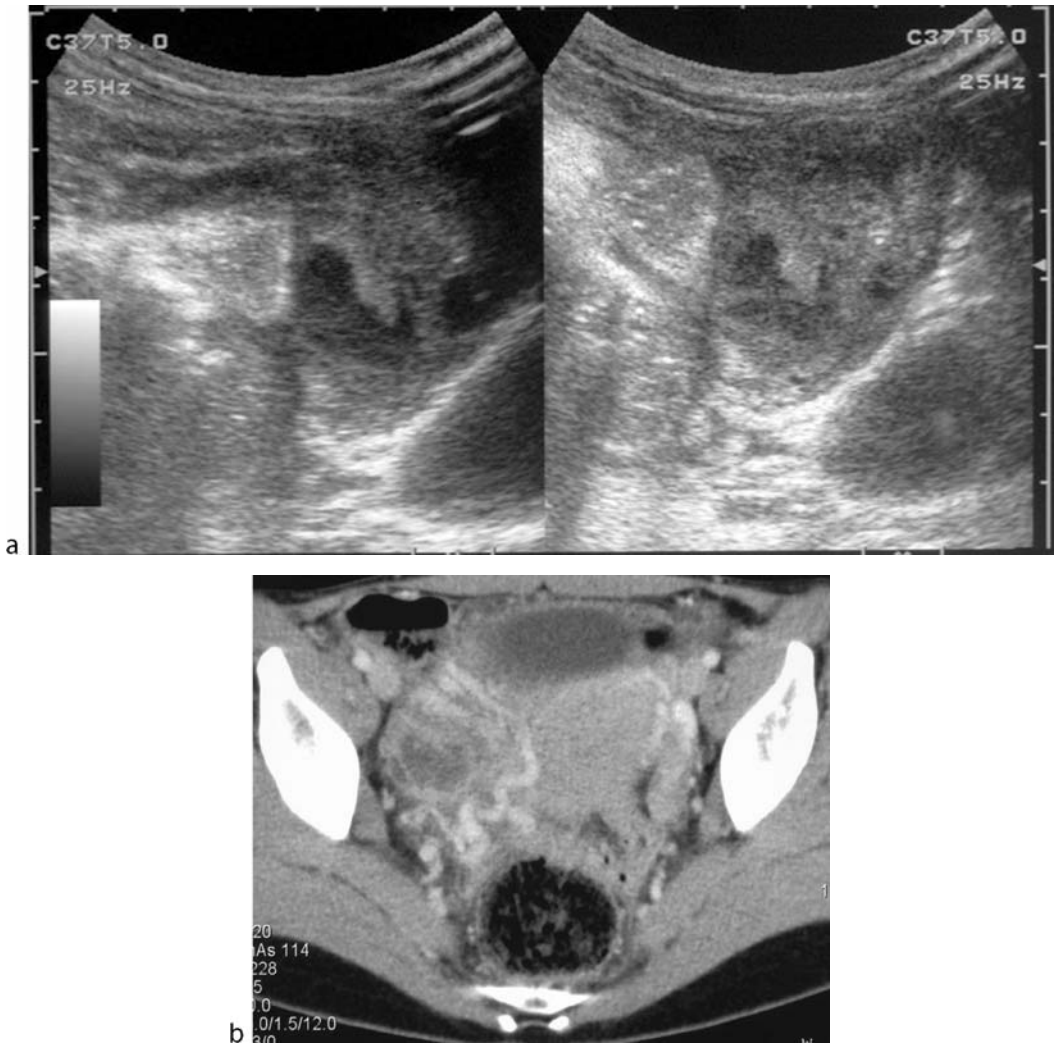

Abscess Tubo-Ovarian. Figure 1 TOA in sonography (a) and CT (b). Transabdominal sonography in two planes (a) shows enlargement of the right ovary with inhomogenous morphology of irregular cystic and solid areas. Contrast enhanced CT (b) reveals a right adnexal mass with peripheral rim enhancement, central liquid areas, and ill-defined margins. Obscured pelvic fat planes and engorgement of parametrial vessels support the diagnosis of an inflammatory mass. Courtesy of Dr R Kubik-Huch, Baden.

In secondary TOA they may contribute in establishing the source of the abscess. In TOA in postmenopausal further imaging is necessary due to their high association with underlying genitourinary pathologies.

Oral bowel opacification in CT facilitates differentiation of distended paralytic or obstructed small bowel loops, which are adherent to the adnexal region from fluid collections within an abscess. Rectal enema may also contribute to better assess rectosigmoid wall thickening, particularly, in secondary TOA e.g., in diverticulitis (Fig. 2).

MRI is best suited to identify pyosalpinx, especially in complex adnexal masses. Multiplanar imaging allows best demonstration of the anatomical details. The dilated fallopian tube is usually best identified on sagittal and oblique axial images. Similar to IV CT contrast media aids in lesion characterization and in assessing complications, e.g., peritonitis and distant abscesses.

Fluid is found in almost 50% of cases of TOA and small amounts can be better appreciated on MRI (4).

Nuclear Medicine

Nuclear medicine usually does not contribute in the diagnosis of TOA.

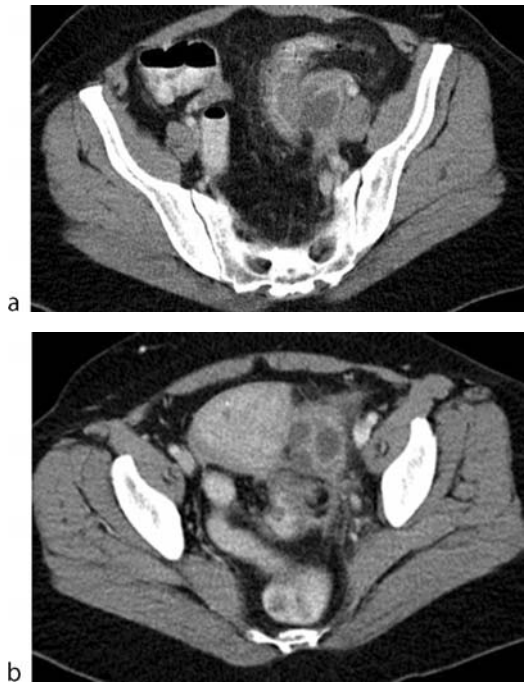

Abscess Tubo-Ovarian. Figure 2 TOA in a 55-year-old female. Transaxial CT scans (a and b) demonstrate ovarian involvement in sigmoid diverticulitis. The left ovary is attached to the sigmoid colon. It is enlarged and shows multiple cystic lesions with mural enhancement. Surrounding stranding and small amounts of ascites are associate findings.

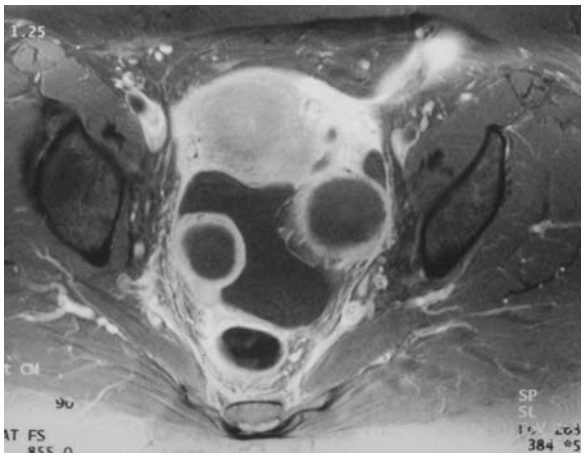

Abscess Tubo-Ovarian. Figure 3 Bilateral TOA in MRI. Transaxial contrast enhanced MRI shows bilateral cystic adnexal masses and ascites. Extensive peritoneal enhancement is demonstrated along the uterus, parametria, left round ligament, uterosacral ligaments, and the mesorectum. Such extensive homogenous contrast enhancement along pelvic ligaments is a finding suggestive of inflammation. Courtesy of Dr A Heuck, Munich.

Diagnosis

The diagnosis of TOA is based upon the clinical presentation and imaging findings on sonography. History of PID is a major risk factor, although up to 20% of cases that progress to TOA have normal leukocyte counts and are afebrile (4). As the majority of TOA is encountered in the same age as ectopic pregnancy, a negative pregnancy test is mandatory before further imaging.

The role of CT and MRI includes establishing the diagnosis and associated complications of TOA, and assessment of underlying disease that may implicate invasive therapy.

Findings in CT and MRI include uni- or bilateral complex adnexal masses with ill-defined margins. In contrast to tumorous adnexal lesions pelvic fat planes are typically obscured (4, 5) (Figs 1b and 3). Adhesions of the uterus, distended or thickened bowel loops, and hydronephrosis may be associated findings. Without the appropriate clinical background, the differential diagnosis from other adnexal pelvic lesions, particularly tumors is difficult by imaging. However, in the typical clinical setting the finding of a dilated tube with pus is pathognomonic for the diagnosis of TOA. Unusual TOA caused by actinomycosis and tuberculosis have nonspecific imaging findings and tend to resemble ovarian malignancies, often with peritoneal seeding (4).

MRI is the best imaging modality to differentiate between a multicystic ovarian mass and an abnormal fallopian tube. The typical findings for the latter include a cystic tortuous tubular structure which extends from the tubal angle and displays multiple incomplete interdigitating septations (5). Wall thickening and mural contrast enhancement aid in the differentiation from hydrosalpinx. The proteinaceous nature of the fluid is characterized by hypointense to intermediate SI on T1WI and intermediate to high SI on T2WI. Abscesses present as complex thick walled masses with uni- and often multilocular appearance (4, 5). Intense enhancement or thickening of adjacent peritoneum and pelvic ligaments are findings underlining the inflammatory character (Fig. 3). Large amounts of fluid tend to be present only in peritonitis.

MRI is superior to CT in characterization of sonographically indeterminate lesions, particularly in the differential diagnosis of ovarian neoplasm, endometriomas, and hemorrhagic cysts which may resemble TOA (5). Adnexal torsion which occurs in the same age population as TOA is typically associated with cystic adnexal lesions.

The tubular nature of pyosalpinx is more difficult to assess by CT, however this problem may have been overcome by multihelical CT. CT is widely performed in an acute setting especially to diagnose secondary TOA or

multiple abscesses after perforation of TOA. Other indications for CT include assessment of fever and pain of uncertain origin. CT serves also as guidance for percutaneous abscess drainage.

Interventional Radiological Treatment

Image guided drainage of TOA refractory to 24–48 h of intravenous antibiotic treatment is a safe alternative to laparoscopy (1). Technique and approach depend on the location and size of the TOA and the local expertise (5). Lesions with deep pelvic location are best treated by a transvaginal approach. Alternative approaches guided by ultrasonography and more commonly by CT use a transabdominal or transgluteal route (Fig. 4). In lesions up to 3–4 cm in diameter, and in unilocular abscesses needle aspiration, which often requires a series of interventions, is usually performed. If an access is possible, in larger TOA, especially if they are multiloculated catheter drainage by trocar or Seldinger technique is usually performed.

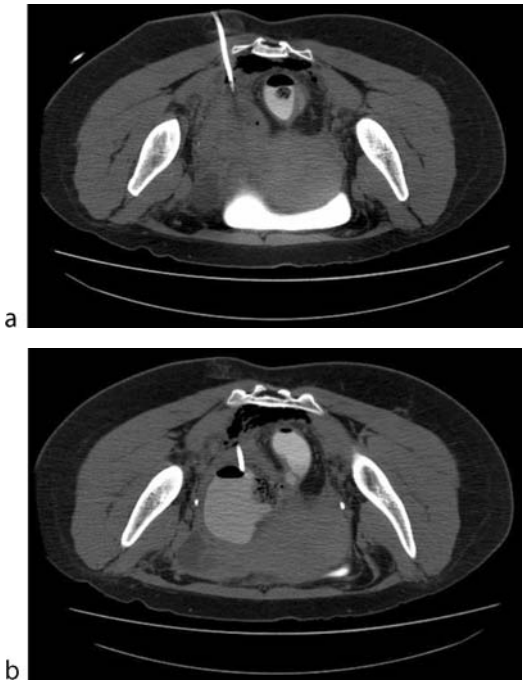

Abscess Tubo-Ovarian. Figure 4 CT guided drainage of a pelvic abscess. Pelvic abscess involving the adnexa developed as complication of pelvic surgery. The large left cystic lesion containing fluid and air was drained via a transgluteal parasacral approach. The abscess is shown before (a) and after opacification (b) through the drainage. Rectal opacification was performed before the procedure.

Bibliography

1. Livengood CH (2006) Tuboovarian abscess www.uptodate.com
2. Clement PB (2002) Anatomy and histology of the ovary. In: Kurman RJ (ed) 2Blaustein's Pathology of the Female Genital Tract. Springer, New York, pp 649–674
3. Varras M, Polyzos D, Perouli E et al (2003) Tubo-ovarian abscess: spectrum of sonographic findings with surgical and pathological correlations. Clin Exp Obstet Gynecol 30:117–121
4. Kim HS, Kim SH, Yang DM et al (2004) Unusual causes of tubo-ovarian abscess: CT and MR imaging findings. RadioGraphics 24: 1575–1589
5. Ghiatas AA (2004) The spectrum of pelvic inflammatory disease. Eur Radiol 14: E184–E192

Accessory Biliary Ducts

Their occurrence in general population has been estimated ranging from 2% to 5%. These ducts may extend from the liver parenchyma toward different structures (gallbladder, common hepatic duct, cystic duct, or the common biliary duct).

▶Congenital Malformations, Liver and Biliary Tract

Accessory Spleen

Accessory spleens are masses of additional splenic tissue. They represent by far the most common congenital abnormality of the spleen. Accessory spleens are round small masses that resemble splenic structure. They may be located anywhere in the abdomen, but the most common sites are near the splenic hilum and the tail of the pancreas. Intrapancreatic accessory spleen can mimic a neoplastic mass. Other possible locations are along the splenic vessels, in the gastrosplenic and splenorenal ligaments, in the mesentery, and in the omentum. Any accessory splenic tissue may become hypertrophic. When splenectomy is performed for hypersplenism, hypertrophy of an accessory spleen may cause recurrent disease. Ectopic splenic tissue may mimic neoplasms and lymphadenopathies. Ectopic splenic tissue shows imaging features identical to those of the normal spleen at US, CT, and MR. The enhancement pattern, especially the characteristic inhomogeneity in the arterial phase, is very specific. The use of a wide number of different MR sequences increases the confidence in diagnosis. MR reticuloendothelial-targeted contrast media can confirm the splenic nature of the mass. 99m-Technetium sulfur colloid scintigraphy and 99m-technetium-labeled heat-damaged red blood cells

represent the most specific imaging techniques to confirm the presence of functioning splenic tissue.

▶Congenital Abnormalities, Splenic

Accidental Clinical Findings

▶Incidental Neuroradiological Findings

Acetabular Fractures

The most common mechanism for acetabular fractures is motor vehicle accidents. These fractures are often associated with pelvic ring fractures, femoral head fractures, and hip dislocations. The most widely used classification system for acetabular fractures is the Judet–Letournel system. This system describes basic injuries to the acetabulum as column, rim, and transverse fractures as elementary fractures (see Pelvic Fractures). Five additional combinations of these elementary fractures are described and are classified as associated injuries. Most acetabular fractures require surgery to maintain the congruency of the hip joint. The most common long term complication is degenerative joint disease.

▶Fractures, Pelvis

Achalasia

▶Oesophageal Disease, Childhood

Achondroplasia

The most common enchondrally slowed systematic short stature dysplasia. A mutation in the FGFR3 gene is responsible. Its "family" includes the more severe thanatophoric dysplasia and the less severe hypochondroplasia.

▶Osteodysplasia

Acinar Cell Carcinoma, Pancreatic

Acinar cell carcinoma is a malignant epithelial tumor with acinar differentiation. It is uncommon, accounting for 1–2% of all exocrine pancreatic tumors. These tumors tend to reach a large size at presentation and frequently have multiple areas of hemorrhage and necrosis or cystic degeneration. Typical microscopic findings include a gross lobulation of markedly cellular tissue by fibrous strands. In most tumors acinar areas alternate with trabecular and solid formations. A capsule often surrounds these tumors. Vascular infiltration and other adjacent structures invasion are frequent. Typical clinical presentation is related to increase of lipase and includes subcutaneous fat necrosis, rash, polyarthralgias, and eosinophilia. An association with elevated serum alpha-fetoprotein and carcinoembryonic antigen levels has been reported, a unique feature among the pancreatic exocrine tumors. At imaging, most of these tumors appear as a well circumscribed, homogenous or heterogeneous mass with minimal biliary obstruction. Areas of necrosis and hemorrhage can also be seen. CT scans show an intense enhancement during the arterial phase correlating with the hypervascular nature of these tumors. More than half of the patients with acinar cell carcinoma present with metastases at the time of diagnosis; the prognosis of this tumor is usually better than that of adenocarcinoma, but worse than islet cell tumors.

▶Carcinoma, Pancreatic

ACKD

▶Acquired Cystic Kidney Disease

ACKD, Differential Diagnosis

The most difficult differential diagnosis of acquired cystic kidney disease (ACKD) is the presence of multiple simple cysts. The size of the cysts and their location are not helpful to differentiate between the two diseases. When the renal function is preserved, the diagnosis is likely to be ACKD, but multiple renal cysts can be found in patients with chronic renal failure.

In medullary cystic disease, cysts are small and strictly located within the medulla.

At the moment of diagnosis of ACKD, the size of the kidneys is normal or reduced, in contrast to autosomal dominant polycystic kidney disease (ADPKD). In ADPKD, the renal cysts are much bigger than in ACKD, as they typically exceed 5 cm. Cysts can be detected in other locations such as the liver, the spleen, and the pancreas.

Other diseases such as von Hippel Lindau and tuberous sclerosis are easily ruled out with the context (family cases), the presence of associated tumors (hemangioblastoma of the central nervous system, pheochromocytoma, pancreatic cysts, or angiomyolipoma).

▶Cystic Renal Disease, Acquired

Acoustic Standoff Pad

Sonolucent gel pad enabling examination of the skin and immediately underlying structures within the optimal short-axis focal point of the transducer.

▶Cutaneous Lesions, Breast

Acquired Cystic Kidney Disease

The development of multiple renal cysts in patients with end-stage renal disease, before or after starting dialysis, without hereditary cystic disease.

▶Cystic Renal Disease, Acquired

Acquired Hyperostosis Syndrome

▶Spondyloarthropathies, Seronegative

Acquired or Secondary Hemochromatosis

▶Hemochromatosis, Skeletal

ACR

American College of Radiology.

▶Calcifications, Breast

ACR Type

The American College of Radiology (ACR) type refers to different parenchymal densities of the breast, implying a more or less high diagnostic accuracy.

▶BI-RADS, Lexicon

Acral Osteolysis

Acral osteolysis is a feature of systemic scleroderma and is accompanied by soft tissue fading of the finger tips. The differential diagnosis consists of hyperparathyroiditis, arteriosclerosis obliterans, freezing, burns, epidermolysis bullosa, and pycnodysostosis.

▶Connective Tissue Disorders, Musculoskeletal System

Acromegaly

Giuseppe Guglielmi
Professor of Radiology, University of Foggia
Ospedali Riuniti – Viale Pinto – 71100 Foggia
g.guglielmi-g@unifg.it

Synonym

Gigantism

Definitions

Acromegaly (from Greek akros "end" and megalos "large"-extremity enlargement) is a very rare disease (annual incidence: 3.4/1,000,000 and prevalence: 60/1,000,000) characterized by chronic growth hormone (GH) and insulin-like growth factor-I (IGF-I) excess

caused by a pituitary chromophobic or eosinophilic adenoma (usually macroadenoma), rarely by ectopic production of growth hormone (tumors of pancreas, lungs and adrenal glands) or somathotropin-releasing hormone. These tumors either produce GH or growth hormone releasing hormone (GHRH), which stimulates the pituitary gland to produce GH.

Several rare hereditary syndromes may also cause acromegaly: multiple endocrine neoplasia (MEN1), McCune–Albright syndrome, Carney syndrome, and familial acromegaly.

The rate of GH production and the aggressiveness of the pituitary tumor vary from patient to patient; more aggressive tumors are seen in younger patients.

Acromegaly most commonly affects middle-aged adults (30–40 ages). When GH-producing tumors occur in childhood, before closure of the cartilage epiphysis, an excessive growth of the entire skeletal system results. This condition is called gigantism.

Acromegaly can result in serious illness and premature death, in fact the acromegalic patients have a reduced life expectancy, with a two-to-four-fold increased mortality rate. Life expectancy for inadequately treated patients is approximately 60 years. The duration of symptoms before diagnosis, older age at diagnosis, duration of disease, and presence of diabetes, hypertension, and cardiovascular disease are other factors associated with increased mortality. A decrease in the level of GH to <2.5 μg/L reduces mortality.

Pathology/Histopathology

The most common (98%) acromegaly is a well-encapsulated, benign GH-secreting adenohypophysial adenoma. Most pituitary tumors arise spontaneously and are not genetically inherited, but result from a genetic alteration in a single pituitary cell. The mutation occurs in a gene that regulates the transmission of chemical signals within pituitary cells, permanently switching to "on" the signal for cell division and secrete GH. Multiple genetic alterations probably cooperate in the progression toward neoplastic transformation and tumor growth. The most important oncogenes and tumor suppressor genes implicated in the pathogenesis of acromegaly are: oncogenes (gsp (GNAS1), H-ras, and pttg) and tumor suppressor genes (Men1, p16INK4a (CDKN2 or MTSI). Hypothalamic disorders, including aberrant GH-releasing hormone (GHRH) secretion, are being discovered (1). However the fundamental intrinsic defect initiating somathotroph adenoma formation remains unknown (2).

The effects of GH are mediated primarily through the hepatic production of IGF-1 (or somatomedin C). The liver is the main source of circulating IGF, even though there is physiologically important production in other tissues with various autocrine and paracrine functions (3).

IGF-1 acts on a variety of tissues to stimulate proportional body growth. A number of nonhepatic tissues produce IGF-1, including smooth muscle, skin, lung, bone, and cartilage. GH acts directly on bone to promote differentiation of specific precursor cells; promotes IGF-1 production, which stimulates clonal expansion of the differentiated bone cells; the physiological effect of GH is lipolytic in mature adipocytes. GH decreases body fat by increasing the hydrolysis of triglycerides, releasing free fatty acids and glycerol while decreasing free fatty acid re-esterification. Another major target of GH action is muscle, where GH enhances amino acid uptake and nitrogen retention (4).

The excess of GH and IGF-1 results in: osseus enlargement (phalangeal tufts and vertebrae); flared ends of long bones; cystic changes in carpal bones; femoral trochanters; ►osteoporosis; spade-like hands; prognathism (elongation of mandible) in a few cases; sellar enlargement and erosion; enlarged paranasal sinus (especially frontal: 75%); calvarial hyperostosis (especially inner table); enlarged occipital protuberance; posterior scalloping vertebrae (30%), anterior new bone formation of vertebrae and the loss of disc space; heel pad >25 mm; and premature osteoarthritis (most common: knees). GH has profound effects on linear bone growth, bone metabolism, and bone mass (5).

Clinical Presentation

Symptoms of acromegaly depend on how long the patient has had the disease. Soft tissue swelling of the hands and feet is often an early feature (acral enlargement), with patients noticing a change in ring or shoe size. Gradually, bony changes modify the patient's facial features: the brow and lower jaw protrude, the nasal bone enlarges, and spacing between teeth increases. Overgrowth of bone and cartilage often lead to arthritis. When tissue thickens, it may trap nerves, causing carpal tunnel syndrome, characterized by numbness and weakness of the hands. Other symptoms of acromegaly include thick, coarse, oily skin; skin tags; enlarged lips, nose and tongue; deepening of the voice due to enlarged sinuses and vocal cords; snoring due to upper airway obstruction; excessive sweating and skin odor; fatigue and weakness; headaches; and impaired vision. Endocrine disturbances such as decreased libido, menstrual abnormalities, galactorrhoea in women, and impotence in men may also be found.

There may be enlargement of organs, including the liver, spleen, kidneys, and heart. The most serious health consequences of acromegaly are diabetes mellitus, hypertension, and increased risk of cardiovascular

disease (cardiomegaly, premature coronary artery disease, arrhythmias, and heart failure).

Recent studies suggest that acromegaly may increase the risk of benign and malignant neoplasms, thus influencing the final outcome of the disease. The exact mechanism is unknown, but several studies indicate an important role is played by GH and IGF-1 in the tumorgenesis and mitogenesis in many neoplastic tissues. These studies also indicate that these hormones have an autocrine–paracrine role in the proliferation of normal and neoplastic cells. Patients with acromegaly are in fact at increased risk for developing neoplasia of colon, breast, prostate, and lung (3).

Imaging

A lateral radiograph of the skull demonstrates an enlarged sella turcica. At earlier stages of disease osteophytes may be found along with a paradox widening of joint space due to cartilage proliferation. At later stages, the radiographic features of joint involvement are joint space narrowing bone sclerosis, cyst formation, and osteophytosis. These features resemble the changes of primary ►degenerative joint disease. Acromegaly can result in periosteal bone formation, leading to the widening of osseus structure and enlargement of soft tissues, particularly in the hands, feet, and lower jaw. Other features include: enlargement of costochondral junctions, thickening of intervertebral discs, mandibular enlargement, thickening of the cranial vault (Fig. 1), prominence of the supraorbital ridges and facial structure, and cortical thickening of tubular bones.

Nuclear Medicine

No typical diagnostic findings.

Diagnosis

Although the disease is uncommon, it is believed to be widely under diagnosed due to its insidious nature and a general low level of disease awareness in the medical community. As a result, despite the well-described features of the syndrome, patients often live with active disease for up to 10 years before a diagnosis is made (6).

A 2-step screening is recommended if there is a suspect of acromegaly. To confirm the diagnosis, measurements of GH and/or IGF-1 levels can be taken. Since the concentration of GH may vary over time and a patient with acromegaly may have a normal GH level at any time, the most accurate measurement of GH is obtained when the hormone is normally suppressed. Thus, an oral glucose tolerance test is recommended to diagnose acromegaly. A physiological decrease in GH is observed after the ingestion of glucose. This is not the case

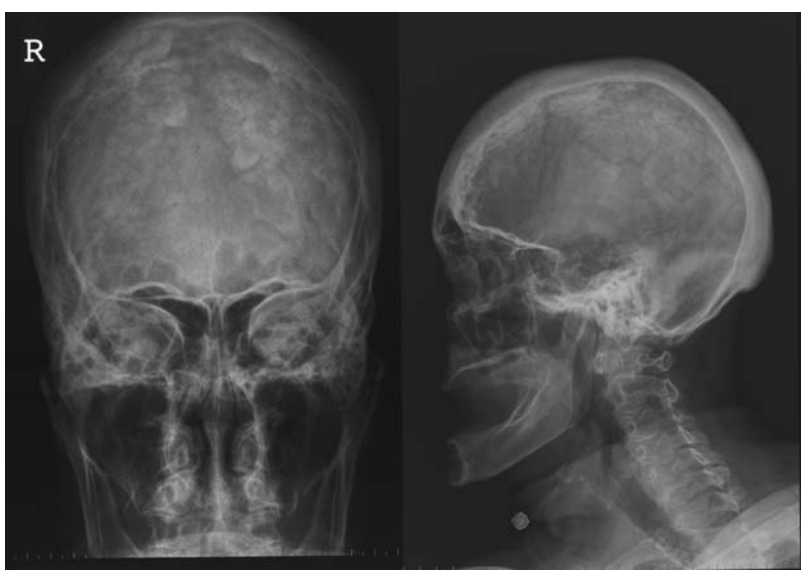

Acromegaly. Figure 1 A.p. and lateral cranial radiographs of a 66-year-old woman. Diffuse thickening of the skull with signs of internal hyperostosis (predominately of the frontal region) can be seen. The sella turcica appears enlarged, hyperpneumatization of the maxillary and sphenoidal sinuses, hypertrophy of the external occipital proturbance, complete dental loss associated with alveolar atrophy, enlargement of the mandible and osteoporosis of the cervical vertebrae are also present.

for patients with acromegaly. The IGF-1 level in the blood is increased and is more stable over the course of the day than GH levels. After a diagnosis of acromegaly has been made it is necessary to proceed by locating the pituitary adenoma using CT and/or MRI. If these exams are negative, a nonpituitary tumor of the chest, abdomen, or pelvis may be the cause of GH production.

During follow-up, it is important to obtain serial photographs taken over years to observe physical changes in the patient; blood tests to check the growth hormone and IFG-1 levels; and it is important to follow the skeletal effects of chronic GH excess by evaluating bone mineral density (7).

A series of diagnostic tests are also necessary to define the complications caused by the disease.

References

1. Metabolism, vol 45, No 8, Suppl1 (August), 1996:pp 51–52
2. Molecular pathogenesis of acromegaly, Marlys R (1999) Drange and Shlomo Melmed (Pituitary) 2:43–50
3. Acromegaly and the risk of cancer; Bogdan Marek, Dariusz Kajdaniuk et al (2001) Pathophysiology 8; 69–75
4. Biological effects of growth hormone and its antagonist. Shigeru Okada and JJ Kopchick. Trends in Molecular Medicine, Vol 7 No.3 March 2001
5. The effect of growth hormone on cortical and cancellous bone. J Muscoloskelet neuronal Interact. 2001 Sep; 2 (1):49–58
6. Medical management of growth hormone-secreting pituitary adenomas. Racine and Michael S. Barkan Ariel L. (2002) Pituitary 5: 67–76
7. Long-term maintenance of the anabolic effects of GH on the skeleton in successfully treated patients with acromegaly. Biermasz NR, NA Hamdy et al (2005) Eur J Endocrinol Jan; 152 (1):53–60
8. Hennessey JV, Jackson IM. "Clinical features and differential diagnosis of pituitary tumors with emphasis on acromegaly". Baillieres Clin Endocrinol Metab 1995; 9 (2): 271–314

Acromegaly

The differential diagnosis of acromegaly includes a several heterogeneous disorders; among them the most important ones are degenerative joint disease, secondary hypertrophic arthropathy, osteoporosis and Paget's disease. In most cases, the different diagnostic imaging modalities are able to make the diagnosis.

▶Important Differential Diagnoses

Activatable Probe

▶Molecular Probes, Optical Probes

Active Targeting

Active targeting (specific targeting) requires modification of the bubble shell to allow selective binding to cellular epitopes or receptors of interest. In general, specific USCAs consist of stabilized microbubbles as signaling moiety and shell-surface-bound ligands (such as antibodies, peptides, polysaccharides, or aptamers) as binding moiety.

▶Targeted Microbubbles

Acute Abdomen

Acute Abdomen can be defined generally as an intraabdominal process causing severe abdominal pain and often requiring surgical intenvetion. There are different causes of an acute abdomen. Leiomyomas especially when they ruptured may present as an acute abdomen. It is a condition that requires immediate judgement or decision as to management.

Acute Abdomen, Genital Causes

PATRICK R. KNÜSEL
Institut für Radiologie,
Kontonsspital Baden, Baden, Switzerland
patrick.knuesel@ksb.ch

Synonyms

Acute abdominal pain, Abdominal cramps, Peritonitis

Definition

The acute abdomen is a frequently encountered clinical finding with a variety of possible etiologies. This chapter highlights the most frequent genital pathologies that may cause an acute abdomen.

Genital causes of an acute abdomen include complications of leiomyoma, uterine rupture, adnexal torsion, hemorrhagic cyst, ruptured dermoid cyst, ovarian hyperstimulation syndrome, pelvic inflammatory disease (PID), endometriosis, extrauterine gravidity (EUG),

uterine perforation, ovarian vein thrombosis, endometritis, and HELLP syndrome.

Placental abruption and postpartal hematoma are among the most common obstetrical causes of acute abdomen. Imaging may play a role in defining the extent of hematoma. However, in most cases, the clinical presentation is straightforward and therefore no further details are discussed here.

Rarely, genitourinary tuberculosis may present as an acute abdomen (1) due to peritonitis, but tuberculosis is usually known from the patient's history. This condition is not further discussed here, but should be kept in mind in the appropriate clinical setting.

Pathology/Histopathology

Uterine Causes

Fibroids, or *leiomyomas*, are the most common benign tumors in the female pelvis, having been reported in 25–40% of women over 35 years of age. They are classified according to their localization as submucosal, intramural, subserosal, and extrauterine (i.e., mostly broad ligament). Leiomyomas may undergo hyaline degeneration and show varying degrees of liquefaction. Hyaline degeneration or necrosis typically gives fibroids a more cystic appearance. Malignant sarcomatous transformation has been described as a rare condition. Only 10% of leiomyomas show calcifications. Submucosal, subserosal, and extrauterine leiomyomas may be pedunculated and therefore may undergo torsion of the pedicle with subsequent infarction, degeneration, necrosis and, ultimately, suprainfection.

In pregnancy, *red degeneration* of leiomyomas is known to show symptoms of acute pelvic pain with labor-like contractions. This occurs when a fibroid's arterial blood supply is insufficient, causing it to turn red because of infarction. It can also happen outside of pregnancy, but it usually occurs during midterm pregnancy.

Uterine rupture is mostly a peripartum complication after spontaneous delivery or cesarean section. Pregnant women with previous cesarean section are more prone to uterine ruptures. Perforation of the uterus may also result from dilatation and curettage.

Adnexal Causes

Adnexal torsion is considered a partial or complete rotation of the ovary, the ipsilateral fallopian tube, or both around the axis of their vascular pedicle. As a result, untreated torsion may result in vascular compromise progressing from venous stasis and edema to arterial occlusion and finally gangrenous and hemorrhagic necrosis with increasing severity and duration of torsion. In addition, secondary infection and peritonitis or rupture as well as concomitant hemoperitoneum may occur, particularly in patients presenting late. Accordingly, immediate adnexectomy is mandatory. If adnexal torsion is diagnosed and treated in time, the ovary can possibly be salvaged surgically by untwisting the pedicle and resecting the cyst or tumor.

Ipsilateral ovarian neoplasia or cysts are associated with 50–81% of cases of adnexal torsion (2), but torsion can also be spontaneous, particularly in children. The most frequent neoplastic association in young women and girls is teratoma.

Hemorrhagic cysts are known to occur spontaneously or following trauma to a follicular or corpus luteal cyst. If there is cyst rupture, the resulting hemoperitoneum can be life-threatening, especially in patients undergoing anticoagulation therapy.

Dermoid cysts or mature (cystic) teratomas are considered to derive from the ecto- and mesoderm that contain fat and may contain any combination of sebaceous glands, hair, teeth, and even thyroidal stroma. Although rare, rupture of such a cyst results in hemoperitoneum and chemical peritonitis.

Ovarian hyperstimulation is usually iatrogenic and is the most feared complication in gonadotropin therapy for infertility. However, spontaneous cases also occur in pregnancy. The syndrome includes rapid weight gain, ascites, pleural effusions, intravascular volume depletion with hemoconcentration, and oliguria.

Pelvic Inflammatory Disease

PID is the most common cause of acute pelvic pain in women and imaging findings vary with the stage of disease. It affects sexually active girls and women. Most cases result from ascending infection, usually a mixture of anaerobic and aerobic organisms. Women are more prone to be affected by *adnexitis* shortly after menstruation, abortion, or gynecologic instrumentation. Most infections are ascending and bilateral. Unilateral affection has been observed in women with intrauterine contraceptive devices (IUDs). Descending spread most often results in appendicitis, ileitis, or diverticulitis.

Tubo-ovarian abscess (TOA) is the complication of a persistent or relapsing adnexitis. Ovarian parenchyma is usually preserved. Pure ovarian abscess usually occurs only in complicated pelvic surgery.

An ascending PID may lead to inflammation of the liver capsule or diaphragm *(Fitz-Hugh-Curtis syndrome)*. The patient reports right upper quadrant pain. The spread of bacteria (*Chlamydia trachomatis*, *Neisseria gonorrhoeae*) from the pelvis to the liver capsule most likely results from the circulation of abdominal fluid over the right paracolic gutter.

Endometriosis

Endometriosis results from the implantation of functional endometrium outside the uterus. A spectrum of small endometriotic implants to large cysts ("chocolate cysts" or endometriomas) may be seen. Endometriosis primarily affects women during their reproductive years. The prevalence of this important gynecologic disorder is estimated to be 5–10%. Retrograde menstruation, lymphatic spread, hematogenous spread, and coelomic metaplasia are some theories of potential pathogenesis in endometriosis. The most common implantation sites are the ovaries, cul-de-sac, and uterine ligaments. Rare locations also include the colon (sigmoid), small intestine, and ureter.

Extrauterine Gestation (EUG or Ectopic Pregnancy)

EUG occurs in interstitial (cornual), cervical, and intra-abdominal sites. However, the isthmic or ampullary portions of the fallopian tube are the most frequent locations. The physiologic needs for the normal development of a fetus are not provided outside of the uterus, resulting in fetal demise. The most feared complication is rupture of the gestational sac, which often results in intraperitoneal hemorrhage. Ectopic pregnancies constitute 9% of all pregnancy-related deaths in the first trimester [USA: National Center for Health Statistics (NCHS), 1994]. Another rare complication of early pregnancy is septic abortion with peritonitis.

Postoperative or Peri- and Postpartum Complications

Ovarian vein thrombosis (synonym *ovarian thrombophlebitis*) is an uncommon but potentially serious disorder associated with a variety of pelvic conditions, most notably recent childbirth. Nonpuerperal ovarian vein thrombosis is infrequent but associated with contraceptive medication.

Venous stasis and hypercoagulability are common in the immediate postpartum period. Other conditions associated with hypercoagulability include recent surgery, trauma, malignancy (treated with chemotherapy), and Crohn's disease. In 80–90% of cases, ovarian thrombosis occurs on the right side. If complicated by infection, ovarian thrombosis becomes a serious condition. Sepsis and propagation of thrombosis to the renal and caval veins with pulmonary embolism may be fatal.

Endometritis is an infection of the endometrium or decidua, which may extend into the myometrium and parametrial tissues. Endometritis is divided into obstetric and nonobstetric types. After vaginal delivery, 1–3% of patients develop endometritis. In nonobstetric endometritis precedent instrumentation, PID, or cervical stenosis may be the cause.

HELLP is an acronym *(hemolysis, elevated liver enzymes and low platelets)* given to a syndrome occurring in 4–12% of preeclamptic patients. Pathologic intravascular coagulation results in end-organ damage in the peripartal period. The associated morbidity and mortality are high. Major complications include placental abruption, acute renal failure, and cerebral hemorrhage. The most common serious intra-abdominal complications include hepatic hemorrhage with infarction and/or rupture. Histopathologic examination demonstrates small vessel fibrin deposits, periportal hemorrhage, and hepatocellular necrosis.

A *pelvic abscess* may be the result of a descending infection such as appendicitis, psoas abscess, or diverticulitis. An iatrogenic abscess may occur after genital and nongenital operative procedures in the pelvis (e.g., hysterectomy, Wertheim procedure, sigmoidectomy, etc.). Regarding genital causes of acute abdomen, only TOA is further discussed in detail.

Clinical Presentation

The age of the patient and exclusion of pregnancy are the first criteria to be considered in narrowing down the differential diagnosis. Most of the genital causes of acute abdomen have similar presenting symptoms. Pelvic pain, nausea, vomiting, tenderness, and peritoneal signs are nonspecific findings that make a straightforward clinical diagnosis difficult. In general, a rapid onset of pelvic pain is likely to be caused by a ruptured tumor (e.g., cyst, teratoma, TOA), tubal abortion, ruptured EUG, torsion (e.g., pedunculated myoma, adnexal torsion), or infarction/necrosis (e.g., red degeneration). A colicky type of pain is typical for adnexal torsion. Tumor, infection (salpingitis, TOA), EUG, or ovarian hyperstimulation are characterized by a slower onset. Acute pain and vaginal bleeding indicate a uterine or adnexal origin as in pedunculated submucosal or torsed leiomyoma, EUG, red degeneration, placental abruption, or postpartal complications (e.g., uterine rupture, postpartal hematoma). Red degeneration and placental abruption present with uterine contractions and can lead to early labor or miscarriage.

Severe hypotension with hemodynamic shock may occur after rupture, especially with concomitant coagulation disorders such as HELLP syndrome.

Fever and/or leukocytosis suggest infection (e.g., PID, endometritis) but are also frequently observed in torsion (necrosis) and ovarian thrombosis ("thrombophlebitis" with evolving sepsis).

If the patient presents with right upper quadrant pain and a history of PID, Fitz-Hugh-Curtis syndrome should be considered.

Endometriosis has been reported in asymptomatic women undergoing laparoscopic tubal ligation, as well as in 20% of women with infertility and 24% with pelvic pain (3).

Involvement of the gastrointestinal tract may result in catamenial diarrhea, rectal bleeding, or constipation. Flank pain, pleuritic chest pain, and cyclic headaches are other symptoms associated with atypical implant location. Rarely, endometrial cysts can rupture and present with symptoms of an acute abdomen.

Imaging

In general, conventional radiographs (CR) are not suited for a definite diagnosis of genital causes in acute abdomen, but are often performed to exclude other conditions and to evaluate important findings such as free air, bowel obstruction, bowel perforation, or obstipation. Therefore, in this chapter CR findings are only mentioned when specific findings are relevant.

In premenopausal women, pregnancy must be excluded before X-ray based-examinations (CR or CT) are performed. As in children, sonography (US) is usually the first imaging study of choice. Transabdominal US is well-suited for characterizing processes in the upper abdomen or pelvis and may be followed by transvaginal US (TVUS) to further limit or delineate pathology. Due to its inherent high soft tissue contrast, magnetic resonance imagine (MRI) is the most sensitive and specific examination for pelvic imaging. MRI without gadolinium contrast enhancement is the cross-sectional modality of choice in pregnant woman (relative contraindication in first trimester). If pregnancy is excluded or in life-threatening situations, computed tomography (CT) may be considered initially in the setting of an acute abdomen.

Complicated Leiomyoma

US or TVUS is usually diagnostic, particularly if one or more rounded masses of the uterus show iso- or slightly hypoechoic signal. Hyperechoic signal suggests hemorrhage ("red degeneration") or calcification if there is dorsal acoustic shadowing. Calcification is uncommon, seen only in 10% of leiomyomas, but very specific. Large degenerated fibroids may appear cystic.

In CT, fibroids are mostly found incidentally and contour deformity is the most common finding. Leiomyomas in general show inhomogeneous contrast enhancement and, depending on the degree of degeneration and necrosis, areas of diminished contrast enhancement and low attenuation. The latter is typical for torsion of a pedunculated leiomyoma with infarction (4).

In MRI, uncomplicated fibroids show homogeneous hypointense signal, whereas degenerating leiomyomas show a hyperintense signal on T2-weighted imaging (T2-WI) and sarcomatous transformation typically shows contrast enhancement in addition. A typical pattern is described in red degeneration where fibroids display a hyperintense rim on T1-WI and hypointense rim on T2-WI. These findings correspond with numerous dilated vessels filled with red blood cells at the periphery of the lesion. The signal characteristics of the rim are best explained as an effect of abundant intracellular methemoglobin in these vessels (5).

Patients present with an acute onset of localized lower abdominal pain. Patients may experience vomiting and/or a low-grade fever. Red degeneration usually occurs in pregnant patients between 12 and 20 weeks of gestation (Fig. 1).

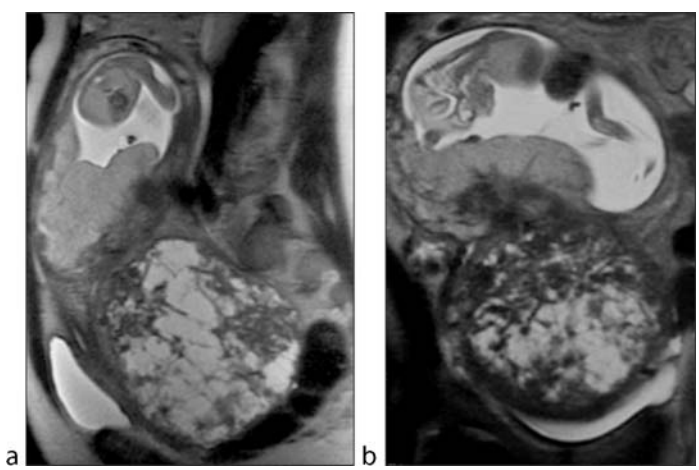

Acute Abdomen, Genital Causes. Figure 1 T2-WI MR in (a) sagittal and (b) coronal planes: pregnancy with fetus in utero and below adjacent, hyperintense, cystic mass corresponding to a necrotizing uterine leiomyoma, probably due to red degeneration.

Uterine Perforation

US, CT, and MRI are all adequate for showing discontinuity of the uterus and hemorrhage. CT and MRI are better suited at depicting a distended postpartal uterus because of their larger field of view.

Adnexal Torsion

Doppler US is the study of choice for adnexal torsion. US findings have been described well (2) and include ascites, an enlarged ovary with peripherally distributed follicles, an associated cyst or mass, and lack of central parenchymal vascularity.

CT and MRI are useful additional imaging modalities when US findings are nonspecific or for preoperative planning.

Common CT and MRI findings include fallopian tube thickening, smooth wall thickening of the torsed adnexal cyst, ascites, an enlarged ovary displaced form its anatomic location (Fig. 2), and uterine deviation to the torsed side.

If unenhanced CT is performed, hemorrhagic infarction, hemorrhage into a cystic mass, or hemoperitoneum may be considered if attenuation exceeds 50 HU. After intravenous contrast medium administration, lack of enhancement is observed in hemorrhagic infarction.

In addition to CT findings, MRI is able to nicely depict fat-containing tumors (e.g., teratoma) with fat-suppressed T1-WI or in-phase and opposed-phase sequences, alternatively. In MRI, small areas of hemorrhage are discerned as T2-WI low and T1-WI high signal intensities, whereas large hemorrhagic areas usually show intermediate to low signal.

According to a study by Rha and coworkers (2), ascites was found in adnexal torsion with and without hemorrhagic infarction, whereas hemoperitoneum always accompanied infarction.

If the diagnosis is uncertain, diagnostic laparoscopy can be done.

(Ruptured) Hemorrhagic Cyst

US can help detect the presence of fluid in the cul-de-sac. CT and MRI may be helpful in ruling out active bleeding or other causes of free fluid in the abdomen. Hemoperitoneum or hemorrhagic cysts may be better demonstrated by CT (Fig. 3) or MRI.

Ruptured Dermoid Cyst (Teratoma)

CR may show calcifications, particularly teeth-like structures, which are highly specific for mature teratomas. In CT or MRI, a heterogeneous pelvic mass with various amount of fat density or fat signal in young female patients is pathognomonic (see example in Fig. 4). In ruptured teratomas, considerable ascites results from chemical peritonitis.

Ovarian Hyperstimulation

US, CT, and MRI show similar findings of bilateral ovarian enlargement due to numerous distended corpora lutea cysts of varying sizes. Cysts are typically located in the periphery of the stromal ovarian tissue resulting in the classic "wheel spoke" sign. Another key finding is rapid accumulation of ascites in the abdomen and variable pleural effusions (Fig. 5). Diagnosis is usually made clinically and may be confirmed by US, especially in order to evaluate for drainage of peritoneal fluid.

Pelvic Inflammatory Disease

In uncomplicated acute *salpingitis*, CR, US, and CT findings are usually normal or demonstrate a small amount of fluid in the cul-de-sac. A *pyosalpinx* may be seen as a tubular fluid-containing structure with thickened walls. With progression to TOA, CT findings often

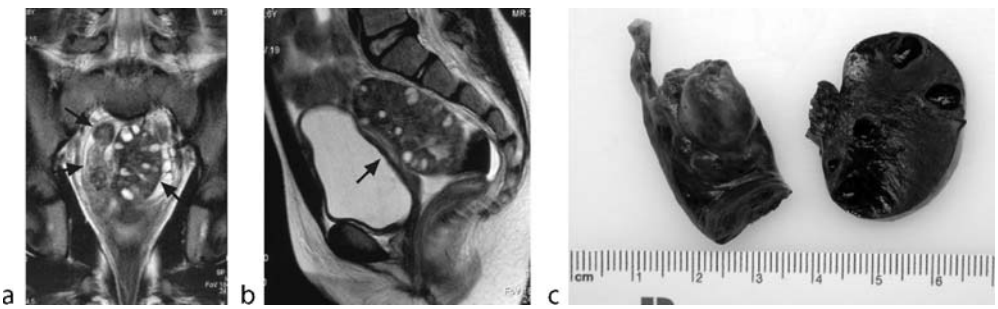

Acute Abdomen, Genital Causes. Figure 2 Six-year-old girl with right-sided ovarian torsion. T2-WI MR in (a) coronal and (b) sagittal planes with enlarged right ovary (*open arrow*) displaced form its anatomic location to a more medial and cranial position. Multiple small excentric cysts but no specific signal changes indicating infarction or necrosis are present. Thickened and contorted vascular bundle is shown in the coronal plane (*arrows*). Small peritoneal fluid collection. (c) Macropathologic specimen shows a twisted vascular bundle and hemorrhagic infarction of ovarian parenchyma.

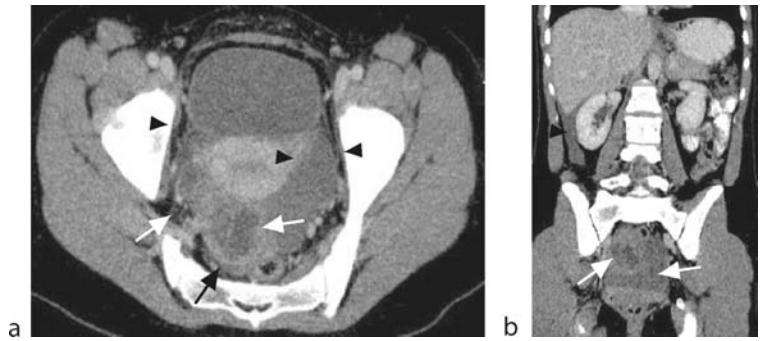

Acute Abdomen, Genital Causes. Figure 3 A 24-year-old nonpregnant woman with acute deep right pelvic pain. (a) axial and (b) coronal reformatted CT images illustrate a hypodense cystic mass with some irregular, ill-defined hyperdense borders (*open arrows*) as well as a normally contrasted uterus and urinary bladder ventrally. Concomitant free fluid (*arrowheads*) shows a slightly higher density than the urinary bladder and is, therefore, suggestive of hemoperitoneum.

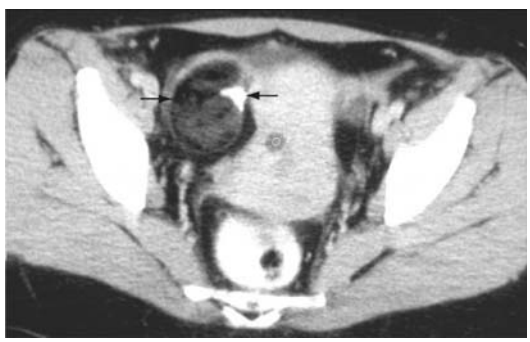

Acute Abdomen, Genital Causes. Figure 4 Teenage female patient with nonruptured typical appearance of a teratoma (dermoid cyst) containing calcified teeth (*arrow*), fatty (*arrowhead*) and low density components, as well as some enhancing parenchyma of the right ovary. If fat is present in a ruptured ovarian lesion with accompanying ascites, a ruptured teratoma must be considered.

include thick-walled, low-attenuation adnexal mass or masses with internal septations (demonstrated in Fig. 6c). An associated serpiginous structure may be found, corresponding to a dilated, pus-filled fallopian tube (4). CR is usually unspecific, but may show gas-containing pelvic mass. US shows a cystic, hypoechoic adnexal mass with irregular contours and irregular thickened walls. Fluid is mostly demonstrated in the cul-de-sac and an increasing amount of fluid indicates rupture. MRI of a TOA depicts a mass with low signal intensity on T1-WI and heterogeneous high signal intensity on T2-WI (Fig. 6a, b). A thickened wall and "stranding" of the pelvic fat is well enhanced after contrast.

In Fitz-Hugh-Curtis syndrome, perihepatic adhesions or fluid may be seen in US. CT and MRI findings may help delineate a loculated perihepatic peritoneal collection. Diagnostic laparoscopy remains the gold standard.

Endometriosis

Laparoscopic exploration remains the gold standard for the diagnosis of endometriosis. Although variable, more or less specific findings of endometriosis can be found. Sonography, especially transvaginal US, can depict cystic changes, whereas implants and adhesions remain undetectable. Low-level internal echoes and echogenic small wall foci are more specific findings for endometriomas. Unilocular and multilocular forms (with septations) are also described (4).

However, functional or hemorrhagic ovarian cysts, dermoid cysts, and cystic neoplasms are the usual overlapping entities in US and CT. Findings are variable, from a rather solid to a rather cystic mass, and therefore nonspecific.

MRI is reported to be more specific for endometrial cysts, but adnexal masses may remain difficult to differentiate at times. An endometrioid lesion typically demonstrates a T1-WI high signal without signal loss in fat-saturated T1-WI sequences. Classically, T2-WI sequences show signal loss, so-called shading. This phenomenon results from cystic bleeding and resultant methemoglobin and/or protein content.

Bilaterality and multiple lesions are ancillary findings that support the diagnosis with any imaging modality.

Extrauterine Gravidity

Transabdominal or transvaginal US is recommended in all studies. Findings in ectopic pregnancy include the following: live extrauterine embryo, absence of an intrauterine gestational sac, free fluid (particularly hemorrhagic) in the pelvis or peritoneum, adnexal mass, hematosalpinx, adnexal ring sign and a "ring-of-fire" sign on color Doppler image, and absence of low-resistance endometrial arterial flow. In contrast, an endometrial color Doppler finding is highly suggestive of intrauterine pregnancy.

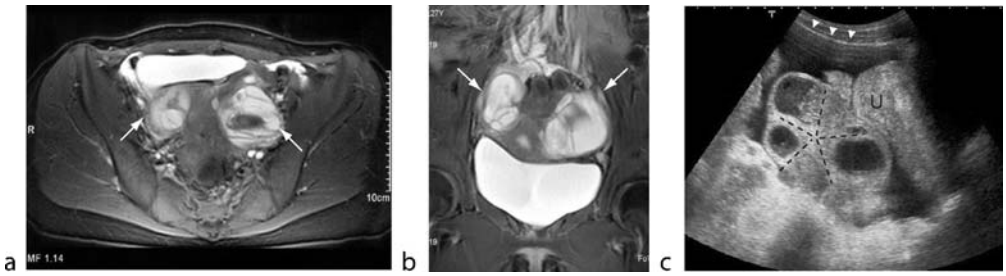

Acute Abdomen, Genital Causes. Figure 5 Ovarian hyperstimulation syndrome. Axial (a) and coronal (b) plane of the pelvis with bilateral cystic enlargement of both ovaries (arrows) with ascites in the context of *in vitro* fertilization. (c) Transabdominal sonography of the right ovary demonstrates large cysts around a starlike parenchymal center ("wheel spoke" sign: dashed lines) and anechoic ascites (*arrowheads*). Uterus (U).

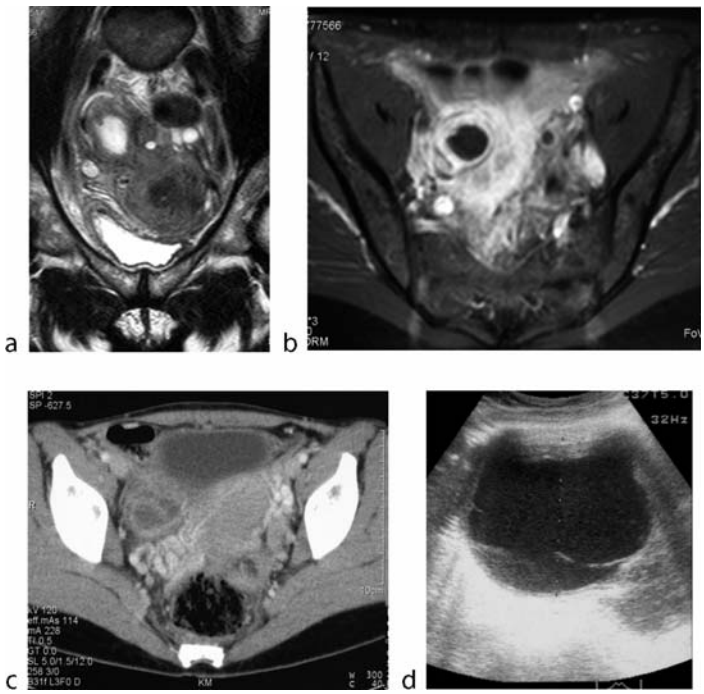

Acute Abdomen, Genital Causes. Figure 6 Tubo-ovarian abscess. T2-WI MR (a) shows a cystic right adnexal mass with wall-thickening (*arrow*) and high signal internally (*x*). Small rim of free fluid (*open arrows*). Fat-suppressed T1-WI sequence after intravenous contrast (b) depicts thick-walled cystic structure with high signal due to peripheral contrast enhancement of the abscess and low signal internally (*x*). Note also contrast enhancement of the surrounding pelvic fat (*arrowheads*). Contrast-enhanced CT also demonstrates abscess with enhancing, thickened walls and low-density fluid and septations in the center (*x*). Transabdominal US (d) shows internal septations and anechoic fluid.

CT is generally contraindicated in these cases due to the potential of a viable pregnancy and the typically nonspecific findings.

MRI findings suggestive of an ectopic pregnancy include a tubal gestational sac, a tubal hematoma with a ring sign (peripheral hyperintensity on T1-WI), tubal wall enhancement, and an adnexal mass with hemorrhagic fluid in the peritoneum. MRI can additionally delineate confounding adnexal findings seen on US, such as follicular or corpus luteum cysts.

Ovarian Vein Thrombosis

US is a useful initial study; however, US is generally limited due to overlying bowel gas. Color Doppler is a helpful tool for the assessment of flow in imaged vessels.

CT and MR findings usually allow a definitive diagnosis and the exclusion of many other pathologies. CT findings consist of a tubular structure with wall enhancement and low-attenuating thrombus in the vein (Fig. 7).

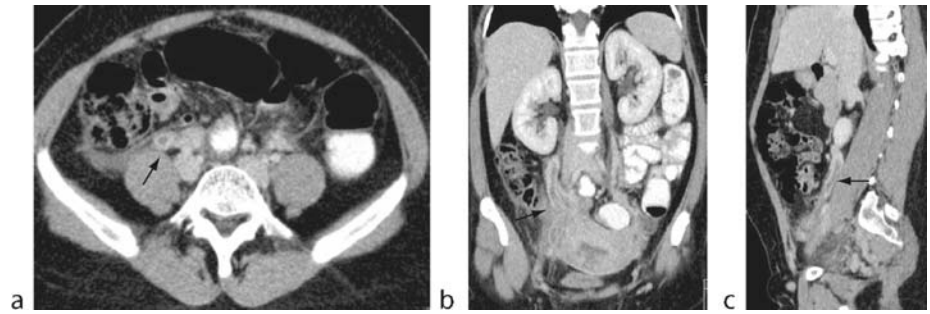

Acute Abdomen, Genital Causes. Figure 7 Nonpuerperal ovarian vein thrombosis. Two-dimensional multiplanar reconstructions in (a) axial, (b) coronal, and (c) sagittal planes show a tubular hypodense thrombus in the thickened right ovarian vein associated with wall thickening and enhancement (*arrow*). Right adnexal and parametrial structures are also ill-defined due to edema.

Endometritis

CT and MRI are the imaging modalities of choice. Small amounts of fluid or air in the uterine cavity may persist for several weeks after vaginal delivery. Therefore, the presence of air is not a specific sign. Enhancing soft tissue within the cavity is suggestive of retained products of conception. US may also be an alternative, but is generally less suited to identifying parametrial inflammation or extrauterine abscess.

HELLP

US may be the initial imaging method to identify intrahepatic or subcapsular hemorrhage. However, contrast-enhanced CT is excellent for excluding active arterial bleeding and for serial follow-up. MRI is a very sensitive and specific method for demonstrating subcapsular or intrahepatic hematoma as well as areas of infarction (6).

Bibliography

1. Kim SH, Kim SH, Yang DM et al (2004) Unusual causes of tubo-ovarian abscess: CT and MR imaging findings (review). Radiographics 24:1575–1589
2. Rha SE, Byun JY, Jung SE et al (2002) CT and MR imaging features of adnexal torsion. Radiographics 22:283–294
3. Anonymous (1997) Revised American society for reproductive medicine classification of endometriosis. Fertil Steril 67:817–821
4. Bennett GL, Slywotzky CM, Giovanniello G (2002) Gynecologic causes of acute pelvic pain: spectrum of CT findings (review). Radiographics 22:785–801
5. Kawakami S, Togashi K, Konishi I et al (1994) Red degeneration of uterine leiomyoma: MR appearance. J Comput Assist Tomogr 18:925–928
6. Leyendecker JR, Gorengaut V, Brown JJ (2004) MR imaging of maternal diseases of the abdomen and pelvis during pregnancy and the immediate postpartum period (review). Radiographics 24:1301–1316

Acute Abdominal Pain

▶Acute Abdomen, Genital Causes

Acute Arterial Occlusion

▶Ischemia, Limb, Acute

Acute Ischemic Limb

▶Ischemia, Limb, Acute

Acute Lung Injury (ALI)

▶Diffuse Alveolar Pulmonary Damage and Acute Respiratory Distress Syndrome

Acute Parenchymatous Jaundice

▶Budd–Chiari Syndrome

Acute Upper Extremity Ischemia

▶Ischemia, Brachial

ADC

▶Apparent Diffusion Coefficient

Adenoacanthoma, Gallbladder

Adenosquamous carcinoma, gallbladder
▶Neoplasms, Gallbladder

Adenocarcinoma of the Pancreas

▶Carcinoma, Pancreatic

Adenocarcinoma, Gallbladder

Malignant tumor originating from columnar cells of the gallbladder epithelium. It is the most common primary malignant epithelial form, with a pattern similar to those of other bile duct carcinomas.
▶Neoplasms, Gallbladder

Adenoma, Breast

Luis Pina
Department of Radiology
Clínica Universitaria de Navarra
Spain
ljpina@unav.es

Definition

Adenomas of the breast are benign tumors composed of epithelial cells and sparse, inconspicuous stroma. For practical purpose, two types are considered: tubular and lactating adenomas. Both are variants of fibroadenoma (1, 2). Other types, such as apocrine adenomas, pleomorphic adenomas, ductal adenomas, and ▶nipple adenomas, are very infrequent lesions (3).

Pathology

Tubular adenomas are macroscopically similar to fibroadenomas. The lesions are composed of small, round tubules and little stroma (2).

Lactating adenomas are compact aggregates of lobules exhibiting secretory hyperplasia (1).

Apocrine adenomas consist of nodular adenosis with extensive apocrine metaplasia (3).

Pleomorphic adenomas are similar to those found in the salivary glands.

Ductal adenomas are well-circumscribed benign lesions that consist of a proliferation of tubules surrounded by fibrosis and are located, at least in part, inside the duct lumen (3).

Nipple adenomas are not true adenomas of the breast, because of its dominant stromal component. These lesions are located around the collecting ducts of the nipple.

Clinical Presentation

Tubular adenomas are rare tumors found in young women, accounting for 0.13 to 1.7% of all benign breast lesions (3). These adenomas are well-delimited, freely movable nodules, resembling fibroadenomas.

Lactating adenomas occur during pregnancy or the puerperal period, and consist of palpable, soft, well-circumscribed masses (2).

Nipple adenomas usually present as sanguineous or serous nipple discharge.

The remaining types of adenomas are infrequent lesions that may present as masses or as nipple discharges.

Imaging

Mammography

Mammographic features of tubular and lactating adenomas are similar to those of fibroadenomas. These lesions are found as ovoid or lobulated masses with well-delimited margins if they are surrounded by fat (Fig. 1). In dense breasts, adenomas may have occult margins or may be invisible. Calcifications may be observed (4).

Adenoma, Breast. Figure 1 Ovoid, dense mass with well-circumscribed and obscured margins. Craniocaudal view (detail). Pathology: ►tubular adenoma.

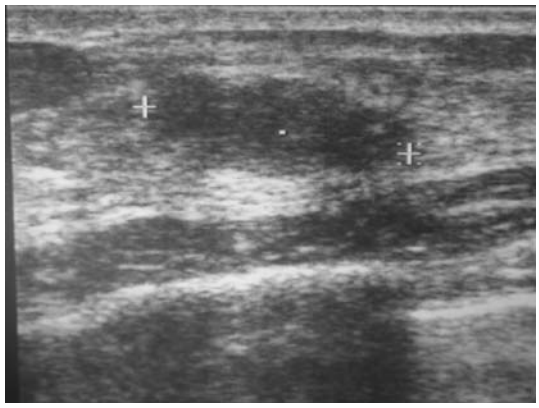

Adenoma, Breast. Figure 2 Ultrasound showing an ovoid, hypoechoic, solid mass with well-circumscribed margins. Tubular adenoma.

Ultrasonography

As with fibroadenomas, adenomas are usually hypoechoic, homogeneous, well-circumscribed masses with posterior acoustic enhancement (Fig. 2). However, they may also be ill-delimited, irregular, heterogeneous masses with posterior shadowing (5).

Magnetic Resonance

Adenomas, as well as fibroadenomas, may enhance after the administration of paramagnetic contrast medium. These lesions may be seen as well-circumscribed masses with heterogeneous structure and suspicious enhancement curves (Fig. 3).

Nuclear Medicine

Nuclear medicine studies are not indicated for this pathology.

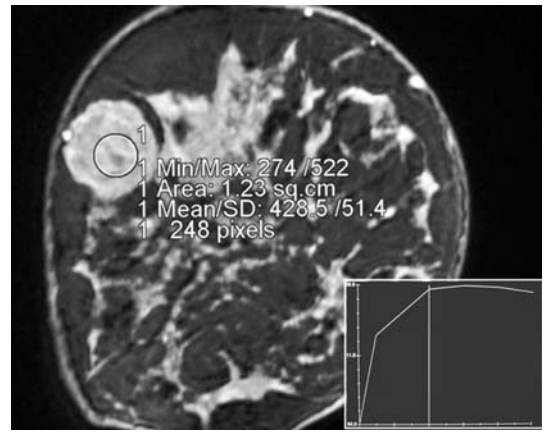

Adenoma, Breast. Figure 3 Contrast-enhanced magnetic resonance image of a 32-year-old woman during the puerperal period. The patient had an infiltrating ductal carcinoma in the contralateral breast. A round mass with smooth margins is seen in the right breast, coincident with a smooth, palpable lesion. Time–signal intensity curve type 3. Pathology: ►lactating adenoma.

Diagnosis

The diagnostic approach of tubular adenomas is similar to that for fibroadenomas. The lesions can be differentiated from one another only on the basis of a biopsy.

The diagnosis of lactating adenoma is suspected clinically when patients present with a palpable mass during pregnancy or the postpartum period. Ultrasound is useful in order to differentiate a solid lactating adenoma from a galactocele. Nevertheless, if the lesion is solid, a biopsy is indicated to rule out malignancy.

Bibliography

1. Rosen PP (2001) Fibroepithelial neoplasms. In: Rosen PP (ed) Rosen's Breast Pathology. Lippincott Williams & Wilkins, Philadelphia, pp 163–200
2. Schnitt S, Connolly JL (2004) Pathology of benign breast disorders. In: Harris JR, Lippman ME, Morrow M et al (eds) Diseases of the Breast. Lippincott Williams & Wilkins, Philadelphia, pp 77–99
3. Bussolati G, Tavassoli FA, Nielsen BB et al (2003) Benign epithelial proliferations. In: Tavassoli FA, Devilee P (eds) Pathology and Genetics of Tumours of the Breast and Female Genital Organs. International Agency for Cancer, Lyon, pp 81–85
4. Cardeñosa G (2001) Lobules. In: Cardeñosa G (ed) Breast Imaging Companion. Lippincott Williams & Wilkins, Philadelphia, pp 272–279
5. Rosenfield Darling ML, Smith DN, Rhei E et al (2000) Lactating adenoma: sonographic features. Breast J 6:252–256

Adenoma, Gallbladder

Rare benign tumor originating from the epithelium of the gallbladder that can be an isolated finding or associated with familial adenomatous polyposis and Peutz-Jeghers syndrome. Macroscopically, these lesions appear as polypoid structures projecting into the gallbladder lumen.
▶Neoplasms, Gallbladder

Adenoma, Hepatic

Riccardo Lencioni, Marzio Perri
Department of Diagnostic and Interventional Radiology, University of Pisa, Italy
lencioni@med.unipi.it

Definition

Hepatocellular (hepatic) adenoma is a rare, frequently encapsulated nodular lesion of the liver characterized by the benign proliferation of liver cells.

Epidemiology

Hepatocellular adenoma occurs predominantly in young women, more commonly in reproductive age women, who use oral contraceptives. Though the female:male ratio is 4:1, the incidence of hepatocellular adenoma appears to have increased in males, because the use of anabolic drugs has become widespread in sports. In a few patients, the tumor may present multiplicity (more than ten lesions) in an otherwise normal liver (liver adenomatosis).

Pathogenesis

The pathogenesis of adenomas is not fully understood. Clonality studies indicate that this tumor results from benign proliferation of a clone of hepatocytes. Limited genetic alterations have been found in patients with hepatocellular adenoma, such as gain of chromosome 7p, 17q and 20q and deletions from exon 3 to exon 4 of the beta-catenin gene. At variance with hepatocellular carcinoma, no genetic changes for the p53, axin and adenomatous polyposis colon genes, have been detected in adenomas. Adenoma, therefore, is not pathogenically linked to the sequence adenoma–carcinoma as it is intestinal polyposis. Oral contraceptives have a role in the evolution of some forms of liver adenomatosis, and vascular liver damage due to altered liver cell proliferation, intrahepatic vascular shunts, or an association with FNH, have been postulated.

Pathology and Histopathology

Hepatic adenomas are soft, yellow lesions often with a highly vascularized surface and a capsule, and focal areas of hemorrhage in the parenchyma. The histologic features are two or more cell thick sheets of hepatocytes without cellular atypia (to differentiate from adenocarcinoma), portal tracts (to differentiate from liver cell regeneration), and biliary ductules and fibrosis (to differentiate from FNH). There may be fatty infiltration at the periphery of small areas of liver cell proliferation (adenomatous hyperplasia) seen between large adenomas. Some degree of liver cell dysplasia may be present in adenomas, particularly in those with a pseudofollicular pattern. Foci of malignant transformation have been described that may escape detection in small specimens obtained with a thin-needle liver biopsy.)

Clinical Presentation

Hepatocellular adenomas are usually solitary. Approximately 30% of the patients have multiple nodules and the presence of more than ten adenomas defines liver adenomatosis. Approximately half of the cases of adenomas have been discovered incidentally whereas the remaining have had such symptoms as pain or abdominal mass. Patients with hepatocellular adenoma have a higher prevalence of symptoms at first presentation compared to patients with hemangioma or FNH, probably caused by the high rate of intratumoral or intra-abdominal hemorrhage. The diagnosis of liver adenomatosis is made because of complications of adenomas (intraperitoneal bleeding, intratumoral hemorrhage or necrosis producing acute pain), because of hepatomegaly with or without symptoms, or as an incidental finding. While the massive form of liver adenomatosis is rare and can be unilobular, most patients have multifocal liver adenomatosis spread in both lobes.

Imaging

Ultrasound and Contrast-Enhanced Ultrasound

Hepatocellular adenoma has variable sonographic appearances. The lesion may appear as slightly hypoechoic, isoechoic, or hyperechoic. When necrotic or hemorrhagic changes occur, adenoma appears as a complex mass with a large cystic components. Using color or power Doppler,

the arterial hypervascularity is well demonstrated by arterial vessels running along the border of the lesion in a "basket" pattern (1). At contrast-enhanced ultrasound (CEUS), adenoma shows intense enhancement during the arterial phase. During the portal venous and equilibrium phases adenomas may appear as isoechoic or slightly hyperechoic mass (2). None of these features, unfortunately, is specific enough for the diagnosis.

Computed Tomography

Baseline computed tomography (CT) scans can easily detect the presence of fat or recent hemorrhage within the lesion, features that can suggest the diagnosis of adenoma (3). During dynamic contrast-enhanced CT scanning, noncomplicated adenomas may enhance rapidly and appear homogeneously hyperdense compared to the liver. The enhancement usually does not persist in adenomas because of arteriovenous shunting within the lesion. Larger or complicated adenomas may be highly heterogeneous because of necrotic phenomena or intralesional hemorrhage (Fig. 1).

Magnetic Resonance

On magnetic resonance (MR) images, hepatocellular adenoma can show variable signal intensity. It has been reported that 59–77% of adenomas are hyperintense on T1-weighted images due to intralesional content of fat or glycogen, or because of recent hemorrhage (3). In contrast, low signal intensity areas are related to necrosis. The neoplasm may appear homogeneously or heterogeneously hyperintense on T2-weighted images (Fig. 2). With dynamic MR study, adenoma shows early enhancement during the arterial phase and becomes isointense to liver in the portal venous and delayed phases, features that overlap with those of other hypervascular tumors. On the other hand, the usefulness of tissue-specific MR agents is not fully established. After administration of Mn-DPDP, adenoma shows positive enhancement, but contrast uptake may not occur with Gd-BOPTA (3). Adenomas, in some cases, may take up superparamagnetic iron oxide particles, resulting in decreased signal intensity on T2-weighted images. However the uptake of SPIO in adenoma is variable, depending of Kupffer cells content or function (4).

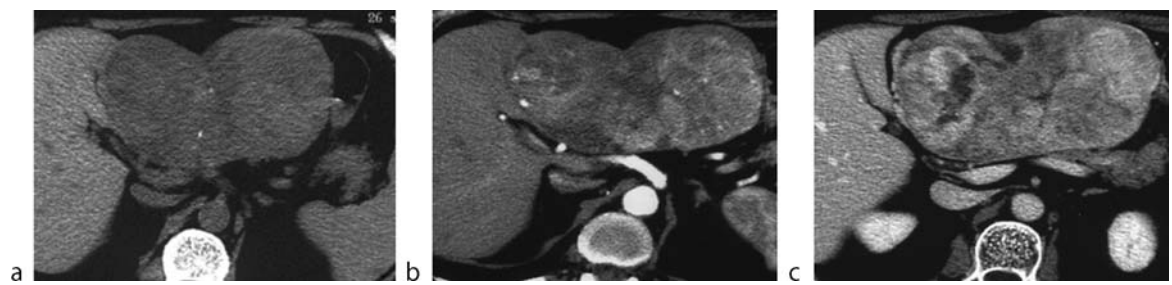

Adenoma, Hepatic. Figure 1 Hepatocellular adenoma—spiral CT. Nonenhanced CT scan (a) demonstrates a large, heterogeneous, predominantly hypoattenuating mass replacing the lateral segment of the left hepatic lobe. After contrast medium administration, in the arterial (b) and portal venous (c) phases, the lesion shows heterogeneous enhancement. Note the presence of focal hypoattenuating areas within the lesion due to internal necrosis.

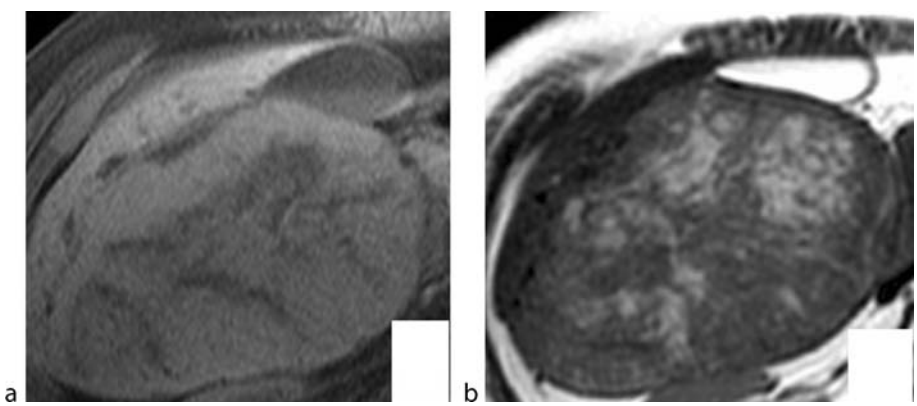

Adenoma, Hepatic. Figure 2 Hepatocellular adenoma—MR. MR shows a large, exophytic mass in the right hepatic lobe. The lesion is heterogeneously isointense to liver parenchyma on T1-weighted image (a) and heterogeneously hyperintense on T2-weighted image (b).

Diagnosis

Laboratory tests are not helpful during the diagnostic work-up. However, negative tests for serum AFP and hepatitis B and C corroborate the exclusion of malignant disease. Radiologic diagnosis of adenoma is very difficult. Unfortunately, CT and MR imaging features of adenoma are nonspecific, and the only finding that may suggest the diagnosis is the detection of intratumoral hemorrhage. Even with the use of MR and liver-specific contrast agents, a final diagnosis can hardly be made in nonhemorrhagic adenoma. Percutaneous liver biopsy is of little value because of the possible lack of specific features in a small specimen, while the procedure carries the risk of needle-induced bleeding in hypervascular nodes. In liver adenomatosis, two- or threefold increase of alkaline phosphatase or gammaglutamyl transpeptidase levels have been described.

Bibliography

1. Bartolozzi C, Lencioni R, Paolicchi A et al (1997) Differentiation of hepatocellular adenoma and focal nodular hyperplasia of the liver: comparison of power Doppler imaging and conventional color Doppler sonography. Eur Radiol 7:1410–1415
2. Nicolau C, Bru C (2004) Focal liver lesions: evaluation with contrast-enhanced ultrasonography. Abdom Imaging 29:348–359
3. Grazioli L, Federle MP, Brancatelli G et al (2001) Hepatic adenomas: imaging and pathologic findings. Radiographic 21:877–894
4. Reimer P, Balzer T (2003) Ferucarbotran (Resovist): a new clinically approved RES-specific contrast agent for contrast-enhanced MRI of the liver: properties, clinical development, and applications. Eur Radiol 13:1266–1276

Adenomatous Hyperplasia, Gallbladder

This condition is characterized by the presence of hyperplasia of the gallbladder wall, limited to the epithelial elements of the mucosa without the involvement of the muscular layer. Two types are described: a villous form with long papillary mucosal projections and a spongy type with branching and dilated glands occasionally with cystic features. Inflammation and stones are frequently associated. This condition is considered an in situ carcinoma when atypical mitoses are detected.

▶Cholecystoses

Adenomegaly

Indicates enlargement of lymph nodes

▶Lymphadenopathy

Adenomyoepithelioma

Benign tumour composed of epithelial and myoepithelial cells.

▶Breast, Benign Tumours

Adenomyoma, Gallbladder

Circumscribed form of adenomyomatosis, with a characteristic umbilication on the center of the surface top, usually located in the gallbladder fundus. Cholecystograms show a small, smooth, filling defect with a central opaque dot corresponding to the surface umbilication.

▶Cholecystoses

Adenomyomatosis, Gallbladder

▶Cholecystoses

Adenomyomatosis, Gallbladder

Benign condition characterized by hyperplastic changes of the gallbladder wall and therefore named hyperplastic cholecystosis. Typical features include the overgrowth of the surface epithelium with associated formation of intramural diverticula or sinus tracts termed Rokitansky–Aschoff sinuses. Adenomyomatosis may be focal, segmental, or diffuse. It occurs most frequently in middle-aged females, its etiology is unclear, and it is usually asymptomatic. US is the examination of choice, showing the mural thickening with cystic spaces visible as small anechoic structures outside the gallbladder wall. CT and MR can be used as problem-solving modalities, especially to differentiate hyperplastic cholecystosis from gallbladder carcinoma.

▶Cholecystoses

Adenosis

Increase in the number or size of glandular elements.

▶Fibrocystic Disease, Breast

Adenosis Tumor

►Sclerosing Adenosis, Breast

Adenosquamous Carcinoma, Gallbladder

Malignant lesion originating from areas of squamous metaplasia of the gallbladder epithelium. This tumor represents about 5–10% of cases of gallbladder carcinoma. Rapid growth and early metastatic spread associated with wide infiltration and dissemination are characteristic.
►Neoplasms, Gallbladder

Adrenogenital Syndrome

Rosemary Arthur
Department of Pediatric Radiology, Leeds General Infirmary, Clarendon Wing, Leeds, UK
r.arthur@ukonline.co.uk

Synonyms

Congenital adrenal hyperplasia; 21-hydroxylase deficiency

Definition

►Congenital adrenal hyperplasia is a group of inborn errors of metabolism arising from enzyme defects in the biosynthesis pathways of adrenal corticosteroids, resulting in inadequate production of glucocorticoids and mineralocorticoids and excess production of adrenal androgens.

Pathology/Histopathology

The adrenal cortex produces three principle groups of corticosteroids: mineralocorticoids responsible for electrolyte balance, glucocorticoids necessary for carbohydrate mobilization and potentiation of catecholamine action in response to stress, and adrenal androgens necessary for growth and sexual development. Adrenal corticosteroid production begins with the uptake of serum cholesterol and transport into the mitochondrium of the cells of the adrenal cortex, under the stimulation of adrenocorticotropic hormone (ACTH), gonadotropins, and steroidogenic acute regulatory protein (StAR). Hormone production proceeds by a series of steps enabled by steroidogenic enzymes; following the conversion of cholesterol to pregnenolone, a number of alternative pathways lead to the production of aldosterone, cortisol, or androgenic steroids (Fig. 1) (1, 2). Several autosomal recessively inherited disorders result in a deficiency of one of the enzymes or regulatory proteins essential for hormone production, leading to a partial or complete block in normal corticosteroid biosynthesis and overproduction of other steroid hormones. This in turn gives rise to a number of distinct clinical syndromes generically referred to as congenital adrenal hyperplasia (CAH).

Clinical Presentation

21-hydroxylase deficiency (21-OHD) accounts for 90–95% of individuals with CAH and is due to genetic mutations in the gene encoding the enzyme P 450c21 (21-hydroxylase), which catalyzes the hydroxylation of progesterone to deoxycortisone in the production of the aldosterone, and 17OH progesterone to 11-deoxycortisol in the production of cortisol (Fig. 1). The enzyme block results in a buildup of progesterone and 17-OH progesterone, which are diverted along the pathway for androgenic steroid production. The resulting low levels of cortisol stimulate the production of ACTH through the hypothalamic–pituitary feedback mechanism to further stimulate overproduction of androgenic steroids. Although originally recognized in its severe classic form with an incidence of 1 in 14,000 individuals, milder forms with an incidence of about 1 in 100–1,000 are now well recognized. Approximately 50–75% of those with CAH are unable to synthesize sufficient aldosterone and are termed salt losers. The clinical manifestations of CAH depend on the severity of 21-OHD deficiency, giving rise to a wide spectrum of disease presentation.

Classical salt-wasting CAH: In females, classic CAH presents at birth, being the most common cause of ►ambiguous genitalia *(cross reference Ambiguous genitalia essay)*. The degree of ambiguity varies but may be severe enough for incorrect gender assignment. Milder cases may show just minor cliteromegaly and partial fusion of the labioscrotal folds (Fig. 2). Increased ACTH levels often cause hyperpigmentation of the genitalia and areolae. The ovaries, uterus, and fallopian tubes develop normally because sexual differentiation of the female

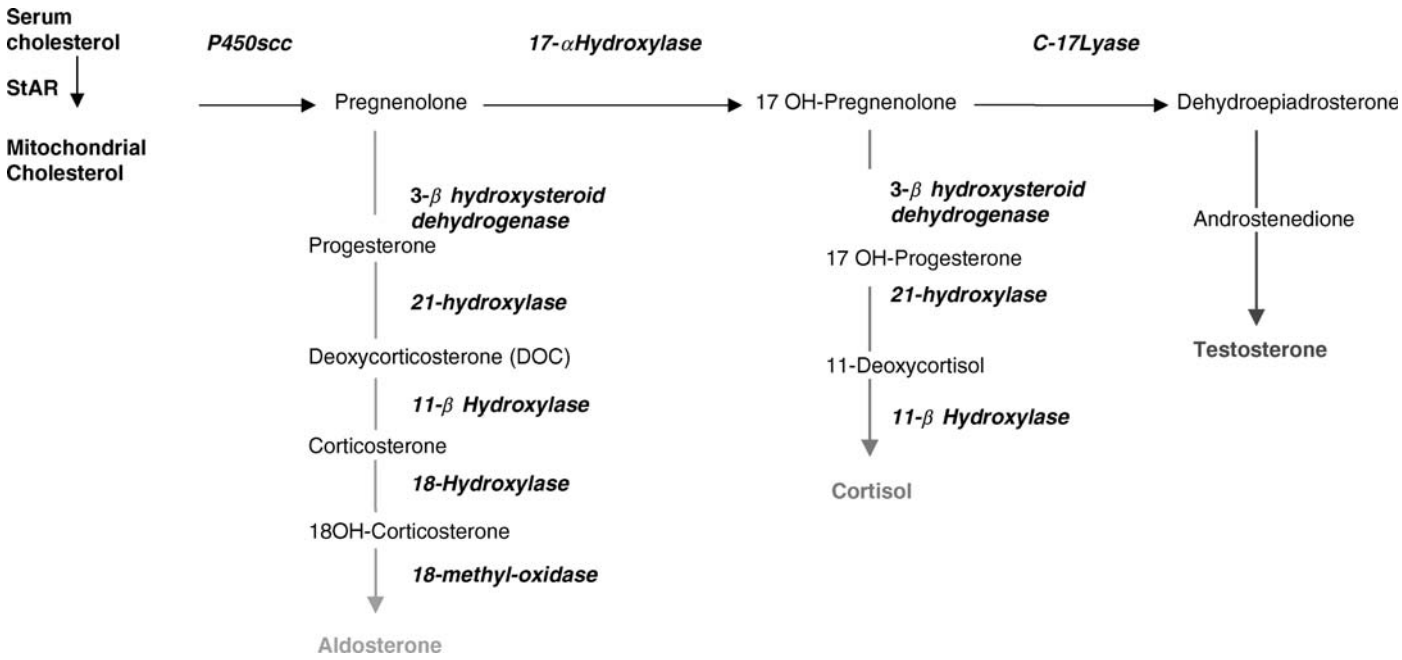

Adrenogenital Syndrome. Figure 1 **Illustrating main pathways for adrenal steroidogenesis. (adapted from Deaton MA, Glorioso JE, Mclean DB. (1999) Congenital adrenal hyperplasia: Not really a Zebra):**

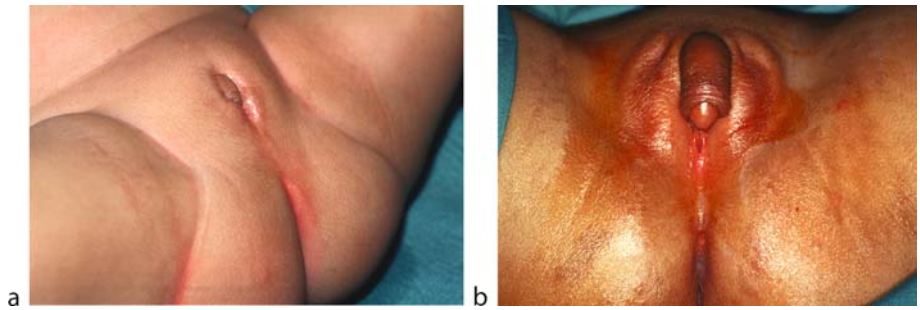

Adrenogenital Syndrome. Figure 2 **Masculinization in a 46XX female with congenital adrenal hyperplasia. (a) Minor clitoral enlargement. (b) More severe virilization with a phallic urethra and a single perineal opening of a urogenital sinus.**

Adrenogenital Syndrome. Table 1 **Key clinical features and enzyme deficiencies in congenital adrenal hyperplasia**

Enzyme Deficiency	Salt losing/ Hypertension	External genitalia and sexual development		Laboratory
		Male 46XY	Female 46 XX	
21-hydroxylase deficiency, classical	50% salt losing crisis	Male Postnatal virilization No testicular enlargement	Masculinized female – to complete sex reversal Postnatal virilization	Raised 17-OHP before and after ACTH Raised serum androgens
Non-classical		Premature adrenarche Disordered puberty	Premature adrenarche Disordered puberty	Salt wasting: low serum aldosterone Elevated plasma renin
11β-hydroxylase deficiency	Neonatal salt losing Hypertension >2 years	Male Premature adrenarche Postnatal virilization	Masculinized female Premature adrenarche Postnatal virilization	Raised ACTH, 11-dextcortisol and DOC. Raised androgens Salt wasting: low serum aldosterone Low plasma renin
Lipoid CAH StAR deficiency	Salt losing crisis	Female (sex reversal, undermasculinized male)	Female Disordered puberty	Low/absent all steroids hormones Decreased or absent response to ACTH
3β-hydroxysteroid dehydrogenase deficiency	Salt losing crisis	Undermasculinized male Postnatal virilization	Masculinized female – mild Postnatal virilization	Raised ACTH Increased ratio of 17-OH hydroxypregnenolone to 17-OH hydroxyprogesterone and of DHEA to androstenedione
17α-hydroxylase/ 17,20-lyase deficiency	Hypertension	Undermasculinized male–to complete sex reversal Sexual infantilism Disordered puberty	Female Sexual infantilism Disordered puberty	Raised DOC, corticosterone, 18-OHDOC, 18-Ohcorticosterone and hyperresponse to ACTH Salt wasting: low serum aldosterone. Low plasma renin

internal organs does not depend on normal sex hormone production. Although large amounts of testosterone are produced in the male fetus, this has little effect on genital development, and males remain unrecognized until they present with a ►salt-losing crisis with severe dehydration, shock, hypotension, and cardiovascular collapse, with evidence of hyponatremia and hyperkalemia. Significant salt losing becomes apparent only at about 2–4 weeks of age because electrolyte balance in the fetus is maintained by the maternal kidneys and placenta.

Simple virilizing 21-OHD refers to individuals with a deficiency of 21-OHD in the absence of salt wasting. Males escape diagnosis until age 3–7 years, when the effect of an excess of androgenic steroids becomes clinically apparent with the development of ►precocious puberty, acne, pubic hair, and phallic growth. Chronic androgen excess disrupts the hypothalamic pituitary axis, and the testes remain prepubescent. Females generally present at birth on account of ambiguous genitalia, but if ambiguity is mild, the condition may present later in childhood with

premature adrenarche. Skeletal maturation proceeds rapidly in both boys and girls before treatment, but advanced skeletal maturation leads to early epiphyseal fusion and cessation of growth, resulting in short stature.

Nonclassic 21-OHD refers to clinically mild CAH that may escape early diagnosis. Reduced cortisol production and the body's inability to generate appropriate responses to stress often result in recurrent sinus and severe pulmonary infections. Other symptoms include orthostatic syncope, short stature, acne, hirsutism, polycystic ovarian syndrome, menstrual irregularities, and infertility.

11-β hydroxylase deficiency (*11-β OHD)* accounts for about 8–10% of cases of CAH. Both glucocorticoid and mineralocorticoid production is affected; the blocked metabolites are redirected to excessive androgenic hormone production, giving rise to a clinical presentation similar to 21-OHD. However, there is also an accumulation of deoxycortisol (DOC), a mineralocorticoid ameliorating the salt-losing features of this deficiency but resulting in the development of hypertension from about 2 years of age.

StAR deficiency–congenital lipoid adrenal hyperplasia is the most severe inherited disorder of steroid hormone synthesis, affecting the transport of cholesterol into the mitochondria under the control of StAR. This results in severe reduction in the levels of mineralocorticoids, glucocorticoids, and androgenic steroids, with resulting high levels of ACTH and plasma renin and a buildup of cholesterol within the adrenal glands, causing massive enlargement. Steroidogenesis also occurs in the fetal testis, and the accumulation of cholesterol causes Leydig cell destruction, eliminating testosterone biosynthesis. As a result, a 46XY male undergoes phenotypic gender reversal with female external genitalia and a blind vaginal pouch, but Mullerian inhibiting hormone is still produced by the Sertoli cells, and the cervix, uterus, or fallopian tubes regress. Salt losing generally develops after several weeks. In the 46XX genetic female, the ovary does not engage in steroidogeneis and remains unaffected until stimulated at puberty by gonadotropins. Cholesterol then accumulates within the ovary, impairing progesterone production and resulting in disordered puberty and infertility (1, 3).

Several other distinct syndromes are recognized. The most important of these are 3β-hydroxysteroid dehydrogenase deficiency (3β-HSD) and 17-hydroxylase/17,20–lyase deficiency, as indicated in Table 1.

Imaging

Al-Alwan et al reported high sensitivity of 92% and specificity of 100% for the ultrasound diagnosis of CAH in neonates based on the presence of two or three abnormalities including size, i.e., limb width >4 mm, outline, and echotexture (5) (Fig. 3). Use of a high-frequency transducer is essential (see Figure 1 of chapter Essay on congenital malformations, adrenals). In CAH, the gland may develop an abnormal crenated or lobulated outline, and the normal central echogenic stripe may be replaced by a more diffuse echotexture. However, the adrenal glands may appear entirely normal, and in some centers ultrasound imaging is not routinely performed. Ultrasound features of less common forms of CAH are not well documented with the exception of the StAR syndrome, in which the adrenal glands are grossly enlarged due to the accumulation of cholesterol and its esters. Computed tomography is rarely indicated, but if performed in StAR, the enlarged adrenal glands show a decrease in attenuation.

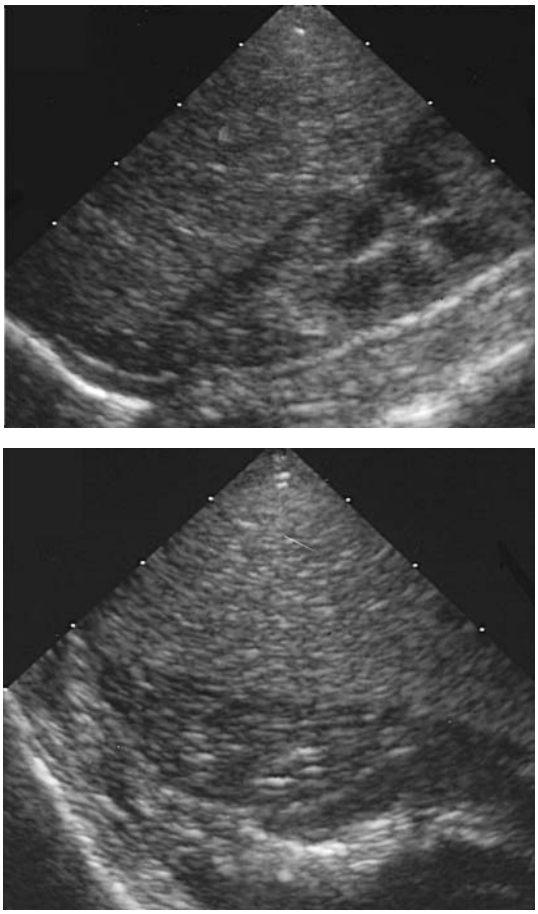

Adrenogenital Syndrome. Figure 3 Longitudinal and transverse images of the adrenal gland of an infant with classic congenital adrenal hyperplasia. Note the diffuse echogenicity of the gland with loss of central echogenic stripe.

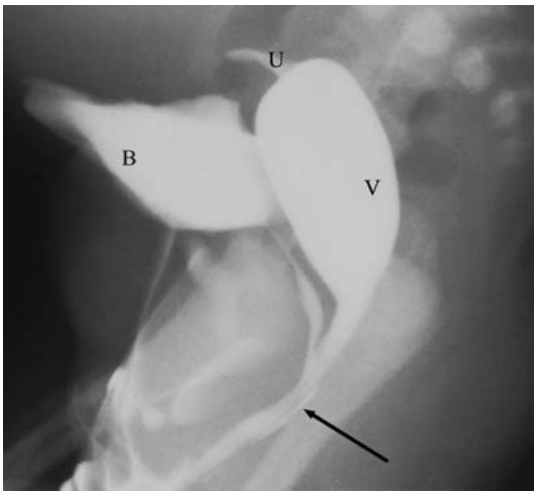

Adrenogenital Syndrome. Figure 4 Genitogram demonstrating a phallic urethra and urogenital sinus (*arrow*) in a female with classic congenital adrenal hyperplasia. (*B* bladder, *V* vagina, *U* uterine cavity)

When there is genital ambiguity, ultrasound is particularly helpful to document the presence of the uterus and ovaries and to demonstrate a hydrocolpos and a urogenital sinus *(cross reference Ambiguous genitalia essay Fig. 2). Genitography is necessary before reconstruc*tive surgery in girls with ambiguous genitalia to characterize the length of the urogenital sinus (Fig. 4). MRI scanning is particularly helpful in delineating pelvic anatomy in teenagers who present with disordered puberty, especially when ultrasound fails to demonstrate normal internal organs in phenotypic females (Fig. 5).

During childhood, it is necessary to regularly estimate skeletal maturity by performing bone age estimation.

Diagnosis

The diagnosis of CAH is made on the basis of clinical features, including the presence of sexual ambiguity, a salt-losing state, hypertension, growth and pubertal disorders in conjunction with identification of hormone deficiencies, and demonstration of excess metabolites (Fig. 1 and Table 1). Karyotyping is essential when there is any concern about sexual ambiguity. Cytogenetic testing is rarely necessary to confirm the diagnosis.

Prenatal diagnosis is possible on the basis of HLA typing when the parents are known to be heterozygotes following the birth of an earlier affected child. In parents at risk but with no previous children, DNA analysis of chorionic villous or amniotic fluid cells or measurement

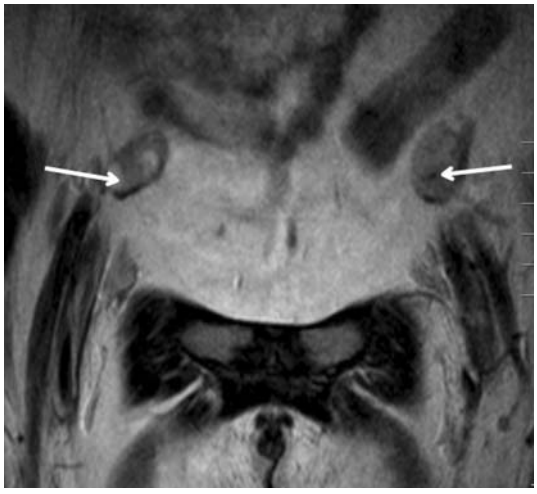

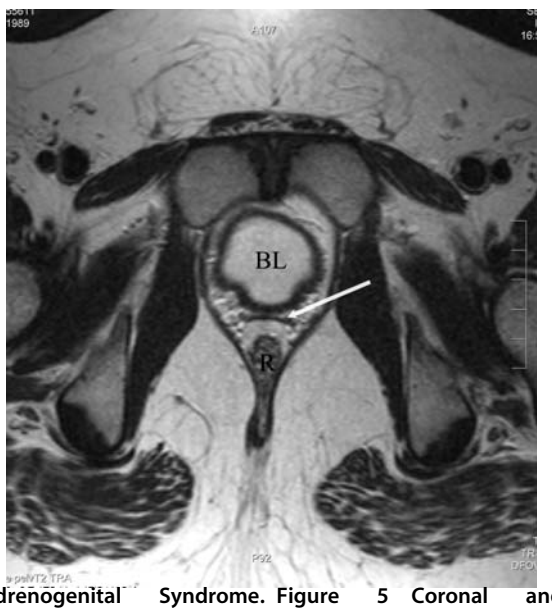

Adrenogenital Syndrome. Figure 5 Coronal and transverse T2-weighted images through pelvis of a 16-year-old "girl" presenting with delayed puberty having been previously treated for congenital aldosteronism. Investigation revealed XY karyotype, and biochemical analysis confirmed StAR deficiency. The coronal magnetic resonance (MR) image demonstrates intraabdominal gonads (*arrows*) confirmed to be testes on histology. The transverse MR image demonstrates a thin residual uterovaginal anlagen (*arrow*) with absence of a normal uterus and vagina. (*BL* bladder, *R* rectum)

of 17-hydroxy steroids in amniotic fluid can be undertaken. Prenatal treatment with dexamethasone treatment for the mother must begin as soon as pregnancy is confirmed (before 6–8 weeks) to prevent abnormal genital development. Once the diagnosis and karyotype

are confirmed, treatment can be stopped in males until after birth but must be continued throughout pregnancy in affected females to prevent excessive androgenic steroid production.

Bibliography

1. Miller WL (1997) The adrenal cortex and its disorders. In: Brook C, Clayton P, Brown R (eds) Brook's Clinical Pediatric Endocrinology. Blackwell Publishing. pp 293–351
2. Deaton MA, Glorioso JE, Mclean DB (1999) Congenital adrenal hyperplasia: not really a zebra. Am Fam Physician 59:1190–1196
3. Saenger P (1997) New developments in congenital lipoid adrenal hyperplasia and acute steroidogenic acute regulatory protein. Pediatr Clin North Am 44:397–421
4. Daneman A (2004) The adrenal gland. In: Kuhn JP, Slovis TL, Haller JO (eds) Caffey's Paediatric Diagnostic Imaging. Mosbypages 239–251
5. Al-Alwan I, Navarro O, Daneman D et al (1999) Clinical utility of adrenal ultrasonography in the diagnosis of congenital adrenal hyperplasia. J Pediatr 13571–75

Adult Respiratory Distress Syndrome (ARDS)

►Diffuse Alveolar Pulmonary Damage and Acute Respiratory Distress Syndrome

Adverse Events to Ultrasound Contrast Media

►Contrast Media, Ultrasound, Safety and Adverse Reactions

Adverse Reaction

Adverse (drug) reactions concern noxious and unintended responses to a medicinal product. The phrase "responses to a medicinal product" means that a causal relationship between a medicinal product and an adverse event is at least a reasonable possibility.

►Adverse Reactions, Barium

Adverse Reactions, Barium

Emmanuelle Pinès
Pharmacovigilance Department, Guerbet, Roissy CDG, France
emmanuelle.pines@guerbet-group.com

Characteristics

Provided they are used with some precautions, barium-based contrast media carry the reputation of having a satisfactory safety profile with respect to the benefit they afford in diagnostic imaging. The notion of a satisfactory safety profile is to be alleged with caution because barium sulfate can sometimes be responsible for serious and unpredictable ►adverse reactions. In clinical trials, barium has usually been reported to be responsible for no or minor digestive discomfort. Larger postmarketing authorization surveys allowed for a more accurate picture of very rare complications such as barium extravasation or intravasation. In such a survey, 82 complications including 13 deaths were reported through retrospective questionnaires based on more than 730,000 examinations performed between 1992 and 1994 (1). In that survey, the most frequently reported reactions attributed to barium sulfate consisted of abnormal diffusion into or outside the peritoneum, barium impaction, and barium intravasation. Only one case of ►allergy was mentioned.

Allergic Reactions

Allergic reactions to barium sulfate have been reported to be in the range of several cases per several hundred thousand examinations (1/750,000), with serious cases being reported in millions. Cases of allergy to barium sulfate have been reported after barium enema and upper gastrointestinal tract examinations. Allergy in these cases is most probably due to one of the multiple ingredients contained in the barium mixture, including additives, preservatives, flavoring agents, dyes, antifoaming agents, vegetable gum, and so on. Glucagon given for its hypotonic effect has been incriminated in some cases, but was not administered in all published cases of allergy supposedly related to barium sulfate. In the same manner, latex contained in medical gloves or balloons may be responsible for serious allergic reactions that need to be identified as such before incriminating the contrast medium. The potential responsibility of lubricating agents also must not be neglected.

Allergic symptoms reported in cases of barium allergy usually involve the skin, with skin rash, urticaria, and pruritus, followed by effects on the respiratory tract and level of consciousness. Barium allergy can also take the form of a digestive angioedema, and cases of anaphylactic shock have been reported. A history of food allergy in children is certainly a risk factor. Finally, allergy to the barium entity itself remains to be proven (2, 3).

Barium Aspiration

Classical toxic complications of barium sulfate include inadvertent pulmonary inhalations that are responsible for toxic lesions of the respiratory tract. These complications usually occur in patients with altered respiratory function, head and neck cancer, bronchoesophageal fistula, or swallowing disorders, usually of neurological origin (1). Clinical consequences range from minor respiratory symptoms with visible barium on chest X-ray to severe chemical interstitial pneumopathy of possibly fatal evolution, particularly in elderly patients. Although diluted barium was the contrast medium used for bronchography in the past, it has a recognized toxicity for pulmonary tissues, and it induces, as attested by postmortem examinations and animal studies, an acute inflammatory edematous macrophagic reaction followed by fibrosis.

The density of barium is a factor of poor tolerance. The potential toxicity of gastric liquid, which may be inhaled together with the contrast medium, has also been evoked, based on what is seen in Mendelson's syndrome. Barium particles have been found in macrophagic cells associated with intraalveolar granuloma as well as septal and intraalveolar fibrosis. Indeed, after aspiration, barium particles that accumulate in the alveolar spaces are phagocytosed by alveolar macrophages. Others may pass directly across the alveolar epithelium into the alveolar or peribronchiolar interstitial tissue. Some are then transported *via* the lymphatic system in the interlobular septa and pleura. Radiological investigations have shown pulmonary opacities caused by the high atomic number of barium. Regions of involved lung depend on the patient's position during and after the aspiration. The basal segments of the lower lobes are most often involved when the patient is in the erect position, the middle lobes if the patient is leaning forward, and the posterior segments of the upper lobes or the superior segments of the lower lobes when the patient is in the recumbent position.

Asymptomatic fibrosis has even been reported to possibly last over 1 year after accidental barium inhalation. Depending on the patient's status and extension of the lesions, management includes one or more of the following measures: postural physiotherapy, oxygen therapy, antibiotic therapy, and bronchoscopic aspiration of the contrast medium (4, 5).

Barium Peritonitis

When perforation occurs during digestive opacification using barium sulfate, serious and possibly fatal complications may occur. The frequency of colon perforation following barium enema has been reported to be of 2–4 cases per 10,000 examinations with a mortality rate ranging from 20 to 100%. The nature of the extravasated digestive content is an important factor because the highest mortality rates have been reported in animals during barium-plus-feces-induced peritonitis. This mixture was shown to be more toxic than either barium or feces alone. The volume of contrast medium is also a major prognostic factor. Extraluminal barium toxic diffusion is more frequently observed after enema than during esophagastric perforating procedures.

The clinical presentation of barium peritonitis is that of classical peritonitis with subsequent loss of water and electrolytes, as well as sepsis. When barium comes in contact with the peritoneum, adhesions form very quickly, leading to obstruction that often requires surgical intervention. Fibrosis and barium granuloma occur as a result of foreign body reaction. Urgent surgical management aimed at removing as much barium as possible is usually required.

The systemic release of barium has been identified in some cases in which, following barium peritonitis, elevated levels of barium in the cerebral spinal fluid or plasma were found, which could explain the patients' altered neurological status. Barium poisoning may indeed be responsible for hypokalemia, arrhythmia, QT prolongation, pulmonary edema, digestive hypermotility, and myoclonus. It has also been deemed responsible for neurological damages provoking abnormal movements, coma, and even death following cerebral edema. It has been suggested that the unbound part of the barium was the toxic entity. The following mechanisms have been suggested for explaining the release of the free compound, particularly in cases of toxicity occurring a long time after a barium enema was done: sequestration of barium into the bone and subsequent release due to bone turnover; conversion of insoluble barium to a soluble form, $BaCl_2$, following digestive conversion from $BaSO_4$ by cationic exchange in the digestive tract; and finally, binding of barium to plasma proteins and release in its free form if plasma acidosis is present.

Hemofiltration aiming at removing barium in those cases produced some results. Barium extravasation has also been discovered years after the accidental diffusion around peripyloric soft tissues after unrecognized perforation. It may be responsible for retroperitoneal fibrosis when it takes place in that region (6, 7).

Barium Obstruction

Colonic obstruction following barium sulfate administration usually occurs in patients with underlying constipation, colonic stenosis, or diverticulosis. Any factor for colon atonicity such as hypothyroidism or the atonicity observed in elderly patients may be a risk factor because it is associated with a prolonged transit time. Barium obstruction is due to resorption of water from the barium mixture, which may stay in the digestive tract for several months and not be discovered until long after the examination. Barium inspissations take the form of a sometimes significant digestive mass, which usually requires radical surgical treatment. In less serious cases, medical treatment using lactulose may be sufficient. The possibility of barium obstruction, which is reported even with modern preparation, justifies precautions such as preventing dehydration before the examination, avoiding preexamination fasting, favoring patient mobility, and providing postexamination alimentation (8, 9).

Barium Granuloma

Barium granuloma may develop when the medium is administered to examine a digestive mucosa presenting with areas of discontinuity, either for pathological reasons such as inflammatory colitis or due to injury from tip insertion. Barium can thus be stocked in the submucosal layer or even move further down, possibly leading to, in cases of enema, proctitis and abscess. Granulomas occur as a result of foreign body reaction with chronic inflammation including fibroblastic proliferation and fibrosis. Histology shows macrophages and multinucleated foreign body giant cells with intracytoplasmic barium sulfate crystals. Granuloma takes the form of polypoid masses of variable sizes. Digestive damage may also take the form of large necrotic ulcers and may even mimic rectal carcinoma. Diagnosis is based on X-ray examination and biopsy results. Treatment depends on the extent of the lesions and eventual complications. It may consist of mucosa excision (10).

Venous Intravasation

Intravasation of barium is one of the most serious but fortunately extremely rare complications of barium examinations and is usually reported after barium enema but also has been observed after upper gastrointestinal tract examination. Intravasation has a fatal outcome in up to more than 67% of cases. Death occurs as a consequence of massive pulmonary embolisms within minutes of the accident. Intravasation after barium enema usually occurs in elderly patients who have weak sphincter tone, in patients with pathological or traumatic mucosal discontinuity, and after a balloon has been too highly inflated. It may also follow an inadvertently inappropriate positioning of the rectal tube in the vagina. Intravasations leading to portal vein embolization are said to be less serious than those with systemic vein embolization because in the former, the liver filters barium particles, and a very small amount of barium thus goes into the lung.

The territory of venous embolization depends on the site of barium intravasation. Intravasation in the small intestine, colon, or proximal part of the rectum results in barium embolization *via* the superior hemorrhoidal or mesenteric veins into the portal system. Intravasation in the distal part of the rectum results in embolization *via* the inferior and middle hemorrhoidal veins to the systemic circulation. Clinical symptoms may include respiratory distress, hypotension, shock, fever, and disseminated intravascular coagulation. Apart from showing the vascular thrombosis, computed tomography scanning reveals high density of organs such as the liver, spleen, lungs, renal cortex, and brain due to the presence of barium captured in the reticuloendothelial system. Depending on the situation, barium may also be seen in the inferior vena cava, heart, pulmonary arteries, and brain. After lung passage, thrombogenic barium particles are delivered into the systemic circulation, enter the lymphatic system, and are finally captured in the bones, where they are stocked.

Histological findings are those of classical reaction to barium sulfate, including granulomatous reaction, fibrosis, and stenosis. Treatment is symptomatic and includes respiratory assistance, antibiotic therapy, and vascular filling. Draining as much barium as possible in cases of early diagnosis may prevent further toxic diffusion.

Precautions such as identification of patients at risk, insertion of the tube by a radiologist or under a radiologist's control, careful assessment of rectal sphincter tone, radiological follow-up of tube positioning, and inflation of the balloon with great care should be respected. However, if intravasation does occur, early recognition and very quickly available resuscitation equipment are key factors for a favorable outcome. Barium intravasation leading to portal vein embolization may also mimic biliary fistula. The distribution of barium sulfate in the reticuloendothelial system has been compared with that of thorium dioxide. Finally, the potential consequences of an associated air embolism in cases of double-contrast examination must not be neglected (11, 12).

Miscellaneous

Isolated reports of acute appendicitis due to fecalith following barium enema have been published; these must be distinguished from barium appendicitis cases related

to local retention of barium. Baritosis of mediastinal lymph nodes has also been reported.

Bibliography

1. Blakeborough A, Sheridan MB, Chapman AH (1997) Complications of barium enema examinations: a survey of UK consultant radiologists 1992 to 1994. Clin Radiol 52:142–148
2. Seymour PC, Kesack CD (1997) Anaphylactic shock during a routine upper gastrointestinal series. Am J Roentgenol 168:957–958
3. Stringer DA, Hassall E, Ferguson AC et al (1993) Hypersensitivity to single contrast barium meal studies in children. Pediatr Radiol 23:587–588
4. Voloudaki A, Ergazakis N, Gourtsoyiannis N (2003) Late changes in barium sulfate aspiration: HRCT features. Eur Radiol 13:2226–2229
5. Tamm I, Kortsik C (1999) Severe barium sulfate aspiration into the lung: clinical presentation, prognosis and therapy. Respiration 66:81–84
6. Akinpelu S, Aw Yeang HW, Dean P et al (2001) Barium toxicity following intraperitoneal barium extravasation. Care of the Critical Ill 17:137–139
7. Kozianka Kielan W, Waleczek H (2003) Barium peritonitis—a study in pigs. Adv Clin Exp Med 12:569–573
8. Kounis NG, Zavras GM, Papadaki PJ et al (2003) Late colonic obstruction after barium meal examination in a myxoedematous patient. Int J Clin Pract 57:68–69
9. Pai ML, Acharya BS, Bapat RD (1997) Colonic chemobenzoar—intestinal obstruction due to barium inspissation. Indian J Gastroenterol 16:114–115
10. Lewis JW, Morris D, Kerstein MD et al (1975) Barium granuloma of the rectum: an uncommon complication of barium enema. Ann Surg 181:418–423
11. Steinman RM, Torres G, Stoupis C (1994) CT of abdominal barium intravasation. J Comput Assist Tomogr 18:149–151
12. Zalev AH (1997) Venous barium embolization, a rare, potentially fatal complication of barium enema: 2 case reports. Can Assoc Radiol J 48:323–326

Adverse Reactions, Iodinated Contrast Media, Acute Renal

James H. Ellis
Department of Radiology, University of Michigan, Ann Arbor, Michigan, USA
jimellis@umich.edu

Synonyms

Contrast induced nephrotoxicity (CIN); Contrast induced renal dysfunction; Contrast induced renal failure

Definition

Contrast induced nephrotoxicity (CIN), defined as a temporary or permanent reduction in renal function, is the acute renal adverse reaction to the administration of radiographic iodinated contrast medium (RICM). In practice, this can be a difficult definition to apply. In an occasional case, the administration of contrast medium is clearly the inciting event for the subsequent reduction in renal function. However, in many cases, patients receiving contrast medium have underlying illnesses that might lead to renal dysfunction, experience events that may damage the kidney (e.g., hypotension), and/or undergo other interventions (e.g., medications, surgery) that might contribute to a decline in renal status. Regardless, when renal dysfunction follows shortly upon the administration of a contrast medium that is known to be potentially nephrotoxic, and no other obvious acute events have occurred that are likely to be the cause, the etiology is usually assigned to the contrast medium.

Another issue with the definition of CIN is the degree of renal dysfunction that must occur, and how that dysfunction is to be measured, before the patient is deemed to have experienced nephrotoxicity. Assessment of glomerular filtration rate is considered the most accurate way to evaluate renal function, but direct measurements are difficult. Estimates of glomerular filtration rate can be obtained from measurements of serum creatinine levels. In most studies of CIN, however, raw serum creatinine levels are used, and CIN is defined as a specific increase of serum creatinine within a specified duration of observation. The increase in serum creatinine occurs not just from the reduction in renal excretion of creatinine that occurs essentially immediately after the contrast medium administration; the rise in serum creatinine also requires the body to produce creatinine, which takes time. Thus, it is typical to measure creatinine at some combination of 24, 48, and 72 h after contrast medium administration to detect a rise. The necessary increase is not uniformly agreed upon. One common definition is a rise in serum creatinine of 0.5 mg/dl (44 μmol/L) or an increase of 25% from baseline (1) but other values for the absolute and/or relative increases have been used. CIN defined by lab values may be necessary for scientific investigation but may not directly relate to clinically significant events at the patient level.

Indications

The indications for the use of contrast media are legion and will not be described here. However, no drug is without risk, and the administration of contrast media must be put to the same test as other medications, that is, do the potential benefits outweigh the potential risks? One of the risks of contrast medium administration is CIN, which varies with the amount and type of contrast medium administered as well as with patient condition (i.e., risk factors). With limited exceptions, the contrast

medium that causes CIN is almost always a RICM. Hence most of the information on CIN incidence, clinical significance, and methods for mitigating CIN risk come from studies on RICM.

Contraindications

A number of conditions can put a patient at higher risk of CIN than the population without such risk factors, and hence these conditions are considered relative contraindications to the administration of RICM.

Preexisting renal insufficiency is the most important of the many risk factors for the development of CIN(2) (ACR). Diabetes as the cause of nephropathy puts the patient at even greater risk, and when renal dysfunction occurs, it is more likely to be irreversible. However, the presence of diabetes mellitus alone is probably not a risk factor for CIN when renal function is normal. Other described risk factors include American Heart Association class IV congestive heart failure, hyperuricemia, dehydration, concurrent use of nephrotoxic drugs such as aminoglycoside antibiotics and nonsteroidal antiinflammatory agents, advanced age, and administration of large or repeated doses of contrast media (1–3). Multiple myeloma may not be an important risk factor if the patient is hydrated. The incidence of contrast induced renal failure is greatest when multiple risk factors are present.

Pregnancy/Lactation

Usually pregnant or lactating patients are excluded from studies on CIN or simply do not have the risk factors required for entry into the study. Thus, it is not known whether pregnant or lactating patients are at different risk for CIN than the general population. Typically for pregnant or lactating patients, the issues concerning RICM administration revolve around potential adverse effects on the fetus or neonate respectively. There is no evidence that administering RICM to pregnant patients causes CIN in the fetus. Studies have shown that, if a lactating mother is administered RICM or gadolinium contrast medium, the amount of contrast medium that is excreted in breast milk and absorbed by the breast-feeding neonate is small and much lower than the typical pediatric dose; consequently, there is no appreciable risk of CIN.

Use and Dosage

CIN results from direct toxicity to the kidneys and thus is dose related, with greater risk when larger doses of RICM are administered over shorter periods of time.

Low osmolality contrast media (LOCM) are less nephrotoxic than high osmolality contrast media (HOCM) in patients with preexisting renal impairment. Preliminary evidence has suggested that the use of iso-osmolality contrast media (IOCM) may further reduce the risk of CIN from RICM administration (2). At the time of this writing, this remains controversial as a general conclusion because the investigations to date involve only a single IOCM and LOCM. Comparable studies comparing various IOCM and LOCM are not yet available.

Gadolinium-based contrast media are considered nonnephrotoxic at the low doses used for MR. They are radiopaque (though less so per unit volume than standard RICM) and can be used as a RICM substitute. However, at equiattenuating doses, gadolinium agents are likely more nephrotoxic than LOCM (1).

Adverse Reactions

Most patients who receive contrast medium do not have their renal function assessed shortly before and at regular intervals in the few days after their imaging test. Thus the true incidence of CIN is unknown, though it is generally estimated at 2–7%, with the incidence varying with the population studied and the criteria used for diagnosis, as discussed above.

Many of the assumptions concerning CIN have been challenged in a review of the literature (4) that found that most studies of CIN involved cardiac catheterization and exceedingly few included a control group that did not receive RICM; it is possible that the incidence of CIN from intravenous RICM use has been overestimated.

In patients who suffer CIN, a rise in serum creatinine elevation is first detectable 1–3 days from RICM injection, typically peaks at 3–7 days, and usually returns to baseline within 10–14 days. Some patients may suffer permanent reduction in renal function. There is no effective treatment for established CIN, hence prevention is key. Avoiding large or repeated doses of RICM or switching to imaging studies that do not employ potentially nephrotoxic agents reduces the risk, as does discontinuing other concomitant nephrotoxic drugs if possible.

Interactions

Various interventions have been tried to reduce CIN risk, with little success. One of the most clearly efficacious is hydration, which can be oral or (and more commonly studied) intravenous. Intravenous normal saline is superior to half-normal saline as a hydrating agent. Perhaps hydration

with sodium bicarbonate solutions may be even more effective in reducing CIN risk; the evidence is very limited.

Whether the addition of other drugs improves on saline hydration alone is controversial. Acetylcysteine, typically administered orally but also tested as an intravenous drug, has been widely studied with mixed results; many investigations have shown a protective effect and others have not. Even metaanalyses have come to opposite conclusions regarding the efficacy of acetylcysteine. Several possible reasons for these varying results have been discussed (5). In part because of low risk, acetylcysteine is widely used. Intravenous theophylline may reduce CIN risk, but only limited evidence is available.

A substantial limitation to our knowledge is that some drugs simply lower serum creatinine during short term administration. Administering such a drug would appear to reduce CIN by the typical criteria used, even if long term renal function alterations were not affected. Studies to date have not employed a control group that receives the premedication but not the contrast medium, and in addition most studies do not include long term follow up. These issues compound the problems of how much clinical significance there is to a transient rise in laboratory values, how important it is to minimize that rise, and what, if any, is the relationship between that initial rise and clinically significant renal dysfunction caused by RICM.

There is no direct interaction between RICM and metformin, an oral antihyperglycemic medication. Metformin itself is not nephrotoxic, but it is excreted by the kidneys. If a patient develops CIN renal dysfunction, and if metformin continues to be administered, the patient's blood levels of metformin may rise, putting the patient at elevated risk for lactic acidosis, a rare but often fatal complication of metformin therapy. It is recommended that metformin be discontinued at the time that RICM is administered and be resumed only after the patient's renal function has been determined to be normal a minimum of 48 h later (to allow time to detect CIN if it occurs) (1, 2).

Bibliography

1. Contrast Media Safety Committee (2006) Guidelines on Contrast Media: Version 5.0. European Society of Urogenital Radiology, Vienna, Austria
2. Committee on Drugs and Contrast Media (2004) Manual on Contrast Media: Version 5.0. American College of Radiology, Reston, Virginia, USA
3. Morcos SK (2004) Prevention of contrast media nephrotoxicity—the story so far. Clin Radiol 59:381–389
4. Rao QA, Newhouse JH (2006) Risk of nephropathy after intravenous administration of contrast material: a critical literature analysis. Radiology 239:392–397
5. Fishbane S, Durham JH, Marzo K et al (2004) N-Acetylcysteine in the prevention of radiocontrast-induced nephropathy. J Am Soc Nephrol 15:251–260

Adverse Reactions, Iodinated Contrast Media, Acute, Non renal

William H. Bush, Jr.
Department of Radiology, University of Washington, Seattle, USA
whbush@u.washington.edu

Synonyms

Allergic reactions; Allergic-like reactions; Anaphylactic reactions; Anaphylactoid reactions; Anaphylaxis-like reactions; Contrast reactions; Hypersensitivity contrast reactions; Idiosyncratic contrast reactions.

Definition

Clinical manifestations of an acute reaction to a contrast medium vary considerably from a mild reaction causing mild urticaria/hives to a serious reaction that is indistinguishable from anaphylaxis. Etiology of these reactions is uncertain; they appear to involve a complex relationship between the contact, immune, coagulation, and complement systems of the body. As to whether these reactions to iodinated contrast agents are true allergic reactions is still unsettled. Supporting an "allergic theory" is the observation that contrast reactions mimic true anaphylaxis. Like true allergic reactions, a small amount of contrast, even a "test dose," can elicit a severe, life-threatening reaction. Conversely, demonstration of IgE antibodies directly to the contrast agent has been questioned (1). Additionally, contrast reactions fail many of the relationships defining true allergic reactions: preexposure to the offending agent (contrast medium) often has not occurred; pretesting is not reliably consistent; reactions do not occur consistently or do not occur with the same severity on repeat exposure to the same contrast agent that caused an initial reaction. Hence, the term "idiosyncratic" (Greek: one's own peculiar susceptibility) has been used to describe these unpredictable events. The relationship of iodine to the initiation of a contrast reaction is open to debate and seems unlikely to be the causative agent; more likely it is the molecule to which the iodine is bound that is the culprit. For example, seafood is often used as the example of an iodine-containing substance that causes anaphylactic reactions in some individuals; however, many other foods containing large amounts of iodine do not cause allergic-like reactions. Furthermore, gadolinium MR contrast agents cause anaphylactic-like reactions, albeit less frequently, that are identical to those caused by iodinated contrast agents.

Characteristics

Mechanism

The process by which contrast agents cause reactions seems multifactorial.

Interaction of contrast agents with biological molecules appears to relate to the hydrophilicity of these iodine-bound benzene ring molecules. It is suggested that the toxicity of a contrast agent is less if the benzene ring is shielded by large hydrophilic groups and the arrangement of the hydroxyl groups. There is variation in the prevalence of reactions associated with various iodinated contrast agents.

From his extensive research, Elliot Lasser (1) has proposed a mechanism to help understand reactions to iodinated contrast media: the large contrast-containing molecule causes steric hindrance or overload effect on the antigen-binding sites on IgE. The contrast medium (CM) does not bind to the antigen binding site on IgE; instead it binds to the Fc (constant) portion of the molecule. In diluted concentrations, CM activates the IgE, but in higher concentration it inhibits the antigen-binding site on IgE. This varies with the particular contrast medium. Since the immunoglobulin binding is nonspecific, the resultant reaction depends on the quantity of IgE that a particular patient has in his/her circulation and on his/her mast cells at the time the contrast medium is administered. This nonspecific binding helps explain why allergic patients are at particular risk and why previous CM administration is not necessary for a reaction to occur. Since mast cell activation, when occasioned following CM injection, depends on the interaction of the antigen (CM: pseudoantigen) with an antibody (IgE), albeit an interaction with the Fc part of the IgE, one can argue that reactions to contrast media should be considered true anaphylaxis.

Additionally, direct contact of the contrast agent with the endothelium of blood vessels is postulated to activate Factor XII; this substance in turn activates kallikrein; kallikrein activates bradykinin; bradykinin activates prostaglandin and the leucotrienes (1, 2). The activation/release of these potent mediators can lead to a contrast reaction. Bradykinin can mimic all the significant pathophysiological effects of histamine but is far more potent; this sequence of events or pathway would not be "blocked" by antihistaminic drugs.

As proposed by Lalli, contact by intravascularly injected contrast on the bare areas of the brain/area postrema/limbic can stimulate the central nervous system to produce many of the effects associated with contrast reactions: nausea, vomiting, change in blood pressure. Iodinated contrast agents exhibit much more toxicity when intraventricular contact occurs than when the contrast is administered intravascularly.

The exact mechanism of the acute, anaphylactic/anaphylaxis-like reaction to iodinated contrast agents is, therefore, complex and yet to be fully elucidated.

Incidence

Overall, about 3% of patients who receive nonionic, lower-osmolality monomeric contrast media (LOCM) experience a contrast reaction, though the vast majority of reactions are mild and require no treatment (2, 3). Moderate reactions, such as bronchospasm or hypotension, occur with approximately 1 of 250 patient injections (0.4%). Severe, like-threatening reactions are very uncommon, occurring with 1 of 2500 patient injections (0.04%) (4). The occurrence of a severe reaction with LOCM is much less frequent (1/5th) than caused by the older conventional ionic higher-osmolality agents (HOCM). With the newer nonionic iso-osmolal dimers, acute idiosyncratic reactions seem to occur about as frequently as with the LOCM; some nonionic dimers have an increased frequency of delayed reactions, though invariably mild.

Occurrence of a fatal reaction is much less frequent than 30 years ago. Exact numbers are difficult to obtain, but using the largest series of reported reactions, the risk of a fatal reaction after an injection of iodinated LOCM is approximately 1:170,000 injections (4). The change over 30 years from a risk of 1:30,000 to 1:170,000 likely reflects the increasing use of nonionic LOCM and the increased emphasis and training about the treatment of reactions by radiologists.

Adverse Reactions

Acute Contrast Reactions

Key to treating a contrast reaction is recognition of what adverse effect or reaction is occurring in the patient (5). Some patients are uncomfortable but calm: those experiencing nausea, vomiting, hives, itching, redness. Other patients are anxious and agitated, usually caused by hypoxia: those experiencing edema of airways, bronchospasm, laryngeal edema, pulmonary edema. And still other patients are less responsive, subdued, or unresponsive: those who have become hypotensive. Recognition of these signs and the patient's behavior helps direct search for identification of the exact reaction and, thereby, the more specific and effective treatment (discussed in a later chapter in this section).

Nausea and vomiting: Less common with nonionic LOCM; rarely of significance; however, may be the initial component of a more serious reaction.

Urticaria/hives, itching, diffuse erythema: More common than nausea and vomiting; varies in severity; may be a

component of a more generalized, acute systemic reaction; treated symptomatically if occurs as an isolated event.

Angioedema: A significant reaction since it can narrow the airways; a contrast reaction with angioedema of the face and lips should alert the radiologist that edema of the lower airway, including the larynx, may also be occurring.

Laryngeal edema: A serious, life-threatening event requiring prompt and aggressive treatment; anxious patient; signs include coughing, trying to clear throat, hoarseness, squeaky voice; sense of lump in throat; patient has difficulty getting air "in."

Bronchospasm: Resembles the classic "asthma attack;" anxious patient; chest tightness, shortness of breath, wheezing; patient has difficulty getting air "out;" often history of similar attacks.

Hypotension with responsive tachycardia: Usually a component of an acute, generalized systemic anaphylaxis-like reaction; can complicate and slow absorption of treatment medications used to treat the reaction.

Hypotension with vagal-induced bradycardia (vaso-vagal reaction): Presents with symptoms of hypotension plus a very slow heart rate; calm, subdued patient; diaphoretic, cool skin. Since patients are already supine/recumbent, the severity of the reaction encountered is usually much worse than when a vaso-vagal reaction or "fainting spell" occurs in an upright patient. Key to diagnosis is recognizing the bradycardia.

Acute, generalized systemic reaction: Usually has many of the above components—hives, redness, angioedema, airway compromise, hypoxia, hypotension; requires early, active, and aggressive treatment.

Acute pulmonary edema: Uncommon; may be due to a reaction directly in the airways and lungs or may reflect cardiac decompensation and/or myocardial infarction.

Cardiopulmonary collapse/cardiac arrest: May occur suddenly without preliminary signs; may evolve rapidly from initial nausea and vomiting or from a moderate contrast reaction to complete cardiovascular collapse.

Other Adverse Contrast Reactions

Neurotoxicity: Neurotoxicity can be caused by direct contact of a contrast medium with the central nervous system (intrathecal or intracisternal); may occur from "indirect" contact *via* intravascular injection. After intrathecal injection (e.g., in the lumbar subarachnoid space), some contrast normally diffuses rostrally in the spinal canal by cerebrospinal fluid (CSF) circulation and/or gravity; neurological manifestations of contrast toxicity may not appear for 2–24 h after spinal canal injection. Neurotoxicity varies with the contrast agent (6). Conventional ionic contrast media cause severe toxic reactions when injected inadvertently into the CSF.

Effect on the thyroid gland and function: Early studies from the 1970s showed transient hypothyroidism in the fetus when ionic HOCM was administered in amniotic fluid. Intravascularly administered contrast crosses the placenta. A more recent, though single, study showed no adverse affect on the neonatal thyroid by nonionic LOCM (7). In older patients with hyperthyroidism, thyrotoxicosis may occur in a delayed (days to weeks) manner, even after LOCM.

Hypertensive reaction: Very uncommon; sudden onset of severe headache; sudden change in mentation; seizure.

Adverse Effects in Children

Children have a lower incidence of contrast reactions. The reactions that they experience tend to be anaphylaxis-like and/or involve the airway (8). Children have strong hearts, so cardiovascular-type reactions are very uncommon. The current use of lower osmolality contrast agents minimizes the osmotic effect that could be experienced with older HOCM; nonionic LOCM are also much less toxic if inadvertently aspirated.

Nonvascular Routes of Administration that can Result in an Acute Contrast Reaction

Both high-osmolality ionic (HOCM) water-soluble contrast and lower-osmolality contrast (LOCM) are used to opacify the GI tract if barium is not desired. If iodinated contrast is absorbed into the bloodstream, the risk of an allergic-like contrast reaction can be just as significant and severe as if the iodinated contrast were administered directly intravascularly. Contrast media are absorbed rapidly from the peritoneal cavity or severely inflamed intestinal mucosa. Situations of potential significant absorption occur when water-soluble iodinated contrast is used to opacify the GI tract in patients with inflammatory bowel disease, bowel perforation, and potentially during high-grade intestinal obstruction when ischemia of the bowel wall is present. Reactions can be similar in presentation and severity as when they occur after intravascular administration.

Anaphylactic-like reactions to contrast media are not considered to be dose related. Therefore, other routes of administration that can lead to systemic absorption and an allergic-like, acute contrast reaction include: endoscopic retrograde pancreatography (ERCP) with aggressive injection; retrograde ureteropyelography with injection that results in pyelo-venous backflow; extensive leak into the retroperitoneum; cystography with bladder rupture or leak.

Summary

Mild reactions to iodinated contrast media are relatively common but severe reactions are rare. The exact etiology

and mechanism of these allergic-like reactions are not fully defined though they appear to be caused by the contrast molecule, rather than the iodide itself, through a complex series of events that affects IgE plus activation of other mediators such as the leucotrienes and bradykinin. Reactions to contrast media appear relatively unique to the individual patient and are not consistently predictable. These reactions present in many fashions and severities. Recognizing the signs and presentations allows the radiologist and clinician to identify the type of reaction which, in turn, facilitates rapid treatment and reversal of the reaction.

Pregnancy and Lactation

Iodinated contrast agents cross the placenta. Iodinated contrast media are approved by the Food and Drug Administration (FDA) of the USA for use during pregnancy and in infants and pediatric patients. The over-riding decision about the use of iodinated contrast in the pregnant patient usually relates to the radiation necessary to generate the image and risk of radiation to the fetus.

Iodinated contrast and lactation become of concern only because the nursing infant is an "innocent bystander"—the mother, not the infant, needs the contrast medium for the imaging study. Iodinated contrast is approved for use in infants. Studies have shown that less than 1% of contrast administered intravascularly to the mother appears in her breast milk and less than 1% of that is absorbed from the infant's gastrointestinal tract; this represents less than 1% of recommended dose for an infant undergoing an imaging study (8). An option to avoid any contrast exposure to the infant is for the lactating mother to use a breast pump for days prior to the contrast study to obtain and store (freeze) breast milk; then she pumps and discards the breast milk for 2 days after her contrast study.

In the USA, gadolinium agents are not approved by the FDA for use in pregnancy or in pediatric patients under age 2. However, for lactating/nursing mothers after pregnancy, the same principles for contrast use as with iodinated contrast can be applied since less than 0.04% of intravascularly administered gadolinium appears in the breast milk and less than 1% is absorbed by the nursing infant (8).

Bibliography

1. Lasser EC (2004) Chasing contrast molecules: A 45 year quixotic quest. Acad Radiol 11:1190–1196
2. Bush WH and Lasser EC (2000) In: Pollack HM and McClellan BL (eds) Clinical Urography. 2nd edn. WB Saunders Co., Philadelphia, pp 43–66
3. Thomsen HS and Morcos SK (2004) Contrast media safety committee of the European Society of Urogenital Radiology (ESUR). Management of acute adverse reactions to contrast media. Eur Radiol 14:476–481
4. Katayama H, Yamaguchi K, Kozuka T et al (1990) Adverse reactions to ionic and nonionic contrast media: a report from the Japanese Committee on the Safety of Contrast Media. Radiology 175:621–628
5. Krecke KN (1999) Presentation and early recognition of contrast reactions. In: Bush WH, Krecke KN, King BF et al (eds) Radiology Life Support (Rad-LS). Hodder Headline/Arnold Publishers, London, pp 22–30
6. Leonardi M and Agati R (1999) Neurotoxicity. In: Thomsen HS, Muller RN, and Mattrey RF (eds) Trends in Contrast Media. Springer Verlag, Berlin, pp 95–116
7. Cohan RH and Ellis JH (1999) Adverse reactions to iodinated radiographic contrast media. In: Thomsen HS, Muller RN, and Mattrey RF (eds) Trends in Contrast Media. Springer Verlag, Berlin, pp 117–132
8. Committee on Drugs and Contrast Media of the American College of Radiology. Manual on Contrast Media, Version 5.0. American College of Radiology, 2004, Reston, pp 7–11, 35–39, 45–50

Adverse Reactions, Iodinated Contrast Media, Delayed

Fulvio Stacul[1,*], Judith A. W. Webb[2], Henrik S. Thomsen[3], Sameh K. Morcos[4]
[1]Institute of Radiology, Ospedale di Cattinara, Trieste, Italy
[2]Department of Diagnostic Imaging, St Bartholomew's Hospital, London, UK
[3]Department of Diagnostic Radiology, Copenhagen University Hospital at Herlev, Herlev, Denmark
[4]Department of Diagnostic Imaging, Northern General Hospital, Sheffield Teaching Hospitals NHS Trust, Sheffield, UK
*U.C.O. di Radiologia, Ospedale di Cattinara, Strada di Fiume, Trieste, Italy
fulvio.stacul@aots.sanita.fvg.it

Synonyms

Delayed adverse reactions; Late adverse reactions

Definition

Delayed adverse reactions to intravascular iodinated contrast media are defined as reactions occurring between 1 h and 1 week after contrast medium injection.

Characteristics

Many aspects of delayed adverse reactions remain controversial and there is widespread uncertainty among radiologists about the incidence, significance, and management of delayed reactions.

Reaction Type and Severity

The symptoms of delayed reactions most commonly described are headache, skin rash, itching, nausea, dizziness, urticaria, fever, arm pain, and gastrointestinal disturbances. However delayed reactions to enhanced and unenhanced CT were compared, only the skin reactions occurred more frequently in the group who received contrast medium (nonionic monomer or dimer) and skin reactions appear to account for the majority of true delayed reactions. The types of delayed skin reactions and their relative frequencies are similar to those, which occur with many other drugs. Maculopapular rash is observed in the majority of affected patients. Other frequently occurring skin reactions are angioedema, urticaria, erythema, macular exanthema, and scaling skin eruption.

In most cases the skin reactions are mild or moderate, that is they may be discomforting and require specific treatment (steroids, antihistamines, topical emollients). Depending on their localization, these reactions may be more or less disturbing, the most troublesome being those confined to the palms, soles of the feet, or face. Severe delayed reactions needing hospital treatment and/or leading to persistent disability or death have been reported, but are very rare. Furthermore, often patients who experienced delayed reactions had underlying serious medical conditions.

A number of pathophysiological mechanisms have been proposed for delayed skin reactions. Although the pathogenesis is still not fully understood, it appears that many are type IV hypersensitivity reactions, that is they are T-cell mediated (1, 2). The skin reactions often show typical features of delayed hypersensitivity including exanthematous rash, positive skin tests, and lymphocyte rich dermal perivascular infiltrate sometimes accompanied by eosinophils on skin biopsy.

If there is doubt about whether contrast medium is responsible for the skin reaction, skin testing (patch and delayed intradermal tests) may be attempted (1). However, the low negative predictive value of such tests should be reminded and it remains to be established if skin testing is also a suitable tool for selection of an alternative contrast medium.

Frequency

Determining the true frequency of delayed adverse reactions to contrast media from the literature is difficult. First, a variety of different methodologies have been used, with different methods of data collection (questionnaires, patient interviews in person or by phone), different start points (at a variety of times from 30 min after contrast medium injection) and different data collection periods (from 1–7 days). A further problem is the fact that the greater the time interval between the contrast medium injection and the onset of symptoms, the more difficult it is to be sure that the symptoms are contrast medium-induced. This has been highlighted by studies of "background noise" by several investigators who have shown a high incidence of delayed symptoms after radiological investigations not using contrast medium.

The frequency of delayed adverse reactions to nonionic monomers has been reported to be between 0.52 and 23%. Several studies suggest that the incidence in the 1–24 h period is 4% or less and in large studies the frequency of delayed skin reactions was 1–3% over a period of 7 days. There do not appear to be significant differences in the incidence of delayed reactions between ionic and nonionic agents, nor between the different nonionic monomers. No significant differences have been found between the nonionic monomers and the ionic dimer ioxaglate either.

The available evidence suggests that delayed skin reactions are more common with nonionic dimers. The nonionic dimer iodixanol caused more delayed skin reactions than either the ionic dimer ioxaglate or the nonionic monomers iopamidol and iomeprol (4). In another study, the frequency of delayed skin reactions with iodixanol was similar to that with nonionic monomer, but more of the iodixanol patients were treated with hydrocortisone or antihistamine (3). The nonionic dimer iotrolan was withdrawn in 1995 because of the high incidence of delayed reactions, particularly skin reactions, initially reported from Japan but subsequently also from the USA.

Reaction Onset and Duration

Delayed skin reactions after contrast medium develop within 1–7 days with the majority occurring within the first 3 days. Most reactions are self-limiting and have resolved by 7 days, with up to three-quarters resolving within 3 days.

Predisposing Factors

A number of factors appear to predispose to the development of delayed adverse reactions. A previous reaction to contrast medium is an important predisposing factor increasing the risk by a factor of 1.7 to 3.3. However, there is no evidence that patients with a

Adverse Reactions, Iodinated Contrast Media, Delayed. Table 1 ESUR guidelines for late adverse reactions to intravascular iodinated contrast media

Definition	A late adverse reaction to intravascular iodinated contrast medium is defined as a reaction, which occurs 1 h to 1 week after contrast medium injection
Reactions	A variety of late symptoms (e.g., nausea, vomiting, headache, musculoskeletal pains, fever) have been described following contrast medium, but many are not related to contrast medium
	Skin reactions of similar type to other drug eruptions are true late adverse reactions. They are usually mild to moderate and self-limiting
Risk factors for skin reactions	Previous contrast medium reaction Interleukin-2 (IL-2) treatment
Management	Symptomatic and similar to the management of other drug-induced skin reactions
Prophylaxis	Generally not recommended Patients, who have had a previous serious late adverse reaction, can be given oral steroids (see ESUR Guidelines on prevention of generalized adverse reactions)
Recommendations	Tell patients who have had a previous contrast medium reaction or who are on IL-2 treatment that a late skin reaction is possible and that they should contact a doctor if they have a problem

previous delayed reaction are at increased risk for a subsequent immediate anaphylactic reaction. A history of allergy is a further risk factor, increasing the likelihood of a reaction approximately twice. Especially, a history of drug and contact allergy seems to predispose to delayed skin reactions after contrast medium exposure. A seasonal variation in the incidence of delayed skin reactions has been described: a significantly higher incidence of delayed adverse reactions during the pollinosis period was observed. Females are more likely to develop delayed adverse reactions than males. Coexisting diseases also appear to predispose to delayed reactions, especially renal disease, but also cardiac and liver disease and diabetes mellitus. Some of the most severe skin reactions reported occurred in patients with systemic lupus erythematosus or patients who were taking hydralazine, which induces a lupus-like syndrome in some patients. Bone marrow transplantation patients were reported to be another risk group for severe contrast medium induced skin eruptions.

The increased incidence of delayed reactions to contrast media in patients who have received interleukin-2 (IL-2) immunotherapy is well documented, with an increased frequency of 2 to 4 times. Skin rash, pruritus, and flu-like syndrome were all more frequent in patients who had received IL-2.

Prophylaxis

In view of the infrequent and self-limiting nature of the great majority of delayed reactions, it does not seem appropriate to warn patients with no special risk factors about the possibility of a delayed reaction. However, it is recommended that patients who have had either a previous delayed skin reaction after contrast medium administration or suffer from major drug or contact allergy are warned about the possibility of a delayed skin reaction and told to contact a doctor if they have a problem.

If patients who have previously had a delayed skin reaction to iodinated contrast medium require further contrast medium, it is recommended that an alternative contrast medium is chosen and steroid prophylaxis is given. However, because of frequent cross-reactivity among different contrast media, change of contrast agent is no guarantee against a repeat reaction (1).

Conclusion

Delayed adverse reactions to iodinated contrast media have been recognized for 20 years. They are mainly mild or moderate skin reactions, which develop from 1 to 7 days after contrast medium administration and usually resolve with 3 to 7 days. The majority of these cutaneous reactions are T-cell mediated allergic reactions. Simple guidelines were proposed by the Contrast Media Safety of the European Society of Urogenital Radiology (ESUR) (5) and are reported here (Table 1).

Bibliography

1. Brockow K, Christiansen C, Kanny G et al (2005) Management of hypersensitivity reactions to iodinated contrast media. Allergy 60:150–158
2. Christiansen C, Pichler WJ, Skotland T (2000) Delayed allergy-like reactions to X-ray contrast media: mechanistic considerations. Eur Radiol 10:1965–1975
3. Rydberg J, Charles J, Aspelin P (1998) Frequency of delayed allergy-like adverse reactions following injection of intravascular non-ionic contrast media. A retrospective study comparing a non-ionic monomeric contrast medium with a non-ionic dimeric contrast medium. Acta Radiol 39:219–222
4. Sutton AGC, Finn P, Campbell PG et al (2003) Early and delayed reactions following the use of iopamidol 340, iomeprol 350 and iodixanol 320 in cardiac catheterization. J Invas Cardiol 15:133–138
5. Webb JAW, Stacul F, Thomsen HS et al (2003) Delayed adverse reactions to intravascular iodinated contrast media. Eur Radiol 13:181–184

Adverse Reactions, Iodinated Contrast Media, Predisposing Factors

Judith A W Webb
Diagnostic Radiology Department, The London Clinic, London, UK
jawwebb@btopenworld.com

Characteristics

Predisposing Factors

The choice of contrast medium and certain patient-related factors may predispose to an acute idiosyncratic reaction to intravascular iodinated contrast medium.

a. Contrast medium type
   The use of low osmolality nonionic agents reduces reaction rates by a factor of 4 to 5 compared to high osmolality ionic agents (1).
b. Patient factors (2)
   A previous reaction to contrast medium is the most important factor predisposing to an acute idiosyncratic reaction. Asthma is another significant risk factor. A history of drug or food allergy, or of hayfever or eczema, all increase the risk of reaction but less than asthma. Allergy to seafood is not a more significant risk factor than allergy to other foods. Allergy to topical iodine skin preparations does not seem to predispose to acute contrast medium reactions. There is controversy about whether β-blockers increase the incidence of contrast medium reactions. However, β-blockers can impair the response to treatment if a reaction occurs.

Prevention Measures

Measures to reduce the risk of acute idiosyncratic reactions to iodinated contrast media should be used in all patients, with special precautions taken in patients considered to be at increased risk.

a. In all patients, the key measures to reduce the risk of reaction are
   - use a low osmolality nonionic agent
   - keep the patient in the Radiology Department for 30 min after contrast medium injection, since most reactions occur during this time
   - have the drugs and equipment for resuscitation readily available
b. Patients at increased risk of an acute reaction give a history of
   - previous generalised contrast medium reaction, either moderate or severe
   - asthma
   - allergy requiring medical treatment

In patients at increased risk, the key measure to reduce the risk of reaction are:

- Check that iodinated contrast medium is essential. Would another test (e.g. ultrasonography, magnetic resonance imaging) give the required diagnostic information?
- Choose a different iodinated agent for previous contrast medium reactors.
- Consider the use of pre-medication, especially in previous contrast medium reactors and high-risk patients.
- A suitable pre-medication regime is prednisolone 30 mg (or methylprednisolone 32 mg) orally given 12 and 2 h before contrast medium.
- H2 antihistamines may also be used

Pre-medication

The use of steroid pre-medication is controversial and opinion is divided (2). Evidence for a beneficial effect of steroids was greater with the high osmolality ionic agents, but the available evidence does suggest that steroids reduce the chance of a reaction to low osmolality nonionic agents (3). If an anaphylactic reaction occurs, steroids are beneficial because they reduce the release of chemical mediators. To be effective, steroids must be given at least 6 (and preferably 12) h before contrast medium.

Treatment

First-line drugs and instruments should be available in the examination room so that acute idiosyncratic adverse reactions can be managed promptly (4):

- Oxygen
- Adrenaline 1:1,000
- Antihistamine H1, suitable for injection
- Atropine
- β-2-agonist metered dose inhaler
- Intravenous fluids—normal saline or Ringer's solution
- Anti-convulsive drug (e.g. diazepam)
- Sphygmomanometer
- One-way mouth breather apparatus.

If there is a significant acute reaction, important early measures are:

- Maintain an adequate airway

- Check the pulse and blood pressure. Differentiation between hypotension due to bradycardia (indicating a vagal reaction) or tachycardia (indicating possible anaphylaxis) is important.
- Give oxygen at 6–10 L/min by mask
- Give normal saline intravenously.

The first-line treatment of acute reactions to contrast media is largely symptomatic and is outlined in Table 1 (4).

Adverse Reactions, Iodinated Contrast Media, Predisposing Factors. Table 1 Simple guidelines for the first-line treatment of acute reactions to contrast media (Thomsen HS, Morcos SK and Members of Contrast Media Safety Committee of ESUR, 2004)

Reaction	Treatment
Nausea/ vomiting	Transient: supportive treatment
	Severe: protracted: appropriate antiemetic drugs should be considered
Urticaria	Scattered, transient: supportive treatment including observation
	Scattered, protracted: appropriate H1-antihistamine intramuscularly or intravenously should be considered. Drowsiness and/or hypotension may occur
	Profound: consider adrenaline 1:1,000, 0.1–0.3 mL (0.1–0.3 mg) intramuscularly in adults, 0.01 mg/kg intramuscularly up to 0.3 mg maximum in children. Repeat as needed
Bronchospasm	1. Oxygen by mask (6–10 L/min)
	2. β-2-agonist metered dose inhaler (2–3 deep inhalations)
	3. Adrenaline
	Normal blood pressure
	Intramuscular: 1:1,000, 0.1–0.3 mL (0.1–0.3 mg; use smaller dose in a patient with coronary artery disease or elderly patient)
	In paediatric patients: 0.01 mg/kg up to 0.3 mg maximum
	Decreased blood pressure
	Intramuscular: 1:1,000, 0.5 mL (0.5 mg) in adults: in paediatric patients: 0.01 mg/kg intramuscularly
Laryngeal oedema	1. Oxygen by mask (6–10 L/min)
	2. Intramuscular adrenaline (1:1,000), 0.5 mL (0.5 mg) for adults, repeat as needed
Hypotension	Isolated hypotension
	1. Elevate patient's legs
	2. Oxygen by mask (6–10 L/min)
	3. Intravenous fluid: rapidly, normal saline or lactated Ringer's solution
	4. If unresponsive: adrenaline: 1:1,000, 0.5 mL (0.5 mg) intramuscularly, repeat as needed
	Vagal reaction (hypotension and bradycardia)
	1. Elevate patient's legs
	2. Oxygen by mask (6–10 L/min)
	3. Atropine 0.6–1.0 mg intravenously, repeat if necessary after 3–5 min, to 3 mg total (0.04 mg/kg) in adults. In paediatric patients give 0.02 mg/kg intravenously (maximum 0.6 mg per dose), repeat if necessary to 2 mg total
	4. Intravenous fluids: rapidly, normal saline or lactated Ringer's solution
Generalised anaphylactoid reaction	1. Call for resuscitation team
	2. Suction airway as needed
	3. Elevate patient's legs if hypotensive
	4. Oxygen by mask (6–10 L/min)
	5. Intramuscular adrenaline (1:1,000), 0.5 ml (0.5 mg) in adults: Repeat as needed. In paediatric patients 0.01 mg/kg to 0.3 mg maximum dose)
	6. Intravenous fluids (e.g., normal saline, lactated Ringer's)
	7. H1-blocker, e.g., diphenhydramine 25–50 mg intravenously
	8. β-2-agonist metered dose inhaler for persistent bronchospasm: 2 or 3 inhalations

References

1. Katayama H, Yamaguchi K, Kozuka T et al (1990) Adverse reactions to ionic and nonionic contrast media. Radiology 175: 621–628
2. Webb JAW (2006) Prevention of acute reactions. In: Thomsen HS (ed) Contrast Media—Safety Issues and Guidelines. Springer-Verlag, Heidelberg, pp 11–17
3. Lasser EC, Berry CC, Miskin MM et al (1994) Pretreatment with corticosteroids to prevent adverse reactions to nonionic contrast media. Am J Roentgenol 162:523–526
4. Thomsen HS, Morcos SK and Members of Contrast Media Safety Committee of ESUR (2004) Management of acute adverse reactions to contrast media. Eur Radiol 14:476–481

Aganglionosis

A complete absence of ganglion cells in the myenteric and submucosal plexuses of the colon.
►Hirschsprung's Disease and Related Disorders

Aganglionosis of the colon

►Hirschsprung's Disease and Related Disorders

Agenesis of the Corpus Callosum

Agenesis of the corpus callosum there is no development of the corpus callosum, one of the cerebral commissures. The lack of formation of callosal axons, or when the axons fail to cross the midline, will lead to several alterations in this region.
►Congenital Malformations, Cerebrum

Agenesis of Dorsal Pancreas

►Congenital Anomalies of the Pancreas

Agenesis, Pancreatic

Congenital absence of the pancreatic gland. Complete pancreatic agenesis is extremely rare and usually incompatible with life. In agenesis of the dorsal pancreas only the pancreatic head is present. Agenesis of the ventral pancreas and uncinate process has also been described.
►Congenital Abnormalities, Pancreatic

Aging Brain

Massimo Filippi[1,2], Federica Agosta[1], Maria A. Rocca[1]
[1]Neuroimaging Research Unit, Department of Neurology, Scientific Institute and University Ospedale San Raffaele, Via Olgettina, Italy
[2]MRI Research Group, Scientific Institute Fondazione Don Gnocchi, Milan, Italy
m.filippi@hsr.it

Definitions

Normal aging of the brain can be defined as a set of structural, metabolic, and functional abnormalities of both the gray matter (GM) and white matter (WM). All those magnetic resonance (MR) sequences which are sensitive to the detection of focal areas of tissue abnormalities and which provide reliable estimate of atrophy, such as dual-echo, T1-weighted, and fast fluid-attenuated inversion recovery (FLAIR), are usually referred to as conventional MR imaging (MRI). Conventional MRI, however, does not provide information about the nature of tissue changes occurring both inside and outside focal macroscopic lesions. ►Magnetization transfer (MT) MRI, ►diffusion-tensor (DT) MRI, ►functional MRI (fMRI), and ►proton MR spectroscopy (^{1}H-MRS) have the potential to provide at least partial information about the nature of structural and metabolic changes occurring in the normal aging brain.

Characteristics

Imaging ►White Matter Hyperintensities (WMHs)

Incidental WMHs can be seen on computed tomography scans, but they are better visualized on conventional MR images of the brain in about 30% of healthy subjects older than 60 years (Fig. 1) (1). Their prevalence rises steadily with increasing age. Other established risk factors for WMHs are female sex, aortic atherosclerosis, and high-systolic blood pressure. The genetic background may also be important (a gene influencing WMHs volume has been recently located on chromosome 4).

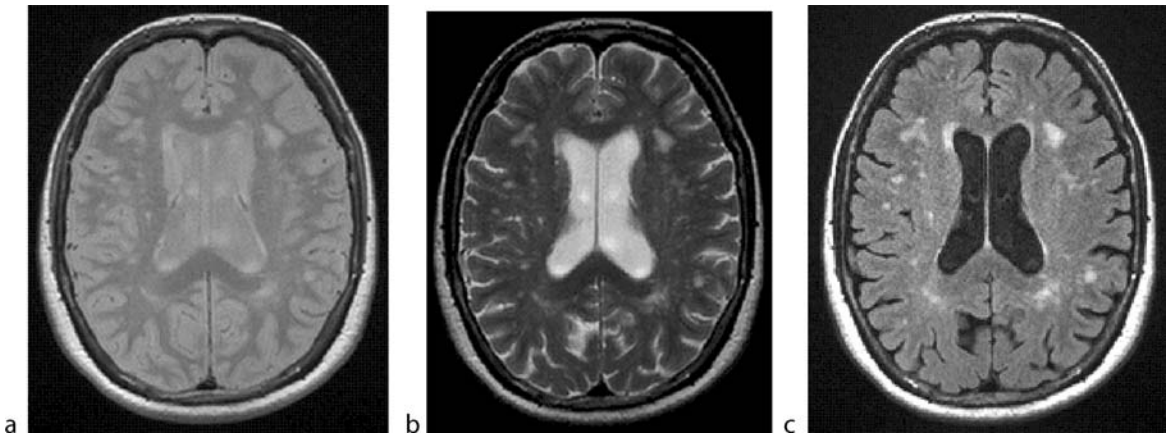

Aging Brain. Figure 1 Axial proton density-weighted (a), T2-weighted (b), and fluid-attenuated inversion recovery (c) magnetic resonance images of the brain from a 73-year-old healthy subject. Multiple hyperintense lesions, suggestive of multifocal white matter pathology, are visible. In c, the suppression of the signal of the cerebrospinal fluid allows a better identification of the lesions located in the periventricular and juxtacortical regions.

Age-related WMHs are usually located in the deep and subcortical WM and around the ventricles. They have different features on MRI scans, the most typical of which are punctate hyperintensities, periventricular caps and halos, and large lesions (which can be confluent). Punctate hyperintensities are associated with highly variable pathological findings, ranging from no detectable pathology to an enlargement of the perivascular spaces. Periventricular caps and halos are associated with discontinuation of the ependymal lining leading to infiltration of water among axons and chronic edema of the WM immediately adjacent to the ventricles, but no axonal damage. The major vascular pathological finding of (confluent) macroscopic lesions is the one that has been termed as "segmental arterial wall disorganization" or as "lipohyalinosis". The loss of the arterial architecture consists of "whorls, tangles, or wisps of more or less fine connective tissue that entirely replaces the vessel wall and obliterates the normal vascular coats". The main consequences of lipohyalinosis are thickening of the small-vessel walls and luminal narrowing (arteriolosclerosis).

The extent of WMHs has been associated with age-related global cognitive impairment. However, the magnitude of this association is relatively weak. Severe WMLs are associated, on a cross-sectional basis, with 0.6–0.7 point reduction of the Mini Mental State Exam (MMSE) score, and predict faster than normal cognitive deterioration of 0.20–0.27 MMSE points per year (a rate 2 –3 times greater than that of persons with no or only mild WMHs, while that of patients with Alzheimer's disease [AD] is 34–38 times faster).

The MTR of WMHs is significantly lower than that of normal appearing WM (NAWM), thus confirming the presence of a significant intralesional destructive component. Average MTR of WMHs has also been shown to correlate with the extent of such abnormalities, thus suggesting similar causative mechanisms (1).

Imaging ▸Brain Atrophy

Age-related changes in brain volume are apparent in both postmortem and *in vivo* MRI studies (Fig. 2). Postmortem studies reported an age-related decrease of brain volume close to 2 cm^3/year between the third and eight decades, whereas MRI studies performed over the entire life span set the average atrophy rate at around 2.5 cm^3/year. GM volume starts to decrease early in life (at the end of the first decade), whereas WM volume starts to decrease at the fourth decade. Risk factors for age-related brain tissue loss include hypertension, diabetes mellitus, alcohol, hyperlipidemia, cigarette smoking, elevated plasma homocysteine, and the ε4 allele of the apolipoprotein (APOE) gene.

On average, GM volume loss is greater in the cortex than in subcortical structures. Age-related cortical density decrease seems to follow a gradient, with greatest and earliest changes occurring in association areas, especially those of the prefrontal cortex (2). However, recent MRI studies have described, in addition to an age-related atrophy of associative cortices, a widespread age-related thinning of a large portion of the cortical ribbon, including several primary areas, which were previously considered to be spared by aging (2).

Although the hippocampus is considered to be one of the most important targets of age-related memory changes, the majority of the studies failed to demonstrate significant age-related hippocampal atrophy in absence of AD. Only recently, a few MRI studies have suggested a nonlinear relationship between age and hippocampal atrophy, being the rate of hippocampal atrophy modest until the sixth decade and higher afterwards. Modern

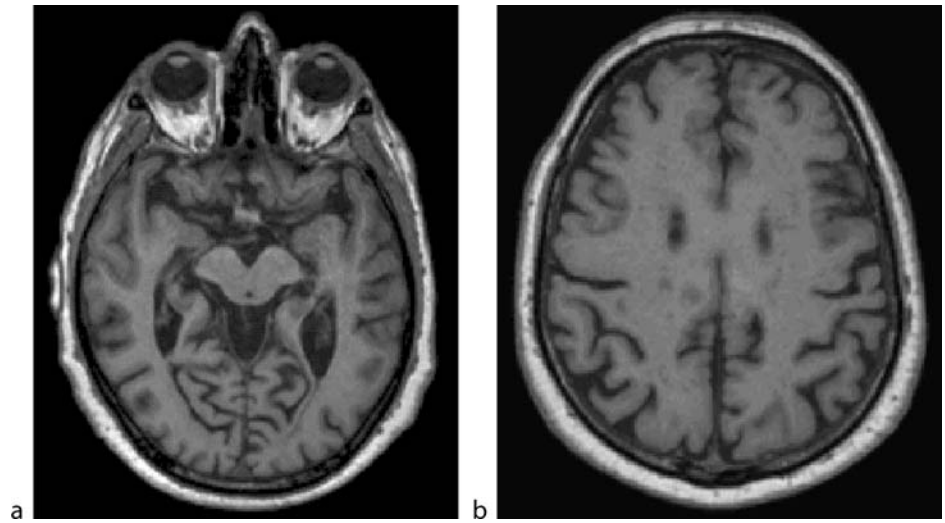

Aging Brain. Figure 2 Axial T1-weighted magnetic resonance images of the brain from an 82-year-old healthy subject. An enlargement of the cortical sulci and ventricular size is evident.

stereological techniques suggest that only minimal age-associated neuronal loss occurs in the entorhinal cortex, whereas a significant age-associated neuronal loss can be found in hippocampal subiculum and CA1. Conversely, recent structural MRI studies found an increased rate of entorhinal cortex atrophy with age. This discrepancy may be due to the fact that MRI measures of brain volume reflect the contributions of all tissue types, whereas stereological techniques quantify only the number of neurons.

Imaging ▸Normal Appearing Brain Tissue (NABT) Damage

Several DT-MRI studies have demonstrated that, in the NABT, MD increases and FA decreases with age, suggesting tissue deterioration over time, which goes undetected when using conventional MRI. Although not confirmed by all studies, a decrease of NABT-MTR with age has been found (3). The relation between volumetry changes, microstructural modifications and aging in the GM and NAWM (taken in isolation) has also been investigated. In a study of a large cohort of healthy individuals spanning seven decades of life, subjects' age was significantly correlated with all GM MT- and DT-derived quantities, whereas only the MD peak height of the WM histogram did so, suggesting that brain WM and GM have different vulnerabilities to aging (Fig. 3). DT-MRI studies also revealed reduced WM integrity in elderly people, especially in the frontal lobes (4). ^{1}H-MRS has demonstrated a decline with age of *N*-acetyl aspartate (NAA) levels in different brain regions, including the hippocampus (3). More recently, an increase of myoinositol, which is thought to be a marker of glial activity and a reduction of glutamate in the motor cortex, a finding consistent with neuronal loss have also been described.

Imaging Cortical Functional Reorganization

Functional imaging techniques in normal elderly people showed changes in brain activity during both cognitive and motor tasks. Many of these studies found an increase and a bilateralization of activations with increasing age. The interruption of the normal neural networks subserving cognitive performance by age-related structural and metabolic changes might, therefore, underlie decline in function (5). Cognitive reserve and brain plasticity have been shown to be affected by the educational level and to be reduced in carriers of the ε4 allele of the APOE gene. fMRI may be useful in predicting subsequent decline in those people at risk of developing AD.

A consistent observation from functional neuroimaging studies of cognitive tasks is that, in elderly people, there is an increased activity of several cortical regions, particularly in the frontal lobe, relative to young adults performing the same task (5). The recruitment of additional regions, which are not activated in young people to perform a given task, has also been described. Furthermore, an increased volume of WMHs located in dorsal prefrontal areas has been correlated with decreased activity of the prefrontal cortex during performance of memory tasks. These findings suggest that age-related decline in the performance of cognitive tasks might also reflect changes of functional integration of different GM regions, due to the disruption of the WM tracts, and not only a dysfunction of critical cortical areas.

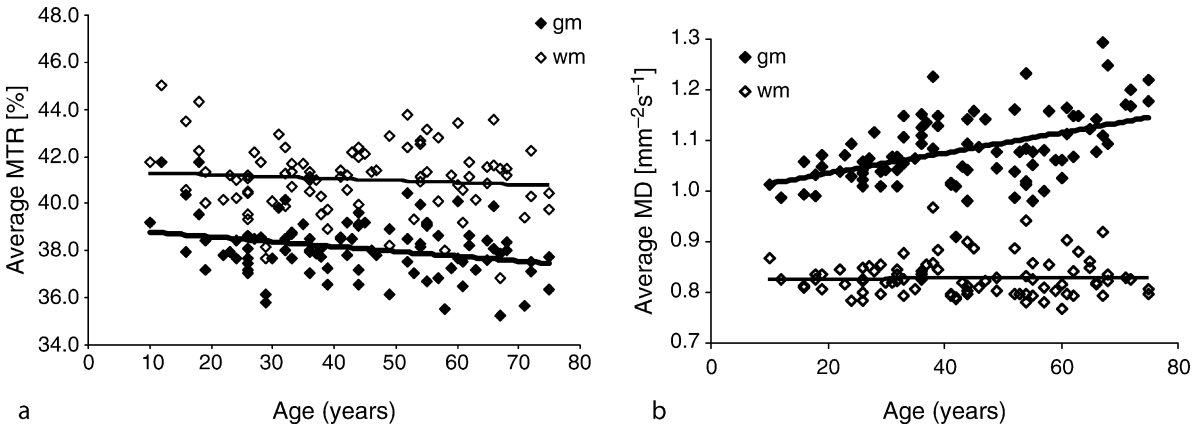

Aging Brain. Figure 3 Scatterplots and regression lines for the relationship between age and average MTR (a) and average MD (b) for both gray (thick line) and white (thin line) matter in 89 healthy subjects (age range from 11 to 76 years). Modified from Benedetti B, Charil A, Rovaris M et al (2006) Neurology 66:535–539 permission to reproduce the already published figure has been requested (but not yet obtained).

The majority of the fMRI studies, which assessed the effects of normal aging on movement-associated cortical activations, demonstrated an age-related overactivity of several regions of the sensorimotor network (6) and a reduced functional lateralization of the primary motor cortex. An altered functional connectivity among various sensorimotor regions has also been reported in elderly people without overt neurological disorders as well as a heterogeneous effect of aging on local and distributed neuronal subpopulations of the motor network.

References

1. Fazekas F, Ropele S, Enzinger C et al (2005) MTI of white matter hyperintensities. Brain 128:2926–2932
2. Salat DH, Buckner RL, Snyder AZ et al (2004) Thinning of the cerebral cortex in aging. Cereb Cortex 14:721–730
3. Benedetti B, Charil A, Rovaris M et al (2006) Influence of aging on brain gray matter and white matter changes assessed by conventional, MT, and DT MRI. Neurology 66:535–539
4. Wozniak JR, Lim KO (2006) Advances in white matter imaging: A review of *in vivo* magnetic resonance methodologies and their applicability to the study of development and aging. Neurosci Biobehav Rev 4; Epub ahead of print
5. Grady CL, Springer MV, Hongwanishkul D et al (2006) Age-related changes in brain activity across the adult lifespan. J Cogn Neurosi 18:227–241
6. Ward NS, Frackowiak RS (2003) Age-related changes in the neural correlates of motor performance. Brain 126:873–888

Agyria-pachygyria Complex

Agyria-pachygyria complex neuronal migration disorder that may be limited to a focal pachygyria or may involve a larger area of the cerebral cortex. Agyria is defined as an absence of gyri and is also called complete lissencephaly.

▶Congenital Malformations, Cerebrum

AIDH

Atypical intraductal hyperplasia.

▶Carcinoma, Ductal, *In Situ*, Breast

AIDS Cholangiopathy

AIDS cholangiopathy, also called AIDS-related cholangitis, is an emerging form of cholangiopathy described in patients affected by AIDS and is characterized by extrahepatic biliary edema, ulceration, and obstruction. It is considered an infectious cholangitis, although its etiology is uncertain. Opportunistic organisms that overgrow the duodenum and proximal small intestine, such as cryptosporidium and cytomegalovirus, may gain access to the biliary system via the major papilla. Cholangiographic findings include strictures of the distal common bile duct, which are a result of papillitis, or intrahepatic ductal abnormalities simulating primary sclerosing cholangitis, such as short strictures and irregular contours due to mucosal thickening. In the biliary system, AIDS may cause other affections such as papillitis, acute acalculous cholecystitis, and, more rarely, lymphoma or Kaposi's sarcoma. Acute acalculous cholecystitis may be caused by cytomegalovirus infection or fungal or protozoal

parasitic infection. US, CT, MR imaging depict a thickened gallbladder wall in the absence of stones.
▶Cholangitis

AIDS-Related Cholangiopathy

AIDS-related cholangiopathy is an infective complication of the biliary tree in patients with advanced-stage AIDS. It is thought to be a form of secondary sclerosing cholangitis resulting from a variety of opportunistic infections. Cryptosporidium and cytomegalovirus are the most commonly isolated infectious organisms in patients with AIDS-related cholangiopathy. Clinical manifestations are right upper quadrant abdominal pain, cholestasis, and symptoms of cholangitis. Various cholangiographic abnormalities have been described at ERCP; the most common findings are papillary stenosis and intrahepatic ductal abnormalities, which resemble sclerosing cholangitis. Endoscopic sphincterotomy may provide symptomatic relief for patients with papillary stenosis. Balloon dilation of strictures and stent placement may be also performed as symptomatic treatments.
▶Occlusion, Bile Ducts

AIDS-Related Lymphoma, Hepatic

Aggressive primary lymphomatous involvement of the liver with characteristic features, occurring in patients affected by acquired immunodeficiency syndrome.
▶Lymphoma, Hepatic

Air Agents

▶Contrast Media, Ultrasound, High Solubility Gas

Air Bronchogram

An air bronchogram is produced by air within bronchi or bronchioli that pass through airless parenchyma (due to absorption or replacement of air or both). It becomes visible as a branching linear lucency within a consolidation. The presence of an air bronchogram indicates the intrapulmonary location of opacity as opposed to a pleural or mediastinal location. It is generally regarded as evidence of the patency of the more proximal airways. It is most commonly seen in pneumonia and edema but also in ARDS, in nonobstructive forms of atelectasis, and in certain neoplasms (notably lymphoma and bronchioloalveolar carcinoma).
▶Atelectasis

Air Crescent Sign (Synonym: Air Meniscus Sign)

Air in a crescent shape in a nodule or a mass, separating the outer wall of the lesion from an inner sequestrum. It is most frequently seen in an aspergillus infection and interpreted as sign for an increasing recovery of the immune reaction of the host against the pathogen.
▶Nodules, Pulmonary, Solitary

Air Enema

A radiological technique used to reduce an ileo-colic intussusception whereby air is introduced to the rectum under preset pressures and under fluoroscopic guidance.
▶GI Tract, Pediatric, Specific Problems

Air Meniscus Sign

▶Air Crescent Sign

Air Trapping

Retention of air in all or parts of the lung as a result of complete or partial airway obstruction, best seen on expiratory HRCT. Most often found in patients with bronchiolitis obliterans, cystic fibrosis, asthma, or bronchiectasis.
▶Bronchitis and Bronchiolitis in Childhood
▶Airway Disease

A

Airway Disease

Philippe A. Grenier
Hôpital Pitié-Salpêtrière, Paris, France
philippe.grenier@psl.ap-hop-paris.fr

Synonyms

Asthma; Bronchiectasis; Bronchiolitis; Chronic bronchitis; Chronic obstructive pulmonary disease (COPD); Small airway disease; Tracheobronchomegaly; Tracheobronchomalacia

Definitions

Tracheobronchomegaly refers to marked dilatation of the trachea and mainstem bronchi.

Tracheobronchomalacia is defined by an abnormal softening of the supportive cartilage rings, producing abnormal tracheal and proximal bronchi flaccidity.

Bronchiectasis is a chronic condition characterized by local, irreversible dilatation of bronchi, usually associated with inflammation which is secondary to infection, mechanical obstruction (inflammatory bronchial stenosis, bronchial tumour, ►broncholithiasis), inflammatory disorder, immunological overresponse [►allergic bronchopulmonary aspergillosis (ABPA)] or immunodeficiency.

Chronic bronchitis is defined as a clinical disorder characterized by excessive mucus secretion by the bronchial tree, manifested by chronic or recurring productive cough on most days in more than 3 months of each of the 2 successive years.

Chronic obstructive pulmonary disease (COPD) includes chronic bronchitis and is characterized by a persistent reduction in expiratory airflow. It is often associated with ►sabre-sheath trachea and emphysema.

Asthma is a chronic inflammatory condition involving the airways characterized by bronchial hyperreactivity with variable degrees of airway obstruction.

Bronchiolitis, or small airway disease, is a group of disorders in which the pathological lesion is primarily in the small airways including the terminal bronchiole, respiratory bronchiole and alveolar ducts. Bronchiolitis include infectious or inflammatory disorders that may be reversible under specific or anti-inflammatory treatment and/or subsequent scaring and obliteration.

These entities may be variably associated in a given patient.

Pathology/Histopathology

Tracheobronchomegaly is often associated with tracheal diverticulosis and bronchiectasis. Atrophy affects the elastic and muscular elements of both the cartilaginous and membranous parts of the trachea.

Tracheobronchomalacia results from weakened tracheal cartilages, often seen in association with a number of disorders including tracheobronchomegaly, COPD, diffuse tracheal inflammation such as ►relapsing polychondritis, as well as following trauma.

Bronchiectasis has been classified into three subtypes, reflecting increasing severity of disease: cylindrical, characterized by relatively uniform airway dilatation, varicose, characterized by non-uniform and somewhat serpiginous dilatation, and cystic. As the extent and degree of airway dilatation increase, the lung parenchyma distal to the affected airway shows increasing collapse or fibrosis.

The histological abnormalities seen in chronic bronchitis include bronchial submucosal hyperplasia, smooth muscle hypertrophy, chronic inflammation and the obstruction of small airways.

In asthma, the chronic inflammatory process of the airways leads to structural changes, such as new vessel formation, airway smooth muscle thickening and fibrosis, which may result in irreversible airway narrowing (airway wall remodelling).

Obliterative bronchiolitis is characterized by bronchiolar and peribronchiolar inflammation and irreversible circumferential submucosal fibrosis that ultimately leads to luminal obliteration affecting membranous and respiratory bronchioles.

Clinical Presentation

Tracheobronchomegaly, tracheobronchomalacia and bronchiectasis are often associated with recurrent lower respiratory tract infection. Tracheobronchomalacia often leads to dyspnea and expiratory stridor. Bronchiectasis remains an important cause of haemoptysis and chronic sputum production. Chronic or recurrent productive cough on most days is a clinical criterion that defines chronic bronchitis. The main clinical symptom of COPD is dyspnea associated with a chronic airflow obstruction at functional pulmonary tests, which is not completely reversible.

Asthma is characterized by recurrent episodes of wheezing, chest tightness, breathlessness and coughing usually associated with widespread but variable airflow obstruction that is often reversible either spontaneously or with treatment. When asthma has become persistent, the clinical symptoms overlap with those of COPD.

In obliterative bronchiolitis, patients may be asymptomatic or present with progressive shortness of breath when the large proportion of the airways are affected.

Imaging

Tracheobronchomegaly is characterized on radiographs and CT scans by an immediately subglottic trachea having a normal diameter that expands as it passes to the carina and this dilatation often continues into the major bronchi. Atrophic mucosa prolapses between cartilage rings and gives the trachea a characteristically corrugated outline on radiographs and CT scan. Corrugations may become exaggerated to form sacculations or diverticula (1–3).

The radiographic diagnosis of tracheobronchomalacia is based on a reduction by almost 300% of the sagittal diameter at expiration. At CT, the diagnosis is based on a narrowing of the lumen of diameter by more than 50% on expiration compared with that on inspiration. The coronal diameter of the trachea becomes significantly larger than the sagittal one. The flaccidity of the trachea or bronchi is usually most apparent during forced expiration (Fig. 1).

Bronchiectasis induces abnormalities on chest radiographs in the majority of cases (2). Thickened bronchial walls are visible either as single thin lines or as parallel line opacities (►tramline). When seen end-on, bronchiectatic airway appears as poorly defined ring or curvilinear opacities. Dilated bronchi filled with mucous or pus result in tubular or ovoid opacities of variable size. Cystic bronchiectasis manifests as multiple thin-walled ring shadows often containing air-fluid levels. Pulmonary vessels may appear increased in size and may be indistinct because of adjacent peribronchial inflammation fibrosis. Localized forms are frequently accompanied by atelectasis which may be mild and detected only because of vascular crowding, fissure displacement or obscuration of part of the diaphragm.

The CT findings of bronchial dilatations and bronchiectasis include lack of tapering of bronchial lumina, internal diameter bronchi greater than that of the adjacent pulmonary artery (►signet ring sign) (1–3) (Fig. 2), visualization of bronchi within 1 cm of the costal pleura or abutting the mediastinal pleura, and mucus-filled dilated bronchi. In varicose bronchiectasis, the bronchial lumen assumes a beaded configuration. Cystic bronchiectasis is seen as a string of cysts caused by sectioning irregular dilated bronchi along their lengths, or a cluster of cysts, caused by multiple dilated bronchi lying adjacent to each other. Secretion accumulation within bronchiectatic airways is generally easily recognizable as

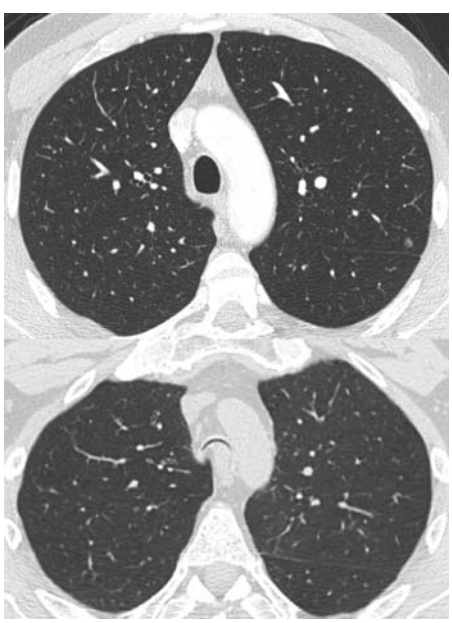

Airway Disease. Figure 1 Tracheomalacia. The tracheal lumen has a normal appearance on the inspiratory transverse CT scan (*top*). This lumen collapses on the expiratory transverse scan (*bottom*). The posterior tracheal wall bows anteriorly tremendously reducing the airway lumen.

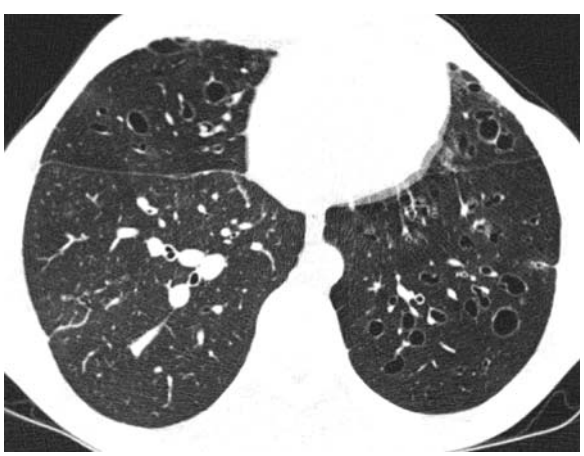

Airway Disease. Figure 2 Bilateral bronchiectasis and obliterative bronchiolitis. Cystic and thin-walled dilated bronchi are present in the right middle lobe, the lingula and the left lower lobe. The lung parenchyma in the right middle and the left lower lobes appears hypoattenuated and hypoperfused. This appearance results from the presence of obliterative bronchiolitis lesions in these areas inducing hypoventilation and reflex vasoconstriction. Notice the large size of the pulmonary vessels in the right lower lobe resulting from the phenomenon of pulmonary blood flow distribution in the normal ventilated areas.

lobulated glove-finger, V- or Y-shaped densities. CT may show completely collapsed lobe containing bronchiectatic airways. Subtle degrees of volume loss may be seen in lobes in relatively early disease. This is most evident in the lower lobes on the basis of crowding of the mildly dilated bronchi and posterior displacement of the oblique fissure.

The majority of patients with symptoms of chronic bronchitis or COPD have a normal chest radiograph. When radiographic abnormalities are present, they can include hyperinflation, oligaemia, bronchial wall thickening and accentuation of linear lung markings. A sabre-sheath trachea appearance may be present (Fig. 3). In hypoxic patients, with the onset of right-heart failure the heart and hilar and intermediate lung vessels become enlarged (2).

On CT scans, bronchial wall thickening is present. Air-filled outpouchings are seen in addition to the lumen of main, lobar, or segmental bronchi. The extent of lung hypoattenuation at expiration probably reflects ►air trapping more than reduction of the alveolar wall surface (1).

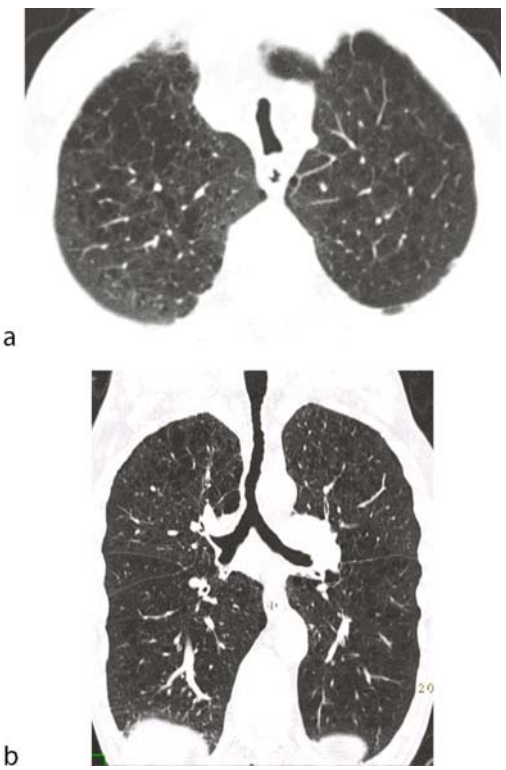

Airway Disease. Figure 3 COPD patient with sabre-sheath trachea and emphysema. Transverse thin section CT (a) and coronal reformat (b) demonstrate the abnormally small coronal diameter of the tracheal lumen. Presence of bilateral centrilobular emphysema predominantly distributed in the upper lobes.

In asthma, hyperinflation is often transient but may be a permanent change. When present, bronchial wall thickening is usually an irreversible phenomenon. Chest radiograph may depict complications including consolidation, atelectasis, mucoïd impaction, pneumothorax and pneumomediastinum. Consolidation is commonly infective but in some cases, it is due to eosinophilic consolidation probably associated with allergic aspergillosis. Subsegmental or lobar collapse is due to mucoïd impaction in large airways or more commonly mucus plugging in many small airways (2).

CT scans may show bronchial dilatation, bronchial wall thickening, ►mucoid impaction, decreased lung attenuation and air trapping. These abnormalities may or may not be reversible with steroid treatment. Bronchial wall thickness measured at CT has proved to be prominent in patients with more severe asthma. It is correlated with the duration and severity of disease and the degree of airflow obstruction (1, 3).

In obliterative bronchiolitis, chest radiograph is often normal or show mild hyperinflation, subtle peripheral attenuation of the vascular makings and central bronchiectasis may be seen.

CT findings usually consist of areas of decreased lung attenuation associated with vessels of decreased calibre on inspiratory scans and air trapping on expiratory scans (Fig. 2). Bronchial wall thickening and bronchiectasis, both central and peripheral, are also commonly present. Redistribution of blood flow to the normally ventilated areas causes increased attenuation of lung parenchyma in these areas increased in size, and the resulting pattern is called '►mosaic perfusion' (Fig. 2) (1–3).

Nuclear Medicine

Perfusion/ventilation scanning has a limited role in the assessment of chronic airway disease. The technique however may be useful to pre-operatively assess the distribution of lung perfusion and the extent of perfusion/ventilation defects.

Diagnosis

Diagnosis of chronic airway disease is made on the basis of clinical symptoms, functional abnormality and imaging features.

Tracheal disorders are suggested on chest radiographs and definitely recognized on inspiratory and expiratory CT scans. In patients with bronchiectasis, clinical symptoms and functional abnormalities may be present or absent. In the majority of cases, chest radiographs reveal abnormalities but the definitive diagnosis in

entirely based on CT features. MDCT has become the gold standard to assess the presence and extent of bronchiectasis.

The diagnosis of chronic bronchitis is only clinical. The diagnosis of COPD is based on clinical and functional abnormalities (chronic airflow obstruction) and supported by imaging findings, especially by the detection, characterization and assessment of extent of associated emphysema.

The diagnosis of asthma is established on the basis of pulmonary tests showing wide variations (15–20%) of predictive values over short period of time in resistance to airflow in intrapulmonary airways. The chest radiography is usually recommended in all asthmatic patients who are ill enough to justify admission to a hospital. The clinical indications for CT in patients with asthma include: to detect bronchiectasis in patient with suspicion of ABPA; to document the presence and extent of emphysema in smokers with asthma and to identify condition that may be confused with asthma, such as hypersensitivity pneumonitis.

The diagnosis of obliterative bronchiolitis is always challenging for the clinician because there is no pathognomonic, clinical or functional abnormality. Thin collimation CT has become the best modality of choice to diagnose and to assess the extent of bronchiolar lesions.

Bibliography

1. Grenier PA, Beigelman-Aubry C, Fétita C et al (2002) New frontiers in CT imaging of airway disease. Eur Radiol 12:1022–1044
2. Hansell DM, Armstrong P, Lynch DA et al (2005) Airway diseases. In: Imaging of the Diseases of the Chest. 4th edn. Elsevier Mosby, Philadelphia, pp 711–783
3. Naidich DP, Webb VR, Grenier PA et al (2005) Bronchiectasis and small airway diseases. In: Imaging of the Airways. Functional and Radiologic Correlations. Lippincott Williams and Wilkins, Philadelphia, pp 106–176

Alagille Syndrome

Alagille syndrome is a syndrome with autosomal dominant transmission associated with dysmorphic facies, ocular abnormalities, cardiovascular anomalies, and vertebral defects (butterfly vertebrae). At the level of the liver, there is a hypoplasia of the intralobular bile ducts leading to neonatal cholestasis, progressive portal hypertension, cirrhosis, and hepatocarcinoma.

▶Congenital Malformations, Bile Ducts
▶Congenital Malformations, Liver and Biliary Tract

ALARA Principle

The acronym for ALARA denotes *as low as reasonably* achievable. The ALARA principle dictates that all radiologists take steps to limit the radiation dose received by both staff and patients during any radiological procedure, whilst at the same time maintaining the diagnostic quality of the images obtained.

▶Radiation Issues in Childhood

Alcoholic Hepatitis

Ethanol can be responsible both for acute and chronic hepatitis. Alcoholic hepatitis is an acute inflammation of the liver due to alcohol abuse. Alcoholic hepatitis may have various presentations, although typically the patient has a long history of alcohol consumption with a recent episode of heavy assumption. Alcoholic hepatitis occurs very frequently in patients with underlying chronic alcoholic liver disease and alcoholic cirrhosis. Alcoholic hepatitis can range from a mild form, characterized by isolated laboratory abnormalities, to severe liver dysfunction with complications such as hepatic encephalopathy, ascites, bleeding esophageal varices, coagulopathy, and coma. Histologically, the characteristic features are ballooning degeneration of hepatocytes, inflammatory infiltrates with neutrophils, and Mallory's hyalin. Acute alcoholic hepatitis by itself does not lead to cirrhosis and is reversible in several months if the patient stops drinking. In case of prolonged alcohol consumption, alcoholic hepatitis can lead to liver cirrhosis.

▶Hepatitis

ALL

Acute lymphoblastic leukemia is a rapidly progressing cancer of the blood involving lymphocytes. It is the most common form of childhood leukemia.

▶Leukemia

Allergic Bronchopulmonary Aspergillosis (ABPA)

It is a condition that occurs in patients with pre-existing asthma, characterized by pulmonary infiltration with eosinophils, mucoïd impaction and central bronchiectasis. To establish the diagnosis of ABPA, patients must exhibit all the following criteria: history of asthma, immediate skin test reactivity to *Aspergillus f.*, and elevated serum IgE and precipition antibodies against *Aspergillus f.*

▶Airway Disease

Allergic Reactions

▶Adverse Reactions, Iodinated Contrast Media, Acute, Non renal

Allergic-Like Reactions

▶Adverse Reactions, Iodinated Contrast Media, Acute, Non renal

Allergy

Inappropriate or exaggerated reaction of the immune system to substances that cause no symptoms in most people. It includes reactions to chemical exposure; respiratory reactions to dust, pollen, or other substances; and reactions to food.

▶Adverse Reactions, Barium

Alpha-1-Antitrypsin Deficiency

Results from a genetic defect. The mechanism that causes associated liver disease and emphysema in some people with this deficiency is not known. Alpha-1-antitrypsin is a protein that blocks the destructive action of neutrophil elastase on lung elastin fibers, and the resulting imbalance of lung proteases and antiproteases probably plays an important role in the development of emphysema. Individuals with a homozygous deficiency who also smoke have a greatly increased risk of developing severe panlobular emphysema with a basal predominance before the age of 35. Such a homozygous deficiency accounts for less than 1% of emphysema.

▶Emphysema and Bulla

Ambiguous Genitalia

Arthur Rosemary
Department of Pediatric Radiology, Leeds General Infirmary, Clarendon Wing, Leeds, UK
r.arthur@ukonline.co.uk

Synonyms

Intersex; Intersexuality; XX or XY sex reversal

Definition

Ambiguous genitalia is a generic term applied to newborn infants who cannot be assigned a sex immediately after birth as a result of abnormal genital development and includes infants whose phenotypic appearance is incongruent with a ▶karyotype established prenatally. The term has also been used to encompass a spectrum of milder genital abnormalities, e.g. severe scrotal hypospadia or isolated cliteromegaly, even though their sex assignment is not initially considered in doubt. The development of ambiguous genitalia is the 'end' result of a number of disorders with varying aetiologies.

Pathology/Histology

Interruption of normal genital development in the first trimester may result in the development of ambiguous genitalia. Chromosomal sex is determined at fertilisation normally XX (female) and XY (male) although various deletions, translocations and mosaic combinations occur. Sex determination genes sited on the sex chromosomes influence the development of the bipotential gonads to

Ambiguous Genitalia. Table 1 Outlines the most frequent causes of genital ambiguity

	Diagnosis	Karyotype	Internal organs	Gonads	Comment
Masculinised female	CAH, foetal androgens	46,XX	Normal uterus UG sinus	Ovaries	Impalpable gonads
Under-masculinised male					
Testis determination	Gonadal dysgenesis (GD)	Partial GD XY or Mixed GD XO/XY	Uterus—may be rudimentary UG sinus	streak gonad/testis (dysgenetic or normal)	±Impalpable gonads
		Complete GD Swyer XY	Uterus—ay be rudimentary	Bilateral streak gonads	Impalpable gonads
Androgen biosynthesis	17β-OHS Dehydrogenase deficiency 5α-reductase deficiency	XY	Absent uterus Perineoscrotal hypospadias Pseudoperineal vagina/utricle	Testes	±Impalpable gonads Gonadal neoplasm rare
Androgen insensitivity	Complete or partial androgen insensitivity syndrome	XY	Absent uterus Perineoscrotal hypospadias Pseudoperineal vagina/utricle	Testes	±Impalpable gonads Risk of gonadal neoplasm
True hermaphroditism	True hermaphroditism	XX, XY, XX/XY	Uterus-rudimentary or bicornuate rarely normal	testes and ovarian tissue ±ovotestes	±Impalpable gonads
Syndromal	e.g. DRASH	Gonadal dysgenesis	No uterus	Intra-abdominal dysgenetic testes	Impalpable gonads Wilms' tumour 50% Nephropathy

develop into testes or ovaries, which produce hormones and peptides giving rise to differentiation of the primitive internal ducts and external genitalia and subsequent development of phenotypic sex. In the male, sertoli cells in the foetal testis produce anti-Mullerian hormone (AMH) causing regression of the Mullerian structures whereas Leydig cells secrete androgens including testosterone. The androgens act to develop the Wolffian duct structures to form the epididymes, vasa deferentia and seminal vesicles. 5α-reductase converts the testicular testosterone into dihydroreductase which virilises the developing external genitalia. During this time the testes begin to descend to the scrotum although the process is not fully understood (1).

In the female, in the absence of AMH, the Mullerian ducts persist to develop into the uterus, fallopian tubes and upper two-thirds of the vagina. In the absence of androgens, the Wolffian duct system involutes and the ►urogenital sinus becomes the urethra and lower vagina.

Traditionally ambiguous genitalia has been subdivided into four types; female pseudohermaphroditsm, male pseudohermaphroditsm, gonadal dysgenesis and true hermaphroditism (2, 3). It has been argued that these terms cause confusion to patients and clinicians and that a more descriptive and functional classification has been suggested as outlined in Table 1 (4).

Masculinised Female XX

Congenital adrenal hyperplasia is the commonest cause of ambiguous genitalia in the newborn (►congenital adrenal hyperplasia). The phenotypic appearance varies from

mild cliteromegaly to advanced virilisation, with hypospadias, penile urethra but empty scrotum. There is usually a single perineal opening with the vagina and urethra forming a urogenital sinus (UGS) which opens at the base of the phallus. The vagina may become quite distended as a result of vaginal stenosis at the junction with the UGS.

Under-Masculinised Male Y Chromosome Present

These conditions can be subdivided into three broad categories, i.e. defects in testis determination, androgen biosynthesis or androgen action.

Gonadal dysgenesis (GD) results from a failure in testis determination as a result of sex or autosomal chromosomal abnormality. Partial GD (XY karyotype) and mixed GD (45,XO/46,XY) are associated with a streak gonad on one side and a testis which is often dysgenetic on the other. Failure of Sertoli cell function results in preservation of Mullerian remnants, and a rudimentary uterus is present in all cases. Partial genital ambiguity results from androgen secretion reflecting residual Leydig cell function in a normal or dysgenetic testis. Most infants have ambiguous genitalia, often with severe under-masculinisation. There is a high risk of gonadal neoplasia and gonadectomy recommended. A number of syndromes are also associated with gonadal dysgenesis and ambiguous genitalia, e.g. the DRASH syndrome is characterised by XY karyotype, ambiguous genitalia, nephropathy and a predisposition to Wilms' tumour.

In defects in androgen biosynthesis, e.g. deficiency in 17β-hydroxysteroid dehydrogenase and 5α-reductase, the testes are histologically normal and produce AMH with involution of Mullerian structures, but defects in androgen biosynthesis result in under-masculinisation of the external genitalia. This is often severe and may result in complete ▶sex reversal. Gonadal neoplasms may occur but are uncommon.

Complete androgen insensitivity syndrome (CAIS, testicular feminisation syndrome) is inherited as an X-linked recessive condition and occurs in XY individuals due to defective binding of androgens to tissue receptors. There may be complete sex reversal. The testes are normal although often intra-abdominal producing AMH resulting in Mullerian regression and absence of the uterus and upper 2/3 vagina. A pseudo-perineal blind vaginal opening may be present or a prostatic utricle may be noted on an micturating cystourethrogram (MCUG). Partial androgen insensitivity syndrome (PAIS) is less severe and may only be associated with isolated hypospadias or impaired fertility although ambiguous genitalia may occur. Patients with PAIS and CAIS are at risk of developing gonadoblastoma and should undergo gonadectomy.

True Hermaphroditism

In true hermaphroditism both testicular and ovarian tissue are in the form of ovary and or testis and or ovotestes. Karyotype is variable with XX; mosaics XO/XY, XX/XXY, XX/XY and XY karyotype most frequent. Testes/ovotestes may be intra-abdominal, inguinal or labio-scrotal although ovaries are nearly always intra-abdominal. The internal ducts associated with ovotestes are usually fallopian tubes, whereas an isolated testis is associated with an ipsilateral vas, and isolated ovary with ipsilateral fallopian tube. A uterus is usually present but may be rudimentary, or bicornuate. External genitalia are variable but most individuals have hypospadias and a bifid scrotum and a normal sized phallus. Gonadal neoplasms are rare.

Clinical Presentation

Clinical presentation ranges from pronounced genital ambiguity to mild virilisation of the female and minor under-masculinisation of the male (Fig. 1). In severe cases, (presence of cliteromegaly/micropenis, bifid scrotum, severe perineoscrotal hypospadias, and bilateral undescended or impalpable gonads), difficulty of sex assignment is encountered at birth whereas in others the clinical signs may be more subtle. Complete sex reversal, e.g. severe under-masculinised male may occur where there is no clinical suspicion of ambiguous genitalia until much later in life when puberty fails to proceed normally.

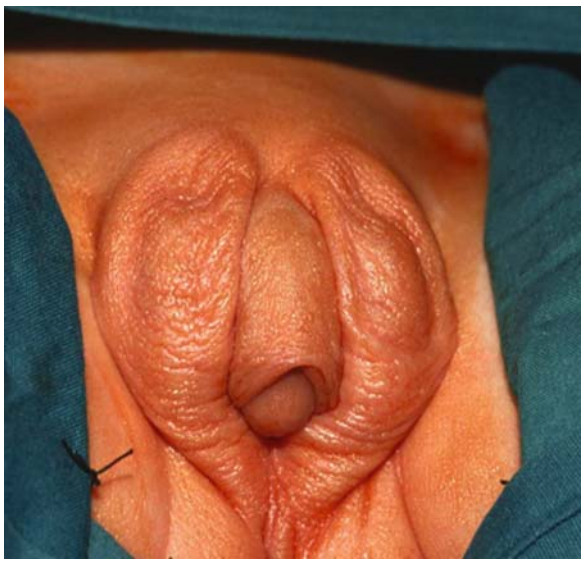

Ambiguous Genitalia. Figure 1 Under-masculinised infant showing external genitalia, with bifid scrotum (labio-scrotal folds) that contain palpable gonads, and under-developed penis.

The diagnosis of ambiguous genitalia should be considered a medical emergency on account of the serious social, psychological and medical implications for the child and their family. Although initial discussions with the family will need to take place at the base hospital, in most cases referral to a specialist centre for more detailed investigation is appropriate. Clinical history should include detailed family history, and history of drug exposure during pregnancy and any signs of maternal virilisation should be noted. On examination the size and nature of the phallus, scrotum or labio-scrotal folds, site of urethral meatus and any other perineal openings, and the presence of palpable gonads should be documented.

Immediate steps should be taken to confirm the infant's karyotype by fluorescence in situ hybridization (FISH) analysis, followed by a more detailed karyotype analysis to determine whether there is female masculinisation, male under-masculinisation or true hermaphroditism. Urea and electrolyte estimation and 17-OH-progesterone should establish whether the infant has evidence of congenital adrenal hyperplasia. Pelvic ultrasound should be arranged to identify internal genital anatomy. Other investigations may include detailed endocrinological studies, genitography, magnetic resonance imaging, laparoscopy, laparotomy and gonadal biopsy.

Imaging

The aim of imaging is to identify the internal genital anatomy, so that the results can be correlated with the karyotype and clinical features to enable a prompt diagnosis be made, to assist in rapid gender assignment and to inform discussions with regard to the feasibility of reconstructive surgery.

Ultrasound

Identification of a normal uterus is generally straightforward although a rudimentary uterus may be difficult to identify. The transducer should be angled caudally to visualise the vagina and identify any cystic dilatation due to a urogenital sinus (UGS) (Fig. 2). Scanning directly from the perineum using a linear transducer can be useful. Normal ovaries are usually easily identified in newborn females and can generally be differentiated from intra-abdominal testes by the presence of small follicles seen in over 80% of normal female neonates. Intra-abdominal testes are often difficult to visualise by ultrasound, but when seen are usually small solid masses, more easily identified when close to the internal inguinal ring. The inguinal regions should also be examined since testes may be seen in the inguinal canal even when clinically impalpable.

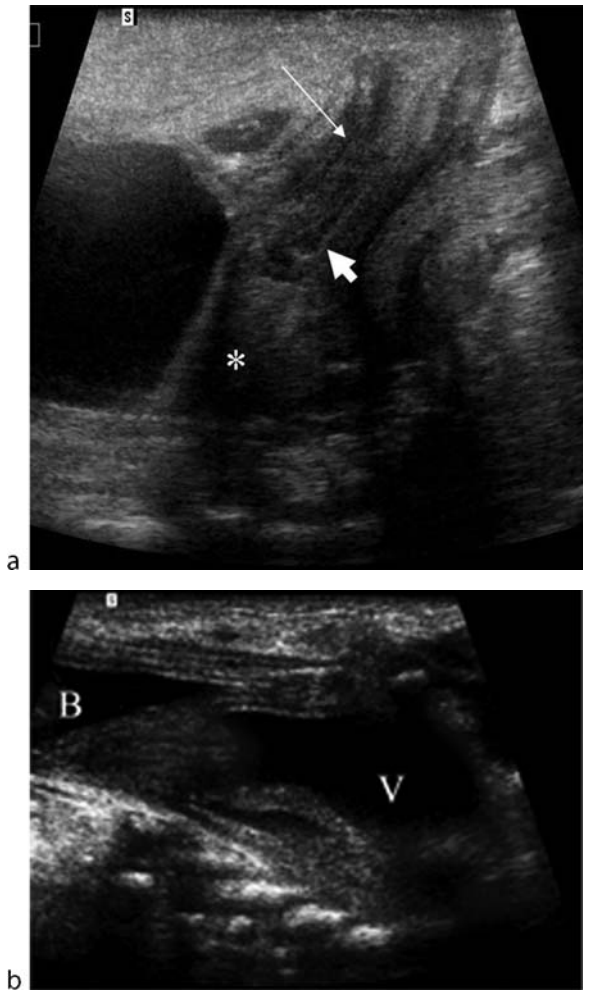

Ambiguous Genitalia. Figure 2 (a) Normal perineal scan in a female infant showing base of fluid-filled bladder, with the urethra anteriorly (arrow) and a trace of fluid in the vagina (short arrow), * is the uterine body. The rectum is seen posteriorly. (b) Perineal scan in a female with a persistent UG sinus, with dilatation of the fluid-filled vagina. The body of the cervix can be seen indenting the vagina vault. (B is bladder and V is vagina)

Genitography

Genitography is often performed to clarify the anatomy and identify the presence of any Mullerian remnants such as vagina and prostatic utricle, and may be performed fluoroscopically or by ultrasound. The two examinations may be complimentary, with fluoroscopic images often being preferred as a roadmap at the time of surgery, whereas as ultrasound examination will give more precise information with regard to uterine morphology, will usually accurately demonstrate the union of the vagina and urethra to form the UGS and avoids ionising

radiation. During a fluoroscopic examination a urethral catheter is passed retrogradely into the urethra, or other perineal opening and the infant imaged in the lateral position (3). In the case of a UGS the catheter often enters the vagina rather than the bladder but gentle injection of contrast will normally outline the important anatomical details. If the bladder is successfully catheterised the anatomy is usually well demonstrated on micturition. The length of the common channel should be identified as the vagina and urethra may join to form the UG sinus close to the perineal surface or more proximally making reconstructive surgery more difficult (Fig. 3). The vaginal vault may show an indentation due to the cervical impression of the uterus, but this may not be identified if the uterus is rudimentary or the vagina inadequately distended. Contrast may reflux into the uterine body and fallopian tubes if present. The overall size of the vagina should be assessed as the size may vary from small to large, and marked vaginal distension may occur if there is a distal vaginal stenosis, particularly in congenital adrenal hyperplasia. An ultrasound genitogram can be performed similarly by retrograde injection of saline into the UGS at the time of sonography using both perineal and transabdominal scan planes.

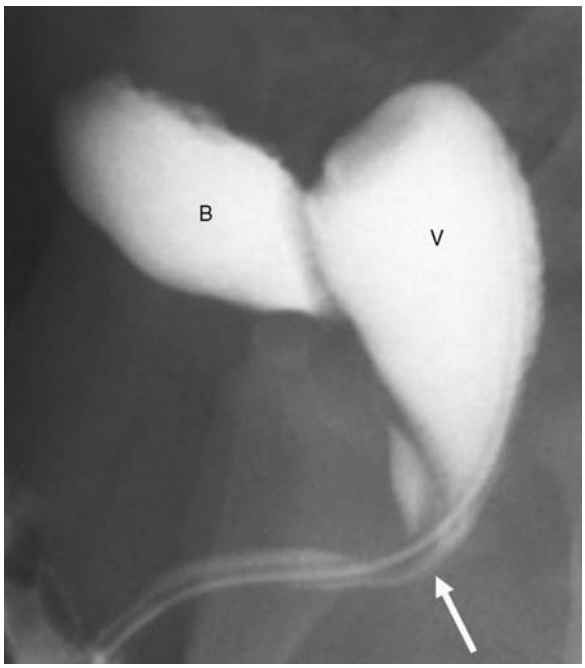

Ambiguous Genitalia. Figure 3 Genitogram. The catheter has been passed retrogradely through the UG sinus into the vagina and contrast injected. The UGS is long with high entry of the vagina (*arrow*). There is a clear indentation from the cervix into the vaginal vault. B is bladder, V is vagina.

Magnetic Resonance Imaging

Magnetic resonance imaging is particularly useful in the older child to obtain detailed assessment of the uterus and vagina and may identify the presence of intra-abdominal gonads not seen on ultrasound. We have found MR helpful in the assessment of children who present later in

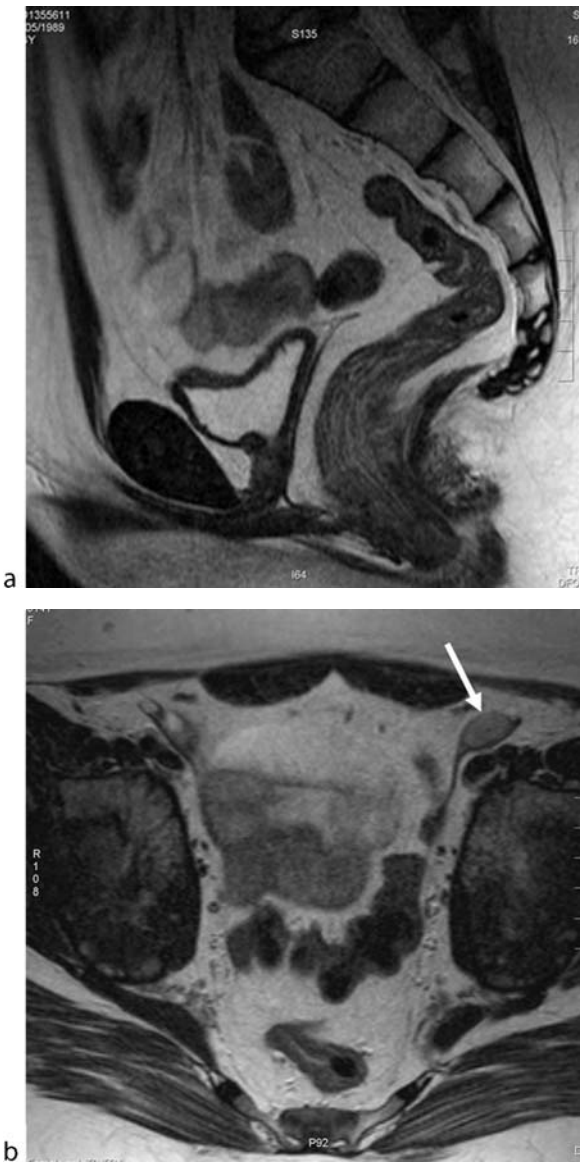

Ambiguous Genitalia. Figure 4 Sagittal and transverse MRI images in a teenage girl presenting with amenorrhea. Karyotype was found to be XY and a defect in androgen synthesis was identified. The uterus and vagina were absent although a thin membranous structure is seen posteriorly to the bladder though to represent a vestigial Mullerian remnant. A gonad (testis) is seen close to the right internal inguinal ring (*arrow*).

life around adolescence to identify any uterine remnant, the vagina and gonads that may not have been well visualised by ultrasound (Fig. 4).

Diagnosis

Diagnosis is reached on the basis of karyotype determination, internal and external genital anatomy and endocrinological studies in most cases. The appearance of the external genitalia is rarely diagnostic but the presence of palpable gonads is a particularly important sign excluding the diagnosis of either female masculinisation or complete gonadal dysgenesis. Bilaterally palpable gonads indicate that androgen insensitivity, androgen biosynthesis defects or true hermaphroditism are the most likely causes. Absence of palpable gonads may occur in all major types of ambiguous genitalia. The identification of the uterus on US will be seen in all cases of masculinised female intersex conditions when associated with XX karyotype will usually prove to be due congenital adrenal hyperplasia. A uterus may be identified in some infants with gonadal dysgenesis (XY or XO/XY) and true hermaphroditism, but is not seen in other causes of undermasculinised males. Laparoscopy and gonadal biopsy will be necessary to confirm gonadal dysgenesis and the nature of gonads and internal organs in true hermaphroditism. In a few cases a precise diagnosis and explanation for ambiguous genitalia will not be made.

Bibliography

1. Achermann JC (2005) Development of the reproductive systems. In: Brook C, Clayton P, Brown R (eds) Brook's Clinical Pediatric Endocrinology. Blackwell Publishing, pp 153–170
2. Hyun G, Kolon F (2004) A practical approach to intersex in the newborn period. Urol Clin North Am 31:435–443
3. Cohen HL, Haller JO (2004) Anomalies of sex differentiation. In: Kuhn JP, Slovis TL, Haller JO (eds) Caffey's Pediatric Diagnostic Imaging. Mosby, pp 1967–1979
4. Hughes IA (2005) Ambiguous genitalia. In: Brook C, Clayton P, Brown R (eds) Brook's Clinical Pediatric Endocrinology. Blackwell Publishing, pp 153–170

Amebic, Abscess, Hepatic

Amebic abscess is the most common type of hepatic abscess worldwide and is particularly frequent in developing countries. It is the most frequent extraintestinal manifestation of *Entamoeba histolytica* infection. The incidence of amebic liver abscess in patients with amebic colitis is about 4%. Fever and pain are the most commonly encountered symptoms. Anorexia, nausea, vomiting, weight loss, and pleural effusion are often present. Furthermore, diarrhea may be present in these patients at the time of diagnosis or within the previous few months, sometimes with bloody feces.

Both CT and US are sensitive in the detection of amebic abscesses. At US, an amebic abscess usually appears as a large, well-defined, hypoechoic lesion, and contains low-level internal echoes. At CT, amebic abscesses do not have a specific appearance; they usually are round or oval well-defined lesions with water-like attenuation values. The demonstration of a wall and a peripheral edema surrounding the abscess is a common finding. The wall may be hyperdense on unenhanced scans and always shows enhancement after contrast medium administration. The central abscess cavity may show multiple septa or fluid-debris levels and nodularity at the margins. MRI is a sensitive technique in detecting amebic abscesses, but the findings are not specific. Amebic abscesses have a homogeneous or inhomogeneous aspect with decreased signal intensity on T1-weighted images and increased signal intensity on T2-weighted images. Perilesional edema is often seen on T2-weighted image. The central necrosis does not show any enhancement after contrast medium administration, while the periphery strongly enhances, due to the presence of inflammatory tissue.

▶Abscess, Hepatic

Ameloblast

A cylindrical epithelial cell in the innermost layer of the enamel organ, which takes part in the elaboration of the enamel prism.

▶Neoplasms, Odontogenic

AML

Acute myeloid leukemia is a rapidly progressing cancer of the blood affecting immature bone marrow cells, usually of the white blood cell population. It is less common in children than adults.

▶Leukemia

Amplitude Modulation Imaging

Multi-pulse ultrasound imaging approach similar to phase modulation imaging that employs a series of pulses with alternating amplitudes and enables selective detection of the non-linear echoes arising from microbubble contrast agents.

▶Specific Imaging Techniques (Contrast Media, Ultrasound)

Amyloidosis

Accumulation of various insoluble fibrillar proteins (amyloid) in amounts sufficient to impair normal function. Symptoms are hoarseness and dyspnoea.

▶Larynx, Inflammatory Diseases

▶Diffuse Infiltrative Disease, Hepatic

Anal Atresia

▶Anorectal Malformation

Anal Sphincter Weakness

Anal sphincter weakness is defined as a reduced anal resting and/or squeeze pressure, resulting in recurrent uncontrolled passage of fecal material.

▶Pelvic Floor Dysfunction, Anorectal Manifestations

Anaphylactic Reactions

▶Adverse Reactions, Iodinated Contrast Media, Acute, Non renal

Anaphylactoid Reactions

▶Adverse Reactions, Iodinated Contrast Media, Acute Non renal

Anaphylaxis-Like Reactions

▶Adverse Reactions, Iodinated Contrast Media, Acute, Non renal

AND

▶Axillary Node Dissection

Andersson Lesion Type A or Inflammatory Type

Andersson lesion type A or inflammatory type is a subdiscal osteitis of the central part of the intervertebral space with mild erosion and even milder sclerosis. It is a rare but characteristic feature of ankylosing spondylitis. In contrast to bacterial inflammation of the discovertebral junction, it can persist unchangingly for months and years, and it never exhibits perivertebral abscesses.

▶Spondyloarthropathies, Seronegative

Andersson Lesion Type B

Andersson lesion type B is a transdiscal insufficiency fracture in ankylosing spondylitis (rare but typical), mainly in the thoracolumbar junction in osteoporotic, kyphotic, multisegmentally ankylosed vertebral columns. It is often promoted by minor trauma.

▶Spondyloarthropathies, Seronegative

Anemia

►Erythropoietic System, Diseases of the

Aneurysm

Abnormal dilation of any vascular structure with the risk of rupture.
►Stroke, Interventional Radiology

Aneurysm, Aortic and Thoracic

Robert Morgan
St George's NHS Trust, Blackshaw Road,
London, UK
robert.morgan@stgeorges.nhs.uk

Synonyms

Thoracic aneurysm; thoracic aortic aneurysm

Definition

Aneurysmal enlargement of the ►thoracic aorta is normally defined as permanent dilatation to at least 150% of normal size.

Pathogenesis/Histopathology

Similar to abdominal aortic ►aneurysms, the majority of thoracic ►aortic aneurysms (TAAs) are caused by atherosclerosis. Aneurysmal dilation may involve only a portion of the thoracic aorta or the entire aorta may be aneurysmal. TAAs can be classified by site, morphology, and etiology. True aneurysms involve all the layers of the aortic wall, while false aneurysms are essentially contained ruptures and involve just the outer layers of the wall, usually only the adventitia, surrounded by fibrosis related to a previous hematoma. The majority of aneurysms, including those due to atherosclerosis and Marfan's syndrome, are of the fusiform type. Saccular aneurysms refer to aneurysms where there is localized dilatation, which is often confined to one side of the aortic wall. Thoracic aneurysms are associated with hypertension, coronary artery disease, and abdominal aortic aneurysms.

The main causes of TAA are atherosclerosis, hypertension, Marfan's syndrome, Ehlers–Danlos syndrome, and syphilis, mycotic aneurysms and connective tissue disorders, e.g., ankylosing spondylitis, rheumatoid arthritis, Reiter's disease, systemic lupus erythematosus.

The most frequent site of a TAA is the descending aorta. In most patients, atherosclerosis is the underlying cause of descending aortic and aortic arch aneurysms. Aneurysms of the ascending aorta are often due to cystic medial degeneration. These commonly start at the aortic root and extend distally into the ascending aorta. Ascending aortic aneurysms are commonly seen in patients with Marfan's syndrome, although in the majority of patients atheroma is also the underlying cause. False aneurysms are usually the result of previous trauma that was not diagnosed at the time of the injury. Such aneurysms usually occur around the aortic isthmus just beyond the origin of the left subclavian artery. They often involve the inferior surface of the aortic arch as it becomes the descending aorta and a saccular configuration is not uncommon. Mycotic aneurysms are almost all due to bacterial infection and in most cases are also false aneurysms. Aneurysms of the descending aorta may extend into the abdomen and are referred to as thoracoabdominal aortic aneurysms.

Clinical Presentation

Aneurysms of the thoracic aorta are a disease of increasing age and occur in males three times as commonly as in females. They occur in 1:1,000 of the population.

Thoracic aneurysms are usually discovered by chance on a routine chest radiograph. Clinical presentations include substernal, back or shoulder pain, superior vena cava syndrome (due to compression of the SVC), dysphagia (due to esophageal compression), dyspnea, stridor (due to airway compression), and hoarseness (due to laryngeal nerve compression). Although TAAs may present because of pressure effects on adjacent structures as described, the main problem is rupture, which is usually catastrophic and fatal. Around half of patients die from the actual rupture, and coexisting medical disease accounts for the rest. Natural history studies of patients with untreated TAA estimate mortality rates of 50% after 5 years and 70% after 10 years. Eighty percent of thoracic aneurysms detected at autopsy have ruptured. The risk of rupture increases with aneurysm size and most aneurysms rupture when they reach 10 cm in diameter (1).

Imaging of TAA

TAAs are the most common cause of a mediastinal mass on chest radiography. Other chest radiographic findings include a widened tortuous aorta and curvilinear peripheral calcifications within the mediastinal mass. The main modalities used to image the thoracic aorta are computed tomography (CT) and magnetic resonance imaging (MRI)/magnetic resonance angiography (MRA). Most radiologists prefer CT to MR, although the relative advantages of MR with respect to the non-use of ionizing radiation and iodinated contrast media are obvious. Both axial images and multiplanar (MIP) reconstructions are necessary for an adequate assessment of the thoracic aorta.

The normal diameters of the thoracic aorta are:

Aortic root	36 mm
Ascending aorta 1 cm proximal to arch	35 mm
Proximal descending aorta	26 mm
Distal descending aorta	24 mm

Transesophageal echocardiography is used as a supplementary technique in some patients, mainly those who have aneurysmal aortic dissections, so as to locate the main proximal fenestration when this is not clear from either the CT or MR images.

The size criteria for treatment of TAAs vary widely from center to center, which is often due to the individual interventionalist's enthusiasm, ability, and experience in treating TAAs. Most operators would consider treating fusiform aneurysms if they were 6 cm or larger. Because of the relative paucity of data on the rupture rates of saccular aneurysms, these types of aneurysms are often treated when they are smaller than 6 cm.

Diagnosis

Thoracic aneurysms are diagnosed by imaging. In the majority of patients, thoracic aneurysms are discovered as a chance finding on chest radiographs that have been obtained for other clinical indications. Patients presenting with symptoms referable to the aneurysm undergo chest radiography at first, followed by either CT or MRI to evaluate the identity of mediastinal enlargement seen on the chest x-ray.

Interventional Radiology Treatment

Since the early 1990s, many patients with aneurysms of the descending aorta and some patients with aneurysms involving the aortic arch have been treated by the insertion of ►stent grafts into the aorta *via* small arteriotomies in the femoral arteries.

The aim of therapy is to exclude the aneurysm sac from the circulation to prevent further growth and rupture. This is achieved by placing one or more stent grafts in the aorta extending from the normal-caliber proximal aorta through the aneurysm to the normal-caliber aorta inferiorly. Short aneurysms may only require a single device; more extensive aneurysms may require several overlapping devices (2).

While it is difficult to envisage aneurysms of the ascending aorta being treated in this way in the near future, with increasing physician experience and advances in stent graft technology, it is predicted that most patients with nonascending TAA will be treated by endografts within a few years.

Stent Graft Designs

All stent grafts for use in the thoracic aorta consist of a metallic mesh (the stent) made up of either nitinol or stainless steel with a covering material (the graft) consisting of either polyester, polytetrafluoroethylene (PTFE), or dacron along the length of the stent. The graft material is affixed to the stent either by multiple small sutures or by enclosing the stent between two layers of graft material. All stent grafts are of the self-expanding type and are mounted on a delivery system whose function is to advance the stent in a compressed state from the site of access into the vascular system, usually the femoral arteries, to the desired site of deployment. The stent graft is compressed on the delivery system by a covering outer sheath. When the outer sheath is retracted, the stent graft is released and expands to its predetermined diameter by its own radial force.

Several types of stent graft for use in the thoracic aorta are currently available. The main types are the Valiant endograft (Medtronic, Santa Rosa, CA) (Fig. 1), the Gore TAG endograft (WM Gore, Flagstaff, AZ), and the Zenith TX2 endograft (William Cook, Bjaeverskov, Denmark). The devices are available in a range of lengths and diameters. The range of diameters is from 22 mm to 46 mm and lengths vary from 100 mm to 200 mm.

Inclusion Criteria for Endografting

Suitability for treatment with a stent graft depends on the presence of proximal (upper) and distal (lower) landing zones of the normal-caliber aorta to place the ends of the devices so that an effective seal can be achieved between the stent graft and the aortic wall. The diameter criteria

Aneurysm, Aortic and Thoracic. Figure 1 A Valiant endograft.

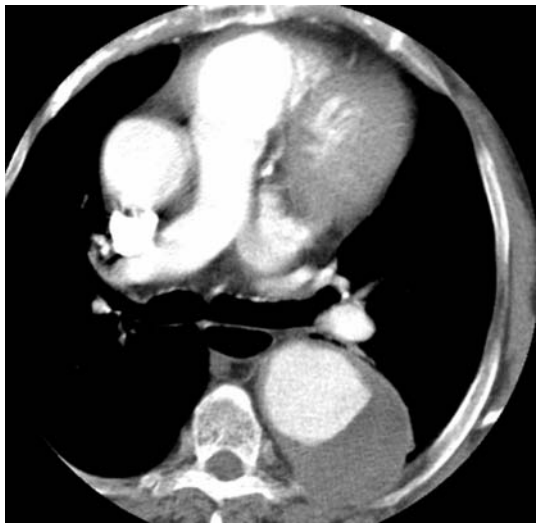

Aneurysm, Aortic and Thoracic. Figure 2 A patient with a 65-mm diameter aneurysm of the descending thoracic aorta.

for suitable landing zones are decided by the available sizes of endografts. In general, devices should be oversized by 10–20% in relation to the landing zones to provide an adequate seal. In practice, the maximum diameter for a landing zone is 42 mm and the minimum landing zone diameter is 18 mm. The landing zones should be at least 20 mm in length.

When aneurysms are close to or involve the aortic arch, it is possible to extend the length of the proximal landing zone by intentionally covering the left subclavian artery with the stent graft. If this maneuver is still not likely to produce a landing zone of adequate length, the landing zone can be elongated by elective bypass of the left common carotid artery to the right common carotid artery. It is even possible to treat patients with aneurysms of the mid-aortic arch, by elective bypass of the left common carotid and innominate arteries to the mid-ascending aorta before insertion of an endograft. If aneurysms extend into the upper abdomen, the distal landing zone length can be increased, if necessary, by bypass of one or more of the celiac, superior mesenteric, and renal arteries.

The access arteries (iliac and femoral) should be assessed for their ability to convey a stent graft delivery system. If they are too diseased or tortuous to accept passage of devices from a femoral arteriotomy, stents can be introduced *via* other access arteries (often using a surgical prosthetic conduit) including the common iliac arteries, the abdominal aorta, the axillary arteries, the subclavian arteries, or even the common carotid arteries.

Stent Graft Insertion Procedure

The devices are inserted as a combined procedure by an interventional radiologist and a vascular surgeon. The procedure is performed with the patient under general or regional anesthesia, although stents can also be inserted with the aid of local anesthesia alone. A diagnostic flush catheter is placed in the proximal aorta *via* a brachial artery or the contralateral femoral artery. Femoral arteriotomy is performed, and an exchange length extra stiff guidewire (e.g., Lunderquist wire, William Cook) is advanced so that the tip is placed in the low ascending aorta. The stent graft delivery system is advanced over the guidewire to the desired site of deployment. Accurate positioning is achieved by serial aortography. When the correct position is achieved, the stent graft is released. The stent graft should be molded by balloon dilatation to achieve its full diameter and to eliminate folds in the device (Figs. 2 and 3).

Results of Endografting

The technical success rates of stent grafting with immediate exclusion of the aneurysm sac are 81–100%. Mortality rates are 2–10% for elective procedures and increase to 28% for emergency procedures. These results are better than the mortality rates reported in most surgical series, which are around 15–25%. Morbidity after endovascular repair is substantially less than for open surgery. In most cases, patients are discharged from hospital a few days after the

Aneurysm, Aortic and Thoracic. Figure 3 The aneurysm has been treated by the insertion of endografts into the thoracic aorta.

procedure and in many cases they are not required to spend time on the intensive care unit (3,4).

Similar to abdominal aortic aneurysm stent-grafting, endoleaks are a problem with endovascular therapy for thoracic aneurysms. The most common endoleak is an attachment site (or type 1) endoleak. These may occur immediately or during follow-up and should be treated with additional overlapping devices. Type 3 leaks (between adjacent devices or through disrupted grafts) may occur and should also be treated with additional devices. Type 2 leaks from intercostals vessels supplying blood retrogradely into the aneurysm sac occur but are uncommon as are other types of leak. The paraplegia rates are 1–2% and are much lower than open surgery. The treatment of acute paraplegia following thoracic stenting is immediate catheter drainage of cerebrospinal fluid. Stroke is a more common complication occurring at least twice as commonly as paraplegia in most series.

The development of endografting revolutionized the diagnosis and treatment of TAAs. Many patients with life-threatening aneurysms of the descending aorta and aortic arch who would hitherto have been refused surgery are now treated with high success rates and low mortality and morbidity at most large hospitals. Further research into combined endografting and surgery, and the development of fenestrated and branched endografts, may in the future enable the majority of TAAs in all locations to be treated without the need for a thoracotomy and cardiopulmonary bypass.

References

1. Ogilvie BC. The thoracic aorta. In: Grainger RG, Allison DJ, Adam A, Dixon AK (eds) Diagnostic Radiology – A textbook of medical imaging. Churchill Livingstone, pp 953–956
2. Dake MD, Miller DC, Mitchell RS et al (1998) The "first generation" of endovascular stent-grafts for patients with aneurysms of the descending thoracic aorta. J Thorac Cardiovasc Surg 116:689–703
3. Black JH, Cambria RP (2006) Current results of open surgical repair of descending thoracic aortic aneurysms. J Vasc Surg 43 Suppl A:6–11
4. Ouriel K, Greenberg RK (2003) Endovascular treatment of thoracic aortic aneurysms. J Card Surg 18:455–463

Aneurysm, Artery, Iliac

Tony Nicholson
Leeds Teaching Hospitals NHS Trust
Leeds, UK
Tony.Nicholson@leedsth.nhs.uk

Definition

Iliac aneurysms are pulsatile swellings of the iliac arteries in the pelvis. An actual size definition is difficult and an artery is usually said to be aneurysmal when it is more than 50% larger than its counterpart but this is a gray area.

Characteristics

Ninety percent are caused by atherosclerosis where a marked decrease in aortic elastin, an increase in collagen production and degradation, inflammatory changes, and imbalances of matrix metalloproteinases and their inhibitors have been noted in pathologic studies. Ten percent are mycotic, syphilitic, traumatic, iatrogenic, congenital (due to persistence of the sciatic artery), or vasculitic. Genetic predisposition plays some role, especially in disorders such as Marfan disease and type IV Ehlers-Danlos syndrome. Familial clustering of cases also have been documented.

They are found in 16% of patients with abdominal aortic aneurysms (1). Isolated iliac artery aneurysms are rare, being found in only 2% of patients (2) but rupture has a high mortality rate. Eighty-nine percent occur in the common iliac artery, 10% in the internal iliac artery, and only 1% in the external iliac artery.

Clinical risk factors that predispose individuals to these degenerative changes in the arterial wall include smoking, advanced age, male sex, chronic obstructive pulmonary disease (COPD), hypertension, and family history.

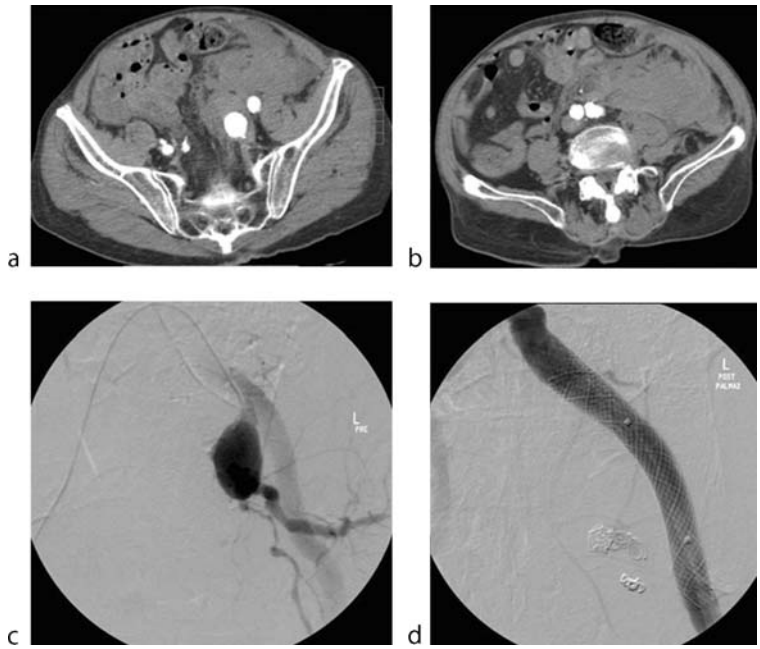

Aneurysm, Artery, Iliac. Figure 1 A ruptured left internal iliac aneurysm, diagnosed by CECT (Fig. 1a and b) was successfully treated by coil embolising the outflow arteries and covering the inflow with a stent graft (Fig. 1c and d).

A literature review suggests that for atherosclerotic aneurysms, the median (range) age at presentation is 71.9 (47–89) years and 95% are male. The natural history is unclear but is probably one of increasing size, with corresponding increased risk of rupture. Presentation is with rupture in 40%, leading to rapid death if untreated. The median size (range) of aneurysms at diagnosis is 7.7 (2–13) cm.

Symptoms included abdominal pain (31.7%), urological symptoms (28.3%), neurological symptoms (18.3%), groin pain (11.7%), hip or buttock pain (8.3%), and gastrointestinal symptoms (8.3%). Diagnosis may also be coincidental as a result of investigation for other conditions. Ultrasound, CT, and MRA are the most useful diagnostic tools.

Surgical treatment is difficult but can be achieved by ligation, excision, or endoanneurysmorrhaphy. More recently, radiological treatments include coil embolization and endoluminal stenting (often in combination) with the established advantages of endovascular repair have yielded promising results (Fig. 1).

Bibliography

1. Walter JF, Stanley JC, Mehigan IT et al (1978) External iliac artery fibroplasias. Am J Roentgenol 131:125–128
2. Richardson JW, Greenfield LJ (1988) Natural history and management of iliac aneurysms. J Vasc Surg 8:165–171

Aneurysm, Artery, Visceral

Tony Nicholson
Leeds Teaching Hospitals NHS trust
Leeds, UK
Tony.Nicholson@leedsth.nhs.uk

Definition

Visceral artery aneurysms are focal swellings of the arteries that supply the gastrointestinal tract, namely the coeliac trunk, superior mesenteric artery, inferior mesenteric artery and their branches. The splenic artery is the most common site of visceral aneurysm, accounting for 60% of the cases.

Characteristics

Visceral artery aneurysms are caused by or are associated with:

1. Pancreatitis (up to 10% of cases of pancreatitis)
2. Pregnancy (not a cause of aneurysm formation but associated with a greater risk of rupture)
3. Portal hypertension

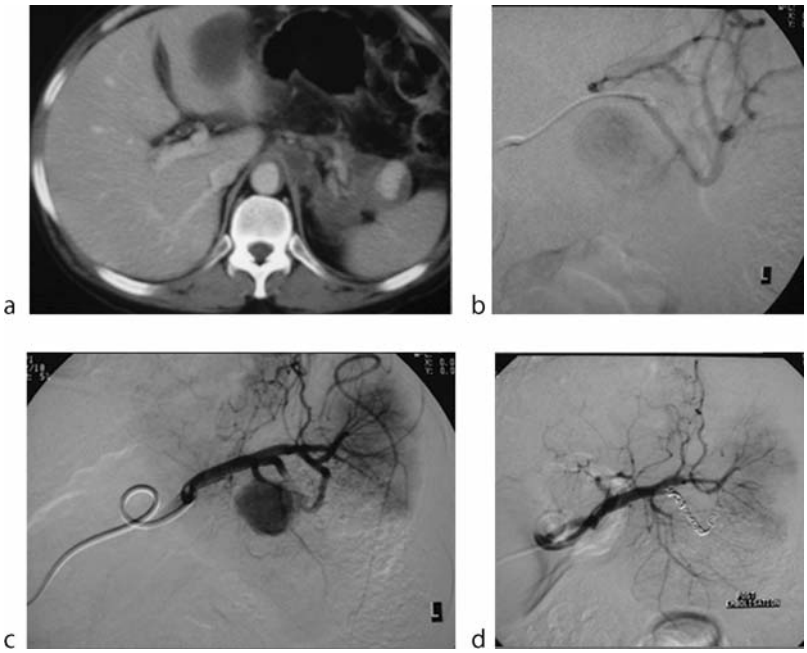

Aneurysm, Artery, Visceral. Figure 1 **A CT scan in a 65-year-old patient who presented with abdominal pain and haematemesis reveals a pseudoaneurysm close to the hilum of the spleen (a). Angiography confirms an aneurysm of the pancreatica magna artery which has ruptured into a splenic hilar branch (b and c). Proximal and distal coil embolization (d) occluded the aneurysm and maintained the viability of both spleen and pancreas.**

4. Medial fibrodysplasia
5. Splenomegaly
6. Iatrogenic (after orthotopic liver transplantation)
7. Polyarteritis nodosa (diffuse involvement of main artery and branches)
8. Infection (including TB)
9. Hyperdynamic flow (as occurs in isolated coeliac artery dissection)
10. Atherosclerosis is only a very rare cause of visceral aneurysms.

Patients do not usually present with rupture but the significance of these lesions lies in that risk, which has been reported between 3.0 and 9.6%. Rupture carries a 36% mortality rate. Patients with ruptured visceral aneurysms typically have signs and symptoms of an abdominal catastrophe and may be in frank shock though if a splenic artery aneurysm ruptures haemorrhage is sometimes contained temporarily in the lesser sac, affording an opportunity for diagnosis and intervention. If rupture occurs into an adjacent viscus patients may present with haematemesis or melaena. Most lesions found incidentally are repaired electively (Fig. 1).

The indications for intervening include:

- Rupture
- Abdominal pain: This may be indicative of a rapidly expanding aneurysm or impending rupture
- Aneurysms found incidentally in females who are pregnant or in those contemplating pregnancy
- Diameter greater than 2 cm: Currently, no consensus exists for the size at which a visceral aneurysm should be repaired in an asymptomatic patient. Diameters range from 1.5–3 cm, although most are approximately 2 cm. However, reports of aneurysm rupture at 1.5 cm diameter do exist. Calcification probably does not confer protection.
- Enlarging aneurysm
- Mesenteric ischemia or infarction secondary to embolization from the aneurysm sac
- Inferior pancreaticoduodenal artery aneurysms associated with acute dissection of the coeliac origin.

Surgery carries a high morbidity and mortality and wherever possible endovascular treatment should be used either by embolization or stenting.

Bibliography

1. Messina and Shanely, Visceral artery aneurysms. Surg Clin North Am 77(2):425–42, April 1997

Aneurysm, Hepatic Artery

Focal dilatation of the lumen of the hepatic artery caused by vasculitis (polyarteritis nodosa, cystic medial necrosis, fibromuscular dysplasia), infection (mycosis, tuberculosis, syphilis), Rendu–Osler–Weber disease, atherosclerosis, or following liver transplantation at the site of the arterial anastomosis. Hepatic artery aneurysms are the second most common splanchnic aneurysms after those of the splenic artery. They are usually asymptomatic and the classic triad of abdominal pain, hemobilia, and obstructive jaundice is observed in only 30% of patients. On US, hypoechoic masses in the pancreaticoduodenal area may be observed and the Doppler spectrum shows a typical arterial waveform within the lesion.

On CT, the lesion is hypodense on precontrast images and shows an intense contrast enhancement during the arterial phase following intravenous contrast medium administration. Both CT angiography and MR angiography allow an accurate evaluation of the aneurysmal site and the size, whereas selective hepatic angiography and subsequent embolization may be used in selected cases.

▶Transplantation, Hepatic

Aneurysm, Intracranial

Johannes Weber
Section of Neuroradiology, University of Freiburg Medical School, Freiburg, Germany
johannes.weber@uniklinik-freiburg.de

Synonyms

Aneurysm; Cerebral

Definitions

Intracranial aneurysms are classified based on morphology, size, location, and etiology:

1. Saccular aneurysms
2. Fusiform aneurysms
3. Dissecting aneurysms

Saccular aneurysms are the most common types of intracranial aneurysms. Causes of intracranial aneurysm include hemodynamically induced or degenerative vascular injury, atherosclerosis, underlying vasculopathy, and high-flow states, as in arteriovenous malformation (AVM) and fistula. Trauma, infection, drug abuse, and neoplasms represent uncommon causes.

Characteristics

Epidemiology

The incidence of intracranial aneurysms is estimated at 1–6% of the population. A reasonable prevalence is about 2.3%. The frequency of aneurysms increases beyond the third decade of life. Women have an approximately 1.6 higher risk for cerebral aneurysms than men. Familial intracranial aneurysms have been reported.

Intracranial aneurysms are uncommon in children and account for less than 2% of all cases.

Etiology

Most saccular or intracranial berry aneurysms show evidence of congenital, developmental, or inherited weakness of the arterial wall. Most intracranial aneurysms probably result from hemodynamically induced degenerative vascular injury. The occurrence, growth, thrombosis, and even rupture of intracranial saccular aneurysms may be caused by abnormal hemodynamic shear stresses on the walls of large cerebral arteries, particularly at bifurcation points.

Genetic conditions are associated with an increased risk of aneurysm development, where autosomal dominant polycystic kidney disease (ADPKD) is by far the most common genetic abnormality. Between 5% and 40% of ADPKD patients have cerebral aneurysms.

Vasculopathies such as fibromuscular dysplasia (FMD), connective tissue disorders (e.g., Ehlers-Danlos), and spontaneous arterial dissection are associated with an increased incidence of intracranial aneurysm.

Pathology

Saccular aneurysms are rounded berrylike outpouchings that arise from arterial bifurcation points, most commonly in the circle of Willis. These are true aneurysms, that is, they are dilatations of a vascular lumen caused by weakness of all vessel wall layers. The aneurysmal sac itself is usually composed of only intima and adventitia. The intima is typically normal, although subintimal cellular proliferation is common. The internal elastic membrane is reduced or absent, and the media ends at the junction of the aneurysm neck with the parent vessel. Lymphocytes and phagocytes may infiltrate the adventitia. The lumen of the aneurysmal sac often contains thrombotic debris.

Location

Saccular aneurysms commonly arise at the bifurcations of major arteries.

Approximately 85% of all intracranial aneurysms arise in the anterior (carotid) circulation. Common locations include the anterior communicating artery (30%), the internal carotid artery (ICA) at the posterior communicating artery origin (25%), and the middle cerebral artery (MCA) bifurcation (20%). The ICA bifurcation (7.5%) and the pericallosal/callosomarginal artery bifurcation are rare sites (4%).

About 15% of all intracranial aneurysms are located in the posterior (vertebrobasilar) circulation. The majority arise from the basilar artery bifurcation. However, the origin of the posterior inferior cerebellar artery (PICA) and the superior cerebellar artery (SCA) as well as the anterior inferior cerebellar artery (AICA) are also common sites for saccular aneurysms.

Intracranial aneurysms are multiple in 10–30% of all cases, with a strong female predilection. They are often associated with vasculopathies such as FMD and other connective tissue disorders.

Clinical Presentation

Most aneurysms do not cause any symptoms until they rupture. On presentation, patients typically report "the worst headache of their lives." Meningeal signs increase suspicion of subarachnoid hemorrhage (SAH). Acute hemorrhage can be subarachnoid, subdural, intraventricular, and/or intraparenchymal. Acute brain swelling, acute ventricular dilatation, and brain shift are other possible sequelae.

Other symptoms such as cranial neuropathies are uncommon. Cranial nerve affections typically are due to pulsatile irritation and compression caused by usually medium to large aneurysms. Giant aneurysms (diameter >2.5 cm) are more often symptomatic because of their mass effect.

The most widely used grading scale assessing the clinical severity of SAH is the five-step Hunt and Hess scale. The Fisher grade describes the amount of blood on a noncontrast computed tomography (CT) study of the head. Both scales correlate with patient outcome.

Delayed sequelae of SAH are hydrocephalus (10–20% of cases), vasospasm, brain infarction (due to direct pressure from space-occupying lesion, vessel compression from brain shift, severe diffuse vasospasm, or systemic hypotension, decreased cardiac output, hypoxia), hemorrhage, and seizures (15%).

Natural History and Clinical Outcome

The risk of rupture among incidental aneurysms was formerly estimated as 1–2% per year. The International Study of Unruptured Intracranial Aneurysms (ISUIA) study published in 1998 (retrospective component) and 2003 (prospective component) found that the risk of rupture in patients with unruptured aneurysms smaller than 7 mm in the anterior circulation without a hemorrhage from another aneurysm is extremely small. Aneurysms such as those of the basilar tip and the posterior communicating artery, aneurysms larger than 10 mm, and aneurysms that are found in patients who had bled from a prior aneurysm were found to have higher risks.

In general, bleeding risk varies between 7–10 ruptures/100,000 people in the USA and 15–25 ruptures/100,000 people in Finland and Japan. A quarter of cerebrovascular deaths are caused by SAH due to rupture of a cerebral aneurysm. Rupture is associated with significant morbidity and mortality. One-third of patients die immediately, one-third will be disabled, and another third will not suffer significant sequelae. Rebleeding has a peak incidence within the first 24 h after rupture. In the case of nontreated ruptured aneurysms, rebleeding occurs in 50% of patients within the first 6 months with a mortality of 50%.

The leading cause of disability and death from aneurysm rupture is vasospasm. Three important factors that influence outcome positively are early referral to a hospital that has experienced physicians in treating intracranial aneurysms, early treatment (surgical clipping or endovascular coiling), and aggressive treatment of vasospasm.

Outcomes associated with unruptured aneurysms are based primarily on whether they are treated and the results of that treatment. Unruptured aneurysms that have manifested with other symptoms such as cranial nerve palsy, brain stem compression, or visual loss should be treated because the natural history risk of rupture is believed to be significantly higher (6% per year) than that of incidentally discovered lesions.

Cigarette smoking, female sex, and younger age have recently been shown to correlate with aneurysm growth and rupture.

Imaging

Basically, three major modalities are used to for the diagnosis and follow-up of intracranial aneurysms. CT angiography (CTA), today used as a thin-section bolus-tracking technique with an excellent spatial submillimeter resolution, magnetic resonance angiography (MRA) either as time of flight (TOF) or as a contrast-enhanced technique

(CE-MRA), and finally catheter angiography. MRA or CTA is the preferred initial methods for evaluation of unruptured intracranial aneurysms, whereas digital subtraction angiography (DSA) is the preferred modality in patients with an acute SAH.

The ability of CT to reveal SAH in the acute phase is approximately 100%, and therefore CT is the standard method of choice (Fig. 1). Currently, CT involves multidetector techniques (MDCT) that allow fast scanning covering large field of views in submillimeter spatial resolution. CTA using a bolus-tracking technique after intravenous injection of contrast agent in combination with MDCT has the potential to even detect small aneurysms (Fig. 2). CTA and nonenhanced CT (NECT) may show calcifications in the neck of an aneurysm, which provides important information for the surgeon.

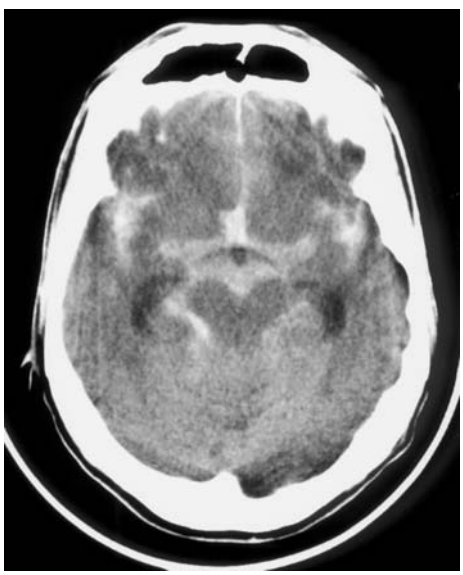

Aneurysm, Intracranial. Figure 1 NECT of acute SAH. Basal cisterns show hyperdense acute bleeding along vessel course.

DSA still remains the gold standard for detecting and assessing the size, morphology, and location of an intracranial aneurysm. Three-dimensional rotational angiography contributes fundamentally in the understanding of aneurysm anatomy, even in complex situations. This technique allows accurate depiction of the aneurysm morphology and helps in the planning of treatment strategies. Generally, the aim of DSA in SAH is to identify the presence or absence of any aneurysms, to delineate the relationship of an aneurysm to its parent vessel and adjacent penetrating branches, to assess the collateral circulation, to depict vasospasm, and to determine treatment modalities. In approximately 15% of patients with SAH, no aneurysm is found. An important contributor of this group is nonaneurysmal perimesencephalic SAH, where bleeding on a CT scan or MR image is localized anterior to the brain stem and adjacent areas such as the interpeduncular fossa and ambient cisterns.

Aneurysm appearance in magnetic resonance imaging (MRI) is highly variable and may be quite complex. The signal depends on the presence, direction, and flow rate, as well as the presence of clot, fibrosis, and calcification within the aneurysm itself. Currently, the two major MRA techniques in the depiction of cerebral aneurysms are TOF or contrast-enhanced (CE-)MRA.

TOF is generally used as a multislab three-dimensional technique. This sequence delineates the parent artery and depicts the size and orientation of an aneurysm dome and neck and is well suited for follow-up examinations after coiling. Aneurysms smaller than 3 mm may be difficult to detect, because TOF is a flow-dependant technique and flow in small aneurysms is low.

Treatment

The two treatment methods are surgery (clipping or wrapping) or endovascular coiling.

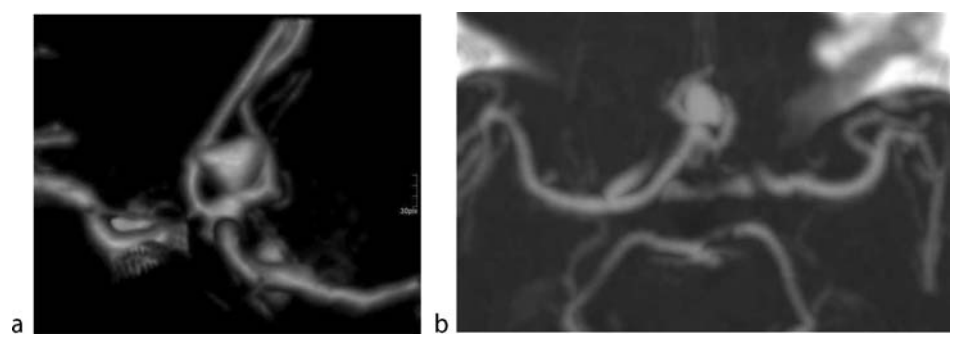

Aneurysm, Intracranial. Figure 2 (a, b) CTA of an AcomA aneurysm. Three-dimensional MIP reconstruction (a), and transverse (b) source image of a CTA, all depicting the pathology.

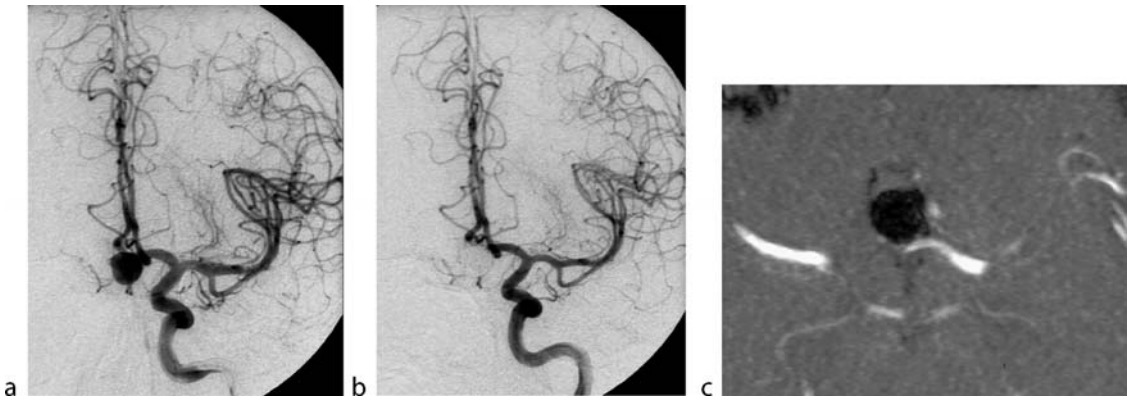

Aneurysm, Intracranial. Figure 3 (a–c) DSA of an AcomA aneurysm that was treated endovascularly using coils (b). Complete obliteration is shown on conventional DSA and TOF-MRA images (c).

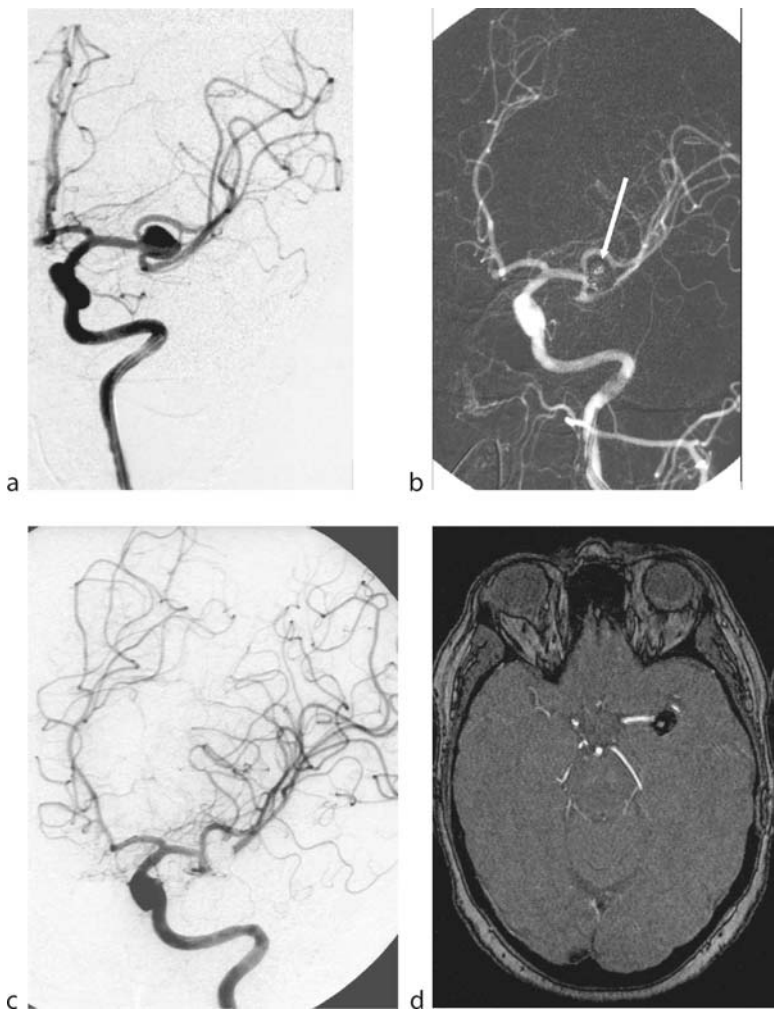

Aneurysm, Intracranial. Figure 4 (a–d) DSA of an aneurysm of MCA bifurcation. Incomplete coiling (b, *arrow*) was spontaneously abolished in the control DSA after 6 months (c). Residual flow in the cavity of the MCA aneurysm is shown on a TOF source image as central white spot (d).

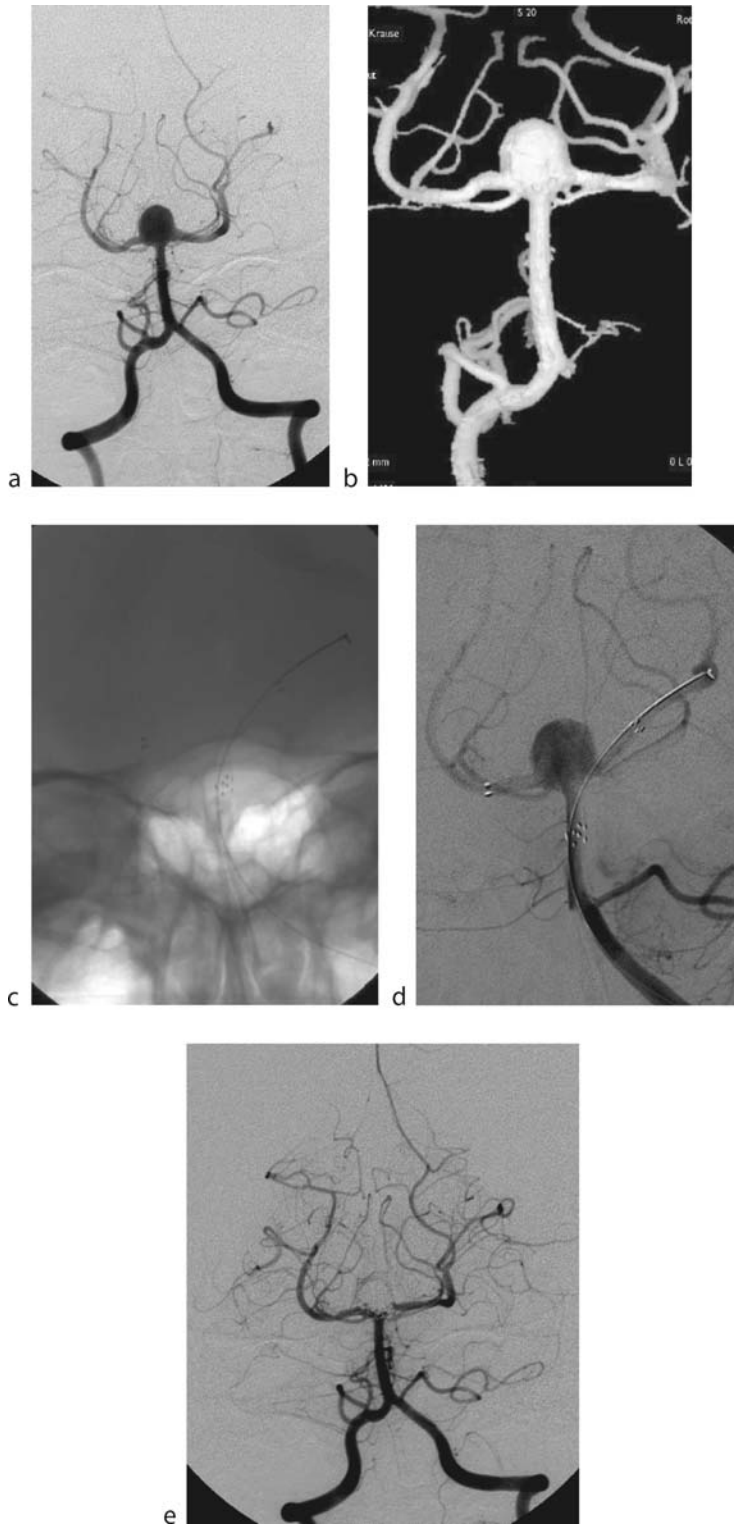

Aneurysm, Intracranial. Figure 5 (a–e) Broad based aneurysm of the basilar tip in DSA (a) and three-dimensional reconstruction (b) from a rotational angiography series. Both posterior communication arteries (PCAs) are embraced in the neck of the aneurysm. Y-shaped implementation of two intracranial stents, reaching from the basilar trunk to the PCA on both sides (c, d). Complete coiling of the basilar tip aneurysm obtaining patency of the right and left PCA (e).

The goal of surgical treatment is usually to place a clip across the neck of the aneurysm to exclude the aneurysm from the circulation without occluding brain-supplying vessels. MRI-compatible clips are manufactured in various types, shapes, sizes, and lengths. When the aneurysm cannot be clipped, wrapping is another choice that aims to protect the aneurysm sac to prevent bleeding. Wrapping can be performed with cotton or muslin, with muscle, or with plastic or other polymer.

The operative morbidity and mortality associated with clipping depends on whether the aneurysm has ruptured; surgery of ruptured aneurysms is more difficult and therefore morbidity is higher. The risk of surgery for unruptured aneurysms is estimated at 4–10.9% morbidity and 1–3% mortality.

During the past 15 years, endovascular methods have been developed and refined to treat intracranial aneurysms. Initially, endovascular balloon occlusion of a feeding artery was performed. This procedure was soon followed by direct obliteration of the aneurysmal lumen, first by detachable balloons and later by microcoils, first described by Guglielmi and colleagues (Figs. 3 and 4). They used detachable platinum microcoils that were placed in intracranial aneurysms. These days, coiling has become the primary treatment modality for aneurysms in many centers. It can be used to treat most aneurysms. Former limitations, such as aneurysms with wide necks or complex morphologies and high rates of recurrence secondary to coil compaction, have been addressed with complex shaped coils, balloon ("remodeling") and stent technology, and biologically active coils (Fig. 5).

The purpose of the coil is to induce thrombosis at the site of deployment *via* electrothrombosis. Newer biologically active coils are coated with various substances to enhance permanency of the thrombus within the coiled aneurysm by permitting a denser packing or engendering a tissue response at the neck of the aneurysm that decreases blood flow into the aneurysm and subsequent recanalization.

For the embolization procedure, a guiding catheter is placed in the cervical internal carotid or VA. Microcatheters of varying sizes can then be navigated into the aneurysm cavity using road-mapping technique. Coils of decreasing sizes are delivered into the aneurysm cavity and electrolytically detached. This process is continued until maximal angiographic obliteration of the aneurysm cavity is achieved.

Estimated risks associated with coiling based on several large studies are on the order of 3.7–5.3% morbidity and 1.1–1.5% mortality. One of the major drawbacks associated with coiling is that, over time, the coils can compact, leading to reopening or recanalization of the aneurysm. A reopened aneurysm has a certain risk of hemorrhage that is believed to be low. Newer technologic advances such as biologically active coils and stents designed to prevent recanalization are currently developed and in clinical use. Severe spasms can be treated with intra-arterially administered nimodipine or papaverine (Fig. 6).

Increased safety of coiling over clipping was demonstrated in the International Subarachnoid Aneurysm Trial (ISAT). The study was stopped prematurely after a planned interim analysis found a 23.7% rate of dependency or death in the coiling cohort versus a 30.6% rate in the clipping cohort. Continued follow-up from the ISAT study has recently been published: the original results were confirmed, with a higher rate of seizures in the

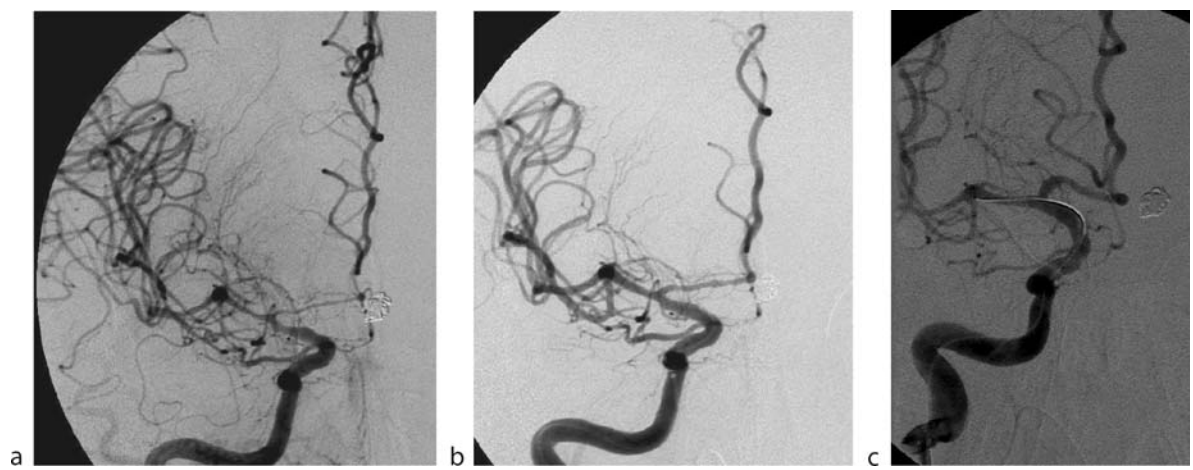

Aneurysm, Intracranial. Figure 6 (a–c) Severe vasospasms of the right A1, M1, and distal ICA (a). Partially resolved spasms after superselective intra-arterial administration of papaverine and nimodipine (b). Percutaneous transfemoral angioplasty (PTA) was finally performed in the A1 and M1 segments (c), resulting in restoration of approximate original vessel diameters.

clipping group and a slightly higher rate of rebleeding in the coiling group.

Ultimately, the decision to clip or coil should be made on an individual basis and may often involve difficult-to-quantify variables such as patient interest in one technique over the other or the experience or availability of physician operators.

Bibliography

1. Molyneux A, Kerr R, Stratton I et al (2002) International subarachnoid aneurysm trial (ISAT) of neurosurgical clipping versus endovascular coiling in 2143 patients with ruptured intracranial aneurysms: a randomised trial. Lancet 360:1267–1274
2. Wanke I, Egelhof T, Dorfler A et al (2003) [intracranial aneurysms: Pathogenesis, rupture risk, treatment options]. Rofo Fortschr Geb Rontgenstr Neuen Bildgeb Verfahr 175:1064–1070
3. Wiebers DO, Whisnant JP, Huston J et al (2003) Unruptured intracranial aneurysms: natural history, clinical outcome, and risks of surgical and endovascular treatment. Lancet 362:103–110
4. ISUIA (1998) Unruptured intracranial aneurysms—risk of rupture and risks of surgical intervention. International study of unruptured intracranial aneurysms investigators. N Engl J Med 339:1725–1733

Aneurysm, Splenic Artery

The splenic artery is the third most common site of intra-abdominal aneurysm formation after the abdominal aorta and iliac arteries, representing approximately 60% of all visceral arterial aneurysms. It is usually caused by atherosclerosis; however, it may also have congenital or infective origins, and a significant relation with pregnancy, multiparity, and portal hypertension have been reported. The majority of splenic artery aneurysms are single and saccular in shape, and are located in the middle and distal parts of the splenic artery.

In most cases, splenic artery aneurysm is asymptomatic although rupture of the aneurysm may occur in 5–10% of cases leading to massive intraperitoneal hemorrhage.

On US examination, splenic artery aneurysm appears as a hypoechoic mass in the left upper part of the abdomen with an arterial waveform at Doppler evaluation.

On CT scans, splenic artery aneurysm appears as well-defined low-density mass with or without calcifications and an intense enhancement within the residual patent lumen is observed after the administration of intravenous contrast medium. Moreover, both CT angiography and MR angiography allow an accurate evaluation of the aneurysmal site and the size, while selective splenic angiography and subsequent embolization may be considered in lesions larger than 2 cm.

▶Transplantation, Hepatic

Aneurysmal Bone Cyst

ABC is a nonneoplastic bone lesion of uncertain origin capable of marked expansion and rapid bone destruction and characterized by multiple blood-filled channels or spaces separated by fibrous septa.

▶Neoplasm-Like Lesions, Bone

Aneurysms, Cerebral

JY Gauvrit
Neuroradiology Department
Salengro Hospital
Lille
France
jygauvrit@gmail.com

Definitions

Abnormal outpouching of an intracranial blood vessel wall.

Aneurysms develop during the course of life. They are almost never found in neonates and they are also rare in children (1). The exact prevalence of unruptured aneurysms is unknown but autopsy series estimate the prevalence at 1.3 to 7.9%, the prevalence tending to increase with age. The morphological appearance is saccular or fusiform, the most common type being the saccular ('berry') aneurysm, constituting about 90% of all intracranial aneurysms. Fusiform aneurysms account for between 5 and 10% of cases. The latter are characterised by the absence of a defined neck, circumferential involvement of the parent artery and a longish course. Aneurysms are located intradurally or extradurally. Intradural aneurysms most often involve the bifurcation of vessels at the base of the brain, especially the anterior and middle cerebral artery, distal internal carotid artery and the vertebrobasilar trunk. Anterior circulation aneurysms constitute about 85% of cases. They can occur as solitary (70%) or multiple aneurysms (30%). While the majority of aneurysms are small in size (<10 mm), some 5 to 7% of intracranial aneurysms are defined as giant aneurysms, with a maximum diameter of more than 2.5 cm.

Pathology/Histopathology

It is not known why some adults develop aneurysms and most do not. Although aneurysms are not in the strict

sense congenital, there are specific conditions under witch they may occur: disorders of connective tissue, disorders of angiogenesis, associated hypertension and local haemodynamic stress.

Some classical acquired risk factors for stroke also apply to aneurysm development and SAH. Smoking, hypertension and heavy drinking emerge as significant risk factors with odds ratios of about two or three.

Clinical Presentation

Most intracranial aneurysms remain undetected until the time of rupture.

SAH is the most common initial clinical presentation. About 85% of cases of spontaneous SAH are due to the rupture of an intracranial saccular aneurysm, 10% to perimensencephalic non-aneurysmal haemorrhage and 5% to other, rare causes. The risk of rehaemorrhage is very high during the first five days and early imaging is therefore important for any therapeutic decision and for the outcome. Other findings are cerebral infarction and intracerebral hemorrhage.

Unruptured aneurysms usually remain asymptomatic. Additional aneurysms can sometimes be found in patients with a symptomatic aneurysm. Aneurysms may also be found unexpectedly in patients undergoing investigation for another pathology (e.g. vertigo, headache). Unruptured aneurysms, especially large or giant aneurysms, can sometimes cause neurological symptoms: cranial nerve palsy (oculomotor nerve or optic nerve) visual disturbances and pain. The findings of an international study on unruptured intracranial aneurysms evaluated the annual risk of rupture for aneurysms less than 10 mm in diameter as 0.05% (2). Moreover, the risk of bleeding is relatively high for aneurysms larger than 10 mm and for posterior circulation aneurysms.

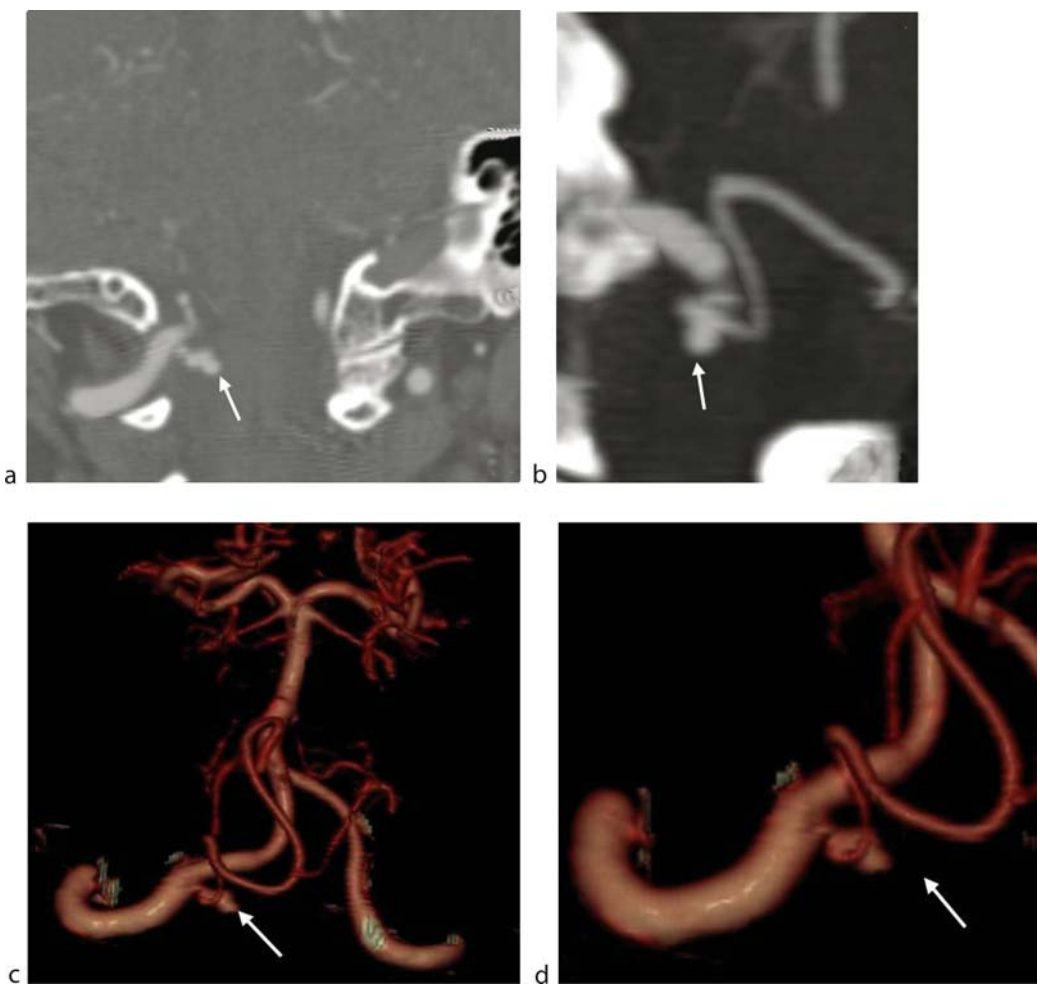

Aneurysms, Cerebral. Figure 1 CT angiography data displayed as MIP (maximum intensity reconstructions) (a-b) and VRT (volume rendering technique) (c-d) reveals an aneurysm of the right PICA (arrow).

Imaging

The imaging evaluation of aneurysms has to include the location, size, number and morphologic appearance and, in the case of saccular aneurysms, the architecture of their neck. The exact characterisation of the aneurysm including its maximum diameter and neck size, and any branches arising from the aneurysmal sac, as well as variations in the circle of Willis are important issues for the pre-therapeutic risk assessment.

Computed Tomography (CT) Angiography

Parameters for CT angiography acquisition with a multidetector row scanner provide a section thickness of 0.5 to 0.75 mm, with a scanning time of approximately 20 s. The scanned volume includes the entire head from the dens axis to the vertex. A total of 80 mL of contrast media at a rate of 3.5 mL/s is injected *via* a venous line. CT data from different sources are examined, 2D maximum intensity projection (MIP) reconstructions providing a study of the size of the vessel, neck, sac and the 3D volume rendering technique (VRT) providing a true volumetric view (Fig. 1).

Teksam et al (3) found a sensitivity of 84% for the detection of intracranial aneurysms less than 4 mm in diameter, 97% for the detection of intracranial aneurysms between 4 and 10 mm in diameter and 100% for those with a diameter greater than 10 mm. These results justify the application of CT angiography for the detection of intracranial aneurysms in patients presenting with SAH. Despite its limitations for detecting branches originating from the aneurysmal sac, CT angiography is a more practicable option and a reliable tool for the detection of

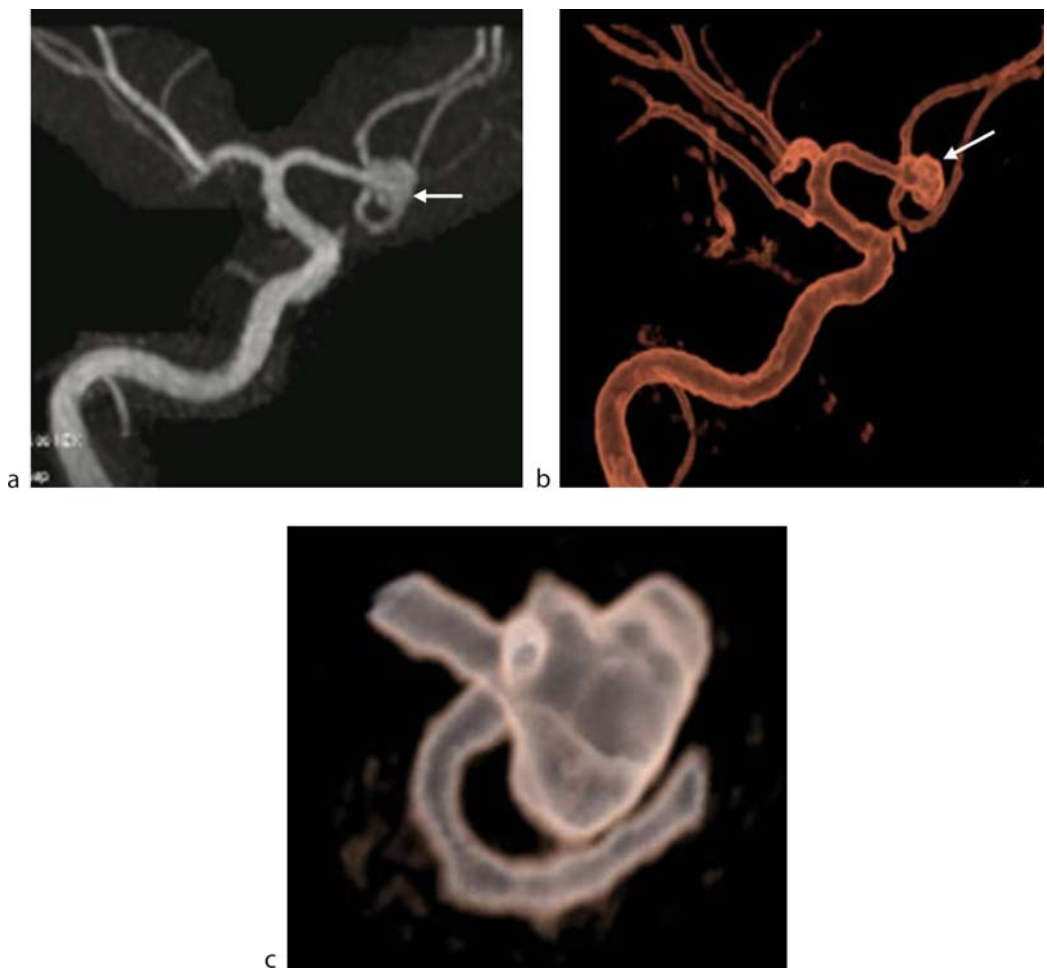

Aneurysms, Cerebral. Figure 2 Time-of-flight MR angiography with MIP (maximum intensity reconstructions) (a) and global view (b), centred views (c) VRT (volume rendering technique) reconstructions reveal an aneurysm of the middle communicating artery (*arrow*).

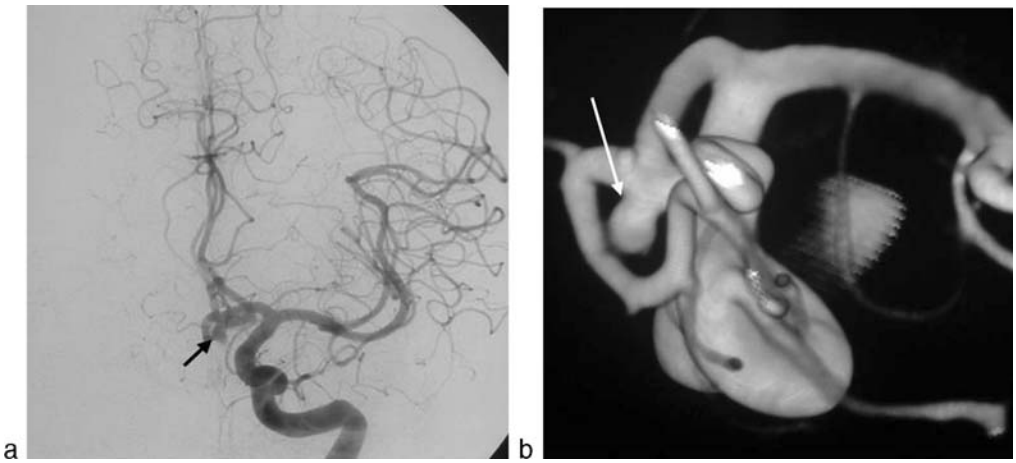

Aneurysms, Cerebral. Figure 3 Conventional catheter angiography (a) with 3D reconstructions (b) reveal an aneurysm of the anterior communicating artery (*arrow*).

intracranial aneurysms in patients presenting with acute non-traumatic SAH, because it is widely available, less expensive and offers great procedural safety.

Post-operative confirmation is generally done using ►DSA because the artefacts from surgical clips interfere with the image quality of magnetic resonance (MR) angiography and 3D-CT angiography. The advent of paramagnetic titanium clips is, however, expected to alleviate the problem of artefacts, allowing evaluation by multi-detector row CT angiography.

MR Angiography

The spatial resolution of 3D time-of-flight (TOF) MR angiography is approximately 0.8 mm and is sufficient to detect aneurysms 2 to 3 mm in size. MR angiography studies have found sensitivity rates of more than 95% for large aneurysms (>6 mm) but lower rates for smaller aneurysms, with detection rates averaging 60%. However, the combined evaluation of axial source images and MIP reconstructions increases the sensitivity of detection in comparison with MIP reconstructions alone (95 versus 75%). MR angiography is safe and reasonably sensitive (90%), which makes it well suited to screening people at risk of intravascular aneurysms (Fig. 2).

Another excellent indication for MR angiography is the follow-up of patients who have undergone endovascular treatment. It provides an effective way of detecting aneurysm recanalisation requiring retreatment. DSA is the method of reference, but this technique is invasive, limiting its use in clinical practice. Contrast-enhanced (CE) MR angiography, the reference technique for extracranial carotid disease, can be performed to image intracranial vessels and to follow-up aneurysms treated with Guglielmi detachable coils (4).

Digital Subtraction Angiography

DSA is the gold standard and is usually performed for the detection of a cerebral aneurysm because of its inherent high-spatial resolution. Due the frequency of multiple aneurysms, complete four-vessel angiography is necessary.

DSA can localize the lesion, reveal aneurysm shape and geometry, determine the presence of multiple aneurysms, define vascular anatomy and collateral circulation and assess the presence and degree of vasospasm. Using rotational angiography, multiple oblique views are obtained as the source for 3D reconstructions, thereby further increasing the performance of DSA (Fig. 3). Several 2D working views are performed after the 3D reconstructions and are used during the surgical or endovascular procedure (5).

However, catheter angiography is not an entirely innocuous procedure. A systematic review found a transient or permanent neurological complication rate of 1.8%. The aneurysm may re-rupture during the procedure, as occurs in 1 to 2% of cases.

References

1. Rinkel GJ, Djibuti M, Algra A et al (1998) Prevalence and risk of rupture of intracranial aneurysms: a systematic review. Stroke 29:251–256
2. Wiebers DO, Whisnant JP, Huston J 3rd et al (2003) Unruptured intracranial aneurysms: natural history, clinical outcome, and risks of surgical and endovascular treatment. Lancet 362:103–110
3. Teksam M, McKinney A, Casey S et al (2004) Multi-section CT angiography for detection of cerebral aneurysms. AJNR Am J Neuroradiol 25:1485–1492
4. Farb RI, Nag S, Scott JN et al (2005) Surveillance of intracranial aneurysms treated with detachable coils: a comparison of MRA techniques. Neuroradiology 507–515
5. Anxionnat R, Bracard S, Ducrocq X et al (2001) Intracranial aneurysms: clinical value of 3D digital subtraction angiography in the therapeutic decision and endovascular treatment. Radiology 218:799–808

Angel Wings Sign, Spinnaker Sign

In younger persons, the thymus may be outlined by air and this finding is specific for pneumomediastinum. These signs have been suggested as descriptive terms.
▶Pneumomediastinum

Angina Pectoris

Angina pectoris is the name for a clinical syndrome due to myocardial ischemia experienced as pain or tension in the middle of the chest. Radiation into the jaw and, especially, the left arm may occur.
▶Ischemic Heart Disease, Nuclear Medicine

Angiodysplasia

Acquired vascular malformation of the bowel wall.
▶Vascular Disorders of the Gastrointestinal Tract

Angiogenesis

The formation of new blood vessels.
▶Perfusion, Neoplasms

Angiomyolipoma

▶Lipomatous Neoplasms, Hepatic

Angiomyolipoma, Hepatic

Very uncommon benign mesenchymal tumor composed of a variable amount of proliferating blood vessels, muscle elements, and fat. It can occur as a solitary mass or as multiple lesions in the case of tuberous sclerosis. This tumor usually presents a combination of fat and soft tissue. Imaging features of angiomyolipoma are related to the distribution and amount of fat and to the relative proportion of its three histological components.
▶Lipomatous Neoplasms, Hepatic

Angioplasty

Or percutaneous transluminal angioplasty (PTA) is the dilation of a vessel with the use of a balloon catheter.
▶Stroke, Interventional Radiology

Angiosarcoma

▶Hepatic Sarcoma

Angiosarcoma, Hepatic

Primary malignancy of the liver occurring in adults, with a male predominance, arising from vascular endothelial cells of the liver. This form although rare represents the most common primary mesenchymal malignancy of the liver. Tumor onset seems to be related to chronic exposure to toxic agents such as inorganic arsenic and vinyl chloride or to long-term irradiation with thorium oxide. In some cases an association with hemocromatosis, von Recklingausen's disease, alcoholic cirrhosis and anabolic, steroid intake has been described. Tumor size may vary from a few millimeters to several centimeters. The presence of internal hemorrhage determines the red-brown appearance of the nodules. Larger tumors are usually not capsulated and may contain cystic areas with blood debris filling. This tumor is composed of malignant endothelial cells organized to form vessels that may range from abortive or cavernous forms to structured, frequently dilated sinusoids. Early metastatic spreading to lungs and spleen is common.
▶Hepatic Sarcoma

Aniridia

Congential absence of the retina of the eye.
▶Neoplasms, Kidney, Childhood

Anismus

Anismus is an abnormal activity of pelvic floor musculature that results in an outlet obstruction characterized by difficulties in rectal evacuation.
▶Pelvic Floor Dysfunction, Anorectal Manifestations

Anismus - spastic pelvic floor syndrome - diskinetic puborectalis muscle - pelvic floor dyssynergia

▶Pelvic Floor Dysfunction, Anorectal Manifestations

Ankylosis

Loss of motion until complete immobility of a joint is referred to as ankylosis and can be due to alterations around ("false") or in the joint itself ("true"). When there is bony bridging across the joint space and complete immobility, it is termed "osseous" or "complete." Ankylosis can also be applied to an osseous junction between neighboring bones.
▶Dish

Annexin V

A 36-kDa protein, which binds in the presence of Ca^{2+} to externalized phosphatidyl serine (PS).
▶Apoptosis

Annular Fissures

▶Degenerative Conditions, Spine

Annular Pancreas

The annular pancreas represents a congenital anomaly characterized by a ring of normal pancreatic tissue that arises from the head of the pancreas encircling the descending portion of the duodenum.
▶Congenital Abnormalities, Pancreatic
▶Congenital Anomalies of the Pancreas

Annular Tears

The tears in the annulus fibrosus caused by aging, acute or repetitive trauma or overloading. There are three types of fissures: concentric, transverse, and radial. Annular fissures are present in almost all individuals over 40 and in virtually all bulging disks. Therefore, they could be considered as paraphysiological, however some of them result in disk herniation. Annular tears can be visualized on both sagittal and axial planes on T2-weighted and postcontrast T1-weighted MR images as bands of increased signal (high intensity zones – HIZ) in the annulus fibrosus.
▶Degenerative Conditions of the Spine

Anomalies of Cortical Development

▶Gyration Disorders, Cerebral

Anomalies of the Cerebral Commissures

▶Congenital Malformations, Cerebrum

Anomalous Termination of Bile Ducts

Anomalous termination of the hepatic ducts into the gallbladder or anomalous end of the common bile duct into the pylorus, stomach, pancreatic duct. In the second case the refluxes of gastric contain may appear.

▶Congenital Malformations, Liver and Biliary Tract

Anophthalmia

▶Congenital Malformations, Orbit

Anorectal Malformation

Erich Sorantin
Department of Radiology, Division of Pediatric Radiology, University Hospital Graz, Graz, Austria
erich.sorantin@meduni-graz.at

Synonyms

Anal atresia; Imperforate anus; Rectal atresia—most of them are variants of anorectal malformations and therefore should not be used as synonyms

Definition

Several definitions exist, the two most frequent are listed later.

Gans classification (1):

1. *Rectal atresia*: The anus is open and a variable segment of the rectum superior to the anus is atretic, no fistula is present.
2. *Ectopic anus:* Most common abnormality of the anorectal segment. It occurs when the terminal bowel fails to descend normally, resulting in a lack of communication with the anus and in an abnormal bowel opening *via* a fistula (perineal, vestibule, vagina, urethra, bladder, or cloaca).
3. *Imperforate anus:* Terminal bowel ends blindly and no fistula exists.
4. *Anal or rectal stenosis:* Mildest form, represents cases of incomplete anal or rectal atresia.

Wingspread workshop classification of anorectal malformations (ARM) (2). Basically, high, intermediate, and low groups are distinguished as well as male and female subgroups:

1. ▶*High ARM:* The blind pouch ends above the sling of the hypotrophic puborectalis muscle. There can be associated rectobulbar fistulas in males or rectovaginal fistulas in females.
2. ▶*Intermediate ARM:* The rectal pouch enters the sling of the puborectalis muscle; depending on the gender, either rectobulbar or rectovaginal fistulas can exist.
3. ▶*Low ARM:* The rectum passes through a well-developed puborectalis muscle sling. The aboral ending is an anocutaneous fistula in males, whereas in females this is represented by an anocutaneous or anovestibular fistula.

Female cloacae were placed in a separate group, because they may be considered high, intermediate, or low depending on the length of the common channel.

Regarding outcome it is clear that results are best in the low ARM group, where associated malformations occur less frequently. In the other forms, results are less satisfying and malformations as well as urinary tract disorders are more frequent (2).

Associated Anomalies

Associated malformations can be found in about 20–70% of patients with ARMs (2). Höllwarth et al studied these associated malformations in 75 patients, finding an overall incidence of 72% (details are given in Table 1).

Anorectal Malformation. Table 1 ARM associated malformations in 75 children

Anatomical System	Total in %
Skeleton	46.6
Urinary tract	41.3
Cardiac system	18.6
Intestinal tract	18.6
Cerebral	13.3
Genitalia	12.0
Others	22.6

Source: Höllwarth ME, Sorantin E (2001) Urinary problems associated with imperforate anus. In: Fotter R (ed) Pediatric Uroradiology, Chapter 6, Springer, Berlin, pp 105–110

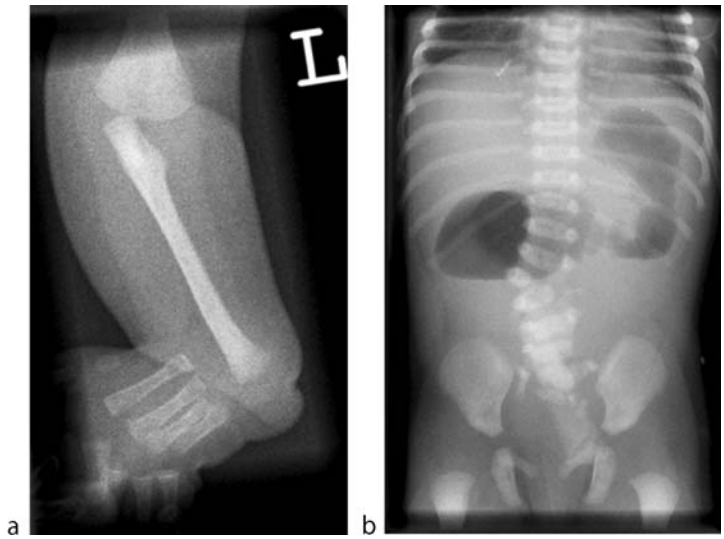

Anorectal Malformation. Figure 1 Male, 1 day old, imperforate anus and VACTERL association, plain films. (a) Left upper extremity—radial aplasia is shown. (b) Abdomen—sacral aplasia, severe vertebral malformation as well as a right-sided pelvic rib is presented.

As can be seen, frequently more than one organ system is involved. Boemers created the acronym ▶ARGUS for children suffering from the association of AnoRectal, GenitoUrinary, and Sacral anomalies (3). Another acronym is the so-called *VATER* or *VACTERL* association, combining Vertebral anomalies, Anorectal atresia, Cardiac anomalies, Tracheoesophageal fistula, Esophageal atresia, Renal dysplasia, and Limb malformation (Fig. 1) (2).

Vertebral anomalies occur more frequently in the lumbar and sacrococcygeal spine. Partial or complete sacral agenesis is part of the caudal regression syndrome and is a strong indicator of neurogenic bladder dysfunction. Imperforate anus is also included in the Currarino triad, where it is found in combination with sacral dysplasia and an anterior sacral mass (e.g., teratoma, anterior meningomyelocele). As a general rule, associated malformations occur more frequently in the high ARM or intermediate ARM groups than in the low ARM group.

Urologic Problems

The outcome of ARM patients is determined by the associated malformations, especially by the structural and functional anomalies of the urinary tract, as well as complications of surgical procedures (2).

Structural

In males, rectourethral fistulas can be detected in about 80% of patients in the high ARM or intermediate ARM groups, whereas rectovesical fistulas are only present in 8% (Fig. 2). Renal dysplasia, renal agenesis, renal ectopia, duplications, and hydronephrosis are the most common anomalies of the upper urinary tract. In addition, 47% of

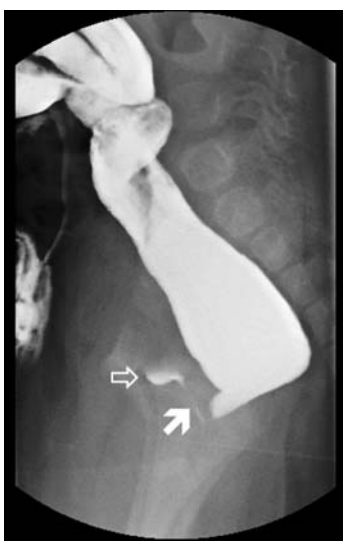

Anorectal Malformation. Figure 2 Male, 8 months old, imperforate anus with rectourethral fistula, loopography, last image hold, lateral projection. Loopography is performed by instillation of the contrast medium into an existing colostomy. *Solid*, *white arrow* points to the rectourethral fistula, contrast medium is accumulating within the bladder (*nonsolid white arrow*).

patients in the high ARM group and 35% in the low ARM group exhibit a vesicoureteric reflux, caused be either malformations of the vesicoureteric junctions or more commonly by neurogenic bladder dysfunction (4). In the lower urinary tract hypospadias, epispadias and exstrophy, urethral diverticula, valves, strictures, or duplications can be found (2).

Functional

The most important functional disorder is represented by any kind of neurogenic bladder, which is either related to the surgical reconstruction procedure or inherent to the associated sacral malformation. This was confirmed by Boemers et al, who investigated ARM patients with/without sacral anomalies urodynamically. Patients with a normal-appearing sacrum or only minor dysplasia will exhibit a normal bladder and sphincter function in 98% of cases. In contrast, almost all patients with major sacral dysplasia will suffer from neurogenic bladder.

Embryology/Pathology

Simply speaking, ARM are thought to represent the failure of the hindgut to descend properly.

Clinical Presentation

Abdominal distension. No evidence of an anal opening on physical examination. Incidence is about 1 in 5,000 live births.

Imaging

Recently, Boemers et al published guidelines for diagnostic screening and initial management in children with ARM ("ARGUS" protocol) (3).

1. *Sacral anomalies*: Plain films of the spine including the sacrum in two projections. Spinal ultrasound is mandatory in almost all patients where any kind of sacral dysplasia is found. Special care must be taken in patients with suspected Currarino triad not to overlook a presacral mass such as an anterior myelomeningocele. Magnetic resonance imaging (MRI) is indicated whenever spinal ultrasound depicts an abnormality. This MRI investigation should also serve as a baseline study for the future, where spinal ultrasound can no longer be performed due to increasing vertebral ossification (usually after the first half year, and definitely after the first year of life).
2. *Urinary tract*: Renal ultrasound and pelvic ultrasound should be performed as soon as possible. In the first days of the life it should be noted that due to the physiological oliguria in neonates, dilatations of the collecting system can be missed. Special attention should be given to the bladder. Pathological bladder wall thickness, trabeculation, a dilated posterior urethra in combination with frequent bladder neck openings and closings point to neurogenic bladder dysfunction with uninhibited detrusor contractions (3). Voiding cystourethrography (VCU) is recommended in all patients with upper urinary tract dilatation. Furthermore, VCU should be performed on male patients without a perineal bowel opening in order to detect a rectourethral fistula (2, 3). Functional assessment of the lower urinary tract by urodynamics is mandatory in all patients with sacral dysplasia during the first 3 months of life (3). Whenever VCU is necessary, a modified VCU technique, or better still video urodynamics (VUD), should be used (5). In boys with a rectourethral fistula and no perineal opening, for VUD the abdominal pressure can be recorded either by using an existing colostomy or by placing a microtip catheter in the stomach (2). Routine intravenous urography (IVU) can now be replaced in many cases by ultrasound and isotope studies. However, there is still a role for IVU whenever detailed anatomical information is necessary as well as in the postoperative care of urologic procedures. In the future, there will also be a role for MR urography.
3. *Genitals:* Ultrasound provides an excellent overview of the uterus and ovaries in newborn girls. A genitogram has to be performed on all newborn girls with persistent cloaca (3).
4. *CNS:* Cranial ultrasound is part of the neonatal work-up whenever a malformation is discovered; MRI should be performed electively.
5. *Heart:* Chest films are taken routinely in the preoperative phase. Whenever there is a cardiac abnormality or a heart murmur further work-up is indicated.

Nuclear Medicine

As already mentioned, renal isotope studies can be used to examine split renal function and urine drainage.

Diagnosis

The diagnosis is made clinically. The associated malformations are diagnosed by imaging and further clinical

work-up such as endoscopy. In case of complex syndromes, genetic counseling is mandatory.

►EI Tract, Pediatric, Congenital Malformations

Bibliography

1. Berrocal T, Lamas M, Gutierrez J et al (1999) Congenital anomalies of the small intestine, Colon and rectum. Radiographics 19:1219–1236
2. Höllwarth ME, Sorantin E (2001) Urinary problems associated with imperforate anus. In: Fotter R (ed) Pediatric Uroradiology, Chapter 6, Springer, Berlin, pp 105–110
3. Boemers T, Beek F, Bax N (1999) Guidelines for the urological screening and initial management of lower urinary tract dysfunction in children with anorectal malformations the ARGUS protocol. BJU Int 83:662–671
4. Ralph D, Woodhouse C, Ransley P (1992) The management of the neuropathic bladder in adolescents with imperforate anus. J Urol 148:366–368
5. Sorantin E, Lindbichler F, Fotter R (2005) Imaging in Children, 2nd edn, vol 1, Chapter 4.16, Elsevier Churchill Livingstone, Edinburgh, pp 863–869

Anorectal Malformation

►GI Tract, Paediatric, Congenital Malformations

Anterior Mediastinum

The narrow region between the pericardium and the sternum containing the thymus or its remnants, some lymph nodes and vessels and branches of the internal thoracic artery.

►Neoplasms of the Chest in Childhood

Antibodies

Proteins used by the immune system to identify and neutralize foreign objects. Each antibody recognizes a specific binding site, called an antigen. Five different isotypes are known: IgA, IgD, IgE, IgG, and IgM. For imaging and therapeutic purposes in medicine, IgG is the relevant isotype.

►Receptor Studies, Neoplasms

Aorta and Large Vessel Disease, MRI

Rossella Fattori
Department of Radiology, Cardiovascular Unit, University Hospital S. Orsola, Bologna, Italy
ross@med.unibo.it

Magnetic Resonance Imaging Techniques for Studying the Thoracic Aorta

Spin-Echo MRI

Spin-echo (SE) T1-weighted imaging provides the best anatomic detail of the aortic wall and of pathologic conditions, such as atheromatous plaques, intimal flaps, and intramural hemorrhage, and is still the basis of any aortic study (1), whereas T2-weighted images (TR = 2-3 R-R'; TE, 80–100 msec) can be used in tissue characterization of the aortic wall or blood components. A superior black-blood effect is achieved by using preparatory pulses such as presaturation, dephasing gradients, and preinversion, with one or more additional RF pulses outside the plane to suppress the signal intensity of inflowing blood and to nullify the blood signal (black-blood SE sequences).

Gradient-Echo MRI

Gradient-echo (GE) techniques provide dynamic and functional information, although with fewer details of the vessel wall. The bright signal of the blood pool on GE images results from flow-related enhancement obtained by applying radio-frequency pulses to saturate a volume of tissue. With a short TR (4–8 msec) and low flip angle (20–30°), maximal signal is emitted by blood flowing in the voxel, with a high degree of temporal resolution throughout the cardiac cycle (up to 20–25 frames).

Flow Mapping

Accurate quantitative information on blood flow is obtained from modified GE sequences with parameter reconstruction from the phase rather than the amplitude of the MR signal. Vector mapping has been used to describe flow patterns in different aortic diseases (including hypertension, aneurysms, dissection, Marfan syndrome, and coarctation). MR maps of flow velocity are obtained two-dimensionally, which is particularly important in profiles of nonuniform flow, such as that in the great vessels (2).

MR Angiography

Three-dimensional (3D) contrast-enhanced MR angiography (MRA) constitutes the most common angiographic method for evaluation of the great vessels (3). The technique relies on the contrast-induced T1-shortening effects of the contrast medium, and saturation problems with slow flow or turbulence-induced signal voids are avoided. During the short intravascular phase, the paramagnetic contrast agent provides signal in the arterial or venous system, enhancing the vessel-to-background contrast-to-noise ratio irrespective of flow patterns and velocity. Pulsatility artifacts are minimized, even in the ascending aorta and without electrocardiographic gating. With the support of maximum intensity projection (MIP) images and of 3D multiplanar reformation (MPR), this technique delineates all the morphologic details of the aorta and its side branches in any plane in a 3D format.

Acquired Aortic Disease

Aortic Dissection

Aortic dissection is characterized by a laceration of the aortic intima and inner layer of the aortic media that allows blood to course through a false lumen in the outer third of the media extending from the ascending aorta to the iliac arteries (type A) or involving the descending aortic segments exclusively (type B).

Using a magnetic resonance imaging (MRI) SE black-blood sequence in the axial plane, the intimal flap is detected as a straight linear image inside the aortic lumen. The true lumen can be differentiated from the false by the anatomic features and flow pattern: the true lumen shows a signal void, whereas the false lumen has higher signal intensity. In addition, visualization of remnants of the dissected media as cobwebs adjacent to the outer wall of the lumen may help identify the false lumen. A detailed anatomic map of aortic dissection must indicate the type and extension of dissection and also distinguish the origin and perfusion of branch vessels (arch branches, celiac, superior mesenteric, renal arteries, and coronary arteries) from the true or false channels. High signal intensity of effusion (pericardial, periaortic, or pleural) indicates a bloody component and is considered a sign of impending rupture of the ascending aorta into the pericardial space or of the descending aorta into the mediastinal or retroperitoneal space. In stable patients, adjunctive GE sequences or phase contrast images can be instrumental in identifying aortic insufficiency in type A dissection, entry, or re-entry sites as well as in differentiating slow flow from thrombus in the false lumen. Gadolinium-enhanced 3D MRA enhances visualization of the intimal flap and its relationship with aortic vessels in a 3D format.

Intramural Hematoma

Intramural hematoma (IMH) derives from spontaneous rupture of the aortic vasa vasorum of the media layer as the initiating process, which is confined in the aortic wall without intimal tear. This results in a circumferentially oriented blood-containing space seen on tomographic imaging studies. IMH may occur spontaneously or as a consequence of penetrating aortic ulcer in intrinsically diseased media. T1-weighted images reveal a crescent-shaped area of abnormal signal intensity within the aortic wall. In the acute phase (0–7 days after the onset of symptoms), oxyhemoglobin shows intermediate signal intensity on T1 SE images and high signal on T2 SE, whereas in the subacute phase (>8 days) methemoglobin shows high signal intensity in both T1 and T2 SE images (Fig. 1). The progression of IMH to overt dissection and rupture has been reported in 32% of cases, in particular with involvement of ascending aorta.

Aortic Ulcer

Aortic ulcer is characterized by rupture of the atheromatous plaque, disrupting the internal elastic lamina. The MRI diagnosis of aortic ulcer is based on visualization of a crater-like ulcer located in the aortic wall. Mural thickening with high or intermediate signal intensity on SE sequences may indicate extension of the ulcer into the media and formation of an intramural hematoma. MRA is particularly suitable for depicting aortic ulcers along with the irregular aortic wall profile seen in diffuse atherosclerotic involvement. The aortic ulcer is easily recognized as a contrast-filled outpouching of variable extent with jagged edges, which may result even in large pseudoaneurysm. The disadvantage of MRI with respect to computed tomography (CT) is failure to visualize dislodgment of the intimal calcifications that are frequently observed in aortic ulcers.

Aortic Trauma

A long examination time as well as difficult access to the patient has been considered the main limitation of MRI in acute aortic pathology. The development of fast MRI techniques has shortened the examination time to a few minutes, thus MRI can be used even in critically ill patients. On SE images in the sagittal plane, a longitudinal visualization of the thoracic aorta makes it possible to distinguish a partial lesion (a tear limited to the anterior or the posterior wall) from a lesion encompassing the entire aortic circumference. The presence of periadventitial hematoma and/or pleural and mediastinal hemorrhagic effusion may also be considered a sign of instability (Fig. 2). In the same sequence used to evaluate the aortic

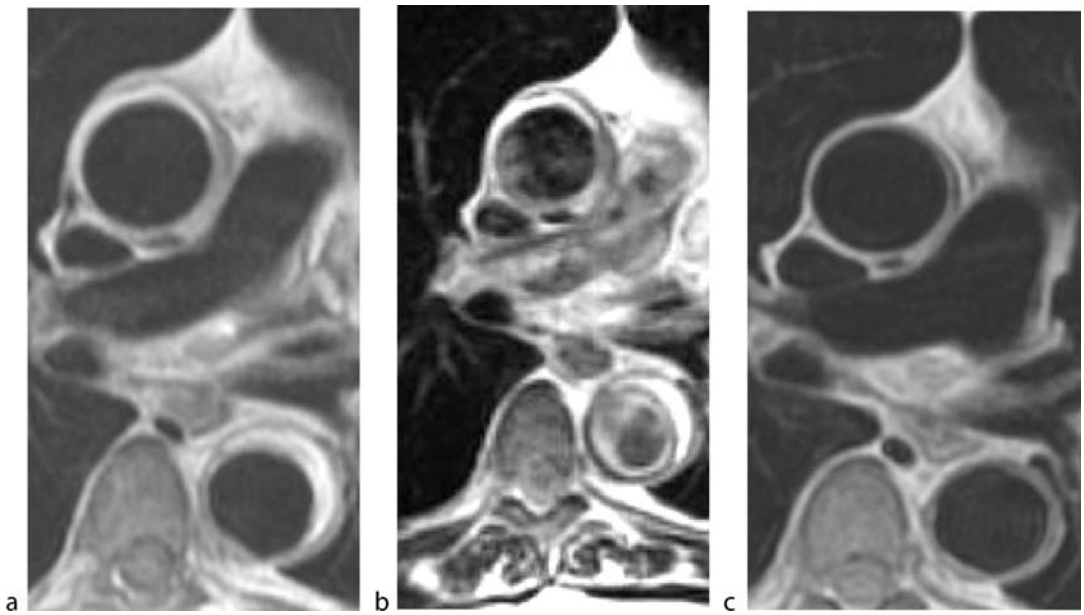

Aorta and Large Vessel Disease, MRI. Figure 1 MRI study of type A intramural hematoma involving the ascending and descending aorta performed few days (a, b) and two months (c) after symptoms onset. Black-blood spin-echo T1 image (a) showing a high signal intensity of the hematoma, which increases in black-blood spin-echo T2 (b), due to the presence of methemoglobin in the subacute phase. Two months later the hematoma is completely reabsorbed (c).

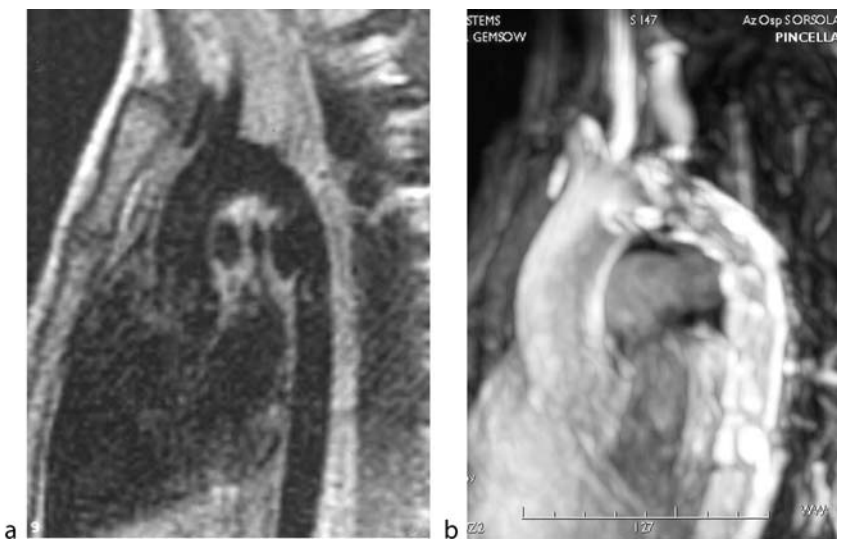

Aorta and Large Vessel Disease, MRI. Figure 2 Traumatic aortic injury before (a) and after endovascular stent-graft treatment (b) SE sagittal MR image of the traumatic injury providing a diverticular aneurysm with mediastinal and periaortic hematoma along the descending aortic segment. MRA after stent-graft treatment (b) the lesion is covered by the stent-graft; the metallic springs are visible like artifacts.

lesion, without the need for any additional time, the wide field of view of MRI provides a comprehensive evaluation of chest trauma, such as lung contusion and edema, pleural effusion, and rib fractures.

Thoracic Aortic Aneurysms

MRI is effective in identifying and characterizing thoracic and abdominal aortic aneurysms. SE sequences are helpful in evaluating alterations of the aortic wall and periaortic

space. Periaortic hematoma and areas of high signal intensity within the thrombus may indicate instability of the aneurysm and are well depicted on SE images. Atherosclerotic lesions are visualized as areas of increased thickness with high signal intensity and irregular profiles. With fat suppression technique, the outer wall of the aneurysm can be easily distinguished on MR images by the periadventitial fat tissue, hence the aneurysm diameter can be accurately measured. The high level of reproducibility of MRI measurements ensures optimal reliability in monitoring expansion rate. MRA may play an important role in preoperative evaluation. Contrast-enhanced 3D MRA can provide precise topographic information about the extent of an aneurysm and its relationship to the aortic branches. The capability of contrast MRA to visualize the artery of Adamkiewicz represents an important advance in planning the surgical repair of a thoracic aneurysm.

Aortitis

Contrast-enhanced T1- and T2-weighted SE MRI has been shown to be highly effective in the evaluation of Takayasu arteritis even in the early phases, providing important information on the activity of the disease. Active inflammatory disease appears as variable thickening of the aortic wall, enhanced after gadolinium administration. The chronic, quiescent stage is characterized by extensive perivascular fibrosis without contrast enhancement. MRA can replace invasive angiography in the study of aortic and branch vessel stenosis, and avoidance of angiography is highly desirable in patients affected by aortitis because it carries a risk of pseudoaneurysm formation at the site of arterial puncture.

Congenital Aortic Disease

Aortic Arch Anomalies

Aortic arch anomalies result either from abnormal regression of an embryonic arch that normally remains patent or from persistent patency of a structure that normally regresses during fetal life.

Usually, SE MRI in axial or coronal and sagittal planes and thin slice thickness provides excellent visualization of the vascular structure and their relationship with mediastinal organs, whereas MRA is useful for defining the complex anatomy of the arch and supraaortic vessels (4).

An aberrant right subclavian artery (*arteria lusoria*) is the most common type of vascular anomaly. The right subclavian artery may also arise from an outpouching, known as the diverticulum of Kommerell, which represents persistence of the most distal portion of the embryonic right arch. On MRI SE or GE sequences, the aberrant right subclavian artery is defined as a tubular structure crossing the mediastinum from right to left, behind the trachea and the esophagus, in an oblique ascending direction. An extrinsic compression of the esophagus, as typically shown on barium swallow, can also be seen on axial and sagittal SE MR images.

A right aortic arch (0.1% of population) passes to the right of the trachea and may descend either to the right or the left of the thoracic spine. Two types of right aortic arch are described: right aortic arch with mirror image brachiocephalic branching, and right aortic arch with aberrant left subclavian artery.

A double aortic arch is characterized by the presence of both a left and a right aortic arch; these arise from a branching of the ascending aorta, pass on both sides of the trachea and esophagus, and join posteriorly to form the descending aorta, which may lie to the right or left of the vertebral column. The luminal size of the two arches in relation to each other varies considerably, and one of them (usually the left) may be partially or completely atretic. The double aortic arch is a vascular ring that can produce severe symptoms if it compresses the trachea and esophagus.

Cervical arch is a rare anomaly in which the aortic arch extends into the soft tissues of the neck before turning down on itself, forming the descending aorta.

Aortic Coarctation

Coarctation is a common congenital anomaly in which an abnormal plication of the tunica media of the posterior aortic wall proximal to the ligamentum arteriosum causes a fibrous ridge to form, which protrudes into the aorta and causes an obstructive lesion. The stenotic segment can be focal (aortic coarctation), diffuse (hypoplastic aortic isthmus), or complete (aortic arch interruption).

MRI axial and sagittal SE sequences are useful for quantify morphologic indexes of coarctation expressed as the ratio of diameter at the isthmus and above the diaphragm. However, although detection of anatomic narrowing of the aorta establishes the diagnosis of coarctation, an assessment of its clinical significance depends on determining its hemodynamic effects. GE MRI has been applied to evaluate flow turbulence across the coarctation; the severity of coarctation is quantified on the basis of the length of flow void. Further functional information can be provided by MR flow mapping, which can define the severity of the stenosis by measuring velocity jets at the level of coarctation and mean flow deceleration in the descending aorta. With this technique, it is possible to predict the coarctation severity with good sensitivity and specificity (95 and 82%, respectively) compared to catheter angiography. Flow mapping is also able to quantify the flow pattern and volume of collateral flow in the descending

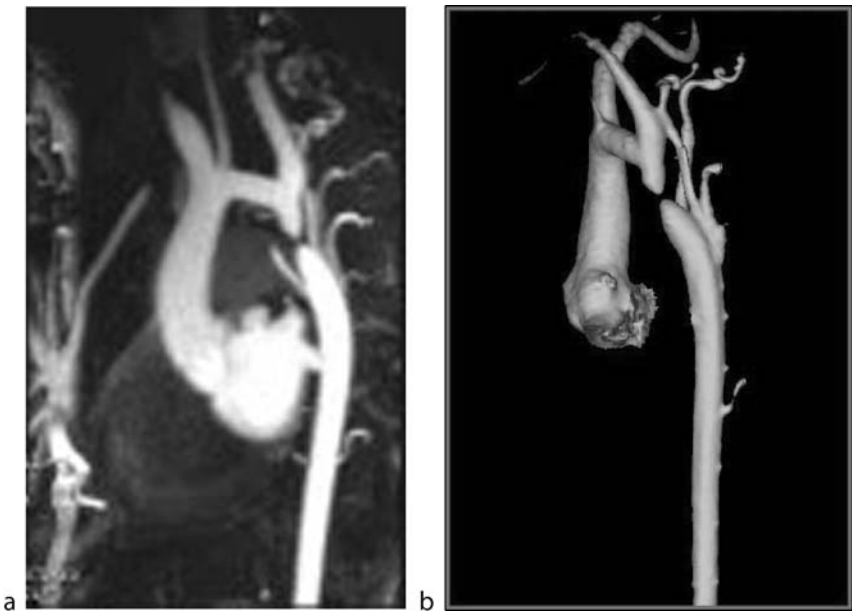

Aorta and Large Vessel Disease, MRI. Figure 3 MRA of aortic coarctation. The stenotic isthmic aortic segment as well as the collateral circulation throughout the intercostal arteries is well visible both in MIP (a) and VR reconstruction (b).

aorta, which are other important parameters of the severity of coarctation, and this information may be crucial in the choice of surgical strategy. Finally, MRA provides excellent visualization of the stenotic segment and of the collateral circulation (Fig. 3).

Aneurysms of the Valsalva Sinus

Aneurysm of the Valsalva sinus is a rare congenital anomaly of the structural layers of the aortic wall and is characterized by the absence of the medial layer. This abnormality is usually limited to one of the Valsalva sinuses, most frequently the right coronary one. Because of the absence of the elastic components of the medial layer, the Valsalva sinus is asymmetrically dilated, even in the neonate. The aortic abnormality is visible on SE and MRA images. Rupture of sinus aneurysm is usually into the right atrium and creates a left-to-right shunt, which can be visualized by GE sequences.

Bibliography

1. Reddy GP, Higgins CB (2000) MR imaging of the thoracic aorta. Magn Reson Imaging Clin N Am 8(1):1–15
2. Debatin JF, Hany TF (1998) MR-based assessment of vascular morphology and function. Eur Radiol 8:528–539
3. Krinsky G, Rofsky N, Flyer M et al (1996) Gadolinium-enhanced three dimensional MR angiography of acquired arch vessels disease. Am J Roentgenol 167:981–987
4. Russo V, Renzulli M, La Palombara C et al (2005) Congenital diseases of the thoracic aorta. Role of MRI and MRA. Eur Radiol 26:1–9

Aorta, Grafts, and Prostheses

The aorta is the largest artery in the body. A graft is used in vascular procedures to patch blood vessels, to line aneurysms, or to bypass blood across blocked blood vessels. A prosthesis is an artificial device used to mimic another device or part of the body. Prostheses are often placed within a part of the body. A stent graft is an example of a prosthesis. Prostheses are often used during interventional procedures.

▶Aneurysm, Aortic and Thoracic

Aortic Aneurysms

An aortic aneurysm occurs when the aorta dilates to more than one and a half times its normal diameter.

▶Aneurysm, Aortic and Thoracic

Aortic Dissection

Separation of the layers within the aortic wall.

▶Dissection, Aortic, Thoracic

Aortic Obstruction

▶Stenosis, Aortic, Abdominal

Aortic Syndrome

▶Stenosis, Aortic, Abdominal

Apert Syndrome

Apert syndrome (acrocephalosyndactyly type I) is characterised by bilateral coronal synostosis with brachycephaly, widened metopic and sagittal sutures, hypertelorism, shallow orbits with proptosis, maxillary hypoplasia with downturned mouth and severe symmetric syndactylism of the hands and feet. The central nervous system may demonstrate megalocephaly, giral abnormalities, hypoplastic white matter, heterotopic gray matter, frontal encephalocele, corpus callosal agenesis and/or ventriculomegaly. Choanal stenosis, cleft palate, cervical spine fusion (usually C5 and C6), otitis media, Eustachian tube dysfunction and conductive hearing loss are common. Concurrent problems with the cardiovascular, genitourinary, gastrointestinal and respiratory systems may contribute to morbidity. There may be ankylosis of the elbows, hips and shoulders. The stylohyoid ligament calcifies in 38–88% of patients.

▶Congenital Malformations, Nose and Paranasal Sinus

Apocrine Metaplasia

Histologic lesion that characterizes areas of cystic change in the breast.

▶Fibrocystic Disease, Breast

Apophyseal Joint Arthritis

Apophyseal joint arthritis is seen in rheumatic disease. In spondylarthropathies the lumbar spine is most commonly affected, whereas in rheumatoid arthritis it is virtually confined to the cervical spine. In spondylarthropathies, late stages of apophyseal joint arthritis often show postarthritic ankylosis, in contrast to rheumatoid arthritis, in which postarthritic degenerative osteoarthritis is common.

▶Rheumatoid Arthritis

▶Spondyloarthropathies, Seronegative

Apoptosis

Michael Eisenhut, Walter Mier, Uwe Haberkorn
Abteilung Radiopharmazeutische Chemie Deutsches krebsforschungszentrum Heidelberg, Germany
m.eisenhut@dkfz.de

Definition

The cell biological phenomenon termed *apoptosis* (programmed cell death) represents an energy-dependent elimination process for cells that have been injured, infected, or immunologically recognized as harmful or superfluous. This mechanism controls the fate and life expectancy of cells that play important roles in a large number of disorders such as myocardial infarction and neurodegenerative diseases or in transplanted organs. Apoptosis is also observed in cancer tissue, which might be enhanced after treatment with cytostatic drugs or ionizing radiation. This phenomenon was already described in the nineteenth century, but was termed "*apoptosis*" in 1972 by Kerr and colleagues: "*A basic biological phenomenon with wide ranging implications in tissue kinetics*" (1).

Apoptosis is initiated by a series of events including receptor-mediated activation of the death-inducing signaling complex (DISC). As illustrated in Fig. 1, the main triggers of DISC are ▶FasL (CD95L), TRAIL, or tumor necrosis factor alpha (TNFα). Once activated through an autocatalytic cleavage/activation mechanism, the destruction of the cell starts off in the DISC releasing caspase 8, which triggers the activation of other downstream ▶caspases, the so-called executioner caspases. The 15 caspases known to date belong to the family of aspartyl-specific cysteine proteases that are not only essential for the starting event in the DISC but also for the execution of apoptosis. Substrates of downstream-acting caspases are molecules involved in DNA repair, ribonucleoproteins, signaling molecules, structural proteins, and oncoproteins. Cleavage of structural proteins accounts for some of

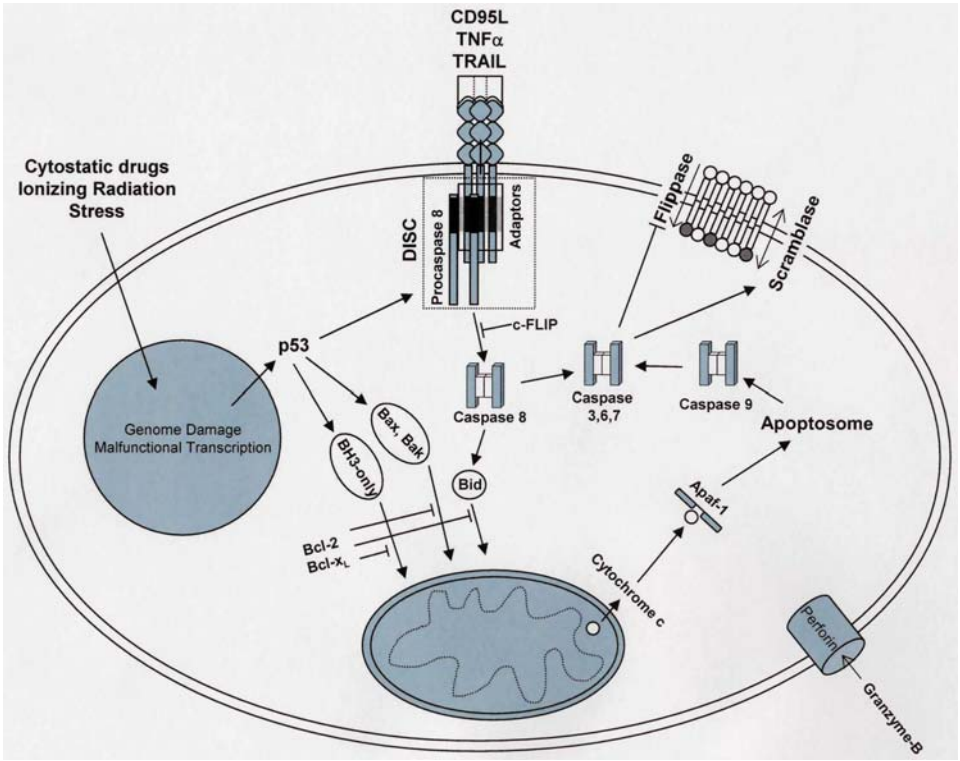

Apoptosis. Figure 1 Overview of the various pathways described in the Definition section.

the massive morphological changes such as membrane blebbing, nuclear fragmentation, and the formation of apoptotic bodies during apoptosis. However, caspase activation does not necessarily lead to apoptosis, but can occur even without inducing cell death.

Cytostatic drugs are less well characterized with regard to the apoptosis-inducing mechanism. They act as DNA-damaging agents, antimetabolites, mitotic inhibitors, nucleotide analogs, or inhibitors of topoisomerases. Some drug-induced DNA damage is sensed by p53, suggesting that p53 may be considered a master switch for apoptosis. It is also suggested that anticancer drugs trigger CD95L/CD95, TRAIL, and TNFα expression through p53 stimulation (2). The same should hold for the cytotoxic action of ionizing radiation, which injures the DNA by forming double-strand breaks. In this context, it is necessary to note that the hypothesis about tumor response to radiation is determined not only by tumor cell phenotype but also by microvascular sensitivity, because endothelial apoptosis regulates angiogenesis-dependent tumor growth (Garcia-Barros, et al, 2003).

Another initiator of apoptosis is granzyme B, which assisted by the transmembrane pore-forming protein ►perforin, penetrates into the cell where it shares the primary specificity of caspases to cleave at the carboxyl terminal of aspartate residues in their substrates. ►Granzyme B together with perforin is released by cytotoxic T cells upon specific interaction with the target cell and belongs, therefore, to the cellular immune response machinery.

Mitochondria-associated proteins of the ►Bcl-2 family play a major role in apoptosis induced by anticancer drugs and radiation therapy. While Bax and Bak promote cell death, Bcl-2 and Bcl-x_L act against it. A third group of indirect promoters represent Bad, Bid, Bik, and Bim, so-called BH3-only proteins, docking to an extended hydrophobic groove on the prolife Bcl-2-like proteins, thereby abrogating the antiapoptotic functions of, for example, Bcl-x_L. This leads to an imbalance in favor of Bax and Bak, which induce mitochondrial membrane permeabilization releasing among others ►cytochrome *c* from the mitochondrion. Cytochrome *c* binds to apoptosis protease activating factor (Apaf-1) and aggregates to the heptameric apoptosome. Procaspase 9 dimerizes at the apoptosome scaffold, thereby activating itself. Active caspase 9 in turn activates downstream caspases 3, 6, and 7, the executioner caspases, leading to the vast degradation of the proteome.

The mitochondria-involving intrinsic pathway of apoptosis is also active in the type II extrinsic pathway induced by the DISC. In this case, caspase 8 originating from the DISC cleaves Bid into its truncated form which then translocates into the mitochondrion where it is involved in the release of apoptogenic factors (*vide supra*).

Pathology/Histopathology

In normal tissues, cell proliferation and cell death are balanced. If this balance is disturbed by a variety of stimuli, too much or too little apoptosis is observed. Blood precursor cells, for example, need colony-stimulating factor (CSF) or direct contact with stromal cells to survive and differentiate. In the absence of these stimuli, the cells are eliminated *via* programmed cell death. The same happens to hormone-dependent organs, which develop atrophy through the absence of hormones.

On the cellular level, various mechanisms of apoptosis lead to well-defined morphological changes in the cell. These include nuclear membrane breakdown, cytoskeletal reorganization, plasma-membrane blebbing, and loss of cell adhesion. The nucleus shrinks with condensation of chromatin, followed by disintegration of nuclear residues. This effect can be visualized by electrophoresis indicating a ladder pattern of fragmented DNA. Under the microscope, some of these effects might be visible. An often used indicator for DNA fragments is the terminal transferase dUTP nick end labeling (►TUNEL Assay). This assay relies on the formation of nicks in DNA that can be identified by terminal transferase, an enzyme that catalyzes the addition of dUTPs that are secondarily labeled with a marker. In combination with immunocytochemistry or flow cytometry, this assay reproducibly labels cells in the final stages of apoptosis.

Other indicators are artificial substrates for activated caspases that become fluorescent after cleavage and fluorescent ►annexin V that binds in the presence of Ca^{2+} with externalized ►phosphatidyl serine (PS). Processes leading to the activation of caspases have been described earlier, and the apoptosis-induced presentation of PS is a result of flippase inactivation responsible for the asymmetric lipid distribution in the double-layered cell membrane. In addition, scramblase promoting externalization is activated. This occurs during blood coagulation, thrombosis, and apoptotic cell death (*vide infra*).

Clinical Presentation

The following diseases involve apoptosis: cancer, myocardial infarction (partly), viral infections, hematopoietic disorders, inflammation, and neurodegenerative disease. A prominent example of neoplastic disease is the t(14;18) translocation of follicular lymphoma, which driven by the Ig heavy chain promoter leads to overexpression of the antiapoptotic player Bcl-2. The resulting resistance to chemotherapy leads to a poorer prognosis.

In myocardial infarction, an increased programmed cell death rate has been reported. Besides necrosis, apoptosis occurs in border areas of ischemia.

Viral infections may cause activation of cytotoxic T cells, recognizing viral peptides in combination with MHC class II molecules on the surface of infected cells. Consequently, cytotoxic T cells release granzyme B/porin and present CD95L on their plasma membrane, both triggering the proteolytic-driven death machinery (Fig. 1). Viruses have, however, developed molecular mechanisms to escape this lethal fate, producing serious clinical problems.

Diseases related to hematopoietic disorders that are attributed to apoptosis may arise in the absence of growth factors. These factors are needed to develop differentiated blood cells. Thus, chronic hematological disorders, such as anaplastic anemia and myelodysplastic syndromes, may partly be caused by the activation of cell death genes.

In chronic inflammatory reactions, excess lymphocytes are removed by apoptosis. This occurs through the CD95L/CD95 system. Insufficiencies in this mechanism can lead to autoimmune diseases such as lupus erythematosus. Here, circulating soluble CD95 competes with cell-bound CD95, thus preventing the necessary death signal.

Loss of neurons may be induced by oxidative stress, excitatory toxicity, calcium toxicity, and survival factor deficiency. Direct evidence for an apoptosis-mediated cell death of neurons was found in Alzheimer disease. It could be demonstrated that β-amyloid induces apoptosis in cultured central nervous system neurons. Other diseases such as retinitis pigmentosa and amyotrophic lateral sclerosis are related to genetic alterations leading to apoptosis-mediated degeneration of functional cells. All mechanistic aspects on which the various diseases rely are briefly described in the "Definition" section.

Imaging

Visualization of tissues with apoptotic cells is not possible with conventional radiography, computed tomography (CT), and ultrasound. Merely secondary effects on organs affected by this process can be seen, which are morphological shrinking and/or changes in the signal intensity induced by alterations of mass density. Apart from radionuclide imaging, magnetic resonance spectroscopy (MRS) is currently the clinically available method for noninvasive *in vivo* detection and quantification of apoptosis. The changes in lipid structure and fluidity of the cell membrane that take place during the apoptotic process generate a number of small molecules (e.g., cytoplasmic lipid bodies, choline metabolites) that can be directly monitored by water-suppressed lipid ^{1}H-MRS techniques (3).

Nuclear Medicine

As already mentioned in the previous section, radiolabeled compounds are the preferred agents for imaging apoptosis. This is due to the comparatively tiny mass amounts of carrier molecules necessary to obtain ample signal intensities. For the detection of apoptosis, radiolabeled annexin V, a human 36-kDa protein, is currently the most promising agent for detecting apoptosis *in vivo* (3). This agent allows the imaging of an early event in apoptosis, involving the externalization of phosphatidyl serine from the inner to the outer leaflet of the plasma membrane. The high affinity of annexin V for cells with exposed phosphatidyl serine ($K_d < 10^{-10}$ M) is the basis of detecting apoptosis *in vivo*.

This phenomenon was originally exploited for the detection of apoptotic cells by flow cytometry, using the binding of fluorescein isothiocyanate-labeled annexin V to phosphatidyl serine. The success of this method suggested the replacement of the fluorescent tag by a radioactive tracer. Consequently, ^{99m}Tc-labeled annexin V was used several years later to image apoptosis in animals. An increased accumulation was found in Jurkat cells where programmed cell death was initiated by growth factor deprivation, anti-CD95 antibody, and doxorubicin treatment. In addition, anti-CD95-treated mice showed a threefold rise in hepatic ^{99m}Tc-annexin V accumulation in response to severe liver damage with histological evidence of apoptosis. Increased uptake was also detected in animal models using the acute rejection of transplanted heterotopic cardiac allografts or transplanted murine B cell lymphomas treated with cyclophosphamide. Radiolabeled annexin V is, therefore, a biological marker which gives, for the first time, direct information about the cytotoxic therapy response of tumors.

Several ^{99m}Tc-labeled annexin V compounds have been studied in humans, differing in bifunctional chelators. The most successful agent is hydrazinonicotinamide-conjugated annexin V, which binds ^{99m}Tc efficiently at very low molar concentrations. The investigation of ^{99m}Tc-HYNIC-annexin V for human application revealed favorable biodistribution characteristics. In addition, ^{99m}Tc-HYNIC-annexin V is easily obtained by a kit formulated preparation (Figs. 2 and 3).

Other targets for receiving information about the biological fate of tissue undergoing apoptosis are cysteine proteases of the caspase family. As described earlier, these enzymes play a key role during apoptosis. Besides

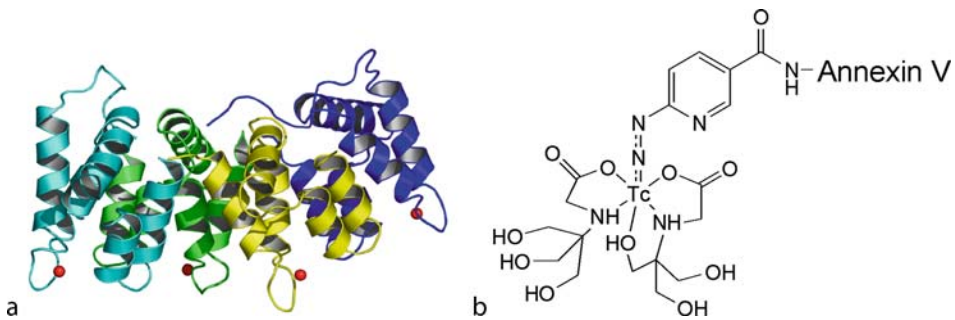

Apoptosis. Figure 2 Perpendicular views of annexin A5. (a) Each structural domain is colored differently; the calcium ions are red (taken from http://www.lbpa.ens-cachan.fr/bentley/index.html). ^{99m}Tc complex of hydrazinonicotinamide-conjugated annexin V (b).

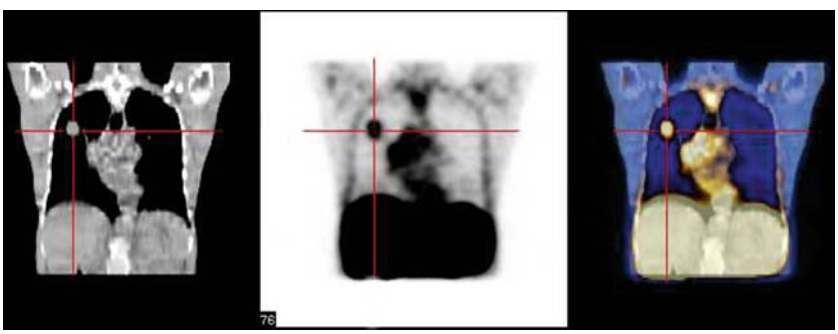

Apoptosis. Figure 3 Images of an untreated patient with a lung tumor showing intense uptake of [^{99m}Tc]HYNIC-annexin V. CT left, scintigram middle, fusion image right. The intensity of uptake may increase after chemo- or radiation therapy. The intraindividual change of uptake correlates with therapy response.

irreversible inhibitors, synthetic caspase substrates have been investigated for their potential as apoptosis-selective imaging agents. Although selective uptake in apoptotic cells was observed, imaging could not be demonstrated with these agents until now.

Diagnosis

Clinical imaging studies with ^{99m}Tc-labeled annexin V have demonstrated the feasibility of delineating cell death in acute myocardial infarction, in tumors with a high apoptotic index, and in response to antitumor chemotherapy. Most anticancer agents act by inducing apoptosis in sensitive tumor cells. Hence, in many types of cancers, a significant increase of apoptosis after chemotherapy correlates with tumor chemosensitivity. Theoretically, a reliable evaluation of apoptotic changes, after chemotherapy to baseline, may provide valuable insights into the treatment prospect of cancers. The tumors that were investigated to date were squamous head and neck carcinomas, non-small-cell lung cancer, small-cell lung cancer, breast cancer, lymphoma, and sarcoma. Increased localization of ^{99m}Tc-labeled annexin V within 1 to 3 days of chemotherapy has been noted in some, but not all, subjects with these tumors. Most subjects with increased ^{99m}Tc annexin V uptake after the first course of chemotherapy have shown objective clinical responses. It is suggested that increased posttreatment ^{99m}Tc annexin uptake is associated with improved time to progression of disease and survival time (4).

Bibliography

1. Kerr JFR, Wyllie AH, Currie AR (1972) Apoptosis: a basic biological phenomenon with wide ranging implications in tissue kinetics. Br J Cancer 26:239
2. Krammer PH (1999) CD95(APO-1/Fas)-mediated apoptosis: live and let die. Adv Immunol 71:163–210
3. Lahorte CMM, Vanderheyden J-L, Steinmetz N et al (2004) Apoptosis-detecting radioligands: current state of the art and future perspectives. Eur J Nucl Med Mol Imaging 31:887–919
4. Green AM, Steinmetz ND (2002) Monitoring apoptosis in real time. Cancer J Mar–Apr 8(2):82–92
5. Garcia-Barros M, Paris F Cordon-Cardo et al (2002) Tumor response to Radiotheraphy Regulated by Endothelial Cell Apoptosis. Science 300: 1155–1159

Apparent Diffusion Coefficient (ADC)

ADCs are obtained by calculating and measuring signal intensity in a series of diffusion-weighted MR images. ADCs of the tissues vary according to microstructure and physiologic state of the tissues.

▶Lymphadenopathies, Head and Neck

Appendicitis

Patrice Taourel
Service d'Imagerie Médicale Hôpital Lapeyronie,
371 avenue du Doyen Gaston Giraud,
34295 MONTPELLIER CEDEX 5.
p-taourel@chu-montpellier.fr

Definition

Acute appendicitis is the inflammation of the appendix, which is a long intestinal diverticulum arising from the cecum approximately 3 cm below the ileocecal wall. It constitutes the most common cause of acute abdominal pain requiring surgical intervention in the Western world.

Pathology

The primary pathogenic event in the majority of patients with acute appendicitis is luminal obstruction, which may result from fecaliths, lymphoid hyperplasia, and more rarely foreign bodies, parasites, and both primary and metastatic tumors. Fecaliths which result from the inspissation of fecal material and inorganic salts within the appendiceal lumen constitute the most common cause of appendiceal obstruction.

Once appendiceal obstruction occurs, the continued secretion of mucus results in elevated intraluminal pressure and luminal distention. Increased intraluminal pressures may lead to venous engorgement, arterial compromise, and tissue ischemia and may result in appendiceal perforation. The appendiceal perforation is associated with a localized peritonitis since the terminal ileum, cecum, and omentum are generally able to "wall off" the inflammation or more rarely it is associated with a generalized peritonitis. Perforation is a relatively common complication of appendicitis with a median incidence of 20%, and it constitutes the major factor of morbidity and mortality in appendicitis.

Clinical Presentation

The clinical presentation of patients with appendicitis depends on the location of the appendix, on the pathologic

state of the inflamed appendix, and on the age and sex of the patient. Although the base of the appendix arises from the posteromedial wall of the cecum, the appendix may lie in a retrocecal, subcecal, retroileal, preileal, pelvic, or subhepatic site. Consequently, this variability in location may greatly influence the clinical presentation in patients with suspicion of appendicitis and the differential diagnoses discussed in such patients. The most accurate clinical signs of appendicitis are the presence of right lower quadrant pain, rigidity, and migration of the initial periumbilical pain to the right lower quadrant. The most reliable sign of perforation is a patient's temperature being higher than 38.5°C. By using only clinical diagnosis, the mean false-negative appendicectomy rate is approximately 20%; in women of childbearing age it is higher, because symptoms of acute gynecologic conditions such as pelvic inflammatory disease may have a similar manifestation.

Imaging Modality

Ultrasound

Ultrasound (US) in well-trained hands is highly accurate in the diagnosis of appendicitis. The US approach to the right lower quadrant includes graded compression with slow and gentle maintained pressure, by using a high-frequency linear or curvilinear probe. In women, when examination *via* the suprapubic approach is inconclusive, endovaginal US should be added, because it may reveal a gynecologic explanation for the symptoms and it may identify the appendix in a pelvic location.

The diagnosis of appendicitis is based on the identification of the inflamed appendix as a blind-ended, tubular structure with a laminated wall that arises from the base of the cecum. The appendix is aperistaltic and noncompressible. A threshold of 6 mm in anteroposterior diameter of the appendix under compression is the best finding of appendicitis (Fig. 1), with both a high negative predictive value and a high positive predictive value. When the appendix is identified, the evaluation of a periappendicular finding does not improve the accuracy of US. However, inflammatory changes in the perienteric fat are often the first and more obvious finding at US examination. Inflamed fat appears as a badly limited echogenic mass that separates the inflamed appendix from the surrounding gut and other organs. Secondary appendicular findings such as appendicoliths seen as bright, echogenic foci with clean distal acoustic shadowing (Fig. 2), Doppler enhancement of the appendicular wall, or absence of gas in the appendicular lumen are ancillary signs that may be useful in equivocal cases.

There are two main pitfalls in the diagnosis of appendicitis. The first is the misinterpretation of the terminal ileum as the appendix, which may lead to over

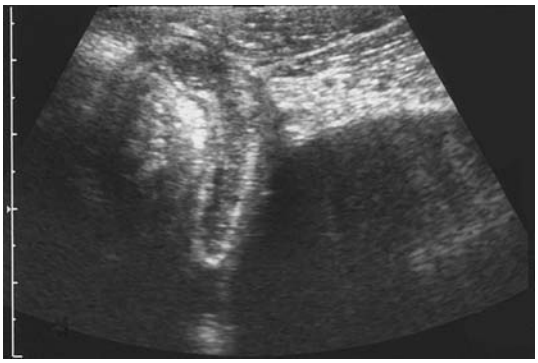

Appendicitis. Figure 1 US of an appendicitis.

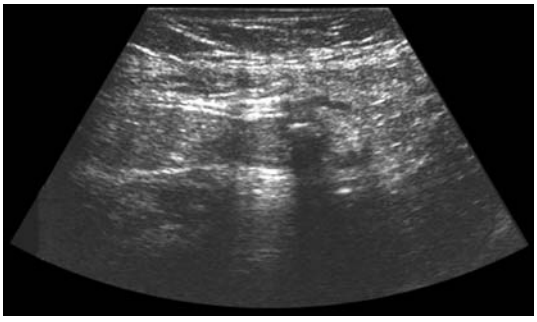

Appendicitis. Figure 2 US of appendicitis with appendicolith.

diagnosis of appendicitis. In contrast to the appendix, the terminal ileum does not attach to the base of the cecum, is not blind-ended, shows frequent peristaltic activity, and is usually oval in cross section. The second pitfall is the nonvisualization of the normal appendix, which is classically considered as a major weakness of US in the exploration of patients with suspected appendicitis. However, technological advances combined with increased radiologist experience have dramatically improved the US visualization of the normal appendix, which is now identified in more than two-thirds of cases in well-trained teams.

US diagnosis of appendicitis after perforation can be difficult since the distended appendix may no longer be visualized at US examination. Perforated appendicitis must be considered in patients without a history of appendicectomy when a collection is identified in the right lower quadrant.

Computed Tomography

Computed tomography (CT) is a highly accurate and effective cross-sectional imaging technique for the diagnosis and staging of appendicitis.

CT protocols used in patients with suspected appendicitis differ considerably with regard to the anatomic area to be included in the scan and the use of intravenously, orally, and rectally administered contrast material. Most teams use thin slices without intravenous contrast material and only administer contrast material in equivocal cases when the appendix is not identified such as in patients with mild appendicitis, patients with a paucity of mesenteric fat, or patients with perforated appendicitis. Some teams have promoted a more invasive protocol which involves scanning after the rapid administration of colonic contrast material to fill the cecum and the appendiceal lumen.

The main finding of appendicitis is the identification of an inflamed appendix, which is dilated measuring more than 7–8 mm in diameter, with a circumferential and symmetric wall thickening, better demonstrated after intravenously administered contrast material with an enhancement of the thickened appendiceal wall. Reformatting (Fig. 3) and cine mode are very helpful in identifying the appendix on its entire length. Periappendiceal inflammation is present in 98% of patients with acute appendicitis with linear fat stranding, local fascial thickening, or clouding of the peri-ileal fat.

Perforated appendicitis is usually accompanied by pericecal phlegmon or abscess. Although a pericecal phlegmon or abscess is strongly suggestive of appendicitis, these are nonspecific findings that may be seen in other diseases entities. The most specific finding of perforated appendicitis is the identification of extraluminal air, which, however, may be seen in other causes of bowel perforation in the right lower quadrant such as cecal diverticulitis or Crohn's disease, and the identification of an appendicolith within a appendiceal abscess or phlegmon.

Magnetic Resonance Imaging

The indication of magnetic resonance imaging (MRI) in patients with suspicion of appendicitis is only limited to pregnant women with the same signs on CT, a poorer spatial resolution, and limitations in the identification of the extraluminal air.

Diagnosis

There is not a univocal strategy in patients with suspicion of appendicitis. The elaboration of a triage strategy needs to address two questions: (i) which patients need imaging? and (ii) which imaging modality should be used: US versus CT?

Although the use of imaging in clinically equivocal cases of appendicitis is universally admitted, the systematic use of imaging in patients with a clinical suspicion of appendicitis is still controversial. Several studies have been

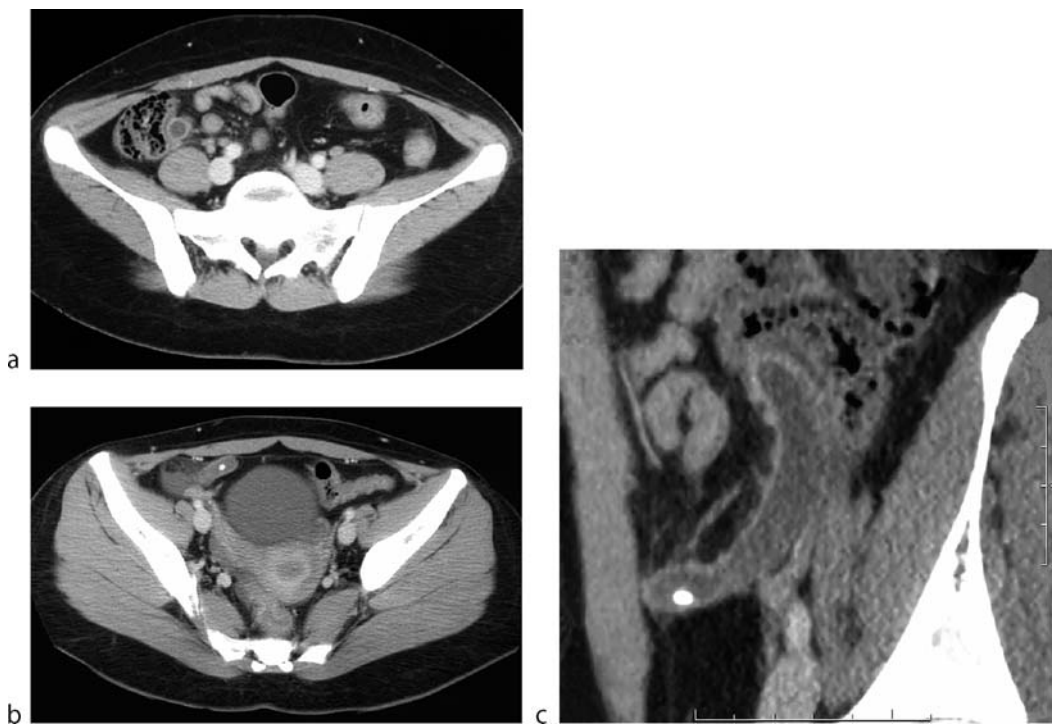

Appendicitis. Figure 3 CT of appendicitis with oblique reformating.

published in which the medical and financial implications of the systematic use of imaging have been assessed. It has been shown that the use of imaging improved patient care both by averting unnecessary appendicectomy and by averting delays before necessary medical or surgical treatment. The cost analysis demonstrated that routine use of imaging was cost-effective because savings achieved by eliminating unnecessary surgery and in-hospital observation outweighed the cost of performing routine imaging of appendicitis.

The choice between US and CT depends on the institution's preference and on the available experience. In most teams, particularly in the USA, CT is considered as the modality of choice. It has the advantage of being more sensitive in demonstrating a normal appendix and in excluding acute appendicitis. It is more accurate in staging periappendiceal inflammation and its extent and in differentiating periappendiceal phlegmon from abscess. The accurate staging of acute appendicitis is of importance for the management of patients, with the option of using an antibiotic therapy or a percutaneous drainage before surgery in complicated appendicitis and of triaging patients appropriately for laparoscopic versus open surgery since the laparoscopic approach may not be optimal in patients with complicated appendicitis. Moreover, CT is more useful in providing alternative diagnoses such as a Crohn's disease, cecal diverticulitis, right ischemic colitis, sigmoid diverticulitis with the sigmoid loop located in the right lower quadrant, or a urologic condition. Conversely, US is more accurate in diagnosing a gynecologic condition and is equally accurate in diagnosing mesenteric lymphadenitis, which is the main differential diagnosis of appendicitis. In our experience, the patient's age, sex, and body habitus as well as the clinical presentation are important influencing factors and we use the following diagnostic triage both in the decision of imaging and in the choice between US and CT (Fig. 4).

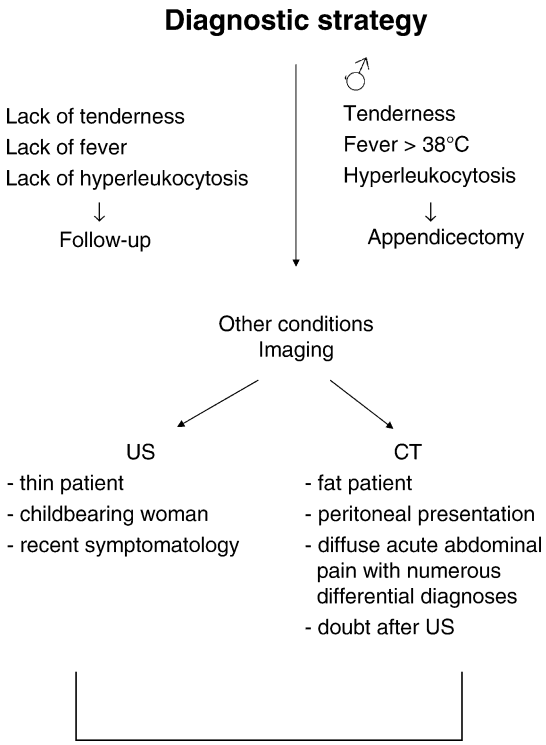

Appendicitis. Figure 4 Diagnostic algorythm for patients with suspicion of appendicitis.

Bibliography

1. Birnbaum BA, Wilson SR (2000) Appendicitis at the millenium. Radiology 215:337–348
2. Kessler N, Cyteval C, Gallix B et al (2004) Appendicitis; evaluation of sensitivity, specificity and predictive values of Us, Doppler US, and laboratory findings. Radiology 230:472–478

APUD

Amine precursor uptake and decarboxylation—Paracrine cells of which argentaffin cells are an example.

▶Neoplasms of the Chest in Childhood

Archnoid Cyst

▶Cysts, Cerebral and Cervical, Childhood

Architectural Distortion

Disruption of the normal breast architecture with no definite mammographically visible mass

▶Carcinoma, Breast, Imaging Mammography, Primary Signs
▶Sclerosing Adenosis, Breast

ARCO

▶Association Recherche Circulation Osseous

ARGUS

Acronym for children suffering from the association of AnoRectal, GenitoUrinary, and Sacral anomalies.
▶Anorectal Malformation

Arm Claudication

▶Claudication, Brachial

ARPKD and ADPKD

Autosomal recessive or dominant polycystic kidney disease: An inherited progressive condition that may manifest in different ages and with varying expression, potentially deleterious to renal function.
▶Cystic Renal Disease, Childhood

Arterial Ischemic Stroke

▶Stroke, Children

Arterio-venous Malformation, Hepatic

Hepatic arterio-venous malformation (AVM) is a rare vascular disorder characterized by direct arterial connection to the venous drainage system within the liver. Arterio-venous fistulae may be congenital (vascular malformations in Rendu–Osler disease) or acquired. Iatrogenic causes (percutaneous liver biopsy, percutaneous liver tumor ablation procedures), trauma, and cirrhosis are mostly involved for acquired fistulae. The condition results in a high-flow, low-resistance shunt that can cause high-output cardiac failure and hydrops. Diagnosis is usually achieved by means of color Doppler US, while selective hepatic angiography and following embolization may be useful in symptomatic cases.
▶Vascular Disorders, Hepatic

Arteriohepatic Dysplasia

Synonym for Alagille syndrome.
▶Congenital Malformations, Liver and Biliary Tract
▶Congenital Malformations, Bile Ducts

Arterioportal, Fistula

Arterioportal fistulas consist of a communication between the hepatic artery and the portal venous system. Arterioportal shunts may be intra-hepatic or extra-hepatic and acquired or congenital. The most common causes of acquired arterioportal fistulas are cirrhosis and hepatic neoplasms, blunt or penetrating trauma, iatrogenic injuries, rupture of an aneurysm of the hepatic artery. Congenital arterioportal fistulas can be associated with Rendu–Osler disease, hereditary haemorrhagic telangiectasia, Ehlers–Danlos syndrome. Arterioportal shunts may be minute or large. Large arterioportal fistulas themselves may cause portal hypertension and high-output heart failure.

Doppler US usually allows an accurate diagnosis. Enlargement of the hepatic artery and dilatation of the involved portal venous segment can be observed at US examination. Doppler US shows pulsatile hepatofugal flow in the portal vein. Both contrast-enhanced CT and contrast-enhanced MR imaging may demonstrate marked enhancement of the main portal vein, segmental branches or major tributaries, with attenuation or signal intensity approaching that of the aorta on arterial-phase images. Arteriography can be performed to confirm the diagnosis and embolization may be considered.
▶Portal Hypertension

Arteriovenous Malformation

A mass consisting of tightly packed arteries, capillaries, and veins.
▶Congenital Malformations, Vascular, Brain
▶Stroke, Interventional Radiology
▶Vascular Disorders of the Gastrointestinal Tract

Arteriovenous Shunting

Pathological vascular channels between arteries and veins, bypassing the capillaries with high-volume blood flow; common in tumors.

▶Contrast Media, Ultrasound, Applications in Kidney Tumor

Arthritis

Inflammation of a joint. With the use of bone scintigraphy, the floridity of arthritis or response to treatment may be judged early.

▶Bone Scintigraphy

Arthritis of the Costotransversal and Costovertebral Joints

Arthritis of the costotransversal and costovertebral occurs in ankylosing spondylitis and is the main cause of respiratory movement restriction. In X-ray imaging, it is most often occult. Magnetic resonance imaging, however, shows typical arthritic features: adjacent bone marrow and soft tissue edema, contrast material enhancement of the synovial membrane, and bony destruction or ankylosis.

▶Spondyloarthropathies, Seronegative

Asbestos Related Diffuse Pleural Thickening

According to the International Labour Organisation (ILO), chest radiograph criteria for defining diffuse pleural thickening includes; pleural thickening greater than 5 mm at any site, bilateral pleural thickening involving at least 25% of the chest or 50% if unilateral, or obliteration of the costophrenic angle.

▶Pleural Plaques

Ascites

An accumulation of transudate, exudate, or chyle in the peritoneal cavity.

▶Peritoneal Collections

Ascites, Pancreatic

Ascites is an abnormal accumulation of fluid in the abdomen. Pancreatic ascites develops when a pseudocyst bursts releasing pancreatic juices. Abdominal paracentesis is the most rapid and perhaps the most cost-effective method of diagnosing the pancreatic ascites.

▶Pancreatitis, Acute

Aseptic Bone Necrosis

▶Osteonecrosis, Adults

Aspergilloma

Colonization with aspergillus of a previous TB cavity.

▶Tuberculosis, Lung

Aspergillosis

Cerebral aspergillosis usually occurs after hematogenous dissemination from an extracerebral focus, or is a result of contiguous spread of the infection from the paranasal sinuses.

▶Infection, Opportunistic, Brain

Asplenia

The absence of the spleen is a rare condition usually associated with other congenital malformations, especially cardiovascular and pulmonary anomalies. Asplenia

may be seen in association with abdominal situs ambiguous and has been classically called asplenia syndrome. The asplenia syndrome is most frequently encountered in males and is associated with severe cyanotic congenital heart diseases. The typical anatomic features of classic asplenia syndrome are trilobed lungs with bilateral minor fissures and eparterial bronchi, bilateral systemic atria, midline liver, absent spleen, and variable location of the stomach. Scintigraphy is the standard examination in documenting the absence of the spleen.

▶Congenital Abnormalities, Splenic

Asplenia Syndrome

Asplenia syndrome is characterized by asplenia, or absence of the spleen, associated with abdominal situs ambiguous. The syndrome is most frequently encountered in males and is associated with severe cyanotic congenital heart diseases. The typical anatomic features of classic asplenia syndrome are trilobar lungs with bilateral minor fissures and epiarterial bronchi, bilateral systemic atria, midline liver, absent spleen, and variable location of the stomach.

▶Splenic Anomalies

Asplenia, Polysplenia Syndromes

▶Congenital Malformations, Splenic

Association Recherche Circulation Osseous (ARCO)

ARCO is an international organization and published the widely accepted staging criteria for osteonecrosis: committee on terminology and classification.

▶Osteonecrosis in Adults

Asthma

▶Airway Disease

Asymmetric Density

An asymmetry of the glandular breast tissue, visible mammographically on two views. Asymmetry is common but should be evaluated as uncommonly there may be an underlying mass or architectural distortion.

▶Carcinoma, Breast, Imaging Mammography, Primary Signs

Atelectasis

Cornelia Schaefer-Prokop
AMC, Amsterdam
c.m.schaefer@amc.uva.nl

Synonyms

The word atelectasis is of Greek origin and means "lack of stretch." "Loss of volume" and "collapse" are used synonymously (caveat: collapse may refer to the complete atelectasis of one lobe)

Definition

Collapse or decrease in the volume of a lung or a portion of the lung. The term refers to the region and amount of lung that is collapsed or to the underlying pathophysiology.

Pathology/Histopathology

There are various *pathological* mechanisms causing atelectasis:

1. *Postobstruction or resorption atelectasis*: the intra-alveolar air is resorbed distal to a bronchial obstruction. The latter may be endobronchial (e.g., neoplasm, mucoid impaction, foreign body) or extrabronchial (e.g., lymphadenopathy). A mucoid or fluid bronchogram, seen on computed tomography (CT) as a low-density branching structure, should prompt the search for a central obstructing lesion (Fig. 1).

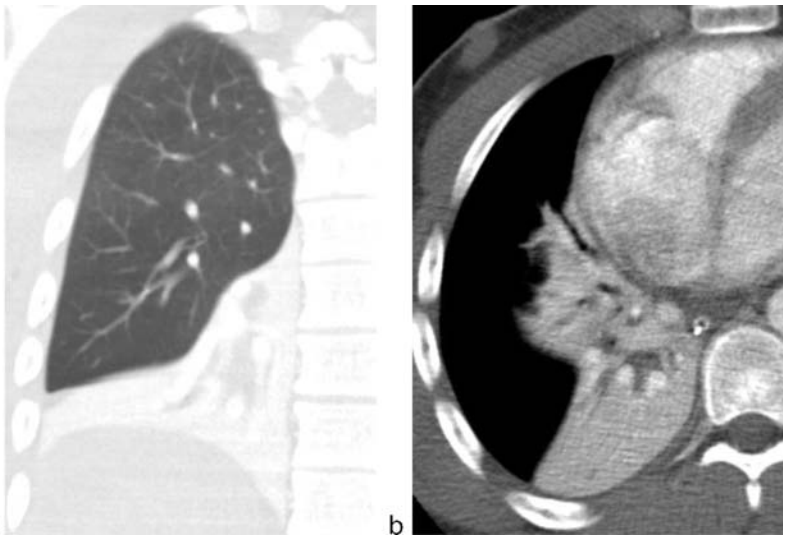

Atelectasis. Figure 1 Patient with obstruction (resorption) atelectasis due to a large central mucous plug. Note the bronchi filled with mucus next to the contrasted arteries.

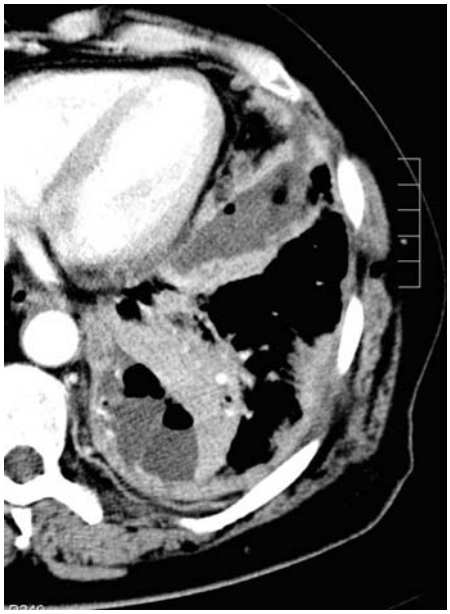

Atelectasis. Figure 2 Patient with pleural empyema (note pleural split sign and air inclusions after pleurodesis) with a compression atelectasis of the lung parenchyma.

2. *Passive or compression atelectasis*: pulmonary collapse as a result of a space-occupying lesion within the pleural space, such as pneumothorax or pleural effusion, or within the lung, such as bulla or mass (Fig. 2). The lung collapse seen with a pneumothorax is also described as relaxation atelectasis.
3. *Adhesive, nonobstructive atelectasis* (or microatelectasis) caused by surfactant deficiency and seen postoperatively or in acute respiratory disease syndrome (ARDS).
4. *Cicatrization atelectasis*, focal or more diffuse collapse resulting from fibrosis or scarring. It is frequently associated with bronchiectasis and also seen in granulomatous diseases.

A *rounded atelectasis* (synonym: folded lung, atelectatic pseudotumor) represents a compression atelectasis seen after resorption of a pleural exudate and reactive fibrosis formation. It is most frequently seen in asbestos-related pleural disease, but is also seen in association with any (exudative) pleural effusion.

A *platelike atelectasis* (*synonym: discoid atelectasis*) is a linear or planar opacity representing a portion of the lung with decreased volume, usually seen in lower lung zones.

Clinical Presentation

Physical changes and symptoms depend on the size of the atelectasis and on the underlying and accompanying respiratory diseases. In most cases there will be no clinical findings at all. In patients with ▶right middle lobe atelectasis, the upper and lower lobe will fill the space occupied by the collapsed lung, and breath sounds can be

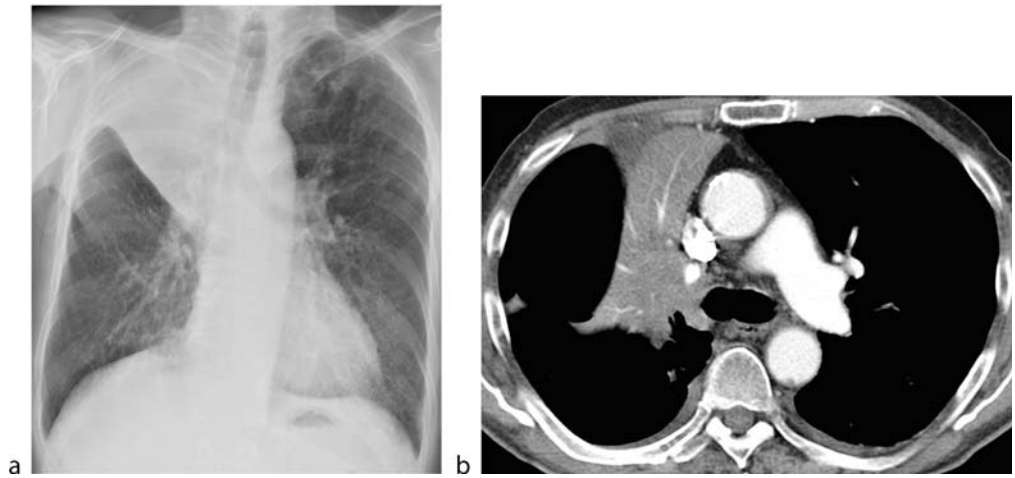

Atelectasis. Figure 3 Patient with a central perihilar tumor and upper lobe atelectasis: the curvilinear delineation of the atelectasis of the upper lobe indicates a central tumor as underlying disease (▶Golden S-sign).

normal. Atelectasis of the lower lobe may result in absent breath sounds. If atelectasis is caused by intrabronchial obstruction (e.g., tumor, mucous plugging), crackles distal to the obstruction may be heard (Fig. 3).

Imaging

The collapse of one or multiple complete lung lobes causes distinct imaging features based on the volume loss on one side, the displacement of fissures and elevation of the ipsilateral diaphragm (juxtaphrenic peak), the mediastinal and hilar structures, and the compensatory overinflation of the remaining lung.

On CT images, atelectasis shows a strong and homogeneous enhancement after intravenous injection of contrast media. This represents a valuable finding for differentiating atelectasis from a tumor or pneumonia, both showing a less intense and more inhomogeneous enhancement.

Postobstruction or resorption atelectasis: A mucoid or fluid bronchogram, seen on CT as low-density branching structures, should prompt the search for a central obstructing lesion.

A *rounded atelectasis* describes a peripherally located, rounded or wedge-shaped atelectasis (sometimes mimicking a bronchogenic neoplasm) that is always adjacent to pleural thickening. As opposed to a tumor, it demonstrates the characteristic homogeneous enhancement after contrast medium injection at CT; vessels and bronchi located more centrally are crowded and course in a characteristic curvilinear fashion like a "comet tail."

Diagnosis

The diagnosis of atelectasis is based on typical imaging findings. In most cases the type of atelectasis and the underlying disease can also be determined.

Bibliography

1. Proto AV (1996) Lobar collapse: basic concepts. Eur Radiol 23:9
2. Stark P, Leung A (1996) Effects of lobar atelectasis on the distribution of pleural effusion and pneumothorax. J Thorac Imaging 11:145
3. Ashizawa K, Hayashi K, Aso N et al (2001) Lobar atelectasis: diagnostic pitfalls on chest radiography. Br J Radiol 74:89
4. Raasch BN, Heitzman ER, Carsky EW et al (1984) Computed tomographic study of bronchopulmonary collapse. Radiographics 4:195

Atheromatous RAS

RAS secondary to the presence of atheromatous plaque(s) in the arterial wall.

▶Stenosis, Artery, Renal

Atherosclerotic Nephropathy

A complex entity. It is an important cause of end-stage renal failure, a consequence of the association of multiple

factors, including decreased renal blood flow, intrarenal atherosclerotic arterial disease, atheroembolism, diabetes, increased oxidative stress, medullary hypoxia, endothelial dysfunction, and inflammation.
►Hypertension, Renal

Athyroid

The physiological manifestation where there is a complete absence of thyroid function or hormone production.
►Congenital malformations, Thyroid, and Functional Disorders

ATN

►Tubular Necrosis, Kidney, Acute

Atypical Ductal Hyperplasia

Breast lesion with some of the architectural and cytologic features of low-grade ductal carcinoma *in situ* in part of the affected areas.
►Radial Scar, Breast

Atypical Lobular Hyperplasia

Proliferation of lobular epithelium with some of the features of lobular carcinoma in situ.
►Hyperplasia, breast

Auditory Ossicles

The middle ear ossicles are the malleus, incus, and stapes.
►Temporal Bone, Inflammatory Diseases, Acute, Chronic

Autogenous Dialysis Fistula

A surgically created, direct communication in between an artery and a corresponding superficial vein allowing increased blood flow through the vein in order to provide luminal dilatation and thickening of the vein wall.
►Fistula, Hemodialysis

Autoimmune Hepatitis

Chronic inflammatory disease of the liver due to a cell-mediated immune response against the body's own liver. The histologic and clinical features are virtually indistinguishable from chronic viral hepatitis. Women are more often affected than men (8:1). The cause is unknown, but a genetic predisposition or an acute liver infection has been advocated as possible factor. Autoimmune hepatitis can progress to cirrhosis. It can also sometimes occur as acute hepatitis. The diagnosis is achieved with a combination of clinical and laboratory findings. Various specific autoantibodies are routinely used. However, the definite diagnosis of autoimmune hepatitis always requires a liver biopsy. Imaging has a poor role in the diagnostic work-up, but is used to follow the progression to cirrhosis and to detect complications such as portal hypertension and development of hepatocellular carcinoma. The findings at ultrasound, computed tomography, and magnetic resonance do not differ from those observed in other forms of chronic hepatitis.
►Hepatitis

Autoimmune Pancreatitis

Autoimmune pancreatitis (AIP) is a unusual type of chronic pancreatitis having an underlying autoimmunity mechanism. It is reported to represent about the 5% of cases of chronic pancreatitis, but its real incidence and prevalence are not well known. AIP is a recently defined disease, which appears to be a unique clinical entity characterized by peculiar pathologic and imaging findings, laboratory data and effectiveness of

corticosteroid therapy. In 2002, the Japan Pancreas Society proposed diagnostic criteria of AIP, including findings of imaging studies (diffuse narrowing of the main pancreatic duct with diffuse enlargement of the pancreas), laboratory data (elevated levels of serum IgG or the presence of autoantibodies) and histopathological findings (fibrotic changes with lymphocyte and plasma cell infiltration).

Association with other autoimmune diseases (as Sjogren syndrome, primary sclerosing cholangitis and biliary cirrhosis,) has been reported in about 50% of patients.

AIP can be classified in diffuse (more common) and focal type, which usually involves the pancreatic head and/or the uncinate process. Pathological findings include diffuse lymphoplasmacytic infiltration, variable degree of parenchymal atrophy and fibrotic changes of the gland and contiguous soft tissues. Sometimes the fibro-inflammatory process involves also the intrapancreatic tract of the common bile duct and small venous vessels.

Clinical features are non-specific and include slight upper abdominal pain, obstructive jaundice, weight loss and easy fatigability. Laboratory tests may show an increased levels of IgG (especially the IgG4 subtype) and the presence of autoantibodies (anti-nuclear antibodies, anti-carbonic anhydrase anti-bodies, etc.) pointing out the autoimmune origin of this disease. Serum levels of amylase, lipase and bilirubin may be increased.

US examination shows a homogeneous, hypoechoic, diffuse or focal enlargement of the pancreas, sometimes associated with dilation of the intra-hepatic and common bile ducts. After US contrast-media administration, the involved pancreatic parenchyma shows from mild to moderate enhancement, which is thought to be directly related to the inflammatory involvement and inversely related to the degree of fibrosis.

On CT, the diffuse type of AIP appears as a uniform swelling of the pancreas with well-defined outline. A hypodense rim-like capsule surrounding partially or completely the pancreas and showing a delayed post-contrast enhancement can be observed; this finding is related to fibro-inflammatory changes involving the peripancreatic adipose tissue and it is characteristic of AIP. In the focal type, CT examination depicts a mass-like lesion usually located in the head and/or in the uncinate process. Before contrast-medium administration, this focal enlargement typically has smooth margins and it appears homogeneous and iso- or hypodense with respect to the surrounding pancreas. On contrast-enhanced images, the lesion usually shows a hypodense appearance in pancreatic phases with a delayed enhancement. Dilation of the main pancreatic duct and biliary tree may be depicted. Sometimes wall thickening of the distal common bile duct showing enhancement is present. Parenchymal calcifications, pseudocysts, vascular invasion, inflammatory involvement of the mesentery, the anterior pararenal fascia and the lateroconal fascia are typically absent.

MR examination can demonstrate a homogeneous, focal or diffuse pancreatic enlargement, which generally is hyper-isointense in T2-weighted images and hypointense in T1-weighted sequences compared with the liver. In gadolinium-enhanced T1-weighted images, the involved pancreatic parenchyma shows a homogeneous enhancement. A capsule-like rim surrounding the pancreas may appear as a hypointense peripheral band on both T1 and T2-weighted images and may show delayed enhancement.

MR cholangiopancreatography (MRCP) and endoscopic retrograde cholangiopancreatography (ERCP) often show diffuse or focal narrowing of the pancreatic duct.

Corticosteroid therapy can determine resolution of clinical manifestation, normalization of pancreatic function, and complete or partial regression of morphologic pancreatic abnormalities. However, in the absence of an appropriate clinical setting, the focal form of AIP can be extremely difficult to differentiate from pancreatic cancer on the basis of imaging features alone and biopsy or surgical resection may be necessary.

▶Pancreatitis, Chronic

Avascular Necrosis

Ischemic death of the cellular elements of bone and marrow. Ischemic necrosis is a term usually reserved for epiphyseal and subarticular involvement. Bone infarcts describe a similar process occurring in the metaphysis and epiphysis. Etiologies include intraluminal occlusion (thromboembolic, Caisson's disease), vessel abnormality (vasculitis, radiation, disruption secondary to trauma), or compression from external mechanical pressure (fatty deposition secondary to hypercortisolism, Gaucher's). MRI and scintigraphy are sensitive early in the disease. Early MRI changes include T2-prolongation or decreased areas of enhancement. The most characteristic MRI abnormality is the double line sign with an inner border of T2 high signal surrounded by a low signal border. Radiographic abnormalities occur late in the course of disease and are characterized by patchy lucent areas of sclerosis, lucency, and osseous collapse.

▶Fractures, Peripheral Skeleton
▶Juvenile Osteonecrosis
▶Osteonecrosis, Adults
▶Osteonecrosis, Childhood

Avulsion

A pulling away of a secondary growth center bone or cartilage by tendon, ligament, or muscle.
▶Fractures, Bone, Childhood

Axillary Lymphadenopathy

Enlargement of lymph nodes in the axilla
▶Carcinoma Breast, Imaging Mammography, Secondary Signs

Axillary Node Dissection (AND)

Standard surgical removal of the whole axillary lymph nodes, levels I and II.
▶Breast Conserving Therapy

Azotemia

Elevation of the blood urea nitrogen (BUN) and serum creatinine levels.
▶Glomerulonephritis

B-cell Lymphoma

Malignant transformation of B-lymphocytes. Various subtypes can occur, depending on the moment of transformation during the B-cell life cycle. Represents the largest subset of non-Hodgkin lymphoma and is the most frequent cause of mammary lymphomatous involvement.
►Lymphoma, Breast

Background Radiation

Ionizing radiation is part of the environment. Eighty percent of background radiation comes from natural sources including radon gas, cosmic rays, the earth's crust, and radioisotopes in the human body and within the food chain. Industrial sources account for approximately 1% and medical sources of radiation for the remaining 19%. The average background radiation dose to the world's population is 2.4 mSv/year.
►Radiation Issues in Childhood

Backwash Ileitis

This term indicates the rare involvement of the distal ileum in UC, which may occur only when the disease involves the entire colon (pancolitis). Whenever present, the differential diagnosis with Crohn's disease can be difficult.
►Colitis, Ulcerative

Banti's Syndrome

Banti's syndrome, or non-cirrhotic idiopathic portal hypertension, is a condition characterized by congestive splenomegaly in the absence of intra-hepatic or extra-hepatic obstruction. The syndrome is characterized by signs of portal hypertension. Signs of hyper-splenism, with anaemia, leukopenia and thrombocytopenia, are often present. The advanced stage of Banti's disease may be complicated by upper gastrointestinal haemorrhages.
►Portal Hypertension

Barium Meal

A radiographic examination of the upper GI tract that may be tailored to focus on peptic ulcer disease, on gastric cancer detection, or on evaluation of the gastro-oesophageal reflux disease.
►Gastroesophageal Reflux in Adult Patients: Clinical Presentations, Complications, and Imaging

Barium, Indications and Contraindications

Bruno Bonnemain
Villeparisis, France
bruno.bonnemain@wanadoo.fr

Definition

It was rapidly recognized after the discovery of X-rays that a radio-opaque product would be needed to opacify the alimentary tract. A number of agents were tried until Bachem and Günther, in Germany, first used barium sulfate in 1910, and this has remained the agent of choice ever since. Various formulations have been commercialized to take into account the region of interest, the site of administration (oral versus rectal route), the mode of administration (single-versus double-contrast examination), and the type of equipment used (conventional versus CT). Barium sulfate (or iodinated contrast agents)

are administered orally to evaluate abnormalities of the mouth, pharynx, oesophagus, stomach, duodenum, and proximal small intestine. These contrast media are also administered rectally for retrograde examinations of the colon and distal small intestine. A specific, antegrade examination of small intestine may also be performed following ingestion (small bowel follow through) or direct-infusion into the distal duodenum *via* an intubation tube (small bowel enteroclysis).

Indications

As a general statement, the indications mentioned concern radiographic visualization of the gastrointestinal tract. The approved indications may vary from country to country, and according to the product final formulation.

1. Basic formulation (oral or rectal route): Barium sulfate is indicated for conventional radiological examination of the oesophagus, stomach, duodenum, and colon in double contrast or complete filling, as well as small bowel follow-through.
2. Formulation for colon: Barium sulfate is indicated for opacification of the colon for radiological explorations by the double-contrast technique or with barium filling.
3. Formulation for CT (oral route): Barium sulfate is indicated for opacification of the gastrointestinal tract in CT examination.
4. Oral pastes of barium sulfate are indicated for opacification of upper gastrointestinal tract: pharynx, hypopharynx, and oesophagus during radiological explorations.
5. Specific double-contrast formulations of barium sulfate (high-density products) are indicated for opacification of the oesophagus, stomach, and duodenum for double-contrast radiological examination.

Contraindications

Barium sulfate—when used properly—is a remarkably safe contrast agent. There are, however, certain contraindications, both absolute and relative, which need to be considered (the wording can vary from one country to another). These include:

1. Leakage into the pleural or peritoneal spaces
2. Leakage into the mediastinum
3. Possible pulmonary aspiration
4. Known gastric perforation
5. Barium given orally in suspected distal large bowel obstruction.
6. Suspected or known intestinal perforation or obstruction.
7. Toxic megacolon
8. Hypersensitivity to barium sulfate or any component of the formulation
9. Within 6 days of large forceps or "hot" colonic biopsy or snare polypectomy.

In addition, for Barium pastes, esophageal atresia is considered as a contraindication.

Finally, caution should be exercised in patients with preexisting constipation due to the risk of barium stercoroma, particularly in elderly subjects. Since some formulations contain potassium sorbate, the potassium intake should be taken into account for patients with a low-potassium diet. Patients with gastrointestinal reflux should be monitored closely for any intensification of this symptom when barium sulfate is given orally.

In conclusion, barium sulfate is helpful in radiology for gastrointestinal examinations and the benefit–risk ratio is clearly favorable if properly used.

Barium Interactions

Jean-Marc Idée
Guerbet Research Division, Aulnay-sous-Bois, France
jean-mar.idee@guerbet-group.com

Definition

To date, no extensive studies have been reported in the literature about a deleterious interaction of barium sulfate with drugs, chemical agents, or ions. In fact, two situations should be considered: (a) potential deleterious interactions of barium sulfate with drugs, (b) interactions aimed at improving the imaging efficacy of the gastrointestinal tract. Although the latter situation refers to a rather broad definition of "interaction," we believe it is worth mentioning here.

Interactions

Side Effects Resulting from Interactions of Barium Sulfate with Drugs

Barium sulfate shows negligible absorption from the gastrointestinal tract following either oral or rectal administration (1), and, consequently, is not metabolized by the liver. Therefore, traditional interactions involving

the group of cytochrome P450 enzymes or other pathways cannot be expected in this case.

Barium sulfate suspensions can be considered as unstable adsorption complexes that have the potential to bind many chemical substances, including drugs. Consequently, this may interfere with the intestinal absorption of orally-administered drugs (1). In such cases, the barium coating would lead to the inhibition of the drug absorption by the gastrointestinal tract, thus constituting a "mechanical interaction" which, in turn, would reduce or completely inhibit the drug-induced effects. However, the probability for simultaneous administration of barium and a drug is low and, to the best of our knowledge, no clinical studies have been published so far. Nevertheless, clinicians should be aware of such potential risk and take all necessary measures to prevent it.

Interactions with Compounds to Improve Imaging Efficacy

Among numerous additives, gums such as tragacanth are used to promote adherence of the barium sulfate to the mucosa. Because different manufacturers use different additive agents, these may be incompatible. Consequently, barium sulfate suspensions should not be mixed together during the same examination, to avoid flocculation (2).

An excess in mucus can be detrimental to the barium sulfate coating. Schematically, two categories of methods have been used to control the local production of mucus and consequently improve the quality of barium coating: (a) systemic administration of drugs such as histamine H2 receptor antagonists or *N*-acetylcysteine and (b) topical treatment with mucolytic drugs. The efficacy of histamine H2 receptor antagonists is an object of debate. The mucolytic drug *N*-acetylcysteine has not been found to improve the quality of double-contrast barium meal whereas double-contrast barium enema has been shown to be of better quality in patients receiving this agent (3).

The divalent cation magnesium has been shown to improve the quality of barium coating during double-contrast enema, an effect that cannot be attributed to the increase in viscosity (4).

Finally, antispasmodic drugs (hyoscine-*N*-butylbromide or glucagon) are widely used in barium enema examinations to minimize patient discomfort and to improve the quality of the examination (5).

Bibliography

1. Swanson DP and Halpert RD (1990) Gastrointestinal contrast media: barium sulfate and water-soluble iodinated agents. In: Swanson DP, Chilton HM, and Thrall JH (eds) Pharmaceuticals in Medical Imaging. Radiopaque Contrast Media. Radiopharmaceuticals. Enhancement Agents for Magnetic Resonance Imaging and Ultrasound. Macmillan Publishing Co. Inc., New York, pp 155–183
2. Freeman A (1999) Contrast agents and the gastrointestinal tract. In: Dawson P, Cosgrove DO and Grainger RG (eds) Textbook of Contrast Media. ISIS Medical Media, Oxford, pp 181–189
3. Van Damme W and Gunawan OH (1981) The use of *N*-acetylcystein in double-contrast radiography of the colon: a clinical trial. J Belge Radiol 64:171–173
4. Cittadini Jr, Gallo A, De Cicco E et al (2001) Magnesium ions and barium coating of colonic mucosa: is it a simple question of viscosity? Eur Radiol 11:1429–1532
5. Goei R, Nix M, Kessels AH et al (1995) Use of antispasmodic drugs in double contrast barium enema examination: glucagon or buscopan? Clin Radiol 50:553–557

Barium, Presentations

Jean-Philippe Barraud
Guerbet, Roissy,
France
barraudj@guerbet-group.com

Definition

Manufacturers have developed a large number of barium preparations to optimize the quality and facilitate the use of barium sulfate contrast media. Their availability is subject to the locally prevailing regulations. The following information has been obtained from a selection of manufacturers who kindly accepted to send the author the relevant data.

Characteristics

Paste

Most pastes are thick containing more than 100% barium sulfate (w/v).

They are mainly used to opacify the esophagus, the rectum, and the sigmoid colon.

Manufacturers add functional excipients to obtain the characteristics of the paste and flavoring agents to improve their palatability and therefore patient compliance in explorations of the esophagus.

The following list is representative of excipients mentioned by manufacturers. It is not exhaustive, because of the large number of manufacturers present worldwide.

Functional excipients: xanthan gum, natural gums, potassium sorbate, sorbitol, glycerol, saccharin sodium, cellulose, carboxymethylcellulose, simethicone, polyoxyethylene glycol monooleate, polyoxyethylene glyceryl monooleate, citric acid, sulfuric acid, sodium methylparabenzoate, sodium propylparabenzoate.

Flavoring agents: strawberry, vanilla, caramel.

Examples of brand names and composition:

Pastes are usually available in tubes.
Evacupaste 100: 100% w/v, that is 70 g of barium sulfate per 100 ml of paste or 56% w/w.
Microtrast: 154 g of barium sulfate per 100 ml, that is 154% w/v, or 70% w/w, that is 70 g of barium sulfate per 100 g of paste.
Prontobario Esofago: 113% w/v.
Esopho-Cat: 3% w/v

Powder

Barium sulfate contrast media in powder form contain mainly barium sulfate powder. Excipients are selected by manufacturers for the various preparations depending on the administration route (oral or rectal) and the respective indications. The final preparation of the contrast media requires addition of water, which usually has to be mixed vigorously before use.

There are two main families of barium contrast media in powder form: colon products and upper gastrointestinal (GI) tract products.

Colon powder products contain from 92 to 99% w/w barium sulfate.

The list and the choice of excipients stem from the need of creating homogeneous films for double contrast studies or homogeneous volumes of barium sulfate for repletion studies: natural gums, sodium citrate, citric acid, sorbitol, ethyl maltol, simethicone, polyoxyethylene glyceryl monooleate, polypropylene glycol, bentonite, titanium dioxide, sodium carmellose, sodium carragenine, carboxymethylcellulose.

These products are often available in soft or semirigid enema bags to which water is added for constitution of the corresponding contrast media. The final concentration of barium sulfate is higher for double contrast barium enemas than for repletion studies.

Examples of brand names and composition:

E-Z-Paque: 95% w/w, that is 95 g barium sulfate per 100 g of product.
Micropaque colon: 92% w/w.
Prontobario colon: 94% w/w.
SOL-O-PAKE: 99% w/w.

Upper GI tract powder products contain from 81 to 98% barium sulfate powder w/w.

Excipients: natural gum, citric acid, sorbitol, simethicone, polyoxyethylene glyceryl monooleate, polyethylene glycol oleate, polypropylene glycol, bentonite, saccharin sodium, sodium carmellose, sodium citrate, sorbitol.

Flavoring agents are selected to ensure the maximum compliance of patients, who have to drink the constituted product: strawberry, vanilla, caramel, marshmallow.

High-density (HD) products allow preparation of contrast media containing up to 250% w/v barium sulfate for double contrast examination of the stomach.

These products are usually available in single-dose beakers to which water is added depending on the final concentration.

Examples of brand names and composition:

E-Z-Paque: 95% w/w, that is 95 g barium sulfate per 100 g of product.
Digibar 190: 97% w/w.
E-Z-HD: 98% w/w
Prontobario HD: 98% w/w.
Entero Vu: 81%w/w.

Suspension

Barium sulfate suspensions in water are the most widely used preparations, because they are ready or nearly ready to use.

Medium- and HD suspensions are used for conventional radiological GI tract imaging. Suspensions contain from 13 to 210% barium sulfate (w/v), depending on the main indication of each product. The concentration of the product is often adjusted by the user by addition of water to obtain the optimal barium sulfate concentration for a given examination.

Excipients: natural gums, xanthan gum, cellulose, potassium sorbate, sorbitol, ethyl maltol, sodium citrate, citric acid, simethicone, saccharin sodium, carmellose sodium, magnesium aluminum silicate, methylcellulose, sodium carboxy methylcellulose, polyoxyethylene glyceryl monooleate, potassium chloride, sodium citrate, sulfuric acid, acetic acid, hydrochloric acid, sodium methylparabenzoate, sodium propylparabenzoate

Flavoring agents: strawberry, vanilla, caramel, lemon cream, blueberry, orange, apple.

Examples of brand names and composition:

Liquid E-Z-Paque: 60% w/v, that is 60 g barium sulfate per 100 ml of suspension.
Entero-H: 80% w/v.
Liquid Polibar: 100% w/v
Liquid Polibar Plus: 105% w/v
Maxibar: 210% w/v
Micropaque: 100% w/v
Prontobario 60%: 60% w/v.

Lower-density suspensions have been designed for delineation of the GI tract during computed tomography (CT) examinations. Their barium sulfate concentration ranges from 0.1 to 5% w/v.

Some preparations are ready to use. Other preparations must be diluted with water to reach the appropriate radiological density measured in Hounsfield units.

Excipients: natural gum, xanthan gum, sodium carragenine, potassium sorbate, sorbitol, sodium citrate, citric acid, benzoic acid, pectin, simethicone, saccharin sodium, polyoxyethylene glyceryl monooleate, sodium methylparabenzoate.

Flavoring Agents: Vanilla, Caramel, Blueberry, Banana, Apricot, Apple

Examples of brand names and composition:

E-Z-Cat: 4.9% w/v, that is 4.9 g barium sulfate per 100 ml of suspension.
Microcat: 5% w/v
Micropaque CT/Scanner: 5% w/v.
Ready-Cat 2: 1.2% w/v
Volumen: 0.1% w/v

Barrett's Oesophagus

Progressive columnar metaplasia of the distal oesophagus due to long-standing gastro-oesophageal reflux and reflux oesophagitis. The risk of developing oesophageal adenocarcinoma is greatly increased in the presence of these changes.

▶Neoplasms Oesophagus
▶Reflux, Gastroesophageal in Adults

Basal Cell Nevus Syndrome

Genetic disorder, also known as Gorlin's or Gorlin–Goltz syndrome, characterized by the development of multiple odontogenic keratocysts in association with a symptom complex including skeletal (bifid ribs, synostosis of ribs, kiphoscoliosis, vertebral fusion, polydactyly, hypertelorism, relative frontal bossing and prognathism, midface hypoplasia), cutaneous (multiple basal cell carcinomas), ophthalmologic, neurologic, sexual abnormalities, and ectopic calcifications.

▶Neoplasms, Odontogenic

Basal Ganglia and Thalamic Lesions

The most common site of injury in neonates with HIE. The hallmark of an acute hypoxic-ischaemic event such as may occur following a uterine rupture or placental abruption. They are associated with the later development of cerebral palsy. The severity of the impairment relates to the extent of the lesions.

▶Hypoxic, Ischaemic Brain Injury

Basedow Goiter

▶Thyroid Autoimmune Diseases

Basedow's Disease

▶Thyroid Autoimmune Diseases

Battered Child Syndrome

Alan E. Oestreich
Cincinnati Children's Hospital Medical Center, Cincinnati, Ohio, USA
Alan.Oestreich@cchmc.org

Synonyms

Child abuse; Nonaccidental trauma; Shaken baby

Definitions

Injury inflicted on a child, most typically in the first year of life, by one or more adults or older children. The trauma results from anger, frustration, aggression, misguided discipline, or occasionally ignorance. Sexual abuse can occur throughout childhood. Neglect or emotional deprivation can also occur at any age. The radiologic findings of child abuse may be simulated by a large variety of diseases, conditions, or situations. It is required of healthcare workers to report the *suspicion* of child abuse to appropriate authorities.

Pathology/Histopathology

If a battered child dies, forensic autopsy is directed initially toward investigating intracranial, intraabdominal,

and genital trauma. Photographic documentation of surface lesions is also pertinent, including any recognizable teeth patterns (also in the living battered child). Radiology postmortem can contribute to identifying fractures. Histopathology has value in evaluating the duration of reparative response to fracture. Since periosteal reaction and callus are not visible on radiographs (except on the lung-side of ribs) before about 10 days, uncalcified hemorrhage and early callus may be documented on pathology investigation.

As a sequel to abusive injury affecting growth plate and metaphyses, columns or tubes of unossified (formerly physeal) cartilage may persist into the metaphysis during further bone growth. The length of that column on pathology section is a measure of timing since a traumatic event. Pancreatic trauma from abuse may lead to long bone infarction, which may be evident histologically earlier than radiographically.

The corner fractures of abuse tend to be Salter II fractures through the junction of the straight bone bark (metaphyseal collar) with the curved bone cortex, and then extend into the physis. Occult rib fractures are often quite posterior and might be sought at autopsy.

An important gross and microscopic finding to distinguish Menkes syndrome (congenital copper deficiency) from abuse in infant boys is ▶*pili torti*, the characteristic kinky hair, which is also brittle. Emergency physicians and pediatricians (and knowledgeable pediatric radiologists) should be alert for this microscopic finding and know its microscopic appearance, lest abuse be diagnosed instead. The appearance is particularly well illustrated in a recent textbook (1). On autopsy, the highly tortuous arteries of this disease would also be evident. Do not do diagnostic angiography injections in boys known to have Menkes. Histology in suspected battering may reveal osteoporosis, hyperparathyroidism, or osteopetrosis as alternate diagnoses for multiple fractures.

Clinical Presentation

The battered child is generally brought to medical attention in one of the four ways: (1) a person in authority suspects something is amiss; (2) a parent or caretaker seeks medical assistance, often not acknowledging that abuse may have occurred; or (3) a clinical or radiographic finding serendipitously leads a physician or other healthcare worker to suspect the condition. The most extreme presentation is (4) child's death. Whenever the question of abuse is raised, two things are necessary to do: (1) a thorough clinical and radiologic investigation for findings of abuse and (2) a thorough consideration of alternate (nonabuse) explanations for the findings. Specialized pediatric social workers can play a major role in the investigation, especially in interviewing the parents, caretakers, and other pertinent individuals. Criminal justice persons can also be involved and helpful in looking into a suspected diagnosis.

The child with abuse fractures is most often under one year of age. An abused child may evidence behavior of fear or avoidance of the parent/caretaker, and the parent/caretaker may evidence inappropriate behavior toward the child; an alert radiology technologist should communicate any opinion about such interactions promptly to the radiologist. A starved child may eat and drink excessively if permitted in the medical setting. A child may favor a fractured part or limb.

The presence of blue sclerae would hint at the alternate diagnosis of osteogenesis imperfecta. Kinky brittle hair in a boy would reflect Menkes disease (Fig. 1). A rachitic "rosary" at the anterior ends of ribs and swollen wrists and knees may signify rickets, usually with secondary hyperparathyroidism.

A bogus diagnosis of "temporary brittle bone disease of infancy" or similar names has been proposed to avoid the diagnosis of battered child in some legal cases (2). It is not a medically supported diagnosis. Sometimes, bone densitometry using inappropriate adult standards had been used for documentation.

The entire past radiologic record should be rapidly available, to check for evidence of prior trauma or

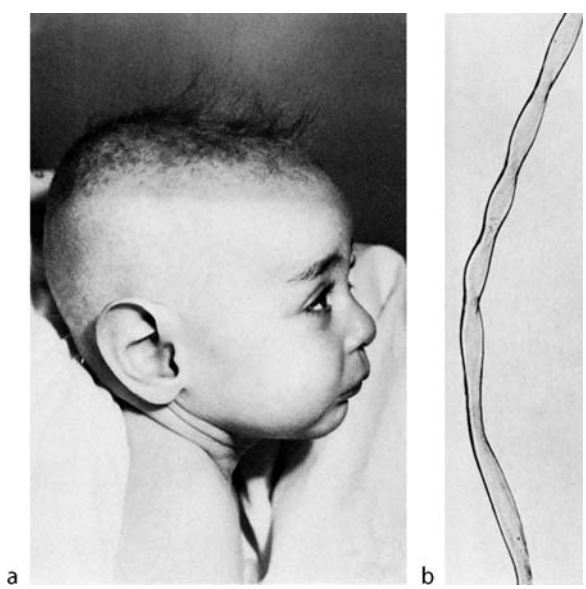

Battered Child Syndrome. Figure 1 Menkes kinky hair syndrome in a 4-month-old boy with characteristic hair and the diagnostic microscopic pili torti of a hair strand. (From Canepa G, Maroteaux P, Pietrogrande V (2001) Menkes Disease. Dysmorphic-Syndromes and Constitutional Diseases of the Skeleton. Piccin, Padova, pp 1049–1053.)

suspicion of battering. Abnormal eyegrounds should imply a rapid need for head CT, looking for intracranial hemorrhage. Once abuse is suspected, a complete accurately annotated skeletal radiographic survey should be obtained and reviewed straightaway by a radiologist to look for other, occult, fractures.

Other children in the same household or nursery as an abused child are also candidates for having been battered.

Unfortunately, one presentation of the battered child is the dead child.

Imaging

The complete skeletal survey for possible abuse should include at least one view of every bone. A radiologist should immediately review the first set of radiographs, so that orthogonal (90° to the original view) images can be added for any area that is suspicious, but not definite, for fracture. For ribs, an appropriate oblique should be requested instead. Confirmation of proper image labeling (name, date, or side of body) at the time of first review is important; especially should eventual testimony become necessary. Important when looking for fractures is appropriate magnification of the images, either routinely or when a site is suspected. In particular, viewing of the small tubular bones is improved. With film, a handheld magnifying glass of at least 2×× is useful; with PACS, as much magnification as needed should be employed. An alternative diagnostic method to seek occult fractures is coronal whole-body STIR MRI, which also may reveal soft tissue injuries.

One should record an estimated bone age for the subject and look carefully for metabolic bone disease (is the ►lamina dura around teeth well-defined? are zones of provisional calcification sharply different in density from adjoining bone? or uncalcified?) Do not forget to look for stomach distention, free gas in the abdomen, or other visceral abnormality. On the long bones, the normal ►step-off (Fig. 2), between the straight metaphyseal collar, generally 1–3 mm long, and the curved metaphyseal shape beyond it toward the shaft is not to be mistaken for fracture; images centered at that metaphysis may improve the differentiation. Carefully check for contour changes in diaphyses that might reflect old, healed fractures. Ultrasound can also document cortical breaks and periosteal reaction from abuse fractures.

If the question of intracranial hemorrhage arises because of abnormal eyegrounds, behavior, or history, a CT of the head should be rapidly obtained. On follow-up, a head MRI may document hemorrhage and better define injury to the underlying brain. The abdomen may require emergency ultrasound, CT, or contrast fluoroscopy for clinical questions as well.

Since it takes 10 days for periosteal reaction to occur after trauma, even in infants, a repeat skeletal survey after 10–14 days is in order if diagnosis is not certain. Depending on the initial level of suspicion and social circumstances, a bone scan may be employed without waiting those 10 days.

It is always prudent to include technologists' observation of parent (caretaker)–child interaction or unusual parental behavior within the radiology report. The radiologists' overall impression of the probability or possibility of battering belongs in the formal report.

Nuclear Medicine

Bone scanning is helpful both in confirming if a lesion suspected of being a fracture on skeletal radiographic survey is indeed one, and in revealing possible additional fractures. Because physes and other growth plates are

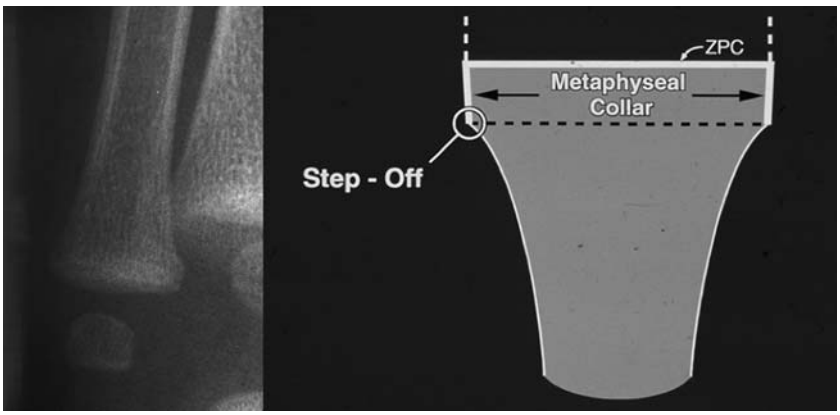

Battered Child Syndrome. Figure 2 Do not mistake the normal step-off at the junction of metaphyseal collar with the curved portion of the metaphysis. A normal step-off at distal fibula of a 1 1/2-year-old child with a diagrammatic representation. (The latter adapted from Oestreich AE, Ahmad BS (1992) Skeletal Radiol 21:283–286(4).)

normally hot on bone scanning, and because many abuse fractures are localized in the metaphyses at the epiphyses, results may be equivocal at those sites, especially in subjects less than 2 years old. Careful, and perhaps quantitative, comparison of the same site of the contralateral limb may help. Carefully observe also the small tubular bones of hands and feet, vertebral bodies and spinous processes, and especially the ribs for occult fracture activity. Healed fractures can show deformity on radiographs without abnormal activity on nuclear images.

Pancreatic scanning may contribute to evaluation of injury of that organ, but ultrasound is more easily performed and often diagnostic, as is CT, which is more frequently done in the United States.

Diagnosis

Always be alert for evidence of child battering. Once abuse is suspected be skeptical that another reason may account for the findings. Do not miss abuse and do not overcall abuse.

Many skeletal survey findings raise the question of abuse: metaphyseal corner fractures, bucket-handle metaphyseal fractures, fractures of different ages, spiral or transverse shaft fractures in the first year of life, fractures not compatible with the stated history, fractures of small tubular bones in infancy, fractures of ribs, in particular of the first rib, fractures of unusual sites (acromion, clavicle, other scapular, for example), sometimes delay in bone age, occasionally "leukemic" metaphyseal bands, multiple skull fractures, unexplained fractures of vertebral bodies or spinous processes, and otherwise unexplained long bone infarcts (the latter secondary to traumatic pancreatitis).

A fracture less than 10 days old will not show callus or periosteal reaction; a fracture more than 10 days old will. The normal physiologic periosteal reaction of infants about 1–6 months of age should not be mistaken for fracture callus, even if the bone is fractured. Note that the portions of ribs adjacent to lung *will* show soft tissue periosteal reaction before 10 days because it will be soft tissue interfacing with air.

Since metaphyseal corner fractures are a characteristic feature of abuse, it is necessary to differentiate them from the normal step-off between the 1–3 mm long straight metaphyseal collar (first described by Laval-Jeantet) adjacent to the physes and the monotonically curved remainder of the metaphysis and diaphysis that has a periosteum. The bucket handle appearance at the metaphyseal region is a corner fracture, perhaps with periosteal reaction, viewed at a different angle than merely perpendicular to the incident X-ray beam.

In the differential diagnosis of child abuse, remember that birth trauma simulates most of the findings, with the exception of fractures of different ages. Similarly, rescue trauma, to pull a baby out of danger, may also simulate abuse, again except for fractures of different ages. A simulator of suspicious first rib fracture is the hox gene variation in which a cervical rib seemingly articulates with an upward process of the subjacent rib; the articulation interface simulates fracture (Fig. 3). Typical toddler fractures once a child begins to walk should not be suspicious, nor should a simple linear skull fracture with appropriate history and no signs of intracranial hemorrhage. Another pitfall would be to mistake the result of emergency intraosseous vascular access radiologic defect in the tibia for battering fracture; history is critical (3).

Seek evidence of metabolic or other generalized bone disease with increased fracturability. Most osteogenesis imperfecta patients show osteoporosis and multiple (more than 7–10) wormian intrasutural bones of the skull. Multiple ►wormian bones and increased bone fracturing are also seen in the rare pycnodysostosis (with broad mandibular angles) and the uncommon Menkes syndrome—congenital copper deficiency, the latter only in boys. If bones are abnormally dense, at least in portions, consider osteopetrosis. Hyperparathyroidism shows loss of the lamina dura around erupted and unerupted teeth; most cases of hyperparathyroidism are secondary to rickets, which should also be manifest on the survey. Scurvy is manifested by generalized osteoporosis, vigorous callus, and Salter I epiphyseolysis, especially at the knee. Periosteal reaction of hypervitaminosis A has an unusual distribution of ulnas, fibulas, and fifth metatarsals, and skull sutures may be separated. Do not forget leukemia as a cause of unexplained fractures, often with osteoporosis or leukemic lucent metaphyseal bands due to generalized illness.

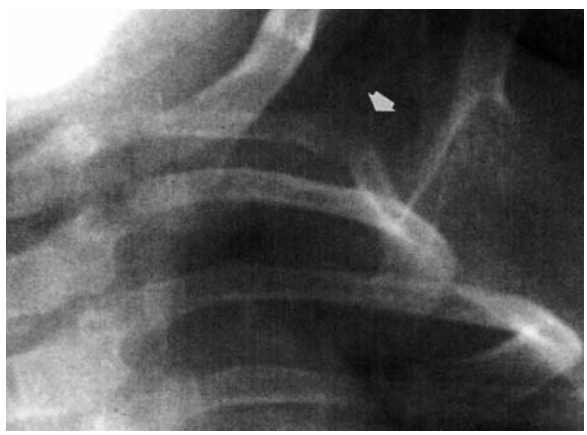

Battered Child Syndrome. Figure 3 Cervical rib simulating abuse. Seven month old girl being examined for possible abuse. The cervical rib nearly synostosing with a process extending upward from the subjacent rib should not be called a rib fracture; it is a hox gene abnormality of rib segmentation. (From Oestreich AE (1996) Radiology 199:582(5).)

Careful perusal of imaging and medical records of an infant may give evidence of prior suspicious episodes. It may even reveal otherwise inexplicable multiple visits for medical care with unusual findings, which would be suspicious of Munchhausen-by-proxy syndrome, in which a parent imposes symptoms or signs upon the child.

Bibliography

1. Canepa G, Maroteaux P, Pietrogrande V (2001) Menkes Disease. Dysmorphic-Syndromes and Constitutional Diseases of the Skeleton. Piccin, Padova, pp 1049–1053
2. Mendelson KL (2005) Critical review of temporary brittle bone disease. Pediatr Radiol 35:1036–1040
3. Harty MP, Kao SC (2002) Intraosseous vascular access defect: fracture mimic in the skeletal survey for child abuse. Pediatr Radiol 32:188–190
4. Oestreich AE, Ahmad BS (1992) The periphysis and its effect on the metaphysis: I. Definition and normal radiographic pattern. Skeletal Radiol 21:283–286
5. Oestreich AE (1996) Cervical rib simulating fracture of the first rib in suspected child abuse. Radiology 199:582

Bcl-2 Family

Antiapoptotic family members (Bcl-2 and Bcl- x_L) and a subgroup of proapoptotic proteins (Bax and Bak) are structurally similar and form a balancing equilibrium in normal cells.

▶Apoptosis

Beckwith Wiedeman syndrome

Complex syndrome that is mainly characterized by gigantism and visceromegaly. Craniofacial dysmorphism, macroglossia, omphalocele, and tumors of various organs (liver, kidneys, pancreas, adrenals, SNC, and so on) have been reported. At the level of the pancreas, cysts, pancreatoblastoma, and nesidioblastosis have all been reported in association with the syndrome.

▶Congenital Anomalies of the Pancreas

Bed Rest

Conservative measure aimed at reducing disc herniation by axial unloading of the spine.

▶Conservative Therapy for Lumbosacral Radicular Syndrome

Bed-Side Imaging

As severly sick patients, particularly those on ECMO, are extremely difficult to transport, imaging is nearly entirely performed at the patients' bed-side using mobile devices.

Bell's Palsy

Isolated, sudden, unilateral, peripheral facial nerve paralysis caused by a viral-induced neuronitis. The induced inflammatory response leads to compression of the nerve against the rigid walls of the fallopian canal, ischemia and axonal degeneration HSV is the most commonly implicated agent thought to be in a latent state in the geniculate ganglion, reactivated by non-specific triggering events. It is the most common cause of FNP, with a reported annual incidence of 15 to 40:10,000 people.

▶Facial Nerve Palsy

Benign and Malignant Nodes in the Neck

▶Lymphadenopathies, Head and Neck

Benign and Malignant Ovarian Tumors

▶Masses, Ovarian

Benign Bone Tumors

▶Neoplasms, Bone, Benign

Benign Central Venous Thrombosis

Thrombosis on the basis of a benign etiology, often hemodialysis related. Nowadays also increasingly

observed in patients with permanent central venous access catheters and pacemakers.
▶Occlusion, Venous Central, Benign

Benign Peripheral Sheath Tumours

Benign tumours originated from the peripheral nerves or soft tissues. This term includes schwannomas, neurofibromas and perineuromas.
▶Breast, Benign Tumours

Benign Prostatic Hypertrophy

▶Hyperplasia Benign Prostate

Benign Teratoma

▶Teratoma, Ovaries, Mature, Ovalar

Bezoar

A ball or clump of swallowed foreign matter, most often hair or vegetable fibrous material, and usually retained within the stomach although they can occur at any point in the gastro-intestinal tract.
▶GI tract, Pediatric, Foreign Bodies

BI-RADS MRM

When evaluating MR mammography, morphologic and dynamic criteria should be taken into account as classified by the MRM-BI-RADS.
▶MR Mammography

Bile Duct Adenomas, Extrahepatic

Rare benign tumor usually located in the common bile duct and the common hepatic duct. The majority of extrahepatic bile duct adenomas are tubular. They are composed of intestinal-type glands and are lined by pseudostratified columnar epithelium appearing as intraluminal, isoechoic relative to liver parenchyma, non-shadowing masses on US images. On direct MR or MR cholangiography images a biliary adenoma appears as a polypoid filling defect within the bile duct with lobular (in the case of tubular adenoma) or cauliflower-like (in the papillary type) contour.
▶Neoplasms, Bile Ducts

Bile Duct Cyst

When evaluating MR mammography, morphologic and dynamic criteria should be taken into account as classified by the MRM-BI-RADS.
▶Congenital Malformations, Bile Ducts

Bile Duct Cystadenocarcinomas

Biliary cystadenocarcinoma is a rare cystic malignant tumor arising from bile duct epithelium. It typically occurs in middled-age women and causes no symptoms until it grows to a huge mass compromising adjacent anatomical structures. Since local or metastatic spread is rare, patients are usually referred for surgery.

It usually appears as a large cystic lesion with intralesional septa on US, CT, and MR images, although there are no specific imaging features allowing a reliable differentiation of biliary cystadenoma from cystadenocarcinoma; the demonstration of mural nodules is suggestive of a malignant form. However, the diagnosis is usually obtained by histological analysis of the resected cystic mass.
▶Neoplasms, Bile Ducts

Bile Duct Cystadenomas

Biliary cystadenomas are uncommon unilocular or multilocular benign cystic neoplasms that may occur within the liver, extrahepatic biliary tree, or gallbladder. Biliary cystadenomas range in size from 3 to 40 cm. On US they appear as unilocular or multilocular cystic lesions with intralesional septa containing low-level echoes from blood products, mucin, or proteinaceous fluid. On CT a

large, low-attenuating mass with lobulated margins and irregular walls with fibrous septa enhancing after contrast medium injection is usually observed.

On MR imaging the tumor appears as a uniloculated or multiloculated cystic mass. The MR signal intensity of biliary cystadenoma may vary on both T1- and T2-weigthed images, depending on the content of the cystic fluid.

▶Neoplasms, Bile Ducts

Bile Duct Obstruction

▶Occlusion, Bile Ducts

Bile Duct Papillomatosis

Biliary papillomatosis is a rare disorder characterized by multiple and recurrent papillary adenomas in the biliary tract. The extrahepatic bile ducts are involved in most cases. The most common imaging feature is intra- and extrahepatic dilatation. Complete surgical excision of biliary papillomatosis is difficult and local recurrence is common. Papillomatosis has a greater potential for malignant transformation than solitary adenoma.

▶Neoplasms, Bile Ducts

Bile Duct Tumors

Bile duct tumors include both benign (bile duct adenoma, bile duct cystadenomas) and malignant (bile duct cystadenocarcinomas, cholangiocellular carcinoma) neoplasms arising from the bile duct epithelium.

▶Neoplasms, Bile Ducts

Bilhemia

Bilhemia is a rare clinical entity usually caused by a pathologic communication between intrahepatic bile ducts and the hepatic venous system following the formation of an extensive hematoma within necrotic tissue. Passage of bile into the bloodstream is due to an increased biliary-venous gradient and occurs during the resorption of the biliohematoma.

Clinically, bilhemia is characterized by the rapid development of jaundice with a marked increased in the total serum bilirubin level. When a considerable amount of bile enters the bloodstream, it may cause an embolism in the lungs and kidneys. If untreated, bilhemia has a high mortality. Endoscopic retrograde or direct cholangiography is the imaging modality of choice for the demonstration and localization of a biliovenous fistula. Magnetic resonance cholangiography and biliary scintigraphy may also be useful, whereas arteriography is usually nondiagnostic. Currently, interventional radiological procedures, particularly percutaneous biliary stenting, are frequently employed for the treatement of posttraumatic bilhemia.

▶Trauma Hepatobiliary

Biliary Anatomy

Davide Caramella, Paola Vagli, Carlo Bartolozzi
Department of Diagnostic and Interventional Radiology, University of Pisa, Italy
caramella@do.med.unipi.it

Synonyms

Diagnostic imaging of the biliary tree (bile ducts; gallbladder)

Definition

Modality of depiction of the normal biliary structures by means of diagnostic imaging.

Characteristics

Gross Anatomy

The right and the left hepatic ducts are formed by the junction of the intrahepatic bile ducts, and these join at the porta hepatis to form the common hepatic duct. The common hepatic duct, about 2.5 cm below its origin, is connected with an acute angle to the gallbladder by means of the cystic duct, forming the common bile duct or choledochal duct. The cystic duct runs almost parallel to

the common duct and usually joins it at the inferior aspect of the porta hepatis or sometimes at a lower level. The choledochal duct extends for about 7 cm from the cystic duct to the duodenal papilla, running downward in the right free edge of the gastrohepatic ligament or lesser omentum (on the left of the Winslow foramen), with the hepatic artery to its left and the portal vein behind it. Inferiorly, its course is firstly located behind the duodenum and then in a groove of the head of pancreas before entering the second part of the duodenum. At the duodenal papilla it joins to the pancreatic duct, although occasionally they remain separate. Branches from the hepatic artery provide arterial supply to the biliary tree, while venous drainage is by means of the portal venous system. The gallbladder lies at the inferior edge of the right hepatic lobe (in the gallbladder fossa), lateral to the quadrate lobe (segment IV) in relationship to the superior border of the proximal transverse colon. It is also connected to the anterolateral aspect of the gastric antrum, duodenal bulb, and proximal descending duodenum. The gallbladder is held against the bottom surface of the liver by peritoneum, and is surrounded by fat. Its size is about 7 to 10 cm in length and it has a capacity of approximately 30 mL, although it may vary in size and shape often according to the patient's stature. It is subdivided into three portions: the fundus, body, and neck. The neck is S-shaped and connects with the cystic duct within which lies the spiral valve of Heister. The fundus is directed downward, forward, and to the right and it comes into close relationship with the anterior abdominal wall. The body is directed upward and backward to the left, and near the porta hepatis is continuous with the neck. The gallbladder wall is structured into three layers and is composed of the mucosa, the fibromuscular layer, and the serosal layer. The mucosa presents small sulci that combine, generating a honeycomb aspect. Arterial supply is performed by means of the cystic artery that is a branch of the hepatic artery. Veins from the gallbladder join the tributaries of the portal and hepatic veins. The gallbladder and biliary ducts are both reached by parasympathetic and sympathetic nerves (1).

Ultrasound

The larger intrahepatic biliary ducts may be seen arborizing into the hepatic parenchyma and can be differentiated from the intrahepatic veins that have no obvious walls. Distinction between biliary ducts and the other vessels is performed thanks to their typical branching pattern and the presence of Doppler signal. The normal choledochal duct is hard to demonstrate for its small caliber (0.5–1.1 cm) and oblique course. In sagittal sections it can be seen anteriorly to the inferior vena cava and crossing in front of the portal vein. A dilated choledochal duct may be distinguished from the portal vein by means of serial scans demonstrating the communication of the portal vein with the confluence with the mesenteric and splenic veins and the presence of the posterior "dip" of the choledochal duct as it passes downward behind the first part of the duodenum. In transverse scans the small, circular, well-demarcated, echo-free ring produced by the choledochal duct may be recognized medial to the gallbladder, lateral to the inferior vena cava, and in front of the portal vein. Also, transverse scans at the level of the major axis of the pancreas may show the distal end of the choledochal duct on the posterior aspect of the head of the pancreas with the gastroduodenal artery placed anteriorly. Size and position determine the capability to visualize the gallbladder. Normal bile is anechoic allowing us to distinguish the gallbladder from the normal acoustic texture of the liver parenchyma. A normal, physiologically dilated gallbladder should be demonstrated on longitudinal, transverse, and oblique scanning in fasting patients. Intercostal scans in the transverse plane are of particular value for patients in whom the liver lies deeply under the costal margin. The gallbladder shows many variations in location and size. It is usually placed anterior to the right kidney and it can also have different relationships with the liver (subhepatic, intrahepatic, or mesenteric gallbladder). It appears as a well-demarcated, smooth-walled, pear-shaped, and fully transonic area, lying obliquely on the inferior surface of the right lobe of the liver in sagittal scans. The fundus presents a rounded contour, while the body has a semilunar shape and diminishes to a varying degree as it passes upward and backward to form the gallbladder neck. In this region the presence of spiral valves may be revealed in cases of dilatation. The gallbladder neck invariably lies immediately anterior and inferior to the portal vein. It may be difficult to visualize because of the presence of an acoustic shadow at this level (probably due to the collagen arrangement of the spiral valve) that should not be mistaken with stones. On axial sections with the transducer angled cranially, it is possible to show the pear shape of the gallbladder sectioned along its long axis lying anterior to the right kidney (1). Ultrasound (US) shows a three-layered gallbladder wall consisting of a strongly reflective outer layer, a minimally reflective inner layer, and an anechoic layer between. The wall thickness is usually less than 2 mm.

Computed Tomography

The normal intrahepatic biliary radicles are not seen on computed tomography (CT) scans, whereas the normal common hepatic or the common bile duct can be seen as a water-dense structure, varying in diameter from 6 to 8 mm. The common hepatic duct lies anterolateral to the portal vein in the region of the liver hilus, while the caudal

end of the common bile duct lies within the head of the pancreas, medial with respect to the second duodenal portion. Unlike with the hepatic vessels, the intravenous administration of iodinated contrast medium determines no elevation in the attenuation value of the near water-dense biliary tree. However, a better depiction of mild dilatation of the biliary tree may be acquired after contrast medium administration, obtaining parenchymal enhancement. On CT scans the gallbladder is shown as an oval or elliptic sac of near-water density lying in a fossa on the inferior surface of the liver. When its walls are contracted it may be difficult to localize and can appear ill defined. The gallbladder neck is directed superomedially, while the fundus projects inferolaterally. In more caudal scans, the gallbladder assumes a more anterior position and occasionally may extend beyond the inferior margin of the liver near the second duodenal portion. The thickness of normal gallbladder walls is nearly imperceptible. Recent advances in three-dimensional CT (single and multirow CT) in terms of thin section, single breath hold acquisitions, and three-dimensional and multiplanar reformation techniques suggest the possibility of CT ▶cholangiography for an elective visualization of the biliary tree after the intravenous or oral administration of cholangiographic iodinated contrast medium. Because of its high contrast resolution, CT enables visualization of the bile ducts that are also opacified with oral cholecystographic contrast medium before its concentration in the gallbladder (2).

Cholangiography

This technique was firstly introduced in 1954 as intravenous cholangiography for the noninvasive visualization of the common bile duct. It consists in intravenous injection of a dedicated iodinated contrast medium that is excreted by hepatocytes allowing the opacification of biliary ducts. Therefore, to obtain an adequate opacification of the biliary tree, liver function must be reasonably good. Gallbladder visualization was not included in cholangiography studies and in the pre-US/CT era this structure was visualized by means of oral ▶cholecystography, now considered obsolete. Intravenous cholangiography has been replaced by direct cholangiography, representing a way of direct visualization of the biliary tract (intra- and/or extrahepatic), by means of introduction of iodinated contrast medium in the biliary system that is outlined on radiographs. This technique includes different methods:

- ▶Percutaneous transhepatic cholangiography (PTC) (percutaneous catheterization of an intrahepatic bile duct)
- ▶Endoscopic retrograde cholangiopancreatography (ERCP) (endoscopic catheterization of the common bile duct *via* Vater's papilla)
- Perioperative cholangiography (catheterization of the cystic duct during surgical procedures)
- Trans-Kehr cholangiography (injection of iodinated contrast medium directly into the surgical T-tube).

Cholangiography allows the whole course of the biliary tree to be depicted with high fidelity and is usually performed to assess the presence, location, extension, and cause of biliary obstruction, bile extravasation in case of biliary leakage, and less frequently for evaluating congenital malformations of the biliary tract.

Today, cholangiography is usually a part of interventional or endoscopic procedures and has been replaced by noninvasive methods [US, CT, and ▶magnetic resonance cholangiopancreatography (MRCP)] in the diagnostic work-up of biliary tree diseases.

Magnetic Resonance Cholangiography and Magnetic Resonance Cholangiopancreatography

Magnetic resonance cholangiography (MR cholangiography) was introduced in 1991 by Wallner and has emerged as an accurate, noninvasive alternative to diagnostic ERCP in the evaluation of diseases of the biliary tract. MR cholangiography is performed with the use of heavily T2-weighted images obtained with different pulse sequences (gradient echo sequences with the steady-state free precession, two-dimensional and three-dimensional heavily T2-weighted fast spin echo sequences, half Fourier rapid acquisition with relaxation enhancement RARE sequences) without the injection of contrast medium that demonstrate the fluid-containing bile ducts as high-signal-intensity structures. Stationary fluids, including bile and pancreatic secretions, have high signal intensity whereas solid organs have low signal intensity. This combination of imaging characteristics provides optimal contrast between the hyperintense signal of bile and the hypointense signal of the background. This technique also allows visualization of the pancreatic ducts generally after the administration of a secretive agent (secretin) and is then called MRCP.

MRCP combines the benefits of projectional and cross-sectional imaging techniques providing an overview of the entire biliary and pancreatic ductal system by means of data acquisition and image reconstruction rendered on the coronal plane in a conventional cholangiography fashion allowing high-quality imaging comparable to that of ERCP.

A comparable diagnostic accuracy with respect to ERCP in the diagnosis of choledocholithiasis is reported by various authors for MRCP. MR cholangiography may help to establish the diagnosis of malignant obstruction and is useful in evaluating those patients in whom ERCP was unsuccessful or incomplete. Moreover, MR cholangiography plays a crucial role in evaluating postsurgical

biliary tract alterations and can demonstrate a variety of congenital anomalies of the biliary tract (aberrant ducts, choledochal cysts, Caroli disease, pancreas divisum). In addition, intentional or incidental imaging of the gallbladder with MRCP can be used to identify calculi or help determine the presence and extent of neoplastic disease (3).

Image Processing

Biliary tract examinations using rapid three-dimensional volumetric techniques can be performed with three-dimensional CT (single and multirow CT) and MR cholangiopancreatography. CT techniques are especially useful when MR is unavailable or contraindicated, or when the quality of MRCP images is suboptimal (CT cholangiography has a better spatial resolution, hence its clearer depiction of small ducts). However, to date, the use of radiation, the low availability of biliary contrast medium, and the possible adverse reactions to iodinated contrast agents have all had a negative impact on a large-scale diffusion of the technique. Integration of volumetric acquisition and three-dimensional surface and volume rendering techniques facilitates the study of the biliary tract in a noninvasive way. One of the advantages is the possibility to process these volumetric data sets so to generate three-dimensional reconstructions, which can be obtained with both external and endoluminal views of the organ anatomy. Maximum intensity projection (MIP), minimum intensity projection (Min IP), shaded surface display (SSD), and volume rendering (VR) algorithms provide external views of the pancreaticobiliary tract. Endoluminal views can be obtained with ►virtual endoscopy (VE).

MIP and SSD provide a global map of the pancreaticobiliary tree anatomy that can be helpful in the interpretation of two-dimensional MRCP images (particularly postsurgical anatomy, anatomic variants of the pancreaticobiliary ductal system, and large biliary neoplasms).

However, various authors have stressed the limitations of such algorithms in the depiction of small intraductal pathology, and particularly in the detection of small calculi in the common bile duct. VR is the latest development in three-dimensional imaging of the anatomy of the pancreaticobiliary tree, allowing radiologists to display simultaneously different anatomical structures imaged within a single volume. VR has the advantage of providing a clear roadmap of the entire biliary tree, but its real role in demonstrating pathological changes deserves further clinical evaluation. Virtual simulation of fiber-optic endoscopy can be obtained with a new software tool based on surface or volume rendering techniques, called virtual cholangioscopy, when specifically applied to the study of the biliary system. Endoluminal views of the pancreatic and bile ducts can be obtained by rendering CT or MRI data sets. The application of the VE surface algorithm to three-dimensional CT data sets with proper setting of the thresholds allows rendering of the interface pixels only, i.e., those pixels on the border between endoluminal fluid (bile, pancreatic secretions) and surrounding soft tissue that remains undisplayed. Segmentation of MRCP data sets has been made feasible by the high contrast difference between the bile ducts (brightest voxels) and the surrounding tissue (darkest voxels). Navigation sequences can be simulated through the common bile duct, common hepatic duct, left and right hepatic ducts, intrahepatic branches, pancreatic duct, cystic duct, and gallbladder. All these anatomical details appear as tubular structures, with a smooth internal surface. The confluence between these branches can also be represented. In most cases three-dimensional imaging does not add quantitative information to MRCP, but the main advantage over cross-sectional anatomy is represented by a different rendering of data, more familiar to the human eye.

Constant integration between two-dimensional source images and three-dimensional reconstructions, both with external and endoluminal views, represents an added value to the diagnostic potentialities of MRCP in the evaluation of biliary tract diseases (4).

Nuclear Medicine

Hepatobiliary scintigraphy is a physiological test that evaluates hepatic bile formation, excretion, and biliary tree patency. Images are acquired in a dynamic fashion for up to 4 h after the intravenous administration of a technetium-labeled iminodiacetic acid (IDA) derivative that is an organic anion moving from the plasma into bile like bilirubin. Two ^{99m}Tc-IDA agents (disofenin and mebrofenin) are widely used showing a homogeneous liver uptake and an excellent visualization of the gallbladder and the cystic and common bile duct within 60 min of intravenous tracer injection. Following intravenous injection, these organic anion tracers are rapidly bound to plasma protein, circulate to the liver, dissociate from their binding proteins, and are taken up by hepatocytes (peak hepatocyte uptake at 10 min). After processing within the hepatocyte through the ligandin system and possible glucuroconjugation (as occurs for bilirubin), these agents are rapidly secreted into the bile providing excellent visualization of the biliary tract (90% visualization of the common bile duct and gallbladder at 30 min and 100% at 60 min after tracer injection). Patients undergoing cholescintigraphy should have fasted for a minimum of 2–4 h before tracer injection. Anterior images of the liver and biliary tract are routinely obtained at 5 and then at 10–15-min intervals for 1 h after tracer

injection or in dynamic acquisition. Intravenous administration of morphine sulfate can be performed in cases of nonvisualization of the gallbladder when adequate hepatic uptake and excretion into the bowel is documented. Morphine induces contraction of the sphincter of Oddi raising intrabiliary pressure and filling the gallbladder if the cystic duct is patent, followed by imaging at 30 and 45 min. Alternatively, delayed images at 3–4 h can be obtained to confirm the presence or absence of cystic duct patency with similar accuracy. This test may be nondiagnostic in patients with liver failure and intrahepatic cholestasis of any cause because of the inability to conjugate and excrete the radiotracer.

Bibliography

1. Taylor KJW, Rosenfield AT (1979) Ultrasound liver and biliary tract. In: Margulis AR, Burhenne HJ (eds) Alimentary Tract Radiology. Mosby, St. Louis, pp 183–197
2. Chopra S, Chintapalli KN, Ramakrishna K et al (2000) Helical CT cholangiography with oral cholecystographic contrast material. Radiology 214(2):596–601
3. Fulcher AS, Turner MA, Capps GW (1999) MR Cholangiography: technical advances and clinical applications. Radiographics 19 (1):25–44
4. Boraschi P, Lodovigi S, Campori G et al (2002) Biliary tract. In: Caramella D, Bartolozzi C (eds) 3D Image Processing. Springer, Berlin Heidelberg, pp 223–232

Biliary Atresia

Most frequent cause of persisting neonatal cholestasis, characterized by obliteration or discontinuity of the extrahepatic biliary system (extrahepatic biliary atresia). If untreated secondary biliary cirrhosis develops.

▶Congenital Malformations, Liver and Biliary Tract
▶Congenital Malformations, Bile Ducts

Biliary Hamartoma

Bile duct hamartomas are small clusters of slightly dilated bile ducts surrounded by a fibrous tissue. They do not communicate with the biliary tree. At pathologic analysis, they appear as grayish-white nodular lesions 0.1–1.5 cm in diameter scattered throughout the liver parenchyma. Bile duct hamartomas are rather common and usually represent an incidental finding at imaging examinations. At ultrasound biliary hamartomas may present as either hypoechoic or anechoic small nodules; in rare cases they have a hyperechoic appearance. CT shows hypodense small hepatic nodules. At MR the lesions are hypointense on T1-weighted images and markedly hyperintense on T2-weighted images.

Von Meyemburg complexes: Biliary hamartoma.

▶Cystic-Like Lesions, Hepatic

Biliary Hypoplasia

Reduction of the caliber of the intra and extrahepatic ducts or both resulting in an inadequate biliary drainage. The degree of the damage depends on the severity of the hypoplasia.

▶Congenital Malformations, Liver and Biliary Tract

Biliary Lithiasis

▶Gallstones

Biliary Stones

Particulate, sand-like matter that forms from precipitation of solutes in bile. The clinical course is extremely variable. Possible outcomes are complete resolution, progress to gallstone formation, and complications, including intermittent abdominal pain, acute pancreatitis, and acute cholecystitis. Risk factors associated with biliary sludge are rapid weight loss, pregnancy, ceftriaxone therapy, and transplantation. At US biliary sludge is easily diagnosed: it presents as echoic sediment with or without acoustic shadowing in the dependent portion of the gallbladder and shifts slowly with positioning.

▶Gallstones

Biliary Tuberculosis

Tuberculosis infection of the biliary tract is extremely rare. The presence of a high concentration of bile acids, a competent sphincter of Oddi, a rapid passage of bacilli through the duodenum and presence of pancreatic secretions represent protective factors against bile infection by Mycobacterium tuberculosis. The possible etiopathogenesis include: ascending or descending infection through the biliary tract, direct infection from a neighbouring focus,

hematogenous and lymphatic spread. Tuberculous cholecystitis is usually associated with gallstones. In fact, bacilli form a nidus for the stone formation. Biliary tuberculosis has nonspecific clinical and radiological features and therefore its preoperative diagnosis is very challenging. The definite diagnosis is usually based on intraoperative and histopathological findings: evidence of caseating granulomatous inflammation with bile cytology revealing Mycobacterium tuberculosis is confirmatory. Most of the cases present with a clinical setting consistent with cholecystitis, mainly right upper abdominal pain, nausea, vomiting, and low-grade fever. In such cases US usually reveals features of acute or chronic cholecystitis. Bile duct dilatation may be also present. In most cases, it is due to compression by enlarged tuberculous lymph nodes. In some instances, biliary infection may produce multiple irregular biliary strictures. In these cases, the visualization at US and CT of periductal ill-defined soft tissue material may lead to the wrong diagnosis of cholangiocarcinoma.

▶Occlusion, Bile Ducts

Biliary–respiratory Congenital Communication

Rare congenital abnormality where an anomalous tract connects the tracheobronchial tree with the biliary tree. The common sign is foamy bile sputum.

▶Congenital Malformations, Liver and Biliary Tract

Biliary-Vascular Fistula

Biliary–vascular fistula is an abnormal communication between the biliary tree and the intrahepatic vascular system. Biliary–vascular fistulas are rare and usually result from interventional radiology procedures such as percutaneous liver biopsies and biliary stenting. They include both arteriobiliary and venous- or portobiliary communications, and two clinical entities, such as hemobilia and bilhemia, have been distinguished. In fact, the direction of flow through the pathologic biliary–vascular communication depends on the pressure gradient between the two systems (vascular and biliary). Because blood pressure generally exceeds pressure in the bile ducts, hemobilia is, by far, the more common problem. Flow in the opposite direction, bilhemia occurs in the rare patient in whom the normal pressure gradient is inverted, directing bile into the hepatic veins or the portal vein.

▶Trauma Hepatobiliary

Billroth's Gastrectomy Type I

Removal of lower portion of stomach (pylorus) with end to end anastomosis of the remaining stomach with the duodenum.

▶Stomach and Duodenum in Adults Postoperative

Billroth's Gastrectomy Type II

Subtotal excision of the stomach with closure of the proximal end of the duodenum and side-to-side anastomosis of the jejunum to the remaining portion of the stomach.

▶Stomach and Duodenum in Adults Postoperative

Biloma

Biloma is a perihepatic or intrahepatic bile collection resulting from damage of the biliary tree and bile leakage. As a result of the slow rate of leaking, a biloma may take weeks or months to develop after trauma; hence, it usually is diagnosed by using follow-up scans.

Clinical manifestations depend on the location and size of the lesion. At ultrasound, computed tomography (CT), and magnetic resonance (MR) imaging, biloma usually appears as a rounded or ellipsoid, fairly well-defined, loculated cystic mass localized in close proximity to the liver and bile duct. Hepatobiliary scintigraphy and MR cholangiography enable demonstration of the precise site of bile leakage; provide useful information in cases of suspicious biliary leakage. Although minor biloma usually resolves spontaneously, large or increasing biloma may require US- or CT-guided percutaneous drainage.

▶Trauma Hepatobiliary

Bioluminescence

Clemens Löwik, Eric Kaijzel
Endocrinology Research Laboratory and Molecular Imaging, Leiden University Medical Center, The Netherlands
c.w.g.m.lowik@lumc.nl

Definition

Bioluminescence refers to the enzymatic generation of visible light by living organisms. The most commonly used bioluminescent reporter gene for research purposes has been luciferase from the North American firefly *Photinus pyralis*. The enzyme catalyzes the transformation of its substrate D-luciferin into oxyluciferin in an oxygen and ATP-dependent process, leading to the emission of photons (Fig. 1).

Biological sources of light (bioluminescence) have sufficient intensity to cross animal tissues provided that the endogenous light has a wavelength >500 nm. Above this wavelength, tissue absorption of photons decreases. The firefly luciferase/luciferin reaction emits photons at wavelengths from 500 to 620 nm and is therefore suitable for external detection. Apart from fulfilling this criterion, another important finding was that the substrate luciferin, after intravenous or peritoneal injection into animals, diffuses within a few minutes throughout the entire body and is rapidly taken up by cells (1). Luciferin, which is not immunogenic, also crosses the blood–brain barrier, although this takes more time (10–15 min); therefore, luciferase can be used as a reporter in brain-related research. Bioluminescence imaging (BLI) of luciferase reporters provides a relatively simple, robust, cost-effective, and extremely sensitive means to image fundamental biological processes *in vivo* due to exceptionally high signal-to-noise levels. Apart from firefly luciferase, other luciferases with matching substrates have been found useful for molecular imaging, including *Renilla* luciferase, green or red click beetle (*Pyrophorus plagiophthalamus*) luciferases, and *Gaussia* luciferase. *Renilla* and *Gaussia* luciferases use a different substrate, coelerentarazine, and emit mainly blue light. The emission spectrum is very broad, and a part also exceeds the wavelength of 550 nm, making it suitable for BLI. *Renilla* and *Firefly* luciferase can also be used in combination as dual reporters for BLI (2).

Imaging

Recent technical advances for imaging weak visible light sources using cooled charged coupled device (CCCD)

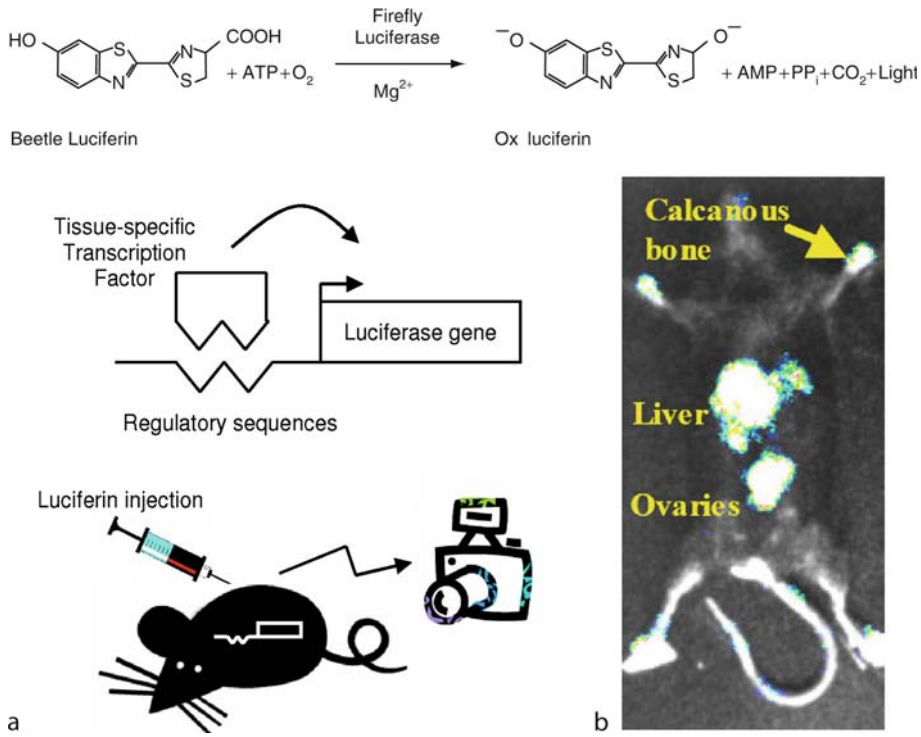

Bioluminescence. Figure 1 Biological principle of bioluminescent imaging of luciferase expression. (a) Firefly luciferase converts the substrate luciferin into oxyluciferin and light. Tissue-specific transcription factors bind to regulatory sequences cloned directly adjacent to the luciferase gene, resulting in tissue-specific expression of luciferase, which can be visualized by injection of luciferin and detection of the emitted light by cooled charged coupled device cameras. (b) Image of a transgenic (ERE-luc) mouse during proestrus expressing the luciferase gene under the control of an estrogen-responsive element. Note the intense staining of the ovaries, which subsides during estrous. Reprinted from de Boer, Blitterswijk, Lowik. *Biomaterials* 27 (2006) with permission from Elsevier.

cameras, peltier-cooled detectors, and microplate channel intensifiers allow detection of bioluminescent emission from inside the tissues of an animal (Table 1).

These technical developments have made it possible to monitor gene expression in the living animal *via* a *luc*-reporter gene linked to specific promoters or to follow in real time the fate of luciferase (*luc*)-transfected tumor cells or immune cells injected in living animals (Fig. 1). One of the many advantages of this methodology is that it is noninvasive and therefore allows investigations in the same animal at different time points. Consecutive analysis of the same animal means that fewer animals are needed for each study and that experimental uncertainties arising from interanimal variations are greatly reduced. This technology is extremely useful in many research areas such as cancer research, as it focuses on detecting primary tumor growth and on micro- and macrometastatic tumor spread (Fig. 2).

Cell Trafficking

BLI can also be used to follow in real time the fate of luciferase-transfected cells injected in living animals. This application is widely applied in cancer research to follow not only tumor progression but also the metastatic process by which tumor cells metastasize to distant tissues or organs. It is also used to follow the migration and fate

Bioluminescence. Table 1 Several currently available BLI systems

Company	System	Technology
Xenogen	IVIS	Liquid nitrogen-cooled CCD camera
Berthold	NightOwl	Peltier-cooled CCD camera
Hamamatsu +	VIM Camera	Intensified CCD camera
Improvision	Model C2400-47	
Roper Scientic	ChemiPro	Cryogenic-cooled CCD camera
Biospace	PhotoImager	Intensified CCD camera
Kodak	*In vivo* FX	Thermoelectric CCD camera

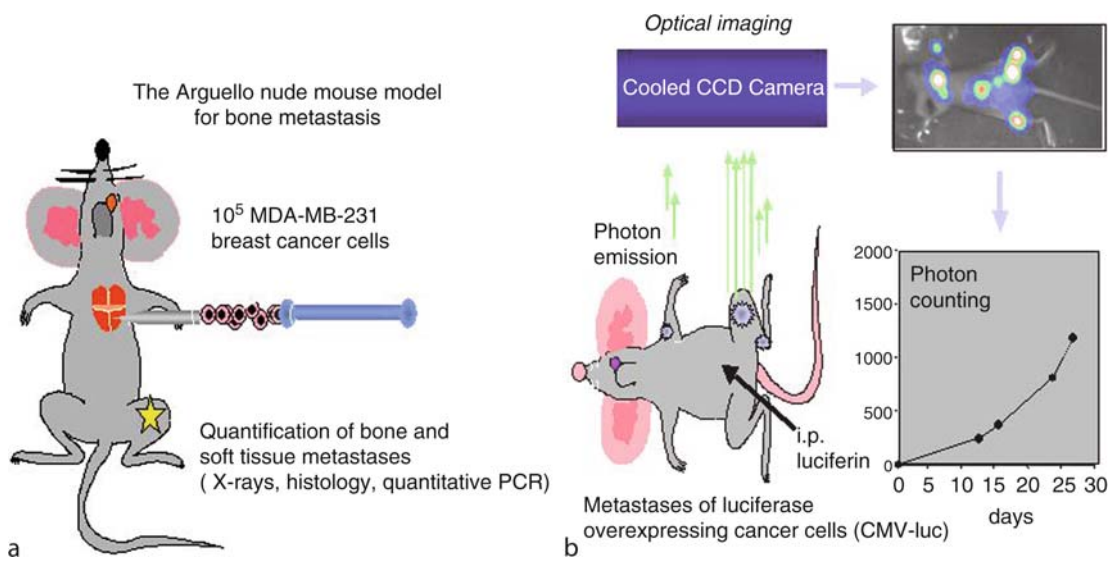

Bioluminescence. Figure 2 The Arguello nude mouse model for bone metastasis (a) Injection of 100,000 human MDA-MB-231 cancer cells into the left cardiac ventricle of immunodeficient (*nu/nu*) mice will lead to bone/bone marrow metastases (From Arguello F, Baggs RB, Frantz CN (1988) A murine model of experimental metastasis to bone and bone marrow. Cancer Res 48:6876–6881). (b) Intracardiac injection of MDA-MB231 cells stably expressing luciferase will lead to metastases of luc-expressing cancer cells, of which progression can be noninvasively monitored using bioluminescent imaging. Reproduced with permission from Lowik, Cecchini, Maggi, Pluijm. Ernst Schering Res Found Workshop 49 (2005).

of immune cells or transplanted stem cells, such as neuronal stem cells in the brain after ischemic stroke or embryonic stem cells in heart regeneration.

Gene Expression

BLI makes it possible to monitor gene expression in living animals *via* a luciferase reporter gene linked to cell-, tissue-, differentiation- or other process-specific promoters. These constructs can be either transfected into cells that can be transplanted into animals or be used to make transgenic gene-reporter mice.

Transgenic Gene-Reporter Mice

Using luciferase-based specific gene reporters, it is possible to transfect embryonic stem cells with such a construct and make transgenic gene-reporter mice. For instance, we generated mice transgenic for the luciferase gene under the control of an estrogen-responsive element (ERE-luc)n (3). Luciferase activity in individual mice could be followed throughout the estrous cycle, and a peak of luciferase activity was observed during proestrus in reproductive tissues (Fig. 1). Using ERE-luc mice, we were able to monitor estrogen receptor activity dynamics in a tissue-specific and quantitative way, demonstrating the power of BLI.

Recent advances in small animal imaging instrumentation, molecular genetics, and reporter gene design have yielded the ability to integrate imageable reporters like luciferase into various transgenic mouse models that resemble human diseases. (Some examples are listed in Table 2).

Bioluminescent Tomography

The current BLI systems use photographic principles to capture light emitted from the animals at sites where luciferase is expressed. Photons are detected at the surface of the animal in two dimensions, also known as planar imaging, the simplest technique for detecting optical reporter molecules *in vivo*. Photon attenuation, however, is strongly nonlinear as a function of depth and of the optical heterogeneity of tissue, which hampers signal quantification. Planar imaging is further complicated by the inability to resolve depth and by tissue scattering and absorption, which limits spatial resolution. A way to circumvent the problems of 2D planar BLI would be a combination of multiview angle imaging (bioluminescence tomography) with *a priori* information on tissue heterogeneity. This can now be achieved using the newly

Bioluminescence. Table 2 Examples of transgenic BLI reporters for models of human disease

Name	Regulatory Element	Application
Transgenic mice		
hOC-luc	Osteocalcin promoter	Bone repair and development
BMP-4	Bone morphogenetic protein-4	Bone repair and development
colI(1)-luc	Bone-specific enhancer of the mouse collagen (α1) I gene	Matrix deposition
BSP-luc	BSP promoter	Matrix deposition
VEGFR2-luc	VEGFR2 gene promoter	Angiogenesis
VEGF-luc	VEGF gene promoter	Angiogenesis
PSA-luc	PSA promoter	Oncology
Epx* or Epo-luc	Epo promoter	Inflammation
Saa1-luc	Serum amyloid A-1 promoter	Inflammation
IL-2-luc	Interleukin-2	Inflammation
TNF-luc	TNF promoter	Inflammation
iNOS-luc	iNOS gene promoter	Inflammation
NFκB-luc	3 NFκB site from the Igκ light chain promoter	Inflammation
Ho1-luc or Hmox1-luc	Heme oxygenase-1promoter	Drug metabolism/toxicology
SOD1-luc	Superoxide dismutase promoter	Drug metabolism/toxicology
Cyp3A4-luc	Cytochrome p450 isoform 3A promoter	Drug metabolism/toxicology
RIP-luc	Rat insulin gene promoter	Metabolic disease
Retn-luc	Resistin promoter	Metabolic disease
GFAP-luc	GFAP-promoter	Neurology
ER-DEVD-luc	Caspase cleavage sequence	Apoptosis

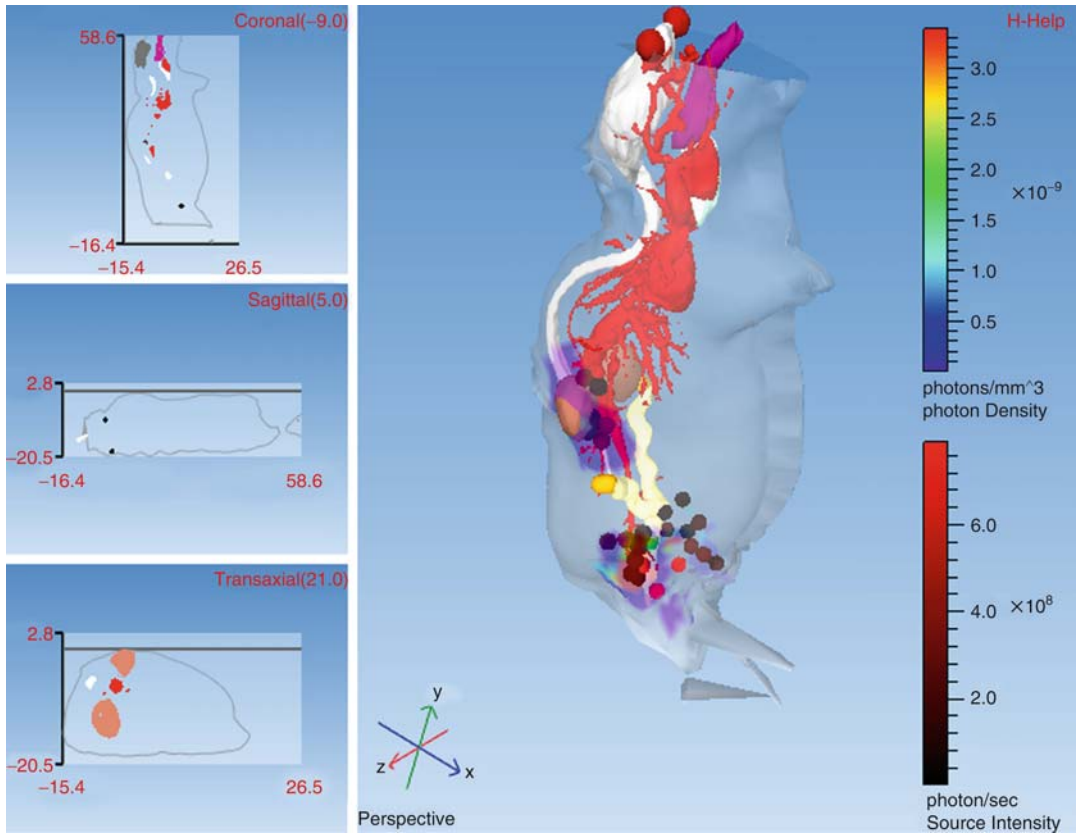

Bioluminescence. Figure 3 Using Xenogen IVIS 3D Living Image Software, reconstructions of a RC21-luc expressing tumor in the right kidney and its metastases in the urogenital area are displayed as voxels (*dots*) with a red–black color bar, red indicating the highest intensity. Cross-sectional planes and depth locations are shown on the left.

developed 3D BLI systems from Xenogen (Fig. 3). If these 3D images are combined with 3D spatial (tissue) information obtained by computed tomography or magnetic resonance imaging, algorithms can be developed to more precisely correct for photon scattering and absorption due to tissue heterogeneity and depth.

Diagnosis

Noninvasive *in vivo* BLI is a powerful tool in small animal models of human biology and disease. BLI is perfectly suited to monitor gene expression in transgenic reporter mice and to detect and follow small numbers of cells noninvasively. In cancer, BLI enables researchers to follow tumor progression and metastasis and can help identify *in vivo* molecular targets of cancer and their metastases. The application of BLI in combination with new animal models for cancer will allow us to study very rapidly and conveniently the efficacy of new therapeutic approaches such as gene therapy, stem cell therapy, and antiangiogenic therapy, and when successful can be a first step toward clinical application.

Bibliography

1. Contag CH, Spilman SD, Contag PR et al (1997) Visualizing gene expression in living mammals using a bioluminescent reporter. Photochem Photobiol 66:523–531
2. Bhaumik S, Gambhir SS (2002) Optical imaging of *Renilla* luciferase reporter gene expression in living mice. Proc Natl Acad Sci USA 99:377–382
3. Ciana P, Raviscioni M, Mussi P et al (2003) In vivo imaging of transcriptionally active estrogen receptors. Nat Med 9:82–86
4. Arguello F, Baggs RB, Frantz CN (1988) A murine model of experimental metastasis to bone and bone marrow. Cancer Res 48:6876–6881

Bioluminescence Imaging

▶Optical Imaging

Biomarker

Biomarkers are tissue or plasma indicators of a specific biological process.
▶PET in Drug Discovery Imaging

Biphasic Barium Study

A modification of the double-contrast technique whereby an additional quantity of dilute barium is given toward the end of the examination, and further films are obtained of the compressible parts of the stomach and duodenum. It shows some lesions better than by double-contrast alone.
▶Ulcer Peptic

Biphasic Magnetic Resonance Contrast Agents

This term refers to substances that exhibit contrary signal intensities on T1-weighted and T2-weighted images. Water is a typical biphasic contrast agent, showing a low signal on T1-weighted and a high signal on T2-weighted magnetic resonance images.
▶Contrast Media, MRI, Oral Agents

BI-RADS, Lexicon

Silvia Obenauer
Department of Radiology, Georg-August-University of Goettingen, Goettingen, Germany
obenauerheuser@yahoo.de

Synonyms

Breast Imaging Reporting and Data System (BI-RADS); classification of the American College of Radiology (ACR)

Definition

The Breast Imaging Reporting and Data System (BI-RADS) of the American College of Radiology (ACR) is a tool to reduce limitations in the terminology of mammographic reports. The ▶BI-RADS lexicon includes illustrations of each feature described, a section on auditing a mammography practice, and sample reports. It is intended to standardize the terminology in mammographic reports, assessments of findings, and recommendations of actions to be taken. The relationship between an assessment and management recommendations has implications for clinical care, teaching, and evaluation of the screening interpretations of radiologists (1–3). Different features of masses and calcifications indicate the categorization. Standardized lexicons for breast ultrasound (US-BI-RADS) and breast magnetic resonance imaging (MRM-BI-RADS) are also available (4–6).

BI-RADS Lexicon for Mammography according to the ACR (1)

The BI-RADS lexicon describes four classes of breast parenchymal density (Table 1, Fig. 1).

The following features are distinguished in the BI-RADS lexicon:

Masses

A mass is defined as a lesion seen in two different projections. If a lesion is seen in only one projection, it should be called a density. Masses are further classified by shape, margin, and density (Fig. 2):

Shape

The shape of a mass can be round, oval, lobular, or irregular (Fig. 2a).

Margin

The margin of a mass can be described as circumscribed (well defined or sharply defined), microlobulated (undulated with short cycles), obscured (hidden by superimposed adjacent tissue), indistinct (ill-defined), or spiculated (Fig. 2b).

BI-RADS, Lexicon. Table 1 Classification of breast tissue density according to the BI-RADS lexicon (ACR, American College of Radiology)

ACR	Description	Diagnostic Accuracy
1	Almost fat	Very high
2	Fibroglandular	High
3	Heterogeneously dense	Limitation
4	Dense	Limitation

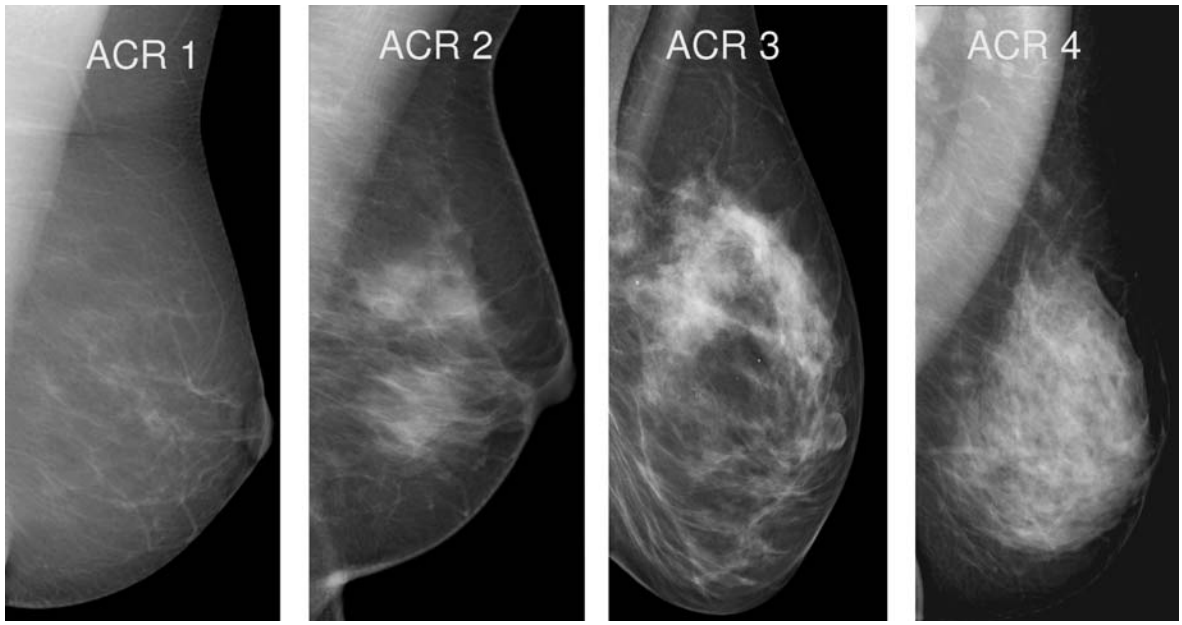

BI-RADS, Lexicon. Figure 1 Different types of breast tissue density according to the American College of Radiology (ACR). ▶ACR type 1 = fatty, type 2 = fibroglandular, type 3 = heterogeneously dense, type 4 = extremely dense breast tissue. From Obenauer S, Hermann KP, Grabbe E (2005). Applications and literature review of the BI-RADS classification. Eur Radiol 15:1027–1036.

Density

The density of a mass can be high, equal (isodense), low, or fat containing (Fig. 2c).

Calcifications

Different types of calcifications are distinguished, and the distribution of the microcalcifications is described (Fig. 3).

Types of calcifications (Fig. 3)

Typically benign calcifications (Fig. 3a)

- Skin calcifications (dermal)
- Vascular calcifications
- Coarse or popcorn-like calcifications
- Large rodlike calcifications
- Round calcifications
- Lucent-centered calcifications
- "Eggshell" or "rim" calcifications
- Milk or calcium calcifications
- Suture calcifications
- Dystrophic calcifications
- Punctuate calcifications

Calcifications of intermediate concern (Fig. 3b)

- Amorphous or indistinct calcifications

Calcifications with a higher probability of malignancy (Fig. 3c)

- Pleomorphic or heterogeneous calcifications (granular)
- Fine linear or fine linear branching (casting) calcifications

The distribution of microcalcifications is shown in Fig. 4.

Architectural Distortion

The normal architecture is distorted with no definite mass visible. Architectural distortion can also be an associated finding.

Special cases include tubular density or a solitary dilated duct, intramammary lymph nodes, asymmetric breast tissue, and focal asymmetric density.

Associated Findings

The associated findings are used with masses or calcifications or alone when no other abnormality is present:

- Skin retraction
- Nipple retraction
- Skin or trabecular thickening
- Skin lesion
- Axillary adenopathy
- Architectural distortion

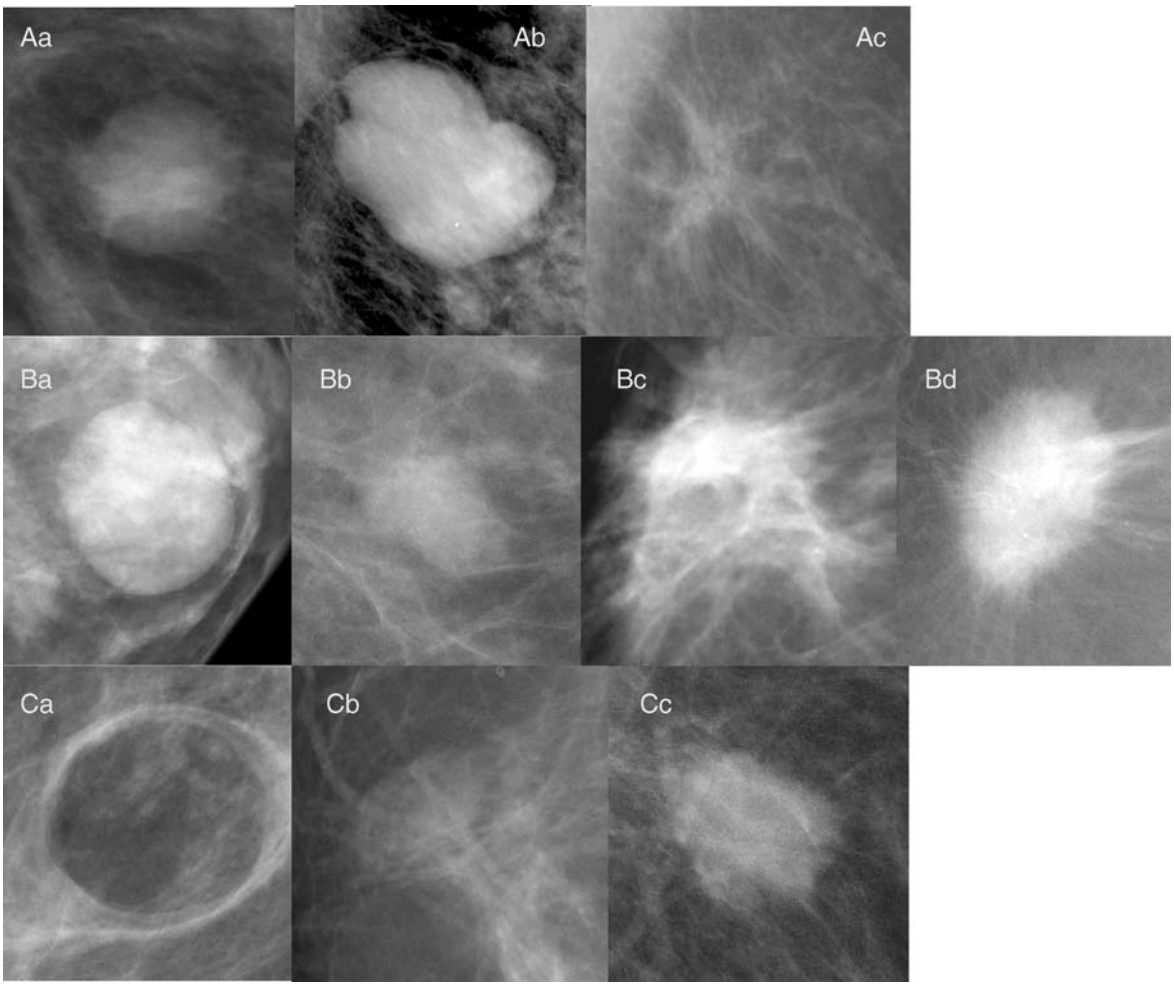

BI-RADS, Lexicon. Figure 2 Shape (A), margin (B), and density (C) of masses according to the BI-RADS lexicon. *Shape*: round/oval (Aa), lobular (Ab), irregular (Ac); *margin*: well-defined (Ba), ill-defined (Bb), obscured (Bc), spiculated (Bd); *density*: fat-containing (Ca), isodense (Cb), high density (Cc). From Obenauer S, Hermann KP, Grabbe E (2005). Applications and literature review of the BI-RADS classification. Eur Radiol 15:1027–1036.

Location of Lesion

The location of a lesion should be expressed by its

- Side (left, right, or both)
- Location (according to the face of the clock and subareolar, central, or axillary)
- Depth (anterior, middle, or posterior)

BI-RADS Categories

After a clear description of the findings according to the above-mentioned parameters, a report with the categorization of a mammogram into the BI-RADS classification is necessary for implementing a suggestion for the next course of action (Table 2).

US-BI-RADS (4)

Features in ultrasound according to the BI-RADS classification are given in Table 3.

MRM-BI-RADS (5, 6)

Features in MRM according to the BI-RADS classification are summarized in Table 4 (Figs. 5–8).

The time–signal intensity curve shows an initial rise, which could be slow (<100%), medium (100%), or fast (>100%). The postinitial curve course could be persistent (>10% further increase), a plateau (between 10% and +10%), or a washout (>10% decrease; Table 4, Figs. 9, 10).

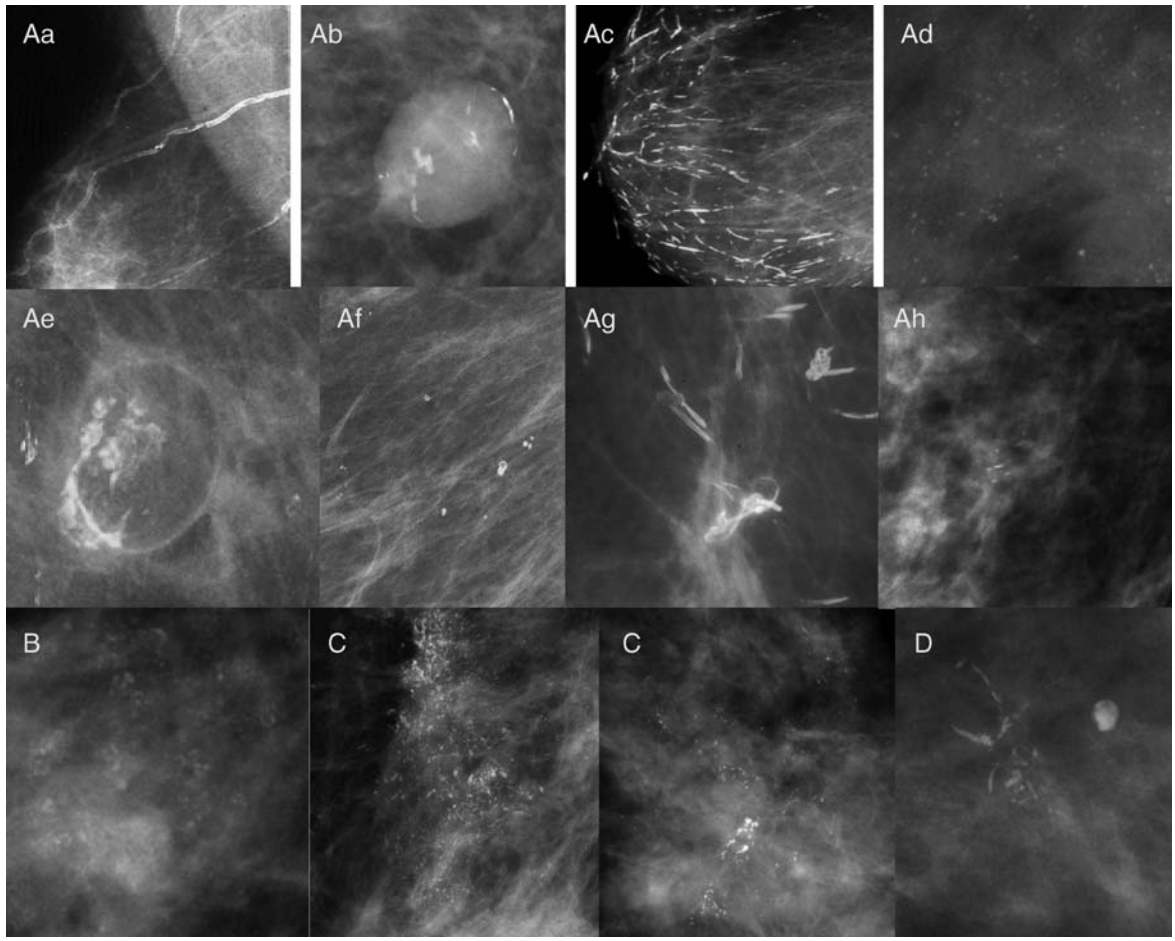

BI-RADS, Lexicon. Figure 3 Types of microcalcifications according to the BI-RADS lexicon. Typically benign findings (A): vascular (Aa), coarse or popcorn-like (Ab), large rodlike (Ac), round (Ad), "eggshell" (Ae), lucent-centered (Af), suture (Ag), and milk or calcium (Ah) calcifications; amorphous calcifications (B); pleomorphic (C) and fine linear branching (D) calcifications.

References

1. American College of Radiology (ACR) (1998) Illustrated Breast Imaging Reporting and Data System (BI-RADS). 3rd edn. American College of Radiology, Reston, VA
2. Liberman L, Menell JH (2002) Breast imaging reporting and data system (BI-RADS). Radiol Clin N Am 40:409–430
3. Obenauer S, Hermann KP, Grabbe E (2005) Applications and literature review of the BI-RADS classification. Eur Radiol 15:1027–1036
4. Mendelson EB, Berg WA, Merritt CRB (2001) Toward a standardized breast ultrasound lexicon, BI-RADS: Ultrasound. Semin Roentgenol 3:217–225
5. Orel SG, Schnall MD (2001) MR imaging of the breast for the detection, diagnosis, and staging of breast cancer. Radiology 220: 13–30
6. Ikeda DM, Hylton NM, Kinkel K et al (2001) Development, standardization, and testing of a lexicon for reporting contrast-enhanced breast magnetic resonance imaging studies. J Magn Reson Imaging 13:889–895

Birth Asphyxia

▶Hypoxic, Ischaemic Brain Injury

Birth Canal

The birth canal consists not only of the bony structure of the pelvis but also of the soft tissue, which can be accessed by magnetic resonance imaging but is not included in pelvimetry.

▶Magnetic Resonance Pelvimetry

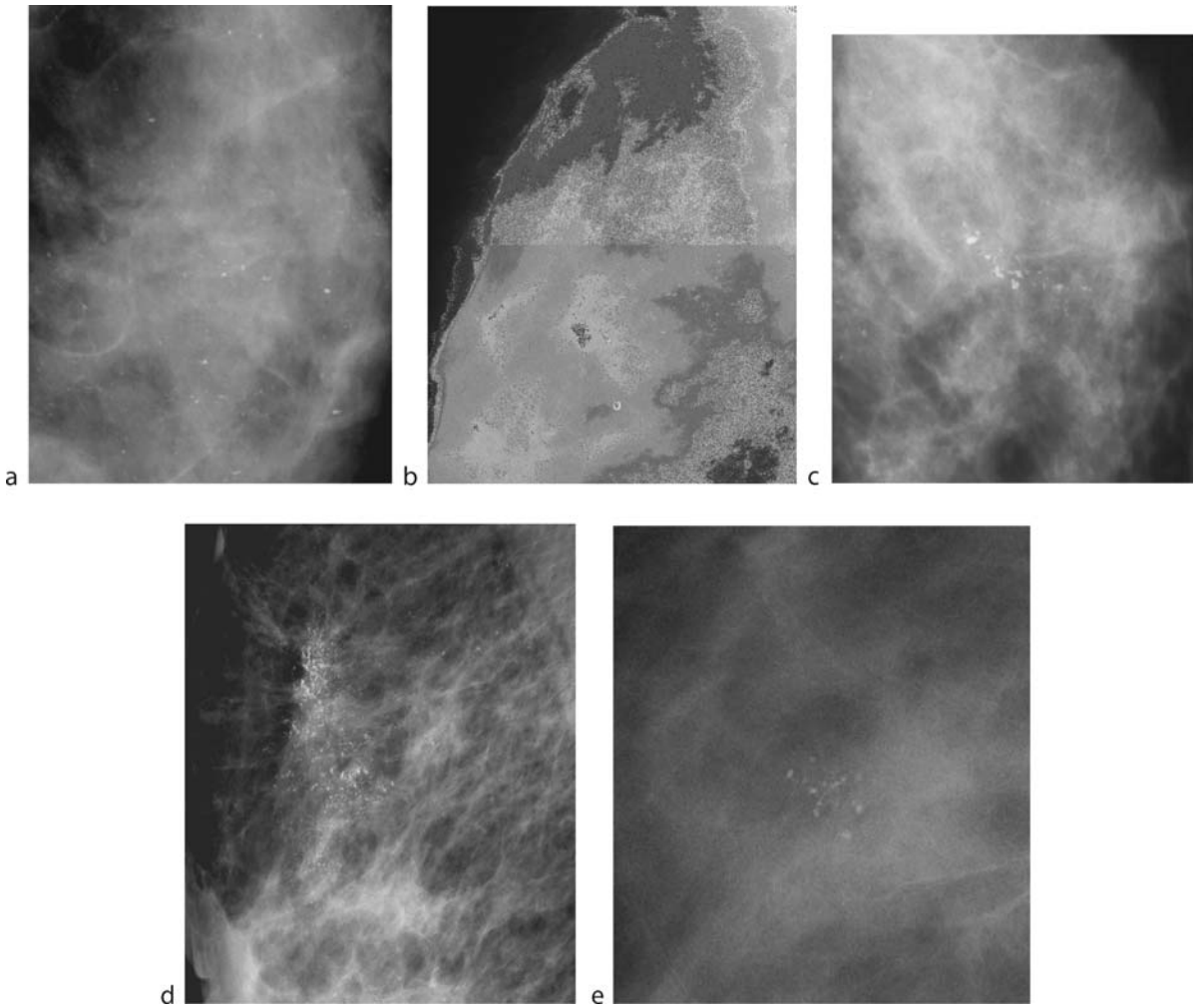

BI-RADS, Lexicon. Figure 4 Distribution of microcalcifications according to the BI-RADS lexicon: diffuse (a), regional (b), linear (c), segmental (d), cluster of microcalcifications (e). From Obenauer S, Hermann KP, Grabbe E (2005). Applications and literature review of the BI-RADS classification. Eur Radiol 15:1027–1036.

BI-RADS, Lexicon. Table 2 American College of Radiology BI-RADS categories for mammography with probability of malignancy and recommendations

Category	Finding	Probability of Malignancy	Recommendation
0	Needs additional imaging evaluation	–	Additional imaging by spot compression, magnification, special mammographic views, ultrasound
1	Negative	0%	Normal interval follow-up
2	Benign	0%	Normal interval follow-up
3	Probably benign	<3%	Short interval follow-up
4	Suspicious abnormality	20–30%	Biopsy should be considered
5	Highly suggestive of malignancy	~90%	Appropriate action should be taken
6	Histologically proven malignancy	100%	Appropriate therapy

Bladder Dysfunction. Table 3 Ultrasound features classified according to the BI-RADS lexicon

Mass	Margin	Circumscribed	
		Irregular	Indistinct
			Angular
			Microlobulated
			Spiculated
	Shape	Oval	
		Round	
		Irregular	
	Orientation	Wider than tall	
		Taller than wide	
	Echo pattern	Anechoic	
		Hyperechoic	
		Complex	
		Hypoechoic	
	Posterior acoustic features	No posterior acoustic features	
		Enhancement	
		Shadowing	
		Combined pattern	
	Surrounding tissue	No effect	
		Ducts	
		Cooper's ligament changes	
		Edema	
		Architectural distortion	
		Skin thickening	
		Skin retraction or irregularity	
		Pectoral muscle seen	
Calcification	No calcification		
	Macrocalcification		
	Microcalcification out of/in mass		
Special cases	None		
	Mass in or on skin		
	Foreign body		
	Lymph nodes, intramammary		
	Lymph nodes, axillary		
Vascularity	None		
	Same as in normal tissue		
	Decreased		
	Increased		

Bitewing Radiographs

Particular radiological film used to highlight upper and lower crowns through a single exposure.

▶Caries and Periodontal Diseases

Bladder Dysfunction

Symptoms with abnormal micturition in all circumstances and urinary loss

▶Bladder, Neurogenic

BI-RADS, Lexicon. Table 4 Breast magnetic resonance imaging features classified according to the BI-RADS categories

Focus/Foci	
Masses	
Margin	Smooth
	Irregular
	Spiculated
Shape	Oval
	Round
	Lobular
	Irregular
Enhancement	Homogeneous
	Heterogeneous
	Rim enhancement
	Dark internal septation
	Enhancing internal septation
	Central enhancement
Non-masslike enhancement	
Distribution modifiers	Focal area
	Linear
	Ductal
	Segmental
	Regional
	Multiple regions
	Diffuse
Internal enhancement	Homogeneous
	Heterogeneous
	Stippled, punctate
	Clumped
	Reticular, dendritic
Contrast media enhancement curve	
Initial rise	Slow
	Medium
	Fast
Delayed phase	Persistent
	Plateau
	Washout

Bladder Exstrophy

A severe congenital malformation of the urinary bladder defined by a failure to close, resulting in a ventrally open bladder, with consecutively usually no proper bladder outlet apparatus and no normal urethra as well as corresponding abdominal wall and pelvic skeleton defects.

▶Urinary Tract

Bladder, Neurogenic

Catherine Roy
Department of Radiology B, University Hospital of Strasbourg, Hôpital Civil, Strasbourg, France
catherine.roy@chru-strasbourg.fr

B

Definition

Neurogenic bladder is a dysfunction voiding urine and maintaining continence in all situations.

Physiopathology (1,2)

Neuromuscular dysfunction of the bladder and urethra is common. It has been estimated that the prevalence in adults of various forms of dysfunction in adults may be as high as 10%. It can be caused by common diseases such as diabetes mellitus, cerebrovascular disease, Alzheimer's and Parkinson's disease, and by drug therapy affecting musculature (antidepressants and cardiovascular treatment), or such as calcium channel blockers (as side effects).

Anatomical Support

The musculature of the bladder is complex. Male continence mechanism is supported by a proximal part involving the bladder neck and a distal part surrounding the veru montanum until the distal urethra and perineal floor. The proximal urethral continence mechanism is basically involuntary, whereas the external distal sphincter mechanism is under voluntary control. The entire urethral wall is considered to contain intrinsic or internal sphincter (involuntary) where as the periurethral striated muscle surrounding the internal sphincter is called the external sphincter (voluntary and around the membranous urethra). But, an anatomic sphincter between bladder and urethra has not been clearly defined. In females, the main sphincter activity is found in the entire proximal three-fourths of the urethra, best developed with smooth and striated muscles in the mid-urethra. The important component of the urethral closure mechanism is the striated muscle, most of which is composed by muscles of the urogenital diaphragm. To sum up, the wall of the entire bladder, the bladder neck and the upper half of the prostatic urethra in male and females contains smooth muscle, whereas the wall of the lower half of the prostatic urethra in male contains striated muscle.

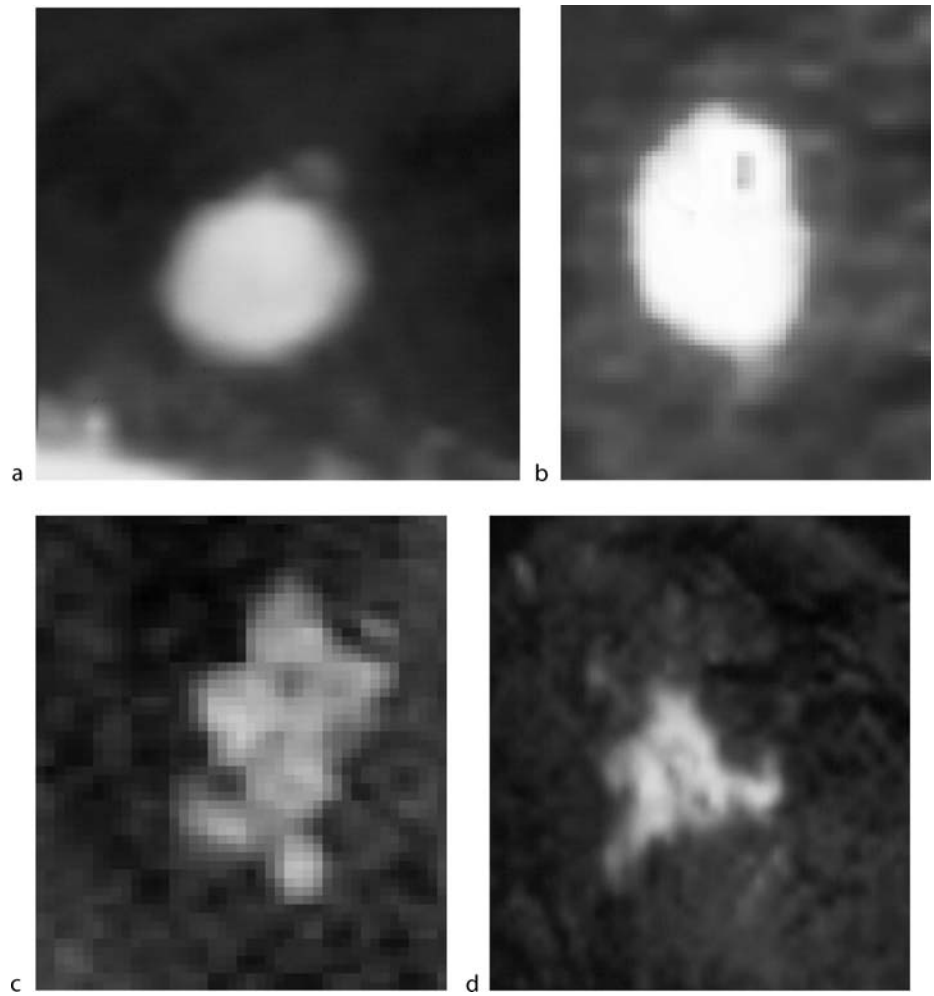

BI-RADS, Lexicon. Figure 5 Shape of mass enhancement in magnetic resonance mammography: round (a), oval (b), lobular (c), irregular (d).

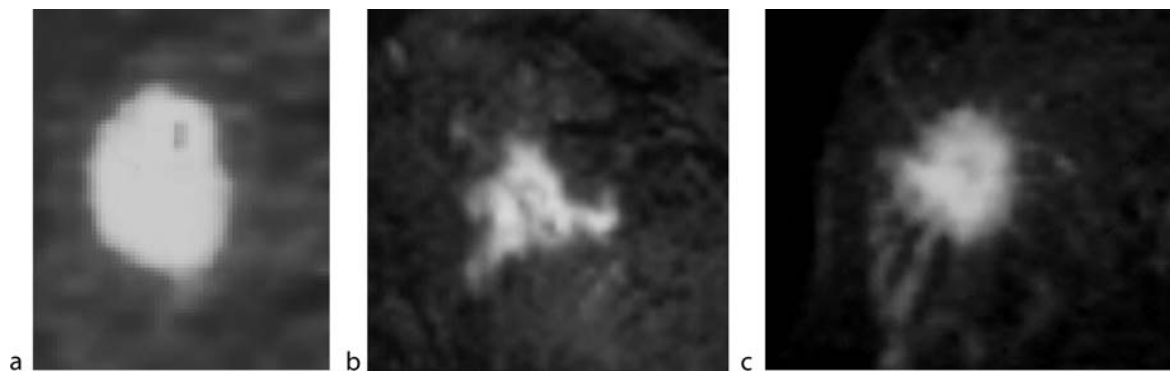

BI-RADS, Lexicon. Figure 6 Margin of mass enhancement in magnetic resonance mammography: smooth (a), irregular (b), spiculated (c).

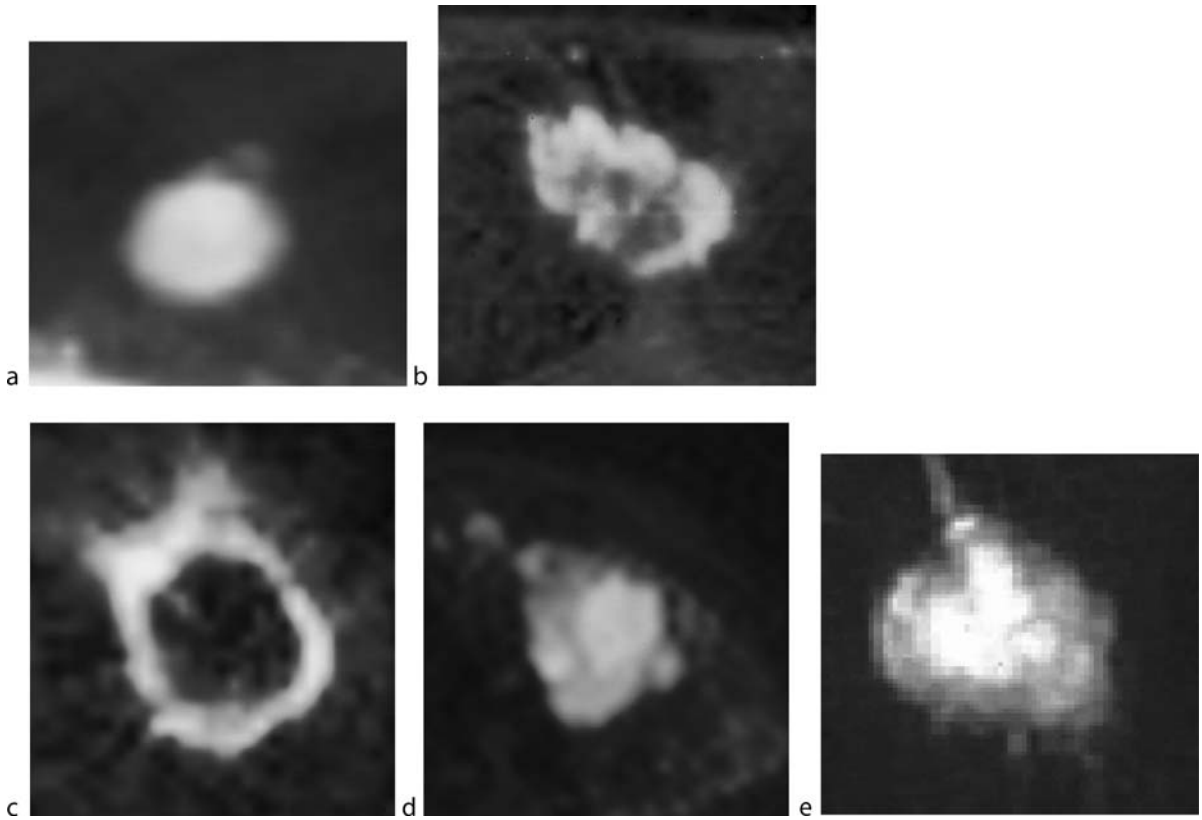

BI-RADS, Lexicon. Figure 7 Mass enhancement: homogenous (a), heterogenous (b), rim enhancement (c), internal septation (d), central enhancement (e).

Physiology

Neural control involves both the central system and peripheral nerves. The central system is rather complex coming from many locations such as cortical, pontine, sacral or conal locations with communications between them. The peripheral control involves three differents groups of nerves:

- the parasympathetic nerve supply arises from the anterior columns at S3, which contracts the detrusor during voiding.
- the pudendal nerve arises from the anterior column of S2 and supply the periurethral striated sphincter.
- the sympathetic nerve supply arises from the anterior of T11-L2. The nerve endings produce norepinephrine during bladder filling. Its effect differ from parts of bladder.

Clinical Presentation

Neurogenic bladder and voiding dysfunction may result from lesions that interrupt the cerebrospinal cord and peripheral nerves (tumors, inflammation, degenerative vascular, myelodysplasia, herniated intervertebral discs, multiple sclerosis). T1 produces destrusor hyperrefleion with marked dilatation of the prostatic urethra during the voiding phase with narrowing at the level of the membranous urethra. It may first manifest recurrent by episodes of urinary tract infection or acute urinary retention. They include symptoms both "irritative" and "obstructive" such as hesitancy, urgency with or without incontinence, urinary frequency, straining to void, sensation of incomplete bladder emptying, nocturia, and intermittent stream. The most widely used non imaging study is a urodynamic with voiding speed including peak voiding flow rate in milliliter per second and electromyogram with urethral pressure registration.

Imaging (3,4)

Imaging plays an important role in the evaluation of patients with neurogenic bladders. Management of neuromuscular dysfunction of the bladder and urethra is to evaluate and prevent deterioration due to infections,

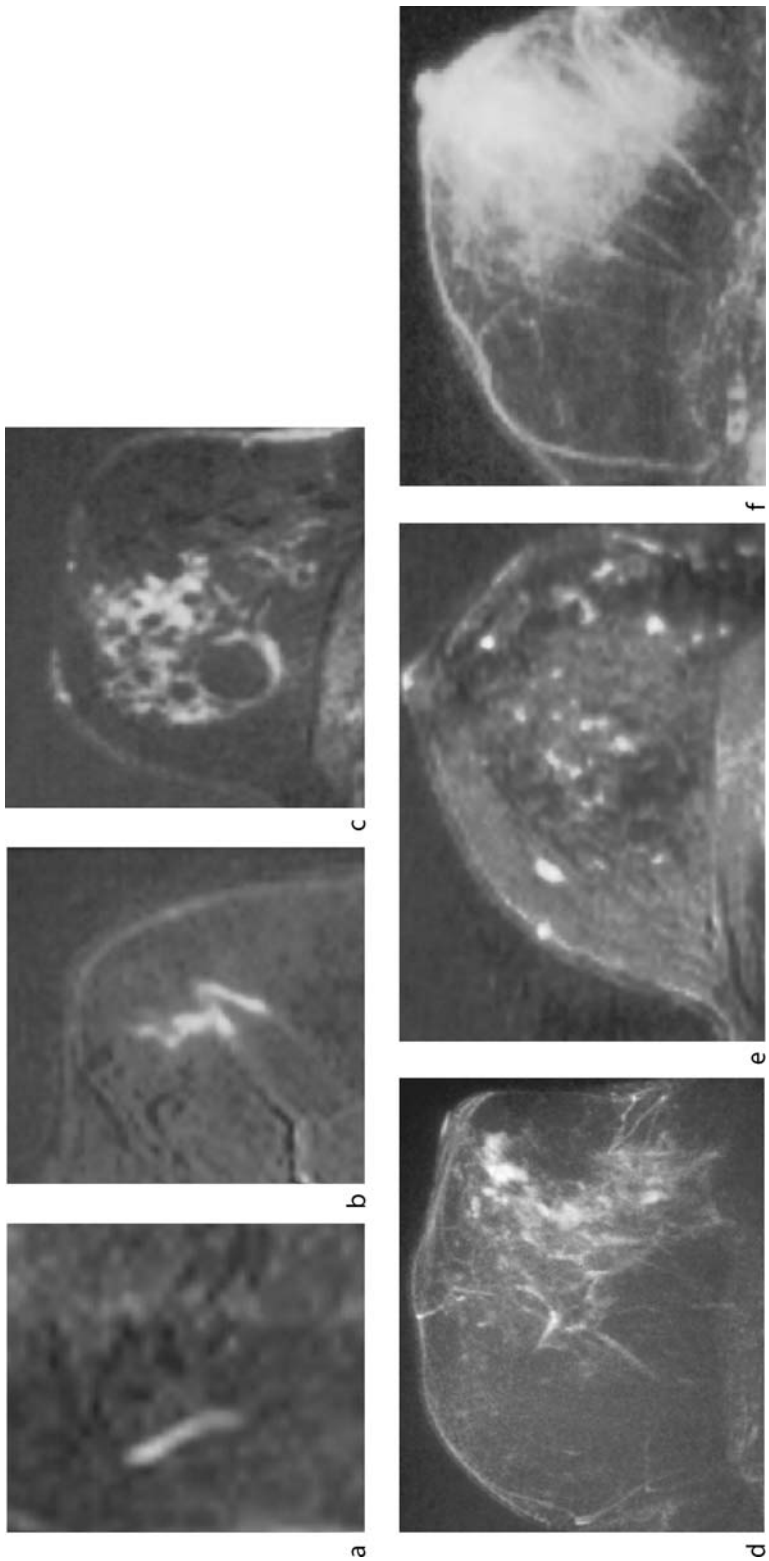

BI-RADS, Lexicon. Figure 8 Non-masslike enhancement: linear (a), dendritic (b), regional (c), segmental (d), multiple regions (e), diffuse (f).

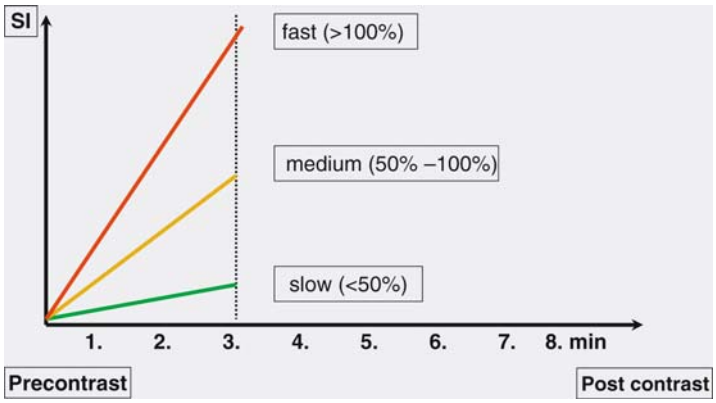

BI-RADS, Lexicon. Figure 9 Contrast media enhancement curve. Initial signal intensity: fast, medium, slow.

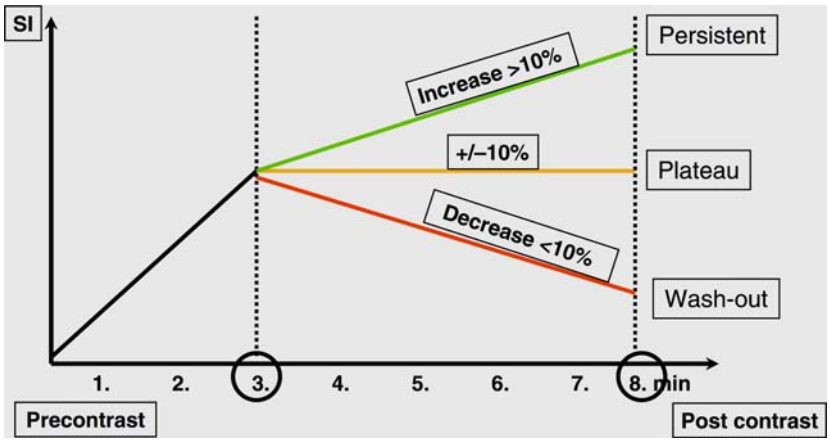

BI-RADS, Lexicon. Figure 10 Contrast media enhancement curve. Postinitial signal intensity: further increase, plateau, washout.

stone formation and renal failure. They are common with increased bladder pressures and vesicoureteric reflux due to untreated detrusor-external sphincter dysynergia. For imaging studies, both US and opacified radiograms are proposed.

Transabdominal US can demonstrate multiple bladder stones and the presence of diverticula (Fig. 1). Of these patients, 10–15% of them will develop urinary tract calculi with bladder the most common site of stone formation. Dilatation of upper urinary tract is established with knowledge of the parenchymal thickness. Evaluation of the post voiding volume is the major step iniatially and for follow-up during treatment. US can be associated with urodynamic studies to localize catheter and dynamics analysis during micturation. It is performed with transrectal or transvaginal probe.

Plain radiograph may demonstrate spinal or pelvic fractures, stones, agenesia or hypoplasia of the sacrum or spinal dysraphism (Fig. 2). There is a characteristic pattern called "eggshell crust" pattern around the balloon of the indwelling Foley catheter or calcification around a foreign body introduce during multiples catheter manipulation, associated with rounded or oval layered or homogeneous radiopaque calcific densities. Stones may be unique and ovoid with multiple with layers of opacities or multiple faceted borders.

IVU may reveal bilateral dilatation of the upper tracts, either as a result of vesicoureteric reflux or functional ureteral obstruction due to hypertrophy of the bladder wall. AIVU is recommended to establish early a baseline for follow-up (to diagnose stones or other unrelated pathology). AIVU voiding cystogram is mandatory to evaluate micturation during in lateral and oblique position. All infection is controlled before the examination is done. It can detect urethral strictures which are better assessed by a retrograde opacification.

A sophisticated evaluation can be achieved by combining the voiding cystourethrogram with simultaneous urodynamic studies (VCUG) and electromyographic monitoring (EMG) of external sphincter activity. These

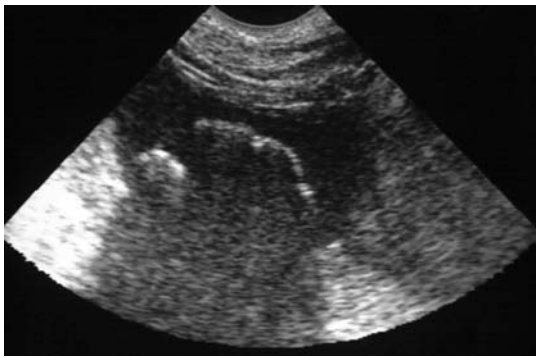

Bladder, Neurogenic. Figure 1 Transabdominal ultrasound. It shows multiple intravesical masses with acoustic shadows which were calcified foreign bodies secondary to numerous catheter manipulations.

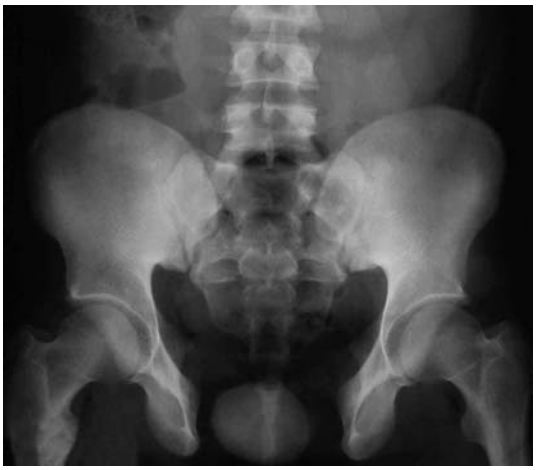

Bladder, Neurogenic. Figure 2 Post voiding plain radiograph after IVU. It shows large dehiscence of the symphysis pubic bone and sacrum atresia typical for bladder exstrophia. Residual volume after bladder reconstruction.

combined parameters are recorded with a system equipped with a video of images and pressure registration during micturation. All infection is controlled before the examination is done. The normal bladder fills to capacity (300–1000 ml) without significant slowing or interruption, indicating that the intravesical pressure remains low. A strong urge to void at small volume associated with a stop in the retrograde infusion of contrast indicates an abnormal elevated pressure inside bladder by involuntary detrusor contraction or a small capacity bladder with low compliance. On the other hand, an abnormally large bladder capacity at low filling pressure indicates an acontractile bladder. After bladder capacity is reached during VCUG, the patient is turned to a 45° oblique position and

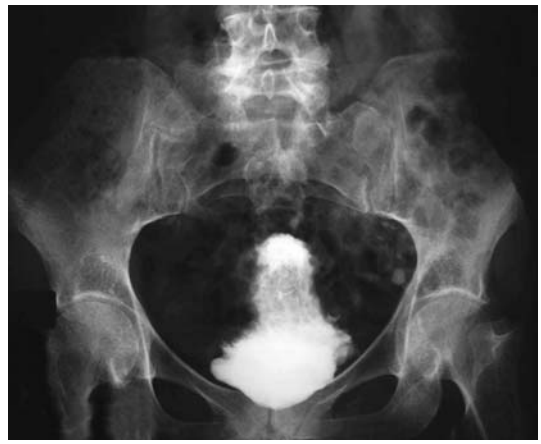

Bladder, Neurogenic. Figure 3 Post voiding film after IVU. It shows moderate residual volume with bladder wall trabeculation. Note the "Christmas tree" shape of the bladder.

radiograph is obtained during removal of the catheter and micturation. A post voiding film, including the renal areas, should always be obtained to check the vesicoureteric reflux and to estimate the degree of bladder emptying. The main advantage of the voiding cysto-urethrogram in patients with neuromuscular bladder dysfunction is to demonstrate vesicoureteral reflux. Patients with detrusor areflexia secondary to lesions affecting the sacral reflex arc (concis medullaris lesions) have a large, smooth-walled bladder because of chronic overdistension with large post void residual. With supra sacral spinal cord lesions, patient may develop detrusor-external sphincter dyssynergia. In this condition there is a lack of coordination between contraction of the bladder detrusor and relaxation of the external sphincter. Marked dilatation of the prostatic urethra is evident during the voiding phase, with marked narrowing at the level of the membranous urethra due to contraction of the external sphincter. The intravesical pressures are typically markedly elevated. This functional bladder outlet obstruction causes bladder wall thickening, trabecular diverticular formation vesicoureteric reflux. The typical bladder of these patients is the so-called pine tree or Christmas tree bladder (Fig. 3). This pattern can also be seen in some patients with poor bladder wall compliance and with bladder outlet obstruction due to other causes. Patients with a sensory paralytic bladder (e.g., diabetes) have a lack of sensation of fullness and they are "infrequent voiders." A large bladder extending into the abdomen is typically seen with large post void residuals.

Scintigraphy with radionuclide cystography is also used to detect vesicoureteral reflux. The goal of radioisotope renography is to assess renal perfusion and function (3, 4).

References

1. Amis ES, Neuwhouse JH (1991) Neurogenic bladder dysfunction and urinary incontinence. In: Essentials of Uroradiology. Little Brown, Boston, pp 307–316
2. Amis SE, Blaivas JG (1991) Neurogenic bladder simplified. Radiol Clin North Am 29:577–580
3. Amis ES, Blaivas JG (1990) The role of the radiologist in evaluating bladder dysfunction. Radiology 175:317–318
4. Yuhico M, Dickno AC (1998) Neurogenic bladder and radiology. In: Jafri SZ, Dickno AC, Amendela MC (eds) Lower Genitourinary radiology; Imaging and Intervention Jafri SZ, Dickno AC, Amendela MC. chap 4. Springer Verlag, pp 80–98

Bleb

The term bleb also refers to a pleural based, thin-walled air space, mostly located in the lung apex. The distinction between bleb and bulla is of little practical significance. The morphological appearances of a pneumatocele, a lung cyst or a bleb are very similar.

▶Pulmonary Opacity, Cystic Pattern

Bleeding Disorders, Osteoarticular

Klaus Woertler
Department of Radiology, Klinikum rechts der Isar, Technical University Munich, Munich, Germany
woertler@roe.med.tum.de

Synonyms

Hemophilic osteoarthropathy

Definition

The term hemophilic osteoarthropathy summarizes alterations of joints and bones that develop as sequelae of repetitive bleeding in patients with systemic blood coagulation disorders. Osteoarthropathy is most commonly observed with hemophilia A (classic hemophilia) and hemophilia B (Christmas disease), which are caused by a hereditary chromosome X-linked recessive deficiency of the antihemophilic factor VIII and the plasma thromboplastic component factor IX, respectively. The level of factor deficiency determines the severity of the disease: Patients with more than 5% of normal factor activity have mild disease, those with 1–5% have moderately severe disease, and those with less than 1% have severe disease.

Pathology/Histopathology

Repetitive hemarthrosis represents the most common musculoskeletal manifestation of hemophilia. In early stages, ▶hemophilic arthropathy is characterized by pathologic alterations of the synovium and articular cartilage. Chronic synovitis with brownish discoloration of the synovial membrane is thought to be initiated by resorption of hemosiderin and other blood breakdown products and progresses to synovial proliferation with extension over the margins of articular cartilage. Villous proliferation and hypervascularization lead to an increased vulnerability of the synovium and increase the risk of further joint hemorrhage. Synovial fibrosis, extensive hemosiderosis, and atrophy represent the final stage of this chronic process observed in the later course of the disease. Destruction of articular cartilage in hemophilic joints occurs as a sequel of different biochemical, cellular, and mechanical factors. The liberation of proteolytic enzymes from abnormal synovium, toxic effects of blood breakdown products, enzymatic reactions of chronic inflammation, and direct cellular destruction have been identified as contributors to articular cartilage degradation. Decreased mechanical capacity of subchondral bone due to intraosseous bleeding and subchondral cyst formation causes localized osteochondral defects, especially in the weight-bearing central areas of the articular surfaces. Direct invasion by proliferating synovial tissue, increased intra-articular pressure, and abnormal loading represent further effects, which, in addition to the latter, contribute to rapid articular cartilage damage, finally leading to complete exposure of subchondral bone. Continued destruction of bone results in formation of crevices and grooves within the osseous surface. In children, repetitive intra-articular bleeding can lead to epiphyseal hypertrophy and accelerated maturation, which are thought to be initiated by chronic hyperemia.

▶Hemophilic pseudotumor represents an extra-articular musculoskeletal manifestation of hemophilia that can develop with intraosseous, subperiosteal, and/or intramuscular bleeding. Histologically, hemophilic pseudotumors equal chronic hematomas, which are encapsulated by fibrous tissue and accompanied by an inflammatory reaction of variable extent. Intraosseous or subperiosteal pseudotumors, in addition to the latter, are characterized by bone resorption and periosteal new bone formation.

Clinical Presentation

Due to its recessive chromosome X-linked transmission, hemophilia almost exclusively occurs in males, although rare cases of clinical manifestations in females have been reported. The disease has an incidence of 8–11:100,000

with approximately 4 severe cases per 100,000 births. Hemophilia A is about ten times more common than hemophilia B. Mild forms are often diagnosed relatively late in life, since bleeding might be apparent only during surgery or following major trauma. Moderately severe and severe forms are characterized by excessive bleeding after minor traumatic events or even by spontaneous hemorrhages. Repeated hemarthroses are a typical complication that occurs in a high percentage of patients (75–90%) with severe hemophilia, with the knee, elbow, and ankle joints representing the most common locations. About 89% of the patients experience the first episode of joint bleeding during their first decade of life, not infrequently before the age of 3 years, followed by repeated hemarthroses that are most common between the ages of 8 and 13 years, and decrease in frequency during adulthood.

Because the general prognosis of the disease could be dramatically improved by factor replacement and, thus, the prevention of life-threatening bleedings, disabling arthropathy due to repeated joint bleedings nowadays represents one of the main problems in clinical management of hemophilic patients. Continuous prophylactic factor replacement has been claimed to reduce the incidence of joint damage in hemophilic patients but is limited by high costs and possible side effects. Hematological treatment on demand, on the other hand, necessitates frequent evaluation for the early diagnosis of joint disease, because even a small number of joint bleedings can cause irreversible osteoarthropathic alterations. Factor replacement has not only decreased the general severity of arthropathy, but also influenced its pattern of distribution by allowing the patients normal physical activity, even on a sportive level. In treated hemophilic children and young adults, the most severe alterations are nowadays usually observed in the ankle joints, followed in frequency by the elbow and knee joints, whereas the knee is still the most severely affected joint region in older patients.

Hemophilic pseudotumor is a rare complication of hemophilia and occurs in 1–2% of patients with severe factor deficiency. The lesion can clinically mimic a neoplasm. Osseous manifestations most often affect the femur, the pelvic bones, the small bones of the hands and feet, and the mandibula, whereas pseudotumors of the soft tissues typically develop within the muscles of the pelvis and the lower extremity.

Imaging

Hemophilic Arthropathy

Conventional radiography (Fig. 1) represents the primary imaging modality to assess hemophilic arthropathy. Relatively dense periarticular soft tissue swelling can be

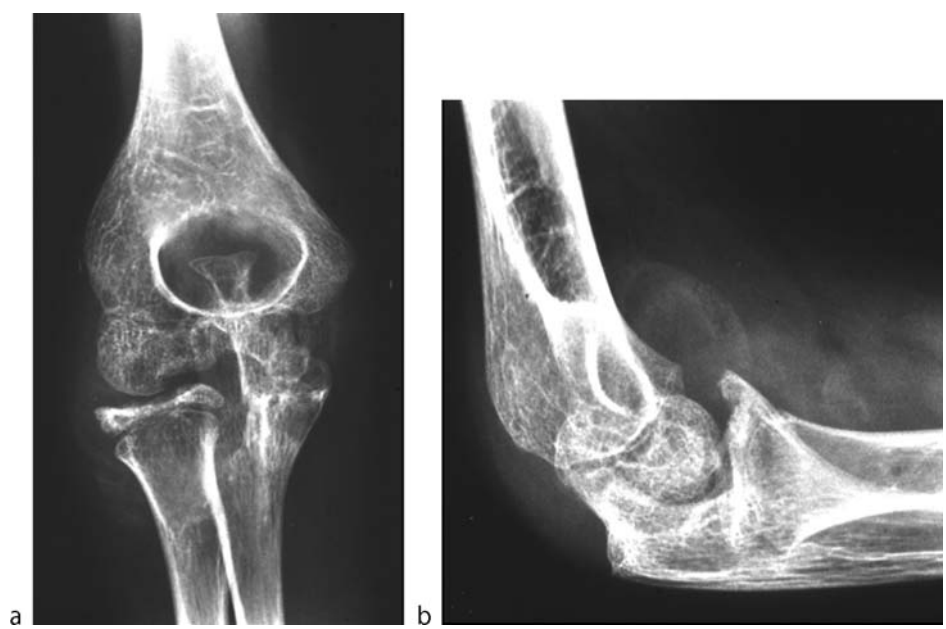

Bleeding Disorders, Osteoarticular. Figure 1 Hemophilic arthropathy of the elbow in an 8-year-old boy (▶Pettersson score: 8). (a) Anteroposterior and (b) lateral radiographs show dense periarticular soft tissue swelling, periarticular osteopenia, pressure erosions of the olecranon, widening of the trochlear and radial notches of the ulna as well as the olecranon fossa of the humerus, enlargement of the radial head, irregularity of the subchondral bone surfaces, and subchondral cysts.

observed due to intra-articular hemorrhage following acute bleeding as well as due to synovial proliferation with hemosiderin deposition in patients with chronic arthropathy. Periarticular osteopenia as a sequel of hyperemia and disuse may be striking and can develop into a "hypertrophic atrophy" with marked rarefaction and thickening of bony trabeculae that might persist into adult life. In children, soft tissue swelling and osteopenia can be associated with premature development of ossification centers and epiphyseal overgrowth (balloon epiphyses). Bone erosions at the joint margins as well as widening of notches and recesses can already be seen in earlier stages of arthropathy. Irregularities of the subchondral bone contours as well as subchondral cyst formation are typical findings that already occurr when the joint space is still preserved. Narrowing of the joint space develops with advanced cartilage loss and can be accompanied by signs of secondary osteoarthritis at later stages of the disease. Severe joint disorganization with incongruency, subluxation, deformity, or even ankylosis might be apparent in patients with end-stage arthropathy.

To allow staging and treatment monitoring of hemophilic arthropathy, several radiographic scoring systems have been proposed. The system suggested by Pettersson and coworkers (1980) is widely used in Europe and has also been adopted by the Orthopedic Advisory Committee of the World Federation of Hemophilia. It includes eight different pathologic findings that are assessed with an additive scale to estimate the level of joint destruction (Table 1). However, because both synovial and articular cartilage abnormalities usually precede irreversible osseous changes, radiographic staging of early hemophilic arthropathy according to the Pettersson score or other scoring systems tends to underestimate the severity of joint alterations that, due to subclinical bleeding, can even be present in asymptomatic joints.

MR imaging (Fig. 2) is more accurate in depicting arthropathic changes at earlier stages when radiographs are still normal or demonstrate only minor abnormalities (Pettersson score 0–4).

Especially in children, MR imaging therefore can provide valuable information for individual implementation of drug treatment as well as for timely decision for synovectomy.

Because acute synovitis, intra-articular blood, and periarticular edema are usually observed following acute joint hemorrhage, MR imaging should not be performed earlier than 6 weeks after a clinically evident bleeding episode to ensure a reliable assessment of the current stage of arthropathy. Synovial alterations in chronic hemophilic arthropathy range from slight thickening to extensive proliferation with expansion of the joint capsule. Due to hemosiderin deposition, the synovial tissue usually shows low signal intensity on both T1- and T2-weighted images. T2*-weighted gradient echo sequences are sensitive to susceptibility effects and can be used to detect smaller amounts of iron. Contrast-enhanced pulse sequences can be useful at initial stages of chronic synovitis when synovial thickening is less conspicuous on unenhanced images. MR imaging can also be used to estimate the extent of cartilage damage and to depict bone erosions, subchondral cysts, and areas of osteonecrosis.

Hemophilic Pseudotumor

On radiographs, most intraosseous hemophilic pseudotumors arise as lytic, well-demarcated, and expansile lesions, often associated with a shell-like neocortex and trabeculations. Thus, giant cell tumor of bone, aneurysmal bone cyst, and fibrous dysplasia represent the most important differential diagnoses. Sclerotic borders and ossifications may appear with healing.

Lesions in subperiosteal locations are radiographically characterized by pressure erosion of bone and various types of periosteal new bone formation and therefore may simulate malignancy or infection.

The MR appearance of both osseous and intramuscular hemophilic pseudotumors (Fig. 3) varies with the age of the hematoma and its stage of organization. The

Bleeding Disorders, Osteoarticular. Table 1 Pettersson score

Radiographic Finding	Score (0–13)		
Osteoporosis	Absent = 0	Present = 1	
Enlarged epiphyses	Absent = 0	Present = 1	
Irregular subchondral bone surface	Absent = 0	Partially involved = 1	Totally involved = 2
Narrowing of joint space	Absent = 0	Joint space > 1mm = 1	Joint space ≤ 1mm = 2
Subchondral cyst formation	Absent = 0	1 cyst = 1	> 1 cyst = 2
Erosions at joint margins	Absent = 0	Present = 1	
Gross incongruence of articulating bone ends (angulation/displacement)	Absent = 0	Slight = 1	Pronounced = 2
Joint deformity	Absent = 0	Slight = 1	Pronounced = 2

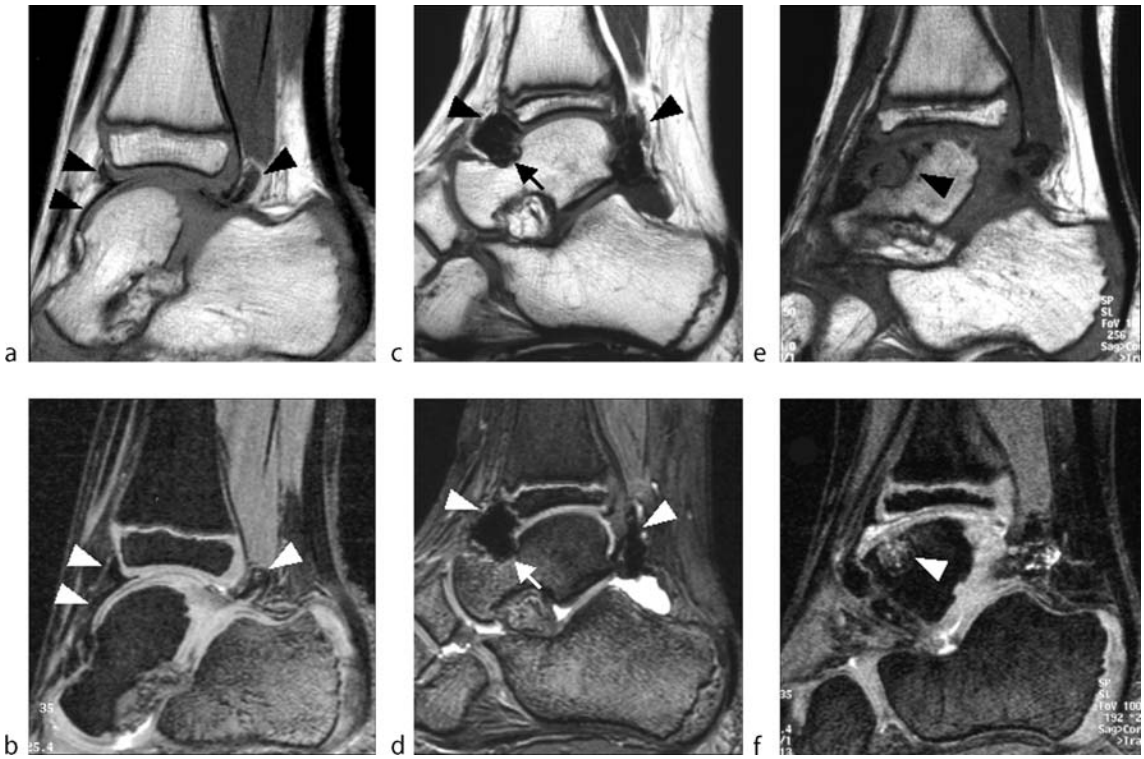

Bleeding Disorders, Osteoarticular. Figure 2 Magnetic resonance imaging findings in hemophilic arthropathy. T1-weighted spin echo (SE) (*first row*) and T2*-weighted gradiant echo (GRE) (*second row*) images of three different hemophilic children with arthropathy of the ankle show (a, b) thickening and low signal intensity of the synovium (*arrowheads*) at the anterior and posterior joint recesses, (c, d) marked synovial proliferation (*arrowheads*) and hemosiderosis with capsular expansion and consecutive pressure erosion (*arrow*) at the talar neck, and (e, f) synovial proliferation associated with diffuse damage of articular cartilage and subchondral cyst formation (*arrowhead*).

surrounding capsule is usually depicted as a peripheral rim of low signal intensity on all pulse sequences, owing to the presence of fibrosis and hemosiderin deposits.

Nuclear Medicine

In the past, skeletal scintigraphy was used to evaluate hemophilic arthropathy as well as hemophilic pseudotumor, but it has been replaced by radiography and MR imaging as more specific methods.

Diagnosis

Hemophilia is diagnosed by laboratory testing of factors VIII and IX, by which the type and severity of the disease can be determined. Genetic testing can uncover carriers and individuals with mild hemophilia.

References

1. Park JS, Ryu KN (2004) Hemophilic pseudotumor involving the musculoskeletal system: spectrum of radiologic findings. AJR Am J Roentgenol 183:55–61
2. Pettersson H, Ahlberg A, Nilsson IM (1980) A radiologic classification of hemophilic arthropathy. Clin Orthop 149:153–159
3. Resnick D (1995) Bleeding disorders. In: Resnick D (ed) Diagnosis of Bone and Joint Disorders. 3rd edn. Saunders, Philadelphia, pp 2295–2322
4. Stein H, Duthie RB (1981) The pathogenesis of haemophilic arthropathy. J Bone Joint Surg Br 63:601–609
5. Yulish BS, Lieberman JM, Strandjord SE et al (1987) Hemophilic arthropathy: assessment with MR imaging. Radiology 164:159–762

Blood Diseases

▶Hemoglobinopathies, Skeletal Manifestations

Blood Flow

▶Perfusion, Neoplasms

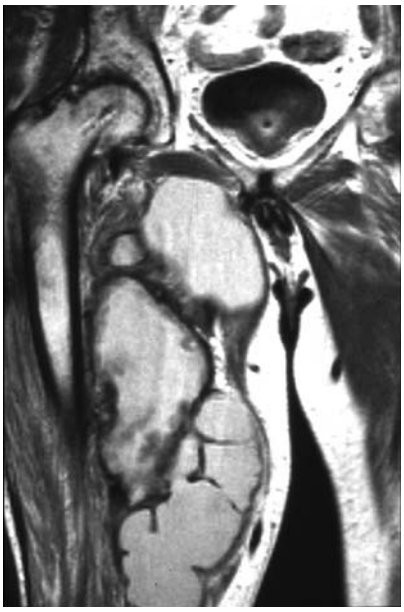

Bleeding Disorders, Osteoarticular. Figure 3 Intramuscular hemophilic pseudotumor of the thigh in a 41-year-old patient. T1-weighted SE image shows a huge intramuscular mass with inhomogeneous predominantly hyperintense signal surrounded by a capsule of low signal intensity. Note also arthropathic alterations of the right hip joint with synovial proliferations. Deformity of the right proximal femur was caused by previous femoral neck fracture.

Blood Oxygenation Level Dependent (BOLD) Contrast

The contrast which is studied in functional magnetic resonance imaging studies and which is dependent of the amount of deoxyhaemoglobin in the blood.

▶Brain, Functional Imaging

Blood Pool Agents

Contrast agents (for ultrasound and magnetic resonance imaging) that are confined to the intravascular fluid compartment and do not leak into the interstitium.

▶Contrast Media, Ultrasound, Applications in Kidney Tumor

Blood Pool Contrast Agent

A contrast agent which, after intravascular injection, is freely distributed in the whole blood volume without leaving the vascular compartment. A blood pool contrast agent is transported with the blood flow, allowing its use as tracer for the inflow, distribution and outflow of blood (wash-in/wash-out kinetics) within a certain organ.

▶Contrast Media, Ultrasound, Commercial Products

Blood Urea Nitrogen

Blood urea nitrogen measures the amount of urea nitrogen, a waste product of protein metabolism, in the blood. Urea is formed by the liver and carried by the blood to the kidneys for excretion. A test measuring how much urea nitrogen remains in the blood can be used as a test of renal function. However, there are many factors besides renal disease that can cause BUN alterations, including protein breakdown, hydration status, and liver failure. Reference values for BUN in adults (values may differ slightly from laboratory to laboratory) are 7–20 mg/100 mL. Men may have values slightly higher than women.

▶Tubular Necrosis, Kidney, Acute

Bloodgood's disease

▶Fibrocystic Disease, Breast

Blue Bloaters

Patients with emphysema who suffer from severe hypoxemia and hypercapnia and have peripheral edema due to right heart failure, but only mild dyspnea.

▶Emphysema and Bulla

Blunt Abdominal injury

▶Trauma, Hepatobiliary

Blunt Abdominal Trauma

▶Trauma, Hepatobiliary

Blunt Hepatic Injury

▶Trauma, Hepatobiliary

Bochdalek Hernia

maldevelopment of the diaphragm resulting in a defect that is characteristically posterior and left sided.
▶Hernia, Diaphragm, Congenital

Bone Age

Alan E. Oestreich
Cincinnati Children's Hospital Medical Center, Cincinnati, Ohio, USA
Alan.Oestreich@cchmc.org

Synonym

(Estimation of) skeletal maturation (by imaging)

Definitions

Bone age estimation methods all relate the appearance of a portion of the subject's ossified skeleton to a set of standards, usually by visual comparison. Bone age is a measure of enchondral bone development (with the exception of the use of the metaphyseal width, which is the result of membranous ossification from the one-cell-layer thick bone bark around portions of the physis and metaphysis). The elements observed in the bone age process consist of (a) are the growth centers in question ossified yet? (b) relative size of growth centers once they are ossified, in relation to the adjacent metaphysis, (c) shapes of growth centers, including nonepiphyseal growth centers, such as carpal or tarsal bones and sesamoids (including patella), and (d) the state of fusion of the physes between epiphyses and metaphyses, and how narrow is the remaining cartilage space between them if not yet fused. Generally, bone age is expressed, or implied, in statistical terms, reflecting numerical deviation from an estimated mean. For example, in our use of the ▶Greulich–Pyle method, "advanced" or "delayed" bone age represents values more than two standard deviations from the expected mean. Technically, each represents a rejection of the null hypothesis that the bone age is within normal limits with 96% confidence. When chronologic bone age is unknown, the bone age serves as a best guess at the subject's true age.

Pathology/Histopathology

Many causes of disturbed bone age have histopathologic or at least gross pathology manifestations. Abnormality of the pituitary, thyroid, adrenals, and ovaries are major examples, although biochemical and radiologic investigation may obviate biopsy in some circumstances. Conditions of high local vascularity, such as juvenile idiopathic arthritis and hemophilic hemorrhage, have biochemical and radiologic manifestations, as well as those amenable to pathology/histopathology. In achondroplasia, in the first decade of childhood, the slow enchondral growth results in more of the growth cartilage surrounding growth centers to not be ossified as soon as would be expected in normals. The result is a delayed bone age. In long-term arthritis, this same cartilage is diminished and ossification increases compared to normals.

Clinical Presentation

The child with delayed bone age is quite often of short stature. The child with advanced bone age often shows signs of sexual precocity. Growth hormone deficient children have normal features despite being proportionately small; hypothyroidism has many other clinical features, including coarse skin and slow reflexes; girls with low estrogen may be tall, as they continue growing for a longer time than their peers, and at the same time have a delay in pubertal features. A malnourished or chronically ill child may also have delayed bone age.

Imaging

For the Greulich–Pyle (1) and several other methods, a frontal PA image of the left hand and wrist is obtained and analyzed. In certain circumstances, the right hand may be

more appropriate (such as unilateral hypoplastic or overgrown left hand). For the ▶Sontag method (2), several images are obtained of the left side of the body to show countable growth centers of upper and lower extremity. We use the Sontag method in the first year of life, and in the second year we use it if hand and wrist show no more than capitate and hamate ossified. Standards are available for the knee (AP and lateral images). The Risser method of iliac crest ossification requires a full view of at least one iliac crest. The Tanner method (3) requires numerical measurement of many centers, a rather tedious task.

In addition to counting, measuring, or comparing growth centers to standards, one should also evaluate bone age images for metabolic bone disease (rickets), dysplasia (such as achondroplasia), or arthritis (juvenile idiopathic, for example Fig. 1)), that might affect maturation, as well as features of any other concomitant condition. The broad terminal tufts of Turner syndrome; the large distal epiphyses, cone epiphyses of small tubular bones, and prominent metacarpal pseudoepiphyses of cleidocranial dysplasia (Fig. 2); and the broad distal thumb phalanges of Rubinstein–Taybi syndrome are examples of findings that may initially suggest diagnoses from bone age studies.

Methods have been proposed using ultrasound images of the hand and wrist as nonradiation methods for obtaining a bone age—I do not feel they have adequate precision at this time.

Measurement of lateral thoracic subcutaneous fat in newborns provides a reasonable estimate of gestational age in the absence of hypoglycemia (4); it exceeds the normal standards in infants of diabetic mothers and in nesidioblastosis.

Nuclear Medicine

The high activity of physes ceases when the epiphysis fuses to the metaphysis. Quantification of the degree of fusion by activity on scan is possible. Similarly, the onset of ossification in a cartilaginous growth center is presaged by "preossification center" activity.

Endocrine causes of abnormal bone age can be investigated by nuclear imaging. They include tumors and nodules of thyroid, pituitary, adrenals, ovaries, and testes. Nuclear medicine is also helpful in locating functioning ectopic thyroid, especially at the base of the tongue, when the customary gland site does not show tissue or activity.

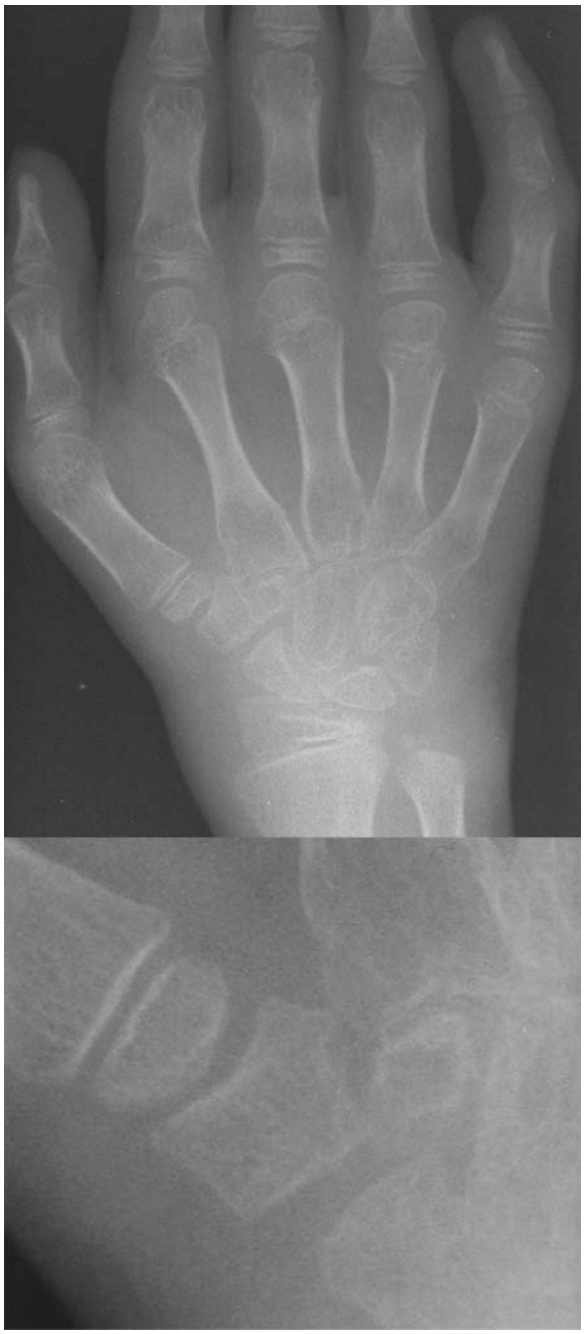

Bone Age. Figure 1 Juvenile idiopathic arthritis with selective acceleration of maturation. The carpal bones are both overdeveloped and crowded and several metacarpal heads are large for age. The proximal lateral corner of the trapezium is squared off, as shown in the enlargement below. (From Oestreich AE, Crawford AH (1985) Atlas of Pediatric Orthopedic Radiology. Thieme Verlag, Stuttgart, p 159(6)).

Diagnosis

Visual comparison of a subject's bone age image to standards such as Greulich–Pyle (1) requires knowledge of the gender, so that the gender-specific standard images be used. However, it is preferable not to know the chronologic age before doing the comparisons, so that, being blinded to that age, one has a better chance not to

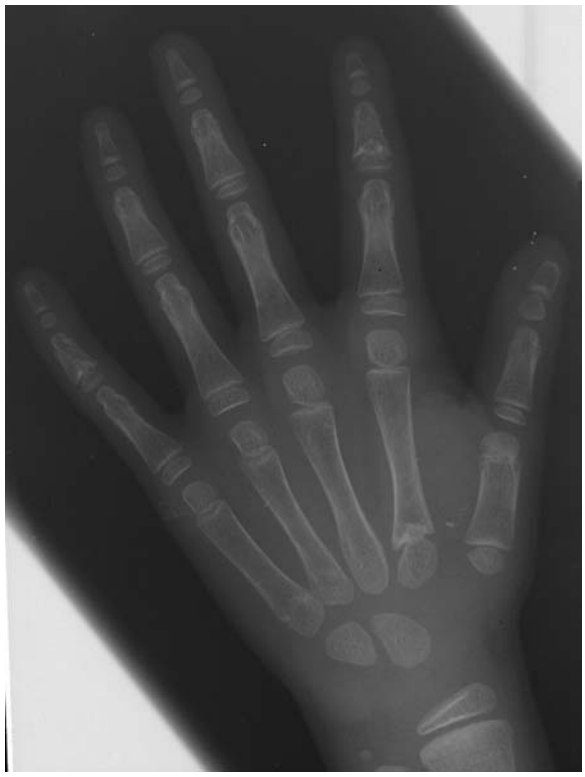

Bone Age. Figure 2 Cleidocranial dysplasia. Seven year old child. Characteristic prominent pseudoepiphysis at the proximal 2nd metacarpal, cone epiphyses of ring and little finger middle phalanges, and oversized epiphyses for the distal phalanges of thumb and other fingers. (From Oestreich AE, Crawford AH (1985) Atlas of Pediatric Orthopedic Radiology. Thieme Verlag, Stuttgart, p 129(6)).

let one's expectations skew the choice of bone age. It is preferable to interpolate bone age between two standards rather than merely selecting the closest. Be sure to understand that bone ages chosen are compared to the mean expected bone age, not the chronologic age itself.

The carpal bones seem much more variable than other hand and distal forearm centers. Thus, they should not be used, after about 18 months of age, as strong measures of bone age. Discordance between "carpal" and "finger" bone age is quite common. My guess is that usual and unusual childhood illnesses affect the carpals disproportionately. Left-to-right discordant bone age suggests disuse of the less mature side, such as associated with brachial plexus palsy, or hypervascularity of the more mature side, such as from diffuse unilateral arthritis. Healing of fractures increases maturation of adjacent growth centers as well.

Delayed bone age may reflect chronic illness or malnutrition; occasionally neglect or abuse; endocrine diseases (thyroid, pituitary, adrenal, or gonad); and locally in bones affected with melorheostosis or other hypovascular situations. Children with Perthes disease seem to have a relatively delayed hand and wrist bone age. Advanced bone age is seen in many premature puberty states, in Marshall syndrome, hypothalamic/pituitary tumors; perhaps, overdose of growth hormone treatment, and locally from hypervascular states, including juvenile idiopathic arthritis (Fig. 1), hemophilia hemorrhage (clearing of which takes vascularity), and, quite dramatically, in neonatal onset (or infant onset) multisystem inflammatory disease (NOMID).

In growth hormone deficiency/hypopituitary/Laron short stature, bones are normally shaped despite the delayed bone age. In hypothyroidism, bones (like the children themselves) are malformed, with epiphyseal and carpal and tarsal irregularity earlier in bone age, and metaphyseal irregularity later in bone age. The hypogonadal Turner syndrome, like most decreased sex hormone conditions, shows bone age delay principally in the second decade. Turner syndrome additionally shows characteristic drumstick distal finger phalanges and a recognizable abnormality in mandible shape (5). In the estrogen deficiency of very high performance athletic teenage girls, bones tend to be long as they continue to grow. Achondroplasia has dysplastic short bones in a rhizomelic pattern.

Bibliography

1. Greulich WW, Pyle SI (1959) Radiographic Atlas of Skeletal Development of the Hand and Wrist. 2nd edn.Stanford University Press, Stanford
2. Keats TE, Sistrom C (2001) Skeletal Maturation: Method of Sontag, Snell, and Anderson. Atlas of Radiographic Measurement. 7th edn. Mosby, St. Louis, p 317
3. Tanner JM, Whitehouse RH, Marshal WA et al (1983) Assessment of Skeletal Maturity and Prediction of Adult Height (TW2 method). 2nd edn.Academic Press, London
4. Kuhns LR, Berger PE et al (1974) Fat thickness in the newborn infant of a diabetic mother. Radiology 111:665–671
5. Rzymski K, Kosowicz (1975) The skull in gonadal dysgenesis. A roentgenometric study. Clin Radiol 26:379–384
6. Oestreich AE, Crawford AH (1985) Atlas of Pediatric Orthopedic Radiology, Thieme Verlag, Stuttgart

Bone Infarction

Ischemic osteonecrosis in the nonweight-bearing regions of bones (metaphyseal and diaphyseal location). This is often an incidental finding and usually does not lead to articular destruction. Most commonly affected are the distal femur and the proximal tibia.

▶Osteonecrosis, Adults
▶Osteonecrosis, Childhood

Bone Infection

Bone infection is in daily practice most frequently caused by bacteria. Invasion and colonization of bone can occur by three principal routes: 1. Spread from a contiguous source as seen in chronic foot ulcers in diabetic patients. 2. Hematogenous spread as typically seen in children and in spondylodiscitis of adults. 3. Direct implantation may occur after accidents with open fractures, direct punctures or after bone surgery.

Bone infection can be separated into osteomyelitis (infection of cortex and bone marrow) and osteitis (infection of cortical bone only). Depending on the duration of bone infection acute or chronic forms can be distinguished which may reveal typical appearances on plain film: Acute osteomyelitis leads to ill defined permeative bone destruction with periosteal reaction and surrounding soft tissue swelling. Chronic osteomyelitis on the other hand may reveal intraosseous abscesses, bony fistula, relatively demarcated bony destruction combined with reactive bone proliferation.

►Osteomyelitis

Bone Marrow Infections

►Osteomyelitis, Neonates, Childhood

Bone Metastases

Bone metastases may either be osteoblastic, osteolytic, or have mixed characteristics. Because bone scintigraphy is sensitive to bone buildup, it visualizes osteoblastic metastases very well and is also sensitive to mixed lesions.

►Bone Scintigraphy
►Metastases, Skeletal

Bone Scan

►Bone Scintigraphy

Bone Scintigraphy

Andreas Bockisch, Monia Hamami, Sandra J. Rosenbaum-Krumme
Klinik fur Nuklearmedizin, Universitaetsklinikum Essen, Germany
andreas.bockisch@uni-essen.de

Synonyms

Bone scan; Skeletal scintigraphy

Definition

Bone scintigraphy is a diagnostic tool in the evaluation of the skeletal system. Depending on bone metabolism, especially turnover and blood flow, bone will incorporate certain radioactive tracers.

Pathology/Histopathology

Physiologically there is a balance of osteoblastic and osteolytic activity. Many metabolic disturbances lead to enhancement of the osteoblastic branch. Bone scintigraphy images osteoblastic activity and allows semiquantitative measurement of it. Therefore, diseases with osteoblastic reactions—especially focal—are the domain of bone scintigraphy. Systemic increased bone turnover may also be detected. For basic measuring reasons, the method is insensitive concerning lytic lesions.

One of the most dominant applications is the search for ►bone metastases (osteoblastic or mixed), which is performed as a static single-phase investigation. Bone scintigraphy is very sensitive to bone buildup—not only due to metastases but also due to active benign diseases such as traumata, active ►arthritis, and benign bone tumors. Rarely, extraosseous accumulation occurs. The experienced nuclear medicine physician is aware of these possible disturbances that need to be differentiated from osseous accumulation, such as by the help of tomography (single photon emission computed tomography, or ►SPECT). Because bone scintigraphy reveals changes in bone metabolism more than changes in bone structure, bone scintigraphy complements rather than replaces plain radiography (X-rays). The changes noted on bone scintigraphy usually precede the changes noted on radiographs because the bone metabolism usually changes before the bone structure changes.

Clinical Presentation

Lower back pain: The typical indication is lower back pain with negative radiographs. Due to its high sensitivity for osteoblastic reactions, bone scintigraphy can detect intravertebral arthritis or infractions very early. Using sectional imaging (SPECT) is advantageous.

Osteomyelitis: In contrast to morphology-based imaging, bone scintigraphy is not or is only slightly influenced by the residues of lapsed changes, but it is very sensitive to present developments. Thus, bone scintigraphy is suitable for differentiating between an acute episode of chronic osteomyelitis and a chronic state, for example. A negative bone scan excludes active osteomyelitis. Newborns or nurslings are the only exceptions in which osteomyelitis may present with indifferent or even reduced activity in the bone scan [2].

Traumata: A bone scan reliably detects the increased osteoblastic activity after fracture or severe injury below the level of the fracture. Depending on the site, there is a calm period of some hours up to a maximum of 7 days in which the bone scan may be negative (or may not be). A high-activity period follows, and finally the increase in bone turnover abates over many weeks and months. In the beginning, the blood pool activity is increased. Considering all these facts, the age of a fracture may be estimated. Applications include identification of (more) acute fractures in the presence of multiple fractures in osteoporosis and determination of the age of a fracture for forensic reasons (such as insurance questions) or suspicion of child abuse. Bone scintigraphy can also give valuable information about the course of posttraumatic healing. Abnormally prolonged repair may be detected after fracture or surgery (implants), and pseudoarthrosis may be characterized as hypo- or hypermetabolic.

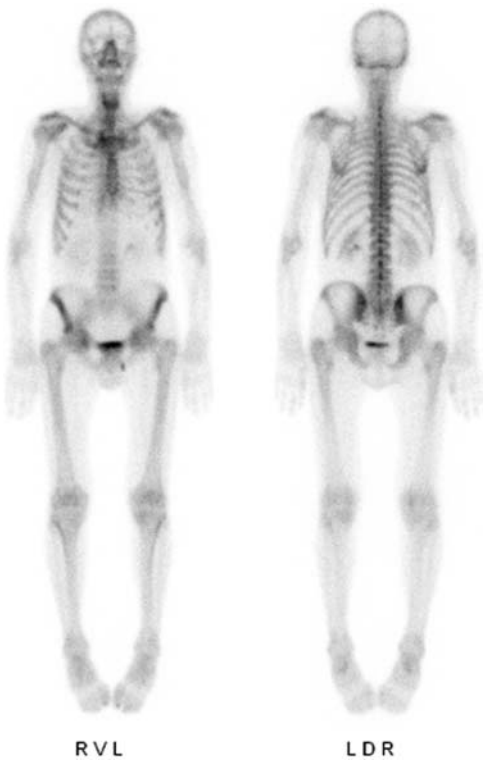

Bone Scintigraphy. Figure 1 Essentially normal bone scintigram. The investigation is performed both in ventral view (*right*) and dorsal view (*left*). Due to the significantly higher thickness of absorbing body tissue between the photon-emitting source (here, the bone) and the gamma camera, detection of structures from the distant side of the body overprojection is negligible. There is no focal abnormality. The kidneys as well as the urinary bladder are contrasted because of the excreted radiotracer. For the same reason, contamination with radioactive urine may be observed inguinally, as in this case (small spot left anterior). Note that the rips are expected to be well separated and it should also be feasible to identify the bodies of the lumbar spine individually, depending on their angulation to the gamma camera collimator.

Imaging

Refer to Figs. 1, 2, and 3 for imaging examples.

Nuclear Medicine

Bone scintigraphy is one of the most frequently applied nuclear medicine procedures. It follows the metabolic bone turnover and allows semiquantitation of osteoblastic activity. In the 1950s, ^{18}F was used as tracer, which was abandoned in the late 1970s when ^{99m}Tc became available (3) and ^{99m}Tc-labeled phosphonates for bone scintigraphy were developed, evaluated, and finally established. Because fluoride intensively takes part in bone turnover, ^{18}F is an identical tracer and from biological aspects is ideal. However, its emission energy is not suitable for gamma camera application. Today, ^{18}F has had a revival in its use with positron emission tomography (PET) scanning. ^{18}F–PET investigations may be referred to as ace bone scintigraphy and may be considered especially in those cases in which improved spatial resolution is needed. The principle of bone scintigraphy—the increased accumulation of suitable radionuclides—is also used for therapeutic purposes. Bone pain due to osteoblastic metastases can be significantly reduced, and bone metastases may be shrunk and small ones even cured using suitable beta-emitting nuclides.

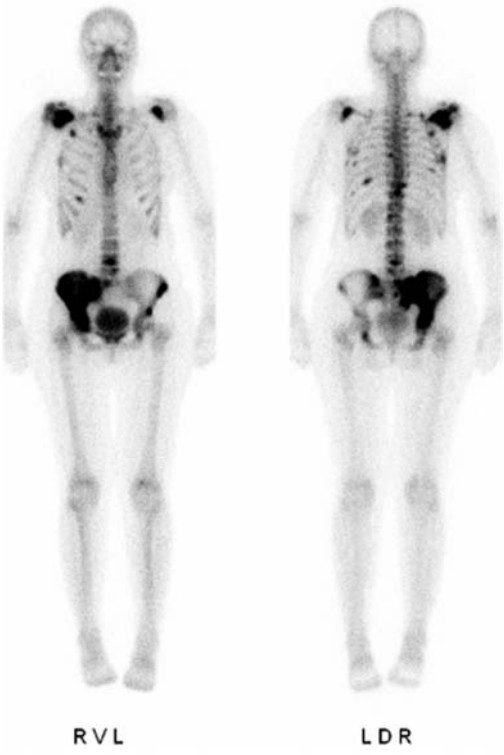

Bone Scintigraphy. Figure 2 Osteoblastic bone metastases in a patient with breast cancer. Whereas the extended involvement of the right side of the pelvis and of the right shoulder was known from X-ray, the additional lesions in the left shoulder and the left side of the pelvis, multiple rips, and some vertebral bodies were diagnosed by the bone scintigraphy demonstrated here.

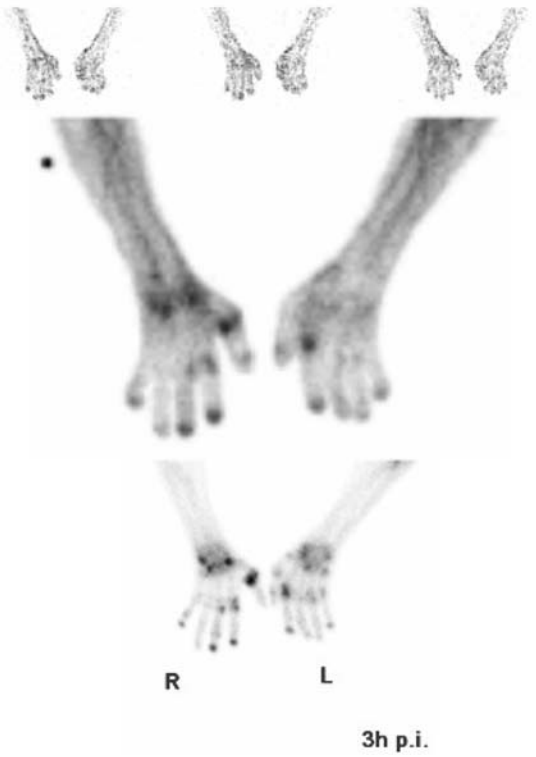

Bone Scintigraphy. Figure 3 Patient with psoriasis arthropathy. (a) Dynamic investigation over 60 s. Each sequential image was recorded over 3 s. (b) Early scintigram (blood pool) and (c) late scintigram of the hands. Diffuse hyperperfusion is seen in the right hand compared with the left one, which is supposedly also hyperperfused—however, to a lesser extent. The blood pool image shows some joints as hyperactive, which also represents increased osteoblastic activity. In addition, other joints are positive in the late image only. In arthritis, the combination of positive early- and late-phase scintigram is suggestive for acute positive late phase only for chronic disease.

Principles of Bone Scintigraphy

The term "bone scintigraphy" is associated with gamma camera imaging and the application of ^{99m}Tc-labeled ▶polyphosphonates. These phosphonates also take part in the bone buildup. In the course of that process, the technetium is separated and remains in an insolvable form at the point of ossification. ^{99m}Tc-diphosphono-propandicarbone-acid (DPD), ^{99m}Tc-hydroxy-ethylene diphosphonate (HDP), and ^{99m}Tc-methylene diphosphonate (MDP) are frequently used.

MDP, DPD, and HM-DPD have basically similar characteristics but somewhat different kinetics. During the time period of investigation—typically up to a maximum of 4 h, and in special cases up to about 24 h—no relevant redistribution of the deposited activity occurs.

In adults of standard weight, 500–750 MBq ^{99m}Tc-labeled polyphosphonates are applied. Depending on the clinical question, the investigation may be performed using one-, two-, three-, or, rarely, four-phase technique.

In the first phase, radionuclide angiography, dynamic imaging is performed of the area of interest with an image frequency of, for example, 2/s for creation of time–activity curves. For visual analysis, these images are summed up for an integral time of 2–3 s each.

The second phase is an early static image taken between about 4 and 10 min as limits. It reflects the blood volume as the tracer is still predominantly dissolved in the blood; however, specific bone turnover also occurs, which might influence the result in spots of very high turnover such as the epiphysis in children. The blood pool investigation is often restricted to one body region. If a whole-body blood pool investigation is considered, the investigation has to be performed with high speed in order to meet the above-mentioned time limitations.

The third phase is literally the bone scintigraphy. At that time, about half of the activity has been renally excreted. The remaining activity has mostly accumulated in the bone proportional to the osteoblastic activity. The minor part of the activity remains in the blood pool or is nonspecifically distributed extracellularly. Especially in patients with low absolute kidney function, the target-to-background ratio may be unfavorable, resulting in images of impaired quality. In this case, further late or very late (24 h) imaging may overcome the problem.

The fourth phase is seldom needed and has its value in differentiating between specific accumulations in the diseased bone and increased soft tissue activity, such as in ulcera in diabetic foot syndrome.

In the mineral phase (phase 3 or 4), the investigation may be performed in cross-sectional imaging technique (SPECT) in addition to planar [3]. The three-dimensional information from SPECT is especially useful when investigating more complex bony structures such as the head or the pelvis, mostly leading to increased sensitivity and specificity. Further improvement may be achieved by correlation with additional morphologic images or by performing a SPECT/computed tomography investigation [4].

Diagnosis

Bone scintigraphy is a quick, reliable, and cost-efficient modality to check the bone status in malignant diseases that frequently present with osteoblastic or mixed bone metastases, including breast carcinoma, lung cancer, prostatic cancer, and gastrointestinal cancer [5]. To evaluate individual diagnostic and therapeutic regimens, screening for bone metastases may be an important component; however, for lack of space, this will not be discussed here.

In primary bone tumors, bone scintigraphy is performed using a three-phase technique. Although today, bone scintigraphy for primary diagnosis of bone tumors has taken a back seat, it might help to make a differentiated diagnosis in uncertain cases. Malignant tumors often show up intensively in all of the three phases. In prediagnosed malignant and benign bone tumors that are known to have a multilocal appearance, bone scintigraphy is used to clarify the extent of disease as the whole-body state is quickly acquired. In a given entity of tumors, the intensity of bone turnover is expected to correlate positively with the degree of malignancy. This experience may be used for directed biopsies, such as in fibrous dysplasia or Paget's disease. As a functional modality, bone scintigraphy is well suited for follow-up and for early detection of response to therapy [1]. In this context, the blood pool changes have been found to be of special value.

A couple of benign diseases apart from benign primary bone tumors are indications for bone scintigraphy. In these investigations, at least a two-phase investigation is mandatory. Due to the comparatively low radiation exposure (typically 4–5 mSv for adults), bone scintigraphy is readily used, as well as in nonmalignant diseases and for children. In the latter case, the activity to apply is chosen according to European Association of Nuclear Medicine recommendations. The nuclear medicine modality allows scanning of the whole skeleton within less than half an hour and with low radiation exposure, which is independent of the extent of the investigation. Bone scintigraphy is performed either to detect disease, to characterize the disease or its clinical course, or to define the extent of disease (such as in a search for metastases of osteomyelitis or fractures in a multitrauma patient). Often, more than one of the indications applies.

References

1. Knop J, Montz R (1983) Bone scintigraphy in patients with osteogenic sarcoma. Cooperative Osteogenic Sarcoma Study Group COSS 80. J Cancer Res Clin Oncol 106: Suppl: 49–50
2. Schauwecker DS (1992) The scintigraphic diagnosis of osteomyelitis. AJR 158:9–18
3. Subramanian GJG, McAffee RE, O'Hara M et al (1971) Mehter: ^{99m}Tc- polyphosphate PP46: A new radiopharmaceutical for skeletal imaging. J Nucl Med 12:399–400
4. Romer W, Nomayr A, Uder M et al (2006) SPECT-guided CT for evaluating foci of increased bone metabolism classified as indeterminate on SPECT in cancer patients. J Nucl Med 47(7):1102–1106.
5. Wang K, Allen L, Fung E et al (2005) Bone scintigraphy in common tumours with osteolytic components. Clin Nucl Med 30(10):655–671

99mTc Bone Scintigraphy

Radioisotope bone scintigraphy is the standard whole-body imaging technique for screening bone metastases. It depicts the tracer accumulation at any skeletal site with an elevated rate of bone turnover as seen in neoplasia, trauma, arthropathy, or inflammation.

▶Metastases, Skeletal

Bony Destructions

Bony destructions in a marginal location of the joint surface is, together with cartilage destruction, one of the three radiologic key symptoms of arthritis (the other two are synovial soft tissue swelling and collateral phenomenon).

▶Rheumatoid Arthritis

BOOP

Bronchiolitis obliterans organizing pneumonia. Proliferative bronchiolitis with granulation tissue in the bronchiolar lumen of the distal airways.
▶Bronchitis and Bronchiolitis in Childhood

Borderline Tumor

Borderline ovarian tumor is a subtype of epithelial ovarian cancer and is classified as a tumor of low malignant potential. Compared to invasive ovarian cancer, it occurs in younger women and has a better prognosis.
▶Masses, ovarian

Botryoid

Rounded swellings resembling a bunch of grapes.
▶Rhabdomyosarcoma

Boutonniere Deformity

Boutonniere deformity is a typical deformity in late-stage rheumatoid arthritis with flexion of the proximal interphalangeal joint and hyperextension of the distal interphalangeal joint.
▶Rheumatoid Arthritis

Bouveret's Syndrome

Duodenal obstruction due to a gallstone migrated through a cholecystoduodenal fistula.
▶Cholecystitis

Bowel Disease, Inflammatory

This term usually indicates both UC and Crohn's disease.
▶Colitis, Ulcerative
▶Crotin's Disease

BPD

▶Dysplasia, Bronchopulmonary

BR14

Microbubble US contrast agent used with low mechanical index. The bubbles consist of perfluorobutane and are stabilized by a phospholipid shell. The agent has a liver-specific late phase. Clinical development stopped (2003). Manufacturer: Bracco SPA, Italy.
▶Contrast Media, Ultrasound, Hepatic

Brachial Ischemia, Chronic

Elias N. Brountzos
Department of Radiology, Athens University, Medical School, Athans, Greece
ebrountz@cc.uoa.gr

Definition

Long-standing reduction in the blood perfusion of the upper extremity as a result of an occlusive arterial lesion. In contrast to the acute upper extremity ischemia, chronic ischemia has a more subtle presentation.

Vascular Anatomy

See also Fig. 1. The main artery supplying the upper extremity is the subclavian artery. The subclavian artery originates from the innominate artery on the right and from the aorta on the left. It is defined distally by the lateral border of the first rib, where it becomes the axillary artery. Branches of the subclavian artery are the vertebral artery, the internal mammary artery, the thyrocervical trunk, and the costocervical trunk. The axillary artery lies between the lateral border of the first rib and the lateral margin of the teres minor muscle, where it becomes the brachial artery. Its branches are the superior thoracic artery, the lateral thoracic artery, the thoracoacromial artery, the subscapular artery, and the circumflex humeral artery. The branches of the subclavian and the axillary

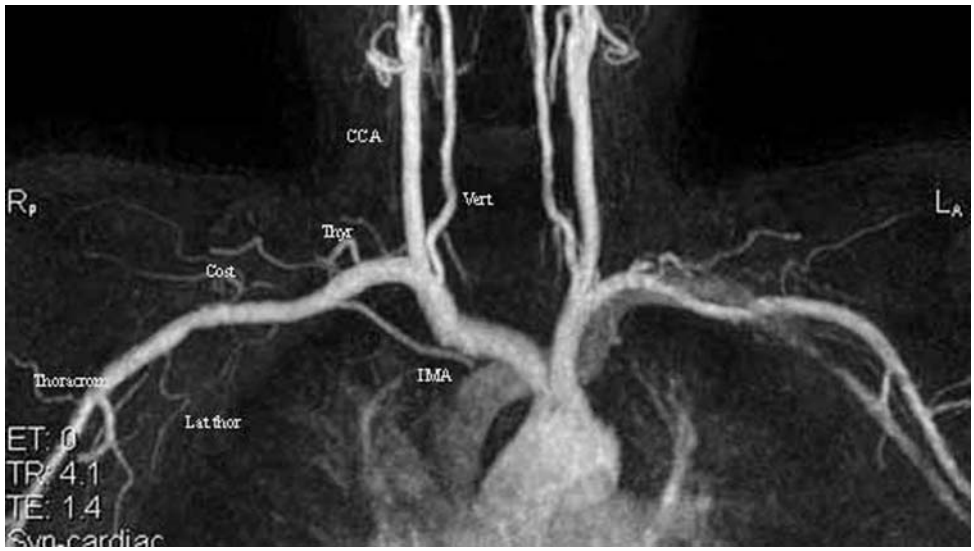

Brachial Ischemia, Chronic. Figure 1 Maximum intensity (MIP) reconstruction from a gadolinium enhanced 3-D magnetic resonance angiography (MRA) of a normal subject in the RAO projection depicts normal upper extremity arterial anatomy. Vert: vertebral artery; CCA: common carotid artery; IMA: internal mammary artery; Thyr: thyrocervical trunk; Cost: costocervical trunk; Lat thor: lateral thoracic artery; Thoracrom: thoracoacromial artery.

arteries serve as a rich network of collateral circulation in any case of subclavian or axillary artery occlusion. The brachial artery ends to its bifurcation in the proximity of the radial head. One of the most consistent branches of the brachial artery is the deep brachial artery, which supplies the muscles of the posterior aspect of the upper arm. The radial and ulnar arteries arise from the brachial artery, the interosseous artery arising from the ulnar artery. A rich collateral network is formed around the elbow from the anastomoses between the recurrent ulnar and radial interosseous arteries and the brachial collaterals. The main arterial supply to the hand is at its volar side. The dorsal side contains veins. The superficial palmar arch is primarily formed by the ulnar artery. The deep palmar arch is formed by the radial artery. The paired proper digital arteries supply the fingers (1).

The extensive collateral supply at the shoulder and the elbow explains the absence of symptoms in many patients with chronic segmental arterial occlusion of the subclavian, the axillary, or the brachial artery.

Pathology

Arterial occlusion may be a result of a fixed lesion, or a result of vasospasm; both mechanisms are not mutually exclusive and may be combined. In 60% of patients with the primarily vasospastic Raynaud's syndrome an underlying disorder is diagnosed producing fixed occlusive lesions of the palmar and digital arteries (2). Different etiologies apply for the large arteries (aortic arch to the wrist), and to the small arteries (distal to the wrist) (Table 1). *Atheroclerotic disease* is more often diagnosed when it is located at the origins of the great arch vessels, e.g., the innominate artery, and the subclavian artery, because at these locations it is more likely to cause symptoms. Innominate artery and subclavian artery occlusive disease occurs in relatively younger patients than other types of atherosclerotic disease. The left subclavian artery is more commonly affected compared to the right side. The prevertebral part of the subclavian artery is usually involved. Atherosclerotic disease in more distal locations is less likely to cause ischemic symptoms. Involvement of the small arteries of the fingers is found in smokers, diabetics, and patients with end stage renal disease (1). *Trauma* is more likely a cause of acute upper limb ischemia, but in some patients treated conservatively, symptoms of chronic ischemia develop later (3). Arterial complications of the *thoracic outlet syndrome (TOS)* are rare compared to the neurologic involvement (less than 5% of the cases). The subclavian artery is compressed in the scalene triangle, or the costo-clavicular space. The initial lesion is an arterial stenosis, but later a poststenotic dilatation is formed not unusually containing mural thrombus. This may result in peripheral microembolization, usually of the thumb or index finger. *Takayasu's arteritis* affects proximal vessels such as the innominate and subclavian arteries. A more distal involvement of the axillary and proximal brachial artery is suggestive of *giant cell arteritis*. Connective tissue disorders include *Systemic lupus erythematosus (SEL), Scleroderma,*

Brachial Ischemia, Chronic. Table 1 Etiology of chronic upper extremity ischemia

Large arteries
1. Atherosclerosis
2. Trauma
a. Blunt, penetrating
b. Iatrogenic
3. Arterial thoracic outlet syndrome (compression by cervical rib, scalenus muscle, etc.)
4. Embolization associated with thoracic outlet syndrome
5. Arteritis
a. Takayasu's
b. Giant cell
c. Buerger's disease
6. Fibromuscular disease
Small arteries
1. Raynaud's syndrome
2. Atherosclerosis
3. Connective tissue disease (Scleroderma, Rheumatoid arthritis, SEL, Mixed connective tissue disorder)
4. Myeloproliferative disease (Essential thrombocytosis, polycythemia vera, Chronic Myeloid Leukemia, Myelofibrosis)
5. Hypercoagulable states (Antithrombin III, protein C, protein S deficiencies, Antiphospholipid syndrome, heparin antibodies, etc)
6. Cold injury
7. Buerger's disease
8. Occupational vascular problems
a. Vibration-induced white finger
b. Hypothenar hammer syndrome
c. Athletic injuries
9. Chronic renal failure

Rheumatoid arthritis, Sjoegren syndrome, Henoch-Shoenlein purpura, Dermatomyositis, Wegener granulomatosis, and Polyarteritis nodosa (PAN). This heterogeneous group of maladies is characterized by tapering of the ulnar, radial, and digital arteries with segmental occlusions and frequently superimposed vasospasm. Arterial lesions are the result of endothelial damage, fibrinoid thickening, and intimal hyperplasia leading to obliterative endarteritis of the digital arteries and caused by antigen–antibody complex deposition (4). *Fibromuscular dysplasia* (FMD) of the upper extremity is more commonly located in the subclavian, the axillary, and the brachial arteries. *Buerger's disease* of the upper limb is found in two-thirds of the patients suffering from this disease. *Raynaud's syndrome (RS)* is the most common cause of upper limb ischemia. It is characterized by episodic attacks of vasospasm caused by closure of the small arteries of the most distal parts of the extremity in response to cold or emotional stimuli. With arterial closure the hand becomes white, then with relaxation of the spasm turns blue due to cyanosis, and finally with reactive hyperemia becomes red. In a large proportion of patients, an underlying disorder can be diagnosed causing fixed arterial lesions. Prolonged professional use of vibratory tools has been associated with symptoms similar to Raynaud's syndrome. This condition is termed "*Vibration-induced white finger.*" Patients with the "*Hypothenar hammer syndrome*" are professionals who use the palm of the hand for pushing, pounding, or twisting (mechanics, carpenters, etc.). Typical symptoms are blanching of the fingers, coolness, paresthesias, more or less similar to Raynaud's syndrome. Similar conditions can develop in athletes using their hands in the same fashion (handball players).

Clinical Presentation

Occlusive arterial disease of the upper extremity arteries is less often symptomatic compared to that of the legs, because less muscular workload falls in arms, and the arterial collateral network in the upper extremity is very extensive to compensate for localized arterial occlusions (1). When symptomatic, chronic ischemia usually presents as arm claudication. This is more usual with *proximal atherosclerotic lesions.* Other symptoms include rest pain and gangrene, but those occur much less frequently and almost invariably in the fingers. Similar clinical presentation occurs in patients with *Takayasu's disease or giant cell arteritis* with proximal lesions. However, these patients similarly to those with *connective tissue disorders* are generally younger than the athero-

sclerotic patient and may also have other symptoms from the underlying disease. Patients with *arterial involvement of TOS* complain of numb hand or tingling associated with activity that compresses the arteries within the thoracic outlet space. In some instances, the initial presentation is with symptoms of microembolization of the digital arteries or the palmar arch. Symptoms include Raynaud's syndrome, paresthesias, cold sensation, or pain. Symptoms of microembolization may last long before a major embolic complication causing acute ischemia takes place. At physical examination, a pulsatile mass may be palpated in the supraclavicular fossa, but it does not always represent the subclavian aneurysm itself, but rather the underlying bony abnormality pushing the artery upward (1). The presenting symptom in patients with FMD maybe distal embolization. *RS* is characterized by episodic ischemic attacks involving the hands and fingers after exposure to cold or emotional stimuli.

Imaging

Duplex or Color Doppler Sonography

The origins of the innominate and the subclavian arteries can be evaluated by color Doppler sonography (CDS) but often not without difficulty because the vessels are situated deep in the thorax. In these cases, transesophageal sonography is more suitable. More distally the vessels become superficial and can be imaged by high-frequency probes. A complete examination of all upper-extremity arteries is accurate but time-consuming.

CT Angiography

This modality is excellent suited for the evaluation of the arch and the origins of the upper extremity arteries. Excellent imaging of the arterial anatomy of the upper limb can be achieved using CT angiography (CTA) with postprocessing, although the resolution does not allow for the evaluation of the digital arteries. A noncontrast scan is initially obtained followed by the contrast scan using thin collimation. Coverage should include the proximal neck to the hand.

Magnetic Resonance Angiography

The origins of the subclavian and innominate arteries and their proximal parts to the shoulder can be imaged with coronal 3-D gadolinium enhanced acquisitions. High quality images of the hand arteries comparable to the conventional invasive angiography are now possible in less than 5 min with the use of dedicated surface coils that provide high spatial resolution (4).

Conventional Angiography

It is still considered the gold standard for the imaging of the upper limb arterial anatomy; everything from the aortic arch to the fingers should be imaged, otherwise significant pathology may be missed. For the imaging of the aortic arch and the origins of the arch vessels digital subtraction angiography (DSA) is performed in the left anterior oblique (LAO) projection with a pigtail catheter positioned in the ascending aorta; imaging in the right anterior oblique (RAO) projection depicts the origins of the right subclavian and common carotid arteries. Imaging of the upper extremity arteries is performed with selective catheterization: the subclavian and axillary arteries are imaged with the tip of the catheter in the subclavian artery; the brachial artery is imaged with the tip of the catheter in the axillary artery; the forearm and hand arteries are imaged with the tip of the catheter in the brachial artery. Magnification views are used for detailed depiction. To avoid vasospasm causing diagnostic pitfalls the hand should be kept warm or the injection of vasodilators is used.

Diagnosis

In patients with *atherosclerotic disease of the proximal upper extremity arteries* angiography typically depicts a localized lesion, concentric or eccentric with or without calcification. Lesions at the origin of the right subclavian artery may involve also the origin of the right carotid artery (1). Not unusually, multiple arch arteries are involved with stenoses and occlusions. Angiography in *Atherosclerotic disease of the distal upper extremity arteries* depicts segmental occlusions of the palmar or digital arteries.

In patients with *TOS with arterial involvement* chest radiograph, CT and MRI may reveal the underlying structural abnormality, such as a cervical rib, or acquired anomalies of the clavicle or the first rib. Imaging with DSA or other modalities is recommended to evaluate the subclavian artery for stenosis, aneurysm and the existence of mural thrombus, and to look for distal embolization. DSA in combination with evocative maneuvers such as 90° abduction and external rotation have been used to reveal the arterial compression; however, these findings are encountered in 50% of normal subjects. Ultrasonography and CTA/MRA better evaluate the vessel lumen, wall, and the surrounding tissues.

In patients with *arteritides,* CTA and magnetic resonance angiography (MRA) characteristically depict wall thickening that enhances after gadolinium injection. *Takayasu's arteritis* affects proximal vessels such as the innominate and subclavian arteries. A more distal involvement of the axillary and proximal brachial artery

is suggestive of *giant cell arteritis*. In addition to imaging, the diagnosis is established on the basis of clinical history and laboratory tests. In patients with *connective tissue disorders* angiographic findings include tapered occlusions without intraluminal filling defects (as opposed to embolization). Angiography is important for the diagnosis of PAN with 89% sensitivity and 90% specificity; without this tool the diagnosis is possible in only 20–30% of the cases whenever tissue pathology yields diagnostic results (4). Angiographic findings of PAN include digital artery occlusions as a common finding with other vasculitides, but the depiction of digital aneurysms is suspicious of PAN.

In patients suspected to suffer from FMD, DSA is essential for the diagnosis depicting the characteristic beaded appearance in the case of medial fibroplasia. Because bilateral disease is often present both arms should be imaged. *In Buerger's disease* angiographic findings of the hand and digital arteries include occlusions and characteristic corkscrew collaterals from the perineural arteries and vasa vasorum (1). *In Raynaud's syndrome* (RS) hand arteriography before and after ice water immersion has been used in the past for the establishment of the diagnosis. After exposure to cold prominent vasospasm of the palmar and digital arteries is a feature of the RS. Today, the diagnosis of RS is based instead on angiography on Nielsen's test and digital plethysmography (2).

In patients with *Vibration-induced white finger*, angiography depicts multiple permanent digital arterial occlusions in these patients. The extent of the involvement is proportional to the duration of the causative activity. Angiographic findings of the *Hypothenar hammer syndrome* include occlusion or aneurysm of the ulnar artery, adjacent to the hook of the hamate bone, and occlusions of digital arteries from microembolization.

Interventional Treatment

Treatment of *atheromatous lesions of the origins of the innominate and subclavian arteries* is warranted in symptomatic patients. Surgical treatment includes transthoracic endarterectomy or bypass graft from the ascending aorta. More often the carotid artery or the contralateral axillary artery are used as inflow vessels for the construction of carotid-subclavian or axillo-axillary bypasses. The results of these operations are excellent with good long-term patency. Because of its minimally invasive nature percutaneous angioplasty with or without stent placement has gained widespread acceptance and is advocated as first line therapy for short isolated lesions. Meticulous technique is required during ostial right subclavian artery stent placement treatment, so to avoid inadvertent occlusion of the right carotid artery. Stent placement is not recommended across the ostium of a patent vertebral artery (Fig. 2). The immediate results are excellent with rare complications; although information on long-term results is scarce, patency appears to be comparable to open surgery. Interventional treatment is also successful in proximal lesions of *Takayasu's arteritis*, provided the patient is also treated medically (5). The management of the *TOS* is surgical and consists of thoracic outlet decompression with resection of the cervical rib or abnormal first rib, or other underlying bone anomaly, and scalenectomy; arterial reconstruction

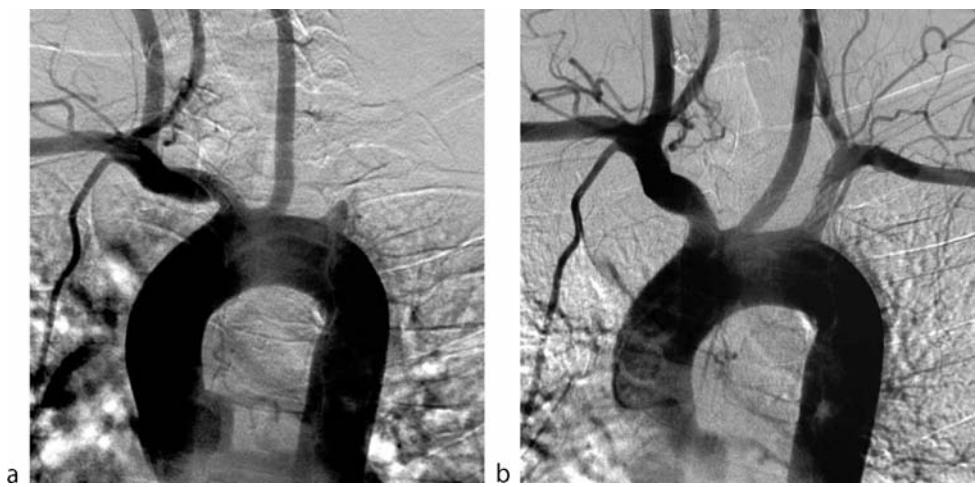

Brachial Ischemia, Chronic. Figure 2 (a) DSA in the LAO projection depicts occlusion of the left subclavian artery. (b) DSA in the LAO projection after percutaneous placement of a balloon expandable stent; note that the stent does not extend to the vertebral artery ostium.

is mandatory in the presence of an aneurysm; embolectomy or sometimes venous bypass maybe required. As an alternative to aneurysmatectomy exclusion of the aneurysm with a stent-graft can be used (1).

Brachial Plexopathy

▶Trauma, Birth

Brachial Plexus Injury

▶Trauma, Birth

Brachial Vein Obstruction

▶Thrombosis, Venous, Brachial

Brachial Vein Occlusion

▶Thrombosis, Venous, Brachial

Brachialgia

▶Clinical Presentation of Spinal Nerve Root Compression

Brain

Philippe Demaerel
Department of Radiology, University Hospital K.U.Leuven, Leuven, Belgium
philippe.demaerel@uz.kuleuven.ac.be

Neuroradiology deals with imaging of the central nervous system. The imaging techniques include ultrasound, computed tomography (CT), magnetic resonance imaging (MRI), X-ray myelography, and digital subtraction angiography (DSA).

The advent of MRI in the early 1980s has radically changed the radiological approach in patients with neurological symptoms. MRI provides higher resolution and tissue contrast than CT. MRI has also resulted in a decrease in the number of more invasive diagnostic techniques such as DSA and X-ray myelography.

This section only deals with neuroimaging of the brain.

MRI has replaced CT for several clinical applications either based on the type of suspected pathology (e.g., multiple sclerosis) or based on the expected area of involvement (e.g., brain stem, cerebellum, and pituitary gland). However, there is poor evidence in the literature that MRI has a therapeutic impact or that it changes patient outcome. Quantitative assessments of the clinical effect of MRI in large-case series or well-controlled comparison trials are still missing.

Due to its superior image quality, the frequent discovery of *incidental abnormalities* of unknown significance, particularly in the older population, should be borne in mind. Knowledge of *normal aging* signs on MRI is important in order to avoid unnecessary additional (possibly invasive) diagnostic or even therapeutic procedures.

Apart from morphological imaging, MRI also has the potential of *imaging brain function* (e.g., spectroscopy, BOLD imaging, perfusion imaging, and diffusion tensor imaging).

In the last decade, therapeutic or interventional endovascular procedures have become the modality of choice in the treatment of cerebral aneurysms. However, other pathologies such as arteriovenous malformations, arteriovenous fistulas, and arterial stenoses are also being treated by endovascular procedures.

Cranial imaging encompasses imaging of the skull, the meninges, the cerebrospinal fluid-containing spaces, the vascular structures, the cranial nerves, and the brain substance (white matter and gray matter). Pathology can be seen in each of these anatomical compartments.

Diagnostic neuroradiology can, to some extent artificially, be divided into an adult and a pediatric subspecialty. In textbooks, the different entities are usually classified into congenital, traumatic, vascular, tumoral, degenerative, metabolic, and infectious pathology.

Pediatric neuroradiology is often discussed separately because the type of pathology encountered is often different from adult diseases. The role of MRI in pediatric neurological disease is even more prominent than in adult neurological diseases. The often subtle congenital cerebral malformations and the more frequent occurrence

of cerebellar pathology are two examples of the prominent role of MRI in pediatric neuroimaging.

Although there seems to be an emerging role for diffusion-weighted imaging in cranial *trauma*, CT remains the modality of choice in daily practice. The close proximity of the CT suite to the emergency department and the need for close monitoring in acute trauma patients are in favor of CT. Bone fractures as well as fresh blood are clearly visible on CT images. MRI is superior in detecting diffuse axonal injuries. Plain skull X-ray is no longer routinely indicated in cranial trauma.

Stroke is a common cause of death in the Western world. Stroke imaging is currently one of the "hot" topics in neuroradiology. The search for an optimal selection of patients who can be considered candidates for (intra-arterial) thrombolysis is still ongoing. Different MR techniques play a role in the work-up of a stroke patient. Diffusion and perfusion imaging are used to demonstrate the presence of a "penumbra" and to assess the viability of this tissue at risk. An area of restricted diffusion on an apparent diffusion coefficient map needs to be correlated to the perfusion defect. When the area on perfusion appears larger than on diffusion imaging, the area of difference corresponds to the penumbra. MR angiography (MRA) or CT angiography can demonstrate the occlusion of a major artery. Some authors will argue that the rapid accessibility of CT for excluding a fresh hemorrhage is sufficient to decide on thrombolytic or conservative treatment, but diffusion-weighted MRI is certainly more sensitive in detecting recent ischemia. MRI is clearly superior to CT in detecting chronic bleeding. Simultaneously, research is being performed on plaque imaging in the *carotid and vertebral arteries*. MRA and CT angiography each have advantages in assessing a stenosis. The advantage of CT is the ability to demonstrate calcification in the plaque. But the advantages of MRI include the absence of ionizing radiation and not having to use iodinated contrast agents. Several systematic reviews have been published and according to the observations, there seems to be a consensus that MRA or CT angiography in combination with ultrasound can replace DSA in the majority of patients.

Stroke can also be caused by a *venous thrombosis* or by arterial dissection. Etiologies of venous thrombosis include oral contraceptives (in combination with smoking), pregnancy, and hypercoagulable states. Venous thrombosis can involve the superficial or the deep venous system. Causes of a nontraumatic dissection include fibromuscular dysplasia, hypertension, and oral contraceptives. In both pathologies, MRI is currently the modality of choice to demonstrate the abnormalities, which will lead to the appropriate treatment.

The incidence of *aneurysms* in the population is 2–7% and the risk of bleeding is 2% per year. About 10% of all intracranial aneurysms are multiple. Aneurysms arising from the vessels forming the circle of Willis account for more than 90% of all intracranial aneurysms. MRA is accepted as a screening modality in relatives of patients with aneurysms. Following endovascular treatment, MRA can be used in the follow-up, but occasionally an additional DSA examination may be necessary. MRA at 3 Tesla (T) currently provides excellent visualization of the large and medium-sized arteries (Fig. 1).

Arteriovenous malformations are rare congenital lesions and usually present in patients older than 40 years. The risk of bleeding is 2% per year, but several factors may increase this risk (e.g., venous aneurysms, deep venous drainage. In the work-up of a patient with an arteriovenous malformation, DSA remains mandatory. Dural arteriovenous malformation and fistula usually develop secondary to a venous thrombosis. They usually occur in the posterior fossa, tentorium, or in the cavernous sinus. These malformations are frequently missed on CT and MRI and only DSA will demonstrate the fistula. Cavernous and venous malformations are more benign lesions with a small to nonexisting risk of a limited bleeding.

MRI has rapidly been accepted as the most important preoperative technique in brain *tumors*. The multiplanar imaging capability is the main advantage of MRI in

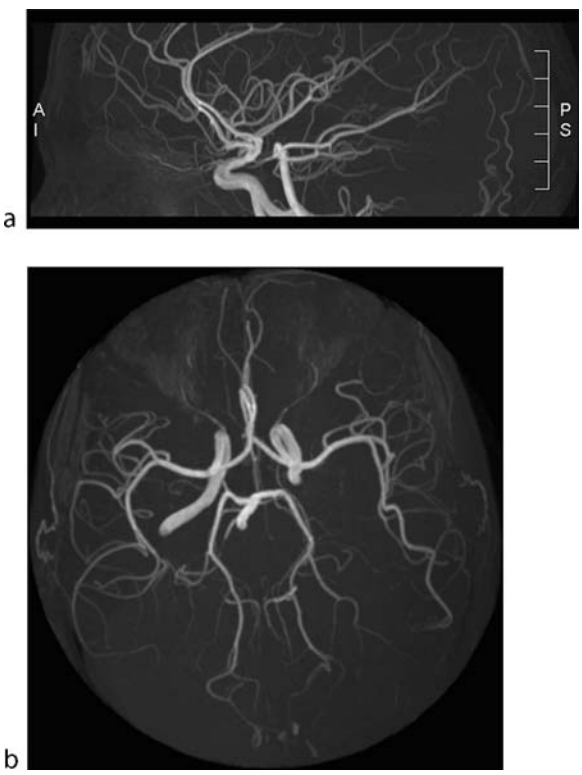

Brain. Figure 1 MR angiogram of the circle of Willis at 3 T. Lateral (a) and cranial (b) view.

visualizing the extent of a tumor. Usually, intracranial tumors are classified as intra-axial (parenchymal) tumors and extra-axial (dural/meningeal) tumors. The most common dural tumor is the meningioma. Gliomas (including the World Health Organization grade 2 and 3 astrocytoma as well as glioblastoma multiforme) are the most common type of intrinsic brain tumors. Up to 30% of brain tumors are metastases from a distant primary tumor. The general rule is that MRI will depict more metastases than CT, particularly when it concerns small lesions (Fig. 2). MRI is also more sensitive in the detection of carcinomatous meningitis. With the onset of newer techniques such as MR spectroscopy, perfusion imaging, and diffusion tensor imaging, our insight into tumors is steadily improving. MR spectroscopy may give an idea of the degree of malignancy in a noninvasive way. Perfusion imaging can assess the vascularity of a tumor without further need for DSA. Functional MRI (using BOLD imaging) will help to locate the tumor in relationship to the surrounding functional cortex, and diffusion tensor imaging will demonstrate the displacement or invasion of white matter tracts by the tumor.

Following treatment, MRI is the modality of choice in the follow-up of cerebral pathology. An accurate assessment of residual tumor tissue or the follow-up after chemo- and/or radiotherapy is best performed using MRI. The success of this examination will depend on the patient's cooperation in the immediate posttherapeutic stage.

The increasing use of high field strengths and 3-D imaging sequences has led to more clinical research on *morphometry* in neurological disease, for example, *Alzheimer's disease*, *Huntington's disease*, and *partial complex seizures*. It has been suggested that early stages of Alzheimer's disease are best distinguished from normal aging by measuring the volume of the hippocampus and/or temporal lobe. Patients with longer duration of disease were best distinguished by pathology of the medial

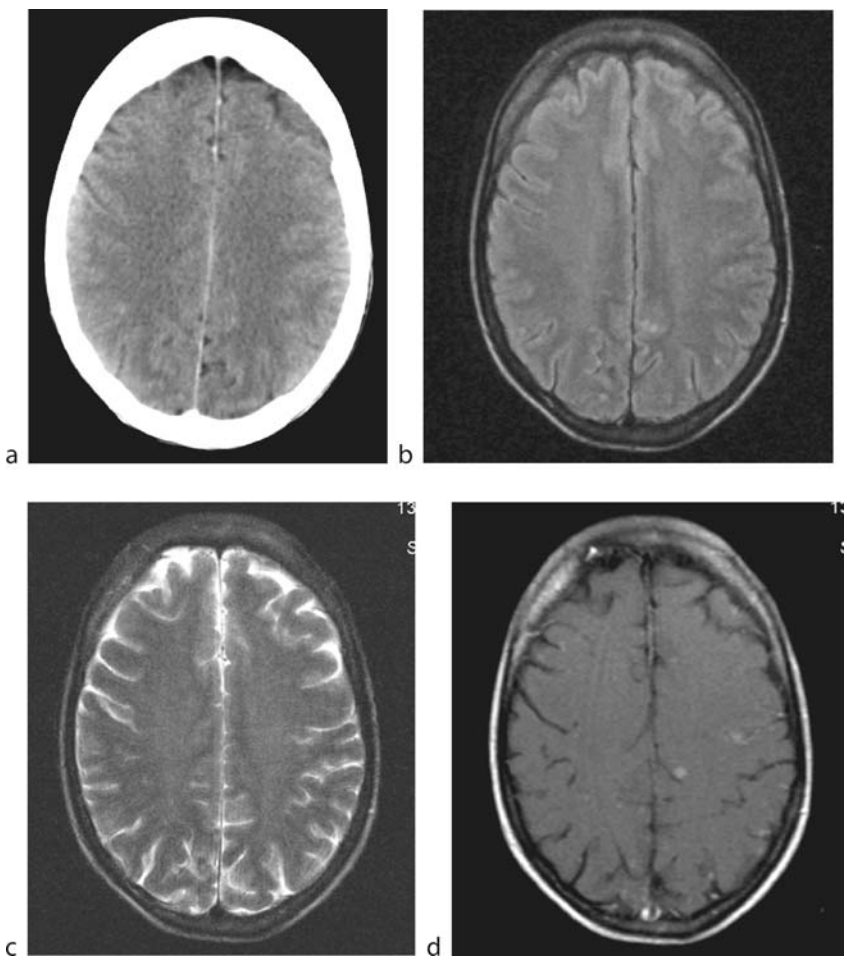

Brain. Figure 2 Axial contrast-enhanced CT (a), fluid-attenuated inversion recovery (b), T2-weighted (c), and Gd-enhanced magnetization transfer T1-weighted (d) MR images in a patient with brain metastases from a lung carcinoma. Note that the metastases are only visible on the Gd-enhanced T1-weighted images (d).

temporal lobe and anterior cingulate gyrus. This appears to be consistent with the progressive clinical presentation of Alzheimer's disease.

In *multiple sclerosis* (*MS*), MRI was rapidly recognized to be far superior to CT. For the clinical diagnosis of MS, the sensitivity of MRI exceeds that of all noninvasive clinical tests. Recently, MRI has been included in the criteria for clinically definite MS. Other MRI techniques with increased specificity to the more destructive aspects of MS pathology, such as magnetization transfer MRI, diffusion-weighted MRI, and proton magnetic resonance spectroscopy, have recently been applied to MS cognitive studies.

In *toxic* and *infectious* diseases, MRI often plays a crucial role in the difficult diagnostic work-up along with the history and laboratory tests. The frequent involvement of deep brain structures, the brain stem, and the cerebellum in toxic and metabolic disorders is far better assessed by MRI than by CT. Staphylococcal brain abscesses can be diagnosed by demonstrating a high signal on diffusion-weighted images, but occasionally necrotic metastases may look similar. Herpes simplex meningoencephalitis will be seen earlier on MRI than on CT. Inflammatory disease of the vessel wall is called *vasculitis* and can be the result of an infectious etiology (bacterial, viral, tuberculous) or noninfectious etiology (polyarteritis nodosa, granulomatous angiitis). In older patients the differential diagnosis with atheromatosis can be difficult. MRA can demonstrate the segmental narrowings, but when MRA is normal or when only one narrowing is seen, catheter angiography will still be necessary and ultimately biopsy confirmation is needed. MRI does not play a role in viral meningitis but is often indicated in patients with acquired immunodeficiency syndrome who are prone to *opportunistic infections*. Toxoplasmosis and cryptococcosis are two common opportunistic infections. The differential diagnosis with lymphoma is particularly important.

The use of dedicated MR techniques in imaging pathology of the *cavernous sinus and pituitary gland* has resulted in a clear preference of MRI over CT. The most common pituitary tumor is the adenoma. Most microadenomas (<1 cm) are diagnosed on the basis of blood test results. Macroadenomas present with compression of the optic chiasm. MRA is usually performed to image the normal vascular anatomy and to exclude aneurysms of the circle of Willis.

The approach to a patient with *epilepsy* has significantly changed with the introduction of MRI. The diagnostic yield depends on several factors. In patients with intractable temporal lobe epilepsy, epileptogenic lesions can be found in 65–83% of the cases. The detection of mesial temporal sclerosis, not visible on CT, is the most typical example. Up to 85% of the patients who are operated on remain seizure free after surgery. In the near future the use of 3-T MR units may further improve the detection of subtle lesions. 3-T MRI yields a higher signal-to-noise ratio (Fig. 3). This can be invested in a higher spatial resolution. Thin slices or a 1024 × 1024 matrix is now routinely feasible. The coregistration of MRI images with single photon emission computed tomography (SPECT) and positron emission tomography (PET) images is an important tool in preparing epilepsy patients for surgery (Fig. 4). In these cases, the morphological information of MRI is combined with the functional information from SPECT or PET.

In pediatric neuroimaging, MRI is indicated whenever there are neurological signs or symptoms. One of the reasons to prefer MRI rather than CT is the more frequent involvement of structures such as the brain stem, the

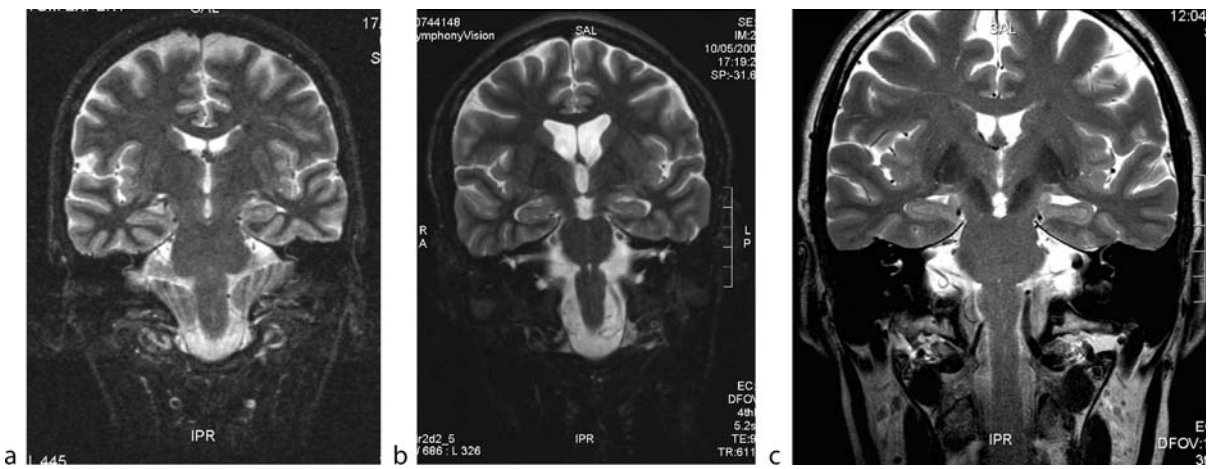

Brain. Figure 3 Coronal T2-weighted MR images obtained at 1.0 T (a), 1.5 T (b), and 3 T (c). Note the increased signal-to-noise ratio with increasing field strength. Internal hippocampal architecture is only seen at 3.0 T (c).

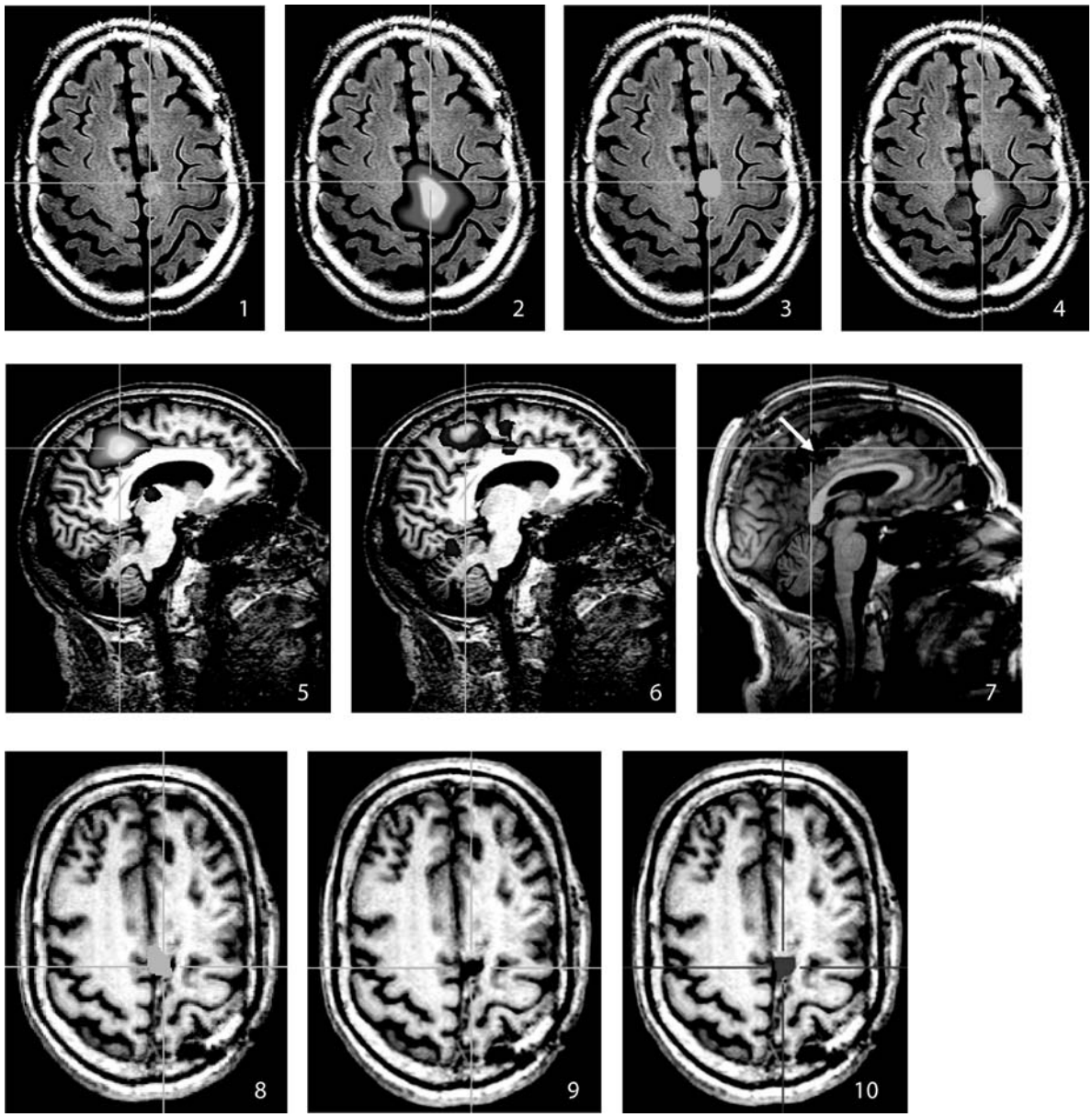

Brain. Figure 4 Fluid-attenuated inversion recovery MR image (1) at 3.0 T shows a suspicious lesion in the left parietal lobe, close to the midline. An ictal SPECT was obtained and coregistration between MRI and the subtraction from the ictal and interictal SPECT (2, 5). The lesion was outlined manually (3) and the SPECT finding was shown in the background (4). Functional MRI shows the cortex responsible for motion of the left foot close to the SPECT area of hyperperfusion (6). A subdural grid with EEG electrodes was placed on the brain during surgery to determine the area where the epileptic attacks first start (7). Electrical stimulation of each of these electrodes confirmed the functional MRI result that the area of hyperperfusion was located next to the motor cortex. Finally, the manual outlining of the lesion is shown (8), the postoperative MR image (9), and the manual outlining of the postoperative site (10) (Courtesy of Demaerel P, Lagae L, Van Paesschen W Azimuz 2005;I(2):4–11).

cerebellum, and the optic chiasm that are more easily assessed on MRI. The use of MRI has led to a new framework for the classification of the *cerebral malformations of the cortex*. More recently, the growing interest in the cerebellum has led to a newly proposed classification of *congenital cerebellar disorders*. CT remains useful for imaging craniosynostosis, and in these patients 3-D CT is performed in the preoperative work-up and in the follow-up after

treatment (Fig. 5). Neurofibromatosis is the most frequent *neurocutaneous syndrome*. This is an autosomal dominant disorder with prominent cutaneous "café au lait" lesions, plexiform neurofibromas, and bilateral optic nerve/optic chiasm gliomas. MRI not only plays a role in the diagnosis but also in the follow-up of patients with optochiasmatic glioma treated with chemotherapy. *Nonaccidental head injury* is a specific condition where both CT and MRI play a role. Generally speaking, CT is always indicated following a suspected nonaccidental cranial trauma. But it is now accepted that diffusion-weighted MR has prognostic value in these infants. MRI has therefore recently been recommended as part of a protocol in suspected nonaccidental cranial trauma and should preferably be performed within 3–10 days after admission.

Pediatric *stroke* is an important pediatric illness. As many children are affected by stroke as by a tumor. A combination of clinical and radiological criteria are needed to define subgroups of patients.

Imaging following a perinatal *hypoxic or anoxic ischemic insult* in a preterm or term-born child is a common neonatal event. Ultrasound is performed in the acute stage and MRI is performed later on to assess the sequelae. The typical finding of "periventricular leukomalacia" occurs in up to 20% of prematurely born infants. Periventricular leukomalacia is currently a research topic in several large centers. Germinal matrix hemorrhage occurs in more than 60% of infants born between 28 and 32 weeks of gestation. Ultrasound is used to grade these hemorrhages and occasionally MRI is indicated.

Metabolic diseases have extensively been studied since the advent of MRI. New diseases have been identified and, using diffusion-weighted imaging, new classification schemes have been proposed. Pattern recognition analysis has led to more rapid analysis of MR examinations. Often, the preferential involvement of either the white or the gray matter is used for classification purposes.

Hydrocephalus can occur in both adults and children, but is relatively more frequent in infants. Cerebrospinal fluid flow imaging has been used to study the pathophysiology of hydrocephalus.

Childhood *neoplasms* are often different from those encountered in adults. Infratentorial and visual pathway neoplasms occur more frequently in children. Medulloblastoma and pilocytic astrocytoma are the most common infratentorial neoplasms. Neoplasms detected before the age of 6 months are considered as a separate category and are often referred to as congenital neoplasms.

Fetal neuroimaging seems to play a role when ultrasound demonstrates pathology. Two studies have shown that MRI may change the diagnosis or provides additional information that alters management in up to one-third of the patients.

The decrease in the number of diagnostic DSA procedures, as a consequence of the ever-increasing quality of noninvasive MR examinations, has to some extent been compensated by an increase in interventional DSA procedures.

Intra-arterial thrombolysis is not unanimously accepted as a treatment modality of stroke patients. The emphasis is on the selection of candidates for thrombolysis beyond a 3-h window. It is likely that MRA/perfusion MR and possibly CT angiography/perfusion CT will play a decisive role in this matter.

Arterial stenting is emerging as an alternative treatment to conventional endarterectomy. Although it is not entirely elucidated which patient may benefit from this therapy, a high revascularization rate has been found in retrospective studies.

Endovascular treatment of aneurysms became rapidly accepted as the treatment of choice in most cerebral aneurysms. Since the introduction of Guglielmi detachable coils, there have been some further improvements.

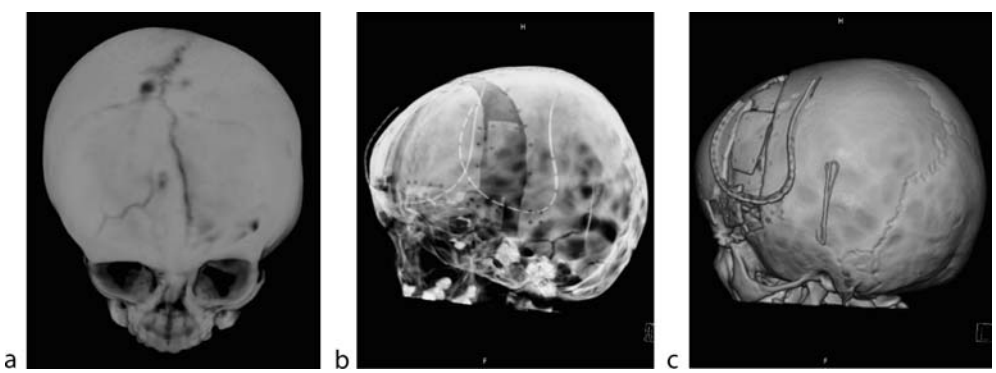

Brain. Figure 5 Preoperative 3-D cranial CT shows the closure of the left frontal suture (a). Postoperative 3-D cranial CT using a volume rendering technique using different densities that are transformed to different transparencies (b, c) give the necessary postoperative information.

Follow-up after endovascular treatment can be performed by MRA in most cases. Occasionally, DSA will remain necessary to assess the degree of coil impaction. Imaging also plays a pivotal role in the diagnostic work-up and/or treatment of *arteriovenous malformations*, which constitute an uncommon disease with a prevalence of approximately 0.1% and an incidence of approximately 0.01%. The most important manifestations are hemorrhage and epilepsy. Although there is still controversy regarding the annual risk of hemorrhage and the identification of high-risk arteriovenous malformations, there seems to be consensus that treatment should aim at total occlusion or complete removal. Several treatment options are available such as microsurgery, radiation therapy, and endovascular treatment using liquid embolic agents.

Caroticocavernous fistulas are most often characterized by a direct communication between the internal carotid artery and the cavernous sinus. They usually occur following a trauma and drain into the ophthalmic vein and inferior petrosal sinus. Clinically this will present as a pulsatile proptosis with a bruit.

Intraoperative MRI is currently changing neurosurgery. Although preoperative MR images of space-occupying lesions are of course useful and necessary to the neurosurgeon, the brain shift caused by these lesions is limiting the use of these images during the neurosurgical procedure. Using intraoperative MRI, the positional error caused by brain shift on the preoperative images has been resolved.

Bibliography

1. Barkovich AJ (2005) Pediatric Neuroimaging. 4th edn. ISBN 0-7817-5766-5. Lippincott Williams & Wilkins
2. Osborn AG, Blaser S, Salzman KL (2004) Diagnostic Imaging: Brain. ISBN 0721629059 Elsevier Mosby Saunders
3. Lasjaunias P, Berensein A, ter Brugge KG (2001) Surgical Neuroangiography. Clinical Vascular Anatomy and Variations. ISBN 3-540-41204-2. Springer, Berlin, Heidelberg, New York
4. Berenstein A, Lasjaunias P, ter Brugge KG (2004) Surgical Neuroangiography. Clinical and Endovascular Treatment Aspects in Adults. ISBN 3-540-41668-4. Springer, Berlin, Heidelberg, New York
5. Lasjaunias P, ter Brugge KG, Berenstein A (2006) Surgical Neuroangiography. Clinical and Interbventional Aspects in Children. ISBN 3-540-41681-1. Springer, Berlin, Heidelberg, New York
6. Von Kummer R, Back T (2006) Magnetic Resonance Imaging in Ischemic Stroke. ISBN 3-540-00861-3. Springer, Berlin, Heidelberg, New York

Brain Atrophy

A significant change in brain volume. Aging is typically associated with brain atrophy, which reflects a decrease of brain weight, due to the loss of both gray matter (starting at the end of the first decade of life) and white matter (starting at the fourth decade), and a corresponding increase of cerebrospinal fluid volume.

▶Aging Brain

Brain, Edema

▶Trauma, Head, Accidental

Brain, Functional Imaging

Stefan Sunaert, Caroline Sage, Silvia Kovacs, Ronald Peeters
Department of Radiology, University Hospital
Stefan.Sunaert@uz.kuleuven.ac.be

Synonyms

BOLD-fMRI; Functional magnetic resonance imaging (fMRI); Functional neuroimaging

Definition

In the broadest sense, functional imaging of the brain refers to any imaging technique that goes beyond the visualization of anatomy to measure aspects of local physiology. In a more specific sense, functional imaging refers to techniques of which the main goal is the mapping of the activity of the living brain elicited by specific tasks.

Two main approaches exist for non-invasive functional neuroimaging, in which neural activity is visualized either directly or indirectly. On one hand, in electrophysiological methods, such as electro-encephalography (EEG) and magneto-encephalography (MEG), signals that represent the summations of electrical events in individual neuronal cells are measured directly. On the other hand, metabolic/vascular methods, such as positron emission tomography (PET) and ▶functional magnetic resonance imaging (fMRI), indirectly infer information on neuronal activity by measuring the metabolic and/or vascular changes that are associated with neural activity.

Characteristics

The Biophysical Basis of fMRI

Activation of a neuronal cell population results in a local increase of the metabolism and the metabolic rate of glucose and oxygen. This increase of metabolism and metabolic rate is accompanied by a local increase of cerebral blood flow (CBF), both of which show a graded response to different degrees of functional activation. This connection—or 'coupling'—between neural activity and energy metabolism/CBF is the foundation of functional neuroimaging and has already been clearly established in animal studies and, to a lesser degree, in human studies.

The function of this 'neurovascular coupling' seems logical: an adequate supply of oxygen and glucose has to be maintained for varying levels of neuronal metabolism. The reality, however, is more complicated (Fig. 1). During neural activity, the increased amount of supplied oxygen does not match the actually increased consumption. As expected, the oxygen level of the blood initially drops slightly during the first second(s) of brain activation (the 'early response'), indicating an increase in cerebral metabolic rate of oxygen ($CMRO_2$). However, this event is followed by a huge increase in CBF that over-compensates the metabolic demand for oxygen, thus resulting in a local increase of oxygen concentration in the blood (the 'late' response). Although it has been demonstrated that the 'early response' corresponds to the neural activity both temporally and spatially, this is difficult to measure directly.

In fMRI, neural activity is measured indirectly using the ▶blood oxygenation level dependent (BOLD) contrast, as it is impossible to determine physiological parameters (such as CBF) directly. This BOLD contrast is a reflection of the complex interplay of blood oxygenation, CBF and $CMRO_2$ (Fig. 1). The first images sensitive to the level of blood oxygenation were first reported on by Ogawa and coworkers at 7T (1).

fMRI has a relatively low temporal resolution compared to electrophysiological methods. This is due to the fact that the response time is relatively slow (range of seconds) compared to the time constant of neural activity (range of tens of hundreds of milliseconds). Spatially, however, the coupling between the physiological response and neural activation is tight and well-localized, allowing the precise localization of task-related neural activity. It should also be noted that the precise mechanisms underlying and regulating the BOLD response remain to be elucidated and are subject of intense research.

When measuring BOLD responses in an fMRI experiment, three parameters can contribute to the recorded fMRI signal: the blood flow velocity, the blood flow volume and the blood oxygenation level. By carefully choosing MR imaging parameters, the contribution of blood flow velocity and blood flow volume can be minimized, while maximizing the blood oxygenation

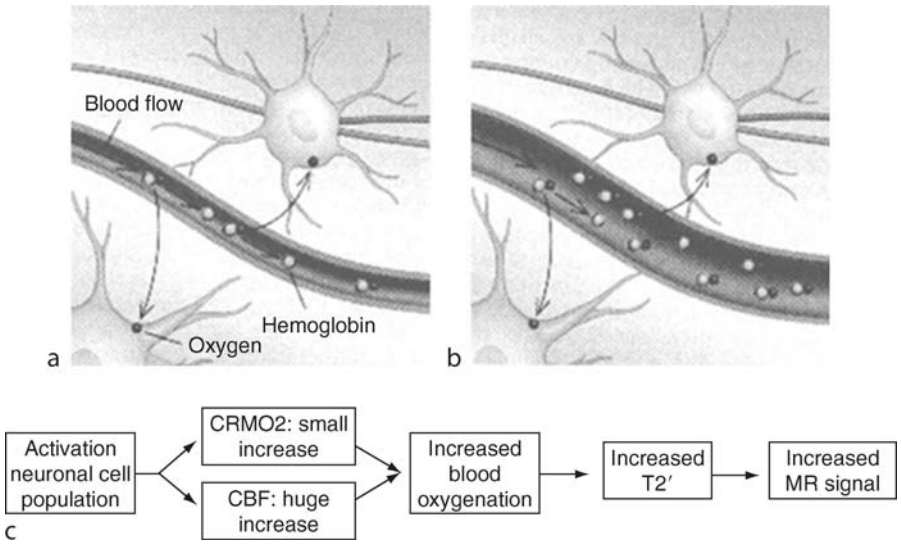

Brain, Functional Imaging. Figure 1 The biophysical basis of fMRI. (a) At rest, neurons extract oxygen from haemoglobin molecules in the blood. The blood flow maintains a constant level of blood oxygenation and oxygen/glucose supply. (b) When activated, the neurons extract a small additional amount of oxygen from the blood, while the cerebral blood flow is hugely increased. This mismatch between oxygen extraction and cerebral blood flow forms the basis of the blood oxygen level dependent contrast. (c) Schematic representation of the events leading to a blood oxygen level dependent response.

dependency of the fMRI signal, hence the name 'blood oxygenation level dependent (BOLD) contrast'.

The BOLD imaging contrast finds its basis in the observation that the transverse relaxation time (T2) of water protons in the blood provides information about the oxygenation state of the blood (2). In the blood, oxygen is transported by haemoglobin (Hb). The presence of deoxyhaemoglobin (dHb) creates magnetic field gradients around the red blood cells and in the tissue surrounding the vessels. These field gradients shorten T2* of the tissue and reduce the MR signal at rest from what it would be if there were no dHb present. The T2 relaxation time of blood is thus dependent on the degree of oxygenation of the blood, providing an endogenous contrast agent detectable with MRI.

Technical Challenges of fMRI

Susceptibility weighted sequences—T2*w images—are very suitable to measure the local susceptibility changes induced by the fMRI BOLD contrast upon neuronal activation. Although BOLD activations have been demonstrated with many different T2*-weighted imaging schemes, most fMRI experiments are performed with gradient echo single-shot echo planar imaging sequences (EPI) (Fig. 2A).

In MRI, an image matrix is built from a series of acquired k-space lines. In conventional sequences, this matrix will be filled over several repeats (shots), while in EPI the complete k-space is filled in a single shot, allowing to, acquire multiple adjacent slices in a very limited amount of time. This technically challenging method makes it possible to form a single slice MR image in as little as 70–100 msec. Multiple adjacent slices (e.g. 30 slices) are thus acquired covering the complete brain in about 2–3 sec. The image acquisition matrix is typically 64×64 voxels, resulting in a poorer spatial resolution than standard MR images, but the temporal resolution is far better. One of the key advantages of single-shot imaging is that the data collection is so short that the images are insensitive to motions that would create artifacts in standard images, such as pulsatile flow or swallowing.

After data acquisition, these data need a reasonable amount of post-processing before activation patterns can reliably be visualized (Fig. 2B). The detailed description of post-processing of fMRI data is beyond the scope of this description and is discussed in detail elsewhere [e.g. see (3)]. Briefly, the processing of fMRI data involves a number of steps which include correction techniques for bulk head motion, spatial normalization to a standard brain, spatial smoothing, statistical techniques for the reliable separation of the relevant fMRI signal change from the noise and visualization techniques for localizing activation foci on the anatomy of individual subjects.

Clinical Applications of fMRI

fMRI has been widely used to uncover the activation patterns elicited by specific tasks in both healthy volunteers and patients with a broad range of neurological disorders (Fig. 3).

In a clinical setting, additional factors may complicate the fMRI experiment. First, due to the presence of brain pathology or alterations of the cerebrovascular system, the physiological BOLD contrast may be altered or even absent. For example, the BOLD response in the vicinity of aglial tumour may not accurately reflect the electrical neuronal activity, as this tumour type can induce abnormal vessel proliferation in adjacent brain tissue, thereby altering regional CBF, CBV, vasoactivity and potentially, the BOLD contrast. Similar effects may be present in the case of congenital vascular malformations, in which aberrant vasculature may disturb a correct BOLD response to be elicited.

Second, other factors, including vasogenic oedema and tumoral haemorrhage, may contribute to the observation of a decreased BOLD response in near-lesion brain tissue. Metabolic changes in some brain tumors could induce environmental changes (e.g. tissue pH changes), which may again eliminate the physiological haemodynamic response.

Finally, the BOLD signal can also be significantly influenced by various pharmacological agents. For example, antihistaminics might reduce the BOLD response, while caffeine is a known booster of the BOLD response.

Considering these additional factors, it is of utmost importance to realize that the observation of an absence of fMRI activity in a particular brain region does not directly imply that electrical activity within this area is non-existing, and thus that it is safe to surgically remove this region.

In neurosurgical settings, traditionally, mapping of eloquent areas is achieved by invasive methods such as intraoperative cortical stimulation in the awake patient, implantation of a subdural grid with extraoperative stimulation or intraoperative recording of sensory-evoked potentials. fMRI can obtain these data preoperatively and completely non-invasively (4). Together with its high sensitivity for visualizing brain lesions, fMRI can define the relation between the margin of a lesion and any adjacent functionally significant brain tissue. fMRI has the potential to predict the possible deficits in cognition, language, motor and/or sensory perceptual functions that would arise from intrinsic lesion expansion, such as bleeding into an arteriovenous malformation, or from therapeutic intervention, such as surgery. Therefore, in a clinical setting, fMRI is mostly used for risk assessment of the treatment options, which should improve therapy with increased life expectancy and decreased morbidity.

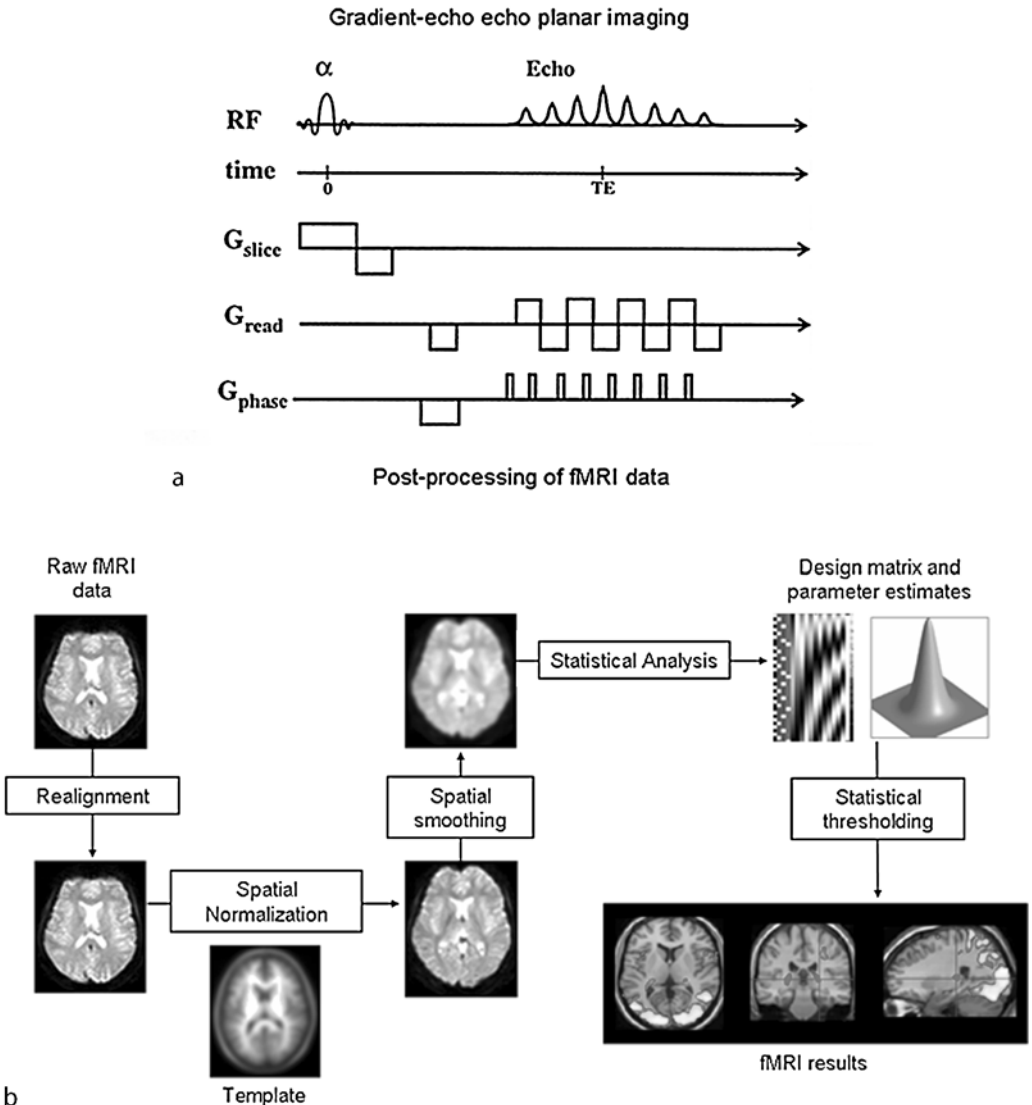

Brain, Functional Imaging. Figure 2 Technical challenges of fMRI. (a) The timing scheme of a gradient-echo single-shot ►echo planar imaging (EPI) sequence. At time zero, a radiofrequency (RF) excitation 90° pulse (α) of a narrow frequency range is transmitted to the subject in the presence of a spatial magnetic field gradient (G_{slice}), thereby exciting protons over a correspondingly narrow range of location (i.e. slice selection). In-plane spatial encoding is achieved by applying magnetic field gradients across this image slice, along the readout (G_{read}) and phase encoding (G_{phase}) directions. An echo train is generated by a rapidly alternating gradient in G_{read}. The phase encoding is achieved by gradient 'blips', small phase encoding gradients that add up in between the echoes. The phase gradient scheme is designed such that the echo with the highest amplitude occurs at the echo time (TE), and the amplitude of this echo is T2* weighted. (b) Schematic summary of post-processing steps of fMRI data.

Other clinical applications of fMRI include the postoperative follow-up of patients that underwent (partial) resection of a brain lesion, the guidance of therapeutical/pharmacological development by monitoring possible changes in activation patterns, and the identification of preclinical expression or the differential diagnosis of certain neurodegenerative or neuropsychiatric diseases (e.g. Alzheimer's disease or schizophrenia) (5).

Bibliography

1. Ogawa S, Lee TM, Kay AR et al (1990) Brain magnetic-resonance-imaging with contrast dependent on blood oxygenation. Proc Natl Acad Sci U S A 87:9868–9872
2. Thulborn KR, Waterton JC, Matthews PM et al (1982) Oxygenation dependence of the transverse relaxation time of water protons in whole blood at high field. Biochim Biophys Acta 714:265–270
3. Turner R, Howseman A, Rees GE et al (1998) Functional magnetic resonance imaging of the human brain: data acquisition and analysis. Exp Brain Res 123:5–12

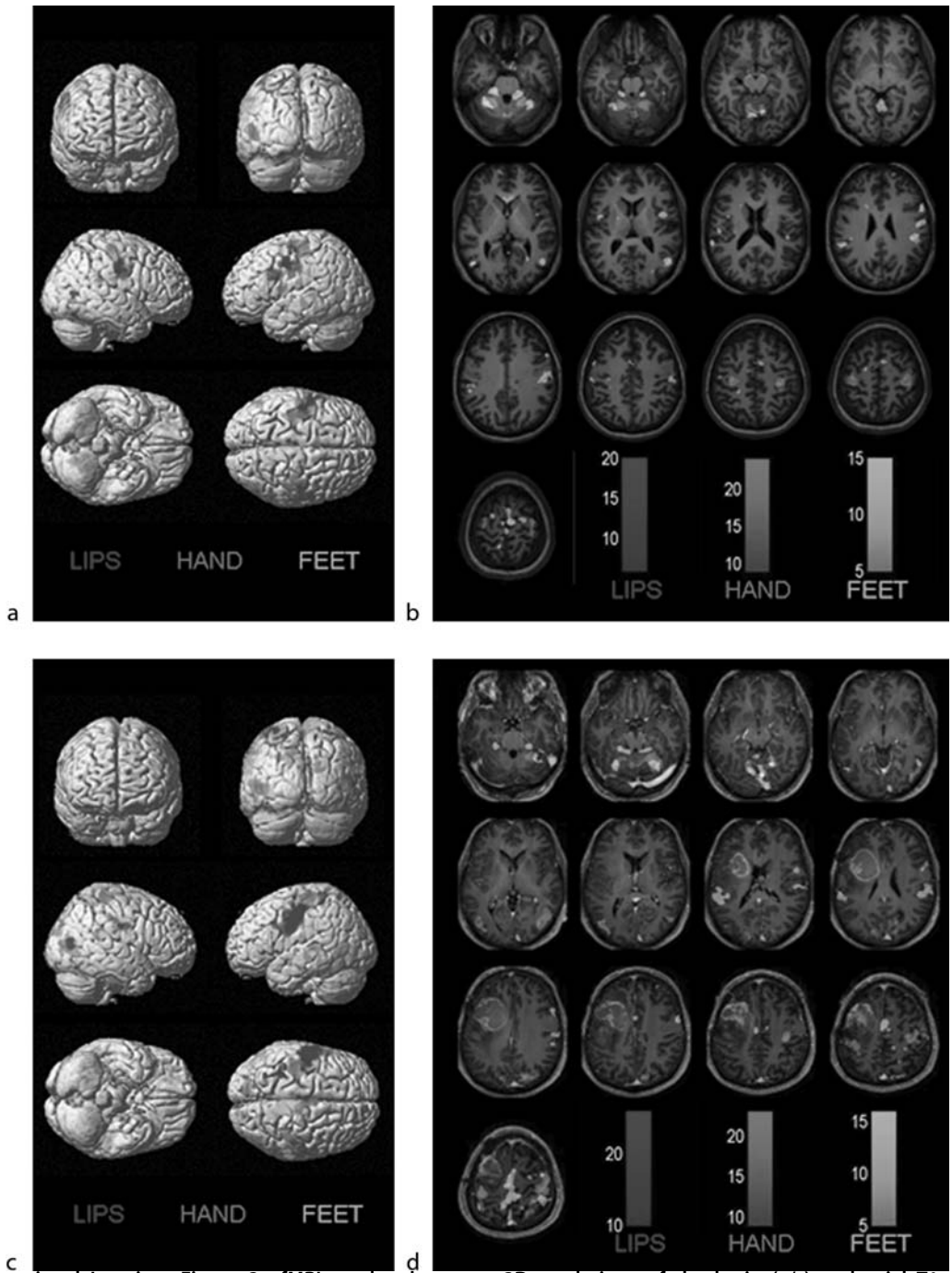

Brain, Functional Imaging. Figure 3 fMRI results shown on 3D renderings of the brain (a/c) and axial T1-weighted 3D-TFE slices (B/D). The subjects performed three series of motor tasks: lip pouting, bilateral finger tapping and bilateral feet movement, shown in blue, red and green respectively. (a/c) results obtained in a healthy volunteer. The somatotopical organization of the primary sensorimotor cortex and cerebellum are clearly demonstrated, with the foot representation located most medially, the lip representation most laterally and the hand representation in between. (c/d) results obtained in a patient with a glioblastoma multiforme (grade IV) located within the right gyrus frontalis medius and considerable perilesional edema. Somatotopy of the primary sensorimotor cortex and cerebellum can also be demonstrated in this patient. Note that due to the mass effect of the lesion the lip and hand representations are shifted posteriorly. Based on these results, minimal to no post-operative motor deficits would be expected, since the locations of activation are sufficiently separated from the lesion.

4. Sunaert S (2006) Presurgical planning for tumor resectioning. J Magn Reson Imaging 23:887–905
5. Weiller C, May A, Sach M et al (2006) Role of functional imaging in neurological disorders. J Magn Reson 23:840–850

Brain, Hematoma

▶Trauma, Head, Accidental

Brain, Injury

▶Trauma, Head, Accidental

Branchial Cleft Anomalies

Branchial cleft anomalies may present pathologically as a *fistula, sinus*, or *cyst*, based on the degree of completion of development of the anomalous structure.

▶Congenital Malformations, Neck

Breast

Silvia Obenauer
Department of Radiology,
Georg-August-University of Goettingen,
Goettingen, Germany
obenauerheuser@yahoo.de

General

The breast is a well-defined apocrine sweat gland. These glands have evolved into an organ whose purpose is to produce and secrete milk during lactation. The knowledge of hormonal influences during the life cycle (physiology) and mammographic anatomy are important prerequisites for interpretation of breast diseases. The breast is a mass of glandular, fatty, and fibrous tissues positioned over the pectoral muscles of the chest wall. Although the majority of breast disorders are benign, breast cancer is the most common cause of cancer death among women in the European Community. The sharp increase in the incidence of breast cancer over the last decades, however, is associated with only a very slight increase in the death rate. One of the disturbing aspects of breast cancer is that little can be done to prevent it. Most risk factors cannot be influenced. This is especially true for genetically determined premenopausal cancers. The best chance to cure breast cancer is to treat it at its earliest stages. There is evidence that biennial screening for breast cancer of women aged 50–70 years leads to mortality reduction, provided that the quality and assessment of mammography are excellent, and the negative effects of screening, such as false-positive results and missed cancers, are limited. To reach this goal, quality assurance of the imaging modalities is of most importance. The performance of triple diagnostic procedures consisting of a physical examination, X-ray mammography, and biopsy, if necessary, are recommended in the breast cancer diagnostic work-up. Abnormal findings in mammograms may require the performance of additional mammographic images and/or ultrasound. Additional mammographic images include spot compression/magnification views, tangential views, rolled views and other individually determined, angled views of the breast designed to solve special problems.

Since the introduction of dynamic contrast-enhanced MR imaging of the breast approximately 15 years ago, its usefulness as a highly sensitive tool in the diagnosis of malignant breast lesions has been confirmed. In spite of its variable specificity, contrast-enhanced MR imaging of the breast can improve diagnostic accuracy if it is used as an adjunct to mammography and ultrasound for specific indications. MRI is particularly useful for the evaluation of breast implants and the detection of cancer in patients with implants. Other indications for contrast-enhanced MRI of the breast are the finding of occult cancer in the presence of positive axillary adenopathy or other metastases, and the follow-up of breast cancer treated by surgery, radiation, or chemotherapy. Advantages also have been demonstrated in the preoperative evaluation and local staging of breast cancer.

Other imaging modalities including nuclear medicine studies (technetium sestamibi, positron emission tomography, sentinel lymph node mapping), thermography, computer tomography laser mammography, electrical impedance imaging, light mammography, and MR elastography are under investigation.

Modern mammography demands high standards in all aspects. These include X-ray equipment, radiographic technique, film-screen combinations, processing, viewing conditions, and interpretation. Shortcomings in any of these areas lead to errors. Several advancements in the last decades, such as grid, screen-film mammography, and anode-filter combinations, have improved the quality of mammography. The introduction of digital imaging was a

step to the digital horizon in mammography with all the advantages of digitization in radiology. As part of ongoing efforts to improve quality in the practice of mammography and to standardize mammographic reporting, the American College of Radiology (ACR) has devised the Breast Imaging Reporting and Data System (BI-RADS), a standardized categorization used for the evaluation of breast lesions according to their morphology. The illustrated lexicon describes mammographic lesion features and includes special cases that are encountered with breast masses. Calcifications are divided according to their individual morphology and their distribution. Typically benign calcifications, calcifications of intermediate concern, and calcifications with a high probability of malignancy are described in detail. The BI-RADS publication includes a section describing a reporting system designed to facilitate communication and outcome monitoring. In a mammographic report, the findings are summarized in the final assessment section. The categorization into one of the five assessment categories (negative, benign finding, probably benign finding, suspicious abnormality, highly suggestive of malignancy) indicates a course of appropriate action.

Ultrasound is an important complementary procedure to mammography. Analysis of sonographic features may aid in the appropriate selection of lesions to be followed-up or biopsied. The ACR has also developed a breast ultrasound lexicon (BI-RADS—ultrasound) to realize consistent terminology and clear communication of findings and results directly affecting patient management.

A BI-RADS lexicon for MRI was developed to encompass the reporting of breast MRI scanning technique, lesion architecture, and region of interest (ROI) kinetic/time–intensity curve interpretation.

Special Procedures

Special procedures such as:

- Cyst aspiration,
- Pneumocystography,
- Fine-needle aspiration cytology,
- Tru-cut biopsy,
- Vacuum assisted biopsy,
- ABBI- and Site-select devices,
- Galactography,
- Presurgical lesion localization, and
- Specimen radiography

will be described in detail.

Biopsy performance can be guided by different methods: ultrasound-guided, mammography-guided (stereotactic), or MR-guided. Stereotactic biopsy is performed in women with nonpalpable mammographic lesions which cannot be located by ultrasound. It is the procedure performed for the evaluation of suspicious microcalcifications. Once the decision to perform biopsy has been made, the physician has a choice of biopsy instruments. The most widely available and least expensive is the 14-gauge tru-cut type needle. Another commonly used biopsy instrument is the vacuum-assisted probe.

Special Disease Entities of the Breast

In accordance with the ACR classification the section of special disease entities of the breast contains essays dealing with:

- Neoplasms (benign, malignant),
- Inflammation,
- Effects of trauma and therapy,
- Duct diseases, mammary dysplasia, cutaneous lesions, lymphadenopathy,
- Metabolic-endocrine-toxic changes, and
- The male breast.

Each essay is divided into:

- General information,
- Pathology,
- Imaging findings in ultrasound, mammography, and contrast-enhanced MR mammography (MRI) with reference to the BI-RADS classification,
- Differential diagnosis, and
- Clinical presentation, treatment, and prognosis of the disease.

Neoplasms

Benign Lesions

There are a number of benign disorders that occur in the breast like:

- Cysts are harmless accumulations of fluid in the breast. Most painless cysts may be left alone. Occasionally a physician may drain them by fine-needle aspiration.
- Fibroadenomas are the most common benign tumor in young women. They are round or oval, movable and firm. Fibroadenoma has no risk of increased malignant transformation and is not associated with an increased risk of breast cancer.
- Benign phyllodes tumors are similar to fibroadenomas.
- Adenomas are rare benign tumors in young women.
- Hamartoma of the breast is a fibroadenolipoma.
- Galactoceles are milk-filled cysts that can occur in pregnant or lactating women.
- Lipomas are usually solitary, asymptomatic, and slow-growing lipid lesions.
- Papillomas are the most common cause of serous/sanguinous nipple discharge.
- Fibrocystic changes include a range of changes within the breast involving both the glandular and stromal tissues.

- Hyperplasias show a proliferation increased cellularity of glandular ductal epithelium.
- Sclerosing adenosis is a proliferation of glandular tissue.
- Radial scar is a benign proliferative lesion with a spiculated appearance on mammography.
- Milk-of-calcium is fine powdery calcifications precipitated into dilated lobules and microcysts.
- Plasma cell mastitis is a rare aseptic inflammation usually located in the subareolar area.
- Hemangioma is benign well-circumscribed vascular neoplasms.
- Mondor's disease is a superficial thrombophlebitis.
- Myoepithelial neoplasms are very rare and arise from myoepithelial cells. There are benign or malignant forms:
  - Adenomyoepithelioma,
  - Myoepitheliosis,
  - Malignant myoepithelioma,
  - Pleomorphic adenoma, and
  - Adenoid cystic carcinoma.

Malignant Lesions

In this section epidemiology of breast cancer and typical signs for malignancy are discussed. The malignant lesions are also described in detail.

Several factors increase the risk of developing breast cancer. These include:

- Demographic factors,
- Reproductive variables,
- Multiple primary cancers,
- Family history,
- Benign breast diseases,
- Mammographic features,
- Radiation exposure, and
- Geography.

Mammographic signs of breast cancer are divided into primary and secondary signs:

Primary signs

- Dominant mass: ill-defined, spiculated, usually dense
- Microcalcifications:
  - amorph or polymorph
  - clustered, linear, or segmental distribution
- Diffuse increase in density
- Architectural distortion

Secondary signs

- Distortion of adjunct tissues, obliteration of the subcutaneous, or retromammary space
- Asymmetric thickening
- Asymmetric ducts, duct dilatation
- Skin or nipple changes
- Edema of all or part of the breast
- Increased vascularity with venous engorgement
- Enlarged axillary lymph nodes.

Malignant Lesions in Detail

Breast cancer is the most common malignant lesion in breast with the following histopathological entities:

- Noninvasive carcinoma
- Ductal carcinoma *in situ* (DCIS)
- Lobular carcinoma *in situ* (LCIS)
- Invasive carcinoma
- Invasive ductal carcinoma
- Invasive lobular carcinoma
- Mucinous/colloid carcinoma
- Medullary carcinoma
- Inflammatory breast cancer
- Ductal papillary carcinoma
- Intracystic papillary carcinoma
- Tubular carcinoma
- Adenocystic carcinoma
- Paget carcinoma of the nipple.

Metastases in the breast occur with the following primaries: melanoma, ovarian carcinoma, leukemia, or lymphoma.

Lymphomas of the breast can be primary or metastatic lymphoma.

Sarcomas of the breast like fibrosarcoma, rhabdomyosarcoma, liposarcoma, and angiosarcoma are very uncommon.

Inflammation

Mastitis is an infection that most often affects women who are breast-feeding or who have an injury of the skin. Some cases progress to form breast abscesses. There are three forms of mastitis: puerperal, nonpuerperal, and granulomatous mastitis.

Abscesses of the breast are usually seen in lactating women.

Posttraumatic and Posttherapeutic Changes

Hematomas/seromas of the breast result from surgery or biopsy, blunt trauma, coagulopathy or after anticoagulant therapy.

Postsurgical or posttraumatic calcifications like

- Fat necrosis and oil cysts of the breast are an aseptic saponification of the fat by tissue lipase after local destruction of fat cells with the release of lipids and
- Dystrophic calcifications.

Scars and architectural distortion after breast-conserving treatment, breast reconstruction or after breast augmentation (enlargement) with implants are often a challenge for radiologists since they are difficult to differentiate from recurrent malignancy.

Imaging findings after breast prostheses implantation including silicone implant rupture will be discussed.

Duct Disease, Mammary Dysplasia, Cutaneous Lesion, Lymphadenopathy

Duct ectasia is a common condition associated with a green or black, often thick, sticky discharge. Other duct diseases as well as mammary dysplasia, and lymphadenopathy will be revealed.

Intramammary lymph nodes are not uncommon.

Furthermore skin lesions like moles and sebaceous cysts can be superimposed over parenchyma and create difficulties in the differential diagnosis from parenchymal lesions.

Metabolic, Endocrine, and Toxic Changes

Changes due to hyperestrogenism, menopause, cycle, and lactation are discussed.

Male Breast

Gynecomastia is a hypertrophy of the male mammary gland.

Breast Abscess

A breast cavity filled with purulent material.
►Duct Disease, Breast

Breast Cancer Recurrence

►Recurrent Neoplasms, Breast

Breast Cancer Relapse

►Recurrent Neoplasms, Breast

Breast Cancer Screening

►Screening, Breast Cancer

Breast Conservation Treatment

►Breast Conserving Therapy

Breast Conserving Therapy

Luis C. Apesteguía
Hospital Virgen del Cashino, Pamplona, Spain
luis.apesteguia.ciriza@cfnavarra.es

Synonyms

Breast conservation treatment; Breast-conserving surgery; Conservative breast surgery; Conservative surgical therapy

Definition

Breast-conserving therapy (BCT) can be defined as a group of surgical procedures that completely remove the breast cancer along with a rim of normal breast tissue around it, saving most of the normal breast tissue. In contrast to the classical treatment, radical mastectomy, the aim of BCT is not only to achieve safe oncological therapy but also to preserve as much as possible of the mammary gland and axillary nodes (1, 2).

Characteristics

Diagnostic and surgical management of breast cancer has changed significantly in recent years. Percutaneous biopsy is used in the diagnostic process, thus avoiding scarring incisions. The preferred method of treatment for many women with early breast cancer is BCT, principally ►lumpectomy and axillary dissection, usually followed by breast ►radiation therapy (RTP). ►Sentinel node biopsy is becoming a valid alternative, thus decreasing morbidity following standard axillary dissection. These techniques allow women with different forms of breast cancer to conserve their breasts and axilla.

Nowadays BCT is widely accepted as an adequate surgical therapy for stages I and II breast cancer, but just two to three decades ago, the pioneers of these techniques had to demonstrate their accuracy versus radical mastectomy, the former gold-standard treatment (1–3). A slightly higher local recurrence rate was reported in some larger studies in women who underwent BCT instead of mastectomy, which usually does not require postoperative RTP. However, in general terms the rates of local recurrence and long-term survival have been demonstrated to be similar for both therapeutic schemes.

Six prospective randomized trials conducted from 1972 to 1989 have shown no difference in survival between mastectomy and BCT plus RTP for stages I and II breast cancer (Table 1) (1–5).

Imaging Issues

Radiology and imaging techniques in general are in the center of these changes. The spread and improvement of mammography (MX), ultrasonography (US), and imaging-guided interventional techniques have been the origin and essential condition for generalization of BCT, first for detection of small lesions and accurate assessment of its extent within the breast, then as a necessary adjunct in surgical procedures, and finally as the most useful methods for follow-up and early detection of local recurrences.

Breast Conserving Therapy. Table 1 Survival rates of breast-conserving therapy plus radiation therapy (BCT + RTP) compared with radical mastectomy alone (RM) [adapted from Winchester DP, Cox JD (1998) Standards for diagnosis and management of invasive breast carcinoma. CA Cancer J Clin 48:85]

Trial	Number	Endpoint (years)	BCT + RTP	RM	*P*-value
Milan Cancer Institute	701	18	65	65	NS
Institut Gustave-Roussy	179	15	73	65	0.19
NSABP B-06	1,843	12	63	59	0.12
National Cancer Institute	237	10	77	75	0.89
EORTC	903	8	54	61	NS
Danish Breast Cancer Group	905	6	79	82	NS

NS = not significant

Population-based screening programs allow detection of very small, invasive, or in situ breast carcinomas, lesions for which BCT is the elective treatment.

Complete evaluation of the breast before BCT may require mammographic additional views, magnification, comparison with prior studies, US, and magnetic resonance imaging (MRI) to detect additional sites of carcinoma, which may change the indication of surgical therapy from BCT to mastectomy. Nonpalpable carcinoma can be diagnosed using needle localization with excisional biopsy or imaging-guided percutaneous biopsy. These procedures use either stereotactic MX, US, or MRI to localize the suspicious lesion. US is preferred if the lesion is clearly identifiable by this technique. A large-core needle or a vacuum-assisted device is then used to obtain several samples from the lesion through a small incision (several millimeters in length) under local anesthesia.

Localization for excisional biopsy or BCT of nonpalpable tumors previously diagnosed percutaneously requires that a hook-wire be placed prior to surgery, again using the most adequate imaging method. Several studies suggest that the percutaneous procedures are faster and less costly than excisional biopsy. Stereotactic MX on digital table may not be possible, as with patients who cannot lie in the prone position or those who have an extremely high body weight. Lesions close to the chest wall may be difficult to remove stereotactically, requiring hook-wire excisional biopsy.

Percutaneous biopsy with malignant results allows the volume of the surgical specimen to be better adjusted to the tumor size, thus avoiding additional operations and the risk of local recurrence. Contrast-enhanced MRI has demonstrated an excellent usefulness in preoperative evaluation and local staging. A more precise evaluation of the tumor size and detection of additional foci not identifiable either by MX or US reduces the number of cases for BCT, but consequently, the rates of local recurrence will be also reduced. Both US and MRI are excellent methods for detecting suspicious axillary nodes that can be punctured by US guidance in order to decide the most appropriate axillary management.

Surgical Techniques

Breast

There are three main surgeries for the mammary gland: lumpectomy, ►quadrantectomy, and segmental mastectomy.

Lumpectomy is the surgical removal of a tumor along with a small margin of the surrounding normal breast tissue. Segmental mastectomy is a wider excision with the aim of achieving better adequation to the morphology of a mammary segment. Quadrantectomy is the term

used when up to one-quarter of the breast is removed, including an ellipse of skin and fascia of the pectoralis major muscle. It is usually indicated for more extended tumors.

After the excision is performed and the specimen is clearly marked by the surgeon, radiography should be done to ensure that the area of concern has been completely removed according to the radiologist's opinion. In this case, both the specimen and the radiograph are sent to the pathology department. The pathologist should carefully mark the resection margins prior to cutting the specimen so that the relationship of the lesion to the surgical margins can be ascertained. If the margins appear free of tumor, the surgical procedure on the breast can be finished. Frozen section is not desirable in this context. However, the final microscopic report may reveal residual cancer cells in the margins. If the margins of the removed specimen are affected either in intraoperative or in definitive histological study, additional surgical reexcision is usually indicated to remove the remaining lesion. If it is not possible to clear the margins on reexcision, then a mastectomy is normally offered. Some controversy remains regarding how large the safety pathologic margins should be, although some consensus has been reached for 2 mm. If a margin is <2 mm. and reexcision is declined or inappropriate, a radiation boost to the tumor bed is recommended.

Axilla

In addition to the local excision, a separate incision is performed during the same procedure in order to include a sampling or removal of the axillary lymph nodes and to determine whether the cancer has begun to spread out of the breast itself.

There are two procedures for removing lymph nodes in breast cancer patients: ►axillary node dissection (AND) and sentinel lymph node biopsy (SLNB).

AND is the standard way to remove axillary lymph nodes. Typically, 10–30 nodes are removed under general anesthesia and are later examined in the pathology laboratory. Standard AND involves levels I and II nodes. Removal of level III axillary nodes is necessary only when obvious disease is present.

The most common side effect of lymph node removal is ►lymphedema of the arm, which affects 10–20% of patients, including some patients who have only SLNB. The risk of lymphedema is greater if the patient also undergoes RTP and/or the lymph nodes contain cancer cells upon final examination. To help manage lymphedema, patients should report symptoms as soon as they occur. In addition, special exercises should be performed shortly after recovering from surgery to encourage and help maintain lymphatic flow. Early signs of lymphedema are a feeling of tightness in the arm, pain, aching or heaviness, swelling, redness, and less movement or flexibility in the affected extremity. In addition to lymphedema, other common side effects of AND include limitations of arm/shoulder movement and numbness of the upper arm skin.

SLNB is a more recent technique that requires a multidisciplinary approach, coordinating the efforts of the radiology, surgery, and pathology departments. Appropriate training and skill development is mandatory. Generally accepted indications include women with T1 and T2, clinically N0 breast cancers.

The sentinel lymph node is the first node in the chain of nodes draining the area containing the malignant lesion. The sentinel node is a key indicator of spread. The technique involves injecting a blue dye, radioactive tracer, or both to identify the "sentinel" lymph nodes. This is done during surgery with a gamma probe (a handheld device) that identifies a "hot spot" representing the node. When the dye techniques are used, the sentinel node is colored blue for visual identification. The sentinel node can then be identified, removed, and examined for tumor cells. In a small percentage of patients, the sentinel node is located in the internal mammary chain.

Using this method, only the first one to three nodes in the lymphatic chain are removed. If the sentinel nodes are affected or if the surgeon is unable to identify a sentinel node, additional surgery is performed to remove the remaining axillary nodes. If the sentinel nodes do not contain cancer cells, then no additional lymph nodes are removed, reducing the side effects. SLNB is rapidly becoming a more common procedure, but AND is still considered standard by many physicians.

The positive predictive value of the SLNB is about 95%. Contraindications include a clinically positive axilla, prior axillary surgery, pregnancy, or lactation. Women who have received preoperative chemotherapy or have multicentric and extensive multifocal carcinomas or tumors >5 cm should not undergo SLNB.

Axillary dissection is not currently recommended for ►ductal carcinoma in situ (DCIS). However, the larger the focus of DCIS, the higher the chance that a focus of microinvasive disease is present. Therefore, SLNB is appropriate in patients with DCIS >5 cm in diameter. Women with well-differentiated DCIS <1 cm and with complete radiographic and pathologic excision do not require axillary dissection and may be managed by wide excision alone.

Radiation Therapy

Randomized trials have compared breast-conservation surgery alone with surgery plus RTP, demonstrating a higher recurrence rate in women who do not receive radiation. Standard BCT should therefore be followed by

adjuvant RTP, either local or systemic. Most commonly, at least six weeks of RTP is carried out to ensure that all cancer cells in the remaining breast have been destroyed. The dose of radiation delivered to the entire breast is between 45 and 50 Gy. A booster dose of 15 Gy is delivered to the tumor site. This treatment is optimally started 2–8 weeks following the surgery, unless adjuvant was given before. Newer studies, still under investigation, are beginning to show that shorter radiation times may be equally effective in preventing local tumor recurrence. Chemotherapy, tamoxifen, or both may also be given as adjuvant therapies.

Concerning DCIS, adjuvant RTP is currently recommended for women with tumors >1 cm in diameter or comedo-type DCIS treated with BCT and in all patients with close margins (<5 mm) of excision.

Common side effects of radiation therapy include fatigue, loss of appetite, nausea, hair loss to the treated area, and, more often, rash or skin redness in the treated area. Acute symptomatic pneumonitis is uncommon, but late radiological changes of lung fibrosis are frequent. Esophagitis may develop if an en face internal mammary field is used. Cardiac toxicity is rare. Most of these effects are temporary and do not occur in all patients.

Indications and Contraindications

Women diagnosed with carcinoma <5 cm are candidates for BCT. Tumor size is not an absolute contraindication, but the presence of a large tumor in a small breast treated with adequate margins might result in an unwanted cosmetic result.

Some other exceptions can be considered. According to the American Cancer Society, BCT should not be indicated for women who have already undergone RTP in the breast/chest area, who have multicentric disease, whose previous lumpectomy did not completely remove the cancer, who have connective tissue diseases such as scleroderma, or who would be pregnant at the time of RTP. The location, size, associated microcalcifications, and any other characteristics of the primary tumor must be carefully determined. Patients with invasive ductal and lobular cancers are candidates for BCT if the tumor is not diffuse and negative margins can be achieved. The presence of positive axillary nodes is not a contraindication to BCT. Tumors close to the nipple-areola complex may require excision of the nipple, but this is not a contraindication.

There has been some controversy about the usefulness of BCT as treatment for DCIS and for invasive carcinomas with an extensive intraductal component because of the discontinuous morphology of this lesion, which can extend through large areas of the breast, sometimes with lack of imaging findings. BCT has finally been considered preferable to radical mastectomy and for not extensive DCIS, proven that its rates of recurrence and survival are similar to those of radical mastectomy. Women with very diffuse areas of DCIS (>5 cm or one-quarter of the breast) have a substantial risk of recurrence after BCT, so mastectomy should be recommended for them. The Van Nuys prognostic index, which incorporates age, margin status, grade, and size, can be useful to estimate the risk of recurrence after BCT in these cases. Invasive lobular carcinomas are also more problematic because of the difficulty in identifying their limits by imaging techniques.

The patient's wishes should always be considered when deciding on treatment. For most patients, mastectomy will not influence the likelihood of survival but may impact the quality of life. Women treated with BCT have fewer episodes of depression, anxiety, and insomnia.

BCT may be performed using a local anesthetic, sedation, or general anesthesia, depending on the extent of the surgery needed. Unlike after mastectomy, a drainage tube is usually not necessary after lumpectomy. A ▶seroma (clear fluid trapped in the wound) usually fills the surgical cavity and helps to naturally remold the breast's shape. Gradually, the seroma is absorbed, and the body replaces it with scar tissue. This natural healing process and formation of scar tissue occur over a period of months, so the final results of the surgery may not be apparent for some time.

Complications of BCT are similar to those of radical mastectomy and RTP. The most frequent are bleeding and infection. In rare instances, women may experience recurring seromas after BCT. These collections are easily drained in the surgeon's office or under radiological guidance. If they recur, several methods may be used, including compression or sclerosis to fill and harden the space in the breast. At times, these treatments can be uncomfortable, but they are rarely needed. Major complications after AND include nerve damage and lymphedema of the arm. Injury to the long thoracic nerve denervates the serratus anterior muscle and causes a winged scapula. Intercostobrachial nerve damage causes loss of sensation in the upper inner arm.

Several strategies are recommended for preventing lymphedema, but these strategies lack scientific proof of effectiveness. Patients should immediately seek treatment for any infection. Blood pressure measurements, venipunctures, and intravenous insertions should be avoided in the arm on the side of the surgery.

Follow-up

The ability to obtain clear surgical margins and the tumor's pathologic characteristics are important considerations

in patient selection for BCT. Complete tumor removal as documented by pathologic margins is associated with optimal local cancer control in most reported series. However, not all cancers are amenable to complete surgical removal, and some pathologic subtypes, such as infiltrating lobular carcinoma, present difficulties in obtaining clear margins and may result in a high incidence of local failure after BCT and RTP.

As for invasive ductal carcinoma with an extensive intraductal component, if adequate surgical margins can be achieved, local recurrences after irradiation are acceptably uncommon. All subtypes of DCIS have been resected with equal success rates in obtaining clear margins. However, the local recurrence rates for intraductal cancer appear somewhat higher than those for invasive tumors. Multifocal intraductal carcinomas with microinvasion have a high local recurrence rate, with recurrences developing within the first 18 months of follow-up.

Local recurrence can occur after surgery. Local recurrence following BCT is usually at the surgical site and can be treated with conservative reexcision or mastectomy. After mastectomy, recurrence is on the chest wall. Clinical history, physical examination, and conventional breast imaging techniques are the most effective means of follow-up. Patients at exceptionally high risk of recurrence or development of a second primary tumor should be watched more closely.

MX is important for the early recognition of recurrence. Unfortunately, changes seen on mammography resulting from surgical therapy and irradiation may mimic the signs of malignancy. Increased density, skin thickening, architectural distortion, and scar formation are the most common findings caused by surgical intervention. Dystrophic and fat necrosis calcifications can be caused by RTP.

A baseline mammogram should be obtained approximately 3–6 months after tumor excision and the completion of RTP. MX should then be done at least annually. US is a well-known adjunctive technique, more necessary to investigate dense breasts or areas where density is higher, so that the sensitivity of MX is lower.

Patients must be routinely followed by physical examination and annual mammograms after BCT. The signs and symptoms of breast cancer recurrence are the same as those in a nonradiated breast and include new cluster calcifications, asymmetric densities, or, occasionally, increasing size of a preexisting scar. Breast fibrosis in the area of the tumor-bed boost can persist for many months and be confused with recurrence. MRI with gadolinium has showed the highest sensitivity in this differential diagnosis.

Frequently, fat necrosis and oil cysts may also appear near the surgical scar, resembling recurrence. In these cases, percutaneous biopsy should be carried out to detect recurrence. The natural history of the postirradiation mammogram includes a slow but progressive return to normal degrees of breast fibrosis and skin thickness.

The recurrence rate outside the immediate tumor bed is negligible until the fifth year, and it then increases 1% per year thereafter.

Bibliography

1. Harris JR, Lippman ME, Morrow M et al (2004) Diseases of the Breast, 3rd edn. Lippincott Williams & Wilkins, Philadelphia, pp 43–50
2. Dershaw DD (2002) Breast imaging and the conservative treatment of breast cancer. Radiol Clin N Am 40(3):501–516
3. Veronesi U, Sarccoci R, Del Vechchio M et al (1981) Comparing radical mastectomy with quadrantectomy, axillary dissection and radiotherapy in patients with small cancers of the breast. N Engl J Med 305:6
4. Fisher B, Anderson S, Redmond CK et al (1995) Reanalysis and results after 12 years of follow-up in a randomized clinical trial comparing total mastectomy with lumpectomy with or without irradiation in the treatment of breast cancer. N Engl J Med 333:14561461
5. Winchester DP, Cox JD (1998) Standards for diagnosis and management of invasive breast carcinoma. CA Cancer J Clin 48:85
6. Fowble B, Rosser C, Hanlon A et al (1998) Conservative surgery and radiation for Stages I and II breast cancer. In: Bland KI, Copeland EM (eds) The Breast: Comprehensive Management of Benign and Malignant Diseases. 2nd edn. W.B. Saunders, Philadelphia, pp 1172–1178

Breast Fistula

Communication between an internal cavity of the breast and the skin.

▶Inflammation, Breast

Breast Imaging Reporting and Data System (BI-RADS);

▶BI-RADS, Lexicon

Breast Mass

Space-occupying lesion seen in two different projections.

▶Neoplasms, Phyllodes, Breast

Breast Metastasis

Secondary deposition of malignant cells from a tumor outside the breast, most commonly melanoma, lung cancer, ovarian cancer, sarcoma, or gastrointestinal carcinoid tumor.

▶Metastases, Breast

Breast Recurrent Neoplasms

Breast neoplasms that are diagnosed during follow-up, several months or years after some kind of treatment; normally, surgical removal has been carried out on the breast and the primary neoplasm has apparently been completely removed or disappeared.

▶Recurrent Neoplasms, Breast

Breast-Conserving Surgery

▶Breast Conserving Therapy

Breast, Architectural Distortion

A term that describes a mammographic lesion whose main features are radiating spicules with no definite mass visible.

▶Radial Scar, Breast

Breast, Benign Tumors

Pina Luis
Clínica Universitaria de Navarra, Spain
ljpina@unav.es

Definition

Several rare benign tumours are included, such as adenomyoepitheliomas, leiomyomas, ▶myofibroblastomas, ▶granular cell tumours, desmoid tumours, chondrolipomas, benign peripheral nerve sheath tumours, haemangiomas and ▶mucocele-like tumours.

Pathology

Adenomyoepitheliomas are benign solid tumours of variable myoepithelial cells growing around small epithelial-lined spaces. Rarely, adenomyoepitheliomas may become malignant (1).

Most leiomyomas arise from smooth muscle in the nipple and areola (2). Parenchymal leiomyomas arise from metaplasia of myoepithelial, myofibroblastic cells or from blood vessels.

Myofibroblastomas are benign spindle cell tumours of the mammary stroma composed of myofibroblasts (2). Granular cell tumours are benign lesions derived from Schwann cells and consist of a poorly circumscribed proliferation of clusters of cells in which the main characteristic is prominent granularity of the cytoplasm. The granularity corresponds to lysosomes (2).

Desmoid tumours, also known as fibromatosis, consist of a locally invasive, non-encapsulated proliferations of spindle fibroblasts and myofibroblasts. Mammary involvement from fibromatosis of the pectoral fascia is excluded (2).

Chondrolipomas are rare benign neoplasms consisting of fat, cartilage and fibrous tissue. ▶Benign peripheral sheath tumours include schwannomas, neurofibromas and perineuromas. Schwannomas are benign tumours originated from Schwann cells. Neurofibromas are benign lesions composed of a mixture of Schwann cells, perineural like cells and fibroblasts. Finally, perineuriomas are benign proliferations of perineural cells.

Haemangiomas are benign tumours or malformations of mature vessels (2). Three subtypes are described: cavernous, capillary and venous.

Mucocele-like tumours include benign and atypical lesions. These tumours originate in cysts distended with mucin that extrudes into the surrounding stroma. The cysts are lined by cuboidal epithelial cells, although a pattern of atypical ductal hyperplasia may be found (3).

Clinical Presentation

All these benign tumours are very infrequent breast lesions. Occasionally these tumours may be palpable and thus simulate breast cancers. Granular cell tumours and desmoid tumours are the most suspicious at palpation. Myofibroblastomas also occur in men.

Imaging

Mammography

Mammography is not able to differentiate these benign tumours from other benign or malignant lesions (4). Granular cell tumours and desmoid tumours usually appear as spiculated masses, similar to carcinomas (Fig. 1). The remaining tumours are seen predominantly as round to oval well-circumscribed masses (4). Mucocele-like tumours may also be seen as clustered microcalcifications (Fig. 2).

Ultrasound

Both granular cell tumours and fibromatosis present as suspicious irregular masses (4). The remaining tumours usually appear as well-circumscribed hypoechoic masses (Fig. 3). Mucocele-like tumours are found as complicated cysts.

Magnetic Resonance

The experience with all these tumours is limited to a few case reports. Desmoid tumours are seen as isointense lesions on T1-weighted sequences and heterogeneous on T2-weighted sequences. On contrast-enhanced fat-suppressed T1-weighted images, desmoid tumours are ill-circumscribed masses with heterogeneous enhancement (4).

Myofibroblastomas are found as isointense lesions compared with the muscle on T1-weighted images and hyperintense on T2-weighted images. On enhanced T1-weighted images, myofibroblastomas enhance homogeneously (5).

Nuclear Medicine

Nuclear medicine studies are not useful to diagnose these rare benign tumours.

Diagnosis

The diagnosis of very infrequent benign lesions may be problematic for the pathologist, even when the lesions are excised *in toto*. The partial sampling of these lesions, as occurs in needle core biopsies, makes the diagnosis more difficult. In most cases, the complete excision of these tumours is recommended to confirm the diagnosis (6).

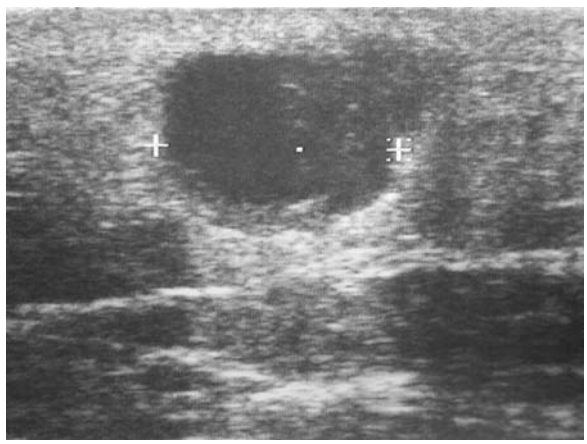

Breast, Benign Tumours. Figure 2 Ultrasonography shows an ovoid well-circumscribed homogeneous mass. Myofibroblastoma.

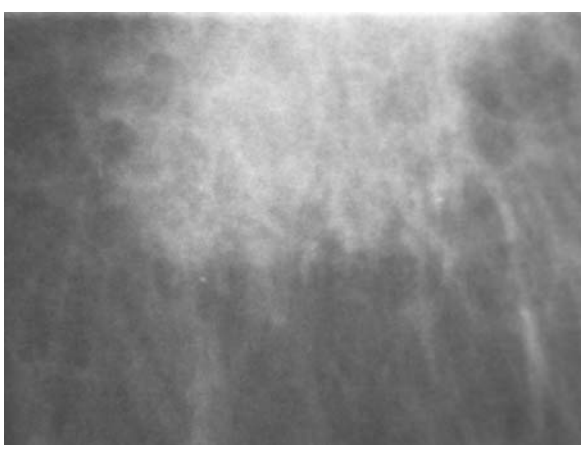

Breast, Benign Tumours. Figure 1 Irregular mass with indistinct margins. Craniocaudal view (detail). Pathology: desmoid tumour.

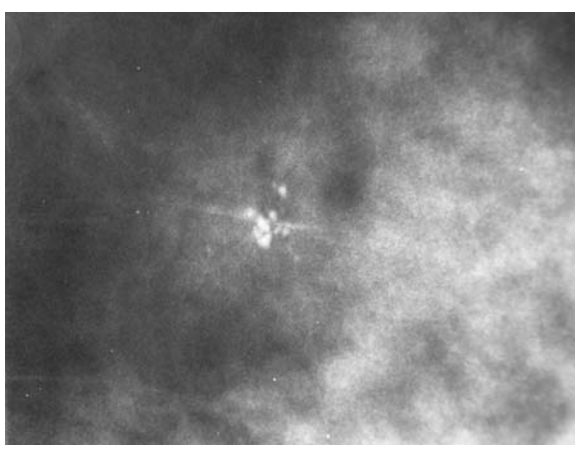

Breast, Benign Tumours. Figure 3 Small cluster of pleomorphic calcifications. Craniocaudal view (detail). Pathology: mucocele-like tumour.

Bibliography

1. Tavassoli FA, Soares J (2003) Myoepithelial lesions. In: Tavassoli FA, Devilee P (eds) Pathology and Genetics of Tumours of the Breast and Female Genital Organs. International Agency for Cancer, Lyon, pp 86–88
2. Drijkoningen M, Tavassoli FA, Magro G et al (2003) Mesenchymal tumours. In: Tavassoli FA, Devilee P (eds) Pathology and Genetics of Tumours of the Breast and Female Genital Organs. International Agency for Cancer, Lyon, pp 89–98
3. Heywang-Köbrunner SH, Schreer I, Dershaw DD (eds) (1997) Benign tumors. In: Diagnostic Breast Imaging. Thieme, Stuttgart, pp 166–193
4. Nakazono T, Satoh T, Hamamoto T et al (2003) Dynamic MRI of fibromatosis of the breast. Am J Roentgenol 181:1718–1719
5. Vourtsi A, Kehagias D, Antoniou A, Moulopoulos LA, Deligeorgi-Politi H, Vlahos L (1999) Male breast myofibroblastoma and MR findings. J Comput Assit Tomogr 23:414–416
6. Hoda SA, Rosen PP (2004) Observations on the pathologic diagnosis of selected unusual lesions in needle core biopsies of breast. Breast J 10:522–527

Breast, Biopsy

R. Schulz-Wendtland, K. Anders, W. Bautz
University of Erlangen-Nürnberg, Institute of Radiology, Gynaecological Radiology, Erlangen, Germany
ruediger.schulz-wendtland@idr.imed.uni-erlangen.de

Interventional methods such as ultrasound- or mammographically guided biopsy/vacuum biopsy constitute valuable tools for complementary diagnostic workup and screening of the (female) breast, otherwise composed of clinical examination, mammography, ultrasound, and—if required—dynamic magnetic resonance imaging (MRI).

As claimed by the European Society of Mastology, to avoid open/surgical (diagnostic) biopsy in at least 70% of all palpable as well as nonpalpable, merely mammographically/sonographically detected lesions, histological assessment should be performed before surgery. Open biopsy ought to be reserved for selected cases exclusively.

Compared with open/excisional biopsy, the transcutaneous approach is cheaper and less time-consuming and entails lower morbidity risks. Furthermore, the rate of false-negative findings of approximately 0.05% is significantly lower than that of open biopsy following presurgical imaging-guided labeling (e.g., wire), with a false-negative rate of 2.6%.

However, unambiguous diagnosis according to the American College of Radiology guidelines/BI-RADS classification must be emphasized (Table 1).

Ultrasound-Guided Core-Cut/Vacuum Biopsy (Large Core Biopsy)

Indications

Indications for transcutaneous sonographically guided biopsy:

1. Histologic assessment of suspicious lesions discernible in ultrasound, beyond 0.5 cm in size, BI-RADS IV.
2. Presurgical proof of malignancy in suspicious lesions discernible in ultrasound, beyond 0.5 cm in size, BI-RADS V.

Contraindications

Absolute contraindications are severe coagulopathy or allergy to local anesthetics.

Ultrasound-Guided Core-Cut Biopsy

Technique

Nowadays, high-speed core-cut biopsy systems with fully automatic or sequential mode are available. According to current guidelines, biopsy needles 10 cm in length with a diameter of 12–14 gauge are used, with a penetration depth of 1.5 or 2.2 cm. Increasing needle diameter and penetration feed increase the weight of the biopsy samples and improve diagnostic reliability.

Breast, Biopsy. Table 1 BI-RADS Mammography-Categories

BI-RAD category	Description	Guidance	Risk of Malignancy
0	Mammographic incomplete	Additional imaging/prior mammography	?
1	Negative	Nothing to comment on	0%
2	Benign finding	Nothing	0%
3	Probably benign finding	Initial short-interval follow-up	<2%
4	Suspicious abnormality	Biopsy	2%–<95%
5	Highly suggestive of malignancy	Biopsy/therapy	>=95%
6	Proven malignancy	Therapy	100%

Following thorough disinfection, aseptic puncture is performed. Surgical and oncological considerations (e.g., access during subsequent surgery) should be taken into account when placing the biopsy cannula. Under local anesthesia, the lesion in question is targeted using a coaxial cannula, and the core-cut biopsy itself is performed under ultrasound view tangential to a linear 7.5-MHz transducer. For documentation purposes, the needle position should be imaged before and after the intervention. At least five samples should be extracted to ensure ample tissue for histologic assessment. To mark the biopsy area for subsequent imaging, a small clip should be placed in the target area *via* the coaxial cannula before removing the latter. Subsequently, biopsy access is sealed with a sterile dressing, and the patient is instructed to apply local compression for the following 30 min. According to the "European Guidelines for Quality Assurance" (pathology), the biopsy samples are microscopically evaluated after rapid embedding (approximately 2 h) and in paraffin cuts (24 h).

In cases of discrepancy between the findings of complementary diagnostics/imaging and histology, either additional biopsy or open/excisional biopsy must be done to achieve clarifying results (Fig. 1a, b).

Follow-Up After Biopsy

Ultrasound should be done after 6, 12, and 24 months, with mammography after 1 and 2 years. When a lesion is progressing, surgery/histological clarification is mandatory.

Ultrasound-Guided Vacuum Biopsy (Large Core Biopsy)

Technique

The hand-guided vacuum biopsy system Mammotome (Ethicon Endo-Surgery, Breast Care; Fig. 2a) can be used for vacuum extraction. Following disinfection and local anesthesia, needle placement is performed within or close to the lesion in question under ultrasound view, the cannula preferably running tangentially to the chest wall.

The basic technologic principles of the vacuum biopsy unit are a vacuum/low-pressure unit and an engine-driven high-speed rotating knife (8–11 gauge). All features of the biopsy unit can be directed *via* handle, foot pedal, or touchscreen.

Tissue extraction starts with intake of adjacent tissue into the biopsy notch at the lateral needle surface. Subsequently, the high-speed knife is advanced into the lesion, and by closing the biopsy notch, the first tissue sample is cut off. As soon as the rotational knife has reached the anterior arrest/lock, tissue suction as well as transection is completed. As soon as the knife is retracted, because of the vacuum technique the tissue sample is drawn into the center of the needle and can thus be withdrawn with tweezers. Meanwhile, the needle itself remains stable within the lesion. By turning the needle clockwise, several additional tissue samples can be extracted. Thus, theoretically, an interrelated tissue bloc of up to 2 cm can be removed. Optionally, the separate extraction steps can be performed manually as well as computer-assisted.

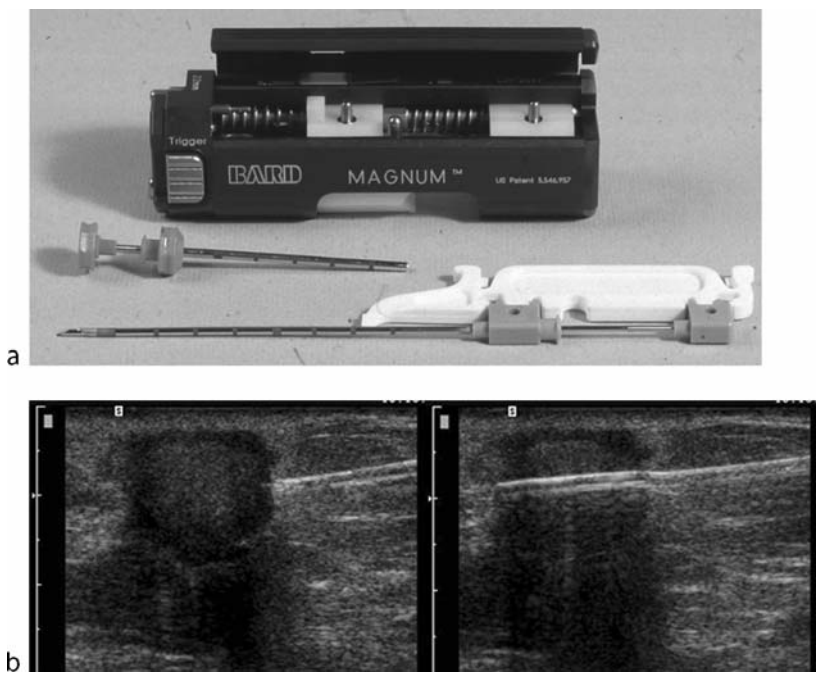

Breast, Biopsy. Figure 1 Care Needle Biopsy (CNB).

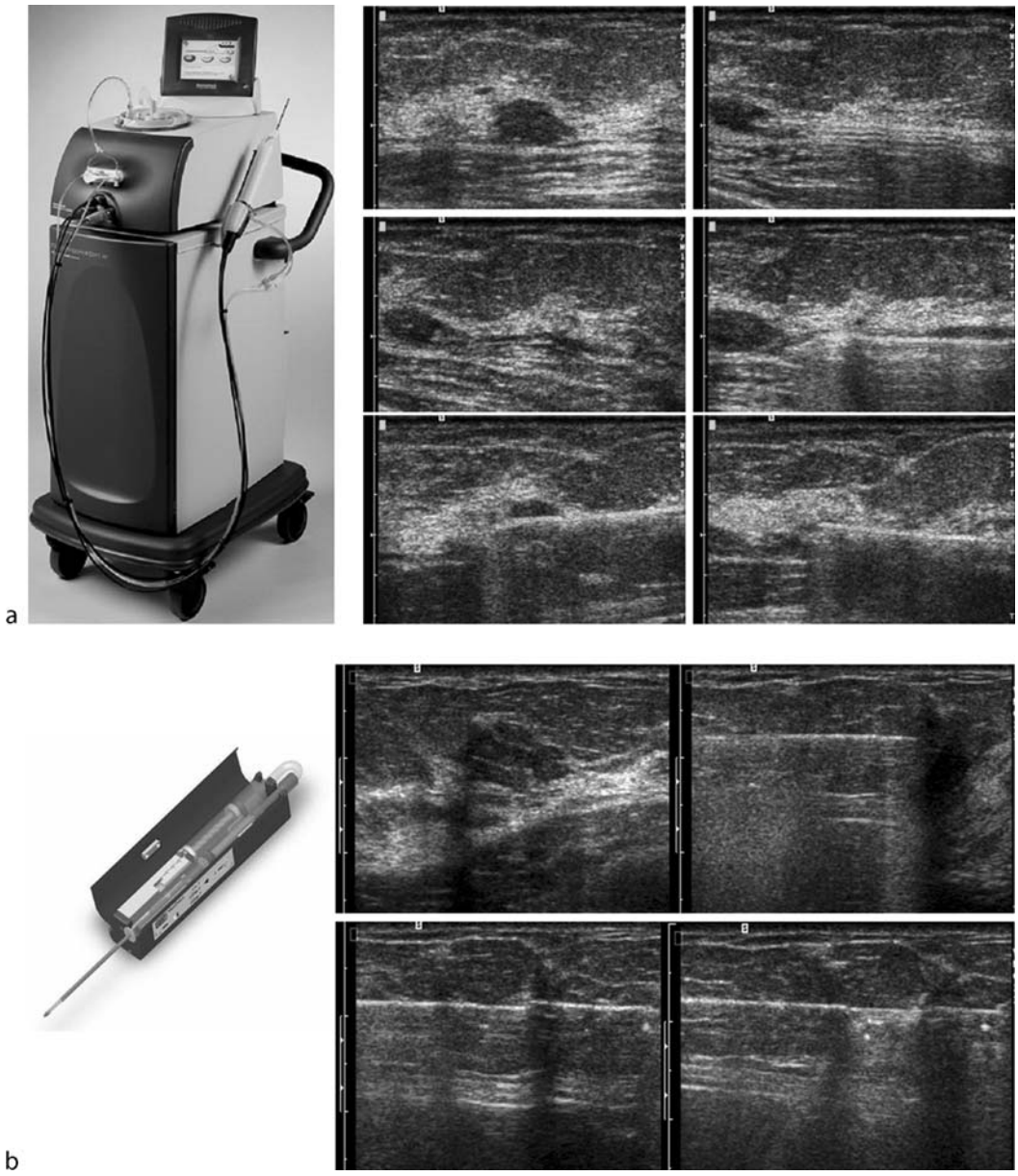

Breast, Biopsy. Figure 2 Large Core Needle Biopsy (L-CNB).

The weight of a single, complete tissue sample is about 75–100 mg. Upon completion of the biopsy (circumscript lesion >10 samples, suspicious calcifications 10–20 samples), a clip is placed within the biopsy area *via* the biopsy needle to mark the biopsy site for subsequent imaging. Following retraction of the needle, the biopsy access is sealed with a sterile dressing, and local compression is applied for about 30 min.

Two years ago, a new vacuum biopsy system was introduced (Vacora, Bard–Angiomed; Fig. 2b). In this system, all components (vacuum and pressure pump, electric engines, processor/control system, and lithium-ion, 7.2-V storage battery) are integrated in a single handle. With this biopsy system, a one-way biopsy cannula consisting of two interleaved cavities and a vacuum/pressure plunger pump is used. The needle diameter is 11-gauge, and the sample weight usually ranges from 150 to 170 mg.

Positive pressure within the system facilitates sample recovery from the biopsy window and is used to clean the vacuum cannula after each sample extraction. A coaxial needle helps to place the biopsy cannula within the lesion

in question. The remaining procedure as well as histologic assessment of the individual samples and follow-up intervals resemble those of ultrasound-guided biopsy.

Thus, in discordant findings of complementary diagnostics versus histology, repeated biopsy or surgery is mandatory. Furthermore, surgical excision and definite histological assessment are essential in cases of lesion progression. As with other biopsy techniques, biopsy access should not interfere with possible subsequent surgery and should follow oncological regulations.

Results

The current literature reports sensitivity and specificity values of 100%.

Mammographically Guided/Stereotactic Vacuum Biopsy (Large Core Biopsy)

Stereotactic Localization

Following calibration of the digital stereotactic equipment, the target area for subsequent intervention is defined according to craniocaudal mammography. The breast tissue is fixed with the compression pads, and the position is recorded with color marks on the patient's skin. With the aid of stereo views (+/−10 and +/−15°, respectively) the x- and y-coordinates of the lesion in question are defined, and the depth of the lesion (z-value) is calculated. Corresponding to the needle length, the matching coordinates are settled.

Indications

Indications for stereotactic vacuum biopsy (large core biopsy) include the following (sampling error in lesions <5 mm):

1. Histologic assessment of suspicious lesions (BI-RADS IV) that can be seen in mammography only.
2. Presurgical proof of malignancy in suspicious lesions (BI-RADS V) that can be seen in mammography only.
3. Histological assessment in differential diagnosis of mastopathy versus ductal carcinoma *in situ* with suspicious calcifications, BI-RADS IV and V.

Contraindications

Absolute contraindications are severe coagulopathy or allergy to local anesthetics.

Technique

For stereotactic biopsy, patient tables (prone position) as provided by Fischer and Lorad are used in combination with the Mammotome biopsy system by Ethicon Endo-Surgery Breast Care or the Vacora system by Bard-Angiomed.

On the basis of stereotactic mapping, exact localization of the lesion in question becomes feasible. Localization is based on digital mammography (10 line pairs/mm, matrix 1,024 × 1,024) performed in the prone position on the biopsy table. The patient's breast is placed within a table opening; with the aid of a fenestrated tube, the breast tissue is compressed and the lesion in question becomes accessible *via* the fenestration. If the lesion is localized in the upper quadrants, craniocaudal compression is used. For lower quadrant lesions, mediolateral, lateromedial, or caudocranial compression is applied. (Caudocranial access is feasible when the patient is positioned laterally.) The direction of the biopsy is chosen according to the shortest skin-to-lesion distance. Nevertheless, in possible malignant lesions (BI-RADS IV/V), oncological and surgical considerations—for instance, transection route in subsequent segmentectomy—have to be taken into account.

Following tissue compression, a 0° sector mammography is first performed. Subsequently, two angulated views (+15 and −15°) are acquired. Based on the lesion shift between those two views compared with a predefined reference point, the three-dimensional localization of the lesion can be calculated. Hence, the lesion center, reference point, and needle length are transferred to a computer (autoguide), and stereotactic positioning of the biopsy unit is performed.

Following disinfection and local anesthesia, the biopsy needle is manually placed at or within the lesion in question.

The basic technologic principles of the vacuum biopsy unit are a vacuum/low-pressure unit and an engine-driven high-speed rotating knife (8–11 gauge). Tissue extraction starts with intake of adjacent tissue into the biopsy notch at the lateral needle surface. Subsequently, the high-speed knife is advanced into the lesion, and by closing the biopsy notch, the first tissue sample is cut off. As soon as the rotational knife has reached the anterior arrest/lock, tissue suction as well as transection is completed. As soon as the knife is retracted, because of the vacuum technique the tissue sample is drawn into the center of the needle and can thus be withdrawn with tweezers.

Meanwhile, the needle itself remains stable within the lesion. By turning the needle clockwise, several additional tissue samples can be extracted. Thus, theoretically, interrelated tissue of up to 2 cm can be removed. The weight of a single complete tissue sample is about 75–100 mg. Upon completion of the biopsy (circumscript lesion >10 samples, suspicious calcifications 10–20 samples) and additional sample X-ray, a clip is placed within the biopsy area *via* the biopsy needle to mark the biopsy site for subsequent imaging.

Following retraction of the needle, the biopsy access is sealed with a sterile dressing, and local compression is applied for about 10–15 min.

Subsequently, orthogonal mammographic views are acquired for documentation purposes. According to the "European Guidelines for Quality Assurance" (pathology), the biopsy samples are microscopically evaluated after rapid embedding (approximately 2 h) and in traditional paraffin cuts (24 h).

In cases of discordant findings, repeated intervention or open/excisional biopsy/resection is mandatory.

Stereotactic vacuum biopsy is performed on an outpatient basis. Usually, patients will be dismissed 3 h after the intervention. In benign findings, follow-up mammography is performed 6 and 12 months following biopsy. In progressive lesions, open biopsy/surgery is absolutely necessary.

Stereotactic vacuum biopsy can also be carried out in the upright position (seated patient). In these cases, a mammography unit combined with additional computerized digital stereotactic device is used (20 or 10 line pairs/mm, matrix 1,024 × 1,024 pixels). The patient's breast is fixed between a receiver and supportive pad and remains fully accessible (360°). Appropriate patient positioning makes it possible to visualize lesions adjacent to the chest wall as well. The further proceedings resemble those mentioned above (Fig. 3a–e).

Results

In the current literature, sensitivity and specificity values of up to 100% are reported.

MRI-Guided Core-Cut or Vacuum Biopsy (Large Core Biopsy)

With the growing use of dynamic magnetic resonance (MR) mammography, more and more lesions will be seen that are reproducible neither clinically nor by mammography or ultrasound.

Indications

Indications for MR-guided core-cut or vacuum biopsy (large core biopsy) are the following:

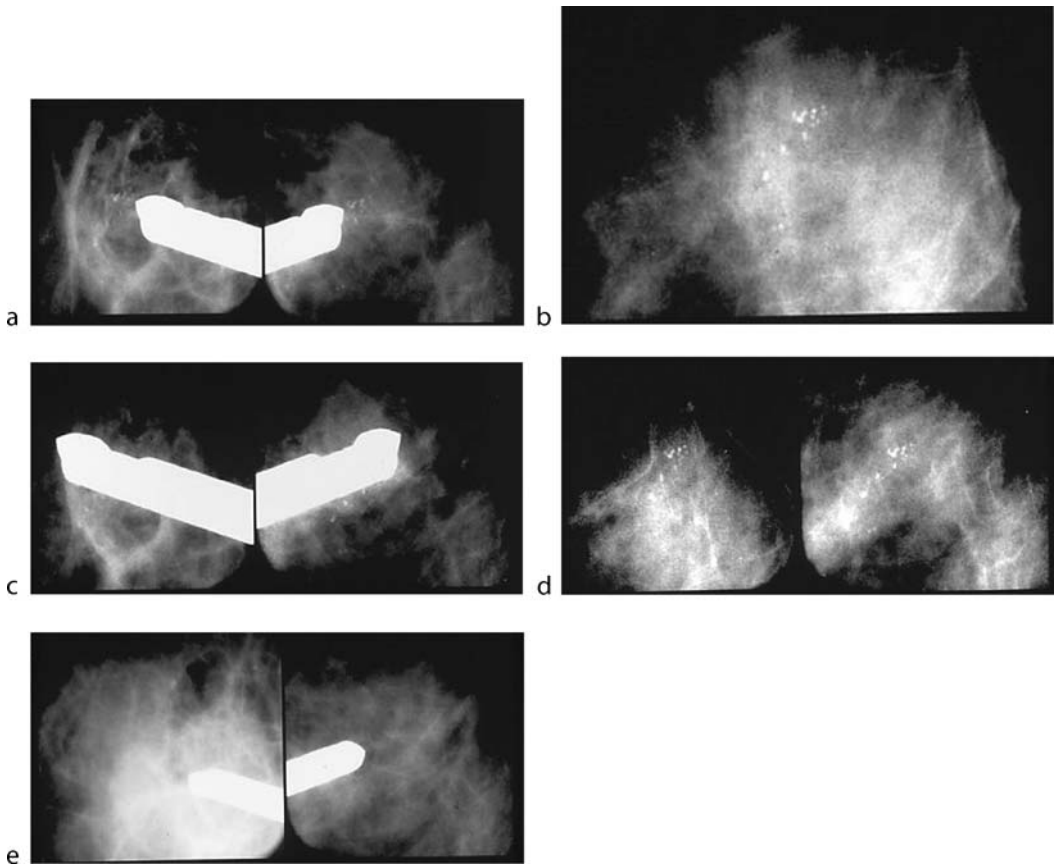

Breast, Biopsy. Figure 3 a, Prefire; b, Scout; c, Post fire; d, Localization; e, Postprocedure.

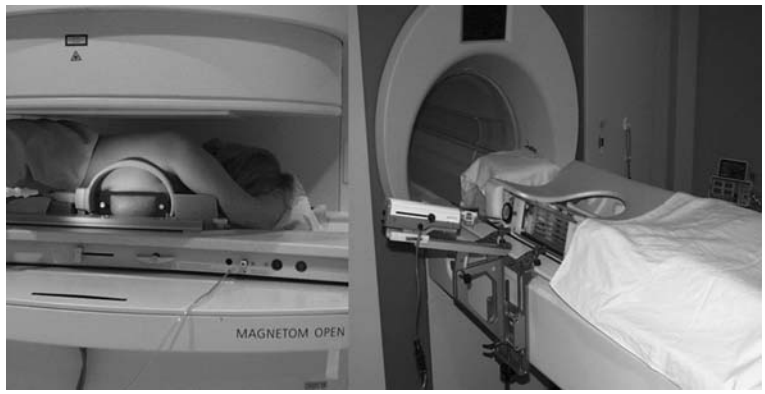

Breast, Biopsy. Figure 4 ***Left*: University of Munich. *Right*: University of Erlangen. Nuremberg.**

1. Histological assessment of suspicious lesions (BI-RADS IV) >5 mm, seen in MRI only.
2. Presurgical proof of malignancy in highly suspicious lesions >5 mm (BI-RADS V) that are seen in MRI only.

Contraindications

Pacemakers and some metal implants constitute contraindications for MRI.

Technique

Different devices for MR-based biopsy of the breast use one or more plastic pads for tissue compression. Through several fenestrations within those compression pads, biopsy needles or markers can be placed following exact three-dimensional localization. In bore magnet or closed systems, real-time control of interventions is impossible; they must be performed outside of the bore instead. Provided that MR-compatible equipment is available, conventional core-cut biopsy as well as vacuum intervention is feasible and is performed as described earlier.

In discordant findings, repeated MR-guided intervention or open biopsy following MR-guided lesion marking is mandatory. Follow-up MRI is recommended 6 months postintervention. In cases of lesion progression, surgery (for definite clarification) is obligatory (Fig. 4).

Results

The literature reports sensitivity and specificity values of up to 100% for MRI-guided punch or vacuum biopsy.

Bibliography

1. American College of Radiology (ACR) (2004) (Hrsg) Breast Imaging—Reporting and Data System (BI-RADS™). Reston, Philadelphia
2. Duda VF, Schulz-Wendtland R (2004) (Hrsg) Mammadiagnostik. Springer-Verlag, Berlin, Heidelberg, New York
3. Fischer U (2003) (Hrsg) Mammographiebefund nach BI-RADS™. Thieme-Verlag, Stuttgart
4. Heywang-Köbrunner SH, Schreer J (2003) (Hrsg) Bildgebende Mammadiagnostik. Thieme-Verlag, Stuttgart
5. Lanyi M (2003) (Hrsg) Brustkrankheiten im Mammogramm. Springer-Verlag, Berlin, Heidelberg, New York
6. Parker SH, Jobe WE (1993) (Hrsg) Percutaneous Breast Biopsy. Raven Press, New York
7. Sickles EA (2001) (Hrsg) Breast Imaging. Lippincott Williams & Wilkins, Baltimore
8. Tabar L, Tot T, Dean PB (2003) (Hrsg) Breast Cancer. Thieme-Verlag, Stuttgart

Breast, Cysts

Fluid-filled structures derived from the terminal duct lobular unit.

▶Fibrocystic Disease, Breast

Breast, Digital Imaging

Klaus-Peter Hermann
Gesellschaft Wissenschaftliche Datenverarbeitung mbH, Göttingen, Germany
kherman@gwdg.de

Traditionally, mammography has been produced as analog images with screen-film combinations. Digital imaging technology has now been introduced in diagnostic radiology, but for many years no adequate digital technique was available for mammography.

There has been much debate about spatial resolution in digital mammography. It was assumed that digital mammography would require spatial resolution similar to that of

screen-film mammography (SFM). However, it has been shown that other features of digital systems could compensate for the lower spatial resolution, leading to better detection of microcalcifications. One characteristic is the detective quantum efficiency (DQE). The DQE is dependent on the radiation dose and the local frequency, and it enables objective comparison between different imaging systems on the basis of image quality and dose efficiency.

In digital mammography, contrast can be changed in postprocessing by windowing and leveling. The further advantage of digital systems is the high dynamic range and the linear relationship between dose at the detector and signal intensity, as opposed to the sigmoid relationship between optical density and dose in screen-film systems. Digital image processing technology can display overexposed or slightly underexposed images with normal image quality.

The main advantage of any digital imaging system is the separation of image acquisition, processing, and display, allowing optimization of each of these steps. It is hoped that this will enable digital mammography to outperform SFM. In addition, advanced applications such as computer-assisted detection/diagnosis can be easily applied to the digital mammogram.

Digital Systems

Various equipment manufacturers have adopted different approaches to digital mammography. Photostimulable phosphor computed radiography was the first digital imaging system to be used for mammography. The imaging plate is contained within a cassette, which can be used in a standard mammography machine without modification. After exposure, the cassette containing the imaging plate is inserted into a reader. The imaging plate is then scanned by a laser. The emitted light is detected by a photomultiplier system, and the resultant electrical signal is digitized. Different high-resolution storage phosphor plates are commercially available (FCR 5000MA, FujiFilm, Tokyo, Japan; CR 850, Kodak, Rochester, NY, USA; Regius 190, Konica-Minolta, Tokyo, Japan; ADC Compact Plus, Agfa, Mortsel, Belgium). Other systems combine digital storage phosphor plates with the direct magnification technique and an X-ray tube with a very small focal spot. This system, however, has failed clinical use. Systems using charge-coupled devices (CCDs) have been used for stereotactic preoperative localizations and percutaneous biopsies. However, CCD chips could not be used for full-field breast imaging due to limitations of the field of view.

The SenoScan Full-Field Digital Mammography System (Fischer Imaging Corporation, Denver, CO, USA) uses an array of four phosphor-coupled CCDs in a rectangular configuration. This gives an overall detector size of approximately 1 × 22 cm. The long axis of the detector is aligned perpendicular to the patient's body. The X-ray beam is collimated to fit the 1-cm width of the detector. The detector then scans over a distance of 30 cm from left to right synchronously with the X-ray beam. This results in an image size of 22 × 30 cm.

The first online system for digital mammography with US Food and Drug Administration approval was the Senographe 2000D (GE Medical Systems, Waukesha, WI, USA). The 19 × 23-cm^2 detector is based on a semiconductor layer of amorphous silicon with a CsI phosphor layer (CsI/a-Si). The pixel size is 100 μm. The detectors used in the Selenia (Hologic, Bedford, MA, USA) and Novation (Siemens, Erlangen, Germany) systems are based on a semiconductor layer of amorphous selenium, which allows direct conversion from absorbed X-ray into electronic charges. The detector is 24 × 29 cm^2, and the pixel size is 70 μm. Further selenium-based systems are being manufacturing by Instrumentarium Imaging (Tuusula, Finland, currently with GE Medical Systems), IMS (Bologna, Italy), and others. The individual counting of each interacting X-ray photon is the technology for a direct converting digital detector, such as the MicroDose system (Sectra Medical Systems, Linköping, Sweden).

Digital mammograms can be printed onto film *via* a laser printer or presented as a soft-copy display on a monitor. Images are typically displayed for soft-copy reporting on two monitor workstations, with each monitor having a resolution of 2,048 × 2,650 pixels. Soft-copy displays provide the reader with much greater freedom to change the appearance of the image, and the workstation enables questionable areas to be quickly evaluated. Windowing can be adjusted manually by mouse click. Measurement and annotation tools are available.

Digital mammography is likely to improve patient throughput. Further new applications include the ability to use picture archiving and communication systems with the possibility of teleradiology. Furthermore, digital tomosynthesis and contrast digital mammography are two new innovative features that are possible with digital mammography.

Bibliography

1. Pisano ED, Yaffe MJ (2005) Digital mammography. Radiology 234:353–362
2. Noel A, Thibault F (2004) Digital detectors for mammography: the technical challenges. Eur Radiol 14:1990–1998
3. Freer TW, Ulissey MJ (2001) Screening mammography with computer-aided detection: a prospective study of 12,860 patients in a community breast center. Radiology 220:781–786
4. Niklason LT, Bradles TC, Niklason LE et al (1997) Digital tomosynthesis in breast imaging. Radiology 205:399–406
5. Jong RA, Yaffe MJ, Skarpathiotakis M et al (2003) Contrast-enhanced digital mammography: initial clinical experience. Radiology 228:842–850

Breast, Fibrosis

Fibrous proliferation of the mammary stroma.
►Fibrocystic Disease, Breast

Breast, Infection

Luis Pina
Department of Radiology
Clínica Universitaria de Navarra,
Navarra, Spain
ljpina@unav.es

Synonyms

Infection of the breast; Mastitis

Definition

►Mastitis Puerperal, Acute is a bacterial infection of the lactiferous ducts occurring during pregnancy and lactation, usually due to *Staphyllococcus aureus* (1–3). Acute nonpuerperal mastitis is seen outside the lactation period, although more rarely. Any acute mastitis may evolve to subacute or chronic mastitis if treatment is not adequate. Abscesses and fistulae may be complications (4).

Granulomatous conditions, such as ►granulomatous lobular mastitis, foreign body granulomas, tuberculosis, fungal infections, sarcoidosis, autoimmune diseases, and parasitic infections, may also affect the breast.

Pathology

Acute puerperal or nonpuerperal mastitis consists of an acute inflammation of the breast that may be accompanied by focal necrosis. This entity may evolve to organized chronic abscesses and fistulae.

Granulomatous lobular mastitis is an inflammation involving the breast lobule with noncaseating granulomata and microabscesses. Microscopic examination in sarcoidosis reveals epithelioid granulomas in the mammary parenchyma, with multinucleated Langhans giant cells that form asteroid or Schaumann bodies. Tuberculous mastitis consists of granulomatous lesions with caseous necrosis. Specific parasitic infections, such as filariasis, may lead to a granulomatous reaction with eosinophilic infiltration and adult filarial worms.

Clinical Presentation

Breast mastitis is less frequent nowadays than several years ago. Most cases occur in women between ages 18 and 50 years (3).

Acute puerperal mastitis is characterized by pain, erythema, swelling, tenderness, and even systemic signs of infection (3) during the lactational period. If an abscess is formed, a fluctuant palpable mass with adjacent red skin may be observed. Puerperal mastitis typically occurs within 2–3 weeks after the beginning of lactation and is caused by *Staphylococcus aureus.* This organism is transmitted from the infant. A history of cracked nipple or skin abrasion may be found.

Nonpuerperal mastitis may be central (periareolar) or peripheric (3). The former is more common and occurs in young women, especially in cigarette smokers and women with previous periductal mastitis, whereas the latter is less frequent and affects women with underlying diseases such as diabetes, rheumatoid arthritis, trauma, and steroid treatment. Central mastitis is seen as a periareolar inflammation that may or may not be associated with a retroareolar mass, nipple retraction, and purulent nipple discharge. This mastitis is usually indolent and relapsing. The pathogen may be *Staphylococcus aureus* but also anaerobes (*Bacteroides, Peptostreptococcus, Propionilbacterium*).

Granulomatous lobular mastitis affects young women. The pathogen is unclear, but corynebacteria may be involved. Clinically it appears as a hard firm mass, similar to breast carcinoma (3).

Tuberculosis is uncommon in our countries. The breast is involved by lymphatic spread from axillary or mediastinal nodes, and the clinical presentation is an acute abscess.

Parasitic infections due to filariasis occur in tropical and semitropical regions. The parasite forms an abscess that is hard and may mimic carcinoma. Axillary nodal enlargement is often found.

Breast involvement in systemic sarcoidosis is rare and may produce a firm mass that can be mistaken for carcinoma.

Imaging

Mammography

Acute mastitis presents as skin thickening, diffusely increased density, reticular edema, and, occasionally, well to ill-defined breast mass (due to abscess formation). Subacute or chronic mastitis may show similar findings on mammography, although scars may also occur (4, 5) (Fig. 1).

Ultrasound

Ultrasonographic findings of acute mastitis are skin thickening, hyperechogenicity of fat lobules, decreased echogenicity of glandular tissue with posterior shadowing, dilated ducts, and abscess formation. ▶Breast abscesses are usually round to oval lesions, with well-circumscribed or ill-defined margins. Breast abscesses may be anechoic, similar to simple cysts, but most of them are hypoechoic with fluctuating internal echoes (Figs. 2 and 3). Ultrasound is valuable for guiding percutaneous drainage of the abscess (4, 5).

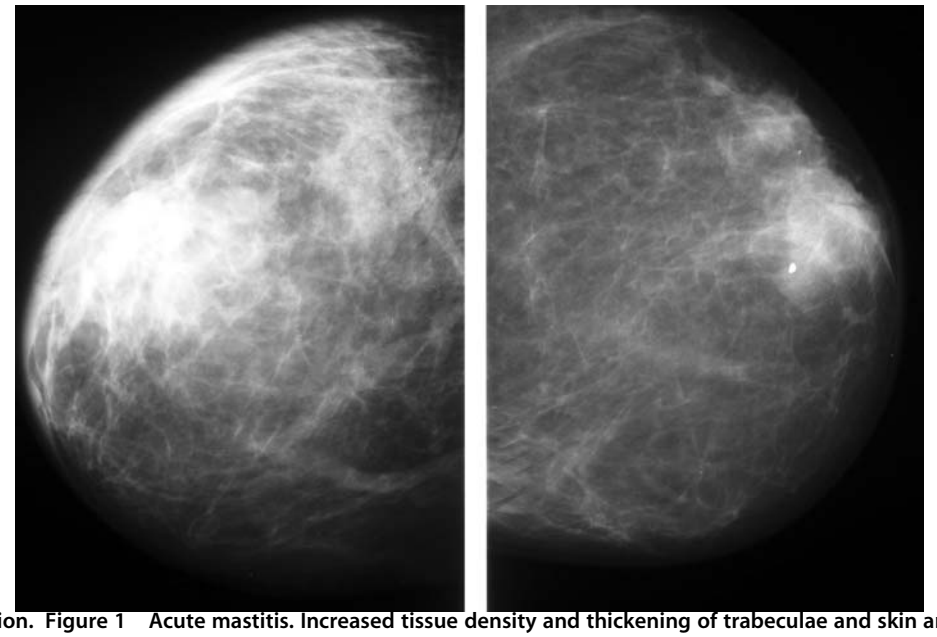

Breast, Infection. Figure 1 Acute mastitis. Increased tissue density and thickening of trabeculae and skin are seen in the left image (craniocaudal view).

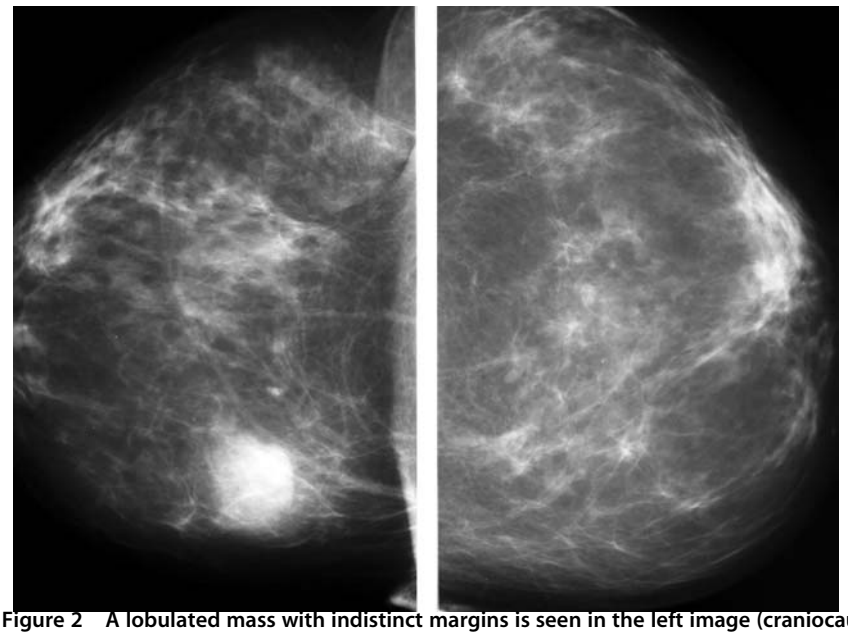

Breast, Infection. Figure 2 A lobulated mass with indistinct margins is seen in the left image (craniocaudal view). Breast abscess.

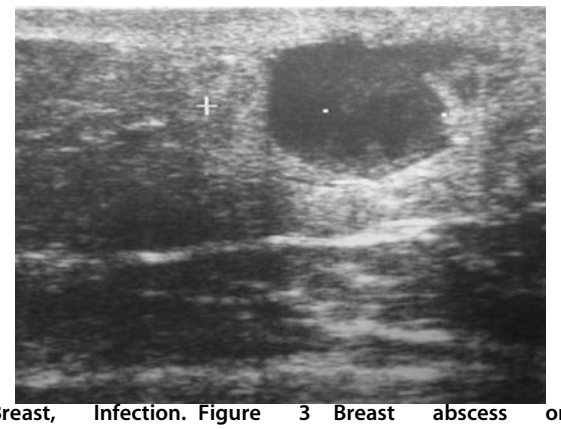

Breast, Infection. Figure 3 Breast abscess on ultrasound. The lesion is hypoechoic, showing internal echoes and posterior acoustic enhancement. Note the hyperechogenicity of the surrounding fat due to inflammatory infiltrate.

Magnetic Resonance

Magnetic resonance imaging is not indicated as a diagnostic tool for breast inflammatory disease, except in selected cases (for instance, silicone implants or free silicone injections). Contrast enhancement may be observed because of the activity of the inflammatory process. Acute inflammation leads to a significant contrast enhancement, while it may be minimal in a chronic phase. Abscesses are seen as fluid-filled cavities with variable signal intensity in T1- and T2-weighted sequences. Characteristically, the wall of abscesses shows intense enhancement after paramagnetic contrast administration (4).

Nuclear Medicine

Diagnosis: The diagnosis of acute mastitis is based on the clinical findings. Ultrasonography may be performed to detect an abscess, to guide drainage of the abscess, and to evaluate the therapeutic response. If the response is inadequate, mammography and skin biopsy are important for excluding inflammatory carcinoma (4).

In subacute or chronic mastitis, ultrasonography is useful to detect abscesses or fistulae. Mammography or skin biopsies are needed to rule out malignancy.

Bibliography

1. Rosen PP (2001) Inflammatory and reactive Tumors. In: Rosen PP (ed) Rosen's Breast Pathology. Lippincott Williams & Wilkins, Philadelphia, pp 29–63
2. Webster DJT (2000) Infections of the Breast. In: Hughes LE, Mansel RE, Webster DJT (eds) Benign Disorders and Diseases of the Breast. Concepts and Clinical Management. Saunders, London, pp 187–197
3. Dixon LM, Bundred NJ (2004) Management of disorders of the ductal system and infections. In: Harris JR, Lippman ME, Morrow M (eds) et al Diseases of the Breast. Lippincott Williams & Wilkins, Philadelphia, pp 47–56
4. Heywang-Köbrunner SH, Schreer I, Dershaw DD (1997) Cysts. In: Heywang-Köbrunner SH, Schreer I, Dershaw DD (eds) Diagnostic Breast Imaging. Thieme, Stuttgart, pp 156–165
5. Cardeñosa G (2001) Stroma. In: Cardeñosa G (ed) Breast Imaging Companion. Lippincott Williams & Wilkins, Philadelphia, pp 307–354

Breast, Physiology

Sue Barter
Cambridge Breast Unit, Addenbrookes Hospital, Cambridge, UK
sue.barter@addenbrookes.nhs.uk

Definition

Breast tissue is responsive to hormonal changes, and an understanding of this is fundamental to the interpretation of breast imaging at particular phases of the menstrual cycle. Hormonal factors also need to be understood in relation to imaging patients before menarche, during pregnancy and lactation, after the menopause, and with hormone replacement therapy (HRT).

It is also important to be familiar with the changes affecting the breast parenchyma in order to understand breast conditions that are so common they can be considered to be aberrations rather than disease. This is particularly relevant when considering fibrocystic change.

Characteristics

Breast Physiology during the Menstrual Cycle

Breast morphology is profoundly affected by cyclical variations in hormonal levels during the normal menstrual cycle. Histological changes have been reported in both stroma and epithelium, and are summarized in Table 1 (1).

During the proliferative phase of the menstrual cycle, increasing levels of oestrogen stimulate breast epithelial proliferation. The epithelium exhibits sprouting with increased mitotic activity, and increased nuclear density. These microscopic changes are attributed to increases in size and number of intracellular organelles, especially the Golgi apparatus, ribosomes, and mitochondria.

Similarly in the luteal phase of the cycle progestogens induce epithelial changes. The breast ducts dilate and the alveolar cells differentiate into secretory cells.

Breast, Infection. Table 1 Breast physiology during the the menstrual cycle

Phase	Days	Stroma	Lumen	Epithelium			
				Cell types	Orientation of epithelial cells	Mitoses	Active secretion
I. Proliferative	3–7	Dense, cellular	Tight	Single mainly pale eosinophilic cells	No stratification apparent	Present, average 4/10 per HPF	None
II. Follicular	8–14	Dense, cellular, collagenous	Defined	Luminal columnar basophilic cell; intermediate pale cell; basal clear cell with hyperchromaticnucleus (myoepithelial)	Radial, around lumen	Rare	None
III. Luteal	15–20	Loose, broken	Open with some secretion	Luminal basophilic cell; intermediate pale cell; prominent vacuolization of basal clear cell (myoepithelial)	Radial, around lumen	Absent	None
IV. Secretory	21–27	Loose, broken, edematous	Open with secretion	Luminal basophilic cell; intermediate pale cell; prominent vacuolization of basal clear cell (myoepithelial)	Radial, around lumen	Absent	Active apocrine secretion from luminal cell
V. Menstrual	27–2	Dense, cellular	Distended with secretion	Luminal basophilic cell with scant cytoplasm	Radial, around lumen	Absent	Rare

Source: Adapted from Vogel PM, Georgiade NG, Fetter BF et al (1981) Am J Pathol 104:23–34.

In the secretory phase, there is an increase in the size of the lobules, and ductules, and the stroma becomes loose and edematous. The basal cells show prominent vacuoles (Fig. 1).

Immediately before the onset of menstruation there is a peak in mitotic activity, with lymphocytic infiltration and apoptosis following the onset of menstruation (2).

Premenstrual breast fullness and tenderness can therefore be explained by increasing interlobular edema and the proliferation of ductules and acini under hormonal influence.

Pregnancy and Lactation

During pregnancy marked proliferation of ducts, alveoli, and lobules occurs under the influence of luteal and placental hormones. Prolactin is released progressively during pregnancy and also stimulates epithelial growth and secretion.

In the first 3 to 4 weeks of pregnancy marked ductal sprouting with some branching, and lobule formation occurs mainly under the influence of estrogen. At 5 to 8 weeks breast enlargement is significant, with dilatation of superficial veins, and increasing pigmentation of the nipple/areolar complex (3).

Secretory activity starts in the early stages with supranuclear vacuolation.

In the second trimester, lobule formation becomes dominant under the influence of progesterone. The alveoli contain colostrum.

From the second half of pregnancy onward, the breasts increase in size due to increasing dilatation of the alveoli, as well as hypertrophy of myoepithelial cells, connective tissue, and fat. (Fig. 2)

At parturition an immediate drop in placental hormones occurs allowing the effects of prolactin to become dominant. This causes the breast epithelial cells to change from a presecretory to a secretory state. With the establishment of lactation, there is even greater distension of the glandular lumina, with obliteration of the stroma. Large fat vacuoles are visible in the secretory cells.

After pregnancy and lactation, involution occurs at a varying rate between individuals, and after a period of about 3 months the breasts return to normal (4).

Postmenopausal Changes or Involution

The term "involution" is used specifically to describe the changes that occur in the breast due to the menopause. These changes begin some years before the cessation of menstrual periods and may start as early as in the 30s in nulliparous women. There is a gradual decrease in the lobular architecture, involving both the stroma and epithelium. The stroma becomes dense, converting into hyaline collagen, resembling normal connective tissue. The basement membrane of the acini becomes thickened, and the epithelium atrophies and becomes flattened. The lumina become narrow with the cessation of secretions. Some acini coalesce with the formation of small cysts. These may later shrink spontaneously and be replaced by fibrous tissue, but may also continue to accumulate fluid and enlarge, presenting symptomatically. The interlobular ducts shrink and some disappear altogether (Fig. 3).

The above changes are not uniform and may vary in degree from segment to segment. The stroma gradually is replaced by fat, and the breast becomes softer. This makes it more radiolucent, and hence mammographic screening becomes more sensitive.

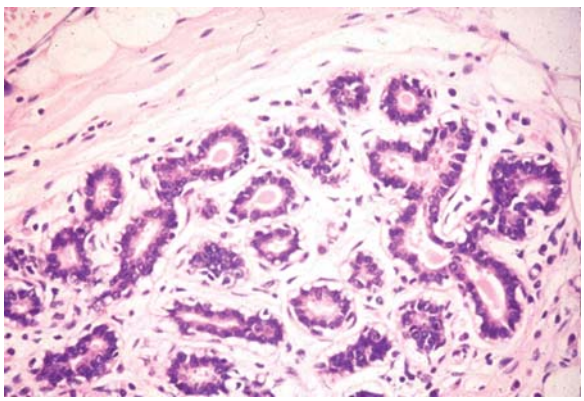

Breast, Physiology. Figure 1 Normal breast lobule in the secretory phase showing vacuolation of basal cells. (Courtesy of Dr Sarah Pinder, Consultant Histopathologist, Addenbrookes Hospital, Cambridge.)

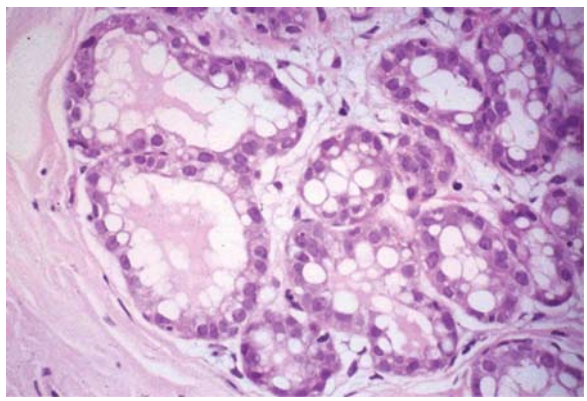

Breast, Physiology. Figure 2 Pregnancy change in the breast. Note prominent vacuolation and secretions in the ducts. (Courtesy of Dr Sarah Pinder, Consultant Histopathologist, Addenbrookes Hospital, Cambridge.)

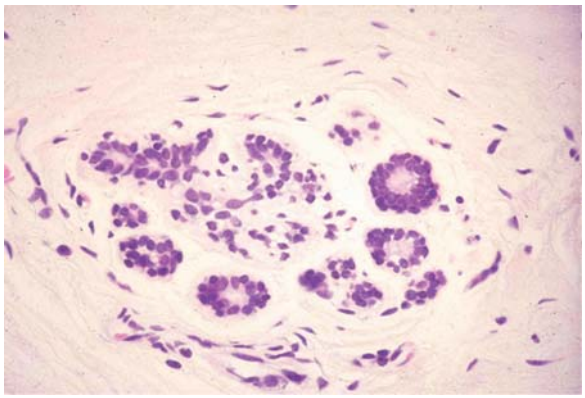

Breast, Physiology. Figure 3 Postmenopausal breast tissue showing atrophy of lobules and dense stroma. (Courtesy of Dr Sarah Pinder, Consultant Histopathologist, Addenbrookes Hospital, Cambridge.)

Premenarche and Puberty

During fetal development, the breast is derived from a modified apocrine or sweat gland. This results in a rudimentary organ, identical in boys and girls, consisting of a few simple branched ducts lying in stroma. At puberty the ducts elongate, divide, and form terminal ductal lobular units (TDLU). TDLU With the onset of puberty, the breasts change in size and shape. Morphologically, there in an increase in size due to an increase in connective tissue and fat. There is elongation and proliferation of the ducts, with budding and branching. New lobules form, and the nipple and areola alter in shape and become more pigmented. All of these changes are hormonally induced. Both estrogen and progesterone stimulate and promote growth of the breast parenchyma.

Hormone Replacement Therapy

After the menopause, without hormone replacement, the breasts are usually collapsed and soft due to the decreased levels of circulating estrogen and progesterone. HRT reverses the physiological changes of breast involution and therefore benign conditions such as fibroadenoma, cysts, and mastalgia may persist after the menopause with its use.

Continuous combined HRT has also been reported to increase the number and size of proliferating breast epithelial cells in tissue biopsies from areas of abnormal mammographic breast density compared with biopsies from women with no history of HRT exposure, or those who are taking unopposed oestrogen (5).

Most studies evaluating the effect of HRT on breast density report higher proportion of relatively radiodense tissue, compared to women who have never used HRT. This is likely to be due to epithelial proliferation (6, 7).

Studies have shown some HRT formulations appear to have a greater effect than others depending upon which progestin is used. Cyproterone acetate and medroxyprogesterone acetate (MPA) seem to produce higher incidences of fibrocystic change and increased density on mammography.

Unopposed estrogen does not increase mammographic breast density, but approximately 25% of women allocated to combined HRT containing MPA are likely to develop an increase in mammographic density within the first year of use, irrespective of whether the MPA administration is cyclical or continuous (5).

Hormonal Contraceptives

The combined oral contraceptive pill has been shown to increase breast epithelial proliferation. Whilst proliferation does not appear to differ according to the progestogen (i.e., comparing levonorgestrel with desogestrel), a positive correlation between increasing serum levonorgestrel and proliferative indices has been reported. Evidence about the effect of progestogen-only pills (POPs), depot progestogens or progestogen-releasing intrauterine systems (IUSs) on epithelial proliferation is lacking. Studies evaluating the effect of combined oral contraceptive pills (COCs) on mammographic density are contradictory (5).

Bibliography

1. Vogel PM, Georgiade NG, Fetter BF et al (1981) The correlation of histologic changes in the human breast with the menstrual cycle. Am J Pathol 104:23–34
2. Rudland PS, Barraclough LR, Fernig DG et al (1998) Growth and differentiation of the normal mammary gland and its tumors. Biochem Soc Symp 63:1–20
3. Rosen PP (2001) Rosen's Breast Pathology. 2nd edn. Lippincott, Williams & Wilkins, Philadelphia
4. Bland KI, Copeland EM (2004) The Breast. 3rd edn. WB Saunders, Philadelphia
5. Marsden J, A'Hern R (2003) Progestogens and breast cancer risk: the role of hormonal contraceptives and hormone replacement therapy. J Fam Plann Reprod Health Care 29(4):185–187
6. Million Women Study collaborators (2003) Breast cancer and hormone-replacement therapy in the Million Women study. The Lancet 362:419–427
7. Million Women Study collaborators (2004) Influence of personal characteristics of individual women on sensitivity and specificity of mammography in the Million Women Study: cohort study. BMJ 329:477–479

Breast, Special Procedures

R. Schulz-Wendtland, K. Anders, W. Bautz
University of Erlangen-Nürnberg Institute of Radiology, Gynaecological Radiology, Erlangen, Germany
ruediger.schulz-wendtland@idr.imed.uni-erlangen.de

Galactography

Galactography is a contrast-enhanced study of the lactiferous duct.

Indication: Galactography is performed in cases of pathologic secretion, i.e., spontaneous, nonmilky (serous, flocculated, or bloody) secretion from a single duct in one breast.

Milky secretion from several ducts or bilateral secretion does not constitute a proper indication.

Contraindications: Inflammatory processes of the breast constitute an absolute contraindication, whereas previous reactions to contrast media constitute a relative contraindication for galactography.

Adverse events/side effects: Mastitis following galactography as well as local pain in cases of paraductal contrast deposits may occur.

Technique: Before galactography, secretion samples for cytologic assessment should be secured. Thorough disinfection of the nipple and the surrounding skin is then followed by careful probing of the nipple after expression of some fluid to mark the lactiferous duct in question. As soon as the probe (e.g., lymphography cannula) hits the ductal orifice, it will sink in without significant resistance. Between 0.3 and 0.5 ml of nonionic contrast medium may be injected, and subsequently orthogonal mammography (craniocaudal and mediolateral) is performed.

Kindermann found merely ductal ectasia without intraductal lesions in 65% of his cases; biopsy was performed in 35%, with malignant lesions found in only 4.3% of all cases. Thus, papilloma and papillomatosis accounted for the majority of secretory findings. In cases of bloody secretion, the frequency/prevalence of malignant disease increases up to 37%.

The most important findings are:

- Regular ducts,
- Ductal ectasia,
- Filling defects/contrast stop, suspected papilloma, differential diagnosis intraductal cancer (further assessment warranted).

Ductal Puncture/Antegrade Galactography

The current widespread use of radial/antiradial ultrasound approaches, oriented along or perpendicular to the lactiferous ducts, has increased the number of morphologically conspicuous ducts without pathological secretion. If further assessment is required, antegrade galactography can be indicated in these cases.

Rissanen et al. introduced antegrade, sonographically guided percutaneous galactography in 1993.

Technique: The conspicuous duct should be punctured with the least possible injury under sonographic guidance. If the tip of the needle can be clearly visualized within the ductal lumen, contrast agent may be carefully instilled, similar to conventional/retrograde galactography. Subsequently, two orthogonal mammographic views are acquired. Image reading criteria are as for retrograde galactography.

Presurgical Lesion Localization

According to European Guidelines (EUSOMA), 70% of all palpable and impalpable lesions are to be assessed histologically before surgery. Additional labeling ahead of therapeutic operation enables the surgeon to exactly predefine oncological/surgical strategies and lesion access. Open biopsy should be undertaken in exceptional cases only.

According to EUSOMA standards, the lesion marker should be placed less than 10 mm from the lesion in question in more than 80% of all labeling procedures. To be able to rely on the most exact needle placement possible is of great concern to the surgeon, who wants to perform tissue-saving yet efficient excision and needs to guarantee adequate safety margins in malignant lesions.

In histologically benign lesions, open biopsy should yield tissue samples of less than 30 g in 90% of all cases.

Before presurgical labeling, apart from standard craniocaudal and oblique views, an additional mediolateral projection should be acquired. Furthermore, the mediolateral projection might be helpful before stereotactic localization. If exact three-dimensional information on lesion position is available, the plausibility of the calculated target area can be verified before needle access.

Freehand Localization

By means of orthogonal mammography views, the reader may localize the lesion in question and advance a localization needle toward the lesion center. Usually this results in the least possible trauma for the patient, and the shortest/direct access is also marked, which may be regarded as true advantages. However, in less-experienced

examiners, the needle position might have to be revised, resulting in additional mammographic views for post-interventional monitoring.

On craniocaudal and mediolateral views, the distance between the nipple and the access incision can be defined, as can the distance between skin surface and the lesion in question. According to these measurements, the needle access can be marked on the patient's skin. Yet, it should be kept in mind that mammography is performed with tissue compression. Following intervention, the needle position should be checked in two orthogonal planes—and adjusted if necessary. As soon as correct needle position is achieved—and documented—wire placement or dye injection may be performed.

Sonographic Localization

Lesion access should be chosen according to the shortest possible skin lesion distance, but it should not interfere with surgical transection pathways. However, to sufficiently visualize the needle and wire during placement, it should be kept parallel to the linear transducer. In circumscribed findings, the marker should penetrate the lesion center and the tip of the wire should be placed and fixed in the tissue distal to the lesion, the maximum tolerable distance being 1 cm. Orthogonal mammographic views following intervention are obligatory. The orientation of the wire as well as the distance between the skin and lesion, the depth of the tip of the wire, and the location of the wire relative to the lesion must be documented. Moreover, information should be given concerning the general extent of the excision and the dimensions in relation to the marker.

In noncircumscribed findings—e.g., ductal/segmental changes—the following options are available:

- The complete extent of the changes in question is marked with a longer wire, or
- The lesion margins are tagged separately with two or more wires, whereas the transverse dimension can be indicated by color marks on the patient's skin.

Localization by Perforated or Tagged Compression Needle

Depending on the lesion site, a craniocaudal, mediolateral, or lateromedial mammogram will be obtained using a perforated compression panel. Needle placement is carried out under tissue compression and according to the lesion is coordinated *via* the perforated/fenestrated compression panel. In doing so, the needle should perforate the lesion to a certain extent, so that after decompression and relaxation of the tissue it still perforates or at least reaches the lesion. The second plane mammogram is then obtained. If necessary, the needle position may be adjusted according to this second view. If correct needle position is achieved, wire placement or dye injection may be performed, and the exact positioning will be documented in orthogonal views.

The major drawback of this method is that, as in stereotactic labeling, the wire/tag does not necessarily mark the ideal lesion access for surgery, but a rather prolonged one.

Stereotactic Localization

Stereotactic lesion localization is carried out according to stereotactic biopsy as described in the previous section. Following exact needle placement, wire placement and/or dye injection is performed. Apart from stereotactic documentation planes (±15°), additional orthogonal views (cc and ml views) should be obtained. Misplacement of just a few millimeters under compression may equal considerable misplacement following tissue decompression. It is thus recommended to advance the needle about 5 mm beyond the calculated target. If these rules are observed, stereotactic localization proves to be a very reliable method.

MRI-Guided Localization

In lesions exclusively definable with magnetic resonance imaging (MRI), presurgical tagging must be carried out in MRI as well. Without additional (specialized) coils, MRI-guided tagging results in marker deviation of ±1 cm from the target lesion because of breathing artifacts. By using dedicated coils, more exact marker placement can be achieved.

Galactographic Localization

Lesions visible on galactographs only should be color-marked on the patient's skin following up-to-date (if necessary, repeated) galactography.

Specimen Radiography/Specimen Ultrasound

In all lesions subjected to presurgical labeling and excision, postsurgery sample X-ray (two planes) or ultrasound must be performed to assure complete removal. Standard and magnification techniques are used. Sample compression may be helpful to increase contrast and facilitate delineation of the resected lesion. In addition, the most suspicious areas (calcifications/solid lesions) should be marked for the pathologist with additional tags/needles. Microcalcifications always warrant additional magnification views, as those will usually give further information about morphology and about more, even smaller, calcifications.

Written notification must be given to the surgeon and the pathologist, about whether

- The lesion has been removed completely;
- The lesion might be incomplete;
- The lesion is definitely incomplete;
- The lesion is not contained in the sample.

In lesions that could be seen and tagged on ultrasound only, additional sample ultrasound may increase confidence concerning successful excision; evaluation obeys the same standards as in sample X-rays (Fig. 7a–e).

Bibliography

1. American College of Radiology (ACR) (2004) (Hrsg.) Breast imaging—reporting and data system (BI-RADS™). Reston, Philadelphia
2. Duda VF, Schulz-Wendtland R (2004) (Hrsg.) Mammadiagnostik. Springer-Verlag, Berlin, Heidelberg, New York
3. Fischer U (2003) (Hrsg.) Mammographiebefund nach BI-RADS™ Thieme-Verlag, Stuttgart
4. Heywang- Köbrunner SH, Schreer J (2003) (Hrsg.) Bildgebende Mammadiagnostik. Thieme-Verlag, Stuttgart
5. Lanyi M (2003) (Hrsg.) Brustkrankheiten im Mammogramm. Springer-Verlag,Berlin, Heidelberg, New York
6. Parker SH, Jobe WE (1993) (Hrsg.) Percutaneous breast biopsy. Raven Press, New York
7. Rissanen T, Typpo T, Tikkakoshki T, Turunen J, Myllymaki T, Suramo, I (1993) Ultrasound-guided percutaneous galactography. J Clin Ultrasound Oct;21(8):497–502
8. Sickles EA (2001) (Hrsg.) Breast imaging. Lippincott Williams & Wilkins, Baltimore
9. Tabar L, Tot T, Dean PB (2003) (Hrsg.) Breast cancer.Thieme-Verlag, Stuttgart

Breast, Therapy Effects

Pinar Balci
Dokuz Eyliil University School of Medicine,
Department of Radiology,
Inciralt-Izmir-Turkey
pinar.balci@deu.edu.tr

Definitions

Breast-conserving treatment involves surgical removal of a breast cancer, often with axillary dissection, usually followed by *breast irradiation*. In addition to postsurgical changes, changes following axillary node dissection and radiotherapy can also occur. The changes induced by breast-conserving treatment with irradiation affect the entire breast and are superimposed on the changes at the surgical site. These changes can mimic and obscure malignancy. Depending on whether a hematoma, a seroma, or fat necrosis is present, postsurgical changes can have variable radiologic presentations. To avoid diagnostic errors, the radiologist's knowledge and experience, systematic interpretation, and selection of supplemental radiologic methods is an important part of following up these patients.

Therapy effects are also seen following *reconstruction, augmentation, and reduction* of the breast. Reconstruction can be achieved by means of implants or myocutaneous flaps. Augmentation refers to enlargement of the breast for to correct congenital or acquired anisomastia or micromastia, or for cosmetic reasons. Reduction is performed to achieve symmetry in anisomastia or following mastectomy. Macromastia is a frequent indication for reduction mammoplasty.

Neoadjuvant systemic ▶chemotherapy is used to enable breast-conserving surgery in patients with large primary operable breast cancers. It is important to be able to assess response to systemic therapy, both for assisting the surgeon and for prognostic purposes (1).

Hormone therapy or hormone replacement therapy (HRT) may affect breast tissue. Use of HRT increases mammographic breast density in 17–73% of women. The incidence of increased density is more frequent with combined estrogen/progestin HRT than with estrogen alone. Breast density changes occur rapidly with HRT, with the greatest changes occurring in the first year. Breast tenderness is also a common side effect of HRT use, particularly at initiation of therapy. Onset of breast pain with HRT initiation is frequently associated with an increase in mammographic breast density, indicating that the onset of breast tenderness associated with initiation of HRT use may signify a proliferative response reflected mammographically as an increase in breast density. While increases in mammographic breast density and breast tenderness are associated with HRT, the method of HRT administration may alter the occurrence and degree of these effects (2). Postmenopausal hormone therapy has been associated with an increased risk of breast cancer, and an increase in mammographic breast density has been reported to occur in a significant proportion of women during such treatment (3).

On the other hand, tamoxifen is a widely used antineoplastic agent, not only for early adjuvant therapy but also for prophylaxis and treatment of breast cancer. It has antiestrogenic effects in the female reproductive organs, especially breast parenchyma (4).

Pathology/Histopathology

Radiation

The breast may be exposed secondarily to radiation during diagnostic procedures such as ▶mammography and fluoroscopy or in the course of radiotherapy administered

to another organ, such as mediastinal radiotherapy for Hodgkin's disease. The radiation exposure in these situations has been associated with an increased risk for subsequent development of breast carcinoma (1).

Radiation of the breast for mammary carcinoma in the course of breast-conserving treatment involves levels of exposure that produce alterations in non-neoplastic as well as neoplastic tissues.

Radiation-induced histologic changes must be distinguished from recurrent carcinoma in the interpretation of a post-treatment biopsy. Compared with a preradiation specimen, major changes in a normal breast are apparent in the terminal ductal units. These include the following: (1) collagenation of intralobular stroma, (2) thickening of periductal and periacinar basement membranes, (3) severe atrophy of acinar and ductular epithelium, (4) cytologic atypia of residual epithelial cells, and (5) relatively prominent acinar myoepithelial cells that seem to be preserved better than the epithelial cells. In a minority of specimens, atypical fibroblastin may also be found in the interlobular stroma. In one study, differences in radiation effects among individual patients were not correlated with radiation dose, patient age, post-treatment interval, or the use of adjuvant chemotherapy.

Fat necrosis and atypia of stromal fibroblasts are more common in proximity to external boosted or radioactive implanted areas. Radiation-induced vascular changes may occur in external boost procedures. Cytologic atypia can create diagnostic problems even if one is aware of the typical appearance of radiation-induced atrophy of the breast, especially in fine-needle aspiration cytology (5).

Chemotherapy

Chemotherapy effects are now most often encountered in the breast when patients with locally advanced or inflammatory carcinoma have been given high-dose systemic therapy preoperatively, as the so-called neoadjuvant therapy. The fundamental manifestation of chemotherapy effects is a decrease in tumor cellularity. The effects may be more pronounced after combined chemotherapy and ►radiation therapy. The cells are enlarged because of increased cytoplasmic volume. The cytoplasm often contains vacuoles or eosinophilic granules. Cellular borders are typically well defined, and the cells tend to shrink away from the stroma. Some carcinoma cells show enlargement, pleomorphism and hyperchromasia of nuclei. In the most extreme situation, no residual carcinoma may be detectable in 6.7–10% cases. Residual degenerated and infarcted necrotic carcinoma may be recognized by the loss of normal staining properties and decreased architectural detail. With the passage of time, degenerated invasive carcinoma is absorbed. Healed sites may be appreciated because of residual architectural distortion characterized by fibrosis, stromal edema, increased vascularity composed largely of thin-walled vessels, and a chronic inflammatory cell infiltrate. Fibrosis and atrophy of lymphoid tissue are characteristic features of chemotherapy effect at sites of metastatic carcinoma in lymph nodes (5).

Hormone Treatment Effect

Hormone therapy has been used to treat mammary carcinoma and postmenopausal replacement for years. In postmenopausal women, normal breast epithelium is stimulated to proliferate, with elongation of small terminal ducts and the formation of lobules. Epithelial changes are accompanied by the accumulation of interlobular connective tissue. The histologic correlates to mammographic breast density during HRT are not fully clear, but they have been suggested to at least partly reflect increased proliferation of epithelium and stroma (5). On the other hand, the main antiproliferative effects of tamoxifen are mediated by competition with estrogen for binding to the cytoplasmic estrogen receptor, with subsequent inhibition by the tamoxifen-estrogen receptor complex of the many activities of endogenous estrogen within tumor cells. Breast parenchyma shows a decrease during tamoxifen therapy (4).

Clinical Presentation

Depending on the extent of postoperative edema, the breast is regionally or diffusely dense and swollen in the early postoperative phase. Palpation has limited value in this situation. Axillary dissection or radiotherapy can lead to acute lymphedema of the breast, with swelling and peau d'orange. Radiotherapy leads to erythema, skin thickening, and swelling of the entire breast. A dry epitheliosis of the skin and an edema-induced induration may develop, as well as hyperpigmentation to a variable degree and, in large breasts, a wet epitheliosis along the inferior mammary fold.

In general, erythema, edema, and skin thickening largely resolve during the first two years, but considerable variations can be observed.

Scar regions may be palpable as flat plateau-like areas, or new nodular and firm areas can develop. Oil cysts are often clinically palpated as movable suspicious nodules or induration. Large dystrophic calcification, oil cysts, and oil granulomas can usually not be distinguished from recurrence. Mammary fibrosis and skin dimpling can be a cause of diagnostic problems clinically or on conventional imaging (1).

HRT-induced breast tenderness typically occurs within the first six months and tend to subside with time. This correlates with the findings of a current study in which more women had breast pain in the first six months, and fewer

noted this problem at one year (2). McNicholas et al (6) found that seven of nine (78%) women who developed moderate or severe breast pain during the first year of continuous combined oral HRT use had an increase in breast density, whereas only two of 21 (10%) women who did not develop breast pain had an increase in breast density.

Imaging

The major goals of imaging are early detection of recurrent breast carcinoma following breast-conserving therapy and achievement of the lowest possible rate of false-positive diagnostic biopsies. *Mammography* combined with clinical examination is the most important diagnostic modality. The highest accuracy can be achieved if both the preoperative and the postoperative studies are available at the time a new mammogram is obtained. *Ultrasound* may be useful as an adjunct in mammographically dense tissue. The selected use of *contrast-enhanced magnetic resonance imaging* (MRI) is important. If the evaluation is impaired owing to increased density and scars, contrast-enhanced MRI permits markedly improved and earlier detection of recurrence and correct identification of scar-related fibrotic changes beginning one year after radiotherapy (1).

Following breast reduction as well as after reconstruction or augmentation with transplanted autogenous tissue, the resultant scar formation and architectural changes are determined by the surgical technique. Tangential mammograms are necessary for evaluating breasts after augmentation or reconstruction with silicone prostheses. Contrast-enhanced MRI has proven to be an important supplemental method for high-risk patients because of its high sensitivity.

HRT increases the density of breast parenchyma, thus rendering precocious diagnosis of small tumors more difficult. Any factor that increases breast density may decrease the sensitivity of mammography and influence the accuracy of its interpretation.

Changes in mammographic breast density can be evaluated in several ways. The most practical means of evaluating large populations for changes in breast density is to use the Breast Imaging Reporting and Data System (BI-RADS) density categories because this information is typically included in standard mammography reports, bypassing the need to retrieve mammograms. Ultrasound may be useful in mammographically dense breasts (1).

Nuclear Medicine

Scintimammography provides functional information by evaluating tracer uptake. Tc-99m sestamibi accumulates preferentially in tumor cells. The sensitivity and specificity of the method are 83–97% and 70–90%, respectively, in palpable masses. FDG-positron emission tomography (PET) can also detect residual tumor, occult metastasis, or local recurrence, but it may not be suitable for mapping. It is sensitive for measuring response to systemic therapy, thus enabling tailoring of an individual's treatment. A definite advantage of PET is its capability to provide a fast overview of the whole body and to detect unsuspected metastases (7).

Diagnosis

Mammography is the most important method following breast-conserving therapy and irradiation. The following changes are seen:

- Diffuse changes, including trabecular coarsening, skin thickening, and diffusely increased breast density secondary to irradiation and axillary dissection
- Localized parenchymal changes of the skin and breast tissue due to surgical scarring
- Localized parenchymal changes secondary to fat necrosis manifested as liponecrosis, oil cysts, or a lipophagic granuloma
- Calcifications

Acute changes (diffuse increased breast density, trabecular coarsening, skin thickening, etc.) can resolve slowly during the first two years after radiotherapy. Chronic edema can resolve or undergo fibrotic transformation, producing a similar mammographic pattern (Fig. 1).

Localized changes may occur with scar formation following surgery or fat necrosis and its forms of transformation. For example, oil cysts are characterized by round and oval radiolucencies of fat density, small capsules, and egg-shell calcifications. Lipophagic granuloma generally presents as a newly developing mass with an irregular outline. Dystrophic calcifications frequently occur in conjunction with therapy-induced cell and tissue necrosis; these are large, elongated, coarse amorphous calcifications and ringlike, egg-shell forms, scattered dystrophic microcalcifications, and fine punctate calcifications at the site of tumorectomy. *Magnification mammography* is necessary for an exact analysis.

On the other hand, recurrences can become mammographically visible as a nodular or ill-defined mass, enlarging scar, microcalcifications, or diffusely increased density.

After the completion of radiation, a baseline mammogram of the treated breast should be done in 3–6 months, followed by a bilateral mammogram after 12 months. In the United States, yearly mammograms are suggested if no suspicion exists. If the cancer contained

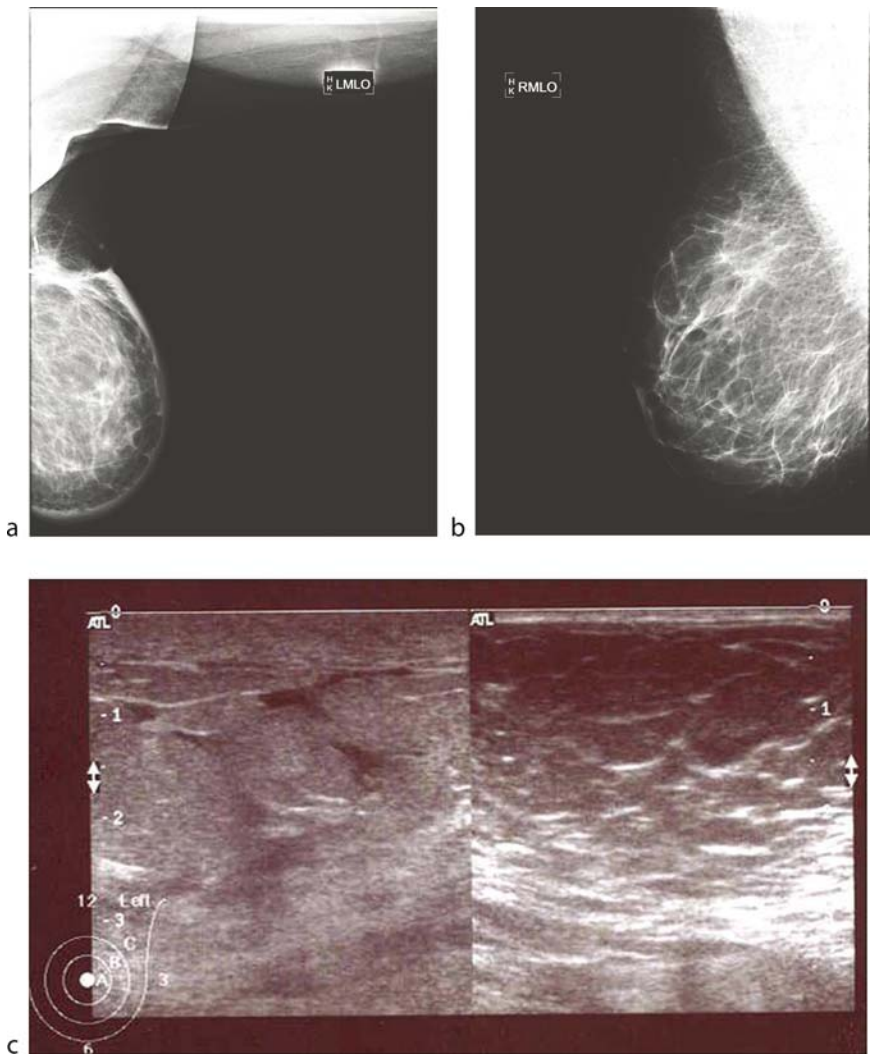

Breast, Therapy Effects. Figure 1 (a) Mammogram (*left*) in MLO position following breast-conserving therapy showing skin thickening, trabeculary coarsening, metallic clips, and scar formation at the operation site. (b) Mammogram (*right*) in MLO position shows normal BI-RADS I breast pattern of the same patient. (c) Ultrasound of both breasts showing skin thickening and lymphatic dilatation on the left. Right side reflects normal echo pattern.

microcalcifications, a postoperative mammogram is obtained before radiotherapy.

In the acute stage, *sonography* evaluates varying degrees of radiation-induced skin thickening. The edema-related echogenicity increases in the subcutaneous space and decreases in the parenchyma, leading to a loss of the normal echo pattern. It can be helpful to distinguish the mammographically visible or palpable hematoma and a simple cyst from a mass. Sonography can detect a recurrence if the breast tissue is very dense.

Within the postoperative 12 months, MRI may indicate false-positive calls because of patchy and focal enhancement. Beginning about 12 months after radiotherapy, supplemental MRI can detect very small recurrent tumors in dense or even irregularly structured tissue with great sensitivity (1).

Because of the partial mammographic visualization of the tissue surrounding the prosthesis, mammography plays a limited role in evaluating any scar formation or detecting recurrent disease. The role of mammography is restricted to detecting suspicious microcalcifications. Rarely, a ruptured implant may be detected by mammography. When performed after breast reconstruction with autogenous tissue transfer, mammographic evaluation of areas with dense scar or muscle tissue is limited. If reduction mammoplasty is done, breast changes may change depending on surgical techniques. The most common findings are parenchymal redistribution, elevation of the nipple,

calcifications, oil cysts, retroareolar fibrotic bands, and skin thickening (Fig. 2). Sonography is suitable for evaluating the tissue surrounding the prosthesis. Its accuracy is limited because of scar formation. MRI has shown that recurrences around implants and small prosthetic defects can be detected earlier with MRI than with other modalities (1).

Preoperative chemotherapy has provided for downsizing and downstaging of breast cancer. In neoadjuvant systemic therapy, conventional techniques of assessing response (clinical examination, X-ray mammography, and ▶breast ultrasound) rely on changes in tumor size, which are often delayed and do not always correlate with pathologic response (8). Improved patient prognosis is a function of pathologic tumor response and residual microscopic disease. These methods are inefficient for monitoring tumor change due to the delay in change noted by clinical examination or current imaging techniques when carcinomas undergo preoperative therapy. The tumors do not necessarily contract in a uniform, spherical way. Pockets of microscopic nests of viable tumor cells may remain scattered throughout the tumor bed. The benefits of enhanced MRI have opened a window for providing evidence of tumor response and residual disease. MRI prediction has been found to be more accurate than clinical examination or mammography in assessing complete response, partial response, or no response. Rieber et al (9) noted that responders had a flattening of the Gd-DTPA uptake curve after the first chemotherapy cycle or a complete absence of Gd-DTPA uptake after the fourth cycle.

Hormone replacement has an impact on the mammographic image. A generalized increase in the extent and density of partially involuted parenchyma is possible (Fig. 3), and a new occurrence or an increase in the size of focal densities can be seen in mammographic images. Estrogen combined with progestins has a stronger association with increased breast density than with the use of estrogen alone and is more commonly observed with the use of continuous combined HRT compared with cyclic HRT. But tibolone is found to have much fewer effects on breast. Tibolone, as a tissue-specific steroid, does not have an estrogenic effect on breast cells. In older women, cysts, fibroadenomas, and other benign breast changes can develop in breasts. Cysts and fibroadenomas can enlarge and simulate a malignant process. After breast-conserving treatment, breast density of healthy breast can increase unilaterally because the irradiated fibrosed breast tissue does not respond to hormones (2).

Sonography is an important diagnostic method for assessing mammographically dense parenchyma. Some focal findings can be detected and interpreted only by ultrasound in these cases. The glandular tissue after hormone stimulation will generally appear homogenous and moderately hyperechoic, but variations because of breast dysplasia are possible. A simple cyst will not require further evaluation, but solid focal lesions that are not

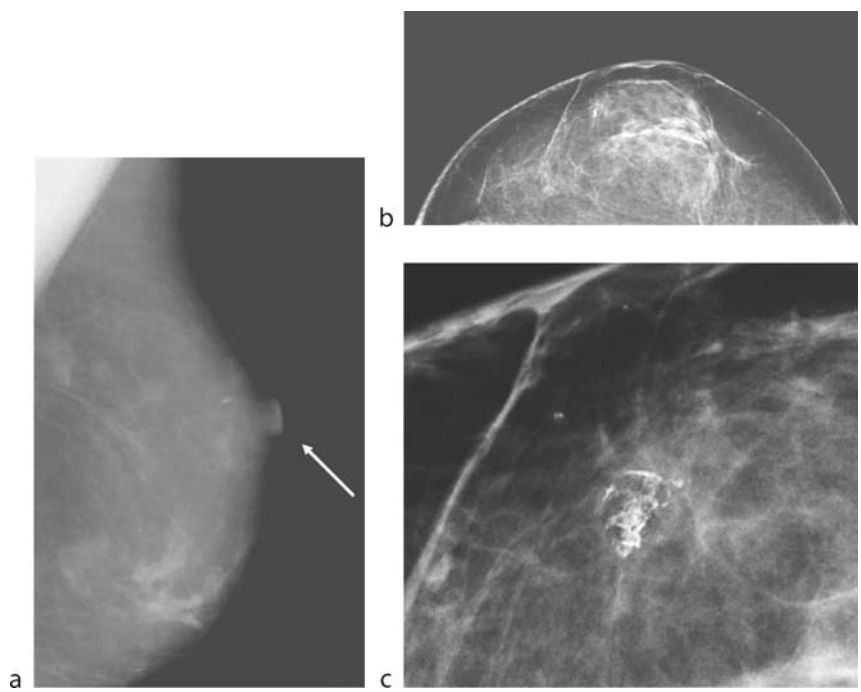

Breast, Therapy Effects. Figure 2 Findings following reduction mammoplasty. (a) Fibrotic bands in lower quadrant and elevation of the nipple (MLO mammogram). (b) Fibrotic bands and fat necrosis in retroareolar region (CC mammogram). (c) Calcification due to fat necrosis (magnification mammogram).

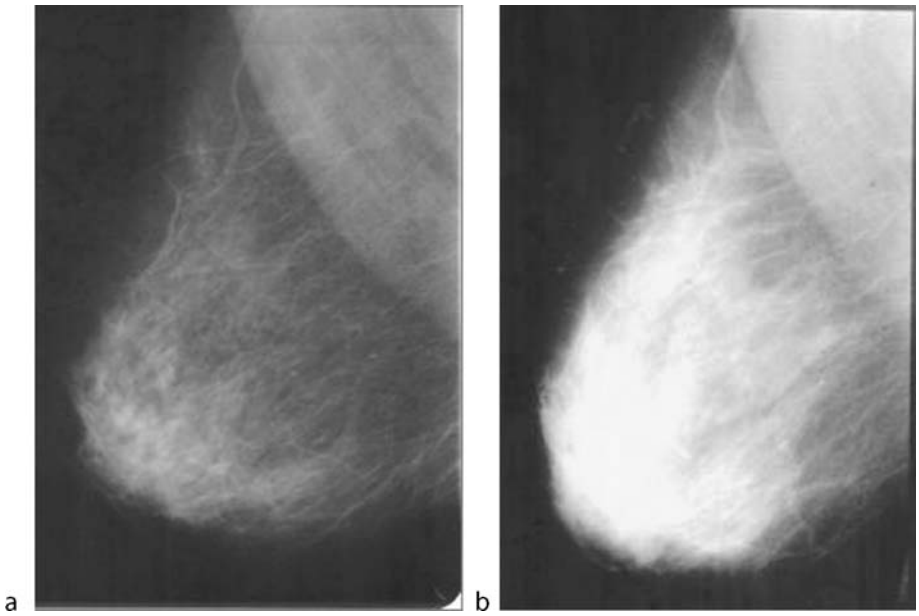

Breast, Therapy Effects. Figure 3 (a) Normal breast pattern of a patient prior to ▶hormone replacement therapy (HRT). (b) Breast pattern of the same patient following two years of HRT, showing a diffuse increase in density.

definitely benign mammographically and sonographically usually require biopsy. The interruption of hormone therapy for 2–3 months may determine whether the lesion is malignant or has regressed. MRI is not indicated for diagnosing changes occurring during HRT. The resulting proliferative changes can be expected to enhance with MRI contrast agents, impairing both detection and exclusion of malignancy (1).

On follow-up mammography of breast cancer patients, breast parenchyma has been shown to be decreased after tamoxifen therapy. A tamoxifen-induced breast parenchymal decrease is more significant in postmenopausal women. Because tamoxifen-induced breast parenchymal decrease is relatively less well shown on mammograms in postmenopausal women with fatty changes of the breast, mammography is the most useful method for evaluating breast parenchymal changes after tamoxifen treatment (9).

Bibliography

1. Heywang-Köbrunner SH, Dershaw D, Schreer I (2001) Diagnostic Breast Imaging. 2nd edn. Thieme, Stuttgart. pp 339–374
2. Harvey J, Kawakami FT, Quebe-Fehling de Palacios PI et al (2005) Hormone replacement therapy and breast density changes.Climacteric 8(2):185–193
3. Million Women Study Collaborators (2003) Breast cancer and hormone replacement therapy in the Million Women Study. Lancet 362:419–427
4. Son HJ, Oh KK (1999) Significance of follow up mammography in estimating the effect of tamoxifen in breast cancer patients who have undergone surgery. Am J Roentgenol 173:905–909
5. Rosen PP (2001) Rosen's breast pathology. In: Rosen PP (ed) Pathologic Effects of Therapy. Lippincott Williams & Wilkins, Philadelphia pp 887–897
6. McNicholas MMJ, Heneghan JP, Milner MH et al (1994) Pain and increased mammographic density in women receiving hormone replacement therapy: a prospective study. Am J Roentgenol 163:311–315
7. Nakamura S, Kenjo H, Nishio T et al (2001) 3D-MR mammography-guided breast conserving surgery after neoadjuvant chemotherapy: clinical results and future perspectives with reference to FDG-PET. Breast Cancer 8(4):351–354
8. Beresford M, Padhani AR, Goh V et al (2005) Imaging breast cancer response during neoadjuvant systemic therapy. Expert Rev Anticancer Ther Oct 5(5):893–905
9. Rieber A, Zeitler H, Rosenthal H et al (1997) MRI of breast cancer: influence of chemotherapy on sensitivity. Brit J Radiol 70:452–458

Bright Liver

Ultrasound finding causes a diffuse increase in echogenicity of the hepatic parenchyma, with regular, tiny, tightly packed echoes. This appearance is typically found in hepatic steatosis, but may also be found in hepatic fibrosis.
▶Steatosis, Hepatic

BRN

▶Breast Recurrent Neoplasms

Brodie's Abscess

A Brodie's abscess represents an intramedullary abscess formation and is a typical complication of chronic osteomyelitis, especially seen in children. Radiographs may reveal a sharply delineated radiolucent lesion surrounded by fine surrounding sclerosis. Frequent locations are the distal and proximal metaphyses of the tibia.

Broken Bones

▶Fractures, Bone, Childhood

Bronchial Adenocarcinoma

▶Neoplasms, Chest, Childhood

Bronchial Adenomas

Low-grade malignant lesions originating from the APUD system.

▶Neoplasms, Chest, Childhood

Bronchial Arteries

In 90% of cases, the source of hemoptysis is the bronchial circulation. The bronchial arteries originate from the proximal portion of the descending thoracic aorta. The right bronchial artery arises from the lateral or dorsolateral aspect of the aorta, most frequently in a common trunk with an intercostal artery (intercostobronchial artery). The left bronchial artery usually originates from the anterior aspect of the thoracic aorta or the concavity of the aortic arch. A left–right bronchial artery may also be seen.

▶Hemoptysis

Bronchial Atresia

▶Congenital Malformations, Tracheobronchial Tree

Bronchial Embolization

Bronchial embolization consists in occluding bronchial and non-bronchial systemic supply to the lung in case of

▶Hemoptysis

Bronchiectasis

Permanent and irreversible dilatation of the bronchial tree as a result of airway obstruction and inflammation.

▶Cystic Fibrosis
▶Airway Disease

Bronchiolitis

Inflammation of the respiratory bronchioles due to viral infection.

▶Bronchitis and Bronchiolitis in Childhood
▶Airway Disease

Bronchiolitis Obliterans

▶Bronchitis and Bronchiolitis in Childhood

Bronchioloalveolar Carcinoma

An uncommon primary malignant pulmonary neoplasm, and it accounts for 2–14% of all pulmonary malignancies. It is a subtype of adenocarcinoma with a commonly peripheral parenchymal location, no distortion of the pulmonary interstitium and neoplastic cells growth along the intra- and interlobular septa. It can have three different radiological patterns: (1) bilateral, multinodular type, (2) diffuse, infiltrative type involving a single lobe or the entire lung simulating pneumonia and (3) solitary peripheral pulmonary nodule. Growing along the septa is appreciated as crazy-paving pattern.

▶Neoplasms Pulmonary

Bronchitis and Bronchiolitis in Childhood

Gundula Staatz
Department of Radiology, Division of Pediatric Radiology, University of Erlangen-Nürnberg, Erlangen, Germany
gu.stz.uni-erlangen@t-online.de

Synonyms

Bronchiolitis obliterans; Tracheobronchitis

Definitions

Tracheobronchitis represents viral lower respiratory tract infection with thickening of the bronchial walls and involvement of the interstitium.

►*Bronchiolitis* is defined as a serious viral infection of the tracheobronchial tree typically due to parainfluenza virus, respiratory syncytial virus or adenovirus occurring in children under 2 years of age.

Bronchiolitis obliterans (constrictive bronchiolitis) is characterized by a necrotising fibrotic bronchiolitis with subsequent obliteration of the bronchioles due to extensive scarring. The distal alveolar ducts and alveoli are primarily not involved. *Swyer–James–McLeod syndrome*, as a variant of postinfectious constrictive bronchiolitis, involves only one lung and develops usually after a pulmonary infection with subsequent alveolar destruction and obliterative bronchiolitis in infancy or early childhood. In bronchiolitis obliterans organizing pneumonia (►BOOP) proliferative granulation tissue polyps are filling the lumens of terminal and respiratory bronchioles and with extension into alveolar ducts and distal alveoli, organizing pneumonia is associated. BOOP is a rare diagnosis in children but increasingly observed following allogeneic lung or bone marrow transplantation.

Asthma is defined as a chronic inflammatory disease of the lower respiratory tract, characterized by repeated episodes of bronchiolitis, reversible airway obstruction, and tracheobronchial mucosal hyperreactivity. Asthma is divided into extrinsic (allergic or atopic), intrinsic (late-onset or nonatopic), and occupational forms. Childhood asthma is usually atopic and often associated with allergic rhinitis and atopic dermatitis.

Pathology/Histopathology

In bronchiolitis, the inflammation of the bronchioles causes thickening of the bronchial wall with involvement of both the mucosa and the peribronchial interstitium. The mucosal edema may lead to complete airway obstruction with atelectasis, but ►air trapping due to partial airway obstruction is more frequent in children. Constrictive bronchiolitis, as a fibrotic bronchiolitis with destruction of the bronchioles, is characterized by histological changes varying from mild bronchiolar inflammation and scarring to concentric fibrosis with complete obliteration of the bronchioles. In BOOP, polypoid masses of granulation tissue in lumens of small airways, alveolar ducts, and some alveoli are identified histologically (1). Asthma is a process involving both central and peripheral airways and is characterized by eosinophilic infiltration and thickening of the airway wall (2). The thickened airway walls show an increased smooth muscle mass, mucous gland hypertrophy, and vascular congestion leading to a markedly reduced airway caliber. Increased amounts of mucus and inflammatory exudate block the airway passages and also cause an increased surface tension favoring airway closure (2).

Clinical Presentation

In children with bronchiolitis the infection usually starts in the upper respiratory tract with rhinitis, pharyngitis, and fever. When the disease progresses to the lower respiratory tract cough, tachydyspnea, expiratory distress, chest retractions, diffuse coarse crackles, and wheezing occur. The coughs may be pertussis-like and increasing dyspnea, and cyanosis indicates hypoxia. The main differential diagnosis is asthma, but also conditions such as foreign body aspiration, cystic fibrosis, pulmonary malformations (cysts, tracheo-esophageal fistulas), vascular rings, or gastroesophageal reflux must be considered. Clinical symptoms in BOOP include persistent nonproductive cough, effort dyspnea, low-grade pyrexia, malaise, and weight loss. Pleuritic chest pain and hemoptysis are less common. Auscultation of the thorax reveals fine, dry, lung crepitations, and typically pulmonary function tests show a restrictive pattern.

Imaging

Although the diagnosis of tracheobronchitis and bronchiolitis is primarily based on the clinical findings, chest radiographs are commonly obtained to differentiate viral from bacterial infection. Even in bronchiolitis obliterans, chest radiographs may be normal or show unspecific findings like hyperaeration. In childhood asthma, chest X-rays are usually obtained to rule out complications like atelectasis, pneumomediastinum, and pneumothorax. In the past years, high resolution computed tomography (HRCT) of the chest has been frequently used in

paediatric lung disease, because this technique offers high spatial resolution and excellent evaluation of the lung parenchyma and especially the interstitium (3). Hyperpolarized gas- and molecular oxygen-enhanced MR imaging are two new techniques for high-resolution MR imaging of pulmonary airspaces, but there is only very little clinical experience with these MR techniques especially in children (4).

Nuclear Medicine

Ventilation and perfusion scintigraphy (VQ scans) provide a relatively noninvasive evaluation of lung function and allow a quantitative assessment of the perfusion of each lung segment. Areas of abnormal aeration and air trapping may be demonstrated, however, VQ scanning gives relatively poor anatomical detail of the lungs and is not commonly used for the assessment of small airways disease in children.

Diagnosis

The typical appearance of viral lower respiratory tract infection (tracheobronchitis) on chest radiographs is a symmetric parahilar peribronchial pattern, resulting from thickening of the bronchial walls with involvement of the mucosa and the interstitium. Parahilar peribronchial infiltrates are often referred as bronchopneumonia and hilar lymphadenopathy is usually associated (Fig. 1). In bronchiolitis markedly hyperinflated lungs with flattening of the diaphragm and peribronchial infiltrates are demonstrated on the chest X-rays (Fig. 2). Atelectatic areas from mucoid plugging and pleural thickening may also be evident. Swyer–James syndrome is characterized by a unilateral hyperlucent lung with normal or reduced volume during inspiration and air trapping during expiration.

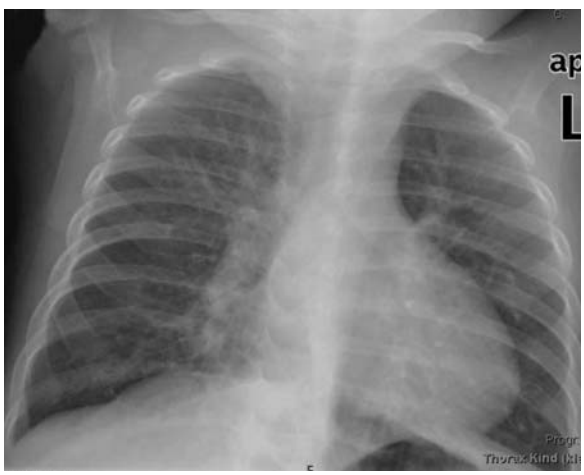

Bronchitis and Bronchiolitis in Childhood. Figure 1 Lower respiratory tract infection in a 3-year-old child. Hyperinflated lungs, parahilar thickening of the bronchial walls, peribronchial infiltrates, and bilateral hilar lymphadenopathy are identified on the plain chest X-ray.

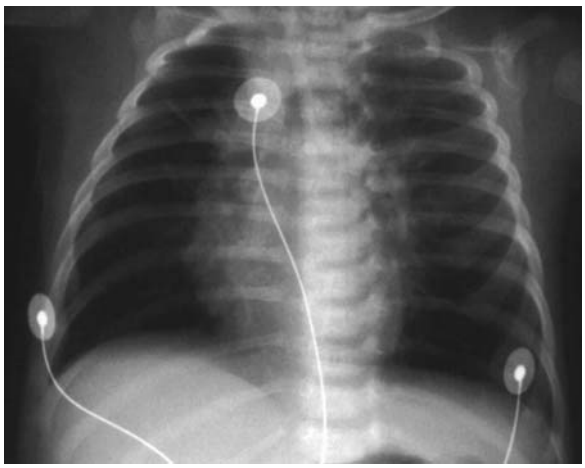

Bronchitis and Bronchiolitis in Childhood. Figure 2 RSV-bronchiolitis. Markedly hyperinflated lungs with flattening of the diaphragm and peribronchial hilar infiltrates are demonstrated on the chest radiograph.

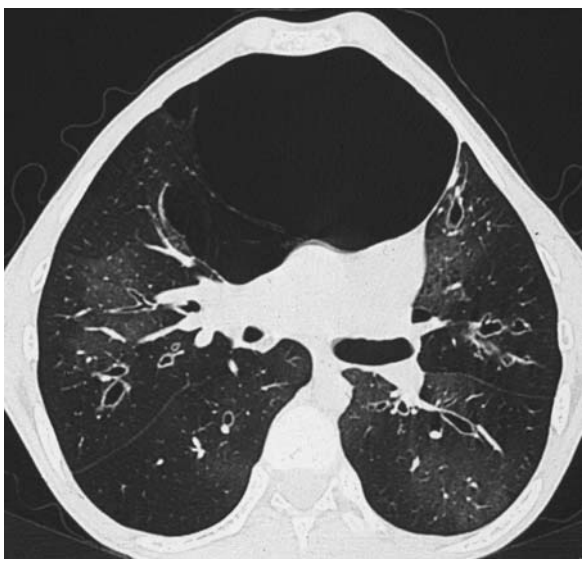

Bronchitis and Bronchiolitis in Childhood. Figure 3 HRCT of bilateral mosaic perfusion pattern in an adolescent with bronchiectasis. A large bulla is visible in the anterior right upper lobe, compressing the upper mediastinum and shifting it to the contralateral side.

High-resolution CT features of small airway disease include air trapping, ground glass opacifications, centrilobar nodules, bronchial wall thickening, bronchiectasis, and ▶mosaic perfusion pattern (5). Mosaic perfusion results from regional perfusion differences caused by a reduced vascularity in lucent lung areas due to secondary hypoxic vasoconstriction (Fig. 3). This pattern is most common in children with asthma, cystic fibrosis, bronchopulmonary dysplasia, and bronchiolitis obliterans. Other HRCT findings in bronchiolitis obliterans are bronchiectasis, bronchial wall thickening, and air trapping in the hyperlucent lung parenchyma. Typical HRCT findings in asthma are air-trapping, bronchial dilatation, bronchial wall thickening, mucoid impaction, and atelectasis. Cystic fibrosis has to be considered as a differential diagnosis to bronchiolitis. Besides air trapping and mosaic perfusion, common findings of cystic fibrosis on HRCT images are bronchiectasis, peribronchial thickening, mucous plugging, centrilobar nodular opacities (mucoid impaction), or cystic and bullous lung lesions.

Bibliography

1. Epler GR, Colby TV, McLoud TC et al (1985) Bronchiolitis obliterans organizing pneumonia. N Engl J Med 312:152–158
2. Saetta M, Turato G (2001) Airway pathology in asthma. Eur Respir J Suppl 34:18–23
3. Copley SJ, Padley SP (2001) High-resolution CT of paediatric lung disease. Eur Radiol 11:2564–2575
4. McAdams HP, Hatabu H, Donnelly LF et al (2000) Novel techniques for MR imaging of pulmonary airspaces. Magn Reson Imaging Clin N Am 8:205–219
5. Franquet T, Muller NL (2003) Disorders of the small airways: high-resolution computed tomographic features. Semin Respir Crit Care Med 24:437–444

Bronchogenic Cyst

Foregut malformation developing from an abnormal budding of the ventral foregut (tracheobronchial tree).
▶Congenital Malformations, Tracheobronchial Tree

Broncholithiasis

It is a condition in which a peribronchial calcified nodal disease erodes into or distorts an adjacent bronchus. This disorder results in airway obstruction. Histoplasmosis and tuberculosis are the most frequent causes, but other infections including actinomycosis, coccidioidomycosis and cryptococcosis, as well as silicosis, have been implicated as possible etiologies. Symptoms are commonly couch, haemoptysis, recurrent episodes of fever and purulent sputum. The diagnosis is most reliably diagnosed with CT scan, which can demonstrate: a calcified endobronchial or peribronchial lymph node; bronchopulmonary complication due to obstruction, and the absence of any associated soft tissue mass.
▶Tuberculosis
▶Airway Disease

Bronchopulmonary Dysplasia

Chronic lung disease, which occurs in premature infants due to the treatment with oxygen and positive pressure ventilation.
▶Dysplasia, Bronchopulmonary

Bronchopulmonary Sequestration

Embryonic mass of lung tissue disconnected from the tracheobronchial tree with a blood supply from the systemic circulation.
▶Congenital Malformations, Tracheobronchial Tree

Bronchoscopy

▶Optical Imaging

Brown Tumors

Osteolytic changes that can mimic secondary or primary bone tumors and are found with primary and secondary hyperparathyroidism.
▶Hyperparathyroidism

Bubbles

▶Microbubbles

Bubbly Lungs

Typical radiographic appearance of bronchopulmonary dysplasia characterized by pseudocysts (bubbles) alternating with interstitial fibrosis and atelectasis.
▶Dysplasia, Bronchopulmonary

Bucket Handle Fracture

Metaphyseal corner Salter II fracture viewed obliquely with respect to the shaft axis, looking like the handle of a bucket, and characteristic of an abuse fracture.
▶Battered Child Syndrome

Buckle (Torus) Fracture

A fracture in childhood with a local bending deformity of the normal monotonically curved contour of diaphysis or metaphysis, or of the equivalent in flat bones.
▶Fractures, Bone, Childhood

Budd–Chiari Syndrome

I. Kaare Tesdal
Department of Radiology and Nuclear Medicine, Klinikum, Friedrichshafen, Friedrichshafen, Germany
k.tesdal@klinikum-fn.de

Synonyms

Hepatic obstruction; Nonthrombotic hepatic vein obstruction; Obliterating hepatic vein endophlebitis; Thrombotic hepatic vein obstruction

Definition

Budd–Chiari syndrome is a rare condition and describes an entity of diseases characterized by thrombotic or nonthrombotic obstruction to hepatic venous outflow (1). The obstruction may completely or partially block the hepatic veins. George Budd (1808–1882) described it in 1845, and Hans Chiari added the first pathologic description of a liver with "obliterating endophlebitis of the hepatic veins" in 1899. The syndrome most often occurs in patients with underlying thrombophilic disorders, including myeloproliferative disorders such as polycythemia vera and paroxysmal nocturnal hemoglobinuria, pregnancy, tumors, chronic inflammatory diseases, clotting disorders, and infections.

Pathology/Histopathology

Obstruction of intrahepatic veins leads to hepatic congestion and hepatopathy as blood flows into, but not out of the liver. Characteristically, the caudate lobe of the liver is spared due to direct venous channels from the inferior vena cava. The blood accumulation in the liver raises the pressure in the nonoccluded hepatic veins and in the portal veins leading to portal hypertension. Hepatocellular injury results from microvascular ischemia due to congestion, and liver insufficiency result.

Clinical Presentation

In the Western world, the Budd–Chiari syndrome is predominantly seen in women. Age at presentation is usually the third or fourth decade of life, although the condition may also occur in children or elderly persons. The symptoms of Budd–Chiari syndrome may begin suddenly and severely, but usually they begin gradually. Hepatomegaly, ascites, and abdominal pain characterize Budd–Chiari syndrome, but all these symptoms are nonspecific. Four main clinical variants have been described: acute liver disease, subacute liver disease, fulminant liver disease, and chronic liver failure. The most common presentation is subacute liver disease complicated by symptoms of portal hypertension and varying degrees of liver insufficiency. A model has been created using the following equation that allows for the prediction of survival of patients with BCS: $1.27 \times$ encephalopathy $+ 1.04 \times$ ascites $+ 0.72 \times$ prothrombin time $+ 0.004 \times$ bilirubin. Based on this model, patients can be separated into three groups with good, intermediate, and poor 5-year survivals. The parameters determining the outcome are accompanying complications such as portal vein thrombosis, thrombosis of inferior vena cava, and renal failure. (a) Acute and subacute forms: these are characterized by rapid development of abdominal pain, ascites, hepatomegaly, jaundice, and renal failure. (b) Fulminant form:

the patients may present with fulminant or subfulminant hepatic failure along with ascites, tender hepatomegaly, jaundice, and renal failure. This form of presentation is uncommon. (c) Chronic form: this is the most common form, and patients present with progressive ascites, and approximately 50% of patients also have renal impairment. Further severe complications in these patients are progressive liver insufficiency, hydrothorax, hepatic encephalopathy, or variceal bleeding.

Imaging

As imaging modalities we use ultrasound, magnetic resonance imaging (MRI), angiography of hepatic veins, and computed tomography (CT) scan to diagnose Budd–Chiari syndrome. Using ultrasound, thrombi can be visualized, and duplex sonography is the preferred mode. The sensitivity and specificity of combining different modes of ultrasound are 85–90%. MRI scanning with pulsed sequencing helps in the assessment of hepatic venous and portal blood flow, and the sensitivity and specificity are more than 90%. Angiography of hepatic veins (hepatic venography) can demonstrate thrombi or membranous webs if the hepatic veins are partially open. CT is the workhorse imaging system in most radiology departments and diagnostic centers dealing with liver diseases (Fig. 1). Contrast CT is fast, patient friendly, and has the unique ability to image all thoracic and abdominal structures. The advances in technology and

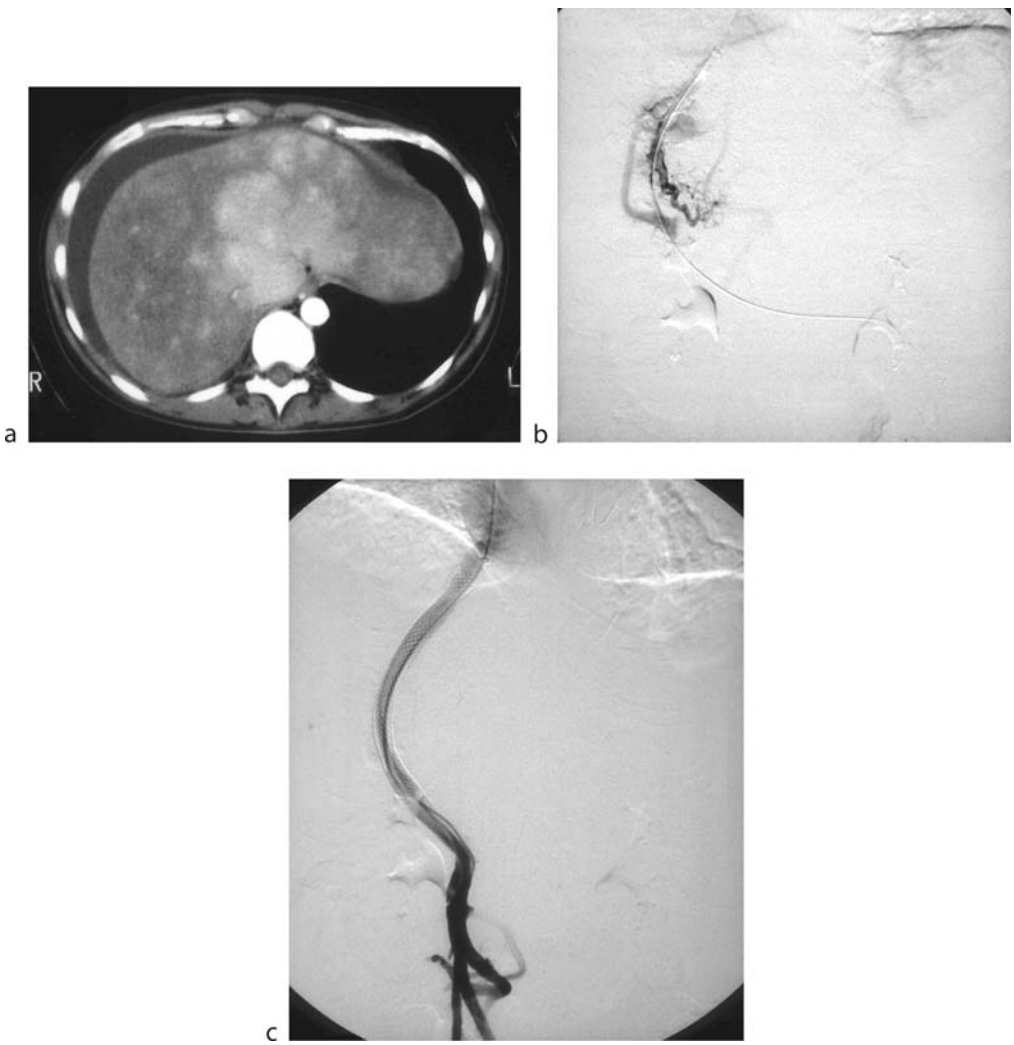

Budd–Chiari Syndrome. Figure 1 CT in a 34-year-old woman presenting symptoms of subacute Budd–Chiari syndrome and severe variceal bleeding. The arterial phase shows a hypertrophy of the liver, and an inhomogeneous parenchyma due to subtotal occlusion of the hepatic veins (venous outflow).

clinical performance using multidetector CT, enables the diagnosis of Budd–Chiari syndrome and the accompanying complications (e.g. liver cirrhosis, ascites, hydrothorax).

Diagnosis

The most important diagnostic workups are the imaging modalities like duplex sonography and CT. In addition to the routine laboratory tests (usually nonspecific), the following tests should be performed to evaluate for a hypercoagulable state: Protein C activity, antithrombin, total and free protein S, activated protein C resistance, prothrombin gene G2021OA mutation, homocysteine concentration, factor V Leiden mutation, lupus anticoagulants, plasminogen, fibrinogen, and heparin antibodies. The diagnosis of bone marrow disorders like polycythemia vera, essential thrombocytosis, myeloproliferative syndrome, and myelofibrosis has to be established or excluded according to international definitions. Examination of ascitic fluid provides useful clues to the diagnosis since patients usually have high protein concentrations (>2 g/dL), but this may not be present in persons with the acute form of Budd–Chiari syndrome. A biopsy of the liver is not compulsory for the diagnosis. The typical histologic findings after liver biopsy are high-grade venous congestion and centrilobular liver cell atrophy and thrombi within the terminal hepatic venules. The extent of fibrosis and cirrhosis can be determined based on biopsy findings.

Interventional Radiological Treatment

Treatment options include medical therapy, balloon dilation (PTA) of hepatic vein, portal systemic shunt surgery, transjugular intrahepatic portosystemic shunt (TIPS), and liver transplantation. Irrespective of the course of the disease, a side-to-side shunt or liver transplantation is indicated if medical treatment fails. In recent years, a number of reports of TIPS as a treatment for Budd–Chiari syndrome (BCS) have appeared.

References

1. Dilawari JB, Bambery P, Chawla Y et al (1994)Hepatic outflow obstruction (Budd–Chiari syndrome). Experience with 177 patients and a review of the literature. Medicine 73:21–36
2. Boyer TD, Haskal ZJ (2005) The role of transjugular intrahepatic portosystemic shunt in the management of portal hypertension. Hepatology 41:385–400
3. Tesdal IK, Filser T, Weiß Ch et al (2005) Transjugular intrahepatic portosystemic shunt: adjunctive embolotherapy of gastroesophageal collaterals in the prevention of variceal rebleeding. Radiology 236:360–367
4. Rössle M, Olschewski M, Siegerstetter V et al (2004) The Budd–Chiari syndrome: outcome after treatment with transjugular intrahepatic portosystemic shunt. Surgery 135:394–403

Bulging Disk

A bulging disk is one in which the contour of the outer annulus extends in the axial plane beyond the edges of the disk space, over greater than 50% of the circumference of the disk and usually less than 3 mm beyond the edges of the vertebral body.

▶Herniation, Intervertebral Disk

Bulla

This has been defined as a sharply demarcated area of emphysema measuring >1cm in size and being delineated by a thin (1 mm) epithelialized wall. It may be difficult to distinguish a bulla from a cyst, but bullae are usually associated with extensive emphysematous changes elsewhere in the lung.

▶Pulmonary Opacity, Cystic Pattern

BUN

▶Blood Urea Nitrogen

Byler Disease

Form of progressive familial intrahepatic cholestasis pertaining to a heterogeneous group of autosomal recessive childhood cholestasis of hepatocellular origin. This form was first described in Amish kindred. It is characterized by cholestasis often arising in the neonatal period that leads to liver failure.

▶Congenital Malformations, Liver and Biliary Tract

Byler's Disease

Familial intrahepatic cholestasis, initially described in Amish descendants of Jacob Byler. The disease is

characterized by the absence of a gene encoding for canalicular transport and bile formation. An autosomal recessive inheritance with two subtypes called respectively low GGT PFIC 1 and 2 has been demonstrated. Clinically patients present with a chronic cholestatic syndrome that begins in infancy and usually progresses to cirrhosis within the first decade of life. Common features are hepatocellular cholestasis with low serum levels of gamma glutamyl transpeptidase activity.

►Hepatic, Pediatric Tumors, Malignant

CA-125

CA-125, a glycoprotein antigen, is currently the most commonly used tumor marker for ovarian cancer. Its value lies in the assessment and monitoring of recurrent ovarian cancer. In primary ovarian cancer it is less specific, particularly in premenopausal women and in early-stage disease.

►Carcinoma, Ovarium

Cacchi-Ricci disease

►Medullary Sponge Kidney

Caffey Disease

Alan E. Oestreich
Cincinnati Children's Hospital Medical Center, Cincinnati, Ohio, USA
Alan.Oestreich@cchmc.org

Synonym

Infantile cortical hyperostosis

Definitions

A skeletal condition in infants and fetuses manifest by periosteal reaction, involving only a few bones, especially tubular bones and the mandible and scapula, associated with warmth and tenderness, and not due to a known specific cause. The condition is generally self-limited and heals. Because of its close simulation of the skeletal effect of long-term use of high dose prostaglandin E, it may well be metabolic in nature; however, others (including, at one time, Caffey) have postulated a viral cause, and sometimes it occurs in several members of a family, raising the question of genetic susceptibility. As a periosteal process, it manifests only at sites of membranous bone growth.

Pathology/Histopathology

The hyperostosis (periosteal reaction) of Caffey disease eventually heals into a somewhat thick cortex, which slowly returns to normal over time. The role of biopsy would be principally to exclude competing diagnoses, such as osteomyelitis or metastases from neuroblastoma, in the unusual circumstance that the diagnosis is in question. The periosteal reaction of Caffey disease will stop short of the short, straight ►metaphyseal collar at the metaphysis, since such reaction only occurs where periosteum is present, and it cannot occur on exclusively enchondral bones (*viz*, tarsal or carpal bones) that do not have a periosteum.

Clinical Presentation

The earliest presentation of Caffey disease is intrauterine polyhydramnios, presumably as a consequence of mandible involvement making swallowing painful for the fetus. After a baby is born, the findings are warmth, tenderness, possible swelling, and reduction in motion of the affected bones.

Similar signs may be found in high dose prostaglandin E use leading to periosteal reaction (1); additionally vomiting may occur from antral narrowing in babies so treated. The Scotch terrier puppies that get a Caffey-like hyperostosis of the mandible refuse food or drink because of pain, but survive nicely if tube fed during the active disease.

If periosteal reaction simulating Caffey disease is due to neuroblastoma, metastases, redness, warmth, and even tenderness may be absent (unless there is a pathological fracture).

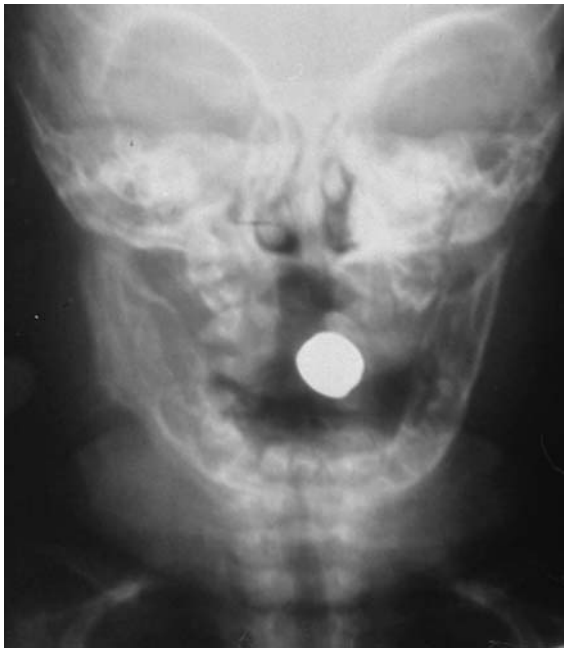

Caffey Disease. Figure 1 Right-sided mandibular periosteal reaction in Caffey disease. From Oestreich AE, Crawford AH (1985) Atlas of Pediatric Orthopedic Radiology. Thieme Verlag, Stuttgart p 104.

Imaging

Careful analysis of long bones, mandible (Fig. 1), scapula, clavicle, and ribs for periosteal reaction on plain radiographs, using magnification of the images in symptomatic areas, is the method to document Caffey disease. In high dose prostaglandin E disease, we have seen similar involvement of small tubular bones of the hand (Fig. 2); perhaps that may also occur in Caffey disease. Periosteal reaction can be shown with ultrasound or CT, but plain images suffice, especially if careful attention is directed to symptomatic sites and 10 days have elapsed since the onset of the disease. On prenatal ultrasound, evaluation for polyhydramnios is pertinent.

Nuclear Medicine

Since it takes about 10 days for periosteal reaction of any etiology to appear on conventional radiographs, nuclear imaging is capable of demonstrating abnormal activity earlier, as early as the first day of the process, in Caffey disease, as well as earlier than 10 days in simulating conditions, including prostaglandin E high dose, hypervitaminosis A, trauma (such as abuse), and tumor (such

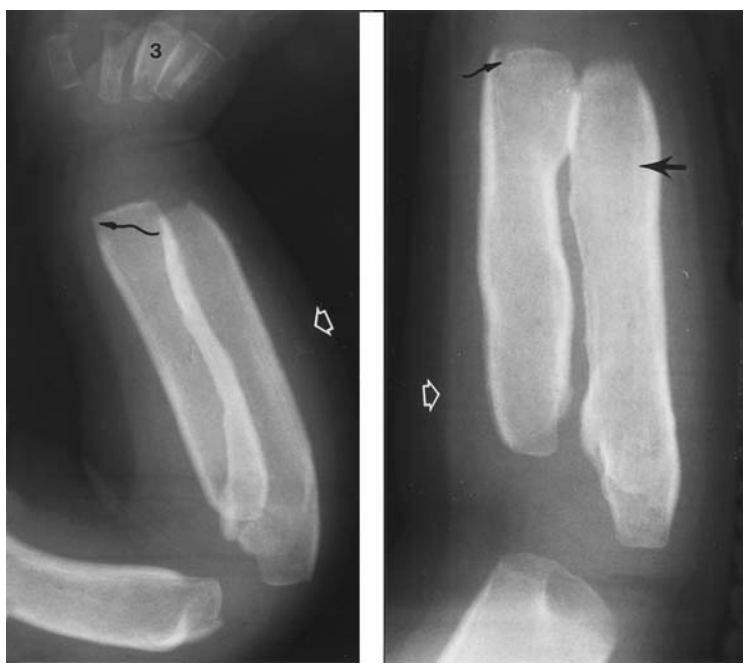

Caffey Disease. Figure 2 Painful swollen forearm following 3 months of prostaglandin E therapy. The deep soft tissues are swollen (white arrows). Note periosteal reaction at metacarpal 3 (3). The metaphyseal collars (curved arrows) are spared from the periosteal reaction. The earlier cortex of the ulna (black arrow) is barely discernable. From Oestreich AE, Shownkeen H (1993) Massive prostaglandin-E periosteal reaction in an infant. Lessons to be learned. Year Book of Pediatr Radiol (Miskolc) 5:49.

as neuroblastoma metastases; once neuroblastoma is suspected, I131MIBG is the nuclear method of choice). Caffey disease is particularly supported by increased mandible activity on bone scan.

Diagnosis

Periosteal reaction along long bones in Caffey disease stops short of the 1–3 mm metaphyseal collar (Fig. 2). For the mandible, clavicle and scapula, it may merely present as enlarged dense bone. Rib disease is best seen if the most lateral portions are involved.

Other causes of diffuse periosteal reaction in infancy or later in childhood include neuroblastoma metastasis, Weismann–Netter Stuhl disease, Erdheim-Chester disease, ▶Melhem hyperostosis and hyperphosphatemia (2), as well as physiologic periosteal reaction found in a significant percentage of normal (and even abnormal) infants 1–6 months of age (3).

Bibliography

1. Benz-Bohm G, Emons D et al (1984) Cortical hyperostoses after long-term prostaglandin E2 therapy [in German]. Radiologe 24:72–78
2. Melhem RE, Najjar SS, Khachadurian AK (1970) Cortical hyperostosis with hyperphosphatemia: a new syndrome? J Pediatr 77:986–990
3. Shopfner CE (1966) Periosteal bone growth in normal infants. A preliminary report. Am J Roentgenol Radium Ther Nucl Med 97:154–163

Calcific Periarthritis

Calcifications within periarticular soft tissues frequently with a history of pain.
▶HADD

Calcific Tendinosis or Calcific Tendinotis

Calcifications within tendons frequently with a history of pain.
▶HADD

Calcification, Intracranial, Neonatal

Veronica Donoghue
Radiology Department, Children's University Hospital, Dublin, Ireland
veronica.donoghue@cuh.ie

C

Synonym

TORCH infections

Definition

Pathological calcification of the newborn brain is detected on plain radiography or CT examination. The numerous causes include perinatal toxoplasmosis, others i.e. HIV, rubella, cytomegalovirus, herpes (TORCH) infections, metabolic abnormalities, vascular disease, brain infarction, tumours and ▶neurophakomatoses.

Pathology/Histopathology

The pathology in neonatal intracranial calcification varies with the underlying cause.

Each one is discussed in more detail elsewhere in this section.

Clinical Presentation

Some infants with *congenital infection*, in particular *cytomegalovirus* present with a small head circumference and infants with toxoplasmosis may have hydrocephalus (1) All these infections are generalised infections and the infants may have skin rashes and haemorrhages, hepatosplenomegaly, chorioretinitis and pneumonitis.

The diagnosis of *tuberous sclerosis* depends on detecting the characteristic cutaneous lesions and the presence of cardiac tumours such as rhabdomyomas which can be diagnosed using antenatal sonography. They can also present with renal cysts and hamartomas.

In *Sturge–Weber disease* a facial haemangioma causing a port-wine stain in the distribution of the trigeminal nerve is characteristic.

In *Von–Hippel–Lindau disease* there are cerebellar and retinal haemangiomas and the patients may also present with polycystic kidney disease and cysts in other organs.

Many of these patients including those with inherited metabolic diseases and brain infarction may also present with seizures.

A ►pseudo-TORCH syndrome has been described such that patients who are microcephalic at birth have delayed motor and cognitive development, long tract signs and their work-up for congenital infections is normal. Many have affected siblings and parental consanguinity has been reported in approximately one-third of patients suggesting an autosomal recessive inheritance (3).

Imaging

Intracranial calcification maybe curvilinear, linear, punctuate or clumpy. If dense it may be seen on plain radiographs but it is more easily identified with CT (Fig. 1). Ultrasonography can identify calcification particularly if it is in the periventricular regions (Fig. 2). MR imaging is a poor tool to detect calcification but it may be seen using gradient-echo sequences and also as reduced signal on T2 and increased signal on T1 sequences.

In cytomegalovirus and less commonly rubella and toxoplasmosis infections, the calcification tends to be periventricular in location (Figs. 1 and 2). It may also involve the basal ganglia. In the other infections the location is non-specific and can occur almost anywhere in the brain. Increased echogenicity of the lenticulostriate regions on sonography, sometimes referred to as *non-calcifying vasculopathy*, has been reported in infants with congenital infection. This however is a non-specific finding and can also be seen in some trisomy syndromes, ischaemia and storage disorders (2).

MR and CT imaging may also detect various brain developmental anomalies such as delayed myelination, lissencephaly, polymicrogyria, cerebellar hypoplasia and schizencephaly, depending on the gestational age at the time of infection.

Infants with pseudo-TORCH syndrome also demonstrate calcification which is mainly periventricular in location but may also involve the basal ganglia. They also have ventricular dilatation secondary to white matter volume loss and the cerebellum and brainstem may be small.

Intracranial tubers of tuberous sclerosis are seldom calcified in the newborn period.

In Sturge–Weber syndrome, the calcification characteristically occurs in the cerebral cortex underlying the angiomatosis and typically has a gyriform pattern. The calcification however is seldom seen in the newborn period.

In tumours and areas of infarction the calcification is non-specific.

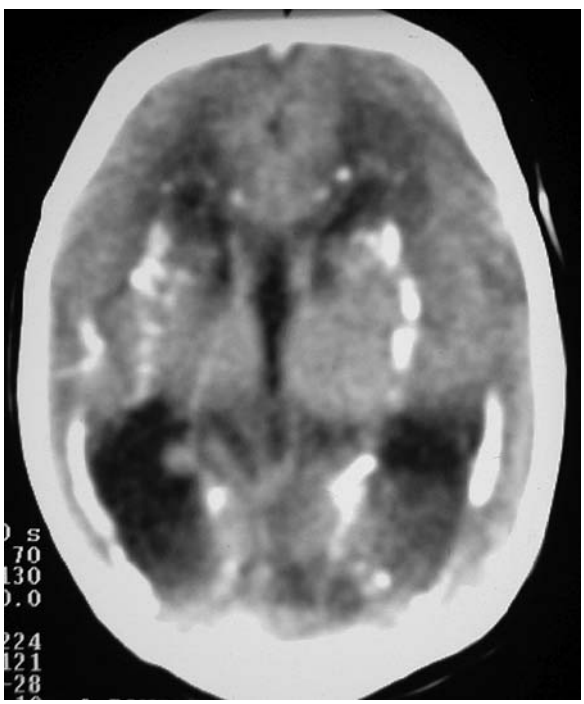

Calcification, Intracranial, Neonatal. Figure 1 CT brain on newborn infant with congenital cytomegalovirus infection. There is extensive intracranial calcification of a punctuate, clumpy and curvilinear nature.

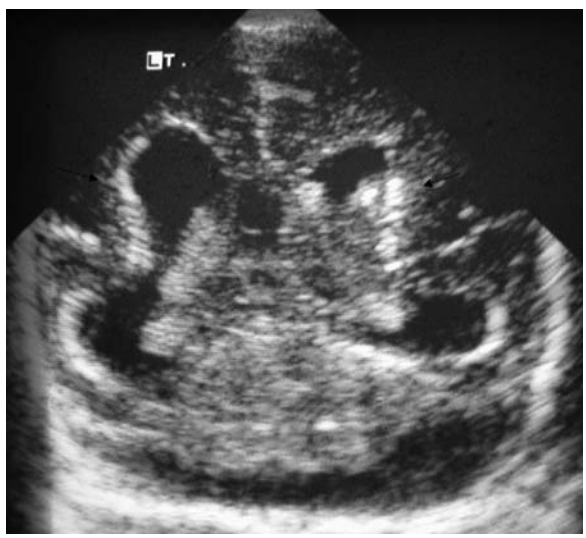

Calcification, Intracranial, Neonatal. Figure 2 Ultrasound image in infant with congenital cytomegalovirus infection. There is extensive increased periventricular echogenicity in keeping with calcification (arrows).

Diagnosis

If dense, intracranial calcification can be seen on plain radiography. It may also be identified on sonography particularly when periventricular in location.

CT is the most sensitive imaging modality.

MR imaging is poor at detecting calcification but it maybe suggested on gradient-echo sequences and also as reduced signal on T2 and increased signal on T1 sequences.

Bibliography

1. Barkovich JA (ed) (2005) Pediatric Neuroimaging. 4th edn. Lippincott Williams and Wilkins, Baltimore
2. El Ayoubi M, de Bethmann O, Monset-Couchard M (2003) Lenticulostriate echogenic vessels: clinical and sonographic study of 70 neonatal cases. Pediatr Radiol 33:697–703
3. Reardon W, Hockey A, Silberstein P et al (1994) Autosomal recessive congenital intrauterine infection-like syndrome of microcephaly, intracranial calcification and CNS disease. Am J Med Genet 52:58–65

Calcifications, Breast

Arne Fischmann
University of Tübingen Department of Diagnostic Radiology, Tübingen, Germany
arne.fischmann@med.uni-tuebingen.de

Synonym

Microcalcifications

Definition

Crystals of calcium phosphate, calcium carbonate, calcium oxalate, and magnesium phosphate developing in different benign or malignant transformations of breast tissue.

Pathology/Histopathology

Calcifications are usually localized in the terminal ductulolobular unit (1). In general, the various calcifications are deposited in areas where compound lipids are present. Calcifications may be psammous, granular, laminar, or amorphous. Sometimes they form circular structures referred to as Liesegang rings within cysts (2).

While most calcifications are easily detectable in H&E-stained sections, calcium oxalate is obscure to standard work-up and only visible in polarized light. As calcium oxalate is mainly associated to benign disease, detection is important to avoid unnecessary follow-up biopsies.

Radiologic–pathologic correlation of calcifications is difficult, as up to 25% of calcifications are lost during embedding and fixation of specimens. Moreover, microcalcifications smaller than 100 are undetectable at mammography. Therefore all specimens taken for microcalcifications should undergo specimen radiography and the pathologist should thoroughly search for calcifications marked radiologically.

Clinical Presentation

Due to their size and distribution, calcifications are impalpable and clinically invisible, therefore only lesions with mass effect and associated calcifications are clinically detectable.

Approximately 40–50% of mammary carcinomas have calcifications that are mammographically detectable. Intraductal comedocarcinoma and infiltrative carcinoma, in particular, are frequently associated with calcifications, whereas lobular carcinomas are rarely calcified. Among the benign lesions, sclerosing adenosis is associated with calcifications with a frequency of 50%.

With 58% positive predictive value in patients treated with breast-conserving therapy, calcifications are a valuable tool in the detection of recurrence.

Imaging

Mammography is the primary imaging modality in the detection and description of calcifications. The widespread use of screening mammography since the 1970s has caused a substantial increase in the incidence of calcifications.

In general, detection of clustered calcifications in mammography should advocate the performance of magnification views, preferably in craniocaudal and mediolateral positioning to localize precisely the calcifications and to detect milk of calcium.

Sonography is useful in showing cystic changes in fibrocystic disease. In some cases microcalcifications can be viewed directly on sonographs.

Despite the characteristic appearance of calcium on magnetic resonance imaging (MRI) with low signal on T1-weighted and T2-weighted images, MRI has no practical use in the detection or classification of calcifications. This is mainly due to the small size of single

calcifications, which is far below the voxel size. MRI is therefore only able to detect the underlying disease. As sensitivity for *in-situ* carcinoma is about 80%, a normal MRI in cases of suspicious microcalcifications cannot rule out malignant disease. In fibroglandular or dense breast tissue, preoperative magnetic resonance tomography can be useful in detecting multifocal disease. This is also true for new calcifications after breast-conserving therapy, where it is difficult to distinguish liponecrotic calcifications *in statu nascendi* from recurrent breast cancer.

Nuclear Medicine

Currently there is no known tracer for classifying calcifications. Nuclear medicine is therefore confined to cases where calcifications lead to a diagnosis of breast cancer and require further work-up.

Diagnosis

Mammography is currently the only imaging modality that can detect and classify microcalcifications with sufficient diagnostic accuracy.

Morphology and distribution are the most important parameters when differentiating benign from malignant calcifications, whereas the number of calcifications is of little importance.

All calcifications should be classified according to the categories described in the Breast Imaging Reporting and Data System (BI-RADS) lexicon by the American College of Radiology (ACR). A summary of these descriptions is given below.

Typically, benign calcifications can rule out malignancy with a high probability and are usually pathognomonic. These include: skin calcifications, vascular (Fig. 1), round, popcorn-like (fibroadenoma), large rod-like (plasma cell mastitis), lucent centered, egg-shell or rim calcifications (lipid necrosis), milk of calcium (Fig. 1), suture, and dystrophic calcifications.

Coarse, heterogeneous calcifications are of intermediate concern and often represent fibroadenoma, fibrosis, or trauma.

Amorphous or punctuate calcifications have a diameter of less than 0.5 mm, and are usually indistinct (Fig. 2). Pathologically they often represent psammoma-like structures (1).

Fine pleomorphic calcifications are of similar shape but vary in size without casting parts, which are more suspicious (3).

Fine-linear or fine-linear branching calcifications are usually associated with comedocarcinoma (Fig. 3).

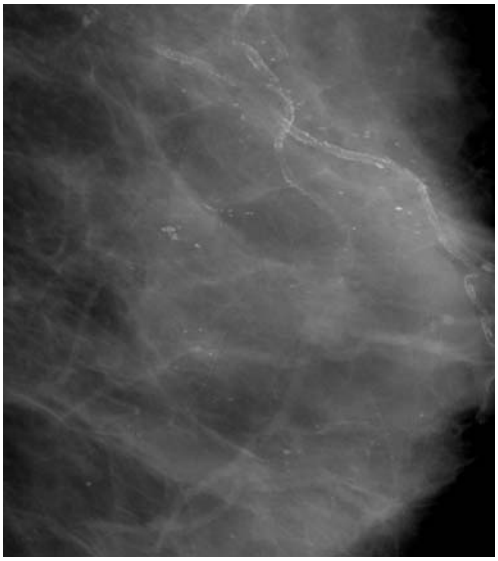

Calcifications, Breast. Figure 1 Multiple crescent shaped calcifications in this lateral view represent milk of calcium. These are typically benign as well as the vascular calcifications in this image.

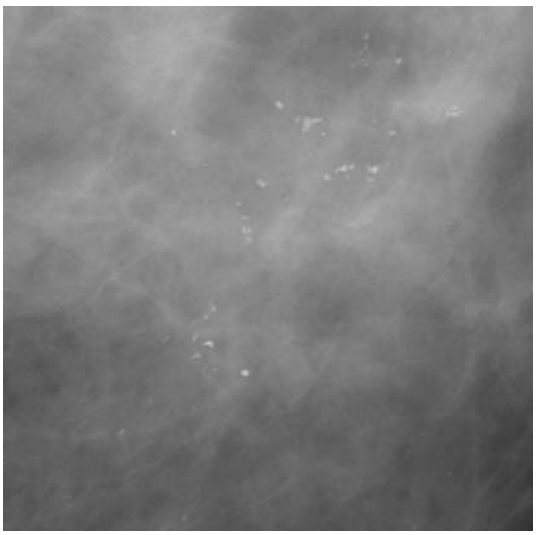

Calcifications, Breast. Figure 2 A small group of amorphous calcifications in a segmental distribution representing ductal carcinoma *in situ*.

Groups can be classified into segmental, linear, multilocular, regional (>2cm^2 in an area that does not suggest a ductal distribution), grouped or clustered (<2cm^2), and diffuse/scattered. In particular, segmental and linear distributions are strongly associated to malignant disease. However, the diagnostic accuracy for calcifications is lower than for solid lesions. Sensitivity is reported to be as low

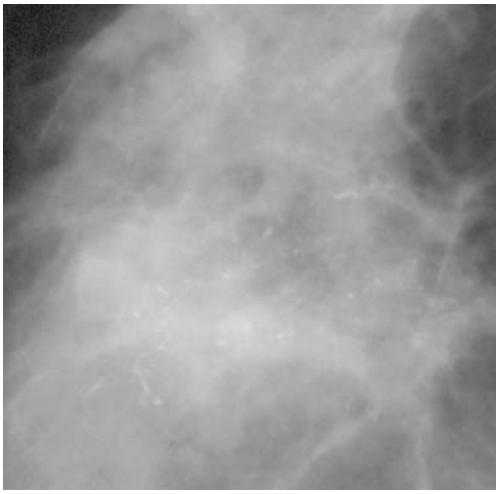

Calcifications, Breast. Figure 3 Polymorphous, casting calcifications in a regional distributions representing typical DCIS.

as 67%. As the specificity is lower, biopsy should be performed more often: the definite diagnosis of the underlying disease in the case of suspicious calcifications can only be obtained by histology.

In addition to this, calcifications tend to either underestimate tumor extent due to uncalcified parts of the lesion, or to overestimate the extent, because benign calcifications are included in the suspicious group.

Interventional Radiology

Biopsy with stereotactic guidance is the preferred diagnostic method for biopsy work-up of suspicious calcifications. Especially in BI-RADS 4 calcifications, vacuum biopsy is superior to core biopsy because underdiagnosis is lower and additional excision biopsies can be avoided. Ultrasound-guided biopsy of calcifications should only be performed if the mammographic and ultrasound-detected lesion can be correlated with certainty. In this case a specimen radiograph and a postbiopsy mammograph are obligatory to verify the correct biopsy.

If open biopsy is necessary, preoperative localization with a guidewire should be performed. Specimen radiography is advocated to verify complete biopsy. The exact localization of the calcifications should be described and communicated to the pathologist to assure correct work-up.

Bibliography

1. Tabar L, Dean PB, Tot T (2001) Teaching Atlas of Mammography. 3rd edn. Thieme Medical Publishers, Stuttgart
2. Tavassoli FA (1999) Microcalcifications. In: Tavassoli FA (ed) Pathology of the Breast. McGraw-Hill, New York, pp 174–186
3. American College of Radiology (2004) Breast Imaging Reporting and Data System (BI-RADS). 4th edn. American College of Radiology, Reston, VA

C

Calcifications, Coronary, Plaque, Calcium Scoring

Christoph R. Becker
Ludwig-Maximilians-Universität, Munich, Germany
christoph.becker@med.uni-muenchen.de

Development of Coronary Atherosclerosis

Coronary atherosclerosis begins as early as in the first decade of life with endothelial dysfunction, proliferation of smooth muscle cells, and deposition of fatty streaks in the coronary artery wall. At the later stage of the still clinically silent disease, which may have already occurred in the first decade of life, these lesions may further accumulate cholesterol within the intima and media coronary artery wall layer, with a fibrous cap separating the lipid pool from the coronary artery lumen. Inflammatory processes with invasion of macrophages and activation of matrix-metallo proteases may cause consecutive weakening of the fibrous cap. Such vulnerable plaques may rupture when exposed to shear stress, and the thrombogenic lipid material may enter the bloodstream. In the most unfortunate event, thrombus progression may turn the vulnerable plaques into culprit lesions that occlude the coronary vessels, leading to myocardial ischemia, ventricular fibrillation, and even death.

In the initial stadium of atherosclerosis, the coronary vessel widens at the location of the atherosclerotic plaques. The phenomenon is called "positive remodeling" and explains why such plaques may not be seen by cardiac catheterization. Nonfatal plaque rupture or erosion at the end stage may heal, organize, and subsequently calcify. Fibrocalcified lesions may reduce vessel lumen diameter by scarring (negative remodeling) with consecutive reduction of blood flow, resulting in myocardial ischemia.

Estimation of Cardiac Event Risk

In many patients, unheralded myocardial infarction associated with a mortality of approximately 20% is the

first sign of coronary artery disease (CAD). Approximately 40% of the general population is considered to have a moderate (10–20%) midterm risk (within the next 10 years) of developing a myocardial infarction. Taking the conventional cardiovascular risk factors (diabetes, hypertension, hypercholesteremia, smoking, family history) into account currently provides the base for myocardial infarction risk assessment according to established risk stratification schemes. All of the currently available risk stratification schemes, however, suffer from lack of accuracy to correctly determine risk, and in particular, uncertainty exists regarding how to treat those who have been identified to be at intermediate risk. Further tools providing information about the necessity to either reassure or treat these individuals are warranted. Computed tomography (CT) is currently the only reliable and practical tool that allows noninvasive investigation of the entire coronary artery tree and quantification of coronary calcium as a surrogate marker of atherosclerotic plaque burden.

Coronary Calcium Screening

As a fundamental requirement for screening for coronary atherosclerosis by CT, the radiation exposure should be reduced to a minimum (about 1 mSv). Any MDCT scanner can perform coronary calcium screening without contrast media by acquiring 3-mm consecutive or better overlapping slices. Even the tiniest calcification will become visible by reconstruction with a no-edge enhancing soft-tissue kernel. After the reconstruction, the image data need to be analyzed and postprocessed by a dedicated workstation. After identification of the specific lesions, the workstation may automatically display the amount of coronary calcium in quantities such as the Agatston score, volume equivalent, and absolute mass.

Coronary calcium is a specific marker for coronary atherosclerosis. In large cohorts of 10,000 asymptomatic persons, it was demonstrated that the amount of calcium depends on gender and increases with age. It was also found that 70% of unheralded myocardial infarction occurred in those patients with a calcium score above the 75th percentile compared with an age- and gender-related asymptomatic cohort. Furthermore, it had been proposed that the amount of calcium detected in an individual asymptomatic person should be seen in conjunction with his or her conventional cardiovascular risk factors. In particular, in persons with an intermediate cardiovascular risk, lower age and lower gender-related calcium in the coronary arteries (<25th percentile) may allow the person to be reassured, whereas any higher amounts of coronary calcium (>75th percentile) may act as a guide to risk factor modification and probably intensive medical therapeutic strategies.

The progression of coronary calcium in subjects with hypercholesteremia may depend on the intensity and efficacy of statin therapy. In asymptomatic hypercholesteremic persons without therapy, ineffective (high-density lipoprotein >120 mg/dL) and effective statin therapy (high-density lipoprotein <120 mg/dL), the annual progression rate was reported to be 52 ± 36%, 25 ± 22%, and −7 ± 23%, respectively. However, it remains unclear how the change in the amount of coronary calcium is related to event risk.

Assessment of Patients with Acute Coronary Syndrome and Acute Chest Pain

The diagnosis, risk stratification, and management of patients with suspected acute coronary syndrome entering the emergency department remains a clinical challenge. Acute coronary syndrome constitutes a broad spectrum of clinical status including ST-elevation myocardial infarction, non-ST-elevation myocardial infarction, and unstable angina. Clinical management with percutaneous intervention, thrombolysis, or medical therapy is clearly established only in a small fraction of patients with acute coronary syndrome. The larger group of patients may present with ambiguous electrocardiogram (ECG) signs or laboratory markers for myocardial ischemia. It has been shown that patients with angina-like chest pain, normal cardiac enzymes, normal or indeterminate ECG, and negative coronary calcium scans as detected by CT may be safely discharged from the emergency department without further testing or observation.

In rare cases, myocardial infarction may occur in patients with no coronary calcium as detected by CT. The entire extent of coronary atherosclerosis with calcified and noncalcified plaques may become visible by the administration of contrast media. The current gold standard for detecting coronary atherosclerosis *in vivo* is intracoronary ultrasound (ICUS). Studies comparing ICUS with MDCT have shown a good correlation between the echogeneity and CT density of coronary atherosclerotic lesions. Plaques with low, intermediate, and high echogeneity may correspond to plaques in MDCT with a density of 14 ± 26 HU, 91 ± 21 HU, and 419 ± 194 HU, respectively. The sensitivity and specificity of CT to detect calcified and noncalcified coronary atherosclerosis is between 78 and 94%, respectively. However, the sensitivity to detect noncalcified plaques in a lesion-by-lesion comparison between CTA and ICUS is only 53%. In heart specimens, the low-density (40 HU) and high-density (90 HU) components of plaques as detected by CT may correspond to lipid and fibrous tissue, respectively. Micro-CT with ultrahigh

spatial resolution is able to distinguish between different plaque components such as lipid, fibrin, and calcium by the different Hounsfield units. In the early stage of atherosclerosis, the proliferation of smooth muscle cells increases the Hounsfield units of atherosclerotic plaques.

In patients with myocardial infarction, noncalcified lesions in the culprit coronary artery may likely correspond to an intracoronary thrombus. Although the entire extent of atherosclerosis is similar in patients with myocardial infarction and stable angina, patients with acute myocardial infarction may present with significantly more noncalcified lesions. On the other side, the extent of calcified lesions was found to be significantly higher in patients with chronic stable angina.

Patients with unstable angina may present with noncalcified low-density plaques in their coronary arteries that may correspond to vulnerable plaques. The vulnerable plaque that had been detected before its rupture may present with a low-density center surrounded by a high-density rim, most likely corresponding to a lipid pool and a fibrous cap, respectively. In due course these plaques may rupture, resulting in a culprit lesion with subsequent myocardial infarction.

As mentioned earlier, large lipid components may be found predominantly in vulnerable plaques that are prone to rupture, with subsequent thrombosis and occlusion of the coronary artery. Currently, however, it appears unlikely that coronary CTA may be used as a screening tool for vulnerable plaques in asymptomatic subjects because of the necessity of administering contrast media and the comparably high radiation exposure for this application. Furthermore, the prospective value for the detection of noncalcified lesions has not been demonstrated so far and needs to be further investigated in clinical studies. If the ability of coronary CTA to detect vulnerable plaques in patients with acute coronary syndrome holds true, new strategies need to be considered for appropriate management of these patients. The noninvasive detection of vulnerable plaques may probably justify intensive medical treatment and follow-up or, alternatively, may lead to invasive approaches, such as plaque sealing. Moreover, in patients with atypical chest pain, CTA may soon serve as a tool for comprehensive diagnostic work-up. A single CTA investigation will allow differential diagnosis for a variety of diseases that need to be taken into account for acute chest pain, including ruling in or out pulmonary embolism, aortic dissection, and CAD.

In the near future, coronary CTA may become a valid pretest before cardiac catheterization for patient triage for conservative, interventional, or surgical therapy, and may reduce the use of invasive diagnostic procedures to preselected patients in whom coronary interventions are essentially required.

Calcinosis Cutis

Calcinosis cutis is a feature of scleroderma, and especially of its subset CREST syndrome. Grouped and speckled calcium deposits are found subcutaneously mainly at pressure-exposed locations like the fingertips. Calcification in hydroxylapatite deposition disease or in polymyositis/dermatomyositis must be considered as the differential diagnosis and can be distinguished by location and morphology as well as additional features (clinical, radiologic).

▶Connective Tissue Disorders, Musculoskeletal System

Calcium Hydroxyapatite Deposition Disease

▶HADD

Calcium pyrophosphate Deposition Disease

▶CPPD

Calcium Pyrophosphate Dihydrate Crystals Deposition Disease (CPPD)

Calcium pyrophosphate dihydrate crystals deposition disease or pseudogout is a joint disease caused by calcium pyrophosphate dihydrate crystal deposits with intermittent attacks of acute arthritis and degenerative arthropathy. A radiographic feature is a linear calcification of articular cartilage, especially fibrocartilage. CPPD is an important differential diagnosis to hemochromatosis.

▶Hemochromatosis, Skeletal

Cane-of-Bamboo Fragment

Cane-of-bamboo fragment describes the complete syndesmophytic bridging of only a few segments, contrasting

with the otherwise normal radiologic appearance of the vertebral spine; it is relatively typical in SAPHO.
▶Spondyloarthropathies, Seronegative

Cane of Bamboo

Cane of bamboo is a typical late-stage radiographic appearance of the lumbar vertebral spine in patients suffering from ankylosing spondylitis. Multisegmentally, the discs are completely bridged by circular ossification of the annulus fibrosus.
▶Spondyloarthropathies, Seronegative

Capillary Telangiectasia

Small nests of dilated capillaries with normal intervening brain tissue. Also known as capillary angioma.
▶Congenital Malformations, Vascular, Brain

Capsule of Ultrasound Contrast Media

▶Contrast Media, Ultrasound, Shell of, Influence on Pharmacology and Acoustic Properties

Caput Medusae Sign

A classic sign of developmental venous anomaly on digital subtraction angiography and magnetic resonance imaging. It is characterized by a nest of small vessels converging toward a bigger enlarged transcortical vein.
▶Congenital Malformations, Vascular, Brain

Carbon Monoxide

Carbon monoxide (CO) is a colorless, odorless gas produced from incomplete fuel combustion. It has a high affinity for hemoglobin and other heme-containing molecules, and severe or prolonged exposure can result in hypoxic brain injury, most commonly affecting the globi pallidi.
▶Toxic Disorders, Brain

Carcinoid Tumor

The term carcinoid covers a broad spectrum of neoplasms that originate from a variety of neuroendocrine cells. The most common carcinoid tumors of the small intestine secrete serotonin or serotonin precursors.
▶Neoplasms Small Bowel

Carcinoid Tumor, Pancreatic

A rare neuroendocrine tumor of the pancreas that originates from the enterochromaffin cells that produce serotonin. It causes a syndrome caused by the increased secretion of serotonin, called carcinoid syndrome. Carcinoid syndrome includes flushing, diarrhea, bronchoconstriction, and cardiac disease. Most patients with carcinoid tumors do not develop carcinoid syndrome.
▶Islet Cells Tumors, Pancreatic

Carcinoma, Breast, Imaging Mammography, Primary Signs

Sue Barter
Cambridge Breast Unit,
Addenbrookes Hospital,
Cambridge, UK
sue.barter@addenbrookes.nhs.uk

Definition

The primary signs of malignancy on mammography are defined as follows:

- Dominant mass
- Microcalcification
- Asymmetric density
- Architectural distortion
- Carcinoma usually appears on a mammogram as a mass, cluster of microcalcification or architectural distortion.

Characteristics

Dominant Mass

A mass as defined by the BIRADS Breast Imaging Lexicon (1) is a space-occupying lesion seen on two different projections. Masses may be irregular, ill-defined, dense or have a spiculated margin, where the lesion is characterised by lines radiating from the margin of the mass. A dense irregular mass with a spiculated margin that is not related to previous surgery is virtually diagnostic of malignancy.

The spicules may radiate out from an ill-defined mass for several centimetres or appear as a 'brush border'. They may be readily visualised when the breast tissue is fatty, but difficult to detect in dense breast tissue (Fig. 1a).

Magnification/paddle mammographic views of ill-defined masses are invaluable for demonstrating spiculation that may be partially obscured by overlying glandular breast tissue.

Pathologically, the spicules represent strands of fibro-malignant tissue that is related to the generalised desmoplastic response produced by cancer in the surrounding tissue.

A mass with spiculated margins should be considered malignant even if it remains stable over time, and biopsied.

Poor definition of the margin of a mass is a common feature of malignancy, though not as specific as a spiculated margin. Cancer should always be considered when a mass has poorly defined margins. Many cancers do not elicit the desmoplastic reaction in the surrounding tissue that produces spiculation, but the lack of definition of the borders raises concern that there is invasion of the surrounding tissue by the malignant process (Fig. 1b).

A mass with microlobulated margins where the lobulations are multiple and measure a few millimetres in diameter is suspicious of malignancy (Fig. 1c).

Some malignant masses contain irregular malignant-type microcalcification (see later). This is usually due to necrosis within the tumour mass, or an associated intraductal component. It is important to identify calcification associated with a malignant mass, especially if it extends beyond the margins of the mass, since there is a high risk of recurrence if the intraduct component is not also excised.

Microcalcifications

Certain shapes and patterns of microcalcification are strongly associated with breast cancer (Fig. 2).

BIRADS defines microcalcification associated with malignancy into the following categories:

- Amorphous or indistinct calcifications. These are often round- or flake-shaped calcifications that have a sufficiently small or indistinct appearance that a more specific morphological classification cannot be determined. They do not layer on horizontal beam magnification lateral images, and are therefore not microcystic. They are of intermediate suspicion and may be associated with malignancy (Fig. 2a).
- Pleomorphic or heterogeneous calcifications. These are usually more conspicuous than the amorphic forms and are neither typically benign, nor malignant in appearance, being irregular in shape with varying sizes and density. They are usually less than 0.5 mm in diameter. They should be regarded as suspicious of malignancy (Fig. 2b).
- Fine, linear or fine, linear and branching (casting) calcifications. These are thin irregular calcifications that appear linear, but are discontinuous and under 0.5 mm in width. Their distribution follows the course of the duct system involved, and the casting appearance is due to filling of the lumen of the duct involved irregularly with necrotic carcinoma cells. This pattern of microcalcification is most often seen with comedo-type ductal carcinoma *in situ* (DCIS), and is virtually diagnostic (Fig. 2c).

Distribution of suspicious microcalcification

The ACR BIRADS defines four patterns of distribution:

1. Clustered
2. Segmental
3. Regional
4. Diffusely scattered

Clustered microcalcification is suspicious, especially if the cluster has a triangular shape. A cluster of five or more particles of pleomorphic microcalcification, which is demonstrated in a volume of 1 cc has a 20–25% risk of malignancy.

Microcalcification that falls into any of the above categories should be investigated further with core biopsy or wide-bore needle (mammotome) biopsy.

Asymmetric Density

This is a density that cannot be accurately described by shape. It is visible as asymmetry of tissue density with similar shape on two views, but completely lacks borders or the definition of a true mass.

It may represent an island of normal breast tissue but its lack of specific benign characteristics warrants further investigation by magnification/paddle views and ultrasound.

Additional imaging may reveal an underlying true mass or significant architectural distortion (Fig. 3).

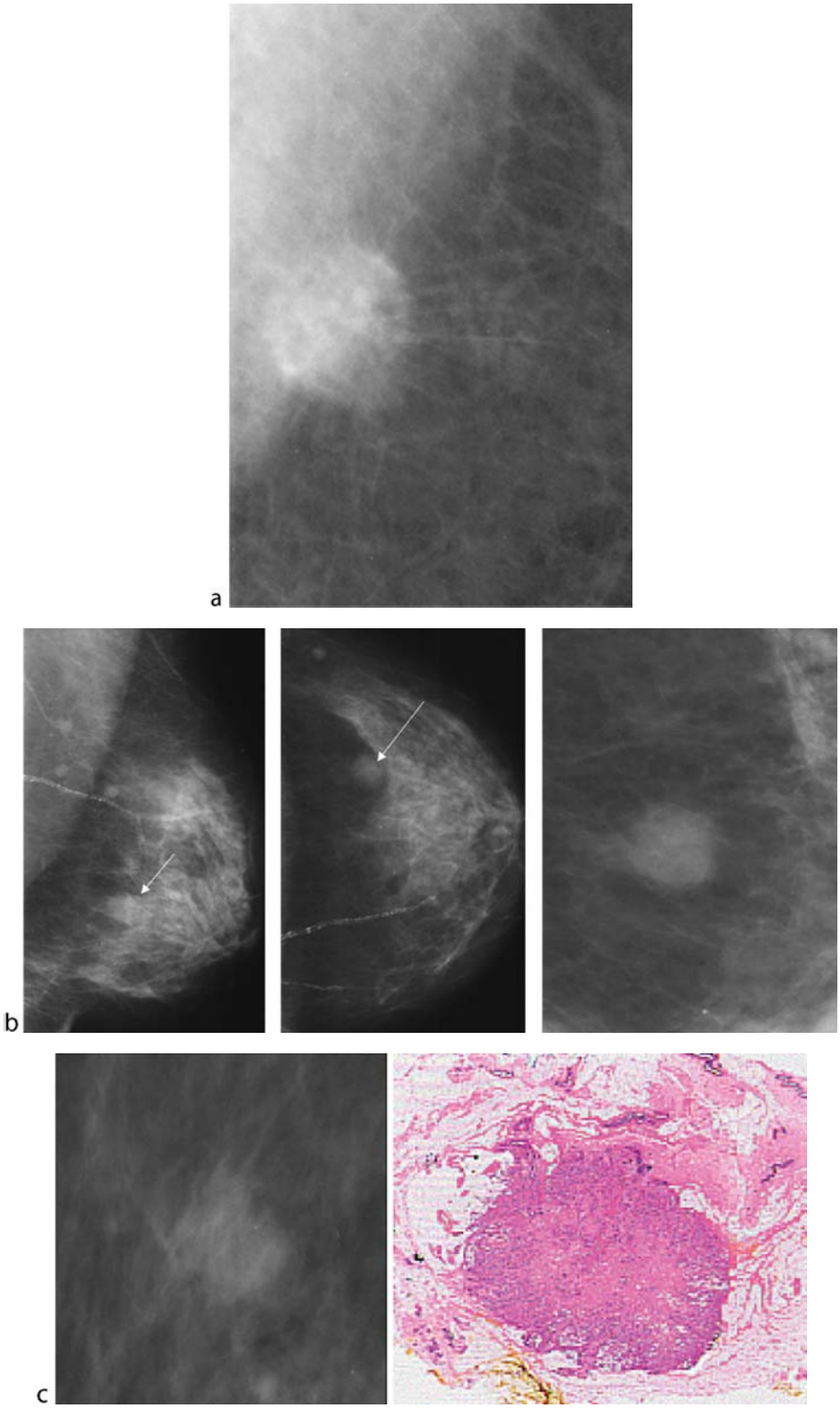

Carcinoma, Breast, Imaging Mammography, Primary Signs. Figure 1 (a) Spiculate mass due to 11 mm invasive ductal carcinoma. (b) Poorly defined mass due to invasive ductal carcinoma Grade 3. (c) Lobulated mass due to Grade 3 infiltrating ductal carcinoma.

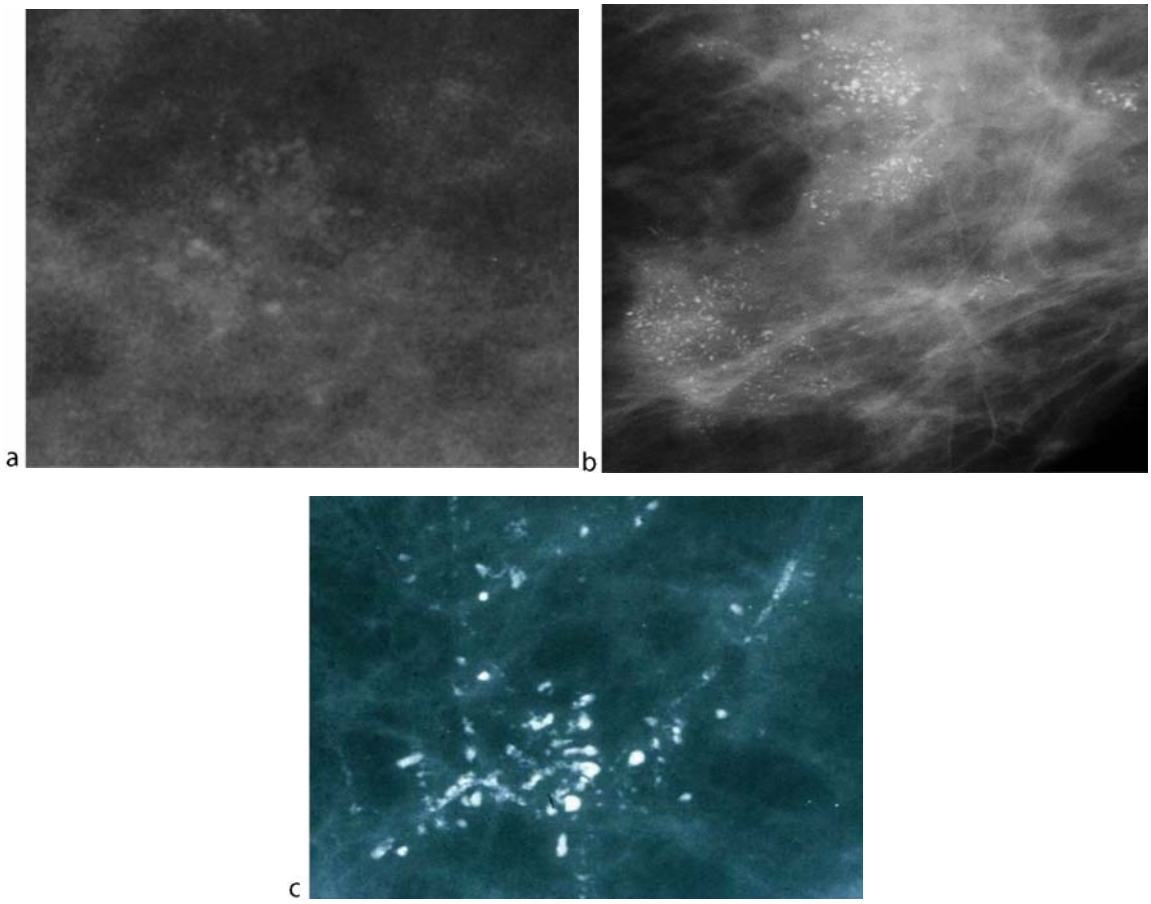

Carcinoma, Breast, Imaging Mammography, Primary Signs. Figure 2 (a) DCIS: Amorphous microcalcification. (b) DCIS: Pleomorphic-type microcalcification. (c) DCIS: Casting-type microcalcification.

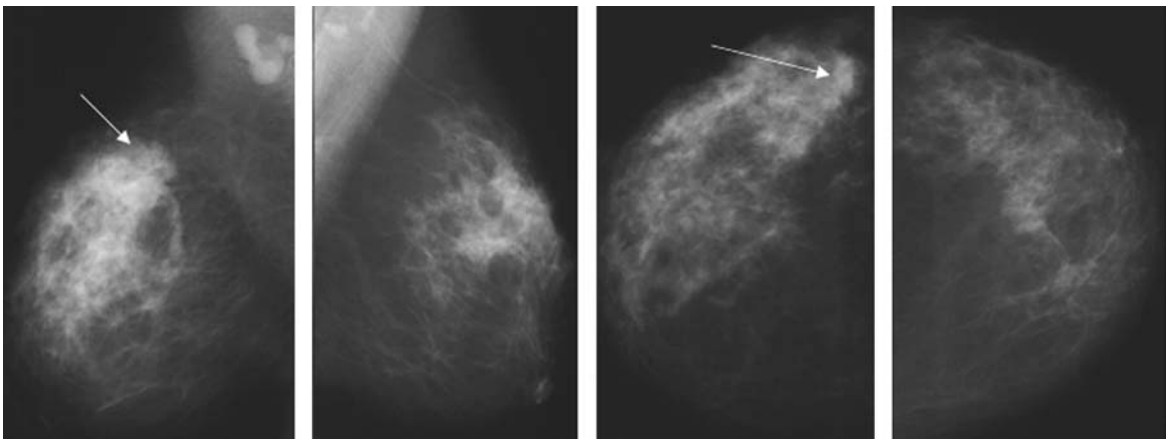

Carcinoma, Breast, Imaging Mammography, Primary Signs. Figure 3 Asymmetric density, Grade 2 38 mm IDC and ILC.

Architectural Distortion

Normal breast architecture is distorted with no definite mass visible. This includes spiculation radiating from a point. Architectural distortion is often visible at the parenchyma/subcutaneous fat interface as a flattening or retraction of the parenchyma.

The posterior margin of the parenchyma is the other site that should be carefully examined for signs of

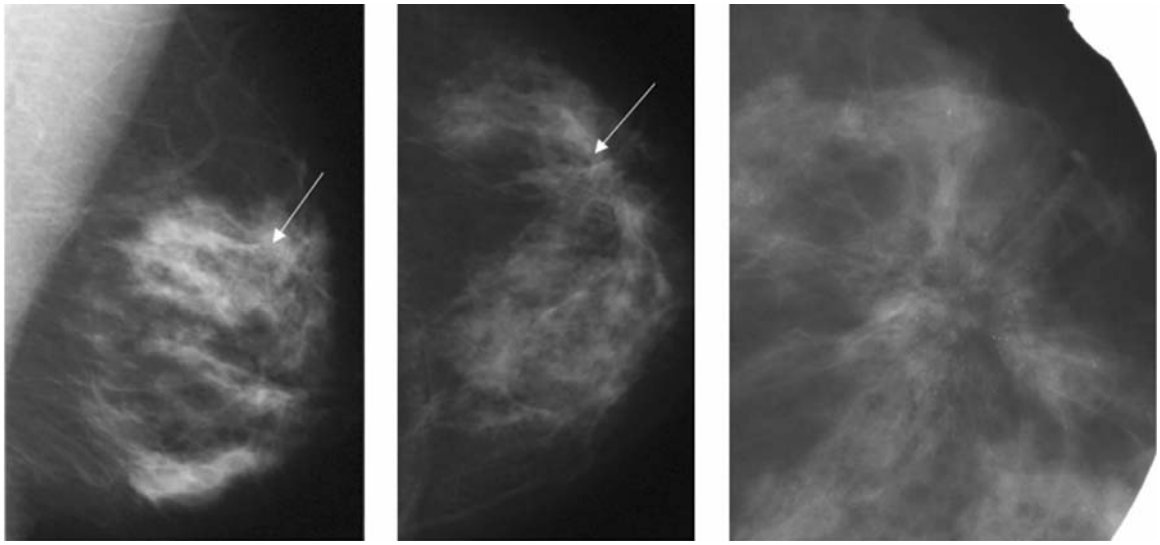

Carcinoma, Breast, Imaging Mammography, Primary Signs. Figure 4 Parenchymal distortion, Grade 1 tubular carcinoma.

architectural distortion. Focal retraction or distortion of the parenchymal edge should be investigated further with magnification/paddle views and high-resolution ultrasound (Fig. 4).

Breast cancer does not always produce a mammographically visible mass but frequently disrupts the normal surrounding tissue. This is an important but often subtle sign of malignancy.

Post-surgical scarring and fat necrosis are the most common non-malignant causes of architectural distortion. Radial scars may also produce architectural distortion.

If any of the primary signs of malignancy are detected on mammography, full breast assessment should be carried out, including needle biopsy.

Bibliography

1. American College of Radiology (ACR) (2003) Breast Imaging Reporting and Data System Atlas (BI-RADS Atlas). Reston, Virginia

Carcinoma, Breast, Imaging Mammography, Secondary Signs

Sue Barter
Cambridge Breast Unit,
Addenbrookes Hospital,
Cambridge, UK
sue.barter@addenbrookes.nhs.uk

Definition

The secondary signs of malignancy on mammography are defined as

- Enlarged axillary lymph nodes
- Asymmetric ducts or duct dilatation
- Skin and nipple changes
- Oedema of all or part of the breast
- Asymmetric breast tissue
- Increased vascularity with vascular engorgement
- Distortion of parenchymal edge, obliteration of the subcutaneous or retromammary space.

Enlarged Axillary Lymph Nodes

Enlarged axillary lymph nodes as the sole indicator of underlying malignancy in the breast are uncommon. Mammography only gives a limited view of the axilla, with the lower level 1 lymph nodes visible on the MLO view (Fig. 1).

Normal axillary nodes are less than 2 cm in size and have a hilar notch or lucent centre due to fat in the hilum. They may be almost replaced by fat so that only a thin rim of lymphoid tissue is visible around a lucent centre. When fatty replacement of a node occurs, the node may be enlarged, reaching up to 3–4 cm in size.

Lymph nodes that are 1.5–2 cm in size without a fatty hilum or lucent centre should be considered suspicious and investigated. Such findings are however non-specific, and may be secondary to reactive hyperplasia, lymphoma, collagen/vascular disease or metastases from other sites. It is not possible mammographically to differentiate benign lymphadenopathy from secondary involvement with breast cancer on mammography, and ultrasound and core biopsy or fine needle aspiration cytology of abnormal nodes is indicated (1, 2).

When malignancy suspicious for a breast primary is detected in axillary nodes, without any evidence of a

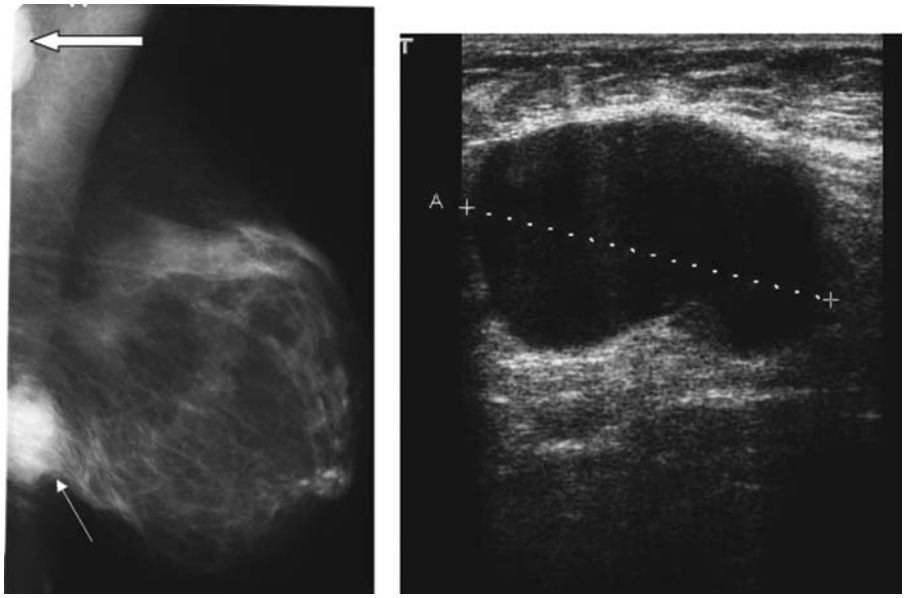

Carcinoma, Breast, Imaging Mammography, Secondary Signs. Figure 1 Diffuse breast oedema: note skin and trabecular thickening. Inflammatory carcinoma with axillary lymph node involvement.

primary lesion on mammography, MRI has become the investigation of choice for demonstrating occult breast malignancy (3).

Asymmetric Ducts or Duct Dilatation

Breast tissue may contain serpentine or nodular structures on mammography, and these represent asymmetric ducts or duct dilatation. Wolfe suggested that the presence of such findings was an indicator of malignancy, but other authors have found that asymmetric ducts are fairly common and part of the spectrum of benign breast change. Unless asymmetric or dilated ducts are associated with a palpable abnormality or mammographic sign of malignancy such as a mass or microcalcification, they should be considered a normal variant (4, 5).

A group of ducts converging on the nipple, and asymmetric compared to the contralateral breast is striking mammographically, but usually represents benign duct ectasia (5).

Skin and Nipple Changes

Skin changes associated with breast cancer are generally late changes due either to direct invasion by tumour, or obstruction of draining veins or lymphatics. Generally skin and nipple changes are best evaluated clinically.

Nipple retraction or inversion is usually long standing and due to benign changes such as involution or duct ectasia. When associated with malignancy it occurs over a short period of time, and is usually associated with a cancer lying close beneath the nipple, readily visible on the mammogram. It is very rarely the only mammographic sign of malignancy and scrutiny of the retroareolar region in such cases, augmented by magnification/paddle views will invariably demonstrate the underlying tumour.

When skin retraction is visible clinically, the tumour mass is usually readily seen on the mammogram. Sometimes a deep cicatrizing tumour deeper within the breast can cause skin retraction through involvement with Cooper's ligaments.

Diffuse skin thickening associated with cancer indicates advanced disease. There is usually associated diffuse thickening of the trabecular pattern. (Fig. 2). These appearances are non-specific and may represent oedema due to lymphatic or venous obstruction.

Thickened skin is often demonstrated in inflammatory carcinoma, usually due to diffuse permeation of the dermal lymphatics by tumour. The diagnosis is usually evident clinically with the classic triad of skin oedema, erythema and inflammation, in the absence of infection.

Oedema of All or Part of the Breast

The mammographic features of oedema of the breast are non-specific. There is a diffuse thickening of the trabecular pattern, often associated with skin thickening. If due to malignancy it is usually a late change indicating advanced disease, and is either due to diffuse infiltration, or lymphatic or venous obstruction (Fig. 2).

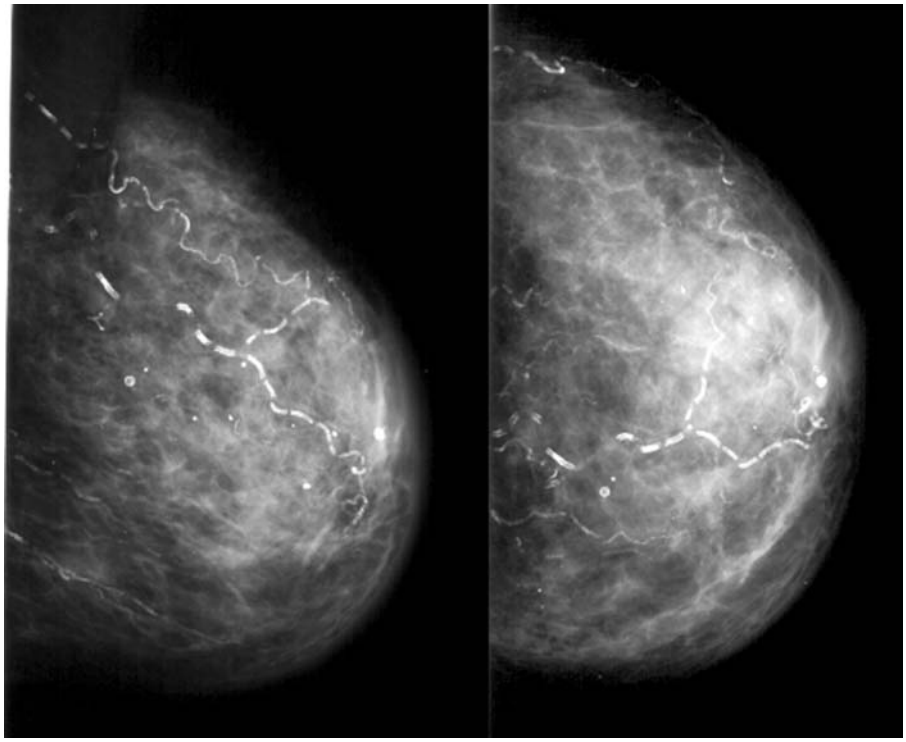

Carcinoma, Breast, Imaging Mammography, Secondary Signs. Figure 2 Mammogram and ultrasound of enlarged axillary node (block arrow) The cancer is readily visible inferiorly (small arrow).

Radiotherapy may also be a cause of diffuse breast oedema in the treated breast and should not be mistaken for recurrence. Oedema may be evident on the baseline post-treatment mammogram, but usually improves over time.

Asymmetric Breast Tissue

This should not be confused with focal asymmetric density (see primary signs of malignancy). Asymmetric breast tissue is a variant of normal, where there is a greater volume of glandular breast tissue in either the whole breast or part of the breast when compared to the other side. It is rarely due to an underlying breast cancer, usually a diffuse invasive lobular cancer.

Some palpable cancers do not produce a mammographically discreet lesion, or microcalcification, and the only visible finding may be an increase in density usually in part and rarely in all of the mammogram.

A progressive increase occurs in asymmetric density, particularly when focal should be investigated further; but it should be borne in mind that hormone replacement therapy (HRT) can often cause a diffuse or focal increase in breast density.

If the breast architecture is preserved, and there is no underlying mass or microcalcification, and the patient is clinically normal, then the asymmetry is almost always a normal variation (5).

Increased Vascularity with Vascular Engorgement

Increased vascularity as the only sign of breast carcinoma is extremely uncommon. Asymmetric prominence of veins in the breast is usually caused by under-compression during acquisition of the mammogram. Advanced breast cancer causing venous obstruction in the axilla may cause venous engorgement of the affected breast.

Distortion of Parenchymal Edge, Obliteration of the Subcutaneous or Retromammary Space

In the normal breast, the interface between the subcutaneous fat and the breast parenchyma shows a

scalloped pattern due to Cooper's ligaments attaching to the skin. Breast cancer, which develops near the edge of the breast parenchyma, can cause distortion of this pattern, either by causing flattening or retraction of the parenchymal edge, or a bulge into the subcutaneous fat. Similarly, the fat/parenchymal interface posteriorly may be distorted or shows a focal bulge due to a carcinoma.

Bibliography

1. Murray GM, Given-Wilson RM (1997) The clinical importance of axillary lymphadenopathy detected on screening mammography. *Clin Radiol* 52(6):458–461
2. Patel T, Given-Wilson RM, Thomas V (2005) The clinical importance of axillary lymphadenopathy detected on screening mammography: revisited. *Clin Radiol* 60(1):64–71
3. Buchanan CL, Morris EA, Dorn PL et al (2005) Utility of breast magnetic resonance imaging in patients with occult primary breast cancer. *Ann Surg Oncol* 12(12):1045–1053
4. Wolfe JN (1967) Mammography: ducts as a sole indicator of breast carcinoma. *Radiology* 89:206
5. Kopans DB, Swann CA, White G et al (1989) Asymmetric breast tissue. *Radiology* 171:639–643

Carcinoma, Breast, Demography

Sue Barter
Cambridge Breast Unit,
Addenbrookes Hospital,
Cambridge, UK
sue.barter@addenbrookes.nhs.uk

Definition

Breast cancer is the third most common cancer in the world, creating a burden of disease comparable with that of colorectal cancer. With over half a million new cases in the world each year, only cancer of the lung and stomach occurs with greater frequency, and breast cancer, overall, accounts for about 9% of cancer cases in the world, and over 18% of cancers occurring in women. It is most common in North America and Western Europe, accounting for about one in four female cancers in these regions, whereas in the Far East (China and Japan) it is very much rarer. It is also common in southern South America. The highest incidence rates of all are found in Hawaii, where a rate of 93.9 per 100,000 female population has been reported, and in US white women. The incidence rises with age from about 30 years, but more slowly after the menopause than before. There are ethnic variations such as a high incidence in Israeli Jews compared with non-Jews in Israel. It is more common in single women, in higher social classes, and in urban rather than in rural areas. About 1% of cases occur in males.

Risk Factors

Breast cancer is a multifactorial disease that may involve life style, environmental and reproductive factors, as well as genetic factors. As with many other cancers, it may also involve as yet unknown factors. One in ten women will develop breast cancer by the age of 80. For most women, as they get older, their risk of breast cancer increases.

Risk Associated with Family History

- The risk of breast cancer in women with an affected first-degree relative (mother, sister, or daughter) is approximately twice the risk to other women.
- The risk of breast cancer is related to the strength of the family history. The risk increases with the number of affected relatives, and increases as the age of the affected relatives decrease.
- Only a minority of this increase risk is due to the known high risk genes BRCA1 and BRCA2.
- The chance of carrying a BRCA1 or BRCA2 mutation is related to the strength of the family history not only of breast cancer but also of ovarian cancer and male breast cancer.
- The risks of breast cancer in carriers of BRCA1 or BRCA2 mutations have been estimated as between 60% and 80% and between 40% and 80%, respectively.

Hormonal Factors

Factors that influence the amount of estrogen produced by a woman's body over her lifetime (such as the ages at the onset of menstruation, pregnancy, and age at menopause) are known to influence breast cancer risk. During the reproductive years, a woman's body produces high levels of estrogen.

- Earlier menarche (aged 12 or younger) and late menopause (aged 55 or older) is associated with an increase in risk of breast cancer Women who start to menstruate at an early age and reach menopause at a late age are exposed to high levels of estrogen for more years than are women who have a late menarche or early menopause.

- Nulliparity and late age at first birth are associated with significant increases in breast cancer risk.
- Women who have their first full-term pregnancy at a relatively early age have a lower risk of breast cancer than those who never have children or those who have their first child relatively late in life.
- Pregnancy may lead to lasting changes in the sensitivity of breast tissue to cancer-causing agents, as well as in the maturation of breast tissue. In addition, several hormonal changes occur after a full-term pregnancy and may persist for years.
- Increased parity has been found to be associated with a decrease in breast cancer risk (38% decrease in risk in women who reported five or more live births, 32% decrease in risk in women who reported three or more births compared to women who reported one birth).

Hormone Replacement Therapy

Evidence suggests that hormone replacement therapy (HRT) is associated with an increase in breast cancer risk.

- The Million Women Study found that the relative risk of breast cancer in current users increased with increasing total duration of use of HRT (1). The risk associated with HRT is small for short duration use (up to 2 years) but is in the region of a two-fold risk for women taking combined HRT for 10 years or more.
- The Million Women Study found that the associated risk was substantially greater for estrogen–progestagen than for other types of HRT, and suggests that there is little or no overall increase in the relative risk of breast cancer in past users of HRT.
- The Collaborative Group (2) has shown that there is 2.3% increase in relative risk for every year used. The risk appears to be confined to current users and women who have used HRT in the last 5 years and that the risk of HRT use disappears 5 years after stopping.

Hormonal Contraceptives

Numerous scientific studies have investigated the relationship between the use of oral contraceptives (birth control pills) and the risk of breast cancer.

- Use of oral contraceptives slightly increases the risk of breast cancer.
- This increase in risk appears to be confined to current and recent use (within 5–10 years, relative risk 1.24 for current users).

Breastfeeding

Breastfeeding confers a protective effect on breast cancer risk.

- The Collaborative Group (3) found that each 12 months of breastfeeding confers a reduction of about 4%.
- The protective effect of breastfeeding is in addition to the protective effect of pregnancy alone.
- The reduction in breast cancer risk is related to total duration of breastfeeding.
- If breastfeeding does protect against breast cancer, it may do so by delaying the resumption of ovulation (with its accompanying high estrogen levels) after pregnancy.

Alcohol Consumption

The risk of breast cancer increases with alcohol consumption.

- The Collaborative Group (4) reported an increase of 7.1% in relative risk for each additional 10 g/day intake of alcohol.
- Women who drink moderate amounts of alcohol have been found to have a slightly higher risk of breast cancer than do those who abstain. It is uncertain, however, whether this association reflects a cause-and-effect relationship.
- The use of alcohol may vary among women who differ with regard to other factors that are known to influence breast cancer risk—such as age, obesity, and reproductive history.

Weight

A high body mass index (BMI) is associated with a significant increase in post-menopausal breast cancer risk in the general population.

- A recent IARC report (5) suggested that more than 100 studies over nearly 30 years in populations in many countries have established that increased body weight increases breast cancer risk among post-menopausal women.
- Almost all of these studies have shown that this association is largely independent of a wide variety of reproductive and life style risk factors.
- The association between being overweight and breast cancer appears to increase in a stepwise fashion with advancing age after the menopause (5).
- This relationship is probably mediated by estrogen production. Fat cells produce some and obese

post-menopausal women, therefore, tend to have higher blood estrogen levels than non-obese women do.

- Obesity does not seem to be a risk factor for breast cancer in pre-menopausal women. In younger women, the ovaries are the main producers of estrogen. The much smaller amount of estrogen produced by the fat cells does not appear to have any significant impact on breast cancer risk.

Physical Activity

Scientific studies have consistently shown that the risk of breast cancer is lower among physically active pre-menopausal women than among sedentary women.

- Moderate physical exercise is associated with a decreased risk in breast cancer. The effect of physical activity on breast cancer risk may be due at least in part to effects of exercise on the female hormones.
- Although the effects of obesity and physical inactivity on breast cancer risk are not as strong as the effects of previous breast disease or family history of breast cancer, they are important risk factors because they are modifiable.
- Exercise and weight control currently represent the most effective life style changes that a woman can make to reduce her risk of breast cancer.
- Lack of physical activity is an established risk factor for pre-menopausal breast cancer and represents part of a complete approach to weight management.

Radiation

Exposure to ionizing radiation, particularly in the young breast, is associated with an increased risk of developing breast cancer.

There is now substantial evidence that women who received radiotherapy at or below the age of 35, which included part of their breast tissue (upper body mantle radiotherapy), have a higher risk of developing breast cancer.

Bibliography

1. Million Women Study Collaborators (2003) Breast cancer and hormone-replacement therapy in the Million Women Study. Lancet 362:419–427
2. Collaborative Group on Hormonal Factors in Breast Cancer (1997) Breast cancer and hormone replacement therapy: collaborative reanalysis of data from 51 epidemiological studies of 52,705 women with breast cancer and 108,411 women without breast cancer. Lancet 350:1047–1059
3. Collaborative Group on Hormonal Factors in Breast Cancer (2002) Breast cancer and breastfeeding: collaborative reanalysis of individual data from 47 epidemiological studies in 30 countries, including 50,302 women with breast cancer and 96,973 women without the disease. Lancet 360:187–195
4. Collaborative Group on Hormonal Factors in Breast Cancer (2002) Alcohol, tobacco and breast cancer—collaborative reanalysis of individual data from 53 epidemiological studies, including 58,515 women with breast cancer and 95,067 women without the disease. Lancet 87:1234–1245
5. International Agency for Research on Cancer (IARC) (2002) IARC Handbooks of Cancer Prevention. Volume 6: Weight Control and Physical Activity. IARC Press, Lyon

Carcinoma, Breast, Inflammatory

Common features of inflammatory carcinomas are skin thickening and diffuse increased breast density. Other findings such as trabecular thickening, axillary lymphadenopathy, architectural distortion, focal asymmetric density, and nipple retraction may be found. Less often, calcifications or masses are present. This tumor entity may be misdiagnosed as benign inflammatory process.

▶Carcinoma, Other, Invasive

Carcinoma, Cervix Uteri

Martin Unterweger
Diagnostic Radiology, Cantonal Hospital Baden, Baden, Switzerland
Martin.Unterweger@ksb.ch

Synonyms

Cervical carcinoma

Definition

Carcinoma of the cervix uteri is 3rd most common tumor of the female pelvis. After the age of 20 years the incidence increases with two incidence peaks around 30 years for *in situ* carcinoma and around 60 years for invasive cancer. Risk factors for the development of cervical carcinoma include early age intercourse, multiple sexual partners, and perhaps the most important exposure to specific subtypes of the human papillomavirus (HPV). Screening is possible with the Papanicolau smear.

Pathology/Histopathology

Approximately 80–90% of cervical malignancies are squamous cell carcinomas. The remaining 10% of cervical cancers consist of adenocarcinomas and rarely sarcomas. The majority of cervical carcinomas occur at the squamocolumnar junction. Cervical carcinoma normally arises from a preexisting dysplastic lesion. Carcinoma *in situ* represents extension of malignant cells to the basal membrane of the epithelium. The metastatic spread is generally lymphatic, first in the iliac lymph nodes and further in the retroperitoneal lymph nodes. Hematogenic metastases are rarely seen. The most common sites of metastasis are the lungs, bones, and liver.

Clinical Presentation

The major symptoms of cervical carcinoma are vaginal discharge and bleeding, but over 20% of patients with invasive cervical carcinoma are asymptomatic. Pelvic or abdominal pain and urinary problems are less common symptoms and occurs normally in advanced cases.

The International Federation of Gynecology and Obstetrics (FIGO) classification is used for staging in most institutions (Fig. 1). This classification is based on clinical findings of the primary tumor as well as on lymphatic spread. Because of good soft tissue contrast MRI was shown to be superior to CT in staging cervical carcinomas, e.g., for diagnosis of parametrial invasions (1, 2). It was shown to be a helpful addition to transvaginal ultrasound especially in tumors exceeding 2 cm *in situ* (3).

Surgery is usually performed in FIGO I-IIA. In FIGO IIB or more adjuvant radiotherapy is regarded as therapy of choice. Therefore, pretherapeutic staging is important for decision-making.

Imaging

MRI with his high soft tissue contrast is an ideal imaging modality for evaluation of cervical carcinoma. Cervical carcinoma will be identified as a high signal intensity mass on T2-weighted images. Cervical carcinomas are lesser conspicuous on T1-weighted images, because of similar signal intensity to the normal cervical tissue. MR contrast medias cause variable tumor enhancement and are rarely indicated. They could be helpful for depiction of bladder or rectal wall infiltration.

TNM	FIGO	MRI findings
Tis	0	Carcinoma in situ (before invasion), no indication for MRI
T1	I	Cervical carcinoma confined to the cervix
T1a	IA	Microscopic diagnosis, no tumor on MRI
T1b	IB	Carcinoma only in cervix uteri, tumor hyperintense compared to cervical stroma
T2	II	Tumor invades beyond uterus, no expansion in the pelvic sidewall
T2a	IIA	Invasion of vagina excluding lower 1/3, parametrium without tumor
T2b	IIB	Infiltration of parametria, disruption of low-signal-intensity stromal ring (T2w)
T3	III	Tumor in the lower vagina, pelvic wall infiltration or hydronephrosis
T3a	IIIA	Tumor infiltrating the lower vagina, best seen on sagittal plane
T3b	IIIB	Tumor infiltrating the pelvis wall or hydronephrosis, dilated ureter (MR urography)
T4	IV	Tumor outside the pelvis, distant metastasis
T4a	IVA	Invasion of the bladder and rectal mucosa, obliteration of fat planes between cervix and bladder or rectum, retrospectively
T4b	IVB	Distant metastasis

Carcinoma, Cervix Uteri. Figure 1 Staging of carcinoma cervix uteri according to TNM and FIGO. (From Pakkal MV, Rudralinbgam V, McCluggage WG et al MR staging in carcinoma of the endometrium and carcinoma of the cervix)

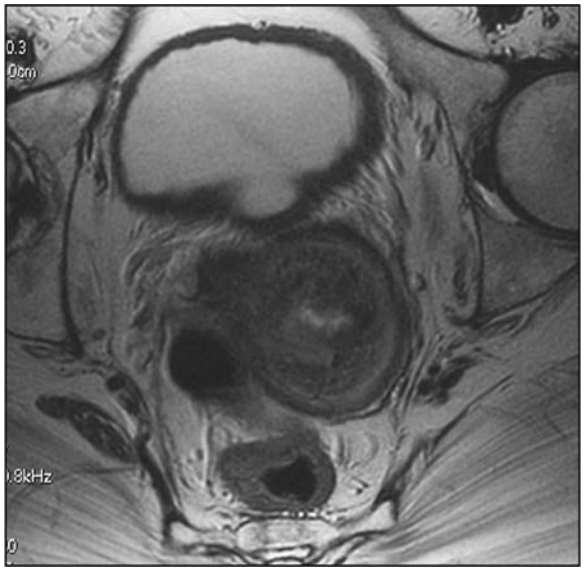

Carcinoma, Cervix Uteri. Figure 2 Axial oblique (perpendicular to the cervical cancel) T2-weighted MRI with a cervical carcinoma in stage IB. The tumor is restricted to the cervix uteri, the hypointense stroma is not disrupted.

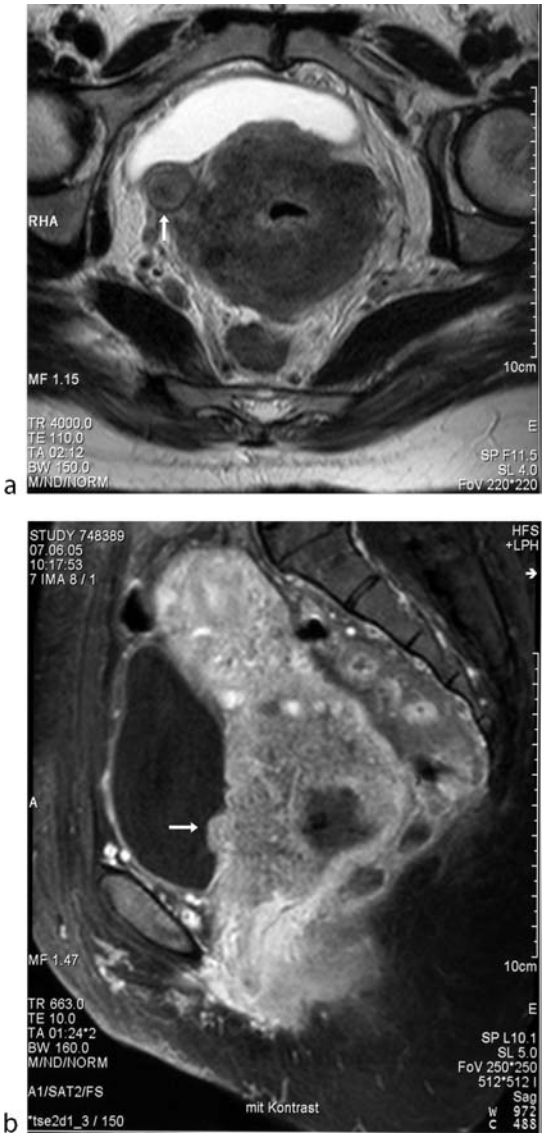

Carcinoma, Cervix Uteri. Figure 3 (a) Cervical carcinoma stage IVA with infiltration of the bladder and rectal wall on a T2-weighted transversal MR image. Enlarged lymph node (arrow). (b) Sagittal contrast-enhanced T1-weighted MR image shows the cervical carcinoma with urinary bladder wall infiltration (arrow) in stage IVA.

The staging of cervical carcinoma with MRI is based on the FIGO criteria. In stage IA there is no MR correlation of the cervical carcinoma because it is a preclinical diagnosis, which can only be demonstrated microscopically. In stage IB the tumor is restricted to the cervix without infiltration of the vagina (Fig. 2) and the stroma surrounding the tumor is intact. In stage IIB the parametria are infiltrated, where the tumor extend over the cervix border into the parametria. The low-signal-stromal ring is disrupted on MRI. In FIGO IIIA tumor infiltrates the lower vagina best seen on sagittal images and in IIIB extend to obturator internal, piriformis or levator ani muscle. Hydronephrosis also is a sign for this stage. In such cases, additional MR urography will be helpful. In stage IVA the tumor infiltrates the bladder or rectal wall, which can be well demonstrated on T2-weighted MRI without fat saturation because of the fat plane obliteration between cervix and bladder or rectal wall (Fig. 3). Distant metastases are seen in stage IVB. In the literature the overall accuracy of MRI staging is reported to be 76–92%.

The most important prognostic criteria are the parametrial infiltration and lymphatic spread. MRI, as CT, has a limited sensitivity for lymph node metastases. CT has become increasingly popular in the staging of cervical carcinomas. CT is able to demonstrate the primary tumor in cases of extensive disease as well as hydronephrosis. Furthermore encasements of the iliac vessels, enlargements of the obturator or piriformis muscles are all signs of stage III disease. But the most important use of CT in cervical carcinoma is the evaluation of lymphatic nodes. However, lymph node size is the only morphological criterion used to determine the presence of metastases. CT has a fairly high specificity (93%) when utilizing criteria of nodal enlargement greater than 1 cm in the short axis as pathologic. However, the overall accuracy of detecting lymph node metastasis varies in the literature between 70% and 75%. In the evaluation of parametrial infiltration, CT has an overall accuracy of 76%, a positive predictive value of 58%, and a negative predictive value of 85%.

Endovaginal sonography is normal directly applied by the gynecologist. Large necrotic tumors can appear as hypoechogenic masses. Sonography can demonstrate urinary obstruction with high degree of accuracy. Invasion of the bladder and parametrium infiltration can sometimes be seen. However, sonography is limited in differentiating between tumor and normal cervical tissue. Furthermore, accuracy for the evaluation of pelvic and retroperitoneal lymph nodes is limited with sonography.

Recurrence of cervical carcinoma occurs normally within 2 years. The difference of fibrosis and recurrence is seldom possible with MRI within 12 month after the end of treatment, since reparative tissue change after radiotherapy will also show contrast enhancement.

Bibliography

1. Durfee SM, Zou KH, Muto MG et al (1996) The role of magnetic imaging in treatment planning of cervical carcinoma. J Woman Imaging :63-68 vol 12(2)
2. Hamm B, Kubik- Huch RA, Fleige B (2001) MR and CT of the female pelvis. Radiological–Pathological Correlation Europ Radiol 11:233–245
3. Akata D, Kerimoglu U, T Hazirolan et al (2005) Efficacy of transvaginal contrast-enhanced MRI in the early staging of cervical carcinoma. Eur Radiol 15:1727–1733
4. Pakkal MV, Rudralinbgam V, McCluggage WG et al MR staging in carcinoma of the endometrium and carcinoma of the cervix (2004) The Ulster medical journal, 73(1), 20–24
5. Tavassoli FA and P Deville (2003) Tumor of the Breast and Female Genital Organs. WHO classification of tumors. Pathology and Genetics Tumor of the Breast and female Genital organs. Lyon: IARC Press

Carcinoma, Ductal, *In Situ*, Breast

Fischmann Arne
Department of Diagnostic Radiology, University of Tübingen, Tübingen, Germany
arne.fischmann@med.uni-tuebingen.de

Synonyms

Ductal intra-epithelial neoplasia (►DIN) type 1c to 3

Definition

DCIS is an epithelial neoplasia originating in the terminal ductulo-lobular unit and progressing into the ductal system that is confined to its natural basement membrane boundaries. The differentiation of the DCIS from premalignant lesions with identical origin (ductal hyperplasia or DIN 1a, atypical ductal hyperplasia or DIN 1b) may often be difficult. DCIS is a precursor of invasive ductal carcinoma but does not invariably lead to invasion and is therefore omitted in the pathologic classification by the concept of ductal intra-epithelial neoplasia. The different patterns are risk factors for invasive growth of different magnitude.

Pathology/Histopathology

DCIS poses an increasing problem to pathology as more lesions are detected with modern imaging methods and mammography screening. Gradual changes with increasing likelihood of malignancy often lead to inter-individual variation of classification.

According to the pathologic pattern in HE-stains DCIS is divided into five groups: comedo type with necrosis, cribriform, papillary, micropapillary and solid mosaic. The comedo subtype is the most common form of DCIS having the highest risk of infiltrative growth. In more than 50% these patterns coexist in the same specimen or sometimes even in the same duct especially in large tumours. The former concept of 'non-invasive' carcinoma is nowadays replaced by cellular and structural changes representing increasing probability of malignant transformation and infiltrating growth.

The following grading system of ductal intra-epithelial neoplasia (DIN) was advocated by the world health organization (WHO). It represents the view that transformation from ductal hyperplasia to intra-epithelial neoplasia is a gradual process and no clear-cut margin of malignant disease can be established

- DIN 1a represents intraductal hyperplasia without atypia
- DIN 1b represents atypical intraductal hyperplasia (►AIDH)
- DIN 1c is a low-grade DCIS or G1 lesion often of the micropapillary or cribriform subtype
- DIN 2 represents an intermediate grade (or grade 2) DCIS
- DIN 3 is a high-grade (or grade 3) DCIS usually of the comedo subtype displaying cellular atypia and necrosis

Microinvasion is described as extension of cancer cells beyond the basement membrane with no single focus larger than 1mm in greatest diameter (T1mic) and is seen in approximately 14% of cancer cases increasing with size (1).

Although this system has many advantages over previous classifications the precise grading of a single

lesion, especially the differentiation of AIDH and DCIS remains difficult and inter-observer variability remains high, e.g. mitotic activity may vary according to age and is of little use in the classification of DCIS and AIDH. Therefore exact grading does not only include histologic changes but also extent of disease: a lesion with the cytologic and architectural features of low-grade DCIS not exceeding 2 mm qualifies to be AIDH (2).

As histologic grading (especially presence of comedonecrosis) and tumour-free margin of less than 1mm are known to be associated with increased risk of recurrence, the so-called Van Nuys Prognostic index was developed that shows a good correlation to the risk of recurrence.

Van Nuys prognostic index

Value	1 Point	2 Points	3 Points
Tumour size	≤15 mm	16–40 mm	>40 mm
Tumour-free margin	≥10 mm	1–9 mm	<1 mm

Values are added and the result correlates to prognosis: An index of 3–4 has a risk of recurrence of about 2%, 5–7 about 19%, 8–9 of more than 50%.

Molecular markers are of increasing importance in the grading of DCIS, as these changes seem to persist in consecutive invasive disease: low-grade DCIS will usually lead to low grade IDC while high-grade DCIS will cause high-grade IDC. Oestrogen receptor is negatively correlated to histologic grading and therefore more likely to be expressed in low grade DCIS, while p53 is mainly expressed in DIN 3. HER2 is negatively correlated with prognosis. Cellular alterations (like loss of oestrogen receptor or actin in the myoepithelium) are often present before morphological changes can be detected by ►H&E-staining, this being true especially in hyperplastic areas adjacent to comedocarcinoma. ►VEGF, Ki-S1 and ►PDGF as well as c-erb are expressed but clinical significance remains obscure.

Clinical Presentation

Most patients with DCIS present without clinical symptoms and are detected during screening mammography, only about 10% of patients with DCIS present with irregularities or lumps in the breast and in rare cases with Paget's disease or nipple discharge.

With the increasing use of mammography, incidence of DIN in breast biopsies increased from 25% to 28%. The overall age-adjusted incidence of DCIS ranges from 10 to 31/100.000. In autopsy series the prevalence of DCIS ranged from 4.3% to 18.2% for women above 60 years. DCIS constitutes about 10–15% of newly diagnosed breast cancers, of which at least 90% are detected by mammography. About 20% (10–77%) of breast cancers detected with mammography screening represent DCIS.

DCIS is a precursor of invasive disease. Unfortunately the natural history of DCIS is not known in an individual lesion, therefore the risk-benefit ratio should be considered carefully in each individual lesion. The rate of progression of untreated DCIS to invasive cancer ranged from 14% to 43%. The relative risk of AIDH to develop into invasive cancer ranged from 1 to 13 (2). DCIS increases the risk to develop breast cancer 8 to 10-fold. Interestingly the risk is increased in the contralateral breast as well, indicating that DCIS is not an unequivocal precursor of IDC but also an important risk factor.

Usually the pathologic extent of DCIS is larger than the clinically and mammographically estimated size. This is not only true for the macroscopic but also for the microscopic extent of disease: 1–2% of patients with DCIS have LN-metastases at the time of diagnosis indicating undetected invasive disease (2). Incidence of bilaterality either as DCIS or as IDC is reported to range from 2.2% to 22% (2). DCIS is also known to be multifocal in about 30%.

Risk factors for the development of DCIS and IDC are similar, hormonal replacement therapy seems to be of minor importance in DCIS, contrary to IDC. Up to now no hormonal or other stimulus for DIN is known and changes seem to be irreversible.

Treatment

Complete excision with or without radiotherapy is currently the treatment of choice for locally confined DCIS. Without radiation, 10–60% of the patients develop recurrences. Several studies showed that radiation reduced the risk of recurrence after breast conservation therapy by about 50%, causing 3.5–23% recurrences. Lumpectomy without radiation should not be considered until several ongoing studies present their data. About 75–100% of patients can be salvaged after recurrence.

Although mastectomy has a lower risk of recurrence than lumpectomy and radiation (1.4% vs. 8.9%) there is no significant difference in survival, making lumpectomy the preferable therapy option. In high-risk patients mastectomy with axillary lymph node resection can be considered as it only shows a recurrence rate of 0.75%. In all other patients axillary resection and sentinel lymph-node is presently investigational and should only be performed in case of a suspected invasion.

Tamoxifen reduced the risk of ipsilateral local failure in patients treated with excision and radiotherapy,

although it seems to be profitable only in ER-positive breast cancers and should not be used in patients with low risk of recurrence.

Imaging

Currently mammography is the only modality able to identify calcifications that are associated with DCIS in 70–90%. Especially linear branching, casting calcifications (Fig. 1) or multiple clusters of fine granular calcifications or calcifications in segmental distribution (Fig. 2) are regularly consistent with DCIS. Still diagnostic accuracy in the classification of MC remains lower than for solid masses. The latter are usually associated with invasive disease. Ductal distribution of calcifications has a positive predictive value of 30–63%, Although mammography can detect up to 83% of DCIS lesions, it is know to underestimate the extent of disease by up to several centimetres (3).

Sonography does usually not show any specific result hence positive predictive value for sonography is only about 50%. About 80–90% of DCIS show enhancement on MRI, which is in 50% unspecific. Contrast enhancement is correlated to the size and density packing of involved ducts and to neoangiogenesis, which is low in most DCIS. The differentiation of high- and low-grade DCIS as well as to IDC is not possible.

Typical signs of DCIS in MRI are irregular ductal enhancement and stippled regional enhancement while spiculated mass and washout seem to be signs of IDC. Ring enhancement is not detectable in DCIS. Ductal enhancement can be assigned to DCIS in about 20% but also to IDC, LCIS and to benign lesion in 55%. Although ductal enhancement is detected in 38–60% of DCIS on MR, specificity remains low with 45% (4). Especially small lesions below 5 mm are easy to be missed by MRI, while it is particularly useful in evaluating residual disease, and multi-centricity.

Nuclear Medicine

^{99m}Tc-sestamibi scintimammography shows areas of diffuse heterogeneous uptake. To improve diagnostic accuracy images should always be evaluated together with the mammograms. It is especially useful in evaluating areas of extensive intraductal carcinoma around IDC and to evaluate palpable masses in dense breasts. Still it is less specific for DCIS than for IDS.

^{18}FDG-PET is especially useful in the detection of invasive and metastatic breast cancer. Up to the present time there was no published study evaluating the role of ^{18}FDG-PET in the detection and classification of DCIS. It should therefore only be used in an experimental setting.

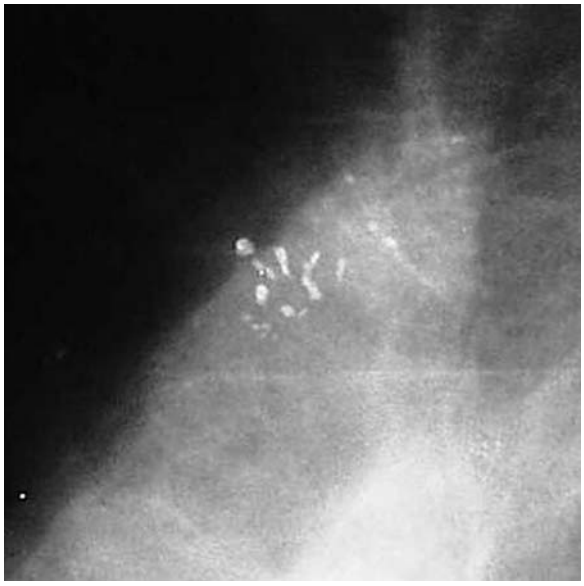

Carcinoma, Ductal, *In Situ*, Breast. Figure 1 Casting calcifications typical for a small DCIS, which was proven by ▶VB.

Carcinoma, Ductal, *In Situ*, Breast. Figure 2 Granular calcifications in a ductal distribution including more than one quadrant of a breast.

Diagnosis

Most DCIS are first detected by screening mammography. Screening intervals correlate strongly with histological grading and extent of disease. As most lesions should be confirmed histologically before treatment, core needle biopsy with stereotactic or sonographic guidance is the usual means to diagnose DCIS.

Interventional Radiology

DCIS is usually diagnosed by stereotactic core needle biopsy or VB, although the former has a higher tendency to underestimate disease: 10% of patients with DCIS in core-biopsy are found to have IDC. Nipple aspirate fluid, ductal lavage and fine needle aspiration are of limited value in the diagnosis.

Several techniques for minimal invasive breast therapy have been described: laser-induced thermotherapy, radiofrequency ablation, high-intensive focused ultrasound, cryotherapy and thermal ablation using magnetic nanoparticles. Especially in the case of pure DCIS these methods remain experimental as imaging modalities tend to underestimate tumour extension and as margins cannot be evaluated.

Bibliography

1. Leonard GD, Swain SM (2004) Ductal carcinoma *in situ*, complexities and challenges. J Natl Cancer Inst 96:906–920
2. Tavassoli FA (ed) (1999) Ductal intraepithelial neoplasia: risk factors for subsequent development of invasive carcinoma. In: Pathology of the Breast. McGraw-Hill, New York, pp 205–312
3. Holland R, Hendriks JH, Vebeek AL et al (1990) Extent, distribution, and mammographic/histological correlations of breast ductal carcinoma *in situ*. Lancet 335:519–522
4. Liberman L, Morris EA, Dershaw DD et al (2003) Ductal enhancement on MR imaging of the breast. Am J Roentgenol 181 (2):519–525

Carcinoma, Ductal, Invasive

Silvia Obenauer
Department of Radiology, Georg-August-University of Goettingen, Goettingen, Germany
obenauerheuser@yahoo.de

Synonyms

IDC; Infiltrating ductal carcinoma; Not otherwise specified (NOS); Scirrhous carcinoma

Definition

An invasive carcinoma is a tumor with extension of tumor cells through the ductal basement membrane. About 65% of breast carcinomas are invasive ductal carcinomas. Invasive ductal carcinomas are classified as 75% NOS, 10% medullary, 10% mucinous, 5% tubular, 5% papillary, under 1% adenoid cystic carcinomas, and others. An ▶interval cancer is a malignant tumor which presents clinically during the interval between routine screenings. This type must be distinguished from missed cancers that were overlooked on prospective initial studies, but were visible on review.

Pathology

Gross pathology often shows a hard mass.

Staging of the tumor depends on the tumor size (TNM of UICC):

Tx tumor not judgeable
T0 no tumor
Tis intraductal carcinoma, carcinoma lobulare *in situ*, M. Paget without tumor
T1 tumor ≤2 cm
T1mic: <1 mm (microinvasion)
T1a: >1mm – ≤5mm
T1b: >5 mm – ≤10 mm
T1c: >10 mm – ≤20 mm
T2 tumor >2 cm – ≤5 cm
T3 tumor ≥5 cm
T4 metastatic disease
T4a infiltration of thoracic wall
T4b infiltration of skin
T4c infiltration of both structures
T4d inflammatory carcinoma
N regional lymph nodes
Nx lymph node not judgeable
N0 no regional lymph nodes
N1 metastases in ipsilateral axillary lymph nodes, moveable
N2 metastases in ipsilateral axillary lymph nodes, not moveable
N3 metastases in ipsilateral lymph nodes of mammaria interna.

Furthermore, peritumoral intraductal tumor components must be distinguished:

PIC predominant intraductal component
More than 80% intraductal component and 20% invasive component
EIC extensive intraductal component
Between 25 and 80% intraductal component
Less than 75% invasive component

SIC small intraductal component
Less than 25% intraductal component
More than 75% invasive component.

Multifocality and multicentricity are discussed in the chapter about multiple carcinomas of the breast.

Clinical Presentation

The patient may present with a hard, palpable mass and/or skin, and/or nipple retraction. More details are described in the section on primary and secondary signs. However, sometimes the tumor is occult.

Imaging

All descriptions of the imaging characteristics of invasive tumors should be made according to the BI-RADS classifications. Furthermore, the localization and size of the tumor must be reported with precision. The differential diagnosis includes invasive lobular carcinoma, radial scar, or scars after surgery. Some fat necrosis or abscesses could mimic an ▶invasive ductal carcinoma. Changes from a previous mammogram should be considered, such as a new density, mass, or microcalcifications.

Mammography

A spiculated mass with irregular margins is a typical sign of invasive ductal carcinomas. The density of the tumor is often higher than that of the parenchyma. In some cases, the tumors also present with amorphous or pleomorphic microcalcifications. Other imaging features may be focal asymmetry or architectural distortion, and therefore changes from a previous mammogram must be interpreted carefully (Figs. 1 and 2).

Ultrasound

The tumor is often characterized by an irregular, hypoechoic mass, typically more tall than wide, with a thick echogenic rim and posterior acoustic enhancement. The tumor is not comprisable.

MR Mammography

Typical findings on magnetic resonance (MR) images are rim-enhancing masses, which are irregular or spiculated with heterogeneous enhancement. Signal intensity curves show a high initial contrast media uptake and a postinitial

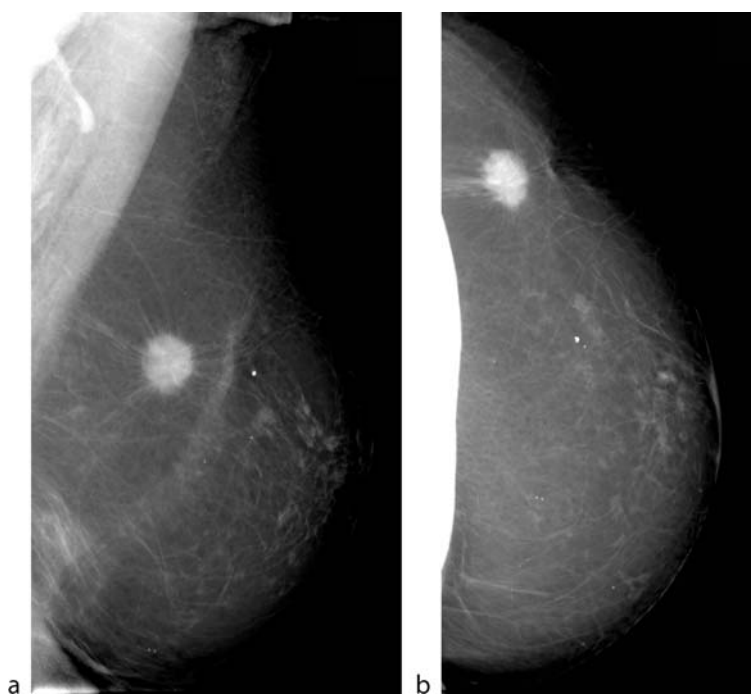

Carcinoma, Ductal, Invasive. Figure 1 Patient with a new, palpable mass in the upper, outer quadrant of the left side. On mammography, an irregular and spiculated mass of 1.5 cm with skin retraction is seen on mediolateral oblique (a) and craniocaudal views (b). Histology revealed an invasive ductal carcinoma, IDC pT1c N0 G2.

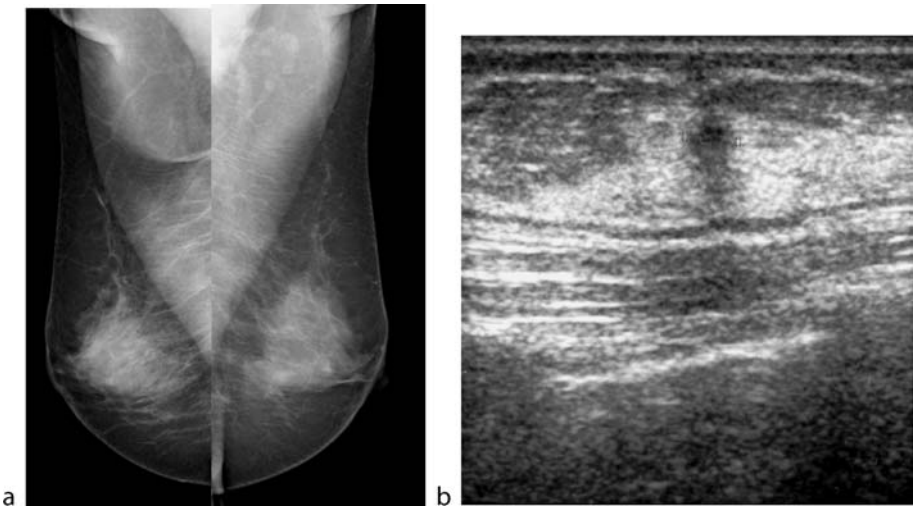

Carcinoma, Ductal, Invasive. Figure 2 Patient with a new, palpable mass on the right side. The tumor is difficult to see on the mammography due to the density of the parenchyma (a). On ultrasound, the tumor is characterized by an irregular, hypoechoic, 1-cm mass, more tall than wide with a thick echogenic rim and posterior acoustic enhancement (b). The tumor is not comprisable. Histology revealed an invasive ductal carcinoma.

plateau or wash-out. On water-sensitive sequences, the tumor has an intermediary signal and on T1-weighted images the tumor is hypointense (Fig. 3).

Bibliography

1. Newstead GM, Baute PB, Toth HK (1992) Invasive lobular and ductal carcinoma: mammographic findings and stage at diagnosis. Radiology 184:623–627
2. Boetes C, Mus RD, Holland R et al (1995) Breast tumors: comparative accuracy of MR imaging relative to mammography and US for demonstrating extent. Radiology 197:743–747

Carcinoma, Endometrium Uteri

Martin Unterweger
Diagnostic Radiology, Cantonal Hospital Baden, Baden, Switzerland
Martin.Unterweger@ksb.ch

Synonyms

Endometrial carcinoma

Definition

Endometrial carcinomas are the most common malignancies of the female pelvis. The mortality of this disease has decreased in the last few years because of earlier detection and advances in tumor treatment. The peak incidence of endometrial carcinoma is around 60 years. The disease is uncommon before the age of 40 years. Risk factors include nulliparity, infertility, obesity, diabetes, and Stein–Leventhal syndrome. One important variable is prolonged stimulation of the endometrium with high-dose estrogen treatment, that is, postmenopausal hormonal replacement or oral contraception. On the other hand, endometrial carcinoma is rarely seen in patients with ovarian agenesis.

Pathology/Histopathology

Endometrial carcinoma arises from the glandular component of the endometrium in the upper uterus. It may grow in a circumscribed pattern, presenting as a focal mass protruding into the uterine cavity and occasionally within an endometrial polyp. However, endometrial carcinomas can also grow diffusely, involving multiple parts of the endometrium. Approximately 90–95% of endometrium carcinomas are adenocarcinomas (Fig. 3). The remaining 10% of nonepithelial uterine cancers comprise sarcomas, mixed tumors, and secondary malignancies. Some less common epithelial varieties include mucinous, secretory, clear cell, and papillary serous carcinomas. The clear cell tumor is highly malignant and has a bad prognosis. Endometrial carcinoma typically arises from the endometrial mucosa. The depth of

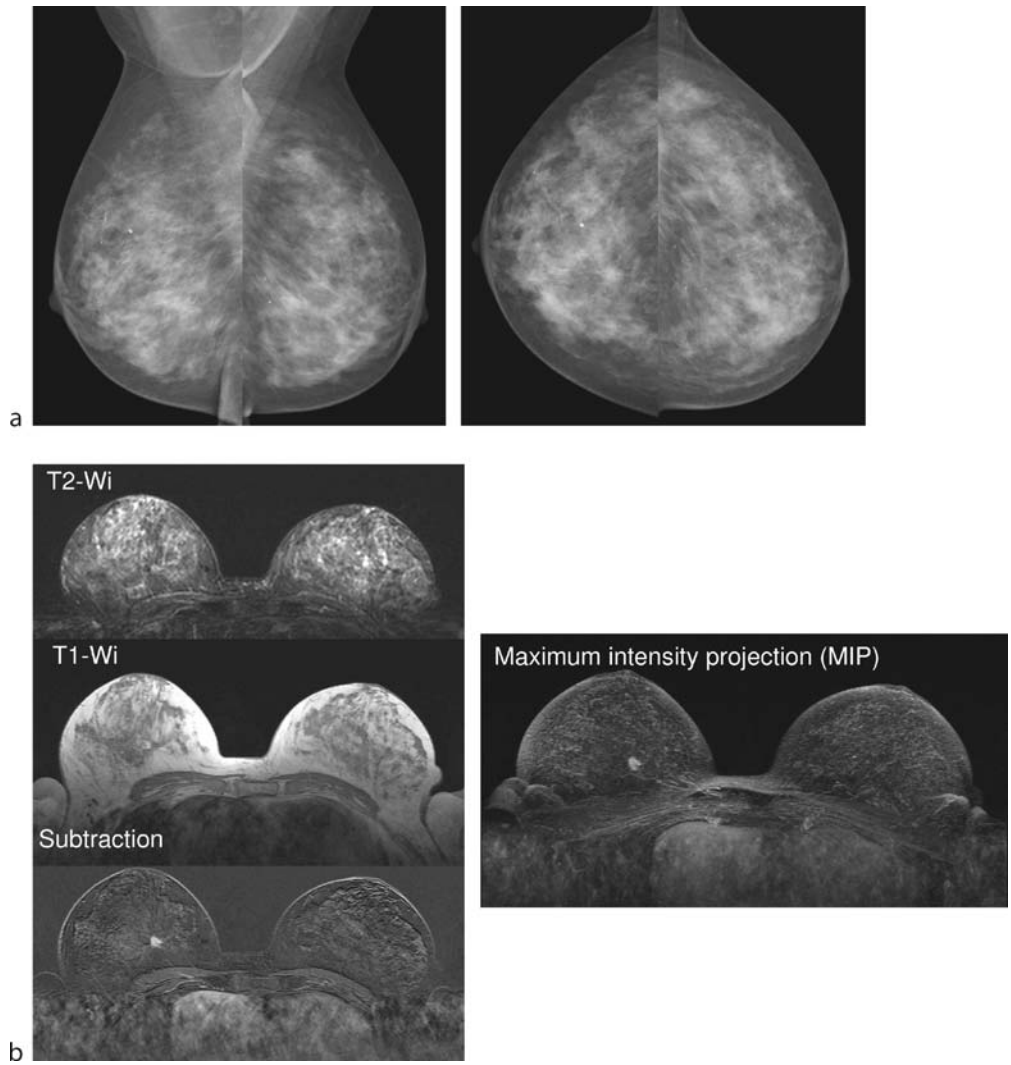

Carcinoma, Ductal, Invasive. Figure 3 Mammography of extremely dense breast tissue (ACR type 4). Tumor is difficult to see on the right side in the inner quadrant (a). MR mammography shows an irregular and spiculated rim-enhancing mass in the right breast (b). The size of the suspected tumor is about 1 cm and it is localized in the inner upper quadrant of the right breast. On T2-weighted imaging, the tumor has intermediary signal. Signal intensity curve shows a rapid initial increase with a plateau in the delayed phase.

myometrial invasion is a very important prognostic factor and correlates with frequency of lymphatic metastasis. The most common sites of distant metastases are the lung, liver, brain, and bone.

Clinical Presentation

Postmenopausal bleeding is the most important presenting symptom of endometrial carcinoma. Because there are multiple benign causes of postmenopausal bleeding, including estrogen therapy, endometrial hypertrophy, atrophic vaginitis, and endometrial and cervical polyps, only 15% of patients with this symptom and endometrial carcinoma will be diagnosed. Less than 5% of patients with carcinoma of the endometrium are asymptomatic at the time of diagnosis. Endometrial carcinoma in premenopausal women usually presents as abnormal uterine bleeding, oligomenorrhea, or menometrorrhagia. The diagnosis of endometrial carcinoma is made histologically with fractional endocervical curettage.

In most institutions, the International Federation of Gynecology and Obstetrics (FIGO) classification is applied for staging of endometrial carcinomas (Fig. 1).

TNM	FIGO	Remarks
T is	0	Carcinoma *in situ*
T1	I	Disease confined to the corpus uteri
T1a	-	Tumor limited to the endometrium
T1b	-	<50% of the myometrium involved
T1c	-	>50% of the myometrium involved
T2	II	Invasion of the uterine cervix, but not extending into the uterus fundus
T2a	IIA	Invasion of the endocervix
T2b	IIB	Cervical stroma invasion
T3	III	Vaginal extension, with spread into the adnexa or parametrium
T3a	IIIA	Invasion into serosa or adnexa or positive peritoneal cytologic finding
T3b	IIIB	Invasion in the vagina
T4	IV	Tumor extention outside the true pelvis, invading the bladder or rectal mucosa
T4a	IVA	Carcinoma involving the rectal mucosa or bladder
T4b	IVB	Distant metastases

Carcinoma, Endometrium Uteri. Figure 1 Staging of endometrial carcinoma according to TNM and the International Federation of Gynecology and Obstetrics (FIGO).

Around 70% of patients are diagnosed with stage I disease. The 5-year survival in this subpopulation is 76%. This survival rate decreases to 59% for stage II and 29% for stage III. Tumor grade also shows a correlation with 5-year survival.

Imaging

On sonography, stage I endometrial carcinoma typically appears as widening of the hyperechogenic endometrium. The postmenopausal endometrium is atrophic and generally measures less than 3 mm. A thickness of greater than 5 mm should always be considered abnormal in women not receiving estrogen therapy. Endovaginal sonography can be useful for screening women with postmenopausal bleeding.

The value of computed tomography (CT) in local staging of endometrial carcinoma is limited, since the spread of endometrial carcinomas is normally small or microscopic to the cervix, parametrium, and lymph nodes.

On magnetic resonance imaging (MRI), the signal intensity of endometrial carcinomas is typically similar to that of normal endometrium on nonenhanced MR images. Tumors are generally hyperintense on T2-weighted images compared to the endometrium and isointense on T1-weighted images. The lesions can be heterogeneous because of necrosis or contents of blood products in the tumor. Large carcinomas are often seen as polypoid masses expanding the endometrial cavity. Secondary signs of small tumors include an increased thickness or lobulation of the endometrium. Endometrial carcinoma enhances variably on dynamic gadolinium-enhanced images. The enhancement is typically different from that of normal myometrium or endometrium. With contrast-enhanced images, the detection of small tumors and differentiation between lesions and fluid or necrosis can be improved. Thus, contrast agents should be routinely applied for staging of endometrial carcinoma. Myometrial invasion is best evaluated on T2-weighted images (Fig. 2) and gadolinium-enhanced scans (Fig. 3). An intact junctional zone is present in stage IA without myometrial invasion. In stage IB, lesions infiltrate the junctional zone and the inner part of the myometrium. Invasion of more than 50% of the myometrium indicates stage IC disease. Cervical invasion (stage II) is best seen on T2-weighted or contrast-enhanced images in the sagittal plane.

In stage III, the local extrauterine disease is demonstrated as extension of tumor outside the myometrium, adnexal masses, vaginal metastases, or pelvic lymphadenopathy. Rectal or bladder wall invasion of tumor (stage IVA) is suspected if the normal fat planes between these organs are interrupted. The overall accuracy of gadolinium-enhanced MRI in the staging of endometrial carcinoma is between 84 and 94%.

Tumor recurrence usually depends on the type of therapy. Patients treated with radiation and surgery typically present with distant metastases. Patients treated only with surgery more often present with pelvic wall, parametrial, or vaginal apex recurrences. Most recurrent tumors will occur within 3 years after initiation of treatment. Early-stage and low-grade tumors often recur late, more than 5 years after initiation of treatment.

Diagnosis

Endocervical and endometrial biopsy is the only reliable option for diagnosis.

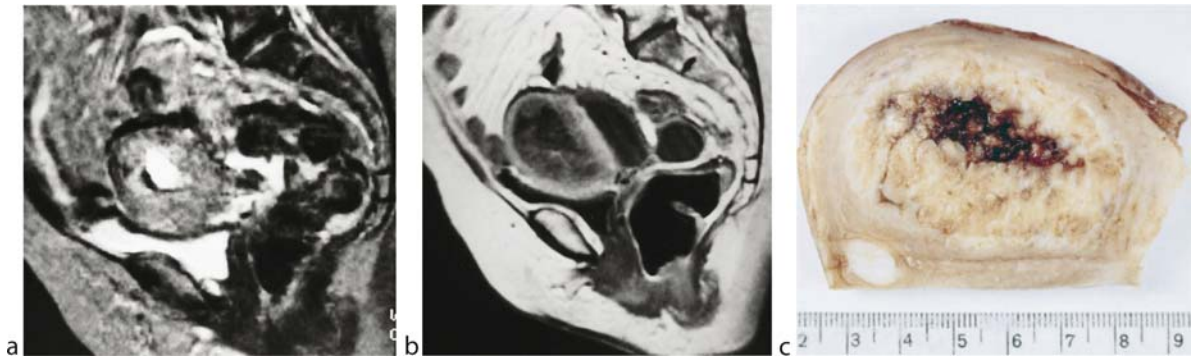

Carcinoma, Endometrium Uteri. Figure 2 (a–c) Pictorial review using MR imaging and CT of the female pelvis. Endometrial carcinoma in stage IC. (a) Sagittal T2-weighted magnetic resonance (MR) image. The T2-weighted image demonstrates only an increased amount of fluid in the uterine cavity. Demarcation of the histologically proven endometrial carcinoma is missing. (b) Sagittal T1-weighted MR image immediately after intravenous contrast administration. Significantly better demarcation of the carcinoma relative to the myometrium is noted. The hypovascularized endometrial carcinoma extends to the outer layers of the myometrium. (c) Gross specimen. Note the good morphologic correlation with the contrast-enhanced MR image. (Figure 9a–c: Reprinted from Hamm, B., Kubik-Huch, R.A., Fleige, B., *Eur. Radiol,*. 9, 3–15, 1999).

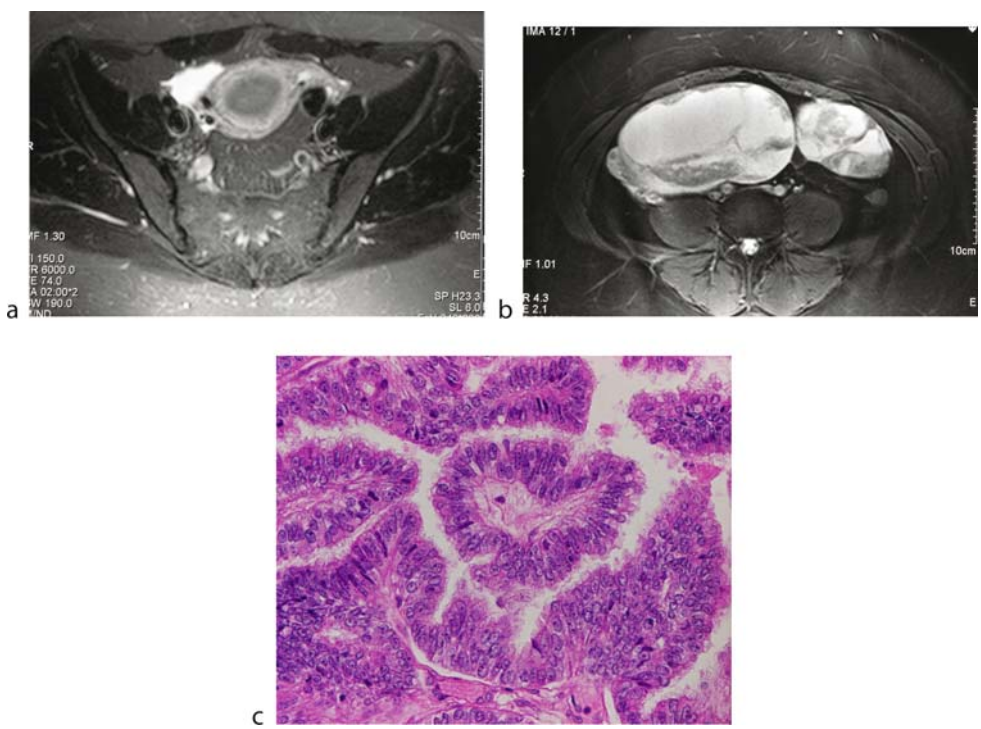

Carcinoma, Endometrium Uteri. Figure 3 (a–c) (a) Axial T2-weighted magnetic resonance imaging (MRI) demonstrates an enlarged nonhomogenous hyperintense uterus, which was histologically proven as an endometrial carcinoma, stage III. (b) Axial T2-weighted MRI shows huge ovaries on both sides, which shows the invasion. (c) Histology of an endometrial adenocarcinoma of the uterus.

Bibliography

1. Frei KA, Kinkel K, Bonel HM et al (2000) Prediction of deep myometrial invasion in patients with endometrial cancer: clinical utility of contrast-enhanced MR imaging a meta analysis and Bayesian analysis. Radiology 216:444–449
2. Seki H, Takan T, Sakai K (1999) Value of dynamic MR imaging in assessing endometrial carcinoma involvement of the cervix. Am J Roentgenol., Jul 2000; 175:171–176
3. Kinkel K, Kaja Y, Yu KK et al (2000) Radiological staging in patients with endometrial cancer: a Meta-analysis. Radiology 1999; 212:711–718
4. Tavassoli FA, and Deville P (2003) Tumor of the breast and female genital organs. WHO classification of tumors
5. Hamm B, Kubik-Huch RA, Fleige B (1999) Eur Radiol 9:3–15

Carcinoma, Gallbladder

Malignant tumor arising from the gallbladder epithelium.
►Neoplasms, Gallbladder

Carcinoma, Hypopharynx

Stefano Cirillo
Institute for Cancer Research and Treatment, Turin, Italy
stefano.cirillo@ircc.it

Definition

Hypopharyngeal carcinoma is a malignant neoplasm originating from the mucosal surface of the hypopharynx.

The ►hypopharynx is a musculomembranous conduit; it lies behind the larynx and extends from its junction with the oropharynx at the tip of the epiglottis (at the level of the hyoid bone) superiorly to the lower border of the cricoid cartilage inferiorly. The muscular-supporting structure is formed by the middle and inferior pharyngeal constrictor muscles. It extends inferiorly down to the cricopharyngeus muscle, where the pharynx joins with the cervical esophagus.

The hypopharynx can be divided into three segments: the *pyriform sinus*, the *postcricoid area*, and the *posterior pharyngeal wall*.

Pathology/Histopathology

The most frequent macroscopic presentation of hypopharyngeal carcinoma is an ulcerative infiltrative lesion (90% of the cases), often associated with a necrotic evolution and erosion of the adjacent cartilaginous, membranous and muscular anatomic structures. The latter represent a form of barrier which hinders further diffusion to the contiguous areas.

Over 95% of malignancies of the hypopharynx are squamous cell carcinomas (well differentiated or undifferentiated); the remaining 5% are squamous cell carcinoma with sarcomatous component, undifferentiated carcinomas, and verrucous and basaloid carcinoma. The hypopharyngeal carcinomas can arise in the pyriform fossa (60%), in the posterior hypopharyngeal wall (25%), and in the postcricoid area (15%).

The cancer spread depends on the site of origin: when the diagnosis is made at a late stage the site of origin is often unrecognizable.

Carcinomas of the *pyriform sinus* are rarely confined. They can extend to the supraglottis larynx involving the aryepiglottic folds, the fatty tissue of the superior paralaryngeal space, and the preepiglottic space; or they can involve the glottic plane anteriorly.

Pyriform sinus tumors originating from the apex and the lateral walls often invade the thyroid cartilage and they may extend directly to the thyroid.

Carcinomas of the *posterior hypopharyngeal wall* can spread in a craniocaudal direction (to the oropharynx or esophagus), in a circumferential direction, or deeply and posteriorly to the prevertebral muscles.

Carcinomas of the *postcricoid area* show a submucosal spread, anteriorly to the posterior cricothyroid muscle and the cricoid cartilage, circumferentially or caudally to the esophagus (1).

Clinical Presentation

Its incidence varies widely. In males, it ranges from 0.3 per 100.000 inhabitants in Iceland to 17 per 100 in France. Among women, the variability is less pronounced. Hypopharynx carcinoma represents approximately 8 and 5% of head and neck epithelial cancers in males and females, respectively, excluding tumors of the skin and the thyroid gland.

Most patients who develop cancer of the hypopharynx have a history of heavy smoking and drinking. Males are about eight times more susceptible to cancer of the hypopharynx than females, In females of Irish and Scandinavian descent who present with Plummer–Vinson syndrome—characterized by esophageal webs, iron deficiency anemia, glossitis, and increased incidence of esophageal cancer—there is also an increased incidence of carcinoma of the postcricoid region.

Hypopharynx carcinoma may remain asymptomatic for a long period; at presentation, the disease is often

advanced. The characteristic symptoms are sore throat, otalgia due to involvement of the Arnolds nerve, a branch of the tenth pair of the cranial nerves, and dysphagia. A "hot potato" voice or hoarseness due to vocal cord paralysis may be present.

Among patients with ►head and neck cancers, hypopharyngeal carcinomas carry a lower survival rate than cancers of other sites. There are several reasons for this poor prognosis: the hypopharynx is a "silent" area and at the time of presentation patients are often at an advanced stage of disease. Seventy-five percent of patients have lymph nodal metastases at the time of diagnosis, 36% have clinically evident adenopathies, 20–40% have distant metastases, and 4–15% show a second synchronous or metachronous tumor.

Tumor size is also associated with metastases to the neck, as they occur in 50% of cases when the tumor is bigger than 4 cm, but in 85% of the cases when it is smaller than 4 cm.

The overall survival of patients with hypopharyngeal carcinoma is about 40% at 5 years. The site, size, and presence or absence of neck metastases have a significant effect on the outcome; in patients with cervical metastases, there is a 20–25% risk of distant metastases within 2 years of treatment. Stage I and II posterior hypopharyngeal wall carcinomas have an excellent prognosis. In contrast, even small pyriform sinus carcinomas are notorious for metastasizing early and carry a poor prognosis. Postcricoid lesions usually present as advanced lesions with extensive paratracheal and mediastinal metastases, and have a poor prognosis (Table 1) (2).

Carcinoma, Hypopharynx. Table 1 T staging for hypopharynx carcinoma

T1	Tumor limited to one subsite of the hypopharynx and ≤2 cm in greatest dimension
T2	Tumor invading more than one subsite of the hypopharynx or an adjacent site, or measuring >2 cm but ≤4 cm in the largest diameter without fixation of the hemilarynx
T3	Tumor measuring >4 cm in largest dimension or fixation of the hemilarynx
T4	Tumor invading the thyroid/cricoid cartilage, hyoid bone, thyroid gland, esophagus, or central compartment soft tissue, which includes prelaryngeal strap muscles and subcutaneous fat
T5	Tumor invading the prevertebral fascia, encasing the carotid artery, or involving the mediastinal structures

Diagnosis

The physical examination should include a thorough head and neck assessment with particular attention given to the oral cavity and the patient's general appearance for signs of severe nutritional deficiencies. The physical examination must be associated with indirect mirror examination and direct endoscopy. The tumor must be confirmed histologically, and any other pathologic data obtained from a biopsy should be included.

The most important goal of the staging endoscopy is to determine the lowermost extent of the tumor and its relation with the pyriform apex and the cervical esophagus.

Esophagoscopy and biopsies should be performed after mapping of the tumor, and complete evaluation of the esophagus down to the gastroesophageal junction is mandatory, as the esophagus is the most frequent site of asymptomatic synchronous primary tumors.

Hypopharyngeal carcinomas arise from the mucosa, thus they are usually visible at the surface, but their submucosal extension cannot be evaluated by endoscopic examination alone. Indeed, clinical and endoscopic examination may underestimate tumor extension. Integration between clinical, endoscopic, and imaging (CT/MR) data is necessary for the correct staging.

Imaging

The disease extent is often endoscopically underestimated because of submucosal tumor spread that can be well visualized with computed tomography (CT) or ►magnetic resonance imaging (MRI). CT and MRI scans are often valuable to further delineate disease extent at the primary site and in the neck. Imaging techniques may, however, underestimate the mucosal growth and overestimate its extension due to difficulty in differentiating cancer tissue from perilesional edematous reaction.

Thus, integration between clinical–endoscopic examination and imaging is necessary.

The role of imaging in hypopharynx carcinoma is as follows:

- Identifying the cancer
- Measuring its volume and dimension
- Evaluating deep tissue diffusion
- Identifying and characterizing of adenopathies
- Follow-up.

Conventional radiography with barium swallow has a limited role for staging, despite a reported sensitivity of 96, 87, 44% in detection of cancer of the pyriform fossa, posterior hypopharyngeal wall, and postcricoid area, respectively.

►Multidetector CT (MDCT) is the first-choice exam for staging hypopharyngeal carcinoma: because of its rapidity, motion artifacts can be erased and scans

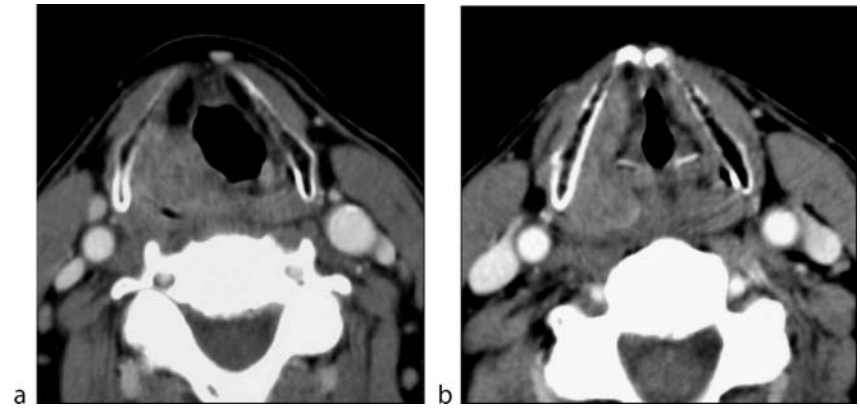

Carcinoma, Hypopharynx. Figure 1 Squamocellular cancer of right pyriform sinus—MDCT: extension anteriorly to paraglottic space, associated with enlargement of thyroarytenoid space.

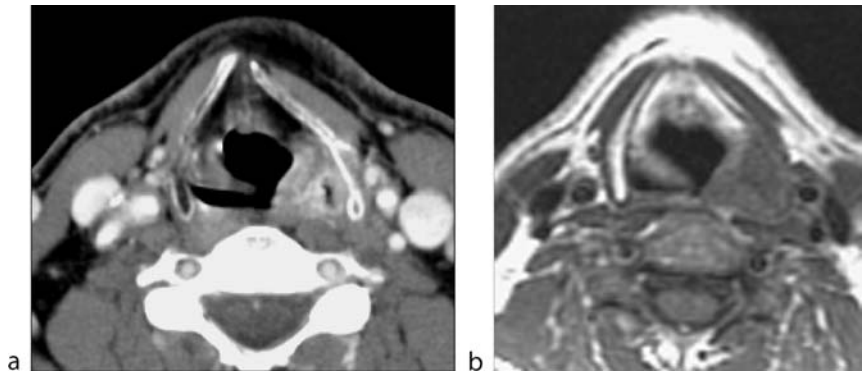

Carcinoma, Hypopharynx. Figure 2 Squamocellular cancer of left pyriform sinus—MDCT (a) shows cancer in contiguity with the left thyroid cartilage, sclerotic. MRI (b) T1-weighted image shows low intensity of left thyroid cartilage for infiltration.

can be performed during functional and dynamic maneuvers, such as phonation or Valsalva, sometimes needed for better visualization of the apex of the pyriform sinus.

MDCT allows the radiologists to make multiplanar reconstruction of excellent quality, obtaining imaging on different planes with optimal tumor visualization and delimitation of tumor volume and of the size of any associated adenopathy.

Identification is possible by evaluation of a space-occupying mass, an area with anomalous enhancement, an obliteration of the adipose space, an asymmetric enlargement of soft tissue, and an asymmetry of the pyriform sinus.

For identification, the sensitivity of MDCT (95%) is higher than that of MRI (87%).

A critical point for hypopharynx carcinoma is the infiltration of the pharyngeal constrictor muscle, the laryngeal cartilages, the paraglottic space, and the prevertebral space (Fig. 1).

The accuracy of MDCT in staging hypopharynx carcinomas is 84–86.4% versus 70–87% of MRI.

Although MRI permits an accurate contrast resolution of the anatomic structure, it can be biased by motion artifacts, due to the long acquisition time, especially in elderly patients with dyspnea, cough, and large expiratory excursions. MRI is necessary when MDCT cannot exclude infiltration of the laryngeal cartilages, the prevertebral muscle, and the cervical esophagus.

MRI has a better sensitivity than MDCT (97 vs. 68% respectively) for assessing cartilage infiltration. Thyroid cartilage infiltration is present in most cancers arising from the apex and in 55% of those arising from the lateral walls (Fig. 2).

For infiltration of the prevertebral muscles, MRI has a sensitivity of 88%, a specificity of 14–29%, and a diagnostic accuracy of 53–60% (Fig. 3).

The MRI criteria useful for determining infiltration of the cervical esophagus show variable accuracy, ranging from 67 to 86%.

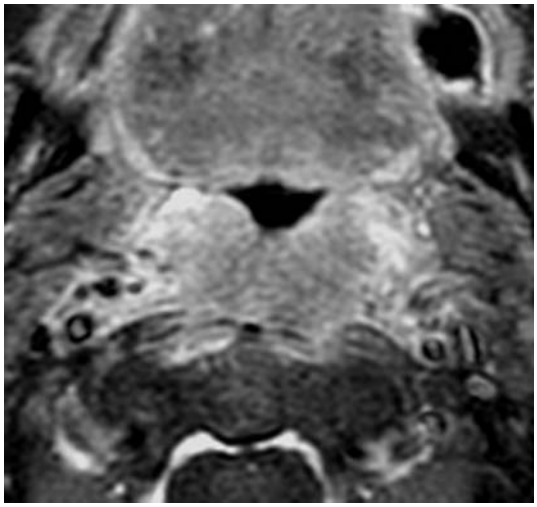

Carcinoma, Hypopharynx. Figure 3 Squamocellular cancer of posterior wall—MRI: T1-weighted image after i. v. gadolinium administration: thickening of posterior wall, associated with involvement of the prevertebral muscles.

The role of imaging is also to identify adenopathies that cannot be assessed by physical examination, by characterizing them and detecting possible capsular rupture.

Ultrasonography is the most useful examination for assessing superficial laterocervical adenopathies, by providing an accurate morphologic and dimensional evaluation. MDCT and MRI evaluation is indicated for deep adenopathies (i.e., retrolateral pharyngeal, which represent an important prognostic factor for local recurrence and distant metastases).

Another imaging objective is to identify lymph node capsular rupture, present in 23% of lymph nodes greater than 10 mm, 40% of those smaller than 20 mm, 50% of those greater 20 mm, and 70% of those greater than 30 mm. Capsular rupture is present in 25% of lymph nodes presenting with normal dimensional criteria (3, 4).

Nuclear Medicine

Nuclear medicine tests are useful in the follow-up of patients who underwent surgery or radiotherapy, for whom there is a clinical suspicion of local recurrence. In this setting, FDG-positron emission tomography (PET) provides a high sensitivity (86–100%) and specificity (69–87%) (5).

PET has some limitations due to its low spatial resolution and the absence of anatomic reference points, which is of particular relevance considering the complexity of the head and neck region. Moreover, uptake is at times present in physiological conditions generating possible false-positive findings. Anatomic limitations can be partially overcome by the combination of CT–PET, which permits simultaneous acquisitions of morphological and metabolic data.

Bibliography

1. American Cancer Society (2006) Cancer Facts and Figures 2006. American Cancer Society, Atlanta, GA
2. Sturgis EM, Wei Q, Spitz MR (2004) Descriptive epidemiology and risk factors for head and neck cancer. Semin Oncol December 31(6):726–733
3. Keberle M, Kenn W, Hahn D (2002) Current concepts in imaging of laryngeal and hypopharyngeal cancer. Eur Radiol July 12(7):1672–1683. Epub 2002 Feb 9
4. Becker M, Hasso AN (1996) Imaging of malignant neoplasms of the pharynx and larynx. In: Taveras JM, Ferruci JT (eds), Radiology: Diagnosis—Imaging—Intervention Lippincott, Philadelphia, PA, pp 1–16
5. Sharon F. Hain (2005) Positron emission tomography in cancer of the head and neck. Brit J Oral Maxillofac Surg 43:1–6

Carcinoma, Lobular, *In situ*, Breast

Arne Fischmann
Department of Diagnostic Radiology, University of Tübingen, Tübingen, Germany
arne.fischmann@med.uni-tuebingen.de

Synonyms

Lobular intraepithelial neoplasia (LIN); Lobular neoplasia (LN)

Definition

Lobular carcinoma *in situ* (LCIS) is carcinoma filling and dilating the intralobular ductuli with loosely aggregated monomorphous cells without stromal invasion. Contrary to prior beliefs describing LCIS as a premalignant lesion, it is nowadays regarded as a risk factor for invasive cancer.

Atypical lobular hyperplasia (ALH) is defined as a lesion that either has some, but not all, of the features of LCIS or has all the features of LCIS but involves up to only 50–75% of a lobule.

Pathology/Histopathology

The cells are uniform, bland, and homogenous without mitosis and are often arranged in a linear file or planar

growth pattern. Pathology is confined to the terminal ductulolobular unit, although a pagetoid involvement of the ducts can sometimes be observed. Necrosis and microcalcifications may occur in LCIS but are rare.

If less than half of one terminal ductulolobular unit is involved, the lesion is called ALH. It remains unclear whether the separation of LCIS and ALH is of clinical relevance because several features used to distinguish ALH and LCIS have no influence on prognosis (1).

Similar to the classification of ductal intraepithelial neoplasia (DIN), ALH, and LCIS are classified as ►lobular intraepithelial neoplasia (LIN) 1–3 depending on the extent of lobular involvement:

1. LIN 1 represents partial or complete filled acini without distention.
2. In LIN 2, multiple or all acini are filled and distended but to a lower degree than in LIN 3. Undermining growth into the terminal ductuli may occur.
3. LIN 3 represents extensive distention of the acini or confluent acini. If goblet cells are detected or the polymorphous form of LCIS is present, the lesion is classified as LIN 3 irrespective of extent.

Coexistence of ductal and lobular neoplasia in one specimen occurs in up to 16% of cases.

Cells are estrogen-receptor positive in up to 60%, a higher rate by far than in invasive carcinoma. A loss of E-cadherin enables the cells to move relatively freely in the ductulolobular system.

LCIS is multicentric in 47–93% and bilateral in 30–67%. Generally, a diffuse involvement of the breast is detected. Therefore, some authors advocate assuming bilateral involvement if LCIS is detected in a specimen.

A finding of lobular hyperplasia, especially with atypia, should mandate further sectioning to exclude invasive lobular carcinoma (ILC), with which it is associated in 5–16% of cases (2).

Clinical Presentation

LCIS does not lead to a palpable mass and is almost always an incidental finding in a specimen retrieved for another reason. Hence, the true incidence of LCIS in the general population is unknown, as it has no clinical or mammographic manifestation. LCIS is found in about 1.1–3% of breast biopsies and in 5.7% of all breast malignancies.

Although ILC is associated with contralateral carcinoma, contralateral malignancy is lower in LCIS (2%) than in DCIS (6%). Generally, LCIS is multifocal (47–93%) and bilateral (30–67%).

The average age of women with LCIS is between 44 and 46, which is 10 years younger than for DCIS. A high proportion (90%) are premenopausal.

LCIS is today considered to be a risk indicator for invasive breast neoplasia rather than being a true precursor lesion: 2.2–7% of patients with LCIS develop invasive carcinoma in 5 years, and 35% develop ipsilateral and 25% contralateral ILC in 20 years, which indicates a fivefold risk of breast carcinoma. A positive family history of breast carcinoma increases this risk to about 11-fold. More than 50% of these malignancies occur more than 15 years after LCIS is diagnosed, in contrast to DCIS, in which more than 90% of recurrences occur within 5 years, indicating the slow growth pattern of LCIS. Most malignancies that follow LCIS are of ductal origin, supporting the view, that LCIS is a risk factor rather than a precursor of malignant disease. One explanation of this fact would be that coexisting DCIS grows faster and becomes invasive sooner than LCIS.

Mortality for LICS is low—less than 7.2% in long-term follow-up, and newer studies even report absent mortality in LCIS.

Risk factors associated with LCIS are comparable to those associated with DCIS or invasive carcinoma: family history or previous history of cancer, late age of pregnancy, or nulliparity. Increasing age actually reduces the risk of subsequent carcinoma in women with LCIS.

Therapy

Because of the wide dissemination of disease, early studies suggested mastectomy for DCIS: after open biopsy, up to 60% of patients were found to have residual LCIS and 6% to have residual ILC in a consecutive mastectomy, in 80% involving a different quadrant. Hence, clear margins cannot resolve the risk of recurrence.

Some groups have suggested bilateral mastectomy on prophylactic grounds. Because initial mastectomy has never been shown to reduce mortality over observation alone, conservative treatment—usually close long-term follow-up—is more advisable, especially considering the relatively young age of the patients.

Ample biopsy in the contralateral breast has been proposed to examine bilateral disease but is nowadays no longer acceptable in the absence of clinical or imaging criteria for biopsy.

LCIS is to be viewed as a risk factor, like a family history of breast cancer, rather than as a premalignant lesion.

There is no evidence that radiation therapy, chemotherapy, or axillary lymph node sampling or dissection have any therapeutic role in LCIS.

Tamoxifen has reduced the risk of invasive breast carcinoma by 56% in women with LCIS and by 86% in women with ALH.

Imaging

Due to the slow growth and infiltrative pattern, neither calcifications nor a solid mass is visible in LCIS. The only mammographic sign is sometimes a parenchyma-like aggregation of breast tissue. Calcifications—usually of the powderish type—are sometimes found in adjacent breast tissue, referred to as "neighborhood calcifications." In rare cases, LIN 3 can present with necrosis and associated microcalcifications, usually of the fine granular type (3). Because these are often associated with ILC, more aggressive treatment should be considered.

Sonography does not show any specific sign.

Although 30% of patients with LCIS show an unsharp region of enhancement on magnetic resonance imaging (MRI), the lesion is not distinguishable from breast parenchyma or mastopathic changes. No prospective signs of malignancy can be detected.

Nuclear Medicine

At the present time, nuclear medicine has no role in the evaluation of LCIS. Diffuse heterogeneous uptake of ^{99m}Tc-sestamibi and ^{99m}Tc-(V)DMSA has been reported. Still, the number of cases was too low to render this method more than experimental.

Because of its slow growth, LCIS does not show increased uptake of ^{18}FDG.

Diagnosis

LCIS is usually a chance finding, detected in specimens taken for evaluation of a neighboring finding. If LCIS is found in a specimen, it must be questioned whether the clinical symptoms can be explained by the LCIS. If not, a further biopsy should be considered to rule out neighboring ILC or DCIS, especially because a rate of underestimation in ►core needle biopsy of 31% has been reported (4).

MRI can be performed to rule out invasive disease associated with LCIS.

Bibliography

1. Tavassoli FA (1999) Lobular neoplasia. In: Tavassoli FA (ed) Pathology of the Breast. McGraw-Hill, New York, pp 373–397
2. Frykberg ER (1999) Lobular carcinoma in situ of the breast. Breast J 5(5):296–303
3. Sapino A, Frigerio A, Peterse JL et al (2000) Mammographically detected in situ lobular carcinomas of the breast. Virchows Archiv 436(5):421–430
4. Elsheikh TM, Silverman JF (2005) Follow-up surgical excision is indicated when breast core needle biopsies show atypical lobular hyperplasia or lobular carcinoma in situ: a correlative study of 33 patients with review of the literature. Am J Surg Pathol 29(4):534–543

Carcinoma, Lobular, Invasive

Silvia Obenauer
Department of Radiology, Georg-August-University of Goettingen,
Goettingen, Germany
obenauerheuser@yahoo.de

Synonyms

Infiltrating lobular carcinoma (ILC)

Definition

About 10% of all breast cancers are invasive lobular carcinomas (ILCs). The cytologic features of the cells suggest that they arise from the lobules.

Pathology

The tumor is more often multifocal or multicentric or controversial (bilaterality). The tumor metastasizes frequently to bone, the peritoneum, adrenals, gastrointestinal tract, ovary, and leptomeninges.

Clinical

The patient may present with a palpable mass and with negative mammography and ultrasound. Sometimes the patient reports a decrease in size of the affected breast ("►shrinking").

Imaging

All descriptions of the imaging of the invasive tumors should be done according to the BI-RADS classifications. Furthermore, localization and size of the tumor must be reported exactly. There are large crossovers with other tumor entities in appearance (Figs. 1, 2).

Mammography

ILCs are often difficult to detect mammographically due to an insidious growth pattern. Therefore, the tumors are often larger at diagnosis than other cancers and may present as palpable masses. ILC is the tumor entity with

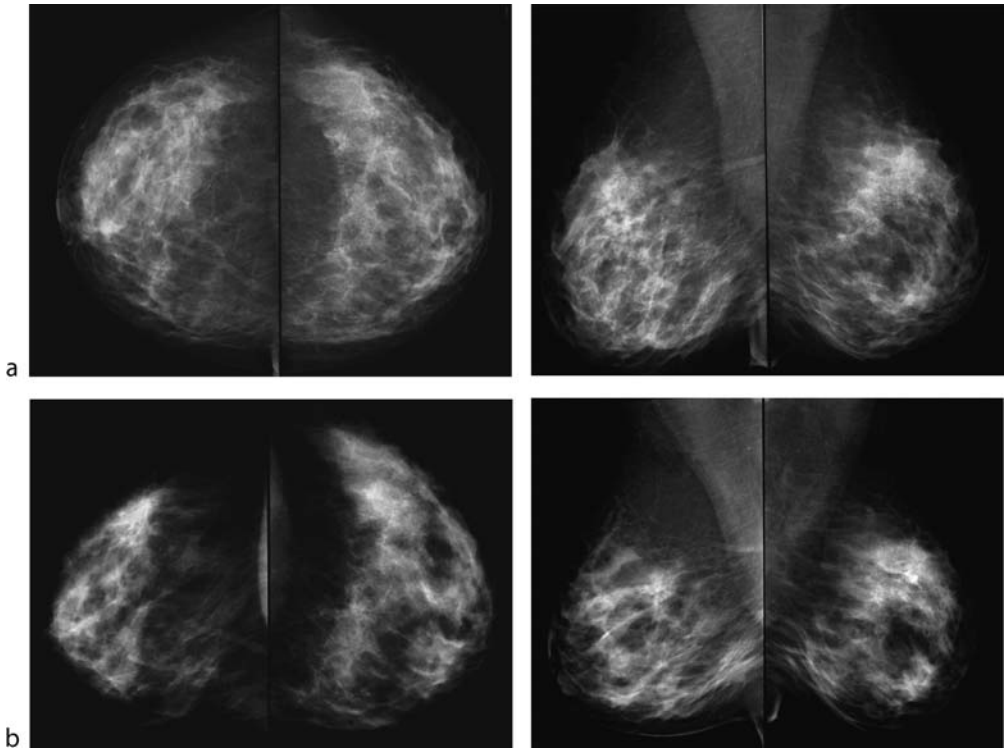

Carcinoma, Lobular, Invasive. Figure 1 (a) Normal mammography. (b) Mammography follow-up after nine months due to a new palpable mass on the right side. Mammography shows only a "shrinking sign" of the right breast in the follow-up. Histology: invasive lobular carcinoma.

the most diagnostic failures, especially in mammography. Most commonly, the tumor presents as a spiculated mass or mass of asymmetric density without definable margins.

Architectural distortion is also possible, whereas calcifications are rare. Sometimes the tumor is seen only in one view. In addition, even when mammography shows the tumor, its extent is often underestimated.

Ultrasound

The tumor is often characterized as a vague area of shadowing without defined borders. But the tumor is often not easily recognized on ultrasound because it grows diffusely.

Magnetic Resonance Mammography

Typical findings in magnetic resonance imaging are rim-enhancing masses that are irregular or spiculated with heterogeneous enhancement. Signal-intensity curves show a high initial contrast media uptake and a postinitial plateau or wash-out. The tumor is presented in water-sensitive sequences by an intermediary signal.

References

1. Boetes C, Veltman J, van Die L et al (2004) The role of MRI in invasive lobular carcinoma. Breast Cancer Res Treat 2773:1–7
2. Hilleren DJ, Andersson IT, Lindholm K et al (1991) Invasive lobular carcinoma: mammographic findings in a 10-year experience. Radiology 178:149–154
3. Newstead GM, Baute PB, Toth HK (1992) Invasive lobular and ductal carcinoma: mammographic findings and stage at diagnosis. Radiology 184:623–627

Carcinoma, Male Breast

Karin Bock
University of Marburg, Marburg, Germany
bock@med.uni-marburg.de

Synonyms

Breast cancer, male; Breast neoplasm, male; Breast tumors, male; Tumors, male breast

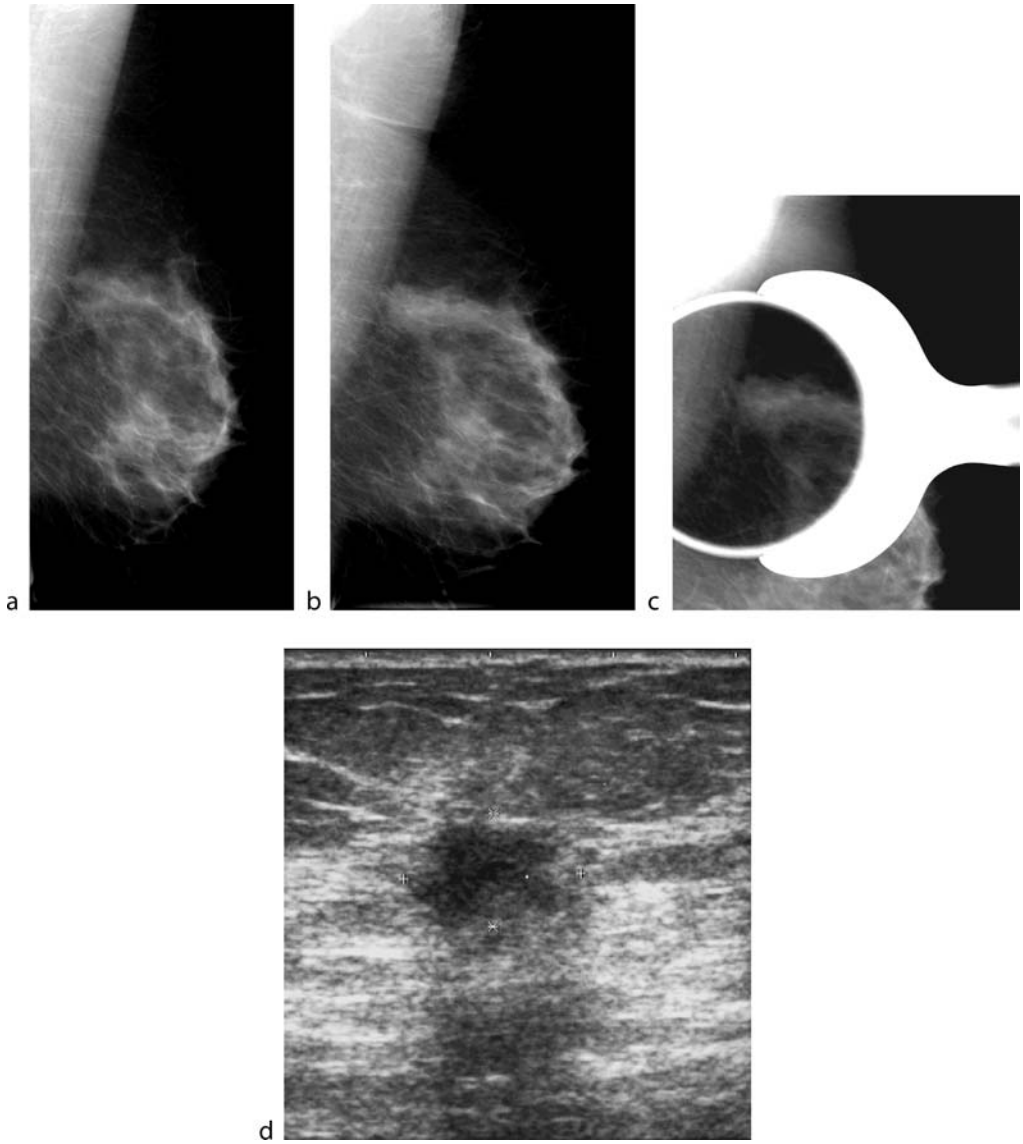

Carcinoma, Lobular, Invasive. Figure 2 (a–d): a Mammography in mlo view without pathology (a). At the six-month follow-up, a new mass in the left upper quadrant is seen, (b) which is most visible in the spot view (c). Ultrasound shows a hypoechoic mass with irregular borders (d).

Definitions

Malignant neoplasms of the male breast that account for approximately 0.7% of all breast cancer diagnoses and less than 1% of all malignant neoplasms in males.

The mean age at diagnosis for men is 67 years, which is 5 years older than the average age at diagnosis for women.

Primary malignant neoplasms with an overall incidence of 0.5–3% must be distinguished from metastases to the breast of extramammary carcinomas (e.g., melanoma, lymphoma, prostate cancer).

Pathology/Histopathology

Physiologically, the male breast consists of fat and a few strands of fibrous and connective tissue behind a small nipple with rudimentary ducts only.

The range of histologic subtypes for male and female breast cancers is similar, but relative distributions differ significantly.

Thus, ductal carcinoma *in situ* compromises approximately 10% of breast cancers in men, while the majority of cases are invasive cancers. Data obtained from more

than 2,000 male patients from the SEER cancer registry demonstrated 93.7% of male breast cancers as ductal or unclassified carcinomas, the others being papillary (2.6%), mucinous (1.8%), or lobular (1.5%).

In comparison to female breast cancers, male breast cancers show higher rates of estrogen receptor expression and equal rates of progesterone receptor expression. Moreover, in contrast to women, the c-erbB2 proto-oncogene is less likely to be overexpressed (approximately 5% only).

Clinical Presentation

As male breast cancer is still considered a rare disease, there is no screening for it and diagnosis is usually made clinically and in an advanced stage of disease.

The most common clinical presenting symptoms in male breast cancer patients are

1. Painless subareolar lumps
2. Nipple retraction
3. Bloody nipple discharge.

Imaging

The most appropriate work-up of suspicious breast findings is diagnostic *mammography*. As for women, the examination should consist of craniocaudal and mediolateral oblique views of each breast (see Fig. 1a, b). A small metal marker can be placed on the skin over the mass to help identify its location on mammographs. In contrast to females, supplementary mammographic views (e.g., spot compression, magnification, exaggerated craniocaudal, cleavage) are rarely needed to clarify lesions. The value of digital mammography has not been evaluated yet.

For evaluation of male mammograms, the breast imaging reporting and data system (BI-RADS) can be used successfully (1, 2).

The sensitivity, specificity, and overall accuracy of mammography in the diagnosis of male breast cancer have been reported by some investigators to be 92%, 89–90%, and 90%, respectively (3,4).

However, although there are characteristic mammographic features that allow breast cancer in men to be recognized, overlap between these features and the mammographic appearance of benign nodular lesions cannot be neglected (5).

Malignant breast tumors are more often eccentric, displacing ill-defined, spiculated, or macrolobulated margins (see Figs 1a, b and 2a, b), but even well-defined margins have been described (4–6). On the other hand, benign breast tumors, such as cysts or fibroadenoma, are seldom found, due to normally rudimentary ducts and glandular tissue.

Calcifications are fewer, coarser, and less frequently rod-shaped than in female breast cancer (5). Secondary features can include skin thickening as well as nipple retraction and axillary lymphadenopathy.

Computer-assisted diagnosis (*CAD*)—Systems do not play a role in the diagnosis of male breast disease, as mammography in men is only performed when clinical findings are present.

Breast ultrasound (7.5–13 MHz, linear arrays) is considered a useful adjunct without radiation hazards,

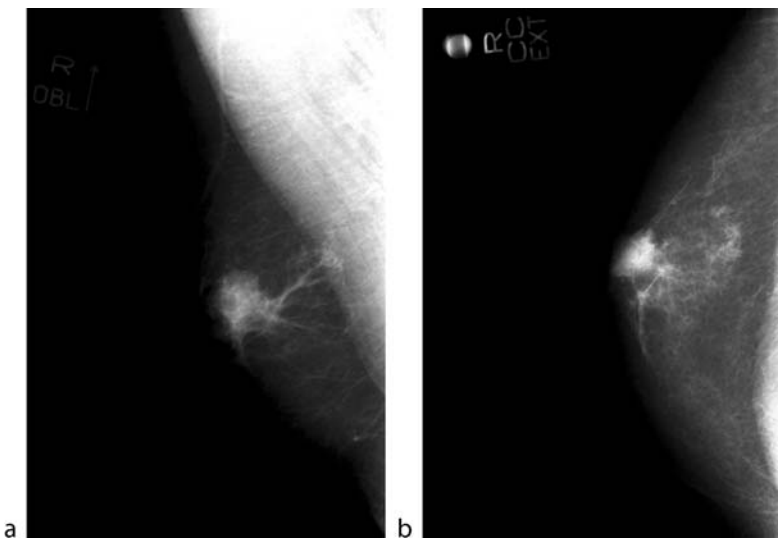

Carcinoma, Male Breast. Figure 1 (a, b) Two standard view mammographs of a man's left breast displaying pseudogynecomastia with retroareolar breast cancer.

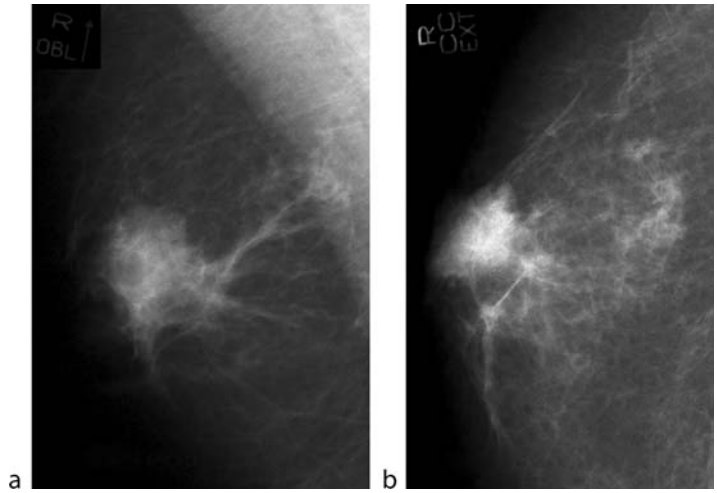

Carcinoma, Male Breast. Figure 2 (a, b) Magnification views (compare Figure 1a, b) displaying male breast cancer. Retroareolar irregular hyperdense lesion with convex borders, satellites toward the chest wall.

increasing the diagnostic specificity and providing additional information regarding nodal involvement, and is an image guide of choice for percutaneous procedures.

The BI-RADS—Ultrasound atlas (6) improves effective use of ultrasound by defining a lexicon of terms and characterizing typical features in the sonographic assessment of lesions.

Sonographic features of malignant tumors of the male breast do not differ substantially from those in female breast cancer (7). The most important features for malignant lesions being irregular shape, architectural distortion, and posterior shadowing (see Fig. 3).

Other imaging techniques such as *MRI* are still investigational in the diagnosis of female breast cancer. Moreover, to date, there are no published data on MRI in male breast cancer.

Studies on molecular imaging such as positron emission tomography (*PET*) or single photon emission computed tomography (*SPECT*) are of distinct diagnostic value in female breast cancer, but have not been tested for male breast cancer. So far, it does not seem feasible to use any of these techniques in the evaluation of clinically apparent breast findings.

Nevertheless, a normal imaging evaluation should never overrule a strongly suspicious finding on physical examination.

Nuclear Medicine

Not applicable in male breast disease, except for sentinel node biopsy in cases of proven breast cancer.

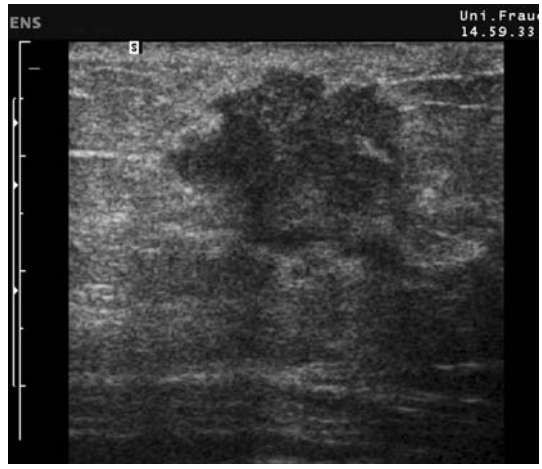

Carcinoma, Male Breast. Figure 3 Male breast cancer (compare Figure 1a, b and 2a, b). B-mode ultrasound (10 MHz, Siemens Sonoline Elegra 10 MHz, linear array) displaying an irregular-shaped, infiltrating mass with disturbed sound transmission as the most reliable characteristic features of malignancy.

Diagnosis

After appropriate local imaging, a suspicious mass requires biopsy to confirm the diagnosis. As in the diagnosis of breast lumps in women, the method of choice should be a minimally invasive procedure, that is, core needle biopsy (≤14G) (8).

Despite limited data, sentinel node biopsy seems feasible in male patients too.

Bibliography

1. ACR BI-RADS (2003) Mammography. 4th edn. Reston, VA
2. Bock K, Iwinska-Zelder J, Duda VF et al (2001) Validity of the Breast Imaging—Reporting and Data System (BI-RADS) for clinical mammography in men. Fortschr Röntgenstr 173:1019–1023
3. Evans GF, Anthony T, Turnage RH et al (2001) The diagnostic accuracy of mammography in the evaluation of male breast disease. Am J Surg 181:96–100
4. Partik B, Mallek R, Rudas M et al (2001) Malignant and benign diseases of the breast in 41 male patients: mammography, sonography and pathohistological correlations. Fortschr Röntgenstr 173:1012–1018
5. Appelbaum AH, Evans GFF, Levy KR et al (1999) Mammographic appearances of male breast disease. Radiographics 19:559–568
6. ACR BI-RADS (2003) Ultrasound. 1st edn. Reston, VA
7. Günhan-Bilgen I, Bozkaya H, Üstün EE et al (2002) Male breast disease: clinical, mammographic, and ultrasonographic features. Eur J Radiol 43:246–255
8. Janes SE, Lengyel JA, Singh S (2005) Needle core biopsy for the assessment of unilateral breast masses in men. Breast July 15 (Epub ahead of print)

Carcinoma, Multiple, Breast

Silvia Obenauer
Department of Radiology, Georg-August-University of Goettingen, Goettingen, Germany
obenauerheuser@yahoo.de

Definition

An invasive carcinoma is a tumor with extension of tumor cells through the ductal basement membrane. About 65% of carcinomas are invasive ductal carcinomas. Multifocal tumors must be distinguished from multicentric tumors.

Pathology

The tumors are classified as already described in the chapter on ductal invasive carcinomas.

Clinical Presentation

The patient could present with many hard, palpable masses and/or skin, and/or nipple retraction.

Imaging

All descriptions of the imaging of invasive tumors should be made according to the BI-RADS classification. Furthermore, the localization and size of the tumor must be reported with precision (Figs. 1 and 2).

Multifocality

One or more masses are found in one quadrant, at a maximum of 2 cm away from the main tumor. The therapy of choice is quadrantectomy.

Multicentricity

One or more tumors are more than 2 cm away from the main tumor, often in different quadrants. Mastectomy is usually performed.

Often a tumor is seen on mammography. Because mutifocal, multicentric, or contralateral tumors have a big influence on the therapy and prognosis, we perform MR mammography preoperatively.

Mammography

A spiculated mass with irregular margins is a typical sign of invasive ductal carcinomas. The density of the tumor is often higher than that of the parenchyma. In some cases the tumors also present with amorphous or pleomorphic microcalcifications. Other imaging features may be asymmetry or architectural distortion, and therefore changes from a previous mammogram must be interpreted carefully.

Ultrasound

The tumor is often characterized by an irregular, hypoechoic mass, typically more tall than wide with a thick echogenic rim and posterior acoustic enhancement. The tumor is not comprisable.

MR mammography

Typical findings on magnetic resonance mammography (MRM) are rim-enhancing masses that are irregular or spiculated with heterogeneous enhancement. Signal intensity curves show a high initial contrast media uptake and a postinitial plateau or wash-out. On water-sensitive sequences the tumor has an intermediary signal.

MRM reveals additional tumors not previously seen on mammography or ultrasound. Therefore, MRM could be performed before therapy to exclude ▶multifocality or ▶multicentricity. Studies have found that MRM reveals about 14% additional findings that were not previously seen.

Bibliography

1. Fischer U (2000) Lehratlas der MR-Mammographie. Thieme Verlag, Stuttgart-New York
2. Heywang SH, Wolf A, Pruss E et al (1989) MR imaging of the breast with Gd-DTPA: use and limitations. Radiology 171:95–103

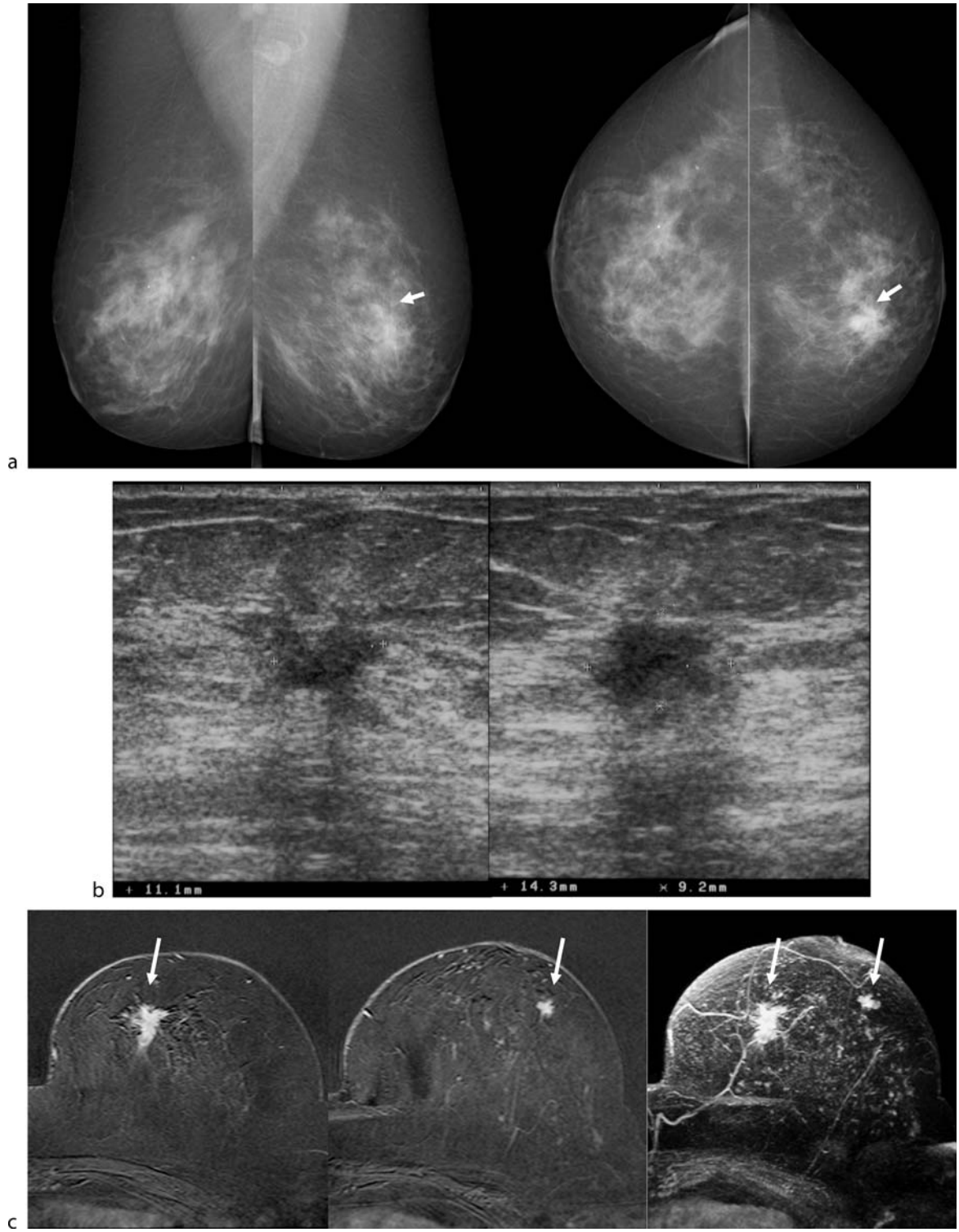

Carcinoma, Multiple, Breast. Figure 1 Mammography of a patient with a palpable mass on the left side. Typical spiculated mass on the left side in mediolateral oblique and craniocaudal views (a). Ultrasound revealing a second mass on the left side (b) which was confirmed by MRM on a subtraction image and maximum intensity projection (c). Histology determined bifocal invasive ductal carcinoma.

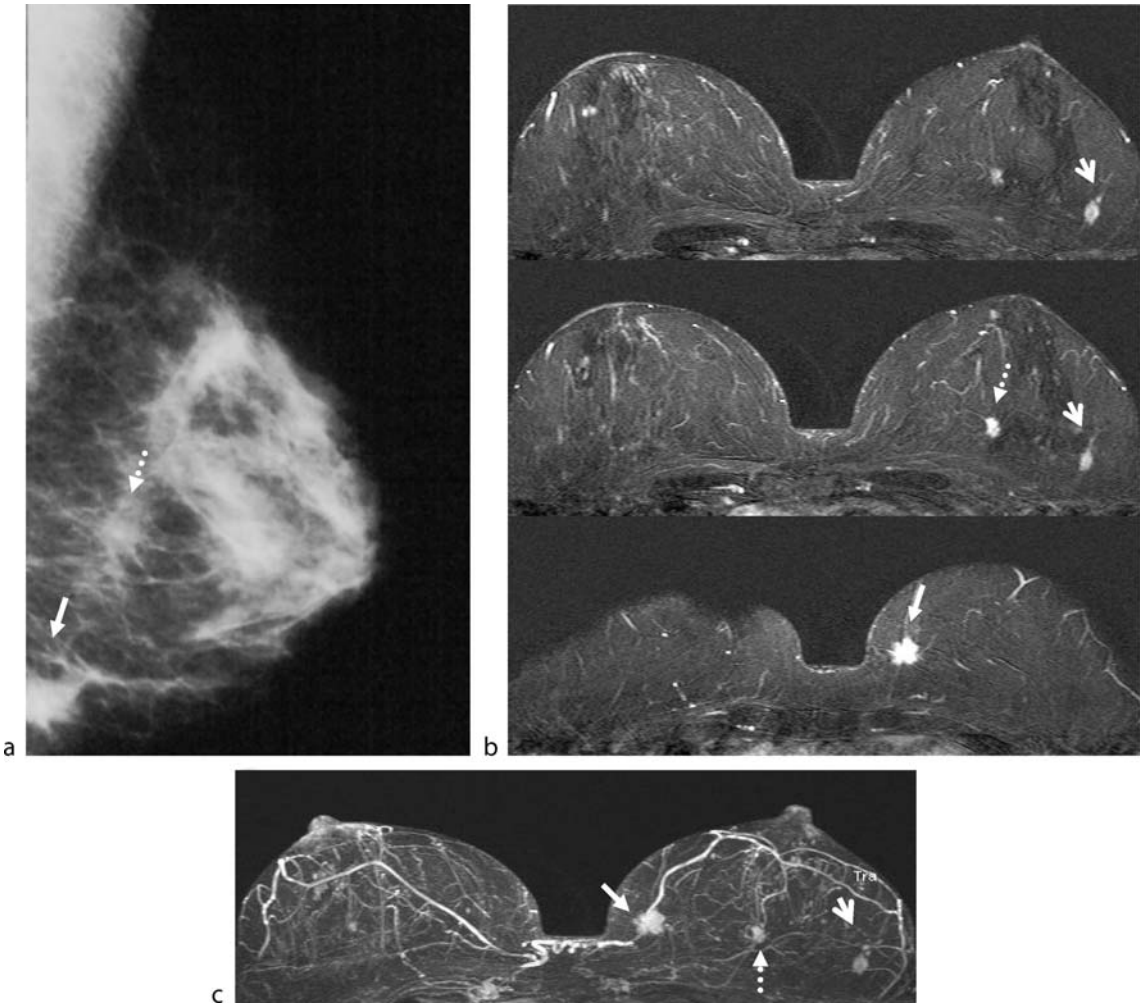

Carcinoma, Multiple, Breast. Figure 2 Mammography of a patient with a palpable mass in the left breast (caudal quadrant). Additional suspicious lesion in the middle of the breast (a). MRM of a multicentric carcinoma in the left breast, on subtraction image (b) and on maximum intensity projection (c).

Carcinoma, Other, Invasive, Breast

Silvia Obenauer
Department of Radiology, Georg-August-University of Goettingen, Goettingen, Germany
obenauerheuser@yahoo.de

Synonyms

Circumscribed carcinoma; Colloid carcinoma; Gallert carcinoma; Gelatinous carcinoma; Infiltrating papillary carcinoma; Inflammatory carcinoma; Intracystic papillary carcinoma with invasion; Medullary carcinoma; Mucinous carcinoma; Papillary carcinoma; Tubular carcinoma

Definition

Invasive carcinomas comprise medullary carcinoma, mucinous carcinoma, tubular carcinoma, papillary carcinoma, and ►inflammatory carcinoma.

Papillary carcinoma is a rare form of specified invasive ductal carcinoma (about 1–2% of all breast cancers). Medullary and mucinous carcinomas are also rare tumors (<5% of all breast cancers). Medullary carcinoma presents with a rapid growth and local aggressiveness. Mucinous

carcinoma is a well-differentiated, invasive adenocarcinoma. Tubular carcinoma is a well-differentiated form of infiltrating ductal carcinoma, which is slow growing. Inflammatory carcinoma typically presents with a rapid onset of diffuse breast changes and aggressive tumor invasion of the dermal lymphatics.

Pathology/Histopathology

Medullary Carcinoma

Medullary carcinoma is often a well-defined expansive mass, which is softer than most breast carcinomas. The cut edge reveals a nodular architecture with hemorrhage and necrosis.

The typical type contains no glandular elements and has an intense lymphoplasmacytic reaction, poorly differentiated nuclear grades with a high mitotic rate, and minimal desmoplastic stromal reaction.

Mucinous Carcinoma

Pathological pure and mixed types are distinguished. The pure type consists of more than 75% mucinous cells and the mixed type of mucinous and invasive, not otherwise specified elements. The pure type is usually smaller than the mixed type. The tumor cells are often found in lakes of mucin.

Tubular Carcinoma

On gross pathology, the tumor shows a tan-to-gray cut surface with ill-defined or spiculated margins. Microscopic features show well-formed tubular elements with often uniform nuclei and a low mitotic rate.

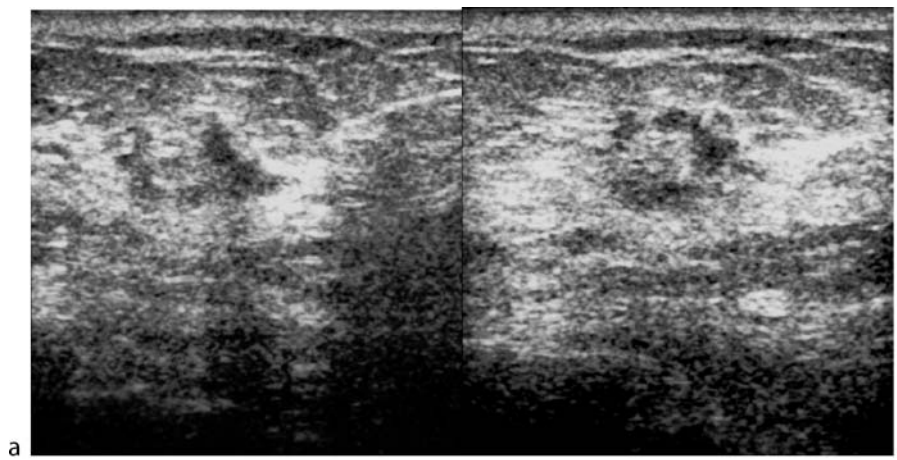

a

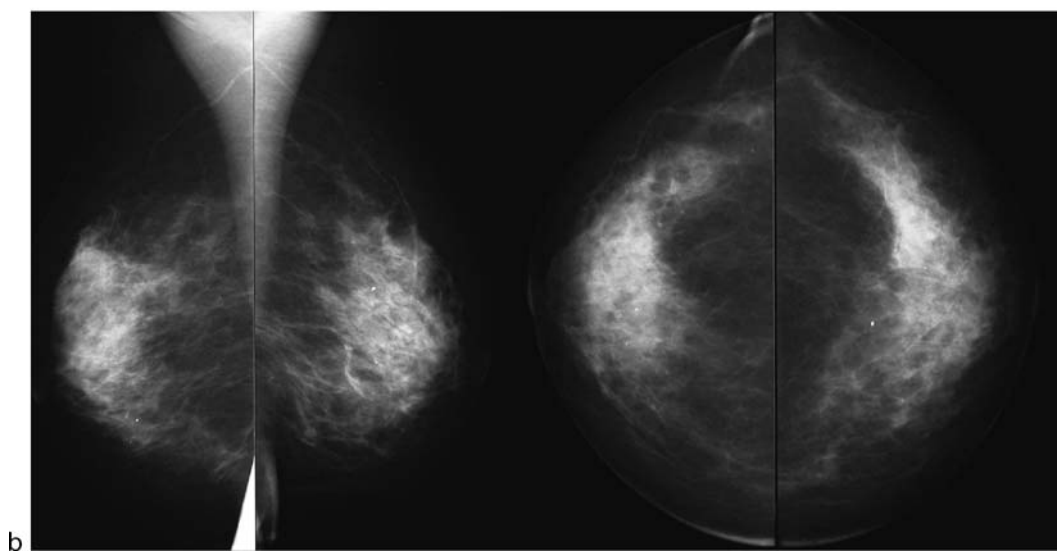

b

Carcinoma, Other, Invasive, Breast. Figure 1 Continued

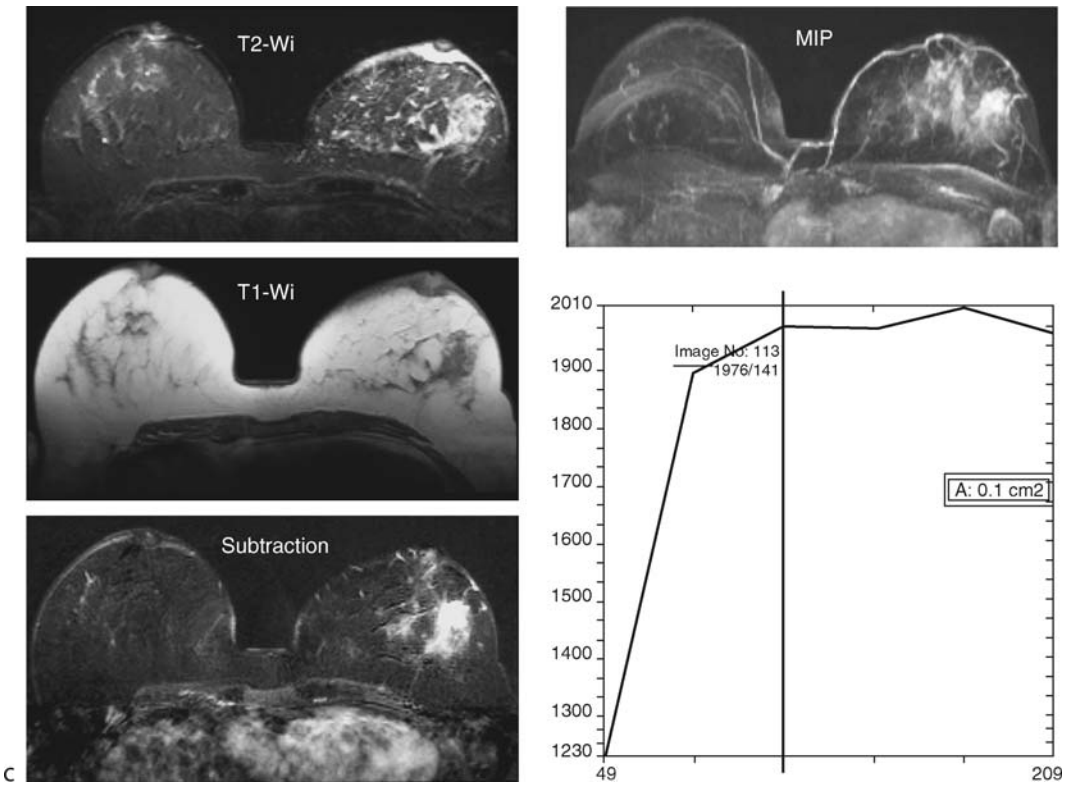

Carcinoma, Other, Invasive, Breast. Figure 1 Mass with irregular border and inhomogeneous echo inside is shown on an ultrasound image (a). Mass on the left side is masqueraded by parenchyma on the mammography. However, higher density on the left outer quadrant is seen (b). MR mammography reveals edema and skin thickening of the left breast on T2-weighted imaging. A mass on the left upper outer quadrant is seen with surrounding edema and contrast media enhancement. On T2-weighted imaging the mass is hyperintense. Signal intensity curves reveal an initial rise of about 100% and a postinitial plateau (c). Histology: papillary carcinoma.

Papillary Carcinoma

Two types are distinguished; the solid form that has a higher tendency to invade and the cystic form that may develop in a dilated lobule or duct. On gross pathology, a well-circumscribed mass is seen, often containing hemorrhage and cystic areas. On microscopy, an absent myoepithelial layer distinguishes the invasive form from a benign papillary lesion. Usually, the lesion is not associated with necrosis or calcifications. Invasive elements are often seen in the periphery of the tumor.

Inflammatory Carcinoma

Breast skin changes such as erythema, thickening, and peau d'orange are common. A diffuse infiltrating tumor without a well-defined tumor mass is found. The tumors are often poorly differentiated, are estrogen-receptor negative, and intralymphatic dermal tumor emboli are seen.

Clinical Presentation

Medullary Carcinoma

Most of these lesions are palpable, soft, and mobile masses usually located in the upper outer quadrant.

Mucinous Carcinoma

The tumors are often soft on palpation and may be perceived as benign.

Tubular Carcinoma

The tumors may be palpable, but most of them are detected on images.

Papillary Carcinoma

A firm, but not hard, mass that may be palpable. Nipple discharge is seen in up to one-third of patients.

Inflammatory Carcinoma

The patient presents with breast erythema, warmth, skin thickening, peau d'orange, pain, and sometimes a palpable mass.

Imaging

Medullary Carcinoma

These tumors are often oval or lobulated circumscribed masses (Figs. 1–3).

Mucinous Carcinoma

This tumor entity often appears as a well-circumscribed and round mass.

Tubular Carcinoma

The tumor is typically a small spiculated mass.

Papillary Carcinoma

The size of the invasive component is often small in relation to the lesion size.

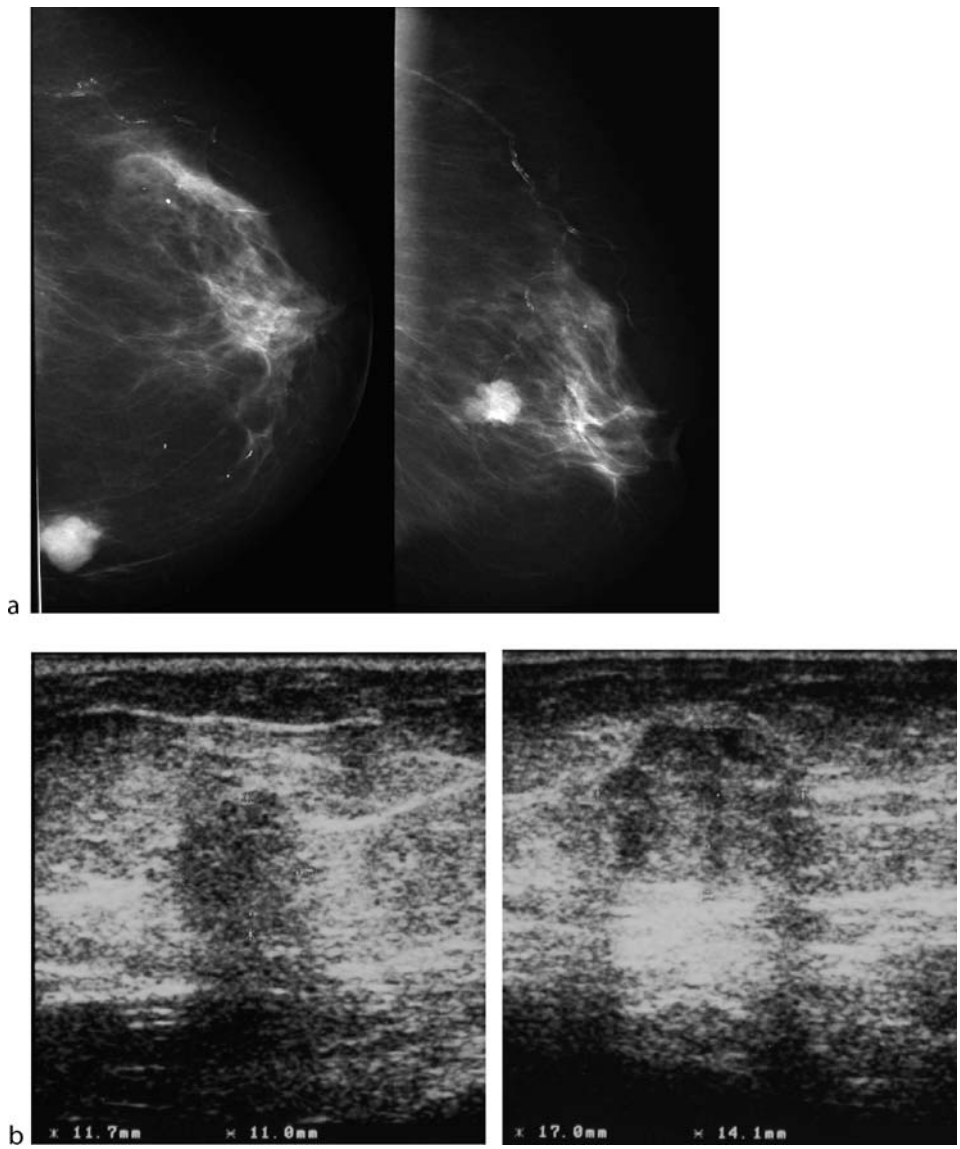

Carcinoma, Other, Invasive, Breast. Figure 2 Continued

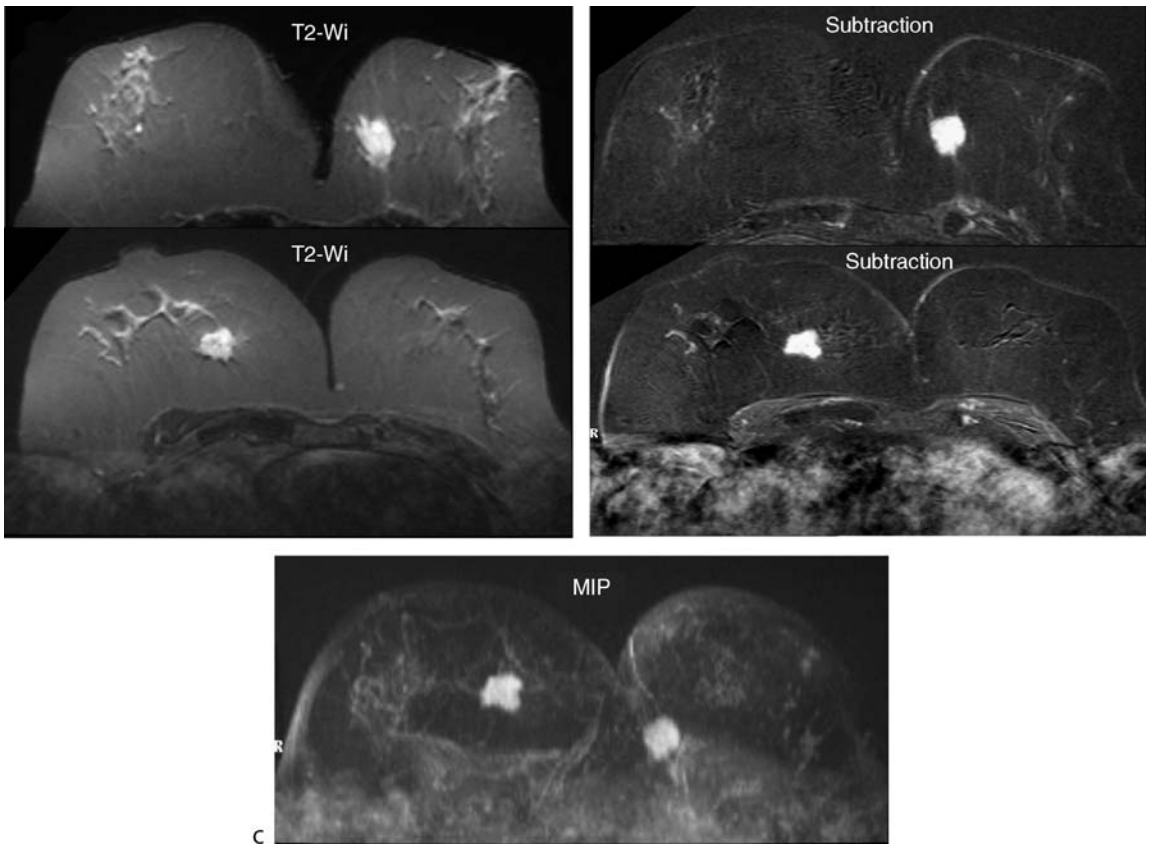

Carcinoma, Other, Invasive, Breast. Figure 2 Mammography of the left side reveals a lobulated mass in the middle inner quadrant without microcalcifications (a). Ultrasound of the lobulated mass with hypoechoic signal and posterior acoustic enhancement (b). MR mammography reveals lobulated masses on both sides of the breasts in the inner quadrant. The masses show hyperintense signal on T2-weighted images and strong contrast media enhancement in the subtraction images (c). Histology shows mucinous carcinomas.

Inflammatory Carcinoma

This tumor entity may be misdiagnosed as benign inflammatory process.

Mammography

Medullary Carcinoma

Typical findings are an oval, lobulated, or round mass with circumscribed margins. Calcifications are very rare.

Mucinous Carcinoma

Typical mammographic findings are a round, well-circumscribed, noncalcified mass. Most commonly the process is solitary at initial presentation and later multiple and bilateral masses are seen as the disease progresses. Spiculations and calcifications are rare.

Tubular Carcinoma

Typical mammographical findings are round or oval masses with spiculations. Sometimes the tumor is seen with architectural distortion, asymmetric density, and microcalcifications.

Papillary Carcinoma

Often a round, oval, or lobulated well-circumscribed mass is seen. Sometimes multiple masses occur. Calcifications and spiculations are rare findings. Pneumocystography may identify an irregular mass. Galactography may be helpful in the evaluation of nipple discharge. Typical findings will be ductal obstruction, wall irregularity, and filling defects.

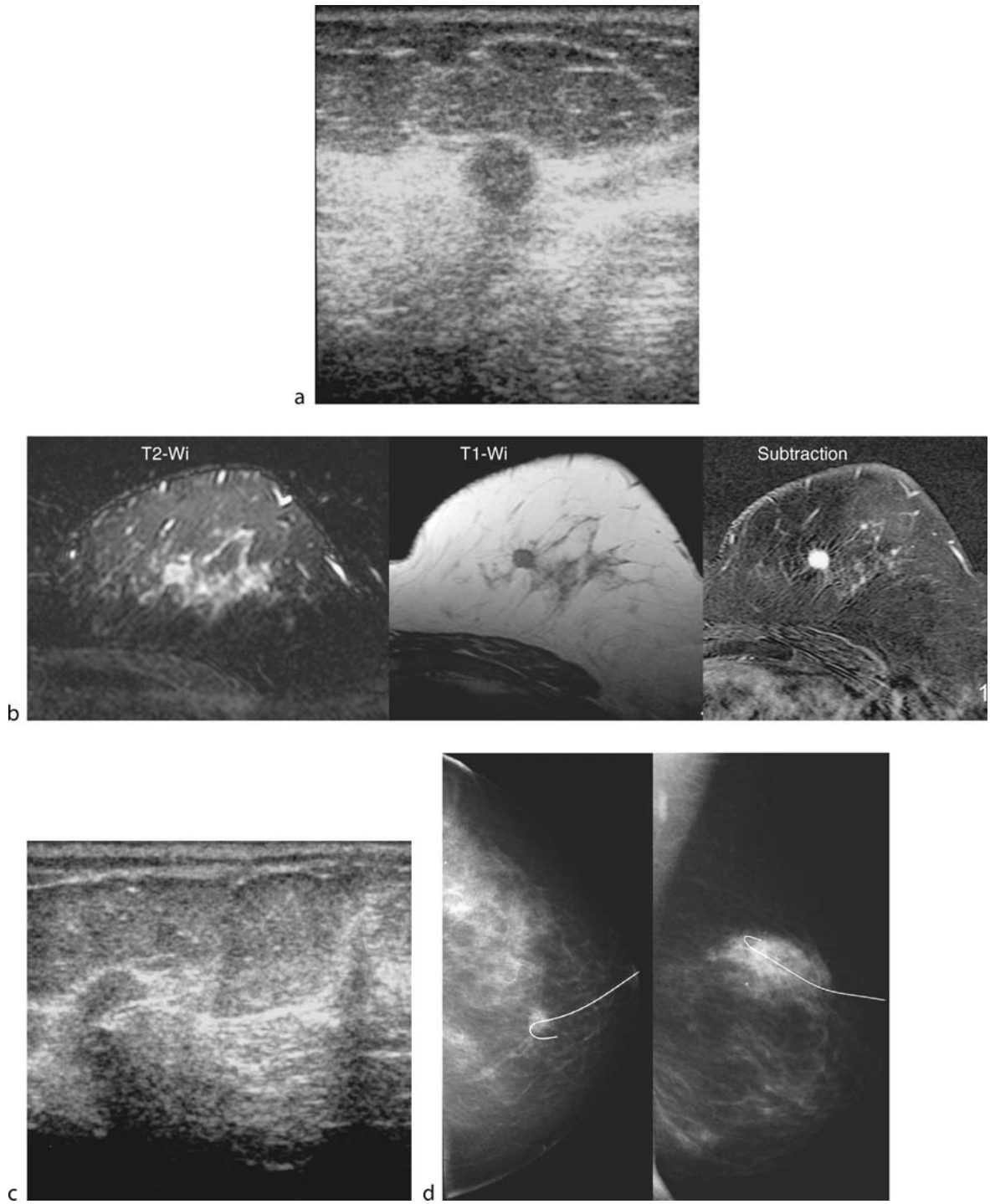

Carcinoma, Other, Invasive, Breast. Figure 3 Ultrasound of a tubular carcinoma revealing a hypoechoic mass, more tall than wide (a). MR mammography shows a round mass on the left side. On T2-weighted images the mass is hyperintense, on T1-weighted images hypointense, and on the subtraction image the mass shows contrast enhancement (b). Preoperative ultrasound-guided localization of the mass was carried out (c). Follow-up mammography after ultrasound-guided wire localization shows a round, partially ill-defined mass in the left upper middle quadrant exactly localized by wire (d). Histology shows tubular carcinoma.

Inflammatory Carcinoma

Common features are skin thickening and diffuse increased breast density. Other findings such as trabecular thickening, axillary lymphadenopathy, architectural distortion, focal asymmetric density, and nipple retraction may be found. Less often, calcifications or masses are found.

Ultrasound

Medullary Carcinoma

Typically, a well-defined, hypoechoic mass is found. Some large lesions may have anechoic areas. A posterior acoustic enhancement is not uncommon.

Mucinous Carcinoma

Typically, a round or oval mass is seen, sometimes with lobulations. The margins are smooth or irregular. There may be internal anechoic echoes. Posterior acoustic enhancement is not common.

Tubular Carcinoma

The tumor shows an ill-defined hypoechoic mass with posterior acoustic shadowing. Sometimes hyperechoic foci represent calcifications.

Papillary Carcinoma

Often a homogeneously solid and cystic mass is seen with posterior acoustic enhancement. Sometimes an intracystic mass or mural nodules can be distinguished. Sequelae of hemorrhage may also be seen.

Inflammatory Carcinoma

On ultrasound, nonspecific findings are seen such as widening of the dermal–subcutaneous fat interface. Edematous changes are, however, indistinguishable from tumor infiltration.

Magnetic Resonance Mammography

Medullary Carcinoma

Often an oval or round, lobulated, heterogeneous, enhancing mass is seen.

Mucinous Carcinoma

Often a round, well-circumscribed, or ill-defined, rim-enhancing mass is seen.

Tubular Carcinoma

The tumor shows the typical enhancement of an invasive ductal carcinoma with an irregular spiculated mass and a strong initial contrast media rim or inhomogeneous enhancement.

Papillary Carcinoma

The solid components show a heterogeneous, well-circumscribed enhancing mass when i.v. contrast media is administered.

In the cystic mass, mural or nodular enhancement with or without hemorrhage is seen.

Inflammatory Carcinoma

Magnetic resonance mammography is not indicated for this tumor entity. Often a diffuse, intense, rapid enhancement is seen, which is indistinguishable from benign inflammatory process.

Bibliography

1. Heywang SH, Wolf A, Pruss E et al (1989) MR imaging of the breast with Gd-DTPA: use and limitations. Radiology 171:95–103
2. Newstead GM, Baute PB, Toth HK (1992) Invasive lobular and ductal carcinoma: mammographic findings and stage at diagnosis. Radiology 184:623–627

Carcinoma, Ovarium

Rosemarie Forstner
Department of Radiology, Paracelsus Private Medical University, Salzburger Landeskliniken, Salzburg, Austria
r.forstner@salk.at

Synonyms

Epithelial ovarian cancer; Epithelial ovarian neoplasm; Malignant ovarian neoplasm; Ovarian cancer; Primary malignant neoplasm of ovary

Definition

Ovarian cancer is the leading cause of death among all gynecologic malignancies. In females, it is the fifth most common cancer. The majority of ovarian carcinomas are epithelial in origin, accounting for approximately 85% of

ovarian malignancies (1). The incidence of ovarian cancer increases with age, with a median age of 61 years at diagnosis (2). Familial evidence of ovarian cancer is the strongest risk factor: ovarian cancer develops in these women when they are one decade younger than the normal population (1). There are significant differences in prognosis between early and advanced ovarian cancer. While early-stage cancer is often curable, advanced-stage ovarian cancer has an overall 5-year survival rate of 38–53% (1). This is attributed to the fact that at the time of diagnosis up to 70–85% of patients present with peritoneal cancer spread outside the pelvis.

Pathology/Histopathology

Macroscopically, ovarian cancer most often presents as uni- or bilateral multilocular cystic tumors with intracystic ►papillary projections or as mixed solid and cystic tumors (3). Rarely, ovarian cancers may be predominantly solid (3). Cystic elements within the tumor may contain serous, hemorrhagic, or turbid fluid. Papillary projections, which are a typical feature of serous ovarian tumors, may fill the cyst cavities. ►Psammoma bodies within the tumor presenting tiny calcifications are detected in 30% of serous adenocarcinomas. Bilateral ovarian involvement is typically found in serous cystadenocarcinoma, which is the most common ovarian cancer; it is rarely encountered in endometrioid cancer (3). Endometriosis is associated with endometrioid cancer and particularly with clear cell cancer (3).

Epithelial ovarian cancers are adenocarcinomas and comprise, depending on their histopathologic features, serous, mucinous, endometrioid, transitional cell, clear cell, undifferentiated, and mixed carcinomas (1). Except for clear cell carcinomas, the histologic type has limited prognostic significance independent of clinical stage (1).

Epithelial carcinomas are characterized by histologic type and the degree of cellular differentiation (grade).

Clinical Presentation

Ovarian cancer usually remains clinically silent in early-stage disease. Rarely, abnormal uterine bleeding may be the first symptom of ovarian cancer. With more advanced stage and tumor masses larger than 10 cm, women often complain of bloating, abdominal discomfort, pelvic pressure, or urinary or rectal discomfort. The disease may also become clinically apparent by ascites-related symptoms including abdominal swelling and pleural effusion with shortness of breath (1).

Imaging

The American College of Radiology (ACR) recommends ►screening for ovarian cancer by ►CA-125 and ultrasound (US) assessment of the ovaries only in high-risk patients (2). These are patients with a positive family history of ovarian cancer or *BRCA1* or *BRCA2* gene mutations.

The role of imaging in suspected ovarian cancer includes characterization of an adnexal mass, ►staging of ovarian cancer, and defining criteria of nonresectability.

Criteria for differentiation between benign and malignant ovarian masses do not differ for the cross-sectional imaging modalities US, computed tomography (CT), and magnetic resonance imaging (MRI). They include tumor size and morphologic criteria of the internal architecture of an adnexal mass including its vascularization (4). Secondary signs supporting the diagnosis of metastatic spread are ascites, peritoneal implants, or lymph node enlargement (4).

Staging of ovarian cancer is based on the extent and location of disease found at explorative laparotomy. The International Federation of Gynecologists and Obstetricians (FIGO) classification system is the most commonly used staging system for ovarian cancer. Although definitive staging of ovarian cancer is based on the findings at surgery, preoperative assessment of the tumor extent by imaging may influence patient management. Accurate preoperative assessment of ovarian cancer may assist in selecting sites for biopsy and may alert to tumor deposits that are difficult to visualize intraoperatively, for example, locations in the upper abdomen and lymph nodes. Furthermore, it may influence surgical strategy, for example, need of subspecialist cooperation or of referral to an oncology center.

Preoperative routine chest radiographs, intravenous urography (IVU), and barium studies have recently been replaced by CT.

In cases of extensive cancer and signs of nonresectability in CT or MRI, candidates who may benefit from neoadjuvant therapy prior to surgery may be selected.

In the assessment of ovarian cancer, *US* is the primary imaging modality for detection and characterization of adnexal masses (2) (Fig. 1).

MRI is currently most commonly used as a problem-solving modality in cases of indeterminate adnexal masses (2). Its advantages over US are superior morphologic assessment of adnexal masses, particularly in hemorrhagic lesions. MRI is superior to US and CT in the evaluation of local pelvic spread of ovarian cancer.

Multidetector contrast-enhanced CT is the modality of choice for preoperative staging and for follow-up of ovarian cancer (2) (Fig. 2). Alternatively, particularly in

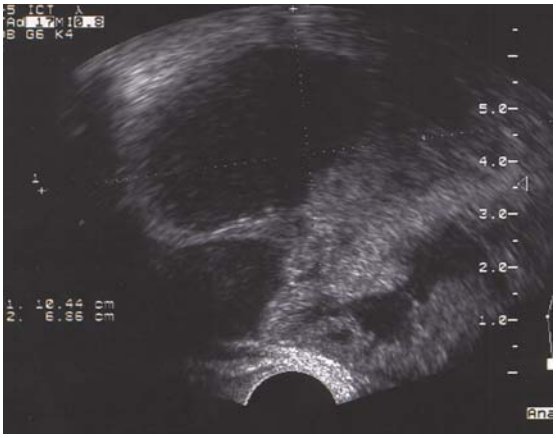

Carcinoma Ovarium. Figure 1 Mucinous adenocarcinoma on US image. A large, complex ovarian lesion consisting of solid and cystic elements is demonstrated in transvaginal sonography. The cyst contains multiple homogeneous echoes presenting hemorrhagic or proteinaceous fluid; the cyst walls are thick and irregular.

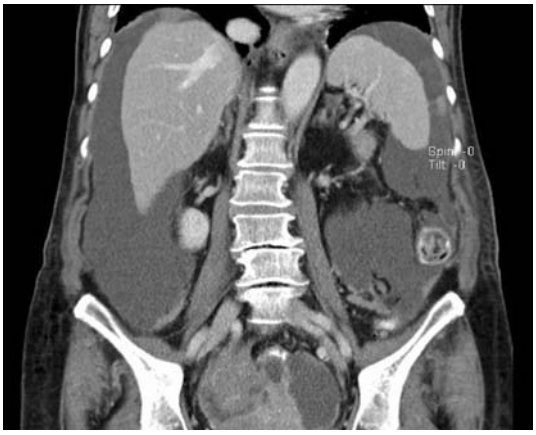

Carcinoma Ovarium. Figure 2 Staging of ovarian cancer by CT. A complex, solid, and cystic ovarian mass is demonstrated on the coronal CT scan. Large amounts of ascites are found throughout the abdomen. Small bilateral diaphragmatic nodules and plaquelike peritoneal thickening in the paracolic gutters show stage IIIb disease.

the case of contraindications for intravenous contrast media, MRI is used for preoperative staging of ovarian cancer. Following the FIGO criteria, CT and MRI perform similarly in staging ovarian cancer, with reported sensitivities of 63–79% and specificity of 100% (5).

Nuclear Medicine

Fluorodeoxyglucose positron emission tomography (FDG PET)-CT is emerging as a new imaging technique for assessing ovarian cancer. Currently it is only recommend complementary to CT for the detection of recurrent ovarian cancer. For preoperative staging of ovarian cancer, recent data suggest that the combination of FDG PET and CT is superior to CT alone.

C

Diagnosis

Ovarian cancers are typically inhomogeneous adnexal masses with a mixed pattern of cystic and solid elements, and are often large at the time of presentation (4). US is the modality of choice for detection and characterization of lesions as yielding a high or low risk for malignancy (2).

MRI is currently used as a problem-solving modality complementary to sonography. Its strength is not to define the exact histology of ovarian cancer, but to predict if a lesion is malignant or not.

The most commonly used imaging criteria suggestive of malignancy in US and MRI are: lesions size larger than 4 cm, thickness of wall or septa exceeding more than 3 mm, papillary projections, necrosis, partially cystic and solid internal architecture, a lobulated solid mass, and presence of tumor vessels (4) (Fig. 3). Doppler assessment in ovarian cancer displays a low resistive index (RI<1) (2).

Contrast-enhanced MRI studies assist in tumor characterization, especially in the depiction of papillary projections and necrosis.

None of these imaging criteria, however, are specific enough as a single factor to diagnose ovarian cancer reliably. The likelihood of malignancy increases with solid nonfibrous elements, thickness of septa, and presence of necrosis. Ancillary findings such as presence of lymphadenopathy, peritoneal lesions, and ascites improve the diagnostic confidence. The combination of tumor size and architecture and ancillary signs improves prediction of malignancy and yields an accuracy of 89–95% in MRI (4).

In a multivariate logistic regression analysis of complex adnexal masses studied by MRI, necrosis within a solid portion of an ovarian mass and vegetations in a cystic lesion were the most predictive signs of malignancy (4). Solid, nonfatty, nonfibrous tissue with or without necrosis has also been reported as a valuable predictor of malignancy. Thick walls and septations are less reliable signs of malignancy, as they may also occur in abscesses, endometriomas, and benign neoplasm such as cystadenofibromas and mucinous cystadenomas.

Large amounts of ascites in a patient with ovarian cancer usually indicate the presence of peritoneal metastases (Fig. 2). Absence of ascites does not exclude ovarian malignancy, as 50% of borderline tumors and 83% of early-stage ovarian cancers are not associated with ascites (2).

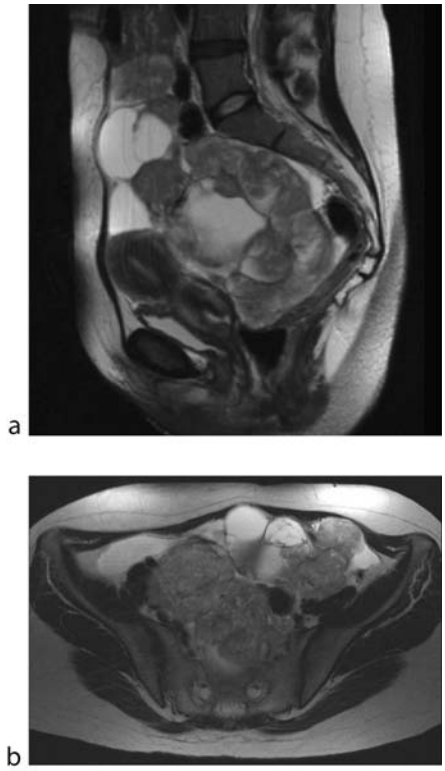

Carcinoma Ovarium. Figure 3 Papillary serous adenocarcinoma in a 46-year-old patient. Sagittal (a) and transaxial (b) T2-weighted MR images demonstrate a complex partly cystic and solid adnexal tumor that is found separate from the uterus and extends to the level of L4. The solid areas are composed of multiple papillary excrescences which also fill the cystic areas. Only small amounts of ascites surround the lesion.

CA-125 is currently the most commonly used tumor marker for ovarian cancer. However, elevation of CA-125 can be observed in other malignant epithelial cancers and in benign conditions, including cirrhosis, pancreatitis, endometriosis, and pelvic inflammatory disease as well as in different stages of the menstrual cycle. More than 80% of women with advanced epithelial ovarian cancer present with CA-125 elevations. However, the sensitivity of CA-125 elevation in early-stage disease is only 25% (2).

Bibliography

1. Hensley ML, Alektiar KM, Chi DS (2001) Ovarian and fallopian-tube cancer. In: Barakat RR, Bevers MW, Gershenson, Hoskins WJ (eds) Handbook of Gynecologic Oncology. Martin Dunitz, London, pp 243–263
2. Togashi K (2003) Ovarian cancer: the role of US, CT and MRI. Euro Radiol 13 (Suppl 4):L87–104
3. Seidman JD, Russell P, Kurman RJ (2002) Surface epithelial tumors of the ovary. In: Kurman RJ (ed) Blaustein's Pathology of the Female Genital Tract. Springer Verlag, New York, pp 791–904
4. Hricak H, Chen M, Coakley FV et al (2000) Complex adnexal masses: detection and characterization with MRI—multivariate analysis. Radiology 214:39–46
5. Tempany CM, Zou KH, Silverman et al (2000) Staging of advanced ovarian cancer: comparison of imaging modalities—report from the Radiology Oncology Group. Radiology 215:761–767

Carcinoma, Pancreatic

Carlo Bartolozzi[1], Laura Crocetti[1], Piero Boraschi[2], Carla Cappelli[1]
[1]Department of Diagnostic and Interventional Radiology, University of Pisa, Italy
[2]2nd Department of Radiology, University Hospital, Pisa, Italy
l.crocetti@med.unipi.it

Synonyms

Adenocarcinoma of the pancreas; exocrine carcinoma of the pancreas; pancreatic ductal adenocarcinoma

Definitions

Pancreatic ductal adenocarcinoma accounts for 90% of all primary malignant tumors arising from the pancreatic gland. It represents the fourth leading cause of cancer death and its incidence tripled over the past 40 years. The peak of incidence occurs in the seventh and eighth decades of life, with an incidence rate slightly higher in men than in women. Despite improvements in diagnostic and surgical techniques and perioperative management, pancreatic carcinoma represents a major health problem and it remains a significant challenge, being the tumor at the time of diagnosis confined to the pancreas in about 10% of patients, locally advanced in 40% of cases, and metastatic in 50% of cases. The poor survival of patients with pancreatic cancer is caused by the late diagnosis and the low resection rate. For all stages combined, the 1-year survival rate is 19% and the 5-year survival rate is 4%. Overall, fewer than 5% of patients undergo resection, but among these, as many as 20% survive 5 years. The median survival is less than 18 months after surgery.

The definitive causative factors that lead to an increased incidence of pancreatic cancer are unknown. Many environmental factors are associated with increased risk of pancreatic cancer, including high-protein and high-fat diets and the exposure to aromatic amines, such as in cigarette smoking or occupations including chemistry or petrochemical work.

The association of pancreatic adenocarcinoma with chronic pancreatitis is still unclear, but individuals with the hereditary type of chronic pancreatitis seem to have a predisposition for pancreatic cancer stronger than that of the general population. Alcohol abuse is seen in 4% of patients and association of alcohol and pancreatic cancer is indirectly related to the development of alcohol-induced pancreatitis. Whether or not diabetes is a risk factor for pancreatic adenocarcinoma remains controversial. Diabetes or impaired glucose tolerance occurs in about 80% of cases at the time of the diagnosis, but recent evidence suggests that diabetes is a consequence of carcinoma rather than a predisposing factor, because of the production of a diabetogenic factor.

There is increasing evidence that some pancreatic cancers are inherited and that genetic predisposition plays a significant role in pancreatic cancer risk. Furthermore some genetic syndromes associated with an increased risk of pancreatic cancer have been identified and these include the familial atypical multiple mole melanoma syndrome (FAMMM), characterized by the germline mutation in the p16 gene; the Peutz-Jeghers syndrome; the hereditary nonpolyposis colorectal cancer (HNPCC) with germline mutations in the DNA mismatch repair genes; the hereditary pancreatitis, caused by mutations in the PRSS1 gene (cationic trypsinogen gene); and the familial breast cancer caused by a mutation of the BRCA2 gene.

Pathology and Histopathology

In the past, numerous classification schemes for pancreatic tumors were proposed. Presently, the most widely adopted is the AFIP classification system, published by the Armed Forces Institute of Pathology in 1995. According to the AFIP system, pancreatic tumors are classified into primary tumors, secondary tumors, and tumor-like lesions. Primary tumors are then classified into exocrine lesions, endocrine lesions, and nonepithelial tumors. All the pancreatic tumors are divided according to their biologic behavior into benign, borderline (with an uncertain malignant potential), and malignant.

The ductal adenocarcinoma and its variants account for the vast majority (about 90%) of malignant pancreatic neoplasms. Microscopically ductal adenocarcinoma is composed of epithelial cells forming glands surrounded by dense fibrous connective tissue. Most adenocarcinomas infiltrate into perineural, lymphatic, and vascular spaces. Some variants of ductal adenocarcinoma include the mucinous noncystic adenocarcinoma or colloid carcinoma, which is characterized by abundant extracellular mucin production; the adenosquamous carcinoma with glandular and squamous components; the signet-ring cell carcinoma composed almost exclusively of cells filled with mucin; and the undifferentiated or anaplastic carcinoma, composed of large cells showing extreme anaplasia.

Between 60% and 70% of ductal adenocarcinomas are located in the head of the pancreas. Carcinomas of the pancreatic head have an intimate relationship with the distal common bile duct and the main pancreatic duct, producing stenosis and eventually obstruction with duct dilatation and fibrous atrophy of the parenchyma (obstructive chronic pancreatitis).

It is now widely accepted that ductal pancreatic adenocarcinomas arise from lesions which represent precursors of the carcinomas, called PanINs (►pancreatic intraductal neoplasms); the development of carcinoma from PanINs lesions involves accumulation of multistep genetic alterations. PanINs lesions are composed of mucin-producing epithelial cells with varying degrees of cytological and architectural atypia that involve the small pancreatic ducts. PanINs can be flat 1A, papillary without atypia 1B, papillary with atypia 2, or may be a carcinoma *in situ* 3. PanINs display some of the genetic changes which are founded in infiltrating carcinomas (mutations in K-ras gene, p16, p53, BRCA2 and DPC4), suggesting that there is a progression from PanIN 1 to PanIN 2 and PanIN 3 to infiltrating adenocarcinoma.

A number of schemes have been proposed in the past for the staging of pancreatic carcinoma. By 1977, they were replaced by the UICC (Union Internationale Contre le Cancer) staging system, which is a TNM staging system. The newest revised version was published in 2002 by the American Joint Committee for Cancer. A more complex stage classification system had been proposed by the Japan Pancreas Society (JPS) in 1987; this classification system primarily relies on the prognostic value of tumor size and local spread, adding other factors to the classification such as serosal invasion, retroperitoneal invasion, and invasion of the portal vein. An important prognostic factor is also the possible presence of residual neoplastic tissue at the level of margins of surgical resection; the extent of resection is graded into R0 (complete resection), R1 (grossly negative but positive microscopic margins of resection), and R2 (grossly and microscopically positive margins of resection).

Clinical Presentation

Clinical symptoms and signs develop late, particularly in tumors of the pancreatic body and tail, thus the vast majority of pancreatic cancers are diagnosed at an advanced, incurable stage. The most common, even nonspecific, symptom associated with carcinoma is abdominal pain, especially in patients with a locally advanced lesion, because it indicates spread of tumor to perineural lymphatics. The typical epigastric pain is frequently accompanied by back pain. Obstructive

jaundice represents the most common finding in patients with a neoplasm arising in the head of the pancreas and obstructing the common bile duct. Dark urine, light stools, pruritis, and palpable gallbladder (Courvoisier's sign) may be present together with jaundice; laboratory tests reveal elevated conjugated bilirubin concentrations and alkaline phosphatase and γ-glutamyl transpeptidase levels. Obstruction of the pancreatic duct or its side branches results in symptoms related to an obstructive pancreatitis. It is important to suspect a pancreatic carcinoma when there are not obvious causes for the acute pancreatitis (such as gallstones, alcohol abuse etc.). Other signs include new onset of diabetes or instability of diabetes that was previously well-controlled and thrombophlebitis (Trousseau syndrome). Weight loss, weakness, and anorexia may be present. Nausea and vomiting can be related to a gastroduodenal obstruction.

The carbohydrate antigen 19.9 (Ca 19.9) blood levels can be increased in patients with pancreatic adenocarcinoma; however 10–15% of individuals do not secrete the Ca19.9. In addition, Ca19.9 levels can be elevated in benign biliary or pancreatic diseases.

Imaging

Ultrasound (US) examination often represents the first level imaging modality performed in patients with pancreatic lesions, the symptoms usually being the symptoms usually nonspecific. Direct visualization of the tumor by US is often difficult and depends on the size and location of the tumor. The lesion may have a variable appearance on US, however the large majority of pancreatic cancers present as hypoechoic, nonhomogeneous lesions with irregular margins. US examination is less sensitive than other modalities in the detection of pancreatic malignancy, particularly when the lesions are smaller than 2 cm. In some cases, the intravenous administration of a contrast medium during the examination can improve the depiction of the pancreatic tumor, showing the lesion a much lower contrast enhancement than the normal pancreatic parenchyma. Indirect signs include dilatation of biliary and pancreatic ducts associated to dilatation of the gallbladder. US can also demonstrate the presence of locoregional lymph nodes enlargement, distant metastases (in particular liver metastases) or peritoneal carcinosis. Despite the advances in US technology, including the employment of US contrast media, the local staging of pancreatic cancer results difficult in the majority of cases. In particular, the relation of the tumor to peripancreatic vessels is demonstrated less reliably with US than with other modalities.

Endoscopic ultrasound (EUS) has been used for early detection of small carcinomas as well as local staging. The close proximity of the transducer to the region of interest permits the use of high ultrasound frequencies, then improving the image resolution. EUS can determine the size and local extent of a pancreatic cancer, also assessing the peripancreatic vascular and lymph node involvement. EUS can also enable the fine needle aspiration.

Intraoperative ultrasound (IOUS) allows to easily identify pancreatic lesions and to precisely define the staging of the tumor, demonstrating the relationships between the tumor itself and adjacent structures (in particular vascular structures) and also highlighting with high sensitivity small hepatic metastases.

Presently, computed tomography (CT) is the most widely used and most sensitive technique for the evaluation of the pancreas. High-resolution spiral CT has represented the preferred noninvasive imaging modality for the diagnosis and staging of pancreatic cancers. However state-of-the-art CT scanning is actually based on multidetector CT, which has allowed a further improvement in resolution and in scan timing, thus obtaining acquisitions in multiple selective phases of contrast distribution. Multidetector CT should be the first-line study for the detection of pancreatic tumor and for evaluating its resectability. Before the CT examination, the distension of stomach and duodenum must be obtained. Water represents the oral contrast agent of choice, associated with the intravenous administration of a hypotonizing drug, just before the scan. Acquisition is performed before and after the intravenous administration of the iodinated contrast medium. After the contrast administration, acquisition with thin slices (1–2 mm) must be performed in the pancreatic phase (delay 35–40 sec) and in the venous phase (delay 70–80 sec). Typically, pancreatic adenocarcinoma is more hypodense than pancreatic parenchyma, especially during the pancreatic phase when the parenchyma shows the highest contrast enhancement. The margins of the lesion usually are poorly defined; central necrosis can be present. Features suggestive of pancreatic cancer include also alterations in morphology of the gland, such as focal enlargement or, more rarely, diffuse enlargement and obliteration of peripancreatic fat (which is suggestive of invasion beyond the margins of the gland). Pancreatic ductal dilatation is often present, associated with a dilatation of the biliary ducts and of the gallbladder when the tumor is localized in the pancreatic head. Chronic obstruction of the pancreatic duct leads to atrophy of the parenchyma distal to the obstruction (Fig. 1) (1–4).

In order to define the staging and resectability of the tumor, the possible infiltration of the adjacent structures (including retroperitoneal fat infiltration), and the presence of lymph node metastases, distant metastases, or peritoneal carcinosis must be identified. Spread to surrounding organs may typically involve the

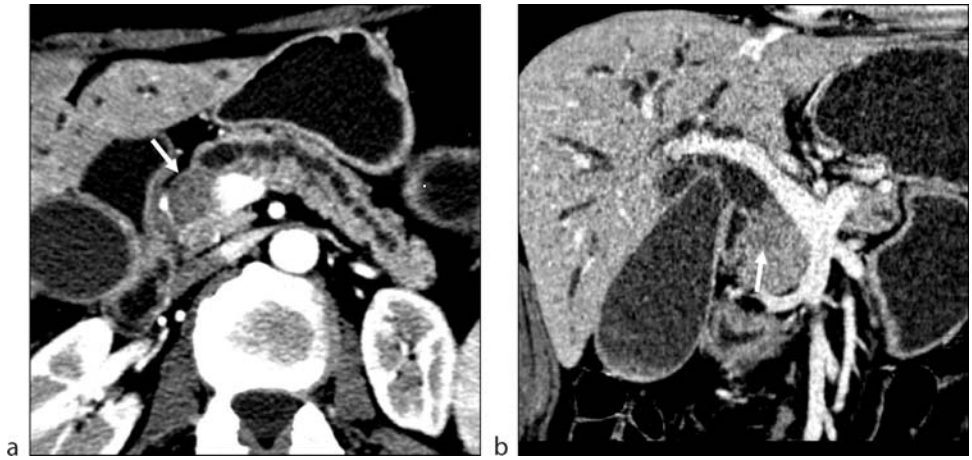

Carcinoma, Pancreatic. Figure 1 Multidetector CT study in a case of ductal adenocarcinoma of the pancreatic head. The lesion causes obstruction of the pancreatic duct which appears dilated; atrophy of the parenchyma distal to the obstruction is associated (a). The multiplanar reconstruction on the coronal plane shows dilatation of the biliary system and the gallbladder in the same case (b).

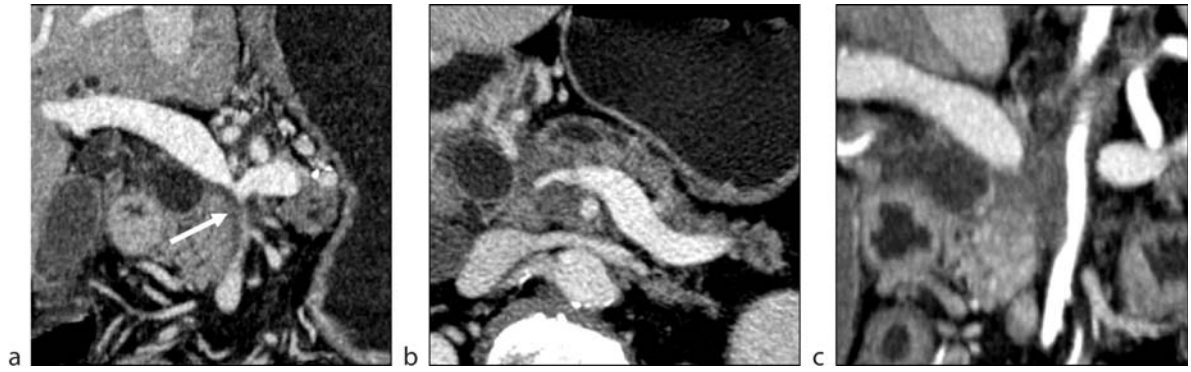

Carcinoma, Pancreatic. Figure 2 Multidetector CT study in a case of ductal adenocarcinoma of the pancreatic head and uncinate process. Stenosis of the portomesenteric junction and the superior mesenteric vein, which suggests infiltration, can be observed (*arrow*, a). The neoplastic tissue obliterates also the retroperitoneal tissue corresponding to the retroportal pancreatic margin reaching the right wall of the superior mesenteric artery (b, c).

duodenum, spleen, stomach, and colon. Pancreatic cancers can involve local vessels, such as the celiac axis, superior mesenteric artery, and venous vessels, including the portal vein, the splenic vein, and the superior mesenteric vein (Fig. 2). When the lesion shows no contact with the vessel, the fatty plane around the vessel result intact, while the presence of neoplastic tissue reaching the vascular wall or variably surrounding the vessel can suggest a vascular involvement. However, the presence of soft tissue surrounding a vessel may also be due to a desmoplastic inflammatory reaction. Vascular encasement is suggested when the vessel occlusion or stenosis is present, sometimes associated to collateral circulation. Initial reports suggested that any degree of tumor to vessel contiguity indicated tumor unresectability. Since the introduction of helical CT, several classifications have been proposed to grade the degree of vascular infiltration, to relate the vascular involvement with the resectability of the tumor, and to establish when the encasement of the vessel represents a certain sign of vascular infiltration. For instance, Lu et al in 1997 proposed a classification including four different grades on the basis of the vascular surrounding, and identified a cut-off of resectability, demonstrating that the mere contiguity between tumor and vascular structure does not automatically mean vascular invasion, while when the tumor surrounds the vessels for more than 50% of its circumference, there is a high likelihood of vascular infiltration. Multidetector CT has further improved the staging of vascular invasion, because of the increased spatial

resolution and the possibility to associate multiplanar and maximum intensity projection reformations and volume rendering images.

Another fundamental aspect in order to stage pancreatic tumors is to value the infiltration of the fat peripancreatic retroperitoneal tissue. In particular, for tumors of the head/uncinate process, it is fundamental to evaluate the fat retroperitoneal tissue infiltration in correspondence of the retroperitoneal resection margin (retroportal margin), which corresponds to the fatty layer localized behind the portal and superior mesenteric vein and comprised between the right margin of the proximal 3–4 cm of the superior mesenteric artery and the left margin of the head/uncinate process of the pancreas, near the origin of the postero-inferior pancreatic arch. Multidetector CT is an accurate technique in order to evaluate retroportal margin involvement, and the suspicion of infiltration arises at CT when the fatty retroperitoneal tissue appears obliterated, irregular, or with abnormal density. Neoplastic infiltration is in fact a critical factor in tumor staging and in surgical planning because it frequently represents a site of persistence and recurrence of disease and it is related to half postsurgical survival (1–4).

Regional lymph node metastases can be suspected at CT only when there is a lymph node enlargement; for this reason nodal staging with CT is reported to be often incorrect. Distant metastases usually involve the liver, while lungs and other organs are less commonly involved. The peritoneal nodules are rarely demonstrated by means of CT, while omental thickening or ascites are often the only finding suggesting the peritoneal carcinosis (1–4).

Recent advances in magnetic resonance (MR) imaging (including high resolution and fast imaging, tissue-specific contrast media, MR colangiopancreatography (MRCP), and functional imaging) improved its ability in diagnosing and staging pancreatic cancer. MR offers the advantage of the simultaneous evaluation of pancreatic parenchyma, vessels, and ductal system during the same examination (5,6).

The normal pancreas shows low signal intensity on T1-weighted images and intermediate signal on T2-weighted images, with a variable amount of fat in the gland parenchyma. Owing to the desmoplastic nature of ductal adenocarcinoma, at MR the tumor is visible as an area of lower signal intensity on T1-weighted images. On T2-weighted images it has variable signal intensity, depending on the degree of desmoplastic reaction, hemorrhage, necrosis, and associated inflammatory changes. Pancreatic cancer can cause pancreatitis distal to the lesion, because of ductal obstruction; this causes a low signal intensity of the pancreatic tissue on T1-weighted images, which results in poor contrast between the tumor and the parenchyma surrounding the lesion (Fig. 3). Following intravenous administration of gadolinium, the tumor may become more conspicuous, since the parenchyma enhances in the early phase but the tumor exhibits poor enhancement. On delayed images pancreatic adenocarcinomas show variable appearance depending on the size of the interstitial space and venous drainage. The administration of the Mn-DPDP can further improve the lesion conspicuity, particularly in case of small tumor, increasing the contrast between the high enhancing pancreatic parenchyma and the lesion; furthermore assessment of the liver is an important factor in the staging of pancreatic cancer patients, since pancreatic tumors tend to metastasize early into the liver. MR examination with Mn-DPDP has been found to be superior to CT in the detection of liver metastases (5,6).

MR colangiopancreatography (MRCP) sequences can be performed, to visualize the pancreatic and biliary ductal systems. When both the common bile duct and the pancreatic duct are involved, two adjacent ring-like ducts (known as the "double duct" sign) are visible within the pancreatic head. Furthermore, dilatation of the

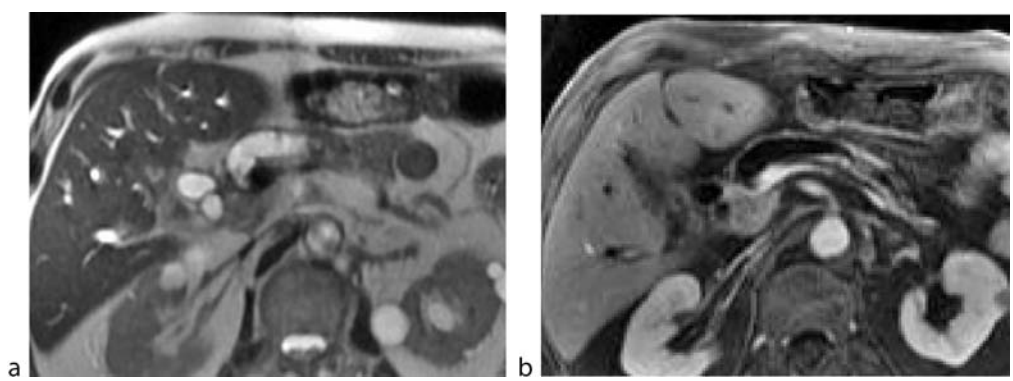

Carcinoma, Pancreatic. Figure 3 MR in a case of ductal adenocarcinoma of the pancreatic head. Axial single-shot fast spin-echo T2w (a) and gadolinium-enhanced fat-suppressed SPGR T1w (b) images demonstrate a hypointense lesion in the pancreatic head causing an abrupt cut-off of the pancreato-biliary system, which is markedly dilated.

intrahepatic bile ducts and of the gallbladder can be seen. The intravenous administration of secretin allows the improvement of the pancreatic ducts delineation; the presence of a ductal obstruction persistent after the secretin administration, sometimes with associated dilatation of the duct proximal to the obstruction, is suggestive for a neoplastic stenosis. MR angiographic sequences can be performed to demonstrate the vascular patency and to assess the vascular involvement (5,6).

Lymph node metastases can be suspected when there is a lymph node enlargement; nodal disease is shown using fat-suppressed T2-weighted images and Gd-enhanced images.

Although the sensitivity of endoscopic retrograde cholangiopancreatography (ERCP) for the diagnosis of pancreatic cancer is quite high, it is now rarely necessary and should not be routinely used. Because of its invasiveness and the high risk of complications, it has been replaced by MRCP, which provide a good alternative. ERCP plays, however, a very important role when used in combination with interventional radiological procedures such as biliary drainage and stent placement. ERCP findings include narrowing of the duct by tumor encasement, duct erosion with contrast extravasation, or complete obstruction associated to dilatation of ducts proximal to the point of obstruction. The pancreatic ducts between the obstruction and the papilla of Vater are usually normal; this finding may help to distinguish pancreatic carcinoma from pancreatitis. Involvement of both the pancreatic and common bile duct, termed double-duct sign, was originally described as being specific for carcinoma, while it also may be seen in pancreatitis.

The use of pancreatic biopsy (percutaneous or endoscopic) in the diagnostic work-up of a patient with a suspected pancreatic cancer is controversial. Complications such as hemorrhage, pancreatitis, fistula, and abscess have been reported and there are reports of tumor seeding along the tract of the needle. Additionally, malignancy cannot be excluded with certainty when malignant cells are not found in the specimen. For these reasons biopsy has no role in patients with a resectable pancreatic mass. Pancreatic biopsy is mandatory in patients excluded for a surgical resection and candidates for palliative treatment. Further biopsy may be performed in the suspicion of more uncommon lesions, such as ▶pancreatic lymphoma, which can be susceptible of chemotherapy treatment.

Nuclear Medicine

Positron emission tomography (PET) with the administration of 18F-FDG has been successfully used in the management of patients with pancreatic cancer for initial diagnosis, pretreatment staging, detection of distant metastases, evaluation of treatment response, and detection of recurrence (1, 7).

Diagnosis

Surgical resection remains the treatment of choice for pancreatic adenocarcinoma. To date, a curative treatment of pancreatic cancer can be achieved only with complete surgical resection. Vascular invasion, infiltration of the adjacent structures, and the presence of lymph node metastases, distant metastases, or peritoneal carcinosis are generally accepted reasons for unresectability. On the other hand, the diagnosis of vascular invasion by pancreatic cancer is one of the most critical issues in imaging; in fact, while in some institutions surgery is precluded in cases of vascular invasion, other surgeons perform aggressive surgery with vascular resection. For these reasons the role of diagnostic imaging is not only to demonstrate the tumor but also to accurately assess the resectability of the lesion, for identifying patients who might benefit from surgery and to avoid unnecessary interventions.

There is much debate concerning the sensitivity and specificity of imaging investigations in the diagnosis and staging of pancreatic carcinoma. Contrast-enhanced multidetector CT is generally accepted to be the first line of investigation in a patient with suspected pancreatic cancer. The reasons for this preference include its wide availability, speed, and the possibility to perform thin sections with high spatial resolution. Several studies have compared CT with MR regarding tumor detection and staging, obtaining similar results with both modalities. The current role of MR is probably more important for the detection and characterization of the lesion, particularly when the lesion is not easily demonstrable with CT. MR is also helpful in evaluating and characterizing liver lesions in patients with pancreatic cancer. In the detection and staging of small tumors, EUS and IOUS can be reliable. In conclusion, multidetector CT or MR should be used first in the detection and staging of pancreatic adenocarcinoma. When CT or MR findings are doubtful, EUS or IOUS should be applied for detection and for the assessment of resectability. PET imaging is usually reserved to confirm the malignancy, to differentiate between a carcinoma and a focal nodular pancreatitis and to recognize distant metastases.

References

1. Saisho H, Yamaguchi T (2004) Diagnostic imaging of pancreatic cancer. Computed tomography, magnetic resonance imaging, and positron emission tomography. Pancreas 28(3):273–278

2. Lepanto L, Arzoumanian Y, Gianfelice D et al (2002) Helical CT with CT angiography in assessing periampullary neoplasms: identification of vascular invasion. Radiology 222:347–352
3. Lu DS, Reber HA, Krasny RM et al (1997) Local staging of pancreatic cancer: criteria for unresectability of major vessels as revealed by pancreatic-phase, thin-section helical CT. AJR Am J Roentgenol 168(6):1439–1443
4. Mc Nulty NJ, Francis IR, Platt JF et al (2001) Multi-detector row helical CT of the pancreas: effect of contrast-enhanced multiphasic imaging on enhancement of the pancreas, peripancreatic vasculature, and pancreatic adenocarcinoma. Radiology 220:97–102
5. Schima W, Fugger R (2002) Evaluation of focal pancreatic masses: comparison of mangafodipir-enhanced MR imaging and contrast-enhanced helical CT. Eur Radiol 12(12):2998–3008
6. Semelka RC, Marcos HB (1998) Nonendocrine Tumors of the pancreas. In: Heuck A, Reiser M (eds) Abdominal and Pelvis MRI. Springer, Berlin-Heidelberg, pp 51–58
7. Diederichs CG, Staib L, Vogel J et al (2000) Values and limitations of 18F-fluorodeoxyglucose-positron-emission tomography with preoperative evaluation of patients with pancreatic masses. Pancreas 20:109–116

Carcinoma, Rectal

S. M. E. Engelen[1,2], G. L. Beets[2]
M. J. Lahaye[1,2], R. G. H. Beets-Tan[1]
[1]Department of Surgery, University Hospital Maastricht, Maastricht, Netherlands
[2]Department of Surgery, University Hospital Maastricht, Maastricht, Netherlands
Rbe@rdia.azm.nl

Definition

In Western countries, colorectal cancer is the second most common malignancy. There are 940,000 new cases yearly worldwide, of which about one-fourth are adenocarcinomas of the rectum (1). The rectum is arbitrarily defined as the distal 12–15 cm of the large bowel. The incidence of rectal carcinoma is increasing.

Pathology/Histopathology

The vast majority of rectal carcinomas are adenocarcinomas originating from adenomatous polyps or glands. The remainder are rare entities i.e. neuroendocrine tumours. Tumours start as intramucosal lesions, gradually growing outward through the rectal wall, invading the muscularis propria, blood and lymphatic vessels, surrounding mesorectal fat, mesorectal lymph nodes and eventually the surrounding structures.

Rectal cancer metastasizes *via* lymphatic and hematogenous routes. Lymphatic spread is mainly to mesorectal nodes, and from there on to the para-aortic nodes in advanced cases. In distal tumours, internal iliac nodes can be involved. Hematogenous spread is through the superior rectal vein, draining into the inferior mesenteric and portal vein. Distant metastases in rectal cancer are therefore most often located in the liver. For distal tumours, venous drainage is *via* the middle and inferior rectal vein into the internal iliac vein into inferior vena cava. Pulmonary metastases are therefore more common in rectal cancer than in colon cancer. Other sites of metastases in rectal cancer are retroperitoneum, ovaria, peritoneal cavity, adrenals, bone and brain.

There are several risk factors for developing rectal carcinoma: age (>50 years), high-fat and low-fibre diet, personal or family history (first degree relative) of colorectal cancer, inflammatory bowel diseases (M. Crohn, Ulcerative Colitis), familial adenomatous polyposis (FAP) and hereditary non-polyposis colorectal cancer (HNPCC). Alcohol consumption, smoking, little physical activity and diabetes mellitus are less well-defined risk factors. Risk factors for rectal carcinoma are mostly associated with Western lifestyle, explaining large variation in incidence of rectal cancer worldwide.

Clinical Presentation

Rectal bleeding and changed bowel habits can be early symptoms of rectal carcinoma. Rectal bleeding of cancer often resembles haemorrhoidal blood loss. Other symptoms include mucus discharge, narrowing calibre of stool, increased frequency of defecation, feeling of rectal fullness and tenesmus. Anal canal involvement of tumour mass may lead to anal pain. Bulky tumours can invade sacrum and sacral plexus, causing pelvic pain and sciatic nerve symptoms.

Signs and symptoms of metastatic disease are weight loss, fatigue, abdominal distention, pain in the right upper quadrant, jaundice and ascites.

Imaging

Imaging in rectal cancer is used for local and distant staging. T stage has long been used as a measure for local extent, and has therefore been subjected to many studies. At present, the importance of prediction of the ►circumferential resection margin (CRM) along the ►mesorectal fascia is accepted as an important feature for the surgeon, as incomplete removal of the lateral spread of the tumour is a main cause of local recurrence (Fig. 1). Another risk factor for local recurrence and therefore of interest in local staging is nodal status. Distant staging concerns liver, lung and further extra hepatic sites.

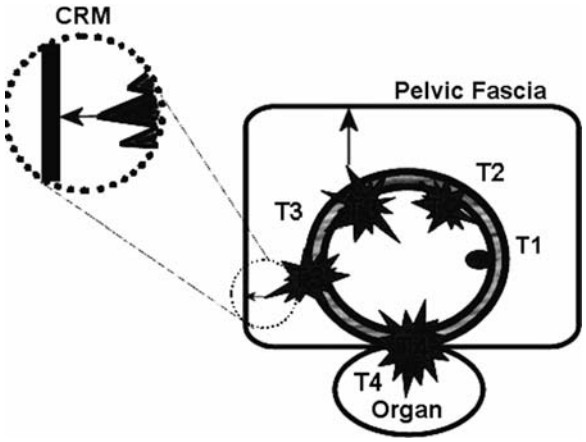

Carcinoma, Rectal. Figure 1 Transverse section through the rectum. Illustration of the circumferential resection margin (CRM) and different T stages. The CRM is defined as the closest distance from tumour to mesorectal fascia (pelvic fascia). This fascia is used as the plane of dissection in rectal cancer surgery. Preoperative identification of a close or involved CRM allows the clinician to use preoperative radiochemotherapy and/or more extensive surgery. The prognostic inhomogeneity of T3 rectal tumours is shown in this figure as well, as T3 tumours can have a wide (upper-left tumour) or close (left-sided tumour) CRM. (Reprint with permission from Lahaye MJ, Engelen SME, Nelemans PJ et al (2005) Imaging for predicting the risk factors—the circumferential resection margin and nodal disease—of local recurrence in rectal cancer: A meta-analysis. Semin Ultrasound CT MRI 26: 259–68.)

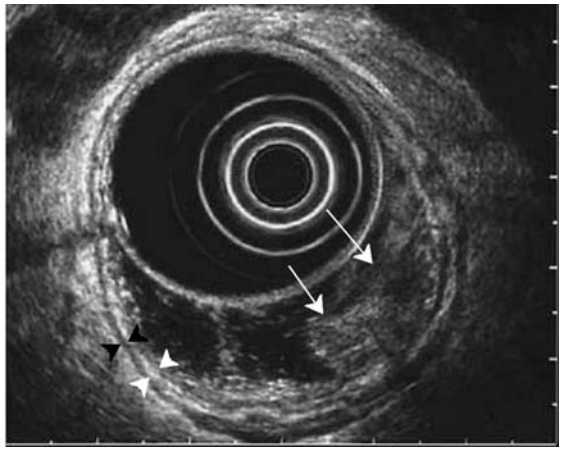

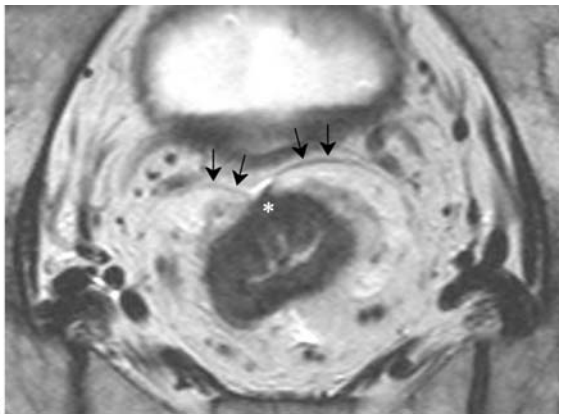

Carcinoma, Rectal. Figure 2 (a) Endorectal sonography of T1 rectal carcinoma confined to mucosa and superficial submucosa. Anteriorly, seminal vesicles are seen (white arrows). (Reprint with permission from Schwartz, DA, Harewood, GC, Wiersema, MJ (2002). EUS for rectal disease. Gastrointest. Endosc. July; 56(1):100–109.) (b) Transverse T2W TSE (TR/TE 3427/150 ms) MR image of a pelvis of a 73-year-old male. T3 rectal carcinoma. Anteriorly, the mesorectal fascia (black arrows), is retracted by the tumour (white asterisk).

Local Extension

Endorectal ultrasound is an accurate modality to depict the bowel wall and therefore to assess superficial tumours, especially T1 and T2 stages (Fig. 2a). Due to its limited field of view, EUS is less useful for non-superficial tumours (T3 and T4) and more proximal or stenosing tumours. Moreover, endorectal ultrasound is an observer-dependent imaging modality with important patient discomfort. This real-time exam is not suitable to be used as road map for the surgeon during operation.

MRI with a dedicated external coil (phased-array coil) has the major advantage of a large field of view, combined with a high spatial and contrast resolution, providing detailed anatomical information on structures in the pelvis. In single-centre studies MRI is a very good tool in preoperative prediction of CRM (2, 3) (Fig. 2b). Multi-centre studies on the routine use of MRI are ongoing. For predicting T-stage, MRI is less accurate in staging superficial tumours, unless an endorectal coil is used, which is however not widely available.

CT can give an impression of the size of the tumour and the proximity of the surrounding structures, and has long been used for staging of fixed tumours. Comparative studies however have shown superiority of MRI in prediction of organ invasion, because of better contrast resolution compared to CT.

Nodal Status

At present, no imaging modality has a sufficient accuracy for reliable prediction of nodal status. This is because current modalities only use morphologic criteria. Furthermore, these morphologic criteria can only be applied in large nodes. It is known however, that small

nodes with metastases are not uncommon in rectal cancer. A recent meta-analysis showed that endorectal ultrasound is slightly but not significantly better than CT and MRI in prediction of nodal status (4).

A new iron specific MR contrast agent (ultra small paramagnetic iron oxide—USPIO) has been developed recently. This contrast agent is taken up by the reticulo-endothelial system of healthy nodal tissue, causing a decrease in signal intensity on T2-weighted MR images. Malignant nodes do not take up the contrast because of lack of normal node anatomy, and therefore appear white (high-intensity) on T2-weighted images. This new contrast agent has been proven to be accurate in prediction of nodal status in prostate, bladder, head and neck malignancies (5). Use of this agent in rectal cancer is under investigation. Results of studies are awaited.

Metastatic Disease

Organs of primary interest in assessing for presence of metastases are liver and lungs. Wide availability as well as low cost make chest X-ray and liver sonography the imaging modalities of first choice. However, CT is more sensitive. Although there are little data on the cost-effectiveness, it is recommended to use CT scanning of liver and lungs at least in high risk patients. The rationale for choosing a more accurate but expensive tool relates to new developments in the treatment of metastatic disease. With combinations of more effective systemic therapy and metastasectomies or local destruction of metastases the prognosis is no longer as grim as it used to be, and some patients even can be cured.

Nuclear Medicine

^{18}FDG PET is a functional imaging method, based on imaging of increased glucose metabolism in neoplastic cells, by detecting fluorine-18 deoxyglucose uptake. So far, there is no consensus about use of ^{18}FDG PET in primary rectal carcinoma.

The main drawback of PET is its low resolution. Therefore, PET can only be used in combination with anatomical imaging such as CT for reliable information on exact tumour localization. A systematic review on hepatic metastases in colorectal cancer has shown that PET is of additional value to CT for the detection of extrahepatic disease which could alter patient management (6). However, randomized controlled clinical trials are lacking on this subject. Drawbacks are inability of PET to localize metastases that are small (<1–2 cm). Also, inflammatory processes have increased glucose metabolism as well, which may cause false-positive findings on PET.

In recurrent rectal cancer, use of ^{18}FDG PET could be valuable to differentiate between recurrent tumour and postoperative fibrosis.

Diagnosis

History taking should include, additional to the specific symptoms mentioned earlier, the family and personal history regarding colorectal polyps and malignancies as well as other malignancies. Only rarely a rectal cancer is diagnosed only by history taking. Digital rectal examination however can be highly specific for mid and distal rectal cancer. Physical examination should also include vaginal examination and palpation of inguinal nodes.

The definitive diagnosis of rectal carcinoma is based on histologic examination of tissue obtained through an endoscopic biopsy. As 3–5% of patients have a synchronous more proximal tumour all patients should have an examination of the complete colon whenever possible.

Treatment Implications

The principal treatment of rectal cancer is surgery. Depending on extension of tumour, surgery consists of local excision (T1 tumours in selected patients), ▶total mesorectal excision (TME) or more extensive surgery (locally advanced tumours). TME is a procedure in which the rectum is removed together with its surrounding mesorectal fat and the enveloping mesorectal fascia. In this way, tumour spread as well as invaded lymph nodes in the mesorectal fat are removed. This surgical technique is at present recognized as standard of care.

Radiotherapy as well as chemotherapy are important as (neo) adjuvant treatment. Preoperative radiotherapy reduces the local recurrence rate significantly. For more extended tumours (Fig. 3), a long course of chemo radiation therapy can provide significant downsizing of the tumour. Adjuvant chemotherapy reduces the likelihood of later metastatic disease, although the evidence is not as strong as in colon cancer. Metastatic disease is treated with chemotherapy with the goal of prolonged palliation. A small number of patients with metastatic disease can be cured with surgical excision of metastases with or without the use of concomitant chemotherapy.

Multi-disciplinary involvement in the decision making is very important for the treatment of rectal cancer. Good quality preoperative imaging plays a key role in this process, leading to an optimal individual treatment.

Bibliography

1. Stewart BW, Kleihues P (eds) (2003) World Cancer Report 2003. Lyon: IARC Press

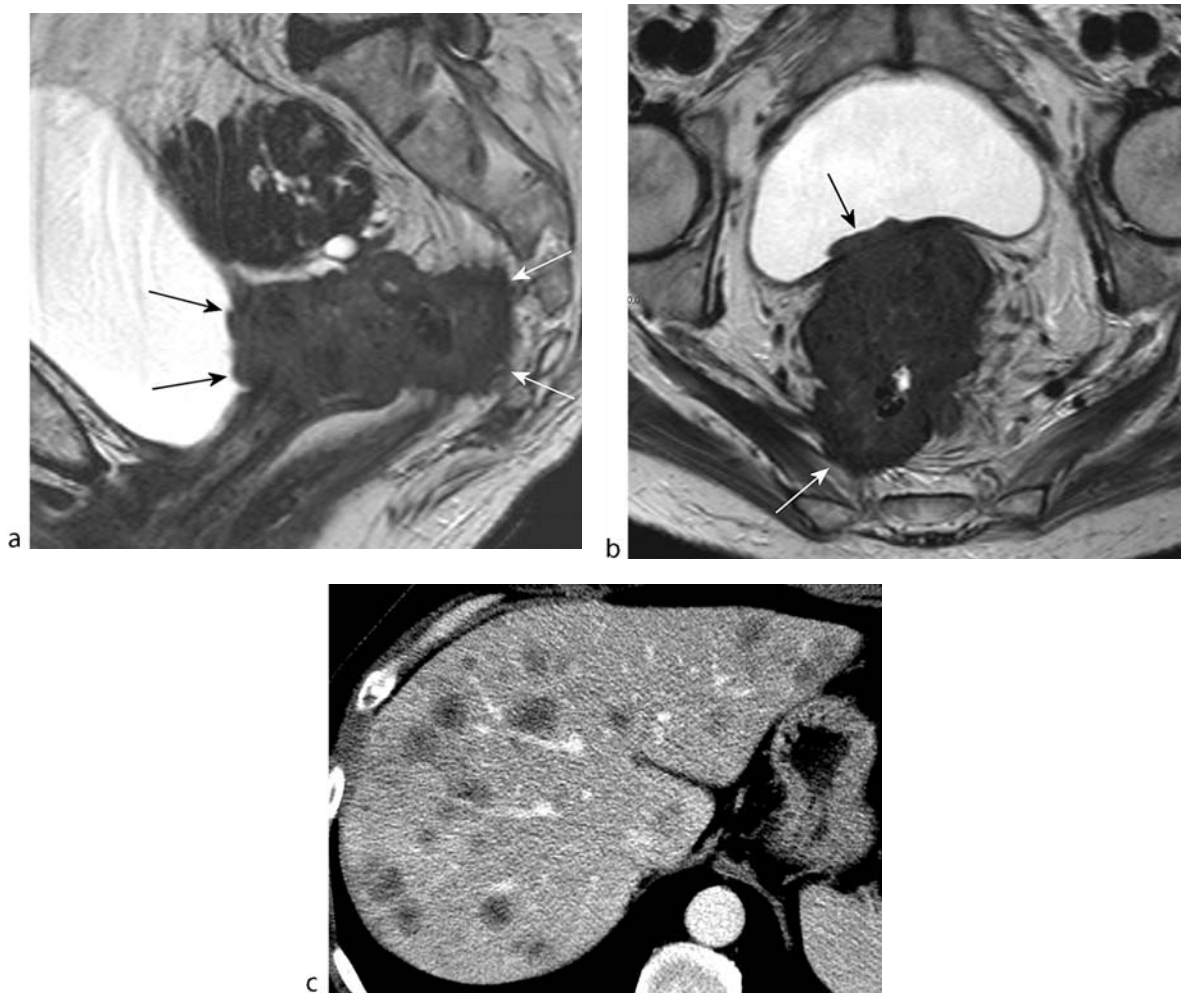

Carcinoma, Rectal. Figure 3 Locally advanced distal rectal cancer. (a) Sagittal T2W TSE (TR/TE 3427/150 ms) MR image of the pelvis of a 77-year-old female. Locally advanced rectal carcinoma, invading the bladder anteriorly (black arrows) and the presacral space posteriorly (white arrows). (b) Transverse T2W TSE (TR/TE 3427/150 ms) MR image of the same patient. Anteriorly, invasion of the bladder is again visible (black arrow). Right posterolateral, invasion of the piriform muscle is indicated by the white arrow. (c) Contrast-enhanced CT scan of a liver (PVP). Multiple liver metastases of a rectal carcinoma in a 59-year-old male.

2. Beets-Tan RG, Beets GL, Vliegen RF et al (2001) Accuracy of magnetic resonance imaging in prediction of tumor-free resection margin in rectal cancer surgery. Lancet 357: 497–504
3. Brown G, Richards CJ, Newcombe RG et al (1999) Rectal carcinoma: thin-section MR imaging for staging in 28 patients. Radiology 211:215–222
4. Lahaye MJ, Engelen SME, Nelemans PJ et al (2005) Imaging for predicting the risk factors—the circumferential resection margin and nodal disease—of local recurrence in rectal cancer: A meta-analysis. Semin Ultrasound CT MRI 26:259–268
5. Harisinghani MG, Barentsz J, Hahn PF et al (2003) Noninvasive detection of clinically occult lymph-node metastases in prostate cancer. N Engl J Med. June 19; 348 (25):2491–2499
6. Wiering B, Krabbe PFM, Jager GJ et al (2005) The impact of fluor-18-deoxyglucose-Positron Emission Tomography in the management of colorectal liver metastases. A systematic review and metaanalysis. Cancer 104:2658–2670

Carcinoma, Renal Cell

Laurence Rocher, Malik Chouli, Yves Menu
Hôpital de Bicêtre, Paris, France
laurence.rocher@bct.ap-hop-paris.fr

Synonyms

Conventional renal carcinoma; Grawitz tumor; Hypernephroma; Kidney cancer

Definitions

Renal cell carcinoma is the most common solid renal neoplasm accounting for 80 to 85% of all malignant renal tumors and for 2% of all cancers. Renal cell cancer (RCC) represents the fifth most common cancer in men (male-to-female ratio is 2:1), with a rising incidence. A solid mass detected in the kidneys can be considered as a renal cell carcinoma until any other possibility is proved. It originates from renal tubular epithelium, usually in the cortex.

Lymphomas, metastases, various sarcomas are other solid rare noncarcinoma malignant tumors of the kidney.

A special group of patients includes those with some hereditary conditions. The most common are Von Hippel–Lindau disease and tuberous sclerosis. Other conditions are the followings: hereditary papillary renal cancer, Birt–Hogg–Dubé syndrome, hereditary leiomyoma renal cell carcinoma, familial renal oncocytoma, hereditary nonpolyposis colon cancer, and medullary carcinoma of the kidney. In these patients, tumor incidence is much higher, multiple synchronous or metachronous tumors are frequent, and age of onset is much lower.

Pathology/Histopathology

Renal cell carcinoma is typically round-shaped, varying from several millimeters to tumors that almost fill the abdomen. A pseudocapsule, related to compressed parenchyma and fibrous tissue is commonly found. Areas of yellowish or brownish components are intermingled with sclerosis, hemorrhage, and necrosis. The tumor can extend into the renal vein and to the inferior vena cava as a tumor cast.

A new histologic classification proposed by the Union Internationale Contre le Cancer (UICC) and the American Joint Committee on Cancer (AJCC) in 1997 is widely accepted. Renal cell carcinoma can be divided into several histologic subtypes like, including clear cell (70–80%), papillary (10–15%), chromophobe cell (5%), collecting duct carcinoma (Bellini duct carcinoma) (1%), medullar carcinoma (1%). Sarcomatoid variant is not considered a type of its own, 4 to 5% are unclassified. Each subtype is associated with a different prognosis indeed: tubulopapillar and chromophobe renal cell carcinomas carry a better prognosis than clear cell renal carcinoma. Since 1998, new entities have surfaced in renal tumor classification included in WHO 2004 classification multilocular renal carcinoma, Xp11 translocation, and low-grade mucinous tubular carcinoma.

Sarcomas included leiomyosarcoma, hemangiopericytoma, liposarcoma, rhabdosarcoma, and malignant fibrous histiocytoma. Sarcomas are usually very large but radiological findings are not specific.

Nuclear grade is the most important microscopic feature that independently correlates with survival for all stages. The most widely used is the Fuhrman classification.

Clinical Presentation

The triad of pain, hematuria, and flank mass is highly indicative for a renal tumor, and generally indicates advanced disease. Other symptoms are related to metastatic disease: pathologic fracture, bone pain, neurologic disorders.

Fever, general status alteration, sudden development of a varicocele, polyglobuly, hypertension, hypercalcemia are other circumstances of diagnosis. Some of them represent paraneoplastic syndromes. Fortuitous detection with US or CT occurs for 40% of renal mass detected. For this reason, the incidence of renal cell carcinoma has apparently increased over the last 20 years, especially concerning small tumors.

Imaging

The aim of any preoperative imaging is to differentiate benign from malignant lesions, to adequately assess tumor size, localization, and organ confinement, to identify visceral metastases and lymph metastatic node, and to reliably predict the presence and extent of any tumor cast into the renal vein and the inferior vena cava.

Imaging Techniques

Intravenous pyelography with nephrotomography is no more the reference standard in case of suspected renal cancer, because of its poor sensibility.

Ultrasonography–Color Doppler

Ultrasound (US) evaluation has a role in the detection of renal masses and has improved recently with technical upgrading of the devices. The sensitivity is 80% for tumors over 3 cm and 60% for tumors less than 2 cm.

The specificity for characterizing solid tumor subtypes is poor but conversely is excellent for distinguishing cystic from solid lesion. When a solid lesion or atypical cystic lesion is detected on US, it must be analysed by CT. Staging with US is nonaccurate as compared with CT, although liver metastases and vein involvement may be confidently detected with US. Contrast-enhanced ultrasonography may facilitate the evaluation of tumor vasculature and venous involvement.

Computed Tomography

CT is the modality of choice for detection, characterization, staging, and follow-up of patients with renal carcinoma.

New technologies, such as multidetector CT (MDCT) with thin collimation and multiplanar reformatting, might result in a diagnostic improvement. Three or four helical phases are required to have the best diagnosis and staging (Fig. 1).

Unenhanced phase provides a baseline from which to measure the enhancement within the lesion after the injection of intra venous contrast material. This enhancement (at least 15 UH) is important in distinguishing hyperdense cysts (no enhancement) from solid tumor. The diagnosis of renal cell carcinoma rests on demonstrating enhancement within a renal mass Renal cell carcinoma usually has an attenuation similar to the surrounding parenchyma but may show higher attenuation in case of hemorrhage. Unenhanced CT scan also demonstrates calcification (30%) in the tumor.

The cortico-medullar phase occurs at about 35–40 sec after the start of injection. This phase is essential for accurate staging of renal cell carcinoma. Maximal opacification of the renal arteries and veins occurs, allowing study of the venous extension of tumoral tissue. This phase allowed vascular reconstruction before partial

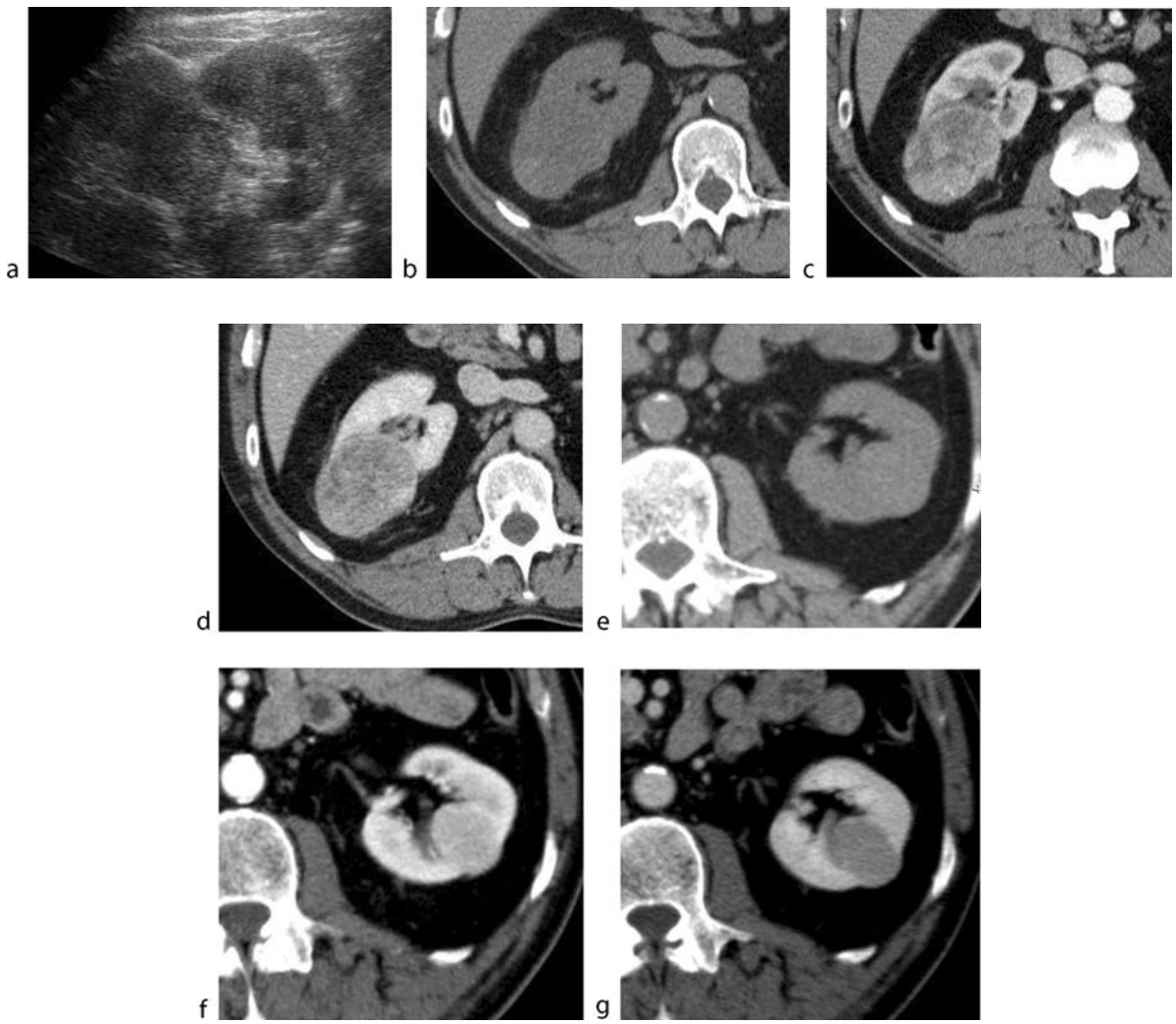

Carcinoma, Renal Cell. Figure 1 US and CT findings in renal clear cell carcinomas. (a) US of the right transverse plane shows a large renal mass. (b, c, d) CT findings. Nonenhanced CT (b) shows slightly high attenuation of the peripheral portion, contrast-enhanced CT in cortical (c) and nephrographic (d) phases show heterogeneous enhancement. (e, f, g): a homogeneous renal tumor in a 71-year-old man. Noncontrast enhanced (e), cortical phase shows an important and early enhancement (f), the tumor is low attenuated on the nephrographic-phase image (g).

surgery. Clear cell carcinoma has a great enhancement at this phase.

Hypervascular metastases of the liver, pancreas, muscles are most visible compared tubular phase. This phase must concern liver and kidney.

The nephrogenic or tubular phase is the more useful phase; it is made up after a scanning delay between 80 and 120 sec after the start of injection. The renal parenchyma enhances homogeneously. That is why the nephrographic phase is the most helpful for detecting renal masses and characterizing indeterminate lesions. The enhancement of papillary tumor is well demonstrated more clearly as at the cortical phase.

The excretory phase is optional. It begins approximately 180 sec after the initiation of injection of iodinated contrast material. This phase is occasionally helpful to better delineate the relationship of a centrally located mass with the collecting system.

Thoracic examination depicts lung or pleural metastasis, mediastinal lymph nodes, and attention is required in axillar regions and thoracic wall.

Pelvic examination may be proposed with the aim to depict peritoneal, pelvic lymph nodes, and pelvic bones metastasis.

Chest and pelvis examination can be carried within a single acquisition, for instance at the cortico-medullar phase, when the examination is performed using MDCT.

Magnetic Resonance Imaging

In the absence of formal contraindications, magnetic resonance imaging (MRI) is helpful in cases of renal failure, because CT with iodine injection cannot be performed. MRI can be a substitute to CT. CT remains mandatory for chest examination that does not require iodine injection. Another advantage of MRI is that it can help in characterizing small and/or cystic lesion.

Abdominal imaging examinations are performed with an abdominal phased array surface coil (which increases signal to noise ratio); breath-hold sequences are helpful to minimize artifacts secondary to respiratory motion and to allow dynamic evaluation after contrast injection.

Precontrast imaging includes axial breath-hold T1-weighted gradient echo sequence performed with in phase and out phase images, to provide anatomical overview, detection of lymphadenopathy, characterization of any associated adrenal mass. Fat-suppressed T1-weighted sequence, which allows differentiation of fat from hemorrhage may also be acquired. A transverse or coronal T2 sequence, usually using a breath-hold technique, is performed to differentiate cystic lesion from hydronephrosis. Fat saturation can be associated as well.

To evaluate the renal vasculature, a high-resolution breath-hold fat-suppressed three-dimensional T1-weighted spoiled GRE sequence is performed in a coronal-oblique or axial plane before and at the arterial phase after dynamic the intravenous administration of gadolinium. Images are displayed either as native two dimensional or reformatted using a maximum-intensity-projection (MIP) algorithm.

Evaluation of the renal parenchyma is subsequently performed with a breath-hold three-dimensional fat-suppressed T1-weighted spoiled GRE sequence in the axial plane at the cortical and tubular phases.

MR urographic images can be provided with a heavily T2-weighted sequence.

Angiography

Today, angiography has a very limited role in renal tumors because CT and/or MRI provide diagnostic images of renal vessels. Angiography is still useful when embolization of the tumor, usually before surgery, is required.

Results

Clear Cell Type

On US, the appearance varies: larger tumors are usually hypoechoic or isoechoic to renal parenchyma, whereas more than half of small renal cell carcinomas are hyperechoic.

On CT, most renal cell carcinomas are solid lesions with attenuation values of 20 HU or greater on plain CT. Small (<3 cm diameter) tumors usually have a homogeneous appearance; whereas larger lesions tend to be more heterogeneous due to hemorrhage or necrosis. Calcifications are detected in up to 30% of cases of renal cell carcinoma. The enhancement is often heterogeneous, important and early, reaching a maximum at the cortico-medullary phase. On nephrographic phase, it appears hypodense compared to the normal renal parenchyma.

On MRI, renal cell carcinomas have variable signal intensity on T1- and T2-weighted sequences, often slightly hypointense on T1-weighted images and isointense to slightly hyperintense on the T2-weighted images, but anyway significantly lower than cystic lesions. Enhancement after gadolinium injection is early and strong.

Renal clear cell carcinoma may have a cystic appearance.

Identification and characterization of complex cystic renal mass relies on Bosniak classification, which is based on CT criteria but is also employed also for MRI. The criteria include the plain attenuation of cyst, the presence of calcifications, number of septae, the thickness (regular

or nodular) of the wall or septae, the presence or absence of enhancing soft tissue components.

The categories I and II are benign lesions, the categories III and IV with thick enhancing walls or septae or thick nodular enhancing soft tissue components, are suspicious of malignant lesions and surgery is therefore indicated (Fig. 2).

Tubulopapillar Carcinoma

It is commonly a small (<3 cm) and sometimes multifocal or bilateral. It can appear hyperechoic at ultrasonography, and mimic an angiomyolipoma: the rule is that any lesion that is not clearly a simple cyst on US must be studied further by CT. Enhancement appears lower and delayed as compared with the clear cell type. It may appear hypointense on T2-weighted sequences, which is an indicator for this diagnosis (Fig. 3).

Chromophobe Renal Cell Carcinoma

It usually appears large, often homogeneous, and lobulated, showing a low enhancement. In some cases, a spoke-wheel-like enhancement with a central scar like an oncocytoma may be seen, but early enhancement is usually lacking.

Bellini Duct Carcinoma, Medullar Carcinoma

They are localized in the renal medulla, show a mass effect on the collecting system but there is no modification of the cortical line. Postcontrast enhancement is weak. It may present as a large infiltrating tumor. Prognosis is poor.

Staging

The prognosis of renal cell carcinoma is related to the tumor stage.

Robson classification has been widely used. The stages are following:

I: tumor within the renal capsule
II: tumor spread to the perirenal fat and/or adrenal gland
IIIA: venous tumor invasion
IIIB: regional lymph node metastasis
IIIC: venous invasion and regional node metastasis
IVA: direct invasion beyond Gerota's fascia
IVB: distant metastasis.

TNMV classification is now more used (from the TNM atlas, 6th edition, 2003):

T0: no evidence of primary tumor
T1a: tumor ≤4 cm in greatest dimension
T1b: tumor >4 cm and ≤7 cm
T2: >7 cm
T3a: tumor invades adrenal gland or perinephritic tissue but not beyond Gerota's fascia
T3b: tumor grossly extends into renal vein or vena cava
T3c: tumor grossly extends into the vena cava above the diaphragm
T4: tumor invades beyond Gerota's fascia

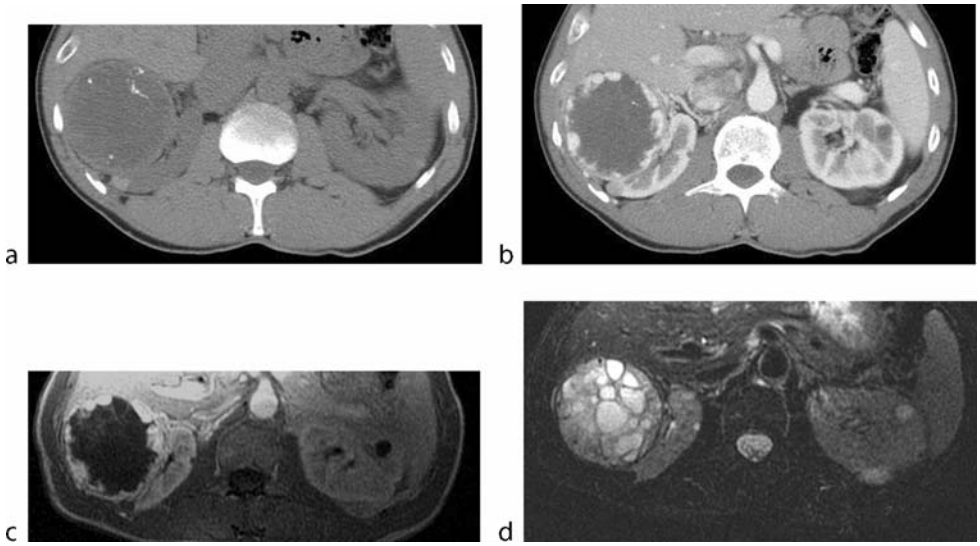

Carcinoma, Renal Cell. Figure 2 Cystic renal cell carcinoma. (a) nonenhanced CT shows small calcifications in the mass. (b, c) contrast-enhanced CT (b) and gadolinium-enhanced T1-weighted MR image (c) show well-enhancing nodules at the peripheral portion, septa are not well seen. (d) T2-weighted MR fat-suppressed image well demonstrate irregular septa.

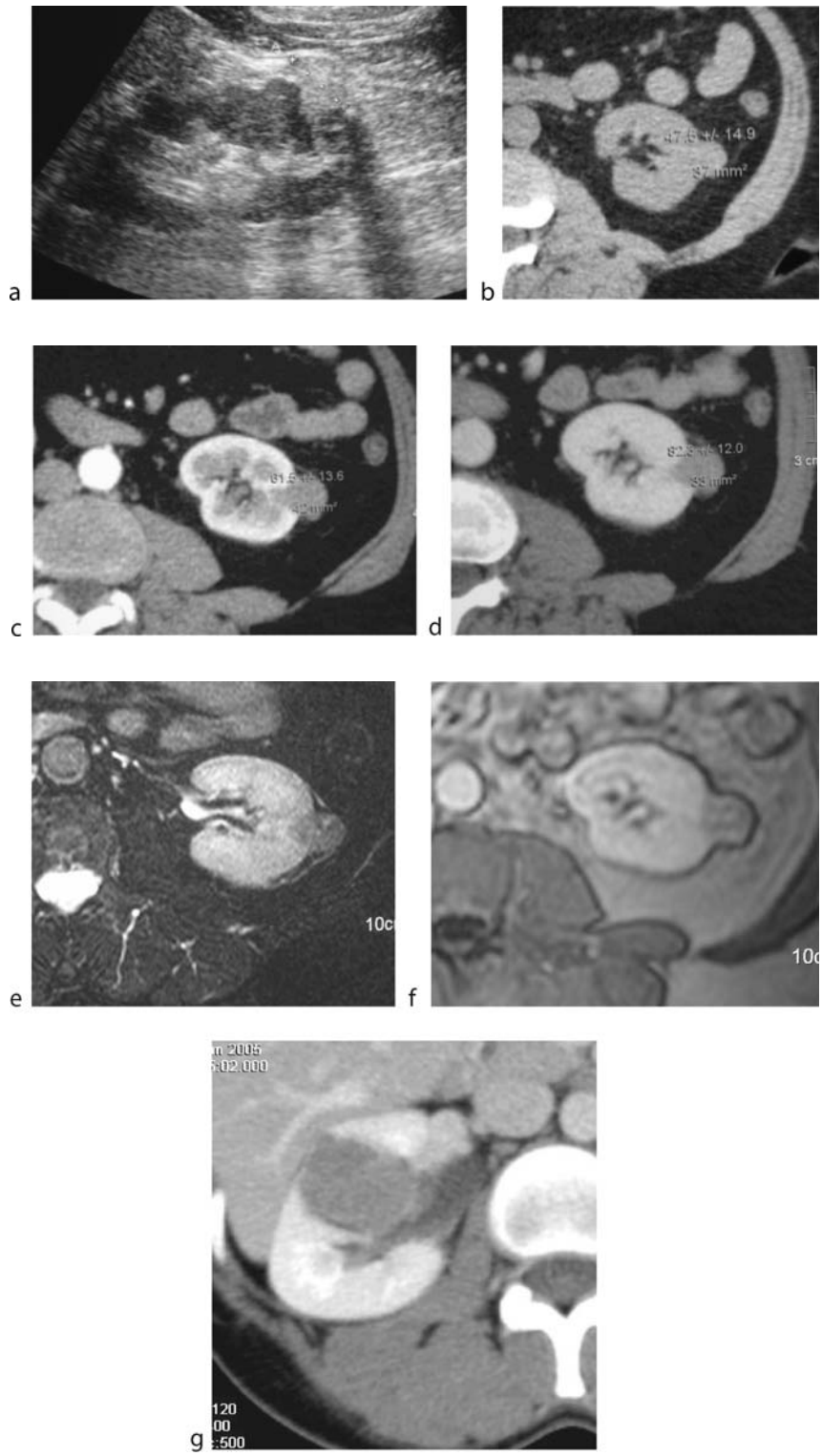

Carcinoma, Renal Cell. Figure 3 US, CT, and MRI in papillary type renal cell carcinomas. (a) US shows a hyperechoic small mass growing exophytically. (b, c, d) CT shows a homogeneous low and delayed enhancement of the tumor. (e) T2-weight MR fat saturation sequence shows the low signal of the mass than that of he renal parenchyma. (f) contrast-enhanced T1-weighted image demonstrates low enhancement of this lesion. (g) Papillary tumor in a 27-year-old woman with hematuria. Contrast-enhanced CT illustrates a low-attenuated lesion growing in the renal sinus.

N0: no regional lymph nodes metastasis
N1: metastasis in a single lymph node
N2: multiple lymph nodes
M0: no distant metastasis
M1: distant metastasis.

Description of the Extension

Local Extension

Perinephric spread of tumor is demonstrated by the presence of an enhancing nodule in the perinephric space. This sign is highly specific but is encountered in only 46% of the cases. Perinephric stranding does not reliably indicate tumor spread; indeed it may be caused by edema, vascular stasis, or previous inflammation.

The involvement of ipsilateral adrenal gland is not frequent, reported at less 5%.

Direct extension of renal cell carcinoma outside the Gerota fascia (stage T4) is difficult to diagnose with certainty unless there is a demonstrable focal change in attenuation within an organ.

The extension into collecting system is evaluated on excretory phase.

Regional Extension

Venous Spread of tumors is very well studied on MDCT and MRI. After detection, precising the exact level of the

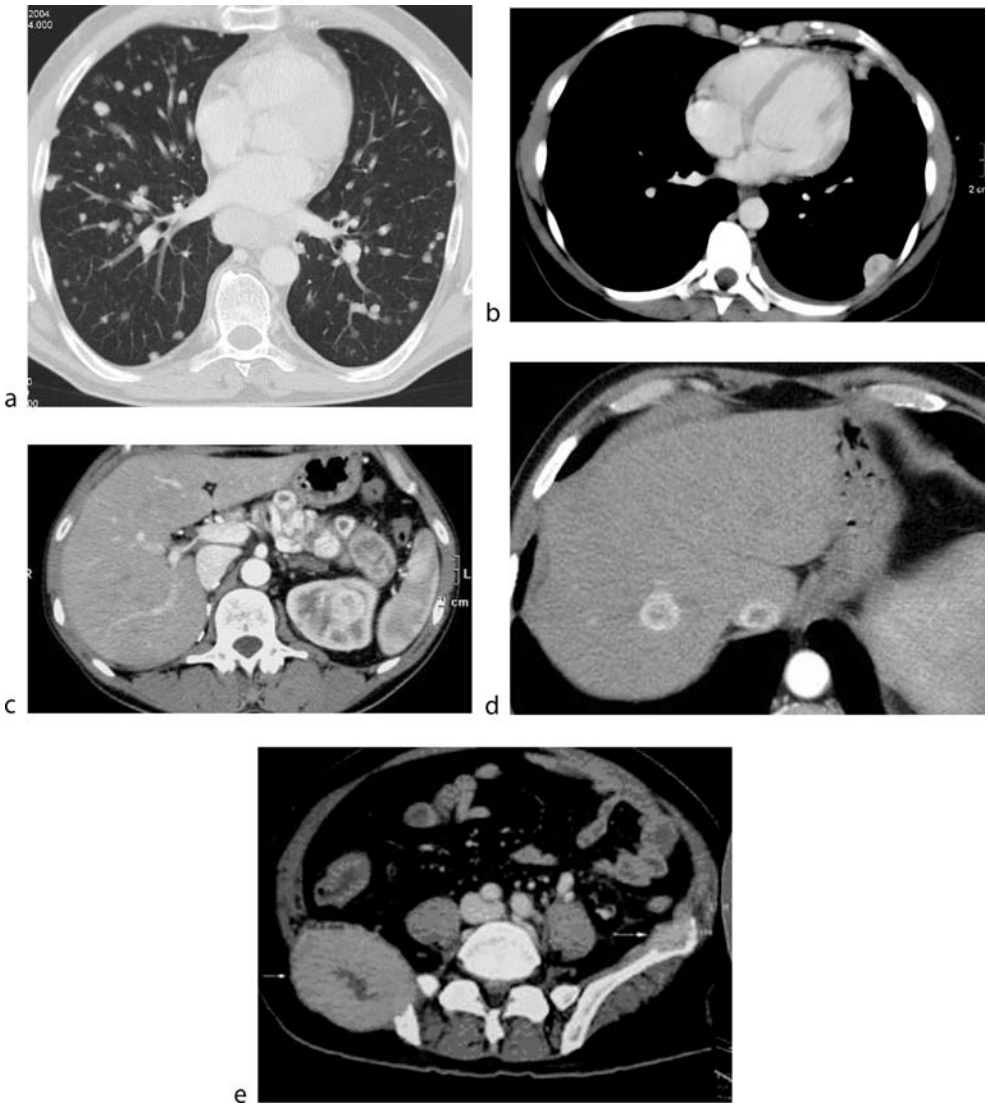

Carcinoma, Renal Cell. Figure 4 Examples of distant and lymph nodes metastasis. Pulmonary (a), pleural (b), pancreatic (c), hepatic (d), and osseous (e) metastasis of renal clear cell type carcinomas.

cast is of dramatic importance. It is mandatory for the surgeon to know if the tumor cast is limited to the renal vein, prolapses in the inferior vena cava, and in this case, how far is the tumor cast from the right atrium. This may have a major impact on surgical technique, some patients requiring extra corporeal circulation and even the combined surgery with a cardiovascular surgeon.

Regional lymphadenopathy should be detected, the number evaluated and the representative size reported.

General Extension

Metastases involve mainly lung parenchyma, pleurae, bone, liver, pancreas, muscle and rarely, thyroid, ovarian, small bowel, colon, peritoneal fat, vagina, bladder. Liver and pancreas metastasis have usually a strong and early enhancement, more clearly visible at an abdominal arterial phase (Figs 3 and 4).

Nuclear Medicine

It does not play a role in the diagnosis of renal tumor. Nevertheless it can predict, before surgery, residual renal function after total or partial nephrectomy.

PET with FDG may be helpful in the evaluation of "equivocal findings" on conventional studies, including bone scan, and also in the differentiation between recurrence and post treatment changes. The value of other PET tracers in renal cell carcinoma is under investigation.

Diagnosis

The final diagnosis requires histopathology and is most often provided by the analysis of material from surgical resection. Percutaneous biopsy is not justified in most cases because surgery will be necessary in most cases, including patients with regional or general extension, who can benefit from the resection of the primary tumor. Percutaneous CT or US guided trucut biopsy may be helpful in selected cases of atypical lesion, multifocality, metastatic patient and/or patient with operative risk.

Renal cell carcinoma can be mimicked by benign tumors like angiomyolipoma (fat component objectived at CT or MRI), oncocytoma (in some cases, cartwheel-like central scar may suggest the diagnosis, but specificity is low).

Chronic infection like xanthogranulomatous pyelonephritis may present as an infiltrative tumor.

Lymphoma or metastasis is usually hypovascular and multiple, but some atypical cases can simulate renal cell carcinoma.

Interventional Radiological Treatment

The number of detected renal cell carcinomas has been increasing, and many are early-stage lesions. Nephron-sparing surgery has been proposed as a more appropriate treatment for small (≤4 cm) renal cell carcinomas. Percutaneous thermal ablation therapies, principally radiofrequency (RF) ablation, have been advocated recently as an alternative to surgery. Preliminary data are promising. Cryotherapy has been performed by using open, laparoscopic, and percutaneous approaches and is likely just as effective in ablating cancerous tissues as is RF ablation. In palliative or not operable cases, embolization arteriography can be used in bleeding lesion. In cases of postoperative complications, embolization and percutaneous drainage can be used.

Bibliography

1. Sheth S, Scatarige JC, Horton KM, et al (2001) Current concepts in the diagnosis and management of renal cell carcinoma: role of multidetector CT and three-dimensional CT (review). Radiographics October 21 Spec No:S237–S254
2. Israel GM, Bosniak MA (2005) How I do it: evaluating renal masses. Radiology August 236(2):441–450
3. Kim JK, Kim TK, Ahn HJ, et al (2002) Differentiation of subtypes of renal cell carcinoma on helical CT scans. Am J Roentgenol June 178(6):1499–1506

Carcinoma, Vulva

Martin Unterweger
Diagnostic Radiology, Cantonal Hospital Baden, Baden, Switzerland
Martin.Unterweger@ksb.ch

Synonyms

Vulvar cancer

Definition

Carcinomas of the vulva are rare tumors, which account only for about 35% of female genitourinary malignancies. They present as polypoid vulvar masses and can be easily

reached for biopsy. The patients are normally post-menopausal.

Pathology/Histopathology

Over 90% of vulvar carcinomas are squamous cell carcinomas. The rest are uncommon tumors, e.g. basal cell carcinoma, vulvar intra-epithelial neoplasia, vestibular papilloma and sarcomas.

Clinical Presentation

Staging of vulvar carcinoma depends on local extension and lymphadenopathy (Table 1). Local extension can involve the urethra, vagina, peritoneum and anus. More distant infiltration of the pelvic floor and bladder is also possible. Initially, lymphatic metastatic spread is into the superficial inguinal nodes, in the deeper inguinal nodes and the iliac nodes. If lymph node spread is found, 5-year survival is only 40%. Therapeutic options in vulvar carcinomas

Carcinoma, Vulva. Table 1 Staging of vulvar carcinoma according to TNM and FIGO

TNM	FIGO	
Tis	0	Carcinoma *in situ*
T1	I	Tumor confined to the vulva with a dimension <2 cm
T2	II	Tumor confined to the vulva with a dimension >2 cm
T3	III	Tumor involves the lower urethra, vagina and anus
	III	FIGO III or if regional lymph nodes are present in T1 or T2
T4	IVA	Tumor invades bladder mucosa, rectal mucosa or tumor fixed to bone
	IVA	only in FIGO staging if N2 (retroperitoneal lymph nodes are present) in T1 or T2
	IVB	Any T with a metastasis (M1)

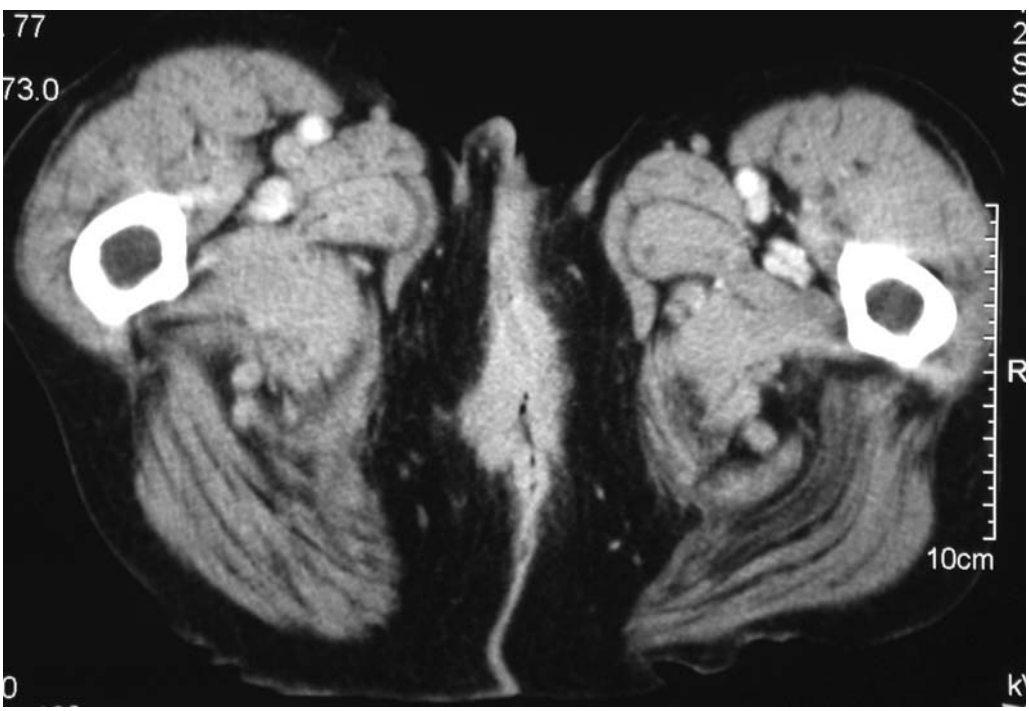

Carcinoma, Vulva. Figure 1 Axial CT demonstrates a contrast-enhanced thickened vulva in an assay of a female patient with histologically confirmed vulvar cancer (*arrow*). No pathological lymph nodes were seen in the abdominal CT.

include a radical vulvectomy or local resection of the tumor in smaller carcinomas. If metastases are present, a combined radio- and chemotherapy could be applied.

Imaging

With CT or MRI the infiltrating of the surrounding soft tissue of the vulva and the lymphatic spread can be demonstrated. However, CT is limited in the evaluation of the primary tumor in the vulva (Fig. 1a). Due to its higher tissue contrast, MRI is more accurate for the assessment of local tumor spread and involvement of surrounding structures. Lymph nodes with a size over 1 cm are defined as pathologic (Fig. 1b).

Diagnosis

The diagnosis is normally clinically suspected and then pathologically confirmed with a biopsy or after the tumor resection.

Bibliography

1. Semelka R (2002) Abdominal Pelvic MRI. Wiley-Liss, New Jersey
2. Sohaib SA, Richards PS, Ind T et al (2002) MR imaging of carcinoma of the vulva. Am J Roentgenol 178(2):373–377
3. Hawnaur JM, Reynolds K, Wilson G et al (2002) Identification of inguinal lymph node metastases from vulva carcinoma by magnetic resonance imaging: an initial report. Clin Radiol 57(11):995–1000
4. Outwater E, Kressel HY (1992) Evaluation of gynaecologic malignancy by magnetic resonance imaging. Radiol Clin North Am 30(4):789–806 (Review)
5. Tavassoli FA, Deville P (2003) Tumor of the Breast and Female Genital Organs. WHO classification of tumors

Carcinomatous Cirrhosis

Desmoplastic reaction induced by a diffusely infiltrative cancer of the liver.

▶Cirrhosis, Hepatic

Carcinosarcoma

The main presentation of this rare malignant tumor is a polypoid lesion in the lower esophagus. Rarely, this tumor has been described in the gallbladder and stomach. Both carcinomatous and sarcomatous tissues are involved in this malignancy.

▶Neoplasms, Gallbladder

Cardiac Enlargement

Increase of size of cardiac Chambers that could produce esophageal compression due to the close relationship between them.

▶Compression, Extrinsic, Esophagus

Cardiac Radiology

Albert de Roos
Department of Radiology, C2-S,
Leiden, The Netherlands
A.de_Roos@lumc.nl

Cardiac radiology encompasses the use of several imaging technologies, including conventional chest radiography, ultrasound, X-ray angiography, nuclear medicine techniques, and more recently computed tomography (CT) and magnetic resonance imaging (MRI). Traditionally, in many countries cardiac ultrasound and coronary X-ray angiography are performed by cardiologists, although exceptions may exist. A discussion of the anatomy and pathology as defined with X-ray angiography constitutes a basis for the interpretation of other technologies that depict the left ventricle and coronary artery tree. Some understanding of functional aspects as assessed by cardiac ultrasound may provide a basis for understanding similar pathophysiological concepts with MRI and CT.

In this review these imaging technologies are discussed with special emphasis on chest radiology, multidetector CT, and MRI.

1. Chest radiology: Chest radiographs are routinely obtained in patients with suspected cardiac disease. A number of useful observations on the presence of heart failure and underlying valvular and other cardiac pathologies can be made from chest radiographs. The size and shape of the heart can provide a clue as to the presence of certain valvular abnormalities. The size and position of the great arteries may also provide diagnostic clues. Abnormal calcifications (coronary, valvular, etc.) can help to identify certain valve

abnormalities. The appearance of the lungs and interstitium is routinely interpreted so as to detect imminent or overt heart failure. The presence of signs of heart failure on chest radiographs has clinical importance for the guidance of treatment as well as prognostic implications.

2. Nuclear medicine imaging: A number of advanced nuclear techniques are available [single photon emission CT (SPECT), positron emission tomography (PET)], which have widespread application and are accepted in routine clinical practice as they have proven their clinical value in terms of patient management and predicting prognosis. Rest-stress perfusion is most commonly applied for the detection of ischemic heart disease. Newer techniques also allow accurate evaluation of regional and global left ventricular function. PET scanning has traditionally been the gold standard for the assessment of myocardial viability, but for detailed viability imaging it is currently challenged by MRI.
3. Cardiac ultrasound allows regional and global function assessment both at rest and under pharmacological stress testing. This application is widely used for the detection of wall motion abnormalities as a sign of underlying ischemic heart disease. The accuracy and success rate of MRI have recently challenged ultrasound for rest–stress function analysis. Ultrasound is still the first-line tool for cardiac function analysis. It also allows comprehensive and sophisticated flow analysis across valves and other hemodynamics. For example, tissue Doppler techniques allow detailed analysis of systolic as well as diastolic heart function. Many functional features of ultrasound are now also becoming possible and applicable with MRI. Some structures are better visualized and quantified with MRI than with ultrasound; therefore, MRI can complement ultrasound in complex pathologies or when patients lack adequate acoustic windows.
4. X-ray coronary angiography is the mainstay of coronary artery imaging. Treatment and stent placement are guided by high-resolution X-ray technology. Understanding the anatomy from traditional angiographic projections can provide a good basis for the interpretation of current multidetector CT and MRI images that attempt to present the coronary artery tree in similar projections.
5. MRI has made much progress over the last few years in terms of technology and clinical applications for cardiac imaging. Recent MRI pulse sequences are optimized for cardiac imaging and today allow routine high-quality imaging. Both anatomy and function can be well evaluated by black-blood and bright-blood techniques, respectively. Coronary artery imaging has also become feasible and some clinical indications have become evident. Further technological advancement is still required for reliable imaging of coronary artery stenosis and atherosclerotic plaque in the small-sized coronary vessels. MRI is currently the new gold standard for functional assessment of ventricular function. Another routine application currently is the assessment of myocardial viability by using delayed enhancement imaging. Many aspects of ischemic heart disease are currently assessable by MRI. Furthermore, MRI has proved to be a valuable tool for the assessment of clinically relevant issues in the follow-up of patients with (repaired) congenital heart disease.
6. Multidetector CT has rapidly developed into a reliable tool for coronary and bypass imaging. In particular, 16-row technology has advanced the clinical utility of CT significantly. High-quality coronary imaging is now possible routinely for diagnostic studies, with a high success rate. Cardiac CT is also developing into a tool for functional analysis as well as perfusion imaging. Ultimately, integration of these techniques may allow comprehensive evaluation of ischemic heart disease. In addition, other cardiac applications have shown clinical relevance (e.g., pulmonary vein imaging preablation). In general, thoracic vascular imaging (e.g., aortic dissection, pulmonary embolism) has greatly benefited from recent multidetector CT applications.

Caries

Gino Ghigi
University of Bologna, Bologna, Italy
gghigi@alma.unibo.it

Synonym

Tooth decay

Definition

Dental caries is one of the most common dental diseases for humans, and it consists in a progressive demineralization of the tooth surface.

Pathology/Histopathology

Pathogenesis is due to a combined effect of different factors, such as dental plaque, carbon hydrates, receptiveness, and time. Within the dental plaque several bacteria grow (streptococci and lactobacilli), which usually induce the production of acids and a pH reduction to a value lesser than 5.5. This is the consequence of a combination between bacteria and the fermentation of carbon hydrates, which can lead to the demineralization of the enamel (1).

Clinical Presentation

Enamel carious lesion is asymptomatic and in its initial stage it looks like a white spot that affects only the enamel. During this period, the carious lesion could change its color and become darker, as a consequence of an attempt to mineralize it. Later on, if not treated, the enamel carious lesion could involve dentin and become symptomatic, suffering from physical, chemical, and thermal stimuli.

Imaging

The radiological image of dental caries is a radio transparency because of the loss of mineral tissue. Bitewing radiographs and intraoral dental films, with the central ray perpendicular to the tooth's vertical axis, are the most common techniques. Recently conventional radiographs have been substituted by phosphor images (2).

Plain X-rays are usually the main imaging tools in investigating caries, but sometimes tomography could be useful to highlight small caries at their initial stage.

Nuclear Medicine

Bone scintigraphy has not any role in the assessment of dental diseases such as dental caries.

Diagnosis

Radiology usually subdivides dental caries into four classes, on a penetration level basis:

- 1st class: carious lesion that involves lesser than a half of the enamel
- 2nd class: carious lesion that involves more than a half of the enamel
- 3rd class: carious lesion that involves dentin only in its external portion
- 4th class: carious lesion that involves more than a half of the dentin and perhaps also dental pulp

Interproximal dental caries develops within the area between two contiguous dental crowns, and so it can be well estimated with bitewing radiograms (Fig. 1).

Occlusal dental caries cannot be easily detected by radiology till the carious lesion starts involving dentin. Vestibular and lingual dental caries can be easily recognized by a clinical approach, and radiology is poorly useful.

Radicular caries involves cementum and perhaps dentin. Radicular caries has a radiological aspect of radio transparencies localized where portions of root are exposed because of gingival recession.

Recurrent dental caries develops in proximity to a carious lesion treatment (Fig. 2). Recurrent caries sometimes cannot be easily recognized because of the overlapping radio opacity or radio transparency of the treatment.

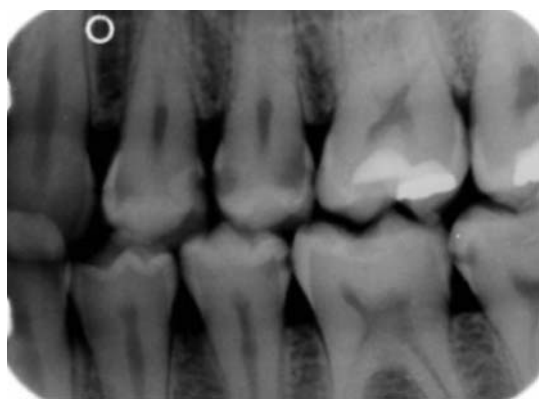

Caries. Figure 1 Digital bitewing radiograph: interproximal caries of different classes.

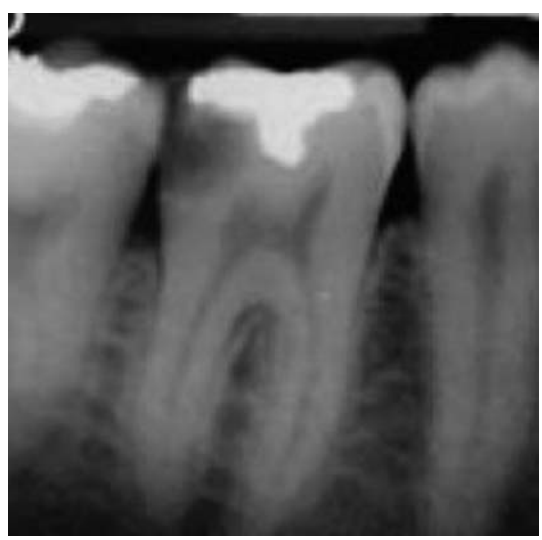

Caries. Figure 2 Recurrent caries.

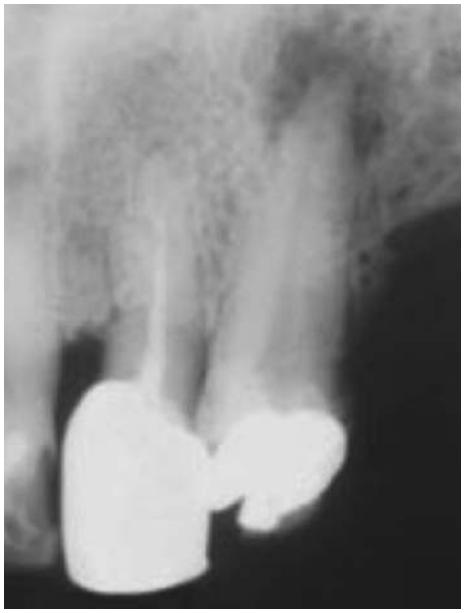

Caries. Figure 3 Periapical granuloma.

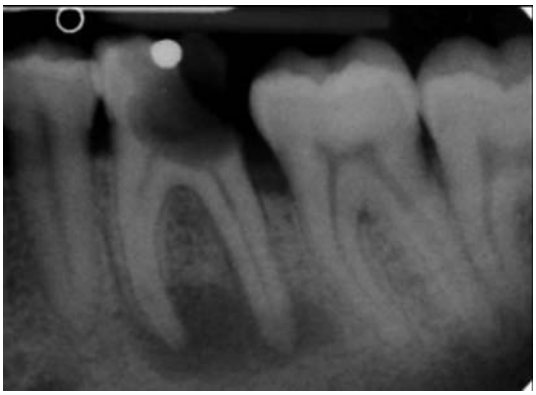

Caries. Figure 4 Periapical roundish granuloma, similar to a cyst.

A pulpal disease, if no treatment is provided, is followed by diffusion of bacteria toward the dental apex, with a phlogosis of the periapical region, the so-called acute periapical diseases. The diffusion could spread also to the structures in proximity.

From a radiological point of view, a homogeneous lacuna with a shaded outline can be observed. If the phlogistic process becomes chronic, in this case an expansion of the apical periodontal region with areas of surrounding osteosclerosis can be observed. Chronic periapical diseases are commonly indicated as apical granuloma.

Granuloma is usually asymptomatic and in radiology it is represented by a periapical transparency (Fig. 3), sometimes roundish and similar to a cyst (Fig. 4). The periapical bone infection can spread to tissues in proximity and can cause odontogenic abscesses, fistulas, and sinusitis.

Bibliography

1. De Florio L, Ghigi G (2005) Compendio di Radiologia Odontostomatologica Napoli, Idelson Gnocchi 2nd ed.
2. Wenzel A (2000) Digital imaging for dental caries. Dent Clin North Am 44:319–338

Carcinoma, Prostate

Jurgen J. Fütterer, Stijn W. T. P. J. Heijmink
Department of Radiology, University Medical Centre Nijmegen, Nijmegen, The Netherlands
j.futterer@rad.umcn.nl

Synonym

Prostatic adenocarcinoma

Definition

Prostate cancer is a malignant tumor of glandular origin in the prostate.

Characteristics

Epidemiology

Prostate cancer is the sixth most common cancer in the world. In 2005, an estimated 232,090 new cases and 30,350 deaths of prostate cancer are expected in the United States (1, 2). The lifetime risk of men developing clinically diagnosed prostate cancer is approximately one in six. With an ever-aging population, these figures are likely to increase in the coming decades. The use of prostate-specific antigen (PSA) testing has facilitated an earlier awareness of abnormalities in prostate health, resulting in a more frequent biopsy diagnosis of this disease (3). There has been an increase in the prevalence of prostate cancer, possibly due to increased importance of etiological factors such as diet and lifestyle.

Prostate Cancer Pathophysiology

Prostate cancer is a multifactorial disease. Age and a positive family history of prostate cancer are the main risk factors. Other factors are the type of diet, lifestyle-related

factors, and certain genetic defects (3). There is also a distinct geographical and racial difference in prostate cancer incidence with higher rates in Western countries and among black men, as compared to Asian countries and white men, respectively.

The main task of the prostate gland is to lubricate the sperm produced in the testes during ejaculation. In healthy prostatic epithelial cells, the enzyme aconitase is inhibited by high levels of zinc present in the cells. This, in turn, blocks the oxidation of citrate in the Krebs cycle, thus accumulating citrate in the prostatic lumina.

The earliest determinable pathological changes in the characteristics of the healthy prostatic cells are atrophic and inflammatory changes. A cascade of these and other factors may lead to the histopathologically defined precursors of prostatic intraepithelial neoplasia.

Normal Prostate Anatomy

On the basis of embryological origins, the prostate is anatomically divided into three zones that are eccentrically located around the urethra: the innermost transition zone, the central zone, and the outermost peripheral zone. Knowledge of the zonal anatomy of the prostate is very useful, considering that many prostatic diseases have a zonal distribution. Up to 70–80% of prostate cancer is located in the peripheral zone, whereas about 20% emerge in the transitional zone, and 10% in the central zone (4). Radiologically, in older patients the transitional zone and central zone cannot be distinguished due to compression of the central zone by benign prostatic hyperplasia and are referred together as the central gland. Most central gland tumors have additional tumor foci in the peripheral zone. Another aspect of the prostate anatomy that is relevant to radiologic imaging relates the prostatic capsule. The prostate is surrounded by a thick layer of fibromuscular tissue corresponding to the capsule. The "true" prostatic capsule, however, is a thin (0.5–2 mm) layer of connective tissue that is located externally to the peripheral zone. Around this layer there is the pelvic fascia, often called the "false" prostatic capsule.

Transrectal Ultrasonography

Nowadays, in regular clinical practice, prostate biopsies are performed under gray-scale transrectal ultrasonography (TRUS) guidance. Although prostate cancer traditionally appears as a hypoechoic lesion in the peripheral zone on TRUS (Fig. 1), nonmalignant conditions such as prostatitis, atrophy, and prostatic intraepithelial neoplasia may also present as hypoechoic lesions (5, 6). Thus, a hypoechoic lesion has a chance of 17–57% of being prostate cancer. More than 40% of prostate cancer lesions are isoechoic whereas only 5% are hyperechoic. Color Doppler imaging detects blood flow by determining its velocity and direction. An increased blood flow related to tumor neovascularity is a characteristic of prostate cancer. Use of Doppler imaging thus increased the accuracy rate of prostate cancer detection to 40–90%, with sensitivity and specificity outcomes being widely spread (52–75% and 40–82%, respectively). Application of gas-filled microbubble contrast agents enhances the visibility of the prostatic vasculature. This may lead to increased prostate cancer detection rate. Reported sensitivities and specificities of prostate cancer detection using contrast agents were 53–87% and 46–79%, respectively (7–9).

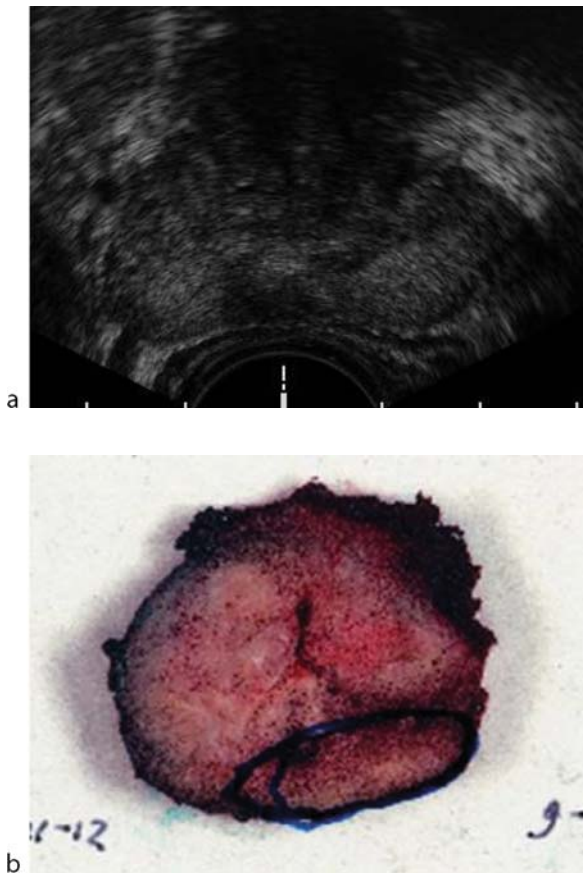

Carcinoma, Prostate. Figure 1 (a) Transrectal ultrasound image through the prostate demonstrating a hypoechoic area in the right peripheral zone indicating prostate carcinoma. This was confirmed with (b) whole mount section histopathology.

Computed Tomography

In general, computed tomography (CT) scanning has too little soft-tissue contrast resolution to differentiate the tissues intraprostatic (Fig. 2a). An additional disadvantage of CT is that the patient is exposed to a significant dose of radiation. Two studies revealed low sensitivity (26–29%) with reasonably high specificity (80–89%) in

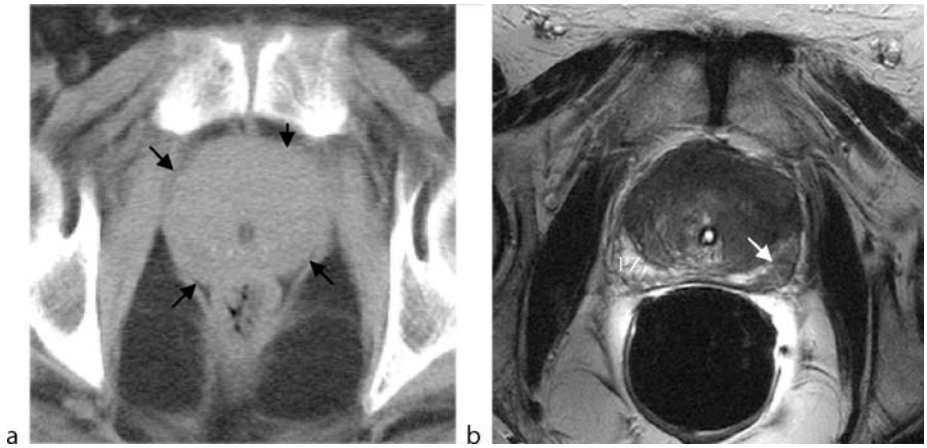

Carcinoma, Prostate. Figure 2 A 56-year-old patient with biopsy-proven prostate cancer. (a) Axial CT slice through the prostate (arrows indicate prostate contour). Prostate tumor is not visible. (b) Axial T2-weighted MR image in the same patient. A low signal intensity (arrows) in the left peripheral zone (PZ) indicating prostate cancer, which was confirmed with whole mount section histopathology.

staging prostate cancer (10, 11). Thus, CT has little value for staging and detection of prostate cancer.

Magnetic Resonance Imaging

Contrary to CT scanning, magnetic resonance (MR) imaging has a high soft-tissue contrast resolution. On T2-weighted MR images, normal prostate tissue displays an intermediate to high signal intensity whereas the central gland has lower signal intensity than the peripheral zone (12, 13). Conversely, the prostate has homogeneous, intermediate signal intensity on T1-weighted images. This means that the differentiation between peripheral and central zone cannot be perceived.

On T2-weighted MR images, prostate carcinoma displays as a low signal intensity area in a bright normal peripheral zone (Fig. 2b). In addition to carcinoma, the differential diagnosis of an area of low signal intensity includes postbiopsy hemorrhage, prostatitis, benign prostatic hyperplasia, effects of hormone or radiation treatment, scars, calcifications, smooth muscle hyperplasia, and fibromuscular hyperplasia (14). Detecting prostate carcinoma in the central gland on T2-weighted images is difficult because this area is often involved with benign prostate hyperplasia, which has signal intensity similar to that of carcinoma and the inner gland structure is more inhomogeneous. Postbiopsy hemorrhage can also appear as a low signal intensity lesion, but can be differentiated from prostate cancer as it is hyperintense using T1-weighted sequences (Fig. 3).

MR imaging obtained high sensitivities (77–81%), whereas specificities were lower (46–61%), in localizing prostate cancer. The addition of 3D proton MR spectroscopic imaging to anatomical MR imaging increased the localization specificity up to 91% (15). Because of typical tumor contrast enhancement characteristics, cancer can be differentiated from normal tissue on fast dynamic contrast enhanced MR imaging (16). Engelbrecht et al. (17) showed that prostate cancer demonstrated different enhancement patterns compared to both onset time, time to peak, peak enhancement, and washout.

The current general opinion is that the localized prostate cancer can be treated successfully by radical prostatectomy in the patient group with a life expectancy of 10 to 15 years or more. Accurate staging is therefore especially important for the proper management of prostate cancer. The most reliable criteria for the detection of extracapsular extension of prostate carcinoma are asymmetry of the neurovascular bundle, obliteration of the rectoprostatic angle, tumor bulge into the periprostatic fat, broad tumor contact with the surface of the capsule, an extracapsular tumor, and the radiologists' overall impression (18, 19). The most common but misleading MR sign of extraprostatic extension, e.g., irregular bulging (especially in nonpalpable tumors), is not often used. Wedge shape, diffuse extension without mass effect, and size are the morphological features of low-intensity lesions in the peripheral zone on prebiopsy T2-weighted MR images that give the best prediction of malignancy. Seminal vesicle invasion can be identified as an asymmetric area of low signal intensity in the seminal vesicles that is visible on T2-weighted MR images (18). Thickening of the tubular walls and asymmetric widening of the seminal vesicles have to be avoided as criteria because these are nonspecific signs. Senile amyloidosis can mimic extraprostatic spread. Prostate MR imaging should be obtained at a minimum of 2 to 4 weeks after prostate biopsy, as hemorrhage decreases staging accuracy. Endorectal MR imaging findings are significant predictors for the detection of extracapsular disease when

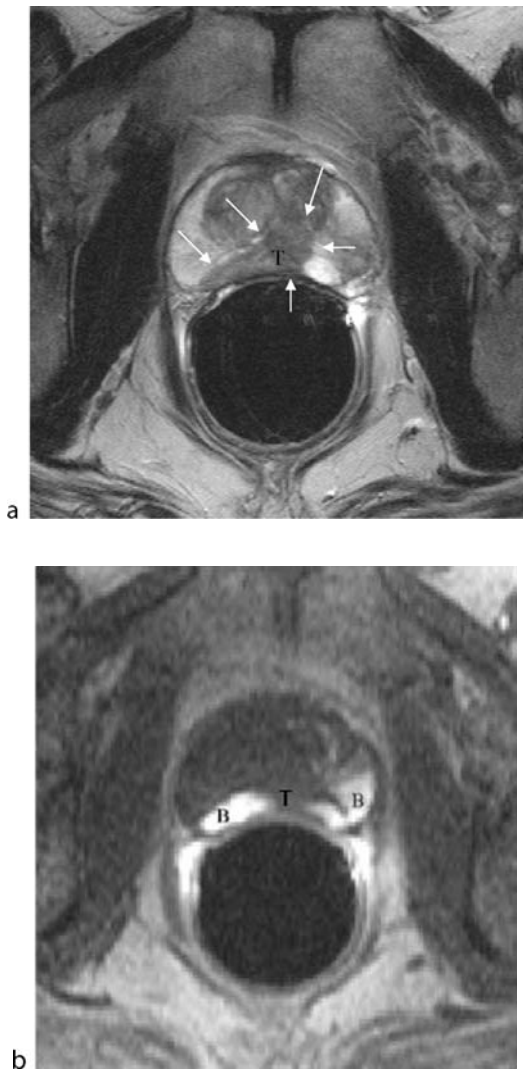

Carcinoma, Prostate. Figure 3 A 64-year-old patient with prostate cancer underwent MR imaging 2 weeks after transrectal ultrasound-guided biopsy. (a) Axial T2-weighted image through the prostate demonstrates a low signal intensity area in almost the whole peripheral zone (arrows). However, the T1-weighted axial image (b) at the same level revealed high signal intensity areas in the peripheral zone which were biopsy artifacts (B). Only in the mid-peripheral zone, tumor (T) was present which was confirmed with whole mount section histopathology.

MR images are interpreted by genitourinary radiologists experienced with MR imaging of the prostate. Engelbrecht et al. (20) suggested in their meta-analysis that the use of turbo spin-echo MR sequences, an endorectal coil, and multiple imaging planes can improve staging performance of MR imaging. Addition of dynamic contrast enhanced MR imaging to the anatomic images revealed a significantly improved staging accuracies for less-experienced readers (21). Addition of 3D proton MR spectroscopic imaging to MR imaging improved staging accuracies, most significantly for less-experienced readers.

Bibliography

1. Jemal A, Murray T, Ward E et al (2005) Cancer statistics 2005. CA Cancer J Clin 55:10–30
2. Parkin DM, Bray FI, Devesa SS (2001) Cancer burden in the year 2000. The global picture. Eur J Cancer 37(Suppl 8):S4–S66
3. Barry MJ (2001) Prostate-specific-antigen testing for early diagnosis of prostate cancer. N Engl J Med 344:1373–1377
4. McNeal JE (1981) Normal and pathologic anatomy of the prostate. Urology 17:11–16
5. Lee F, Gray JM, McLeary RD et al (1986) Prostatic evaluation by transrectal sonography: criteria for diagnosis of early carcinoma. Radiology 158:91–95
6. Meirelles LR, Billis A, Cotta AC et al (2002) Prostatic atrophy: evidence for a possible role of local ischemia in its pathogenesis. Int Urol Nephrol 34:345–350
7. Unal D, Sedelaar JP, Aarnink RG et al (2000) Three-dimensional contrast-enhanced power Doppler ultrasonography and conventional examination methods: the value of diagnostic predictors of prostate cancer. BJU Int 86:58–64
8. Halpern EJ, Rosenberg M, Gomella LG (2001) Prostate cancer: contrast-enhanced US for detection. Radiology 219:219–225
9. Frauscher F, Klauser A, Berger AP et al (2003) [The value of ultrasound (US) in the diagnosis of prostate cancer]. Radiologe 43:455–463
10. Tarcan T, Turkeri L, Biren T et al (1996) The effectiveness of imaging modalities in clinical staging of localized prostatic carcinoma. Int Urol Nephrol 28:773–779
11. Barbieri A, Monica B, Sebastio N et al (1997) [Value and limitations of transrectal ultrasonography and computer tomography in preoperative staging of prostate carcinoma]. Acta Biomed Ateneo Parmense 68:23–26
12. Sommer FG, Nghiem HV, Herfkens R et al (1993) Determining the volume of prostatic carcinoma: value of MR imaging with an external-array coil. AJR Am J Roentgenol 161:81–86
13. Schnall MD, Imai Y, Tomaszewski J et al (1993) Prostate cancer; local staging with endorectal surface coil MR imaging. Radiology 178:797–802
14. Schiebler ML, Schnall MD, Pollack HM et al (1993) Current role of MR imaging in the staging of adenocarcinoma of the prostate. Radiology 189:339–352
15. Scheidler J, Hricak H, Vigneron DB et al (1999) Prostate cancer: localization with three-dimensional proton MR spectroscopic imaging—clinicopathologic study. Radiology 213:473–480
16. Barentsz JO, Jager GJ, van Vierzen PBJ et al (1996) Staging urinary bladder cancer after transurethral biopsy: the value of fast dynamic contrast-enhanced MR imaging. Radiology 201:185–193
17. Engelbrecht MR, Huisman HJ, Laheij RJF et al (2003) Discrimination of prostate cancer from peripheral zone and central gland tissue using dynamic contrast-enhanced MR imaging. Radiology 229:248–254
18. Outwater EK, Petersen, RO, Siegelman ES et al (1994) Prostate carcinoma: assessment of diagnostic criteria for capsular extension on endorectal coil images. Radiology 193:333–339
19. Yu KK, Hricak H, Alagappan R et al (1997) Detection of extracapsular extension of prostate carcinoma with endorectal and phased-array coil MR imaging: multivariate feature analysis. Radiology 202:697–702

20. Engelbrecht MR, Jager GJ, Laheij RJ et al (2002) Local staging of prostate cancer using magnetic resonance imaging: a meta-analysis. Eur Radiol 12:2294–2302
21. Futterer JJ, Engelbrecht MR, Huisman HJ et al (2005) Staging prostate cancer with dynamic contrast-enhanced endorectal MR imaging prior to radical prostatectomy: experienced versus less experienced readers. Radiology 237:541–549

Caroli's Disease

Caroli's disease, first described by Jacques Caroli in 1958, is a rare, autosomal recessive condition characterized by segmental, non-obstructive saccular or fusiform dilatation of the intrahepatic bile ducts. Other typical pathologic features are the presence of intraluminal bulbar protrusions, bridges across the dilated lumina and portal radicles partially or completely surrounded by dilated bile ducts. The abnormality may be segmental or diffuse. The pure form of the disease is quite rare, while a various degree of congenital hepatic fibrosis is usually associated. Caroli's syndrome is the condition in which features of both congenital hepatic fibrosis and Caroli's disease are simultaneously present.

▶Cystic-Like Lesions, Hepatic
▶Congenital Malformations, Bile Ducts

Caroli's Syndrome

Caroli's syndrome is the condition in which features of both congenital hepatic fibrosis and Caroli's disease are simultaneously present.

▶Cystic-Like Lesions, Hepatic

Carotid and Vertebral Artery Pathology

Jonathan Gillard, Daniel Scoffings
Cambridge University Hospitals Foundation Trust, Cambridge, UK
Jhg21@cam.ac.uk

Definitions

Carotid atherosclerosis is characterised by lipid deposition, macrophage infiltration and fibrous cap development in the arterial wall with subsequent luminal narrowing. Stenoses occur most often at the bifurcation of the common carotid artery (CCA). Stenoses are quantified as percentages, which vary according to the method of measurement. The most common methods are those of the North American Symptomatic Carotid Endarterectomy Trial (NASCET) and the European Carotid Surgery Trial (ECST). The NASCET method compares the narrowest luminal diameter of the carotid artery to that of the normal distal internal carotid artery (ICA), beyond any post-stenotic dilatation. The ECST method compares the minimal luminal diameter to the predicted normal luminal diameter at the same level. A 50% NASCET stenosis corresponds to a 70% ECST stenosis. NASCET showed benefit from endarterectomy for symptomatic 70–99% stenoses, with a 17% reduction in ipsilateral stroke at two years. The Asymptomatic Carotid Atherosclerosis Study found some benefit for endarterectomy for asymptomatic stenoses greater than 60%, with a 5.9% reduction in stroke over 5 years.

Dissection indicates intramural haemorrhage in an artery. Typically the blood tracks between the tunica intima and media, less often between media and adventitia.

The term non-atheromatous vasculopathy includes intrinsic arterial diseases such as fibromuscular dysplasia (FMD), systemic diseases that affect the arteries such as neurofibromatosis type 1 and Marfan syndrome, and extrinsic processes such as tumour, infection and radiation injury.

Pathology/Histopathology

Plaques and their precursors can be classified into asymptomatic early lesions and advanced lesions, which may or may not be symptomatic. The earliest lesions, fatty streaks, are composed of layers of lipid-loaded macrophages and intimal smooth muscle cells in a proteoglycan matrix. Advanced lesions are characterised by a thickened, disorganised intima with deformation of the arterial wall. Lesions may have a fibrous cap of connective tissue overlying the lipid core and may be complicated by surface disruption, calcification, hemorrhage or thrombosis.

In a sub-intimal dissection haemorrhage lies between the intima and media and narrows the arterial lumen. In a sub-adventitial dissection the blood may extend beyond the adventitia to form a pseudoaneurysm. The most common site of carotid dissection is the cervical ICA just beyond the bulb. Intracranial carotid dissection is uncommon, but usually involves the supraclinoid ICA. Vertebral artery dissection typically occurs between C2 and the skull base.

Three types of FMD affect medium sized arteries. Medial FMD (90–95%) consists of fibrous proliferation

and smooth muscle hyperplasia in the tunica media. Intimal and adventitial FMD are rare. Marfan syndrome is associated with cystic medial necrosis. Radiation injury causes fibrinoid necrosis, endothelial damage and accelerated atherosclerosis.

Clinical Presentation

Carotid stenoses are often asymptomatic but may be detected by finding a bruit at physical examination. Embolisation of plaque components after ulceration or haemorrhage can result in a transient ischaemic attack or cerebral infarct.

Carotid or vertebral dissection is usually associated with neck pain or headache. Horner's syndrome may occur with ICA dissection. Deficits due to ischaemia in the territory supplied by the dissected artery also occur, dissection underlying 5–20% of strokes in young patients.

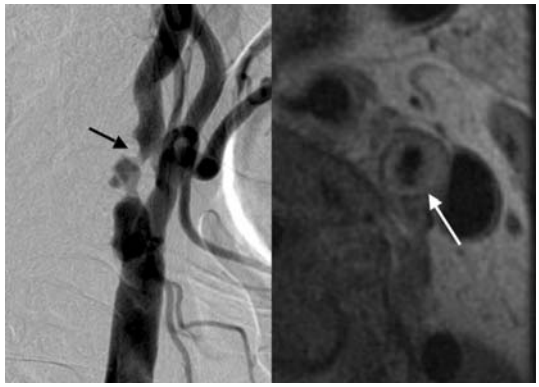

Carotid and Vertebral Artery Pathology. Figure 1 Right carotid stenosis. Catheter angiogram (a) shows an irregular, ulcerated plaque of the proximal internal carotid causing a tight stenosis (*arrow*). High-resolution axial MR (b) shows the extraluminal component of the plaque (*arrow*).

Imaging

Atherosclerosis

Digital Subtraction Angiography (DSA)

This remains the gold standard for measuring carotid stenosis though its use has declined as non-invasive imaging has improved. Studies should include AP, lateral and oblique views of each carotid bifurcation. Views of the distal carotid siphon and the intracranial circulation are necessary to detect tandem lesions, present in 20%, and to evaluate collateral circulation. The lumen at the site of maximum stenosis is often non-circular so that standard angiographic views do not accurately show the true minimum luminal diameter. (Fig. 1) Plaque ulceration is shown as a niche of at least 2 mm, a double density of contrast, or marked luminal irregularity. The detection of plaque ulceration by DSA is sub-optimal.

Ultrasound

A consensus statement has been issued regarding the use of US in the diagnosis of carotid stenosis, requiring the use of gray scale, colour Doppler and analysis of spectral Doppler waveforms (2). The angle of insonation should be 60° or less to the long axis of the artery to reduce measurement errors. The peak systolic velocity (PSV) is the most reproducible measure. Doppler measurements cannot predict the exact percentage stenosis, rather the result is stratified within one of the following groups. Normal: PSV <125 cm/s, no intimal thickening or plaque. Less than 50% stenosis: PSV <125 cm/s with intimal thickening or plaque on gray scale US. 50–69% stenosis: PSV 125–230 cm/s, plaque visible. Greater than 70% stenosis but less than near occlusion: PSV >230 cm/s, plaque and luminal narrowing seen on gray scale and colour Doppler imaging. Total occlusion is diagnosed by absence of flow on colour Doppler. Morphological assessment of plaques with ultrasound has not been conclusively shown to be of clinical value, but fibrous plaques tend to be of homogeneous reflectivity whilst heterogeneous plaques, containing lipid, haemorrhage and calcification, are associated with a greater incidence of neurologic events.

CT

With multislice CT machines, volumetric data acquisition during the injection of iodinated contrast allows fast, minimally invasive angiography of the cervicocephalic arteries. Different post-processing techniques are available: ►*shaded surface display* underestimates stenoses while ►*maximum intensity projections* (MIPs) can be performed quickly but overestimate stenoses. Multiplanar, or curved planar reformats are the preferred post-processing technique, allowing stenosis measurement. An advantage of CT over DSA is its depiction of the plaque and arterial wall beyond the lumen. Plaque calcification can be detected and quantified. Similarly, CT can differentiate between plaques that are lipid-rich or mostly fibrous. Attenuation of 60 HU is the optimal cut off to distinguish lower attenuation lipid-rich plaques from fibrous plaques. With automated methods plaque area and volume can also be measured from CT. Such techniques have yet to reach mainstream clinical practice.

MRI

Carotid magnetic resonance angiography (MRA) allows non-invasive measurement of stenoses without the risks of ionising radiation or iodinated contrast. Two-dimensional ▶time-of-flight (TOF) MRA uses sequential acquisition of thin slices, which are then stacked and MIPs obtained. Flow gaps correlate well with significant stenosis, the method is sensitive to slow flow and background suppression is good. The long TE used results in signal loss in areas of turbulent flow, however. Three-dimensional TOF-MRA excites a slab of tissue and sub-divides it with phase encoding gradients. Advantages over 2D TOF-MRA include better signal to noise ratio due to excitation of a volume of tissue and better through plane resolution because thinner slices can be reconstructed. Progressive saturation of protons as they move into the slab can be avoided by multiple overlapping thin slab acquisition (▶MOTSA). With fast gradient echo sequences images can be acquired during the first pass of a bolus of gadolinium chelate injected at 2–3 mL/sec. A correct timing is vital for contrast-enhanced MRA (CE-MRA).

Dedicated phased array coils enable high-resolution MR of the plaque, using 'black-blood' techniques with T1 and T2 weighting. This allows assessment of the plaque surface and its components.

Dissection

Smooth, or slightly irregular luminal narrowing over a long segment are the typical DSA findings. The degree of narrowing varies from minimal to complete occlusion, which can have a 'rat's tail' appearance. Intimal flaps are specific but seen in only 10%. Similar appearances are shown by CT and MR angiography. Acute intramural haematoma appears as a periarterial cuff of isointense or slightly hyperintense signal on T1 and T2 weighted MR, becoming hyperintense on T1 weighted images after a few days (Fig. 2) (3). Fat-suppressed T1 weighted sequences improve detection of the haematoma. Ultrasound can show a hyperreflective intimal flap, mural haematoma, or absence of colour flow in the false lumen, but dissection is more often inferred from abnormal Doppler indices in the absence of visible plaque.

Non-atheromatous Vasculopathy

Fibromuscular dysplasia results in segments of alternating stenosis and dilatation, the 'string of beads' appearance at angiography. It tends to spare the carotid bifurcation and bulb and is most common at the C2–3 levels. Vasculopathy due to neurofibromatosis type 1 and Marfan's syndrome manifest as areas of fusiform ectasia and tortuosity. Infections, such as retropharyngeal abscess or necrotising otitis externa can also narrow or displace the carotid. Radiation injury produces areas of stenosis or arterial occlusion, with moyamoya vessels intracranially.

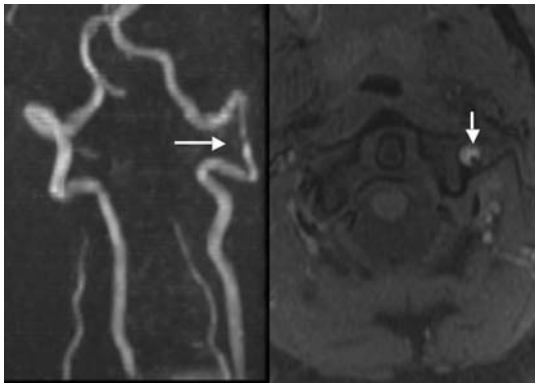

Carotid and Vertebral Artery Pathology. Figure 2 Left vertebral artery dissection. 3D-time-of-flight MR angiogram (a) shows short segment of narrowing of the vertebral artery between C1 and C2 (*arrow*). Fat-suppressed T1-weighted MRI (b) shows intramural haematoma as a crescent of high signal (*arrow*).

Diagnosis

The use of DSA in diagnosing carotid stenosis has declined with improving non-invasive techniques. A cost-benefit analysis using an analytical model recommended use of Doppler US and CE-MRA (4). This has been supported by a recent meta-analysis of the accuracy of non-invasive imaging (5). This showed that for 70–99% NASCET stenosis, sensitivities and specificities were: CE-MRA 94%, 93%; MRA 88%, 84%; Doppler US 89%, 84; CTA 76%, 94%. There was a paucity of reliable data for 50–69% stenosis.

References

1. Gillard J, Graves M, Hatsumaki T et al (eds) (2006) Carotid disease: the role of imaging in diagnosis and management., Cambridge University Press, Cambridge
2. Grant EG, Benson CB, Moneta GL et al (2003) Carotid artery stenosis: gray-scale and Doppler US diagnosis - Society of Radiologists in Ultrasound Consensus Conference. Radiology 229:340–346
3. Provenzale JM (1995) Dissection of the internal carotid and vertebral arteries: imaging features. Am J Roentgenol 165:1099–1104
4. U-King-Im JM, Hollingworth W, Trivedi RA et al (2005) Cost-effectiveness of diagnostic strategies prior to carotid endarterectomy. Ann Neurol 58:506–515
5. Wardlaw JM, Chappell FM, Stevenson M et al (2006) Accurate, practical and cost-effective assessment of carotid stenosis in the UK. Health Technol Assess 10:1–200

Carotid Artery Steal

Reversed flow in the right carotid artery caused by a significant stenosis in the origin of the innominate artery. Similar steal may involve the external carotid artery in the case of ipsilateral common carotid artery occlusion.
▶Steal Syndrome Vertebral

Carotid Endarterectomy

Open Surgery in order to resect atherosclerotic plaques out of the internal carotid artery in order to normalize the arterial diameter and treat a potential source of cerebral emboli.
▶Stroke, Interventional Radiology

Cartilage Destruction

Cartilage destruction in rheumatoid arthritis typically leads to a concentric pattern of joint space diminution, which is, together with bone destruction, one of the three radiologic key symptoms of arthritis (the other two are synovial soft tissue swelling and collateral phenomenon).
▶Rheumatoid Arthritis

Cartilage T2 Relaxation Time

Molecular motion of cartilage water protons and the structure of the extracellular matrix influence spin–spin relaxation. Therefore, quantitative T2 measurements may serve as a non-invasive tool to measure cartilage matrix integrity. In cartilage degeneration an increase in cartilage T2 is observed.
▶Degenerative Joint Disease, Peripheral Joints

Caspases

Proteolytic enzymes belonging to the family of aspartyl-specific cysteine proteases, which are not only essential for the starting event in the DISC but also for the execution of apoptosis.
▶Apoptosis

Cationic Lipophilic Complexes

The cationic lipophilic complexes ^{99m}TC sestamibi and ^{99m}TC tetrofosmin have recently replaced other gamma emitting radiopharmaceuticals with similar biological properties but less favorable physical characteristics. They are used as perfusion and tumor imaging agents.
▶Single Photon Emission Computed Tomography

Cauda Equina Syndrome

Syndrome of muscle paresis, saddle aneasthesia, sphincter disturbance and/or micturition disturbance due to involvement of multiple lumbosacral nerve roots, frequently caused by large median disc herniations.
▶Conservative Therapy for Lumbosacral Radicular Syndrome

Caudal Agenesis—Caudal Regression

▶Congenital Malformations, Spine and Spinal Cord

Caval Vein Occlusion

▶Thrombosis, Caval Vein, Inferior

Cavernous Angioma

Congenital vascular malformation formed by thin-walled, endothelial-lined sinusoidal vascular spaces, filled by slow-flow blood, with no intervening brain tissue. Also known as cavernoma and cavernous hemangioma. The term “occult vascular malformation” is obsolete.
▶Congenital Malformations, Vascular, Brain

Cavitary Necrosis

Multiple fluid- and air-filled cavities without rim-enhancement found in low attenuation lung parenchyma representing necrotizing pneumonia.
▶Pneumonia in Childhood

CCAM

▶Congenital Cystic Adenomatoid Malformation (CCAM)

CDH

▶Congenital Diaphragmatic Hernia (CDH)

Celiac Artery Stenosis

Celiac artery stenosis may be due to atheromatous disease or, in the younger patient, impingement by the diaphragmatic crura or median arcuate ligament. Atherosclerotic lesions tend to occur in the proximal or mid-proximal part of the artery. Clinical features of a severe celiac artery stenosis include postprandial epigastric pain, weight loss, and abdominal bruit. At Doppler US evaluation, the Doppler spectrum shows an elevated peak velocity and spectral broadening, findings consistent with turbulence. The diagnosis is usually confirmed by conventional angiography; however, CT angiography or MR angiography may be also useful.
▶Transplantation, Hepatic

Cell Cycle

The series of stages in which cells proceed from a resting state to cell division. The cell cycle includes interphase (consisting of G1-, S-, and G2-phases) followed by the mitotic phase, in which the replicated DNA is separated into two groups of chromosomes followed by division of the entire cell.
▶Proliferation of Neoplasms

Cell Doubling

▶Proliferation of Neoplasms

Cell Growth

▶Proliferation of Neoplasms

Cell Membrane-based System

Cell membrane-based reporter systems utilize gene products that are associated with the cell membrane.
▶Reporter Systems

Cellulitis

Cellulitis is a diffuse, spreading, acute inflammation within solid tissues, characterized by hyperemia, WBC infiltration, and edema without cellular necrosis or suppuration.
▶Gout
▶Infection, Soft Tissue
▶Oral Cavity, Inflammatory Diseases

Cemento-Ossifying Fibroma

Benign fibro-osseous lesion characterized by fibrous and calcified tissues associated with mature and immature bone/cement. Histologically, this lesion is very similar to fibrous dysplasia and the diagnosis is often difficult. It usually occurs in the jaws; localizations in the paraorbital region are rare.
▶Fibro-Osseous Lesions, Facial Skeleton

Central Facial Nerve Paralysis (CFNP)

Is a clinical condition characterized by paralysis of the muscles of the lower two thirds of the face secondary to supra-nuclear insults. Whereas fibres that project to the part of the motor nucleus that innervate the forehead muscles decussate only partially, those that project to the part of the nucleus that innervate the muscles of the lower two thirds of the face decussate completely. Henceforth, lesions of the upper motor neuron result in contralateral facial palsy sparing the upper face.

▶Facial Nerve Palsy

Central Neurofibromatosis

▶Neurofibromatosis, Musculoskeletal Manifestations

Cephalocele

▶Congenital Malformations, Cerebrum

Cerebellar Dysgenesis

Cerebellar Dysgenesis can involve the vermis and/or the hemispheres. This general term includes entities such as rhombencephalosynapsis, molar tooth malformations, and different abnormalities of foliation and fissuration.

▶Congenital Malformations, Cerebellar

Cerebral Aneurysm

▶Aneurysm, Intracranial

Cerebral Herniation

Secondary traumatic lesion that is the result of increased intracranial pressure. Herniation of the uncus/parahippocampal gyrus and herniation of the tonsils are the two most common types.

▶Trauma, Head, Accidental

Cerebral Infarction

The irreversible damage of the brain caused by inadequate blood supply.

▶Stroke, Children

Cerebral Infections

▶Infection, Opportunistic, Brain

Cerebral Neonatal Disease (Neuro View)

T. A. Huisman
Johns Hopkins University, Baltimore, USA
thierry.huisman@kispi.unizh.ch

Synonyms

Encephalopathy of the newborn; Neonatal diseases of the central nervous system; Perinatal cerebral injury

Definition

Neonatal cerebral disease refers to pathologies of the CNS that are present at birth or become symptomatic within the first weeks of life. These pathologies may have been acquired pre-, peri-, or postnatally.

Pathology and Histopathology

Neonatal cerebral diseases include a wide variety of pathologies like malformation, infection, tumor, hemorrhage, focal or generalized ischemia, and trauma. In addition, the timing of injury may vary, lesion may result

from prenatal (e.g., intrauterine fetal infection), perinatal (e.g., hypoxic-ischemic encephalopathy, HIE), or postnatal (e.g., germinal matrix hemorrhage) events (1, 2).

Hypoxia-ischemia or perinatal asphyxia is one of the leading causes of severe neurological deficit for all gestational ages. The exact etiology and cascade of events in HIE as well as the identification of the principal and supporting/mediating factors that determine severity of brain injury are the focus of ongoing research. Clinical presentation and outcome vary significantly with gestational age. Additional cardio-pulmonary diseases (e.g., congenital heart disease) may aggravate injury. HIE is characterized by the combination of cerebral ischemia (cerebral hypoperfusion) and cerebral injury due to global hypoxia (reduced blood oxygenation). Experimental studies showed however, that ischemia rather than hypoxia is responsible for most of the tissue injury. Neuronal and glial cell death is induced by many factors that are only partially understood. Primary and secondary energy failure with collapse of the normal aerobic pathway of glucose metabolism and shift into an anaerobic glycolysis result in a loss of transmembranous ion exchange, an excessive influx of calcium, failure of the neuronal resting membrane potential, lactic acidosis (anaerobic glycolysis) and cellular damage by release of free radicals and neurotoxic excitatory amino acids (glutamine and glutamate).

In contrast to adult brain, HIE in neonates is characterized by a selective vulnerability of different anatomical areas of the brain. This selective vulnerability is believed multifactorial and is tightly bound with the stage of brain maturation at the time of injury. The rapid biochemical, metabolic, cellular and anatomical changes are factors that determine vulnerability. This explains, at least partially, why the premature brain shows different patterns of injury compared with the term neonate. Generally, in preterm infants the white matter is more vulnerable while in term neonates the central and cortical gray matter is more susceptible. In addition, the maturation of the cerebral vasculature with progressive migration of the watershed zones from the periventricular areas to the subcortical regions explain the periventricular, confluent linear extension of white matter injury in preterm neonates while in term neonates wedge-shaped cortical/subcortical injuries are observed. These wedge shaped lesions match the border zones between the anterior, middle, and posterior cerebral arteries.

Focal infarction in neonates results from acute thrombo-embolic occlusion of major cerebral arteries. Ischemic infarction in neonates is rare. It is most frequently observed in neonates with congenital heart disease, coagulopathies, or hemoglobinopathies. Arterial dissection due to a traumatic birth seldom occurs.

Germinal matrix hemorrhages (GMH) are the most frequent intracranial hemorrhages in the newborn period. Premature born neonates are at increased risk for GMH. Based on their extension, GMH are classified into three different grades. Extension into the ventricular system may result in a hydrocephalus. Compression of the subependymal veins by the hematoma may induce a hemorrhagic venous infarction.

Neonatal infections can be acquired *in utero* due to (a) transplacental maternal–fetal transmission, (b) by ascending vaginal infections, or (c) during the passage through the birth canal during delivery. Neonatal infections may interfere with normal brain development if acquired *in utero*. Timing of infection in relation to the gestational age determines extent and kind of injury. Early in pregnancy, developmental brain anomalies occur with different degrees of migrational disturbances, microcephaly, cerebellar and brainstem hypoplasia as well as injuries/malformations of the eyes, and inner ear. Later in gestation, already developed and differentiated brain structures may become injured resulting into encephaloclastic lesions. Intracerebral calcification frequently develops. Most infections belong to the TORCH acronym. They include Toxoplasmosis, Other (HIV), Rubella, Cytomegalovirus, and Herpes simplex. Neonatal herpes simplex type II infection is typically acquired during birth while passing through an infected birth canal. Pre- and postnatal Herpes simplex-II infections are rare. In the case of a complicating meningoencephalitis, the prognosis is poor. Extensive perivascular infiltrates with ischemic and hemorrhagic infarction are usually fatal.

Metabolic diseases are rare, but initial symptoms may present shortly after birth with poor primary adaptation, seizures, respiratory distress, hypotonia, developmental delay, hypoglycemia, etc.

Clinical Presentation

Neonates with acute perinatal asphyxia present with low Apgar scores, low umbilical cord pH, bradycardia, and respiratory insufficiency. In addition, the amniotic fluid is often meconium stained. Additional signs of neonatal encephalopathy that may develop during the initial days of life include irritability, neonatal seizures, stupor, lethargy, generalized muscular hypotonia (floppy child), and poor reflexes (Moro, Gag, Suck). Clinical symptoms may parallel the cascade of primary and secondary energy failure characterized by an initial period of severe neurological symptoms, followed by a phase of partial recovery which is again followed by a lasting phase of neurological deficits.

Focal infarction in neonates may be clinically silent or present with focal seizures that can become generalized. Focal neurological deficits depend on the anatomical location of infarction respectively on the involved functional center.

Clinical signs in GMHs depend on the location and especially grade of hemorrhage. A grade I GMH is frequently an incidental finding on routine ultrasonography in preterm neonates. Neonates with higher grade GMHs will present with various neurological symptoms that are especially determined by the degree of hydrocephalus.

Clinical findings in neonatal infections are determined by the timing of infection in relation to the gestational age. The earlier the onset of infection, the more extensive the developmental anomalies will be. Clinical symptoms are frequently complex with signs of significant developmental delay as well as deafness, poor vision and seizures. In the case of late infection during gestation, focal neurological deficits and seizures are encountered. Cerebral malformations are discussed in the chapter "Congenital malformations" (cerebral).

Imaging

Patterns of brain injury in acute perinatal hypoxia have been studied extensively and differ between premature and term neonates. In premature neonates, the white matter is predominantly involved while in term neonates the gray matter is involved. These patterns of injury reflect the different vulnerability of different cerebral structures.

Ultrasound

The sonographic imaging of the brain immediately after the ischemic event maybe normal. In the premature infant the periventricular white matter may become echogenic as a result of coagulation necrosis and edema. The distinction between hemorrhagic and nonhemorrhagic periventricular leukomalacia however is difficult. Over the course of the subsequent 1–2 weeks the echogenicity decreases and cysts may develop at 10–14 days and beyond. These cysts usually coalesce and disappear as the ventricles enlarge and the damaged tissue is resorbed. In the term infant the cortex becomes echogenic with moderate to severe edema and this maybe diffuse or focal. Ventricular size is a nonspecific finding as small slit-like ventricles maybe seen as a normal finding in the term infant. Later cystic encephalomalacia, ventricular enlargement, and atrophy may develop in severe cases. Routine sonography through the anterior fontanelle may miss the peripheral areas of the parieto-occipital lobes, the sites of watershed infarction. These areas are now better visualized using the newer high frequency ultrasound probes and all available acoustic windows. In infants with thalamic and basal ganglia infarction there maybe focal or diffuse increased echogenicity in these regions.

Magnetic Resonance Imaging

In hypoxic-ischemic injury, T1-hypointense and T2-hyperintense white matter edema narrows the ventricular system as well as the subarachnoid spaces (Fig. 1a). A T1-hyperintense cortical highlighting following the cortical ribbon is seen due to intracortical petechial hemorrhages. This T1-hyperintensity is matched by a T2-hypointensity. Additional cortical necrosis will result in a diminished cortico-medullary differentiation. Moreover, signal alterations are seen within the basal ganglia/thalamus, hippocampus and posterior limb of the internal capsule (PLIC). In particular, the loss of the normal T1-hyperintense signal of the white matter tracts within the PLIC has been shown to correlate with degree of hypoxic-ischemic injury and outcome. On T2-weighted imaging a corresponding loss of the T2-hypointensity is observed. Finally, in many cases a linear, centripetal T2-hypo- and, T1-hyperintensity is seen within the cerebral white matter due to a stasis/thrombosis within the medullary veins. MR-spectroscopy may identify lactate within the ischemic white or gray matter as well as a reduction of the normal metabolites within the brain (Fig. 1b). Diffusion weighted imaging allows to differentiate between cytotoxic edema and vasogenic edema.

On follow-up after HIE, a multicystic encephalopathy ensues with *ex vacuo* enlargement of the CSF spaces. Depending on the gestational age, a multicystic periventricular leukoencephalopathy (Fig. 2) is seen or a more classical appearance of cortical–subcortical watershed ischemias.

Imaging appearance of GMH is discussed in the chapter titled: hemorrhage, intracranial, neonates. Ultrasonography is the primary imaging modality. In cases where ultrasonography cannot explain neurological symptoms, computer tomography (CT) or even better MRI should be performed.

In neonatal infections MRI is the imaging modality of choice to identify the associated disorders of development (Fig. 3). CT can be helpful to identify parenchymal calcifications, chorioretinitis, and malformations of the inner ear.

In metabolic diseases functional MRI techniques like MR-spectroscopy and diffusion tensor imaging are especially helpful in narrowing differential diagnosis.

Diagnosis

Diagnosis in neonatal disease should always rely on the combined analysis of clinical history, clinical-neurological findings, laboratory tests, and imaging findings. In neonatal encephalopathy without an obvious history or signs of acute perinatal hypoxia/injury other causes of neonatal

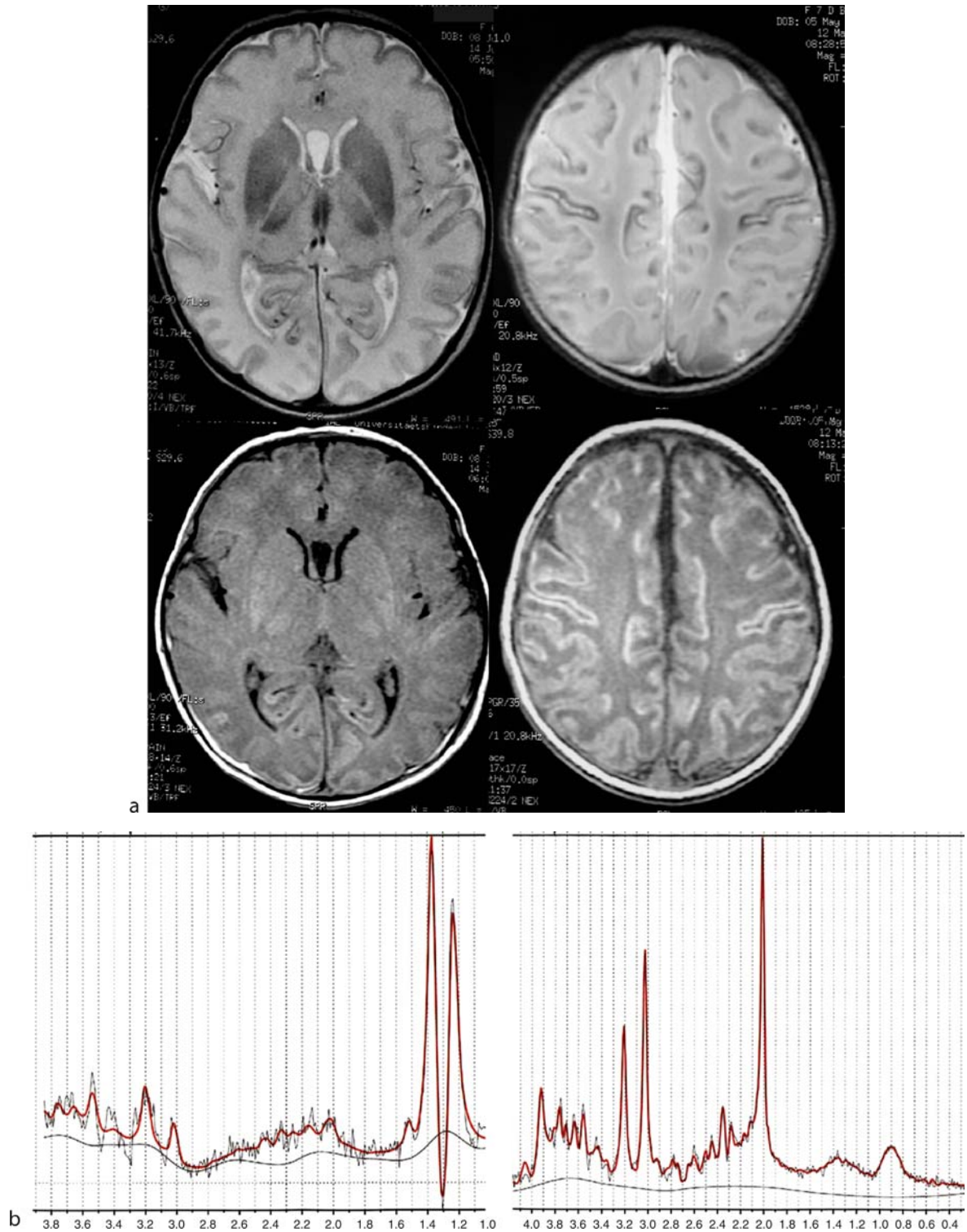

Cerebral Neonatal Disease (Neuro View). Figure 1 (a) Axial T2-FSE (upper row) and T1-SE (lower row) images of a term neonate with HIE. A diffuse white matter edema is seen with narrowing of the adjacent CSF-spaces. In addition, the T1-hyperintense and T2-hypointense signal intensity of the PLIC is missing. Finally, a T1-hyper- and T2-hypointensity is seen within the cortical ribbon of the central region due to intracortical petechial hemorrhages. (b) 1H-MRS of a child with severe HIE (left spectrum) compared with a 1H-MRS of healthy neonate (right spectrum) shows a significant lactate doublet

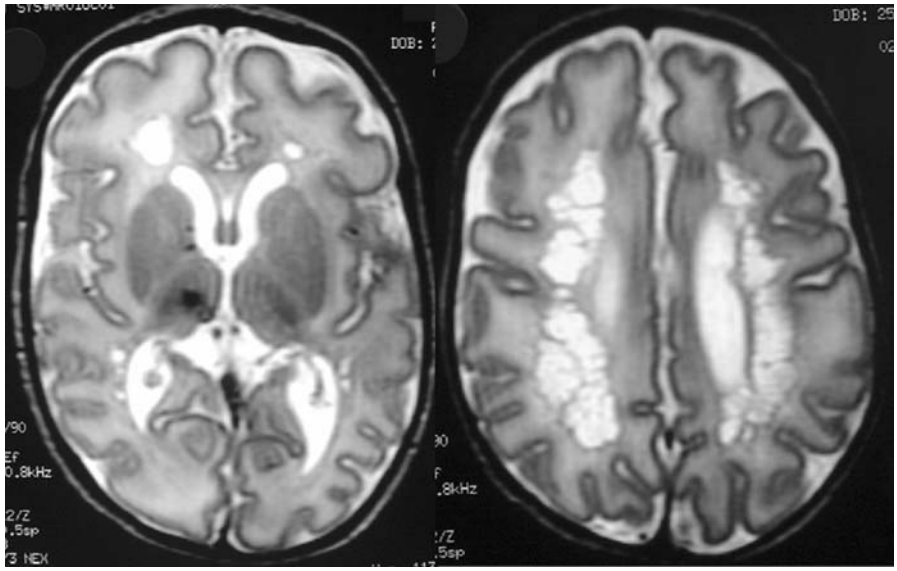

Cerebral Neonatal Disease (Neuro View). Figure 2 Axial T2-FSE in a 4 months old, premature born child with severe HIE. Multicystic leukoencephalopathy within the periventricular white matter is observed with a mild vacuo enlargement of the ventricular system.

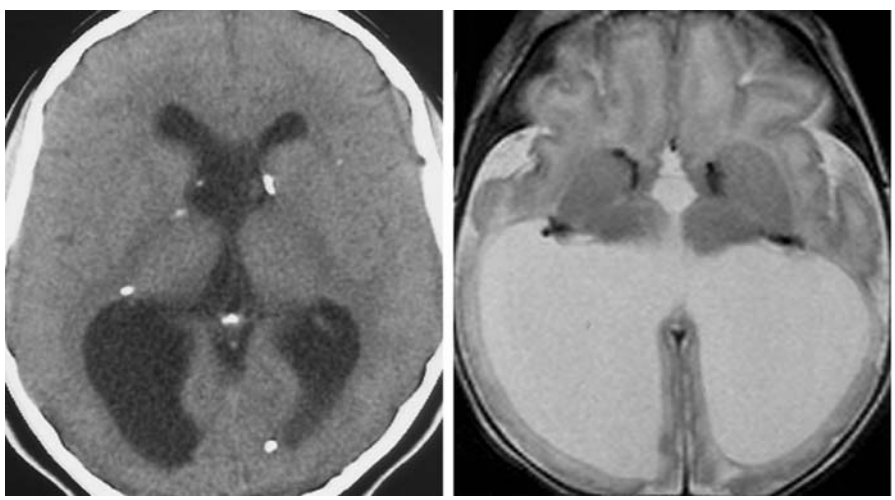

Cerebral Neonatal Disease (Neuro View). Figure 3 Axial CT and T2-FSE in two children with congenital toxoplasmosis infection. CT reveals multiple tiny, subependymal calcifications as well as a ventriculomegaly. MRI shows an identical pattern with T2-hypointense calcifications and a significant ventriculomegaly.

encephalopathy like e.g., neurometabolic diseases, hyperbilirubinemia, congential infections or malformations should be excluded. In addition, dual injury should be considered in complex or unexplained cases of neonatal encephalopathy. Furthermore, additional systemic diseases outside the central nervous system may complicate or aggravate neurological disease (e.g., congenital heart disease). Neuroimaging is increasingly combining anatomical–morphological data with functional results like diffusion tensor imaging, perfusion weighted imaging and qualitative and quantitative proton MR-spectroscopy. The functional data increasingly serves as predictors of outcome.

Bibliography

1. Triulzi F, Baldoli C, Parazzini C (2001) Neonatal MR imaging. Magn Reson Imaging Clin N Am 9(1):57–82
2. Paneth N, Rudelli R, Kazam E et al (1994) Brain Damage in the Preterm Infant (Clinics in Developmental Medicine) pp 22–137

Cerebral Tumors in Childhood

▶Neoplasms, Brain, Supratentorial, Pediatric

Cerebral Vasculature

The blood vessels that supply the brain. The arterial supply comprises the anterior (internal carotid) and posterior (vertebrobasilar) circulations that are linked through the circle of Willis.

▶Stroke, Children

Cerebral Venous Thrombosis

Shelley Renowden
Department of Neuroradiology, University of Bristol, Bristol, UK
shelley.renowden@north-bristol.swest.nhs.uk

Definition

One to two percentage of all adult strokes result from cerebral venous sinus thrombosis (VST). The real incidence of VST is unknown.

The sinuses most commonly affected are the superior sagittal (70–80%), transverse and sigmoid sinuses (70%) and less often, the cavernous and straight sinuses. In one third, more than one sinus is involved and in 30–40%, cerebellar and cortical vein thrombosis is associated. Venous anatomy is illustrated in Fig. 1.

Aetiology

There are many causes of VST but aetiology is unknown in one-third (1). Often multiple factors contribute. The most common are pregnancy and the puerperium, the contraceptive pill, coagulopathies and intracranial infections. Others causes include all causes of deep venous thrombosis, head and neck infections and cranial tumours.

Clinical Features

Presentation varies and may be acute, sub-acute or chronic, dependent upon venous collaterals, thrombus location and rate of progression (1).

Headache is the most common symptom in 74–90% of patients and reflects venous congestion. In 15%, presentation mimics sub-arachnoid haemorrhage (SAH).

Venous occlusion and hypertension may significantly elevate intracranial pressure (ICP) and additionally cause dizziness, nausea, visual disturbance and papilloedema, mimicking idiopathic intracranial hypertension (IIH).

Focal neurological deficits and seizures, which may be focal, occur and may be associated with a Todd's paresis.

Deep venous involvement may result in infarction of the basal ganglia, thalamus, and hypothalamus and these patients may deteriorate rapidly with coma and long tract signs.

Diagnostic Imaging

Cranial CT

Routine cranial CT is normal in 20% but is often the first line of investigation.

Pathognomonic signs of VST are the cord sign (in 25%) and the empty delta sign (in up to 46%) (Fig. 2). Thrombosed cortical veins and sinuses appear dense on plain CT (Fig. 3a). Unfortunately, interpretation is sometimes difficult (2). Flowing venous blood often may mimic dense clot in a sinus. Beam hardening artifact from the skull vault may mimic dense thrombus in the transverse sinuses and partial volume artifact may obscure clot within the horizontal portion of the superior sagittal sinus (SSS) or the transverse sinus (TS).

Other signs include generalised (48%) (Fig. 3) or focal brain swelling (3%), white matter oedema (12%), venous infarction (13%) (Fig. 3), parenchymal haemorrhage (33%), sub-dural haematoma (8%) and tentorial or falcine enhancement indicating venous stasis or dural hyperaemia (19%).

CT Venography

Multichannel helical CT enables 3D vascular imaging. Large volumes of tissue may be scanned during peak venous enhancement with high spatial resolution and triplanar reconstruction clearly demonstrates the veins and sinuses. CTV is unaffected by flow related artifacts

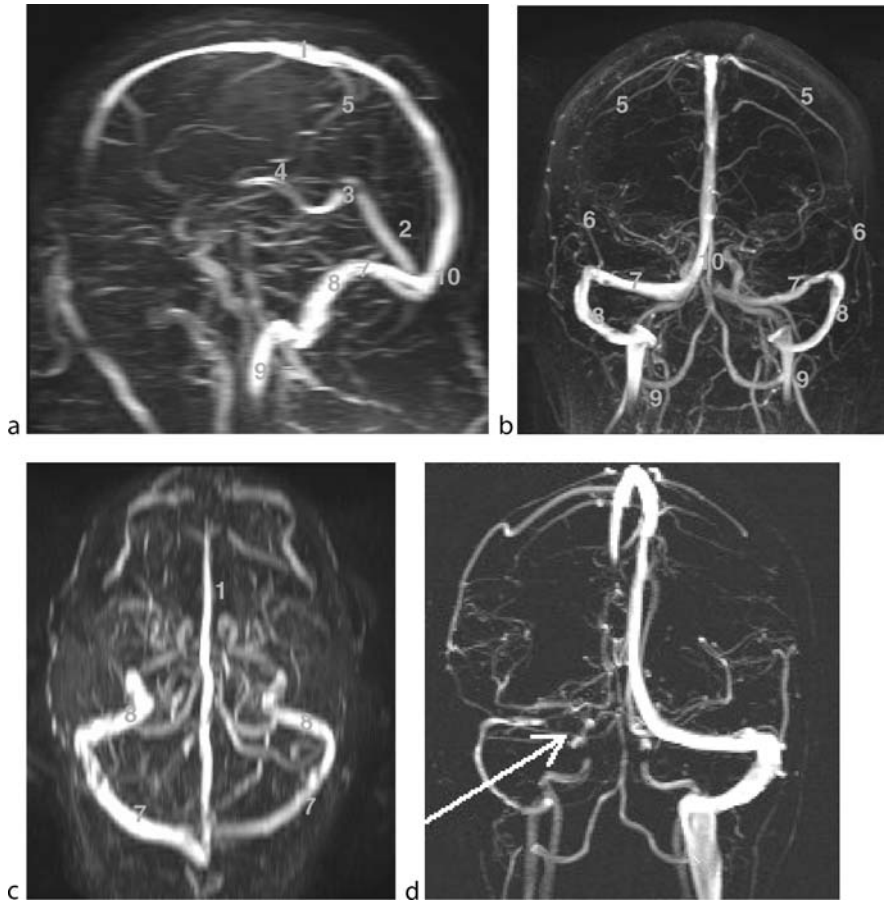

Cerebral Venous Thrombosis. Figure 1 Lateral (a) and frontal (b) 3D phase contrast reformatted MR venograms demonstrate venous sinus anatomy (1 = superior sagittal sinus; 2 = straight sinus; 3 = vein of Galen; 4 = internal cerebral veins; 5 = cortical vein; 6 = vein of Labbe; 7 = transverse sinus; 8 = sigmoid sinus; 9 = jugular vein; 10 = torcula).

(3). It may be used in uncooperative patients as acquisition times are very short and it is clearly useful in those in whom MRI is contraindicated. There may however be problems with background bone suppression and optimal timing of image acquisition is important to minimize arterial and venous superimposition.

Magnetic Resonance Imaging (MRI)

MRI is the preferred method (combined with magnetic resonance volumetry [MRV]) for diagnosis and follow up in our institution. Parenchymal abnormalities are seen more readily on MRI than on CT. It is important, at least for the initial diagnosis, to combine MRI in different planes with MRV. This combination importantly minimises confusion with sinus aplasia/hypoplasia (seen as a flow gap on MRV) and flow related artifacts with thrombus.

On T1W a thrombus appears isointense in the first days, then remains hyperintense during approximately 10 days and becomes isointense again after 2–3 weeks.

On T2W the thrombus appears hypointense during approximately 10 days and then becomes hyperintense (Fig. 4) (4).

MRV

Two dimensional or three dimensional time-of-flight (TOF) or phase contrast (PC) sequences may be used.

The author favours 3D PC sequences. Although TOF sequences have shorter acquisition times, good spatial resolution, and cover a larger volume, optimal signal is only returned when the slices are aligned perpendicular to direction of flow and signal loss arises from the in-plane saturation effect and from slow flow and intravoxel phase

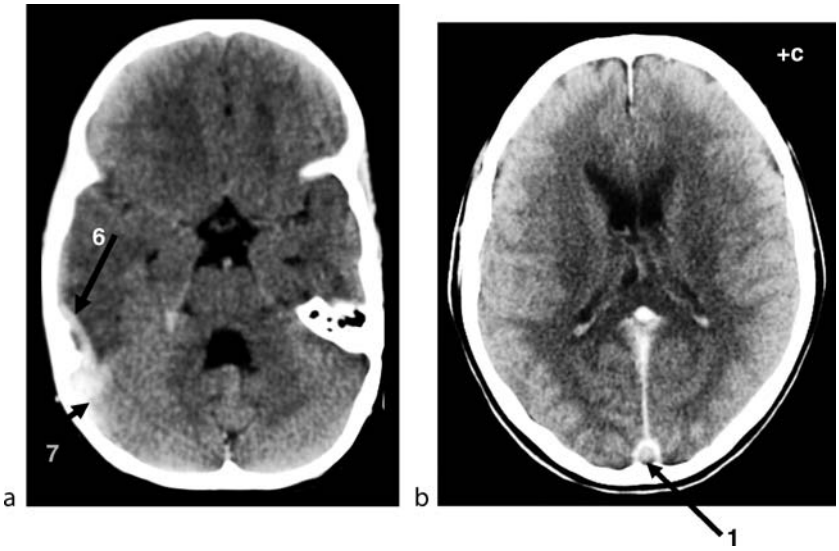

Cerebral Venous Thrombosis. Figure 2 **Axial unenhanced cranial CT scan (a) demonstrates the cord sign as dense thrombus in the right vein of Labbe (6, thin arrow) and right transverse sinus (7, thick arrow). Contrast enhanced axial cranial CT scan (b) demonstrates the "empty data sign" (arrow). Intraluminal thrombus is seen as a filling defect within the enhanced walls of the superior sagittal sinus (I).**

dispersion with turbulent flow. An additional problem associated with TOF MRA is that the hyperintense signal from methaemoglobin within clot may mimic flow.

PC is not associated with maximum intensity projection (MIP) or in plane saturation artifacts but the disadvantages are longer acquisition times, aliasing artifacts and intravoxel phase dispersion.

A hypoplastic/aplastic sinus may mimic sinus occlusion on MRV and must be differentiated by examination of the source images and triplanar MRI. 'Flow gaps' in the transverse sinuses due to hypoplasia may be seen in nearly one third of normals mostly in the non-dominant sinus or co-dominant sinus (5).

Small filling defects may also result from fat, fibrous bands and septae and arachnoid granulations.

Cerebral Angiography

Cerebral angiography is not generally used for diagnosis of VST and is usually only performed as part of local thrombolysis. Partial or complete non-opacification of venous sinuses and veins, dilated cortical collateral veins with a corkscrew appearance, increased cerebral circulation transit time and flow reversal away from the obstructed sinus or vein are signs that may be present.

Treatment

VST is poorly understood, unpredictable, diverse in presentation and causation, with variable sinus/venous involvement, and while potentially life-threatening (see Fig. 3) has a high incidence of spontaneous recovery. Treatment regimens are therefore impossible to compare and should be somewhat individualised.

Although there are few randomised control trials, heparin is considered by most to be the drug of first choice. Complications are rare and haemorrhagic infarction is not a contraindication. Heparin may act by limiting thrombus extension and promote its dissolution and is usually followed by oral anticoagulation for 3–6 months or longer with coagulopathies.

Pharmacological local thrombolysis is performed at our institution if the patient is in coma at the outset or if there is clinical deterioration despite full anticoagulation. It involves the selective delivery of thrombolytic agent directly into the occluded sinus. Local thrombolysis is usually performed *via* the transvenous femoral route. The patient is anticoagulated using heparin. Either urokinase or rt-PA is delivered directly into the clot using either bolus hand injections or an infusion. Recombinant tissue-type plasminogen activator (rt-PA) is often preferred because it has a greater affinity for plasminogen bound to fibrin rather than circulating plasminogen and thus has a reduced systemic effect. Recanalisation is faster with rt-PA than with urokinase. Extensive mechanical disruption of the clot by the micro-guide wire is important and clot maceration may be further enhanced if necessary using a balloon catheter or microsnare device.

The objective in most cases is complete recanalisation but while this is desirable, experience suggests that

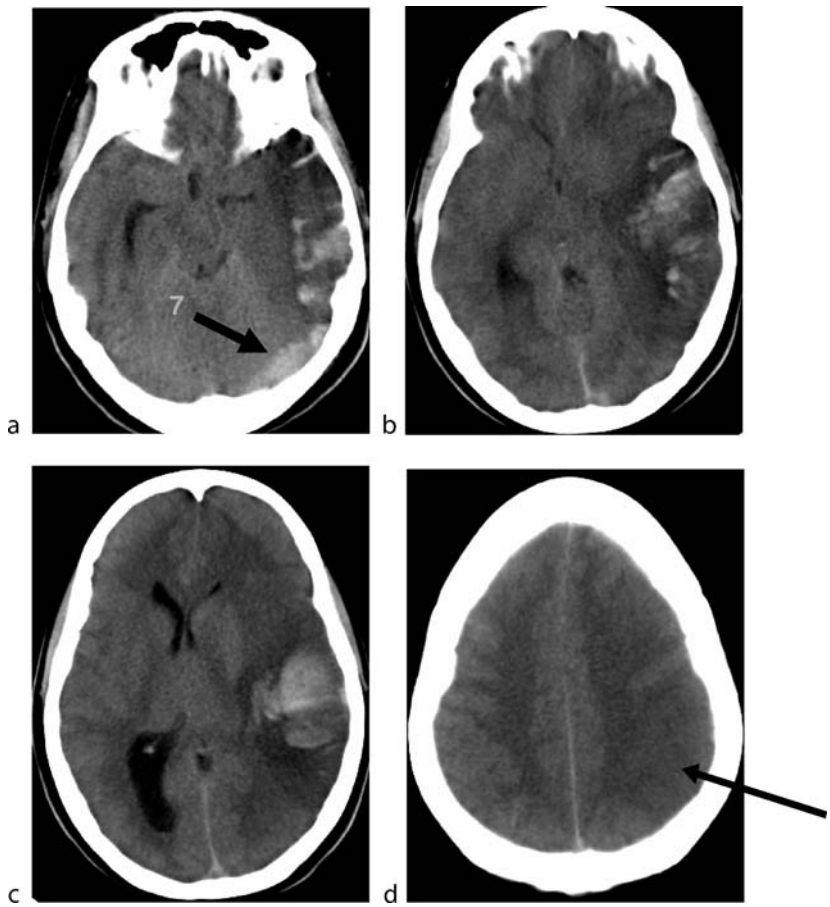

Cerebral Venous Thrombosis. Figure 3 Axial unenhanced cranial CT images (a–d) demonstrate severe consequences of venous sinus thrombosis, rapidly fatal in this 17-year-old girl, despite local thrombolysis. The dominant left TS, sigmoid sinus and jugular vein are occluded. Thrombus extended up to the torcula and then started to propagate in a congested SSS. The right TS is hypoplastic unfortunately. There is generalised cerebral swelling with effacement of the sulci, basal cisterns and third ventricle. There is bilateral uncal herniation with midbrain compression (a, b). Haemorrhagic venous infarction (a–c) involves the left temporal lobe and additional swelling has resulted in compression of the left lateral ventricle, midline shift and contralateral hydrocephalus. Parenchymal oedema reflecting venous hypertension is present in the left parietal and frontal lobes (d, arrow). There is a small amount of blood in the right occipital horn.

complete recanalisation is not always necessary for a good outcome.

Catheter mediated thrombectomy using a saline jet vacuum device has also been described and is used together with local pharmacological thrombolysis. It should probably be reserved for those with extensive thrombosis and malignant intracranial hypertension.

Outcome

Outcome is often favourable. Mortality ranges between 5.5–30% and a further 15–25% will incur permanent neurological deficits. Mortality is high in those presenting with a rapid onset, in coma, in infancy, in the aged and with involvement of the cortical, deep and cerebellar veins. VST recurrence is estimated in about 12% of patients.

Dural and pial arteriovenous fistulae may occasionally occur following VST thrombosis. Venous hypertension may promote growth of microscopic arteriovenous-shunts within the vasa vasorum of the normal pachymeninges and/or may stimulate the release of angiogenic factors.

References

1. Van Gijn J (2000) Cerebral venous thrombosis: pathogenesis, presentation and prognosis. J Royal Society of Medicine 93:230–233
2. Provenzale JM, Joseph GJ, Barboriak DP (1998) Dural sinus thrombosis: findings on CT and MR imaging and diagnostic pitfalls. AJR 170:777–783

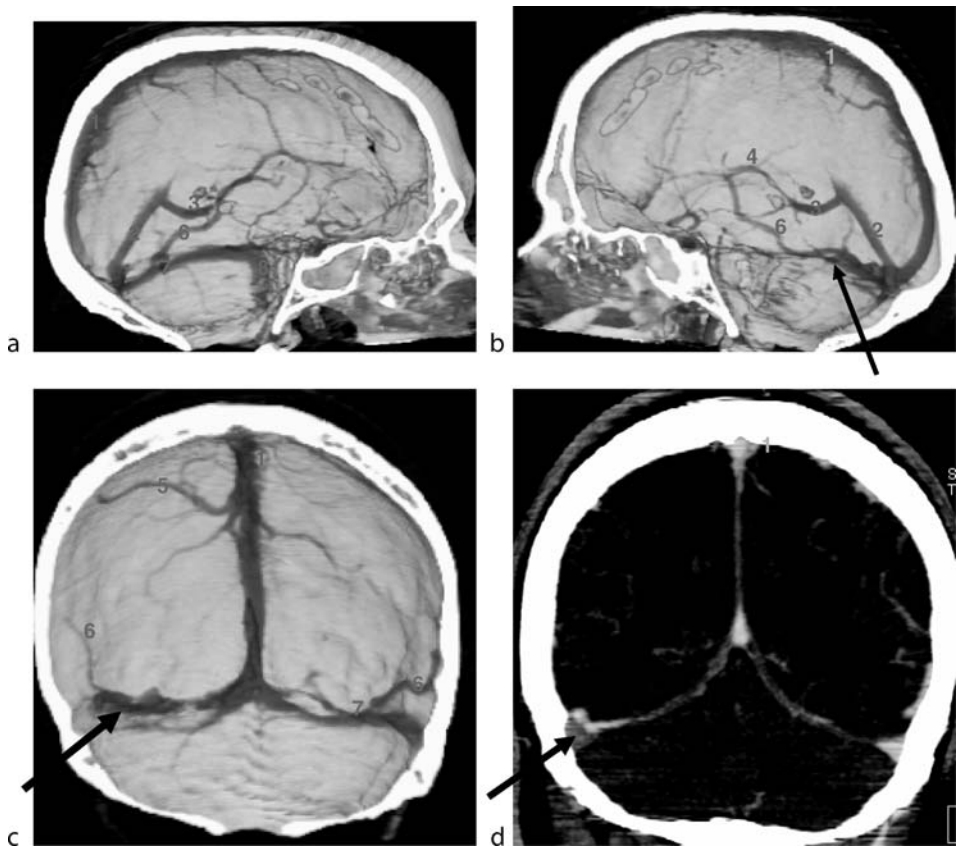

Cerebral Venous Thrombosis. Figure 4 CT venography with sagittal (a, b) and coronal (c) reconstructions and a mipped coronal image (d) demonstrate thrombus in the right transverse sinus. Venous antomy is again well demonstrated and the numbering is as in Figure 1.

3. Ozsvath RR, Casey SO, Lustrin ES et al (1997) Cerebral venography: comparison of CT and MR projection venography. AJR 169: 1699–1707
4. Bianchi D, Maeder Ph, Bogousslavsky J et al (1998) Diagnosis of cerebral venous thrombosis with routine magnetic resonance: an update. European Neurology 40:179–190
5. Ayanzen RH, Bird CR, Keller FJ et al (2000) Cerebral MR venography: normal anatomy and potential diagnostic pitfalls. AJNR 21:74–78

Cervical Carcinoma

▶Carcinoma, Cervix Uteri

Cervicomedullary Angle

Cervicomedullary angle is the angle between two lines on, respectively, the ventral side of the medulla oblongata or brainstem and the cervical cord, in degrees. A decrease <135° is a risk factor for the development of myelopathy in patients with rheumatoid arthritis with cervical spine affection.

▶Rheumatoid Arthritis

Cervix

The cervix is the lower and narrow part of the uterus, which forms a canal that opens into the vagina.

▶Carcinoma, Cervix Uteri

CEUS

Contrast-enhanced ultrasound.

▶Contrast Media, Ultrasound, Safety and Adverse Reactions

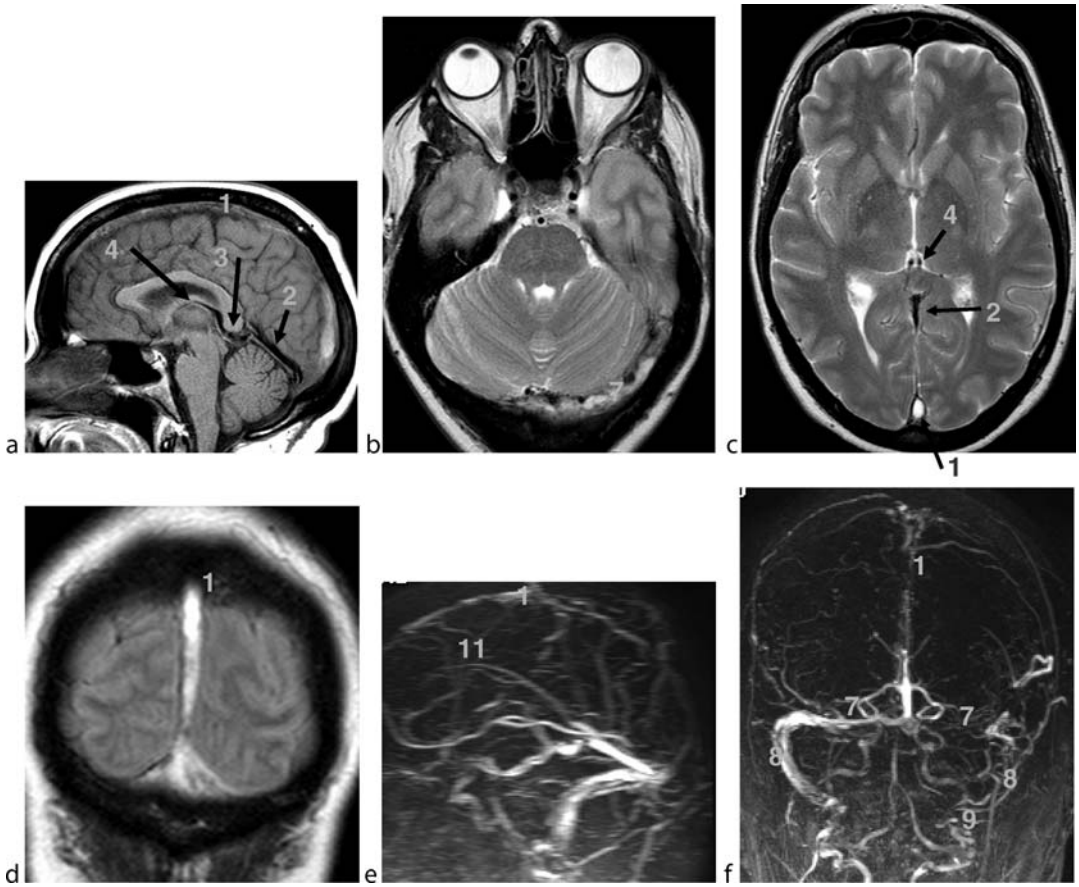

Cerebral Venous Thrombosis. Figure 5 T1W sagittal (a) and T2W (b, c) axial and coronal FLAIR (d) MR images demonstrate signal from sub-acute clot in the SSS and left TS, hyperintense on both T1W and T2W. Note the normal flow voids seen in the SS and deep venous system (a, c). Lateral (e) and frontal (f) projections of a 3D PC MR venogram in the same patient confirm occlusion of these sinuses and the left sigmoid sinus and jugular vein. The patient suffered increasingly severe headaches over 3–4 weeks. The clinical severity here is much less than the patient in Fig. 3 almost certainly reflecting the less rapid onset and superior venous collateralisation.

CEUS – Contrast-Enhanced Ultrasound of the Kidneys

▶Contrast Media, Ultrasound, Applications in Kidney Tumor

CFNP

▶Central Facial Nerve Paralysis (CFNP)

Charcot Neuroarthropathy

▶Neuropathic Joint Disease

CHARGE Association

The acronym refers to a clustering of malformations that occurs more frequently together than expected on the basis of chance. The diagnosis is firmly established when

all major criteria or three major and three minor criteria are present. Major criteria are coloboma (C), choanal atresia (A), typical external ear anomaly and/or hearing defects (E) and brain stem and cranial nerve dysfunction. Minor criteria are heart defects (H), genital hypoplasia (G), orofacial clefting, tracheoesophageal fistula, short stature and developmental delay (R).

▶Congenital Malformations, Nose and Paranasal Sinus

Chelator

Linking molecule between vector and radionuclide. The chelator defines with which radionuclides a vector can be labeled. Stable binding of the radionuclide by the chelator is mandatory for application of a radiopharmaceutical in patients.

▶Receptor Studies, Neoplasms

Chemoembolization

Thomas Rand
Allgeneines Krankenhfus-Universitätzkliniken
Vienna, Austria
thomas.rand@akhwien.at

Synonyms

Liver embolization; TACE

Definition

Transarterial chemoembolization (▶TACE) is based on the injection of a chemotherapeutic agent, mixed with an embolic material, into selected branches of the hepatic arteries feeding a liver tumor. This concept derives from the pathophysiological background of liver perfusion: Hepatocellular carcinoma (HCC) tumors are hypervascular and receive their blood supply from the hepatic artery. Normal liver receives approximately 70% of its blood supply from the portal vein and 30% from branches of the hepatic artery. The rational for TACE is that the infusion of a drug such as Doxorubicin, Mitomycin C, and Cisplatin with a viscous material (e.g. lipiodol) followed by embolization of the blood vessel with Gelfoam, PVA particles or spherical embolic agents will occlude arterial blood supply to the tumor causing an infarct and subsequent necrosis of the tumor. The advantage of TACE is that higher concentrations of the drug can be delivered to the tumor with decreased systemic exposure as compared with systemic chemotherapy.

Other hypervascular malignancies that might be considered derive from gastrointestinal neuroendocrine tumors that have been currently extensively reclassified. Management of these tumors nowadays include a more radical surgical approach of treatable tumor masses and treatment of liver metastases by embolization or thermoablation (1, 2).

Pathology/Histopathology

(HCC is the fifth most common cancer in the world and represents more than 5% of all cancers with an estimated annual incidence of about 1 million cases. Approximately 500,000 cases of HCC are diagnosed each year and it is the third cause of cancer-related deaths (3). There are wide geographical variations in the incidence of the disease with the highest rates in the developing countries of Asia and Africa. However, the incidence of HCC is increasing in North America and Europe (4). HCC tends to develop in cirrhotic livers due to hepatitis B and C virus, iron overload states, or alcohol abuse.

Clinical Presentation

Despite advances in diagnosis and treatment, the overall 5-year survival rate is only 2%. It is generally accepted that surgical resection, liver transplantation, and percutaneous tumor ablation are the only curative treatment options for patients with early stage HCC. Curative surgical resection is not feasible in many patients, therefore palliative approach is frequently considered to limit tumor progression. Today, several treatment modalities are discussed and compared. Multiple specialities are required for optimal treatment. Treatment options and prognosis depend on tumor stage and the cirrhotic background. Untreated HCC carries a poor prognosis and is directly related to the degree of underlying cirrhosis and tumor stage. Early detection offers the only possibility for cure. In patients with large tumor mass and Child C cirrhosis, patient survival is not more than 6 months. Patients with small HCCs (<5 cm diameter) and stable liver function have a better prognosis with 2-year survival rates of up to 56% (5).

Approximately 75% of HCC patients are not candidates for curative treatments either due to poor liver function or the presence of advanced disease. Nonsurgical treatments for unresectable HCC include systemic chemotherapy and radiotherapy, but these treatments have not

been found to prolong survival in randomized clinical studies. Chemotherapeutic agents (e.g. Doxorubicin) can be infused directly into the systemic circulation. However, serious side effects may arise, such as pain, nausea, vomiting, myelosuppression, and alopecia, or even cardiac toxicity.

From therapeutic aspects, arterial embolization achieves partial response in 15–55% of patients and significantly delays tumor progression and vascular invasion (6–9). Two major studies have reported the benefits for chemoembolization in selected patients. Llovet et al reported 1- and 2-year survival probabilities of 82% and 63% with objective response sustained for at least 6 months in 35% of cases (9). Lo et al found significant improvement in survival for Asian HCC patients treated by chemoembolization with a Lipiodol/Cisplatin emulsion and gelatin sponge (8). A systemic review and meta-analysis of randomized clinical trials for unresectable HCC has shown a survival benefit of chemoembolization (10). Innovative studies dealt with potential application of TACE in patients scheduled for liver transplantation: Graziadei and Jaschke et al demonstrated that TACE can be highly effective in preventing tumor progression in patients listed for liver transplantation, but failed to show beneficial effects on patient survival in advanced-stage HCCs (11). Thus, the best candidates for chemoembolization are those with preserved liver function and asymptomatic multinodular tumors without invasion or extrahepatic spread.

New strategies are also in discussion regarding technical aspects and innovations in mixture and application of chemotherapeutic and embolic agents.

Until now, generally superselective application of the chemotherapeutic drug to the tumor was followed by its embolization with microparticles, each procedure done as one step. Recent studies (12) have shown advantages of application of the embolic agents (microspheres) that are already loaded with doxorubicin.

Imaging

The procedure itself is monitored by fluoroscopy and digital subtraction angiography (DSA).

Interventional Radiological Treatment

Before Embolization

Clinical status, residual liver function, and blood parameters must be evaluated before the embolization procedure.

Contraindications for transarterial embolization are advanced tumor stages and/or advanced cirrhotic disease (Child C, Okkuda III) or other stages of uncontrolled liver disease, bacterial infection, presence of complete portal vein thrombosis, and contraindications for arterial access.

Informed consent for the embolization procedure must be obtained and the palliative aspect of chemoembolization should be evident.

Embolization Procedure

Transarterial embolization is performed according to a standardized technique. Hydration, analgesics, and antiemetics are administered before and during treatment. The femoral artery is catheterized under local anesthesia, and diagnostic angiography of the celiac trunk and superior mesenteric artery is usually performed with use of Sidewinder-configurated catheter. After identification of the vascular anatomy, a superselective highly flexible coaxial 3French microcatheter, is advanced into the hepatic arteries.

Arterial embolization is performed, when possible, through catheterization of feeding arteries of the tumor as selectively as possible.

When separately applied, the chemotherapeutic agents are administered prior embolization with microparticles. Embolization particles are then mixed with the contrast media and injected under fluoroscopic control, according to the location of the HCC, using sizes from 100 nm up to 700 nm (Fig. 1). Alternatively, as an innovative technique, microparticles can also be loaded directly with the chemotherapeutic agent and be used as a carrier and embolization agent at the same time. This technique shows very promising results. The procedure ends when complete occlusion of the arteries feeding the tumor is achieved. When injecting contrast agents, stasis is observed. Later embolizations are performed identically when CT follow-up indicates tumor progression or inadequate treatment response.

Dose Selection

The standard doxorubicin dose mixed with Lipiodol is adjusted to the serum bilirubin level as follows: bilirubin value of <1.5 mg/dL-75 mg/m^2 doxorubicin; bilirubin value of 1.5–3 mg/dL-50 mg/m^2. On average, patients receive 50–100 mg of doxorubicin in a single session. Embolization particles are used in sizes from 100 nm up to 700 nm. Treatment is applied periodically after 2–4 months, accounting for 2–4 treatments per year.

Further Medication, Follow-Up

Pain medication and antibiotics are given systematically, further conservative medication might be necessary in

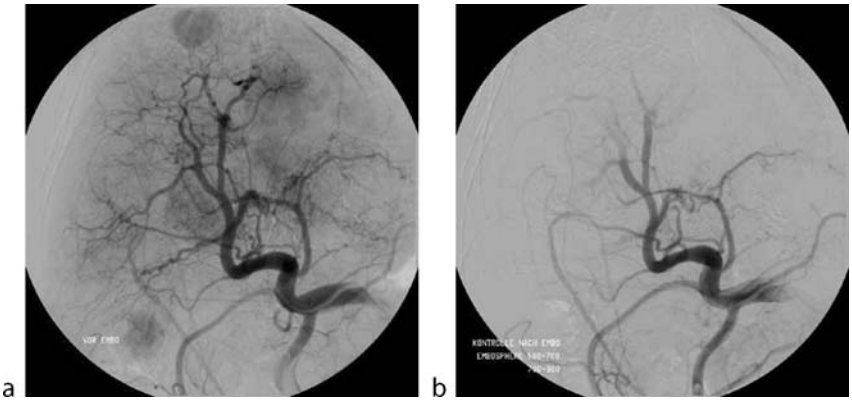

Chemoembolization. Figure 1 Multicentric HCC before (Fig. 1a) and after (Fig. 1b) TACE.

cases of a postembolic syndrome. Follow-up should be performed by CT or MR imaging and is usually applied 5–6 weeks postembolization.

References

1. Marlink RG, Lokich T, Robins SR et al (1990) Hepatic arterial embolization of metastatic hormone secreting tumors. Cancer 65:2227–2232
2. Kloeppel G, Heitz PU, Capella C et al (1996) Pathology and nomenclature of human gastrointestinal neuroendocrine 8carcinoid) tumors and related lesions. World J Surg 20:132–141
3. Parkin DM, Bray F, Ferlay J et al (2001) Estimating the world cancer burden: Globocan 200. Int J Cancer 94(2):153–156
4. El-Serag HB, Mason AC (1999) Rising incidence of hepatocellular carcinoma in the United States. N Engl J Med 340(10):745–750
5. Barbara L, Benzi G, Gaiani S et al (1992) Natural history of small untreated hepatocellular carcinoma in cirrhosis: a multivariate analysis of prognostic factors of tumor growth rate and patients survival. Hepatology 16:132–137
6. Lin DY, Liaw YF, Lee TY (1988) Hepatic arterial embolization in patients with unresectable hepatocellular carcinoma-a randomised controlled trial. Gastroenterology 94(2):453–456
7. Pelletier G, Roche A, Ink O et al (1990) A randomized trial of hepatic arterial chemoembolization in patients with unresectable hepatocellular carcinoma. J Hepatol 11(2):181–184
8. Lo CM, Ngan H, Tso WK et al Randomized controlled trial of transarterial lipiodol chemoembolization for unresectable hepatocellular carcinoma. Hepatology 35(5):1164–1171
9. Llovet JM, Real MI, Montana X et al (2002) Arterial embolization or chemoembolization versus symptomatic treatment in patients with unresectable hepatocellular carcinoma: a randomised controlled trial. Lancet 359(9319):1734–1739
10. Llovet JM, Bruix J (2003) Systemic review of randomised trials for unresectable hepatocellular carcinoma: chemoembolization improves survival. Hepatology 37(2):429–442
11. Graziadei IW, Sandmueller H, Waldenberger P et al (2003) Chemoembolization followed by liver transplantation for hepatocellular carcinoma impedes tumor progression while on the waiting list and leads to excellent outcome. Liver Transpl 9(6):557–563
12. Lammer J (2005) Prospective Study of Doxorubicin in the Treatment of Hepatocellular Carcinoma (HCC) by Drug-Eluting Bead Embolisation (PRECISION V-Study) The Vienna Experience. CIRSE, presentation

Chemonucleolysis

A proteolytic enzyme called chymopapain is injected into the centre of the intervertebral disc in order to induce hydrolysis of the proteoglycan molecules that form the nucleus pulposus. The resulting proteoglycan fragments have limited water-binding abilities, which leave intradiscal water molecules free to diffuse into the surrounding tissues. The resulting loss of water causes a decrease of intradiscal pressure. This causes the herniated portion of the nucleus pulposus to recede towards the centre of the disc, relieving pressure on the nerve root.

▶Percutaneous Interventions for Lumbar Radicular Syndrome

Chemoperfusion

THOMAS RAND
Allgeneines Krankenhfus-Universitätzkliniken
Vienna, Austria
thomas.rand@akhwien.at

Definition

Chemoperfusion is a locoregional treatment used as an adjuvant therapy in locally advanced tumors and as palliation in inoperable tumors. Intra-arterial locoregional chemoperfusion has been performed as a palliative therapy in bleeding bladder cancer, in the therapy of head and neck carcinomas, in inoperable pancreatic

carcinomas and local recurrence, and in hepatic metastases from breast carcinoma (1, 2). However, serious side effects have been observed, and in light of innovative embolic agents with the option of combining chemotherapy and embolic procedures, arterial chemoperfusion is only rarely applied today. As a nonvascular variation, intraperitoneal hyperthermic chemoperfusion is performed in tumors originating from the genital and gastrointestinal systems, in addition to surgical debulking of tumor masses (3, 4).

Characteristics

Locoregional Chemoperfusion

Clinical Background

Locoregional chemoperfusion of inoperable pancreatic carcinoma or of cases of local recurrence has been used to reduce side effects and provide clinical benefits. However, only a small series of patients have been studied (2).

Locoregional therapy of head and neck carcinomas (PEC) has been performed with the superselective application of cisplatin (5). The concept of this therapy is based on the simultaneous transarterial locoregional application of cisplatin and the systemic venous application of sodium thiosulfate. After its arterial passage, cisplatin is bound to the circulating sodium thiosulfate in a complex that makes the cisplatin ineffective and thus prevents systemic side effects of the chemotherapeutic agent. Additional pain medication is mandatory.

Technique

Locoregional application of chemotherapeutic agents is performed *via* superselective arterial catheterization, with the introducer sheet in the femoral artery. Selective angiographies are performed to evaluate the tumor feeding arteries and the arterial vascularization of the neoplasm.

Arterial embolization is performed, when possible, through catheterization of feeding arteries to the tumor as selectively as possible using a highly flexible coaxial 3 French microcatheter, analogous to transarterial chemoembolization (TACE). In contrast to TACE, however, only the chemotherapeutic agent is applied, without further embolization.

Hyperthermic Perfusion Chemotherapy

Clinical Background

Intraperitoneal hyperthermic perfusion chemotherapy (IHCP) is a locoregional treatment modality that is used as adjuvant treatment in locally advanced operable tumors and as palliation in inoperable tumors with the goal of treating peritoneal seedings and peritoneal micrometastases.

The intraperitoneal administration of cytotoxic agents has been used since 1980 (6, 7). The first aim of this method is the eradication of microscopic residual disease. It has the benefit of higher concentrations of drugs being delivered locally to the tumor site, while preventing the systemic toxic effects compared with intravenous administration. The efficacy of a drug is calculated by the ratio of the peritoneal cavity area under the concentration/time curve to the plasma area under the concentration/time curve. This ratio is between 250 and 1400 for 5-fluorouracil, 12 and 20 for cisplatin, and 75 and 80 for mitomycin C. The efficacy is increased with the slow absorption rate of cytotoxic drugs. Hydrophilic drugs like 5-fluorouracil, cisplatin, and mitomycin C are absorbed very slowly from the peritoneal surface, and therefore they are the most useful drugs for IHCP. Beyond this, the direct tumor absorption of drugs occurs up to a level of 5 mm beneath the tumor surface, which means tumor nodules exceeding 5 mm are not suitable for IHCP. In this technique, the cytotoxic effect of hyperthermia also enhances the efficacy by maximizing the diffusion of the drugs to the tumoral nodules.

In gastric cancer, IHCP can also be used as a neoadjuvant (preoperative) substance for down-staging, but the most preferential use is the adjuvant route. Takahashi and Hagiwara used activated carbon particles in the peritoneal cavity, which adsorbed a large amount of mitomycin C, in gastric cancer patients with definite serosal involvement (8, 9). They found a 2- and 3-year survival advantage of 14 and 18%, respectively, compared with control groups. In other studies that used cisplatin or mitomycin C in early postoperative intraperitoneal chemotherapy, statistically significant survival advantages were found against control groups and it was determined that this advantage occurred especially in stage III diseases. Fujimura et al reported 40% complete remission and 1- and 2-year survival rates of 67 and 40%, respectively, after IHCP in gastric cancer patients with peritoneal seeding (10).

Technique

Cytoreductive surgery consists of the removal of all gross tumors and involved organs or peritoneum. At the end of the operation two drains are inserted in the peritoneal cavity and after the closure of the abdomen, an extracorporeal circuit is used to conduct IHCP,

allowing perfusate circulation at 300–500 ml/min and hyperthermia ranging from 40 to 42°C for 60–90 min. The perfusate consists of 3 L of saline solution with cytotoxic drugs, for example, 10 mg/L mitomycin C is recommended because of its high penetration rate to micronodules and low absorption rate across the peritoneal surface. At the end of the perfusion, 1 L of perfusate is emptied and the rest is left in the abdomen for 12 h.

Bibliography

1. Textor HJ, Wilhelm K, Strunk H et al (2000) Locoregional chemoperfusion with mitoxantrone for palliative therapy in bleeding bladder cancer compared with embolization. Rofo 172(5):462–466
2. Vogl TJ, Heller M, Zangos S et al (2003) Transarterial chemoperfusion of inoperable pancreas carcinoma and local recurrence. Rofo 175(5):695–704
3. Reichman TW, Cracchiolo B, Sama J et al (2005) Cytoreductive Surgery and Intraoperative Hyperthermic Chemoperfusion for advanced ovarian carcinoma. J Surg Oncol 90:51–58
4. Erhan E, Haluk A (2004) The effectiveness of adjuvant intraperitoneal hyperthermic chemoperfusion after cytoreductive surgery in locally advanced gastric cancer. Indian J Surg 66:277–280
5. Rohde S, Kovacs AF, Zanella FE et al (2005) [Local chemotherapy for squamous cell cancer of the oral cavity and oropharynx] Radiologe Sep 45(9):843–50
6. Spratt JS, Adcock RA, Muskovin M et al (1980) Clinical delivery system for intraperitoneal hyperthermic therapy. Can Res 40:256–260
7. Howell SB (1980) Pharmacokinetic principles of regional chemotherapy. Contr Oncol 29:1–8
8. Takahashi T, Hagiwara A, Shimotsuma M (1994) Intraperioneal chemotherapy with mitomycin C bound to activated carbon particles for patients with advanced gastric cancer. Eur J Surg Oncol 20:183–184
9. Hagiwara A, Takahashi T, Kojima O et al (1992) Prophylaxis with carbon- absorbed mitomycin against peritoneal recurrence of gastric cancer. Lancet 339:629–631
10. Fujimura T, Yonemura Y, Fushida J et al (1990) Continuous hyperthermic peritoneal perfusion for the treatment of peritoneal dissemniation in gastric cancers and subsequent second-look operation. Cancer 65:65–71

Chemotherapy

This is a treatment with anticancer drugs that may be given intravenously or orally. The drugs travel through the bloodstream to reach cancer cells in most parts of the body. When used as *adjuvant therapy* after breast conservation therapy or mastectomy, chemotherapy reduces the risk of breast cancer recurrence. Chemotherapy given before surgery is called *neoadjuvant therapy.*

▶Breast, Therapy Effects

Chest

Hans-Ulrich Kauczor
Department of Radiology, German Cancer Research Center, Heidelberg, Germany
hu.kauczor@dkfz-heidelberg.de

C

Chest radiology is one of the recognized subspecialty areas of radiology. In the last decade remarkable advances in the ability to vividly image both normal anatomic and pathophysiologic aspects of the lungs and other thoracic structures have been accomplished. All the different imaging modalities, such as projection radiography, computed tomography (CT), magnetic resonance imaging, ultrasonography, angiography, and nuclear medicine examinations are applied to imaging of pulmonary, pleural, and mediastinal diseases. Cardiac and vascular diseases are covered separately. This entry focuses on adult radiology; pediatric radiology is covered separately.

Chest radiology is oriented toward disease entities and not imaging modalities. Thus, readers will become familiar with and understand the utility and limitations of all modalities for each particular disease and clinical situation much easier by retrieving the respective information.

To understand the imaging findings in chest radiology and their interpretation, a profound knowledge base of anatomy, histochemistry, and physiology of the lung as well as pathology and pathophysiology of lung diseases is necessary, because such radiological-pathological as well as structural-functional correlations are important.

The chest consists of three major anatomic compartments: (1) lungs, (2) chest wall, and (3) mediastinum.

1. Lungs. The lungs are divided into lobes by fissures, then further into segments, and continue to divide down to the alveolar space represented by pulmonary lobules and acini. The airspaces are supported by airways that have a continuous dichotomous branching structure starting from the trachea, carina, and main stem bronchi, going down to the small airways and bronchioles. The airways are surrounded by connective tissue, and there are distinct bronchovascular bundles and lymphatic and venous pathways within this lung structure.

2. Chest wall. The chest wall itself consists of the rib cage, respiratory muscles including the diaphragm, and soft tissue. The lung is surrounded by the visceral pleura, which has areas of invagination that give rise to the interlobar fissures. The chest wall is covered by the parietal pleura. Between the pleural surfaces is a small amount of fluid, which allows for smooth sliding of the lung during inspiration and expiration.

3. Mediastinum. Apart from the heart and fat, the mediastinum contains multiple different anatomical structures such as arteries, veins, nerves, and lymphatics as well as the esophagus (which belongs to the gastrointestinal tract), the tracheobronchial tree (which belongs to the respiratory tract) and finally, a primary mediastinal organ, the thymus. All of them can be the origin of disease in the mediastinum and also involve other structures. Additionally, adjacent structures such as lungs, pleura, and pericardium can afflict the mediastinum by means of continuous infiltration. The mediastinum is divided into anterior, middle, posterior, and superior parts.

The regular anatomy of the chest can be visualized by all the different modalities, which have particular advantages and disadvantages related to their respective properties. Abnormalities of the normal anatomy require the depiction of normal variants and the diminishment or enlargement of particular structures or organs. It is important to recognize normal image characteristics, structures, and patterns, which can be solitary, multiple, or disseminated. For radiology of the lungs, specific correlations between normal anatomy and pathological changes as well as image morphology have been established. The observations of individual findings can represent "signs" or they can merge to complex patterns that are based on radiological morphology. Such parameters relate radiological-morphological findings to anatomic-pathological substrates. Additionally, the correlation of abnormalities to particular pathophysiologic phenomena or pathological entities is facilitated by the use of image patterns. To understand image patterns, a profound knowledge base of normal anatomy, pathophysiology, and pathology is mandatory for applying these patterns to detect primary vascular, pulmonary, or pleural disease as well as diseases of the mediastinum or chest wall, and in establishing the differential diagnosis of cardiac diseases.

The lung has only a limited number of possible reactions to the wide array of different noxious substances that are related to different disease entities. The radiological patterns reflect the macroscopic consequences of lung disease, and the number of different patterns is thus also limited. The accurate analysis of imaging findings with regard to size, number, morphology, localization, and distribution is the prerequisite for detecting and using image patterns. Image patterns are first of all divided according to the predominant type of the change of attenuation (increase, decrease), the potential change of structure (destruction of lung architecture) and the morphological appearance, including extensive (alveolar, interstitial) or localized (nodular, reticular, reticulonodular), generalized, or focal. Although the commonly used modalities—radiography, CT, and angiography—mainly focus on visualizing structure, the application of magnetic resonance imaging, ultrasonography, and nuclear medicine is directed at elucidating function. Magnetic resonance imaging and nuclear medicine look for disease activity, vascularization, and blood flow as well as ventilation and perfusion, while ultrasound looks for respiratory motion and blood flow.

Signs and Patterns in Chest Radiology

- Air bronchogram—indicates a parenchymal process, including nonobstructive atelectasis, as distinguished from pleural or mediastinal processes
- Air crescent sign—indicates a lung cavity, often due to fungal infection
- Deep sulcus sign on a supine radiograph—indicates pneumothorax
- Continuous diaphragm sign—indicates pneumomediastinum
- Ring around the artery sign (around the pulmonary artery on lateral chest radiograph)—indicates pneumomediastinum
- Fallen lung sign—indicates a fractured bronchus
- Gloved finger sign—indicates bronchial impaction
- Hampton's hump—indicates a pulmonary infarct
- Silhouette sign—loss of the contour of the heart or diaphragm, used to localize a parenchymal process (for example, a process involving the medial segment of the right middle lobe obscures the right heart border, a lingula process obscures the left heart border, and a basilar segmental lower lobe process obscures the diaphragm)
- Scimitar sign—an abnormal pulmonary vein seen in venolobar syndrome
- CT angiogram sign—enhancing pulmonary vessels against a background of low attenuation material in the lung
- Halo sign—suggests invasive pulmonary aspergillosis in a leukemic patient
- Kerley A and B lines
- Honeycombing
- Cystic pattern
- Nodular pattern
- Reticular pattern
- Septal thickening
- Perilymphatic distribution patterns
- Bronchiolar opacities
- Tree-in-bud
- Air trapping
- Ground-glass opacities
- Egg-shell calcifications of lymph nodes
- Cavitation
- Unilateral hyperlucent lung

Lung Diseases

Lung diseases can be divided into several major groups:

Interstitial Lung Disease

- Scleroderma
- Drug toxicity
- Congestive heart failure—enlarged cardiac silhouette, pleural effusions, vascular redistribution, interstitial and/or alveolar edema, Kerley lines
- Asbestos-related pleural disease and asbestosis
- Pneumoconiosis, silicosis, coal worker's pneumoconiosis
- End-stage lung disease
- Sarcoidosis
- Progressive massive fibrosis
- Langerhans cell histiocytosis
- Lymphangioleiomyomatosis

Alveolar Lung Disease

- Acute alveolar lung disease (ALD)
- Pulmonary-renal syndrome
- Acute respiratory distress syndrome (ARDS)
- Cryptogenic organizing pneumonia (COP; bronchiolitis obliterans organizing pneumonia, or BOOP)
- Fat embolization
- Alveolar proteinosis

Atelectasis and Airway and Obstructive Lung Disease

- Partial or complete atelectasis
- Bronchiectasis, cystic fibrosis
- Asthma
- Chronic obstructive pulmonary disease (COPD)
- Tracheomegaly
- Tracheal and bronchial stenosis
- Emphysema and bulla, alpha-1-antitrypsin deficiency
- Kartagener's syndrome

Solitary and Multiple Pulmonary Nodules

Neoplasms

- Non-small cell lung cancer
- Small cell lung cancer
- Adenoid cystic and carcinoid tumors

Chest Trauma

- Contusion, laceration
- Tracheobronchial tear

Infection

- Bacterial pneumonia, typical, atypical
- Tuberculosis
- Fungal pneumonia, including *Pneumocystis carinii* pneumonia and invasive aspergillosis
- Viral pneumonia, including cytomegalovirus pneumonia
- Acquired immune deficiency syndrome (AIDS)
- Posttransplant lymphoproliferative disorders

Congenital Lung Disease

- Pulmonary venolobar syndrome
- Intralobar and extralobar sequestration
- Bronchial atresia

Pulmonary Vascular

- Acute pulmonary embolism, venous thromboembolic disease
- Pulmonary arterial hypertension

Diseases of the Chest Wall

Chest Wall, Pleura, and Diaphragm

- Pneumothorax, tension pneumothorax
- Pleural effusion
- Pleural calcification, asbestos exposure, tuberculosis
- Subdiaphragmatic abscess
- Diaphragm rupture
- Phrenic nerve paralysis
- Involvement with lung cancer
- Serothorax, fibrothorax
- Malignant mesothelioma
- Pleural metastases
- Fractured ribs, clavicle, spine, scapula

Diseases of the Mediastinum

- Bronchogenic, pericardial, thymic, or esophageal duplication cyst, goiter, lymphoma, germ cell tumors, neurogenic tumors
- Pneumomediastinum

Chest Pain

Chest pain is often a symptom leading to referral of patients for a barium meal study, and for which the diagnostic

concerns include cardiac disease, gastro-oesophageal reflux and musculo-skeletal disorders.

▶Gastroesophageal Reflux in Adult Patients: Clinical Presentations, Complications, and Imaging

Chest Trauma

Jürgen Biederer
German Cancer Research Center, Heidelberg, Germany
j.biederer@dkfz.de

Definitions/Pathology/Histopathology

Chest trauma is defined by lesions to the chest that are induced by physical or chemical force. The chest is considered as a functional unit of the lung parenchyma, visceral pleura, airways, vasculature, and the surrounding structures with parietal pleura, mediastinum, chest wall, and diaphragm. The genuine task of this complex system is to guarantee gas exchange by ventilation and perfusion. Any trauma to single or multiple of these structures directly or indirectly involves all parts of the system. The pattern of lesions and the structures involved is directly related to the mechanism, intensity, and duration of the effective forces. The spectrum of mechanisms covers perforating and blunt trauma, barotrauma and aspiration of foreign bodies or (aggressive) gases and fluids, or any combination of these.

Perforating trauma is typically related to stab trauma or gunshot. Trauma mechanisms are directly related to cut and tear along the path of the impacted material. Impact with high kinetic energy (bullets, etc.) can combine this with mechanisms similar to blunt trauma (shockwaves with compression/decompression mechanisms).

The typical scenarios for *blunt trauma* of the chest are motor vehicle accidents or deep falls with deceleration injury. Blunt trauma to the chest wall may result in soft and bony tissue lesions. Rib fractures for themselves are usually of minimal clinical importance, but dislocated fragments can lacerate the pleura, lung, or abdominal organs thus combining blunt trauma with perforating mechanisms. Paradoxical movement of a ▶flail chest due to multiple rib fractures can impair respiratory mechanics, promote atelectasis, and impair pulmonary drainage. Fractures of the thoracic spine, sternum, clavicle, or scapula are less relevant for the respiratory function of the chest, but indicative of extreme forces and associated with a high probability of life-threatening injury.

▶Traumatic diaphragmatic hernia predominantly occur on the left side (4/5 cases) and may present with acute or delayed herniation of abdominal organs depending on the extent of the initial tear.

The mechanisms of blunt trauma to the lungs are direct or indirect deceleration, compression, or decompression. Deceleration becomes effective at transitions between fixed and elastic structures and results in destructive shear forces, e.g., between bronchovascular structures and blood-filled lung parenchyma. Compression and decompression effects occur along shockwaves with either abruptly elevated or lowered pressure. Both lead to local contusion or even rupture of lung parenchyma (laceration). Injuries may be visible either at the side of trauma or on the opposite side. The leading patterns include contusion (most frequent), laceration, aspiration, and atelectasis. These may even occur with intact chest wall. Conditions affecting primarily extrathoracic sites may have indirect effects on the lungs causing ARDS or fat embolism syndrome. Traumatic pulmonary pseudocysts are relatively rare sequelae of blunt chest trauma with lung contusion. ▶Tracheobronchial lesions are rare (incidence ~1%) in blunt chest trauma but potentially life-threatening. Due to the underlying forces, concomitant blunt aortic injuries and myocardial contusion are frequently found. Cardiac contusion is the most common injury of the heart, but other injuries, including coronary injuries, pericardial tears, rupture of the free wall, septum, and heart valves, tamponade, as well as conduction defects, may be found. Cerebral air embolism is a rare, but severe complication of lung contusion.

Clinical Presentation

Seventy percent of the patients with severe thoracic injury are polytraumatized and present with shock symptoms. In perforating trauma, the combination of relatively small externally visible lesions with life-threatening intrathoracic complications is critical. Patients with blunt trauma present with more or less obvious chest wall injury. Pneumothorax and lung contusions lead to dyspnea, tachypnea, and cyanosis. If a tension pneumothorax is present these are combined with tachycardia and arterial hypotension. Contrarily to lung lacerations, lung contusions usually present without hemoptysis. Patients with massive intrathoracic bleeding (▶hemothorax due to rupture of intercostal arteries or ▶lung laceration) present with signs of respiratory failure, hypovolemia, and finally shock symptoms. The triad of arterial hypotension, elevated central venous pressure and

dampened heart sound can be indicative for cardiac tamponade. Clinical signs of tracheobronchial lesions are hemoptysis, pneumothorax, ►pneumomediastinum, subcutaneous emphysema, or an insufficient expansion of the lungs after drainage of a pneumothorax.

Imaging and Diagnosis

Respiratory failure related to chest trauma is a major cause of mortality during the "golden hour" of polytrauma. Immediate, life-threatening conditions that require prompt diagnosis are airway obstruction, pneumothorax (simple, open or tension pneumothorax), flail chest, cardiac tamponade, and massive hemothorax ("the lethal six"). Very often, initial treatment requires just simple procedures, such as chest tube insertion or pleural drains. Algorithms of polytrauma management therefore include chest X-ray and ultrasound as the primary survey with CT as second line imaging modality for the hemodynamically stable patient (Fig. 1). An alternative concept is based on initial whole body Multislice CT as the primary survey ("emergency room CT"). It is superior for the fast diagnosis of the "lethal six" when the dedicated workflow for transportation, scanning, data management, reading and reporting is fulfilled. Contrast administration is mandatory to exclude blunt vessel injury since CT-Angiography has replaced diagnostic DSA.

Further, potentially life-threatening injuries to be detected by CT ("the hidden six") are pulmonary contusion, tracheobronchial rupture, diaphragmatic tear, thoracic aortic rupture, ►esophageal rupture, and myocardial contusion. Further, impact from CT comes from the detection of pericardial hemorrhage, major thoracic vascular injury, small pneumothorax, and from the definition of the extent of contusion, laceration, and pulmonary pseudocysts, which is considered an important prognostic factor (Figs. 2, 3). Catheter misplacements can also be clearly identified. On chest X-ray and CT, the

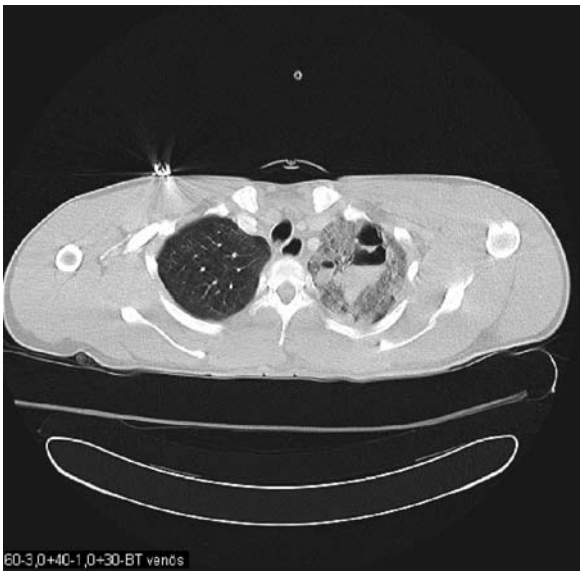

Chest Trauma. Figure 2 Lung laceration and severe lung contusion in the left upper lobe after blunt chest trauma with formation of hematopneumoceles.

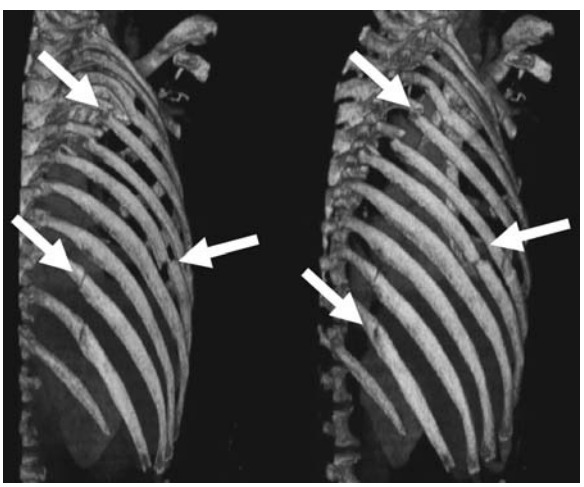

Chest Trauma. Figure 1 Volume renderings in posterior and latero-posterior views of the right chest wall indicating flail chest after blunt chest trauma with serial rib fractures and rib fragmentation (*arrows*).

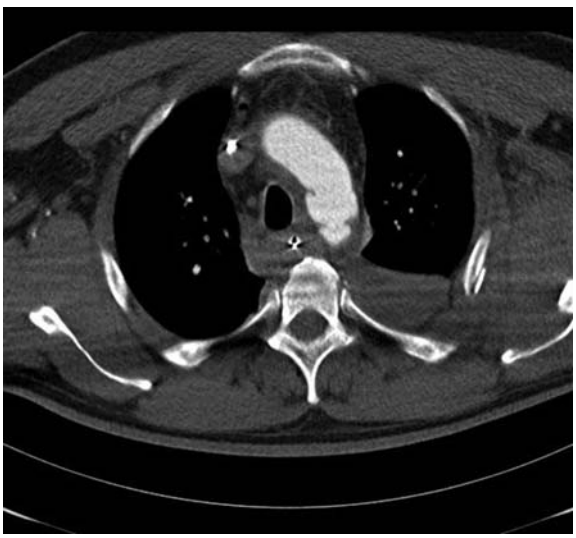

Chest Trauma. Figure 3 Traumatic aortic dissection at the typical location in the upper descending aorta with concomitant left-sided hemothorax and small mediastinal hematoma.

"fallen lung sign" is indicative for main stem bronchial rupture, but incomplete tracheobronchial rupture may be overlooked and definite diagnosis of airway lesions is usually made by endoscopy. A pneumomediastinum is not necessarily related to direct rupture of the tracheobronchial tree (►Macklin effect). The usual procedure for follow-up of chest trauma is chest X-ray with additional CT as far as necessary.

Nuclear Medicine

Nuclear medicine does not contribute to the diagnostic procedures of acute chest trauma.

Interventional Radiological Treatment

Except for endograft implantation for the treatment of thoracic aortic rupture, endovascular procedures do not contribute to the treatment of chest trauma. Endobronchial stenting for tracheobronchial lesions might replace surgical repair in selected patients.

Bibliography

1. Gavant ML (1999) Helical CT grading of traumatic aortic injuries. Impact on clinical guidelines for medical and surgical management. Radiol Clin North Am 37:553–574
2. Gavelli G, Canini R, Bertaccini P, et al (2002) Traumatic injuries: imaging of thoracic injuries. Eur Radiol 12:1273–1294
3. Miller LA (2006) Chest wall, lung, and pleural space trauma. Radiol Clin North Am 44:213–224
4. Reuter M (1996) Trauma of the chest. Eur Radiol 6:707–716
5. Stahel PF, Schneider P, Buhr HJ, et al (2005) Emergency management of thoracic trauma [Article in German]. Orthopäde 34:865–879

Chest, Neonatal

Veronica Donoghue
Radiology Department, Children's University Hospital, Dublin, Ireland
veronica.donoghue@cuh.ie

Synonyms

Congenital Neonatal Pneumonia; Hyaline Membrane Disease; Idiopathic Respiratory Distress Syndrome; Meconium Aspiration Syndrome; Pleural Effusions; Transient Tachypnoea of the Newborn

Definitions

The various medical causes of newborn respiratory distress depend largely on the gestational age of the infant. In the premature infant, the commonest abnormality is ►hyaline membrane disease, sometimes referred to as idiopathic respiratory distress syndrome or surfactant deficiency disease.

In the term infant, the causes include ►transient tachypnoea of the newborn, also referred to as retained foetal lung fluid or wet lung syndrome, amniotic fluid aspiration, ►meconium aspiration syndrome, which is defined as respiratory distress in an infant born through meconium stained amniotic fluid where symptoms cannot be otherwise explained, ►neonatal pneumonia, spontaneous pneumothorax/pneumomediastinum and ►pleural effusions.

Congenital abnormalities of the lung bud and vascular development include pulmonary agenesis and hypoplasia, pulmonary venolobar or Scimitar syndrome, horseshoe lung, congenital lobar emphysema, bronchial atresia, congenital cystic adenomatoid malformation, pulmonary sequestration, bronchopulmonary foregut malformations, oesophageal lung, bronchogenic cysts, neuroenteric cysts, pulmonary vascular malformations, congenital pleural effusions which include chylothorax, and situs abnormalities.

Abnormalities of the diaphragm include congenital diaphragmatic hernia of the Bochdalek and Morgagni types, eventration of the diaphragm and accessory diaphragm. The majority of these congenital and diaphragmatic abnormalities are discussed elsewhere.

Pathology/Histopathology

Hyaline Membrane Disease: In this condition, the abnormality is a deficiency of the lipoprotein surfactant superimposed on structural immaturity of the lungs. The surfactant is produced by the alveolar cells. Without it alveolar surface tension is raised, there is a reduction in alveolar distensibility and as a result collapse of the alveoli. The alveolar ducts and terminal bronchioles are distended and lined by hyaline membranes containing fibrin, cellular debris and fluid. Hyaline membranes are thought to result from a combination of ischaemia, barotrauma and increased oxygen concentrations delivered by assisted ventilation. In the very premature infant in particular there is also associated pulmonary haemorrhage and interstitial and airspace oedema later in the course of the disease. It is suggested that the presence of oedema is due to the fact that immature arterioles in these infants have a highly permeable basement membrane

which is aggravated by anoxia and acidosis. In addition immature vessels in these infants may lack sufficient smooth muscle to compensate for haemodynamic and osmotic changes. As a result there is capillary leaking and water is drawn into the alveoli. At low lung volumes negative interstitial pressure reduces fluid movement into the lymphatics.

Pulmonary Haemorrhage occurs because of an immature sequence of clotting factors, platelet sequestration or vitamin K and enzyme deficiency (1).

Transient Tachypnoea of the Newborn: During foetal life the lungs are expanded with fluid, an ultrafiltrate of foetal serum which contributes to amniotic fluid volume. During and after birth the fluid is removed by the pulmonary lymphatics and capillaries. In transient tachypnoea of the newborn there is slow or incomplete removal of the lung fluid. The incidence is increased in infants delivered by caesarian section. It is postulated that the absence of squeezing of the thorax during passage through the vaginal canal results in retention of lung fluid. The condition is also reported in infants with hypoproteinaemia, hyponatraemia, maternal fluid overload, small hypotonic or sedated infants and infants who have experienced a precipitous delivery (2).

Amniotic Fluid Aspiration: If intra-uterine foetal distress occurs the foetus may gasp and aspiration of amniotic fluid may occur. Debris in the amniotic fluid may contain squames and lanugo hair.

Meconium Aspiration Syndrome: Passage of meconium in utero is associated with ante- or intrapartum foetal acidaemia. It is widely accepted that foetal hypoxia causes an increase in intestinal peristalsis with anal sphincter relaxation and as a result passage of meconium. It is also thought that oligohydramnios may result in compression of the foetal head and umbilical cord, which may precipitate a vagal response and passage of meconium. Meconium aspiration syndrome may be secondary to aspiration of meconium *in utero* or at birth, maybe related to alterations in the pulmonary vascular system, which occurs as a result of asphyxia or indeed the presence of meconium itself. It appears that the degree of symptomatology is directly related to the viscosity of the meconium and large amounts of thick meconium can completely obstruct the airways. It is however more common for the meconium to migrate distally into the peripheral airways causing complete or partial obstruction. Complete obstruction causes atelectasis and ventilation—perfusion mismatch and partial obstruction causes a 'ball-valve' effect, whereby gas flows into the distal airways during inspiration, but becomes trapped distally during expiration due to the smaller diameter. After several hours there is an inflammatory response to the presence of meconium resulting in the presence of polymorphonuclear leucocytes diffusely throughout the lungs. These cells release chemical mediators which adversely affect the tissues. In addition the presence of bile salts in the meconium causes specific toxicity in type (II) pneumocytes. All contribute to the picture of chemical pneumonitis which leads to pulmonary vasoconstriction and in turn persistent pulmonary hypertension of the newborn (3).

Neonatal Pneumonia: Although the foetal environment is considered relatively protected neonatal sepsis can occur even in the presence of intact amniotic membranes. Congenital infections can occur through transplacental spread of organisms most commonly the 'TORCH' group (cytomegalovirus, herpes, rubella, toxoplasmosis) and are rare. Perinatal infections can be acquired *via* ascending infection from the vaginal tract which also causes chorioamnionitis sometimes referred to as amnion infection syndrome, transvaginally during the birth process and nosocomially in the neonatal period. It is postulated that most organisms causing neonatal pneumonia gain entry during the birth process as the foetus takes the first gasping efforts at breathing. This may occur earlier in the asphyxiated infant who may aspirate in response to non-specific stressful events. It is important therefore to treat chorioamnionitis aggressively once diagnosed. Approximately half of all the infections are due either to group B streptococcus or *E. Coli* (3).

Spontaneous Pneumothorax/Pneumomediastinum: This condition maybe the result of the infants own forceful initial respiratory effort or may result from resuscitation.

Pleural Effusions in the neonatal period are most likely due to chylothorax. Less common causes include hydrops foetalis, non-immune hydrops and cardiac disease.

The cause of chylothorax is unknown. Birth trauma to the thoracic duct has been suggested but is unlikely, as the effusion is seen on antenatal ultrasonography. Late maturation of the thoracic duct has also been suggested.

Hydrops Foetalis most commonly results when a Rhesus-negative mother becomes sensitised to Rhesus-positive blood. This results in the development of antibodies which enter the foetal circulation causing haemolysis and anaemia. When severe this may result in soft tissue oedema, pleural effusions, ascites and pericardial effusions.

The commonest causes of non-immune hydrops are twin–twin transfusion, foetomaternal transfusion, cardiac arrhythmias and tumours, cystic adenomatoid malformations, pulmonary arteriovenous malformations, lymphangiectasia and intra-uterine infection.

Clinical Presentation

Hyaline Membrane Disease: Clinically these infants are usually symptomatic within minutes of birth, with grunting, nasal flaring, intercostals retraction, tachypnoea

and cyanosis. The degree of symptomatology varies with the severity of disease. Prenatal steroid administration to mothers during the 2 days prior to delivery is safe and significantly reduces the incidence of the disease in premature infants. It promotes endogenous surfactant production and lung maturation in addition to inducing anti-oxidant enzymes. A similar response can occur when maternal steroid production is increased because of stress caused by prepartum maternal infection, toxaemia or other forms of prepartum stress. These situations however need to exist for 24 h or more prior to delivery. The condition results in poor gas exchange, hypoxia, hypercarbia and acidosis.

Transient Tachypnoea of the Newborn: Mild to moderate respiratory distress without cyanosis is typically present at birth or in the first couple of hours in this condition. Clinically resolution usually occurs within 48 h and often within 24 h.

Amniotic Fluid Aspiration: Tachypnoea is the most common clinical finding and its severity varies with the degree of aspiration.

Meconium Aspiration Syndrome: Clinically these infants demonstrate pallor, cyanosis, apnoea, grunting and intercostal retraction. Respiratory and metabolic acidosis may develop due to hypoxaemia and hypercarbia secondary to ventilation—perfusion mismatch.

Neonatal Pneumonia: The clinical signs and symptoms in neonatal pneumonia are frequently non-specific. The infant maybe listless, have pallor, apnoea, tachypnoea, tachycardia, bradycardia or feeding intolerance. Laboratory tests may also be non-specific. These infants usually present after 48 h of birth and have a less fulminant course. Those infants who present in the first 48 h of life tend to have a more severe clinical picture of hypotension, shock, disseminated intravascular coagulation and multi-organ failure. Mortality rates are high in this form of the disease especially when due to *B. streptococcus*.

Spontaneous Pneumothorax: Pneumothorax causes varying degrees of respiratory distress. They are usually transient and do not need intervention.

Pneumomediastinum is for the most part asyptomatic.

Pleural Effusions: This condition is frequently diagnosed by antenatal ultrasonography and if large may be treated antenatally by thoracocentesis and/or thoracoamniotic shunt.

After birth if the effusion is large the infants present with respiratory distress. The condition maybe bilateral.

Imaging

The chest radiograph is the most useful imaging modality in the investigation of the various medical conditions which cause respiratory distress in the newborn period.

It is also very important in determining the position of various tubes which are introduced during therapy, together with their complications. The most common of these is a misplaced endotracheal tube which ideally should be positioned above the level of the carina and the origin of the right upper lobe bronchus. Failure to do this may result in bronchial occlusion and atelectasis. Endotracheal and nasogastric tubes may perforate the trachea or oesophagus and cause a pneumothorax or pneumomediastinum.

The position of pleural chest tubes to drain pneumothoraces and pleural effusions can also be assessed on the chest radiograph. Misplacement may result in diaphragmatic paralysis as a result of phrenic nerve damage.

Positioning of intravenous and intra-arterial lines in the heart is not ideal as they may predispose the infant to thromboembolism. The venous catheters are best positioned in either the superior or inferior vena cava. Perforation of the superior vena cava resulting in hydrothorax and haemothorax has been reported. Umbilical arterial line tips are best located in the aorta proximal to the origins of the main arterial branches in order to avoid thrombosis and ischaemia to the dependant organs.

Hyaline Membrane Disease: Although the initial radiographic findings maybe noted shortly after birth, occasionally the maximum findings are not present until 6–24 h of life. Prior to commencement of assisted ventilation, typically the radiographic findings are those of underaeration of the lungs with fine granular opacification and air bronchograms which are diffuse and symmetrical. This is due to collapsed alveoli with distended terminal bronchioles and alveolar ducts. When distension is very poor there is more generalised opacification and a frank whiteout of the lungs (3) (Fig. 1a). Very small infants less than 26 weeks gestation may have clear lungs initially or mild perihilar haziness (4). Their lungs are biochemically and structurally immature and require prolonged ventilatory support. Several technologies have significantly altered the radiographic evolution. The clinical use of artificial surfactant is a very important recent therapeutic advance. It is given at birth, frequently prior to performing the first chest radiograph with up to 3–4 additional doses in some patients. It is given through the endotracheal tube and radiographic improvement can occur quickly. It is often not evenly distributed throughout the lungs and it is common to see residual areas of atelectasis alternate with areas of improved aeration. In addition the surfactant may reach the level of the acini causing sudden distension which produces a radiographic picture similar to interstitial pulmonary emphysema (3). It is therefore essential to correlate the image closely with the clinical findings

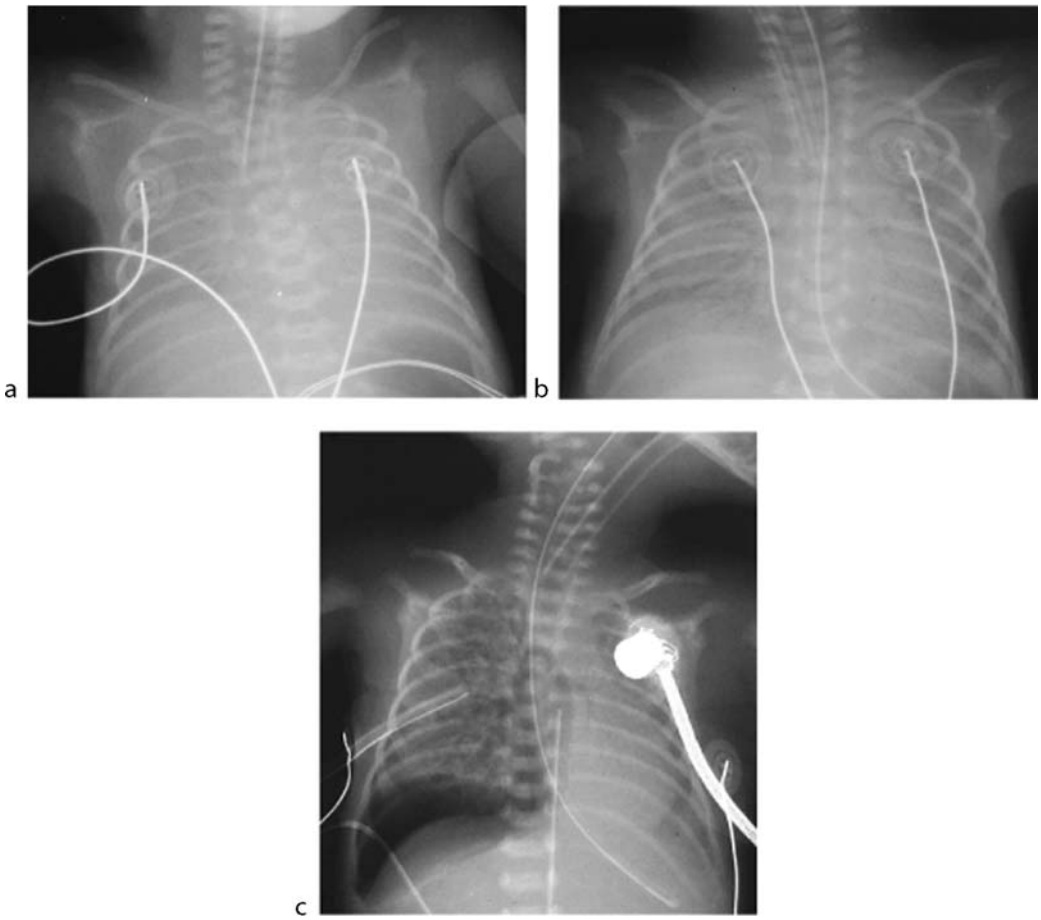

Chest, Neonatal. Figure 1 (a) Severe hyaline membrane disease showing almost complete 'whiteout' of both lungs with some air bronchogram visible bilaterally. (b) Premature infant with patent ductus arteriosus. The heart is bulky. There is distortion of the left main bronchus and marked pulmonary opacification due to pulmonary oedema. (c) Ventilated premature infant. There is right pulmonary interstitial emphysema and a right inferior and medial pneumothorax. A right chest drain is in position.

when interpreting the radiographs. Smaller infants, less than 27 weeks gestation may not respond well to surfactant therapy. Their lungs, although becoming clear with surfactant therapy are very immature with fewer alveoli than normal, leading to inadequate gas exchange and the need for prolonged ventilation which in turn leads to chronic lung problems, most commonly a hazy to opaque appearance on the chest radiograph. This is due to the presence of haemorrhage and pulmonary oedema, the latter is sometimes referred to as the 'leaky-lung' syndrome (2). Less commonly the radiograph demonstrates a much coarser irregular pattern similar to that seen in *bronchopulmonary dysplasia*.

A *patent ductus arteriosus* is common in premature infants and is thought to contribute to the lung disease. In the early stages of hyaline membrane disease the rigid lungs together with hypoxia and hypercarbia result in persistent pulmonary vasoconstriction. This may lead to right-to-left shunting through the ductus. With surfactant therapy and improved oxygenation there is a reduction in pulmonary resistance and left-to-right shunting may occur leading to pulmonary oedema. Radiographically in addition to pulmonary oedema there may be evidence of sudden cardiac enlargement with left atrial enlargement causing elevation or distortion of the left main bronchus (Fig. 1b). Treatment with indomethacin may result in ductal closure but occasionally surgery is necessary.

High frequency ventilation may also be employed to reduce the incidence of barotrauma. This method employs supra-physiological breathing rates and tidal volumes frequently less than dead space. This allows oxygenation and carbon dioxide removal without pressure induced injury. The aim is to achieve maximum alveolar recruitment without overdistending the lungs as

overdistended lungs compromise the systemic circulation. The chest radiograph in infants on high frequency ventilation is the best diagnostic tool for assessing overinflation of the lungs. Ideally the dome of the diaphragm should project over the 8–10th posterior ribs if the main airway pressure is appropriately adjusted. Otherwise the chest radiograph is not different from those infants receiving conventional ventilation.

Positive pressure ventilation in these premature infants is the most common cause of complications such as pneumothorax, pneumomediastinum, pneumopericardium and pulmonary interstitial emphysema. These air leaks are less common since the more routine use of artificial surfactant and high frequency ventilation. When a terminal airway ruptures—most often as a result of air being forced into the collapsed alveoli of hyaline membrane disease—air leaks into the pulmonary interstitial tissues and lymphatics and results in pulmonary interstitial emphysema. This causes stiff lungs which do not empty with expiration. Gas exchange is poor as a result and pulmonary blood flow maybe compromised and there is a need to increase ventilatory requirements. Radiographically, pulmonary interstitial emphysema is seen as bubbles often radiating from the hilum to the lung periphery (Fig. 1c). It maybe unilateral, bilateral or confined to part of a lung and may cause mass effect and mediastinal shift. If interstitial air reaches the pleural surface of the lungs and if a bleb bursts, a pneumothorax develops (Fig. 1c). If air dissects centrally it may leak into the mediastinum, pericardial space or downwards into the peritoneal cavity. Large pneumothoraces are easily identified radiographically but smaller pneumothoraces maybe subtle as sick infants are nursed in the supine position and free air may accumulate over the anterior surface of the lung producing a large hyperlucent lung and increased sharpness of the mediastinal edge. A pneumopericardium is recognised radiographically by the presence of air completely surrounding the heart and the pericardial sac maybe visible as a white line. Skin folds should not be mistaken for pneumothoraces. They can be seen to continue beyond the lung edge.

Focal atelectasis, due to malposition of the endotracheal tube, poor clearance of secretions or mucous plugging is also a common complication of surfactant deficiency.

Radiographically there is pulmonary opacification with volume loss or ipsilateral mediastinal shift proportional to the degree of atelectasis.

Infants with hyaline membrane disease are also at risk of pneumonia. The radiographic picture may be identical to that of the underlying condition. However, the lungs are usually more compliant and the infants require lower levels of ventilation relative to the degree of opacification present. More commonly however, there is evidence of patchy pulmonary opacification (5).

Pulmonary haemorrhage may also develop in infants with hyaline membrane disease secondary to severe hypoxia and capillary damage. Mild cases are difficult to detect on the chest radiograph. In severe cases blood may ooze from the nose, mouth or endotracheal tube. Radiographically the lungs may show homogeneous opacification and appear airless (3).

Bronchopulmonary dysplasia, a long-term consequence of neonatal lung disease is discussed elsewhere.

Though it does not serve as a substitute for the chest radiograph ultrasonography has been shown to be useful for assessing the severity of hyaline membrane disease and documenting the success of artificial surfactant. The persistence of retrodiaphragmatic hyperechogenicity beyond day 9–18 has also been demonstrated as a predictor for the development of bronchopulmonary dysplasia.

Transient Tachypnoea of the Newborn: The most common appearance is mild overaeration of the lungs, perihilar interstitial shadowing, prominent blood vessels and the presence of fluid in the horizontal fissure (Fig. 2). Occasionally there is a small pleural effusion and mild cardiomegaly. The radiographic findings maybe more marked on the right side and to date this finding remains unexplained. When the changes are marked there should be close clinical correlation to help distinguish this condition from meconium aspiration syndrome and neonatal pneumonia. Typically the appearances clear rapidly within 24–48 h.

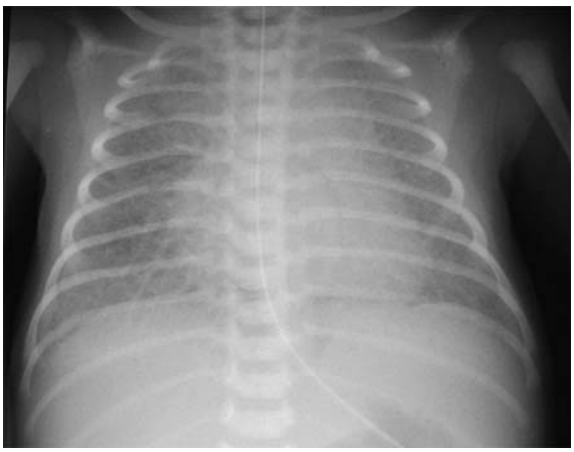

Chest, Neonatal. Figure 2 Transient tachypnoea of the newborn. There is mild cardiomegaly, bilateral perihilar shadowing most marked on the right and a small right basal pleural effusion.

Amniotic Fluid Aspiration: The radiographic findings vary with the volume of fluid aspirated and the amount of debris it contains. If aspiration is severe the chest radiograph may show marked nodular opacification. This however clears rapidly over the next 24 h which helps distinguish the condition from meconium aspiration.

Meconium Aspiration Syndrome: The chest radiographic picture includes any combination of diffuse patchy coarse infiltrates which maybe asymmetric or symmetric and focal or general, overinflation, air leaks, pleural effusions and cardiomegaly (Fig. 3).

Infiltrates are the result of atelectasis due to airway occlusion and alveolar oedema as a consequence of inflammation. The hyperinflation and air leaks result from partial airway occlusion and air trapping. Alveoli may rupture with free air dissecting into the pleural spaces and mediastinum. Pleural effusions are also the result of the inflammatory process.

Cardiomegaly may be the result of direct intra-uterine asphyxia or *persistent pulmonary arterial hypertension* (3). One-third of infants with meconium aspiration syndrome require assisted ventilation. As air leaks are a common complication they are exacerbated by using positive end expiratory pressure or continuous positive airway pressure ventilation. High frequency ventilation is also used and has the benefits of less barotrauma and better attainment of respiratory alkalosis in an attempt to achieve pulmonary vascular vasodilatation in those infants with associated persistent pulmonary arterial hypertension. The latter is also treated with inhaled nitric oxide. Surfactant deficiency is also seen in infants with meconium aspiration syndrome and this may be treated with artificial surfactant. It is probably caused by inhibited surfactant function or alterations in its composition. Infants who are resistant to the above therapies are treated with extra-corporeal membrane oxygenation. The technique is discussed elsewhere in this section.

Neonatal Pneumonia: The radiographic changes in neonatal pneumonia are non-specific to the extent that it is not possible to determine a causative organism from the appearances. In addition many neonates do not suffer from pneumonia in isolation but it may complicate other conditions. The radiographic pattern may mimic hyaline membrane disease or transient tachypnoea of the newborn. The presence of some overinflation associated with airspace disease has been reported as suggestive of pneumonia. Also the presence of pleural effusions with opacification is more suggestive of pneumonia especially group B streptococcus. A diffuse, bilateral alveolar pattern which develops in the first 4–6 h of life is characteristic though not specific (3) (Fig. 4).

Spontaneous Pneumothorax: Large pneumothoraces are easily identified radiographically, but smaller pneumothoraces may be subtle as sick infants are nursed in the supine position and free air may accumulate over the anterior surface of the lung producing a large hyperlucent lung and increased sharpness of the mediastinal edge. The thymus may also be compressed and elevated giving the appearance of a superior mediastinal mass. A medial

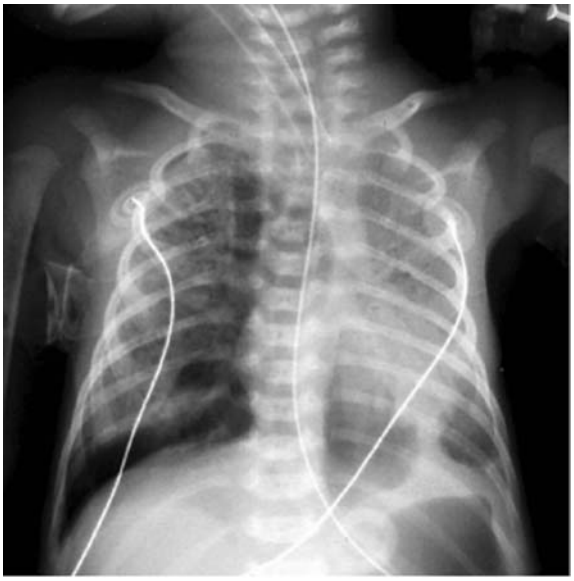

Chest, Neonatal. Figure 3 Meconium aspiration syndrome. There is coarse bilateral pulmonary opacification, hyperinflation and bilateral air leaks with some mediastinal shift to the left side.

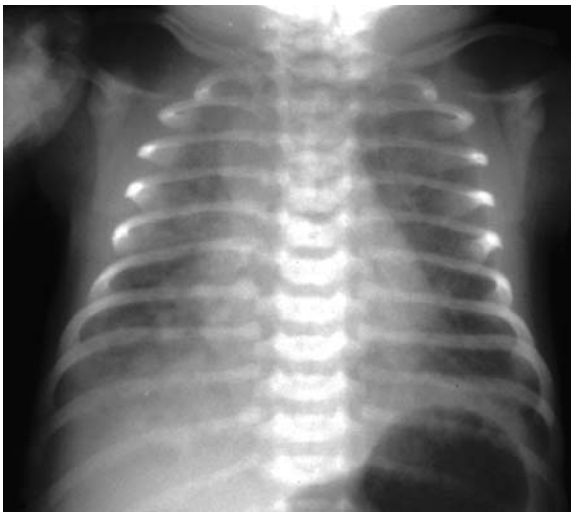

Chest, Neonatal. Figure 4 Group B streptcoccus neonatal pneumonia. There is diffuse bilateral coarse pulmonary opacification.

pneumothorax may be difficult to differentiate from a pneumomediastinum.

Pleural Effusions: The condition maybe diagnosed antenatally using ultrasonography. Antenatal MR imaging may also be helpful to delineate the extent of the effusion and to assess the presence of an underlying abnormality such as *cystic adenomatoid malformation*. After delivery radiography will demonstrate the effusion which maybe bilateral. If large enough it may opacify the entire hemithorax and cause shift of the mediastinum to the contralateral side.

Ultrasonography is the easiest way to confirm the presence of an effusion and is useful to guide thoracocentesis. Underlying causes such as cardiac abnormalities and cystic adenomatoid malformation may also be detected prior to aeration of the cysts. CT scan may be necessary to delineate the extent of conditions such as cystic adenomatoid malformation and rarer anomalies such as pulmonary lymphangiectasia, arteriovenous malformations and arteriovenous malformations. The latter can also be imaged using MR imaging. The treatment of chylothorax is by thoracocentesis and multiple aspirations may be necessary prior to resolution.

Diagnosis

In neonatal chest disease close correlation with the clinical history is very important in arriving at the correct diagnosis. In the premature infant hyaline membrane disease is the most serious pulmonary abnormality. The presence of the classic chest radiographic findings as described above, in these premature infants is diagnostic. In the term infant tachypnoea of the newborn, amniotic fluid aspiration, meconium aspiration syndrome and neonatal pneumonia may be difficult to distinguish radiographically. A finding of meconium below the vocal cords on laryngoscopic examination together with the presence of coarse pulmonary opacification and air leaks on the chest X-ray is highly suggestive of meconium aspiration syndrome. A history of prolonged rupture of the membranes during later pregnancy or the diagnosis chorioamnionitis in the mother together with coarse patchy pulmonary opacification is a strong pointer towards neonatal pneumonia. Transient tachypnoea of the newborn and amniotic fluid aspiration are benign conditions causing mild clinical symptoms that are transient and seldom require ventilatory support despite the fact that the radiographic changes are occasionally quite marked. Resolution is usually complete in 24–48 h.

The definitive cause of a pleural effusion may be made by examining the aspirated fluid. In infants with a chylothorax the fluid will have a high lymphocyte count. After feeding has been established the fluid will have a milky appearance.

Bibliography

1. Wood BP, Davitt MA, Metlay LA (1989) Lung disease in the very immature neonate: radiographic and microscopic correlation. Pediatr Radiol 20:33–40
2. Swischuk LE (2003) Respiratory system. In: Swischuk LE (ed) Imaging of the Newborn, Infant and Young Child. 5th edn. Williams and Wilkins, Baltimore
3. Donoghue V (ed) (2002) Radiological Imaging of the Neonatal Chest. Springer-Verlag, Berlin Heidelberg New York
4. Newman B (1999) Imaging of medical disease in the newborn lung. Radiol Clin North Am 37:1049–1065
5. Cleveland RH (1995) A radiologic update on medical disease of the newborn chest. Pediatr Radiol 25:631–637

Chest, Thromboembolic Diseases

Edwin J. R. van Beek
Department of Radiology
Carver College of Medicine, University of Iowa Hospitals and Clinics,
Iowa City, USA
Edwin-vanbeek@uiowa.edu

Synonyms

Chronic thromboembolic pulmonary hypertension (CTEPH); Fat embolism syndrome; Pulmonary embolism (PE); Venous thromboembolic disease

Definition

Thromboembolic pulmonary arterial diseases are a spectrum involving the embolization of either blood clot or fat/marrow droplets into the pulmonary arterial circulation.

The vast majority of the spectrum relates to *acute pulmonary embolism (PE)*. This is a syndrome caused by the dislodgement of thrombus within the context of deep vein thrombosis (1). The thrombus material will be caught in the pulmonary arteries, and depending on size and extent of the thrombotic material lung perfusion will be impaired.

Chronic Thromboembolic Pulmonary Hypertension (CTEPH) is the condition that results from recurrent PE or incomplete resolution of significant or extensive acute

pulmonary emboli. The pulmonary arterial bed becomes obstructed, and the result is an increase in pulmonary arterial pressure.

The more generic term for acute pulmonary embolism and deep vein thrombosis is *venous thromboembolic disease* (1) in the acute form. Chronic forms include postphlebitic syndrome, varicose veins, and chronic thromboembolic pulmonary hypertension.

Fat embolism syndrome is a specific type of pulmonary embolism, which occurs in the course of large bone fractures and/or orthopedic manipulations and surgery. This syndrome usually occurs subclinical, but in multiple fractures or with extensive bone marrow surgery (such as the introduction of intramedullary nails), the bone marrow fat will enter the venules from where the central venous system will be reached. As a result, fat droplets will obstruct the pulmonary vascular bed and a rise in pulmonary artery pressure will occur. There is also a humoral response, leading to acute respiratory distress syndrome and (often extensive and fatal) pulmonary edema.

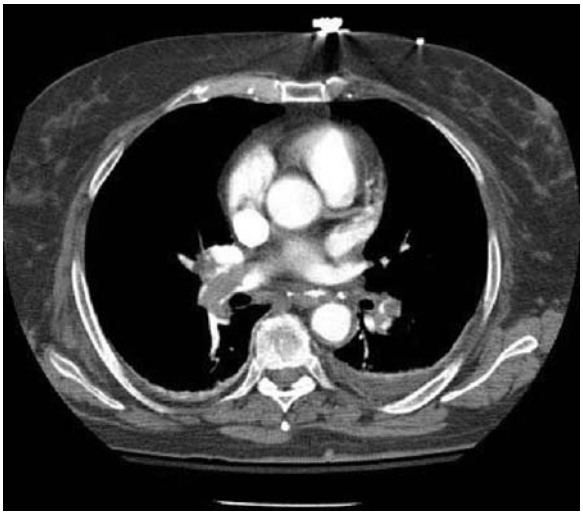

Chest, Thromboembolic Diseases. Figure 1 CT pulmonary angiography demonstrating filling defects in the right main and bilateral lobar pulmonary arteries.

Pathology/Histopathology

The pathology and histopathology depends on the clinical syndrome. The main pathological findings are:

1. Acute pulmonary embolism: this will cause a thrombus mass occluding the lumen of the pulmonary arterial tree. Depending on the extent of the emboli, the heart may also demonstrate acute right over-load, including atrial and ventricular dilatation. A saddle embolus is the term applied to a central large embolus that straddles the main pulmonary artery bifurcation. This type of PE is often (but not always!) immediately fatal. (Fig. 1) demonstrates acute embolism as seen on CT pulmonary angiography.
2. Chronic thromboembolic disease: this will cause mural adherent thrombus mass and intimal hyperplasia due to the incorporation of thrombus material into the vessel wall. This type of disorder will also cause webs (fibrous bands), vessel wall fibrosis, and stenosis as part of the recanalization of thrombus material. (Fig. 2) demonstrates the findings of a mural thrombus in an extremely dilated pulmonary artery as part of the CTEPH spectrum on CT pulmonary angiography (2a) and on MR pulmonary angiography in a different patient (2b). Other examples of findings in CTEPH are included in the Chapter on pulmonary hypertension.CT pulmonary angiogram in a patient with CTEPH demonstrates aneurysmal dilatation of the left upper lobe pulmonary artery with vessel remodeling in the presence of extensive mural thrombus. CTEPH in a different patient demonstrates similar findings as above in a MR angiogram, this time involving the right main pulmonary artery.
3. Fat embolism syndrome is diagnosed by demonstration of fat droplets in the pulmonary capillary bed. In significant fat embolism, there is rapidly increasing obstruction of the peripheral pulmonary arterial bed, resulting in a rapid rise of pulmonary arterial pressure and acute right heart failure and death. To deal with this new pressure gradient, right-to-left shunts may become apparent, such as seen in patients with patent foramen ovale. In these circumstances, paroxysmal embolization and a clinical course similar to that seen in septic endocarditis may develop.

Clinical Presentation

The clinical presentation of thromboembolic pulmonary arterial diseases is highly variable. For PE, it can be divided into acute major events, acute minor events, and chronic insidious development of symptoms. This has led to the introduction of the terminology acute massive PE, acute submassive PE, acute nonmassive PE, and chronic PE (2).

a. Acute massive PE: Patients with large pulmonary embolism or with occlusion of a significant portion of the vascular tree will present with symptoms that are acute in onset and the result of perfusion decrease and strain on the right ventricle. Up to 10% of patients suffer acute coronary arrest or will die within the first

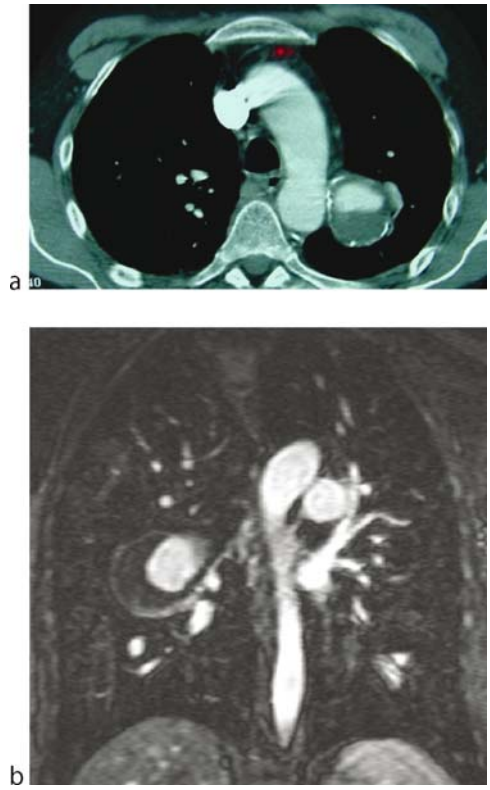

Chest, Thromboembolic Diseases. Figure 2 Chronic thromboembolic pulmonary hypertension. (a) CT pulmonary angiogram in a patient with CTEPH demonstrates aneurysmal dilatation of the left upper lobe pulmonary artery with vessel remodelling in the presence of extensive mural thrombus. (b) CTEPH in a different patient demonstrates similar findings as above in a MR angiogram, this time involving the right main pulmonary artery.

hour of this catastrophic embolism syndrome. Patients will present with circulatory instability (shock), dyspnea and/or chest pain and the "fear of dying."

b. Acute submassive PE: Patients with this level of embolism will present similarly to those with massive PE, with the exception that they are not suffering from hemodynamic instability using routine measures of blood pressure and heart rate. However, right heart strain and right ventricular dysfunction may be diagnosed using echocardiography.

c. Acute nonmassive PE: Many patients with nonmassive PE will present with a plethora of symptoms, ranging from asymptomatic to chest pain, dyspnea, tachycardia, and hemoptysis.

d. Chronic thromboembolic pulmonary hypertension (3): Patients with chronic thromboembolism often present with gradual, progressive shortness of breath, dyspnea on exertion and general lack of energy. They may suffer intermittent episodes of more significant symptoms as discussed above.

e. Deep vein thrombosis and clinically silent PE (1): A significant number of patients will present with leg symptoms, rather than chest symptoms. This is the group of patients who will present with deep vein thrombosis: swelling, calf pain, and red discoloration. Upon further questioning, many will have symptoms of PE, but a significant proportion of PE in this group of patients will be completely asymptomatic.

f. Fat embolism syndrome always presents in the presence of long-bone and/or pelvis fractures. It is often an acute progressive syndrome, leading to right heart failure and in the presence of patent foramen ovale will yield systemic fat embolism (petecchiae, neurological syndromes) similar to left-sided endocarditis.

Imaging

Chest radiography is only helpful in detecting disorders that may mimic PE: pneumothorax, heart failure, pleural effusions, and rib fractures (1, 3). PE can present with pulmonary infarction in 10–15% of patients (usually those with limited cardiorespiratory reserve), which will demonstrate a peripheral area of lung consolidation (►Hampton hump). Other findings include pleural effusions and hyperlucency of lung areas due to vascular obstruction more centrally (►Westermark sign). However, the vast majority of patients with proven PE will have a (nearly) normal chest radiograph.

Pulmonary angiography has long served as the reference method for the diagnosis of PE. However, as it is an invasive technique, this method never gained much popularity. With the increased capabilities of CT, invasive pulmonary angiography has all but vanished from the radiological arsenal (1, 3, 4).

The technique is still important for interventions in extremely sick patients with massive PE (thromboendarterectomy and fragmentation devices have been successfully developed) and as part of the work-up during right heart catheterization in patients with pulmonary hypertension.

CT pulmonary angiography is now the method of choice for the diagnostic management of PE (3, 4). Not only is it capable of detecting PE in central down to subsegmental vessels (Fig. 1), it can also give important alternative diagnoses that help in the management of patients with chest symptoms. It is not surprising, therefore, that there has been a huge demand for this technology in the acute hospital setting. As a result, the prevalence of PE using CT-pulmonary angiography

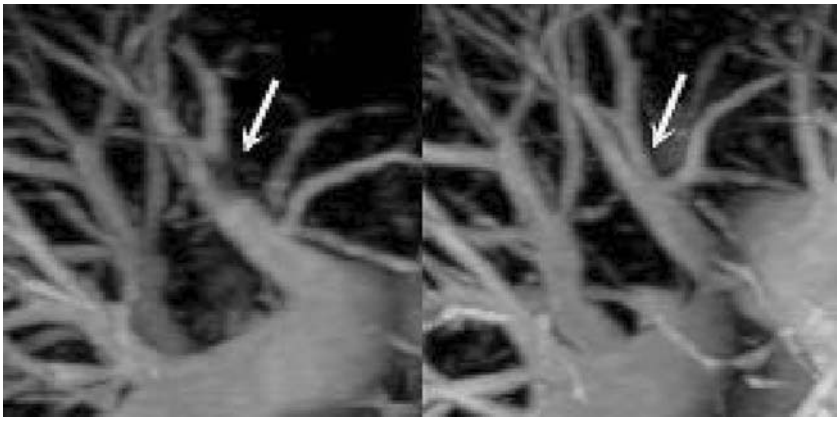

Chest, Thromboembolic Diseases. Figure 3 MR pulmonary angiogram (detail) of patient with pulmonary embolism (left) and following treatment (right).

has decreased from 40–50% in early studies to less than 10–15% in current clinical practice.

Important studies have shown that it is safe to withhold anticoagulant therapy in patients with suspected PE and normal CT pulmonary angiography provided the quality of the study was good. Unfortunately, up to 7% of studies will suffer from technical problems, although this number is decreasing with increasing detector rows in the CT systems.

Echocardiography is the method of choice in patients with massive PE, as it is both bed-side and capable of demonstrating large PE and the sequellae on the heart (1, 2). It has also been applied for assessment of patients with submassive PE and for evaluation of fibrinolytic therapy effectiveness.

Ultrasonography of the leg veins may be applied to detect deep vein thrombosis in the context of venous thromboembolism (1, 2, 4). Both compression and Doppler color ultrasonography have excellent sensitivity and specificity for detection of thrombi in symptomatic patients. However, in asymptomatic patients the diagnostic accuracy of this technique is less favorable, and may not be cost-effective (5).

Magnetic Resonance Imaging has many different techniques, which may be employed for the diagnosis of pulmonary vascular diseases, including MR perfusion, MR angiography, and direct clot imaging (6). Excellent anatomical detail can be obtained (Fig. 3), but presently the technique is usually reserved for difficult cases or where ionizing radiation or iodine contrast agents must be avoided.

Nuclear Medicine

Traditionally, perfusion (-ventilation) lung scintigraphy was the main diagnostic test for pulmonary vascular disease demonstrating the typical mismatch of a perfusion defect and preserved ventilation. With the advent of CT and MRI, this technology has been largely omitted from the diagnostic work-up of acute pulmonary embolism.

Diagnosis

The diagnosis of acute PE is based on demonstration within the pulmonary artery of a filling defect within a pool of contrast. Secondary signs include a cut-off vessel (no contrast at all), (sub) segmental consolidation, or nonenhancement of lung parenchyma.

In CTEPH, both the wall-adherent thrombus material and the secondary signs, including pulmonary artery dilatation, right ventricular and atrial dilatation, right ventricular hypertrophy, and bronchial artery hypertrophy may be demonstrated using CT or MRI.

Fat embolism syndrome is generally diagnosed at autopsy or by broncho-alveolar lavage. Acute right heart failure, ARDS and multiple organ failure are the most common findings, within a setting of long bone and/or pelvis fractures.

Interventional Radiological Treatment

The main interventional treatments for pulmonary vascular diseases are reserved for patients with acute massive PE (thrombo-endarterectomy and fragmentation devices) and for the treatment of right-left shunts in patent foramen ovale with paroxysmal embolization.

Inferior vena cava filters may be employed to support patients with contraindications for anticoagulant therapy, those in whom this therapy fails or in patients who are scheduled to undergo or already underwent pulmonary thrombo-endarterectomy.

Bibliography

1. Oudkerk M, van Beek EJR. Ten Cate JW eds (1999) Pulmonary embolism - epidemiology, diagnosis and treatment. Blackwell Science Publishers, Berlin
2. ESC Task Force on Pulmonary Embolism (2000) Guidelines on management of acute pulmonary embolism. Eur Heart J 21:1301–1336
3. Schoepf UJ, Costello P (2004) CT angiography for diagnosis of pulmonary embolism – state of the art. Radiology 230:329–337
4. Sohne M, ten Wolde M, Buller HR et al (2005) Pulmonary embolism. In: Lipson DA, van Beek EJR. Functional lung imaging. Taylor and Francis, New York, pp 480–498
5. Turkstra F, Kuijer PMM, van Beek EJR et al (1997) Value of compression ultrasonography for the detection of deep venous thrombosis in patients suspected of having pulmonary embolism. Ann Intern Med 126:775–781
6. Van Beek EJR, Wild JM, Fink C et al (2003) MRI for the diagnosis of pulmonary embolism. J Magn Reson Imaging 18:627–640

Chiari Malformation

Chiari Malformation comprises three different cerebellar malformations. The Chiari 1 malformation can occasionally be acquired, but all Chiari malformations are usually congenital. They are due to a lack of expression of the surface molecules, and imaging shows an abnormally small posterior fossa.

►Congenital Malformations, Cerebellar

Child Abuse

►Battered Child Syndrome

Children, Imaging Techniques

Anne Paterson
Royal Belfast Hospital for Sick Children, Belfast, UK
annie.paterson@royalhospitals.n-i.nhs.uk

Definition

The selection of an imaging modality depends largely upon the clinical question that is being asked, but local availability of equipment, the potential risks to the patient from the possible use of sedation or anaesthesia, and the radiation dose involved all need to be considered before the patient is investigated. Communication between radiologists and their clinical colleagues, the use of imaging protocols in common clinical scenarios and the review of request forms by senior radiologists also play an important role in the choice of a particular imaging technique.

Pathology

Imaging

Projection Radiography (Plain Films)

Over a 100 years have passed since the discovery of X-rays by Wilhelm Röntgen and since that time there have been considerable advances in diagnostic imaging techniques, yet plain film radiography remains the most frequently requested radiological investigation.

Basic principles: X-rays are generated, attenuated as they pass through the patient and the resultant X-ray beam emerging from the patient is then made visible by a variety of detectors:

- ►Film-screen (FS): Photographic film is sandwiched between two intensifying screens (made of rare earth materials). The screen fluoresces when it is irradiated and exposes the film. The latent image produced can only be 'read' when the film is (chemically) developed.
- ►Computed radiography (CR) uses a radiographic screen containing a type of phosphor (photostimulable phosphor plate, storage phosphor imaging plate, digital cassette). When the plate is exposed to X-rays, a latent image is formed and stored as electronic charges. A laser beam is used to stimulate the plate and the emitted light is directed to a photomultiplier tube, the electrical output signal of which is digitised. The digitised image can then be read by the radiologist (either on 'hard-copy' laser-printed films or 'soft-copy' workstations). A host of post-processing techniques can be used to improve the quality and appearance of the soft-copy image.
- ►Digital radiography (DR) makes use of caesium iodide (CsI) layered onto an amorphous silicon photodiode panel as a detector. When the CsI crystals absorb X-ray photons, they emit light, which is immediately converted into an electronic charge by the photodiode (no latent image is formed by this technique). Read-out electronics convert this information into an image (which can be printed onto film or viewed on a monitor). As with CR systems, the soft-copy image can be post-processed by the reporting radiologist.

CR and more recently DR are now replacing FS systems. One of the main reasons for this, is the potential

to reduce the rate of repeat films due to poor exposure technique (1), making them a popular choice in paediatric radiology. Both CR and DR systems operate over a wide dynamic range, in contrast to FS systems. An underexposed FS radiograph produces a 'white' film, an overexposed one the familiar 'black' film. The radiologist can read neither and the image must be repeated, increasing the radiation dose to the patient. The separation of image acquisition from display in both CR and DR allows these systems to compensate for inappropriate exposure factors and produce an image of consistent appearance. The phenomenon of 'exposure factor creep' is becoming increasingly recognised in the literature (2); radiographers often choose higher exposure factors, as the images produced are less grainy, and the increased radiation dose can go unnoticed unless regular quality assurance (QA) checks are in place. DR systems perform more efficiently than CR and the potential for dose reduction is greater (3).

Advantages, limitations and uses of projectional radiography: Regardless of the detector system used, projectional radiography is considered a low dose imaging technique. The risk to the patient can be further reduced by the judicious use of lead shields (e.g. for the breast and gonads). Radiographs are rapidly obtained, require no patient preparation, are painless, readily available and relatively cheap.

Projectional radiography is principally used to investigate the skeleton and chest. Only four different anatomical densities can be detected by the radiologist:

- Bone (and other calcifications)
- Soft tissue/fluid
- Fat
- Air

It is also possible to distinguish other densities foreign to the body, such as metal or radiographic contrast media (containing barium or iodine). The radiologist can only appreciate the outline of a structure on a plain radiograph when it is adjacent to a different density: blood vessels (fluid density) are seen coursing through the lungs on a chest radiograph because the surrounding alveoli are filled with air. Many disease processes (particularly those involving the soft tissues) have similar appearances on plain radiographs, and the possible differential diagnoses are vast. Relevant clinical findings and laboratory data help to tailor this list.

Fluoroscopy

Basic principles: Fluoroscopy is an enhanced X-ray technique that utilises an image intensifier tube connected to a closed circuit television system. The function and structure of body systems can be evaluated in real time, for both diagnostic examinations and as a prelude to interventional procedures. In addition, stationary images may be captured and can be viewed immediately on the television monitor. The static images may be radiographic exposures (if high spatial resolution is required), 'fluorograb' images taken during screening or as 'last image hold' from the television monitor. The latter techniques do not involve any further radiation to the patient and are commonly employed in paediatric radiology. Pulsed (as opposed to continuous) fluoroscopy is now considered imperative in paediatric radiology, as radiation dose reductions of over 90% can be achieved, whilst still maintaining imaging quality (4).

Uses: Fluoroscopy is most commonly used to evaluate the gastrointestinal and genitourinary tracts. Contrast media containing either barium sulphate or iodine in solution, can be ingested or introduced per rectum (or via stomas) to give detailed images of bowel anatomy, or instilled via a urinary catheter to outline the bladder. Iodine containing contrast media can also be injected intravenously or intra-arterially to demonstrate vascular anatomy. Angiographic examinations are improved by the use of digital subtraction techniques, whereby the anatomic background detail is removed to leave images showing only the contrast-enhanced vascular tree.

Interventional procedures in paediatric radiology usually require that the patient be sedated or receive an anaesthetic. Fluoroscopic guidance may be employed to place drainage catheters (e.g. into abscess cavities or nephrostomy tubes), for hydrostatic or pneumatic reduction of intussusception, during oesophageal, vascular or tracheal dilatations, and for vascular embolisation procedures.

Computed Tomography

Computed tomography (CT) is now estimated to account for around 15% of a radiology department's workload, but it is a high radiation dose technique and is responsible for 70–75% of the collective population dose from medical radiation (5, 6). Baseline axial 2D image sets are created by this technique, but newer single and multi detector helical scanners allow the radiologist to produce 2D images in any plane, using a workstation. Post-processing techniques can also be used to produce sophisticated 3D reconstructions, which can be of huge benefit to surgical colleagues in operative planning, and have also led to CT being utilised to perform non-invasive peripheral and cardiac angiography, and virtual endoscopy (both bronchoscopy and colonoscopy) examinations.

Basic principles: CT scanners consist of a rotating X-ray tube and a curved bank of detectors both housed within a gantry. The X-ray beam passes through the patient, is recorded by the detectors and an electronic

signal is generated, which is then used to reconstruct the image. In CT, there is a complex relationship between the radiation dose received by the patient and image quality, and the radiologist and radiographer must carefully plan each examination. This is of particular relevance in paediatric CT studies, given the stochastic risks from ionising radiation (7).

The anatomic detail given by CT images is excellent and post-processing techniques can be used to study the different body tissues. Modern CT scanners acquire image data rapidly, lessening the need for sedation and anaesthesia in younger children. Patient preparation is minimal; for some examinations, the child may be required to drink oral contrast medium (a dilute solution of barium or a water-soluble iodinated agent), though this can generally be mixed with juice or flavourings to improve palatability. An indwelling IV cannula is also commonly required and the distress at its insertion can be minimised by the use of topical anaesthetic agents. The cannula allows IV contrast medium to be injected during the examination, for easier inspection of solid organs and for direct visualisation of blood vessels. Contrast agents are valuable in paediatric CT scanning, not least because many children lack body fat, making interpretation of the abdomen and pelvis difficult without the benefits of contrast media.

Uses: Traditionally, CT has been particularly useful in the staging and follow-up of tumours, for evaluating trauma and infections, to study the lung parenchyma and mediastinal structures, and for cranial imaging. More recently, CT use has increased to include the investigation of suspected appendicitis or renal calculi, and to provide detailed anatomy of fracture sites (both acutely and following surgery).

Ultrasound

Basic principles: Piezoelectric crystals, contained within an ultrasound (US) probe (transducer), emit high-frequency sound waves when subjected to an alternating current. These sound waves pass through the patient's body, being reflected back towards the probe when tissues of different acoustic properties interface. The sound 'echoes' generate a signal within the crystal that is used to form the image. This process occurs so rapidly, that the images can be generated in real time. Bone absorbs the sound completely, air reflects it, which is why acoustic 'shadows' are seen behind them. Fluid-filled structures, such as the bladder transmit sound well, which is why a stronger 'echo-signal' is seen behind them. The time taken for the echoes to return to the crystal is used to determine a tissue's location in the body.

Techniques, advantages and uses: In medical US, transducer frequencies of between 1 and 15 MHz are used. Higher frequency probes provide exquisite detail, but have only limited tissue penetration. The converse is true for lower frequency probes, which are needed to image larger patients or deeper structures. The small size and lack of obesity in many children mean US images of excellent quality can be obtained. In addition, the anatomy of the growing skeleton, means that non-ossified bone can be imaged, e.g. to allow visualisation of the spinal cord or the hip joints. The fontanelles in an infant's skull allow imaging of the brain that is not possible in adult patients. US is commonly used to examine the solid intra-abdominal organs, the heart in echocardiography, superficial organs such as the thyroid gland and testes, and soft tissue masses. Bowel US for suspected hypertrophic pyloric stenosis and appendicitis are regularly requested, and the use of US as a guidance imaging modality for interventional procedures, voiding cystourethrograms and reduction of intussusception are common. The choice of US as the imaging modality for some of these clinical problems will be largely dependent upon local expertise.

The major advantage of US in paediatric radiology is that it does not involve ionising radiation, meaning it is safe to use in all patients, and can be performed repeatedly. US is portable and widely available. It is painless, requires little in the way of patient preparation and patient sedation is unnecessary, given that the examinations can generally be performed rapidly. High-quality US images do, however, require a skilled paediatric sonographer to perform the examination.

Newer developments in the field of US include tissue harmonics, which particularly improve the image quality in larger patients and the increased use of 3D imaging. The term '4D' US has been coined; it simply refers to 3D images being obtained in real time, with time representing the fourth dimension.

Colour Doppler and Doppler Interrogation

Basic principles and uses: The information obtained from an US examination can be increased with a technique that utilises the Doppler effect (a perceived change in the frequency of a sound emitted by a moving source). In US exams, the moving sources are erythrocytes, with the echo undergoing a frequency shift depending upon the speed and direction of blood flow within a vessel. This data can be colour-coded (by convention, flow towards the probe is red and away from the probe is blue, but this is arbitrary) or can be presented in graphical form to show the shape of the pulse wave and the velocity of the flowing blood. In paediatric radiology, Doppler is especially useful to look for vessel patency in children with central lines (before and after insertion), to assess vessels in relation to

new and known malignancies, following organ transplantation, for assessment of renal blood flow in children with suspected acute pyelonephritis and also during echocardiography. US contrast media are also available, though their use in paediatric radiology is currently limited. They may be used in echocardiography, particularly in the assessment of suspected arteriovenous malformations, in sonocystography, to aid the detection of vesicoureteric reflux and in the assessment of organ and tumour perfusion. These agents are injected intravenously and contain numerous microbubbles, which act as strong reflectors of the US beam.

Magnetic Resonance Imaging

Basic principles: Magnetic resonance imaging (MRI) is technically the most complex of the currently available imaging modalities, and gives vast anatomic and physiological detail of the body. In their most simplistic terms, the physics of MRI involve the patient being placed in a strong magnetic field. Here, those atoms in the body, which have magnetic moment (more protons than neutrons in the nucleus), align themselves with the magnet. A radiofrequency (RF) pulse is then applied to disturb this formation. When the RF pulse is switched off, the atoms realign with the main magnetic field and give off a signal as they do so. This signal is minute, but multiplied many millions of times, due to the number of (hydrogen) atoms within the human body; it is this signal that is used to create the image. Many RF pulses are required to form the image, and the timing, length and type of the RF pulses, give the different sequences used in modern MRI. An individual MR sequence can take less than 1 to longer than 15 min, and each examination is comprised of several sequences. The total time taken for an MR study is between 30–60 min. Small amounts of patient motion can destroy the images, as they cannot be reconstructed until an entire sequence is complete. Many children cannot hold still for the length of time required and frequently require sedation or general anaesthesia for this type of examination.

Both oral and IV contrast media are utilised in MRI, though not frequently in children. Oral MR contrast agents consist of ferrite compounds that accumulate in the reticuloendothelial system. Gadolinium chelates are the most common IV contrast agents; they work by shortening the T1-relaxation times of protons, increasing the signal from tissues and organs on T1-weighted sequences.

Advantages and uses of MRI: Excellent contrast resolution and multiplanar imaging are the major benefits of MR. The most commonly performed MR examinations are those of the central nervous system; posterior fossa detail and grey/white matter differentiation are well demonstrated. MR is also the imaging modality of choice to evaluate many musculoskeletal problems: trauma, tumours (both benign and malignant, pre- and post-operatively), bone marrow disorders and joint disease. Other indications include tumour staging and follow-up, the mapping of vascular malformations and their blood supply, assessment of the airway, examination of both children and adults with congenital heart disease, the study of genito-urinary tract anatomy and in the case of the kidneys themselves, function.

Newer techniques include diffusion-weighted MR studies (based upon the Brownian motion of the water molecules in a tissue), which are useful in the detection of tissue ischaemia, functional MRI (based upon the increase in blood flow to the local vasculature that accompanies neural function), as an adjunct to neurosurgical planning and contrast-enhanced dynamic MRI. The latter technique is useful in cardiac studies, to calculate for example, the ventricular ejection fraction and blood flow across septal defects, within shunts and in stenotic vessels. Contrast-enhanced dynamic MRI is also useful in MR urography (often in conjunction with a dose of diuretic), where renal function can be mapped to provide information analogous to a radioisotope MAG 3 study.

Nuclear Medicine

Basic principles: A radiopharmaceutical is a minute quantity of a drug to which a radionuclide is tagged. This compound may then be injected, ingested or inhaled and is delivered to a specific organ or body tissue. Once it reaches its target, the radionuclide emits gamma radiation, which is detected by a scintillation (gamma) camera. Computer software aids in image reconstruction, based upon the position in the body from which the radiation was emitted. Using nuclear medicine techniques, it is possible to study the function of different organs, tissues and bones. Most commonly, 2D planar images are produced, but using a technique called SPECT (▶single photon emission computed tomography), the images can be reconstructed in multiple planes. The anatomic detail obtained in nuclear medicine is limited.

Advantages and uses of nuclear medicine: Nuclear medicine studies are divided broadly into two types: dynamic and static. The former may be used to study, for example gastro-oesophageal or vesicoureteric reflux, regional blood perfusion, gastric emptying, biliary or renal excretion. Static studies may be used to study more specific radiotracer absorption, such as by the kidneys to evaluate for acute pyelonephritis or focal renal scars, or by the bone cortex when evaluating for metastatic disease, osteomyelitis or fractures. Other commonly requested paediatric radioisotope studies include the study of

primary tumours, such as neuroblastoma, lung function assessment and to aid in the evaluation of children with epilepsy.

New developments: Probably the fastest developing area in nuclear medicine is the use of PET (►positron emission tomography) and PET-CT. These techniques make use of short-lived, positron-emitting isotopes, to study biochemical and physiological processes within the body. The most commonly used isotope is ^{18}F-fluorodeoxyglucose (FDG), which is a glucose analogue that accumulates in normal cells, inflammatory lesions and malignant tumours. The technique works upon the principle that the abnormal tissues take up and metabolise the isotope at a faster rate than do normal tissues. In common with other nuclear medicine examinations, the anatomical information from a PET scan is limited, but fusing the axial PET images with the corresponding CT study, is a sensitive technique for localising a lesion. PET and PET-CT are not yet widely available. They rely upon on-site or regional isotope production in a cyclotron; with express delivery of the isotope to the nuclear medicine department (the isotopes are very short-lived). The technique is expensive and delivers a higher radiation dose to the patient, than do the more common nuclear medicine examinations. Due to the length of time a study takes, a child is likely to require sedation or anaesthesia. In paediatric radiology, PET has mainly been used in the staging and follow-up of children with lymphomas and in the pre-operative assessment of children with epilepsy.

Diagnosis

There are important anatomic, physiological and psychological differences between children and adults, and whilst the paediatric radiologist has all of the imaging modalities his or her adult colleagues have at their disposal, the choice of which modality to use in a given clinical scenario, will be governed in part by the special needs of an individual child. Communication skills are vital to all radiologists, but a paediatric radiologist must be able to explain procedures and answer questions in a language that is comprehensible to both a patient's (adult) carers, and to the child himself. The cooperation of a child for a particular study is likely to depend upon how successful the radiologist has been in this task, and dictates whether or not the images obtained are of diagnostic quality.

Bibliography

1. Don S, Albertina MJ, Ammann DL et al (1995) Soft-copy computed radiography in neonatal and pediatric intensive care units: cost savings analysis. Radiology 197:501–505
2. Willis CE, Slovis TL (2004) The ALARA concept in pediatric CR and DR: dose reduction in pediatric radiographic exams—a white paper conference executive summary. Pediatr Radiol 34 (Suppl 3): S162–S164
3. Samei E, Hill JG, Frey GD et al (2003) Evaluation of a flat panel digital radiographic system for low-dose portable imaging of neonates. Med Phys 30:601–607
4. Brown PH, Thomas RD, Silberberg PJ et al (2000) Optimization of a fluoroscope to reduce radiation exposure in pediatric imaging. Pediatr Radiol 30:229–235
5. Linton OW, Mettler FA (2003) National conference on dose reduction in CT, with an emphasis on pediatric patients. Am J Roentgenol 181:321–329
6. Wiest PW, Locken JA, Heintz PH et al (2002) CT scanning: a major source of radiation exposure. Semin Ultrasound CT MR 23:402–410
7. Brenner DJ, Elliston CD, Hall EJ et al (2001) Estimated risks of radiation-induced fatal cancer from pediatric CT. Am J Roentgenol 176:289–296

Chloroma

►Hepatic Sarcoma

Cholangiocarcinoma, CC

►Neoplasms, Bile Ducts

Cholangiocellular Carcinoma, CCC

►Neoplasms, Bile Ducts

Cholangiography

Introduced in 1954 as intravenous cholangiography for the visualization of the common bile duct, it consists in intravenous injection of an iodinated contrast medium that is excreted by hepatocytes allowing the opacification of the biliary ducts. Gallbladder visualization was not included in cholangiography. Intravenous cholangiography has been replaced by direct cholangiography, which includes percutaneous transhepatic cholangiography

(PTC), endoscopic retrograde choledochopancreatography (ERCP), perioperative cholangiography, and trans-Kehr cholangiography.
►Biliary Anatomy

Cholangitis

Thomas Helmberger[1], Carlo Bartolozzi[2], Paola Vagli[2]
[1]Clinic of Radiology and Nuclear Medicine, University Hospitals Schleswig-Holstein Campus, Luebeck
[2]Department of Diagnostic and Interventional Radiology, University of Pisa, Italy
thomas.helmberger@uni-luebeck.de
bartolozzi@do.med.unipi.it

Synonyms

Acute cholangitis; AIDS cholangiopathy; Ascending cholangitis; Bacterial cholangitis; Bile duct inflammation; Chemotheraphy-induced cholangitis; Cholangitis due to scolicidal agents; Clonorchiasis; Eosinophilic cholangitis; fascioliasis; Fungal cholangitis; Ischemic cholangitis; Primary sclerosing cholangitis; Recurrent pyogenic cholangitis

Definition

Cholangitis means inflammation of the bile ducts. The term applies to inflammation of any portion of the biliary ducts, from the liver to the gallbladder and intestine. The inflammation is produced by infection or some other cause (toxic agents or ischemic or autoimmune disorders). Bile duct inflammation, in either the acute or chronic form, may result in a fibrosing process in some instances (primary or secondary sclerosing cholangitis).

Pathology/Histopathology

Cholangitis, Bacterial

►Cholangitis, bacterial also called ►cholangitis, ascending or ►cholangitis, acute is an acute infection of the biliary tree with the potential to cause significant morbidity and mortality. The pathogenesis of cholangitis requires stasis or obstruction of bile flow, which predispose to subsequent infection. Choledocholithiasis is the most common cause of obstruction. Strictures, stenosis, tumors, choledochal/biliary cysts, and ►sump syndrome have also been described as causes of bile stasis and cholangitis. Recently, endoscopic manipulation and stents placement have increasingly been reported as causes of benign strictures and subsequently of cholangitis. Hepatobiliary or pancreatic head malignancies are less common causes of biliary obstruction and subsequent bile contamination.

Bacteria are not normally present in bile or are present only in very small amounts; however, the incidence of bactibilia increases in cases of gallbladder and common bile duct stones. The most common organisms found are *Escherichia coli*, *Klebsiella*, *Enterobacter* species, enterococci, and group D streptococci. Bacteria most frequently infect the bile directly from the gut or through the lymphatics or vascular supply; infection thereby ascends into the hepatic ducts. The development of increased biliary pressure pushes the infection into the biliary canaliculi, hepatic veins, and perihepatic lymphatics, leading to bacteremia. The infection can present suppurative features.

Cholangitis is reported in all races but is relatively uncommon in Western countries, where it occurs in association with other diseases that cause biliary obstruction and bactibilia. The condition is reported in both females and males and has no clear predominance. Otherwise, gallstones are more common in women, and cholangitis due to gallstones shows a higher prevalence in females. The condition mostly occurs in adults, with a reported median age at onset of 50–60 years (1, 2).

Cholangitis, Sclerosing Primary

►Primary sclerosing cholangitis (chol, PS) (PSC) is a chronic, idiopathic, fibrosing inflammatory disorder affecting the bile ducts (both intrahepatic and extrahepatic) leading to bile duct obliteration, cholestasis, and biliary cirrhosis. The term "primary" is used to differentiate this condition from biliary strictures due to bile duct injury, cholelithiasis, ischemia, and chemical injury (secondary sclerosing cholangitis). Peak incidence occurs in the third and fourth decades of life, and a male predominance appears to exist. The etiology remains unknown, although most authors believe it to be an autoimmune process because it may be associated with other autoimmune diseases such as retroperitoneal fibrosis, mediastinal fibrosis, and Sjögren syndrome. A strong association with inflammatory bowel disease, especially ulcerative colitis, has also been noted.

Pathophysiologically, the biliary injury may be initiated by an immune-mediated destruction of the hepatobiliary tract that is perhaps caused by transient infection or the absorption of bacterial products in genetically predisposed individuals with colonic disease.

Bacteria, toxins, viral infections (reovirus and cytomegalovirus), and genetic factors (increased frequency of HLA-B8 and HLA-DR3) have also been proposed as predisposing agents. These lend support to the theory that immunologic and genetic mechanisms may both be involved in the pathogenesis. Histological findings include nonspecific features such as periductal concentration of mononuclear cells, ductular proliferation, aspects resembling chronic active hepatitis, and specific findings including concentric obliterative fibrosis of interlobular bile ducts with the presence of intrahepatic cholangiectasis and ductal obliteration. Bile ducts grossly display multiple short strictures, pseudodiverticula, and wall thickening. Saccular dilatations like those seen in Caroli's disease are uncommon.

The diagnosis is based on a combination of clinical features and a cholestatic biochemical profile, along with typical cholangiographic abnormalities confirmed by liver histology and the exclusion of secondary causes of sclerosing cholangitis. PSC is usually progressive, leading to cirrhosis, portal hypertension, and liver failure. An increased incidence of cholangiocarcinoma and gallbladder carcinoma is reported in these patients. In adult patients, the median period of survival from the time of diagnosis is 9–11 years but is shorter for patients who are symptomatic at the time of diagnosis. Treatment is usually palliative and includes medical therapy with choleretic or immunosuppressive therapy or endoscopic or percutaneous mechanical dilation of dominant strictures. Liver transplantation remains the only effective therapeutic option for patients with end-stage liver disease from PSC (3).

Cholangitis, Recurrent Pyogenic

Recurrent pyogenic cholangitis, also called oriental cholangiohepatitis, intrahepatic pigmented calculus disease, or hepatolithiasis, is a complex hepatobiliary disease characterized by chronic inflammation of the bile ducts attributed to parasite influx. In endemic areas (Southeast Asia), parasites such as *Clonorchis sinensis* and *Ascaris lumbricoides* can inhabit the bile ducts, causing ductal damage and strictures. Other parasites such as *Opistorchis viverrini*, *Fasciola hepatica*, and *Entamoeba* have also been implicated. Recurrent pyogenic cholangitis is rarely observed in Western countries but may be diagnosed in native Asian people, in whom it tends to be less severe. The infection is typically chronic and recurrent, leading to progressive destruction of the bile ducts and secondary biliary cirrhosis. The primary histopathologic changes of recurrent pyogenic cholangitis are proliferative fibrosis of bile ductal walls, with inflammatory infiltration of the portal tracts and periductal abscesses. Grossly multiple strictures associated with marked dilatation upstream from the stenotic tracts can be observed both in the intrahepatic and extrahepatic bile ducts. Marked enlargement of intrahepatic and extrahepatic ducts may be present. The nidus for stone formation is provided by the presence of secondary bacterial infection, whereas brown-pigmented bile stones can be frequently observed inside bile ducts. Intraductal stones can lead to progressive biliary obstruction and recurrent infection, resulting in the formation of multiple cholangitic hepatic abscesses, biliary strictures, and, eventually, severe hepatic destruction, cirrhosis, and portal hypertension. An increased incidence of cholangiocarcinoma is also reported (4).

Clinical Presentation

Cholangitis, Bacterial

Cholangitis ranges from light forms to fulminant destructive sepsis associated with multiple organ failure. In 1877, Charcot described a triad of findings related to cholangitis: right upper quadrant pain, fever, and jaundice. In 1959, Reynolds and Dargon described a more severe form, adding two other signs: septic shock and mental confusion (Reynolds pentad). A history of past symptoms of gallbladder colic or recent biliary tract manipulation associated with fever, right upper quadrant pain, and jaundice is highly suggestive of cholangitis. Other signs and symptoms include chills, rigor, itching, acholic or hypocholic stools, and mild hepatomegaly. Laboratory findings include leukocytosis, hyperbilirubinemia (patients with malignant obstruction generally have significantly higher bilirubin levels than those with benign obstruction), and elevated alkaline phosphatase levels. Elevation of transaminases and serum amylase levels is possible in cases of concurrent pancreatitis due to stone impaction at the ampulla of Vater and secondary obstruction of the pancreatic duct. Blood culture findings are positive in nearly half of the patients. Bile culture findings are positive in nearly all patients. With increasing degrees of sickness, there is an increased likelihood of complications such as liver failure, hepatic abscesses, bacteremia, gram-negative sepsis, and acute renal failure. The prognosis is usually severe, although it improves with early antibiotic treatment and appropriate drainage and decompression of the biliary tract as needed. Factors associated with poor prognosis include advanced age, female gender, acute renal failure, preexisting cirrhosis, and malignant biliary obstruction (1, 2).

Cholangitis, Sclerosing Primary

The onset and progression of PSC tend to be insidious, and some patients may be affected without having

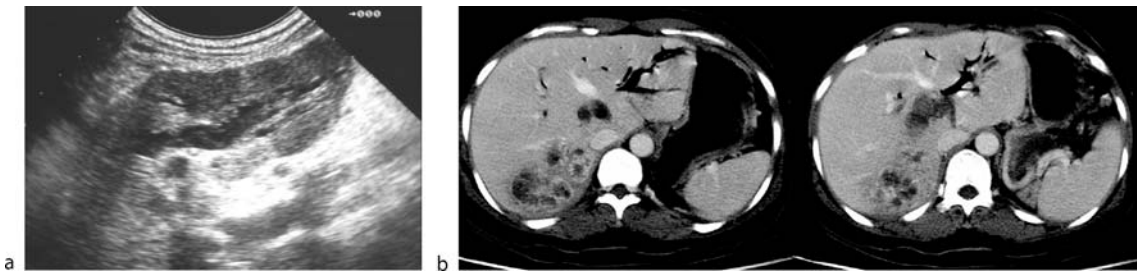

Cholangitis. Figure 1 (a) Bacterial cholangitis. Ultrasound examination shows echogenic material within a dilated bile duct in the left lobe. (b) Bacterial cholangitis. Computed tomographic image displays aerobilia in the left lobe and inflammed, dilated bile ducts in the right lobe. Inflammed biliary walls are concentrically thickened, enhancing after contrast medium administration and surrounded by parenchymal hypodensity due to edema.

symptoms. Patients may present with nonspecific signs, including progressive fatigue, abdominal pain, fever, and intermittent jaundice, or with cholestasis and complications of cholestasis such as pruritus, cholangitis, and fat malabsorption. Additionally, some patients may show the stigmata of chronic liver disease and cirrhosis at the time of presentation.

Biochemical analysis reveals increased levels of serum bilirubin and alkaline phosphatase in most patients, with a mean increase in the alkaline phosphatase level to three times the upper limit of normal. Serum transaminase levels may be normal or elevated. Perinuclear antineutrophil cytoplasmic antibodies (pANCAs) have been found in most patients with PSC. The presence of pANCAs is associated with a more severe course of autoimmune liver disease (3).

Cholangitis, Recurrent Pyogenic

Clinical presentation is characterized by recurrent attacks of abdominal pain, fever, and jaundice caused by intrahepatic ductal strictures and calculi. The therapeutic approach is ruled by the complete clearance of calculi and debris from the biliary tract and the elimination of bile stasis to prevent recurrent attacks of the disease. Therefore, hepatolithiasis is difficult to eradicate, and for effective treatment, accurate topographic cholangiographic evaluation of disease distribution is required before surgical intervention (surgical resection of the affected portion of the liver and the creation of biliary–enteric anastomosis to allow adequate biliary drainage) (4).

Imaging

Cholangitis, Bacterial

Computed tomography (CT) and ultrasound (US) are commonly employed to diagnose biliary dilation. Endoscopic retrograde cholangiopancreatography (ERCP) or percutaneous transhepatic cholangiography (PTC) may directly visualize the biliary ducts and treat the obstruction in a unique session. A paramount view of the biliary tree may also be achieved by means of magnetic resonance cholangiopancreatography (MRCP). Conventional radiography plays an inferior role in the diagnosis of acute cholangitis, showing only indirect signs such as adynamic ileus, radiopaque gallstones, and aerobilia after endoscopic manipulation or in cases of bilioenteric fistula.

US is the modality of choice for gallstones and cholecystitis but is not completely reliable for choledocholithiasis in all patients. US is also sensitive for diagnosing and differentiating intrahepatic from extrahepatic dilatation, including common bile duct dilatation, but it may fail in establishing the cause of stenosis (stone vs. stricture). Purulent bile can be identified as intraluminal echogenic material within dilated bile ducts (Fig. 1a). Furthermore, US can display other abdominal organs (gallbladder, aorta, pancreas, liver), thereby excluding other potential causes of acute abdominal pain. Complications such as liver abscess can also be detected.

CT depicts biliary dilatation and adds further information to provide the precise site of obstruction and also displays inflammation of the biliary tree walls or eventual aerobilia. Thickening of the bile duct walls, either concentric or diffuse, may be underlined after contrast enhancement; increased attenuation of bile or aeroblia may also be displayed (Fig. 1b). Cholangitis may also be present with no visible sign on CT. Potential causes and complications of cholangitis (ampullary tumors, liver abscesses) or pathologies that clinically mimic cholangitis and must be distinguished from cholecystitis, biliary colic, mesenteric ischemia, or ruptured appendix may be displayed by CT.

Magnetic resonance (MR) imaging resembles CT findings without further specific contribution to the diagnosis. Cholangiographic acquisitions depict irregularities of the walls of the bile ducts associated with filling

defects that may be due to stones or sludge, and can accurately determine the site of blockage.

ERCP and PTC may be used for diagnostic and therapeutic purposes, allowing stones to be removed and strictures resolved. Endoscopic biliary drainage and decompression have mostly replaced surgery as the initial treatment of severe cholangitis. In unstable patients, a reasonable option for decompressing the biliary tract is percutaneous biliary drainage (2).

Cholangitis, Sclerosing Primary

US findings may be normal in about half of the patients. In some patients, US may show only unspecific features, including intrahepatic and extrahepatic ductal dilatation, or signs of cirrhosis such as increased echogenicity and heterogeneity of liver parenchyma. Splenomegaly and ascites are observed in cases of portal hypertension. US cannot display bile duct abnormalities unless there is dilatation. Sludge or stones may be present in long-standing cases, presenting as echogenic intraductal structures. Wall thickening and intraductal protrusions may be depicted in the common bile duct. CT signs of primary sclerosing cholangitis are quite specific, including randomly dilated small peripheral ducts without apparent connection to the central duct, which are referred to as skip dilatation or knoblike appearance. After contrast medium administration, regular or nodular wall thickening may be appreciated.

Peripheral wedge-shaped areas of high T2 signal intensity and dilatation of bile ducts are characteristic MR findings in PSC.

Cholangiographic techniques (both invasive PTC/ERCP and noninvasive MRCP) may depict typical changes in intrahepatic and extrahepatic bile duct morphology.

The cholangiographic findings depend on the stage of the disease and include multifocal, intrahepatic bile duct strictures alternating with normal-caliber ducts, which sometimes produce a beaded appearance. Early phases present with short annular intrahepatic strictures, randomly distributed, alternating with normal or slightly dilated segments, with a distinctive acute-angle branching pattern. Strictures usually occur at the bifurcation of ducts and are out of proportion with respect to proximal ductal dilatation. Progressive fibrosis and periductal inflammation cause an increase in strictures and duct obliteration, avoiding opacification of peripheral ducts on ERCP, and producing a "pruned tree" appearance. Irregular narrowing with small diverticular marginal protrusions or shaggy contours is typically found in extrahepatic ducts. Nonspecific cholangiographic findings include webs, diverticula, and stones.

ERCP shows a higher success rate in the absence of dilated intrahepatic ducts with respect to PTC and represents the standard of reference for diagnosing PSC because the clinical, biochemical, and hepatic histological findings are usually nonspecific. ERCP provides a high sensitivity regarding peripheral intrahepatic duct abnormalities and allows interventional procedures such as mechanical dilation of obstructing strictures, stent placement, and biopsy.

MRCP is a suitable noninvasive alternative method for detecting and localizing bile duct obstruction and choledocholithiasis. By using heavily T2-weighted sequences, the signal of static or slow-moving fluid-filled structures such as biliary and pancreatic ducts is greatly increased, resulting in increased duct-to-background contrast. Advantages of MRCP include better demonstration of ducts proximal to an obstruction or tight stenosis, and when combined with conventional T1- and T2-weighted sequences, the ability to generate an anatomical imaging of extraductal disease. However, MRCP provides less spatial resolution than ERCP, thereby decreasing the sensitivity to peripheral ductal abnormalities. On MRCP, the presence of stenoses is usually deduced when there is prestenotic dilatation (Fig. 2); however, in the initial stages of stenosis, there is only temporary dilatation. As a result, these early stenoses may remain undetected at MRCP. In addition, the extent of a focal short stricture, especially of the common hepatic duct, may be overestimated at MRCP for the ducts collapsed downstream of the stenosis. The visualization of mildly dilated peripheral ducts that do not connect to the central ducts is a characteristic sign on MRCP (3).

Cholangitis, Recurrent Pyogenic

Pigmented intrabiliary calculi are hardly visualized by conventional radiography due to their low opacity. US

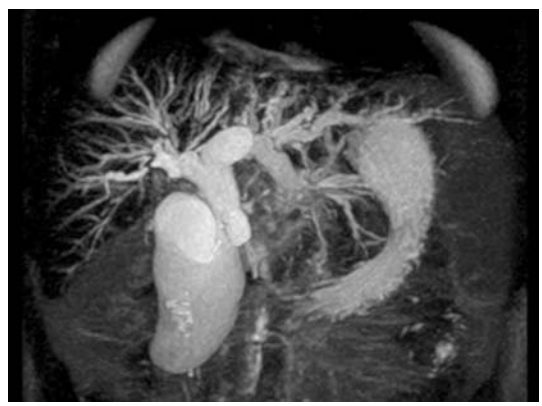

Cholangitis. Figure 2 Magnetic resonance cholangiography. This three-dimensional MIP reconstruction shows the typical aspect of sclerosing cholangitis. (Courtesy of Dr. Piero Boraschi)

can visualize intrahepatic and extrahepatic bile duct dilatation, biliary stones, and coexisting parenchymal abnormalities, such as hepatic atrophy, abscess, and biloma. Other suggestive US features are localized dilatation of the lobar or segmental bile ducts, increased periportal echogenicity, and fibrous thickening of the duct walls with increased wall echogenicity. Pigmented stones usually show a medium echogenity with a variable degree of acoustic shadowing, and the association in some instances of aerobilia determines a low capacity of US for detecting ductal stones. Also, US poorly visualizes dilated ducts completely filled by sludge or calculi.

CT may depict pigment stones as hyperdense to isodense structures relative to their degree of calcification. CT can also better appreciate on precontrast scans the presence of calculi inside significantly dilated ducts and provides assessment of the spatial extent of ductal involvement. A significant enhancement of the involved ductal walls as well as of periductal tissues, suggesting inflammation, can be observed after contrast medium administration. CT even allows accurate depiction of coexisting hepatic parenchymal complications such as intrahepatic abscesses, biloma, and segmental or lobar atrophy.

Cholangiographic findings include multifocal strictures and dilatation of the intrahepatic bile ducts, disproportionate dilatation of the extrahepatic bile ducts unrelated to strictures or stones, straightening and rigidity of the ducts, a right-angle branching pattern, and decreased arborization. In rare instances, cholangiectasis or "bile lakes" can occur from progressive obstruction and inflammation. Stones determine filling defects in the opacified bile ducts. When the calculi completely obstruct the orifice of the segmental or subsegmental bile ducts, they cannot be detected (missing duct sign). Direct cholangiography, such as ERCP and PTC, has been the most accurate way to obtain an accurate topographic description of the biliary tree by depicting the full spectrum of ductal changes and calculi. However, these techniques have limitations, especially in cases of high-grade stenosis, impacted calculi, and complete ductal obstruction, and are invasive with an increased risk of septic complications. Conversely MRCP rendering of the stationary fluids allows noninvasive depiction of the entire biliary tree despite obstruction or stenosis. Parenchymal atrophy is seen as slightly hyperintense areas with reduced volume, while bile duct dilatation and biloma may be depicted regardless of their communication with the bile duct (4).

Nuclear Medicine

Cholangitis, Bacterial

Biliary scintigraphy with ^{99m}Tc-radiolabeled molecules such as iminodiacetic acid derivatives is a functional study showing high sensitivity. It is associated with positive results before the ducts result in enlargement on US, but high bilirubin levels may decrease the study's sensitivity. Obstruction of the common bile duct causes a lack of visualization of anatomic details and of activity within the small intestine.

Diagnosis

Cholangitis, Bacterial

The diagnosis is obtained in most cases on the basis of clinical and laboratory findings and should be suspected in patients with a history of past symptoms of gallbladder colic or recent biliary tract manipulation. A diagnostic imaging work-up must be done to confirm the diagnosis and to depict potential causes and the site of biliary obstruction.

Cholangitis, Sclerosing Primary

Diagnosis is usually achieved by means of the typical cholangiographic pattern. Histological analysis is used only for confirmation because it shows only nonspecific inflammatory fibrosis of the portal triads and a paucity of bile ducts. Differential diagnosis must encompass other causes of secondary sclerosing cholangitis or nonsclerosing processes that mimic primary sclerosing cholangitis at cholangiography. These include strictures or stones complicating chronic bacterial cholangitis, parasitic or ►fungal infection of the bile, cholangitis related to acquired immunodeficiency syndrome (AIDS), ischemia due to treatment with chemotherapeutic agents or to hepatic arterial thrombosis complicating liver transplantation, previous bile duct surgery, congenital biliary anomalies, and rare entities such as ►eosinophilic cholangitis.

In definitely dilated ducts that simulate primary sclerosing cholangitis, one should consider other sclerosing ductal processes, such as ascending cholangitis or primary sclerosing cholangitis complicated by cholangiocarcinoma (3).

Cholangitis, Recurrent Pyogenic

In patients from endemic areas, the presence of a characteristic clinical history associated with imaging features including predominantly left-sided findings should prompt consideration of this diagnosis. Diffuse, uniform dilatation of the intrahepatic bile ducts, particularly in the periphery of the liver, with thick enhancing walls and the absence of extrahepatic biliary dilatation, should also raise suspicion for ►clonorchiasis. Other causes of sclerosing and chronic cholangitis must be excluded (4).

Bibiliography

1. Lipsett PA, Pitt HA (1990) Acute cholangitis. Surg Clin North Am 70(6):1297–1312
2. Balthazar EJ, Birnbaum BA, Naidich M (1993) Acute cholangitis: CT evaluation. J Comput Assist Tomogr 17(2):283–289
3. Vitellas KM, Keogan MT, Freed KS et al (2000) Radiologic manifestation of sclerosing cholangitis with emphasis on MR cholangiopancreatography. Radiographics 20(4):959–975
4. Park MS, Yu JS, Kim KW et al (2001) Recurrent pyogenic cholangitis: comparison between MR cholangiography and direct cholangiography. Radiology 220(3):677–682

Cholangitis due to Scolicidal Agents

Form of secondary sclerosing cholangitis due to injection of scolicidal agents into hydatid liver cysts directly communicating with the bile duct system.
▶Cholangitis

Cholangitis, Acute

Acute bacterial infection of the bile ducts
▶Cholangitis

Cholangitis, Ascending

Also called bacterial cholangitis, ascending cholangitis is usually determined by bacterial (gram-negative) contamination of an obstructed biliary system. The role of MRCP or ERCP is to enable diagnosis of the underlying cause of the obstruction, while the diagnosis of ascending cholangitis is clinical. Clinical presentation usually occurs with the classic Charcot triad of abdominal pain, fever, and jaundice. Complications such as liver abscess and sepsis can occur when increased ductal pressure causes necrosis of the duct wall with reflux of infected bile into the portal triads.
▶Cholangitis

Cholangitis, Bacterial

Also called ascending cholangitis or acute cholangitis, this is a bacterial infection of the biliary tree. Development of cholangitis requires stasis or obstruction of bile flow, which subsequently becomes infected. Diagnostic imaging may confirm diagnosis and reveal the causes or the site of obstruction.
▶Cholangitis

Cholangitis, Chemotherapy-induced

Secondary sclerosing cholangitis characterized by the presence of strictures in the common hepatic duct occurring in patients with metastatic liver disease, treated by means of hepatic arterial infusion of chemotherapeutic agents such as floxuridine. Hepatic toxic effects can develop because of a high rate of extraction on the first pass through the liver. Characteristic features include an inflammatory, fibrosing process in the portal triads, causing narrowing or occlusion of the bile ducts that simulates primary sclerosing cholangitis at conventional cholangiography. The mechanism of injury is either a direct effect of treatment or ischemia secondary to thrombosis of the intrahepatic arterial branches. According to the specific arterial supply of the biliary ducts, intrahepatic bile ducts and the lower portion of the common bile duct are unimpaired in most cases. Bile duct strictures occur as early as 2 months after therapy and may decrease if the intraarterial infusion is interrupted. The most common cholangiographic findings are narrowing of the bifurcation of the common hepatic duct with sparing of the distal common bile duct. Cross-sectional imaging is usually required to exclude worsened metastatic disease in these patients.
▶Cholangitis

Cholangitis, Eosinophilic

Presence of multiple strictures of the bile ducts due to eosinophilic infiltration of the hepatobiliary system usually associated with eosinophilic gastroenteritis. This rare condition is reversible, responds rapidly to corticosteroid therapy, and may result in radiographic and histological features in accordance with cholangitis, cholecystitis, or chronic hepatitis.
▶Cholangitis

Cholangitis, Fungal Infection

Form of secondary sclerosing cholangitis characterized by diffuse inflammation and strictures determined by various fungal infections of the liver and the biliary tree. Imaging features resemble those of primary sclerosing cholangitis.
▶Cholangitis

Cholangitis, Ischemic after Liver Transplantation

Biliary strictures occurring in liver recipients can be classified into anastomotic and nonanastomotic types and can be caused by iatrogenic injury, hepatic arterial thrombosis or stenosis, prolonged preservation time, recurrence of primary liver disease, chronic rejection, or cholangitis. Anastomotic strictures are mostly extrahepatic ductal, due to iatrogenic trauma with consequent ischemia and scar formation. In these cases, ascending cholangitis may result in formation of intrahepatic bile duct strictures that simulate primary sclerosing cholangitis. Nonanastomotic strictures are mostly due to arterial ischemia and are unrelated to iatrogenic bile duct injury. The hepatic artery represents the unique arterial supply to the transplanted liver, since the peribiliary collaterals from the hepatic, gastroduodenal, celiac, and superior mesenteric arteries are absent in the transplanted liver. Therefore, the presence of hepatic artery obstruction, mostly determined by arterial thrombosis, may result in severe ischemia and bile duct or hepatocyte necrosis. Other causes of nonanastomotic strictures are prolonged preservation time, bacterial or viral cholangitis, and rejection.
▶Cholangitis

Cholangitis, Recurrent Pyogenic

Also called oriental cholangiohepatitis, intrahepatic pigmented calculus disease, or hepatolithiasis, this is a complex hepatobiliary disease characterized by chronic inflammation of the bile ducts and is attributed to parasite invasion. In endemic areas (Southeast Asia), parasites such as Clonorchis sinensis and Ascaris lumbricoides can inhabit the bile ducts, causing ductal damage and strictures. Other parasites such as Opistorchis viverrini, Fasciola hepatica, and Entamoeba have also been found.
▶Cholangitis

Cholangitis, Sclerosing Primary

Chronic, idiopathic, fibrosing inflammatory disorder affecting the bile ducts that eventually leads to bile duct obliteration, cholestasis, and biliary cirrhosis. The term "primary" is used to differentiate this condition from bile duct strictures due to bile duct injury, cholelithiasis, ischemia, or chemical injury (secondary sclerosing cholangitis). The peak incidence occurs in the 3rd and 4th decades of life, and a male predominance appears to exist. It is believed to be an autoimmune process because it is frequently associated with other autoimmune diseases such as ulcerative colitis.
▶Cholangitis

Cholecystitis

Thomas Helmberger[1], Carlo Bartolozzi[2], Paola Vagli[2], Giuliano Mariani[2]
[1]Clinic of Radiology and Nuclear Medicine, University Hospitals Schleswig-Holstein, Campus Luebeck, Germany
[2]Department of Diagnostic and Interventional Radiology and of Nuclear Medicine, University of Pisa, Italy
thomas.helmberger@uni-luebeck.de
bartolozzi@do.med.unipi.it

Synonyms

Cholecystitis acute; Cholecystitis acute acalculous; Cholecystitis chronic; Cholecystitis emphysematous; Cholecystitis gangrenous; Cholecystitis necrotizing; Cholecystitis xanthogranulomatous; Inflammation of the gallbladder

Definition

Cholecystitis is the inflammation of the gallbladder occurring most commonly in cases of obstruction of the cystic duct caused by gallstones. In a very small percentage

(about 10%) of cases, cholecystitis occurs without gallstones (►acalculous cholecystitis). The inflammation often initiates without contamination, and infection may develop later; therefore, bacterial proliferation may be a result of cholecystitis and not the precipitating factor. Severe disease, alcohol abuse, and rarely, tumors of the gallbladder can also be the cause of cholecystitis. Cholecystitis may develop either as an acute or a chronic process. ►Acute cholecystitis is the abrupt onset of inflammation of the gallbladder, resulting in severe upper abdominal pain (biliary colic), which may occur repeatedly. ►Chronic cholecystitis is a long-standing inflammation of the gallbladder characterized by repeated episodes of pain (gallbladder attacks) over a prolonged period.

Pathology and Histopathology

Cholecystitis, Acute

Acute calculous cholecystitis is the acute inflammation of the gallbladder, caused in most instances by obstruction of the cystic duct (usually by gallstones or sludge), leading to distension of the gallbladder and resulting in acute inflammation of the gallbladder wall. As the gallbladder becomes distended, blood flow and lymphatic drainage are compromised, leading to mucosal ischemia and necrosis. Cholelithiasis is the major risk factor for cholecystitis; therefore, risk factors for cholecystitis reflect those for cholelithiasis and include age, female gender, certain ethnic groups (native Americans), obesity or rapid weight loss, and some drugs. Acute cholecystitis complicates the course of symptomatic gallstones in 10–20% of patients. Early acute histological findings include edema and venous congestion. Signs of acuteness are usually overlapped by histological features suggestive of ►chronic cholecystitis. Specific findings include fibrosis, flattening of the mucosa, and chronic inflammatory cells. Mucosal herniations known as Rokitansky–Aschoff sinuses are related to increased hydrostatic pressure and are present in half of the cases. Focal necrosis and infiltration of neutrophils may also be present. In advanced cases, gangrene or perforation may develop (1–4).

Cholecystitis, Acute, Acalculous

Acalculous cholecystitis is defined as an acute inflammation of the gallbladder in the absence of visible stones. It occurs most likely in elderly men secondary to major injuries such as major surgery, trauma, sepsis, burns, cardiac events, and a widespread severe disease particularly in people receiving prolonged intravenous feeding. The most common predisposing factors are biliary stasis associated to prolonged fasting, immobility, and hemodynamic instability. About half of the cases of acute cholecystitis in pediatric patients are acalculous disease, perhaps originating as an infection (viral or other). The exact pathogenesis of acalculous cholecystitis is unclear, although current theory is related to the histotoxicity of concentrated, stagnant, retained bile developing in cases of prolonged fasting where the gallbladder never receives a stimulus to empty. Ischemia is considered another potential cause of direct injury. In some patients, infection may be the primary event, as has been described in cases of typhoid fever or AIDS cholangiopathy. Complications such as gallbladder wall necrosis, gangrene (diffuse or focal), and perforation are common. The mortality is very high because of the fulminant course and coexistent disease (1,4).

Cholecystitis, Emphysematous

►Emphysematous cholecystitis is a severe condition associated with a high mortality and characterized by the presence of gas within the wall and the lumen of the gallbladder.

It can be considered either as a complication of acute cholecystitis (occurring in about 1% of cases), in particular acalculous, or as a separate entity. It occurs most commonly in elderly males and diabetics and is less frequently associated with cholecystolithiasis than other forms of acute cholecystitis. Pathogenesis of this type of disease is related to ischemia (obstruction of the cystic artery) and bacterial overgrowth with gas-forming agents such as *Escherichia coli*, *Clostridium perfringens* or *Clostridium welchii*, anaerobic streptococci, and *Klebsiella* species. Whether these bacteria represent the primary cause of the disorder or are secondary invaders remains unclear. Histologically the layers of the gallbladder wall become separated, leading to the characteristic tissue crepitus, while colonies of bacteria can be observed forming intramural abscesses and the gallbladder content is often purulent. The frequent occurrence of gangrenous evolution and perforation, associated to the septic course and comorbidities, explains the high morbidity and mortality rate (1).

Cholecystitis, Chronic

►Chronic cholecystitis represents the chronic inflammation of the gallbladder wall associated to recurrent mild attacks of acute cholecystitis. This condition occurs predominantly in patients with long-standing cholecystolithiasis and shows a female predominance with an increased incidence in elderly patients. Although rare, cases of chronic acalculous cholecystitis have been reported. Repeated attacks of acute inflammation, usually caused by stones, lead to a progressive damage of the

gallbladder that becomes deformed (scarred, and shrink) with wall thickening due to the fibrosing inflammatory reaction. Additionally, the gallbladder may lose its function of concentrating and storing bile. The gallbladder usually contains sludge or gallstones that often cause obstruction of the gallbladder neck or the cystic duct. Long-standing gallstones may determine erosion of the gallbladder walls causing complications such as bilioenteric fistulas and ►gallstone ileus, and they are also considered the most important risk factor for gallbladder carcinoma.

Cholecystitis, Xanthogranulomatous

►Xanthogranulomatous cholecystitis (XGC) is an uncommon form of chronic cholecystitis, formally characterized by Christensen and Ishak, and previously called by many pseudonyms such as "ceroid granulomas," "ceroid-like histiocytosis," and "fibroxanthogranulomatous inflammation". XGC was initially reputed as a malignant disease for its pseudotumoral appearance. Currently, it is considered benign, showing similar behavior and histological pattern to other xanthogranulomatous lesions occurring in other organs such as the kidney (xanthogranulomatous pyelonephritis), female genital tract, lymph nodes, and urinary bladder. It occurs predominantly in middle-aged females, and frequently the patients are misdiagnosed as having cholelithiasis or a primary cancer. Early phases are histologically characterized by the collection of lipid-loaded macrophages with acute and chronic inflammatory cells in areas of destructive phlogosis, replaced by increasing fibrosis in the late stages. The gross appearance is that of yellowish tumor-like masses in the gallbladder wall typically extending into the adjacent structures (liver bed and surrounding viscera) and leading to perforation, fistula formation, abscess, biliary ductal stricture or obstruction, and ascending cholangitis. An increased association of underlying carcinoma in patients with XGC than in those with ordinary cholecystitis has been reported. Associated cholesterol gallstones are a common finding. The pathogenesis is not clear but it is assumed that a chronic inflammation determined by stones or obstruction of gall flow determines the formation of lysolecithin in bile, resulting in further damage to the gallbladder mucosa. The upgrading from cholecystitis to XGC is related to the occlusion by means of inspissated bile and mucin of the Rokitansky–Aschoff sinuses. These develop into rupture when the wall tension of the distended gallbladder exceeds its natural compliance, leading to the spreading of inflammation into the adjacent tissues. Histiocytes add to the catabolism of bile phagocyting insoluble cholesterol and bile salts, generating the characteristic XGC appearance of loaded macrophage and foamy histiocytes, and resulting in the formation of xanthoma cells (5).

Clinical Presentation

Cholecystitis, Acute

Upper abdominal pain, often radiating to the right scapula in patients with a history of biliary pain or documented gallstones, is the most common presenting sign. Signs of peritoneal irritation consisting of tenderness in the right upper quadrant or in the epigastric region may be present, often with guarding or rebound and positivity of the Murphy sign.

Characteristically, the pain begins in the epigastric region and then localizes to the right upper quadrant. Initially it is described as intermittent, becoming persistent in nearly all cases. Other common signs include nausea, vomiting, and fever that can be less evident in elderly or diabetic patients. Jaundice indicates common bile duct obstruction and is not commonly reported. The persistence of constant severe pain for more than 6 h helps to differentiate cholecystitis from biliary colic. A complete remission is achieved in most cases, although some patients require surgery or develop important complications such as pericholecystic abscess, empyema of the organ, bilioenteric fistulas and gallstones ileus, ►emphysematous cholecystitis, sepsis, perforation, and gangrene. These complications are often suggested by the persistence of the abdominal pain for more than 2–3 days and the appearance of high fever, chills, ileus, and a marked increase in the white blood cell count. If the diagnosis is certain and the risk of surgery is low, the gallbladder is usually laparoscopically removed during the first 2 days from the onset. If a complication is suspected, immediate surgery is required. After gallbladder removal for cholecystitis with gallstones, a small percentage of people develop new or recurring episodes of pain, like gallbladder attacks, probably resulting from an abnormal function of the sphincter of Oddi or from residual stones in the biliary tree.

Cholecystitis, Acute, Acalculous

Individuals presenting with acalculous cholecystitis are typically older hospitalized patients with microvascular disease or other severe comorbidities without prior history of gallbladder disease. Usually the onset is characterized by abrupt excruciating pain in the upper abdomen, although often patients may present with fever and sepsis alone, without signs of acute cholecystitis. The most frequent physical and laboratory findings are nonspecific including fever, right upper quadrant pain, nausea, leukocytosis, and elevation of liver-associated enzymes and bilirubin. Abdominal pain is present in nearly all patients; however, the pain is often not localized to the right upper quadrant. Surgical removal of the diseased gallbladder is required in almost all cases and is considered the reference treatment (2).

Cholecystitis, Emphysematous

The clinical scenario is not significantly different from that of acute cholecystitis, consisting of right upper quadrant pain radiating to the back, unrelated to the patient's position. Other unspecific signs include leukocytosis, fever, tachycardia, tenderness in the right upper quadrant, diminished bowel sounds, or a palpable mass. However, in elderly and diabetic patients this condition may present with few or no localizing symptoms or signs. The transient decrease of abdominal pain associated to peritoneal signs suggests perforation.

Cholecystitis, Chronic

Chronic cholecystitis is usually asymptomatic if there are no associated complications. A clinical history or recurrent attacks of acute cholecystitis or biliary colic may be reported. A palpable mass in the right upper quadrant due to fibrous involvement of the gallbladder is uncommon. The reduced ability of the gallbladder in concentrating bile may hinder the ingestion of a fatty meal. Recommended therapy includes surgical removal of the gallbladder, usually in a laparoscopic fashion, once the acute episode subsides.

Cholecystitis, Xanthogranulomatous

Clinical features resemble those observed in acute or chronic inflammation of the gallbladder, such as acute or chronic pain in the right upper quadrant, fever, and anorexia.

Imaging

Cholecystitis, Acute

Conventional radiography does not play a primary role in the diagnosis of cholecystitis, allowing only detection of indirect signs, such as calcified gallstones that suggest cholelithiasis with or without cholecystitis. The presence of gas limited to the gallbladder wall or lumen indicates gangrenous or ▶emphysematous cholecystitis. Ultrasound (US) suggests the diagnosis of cholecystitis in most instances showing a very high sensitivity and specificity for detecting gallstones and gallbladder sludge that is usually visualized as nonshadowing and inhomogeneous echogenic material, which tends to form a fluid–fluid level. The main US features suggestive of acute cholecystitis include pericholecystic fluid from perforation or exudation, gallbladder distension (diameter >4 cm, length >10 cm), gallbladder wall thickening greater than 3–4 mm, and sonographic Murphy's sign. The thickened wall usually shows a multilayered aspect due to the visualization of a hypoechoic middle layer between two outer hyperechoic layers, which is related to the edema and cellular infiltration of subserosa and submucosa (Fig. 1). A sonographic Murphy's sign is the presence of pain (not related to breathing), evoked by direct pressure of the probe over a sonographically localized gallbladder. The presence of gallstones also aids to confirm the diagnosis, and a dilated common bile duct or dilated intrahepatic ducts indicate common bile duct stones. US also identifies complications (perforation, empyema, abscess). Color Doppler US of the cystic artery at the level of the anterior wall of the gallbladder may demonstrate increased flow. However, this finding may also be observed in other conditions associated with gallbladder wall thickening. Computed tomography (CT) may be adequate for detecting complications such as empyema or suppurative cholecystitis, and it also provides more accurate information of the surrounding structures than US. In particular, the extent and the exact anatomical localization of the pericholecystic abscesses are well visualized on CT. CT is also superior to US in correctly identifying small pericholecystic gas collections

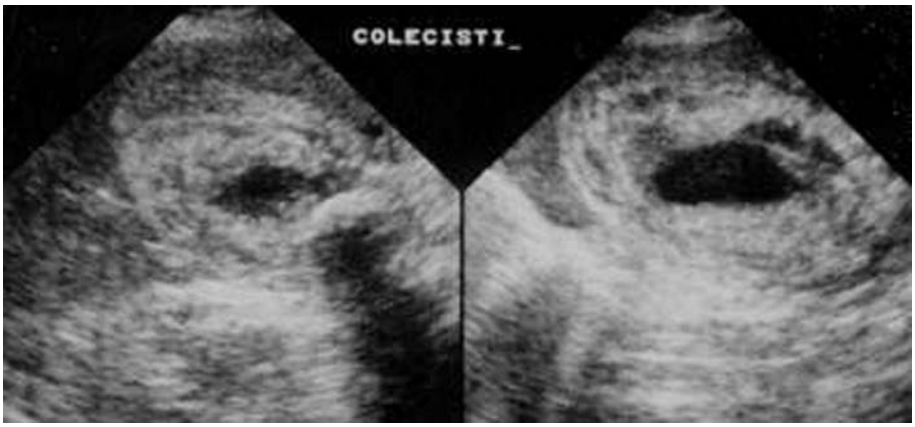

Cholecystitis. Figure 1 Acute cholecystitis. US shows a thickened wall with a multilayered aspect due to the visualization of a hypoechoic middle layer between two outer hyperechoic layers.

and distinguishing them from bowel gas as well as in detecting a gallstone lying outside the lumen of the gallbladder. CT may also depict calcified stones in the gallbladder or in the cystic duct, biliary tree dilatation, focal or diffuse thickening of the gallbladder wall (more than 3–4 mm in cases of noncontracted gallbladder), fluid in the gallbladder fossa, enlargement of the gallbladder, and infiltration of the surrounding fat. The presence of a hypodense concentric band surrounding the gallbladder may indicate fluid collection in the gallbladder bed (in the absence of ascites) or edema in the outer layers of the gallbladder wall. The gallbladder content may show an abnormally elevated density indicating hemobilia. After contrast medium administration, a significant increase in attenuation values of the gallbladder wall as well as increased contrast accumulation in the inflamed hyperemic area surrounding the liver parenchyma can be observed (Fig. 2). The presence of an inflammatory reaction in the pericholecystic fatty tissue is a specific CT sign and appears as a band-like structure with soft tissue density around the gallbladder. Nevertheless, CT misses 20% of gallstones because the stones may be of the same radiographic density as bile. Morphological features of acute cholecystitis in magnetic resonance imaging (MRI) resemble those of CT. On T2-weighted images, inflammatory pericholecystic changes are displayed as high-signal linear structures around the gallbladder. Gadolinium-enhanced T1-weighted images show the same inflammatory changes of the gallbladder wall, pericholecystic fat, and intrahepatic periportal tissues as those displayed on enhanced CT.

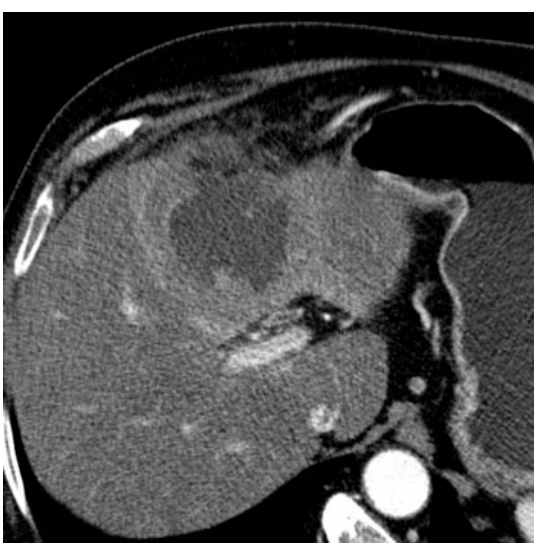

Cholecystitis. Figure 2 Acute cholecystitis. CT shows a diffuse thickening of the gallbladder wall and infiltration of the surrounding fat. A significant enhancement of the gallbladder wall as well as increased contrast accumulation in the inflamed hyperemic surrounding liver parenchyma can be observed.

Endoscopic retrograde cholangiopancreatography (ERCP) provides both endoscopic and radiographic visualization of the biliary tract. ERCP can be diagnostic and therapeutic by direct removal of common bile duct stones and may be particularly useful in patients at high risk for common duct stones if signs of common bile duct obstruction are not present (1–4).

Cholecystitis, Acute, Acalculous

Conventional radiography is of limited use (as stated for acute calculous cholecystitis), allowing detection of indirect signs such as the presence of air in emphysematous complications. The presence of gas has a high association with gangrene and perforation. US is the first approach and may depict nonspecific signs of distension of the gallbladder and sludge (echogenic bile), while more specific signs include gallbladder wall thickening with hypoechoic regions within the wall (striated gallbladder, i.e., gallbladder wall edema) and the presence of pericholecystic fluid or intraluminal membranes. Gangrenous and emphysematous complication is characterized by the presence of gas. Major criteria for US diagnosis are gallbladder wall thickening greater than 3–4 mm (measured in the transverse plane in a noncollapsed gallbladder), the presence of pericholecystic fluid (that suggests advanced disease or perforation), and mucosal sloughing, whereas gallbladder distension (more than 4 cm transverse), and echogenic bile (sludge) are considered minor criteria.

CT is the imaging technique of choice in patients with abdominal pain with fever or leukocytosis of undefined etiology, offering the advantage of evaluating the entire abdomen. The normal gallbladder wall is barely perceptible as a thin enhancing rim on contrast-enhanced CT and the following CT signs in the appropriate clinical setting are suggestive of the diagnosis: gallbladder wall thickening, subserosal halo (i.e., gallbladder wall edema), mucosal irregularity and sloughing, intraluminal hemorrhage, localized pericholecystic fluid collections, perforation of the gallbladder wall or inflammation of pericholecystic fat, and indistinctness of the liver–gallbladder interface. Mucosal sloughing and intramural gas are infrequent specific findings. Isolated local pericholecystic fluid collections and pericholecystic inflammatory changes are relatively specific and suggest advanced disease, but they lose specificity in the setting of concurrent ascites or recent abdominal surgery (1, 4).

Cholecystitis, Emphysematous

Conventional radiography contributes to the diagnosis by showing the presence of an air–fluid level in the right

upper quadrant representing gas in the gallbladder lumen, a curvilinear gas collection conforming to the gallbladder wall in the case of intramural gas, or multiple small air bubbles in the Rokitansky–Aschoff sinuses. The classic picture observed on abdominal radiographs is believed to represent a late phase in the evolution of ►emphysematous cholecystitis and may predict a poor outcome. If perforation occurs, mottled pericholecystic air accumulation is visible. Aerobilia can be associated in rare instances. US shows the gallbladder lumen as containing hyperechoic structures with blunt acoustic shadowing that cause obscuration and render differentiation from intestinal gas difficult. Gas within the gallbladder wall is usually depicted as a ring due to hyperechoic tiny structures located around the fluid-filled gallbladder. Curvilinear gaseous artifacts in the gallbladder, the "ring down effect" or "comet tail" signs, are diagnostic but not frequent signs of emphysematous cholecystitis. An original feature called "effervescent bile" may be observed if the gas leaks from the wall of the gallbladder into the bile. CT should be performed if US and conventional radiography are not diagnostic. CT can better depict the presence of extra- and intraluminal gas and may also demonstrate possible extension into the pericholecystic tissue and the hepatic ducts (1, 4).

Cholecystitis, Chronic

Imaging features (both US and CT) of ►chronic cholecystitis are not specific, including a contracted gallbladder associated with gallbladder wall thickening and cholelithiasis. US can show a diffuse gallbladder wall thickening with shadowing or nonshadowing particles within the gallbladder lumen.

Cholecystitis, Xanthogranulomatous

US and CT features are nonspecific and frequently suggestive of malignancy. Suspect findings include irregular or nodular marked thickening of the gallbladder wall with an indistinct separation from the liver parenchyma especially when the inflammatory process extends to involve the adjacent liver. US shows hypoechoic bands or nodules within the thickened gallbladder wall. These hypoechoic nodules represent abscesses or foci of xanthogranulomatous inflammation. Other findings include disruption of the mucosal line, pericholecystic fluid, stones, and intrahepatic biliary dilatation. CT shows low attenuation foci in the gallbladder wall corresponding to the hypoechoic nodules seen at US. CT can also depict the presence of a mass in the gallbladder wall with inhomogeneous density and moderate to marked enhancement after contrast medium administration, which may extend to the liver or to other adjacent organs. Associated infiltration of the surrounding fatty tissue that presents a striate appearance is commonly reported (2, 5).

Nuclear Medicine

Cholecystitis, Acute

Hepatobiliary scintigraphy with ^{99m}Tc-labeled iminodiacetic acid (IDA) derivates has been found to be very accurate in diagnosing ►acute cholecystitis. These tracers are intravenously administered and secreted by hepatocytes into the bile, enabling a morphofunctional study and the visualization of the gallbladder, biliary tree, and small bowel filling in about 30 min. Since acute cholecystitis is initiated and characterized by cystic duct obstruction, cholescintigraphy that detects cystic duct obstruction should correlate better with acute cholecystitis with respect to the presence of cholelithiasis. In the case of cystic duct obstruction, on radionuclide scans there is no visualization of the gallbladder at 60 min as the bile is excreted directly into the duodenum. If the gallbladder is not visualized, morphine may be administered intravenously causing increased resistance to flow through the sphincter of Oddi, resulting in a filling of the gallbladder if the cystic duct is patent, thus reducing the number of false positives in patients who are critically ill and immobilized with viscous bile. The persistent nonvisualization of the gallbladder within 60 min after tracer administration, despite morphine injection or delayed images, is the characteristic pattern of acute cholecystitis. The reported negative predictive value of a normal cholescintigraph in excluding acute cholecystitis is greater than 98%. In patients with persistent gallbladder nonvisualization, it is important to detect the rim sign on the 45–60-min post-morphine images, because this connotes a complicated cholecystitis (gangrenous forms with or without perforation) indicating inflammatory spread into adjacent liver parenchyma with impairment of local hepatic tracer excretion. Radionuclide studies also have the advantage of revealing an obstructed cystic duct in the case of a normal gallbladder appearance on US imaging.

Cholecystitis, Acute, Acalculous

Cholescintigraphy is considered very sensitive but not specific. The absence of the gallbladder filling can be a manifestation of both mechanical and functional obstruction. The gallbladder filling can also be observed, although an early filling excludes acalculous cholecystitis. Additional findings include the presence of an area of increased pericholecystic radiotracer accumulation in the gallbladder fossa (rim sign) that is associated with complications such

as gangrene. Radiotracer extravasation can rarely be visualized in the setting of perforated ►gangrenous cholecystitis if the cystic duct remains patent.

Cholecystitis, Chronic

In patients with signs and symptoms suggestive of biliary induced pain, but normal US examination for the presence of biliary stones, cholescintigraphy can document gallbladder dysfunction even before stone formation. Signs suggestive of gallbladder dysfunction include delayed gallbladder visualization, persistent gallbladder nonvisualization, or abnormal responses to cholecystokinetic agents. The visualization of the gallbladder within 30-min after morphine injection or in delayed images is a sign of chronic cholecystitis. Hepatobiliary scintigraphy has been used to assess whether chronic ►acalculous cholecystitis is present and to predict the symptomatic response to cholecystectomy. The determination of maximum gallbladder ejection fraction (GBEF) response to a 3-min infusion of sincalide (0.02 μg/Kg) is useful in detecting symptomatic acalculous biliary disease (GBEF > 35% suggests that the patient's symptoms are not related to chronic acalculous biliary disease, 91% NPV), thus confirming the current role of cholescintigraphy in the assessment of patients with chronic biliary pain and normal US.

Diagnosis

Cholecystitis, Acute

The patient's symptoms, associated to the laboratory tests that suggest gallbladder inflammation, together with US features of gallstones or gallbladder wall thickening may lead to the diagnosis. However, many conditions unrelated to gallbladder disease may cause thickening of the gallbladder wall. The most frequent are hepatitis, hypoalbuminemia, ascites, congestive heart failure, and carcinoma. Diagnostic imaging has to contribute substantially to the differential diagnosis and to the detection of complications. Particular attention should be paid to complicated cases in which imaging features such as diffuse or focal wall thickening, as well as infiltrative changes in the pericholecystic lipomatous tissue, can be similar to the findings present in gallbladder carcinoma (1–4).

Cholecystitis, Acute, Acalculous

Often, the diagnosis is difficult and delayed because of the presence of comorbidities that decrease the diagnostic accuracy of both clinical and imaging evaluation. Early imaging evaluation is required, although no single imaging study is sufficient. The different imaging techniques are usually complementary and better suited to excluding, rather than confirming, the disease. It is unusual for ►acalculous cholecystitis to develop in the presence of a normal gallbladder, although this finding can occur early in the course of the disease (4). The differential diagnosis is broad for the presence of nonspecific signs in patients with many co-morbidities. Almost any infectious or inflammatory process can result in such nonspecific findings. In patients with more localized symptoms, the primary differential diagnoses include calculous cholecystitis, ascending cholangitis, acute hepatitis, and pancreatitis.

Cholecystitis, Emphysematous

Clinically, the differential diagnosis must include acute cholecystitis (nonemphysematous), both calculous and acalculous. The radiologic differential diagnosis includes all causes of gas in the biliary tree such as bilioenteric fistula, after ERCP or in cases of cholangitis caused by gas-producing agents.

Cholecystitis, Chronic

US and CT findings may resemble those seen in gallbladder carcinoma. Although the presence of a diffuse mural thickening instead of a focal involvement associated to specific clinical features may help to differentiate benign from malignant affections, pronounced or focal wall thickening when associated to irregularity and lymphadenopathy should suggest malignancy.

Cholecystitis, Xanthogranulomatous

Imaging techniques are well suited for diagnosing complications, while only a histological examination of a surgical specimen will accurately give the final diagnosis of XGC excluding malignancy or a ►gallbladder abscess. It should also be considered that XGC can coexist with malignancy (2, 5).

References

1. Bennett GL, Balthazar EJ (2003) Ultrasound and CT evaluation of emergent gallbladder pathology. Radiol Clin North Am 41 (6):1203–1216
2. Zissin R, Osadchy A, Shapiro-Feinberg M et al (2003) CT of a thickened-wall gallbladder. Br J Radiol 76(902):137–143
3. Adusumilli S, Siegelman ES (2002) MR imaging of the gallbladder. Magn Reson Imaging Clin N Am 10(1):165–184
4. Hanbidge AE, Buckler PM, O'Malley ME et al (2004) From the RSNA refresher courses: imaging evaluation for acute pain in the right upper quadrant. Radiographics 24(4):1117–1135
5. Chun KA, Ha HK, Yu ES et al (1997) Xanthogranulomatous cholecystitis: CT features with emphasis on differentiation from gallbladder carcinoma. Radiology 203:93–97

Cholecystitis, Acute

Acute inflammation of the gallbladder due to obstruction of the cystic duct, usually caused by gallstone or sludge, and leading to distension of the gallbladder. Advanced cases may develop gangrene or perforation.
▶Cholecystitis

Cholecystitis, Acute, Acalculous

Acute inflammation of the gallbladder in the absence of demonstrated stones occurring most likely in elderly adults affected by severe comorbidities. Complications such as gallbladder wall necrosis, gangrene (diffuse or focal), and perforation are common and mortality is very high.
▶Cholecystitis

Cholecystitis, Chronic

Chronic inflammation of the gallbladder caused by repeated attacks of ▶acute cholecystitis in patients with long-standing gallstones. Chronic ▶acalculous cholecystitis has rarely been reported. The gallbladder presents a deformed and thickened wall due to fibrous involvement. Complications include bilioenteric fistulas and ▶gallstone ileus.
▶Cholecystitis

Cholecystitis, Emphysematous

Severe condition associated with a high mortality, characterized by the presence of gas within the wall and the lumen of the gallbladder. It can be considered either as a complication of ▶acute cholecystitis, in particular acalculous, or as a separate entity. It occurs most commonly in elderly males and diabetics. Pathogenesis is related to ischemia and bacterial overgrowth with gas-forming agents. The development of gangrene and perforation are frequently reported.
▶Cholecystitis

Cholecystitis, Gangrenous

Gangrenous or necrotizing cholecystitis is a severe advanced form of ▶acute cholecystitis with a higher morbidity and mortality rate than uncomplicated acute cholecystitis. It results from marked distension of the gallbladder with increased tension of the wall. Associated inflammation leads to ischemic necrosis, with or without associated cystic artery thrombosis. Clinical and laboratory findings are often nonspecific and indistinguishable from those of patients with acute cholecystitis without gangrene. A typical US sign of gangrenous cholecystitis is the presence of heterogeneous or striated thickening of the gallbladder wall, which is often irregular with projections into the lumen and the pericholecystic fluid collections. The presence of intraluminal membranes representing desquamative gallbladder mucosa is a specific finding but is less common. US findings, typically for uncomplicated acute cholecystitis, may be absent in this subset of patients. CT findings in gangrenous cholecystitis are better appreciated after contrast medium administration, and include intraluminal membranes, intraluminal hemorrhage, and an irregular or absent wall.
▶Cholecystitis

Cholecystitis, Necrotizing

Complicated form of acute cholecystitis (both calculous and acalculous) synonymous to gangrenous cholecystitis.
▶Cholecystitis

Cholecystitis, Xanthogranulomatous

Uncommon form of chronic cholecystitis occurring predominantly in middle-aged females characterized by the collection of lipid-loaded macrophages and a gross appearance of yellowish tumor-like masses in the gallbladder wall, typically extending into the adjacent structures (liver bed and surrounding viscera) and leading to perforation.
▶Cholecystitis

Cholecystography

This radiological technique, now considered obsolete, allowed the opacification and visualization of the gallbladder with an orally administered agent owing to the ability of the gallbladder to concentrate the oral medium.

▶Biliary Anatomy

Cholecystoses

Thomas Helmberger[1], Carlo Bartolozzi[2], Paola Vagli[2]
[1]Clinic of Radiology and Nuclear Medicine, University Hospitals Schleswig-Holstein, Campus Luebeck, Luebeck, Germany
[2]Department of Diagnostic and Interventional Radiology, University of Pisa, Italy
thomas.helmberger@uni-luebeck.de
bartolozzi@do.med.unipi.it

Synonyms

Adenomyomatosis gallbladder; Cholesterolosis; Hyperplastic cholecystosis; Porcelain gallbladder; Strawberry gallbladder

Definition

Cholecystosis is a generic term introduced by Colesson and Jutras used to describe a group of noninflammatory, nonlithiasic benign diseases of the gallbladder wall. However, a chronic aspecific inflammatory process seems to be much more frequent than is believed and often this condition is associated with lithiasis. Cholecystoses have been classified into hyperplastic or accumulating forms. The hyperplastic forms are characterized by normal growth with hyperplasia of the cellular wall components, while in the accumulating forms there is an overload of the wall with organic substances or minerals such as lipids or calcium salts (thesaurismosic forms). The hyperplastic forms include both the presence of limited thickening of the wall (focal and segmental cholecystosis) and more extensive thickening. The most common forms of cholecystoses are adenomyomatosis and cholesterolosis (hyperplastic forms) and calcified or ▶porcelain gallbladder (thesaurismosic forms). The clinical picture resembles that of inflammation of the gallbladder caused by stones.

Pathology and Histopathology

Adenomyomatosis, Gallbladder

Adenomyomatosis of the gallbladder is a common, benign condition, with tumor-like features, of unknown cause, characterized by hyperplastic changes of the wall and therefore named hyperplastic cholecystosis. This condition is characterized by overgrowth of the surface epithelium with associated glandular formation and out-pouching into or through the thickened muscular wall, causing formation of intramural diverticula or sinus tracts termed Rokitansky–Aschoff sinuses. Adenomyomatosis of the gallbladder and the associated Rokitansky–Aschoff sinuses may involve the gallbladder in a focal, segmental, or diffuse form. A septum or an annular thickening causing circumferential narrowing of the lumen is frequently associated with adenomyomatosis and must be differentiated from a congenital fold of the gallbladder wall (▶Phrygian cap), which is usually thinner and smoother and localized to the fundus, whereas adenomyomatosis may involve any portion of the gallbladder. Adenomyomatosis occurs most frequently in middle-aged females and its etiology remains unclear (1, 2).

Cholesterolosis, Gallbladder

Cholesterolosis is a benign condition and represents a type of hyperplastic cholecystosis, resulting from the macrophage accumulation of triglycerides and cholesterol esters mainly in the submucosal layer or lamina propria of the gallbladder wall. The true incidence and etiology of cholesterolosis remain unclear, and a causal association with cholesterol gallstones, super saturation of bile with cholesterol, hyperlipidemia, obesity, or atherosclerosis remains unconfirmed. Nevertheless, this condition is often seen in gallbladders containing stones. Two types have been described: a diffuse form, also called "strawberry" gallbladder, and a polypoid form.

The gross appearance of ▶strawberry gallbladder includes a diffuse thickening and the presence of yellowish, diffuse, granular, lipid deposits, varying in distribution and size, in the gallbladder mucosa that resemble a strawberry. The polypoid form is characterized by single or multiple, small (up to 1 cm in some cases), discrete polypoid excrescences composed of cholesterol-filled macrophages. Malignant degeneration has not been described (2).

Porcelain Gallbladder

This condition also called calcified gallbladder, calcifying cholecystitis, and cholecystopathia chronica calcarea refers to the presence of extensive dystrophic calcifications within the chronically inflamed gallbladder wall with associated fibrosis in the muscular layer. The term porcelain gallbladder emphasizes the brittle consistency and blue discoloration of these calcifications that may appear as a broad continuous band in the muscularis conferring a sac-like appearance or multiple punctate calcifications in the mucosal glandular spaces. The most accredited origin of the calcification is secondary to the chronic inflammation of the gallbladder wall due to cholecystitis, but intramural hemorrhage and an imbalance in calcium metabolism also seem to be implicated.

Gallstones are documented in 90% of cases. Porcelain gallbladder has a low prevalence but its clinical importance lies in a significant association with gallbladder carcinoma especially in cases of diffusely calcified gallbladder. A significant female prevalence has been reported with a male-to-female ratio of 1:5.

Clinical Presentation

Adenomyomatosis, Gallbladder, Cholesterolosis, Gallbladder

Usually these conditions remain asymptomatic or are characterized by aspecific features such as vague abdominal pain. Cholecystectomy is rarely required to treat these affections, and may be considered for patients with convincing symptoms or coexisting cholelithiasis.

Porcelain Gallbladder

This condition is usually asymptomatic and incidentally diagnosed. Although asymptomatic, surgical removal of the gallbladder is recommended because the occurrence of carcinoma in porcelain gallbladder is remarkably high.

Imaging

Adenomyomatosis, Gallbladder

Conventional radiography by means of cholecystography is considered obsolete and has been replaced by other imaging modalities. On cholecystograms, the patent Rokitansky–Aschoff sinuses appear as single or multiple oval or rounded extraluminal pouches filled with contrast medium, ranging in size (between 1 and 10 mm), and separated from the lumen by at the most 2-cm-thick band representing both the mucosa and the muscular wall ("pearl necklace" sign).

Ultrasound (US) is the examination of choice showing the mural thickening, especially if the cystic spaces are visible as small anechoic extraluminal structures. These cystic spaces appear as anechoic diverticula and may show echoic foci and/or reverberation artifacts together. Association of cystic spaces with full or partial thickening of the gallbladder wall is considered to be the key diagnostic findings (Fig. 1). Intradiverticular echoic foci are caused by the presence of sludge or stones, and reverberation artifacts due to cholesterol crystals are "V" shaped and shorter in length than artifacts from air. If intramural diverticula are not identified, differentiating adenomyomatosis from other causes of gallbladder wall thickening especially if segmental or focal, such as cholecystitis or carcinoma, is difficult. Exceptionally bright echogenic dots due to debris-filled Rokitansky–Aschoff sinuses may be detected. Gallstones are often associated with adenomyomatosis (1).

Computed tomography (CT) and magnetic resonance imaging (MR) can be used as problem-solving modalities, especially to differentiate hyperplastic cholecystosis from gallbladder carcinoma.

CT shows a thickened gallbladder wall with the "string of beads" sign when the multiple intramural cystic spaces are visualized crossways. This sign is caused by the enhanced proliferative mucosal epithelium of the intramural diverticula surrounded by the unenhanced hypertrophied muscular layer of the gallbladder.

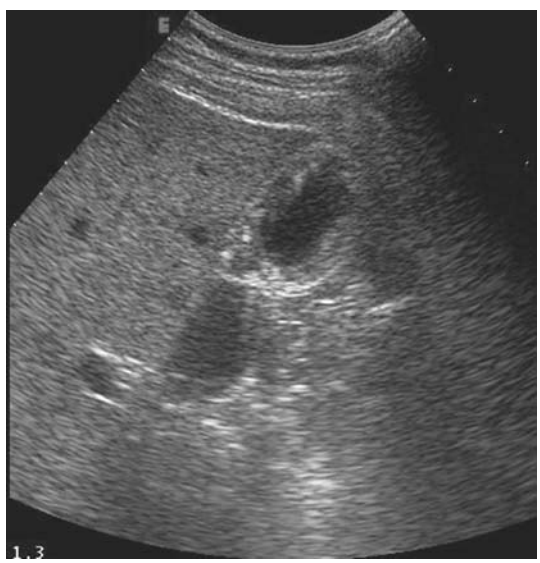

Cholecystoses. Figure 1 ►*Adenomyomatosis gallbladder*. **US shows a segmental mural thickening involving the fundus and partially the body. Rokitansky–Aschoff sinuses appear as anechoic diverticula associated with echoic foci and short reverberation artifacts.**

MR helps to differentiate adenomyomatosis from cholesterolosis and benign from malignant thickening of the gallbladder wall. MR signs suggestive of adenomyomatosis are gallbladder wall thickening with multiple intramural cystic components from Rokitansky–Aschoff sinuses, readily visualized as markedly hyperintense spots on the images, especially using heavily T2-weighted MR breath-hold sequences. Early mucosal enhancement, followed by a serosal enhancement, is a typical feature of the diffuse type of adenomyomatosis. Localized adenomyomatosis displays homogeneous enhancement, showing smooth continuity with the surrounding gallbladder epithelium (3).

Cholesterolosis, Gallbladder

Today, oral cholecystography has been largely replaced by US and to a lesser degree by MR cholangiopancreatography for the evaluation of cholesterolosis. This technique usually shows a functioning gallbladder with single or multiple, fixed, filling defects with a slightly irregular surface caused by the larger, polypoid cholesterol deposits. These filling defects may occur anywhere in the gallbladder and project into the lumen rendering the edges of the gallbladder unsharp. These excrescences appear as fixed lucencies in the opacified gallbladder lumen and are distinguished from calculi thanks to their fixity with compression and positional change.

US shows the lesions as nonshadowing, immobile, intraluminal echoic structures. In fact, cholesterol polyps rarely produce a degree of shadowing. However, in some cases acoustic shadowing may occur, mimicking adherent stones. A comet tail pattern due to parietal deposits of cholesterol may also be detected. US features of the diffuse form of cholesterolosis are not specific and more difficult to recognize (2).

Porcelain Gallbladder

Conventional radiography and CT exhaustively depict calcifications shaped by the gallbladder globular contour in the right upper quadrant, with superior characterization by CT. On conventional radiograms these calcifications appear rather pathognomonic enabling the differentiation from other causes of calcifications in the right upper quadrant. US features are unspecific, referring to extensive gallbladder calcifications and the presence of a nonfunctioning gallbladder. Gallbladder calcifications may show different sonographic patterns including hyperechoic linear or semilunar structures with posterior acoustic shadowing that simulates a stone-filled gallbladder, biconvex curvilinear echoic structures with variable acoustic shadowing, irregular conglomeration of echoes with posterior acoustic shadowing, and an echogenic gallbladder wall without acoustic shadowing. Usually a well-demarcated shadow is associated to this condition, although in the case of heavy calcifications or emphysematous cholecystitis a fuzzy shadowing with reverberation may be observed (4–5).

Nuclear Medicine

Cholesterolosis, Gallbladder

Fluorodeoxyglucose positron emission tomography (FDG-PET) can easily differentiate small polypoid lesions of diffuse cholesterolosis from gallbladder carcinoma, showing a focal tracer uptake at the site of gallbladder carcinoma, whereas there is no marker uptake in cholesterol polyps.

Porcelain Gallbladder

Radionuclide scans, with hepatobiliary tracers (^{99m}Tc imminodiacetic acid analog), provide unspecific features depicting a nonfunctioning gallbladder.

Diagnosis

Adenomyomatosis, Gallbladder

The differential diagnosis includes all conditions causing intraluminal polypoid masses such as adenomatous, hyperplastic, and cholesterol polyps, intramural hematoma, and malignancies (gallbladder carcinoma, carcinoid tumor, metastases). The differential diagnosis is mandatory especially in the case of lesions larger than 10 mm and/or associated to focal gallbladder thickening. A typical enhancement pattern on MR images may lead to the diagnosis (3). The clinical setting may aid in excluding other causes in cases of diffuse thickening such as cholecystitis (acute or chronic), nonfasting state, chronic hypoalbuminemia, hepatitis, and congestive heart failure.

Cholesterolosis, Gallbladder

Differentiating between adenomyomatosis and cholesterolosis can be difficult. Solitary polyps located in the fundus of the gallbladder usually cannot be differentiated from adenomyoma. Also, in cases of diffuse forms the preservation of the multilayered pattern of the gallbladder wall may help to differentiate from carcinoma.

Porcelain Gallbladder

Porcelain gallbladder must be differentiated from large, solitary, calcified gallstones, and milky bile syndrome, where the radiopaque content produces features comparable to

porcelain gallbladder both on conventional radiography and US. Calcified hydatid cysts can mimic porcelain gallbladder on plain abdominal radiograms; however, US or CT images promptly lead to the diagnosis. Regarding the differential diagnosis, other causes of calcifications in the right upper quadrant including schistosomiasis, other granulomatous disease, old healed liver infarcts, calcified renal cysts, calcified nonparasitic liver cysts, calcific primary, and metastatic liver tumors must be excluded.

The US appearance alone may lead to the erroneous diagnosis of emphysematous cholecystitis or a stone-filled gallbladder. However, emphysematous cholecystitis usually causes "dirty" shadowing that can be separated by ring down shadows caused by gas within the gallbladder wall or lumen, while a stone-filled gallbladder produces the wall echo shadow sign that is characterized by two parallel echoic bands separated by a hypoechoic space with distal shadowing. The echoic bands correspond to the interface of the gallbladder wall and the liver and the anterior surface of the gallstone, while the hypoechoic one corresponds to the gallbladder wall itself.

Bibliography

1. Hwang JI, Chou YH, Tsay SH et al (1998) Radiologic and pathologic correlation of adenomyomatosis of the gallbladder. Abdom Imaging 23(1):73–77
2. Berk RN, van der Vegt JH, Lichtenstein JE (1983) The hyperplastic cholecystoses: cholesterolosis and adenomyomatosis. Radiology 146 (3):593–601
3. Yoshimitsu K, Honda H, Jimi M et al (1999) MR diagnosis of adenomyomatosis of the gallbladder and differentiation from gallbladder carcinoma: importance of showing Rokitansky-Aschoff sinuses. Am J Roentgenol 172(6):1535–1540
4. Kane RA, Jacobs R, Katz J et al (1984) Porcelain gallbladder: ultrasound and CT appearance. Radiology 152(1):137–141
5. Versaci A, Terranova M, Rossitto M et al (1999) Authors' experience with the role of preoperative ultrasonography in the study of benign lesions of the gallbladder. G Chir Aug-Sep 20(8–9):354–358

Cholecystosis, Hyperplastic

This term is used to describe both cholesterolosis and adenomyomatosis of the gallbladder.

▶Cholecystoses

Choledochal Cyst Type V

▶Congenital Malformations, Bile Ducts

Choledochal Cysts

Congenital anomalies of the bile ducts consisting of cystic dilatations (saccular or fusiform) of the extrahepatic biliary tree, intrahepatic biliary radicles, or both.

▶Congenital Malformations, Liver and Biliary Tract
▶Congenital Malformations, Bile Ducts

Choledochocele

Type III choledochal cysts arising from the intraduodenal portion of the common bile duct.

▶Congenital Malformations, Liver and Biliary Tract
▶Congenital Malformations, Bile Ducts

Cholestasis

▶Occlusion, Bile Ducts

Cholesterolosis, Gallbladder

A type of hyperplastic cholecystosis resulting from the accumulation of triglycerides within macrophages and cholesterol esters mainly in the submucosal layer or lamina propria of the gallbladder wall. A causal association with cholesterol gallstones, super saturation of bile with cholesterol, and hyperlipidemia remains unconfirmed. Two types have been described: a diffuse form, also named "strawberry" gallbladder, and a polypoid form. The gross appearance of strawberry gallbladder includes a diffuse thickening and the presence of yellowish, diffuse, granular, lipid deposits, varying in distribution and size, in the gallbladder mucosa that resemble a strawberry. The polypoid form is characterized by single or multiple, small, discrete polypoid excrescences composed of cholesterol-filled macrophages.

▶Cholecystoses

Chondroblastoma

Chondroblastoma (Codman tumor) is a benign chondroid tumor with a chondroblast-like cellular component and limited matrix production.

▶Neoplasms, Bone, Benign

Chondrocalcinosis

A condition characterized by deposits of calcium pyrophosphate dihydrate (CPPD) crystals in one or more joints that eventually results in damage to the affected joints. It most often affects the knee, wrist, and pubic symphysis.
▶CPPD

Chondrolysis (of Cartilage)

▶Osteonecrosis, Childhood

Chondrosarcoma

Chondrosarcoma is the second most frequent malignant bone tumour and produces cartilage matrix. Frequently arises from benign cartilage lesions such as osteochondroma or enchondroma (secondary chondrosarcoma). It is usually found in middle aged and older adults. Matrix calcifications may be found and cortical bone destruction is a typical finding.
▶Neoplasms, Bone, Malignant

Chronic Bronchitis

▶Airway Disease

Chronic Cystic Mastitis

▶Fibrocystic Disease, Breast

Chronic Intestinal Pseudo Obstruction

▶Hirschsprung Disease and Related Disorders

Chronic Liver Disease

▶Cirrhosis, Hepatic

Chronic Lung Disease of Prematurity

▶Dysplasia, Bronchopulmonary

Chronic Lymphatic Thyroiditis

▶Thyroid Autoimmune Diseases

Chronic Obstructive Pulmonary Disease (COPD)

▶Airway Disease

Chronic Polyarthritis

▶Rheumatoid Arthritis

Chronic Thromboembolic Pulmonary Hypertension (CTEPH)

▶Chest Thromboembolic Diseases

CIN

▶Contrast Induced Nephrotoxicity

Circumferential Resection Margin

The circumferential resection margin is the distance from rectal tumour to the resection plane (mesorectal fascia) when viewed in a transverse section through the rectum. A complete resection of rectal cancer is defined as a CRM of >2 mm. The CRM can be predicted preoperatively on MRI. In this way, radiologist can predict a narrow margin and indicate at which location a wider excision is needed for radical resection.

▶Rectal Carcinoma

Circumscribed Carcinoma

▶Carcinoma, Other, Invasive, Breast

Cirrhosis, Hepatic

Massimo Bazzocchi, Bartolozzi Carlo, Giuseppe Como, Chiara Franchini
Università degli Studi di Udine, Udine, Italy
massimo.bazzocchi@med.uniud.it

Synonyms

Chronic liver disease; Liver cirrhosis

Definition

Chronic liver disease characterized by diffuse widespread disruption of normal liver architecture with necrosis, fibrosis and formation of ▶regenerative nodules that is caused by various aetiology.

Pathology and Histopathology

Cirrhosis is the final result of chronic liver injury characterized by extensive fibrosis and regenerative nodules replacing the normal liver parenchyma. The process is initiated by necrosis, followed by connective tissue formation and nodular regeneration, leading to distortion of the lobar and vascular liver architecture (1). Regenerating nodules may vary from micronodules (lesser than 3 mm in diameter) to macronodules (3 mm to several centimeters in diameter). The causes of liver cirrhosis could be divided into toxic, inflammation, biliary obstruction, vascular, nutritional, hereditary and idiopathic. The most common causes of liver cirrhosis are chronic viral hepatitis C (HCV) and B (HBV) and alcoholic liver disease. Less frequent are biliary diseases, haemochromatosis, Wilson's disease, galactosemia, tyrosinosis and drug-induced cirrhosis. Cirrhosis is the most important cause of portal hypertension. The obstacle to the portal flow is intrahepatic, being related to compression of hepatic sinusoids caused by regenerative nodules and fibrosis.

Cirrhosis is a premalignant condition: the development of hepatocellular carcinoma (HCC) represents a common long-term complication. Different types of hepatocellular nodules can be found in the cirrhotic liver: regenerative nodule, low-grade and high-grade ▶dysplastic nodule hepatic, HCC. A stepwise carcinogenesis for HCC has been proposed. Ordinary cirrhotic nodules are termed regenerative nodules. The term dysplastic nodule replaces older terms like adenomatous hyperplasia and refers to a nodular region of hepatocytes with dysplasia but without definite malignancy. They are considered premalignant nodules. In the de novo pathway, a single cell may give rise to a focus of small HCC that will develop into a large HCC (2). In the progression from regenerative nodule to overt HCC, there is a reduction in portal blood supply and development of new arterial anomalous vessels, called non-triadal arteries.

Clinical Presentation

Cirrhosis may be clinically silent. It gives non-specific symptoms such as anorexia, weight loss and weakness. Clinical manifestations may be related to portal hypertension: ascites, oesophageal varices, splenomegaly, hepatic encephalopathy. Death usually occurs for progressive liver failure, complications related to portal hypertension, development of HCC.

Imaging

The role of imaging is assessing intrahepatic and extrahepatic signs of cirrhosis and, above all, revealing the presence of HCC.

Ultrasound

Intrahepatic signs of cirrhosis are related to changes in size, morphology, margins and echostructure of the liver. In the early-stage of the disease, the liver may show normal or slightly increased dimensions. In more advanced

stages, hypertrophy of the caudate lobe and the lateral sector of the left lobe associated to atrophy of the right lobe can be observed. This leads to an increased ratio of the size of the caudate lobe to the right lobe that is widely accepted as a sign of cirrhosis (caudate lobe to right lobe size ratio >0.65) (3). The atrophy of the right lobe may result in a widening of the great interlobar fissure and prehepatic colonic interposition. The medial segment of the left hepatic lobe may also be atrophic; this results in enlargement of periportal and pericholecystic spaces (gallbladder fossa), filled by adipose tissue (4). Peculiar sign of cirrhosis is superficial nodularity, best demonstrated using high-frequency probes (Fig. 1). Nodular regeneration may also determine alteration of the profile of hepatic vessels, particularly hepatic veins (5). Cirrhotic liver may show a normal homogeneous parenchymal echostructure, or have an aspecific 'bright liver pattern', with fine, tightly packed echoes distributed throughout the liver parenchyma, as observed also in hepatic steatosis and hepatic fibrosis. The so-called 'coarse pattern' is considered a specific sign of cirrhosis: it consists in inhomogeneous, coarse, thick, echoes, with or without multiple small hypoechoic nodules in the liver tissue (5). A common finding is enlarged lymph nodes at the porta hepatis.

Extra-hepatic signs are related to the portal hypertension: they include ascites, splenomegaly, dilatation and reversal of flow in portal, splenic and superior mesenteric veins, portal vein thrombosis and demonstration of portosystemic collaterals. The diameter of the main portal vein should not exceed 13 mm. In portal hypertension, the normal calibre variation during respiration is not present. Doppler US gives information about flow direction and velocity in the portal vein. A mean velocity <16 cm/sec in the portal trunk suggests portal hypertension. The presence of hepatofugal flow within the main portal vein or reversal of flow in the splenic vein is the indicative for portal hypertension. Patients with cirrhosis are at high risk of developing portal thrombosis. At conventional US chronic portal thrombosis is depicted as hyperechoic material within the portal veins. Recent thrombosis is anechoic and could be not appreciated on conventional US, while can be detected with colour-Doppler US. US is able to demonstrate portosystemic collaterals, such as paraumbilical vein, gastro-oesophageal veins and spleno-renal shunt. The spleen may be enlarged, usually with a homogeneous parenchymal echostructure. Ascites is a common and serious complication of advanced cirrhosis. Gallbladder and stomach wall oedema resulting from portal hypertension may also been observed.

US is the imaging modality of choice in the screening for HCC in cirrhotic patients. The detection of a nodule at US in a cirrhotic liver should raise the suspicion of HCC and require further imaging investigations. The imaging criterion which allows the diagnosis of HCC is the

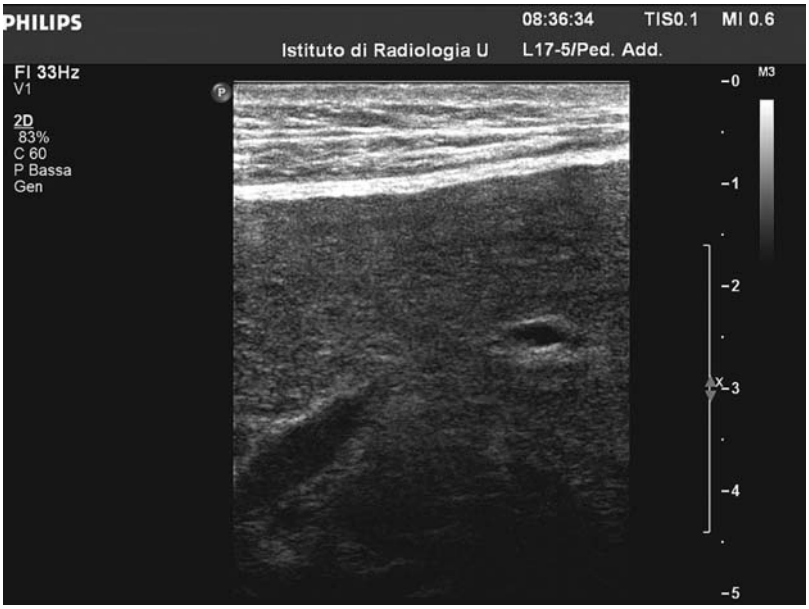

Cirrhosis, Hepatic. Figure 1 US scan with high frequency linear probe. Peculiar sign of cirrhosis is superficial nodularity, best demonstrated using high-frequency probes. We can see so called 'coarse pattern' that is considered a specific sign of cirrhosis: it consists in inhomogeneous, coarse, thick, echoes, with multiple small hypoechoic nodules in the liver tissue.

demonstration of arterial hypervascularization. The use of US contrast media can reliably demonstrate the hypervascularity of HCC.

Computed Tomography

At CT, the cirrhotic liver may appear normally sized or slightly enlarged in the early-stage disease; in advanced stage the global size tends to decrease and the typical is atrophy of the right lobe and hypertrophy of the caudate lobe and of the lateral sector of the left lobe. Atrophy of the medial sector of the left lobe (IV segment) may occur, with consequent enlargement of the gallbladder fossa and the periportal space, filled by adipose tissue. The margins may be irregular, with a nodular appearance. The parenchymal structure may be normal or inhomogeneous. The density of the regenerative nodules rarely differs from that of the cirrhotic liver tissue. Sometimes they show a slight hyperdensity on unenhanced scans, due to their iron content, or a slight hypodensity, due to fatty changes. Regenerative nodules may also become evident for causing mass effect on intrahepatic vessels, which appear compressed or displaced. Contrast-enhanced CT study in cirrhotic liver always includes the arterial phase and the portal–venous phase. The arterial phase is crucial in detecting HCC nodules which typically have a hypervascular pattern. Regenerative nodules do not have a prevalent arterial blood supply. In the arterial phase they usually appear hypodense, sometimes isodense, in the portal–venous phase they are hypo-isodense. A frequent finding is the presence of areas of anomalous perfusion during the arterial phase. These anomalies are called 'transient hepatic attenuation differences' (THAD), because the hyperdensity observed in the arterial phase disappears in the portal–venous scans. THAD are due to small arterial–portal fistulas and have a triangular shape, a peripheral location and do not show mass effect. The portal–venous phase is important in assessing the patency of portal system's veins and the presence of porto-systemic collaterals. Portal thrombosis appears as a defect of contrast enhancement within portal vessels. Large oesophageal varices are often recognizable. Splenomegaly and ascites are accurately demonstrated at CT (Fig. 2).

Magnetic Resonance

Cirrhosis alone does not markedly alter the T1 and T2 relaxation times because fibrous bands and scars constitute a small fraction of liver volume. Cirrhosis is diagnosed by MR using morphologic features analogous to those at US and CT: hypertrophy of the left hepatic and caudate lobes (caudate lobe to right lobe size ratio >0.65), a nodular appearance of the liver surface, and distortion or compression of intrahepatic vessels. In the micronodular form of cirrhosis, the liver surface shows a subtle irregular appearance. MR is much more sensitive than CT in demonstrating regenerative nodules. Regenerative nodules appear as small (<2 cm) nodular lesions, with low signal intensity on T2-weighted images and variable signal intensity on T1-weighted images (Fig. 3). When they contain iron (siderotic nodules) they appear hypointense both on T1-weighted and in T2-weighted

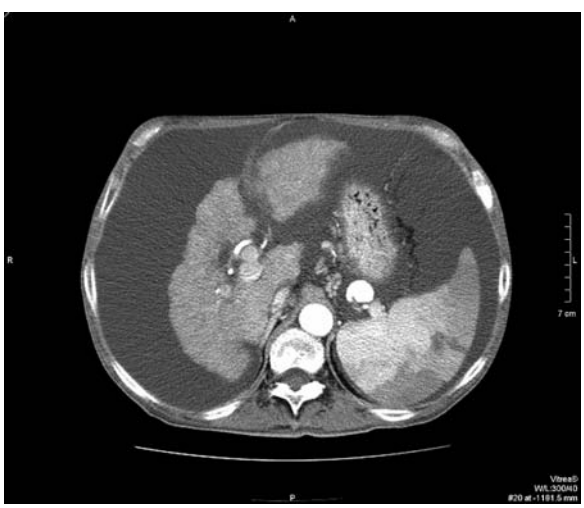

Cirrhosis, Hepatic. Figure 2 CT axial scan of cirrhotic liver in advanced stage: the global size decrease. The margins are irregular, with a nodular appearance. The parenchymal structure is inhomogeneous. There are signs of portal hypertension with the spleen that is enlarged and with inhomogeneous density.

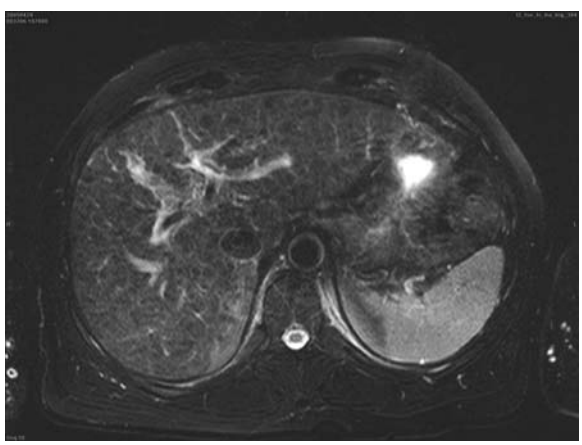

Cirrhosis, Hepatic. Figure 3 MR TSE T2 axial scan: We can see a nodular appearance of the liver surface with distortion of intrahepatic vessels. MR is much more sensitive than CT in demonstrating regenerative nodules. Regenerative nodules appear as small nodular lesions, with low signal intensity on T2-weighted images.

scans. Regenerative nodules may present increased signal intensity on T1-weighted images due to high triglyceride content in zones of fatty degeneration. They are never hyperintense on T2-weighted images. Regenerative nodules show no enhancement on arterial phase gadolinium-enhanced images (2). They appear hypointense with a better demarcation in contrast to the surrounding liver parenchyma using delayed images. Dysplastic nodules and early HCCs show similar features regarding signal intensity, although the latter may be hyperintense on T2-weighted images. Like regenerative nodules, dysplastic nodules can be siderotic. HCC may arise within a high-grade dysplastic nodule. These lesions have a nodule-within-a-nodule appearance on MR images, consisting of one or more hyperintense internal foci within a low signal intensity nodule on T2-weighted images. The central nodule usually also shows enhancement during the arterial phase at gadolinium-enhanced dynamic study (1, 2). HCC shows high signal intensity on T2-weighted images and variable signal intensity on T1-weighted images. However, the differentiation of HCC from regenerative nodules and dysplastic nodules relies on the arterial blood supply of HCC responsible of the typical intense enhancement during the arterial phase of dynamic gadolinium-enhanced imaging of HCC (2). Findings in portal hypertension include enlargement of the extrahepatic portal–venous system (portal vein diameter >13 mm), presence of portosystemic collaterals and splenomegaly. Siderotic nodules in the spleen, called Gandy-Gamna nodules, appear as tiny hypointense foci on T2-weighted images. They are pathognomonic of portal hypertension. Ascites, gallbladder and small bowel wall oedema are manifestations of associated hepatic failure (1).

Interventional Radiology

In cirrhotic patients, hepatic resection for HCC may worsen the hepatic function so interventional procedures can be performed for the treatment of HCC. The rationale is destroying the tumoural tissue, sparing the non-tumoural tissue. Percutaneous ethanol injection (PEI), thermal ablation and transcatheter chemioembolization (TACE) are the main non-surgical therapeutic tools for the treatment of HCC.

Transjugular intrahepatic porto-systemic shunt (TIPSS) is used for the treatment and the prevention of oesophageal variceal bleeding in portal hypertension.

Diagnosis

Cirrhosis may be suspected on the basis of symptoms and laboratory. The diagnosis can be suggested at imaging. Imaging techniques (US, CT, MR) are able to identify hepatic and extrahepatic manifestations of liver disease. The definite diagnosis of cirrhosis is traditionally established with biopsy.

Bibliography

1. Lencioni R, Bartolozzi C (2003) Diffuse liver disease. In: Magnetic Resonance Imaging in Liver Disease, pp 163–197. Thieme: Stuttgart-New York
2. Hussain SM, Zondervan PE, IJzermans JNM et al (2002) Benign versus malignant hepatic nodules: MR imaging findings with pathologic correlation. Radiographics 22:1023–1036
3. Awaya H, Mitchell DG, Kamishima T et al (2002) Cirrhosis: modified caudate-right lobe ratio. Radiology 224(3):769–774
4. Ito K, Mitchell DG, Gabata T et al (1999) Expanded gallbladder fossa: simple MR imaging sign of cirrhosis. Radiology 211(3):723–726
5. Caturelli E, Castellano L, Fusilli S et al (2003) Coarse nodular US pattern in hepatic cirrhosis: risk for hepatocellular carcinoma. Radiology 226(3):691–697

Classification of the American College of Radiology (ACR)

▶BI-RADS, Lexicon

Claudication Brachial

Elias N Brountzos
2nd Department of Radiology, Athens University, Medical School, Greece
ebrountz@cc.noa.gr

Synonyms

Upper extremity claudication; Arm claudication

Definition

Arm, hand, or brachial claudication is described as forearm or hand pain or disabling discomfort arising during exercise.

Pathology

This symptom is characteristic of chronic ischemia of the upper extremity.

Clinical Presentation

Depending on the degree of the reduction of arterial perfusion, the claudication appears with minimal activity such as hair combing, or requires prolonged activity. Brachial claudication represents the most common indication for upper extremity arterial revascularization (1).

See ►Brachial Ischemia

Bibliography

1. Whitehouse Jr (2000) Upper extremity revascularization. In: Rutherford RB (ed) Vascular Surgery, WB Saunders, Denver, Colorado, pp 1162–1170

CLD

►Dysplasia, Bronchopulmonary

Clear Cell Renal Carcinoma

The most common type of RCC, accounting 70% to 80% of the cases in surgical series. This type is diagnosed by histologic and cytogenetic criteria.

►Nodules, Pulmonary, Solitary

Cleft Lip, Palate, and Alveolus Defects

Cleft abnormalities of the lip, palate, and alveolus are the most common congenital disorder of the oral cavity and result from developmental defects with incomplete fusion of the lips, palate, and/or alveolus.

►Congenital Malformations, Oral Cavity

Cloaca

A cloaca is defined as an opening in an involucrum. Pus or sequestra can be discharged through a cloaca in chronic Osteomyelitis.

►Osteonecrosis, Adults

Clonorchiasis

Parasitic infestation by a metacercaria (Clonorchis sinensis) endemic in Southeast Asia and China that most frequently causes a fibrosing cholangitis. The ingestion of contaminated uncooked fresh fish can cause infection in humans.

►Cholangitis

Closed Loop Obstruction

Closed loop obstruction occurs when a segment of bowel is obstructed at both ends, such as in a hernia or by a dense adhesion and becomes distended with a potential to twist on its mesentery.

►Occlusion and Subocclusion, Small Bowel in Adults
►Small Bowel, Postoperative

Clubbed Digits

Digital clubbing is a bulbous digital deformity with a watch-crystal deformity of the fingernail, associated with intrathoracic malformations, neoplastic or inflammatory conditions, as well as with hypertrophic osteoarthropathy.

►Hypertrophic osteoarthropathy

CM

►Spinal Cord Cavernous Malformation

CNS

Central nervous system.

►Tumors, Spine, Intradural, Extramedullary

CNS Toxicity

►Toxic Disorders, Brain

Coarse Liver

Ultrasonographic finding consisting with hepatic cirrhosis. It is characterized by the presence of inhomogeneous, coarse, thick, echoes, with or without evidence of multiple small hypoechoic nodules diffusely distributed throughout the liver tissue.

▶Cirrhosis, Hepatic

Coating of Ultrasound Contrast Media

▶Contrast Media, Ultrasound, Influence of Shell on Pharmacology and Acoustic Properties

Cobb Angle

Standard technique to measure the angle of scoliosis. Lines are drawn in extension of the uppermost and lowermost endplates of the neutral vertebrae. Neutral vertebrae have parallel endplates with—in contrast to the other vertebrae—minimal or no change in shape and are maximally tilted to the horizontal line.

▶Scoliosis

Codman's Angle

Usually suggests an aggressive lesion, found in rapidly growing lesions that penetrate through the cortex causing separation of the periosteum and formation of lamellated new bone, once the periosteum elevates to a significant degree, it can break forming an acute angle. However, findings similar to Codman's angle may also be shown in benign pathologies such as osteomyelitis and subperiosteal hematoma.

▶Neoplasms, Bone, Malignant

Coiling

Application of wire-coils with special configurations and sizes into vascular malformations, mainly into saccular aneurysms, in order to decrease the risk of rupture and hemorrhage.

▶Stroke, Interventional Radiology

Colic

According to Dorland's Medical Dictionary, colic is an acute abdominal pain; characteristic intermittent visceral pain with fluctuations corresponds to smooth muscle peristalsis. Renal colic is pain produced by thrombosis or dissection of the renal artery, renal infarction, intrarenal mass lesions, the passage of a stone within the collecting system, or thrombosis of the renal vein; called also nephric colic.

▶Colic, Acute, Renal

Colic, Acute, Renal

Darja Babnik Peskar, Eveline Smrtnik
University Medical Center Ljubljana,
Ljubljana, Slovenia
darja.babnik@kclj.si

Synonyms

Kidney stones; Renal colic; Ureteral colic; Urinary stones

Definition

Renal colic is a symptom complex characteristic for the presence of obstructing urinary tract calculi. It is defined as pain caused by stone passage within the collecting system (1). According to Dorland's Medical Dictionary, it may also be caused by thrombosis or dissection of the renal artery, renal infarction, intrarenal mass lesions, or thrombosis of the renal vein.

Acute renal colic is more correctly termed ureteral colic, as it is predominantly the result of a ureteral calculus. It is characterized by an abrupt onset of severe pain in the flank or kidney area, radiating anteriorly and caudally to the groin and anterior thigh. During passage, stones cause partial or complete obstruction,

local spasm, proximal dilatation, and stretching of the collecting system, which are responsible for the pain characteristics.

Pathology/Histopathology

►Urinary stones affect 2–3% of the population, usually the middle age group, with a 2:1 male predominance (1, 2). Up to 75% of stones are composed of calcium oxalate, the rest of struvite (magnesium ammonium phosphate), uric acid, hydroxyapatite, or cystine. Stone formation can be associated with primary metabolic abnormalities, primary hyperparathyroidism, prolonged immobilization, recurrent urinary tract infection, malignancy, sarcoidosis, Crohn's disease, laxative abuse, jejuno-ileal bypass, renal tubular acidosis, and gout.

The typical pain of renal colic is caused by distension of the renal pelvis and calices and stretching of the renal capsule in the acutely enlarged kidney. Nausea and vomiting occur due to the common innervations of the renal pelvis, stomach, and intestines through the celiac axis and vagal nerve afferents. In the midureter and lower ureter, pain is predominantly generated by increased peristalsis, muscle spasm, local irritation, and edema.

In ►Urinary Obstruction, Acute, autoregulatory changes of renal blood flow, glomerular filtration rate, and tubular function affect intrarenal hydrostatic pressure (1, 2). The initially increased renal blood flow preserves the glomerular filtration rate in the first hour. Together with an increase of hypotonic urine production and hyperperistalsis, they make an attempt to overcome obstruction. If passage is not attained after 3–5 h, preglomerular arteriolar vasoconstriction causes blood flow to decrease, while hydrostatic pressure continues to rise. After 5 h, both renal blood flow and pressure start to decrease, gradually leading to reduction of pain. Other changes that reduce renal pelvic hydrostatic pressure in the early phase are pyelolymphatic or pyelovenous backflow, and urine leakage into the renal parenchyma and perinephric soft tissues from forniceal rupture in 20% of cases (1, 2). In complete ureteral obstruction, irreversible loss of renal function will already be present after 48 h. Interstitial nephritis and fibrosis may cause atrophy of renal tissue.

Obstructive uropathy from ureteral calculus refers to acute, partial and one-sided obstruction, where renal function is preserved but lowered. A complete recovery of function is expected if blockade is eliminated in time. If obstruction is eliminated after 24 h renal function may recover in 7 to 10 days. Obstruction that lasts 2 to 3 weeks causes renal tubular function to be permanently damaged, thus leading to obstructive nephropathy. Four to eight weeks from onset of obstruction, renal function ceases and we speak of the afunctional kidney.

Clinical Presentation

The classic presentation of renal colic (1) is the acute onset of severe flank or kidney pain radiating to the groin or testicle in the male, and in the labia majora in the female, or in the anterior thigh, with either gross or microscopic hematuria (85%), nausea and vomiting (50%), tachycardia, hypertension, and costovertebral angle tenderness. When ureteral stones are near the bladder urinary frequency and urgency develop. Fever and the presence of leukocytosis, pyuria, or bacteriuria suggest the possibility of infected urinary lithiasis or pyonephrosis. Urinanalysis may reveal original urine crystals. Patients should be encouraged to retrieve stones for analysis.

Pain in renal colic is constant, and lasts for minutes to hours; however, exacerbation of pain with intervals of no pain may occur due to stone passage. Patients tend to move constantly to relieve pain, while patients with an acute abdomen try to be motionless.

Most symptomatic upper urinary tract stones are less than 5 mm in diameter, and the majority of them pass spontaneously in 24–48 h (1). Spontaneous stone passage depends on stone diameter, shape, location, and anatomy of the urotract. In absence of ureteropelvic junction (UPJ) obstruction or ureteral stricture, 4 mm or smaller stones may pass spontaneously in 90%, calculi between 5 and 10 mm in 50% of cases, while larger stones usually require intervention.

Imaging

►Plain film of the kidney, ureter, and bladder (KUB) can be diagnostic of urinary stones, since 90% are radiopaque (1). KUB is necessary for the follow-up of stones that do not pass spontaneously, and for lithotripsy planning and survey. KUB can miss small stones, radiolucent stones (uric acid, xanthine, dihydroxyadenine, indinavir, triamterene stones), or stones overlying bone. Phleboliths, vascular calcifications, calcified lymph nodes, appendicoliths, granulomas, various calcified masses, and even bowel contents can sometimes be confused with urinary tract stones.

When clinical presentation and KUB are not diagnostic, other imaging methods help in the early diagnosis of renal colic. ►Intravenous urography (IVU) is still the gold standard (1), and is preferred by urologists. The main advantages of IVU are the demonstration of renal

function, the precise outlining of the urinary collecting system, the detection of mild or local dilatation, and the differentiation of the obstructing stone from calcium deposits in medullary sponge kidneys (MSK), from abdominal calcifications, and from other intra- or extraluminal pathology. Indirect signs, such as delayed excretion and persisting nephrogram, pyelosinus backflow and extravasation of contrast around the collecting system, are highly suggestive or positive for acute stone obstruction (Fig. 1). After obtaining a KUB and 5 min postcontrast film, either a 10–15 min supine, full abdomen film is obtained to visualize the normally functioning urotract, or a prone film is obtained to spill contrast in the collecting system from the opacified calices on the affected side. A standing oblique film should be obtained under fluoroscopic control, to opacify the ureter to the level of obstruction and to differentiate ureteral stones from other calcifications. If the collecting system is not ready opacified, 1–2 delayed films are required up to a few hours later, and rarely after 24 h. A conducted IVU consists of 4–6 films, depending on the delay. IVU remains price and radiation risk competitive with unenhanced CT (UHTC).

►Ultrasound (US) is a noninvasive, radiation-free method, and may be the initial method in the evaluation of renal colic. It is accepted as a follow-up investigation for monitoring spontaneous stone passage after extracorporeal shock wave lithotripsy (ESWL) or surgical treatment. US can demonstrate obstruction and the obstructing stone based on its echogenicity and dorsal acoustic shadowing. It has certain limitations in evaluating obstruction and depicting small midureteral stones. Its effectiveness is also operator-dependent. In acute colic, with or without a dilated collecting system, duplex ►Doppler US suggests stone obstruction by the assessment of an elevated intrarenal resistive index (RI > 0.7; 92% sensitivity, 88% specificity) or a difference of RI between both kidneys larger than 0.04 (1, 3). False-negative RI results in the first hours after onset may be explained by initial vasoregulation and spontaneous pelvocaliceal rupture (4) (Fig. 3). A characteristic slow or absent ureteral jet in the bladder, and the twinkling artifact behind stones help in the diagnosis of stone obstruction.

►Retrograde pyelography refers to direct ureteral contrast injection through a catheter inserted at cystoscopy. It is the most precise imaging method for diagnosing any type of ureteral pathology, but is rarely performed; mostly when obtaining material for cytology, and prior to ureterorenoscopy (URS) or the placement of double-J stents. When the insertion of double-J stents fails, therapeutically inserted percutaneous nephrostomes (PNS) can also be used for *anterograde pyelography* (1, 2) (Fig. 2).

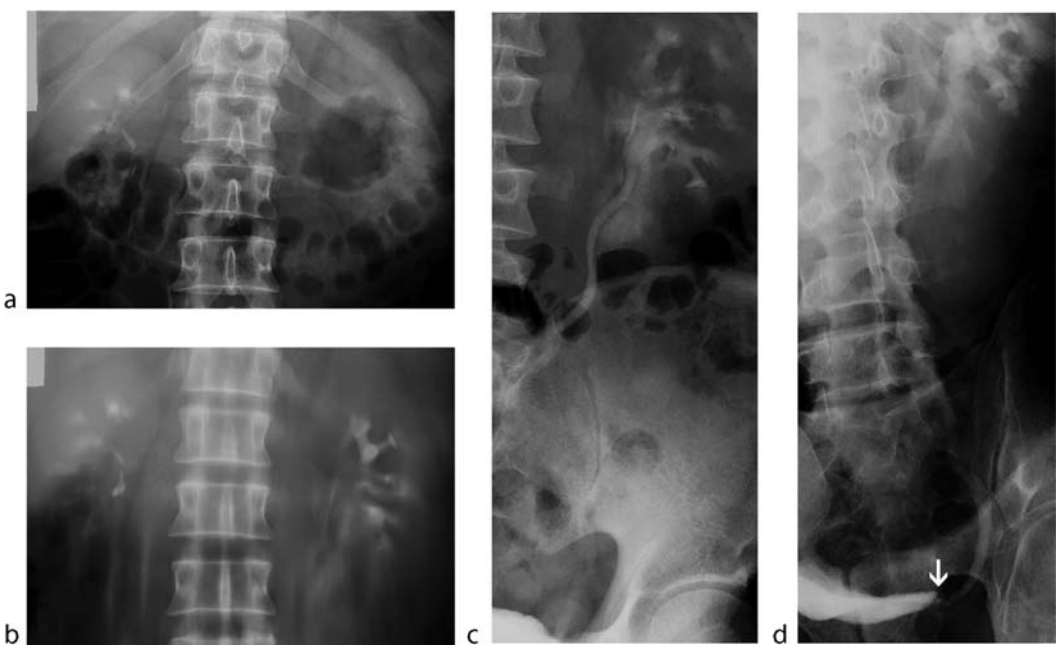

Colic, Acute, Renal. Figure 1 IVU examination in a 55-year-old man with acute renal colic demonstrates (a) slightly delayed excretion on the left 5 min after 30 mL nonionic contrast injection, (b) extravasation around the nonopacified pyelon and proximal ureter after spontaneous caliceal rupture on tomography, (c) in prone position pyelon and ureter opacify 10 min postcontrast, (d) visible level of obstruction at the UVJ due to a small left ureteral calculus *(arrow)*.

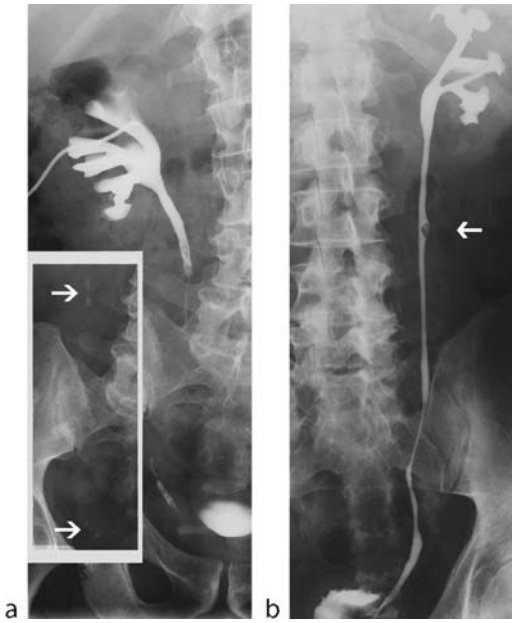

Colic, Acute, Renal. Figure 2 (a) Small radio-opaque right-sided urinary stones detected at KUB *(arrows)* in a female with acute renal colic after ESWL. Percutaneous nephrostoma was inserted after unsuccessful double-J insertion. On anterograde urography these radiopaque and severely obstructing stones were demonstrated as less radiopaque than contrast. (b) Retrograde urography in 64-year old man with acute renal colic and suspected radiolucent left ureteral calculi. An atypical eccentric filling defect is delineated *(arrow)*. IVU was inconclusive, but US confirmed a ureteral stone.

UHCT has proved to be more accurate than IVU for the diagnosis of urinary calculi and equal in demonstrating dilatation (5). It is indicated in patients with a high risk for use of contrast media, in nonfunctioning kidneys, or when urography is inconclusive. Other advantages of CT over IVU are the demonstration of other abdominal pathology. Thin section (3.5 or 5 mm) UHCT has a sensitivity of 97%, and specificity of 96% for the investigation of renal colic (1). Secondary signs typical for the acute phase are periureteral or perirenal tissue stranding and the tissue rim sign due to edema in the ureter wall around small calculi. A split bolus technique of contrast administration and scanning during the nephrographic and excretory phase provides evaluation of renal function and parenchymal alterations, and delineates the collecting system. The advent of multislice-computed tomography (MSCT) provides the ability to perform CT urography with a spatial resolution closer to that obtained at IVU. High-resolution multiplanar (MPR), maximum-intensity (MIP), and average-intensity (AIP) images of the collecting system are generated from unenhanced and enhanced CT data (Fig. 4a).

MR urography is regarded as a diagnostic test of secondary reference following IVU, US, and CT (6). Two different techniques of MRI, depending on the clinical situation, are available. Static-fluid MR urograms are obtained with heavily T2-weighted turbo spin-echo sequences. Dynamic or excretory MR urograms are obtained with gadolinium contrast agent administration and T1-weighted gradient-echo sequences (Fig. 4b, c).

Diagnosis

The diagnosis of an obstructive urinary stone is essential for the exclusion of acute surgical abdominal pathology (appendicitis or abdominal aortic aneurysm). Urinary tract infection, cardiac ischaemia, bowel ischaemia or obstruction, hepatic capsulitis, musculo-skeletal pain, and biliary colic, are also considered in the differential diagnosis.

In patients with acute flank pain, the diagnosis of ureteral calculi can be apparent according to positive history, physical examination, and laboratory studies. In presence of hematuria, calculi are confirmed with 96% accuracy by a positive KUB. Radiological imaging is required to evaluate the location of the stone, the exact size, shape, orientation, radiolucency, all necessary for treatment planning. Kidney function and the presence of infection are assessed. Until recently, IVU was performed to evaluate stone obstruction in inconclusive cases, with a sensitivity of 95%. Recently, abdominal US supersedes IVU in patients with positive KUB. It is the test of choice if KUB is negative, since it can effectively demonstrate radiolucent stones, or exclude other causes of abdominal pain. The reported sensitivity of US for stone detection varies, the highest is 98%. US easily demonstrates larger stones within the renal pelvis and stones in the dilated ureter near the UPJ and ureterovesical junction (UVJ). In the absence of dilatation (35%), duplex Doppler US can assess an elevated RI in the affected kidney, and asymmetry of ureteral jets, thus helping to exclude false-negative cases. It reduces the number of false-positive results by assessing nonobstructive dilatation in cases of extrarenal pelvis, UPJ obstruction, prominent vasculature, residual dilatation, vesicoureteral reflux, megacalices, papillary necrosis, pyelonephritis, full bladder, and diabetes insipidus (2).

UHCT of the abdomen may be helpful as an alternative or in the clarification of equivocal US findings. UHCT of the abdomen is more sensitive and more likely to yield a diagnosis than plain radiographs and US.

Management of urinary stones (1) comprises the insertion of a double-J stent in cases of uncontrollable

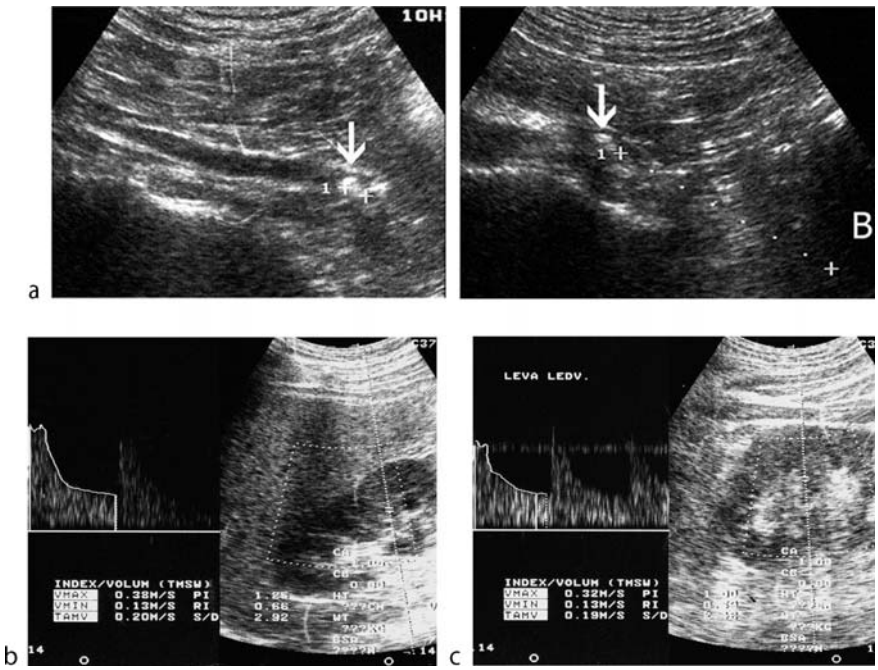

Colic, Acute, Renal. Figure 3 US examination in acute renal obstruction showing (a) ureteral dilatation due to calculus *(arrow)* 6.8 cm from the bladder *(B)*, and (b, c) increased RI in the affected kidney with a significant RI difference of 0.07 between both kidneys. (Contributed by A. Visnar-Perovic)

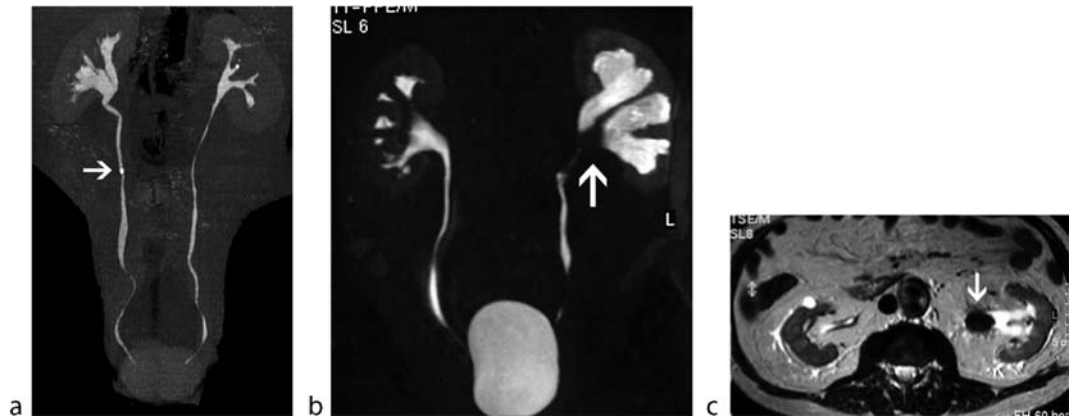

Colic, Acute, Renal. Figure 4 (a) CT urography in 40-year old patient presenting with right-sided flank pain and gross hematuria was performed in a pain-free interval. The MIP image shows a calculus (*arrow*) within the right ureter with sufficient contrast material passage and only slight dilatation of the pelvicaliceal system. In addition, a small infundibular concrement can be appreciated on the left side. (Contributed by J. Kemper) (b, c) MRU case showing a calculus inside the left renal pelvis obstructing the UPJ in a 64-year old man with recurrent left-sided flank pain. (b) MIP from a gadolinium-enhanced T1-weighted breath-hold 3D-gradient-echo-sequence displaying the urographic overview and (c) axial standard T2-weighted TSE-image showing the signal void of the calculus (*arrows*). (Contributed by C. Nolte-Ernsting)

pain, complete obstruction with severe urinary infection or urosepsis, in solitary obstructed kidneys, in large stones that are considered unlikely to pass spontaneously, or in suspected ureteral strictures. Percutaneous nephrostomes are inserted when the insertion of double-J fails. Ten to twenty percent of all urinary stones require surgical removal. Percutaneous nephrostolithotomy (PNL), URS, and ESWL successfully compete to open surgery. Most

urinary stones pass spontaneously in 24–48 h and do not require special treatment other than pain relief, hydration and antiemetics.

Bibliography

1. Menon M and Resnic MI (2002) Urinary lithiasis: etiology, diagnosis, and medical management. In: Campbell MF, Walsh PC, and Retik AB (eds) Campbell's Urology. Urinary Lithiasis and Endourology. WB Saunders Company, Philadelphia, pp 3229–3305
2. Platt JF (1996) Urinary obstruction. Radiol Clin North Am 34 (6):1113–1129
3. Platt JF, Rubin JM, Ellis JH, et al (1989) Duplex Doppler US of the kidney: differentiation of obstructive from nonobstructive dilatation. Radiology 171:515–517
4. Roy C, Tuchmann C, Pfleger D, et al (1998) Potential role of duplex Doppler sonography in acute renal colic. J Clin Ultrasound 26:427–432
5. Smith RC, Verga M, McCarthy S, et al (1996) Diagnosis of acute flank pain: value of unenhanced helical CT. Am J Roentgenol 166:97–101
6. Nolte-Ernsting CC, Staatz G, Tacke J, et al (2003) MR urography today. Abdom Imaging 28:191–209

Colitis, Ulcerative

Francesca Maccioni[1], Sara Parlanti[1], Francesca Siliquini[1], Viola Garbarino[1], Valeria D'Ovidio[2]
[1]Department of Radiological Sciences, Policlinico Umberto I, University of Rome "La Sapienza", Italy
[2]Department of Clinical Sciences, Gastroenteroly Unit, Policlinico Umberto I, University of Rome "La Sapienza", Italy
francesca.maccioni@uniroma1.it

Synonyms

Ulcerative colitis; Ulcerative proctitis; Ulcerative sigmoiditis; Ulcerative pancolitis

Definitions

Ulcerative colitis (UC) was described in 1859 by Sir Samuel Wilks (1824–1911), a British physician who firstly differentiated it from bacterial dysentery.

The greatest incidence of chronic UC is in the second, third and fourth decades of life. The condition is more common in white women. The disease may vary greatly in its severity, course, and prognosis. It has an unknown etiology and a chronic relapsing–remitting course. To date, the pathogenesis of UC still remains unknown, although recent studies showed an important role of environmental enteric, immune, and genetic factors. These studies suggest that UC may result from the loss of tolerance of the immunocompetent intestinal system versus the normal intestinal flora, in genetically susceptible individuals.

UC is characterized by a predictable course and localization, extending continuously from the rectum to the colon, involving first the left colon, then the transverse and right colon, and very rarely the distal ileum. The different patterns of ulcerative colitis are commonly called as "ulcerative proctitis," "ulcerative sigmoiditis," "left-sided colitis," or "pancolitis." A recto-sigmoid localization is present in up to 95% of the patients. The mucosal inflammation of the terminal ileum, is rarely observed in UC, developing only in presence of a pancolitis (the so-called "►backwash ileitis"); in those cases, UC can be hardly differentiated from Crohn's disease (CD).

Pathology/Histopathology

Cryptitis or abscesses of the crypts of Lieberkühn are hallmarks of ulcerative colitis. They form ulcerations that reach the lamina propria, or may produce excrescences also called as "pseudopolyps." With the lateral extension of the ulcers, large areas of bowel wall muscle may be almost completely denuded. Microscopically, UC is characterized by moderate wall thickness, leukocyte infiltrates in the mucosal and submucosal layer, disruption of mucosal elements and aphthoid ulcers, mucosal edema, inflammatory pseudopolyps, without extra-wall lesions neither significant signs of perivisceral inflammations in the majority of cases. Fatty deposition in the submucosal layer is a common finding in long-standing disease. Macroscopically, the chronic inflammatory bowel process of UC determines loss of haustration, moderate strictures, mild diffuse colonic wall thickening, widening of the presacral space, and occasionally severe complications such as massive bleeding, toxic megacolon, tight bowel strictures, or perforation.

The disease is intermittently acute and in the quiescent phase the mucosa may completely heal, but more frequently it appears atrophic with rare crypts, with distorted mucosal architecture and thickening of the lamina propria.

Clinical Presentation

Three degrees of severity are distinguished as mild (about 60–80% of cases), moderate (25%), and severe or fulminant.

Eighty percent of patients have only proctitis or proctosigmoiditis in the early phases of the disease, although in 50% of them a proximal extension later occurs. Only 20% have extensive colitis at the onset of symptoms, the course of the disease can vary widely. Spontaneous remission from a flare-up occurs in 20% to 50% of the patients, although 50% to 70% have a relapse during the first year after diagnosis. The relapse rate is higher in younger patients.

In acute phases, bleeding results from friable and hypervascular granulation tissue; diarrhea with urge incontinence results from damage that impairs the ability of the mucosa in reabsorbing water and sodium. If the disease is more severe, it may extend beyond the mucosa and submucosa into the muscularis mucosa (rarely to serosa) and this explains the dilation of the colon, by loss of motor tone, in cases of toxic megacolon.

Severe disease is indicated by large volumes of diarrhea, weight loss, large amount of blood in the stool, high fever, elevated C-reactive protein, elevated erythrocyte sedimentation rate, low hematocrit value, and hypoalbuminemia. Approximately 65% of patients with UC have positive perinuclear antineutrophil cytoplasm antibodies (pANCA), also present in patients with primary sclerosing cholangitis.

The prevalence of the extraintestinal manifestations such as arthritis, uveitis, pyoderma gangrenous, sacroiliitis, spondylitis, or erythema nodosum, may vary depending on the geographic area, population, location and duration of the disease, medication, and diagnostic accuracy. Patients with ulcerative colitis have an increased risk of developing colorectal cancer. The current procedure to diminish this risk is colonoscopy surveillance and histopathological evaluation of biopsy specimens. This method is not unquestioned and is undergoing continuous evaluation.

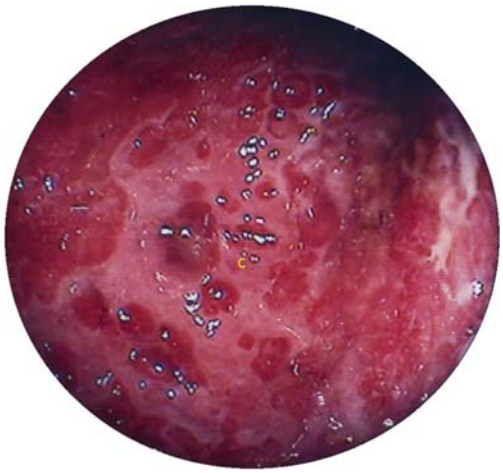

Colitis, Ulcerative. Figure 1 Endoscopic view of the colonic mucosa, as appears in severe ulcerative, very friable, with spontaneous bleeding. Furthermore, loss of vascularity, hemorrhage, and ulcers with fibrin and mucous are well appreciable.

Imaging

Endoscopy

Endoscopy (ES) is definitely a primary examination in the evaluation of UC. The disease is, in fact, usually confined to the colonic mucosa, which is completely accessible to endoscopy. Moreover, endoscopic biopsies, although confined to the mucosa and submucosa layer, may adequately evaluate the severity of colonic wall inflammation, which usually spares the outer muscular and serosa layers.

Typical endoscopic findings include reddening of the mucosa, increased vulnerability, mucosal bleeding, irregular ulcers, pseudopolyps, granularity, loss of vascular architecture, loss of haustration, and occasionally strictures. These changes are continuous in the colon, and the rectum is always involved (Fig. 1).

However, although ES is widely considered the first examination for the diagnosis UC, it can be contraindicated, refused or incomplete in up to 30% of patients with UC. It is an invasive examination causing patient discomfort and associated with possible complications, above all colonic perforation, whose incidence may vary according to the operator's experience, ranging between 0.1% and 3%. Moreover, ES is absolutely contraindicated in the acute phases of severe colitis, due to the higher risk of perforation; in these phases, however, a diagnostic support is crucial to plane an effective treatment. Finally, late complications of UC, particularly tight strictures, can partially or completely prevent the passage of an endoscope. In all these cases other imaging modalities, including barium studies and ►cross-sectional imaging, may add important information on the disease (Fig. 2).

Conventional Radiographs

Barium studies may be an alternative modality to endoscopy to assess luminal changes, particularly when performed with a double-contrast technique. Single- or double-contrast barium enema (BE) may easily visualized the typical mucosal changes of the disease.

In the first phase, BE may show superficial changes related to edema and granulation tissue; occasionally the only sign of inflammation in the early phases is the blunting of the normally acute angles of the rectal valves.

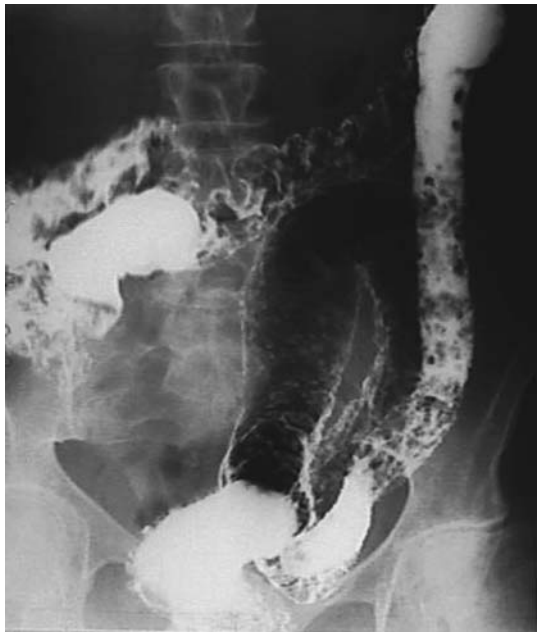

Colitis, Ulcerative. Figure 2 Barium studies, performed with a double contrast technique, shows lack of haustrations and tubular narrowing of the left-side colon, characterized by multiple pseudopolyps and ulcers showing a "collar-button" appearance. (Courtesy of Panzironi G, Department of Radiology, Policlinico Umberto I. Rome, Italy.)

When the disease progresses, using a double-contrast BE, ulcers seen in profile have a "collar-button" appearance. The demonstration of ulcerations by radiographic means is important because these changes indicate clinically and pathologically severe diseases. Between denudated and ulcerated areas, a large number of pseudopolyps may be observed, representing elevation of inflamed mucosa. Secondary changes can be easily seen on both single- and double-contrast BE examinations. Main signs of chronic disease are foreshortening of the colon, lack of haustrations, and tubular narrowing of the colon that gives the large bowel the appearance of a garden hose or stovepipe. Barium studies, although not useful in assessing the clinical activity of UC, can be indispensable in distinguishing between the two diseases (Goldberg et al. 1979; Gore et al. 1997).

In very severe hyper acute phases, a BE may be contraindicated. In such phases a plain film of the abdomen is the best option, being crucial in the identification of the toxic megacolon. This complication is usually well identified at plain films as a severe colonic distention exceeding the 8 cm in diameter in the left colon and the 10 cm in diameter in the right colon. Colonic perforation and free peritoneal air can be easily identified at plain films in upright position as well.

Cross-Sectional Imaging: Ultrasonography, Computed tomography, and Magnetic Resonance Imaging

Cross-sectional studies may play a complementary role in the assessment of UC.

Transabdominal ultrasonography (TUS) is a non-invasive cross-sectional imaging modality that can be helpful in the diagnosis of ▶inflammatory bowel disease (IBD). The main purpose of US is to exclude the involvement of the distal ileum, in order to distinguish UC from CD. High-resolution US, performed with a 7.5 MHz probe, is a well accepted modality to evaluate the wall thickening of the distal ileum in Crohn's disease, therefore it may be extremely useful to differentiate the two diseases, whenever ES or histology are doubtful. Moreover, in more severe colitis, the mild wall thickening, particularly the left and sigmoid colon, if equal or superior to 4 mm, can be well-depicted at high-resolution US. Finally US can be useful in the investigation of biliary complications of the disease, including biliary stones, cholangitis, and cholangiocarcinoma.

Usually cross-sectional modalities cannot assess the typical mucosal changes of UC, but they (CT and MRI above all) can evaluate the mild wall thickening, the increased wall vascularity associated with an active disease, as well the changes in the morphology of the colon. In some cases, cross-sectional imaging may substitute ES and BS, particularly when they are contraindicated in very severe phases.

Thanks to their panoramic and multiplanar capability, both CT and MRI are usually able to distinguish between a proctitis, a left-sided colitis or a pancolitis, according to the findings observed either on axial and coronal planes. MRI Coronal or CT multiplanar reconstructions are very useful to exclude involvement of the terminal ileum, thus helping in differentiating UC from CD, similarly to US. In the evaluation of rectal disease, the mid-sagittal imaging plane offered by MRI better displays the typical widening of the recto-sacral space.

Recently, MRI has been proposed to evaluate the degree of wall inflammation (disease activity) especially in the follow up of patients (thanks to lack of radiations) (Fig. 3). At MR, wall gadolinium enhancement is frequently observed in severe active UC associated marked wall thickening; on the other hand, in moderate disease a moderate wall enhancement can still be present, but

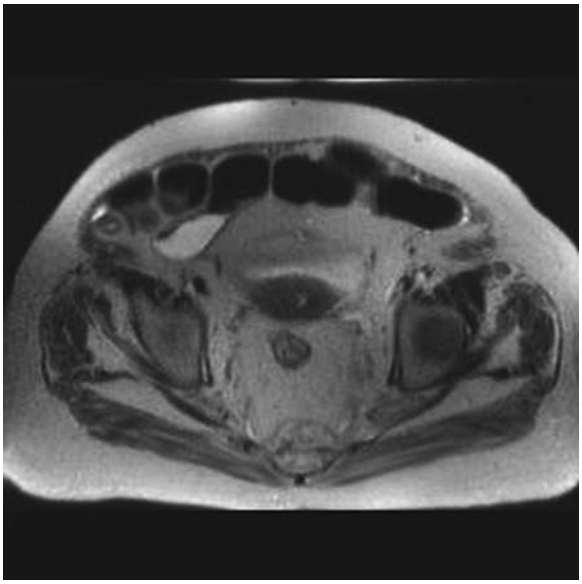

Colitis, Ulcerative. Figure 3 Colitis, Ulcerative. The T2-weighted MR image, acquired on the axial plane, shows a mild case of ulcerative colitis, localized on rectum, demonstrating diffuse thickening and high wall T2 signal of the rectal wall, which is surrounded by abundant fat tissue proliferation, both signs of chronic inflammatory disease.

associated with lower thickening; finally, inquiescent disease, wall enhancement can be very low or absent.

CT and MRI can detect complications of UC requiring surgery, such as diffuse dilatation of the colonic lumen (toxic megacolon), tight strictures, and rectal cancer.

The toxic megacolon can be diagnosed with the same criteria of conventional abdominal plain films: a marked and diffuse colonic dilation (upper normal limit 5.5–6.5 cm in the transverse and left colon) with severe mucosal disease is the typical appearance.

Nuclear Medicine

Radionuclide studies have a useful role in acute fulminant colitis when colonoscopy or BE study is contraindicated, similarly to CT or MRI. Radionuclide studies are also useful in depicting disease activity and the extent of disease and in monitoring the response to therapy. Promising results have been published about the clinical use of technetium 99m white blood cells (WBC) in the assessment of IBD in adults and in a small series of children. In patients with active UC, inflammation is visualized with 99mTc-exametazime-labeled leucocytes or 99mTc-labeled antigranulocyte antibodies. The antibody technique offers the advantage of *in vivo* labeling, but is less reliable than the exametazime method for imaging of colonic inflammation.

Treatment

The treatment of patients with IBD depends on knowledge of the location, extent, and activity of the inflammation. Clinical evaluation (Truelove and Witts classification or the more recent Powell–Tuck index) and ES are usually sufficient to assess the extent and severity of UC, since the inflammatory process involves the colon only, sparing the small bowel. Moreover, biopsy specimens obtained during ES, necessarily limited to the mucosa and submucosa layer, can usually detect most of the pathologic features of UC, since the inflammatory process does not extend beyond the submucosa layer. Clinical data (acute phase reactants, etc.) together with endoscopic evaluation are usually adequate to estimate the disease extent in most of patients with mild to moderate disease. In case of complicated or very severe disease, if endoscopy is limited or contraindicated, or in case doubtful cases, the diagnostic modalities above mentioned may complete the diagnostic procedure, helping to reach a final correct diagnosis.

Generally, most patients with mild to moderate disease are effectively treated with drugs. Occasionally, however, the disease may be extremely severe, thus requiring urgent colectomy if it does not respond to pharmacological therapy promptly.

The drugs of first choice for the treatment of an acute flare-up of UC are 5-ASA-releasing preparations and glucocorticoids.

The efficacy of glucocorticoids and the beneficial effects of sulfasalazine have been known for half a century. The 5-ASA influences a wide variety of immunologic and inflammatory reactions, such as a chemotaxis of white blood cells, cytokine release, and release of reactive oxygen species.

The extent of the disease influences the strategy of treatment.

Left-sided colitis is better treated with rectal administration of drugs, whereas more extensive colitis requires oral or intravenous treatment, depending on the disease severity.

Active distal UC should initially be treated with 5-ASA. If treatment is otherwise

ineffective, steroid enemas and preferably steroid foams, can be used.

If the colitis involves the left colic flexure, rectal treatment is not sufficient. In patient with mild or moderate disease oral administration of 5-ASA preparation is effective.

In more severe cases, or if 5-ASA fails, glucocorticoids should be used orally or intravenously and 60–100 mg of prednisolone equivalent is useful in the majority of patients.

Among those with very severe colitis, however, only half of the patients respond.

When adequate doses of glucocorticoids fail to improve severe UC, a colectomy should be performed, particularly in patients with fulminant colitis and toxic megacolon.

Azathioprine or 6-mercaptopurine is effective in chronic active colitis. However, considering the possible side effects and the need for long term therapy this option should be weighted against colectomy and ileoanal pouch surgery.

Maintenance of remission with sulfasalazine should be used and decreases the relapse rate by about 50%. Azathioprine should be used only in patients who cannot be kept in remission with 5-ASA and who are not willing or able to undergo colectomy.

The most frequent indication for surgical resection in UC is severe inflammation of the large intestine and rectum that is refractory to conservative therapy, also in patients who suffer from the side effects of the medication.

Toxic colitis with or without megacolon can be complicated by perforation. Operation within 3.5 days is prognostically associated with a better outcome than operation after a long, futile treatment attempt with considerable worsening of the patient's general conditions.

Three classic surgical interventions are performed in UC: conventional proctocolectomy with terminal ileostomy (without preservation of the anal sphincter), ileorectal anastomosis (only if the rectum is not extensively involved), or restorative proctocolectomy with ileo-anal pouch, which is nowadays considered the first choice procedure. In the last procedure (total colectomy with ileo-anal pouch), the rectum is completely resected whereas the anal sphincter muscles apparatus is spared; therefore there is no risk of recurrence, and at the same time the ileo-anal pouch ensures a reservoir function. Sometimes the ileal pouch may undergo to chronic wall inflammation, and the so-called "pouchitis" endoscopy is the modality of choice to evaluate the degree of wall inflammation in a pouch. Cross-sectional imaging, particularly MRI or CT, may be useful in evaluating the morphology of the pouch and possible complications.

Bibliography

1. Goldberg HI, Caruthers SB Jr, Nelson JA et al (1979) Radiographic findings of the National Cooperative Crohn's Disease Study. Vol 77: 925–933, Gastroenterology
2. Gore RM (1995) Characteristic morphologic changes in chronic ulcerative colitis: Abdom Imaging. Vol 20:275–278
3. Gore RM, Ghaharemani GG, Miller FH et al (1997) Inflammatory Bowel Disease: Radiologic Diagnosis. In Syllabus of the radiological Society of North America, Categorical Course in Gastrointestinal radiology: 95–109, RSNA Publications
4. Miner PB (2000) Clinical Features, course, laboratory findings, and complications in ulcerative colitis. In: Kirsner JB (ed) Inflammatory Bowel Disease. 5th edn. WB Saunders, Philadelphia, pp 299–304
5. Maccioni F (2004) In: Chapmann AH (ed) MRI of Colitis in Radiology and Imaging of the Colon. Springer-Verlag, Heidelberg, pp 201–214
6. Maccioni F, Colaiacomo MC, Parlanti S (2005) Ulcerative colitis: value of MR imaging. Abdom Imaging 30:online (May)
7. Scholmerich J, Herfarth C In: Cremer M et al (eds) (1999) Ulcerative colitis in Gastroenterology and Hepatology. McGraw-Hill, New York, pp 382–392

Collateral Phenomenon

Collateral phenomenon is an nonspecific finding of periarticular demineralization, which occurs, for example, due to disuse or neighborhood inflammation. Today the terms "regional osteoporosis" and "periarticular demineralization" are more common.

▶Rheumatoid Arthritis

Collimator

In a radionuclide imaging device, a collimator is a block of radiation-attenuating material with one or more apertures defining the field of view and limiting the angular spread of the radiation that can reach the radiation detector assembly.

▶Scintigraphy

Colloid Carcinoma

▶Carcinoma, Other, Invasive, Breast

Coloboma

▶Congenital Malformations, Orbit

Colon, Postoperative

Ashley S. Shaw[1], Alan H. Freeman[2]
[1]Consultant Radiologist
Cambridge University Hospitals NHS Trust
Cambridge, UK
[2]Consultant Radiologist
Cambridge University Hospitals NHS Trust
Cambridge, UK

Synonyms

Abdominal Surgery; Complications; Abdomen; Post-operative

Colonic resection may be performed for a number of conditions, most commonly malignancy, diverticular disease, inflammatory bowel disease (ulcerative colitis, Crohn's disease) or ischaemic bowel. Equally, a wide variety of procedures may be performed, from short segmental resection to complete pan-proctocolectomy. When imaging patients who have undergone colonic surgery, it is important for the radiologist to establish what the underlying condition is, when and what procedures have been performed, and whether there has been any adjuvant chemo- and/or radiotherapy (1). It is only with this information to hand that one is able to identify the most likely pathology, perform the most appropriate study and interpret the images.

Paralytic Ileus

Often referred to simply as 'ileus' (alternatively adynamic or non-obstructive ileus), paralytic ileus is atony of the intestine resulting in failure to propel the bowel contents distally. Ileus is common after any operation where the stomach, small or large bowel have been handled, although the aetiology is complex. It may be exacerbated by biochemical abnormalities (e.g. renal failure, diabetes mellitus, hypokalaemia), anti-cholinergic drugs, reflex sympathetic inhibition (e.g. retroperitoneal haematoma), sepsis or other systemic illness.

Clinical Presentation

Ileus is considered normal for the first few days following colonic surgery. The patient will have little appetite, absent bowel sounds on auscultation and will not pass any flatus or faeces. If this persists for greater than 4–5 days, particularly in the absence of any of the correctable causes detailed above, it may herald the presence of intra-abdominal sepsis or haemorrhage and require investigation.

Imaging

The key differential diagnosis is large bowel obstruction. The supine abdominal radiograph typically demonstrates distension of both small and large bowel (±gastric distension). Ileus, unlike obstruction, often demonstrates multiple loops of dilated bowel with normal calibre bowel in between. In addition, the presence of a gas filled dilated rectum is strongly suggestive of ileus. Serial films often show the degree of bowel dilatation to reduce over time. Oral contrast medium will pass slowly through the dilated bowel, being increasingly diluted by small bowel fluid and is usually unhelpful. Rectal contrast medium may be used to confirm the absence of a colonic stricture (free passage of contrast into the most distal dilated bowel loop confirms ileus). Where ileus persists, cross-sectional imaging with computed tomography (CT) may be helpful to determine whether there is a surgically remediable cause (e.g. abscess or haematoma).

Anastomotic Leak

Following the resection of a segment of colon, the two free ends are usually joined together using sutures or staples. The exceptions to this are Hartmann's procedure, complete pan-proctocolectomy and abdomino-perineal resection, where an ileostomy or colostomy is fashioned. Failure of the anastamosis occurs in a small proportion of patients, but is significantly more common when there is active inflammation or infection at the time of surgery. Segmental ischaemia or radiotherapy also contribute to friable tissue. For this reason, many surgeons may either electively perform a loop ileostomy to temporarily rest or 'defunction', the colon or perform the operation in two stages.

Clinical Presentation

Breakdown of the surgical anastomosis usually occurs towards the end of the first post-operative week. The patient commonly presents with a fever and/or pelvic pain, indicating the presence of an underlying abscess. Preliminary investigations may demonstrate an elevation of the white blood cell count and inflammatory markers.

The presence of a pelvic abscess may lead to an ileus, development of a fistula, peritonitis or mechanical obstruction.

Imaging

A supine abdominal radiograph is often the first investigation but is non-specific. It may show dilated loops of bowel from either ileus or obstruction. A *gastrografin* enema will delineate any ongoing leaks at the anastomosis (Fig. 1) and perhaps identify a fistula. It should be borne in mind that a proportion of leaks will seal spontaneously, but may leave the patient with a pelvic abscess. To assess the pelvis for a collection, cross-sectional imaging with CT is indicated (Fig. 2). CT may be performed following administration of rectal contrast in order to help define the often complex post-operative anatomy. Whilst CT will demonstrate the anatomy, it may be difficult to differentiate haematoma from abscess, particularly when there is often a combination of the two. Where there is clinical concern, percutaneous drainage of any fluid collections is often required, both to confirm the diagnosis and treat the abscess. Failure of radiological management or the development of peritonitis will usually necessitate a repeat laparotomy.

Nuclear Medicine

Occasionally, it may not be possible to clearly demonstrate ongoing infection within the pelvis on cross-sectional imaging, particularly where there is no discrete abscess. In these cases, particularly where there is delayed presentation, a radiolabelled white cell scan may be of use in proving the diagnosis before committing the patient to a prolonged course of antibiotics or further surgery.

Tumour Recurrence

Following diagnosis of colorectal carcinoma, approximately 70% of patients will undergo 'curative' surgery. The reported rates of tumour recurrence vary considerably, with the liver the most common site of metastatic disease (2). Local recurrence, at or near the surgical anastomosis or within the surgical bed, is seen in approximately 10–15% of cases and is more common in rectal than colonic tumours.

Clinical Presentation

The majority of recurrences occur within the first 2 years following surgery. Tumour recurrence at the surgical anastomosis may lead to rectal bleeding or even mechanical obstruction. However, more often there are no local symptoms and it is identified on routine post-operative surveillance, either at CT or endoscopy.

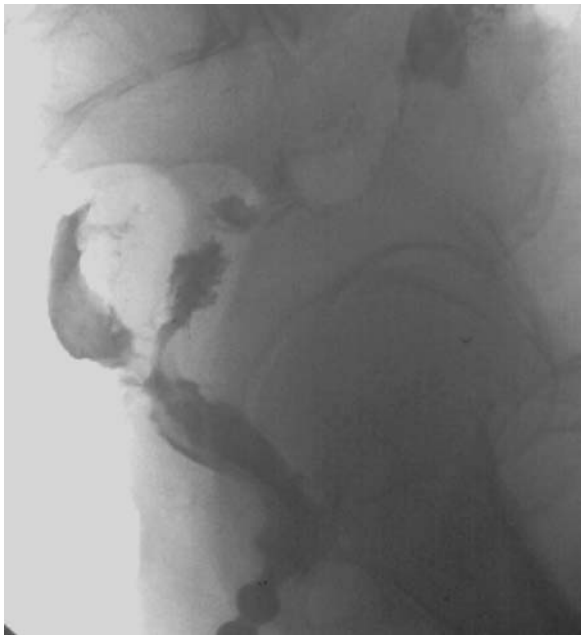

Colon, Postoperative. Figure 1 Contrast enema demonstrating an anastomotic leak in a patient shortly after undergoing an anterior resection.

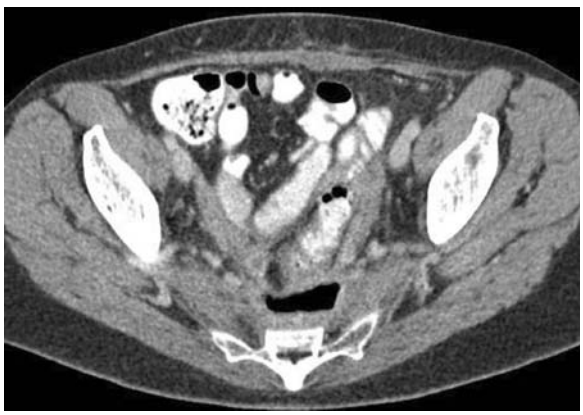

Colon, Postoperative. Figure 2 CT demonstrates a cavity in the pre-sacral space containing air and fluid, indicating the presence of an abscess. The patient had recently undergone an anterior resection.

Imaging

CT is the mainstay of post-operative surveillance following resection of colorectal cancer, usually performed at

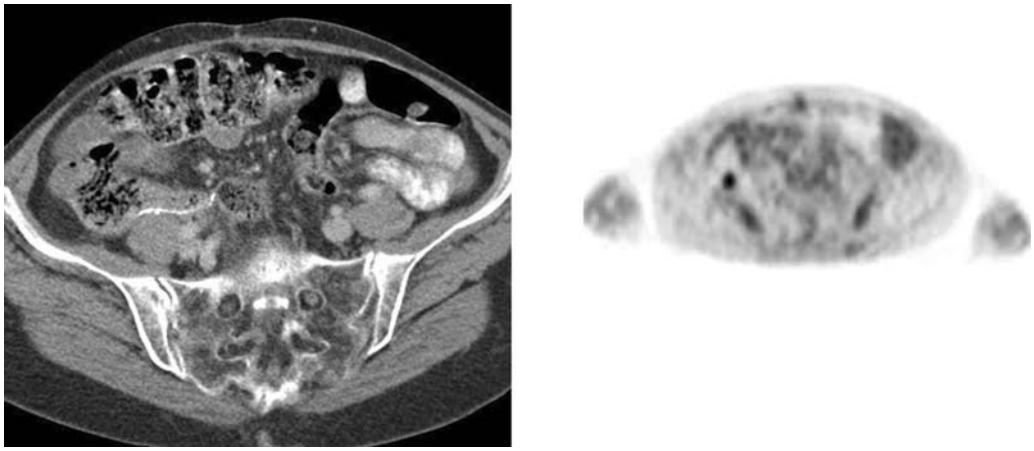

Colon, Postoperative. Figure 3 Patient with previous right hemicolectomy for Dukes B adenocarcinoma. CT does not show any abnormality, but the PET study demonstrates a focal area of recurrence at the anastomosis, confirmed at surgery.

6–12 monthly intervals for 2–3 years after surgery. This will reliably detect liver, peritoneal and nodal metastases. Recurrence at the anastomotic site will be seen as a nodule or plaque of abnormal soft tissue. The difficulty lies in differentiating such areas from post-operative fibrosis or haematoma. Previously, one could either choose to 'watch and wait' or attempt a biopsy of such lesions. This has been superseded in many centres by the use of functional imaging (Fig. 3).

Nuclear Medicine

Positron emission tomography (PET) uses radiolabelled isotopes (principally ^{18}fluoro deoxyglucose-FDG) to identify areas of abnormally increased metabolism within the body. This complements the anatomical imaging offered by CT, enabling differentiation of abnormal soft tissue, and often identifies hitherto unsuspected disease. Sites of recurrent colorectal cancer are detected with a sensitivity of 97% and specificity of 76%, resulting management changes in between one quarter and one third of patients (3). False positive results may occur at sites where there is active inflammation or infection, thus PET may be more difficult to interpret in the early post-operative period.

Bowel Obstruction

Obstruction following colonic surgery has a number of possible causes: recurrence of disease (tumour, Crohn's disease); adhesions; and fibrous strictures at the surgical anastomosis.

Clinical Presentation

Increasing abdominal distension, abdominal pain and the absence of flatus or bowel motions are the typical presenting symptoms of bowel obstruction, with 'tinkling' bowel sounds on auscultation. Bowel obstruction following resection is typically a late complication and occurs at the anastamosis site with an incidence of 2–8% (1). The use of staples, rather than hand sewing the anastamosis, appears to increase the frequency of stricturing.

Imaging

Anastomotic strictures may be evaluated by a number of methods, including double-contrast barium enema (DCBE), colonoscopy and CT. DCBE will allow evaluation of the mucosal surface and identify any fistulae, whereas CT permits evaluation of the extracolonic structures. Recent advances in CT colonography increasingly allow evaluation of the mucosal surface, but in cases where there is suspicion of tumour recurrence, evaluation with FDG-PET or direct visualisation with endoscopy will be required.

Crohn's Disease

Crohn's disease may affect any part of the gastrointestinal tract, most commonly the terminal ileum and not infrequently the colon. A significant proportion of patients with Crohn's disease will require abdominal surgery at some point during the course of their disease, either to resect a fistula or a symptomatic intestinal stricture.

Clinical Presentation

Following surgery for colonic Crohn's disease, approximately one-third will relapse within the next 10 years. Most typically, this involves the neo-terminal ileum leading up to the anastomosis following an ileo-colic resection. However, recurrence may occur elsewhere. The patient will often present with abdominal pain or bleeding per rectum and has often lost weight. Fistulae may extend to the skin surface and result in severe perianal pain.

Imaging

The plain abdominal film may demonstrate mechanical obstruction, but a barium enema is the investigation of choice to evaluate the colonic mucosa. Cross-sectional imaging with CT or MRI will enable imaging of any associated abscesses and fistulae. Imaging perianal and rectal fistulae are now performed using MRI. Suppression of the signal from the pelvic fat allows the demonstration of any abnormal fluid tracks and collections, together with their relationship to the sphincters.

Bibliography

1. Scardapane A, Brindicci D, Fracella MR et al (2005) Post colon surgery complications: imaging findings. Eur J Radiol 53:397–409
2. Faria SC, Tamm EP, Varavithya V et al (2005) Systematic approach to the analysis of cross-sectional imaging for surveillance of recurrent colorectal cancer. Eur J Radiol 53:387–396
3. Huebner RH, Park KC, Shepherd JE et al (2000) A meta-analysis of the literature for whole body FDG PET detection of recurrent colorectal cancer. J Nucl Med 41:1177–1189

Colonic Atresia

A congenital abnormality, usually due to an ischaemic insult in embryological development resulting in complete occlusion of the lumen of the colon.

▶GI Tract, Paediatric, Congenital Malformations

Colonoscopy

Colonoscopy is the "gold standard" for the detection of colonic neoplasms and the preferred colorectal cancer screening strategy.

▶Neoplasms, Benign, Large Bowel
▶Neoplasms, Large Bowel, Malignant

Color Doppler Ultrasound

This uses standard ultrasound methods to produce a picture of a blood vessel. In addition, a computer converts the Doppler sounds into colors that are overlaid on the image of the blood vessel and that represent the speed and direction of blood flow through the vessel.

▶Breast, Therapy Effects
▶Lymphadenopathy

Colorectal Adenomas

Colorectal adenomas are benign polypoid neoplasms, pedunculated or sessile arising from the epithelial cells of the colorectum, with varying degrees of cellular atypia. Although benign, they are the direct precursors of adenocarcinomas and follow a predictable cancerous temporal course unless interrupted by treatment.

▶Neoplasms, Benign, Large Bowel

Colorectal Cancer

Colorectal cancer is the most common cancer of gastrointestinal tract with approximately 150,000 new cases every year. Despite these statistics, mortality from colon cancer has decreased over the past 30 years, possibly because of earlier diagnosis through screening and better treatment modalities.

▶Neoplasm, Large Bowel, Malignant

Colovescical Fistula

Complication of sigmoid diverticulitis presenting with frequency, UTI and pneumoturia. CT confirms diagnosis with findings of thickened bladder mucosa, fistulous track and gas in the bladder.

▶Diverticulitis

Colpocystogram

Invasive radiological technique to assess pelvic floor descent. Progressively replace by MRI.

▶Incontinence, Urinary

Column of Bertin

Normal variant of the renal cortex, which may simulate tumors (pseudotumor).
▶Contrast Media, Ultrasound, Applications in Kidney Tumor

Columnar Lined Oesophagus

▶Reflux, Gastroesophageal in Adults

Comedomastitis

▶Duct Disease, Breast

Communicating Dissection

Dissection with dual lumen and visible tears in the intimal flap.
▶Dissection, Aortic, Thoracic

Compartment Anatomy

Is the concept of tumor anatomical site and definition of borders. The intracompartmental remaining tumor, which respects anatomical borders such as adjacent fascia, has a better prognosis over the tumor, which is already extracompartmental at presentation. The extracompartmental tumor is one that has already spread beyond the anatomical site of origin and requires more extensive surgery. Involvement of an adjacent joint or space such as the popliteal fossa, is extracompartmental, and may necessitate amputation, if limb salvage procedures are not possible.
▶Neoplasms, Soft Tissues, Malignant

Complex Cyst

Cyst with internal masses, thick septations, or thick or irregular wall.
▶Cyst, Breast

Complex Partial Epilepsy (CPE), Focal Epilepsy: Temporal lobe epilepsy (TLE): TLE accounts for approximately 70% of all chronic CPE

▶Seizures, Complex, Partial

Complex Regional Pain Syndrome

Characteristic disabling joint and soft tissue abnormalities of poorly understood etiology. Also known as reflex sympathetic dystrophy, the most common theory of its pathogenesis is an injury to nerves resulting in painful afferent stimuli. These afferent stimuli are thought to activate increased sympathetic tone and other efferent discharge. Symptoms include pain, dysesthesia, swelling, and vasomotor instability. Early changes on scintigraphy are characteristic and demonstrate bilateral asymmetric increased activity in the affected juxta-articular region on all three phases of bone scanning. Decreased unilateral activity occurs in chronic disease. Radiographs may demonstrate periarticular swelling, osteopenia, and subchondral resorption. Preservation of joint space is an important feature in differentiation from an inflammatory arthritis.
▶Fractures, Peripheral Skeleton

Complex Sclerosing Lesion

▶Radial Scar, Breast

Complicated Cyst

Cyst with diffuse internal echoes.
▶Cyst, Breast

Complication of Kidney Graft

▶Transplant Kidney, Complications

Compression, Extrinsic, Esophagus

Luis H. Ros Mendoza,
M[a] Eugenia Guillén Subirán,
Cristina Gutiérrez Alonso
University Hospital Miguel Servet, Department of Radiology, Zaragoza, Spain
lhros@wanadoo.es

Synonyms

Contour wall alteration; Notches; Wall displacement

Definition

Morphologic alteration of the esophagus related to a neighboring mass or space-occupying lesion.

Pathology/Histopathology

Pathology depends on the cause of the extrinsic compression, with the main causes classified as congenital, inflammatory, or tumoral.

In congenital cases, the pathologic findings are related only to the compressive phenomena without the presence of inflammatory signs or tumoral infiltration, which might be present in the two other groups.

Non-neoplastic mediastinal cysts form a group of uncommon benign lesions of congenital origin (1). Neuroenteric and duplication esophageal cysts are localized in the posterior mediastinum, and they might cause this kind of alteration (Fig. 1).

Other cases present an inflammatory origin, such as retropharyngeal abscesses or mediastinal pancreatic pseudocysts. Mediastinal masses associated with chronic pancreatitis should raise suspicion for the extension of the inflammatory process to the mediastinum (Fig. 2).

Tumoral masses located between the esophagus and the tracheobronchial tree, mainly related to bronchogenic carcinoma, can lead to esophageal infiltration and compression (2). Neurogenic tumors (neurilemmoma, paraganglioma, neuroepithelioma, and neurogenic sarcoma) might also compress the esophagus because of their frequent posterior mediastinal location. Leiomyoma, the most frequent benign tumor of the esophagus, can sometimes grow in an eccentric way, making it difficult to differentiate from an extramural mass (Fig. 3).

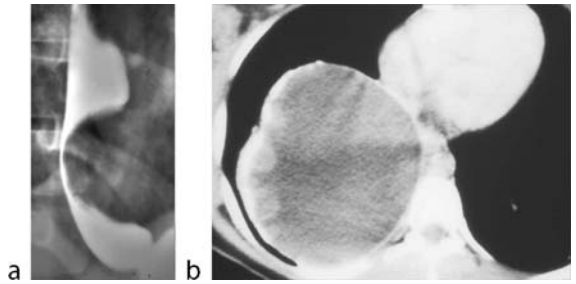

Compression, Extrinsic, Esophagus. Figure 1 Extrinsic esophageal compression related to a noncommunicating esophageal duplication cyst. The barium study (a) shows a significant compression over the esophagus with smooth contours and obtuse angles. Computed tomography (b) identifies a cystic mass, with thick walls and well-defined contours, located in close relationship to the anatomic area of the esophagus.

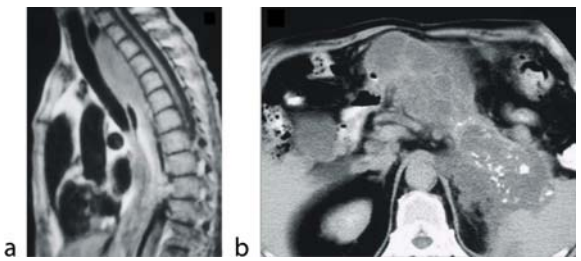

Compression, Extrinsic, Esophagus. Figure 2 Extrinsic compression of the esophagus related to a mediastinal pancreatic pseudocyst. The sagittal plane of the magnetic resonance study (a) shows a mass in the posterior mediastinum that is compressing the thoracic esophagus. The mass corresponds to a pancreatic pseudocyst. Abdominal computed tomography (b) demonstrates the inflammatory pancreatic involvement. Magnetic resonance imaging by means of the sagittal and coronal planes is a very useful tool for studying the esophagus, as it shows this structure in its major longitudinal plane.

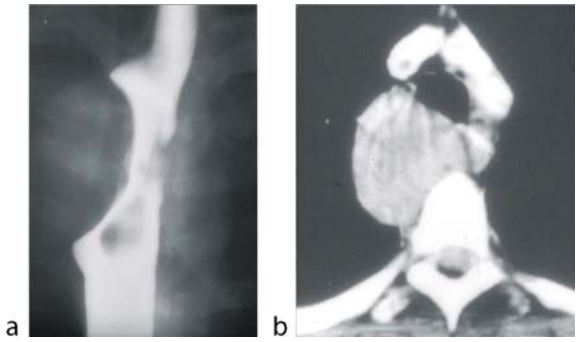

Compression, Extrinsic, Esophagus. Figure 3 Esophageal compression due to an intramural leiomyoma. The barium study (a) shows an esophageal compression that is difficult to classify as intrinsic or extrinsic by only the classic semiological criteria. The compression presents smooth contours and the marginal angles are wide open, almost obtuse. Computed tomography (b) defines a tumoral mass, located in the anatomic area of the esophagus, which is also compressing the trachea, with attenuation values very similar to those of the muscular structures.

Apart from the three groups mentioned earlier, there are other causes for esophageal extrinsic compression:

1. *Vascular compression*: Aberrant right subclavian artery (ARSA) is an anomaly with a reported incidence of 0.5–2%. The aberrant artery usually follows a retroesophageal course; it rarely takes an anterior course to the esophagus or trachea. Anomalies associated with ARSA are nonrecurring inferior laryngeal nerve paralysis, aortic coarctation, right-sided aortic arch, and a common origin of the carotid arteries.
   Other vascular causes of compression include anomalies of the aortic arch, an enlarged ascending aorta, a malpositioned descending aorta, and enlarged pulmonary arteries.
   Enlargement of the left atrium causes compression of the superior part of the distal esophagus, whereas global cardiomegaly can produce compression of the inferior part.
2. *Lymphadenopathies*: Mediastinal lymphadenopathies (from a tuberculous, metastatic, or lymphomatous origin) can also compress the esophagus and cause dysphagia (3).
3. *Thyroid and parathyroid gland enlargement*: Enlargement of the thyroid gland, with either a benign or malignant origin, might produce lateral displacement of the esophagus, which is well seen on the anteroposterior view of a barium swallow study. In secondary hyperparathyroidism, there is a generalized hyperplasia of parathyroid glands that, in some cases, can produce esophageal compression (4).
4. *Cervical osteophytes*: These are found in approximately 20–30% of the aged population. In most of these patients bony spurs are asymptomatic, although they may be associated with neck stiffness and localized or radiating pain. However, large osteophytes that protrude from the anterior edge of the cervical vertebrae can impinge on the upper esophagus, causing dysphagia and odynophagia.
5. *Zenker's diverticulum*: This is a protrusion of the mucosal wall of the hypopharynx through the weakened muscular layer between the oblique fibers of the inferior constrictor of the pharynx and the transverse fibers of the cricopharyngeal muscle. When large, it might compress the cervical esophagus.
6. *Retropharyngeal hematoma*: If this occurs, it is located just in front of the cervical spine. Trauma or anticoagulant therapy can lead to its development.
7. *Esophageal pseudomass*: A narrowed sagittal diameter of the thoracic inlet is recognized as an anatomic variant that causes dysphagia because of extrinsic compression of the esophagus between the trachea and vertebral bodies, resulting in a pseudomass appearance.
8. *Pleural, lung or mediastinal scars*: These can retract the esophagus to the involved side.

Clinical Presentation

The most frequent symptom related to extrinsic esophageal compression is mechanical dysphagia, first for solids and in cases of advanced obstruction, for both solids and liquids. The point at which the patient experiences this symptom is useful for localizing the level and cause of the compression.

Some of the illnesses responsible for the esophageal compression can present specific manifestations:

- Coughing is frequent in patients with ARSA, and stridor is frequent in those with right-sided or double aortic arch.
- Hiccups suggest involvement of the distal esophagus.
- Zenker's diverticulum is characterized by regurgitation, gurgling sounds, and aspiration.
- Large osteophytes (greater than 10 mm) can produce aspiration.
- Mediastinal masses, when large, might produce unilateral sibilants and dysphagia because they compromise both the esophagus and the tracheobronchial tree.
- Thyroid and parathyroid gland alterations can present endocrine symptoms associated with esophageal manifestations (4).

- Fever, night sweats, odynophagia, and weight loss are common manifestations of lymphoma.
- Chronic pancreatitis produces chronic abdominal pain.

Imaging

In some cases, conventional chest radiology might show findings that are suggestive of this condition, including intrathoracic goiter; posterior mediastinal masses; pleural, lung or mediastinal retractions; left atrium enlargement; cardiomegaly; aortic arch anomalies or other vascular alterations.

Lateral neck radiographs can also be useful for showing the presence of osteophytes, localized retropharyngeal masses, or posttraumatic vertebral fractures.

But the most specific semiological criteria are obtained by means of a barium swallow study (5). An intraluminal or intramural mass usually presents its center within or along the contour of the esophageal lumen; as a result, the angles produced by the esophageal wall and the lesions are acute. An extramural mass presents its center out of the contour of the lumen, with these angles being obtuse (Fig. 1a). This is called the spheroid sign.

In some cases, the barium swallow shows fixation and traction of the mucosal folds with a teething appearance suggestive of parietal infiltration.

By means of a barium swallow, it is also possible to differentiate between the esophageal displacement due to a mediastinal mass, which usually causes a narrowing of the lumen, and the retraction due to a neighboring scar, which produces a widening of the esophageal lumen.

In general, the filling defects with smooth or slightly lobulated edges correspond to extramural masses.

On some occasions, ultrasound (US) can be useful for characterizing a posterior mediastinal mass as solid or cystic or an enlargement of the thyroid gland. US-guided fine needle aspiration can be performed in selected cases.

Endoscopic ultrasound (EUS) is being increasingly used as a less invasive alternative to mediastinoscopy to obtain a diagnosis of mediastinal involvement; EUS-guided fine needle aspiration can provide material to establish the histologic diagnosis.

Cross-sectional imaging modalities, computed tomography (CT) and magnetic resonance imaging (MRI), are also very useful tools for evaluating this situation. They confirm the presence of the extrinsic compression and allow a precise evaluation of its cause in the different spatial planes (Figs 1 and 2). MRI angiography demonstrates with great accuracy the different vascular causes of dysphagia and allows a definite evaluation of the cardiac chambers.

Nuclear Medicine

Nuclear medicine techniques might be useful in studying some entities that can produce an extrinsic esophageal compression. Thyroid pathology is well defined by means of nuclear scintigraphy, and mediastinal lymphomatous masses or adenopathies might be identified by means of gallium citrate scintigraphy. The radionuclide study of choice for parathyroid location is single photon emission CT using technetium-99m sestamibi (2-methoxyisobutylisonitrile).

Diagnosis

The initial diagnosis of extrinsic esophageal compression, which can be suspected when the clinical symptoms suggest it, is commonly made during a barium contrast study or during an upper digestive endoscopy that shows a mass or impression covered by normal-appearing epithelium.

The first problem to solve is to differentiate between an extrinsic compression versus a lesion arising from the wall itself. The semiological criteria previously defined—spheroid sign, characteristics of the edges of the compression, teething appearance—can be the key findings to establish the differential diagnosis, although this is not always easy (Fig. 3). Some entities can present specific manifestations on the barium swallow that help determine the specific diagnosis:

- ARSA appears as a characteristic posterior compression, an oblique notch "in bayonet."
- Intrathoracic goiter presents the cervicothoracic sign, compressing and displacing both trachea and esophagus.

The second problem is to determine the origin (cause) of the extrinsic compression. CT and MRI are very useful tools for this because they allow not only identification of the esophageal compression but also identification of its etiology, with the possibility of a detailed evaluation in the different spatial planes. Some entities show specific findings:

- Tuberculous mediastinal adenopathies show a hypodense, necrotic center.
- Narrowing of the thoracic inlet diameter (normal: 6.2 cm in the sagittal plane, range 5–8.7 cm) occurs in cases of esophageal pseudomass (apparent external compression on the upper esophagus from the right side with displacement to the left and narrowing of the esophageal lumen, which is suggestive of a mass that should be excluded with CT).

In some cases, the diagnostic algorithm might be completed by means of a percutaneous puncture under US or CT guidance to obtain sample material for pathologic study.

Interventional Radiological Treatment

Nonresectable malignant esophageal stenosis, in some cases related to parietal infiltration from a neighboring tumor, might be treated using self-expanding stents. The self-expanding plastic stent is removable, induces less hyperplasia than metal stents, and can be used to treat benign esophageal conditions.

Bibliography

1. Trojan J, Mousset S, Caspary WF et al (2005) An infected esophageal duplication cyst in a patient with non-Hodgkin's lymphoma mimicking persistent disease. Dis Esophagus 18(4):287–289
2. Simchuk EJ, Low DE (2001) Direct esophageal metastasis from a distant primary tumor is a submucosal process: a review of six cases. Dis Esophagus 14(3–4):247–250
3. Nagi B, Lal A, Kochhar R et al (2003) Imaging of esophageal tuberculosis. Acta Radiol 44(3)329
4. Weber AL, Randolph G, Aksoy FG (2000) The thyroid and parathyroid glands. CT and MR imaging and correlation with pathology and clinical findings. Radiol Clin North Am 38(5):1105–1129
5. Levine MS, Rubesin SE (2005) Diseases of the esophagus: diagnosis with esophagography. Radiology 237(2):414–427

Compression, Extrinsic, Stomach and Duodenum

Luis H. Ros Mendoza,
Cristina Gutiérrez Alonso,
M[a] Eugenia Guillén Subirán
University Hospital Miguel Servet, Department of Radiology, Zaragoza, Spain
lhros@wanadoo.es

Synonyms

Contour wall alteration; Notches; Wall displacement

Definition

Extrinsic compression of the stomach and duodenum is a morphologic alteration of the gastric and duodenal contour related to a neighboring space-occupying lesion.

Pathology/Histopathology

Pathology depends on the cause of the compression. The most frequent etiologic factors in gastric compression are liver and spleen enlargement, pancreatic pathology (tumors, cysts, and pancreatitis), gallbladder alterations, retroperitoneal lymphadenopathies, renal masses, and collections in the lesser sac.

In duodenal compression, the main causes include hepatomegaly, gallbladder enlargement, coledocal compressions, right renal and adrenal masses, periportal adenopathies, and hepatic angle and transverse colon alterations (1).

According to the histological characteristics, compressions can be classified as congenital (duplication cysts of the stomach or duodenum), inflammatory (acute and chronic pancreatitis, Morrison pouch abscesses), or tumoral (pancreatic adenocarcinoma, hepatic carcinoma, renal cell tumor).

In the first case, the pathologic findings will be related only to the compressive phenomena without the presence of inflammatory signs or tumoral infiltration, which might be present in the two other groups.

Special attention should be given to *gastric duplication* with its special pathologic characteristics: it can be cystic (the most frequent type), tubular, or tubulocystic. The duplication wall is close to the gastric wall, and its muscular layer fuses with the gastric one, although it rarely communicates with the gastric lumen. The duplication contains gastric epithelium (which can become ulcerated) or ectopic pancreatic epithelium (which can develop into pancreatitis).

Clinical Presentation

The patient can have no symptoms, with the extrinsic compression being a casual finding.

If symptoms are present, obstruction is the most frequent one, causing epigastric pain, abdominal distension, early satiety, and nausea and vomiting during or immediately after food intake. Vomiting usually alleviates the symptoms. Significant weight loss may occur (2). In low gastric and duodenal obstructions, "gastric splashing" can be found during clinical examination.

Some illnesses causing extrinsic compression have special clinical manifestations:

- Acute pancreatitis: Nonstop superior abdominal pain that radiates to the back.
- Chronic pancreatitis: Severe abdominal pain that is relieved at the genupectoral decubitus and when the patient sits leaning to the front, together with appetite loss, steatorrhea, and diabetes. Duodenal obstruction is more frequent in cases of alcohol-related pancreatitis.

- Annular pancreas: Bilious vomiting, growth failure, abdominal pain, duodenal obstruction, pancreatitis, and obstructive jaundice.
- Duodenal and gastric duplications: In neonates and infants, they produce vomiting, abdominal distention, volvulus, intussusception, and an abdominal mass. In adults, peptic ulcer or pancreatitis of the ectopic pancreatic tissue may occur. A duplication might get infected, and if it ruptures in the peritoneal cavity, peritonitis occurs.
- Duodenal diverticula: About half of the diverticula are found incidentally. When they are symptomatic, the most common clinical presentation is abdominal pain, gastrointestinal bleeding, and perforation.
- Internal hernias: Might cause small bowel obstruction (closed-loop or strangulating obstruction). They can also produce chronic intermittent intestinal obstruction.
- Superior mesenteric artery syndrome: Appears in cases of significant weight loss, sometimes postsurgical, and in cases of severe burns. The symptoms are a sensation of gastric fullness and abdominal distention after food intake, bilious vomiting, and colicky pain in the middle part of the abdomen, which eases in the prone decubitus and in genupectoral positions.

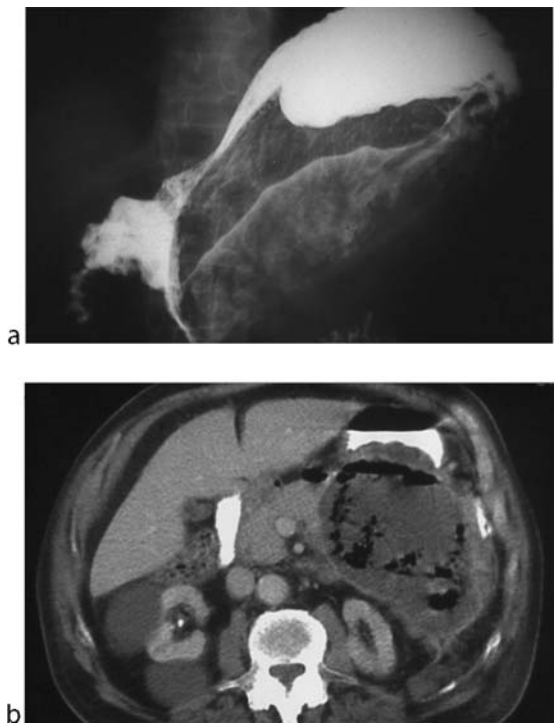

Compression, Extrinsic, Stomach and Duodenum.
Figure 1 Extrinsic compression of the stomach related to a pancreatic abscess. The upper gastrointestinal tract barium study (a) shows a significant extrinsic compression of the posterior gastric wall, with smooth contours and obtuse angles. Computed tomography (b) demonstrates the presence of a large pancreatic abscess as the cause of the extrinsic gastric compression. The stomach is identified by the presence of positive oral contrast within its lumen; the abscess, identified by the presence of gas bubbles, is located in close relationship to the posterior gastric wall.

Imaging

In an *abdominal plain film*, displacement of the gastric luminogram can be identified in some cases.

In *barium contrast examination*, the most common findings are a wide base compression or notch in the luminal contour of the stomach or duodenum, usually accompanied by displacement of the organ, along with a poorly defined area of low density (Fig. 1a). The location of the barium column alteration depends on the cause of the compression (Tables 1 and 2).

By means of *computed tomography* (CT) and *magnetic resonance imaging* (MRI) in the different spatial planes (axial, coronal, sagittal), these same vectors of displacement can be identified, enabling evaluation not only of the extrinsic compression but also of its cause (Figs 1b and 2).

Nuclear Medicine

Gastrointestinal duplications that contain gastric mucosa can be identified with technetium-99m-pertechnetate or

Compression, Extrinsic, Stomach and Duodenum. Table 1 Causes of gastric extrinsic compression

Body: right anterior wall	Hepatomegaly, gastric varicose veins
Body: left posterior wall	Splenomegaly
Body: posterior wall	Paraduodenal and lesser sac hernias
Antrum: anterolateral face	Enlargement of the gallbladder
Antrum: posterolateral face	Internal hernias through Winslow's hiatus
Antrum: posterior face ("antral pad")	Pancreatic masses (tumors, cysts, pancreatitis), retroperitoneal adenopathies, left renal masses, lesser sac collections
Great curvature	Gastric duplication

Compression, Extrinsic, Stomach and Duodenum. Table 2 Causes of duodenal extrinsic compression

First and second portions: medial displacement	Common bile duct (lineal notch), distended gallbladder (carcinoma), hepatomegaly (caudate lobe), focal hepatic lesions, periportal adenopathies, Morrison pouch collections, colonic hepatic angle distension or neoplasms, internal hernias through Winslow's hiatus
Second portion: posterolateral compression	Right renal and adrenal tumors, right renal ptosis
Second portion: annular compression	Annular pancreas
Second portion: medial wall compression (widening of the duodenal arch)	Pancreatic masses (tumors, cysts, pancreatitis), peripancreatic adenopathies (metastatic, lymphomatous), retroperitoneal masses
Second and third portions	Duodenal duplication cysts
Third portion: anterior compression	Pancreatitis (mesenterium involvement), mesenteric masses, superior mesenteric artery syndrome
Third portion: posterior compression	Retroperitoneal hematoma, aortic aneurysms
Fourth portion: medial displacement	Abdominal aortic aneurysms
Fourth portion: anterior compression	Transverse colon distension or neoplasms

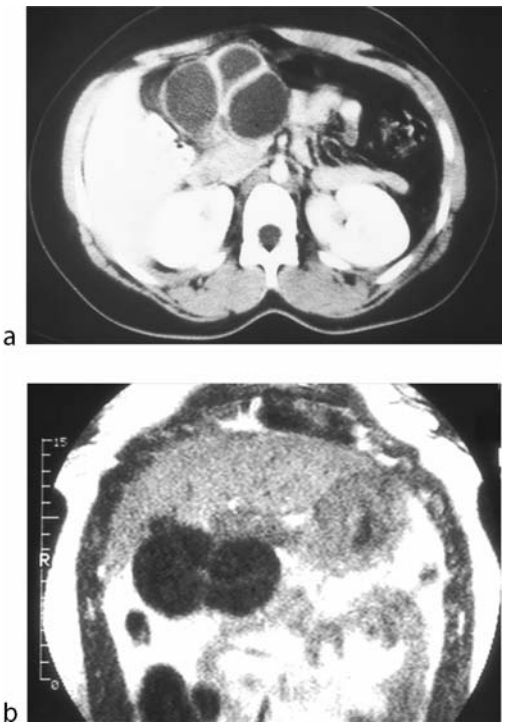

Compression, Extrinsic, Stomach and Duodenum. Figure 2 Extrinsic compression of the duodenum due to a cystic duodenal duplication. Computed tomography (a) shows the presence of a cystic mass with thick walls in the anatomic area of the pancreatic head. The patient had no antecedents of pancreatitis. The coronal plane of the abdominal magnetic resonance study (b) shows that the cystic mass is closely related to the duodenal walls. This and the thick walls (because congenital duplications "duplicate" all the layers of the wall of the digestive tube) are the key findings for suspected duodenal duplication cyst.

technetium-99m diethyltriamine pentaacetic acid scintigraphic evaluation, visualizing the functioning ectopic gastric mucosa simultaneously with the stomach in gastric duplications and even earlier in the case of duodenal duplications (3).

Diagnosis

The initial diagnosis of extrinsic compression of the stomach or duodenum is commonly suspected during an upper digestive endoscopy, with the visualization of a mass or impression covered by normal-appearing epithelium, or during a barium contrast study that presents the findings previously described.

The *first problem* to be solved is the differential diagnosis between extrinsic compression—caused by a normal or abnormal structure adjacent to the involved organ—versus a lesion arising from the wall itself.

In the upper gastrointestinal tract barium study, if the largest part of the lesion projects out of the gastric or duodenal lumen, and if the angle produced by the gastric or intestinal wall and the mass is obtuse, then the cause is more likely extrinsic (Fig. 3). In addition, the notches related to an extrinsic compression are not constant, changing under the actions of gravity and breathing.

Although during the upper endoscopy the finding can be evaluated by means of endosonography and, in some cases, an endosonographically guided fine needle aspiration can be performed (4), transabdominal ultrasound, CT, and MRI are more useful for defining the origin and extent of the extramural masses.

The *second problem* is to determine the origin of the extrinsic compression. In the barium study, the location and characteristics of the extrinsic compression (tubular,

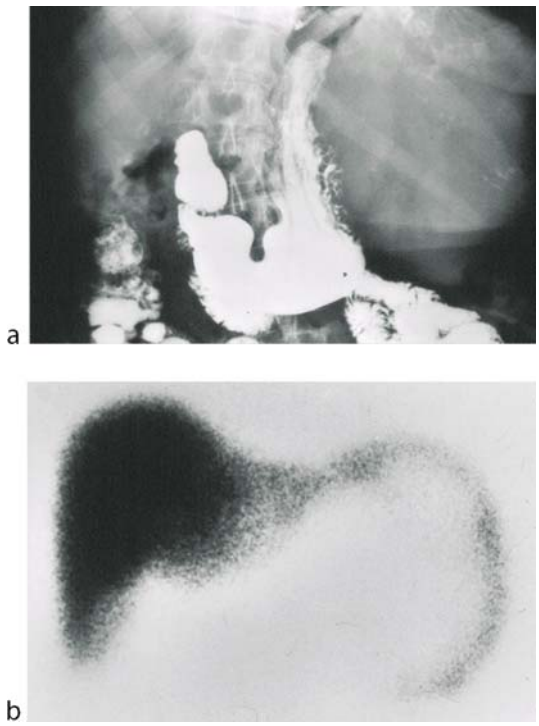

Compression, Extrinsic, Stomach and Duodenum.
Figure 3 Extrinsic compression of the stomach related to a massive splenomegaly. The upper gastrointestinal tract barium study (a) shows the deformity of the great curvature of the stomach, which suggests an extrinsic compression depending on the spleen. A mass effect, with high radiologic density, could be identified in the splenic area. The isotopic study (b) shows the absence of the radioisotope uptake by the spleen due to a massive acute splenic infarct. Edema at this acute stage of the splenic infarct results in the splenomegaly.

serpiginous notches in the case of gastric varicose vein) can be indicative of the cause (Tables 1 and 2), but in general, the cross-sectional imaging modalities, CT and MRI, are more useful in this respect, confirming the findings of the barium study, differentiating intrinsic from extrinsic compression in doubtful cases, and showing the cause of the compression.

Some entities, which are detailed later, present more diagnostic difficulties:

- *Gastric duplications* are more frequently found in the great curvature and duodenal duplications in the anteromedial contour of the first and second portions, and they are usually noncommunicating duplications. They appear on CT as rounded lesions that present a water density and are closely related to the gastrointestinal lumen (Fig. 2). On ultrasonography they appear as cystic structures, with the internal mucosal wall presenting a bright appearance, being the external muscular layer hypoechoic. In doubtful cases, a fine-needle aspiration biopsy under endoscopic ultrasound guidance or nuclear medicine techniques that allow the identification of gastric mucosa can be performed.
- The preoperative diagnosis of *internal hernia* can be made with barium studies, but in the presence of small bowel obstruction, CT plays an important role, allowing the identification of a sac-like mass or cluster of small bowel loops at an abnormal anatomic location, with a stretched and displaced mesenteric vascular pedicle and converging vessels at the hernial orifice.
- *Superior mesenteric artery syndrome* appears on CT as a sharpening in the middle of the third duodenal portion, with retrograde distension. On barium study there is an abrupt lineal compression with dilatation of the first and second duodenal portions and a fluctuant appearance of the barium column, as well as delayed gastric emptying.
- *Gastric varicose* veins are easy to identify on CT. They appear as serpiginous lesions that present intense enhancement after the intravenous contrast administration.
- *Annular pancreas* causes, in the barium study, a filling defect with annular morphology in the descendent portion of the duodenum at the level of the Vater ampulla, with a homogeneous dilatation of the proximal duodenum and inverted peristalsis of this area. To establish the diagnosis of this entity, endoscopic retrograde cholangiopancreatography, pancreatic CT, and MRI are very useful tools.
- *Pancreatic neoplasms* produce characteristic signs in the barium study when they have a long evolution. Enlargement of the duodenal arch and the Frostberg inverted-three sign (compression of the duodenal loop with fixation of the middle portion at the level of Vater papilla) are very well known. In cases with muscular infiltration or mucosal edema, contour spiculation and blurring of mucosal folds are produced; however, these signs are not specific to tumoral lesions, also appearing in acute and chronic pancreatitis.

Interventional Radiological Treatment

In patients with advanced neoplasms that compress the stomach or duodenum, an alternative to traditional surgical palliative treatment (gastrojejunostomy and duodenojejunostomy) is gastroduodenal stent placement, which can be done under fluoroscopic guidance or with a combination of fluoroscopic and endoscopic techniques. Stent placement reduces postsurgical complications, provides better gastric emptying, and is more cost-effective than surgical palliation (5).

Bibliography

1. Martín ES, Pedrosa CS (2000) El tubo digestivo: semiología radiológica. In: Pedrosa CS, Casanova R (eds) Diagnóstico Por Imagen. Tratado de Radiología Clínica. McGraw-Hill-Interamericana de España, Madrid, pp 335–378
2. Feldman M, Friedman LS, Sleisenger MH (2004) Enfermedades Gastrointestinales Y Hepáticas: fisiopatología, Diagnóstico Y Tratamiento. Editorial Médica Panamericana, Buenos Aires
3. Kumar R, Tripathi M, Chandrashekar N et al (2005) Diagnosis of ectopic gastric mucosa using 99Tcm-pertechnetate: spectrum of scintigraphic findings. Br J Radiol 78(932):714–720
4. Hwang JH, Kimmey MB (2004) The incidental upper gastrointestinal subepithelial mass. Gastroenterology 126:301–307
5. Lopera JE, Brazzini A, Gonzales A et al (2004) Gastroduodenal stent placement: current status. Radiographics 24:1561–1573

Computed Radiography (CR)

After passing through the patient, the emergent X-ray beam is detected by a photostimulable phosphor plate, forming a stable latent image. A laser then stimulates the plate, light is emitted and a digital signal produced (via a photomultiplier tube) than is converted into the image. The resultant image can be read either on laser-printed film or as soft copy on a workstation.

▶Children, Imaging Techniques

Computed Tomographic Colonography

CTC is a novel imaging modality for the evaluation of the colonic mucosa in which thin-section spiral CT provides high resolution two-dimensional (2D) axial images; CT data sets are edited off-line in order to produce multiplanar reconstructions (coronal and sagittal images) as well as three-dimensional (3D) modeling, including endoscopic-like views.

▶Neoplasms, Benign, Large Bowel

Computed Tomography

Diagnostic modolity based on X-rays able to obtain cross-sectional images of the human body is a non invassive manner.

▶Ischemic Heart Disease, CT

Congenital (or Dysgenetic) Pancreatic Cyst

Congenital pancreatic cyst is an intrapancreatic cystic lesion non-communicating with the duct system and lined by a single layer of flat epithelium. The cysts are usually enclosed in a thin fibrous capsule and they are filled with a mucoid or serous fluid. They may range from microscopic lesions up to 3–5 cm in diameter. They are believed to result from anomalous development of the pancreatic ducts. Unlike cysts in the liver and kidneys, asymptomatic simple pancreatic cysts are uncommon. Most of these cysts are multiple and associated with von Hippel–Lindau disease or, rarely, with inherited polycystic kidney disease. Macroscopic pancreatic cysts are occasionally seen in patients with cystic fibrosis. At imaging, congenital cysts appear as well-defined cystic lesions with smooth walls and without intramural excrescences or septations. Associated renal and hepatic cysts may be seen.

▶Cystic Neoplasms, Pancreatic

Congenital Abnormalities, Pancreatic

Huisman TA[1], Carla Cappelli[2]
[1]Johns Hopkins University, Baltimore, USA
[2]Department of Diagnostic and Interventional Radiology, University of Pisa, Italy
thierry.huisman@kispi.unizh.ch
bartolozzi@do.med.unipi.it

Synonyms

Pancreatic congenital anomalies; Pancreatic congenital variants; Pancreatic developmental anomalies

Definitions

The pancreas arises from dorsal and ventral anlages that fuse at 6 weeks of gestation. The ventral anlage develops into a part of the pancreatic head and the uncinate process while the dorsal part gives rise to the pancreatic body and tail as well as a second part of the pancreatic head. Congenital variants of the pancreas are seen in

approximately 10% of children and include pancreatic agenesis, hypoplasia, ectopia, ►pancreas divisum, and ►annular pancreas.

Complete pancreatic agenesis is extremely rare and is usually associated with other major malformations. In agenesis of the dorsal anlage only the pancreatic head develops, e.g., in combination with polysplenia syndrome.

In pancreatic hypoplasia, the exocrine elements or more rarely also the endocrine elements are underdeveloped.

Pancreatic ectopia is defined as pancreatic tissue in ectopic locations (e.g., stomach, duodenum, jejunum, appendix, Meckel's diverticulum). These lesions have no contact with the normal pancreas and possess its own ductal system and blood supply. It is usually found at autopsy or as an incidental finding at laparotomy. The incidence varies between 1% and 15%.

In pancreas divisum, the dorsal and ventral anlages did not fuse resulting in two separate pancreatic portions which drain separately into the duodenum: the major drainage (body and tail) is performed by the duct of Santorini through the minor papilla, while the main duct of Wirsung drains only the posterior part of the pancreatic head through the major papilla. The accessory duct of Santorini becomes the main excretory pathway of the gland. This anomaly is the most common pancreatic anomaly (4–14% of all children).

The annular pancreas results from a premature fusion of the dorsal and ventral anlages. This anomaly is characterized by a ring of pancreatic tissue that encircles the second portion of the duodenum. A second embryological theory is that an annular pancreas may also result from an anomaly of the ventral bud rotation. Duodenal obstruction may occur. Incidence is increased in children with Down syndrome and other congenital anomalies.

Pathology and Histopathology

While in complete pancreatic agenesis no pancreatic tissue is found at all, in partial agenesis parts of the pancreas can be identified in the pancreatic region. The histology of the pancreatic tissue is normal.

In pancreatic hypoplasia, lipomatous hypertrophy of the pancreas with extensive atrophy of the exocrine acinar tissue is seen while the endocrine system is preserved; in cases of an associated endocrine hypoplasia the Langerhans cells are also atrophic.

Ectopic pancreatic tissue includes all histological elements of the exocrine and the endocrine pancreas, although the ducts of the exocrine pancreatic tissue are not arranged in the normal anatomical pattern. In gastrointestinal ►ectopic pancreas, the pancreatic tissue is usually found in the submucosa. The ectopic pancreatic tissue may be functionally active and secreting, causing local ulceration of the mucosa. Inflammation of the ectopic pancreas with pseudocyst formation or the development of benign or malignant pancreatic tumor has also been described.

Pancreas divisum occurs when the ductal systems of the ventral and dorsal pancreatic ducts fail to fuse. Grossly pancreas divisum is characterized by a completely separated pancreatic ductal system in an undivided gland. In pancreas divisum the predominant drainage is performed by the dorsal duct of Santorini through the minor papilla. In patients with pancreas divisum, signs of acute or chronic pancreatitis can be found in the dorsal duct distribution while normal pancreatic tissue is seen in the ventral duct distribution. It is suggested that the duct of Santorini and the minor papilla are too small to adequately drain the large amount of secretions which may lead to a relative outflow obstruction with resulting pancreatitis.

Annular pancreas is believed to result from an early fusion of the ventral and dorsal anlages or from a failure of normal pancreatic tissue to rotate around the duodenum. The annulus represents the ventral part of the pancreas that remains fixed to the duodenum. In the extramural type, the pancreatic tissue is drained by a duct originating at the anterior surface of the duodenum, passing posteriorly around the duodenum and opening into the main pancreatic or common bile duct near the ampulla. In the intramural type, pancreatic tissue is found within the duodenal wall and small ducts drain directly into the duodenum.

Clinical Presentation

Pancreatic agenesis is usually associated with severe forms of intractable neonatal diabetes mellitus. Complete pancreatic agenesis is usually characterized by severe morbidity and mortality.

In pancreatic acinar hypoplasia the endocrine pancreatic function is usually intact while the exocrine cells are atrophic. The exocrine pancreatic insufficiency results in malabsorption with weight loss and chronic diarrhea. Congenital pancreatic hypoplasia should always be kept in mind when a child manifests with gross steatorrhea and responds well to pancreatic enzyme replacement therapy. ►Shwachman–Diamond syndrome (SDS) is a rare autosomal recessive disorder characterized by exocrine pancreatic insufficiency associated with bone marrow dysfunction and skeletal anomalies (metaphyseal chondrodysplasia). In affected children the pancreatic acinar cells do not develop in utero and are replaced by fatty tissue.

Ectopic pancreas is a relatively rare entity, usually of no clinical importance and found incidentally during laparotomy or in autopsy. If present, symptoms are nonspecific, including abdominal pain, nausea, vomiting, and gastrointestinal bleeding. Specific symptoms can develop in case of complication. Pancreatitis can occur in ectopic pancreas, leading to typical symptoms and laboratory findings; the ectopic insulin secretion may cause hypoglycemia. Exocrine or endocrine tumors may develop in the ectopic pancreatic tissue. Obstructive symptoms are mainly related to the localization of the ectopic pancreas (gastrointestinal obstruction, obstructive jaundice); intestinal mechanical obstruction can be related to intussusception.

Most patients having pancreas divisum are asymptomatic, although some reports have suggested a high incidence of abdominal pain and acute and chronic pancreatitis with typical clinical and laboratory findings. It has been suggested that the relative stenosis of the accessory papillary orifice, the major outflow tract for pancreatic secretions, is the cause of problems.

In many instances annular pancreas is discovered incidentally during radiological imaging studies performed for other reasons. Symptoms develop when complications occur, including pancreatitis, biliary obstruction, and peptic ulcer. If the annular pancreas forms a complete ring, there may be total obstruction of the duodenum and diagnosis is rapidly evident in the neonate; if the ring is incomplete, obstruction may occur later in life or may never produce symptoms. A history of polyhydraminos and other anomalies such as intestinal malrotation, duodenal atresias, and cardiac anomalies are often associated.

Imaging

Ultrasound (US) is a highly sensitive, nonionizing bedside primary imaging modality that can locate, identify, and characterize pancreatic tissue. Computed tomography (CT) and magnetic resonance imaging (MRI) are second line imaging modalities; dynamic contrast-enhancement pattern may increase sensitivity and specificity. Magnetic resonance cholangiopancreatography (MRCP) can be a noninvasive alternative for endoscopic retrograde cholangiopancretography (ERCP).

In complete pancreatic agenesis, no pancreatic parenchyma can be found in the expected locations. In partial agenesis the pancreatic tissue has a normal aspect on US, CT, and MRI.

Pancreatic hypoplasia can be demonstrated by imaging because of the presence of pancreatic lipomatosis with the replacement of the normal pancreatic parenchyma by fat.

Ectopic pancreatic tissue is unlikely to be identified by US, CT, or MRI. Ectopic pancreas in the stomach and duodenum can occasionally be identified on barium studies as submucosal masses. Their appearance is however nonspecific mimicking any kind of submucosal mass in the gastrointestinal tract. Ectopic pancreatic islands in the stomach and duodenum can display a central depression, which corresponds to the opening of a duct. Gastric locations are typically located along the greater curvature in the proximity of the pylorus, whereas in the duodenum, they are mostly found proximally between the bulb and the ampulla of Vater. Ectopic pancreas located in the gallbladder can be visualized by US, which will display hyperechoic nodular mural thickening without acoustic shadowing; however this appearance is not specific.

In pancreas divisum CT and MRI can occasionally demonstrate a separate dorsal and ventral pancreatic portion divided by a thin fat plane. Definite diagnosis of pancreas divisum is obtained by MRCP or ERCP. MRCP may demonstrate a short (1–6 cm) and thin main duct of Wirsung and a larger accessory duct of Santorini which drains almost the entire pancreas from the tail to the anterior part of the head. The identification of the separated ducts can be enhanced by secretin stimulation. In rare cases, pancreas divisum is associated with a focal dilatation of the duct near the papilla, called santorinicele.

Annular pancreas is usually demonstrated by barium enema studies. Asymmetric extrinsic narrowing of the lateral and medial borders of the second portion of the duodenum with normal mucosal pattern is a typical finding. On US, CT, or MRI the annular pancreas may appear as duodenal wall thickening, as an apparent enlargement of the pancreatic head or as a well-defined ring of pancreatic tissue encircling the duodenum. The presence of calcification can suggest an associated chronic pancreatitis. MRCP demonstrates the presence of the annular duct which drains into the main pancreatic duct.

Nuclear Medicine Diagnosis

In patients with unexplained and persisting signs of cholangitis, pancreatitis, jaundice, recurrent abdominal pain, nausea, and vomiting, a congenital anomaly of the pancreatic or bile duct must be considered. Because clinical findings are usually nonspecific, US, CT, and MR are essential for diagnosis. In case of ectopic pancreatic tissue, diagnostic imaging can fail in detection because of the presence of obscuring complications such as pancreatitis and duodenal perforation. In such cases only the histopathological findings can demonstrate the presence of pancreatic tissue. There is however limited value for nuclear medicine imaging in congenital anomalies of the pancreas.

Interventional Radiological Treatment

ERCP is used for therapeutic intervention in patients with pancreas divisum. Several endoscopic and/or surgical procedures have been proposed in an attempt to improve the pancreatic outflow through the minor papilla in patients with acute recurrent pancreatitis. These include endoscopic sphincterotomy, ductal balloon dilatation, and pancreatic duct stent placement.

Bibliography

1. Leyendecker JR, Elsayes KM, BI Gratz et al (2002) MR cholangiopancreatography: spectrum of pancreatic duct abnormalities. Am J Roentgenol 179:1465–1471
2. Fulcher AS, Turner MA (1999) MR pancreatography: a useful tool for evaluating pancreatic disorders. Radiographics 19:5–24
3. Roberts- Thomson IC (2004) Images of interest. Hepatobiliary and pancreatic: annular pancreas. J Gastroenterol Hepatol 19:464
4. Nijs E, Callahan MJ, Taylor GA (2005) Disorders of the pediatric pancreas: imaging features. Pediatr Radiol 35:358–373
5. Nagi B, Kochhar R, D Bhasin et al (2003) Endoscopic retrograde cholangiopancreatography in the evaluation of anomalous junction of the pancreaticobiliary duct and related disorders. Abdom Imaging 28:847–852

Congenital Adrenal Hyperplasia

A group of inborn errors of metabolism arising from enzyme defects in the biosynthesis pathways of adrenal corticosteroids, resulting in inadequate production of glucocorticoids and mineralocorticoids and excess production of adrenal androgens.

►Adrenogenital Syndrome
►Ambiguous Genitalia

Congenital Anomalies of the Pancreas

F.E. Avni[1], C. Matos[1], J.-F. Chateil[2]
[1]Department of Medical Imaging, University Clinics of Brussels—Erasme, Brussels, Belgium
[2]Department of Pediatric Imaging, Hospital Pellegrin, Bordeaux, France
favni@ulb.ac.be

Synonyms

Agenesis of dorsal pancreas; Annular pancreas; Congenitally short pancreas; Ectopic pancreas; Pancreatic cyst(s); Pancreas divisum; Pancreatic lipomatosis

Definitions

Anatomical Anomalies (1–4)

- Pancreas divisum is the most common anatomic variant of the pancreas. Its incidence varies from 4–14% of autopsies. It is characterized by an incomplete fusion between the dorsal and ventral ducts. Only the duct of Wirsung drains into the ampulla of Vater. The duct of Santorini drains into the minor papilla. Stenosis and pancreatitis may ensue.
- Annular pancreas possibly results from abnormal adherence of the ventral duct to the duodenum that results in a complete ring of pancreatic tissue around the duodenum. About 50% of the patients are present in the neonatal period with an associated duodenal obstruction. Other associated anomalies are Trisomy 21, congenital heart disease, and tracheo-esophageal fistula.
- Congenitally short pancreas corresponds to an absence of the pancreatic neck, body, and tail. There is an increased risk of diabetes and associated malformations.
- Ectopic Pancreas: ectopic pancreatic tissue is an aberrant rest of "normal" pancreatic tissue that can be seen in various locations (stomach, jejunum, liver, spleen, umbilicus, Meckel's diverticulum, and so on). It may ulcerate or remain asymptomatic.
- True single congenital cyst of the pancreas may be isolated or associated to ano-rectal, kidney or limbs anomalies. Intestinal duplication cysts may be sequestrated within the pancreas.

Congenital anomalies resulting from systemic diseases that affect the pancreas (1–4)

- Pancreatic lipomatosis is characterized by fatty infiltration of the pancreas associated with deficient secretion of pancreatic enzymes. It is a common finding in the ►Shwachman–Diamond and ►Johanson–Blizzard syndromes already in infants. The lipomatosis develops progressively in cystic fibrosis (CF). In CF, multiple cysts may develop in late childhood (cystosis).

These congenital causes must be differentiated from acquired causes such as lipomatosis following steroid therapy.

- Multiple cysts in the pancreas are seen in Von Hippel Lindau disease and in Dominant Polycystic kidney disease, but usually in adult patients.
- Pancreatomegaly is observed in ►Beckwith–Wiedemann syndrome.
- Congenital tumors: congenital tumors are very rare but perinatal diagnosis of pancreatoblastoma (exocrine tumor) and insulinoma (endocrine tumor) has

been reported. Among endocrine tumors, nesidioblastosis corresponds to ill defined tumors leading to intractable neonatal hypoglycemia.

Pancreatic cysts may be acquired and appear in the course of cystic fibrosis (cystosis).

Pathology/Histopathology

The histopathological anomalies observed on the pancreas will depend upon the type of the primary lesion and complications that have occurred. For instance, inflammatory lesions or fibrosis will be observed in case of pancreatitis associated to pancreas divisum. Fatty infiltration of the gland will be observed in case of Shwachman disease. Islet cells hypertrophy or a circumscribed tumor can be identified in case of nesidioblastosis.

Clinical Presentation

Congenital anomalies of the gland will be clinically evident either because of an antenatal diagnosis of pancreatic tumor (cyst) or because of an abdominal mass palpated at clinical examination. Other symptoms that orient toward a pancreatic anomaly are evidence of pancreatic insufficiency (fatty diarrhea, failure to grow, diabetes) or abdominal pain related to complications of the malformation.

A pancreatic endocrine tumor should be suspected in case of seizures associated with neonatal hypoglycemia (1–4).

Imaging

Ultrasound is the primary screening tool to evaluate the pediatric pancreas. Its size varies with age. The head and the tail increase ±1.0 cm at birth and 2 cm at 10–15 years. The body varies from 0.5 to 1 cm. The gland's echogenicity is slightly hyperechoic to liver at birth, relatively hypoechoic in children.

The width of the pancreatic duct should not measure above 1.5 mm at 1 year and 2.2 mm at 15 years.

The pediatric pancreas is well seen on contrast-enhanced CT. The technique is well suited to visualize pancreatic calcifications, tumors, or complication of traumatism.

MRI can be used for similar indications than CT. Furthermore, the technique using special ▶MRCP sequences provides important supplementary information about the pancreatic duct and biliary tract. A normal MRCP may obviate the need for ▶ERCP.

ERCP is useful whenever MRCP does not provide sufficient information or when a therapeutic maneuver is planned.

In selected cases, peripancreatic venous sampling can be performed in order to localize nesidioblastosis or other ill defined pancreatic endocrine tumors (1–5).

Nuclear Medicine

Not applicable

Diagnosis

The first imaging tool for evaluating the pancreas is ultrasound. The technique will allow evaluation of its size, form, and echogenicity. Its relation with the portal system will be evaluated. Whenever a mass is observed, CT or MRI should be performed.

Whenever a dilatation of the pancreatic duct is observed and whenever an anomaly of the gland morphology is observed, MRCP should be performed (Figs 1 and 2).

Abnormal hyperechogenicity should suggest lipomatosis (Fig. 3) and other symptoms of an associated syndrome should be looked for (1–5).

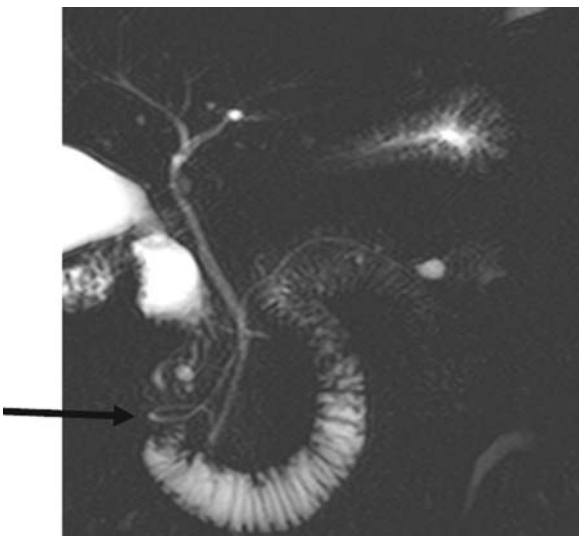

Congenital Anomalies of the Pancreas. Figure 1 Annular pancreas: MRCP demonstrating the pancreatic ducts and the typical annular appearance of the pancreatic duct (arrow).

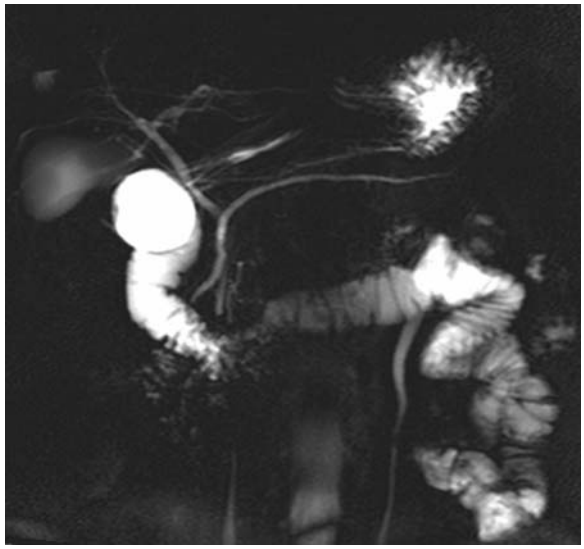

Congenital Anomalies of the Pancreas. Figure 2 Pancreas divisum: MRCP demonstrating separately the main pancreatic and Sontorini ducts.

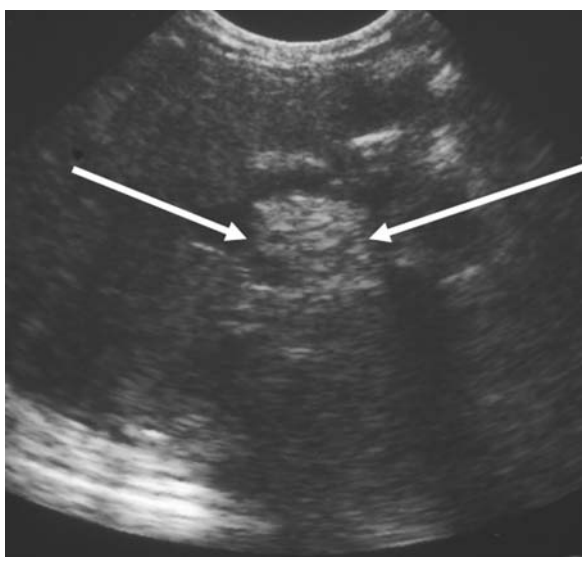

Congenital Anomalies of the Pancreas. Figure 3 Pancreatic lipomatosis in a case of Shwachman syndrome. Ultrasound of the pancreas; the hyperechogenicity of the pancreatic head is striking (between arrows).

Bibliography

1. Enriquez GE, Vasquez E, Aso C (1998) Pediatric Pancreas: an overview. Eur Radiol 8:1236–1244
2. Nijs E, Callahan MJ, Taylor GA (2005) Disorders of the pediatric pancreas: imaging features. Pediatr Radiol 35:358–373
3. Synn AY, Mulvihill SJ, Fonkalsrud EW (1988) Surgical disorders of the pancreas in infancy and childhood. Am J Surg 156:201–205
4. Lerner A, Branski D, Lebenthal E (1996) Pancreatic disease in children. Pediatr Clin North Am 43:125–156
5. Arcement CM, Meza MP, Arumanla S et al (2001) MRCP in the evaluation of pancreatico-biliary disease in children. Pediatr Radiol 31:92–97

Congenital Anomalies of the Uterus

▶Congential Malformations, Mullerian Duct

Congenital Anomalies or Malformations of the Urinary Tract

▶Congential Malformations, Genitourinary Tract; Including Ureter and Urethra

Congenital Abnormalities, Splenic

Huisman TA, Chiara Franchini
Johns Hopkins University, Baltimore, USA
thierry.huisman@kispi.unizh.ch

Synonyms

Inborn Splenic Abnormalities; Splenic Congenital Abnormalities; Splenic Malformations

Definition

Congenital splenic anomalies include inborn anomalies of shape, location, number, and size of the spleen due to aberrant embryologic development.

Pathology and Histopathology

Accessory Spleen

The spleen is a mesodermal derivative, which first appears as a mesenchymal cell condensation inside the dorsal mesogastrium. Sometimes, additional smaller splenic condensations appear and give origin to ▶accessory spleens, representing by far the most common congenital

abnormality of the spleen. Accessory spleens resemble the splenic structure. They may be located anywhere in the abdomen; the most common sites are near the splenic hilum and the tail of the pancreas. Other possible locations are along the splenic vessels, in the gastrosplenic and splenorenal ligaments, in the mesentery, and in the omentum. When splenectomy is performed for hypersplenism, hypertrophy of an accessory spleen may cause recurrent disease (1, 2) (Fig. 1).

Shape Abnormalities

Splenic clefts, notches, and lobules may persist in adult life as variations of the normal shape and are common (1) (Fig. 2).

Abnormal Location

The spleen may be seen in a variety of locations. In congenital diaphragmatic hernia, in Bochdalek diaphragmatic hernia and in eventration of the diaphragm, the spleen may be intrathoracic. If the lateral peritoneal recess is particularly deep the spleen is found posteriorly to the left kidney. The spleen may also be located in the right hypochondrium (1).

Spleno-Gonadal Fusion and Spleno-Renal Fusion

►Spleno-gonadal fusion is a rare anomaly. Due to the close relationship between the developing spleen and

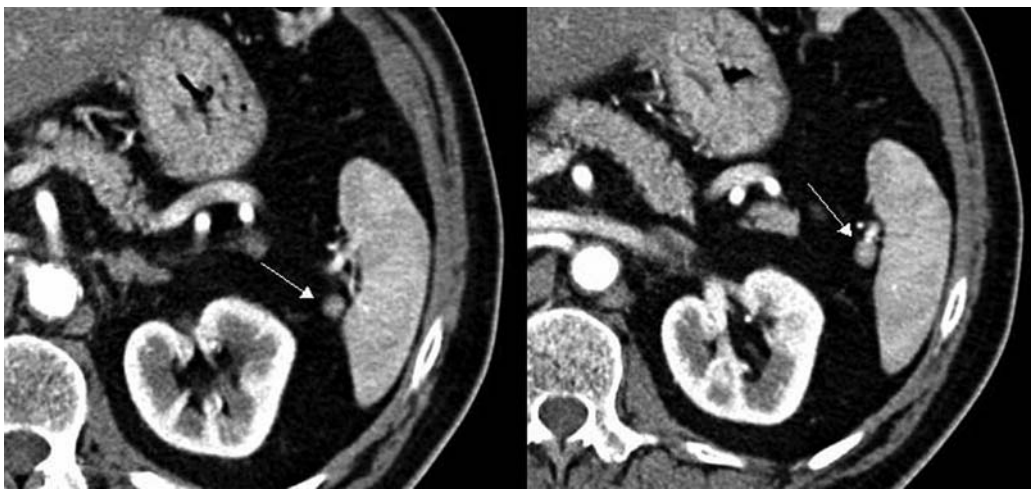

Congenital Abnormalities, Splenic. Figure 1 Accessory spleen CT study shows two small round masses near the splenic hilum (arrows). In the contrast-enhanced arterial phase, they have a strong inhomogeneous enhancement, analogous to that of the normal spleen.

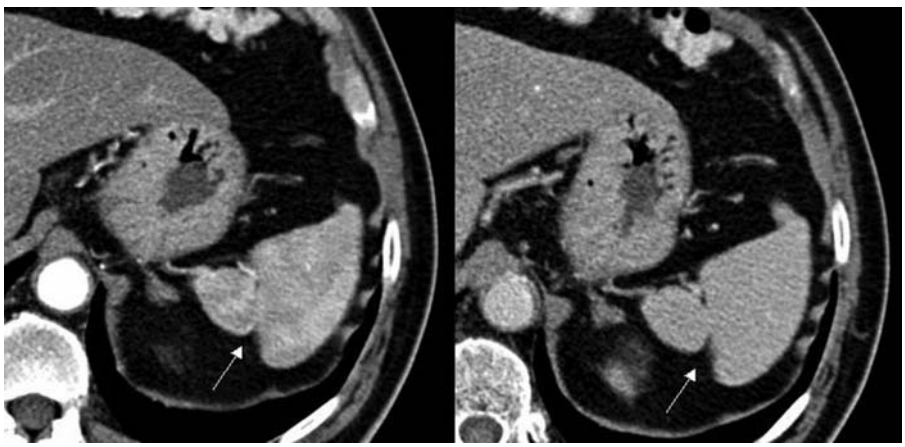

Congenital Abnormalities, Splenic. Figure 2 Splenic cleft CT contrast-enhanced arterial phase. A fissure is appreciable along the posterior margin of the spleen. The smooth edges and the absence of contrast extravasation suggest a congenital splenic cleft.

left gonadal-mesonephric structures, an accessory spleen may be found attached to the left ovary or kidney or may be located within the scrotum. Spleno-gonadal fusion can be classified into two types: continuous (direct connection between the spleen and gonad) and discontinuous (no anatomic connection between ectopic splenic tissue and the principal spleen). This anomaly predominates in males. It can occur as an isolated condition or can be associated with other abnormalities, such as cryptorchismus and orofacial or limb abnormalities (1, 3).

Wandering Spleen

Absence, laxity, or excessive length of ligaments of the spleen leads to an abnormal mobility of the organ. Torsion of the long vascular pedicle may occur, followed by vascular occlusion and splenic infarction (1, 4).

Asplenia and Polysplenia

The absence of the spleen (►asplenia) or the presence of multiple small spleens (►polysplenia) is a rare condition usually associated with other congenital malformations, especially cardiovascular anomalies. Polysplenia or asplenia may associate with abdominal situs ambiguous and are known as asplenia and polysplenia syndrome. Asplenia syndrome is most frequently encountered in males and may be associated with severe cyanotic congenital heart diseases. The typical anatomic features of asplenia syndrome are trilobed lungs with bilateral minor fissures and epiarterial bronchi, bilateral systemic atria, midline liver, and a variable location of the stomach. Polysplenia syndrome is more common in females. The typical anatomic features of classic polysplenia syndrome are bilobed lungs with bilateral hypoarterial bronchi, bilateral pulmonary atria, midline liver, and multiple spleens of variable size and number that may be located in either the left or right abdomen. In rare cases these patients have a single, lobulated spleen or even a normal spleen. Malrotation of the bowel is a frequent finding in heterotaxy syndrome (1, 5).

Splenic Atrophy

Congenital ►splenic atrophy is quite uncommon and is associated with recurrent bacterial infections (1).

Clinical Presentation

Accessory spleens and splenic shape abnormalities are typically an incidental finding at imaging.

Spleno-gonadal fusion may manifest as a mobile and painless left scrotal mass. Other presentations include cryptorchismus, testicular torsion, and inguinal hernia. Spleno-gonadal fusion is often asymptomatic in females.

In case of an intrathoracic location of the spleen, patients usually have respiratory symptoms.

The ►wandering spleen usually is symptomatic in the childhood and may present with an abdominal mass and acute, chronic, or intermittent symptoms due to torsion of the vascular pedicle.

In children with asplenia and polysplenia syndromes, the clinical manifestations may be related to congenital heart disease, immune deficiency (splenic absence), or volvulus due to intestinal malrotation (1).

Imaging

Accessory Spleen

Accessory spleens may vary in number and size, usually ranging from a few millimeters to several centimeters in size. Typically, they appear as round or oval masses near the splenic hilum, but they may be found anywhere in the abdomen. Intrapancreatic accessory spleen, typically in the tail, can mimic a neoplastic mass. Imaging features are identical to those of normal splenic tissue. At computed tomography (CT), the attenuation values before and after contrast administration are identical to those of the spleen. The characteristic inhomogeneous enhancement during the arterial phase is crucial to demonstrate the nature of the mass. On magnetic resonance images (MRI), the spleen is hypointense on T1-weighted scans and hyperintense on T2-weighted scans with respect to the liver and the pancreas. The use of reticuloendothelial-targeted contrast media can confirm the splenic nature of the mass (1, 2).

Shape Abnormalities

Splenic clefts, notches, and lobules are quite common findings and must be distinguished from traumatic lesions. The demonstration at US and CT of characteristic smooth edges and the absence of contrast extravasation suggests a congenital splenic cleft (1).

Spleno-Gonadal Fusion and Spleno-Renal Fusion

In case of left scrotal mass, US is usually the first examination; the splenic tissue appears as a homogeneous, well-encapsulated mass with the same echotexture as the normal spleen. At Doppler US, a vascular architecture analogous to that of the spleen is seen. If spleno-gonadal

fusion is suspected, a cord-like structure connecting the spleen to the mass should be searched for. CT may be helpful to demonstrate associated splenic-renal fusion or cryptorchismus. The typical enhancement pattern confirms diagnosis. In women, spleno-gonadal fusion is usually an incidental finding at US or CT (1, 3).

Wandering Spleen

On plain abdominal X-ray, the absence of the normal splenic outline in the left upper quadrant in association with a soft-tissue mass in the abdomen or pelvis may be noted. US and CT confirm the absence of the spleen in its expected location and the presence of an ectopic splenic location. Torsion of the vascular pedicle may lead to infarction. The congested or infarcted spleen may have a normal echotexture or may be hyperechogenic due to secondary hemorrhage. The spleen's comma-shaped configuration is usually preserved. Splenomegaly with rounded edges of the organ is suggestive for torsion and is attributed to venous congestion. The lack of a flow signal on Doppler US will confirm hypoperfusion. US contrast media can increase sensitivity. Doppler spectral analysis may show a low diastolic velocity with an elevated resistive index in the splenic artery. Unenhanced CT usually shows a decreased density of the spleen; after contrast medium injection a partial or total lack of enhancement may be seen. A whirlpool appearance of the splenic vessels within the splenic hilum indicates torsion (1). Dense splenic vessels (dense artery sign), corresponding to acute thrombosis, are occasionally observed. MR can provide useful information about the precise location of the wandering spleen, the viability of the splenic parenchyma and the splenic vessel anatomy (MR angiography) (4).

Polysplenia and Asplenia

In polysplenia, numerous small splenic masses can be seen predominantly in the right upper quadrant at US, CT, MR, or scintigraphy.

Identification of a missing spleen is more difficult than confirmation of its presence. Scintigraphy remains the gold standard (1, 5).

Nuclear Medicine

99m-Technetium sulfur colloid scintigraphy and 99m-technetium-labeled heat-damaged red blood cells offer functional images and are highly specific for differentiating splenic tissue from other masses. Although nuclear medicine offers the most specific imaging techniques for identifying ectopic splenic tissue, CT and MR offer superior anatomic resolution (2). Scintigraphy is used to confirm the presence of normally functioning splenic tissue in cases of accessory spleens, ectopic spleen, spleno-gonadal and ▶spleno-renal fusion or polysplenia. Scintigraphy is also the examination of choice in documentating the absence of the spleen. However, the absence of a detectable radiotracer uptake can also occur in so-called "functional asplenia," in which the splenic phagocytic function is markedly reduced, despite the presence of

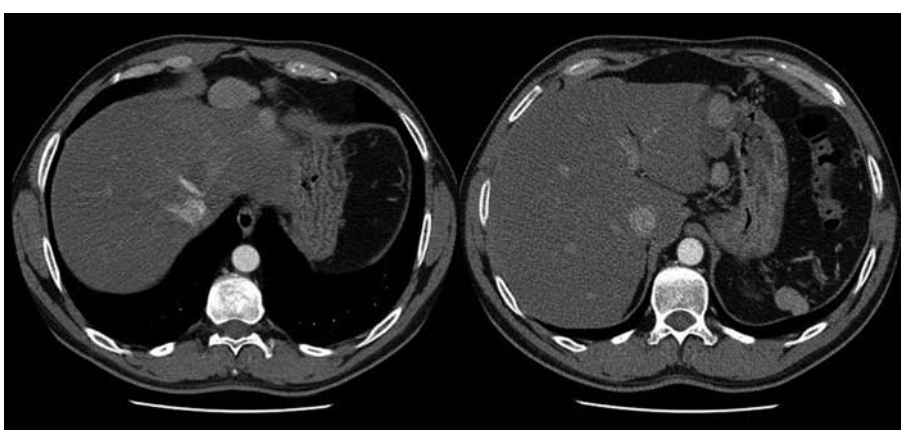

Congenital Abnormalities, Splenic. Figure 3 Splenosis CT study demonstrates multiple masses scattered throughout the abdomen (liver surface, liver hilum, and left hypochondrium) in a patient who had a posttraumatic splenectomy several years before. The masses have regular margins. In the contrast-enhanced arterial phase, the masses typically have a strong inhomogeneous enhancement, analogous to that of the normal spleen.

splenic tissue. Functional asplenia may occur in sickle cell disease, secondary to radiation therapy and chemotherapy, secondary to tumor invasion of the spleen, in splenic anoxia or after bone marrow transplantation (1).

Diagnosis

Ectopic splenic tissue may mimic neoplasms and lymphadenopathies. Imaging can make a definite diagnosis avoiding biopsy. Ectopic splenic tissue shows imaging features identical to those of the spleen in all imaging modalities. The enhancement pattern, especially the inhomogeneity in the arterial phase, is very specific. The combination of different MR sequences increases the confidence in diagnosis. MR reticuloendothelial-targeted contrast media can confirm the splenic nature of the mass. 99m-Technetium sulfur colloid scintigraphy and 99m-technetium-labeled heat-damaged red blood cells represent the most specific imaging techniques to confirm the presence of functioning splenic tissue.

In spleno-gonadal fusion presenting with scrotal mass, US is the first examination to be performed. The homogeneity of the echotexture, the regularity of the vascular architecture and the presence of well-defined margins suggest a nonneoplastic nature of the mass. When spleno-gonadal fusion is suspected, a comparison with the US appearance of the spleen and a study directed to the visualization of a cord-like structure connecting the mass with the normal spleen should be performed. A definitive diagnosis cannot be made solely on the basis of US findings. Nuclear medicine imaging can confirm the presence of splenic areas of activity. However, surgical exploration is generally required to rule out malignancy. Nevertheless, orchiectomy can be avoided because splenic tissue can be dissected away from the tunica albuginea (3).

Accurate preoperative diagnosis of wandering spleen with or without torsion represents an imaging challenge and can be made with US, CT, and MR. Perfusion and viability of the splenic parenchyma can be assessed by contrast-enhanced CT and MR, Doppler ultrasonography, and scintigraphy. Information concerning splenic perfusion and viability is important for the surgeon, especially in younger children where splenopexy instead of splenectomy is the treatment of choice in uncomplicated wandering spleen.

Multiple splenic masses, usually in the abdomen, may be seen in case of multiple accessory spleens, polysplenia, and ►splenosis (autotransplantation of splenic tissue occurring after splenic trauma or after splenectomy) (Fig. 3). History of previous splenectomy suggest the diagnosis of splenosis; in case of polysplenia, other congenital abnormalities are associated.

Bibliography

1. Paterson A, Frush DP, Donnelly LF et al (1999) A pattern-oriented approach to splenic imaging in infants and children. Radiographics 19(6):1465–1485
2. Miyayama S, Matsui O, Yamamoto T et al (2003) Intrapancreatic accessory spleen: evaluation by CT arteriography. Abdom Imaging 28(6):862–865
3. Pomara G (2004) Splenogonadal fusion: a rare extratesticular scrotal mass. Radiographics 24(2):417
4. Deux JF, Salomon L, Barrier A et al (2004) Acute torsion of wandering spleen: MRI findings. Am J Roentgenol 182 (6):1607–1608
5. Applegate KE, Goske MJ, Pierce G et al (1999) Situs revisited: imaging of the heterotaxy syndrome. Radiographics 19(4):837–852; discussion 853–854

Congenital Cystic Adenomatoid Malformation

Intrapulmonary multicystic mass of pulmonary tissue with an abnormal proliferation of bronchial structures.

►Congenital Malformations, Tracheobronchial Tree

Congenital Diaphragmatic Hernia (CDH)

A congenital defect in the diaphragm that allows abdominal contents including bowel and solid abdominal organs to herniate into the chest, most commonly occurring in utero, and resulting in lung hypoplasia on the affected side (left sided in 90%).

►Hernia, Diaphragm, Congenital

►Contrast Media, Ultrasound, Influence of shell on Pharmacology and Acoustic Properties

Congenital Duplication Cyst

Space-occupying lesion of a congenital origin that "duplicates" the different layers of the wall of the digestive tube. It can be communicating or noncommunicating. It is more frequent in the gastric great curvature and in the anteromedical contour of the first and second portions of the duodenum. It presents a water density on CT and a hypoechoic appearance on ultrasonography.

Congenital Heart Disease and Great Vessel Disease, MRI

A. van Straten, G. L. Guit, A. de Roos
Radiology Department, Kennemer Gasthuis, Haarlem, Noord-Holland, The Netherlands
straten@knmg.nl

Definition

Congenital heart diseases (CHD) form a wide range of cardiac malformations. The most common cyanotic congenital heart disease is Tetralogy of Fallot (TOF). Other relatively common CHD are: transposition of the great arteries, atrioventricular septal defects and various kinds of valvular diseases. The most widely used classification is based on the sequential segmental analysis in which the heart is divided into three segments: the atrial chambers, the ventricular mass and the great arteries. In this model, the first step is identification of the arrangement of the atrial chambers (situs). Then ventricular morphology and topology are determined, for example type of atrioventricular connection and morphology of atrioventricular valves. Thirdly, the morphology of the great arteries is assessed (type of ventriculoarterial connection, morphology of arterial valves and infundibulum). Associated cardiac malformations are also noted as well as the cardiac position (position of the heart within the chest and the orientation of the cardiac apex).

Pathology

Most cases of CHD occur spontaneously and aetiology is multifactorial. However, a recent prospective study has shown that patients with CHD have an increased risk of having offspring with a similar CHD (1). The recurrence risk varies between 3 and 8% and is dependent on the cardiac defect and the gender of the involved parent. In general, the risk of recurrence is highest for atrioventricular defects and lowest for TOF. Further evidence of a genetic aetiology is provided by numerous reports of families comprising multiple members with CHD that follow a mendelian pattern of inheritance. This suggests a single gene defect as the specific cause of the CHD. An example of a specific disorder in which the gene defect has been elucidated is the Holt–Oram syndrome. This is an autosomal dominant disorder characterized by atrial and ventricular septal defects as wells as upper limb abnormalities. The affected gene (TBX5) is a member of the T-box family of transcription factors.

Clinical Presentation

Patients with CHD usually present shortly after birth (e.g. transposition of the great arteries), or in (early) childhood. The clinical symptoms are usually failure to thrive and cyanosis. In some cases, patients present at a much later stage or even in adulthood, for example 'pink Fallots', when right ventricular outflow tract obstruction is only mild. When a patients presents with symptoms that would suggest a CHD, history is very important. In the workup of these patients, the electrocardiogram and chest film may provide further insight into the type of cardiac malformation, however, for a definite diagnosis, echocardiography or cardiac magnetic resonance (CMR) imaging is often needed.

With an incidence of 0.3–0.5 per 1,000 live births, TOF is the most common cause of cyanotic CHD (Fig. 1) (2). Traditionally, corrective surgery was preceded by a palliative shunt connecting the systemic arterial circulation to the pulmonary arterial system. It was thought that these shunts would promote growth of the pulmonary arteries and total correction could be delayed until the patient was larger. Nowadays, patients undergo total repair in infancy, which may decrease the risk of late sudden death, but may increase the severity of residual pulmonary regurgitation (PR) in some patients, due to the higher number of trans-annular patch procedures needed in young infants.

Imaging

The clinical role of MR imaging in diseases of the heart and great vessels is rapidly evolving. CMR has become an established non-invasive imaging modality for the assessment of various cardiac disorders, such as cardiac masses, cardiomyopathies, aortic and pericardial diseases and congenital heart diseases. Moreover, due to its accuracy

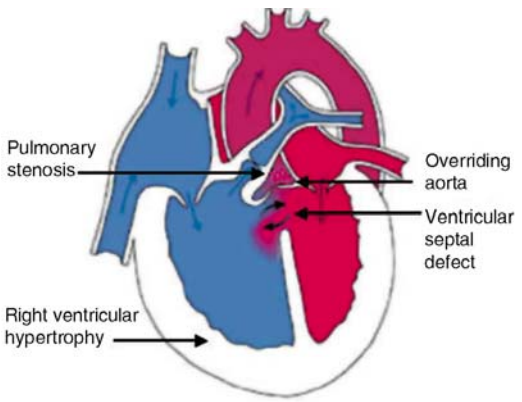

Congenital Heart Disease and Great Vessel Disease, MRI. Figure 1 Schematic view of the Fallot heart.

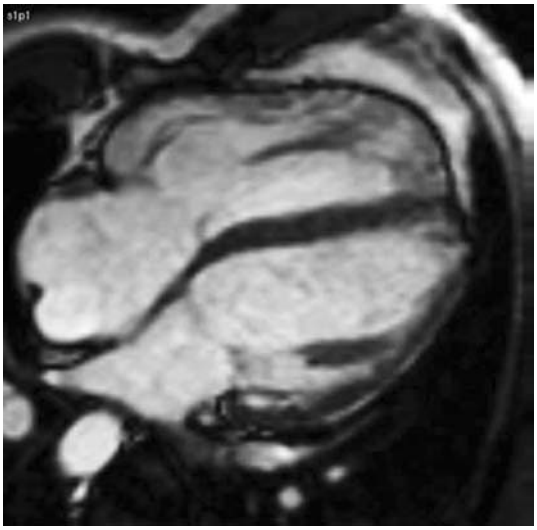

Congenital Heart Disease and Great Vessel Disease, MRI. Figure 2 MR four-chamber view of an adult with TOF and RV hypertrophy due to residual pulmonary stenosis.

and reproducibility, CMR is currently considered the gold standard for quantification of ventricular volumes, function and mass (Fig. 2) (3). Comprehensive functional assessment is possible by CMR due to its capability to measure flow velocity and flow volume, which is a basic requirement to quantify lesion severity in valvular heart disease. Over the past few years, major technical advances have considerably improved acquisition speed and image quality making CMR a useful tool for the evaluation of patients with ischemic heart disease as well. Although the clinical robustness of coronary magnetic resonance angiography still needs improvement, CMR currently provides valuable information to detect reversible ischemia, myocardial infarction and residual viability.

Transthoracic echocardiography is still the most commonly used technique in the non-invasive assessment of CHD, especially in young children whose small thoracic diameter provides an optimal acoustic window. After surgical intervention, however, the use of ultrasound is often restricted because of scar tissue and thoracic deformations. Unlike echocardiography, CMR provides unlimited access to the thoracic cavity and different techniques are available for detailed visualization and accurate measurement of the complex post-surgical morphology and functional status. Biventricular volumes and blood flow can be accurately measured during a single examination, allowing complete evaluation of both right and left ventricular systolic and diastolic function as well as intracardiac and vascular flow.

In the seriously ill or uncooperative patient CMR imaging is often limited, and it is contraindicated in patients with pacemakers. CMR studies are also time-consuming and may require patient sedation. Ultrasound has been the imaging modality of choice for many years, however, recently the role of electron beam CT and multidetector CT (MDCT) has been established in the evaluation of congenital heart disease.

The advantages of MDCT compared to MR imaging should be considered in selecting the optimal imaging modality for a child with CHD. Because MDCT takes less time and has fewer requirements for sedation than does MR imaging, it can be more easily performed in an unstable patient who needs intensive monitoring and care. Failure to wean the patient off the ventilator post-operatively may result from the airway compression caused by the vascular structure. The relationship between the airway and vessel can be accurately evaluated at MDCT. This information is useful for surgical management and cannot be provided by any other imaging modality. On the other hand, MDCT has several disadvantages, such as the need for iodinated contrast agents and radiation exposure, although the latter can be minimized by using a low-dose MDCT protocol.

Nuclear Medicine

The role of radionuclide angiography is limited nowadays since non-invasive imaging modalities such as cardiac CMR and MDCT offer detailed information on cardiac morphology as well as biventricular function.

Diagnosis

Presently, the vast majority of CHD can be surgically repaired. However, even after corrective surgery, the right ventricle (RV) may remain subject to an abnormal pressure and/or volume overload, due to longstanding residual pulmonary stenosis and/or PR. Hence, RV function has shown to be a major determinant of clinical outcome in CHD patients. With the growing number of long-term survivors amongst CHD patients, the need for accurate follow-up becomes increasingly important in clinical management. Careful monitoring of functional parameters such as cardiac function and vascular flow will help to allow early detection of the most important post-operative complications and aid in the timing of re-interventions (4). Timely detection of late complications requires adequate assessment of right ventricular size and function as well as quantification of intracardiac blood flow in these patient groups. Widely used techniques, such as echocardiography and radionuclide studies, have limitations when applied for this purpose, especially in patients with abnormal RV morphology.

Interventional Radiological Management

The recent implementation of fast CMR sequences along with the ability of MR imaging to acquire images in any given orientation and with high soft-tissue contrast makes this technique attractive for guiding interventional procedure. Razavi et al showed that cardiac catheterization guided by MR imaging is safe and practical in a clinical setting, allows better soft-tissue visualization, provides more pertinent physiological information, and results in lower radiation exposure than do fluoroscopically guided procedures (5). MR guidance could become the method of choice for diagnostic cardiac catheterization in patients with CHD, and an important tool in interventional cardiac catheterization and radiofrequency ablation. MR guided cardiopulmonary interventions, however, are challenging due to motion artefacts caused by the beating heart and respiration. Moreover, the tortuous anatomy of the right cardiac chambers and pulmonary arteries makes monitoring of the passage of guide wires and endovascular catheters and the deployment of stents with MR imaging more difficult. Kuehne et al showed that interactive real-time MR imaging has the potential to guide stent placement in the pulmonary valve or main pulmonary artery and measure blood flow volume in the stent lumen immediately after the intervention (6). Several other authors have reported the use of MR imaging—compatible catheters and guide wires. However, none of the investigated instruments contained properties required for complex cardiovascular interventions, such as (a) fast and reliable detection of the tip; (b) curvature of the shaft and (c) material properties such as tip flexibility, torque and tracking ability, shaft strength and flexibility. More work is needed to develop new MR imaging—compatible catheters and guide wires that are appropriate for use in cardiovascular interventions. In the future, research methods such as use of resonance circuits as fiducial markers should be investigated to provide tip and shaft detection without incorporating the risk of heating effects inherent with active catheter tracking methods.

Bibliography

1. Burn J, Brennan P, Little J et al (1998) Recurrence risks in offspring of adults with major heart defects: results from first cohort of British collaborative study. Lancet 351:311–316
2. Ferencz C, Rubin JD, McCarter RJ et al (1985) Congenital heart disease: prevalence at livebirth. The Baltimore-Washington Infant Study. Am J Epidemiol 121:31–36
3. de Roos A, Doornbos J, van der Wall EE et al (1995) Magnetic resonance of the heart and great vessels. Nat Med 1:711–713
4. Vliegen HW, Van Straten A, de Roos A et al (2002) Magnetic resonance imaging to assess the hemodynamic effects of pulmonary valve replacement in adults late after repair of tetralogy of Fallot. Circulation 106:1703–1707
5. Razavi R, Hill DL, Keevil SF et al (2003) Cardiac catheterisation guided by MRI in children and adults with congenital heart disease. Lancet 362:1877–1882
6. Kuehne T, Saeed M, Higgins CB et al (2003) Endovascular stents in pulmonary valve and artery in swine: feasibility study of MR imaging-guided deployment and postinterventional assessment. Radiology 226:475–481

C

Congenital Hepato-Biliary Anomalies

▶Congenital Malformations, Liver and Biliary Tract

Congenital Lesions of the Adrenal Gland

▶Congenital Malformations, Adrenals

Congenital Lobar Emphysema

Congenital progressive overdistension of a lung lobe.
▶Congenital Malformations, Tracheobronchial Tree

Congenital Lymphatic Malformation

▶Lymphangioma

Congenital Malformations, Adrenals

ROSEMARY ARTHUR
Department of Pediatric Radiology, Leeds General Infirmary, Clarendon Wing,
Leeds, UK
r.arthur@ukonline.co.uk

Synonyms

Congenital lesions of the adrenal gland

Definition

Congenital lesions of the adrenal gland arise from disordered embryogenesis, ►inborn errors of metabolism, or the occurrence of disease processes identified in the fetus or early neonatal period.

Histology/Pathology

The fetal adrenal cortex develops around 6 intrauterine weeks from coelomic mesodermal tissue and between 8 and 12 weeks it is invaded by ectodermal sympathetic cells of the neural crest to form the adrenal medulla producing catecholamines. The fetal adrenal cortex differentiates into an outer definitive zone and a larger inner fetal zone producing androgenic precursors for the placental synthesis of estriol. The fetal adrenal gland is proportionately very large, but soon after birth the fetal zone involutes disappearing by 1 year. At the same time the definitive zone of the cortex differentiates to form the glomerulosa (15%), lying peripherally and producing aldosterone, and the fasciculata (75%) and the reticularis (10%), lying next to the medulla both producing glucocorticoids and androgens. The glomerulosa becomes fully differentiated around 3 years of age, whereas the reticularis is not fully differentiated until approximately 15 years. In the adult a normal adrenal gland weighs approximately 4–5 g (1, 2).

Abnormalities in Embryogenesis

A number of developmental abnormalities of the adrenal gland result from disordered embryogenesis. Most are asymptomatic and discovered incidentally, although some are associated with other developmental anomalies (2–5).

Adrenal agenesis is rare and usually occurs in conjunction with ipsilateral renal agenesis. Ten percent of infants with renal agenesis will have adrenal agenesis. In these cases, the renal/adrenal agenesis is thought to be due to the failure of the mesonephric ridge to develop, whereas the majority of cases of renal agenesis (i.e., those not associated with adrenal agenesis) develop as a result of the failure of the ureteric bud to develop normally.

Adrenal hypoplasia of the adrenal glands in anencephalic infants is associated with triploidy and prenatally acquired pituitary and CNS degenerative disorders due to ACTH deficiency. Hypoplasia is also seen in neonatal adrenoleukodystrophy and Zellweger's syndrome.

Accessory adrenal glands are found in up to 50% of autopsies in children, and contain both adrenal cortical and medullary tissue. They may be hormonally active becoming overproductive following adrenalectomy. They are found around the celiac axis, along the line of the gonadal vessels and around the ovaries in girls and around the testes, epididymis, and hernial sacs in boys.

Straight adrenal refers to a discoid-shaped adrenal gland that appears elongated and straight on both longitudinal and transverse imaging rather than having the normal Y, Z, or V shape. This anomaly is seen in association with renal agenesis, hypoplasia, or ectopia and is thought to result from the failure of the renal tissue to indent into the adrenal gland during early development.

Horseshoe adrenal is a single mass of adrenal tissue that lies across the midline, generally posteriorly to the aorta and anteriorly to the inferior vena cava (IVC), but when associated with asplenia is always seen anteriorly to the aorta. Coexisting anomalies occur frequently including 52% asplenia, 37% neural tube defects, 29% renal anomalies, and in 3% Cornelia de Lange syndrome. Horseshoe adrenal does not occur in association with polysplenia, a differentiating feature from asplenia.

Circumrenal adrenal gland is a further anatomical variant describing the finding where there is fusion of two limbs of one gland extending down and around the kidney.

Adrenohepatic fusion and adrenorenal fusion are uncommon anomalies. These occur when the adrenal gland becomes incorporated within the capsule of the liver or kidney and is thought to be due to the disruption of intervening coelomic epithelium allowing these adjacent organs to fuse.

Clinical Presentation

With the exception of adrenal agenesis and severe hypoplasia, these anatomical variants of fusion are associated with normal adrenal function and histologically normal tissue. Adrenal tissue in ectopias, straight adrenal, and fusion anomalies usually show the characteristic pattern of normal adrenal glands on ultrasound (Figs 1 and 2).

Congenital adrenal hyperplasia is a group of inborn errors of metabolism arising from enzyme defects in the biosynthetic pathways of adrenal corticosteroids resulting in inadequate production of glucocorticoids and mineralocorticoids and the excess production of adrenal androgens. (*Give link to CAH/Ambiguous genitalia essays*)

►*Wolman's disease* is an inborn error of metabolism due to a deficiency of the enzyme acid esterase leading to an accumulation of triglycerides, cholesterol, and its esters within many organs particularly the inner layers of the adrenal cortex. The infants develop massive enlargement of the adrenal glands, hepatosplenomegaly, jaundice, vomiting, steatorrhea, abdominal distension, and failure to thrive.

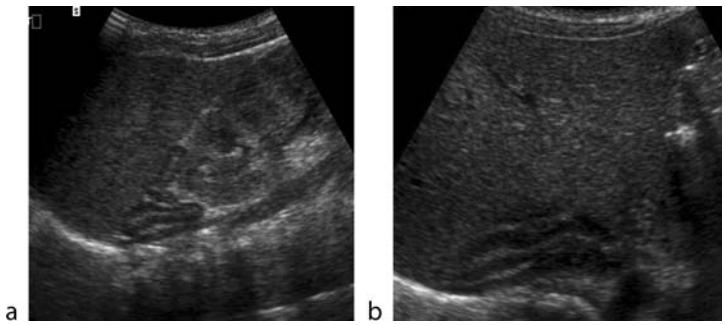

Congenital Malformations, Adrenals. Figure 1 (a) US (longitudinal US) and (b) (transverse US), of a normal, right neonatal adrenal gland.

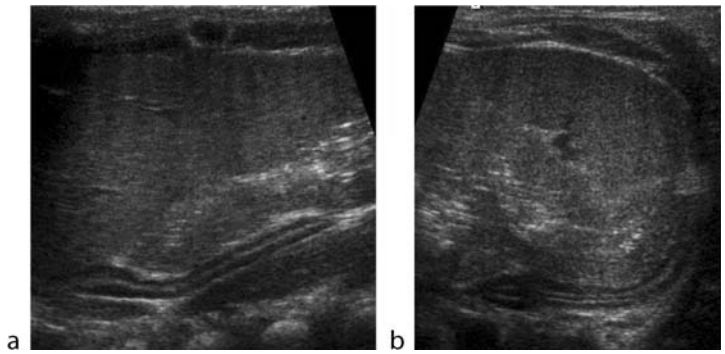

Congenital Malformations, Adrenals. Figure 2 (a) US (longitudinal US) and (b) (transverse US; both same patient as Figure 1), the straight or discoid left adrenal gland associated with left renal agenesis.

The condition generally presents early in infancy and is rapidly progressive resulting in death during the first year.

A number of pathological processes result in *cystic adrenal lesions* that need to be differentiated from simple adrenal cysts and include cystic ▶neuroblastoma, adrenal hemorrhage, adrenal abscess, epidermoid cysts, and intraabdominal extralobar pulmonary sequestration (ELPS) that may be sited within or adjacent to the adrenal glands. Careful imaging should help to differentiate these lesions from the cystic or dysplastic upper moiety of a duplex kidney.

Adrenal congestion and hemorrhage occur in the perinatal period in response to perinatal asphyxia and stress. Hypoxic damage to the endothelial cells results in adrenal congestion which may be followed by hemorrhage and hemorrhagic infarction. Prolonged abdominal compression in labor, particularly in infants born to diabetic mothers, and underlying bleeding diatheses and are also considered etiological factors. Adrenal hemorrhage may be bilateral but is more commonly unilateral affecting the right gland in 70% of cases on account of direct drainage of the right adrenal vein into the IVC. The condition is often asymptomatic, recognized as a result of a palpable kidney displaced by an enlarged adrenal gland, or may present clinically with jaundice, anemia, and rarely hypovolemic shock. If hypertension and/or impaired renal function is present, the possibility of a coexistent ipsilateral renal vein thrombosis should be considered. This occurs more commonly on the left where the adrenal vein drains into the left renal vein. Hemorrhage may track down the retroperitoneal tissues and into the scrotum causing scrotal swelling. Long-term adrenal insufficiency is unusual but may develop when more than 90% of both glands are affected.

Neuroblastoma is the commonest extracranial solid pediatric neoplasm and may present prenatally or be diagnosed at birth, although more commonly it presents in the preschool years. The tumor is variable in size at presentation, and is more commonly cystic than tumors presenting later in childhood. The tumor may be

asymptomatic and discovered incidentally, but when large or associated with hepatomegaly it may result in early neonatal respiratory distress. Neonatal metastatic spread to the liver, skin, and bone marrow sometimes occurs, and when found in association with a localized adrenal primary is staged 4S. These 4S tumors have a favorable prognosis, in contrast to prenatal presentation with hydrops and intraspinal extension, which is associated with a poor prognosis. (*Link to tumors/neuroblastoma essay*)

Adrenal endothelial cysts are seen infrequently in the adrenal glands and are often found incidentally during an ultrasound examination for an unrelated problem. Cysts can be huge and multiloculated, and they are generally filled with blood. They are usually unilateral but may be bilateral and generally decrease in size over time.

Adrenal abscess is unusual in the neonate and is most commonly seen in association with a resolving adrenal hemorrhage following *Neisseria meningitidis*, *Escherichia coli*, β-hemolytic streptococcal, or *Staphylococcus aureus* septicemia.

Imaging

The normal adrenal gland is Y, Z, or V shaped, closely related to the upper pole of the kidneys, and is easily seen in the neonate on *ultrasound imaging* using a high-frequency transducer (Fig. 1). The adrenal gland is a difficult organ to measure on account of its shape, but the thickness of the adrenal limbs should be approximately equal and less than 4 mm in width. Ultrasonically, the neonatal gland has a thin central hyperechoic stripe representing the medulla, central veins, and connective tissue with a surrounding hypoechoic cortex. With increasing age, the differentiation between the cortex and medulla disappears. The contour should be smooth or gently undulating but should not show any marked nodularity (4, 5).

Imaging findings in *Wolman's disease* are fairly characteristic, demonstrating a massive increase in the size of both glands that tend to retain their overall shape in conjunction with areas of calcification. Lymph node enlargement and bowel wall thickening may also be noted (Fig. 3).

A number of *cystic abnormalities* develop in the adrenal glands as discussed earlier and these may be difficult to differentiate on the basis of imaging characteristics alone. Simple adrenal cysts usually appear as simple, thin-walled cysts, whereas resolving hemorrhage and abscess will usually have a thicker wall, and the fluid may contain echoes or even a fluid–fluid level. *Adrenal hemorrhage* presents as an echopoor mass within a mildly enlarged adrenal and tends to become smaller and resolve over 2–4 weeks, often leaving a densely calcified involuted adrenal gland (Fig. 4). Neuroblastoma may also present as a cystic mass, and should be suspected if the wall shows some nodularity. However, the mass may be homogeneous and indistinguishable from other benign or malignant tumors. The differential diagnosis of a complex cystic/solid adrenal lesion should also include an ELPS. These are commonly left-sided and are often first seen in the second trimester on ultrasound, whereas a congenital neuroblastoma is generally first seen in the third trimester

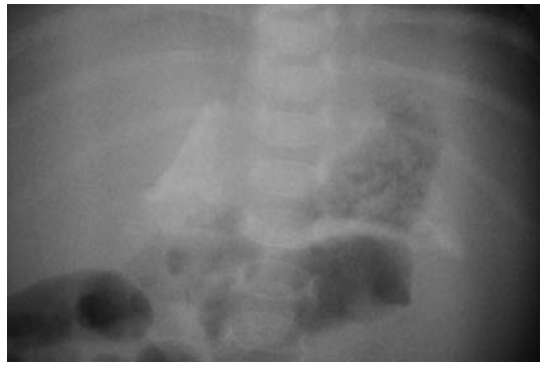

Congenital Malformations, Adrenals. Figure 3 Abdominal X-ray demonstrating calcification in enlarged adrenal glands. Normal overall shape is maintained. (From Paterson A (2002) Adrenal pathology in childhood: a spectrum of disease 12:2491–2508).

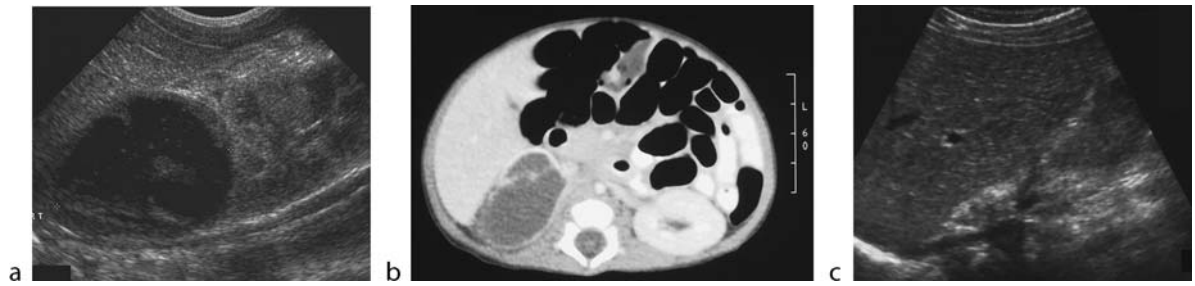

Congenital Malformations, Adrenals. Figure 4 (a) Early US (b) CT, and (c) later ultrasound images of large adrenal hemorrhage, which involutes and become calcified.

following a normal second trimester scan and is more commonly right-sided. EPLS may show increased vascularity, and the identification of a systemic arterial supply helps to clinch the diagnosis.

Abdominal radiography is useful in the assessment of abdominal distension, and in Wolman's disease it will show enlarged and densely calcified adrenal glands, whereas in neuroblastoma the calcification is more focal. In the older child a triangular, dense, calcified adrenal gland may be noted following perinatal adrenal hemorrhage.

CT and MRI scanning of the neonate are rarely helpful in clearly differentiating hemorrhage from a cystic neuroblastoma or adrenal abscess, although helical CT and MRI may be useful to further delineate a mass lesion, particularly when solid and large, and to identify any metastases associated with neuroblastoma. Helical CT and MRI are also useful for the detection of aberrant vessels suggesting the presence of an ELPS. Metaiodobenzylguanidine scintigraphy is only indicated in cases of neuroblastoma.

Diagnosis

The main difficulty in diagnosis is differentiating between the various cystic, complex, or homogeneous masses. A clinical history of perinatal hypoxia should point to the possibility of adrenal congestion and/or hemorrhage, and these lesions should gradually become smaller over the first few weeks of life. Failure to involute is suggestive of more significant pathology, for example, neuroblastoma. Although the potential diagnosis of neuroblastoma is of concern in the case of both cystic and solid congenital adrenal lesions, the outlook for 4S lesions is very good and it is generally considered safe to wait several weeks, particularly in cystic lesions, to see if they involute. Percutaneous/open biopsy will be required for a definitive diagnosis in solid lesions or cystic lesions that fail to involute. Unfortunately, vanillylmandelic acid estimations, a noradrenalin metabolite, are generally unhelpful in the neonatal period.

Bibliography

1. Miller WL (1997) The adrenal cortex and its disorders. In: Brook C, Clayton P, Brown R (eds) Brook's Clinical Pediatric Endocrinology. Blackwell Publishing, pp 293
2. Paterson A (2002) Adrenal pathology in childhood: a spectrum of disease. Eur Radiol 12:2491–2508
3. Strouse PJ, Haller JO, Berdon WE et al (2002) Horseshoe adrenal gland in association with asplenia: presentation of six new cases and review of the literature. Pediatr Radiol 32:778–782
4. Daneman A (2004) The adrenal gland. In: Kuhn JP, Slovis TL, Haller JO (eds) In Caffey's Paediatric Diagnostic Imaging. Mosby, pp 239–251
5. Siegel MJ (2002) Adrenal glands, pancreas and other retroperitoneal structures. In: Siegel MJ (ed) Pediatric Sonography, Raven Press, pp 475–527

Congenital Malformations, Bile Ducts

F.E. Avni, C. Matos, M. Cassart
Department of Medical Imaging, University Clinics of Brussels, Erasme Hospital, Brussels, Belgium
favni@ulb.ac.be

C

Synonyms

Alagille syndrome: Ductular paucity of intrahepatic bile ducts; Bile duct cyst; Biliary atresia; Caroli's disease; Choledochal cyst; Choledochocele; Choledochal cyst type V; Communicating cavernous ectasia of the intrahepatic bile ducts; Extrahepatic atresia; Progressive familial cholestasis; Syndromic hepatic ductular hypoplasia; Watson-Alagille syndrome

Definition

In the infant/neonatal age group, biliary atresia (BA) is the predominant surgical malformation followed by choledochal cyst (CC) and spontaneous perforation of the common bile duct (CBD) (1, 2).

BA consists of a severely complete or partial interruption of the extrahepatic biliary tree (EHBT). It occurs in 1:10,000 to 1:25,000 births. It is thought to result from a progressive *in utero*, inflammatory disease of the entire biliary tract.

There are multiple different anatomic types depending on the extent of the inflammatory and fibrotic process. This leads to numerous variants including (partial) patency of the CBD or gallbladder but also some cystic dilatation of bile ducts (3, 4).

CC consists of a spectrum of malformations of the extrahepatic and intrahepatic bile ducts. The primary anomaly is apparently related to an abnormal pancreaticobiliary junction. There is a common segment that is too long, with reflux of pancreatic juice into the CBD. It occurs in 1:100,000 births.

An early classification indicated three groups of CC. Type I, fusiform or cystic dilatation of the CBD, represents 90% of the patients. Type II corresponds to a diverticulum of the CBD. Type III represents a choledochocele that protrudes into the duodenal lumen.

More recently, two types have been added: type IV corresponds to the presence of multiple extrahepatic bile duct cysts, either as an isolated anomaly (IVa) or in association with intrahepatic biliary cysts (IVb; Caroli's-like disease). Type V is a cystic dilatation of the

intrahepatic bile ducts equivalent to Caroli's disease. Caroli's disease itself is a congenital cystic dilatation of the intrahepatic bile ducts that communicate with the biliary system. The disease can be associated with autosomal recessive polycystic kidney disease, hepatic fibrosis, or both; the condition is then referred as Caroli's syndrome (1–3).

Spontaneous perforation of the CBD is a very rare condition of unknown origin (ischemic lesion is a possible explanation). The perforation is always located at the junction of the cystic duct and the CBD. It may or not be associated with the very rare neonatal biliary lithiasis or biliary plug syndrome.

Intrahepatic bile duct tree congenital anomalies include Byler's disease (progressive familial cholestasis) and ►Alagille syndrome (intrahepatic ductular paucity).

The spectrum of congenital anomalies of the biliary tree also includes rare cases of agenesis, duplication, and septation of the gallbladder (anomalies that are usually without clinical consequences) (1, 2).

Pathology/Histopathology

In BA, the entire EHBT is involved. The biliary ducts are atretic and hypoplastic. Early in the course of the disease, there are tiny but patent biliary structures in the perihilar tissue at the porta hepatis that disappear progressively after 4 months. Some infants may have sparing of the distal BD (patent gallbladder, cystic duct, and CBD). Some others present segmental patency with a pseudocyst-like structure at the level of the CBD or liver hilum. Microscopic evaluation of the liver reveals cholestasis, distorted bile ducts, and a distorted portal vascular system. Extensive fibrosis is also visible (1, 2).

In CC, a long common biliopancreatic channel is observed with partial obstruction of the CBD. The CBD is thickened and fibrotic without a muscular layer. The mucosa is ulcerated. In the case of Caroli's disease, pathology demonstrates saccular or fusiform ductal dilatation of the intrahepatic biliary tree (IHBT). Depending on the age of the patient, evidence of cholangitis, periductal fibrosis, and cirrhosis may be demonstrated as well.

Clinical Presentation

In the neonatal period, most congenital malformations of the BT will be suspected in cases of persistent jaundice, hepatomegaly, and acholic stools. This is the case for up to 80% of patients with BA.

CC is classically suspected with the association of abdominal pain, a right upper quadrant mass, and fluctuant jaundice. Antenatal diagnoses have been reported.

Other clinical symptoms are related to the (later) complications of the congenital malformations (cirrhosis, biliary stones, or rupture of varices).

Imaging

Various imaging techniques provide information about the biliary tract.

1. Conventional X-ray of the spine can be done to demonstrate butterfly vertebrae (Alagille syndrome).
2. Ultrasound (US) is the primary technique used to image the biliary tract, especially in neonates.

The first structure to be identified is the CBD. Yet a normal CBD is difficult to visualize; it has to be differentiated from the hepatic artery. Dilatation should be considered when the diameter is >2 mm, and CC when >7 mm.

The intrahepatic bile ducts are dilated when their diameter exceeds the diameter of the parallel portal branch.

Evaluation of the gallbladder (GB) is more controversial because, even in cases of BA, it may be present and normal in size (2.5–3.5 cm in length). An empty GB after a meal does not exclude the diagnosis; on the contrary, an enlarging GB after 4 h of fasting excludes BA. Ultrasound is helpful in detecting intrahepatic or extrahepatic biliary cysts. It is also important when the triangular cord sign is demonstrated; this consists of a triangular echogenic irregular structure (the fetal biliary duct) at the level of the porta hepatis. Color Doppler analysis is important to detect frequently associated vascular anomalies (preduodenal portal vein, interrupted inferior vena cava).

Periportal fibrosis, portal hypertension, and polysplenia are other possible anomalies demonstrable by US (4).

Magnetic resonance imaging (MRI) can be used in infants and even neonates to demonstrate a normal or abnormal biliary tract. Using T2-weighted MR cholangiography (MRCP), images of the normal or dilated biliary tract can be easily obtained as in adults, and the technique helps to exclude BA.

In cases of BA, the MR equivalent of the US triangular cord sign has been described: a triangular area of high intensity at the level of the porta hepatis can be observed. The status of the liver (periportal fibrosis) and/or vascular anomalies can be analyzed using T1 (without and with gadolinium) and echogradient sequences (5).

Endoscopic retrograde cholangiopancreatography (ERCP) can be performed at any age to assess the patency of the EHBT or IHBT. Its yield is greater in cases of dilated biliary ducts where it has replaced transhepatic opacification of the biliary tract. Its advantage lies in a possible therapeutic maneuver and an easier interpretation than with the imaging.

A perioperative cholangiogram is mandatory to confirm the diagnosis of BA, to determine its type and to differentiate BA with biliary cysts from CC.

Nuclear Medicine

Nuclear medicine scans are of utmost importance for the differential diagnosis of ►neonatal cholestasis and a presumptive diagnosis of BA.

^{99m}Tc-disofenin (DISIDA) has the highest hepatic extraction and the highest diagnostic yield. After proper preparation with phenobarbital (for 5 days), the examination can be performed in neonates. Lack of hepatic captation of the tracer favors hepatic insufficiency (i.e., neonatal hepatitis), and lack of excretion into the intestine on a 24-h delayed scan is highly suggestive of BA. Excretion into the intestine excludes the diagnosis (1, 2).

Diagnosis

Once neonatal cholestasis or obstructive jaundice is suspected, US should be performed to evaluate the liver and biliary tract.

Absence of a visible GB despite 4 h of fasting, a nondilated CBD, the presence of triangular cord sign (Fig. 1), a periportal biliary cyst, echogenic kidneys, and polysplenia are signs suggestive of BA. In equivocal cases, MRCP may provide additional information and eventually exclude the diagnosis.

Nuclear medicine scanning should rapidly be performed (Fig. 2), and during surgery a cholangiogram is mandatory.

If the EHBT or IHBT is dilated on US, MR imaging may be performed to better understand the biliary tract and liver anatomy. Whenever an obstructive jaundice is confirmed, ERCP can be proposed as an alternative to surgery to precisely assess the diagnosis and eliminate any obstructive sludge or lithiasis.

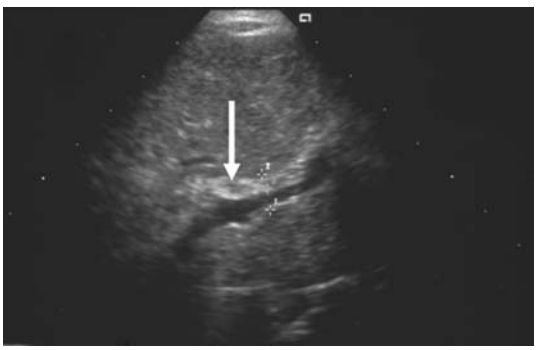

Congenital Malformations, Bile Ducts. Figure 1 Biliary atresia in a neonate. Ultrasound demonstrating the triangular cord sign (*arrow*). Oblique view through the porta hepatic.

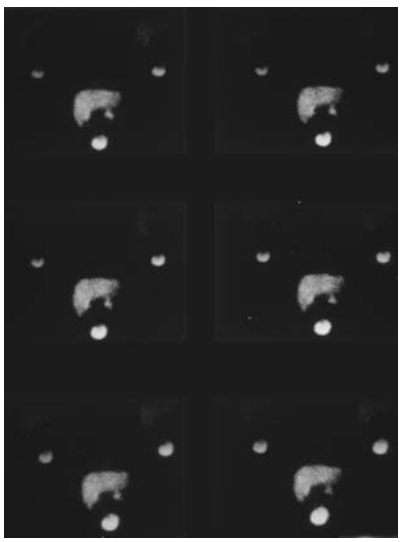

Congenital Malformations, Bile Ducts. Figure 2 Biliary atresia. DISIDA hepatic scan in a neonate. The tracer has been correctly metabolized by the liver but not excreted because no bowel has opacified, despite delayed views.

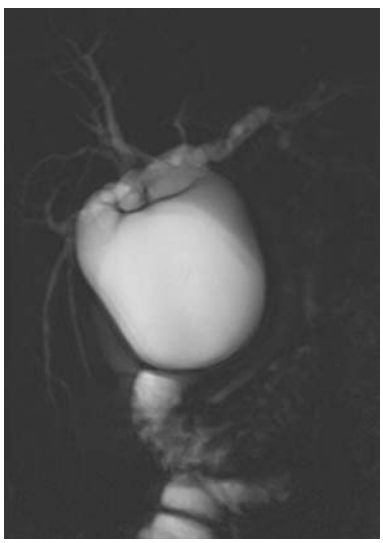

Congenital Malformations, Bile Ducts. Figure 3 Choledochal cyst type 1. Magnetic resonance cholangiopancreatographic demonstration (heavily T2-weighted sequence) of the typical cystic dilatation of the common bile duct.

Both MRCP and ERCP are useful for assessing communication between intrahepatic or extrahepatic cysts and the biliary tract as observed in CC (Fig. 3) or Caroli's disease.

Again, when surgery is elected, a preoperative cholangiogram will be necessary.

Whenever Caroli's disease or syndrome is suspected, the kidneys should be assessed to confirm associated kidney disease.

Bibliography

1. Karrer FM, Hall RJ, Stewart BA et al (1990) Congenital biliary tract disease. Surg Clin North Am 70:1403–1418
2. Benya EC (2002) Pancreas and biliary system: imaging of developmental anomalies and diseases unique to children. Radiol Clin North Am 40:1355–1362
3. Levy AD, Rohrmann CA Jr, Murakata LA et al (2002) Caroli's disease: radiologic spectrum with pathologic correlation. Am J Roentgenol 179:1053–1057
4. Lee HC, Yeung CY, Chang PY et al (2000) Dilatation of the biliary tree in children: sonographic diagnosis and its clinical significance. J Ultrasound Med 19:177–182
5. Norton KI, Glass RB, Kogan D et al (2002) MR cholangiography in the evaluation of neonatal cholestasis: initial results. Radiology 222:687–691

Congenital Malformations, Bone

Alan E. Oestreich
Cincinnati Children's Hospital Medical Center, Cincinnati, Ohio, USA
Alan.Oestreich@cchmc.org

Synonym

Deformity or other structural abnormality of skeletal elements present at (or before) birth

Definitions

Abnormality such as deformity of skeletal elements that is present at or before birth. It may be due to a genetic cause, intrauterine position, or effects of adverse intrauterine conditions, including amniocentesis physical injury, other trauma, prenatal surgery, irradiation, infection substances including medicines ingested by the pregnant mother, or maternal metabolic disease or malnutrition. The abnormalities may affect bone, cartilage, joints, and muscles and tendons, as well as vessels, nerves, and surrounding soft tissues. Those conditions that manifest later in childhood, but are due to causes already present at birth, may be considered as related to congenital malformations.

Pathology/Histopathology

Malformations of bone do not have a specific histopathologic abnormality in general. What one sees on imaging is what the malformation would be on gross pathological examination. Associated vascular and neuromuscular changes are also generally matters of gross pathology, such as the small anterior tibial artery associated with clubfoot. One exception is congenital bony malformation in neurofibromatosis-1, in which mesodermal tissue abnormality is found.

Clinical Presentation

The clinical presentations of congenital malformations are as varied as the malformations. Limp and leg length discrepancy are common to many. Some, including Down syndrome and Williams syndrome, have characteristic associated facies. Skin lesion (such as café-au-lait spots), small rib cage, and fingernail abnormalities are present in some conditions.

Imaging

Although malformations are initially evaluated on plain radiographs, additional modalities are appropriate for specific situations. For example, not yet ossified growth center bones of the foot may be revealed by ultrasound, computed tomography (CT), or magnetic resonance imaging (MRI). For positional relationships of the lower extremity, weight-bearing or simulated weight-bearing images are necessary. For vertical talus diagnosis and evaluation, a maximum plantar flexion lateral view is necessary. The anterior nose or anterior protrusion of the calcaneus on lateral images (1) predicts presence of calcaneonavicular coalition, which is then demonstrated nicely with the everted oblique view (of Slomann) of the foot; CT is not required. The inverted oblique view of the foot, incidentally, nicely shows accessory navicular centers of the foot, although the weight-bearing anteroposterior (AP) view that shows alignment abnormalities should also be obtained.

Scoliosis evaluation requires upright images whenever possible. The flexibility of curves may be checked with supine maximal passive bending of the patient as additional views. Cervical spine evaluation for C1 or C2 malformation or for transverse ligament weakness uses flexion and extension lateral images. To evaluate for

lateral clavicle hook (a sign of upper extremity reduction deformity or weakness); the arms should be at the side of the chest (2). To evaluate an area of upper or lower extremity for unilateral growth disturbance, comparison with the contralateral side is appropriate.

In proximal focal femoral dysplasia, MRI is advisable early in life to determine the presence of cartilaginous centers and to reveal if seemingly nonconnected bony parts of the femur might be connected by cartilaginous (or fibrous) tissue. Ultrasound can yield similar information, but in less exquisite detail.

For pectus excavatum, CT images allow documentation of the severity of the deformity as well as its effects on the heart and other thoracic structures.

In utero imaging for malformation begins with high-detail ultrasound, including 3D imaging. Questions that arise may then be further investigated with fetal MRI. If the answer is still not given, but is important, selected radiographs of the mother's abdomen may be considered, under close supervision by a specialized pediatric radiologist. If possible, radiographs of one twin should be avoided if the other is considered unaffected, for radiation protection considerations.

Nuclear Medicine

If, in malformation, the question arises of whether a bone has capability of growth at a site, bone scanning can indicate the presence of a functioning growth plate. Furthermore, it may be of use in determining if two adjacent carpal or tarsal centers are fused to each other, and if less than normal, or no, growth plate activity occurs between them.

Diagnosis

Several congenital malformations arise related to intrauterine position, including clubfoot, kyphoscoliosis of the tibia, manifestations of amniotic bands, and perhaps developmental dysplasia of the hip and ▶Poland syndrome. Clubfoot is a combination of varus of hindfoot and forefoot, equinus position of the ankle, retarded maturation/small size of tarsal bones, and hypoplasia (or absence) of the anterior tibial artery. The angulation relationship of the talus and calcaneus is observed especially on maximal dorsiflexion lateral images and simulated weight-bearing frontal images. Kyphoscoliosis of the tibia is a posteriorly and medially convex deformation, seen also in the fibula, which improves as a child gets older. Amniotic bands, from damage to a fetal part that was trapped through a gap in the amniotic cavity, cause constriction of bony and soft-tissue elements

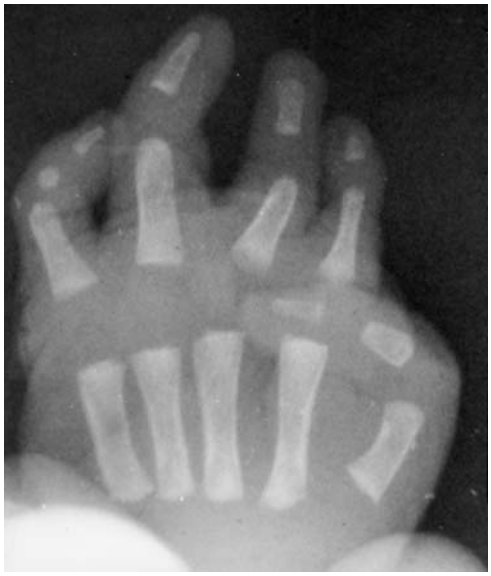

Congenital Malformations, Bone. Figure 1 Poland syndrome. This infant had ipsilateral pectoral muscle hypoplasia. Note the absent middle phalanges 2–4 and hypoplastic middle phalanx 5, with some soft-tissue syndactyly between the middle three fingers. (From Oestreich AE, Crawford AH (1985) Atlas of Pediatric Orthopedic Radiology. Thieme Verlag, Stuttgart p 167)

and perhaps hypoplasia or aplasia distal to the (Streeter) band site. In Poland syndactyly (Fig. 1), middle phalanges of one hand are absent or hypoplastic, soft-tissue syndactyly occurs between involved fingers, ipsilateral ribs are small, the pectoral muscle is small on that side, sometimes with nipple hypoplasia, and a dextroposition of the heart sometimes accompanies left-sided disease. Dr. Josef Warkany suggested that the clenched fist repeatedly beating on the chest in utero may be the causative factor for the unusual combination of findings.

Some congenital malformations may be acquired from intrauterine intervention or the intrauterine environment. For damage from amniocentesis, history of the event is important, as is the case for other trauma or surgery. Heavy metal burden from the mother, lead or bismuth, can yield dense metaphyseal and metaphyseal-equivalent bands in the fetal bones. Magnesium citrate therapy of the mother late in pregnancy yields instead similar lucent bands. Malformations in fetal alcohol syndrome include narrow distal phalanges.

Variation in bone number or connectiveness results from homeobox (hox) gene variations. More complex genetic conditions have recognizable patterns: in cerebrocostomandibular syndrome, gaps appear within ribs and the mandible is small. The mandible is also small in Seckel's syndrome and camptomelic dysplasia, as well as

in ►Pierre-Robin sequence. In cleidocranial dysplasia, a portion or all of the clavicles are missing, wormian bones are present, the pubic symphysis is wide, pseudoepiphyses of the metacarpals and metatarsals are prominent, and vertebral bodies are biconvex. In Down syndrome, trisomy 21, the middle phalanx of the little finger is small, acetabular and iliac angles are low, the sternal manubrium has two centers in series, and the spinal canal behind the dens may be small. About 15–20% of normal children also have two manubrial centers in series. Dislocation of the proximal radius is seen in several genetic syndromes, including Williams syndrome and 4p- (Wolf-Hirschhorn) syndrome. Many upper cervical column abnormalities are seen in ►22q11.2 deletion, including fusions of C2 and C3, platybasia, unfused posterior arch of C1, and upswept posterior lamina and other posterior elements (the C2 swoosh) (3). Wide distal phalanges of the great toes and thumbs, wide tufts of distal phalanges, high incidence of azygos fissure, and low acetabular and iliac angles are findings in Rubinstein-Taybi syndrome. The ►domed talus association (4) includes the ball-in-socket ankle, tarsal bone coalitions (seen on plain images in the second decade of life; on MRI detectable earlier), less than five rays of the feet, short fibula (and often tibia with absent superior tibial spines), and proximal focal femoral dysplasia, in various combinations.

In this article, we were only able to cite a few of hundreds of malformations, which are increasingly being associated with specific genetic findings.

In the equinus tibiocalcaneal relationship, often due to a tight heel cord, the front of the calcaneus is lower than normal in its relationship to the tibia, resembling the "q" in the front of the lower case word equinus that extends below the row of the other letters; in the calcaneus tibiocalcaneal relationship, the front of the calcaneus is higher than normal, like the "l" of the lower case word calcaneus (Fig. 2). In a *valgus* relationship, the distal part heads further from the midline than normal compared to the proximal part, judged with the proximal part in anatomic position; in *varus*, the distal part heads closer to the midline than normal. Mnemonic: the va**r**us proximal right femur looks like a lower case "r" and the valgus right femur looks like a lower case "l."

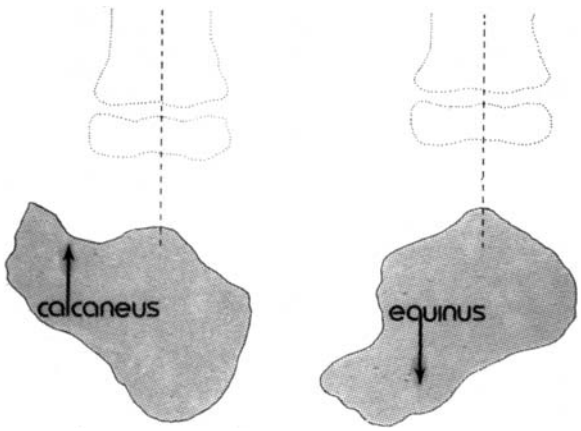

Congenital Malformations, Bone. Figure 2 Calcaneus and equinus mnemonic diagram, by Tamar Kahane Oestreich, see text. (From Oestreich AE, Crawford AH (1985) Atlas of Pediatric Orthopedic Radiology. Thieme Verlag, Stuttgart p 115)

Bibliography

1. Oestreich AE, Mize WA, Crawford AH et al (1987) The "anteater nose"; a direct sign of calcaneonavicular coalition on the lateral radiograph. J Pediatr Orthop 7:709–711
2. Oestreich AE (1981) The lateral clavicle hook-an acquired as well as a congenital anomaly. Pediatr Radiol 11:147–150
3. Ricchetti ET, States L et al (2004) Radiographic study of the upper cervical spine in the 22q11.2 deletion syndrome. J Bone Joint Surg Am 86-A:1751–1760
4. Pistola F, Ozonoff MB, Wintz P (1987) Ball-and-socket ankle joint. Skeletal Radiol 16:447–451

Congenital Malformations, Cerebellar

Philippe Demaerel
Department of Radiology, University Hospitals, Leuven, Belgium
philippe.demaerel@uz.kuleuven.ac.be

Synonyms

Congenital malformations; Hindbrain; Posterior fossa

Definition

Congenital cerebellar malformations involve all malformations of the vermis and cerebellar hemispheres. They are classified on the basis of anatomical and embryological knowledge. Several genes, proteins, and molecules are involved in the various stages of cerebellar development, and it is expected that this knowledge will influence the classification of congenital cerebellar malformations in the future.

Pathology/Histopathology

Although the anatomy of the cerebellum is straightforward, the understanding of embryology is still limited.

Approximately during the fourth week of gestation, the rhombencephalon divides into the metencephalon (pons and cerebellum) and the myelencephalon (medulla oblongata). The metencephalon will give rise to the vermis and the hemispheres, while the cavity in the rhombencephalon will expand to become the fourth ventricle. The roof of the fourth ventricle is divided into an anterior and a posterior membranous area; the posterior membranous area will ultimately communicate with the subarachnoid space at the foramen of Magendie. The posterior membranous area plays a role in several forms of cerebellar hypoplasia related to the ▶Dandy–Walker malformation.

In the formation of the cerebellar cortex, there is first an outward migration of the Purkinje cells and granular cells. Later an inward migration takes place, forming the internal granular cell layer.

The vermis has formed by the 16th week of gestation and the hemispheres 4–8 weeks later. The formation of the vermis is closely related to formation of the hemispheres. The foliation and fissuration occur at least partly simultaneously and are triggered by the migration of Purkinje and granular cells. These processes explain at least to some extent the malformations of fissuration and foliation.

Clinical Presentation

The role of the cerebellum as a center for coordination, motor learning, and higher cognitive functions is well known. Cerebellar abnormalities will usually cause cerebellar signs and symptoms, such as ataxia, cranial nerve palsies, delayed language and speech development, eye movement disorders (nystagmus, oculomotor dyspraxia, and so on), and head/body turning attacks. Epilepsy and mild cognitive deterioration can also be part of the clinical spectrum.

The Chiari I malformation appears to be asymptomatic in up to 14% of the patients in a large series. Magnetic resonance (MR) imaging is not useful in differentiating these patients from symptomatic patients. The typical symptom is occipital headache when coughing or otoneurological disturbances, but the presentation is often more ambiguous.

Joubert syndrome is a separate entity within the molar tooth malformations and is characterized by episodic hyperpnea, abnormal eye movements, ataxia, and mental retardation.

Imaging

MR imaging is the modality of choice in the diagnostic work-up of cerebellar malformations. Computed tomography is not suited to assess intrinsic cerebellar abnormalities. Imaging in different planes is required, and if available, three-dimensional T2-weighted images can be helpful.

A classification is not yet available today, but using knowledge of anatomy, embryology, and histopathology, a provisional classification can be presented.

The two groups of cerebellar malformations are cerebellar hypoplasia and ▶cerebellar dysgenesis. Cerebellar hypoplasia includes the Dandy–Walker malformation. Cerebellar dysgenesis can further be divided into vermian and/or hemispheric dysgenesis. It seems inevitable that there will be some overlap between the two groups of malformations.

The ▶Chiari malformations are not included in the classification and are discussed separately.

Diagnosis

The imaging aspects of the common cerebellar malformations will be briefly reviewed.

The *Chiari I malformation* is defined as a caudal herniation of the cerebellar tonsils over a distance of at least 5 mm through the foramen magnum (below a line from the basion to the opisthion on a sagittal image; Fig. 1a). When the herniation is less than 5 mm, the term "tonsillar ectopia" can be used. This malformation is likely to be the result of an abnormally small posterior fossa and/or the occurrence of craniovertebral anomalies.

The *Chiari II malformation* is a complex entity thought to be due to a lack of expression of surface molecules that cause a persistent aperture of the posterior neuropore. The posterior fossa remains too small, and the cerebellum extends downward, upward, and around the brainstem. Not only the tonsils but parts of the vermis and even the fourth ventricle can herniate through the foramen magnum (Fig. 1b). A lumbar myelomeningocele is associated in more than 85% of cases.

The *Chiari III malformation* consists of a Chiari II malformation with an associated cephalocele (Fig. 1c).

The *Dandy–Walker malformation* is a typical example of vermian and/or hemispheric hypoplasia. It consists of (i) a variable degree of vermian agenesis, (ii) a dilatation of the fourth ventricle with cyst formation, and (iii) an enlarged posterior fossa (Fig. 2a, b). It is thought that a genetic mutation causes an abnormal development of the roof of the fourth ventricle. The posterior membranous area of the roof normally forms the foramen of Magendie. This does not happen in the Dandy–Walker malformation. The Dandy–Walker malformation can be associated with other congenital malformations and has been reported in several syndromes. In the differential diagnosis, one should consider the *persisting Blake's pouch*, the result of a nonperforation of the foramen of

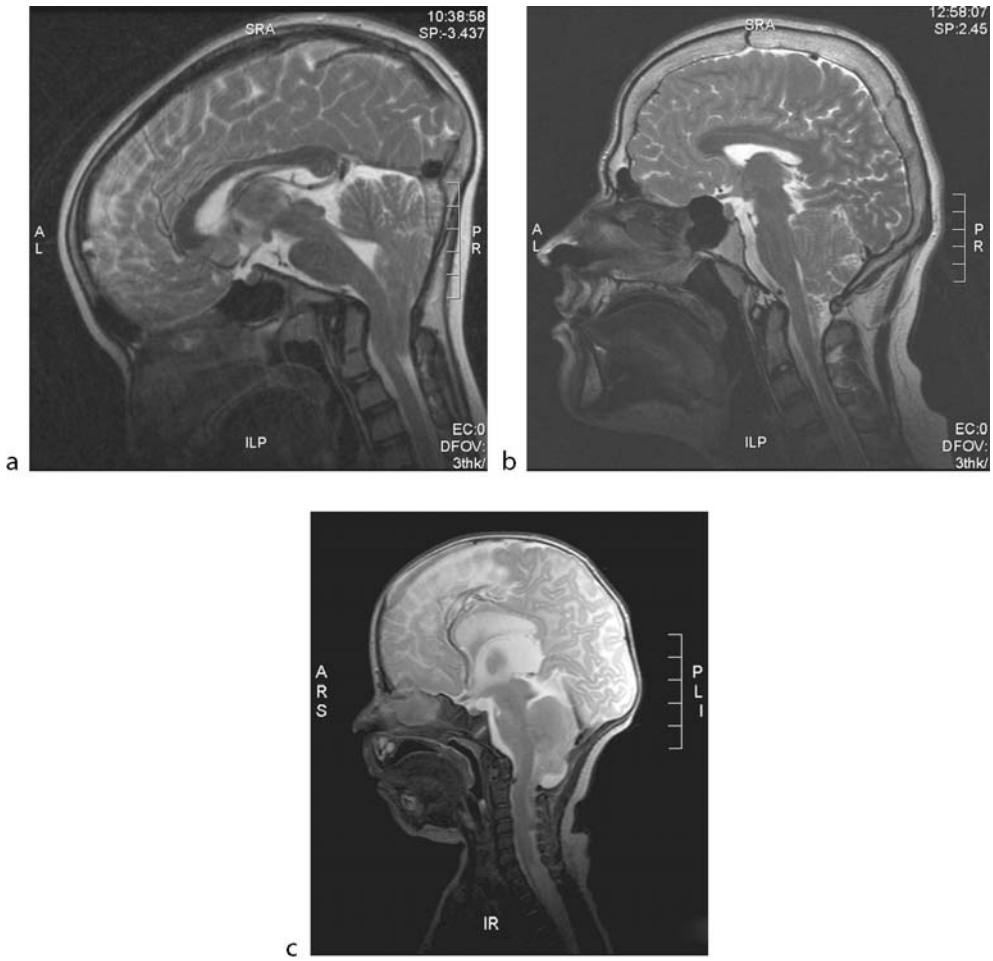

Congenital Malformations, Cerebellar. Figure 1 (a) Sagittal T2-weighted image, Chiari I malformation. Note the herniation of the cerebellar tonsils through the foramen magnum reaching the level of the endplate of C2. (b) Sagittal T2-weighted image, Chiari II malformation. Note the displacement of the fourth ventricle and the herniation of cerebellar tissue to the level of C3. There is tectal beaking and a concave lining of the clivus. The posterior fossa is small. (c) Sagittal T2-weighted image, Chiari III malformation. In addition to the typical finding of a Chiari II malformation, there is a craniocervical cephalocele.

Magendie (Fig. 2c). This malformation resembles *megacisterna magna*, but hydrocephalus is not seen in the latter. Megacisterna magna is asymptomatic but is sometimes considered a mild form of Dandy–Walker malformation. A late opening of the foramen of Magendie has been suggested as an underlying cause. *Arachnoid cysts* in the posterior fossa can resemble a megacisterna magna, but they usually cause symptoms and are often located laterally in the posterior fossa.

Cerebellar dysgenesis can involve the vermis only, the hemispheres only, or both.

The *molar tooth malformations* include several syndromes with *vermian dysgenesis*. Joubert syndrome is the best-known entity. A midline cleft is seen together with a peculiar shape of the fourth ventricle. These malformations are named after the molar tooth appearance of the midbrain on axial images (Fig. 3a, b). This is due to the horizontal course of the superior cerebellar peduncles (due to a lack of decussation of the superior cerebellar peduncles) and a narrow pontomesencephalic junction.

Rhombencephalosynapsis consists of vermian agenesis or severe hypogenesis, fusion of the hypoplastic cerebellar hemispheres, and fusion of the dentate nuclei. Dilated lateral ventricles, fusion of the thalami, and absence of the septum pellucidum can be associated. The disorder is possibly induced by a genetic mutation of the Lmx 1a gene, which regulates events at the pontomesencephalic junction between the fourth and the sixth weeks of gestation. Because of this early timing, metencephalosynapsis might be a more appropriate term. The vermis fails to differentiate, while the hemispheres remain undivided.

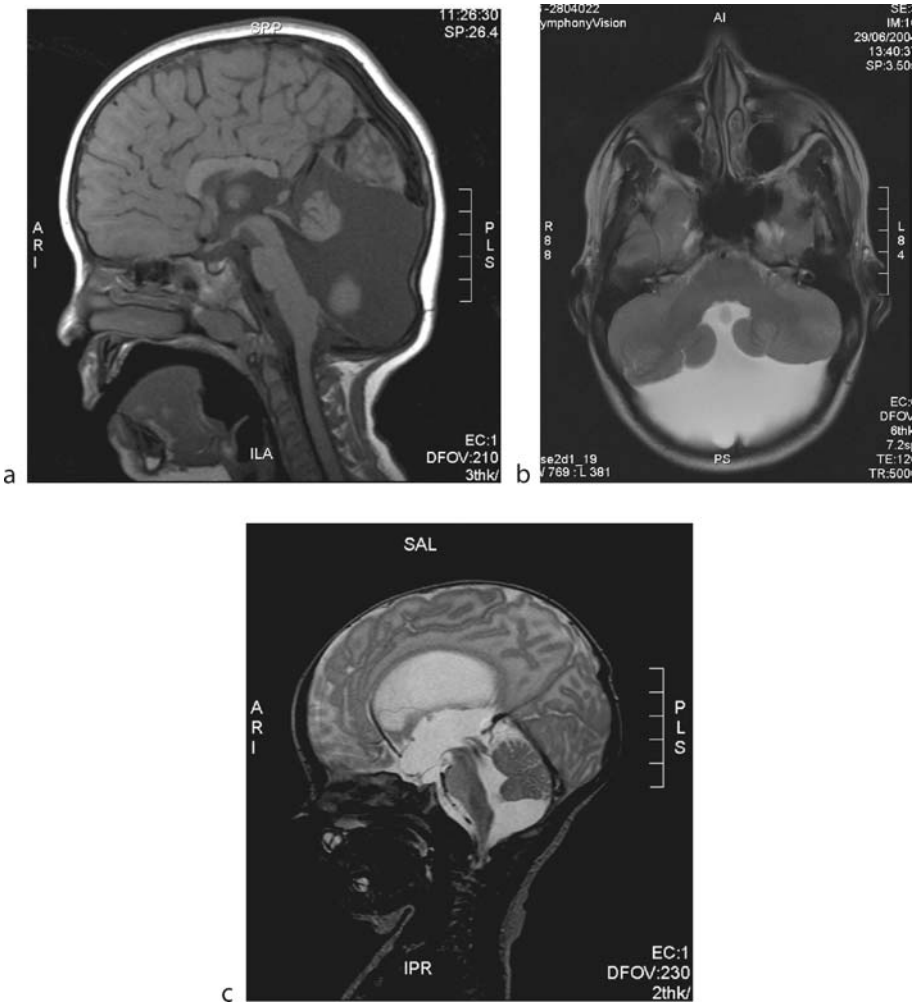

Congenital Malformations, Cerebellar. Figure 2 (a) Sagittal T2-weighted image, Dandy–Walker malformation. The posterior fossa is enlarged. There is an upward rotation of the remaining part of the superior vermis, and there is a large posterior fossa cyst. Note the displacement of the sinus rectus and the hypogenesis of the corpus callosum. (b) Axial T2-weighted image, Dandy–Walker malformation. There is a large communication between the fourth ventricle and the posterior fossa cyst. The hypoplastic cerebellar hemispheres appear "winged outward." (c) Sagittal T2-weighted image, persisting Blake's pouch. There is a large communication between the fourth ventricle and the subarachnoid space, and there is supratentorial hydrocephalus. The vermis is reasonably developed.

Recently, a series of abnormalities have been reported consisting of *vermian and/or hemispheric dysgenesis*.

When only the vermian fissures are involved, this is almost always an asymptomatic incidental finding (*type 1a*; Fig. 3c). Some patients also have an abnormal foliation of the anterior lobe and part of the posterior lobe of the vermis (*type 1b*). Hemispheric extension can occasionally be encountered. Cerebellar signs are frequently seen in this subgroup.

In abnormalities of foliation and fissuration *type 2*, three different hemispheric malformations can be recognized: (i) cortical dysgenesis, (ii) cortical hypertrophy, and (iii) aberrant orientation of the folia. These abnormalities can be seen together or separately. Cortical dysgenesis can be associated with small cyst-like inclusions (Fig. 3d, e). Similar abnormalities have been described in rare syndromes, including Fukuyama muscular dystrophy and Walker–Warburg syndrome, but they can also be observed in the absence of these syndromes. In 60% of the children with type 2 abnormalities, type 1b abnormalities are present, and more than 50% of these children have congenital cerebral anomalies.

The pathogenesis of Lhermitte–Duclos–Cowden remains incompletely elucidated. Although the lesion is classified as a dysplastic gangliocytoma according to

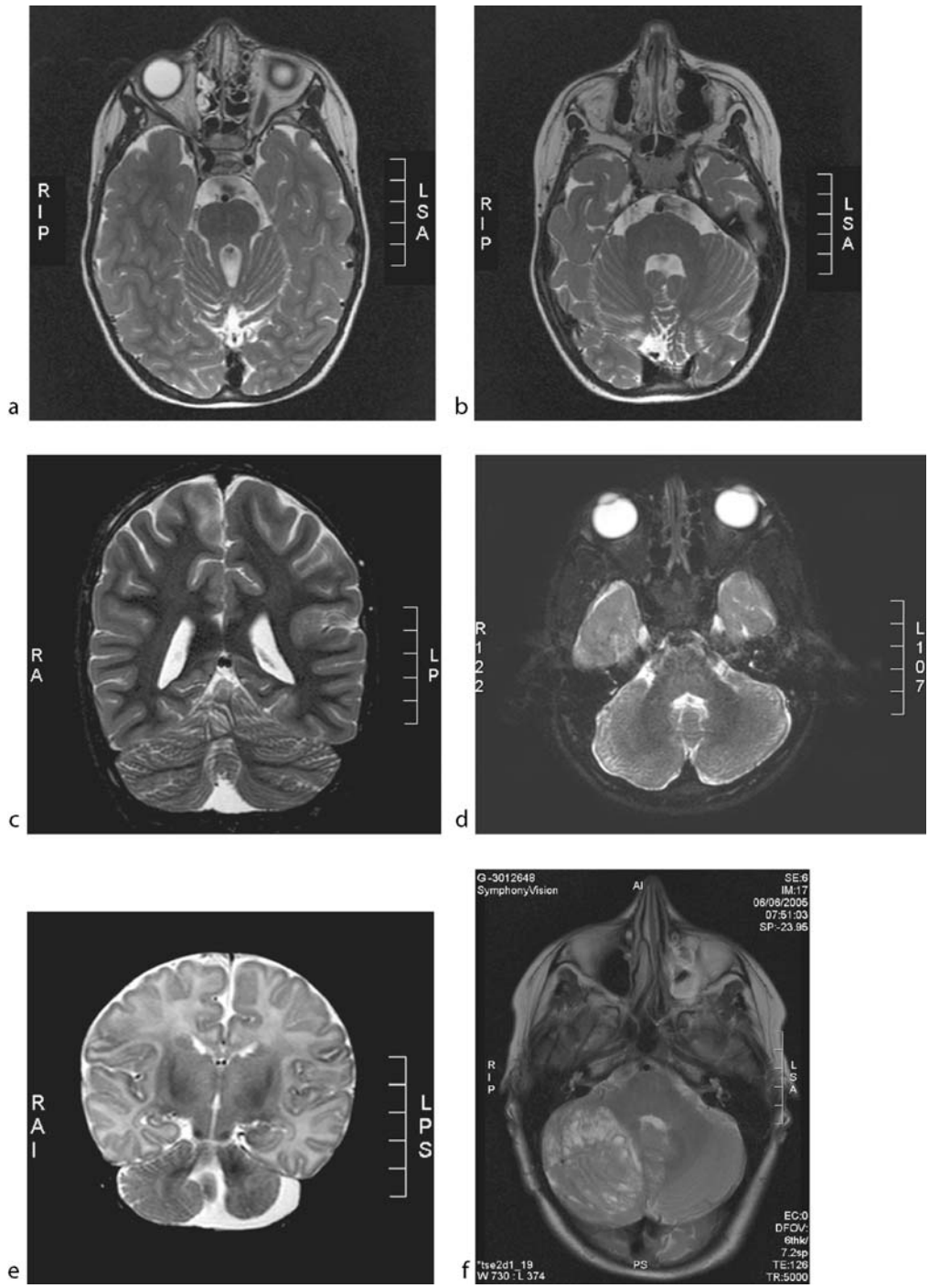

Congenital Malformations, Cerebellar. Figure 3 (a) Axial T2-weighted image, molar tooth malformation. Note the molar tooth appearance due to the horizontal course of the hypoplastic superior cerebellar peduncles. (b) Axial T2-weighted image, molar tooth malformation. The vermian cleft is seen with the "bat wing" appearance of the fourth ventricle. (c) Coronal T2-weighted image, type 1 abnormality of fissuration. The abnormal orientation of the fissures is noted. (d) Axial T2-weighted image, type 2 abnormality of foliation and fissuration. An abnormal foliation is seen, with multiple cyst-like inclusions in the cortex. (e) Coronal T2-weighted image, type 2 abnormality of foliation and fissuration. The cortical dysgenesis is clearly visible in the left hypoplastic cerebellar hemisphere compared with the normal right hemisphere. (f) Axial T2-weighted image, Lhermitte–Duclos–Cowden disorder. A masslike lesion is observed in the right cerebellar hemisphere with a striated folial pattern.

the World Health Organization, there are indications that it might represent a congenital malformation. The imaging appearance is that of a masslike abnormality with, to some extent, a striated pattern of the enlarged folia (Fig. 3f).

Bibliography

1. Barkovich AJ (2005) Pediatric Neuroimaging. 4th edn. Lippincott Williams & Wilkins Philadelphia, Baltimore, New York, London, Buenos Aires, Hong Kong, Sydney, Tokyo
2. Tortori-Donati P, Rossi A (2005) Pediatric Neuroradiology. Springer, Berlin, Heidelberg, New York
3. Demaerel P (2002) Abnormalities of cerebellar foliation and fissuration: classification, neurogenetics and clinicoradiological correlations. Neuroradiology 44:639–646

Congenital Malformations, Cerebral (Neuro View)

Thierry T. A.[1], Veronica Donoghue[2]
[1]Johns Hopkins University, Baltimore, USA
[2]Children's University Hospital, Dublin, Ireland
thierry.huisman@kispi.unizh.ch
veronica.donoghue@cuh.ie

Synonyms

Developmental cerebral anomalies; Disorders of neurulation

Definition

Congenital cerebral malformations result from an erroneous organogenesis, histiogenesis or cytogenesis of the central nervous system (CNS). The aetiology is multifactorial and includes genetic defects, intrauterine destructive events, ischaemia, infections and environmental agents (1–3).

Pathology and Histopathology

Malformations of the CNS are frequent (1:100 births) and may have a significant impact on the quality of life. Cerebral malformations encompass a wide variety of lesions ranging from tiny cortical dysplasias to extensive, highly complex pathologies.

The development of the brain is a highly complex, programmed sequence of interacting processes in which up to 100 billion neurons connect and communicate with each other using countless synapses. While the embryogenesis is most active during the first trimesters of gestation, maturational processes may extend into the second decade of life. The exact anatomical, maturational and functional development of the brain remains the focus of countless research projects.

Classical cerebral malformations should be distinguished from acquired cerebral malformations. Classical malformations result from an erroneous development of the brain which may be genetically encoded while acquired malformations relate to secondary malformations due to a destruction of initially correctly developed brain structures.

A significant overlap between these categories is present. Identical malformations may have different etiologies (e.g. infection, focal hypoperfusion or haemorrhage). In addition, identical 'destructive events' (e.g. focal hypoperfusion due to an arterial embolus) can result in a spectrum of pathologies. The timing of the 'event' in relation to the gestational age is a key feature. Moreover, an increasing number of gene defects are identified in congenital and so-called acquired cerebral malformations. Variable expressions of genetically mediated malformations may result in a spectrum of malformations. Finally, it is increasingly recognized that a predisposition for the development of malformations may be encoded in the chromosomes, a trigger is however necessary to induce the cascade of events.

Cerebral malformations are typically classified into disorders of (a) organogenesis, (b) histiogenesis and (c) cytogenesis. In disorders of organogenesis an altered brain development is combined with a normal histiogenesis while in disorders of histiogenesis, the overall brain structure is normal however anomalous cells persist and continue to differentiate. Inborn errors of metabolism or leukodystrophies represent disorders of cytogenesis.

Clinical Presentation

The spectrum of neurological symptoms varies widely and is often unpredictable. The extent of malformation correlates inconsistently with the severity of neurological symptoms or deficits. Large lesions may be discovered as incidental findings on neuroimaging. Neuronal and functional plasticity of the developing brain with relocation of functional centre may prevent overt neurological deficits. On the other hand, small lesions may present with significant neurological symptoms, e.g. a discrete cortical dysplasia may be causative for intractable seizures preventing normal development. Next to focal neurological deficits, many malformations result in cognitive deficits with different degrees of mental retardation.

Posterior fossa malformations may be present with ataxia. In combined brainstem and cerebellar malformations (e.g. Joubert syndrome) brainstem symptoms may accompany cerebellar symptoms. In callosal malformations and disorders of diverticulation hypothalamic–pituitary malfunction and facial malformations — '*the face predicts the brain*' — occur.

Imaging

Frequent disorders of organogenesis include posterior fossa malformations, callosal or commissural malformations. Disorders of diverticulation or cleavage disorders are less frequently encountered. Malformations of cortical development are described in the chapter on gyration disorders. Ultrasound (US) may serve as a first line imaging tool in neonates. Magnetic resonance imaging is applied when US or CT suspected complex malformations.

Posterior Fossa Malformations

Chiari I Malformation. The cerebellar tonsils herniate into the upper cervical spinal canal (>5 mm below the level of the foramen magnum). The tonsils may be compressed/deformed. Associated syringohydromyelia is seen in 20–25% of cases. There is no increased risk for additional cerebral malformations.

Chiari II Malformation. Complex malformation most probably resulting from too small a posterior fossa in patients with open neural tube defects. The spectrum of findings include varying degrees of downward displacement of the cerebellum with herniation of cerebellar structures into the upper cervical spinal canal, kinking of the upper cervical spinal cord, embracement of the brainstem by the cerebellar hemispheres, tectal plate deformation, supratentorial hydrocephalus, prominent interthalamic adhesion and fenestrations of the falx cerebri with interdigitation of the cerebral hemispheres. Frequently an associated callosal dysgenesis is observed (Fig. 1).

Chiari III Malformation. Very rare malformation of the posterior fossa represented by the spectrum of findings encountered in Chiari II malformation in combination with a low occipital or high cervical meningo-encephalocele.

Rhomboencephalosynapsis. Single lobed cerebellum with vermian agenesis, fusion of both cerebellar hemispheres, dentate nuclei and superior cerebellar peduncles. The cerebellar fissures typically course over the entire cerebellar surface without interruption. Additional malformations are frequent.

Joubert syndrome. Congenital vermian hypoplasia or aplasia. The IV ventricle is deformed and resembles a bat-wing or umbrella while the brainstem resembles a molar tooth on axial imaging. Associated ocular and renal lesions are known.

Cystic Posterior Fossa Malformations

Dandy Walker Malformation. Cystic dilatation of the IV ventricle in combination with varying degrees of vermian hypoplasia. The posterior fossa may be normal in size or enlarged, the torcula is frequently elevated and the vermian remnant rotated upward. The brainstem may be compressed against the clivus. The choroid plexus within the IV ventricle is usually absent, the tentorium cerebelli hypoplastic. Associated malformations are seen in up to 60% of patients, most frequently including callosal dysgenesis, polymicrogyria, cephaloceles and ventricular dilatation. The wide open IV ventricle often resembles a keyhole (Fig. 2). Dandy Walker malformations are believed to result from a combined defective development of the velum medullare anterior and posterior.

Blake's Pouch Cyst. Outpouching of the velum medullare posterior most probably resulting from an incomplete or absent rupture of the velum medullare posterior during development. The posterior fossa may be enlarged, the torcula elevated. The vermis and falx cerebelli is normally developed, the IV ventricle choroid plexus may be displaced dorsally. Associated cerebral malformations are rare.

Retrocerebellar Arachnoid Cyst and Mega Cisterna Magna. The differentiation between an arachnoid cyst and a mega cisterna magna can be difficult. The posterior fossa may be enlarged the cerebellar hemispheres and vermis can be displaced. The IV ventricle choroid plexus is in its normal location. Associated cerebral malformations are rare.

Callosal or Commissural Malformations

In the evaluation of callosal malformations it should be noted that the normal corpus callosum (CC) has a wide variability in size and shape. In addition, it is essential to determine if the encountered callosal anomaly is a primary malformation or a secondary anomaly in shape due to e.g. an adjacent white matter ischemia with focal callosal atrophy or a callosal thinning in chronic severe hydrocephalus.

The CC develops in a programmed sequence (genu, truncus, splenium, rostrum). Callosal agenesis may be partial or complete. Associated cerebral malformations are seen in 50% of cases.

On sagittal images the defective CC is easily identified. In addition, the medial surface of the cerebral hemisphere reveals a radiating pattern of sulci due to the missing cingulate sulcus (no inversion of the cingulate gyrus). On coronal images, the III ventricle may extend superiorly between the hemispheres. The lateral ventricles are displaced laterally and show a trident shape due to the impression by the Probst bundles. The hippocampi may be malrotated. On axial images, the lateral ventricles show

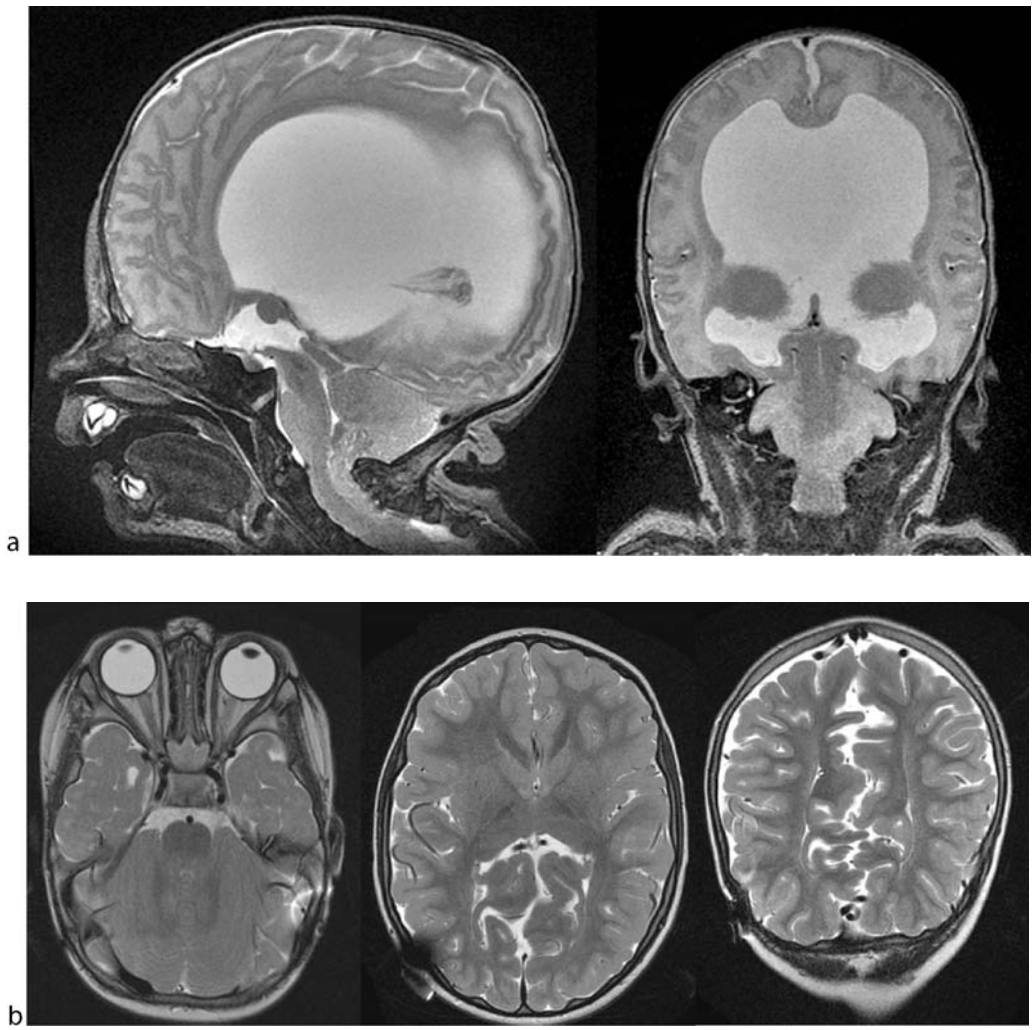

Congenital Malformations, Cerebral (Neuro View). Figure 1 (a) Chiari II malformation: Sagittal, and coronal T2-FSE MRI reveals a small posterior fossa with herniation of the cerebellar tonsils into the upper cervical spinal canal, displacement and compression of the brainstem against the clivus and supratentorial hydrocephalus. (b) Chiari II malformation: Axial and coronal T2-FSE MRI shows a characteristic embracement of the brainstem by the cerebellar hemispheres, a prominent adhesion interthalamica and a fenestration of the falx cerebri with interdigitations of both cerebral hemispheres.

a parallel course, the occipital horns may be enlarged (Fig. 3). Occasionally, an associated interhemispheric lipoma is encountered.

Callosal agenesis is frequently only one component of a more extensive commissural malformation. Consequently, in callosal anomalies, the anterior and posterior commissure as well as the fornix and hippocampi should be studied.

Disorders of Diverticulation or Cleavage Disorders

These anomalies are also known as disorders of ventral induction. They include the holoprosencephaly spectrum. An increasing number of gene defects are identified in holoprosencephaly. Basically, holoprosencephaly results from an incomplete or absent cleavage of the prosencephalon. The spectrum of malformation depends on the degree of cleavage.

Alobar Holoprosencephaly. Most severe form characterized by a small holosphere, monoventricle, fused thalami, missing III ventricle, no falx or CC and no interhemispheric fissure. Frequently, associated malformations of the circle of Willis are encountered.

Semilobar Holoprosencephaly. Partial cleavage of the prosencephalon. The anterior parts of the brain are fused while the posterior brain is split. The thalami are partially separated, a small III ventricle is present, rudimentary temporal horns are seen. The falx cerebri

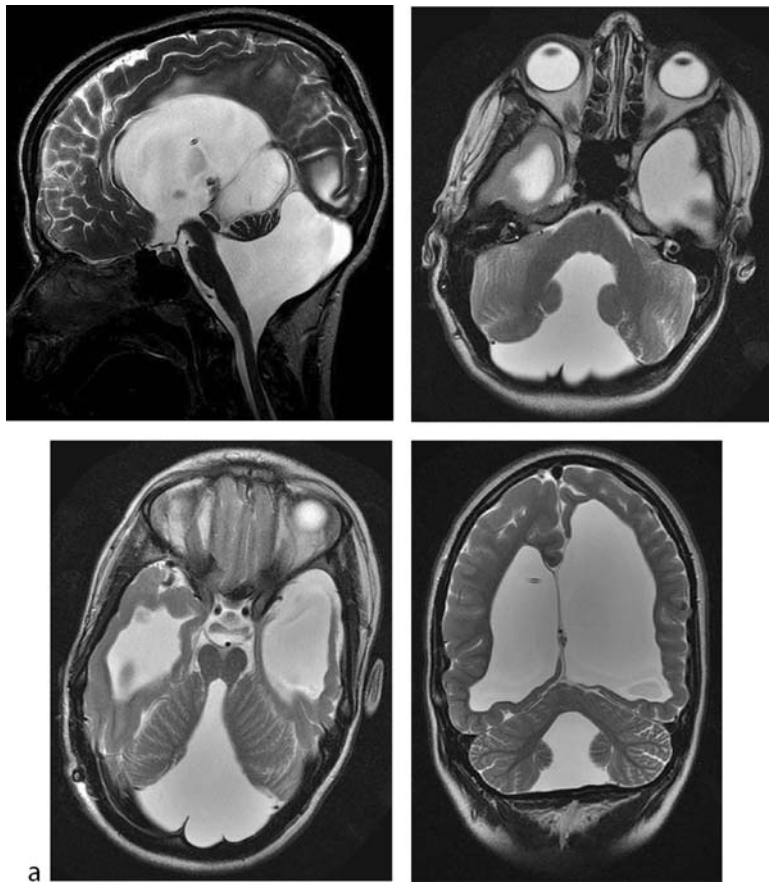

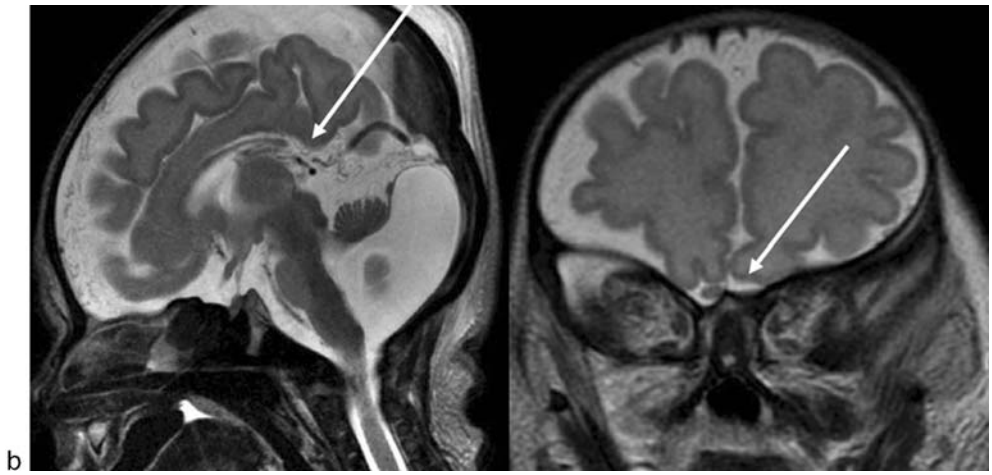

Congenital Malformations, Cerebral (Neuro View). Figure 2 (a) Dandy Walker malformation: Sagittal, axial and coronal T2-FSE MRI reveal a classical Dandy Walker malformations with a cystic dilatation of the IV ventricle, in combination with a hypoplastic, upward rotated superior vermis. No IV ventricle choroid plexu is seen. The brainstem is hypoplastic. On axial images the IV ventricle mimics a key hole. In addition, a supratentorial hydrocephalus is seen. (b) Dandy Walker malformation: Sagittal and coronal T2-FSE MRI may identify a variety of coexisting malformations like e.g. a hypoplastic corpus callosum or a hypoplastic olfactory bulb.

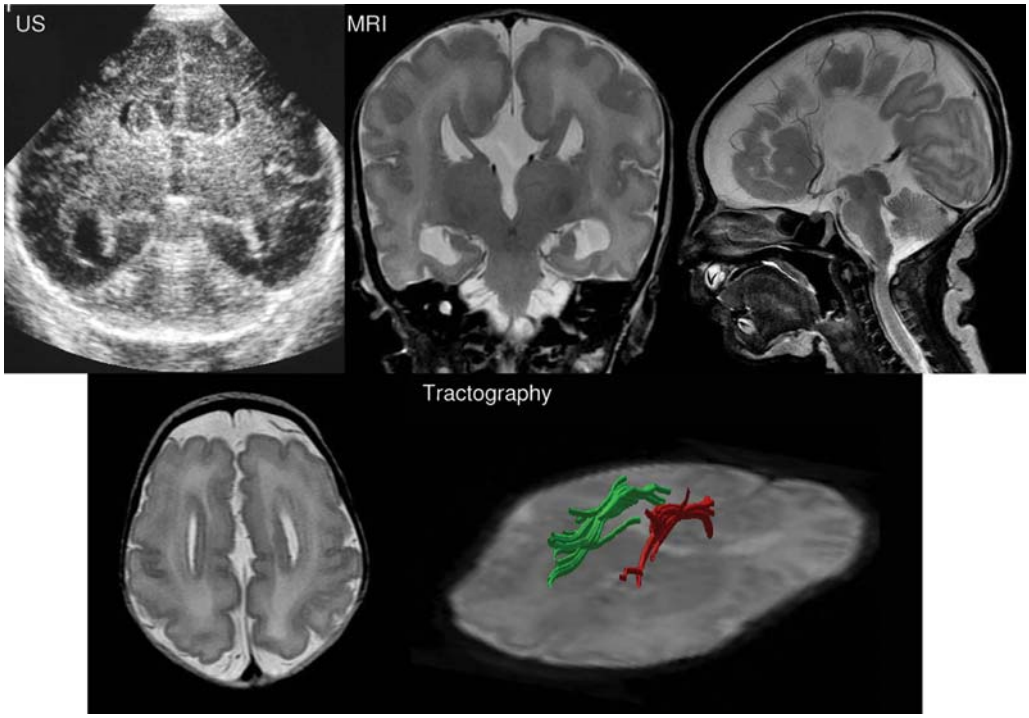

Congenital Malformations, Cerebral (Neuro View). Figure 3 Callosal dysgenesis: Coronal US identifies the characteristic trident shape of the lateral ventricles due to callosal dysgenesis. Coronal, sagittal, and axial T2-FSE reveal the characteristic findings of a callosal dysgenesis including an enlarged, interhemispheric extending III ventricle, a radial gyral pattern of the medial brain surface, a trident shape of the lateral ventricles on coronal images, a parallel course of the lateral ventricles on axial images and T2-hypointense Probst bundles along the medial surface of the lateral ventricles. Tractograhy reconstructions based on diffusion tensor imaging confirms the anterior–posterior course of the Probst bundles.

and interhemispheric fissure is present in the dorsal parts of the brain. This is the only callosal malformation where the dorsal parts of the CC may be present without the anterior part. The optic nerves and olfactory bulbs are frequently hypoplastic.

Lobar Holoprosencephaly. Near complete cleavage of the prosencephalon results in a lobar brain with hypoplastic frontal lobes and rudimentary frontal horns. The falx cerebri extends frontally, the temporal horns are formed.

Septo-Optic Dysplasia. Septo-optic dysplasia is considered to be the mildest variant of lobar holoprosencephaly characterized by an absent septum pellucidum, hypoplastic optic nerves and chiasm. The olfactory bulbs are frequently hypoplastic. Associated cerebral malformations are seen in up to 60% of cases.

Diagnosis

Ultrasound may serve as a first line imaging tool in neonates. Especially when a hydrocephalus is suspected, ultrasound is highly sensitive and may show additional gross parenchymal abnormalities next to the ventricular enlargement. A complete identification of the exact extent and degree of cerebral malformation is essential to guide treatment, may give information concerning prognosis and outcome and should be used for counselling of future pregnancies. Definite diagnosis consequently relies on high resolution triplanar neuroimaging. MRI has proven to be most reliable. With the advance of functional MRI techniques, such as diffusion tensor imaging and tractography (Fig. 3) detailed structural-functional informations can be collected. In the evaluation of malformations of the central nervous system, each radiologist should be aware that if they find one malformation they should look for additional malformations. Frequently, the most obvious lesion is just the tip of the iceberg. A proper knowledge of the complex embryology and maturation of the brain is mandatory.

Bibliography

1. Barkovich AJ (2000) Pediatric neuroimaging, 3rd edn. Lippincott Williams & Wilkens, Philadelphia, pp 251–381
2. Osborn AG (2004) Diagnostic imaging: brain. Amirsys, Salt Lake City, pp I-1–4–78
3. Tortori-Donati P (2005) Pediatric Neuroradiology: Brain. Springer Verlag, Berlin, Heidelberg, pp 41–198

Congenital Malformations, Cerebrum

Pieter Waer, Philippe Demaerel
Dept of Radiology, University Hospitals K.U. Leuven, Leuven, Belgium
philippe.demaerel@uz.kuleuven.ac.be

Synonyms

Anomalies of the cerebral commissures; Cephalocele; Dorsal induction anomalies; Neuronal migration disorders; Ventral induction anomalies

Definition

Depending on the time of insult, different malformations may occur during cerebral development. Often, this will be multifocal involving several brain structures.

It is important to realize that most malformations can display mild, moderate, or extensive changes and that different malformations often occur simultaneously.

Cortical developmental malformations are by far the most common cerebral malformations. Terminology has not always been straightforward, but nowadays a good and flexible classification for the cortical developmental malformations is available which allows the inclusion of new observations (1).

Pathology/Histopathology

A brief review of the embryology of the brain is necessary in the understanding of the pathology of cerebral malformations (2, 3).

Although the cause of cephaloceles remains not fully elucidated, it is believed they may result from a failure of neural tube closure. Other authors have suggested that they might be due to an event occurring after the closure of the neural tube.

The anterior part will form the prosencephalon, mesencephalon, and rhombencephalon at around 30 days of gestation. At this time, the corpus callosum will develop from the commissural plate at the rostral end of the neural tube. The genu of the corpus callosum is formed before the truncus and the splenium. At the end, a more anterior part of the genu and the rostrum become visible. This sequence of formation will be important in analyzing partial agenesis of the corpus callosum. Remnants of the meninx primitiva give rise to the interhemispheric lipomas.

In holoprosencephaly there is a failure of cleavage into hemispheres and sometimes even a failure of separation of the telencephalon from the diencephalon.

The most commonly encountered cerebral malformation is the cortical developmental malformation. The formation of the cerebral cortex begins during the seventh week of gestation with the period of neuronal and glial proliferation in the germinal matrix. The second period consists of a migration of the neurons from the germinal zone along the so-called guiding radial glial fibers. This process takes place between the eighth and twenty-fourth week of gestation. The six-layered cortex can be recognized in the sixteenth fetal week. The thickness does not exceed 4.5 mm. The period of migration is followed by cortical organization, leading to the complex three-dimensional structure of the mature cortex.

Up to the eighteenth week, the hemispheric surface is smooth. At this time, the callosal and parieto-occipital sulci and the calcarine fissure are visible. From 20 weeks onwards, a progressive sulcation can be observed until the thirty-second to thirty-fourth week of gestation.

Clinical Presentation

Minor congenital cerebral malformations can remain asymptomatic. However, often developmental delay, mental retardation, spasticity, hypotonia, epilepsy, hemiplegia, or diplegia are seen in children with a cerebral malformation.

Macro- or microcephaly can also be a sign of an abnormal development.

When the cerebral malformations are part of a syndrome, extracranial anomalies can be encountered.

Imaging

In imaging cerebral malformations, one should always obtain T1- and T2-weighted images, because the ongoing myelination may mask possible malformations during the first 2 years of life on one of these sequences. Additional three-dimensional imaging, using either a T1-weighted gradient-echo sequence or a T2-weighted sequence, will be extremely helpful in displaying the abnormalities.

Diagnosis

The list of cerebral malformations is very extensive and detailed. Here, only the most common malformations are discussed.

Skull and skull base defects are often referred to as "*cephaloceles*." The defect can contain meninges, brain tissue, and/or cerebrospinal fluid.

The terms hypogenesis or complete agenesis are preferably used for partial or complete absence of the corpus callosum. In hypogenesis, the anterior part of the corpus callosum is usually present. The imaging findings of agenesis are quite specific. A radial pattern can be seen on sagittal images (Fig. 1). This is due to the eversion of the cingulate gyri and radial orientation of the medial hemispheric sulci from the region of the roof of the third ventricle. Colpocephaly, corresponding to the dilatation of the trigones and posterior horns of the lateral ventricles, is typically seen on axial images. The third ventricle is widened and extends superiorly. Interhemispheric cysts can be found, and different subtypes have been recognized. Interhemispheric lipomas have frequently been described in association with partial or complete absence of the corpus callosum (4). A curvilinear type of lipoma often appears to be an incidental finding, while the tubulonodular lipoma is usually associated with a more severe abnormality of the corpus callosum and tends to be symptomatic.

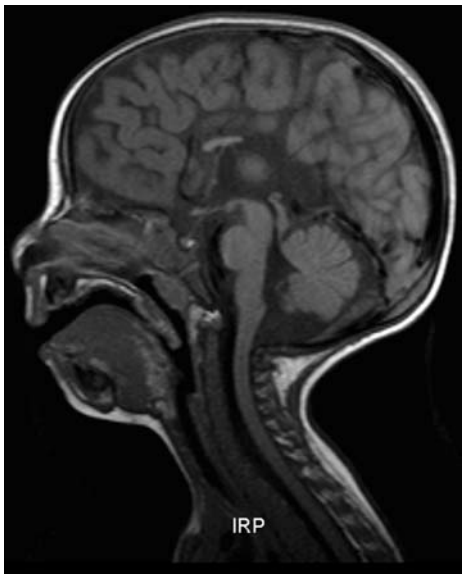

Congenital Malformations, Cerebrum. Figure 1 Agenesis of the corpus callosum. Sagittal T1-weighted image. The typical radial pattern on a mid-sagittal image is due to the radial orientation of the medial hemispheric sulci. The structure visualized is an enlarged hippocampal commissure and does not correspond to the genes of the corpus callosum.

Alobar, semilobar, and lobar *holoprosencephaly* have been distinguished, but significant overlap exists between the different types. The septum pellucidum and the olfactory bulb are always absent in the three subtypes. The lobar form is the least severe from the clinical point of view and the abnormalities can sometimes be very subtle. This latter form is also closely related to septo-optic dysplasia. *Septo-optic dysplasia* or de Morsier's syndrome consists of hypoplasia of the optic nerves and chiasm with absence of the septum pellucidum (Fig. 2). Magnetic resonance (MR) imaging has been used to further classify patients with optic nerve hypoplasia. In 25% of the patients, no associated abnormalities could be demonstrated. The septum pellucidum was absent in 20% of the children. An ectopic neurohypophysis was observed in 15% of the patients. An associated cortical developmental anomaly was found in 15% of the patients with optic nerve hypoplasia. There was evidence of antenatal or prenatal brain injury in the remaining 25% of the children.

Three groups of *cortical developmental malformations* are distinguished: (i) abnormalities of neuronal and glial proliferation, (ii) abnormalities of neuronal migration,

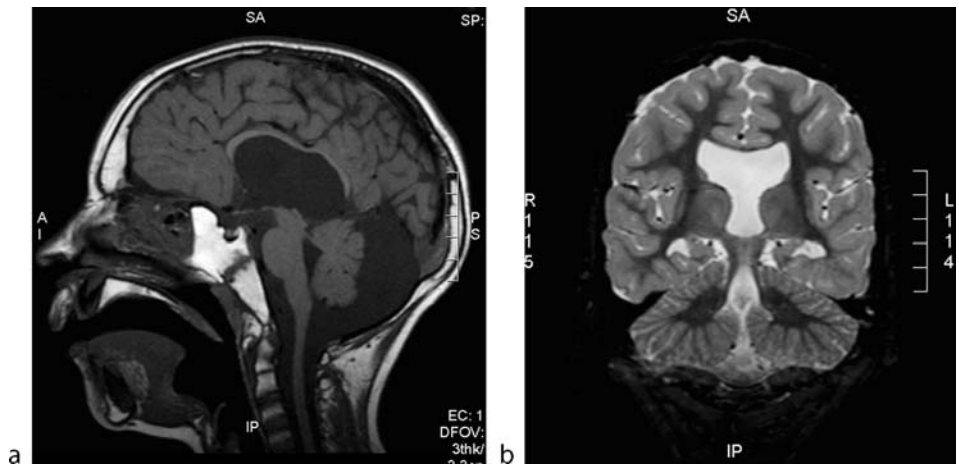

Congenital Malformations, Cerebrum. Figure 2 Septo-optic dysplasia. Sagittal T1-weighted (a) and coronal T2-weighted (b) images. The optic chiasm is hypoplastic (a). The septum pellucidum is absent (b).

and (iii) abnormalities of cortical organization. These malformations can result from several environmental factors including maternal exposure to ethanol and radiation, ischemia, or *in utero* infection, but an increasing number of genetic causes are being identified (5, 6).

The *abnormalities of neuronal proliferation* occur in the early days of cortical development and they often show a high signal on T2-weighted images. Focal cortical dysplasia, first described by Taylor, consists of a focal disorganized cortex with abnormally large neurons, called balloon cells because of their histopathological appearance. On imaging the cortex may appear normal or thinner, usually with blurring of the gray–white matter interface, a useful sign for differentiating focal cortical dysplasia from polymicrogyria (Fig. 3). The high signal on T2-weighted images may be due to gliosis and/or the presence of balloon cells.

Hemimegalencephaly may involve part of one hemisphere or the whole hemisphere and hemicranium. The affected area appears strongly enlarged and has heterogeneous signals reflecting dysmyelination and abnormalities of proliferation, migration, and cortical organization. The abnormalities may undergo changes over time.

The *abnormalities of neuronal migration* occur during the migration of the neurons from the germinal matrix to their final destination, the cortex. They typically have a signal similar to that of gray matter. Lissencephaly is also referred to as agyria-pachygyria complex. Some patients have been shown to have chromosomal mutations, the best known clinical entity being the autosomal dominant form of the Miller–Dieker syndrome. A variable involvement of the cortex can be observed, usually correlating with the severity of the symptoms. In pachygyria the cortex is thickened and the sulci are incompletely formed (Fig. 4). The junction between gray and white matter is regular as opposed to the junction in polymicrogyria.

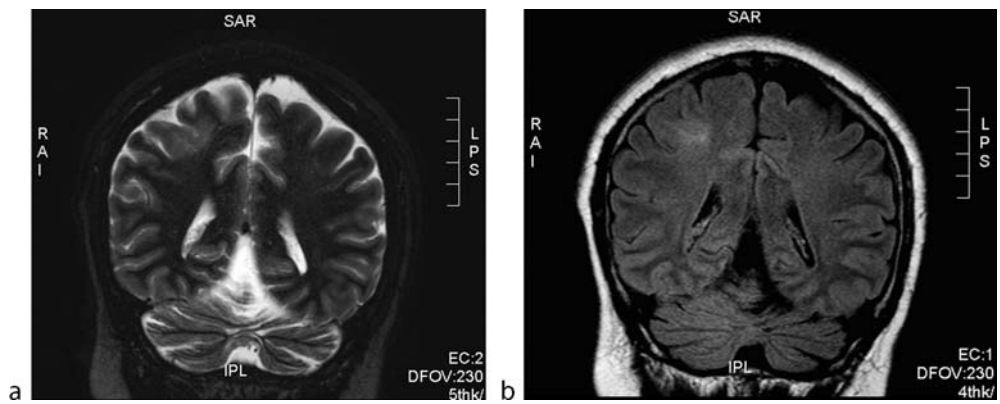

Congenital Malformations, Cerebrum. Figure 3 Focal cortical dysplasia of Taylor. Coronal T2-weighted (a) and fluid-attenuated inversion recovery (b) images. The abnormalities in the cortex and in the subcortical white matter of the right parietal lobe are better seen on the second image (b).

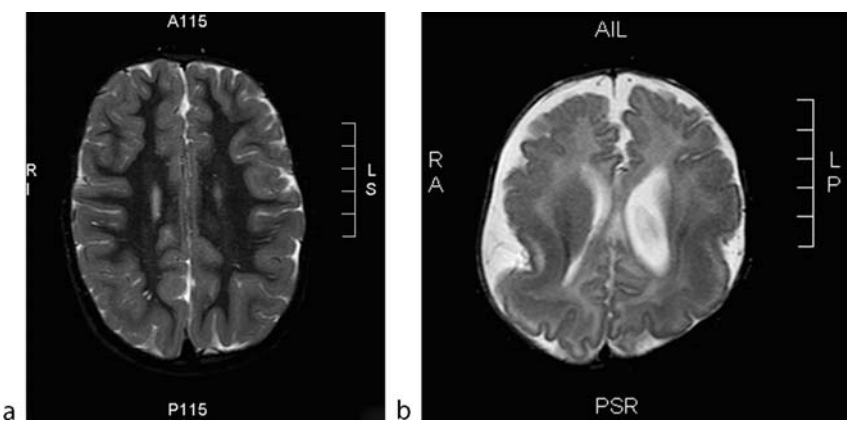

Congenital Malformations, Cerebrum. Figure 4 Pachygyria. Axial T2-weighted (a, b) images. Bilateral focal pachygyria in the parietal lobe (a) and more extensive pachygyria in a 3-month-old infant (b).

Heterotopic gray matter can be located in the subependymal region, in the subcortical region, or in between at any point along the route of migration from the subependymal region to the subcortex (Fig. 5). Heterotopia refers to normal structures in an abnormal site.

Later during gestation, *malformations of cortical organization* can be observed. Polymicrogyria refers to an abnormal gyration consisting of an increased number of gyri. Cortical maldevelopment is due to a process affecting mainly the deep cortical layers, reducing vascularization and arresting growth. Excessive proliferation of the outer layers results in the increased number of gyri. Whereas in the past it was debatable whether polymicrogyria could be diagnosed on MR imaging or only histopathologically, it is now accepted that the diagnosis can be given on imaging (Fig. 6). The inner border is sharp but irregular, which allows the differential diagnosis with pachygyria to be made, where the inner border is sharp but smooth. Bilateral perisylvian polymicrogyria is a well-recognized entity. Usually the opercular and perisylvian cortex are involved.

The term schizencephaly merely refers to an abnormal cleft. The cleft is lined by a polymicrogyric cortex and extends from the subependymal region to the pia. Bilateral and unilateral schizencephaly can be observed, most often in the perisylvian area. The terms open and closed lip schizencephaly refer to the separated and adjacent walls of the cleft.

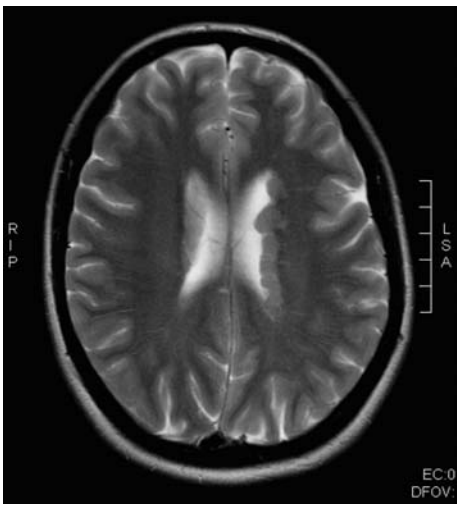

Congenital Malformations, Cerebrum. Figure 5
Subependymal heterotopia. Axial T2-weighted image. Heterotopic gray matter nodules are seen in the subependymal region on the left side.

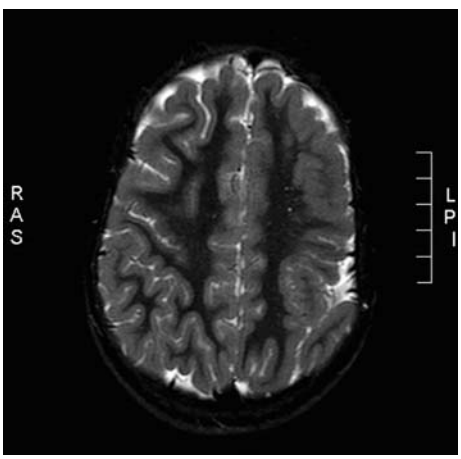

Congenital Malformations, Cerebrum. Figure 6
Polymicrogyria. Axial T2-weighted image. Numerous small abnormal gyri are seen in the left parietal lobe. Note the difference with pachygyria.

Bibliography

1. Barkovich AJ, Kuzniecky RI, Dobyns WB et al (1996) Classification scheme for malformations of cortical development. Neuropediatrics 27:59–63
2. Barkovich AJ (1996) Congenital malformations of the brain and skull. In: Barkovich AJ (ed) Pediatric Neuroimaging. 2nd edn. Lippincott-Raven Publishers, Philadelphia, pp 177–276
3. Sidman RL, Rakic P (1982) Development of the human central nervous system. In: Haymaker W, Adams RD (eds) Histology and Histopathology of the Central Nervous System. Thomas, Springfield, pp 3–145
4. Vandegaer Ph, Demaerel Ph, Wilms G et al (1996) Interhemispheric lipoma with variable callosal dysgenesis: relationship between embryology, morphology, and symptomatology. Eur radiol 6:904–909
5. Barkovich AJ (2002) Magnetic resonance imaging: role in the understanding of cerebral malformations. Brain Dev 24:2–12
6. Blaser SI, Jay V (2002) Disorders of cortical formation: radiologic-pathologic correlation. Neurosurg Clin N Am 13:41–62

Congenital Malformations, Liver and Biliary Tract

Huisman TA[1], Paola Vagli[2]
[1]Johns Hopkins University, Baltimore, USA
[2]Department of Diagnostic and Interventional Radiology, University of Pisa, Italy
thierry.huisman@kispi.unizh.ch
bartolozzi@do.med.unipi.it

Synonyms

Congenital hepato-biliary anomalies; Hepato-biliary malformations

Definition

Congenital anomalies of the liver and biliary system present early in life and may result from hereditary or developmental errors.

Introduction

Congenital hepato-biliary anomalies include a wide spectrum of malformations involving the liver, the biliary tree, and the gallbladder. Children may be asymptomatic or suffer from significant disease, e.g., neonatal jaundice. The most frequent congenital anomalies include ►biliary atresia, ►Alagille syndrome, ►choledochal cysts, ►Caroli's disease, congenital hepatic fibrosis, ►polycystic liver disease, and ►gallbladder anomalies. In neonates with unexplained persisting jaundice hepato-biliary anomalies should be excluded.

Pathology and Histopathology

Biliary Atresia

Persisting neonatal jaundice results in one-third of cases from biliary atresia. Biliary atresia is characterized by a (sub-) total obliteration of the extrahepatic biliary system. Fetal cholangitis due to a malformed biliary tree is believed to be the causative. To prevent permanent hepatic damage, early surgical correction is mandatory. Biliary atresia is associated with situs inversus, congenital heart disease, vascular anomaly, trisomy 17, 18, 21, and polysplenia syndrome.

Alagille Syndrome

Autosomal dominant disorder with chronic cholestasis is due to a hypoplasia of interlobular bile ducts. Associated congenital abnormalities include an abnormal facies, ocular anomalies, butterfly vertebrae, and complex cardiac malformations. Second most common cause of cholestasis in neonates. The incidence is 1 per 100,000 live births. Liver biopsy confirms diagnosis.

Choledochal Cysts

Choledochal cysts encompass a spectrum of common bile duct dilatations that may present with cholestatic jaundice or recurrent cholangitis. The different forms have been classified by Todani. Choledochal cyst type I is the most frequent form (80–90% of cases) characterized by a focal dilatation of the common bile duct. Type I choledochal cysts most probably results from an anomalous proximal insertion of the pancreatic duct into the common bile duct. Reflux of pancreatic enzymes will induce a localized cholangitis with resulting obstruction of the distal common bile duct and proximal dilatation.

Type II choledochal cysts are characterized by focal diverticula of the common bile duct. Type III choledochal cysts are basically ►choledochoceles that protrude into the duodenal lumen. Todani's type IVA shows multiple intra- and extrahepatic cysts while type IVB shows multiple extrahepatic cystic dilatations of the common bile duct. Todani's type V, also known as Caroli's disease, is characterized by segmental nonobstructive dilatations of the intrahepatic bile ducts. This form is associated with stone formation, recurrent cholangitis, and hepatic abscesses. Hepatic fibrosis may develop. Caroli's disease is frequently associated with medullary sponge kidneys, polycystic kidney disease, and nephrothisis. Portal hypertension may develop in disease progress.

Congenital Hepatic Fibrosis

Autosomal recessive disorder occurs with or without associated biliary duct ectasia and infantile or adult polycystic kidney disease. Periportal fibrosis and the presence of irregularly shaped, partially cystic, dilated small bile ducts are the primary pathologic findings. During the course of the disease, hepatomegaly with signs of portal hypertension develops (1).

Polycystic Liver Disease

Two forms are described: the infantile type and the adult type. The infantile type is less common and has an autosomal recessive inheritance while the adult type is autosomal dominant. Children usually present with renal disease are due to the associated polycystic kidney disease. Hepato-biliary cysts may be intrahepatic and/or peribiliary near portal triads or the hepatic hilum.

Gallbladder Anomalies

The gallbladder may be congenitally absent, ectopically located, duplicated, or septated. An absent gallbladder may be an associated finding in polysplenia syndrome. Ectopically located gallbladders are seen within the left hemiabdomen (e.g., situs inversus), in the midline (e.g., asplenia syndrome), intrahepatic, within the abdominal wall, in the falciform ligament ,and in the retroperitoneal area.

Clinical Presentation

Biliary Atresia

Clinical symptoms are related to the neonatal cholestasis. Key findings include jaundice, dark urine, and pale stools. Hepatomegaly may present early, splenomegaly is common

on follow-up due to liver cirrhosis and portal hypertension. Conjugated hyperbilirubinemia and increased levels of alkaline phosphatase, gamma glutamyl transpeptidase and serum aminotransferases may be present.

Alagille Syndrome

The combination of a chronic cholestasis, abnormal facies, ocular abnormalities, butterfly vertebrae, and complex cardiac anomalies are highly suggestive for Alagille syndrome. Most patients if not treated by means of orthotopic liver transplantation will die before the third decade.

Choledochal Cysts

In young children, the lead feature is chronic cholestatic jaundice while clinical presentation in older children may include abdominal pain, obstructive jaundice, and fever. In addition, acholic stools, hepatomegaly, and intermittent episodes of cholangitis and pancreatitis are seen. In untreated cases, recurrent ductal inflammation and biliary stasis may be complicated by hepatic abscesses, cirrhosis, portal hypertension, and cholelithiasis. Laboratory findings are nonspecific. Surgical treatment with complete excision of the cyst and creation of a biliodigestive anastomosis is recommended.

Congenital Hepatic Fibrosis

Principal clinical symptoms are related to the associated renal abnormalities. Initially, liver function may remain preserved, on follow-up hepatomegaly and portal hypertension may develop. Complicating cholangitis occurs.

Polycystic Liver Disease

Most children initially present because of the associated renal disease. Clinical symptoms that are related to the liver include hepatic enlargement by the multiple cysts with compression of adjacent organs as well as the intrinsic bile ducts. In addition, cysts may rupture or hemorrhage. In late stages, hepatic fibrosis may result in portal hypertension.

Gallbladder Anomalies

Gallbladder anomalies are usually asymptomatic and incidentally discovered. Clinical symptoms are related to gallstone formation (2–3).

Imaging

Biliary Atresia

In the majority of children, ultrasound (US) will fail to identify the gallbladder and extrahepatic bile ducts. The intrahepatic bile ducts are usually unremarkable. Because in a minority of affected children, US will show a gallbladder, hepato-biliary scintigraphy is recommended as second imaging modality to rule out biliary atresia. Endoscopic retrograde cholangiopancreatography (ERCP) can be used to confirm diagnosis.

Alagille Syndrome

Imaging features in the newborn period are similar to those in biliary atresia but the identification of the additional components of this syndrome (hypertelorism, butterfly vertebrae, complex cardiac malformations) lead to the correct diagnosis. US of the liver can show hepatomegaly, periportal fibrosis/cirrhosis, and splenomegaly. In less severe forms, US will show a normal liver. Magnetic resonance cholangiopancreatography (MRCP) and ERCP or intraoperative cholangiography may show the patency of the extrahepatic biliary tract.

Choledochal Cysts

Most choledochal cysts are easily identified by US. In addition, sludge and gallstones within the cysts can be seen. US is also helpful in diagnosing complications such as intrahepatic biliary dilatation, portal vein thrombosis, gallbladder or biliary neoplasms, pancreatitis, and hepatic abscesses. On computed tomography (CT), choledochal cysts appear as well-circumscribed hypodense cystic lesions which are separated from the gallbladder. The cyst wall can be thickened due to recurrent cholangitis. On magnetic resonance imaging (MR), choledochal cysts are T2-hyperintense (Fig 1–3). MRCP or ERCP are helpful in classifying the cysts.

Congenital Hepatic Fibrosis

US shows an enlarged hyperechoic liver. Intrahepatic bile duct ectasia and gallbladder enlargement may be seen in case of an associated Caroli's disease. Splenomegaly may result from portal hypertension. Color Doppler sonography should be performed to rule out cavernous transformation. CT and MR show an inhomogeneous pattern with areas of heterogeneously increased or decreased attenuation values or signal intensities.

Polycystic Liver Disease

US reveals multiple, variably sized hypoechoic hepatic cysts. Cysts may show an internal echo due to hemorrhage. The cysts are hypodense on CT, well circumscribed and nonenhancing. On MR, the cysts are T1-hypo and T2-hyperintense without enhancement.

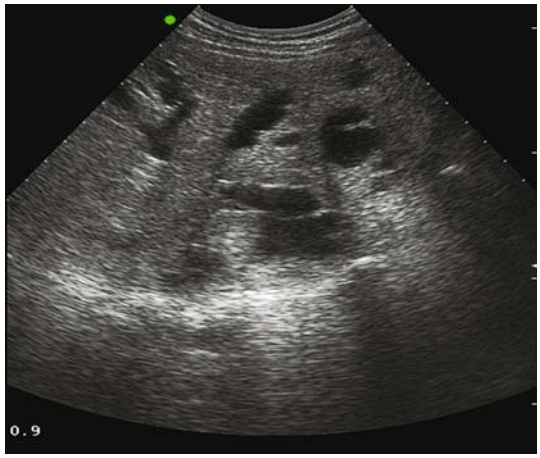

Congenital Malformations, Liver and Biliary Tract. Figure 1 US scan displays the presence of anechoic saccular dilatations of the bile ducts involving both lobes containing intraluminal bulbar protrusions and cross-bridges. The surrounding liver parenchyma shows a normal echostructure.

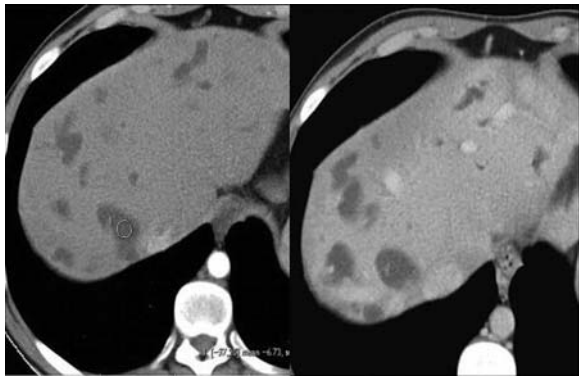

Congenital Malformations, Liver and Biliary Tract. Figure 2 Unenhanced CT scan shows marked intrahepatic ductal dilatation with cystic appearance (*left*). Enhancing central fibrovascular bundles (central dot sign) are identified in many of dilated ducts. These intraluminal dots correspond to intraluminal portal veins, indicating portal radicles surrounded by dilated intrahepatic bile ducts (*right*).

Gallbladder Anomalies

MRCP and US may identify and depict the whole spectrum of these anomalies. In case of an absent gallbladder an ectopic location or an atrophic gallbladder should be excluded.

The spectrum of anomalies can ideally be depicted by MRCP (1–5).

Nuclear Medicine

Biliary Atresia

^{99m}Tc labeled iminodiacetic acid derivates are very sensitive in diagnosing biliary atresia. In case of biliary atresia the liver will show a tracer uptake without excretion into the extrahepatic bile ducts or bowel. Conversely, evidence of intestinal excretion of the radiotracer confirms the patency of the extrahepatic biliary system. The absence of bowel activity after 24 h is an indication for liver biopsy.

Alagille Syndrome

Typically, biliary imaging performed with ^{99m}Tc labeled iminodiacetic acid derivates, fails to show normal excretion of radioisotope into the bowel resembling biliary atresia.

Choledochal Cysts

^{99m}Tc labeled iminodiacetic acid derivates scintigraphy may show the absence of drainage into the intestine in case of complete obstruction of the distal bile duct or the presence of a dilated duct acting as a collecting reservoir (2–4).

Diagnosis

Biliary Atresia

Diagnosis of biliary atresia emerges from recognizing clinical features and imaging findings. US represents the first choice but a normal examination does not exclude diagnosis. Neonatal hepatitis is the number one differential diagnosis. Typically in neonatal hepatitis, US will show a normal gallbladder. Scintigraphy may show a poor tracer uptake in combination with a delayed excretion into the bowel.

Alagille Syndrome

Definitive diagnosis is usually achieved by liver biopsy. The differentiation from biliary atresia can be made by demonstration of an intact extrahepatic biliary tree.

Choledochal Cysts

US findings are diagnostic in many patients, however, in the preoperative setting, complementary studies, such as ERCP, CT, or MR/MRCP may be helpful. Choledochal cyst may resemble hepatic cyst, hepatic abscess, pancreatic pseudocyst, or gallbladder duplications.

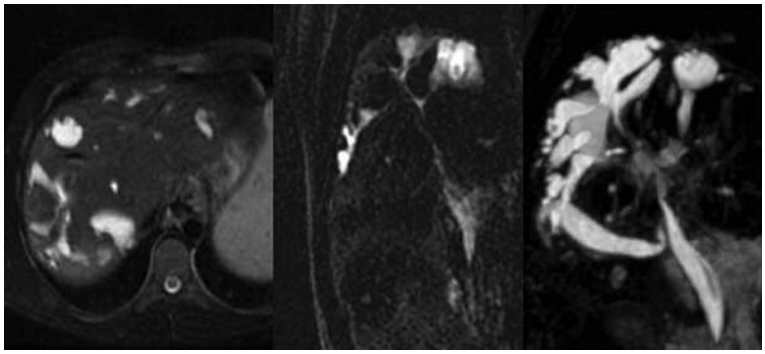

Congenital Malformations, Liver and Biliary Tract. Figure 3 Axial T2-weighted MR image shows multiple hyperintense cystic ectasias involving the entire liver (*left*). MR cholangiogram shows a connection between the saccular dilated segmental bile ducts and the central biliary tree (*middle*). The cystic dilatations communicate with the major biliary tree, and focal narrowing of the major intrahepatic and common bile ducts are depicted by reformatted images (*right*).

Congenital Hepatic Fibrosis

This affection should be suspected in young patients with portal hypertension of unknown origin. Evidence of nephromegaly and renal increased echogenity with polycystic changes support diagnosis. The final diagnosis is dependent on histological findings (biopsy).

Polycystic Liver Disease

The presence of multiple congenital liver cysts in patients with renal disorders suggests diagnosis.

Gallbladder Anomalies

These anomalies are usually an incidental finding on cross-sectional imaging. Most cases are asymptomatic. US may depict the hepato-biliary system anomaly and associated complications. MRCP provides a precise evaluation of the anatomy of the lesions (1–5).

Bibliography

1. Zeitoun D, Brancatelli G, Colombat M et al (2004) Congenital hepatic fibrosis: CT findings in 18 adults. Radiology 231(1):109–116
2. Silverman FN, Kuhn JP (1993) Congenital abnormalities. In: Silverman FN (ed) Caffey's Pediatric X-ray Diagnosis: An Integrated Imaging Approach. Mosby, St. Louis, pp 919–930
3. Taybi H (1979) The biliary tract in children. In: Margulis AR, Burhenne HJ (eds) Alimentary Tract Radiology. Mosby, St. Louis, pp 1504–1516
4. Rizzo RJ, Szucs RA, Turner MA (1995) Congenital abnormalities of the pancreas and biliary tree in adults. Radiographics 15(1):49–68
5. Mortele KJ, Ros PR (2001) Anatomic variants of the biliary tree: MR cholangiographic findings and clinical applications. AJR Am J Roentgenol 177(2):389–394

Congenital Malformations, Musculoskeletal System

Heike E. Daldrup-Link
Department of Radiology, Pediatric Radiology section and Director, Contrast agent Research Group
University of California in San Francisco
USA
daldrup@radiology.ucsf.edu

Congenital malformations are the leading cause of infant mortality in the United States and a major cause of morbidity and mortality throughout childhood. The children with major congenital malformations represent approximately 4% of live births with a higher rate in males than females (4.6% vs. 3.1%), and a higher rate in black children than white children (4.4% vs. 3.8%) (1). Twenty percent of infant deaths are attributed to congenital malformations, a percentage that has increased over time.

Little is known about the causes of congenital malformations. Twenty percent may be due to a combination of heredity and other factors; 7.5% may be due to single-gene mutations; 6% to chromosome abnormalities; and 5% to maternal illnesses, such as diabetes, infections, or anticonvulsant drugs. Fourty to sixty percent of congenital malformations are of unknown origin.

Associations between congenital malformations and environmental agents have been described for radiation

exposure, intrauterine infections (e.g., particular rubella), medications (e.g., thalidomide and anticonvulsants), and toxic waste dumps (e.g., Love Canal and accidents such as Three Mile Island and Seveso). In response, many states began to develop birth defects registries in order to track trends in malformation rates (1).

The musculoskeletal system represents the third most common organ system involved in major congenital malformations (16%). Other potentially involved organ systems are cardiovascular (26%), genitourinary (21%), digestive and clefts (9%), CNS (5%), respiratory (3%), and others (20%). The most common congenital musculoskeletal malformations are dislocation of the hip (22%), varus deformities of the feet (20%), other limb anomalies (10%), anomalies of the skull and face (10%), reduction deformities (6%), valgus deformities of the feet (6%), other feet deformities (3%), and others (23%). A more specific overview over relatively frequent congenital malformations that involve the musculoskeletal system is given in Table 1. The following article provides a brief overview over frequent congential musculoskeletal malformations. Due to its limited length, it cannot be comprehensive. For more detailed information, the reader should consult specific literature for the individual pathologies, mentioned later.

Congenital Malformations of the Hip

►*Hip dysplasia* is the most common congenital malformation and represents an abnormal growth or development of the acetabulum, femoral head, and associated ligaments and soft tissues. It can be associated with instability and/or dislocation of the femoral head. Ultrasonography is the method of choice for the diagnosis and treatment of hip dysplasia and instability in newborns and young infants. The evaluation is typically performed by assessing the alpha angle (which outlines the superior bony acetabulum) and the beta angle (which represents the cartilaginous part of the acetabulum). A normal alpha angle should be greater than 60° and a normal beta angle should be less than 55°. In older children with ossified

Congenital Malformations, Musculoskeletal System. Table 1 Relatively frequent major congenital malformations, that involve the musculoskeletal system

ICD-9	Malformation	Prevalence	Ratio: M/F
090	Congenital syphilis	22.8	1.0
243	Congenital hypothyroidism	3.0	1.1
658.8	Amniotic bands	0.3	0.3
741.0	Spina bifida with hydrocephalus	1.9	0.9
741.9	Spina bifida without hydrocephalus	1.8	0.9
742.1	Microcephalus	5.8	0.8
749.0	Cleft palate	5.8	0.7
749.2	Cleft palate & lip	4.6	1.4
754.3	Congenital dislocation of hip	14.6	0.3
754.51	Talipes equinovarus	11.6	1.7
755.2	Reduction deformities of upper limb	3.0	0.9
755.3	Reduction deformities of lower limb	1.9	1.3
755.8	Arthrogryposis multiplex congentia	1.5	0.9
756.0	Craniosynostosis	4.0	2.1
756.4	Chondrodystrophy	1.1	1.0
756.51	Osteogenesis imperfecta	0.3	0.4
758.0	Down syndrome	10.1	1.0
758.1	Patau syndrome	0.8	1.3
758.2	Edwards syndrome	1.2	0.5
758.7	Klinefelter syndrome	0.6	-
760.71	Fetal alcohol syndrome	2.1	1.4
771.0	Congenital rubella	0.1	1.0
771.1	Congenital cytomegalovirus infection	1.4	1.1
771.2	Other congenital infections	2.3	0.8

Source: From The New York State Department of Health Congenital Malformations Registry: //www.health.state.ny.us.

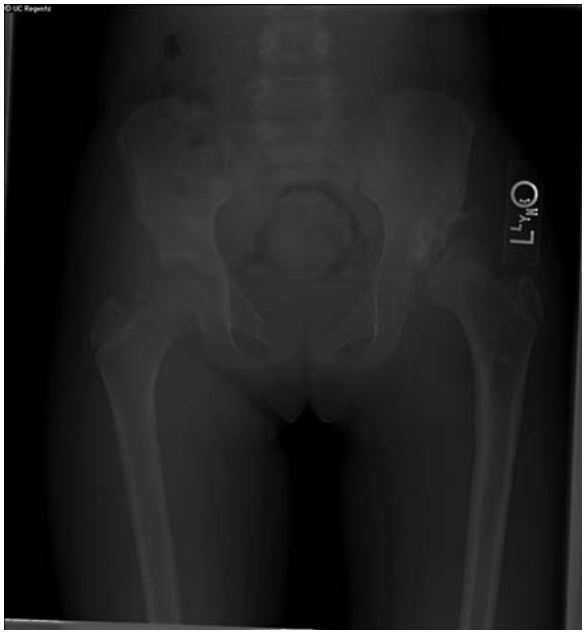

Congenital Malformations, Musculoskeletal System. Figure 1 Hip dysplasia: The left acetabulum is markedly shallow. There is extensive subchondral lucency and sclerosis. There is marked malformation of the left femoral epiphysis. These changes are consistent with congenital hip dysplasia and are unchanged compared to prior study. Ossific fragment is again seen superior to the left femoral head, likely avulsion injury versus heterotopic bone. Several calcific densities are present in the proximal left femoral shaft, which may represent exaggerated trabeculae versus enchondromas.

femoral heads, radiographs are obtained to profile the anterior aspect of the acetabulum (Fig. 1). If any evidence of hip subluxation is present, an additional abducted internal rotation view is added to determine the true neck-shaft angle of the proximal femur. Typical measures for hip joint assessment are the Hilgenreiner line, Perkin line, Shenton Menard line, and acetabular angle (<30° in newborns, decreases with increasing age).

►*Coxa valga* represents an increased angle between the femoral neck and shaft (normal 150° at birth, then gradually decreasing up to 120–130° in adults). The coxa valga usually results from weakness of the abductor muscles and lack of normal weight-bearing forces; it is most commonly associated with neuromuscular disorders such as cerebral palsy, spinal dysraphism, and poliomyelitis, less commonly with some skeletal dysplasias.

►*Coxa vara* represents a decreased angle between the femoral neck and shaft (<120°) and is often associated with shortening of the affected leg, vertical orientation of the capital femoral physis, and femoral anteversion. The congenital coxa vara shows a characteristic radiographic finding of a fragment of bone inferolateral to the proximal femoral physis, which represents a contained area of abnormal calcification.

Congenital Malformations of the Limbs

Congenital malformations of the feet include pes valgus (flat foot) and pes varus (abnormally increased angle between the axis of the calcaneus and second metatarsal), pes planus and pes cavus (decreased or increased longitudinal arch), talipes varus and valgus (abnormally decreased or increased angle between the axes of the ankle and foot), metatarsus varus and adductus (outward or inward bending of the forefoot), and tarsal coalition (abnormal union of two or more tarsal bones).

►Talipes equinovarus (clubfoot) (Fig. 2) involves the talus (ankle) and pes (foot), the heel is elevated (equino—like a horse's) and turned inward (varus). Talipes equinovarus can be idiopathic (most frequent), due to exogenous causes (oligohydramnion, teratogenic agents, e.g., sodium aminopterin, congenital constriction rings) or inherited (autosomal recessive and associated with various syndromes, e.g., diastrophic dwarfism). Radiographic features include parallelism of talus and calcaneus with an AP talocalcaneal angle <20° (normal 25–40°) and lateral talocalcaneal angle of 10–35° (normal 35–50°).

A Rocker bottom foot may occur after inadequate treatment of talipes equinovarus or, more rarely, due to cerebral palsy and other neuromuscular disorders, or due to genetic syndromes, such as trisomy 13, 15, or 18 syndromes. The Rocker bottom foot is diagnosed based on a lateral radiograph, which shows a dorsiflexed forefoot, a plantar flexed calcaneus, a reversed angle between calcaneus and 5th metatarsal, and a reversed angle between a relatively vertical talus and 1st metatarsal.

Reduction defects represent congenital limb malformations (dysmelia), complete absence of a whole limb (amelia) or parts of a limb with only a proximal rudimentary part present (Peromelia), congenital absence of upper and lower arm (leg) with hand (foot) present (phokomelia) or absence of specific bones, e.g., absence of radius/ulna or tibia/fibula (hemimelia). The cause is, in most instances, an exogenous interference with the limb-bud formation in the 3rd–6th week of pregnancy. For example, an increased incidence of dysmelias was noted during the 1950s due to Thalidomide and due to uran intoxication after the wars in Bosnia, Kosovo, and Iraq. Imaging studies of at least the whole affected limb are necessary to fully evaluate dysmelias, since malformations of one bone (e.g., the partial or complete absence of the fibula) are often associated with other malformations of

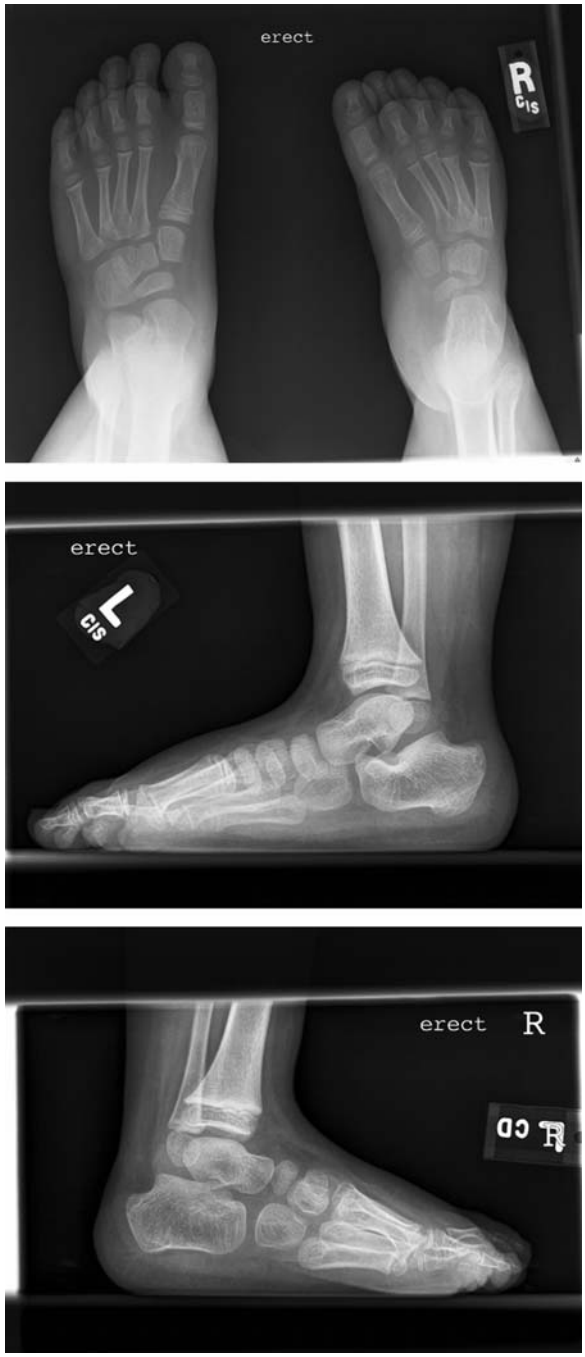

Congenital Malformations, Musculoskeletal System. Figure 2 **Talipes equinovarus.**

Congenital Malformations, Musculoskeletal System. Figure 3 **►Polydactyly: Frontal projection of the left hand demonstrates a well-formed bilateral sixth digit, compatible with polydactyly. This finding can be associated with Ellis-Van Creveld, Meckel-Gruber syndrome, or trisomy syndromes.**

other bones of the same limb (e.g., associated malformations of the femur).

The "lobster claw hand," congenital cleft hand, or split hand (synonyms) may occur isolated or, more frequently, as part of a syndrome with autosomal dominant inheritance and variable penetrance. The split hand is characterized by an absence of the third digital ray, with a deep cleft extending to the carpal bones, dividing the hand into two parts. The syndrome is associated with malformations of the lower legs, especially tibial aplasia.

Other, relatively frequent congenital malformations of the limbs include polydactylies (accessory or supernumerary fingers or toes) (Fig. 3), syndactylies (fused fingers or toes with or without synostosis, webbed fingers or toes) or a combination of both (►polysyndactyly) (3). These may also occur solitary or associated with other abnormalities, e.g., such as in Acrocephalosyndactyly (Apert's syndrome, ►syndactyly and premature closure of sutures of the skull). In addition, fingers or toes may present abnormally short (brachydactyly), abnormally curved (clinodactyly: curving of the fifth finger toward the fourth finger or camptodactyly: fixed in a flexed position), or bifid (bifid digits).

Madelung deformity is characterized by dorsal and lateral bowing of the distal radius, and lateral bowing of the distal radius, shortening of the radius and subluxation of the inferior radio ulnar joint. If congenital, causes are most frequently genetic or dysplastic, less frequently posttraumatic or idiopathic. The most frequently associated genetic syndrome is Turner's syndrome. Associated bone dysplasias are hereditary osteochondromatosis,

achondroplasia, multiple epiphysial dysplasias, and the mucopolysaccharidoses (Hurler and Morquio). The most important associated dysplasia is dyschondrosteosis, a form of mesomelic dwarfism.

Other relatively frequent congenital malformations of the lower limbs include accessory bones, absence of the patella, congenital dislocation of the knee and genu valgum, varum, and recurvatum.

Arthrogryposis multiplex congenita is a rare disease, characterized by multiple limb deformities at birth with gross stiffening of joints and hypotonia or wasting of muscle. The hips are usually dislocated, knees flexed, clubfeet may be present as well as upper extremity deformities similar to Erb's palsy deformity.

Larsen Syndrome represents multiple joint dislocations, mainly hips, and hyperextended or dislocated knee joints. It is associated with cervical kyphosis, which may be life-threatening because of the impingement on the spinal cord at the apex of the kyphosis.

Congential Malformations of the Head and Neck

Deformities of the skull in young babies and infants are most often exogenous, such as forceps delivery or due to positioning (e.g., constant sleeping position on the back causes a flat occiput). Much more rarely, deformities of the skull are due to congenital syndromes with congenital craniosynostosis, such as Apert's syndrome, Crouzon syndrome, Pfeiffer syndrome, or Carpenter syndrome (3). Congenital nose deformities include squashed or bent nose in babies of mothers with oligohydramnion (considered to be due to intrauterine malposition and pressure) and saddle nose in patients with congenital syphilis. A hemicraniofacial microsomia has been associated to exogenous drugs or toxins, such as Thalidomide. Goldenhar syndrome (oculo-auriculo-vertebral syndrome) represents hemifacial microsomia, microtia, abnormal or missing eye, and hemivertebrae (3). ►Hypertelorism, a lateral shift of the orbits, may be due to excessive ethmoid sinus or a midline cleft. In patients with ►hypotelorism, the intercanthal area is narrowed and may be associated with varying degrees of frontonasal hypoplasia. Hypotelorism may be associated with a premature closure of the metopic suture. In the extreme form, the infant looks like a cyclops, this condition is not compatible with life.

Congenital sternocleidomastoid torticollis is the most frequent congenital malformation of the neck, characterized by tilting of the head to one side, rotation of the occiput to that side and the chin to the opposite side due to a unilateral contracture of the sternomastoid muscle. There may be also a facial asymmetry. X-rays may show congenital hemivertebrae or partial fusion of cervical vertebrae, especially in cases where the sternocleidomastoid is normal.

Congenital Malformations of the Spine

►*Congenital scoliosis* is characterized by a lateral curvature of the spine due to congenital vertebral anomalies, such as vertebral absence, partial formation, or lack of separation. Patients with congenital scoliosis require a renal ultrasound to rule out renal anomalies such as a single kidney which is the most common associated finding. MR imaging may be necessary to rule out suspected associated abnormalities of the spinal cord or spinal nerves if clinical neurologic examination findings are present. Early surgical intervention may be required to prevent deformity progression. Other, less frequent patterns of congenital spinal deformity are hyperlordosis and kyphosis.

►*Spina bifida* is a developmental defect of the neuroectodermal tube at the fetal stage, resulting in various degrees of defective closure of the neural arch of the spinal canal. The condition is more common in the western countries. Two main forms should be distinguished: the closed spina bifida (spina bifida occulta), which is usually asymptomatic, and the open spina bifida with meningomyelocele, which is usually associated with neurological deficiencies and sometimes a hydrocephalus.

Congenital spondylolisthesis or dysplastic spondylolisthesis is characterized by presence of dysplastic sacral facet joints, which cause a forward translation of one vertebra relative to another. There is usually no defect in the pars interarticularis. Congenital spondylolisthesis comprise about 14–21% of all cases of spondylolisthesis, occur with a 2:1 female-to-male ratio and typically present around the adolescent growth spurt.

Congenital Platyspondyly is defined as two or more flattened vertebral bodies (single involved vertebra known as vertebra plana) with reduced distance between the endplates and occurs in thanatophoric dysplasia, metatropic dwarfism and osteogenesis imperfecta type IIA. Platyspondyly developing in later childhood occurs in Morquio's disease, spondyloepiphyseal dysplasia tarda, and Kniests dysplasia.

Sacral agenesis or *caudal regression syndrome* refers to a wide range of absent lower portions of the spinal column and pelvis. The incidence is increased in children of diabetic mothers. Sacral agenesis is associated with bowel, bladder or lower extremity motor dysfunction, anorectal malformations, and presacral teratomas or myelomeningoceles.

Klippel Feil syndrome describes a continuity of cervical and upper thoracic vertebrae. It maybe associated with renal

anomalies (38%), sensineural or conductive hearing loss (36%), cardiovascular anomalies (18%) or, less common, limb deficiencies, craniosynostosis, and craniofacial abnormalities.

Malformations of the Chest Wall

Cleidocranial Dysostosis is a developmental and familial disorder of membranous ossification with involvement of the clavicle and the cranial bones. In the typical case, the clavicle may be totally or partially absent and this may be bilateral so that the patient's two shoulders could be brought forward toward the midline to touch each other. The skull is abnormally large with bossing of the parietal and frontal bones. The closure of fontanelles is delayed. The face is small with a relatively large and prognathous mandible and a poorly developed maxilla. The pelvic bones also show poor development with nonfusion of the symphysis pubis and poor development of the sacrum.

►*Sprengel's Shoulder* is characterized by a congenital elevation of the scapula. Developmentally, the scapula has failed to descend from its embryological position in the neck. Radiographs show the elevated position and diminished size of the scapula. It may also show a bony bar connecting the low cervical vertebra with the supero medial angle of the scapula and it is called as the *omovertebral bone.*

Other common congenital malformations of the chest wall are pectus excavatum, funnel chest, and sternum bifidum. Supernumerary ossification centers of the sternum are most commonly seen in association with Down's syndrome.

Osteochondrodysplasias

Relatively common congenital osteochondrodysplasias are osteogenesis imperfecta, McCune Albright Syndrome (polyostotic fibrous dysplasia), osteopetrosis, progressive diaphyseal dysplasia (Camurati Engelmann), enchondromatosis, exostoses, achondrogenesis, thanatophoric dwarfism, chondrodysplasia punctata, achondroplasia, chondroectodermal dysplasia, and spondyloepiphyseal dysplasia. The reader may be referred to the literature for detailed descriptions of these diseases (4).

Bibliography

1. The New York State Department of Health Congenital Malformations Registry: ►//www.health.state.ny.us
2. Graf R (1980) The diagnosis of congenital hip-joint dislocation by the ultrasonic Compound treatment. Arch Orthop Trauma Surg; 97(2):117–133
3. Jones KL, Smith DW (1997) Smiths Recognizable Patterns of Human Malformation. WB Saunders, Philadelphia
4. Spranger JW, Brill PW, Poznanski AK (2003) Bone Dysplasias: An Atlas of Genetic Disorders of Skeletal Development. Oxford University Press, Oxford, England

Congenital Malformations, Neck

Carlos H. Buitrago-Tellez
University of Basel, Head Radiological Institute, Zofingen Hospital, Switzerland
carlos.buitrago@spitalzofingen.ch

Definitions

Malformations of the neck region may initially not be clinically significant but according to their natural history they may change their manifestation and become symptomatic. Generally, congenital malformations can be divided into branchial arch anomalies, ►thyroid malformations, congenital vascular lesions, laryngeal malformations, and congenital dysontogenetic tumors or tumor-like conditions such as the sternocleidomastoid tumor of infancy. The most common anomalies are those associated with abnormal development of the branchial apparatus (1).

Pathology/Histopathology

Branchial Arch Anomalies

First branchial arch anomalies include either cleft cysts or syndrome-associated external auditory canal anomalies. First branchial cleft cysts (BCCs) can be classified according to Arnot (2). In Arnot type I the cleft cyst is located in the parotid gland without communication to the external auditory canal. In type II the cyst is usually located inferiorly to the parotid gland and the cyst tract communicates with the external auditory canal.

First branchial arch anomalies with associated abnormal external ear, external auditory canal stenosis, atresia, or further mandibular malformations include syndromes such as Goldenhar syndrome (Fig. 1), Franceschetti–Treacher-Collins syndrome, Pierre Robin syndrome, or even thalidomide toxicity.

Second branchial arch anomalies include either a persistent stapedial artery or the most common remnants of the second branchial arch. Second BCCs are the most

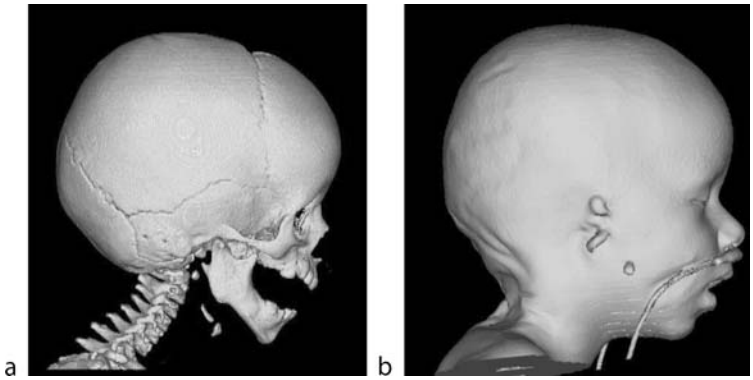

Congenital Malformations, Neck. Figure 1 First branchial arch congenital anomaly: atresia of external auditory canal and abnormal external ear in a 10-month year old baby with Goldenhar syndrome. Note also an accessory apophysis at the ascending ramus of the mandible. (a) Three-dimensional CT reconstruction (Volumen Rendering technique) with osseous display, (b) Three-dimensional CT reconstruction using surface rendering technique with a threshold of −100 HU.

common remnants of the branchial arches, making up around 90% of detected cleft cysts. The Bailey classification system (3) distinguishes four types of second BCC: type I when the cyst lies superficial to the anterior border of the sternocleidoid muscle beneath the cervical fascia and without contact to the internal jugular vein or the carotid arteries.

Type II shows a varying degree of adherence to the internal jugular vein, but no contact with the carotid sheath. In type III the cyst passes between the external and internal carotid arteries and extends further along the lateral pharyngeal wall. Type IV second BCC consist of those cysts located medially to the carotid vessels along the pharyngeal wall.

Third branchial arch anomalies include either the rare DiGeorge's syndrome (absent thymus and third parathyroid gland) or the third BCC. This cyst is located posterior to the sternocleidomastoid muscle and has a sinus tract ascending along the internal carotid artery, passing over the hypoglossal nerve and inferiorly to the glossopharyngeal nerve and then draining into the pyriform sinus.

Fourth branchial arch anomalies may include ►vascular anomalies such as aberrant subclavian artery or the fourth BCCs. These cysts are located around the aortic arch, usually anteriorly on the left, and around the subclavian artery on the right, and their sinus tract may ascend up to the level of the carotid bifurcation draining into the pyriform apex.

►Branchial cleft anomalies may present pathologically as a *fistula*, *sinus*, or *cyst*, based on the degree of completion of development of the anomalous structure. *Fistulae* appear in the case of persistence of both the cleft and the corresponding pouch, thereby forming a communication (i.e., fistula) that is epithelial lined. The fistula lies caudal to the structures derived from that particular arch and has a communication to the skin externally and to the pharynx internally. *Sinuses* may be considered partial fistulae, usually opening externally, with no internal opening.

Congenital Malformations, Neck. Table 1 Vascular congenital lesions of the neck according to the classification of Mulliken and Glowacki (1982)

Hemangiomas
• Capillary hemangioma (superficial)
• Cavernous hemangioma (deep)
• Combined hemangioma
Vascular malformations
• "Low-flow" lesions
Venous malformations
Capillary malformations
Lymphatic malformations (Lymphangioma)
• "High-flow" lesions
Arterial malformations
Arteriovenous malformations
AV Fistulas

Vascular Anomalies

Mulliken and Glowacki (4) proposed a biological classification of vascular birthmarks considering histologic features and clinical behavior. According to their classification system (Table 1), two major categories are distinguished in this setting: vascular tumors and vascular malformations. Vascular tumors include hemangiomas, Kaposiform hemangioendothelioma, and tufted angioma. Vascular malformations comprise high-flow malformations and slow-flow malformations.

High-flow malformations may be arterial or arteriovenous. Slow-flow malformations include venous malformations and capillary and lymphatic malformations. Lymphatic malformations are also known in the literature as lymphangiomas.

The most common vascular tumor is the hemangioma, which in around 30% of cases is visible at birth, the remaining appearing at age 2–4 years. Hemangiomas are most commonly located on the head and neck region. Postnatal growth is rapid and involution is slow.

In contrast, vascular malformations are present at birth in approximately 90% of cases, and depending on their type may manifest clinically at a later age in response to trauma, following incomplete surgical resection, or in altered hormonal states. They also do not involute as hemangiomas and tend to grow with the child.

Hemangiomas can be classified into capillary, cavernous, and capillary cavernous types.

Capillary malformations are groups of tortuous blood vessels in the upper layers of the dermis.

Lymphangiomas or lymphatic malformations are collections of lymph vessels filled with serous fluid. The histology ranges from capillary-sized vessels to macroscopic fluid-filled vessels. They can be divided into four classes clinically and histologically: capillary, cavernous, cystic (hygroma), and lymphangiohemangioma.

Venous malformations grow commensurately with the child. They may expand in response to trauma or hormonal factors. The following histologic characteristics are present: flat endothelium, slow turnover, dysplastic walls in ectatic venous vessels, and thin basement membranes.

Vascular malformations enlarge by hypertrophy. Flat, normal-appearing endothelial cells and ectatic vessels are characteristic findings in vascular malformations.

Hemangiomas rarely affect bone, whereas malformations affect bone in approximately 35% of cases.

Thyroid Malformations

The most common congenital thyroid anomaly is the persistent thyroglossal duct cyst. It occurs along the tract of the thyroglossal duct and is usually in an infrahyoidal location and in the midline. The thyroid gland is usually present and functions normally.

Ectopic thyroid tissue may be located at the base of the tongue in the midline dorsum, but it may also be located along the migration pathway of the thyroid. It is important to consider that in the presence of a lingual ectopic thyroid, the gland is often up to 70% not present at its usual position, so that a preoperative diagnosis is essential to avoid thyroid hormone insufficiency.

Thyroglossal duct cysts may be diagnosed by cytopathological analysis. The cytomorphologic features include colloids, macrophages, lymphocytes, or predominantly neutrophils. The epithelium may be ciliated columnar, metaplastic squamous, or of mature squamous type.

Laryngeal Malformations

The most common congenital anomalies of the larynx are laryngomalacia, bilateral vocal cord paralysis, and congenital subglottic stenosis. Less frequent anomalies comprise laryngeal atresia, laryngeal congenital webs, or vascular anomalies such as subglottic hemangioma or vascular malformations, especially of lymphatic origin (lymphangioma). Congenital laryngeal cysts are very uncommon.

Laryngomalacia is defined as a congenital disorder of the larynx characterized by inspiratory stridor and airway obstruction. It is due to a congenital weakness of the aryepiglottic folds and epiglottis, which are sucked into the airway during inspiration.

Congenital vocal cord paralysis is considered idiopathic. In certain cases, paralysis may occur secondary to central neuromuscular immaturity.

Congenital subglottic stenosis results from incomplete recanalization of the laryngotracheal tube during the third month of gestation. The extreme form of this anomaly is laryngeal atresia. Congenital subglottic stenosis can be classified into two types, membranous or cartilaginous.

Dysontogenetic Tumors or Tumor-Like Conditions

Dysontogenetic cervical tumors include those tumor conditions present at birth and include cervical teratomas, dermoid tumors, and tumor-like conditions as the sternocleidomastoid tumor of infancy or the midline cleft.

The sternocleidomastoid tumor of infancy represents a congenital fibrosis within the muscle and may manifest clinically as a tumor-like mass in the perinatal period.

The midline cervical cleft is a rare congenital anomaly presenting as a midline mass in the form of a pseudonipple located infrahyoidal caudally.

Dermoid cysts are considered the most common form of teratoma and are characterized by a predominance of ectodermal content. Congenital midline cleft histologically consists of a stratified keratinized squamous epithelium with hyperkeratosis, dermal fibrosis, and little or no skin appendages.

Clinical Presentation

Branchial Arch Anomalies

First branchial anomalies associated with external auditory canal atresia or stenosis may present clinically with marked difficulty in hearing, especially if the malformation is bilateral.

First branchial cysts manifest clinically as masses in the parotid gland region, in some cases even up to the submandibular region.

Second to fourth branchial cysts present in a similar way, although the location may be important for diagnosis. Second BCC are typically manifested in the neighborhood of the sternocleidomastoid muscle in the second decade of life. Inflammatory changes may be associated with fistulae formation. Third BCC may also cause an irritation of the hypoglossal or glossopharyngeal nerve in the presence of the typical draining tract.

Vascular Anomalies

Clinically, hemangiomas manifest typically superficially and can exhibit a varied appearance, from a hypopigmented macule to a bruise-like macule. The course of these lesions includes a proliferative postnatal growth phase that lasts for 3–9 months with a gradual involution occurring over 2–6 years. Involution is usually complete by age 7–10 years.

Vascular malformations are by definition present at birth, although in clinical practice 10% may manifest later in the postnatal period. Capillary vascular malformations (i.e., port-wine stains) are the most common type of vascular malformations. The lesions are presents in neonates but darken during adolescence and middle age.

Lymphangiomas present clinically as soft doughy masses that are located in the head and neck region. They may manifest as lymphedema and larger lesions may compromise the airway or the skeletal development of involved structures, such as the mandible. Venous malformations present in a variety of ways, from a slight blue patch to a recurrent growing compressible, soft, blue mass. Episodic painful thrombosis may also occur. Arterial malformations may present with bleeding.

Thyroid Malformations

Thyroglossal duct cysts present as asymptomatic midline masses, although they may occur off the midline in up to 25% of cases. A carcinoma developing in a thyroglossal duct cyst is very rare, but can be responsible for atypical presentation infiltrating surrounding tissues.

A lingual ectopic thyroid gland may manifest with dysphagia, hemorrhage, or airway obstruction.

Laryngeal Malformations

Laryngomalacia may present with noisy respiration and inspiratory stridor that is accentuated by being in the supine position, feeding, and agitation. Vocal cord paralysis also causes an inspiratory stridor and increasing respiratory distress if it is bilateral. Unilateral vocal cord paralysis may cause a hoarse cry.

Congenital subglottic stenosis presents with biphasic stridor with respiratory distress symptoms that may worsen in the case of an upper way infection.

Dysontogenetic Tumors or Tumor-Like Conditions

Cervical teratomas or dermoid tumors as a special form of teratoma present as large masses that may compromise the airway. The sternocleidomastoid tumor of infancy presents as a firm, painless mass in the inferior to the middle third of the muscle in neonates. Congenital midline cleft presents as a midline mass that may be associated with thyroglossal duct cysts, cleft lip/mandible/sternum, cervical contractures, mandibular spurs, microgenia, or bronchogenic cysts.

Imaging

Branchial Arch Anomalies

Branchial cleft anomalies are usually studied by imaging methods, including ultrasound (US) as a basic approach followed by computed tomography (CT) and magnetic resonance imaging (MRI) in more complex anatomic situations.

On US, BCCs present characteristically with a pattern of homogeneous, anechoic, smooth reflections within a well-demarcated, thin and elastic, deformable wall when using a high-resolution transducer. However, some BCCs may present with an inhomogeneous texture and/or irregular walls and hypoechoic characteristics, so that a distinction from inflammatory or neoplastic processes with central necrosis may not be possible. In these cases, CT or MRI may be more useful to rule out associated pathology.

A definitive CT diagnosis of second BCC may be possible in 80–90% of cases. BCCs present a CT appearance of a mass with an enhancing capsule and a lucent center measuring between 20 and 35 HU. To detect sinus or cyst tracts, CT using intravenously administered contrast material, and air as a contrast agent with Valsalva test, may show air along the draining tract proving communication between the internal drainage and the branchial remnant. Three-dimensional CT may be useful in the preoperative planning of craniofacial malformations, including first branchial anomalies, such as the Goldenhar syndrome (Fig. 1).

MRI allows a more detailed analysis of lesion size, morphology, location, relation to the expected course of neurovascular structures, enhancement pattern, attenuation compared to the cerebrospinal fluid (CSF), and T1- and T2-weighted signal intensity (5). This may allow identification of tiny fistulous tracts, especially when using three-dimensional sequences.

Vascular Anomalies

The predominant sonographic features of cavernous *hemangiomas* are well-defined hypoechoic mass lesions with heterogeneous echotexture and the presence of cystic and sinusoidal spaces within, as well as the occasional presence of phleboliths. Color Doppler imaging demonstrates flow inside the mass. MRI is very accurate in detecting hemangiomas, although capillary and cavernous hemangiomas cannot always be differentiated. They show bright signal on T2-weighted, low signal on T1-weighted, and enhancing diffusely without distorted dilated venous vessels.

US with high-resolution transducers can confidently suggest the diagnosis of neck *venous malformations* in up to 90% of cases. The lesions may show well-defined margins, heterogeneous and hypoechoic echo pattern, with sinusoidal spaces and phleboliths on gray-scale imaging, and flow signal on Doppler. In contrast to hemangiomas, large slow-flow venous vessels are present. MRI is superior in the overall characterization of the extent of the venous malformation, showing slow-flow vascular channels, dark on T1-weighted images, bright on T2-weighted images, and enhancing after contrast medium administration. A three-dimensional contrast-enhanced MR angiograph with time resolution or late imaging demonstrates the dilated venous vessels of the malformation.

High-flow vascular malformations contain an arterial component that may be detected by color Doppler US. This may be documented by time-resolved MR angiography, but conventional angiography with selective injection of contrast medium in the involved branch of the external carotid artery or vessels involved is mandatory before therapeutic decisions.

Three-dimensional CT angiography allows detailed description of vascular lesions of the head and neck and offers another effective means of imaging these complex lesions.

Lymphangiomas may be documented by US, CT, or MRI. US may show superficial hypoechogenic multilocular cystic masses with septa of variable thickness, but may fail to demonstrate retropharyngeal, axillary, or mediastinal extensions in all patients. MRI allows a better tissue characterization and lesion extent (Fig. 2).

Lymphangiomas may present as microcystic or macrocystic forms and may be differentiated by MRI. The cysts may usually have variable signal on T1-weighted sequences, from hypointense to brighter signal as CSF, and high signal on T2-weighted sequences. Fluid–fluid levels may be present, especially on the T1-weighted images (see Figs 2a and b).

Thyroid Malformations

The imaging work-up of ectopic thyroid gland requires a thyroid scintigraphy. For further diagnosis of thyroglossal duct cysts, US represents the basic imaging method, followed by CT and MRI. US findings may show anechoic, homogeneous hypoechoic, solid appearing or even heterogeneous midline cervical mass. On MRI the mass may reveal high signal intensity on T2-weighted images and sometimes also on T1-weighted sequences.

Laryngeal Malformations

Plain film radiographs of the cervicothoracic region in the neonate may suggest a diagnosis of laryngomalacia and can exclude anomalies with similar presentation. Inspiratory plain films of the neck may show inferior and medial displacement of the epiglottis and arytenoids. Fluoroscopy may reveal supraglottic collapse and hypopharyngeal dilatation. CT of the larynx region may be necessary if a partial subglottic stenosis or laryngeal atresia is suspected.

Dysontogenetic Tumors or Tumor-Like Conditions

The demonstration of a fat–fluid level on MRI or CT is diagnostic of a cervical dermoid cyst. Other teratomas or tumor-like conditions are also best delineated by CT.

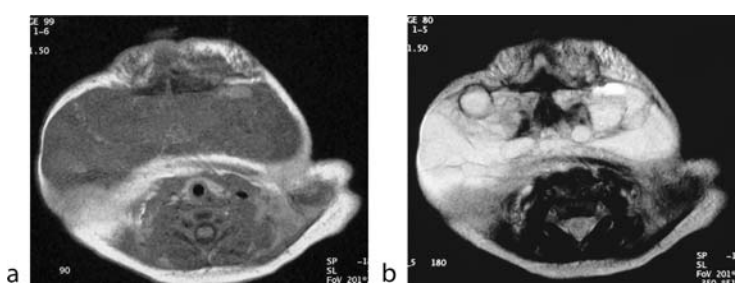

Congenital Malformations, Neck. Figure 2 Lymphangioma of the neck in a 3-day old newborn. (a) T1-weighted axial image at the level of the mandibular symphysis showing a hypointense inhomogeneous mass from the lateral neck crossing the midline. Note hyperintense cysts on the left adjacent to the mandibular body. (b) T2-weigthed image demonstrating high signal intensity together with multiseptate cystic configuration.

Nuclear Medicine

The indications for thyroid scintigraphy pertechnetate using Tc-99m in the setting of congenital thyroid anomalies include investigation of hyperthyroidism, nodularity of the gland, cause of thyroid stimulating hormone elevation, and localization of an ectopic thyroid gland and in the evaluation of a thyroglossal duct cyst.

Diagnosis

Branchial Cleft Anomalies

While the history, physical examination, and imaging findings are the most important parts of the evaluation of neck masses in children, biopsy may be necessary to establish the diagnosis. Image-guided fine-needle aspiration (FNA) is a useful tool in the management of neck masses in children.

Vascular Anomalies

By history and physical examination, 96% of vascular lesions can be classified as hemangiomas or malformations. Knowledge of their natural history as well as their clinical and imaging presentation is essential for making the diagnosis. A biopsy may be accompanied by bleeding.

Thyroid Malformations

As a number of other nonneoplastic and neoplastic lesions can cause cystic midline masses in the neck, FNA may be useful in making a preoperative diagnosis of thyroglossal duct cyst for a more accurate and timely clinical intervention. Histological confirmation is necessary for diagnosis, including the very rare association with carcinoma.

Laryngeal Malformations

A classic history and endoscopic examination usually suffice to establish a diagnosis of laryngomalacia or congenital vocal cord paralysis or congenital subglottic stenosis.

Dysontogenetic Tumors or Tumor-Like Conditions

Surgery with histological evaluation is necessary to establish a diagnosis of dysontogenetic tumors or tumor-like conditions, such as the congenital intramuscular fibrosis present in the sternocleidomastoid tumor of infancy.

Interventional Radiologic Treatment

Patients with hemangiomas are treated surgically by cryosurgery or laser surgery or conservatively according to lesion size and behavior. In patients with venous malformations, percutaneous sclerotherapy is combined with surgical reduction; patients with arteriovenous malformations undergo transarterial embolization before surgical excision of the nidus.

Percutaneous transcatheter arterial embolization plays an increasingly important role in the management of vascular lesions in the neck. Embolization can promote thrombosis within the malformations, reduce bleeding, and decrease the need for transfusion intraoperatively. Moreover, it can facilitate surgical approaches to otherwise unresectable lesions.

Bibliography

1. Mukherji SK, Fatterpekar G, Castillo M et al (2000) Imaging of congenital anomalies of the branchial apparatus. Neuroimaging Clin N Am 10:75–93
2. Arnot RS (1971) Defects of the first branchial cleft. S Afr J Surg 9:93–98
3. Ford GR, Balakrishnan A, Evans JN et al (1992) Branchial cleft and pouch anomalies. J Laryngol Otol 106:137–143
4. Mulliken JB, Glowaki J (1982) Hemangiomas and vascular malformations in infants and children: a classification based on endothelial characteristics. Plast Reconstr Surg 69:412–422
5. Mukherji SK, Tart RP, Slattery WH et al (1993) Evaluation of first branchial anomalies by CT and MR. J Comput Assist Tomogr 17:576–581

Congenital Malformations, Nose and Paranasal Sinus

Fabio Minutoli
Department of Radiological Sciences, University of Messina, Italy
fminutoli@unime.it

Definition

Congenital malformations of the nose and paranasal sinuses are due to discrete faults in the embryological development of the face (1). On the basis of embryogenesis and anatomic location, they can be grouped into four categories: anomalies related to the nasal cavity, nasolacrimal apparatus, nasofrontal region and craniofacial malformations (2).

Pathology/Histopathology

Anomalies Related to the Nasal Cavity

Choanal atresia, the most common congenital abnormality of the nasal cavity, is a developmental defect characterised by lack of communication between the nasal cavity and nasopharynx. Nowadays, it is known that most if not all patients with choanal atresia have bony abnormalities: a combined bony and membranous malformation occurs in about 70% of cases and purely bony atresia is found in about 30% of cases. Choanal atresia seems to be due to persistence of the mesodermal plate, which separates the stomodeum (primitive mouth) from the ectoderm which forms the cranium and brain or of the buccopharyngeal membrane (which separates the stomodeum from the end of the pharyngeal gut). Choanal atresia may be uni- or bilateral. Approximately 75% of children with bilateral choanal atresia have other congenital abnormalities, as exemplificated by the ►*CHARGE association* (1, 3).

Nasal pyriform aperture stenosis is a rare anomaly characterised by narrowing of the anterior bony nasal apertures. It may occur as an isolated anomaly or in association with alobar or semilobar forms of ►*holoprosencephaly*, facial hemangiomas, clinodactyly, hypotelorism, cleft palate, pituitary dysfunction and central megaincisor. Patients with a central megaincisor have an increased incidence of intracranial defects (3).

Congenital absence of the nose (arhinia) with failure of formation of the nose, nares and nasal cavities is rare. It can be associated with various anomalies including maxillary hypoplasia, high arched or cleft palate and ocular and intracranial anomalies.

Nasopharyngeal atresia is an extremely rare malformation that results in complete isolation of the nasal cavity from the oropharynx (3).

Anomalies Related to the Nasolacrimal Apparatus

Congenital nasolacrimal mucocele, a lacrimal sac mucocele with intranasal extension, is an uncommon mass arising in the medial canthal region of the orbit. In such cases, impatency of the distal portion of the nasolacrimal duct results in ballooning of the distal membrane into the nasal cavity, forming a dumbbell-shaped nasolacrimal mucocele. It can become infected determining a dacryocystitis (2).

Anomalies Related to the Nasofrontal Region

In early life, the frontal bone is separated from the nasal bones by the fonticulus frontalis (nasofrontal fontanelle). The nasal bones are separated from the underlying cartilaginous nasal capsule by the prenasal space, which contains a dural diverticulum. This diverticulum regresses, leaving behind the foramen cecum (located anterior to the crista galli).

Congenital herniation of intracranial contents through a defect in the skull with a persistent connection to the subarachnoid space is consistent with cephalocele. Only meninges (meningocele) or both meninges and brain (meningoencephalocele or simply encephalocele) can herniate. According to location, encephaloceles are classified as either occipital (75%), sincipital (15%) or basal (10%). Sincipital encephaloceles occur about the dorsum of the nose, the orbits and the forehead; they are typically either frontonasal (40–60%), nasoethmoidal (30%) or a combination of the two. If brain protrudes through the fonticulus frontalis, a frontonasal encephalocele is formed, whereas brain extending in the prenasal space gives origin to nasoethmoidal encephalocele (the nomenclature is based on the origin of their roof and floor). They have a high prevalence of associated intracranial anomalies.

Midclosure of the dural diverticulum sequestering brain in its distal aspect gives rise to a nasal glioma (nasal cerebral heterotopia). It is composed of dysplastic neurogenic tissue that has become isolated from the subarachnoid space: by definition, it does not contain any CSF-filled space that is connected with either the ventricles or the subarachnoid space of the head. It has no neoplastic features. Nasal gliomas may be intranasal (30%), extranasal (60%) or a combination of the two (10%). Up to 15% of patients with nasal gliomas show multiple cerebral heterotopias.

If the dural diverticulum touches the skin of the nose, it will drag ectoderm with it as it regresses. In 50% of these cases, a dermal sinus will form; in the remaining 50% of cases, an epidermoid or dermoid will be found. Nasal dermal sinuses are thin, epithelium-lined tubes that arise at external ostia situated along the nose and extend deeply for a variable distance, sometimes reaching the intradural intracranial space. Dermoid cysts contain ectoderm with skin appendage and are usually midline with tendency to occur at the glabella. Epidermoid cysts contain ectodermal elements without skin appendages, are usually paramidline and tend to occur near the columella. They may occur in isolation or associated with concurrent malformations (1, 2, 4).

Craniofacial Malformations

Midfacial clefts, the most common craniofacial anomalies, result from deranged development of the frontonasal process and/or failure of adjacent processes to merge successfully. They include the typical unilateral or bilateral common cleft lip and/or cleft palate (98.8% of all facial clefts), the midline craniofacial dysraphisms, an

oblique facial cleft, a transverse facial cleft ('wolf mouth' or macrostomia) and the facial anomalies (including hypoplasia or absence of the nose and intermaxillary segment, and pseudomedian cleft lip) associated with *holoprosencephaly* (4). Midline craniofacial dysraphisms can be divided into two groups: the low group (midline cleft lip), in which the cleft involves the upper lip, hard palate and occasionally the nose; and the high group (median cleft face syndrome or frontonasal dysplasia) in which the cleft involves primarily nose and forehead and, less commonly, upper lip and hard palate (1). Both groups are associated with intracranial anomalies and different kinds of cephalocele.

Many other different syndromic associations involving the midface exist: the syndromes of the first and second branchial arches (including ►*hemifacial microsomia* and ►*mandibulofacial dysostosis*) manifest as deficiencies of tissue and as hypoplasias of the maxillary and mandibular arches; the syndromic craniosynostoses (craniofacial dysostoses) are a group of syndromes (►*Crouzon syndrome* and ►*Apert syndrome* being the most frequent two) that exhibit premature synostoses of cranial sutures as one prominent feature and are frequently associated with maxillary hypoplasia and central nervous system malformations (2, 4).

Clinical Presentation

Congenital arhinia, nasopharyngeal atresia and, when bilateral, choanal atresia, pyriform aperture stenosis and nasolacrimal mucocele determine respiratory obstruction with respiratory distress and cyclical cyanosis. Characteristically, respiratory distress is aggravated by feeding and relieved by crying, since neonates are obligate nose breathers for the first 2–6 months of life. Grunting, snorting, low-pitched stridor and rhinorrhea are other common presenting signs of nasal airway obstruction in neonate or infant. In patients with nasolacrimal mucocele, a tense blue-gray medial canthal mass (due to dilatation of the lacrimal sac) associated with epiphora is appreciable (2, 3).

Anomalies related to the nasofrontal region are usually not associated with airways obstruction. Midface disfigurement, nasal destruction, meningitis and anterior cranial fossa abscesses may occur. Depending on the size of the intracranial connection, cephaloceles may be pulsatile or change in size during crying, the Valsalva maneuver or jugular compression, whereas nasal gliomas, dermoid and epidermoid cysts do not. Dermal sinuses may be associated with intermittent discharge of sebaceous material and/or pus (4).

Clinical presentation of craniofacial malformations is dominated by facial deformities, variously associated with auricular, ocular, musculoskeletal and skin deformities. Moreover, the presence of central nervous system anomalies may be responsible for IQ affection. Midline craniofacial dysraphisms and many syndromic malformations are characterised by hypertelorism, whereas hypotelorism is typically associated with *holoprosencephaly* (1). The nasal and pharyngeal airways may be compromised, increasing the risk of respiratory distress.

Imaging

Computed tomography (CT) is the imaging modality of choice in children with possible malformations related to the nasal cavity or to the nasolacrimal duct. *Magnetic resonance (MR) imaging* is the modality of choice for evaluation of lesions with potential intracranial extension or associated intracranial anomalies, such as congenital midface masses (e.g. dermoid and epidermoid cysts, nasal gliomas, cephaloceles) and craniofacial malformations. However, in many cases, both CT and MR imaging are required to obtain an adequate evaluation of bone, brain and soft-tissue components of midface anomalies (2).

Key imaging features in choanal atresia include narrowing of the posterior choanae to a width of less than 0.34 cm in children under 2 years old, inward bowing of the posterior maxilla, fusion or thickening of the vomer (in children less than 8 years of age the width of the inferoposterior vomer should not exceed 0.34 cm) and the presence of a bone or soft-tissue septum extending across the posterior choanae. Choanal stenosis may appear similar to choanal atresia depending on the degree of narrowing (2).

Imaging features of pyriform aperture stenosis include a shelf of tissue extending across the nostril, just inside the nares, overgrowth and medial displacement of the nasal processes of the maxilla and narrowing of the pyriform aperture (2). A pyriform aperture width less than 11 mm in a term infant has been suggested to be diagnostic of pyriform aperture stenosis (5).

In patients with nasopharyngeal atresia, the posterior choanal passages end blindly, the posterior vomer is wide and both the vomer and the hard palate are fused to the central skull base (3).

The triad of cystic dilatation of the lacrimal sac, dilatation of the nasolacrimal duct and an intranasal cystic mass (homogeneous, well defined, thin-walled) with fluid attenuation is diagnostic of nasolacrimal mucocele. Often, thinning and superior displacement of the inferior turbinate bone occur. Intravenous administration of contrast material may demonstrate slight enhancement of the cyst wall that is more pronounced in dacryocystitis (2).

Imaging features of nasal encephaloceles include a soft-tissue mass that is connected to the subarachnoid

space *via* an enlarged foramen cecum and extends to the glabella or into the nasal cavity. Encephaloceles are isointense relative to gray matter with most MR imaging sequences, but may be hyperintense with T2-weighted sequences because of gliosis. CT may be useful in evaluating bone changes. MR cisternography (hydrographic imaging) may be useful in demonstrating a subarachnoid connection (2).

Nasal gliomas appear as non-enhancing soft-tissue masses; they are isointense to hypointense to gray matter with T1-weighted sequences and hyperintense with proton-density and T2-weighted sequences (2). Extranasal gliomas most commonly lie external to the nasal bones and nasal cavities, typically at the bridge of the nose, to the left or the right of the midline; moreover, they can extend into the maxillary antrum. Intranasal gliomas lie within the nasal or nasopharyngeal cavities, usually between the middle turbinate and the nasal septum. Mixed nasal gliomas consist of extranasal and intranasal components that communicate *via* a defect in the nasal bones or around their lateral edges or, rarely, through defects in the orbital plate of the frontal bone or the frontal sinus (4).

Imaging studies successfully display the course of dermal sinus tracts. They usually appear as isodense fibrous channels or as lucent dermoid channels that extend inward for a variable distance (4).

The imaging of dermoid and epidermoid cysts may overlap, although dermoid cysts are more likely to be midline and fatty, whereas epidermoid cysts usually have fluid attenuation at CT and are isointense relative to fluid at T1- and T2-weighted MR imaging (Fig.1).Diffusion-weighted and magnetization transfer sequences can aid in differentiating solid epidermoid cysts from fluid-containing lesions. In this field, it is very important to recognise normal findings, like septal tubercle (a focal bulge of the anterior nasal septum at the level of the middle turbinate bone) or fatty change within crista galli that may simulate disease (2). Demonstration of an enlarged foramen cecum (normal width: up to 10 mm; avg: 4mm) and distorted crista galli suggests intracranial extension, however it does not prove it (4).

Craniofacial malformations include developmental anomalies of the face and skull that are associated with central nervous system malformations (2). Median cleft face syndrome is characterised by hypertelorism and bony clefting of the nose (with or without cleft upper lip, premaxilla and palate). Associated anomalies may be frontoethmoidal and intraorbital cephalocele, cranium bifidum occultum frontalis, microphthalmos, anophthalmos, intracranial lipomas and callosal agenesis (1, 4).

Midface anomalies in patients with syndromes of the first and second branchial arches or syndromic craniosynostoses are mainly represented by maxillary hypoplasia. It may result in stenosis within the nasal

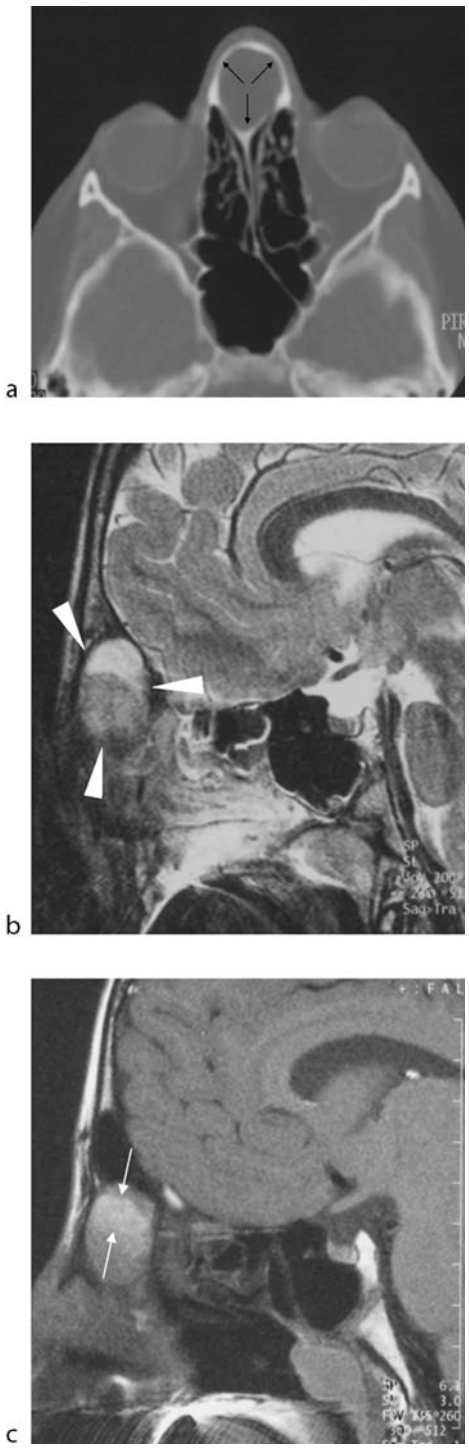

Congenital Malformations, Nose and Paranasal Sinus. Figure 1 Nasal dermoid cyst. Axial CT scan (a) reveals nasal swelling due to a sharply marginated midline lesion with soft-tissue attenuation, which determines broadening of the neighbouring bony structures (*arrows*). Sagittal T2-weighted (b) and sagittal T1-weighted (c) MR images show a inhomogeneous iso- to hyperintense lesion (*arrowheads)* containing areas of fatty-like signal (*arrows*).

cavity; in children with syndromic craniosynostosis, midfacial retrusion is generally associated with narrowing of the entire nasal and nasopharyngeal passages as well as some reduction in choanal dimensions (3).

Nuclear Medicine

Nuclear medicine is of no help in the assessment of congenital malformations of nose and paranasal sinuses.

Diagnosis

Diagnosis of congenital malformations of nose and paranasal sinuses is mainly based on physical examination and imaging. Most patients with craniofacial syndromes can be diagnosed on the basis of the type of anomalies involving the central nervous system and extremities and the presence of similar malformations in relatives (2).

When a congenital midface mass is found, biopsy should not be performed before an intracranial connection is ruled out because of the risk of causing meningitis or cerebrospinal fluid leak.

Only in few cases, the final diagnosis is reached after surgical treatment.

Bibliography

1. Castillo M (1994) Congenital abnormalities of the nose: CT and MR findings. Am J Roentgenol 162:1211–1217
2. Lowe LH, Booth TN, Foglar FM et al (2000) Midface anomalies in children. Radiographics 20:907–922
3. Robson CD, Hudgins PA (2003) Pediatric airway disease. In: Som PM and Curtin HD (eds) Head and Neck Imaging. Mosby Inc., St. Louis, pp 1521–1593
4. Naidich TP, Blaser SI, Bauer BS et al (2003) Embryology and congenital lesions of the midface. In: Som PM and Curtin HD (eds) Head and Neck Imaging. Mosby Inc., St. Louis, pp 3–86
5. Belden CJ, Mancuso AA, Schmalfuss IM (1999) CT features of congenital nasal piriform aperture stenosis: initial experience. Radiology 213:495–501

Congenital Malformations, Oral Cavity

Carlos H. Buitrago-tellez
University of Basel, Head Radiological Institute, Zofingen Hospital, Switzerland
carlos.buitrago@spitalzofingen.ch

Definition

Malformations of the oral cavity may manifest at birth or later, after development of the involved disturbed structures. The oral cavity comprises the anterior two-thirds of the tongue, the buccal mucosa, the gingiva, the soft and hard palate, the retromolar trigone, and the floor of the mouth and is bordered by the maxilla and mandible. Congenital malformations of the oral cavity include ▶cleft lip, palate, and alveolus defects, developmental anomalies of the tongue, vascular anomalies, developmental disturbances of the teeth and/or tooth structure, and congenital dysontogenetic tumors or tumor-like conditions. Most common anomalies of the oral cavity are cleft lip and/or palate and alveolus defects (1).

Pathology/Histopathology

Cleft Lip, Palate, and Alveolus Defects

Cleft abnormalities of the lip, palate, and alveolus are the most common congenital disorder of the oral cavity and result from developmental defects with incomplete fusion of the lips, palate, and/or alveolus. Depending on the association with further malformations, they may be divided into syndromic and nonsyndromic conditions. Among more than 300 syndromes associated with clefts the Pierre-Robin sequence (cleft palate, micrognathia, glossoptosis) and Treacher-Collins malformations (bilateral symmetric anomalies of the structures within the first and second branchial arches) may be mentioned. Nonsyndromic cleft anomalies are considered to be of multifactorial inheritance. Failure of merging of the medial nasal and maxillary processes at the 5th week of embryonic development on one or both sides results in cleft lip. Cleft palate is a partial or total lack of fusion of the palatal shelves.

Complete clefts of the lips and alveolus involve extension into the nose. Incomplete lip clefts do not extend to the nose. Complete clefts of the secondary palate involve both the hard and soft palate. Cleft lips may also be unilateral or bilateral. Unilateral cleft lips result from a failure of mesodermal proliferation, leading to complete or incomplete defects. A complete unilateral cleft lip includes the orbicularis oris muscle where the medial portion of the muscle attaches to the columella and the lateral portion to the nasal ala cartilage. In the bilateral type of cleft, the central part of the muscle is missing.

Clefts of the palate may be of the primary palate (anterior to the incisive foramen through the alveolus) or of the secondary palate, which may have many variants, from bifid uvula to a complete cleft of the hard and soft palate.

Developmental Anomalies of the Tongue

Congenital abnormalities of the tongue include processes that diffusely enlarge the tongue (macroglossia) and processes that cause focal masses.

There are multiple causes of diffuse macroglossia in children, including Down syndrome, hypothyroidism,

mucopolysaccharidosis, Beckwith-Wiedemann syndrome, and congenital duplication. The tongue may be relatively large in patients who have a small mandible (micrognathia), which is seen in children with Pierre-Robin sequence.

Focal masses of the tongue can be caused by vascular malformations or by congenital abnormalities such as thyroglossal duct cyst, lingual thyroid, duplication cyst, or even dysontogenetic congenital tumorous processes such as teratomas (Fig. 1). The most common congenital thyroid anomaly involving the tongue is the persistent thyroglossal duct cyst (see *Congenital Malformations, Neck*).

Ectopic thyroid tissue may also be located at the base of the tongue in the midline dorsum.

Although an intraoral location for duplication cysts is uncommon, when the cysts appear in the oral cavity they usually occur in the tongue. These lesions are usually large and present at birth or on prenatal imaging.

Other congenital malformations of the tongue include aglossia, bifid tongue, adhesions or fissures, hypoglossia or microglossia, which may be associated with skeletal anomalies in the setting of malformation syndromes of the oromandibular region and limbs. Ankyloglossia represents a developmental anomaly defined by the abnormal attachment of the frenum to the floor of the mouth.

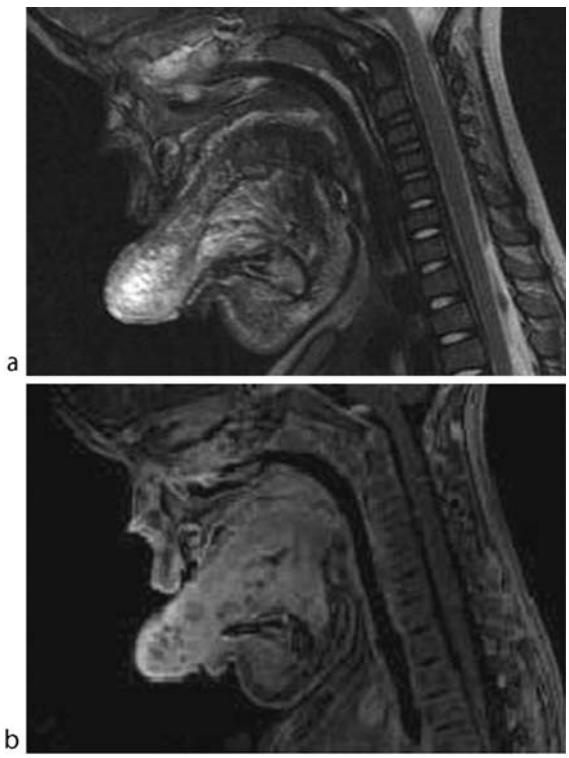

Congenital Malformations, Oral Cavity. Figure 1 Vascular malformation of the tongue with combined lymphangiomatous and venous components: (a) T2-weighted sagittal image showing macroglossia with high signal intensity at the tip of the tongue corresponding to microcystic component, (b) T1- weighted gradient echo sequence image revealing diffuse enhancement with hypointense spaces at the level of the microcystic component and flow voids at the base of the tongue. Patient underwent surgery to relieve macroglossia without complications.

Vascular Anomalies of the Oral Cavity

Mulliken and Glowacki (3) proposed a classification of vascular birthmarks considering histologic features and clinical behavior. Two major categories are distinguished in this setting: vascular tumors and vascular malformations. Vascular tumors include hemangiomas. Vascular malformations comprise high-flow malformations and slow-flow malformations.

High-flow malformations may be arterial or arteriovenous; slow-flow malformations include venous, capillary, and lymphatic malformations. Lymphatic malformations are also known in the literature as lymphangiomas.

The most common vascular malformation in the oral cavity is ▶lymphangioma. Lymphangiomas are collections of lymph vessels filled with serous fluid. The histology ranges from capillary-sized vessels to macroscopic fluid-filled vessels. They can be divided into four classes clinically and histologically: capillary, cavernous, cystic (hygroma), and lymphangiohemangioma.

Cystic lymphangiomas are generally characterized by large sinusoidal spaces, which may have high protein content or hemorrhage within them. Vascular malformations with combined lymphangiomatous and venous components may occur, especially in the tongue, resulting in macroglossia (Fig. 1). Venous malformations grow commensurately with the child. They may expand in response to trauma or hormonal factors.

Developmental Disturbances of the Teeth

Anodontia is a complete lack of tooth development, and hypodontia is a lack of some tooth development. Anodontia is rare, most often occurring in a condition called hypohidrotic ectodermal dysplasia. This is an inherited disease that affects deciduous or permanent teeth. Hypodontia is one of the most common developmental abnormalities. It is often associated with the absence of a dental lamina, which is also associated with many syndromes including Down syndrome and Crouzon syndrome. Hyperdontia is the development of

extraneous teeth. It is believed to be associated with an excess of dental lamina.

Regional odontodysplasia is rare but is most likely to occur in the maxilla and anterior teeth. The cause is unknown. Teeth affected by regional odontodysplasia never erupt into the mouth, have small crowns, are yellow-brown, and have irregular shapes. Supernumerary teeth represent extra teeth found in the dental arches, which result either from formation of extra tooth buds in the dental lamina or from the cleavage of already existing tooth buds. Mesiodens (midline of the maxilla) are the most common supernumerary teeth, and the second most common are the distomolars (distal to the third molar). Abnormalities in the size of teeth include microdontia, in which one or more teeth are smaller than normal, usually the incisors and three molars. In true generalized microdontia, teeth are extremely small, as in midgets. In generalized relative microdontia, teeth are not really small, but they are small compared to the jaw. Macrodontia is uncommon and may appear in the setting of puberty gigantism.

Abnormalities in the shape of teeth include gemination, fusion, concrescence, dilaceration, taurodontism, dens invaginatus, dens evaginatus, and teeth with supernumerary roots. Gemination represents an incomplete twin process with two crowns and one root. Fusion represents union of two normally separated adjacent tooth germs, resulting in one tooth less in dentition. Concrescence means that two adjacent teeth are united by cementum only, and it takes place after tooth formation is complete. In dilaceration, an angle in the root is present. Taurodontism describes elongated, enlarged pulp cavities with short roots. Dens in dente or dens invaginatus represents a tooth in a tooth, meaning an invagination of the enamel organ into the crown before crown formation. In dens evaginatus, an accessory cusp on the occlusal surface is present. Supernumerary roots may result secondary to metabolic dysfunction during root development after birth.

Developmental Tooth Structure Disturbances

Amelogenesis imperfecta is a genetic disorder that results in defective formation of enamel, the hard surface covering the crowns of teeth. Amelogenesis imperfecta either causes problems in the hardening of normal amounts of enamel or causes a smaller amount of normal enamel to be produced. Enamel hypoplasia is associated with a developmental disorder of ameloblasts and may be related not only to amelogenesis imperfecta but also to other factors such as vitamin A, C, or D deficiency or even congenital syphilis. Characteristic teeth changes in the setting of congenital syphilis also include mulberry molars or Hutchinson (screwdriver-like) incisors.

Dentinogenesis imperfecta is a genetic disorder that results in defective formation of dentin, a mineralized material forming the bulk of each tooth. Defective dentin causes the normal enamel layer that covers the tooth to flake off.

Amelogenesis imperfecta and dentinogenesis imperfecta are linked to defects in structural genes that code for proteins necessary for the development of enamel and dentin. Osteogenesis imperfecta is a hereditary disease caused by mutations of genes that produce collagen. A complication of osteogenesis imperfecta that involves the oral cavity in addition to the more generalized effect of fragile bones is a painful dentinogenesis imperfecta-like change in the teeth.

Dysontogenetic Tumors or Tumorlike Conditions

Congenital tumorous lesions of the oral cavity are mainly due to dermoid, epidermoid, or teratoid cysts.

Dermoid cysts are considered the most common form of teratoma and are characterized by a predominance of ectodermal content. The dermoids contain fat or fluid and are usually in the floor of the mouth. Epidermoid cysts usually occur in the sublingual space.

Teratomas involving the tongue are rare. Most cases present at birth with an extremely large mass extruding from the mouth.

Choristomas and mixed hamartomas of the oral cavity are further uncommon lesions that show a variety of clinical presentations, histological appearances, and growth patterns.

Clinical Presentation

Cleft Lip, Palate, and Alveolus Defects

The clinical diagnosis of an orofacial cleft is evident at birth. Clinical problems and manifestations include the risk of aspiration because of communication between the oral and nasal cavities, possible airway obstruction, and potential difficulties in feeding a baby with a cleft and nasal regurgitation.

Developmental Anomalies of the Tongue

When either a diffuse process or a focal mass enlarges the tongue, the tongue may become dysfunctional or obstruct the airway. Thus, airway obstruction may be the basic clinical manifestation of tongue abnormalities. Troubles with eating may also be present.

Thyroglossal duct cysts involving the tongue present as asymptomatic midline lingual masses, although they

may occur off the midline in up to 25% of cases. A carcinoma developing in a thyroglossal duct cyst is very rare, but it may be responsible for an atypical presentation infiltrating surrounding tissues.

A lingual ectopic thyroid gland may manifest with dysphagia, hemorrhage, or airway obstruction. Individuals with ankyloglossia may have speech problems.

Vascular Anomalies

Hemangiomas involving the oral cavity may be asymptomatic but may also manifest clinically with recurrent bleeding, especially if the gingiva or oral mucosa of the soft palate are involved (Fig. 2). The course of these lesions includes a proliferative postnatal growth phase that lasts for 3–9 months, with a gradual involution occurring over 2–6 years. Involution is usually complete by age 7–10 years.

Vascular malformations are by definition present at birth, although in clinical practice 10% may manifest later in the postnatal period.

Lymphangiomas present clinically as soft doughy masses located in the orofacial region. They may manifest intraorally as macroglossia or larger lesions in the mouth floor and can compromise the airway or the skeletal development of involved structures, such as the mandible or maxilla. Venous malformations present in a variety of ways, from a slight blue patch to a recurrent, growing, compressible soft blue mass. Episodic painful thrombosis may also occur. Arterial malformations may present with bleeding.

Developmental Disturbances of the Teeth

There are a number of tooth abnormalities that are not initially clinically evident at birth but are related to development disorders that manifest later on. They may represent not only esthetic problems but also functional disturbances.

Developmental Tooth Structure Disturbances

Dentinogenesis imperfecta causes the teeth to be opalescent and affects both the primary and permanent dentition.

Amelogenesis imperfecta manifests with teeth varying in colors from white opaque to yellow to brown. All teeth are affected, small, and pitted. Teeth have normal pulps and dentin but affected enamel with uneven surfaces. Individuals with amelogenesis imperfecta may be prone to early tooth loss and/or disease of the structures that surround and support the teeth (periodontal disease).

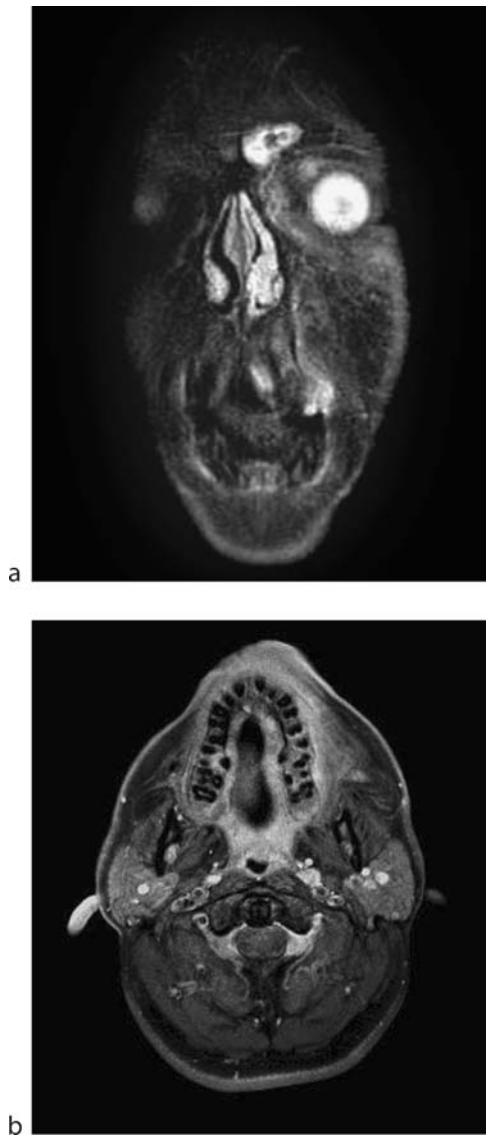

Congenital Malformations, Oral Cavity. Figure 2 Left-sided orofacial hemangioma involving the soft and hard palate on the left. (a) TIRM coronal image at the level of anterior alveolar ridge showing increased signal at the soft palate and gingiva on the left with bone infiltration of the alveolar process marked by high signal intensity. (b) T1-weigthed image after GdDTPA demonstrating diffuse enhancement at the level of the soft-tissue component on the left and the involved alveolar process on the maxilla. Note also the involvement of the upper lip, which was also clinically evident.

Dysontogenetic Tumors or Tumorlike Conditions

Dermoid tumors as a special form of teratoma present as large masses in the floor of the mouth that may compromise the airway.

Imaging

Cleft Lip, Palate, and Alveolus Defects

Cleft lip imaging approaches include ultrasound beyond the second trimester of pregnancy, when the position of the fetal face is located correctly (Fig. 3). Ultrasound diagnosis of cleft palate needs more experience by the examiner to detect atypical movement of the fetal tongue into an open space (cleft) in a lateral view.

Real-time four-dimensional ultrasound has been introduced to prenatal diagnostics of cleft anomalies and may be a useful diagnostic technique in this setting (Fig. 3). Three-dimensional computed tomography (CT) may be useful in preoperative planning in secondary corrections of osseous defects of the hard palate in children.

Developmental Anomalies of the Tongue

Because the tongue is superficially located and presents the initial manifestation of most diseases occurring in the mucosal or lingual surface, these lesions can be easily accessed and diagnosed without imaging analysis. Most congenital lesions of the tongue, however, can manifest as a submucosal bulge and be located in a deep portion of that organ, such as its base. The initial imaging approach is ultrasound. However, the lesions' true characteristics and extent may be recognized only on cross-sectional images such as those obtained by CT or magnetic resonance imaging (MRI).

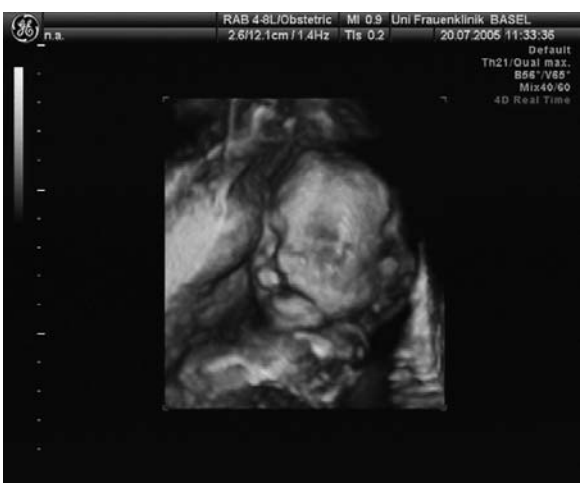

Congenital Malformations, Oral Cavity. Figure 3 Cleft lip palate. Prenatal four-dimensional real-time ultrasound examination showing the right-sided unilateral cleft lip defect clearly. (Image courtesy of PD Dr. S. Tercanli, Department Of Ultrasound, Women's University Clinic, University Hospital Basel)

MRI is superior to CT for evaluating soft tissue lingual lesions. In addition, because it is usually difficult to differentiate congenital lesions from other submucosal neoplasms on the basis of imaging findings alone, clinical history and local examination should be considered when interpreting CT and MR images of the tongue. The imaging work-up of ectopic thyroid gland requires thyroid scintigraphy. For further diagnosis of thyroglossal duct cysts, ultrasound represents the basic imaging method, followed by CT and MRI. Ultrasound findings may show an echoic, homogeneous hypoechoic, solid-appearing, or even heterogeneous midline cervical mass. On MRI the mass may reveal high signal intensity on T2-weighted images and sometimes also on T1-weighted sequences.

Prenatal sonography may be helpful in diagnosing intraoral cystic lesions such as duplication cyst of the tongue. Furthermore, T2-weighted MRI can reveal homogeneous masses that have high signal intensity and variable rings of signal intensity corresponding with mucosa and submucosa in the case of a duplication cyst.

Vascular Anomalies

The predominant sonographic features of cavernous hemangiomas are well-defined hypoechoic mass lesions with heterogeneous echotexture and the presence of cystic and sinusoidal spaces within them, as well as the occasional presence of phleboliths. Color Doppler imaging demonstrates flow inside the mass. MRI is very accurate for detecting hemangiomas, although capillary and cavernous hemangiomas and combined lymphangiohemangioma or lymphatic and venous malformation cannot always be differentiated. They show bright signal on T2-weighted or TIRM sequences (Fig. 2a), low signal on T1-weighted images, and enhance diffusely without distorted dilated venous vessels (Fig. 2b). CT may confirm the infiltration of adjacent bone of the alveolar process of the maxilla.

Lingual venous malformations present on MRI as lobulated masses highly hyperintense on T2-weighted images with respect to normal tongue and slightly hyperintense or isointense on T1-weighted images and/or surrounding muscles. They show a slow and homogeneous filling following intravenous injection of contrast medium. Millimeter-sized hypointense foci and linear hypointense strands are present and may be caused by phleboliths, flow void, or septation.

Lymphangiomas may be documented by ultrasound, CT, or MRI. Ultrasound may show superficial hypoechogenic multioccular cystic masses with septa of variable thickness, but it can fail to demonstrate retropharyngeal, axillary, or mediastinal extensions in all patients. MRI allows better tissue characterization and lesion extent.

Developmental Disturbances of the Teeth

For documentation of developmental disturbances of the teeth, single-tooth radiographs of the suspected anomaly are often adequate. For overall analysis of multiple supernumerary teeth, an orthopantomogram or even CT with three-dimensional reconstructions and dental CT parasagittal reconstructions may be more accurate for therapy planning.

Developmental Tooth Structure Disturbances

Imaging of amelogenesis imperfecta is based on radiographs, including orthopantomogram, palatinal view, and single-tooth images. Radiographically, enamel appears reduced in bulk.

Dysontogenetic Tumors or Tumorlike Conditions

The demonstration of a fat–fluid level on MRI or CT is diagnostic for a dermoid cyst at the mouth floor. Other teratomas or tumorlike conditions are also well delineated by MRI regarding extension and infiltration. CT is superior for detecting calcifications and osseous changes.

Nuclear Medicine

The indications for thyroid scintigraphy pertechnetate using Tc-99m in the setting of congenital disease of the oral cavity include localization of an ectopic thyroid gland and evaluation of a thyroglossal duct cyst to rule out functioning thyroid tissue in other locations.

Diagnosis

Cleft Lip, Palate, and Alveolus Defects

The diagnosis of an orofacial cleft is made based on clinical evidence of the cleft anomaly at birth. Imaging diagnosis using ultrasound allows early detection during pregnancy, especially beyond the second trimester (Fig. 3).

Developmental Anomalies of the Tongue

Because the tongue is superficially located, and the initial manifestation of most diseases occurring there is mucosal change, these lesions can be easily accessed and diagnosed without imaging analysis. However, as previously stated, imaging is necessary to confirm the clinical impression and to delineate lesion extension and characteristics before a surgical or bioptic diagnosis is performed. Because a number of other nonneoplastic and neoplastic lesions can cause cystic midline masses in the neck, fine-needle aspiration may be useful in making a preoperative diagnosis of thyroglossal duct cyst for a more accurate and timely clinical intervention.

Vascular Anomalies

By history and physical examination, 96% of vascular lesions can be classified as hemangiomas or vascular malformations. Knowledge of their natural history and the clinical and imaging presentation is essential for making the diagnosis. Lymphangiomas are the most common soft compressible mass in the orofacial region of children. However, for definite diagnosis a biopsy may be necessary and should be planned based on imaging methods to reduce bleeding risks, especially with associated venous or arterial components.

Dysontogenetic Tumors or Tumorlike Conditions

Surgery with histological evaluation is necessary to establish a diagnosis of dysontogenetic tumors or tumorlike conditions, such as congenital dermoid cyst.

Interventional Radiologic Treatment

Patients with hemangiomas are treated surgically by cryosurgery or laser surgery or conservatively according to lesion size and behavior. In patients with venous malformations, percutaneous sclerotherapy is combined with surgical reduction; patients with arteriovenous malformations undergo transarterial embolization before surgical excision of the nidus.

Lymphangiomas are usually surgically removed. Unfortunately, due to lack of encapsulation, the recurrence rate is high. Alternative treatments include aspiration, percutaneous sclerotherapy, diathermy, and radiation.

Bibliography

1. Eppley BL, van Aalst JA, Robey A et al (2005) The spectrum of orofacial clefting. Plast Reconstr Surg 115:101e–114e
2. Donnelly LF, Jones BV, Strife JL (2000) Imaging of pediatric tongue abnormalities. Am J Roentgenol 175:489–493
3. Mulliken JB, Glowaki J (1982) Hemangiomas and vascular malformations in infants and children: a classification based on endothelial characteristics. Plast Reconstr Surg 69:412–422
4. Lo Casto A, Salerno S, Cannizzaro F et al (2003) MRI findings in lingual venous malformations. Dentomaxillofac Radiol 32:333–336

Congenital Malformations, Orbit

Emanuele Neri, Francesca Cerri, Francesca Turini
Diagnostic and Interventional Radiology, University of Pisa, Pisa, Italy
neri@med.unipi.it

Synonyms

Anophthalmia; coloboma; Cyclopia and synophthalmia; microphthalmos; Septo-optic dysplasia

Definition, Pathology/Histopathology

Anophthalmia, or congenital absence of the eye(s), is a rare, sporadically occurring abnormality usually associated with trisomy syndromes 13–15, Klinefelter's syndrome, and complex craniofacial malformations.

Primary anophthalmia occurs when the optic vesicle does not form. Secondary anophthalmia and congenital cystic eyeball are caused by the same congenital defect: the partial or complete failure of involution of the primary optic vesicle early in the formation of the eye. A small or nonexistent cyst yields the classic appearance of anophthalmia, whereas a large cyst will lead to a congenital cystic eyeball.

Anophthalmia may be difficult to differentiate from severe microphthalmos or orbital hypoplasia. Unlike a child with anophthalmia, a child with microphthalmos, however, has a formed eyeball with lens.

Congenital microphthalmos is a common malformation encountered clinically. Microphthalmos in adults is here defined as eyes of which the axial length is less than 20.4 mm in males and 20.1 mm in females; in children younger than 14 years, it refers to eyes at least three square roots of two-thirds below the mean for age-similar controls.

Although microphthalmos may occur as an isolated event, it is frequently associated with other ocular–orbital abnormalities such as coloboma, glaucoma, cataracts, septo-optic dysplasia, and maternal infections.

Cyclopia and synophthalmia result from total and partial fusion of the optic vesicles, respectively, preventing normal orbital separation.

Cyclopia is the most grotesque developmental abnormality in ophthalmology. The term is commonly used to describe either the abnormality of true cyclopia, in which a single median eye is the only ocular structure present, or synophthalmia, in which two globes are partially fused in a median position. The cause of this malformation is obscure.

Familial occurrence and occurrence in twins and in consanguineous marriages have been documented and would be consistent with a single gene abnormality. However, cyclopia has been produced experimentally in numerous species following exposure to various teratogenic agents, and this has been interpreted as evidence for an environmental cause of cyclopia. In recent years, several isolated case reports of cyclopia in humans have been associated with abnormal chromosomes.

The incidence of the cyclopia/synophthalmia deformity in humans is unknown. By 1963, more than 250 published case reports had been collected. In one hospital, an incidence of approximately 1/40,000 births was reported.

Septo-optic dysplasia is a rare anomaly associated with decreased vision and hypoplasia of the optic nerves. A prominent anterior recess of the third ventricle and a small optic canal are typical. Pituitary insufficiency and absence of or defects in the septum pellucidum are also present. A number of patients with septo-optic dysplasia have schizencephaly and seizures.

Coloboma is a rare congenital abnormality resulting from failure of the embryonic choroid fissure to close properly. It may affect any part of the eye. Morning glory syndrome is a coloboma that affects the optic nerve at the optic disk.

The incidence in the general population, therefore, is probably less than 1/1,000. Typical colobomas are inherited as an autosomal dominant trait, with both variable penetrance (30%) and expression, and they are bilateral in more than 60% of cases. Males and females are affected equally.

A wide variety of environmental agents has been shown to induce the development of coloboma in laboratory animals, but no such association has been proved in humans, although coloboma has been described in a baby whose mother was given thalidomide during pregnancy.

Coloboma at the optic nerve entrance is not uncommon but usually extends to involve a portion of the adjacent retina and choroid. In a relatively small subset of patients, only the proximal part of the fetal cleft fails to close, which results in an isolated defect in the immediate region of the optic disk. Most such colobomas are unilateral, unlike the more extensive defects, although there may be minor cupping of the contralateral optic disk.

Clinical Presentation

The cyclopian deformity is characteristically accompanied by numerous systemic malformations. The infant is small

for estimated age. A microcephalic head has a proboscis over a midline diamond-shaped opening for the single or fused eyes. The ears and mouth are usually of abnormal shape and position. Postaxial hexadactyly may be observed.

At postmortem examination, the forebrain is fused with a single ventricle and a single or absent optic nerve. The olfactory bulbs and tracts are absent, and other cranial nerves may be absent. A significant cardiac abnormality is almost always present (patent foramen ovale, interventricular septal defect, patent ductus arteriosus, dilated atrium or ventricle, or abnormal cardiac valves). The lungs may be atelectatic, edematous, or small. Intestinal lesions range from a small, low-positioned mouth to a high-arched palate; malrotation or Meckel's diverticulum; or a posteriorly located anus. The kidneys may be duplicated, small, polycystic, or hydronephrotic. The data available with these case reports does not permit statistical evaluation of the incidence of specific tissue disorders or of any possible significant differences between the abnormalities present in trisomy D and other different chromosome aberrations, or between trisomy D and the cases with "normal" chromosomes.

A wide variety of clinical findings may be noted at fundoscopic examination of isolated optic nerve head colobomas; they range from slightly increased physiologic cupping to large excavations. The term "morning glory syndrome," first used by Kindler in 1970, refers to the fundoscopic appearance, similar to that of the morning glory flower of the optic nerve head coloboma that involves part of the surrounding retina. There is enlargement and excavation of the optic disk, which has pale glial tissue in its floor and is surrounded by variably pigmented choroid. The remainder of the eye may be normal, but most eyes have associated abnormalities, the most common being microphthalmia and atypical coloboma (i.e., coloboma not originating in the fetal cleft). Other associated abnormalities include optic nerve atrophy, basal (particularly sphenoid) encephalocele, midline craniocerebrofacial clefting, agenesis of the corpus callosum, and many abnormalities not affecting the central nervous system. Vision may be unimpaired or affected by scotomas (blind spots) of varying degree, but blindness is more usual. This leads to strabismus, noted in few patients. Leukokoria may be noted and is important because the differential diagnosis will include retinoblastoma and congenital cataract.

Diagnosis

In most of these syndromes, diagnosis can be made with fetal ultrasound (US). Although the vast majority of these syndromes are exceptionally rare, diagnosis using US cannot be expected without reference values. Eye measurements are easy to obtain and are highly reproducible. Intraocular details such as the lens can also be seen starting from the 22nd week of gestation. In late pregnancy, fetal ocular movements and palpebral movements can be observed. Their significance is not yet established; if there is a relationship between fetal ocular movements and brain maturation, more investigations are clearly needed before fetal ocular movements could be used to assess fetal maturity and development.

Imaging of children with congenital microphthalmos reveals both a small globe and a small, poorly formed orbit. Microphthalmos can be associated with a retrobulbar duplication cyst resulting from a defective closure of the embryonic fissure.

Imaging of children with anophthalmia reveals a poorly formed, shallow orbit with only rudimentary orbital tissue.

The diagnosis of septo-optic dysplasia cannot be made with magnetic resonance (MR) imaging alone. Dysgenesis of the septum is more easily recognized than optic nerve hypoplasia because the chemical shift artifact generated by the interface of orbital fat and the optic nerve obscures the nerve, making accurate assessment of nerve size impossible unless special techniques are used to correct for chemical shift.

In addition, the optic chiasm is difficult to evaluate because its apparent size on MR images is dependent on section thickness, gap, and angle of the chiasm with respect to the plane of the section. Moreover, the intracranial optic nerves, optic chiasm, and optic tracts can be subjectively normal in size on MR images, despite the fact that clinically apparent optic nerve hypoplasia is present.

It appears, therefore, that MR imaging is not sensitive to the small degrees of optic nerve hypoplasia that can be detected clinically. In conclusion, septo-optic dysplasia is a difficult diagnosis to make with MR imaging alone; it requires correlation of the results of ophthalmologic examination with endocrinologic and neuroradiologic studies.

Diagnosis of colobomas is made at fundoscopic examination and is confirmed by imaging, which is indicated to demonstrate the extent of the defect and to exclude associated abnormalities such as those described above. US examination and MR imaging have been suggested as possible modalities. Both techniques, however, require that the patient remain still for relatively long periods with the eyes in a fixed position, as any eye movement will degrade the images obtained and hamper confident interpretation of small scleral defects. For this reason, it is difficult to perform these techniques in children. Also, results of US may be less than satisfactory

due to a variety of technical problems that may make it difficult to image the entire length of the optic nerve. No information is obtained about the brain and the skull base.

MR imaging provides no information that is not readily available with computed tomography (CT), although its lack of ionizing radiation to the eyes is an obvious advantage. The spatial resolution of CT is superior to that of MR imaging, and the inherent contrast between ocular structures and orbital fat permits acquisition of images of excellent quality. Use of the newer fast spin–echo MR imaging sequences, when available, may reduce the overall time required to image the eyes, but the need for multiple sequences, including T1-weighted images, still makes this technique time-consuming. The loud noises produced by the imager during image acquisition cause further difficulties in the sleeping child. CT, with its potential for fast scanning and high resolution is, therefore, presently the technique of choice in children.

Descriptions of the use of CT in diagnosing coloboma are few. These reports describe the findings in several patients with ocular coloboma, but only a small minority confirms the presence of morning glory syndrome at fundoscopic examination. CT findings relate to the extent of the defect. The globe is misshapen, and there is widening of the optic nerve head, which is of water density and is continuous with the vitreous humor. Thinning and eversion of the sclera at the margin of the defect may also be identified. Heterotopic adipose tissue and smooth muscle within the disk have been reported, and these should not be mistaken for tumor. Associated anomalies, including microphthalmos, may be present. CT scans of the brain may demonstrate further associations, including encephalocele and agenesis of the corpus callosum.

Two conditions that may be confused with coloboma at CT are staphyloma at the posterior pole of the globe and microphthalmos with cyst. Staphyloma is an inflammatory condition in which there is localized ectasia of the globe. This is not limited to the inferonasal aspect of the globe, nor does it lead to the classic fundoscopic appearance. Microphthalmos with cyst is a severe malformation of the globe with gross ectasia of the sclera, which results in a cystic structure beside the globe that may be much larger than the globe itself. The important differentiating feature is that the neck of the cyst where it connects with the globe is much smaller than the actual cyst. With thin CT sections confined to the optic nerves, a minimal number of scans will demonstrate the features of optic nerve coloboma. The choroidoscleral defects with cystic expansion of the optic nerve, together with the typical fundoscopic findings, confirm the diagnosis.

References

1. Hopper KD, Sherman JL, Boal DK et al (1992) CT and MR imaging of the pediatric orbit. Radiographics 12:485–503
2. Barkovich AJ, Fram EK, Norman D (1989)Septo-optic dysplasia: MR imaging. Radiology 171(1):189–192
3. Murphy BL, Griffin JF (1994) Optic nerve coloboma (morning glory syndrome): CT finding. Radiology 191:59–61
4. Nippon Ganka Gakkai Zasshi (1994) Microphthalmos and its pathogenic classification. 98(12):1180–2000
5. Benacerraf BR, Frigoletto Jr, Bieber FR (1984)The fetal face: ultrasound examination. Radiology 153:495

Congenital Malformations, Spine and Spinal Cord

Andrea Rossi, Paolo Tortori-Donati
Department of Pediatric Neuroradiology, G. Gaslini Children's Research Hospital, Genoa, Italy
andrearossi@ospedale-gaslini.ge.it

Synonyms

Caudal agenesis—caudal regression; Diastematomyelia—split cord malformation; Lipomyelocele—lipomyeloschisis; Myelocele—myeloschisis; Spinal dysraphism—spina bifida

Definition

Spinal dysraphism is the term used to describe congenital malformations of the spine and spinal cord. Classification of spinal dysraphisms requires a rational correlation of clinical, neuroradiological, and embryological information. Spinal dysraphisms are categorized into open or closed depending on whether the abnormal nervous tissue is exposed to the environment or is covered by the integuments (Table 1).

Spinal dysraphisms are caused by derangements that occur during the three consecutive stages of *gastrulation* (weeks 2–3), *primary neurulation* (weeks 3–4), and *secondary neurulation* (weeks 5–6) (1–5). During gastrulation, the bilaminar embryonic disk, formed by epiblast (future ectoderm) and primitive endoderm, is converted into a trilaminar disk because of formation of an intervening third layer, the mesoderm. Epiblastic cells start migrating toward the primitive streak, a stripe of thickened epiblast composed by totipotential cells, pass inward at the Hensen's node (the cranial termination of the primitive streak), to ingress the interface between the epiblast and the primitive endoderm. Subsequent waves

Congenital Malformations, Spine and Spinal Cord. Table 1 Classification of spinal dysraphisms

Open	Closed				
	With subcutaneous mass		Without subcutaneous mass		
	Lumbosacral	Cervico-thoracic	Simple dysraphic states	Complex dysraphic states	
1. Myelomeningocele	1. Lipomas with dural defect	1. Nonterminal Myelocystocele	1. Intradural lipoma	Disorders of midline notochordal integration	Disorders of segmental notochordal formation
2. Myelocele	1a. Lipomyelomeningocele	2. Meningocele	2. Filar lipoma	1. Diastematomyelia	1. Caudal agenesis
3. Hemimyelomeningocele	1b. Lipomyelocele		3. Tight filum terminale	2. Neurenteric cysts	2. Segmental spinal dysgenesis
4. Hemimyelocele	2. Terminal myelocystocele		4. Persistent terminal ventricle	Dorsal enteric fistula	
	3. Meningocele		5. Dermal sinus		

of epiblastic cells migrating laterally along the interface form the interposed mesoderm, whereas cells migrating along the midline form the notochord, the foundation of the axial skeleton. Establishment of the neural plate under the induction of the notochord marks the onset of primary neurulation on about day 18. Subsequently, the neural plate starts bending, forming paired neural folds that increase in size and approach each other to eventually fuse in the midline to form the neural tube. This process occurs bidirectionally toward the two extremities of the embryo. The cranial extremity of the neural tube (anterior neuropore) closes at day 25, whereas the caudal extremity (posterior neuropore) closes at day 27 or 28. The posterior neuropore corresponds to the 32nd somite, i.e., the future third sacral metamere. The segment of the spine and spinal cord caudad to somite 32 is formed by secondary neurulation. The tail bud, a mass of cells deriving from the caudal portion of the primitive streak, lays down an additional part of the neural tube caudad to the posterior neuropore that undergoes a process of regression, degeneration, and further differentiation, which results in the formation of the tip of the conus medullaris and the filum terminale. The conus medullaris contains a focal expansion of the ependymal canal called terminal ventricle.

Pathology

Myelomeningocele

Myelomeningocele is the principal form of open spinal dysraphism (OSD). In myelomeningocele, the ▶placode herniates, together with the meninges, through a more or less large defect in the midline of the back, typically at a lumbosacral level, and is therefore exposed to the environment. Expansion of the underlying subarachnoid space causes elevation of the surface of the placode above the surface of the skin.

Myelocele

The uncommon myelocele is differentiated from myelomeningoceles by the absence of expansion of the subarachnoid spaces ventrale to the placode. Thus, the placode is flush with the cutaneous surface.

Hemimyelocele and Hemimyelomeningocele

In the setting of a longitudinal cord splitting or diastematomyelia (see later), failure of neurulation of one hemicord produces two additional, very rare forms of OSD, called hemimyelocele and hemimyelomeningocele depending on whether the placode is flush with the skin surface or is elevated.

Lipomyelocele and Lipomyelomeningocele

These are the most common forms of CSD with subcutaneous mass. In both instances, the mass is represented by a lipoma, and the spinal cord is connected to the lipoma at the level of a placode. Differentiation

between the two entities is based on the position of this attachment, the so-called placode–lipoma interface. In lipomyeloceles, the lipomatous tissue creeps into the spinal canal through a posterior bony ▶spina bifida and attaches to the neural placode, i.e., the placode–lipoma interface lies within the spinal canal, whereas in lipomyelomeningoceles, expansion of the subarachnoid spaces pushes the neural placode out of the spinal canal, i.e., the placode–lipoma interface lies outside the spinal canal.

Meningocele

Meningoceles are herniations of a CSF-filled meningeal outpouching through a posterior bony spina bifida. By definition, they do not contain neural elements with the possible exception of redundant nerve roots or the filum terminale.

Myelocystocele

Myelocystoceles are categorized into terminal and nonterminal based on their location along the neuraxis. Terminal myelocystoceles are characterized by herniation of a hydromyelic cavity that involves the terminal portion of the cord into a meningocele. Nonterminal myelocystoceles, either full blown (i.e., containing a hydromyelic cavity) or abortive (i.e., composed of a fibroneural stalk that fans out from the posterior aspect of the spinal cord and crosses a skin-covered meningocele), are located at cervical, thoracic, or high lumbar level.

Intradural and Intramedullary Lipoma

Intradural and intramedullary lipomas are contained within an intact dural sac but are otherwise similar. Large lipomas may displace the cord laterally, resulting in an off midline, flattened, or bumped placode–lipoma interface. In rare instances, lipomas are completely intramedullary.

Filar Lipoma

Filar lipoma is an elementary anomaly of secondary neurulation characterized by a fibrolipomatous thickening of the filum terminale. The incidental finding of fat within the filum terminale in the normal adult population is estimated to be 1.5–5% in unselected MRI studies. In the absence of a ▶tethered cord syndrome (TCS), a fatty filum is therefore considered an anatomic variant.

Tight Filum Terminale

A tight filum terminale is a short, hypertrophic filum that produces tethering and impaired ascent of the conus medullaris. Isolated cases are extremely uncommon, while the abnormality is more frequent in patients with diastematomyelia or dermal sinuses. A low-lying conus medullaris is frequently, albeit not necessarily, associated.

Dermal Sinus

It is an epithelium-lined fistula that extends from the skin surface inward to a variable depth, and sometimes pierces the dura to reach the intradural compartment. The lumbosacral region is the most common location, although cervical, thoracic, and occipital locations are also found. Embryologically, dermal sinus tracts are traditionally believed to result from focal incomplete disjunction of the neuroectoderm from the cutaneous ectoderm.

Persistent Terminal Ventricle

Persistence of the terminal ventricle is embryologically related to preservation of the continuity of the terminal ventricle of secondary neurulation with the central canal of the spinal cord. Differentiation of a persistent terminal ventricle from hydromyelia is based on the location within the conus medullaris immediately above the filum terminale. The size of the cavity usually does not change on follow-up exams.

Diastematomyelia

Diastematomyelia (literally, split cord) refers to a variably elongated separation of the spinal cord in two, usually symmetric halves. There is in fact a continuous spectrum of abnormality ranging all the way between a partially cleft cord contained in a single dural tube at one end, and completely duplicated spinal cord contained within dual dural tubes with an intervening bony spur at the other end. Embryologically, abnormal midline notochordal integration results into a variably elongated segment in which the midline notochord is replaced by two paired notochordal processes separated by intervening primitive streak cells. Each "heminotochord" induces a separate "hemi"-neural plate, which will then neurulate independently to form a "hemi"-neural tube. The resulting malformation essentially depends on the developmental fate of the intervening primitive streak tissue, which is a totipotential tissue capable of differentiating into ecto-, meso-, and endodermal lineages. If this intervening tissue differentiates into cartilage and bone, the two hemicords eventually will be contained into two individual dural sacs separated by an osteocartilaginous spur (type I diastematomyelia). Conversely, if the primitive streak tissue is reabsorbed or only results into a thin fibrous septum, the two hemicords eventually will lie within a single dural tube (type II diastematomyelia).

Caudal Agenesis Syndrome

Caudal agenesis syndrome, also called caudal regression, is a heterogeneous constellation of anomalies that comprise total or partial agenesis of the caudal portion of the spinal column, anal imperforation, genital anomalies, bilateral renal dysplasia or aplasia, pulmonary hypoplasia, and lower limb abnormalities. There is a known association with maternal diabetes mellitus (1% of offspring of diabetic mothers). The degree of vertebral abnormality in CA may range extensively, from isolated agenesis of the coccyx to absence of the sacral, lumbar, and lower thoracic vertebrae. However, the vast majority of these anomalies involve absence of the coccyx and part of, or the whole, sacrum. Caudal agenesis is categorized into two variants depending on the location and shape of the conus medullaris: either high and abrupt (type I) or low and tethered (type II) (23). Embryologically, CA is consistent with abnormal formation of a caudal segment of the notochord and corresponding paraxial mesoderm, resulting in a correspondingly segmental abnormality of neural induction.

Segmental Spinal Dysgenesis

Segmental spinal dysgenesis is defined as the association of (i) segmental agenesis or dysgenesis of the lumbar or thoracolumbar spine; (ii) segmental abnormality of the underlying spinal cord and nerve roots; (iii) congenital paraplegia or paraparesis; and (iv) congenital lower limb deformities. Embryologically, it is related to failure of development of an intermediate segment of the notochord. The spinal cord at level of the abnormality is thoroughly absent, and the bony spine is focally aplastic. As a result, the spine and spinal cord are "cut in two," with resulting acute angle kyphosis.

Clinical Presentation

Because placode ulceration and infection are leading causes of mortality in the untreated newborn, patients with OSDs, including myelomeningoceles, are operated on soon after birth. Unfortunately, surgery cannot restore complete functional recovery, and operated patients usually exhibit a variable association of sensorimotor deficits of the lower extremities, bowel and bladder incontinence, hindbrain dysfunction, hydrocephalus, as well as intellectual and psychological disturbances. Intrauterine myelomeningocele repair has been shown to reduce the incidence of shunt-dependent hydrocephalus and the severity of the Chiari II malformation that is typically associated with OSDs. It is also estimated that 20–40% of individuals with OSDs are allergic to latex. Allergic responses can vary from mild to anaphylaxis, and occur when latex products touch the skin or mucous membranes. Latex-free devices must therefore be used in the MR environment when these patients are studied.

Closed spinal dysraphisms (CSD) are much more heterogeneous than OSDs, and some are not clinically evident at birth. Clinical examination is significantly helpful to restrict the differential diagnosis. A critical factor in this evaluation is the presence of a subcutaneous mass on the patient's back. This will categorize CSDs into those with, and those without, a subcutaneous mass. Affected children usually present with a TCS. TCS includes sensorimotor dysfunction, muscle atrophy, decreased or hyperactive reflexes, urinary incontinence, spastic gait, and orthopedic deformities such as scoliosis or foot and hip deformity. TCS is the main clinical complaint in patients with lipomyeloceles/lipomyelomeningoceles, intradural or filar lipomas, tight filum terminale, diastematomyelia, and caudal agenesis. Several birthmarks are associated with underlying dysraphisms. Among these, focal hirsutism is significantly associated with diastematomyelia. Capillary hemangioma is the least sensitive in predicting underlying malformation, although capillary hemangiomas of the lumbar region are associated with spinal dysraphisms in greater than 10% of cases. Dorsal dimples or ostia can indicate either a dermal sinus or a sacrococcygeal fistula. All fistulas opening above the gluteal crease should be presumed to violate the subarachnoid space until proven otherwise. Conversely, skin pits located within the intergluteal cleft need no further investigation as they are related to simple sacrococcygeal cysts or fistulas. Patients with caudal agenesis may have a rudimentary tail, lower limb abnormalities, or anorectal malformations. Imperforate anus is associated with surgically correctable intradural pathology in at least 10% of patients. Therefore, all patients with imperforate anus should undergo MR imaging studies. Clinically, children with the type I caudal agenesis typically have a stable neurological defect that is due to their "fixed" spinal cord dysplasia, whereas those with the type II will present with a TCS. Patients with segmental spinal dysgenesis typically have a protuberance of bony consistence along their back, corresponding to the apex of a kyphotic gibbus at level of the focal bony aplasia, and are congenitally paraplegic or paraparetic.

Spinal dysraphisms may be part of complex syndromic associations. The OEIS constellation (omphalocele, exstrophy of the cloaca, imperforate anus, and spinal anomalies) can be found in patients with terminal myelocystoceles and caudal agenesis. The latter can also be a part of VACTERL (vertebral abnormality, anal imperforation, cardiac anomalies, tracheoesophageal fistula, renal abnormalities, and limb deformities) and the Currarino triad (partial sacral agenesis, anorectal malformation, and presacral mass: teratoma and/or meningocele).

Imaging

Magnetic resonance imaging (MRI) has greatly ameliorated the diagnosis of these disorders and has enhanced the possibility of earlier and case-tailored treatment, mainly thanks to its multiplanar imaging and tissue characterization capabilities.

Because patients with OSDs (among which myelomeningoceles) are usually operated on soon after birth, only rarely are MRI studies performed prior to surgery. However, preoperative MRI investigation should be performed whenever possible, so as to obtain: (i) anatomic characterization of the various components of the malformation, especially regarding the relationships between the placode and nerve roots; (ii) presurgical evaluation of the entity and morphology of the malformation sequence (hydromyelia, Chiari II malformation, and associated hydrocephalus); and (iii) identification of rare cases with associated cord splitting (hemimyelomeningoceles and hemimyeloceles). MRI of untreated myelomeningoceles shows dehiscence of the subcutaneous fat, fascia, bone, and muscle at level of the spina bifida, and a low position of the spinal cord that forms the dorsal wall of the defect.

On MRI, lipomas are detected as masses that are isointense with subcutaneous fat in all sequences, including those acquired with fat suppression. The appearance of spinal lipomas is variable depending on the presence of dural defects (i.e., lipomyeloceles lipomyelomeningoceles) or absence of them (i.e., intradural and filar lipomas). Lipomyeloceles are characterized by a placode–lipoma interface located within the spinal canal. MRI is the imaging modality of choice to demonstrate both the bony defect and the subcutaneous fat extending into the spinal canal and attaching to the spinal cord. The latter is typically low lying, and the placode–lipoma interface may extend over several vertebral levels. It may be smooth and regular or large and irregular, with stripes of adipose tissue that permeate the spinal cord and penetrate into the ependymal canal. Hydromyelia is usually present in these cases. The size of the spinal canal may be increased in relation to the size of the lipoma, but the size of the subarachnoid space ventral to the cord is consistently normal. Lipomyelomeningoceles may produce a constellation of MRI features and individual cases typically differ from one another because of the variable size of the meningocele and lipoma, as well as the variable orientation of the placode. An archetypal condition in which the placode–lipoma interface lies exactly along the midline is not the rule but, rather, an exception. In most cases, the placode is stretched and rotated eccentrically toward the lipoma on one side, whereas the meningocele develops on the other side. In such an instance, the spinal roots that emerge from the side facing the meningocele have a redundant course and may be at greater risk for damage during surgery, whereas those lying on the side of the lipoma are shorter and cause cord tethering. Unlike with lipomyeloceles, the spinal canal is dilated because of expansion of the ventral subarachnoid spaces. Filar lipomas are detected as hyperintense stripes of adipose tissue with resultant thickening of the filum terminale. Intradural lipomas are larger lipomatous masses that typically connect with an unneurulated spinal cord segment.

In terminal myelocystoceles, MRI shows the terminal portion of the spinal cord that is distended by focal hydromyelia that herniates posteriorly through a wide spina bifida into a meningocele. A subcutaneous lipoma is often associated. Nonterminal myelocystoceles are located along the cervical or thoracolumbar spine; only a thin fibroneurovascular stripe emanating from a limited dorsal myeloschisis and possibly distended by focal hydromyelia enters the meningocele, while the spinal cord remains within the spinal canal. A simple meningocele is detected on MRI as a CSF filled cavity that does not contain the spinal cord. Dehiscence of the subcutaneous fat over the dome of the protruding sac is a common finding to both myelocystoceles and meningoceles.

Diastematomyelia is categorized into two types (see earlier), and a combination of CT and MRI is best suited to evaluate this complex abnormality. In the type I, the radiological hallmark is the osseous or osteocartilaginous septum (the "spur"), which dissects the spinal canal into two separate halves, each containing an independent dural tube, in turn containing a hemicord. Although in the archetypal case the spur connects the vertebral body to the neural arch along a midsagittal plane, "atypical" spurs are common. The spur may course obliquely and may be incomplete, in which case it may originate either from the vertebral body or from the neural arch. In some cases, the spinal canal is divided unequally, resulting in two asymmetric hemicords. There is an indication to CT in order to obtain a three-plane evaluation of the spur for surgical purposes. However, especially in young children, the spur may be mostly cartilaginous, therefore being inadequately visualized on CT; it progressively ossifies as the child grows. MRI is the imaging modality of choice for a thorough investigation of this abnormality. In most cases, the spur is located at the thoracic or lumbar level and lies at the caudal end of the cord splitting. As a consequence, the two hemicords usually surround the spur tightly before fusing with each other to form a normal spinal cord below, whereas rostrally the splitting is much more elongated. Therefore, there is a craniocaudal sequence of partial clefting, complete diastematomyelia within a single dural tube, diastematomyelia with dual dural tubes with intervening spur, and reunion of the two hemicords, an appearance that may recall railway points.

In the type II, there is not an osteocartilaginous spur to divide the spinal canal. As a consequence, there is a single dural tube housing both hemicord. Three variants of diastematomyelia type II exist, i.e., absence of a septum, presence of an intervening fibrous septum, and partial cord splitting. Of these, absence of whatever septum is, by far, the most common. In such case, the diagnosis is relatively straightforward both on correctly placed axial and coronal MRI sequences; on sagittal MR images, the only indicative sign is an apparent thinning of the spinal cord resulting from partial averaging with the intervening subarachnoid space between the two hemicords. A midline, nonrigid, fibrous septum sometimes is detected at surgery; these septa may be identified on axial and coronal T2-weighted images as thin hypointense stripes interposed between the two hemicords. Rare cases of partial cord splitting are characterized by an incomplete separation of the two hemicords, which remain joined by a midline bridge. The conus medullaris is typically low, and there is a strong association with tight filum terminale.

The caudal agenesis syndrome is characterized by a degree of vertebral abnormality that may range extensively, from isolated agenesis of the coccyx to absence of the sacral, lumbar, and lower thoracic vertebrae. However, the vast majority of these anomalies involve absence of the coccyx and part of, or the whole, sacrum. The degree of sacral agenesis may vary, with S1 through S4 present in individual cases. Sacral aplasia may also be asymmetric, with resulting total or subtotal hemisacrum that may, in turn, be unilateral or bilateral. Full appreciation of the heterogeneous spectrum of vertebral malformation requires anteroposterior and lateral X-ray films, which constitute an essential part of the neuroradiological workup. CT may be necessary for clarification of particularly complex conditions. Caudal agenesis is categorized into two variants depending on the location and shape of the conus medullaris: either high and abrupt (type I) or low and tethered (type II).

Bibliography

1. Tortori-Donati P, Rossi A et al (2000) Spinal dysraphism: a review of neuroradiological features with embryological correlations and proposal for a new classification. Neuroradiology 42:471–491
2. Rossi A, Biancheri R, Cama A et al (2004) Imaging in spine and spinal cord malformations. Eur J Radiol 50:177–200
3. Tortori-Donati P, Rossi A, Biancheri A et al (2005) Congenital malformations of the spine and spinal cord. In: Tortori-Donati P (ed) Pediatric Neuroradiology. Heidelberg: Springer Verlag, pp 1539–1596
4. Tortori-Donati P, Cama A, Rosa ML et al (1990) Occult spinal dysraphism: neuroradiological study. Neuroradiology 31:512–522
5. Dias MS, Walker ML (1992) The embryogenesis of complex dysraphic malformations: a disorder of gastrulation? Pediatr Neurosurg 18:229–253

Congenital Malformations, Splenic

F. E. Avni[1], J.-F. Chateil[2]
[1]Department of Medical Imaging, University Clinics of Brussels—Erasme, Brussels, Belgium
[2]Department of Pediatric Imaging, Hospital Pellegrin, Bordeaux, France
favni@ulb.ac.be

Synonyms

Asplenia, polysplenia syndromes; Heterotaxia syndromes, ambiguous situs abdomen; Splenogonadal fusion, wandering spleen

Definitions

A variety of developmental malformations of the spleen may be detected during infancy and childhood (1–3).

- Asplenia: Asplenia is the congenital absence of a spleen. The condition can be isolated or associated with abdominal situs inversus or ▶situs ambiguous and accompanied by congenital heart disease. It is more common in male. In asplenia syndrome, the inferior vena cava (IVC) and the aorta are on the same side. Midgut malrotation, microgastria, and gallbladder duplication may be present.
- Polysplenia: Polysplenia can be isolated or associated with abdominal situs inversus or situs ambiguous and

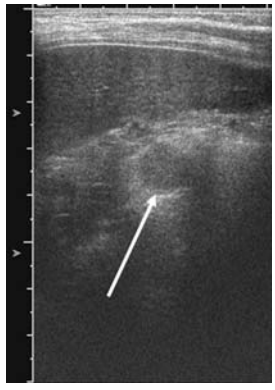

Congenital Malformations, Splenic. Figure 1 Accessory spleen. Incidental finding on ultrasound. Transverse scan of the spleen; the accessory spleen appears as a round well-delineated mass (*arrow*).

accompanied by congenital heart disease. It is more common in females. Polysplenia syndrome includes interruption of the infrahepatic portion of the IVC with azygos continuation, malrotation of the bowel, and absence of gallbladder.

- Splenogonadal fusion: The spleen and/or ectopic splenic tissue may be located anywhere in the abdomen, including attached to the left ovary or within the scrotum, leading to a splenogonadal fusion.
- ►Accessory spleen, cleft notches, and lobules should be considered normal variants.
- In wandering spleen, the ligamentous attachment of the spleen may be lax or absent, leading to an abnormal mobility of the spleen that may undergo torsion.
- True cysts of the spleen may be present in utero and disappear in utero or after birth.
- Lymphangioma and hemangiomas may develop into the spleen. The lesions may be isolated, part of diffuse abdominal disease, or part of syndromes (Klippel Trenaunay Weber, Kasabach–Merritt, Beckwith–Wiedemann, or Turner Syndrome).
- Storage diseases may involve the spleen (►Gaucher disease).

Clinical Presentation

Splenic anomalies by themselves do not produce clinical symptoms unless a mass is present and palpated or unless complications (such as torsion) occur.

Imaging

- *Ultrasound* (*US*): The spleen has a homogeneous pattern, usually hyperechoic compared to the adjacent renal cortex. Its contour is smooth. The technique determines the exact location of the spleen and the presence of accessory glands. Color Doppler evaluation is helpful for evaluation of the vascular anatomy (1, 2). The splenic length measures about 6 cm at 3 months, 7 cm at 12 months, 9 cm at 3 years, and 11 cm at 10 years.
- *Computed tomography* (*CT*): On CT without contrast injection, the spleen appears homogeneous, and its density is around 40 HU. After contrast injection, the helical CT appearance of the spleen depends on the timing of intravenous bolus administration. On early images, the spleen may demonstrate heterogeneous aciform enhancement or a more diffuse pattern that should not be interpreted as disease. This heterogeneity resolves within 70 sec (4).
- *Magnetic resonance* (*MR*) *imaging*: Splenic intensity varies with age in relation with the ratio of white to red blood. In the neonate, before maturation of the lymphoid system and proliferation of white pulp, the spleen is isointense relative to the liver on T1-weighted sequences and isointense to hypointense relative to the liver on T2-weighted sequences. In children older than 8 months, the spleen appears hypointense to the liver on T1-weighted sequences but hyperintense on T2-weighted sequences (5).

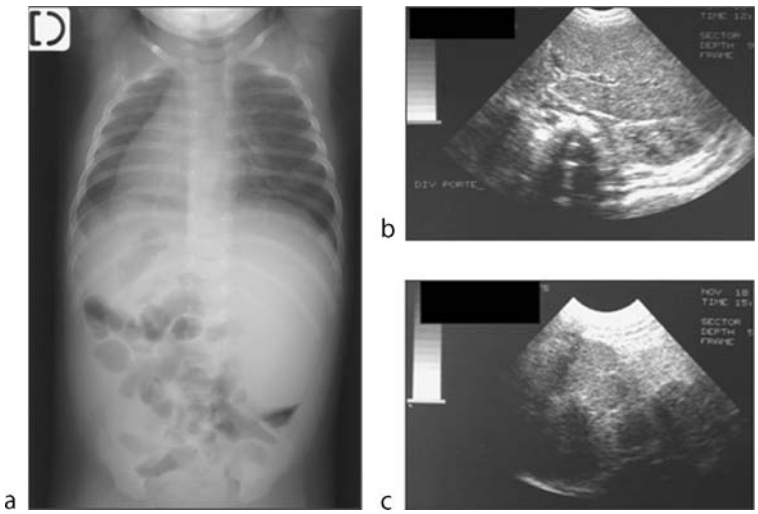

Congenital Malformations, Splenic. Figure 2 Situs inversus and polysplenia. (a) Chest X-ray demonstrating the situs inversus. (b) Ultrasound of the upper left quadrant demonstrating the liver. (c) Ultrasound of the right upper quadrant demonstrating the polysplenia.

Nuclear Medicine

The spleen in normal or abnormal location can be easily identified using Tc99m sulfur-colloid scintigraphy. An accessory or ectopic spleen has imaging characteristics similar to splenic tissue in normal location.

Diagnosis

The diagnosis of splenic anomalies will usually be incidental (Fig. 1), possibly noted on prenatal US examination. Splenic anomalies will be detected on US of the upper abdomen performed as complementary examination in cases of situs inversus or situs ambiguous (Fig. 2).

The spleen is present or absent, unique, or multiple. If absent, nuclear scanning can be done to diagnose ectopic spleen. Isotopic studies can be performed as well in case of splenogonadal fusion.

The diagnosis of a wandering spleen can be suspected on US (Fig. 3). When torsion of a wandering spleen is suspected, CT can be performed to determine the absence of the spleen in its normal location and lack of enhancement of the torsed spleen after contrast injection.

Whenever cystic lesions are demonstrated by US, the differential diagnosis includes benign congenital isolated cyst, ►epidermoid cyst, hydatic cyst, and vascular tumors (lymphangioma, hemangioma).

CT and MR imaging are useful to differentiate between these various diagnoses by showing calcifications, daughter cysts, septa, or abnormal enhancement. In doubtful cases, surgery and histology will be necessary to obtain a definitive diagnosis (3–5).

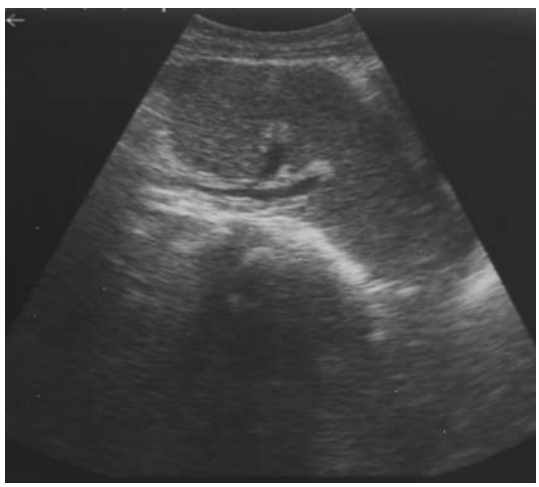

Congenital Malformations, Splenic. Figure 3 Noncomplicated wandering spleen. Ultrasound of the hypogastric area demonstrating a solid mass corresponding to the unattached spleen.

Bibliography

1. Patterson A, Frush DP, Donnelly LF et al (1999) Pattern-oriented approach to splenic imaging in infants and children. Radiographics 19:1465–1485
2. Benya EC (2000) Splenic imaging in infancy and childhood. JBR-BTR 83:217–219
3. Applegate KE, Goska MJ, Pierce G et al (1999) Situs revisited: imaging of heterotaxy syndrome. Radiographics 19:837–852
4. Freeman JL, Kafri ZH, Roberts JL et al (1993) CT of congenital and acquired abnormalities of the spleen. Radiographics 13:597–610
5. Donnelly LF, Emery KH, Bove KE et al (1996) Normal changes in the MR appearances of the spleen during early childhood. Am J Roentgenol 166:635–639

Congenital Malformations, Temporal Bone

Gabriele A. Krombach
Department of Radiology, University Hospital, Aachen, Germany
krombach@rad.rwth-aachen.de

Definitions

Congenital malformations are defined as deviations from the normal anatomical development that lead to functional disorders. They must be differentiated from anatomical variations, which do not cause functional deficiencies and occur more frequently. Congenital malformations can be nongenetic (transplacental) or genetic. In the latter case they may be isolated or syndromal.

Malformations can be classified according to the anatomical structures involved.

Pathology/Histopathology

With respect to the observation that there is a striking resemblance between the various morphological patterns and the stages of inner ear embryogenesis, it has been suggested that malformations result from an arrest of development at a particular stage. Combined malformations of the inner ear and the middle ear with the external ear are rare, since both evolve from mutually independent embryonic origins, namely, from the ectodermal neural crest and the first pharyngeal pouch, respectively.

The bony labyrinth develops between the 4th and 8th week of gestation, grows from the 8th to the 16th week, and ossifies from the 16th to 24th week. The development of the sensory epithelium proceeds until the 25th week. Malformations of the inner ear structures are due to insults between the 4th and 8th week, whereas later injuries affect the sensory epithelium. Owing to these time windows, the majority of patients with sensorineural hearing loss (SNHL) have defects limited to the membranous labyrinth beyond the resolution of the current imaging techniques. Only 20% of patients with congenital hearing loss have anomalies visible on cross sectional imaging.

Microtia, Stenosis, or Atresia of the External Auditory Canal

Microtia indicates a small, abnormally shaped or absent external ear. In approximately 90% of patients it is unilateral. Stenosis (diameter of the external auditory canal 4 mm or less) or atresia of the external auditory canal can be associated with deformities of the middle ear. Microtia is usually divided into four grades: Grade I is a small ear with identifiable structures and a present external auditory canal. Grade II is a partial or hemiear with a stenotic external auditory canal. Grade III is a rudimentary soft tissue structure and atresia of the external ear canal. Grade IV represents absence of the ear, atresia of the external auditory canal, and underdevelopment of the middle ear and deformity of the malleolus and incus.

An *in utero* insult is presumed to cause this malformation. The epithelial cells of the first branchial groove fail to split and canalize, which results in atresia of the external auditory canal.

Ossicular Abnormalities

Congenital abnormalities of the ossicular chain are classified as follows: Class I is the isolated stapedial ankylosis; Class II is the stapedial ankylosis with other ossicular anomalies; Class III is the ossicular anomalies with a mobile stapes; Class IV is the dysplasia of the oval and/or round window.

Nonunion of the incus and stapes is the most common isolated ossicular abnormality and is a result of defects of the long process of the incus.

Oval Window Atresia

The absent cleavage plane between the lateral semicircular canal and the cochlear promontory is associated with a deformed stapes.

Oval window atresia is due to failure of fusion of the primitive stapes with the footplate. If the annular ligament only does not develop, congenital stapes fixation results.

Congenital Cholesteatoma

A cholesteatoma located behind the intact tympanic membrane in a patient with no history of otitis media is presumed to be congenital. Within the temporal bone, it can occur at the petrous apex, mastoid, or middle ear.

Embryonic debris, that is, aberrant epithelial rests of exfoliated keratin within the stratified squamous epithelium, left at the time of closure of the neural tube, can give rise to congenital cholesteatoma.

Michel Aplasia

Michel aplasia is the complete absence of the entire inner ear.

Malformations of the cochlea best demonstrate the "arrest theory," since the distinct anatomical patterns show a remarkable similarity to the appearance of the inner ear at the consecutive stages of embryogenesis. Michel aplasia is the consequence of an arrest of otic placode development in the third gestational week. This extreme form of malformation is very rare and represents less than 1% of inner ear malformations.

Common Cavity Deformity

The common cavity deformity is a single cavity, created from the cochlea and vestibule without the presence of internal architecture.

Arrest of inner ear development between the 4th and 5th week of gestation causes common cavity deformity. At this time, the otic placode has differentiated into the otocyst, but the primordia of the cochlea, vestibule, and semicircular canals have not yet been formed.

Cochlear Aplasia and Cochlear Hypoplasia

In cochlear aplasia the cochlea is absent, whereas in cochlear hypoplasia the cochlea consists of a single turn or less. In both conditions, the vestibule and semicircular canals are present.

An arrest in the development of the cochlear bud during the 5th week of gestation causes cochlear aplasia. Cochlear hypoplasia is due to an arrest during the 6th week.

Mondini Deformity

The cochlea has only 1.5 turns, due to fusion of the middle and apical turns of the cochlea. The osseous spiral lamina and the interscalar septum are missing.

The arrest of inner ear development during the 7th week of gestation causes Mondini deformity. In 20% of patients, it is associated with malformations of the vestibule, semicircular canals, or endolymphatic duct and sac.

Semicircular Canal Aplasia and Dysplasia

This entity refers to partial or complete lack of the development of one or all semicircular canals.

The lateral semicircular canal forms after the superior and posterior semicircular canals have already been formed, between the 6th and 8th week of gestation. The mildest and most common malformation of the inner ear is caused by a late interruption of development and presents as an enlargement of the lateral semicircular canal and the vestibule (Fig. 2a). If development is interrupted at an earlier stage, all three semicircular canals are affected.

Large Vestibular Aqueduct Syndrome

Large vestibular aqueduct syndrome (LVAS) is present if the diameter of the vestibular aqueduct is smaller than 1.5 mm, measured in the middle of the aqueduct (between the common crus and the external aperture). Associated inner ear abnormalities are identified in 60% of the patients, and usually all patients have deficiencies in the modiolus.

LVAS is the most common abnormality in children with SNHL. It results from an arrest of inner ear development in the 7th week of fetal development and follows an autosomal recessive inheritance. There is a female to male predominance of 3:2.

Several mechanisms have been proposed to explain the slow increase of SHNL. Direct transmission of intracranial pressure *via* the vestibular aqueduct to the cochlea can explain deterioration after minor head trauma or barometric pressure changes. Second, accumulation of toxic metabolites in the endolymph might result from dysfunction of the endolymphatic sac and cause cell damage. Third, reflux of hyperosmolar fluid from the endolymphatic sac into the inner ear may cause injury of the cochlear cells. Accordingly, patients with LVAS must be advised to avoid contact sports and scuba diving. They may also benefit from a low-salt diet. In end-stage disease, cochlear implantation is necessary.

Aplasia and Hypoplasia of the Vestibulocochlear Nerve

The normal four nerve branches in the internal auditory canal are lacking.

The internal auditory canal is created by inhibition of cartilage formation at the medial aspect of the otic vesicle in the 9th week of gestation and requires the presence of a vestibulocochlear nerve. The size of the cochlear nerve directly depends on the number of spiral ganglion cells. If the eighth cranial nerve is aplastic, the internal auditory canal will obtain a caliber that depends on the size of the seventh cranial nerve.

Vascular Variants

An aberrant internal carotid artery enters the posterior middle ear cavity and runs along the promontory.

Partial persistence of the stapedial artery represents the intratympanic origin of the middle meningeal artery. It originates from the internal carotid artery between the vertical and horizontal part of the carotid canal, enters the middle ear anteroinferiorly, runs along the promontory, passes between the crura of the stapes, and enters the facial canal. At the level of the first genu, it leaves the facial canal and enters the middle cranial fossa.

Aberrant internal carotid artery: Because of absence of the cervical part of the internal carotid artery and subsequent absence of the vertical part of the bony carotid canal, the tympanic branch of the ascending pharyngeal artery serves as collateral to the horizontal part of the internal carotid artery. Apparently, the vertical segment of the carotid artery enters the temporal bone through the enlarged inferior tympanic canaliculus.

Partial persistence of the stapedial artery: The stapedial artery fails to involute during the third fetal month, so that the developing vessels have to change their course.

Clinical Presentation

Microtia, Stenosis or Atresia of the External Auditory Canal

Conductive hearing loss is the leading symptom in patients with grade II–IV microtia. Up to 90% of patients with stenosis of the external auditory canal develop cholesteatoma as young adults.

Ossicular Abnormalities and Oval Window Atresia

Patients present with congenital conductive hearing loss.

Congenital Cholesteatoma

The most striking finding is a white mass behind an intact tympanic membrane in a young patient with conductive hearing loss. Symptoms depend on the location of the mass if it is not located in the middle ear.

Michel Aplasia, Common Cavity Deformity, and Cochlear Aplasia

Patients present with sensorineural deafness from birth.

Cochlear Hypoplasia

Patients present with a hearing deficit. The severity depends on the degree of membranous labyrinthine development.

Semicircular Canal Aplasia and Dysplasia

If isolated, malformation of the semicircular canals might be asymptomatic.

Mondini Deformity

Mondini deformity is characterized by a low-frequency hearing deficit, due to fusion of the middle and apical turns of the cochlea. High-frequency hearing usually persists to a variable degree.

Large Vestibular Aqueduct Syndrome

The leading symptom is SNHL, which is moderate in early childhood, but gradually deteriorates over a period of years. Usually SNHL deteriorates to profound sensorineural deafness after apparently minor head trauma or sudden changes in barometric pressure.

Aplasia and Hypoplasia of the Vestibulocochlear Nerve

The leading symptom is deafness from birth without change.

Vascular Variants

Aberrant internal carotid artery: Objective or subjective pulsatile tinnitus and conductive hearing loss are common symptoms of an aberrant internal carotid artery. On otoscopy there is a retrotympanic mass that mimics paraganglioma. Biopsy or operation must at all costs be avoided, since it may end disastrously.

Partial persistence of the stapedial artery: Most patients are asymptomatic. In rare cases, pulsatile tinnitus may be present.

Imaging

In general, the history (young age at initial presentation, congenital symptoms) will raise the suspicion of a congenital malformation. High-resolution (HR) thin-slice (1 mm) CT is the imaging technique of choice for patients with suspected congenital malformations of the temporal bone, since it delineates the middle ear and the inner ear. However, neural structures and the fluid-filled labyrinth are only accessible with T2-weighted HR MRI.

Microtia, Stenosis, or Atresia of the External Auditory Canal

CT shows the extent of the malformation with respect to the middle ear (Fig. 1) and provides a roadmap for surgical reconstruction.

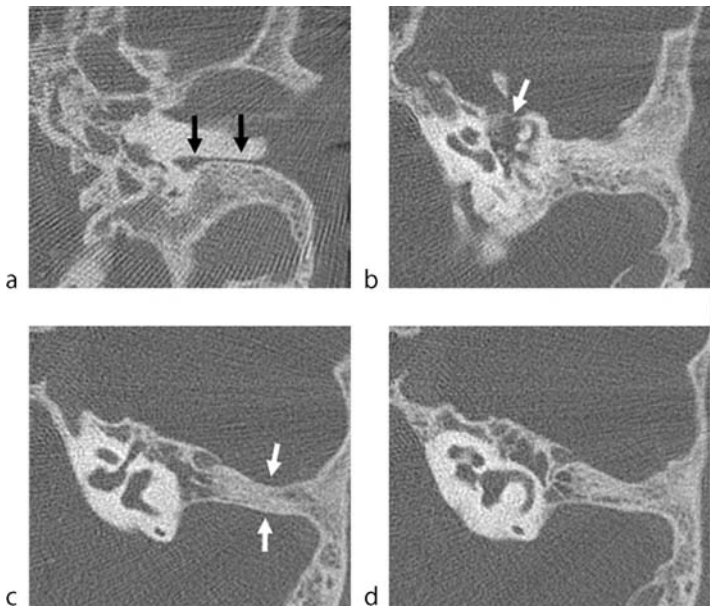

Congenital Malformations, Temporal Bone. Figure 1 Axial HRCT images from a patient with Crouzon syndrome. Stenosis of the external auditory canal is demonstrated (a, *black arrows*). Middle ear opacification is present, due to cholesteatoma (b, *arrow*). The temporal bone itself is small (c, *arrows*), and the inner ear is located near the apex of the temporal bone (d).

Ossicular Abnormalities

HRCT in the axial and coronal plane is required for assessment of the extent of deformities of the ossicular chain.

Oval Window Atresia

HRCT shows the obliteration of the oval window, which is best appreciated in the coronal plane. However, in congenital stapes fixation, which is characterized by absent annular ligament, imaging findings are normal.

Congenital Cholesteatoma

Congenital cholesteatomas of the middle ear present as well-circumscribed masses. The tympanic membrane is intact and the mastoid is well pneumatized. CT without administration of contrast medium is the imaging modality of choice. If glomus tympanicum tumor or facial nerve schwannoma are within the differential diagnosis, contrast enhanced T1-weighted MR images, where congenital cholesteatoma shows a rim enhancement, may be considered.

Michel Aplasia

HRCT demonstrates absence of the cochlea, vestibule, and semicircular canals. The lateral wall of the otic capsule is flat. T2-weighted MR images also do not show inner ear structures; however, complete fibrous or osseous obliteration of the labyrinth is a differential diagnosis in MRI. CT clearly reveals the diagnosis, since in osseous obliteration of the labyrinth, the labyrinthine structures are usually seen with a faded appearance and the lateral wall of the otic capsule is convex, while in Michel aplasia the lateral wall of the inner ear remnant is flat.

Common Cavity Deformity

CT and T2-weighted MRI show a cystic cavity that represents the cochlea and vestibule (Fig. 2a, b). The semicircular canals are absent.

Cochlear Aplasia and Cochlear Hypoplasia

The cochlea is missing (aplasia) or it consists of a single turn or less (hypoplasia). The vestibule and the semicircular canals can be delineated but might be hypoplastic.

Mondini Deformity

The basal turn of the cochlea is normal, whereas the middle and apical turns are fused (Fig. 2c).

Semicircular Canal Aplasia and Dysplasia

Most commonly, the semicircular canals are short and wide (Fig. 2d). They may also be absent or appear as small protrusions in more severe cases.

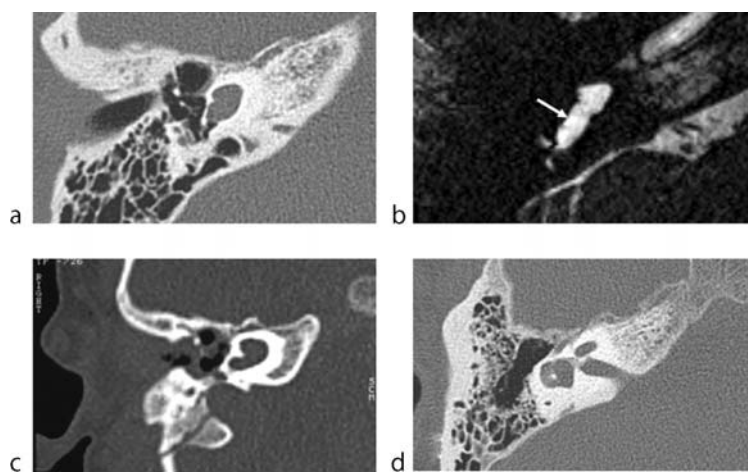

Congenital Malformations, Temporal Bone. Figure 2 Malformations of the inner ear: common cavity deformity (a and b): The axial HRCT image (a) and axial T2-weighted MR image (b) show a cystic cavity (*arrow*, b); Mondini malformation (c). The CT image shows the basal turn, whereas the middle and apical turn are fused. Dysplasia of the lateral semicircular canal. The axial CT image demonstrates the dilated lateral semicircular canal (d).

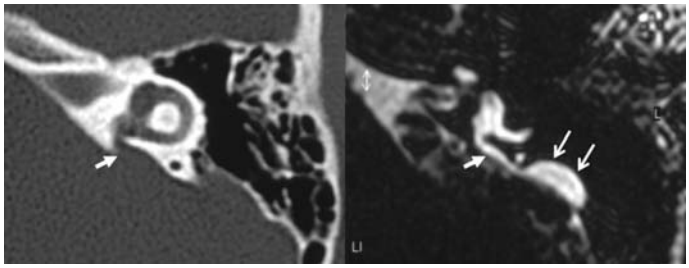

Congenital Malformations, Temporal Bone. Figure 3 Large vestibular aqueduct. The enlarged vestibular aqueduct is visible on the axial CT image (left image, *arrow*) and the axial T2-weighted MR image (right image, *closed arrow*). Only the MR image demonstrates the enlarged endolymphatic sac (*open arrows*).

Large Vestibular Aqueduct Syndrome

Axial HRCT slices show the enlargement of the vestibular aqueduct. Axial T2-weighted MR images demonstrate the enlarged endolymphatic duct within the bony canal and the endolymphatic sac (Fig. 3).

Aplasia and Hypoplasia of the Vestibulocochlear Nerve

HR T2-weighted MRI demonstrates hypoplastic nerves and the narrow internal auditory canal. CT can only show the narrow canal.

Vascular Variants

Aberrant internal carotid artery: CT or MR angiography shows the course of the carotid artery. The vertical part of the carotid canal is missing.

Partial persistence of the stapedial artery: Absent foramen spinosum and enlargement of anterior tympanic facial nerve canal on CT.

Nuclear Medicine

Nuclear medicine is not applied in congenital malformations of the temporal bone.

Diagnosis

Diagnosis of congenital malformations is based on the clinical findings. Congenital conductive hearing loss should raise the suspicion of ossicular abnormalities or oval window atresia. In patients with congenital cholesteatoma, otoscopy shows a white mass behind the intact tympanic membrane. CT shows the extent of the cholesteatoma and possible involvement of the ossicular chain. In patients with SNHL, CT demonstrates the degree of cochlear development. In patients with hypoplasia or aplasia of the vestibulocochlear nerve, sensorineural deafness may raise the suspicion, whereas T2-weighted MRT demonstrates hypoplasia of the nerve. If a very small nerve is present, transtympanic stimulation of the promontory or intracochlear stimulation may be helpful for differentiation between aplasia and hypoplasia.

Bibliography

1. Jackler RK, Luxford WM, House WF (1987) Congenital malformations of the inner ear: a classification based on embryogenesis. Laryngoscope 97(3 Pt 2 Suppl 40):2–14
2. Bamiou DE, Phelps P, Sirimanna T (2000) Temporal bone computed tomography findings in bilateral sensorineural hearing loss. Arch Dis Child 82(3):257–260
3. Casselman JW, Kuhweide R, Ampe W, et al (1996) Inner ear malformations in patients with sensorineural hearing loss: detection with gradient-echo (3DFT-CISS) MRI. Neuroradiology 38(3):278–286
4. Koesling S, Kunkel P, Schul T (2005) Vascular anomalies, sutures and small canals of the temporal bone on axial CT. Eur J Radiol 54(3):335–343

Congenital Malformations, Thymus

Gundula Staatz
Department of Radiology, Division of Radiology
University of Erlangen–Nürnberg, Loschgestr. 15
91054 Erlangen
gu.stz.uni-erlangen@t-online.de

Synonyms

DiGeorge syndrome; Thymus aplasia

Definitions

Congenital malformations of the thymus are rare and include thymus aplasia or hypoplasia, ►ectopic thymus and thymic cysts. *Thymic aplasia or hypoplasia* is defined as an absent or very small thymus, due to an abnormal development of the third and fourth branchial arches encountered in certain immunologic disorders. An absent thymus is most commonly associated with ►*DiGeorge Syndrome*, which is defined as an immunologic disorder characterized by dysmorphic facies, hypoparathyroidism, congenital heart defects and a deficiency in cell-mediated immunity. *Ectopic thymus* is characterized by an aberrant migration of thymic tissue in the superior and posterior mediastinum, bases of the skull, tracheal bifurcation or the cervical region. Ectopic thymus is most frequently located in the cervical region, where it may present as a solid or cystic (*thymus cyst*) mass.

Pathology/Histopathology

Biopsy of the thymus in DiGeorge syndrome reveals no specific histopathologic findings with exception of evidence for thymic hypoplasia. Aberrant cervical thymic tissue histologically contains thymic lobules, lymphoid follicles, Hassell corpuscles, and cysts (1). The cysts can be small or quite large and are lined by a variety of cell types, including non-keratinising squamous, cuboidal, or columnar cells. Cyst contents range from straw-coloured proteinaceous fluid to necrotic debris or old haemorrhage. Cholesterol crystals may be found in the luminal fluid or embedded in the cyst wall. Occasionally parathyroid tissue (also derived from the third pharyngeal pouch) is found in the lesions (1).

Clinical Presentation

The clinical presentation of children with DiGeorge syndrome is primarily characterized by cardiac anomalies, such as tetralogy of Fallot, ventricular septal defect, interrupted aortic arch, pulmonary atresia or truncus arteriosus (2). Arhinencephaly, cleft lip, palate, or uvula, diaphragmatic abnormalities, hydronephrosis, malrotation of the gut and imperforate anus are other anomalies found in DiGeorge syndrome. Hypocalcaemia due to hypoparathyroidism usually begins in the neonatal period and may present with tetany or tonic convulsions. Due to T-cell dysfunction recurrent viral and fungal infections as well as mycobacterial and *Pneumocystis carinii* infections are observed. Ectopic thymus may present as a cervical palpable mass, because it is often located along the anterior border of the sternocleidomastoid muscle lateral to the thyroid gland and near the carotid sheath.

Imaging

The thymus gland can be visualised with use of ultrasound, radiography, CT, MRI and nuclear medicine.

Ultrasound is the modality of first choice for the evaluation of thymic malformations. In fetuses with congenital heart defects, particularly conotruncal anomalies, fetal echocardiography is reliable in diagnosing thymic hypoplasia or aplasia (3). In children below the age of 1 year the incomplete ossification of the sternum and its manubrium provides a comfortable access to the anterior mediastinum, in older children ultrasound of the thymus is performed *via* the jugulum or with use of a parasternal access. Ultrasound is also a reliable tool for the diagnosis of ectopic thymus, especially when the aberrant thymic tissue is located in the neck.

On radiographs the appearance of the thymus is evaluated by the size, configuration and density of the anterior mediastinum.

Computed tomography is a most valuable method for the cross-sectional evaluation of the mediastinum in children, however, because of ionizing radiation, MR imaging is the method of choice for further assessment of thymic malformations beyond ultrasound.

Nuclear Medicine

Fluorine-18 fluorodeoxyglucose (FDG) positron emission tomography (PET) is established as an important diagnostic tool for the diagnosis, staging, and restaging of neoplasms in the mediastinum (4). It plays no role for the assessment of congenital thymic malformations.

Diagnosis

The size and shape of the normal thymus varies considerably with age. In children under 5 years of age, the thymus has a quadrilateral shape with convex lateral contours and gentle undulating borders. In older children and adolescents the thymus shows a triangular configuration with straight lateral margins (5). On chest X-rays the normal thymus presents as a bilateral smoothly outlined mediastinal mass, and particularly on the right side, a characteristic sail-like shadow with a well-defined lateral and inferior margin is often visible (Fig. 1). An absent thymic shadow on the chest X-rays of newborns is

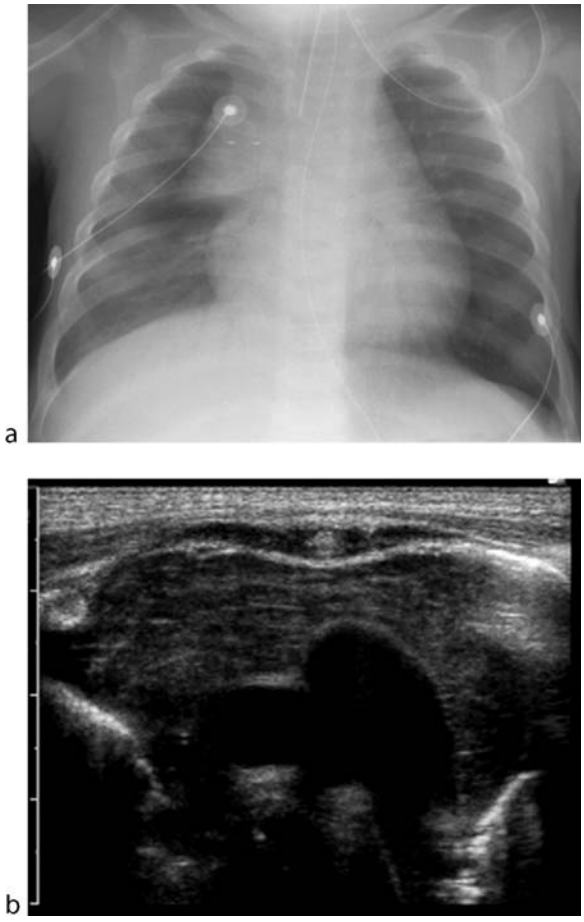

Congenital Malformations, Thymus. Figure 1 (a) Chest radiograph of an intubated neonate from the ICU. Typical sail-like appearance of the right lateral shadow of the thymus with smooth and well-defined margins. (b) US of a normal structured, slightly large thymus in a neonate

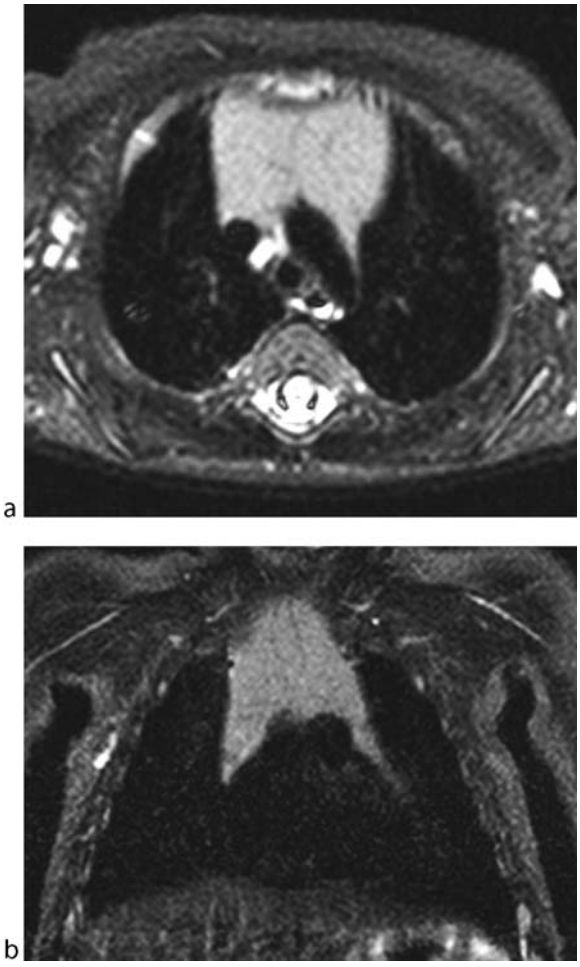

Congenital Malformations, Thymus. Figure 2 Axial (a) and coronal (b) T2-weighted fat-suppressed MR-images of the chest in a 3-month-old girl. The quadrilateral shape of the thymus and the hyperintense signal intensity on T2 weighted images, characteristic for this age group, is demonstrated.

suspicious of thymus hypoplasia or aplasia but the diagnosis has to be confirmed by ultrasound or with MR imaging. On CT images, the normal thymus shows homogenous soft tissue attenuation, with the highest density during infancy, and a homogenous contrast enhancement after intravenous contrast material administration. On MRI, the thymus appears with a signal intensity slightly greater than that of muscle on T1-weighted images, and with a high signal on T2-weighted images (Fig. 2). DiGeorge syndrome is diagnosed by the assessment of the immune system (T-cell function), parathyroid function (parathyroid hormone, PTH) levels, chromosome analysis (microdeletion of 22q11.2), and imaging studies (thymus hypoplasia/aplasia). The diagnosis of aberrant thymus is based on the similar imaging appearance compared to normal thymus. Aberrant thymic tissue may be solid, cystic, or mixed. Cystic lesions are most common and third branchial cleft cysts, lymphangiomas, venous malformations, necrotic or suppurative lymphadenopathy, thyroglossal duct cysts, and epidermoid and dermoid cysts have to be considered as differential diagnosis (1).

Bibliography

1. Cure JK, Tagge EP, Richardson MS et al (1995) MR of cystic aberrant cervical thymus. AJNR Am J Neuroradiol 16:1124–1127
2. Conley ME, Beckwith JB, Mancer JF et al (1979) The spectrum of the DiGeorge syndrome. J Pediatr 94:883–890
3. Chaoui R, Kalache KD, Heling KS et al (2002) Absent or hypoplastic thymus on ultrasound: a marker for deletion 22q11.2 in fetal cardiac defects. Ultrasound Obstet Gynecol 20:546–552
4. Ferdinand B, Gupta P, Kramer EL (2004) Spectrum of thymic uptake at 18F-FDG PET. Radiographics 24:1611–1616
5. Siegel MJ, Glazer HS, Wiener JI et al (1989) Normal and abnormal thymus in childhood: MR imaging. Radiology 172:367–371

Congenital Malformations, Thyroid, and Functional Disorders

Arthur Rosemary
Department of Pediatric Radiology Leeds General Infirmary, Clarendon Wing, Leeds, UK
r.arthur@ukonline.co.uk

Synonyms

Cretinism; Goitre; Grave's disease; Myxoedema

Definition

Congenital disorders of the thyroid gland are developmental disorders, which may present at birth or later in life as a result of abnormal development of the thyroid gland or to inborn errors of metabolism resulting in abnormal hormone production.

Functional disorders of the thyroid gland refer to conditions associated with abnormal production (increased or decreased) or an abnormal somatic response to thyroid hormone or thyrotropin (TSH) and may be the result of a congenital abnormality or be acquired later in childhood.

Pathology and Histology

Development and Hormonogenesis

The thyroid gland develops during the third week of foetal life as a midline outpouching from the floor of the pharynx. During descent into the neck the thyroid gland maintains a connection, the thyroglossal duct, with the base of the tongue until it is obliterated at approximately the seventh intra-uterine week.

During hormonogenesis under the influence of pituitary TSH, thyroid hormone is synthesised by a complex process, where iodine is concentrated from the blood into the follicular cells, oxidised and bound in an organic form to thyroglobulin to produce T3 and T4, the main thyroid hormones. The foetus depends upon low levels of a transplacental maternal thyroid hormone until significant thyroid hormone production begins at about 20 weeks of gestation. Following birth there is a sudden rise in TSH, T4 and T3, followed by a slow progressive fall in childhood to adult levels.

Although thyroid hormone has a number of actions, e.g. thermogenesis, ion transport, and metabolism of amino acids throughout life, it has several unique properties in childhood, being essential for the normal development and maturation of the brain and skeleton. Table 1 indicates the range of thyroid disorders occurring in childhood and the most important congenital and functional disorders will be discussed later.

Congenital Abnormalities

Failure of normal development of the thyroid gland results in *partial or complete agenesis* of one or both lobes, whereas interruption to the normal descent of the thyroid gland will result in the development of *ectopic thyroid tissue* and *thyroglossal duct cysts* (TDC).

Ectopic thyroid tissue maybe found anywhere along the normal descent pathway and maybe found as low as the anterior mediastinum, although a sublingual position is the most common site. Ectopic thyroid tissue is usually associated with a significant degree of hypothyroidism often having poor function, but may enlarge due to compensatory TSH stimulation.

TDC arise from failure of obliteration of the thyroglossal duct in the foetus. They are usually solitary and occur anywhere from the foramen caecum at the base of the tongue to the thyroid gland. Approximately 20% occur above the hyoid bone. In most cases a TDC is

Congenital Malformations, Thyroid, and Functional Disorders. Table 1 Thyroid disorders in children

Congenital
▶Thyroglossal duct cyst
Thyroid dysgenesis
Functional
Hypothyroidism
Congenital hypothyroidism (CH)
Chronic lymphocytic thyroiditis (CLT)
Iodine deficiency
Secondary hypothyroidism (e.g. pituitary disorders)
Hyperthyroidism
Neonatal
Diffuse toxic goitre—Grave's disease
TSH-induced hyperthyroidism
Thyrotoxicosis without hyperthyroidism
Euthyroid
Goitre
Neoplasia
Benign nodules
Adenomas
Cysts
Malignant nodules
Carcinoma—papillary 70%
Lymphoma
Infection
Thyroiditis—pyriform sinus abnormality

present in conjunction with a normally sited and functioning thyroid gland, although in fewer than 5% of TDC, the cyst may contain the only functioning thyroid tissue in the individual.

Clinical Presentation

The clinical presentation dsepends on the underlying condition and usually reflects either a hormonal disorder or consequences of mass effect. Beside the clinical examination, laboratory investigations are essential. Biochemical tests are fundamental in the evaluation of all babies and children with a suspected thyroid abnormality (1). Serum TSH, T3, T4, free T3 and free T4 levels being most important to diagnosis and the results must be related to normal values for age. More complex investigations may be necessary including the identification of TSH receptor antibodies, cytogenetic testing and biochemical investigations to determine the nature of any inborn error of metabolism, thyroid antibody, other autoimmune antibody tests and pituitary function and TRH testing. Screening programmes for congenital hypothyroidism are based on the detection of low levels of thyroxine, and or high levels of TSH in cord blood or a dried blood spot from a heel prick. Programmes based on thyroxine estimation detect both primary and secondary congenital hypothyroidism (CH) but have a low specificity with a high recall rate, whereas those measuring TSH alone will only detect primary CH but are more specific. In those infants with a low TSH, serum TSH and T4 levels are estimated and if confirmed to be abnormal are referred for clinical evaluation (2).

TDC and ►goitre usually present by their mass effect, potentially causing respiratory problems; TDC may also become secondarily infected and present acutely with a painful midline neck mass. The main concern usually affects functional disorders of the thyroid gland.

Functional Disorders

Congenital Hypothyroidism (CH) is the commonest treatable cause of mental retardation world wide, with iodine deficiency as the most important cause. Thyroid dysgenesis is the most frequent cause in Europe where iodine deficiency is rare, occurring in approximately one in 4,000 live births. Table 2 outlines the most common causes of congenital hypothyroidism. In approximately 10% of cases of CH detected by neonatal screening, the condition is transient and resolves within a few weeks of birth. Thyroid dysgenesis accounts for 85–90% of cases of CH with females more commonly affected than males. Most cases are sporadic although the condition is more frequent in children with Down's syndrome. Dysgenesis ranges from agenesis, to hypoplasia of one or both lobes. Unilateral dysgenesis is not usually associated with CH as sufficient thyroid hormone is still being produced. Inborn errors of metabolism resulting in dyshormonogenesis account for a further 10–15% of cases of CH. In contrast to thyroid dysgenesis most cases have an autosomal recessive pattern of inheritance.

Screen detected babies with CH often have no overt clinical manifestations, although severe cases may show clinical signs at birth, including, large tongue, hoarse cry, umbilical hernia, hypotonia, cold extremities, prolonged jaundice, constipation and large fontanelles. Untreated CH will result in severe irreversible developmental and

Congenital Malformations, Thyroid, and Functional Disorders. Table 2 Congenital hypothyroidism

'Transient'
Thyroid dysgenesis (85–90%)
Inborn errors of metabolism (10–15%)
Secondary/tertiary hypothyroidism
Hypothalamic
TRH deficiency
Midline facial brain dysmorphism
Pituitary
TSH deficiency
Multiple hormone deficiencies
TSH resistance
Thyroid hormone resistance

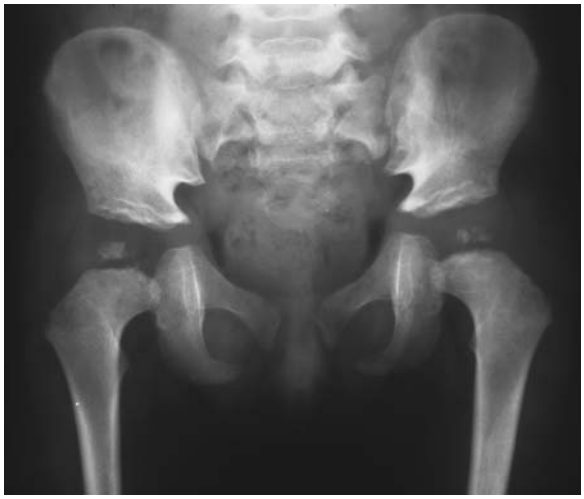

Congenital Malformations, Thyroid, and Functional Disorders. Figure 1 Pelvic X-ray of a young boy presenting with overt signs of ►hypothyroidism, showing delayed and fragmented ossification of the femoral capital epiphyses.

intellectual delay. CH secondary to pituitary or hypothalamic dysfunction may have signs suggestive of hypopituitarism, and can be seen in association with midline facial defects or cerebral malformation; boys may have a micropenis. The presence of a palpable goitre excludes the diagnosis of thyroid dysgenesis, and indicates that the CH is likely to be transient or due to abnormal hormone synthesis resulting in excessive stimulation of the thyroid gland by raised levels of TSH.

The onset of *hypothyroidism in older children* is often insidious, with the development of a *goitre* or identification during child health surveillance due to poor linear growth.

Chronic lymphocytic thyroiditis (CLT) is the most common cause of hypothyroidism presenting beyond infancy although many affected individuals with CLT may initially be euthyroid and present with an asymptomatic goitre. CLT is an autoimmune disorder often affecting adolescent girls with 30–40% having an inherited predisposition to autoimmune disease. The disease is characterised by a destructive process with lymphocytic infiltration and atrophy and fibrosis of the follicles. Goitre occurs in approximately 5% of all children and it is important to distinguish children with goitre due to CLT from those with a simple colloid goitre, by the demonstration of thyroid antibodies in CLT, as the former are at risk of developing hypothyroidism later in life unlike those with a colloid goitre who will remain euthyroid. Children and adolescents with hypothyroidism have an increased incidence of slipped upper femoral epiphyses and puberty may be delayed. In contrast to untreated neonatal hypothyroidism affecting brain development hypothyroidism developing after 3 years of age mainly affects growth and causes delayed skeletal maturation, with no permanent effect on cognitive or neurological development.

Neonatal hyperthyroidism is rare occurring in 2–3% of babies born to mothers with Grave's disease due to the transplacental passage of maternal TSH receptor stimulating antibodies. The condition usually presents towards the end of the first week of life as maternal antithyroid drugs are cleared and is generally transient lasting up to 3 months. The salient features include tachycardia >160, congestive cardiac failure and cardiac arrhythmia. The infant may be irritable, fail to thrive, develop prominent eyes and a goitre may cause airway obstruction. Untreated neonatal ▶hyperthyroidism has a high mortality of approximately 20%. Permanent neonatal hyperthyroidism also occurs as a result of an inherited autosomal dominant genetic mutation in the TSH receptor.

In *older children and adolescents* with hyperthyroidism a large fleshy goitre is common.

Grave's disease, diffuse toxic goitre accounts for 95% of hyperthyroidism in older children generally presenting in adolescent girls with a genetic predisposition to autoimmune disease. Other causes of hyperthyroidism are rare, and include a functioning *thyroid adenoma*, thyrotoxicosis factitia, i.e. ingestion of thyroxine in adolescent girls attempting to lose weight or high levels of TSH secretion, e.g. due to a pituitary adenoma. The absence of a goitre in a thyrotoxic adolescent girl should raise the possibility of thyrotoxicosis factitia. A solitary palpable nodule indicates that an adenoma is the most likely cause. Classical symptoms and signs of thyrotoxicosis develop although ophthalmological signs are less common in children than in adults. Secondary amenorrhoea may occur in association with accelerated bone maturation and linear growth. Cafe au lait spots seen in conjunction with thyrotoxicosis should raise the possibility of McCune Albright Syndrome.

Imaging

X-ray

A number of radiological abnormalities have been described in association with thyroid disease that may serve to point to an underlying thyroid disorder. These include delayed skeletal maturation i.e. bone age, flattened and fragmented femoral epiphyses in hypothyroidism and periostitis and accelerated bone age in hyperthyroidism (Fig. 1). A lateral soft tissue neck may

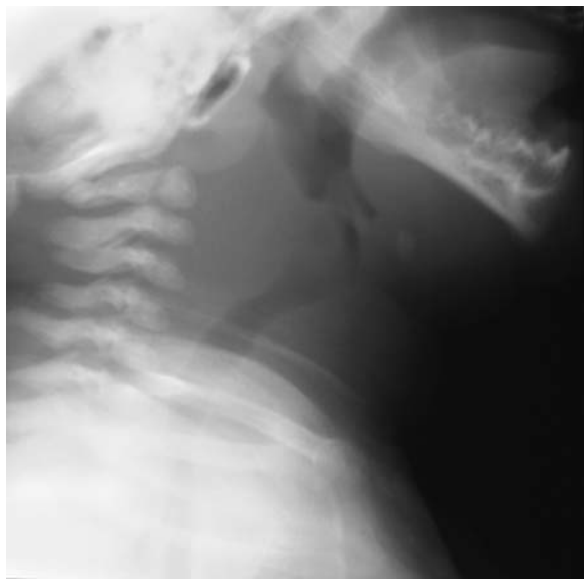

Congenital Malformations, Thyroid, and Functional Disorders. Figure 2 Posterior displacement of the trachea causing mild respiratory distress in a neonate with an enlarged thyroid gland (goitre) due to neonatal hyperthyroidism.

help to demonstrate airway compression in rare cases of airway obstruction, due to an enlarged ectopic thyroid or goitre (Fig. 2).

Thyroid Ultrasound

Ultrasound imaging forms the mainstay of thyroid imaging, to identify the presence or absence of a normal thyroid gland in hypothyroidism, to evaluate any midline swelling thought to be a TDC, and to evaluate a palpable thyroid nodule (Fig. 3). A high frequency transducer is essential (12–15 MHz) and Doppler sonography is useful to assess vascularity of a palpable nodule or ectopic thyroid tissue which is often of increased vascularity (3). A normal thyroid gland in a young child has a lateral lobe measuring approximately 1–1.5 cm in width, 2–3 cm in length and a depth of 0.2–1.2 cm. In CH the finding of a normal thyroid gland indicates that dyshormonogenesis is the most likely cause. In older hypothyroid children where thyroid antibodies are negative and there is no palpable goitre, ultrasound can be helpful to distinguish primary myxoedema i.e. non-goitrous CLT from late presenting thyroid dysgenesis.

There is rarely an indication for ultrasound in a goitre, unless possible mediastinal extension needs to be clarified. The investigation and treatment of solid nodules follows the pathways well established for adult patients, although in children a solitary nodule is more likely to be carcinomatous, particularly papillary carcinoma; functioning adenomas and colloid cysts also occur.

A thyroglossal duct cyst is usually midline but may be found embedded in the strap muscles just to the left of the midline. The wall may be thin and the fluid anechoic, but if there has been previous infection or haemorrhage, the wall may be thickened and the cyst contents may contain echoes. A thyroglossal duct tract may be identified extending deeply to the hyoid bone (Fig. 4).

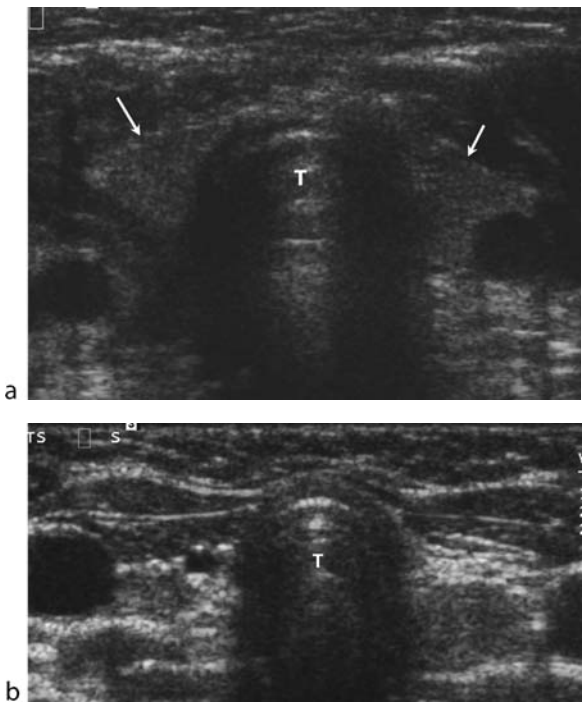

Congenital Malformations, Thyroid, and Functional Disorders. Figure 3 Transverse ultrasound images through the neck. (a) Transverse ultrasound image demonstrating a normal thyroid gland (arrows) in an infant with screen detected congenital hypothyroidism due to an inborn error of metabolism. (b) No thyroid gland could be demonstrated in this infant with thyroid agenesis

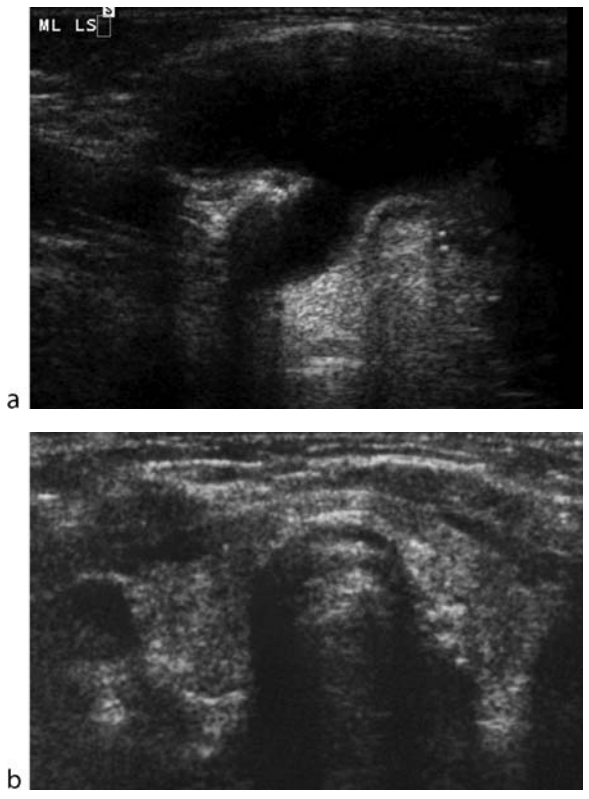

Congenital Malformations, Thyroid, and Functional Disorders. Figure 4 Four year old girl presenting with a high midline neck swelling: (a) Sagittal ultrasound image demonstrating an elliptical cystic structure with posterior and cranial extension towards the hyoid bone typical of a thyroglossal duct cyst (TDC). (b) Demonstrates a normally sited thyroid gland indicating that the TDC can be safely excised.

Thyroid Scintigraphy

Thyroid scintigraphy using technetium-99m pertechnetate and iodine-123 is useful to evaluate both anatomical and functional aspects of a thyroid disease (5). Scintigraphy is essential for the further evaluation of a possible TDC or ectopic thyroid tissue when a normal thyroid gland cannot be identified on ultrasound, as removal of the cyst/ectopic tissue may result in rendering the patient athyroid and dependent on life long thyroid hormone replacement (Fig. 5). Although iodine-123 is more specific and better to quantify dysfunction and inborn errors of metabolism, pertechnetate is cheaper and more readily available, and is the tracer of choice for the initial scan with iodine-123 reserved for further evaluation where the technetium scan is abnormal. In most inborn errors of metabolism the gland is usually enlarged, normally sited and shows increased tracer uptake. Scintigraphy is also used in the evaluation of the solitary thyroid nodule. Identification of a 'hot' nodule suggests the presence of a functioning adenoma and ultrasound

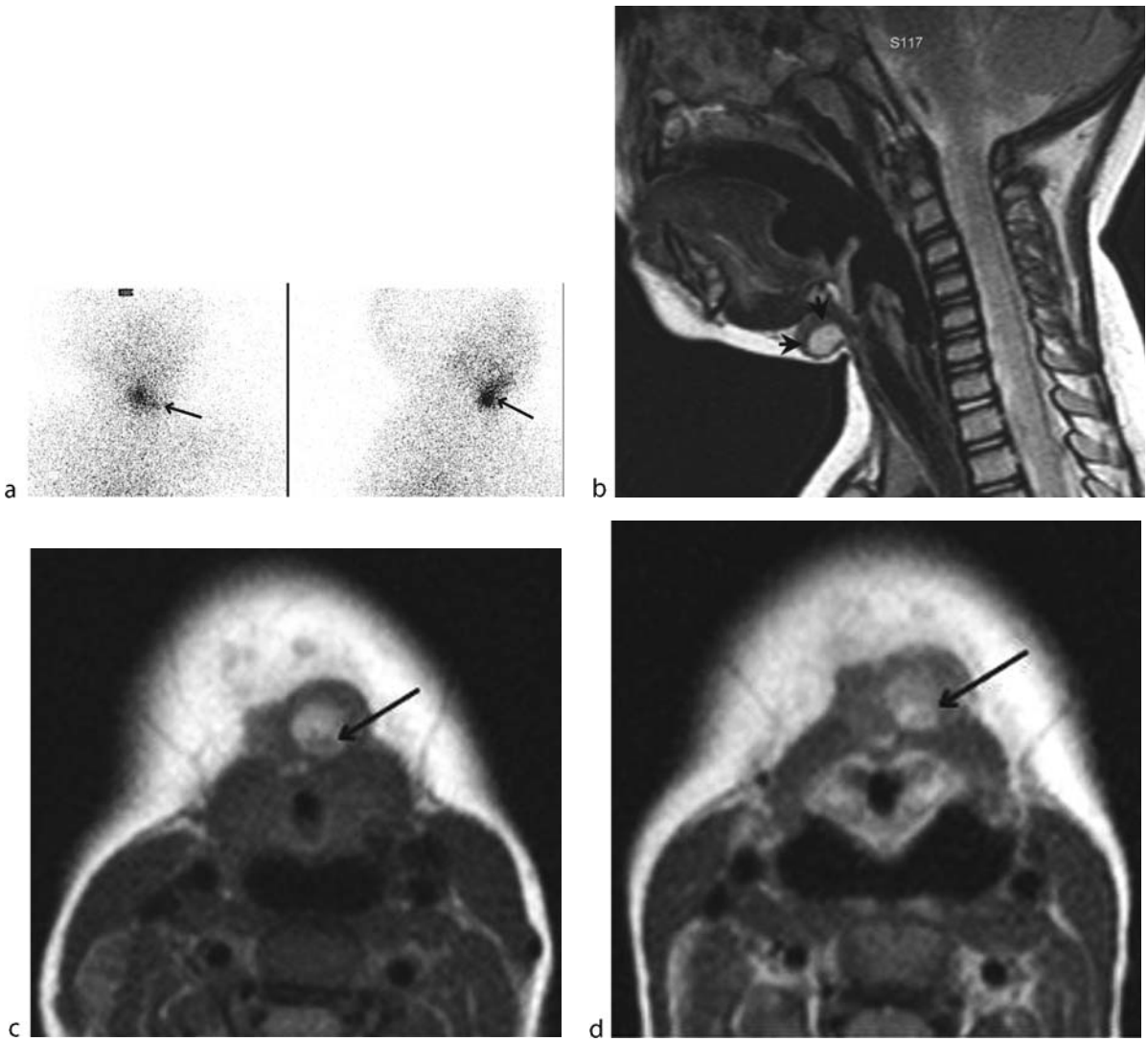

Congenital Malformations, Thyroid, and Functional Disorders. Figure 5 Thyroglossal duct cyst with ectopic thyroid tissue. (a) Thyroid scintigraphy using technetium-99m pertechnetate showing relatively low level uptake of isotope, in frontal and lateral projections, corresponding to the position of the TDC (arrows). No other functioning thyroid tissue was identified, indicating that excision of the TDC would render her athyroid. b-d MRI scans. (b) T2 sagittal, (c) T1 transverse, (d) Contrast enhanced T1 transverse demonstrating a thick walled cystic structure containing proteinaceous fluid in a midline submental region (arrows). No thyroid gland demonstrated elsewhere. There is enhancement of the posterior wall of the TDC following contrast injection (arrows).

Congenital Malformations, Thyroid, and Functional Disorders. Table 3 Important diagnostic features in functional and congenital thyroid disorders

	Disorder	TSH levels	T4 levels	Thyroid gland
Hypothyroidism				
	Dysgenesis	High	Low	Absent/ectopic
	Inborn error of metabolism	High	Low	Normal or enlarged
	TSH resistance	High	Low	Normal/small or not visible
NB (may also be euthyroid or hyperthyroid)	Chronic lymphocytic thyroiditis	High	Normal or low	Enlarged/normal
	Secondary—pituitary or hypothalamic disease	Low	Low	Normal or small
	Thyroid hormone resistance	Normal or low	High	Normal or enlarged
Hyperthyroidism	Neonatal/Graves	Low	High	Normal or enlarged +/– bruit
	Adenoma	Low	High	+/– palpable nodule
	TSH-induced	Normal/ high	High	

fine needle aspiration can then be reserved for evaluation of 'cold' nodules. Open biopsy may be necessary in the younger child.

Cross Sectional Imaging

Cross sectional imaging, i.e. CT or preferably MRI scanning is reserved for the evaluation of more difficult cases, particularly the ectopic sublingual thyroid gland and TDC particularly when recurrent. TDC may be noted to contain contents of intermediate signal intensity on T1 and high signal on T2 if the contents are proteinaceous. Wall enhancement is likely to occur if ectopic thyroid tissue is present (Fig. 5). Nodularity within the mass and the presence of calcification may be an indicator of the development of papillary carcinoma, a complication occurring in approximately 1% of TDC generally during adulthood.

Diagnosis

The diagnoses of the various thyroid disorders depend upon correlation between clinical signs, mode of presentation and the functional status of the thyroid gland, and have been discussed in relation to specific entities earlier. Table 3 summarises the most important findings. The precise pathway for investigation and imaging will depend on the suspected diagnosis. Although initial investigations can be undertaken in a general hospital setting, more complex cases particularly when presenting in the neonate should be referred for specialist investigation and management.

Bibliography

1. Brown RS, Huang S (2005) The thyroid and its disorders. In: Brook C, Clayton P, Brown R (eds) Brook's Clinical Pediatric Endocrinology. Blackwell Publishing, pp 218–253
2. Pollitt RJ, Green A, CJ McCabe et al (1997) Neonatal screening for inborn errors of metabolism: cost, yield and outcome. Health Technol Assess 1:31–35
3. Siegel MJ (1991) Neck. In: Siegel MJ (ed) Pediatric Sonography. Raven Press, pp 63–89
4. Effmann EL (2004) Neck and upper airway. In: Kuhn JP, Slovis TL, Haller JO (eds) Caffey's Paediatric Diagnostic Imaging. Mosby, pp 777–809
5. Schoen EJ, Clapp W, Trinh T (2004) The key role of newborn thyroid scintigraphy with isotropic iodide (123 I) in defining and managing congenital hypothyroidism. Pediatrics 114:683–687

Congenital Malformations, Tracheobronchial Tree

Gundula Staatz
Department of Radiology, Division of Pediatric Radiology, University of Erlangen-Nürnberg Erlangen
gu.stz.uni-erlangen@t-online.de

Synonyms

Bronchial atresia; Bronchogenic cyst; Bronchopulmonary sequestration; Congenital cystic adenomatoid malformation (CCAM); Congenital lobar emphysema; Foregut

malformations, pulmonary and tracheobronchial anomalies such as: bronchial atresia; hypogenetic lung syndrome; Pulmonary arteriovenous malformation; Pulmonary varix; Tracheal bronchus; Tracheal stenosis

Definitions

Congenital malformations of the tracheobronchial tree consist of a heterogeneous group of anomalies, which may be divided into two groups, one with a normal vascular supply, the second group with anomalous vasculature. The most frequent malformations will be addressed in the following chapter.

A *tracheal bronchus* is defined as a right upper bronchus originating in the trachea.

Congenital lobar emphysema is characterised by a progressive overdistension of lung tissue (lobe) without destruction of alveolar septa.

Bronchogenic cysts are foregut duplication cysts developing from an abnormal budding of the ventral foregut and may be located mediastinal, intrapulmonary, or less frequently in the lower neck (1).

Congenital cystic adenomatoid malformation (CCAM) is characterised by an intrapulmonary multicystic mass of pulmonary tissue with an abnormal proliferation of bronchial structures (1). The cysts communicate with the bronchial tree and the vascular supply as well as venous drainage is normal.

Bronchopulmonary sequestration is an embryonic mass of lung tissue disconnected from the tracheobronchial tree with a blood supply from the systemic circulation. Sequestration is divided into an *intralobar* and *extralobar* type. Intralobar sequestration is incorporated within the normal visceral pleura of the lung, has arterial blood supply from the aorta or major aortic branches and drains usually into pulmonary veins. Extralobar sequestration has a separate pleural investment, an arterial blood supply from the aorta or aortic branches and a systemic venous drainage (2).

Pathology/Histopathology

A tracheal bronchus is usually arising from the right lateral wall of the trachea, less than 2 cm above the carina, and is defined as a displaced bronchus, if a single branch of the upper lobe bronchus is missing, and as a supranumary bronchus, if the trifurcation of the right upper lobe is normal (1).

Congenital lobar emphysema is due to a bronchial narrowing, usually caused by an absence or hypoplasia of bronchial cartilage, which leads to an air trapping in the affected lobe. In case of extrinsic compression of a bronchus (e.g. aberrant pulmonary artery), the cartilage rings are malformed, soft and collapsible. The left upper lobe is most often affected, followed by the right middle lobe and the right upper lobe.

The histopathology of a bronchogenic cyst demonstrates a cystic lesion with fibrous walls, which occasionally contain cartilage, lined by ciliated columnar epithelium.

CCAM has been subdivided into three major histological types:

Type 1 (50%)	One or more cysts measuring 2–10 cm in diameter
Type 2 (40%)	Multiple small relatively uniform cysts resembling bronchioles, measuring 0.5–2 cm in diameter
Type 3 (<10%)	Microscopic, adenomatoid cysts, grossly a solid mass without obvious cyst formation

Type 2 and type 3 CCAM may be associated with extralobar sequestration, and receive blood supply from the systemic circulation. The larger cysts of type I lesions are frequently lined by pseudo-stratified columnar epithelial cells, which produce mucine. The cysts of type II lesions are lined by cuboid-to-columnar epithelium and have a thin fibromuscular wall, type II lesions consisting of microscopic, adenomatoid cysts.

Bronchopulmonary sequestration is classified as intra- or extralobar sequestration. Extralobar sequestration is predominantly located on the left side between the lower lobe and the mediastinum and has its own pleural coating; it may occur extra-thoracic, i.e., intra-abdominal. The lesion is composed of non-functioning primitive pulmonary parenchymal tissue without connection to the tracheobronchial tree. Dilated bronchioles, alveolar ducts, and alveoli are found histologically. Intralobar sequestration, which is surrounded by normal lung and incorporated within the normal visceral pleura, is almost exclusively located in the lower lobes, most often on the left side (60%). A bilateral involvement is rarely seen. Intralobar sequestration is characterised by chronic inflammatory tissue replacing the normal pulmonary parenchyma, and multiple cysts filled with viscid fluid or gelatinous material. The pleura is thickened by adhesions to mediastinal and diaphragmatic parietal pleura.

Clinical Presentation

Patients with a tracheal bronchus are usually asymptomatic, but persistent or recurrent upper lobe pneumonia, atelectasis or air trapping, and chronic bronchitis may

occur. Infants with congenital lobar emphysema present with respiratory distress and the clinical examination reveals a hyperresonant thorax with absent breath sounds. A bronchogenic cyst usually causes symptoms due to tracheal or bronchial compression, such as cough, wheezing, stridor, dyspnea, cyanotic spells, and pneumonia (1). Most neonates with CCAM present with respiratory distress. In older infants cough, fever and recurrent pulmonary infections are common findings.

The clinical manifestation of bronchopulmonary sequestration depends on the two different forms of this malformation. Children with intralobar sequestration present more often with pulmonary infection compared to children suffering from extralobar sequestration. Extralobar sequestration is usually an incidental finding, when imaging studies are performed for the evaluation of associated congenital anomalies, such as cardiovascular malformations or diaphragmatic hernia. A communication to the gastrointestinal tract is possible, which can be the cause of feeding problems.

Imaging

Congenital lung malformations are increasingly diagnosed antenatally with use of prenatal ultrasound and foetal MR imaging. After birth, the diagnostic modalities include chest radiographs, ultrasound, scintigraphy, computed tomography (CT), magnetic resonance imaging (MRI), arteriography and bronchoscopy. In children with tracheobronchial malformations, such as tracheal stenosis or tracheal bronchus, bronchoscopy is usually the first method of choice, but recently multidetector spiral computed tomography (MDCT) with the capability of virtual tracheobronchoscopy and bronchography is sometimes used as an alternative.

The diagnosis of congenital lobar emphysema is based in most cases on the clinical examination and the findings of the plain radiographs. CT, and occasionally ventilation/perfusion scintigraphy, is helpful in confirming the diagnosis and in guiding management decisions.

Bronchogenic cysts are best studied with use of CT, but MRI may reveal additional information concerning the haemorrhage, protein or calcium content of the cysts. CCAM can be early identified by prenatal or perinatal ultrasound and MRI (3). Thereafter chest radiographs and CT examinations are the imaging modalities of choice.

Bronchopulmonary sequestration can be suspected on chest radiographs, when a persistent lower lobe opacity or mass is visible in children with recurrent respiratory tract infection. Ultrasound with colour-coded Doppler, CT and MRI provide most helpful information by identifying the anomalous arterial blood supply (4). Especially with the development of MDCT and high-resolution 3D reconstruction techniques, such as volume rendering techniques or maximum intensity projections, the visualisation and identification of the feeding arterial vessel and the venous drainage is accurately performed. Arteriography is only indicated for (pre-operative) embolisation of the systemic feeding artery.

Nuclear Medicine

Radionuclide scintigraphy has an ancillary role in assessing foregut anomalies. Many findings from scintigraphy are relatively non-specific. In infants with congenital lobar emphysema ventilation–perfusion scintigraphy demonstrates restricted ventilation in the affected lobe with ultimate isotope retention due to delayed emptying of alveoli, and a decreased perfusion caused by the markedly attenuated vascularity of the involved lobe.

Diagnosis

A tracheal bronchus is difficult to identify on plain radiographs, but a CT examination is most efficient in demonstrating the aberrant bronchus arising from the lateral tracheal wall (Fig. 1).

Congenital lobar emphysema presents in utero with a fluid-filled over-distended lobe, which may be identified by prenatal ultrasound. On postnatal chest radiographs an over-distended hyperlucent lobe, herniating across the midline, is characteristic. The mediastinum is shifted to

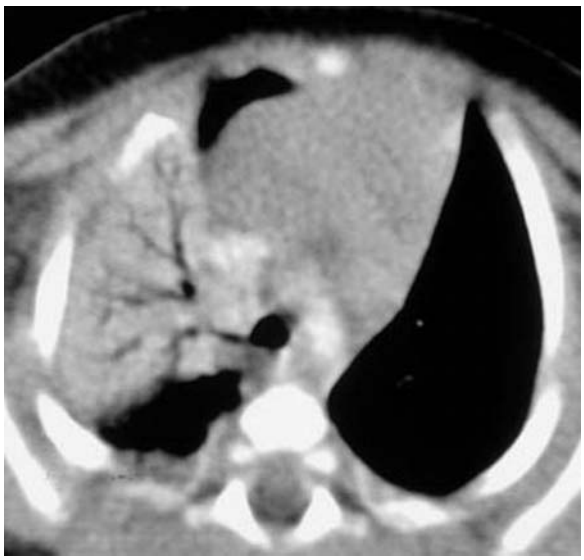

Congenital Malformations, Tracheobronchial Tree.
Figure 1 Chest-CT of a 6-week-old infant with persistent right upper lobe atelectasis demonstrates a tracheal

the contralateral side, the ipsilateral hemidiaphragm is flattened with no movement under fluoroscopy, and the extension of the lobe remains unchanged during exhalation. CT scans demonstrate the hyperlucent, hyperexpanded lobe with attenuated vessels, a midline substernal lobar herniation and compression of the remaining lung (Fig. 2).

A bronchogenic cyst may be identified on chest radiographs by a sharply delineated mass with close contact to the mediastinum, especially to the carina. CT reveals a well-defined round to oval mass with a smooth, thin wall, and a water- or soft-tissue attenuation (5) (Fig. 3). If the cyst is infected or contains secretions, the cyst may appear hyperdense. On T2-weighted MRI images, bronchogenic cysts show homogeneous and markedly high-signal intensity, whereas on T1-weighted MR images the signal intensity can vary between hypo-, iso- and hyperintense due to the fluid content of the cyst, which may consist of protein, blood or calcium (5).

CCAM appears on chest radiographs as a multiple air-filled cystic mass of varying size, which can rapidly expand a lobe due to air trapping with subsequent shift of the mediastinum to the contralateral side. In some patients a pneumothorax occurs. CT provides additional information with depiction of the exact size and extension of the multiple thin-walled, air-filled cysts (Fig. 4). Variable fluid contents in infected or haemorrhagic cysts can also be identified. As a differential diagnosis congenital diaphragmatic hernia, pulmonary sequestration, and bronchogenic cysts has to be considered.

Bronchopulmonary sequestration is visible on plain chest radiographs as a well defined homogeneous or sometimes cystic mass usually located in the posterior portion of the lower lobe. Intralobar sequestration may contain aerated areas due to collateral ventilation and air-trapping (4). Colour-coded Doppler sonography is an elegant method to identify the feeding arterial vessel and the venous drainage, but CT and MRI are often additionally performed, particularly pre-operatively or if

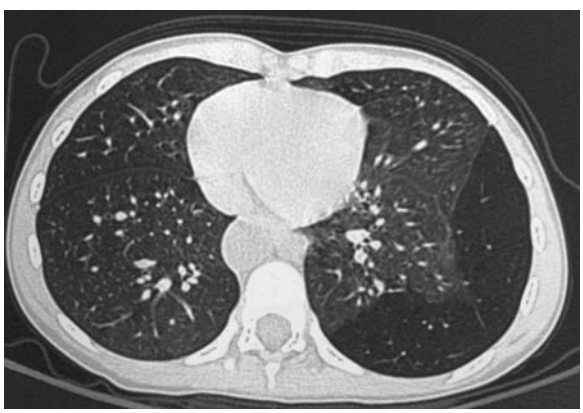

Congenital Malformations, Tracheobronchial Tree.
Figure 2 Congenital lobar emphysema of the left lower lobe. On the chest CT image an overdistended hyperlucent lower lobe on the left side is visible, which leads to a shift of

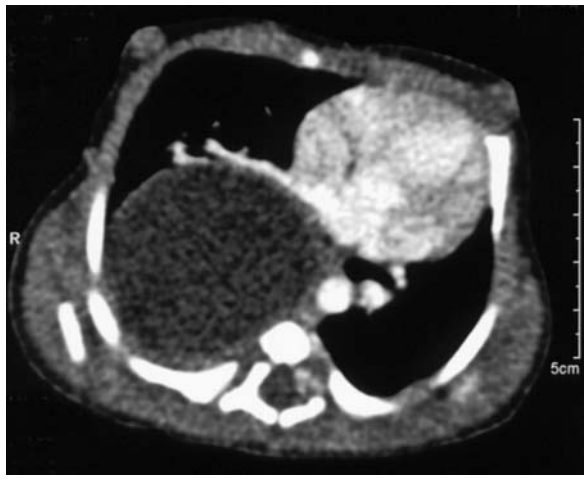

Congenital Malformations, Tracheobronchial Tree.
Figure 3 Contrast-enhanced CT of a newborn with a prenatally diagnosed intrathoracic cyst. A large oval-shaped cystic mass, with a sharply delineated smooth wall and close connection to the mediastinum is identified in the right lower lobe. The left-sided central pulmonary

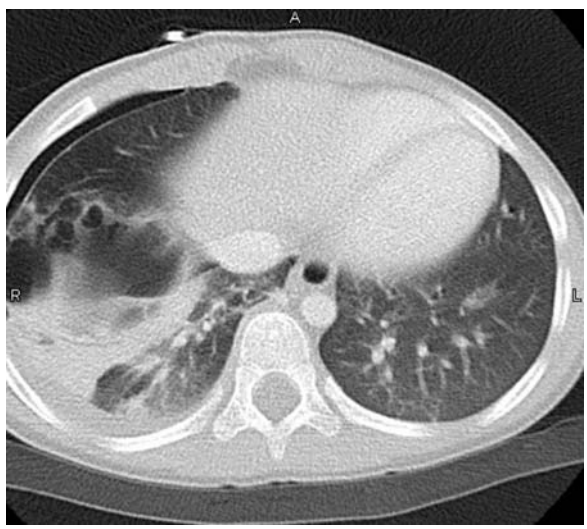

Congenital Malformations, Tracheobronchial Tree.
Figure 4 Chest CT of an adolescent with a CCAM located in the right lower lobe. Multiple air-filled cysts of various sizes are visible. Associated atelectasis in the posterior segments of the right lower lobe, pleural effusion, and a small pneumothorax are also present. (Image from Prof. R. Buchmann, Dept. of Pediatric Radiology, Arkansas

ultrasound cannot accurately delineate the anatomy or remains equivocal. On CT, the lesion enhances after intravenous contrast-material administration and CT-angiography (3D reconstruction) reveals exactly the course and configuration of the anomalous feeding vessel (Fig. 5). Typically the blood supply of bronchopulmonary sequestration arises from the aorta or its major branches such as subclavian, splenic, gastric and intercostal arteries. Venous drainage of extralobar bronchopulmonary sequestration occurs through the systemic circulation, usually via the azygos or hemiazygous veins or the IVC. Intralobar bronchopulmonary sequestration usually drains into pulmonary veins, but also alternative drainage routes via azygos, hemiazygos or IVC are possible. MR angiography is an excellent alternative to contrast-enhanced CT, and provides similar information for the diagnosis of bronchopulmonary sequestration without ionising radiation. For differential diagnosis various diseases have to be considered, such as pulmonary arterio-venous fistula, CCAM, hernias, some pneumonias or neoplasms.

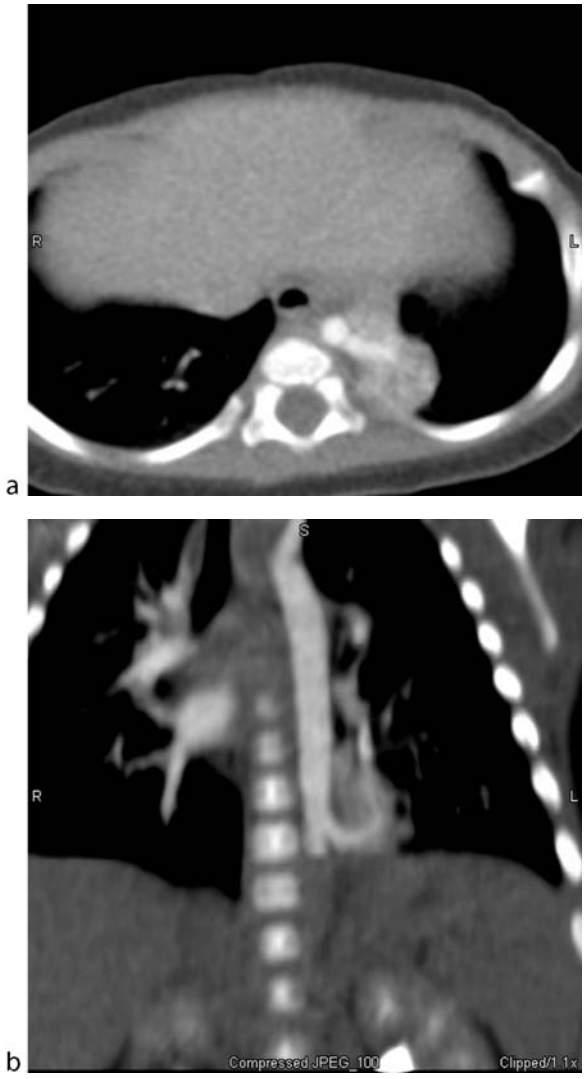

Congenital Malformations, Tracheobronchial Tree.
Figure 5 Arterial phase of contrast-enhanced, axial chest CT (a) and coronal multiplanar reformation (b) of intralobar lung sequestration. A well-defined homogeneously enhancing mass is visible in the posterior basal segment of left lower lobe. The arterial phase clearly depicts the anomalous feeding vessel, arising directly from the thoracic aorta. (Images from Prof. R. Buchmann, Dept. of Pediatric

Interventional Radiological Treatment

Interventional treatment is an interesting therapeutic option in bronchopulmonary sequestration. Transcatheter arterial embolisation (TAE) of the aberrant feeding artery has been performed as a curative therapy or as a pre-operative procedure to minimise the risk of vascular complications during resection.

Bibliography

1. Berrocal T, Madrid C, Novo S et al (2004) Congenital anomalies of the tracheobronchial tree, lung, and mediastinum: embryology, radiology, and pathology. Radiographics 24:e17 (Epub 2003 Nov 10)
2. Siegel MJ (1999) Lung, Pleura and chest wall. In: Pediatric Body CT. Lippincott Williams and Wilkins, Philadelphia, pp 101–140
3. Hubbard AM, Adzick NS, Crombleholme TM et al (1999) Congenital chest lesions: diagnosis and characterization with prenatal MR imaging. Radiology 212:43–48
4. Mata JM, Castellote A (2002) Pulmonary malformations beyond the neonatal period. In: Lucaya J, Strife JL (eds) Pediatric Chest Imaging, Chest Imaging in Infants and Children. Medical Radiology, Diagnostic Imaging (Baert Al, Sartor K (eds)). Springer, Berlin, Heidelberg, New York, pp 93–111
5. McAdams HP, Kirejczyk WM, Rosado-de-Christenson ML et al (2000) Bronchogenic cyst: imaging features with clinical and histopathologic correlation. Radiology 217:441–446

Congenital Malformations, Vascular, Brain

Massimo Gallucci, Nicola Limbucci
Department of Neuroradiology, University Of L'Aquila, L'Aquila, Italy
massimo.gallucci@cc.univaq.it

Synonyms

Arteriovenous malformation; Capillary angioma; Cavernous angioma; Cavernoma; Capillary telangiectasia; Cryptic/occult vascular malformations; Developmental venous malformation; Venous angioma

Definition

Intracranial congenital vascular malformations are classified as arteriovenous malformations (AVMs), cavernous angiomas (CAs), developmental venous anomalies (DVAs), and capillary telangiectasias (CTAs). Mixed lesions are often shown by imaging.

The definition of intracranial vascular malformation is univocal. Old terminology referred to these lesions as different patterns of occult vascular malformations (2); this terminology is based on angiographic features and should be considered obsolete.

CAs are vascular lesions formed by endothelial-lined sinusoidal vascular spaces, filled by slow-flow blood, with no intervening brain tissue.

AVMs can be pial or dural (the latter known as arteriovenous fistulas). Pial AVMs are collections of dysplastic plexiform vessels supplied by arterial feeders and drained by venous channels, with an intervening vascular network.

An arteriovenous dural fistula is a direct shunt without an intervening vascular network. For further details about AVMs please consult the relative chapter.

DVAs are composed of dilated, radially arranged veins draining into an enlarged vein with normal intervening brain. They are considered variations of normal venous drainage (1).

CTAs are small nests of dilated capillaries with normal intervening brain tissue.

Pathology/Histopathology

CAs appear as circumscribed, lobulated, berry-like masses, ranging from a few millimeters to some centimeters. They are composed of thin-walled endothelial-lined sinusoidal vascular channels, without the presence of tunica muscolaris or elastica. Calcifications are common. No intervening brain tissue is present among the channels. The vessels are filled by blood showing different stages of thrombosis. The lesion is surrounded by macrophages and astrocytes containing ferritin and hemosiderin; gliosis is sometimes present. In 23% of patients, CAs are associated with other malformations, usually DVA (3). CAs may occur in any location. About 80% of them are supratentorial and are frequently found at the corticomedullary junction; deep white matter and basal ganglia are also common locations.

DVAs are composed of tufts of dilated, radially arranged veins converging toward an enlarged collector vein that drains into the deep or superficial venous system. Venous walls and intervening brain are normal. DVAs are considered by most as extreme variations of normal venous drainage. In about 30% of cases, the lesions are associated with CAs. The most common location is cerebral or cerebellar deep white matter, often near the ventricles.

CTAs are formed by small nests of dilated capillaries. Vessels are thin-walled and lack muscolaris and elastica. The lesions are often multiple, and the most typical location is the pons.

AVMs usually consist of arterial feeders, collaterals, a nidus, and enlarged veins. In dual AVMs the nidus is absent.

Pathogenesis

Most CAs are congenital; however, *de novo* lesions have been described in familiar forms, in patients with an existing DVA, and after radiation therapy. The relationship among the various malformations is still debated. Some authors suggest that CA and CTA are different stages of the same process. Another theory is that small preexisting DVAs or CTAs induce flow and venous pressure alterations, leading to DVA formation (2). However, different gene mutations have been found in patients with CA and DVA, suggesting a distinct pathogenesis (4).

Pial AVMs are congenital, whereas dural AVMs often occur following recanalization of a venous sinus thrombosis.

Clinical Presentation

The prevalence of *CA* is estimated to be 4% (5–13% of all vascular malformations). CAs are multiple in at least 20–30% of patients, and in 10–15% of cases a familiar pattern is recognized. In familiar forms, the lesions are usually multiple. CAs are symptomatic in about 50–60% of cases, and their clinical course is more severe than for DVA and CTA. Symptoms include seizures, headache, and focal deficits, and they usually occur in young people (20–40 years). Seizures, often refractory, are the most common symptom (50–70%).

The most feared complication of CA is significant intraparenchymal hemorrhage (0.1–1% per year). Subclinical hemorrhage is more common and is responsible for the typical magnetic resonance imaging (MRI) features.

DVAs are considered the most common intracranial vascular malformation (63%) and are almost always clinically silent, representing an incidental finding. Seizures and focal deficits can occasionally be attributed to DVA, but surrounding brain and the venous drainage are normal. Hemorrhage has been described, but it should be considered exceptional. Most symptomatic patients have a mixed malformation, with a CA contiguous to the DVA, and the symptoms depend on the CA.

CTAs are very common and often multiple. They are usually incidentally detected at MRI or autopsy, and they are almost always clinically silent. Sometimes the lesion is part of a mixed malformation: in this case, it can, rarely, bleed.

AVMs present with hemorrhage in 50% of cases and with seizures in 25%.

Imaging

Cavernous Angioma

Digital subtraction angiography (*DSA*): CAs are typically defined as angiographically occult lesions. A faint contrast stain is rare.

Computed tomography (*CT*): CA appears as a small isodense or hyperdense mass, without edema or mass effect, usually with calcifications. After contrast administration the lesion often enhances. In bleeding lesions, CT shows the hematoma with mass effect, but the CA is not usually distinguished.

MRI: CAs have characteristic features. The typical lesion is a nodular mass with a popcorn-like shape and a central core containing areas with heterogeneous signal. The core mixed signal depends on blood clots with different stages of evolution, especially methemoglobin, which is hyperintense on T1. Fluid–fluid levels are sometimes seen in the biggest lesions. Typically, the lesion is surrounded by a complete ring, hypointense on all sequences, corresponding to ferritin and hemosiderin deposits (Fig. 1). The lesion "blooms" on gradient-echo (GE) sequences because of their high sensitivity to susceptibility artifacts. GE sequences should always be acquired because they allow identification of very small

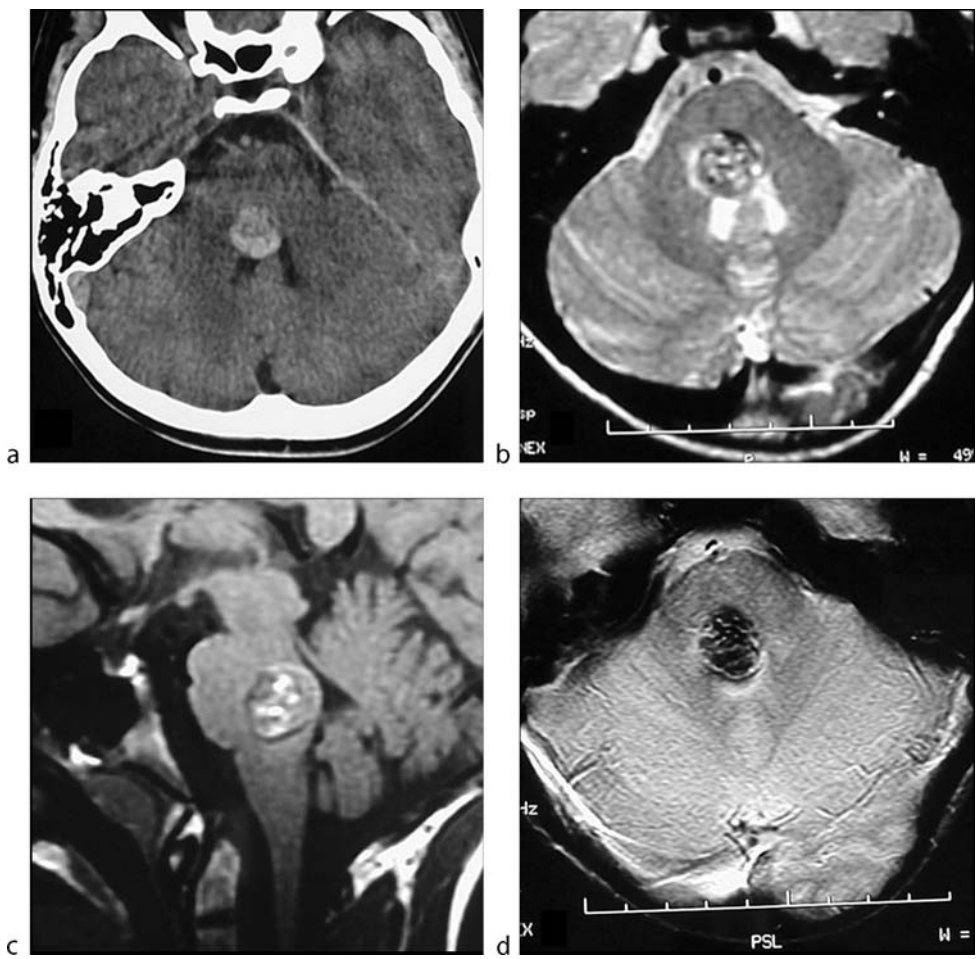

Congenital Malformations, Vascular, Brain. Figure 1 Giant ▶cavernous angioma of the pons. Computed tomography shows a well-defined hyperdense mass (a). On magnetic resonance imaging, the lesion exhibits the classic popcorn-like appearance, with nonhomogeneous aspects on fast-spin-echo T1-weighted (c) and T2-weighted (b) sequences. On gradient-echo sequences, (d) the lesion classically "blooms."

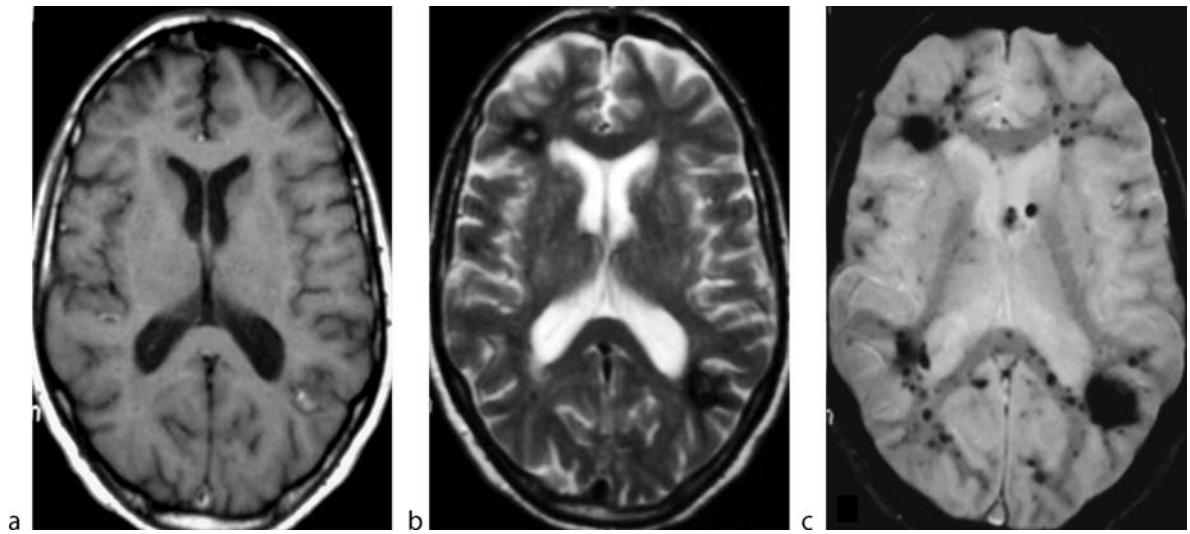

Congenital Malformations, Vascular, Brain. Figure 2 Multiple cavernous angiomas. Fast-spin-echo (FSE) T1-weighted sequence shows multiple round lesions with mixed signal (a). On FSE T2-weighted sequencing, most of the visible lesions are surrounded by a peripheral hypointense rim (b). On gradient-echo T2-weighted sequencing (c), the lesions are more clearly hypointense, and it is possible to detect many small lesions not visible on FSE sequences.

CAs as small hypointense spots that are otherwise not visible with other sequences, especially in multiple forms (Fig. 2).

CAs usually enhance after contrast administration. However, the characteristics of the lesion allow diagnosis without contrast. It is sometimes useful to detect possible associated DVA. Edema and mass effect are absent except in cases of acute bleeding. In this situation, it can often be difficult to identify the lesion within the hematoma.

Developmental Venous Anomaly

DSA: DVAs have a typical angiographic pattern. The arterial and capillary phases are normal, but in the venous phase the lesion becomes evident as a tuft of medullary veins converging toward an enlarged methemoglobin collector vein (caput medusae). The collector drains into a cortical vein, a sinus, or a subependymal vein. However, DSA is not required in the work-up of DVA.

CT: Unenhanced CT is usually normal, although a faint hyperdense area can be seen. After contrast injection, CT shows an intraparenchymal linear vessel corresponding to the collector vein, which can be followed until its entry in a sinus or cortical vein. Also, the venous nest converging toward the collector can usually be detected. Edema and mass effect are absent.

MRI: Unenhanced MRI is able to show the lesion in many cases. The large collector vein appears as a hypointense line on T1 and T2 because of flow void. Sometimes the vein is hyperintense on PD and T2 sequences because of flow-related enhancement due to flow misregistration artifact. Seldom, the radially converging veins can be seen. After contrast, caput medusae can be more easily detected as a tuft of hyperintense thin vessels converging toward a large vein (Fig. 3). On GE sequences an obvious hypointensity can be seen: this has been thought to be related to hemorrhage, but it could simply depend on deoxyhemoglobin in the venous blood. GE sequences are also useful for recognizing associated CA. A Magnetic resonance angiography (MRA) is not necessary but sometimes can show the converging veins. The adjacent parenchyma usually has normal intensity, although hyperintensity suggestive of gliosis has been described.

Capillary Telangiectasia

DSA and CT: Usually normal.

MRI: MRI occasionally shows a solitary hyperintense lesion on T2-weighted sequences, but the lesion is not visible on T1-weighted sequences. More commonly, CTA can be detected as a lacelike region of spotted contrast enhancement with no or minimal signal change on unenhanced images (Fig. 4). GE sequences show a hypointense spot and are more sensitive than unenhanced spin echo (SE) and fast spin echo (FSE) because the lesion often contains hemoglobin degradation products.

Arteriovenous Malformation

DSA: Both the enlarged feeding vessels as well as the nidus and the dilated draining veins can be visualized. Pial AVM

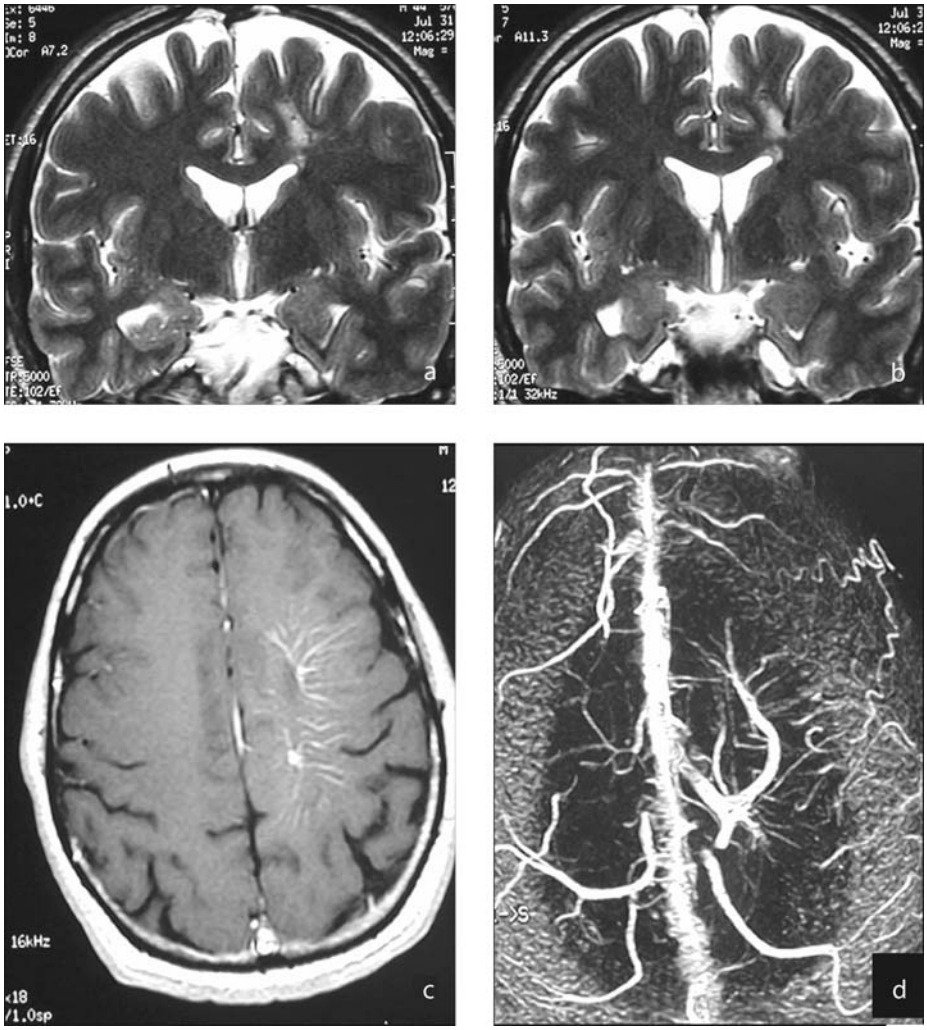

Congenital Malformations, Vascular, Brain. Figure 3 Developmental venous anomaly (DVA). FSE T2-weighted sequence (a, b) shows a left frontal hyperintense area contiguous with an enlarged cortical vein, recognized for the presence of flow void. After contrast administration (c), the DVA is evident by the classic medusae caput sign. MRA imaging (three-dimensional time-of-flight) offers a suggestive visualization of the enlarged veins converging toward a cortical vein (d).

often appears wedge-shaped with a broad cortical base. Dural AVM may have multiple dural feeders.

CT: Pial AVMs will appear slightly hyperdense on unenhanced CT with possible calcification. There is strong enhancement after contrast injection. CT often remains normal in dural AVM.

MRI: Pial AVMs will be visible on T2-weighted images, and different stages of associated hemorrhage can be assessed (Fig. 5). In dural AVM, dilated cortical veins can occasionally be detected.

Diagnosis

Classic CAs are easily diagnosed with MRI. An effort in determining anatomic location is important for surgical planning because eloquent areas could be damaged during surgery. Therefore, f-MRI is often performed to recognize eloquent areas, and MRI-based neuronavigation systems are used during surgery. Other important preoperative information is the presence of an associated DVA that should be spared by surgery.

In patients with acute hematoma, it is difficult to make out the CA, but it becomes obvious at follow-up. A bleeding CA must also be differentiated by hemorrhagic tumors: Useful tips are the complete peripheral ring and the absence of edema and tumoral tissue.

The differential diagnosis can be difficult for the smallest lesions appearing as focal hypointensity on T2-weighted FSE and GE sequences, as the same pattern could be related to residua of hemorrhage.

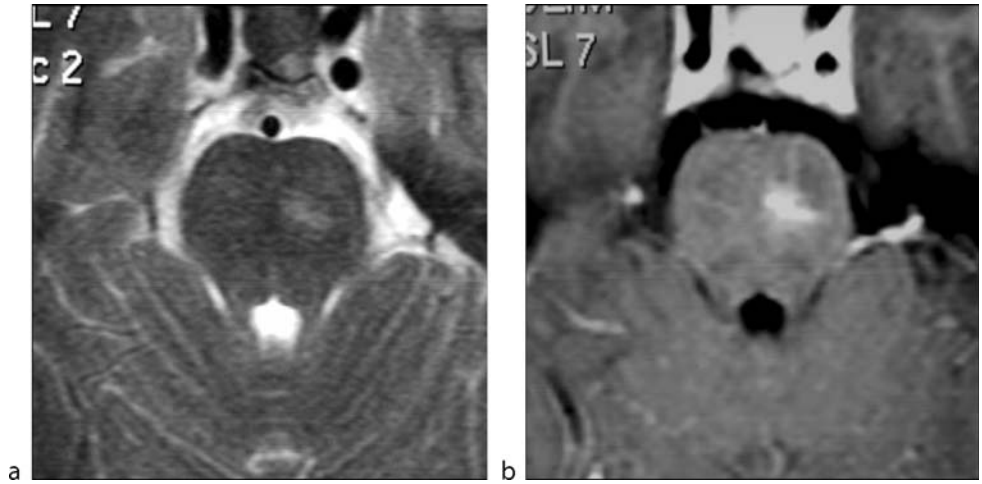

Congenital Malformations, Vascular, Brain. Figure 4 ►**Capillary telangiectasia**. The lesion appears as a smooth hyperintense area on T2-weighted image (a) that, after contrast administration (b), shows a faint contrast enhancement.

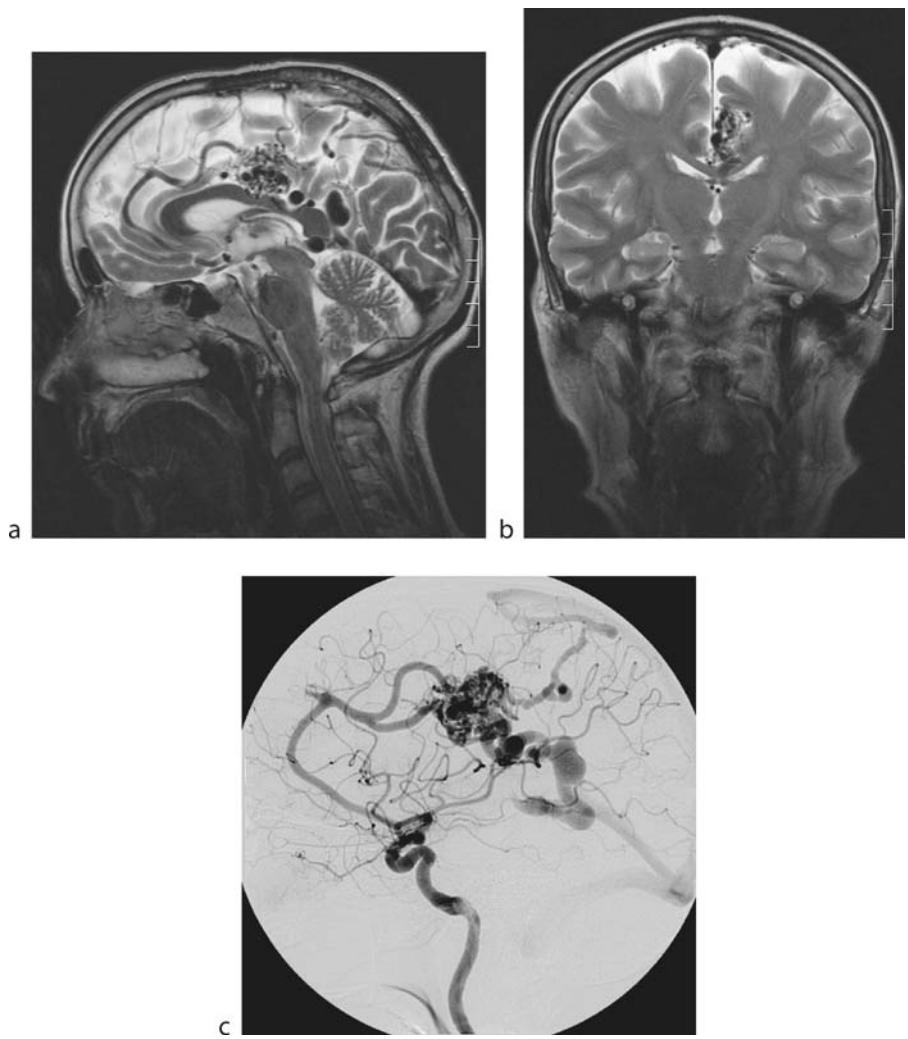

Congenital Malformations, Vascular, Brain. Figure 5 ►**Arteriovenous malformation** in the left cerebral hemisphere on magnetic resonance angiography (a). Dilated venous structures are seen on the axial (b) images as well as the nidus (c).

When multiple lesions are found, the diagnosis is easy if the lesions are typical for CA. However, if multiple hypointense foci are found and no typical lesion is recognized, the differential diagnosis with amyloid angiopathy, disseminated intravascular coagulation, and hypertensive angiopathy is difficult. In these cases, clinical information is essential.

Extraaxial CA can be difficult to differentiate from neurinoma or meningioma.

DVA imaging findings are very typical, so DVAs are rarely misdiagnosed. With perfusion MRI, an increased perfusion in the territory of the DVA can be evident; it is supposed to not correlate with symptoms and should not be interpreted as a complication.

The diagnostic work-up of AVMs includes DSA, MRI, and often fMRI to localize eloquent areas.

Bibliography

1. Lasjaunias P, Burrows P, Planet C (1986) Developmental venous anomalies (DVA): the so-called venous angioma. Neurosurg Rev 9:233–242
2. Dillon WP (1997) Cryptic Vascular malformations: controversies in terminology, diagnosis, pathophysiology, and treatment. Am J Neuroradiol 18:1839–1845
3. Guclu B, Ozturk AK, Pricola KL et al (2005) Cerebral venous malformations have distinct genetic origin from cerebral cavernous malformations. Stroke 36:2479–2480
4. Abe T, Singer RJ, Marks MP et al (1998) Coexistence of occult vascular malformations and developmental venous anomalies in the central nervous system: MR evaluation. Am J Neuroradiol 19:51–57

Congenital Metabolic Disorders

►Neurometabolic Disorders

Congenital Neonatal Pneumonia

►Chest, Neonatal

Congenital Scoliosis

Lateral curvature of the spine due to congenital vertebral anomalies.

►Congenital Malformations of the Musculoskeletal System

Congenitally Short Pancreas

►Congenital Anomalies of the Pancreas

Congential Malformations, Genitourinary Tract; Including Ureter and Urethra

M. Riccabona, R. Fotter
Department of Radiology
Division of Pediatric Radiology
University Hospital Graz, Graz, Austria
michael.riccabona@klinikum-graz.at
richard.fotter@meduni-graz.at

Synonyms

Congenital anomalies or malformations of the urinary tract

Definition

Urinary tract malformations include congenital anomalies that cause disease and potential sequelae. Differentiation of some anatomic variants from malformations is difficult and seen differently at different centres; in some conditions a clear differentiation of a 'variation' versus a 'malformation' can only be established retrospectively, with knowledge of the patient's history. Thus—in addition to 'real malformations'—a number of conditions and abnormalities have to be listed that may partially present as a non-symptomatic variants such as ►duplex kidneys (Table 1). These and rotational, positional as well as ►fusion anomalies of the kidneys have been addressed in the chapter ►Urinary Tract-anatomic variants, though some forms rather represent a malformation such as the rare 'cross fused ectopic duplex kidney'. Other variants may eventually cause disease and thus need to be mentioned here, such as an unusual course of the left renal vein (retroaortal left renal vein with nutcracker syndrome) or a prominent or accessory (segmental) renal artery obstructing the ureter, the uretero-pelvic junction or the calyceal neck causing a (disproportional) dilatation of the affected part. Malformations of the renal parenchyma include cysts (see entry ►Cystic Renal Disease, Childhood), ►dysplasia of various degrees as well as some syndromal or inherited

Congential Malformations, Genitourinary Tract; Including Ureter and Urethra. Table 1 List of common renal malformations

Duplex and triplex kidneys[a]
with orthotopic or ectopic ureteral insertion, duplex or triple ureter or ureter fissus
with or without partially dilated collecting system (refluxing or obstructive)
with or without (partial or segmental) dysplasia
bifid collecting system ('incomplete duplication')
Malrotation, malposition, and ectopia (abdominal, thoracic) and renal agenesis[a]
Fusion anomalies: horseshoe kidney (pre-aortal isthmus), crossed fused renal ectopia[a]
Persisting or unusual course of (accessory) renal vessels[a]
accessory renal arteries and/or veins, retro-aortal (left) renal vein
retro-/circumcaval ureter; compression of the ureter in a horseshoe kidney
Calyceal abnormalities: calyceal diverticulum, tertiary calyx, hydro- and megacalicosis[a]
(generalised or focally/isolated),
Dilatation of the renal pelvis:
laxity, non-symptomatic variation (extra-renal pelvis)[a]
secondary to
obstruction: megaureter, uretero-pelvic- and uretero-vesical junction obstruction
dilating VUR
Renal parenchymal malformations:
Cysts and cystic diseases (see also entry …)
Dysplasia, hypoplasia, nephronophthisis, nephroblastomatosis
Involvement in systemic or syndromal disease (Tyrosinosis, Alport syndrome …)

[a]These entities may be non-symptomatic, then considered a variant (see entry ▶Urinary tract, childhood, normal anatomy and variants) or may cause symptoms and sequelae and then considered a malformation.

conditions (Table 1). Furthermore, some variants may cause impaired urinary drainage and hydronephrosis such as an abnormal course and position of the ureter (i.e. in retro-caval ureter or compression of the ureter by a horseshoe kidney).

In the lower urinary tract, a number of conditions must be mentioned such as malformations of the uretero–vesical junction, an ureterocele, ectopic ureteral insertion, a persisting urachus, bladder diverticula, bladder septation and—in rare cases—duplication (Table 2). The most severe bladder malformation is ▶bladder exstrophy. The urethra as well has a number of malformations, the most common and most dreadful malformation being congenital posterior urethra valves (Table 2). Furthermore there are urethral diverticula as well as pathologic opening and fusion of the urethra leading to various degrees of hypospadia and epispadia. Other rare conditions which need to be mentioned are the prune belly syndrome, the megacystis–megaureter–hypoperistalsis syndrome and urinary tract malformations associated with other systemic or syndromal disease.

Embryology and pathogenesis: The embryology of the urinary tract is described in the entry ▶Urinary Tract, Normal Anatomy and Variations. The various malformations mostly are caused by disruption of the physiological development, and cannot be defined in detail for all these conditions. Due to the common development of the genital and the urinary tract, urinary tract malformations are frequently associated with genital anomalies, typically presenting on the same side as the urinary tract pathology (for more details see entry ▶Genital tract, Childhood). This association needs to be remembered and properly addressed by imaging, particularly as the female genitalia may be difficult to image after the initial months of life until late childhood. Typical anomalies are cystic seminal vesicles, vaginal and uterine duplications, uterine hypo- or aplasia, ovarian hypo- and dysplasia or agenesis and cystic remnants of the Wolffian and Müllerian duct. The most complex entity of these is the cloacal malformation, which usually involves not only the urinary, but also the genital and the anorectal tract, often associated with lower spinal malformations and neurological impairment, which are beyond the scope of this chapter to describe.

Imaging

Depending on the level and severity of the malformation, different modalities will become indicated. Ultrasound (US) in general constitutes the basic imaging tool that then helps to decide on further imaging needs. Depending on the underlying condition nearly all imaging modalities

Congential Malformations, Genitourinary Tract; Including Ureter and Urethra. Table 2 List of most important lower urinary tract malformations

Duplications of bladder, ureter, urethra, ureter fissus[a]
bladder septations[a]
Uretero-vesical junction pathology:
Megaureter (refluxing and/or dysplastic and/or obstructive)
ostial diverticula, atypical ostium (golf hole ostium …)
malpositioned or ectopic ureteric course and insertion[a]
draining into bladder neck, urethra, rectum and perineum genitalia (vagina)
Persisting urachus, urachus cyst/-diverticula[a]
Diverticulum and sacculation[a]
Megacystis[a]
Posterior urethral valve, urethral webs other urethral stenoses
hypo- and episadia, and strictures
Urethral, vesical and ureteral polyps, valves and folds
Complex cloacal malformations, urogenital sinus
Bladder extrophy
Agenesis of the bladder

Note: There may be numerous associated anomalies of the genital tract (see entry ▶genital tract, childhood).

[a]These entities may be non-symptomatic, then considered a variant (see entry ▶Urinary tract, childhood, normal anatomy and variants), or may cause symptoms and sequelae and then considered a malformation.

may become indicated and are used for complete—particularly pre-operative—workup of children with (complex) urinary tract malformations.

Imaging modalities: In mild forms and for pre-natal examinations imaging consists simply of US; post-natally this maybe complemented by voiding cystourethrography (VCUG) and scintigraphy. In more complex cases a more detailed renal imaging by intravenous urography (IVU) in former times and *MR-urography* (MRU) today commonly becomes necessary. *Renal scintigraphy* provides an excellent assessment of renal function and drainage and can be particularly useful for follow-up comparison. If associated skeletal anomalies need to be assessed and evaluated for planning surgical procedures like in complex bladder exstrophy, plain films (to look at the spine, pelvis) and a pelvic CT may become valuable, particularly using 3D reconstruction and viewing techniques of modern *multi-slice CT. Interventional radiology* may offer treatment options in severe obstruction—particularly as a bridging measure—till completion of diagnoses and definite surgery, or may serve as a tool for managing post-operative complications. While these interventional procedures were more frequently performed some decades ago, the change in paradigms based on modern insights in development and prognosis of urinary tract malformations has significantly reduced indication for these procedures, which today are considered helpful mostly for severe bilateral obstruction or intractable infection in an obstructed system. Today measures for remodelling the collecting system without impact on future renal development are deemed less important; the final goal of treatment is preservation of renal function. Therefore—in all these malformations—this final goal becomes the only evidence based driving force that indicates imaging and allows deciding on an individually adapted imaging algorithm.

Imaging algorithms: The task of imaging is often to confirm a pre-natally suspected condition and then to identify the entity. A thorough investigation of the entire genito-urinary tract for depiction of or ruling out associated malformations and dysfunctions needs to be performed in more severe findings such as severe dilatation (e.g. uretero-pelvic—and uretero-vesical junction obstruction, posterior urethral valve), cystic and dysplastic kidneys, duplex systems with disproportional widened moieties or focal dysplasia, ureteroceles, ▶ectopic kidneys and ureters, severe hypo-/epispadia and bladder exstrophy. Finally imaging must provide some grading, not only for initial estimation of the severity of the disease and consecutive implications on treatment, but also for comparison during follow-up, particularly in the increasing number of patients who are treated conservatively. And imaging should provide the pre-operative anatomic information as necessary for the surgeon.

Taking all these tasks into consideration imaging usually starts with a detailed US in a well hydrated child. US not only provides a basic information and overview, but very often is able to establish a definite diagnosis and —to a certain extent—rate the degree of disease. Further imaging is defined by these initial US findings: In a neonatal boy with significant urinary tract dilatation or bladder anomaly, an additional VCUG is recommended for assessment of urethral pathology. (Delayed) renal scintigraphy is usually performed for a baseline assessment of renal function and potential scarring. Diuretic renal scintigraphy and MRU are performed in obstructive and dilative uropathy that potentially need surgery. IVU is rarely used today, sometimes—if MR is unavailable—for pre-operative imaging (to provide basic anatomic information or to rule out a duplex system) and in the post-operative setting for diagnosing post-operative complications. Note, that these investigations should be tailored to the individual query with an adapted imaging protocol (contrast- and X-ray-dose, adapted timing of the individual exposures …). For follow-up, US supplemented by VCUG or contrast-enhanced cystosonography (for refluxing disease) or by diuretic renography

and functional semi-quantitative MRU (for obstructing uropathy) are generally recommended.

Diagnosis

Diagnosis is made by imaging as described above, using the criteria listed in the definition and imaging sections.

Bibliography

1. Barnewolt CE, Paltiel HL, Lebowitz RL et al (1998) The genito-urinary tract. In: Kirks DR (ed) Practical Pediatric Imaging. 3rd edn. Lippincot-Raven publishers, Philadelphia, pp 1005–1175
2. Berdon WE (1991) Contemporary approach to pediatric urologic problems. Radiol Clin North Am 29:605–618
3. Currarino G, Wood B, Majd M (1993) The genitourinary tract and retroperitoneum. congenital renal anomalies. In: Silverman FN, Kuhn JP (eds) Caffey's Pediatric X-Ray Diagnosis: An Integrated Imaging Approach. Vol. 2., 9th edn. Mosby St. Louis, Baltimore, Boston, Chicago, London, Philadelphia, Sydney, Toronto, pp 1223–1243
4. Daneman A, Alton DJ (1991). Radiographic manifestations of renal anomalies. Radiol Clin North Am 29: 351–363
5. Ritchey M (1992) Anomalies of the kidney. In: Kelalis PP, King LR, Belman AB (eds) Clinical Pediatric Urology. Vol. 1, 3rd edn. WB Sounders Company Philadelphia, London, Toronto, Montreal, Sydney, Tokyo, pp 500–528

Congential Malformations, Mullerian Duct

Justus E. Roos
Department of Radiology
Stanford University Medical Center, Stanford, USA
justus.roos@stanford.edu

Synonyms

Congenital anomalies of the uterus

Definition

The female reproductive system develops from the two paired müllerian ducts (synonym: paramesonephric duct) that originate in the embryonal mesoderm lateral to each wolffian duct (synonym: mesonephric duct). The paired müllerian ducts grow in medial and caudal directions, and at 9 weeks of gestation, the cranial part remains nonfused and forms the fallopian tubes. The caudal part fuses to a single canal forming the uterus and the upper two-thirds of the vagina. This is called lateral fusion. In a process called vertical fusion, the intervening midline septum undergoes regression. The caudal part of the vagina arises from the sinovaginal bulb and fuses with the lower fused müllerian ducts. The ovaries originate from the gonadal ridge, a completely different tissue than the mesoderm forming both the urinary and genital systems. Pathogenesis of müllerian duct anomalies (MDA) can be basically classified into the presence of agenesis, hypoplasia, and defects in vertical and lateral fusion of the paired ducts. In 1988, the American Fertility Society (AFS) (1) presented a consensus in classification of uterovaginal anomalies and published a schematization system that is widely accepted among specialists. Most MDA are considered to occur sporadically and some reports give descriptions of the patterns of inheritance. The most well-known anomalies are those induced by exposure to teratogenic agents such as di-ethyl-stilbestrol (DES) and thalidomide (2).

Pathology

According to the classification of the AFS (1), MDA can be classified into seven different classes of uterine anomalies (Fig. 1). Because of the wide variability and overlap of associated cervical and vaginal anomalies, the classification primarily describes uterine defects, whereas cervicovaginal defects must be added separately in the form of a subset. The diagnosis of MDA is based on the clinical presentation and physical examination. This examination consists mainly of the work-up with different imaging methods (3, 4), in which magnetic resonance imaging (MRI) takes a leading role, especially in complex uterine malformation. The different types of MDA and their definition based on their presentations are described in the diagnosis section.

Clinical Presentation

To state the real prevalence, incidence, and distribution of MDA is difficult because of the use of nonstandardized classification systems, different datasets, and varying patient populations examined in clinical studies. The overall data suggest that the prevalence of uterovaginal anomalies approximates 1% in the general population among women with normal and abnormal fertility (3, 4). While the majority of women with MDA have little problem conceiving, they run the risk of spontaneous abortion, premature delivery, abnormal fetal position, and difficulties during delivery. The prevalence of MDA among women with repeated pregnancy loss is around 3% (3–5).

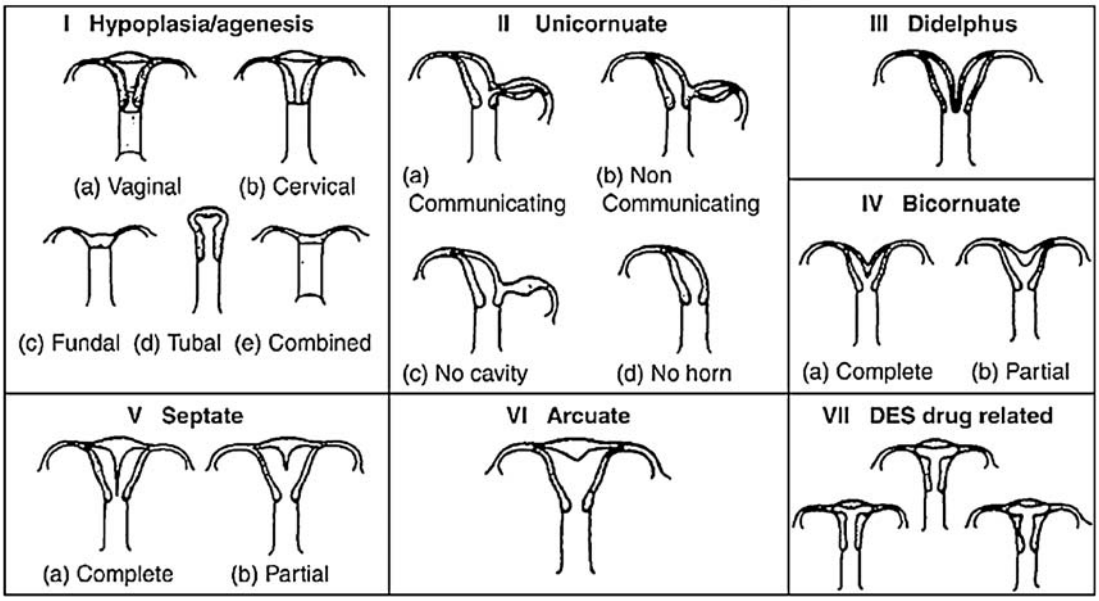

Congential Malformations, Mullerian Duct. Figure 1 Classification system of müllerian duct anomalies (American Fertility Society) (Anonymous, 1998 The American Fertility Society classifications of adnexal adhesions, distal tubal occlusion, tubal occlusion secondary to tubal ligation, tubal pregnancies, müllerian anomalies and intrauterine adhesions. Fertil Steril 49:944–955).

Imaging

The three imaging pillars of MDA are ultrasonography (US), conventional hysterosalpingography (HSG), and MRI.

US imaging should be performed during the secretory phase for the best evaluation of the endometrium cavity, external uterine contour, and surrounding tissue. Transabdominal US (performed with a 2.5.–5-MHz probe) provides information about the entire abdomen, especially of the kidney and the genital organs. Transvaginal US (performed with a 5–8-MHz endovaginal transducer) has the advantage of increased spatial resolution, although at the expense of a decreased field of view. Hysterosonography, which consists of endovaginal US with prior infusion of saline or ultrasound contrast agent into the endometrial canal, allows a better delineation of the endometrial cavity and is performed only for selected indications, that is, in patients with a history of infertility. It is approximately 92% accurate for the detection of MDA. Newer techniques, such as three-dimensional US, further improve the imaging diagnostics by giving better information about the external contour of the uterus and its volume.

HSG provides a morphological assessment of the endometrium cavity and supplies information regarding tubal patency. Because only the internal contour of the uterus can be assessed and the outer contour remains unclear, the characterization of uterine anomalies is somehow difficult, especially in the common case of differentiation between bicornuate and septate uterus.

MRI has the best accuracy in the evaluation of uterine anomalies among the three major imaging methods. Accuracy of up to 100% has been reported. MRI allows an excellent delineation of the entire uterus anatomy including the internal and external uterine contour as well as the diagnosis of secondary findings, that is, endometriosis.

The MRI parameter for a complete evaluation of uterine malformations should include the use of: (i) phased array MR surface coil; (ii) acquisition of oblique T2-weighted (T2-W) and T1-weighted (T1-W) fast spin-echo (FSE) images parallel to the long axis of the uterus; (iii) transverse T1-W and T2-W images of the entire pelvis; and (iv) coronal single shot FSE (SSFSE T2-W) or spoiled gradient-echo images (FSPGR) with the kidney in the field of view (3, 4).

Diagnosis

Class I Anomalies

Class I anomalies are characterized by *dysgenesis* (segmental agenesis and variable hypoplasia) of the müllerian ducts (uterus and upper two-thirds of the vagina). Mayer–Rokitansky–Küster–Hauser syndrome is the most common form of Class I anomaly and includes agenesis of the uterus and vagina.

Class II Anomalies

Unicornuate uterus is a result of partial or complete hypoplasia of one müllerian duct (Fig. 2).

Variants: Unicornuate uterus may be isolated (35%) or associated with a contralateral rudimentary horn. The rudimentary horns present with or without communication to the endometrial cavity and may be associated with or without endometrium, which is also called no cavity rudimentary horn. The variable forms of the rudimentary horns determine the surgical procedure.

Class III Anomalies

Uterus didelphys is a result of complete nonfusion of the müllerian ducts forming a complete uterine duplication (Fig. 3).

Variants: Uterus didelphys may be associated with a longitudinal (75%) or, more rarely, with a transverse vaginal septum, the latter causing obstructive hematometrocolpos. A nonobstructive uterus didelphys is usually asymptomatic.

Class IV Anomalies

Bicornuate uterus is the result of incomplete fusion of the cranial parts of the müllerian ducts (Fig. 4).

Variants: Bicornuate uterus occurs with a wide variability. Extension of the intervening fundal cleft to the internal cervical os characterizes the complete bicornuate uterus with a single cervix (bicornuate, unicollis uterus), whereas variants of partial bicornuate uterus exist if the cleft is of variable length. Bicornuate uterus may be associated with a duplicated cervix (bicornuate bicollis uterus) as well as with a longitudinal vaginal septum, which coexists in up to 25% of cases of bicornuate uterus.

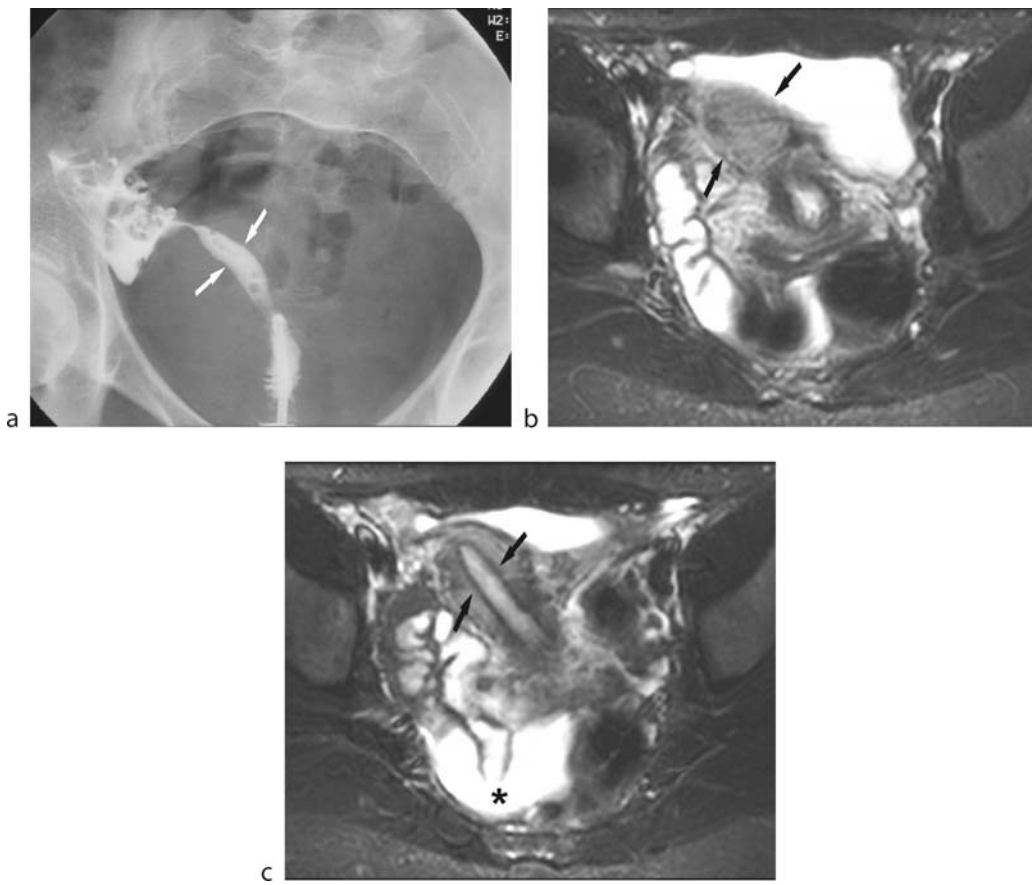

Congential Malformations, Mullerian Duct. Figure 2 A 28-year-old female patient with infertility. HSG (a) shows a fusiform configuration of one endometrial cavity (*arrow*) draining into one fallopian tube. Note the small uterus, which is deviated to one side suggesting the diagnosis. Iatrogenic filling defects in the uterine cavity by air bubbles. Oblique T2-W MR images (b, c) confirm the diagnosis of a unicornuate uterus with presence of a small but elongated uterus that shows normal zonal anatomy (*arrows*). No rudimentary horn is present in this case. Some fluid is present in the pouch of Douglas (*asterisk*).

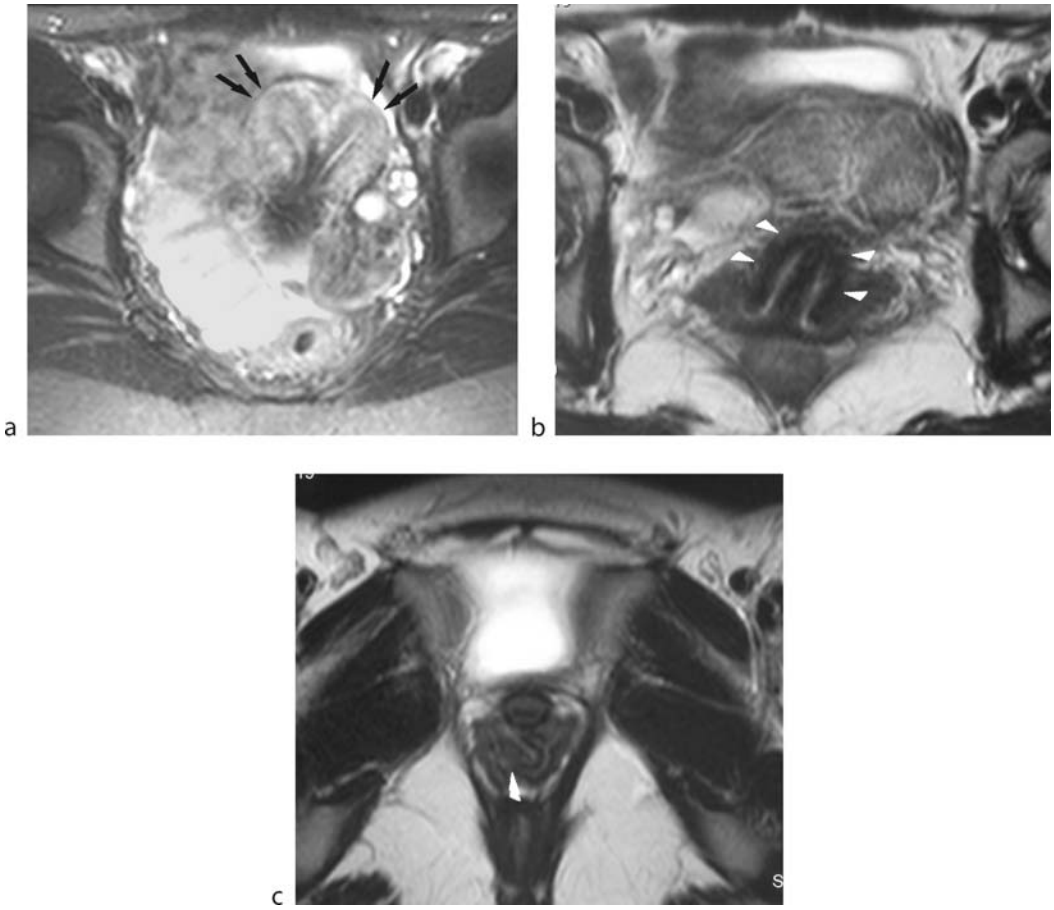

Congential Malformations, Mullerian Duct. Figure 3 A 33-year-old female patient with history of partially resected longitudinal vaginal septum. Transverse oblique T2-W MR images (a, b) show complete duplication of the uterine horns (*arrows*) as well as two duplicated cervices (*arrowheads*). No communication between the two endometrial cavities is present; the cavities show their normal zonal anatomy. Note the longitudinal vaginal septum (c) which appears in 75% of uterus didelphys (*double arrowhead*).

Class V Anomalies

Septate uterus is the result of partial or complete nonregression of the midline uterovaginal septum. According to its definition, the external contour of the uterine fundus may be either convex or mildly concave (<1 cm). This distinction determines whether it is a septate uterus or a bicornuate or didelphic uterus (Fig. 5).

Variants: Septate uterus is the most common MDA and is unfortunately associated with the poorest reproductive outcome (Table 1). Because of different treatment options, septate uterus must be differentiated from bicornuate and didelphic uterus. A widely accepted definition therefore—empirically invented during laparoscopy procedures—states that a uterus is septate if the outer contour of the uterine fundus is only mildly concave in the presence of a septum. The cutoff of concavity is 1 cm; deeper concavity is associated with bicornuate uterus and uterus didelphys. In a complete septate uterus, the septum extends to the external cervical os. In 25% of septate uteri, the septum extends even further into the upper part of the vagina.

Class VI Anomalies

Arcuate uterus is the result of a near complete regression of the uterovaginal septum forming a mild and broad saddle-shaped indentation of the fundal endometrium. Differentiation from bicornuate uterus is based on the complete fundal unification; however, a broad-based septate uterus is difficult to distinguish from an arcuate uterus. There is much controversy as to whether an arcuate uterus should be considered a real anomaly or an anatomic variant.

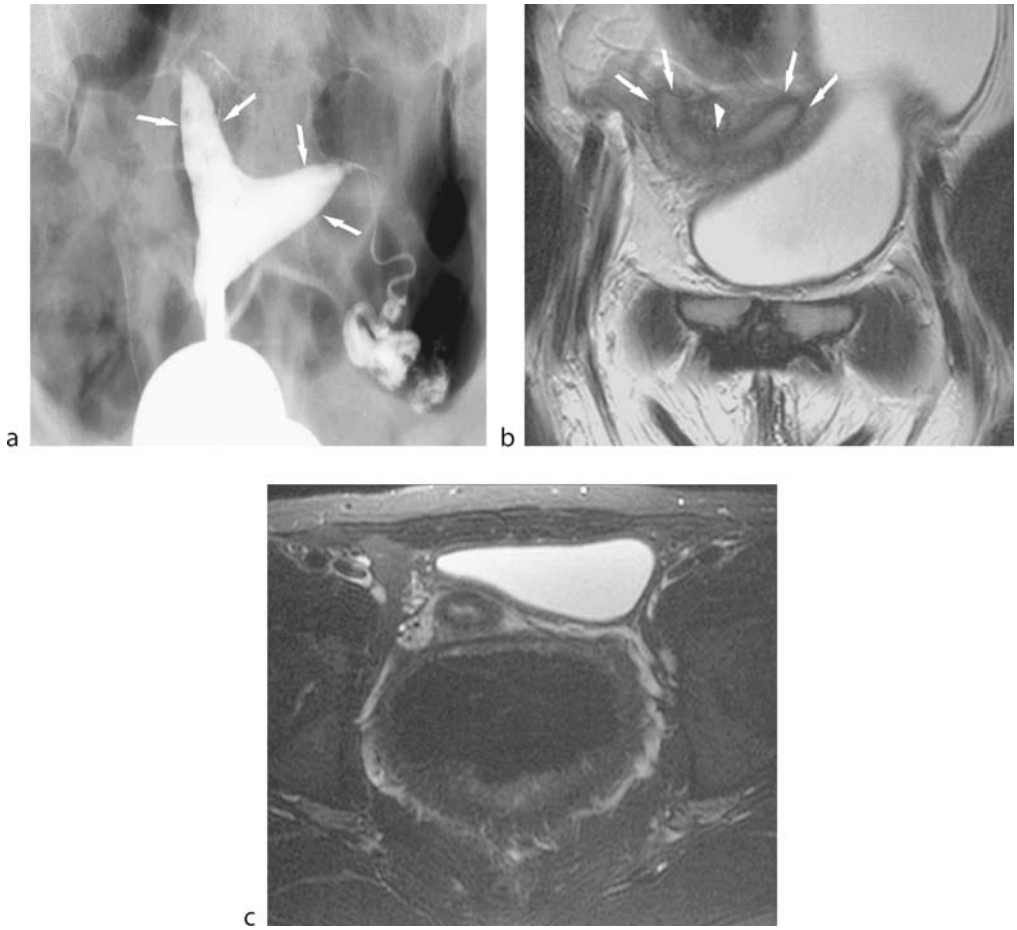

Congential Malformations, Mullerian Duct. Figure 4 A 17-year-old female patient with chronic obstipation and a history of anal surgery as a neonate. HSG (a) shows one cervix, but two separated endometrial cavities (*arrows*), (b) T2-W MR image shows the two separated uterine horns (*arrows*) with communication of their endometrial horns in the mid to lower portion of the uterus. Note the deep (>1 cm) external fundal cleft (*arrowhead*) between the endometrial cavities (*arrows*), a specific characteristic allowing differentiation from a uterus septus. Transverse T2-W MR image at the level of the cervix demonstrates a single cervix, called the bicornuate unicollis uterus.

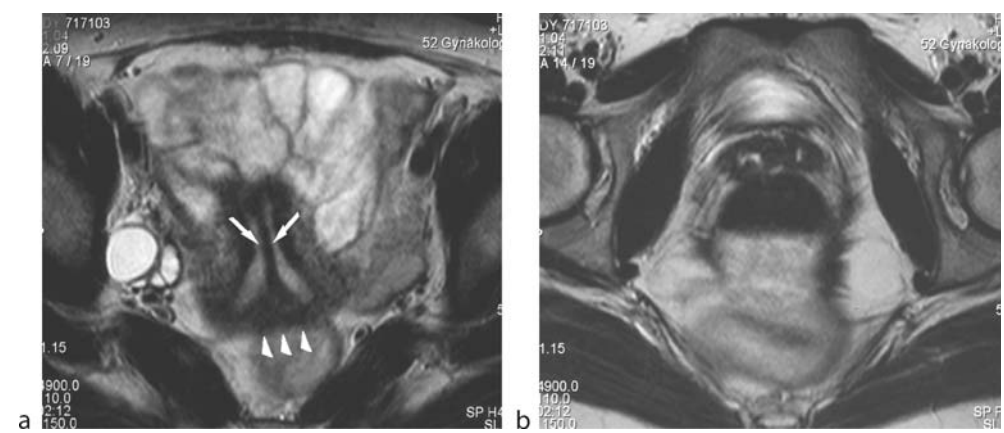

Congential Malformations, Mullerian Duct. Figure 5 A 29-year-old female patient with infertility. Transverse oblique T2-W MR image (a) demonstrates a retroverted uterus with convex uterine fundal contour (*arrowheads*) and a hypointense thin septum dividing the endometrial cavity (*arrows*). The se•ptum extends to the external cervical os (b).

Congential Malformations, Mullerian Duct. Table 1

Müllerian duct anomalies (MDA)	Influence on reproductive/obstetric outcome			Other major associations
	Spontaneous abortion	Premature delivery	Fetal survival rate	
Class I: Dysplasia (4–10%)	No potential for reproduction			Mayer–Rokitansky–Küster–Hauser syndrome
Class II: Unicornuate uterus (5%–20%)	50% (41–62%)	15% (10–20%)	40% (38–57%)	Renal agenesis 67%
Class III: Uterus didelphys (5–11%)	45% (32–52%)	38% (20–45%)	55% (41–61%)	Longitudinal vaginal septum 75%
Class IV: Bicornuate uterus (10–39%)	30% (28–35%)	20% (14–23%)	60% (57–63%)	High cervical incompetence 38%
Class V: Septate uterus (34–55%)	65% (26–94%)	20% (9–33%)	30% (10–75%)	Vaginal septum 25%
Class VI: Arcuate uterus (7%)	Mostly compatible with normal-term gestation			
Class VII: DES-exposed uterus	Increased	Increased	Decreased	Cervical anomalies 44%

Note: All percentages data are pooled from the current literature (4, 5), values in brackets represent percentages ranges (4, 5).

Class VII Anomalies

DES-exposed uterus. DES (synthetic estrogen, 1948–1971) may induce abnormal myometrial hypertrophy in the fetal uterus forming small T-shaped endometrial cavities as well as increase the risk of developing a clear cell carcinoma of the vagina (2). The characteristic uterine abnormalities must be categorized in the group of complex uterine anomalies and may occur with or without exposure to DES.

Bibliography

1. Anonymous (1998) The American Fertility Society classifications of adnexal adhesions, distal tubal occlusion, tubal occlusion secondary to tubal ligation, tubal pregnancies, müllerian anomalies and intrauterine adhesions. Fertil Steril 49:944–955
2. Kaufman RH, Adam E, Hatch EE et al (2000) Continued follow-up of pregnancy outcomes in diethylstilbestrol-exposed offspring. Obstet Gynecol 96:483–489
3. Saleem SN (2003) MR imaging diagnosis of uterovaginal anomalies: current state of the art. Radiographics 23:e13
4. Troiano RN, McCarthy SM (2004) Müllerian duct anomalies: imaging and clinical issues. Radiology 233:19–34
5. Nahum GG (1998) Uterine anomalies. How common are they, and what is their distribution among subtypes? J Reprod Med 43:877–887

Congestive Cardiac Cirrhosis

Cardiac cirrhosis includes a spectrum of hepatic derangements that occur in the setting of right-sided heart failure. Clinically, the signs and symptoms of congestive heart failure (CHF) dominate the disorder. Cardiomegaly, pulmonary venous hypertension, pulmonary edema, or pleural effusion may be observed on chest radiography, while hepatomegaly, splenomegaly, and ascites are usually shown at abdominal US, CT, or MR examination.

▶Vascular Disorders, Hepatic

Connective Tissue Disorders, Gastrointestinal Tract

Frank Pilleul
Gastro-intestinal and Emergency Imaging Department, Hôpital Universitaire Edouard Herriot, Lyon-France
frank.pilleul@chu-lyon.fr

Definition

A family of more than 200 disorders affects the connective tissues. These disorders can result either from alterations in genes responsible for building tissues, known as heritable connective tissue disorders (HCTD), or from chronic degenerative and/or inflammatory conditions that result from abnormal immune reactions to compounds absorbed from the environment, known as connective tissue diseases (CTD) or autoimmune diseases (AID).

In cases of HCTD, the structure and development of skin, bones, joints, heart, blood vessels, lungs, bowel wall, eyes, and ears may change directly related to mutations in genes. Ehlers–Danlos syndrome and Marfan syndrome, which affect large blood vessels including the splanchnic arterial system, are two common HCTD indirectly involving the gastrointestinal (GI) tract by ischemia, hemorrhage, or both.

CTD affect approximately 8% of the population, 78% of whom are women (1). The reasons for the high prevalence in women are unknown. AID can affect virtually every site in the body, including the endocrine system, connective tissue, GI tract, heart, skin, and kidneys. At least 15 diseases are known to be the direct result of an autoimmune response, while circumstantial evidence

implicates more than 80 conditions involving autoimmunity. Some of these CTD can involved the GI tract, such as systemic lupus erythematosus (SLE), vasculitis (Behçet's disease, polyarteritis nodosa, microscopic polyangiitis, rheumatoid vasculitis, Buerger's disease, Takayasu arteritis), and scleroderma.

Pathology/Histopathology

The pathogenesis of AID or CTD is not completely known. AID tend to cluster in families and in individuals, which indicates that common mechanisms are involved in disease susceptibility. Studies of the prevalence of AID in monozygotic twins show that genetic as well as environmental factors (such as infection) are necessary for the disease to develop (2).

Because infections generally occur well before the onset of symptoms of AID, clinically linking a specific causative agent to a particular AID is difficult. AID occurs when a response against one or more self-antigens involving T cells, B cells, or autoantibodies induces injury systemically or against a particular organ (2).

In most animal models of autoimmunity, disease has been transferred to naïve animals with autoimmune cells (splenocytes or T cells), autoantibodies, or both, which provides compelling evidence that infections induce AID by immunomediated mechanisms.

Furthermore, some hypotheses suggest that individuals who express specific human leukocyte antigens (HLA) such as HLA-DR4 or HLA-DQB1 are genetically predisposed. The frequency of HLA-DR4 in patients with CTD is estimated to be 52%. The specific nature of the HLA associations that occur in patients with CTD may vary depending on the ethnicity of the population studied.

Clinical Presentation

GI tract involvement is nonspecific in connective tissue disorders and includes dysphagia, abdominal pain, nausea, vomiting, constipation, diarrhea, and malabsorption. Some complications such as ischemia, infarction, occlusion, perforation, and bowel hemorrhage have been described in the literature as being due to focal or diffuse necrotizing vasculitis in the systemic vasculature.

In cases of HCTD such as type IV Ehlers–Danlos syndrome, GI complications include diverticula, rectal prolapse, GI bleeding, and spontaneous perforation of the bowel. Spontaneous bowel perforation is a rare, but particularly troublesome complication because of its tendency to recur despite aggressive surgical management. Bowel rupture typically occurs in young adults and is usually situated in the sigmoid colon (3).

In SLE, inflammation of the small blood vessels of the gut produces a variety of complications including intestinal ischemia, hemorrhage, ileus, ulceration, infarction, and perforation (4). SLE may involve any part of the GI tract from the esophagus to the rectum. However, the territory of the superior mesenteric artery is most commonly affected.

In general, in CTD with necrotizing vasculitis, the vasa recta and intramural arteries can affect all sizes of blood vessels. The clinical course of disease depends on the size and location of the affected vessel and may be indistinguishable from signs of mesenteric ischemia, GI or intraabdominal hemorrhage, ulceration, or stricture formation.

Digestive involvement in systemic sclerosis is frequent and serious. Esophageal disorder is common with the occurrence of gastroesophageal reflux disease. Gastric involvement is rarely recognized, nor is small intestinal involvement, which may lead to malabsorption, pseudo-obstruction, and bacterial overgrowth. Anorectal involvement is frequent and leads to fecal incontinence and rectal prolapse.

Imaging

Barium Examination

In cases of systemic sclerosis or SLE, a double-contrast examination of the upper GI tract can demonstrate signs of esophagitis, showing "smudged" or "cobblestone" mucosa with thickened and distorted longitudinal folds and sometimes stenosis (Fig. 1).

In cases of CTD with necrotizing vasculitis and SLE, small bowel follow-through can demonstrate irregular thickening and spiculation in the folds of the multiple segments of the duodenum to the terminal ileum, thumbprinting suggestive of ischemic change, and multiple submucosal nodules. Furthermore, in some cases large ovoid or irregular ulcers with marked thickening or multiple small, discrete, "punched-out" ulcers can be identified.

Computed Tomography

Computed tomography (CT) has recently proved to be effective not only for detecting primary lesions, but also for excluding extraluminal complications. Ischemia due to SLE or CTD produces various morphologic changes, including homogeneous or heterogeneous hypoattenuating or hyperattenuating wall thickening, dilatation, abnormal wall enhancement (Fig. 2), mesenteric stranding, vascular engorgement, ascites, pneumatosis, and portal venous gas, particularly in the distribution of the superior mesenteric artery. The bowel wall thickening

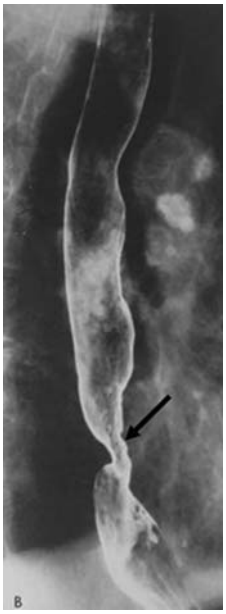

Connective Tissue Disorders, Gastrointestinal Tract. Figure 1 Esophageal stenosis (*black arrow*) postesophagitis in a case of systemic lupus erythematosus identified on upper gastrointestinal follow-through.

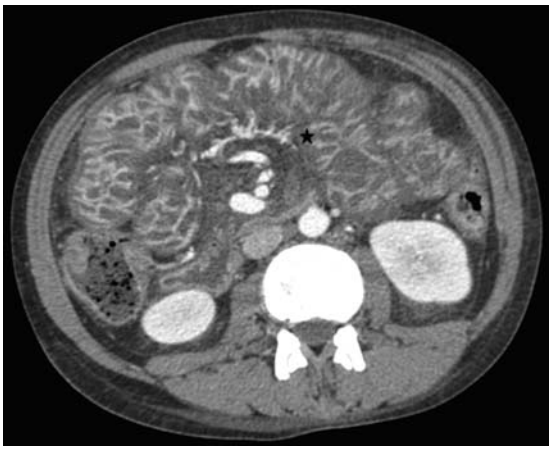

Connective Tissue Disorders, Gastrointestinal Tract. Figure 2 Contrast-enhanced computed tomography scan shows diffuse small bowel wall thickening (*black star*) in a patient with systemic lupus erythematosus.

detected on CT is due to mural edema, hemorrhage, and/or superinfection of the ischemic bowel wall (5). The greatest incidence of bowel wall thickening is observed in cases of reversible mesenteric ischemia (80%).

Furthermore, CT is very sensitive for detecting abdominal complications such as perforation, occlusion, GI hemorrhage, visceral arterial aneurysm (Fig. 3), and

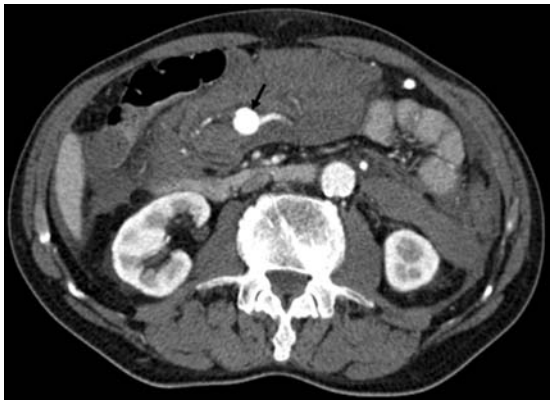

Connective Tissue Disorders, Gastrointestinal Tract. Figure 3 Contrast-enhanced computed tomography scan demonstrates aneurysms of the superior mesenteric artery complicated by mesenteric hematoma in a patient with Behçet's disease.

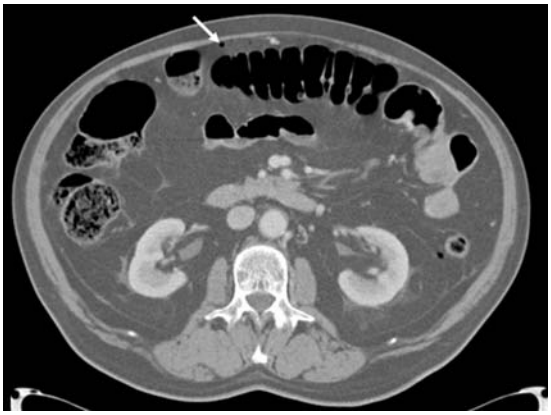

Connective Tissue Disorders, Gastrointestinal Tract. Figure 4 Contrast-enhanced computed tomography scan identifies free air within the peritoneum in a case of systemic lupus erythematosus with small bowel involvement.

peritonitis; CT can easily demonstrate a small amount of intraperitoneal air (Fig. 4), extravasation of contrast within the abdomen, and evident signs of small bowel obstruction.

Diagnosis

The diagnosis and classification of the vasculitis subgroup of CTD relies on a combination of clinical, serological, hematological, radiological, and histological findings. The

Chapel Hill International Consensus Conference classified 10 selected vasculitides depending on the type of vessel predominantly affected.

A diagnosis of SLE can be made with 98% specificity and 97% sensitivity if at least four of the 1982 revised criteria for the classification of SLE are present (7).

Diagnosis of HCTD is often difficult due to the complexity of symptoms and the lack of specific genetic tests. In adulthood, four main clinical findings—a striking facial appearance; easy bruising; translucent skin with visible veins; and ruptured vessels, gravid uterus, or intestines—contribute to the diagnosis, which can be confirmed by the identification of a mutation in the COL3A1 gene coding for type III procollagen.

Bibliography

1. Jacobson DL, Gange SJ, Rose NR et al (1997) Epidemiology and estimated population burden of selected autoimmune disease in the United States. Clin Immunol Immunopathol 84:223–243
2. Rose NR (2002) Mechanisms of autoimmunity. Semin Liver Dis 22:387–394
3. Stillman AE, Painter and R, Hollister W (1991) Ehlers–Danlos syndrome type IV: diagnosis and therapy of associated bowel perforation. Am J Gastroenterol 86:360–362
4. Kistin MG, Kaplan and MM, Harrington JT (1978) Diffuse ischemic colitis associated with systemic lupus erythematosus: response to subtotal colectomy. Gastroenterology 75:1147–1151
5. Ha HK, Lee SH, Rha SE et al (2000) Radiologic features of vasculitis involving the gastrointestinal tract. Radiographics 20:779–794
6. Tan EM, Cohen AS, and Fries JF (1982) The 1982 revised criteria for the classification of systemic lupus erythematosus. Arthritis Rheum 25:1271–1277

Connective Tissue Disorders, Musculoskeletal System

G M Lingg, C Schorn
Department of Radiology
Sana Rheumazentrum Rheinland Pfalz
Bad Kreuznach, Germany
dr.lingg@sana-rheumazentrum-rlp.de

Synonyms

Connectivitis

Definition

Connective tissue diseases (CTDs) consist of the following entities: Systemic lupus erythematosus (SLE), panarteritis nodosa (PAN), systemic scleroderma (SSc), dermatomyositis/polymyositis (DM/PM), and mixed connective tissue disease (MCTD, Sharp's disease). In a more general sense, Sjögren's syndrome and vasculitis (Wegener's granulomatosis, Churg–Strauss syndrome) also belong to this group. The common histologic finding of all these diseases is fibrinoid necrosis and immunocomplex deposition.

Pathology/Histopathology

Immunocomplex deposition in the basal membranes, vascular walls, and interstitial tissue leads to inflammatory and necrotic foci in different organs. Thus multiple organ manifestations are possible among which musculoskeletal disease is seen with various degrees of severity.

Systemic Lupus Erythematosus

Clinical Presentation

The general clinical course is characterized by periods of severe illness and remission. Disease onset is often acute with skin rash after a sun bath indicating photosensibility. Typically, the rash is found on the face in the form of the so-called butterfly erythema. Scalp involvement leads to alopecia. ▶Raynaud's phenomenon may occur. Temperature rise, weakness, weight loss, and polyarthralgia are common. Gastrointestinal involvement is frequent. Neurologic dysfunctions such as mental disorders, seizures, cerebral nerve palsies, or cerebral infarction are facultative but not uncommon symptoms. Lupus nephritis can cause nephrotic syndrome and glomerulonephritis with proteinuria and erythrocyturia and may indicate a serious disease course. Interstitial pneumonitis with dyspnea and cough is a typical feature. Some patients suffer from relapsing pleuritis with pleural pain. Heart manifestations consist of myocarditis, pericarditis, and endocarditis. Hematological disorders include hemolytic anemia and thrombocytopenia.

Reasons for death are mainly cardiovascular diseases, thromboembolic events, and infections. The patients with unfavorable prognosis show rapid development of severe prognostic signs in relation to the mean duration of the disease and frequent and severe complications. Risk factors at disease onset are male sex, nephritis, heart disease, and central nervous system disease.

Laboratory findings are positive LE cells, anti-DNA antibodies, and anticardiolipin antibodies.

Imaging

In the case of polyarthralgia, X-ray imaging is used in order to exclude arthritis. However, in SLE findings are

unspecific. For myalgia/►myositis, magnetic resonance (MR) imaging may be employed.

Signs and Patterns in SLE

Typically, there are rarely objective radiological findings. In fact, in the setting of no or few radiologic signs despite massive clinical symptoms, SLE should be considered as the differential diagnosis. ►*Regional osteoporosis* is unspecific but not uncommon and may progress to general osteoporosis. It may be the only finding. Rarely, *small subchondral cysts* in the metacarpal and metatarsal heads as well as in the carpal and tarsal bones occur and are thought to be micronecrotic foci. Periosteal ossification, tiny soft tissue calcifications, and acroosteolysis are rare findings. Capsular and muscular contractions are the cause of severe sub-/luxations of the finger joints resembling the "*Jaccoud hand*," which was originally described in rheumatic fever after streptococcal infection. Typically, the grave deformities contrast the absence of destructive arthritis (Fig. 1). Pressure erosion following the deformity may occur and should be distinguished from destructive arthritis. Destructive arthritis is a sign of an overlap syndrome with rheumatoid arthritis and is seen in approx. 10% of cases. Epiphyseal necrosis with or without steroid therapy is a relatively common feature and does not differ from its usual aspect in patients with different conditions.

In cases with polyarthralgia, MR imaging shows synovial hyperplasia and joint capsule edema or mild joint effusions, but no specific findings. Epiphyseal necrosis

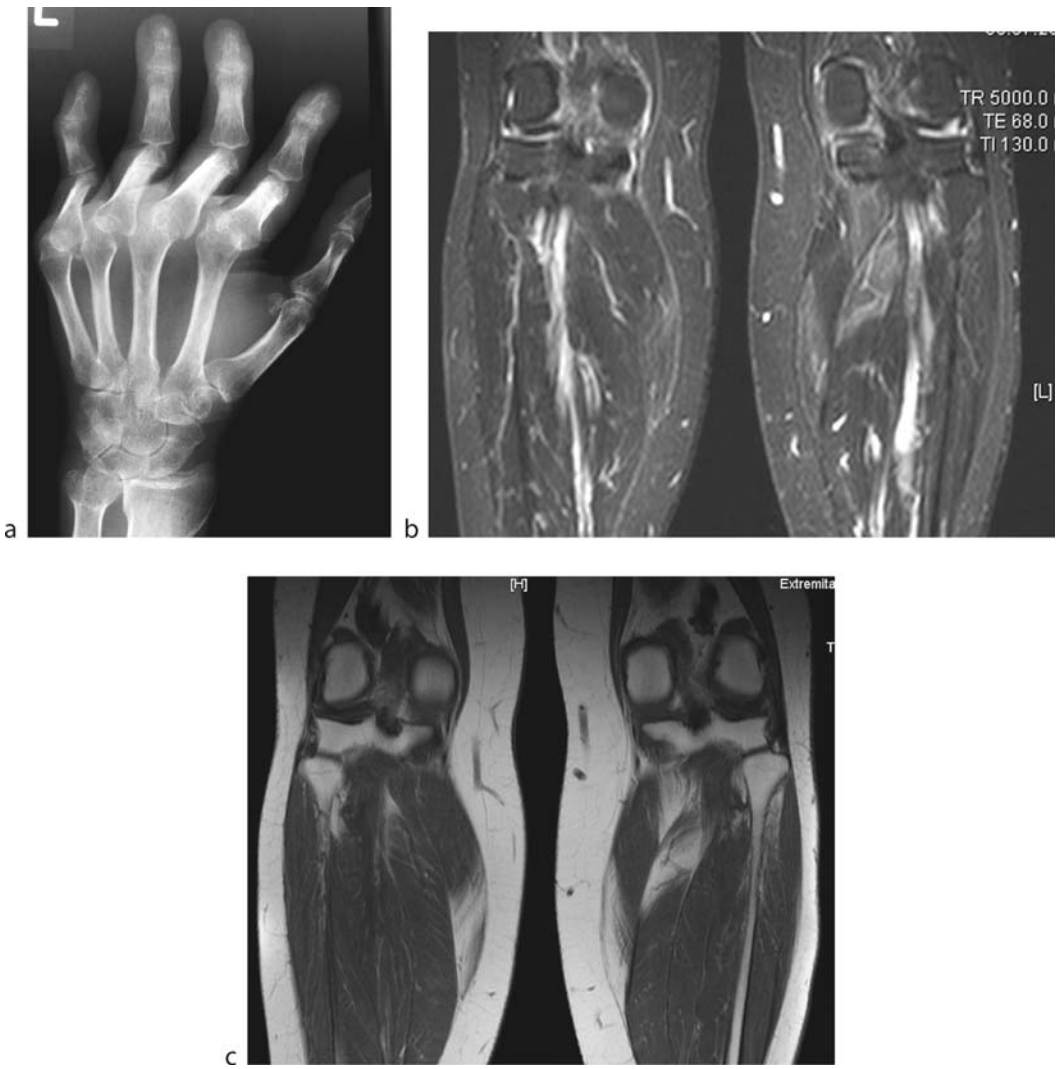

Connective Tissue Disorders, Musculoskeletal System. Figure 1 SLE. (a) "Jaccoud hand" with irregular deformities but without arthritic destructions. (b) Mild myositis of the lower leg with faint edema in the triceps surae and medial head of m. gastrocnemius, STIR image. (c) Short TE TR images show already fatty atrophy of the involved muscles.

can be diagnosed earlier and with more conspicuity in comparison to plain X-ray imaging. Polymyalgia and *myositis* most often affect muscles of the thigh with sparing of the m. sartorius. The lower leg is the second most frequent location (Fig. 1). STIR and T1-weighted images in the coronary and the transverse plane should be acquired. Application of contrast material is not necessary. The most prominent finding in the acute phase of disease is muscle edema and contrast material enhancement if it is applied. Long-standing myositis leads to fatty atrophy. Hemorrhages may occur.

Diagnosis

The clinical picture is most variable and often unspecific. It depends on the organ systems that are affected. Some patients show only mild symptoms at disease onset, others suffer severely and early diagnosis is mandatory. Schematic diagnosis criteria are therefore employed (Table 1) with reasonable sensitivity and specificity. Laboratory findings are important for classification and are included in the classification set.

Systemic Scleroderma

Clinical Presentation

SSc is characterized by an insidious onset mostly in the fourth to fifth decade. There is a twofold female predominance. *Raynaud's phenomenon* is frequently present months or years before actual disease onset. Edema and skin thickening of the hands and feet, the face, or the trunk are often one of the first symptoms. Polyarthralgia is frequent. Within months or years the skin hardens and shrinks leading to joint contractures and trophic deterioration with acral cutaneous necrosis. Teleangiectasias appear, and sweat glands and hair follicles become atrophic. ▶*Calcinosis cutis* can be felt as hard subcutaneous nodules. Dysphagia is a result of esophageal sclerosis with loss of peristalsis and stasis and gastroesophageal reflux. Abdominal distension may be a sign of small bowel involvement. Dyspnea and cough occur in patients with pulmonary fibrosis. Cardiomyopathy (myocardial fibrosis) is possible. Proteinuria or microhematuria is a sign of renal manifestation.

Limited cutaneous and diffuse cutaneous SSc with different severity and survival have been recognized as distinct subsets (Table 2). The features of ▶CREST syndrome (calcinosis, Raynaud's, esophagus dysmotility, sclerodactyly, teleangiectasias) are not confined to the limited subsets of SSc.

Connective Tissue Disorders, Musculoskeletal System.
Table 1 ARA criteria (1982) for the diagnosis of SLE

Skin and mucosal manifestations	Butterfly erythema
	Discoid lupus
	Photosensibility
	Oral ulcerations/aphthae
Lung, abdominal manifestation	Serositis, pleuritis, pneumonitis
Renal manifestation	Nephrotic syndrome, nephritis
	Polyarthralgia, nonerosive arthritis
Cerebral manifestation	Seizures, cerebral nerve palsy, mental disorders
Hematological manifestation	Hemolytic anemia, thrombo-/leukopenia
Immunologic findings	Anti-ds-DNS, Anti-sm, LE-cell-phenomenon, Phospholipid antibodies
	Antinuclear antibodies (ANA)

Definite diagnosis requires 4 of 11 criteria.

Imaging

Patients with scleroderma exhibit marked osteoporosis. Specific findings are fading of the acral soft tissue. Conical deformation of the finger tips and extension deficit lead to the aspect of "*prayer's hand*." ▶*Acral osteolysis* (unguicular process) and ▶*cutaneous necrosis at the finger tips like rat bites* occur later in the disease course. Osteolytic changes can manifest at the distal interphalangeal joints. *Calcinosis cutis* is found especially at mechanically exposed locations, for example, the finger tips or osseous prominences (Fig. 2). However, a peri- or intraarticular location is not uncommon. The calcification is speckled and grouped. It is a characteristic feature of CREST syndrome but can also be seen without CREST. Nondestructive joint deformities with flexion contracture due to skin shrinking are late findings. Erosive arthritis resembling rheumatoid arthritis is possible.

MR imaging shows skin thickening and edema in the early stages, shrinking and atrophy in late stages. Synovial and capsule edema as well as tenosynovitis may be present in symptomatic joints. A rare finding is epimysial edema. In patients with destructive arthritis, joint effusion, synovial thickening, and pannus as well as erosion are found.

Diagnosis

The following set of criteria for the classification of SSc was proposed: (i) autoantibodies to centromere proteins, Scl-70 (topo I), fibrillarin; (ii) symmetric basilar pulmonary fibrosis; (iii) contractures of the digital joints or prayer sign; (iv) dermal thickening proximal to the wrists; (v) calcinosis cutis; (vi) Raynaud's phenomenon; (vii) esophageal distal hypomotility or reflux-esophagitis;

Connective Tissue Disorders, Musculoskeletal System. Table 2 Scleroderma: limited and diffuse disease subsets

Clinical symptom	Limited disease	Diffuse disease
Raynaud's phenomenon	Long standing	Acute onset
Nailfold capillaroscopy	Tortuous, widened	Widened, microinfarction
Skin	Facial and acral skin thickening, dactylitis, teleangiectasia, calcinosis	Hands, forearms, face, feet, corps:
		Skin thickening, dactylitis, teleangiectasia, acral necrosis
Joints	Arthralgia, deformity	Arthralgia, deformity
Muscles	Myositis	Myositis
Lungs	Interstitial pneumopathy, primary pulmonary hypertonia	Interstitial pneumopathy, Secondary pulmonary hypertonia
Gastrointestinal tract	Esophageal dysfunction, dilatation	Esophageal and intestinal dysfunction, dilatation, ulceration
Heart	Pericarditis	Pericarditis, myocarditis, myocardial fibrosis
Autoantibodies	Anticentromere antibodies	Anti-scl-70-antibodies

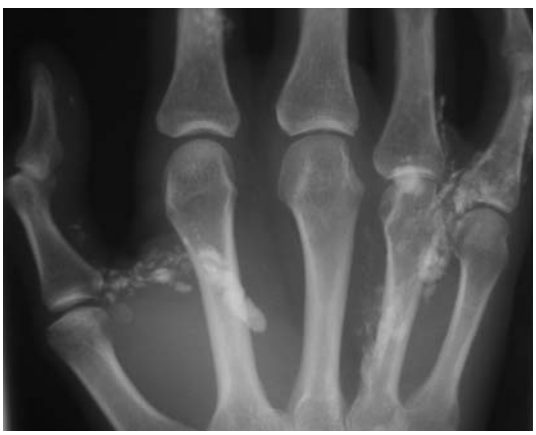

Connective Tissue Disorders, Musculoskeletal System. Figure 2 Scleroderma. Typical calcinosis subcutaneously, peritendinously, periarticularly in a patient with CREST syndrome.

(viii) sclerodactyly or nonpitting digital edema; (ix) teleangiectasias. The diagnosis of definite systemic sclerosis requires at least three of the above criteria.

Microvascular lesions (enlarged and giant capillaries together with hemorrhages, loss of capillaries, and ramified capillaries and vascular architectural disorganization) are a predominant feature in systemic sclerosis and are detected and graded by means of nailfold capillaroscopy.

Overlap Syndromes, Mixed Connective Tissue Disease

Definition

Many patients presenting with symptoms suggestive of a CTD do not fulfill criteria for a specific diagnosis at the initial presentation. Such patients have been designated as having undifferentiated CTD. In time, some of them will develop a specific CTD, whereas others will have a stable clinical course or show overlapping features of two or more CTDs. MCTD is the prototype of a rheumatic diseases overlap syndrome characterized by overlapping features of SLE, scleroderma, polymyositis, and rheumatoid arthritis in the presence of antibodies to U1-ribonucleoprotein (anti-U1-RNP). There is evidence that the clinical and serological features of MCTD represent a distinctive subset of CTD; however, this subject has not been settled yet.

Clinical Presentation

Common features are: Raynaud's phenomenon, sclerodactyly, isolated keratoconjunctivitis sicca, swollen hands, unexplained polyarthritis, myalgia, myositis, rash, pleuritis, pericarditis, central nervous system symptoms, pulmonary symptoms, peripheral neuropathy, raised erythrocyte sedimentation rate. In addition to clinical overlap, serological overlap has also been recognized in patients with CTDs.

Imaging

X-ray imaging is required for the differential diagnosis of synovitis and arthralgia. In cases of MCTD, however, no specific radiologic sign is found. The soft tissue swelling is not necessarily in a synovitic pattern. Calcifications like those found in SSc are possible. MR imaging can assist in the assessment and localization of myositis. Muscle edema is present in the acute phase; later, fatty muscle atrophy develops.

Diagnosis

Multiple sets of criteria for the diagnosis of MCTD have been proposed, indicating how difficult it is to give a precise definition. The presence of anti-U1-RNP antibodies is indispensable but not in itself sufficient. However, its specificity is moderate, accounting for the fact that there may be high titers in SLE, SSc, and RA, too. Reasonable sensitivity and specificity are provided with the Alarcon-Segovia Criteria, when in addition to high titers of anti-U1-RNP, three of five clinical manifestations (edema of the hands, synovitis, myositis (myalgia), Raynaud's phenomenon, and acrosclerosis) are present.

Idiopathic Inflammatory Myopathies

Definition

The idiopathic inflammatory myopathies are characterized by chronic muscle inflammation and involvement of internal organs, which contribute considerably to the morbidity and mortality of the disease. Seven types are described. Type 1: Polymyositis; Type 2: Dermatomyositis; Type 3: Polymyositis or dermatomyositis associated with cancer; Type 4: Childhood polymyositis or dermatomyositis; Type 5: Polymyositis or dermatomyositis in CTD; Type 6: Inclusion body myositis; Type 7: Unspecified myositis: nodular, eosinophilic, granulomatous myositis.

Clinical Presentation

Proximal muscle weakness and also pain which increases with exercise most often affecting the thigh are the clue symptoms. Muscle atrophy, fibrosis, and contracture are late-stage features. Arthralgia and arthritis are relatively common, especially in polymyositis with CTD. Erosion and cartilage destruction, however, are rarely seen. Pericarditis and myocarditis may occur and cause arrhythmia. Skin involvement predominates dorsally at the metacarpophalangeal and proximal interphalangeal joints with papules and livid erythemas. Raynaud's phenomenon and teleangiectasia of the nailfold are similar to scleroderma. Calcinosis is mainly seen in children.

Pulmonary complications (i.e., aspiration pneumonia due to myositis-related esophageal dysfunction and ventilatory insufficiency) and cardiac complications are the most frequent causes of death. Variables associated with poor outcome are older age, pulmonary and esophageal involvement, and cancer.

Imaging

In plain X-ray imaging, indistinct soft tissue findings predominate. The favorite sites of edema are the subcutis and muscles, with swelling, slight attenuation, and fat line disappearance. Fibrosis and contractures lead to atypical projections. In the late stage, muscle volume is decreased as a result of atrophy. The most characteristic finding is ►*soft tissue calcification* mainly muscular or epifascial, sometimes intratendinously or in fat. Subcutaneous linear calcifications are common at the knee, elbow, and fingertips. Blane and coworkers described four distinct patterns of calcification in childhood dermatomyositis: deep calcareal masses, superficial calcareal masses, deep linear deposits, and a lacy, reticular, subcutaneous deposition of calcium encasing the torso. Soft-tissue calcification was identified in 40–60% of cases.

Arthralgia in polymyositis and dermatomyositis does not result in erosion and cartilage destruction. Periarticular osteoporosis and soft tissue swelling, however, may occur.

MR imaging is employed for localization of inflammatory affected muscles in order to find a promising biopsy location. In the acute stage, excessive edema and contrast material enhancement of the affected muscles are seen. Fasciitis in the neighborhood is common. In dermatomyositis, subcutaneous edema and contrast material enhancement of reticular pattern are present. In the chronic phase, edema in muscles, epifascially and subcutaneously resolves. Muscle atrophy with fat interposition and fascial undulation develops.

Diagnosis

According to the widely used criteria (Bohan and Peter criteria 1975), DM is differentiated from PM only by skin changes. Following new diagnostic criteria including histopathological characteristics, dermatomyositis is a microangiopathy affecting skin and muscle; activation and deposition of complement cause lysis of endomysial capillaries and muscle ischemia. In polymyositis and inclusion body myositis, cytotoxic T cells invade muscle fibers that express MHC class I antigens, which leads to fiber necrosis. In inclusion body myositis, vacuolar formation with amyloid deposits coexists with the immunological features.

Diagnosis is definite in the presence of the following criteria: proximal muscle weakness, elevated muscle enzymes (CK, LDH, aspartatransferase, alanine aminotransferase, aldolase), electromyography findings, myositis in muscle biopsy, typical skin manifestation.

Bibliography

1. Fernando MM, Isenberg DA (2005) How to monitor SLE in routine clinical practice. Ann Rheum Dis 64:524–527
2. Masi AT, Rodnan GP, Medsger TA (1980) Preliminary criteria for the classification of systemic sclerosis (scleroderma). Arthritis Rheum 23:581–590

3. Alarcón-Segovia D, Villareal M (1987) Classification and diagnostic criteria for mixed connective tissue disease. In: Kasukawa R, Sharp GC (eds) Mixed Connective Tissue Diseases and Antinuclear Antibodies. Elsevier, Amsterdam, pp 33–40
4. Bohan A, Peter JB, Bowman RL (1977) A computer assisted analysis of 153 patients with polymyositis and dermatomyositis. Medicine (Baltimore) 56:255–261
5. Mastaglia FL, Phillips BA (2002) Idiopathic inflammatory myopathies: epidemiology, classification and diagnostic criteria. Rheum Dis Clin North Am 28:723–741
6. Bohan A, Peter JB (1975) Polymyositis and Dermatomyositis. N Engl J Med 292:344–347, 403–407

Connectivitis

▶Connective Tissue Disorders, Musculoskeletal System

Conservative Breast Surgery

▶Breast Conserving Therapy

Conservative Surgical Therapy

▶Breast Conserving Therapy

Contrast Media, Ultrasound, Phase Modulation

Robert Eckersley
Imaging Sciences Department, Imperial College London, London, UK
r.eckersley@imperial.ac.uk

The compromise of sensitivity against spatial resolution in harmonic mode imaging led to the development of phase modulation imaging (1). This mode is now widespread and available on many commercial clinical systems. The form of phase modulation imaging which has now become standard, and is often referred to as pulse

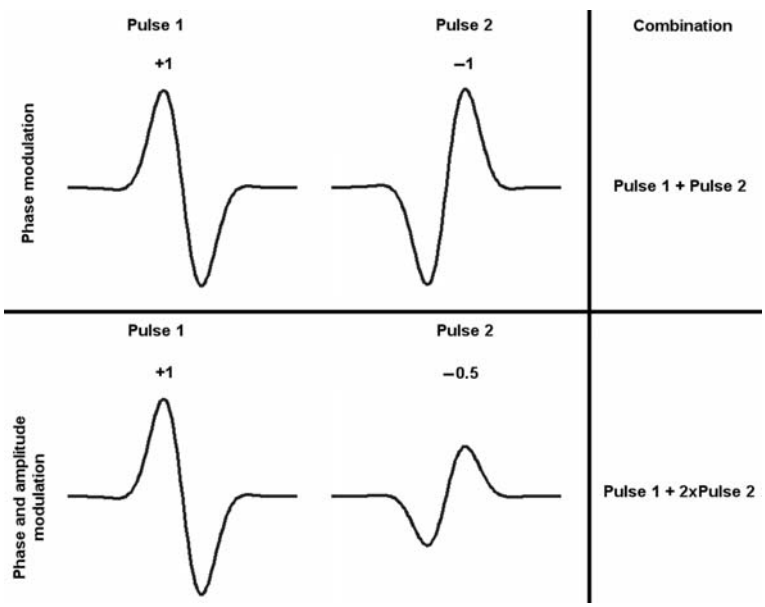

Contrast Media, Ultrasound, Phase Modulation. Figure 1 This figure shows (upper panel) a simple two pulse phase modulation sequence. When the echoes of pulse 1 and pulse 2 are summed, any linear signals will be canceled. The second harmonic signals in the echoes from microbubbles are preserved by this approach. Also presented (lower panel) is a two pulse sequence with combined phase and amplitude modulation. Linear signals can again be removed by appropriate combination of the echoes. This approach can detect nonlinear signals at the fundamental frequency as well as the second harmonic.

inversion imaging is based on alternating the polarity between successive pulses, that is, +1,−1 and so on. (see Fig. 1). When these pulses are scattered linearly from tissues, the echoes of subsequent pulses will cancel when combined. The response of the microbubbles to the +1 and −1 pulse is significantly different, and when the echoes are combined, a residual signal arising from the nonlinearity of the bubbles remains. The nonlinear signal detected by phase modulation imaging comes from the second harmonic signals in the echoes. Broadband imaging pulses can be used, and, unlike harmonic imaging, this multipulse approach does not suffer from the same compromise in specificity and sensitivity to microbubbles against resolution. This approach can be extended (by using more than two pulses) to allow detection target motion using Doppler processing. Successful phase modulation imaging requires precise pulse shaping within the ultrasound equipment to ensure good cancellation of the linear echoes. The specificity of this approach is limited by the generation of harmonic signals during the propagation of the sound through tissues especially at higher MI.

Bibliography

1. Hope Simpson D, CT Chin, Burns PN (1999) Pulse inversion Doppler: a new method for detecting nonlinear echoes from microbubble contrast agents. IEEE Trans Ultrason Ferroelectr Freq Control 46(2):372–382

Continuous Diaphragm Sign

In pneumomediastinum, mediastinal air may also track extrapleurally along the upper surface of the diaphragm and air beneath the heart combines the margins of the bilateral diaphragms.

▶Pneumomediastinum

Contour Wall Alteration

▶Compression, Extrinsic, Esophagus
▶Compression, Extrinsic, Stomach and Duodenum

Contrast Echo

▶Contrast Media, Ultrasound, Applications in Echocardiography

Contrast Echocardiography

This technique consists in injecting 5–10 cc of agitated saline into a peripheral vein while simultaneously imaging the right and left atria using echocardiography. In patients without right-to-left shunting, the contrast is visualized in the right atrium as a cloud of echoes and gradually dissipates as the bubbles become trapped in the pulmonary circulation. In patients with intracardiac or intrapulmonary shunting, the contrast is visible in the left atrium within one cardiac cycle or 3–8 cardiac cycles, respectively.

▶Fistula, Arteriovenous, Pulmonary
▶Contrast Media, Ultrasound, Applications in Echocardiography

Contrast Enhancement

After intravenous injection of contrast medium there is an increased density on CT and increased signal intensity on T1-weighted sequences in MRI. Contrast-enhanced structures appear bright on these images.

▶Neoplasms, Oral Cavity

Contrast Induced Nephrotoxicity

Contrast induced nephrotoxicity is defined as a temporary or permanent reduction in renal function caused by the administration of an imaging contrast medium. In most scientific investigations, this is determined on the basis of laboratory, rather than clinical, grounds. The lower border of what constitutes clinically significant nephrotoxicity is poorly defined.

▶Adverse Reactions, Iodinated Contrast Media, Acute Renal

Contrast Induced Renal Dysfunction

▶Adverse Reactions, Iodinated Contrast Media, Acute Renal

Contrast Induced Renal Failure

▶Adverse Reactions, Iodinated Contrast Media, Acute Renal

Contrast Media MR, Organ Specific

Peter Reimer
Deaprtment of Radiology, Klinikum Karlsruhe, Academic Teaching Hospital of the University of Freiburgh, D-76133 Karlsruhe
Peter.Reimer@klinik.um-karlsruhe.com

Synonyms

Currently, three organ-specific contrast agents with uptake into hepatocytes followed by variable biliary excretion represent the only clinically approved organ-specific contrast agents besides iron oxides:

- Mangafodipir trisodium (Teslascan, GE-Amersham Health, Oslo, Norway)
- Gadobenate dimeglumine (MultiHance, Bracco Imaging S.p.A., Milan, Italy)
- Gadoxetic acid (Primovist, Schering AG, Berlin, Germany).

Enhancement during the distribution phase of contrast agents mainly depends on tumor vascularity (hypovascular vs. hypervascular) and its blood supply while enhancement on delayed images is characterized by the cell specificity of magnetic resonance (MR) contrast agents (extracellular vs. intracellular). Therefore, enhancement characteristics of hepatobiliary contrast agents are applicable to the diagnosis of primary benign and malignant hepatocellular liver tumors (1).

Definition

Mangafodipir Trisodium "Teslascan"

Mangafodipir trisodium is a manganese (Mn) chelate [manganese(II)-*N*,*N*′-dipyridoxylethylenediamine-*N*,*N*′-diacetate-5,5′-bis(phosphate)sodium salt]. Mangafodipir has two components: fodipir and a manganese(II) ion. When mangafodipir is labeled with the ^{14}C-label residing in the fodipir, after a single intravenous dose of 5 μmol/kg of ^{14}C-mangafodipir, the mean ± SD area under the radioactivity plasma concentration curve (AUC) is 22.7 ± 3.2 μg h/mL. Generally, the total body store of manganese in adults is 20 mg. Most of this is from dietary intake (2–5 mg/day). Mangafodipir contains 2.75 mg/mL of chelated manganese. In a 70 kg adult, 5 μmol/kg of mangafodipir injection contains 19.2 mg of chelated manganese. Therefore, single injections will approximately double the total body store of manganese before excretion occurs. Manganese is an essential trace metal in humans with a normal whole body content of 12–20 mg.

Mangafodipir trisodium is a paramagnetic complex and following IV administration, mangafodipir is metabolized by dephosphorylation to Mn-DPMP and Mn-PLED and transmetallated by zinc (Zn) to the corresponding compounds. Mn^{2+} ions released from mangafodipir trisodium are most probably bound by alpha2-macroglobulin and transported to the liver. Its T1 relaxivity in aqueous solution is similar to gadolinium, however, due to the intracellular uptake of Mn^{2+}, its T1 relaxivity in liver tissue is three times greater than that of gadolinium (21.7 mmol/L^{-1}sec^{-1} vs. 6.7 mmol/L^{-1}sec^{-1}). In humans, the manganese(II) ion of mangafodipir is eliminated in the urine by 15% within 24 h and by 59% in the feces in 5 days (2).

Gadobenate Dimeglumine "MultiHance"

Gadobenate dimeglumine [(Gd) benzyloxy-propionic tetraacetic acid (Gd-BOPTA)] is an octadentate chelate of the paramagnetic ion gadolinium. Its kinetic properties resemble those of conventional iodinated contrast media and can be described by a biexponential function comprising a distribution phase and an elimination phase. This agent differs from other available gadolinium-chelates in that it distributes not only to the extracellular fluid space (ECF), but is selectively taken up by functioning hepatocytes and excreted into the bile. The biliary excretion rate is only 3–5% in humans (renal 78 to 96% and feces 0.6 to 4%). The uptake of gadobenate dimeglumine by hepatocytes and excretion into the bile is accomplished *via* the adenosine triphosphate (ATP)-dependent bile-canalicular multispecific organic anion transporter (cMOAT), which is shared by bilirubin and inhibited by bromosulfophthalein (BSP). Gadobenate dimeglumine has a higher relaxivity than equimolar formulations of other approved extracellular contrast agents due to its more lipophilic structure and its capacity for weak and transient interaction with serum albumin. In the liver, the estimated relaxivity is about 30 mmol^{-1}sec^{-1}, compared with calculated values of 16.6 mmol^{-1}sec^{-1} for gadoxetic acid and 21.7 mmol^{-1}sec^{-1} for mangafodipir trisodium. Gadobenate dimeglumine is not metabolized with an elimination half-life of 1.17 to 2.02 h (3).

Gadoxetic Acid

Gadolinium-ethoxybenzyl-diethylenetriamine-pentaacetic-acid is a paramagnetic contrast agent with hepatocellular uptake *via* the anionic-transporter protein and a molecular weight of 725.71 Da ($C_{23}H_{28}GdN_3Na_2O_{11}$). Gadoxetic acid is a highly water-soluble, hydrophilic compound with a lipophilic moiety due to the ethoxybenzyl group. T1-relaxivity as measured in water at 0.47 T of 4.9 $mM^{-1}sec^{-1}$ is comparable to gadopentetate dimeglumine with 3.7 $mM^{-1}sec^{-1}$. The T1-relaxivity in human plasma ($R1$ 8.7 $mM^{-1}sec^{-1}$) is higher than for gadopentetate dimeglumine ($R1$ 5.0 $mM^{-1}sec^{-1}$) and displays only slight dependency on the strength of the magnetic field. This may be explained by the greater degree in protein binding (10.7±3.4%) compared to gadopentetate dimeglumine (1.6±4.2%). At 37°C, the solution has an osmolality of 0.89 osmol/kg H_2O and a viscosity of 1.22 mPasec. Gd-EOB-DTPA is an aqueous formulation with a concentration of 0.25 mol/L and a high thermodynamic stability (log KGdl = −23.46). Gd-EOB-DTPA is equally eliminated *via* the renal and hepatobiliary routes with a half-life of approximately 60 min. The pharmacokinetics is dose-linear up to the dose of 0.4 mL/kg (100 µmol/kg). A total serum clearance (Cltot) of about 250 mL/min was recorded, whereas the renal clearance (Clr) corresponds to about 120 mL/min. Gadoxetic acid is not metabolized and may be bolus-injected at a flow rate of 2 mL/sec (4).

Indication

All three contrast agents are approved for MR imaging of suspected liver tumors. In addition, gadobenate dimeglumine has also been approved for magnetic resonance imaging (MRI) of the central nervous system (CNS) and mangafodipir for pancreatic MRI.

Contraindication

Safety and effectiveness have not been established in pediatric patients for any of the contrast agents. Specific contraindications and precautions for the three contrast agents are as follows.

Mangafodipir

Mangafodipir is contraindicated in patients with known allergic or hypersensitivity reactions to manganese, fodipir or any of the inert ingredients. The dialysability of mangafodipir and its metabolites has not been studied. Pharmacokinetic differences due to drug interactions or race after intravenous of mangafodipir were not studied. Patients with a history of drug reactions to contrast media, other allergies, or immune system disorders should be observed for several hours after drug administration. Caution should be exercised before administering to patients who have or cannot tolerate nausea or vomiting. The possibility of complications from nausea and vomiting should be considered when administering mangafodipir to patients who cannot tolerate vomiting, who have reflux esophagitis or who cannot roll over to prevent aspiration.

Mangafodipir is cleared from the body partially by glomerular filtration and partially by hepatobiliary excretion. Dose adjustments in renal or hepatic impairment have not been studied. The safety of repeated doses has not been studied. If the physician determines those imaging needs to be repeated, repeat images could be obtained up to 24 h after the original injection without reinjection. Safety, effectiveness, or pharmacokinetics of mangafodipir injection in pediatric patients below the age of 12 years has not been established.

Gadobenate Dimeglumine

A known allergic or hypersensitivity reactions to gadolinium or any other ingredients, including benzyl alcohol represents a contraindication. Further contraindications are sickle cell anemia or other hemoglobinopathies and hemolytic anemias. Precautions should be taken to avoid local extravasation during administration. Gadobenate should not be administered to patients who may be using medications or who may have underlying metabolic, cardiac, or other abnormalities that may predispose them to cardiac arrhythmias.

Gadobenate is not recommended in patients with severely impaired renal function (creatinine clearance <30 mL/min). Small quantities of benzyl alcohol (<0.2%) may be released during storage. Therefore, gadobenate should not be used in patients with history of sensitivity to benzyl alcohol.

Gadoxetic Acid

Hypersensitivity to the active substance or to any of the excipients represents a clear contraindication. Caution should be exercised in patients with severe renal impairment due to reduced elimination capacity of gadoxetic acid. Caution should also be exercised when gadoxetic acid is administered to patients with severe cardiovascular problems because only limited data are available so far. It cannot be excluded that of gadoxetic acid may cause torsade de points arrhythmias in an individual patient.

Intramuscular administration may cause local intolerance reactions including focal necrosis and should therefore be strictly avoided.

Pregnancy/Lactation

It is recommended that breastfeeding be discontinued before administration of any of the contrast agents and not reinitiated until 24 h after administration. Use is recommended only if potential benefit to the pregnant woman outweighs the potential risks to the fetus. However, it is recommended not to use mangafodipir since this may cause harm to the fetus when administered to a pregnant woman. Manganese has caused embryo toxicity and fetal toxicity in various animals. Animal studies have shown that 54Mn manganese crosses the placenta and locates in the fetus. At least 24 h after injection, radioactivity is detected in liver and bones of the fetus. It has been reported that manganese enters nerve terminals, accumulates in nervous tissue, and could be associated with neurotoxicity in fetuses. Adequate and well-controlled studies were not conducted in pregnant women. If mangafodipir is used during pregnancy, or if the patient becomes pregnant while taking this drug, the patient should be told of the potential hazard to the fetus.

Use and Dosage

Mangafodipir is administered at a dose of 5 μmol Mn/kg as a short IV infusion over 10–20 min. Near maximal enhancement is achieved at 20 min after the start of the infusion, and persists for several hours. Postcontrast imaging may start as soon as 20 min after the start of the infusion, but longer time intervals are possible because of a plateau-like enhancement up to and several hours.

Gadobenate dimeglumine is administered as a bolus injection at a dose of 0.05 mmol Gd/kg body weight and can be used for rapid dynamic imaging of the liver following bolus injection in the same way in which nonliver-specific contrast materials are used. This approach exploits the differences in blood flow between lesions and normal liver parenchyma. The fraction of gadobenate dimeglumine taken up into the hepatocytes manifests itself as a strong enhancement of the liver parenchyma signal intensity in T1-weighted images between 40 and 120 min postinjection.

Gadoxetic acid is administered as a bolus injection at a dose of 25 μmol Gd/kg body weight (Fig. 1). Near maximal enhancement is achieved at 20 min after the start of the injection, and persists for several hours. Thus, postcontrast imaging may start as soon as 20 min after the start of the infusion, but longer time intervals are possible because of a plateau-like enhancement (5).

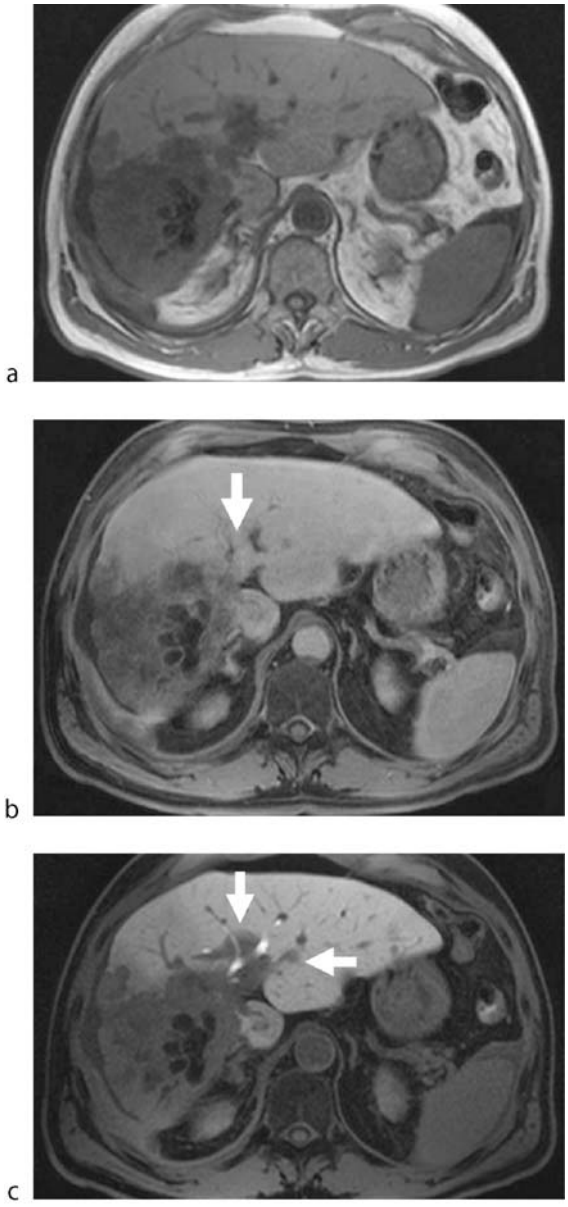

Contrast Media MR, Organ Specific. Figure 1 Patient with Cholangiocarcinoma. The portalvenous system (b) shows weak enhancement following Primovist compared to plain T1 (a). Tumor extension is much better visualized images in the hepatocellular phase (c).

Adverse Reactions

The possibility of a reaction, including serious, life-threatening, or fatal, anaphylactic, or cardiovascular

reactions, or other idiosyncratic reactions, should always be considered, especially in those patients with a history of known clinical hypersensitivity or a history of asthma or allergic respiratory disorders. Caution should be exercised in patients with deoxygenated sickle erythrocytes in all paramagnetic contrast agents.

Mangafodipir showed warmth or flush, nausea, heart pounding (increase in blood pressure and heart rate), and dizziness as the most frequent side effects in clinical studies with facial flushing in 55% of patients. Mild to moderate nausea was observed in 9%. The majority (93%) of adverse events were of mild to moderate intensity: chest pain, dizziness, hot flushes, hypersensitivity, hypertension, palpitation, pruritus, rash, taste perversion, urticaria. A transient increase in blood pressure and heart rate occurred immediately after injection, but returned to baseline after 5 min in all patients. Facial flushing was more often reported after rapid IV bolus injection than after IV infusion. No dosage adjustment is recommended in patients with mild to moderate renal impairment or hepatic impairment.

Gadobenate dimeglumine shows various side effects, which redocumented according to the organ system. Specifically, anemia has occurred in 0.5% of patients. Hypertension (up to 0.7%) and tachycardia (up to 0.5%) have been observed in the cardiovascular system, whereas vital signs remained essentially stable in other studies. The overall incidence of tachycardia in phase II studies ($n = 360$) was less than 1% (doses up to 0.2 mmol/kg). Other rarely reported cardiovascular effects have included acute pulmonary edema, cardiac arrhythmias, electrocardiogram (ECG) abnormalities, hypotension, and syncope. In the CNS, headache (5.8%) and dizziness (3.6%) have been reported following injection. One patient experienced seizures approximately 17 min after administration of gadobenate dimeglumine. The patient had a reported history of seizures. Other rarely reported central nervous system effects have included hemiplegia, hyperonia, paralysis, tremor, and aphasia. Most frequent events in the GI system were nausea, vomiting, and dry mouth in less than 2% of patients. No alteration of renal or liver function has been observed in available studies. Most frequent reactions at the injection site were pain, discomfort, and cold or tingling. Less frequent reactions include pruritus and other allergic-type cutaneous reactions. During postmarketing use of gadobenate dimeglumine, there were reports of anaphylactoid reactions, anaphylactic shock, and loss of consciousness. The observed spectrum is similar to approved extracellular gadolinium chelates.

During the clinical development phase of gadoxetic acid the overall incidence of adverse reactions, which were classified as drug, related was below 5%. Most of the undesirable effects were transient and of mild to moderate intensity. Laboratory changes as elevated serum iron, elevated bilirubin, increases in liver transaminases, decrease of hemoglobin, elevation of amylase, leukocyturia, hyperglycemia, elevated urine albumin, hyponatremia, elevated inorganic phosphate, decrease of serum proteins, leukocytosis, hypokalemia, elevated LDH were reported in clinical trials. ECGs were regularly monitored during clinical studies and transient QT prolongation was observed in some patients without any associated adverse clinical events. In very rare cases, anaphylactoid reactions leading to shock may occur. In the event of excessive inadvertent overdose, the patient should be carefully observed including cardiac monitoring. In this case, induction of QT prolongations is possible.

The most frequent reported definitely, possibly, or probably related AEs were nausea, vasodilatation, headache, taste perversion, and injection site pain. In patients with mild and moderate hepatic impairment, a slight to moderate increase in plasma concentration, half-life, and urinary excretion, as well as decrease in hepatobiliary excretion have been observed in comparison to subjects with normal liver function. However, no clinically relevant differences in hepatic signal enhancement were observed. In patients with severe hepatic impairment, especially in patients with abnormally high (>3 mg/dL) serum bilirubin levels, plasma concentration and half-life are increased with pronounced decrease in hepatobiliary excretion and reduced hepatic signal enhancement. In patients with end-stage renal failure, the half-life is markedly prolonged. Hemodialysis increased the clearance of Gd-EOB-DTPA. In an average dialysis session of about 3 h duration, about 30% of the Gd-EOB-DTPA dose was removed by hemodialysis (6).

Interactions

Transmetallation of manganese may occur. The extent to which this might affect laboratory assays of ferritin, iron, bilirubin, and zinc is not known. Specific interaction studies of mangafodipir, gadobenate dimeglumine, or gadoxetic acid with other medical products have not been carried out during the clinical development. In general, anionic drugs primarily excreted into the bile (such as rifampicin) may compete with the hepatic contrast enhancement and the biliary excretion of hepatobiliary contrast media. Animal studies demonstrated that compounds belonging to the class of rifamycins block the hepatic uptake of hepatobiliary contrast media, thus reducing the hepatic contrast effect. In this case, the expected benefit of an injection of hepatobiliary contrast media might be limited.

Elevated levels of bilirubin or ferritin can reduce the hepatic contrast effect of hepatobiliary contrast media.

Serum iron determination using complexometric methods (e.g., Ferrocine complexation method) may result in false values for up to 24 h after the examination with gadoxetic acid because of the free-complexing agent contained in the contrast medium solution. This has not been studied for gadobenate dimeglumine.

Bibliography

1. Earls JP and Bluemke DA (1999) New MR imaging contrast agents. Magn Reson Imaging Clin N An 7(2):255–273
2. Giovagnoni A and Paci E (1996) Liver. III: Gadolinium-based hepatobiliary contrast agents (Gd-EOB-DTPA and Gd-BOPTA/Dimeg). Magn Reson Imaging Clin N Am 4(1):61–72
3. Huppertz A et al (2004) Improved detection of focal liver lesion at MR imaging: multicenter comparison of gadoxetic acid-enhanced MR images with intraoperative findings. Radiology 230(1):266–275
4. Reimer P, Schneider G, and Schima W (2004) Hepatobiliary contrast agents for contrast-enhanced MRI of the liver: properties, clinical development and applications. Eur Radiol 14(4):559–578
5. Rofsky NM and Earls JP (1996) Mangafodipir trisodium injection (Mn-DPDP). A contrast agent for abdominal MR imaging. Magn Reson Imaging Clin N Am 4(1):73–85
6. Schima W et al (1997) Contrast-enhanced MR imaging of the liver: comparison between Gd-BOPTA and Mangafodipir. J Magn Reson Imaging 7(1):130–135

Contrast Media, Barium

Jean-Philippe Barraud
Guerbet, Roissy,
France
barraudj@guerbet-group.com

Introduction

Barium sulphate contrast media are nearly exclusively used for gastrointestinal tract imaging with conventional X-ray, computed tomography (CT) or less frequently magnetic resonance imaging (MRI) modalities.

The gastrointestinal tract is a succession of hollow organs. Its investigation by means of X-rays requires, in most cases, the use of contrast media, introduced orally or *via* the rectum, because of the small differentiation of soft-tissue permeability to X-rays. The first studies involved various substances, including bismuth sub-nitrate or sub-carbonate, sometimes mixed with bread or gruel, to prepare a meal. Bismuth was sometimes associated with the production of toxic metabolites. In 1910, Bachem and Günther proposed the routine use of barium sulphate, which replaced all other products because of its higher purity and absence of toxicity.

There are two types of contrast media for gastrointestinal tract imaging:

- 'Clarifying' media which are less radio-opaque (to X-rays) than the surrounding tissues: air, gas, e.g. carbon dioxide, water, aqueous solution of methylcellulose.
- 'Opacifying media' which are more radio-opaque than the surrounding tissues.

The opacifying contrast media contain heavy metals with a high atomic number (Z) to increase their radio-opacity: iodine ($Z = 53$) and barium ($Z = 56$) are presently used.

Definitions

Barium and Barium Salts

Barium is normally present in nature as barium carbonate $BaCO_3$ (whiterite) or barium sulphate $BaSO_4$ (barytine).

Barium is a toxic element. Therefore, only those barium salts which are completely insoluble in water, acids and fluids present in the gastrointestinal tract, are devoid of toxicity.

Soluble barium salts are barium chloride, nitrate and carbonate, which are slightly soluble in acids, and barium sulphides and oxides, which are soluble in acids. These salts are heavily toxic: when transported directly to the central nervous system (CNS), they increase CNS excitability and paralyse it.

Non-toxic insoluble barium salts are those salts which are insoluble in water, and remain insoluble after contact with hydrochloric acid in the stomach.

Barium sulphate ($BaSO_4$) is the sole barium salt, which is insoluble in various gastrointestinal tract media and which is therefore not absorbed by the mucosa.

Barium sulphate is obtained from two different pathways:

1. Natural barium sulphate which is extracted from mines and treated by physical (grinding, washing) and chemical processes to reach the specifications of the relevant pharmacopoeia.
2. Precipitated barium sulphate which is obtained by precipitation of other barium salts with sulphuric acid, and thoroughly washed to ensure its purity.

Barium sulphate as a raw material has the following advantages:

- Insolubility in water and acids
- Stability
- High atomic number, generating a good radiological contrast
- Relatively low cost.

The main risks concern the possible passage of barium sulphate into the circulation *via* a breach of the

gastrointestinal tract following trauma or a perforated ulcer, or into the respiratory tract via an oesophageal-bronchial fistula, for example.

Barium sulphate is listed in the European Pharmacopeia and in the US Pharmacopeia, which describe its purity and some physical characteristics, for example its sedimentation rate. Barium contrast media available on most markets are prepared with PE or USP grade barium sulphate.

General Information on Barium Sulphate Contrast Media

Barium sulphate is nearly insoluble in water (2.4 mg/L at 25°C).

Barium sulphate is therefore used as a suspension of two phases:

1. A dispersed phase of barium sulphate particles and excipients used to produce the suspension.
2. A dispersant phase and water-soluble excipients.

The stability and properties of these suspensions, which are usually less stable than solutions are obtained by optimising the parameters of the barium sulphate particles and the formulation of the excipients.

Parameters and Characteristics of the Dispersed Phase

1. The grain size, that is particle size, influences the sedimentation rate, the particulate surface and the viscosity of the suspension.

Grain Size and Sedimentation Rate

The smaller the grain size, the lower the rate of sedimentation will be. Particles of 1 m diameter will have a sedimentation speed of circa 1 cm/h. The sedimentation speed follows approximately Stokes law, which states that the speed of a sphere in a liquid is a function of gravity, the difference of densities of the sphere (d_1) and of the surrounding suspending solution (d_2), the square of radius of the sphere (a) and the viscosity of the solution (η):

$$V = \frac{2ga^2(d_1 - d_2)}{9\eta}$$

Stokes law does not strictly apply because the particles are not perfectly spherical and have different diameters. Nevertheless, the influences of the various parameters are similar: the sedimentation rate decreases if the grain size decreases and if the viscosity increases.

The influence of the grain size is very strong since its square value is implied.

Grain Size and Particle Surface

For a given weight of barium sulphate, a smaller grain size will induce a comparatively larger particulate surface.

For instance, 1 g of $BaSO_4$ will show a particulate surface of

- 1,500 cm^2, if it is divided into particles of 10
- 15,000 cm^2, if it is divided into particles of 1 .

The particle surface is the contact zone between particles and the dispersant phase (water).

This zone is concerned by physical adsorption phenomenon with the water molecules and some ions present in the dispersant phase. The particle size is therefore increased and tends to stick to each other and build some clumps. The homogeneity of the suspension is therefore decreased. Stabilisers are added to prevent the formation of $BaSO_4$ aggregates.

Grain Size and Viscosity

The use of small grain sizes in barium sulphate contrast media induces a high viscosity. Inversely, the use of large grain sizes allows the preparation of lower viscosity barium sulphate contrast media. This is used for preparation of high density (HD) products, which contain particles of up to 30 , and still have a low viscosity for optimal and quick coverage of the stomach mucosa.

2. The electric charge of the particles in suspension and the stabilising excipients.

All solid particles immersed in a liquid have an electric charge which arises from the absorption of certain ions or by the loss of electrons or ions from the particle surface.

This electric charge attracts molecules and ions (sometimes called counter-ions), which are present in the liquid phase. They build a diffuse layer which extends from the fixed layer which sticks to the particle itself to the electrically neutral zone where the electrostatic field has disappeared.

The electrical difference of potential between the fixed layer and the neutral zone is called zeta potential. The zeta potential measures the apparent charge of the particles. It is correlated to the suspension aggregation phenomenon and to the viscosity of the suspension. These electrical phenomena are more important with small size particles. They become negligible for large particles.

Stabilisers are products which are absorbed by $BaSO_4$ particles and which modify their electric charge.

They induce an increase in the apparent negative electric charge of the particles, which consequently creates repulsive forces between particles and thus avoid particulate aggregation and increase the stability of the suspension. One can observe a drop of the value of the zeta potential.

Typology of Commercially Available Barium Sulphate Contrast Media

1. *Powders* contain barium sulphate and excipients, to which water must be added to prepare a suspension of barium sulphate adapted to the concerned radiological examination. The user must adapt the volume of water to the final concentration and derived radioopacity of the contrast media. Thorough mixing is usually necessary. Filtration of the suspension is sometimes recommended.
2. *Suspensions* or gels of a given concentration, to which water might be added within some limits to obtain a different and lower concentration of barium sulphate.
3. *Pastes* mainly designed for studies of the oesophagus and of the rectum, which can be mixed with barium sulphate suspensions to reduce its concentration or viscosity.

Main Features of Barium Sulphate Contrast Media

1. Concentration
   The concentration is expressed in
   - Per cent weight of $BaSO_4$/volume for suspensions and gels
   - Per cent weight of $BaSO_4$/weight for powders and pastes.

   The concentration selected depends on the type of radiological examination performed:
   - Repletion technique of the stomach, small bowel or colon for which the concentration should not exceed 100% w/v.
   - Double-contrast techniques of the stomach for which the concentration can be as high as 250 w/v.
   - Double-contrast technique of the small bowel and of the colon for which concentrations as high as 100% are used.
   - Gastrointestinal tract delineation during CT examinations, for which low concentrations (0.5 to 1.5 w/v) of $BaSO_4$ are used.
2. Fluidity or viscosity
   The required viscosity depends on the concerned examination:
   - Examination of the pharynx and oesophagus require the use of a highly viscous paste which will not fall quickly into the stomach.
   - Double-contrast examination of the stomach requires the use of low-viscosity suspensions to visualise all details of the mucosa, and possibly of high density (in weight and to X-rays) in order to obtain a better contrast.

   Barium sulphate suspensions are non-Newtonian and thixotropic: the relation between shear rate and stress is non-linear and the curves displaying the correspondence between stress and shear rate form a hysteresis loop when shear rates are increased and subsequently decreased. Measurements of viscosity are directly related to the type of apparatus used.

   Viscosity is sometimes measured in seconds needed to empty a standardised cup through a hole.

   Viscosity of the barium sulphate suspension is related to its coating and mucosal adherence performance. The bowel preparation agents prior to double-contrast barium enemas can influence it.
3. Stability
   Stability is usually measured by the sedimentation rate of the suspension, which is expressed by the depth of the supernatant lying over the suspension–supernatant interface after a given period of time.
   Stability of $BaSO_4$ suspension is needed to obtain films free from sedimentation artefacts. The necessary stability will therefore depend on the technique used:
   - Small grain size $BaSO_4$ suspensions (1 m) are mainly used for repletion techniques and double-contrast examinations of the small bowel and of the colon. Their sedimentation rate is usually very low.
   - High density (HD) $BaSO_4$ (1 to 30 and more micrograms grain sizes) are mainly used for double-contrast examinations of the stomach.
4. Hydrophilicity of the $BaSO_4$ suspension is necessary for double-contrast examinations of the colon, because of the very high water adsorption capacity of the colon. The $BaSO_4$ film is therefore subjected to severe dehydration. Hydrophilic resins are used in some products in order to trap the water and avoid drying out of the $BaSO_4$ film. The derived loss of elasticity and uniformity would induce difficulties in image interpretation.
5. Palatability is related to the flavouring agents added in the $BaSO_4$ contrast media for oral use. This is of particular importance for CT barium contrast media used for delineation of the GI tract, which are sometimes self-administered by the patient, outside a strictly medical environment. Pleasant taste and odours lead to an optimal patient compliance to the ingestion of the appropriate dose of $BaSO_4$ contrast media.

Conclusion

Availability of Barium Contrast Media

It is estimated that around 9,000 t of barium sulphate have been used for medical imaging worldwide in 2003.

Barium sulphate contrast media have been made available from more than 20 manufacturers worldwide in forms varying from bulk material to ready-to-use presentations in sophisticated packaging.

Use of Barium Contrast Media

The above-mentioned amount of barium sulphate has been mainly used in conventional fluoroscopic imaging studies in both repletion and double-contrast techniques and in CT studies for GI tract delineation purposes.

Dynamic studies of deglutition and defecation functions are also often based on the use of barium contrast media.

A new and promising field of development concerns CT and MR colonography (also called virtual coloscopy), which are sometimes involving faecal tagging techniques. Barium contrast media absorbed orally have been used for tagging of the faeces in CT (2) and MR (3) colonography.

Bibliography

1. Swanson DP, Chilton HM, Thrall JH (1990) Pharmaceuticals in medical imaging Macmillan Publishing Company
2. Lefère PA, Grypspeerdt SS, Dewyspelaere J, Baekelandt M, Van Holsbeeck BG (2002) Dietary fecal tagging as a cleansing method prior to computed tomographic colonography: Initial results-polyp detection and patient acceptance. Radiology 224:393–403
3. Lauenstein TC, Goehde SC, Ruehm SG, Holtmann G, Debatin JF (2002) MR colonography with barium-based fecal tagging: Initial clinical experience. Radiology 223:248–254
4. Miller RE, Skucas J (1989) Radiographic contrast agents. University Park Press
5. Gallot D. (1983) Le sulfate de baryum: aspects galéniques et formulation, J Pharm Clin
6. Conry BG, Jones S, Bartram CI (1987) The effect of oral magnesium-containing bowel preparation agents on mucosal coating by barium sulphate suspensions. Brit J Radiol 60:1215–1219
7. Bachem C, Gunther H (1910) Bariumsulfat als schattenbildendes Kontrantmittel bei Röntgenuntersuchungen. Z Röntgenk Rad Forschr, 12:369–376

Contrast Media, Extravasation

Marie-France Bellin[1], Jarl Å. Jakobsen[2], Henrik S. Thomsen[3], Sameh K. Morcos[4]
[1]Department of Radiology, University Hospital Paul Brousse, AP-HP. University Paris-Sud 11, Villejuif, France
[2]Department of Radiology, Rikshospitalet, Oslo, Norway
[3]Department of Diagnostic Radiology, Copenhagen University Hospital at Herlev, Herlev, Denmark
[4]Department of Diagnostic Imaging, Northern General Hospital, Sheffield Teaching Hospitals NHS Trust, Sheffield, UK
marie-france.bellin@pbr.ap-hop-paris.fr

Definition

Subcutaneous extravasation is a well-recognized complication of intravenous administration of iodinated and magnetic resonance (MR) contrast media. Most extravasations involve small volumes of contrast material and induce minimal swelling or localized erythema, which rapidly diminish. Extensive tissue necrosis and severe skin and subcutaneous ulceration are rare and usually follow high-volume extravasations. The Contrast Media Safety Committee of the European Society of Urogenital Radiology has produced guidelines for preventing and managing extravasation of contrast media (Table 1) (1).

Contrast Media, Extravasation. Table 1 Contrast Media Safety Committee of the European Society of Urogenital Radiology guidelines for preventing and managing extravasation of contrast media

Risk factors are related to	• The technique
	• Use of a power injector
	• Less optimal intravenous sites, including lower limb and small distal veins
	• Large volume of contrast medium
	• High-osmolar contrast medium
	• The patient is
	• Unable to communicate
	• With fragile or damaged veins
	• With arterial insufficiency
	• With compromised lymphatic and venous drainage
To reduce the risk	• Always use careful intravenous technique, preferably with plastic catheters
	• Use low-osmolar contrast medium
Type of severe injuries	• Most injuries are minor. Severe injuries include skin ulcerations, necrosis of soft tissue, and compartment syndrome
Treatment	• Conservative management is adequate in most cases
	• Limb elevation
	• Application of ice packs
	• Careful monitoring
	• If a serious injury is suspected, seek the advice of a surgeon

Characteristics

Risk Factors

Patient Factors

High-risk patients include noncommunicative patients (infants, small children, and unconscious patients) and patients receiving chemotherapy, because chemotherapy may induce fragility of the vein wall (1, 2). Extravasation injuries are more severe in patients with low muscular mass

and atrophic subcutaneous tissue. In addition, patients with arterial insufficiency (such as atherosclerosis, diabetes mellitus, or connective tissue diseases) or compromised venous drainage (such as thrombosis) or lymphatic drainage (such as radiation therapy, surgery, or regional node dissection) are less able to tolerate extravasation than those with unimpaired circulation (1–5).

Contrast Media Type and Volume

Extravasation of low-osmolar contrast media is better tolerated than extravasation of high-osmolar media. The vast majority of extravasations involve small volumes of contrast material, and symptoms resolve completely within 24 h. Rarely, severe skin ulceration and necrosis can follow extravasation of volumes as small as 10 mL. Large-volume extravasation may lead to severe damage to extravascular tissue and is most likely to occur when contrast medium is injected with an automated power injector and the injection site is not closely monitored.

Factors Due to Injection Technique

Extravasations are more frequent with metallic needles than with plastic cannulae and when indwelling intravenous catheters are used (3). The site of injection also appears to be important: injections into the dorsum of the hand, foot, or ankle are frequently associated with extravasation injury. The frequency of extravasation of contrast medium after mechanical bolus injection is higher than that reported for hand-injection or drip infusion techniques (4) and varies from 0.2 to 0.4%, with power injection rates between 1 and 2 mL. In a study by Jacobs et al (5), the incidence of extravasation (0.6%) did not differ significantly between groups of patients receiving different injection rates of contrast media. In addition, no correlation was noted between the extravasation rate and catheter location, catheter size, or catheter type.

Mechanism

Multiple factors are involved in extravasations. The first factor is osmolality above 1.025–1.420 mOsm/kg water. Both iodinated radiographic and MR contrast agents of low osmolality are better tolerated than high-osmolar iodinated contrast agents. The second factor is the cytotoxicity of contrast media. While Cohan et al (6) found that ionic contrast media were more toxic than nonionic agents, no difference was found by Jacobs et al (5). The presence of meglumine as a cation may also play a role in the cytotoxicity of ionic contrast media (7). The third factor is the volume of extravasated contrast medium. Although severe skin lesions have been described following an extravasation of less than 15 mL, the majority have occurred with large-volume extravasations (8). The fourth factor is the mechanical compression caused by large-volume extravasations that may lead to compartment syndromes. Infection of the extravasated site may increase the severity of local lesions. Extravasation from indwelling intravenous lines is often due to phlebitis that develops in the cannulated veins. Other mechanisms include inadequate placement of the catheter in the vein, multiple punctures of the same vein, and high injection pressure, which can break the vessel wall (1, 2).

Presentation

Symptoms of extravasation are quite variable, and patients may be asymptomatic or complain of stinging or burning pain. At physical examination, the extravasation site appears edematous, erythematous, and tender; swelling may be due to tissue necrosis associated with progressive edema and skin ulceration. Most extravasation injuries resolve spontaneously in 2–4 days; rarely, they lead to long-term sequelae including hypoesthesia, marked weakness, and pain (1, 2, 4). The initial examination does not allow one to predict whether the extravasation injury will resolve or result in ulceration, necrosis, or damage to soft tissue. A number of clinical findings suggest severe injury and justify the advice of a surgeon. These include skin blistering, altered tissue perfusion, paresthesias, and increasing or persistent pain after 4 h (2). Extravasation may also result in acute compartmental syndromes, producing tense and dusky forearms with swelling and diminished arterial pulses. Compartmental syndromes may necessitate emergency fasciotomy to relieve neurovascular compromise (9).

Extravasation injuries must be distinguished from other local reactions to injected fluid, including hypersensitivity reactions and local irritative effects of iodinated contrast agents on the vessel wall. In these reactions, edema and erythema are absent, and the catheter is well positioned in the vein. Extravasated gadolinium is better tolerated than conventional ionic radiographic contrast media and produces a zone of signal void on short relaxation time MR images because of its high local concentration (10). New devices for detecting extravasation are currently under evaluation (11).

Treatment

Elevation of the affected limb: Elevation is often useful to reduce the edema by decreasing the hydrostatic pressure in capillaries.

Topical application of heat or cold: Heat produces vasodilatation and thus resorption of extravasated fluid and edema (12), whereas cold produces vasoconstriction and limits inflammation (13). Cooling can be produced

with ice packs placed at the injection site for 15–60 min three times a day for 1–3 days or until symptoms resolve.
Prevention of secondary infection: Application of silver sulfadiazine ointment is recommended by many plastic surgeons whenever blistering is evident (14).
Hyaluronidase, dimethylsulfoxide (*DMSO*), *corticosteroids, and vasodilators*: Most studies have failed to demonstrate any value of these agents or did not evaluate extravasations of contrast media.
Surgery: Most plastic surgeons believe that the majority of extravasation injuries heal without surgery and that a conservative policy is therefore recommended (15). Surgical drainage or emergency suction applied within 6 h can be effective (16), and the use of emergency suction alone or combined with saline flushing have also been helpful (17, 18).
Aspiration of fluid from the extravasated site: This treatment is controversial, as it usually removes only a small amount of extravasated fluid and carries a risk of infection.

Conclusions

Extravasation of contrast material is a relatively common complication of enhanced imaging studies, but large-volume extravasation may result in severe damage. Early identification is important, and conservative management is effective in most cases. Radiologists should be aware of ways to prevent, recognize, treat, and document extravasation injuries.

Bibliography

1. Bellin MF, Jacobsen JA, Tomassin I et al and members of Contrast Media Safety Committee of European Society of Urogenital Radiology (ESUR) (2002) Contrast medium extravasation injury: guidelines for prevention and management. Eur Radiol 12:2807–2812
2. Cohan RH, Ellis JH, Garner WL (1996) Extravasation of radiographic contrast material: recognition, prevention, and treatment. Radiology 200:593–604
3. Sistrom CL, Gay SB, Peffley L (1991) Extravasation of iopamidol and iohexol during contrast-enhanced CT: report of 28 cases. Radiology 176:65–67
4. Federle MP, Chang PJ, Confer S et al (1998) Frequency and effects of extravasation of ionic and nonionic CT contrast media during rapid bolus injection. Radiology 206:637–640
5. Jacobs JE, Birnbaum BA, Langlotz CP (1998) Contrast media reactions and extravasation: relationship to intravenous injection rates. Radiology 209:411–416
6. Cohan RH, Leder RA, Bolick D et al (1990) Extravascular extravasation of radiographic contrast media: effects of conventional and low-osmolar contrast agents in the rat thigh. Invest Radiol 25:504–510
7. Kim SH, Park JH, Kim YI et al (1990) Experimental tissue damage after subcutaneous injection of water-soluble contrast media. Invest Radiol 25:678–685
8. Upton J, Mulliken JB, Murray JE (1979) Major intravenous extravasation injuries. Am J Surg 137:497–506
9. Benson LS, Sathy MJ, Port RB (1996) Forearm compartment syndrome due to automated injection of computed tomography contrast material. J Orthop Trauma 10:433–436
10. Carrier DA, Ford JJ, Hayman LA (1993) MR appearance of extravasated gadolinium contrast medium. Am J Neuroradiol 14:363–364
11. Birnbaum BA, Nelson RC, Chezmar JL et al (1999) Extravasation detection accessory: clinical evaluation in 500 patients. Radiology 212:431–438
12. Hastings-Tolsma TM, Yucha CB, Tompkins J et al (1993) Effect of warm and cold applications on the resolution of IV infiltrations. Res Nurs Health 16:171–178
13. Elam EA, Dorr RT, Lagel KE et al (1991) Cutaneous ulceration due to contrast extravasation: experimental assessment of injury and potential antidotes. Invest Radiol 26:13–16
14. Heckler FR (1989) Current thoughts on extravasation injuries. Clin Plast Surg 16:557–563
15. Cohan RH, Dunnick NR, Leder RA et al (1990) Extravasation of nonionic contrast media: efficacy of conservative treatment. Radiology 174:65–67
16. Loth TS, Jones DEC (1988) Extravasations of radiographic contrast material in the upper extremity. J Hand Surg 13:395–398
17. Gault DT (1993) Extravasation injuries. Br J Plast Surg 46:91–96
18. Vandeweyer E, Heymans O, Deraemaecker R (2000) Extravasation injuries and emergency suction as treatment. Plast Reconstr Surg 105:109–110

Contrast Media, Iodinated

Henrik S. Thomsen
Department of Diagnostic Radiology, Copenhagen, Denmark, University Hospital, Herlev, Denmark
hentho01@heh.regionh.dk

Iodinated contrast agents are essential in all modern radiographic imaging. The ideal contrast agent should be totally inert, causing no interactions with the organism at any level. Furthermore, it should be excreted rapidly and completely. In reality, none of the current contrast agents is totally inert, but the newer classes of agents are much closer to this state than the old ones.

Iodinated contrast media may be divided into water-soluble and oily contrast media. Oily contrast media include Lipiodol, a stable compound of 40% iodine in poppy seed oil, introduced in the 1920s and later replaced by Lipiodol ultra and Ethiodol, ethyl esters of iodinated fatty acids of poppy seed oil containing 48 and 37% iodine, respectively. These oils are still, to some extent, used for lymphography, hysterosalpingography, and dacryocystography.

Water-soluble contrast agents for use in radiographic techniques are iodinated benzoic acid derivates. They are by

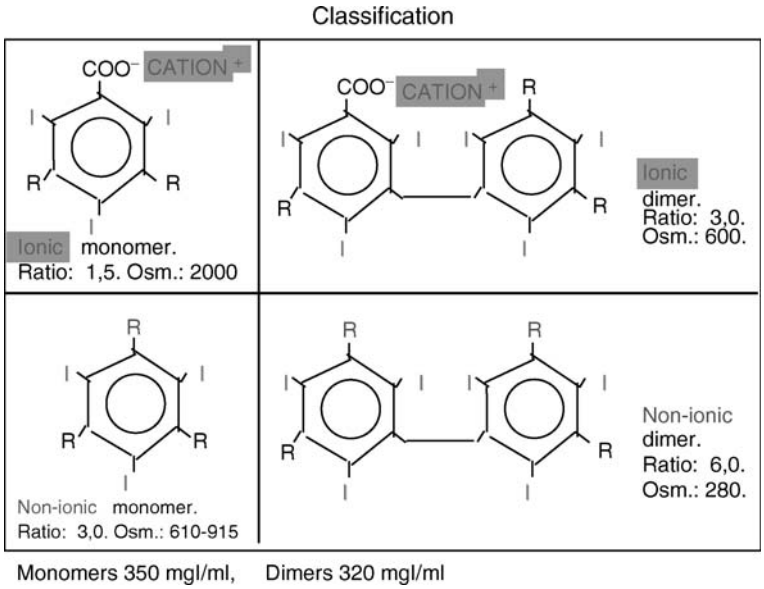

Contrast Media, Iodinated. Figure 1 Classification of water-soluble iodinated contrast media.

far the most used agents for radiography. The current iodinated contrast agents can be divided into four classes (Fig. 1): (a) high-osmolar ionic monomeric agents, (b) low-osmolar nonionic monomeric agents, (c) low-osmolar ionic dimeric agents, and (d) iso-osmolar nonionic dimeric agents. They all are distributed in the extracellular phase, none penetrate an intact blood–brain barrier, and all are excreted *via* glomerular filtration. The high-osmolar ionic monomeric media which are sodium and meglumine salts of tri-iodinated benzoic acid have been available since the 1950s. They are very hyperosmolar, being 5–8 times the osmolality of the blood. The hyperosmolality greatly increases the hemodynamic and toxic effects of these agents. In the 1970s, low-osmolar contrast media became available. This was achieved through converting tri-iodinated benzoic acid into a nonionic molecule by replacing the COOH radical with an amide ($CONH_2$). This molecule in solution will not dissociate, allowing the availability of three atoms of iodine with only one active particle [a ratio of 3:1]. Another development was the introduction of the mono-acid dimer in which two tri-iodinated benzoic rings are linked together with a bridge and the COOH of one ring is converted into an amide. This gives the same iodine: particle ratio of 3:1 in solution, since there are six iodine atoms and two active particles in one molecule. The osmolality of the ionic dimeric contrast media is almost the same as the nonionic monomeric agents and is about two times that of the blood at an iodine concentration of 300 mgI/mL. In the late 1980s the nonionic dimeric contrast media were introduced. This was possible through attaching two nonionic tri-iodinated benzoic rings. These dimers give an iodine:particle ratio of 6:1 since there are six iodine atoms and only one active particle in the molecule. The osmolality of the nonionic dimers at the concentration of 300 mgI/mL is equal to that of the blood. In the 1990s there was a worldwide introduction of nonionic monomeric contrast agents stimulating the conversion. At the turn of the century, both the nonionic monomeric and dimeric agents have firmly established themselves as the agents of choice since they are exceptionally well tolerated by the great majority of patients and are associated with a markedly reduced incidence of life-threatening anaphylactoid reactions as well as moderate and minor adverse reactions. Today more than 90% of all intravascular injections of an iodinated contrast medium in Western Europe and North America are done with a nonionic agent. By far, computed tomography (CT) and cardiac angiography are the examinations where the largest amounts are currently being used.

The benzene ring is, as mentioned earlier, the basis for all iodinated water-soluble contrast agents. One of the purposes of the side chains is to protect the body from the toxic benzene ring with three iodine atoms. The side chains do this well considering the low toxicity of the current iodinated contrast media. The minor variation within one class is mainly for patent protection. The variation in the number of hydroxyl groups may affect the hydrophilicity slightly, but the difference is of minor importance, as several small and large clinical studies have not been able to show any significant difference between

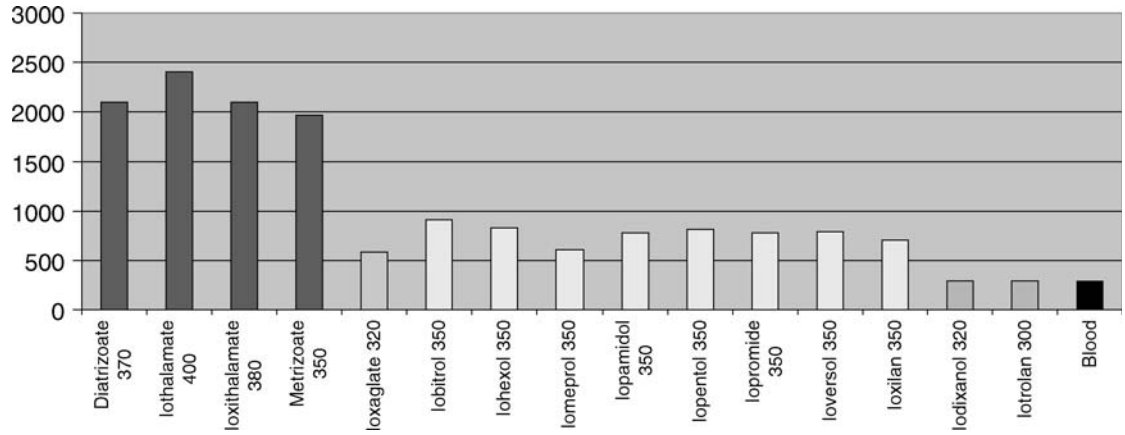

Contrast Media, Iodinated. Figure 2 Osmolality (m Osm/kg water) at 37°C of currently available iodinated contrast media.

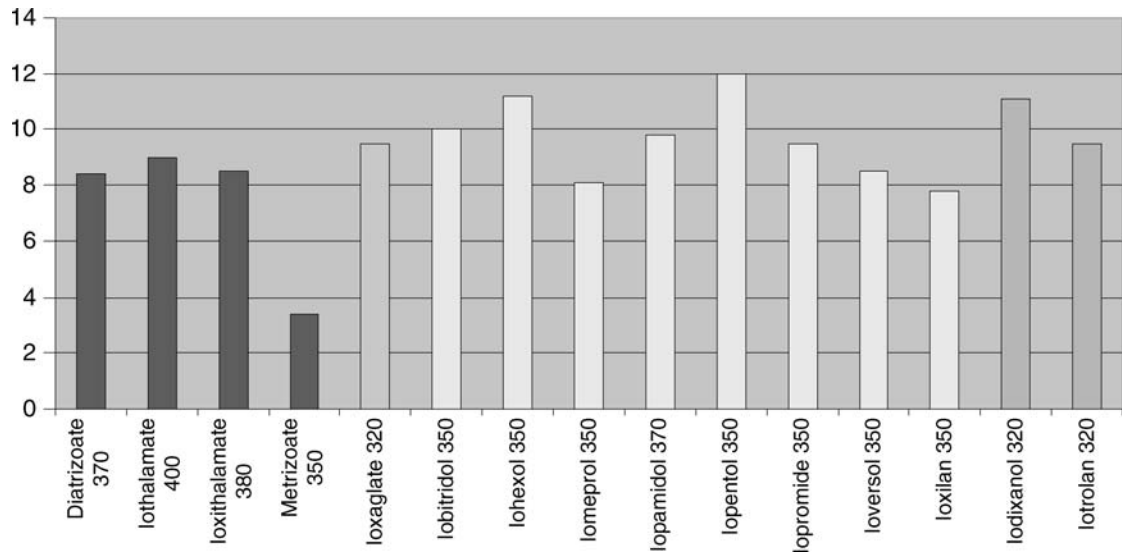

Contrast Media, Iodinated. Figure 3 Viscosity (cP) of current available iodinated contrast media at 37°C.

the various nonionic low-osmolar agents with regard to pharmacokinetics, pharmacodynamics, general safety, renal tolerance, induction of thrombosis, diagnostic effect, and so on. Today many contrast agents are available with various osmolality (Fig. 2) and viscosity (Fig. 3). A decrease in osmolality increases to some extent the viscosity, but there is no linear relationship between osmolality and viscosity. The main disadvantage of increased viscosity is the difficulty it may cause during the intravascular administration of contrast media particularly if a high-flow injection is required or a catheter with very small inner diameter is used.

Attenuation

Iodine has the atomic number 53 and an atomic weight of 127. Attenuation increases with the atomic number of the atom but decreases with the energy (keV) of the X-ray photons, except at the K-edges. The K-edge of iodine is 33 keV. Below 33 keV only very few photons will pass through the body. For CT, the maximal X-ray photon energy is between 120 and 140 keV and the most common photon energies in the spectrum are between 60 and 70 keV. For common radiographic examinations, the maximal X-ray photon energy is

between 70 and 90 keV. Thus, the common photon energies in the spectrum are above the K-edge of iodine (33 keV). The attenuation by the iodinated contrast agent molecule is enhanced by the fact that it contains three iodine atoms.

Administration—Dose

More contrast medium than necessary to confirm the presence or absence of a suspected abnormality or to perform a therapeutic procedure should not be used in any patient. The dose necessary differs from examination to examination. For example, for a dacryocystography a few milliliters of a 350-mgI/mL solution may be needed, for CT of the urinary tract (CT urography) 100 mL of a 300-mgI/mL solution given a split bolus may be more optimal than a single bolus injection of 150 mL, and for coronary angiography it may be diagnostically better to use 250 mL of a 350-mgI/mL solution than 300 mL of a 300-mgI/mL solution. Thus, the dose of contrast medium should be tailored to the actual problem that is being examined. Proper documentation of the intravascular use of contrast media should be included in the patient's records.

Administration—Extravasation

Infants, young children, and unconscious and debilitated patients are particularly at risk of extravasation during contrast media injection. Automated power injection may result in extravasation of large volumes and can lead to severe tissue damage. Fortunately, most extravasations result in minimal swelling or erythema, with no long-term sequelae. However, severe skin necrosis and ulceration may occur. Large volumes of high-osmolar contrast media are known to induce significant tissue damage. Compartment syndrome may be seen associated with extravasation of large volumes. The intravenous technique should always be performed carefully, preferably using plastic catheters for power injection. Conservative management is often adequate, but in serious cases the advice of a plastic surgeon is recommended.

Adverse Reactions

Radiation Versus Contrast Media

For pregnant women, the radiation exposure to the fetus may be a bigger risk than the exposure to contrast media. The same applies to newborns, children, and young adults. For patients over 40 years of age the opposite is the case, as the long-term effects of radiation (e.g., development of solid cancers) diminishes with age and the risk of an adverse reaction to a contrast agent in general increases with age (e.g., nephrotoxicity).

Adverse Reactions to Water-Soluble Contrast Agents

Adverse reactions to intravascular contrast media are nowadays infrequent and generally classified as either idiosyncratic or chemotoxic. Idiosyncratic (i.e., anaphylaxis-like, anaphylactoid) reactions occur unpredictably and independently of the dose or concentration of the agent. Most anaphylaxis-like reactions relate to the release of active mediators. Conversely, chemotoxic-type effects relate to dose, the molecular toxicity of each agent, and the physiological characteristics of the contrast agents (i.e., osmolality, viscosity, hydrophilicity, calcium-binding properties, and sodium content). Some reactions to injection of contrast media (e.g., sudden cardiopulmonary arrest) are difficult to categorize into either of the two major reaction types.

Chemotoxic effects of contrast media are more likely in patients who are debilitated or medically unstable. Hence, patients should be screened for conditions such as renal dysfunction, renovascular disease, severe cardiovascular disease, or recent seizures.

Adverse reactions to intravascular administration of iodinated contrast media are classified into renal and nonrenal. The latter is subdivided into acute (<1 h) and delayed (>1 h) reactions.

Acute Nonrenal Adverse Reactions

An acute reaction to contrast media can be divided into minor, intermediate, and severe life-threatening reactions. The minor reactions include flushing, nausea, arm pain, pruritus, vomiting, headache, and mild urticaria. They are usually mild in severity, of short duration, self-limiting, and generally require no specific treatment. The incidence of these reactions to high-osmolar contrast media is probably between 5 and 15%. Intermediate reactions, more serious degrees of the above symptoms, include moderate degrees of hypotension and bronchospasm. They usually respond readily to appropriate therapy. The incidence of these reactions to high-osmolar contrast media is about 1–2%. Severe life-threatening reactions include severe manifestation of all of the symptoms included under minor and intermediate reactions, convulsions, unconsciousness, laryngeal edema, severe bronchospasm, pulmonary edema, severe cardiac dysrhythmias and arrest, cardiovascular and pulmonary collapse. The incidence of serious reactions with high-osmolar contrast media is around 0.06–0.04%. The prevalence of contrast reactions with low-osmolar

contrast media is lower in comparison to high-osmolar contrast media by a factor of 5. It is mandatory that one is always prepared to treat a reaction.

There are several predisposing factors to contrast reactions. The incidence of severe adverse reactions increases in the presence of these risk factors, particularly allergy or bronchial asthma. A previous reaction to a contrast medium is also an important predisposing factor. For the time being, no medical prevention is recommended; steroid prophylaxis can be administered, but it does not avoid occurrence of adverse reactions in all patients.

Delayed Nonrenal Adverse Reactions to Contrast Media

Most delayed reactions are not serious or life-threatening and include flu-like illness, parotitis, nausea and vomiting, abdominal pain, and headache. Delayed allergy-like reactions with skin manifestation are the most frequent type. Thyrotoxicosis may occur up to 3 months after the injection.

Renal Adverse Reactions to Contrast Media

Contrast medium-induced nephrotoxicity is defined as an impairment in renal function (an increase in serum creatinine by more than 25 or 0.5 mg/dL (44 μmol/L) occurring within 3 days after the intravascular administration of contrast media and the absence of alternative etiology. It is considered an important cause of hospital-acquired renal failure. Diagnostic and interventional procedures using contrast media are performed with increasing frequency. In addition, the patient population subjected to these procedures is progressively older with more comorbid conditions. Prevention of this iatrogenic condition is important to avoid the substantial morbidity and even mortality that can sometimes be associated with contrast medium-induced nephrotoxicity. Even a small decrease in renal function may greatly exacerbate the morbidity and mortality caused by coexisting conditions such as acquired sepsis, bleeding, coma, and respiratory failure, which are more frequent in patients with acute renal failure. Therefore, several measures have been tested to reduce the frequency of contrast medium-induced nephropathy. No measure has yet resulted in avoidance of its occurrence in all patients, but adequate hydration reduces the incidence. When it has occurred, no specific treatment is possible.

Interactions

Several of the *in vitro* studies on the hematologic effects of contrast media have not been confirmed by *in vivo* and clinical studies. Clinical studies indicate that all contrast media possess an anticoagulant effect and that this effect is stronger with ionic contrast media. A meticulous angiographic technique is the most important factor for reducing the thrombotic complications associated with angiographic procedures.

Contrast media may interact with other drugs and may interfere with isotope studies and biochemical measurements. Awareness of the patient's drug history is important to avoid potential hazards.

Contrast Media, Iodinated, Applications in Conventional Radiography and CT

Henrik S. Thomsen, Marie-France Bellin
Université Paris 11, AP-HP, Service de Radiologie, Hôpital Paul Brousse, Villejuif, France
Department of Diagnostic Radiology, Copenhagen, Denmark, University Hospital at Herlev, Herlev, Denmark
hentho01.@heh.regionh.dk

Synonyms

Radiocontrast media; Radiographic contrast media

Definition

Contrast media are drugs that enhance the differences seen on the images between the body tissues. The ideal contrast agent should be totally inert, causing no interactions with the organism at any level. Furthermore, it should be excreted rapidly and completely.

They can be divided into water-soluble iodinated contrast media and non-water-soluble barium agents. The water-soluble iodinated contrast media can be further subdivided according to the number of benzene-rings: monomers (one ring), dimers (two rings). Both types are available as ionic and non-ionic. Thus iodinated contrast agents can be divided into four classes: (i) High-osmolar ionic monomeric agents, (ii) Low-osmolar non-ionic monomeric agents, (iii) Low-osmolar ionic dimeric agents, and (iv) Iso-osmolar non-ionic dimeric agents. Low-osmolar non-ionic monomeric agents are today the most used agents.

Indication

Water-soluble iodinated contrast media, which diffuse throughout the extracellular space after intravascular

administration, are principally used for angiography, during computed tomography (CT) and conventional radiography, notably intravenous urography (IVU). They can also be administered directly into the gastrointestinal tract and urinary tract, or into body cavities to opacify fistulas for example.

Barium sulphate preparations used to visualize the gastrointestinal tract consist of a suspension of insoluble barium sulphate particles which are not absorbed from the gut.

Contraindications

Iodinated Contrast Media

Absolute:

All contrast media: manifest hyperthyroidism

Ionic contrast media: subarachnoidal injection.

Relative:

Reduced renal function, asthma, history of allergy, previous reaction to a iodinated contrast medium

Pregnancy/Lactation

If the examination has been found to be indicated based on a thoroughly analysis of the history, symptoms and signs, one should go ahead and use the contrast media whenever it is necessary in order to confirm the presence or absence of a lesion. In early pregnancy, mutagenic and teratogenic effects may occur but they have never been shown to occur after administration of iodinated contrast media. In late pregnancy, potential harmful effects on fetal thyroid owing to the presence of free iodine are of concern. Therefore, neonates of mothers exposed to iodinated contrast media in the late pregnancy must be checked for thyroid dysfunction within 7 days after birth. In many countries it is already a routine.

It is been recommended to stop lactation for a day or two after administration of iodinated contrast media. However, the neonate will receive between 0.3–0.5% of the maternal dose and again only 1% of those tiny amounts may enter the extracellular fluid of the neonate. Thus, breast feeding may be continued normally when iodinated contrast agents are given to the mother. The baby may notice that the milk has a different taste.

Use and Dosage

The overwhelming majority of iodinated contrast media is used for CT-scanning, cardiac angiography, and interventional radiology. Only a minority is used for the remaining indications. Contrast media are available in various concentrations (140, 150, 180, 200, 240, 250, 300, 350, 370, 400mg/mL). For CT-scanning most radiologists use a contrast medium in a 300mgI/mL solution (monomer) or 270mgI/mL (dimer), whereas for cardiac and coronary angiography most cardiologists prefer concentrations of 350–400mgI/mL of a monomer whereas the dimers are mainly used in concentrations of 320mgI/mL.

The amount of contrast media used depends on the type of examination. For CT fixed doses in mL or in mL/kg body weight are used. The dose varies from country to country for example in some countries only 50mL of a 300mgI/mL solution is used for brain CT studies whereas others give 100mL of the same solution. There is no consensus about the optimal dosage. Regarding the latter not only the total mg of iodine is important, but also speed of injection, size of the bolus, kilovoltage, mAs, pitch affect the resulting image. When it comes to conventional arteriography like coronary angiography and direct injection into body cavities as the renal pelvis, dose depends on many factors including type of the lesion, the skills of the physician, kilovoltage, mAs, body weight, and so on. For an examination like CT urography many protocols have been proposed ranging from 50 to 200mL of 300mgI/mL contrast medium. A split bolus is now advocated by some radiologists, whereas others still recommend the old single injection including a bolus and a much slower follow-up during the first minutes. Optimal dosage is a sensitive area and a consensus has not yet been reached.

For barium studies of the gastrointestinal tract, 300–800mL of barium sulphate preparations are used.

Adverse Reactions

Adverse reactions to iodinated contrast media are more likely to develop in patients with reduced renal function, with asthma, a history of allergy or contrast reaction and in those who are debilitated or medically unstable. These reactions can be divided into renal and non-renal and the later are subdivided into acute and delayed. Acute non-renal adverse reactions can be minor, intermediate or severe. Fatal reactions are rare. The introduction of low-osmolar agents has caused an overall reduction in the number of non-fatal contrast reactions. See the sections: Adverse reactions, contrast media, iodinated, acute, non-renal; Adverse reactions, contrast media, iodinated, delayed; Adverse reactions, iodinated contrast media, acute, renal.

Interactions

See Contrast Media, Iodinated, Interactions with Drugs.

Bibliography

1. Thomsen HS (2006) (ed) Contrast Media: Safety Issues and ESUR Guidelines. Springer Verlag, Heidelberg

Contrast Media, Iodinated, Dose, and Administration

Robert P. Hartman, Bernard King
Department of Diagnostic Radiology, Mayo Clinic, Rochester MN, USA
hartman.robert@mayo.edu

Definition

Computed tomography (CT) utilizing multidetector scanners has introduced many new challenges regarding doses and rates of administration for iodinated contrast to obtain the best quality images of a wide variety of organs and vascular systems in the body. Routine CT of parenchymal organs in many instances requires more volume of contrast material injected at lower rates than CT angiography, which often requires less volume at a higher rate. The exact dose of contrast for any given vascular bed or organ system is becoming standardized but may still vary from institution to institution. In this section, some general principles of contrast administration and dosing will be discussed.

Characteristics

Administration

Whatever exam one wishes to perform the route of contrast material administration is similar. For most multidetector CT protocols, a bolus injection *via* power injectors is superior to IV drip infusion. These power injectors, however, can lead to potential complications including large volume extravasation and/or air embolism. Proper preparation of the injector and IV site as well as communication with the patient is important to limit these potential events. Pain or swelling at the IV site during the injection can be early signs of extravasation and the patient should be monitored for these signs. Whenever possible a nurse or technologist should monitor the site with direct palpation as the injection occurs for signs of extravasation. If detected the injection should be aborted immediately.

The best site for the IV access is an antecubital or forearm vein. Flexible venous cannulas should be used for the access site. Although 22-gauge cannulas can theoretically handle injection rates of 5 cc/sec it is recommended that a 20-gauge or larger IV is used for rates of 3 cc/sec or greater. The more peripheral the IV site the lower the rate of injection. Hand or wrist venipuncture sites may be limited to rates in the 1.5 cc/sec range.

Central venous catheters can be used safely if necessary when peripheral IV access cannot be obtained. The exact specifications and recommendations for any central catheter to be injected should be followed. Often large-bore (9.5 to 10 F) central venous catheters will be able to handle 2.5 cc/sec injection rates without exceeding the manufacturers' specified limitations.

Use and Dosage

Uses

At this time, CT enhanced with iodinated contrast is a wonderful tool for imaging a wide variety of body parts. Imaging of primary tumors of the brain, lung and abdominal organs as well as metastatic disease is a common everyday occurrence. CT angiography is now being routinely performed to detect abnormalities ranging from pulmonary emboli to vascular malformations, arterial stenoses, or acute hemorrhage. Anatomic CT angiography is widely accepted for pretransplant Kidney evaluation as well as pretreatment for peripheral vascular disease. Changes from ischemia, inflammation, and infection in the GI tract can also be readily identified on arterial and venous phase CT imaging. New techniques such as CT perfusion are emerging and will provide even more capabilities in the future.

When determining the dose and timing of the contrast bolus one should first identify the specific body part to be examined. Parenchymal organs are often scanned when the tissue is homogeneously enhancing providing an enhanced background for detecting any abnormalities. However, certain organs including the liver, pancreas, and kidneys, may require multiple phases (arterial, venous, and excretory) imaging to fully evaluate. CT angiography is best performed at the peak of the first pass of the contrast material bolus through the specific vascular bed. Given the wide variety of exams available, it is easy to see that a "one size fits all" dose is not possible but some general dose sizes and timing can be suggested.

Dosing

As mentioned, proper dosing requires a preprocedural determination of the organ system or vascular bed to be studied. Routine examination of the head requires a different dose and rate of injection than a thoracic aorta CT angiogram. In general, routine CT exams for parenchymal organs in the head, chest, abdomen, or pelvis require more volume of contrast injected at a slower rate than CT angiography. The maximal dose of iodinated contrast, in general, is limited to a total of 45 g of iodine. The concentration of the contrast material also may vary. For most examinations, a concentration of 300 mg/mL

Contrast Media, Iodinated, Dose, and Administration. Table 2 Contrast bolus volume, rate of injection, and timing of scan

Area of Interest	Timing (sec)	Bolus Dose (mL) 300 mg/mL concentration [b]350 mg/mL concentration	Injection Rate (mL/sec)
Head and neck			
Carotid/circle of Willis CTA	15[a]	100[b]	4
Routine neck and chest	20	80	3
Routine head	240	100	1
Chest			
Pulmonary arteries (PE study)	15[a]	120	4
Routine chest	20	80	3
Thoracic aorta CTA	20–25[a]	125[b]	4
Abdomen and pelvis			
Abdominal aorta CTA	25–30[a]	125[b]	4
Pancreas arterial phase	40	140	4
Pancreas parenchymal phase	65	140	4
Urogram corticomedullary renal phase	45	100	3
Liver arterial phase	40	140	4
Liver portovenous phase	60	140	4
Urogram nephrographic renal phase	90	100	3
Renal artery CTA	20–25[a]	125[b]	5
Mesenteric CTA	25–30[a]	125[b]	4
Enterography arterial phase	25	150	4
Enterography mucosal phase	60	150	4
Routine abdomen and pelvis	70	140	3
Lower extremity run off CTA	30–35[a]	140[b]	3
Routine chest, abdomen and pelvis	65	140	3

[a]CTA should be performed with bolus timing sequences when available. Times listed are an estimation based on an average individual.
[b]Contrast concentration of 350 mg/mL.

Contrast Media, Iodinated, Dose, and Administration. Table 1 Contrast media volume should be based on patient weight and renal function and can be standardize as in the example below

Volume of Contrast Medium in mL						
	No Diabetes			Diabetes		
Weight	<140 lbs <64 kg	140–240 lbs 64–109 kg	>240 lbs >109 kg	<140 lbs <64 kg	140–240 lbs 64–109 kg	>240 lbs >109 kg
Serum creatinine <1.5 mg/dL	100 mL	140 mL	200 mL	80 mL	120 mL	140 mL
Serum creatinine 1.5–1.9 mg/dL	80 mL	100 mL	140 mL	Consult with Radiologist		
Serum creatinine >1.9 mg/dL	Consult with Radiologist			Consult with Radiologist		

Iodine is sufficient. CT angiography will often be performed with 350–375 mg/mL Iodine.

Contrast volume administered may range from 80–150 cc in the average adult depending on the exam. Certain patient populations however may require adjustment of the overall dose such as diabetics and patients with renal insufficiency. Weight can also be a factor requiring volume adjustments. Table 1 shows one possible method of adjustment in these patients. (Based on a CT exam for an average size healthy patient receiving 1,400 cc of 300 mg/mL). The adjustments are made not only for consideration of image quality but also with the risk of contrast induced nephropathy in mind. As shown, certain situations require consideration of a different modality

Contrast Media, Iodinated, Dose, and Administration.

Table 3 Suggested contrast media dosing rate and volume for bariatric patients

Bariatric Patient (>300 lbs 137 kg)			
Creatinine <1.4 mg/dL			
225 mL of Iodixanol 320 with 50 mL Saline flush			
Injection rate	5 mL/sec	4 mL/sec	3 mL/sec
Scan delay	80	90	100
IV infusion following exam	250–500 mL 0.9 normal saline		

exam or noncontrast exam if it is felt iodinated contrast should not be administered. Alternatively, IV hydration reduced dose of contrast or use of iso-osmolar contrast can be utilized.

As previously mentioned different body, parts require different doses. Although, the type of scanner used and patient health and size play integral roles in the exact dose, some general guidelines for some of the more common exams are provided in Table 2. The volume, rate of injection and timing of the exam are given for contrast material concentration of 300 mg/mL unless otherwise noted.

Pediatric patients are best served by dosing specifically based on weight. In general, 1 mL/2.2 kg (1 mL/lbs) of contrast material up to 100 mL is an excepted dose. Newer scanners allow for examinations on markedly obese patient populations. In these bariatric patients, dosing can be difficult. Some general guidelines for these patients are included in Table 3.

Bibliography

1. Bush WH (ed) (1999) Radiology Life Support. Oxford University Press Inc., New York, NY
2. Katzberg R (ed) (1992) The Contrast Media Manual. Williams and Wilkins, Baltimore, MD
3. King B (ed) (2004) Manual on Contrast Media. American College of Radiology, Reston, VA
4. Thomsen HS (ed) (2004) Guidelines on contrast media, European Society of Urogenital Radiology, Am J Roentgenol 2003; 181: 1463–1471

Contrast Media, Iodinated, Interactions with Drugs

Sameh K. Morcos
Department of Diagnostic Imaging, Northern General Hospital, Sheffield Teaching Hospitals NHS Foundation Trust, Sheffield, UK

Many patients with multiple medical problems who are receiving a variety of drugs are investigated with imaging techniques that require intravascular contrast media. This involves possible interactions between contrast media with other drugs including interference with isotope studies and biochemical measurements.

Drugs that will be Retained in the Body Because of Reduction in Renal Function Induced by Contrast Media

One of the potential adverse effects of iodinated contrast media is reduction of renal function. This leads to retention of drugs that are excreted exclusively through the kidneys. A good example is the indirect interaction between contrast media and metformin. Significant reduction of renal function can be induced by contrast agents in the presence of pre-existing kidney disease particularly diabetic nephropathy. The reduction in renal function induced by contrast media causes retention of metformin potentially leading to the serious complication of lactic acidosis.

Drugs that cause diuresis and natriuresis can be hazardous and should be avoided in patients receiving lithium. Although contrast media especially those of high osmolality can induce significant diuresis and natriuresis, their role of in increasing lithium toxicity is not widely studied.

Drugs that Enhance the Renal Effects of Contrast Media

Nephrotoxic drugs such as non-steroidal anti-inflammatory drugs (NSAIDs) have the potential to increase the renal effects of contrast media. This class of drugs inhibits the intrarenal synthesis of vasodilatory prostaglandins augmenting the renal vasoconstrictor effect of iodinated contrast media and may facilitate the development of contrast media nephrotoxicity. Other nephrotoxic drugs such as gentamicin, cyclosporine and cisplatin may also augment the nephrotoxic effects of contrast media.

Diuretics such as acetazolamide, furosemide, spironolactone, may augment the diuretic effect of contrast media particularly those of high osmolality, leading to dehydration, increased risk of contrast medium nephropathy, electrolyte imbalance and hypotension.

Drugs that Enhance Allergy Like Reactions to Contrast Media

β-Blockers

Patients on β-blockers including the ophthalmic preparations who are given iodinated contrast media are three

times more likely to have an anaphylactoid reaction than matched controls. There is also increased risk of contrast media induced bronchospasm particularly in asthmatics. Anaphylaxis like reaction in these patients is more refractory to conventional treatment because of low reactivity to emergency medication. Adrenaline may be ineffective or promote undesired alpha-adrenergic or vagal effects.

Interleukin-2

In a prospective study of patients undergoing CT who had received Interleukin-2 (IL-2) and intravenous non-ionic low-osmolar or oral-ionic high-osmolar contrast media, or both, there were immediate urticarial reactions in 1.8% of the patients within an hour of contrast administration. No acute reactions were observed in a control group who received contrast media but had not been treated with IL-2. Delayed reactions (erythema, rash, fever, flushing, pruritis and flu-like symptoms) developed in 12% of IL-2 patients and only in 4% of the control group. Two of the IL-2 patients required admission to hospital. The mean onset of symptoms was 4.5 h after injection of contrast media and the mean duration of reaction was 16.4 h. The patients had no risk factor for delayed reactions other than IL-2 therapy and all had previous uneventful exposure to contrast media. None of the patients with immediate reactions developed delayed reactions. The average time since IL-2 therapy was 6 months (range 24 days to 2.4 years). Previous contrast media reaction in an IL-2 patient should be considered a relative contraindication to further contrast media administration. An increased risk of contrast reactions may remain for two years after stopping IL-2 treatment.

The administration of contrast media may also precipitate IL-2 toxicity. Fever, diarrhea, nausea and vomiting have been observed 2–4 h after enhanced CT scanning with non-ionic low-osmolar contrast media. The exact mechanism is not clear but contrast media may generate the release of endogenous IL-2 or reactivate the IL-2 receptors. Patients who develop these reactions should avoid further exposure to contrast media and imaging techniques such as MRI or CT without contrast media injection should be considered for monitoring response to treatment.

Hydralazine

Patients on hydralazine treatment, which can induce systemic lupus erythematosus (SLE) like syndrome may develop cutaneous vasculitis several hours after intravascular administration of non-ionic iodinated contrast medium. Hypersensitivity reactions to iodine-containing compounds have also been described in patients with systemic lupus erythematosus. It was suggested that injection of iodinated contrast media should be avoided in patients receiving hydralazine therapy as they may provoke severe reactions.

Drugs that Interfere with the Hematological Effects of Contrast Media

Effects of Contrast Media on Coagulation

It is well established that contrast media interact with the coagulation mechanism, platelet activation and degranulation and with thrombolytic drugs. Ionic contrast media are more effective than non-ionic agents at increasing the clotting time and give a fourfold increase in the whole blood clotting time when compared to non-ionic agents. Non-ionic contrast media cause less significant alteration of clothing by inhibiting the coagulation cascade after the generation of thrombin at the step of fibrin monomer polymerization. Thus, both ionic and non-ionic contrast media can prolong clotting time and may exaggerate the effects of anticoagulant and antiplatelet drugs.

Effects of Contrast Media on Fibrinolysis

Contrast media impede fibrinolysis and delay the onset of lysis by recombinant tissue-type plasminogen activator (rt-PA), urokinase and streptokinase. This effect is reduced by increasing the concentration of the lysis agent. Contrast media cause fibrin to form in long/thin fibrils, which have a lower mass/length ratio and are more resistant to fibrinolysis. In clinical practice, if coronary angiography is performed before starting thrombolysis the recent administration of contrast media may reduce therapeutic success.

Contrast Media and Drugs Acting on the Central Nervous System

Cerebral angiography with high osmolar contrast media may lower the fit threshold in patients receiving antipsychotics, tricyclic antidepressants, or analeptics. However, this concern does not seem to be important with the routine use of non-ionic low-osmolar contrast media for cerebral angiography.

Drugs that Enhance the Effects of Contrast Media on the Heart

Patients receiving calcium channel blockers may develop hypotension after left ventriculography with high-osmolar

ionic agents. This effect is not significant with low-osmolar non-ionic contrast media, which are less vasoactive and have minimal negative inotropic effect on the myocardium.

Effects of Contrast Media on Isotope Studies

The administration of iodinated contrast media interferes with both diagnostic scintigraphy and radioiodine treatment. The reduced uptake of the radioactive tracer is caused by the free iodide in the contrast medium solution. A delay before undertaking scintigraphy of 4–6 weeks for water soluble and 12 weeks for cholangiographic contrast media is advocated.

Intravascular administration of contrast media shortly after injection of isotope material (Tc-pyrophosphate) for bone imaging can interfere with the body distribution of the Tc-pyrophosphate. Increase uptake of the isotope material in kidneys and liver with low uptake in bones was observed. The diuretic effect of contrast media may increase the elimination of the isotope material in urine so less is available for deposition in skeleton. The increased uptake in the liver is not fully explained.

Intravascular administration of contrast media may also interfere with red blood cell labeling with isotope material. Tc-99m labeling of red blood cells should be performed before contrast media injection. How contrast media interfere with red blood cells labeling is not fully understood.

Mixing Contrast Media with Other Drugs

Contrast media should not be mixed with other drugs before intravascular use. It is also advisable not to inject other drugs through the same venous access used for contrast media injection. If the same venous access is used, there should be adequate flushing with normal saline first.

Effects of Contrast Media on Biochemical Assays

Measurements of clotting time and other coagulation factors can be falsely increased after the intravascular administration of contrast media. Therefore, clotting tests should be avoided for 6 h or more after injection of contrast media.

Iodinated contrast media in the urine may also interfere with some of the protein assay techniques leading to false positive results. Care must be exercised in interpreting tests for proteinuria for 24 h postcontrast media injection.

Gadodiamide and gadoversetamide may cause spurious hypocalcemia particularly at doses of 0.2 mmol/kg or higher in patients with renal insufficiency. These contrast media interfere with calcium measurements obtained by assay using the ortho-cresolphthalein complexone (OOC) method but not with the assays using the Arsenazo III method. The false measurements of serum calcium did not occur with gadopentetate dimeglumine (Gd-DTPA) or gadoteridol. In very high concentrations, Gd-DTPA may interfere with calcium determination when methylthymolblue is used. Awareness of this effect on calcium measurements by some MRI contrast agents is important to avoid incorrect and potentially hazardous treatment.

Iodinated contrast media may interfere with determination of bilirubin, cubber, iron, phosphate and proteins in blood. Caution should be exercised when using colorimetric assays for angiotensin-converting enzyme, calcium, iron, magnesium, total iron binding capacity and zinc in serum samples who have recently received gadolinium based contrast media. Biochemical assays are better performed before contrast media injection or delayed for at least 24 h afterwards or longer in patients with renal impairment. Urgent laboratory tests performed on specimens collected shortly after contrast media injection should be carefully assessed. Accuracy of unexpected abnormal results should be questioned and discussed with colleagues from the hospital laboratories.

Conclusion

Contrast media have the potential for interaction with other drugs and may interfere with biochemical assays. Awareness of these interactions is important to avoid misinterpretation of biochemical data and causing harm to the patient following imaging and interventional procedures. Proper documentation of intravascular use of contrast media should be included in the patient's records.

Bibliography

1. Morcos SK, Thomsen HS, Exley CM et al (2005) Contrast media: interactions with other drugs and clinical tests. Eur Radiol 15:1463–1468

Contrast Media, Iodinated, Oily

Finn Rasmussen
Aarhus University Hospital, Denmark
frasm@as.aaa.dk

Synonyms

Ethiodol; Lipiodol

Definition

Sicard and Forrestier in 1923 first reported the use of iodized poppy seed oil as contrast medium. They injected Lipiodol into an antecubital vein to observe blood flow through the heart and pulmonary arteries.

Oily contrast media include Lipiodol, a stable compound of 40% iodine in poppy seed oil. Lipiodol ultra fluid and *Ethiodol*, ethyl esters of iodinated fatty acids of poppy seed and containing 48 and 37% iodine, respectively, later replaced Lipiodol.

The oily contrast material is phagocytized by polymorphonuclear cells and metabolized to sodium iodide by esterase. After elimination of the oily substance, the foreign-body reaction subsides. Excretion of sodium iodine occurs mainly *via* the kidneys, but the pancreas, liver, and salivary glands take part in its elimination.

Sensitivity reactions occur with an incidence of approximately 0.1%.

After its introduction, iodized oil has been used as a contrast medium in lymphography, bronchoscopy, hysterosalpingography, myelography, and sialography.

Indications

Sialography

Catheterization of the parotid and submaxillary duct using a catheter can be performed after preliminary dilatation of the duct orifice. Injection of 1–2 cc oily contrast media is usually sufficient to outline the main duct and all its branches. Over-distension is avoided by completing the injection when the patient notes a feeling of fullness. Oily contrast media have been replaced by nonionic, low-osmolar, water-soluble contrast media.

Myelography

In 1944, iodophenylundecylic acid (Myodil, Pantopaque) was introduced for myelography. A major drawback of the oily contrast media is the lack of resorption. Complete removal through aspiration is usually not possible after a procedure and the remaining droplets may lead to chronic irritation and arachnoiditis. Low-osmolar, nonionic, water-soluble contrast media for myelography have replaced oily contrast material.

Hysterosalpingography

The injected contrast medium outlines the uterine cavity and fallopian tubes, and spill of contrast medium to the peritoneum can be ascertained. The contrast material is injected through a cannula, a balloon catheter, or a suction device. The contrast medium is injected under image intensifier control. The contrast medium can accidentally be injected through the endometrium and taken up by the interstitial lymph or veins, which outline the uterine wall (Fig. 1).

Oily contrast materials have been used for hysterosalpingography for decades and a low complication rate has been found. In fact, a therapeutic effect of the hysterosalpingography with the use of oily contrast has been observed and pregnancy rates of up to 30% have been reported in infertile couples after the use of oily contrast media. There is still debate on the most superior contrast medium for hysterosalpingography (1, 2).

Lymphangiography

Lymphangiography is performed to visualize lymph vessels in the upper and lower extremities, the thoracic duct, and regional lymph nodes.

The main indication for lymphangiography using oily contrast material is the detection of lymph nodes

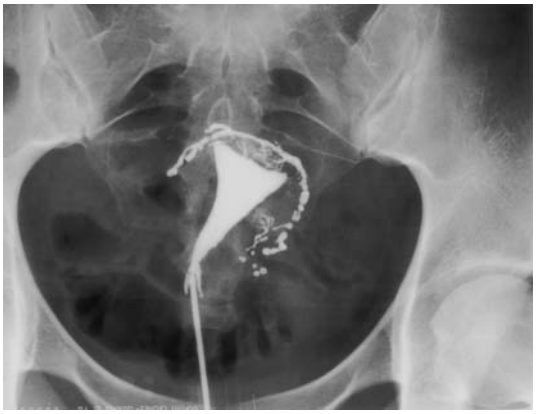

Contrast Media, Iodinated, Oily. Figure 1 Hysterosalpingography demonstrates bilateral tubal occlusion and intravasation.

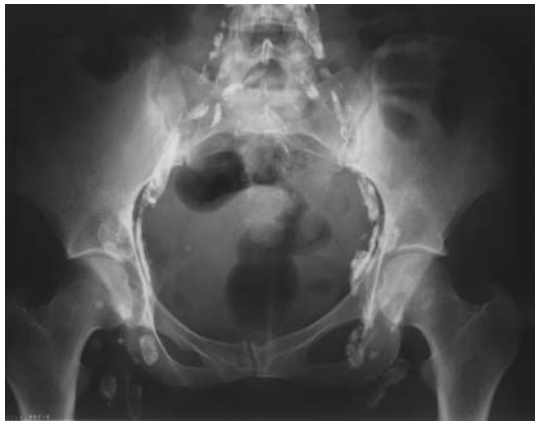

Contrast Media, Iodinated, Oily. Figure 2 Lymphangiography in the nodal phase.

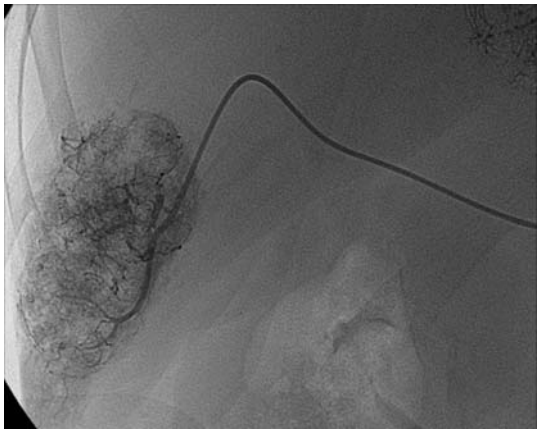

Contrast Media, Iodinated, Oily. Figure 3 The uptake of Lipiodol in a hepatocellular carcinoma after selective catherization and embolization.

metastases in cases of malignant disease, e.g., malignant lymphoma and malignant testicular tumors.

Lymphangiography is performed by demonstrating a lymphatic vessel, dissecting it, and then cannulating it. When the vessel is cannulated, the oily contrast medium is injected slowly with a maximum of 7 mL/h. No more than 10 mL of oily contrast medium should be injected. Images may be obtained in the vascular phase and in the nodular phase (Fig. 2). Contrast medium in excess of that retained in the nodes enters the systemic veins *via* the thoracic duct or lymphatic venous communications. From the veins, it passes into the lung capillaries. The contrast material remains in the lymph nodes for 6 months to 2 years in pathological cases.

Apart from local complications related to the placement of the needle in the lymphatic vessel, the most common complication is embolization to the lung.

Because of the invasiveness of the procedure, the complication rate, and the rather poor imaging impact compared with ultrasound (US), computed tomography (CT), magnetic resonance imaging (MRI), and positron emission tomography (PET)/CT, lymphangiography is no longer performed on a large scale.

Liver Imaging

Oily contrast medium injected into the hepatic artery is taken up by tumors. Normal hepatic parenchyma also takes up the contrast material, but this is cleared from normal liver within a week, whereas it is retained in tumors. Two theories for this phenomenon exist: (1) contrast material is taken up by tumors due to some abnormality of tumor vasculature, making the leakage of contrast into the tumor possible, (2) contrast material is cleaned by the Kupffer cells in normal liver parenchyma, but because such cells do not exist in tumor tissue, contrast material is retained. Usually, 10 mL contrast emulsion is injected into the hepatic artery and a CT scan is performed 7–10 days later. False-negative interpretations of Lipiodol CT may occur in cases of avascular, necrotic, or fibrotic tumors that have not taken up the agent. Focal nodular hyperplasia, hemangioma, cirrhosis, and metastatic lesions may cause false-positive interpretations. However, the pattern of Lipiodol uptake within the lesion is most often characteristic for hepatocellular carcinoma (HCC).

Multirow detector CT and functional MRI with the use of liver-specific contrast agents will probably replace this invasive way of imaging the liver, without the pulmonary side effects seen after injection of oily contrast material.

Liver Chemoembolization

A number of embolic agents have been used to treat liver tumors; one of them is oily contrast material (Fig. 3). With the angiogenesis and parasitization of flow that accompanies hepatic malignancies, no agent is truly permanent. Lipiodol alone has no antitumor effect and must be combined with a cytostatic substance or radioisotope to achieve therapeutic results.

It has been observed that oily contrast material is shunted from arterioles to portal venules before entering the tumor bed. Additional occlusion devices such as coils, Gelfoam, or microspheres can be used. A synergistic effect between embolization and chemotherapy exists. Hypoxia will cause an increased effect of the chemotherapeutic drug. A higher extraction of the drug occurs when passage through the liver is reduced.

Chemoembolization should not be performed if most of the liver is involved by tumor, in the presence of

insufficiency of the liver, significant portal hypertension, occlusion of the portal vein, hepatorenal syndrome, or in significant reduced pulmonary insufficiency.

Randomized studies have shown increased survival in patients with HCC (3). In hormone-producing liver tumors, a reduction in hormone activity has been found after chemoembolization. With regard to colorectal liver metastases, the results are more controversial.

Adverse Reactions

Oily-iodinated contrast materials induce a foreign-body reaction and this can be seen in the form of arachnoiditis in myelography, localized peritoneal fibrosis in hysterosalpingography, localized fibrosis in salivary glands in sialography, and fibrosis and scar reactions in the marginal sinuses and fibrous encapsulation of oil droplets in lymph nodes in lymphangiography. This will also happen in a lymph node that has accidentally been exposed to oily contrast medium in other examinations.

The most important side effect is pulmonary oil embolism. When the iodized oil enters the pulmonary capillaries, lung embolism will appear. Miliary or reticular deposits of oily substance in the lungs are then visible even on a conventional chest image within 24 h after injection. Most of the patients have neither clinical symptoms nor respiratory impairment, but lung scintigraphy reveals that lung embolization has occurred. Twenty-four hours after the oily contrast is injected, it is not found exclusively in the capillary bed of the lung but is scattered in the interstitial tissue of the lung.

The macrophages in the alveolar spaces phagocytize parts of the agent, which is later removed by the sputum. With an increase in the administered dose, the lung becomes a less efficient filter for the oily particles, and the amount reaching other organs such as the liver, spleen, kidneys, and bone marrow is greater. Reactive granulation tissue within the alveolar walls and areas of focal atelectases due to small infarctions are frequently encountered.

Cerebral oil embolism, iodine sialitis and thyroiditis, and hypersensitivity reactions have been reported.

Bibliography

1. Rasmussen F, Lindequist S, Larsen C et al (1991) Therapeutic effect of hysterosalpingography: oil-versus water—soluble contrast media—a randomized study. Radiology 179:75–78
2. Lindequist S, Justesen P, Larsen C et al (1991) Diagnostic quality and complications of hysterosalpingography: oil-versus water—soluble contrast media—a randomized prospective study. Radiology 179:69–74
3. Takayasu K, Arii S, Ikay I et al (2006) Prospective cohort study of transaretrial chemoembolization for unresectable hepatocellular carcinoma in 8510 patients. Gastroenterology 131:461–469

Contrast Media, Iodinated, Water Soluble

Richard H. Cohan, James H. Ellis
University of Michigan, Michigan, USA
rcohan@umich.edu

C

Synonyms

Chemical composition of contrast media; Classification of contrast media; Iodinated contrast media; Pharmacokinetics of contrast media

Definition

Iodinated radiographic contrast media are well tolerated, with large doses routinely administered without significant adverse effects in the vast majority of patients. They are used at higher doses than any other intravascular drug (1). For example, the amount of contrast material administered to a patient for a CT scan and the iodine that the contrast material contains are routinely as high as 90 and 45 g, respectively.

Characteristics

Chemical Composition and Classification

Ionic Monomers: All currently utilized iodinated contrast material is derived from a benzene ring to which have been added three iodine atoms, at the 2-, 4-, and 6-positions.

The earliest of these contrast agents were acids; containing a carboxyl group at the 1-position (required to make the molecule water soluble). These contrast molecules dissociated into two ions in solution: an anion consisting of the carboxylated tri-iodinated benzene ring, and the cation usually consisting of sodium or methylglucamine (or meglumine) or a combination of both (2). Various side chains have been attached to the 3- and 5-positions of these benzene molecules (to further facilitate their water solubility and to minimize toxicity), with variations in these side chains found in the different manufactured agents.

These contrast agents are now termed high-osmolality agents, because at standard concentrations used for CT and angiography, their osmolality is many times that of blood. They are also called ionic monomers, ionic because of the previously discussed dissociation in solution into

Contrast Media, Iodinated, Water Soluble. Table 1 Properties of iodinated contrast media

Type	Ratio (I to particles)	Range in osmolality* (mOsm/kg)	Viscosity* at 37°C (cps)
Ionic monomers	3:2	1,400–1,515	2.3–4.3
Nonionic monomers	3:1	585–672	4.7–6.3
Ionic dimer	6:2	600	7.5
Nonionic dimers	6:1	290	11.8

*Values are given for commercially available iodine concentrations at or closest to 300 mg/mL. These are the concentrations most commonly utilized for excretory urography and CT (but not for angiography)

ions, and monomers because each contrast molecule includes only *one* tri-iodinated benzene ring (3).

One way to compare the properties of various contrast media is to consider the relationship of their X-ray attenuation characteristics to their osmolality. This is done by calculating the ratio of the number of iodine atoms in a contrast molecule to the number of particles that molecule forms in solution. For high-osmolality contrast agents, this ratio is 3:2. For every three iodine atoms in solution, two different particles must be present, the benzene ring analog anion and the cation with which it is conjugated (Table 1).

Nonionic Monomers: Nonionic contrast agents were created using an alternate way to make tri-iodinated benzene ring molecules water soluble: removing the ionizing carboxyl group at the 1-position and replacing it and the side chains at 3-, and 5-positions with much larger components each of which contained several hydrophilic hydroxyl groups. The resulting nonionic monomers are all similar to one another, with mild differences in side-chain composition again accounting for the different brands that are available. Although side-chain modifications can be expected to produce subtle differences in the properties of various nonionic monomers, no significant differences in tolerability or safety among these agents have been identified (1, 3).

Each nonionic monomeric molecule does not dissociate in solution. Hence, one, rather than two, particles are present for each molecule in solution. Thus, the ratio of iodine atoms to particles is 3:1, rather than 3:2. For this reason, the osmolality is halved for a given iodine concentration (Table 1). In fact, the reduction in osmolality is reduced by even more than a factor of two because of the tendency of some of the contrast molecules to associate with one another in solution. Since nonionic monomers have dramatically reduced osmolality compared to ionic monomers, they are referred to as low-osmolality contrast agents. They produce considerably fewer adverse reactions than do ionic monomers.

Ionic Dimers: Another way to reduce the osmolality of contrast media is to replace one of the side chains in an ionic monomer with a side chain containing a second tri-iodinated benzene ring; the result is an ionic dimer. Only one such contrast agent is currently available: ioxaglate. Each ioxaglate molecule contains a cation, and an anion consisting of two tri-iodinated benzene rings, connected to one another by side chains at the 3-position of one molecule and the 5-position of the other. One of these benzene rings still contains an ionizing carboxyl group at the 1-position; however, the other does not (instead containing a nonionizing organic side chain). Ionic dimers contain 6 iodine atoms for every 2 particles in solution. Therefore, they have approximately half the osmolality (at a similar iodine concentration) as do ionic monomers (3) and they are also classified as low-osmolality contrast agents.

The penalty for reducing contrast medium osmolality in this way is that the contrast molecule is still ionic. If ionicity is responsible for some adverse events after contrast media injection, the number of reactions might not be decreased as much when an ionic dimer is injected, compared to a nonionic monomer. Indeed, some adverse reactions, particularly nausea and vomiting, have been observed more frequently after administration of ioxaglate than after administration of nonionic monomers.

Additionally, larger molecules containing more atoms tend to be more viscous. Increased viscosity makes contrast material harder to inject (particularly through long and/or thin catheters), especially when the vessels are small (2).

Nonionic dimers: More recently, nonionic dimers have been produced, in which the lone carboxyl group of an ionic dimer has been replaced with a nonionizing hydrophilic side chain, while the other side chains have also been made increasingly hydrophilic. One nonionic dimer molecule contains 6 iodine atoms for every 1 particle in solution. As a result, at a given iodine concentration, nonionic dimers have the lowest osmolality of all iodinated contrast agents. At traditional concentrations of 250–300 mg I/mL, nonionic dimers have an osmolality nearly equal to that of human blood (290 mOsm/kg). Nonionic dimers are, therefore, termed iso-osmolality contrast agents (Fig.1) (Table 1).

Again, the unwanted result of creating such a large contrast molecule (with two benzene rings and many long side chains) is increased viscosity, a feature which may be responsible for the observation that delayed adverse reactions (reactions beginning at least 1 h after injection), particularly delayed dermatologic reactions, have been reported more frequently in some series when these agents are injected (3).

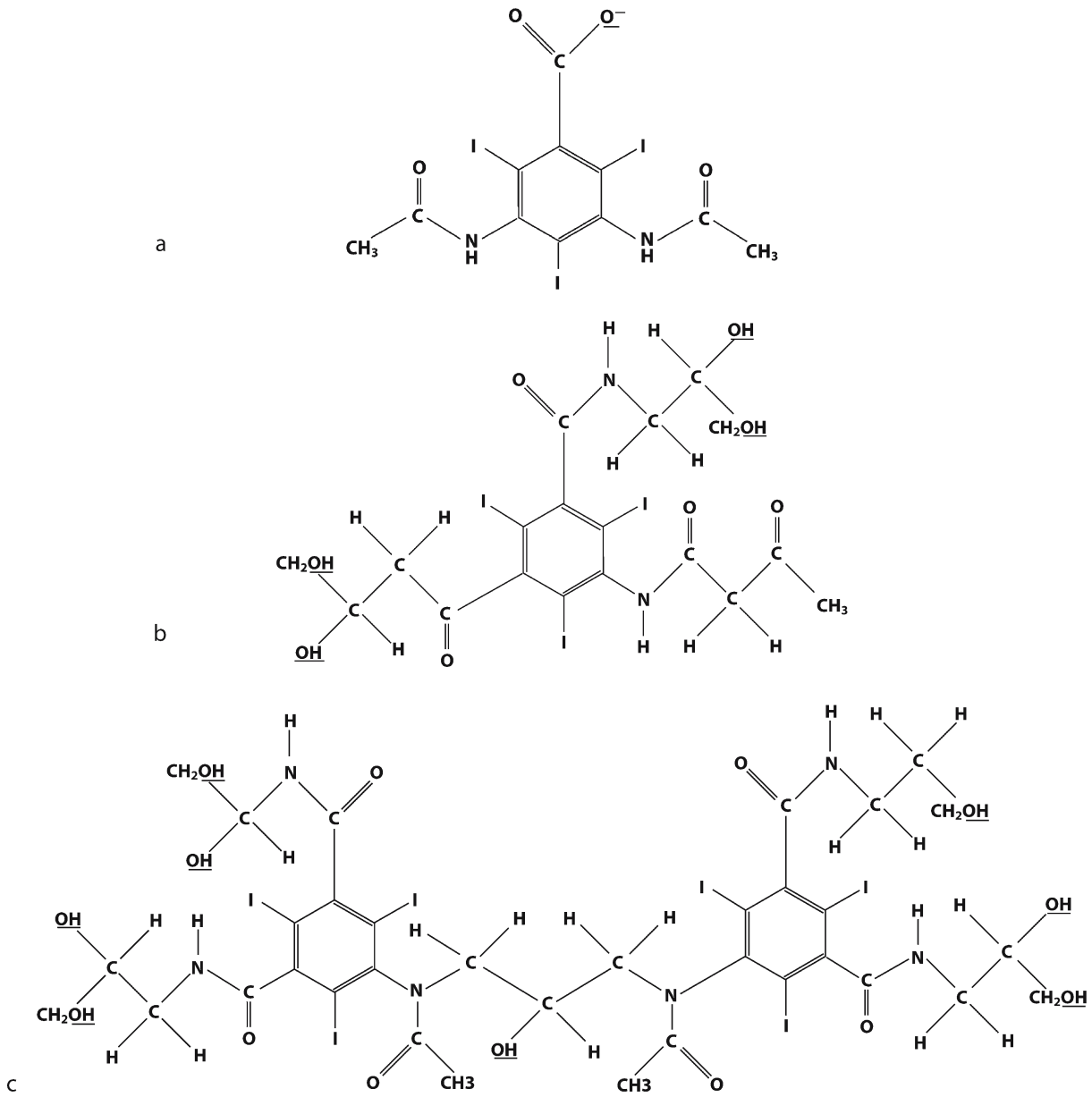

Contrast Media, Iodinated, Water Soluble. Figure 1 **Chemical formulae of several contrast media: (a) Ionic monomer: diatrizoate, (b) Nonionic monomer: iopromide—note that there are many hydroxyl groups (*underlined)* in the side chains, to make this nonionizing molecule water soluble, (c) Nonionic dimer: iodixanol—note again that a large number of hydroxyl groups (*underlined*) have been added to make the molecule water soluble.**

Other Contents in Administered Contrast Material

Free iodide: Although water-soluble iodinated contrast media contain only tiny amounts of free iodide, the amount of administered free iodide still greatly exceeds the recommended daily dose (of 0.15 mg) (4). The maximal amount of free iodide in a bottle of contrast material produced at a concentration of 300 mg I/mL is only 0.05 mg/mL immediately after manufacture (although it rises as shelf-life lengthens) (4). Thus, a 150 mL dose of this agent (as is often administered for CT) would expose a patient to up to 7.5 mg of free iodide. Some additional iodide may also accumulate due to deiodination of contrast material molecules *in vivo* (4).

Additives and Contaminants: Chemical additives are present in all bottles of contrast media. The pH of contrast agents is often adjusted by adding hydrochloric acid or sodium hydroxide. Other additives include tromethamine

(a buffer) and edetate calcium disodium (a "stabilizer"). In addition, calcium chloride dihydrate and sodium chloride are added to iodixanol to provide a sodium/calcium ratio equal to that of blood.

Contaminants may leach into contrast material stored in either vials or prefilled syringes, from chemicals originally located within rubber stoppers or silicone coating (the latter used in prefilled syringes).

Pharmacodynamics

At similar iodine concentrations, all iodinated contrast media produce the same degree of arterial opacification on imaging studies. Venous opacification is slightly diminished, although not to a clinically significant extent, when higher osmolality agents are used, due to a dilutional effect, because high-osmolality agents draw more water into the vascular system.

Postinjection: Following injection of intravenous contrast material, there is gradual equilibrium between extracellular/interstitial and intravascular spaces (3, 5). Contrast molecules are very small, exhibit no significant protein binding, and easily pass outside of the vascular spaces, although they do not enter cells to any significant extent (1).

Vascular enhancement increases with the concentration of injected contrast material and the rate and duration of administration (6). Physiologic parameters that affect the degree of vascular enhancement are cardiac output (directly related) and central blood volume (inversely related). The dynamics of parenchymal organ enhancement are different. The liver, in particular, enhances in a different fashion due to its dual blood supply. Liver enhancement is delayed and its intensity related primarily to the total dose of contrast material injected (6).

Excretion: More than 90% of iodinated contrast media is cleared by renal glomerular filtration and excreted by the kidneys (2, 3, 5). The remainder is eliminated by the liver, bowel, and salivary glands. The normal half-life of contrast material varies between 30 min and 1–2 h in healthy patients (with excretion prolonged in the elderly) (3).

Physiologic Effects of Contrast Media

Aside from their effects on X-ray opacification, iodinated contrast media have a number of normal physiological side effects when injected into patients. Many of these are likely due to hyperosmolality. Thus, many effects are most pronounced when high-osmolality contrast media are used, less so when low-osmolality agents are injected, and absent when iso-osmolality agents are employed.

Cardiac effects: Coronary artery injection with ionic monomers transiently decreases left ventricular contractility (3). In comparison, nonionic monomers produce increased left ventricular contractility and left ventricular systolic shortening (3). Intravenous contrast material injections can lower the threshold for cardiac dysrhythmias, including ventricular fibrillation (3).

Renal effects: Iodinated contrast media produce a brief transient increase (about 1 min long) followed by a longer decrease in renal blood flow (3). The latter is associated with decreased glomerular filtration (3). Potential nephrotoxic effects of high- and low-osmolality agents due to these and/or other factors are usually of little consequence in patients without preexisting renal disease. While small clinical studies found that nonionic dimers produce less nephrotoxicity in patients with underlying renal disease, an *in vitro* study recently demonstrated that they are equally toxic to renal tubule cells at comparable iodine concentrations (7).

Pulmonary effects: Iodinated contrast media produces at least subclinical bronchospasm in all patients (3). Pulmonary vascular resistance may also increase, particularly after injection of high-osmolality agents (3).

Neurologic effects: The most commonly encountered neurologic effects are nausea and vomiting (more often seen with ionic monomers and ionic dimers). In some patients, particularly those in whom the blood brain barrier is disrupted, seizures may be induced (3, 5).

Peripheral vascular effects: Any contrast material with osmolality exceeding that of blood increases circulating blood volume, as it draws in water from the extravascular tissue (3). Vasodilatation also occurs after contrast media injection, resulting in decreased peripheral vascular resistance. These changes may be sensed by the patient as warmth or flushing (5). Blood pressure may transiently decrease, with compensatory increases in cardiac output.

Effects on the thyroid gland: Administered free iodide accumulates in the thyroid gland and can interfere with uptake of any other administered iodide. For this reason, it is often recommended that radioisotope imaging of the thyroid or radioactive iodine treatment for thyroid cancer not be performed within two months of iodinated contrast material injection (4). Clinically apparent adverse affects of contrast media on thyroid function are rare in euthyroid patients, although they are occasionally encountered, most often in the elderly (likely because some older patients have incidental undiagnosed thyroid disease) (4). Exacerbation of hyperthyroidism may be encountered in patients with preexisting thyroid dysfunction (Grave's disease, multinodular goiter, or thyroid autonomy) (4).

Thrombogenic effects: All iodinated contrast media have an inhibitory effect on thrombogenesis. These effects are more pronounced with high-osmolality agents (3, 5).

Local effects: Iodinated contrast media rarely produce local arm pain and erythema even when properly injected into an artery or vein. Local irritation of vascular

endothelium may be responsible (due to chemotoxicity and hyperosmolality). In rare instances, venous thrombosis can occur (3).

Bibliography

1. Christianson C (2005) X-ray contrast media-an overview. Toxicology 209:185–187
2. Morris TW, Fischer HW (1986) The pharmacology of intravascular radiocontrast media. Ann Rev Pharmacol Toxicol 26:143–160
3. Stacul F (2001) Current iodinated contrast media. Eur Radiol 11:690–697
4. Van der Molen A, Thomsen HS, and Morcos SK (2004) Effect of iodinated contrast media on thyroid function in adults. Eur Radiol 14:902–907
5. King BF (1999) Intravascular contrast media and premedication. In: Bush WH, Krecke KN, and King BF (eds) Radiology Life Support. Oxford University Press, New York, pp 10–12
6. Fleischmann D (2003) Use of high-concentration contrast media in multiple-detector-row CT: principles and rationale. Eur Radiol 13: M14–M20
7. Heinrich MC, Kuhlmann KL, Grgic A, et al (2005) Cytotoxic effects of ionic high-osmolar, nonionic monomeric, and nonionic isoosmolar dimeric iodinated contrast media on renal tubular cells *in vitro*. Radiology 235:843–849

Contrast Media, MRI, Blood Pool Agents

Jens Bremerich
Department of Radiology, University Hospital Basel, Basel, Switzerland
jens.bremerich@unibas.ch

Synonyms

Intravascular contrast media

Definition

Biodistribution: Blood pool agents (BPA) are defined by their biodistribution. After intravenous administration, such contrast media extravasate less than standard extravascular agents do. Therefore, BPA are also referred to as intravascular contrast media.

Characteristics and Classification: BPA are retained within the intravascular fluid compartment because of their larger molecular weight, their particle size, or their binding to large intravascular molecules impeding their extravasation, such as albumin. BPA may also be classified with respect to their magnetic properties. Gadolinium (Gd)-based BPA have a predominant T1 effect. Ultrasmall particles of iron oxide (USPIO), on the other hand, are very small coated iron particles with a diameter of ~20 nm. USPIO have a strong T1 effect and a considerable T2 effect. BPA are also classified according to their terminal half-life. While low-molecular agents are eliminated even faster than the extravascular agents (rapid-clearance BPA), high-molecular agents may circulate for several days in the vascular space (slow-clearance BPA).

Gadolinium-Based BPA: The prototype of a large molecular weight BPA is albumin loaded with Gd-DTPA, resulting in a large molecule of 92 kDa with strong T1/T2 relaxivities of 13.7/18.4 $mM^{-1}sec^{-1}$ and an intravascular half-life of 90 min. This compound, however, has unfavorable allergenic properties and clearance pathways and thus cannot be used in humans. Medium molecular weight BPA such as gadomelitol (6.4 kDa; r1/r2 = 27.1/56 L mM^{-1} sec^{-1}; Vistarem) and SHL643A (35 kDa; 13 L $mmol^{-1}$ sec^{-1} gadomer-17) are currently under investigation for use in humans. Reduction of molecular weight not only improves the allergenic properties but also allows renal elimination.

Small molecular weight BPA such as Gadovosfeset trisodium (Vasovist®) reside predominantly in the blood pool because they bind reversibly to various proteins such as albumin and other components of blood plasma. Such binding modifies biodistribution and slows down rotation of the molecule, thus enhancing T1 and T2 relaxivity. Gadobenate dimeglumine (Multihance® Gd-BOPTA) shows some weak protein binding with an *in vivo* blood relaxivity approaching twice the aqueous solution. In 2007 Gadovosfeset trisodium (Vasovist®) gadobenate dimeglumine (Multihance® Gd-BOPTA) is the only intravascular media with intravascular properties approved for use in patients.

Iron oxide BPA: Iron-based BPA are coated USPIO with a strong T1 and T2 shortening effect. Such compounds have a prolonged residence in the intravascular space because of their large particle size of approximately 20 nm and reduced reticuloendothelial system (RES) uptake compared with the larger superparamagnetic particles (SPIO) used for liver imaging (ferumoxides in Endorem®/Feridex® or ferucarbotran in Resovist®). Examples for USPIO are NC100150 injection (Clariscan®), ferumoxtran-10 (Combidex®, Sinerem®), ferumoxytol (Advanced Magnetics), SHU-555C (Supravist®), and very small superparamagnetic iron oxide particles (VSOP). SPIO with a predominant T2 shortening effect have also been referred to as BPA, but they have very short vascular half-lives of less than 10 min due to endocytosis in the liver, spleen, and other RES tissues.

On T1-weighted pulse sequences, USPIO-enhanced angiography vessels appear bright. Sequences with short echo times are required to minimize sensitivity to susceptibility effects.

Indication

General Aspects

Motivation for development of BPA includes the following:

1. BPA with high molecular weight or binding to large molecules provides strong T1 relaxivity because large molecules have a low tumbling rate, resulting in more efficient interaction with water protons.
2. The prolonged intravascular phase of BPA allows for longer acquisition times, which may be useful for angiography with high resolution or in various positions (Fig. 1), double (cardiac and respiratory)-gated coronary angiography, and perfusion imaging at rest and during pharmacologic stimulation.
3. BPA may allow for perfusion quantification because of their well-defined distribution in organ tissue.
4. BPA are used to probe microvascular integrity after myocardial ischemia and infarction; to assess permeability of vessels in tumors, allowing for an estimation of their dignity; and to detect occult bleeding in the gastrointestinal tract.

Angiography

BPA with prolonged vascular enhancement are of particular interest for coronary artery imaging. Debiao et al (1) used SH L 643 A-enhanced magnetic resonance (MR) for free-breathing coronary angiography. The acquisition time of this sequence with prospective cardiac and retrospective respiratory gating was 6–8 min, thus requiring strong and prolonged vascular enhancement. Outside the heart, however, angiography during the equilibrium phase of such BPA is limited by confounding enhancement of both arteries and veins. Wyttenbach et al (2) compared peripheral angiography during the first pass of standard extracellular contrast material versus GdBOPTA. These authors found a comparable diagnostic performance of both compounds in the aortoiliac region. In the distal run-off vessels, however, GdBOPTA yielded higher specificity and a significantly smaller number of nonassessable segments than extracellular contrast media did (2).

Perfusion

BPA enhance normal myocardium to a lesser degree than extracellular agents because the fractional distribution volume of BPA (~5%) is substantially smaller than that of extracellular compounds (~20%). Thus, BPA enhance normal myocardium to a lesser extent than extracellular agents. This might indicate reduced utility of BPA for evaluating myocardial perfusion. An advantage of BPA might be the longer temporal window, which might be used for perfusion imaging during the equilibrium phase. Another advantage might be the improved quantification of perfusion as the first-pass curves return almost to baseline, whereas extravascular agents present an overlap of perfusion and extravasation. Thus, intravascular contrast agents should allow improved qualitative perfusion studies outside the brain. Another potential advantage may be the prolonged acquisition window for imaging at various physiologic conditions. However, the sensitivity of BPA for infarction and the potential for the assessment of myocardial viability is unknown. Bjerner et al (3) assessed myocardial perfusion with first-pass USPIO-enhanced T2-weighted imaging and found a significant signal loss in normally perfused myocardium. Reimer et al (4) used T1-weighted USPIO-enhanced MR for qualitative perfusion imaging. These authors found susceptibility-induced signal loss in the right ventricle,

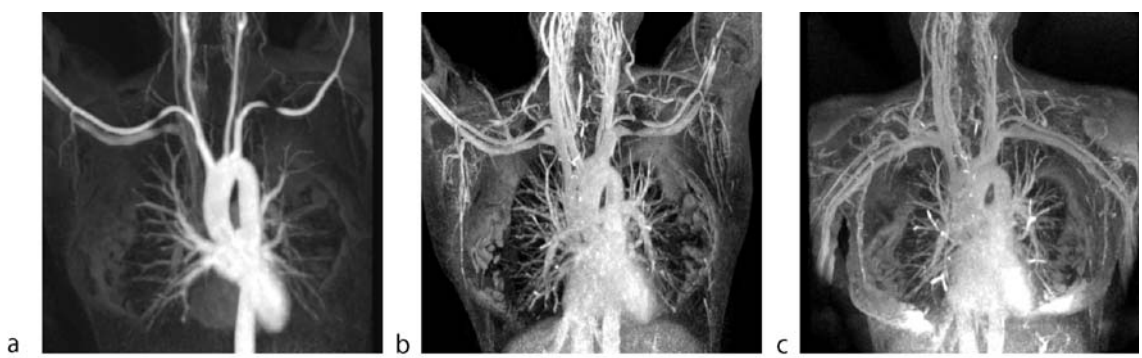

Contrast Media, MRI, Blood Pool Agents. Figure 1 A 42-year-old female with thoracic outlet syndrome. 3D MR Angiograms enhanced with single injection of (Gadovosfeset trisodium, Vasovist©, 0.03 mmol/kg @ 0.8 mL/sec) are shown. Angiograms were acquired with (a) arms-up in arterial phase, (b) arms-up in equilibrium phase, and (c) arms-down in equilibrium phase. With arms-up significant stenoses are present in left subclavian artery (*arrow*) and vein (*arrowhead*), with arm-down stenoses resolve. (Courtesy of Dr. Heyder, Grabs, Switzerland)

which can be explained by a high USPIO concentration, an important limitation of USPIO-based perfusion imaging. Susceptibility effects are most pronounced at high regional concentrations and heterogeneous distribution of USPIO, making quantification difficult.

Tumor Imaging

For grading of breast tumors, Gd-based slow- and rapid-clearance BPA have been used to probe transendothelial permeability of blood vessels, microvascular density, and fractional blood volume using dynamic MR data-fitted to a bidirectional two-compartment model. Transepithelial permeability and microvascular density correlate with tumor grade when using slow-clearance albumin-$(GdDTPA)_{30}$ but not when using rapid-clearance BPA. In a human breast tumor model in mice, a delayed accumulation of gadomelitol after 30 min and 3 h suggests a potential to improve characterization of benign and malignant tumors. On the other hand, USPIO-derived microvascular permeability has been shown to correlate strongly with histopathologic tumor grade in an animal model of breast cancer (5). Thus, BPA may allow tumor grading in the future.

Gastrointestinal Hemorrhage

Attempts to detect and localize intestinal or peritoneal bleedings with BPA have been performed as well, but they lack specificity and do not fulfill all clinical requirements.

Plaque Imaging

After prolonged vascular circulation of USPIO, these are partially taken up by intravascular monocytes or endothelial macrophages, thereby potentially extending pure angiographic imaging to vessel wall imaging and plaque characterization.

Contraindication

The vendors of gadovosfeset trisodium (Vasovist®) and gadobenate dimeglumine (Multihance Gd-BOPTA) mention allergy against Gd chelates as a contraindication. Disturbances of iron metabolism, however, can be expected to be relative contraindications for iron oxide particles.

Pregnancy/Lactation

Gadovosfeset trisodium (Vasovist®) and gadobenate dimeglumine (Multihance Gd-BOPTA) are not recommended in pregnant or lactating women. During lactation, the vendor recommends interrupting lactation for 24 h after contrast administration. In animal experiments, less than 0.5% of the administered dose was transferred to the newborn. This information can be found on the drug information sheet and seems to imply that GdBOPTA may also be administered during lactation. But, the physician is responsible for such administration.

Use and Dosage

Gadobenate dimeglumine (Multihance Gd-BOPTA) can be administered as infusion or bolus injection. The vendor recommends a dose of 0.05 mmol/kg for liver imaging and 0.1 mmol/kg for the central nervous system. Gadovosfeset trisodium (Vasovist®) is approved and has been introduced clinically. Bolus administration or infusion is allowed at a dose of 0.03 mmol/kg. Iron oxide particles such as SHU-555C (Supravist) may be infused or injected as a bolus; a dose of 40 mol Fe/kg seems to be appropriate for first-pass MR angiography and cardiac perfusion.

Adverse Reactions

As with all contrast media, there is a risk of potentially live-threatening adverse reactions. First experiences in controlled studies, however, indicate that the safety profile of such BPA is similar to that for standard extracellular contrast media. In phase III studies with gadovosfeset trisodium (Vasovist®), the incidence of serious or severe adverse events was low.

Interactions

The vendor of gadobenate dimeglumine (Multihance Gd-BOPTA) indicates that no interactions are known for this specific agent. There is a potential risk of drugs competing with gadovosfeset trisodium (Vasovist®) at albumin-binding sites. Caution is required with measurements of iron metabolism with iron oxide particles. Such measurements should not be performed within 15 days after USPIO administration. Moreover, USPIO administration is not recommended in hemosiderosis, when body iron content is already elevated. USPIO has also been reported to interfere with factor XI activity, resulting in changes in thromboplastin time.

Bibliography

1. Debiao L, Zheng J, Weinmann HJ (2001) Contrast-enhanced MR imaging of coronary arteries: comparison of intra- and extravascular contrast agents in swine. Radiology 219:670–678

2. Wyttenbach R, Gianella S, Alerci M et al (2003) Prospective blinded evaluation of Gd-DOTA versus Gd-BOPTA enhanced peripheral MR angiography, as compared with digital subtraction angiography. Radiology 227:261–269
3. Bjerner T, Johansson L, Ercsson A et al (2001) First-pass myocardial perfusion MR imaging with outer-volume suppression and the intravascular contrast agent NC100150 injection: preliminary results in eight patients. Radiology 221:822–826
4. Reimer P, Bremer C, Allkemper T et al (2004) Myocardial perfusion and MR angiography of chest with SH U 555 C: results of placebo-controlled clinical phase I study. Radiology 231:474–481
5. Turetschek K, Huber S, Floyd E et al (2001) MR imaging characterisation of microvessels in experimental breast tumors by using a particulate contrast agent with histopathologic correlation. Radiology 218:562–569

Contrast Media, MRI, Gadolinium Derivates

Bernd Tombach[1], Rolf Vosshenrich[2]
[1]Department of Clinical Radiology, University of Münster (Germany), Institut für Klinische Radiologie, Universitätsklinikum Münster, Münster, Germany
[2]Radiologen-Gemeinschaftspraxis, MRT im Friederikenstift Hannover, Germany, Radiologen-Gemeinschaftspraxis MRT im Friederikenstift, Hannover, Germany
tombach@uni-muenster.de
vosshenrich@t-online.de

Synonyms

Chemical formulas, trade names, and manufacturers of commercially available open chain and cyclic gadolinium (Gd) complexes as magnetic resonance (MR) contrast agents: Gadopentetate dimeglumine (Gd-DTPA, Magnevist, Schering AG, Germany); Gadodiamide (Gd-DTPA-BMA, Omniscan, GE Amersham Health, UK); Gadobenate (Gd-BOPTA, MultiHance, Altana Pharma, Germany); Gadoteridol (Gd-HP-DO3A, Pro Hance, Altana Pharma, Germany); Gadoterate meglumine (Gd-DOTA, Dotarem, Guerbet, France); Gadobutrol (Gd-DO3A-butrol, Gadovist, Schering AG, Germany)

Definition

Water-soluble paramagnetic compounds for magnetic resonance imaging (MRI) signal enhancement detoxified by chelation resulted in a first patent in 1981 covering the composition of paramagnetic complexes (1). The preclinical investigations of Gries, Rosenberg, and Weinmann from Schering AG (Berlin, Germany) included the preparation of the highly soluble T1-MR contrast agent gadopentetate dimeglumine (Gd-DTPA) providing good relaxation properties and an excellent safety profile in animals. In 1983, the clinical development started with the first intravenous injection in humans (phase I clinical trial) resulting in an approval from the health authorities as the first extracellular MR contrast agent (Magnevist) in 1988 (2).

Generally, the image contrast in MRI reflects a complex interaction of intrinsic tissue properties (T1 and T2 relaxation time, proton density, and flow velocity) and extrinsic factors (field strength, gradients, and pulse sequences). Due to the overlap in relaxation times of normal and abnormal tissues, para- or superparamagnetic MR contrast agents specifically altering tissue relaxation times might be beneficial. The paramagnetic gadolinium derivates containing the "magnetic active" ion of Gd^{3+} with seven unpaired electrons shorten both T1 and T2 relaxation times, but predominantly, the longitudinal relaxation of protons (T1) at diagnostically approved doses resulting in a bright signal on T1-weighted images (3, 4). The power of MR contrast agents depend on their concentration in the respective tissue and the resulting intrinsic relaxation times and is called relaxivity R1 and R2 (defined as 1/T1 and 1/T2). For paramagnetic Gd chelates a typical R2/R1 ratio of 1.3 is found, resulting in a decrease of the relaxation time of biological fluids by 50% at a dose of 0.1 mmol/kg body weight.

To reduce the high toxicity for clinical applications, the magnetically active gadolinium ions have to be bound either to open chain (linear) or to cyclic chelators, resulting in highly hydrophilic and stable Gd-chelate complexes with a low molecular weight (MW) of <1 kDa (Fig. 1). Presently, six different compounds with slight differences in their physicochemical properties are approved for clinical use in different countries (Table 1). The similarities of these agents include a strong chelation of the gadolinium ion, comparable effects on tissue signal intensities, and an excellent safety profile in humans. The main differences of these gadolinium chelates are the electrical charge of the chelates, the chemical structure of the ligands, the prepared concentration, and the potential of temporary plasma protein binding (5).

Ionic gadopentetate dimeglumine, nonionic gadodiamide, and ionic gadobenate are open chain Gd complexes. Gadobenate, originally designated as a liver-specific agent with a hepatobiliary excretion rate of approx. 50% in rabbits, is even classified predominantly as an extracellular agent due to the rather low hepatobiliary excretion rate of 2%–4% in humans. This compound offers a temporary serum protein binding resulting in an increased R1 with potential advantages for contrast-enhanced MR angiography (CE-MRA). Nonionic gadoteridol, ionic gadoterate meglumine, and nonionic gadobutrol are macrocyclic

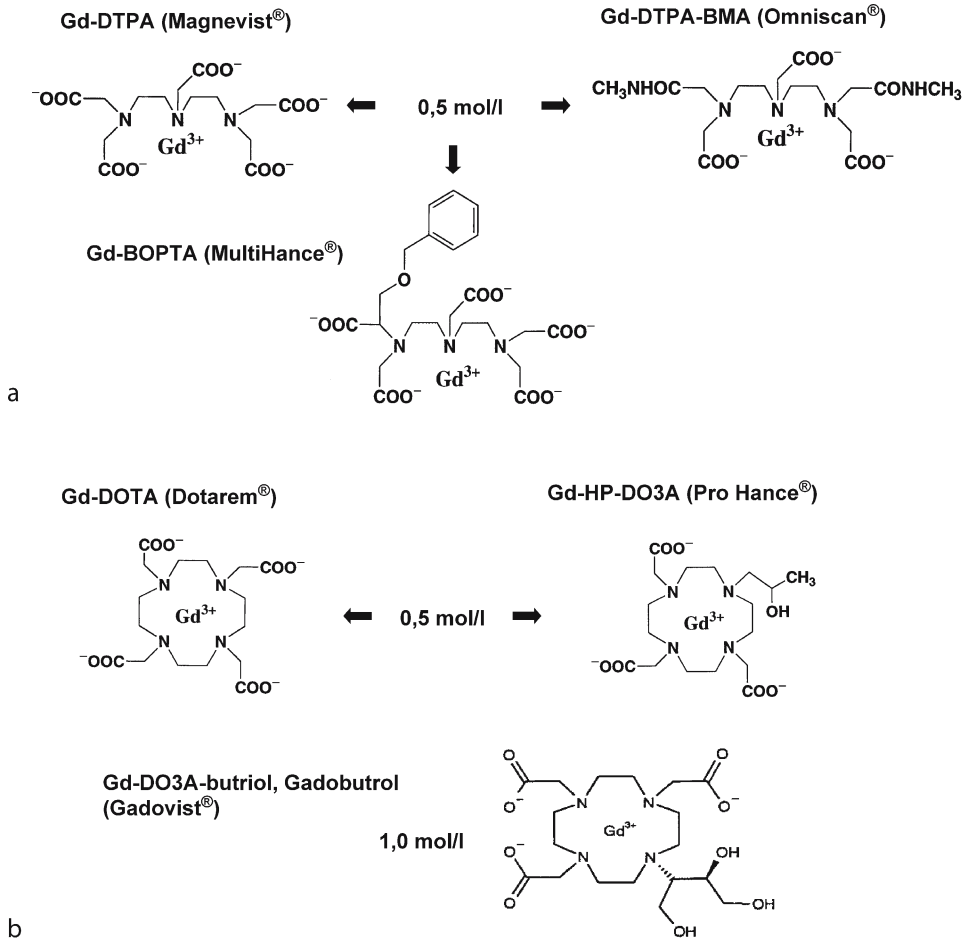

Contrast Media, MRI, Gadolinium Derivates. Figure 1 Chemical structures of gadolinium chelates . Chemical structure of the (a) linear extracellular Gd chelates gadopentetate dimeglumine (Gd-DTPA, Magnevist, Schering AG, Germany) and gadodiamide (Gd-DTPA-BMA, Omniscan, GE-Amersham Health, England), and (b) cyclic extracellular gadoteridol (Gd-HP-DO3A, Pro Hance, Bracco), gadoterate meglumine (Gd-DOTA, Dotarem, Guerbet, France), and gadobutrol (Gadovist, Schering AG, Germany).

complexes with slightly higher complex stabilities of up to 10^{-23} compared with linear chelators with complex stabilities of up to 10^{-18}. Compared to all other commercially available extracellular Gd chelates (0.5 M), gadobutrol is prepared at a 1-M concentration. At the same injection dose, gadobutrol can therefore be applied with half the injection volume and time, which can be advantageous for first-pass imaging like CE-MRA and perfusion studies.

While gadolinium is responsible for the paramagnetic effect of these complexes, the ligand determines the pharmacokinetic behavior. In healthy volunteers, the pharmacokinetic profile of extracellular MR contrast agents is similar to iodinated x-ray contrast agents, indicating a rapid distribution in the extracellular fluid space and a short intravascular phase due to the high hydrophilicity and the low MW. Glomerular filtration is the predominant elimination pathway with a plasma half-life of about 90 min for the unmetabolized Gd chelates. Even in patients with impaired renal function, extracellular Gd chelates can safely be applied without changes of the safety profile. However, the elimination half-life may be prolonged up to more than 20 h in patients with severe renal impairment. In patients requiring hemodialysis treatment, no change in dialysis schedule is required, because low-MW Gd chelates are effectively removable within three dialysis sessions (97–98%) (6, 7).

Indication

The diagnostic power of MRI has been significantly improved since the first intravenously injectable MR

Contrast Media, MRI, Gadolinium Derivates. Table 1 Physicochemical properties of extracellular contrast agents

	Gadobutrol [1 mol/L]	Gadoteridol [0,5 mol/L]	Gadoterate meglumine [0.5 mol/L]	Gadopentetate dimeglumine [0.5 mol/L]	Gadodiamide [0.5 mol/L]	Gadobenate dimeglumine [0.5 mol/L]
Thermodynamic complex stability (log K_{eq})	21.8	23.8	25.8	22.1	16.9	22.6
Osmolality [osmol/kg]	1.60	0.63	1.35	1.96	0.65	1.97
Viscosity [mPa s]	4.96	1.30	2.0	2.9	1.4	5.3
T1 relaxivity [l/mmol s] 0.47 T, plasma	5.6	4.6	4.3	4.9	4.8	9.7

contrast agent came on the market. Worldwide, more than 25% of all MR examinations are performed with contrast agents (8). Typical indications are the detection of tumors and inflammatory processes, whereas degenerative diseases are mostly investigated without contrast agents. Intracranially, contrast-enhanced MRI allows the early detection of a damaged blood–brain barrier. Since high-performance MR scanners are more and more available, newer applications like CE-MRA and organ perfusion studies with extracellular Gd chelates are part of daily clinical routine MR investigations.

Pregnancy/lactation

Since there are only a few safety data available in the literature, the Contrast Media Safety Committee of the ESUR (European Society of Urogenital Radiology) has reviewed the literature and drawn up the following guidelines (9):

Pregnancy: Following the injection of gadolinium agents to the mother, no neonatal tests are necessary.

Lactation: Breast-feeding may be continued normally when gadolinium agents are given to the mother.

Pregnant or lactating women with renal impairment: No additional precautions are necessary for the fetus or neonate. Follow ESUR guidelines for contrast media administration when renal function is impaired.

Use and dosage

The recommended application doses depend on the clinical question and type of MR investigation on the one hand, and the approval status regarding the patient's age and the approved MR indications on the other hand, which are currently extended. However, the approved doses for extracellular contrast agents are in the range of 0.1–0.3 mmol/kg body weight with an accepted standard dose of 0.1 mmol/kg body weight. Compared with low osmolar nonionic x-ray contrast agents, the total osmotic load is much lower and without any effect on safety or tolerability for the extracellular contrast agents used in the approved dose range in MRI.

Adverse Reactions

Controlled clinical trials regarding safety aspects and pre- or postmarketing surveillance studies document an overall incidence of adverse reactions of 1–2% (e.g., nausea, vomiting, local warmth and pain, headache, dizziness), which may be increased by a factor of 2–3 in patients with a history of allergic reactions. However, the incidence of anaphylactic reactions is about six times lower compared to nonionic x-ray contrast agents. Overall, extracellular contrast agents provide by far the safest profile compared to all other contrast agents without any relation to the injected dose up to 0.3 mmol/kg body weight.

Interactions

Gadodiamide and gadoversetamide may cause spurious hypocalcemia, particularly at doses over 0.2 mmol/kg body weight in patients suffering from renal impairment. These contrast agents interfere with calcium measurements using the ortho-cresolphthalein complexone (OOC) method. No false measurements of serum calcium have occurred with gadopentetate dimeglumine or gadoteridol (10). Awareness of this effect is important in order to avoid incorrect and potentially hazardous treatment.

In a study comparing a standard dose gadoteridol and gadodiamide and searching for Gd in human bone tissue by inductively coupled plasma mass spectroscopy gadodiamide left approximately 4 times more Gd behind in bone than did gadotridol (11).Recently, it has been reported that a serious adverse reaction called nephrogenic systemic fibrosis (NSF) may occur after exposure of Gd. Development of NSF was strongly associated with gadodiamide administration in the setting of either acute

hepatorenal syndrome or dialysis-dependent chronic renal insufficiency (12,13). These gadolinium chelates should not be administered in patients with reduced renal function and in general renal function may be considered more closely. Only those gadolinium chelates shall be administered which have been tested and licensed for use in patients with decreased renal function.

References

1. Gries H, Rosenberg D, Weinmann H-J (Schering AG Berlin) (1981). *Paramagnetische Komplexsalze, deren Herstellung und Mittel zur Verwendung bei der NMR Diagnostik.* Patent DE 3129906 (Publication Date of Offenlegungsschrift, February 10, 1983), publication date May 17, 1990; priority date July 24
2. Laniado M, Weinmann HJ, Schorner W et al (1984) Physiol Chem Phys Med NMR 16:157
3. Knopp MV, von Tengg-Kobligk H, Floemer F et al (1999) J Magn Reson Imaging 10:314
4. Bellin MF, Vasile M, Morel-Precetti S (2003) Eur Radiol 13:2688
5. Robert R. Edelman, John R. Hesselink, Michael B. Zlatkin (1996) Clinical Magnetic Resonance Imaging. 2nd edn. W.B. Saunders Company
6. Tombach B, Bremer C, Reimer P et al (2001) Radiology 218:651
7. Tombach B, Bremer C, Reimer P et al (2002) AJR Am J Roentgenol 178:105
8. de Haen C (2001) Top Magn Reson Imag 12, 221
9. Webb JA, Thomson HS, Morcos SK (2005) Eur Radiol 15:1234
10. Morcos SK, Thomson HS, Exley CM (2005) Eur Radiol 15:1463
11. White GW, Gibby WA, Tweedle MF (2006) Invest Radiol 41:272
12. Thomsen HS (2006) Eur Radiol 16:2619
13. Broome DR, Girguis RS, Paron PW et al. (2007) Amer J Roentgenol 188:586

Contrast Media, MRI, Oral Agents

Thomas C. Lauenstein
Department of Radiology, The Emory Clinic
Atlanta, USA
tlauens@emory.edu

Definition

Due to the excellent soft-tissue contrast coupled with the lack of ionizing radiation, magnetic resonance imaging (MRI) of the bowel has emerged as the primary radiological examination tool in many departments. Similar to experiences from computed tomography (CT), the presence of intraluminal contrast facilitates the evaluation of bowel segments.

Contrast agents should fulfill different requirements for oral applications in the clinical routine (1). A homogeneous bowel distension as well as uniform opacification of the lumen should be provided. As for image quality, high contrast between the bowel wall and lumen is necessary, and the presence of intraluminal contrast must not lead to artifact formation. Furthermore, the agents should not be absorbed, or reabsorption must at least be kept to a minimum. Eventually, different aspects should be considered, including high safety (concerning side effects or allergic reactions), sufficient patient acceptance (regarding taste and volume of the agents), and cost-effectiveness.

Similar to all other tissues displayed on MR images, the signal intensity of oral contrast agents mainly depends on the ▶*longitudinal relaxation time* (T1), the ▶*transverse relaxation time* (T2), and the ▶*proton spin density*. Signal intensity can be enhanced as T1 increases, T2 decreases, and/or proton spin density increases. Hence, contrast compounds may modify signal characteristics according to three mechanisms:

1. Agents affecting T1 relaxation times (e.g., paramagnetic chelates).
2. Agents changing T2 relaxation times by disturbing the local magnetic field (e.g., superparamagnetic particles).
3. Agents replacing protons and hydrogen molecules.

Consecutively, substances may be categorized as *positive*, *negative*, or ▶*biphasic agents* (2). A *positive oral contrast compound* produces high signal intensities on both T1-weighted and T2-weighted images, whereas ▶*negative contrast agents* lead to low signal on both T1-weighted and T2-weighted sequences. The term *biphasic* relates to agents with different signal characteristics on different sequence types, such as low signal on T1-weighted images and high signal on T2-weighted images, or vice versa. However, this classification may be confusing because most agents simultaneously influence T1 and T2 relaxation times as well as proton density. Thus, the actual signal intensity may eventually depend on the agents' concentration and the weighting of the image sequence employed (3).

The following substances are clinically used as oral MRI contrast agents:

1. Gadolinium
   Gadolinium-containing agents reduce the T1 relaxation times of all surrounding water molecules. In clinically used concentrations (1 mmol/L), signal intensity of the bowel lumen is rendered bright both on T1- and T2-weighted images due to an only moderate T2-shortening effect. Thus, gadolinium chelates can be considered ▶positive contrast agents. However, in higher concentrations an early T2-shortening effect will be predominant, leading to a signal loss on T2-weighted images. One commercially available oral gadolinium compound is gadopenatetate dimeglumine (Magnevist Enteral,

Schering, Berlin). This agent contains gadolinium at a dosage of 1 mmol/L plus mannitol (15 g/L). Mannitol increases the osmolarity of the formula and thus reduces reabsorption in the gastrointestinal tract.

2. Barium

Barium compounds provide low signal intensities on T1-weighted images. However, signal characteristics on T2-weighted images strongly depend on the concentration of barium. Used in high concentrations (e.g., 1g $BaSO_4$/mL), these formulas lead to low signal of the bowel lumen on T2-weighted images. However, in lower concentrations barium compounds may act like water, providing a higher signal on T2-weighted images. Barium is cheap and commercially available worldwide. A minor drawback might be the relatively long bowel transit times.

3. Superparamagnetic particles

Superparamagnetic iron-based particles may be considered as typical negative contrast agents. They induce local field inhomogeneities, which results in shortening both T1 and T2 relaxation times. However, T2-weighted effects are predominant. Thus, superparamagnetic particles lead to decreasing signal intensity on T2-weighted sequences and on most T1-weighted sequences. This can be considered helpful, especially for labeling bowel fluid and for diminishing the signal of the bowel lumen for MR cholangiopancreatography (MRCP) studies. One commercially available agent (Abdoscan, GE Healthcare) consists of ferrite crystals bound to monodisperse polymer particles. The mean particle diameter is 3.5 m, and the iron contents amount to 20%. This compound is well tolerated when administered orally. Another commercially available formula is Lumirem (Guerbet, Anulay sur Bois, France). It contains iron oxide crystals (Fe_2O_3 and Fe_3O_4) that are coated with silicone, which prevents absorption of the iron. The mean iron content is 175 mg/L, and the average particle diameter is 300 nm (Fig. 1).

4. Manganese-containing agents

Manganese-containing substances are usually biphasic contrast agents. Due to a paramagnetic effect, signal

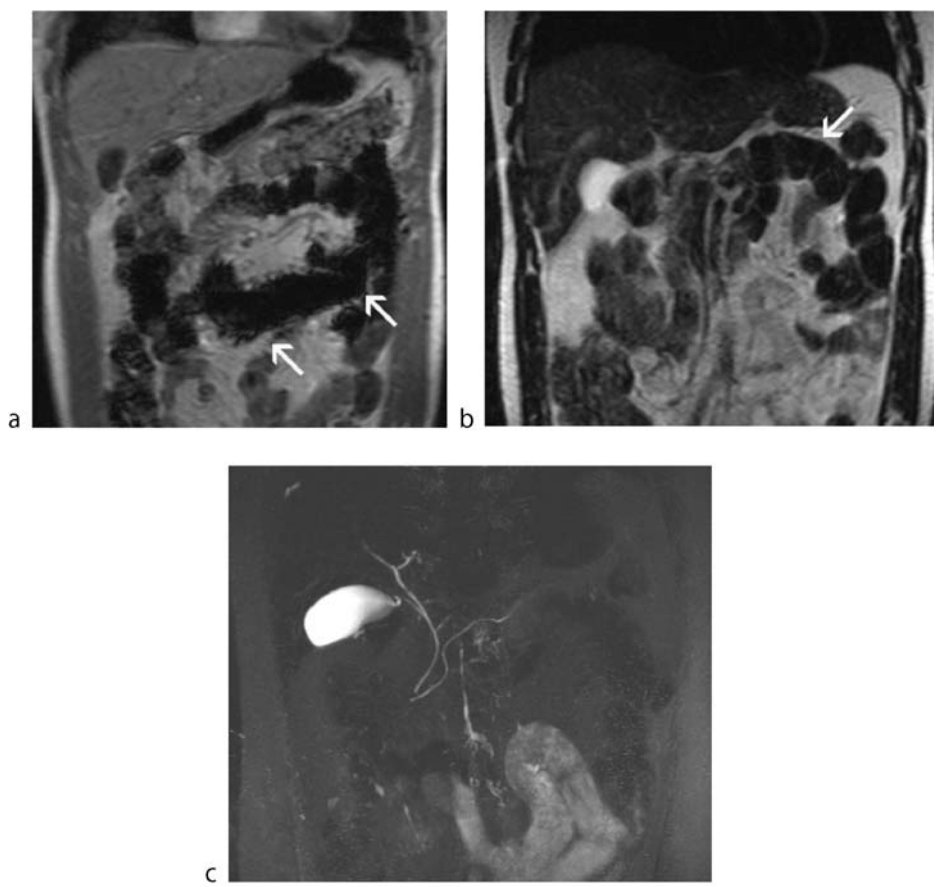

Contrast Media, MRI, Oral Agents. Figure 1 Magnetic resonance (MR) images after the oral ingestion of an agent containing superparamagnetic particles. Signal intensity is rendered dark both on (a) T1-weighted images and (b) T2-weighted images. Therefore, this kind of agent is used to suppress the signal intensity of the duodenum in MR cholangiopancreatography studies (c).

intensity of the bowel lumen is enhanced on T1-weighted images. Furthermore, manganese has a considerable T2-shortening effect, leading to low signal intensity on heavily T2-weighted images. Manganese-containing compounds are commercially available (Lumenhance, Bracco, Milan, Italy). Furthermore, some fruit juices such as pineapple juice and blueberry juice contain a high manganese concentration and therefore may be used as biphasic contrast agents as well (Fig. 2).

5. Water
   Water causes signal increase on T2-weighted images, whereas signal intensities on T1-weighted images are intermediate to low. This biphasic agent is the safest and least expensive oral contrast compound. However, it provides only fair bowel distension, especially in distal bowel segments, because of the fast reabsorption in the small bowel. Thus, it may be used mainly to label the stomach and duodenum and has only a moderate potential to support imaging of the jejunum and ileum.
6. Hydro solutions
   These agents provide signal properties similar to those of water. However, in contrast to pure water, they are not (or only slightly) reabsorbed in the gastrointestinal tract. This is mainly due to additives increasing the agents' osmolarity and/or viscosity. Thus, bowel distension, especially of the jejunum and ileum, is significantly increased. Mannitol, a widely used carbohydrate, mixes well with water, and in concentrations between 1.5 and 2.5%, it has been shown to provide good bowel distension. Sorbitol, another sugar alcohol, has been reported to have similar effects. Another substance is polyethylene glycol 4000 (PEG 4000), a strong hydrophilic molecule, which has no intestinal absorption. PEG 4000 has been shown to provide high luminal distension of small bowel loops.

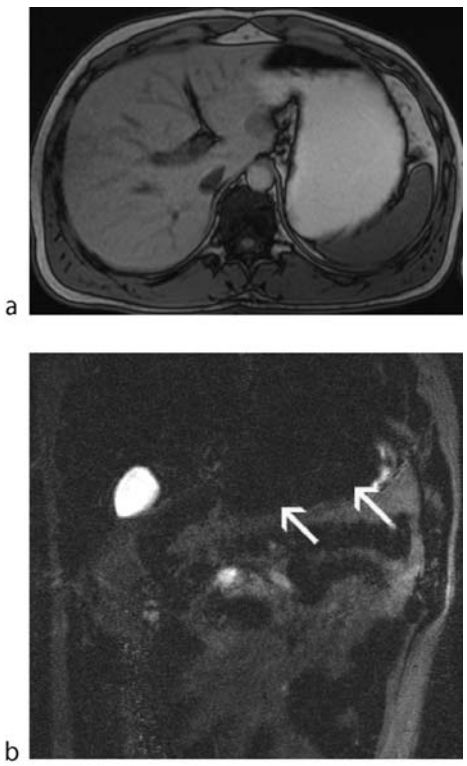

Contrast Media, MRI, Oral Agents. Figure 2
Manganese-containing oral contrast agents are biphasic: while the signal intensity is high on T1-weighted images (a, stomach), signal is reduced on heavily T2-weighted sequences (b, *arrow*).

Indication

Indications to use oral contrast agents for MRI can be divided into three groups.

(1) For the morphological assessment of the stomach or bowel, a high and uniform bowel distension is absolutely mandatory. Collapsed bowel segments may lead to false-positive or false-negative findings; even relatively large lesions may be hidden, or nondistended bowel segments may mimic bowel wall thickening. Therefore, the use of oral MRI contrast agents is obligatory.
(2) Similar to the morphological assessment, functional MRI analysis of the gastrointestinal tract also requires the use of oral contrast. This is especially true for motility studies of the esophagus and stomach. By marking and distending the lumen of these organs, assessment of motility is possible.
(3) Labeling the lumen of stomach and small bowel may be extremely helpful for depicting and analyzing adjacent abdominal organs. This is especially important to image the pancreas, to suppress high bowel signal for MRCP studies, and to facilitate the perceptibility of retroperitoneal and mesenteric lymph nodes.

Contraindication

The consideration of contraindications must be tailored to the specific contrast compounds:

(1) Gadolinium-containing agents must not be used in patients with suspected ileus. Furthermore, their use in dehydrated patients represents a relative contraindication.
(2) Barium-containing agents must not be administered in cases of suspected bowel perforation or before bowel surgery. After endoscopic polypectomy, a

minimal time delay of 7 days should be fulfilled before using barium-containing oral contrast agents.
(3) No contraindications are known for the oral administration of superparamagnetic particles, manganese-containing agents, or hydro solutions.

Pregnancy/Lactation

There are no restrictions on the oral use of barium or water during pregnancy or lactation. As for the administration of all other groups of oral contrast compounds, no definite recommendations are given. However, animal studies have not shown these agents to imply any embryotoxic or teratogenic potential.

Use and Dosage

For labeling of the stomach or the duodenum, relatively low doses of contrast agents (300–600 mL) are sufficient. However, data acquisition should be performed directly after administration of the substances to avoid insufficient marking in patients with fast bowel transit times.

For assessing the small bowel itself, there are technically two different methods for the application of oral contrast agents. To assure high distension of small bowel loops, the MR Sellink technique was developed: A hydro solution (1,000 mL and 2,000 mL) is administered *via* a fluoroscopically placed nasoduodenal or nasojejunal tube at a flow rate of approximately 100 mL/min. Image sets then can be collected following rapid filling of the entire small bowel. This technique provides excellent image quality. However, some patients may perceive the intubation as unpleasant.

The sole oral ingestion of some hydro solutions may also provide high small bowel distension without the need for duodenal intubation. Doses between 1,000 mL (for PEG) and 1,500 mL (for mannitol- or sorbitol-containing agents) should be ingested over 45–60 min before the MR examination.

Adverse Reactions

If applied in recommended doses, there are only mild side effects for all oral MRI contrast compounds. Thus, ingestion of mannitol-containing agents as well as of superparamagnetic particles may lead to flatulence or diarrhea. Regarding the use of barium, cases of constipation have been reported. Barium-containing products have a well-documented safety profile, and allergic reactions or severe side effects are not known.

Interactions

Ingestion of mannitol-containing agents may lead to byproducts such as explosive gases. Therefore, diathermia treatment should not be performed 48 h after the MR examination. Furthermore, bowel surgery in conjunction with electrocautery may not be performed. Interactions with other oral MR contrast compounds are not known.

Bibliography

1. Laghi A, Paolantonio P, Iafrate F et al (2002) Oral contrast agents for magnetic resonance imaging of the bowel. Top Magn Reson Imaging Dec; 13(6):389–396
2. Debatin JF, Patak MA (1999) MRI of the small and large bowel. Eur Radiol 9(8):1523–1534
3. Giovagnoni A, Fabbri A, Maccioni F (2002) Oral contrast agents in MRI of the gastrointestinal tract. Abdom Imaging Jul–Aug; 27 (4):367–375

Contrast Media, MRI, Organ Specific

Peter Reimer
Department of Radiology, Klinikum Karlsruhe, Academic Teaching Hospital of the University of Freiburg, D-76133 Karlsruhe
peter.reimer@klinik.um-karlsruhe.com

A variety of MR contrast agents has been developed to improve the sensitivity and specificity of MR imaging for the diagnosis of disease. Readers will become familiar and understand the indication, contraindication, interactions, and limitations of approved MR contrast agents. Furthermore, candidates, likely to get approval within the near future will be covered.

Contrast agents are administered either orally or intravenously. Oral contrast agents play a minor role and the text will focus on intravenous contrast agents. The mechanism of action is either to increase predominantly (Mn, Gd, or Fe) or to decrease (Fe) signal intensity. Upon intravenous administration, contrast agents leave the intravascular space (unspecific) into the interstitium, are taken up into cells (cell specific), or stay in the intravascular space (blood pool) for some time.

The use of low molecular extracellular nonspecific gadolinium chelates in MRI is well established and quite a number of different contrast agents are clinically approved. These nonspecific contrast agents enhance both normal and diseased tissues. Therefore, contrast agents with tissue specificity to improving the detection and

characterization of disease were developed. Contrast agents may either be directed to normal tissue or to diseased tissue. It turned out that directing contrast agents to normal tissue or to normal structures is much easier than specifically directing contrast agents to diseased tissue such as inflammation, degeneration, tumor, or gene expression. At present, attempts to achieve receptor, optical, or gene specificity propelled the development of a new field called molecular imaging and optical imaging, which is described elsewhere.

The principle of tissue specificity means direction of a contrast agent toward a certain tissue-like liver tissue, splenic tissue, pancreatic tissue, lymph nodes, bone marrow, blood, or inflammation. Contrast agents with this specificity are either superparamagnetic iron oxides (SPIOs) or paramagnetic agents with gadolinium or manganese as magnetic components. As for imaging reticulo-endothelial system (RES) containing organs such as the liver, spleen, lymph nodes, or bone marrow iron oxides of different sizes are used. The larger the iron oxides the higher and faster the uptake in liver and spleen and the lower and slower the uptake in lymph nodes and bone marrow. In addition, ultrasmall iron oxides may also be utilized for vascular imaging based upon their prolonged circulating time and T1-effects as compared to larger iron oxides. Furthermore, by binding specific markers to the magnetic components, further tissue specificity may be achieved. This also applies to paramagnetic-based contrast agents, which are directed to different tissues by means of a modification of the chemical structure resulting in specific attachment to specific tissue.

The most thoroughly investigated and approved tissue specific contrast agents relate to hepatic MRI. A variety of liver contrast agents has been developed for contrast-enhanced MRI of the liver, which is designed to overcome the limitations of unspecific tissue uptake by extracellular low molecular gadolinium chelates. The two main classes of liver-specific contrast agents are SPIO with uptake *via* the RES mainly into the liver and spleen and hepatobiliary contrast agents with uptake into hepatocytes followed by variable biliary excretion. Two hepatobiliary contrast agents, mangafodipir trisodium (Teslascan, 6E, USA) and gadobenate dimeglumine (MultiHance, Bracco Imaging S.p.A., Milan, Italy), are already clinically approved in many Countires. A third hepatobiliary contrast agent, gadoxeficacid, Gd-EOB-DTPA (Primovist, Schering AG, Berlin, Germany), has already been approved in Europe and several other countires. These agents exhibit different features for the detection and characterization of liver tumors. Enhancement during the distribution phase of contrast agents mainly depends on tumor vascularity (hypovascular vs. hypervascular) and its blood supply, while enhancement on delayed images is characterized by the cellular specificity of MR contrast agents (extracellular vs. intracellular—hepatocyte phase or accumulation phase). Therefore, enhancement characteristics of hepatobiliary contrast agents are applicable to the diagnosis of primary hepatocellular liver tumors.

With the advent of rapid three-dimensional imaging sequences combined with existing extracellular gadolinium-based contrast agents, MRA has shown promising signs of becoming a time-efficient and cost-effective tool for the complete assessment of many vascular regions or clinical referrals like peripheral vascular. The use of intravenous low and high molecular gadolinium chelates for contrast-enhanced MRA is limited by the rapid equilibration of these agents between the intravascular and extravascular–extracellular compartments. Alternative paramagnetic and superparamagnetic agents for enhancing MR angiographic images, known as blood-pool agents, are currently being studied. Several blood-pool contrast agents have been designed and some are under clinical investigation. MR contrast agents confined to the intravascular space, so-called blood-pool agents, could change the way vessels are currently imaged by means of MRA. Furthermore, if these agents also exhibited a prolonged plasma half-life, new avenues could be opened to additional applications within the field of MRA but also beyond MRA. Blood-pool agents are particularly promising in contrasting smaller vessel, vessels with slow flow, and vessels with complex flow. In addition, blood-pool agents may be used for perfusion imaging, functional imaging, or imaging of angiogenesis. Two classes of blood-pool agents are under development: paramagnetic gadolinium-based molecules of different size and some ultrasmall iron oxides. Whereas the design of iron oxides suited for blood-pool imaging is well understood and developed, a variety of gadolinium-based agents with different pharmacological profiles is under development.

In the relevant entries we review those concepts of contrast agents which are clinically approved or are in advanced clinical trials. Each of these agents has unique properties that offer advantages for contrast-enhanced MR imaging. Use of these agents, however, requires an understanding of their current and potential clinical indications and inherent limitations. Our purpose is to provide information on the properties, the clinical development, and clinical applications of MR contrast agents which have been approved or are likely to get approval within the near future. Furthermore, since approval is rarely a general approval for whole body MRI and MRA, the approved applications will be explained.

Bibliography

1. Allkemper T et al (2002) Contrast-enhanced blood-pool MR angiography with optimized iron oxides: effect of size and dose on vascular contrast enhancement in rabbits. Radiology 223(2):432–438

2. Balzer JO et al (2003) Safety of contrast-enhanced MR angiography employing gadobutrol 1.0 M as contrast material. Eur Radiol 13 (9):2067–2074
3. Bellin MF, Vasile M, Morel-Precetti S (2003) Currently used non-specific extracellular MR contrast media. Eur Radiol 13 (12):2688–2698
4. Brasch RC (1992) New directions in the development of MR imaging contrast media. Radiology 183(1):1–11
5. Dawson P (1996) Contrast agents in magnetic resonance imaging. Eur J Radiol 23(3):201–204
6. Giovagnoni A, Fabbri A, Maccioni F (2002) Oral contrast agents in MRI of the gastrointestinal tract. Abdom Imaging 27 (4):367–375
7. Hentsch A et al (2003) Gadobutrol-enhanced moving-table magnetic resonance angiography in patients with peripheral vascular disease: a prospective, multi-centre blinded comparison with digital subtraction angiography. Eur Radiol 13(9):2103–2114
8. Laghi A et al (2002) Oral contrast agents for magnetic resonance imaging of the bowel. Top Magn Reson Imaging 13(6):389–396
9. Mitchell DG (1997) MR imaging contrast agents—what's in a name? J Magn Reson Imaging 7(1):1–4
10. Nyman U et al (2002) Are gadolinium-based contrast media really safer than iodinated media for digital subtraction angiography in patients with azotemia? Radiology 223(2):311–318; discussion 328–329
11. Paley MR, Ros PR (1997) MRI of the gastrointestinal tract. Eur Radiol 7(9):1387–1397
12. Reimer P, Tombach B (1998) Hepatic MRI with SPIO: detection and characterization of focal liver lesions. Eur Radiol 8(7):1198–1204
13. Reimer P, Balzer T (2003) Ferucarbotran (Resovist): a new clinically approved RES-specific contrast agent for contrast-enhanced MRI of the liver: properties, clinical development, and applications. Eur Radiol 13(6):1266–1276
14. Reimer P, Schneider G, Schima W (2004) Hepatobiliary contrast agents for contrast-enhanced MRI of the liver: properties, clinical development and applications. Eur Radiol 14(4):559–578
15. Runge VM (2000) Safety of approved MR contrast media for intravenous injection. J Magn Reson Imaging 12(2):205–213
16. Runge VM (2001) Safety of magnetic resonance contrast media. Top Magn Reson Imaging 12(4):309–314
17. Runge VM, Muroff LR, Jinkins JR (2001) Central nervous system: review of clinical use of contrast media. Top Magn Reson Imaging 12(4):231–263
18. Semelka RC, Helmberger TK (2001) Contrast agents for MR imaging of the liver. Radiology 218(1):27–38
19. Spinosa DJ, Kaufmann JA, Hartwell GD (2002) Gadolinium chelates in angiography and interventional radiology: a useful alternative to iodinated contrast media for angiography. Radiology 223(2):319–325; discussion 326–327
20. Tombach B et al (2002) Using highly concentrated gadobutrol as an MR contrast agent in patients also requiring hemodialysis: safety and dialysability. Am J Roentgenol 178(1):105–109
21. Tombach B et al (2002) First-pass and equilibrium phase MRA following intravenous bolus injection of SH U 555 C: phase I clinical trial in elderly volunteers with risk factors for arterial vascular disease. Acad Radiol 9 Suppl 2:S425–427
22. Tombach B, Heindel W (2002) Value of 1.0- M gadolinium chelates: review of preclinical and clinical data on gadobutrol. Eur Radiol 12(6):1550–1556
23. Tombach B et al (2003) Do highly concentrated gadolinium chelates improve MR brain perfusion imaging? Intraindividually controlled randomized crossover concentration comparison study of 0.5 versus 1.0 mol/L gadobutrol. Radiology 226(3):880–888
24. Wang YX, Hussain SM, Krestin GP (2001) Superparamagnetic iron oxide contrast agents: physicochemical characteristics and applications in MR imaging. Eur Radiol 11(11):2319–2331
25. HJ Weinmann et al (2003) Tissue-specific MR contrast agents. Eur J Radiol 46(1):33–44

Contrast Media, MRI, RES Specific Iron Oxide Particles

Peter Reimer
Department of Radiology, Klinikum Karlsruhe, Academic Teaching Hospital of the University of Freiburg, D-76133 Karlsruhe
Peter.Reimer@klinik.um-karlsruhe.com

Definition

Iron oxides possess a large magnetic moment when brought into a magnetic field. A distinguishing feature of superparamagnetic iron oxides (SPIO/USPIO) is that they do not show residual magnetization after removal from the field. Magnetic susceptibility describes the ratio of such induced magnetization to the strength of the applied magnetic field. Typical for all SPIO/USPIO is a non-linear behaviour between induced magnetization and applied field, contrary to paramagnetic agent's which demonstrate a linear behaviour. The effect of superparamagnetic iron oxides (SPIO) on proton relaxation times is best explained by two mechanisms. The large magnetic moment of SPIO generates local field inhomogeneities and promotes dephasing of proton spins and acceleration of transverse relaxation. Second, the large susceptibility difference between particles and the surrounding medium creates magnetic field gradients at microscopic levels. Diffusion in these field gradients leads to an irreversible loss of phase coherence and thus decreases transverse relaxation times of protons.

The iron crystals clustered within phagolysosomes cause a significant superparamagnetic disturbance of the local magnetic field resulting in a pronounced shortening of both T2 and also T1 relaxivity. Therefore, the fundamental principle contrast enhancement after administration of iron oxide particles goes along with the presence or relative absence of Kupffer cells within the normal parenchyma and specific lesions. A significant decrease of the signal in tissue containing Kupffer cells such as normal tissue can be appreciated after SPIO administration, resulting in a relative signal increase in

tissues with a lack of Kupffer cells. Hypovascular liver metastases and cystic lesions are the typical examples for this contrast pattern. Nevertheless, the persistence of Kupffer cells in some hepatocellular tumours can be beneficial in differential diagnostic considerations. These contrast patterns apply to the accumulation phase of SPIO imaged >10 min following injection. Ferucarbotran may be used imaging the perfusion phase of lesions providing additional information especially for lesions characterization especially in hypervascular lesions. However, also due to the much lower dose the contrast yield is lower than observed for low molecular gadolinium chelates.

After intravenous administration, iron oxides circulate in the blood stream for a variable length of time depending on particle size and surface characteristics. Typically, particles accumulate in macrophages of the reticuloendothelial systems (RES; e.g. liver, spleen, lymph nodes, bone marrow etc.). Tissue localization also depends on organ blood flow, opsonisation of iron oxides by plasma proteins, receptor or target cell affinity and relative concentration of binding sites.

Biodegradation of iron oxides is assumed to occur in phagolysosomes within macrophages. Elemental iron from the iron oxide core is incorporated into the body iron pool and can be demonstrated in haemoglobin. In cases of severe hepatic cirrhosis, the splenic signal loss after iron oxide administration is surpassing the signal loss in the liver by far due to the loss of functioning hepatic Kupffer cells. This phenomenon is known as 'colloid shift' from nuclear medicine studies. After ultrasmall iron oxides (USPIO) administration the spleen presents the highest uptake (7.1%/g after 24 h) in comparison to liver (6.3%/g), lymph nodes (3.6%/g) and bone marrow (2.9%/g).

Two different classes of iron oxides are currently clinically approved or have completed phase three trials:

1. SPIO with a high R2/R1 relaxivity ratio and short blood half-life (<10 min). There are currently two clinically approved SPIO ferumoxides (Guerbet, Paris, France) and ferucarbotran (Schering, Berlin, Germany). A high R2/R1 ratio of 5 to 15 is characteristic for superparamagnetic colloids of the SPIO type (Reimer 1998, Reimer 2003, Ros 1995, and Wang 2001).
2. USPIO with a lower R2/R1 relaxivity ratio and longer blood half-life (<3 h) (Harisinghani 2003 and Weissleder 1990). Clinical approval of Ferumoxtran-10 is pending (Guerbet, Paris, France).

Ferumoxides (Feridex, Guerbet, France) consists of crystalline superparamagnetic iron oxide microparticles stabilized as a colloid with low-molecular weight coated with dextran. Ferucarbotran (SH U 555 A, Schering AG, Germany) consists of superparamagnetic iron oxide microparticles coated with carboxydextran. The R1 relaxivity of SPIO varies considerably within the range of diagnostically applied field strengths while the R2 relaxivity is relatively stable within the range of diagnostically applied field strength. Thus, at lower imaging field the T1 effect of these materials is better used. Both contrast agents are approved for hepatic MRI (Reimer 1998, Reimer 2003, Ros 1995 and Wang 2001).

Ferumoxtran-10 [BMS 180549, Sinerem^{TM}], consists of iron-oxide particles coated with dextran (Harisinghani 2003 and Weissleder 1990). It is an ultrasmall superparamagnetic contrast agent that is awaiting registration with Guerbet in Europe. The US FDA has issued an 'approvable letter' for use of Combidex (with Advanced Magnetics in the USA) in the diagnosis of lymph node disease, and the detection, diagnosis and characterisation of benign versus malignant lesions of the liver and spleen. Since, the US FDA has made comments about some data and indications an additional clinical trial may be required to settle the issues. Ferumoxtran-10 has been licensed to Guerbet for Western Europe and Brazil. It is awaiting registration (as Sinerem^{TM}) for imaging cancer in the pelois (uterus, prostal and rectum). Guerbet is also conducting additional clinical trials with ferumoxtran-10 for imaging of multiple sclerosis plaques and breast cancer. Advanced Magnetics has granted exclusive marketing and distribution rights for Combidex for oncology applications in the USA to Cytogen Corporation.

Indication

SPIO and USPIO have been developed for contrast-enhanced MR imaging of the liver, spleen, lymph nodes, bone marrow and other indications. The larger SPIO agents efficiently accumulate in liver with approximately 80% of the injected dose and spleen with 5–10% of the injected dose within minutes after intravenous administration. The smaller USPIO exhibit a longer blood-half life and higher accumulation in the RES within spleen, lymph nodes, bone marrow or vascular plaques.

Both SPIO are approved for imaging of liver tumours (Fig. 1). Benign hepatic lesions derived from hepatocytes such as focal nodular hyperplasia, hepatocellular adenomas, regenerative nodules and dysplastic nodules may embody various amounts of Kupffer cells. Therefore, the relative signal loss after SPIO administration in these lesions may parallel the signal loss in normal hepatic parenchyma indicating a most likely Kupffer cell containing benign lesion. Hemangiomas also show signal changes, which are believed to be based upon the blood pool of hemangiomas and uptake into sinusoidal cells within hemangiomas. Therefore, the relative signal loss after SPIO administration in these lesions may parallel the signal loss in normal hepatic parenchyma indicating a most likely

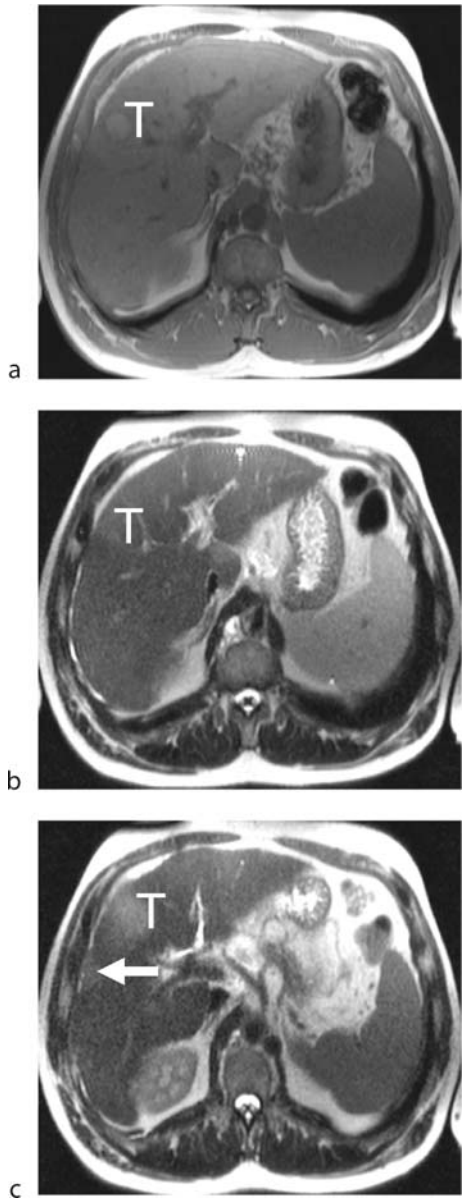

Contrast Media, MRI, RES Specific Iron Oxide Particles. Figure 1 Patient with Hepatocellular Carcinoma. Precontrast imaging (a and b) show a single tumor in the right liver lobe (t). An additional tumor (*arrow*) is visualized following ferucarbotran (c).

Kupffer cell containing benign lesion. On mild to heavily T2-w, images hemangiomas exhibit decreased signal intensity. T1-w sequences may show a signal increase.

The contrast pattern in malignant liver tumours also depends on the hepatocyte content of the lesions. All metastases are devoid of RES cells and thus hypovascular metastases show stable signal and thus increased conspicuity. Hypervascular metastases may exhibit perfusion changes and pooling during the accumulation phase resulting in a temporary signal decrease or increase dependent on T1-effects. Hepatocyte derived malignant lesions reveal more complex patterns. Poorly or moderately differentiated hepatocellular carcinomas are nearly completely devoid of Kupffer cells. Therefore, they exhibit a contrast pattern comparable to metastases going along with their vascularity (hypovascular vs. hypervascular). Well-differentiated hepatocellular carcinomas and hyperplastic regenerative nodules may also contain Kupffer cells. Subsequently, these tumours may show uptake into Kupffer cells and thus proportional to the content and activity a signal decrease on accumulation phase images. This may cause a decreased conspicuity during the accumulation phase compared to plain images. Furthermore, the perfusion phase may be imaged with additional information regarding lesion vascularity.

Ferumoxtran-10 is awaiting registration for imaging cancer in the lymphatic system, perfusion imaging of the brain, heart, liver and spleen, in the delineation of reduced blood flow in damaged tissues following heart attack or stroke, and as an adjunct to magnetic resonance angiography.

Contraindication

Safety and effectiveness have not been established in paediatric patients for any of the contrast agents. Specific contraindications and precautions for the three contrast agents are a prior hypersensitivity to the compounds, dextran or carboxydextran. A known allergic or hypersensitivity reactions to iron-containing products or disorders associated with iron overload represent a contraindication.

An injection should not be considered to patients with asthma, allergies and history of allergic responses to medications, cardiovascular disease or other abnormalities that may predispose them to cardiac arrhythmias or cardiovascular effects.

Iron oxides were not investigated in patients with severe renal or hepatic insufficiency and are thus not recommended in these patients.

Pregnancy/Lactation

The application during pregnancy or lactation is not approved or recommended.

Use and Dosage

Prior to contrast injection T1- and T2-weighted sequences at least in the transverse plane should be obtained. Specific parameters and strategies (breathheld vs. triggered) are somewhat vendor, scanner type and software release dependent. In order to use the information provided by looking at lesion perfusion the weak perfusion effect of Ferucarbotran may be studied by either T1- or T2*-weighted sequences. For T2*-weighting, it appears advantageous not to maximize for T2* in order maintain sufficient signal-to-noise. Initial timing may follow the usual time-points of the arterial-phase and portal-venous-phase followed by delayed acquisitions up to 10 min. Accumulation phase imaging may start as early as 10 min post injection with T2-weighted sequences including a GRE sequence with proton-density characteristics for detection. Mild and heavily T2-weighted TSE-sequences also provide useful information on the signal decrease within RES-containing tumours.

The two SPIO are approved for liver imaging in adult patients. Malignant liver tumours are typically devoid of a substantial number of phagocytic cells so they appear as hyperintense/bright lesions contrasted against the hypointense/dark liver on T2-w sequences. Tumours with a substantial number of phagocytic cells such as focal nodular hyperplasia, hepatocellular adenoma, well-differentiated hepatocellular carcinoma and/or a significant blood-pool (hemangioma or hypervascular lesions) may show sufficient uptake of SPIO with decreasing signal intensity on T2-w sequences. The signal decrease is related to the Kupffer cell activity or tumour vascularity. Furthermore, SPIO show signal changes in T1-w sequences, both during the perfusion phase (ferucarbotran) and accumulation phase (ferumoxides and ferucarbotran) providing additional information.

Ferumoxides is diluted in 100 mL of 5% dextrose solution and drip infused over 30 min, Ferucarbotran may be bolused for dynamic imaging during the vascular phase, however, providing less signal than gadolinium chelates approved at a higher dose. Post-contrast MRI with ferumoxides may start after completion of infusion up to a couple of hours later. For ferucarbotran post-contrast MRI may start as early as 10 min following injection. The post-contrast time window for both agents is probably up to 24–36 h.

Different dosages are approved for use in the USA, Europe and Japan. For ferumoxides, a dosage of 15 µmol Fe/kg is approved in Europe and Japan in contrast to 10 µmol Fe/kg in USA. The different dosages result in considerably varying T1- and T2*-effects especially when gradient-echo sequences are applied. This phenomenon might be even more striking in ferucarbotran, in which dosages up to 16 µmol Fe/kg bodyweight produce maximum contrast effects. Clinically, to simplify contrast injections it was hypothesized that the conventional bodyweight-based injection of iron per kg may be replaced by fixed volumes coming in pre-filled syringes (≤60 kg–0.9 mL and >60 kg 1.4 mL). The effective dose administered per kg bodyweight varies between about 7 and 11 µmol Fe/kg bodyweight.

Ferumoxtran-10 has been given at a dose 0.8 to 1.7 mg Fe/kg bodyweight for suspected hepatic lesions. MRI may be performed as early as after completion of infusion. A dose of 1.7 mg Fe/kg bodyweight was effective for detection of lymph node imaging of patients with prostate cancer, pelvic cancer and head and neck cancer. For the detection of metastases in patients with non-small-cell lung cancer, 2.6 mg Fe/kg bodyweight has been administered. Post-contrast MRI may be performed as early as 24 or 36 h after completion of infusion. An infusion time of 25 to 30 min is required to minimize hypotension or acute lumbar pain.

Adverse Reactions

Adverse reactions vary among the different iron oxides. The two dextran-stabilized compounds show a characteristic reaction when infused rapidly with hypotension, headache, nausea, abdominal pain or lumbar pain (5–30%). Clinical trials with intravenously administered Ferumoxides have been initiated as early as 1987. Early studies were performed with bolus injections of relatively high doses (≤50 µmol Fe/kg bodyweight) of an initial formulation of AMI-25 causing significant hypotension. Subsequently, the agent was reformulated to achieve iso-osmolarity and is currently administered by drip infusion over a period of 30 min since side effects (facial flash, dyspnea, rash, lumbar pain) depend on the dose rate. However, in most cases the administration can be reinitiated after reduction of the injection rate. Dermatologic allergic reactions like urticaria, erythema, pruritus, rash, pain at the infusion site, a sensation or warmth during infusion, or dermatographism have been reported. Non-significant effects are an increase in monocyte counts and mild eosinophilia.

During the clinical development of ferucarbotran, a dose dependent (5–40 µmol Fe/kg bodyweight) increase in PTT was observed, however, the normal range was not exceeded. These minor changes in PTT were attributed to a transient decrease in clotting factor XI activity. The transient decrease of clotting factor XI did not cause any clinical side effects in phases I–III. Previous studies assessing other SPIO or USPIO contrast agents did not report detailed information on clotting parameters. Safety data were obtained during the entire clinical

development. A total of 162 adverse events were documented within 1053 patients, of whom 75 were classified as possibly, probably or definitely drug related. The majority occurred within the first 3 h (73/75) and was of mild intensity. The frequency of adverse events was within the range of other approved MR contrast agents such as gadolinium chelates or placebo medication and no specific pattern was observed, although no direct comparative studies are available so far. Ferucarbotran proved to be a safe contrast agent since no significant cardiovascular changes during close monitoring of blood pressure and heart rate within the magnet bore. Blood tests evaluated revealed minor changes with the increase in iron and ferritin as well as the decrease in total iron binding capacity as a result of the iron injection.

Interactions

The administered free iron is incorporated into the normal iron metabolism, however, the administered dosage of SPIO is not significantly affecting the body's iron pool (e.g. 15 μmol Fe/kg ~840 ng Fe/body weight). Till the degradation of the clustered iron particles the superparamagnetic effects last for several days providing an imaging window of several hours up to several days after administration. Human tissues contain iron in the form of hemosiderin, ferritin and transferrin. Normal liver contains approximately 0.2 mg Fe/g wet weight of liver and total iron stores amount to approximately 3.5 g. The amount of iron oxides that is required for clinical MR imaging (1–2 mg Fe/kg bodyweight; for a 70 kg subject 70–140 mg) is small compared to normal iron stores.

Bibliography

1. Harisinghani MG et al (2003) Noninvasive detection of clinically occult lymph-node metastases in prostate cancer. N Engl J Med 348 (25):2491–2499
2. Reimer P and Tombach B (1998) Hepatic MRI with SPIO: detection and characterization of focal liver lesions. Eur Radiol 8(7): 1198–1204
3. Reimer P and Balzer T (2003) Ferucarbotran (Resovist): a new clinically approved RES-specific contrast agent for contrast-enhanced MRI of the liver: properties, clinical development, and applications. Eur Radiol 13(6):1266–1276
4. Ros PR et al (1995) Hepatic MR imaging with ferumoxides: a multicenter clinical trial of the safety and efficacy in the detection of focal hepatic lesions. Radiology 196(2):481–488
5. Wang YX, Hussain SM, and Krestin GP (2001) Superparamagnetic iron oxide contrast agents: physicochemical characteristics and applications in MR imaging. Eur Radiol 11(11):2319–2331
6. Weissleder R et al (1990) Ultrasmall superparamagnetic iron oxide: an intravenous contrast agent for assessing lymph nodes with MR imaging. Radiology 175(2):494–498
7. Weissleder R et al (1990) Ultrasmall superparamagnetic iron oxide: characterization of a new class of contrast agents for MR imaging. Radiology 175(2):489–493

Contrast Media, Ultrasound, Amplitude Modulation

Robert Eckersley
Imaging Sciences Department, Imperial College London, London, UK
r.eckersley@imperial.ac.uk

Amplitude modulation imaging is a bubble-specific mode which uses alternating pulse amplitudes, that is, +1, +1/2 and so on. (see Fig. 1). This approach works in a similar manner to phase modulation in which appropriate combination of the echoes will result in a complete cancellation for linear scatterers, while non-linear microbubble echoes will show residual signals. These residual signals arise because the microbubbles respond non-linearly to the different amplitude pulses, that is, the double amplitude pulse does not elicit an echo with twice the amplitude, whereas for tissue this would be the case. An advantage of amplitude modulation over phase modulation is that it is able to detect non-linear signals at the fundamental frequency and not just the second harmonic. However, the use of alternating lower power pulses does reduce the sensitivity of this approach. A combination of pulse inversion and amplitude modulation has been shown to improve the sensitivity to microbubbles over tissues still further (1). As with phase modulation, this sequence can be extended to more that two pulses to improve the sensitivity and to enable the use of Doppler processing for motion detection.

Bibliography

1. Eckersley RJ, Chin CT, Burns PN (2005) Optimising phase and amplitude modulation schemes for imaging microbubble contrast agents at low acoustic power. Ultrasound Med Biol 31(2):213–219

Contrast Media, Ultrasound, Applications in Blunt Abdominal Trauma

David Cosgrove
Imaging Sciences Department, Imperial College, Hammersmith Hospital, London, UK
d.cosgrove@csc.mrc.ac.uk

Synonyms

Contrast-enhanced sonography in abdominal trauma; Contrast-enhanced ultrasound in abdominal trauma

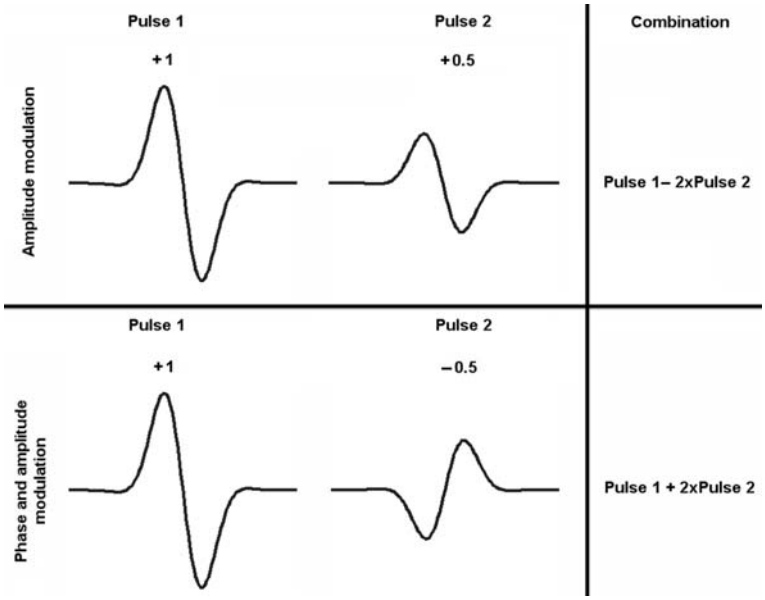

Contrast Media, Ultrasound, Amplitude Modulation. Figure 1 This figure shows (upper panel) a simple two-pulse amplitude modulation sequence. When the echoes of pulse 1 and pulse 2 are combined by doubling pulse 2 and subtracting the result from pulse 1 any linear signals will be cancelled. Both non-linear signals at the fundamental and second harmonic signals in the echoes from microbubbles are preserved by this approach. Also presented (lower panel) is a two-pulse sequence with combined phase and amplitude modulation. Linear signals can again be removed by appropriate combination of the echoes. Combing the two modulation approaches can improve the sensitivity to microbubbles.

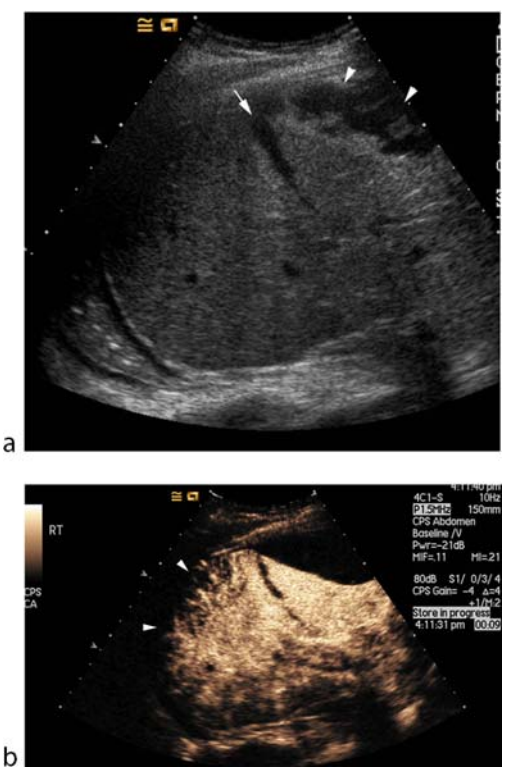

Contrast Media, Ultrasound, Applications in Blunt Abdominal Trauma. Figure 1 Abdominal trauma in a road crash. This patient presented with upper abdominal pain following a car crash. The B-mode ultrasound scan showed a wedge-shaped defect in the right liver (*arrow* in a), suggestive of a tear, as well as an echopoor region (*arrowheads*) that could not confidently be assigned to liver or peritoneum. Following i.v. SonoVue and working in the CPS mode (Sequoia, Siemens), this could be seen to lie outside the liver, which was compressed by it. The liver tear was confirmed, but in addition, there was extensive devascularised liver tissue superiorly (*arrowheads* in b). In this case, the contrast-enhanced scan revealed the full extent of the liver injury as well as the presence of intra-peritoneal bleeding. (Images courtesy of Dr Paul Sidhu, King's College Hospital,

Definition

The use of ultrasound (US) microbubble contrast agents combined with contrast-specific imaging techniques for the detection of traumatic lesions of the abdomen (mainly spleen, liver and kidney)

Introduction

Conventional ultrasound is poor at detecting trauma to abdominal organs because freshly cut tissue has the same appearances as viable tissue on grey scale imaging (1). Large haematomas can be detected, but the extent of tissue damage is under-estimated (2). Colour Doppler might be expected to offer an improvement by depicting non-perfused tissue but, though it does improve sensitivity somewhat overall it has proved disappointing in trauma (3). The critical limitation of Doppler is its inability to detect flow in small vessels where flow is slow, because Doppler cannot distinguish tissue movement from blood flow.

Thus, the role of ultrasound as a means to triage patients according to the severity of their injury is mostly restricted to detecting free fluid in the peritoneum, which in the context of abdominal trauma, is assumed to represent blood, though fresh blood cannot be distinguished form serous fluid using ultrasound. The method, known as focused assessment with sonography in trauma (FAST), examines the right and left upper quadrants and the pelvis for free fluid as a measure of intra-abdominal bleeding and forms a baseline for comparison with subsequent scans to detect deterioration. However, FAST has major limitations, including its inability to pinpoint the source of bleeding and the fact that up to 10% of parenchymal trauma does not result in bleeding into the peritoneum (4). Therefore, in general, contrast-enhanced CT is the preferred technique and it also has the important advantage of being able to assess the head thorax and spine, and so all stable trauma patients are referred for CT unless the injury seems to be trivial.

While an improved ultrasound approach, such as the use of contrast enhancement would have many advantages (performed at the bedside, repeatable, no risk form ionising radiation), CT would always be required to detect head, chest and skeletal injuries.

Contrast Agents and Parenchymal Trauma

Almost all instances of soft tissue injury produce non-perfused regions of tissue, often together with haematomas. Detecting unperfused tissue requires demonstration of the integrity of the microvasculature and this is now possible with microbubble contrast agents (5, 6). Multi-pulse methods with software designed to detect their resonance signals, display the contrast image separately from the grey-scale image, either as a side-by-side display or as a colour-coded overlay. The ability to detect contrast in the microcirculation sets contrast ultrasound apart from Doppler, which can only detect flow in vessels down to arteriolar calibre.

Operation at a low transmit power (using a mechanical index of less than about 0.4) allows real time scanning after administration of contrast. In the kidney, for example, the high perfusion of the cortex is shown as a rapidly developing enhancement that intensifies to a complete colour fill, usually commencing after 15–30 sec, depending on the patient's cardiac output, before washing out over the next few minutes. In the liver and spleen, the microbubbles arrive in the arteries in the same way but less strikingly because of their lower overall blood flow; in the liver the portal supply dominates the wash-in phase and in both, the microbubbles linger within the capacious

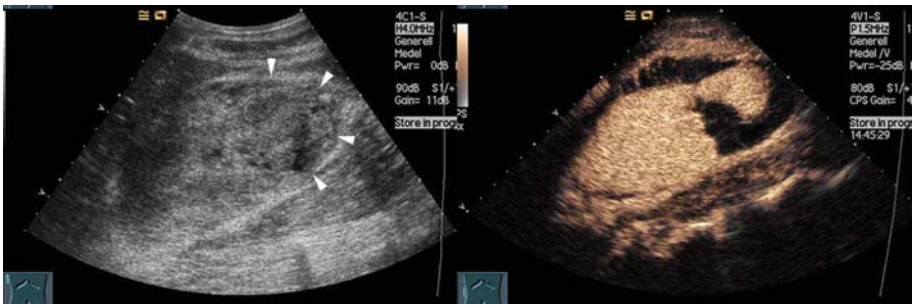

Contrast Media, Ultrasound, Applications in Blunt Abdominal Trauma. Figure 2 Blunt trauma to the right upper abdomen. Following a road traffic crash, this patient was admitted with right flank pain. The grey-scale ultrasound did not reveal any free fluid but an ill-defined irregularity of the texture of the lower pole of the right kidney was noted (arrowheads in A). Following i.v. SonoVue and using the CPS mode (Sequoia, Siemens) complete enhancement in the renal cortex revealed a large defect in the posterior portion of the kidney. A laceration was confirmed on contrast-enhanced CT scanning. (Images courtesy of Dr Anders Knutsson and Dr Lars Thorelius, University Hospital, Linköping, Sweden)

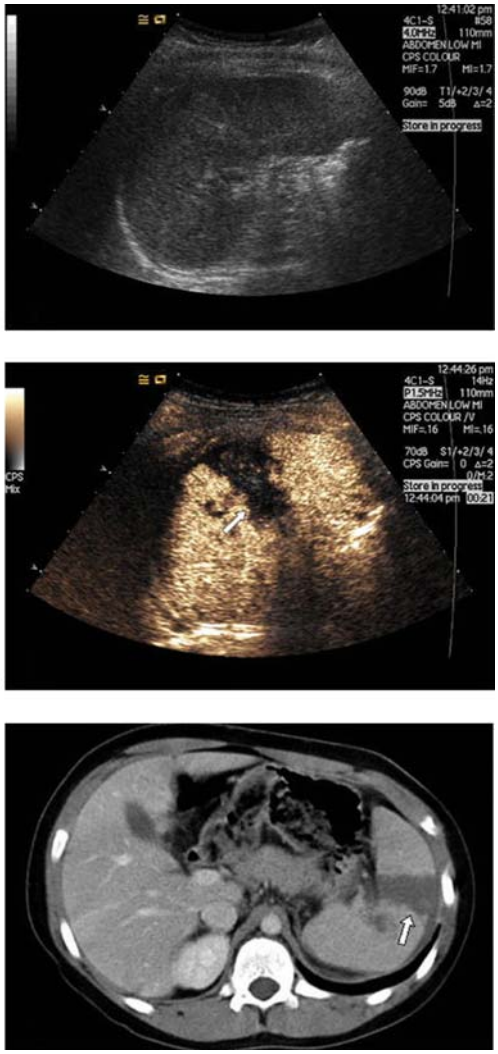

Contrast Media, Ultrasound, Applications in Blunt Abdominal Trauma. Figure 3 Twelve-year old boy with blunt abdominal trauma. (a) Unenhanced oblique intercostal B-mode US 1 day after blunt abdominal trauma. The spleen shows homogeneous parenchyma and regular contour with no focal abnormality. (b) Contrast-enhanced coherent pulse sequencing (CPS) scan in oblique intercostal section 1 day after BAT. Contrast enhancement in normal perfused parenchyma is represented by the gold-coloured overlay, whereas the haematoma appears as a wedge-shaped enhancement defect (*arrow*). (c) Axial contrast-enhanced CT in the portal-venous phase confirming the splenic parenchymal laceration seen on CEUS (*arrow*). (Images courtesy of Dr Thomas Albrecht, Charité—Campus Benjamin Franklin, Berlin, Germany).

microcirculation where they persist for several minutes in the so-called 'sinusoidal' or 'late' phase.

Thus, the arterial phase is critical for demonstrating renal trauma (and other renal abnormalities). The cortical enhancement washes out after around a minute and this allows time for a sweep through the entire renal volume. A second injection is required for the contralateral kidney and usually these can both be drawn from the same ampoule of contrast agent. For the liver and spleen, the sinusoidal phase is the most useful time to scan. It begins at around 30 sec after injection and develops fully over the next 30–60 sec. This leads to a natural protocol for scanning these four organs in which the kidneys are studied first using separate injections, after which the liver and spleen are interrogated with no further injection required in most cases. Thus, the examination can be completed in less than 5 min. Since the microbubble contrast agents used are not cardio- or nephrotoxic, there are generally no contra-indications even in unstable patients and they can be repeated as often as needed, dictated by changes in the patient's vital signs.

Large prospective studies of the potential for contrast-enhanced ultrasound in trauma are underway. Pending completion and publication of the results, only anecdotal reports and pilot studies are available on which to form impressions of the potential role of contrast-enhanced ultrasound in trauma. Several case reports have been presented (7, 8). They often show dramatic images of arterial and sinusoidal phase defects in the kidneys, liver or spleen that were impossible to demonstrate using conventional modes. One report of results in abdominal trauma presented several cases, mostly following road traffic incidents, and demonstrated that lesions could be clearly seen with good correspondence with CT (9) (Fig. 1). A study of 25 patients with presumed splenic trauma using a recently introduced contrast agent and non-linear imaging showed good correlation with CT, only one of 18 lesions being missed, and this was a minor lesion (10). However, only patients with ultrasonographic abnormalities were recruited and this probably biased the results in favour of ultrasound; nevertheless, it is an encouraging result (Figs. 2 and 3).

Active Bleeding

Animal studies have shown that active bleeding from the kidney following experimental injury can be detected as extra-parenchymal enhancement. No systematic human studies have been reported but incidental demonstration of active bleeding from a recently biopsied kidney (Correas J-M, 2002, personal communication) have been reported.

Clinical Role

Clearly, the clinical role of contrast-enhanced ultrasound for the detection of abdominal trauma has not yet been defined but, in many trauma units in countries where

these agents are licensed, the method is acquiring respectability as a means for demonstrating injury to the liver, spleen and kidneys following both blunt and penetrating injuries. However, thus far it has found most use as a means to follow trauma for example, to check for stability before a patient is discharged. It is also useful in children where there is a strong reason to minimise the dose of ionising radiation that is inevitable with CT.

Because ultrasound cannot examine the brain and thorax, or the skeleton, whole-body CT will remain the definitive imaging test in polytrauma. Contrast-enhanced ultrasound may well find a role in follow-up and where trauma is considered to be limited to the abdomen (especially in children).

Bibliography

1. Stengel D, Bauwens K, Sehouli J et al (2001) Systematic review and meta-analysis of emergency ultrasonography for blunt abdominal trauma. Br J Surg 88(7):901–912
2. Brooks A (2001) The role of ultrasound in trauma. J R Army Med Corps 147(3):268–273
3. Nilsson A, Lorén I, Nirhov N et al (1999) Power Doppler ultrasonography: alternative to computed tomography in abdominal trauma patients. J Ultrasound Med 18:669–672
4. Miller M, Pasquale M, WJ B et al (2003) Not so fast. Trauma 1:52–60
5. Cosgrove D (ed) (2004) Advances in Contrast Agent Imaging Using Cadence Contrast Pulse Sequencing Technology (CPS) and Sono-Vue, vol 14, Springer Verlag, Heidelberg, Germany p 124
6. Quaia EE (2005) Contrast Media in Ultrasonography. Springer Verlag, Heidleberg
7. Kraemer N, Cosgrove D, and Blomley M (2004) Microbubble ultrasound demonstrates liver trauma. J Trauma 56(4):913–914
8. Oldenburg A et al (2004) Imaging of paediatric splenic injury with contrast-enhanced ultrasonography. Pediatr Radiol 34(4):351–354
9. Thorelius L (2004) Contrast enhanced ultrasound in trauma. Eur Radiol 14(S8):P43–P52
10. Catalano O, Lobianco R, Sandomenico F et al (2003) Splenic trauma: evaluation with contrast-specific sonography and a second-generation contrast medium. J Ultrasound Med 22:467–477

Contrast Media, Ultrasound, Applications in Echocardiography

Harald Becher[1,*], Robert Olszewski[2]
[1]Oxford University, John Radcliffe Hospital, Oxford, UK
*Cardiac Investigation Annexe, John Radcliffe Hospital, Oxford, UK
[2]Department of Cardiology, Military Medical Institute, Warsaw, Poland
harald.becher@orh.nhs.uk

Synonyms

Contrast echo; Contrast echocardiography; Contrast-enhanced echocardiography

Definition

Contrast in echocardiography is used mainly for three purposes: detection of intracardiac and intrapulmonary shunting, left ventricular opacification and myocardial perfusion. The contrast effect is based on the use of gas microbubbles as blood tracers exploiting their acoustic behaviour during exposure to ultrasound.

Characteristics

The first agents to be used for echocardiography were hand-agitated saline or glucose. These are still used to detect intracardiac shunts. The more recent second generation contrast agents consists of different types of perfluorocarbon gases encapsulated by modified phospholipids, albumin or galactose crystals. These agents are used for left ventricular opacification and myocardial perfusion imaging.

The agitated contrast media used for shunt detection provide intensive opacification of the right heart after intravenous injection. However, agitated agents are unable to cross the pulmonary vasculature. Only, if there is a right to left shunt contrast agent can be displayed in the left heart chambers. The most frequent application of agitated saline is the detection of right to left shunting in atrial septal defects and patent foramen ovale (1) (Fig. 1).

The second generation of contrast agents provide intensive opacification of the right and left heart chambers when administered intravenously. Two techniques for contrast applications are introduced: infusions are preferential for assessment of myocardial perfusion and bolus injections of agents may be satisfactory for left ventricular

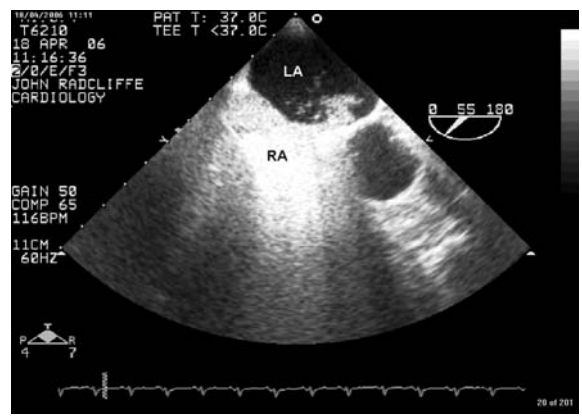

Contrast Media, Ultrasound, Applications in Echocardiography. Figure 1 Contrast transesophageal echocardiography. Contrast is seen mostly in right atrium (RA) and entering to left atrium (LA) via patent foramen ovale.

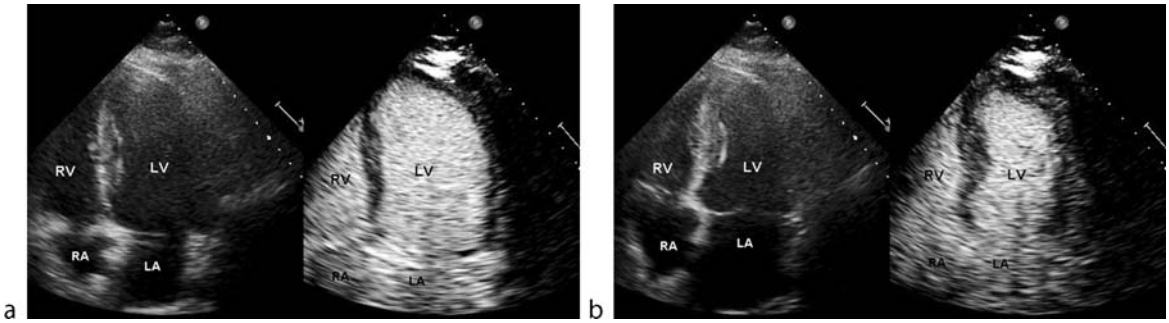

Contrast Media, Ultrasound, Applications in Echocardiography. Figure 2 Transthoracic echocardiographic images of the apical four-chamber view obtained from a patient before (*left*) and after (*right*) the administration of contrast agent. (a) enddiastolic, (b) endsystolic frames. The endocardial border is not well seen at baseline but becomes readily apparent with contrast enhancement. LV—left venticle, RV—right ventricle, LA—left atrium, RA—right atrium.

opacification in many cases. The dosages of contrast needed for LV opacification are minimal—0.1–0.3 ml—compared to those in other imaging modalities like X-ray. These small dosages are possible because of very sensitive contrast specific imaging technologies, which have been implemented in all state of the art ultrasound systems (2).

The major indication for the second generation contrast agents is left ventricular opacification and endocardial border definition. Although image quality has been improved with the introduction of harmonic imaging, there are still a number of studies remaining of inadequate quality, and it is here that the use of contrast agents comes into its own. Even with high-end ultrasound equipment, without contrast, the percentage of suboptimal images ranges from 10 to 15% (Fig. 2). The recent guidelines of the European Association of Echocardiography (EAE) and the American Society of Echocardiography (ASE) suggest to use the delineation of the endocardium as a selection criterion (3). Contrast agents should be considered when less the 80% of the circumference of the LV endocardium is not clearly seen. This is of major importance in stress echocardiography where there is always the need for optimal image quality. Clinical studies have shown the benefit of contrast in improving image quality, percentage of wall segments visualized, and confidence of interpretation of regional and global function both at rest and at peak stress (4).

Less frequently contrast agents are needed for better delineation of thrombi and masses.

In tandem with the development of contrast agents there have been advances in imaging modalities. The first contrast specific modality was harmonic imaging.

Second harmonic imaging enhances contrast effect compared to fundamental imaging and has been used for border definition using real-time imaging. However, it also leads to bubble destruction and artefacts. Latest developments such as power modulation and power pulse inversion, use less transmitting power than harmonic imaging and are almost non-destructive for bubbles and can be performed real-time imaging without the limitations of harmonic imaging and with less contrast. As tissue returns are not displayed, unlike with harmonic imaging, they are ideal for accurately delineating the left ventricular borders and assessing myocardial perfusion.

Harmonic Power Doppler is another method for perfusion imaging. It takes advantage of the signals obtained from bubble destructions during exposure to ultrasound. Power Doppler provides the highest signal to noise ratio for detecting contrast media, but has to be used with trigged mode. That means intermitted power of scanning to replenish the contrast in the myocardium.

Myocardial contrast echocardiography (MCE) is an imaging tool for the assessment of the myocardial microcirculation. Myocardial perfusion is defined as tissue blood flow at the capillary level. The two components of tissue blood flow—capillary blood volume and blood velocity—can be assessed by MCE.

Contrast perfusion imaging can be used to assess inducible myocardial ischemia and viability. The advantage of using perfusion imaging in stress echocardiography is higher accuracy in detecting coronary stenoses. In addition shorter and simple stress protocols can be used.

MCE can be used to determine the spatial extent of viable tissue post-infarction. It has been shown to be superior for detection of acute coronary syndromes in the emergency department compared with routine evaluation. MCE, a rapid bedside method, can be used to define the extent of collateral perfusion during coronary occlusion and hence to predict the ultimate infarct size. It has been performed safely in several thousand patients (5) (Fig. 3).

Current research focuses on using the microbubbles of ultrasound contrast media as drug and gene carriers and applying targeted ultrasound for local drug delivery. Another promising application is the use of the microbubbles to target arteriosclerotic vascular lesions.

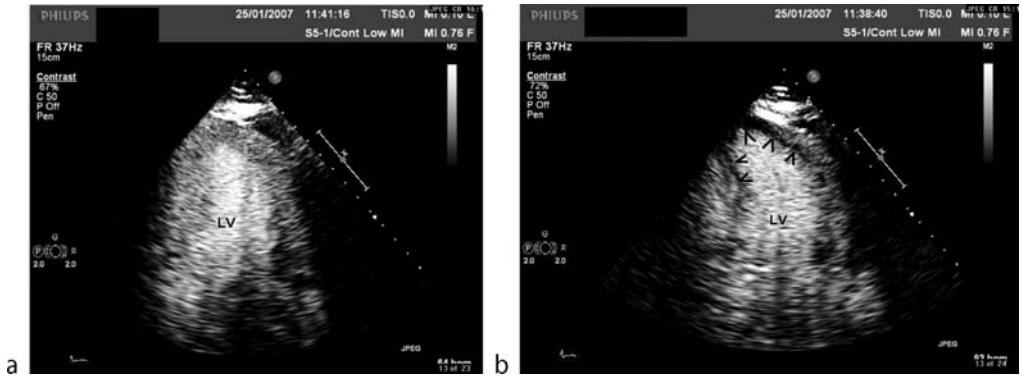

Contrast Media, Ultrasound, Applications in Echocardiography. Figure 3 Contrast study with adenosine. (a) Apical two chamber view in systole at rest showing normal perfusion. (b) After adenosine injection a perfusion defect is displayed in apical anterior and inferior wall (*arrows*) LV—left venticle.

Bibliography

1. Woods TD, Patel A (2006) A critical review of patent foramen ovale detection using saline contrast echocardiography: when bubbles lie. J Am Soc Echocardiogr 19(2):215–222
2. Becher H, Burns P (2000) Handbook of Contrast echocardiography. Springer Verlag. Free download ▶//www.sunnybrook.utoronto.ca/EchoHandbook
3. Lang RM, Bierig M, Devereux RB et al (2006) Recommendations for chamber quantification. Eur J Echocardiogr 7:79–108
4. Olszewski R, Timperley J, Szmigielski C et al (2007) The clinical applications of contrast echocardiography. Eur J Echocardiogr in press
5. Lepper W, Belcik T, Wei K et al (2004) Myocardial contrast echocardiography. Circulation 109(29):3132–3135

Contrast Media, Ultrasound, Applications in Focal Splenic Lesions

Christopher J. Harvey, Adrian K. P. Lim, Martin J. K. Blomley, David O. Cosgrove
Hammersmith and Charing Cross Hospital NHS Trust & Imperial College, London, UK
charvey_99@yahoo.com

Synonyms

Contrast-enhanced ultrasound of the spleen; Microbubble-enhanced ultrasound of the spleen

Definition

The use of microbubble agents and contrast-specific ultrasound (US) imaging modes for detecting splenic pathology. This technique also allows the further evaluation and characterisation of ▶focal splenic lesions, ranging from malignant tumours to benign entities such as splenic infarcts, haemangiomata or abscesses based on patterns of perfusion and splenic parenchymal contrast uptake.

Characteristics

Introduction

The advent of ▶microbubbles has allowed more accurate ultrasonic characterisation of focal splenic lesions to rival that of computed tomography (CT), magnetic resonance imaging (MRI) and nuclear medicine techniques.

Microbubbles were initially thought to be purely vascular agents. However, three agents demonstrate hepatosplenic-specific uptake after their disappearance from the blood-pool phase. They are Levovist, Sonavist (both Schering AG, Germany) and Sonazoid (NC100100; GE Amersham, Norway), of which only Levovist is currently in clinical use. Interestingly, the most widely used microbubble in Europe, SonoVue (Bracco, Italy), demonstrates splenic specificity only (1–3).

In the arterial phase, the spleen demonstrates heterogeneous and patchy ▶enhancement from 0 to 20 sec with the spleen then becoming homogeneous throughout within 50 sec. These enhancement characteristics are similar to those reported with iodinated contrast agents within the spleen on CT and MR imaging and are thought to be due to variable flow rates through the cords and sinuses of the red pulp. Therefore, it is recommended that lesion detection and assessment of the spleen with microbubbles should include the late phase, at least 60 sec post-intravenous injection.

Technological advances combined with the availability of more stable microbubbles (e.g. SonoVue) have facilitated the development of real-time non-destructive (low mechanical index (MI)) ▶microbubble-specific imaging modes that are widely used for focal splenic lesion assessment. Contrast-enhanced imaging of focal splenic lesions may be divided into arterial (20–25 sec) and portal (45–90 sec) phases and sinusoidal (>90 sec). Real-time imaging allows these phases to be followed successively, so that the dynamic enhancement pattern and vascular morphology may be assessed (1–3). The low MI means that continuous imaging can be performed for as long as the agent persists (5–10 min after a full dose of SonoVue). The fundamental and enhancement characteristics of splenic lesions are described later.

Focal Splenic Lesions

Congenital Lesions

A splenunculus is accessory splenic tissue, which is present in 10–30% of the population. They may be single or multiple and most commonly occur at the splenic hilum (75%). They typically have a round contour and their echogenicity is identical to that of the parent spleen. Splenunculi have identical enhancement patterns with ultrasound microbubbles to the adjacent spleen. Splenunculi and the parent spleen enhance simultaneously in the arterial phase and exhibit a heterogeneous sinusoidal phase. Some agents (Levovist, Sonovue) have a delayed splenic-specific parenchymal phase, which is useful in differentiating splenunculi from lymph nodes or pancreatic masses.

Cystic Lesions

Cystic splenic lesions may be subdivided into primary cysts, which are either non-parasitic (epithelial) or parasitic (echinococcosis infection), or secondary cysts, which are thought to be traumatic in aetiology. They contain blood, debris and may exhibit mural calcification.

Non-parasitic cysts show the classic ultrasound features of anechoic contents with posterior acoustic enhancement and smooth walls. Microbubble contrast agents may be helpful in defining the thin wall of the cyst and demonstrating the absence of central enhancement to differentiate benign simple cysts from infective or neoplastic cystic lesions.

Hydatid cysts are rare in the spleen (less than 5% of echinococcus infections). They may be anechoic or have heterogeneous echogenecity. The 'water-lily sign' is characteristic of the condition and is caused by separation of the membranes of the cyst. With intravenous (IV) microbubbles, hydatid cysts show peripheral but not internal enhancement.

Haemangiomas

Haemangiomas are the commonest benign primary splenic neoplasm with a prevalence of 0.3–14% at autopsy. They are tumours of the epithelium of the vascular sinuses and are more commonly cavernous than capillary in pattern. Cavernous haemangiomas are usually small (<2 cm) and are incidental findings on imaging. They are slow growing. Occasionally, haemangiomas may be large and may present as a mass or with rupture and bleeding.

Multiple splenic haemangiomas occur in Klippel–Trenaunay syndrome and may be complicated by rupture, hypersplenism and malignant change.

On ultrasound, haemangiomas typically appear as well-defined avascular echogenic lesions. Atypical features, which are more commonly present in large cavernous haemangiomas, include cystic change and calcification. Small haemangiomas uniformly enhance with microbubbles whereas larger lesions exhibit centripetal filling in on delayed imaging (Fig. 1). However, larger lesions with cystic/necrotic/thrombotic components may show heterogeneous enhancement rather than the centripetal pattern (4). This is due to the fact that cystic spaces (often central) do not possess blood-filled vascular spaces.

Hamartomas

Splenic hamartomas, also known as splenomas, splenadenomas and nodular hyperplasia of the spleen are rare benign tumours occurring with an incidence of 0.024–0.13% in autopsies.

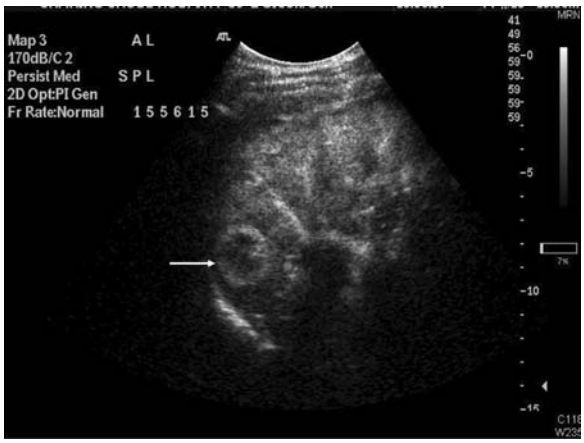

Contrast Media, Ultrasound, Applications in Focal Splenic Lesions. Figure 1 Splenic haemangioma: imaging in the late splenic-specific phase with SonoVue (Bracco, Milan, Italy) using phase inversion mode (HDI 5000, Phillips, USA) shows partial centripetal filling-in of the lesion (arrow) at 3 min post-injection.

Splenic hamartomas are usually found incidentally, although rupture has been described.

On ultrasound, splenic hamartomas are usually solid homogeneous masses and hyperechoic relative to the adjacent splenic parenchyma. However, some may be heterogeneous with cystic changes and areas of calcification secondary to ischaemia or haemorrhage. They are usually hypervascular on colour Doppler. This is thought to reflect the hypervascularity of the red pulp in the hamartoma. Variable enhancement is seen following the intravenous microbubble injection (4, 5).

Lymphangioma

Splenic lymphangioma is a rare slow growing benign tumour. It is characterised by splenic cysts of varying sizes from a few millimeters to several centimeters in size. Splenic lymphangiomas may occur in isolation or with multisystem organ involvement. Complications are associated with the more extensive or larger lymphangiomas and include bleeding, hypersplenism, consumptive coagulopathy and portal hypertension. Malignant transformation is rare but has been described in one case.

On ultrasound, splenic lymphangiomas appear as cystic lesions with septation, echogenic debris and calcification. Lymphangiomas are avascular on colour Doppler and do not enhance with microbubbles.

Lymphoma

Malignant lymphoma is the most common cause of splenic infiltration. The typical ultrasound appearances are of echopoor focal lesions that may be difficult to distinguish from cysts. The borders of the lesions may be poorly defined. 'Target sign' lesions and echogenic lesions have been described. Typically, Hodgkin's and low-grade non-Hodgkin's lymphoma result in diffuse infiltration or focal lesions, which are lesser than 3 cm in size. By comparison, high-grade non-Hodgkin's lymphoma causes focal lesions of greater than 3 cm in size. With microbubbles, irregular peripheral enhancement is seen with the lesions appearing as defects in the late phase (4).

Metastases

Splenic metastases are rare; 7% of post-mortems in patients with metastatic carcinomas and 8% of all splenic lesions were shown to be metastases in one series. The spleen may be involved by direct tumour invasion in pancreatic tail, colon, stomach, bronchus and diaphragmatic carcinomas. The ultrasound appearances are variable with echopoor metastases, being the most common. Echogenic metastases are the least common (5) and target lesions are less common than in the liver. Serosal metastases from ovarian carcinoma result in scalloping of the splenic margin. On Doppler, metastases are usually avascular. Imaging with microbubbles may show variable enhancement in the arterial phase but essentially, all lesions appear as defects surrounded by normally enhancing splenic parenchyma in the late phase (Fig. 2). Metastases may be revealed that are not seen on baseline B-mode/fundamental scanning by increasing their conspicuity. This improves the detection and facilitates the detection of subcentimetre metastases that would otherwise remain occult (4).

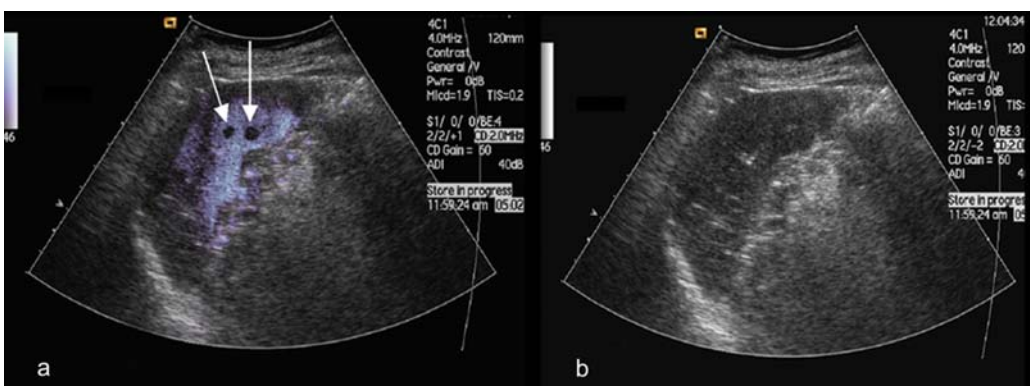

Contrast Media, Ultrasound, Applications in Focal Splenic Lesions. Figure 2 Splenic metastases from melanoma. (a) A duration of 3 min after Levovist (Schering), imaging using a late phase destructive mode (Agent Detection Imaging (ADI), Siemens, USA) demonstrates two metastases as defects (arrows) surrounded by normal splenic microbubble uptake. (b) When the colour overlay is removed, no corresponding B-mode lesions could be identified. This case demonstrates the imaging of the late splenic-specific phase of Levovist that improves the detection of occult metastases by increasing their conspicuity.

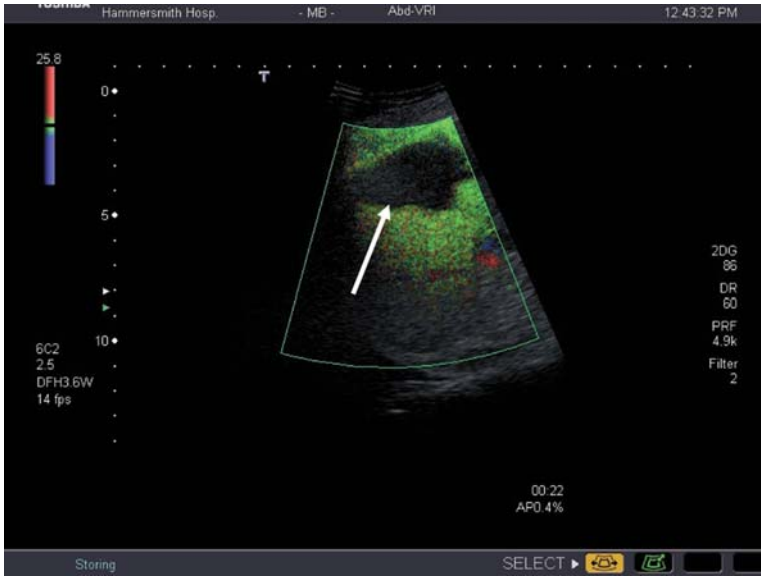

Contrast Media, Ultrasound, Applications in Focal Splenic Lesions. Figure 3 Imaging using Vascular Recognition Imaging (VRI, Aplio, Toshiba, Tokyo, Japan). A duration of 3 min after SonoVue administration shows a wedge-shaped non-enhancing defect consistent with an infarct (arrow) with normal enhancement of the surrounding spleen depicted by stationary microbubbles in green.

Splenic Infarction

Splenic infarction may result from emboli (endocarditis), hyperviscosity syndromes, sickle cell disease and myeloproliferative disorders. On B-mode, acute infarction is ill-defined, characteristically peripheral, wedge-shaped and echopoor. On colour Doppler absent signals confirm the diagnosis. Chronic infarction is seen as an echogenic area due to fibrotic change or calcification with overlying cortical retraction secondary to scarring. Microbubbles improve the ultrasound confidence of diagnosing early infarction (Fig. 3) by delineating an angular geographical hypo-enhancing area in all phases (4).

Splenic Abscesses

Splenic abscesses on ultrasound may be echopoor, septated, irregular walled containing debris and gas. They may have variable peripheral vascularity. Microbubbles may show the vascular rim of the abscesses. Common organisms include *Mycobacterium tuberculosis*, *Pneumocystis carinii* and *Candidiasis*. The latter have been described as showing a characteristic 'bull's eye' appearance with multifocal small lesion (0.5–2 cm in size) consisting of echogenic centres surrounded by echopoor rims. The detection of these lesions is improved by using a high-frequency linear probe. US contrast improves the detection of microabscesses by improving their conspicuity against the normal splenic parenchyma (4).

Heterogeneous Splenic Echotexture

This is seen as multiple tiny (2–3 mm) echogenic foci or just a heterogeneous echopattern on B-mode ultrasound. It is a non-specific finding typically in previous granulomatous infection such as tuberculosis, fungi as well as sarcoidosis, Wegener's granulomatosis, amyloidosis and Crohn's disease. These foci are generally defects in the late phase after microbubble administration.

Summary

Ultrasound is a reliable method of imaging splenic abnormalities. The introduction of microbubbles has further improved the diagnostic capabilities of ultrasound, allowing the investigation of splenic enhancement patterns and characterisation of focal lesions. US imaging in contrast is useful in distinguishing splenunculi from lymph nodes, demonstrating the characteristic enhancement patterns in haemangiomas, improving the visualisation of splenic infarction as well as improving the detection of microabscesses and focal malignancies.

Bibliography

1. Harvey CJ, Blomley MJ, Eckersley RJ et al (2001) Developments in ultrasound contrast media. Eur Radiol 11:675–689

2. Correas JM, Bridal L, Lesavre A et al (2001) Ultrasound contrast agents: properties, principles of action, tolerance, and artifacts. Eur Radiol 11:1316–1328
3. Lim AKP, Patel N, Eckersley RJ et al (2004) Evidence for spleen-specific uptake of a microbubble contrast agent: a quantitative study in healthy volunteers. Radiology 231:785–788
4. Peddu P, Shah M, Sidhu PS (2004) Splenic abnormalities: a comparative review of ultrasound, microbubble-enhanced ultrasound and computed tomography. Clin Rad 59:777–792
5. Abbott RM, Levy AD, Aguilera NS et al (2004) Primary vascular neoplasms of the spleen: radiologic–pathologic correlation. Radiographics 24:1137–1163

Contrast Media, Ultrasound, Applications in Kidney Tumor

Anders Nilsson
Department of Radiology, Ultrasound University, Uppsala University Hospital, Uppsala
anders.nilsson@akademiska.se

Synonyms

CEUS; Contrast-enhanced ultrasound of the kidneys

Definition

Contrast-enhanced ultrasound (CEUS) of the kidneys is mainly dependent on two things: (1) the availability of a contrast agent that will give off strong echoes, by reflection and resonance, and that can be injected intravenously and insonated without significant destruction of the contrast itself, and (2) ultrasound machine software that allows specific recognition of a signal/echo emanating from the contrast agent at an ultrasound output level that will not destroy the agent.

When these requirements are met, we can produce images where the echogenicity is dependent on the contrast agent concentration rather than on the reflectivity and absorption of the insonated tissue. Most contrast agents in clinical use today consist of stabilized gas bubbles, the resonance of which can be distinguished from tissue echoes by dedicated software implemented in the ultrasound machines. Ultrasound contrast agents are so-called ►*blood pool agents*; that is, they do not, in contrast to X-ray contrast media, leave the blood vessels.

Characteristics

Pathology

It is important to understand that the established phases of ultrasound contrast enhancement in the liver (1, 2) do not apply in the kidney because they are dependent on contrast accumulation in normal liver tissue. However, circulation in a capillary bed such as in the kidney is, of course, considerably slower than arterial flow. Because tumor tissue contain pathological vessels with ►*arteriovenous shunting*, it stands to reason that differences in the contrast uptake over time will be different in renal tumors than in normal renal tissue. Preliminary work suggests that the perfusion differences between tissues with a normal capillary bed and the ►*neovascularization* of tumors can be detected if the pattern of contrast enhancement is followed over time, either subjectively or with the aid of analyses programs, preferably built into the ultrasound machine itself (3).

Furthermore, areas completely without blood perfusion will remain dark in a contrast-based image, as no contrast agent will reach these areas. Therefore, images based on contrast concentration can help in the detection of nonperfused focal lesions like cysts, abscesses, infarctions, and post radio-frequency ablation necroses and in their differentiation from tumor tissue. Normal variants, like a ►*column of Bertin*, will have the same enhancement pattern as other normal parts of the renal parenchyma, which may help to make a more confident diagnosis.

Imaging

Normal Kidney

Different stages of renal enhancement exist but are not the same as those described in the liver due to both lack of contrast accumulation and the perfusion differences between the renal cortex and the medulla. The contrast phases must be understood in order to avoid misdiagnosis. The arteries enhance shortly after a bolus injection of contrast agent and are followed closely by a complete fill-in of the cortex. The pyramids, having less vascularity, then gradually enhance over the next 30–40 sec to become isoechoic or almost isoechoic with the cortex. The enhancement then decreases slowly as the contrast concentration in the general circulation falls off (Fig. 1). When this happens, a difference may again appear between the cortex and pyramids, the latter becoming once more hypoechoic. This reappearance of hypoechoic areas corresponding to the pyramids must be remembered because it has a likeness to the enhancement pattern seen in most malignant tumors (see below).

Cysts, Abscesses, and Infarctions

Because structures without perfusion will have no contrast uptake, they will have no brightness in the ultrasound contrast image; they will remain dark with an excellent delineation against surrounding tissues. Simple cysts will thus be unechoic during all the contrast phases even if they

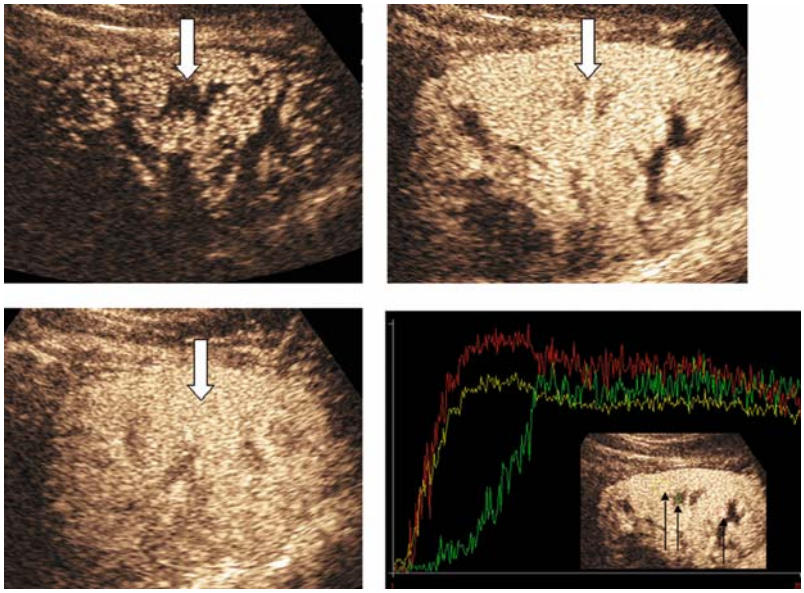

Contrast Media, Ultrasound, Applications in Kidney Tumor. Figure 1 Normal renal enhancement after an intravenous bolus of ultrasound contrast agent. The pyramids (*arrows*) enhance slower but show a complete fill-in after about 60 sec. This is also shown by the quantification graph where regions-of-interest have been placed in a segmental artery, cortex and a pyramid.

are echoic on native ultrasound. In this manner, smaller cysts can be detected and, more importantly, cysts containing echoes (e.g., after a bleeding) can be seen completely without perfusion. The spatial resolution of ultrasound can therefore be used for characterizing indeterminate focal lesions detected on computed tomography (CT), for example (4). New software programs have an excellent sensitivity for detecting even tiny amounts of contrast agents, which makes it possible to detect thin but perfused septae indicative of malignancy rather than simple cysts (Fig. 2).

Similarly, focal lesions that on native ultrasound contain echoes but have no perfusion, such as abscesses and cortical infarctions, can be detected and distinguished from perfused, possibly malignant lesions.

Tumors, Malignant

The contrast enhancement of small hypovascular tumors may be hard to detect on CT, making confident diagnosis of a renal cell carcinoma difficult. It is, of course, an important distinction that can often be made by CEUS, due to the high sensitivity to the presence of contrast agents, even in small quantities. Thus, tumoral vessels can be detected, possibly with the aid of quantification software that can prove an increase in image brightness, assisting the subjective assessment. In addition, small vessels may be depicted in mural nodules, septae, or thickened cyst walls even when they are too small to be detected by Doppler (5) (Fig. 2). Thus, CEUS may be used for evaluating unequivocal CT or magnetic resonance (MR) findings, atypical cysts, or cyst-like lesions with echogenic contents, the existence of contrast within the suspected areas being equivalent to the existence of vessels (i.e., perfused viable tissue).

In the same way, biopsies can be guided to viable areas of a suspected lesion, avoiding necrosis and thus improving the diagnostic yield (6).

Renal tumors often have a contrast enhancement pattern similar to the normal renal parenchyma in the early stages. There may be a rim enhancement in a pseudocapsule (7), but as there is no real accumulation of contrast in the kidneys, the detection rate of small tumors is unlikely to be as much improved by CEUS as is seen with focal liver lesions. However, the vasculature of malignant tumors differs from that of normal tissues, and early experiences indicate that contrast will be washed out of the neovasculature faster than from the renal capillaries, creating a similar but weaker equivalent to the situation in the liver, possibly helping characterization if not detection (8). Thus, malignant tumors tend to be hypoechoic compared with normal parenchyma in the later phases (Fig. 3). This could be helpful in evaluating normal variants, such as a prominent column of Bertin (see above). The suspected area must then be followed to the later stages of the contrast enhancement, at least for 1 min. Most often, a clear difference can be detected by

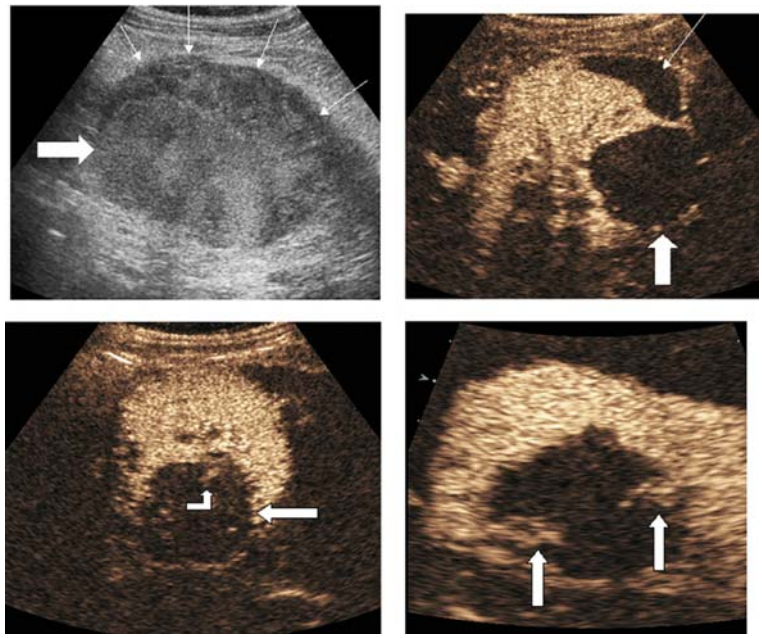

Contrast Media, Ultrasound, Applications in Kidney Tumor. Figure 2 Patient with sudden onset of pain in the right flank. Native ultrasound shows the kidney (*fat arrow*) surrounded by a hematoma (a). On CEUS the hematoma is better delineated (*thin arrow*) and a cyst is seen, probably haemorrhagic as it was not detected on B-mode (b). CEUS also detects small contrast enhancing nodules (*arrows*) within the cyst (c, d). A cystic renal cell carcinoma was later removed.

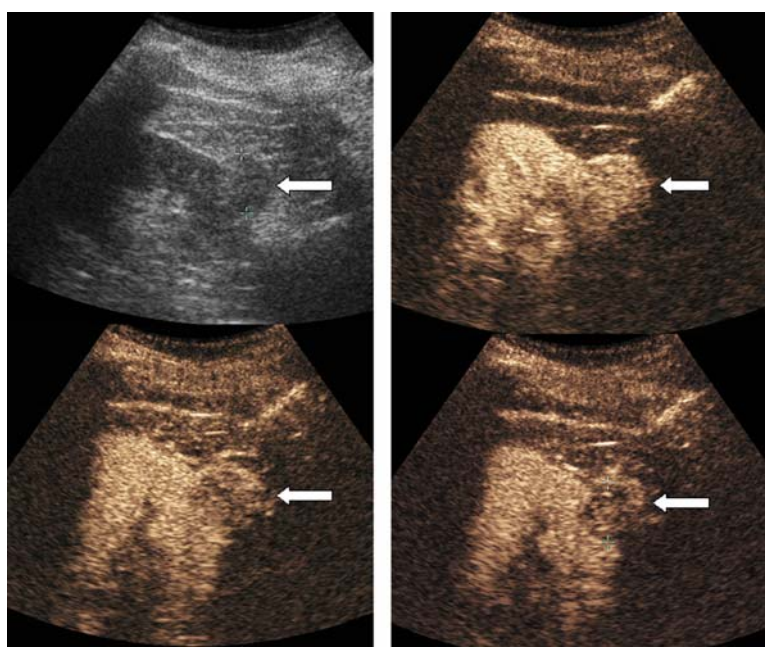

Contrast Media, Ultrasound, Applications in Kidney Tumor. Figure 3 Small renal cell carcinoma seen both on B-mode (a) and CEUS with a contrast enhancement typical of most malignant lesions, i.e. almost isoechoic with the normal parenchyma in the early stages (b = 15 sec) and then increasingly hypoechoic compared to the kidney (c = 30 sec, d = 60 sec).

analysis software at that stage and seen subjectively shortly thereafter. Necrotic areas of the tumor will remain dark, but because partially necrotic tumors tend to be large, they are easily diagnosed on native ultrasound. The detection of necroses is, therefore, of limited importance except as guidance for biopsies.

Tumors, Benign

Vessel anatomy may eventually help distinguish malignancies from benign oncocytomas, but at present, there is not enough scientific evidence to allow us to make that distinction. Lesions such as angiomyolipomas have been shown to enhance less than renal cell carcinomas in the arterial phase (9) and tend to retain the contrast better than a malignant tumor in the later phases, presumably due to vessel anatomy. However, knowledge about how a small, highly differentiated malignant tumor would behave is limited, and differentiation in the individual patient remains difficult.

Diagnosis

It is important to remember that even though the accumulated experience so far indicates that malignant tumors are hypoechoic in the later contrast stages, it cannot be inferred that a lesion that retains contrast is benign. There are as yet no scientific data proving an ability to differentiate between benign and malignant focal lesions, but with improved knowledge of contrast enhancement patterns, this ability may be only a matter of time.

Even though the detection rate of small renal cell carcinomas is unlikely to be improved, CEUS can play an important role in characterizing atypical lesions, detecting small nodules in cystic tumors, and differentiating them from normal variants.

Bibliography

1. Wilson SR, Burns PN, Muradali D et al (2000) Harmonic hepatic US with microbubble contrast agent: initial experience showing improved characterisation of haemangioma, hepatocellular carcinoma and metastasis. Radiology 215:153–161
2. Albrecht T, Hoffmann CW, Schmitz SA et al (2001) Phase inversion sonography during the liver specific late phase of contrast enhancement: improved detection of liver metastases. Am J Roentgenol 176:1191–1198
3. Cosgrove D, Eckersley R, Blomley M et al (2002) Quantification of Blood Flow. Ultrasound. ECR Categorical Course Syllabus. Springer, Berlin Heidelberg New York, pp 84–90
4. Correas JM, Claudon M, Tranquart F et al (2003) Contrast-enhanced ultrasonography: renal applications. J Radiol 84:2041–2054
5. Ascenti G, Zimbaro G, Mazziotti S et al (2001) Usefulness of power Doppler and contrast-enhanced sonography in the differentiation of hyperechoic renal masses. Abdom Imaging 26:654–660
6. Krause J, Nilsson A (2003) Targeted tumor biopsy under contrast-enhanced ultrasound guidance. Eur Radiol 13(Suppl 4):L239–L240
7. Ascenti G, Gaeta M, Magno C et al (2004) Contrast-enhanced second-harmonic sonography in the detection of pseudocapsule in renal cell carcinoma. Am J Roentgenol 182(6):1525–1530
8. Quaia E, Siracusano S, Bertolotto M et al (2003) Characterization of renal tumours with pulse inversion harmonic imaging by intermittent high mechanical index technique: initial results. Eur Radiol 13(6):1402–1412
9. Siracusano S, Quaia E, Bertolotto M et al (2004) The application of ultrasound contrast agents in the characterization of renal tumors. World J Uro 22(5):316–322

C

Contrast Media, Ultrasound, Applications in Transcranial and Intra-Operative Brain Ultrasound

Thilo Hoelscher
Department of Radiology
University of California, San Diego, USA
thoelscher@ucsd.edu

Synonym

Contrast-enhanced ultrasound imaging of the brain

Definition

Transcranial Doppler describes the assessment of flow velocities of intracranial vessels by interpretation of flow spectra while insonating through the intact skull. Other than Doppler flow measurements alone, duplex sonography enables one to combine the visualization of morphological structures with flow velocity assessment using Doppler. Transcranial duplex sonography of the adult brain was introduced in the early 1990s and has been used since then mainly to visualize and assess the circle of Willis. Signal absorption and phase aberration due to insonation through the bone limit the applicability. The introduction of ultrasound contrast agents (UCA) and the development of contrast-specific imaging techniques have improved vascular imaging of the brain significantly. To date, contrast-enhanced ultrasound of the brain includes transcranial macro- and microvascular imaging and assessment as well as intraoperative and therapeutic applications. In this context, the term transcranial Doppler is established and commonly used, whereas new technologies and applications broaden the spectrum of brain ultrasound, exceeding the definition of transcranial Doppler.

Imaging

Macrovascular Imaging

The visualization and assessment of intracranial arteries (circle of Willis) are the domain of transcranial color-coded duplex sonography (TCCS). The main difference compared with conventional transcranial Doppler (TCD) is the color-coded representation of arterial blood flow to allow the unequivocal identification of the circle of Willis within the anatomic grayscale (B-mode) image of the brain parenchyma. Using the Doppler mode, the blood flow can be analyzed semiquantitatively, as in conventional TCD, but with the added advantage of visual control by tracking the target vessel using the color flow map. The major limitation of all transcranial ultrasound techniques has been the massive acoustic signal absorption while insonating through the intact skull. The introduction of UCA improved transcranial vascular imaging significantly, and the diagnostic benefits have been proven in multiple studies (1, 2). Besides the unequivocal advantages of UCA for transcranial ultrasound imaging, contrast-specific artifacts such as "blooming" may limit the diagnostic impact. Strong acoustic signals, encoded as color pixels on the screen, may appear "outside" the anatomical delineation of the vessel, especially in the early phase after UCA injection. The enhancement appears as an overamplification of the color or power Doppler signals on the screen of the ultrasound equipment (Fig. 1). Due to the rapidly increasing knowledge of the acoustic properties of UCA, contrast-specific modalities have been developed to improve transcranial image quality. To date, UCA-specific imaging enables one to visualize intracranial arteries in an angiography-like pattern with higher spatial resolution, fewer artifacts, and lower acoustic output power (Fig. 2) (3). Clinically, contrast-enhanced transcranial ultrasound has the highest impact on stroke diagnosis. The fast and unequivocal assessment of vessel occlusion/patency in the emergency room, or even in the ambulance, may help to optimize the therapeutic strategy for the individual stroke patient.

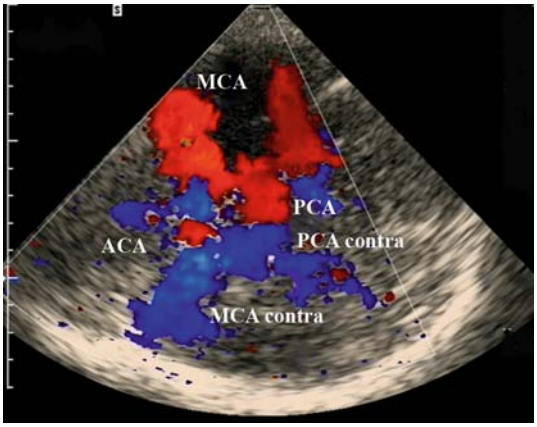

Contrast Media, Ultrasound, Applications in Transcranial and Intra-Operative Brain Ultrasound. Figure 1 "Blooming" artifact contrast-enhanced transcranial ultrasound of the circle of Willis (axial scanning plane *via* the temporal bone window). Vessel delineation is diminished because of the strong contrast signal ("blooming") after intravenous bolus injection of the UCA. *Lighter area* coding represents flow toward the transducer, *darker area* coding flow away from it. MCA: middle cerebral artery, MCA contra: middle cerebral artery contralateral, PCA: posterior cerebral artery, PCA contra: posterior cerebral artery contralateral, ACA: anterior cerebral artery.

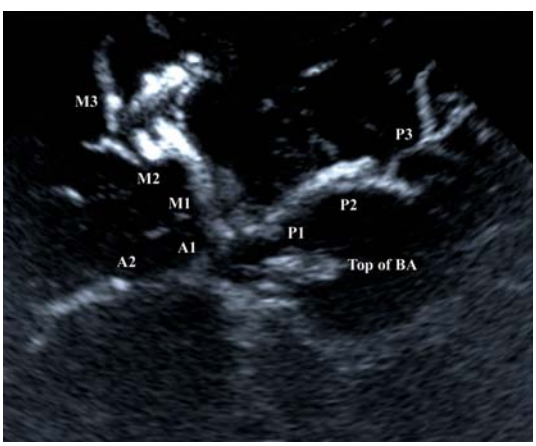

Contrast Media, Ultrasound, Applications in Transcranial and Intra-Operative Brain Ultrasound. Figure 2 Transcranial ultrasound angiography (tUSA) tUSA image of the circle of Willis and its branches after UCA injection. M1, M2, M3: middle cerebral artery segments, A1, A2: anterior cerebral artery segments, P1, P2, P3: posterior cerebral artery segments, BS: brain stem, Top of BA: hyperechogenic distal part of the basilar artery.

Microvascular Imaging

Contrast-specific transcranial ultrasound imaging modalities to assess the parenchymal brain perfusion are mainly based on UCA destruction, due to the high acoustic power used for insonation through the intact skull. Most perfusion techniques applied in brain ultrasound are based on the fact that UCA microbubbles undergo destruction, splitting, and fusion at higher acoustic pressures. These broadband noises partially pass the wall filter used in color and power Doppler and, due to the Doppler shift are interpreted as flow signals, independent of the movement of microbubbles. Three main principles of destructive imaging techniques to assess parenchymal perfusion can be described: (a) bolus kinetic, (b) depletion, and (c) replenishment methods.

Most commonly, the bolus kinetic technique is used to describe the wash-in/wash-out behavior of the UCA after intravenous bolus injection. After data acquisition over time in a predefined scanning plane and using a low frame rate, regions of interests (ROI) are placed in dedicated anatomical areas (Fig. 3). The interpretation of parameters such as signal peak intensity or time to peak intensity is used to semiquantify perfusion patterns and to differentiate between normal (4) or disturbed perfusion (5). Contrast-enhanced brain perfusion

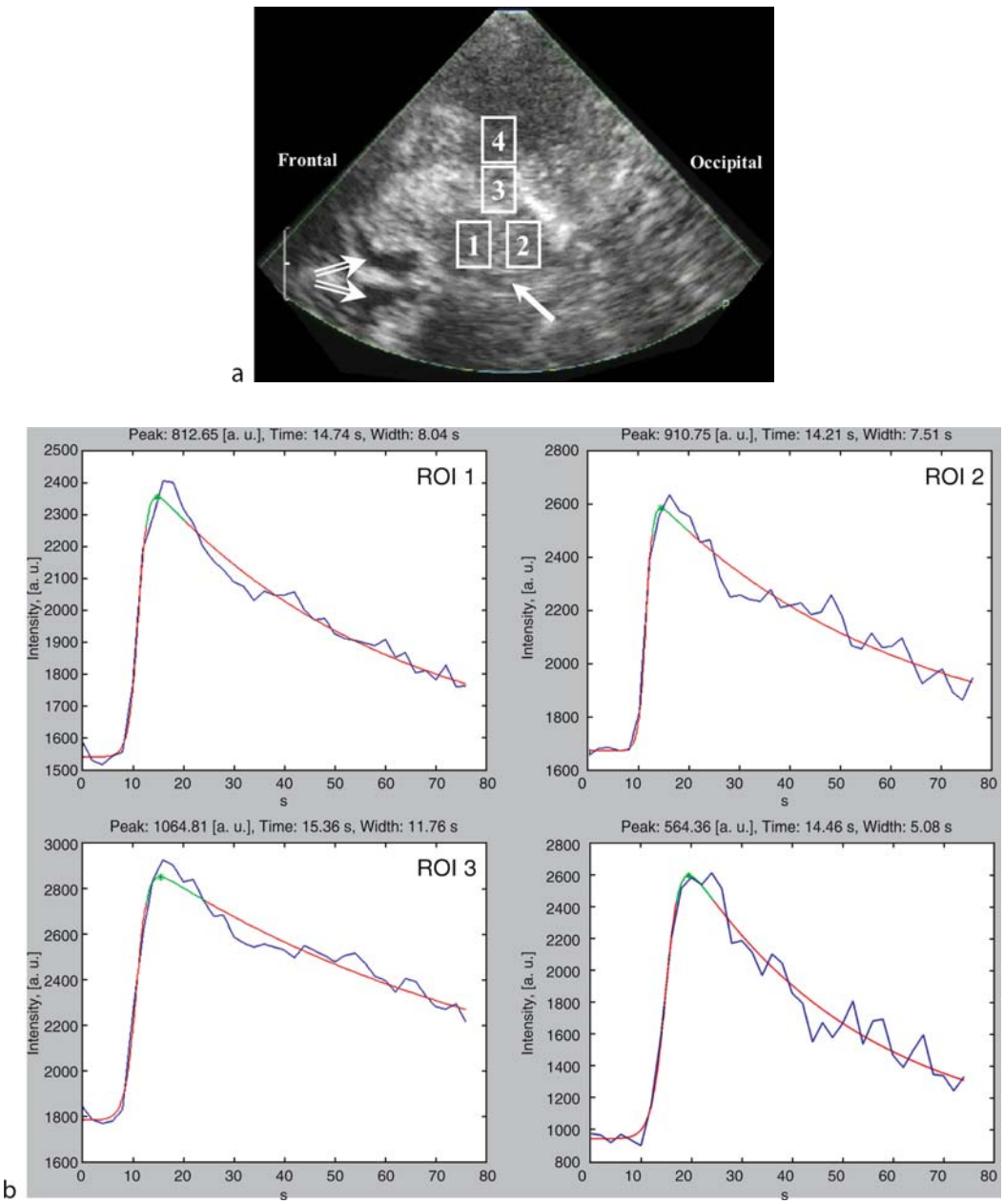

Contrast Media, Ultrasound, Applications in Transcranial and Intra-Operative Brain Ultrasound. Figure 3 Time intensity curves of certain ROIs (a) Axial B-mode image of the diencephalic scanning plane. Visualization of the third (*white arrow*) and the lateral (*dashed white arrows*) ventricles. Projection of the parenchymal ROIs: anterior parts of the thalamus (1), posterior parts of the thalamus (2), lentiform nucleus (3), white matter (4). (b) Corresponding time intensity curves displaying the wash-in/wash-out behavior of the UCA over time in certain ROIs.

imaging achieves clinical importance predominantly in the acute stroke setting and for monitoring the therapeutic effect of thrombolysis (6). Early as well as subsequent information about the microvascular status in the presence or absence of intracranial vessel occlusion may help to optimize the individual therapeutic strategy and extend the therapeutic window for thrombolysis.

Intraoperative Applications

The intraoperative application of ultrasound during neurosurgical interventions has been shown in several studies (7). Although intraoperative magnetic resonance imaging (MRI) and computed tomography (CT) have undoubted benefits, the techniques are costly and therefore not commonly available. In comparison, ultrasound is cost-effective, easy to use, and the only true real-time imaging method. The main goals of intraoperative imaging with ultrasound are the localization of and the navigation to lesions (i.e., tumor, aneurysm, arteriovenous malformation), the assessment of the vascular supply of these pathologies, and the ability to immediately monitor the success of the neurosurgical intervention. The intraoperative use of UCA is of interest, especially in the context of advanced transducer technologies and contrast-specific imaging modalities. To date, vascular structures in the submillimeter range (~100 μm) can be displayed. Single UCA microbubbles can be visualized and tracked, enabling the study of real-time flow dynamics in intracranial aneurysms (Fig. 4). The use of UCA facilitates intraoperative real-time navigation and assessment of the intra- and peritumoral vasculature (8) as well as of aneurysms or arteriovenous malformations. Moreover, the immediate monitoring of the surgical intervention helps to optimize the neurosurgical case management in the operating room.

Interventional Radiological Treatment

Therapeutic Applications

Ultrasound therapy is currently a challenging research field. Therapeutic approaches are mainly based on the well-known physics of ultrasound such as heating or cavitation. Less well known are the biomechanical effects of ultrasound, such as sonothrombolysis or sonoporation.

Sonothrombolysis

Recent studies have demonstrated that ultrasound enables temporary disaggregation of the fibrin structure of thrombotic blood clots and improvement of the enzyme activation of plasminogen in the presence of tissue plasminogen activator (9, 10). Enhanced clot lysis is the key factor for successful stroke therapy. Recombinant tissue plasminogen activator (rt-PA) is currently the only Food and Drug Administration (FDA)-approved drug for acute stroke therapy. To enhance the therapeutic effect of rt-PA in stroke patients with transcranial ultrasound is challenging and the first clinical studies are promising (11). Besides the increasing knowledge of the acoustic properties of UCA microbubbles for diagnostic purposes, their potential as targeted drug carriers for therapeutic applications is of special interest. Specific targeting of thrombotic emboli with UCA as well as rt-PA binding to microbubbles is feasible and the *in vivo* applicability has

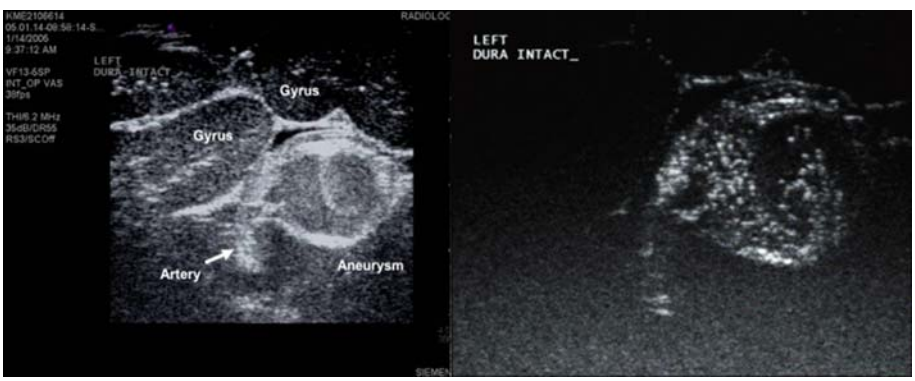

Contrast Media, Ultrasound, Applications in Transcranial and Intra-Operative Brain Ultrasound. Figure 4 Intraoperative aneurysm On the left: Precontrast, the morphology of the aneurysm is visualized in an oblique view through the intact dura mater, posterior to two gyri. The feeding artery can be seen on the left of the aneurysm as a hyperechogenic band (*arrow*). On the right: After contrast injection, acoustic signals from single microbubbles can be visualized as white spots, entering the aneurysm sac in an early systolic phase.

been proven (12). The future goal of transcranial ultrasound in stroke patients is to use clot-targeted rt-PA carrying microbubbles and to enhance thrombolysis with ultrasound while monitoring the therapeutic effect, using the same device.

Sonoporation

Besides sonothrombolysis, ultrasound-mediated gene transfection has opened a new therapeutic avenue. Although the mechanisms are poorly understood, it is evident that ultrasound has the ability to produce nondestructive, transient pores into cell membranes (13), thus enabling the uptake of higher-molecular-weight substances like oligonucleotides. Ultrasound-mediated local gene delivery in tumors (i.e., antisense TGF-β) or tumor-associated neovascularization (i.e., antisense VEGF) is the focus of research (12). Further potential applications are neointimal hyperplasia after arterial balloon injury and gene delivery to infarcted myocardial tissue. The impact of UCA microbubbles in these scenarios is defined by the feasibility of tissue targeting, their use as carriers of genetic sequences, and the positive effect on sonoporation. The future outlook of local drug and gene delivery to treat brain tumors or to enhance neuronal stem cell activity (unpublished data) in neurodegenerative diseases or stroke using acoustically active carriers in combination with brain ultrasound is challenging and remains experimental to date.

Bibliography

1. Bogdahn U, Frohlich T, Becker G et al (1994) Vascularization of primary central nervous system tumors: detection with contrast-enhanced transcranial color-coded real-time sonography. Radiology 192:141–148
2. Gerriets T, Goertler M, Stolz E et al (2002) Feasibility and validity of transcranial duplex sonography in patients with acute stroke. J Neurol Neurosurg Psychiatry 73:17–20
3. Hölscher T, Wilkening WG, Lyden PD et al (2005) Transcranial ultrasound angiography (tUSA): A new approach for contrast specific imaging of intracranial arteries. Ultrasound Med Biol 31:1001–1006
4. Hölscher T, Wilkening W, Draganski B et al (2005) Transcranial ultrasound brain perfusion assessment with a contrast agent-specific imaging mode. Results of a 2-center trial. Stroke 36:2283–2285
5. Postert T, Federlein J, Weber S et al (1999) Second harmonic imaging in acute middle cerebral artery infarction. Preliminary results. Stroke 30:1702–1706
6. Eyding J, Krogias C, Schollhammer M et al (2006) Contrast-enhanced ultrasonic parametric perfusion imaging detects dysfunctional tissue at risk in acute MCA stroke. J Cereb Blood Flow Metab;26(4):572–82
7. Woydt M, Vince GH, Krauss J et al (2001) New ultrasound techniques and their application in neurosurgical intra-operative sonography. Neurol Res 23:697–705
8. Kanno H, Ozawa Y, Sakata K et al (2005) Intraoperative power Doppler ultrasonography with a contrast-enhancing agent for intracranial tumors. J Neurosurg 102:295–301
9. Braaten JV, Goss RA, Francis CW (1997) Ultrasound reversibly disaggregates fibrin fibers. Thromb Haemost 78:1063–1068
10. Devcic-Kuhar B, Pfaffenberger S, Gherardini L et al (2004) Ultrasound affects distribution of plasminogen and tissue-type plasminogen activator in whole blood clots *in vitro*. Thromb Haemost 92:980–985
11. Alexandrov AV, Molina CA, Grotta JC et al (2004) Ultrasound-enhanced systemic thrombolysis for acute ischemic stroke. N Engl J Med 351:2170–2178
12. Unger EC, Matsunaga TO, McCreery T et al (2002) Therapeutic applications of microbubbles. Eur J Radiol 42:160–168
13. Tachibana K, Uchida T, Ogawa K et al (1999) Induction of cell-membrane porosity by ultrasound [letter]. Lancet 353:1409

C

Contrast Media, Ultrasound, Applications in Vesico-ureteral Reflux

Kassa Darge
Department of Pediatric Radiology, Institute of Radiodiagnostic, Bavarian Julius-Maximilians-University Wuerzburg, Wuerzburg, Germany
darge@roentgen.uni-wuerzburg.de

Synonyms

Contrast-enhanced voiding urosonography (VUS); Contrast-enhanced reflux sonography

Definition

►Voiding urosonography (VUS) is an ultrasound (US) examination of the bladder, ureters, and kidneys (± urethra) utilizing intravesically administered US contrast media with the primary purpose to exclude or diagnose reflux into the ureters and pelvi-calyces. ►Vesicoureteral reflux (VUR) a common pediatric problem can, particularly in the presence of urinary tract infection (UTI), result in renal damage and consequently renal function impairment and hypertension. Three different imaging modalities are currently employed for the diagnosis of VUR. The two radiologic modalities, ►voiding cystourethrography (VCUG) and ►radionuclide cystography (RNC) have been in use for several decades. Since the mid-90s the modality without radiation exposure, VUS, has become available as a further diagnostic option for VUR (1).

Indication

Evolvement of US for Diagnosis of VUR

In 1976, the first report appeared on the use of US for the diagnosis of VUR. Further attempts to implement US for reflux diagnosis in children have been underway in two directions (1). The indirect methods were based on the US of the urinary tract, without administration of any kind of substance into the bladder. These included depicting various sonomorphologic changes of the urinary tract as a result of VUR, detecting newly appearing or an increase in existing ureteral or pelvicalyceal dilatation and assessing ureteric jet changes with duplex and color Doppler. The direct means used to diagnose VUR involved instilling various substances intravesically. The most frequently administered fluid was physiological saline solution. The ballooning of the renal pelvis during the filling of the bladder represented the criterion for diagnosis of VUR. Application of air bubbles, by shaking the normal saline before administration or adding carbon dioxide, had also been tried. US studies were also carried out, in which the empty bladder was solely filled with air. In addition to low diagnostic accuracy, all the above methods have major limitations making them impractical for use in routine imaging.

Diagnosis of VUR Using US Contrast Media

The use of an US contrast agent consisting of sonicated albumin (Albunex; Molecular Biosystems, San Diego, USA) for the diagnosis of VUR in a child was reported in 1994 from Japan (1). Utilizing the same US contrast medium, another study compared VUS with both VCUG and RNC in a small group of patients. The sensitivity was found to be 64% and 86% in comparison to VCUG and RNC, respectively. In both cases, the specificity was 100% (1). A further US contrast medium used in the past was a galactose-based microbubbles-containing agent (Echovist, Schering, Berlin, Germany). The comparison of VCUG with VUS using this US contrast medium showed high diagnostic concordance. However, its very short imaging window of approximately 5 min hindered its routine use (1). The "breakthrough" in the US diagnosis of reflux in children came about in the mid-90s with the availability of US contrast agents containing stabilized microbubbles. The US contrast medium Levovist (Schering, Berlin, Germany) was the first of such contrast agents that became available for clinical use in Europe. It is a galactose-based contrast agent that contains microbubbles stabilized with a layer of palmitic acid. The inherent properties of the US contrast medium, resulting in long echo enhancement duration of more than half-an-hour and relatively dense and homogeneous echoes make the search and detection of VUR much easier. In a large number of studies incorporating hundreds of children, the diagnostic accuracy of VUS with the use of Levovist has been compared with that of VCUG (1–4). There is a significant correlation between the two imaging modalities with the concordance rate ranging from 89–97% and more refluxes being detected in the VUS (approximately 10%) (4). Moreover, up to 90% of grade I refluxes in the VCUG are found to be grade II or higher in the VUS (3).

Selection Criteria for VUS

There are mainly two indications for performing a reflux examination in a child: (1) UTI (pyelonephritis) and (2) dilatation of a ureter or renal pelvis. It should be noted that there is a wide variation in practice among all those involved in the diagnosis and management of children with VUR. Consequently, the criteria for the selection of an imaging modality for reflux entail the adaptation to local practices. Currently, the most common criteria applied for performing a VUS or a VCUG as the primary diagnostic modality area are as follows: (a) VUS selection criteria: (i) follow-up examinations, (ii) first examination for VUR in girls, (iii) screening high-risk patients; (b) VCUG selection criteria: (i) first examination for VUR in boys, (ii) specific request for urethral and/or bladder imaging, (iii) inadequate visualization of the bladder or one of the kidneys on US. The selection criteria for RNC are usually as those for VUS.

Contraindication

There are no absolute contraindications for administering the US contrast medium, Levovist, intravesically. Galactosemia, a contraindication for the intravenous administration, is only a relative contraindication. The inability to visualize, for whatever reason, the bladder or one of the kidneys on US excludes the performance of a VUS.

Pregnancy/Lactation

There are no reports regarding the intravesical administration of US contrast media for reflux examination during pregnancy or lactation.

Use and Dosage

VUS Procedure

The VUS examination incorporates four basic steps (2, 3):

1. Precontrast examination: standard US of the urinary tract in supine (±prone) positions.

2. Catheterization or suprapubic puncture of the bladder under sterile condition and administration of normal saline and the US contrast medium.
3. Postcontrast examination: a repeat of the standard US of the urinary tract.
4. Postcontrast voiding examination: US of the renal pelves and terminal ureters (±urethra) during and after micturition.

The necessity and extent of the precontrast examination is determined by the availability of a current US examination of the urinary tract and the type of US imaging modality being used. It is crucial that the normal saline instilled into the bladder is not from a container sealed under vacuum. All plastic containers are not sealed under vacuum but almost all glass containers. The normal saline in the latter is desaturated and the air in the microbubbles diffuses very rapidly in the solution with the consequence of fast decrease of echo-enhancement. The contrast medium is administered slowly into the bladder under sonographic monitoring. Reflux is diagnosed when echogenic microbubbles are detected in the ureters or pelvi-calyces. During the postcontrast examinations, the right and left renal pelves are scanned alternatively. The scan during voiding can be carried out when the patient is lying or sitting on a pan or standing and voiding into a urine bottle. The severity of reflux is graded in a similar manner as the international reflux grading system in VCUG from grade I to V. Comparative studies have shown the high concordance rate of over 85% between the reflux grading system in VCUG and VUS (1, 3).

VUS Imaging Modalities

Depending on the availability, different US imaging modalities are employed in VUS to depict the refluxing microbubbles. These imaging options not only affect the conspicuity of the microbubbles but also the overall diagnostic accuracy of the examination. The most widely employed modality for VUS is conventional (=fundamental) US. This can be combined with color Doppler to enhance the detection of reflux. A recent innovation in US and one with major impact on the application of US contrast media is harmonic imaging. When using harmonic imaging for VUS not only do the microbubbles become strikingly conspicuous compared to fundamental mode but also the sensitivity is significantly increased (Fig. 1) (5). Furthermore, it is possible to visualize intrarenal reflux. Advanced contrast-specific imaging modalities tuned for individual contrast medium, e.g., agent detection imaging (Sequoia, Siemens, Issaquah, USA) have brought about a profound improvement in detecting refluxing microbubbles. The microbubbles are not only enhanced and color-coded but it is also possible to visualize only the refluxing microbubbles blocking out the background gray-scale image (Figs. 2, 3).

Dosage of US Contrast Media for VUS

Currently, the US contrast medium Levovist is the most widely used and the one approved for use in VUS. The concentration of Levovist used for VUS is 300 mg/mL. The dose administered depends on the imaging modality being employed. For fundamental US, the volume of Levovist administered is 5–10% of the filling volume of the bladder (1–3). In case of harmonic imaging or advanced contrast-specific imaging modalities 3–5% of the filling volume of the bladder suffices, i.e., for one cycle of examination just one 2.5-g flask of Levovist will be adequate (5). Recently, a second-generation US contrast agent, SonoVue (Bracco, Milan, Italy), has become

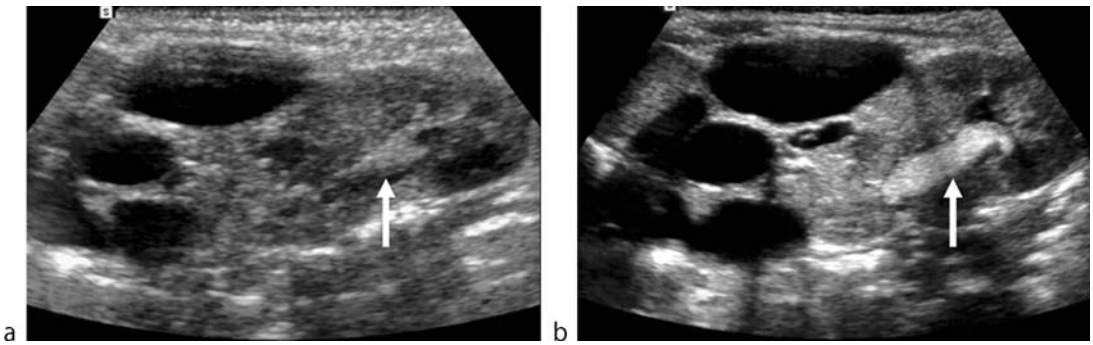

Contrast Media, Ultrasound, Applications in Vesico-ureteral Reflux. Figure 1 Longitudinal scan of a duplex kidney with a multicystic dysplastic upper moiety from ventral after intravesical administration of the US contrast medium Levovist in (a) fundamental and (b) harmonic imaging modalities. The refluxing microbubbles in the lower moiety (arrow) are more conspicuous in the harmonic imaging modality (b).

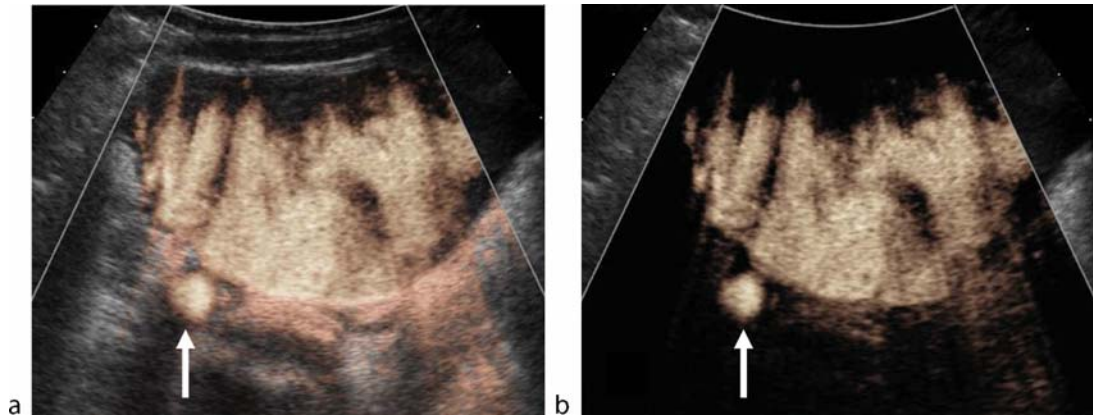

Contrast Media, Ultrasound, Applications in Vesico-ureteral Reflux. Figure 2 Transverse section of the bladder and dilated right terminal ureter (arrow) after intravesical administration of the US contrast medium Levovist using an advanced contrast-specific imaging modality (agent detection imaging). Note the reflux in the right terminal ureter without (a) and after (b) blocking the background gray-scale image.

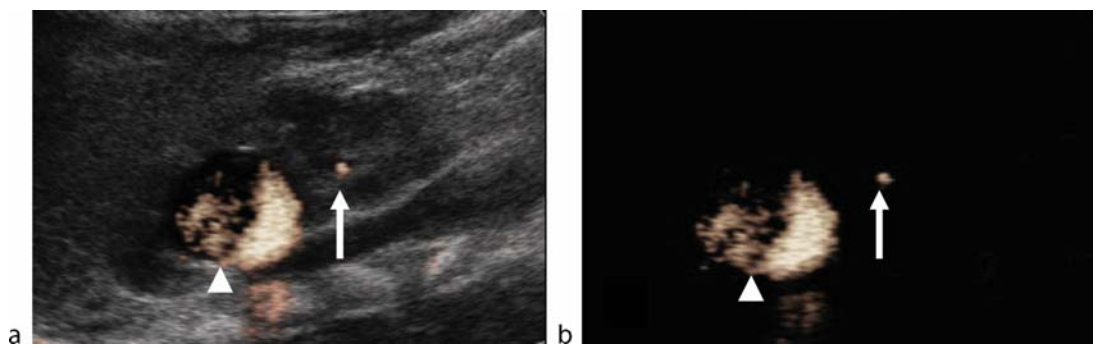

Contrast Media, Ultrasound, Applications in Vesico-ureteral Reflux. Figure 3 Longitudinal section of a duplex kidney from ventral after intravesical administration of the US contrast medium Levovist using an advanced contrast-specific imaging modality (agent detection imaging). Note the reflux in both moieties (arrowhead—upper, arrow—lower) without (a) and after (b) blocking the background gray-scale image.

available in Europe. Preliminary comparative studies have revealed that the dose of this contrast medium for intravesical use is less than 1% of the bladder filling (1). This has a huge potential in the future not only in reducing the amount of contrast medium necessary for an examination but also in markedly lowering the cost for a VUS.

Adverse Reactions

There are no reports of adverse reactions with regard to intravesical instillation of US contrast media, in particular of Levovist.

Interactions

No interactions of intravesically administered US contrast media have been reported.

References

1. Darge K, Riedmiller H (2004) Current status of vesicoureteral reflux diagnosis. World J Urol 22:88–95
2. Darge K, Troeger J, Duetting T et al (2001) Reflux in young patients: comparison of voiding US of the bladder and retrovesical space with echo enhancement versus voiding cystourethrography for diagnosis. Radiology 210:201–207
3. Berrocal T, Gaya F, Arjonilla A et al (2001) Vesicoureteral reflux: diagnosis and grading with echo-enhanced cystosonography versus voiding cystourethrography. Radiology 221:359–365

4. Valentini AL, De Gaetano AM, Destito C et al (2002) The accuracy of voiding urosonography in detecting vesico-ureteral reflux: a summary of existing data. Eur J Pediatr 161:380–384
5. Darge K, Zieger B, Rohrschneider W et al (2001) Contrast-enhanced harmonic imaging for the diagnosis of vesicoureteral reflux. AJR 177:1411–1415

Contrast Media, Ultrasound, Commercial Products

Christian Greis
Bracco ALTANA Pharma GmbH, Clinical Development Ultrasound Contrast Agents, Konstanz, Germany
christian.greis@altanapharma.com

Synonyms

Echo enhancers; Sonographic contrast agent; Sonographic signal enhancers; Ultrasound contrast agents; Ultrasound contrast media; Ultrasound signal enhancers

Definition

An ultrasound contrast medium is a compound that increases the contrast of an ultrasound image. This is obtained by increasing (or decreasing) the echogenicity of a particular compartment within the body. Usually, an ultrasound contrast agent is injected into a blood vessel resulting in an increased echogenicity of the blood and thus in an increased *contrast between blood and tissue*. The currently commercially available ultrasound contrast agents contain ►micro-bubbles with a diameter of a few µm, which consist of an echogenic gas surrounded by a shell for stabilisation. Due to the size of the micro-bubbles, such ultrasound contrast agents are ►blood pool agents not leaving the vascular system. Ultrasound contrast agents of the first generation contain air inside, whereas agents of the second generation contain a gas with low solubility in water (or blood) giving the micro-bubbles a higher stability and longer persistence.

Indication

Currently, there are three major indications described for ultrasound contrast agents:

1. Echocardiography including *left ventricular opacification* (LVO) with the aim to improve *endocardial border delineation* (EBD) and *myocardial contrast echocardiography* (MCE) with the aim to demonstrate and quantify myocardial perfusion,
2. Vascular *Doppler* ►*enhancement* with the aim to overcome insufficient signal-to-noise ratio, especially to obtain higher accuracy in low-flow, no-flow and/or slow-flow conditions,
3. *Sonography of parenchymatous organs* with the aim to detect abnormal vascularity and perfusion.

Not all agents on the market have regulatory approval for all the three indications. To obtain regulatory approval, a significant clinical benefit has to be demonstrated in addition to the sole existence of a contrast effect. In other words, the contrast enhancement should result in diagnostic confidence and not in confusion.

There is a significant difference in the perception of the clinical benefit of contrast enhancement between Europe and the United States. In the United States, the clinical value of contrast enhancement is only recognised for echocardiography and accordingly this is the only indication for ultrasound contrast agents approved by the FDA. In Europe, both echocardiography and vascular/extra-cardiac sonography are accepted indications for contrast enhancement and there are agents with regulatory approval for all the three indications mentioned earlier.

Echocardiography

The improvement of the endocardial border delineation of the heart cavities was the first indication for ultrasound contrast agents. Due to a limited signal-to-noise ratio of the non-digital ultrasound scanners in the early 1990s, the cardiac cavities often appeared not well delineated but obscured by noise signals and signal dropouts in the cardiac wall. Opacification of the blood in the heart cavities resulted in a marked improvement of the endocardial border delineation, allowing a much more reliable determination of *cardiac volumes* and *wall motion*. Even with up-to-date high-end scanners, this clinical advantage is evident (due to the elimination of obscuring echoes from the trabecular structures), as shown in recent controlled multicenter studies (1).

Using recent generations of ultrasound scanners with ►*contrast-specific imaging* modalities (2), the blood distribution can be demonstrated not only in the cavities but also in the micro-vasculature of the myocardium. For this indication called myocardial contrast echocardiography, it is necessary to separate the signals coming from the blood (contrast agent) and those coming from the tissue. This is done by the contrast mode software of the scanner. The visibility and distribution of the contrast enhancement in the myocardium is obvious. However, the evidence for the clinical value of this information has still to be

established and is evaluated in numerous clinical research programs currently ongoing. Up to now, none of the agents available has obtained regulatory approval for the myocardial perfusion indication.

Vascular Imaging

The most sensitive method for vascular imaging is *Doppler sonography*. The demonstration of blood with Doppler sonography is based on the movement of blood cells with a certain velocity (higher than the wall motion velocity) towards or away from the transducer. In some cases, only an insufficient Doppler signal can be obtained, mainly when the blood volume is very small (e.g. in high-grade stenoses) or the vessels are behind highly echogenic structures (e.g. in transcranial Doppler sonography). In such cases, the enhancement of the echogenicity of the blood by an ultrasound contrast agent allows in nearly all cases the demonstration of an adequate flow signal (3).

Parenchymal Vascularity and Perfusion

There is a general limitation for Doppler sonography: it does not work in case of nearly stationary blood (e.g. in capillaries) or indeterminate flow direction (e.g. in complex vascular structures), as found in parenchymal structures or focal lesions. The adequate demonstration of blood in the *micro-vasculature* requires a velocity-independent separation of signals from blood and tissue, which can be obtained during contrast enhancement by the contrast-specific elements in the signal. Using this principle, the micro-vascular distribution and geometry can be demonstrated in B-mode with high spatial resolution and without any movement artefacts. Furthermore, when injected as bolus injection the contrast agent can be used as *tracer* to evaluate the dynamic wash-in and wash-out in the tissue, allowing the assessment of parenchymal *perfusion*. For detection and characterisation of focal liver lesions, the clinical benefit of micro-vascular perfusion assessment has already been demonstrated (4) and the use of contrast enhancement is recommended in respective guidelines (5, 6). Fore some other organs, clinical research programs are still ongoing to establish the clinical value of perfusion assessment for diagnosis or therapeutic monitoring. In Europe, some of the agents available obtained already regulatory approval for micro-vascular imaging.

Commercial Products

Echovist is a 'right heart' contrast agent, i.e. an agent which is not stable enough to survive the pulmonary passage after intravenous injection. The active ingredient of Echovist is Galactose micro-particles containing air. The agent is available in two concentrations with 200 and 300 mg/mL micro-particles in the final suspension. Echovist has been approved in 1991 for the examination of the right heart and venous system and for hysterosalpingo-contrast-sonography after transcervical injection. Echovist is marketed by Schering in Germany and UK.

Levovist is an improved formulation of Echovist, also containing Galactose micro-particles with air but coated with palmitic acid, making the micro-particles more stable. Levovist micro-particles survive the pulmonary circulation and allow the enhancement of the whole circulation. The agent can be prepared in different concentrations (200, 300 and 400 mg/mL micro-particles in the final suspension). In 1995, Levovist has been approved in Germany and until now in more than 40 countries including most European countries, Canada, China and Japan. Levovist obtained regulatory approval for Doppler enhancement including diagnosis of cardiac, vascular and tumour diseases and for diagnosis of vesiculo-ureteral reflux after transurethral injection. Levovist is marketed by Schering.

Albunex has been the first transpulmonary agent on the market, approved 1993 in Japan and 1994 in the United States. It consists of human albumin coated micro-bubbles containing air. In the meantime, Albunex has been replaced by Optison.

Optison contains also human albumin coated micro-bubbles, but containing octafluoropropane gas (perflutren), making the micro-bubbles more stable. The gas concentration is 0.19 mg/mL solution. Optison is the first 'second-generation' contrast agent using gas with low solubility in water to increase stability and persistence. Like Albunex, Optison has been developed only for echocardiography (left ventricular opacification) and obtained first approval in 1998 in the United States and later also in most European countries. Developed by Molecular Biosystems, Optison is marketed now after several transitions by GE Healthcare.

SonoVue consists of sulphurhexafluoride micro-bubbles surrounded by a flexible phospholipid shell. The final solution contains 8 μL/mL SF_6 gas, which is enough to obtain an enhancement of several minutes in the whole vascular system. SonoVue has been approved by the EU medical agency in 2001 for a broad range of indications, including echocardiography (left ventricular opacification), (macro-)vascular Doppler enhancement and assessment of vascularity in focal lesions in liver and breast (micro-vascular enhancement). SonoVue is marketed by Bracco in cooperation with several partners in Europe and China.

Definity consists of octafluoropropane (perflutren) micro-bubbles, surrounded by a phospholipid shell. The final solution contains 150 μL/mL C_3F_8 gas. Definity has been approved by the FDA in 2001 for echocardiography (left ventricular opacification) and in Canada also for liver and kidney imaging. In Europe, a submission for regulatory

approval has been filed. Definity has been developed by ImaRx and is marketed now by Bristol-Myers Squibb.

Imagent consists of tetradecafluorohexane (perflexane) micro-bubbles, surrounded by a phospholipid shell. The final solution contains 92 µg/mL C_6F_{14} gas. Imagent has been developed and approved in the United States in 2003 for echocardiography (left ventricular opacification). Developed by Alliance Pharmaceuticals, Imagent is now marketed by IMCOR Pharmaceutical in the United States.

Contraindication

In general, ultrasound contrast agents are pharmacologically inactive and, with the exception of known hypersensitivity to any of the ingredients, no absolute contraindications exist. They contain no toxic molecules and there are no toxic effects on organs (e.g. the kidneys). However, there may be side effects after the injection of any contrast agent, which require a benefit/risk assessment to assure the best possible safety for the patient. The only significant adverse effects reported are hypersensitivity reactions following the injection of the contrast agent. Such reactions are rare (in about 0.01%) but can be life-threatening. Considering this potential risk (even if the incidence is very low), contraindications were defined for patients having an increased risk in case of a hypersensitivity reaction which is not balanced by a special benefit for this particular patient group (e.g. patients during acute coronary syndrome not having an immediate clinical need for a contrast examination). For the detailed contraindications of the different agents see the respective SPCs approved by the regulatory authorities.

Pregnancy/Lactation

Since the micro-bubbles are not leaving the vascular compartment, there should be no transition into the foetal blood circulation or breast milk. From pharmacological and toxicological studies no special risks are known. However, as for other contrast agents no special clinical studies were performed in pregnant women. Therefore, the experience in this patient group is limited and special care should be taken.

Use and Dosage

Ultrasound contrast agents are usually administered by intravenous *bolus injection*. Due to the low injection volume, a saline injection for flushing directly after the contrast injection is recommended. To avoid high mechanical forces impairing the stability of the micro-bubbles, injection with strong pressure should be avoided and the needle diameter should not be too small (at least 20G).

Recommended doses for one injection are given in the following list:

- Echovist: 3.0–10.0 mL
- Levovist: 6.5–19.5 mL (2.5 or 4.0 g micro-particles)
- Optison: 0.5–3.0 mL
- SonoVue: 2.0/2.4 mL
- Definity: 10 µL/kg BW
- Imagent: 6.25 µL/kg BW

The injection can be repeated, if required. If a longer, continuous contrast enhancement is useful (e.g. for prolonged left ventricular opacification or vascular enhancement), a continuous *infusion* of the contrast agent is possible. In that case, an infusion pump with a rotating syringe holder is preferable, to avoid rising of the micro-bubbles to the superficial layer due to buoyancy.

Adverse Reactions

The most common side-effects reported after the injection of ultrasound contrast agents are mild and resolved within a short time without sequelae. They include local reactions at the injection site, headache, nausea, flush and sensations of heat, coldness or altered taste. In rare cases (about 0.01%), hypersensitivity reactions were reported as known from other colloidal suspensions and contrast agents. Such hypersensitivity reactions (anaphylactoid reactions) can be life-threatening and require immediate treatment. Adequately trained staff and emergency equipment should be available for that reason.

Interactions

Since ultrasound contrast agents are administered only for a short time during the diagnostic examination and the *elimination* from the blood circulation is quite fast (within a few minutes), possible interaction with other medication is limited. Usually, no special interaction studies are performed with contrast agents. From a theoretical point of view, there may be an influence on the bioavailability of drugs given at the same time point, especially if these drugs are able to adhere to albumin or lipid surfaces (depending on the shell of the micro-bubbles). Therefore, it is recommended to use separate intravenous lines if the contrast agent has to be administered simultaneously with another drug (e.g. in case of pharmacological stress echo).

Bibliography

1. Hoffmann R, von Bardeleben S, ten Cate F et al (2005) Assessment of systolic left ventricular function: a multi-centre comparison of cineventriculography, cardiac magnetic resonance imaging, unenhanced and contrast-enhanced echocardiography. Eur Heart J 26:607–616
2. Greis C (2004) Technology overview: SonoVue. Eur Radiol 14(Suppl 8):P11–P15
3. Martegani A, Aiani L, Borghi C (2004) The use of contrast-enhanced ultrasound in large vessels. Eur Radiol 14(Suppl 8):P73–P86
4. Albrecht T, Hohmann J, Oldenburg A et al (2004) Detection and characterisation of liver metastases. Eur Radiol 14(Suppl 8):P25–P33
5. Albrecht T, Blomley M, Bolondi L et al (2004) Guidelines for the use of contrast agents in ultrasound. Ultraschall Med 25:249–256
6. Bruix J, Sherman M (2005) Management of hepatocellular carcinoma. Hepatology 42:1208–1236

Contrast Media, Ultrasound, Hepatic

Thomas Albrecht
Department of Radiology and Nuclear Medicine, Campus Benjamin Franklin, Charité - Universitätsmedizin Berlin, Berlin, Germany
thomas.albrecht@charite.de

Synonyms

Contrast-enhanced sonography of the liver; Contrast-enhanced ultrasound (US) of the liver

Definition

The use of ultrasound (US) microbubble contrast agents combined with contrast-specific imaging techniques for the detection and characterization of liver disease (mainly tumors).

Introduction

Although often the first-line modality for liver imaging, conventional US without the use of contrast agents has a limited role in the diagnosis of liver tumors. Its ability to detect and characterize focal liver lesions is generally inferior to that of other cross sectional imaging modalities [computed tomography (CT) and magnetic resonance imaging (MRI)].

The advent of microbubble contrast agents has greatly enhanced the role of US in liver imaging. Both detection and characterization of liver lesions can be considerably improved by the use of US contrast agents.

US Contrast Agents for Liver Imaging

US contrast agents consist of microbubbles (cross reference) which are less than 10 μm in diameter. They are safe and effective echo enhancers. When given intravenously, microbubbles produce marked augmentation of the US signal for several minutes with up to 25 dB (greater than 100-fold increase) enhancement in echo strength. The signal enhancement is primarily caused by nonlinear bubble behavior (cross reference). Contrast-specific nonlinear imaging modalities (cross reference) such as phase modulation (cross reference) or amplitude modulation (cross reference) or a combination of the two exploiting the nonlinear bubble behavior (cross reference) must be used for contrast-enhanced US of the liver, since the signal enhancement is insufficiently visualized with conventional fundamental US imaging.

With real-time low ▶ *mechanical index* (MI) imaging, the dynamic enhancement pattern and the vascular

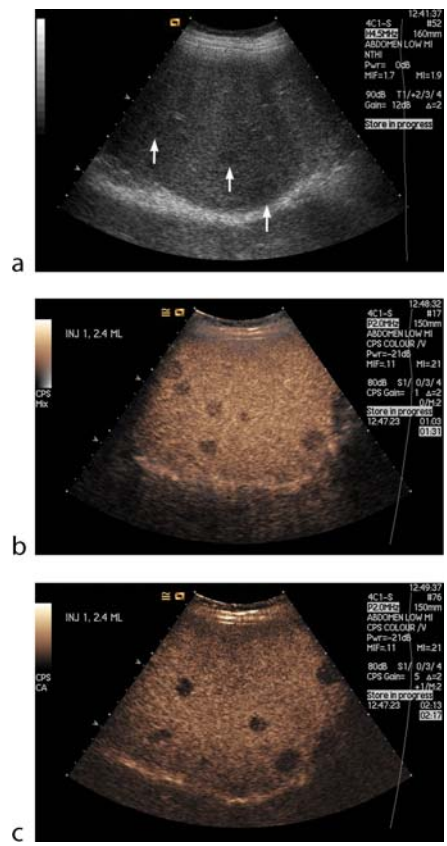

Contrast Media, Ultrasound, Hepatic. Figure 1 Patient with multiple small metastases. (a) Baseline US shows three ill-defined hypoechoic lesions in a slightly heterogeneous liver. (b, c) In the portal venous and delayed phase after SonoVue, multiple lesions are revealed throughout the liver, some of them only a few millimeters in diameter.

morphology of a lesion are assessed during the arterial (starting 10–20 sec and ending 25–53 sec after injection) and portal venous (starting 30–45 sec and ending 120 sec after injection) phases. The delayed phase (>2 min after injection) is particularly useful for detection of metastases because they appear as nonenhancing defects. Characterization is also aided by delayed-phase imaging.

Some agents have a liver-specific late phase where the bubbles accumulate in normal liver parenchyma starting 2–5 min after injection when the vascular enhancement has faded and persisting there for many minutes to hours, analogous to liver-specific contrast agents used in MRI. This late phase is particularly useful for lesion detection and differentiation of benign and malignant tumors. Microbubbles known to exhibit liver-specific behavior are ▶*Levovist*, *Sonavist* (both Schering AG, Germany), ▶*Sonazoid* (NC100100; General Electric, USA), and ▶*BR14* (Bracco SPA, Italy). In the late phase, the bubbles are stationary or extremely slow moving. The mechanism of hepatic accumulation is not completely understood. Possible explanations are mediation by the reticuloendothelial system or pooling and endothelial adherence in the liver sinusoids. For some agents (Sonavist and Sonazoid), Kupffer cell uptake has been demonstrated.

Two contrast agents are currently licensed for liver imaging in Europe: Levovist (Schering AG, Berlin, Germany) and ▶*SonoVue* (Bracco SPA, Milan, Italy). The imaging techniques with these two contrast agents vary considerably. Contrast-specific imaging modes exploiting nonlinear bubble behavior (cross reference) must be used with both agents to achieve clinically useful signal enhancement. Such imaging modes are now available on most medium- and high-end US systems.

Levovist, which was the first agent to be commercially available has liver-specific properties during its late phase; this is advantageous for detection of metastases. High MI imaging (MI>0.7) must be applied when using Levovist. It provides signal enhancement due to strong nonlinear signals from disrupting microbubbles. The disadvantage of this technique is the highly transient nature of the signals, which persist only for a few frames after insonation of an individual area until the bubbles in the imaging plane are destroyed. To exploit the enhancement for clinical use, special scanning techniques such as rapid

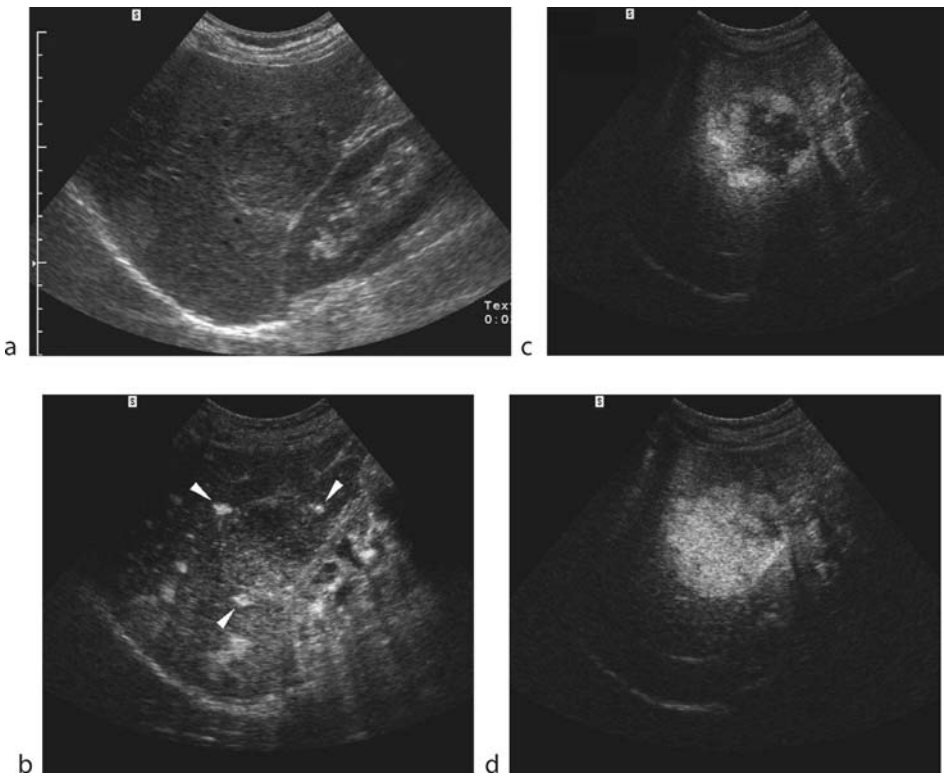

Contrast Media, Ultrasound, Hepatic. Figure 2 Typical dynamic enhancement of a hemangioma using Sonazoid. (a) Atypical baseline appearances: isoechoic lesion (*arrow*) suggestive of metastases in a patient with colon carcinoma. (b) Arterial phase with peripheral nodular enhancement (*arrowheads*). (c) Partial centripetal fill-in in the portal venous phase (45 sec p.i.). (d) Complete filling of the hemangioma in the delayed phase (3, 5 min p.i.).

sweeping through the liver to image intact bubbles with each new frame or intermittent imaging have to be employed. Such scanning techniques are somewhat cumbersome and multiple sweeps through the liver are only possible with repeated injections. For these reasons, Levovist is no longer used on a large scale despite some very good results in the detection and characterization of focal liver lesions.

SonoVue, a more recent agent, provides strong and persistent signal enhancement due to its strong harmonic resonance at low (≤0.2) and very low (<0.1) MI, where minimal or no bubble destruction occurs. This allows for continuous real-time imaging of a lesion during its vascular phase as well as comprehensive surveying of the liver in multiple planes during the delayed phase. Low MI imaging with SonoVue is now preferred in most instances, although it has weaker liver-specific properties than Levovist.

Several experimental agents such as Sonazoid or BR14 combine the advantages of good enhancement at low MI with strong liver-specific properties. Early clinical studies have demonstrated the potential of such agents for detection of metastases. Unfortunately, manufacturers are currently hesitant to continue the clinical development of such agents for commercial reasons.

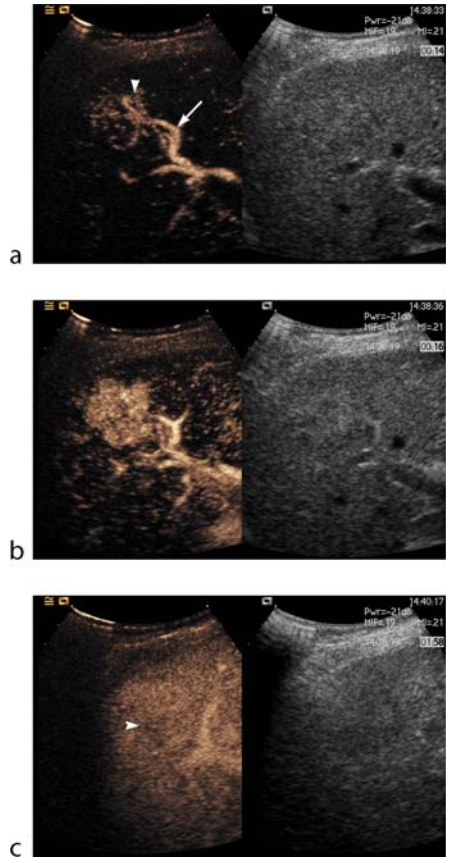

Contrast Media, Ultrasound, Hepatic. Figure 3 Typical focal nodular hyperplasia after SonoVue. (a) Large feeding artery (*arrow*) and spoke-wheel vascular pattern in the lesion (*arrow heads*) during the early arterial phase (14 sec after injection). (b) Two seconds later the lesion is completely filled with contrast and appears hyperenhancing to normal liver. (c) In the portal venous/delayed phase (2 min post injection) the lesion is isoenhancing to normal liver with the exception of a small hypoenhancing central scar (*arrow*).

Indications and Clinical Use

According to the guidelines of the European Federation of Societies for Ultrasound in Medicine and Biology (EFSUMB), the use of contrast agents is indicated in the following clinical situations:

- Detection of focal liver lesions (especially metastases)
- Characterization of focal liver lesions
- Monitoring of liver tumor ablation.

Detection: As with other imaging modalities, the use of contrast agents improves the ability of US to detect liver metastases substantially. As described earlier, metastases are seen as nonenhancing defects in an otherwise homogeneously enhancing liver in the portal venous and particularly in the delayed phase after contrast injection (Fig. 1). The impact on detection is most marked for lesions smaller than 1 cm in diameter and for lesions that are isoechoic on baseline US. Contrast-enhanced US has a sensitivity of approximately 80% in detecting hepatic metastases, which is similar to contrast-enhanced CT. The detection of primary hepatic malignancies such as hepatocellular carcinoma and cholangiocarcinoma is also improved with the use of US contrast agents in comparison to unenhanced US.

Characterization: All common solid liver lesions have rather characteristic dynamic imaging features on contrast-enhanced US (Figs. 2 and 3). Most of these features are analogous to those on dynamic CT and MRI scans. In addition to the vascular phases, the delayed phase is of particular value for differentiating malignant and benign lesions: the great majority of benign lesions show contrast uptake similar to normal liver in this phase, whereas most malignant lesions (especially metastases) appear as enhancement defects. Contrast-enhanced US is an effective tool for liver lesion characterization: approximately 85–90% of liver lesions can accurately be diagnosed as a specific lesion type, and classification of

benign and malignant lesions can be achieved in over 90% of the cases.

Monitoring of liver ablation: Treatment monitoring during or after liver ablation (radiofrequency ablation, laser ablation, percutaneous ethanol injection) is based on the assessment of vascularization and tissue perfusion in the target area to differentiate necrosis from residual viable tumor. Unenhanced US, even when combined with color/power Doppler, does not provide any reliable information about the outcome of ablation treatments, which was an important limitation of US-guided ablative procedures before the advent of US contrast agents. Conversely, with the use of US contrast agents, tissue perfusion can be visualized and crucial information about the extent of the thermal necrosis is thus obtained. Complete ablation is indicated by the disappearance of any previously visualized intralesional enhancement on contrast-enhanced images. Residual viable tumor tissue is suspected when a portion of the original lesion shows persistent enhancement in the arterial or portal venous phase.

Bibliography

1. Albrecht T, Blomley M, Bolondi L et al (2004) Guidelines for the use of contrast agents in ultrasound. Ultraschall Med Jan 2004 25: 249–256
2. Albrecht T, Blomley MJ, Burns PN et al (2003) Improved detection of hepatic metastases with pulse-inversion US during the liver-specific phase of SHU 508A: multicenter study. Radiology 227: 361–370
3. Konopke R, Kersting S, Saeger HD et al (2005) Detection of liver lesions by contrast-enhanced ultrasound—comparison to intraoperative findings. Ultraschall Med 26:107–113
4. Quaia E, Calliada F, Bertolotto M et al (2004) Characterization of focal liver lesions with contrast-specific US modes and a sulfur hexafluoride-filled microbubble contrast agent: diagnostic performance and confidence. Radiology 232:420–430

C

Contrast Media, Ultrasound, High Solubility Gas

N. DE JONG
Erasmus MC, Rotterdam, The Netherlands
n.dejong@erasmusmc.nl

Synonyms

Air agents; First (second) generation contrast agent

Definitions

An agent containing gas bubbles, of which the gas in the bubble easily dissolved in the surrounding liquid (typically water/plasma).

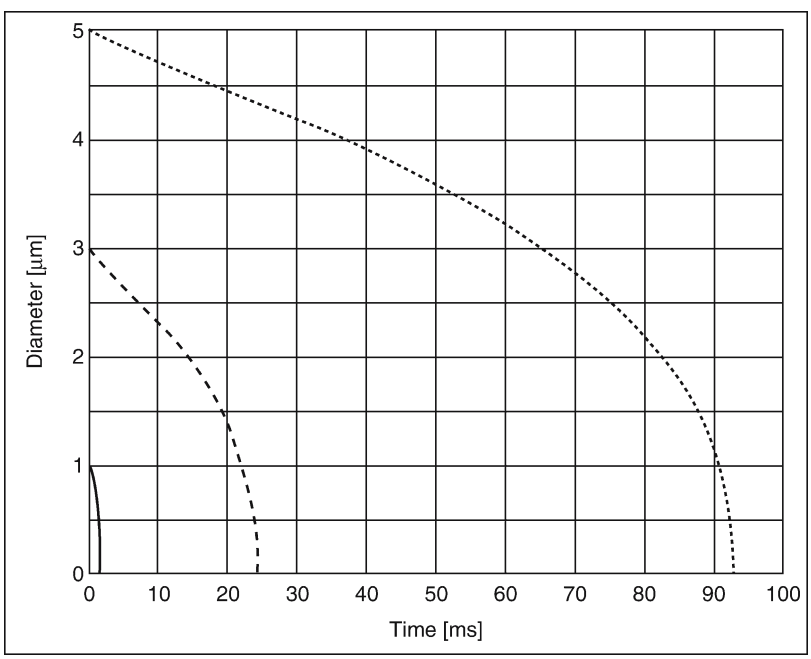

Contrast Media, Ultrasound, High Solubility Gas. Figure 1 Diameter's change versus time for three different sizes; 1, 3, and 5 μm.

Characteristics

Maintaining a gas bubble at a constant size is a technical challenge and many fluctuations in size occur with local environment. Indeed, bubbles suspended in a liquid can coalesce, grow or shrink in response to changes in the environment. Outward diffusion of gases due to surface tension, higher hydrostatic pressures or acoustic pressures induce consequent alterations in bubble size, which can occur very rapidly, within seconds to minutes. Smaller bubbles are more susceptible to these influences. The kinetics of the dissolution of a gas microbubbles is given by the equation of Epstein and Plesset (1):

$$\frac{dR}{dt} = DL\left(\frac{\frac{C_i}{C_0} - 1\frac{2\sigma}{RP_0} - \frac{p_{ov}}{P_0}}{1 + \frac{4\sigma}{3RP_0}}\right)\left(\frac{1}{R} + \frac{1}{\sqrt{\pi Dt}}\right),$$

where, R is the radius of the bubbles, t is the time, D is the diffusion constant, C_i/C_o is the ratio of the dissolved gas concentration to the saturation concentration, σ is the surface tension, P_0 is the ambient pressure, L is the Ostwald coefficient, p_{ov} is the overpressure.

The equation was numerically solved to extract the size variation of a gas bubble. (Fig. 1) shows the change in bubble size as a function of time at three different sizes: 1, 3, and 5 μm diameter. The gas contained in the bubble is air. We can appreciate that the smallest bubble (1 μm) disappears in less than 2 msec, whereas the predicted lifetime of a 5μm air bubble is ∼93 msec. The disappearance of these microbubbles is caused mainly by the diffusion of the contained gas, which dissolves in the surrounding medium.

Bibliography

1. de Jong N, Ten Cate FJ, Lancee CT et al (1991) Principles and recent developments in ultrasound contrast agents. Ultrasonics 29(4):324–330

Contrast Media, Ultrasound, Influence of Shell on Pharmacology and Acoustic Properties

Volkmar Uhlendorf
ETH Zürich, Institut für Pharmazeutische Wissenschaften, Zürich, Switzerland
volkmar.uhlendorf@pharma.ethz.ch

Synonyms

Capsule of ultrasound contrast media; Coating of ultrasound contrast media

Definition

When microbubbles are used as ultrasound contrast media, they usually need some coating—a shell. The shell surrounds the microbubble, stabilises it and thus provides transpulmonary stability. The shell influences both the pharmacological and acoustic properties of the microbubble.

Characteristics

When coated by a protective shell, microbubbles are at least nearly spherical, but as free microbubbles (after removal of the shell) they have an exactly spherical shape. Furthermore the shell has one or several of the following basic functions:

1.1 Reduction of gas exchange (outwards or inwards, depending on type of gases involved),
1.2 Stabilisation against aggregation and fusion of microbubbles (during storage or after administration),
1.3 Control of the surface characteristics on a molecular level (important for immune response, or for targeting),
1.4 Control of elastic and acoustic properties (threshold for acoustic disruption of bubble shell).

A further function might be seen in the encapsulation of drug substances within the bubble or within the shell, but this shall not be considered here in detail.

1.1 together with 1.2 allows providing a sufficiently stable population of small microbubbles. 1.3 is very important for the pharmacology of the bubbles. Finally, 1.4 is important for the acoustic behaviour during ultrasound imaging. These points are discussed in more detail.

The shell material typically belongs to the following classes:

- Fatty acids or lipids,
- Proteins—often denatured,
- Bio-degradable synthetic polymers,
- Combinations of the above,
- Surface-active components of the surrounding body fluid may play some role after administration.

In addition, there may be important functional groups or targeting molecules on the shell surface.

The total mass of shell material differs from agent to agent and also depends on the imaging procedure. For two reasons it usually is very low. First, in nearly all cases the shell is relatively thin when compared to the bubble diameter. Second, the injected amount of contrast agent is typically very low, as bubbles are easily detectable.

1.1 Reduction of Gas Exchange

A small, uncoated microbubble of soluble gas (like air) is not stable, even in a gas-saturated liquid. The surface tension is creating an enhanced pressure within the bubble (up to some atmospheres) which will enforce microbubble dissolution, typically within milliseconds. In a closed vial of contrast media and in a very concentrated bolus there may be a local overpressure or oversaturation, respectively, which temporarily can help to stabilise a microbubble population. But, at least after injection these stabilizing factors no longer exist. A shell can slow down the dissolution process, thus providing sufficient time for contrast imaging.

Several ultrasound contrast media contain hydrophobic (often perfluorated) gases of very low solubility in water. Due to their higher molecular weight compared to air, they also have a reduced diffusivity. In this case, diffusion of soluble low molecular weight gas may lead to a net inflow of gas and some growth of the mean diameter of bubbles without shell. One contrast agent claims to use about the steady-state mixture to prevent such a growth. But, even when insoluble gases or mixtures are used, there remain other reasons for having microbubbles coated.

1.2 Preventing Aggregation and Fusion of Microbubbles

For several reasons, aggregation (coagulation) of microbubbles has to be prevented, both during storage of suspensions and after injection. First, aggregates might become too large for unimpeded passage of capillaries and —in severe cases—would even create a safety risk. Aggregates also could lead to bubble growth by fusion of microbubbles, in particular for hydrophobic gases. Finally, any bubble aggregate is likely to respond acoustically similar to one large bubble and would thus reduce the efficiency. A shell of suitable composition helps to prevent these undesired processes. For this purpose, the shell may contain some (usually negatively) charged groups that lead to repulsion of microbubbles. In addition, there may be molecules preventing fusion for sterical reasons.

During development of a particular contrast agent, the effects should have been studied in detail and an adequate formulation found which guarantees stability during shelf life and *in vivo*. It is therefore not advisable to mix an agent with any other substance (unless allowed by the manufacturer) as this may lead to reduced stability.

1.3 Shell Surface and Microbubble Targeting

There are two relatively simple cases. One is the case of unspecific contrast agents, which remain in the blood pool and do not show uptake in certain organs or attachment to any targets. In the early years of ultrasound contrast agents, this was the intended mode of action. The second 'simple' case is just the opposite, namely purposeful targeting using one of the several techniques, which may not be limited to ultrasound contrast agents. It typically means to provide a bubble shell with a suitable number of targeting molecules, often attached to a linker on the shell surface. In recent years, in several cases the principle could be shown to work as intended.

Unspecific uptake of coated microbubbles in liver and spleen has been observed for several agents. It is expected as a normal response of the immune system, which tends to remove the coated bubbles as foreign particles. The surface properties of the bubble shell are determining the uptake rate, which can be controlled to some degree. This can be important when a long duration of contrast in the blood pool is intended, but also when rapid clearance is desired to get a low background signal for detection of targeted bubbles.

Delayed liver enhancement is a special case of unspecific uptake, mainly observed for Levovist. Its diagnostic applications in tumour imaging are described in a separate entry. The phenomenon is not completely understood and is still subject to research.

1.4 Influence of Shell on Elastic and Acoustic Properties

The acoustic properties of scatterers are determined by their density, elastic properties, shape and size. A bubble shell may have influence on all of these factors.

In nearly all cases, the shells of contrast agent microbubbles are very thin compared to their total diameters. The density of the shell material is very similar to the density of water, plasma or tissue. Therefore, a coated microbubble is essentially a gaseous inclusion in a medium with the density of water, with a size given by the inner diameter of the shell. While density and size are not much affected by the shell, the shell material has a very important influence on the effective elastic—and thus acoustic—properties.

A rigid, inelastic shell will prevent oscillations like those of a 'free' bubble. Therefore, scattering will be weak and about linear. On the other hand, a thin rubber-like, highly elastic shell will allow a bubble response almost like a 'free' bubble, preserving most of their highly desirable nonlinear acoustic behaviour. The same would apply to a shell consisting of smaller, loosely assembled pieces, which do not impede bubble motion.

Actually, most shells have properties between these extreme cases. Some types of thin, but almost rigid shells can be ruptured by sufficiently strong excitation in a

diagnostic ultrasound pulse. This allows controllable switching from weak, linear scattering to much stronger and non-linear scattering. A broken shell also leads to rapid dissolution of microbubbles consisting of air or other soluble gases (see 1.1). Disappearing bubbles can be detected with very high sensitivity in colour Doppler mode, even a single microbubble can be detected with a normal diagnostic ultrasound scanner.

Contrast Media, Ultrasound, Low Solubility Gas

N. DE JONG
ErasmusMC, Rotterdam,
The Netherlands
n.dejong@erasmusmc.nl

Synonyms

Perfluorocarbon gas agents; Second (third) generation contrast media

Definitions

An agent containing gas bubbles of which the gas in the bubble hardly dissolved in the surrounding liquid (typical water/plasma).

Characteristics

The first generation of ultrasound contrast agents were based on air core, whereas the new generations are composed of gases with higher molecular weights. For the kinetics of the dissolution of a gas, microbubble see—High solubility gas ultrasound contrast media. In that equation, the Ostwald coefficient (L) represents the ratio of the gas solubility in liquid to the gas density (1). From the equation, it is clear that microbubbles containing gases with lower Ostwald coefficients persist longer than bubbles containing gases with higher values. (Fig. 1) displays the dissolution in time of a 3 μm diameter bubble containing two different gases: air and sulfur hexafluoride SF_6. The air gas bubble disappears in less than 25 msec whereas the predicted lifetime of an SF_6 gas bubble with the same size is more than 100 msec. Second-generation contrast agents designed with improved lifetime to enable opacification of LV and myocardial microcirculation are composed of less-diffusable gases such as perfluorocarbons, perfluoropropane (optison), or sulfur hexafluoride (sonovue). These types of inert gases have a high molecular weight. Since the diffusion of a gas is inversely proportional to the square root of its molecular weight (2), the higher the molecular weight, the slower the solubility or diffusion of the gas. Table 1 summarizes, for different gases, the Ostwald coefficient and the predicted lifetime of a bubble of 3-m diameter. The gases chosen here are used in commercially available contrast agents or in those under clinical investigations. Clearly, gases with lower solubility provide the bubbles longer persistence. As a matter of fact, not only the Ostwald coefficient plays an important role in the choice of the type of gas for improved stability, but also the saturated vapor pressure at body temperature. Lower vapor pressures will make the bubble to condense into liquid losing therefore the contrast.

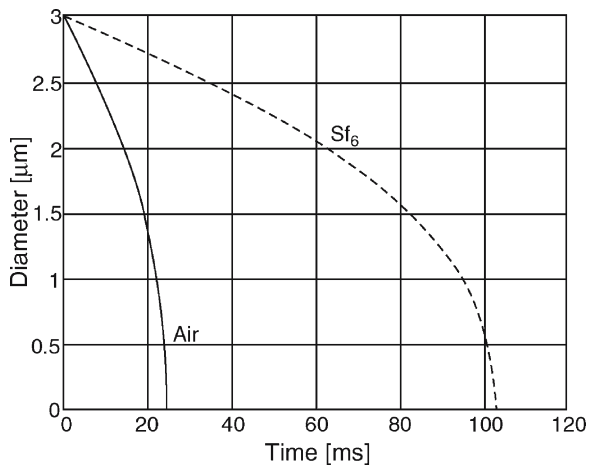

Contrast Media, Ultrasound, Low Solubility Gas. Figure 1 Diameter's change versus time for a bubble of 3 mm diameter; solid: air bubble, dashed: SF_6 gas bubble.

Contrast Media, Ultrasound, Low Solubility Gas. Table 1 Ostwald coefficient and disappearance time for 3-μm diameter bubbles containing different gases

	Ostwald Coefficient ($\times 10^6$)	Disappearance Time (msec)
Air	23,168	24.4
Sulfur hexafluoride (SF_6)	5,950	102.9
Perfluoropropane (C_3F_8)	583	1,110
Perfluorohexane (C_6H_{14})	24	2,000

Bibliography

1. Kabalnov A, Bradley J, Flaim S et al (1998) Dissolution of multicomponent microbubbles in the bloodstream: 2. Experiment. Ultrasound Med Biol 24(5):751–760
2. Porter EA (1995) Effect of blood and microbubble oxygen and nitrogen content on perfluorocarbon-filled dextrose albumin microbubble size and efficacy. J Am Soc Echocardiogr 11:421–425

Contrast Media, Ultrasound, Multipulse Techniques

Multi-pulse techniques are used in microbubble specific imaging for two key purposes. Firstly, a phase and/or amplitude modulated pulse train can be used to preferentially detect the non-linear response of the microbubbles to differing acoustic stimuli against the linear tissue background. Secondly, multiple pulses can be used to provide information on the motion of the microbubbles within the circulation, in the same way that multiple pulses are processed for color or power Doppler imaging.

See under Contrast Media, Ultrasound, Specific Imaging Techniques. ►Contrast Media, Ultrasound, Phase Modulation, for further details.

Contrast Media, Ultrasound, New Clinical Development

Christian Greis
Bracco ALTANA Pharma GmbH, Klinische Entwicklung Ultraschallkontrastmittel, Konstanz, Germany
christian.greis@altanapharma.com

Synonyms

Drug-delivery systems; Microbubbles; Target-specific microbubbles; Ultrasound contrast agents; Ultrasound contrast media

Definition

A classic ultrasound contrast medium consists of echogenic microbubbles, which, after intravenous injection, are distributed freely within the blood compartment. Several of these agents are already in the market and more are under clinical development. These agents differ in the composition of the shell and the encapsulated gas, which has an impact on the stability and the behavior in the sound field. However, microbubble contrast agents can also be used in a broader sense.

One approach is to modify the shell of the microbubbles to obtain an affinity to structures or tissues in the body. Such *target-specific microbubbles* can adhere to cells or specific molecular structures in the body, thereby allowing the imaging of these targets. Since the sensitivity of recent contrast-specific ultrasound technologies is so high that single microbubbles can be detected, such an agent can be used to image individual target molecules on the surface of cells or structures *in vivo* (*molecular imaging*).

Another approach is to incorporate drugs, genes, or other active substances in microbubbles, with the aim of releasing them at a specific location in the body. Such an agent can be used as a *drug-delivery system* allowing local therapy after intravenous administration of the agent. The local release of the active substance can be obtained either with target-specific microbubbles (distributing the encapsulated compound over time) or by local destruction of free circulating microbubbles using local insonation of the target region with high insonation power.

Indication

Standard ultrasound contrast media are used as markers for blood distribution and perfusion. They can help to delineate vascular structures, demonstrate the vascular geometry separated from the tissue background, and act as tracers for the assessment of blood distribution and perfusion.

For some of the existing agents, a certain affinity to endothelial structures has been described, even if they have not been developed for that purpose. Albumin-based contrast agents can attach to activated endothelial cells (1) and the attached microbubbles can be detected there after wash-out of the freely circulating agent. Other agents are captured by the reticuloendothelial system in the liver and spleen (2) or the microbubbles can even be phagocytosed by cells (3), allowing the imaging of phagocytotic active tissue. The attachment and/or phagocytosis of microbubbles in the liver is facilitated by the fenestration of the endothelium in the liver sinusoids, permitting the close contact of microbubbles and perivascular cells. An intracellular uptake of ultrasound contrast agents can also be obtained by using much smaller echogenic nanoparticles, e.g., consisting of biodegradable polymers (4). Such nanoparticles usually have a very high stability and are stored in the tissue for days and weeks.

Usually, ultrasound contrast agents are delivered, after intravenous injection, *via* the vascular system. However, alternative delivery pathways are possible too. For imaging of lymph nodes, the intravenous administration results in the demonstration of lymph node vascularity and perfusion. However, after subcutaneous injection, the agent is delivered *via* the lymphatic pathway to the lymph nodes (5). This allows the demarcation of sentinel nodes without using a radiotracer. Conventional microbubble agents as well as smaller nanoparticle agents can be used for lymphatic delivery.

A more specific attachment of microbubbles to tissues or structures can be achieved by coupling microbubbles to antibodies, binding to specific molecules on the surface of target cells/structures (6). Such agents can be used for targeted imaging down to a molecular level. Possible indications for targeted imaging include the detection of thrombotic material in the vascular system, the demonstration and quantification of neoangiogenesis in tumors, and the imaging of inflammation.

Beyond the diagnostic use, microbubble agents can also be used as therapeutic agents, e.g., to initiate or enhance local therapy. One capability of microbubbles is the local intensification of mechanical forces induced by the ultrasound wave. In combination with high insonation power, this can increase the endogenous or exogenous thrombolytic activity (*accelerated thrombolysis*) or can result in the transient formation of micropores in the capillary vessels (*sonoporation*), facilitating the transport of substances into the target tissue. Furthermore, the microbubble itself can be used simultaneously for the transport and delivery of active substances, acting as a ►drug-delivery system. Using such a system, the local concentration and activity of a drug can substantially be increased, allowing local therapy with reduced systemic effects.

For some pathologies, constant treatment over a long period (or lifelong treatment) is required, creating the need for continuous administration of a drug. In such cases, gene therapy may be preferable, resulting in the repair of pathological functions or induction of protective mechanisms. The first preclinical studies have demonstrated that lipid-coated microbubbles can be used as vectors for the transportation of *genes* or *antisense molecules* instead of using viral vectors. The combination of ►target-specific imaging and local therapy is a very promising opportunity for microbubble contrast agents, and an increasing number of research groups around the world are currently elaborating indications for the diagnostic and therapeutic use of such products. Many positive and encouraging results have already been published, coming from in vitro and animal studies. However, before the first product can be used in clinical studies in humans, extensive pharmacological and toxicological studies have to be performed.

Use and Dosage

Microbubble contrast agents are usually administered intravenously. The shell of the microbubbles ensures stability and integrity until the target region is reached and/or the microbubbles are destructed by a high-power ultrasound pulse. For target-specific imaging, normal doses of the contrast agent can be used. Due to the high sensitivity of contrast-specific imaging modalities, single microbubbles can be detected, so that the current doses used for blood-pool imaging are sufficient. For therapeutic purposes, the dose is mainly dependent on the efficacy of the incorporated drug. However, the lumen in the microbubbles is quite large, and for several drugs as well as oligodendronucleotides (used for gene therapy) it has been shown that effective doses can be obtained.

Adverse Reactions

Since the microbubbles do not contain any toxic substances, no substantial side effects caused by the microbubble carrier are known or expected. As for the current blood-pool imaging agents, allergic reactions can occur due to the colloidal character of the microbubbles. However, such reactions are rare and do not seem to be increased by labeling or loading of the microbubbles. Also for biopolymer nanoparticles, which are accumulated and stored for a long time in the target tissue, no particular side effects have been observed. However, the data available are limited and long-term effects need to be investigated.

Adverse effects of drug-delivery systems seem to be acceptable and are mainly related to the side effects of the encapsulated drug. Due to the local accumulation of the active substance, the side effects of the drug seem to be fewer compared to the systemic administration of the same drug. Therefore, it is expected that higher doses of the drug can be used to increase the local therapeutic effect.

References

1. Villanueva FS, Jankowski RJ, Manaugh C et al (1997) Albumin microbubble adherence to human coronary endothelium: implications for assessment of endothelial function using myocardial contrast echocardiography. J Am Coll Cardiol 30:689–693
2. Blomley MJK, Albrecht T, Cosgrove DO et al (1999) Stimulated acoustic emission to image late liver and spleen-specific phase of Levovist in normal volunteers and patients with and without liver disease. Ultrasound Med Biol 25:1341–1352
3. Takeuchi H, Ohmori K, Kondo I et al (2004) Interaction with leukocytes: phospholipid-stabilised versus albumin-shell microbubbles. Radiology 230:735–742
4. Bauer A, Blomley M, Leen E et al (1999) Liver-specific imaging with SHU 563A: diagnostic potential of a new class of ultrasound contrast media. Eur Radiol 9 [Suppl 3]:S349–352

5. Goldberg BB, Merton DA, Liu JB et al (2004) Sentinel lymph nodes in a swine model with melanoma: contrast-enhanced lymphatic US. Radiology 230:727–734
6. Ellegala DB, Leong-Poi H, Carpenter JE et al (2003) Imaging tumor angiogenesis with contrast ultrasound and microbubbles targeted to $\alpha_v\beta_3$. Circulation 108:336–341

Contrast Media, Ultrasound, Safety and Adverse Reactions

Anders Nilsson
Department of Radiology
Ultrasound University, Uppsala University Hospital, Uppsala, Sweden
anders.nilsson@akademiska.se

Synonym

Adverse events to ultrasound contrast media

Definition

All existing ultrasound contrast agents consist of gas bubbles slightly below the size of red blood cells and are stabilised by a shell. This is to ensure their survival in the blood circulation long enough for an ultrasound examination to be made and, in the case of the newer agents, to enable an examination with a reduced ►mechanical index (MI) to be made without significant destruction of the bubbles. They pass through capillary beds and thus can be injected intravenously. As they can be seen as particles, they do not leave the circulation, i.e. they are so-called blood pool agents. The contrast effect is caused, with increasing ultrasound intensity, by reflection, asymmetrical oscillation and finally bursting. Ultrasound contrast media are generally extremely well tolerated. Like with all drugs, adverse reactions to these agents may occur, but are very rare and seldom clinically relevant.

Indication

Ultrasound contrast media increase the reflectivity of blood. This can be used to enhance Doppler signals, both in spectral and colour Doppler. The asymmetrical oscillation, without significant bubble destruction, is the basis for so-called non-linear imaging techniques where dedicated ultrasound machine software can recognise the non-linear signal from a microbubble and produce an image based on contrast agent concentration rather than basic tissue echogenicity.

Many applications have been developed for this type of imaging, most notably to date the detection and characterisation of the liver and other organs. The ability to differentiate perfused from non-perfused tissue also has many applications in several organ systems.

Contraindications

Ultrasound contrast agents should not be used in patients with previous allergic reactions to the same compounds. Caution should be exercised when microbubbles are used in patients with ischaemic heart disease. Right-to-left ventricular shunts and pulmonary hypertension are also stated as contraindications, see below.

Pregnancy/Lactation

There is no evidence that compounds from ultrasound contrast agents would cause harm in pregnancy or when breastfeeding but as their use in pregnancy and paediatrics is contrary to the product information in most of the contrast agents, experience is limited and contrast used with caution.

Dosage

As different contrast agents have different physical properties and vary in the number of microbubbles per volume unit the dosage varies and must be adjusted with regards to the agent used, the ultrasound machine software and the indication for use.

Adverse Reactions

First, it should be pointed out that both ultrasound within recommended MIs and microbubbles as contrast agents seem to be extremely safe (1). Second, that as ultrasound contrast agents have physical rather than chemical properties in common (stabilised gas bubbles) the adverse reactions may vary more between different agents than is the norm for X-ray contrast media.

The most commonly reported adverse reactions are the same as with other types of contrast media, i.e. headache, a feeling of warmth and flushing. Less often reported are nausea, dizziness, chills, altered taste and dyspnoea. Similar findings were, however, also seen in the placebo groups.

Allergic reactions seem to be very infrequent and mild with general flush and erythema (2). Recently, a small

number of more severe anaphylactic reactions to the agent SonoVue (Bracco SPA, Milano, Italy) have been reported, though, suggesting that repeated exposure over a short period of time should be considered with some care.

As microbubbles are particles they carry a risk of embolisation if they aggregate (individual bubbles are smaller than capillaries and therefore have no embolic potential). This, however, seems extremely unlikely given their extremely low concentration in the blood pool. Contrast injections are given intravenously and thus any such emboli should be filtered out by the capillary beds of the lungs but the existence of right-to-left shunts is usually a contra-indication for the use of microbubble-based contrast agents.

At higher ultrasound intensities a cavitation phenomenon occurs, i.e. the growth and collapse by implosion of microbubbles. This causes significant changes in pressure and temperature and *in vitro*/animal studies have shown local haemolysis, platelet aggregation and damage to endothelial cells (3). Even though these unwanted side effects have not been seen in clinical practise (4), it would be prudent to perform ultrasound contrast examinations with as low an acoustic output as possible. This is not a problem since most modern contrast-specific software use a low MI in order to minimise bubble disrupture.

It should be pointed out that as ultrasound contrast agents are relatively new products, it will take many more years of surveillance to accurately assess the possible existence of other rare adverse reactions.

Bibliography

1. EFSUMB Study Group (2004) Guidelines for the use of contrast agents in ultrasound. Ultraschall Med 25:249–256
2. Correas J-M, Bridal L, Lesavre A et al (2001) Ultrasound Contrast agents: properties, principles of action, tolerance and artefacts. Eur Radiol 11:1316–1328
3. Miller DL, Gies RA (1998) Enhancement of ultrasonically induced hemolysis by perfluorocarbon-based compared to air-based echocontrast agents. Ultrasound Med Biol 24:285–292
4. ter Haar GR (2002) Ultrasonic contrast agents: safety considerations reviewed. Eur J Radiol 41:217–221

Contrast Microbubbles

▶Microbubbles

Contrast Reactions

▶Adverse Reactions, Iodinated Contrast Media, Acute, Non renal

Contrast Reversal

Finding of computed tomography about hepatic steatosis gives a clear evidence of hepatic vessels on unenhanced scans which appear relatively hyperdense compared to the fatty liver, simulating the images obtained after contrast administration.

▶Steatosis, Hepatic

Contrast Specific Imaging Techniques

▶Specific Imaging Techniques, Contrast Media, Ultrasound

Contrast-Enhanced Echocardiography

▶Contrast Media, Ultrasound, Applications in Echocardiography

Contrast-Enhanced Reflux Sonography

▶Contrast Media, Ultrasound, Applications in Vesicoureteral Reflux

Contrast-Enhanced Sonography in Abdominal Trauma

▶Contrast Media, Ultrasound, Applications in Blunt Abdominal Trauma

Contrast-Enhanced Ultrasound (US) of the Liver

▶Contrast Media, Ultrasound, Hepatic

Contrast-Enhanced Ultrasound Imaging of the Brain

▶Contrast Media, Ultrasound, Applications in Transcranial and Intra-Operative Brain Ultrasound

Contrast-Enhanced Ultrasound in Abdominal Trauma

▶Contrast Media, Ultrasound, Applications in Blunt Abdominal Trauma

Contrast-Enhanced Ultrasound of the Spleen

▶Contrast Media, Ultrasound, Applications in Focal Splenic Lesions

Contrast-Enhanced Voiding Urosonography (VUS)

▶Contrast Media, Ultrasound, Applications in Vesicoureteral Reflux

Contrast-Specific Imaging

An imaging modality that allows the selective detection and demonstration of the contrast agent in the body. This requires a separation of signals coming from the contrast agent from those coming from the tissue. The separation of both signals is based on specific characteristics in the contrast agent signal, which are not present in the tissue signal.

▶Contrast Media, Ultrasound, Commercial Products

Contrast-enhanced CT or MRI in ACKD

The gold standard in the diagnosis of acquired cystic kidney disease (ACKD) as well as in the characterization of renal masses (hemorrhagic cysts or solid renal tumors). Can be performed in patients undergoing dialysis but should be replaced by MRI in patients with contraindications to iodinated contrast agents (alteration of renal function or previous allergic reaction).

▶Cystic Renal Disease, Acquired

Contusion, Breast

Reversible infiltration of the breast parenchyma by extravasated blood and edema following trauma.

▶Trauma, Breast

Contusion, Hepatic

Hepatic contusion appears as a hypodense area due to interstitial bleeding, with irregular margins, and is usually associated with major hepatic injuries such as lacerations and hematomas.

▶Trauma Hepatobiliary

Conventional Defecography - Evacuation Proctography

▶Pelvic Floor Dysfunction, Anorectal Manifestations

Conventional Renal Carcinoma

▶Carcinoma, Renal Cell

Core Needle Biopsy

Biopsy in which a histologic specimen is taken, usually with a 14-gauge needle (in contrast to vacuum-assisted biopsy or fine needle aspiration biopsy, FNAB).

▶Carcinoma, Lobular, *In situ*, Breast

Coronary Angiography

Diagnostic modality based on X-rays able to obtain angiographic images of the Coronary arteries by means of a Catheter positioned through the femoral artery.
▶Ischemic Heart Disease, CT

Coronary Angioplasty

Interventional procedure based on transcutaneous placement of a Catheter inside the lumen of a Coronary artery by which it is possible to dilate a stenosis.
▶Ischemic Heart Disease, CT

Coronary Artery Bypass Surgery

Surgical procedure used to revascularize obstructed Coronary arteries.
▶Ischemic Heart Disease, CT

Coronary Artery Disease

Atherosclerotic disease involving the Coronary arteries.
▶Ischemic Heart Disease, CT
▶Ischemic Heart Disease, Ultrasound

Coronary Artery Steal

In patients with internal mammary artery to coronary artery by-pass graft, the presence of a proximal subclavian occlusion may cause coronary artery steal syndrome presenting as angina during arm exercise.
▶Steal Syndrome Vertebral

Coronary Artery Stenosis

Obstruction of a Coronary artery usually determined by atherosclerosis.
▶Ischemic Heart Disease, CT

Coronary Stent

Device used after Coronary artery dilatation to keep the lumen of the Coronary arteries open.
▶Ischemic Heart Disease, CT

Corpus Cavernosum, Thrombosis

Räto T. Strebel[1], Hubert John[2]
[1]Department of Urology, University Hospital Zurich, Zurich, Switzerland
[2]Klinik Hirslanden, Leiter Zentrum für Urologie, Zurich, Switzerland
raeto.strebel@usz.ch

Synonym

Segmental/partial priapism

Definition

A partial priapism of the corpus cavernosum is an exceedingly rare condition. Most frequently, it is characterized by thrombosis within a proximal segment of one corpus cavernosum.

Corpus Cavernosum, Thrombosis. Figure 1 Peyronie's disease with typical penile deformity on erect penis.

Clinical Presentation

Patients complain usually a painful perineal mass some days before seeking medical attention. On physical examination, a tender and painful mass is palpable perineally near the base of the penis.

Imaging

Magnetic resonance imaging of the pelvis should be the imaging modality of choice and reveals the underlying pathology. Frequently, an ultrasound of the perineal region or even a transanal ultrasound is performed beforehand to rule out any perianal abscess. Alternatively, a CT scan may be performed (Fig. 1).

Corpus Luteum Cysts

Corpus luteum cysts have thicker, better vascularized walls than follicular cysts. Similar to follicular cysts, the content varies from watery to proteinaceous to hemorrhagic.

▶Cyst, Follicular, Ovarium

Coxa Valga

Increased angle between the femoral neck and shaft (normal 150° at birth, then gradually decreasing up to 120–130° in adults).

▶Congenital Malformations of the Musculoskeletal System

Coxa Vara

Decreased angle between the femoral neck and shaft (<120°).

▶Congenital Malformations of the Musculoskeletal System

CPPD

Lynne S. Steinbach
Department of Radiology, University of California, San Francisco, USA
lynne.steinbach@radiology.ucsf.edu

Synonyms

Calcium pyrophosphate deposition disease; Chondrocalcinosis; Pseudogout

Definitions

One of the most confusing aspects of calcium pyrophosphate dihydrate (CPPD) arthropathy is the associated nomenclature. A variety of terms have been used. *Chondrocalcinosis* is a more general term that is reserved for pathologically or radiologically evident cartilage calcification. It can include CPPD, dicalcium phosphate dihydrate, or calcium hydroxyapatite crystals, or combinations of the three. CPPD *crystal deposition disease* is a specific term for a disorder characterized by the exclusive presence CPPD crystals in or around joints. The term "*pseudogout*" is not a radiological diagnosis; rather it is reserved for a gout-like clinical syndrome produced by CPPD crystal deposition disease that is characterized by intermittent acute attacks of arthritis. *Pyrophosphate arthropathy* is a term that describes a particular pattern of structural joint damage that occurs in CPPD crystal deposition disease. This arthropathy is similar to osteoarthritis but has some separate distinct features. *Articular and periarticular calcification* can occur with CPPD crystal deposition disease; however, calcium deposits other than CPPD crystal accumulation also may produce this type of calcification.

Pathology/Histopathology

The deposition of various crystals within the articular tissues can cause an acute inflammatory response and acute synovitis and lead to chronic destructive arthritis. First, deposition of CPPD crystals is observed in the articular cartilage, around the chondrocyte lacunae. This may alter biochemistry of cartilage, e.g., proteoglycan concentrations. The acute synovitis of CPPD is probably due to the rupture of preformed deposits of calcium pyrophosphate dihydrate from cartilage into the adjacent synovial cavity.

Clinical Presentation

The clinical presentations of CPPD crystal deposition disease are highly variable, ranging from asymptomatic disease to severe pain associated with a destructive arthropathy. Indeed, this disease has been called a "great mimicker" of other arthritides. Furthermore, occasionally, several of these clinical patterns present at different times during the course of the arthritis.

The *asymptomatic* form of this arthropathy is probably the most common; however, it is difficult to document this because many asymptomatic patients are never seen by a physician. Absence of symptoms occurs in at least 10 to 20% of documented cases of CPPD crystal deposition disease.

Many patients with CPPD crystal deposition disease present with an arthropathy that simulates *osteoarthritis*. An occasional acute inflammatory component is seen in 35 to 60% of such patients. This osteoarthritic form is a chronic and progressive arthritis that is frequently bilateral and symmetric, presenting in the knee, hip metacarpophalangeal, elbow, ankle, wrist, and glenohumeral joints. Flexion contractures are common, especially in the knee and elbow.

Patients with CPPD crystal deposition disease also may have inflammatory symptoms and signs. For example, attacks of *pseudogout* occur in 10 to 20% of symptomatic patients. The pseudogout syndrome is caused by shedding of pyrophosphate crystals into the joint fluid. Although most cases of pseudogout develop spontaneously, situations that trigger acute pseudogout include direct joint trauma, concomitant medical illness such as stroke and myocardial infarction, surgery (especially parathyroidectomy), blood transfusion, parenteral fluid administration, institution of thyroxine replacement therapy, and joint lavage. Hypocalcemia is present in many of these situations and is believed to provoke some attacks of pseudogout. This produces pain, erythema, and tenderness, which can be mistaken for other disorders such as gout or septic joint. The attacks are self-limited and can last from one day to several weeks. They generally are less painful than those of gout and are most common in the knee, but other sites including the hip, glenohumeral, elbow, ankle, wrist, acromioclavicular, talocalcaneal, and metatarsophalangeal joints also are affected. Fever and elevation of the erythrocyte sedimentation rate may accompany pseudogout attacks.

Two to six percent of patients with CPPD crystal deposition disease present with an arthritis that simulates *rheumatoid arthritis*. These attacks are characterized by morning stiffness, fatigue, synovial thickening, restricted joint motion, and an elevated erythrocyte sedimentation rate, and they persist from 4 weeks to several months.

CPPD crystal deposition disease also can have a *pseudoneurotrophic* presentation in as many as 2% of patients. Indeed, CPPD crystalline arthropathy should be considered in the differential diagnosis of rapidly progressive destruction of large joints.

Imaging

Conventional Radiography

Radiographically, chondrocalcinosis usually is apparent in CPPD crystal deposition disease, but the arthropathy can also precede radiographically detectable cartilage calcification, the calcification may not always be dense enough to be visualized on conventional radiographs, or it may be difficult to identify such calcification if the joint is severely deranged. In one study of 3228 patients undergoing knee arthroscopy, a radiographic diagnosis of chondrocalcinosis was made in only 39.2% of patients with pathologically proven CPPD crystal deposition (1).

Computed Tomography and Magnetic Resonance Imaging

Computed tomography (CT) can accurately demonstrate chondrocalcinosis due to the high soft tissue contrast and tomographic nature of this imaging method. However, CT is rarely used to evaluate the painful joint. Magnetic resonance imaging (MRI) is often the cross-sectional imaging procedure performed for painful joints. It is therefore common to encounter CPPD crystal deposition disease in older patients who are being studied with routine MRI. Calcification can be difficult to detect on MRI. Correlation with conventional radiographs is often necessary. Despite this problem, CPPD crystal deposition disease in hyaline cartilage is occasionally detected with standard MRI techniques. Prominent linear or punctate hypointense areas frequently are demonstrated. A small halo of hyperintense signal intensity surrounding the hypointense areas is occasionally seen, probably related to magnetic susceptibility artifact.

Although the low signal intensity calcification can be detected in routine spin echo, fast spin echo, and short tau inversion recovery (STIR) images, the hyaline cartilage calcification is better seen on gradient echo images in which the difference between the magnetic susceptibility of hyaline cartilage and CPPD crystals is enough to create local magnetic field inhomogeneity resulting in signal distortion. In these types of images, foci of cartilage calcification become larger, the so-called "blooming" effect.

Low signal intensity in the hyaline cartilage may be overlooked on MRI if the reader does not include it in a search pattern for chondrocalcinosis. There is also a differential diagnosis for this pattern, which includes hemosiderin from trauma, pigmented villonodular synovitis, and hemophilia; gas related to vacuum phenomenon;

and magnetic susceptibility artifact around postsurgical intra-articular material such as micrometallic debris.

There are also documented cases of CPPD crystal deposition in which the calcification in the hyaline cartilage or menisci was not seen on MRI. This is more common in cases of meniscal calcification in which the short T2 relaxation times of the meniscus and calcification are similar. Occasionally, with MRI, CPPD crystal deposition disease in a meniscus can mimic a meniscal tear. This has important implications and can lead to inappropriate treatment including unnecessary surgery. Gale et al reported areas of high signal intensity in regions of meniscal chondrocalcinosis with T2-weighted spin echo MR sequences (2). This finding may be attributed to the hyperintense halo artifact seen adjacent to calcification of low signal intensity. No reports have described high signal intensity in areas of chondrocalcinosis in T1-weighted images. Such a finding which would potentially simulate a meniscal tear, is theoretically possible given that increased signal intensity of calcium deposits has been found in the discs of the lumbar spine.

Nuclear Medicine

Skeletal scintigraphy may show increased radiotracer uptake in the joints, but these findings are nonspecific.

Diagnosis

CPPD crystal deposition disease is characterized by calcification in and around joints and structural joint changes termed pyrophosphate arthropathy. This arthropathy resembles osteoarthritis; however, it occurs in articulations not usually affected by osteoarthritis, often affecting non-weight-bearing regions such as the radiocarpal, metacarpophalangeal joints, glenohumeral joints, and elbow. It usually is bilateral and symmetric and is most common in the knee, wrist, and metacarpophalangeal joints. Furthermore, CPPD crystal deposition disease has an unusual intra-articular distribution in certain joints such as the knee and wrist where patellofemoral and radiocarpal joint space narrowing may be seen (3).

CPPD crystal deposition disease frequently presents on routine radiography with normal mineralization, narrowing of various articulations, and subchondral sclerosis. Osteophytes are common, but occur with a frequency less than that of osteoarthritis. Subchondral cysts are one of the hallmarks of this arthropathy. The cysts usually are larger, more numerous and widespread than in osteoarthritis. Cysts may form before cartilage loss is evident. Osseous fragmentation and collapse may be related to fracture of these cystic lesions. Intra-articular osteochondral bodies commonly are associated with CPPD crystal deposition disease. These may be free in the joint cavity or embedded in cartilage or synovium.

Cartilage

Chondrocalcinosis is usually caused by CPPD crystal deposition. In 5% of cases, however, it can be related to other crystals such as dicalcium phosphate dihydrate and calcium hydroxyapatite (4). Both hyaline cartilage and fibrocartilage can contain CPPD crystals. The CPPD crystal tends to be deposited in the middle layer of degenerated hyaline cartilage. These deposits are thin and linear and parallel the subjacent subchondral bone (Fig. 1). CPPD crystals are also deposited on the surface of the hyaline cartilage, especially when there is superficial chondral erosion. Hyaline cartilage calcification is most common in the wrist, knee, elbow, and hip.

CPPD crystal deposition in fibrocartilage is most commonly observed in the menisci of the knee, triangular fibrocartilage of the wrist, labra of the acetabulum, symphysis pubis, and annulus fibrosus of the intervertebral disc. Other less common sites of CPPD crystal deposition in cartilage include the articular discs of the sternoclavicular and acromioclavicular joints and glenoid labra.

Synovium and Capsule

Synovial calcification is common in CPPD crystal deposition disease. Synovial calcification can be so widespread that it appears to fill the entire joint cavity,

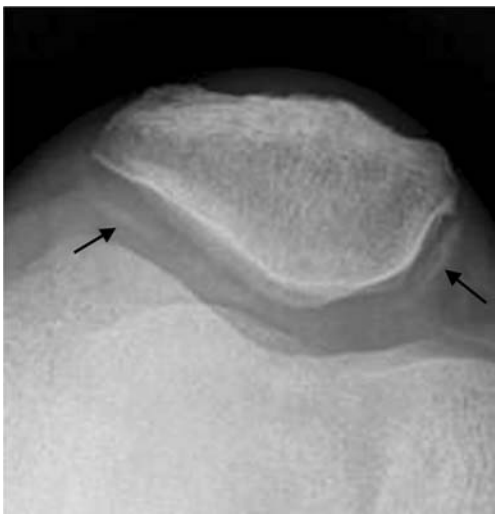

CPPD. Figure 1 Linear calcification is seen along the hyaline cartilage of the medial and lateral facets of the patella (*arrows*) on this Merchant view of the patellofemoral joint.

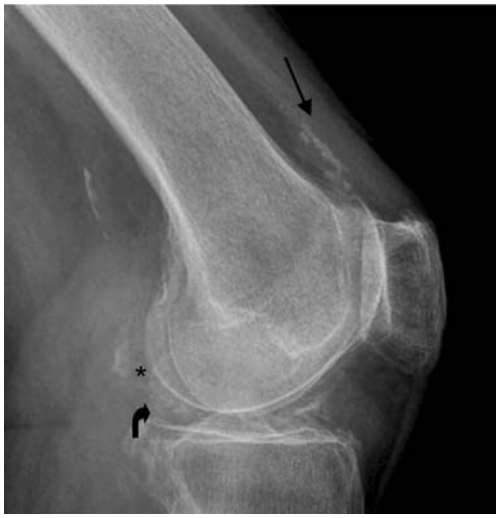

CPPD. Figure 2 Synovial calcification is appreciated along the suprapatellar bursa on this lateral knee radiograph (*arrow*). Hyaline and meniscal calcification is also identified (*curved arrow*). Osteochondral bodies lie posteriorly (*).

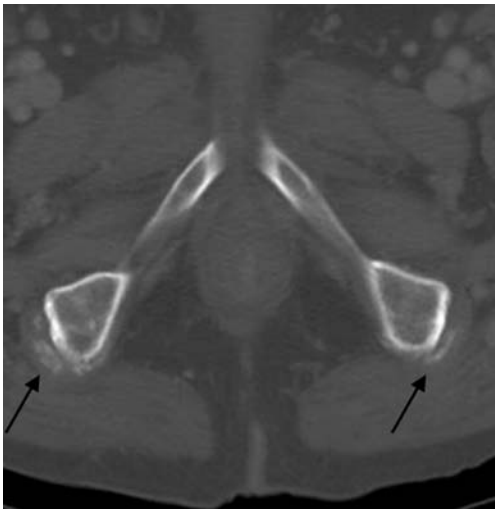

CPPD. Figure 3 Calcium pyrophosphate dihydrate (CPPD) crystal deposition is present in the hamstring tendon origins bilaterally on this CT image (*arrows*).

mimicking synovial osteochondromatosis. Synovial deposits are more common in the wrist, knee (Fig. 2), metacarpophalangeal, and metatarsophalangeal joints. The synovial membrane may demonstrate acute and chronic inflammatory changes in association with CPPD crystal deposition disease. It is not known if the crystals migrate into the synovium from the adjacent cartilage or are deposited directly within the synovium. Capsular calcification may appear as a linear peripheral density and may be difficult to distinguish from early synovial calcification. It is most commonly observed in the elbow, glenohumeral, metatarsophalangeal, and metacarpophalangeal joints.

Tendons, Ligaments, and Bursae

Tendon calcifications are observed with high frequency in patients with CPPD crystal deposition disease. An incidence of 13.5% was reported in such patients in one study (5). Those tendons more frequently involved include the supraspinatus, triceps, quadriceps, gastrocnemius, and Achilles tendons. Hip adductor, rectus femoris, and hamstring tendon calcification may also be seen (Fig. 3). Tendon calcifications commonly are linear or punctate and usually can be distinguished from the more homogeneous, discrete, and nodular calcifications of calcium hydroxyapatite crystal deposition. Calcification often extends far from the tendon attachment. There is a high correlation between the existence of these tendon calcifications and the extent and intensity of calcific deposits in other joints. Direct translocation of CPPD crystals from the articular or bursal surfaces may be responsible for some of the tendinous calcification.

Ligaments can also calcify. Sometimes, the calcification is not dense enough to be visualized on conventional radiographs. The ligamentum flavum and dura mater can contain calcific deposits. Bursal calcification is most common in the olecranon and subacromial bursae.

Other Extra-Articular Soft Tissues

Soft tissue and vascular calcification may be seen in CPPD crystal deposition disease. In particular, tumor-like masses of CPPD crystals can be seen in the extra-articular soft tissues. This manifestation of CPPD crystal deposition disease, known as "tophaceous pseudogout," is rare. In one study, 7 cases of massive focal CPPD crystal deposition disease were identified in atypical locations (6). The patients ranged in age from 31 to 86 years and 6 of them were women. These crystalline masses have been seen near the elbow, finger, jaw, acromioclavicular joint, and hip. Lesions are solitary and usually occur in areas of chondroid metaplasia without predisposing metabolic abnormality. Although the mechanism for development of these masses is not known, it has been postulated that hypertrophic metaplastic chondrocytes accumulating proteoglycans intracellularly provide a seeding site for crystal formation. These calcified masses may initially be mistaken for benign or malignant chondroid or other soft-tissue tumors, tophaceous gout, and tumoral calcinosis. Misdiagnosis sometimes leads to unnecessary surgery. The patterns of calcification usually can be differentiated from the lobular pattern of calcification in tumoral

calcinosis by their granular and more delicate appearance. Calcified soft tissue masses related to CPPD crystal deposition are of intermediate to low signal intensity on MR imaging examinations. They can present as the only manifestation of CPPD crystal deposition disease. Pressure erosion of adjacent osseous structures may be seen. It is important to identify the CPPD crystals, as these masses have also been mistaken for malignant cartilaginous tumors on histologic evaluation because of the presence of chondroid metaplasia.

Bibliography

1. Fisseler-Eckhoff A, Muller KM (1992) Arthroscopy and chondrocalcinosis. Arthroscopy 8:98–104
2. Bencardino JT, Hassankhani A (2003) Calcium pyrophosphate dihydrate crystal deposition disease. Semin Musculoskelet Radiol 7:175–185
3. Steinbach LS, Resnick D (1996) Calcium pyrophosphate dihydrate crystal deposition disease revisited. Radiology 200:1–9
4. McCarty DJ, Hogan JM, Gatter RA et al (1966) Studies on pathological calcifications in human cartilage. I. Prevalence and types of crystal deposits in the menisci of two hundred-fifteen cadavers. J Bone Joint Surg 48A:309
5. Foldes K, Lenchik L, Jaovisidha S et al (1996) Association of gastrocnemius tendon calcification with chondrocalcinosis of the knee. Skeletal Radiol 25:621–624
6. Kaushik S, Erickson JK, Palmer WE et al (2001) Effect of chondrocalcinosis on the MR imaging of knee menisci. Am J Roentgenol 177:905–909

CR

▶Computed Radiography

Cranial Nerves

The cranial nerves (CN) consist of 12 pairs of which the CN III–XII are genuine peripheral nerves.

▶Nerves, Cranial

Cranial Settling

Cranial settling is a characteristic deformity of the occiput-C2 region in rheumatoid arthritis. It is also known as vertical atlantoaxial subluxation or pseudobasilar invagination. Two conditions should be met: (i) the superior aspect of the odontoid process should be even or above the foramen magnum line of McRae and (ii) the anterior arch of C1 should assume an abnormally low position in relation to C2. Cranial settling is a high risk factor for development of myelopathy.

▶Rheumatoid Arthritis

Craniopharyngioma

A tumor located inside the sella turcica, outside in the suprasellar region, or with a sellar and suprasellar component, but always arising from remnants of Rathke's pouch. The tumor often appears cystic, with calcification and irregular peripheral enhancement.

▶Pituitary Gland

Crazy Paving

The superimposition of ground glass opacity and reticular pattern often having the appearance of interlobular septal thickening is described by the term crazy paving. The term was described as being pathognomonic for alveolar proteinosis, in fact it shows a 100% prevalence in patients with alveolar proteinosis. However, it is not specific, because it is also observed in diseases characterized by filling in of the alveolar spaces with liquid or semiliquid and cellular material combined with thickening of the intra- and interlobular septa such as edema, ARDS, hemorrhage, acute interstitial pneumonitis (AIP), or pneumonia.

▶Pulmonary Opacity, Extensive Pattern

CREST

CREST (calcinosis, Raynaud's phenomenon, esophageal dysfunction, scleroderma, teleangiectasia)is a subset of systemic scleroderma. It is not identical to the limited form of systemic scleroderma, but it is thought to show a slightly better prognosis than systemic scleroderma.

▶Connective Tissue Disorders, Musculoskeletal System

Cretinism

▶Congenital Malformations, Thyroid, and Functional Disorders

CRM

▶Circumferential Resection Margin

CRMO

Chronic recurrent multifocal osteomyelitis, usually not associated with organisms and thus not true osteomyelitis. May be a feature of SAPHO (synovitis, acne, pustulosis, hyperostosis [CRMO], and osteitis [CRMO]).
▶Osteomyelitis, Neonates, Infants, Childhood: Including Septic Arthritis and Other Important Soft Tissue Infections/Abscesses

Crohn Disease

Francesca Maccioni[1], Sara Parlanti, Francesca Siliquini, Federica Carrozzo[1]
Department of Radiological Sciences, Policlinico Umberto I-University of Rome La Sapienza, Rome, Italy
francesca.maccioni@uniroma1.it

Synonyms

Crohn disease; Granulomatous enteritis; Granulomatous enterocolitis; Regional ileitis

Definition

Crohn disease is a chronic inflammatory disorder of the alimentary tract of unknown etiology. It is most common in northern Europe, North America, and Japan. The disease most frequently affects the wall of the distal ileum and the right colon, but it may involve any gastrointestinal segment, from mouth to anus, with a typical segmental spreading and a chronic course of relapse and remission.

Generally, the disease has an early onset, around the second to third decade of life, but is not rare in the pediatric age group; a second peak of incidence is observed in an older age group. It can present at virtually any age and lasts for the patient's entire life, with a typical relapsing–remitting course.

Although the pathogenesis of Crohn disease remains unknown, there is an emerging consensus that it results from the complex interaction of multiple genetic, immunologic, and environmental factors. It starts as a breach of the mucosal barrier by a specific infectious agent or environmental toxin, causing inflammation perpetuated by exposure of luminal microflora to the mucosal immune system, and it becomes chronic as a result of a genetically determined failure of immunologic downregulation. Uncontrolled fibrogenesis may lead to stricture formation, and microbial antigens across the mucosa determine the extraintestinal localizations of disease.

Although unpredictable, three main Crohn disease phenotypes (or courses) have been recently identified according to the Vienna classification of Crohn disease (International Working Party for the World Congress of Gastroenterology, 1998): inflammatory (nonfibrostenosing and nonperforating), perforating, and fibrostenosing, with the perforating phenotype being more aggressive and frequently associated with severe complications (1, 2).

Pathology/Histopathology

The disease may involve any part of the gastrointestinal tract, but preferentially the distal ileum, with the majority of patients having an ileitis or ileocolitis.

The small bowel is affected in approximately 80% of cases, particularly the distal ileum, either alone (in 25–35% of cases) or associated with colon localization (in about 30–55% of cases); in only 15–25% of patients is the colon involved alone, frequently at multiple sites.

Involvement of the esophagus, stomach, duodenum, or jejunum in isolation or in association with other common sites is rare. Perianal disease is usually associated with rectal involvement.

Macroscopically, the disease is characterized by a thickened bowel wall and frequently also by a narrowed bowel lumen, which is associated with edematous and thickened mesenteric fat tissue and enlarged local lymph nodes. On the mucosal surface, longitudinal and irregular

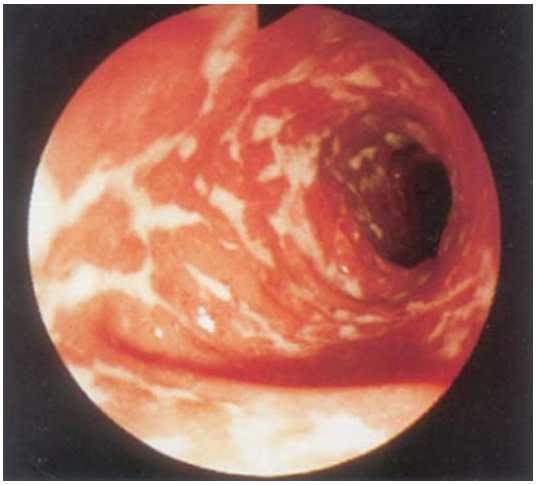

Crohn Disease. Figure 1 Active Crohn disease of the distal ileum. Endoscopic image shows hyperemic mucosa with multiple serpiginous ulcerations, covered by fibrin exudate, at the level of the distal ileum. (Courtesy of Dr. V. D'Ovidio, Department of Gastroenterology, University of Rome La Sapienza.)

ulcerations may be present. At endoscopy, in active disease the mucosal surface is usually hyperemic and is associated with aphthoid or more severe ulcerations—linear, irregular, or serpiginous—usually arising on the mesenteric border (Fig. 1).

Microscopically, the main characteristic of Crohn disease is transmural inflammation, with inflammatory cell infiltrates involving all wall layers. The inflammatory process typically starts in the submucosa layer, consisting of lymphocytes, macrophages, and plasma cells and producing lymphoid hyperplasia and mucosal aphthoid ulcers in the early phases. Aphthoid ulcers develop into linear ulcers and fissures to produce an ulceronodular, so-called cobblestone appearance. In more advanced phases, chronic inflammatory cell infiltrates spread to all wall layers, occasionally producing noncaseating submucosal granulomas consisting of macrophages within the lamina propria in relation to cryptic disruption.

In advanced disease, fibrosis, deep mucosal ulcerations, and transmural fissures are common findings. There is a tendency to involve the serosal surface, which is usually inflamed and hyperemic, associated with involvement of mesenteric fat and adjacent tissues. Typically, the inflammatory process progressively extends outside the intestinal wall, involving first the perivisceral fat tissue (thus producing fibrofatty proliferation and mesenteric adenopathies), and then the adjacent bowel loops, muscles, and genitourinary structures, producing adhesions and enteroenteric, enterocutaneous, and enterovesical fistulas, abscesses, and phlegmons. Toxic megacolon and neoplasms such as lymphoma and carcinoma may also occur.

Clinical Presentation

Crohn disease is characterized by cardinal symptoms, including diarrhea (85%) with variable daily and nocturnal evacuation frequency (three to six times per day), caused by bile salt malabsorption and bacterial overgrowth; bloody diarrhea; abdominal pain (55%); weight loss (65%); and bowel distension, reflecting the typical ileocecal disease localization.

Clinical findings may include a fullness in the right iliac fossa, low-grade fever, tachycardia, and elevated laboratory inflammation findings, such as erythrocyte sedimentation rate, C-reactive protein, and white blood cell count. Other blood tests may be helpful in detecting Crohn disease, such as the antiendomysial antibody test, which is related to the differential diagnosis at initial presentation; the anti-*Saccharomyces cerevisiae* antibody (ASCA) test; and the antiperinuclear neutrophil cytoplasmic antibody (pANCA) test. The ASCA test is thought to be relatively specific to Crohn disease, probably reflecting leakage of the yeast antigen across the mucosal barrier. Conversely, the pANCA test has shown a higher specificity for ulcerative colitis. However, neither of the tests is as specific as originally thought, but they can provide useful discriminatory information when used in combination (ASCA positive, pANCA negative in Crohn disease, and vice versa in ulcerative colitis).

In some cases, the disease can be nonspecific in its presentation, with little more than malaise and weight loss; these cases are a major diagnostic challenge.

Lactose intolerance is common, with milk, cream, and rich cheese foods particularly troublesome. Constipation can reflect an intestinal stricture with subacute obstruction or inflammation confined to the distal colon. Abdominal pain is often localized to the right iliac fossa and suprapubic region, is mild to moderate in intensity and cramping, and is exacerbated by spasm, particularly before passing stool. In the majority of patients, the physical signs of Crohn disease may be evident, represented by anemia, glossitis, aphthous ulceration in the oral cavity, and dehydration requiring prompt medical intervention (1, 2).

The presence of a positive family history of ►inflammatory bowel disease markedly increases the probability of a diagnosis of Crohn disease: 10–20% of Crohn disease patients have an affected first or second-degree relative, compared with less than 1% of the general population. There is also a significant

association of Crohn disease with ankylosing spondylitis, resulting from a shared genetic susceptibility. Major histocompatibility complex associations observed in the subgroup of Crohn disease patients include ankylosing spondylitis (HLA-B27) and primary sclerosing cholangitis (haplotype A1-B8-DR3).

Imaging

Several imaging modalities are used to detect and assess Crohn disease, including barium studies (conventional enteroclysis, small bowel follow-through, and barium enema studies), colonoscopy, ultrasonography, computed tomography (CT), and magnetic resonance imaging (MRI). These modalities can help localize lesions, confirm the clinical diagnosis, assess the extent of disease, and establish inflammatory activity.

Endoscopy and barium studies are widely considered the principal tools for diagnosing and evaluating Crohn disease in the small and large bowel; however, they have a limited capability to demonstrate the transmural extent of disease or extraintestinal complications.

After more than 50 years from their clinical introduction, barium studies of the small bowel are still considered the gold standard for evaluating the small bowel. The contrast agent can be orally administered and its passage followed through the entire small bowel, or it can be administered through a nasojejunal tube. Such administration allows the use of a double-contrast technique, which is otherwise not possible, by adding air or methylcellulose to the barium contrast agent. Barium studies can detect the site and length of lesions, the severity of strictures, and the presence of enteroenteric fistulas with high accuracy. At barium studies, the pathologic segment is usually well separated from the adjacent bowel loops by the fibrofatty proliferation and by bowel wall thickening. However, extraintestinal abscesses, phlegmons, and nonenteric fistulas can be underestimated (Figs 2 and 3).

Colonoscopy allows evaluation of the involvement of colonic mucosa, and in most cases it can be extended to the distal ileum (ileocolonoscopy). Moreover, at endoscopy multiple biopsies are routinely obtained, which is considered extremely important for confirming the diagnosis of Crohn disease.

Cross-sectional imaging, offering three-dimensional visualization and vascular information, has the advantage of identifying the presence of intraperitoneal or extraintestinal complications, such as abscesses and enterocutaneous and extraintestinal fistulas that may require surgical planning. On the other hand, cross-sectional imaging does not allow detection of subtle or advanced mucosal lesions.

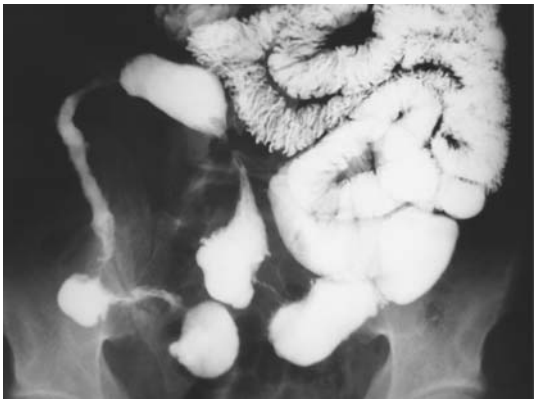

Crohn Disease. Figure 2 Active Crohn disease lesions of the distal ileum. Follow-through barium study shows a long segment of the distal ileum characterized by multiple stenoses and sacculated prestenotic dilations due to the typical segmentary spreading of disease. At the level of the stenotic segments, a cobblestone pattern is also observed.

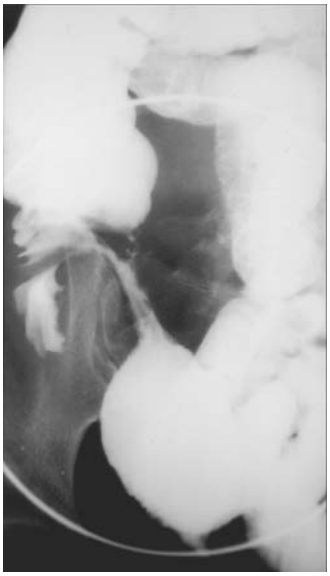

Crohn Disease. Figure 3 Enterocolic fistula. At the barium study, a tight stricture of the distal ileum and irregularity of the cecal fundus are observed, suggestive of ileocecal Crohn disease. A spot view demonstrates a tiny fistulous tract between the terminal ileum and the right colon adjacent to the ileocecal valve, a common extramural bowel complication.

Ultrasound (US), thanks to its noninvasiveness, low cost, and ready availability, is increasingly used as the initial screening modality and as an alternative examination in patients with atypical abdominal symptoms, either

acute or chronic. With modern US equipment, it is possible to make a confident US diagnosis of Crohn disease in most cases.

US can suggest ileocecal Crohn disease quite reliably. The sonographic hallmark is bowel wall thickening that involves all layers of the affected intestinal tract, ranging from 5 to 20 mm. Next to the terminal ileum, the cecum and appendix are not infrequently involved. The layer architecture of the bowel wall is often locally disturbed. In most chronic lesions, the submucosal layer is typically thickened and hyperechoic, likely due to increased submucosal fat either in active or nonactive disease; such submucosal increased thickening and echogenicity produces the typical layered pattern of Crohn disease. The affected bowel shows decreased peristalsis and a narrowed lumen, and it is often surrounded by noncompressible swollen fatty tissue. Mesenteric lymph nodes may be markedly enlarged, and in many cases an abscess, fistula formation, or prestenotic dilatation can be diagnosed as well.

With severe inflammation, the wall may appear diffusely hypoechoic with partial or total loss of layering due to transmural edema, with a central hyperechoic line that corresponds to the narrowed lumen. Peristalsis is reduced or absent, and the diseased segment is noncompressible and rigid, with a loss of haustra. However, the same finding of layering loss may be observed in the presence of diffuse wall fibrosis with nonactive disease.

The accuracy of US is further improved by the use of color Doppler imaging, which is helpful in detecting hyperemia of an inflamed bowel wall and adjacent fat during active disease (Fig. 4).

In conclusion, the liberal use of US in patients with abdominal symptoms constitutes a powerful and reliable tool for the early detection of ileocecal Crohn disease. It decreases the diagnostic delay and prevents unnecessary surgical interventions.

CT is a well-established imaging modality for detecting Crohn disease lesions and is preferred for evaluating the transmural extent of the disease and for diagnosing extraintestinal and intraperitoneal complications. In contrast to US, CT is generally not performed as an initial screening procedure in patients with atypical and protracted and abdominal symptoms. However, because CT is increasingly used as an emergency imaging modality in patients with acute abdominal symptoms, it may undoubtedly help detect clinically unsuspected cases of Crohn disease.

The CT scan is usually obtained in the supine position from the dome of the liver to the level of the perineum to get a panoramic visualization of the entire intestine, with a 5-mm thickness. High-quality multiplanar reformatted images, particularly coronal planes, obtained with multidetector CT equipment can be extremely useful for localizing Crohn disease lesions.

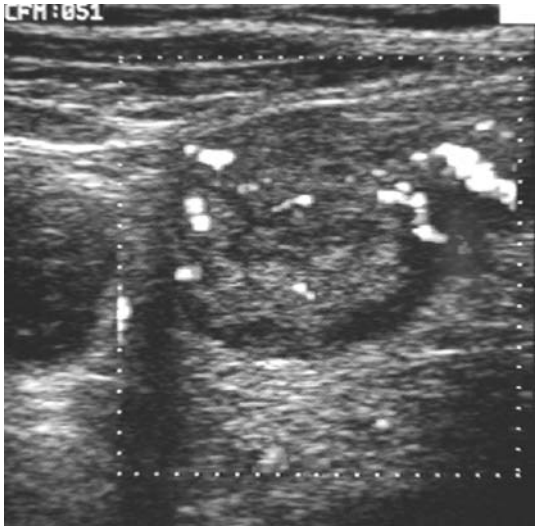

Crohn Disease. Figure 4 Active Crohn disease of the distal ileum. Ultrasound image shows a marked concentric thickening of the bowel wall and a narrowed lumen of the terminal ileum. Increased color Doppler signal suggests a high degree of inflammation of the bowel wall, as well as initial inflammatory involvement of the adjacent mesenteric fat.

To obtain diagnostic CT abdominal images or to provide positive or negative lumen contrast and dilation, various types of intraluminal contrast agents should be administered. Such contrast agents can be administered either orally (about 1–1.5 L given 90 min before the examination) or through a nasojejunal tube (CT-enteroclysis). The contrast agent should provide a homogeneous luminal enhancement, high contrast between the lumen and the bowel wall, and minimal mucosal absorption, and lead to no artifact formation or significant adverse effects.

Positive contrast agents at CT (iodinate or barium solutions) can be helpful for distinguishing bowel loops from enlarged lymph nodes or extramural fluid collections. However, using intraluminal positive contrast agents for bowel wall enhancement after intravenous administration of contrast material may obscure submucosal lesions.

Negative intraluminal contrast agents (methylcellulose or water iso-osmolar solutions) can similarly help detect normal or pathologic bowel wall segments, with the advantage of better visualization of the wall contrast enhancement and submucosal lesions (Fig. 5).

The use of an intravenous contrast agent is extremely important for better visualization of the normal and inflamed bowel wall (3, 4).

MRI is currently considered an emerging cross-sectional modality for evaluating abdominal and intestinal diseases, and is the modality of choice for evaluating

Crohn disease lesions at some institutions. In fact, recent technological advances (increased gradient strength, phased array coils, fast sequences, and so on) have greatly improved the quality of abdominal MR images, allowing acquisition of high-resolution images of the intestine during a single breath-hold, with significant increases in temporal and spatial resolution. In the next years, MRI could become the modality of choice for Crohn disease patients, first because it provides a diagnostic capability similar to CT but without radiation exposure, a fact that is particularly important for younger patients and children, who will have multiple studies during their lives. Moreover, it has an intrinsic higher tissue contrast than CT, allowing better assessment of inflammation in Crohn disease lesions. Finally, the multiplanar panoramic capability of MRI allows, differently from US, evaluation of the entire bowel using multiple planes, similar to multidetector CT images, allowing better identification of Crohn disease lesions and their complications. The lack of radiation exposure justifies and allows the use of MRI for the periodic assessment of Crohn disease activity, for clinical trials, and for follow-up studies.

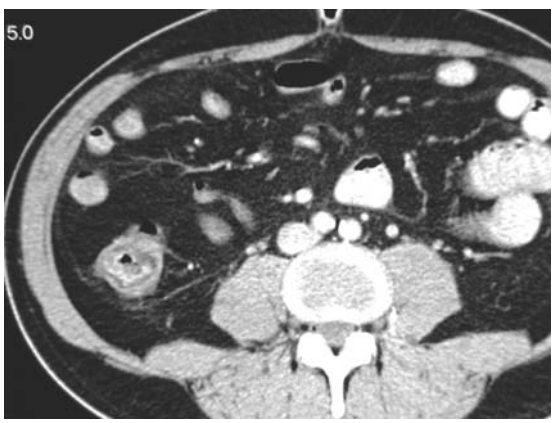

Crohn Disease. Figure 5 Recurrent Crohn disease in a patient who underwent ileocecal resection. The computed tomographic image, on axial plane, shows a marked thickening of the wall of the ileal anastomotic loop, with a narrowed lumen and proliferation of perivisceral fat tissue.

The MRI examination is preferably performed using a high magnetic field (1.5 T) and phased array coil for increased signal-to-noise ratio. The diagnostic imaging protocol should include both T1 and T2-weighted sequences to detect and characterize intestinal lesions, with the acquisition of axial and coronal thin, contiguous images. Acquisition of coronal and axial images is obtained with a 4–6-mm section thickness and a field of view of at least 350350 mm to cover all the bowel loops, adding sagittal plane images if necessary for a complete evaluation of disease.

Various kinds of intraluminal MRI contrast agents have been clinically tested: positive (gadolinium solutions), negative (superparamagnetic), and biphasic (water-like). Negative or biphasic contrast agents are more commonly used for evaluating small bowel diseases. Biphasic intraluminal contrast agents may produce either high or low signal, depending on the pulse sequence used; the more widely used have a water-like behavior, demonstrating low signal intensity on T1-weighted sequences and high signal intensity on T2-weighted sequences.

To assess inflammatory lesion activity, T1-weighted spoiled gradient imaging, after intravenous administration of a gadolinium chelate, and T2-weighted fat-suppressed imaging are used (Fig. 6) (3, 5). On the other hand, to obtain morphologic information, fast T2-weighted sequences (fast half-Fourier acquired single-shot fast spin-echo) and fast T1 and T2-weighted sequences with a steady precession (true-FISP or FIESTA) are preferred. True fast imaging with a steady precession (FISP) sequence provides high-resolution images of the intestine, mesenteric lymph nodes, and vessels. However, this kind of

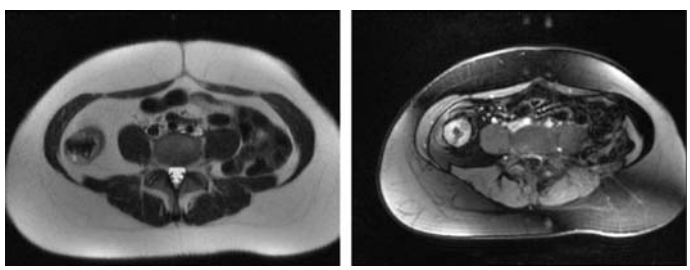

Crohn Disease. Figure 6 Crohn disease of the right colon. T1-weighted magnetic resonance images on axial plane obtained after intravenous administration of gadolinium chelate contrast agent and with suppression of the fat tissue, showing marked bowel wall enhancement with concentric bowel wall thickening at the level of the right colon. The T2-weighted image, obtained at the same level, shows bright bowel wall signal, and wall thickening can be observed as well.

sequence is susceptible to artifacts from intraluminal air due to chemical shift phenomenon, obscuring subtle bowel wall thickening.

The T2-weighted turbo spin-echo sequence provides excellent soft-tissue contrast and is not susceptible to black luminal artifacts; when used with fat suppression, bowel wall edema and mesenteric inflammation can be highlighted, which is useful for assessing the degree of disease activity.

The gadolinium-enhanced fat-suppressed T1-weighted sequences provide excellent visualization of hypervascular inflamed bowel wall, being extremely useful to localize active and complicated intestinal lesions, as well as assess the degree of disease activity (3–5).

Usually, a variable combination of true FISP, T2-weighted turbo spin-echo, and gadolinium-enhanced echo sequences, with or without fat suppression, is used to evaluate the extramural extent of Crohn disease lesions and complications.

Nuclear Medicine

Nuclear medicine plays little role in the initial characterization of Crohn disease. Leukocytes labeled with either technetium-99m-hexamethyl-propylene-amine-oxime (HMPAO) or indium-111 can be used to assess active bowel inflammation in any inflammatory bowel disease.

Once the histological diagnosis of Crohn disease has been established, technetium-99m-HMPAO-labeled white blood cells, with single photon emission CT imaging, may be used to assess disease activity and disease length.

Compared with the indium-111 label, the Tc-99m HMPAO label is preferred due to the better radionuclide availability and better imaging characteristics; moreover, it allows imaging sooner after injection. However, imaging must be done within an hour after injection of Tc-99m-HMPAO-labeled leukocytes because there is normal excretion into the bowel after this time, unlike indium-111-labeled leukocytes, not having bowel excretion.

Advantages over barium studies include the contemporary examination of both large and small bowel, lower radiation exposure (particularly important in younger patients), and higher patient tolerance.

False-positive bowel activity can be found with gastrointestinal bleeding, swallowed leukocytes, or activity related to in-dwelling enteric tubes. In addition, leukocyte uptake is not specific for Crohn disease and will be seen in most infectious or inflammatory bowel processes. As mentioned earlier, there is often normal bowel excretion of Tc-99m-HMPAO leukocytes if imaging is done more than an hour after injection.

Diagnosis

Complete evaluation of Crohn disease is usually difficult because it should include the characterization of the disease, differentiation from other inflammatory bowel diseases, localization within the small and large bowel, the extent of disease, disease severity and possible complications, and the degree of inflammatory activity.

The early phase of the disease is commonly suspected and assessed based on clinical and laboratory findings. Colonoscopy and barium study are the most commonly used imaging modalities in early phases, being able to appreciate enlarged lymphoid follicles, erosions, and aphthoid ulcers. Because of its noninvasiveness, low cost, and ready availability, US should be performed as a primary imaging modality in the clinical evaluation of Crohn disease in association with conventional imaging and laboratory findings.

CT and MRI are preferred when evaluating more advanced phases to assess the transmural extent of the disease and any intraperitoneal complications. Extraintestinal complications are largely detected on cross-sectional imaging. CT and MRI are also useful for characterizing the different disease courses, thus helping with the planning of medical treatment in cases of active inflammatory disease and of ▶surgical treatment in fistulating, fibrostenosing, or perforating disease with abscesses.

Panoramic views and multiplanar images associated with high soft-tissue contrast, static and dynamic imaging capabilities, and the absence of ionizing radiation exposure represent the advantages of the MR modality over CT. On the other hand, CT offers other advantages over MRI, such as shorter examination times, higher availability, higher spatial resolution, and the possibility to choose thickness slices and planes after data acquisition.

Treatment

The ▶medical treatment of Crohn disease varies according to the different disease phases, in particular the acute and the remission phases. During acute exacerbation, the main medical management consists of intravenous administration of glucocorticoids (hydrocortisone or methylprednisolone) in addition to metronidazole. Steroid therapy should be limited because of its various adverse effects, including osteonecrosis, myopathy, osteoporosis, and growth retardation. Intravenous cyclosporine may be used to inhibit cell-mediated immunity for further immune modulation and to increase the corticosteroid response.

The target of chronic therapy is remission of bowel inflammation. Local aminosalicylates have been the main therapeutic agents because of their anti-inflammatory

activity, each one having a different carrier molecule directed to a specific region of the bowel. Sulfasalazine and balsalazide are primarily released in the colon. Dipentum and Asacol are formulations for targeted release in the distal ileum and colon. Pentasa is released in the duodenum to the distal colon, whereas Rowasa is specific for the rectum and distal colon.

Azathioprine, 6-mercaptopurine, and methotrexate are other nonsteroidal immune modulators that are used as alternatives to glucocorticoids for inducing remission. Adverse effects of azathioprine and 6-mercaptopurine are uncommon (incidence of pancreatitis, allergic reactions, infection). The main disadvantage to the use of azathioprine and 6-mercaptopurine is their slow onset of action; response to therapy is usually noted after 3–6 months of treatment. Methotrexate, the long-standing folic acid antagonist, is effective in many patients with disease refractory to azathioprine and 6-mercaptopurine. Nevertheless, it has well-known adverse effects, mainly leukopenia and gastrointestinal upset.

New therapies are targeting tumor necrosis factor-alpha. Biological agents such as infliximab, a monoclonal chimeric antitumor necrosis factor-alpha antibody, are becoming available and showing promising results, with an increased remission rate. Other agents such as mycophenolate have been developed to inhibit guanine nucleotide synthesis and thereby inhibit B and T lymphocytes.

Most patients with Crohn disease undergo surgery within 20 years of diagnosis. Surgical treatment is required in cases of stricture, intractable or fulminant disease, anorectal disease, and intraabdominal abscess. Commonly, half of the patients who have had one surgical treatment will require further surgery for recurrent disease within 10 years. Recurrence occurs more frequently in cases of younger age of onset, enterocutaneous fistulas, multiple sites of disease, and a perianastomotic site of recurrence in stricturoplasty. Recurrence is often defined as detectable active disease associated with reactivation of symptoms (1, 2).

The basic tendency in surgery for Crohn disease is to limit small bowel resection of the involved segments. Stricturoplasty, performed by incising a stricture longitudinally and then suturing it transversely to widen the lumen, is often done when a severe stricture is present to preserve the small bowel and prevent short-bowel syndrome. In the majority of cases, the lack of perioperative deaths with stricturoplasty is a favorable feature compared with surgical resection.

Finally, CT-guided percutaneous abscess drainage may obviate surgery in selected cases. Recently, this has shown great success both as a temporizing measure and as definitive therapy, with a decreased rate of recurrence compared with that of surgery.

Key Points

Crohn disease is a chronic inflammatory bowel disease that commonly involves the distal ileum and the cecum and right colon, characterized by clinical, radiological, and histological features.

Infectious agents or environmental toxins associated with immunological downregulation cause inflammation of the mucosal layer that becomes chronic, until there is uncontrolled fibrogenesis, strictures, lesions, and extramural complications.

Several imaging modalities can detect and assess Crohn disease. Each has distinct advantages and disadvantages, and the decision of which one to use depends on the patient's condition and the phase of the disease.

Medical management is used in the acute or chronic/relapsing phases of the disease. Glucocorticoids (hydrocortisone or methylprednisolone) in addition to metronidazole represent the main acute therapy. Aminosalicylates, methotrexate, azathioprine, and 6-mercaptopurine are used in the chronic phases. Infliximab (a monoclonal antibody) is a new therapy that targets tumor necrosis factor-alpha.

Surgical treatment is indicated in cases of strictures, bleeding, abscesses, perforation, and carcinoma, which are complications not amenable to medical treatment. There is actually a tendency to conservative surgical management; nevertheless, recurrences are common.

Bibliography

1. Derek PJ, Miles P, Neil M (1999) Gastroenterology and Hepatology. McGraw-Hill, New York, Clinical Medicine Series, chapter 42, pp 395–415
2. Thoeni RF (1994) Idiopathic inflammatory disease of the large and small bowel. In: Freeny PC, Stevenson GW (eds) Margulis and Burhenne's Alimentary Tract Radiology. 5th edn. Mosby, St Louis, pp 585–601
3. Furukawa A, Saotome T, Yamasaki M et al (2004) Cross-sectional imaging in Crohn disease. Radiographics 24:689–702
4. Maccioni F, Viscido A, Marini M et al (2002) MRI evaluation of Crohn disease of the small and large bowel with the use of negative superparamagnetic oral contrast agents. Abdom Imaging 27:384–393
5. Maccioni F (2004) MRI of colitis. In: Chapman AH (ed) Radiology and Imaging of the Colon. Diagnostic Imaging. Springer, New York, chapter 20, pp 201–213

Cross-sectional Imaging

Include ultrasonography (US), computed tomography (CT) and magnetic resonance imaging (MRI).

▶Colitis, Ulcerative

Crossing Artery

Accessory renal arteries are frequent at the lower pole of the kidney and may have a close relationship to the ureteropelvic junction.

▶Ureteropelvic Junction Syndrome

Crouzon Syndrome

Crouzon syndrome (acrocephalosyndactyly type II), the most frequent craniofacial dysostosis, is characterised by bilateral coronal synostosis with brachycephalic or oxycephalic vault, maxillary hypoplasia, shallow orbits with proptosis, hypertelorism, cleft palate. Concurrent intracranial anomalies (anomalous venous drainage, hydrocephalus, Chiari I malformation) are common. Other non-obligatory features include calcification of the stylohyoid ligament, cervical spine abnormalities, elbow malformations, minor hand deformities, visceral anomalies, musculoskeletal deformities and skin lesions. Limb anomalies are non-specific.

▶Congenital Malformations, Nose and Paranasal Sinus

Cryotherapy, Hepatic Tumours

Technique for treatment of hepatic neoplasm based on local tumour destruction *in situ* by freezing. The resulting freeze process causes irreversible cellular damage and tissue necrosis is obtained.

▶Interventional Hepatic Procedures

Cryptococcosis

Cryptococcosis is an infection caused by the saprophytic yeast-like fungus Cryptococcus neoformans.

▶Infection, Opportunistic, Brain

Cryptorchidism

Cryptorchidism is the absence of the testis in the ipsilateral hemiscrotum. About 90% of undescended testes are located in the inguinal canal, with the remaining 10% located in the abdomen. Very rarely, the missing testis is ectopic and can be found in the perineum, in the contralateral hemiscrotum, or at the base of the penis.

▶Genital Tract

CSF

Cerebro-spinal fluid.

▶Tumors, Spine, Intradural, Extramedullary

CT

▶Computed Tomography

CT Angiogram Sign

The CT angiogram sign refers to the presence of contrast-enhanced, well-visible vascular structures surrounded by consolidated lung parenchyma with a much lower contrast uptake. Originally it was described as being pathognomonic for bronchioloalveolar carcinoma, but it is also seen in pneumonia and lymphoma. It is not seen in an atelectatic lung (due to the strong enhancement of the atelectatic lung parenchyma) and always indicates a pulmonary process.

▶Atelectasis

CT Dentascan

The CT Dentascan is a special computerized reformatting program that has been developed to obtain true cross section of the mandible and maxilla from CT scan.

▶Neoplasms, Odontogenic

CTA

Computed tomography angiography is based on helical or spiral CT and provides the exploration of one volume with each tube rotation.

Ultra rapid, non-invasive X-ray technique for visualisation of the vascular tree.

▶Cerebral Aneurysms

CTAP

Computed tomography (CT) arterioportography. This technique CT allows a higher level of intrahepatic enhancement to be obtained by means of catheter injection of the contrast medium directly into the celiac axis or hepatic artery. It was introduced to increase the detection rate of CT for small hepatic lesions. The use of CTAP has been largely replaced by multiphase helical scanning and tissue-specific enhanced magnetic resonance imaging.

▶Metastases, Hepatic

CTC

▶Computed Tomographic Colonography

Cubital Tunnel Syndrome

Compression of ulnar nerve in cubital tunnel of elbow region, may be due to sports or occupational injury or tumor.

▶Neoplasms, Soft Tissues, Benign

Cup-and-Saucer Deformity

Cup-and-saucer deformity is a characteristic aspect of inflammatory joint mutilation in the late stage of rheumatic arthritis or psoriatic arthritis, with typical pointed residual bone of the proximal phalanx and grooved destruction of the distal phalanx articulating with each other.

▶Spondyloarthropathies, Seronegative

Cushing's Syndrome

Corresponds to the presence of an adrenocorticotropic hormone (ACTH)-producing tumor. Up to 70% of the pituitary tumors will be visible on magnetic resonance imaging (MRI). To find the source of ACTH overproduction in false-negative MRI cases, bilateral inferior petrosal sinus sampling is recommended to measure the ratio of central to peripheral plasma ACTH levels.

▶Pituitary Gland

Cutaneous Lesions, Breast

Geert M. Villeirs
Division of Genitourinary Radiology
Ghent University Hospital
Ghent, Belgium
geert.villeirs@ugent.be

Definition

The skin of the breast can harbour a number of dermatologic pathologies (e.g. eczema, erythema, keratinization disorders, pigmentation disorders, etc.) and manifestations of systemic disease (e.g. scleroderma, dermatomyositis, polyarteritis nodosa, sarcoidosis, lupus erythematosus, etc.). These abnormalities usually do not significantly differ from similar involvement at other sites in the body.

The breast skin may also be involved in a generalized or focal non-skin disease process. A thickened oedematous skin may be seen especially in the dependent parts of one or both breasts due to cardiac decompensation, renal insufficiency, hypoalbuminaemia and fluid overload. Unilateral skin thickening can also be the result of venous or lymphatic stasis caused by venous thrombosis or lymphatic interruption (e.g. axillary dissection, nodal metastases, radiation therapy, etc.). Skin changes such as thickening, erythema and increased temperature, or thickening, dimpling and retraction may be ancillary findings in an underlying inflammatory (mastitis, abscess), post-traumatic (fat necrosis, scar formation) or malignant disease process. Special types of such reactions are Mondor's disease (band-like skin thickening and erythema due to thrombosis of a superficial vein) and ▶Paget's disease (eczematous involvement of the nipple–areolar complex due to ductal carcinoma *in situ*, see elsewhere in this Encyclopaedia).

Both benign (naevi, warts, sebaceous cysts, keloids, fibromas, haemangiomas, lymphangiomas, etc.) and malignant tumours (melanomas, sarcomas, metastases and cutaneous infiltration by haematologic malignancies) may be encountered as nodular or diffuse lesions of the skin.

Pathology/Histopathology

The skin can react to primary or secondary irritation with only a limited number of symptoms, such as erythema, oedema, diffuse or focal thickening, desquamation, ulceration, etc. Because of its superficial location, it is obvious that most reactions are readily diagnosed clinically and that imaging techniques only play a secondary role. On the other hand, some skin manifestations may trouble the mammographic assessment, because they obscure the underlying tissue due to oedema, or cause nodular densities or (pseudo) calcifications that can be mistaken for intramammary lesions.

Clinical Presentation

Inspection, clinical examination and patient history are of utmost importance for correct diagnosis of dermatologic pathologies, skin tumours and cutaneous manifestations of systemic disease. A detailed description of these pathologies is beyond the scope of this text.

In unilateral or bilateral skin oedema, in which the skin gets swollen and dimpled, the clinical history, general physical examination and lab results are also important to correctly attribute cutaneous thickening to systemic diseases such as cardiac decompensation, renal or hepatic insufficiency. Focal inflammatory disease, post-traumatic status and tumoral lesions underneath the skin of the breast may elicit secondary skin reactions that are readily explainable when the underlying disease is identified, either clinically or with imaging techniques. In ►Mondor's disease, for example, thrombosis of a subcutaneous vein may cause a painful erythematous cord-like skin thickening, often associated with preceding trauma or surgery to the breast. In inflammatory carcinoma, obstruction of the cutaneous lymphatics by tumour deposits causes skin thickening with accentuated pores, resembling the skin of an orange, frequently referred to as ►'peau d'orange'.

Mammography

Except for digital mammography, correctly exposed mammograms do not usually show the skin, especially in high-density breasts. The normal breast skin may measure up to 3 mm in thickness and is usually symmetric, but varies individually and thins with ageing.

Dermatologic pathologies and manifestations of systemic disease may not be visible on the mammogram, except when they are large enough to cause nodular or ill-defined densities, or when they become calcified or pseudocalcified (due to ointments, creams or balms containing X-ray attenuating powders). In both cases, tangential views (with or without a marker on the cutaneous lesion) may be necessary to confirm their dermal origin.

Pathologic skin thickening due to oedema or fibrosis is usually associated with accentuation of the oedematous subcutaneous trabecular framework and may be bilateral, or localized and asymmetric. In the latter case, it can only be well visualized in tangent.

When nodular masses of the skin are visible on the mammogram, they can be distinguished from intramammary lesions by their cutaneous location (on tangential views) and by their characteristic radiolucent rim or fissures caused by soft tissue to air interfaces when the breast is compressed (Fig. 1).

Skin calcifications usually originate in sebaceous glands of the skin. They are characteristically spherical (Fig. 2) and have a lucent centre, but occasionally may be more polygonal or punctate. They are peripherally located (sometimes requiring tangential views) and

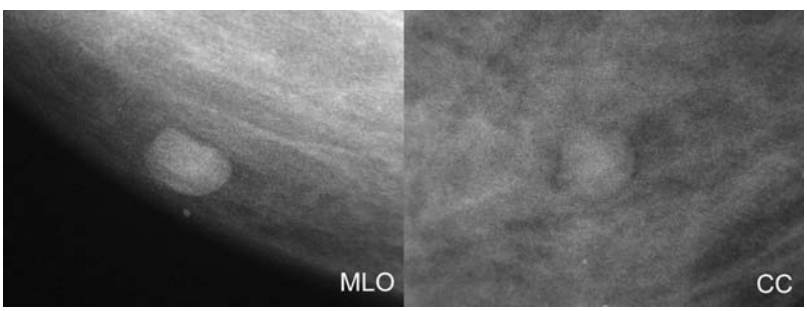

Cutaneous Lesions, Breast. Figure 1 Cutaneous nodule with a radiolucent rim along the boundaries of the lesion in both mammographic projections.

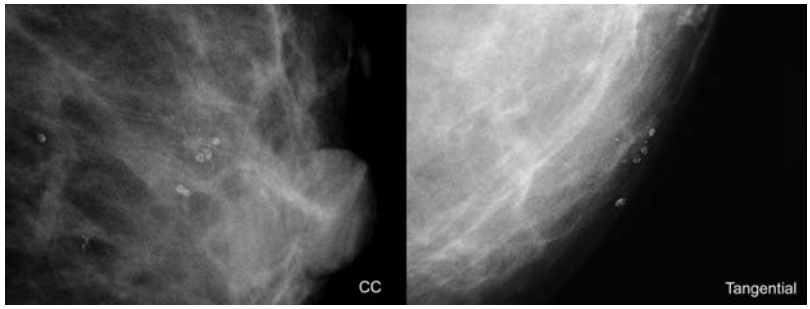

Cutaneous Lesions, Breast. Figure 2 Round lucent-centered calcifications. Their cutaneous origin can be demonstrated on tangential views.

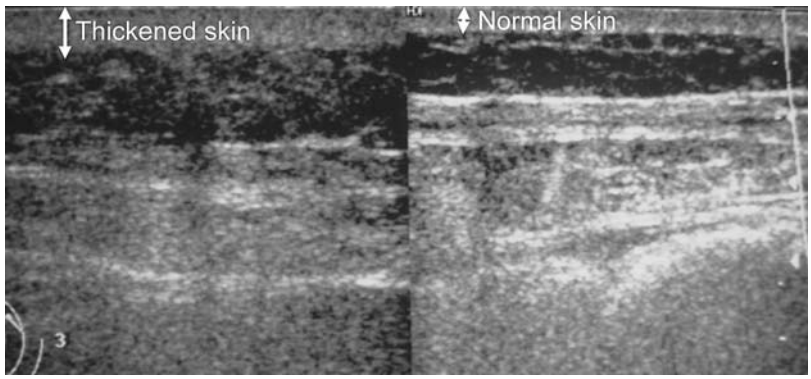

Cutaneous Lesions, Breast. Figure 3 Skin thickening after radiotherapy for breast carcinoma, with indistinct deep margin. Note difference with untreated side.

may be scattered or clustered, but typically maintain a fixed position to one another on different projections or on similar projections at different times ('tattoo sign').

Sonography

The thickened skin is visualized as a broadened hyperechoic rim indistinctly marginated from the underlying isoechoic subcutaneous fat (Fig. 3). The visibility of this area may be improved by using an ▶acoustic standoff pad.

Although sonography can readily demonstrate skin thickening, its role in the diagnostic work-up of cutaneous lesions is limited, except when performed to detect a subcutaneous lesion as the cause of a secondary skin reaction, or to confirm a ▶sebaceous cysts, especially when the latter becomes inflamed. Sebaceous cysts are usually round or oval cutaneous or subcutaneous lesions with varying echogenicity, depending on their relative amount of fluid and echogenic material. Inflamed sebaceous cysts may cause additional skin thickening and increased echogenicity of the surrounding fat.

Magnetic Resonance Mammography

Similar to sonography, MR only plays a minor role in the diagnosis of cutaneous lesions. However, it may be useful for detection or exclusion of underlying disease, especially in mammographically dense breast tissue that could obscure a lesion, or in the post-treatment follow-up to differentiate cutaneous recurrence from post-treatment changes.

Percutaneous Biopsy

Cutaneous lesions that remain indeterminate after inspection, clinical examination, laboratory tests, patient history or even imaging examination(s), may require shave, punch or excisional biopsy for histological

diagnosis. These are usually performed under clinical guidance, although imaging may occasionally be used for selection of the most appropriate biopsy site.

Bibliography

1. Britton CA (1994) Mammographic abnormalities of the skin and subcutaneous tissues. Crit Rev Diagn Imaging 35:61–83
2. Ralleigh G, Walker AE, Hall-Craggs MA et al (2001) MR imaging of the skin and nipple of the breast: differentiation between tumour recurrence and post-treatment change. Eur Radiol 11:1651–1658
3. Sener SF, Milos S, Feldman JL et al (2001) The spectrum of vascular lesions in the mammary skin, including angiosarcoma, after breast conservation treatment for breast cancer. J Am Coll Surg 193:22–28
4. Loffman Felman RL (2002) The tattoo sign. Radiology 223:481–482
5. Ulger H, Erdogan N, Kumanlioglu S et al (2003) Effect of age, breast size, menopausal and hormonal status on mammographic skin thickness. Skin Res Technol 9:284–289

Cutaneous Necrosis at the Finger Tips Like Rat Bites

Cutaneous necrosis at the finger tips like rat bites is a complication of long-standing Raynaud's phenomenon with consecutive ischemia and is relatively common in scleroderma.

"Jaccoud hand" was originally described in rheumatic fever after streptococcal infection. Typically the grave deformities contrast the absence of destructive arthritis. Nowadays, thanks to the rigorous antibiotic treatment of streptococcal infection, it is more often seen in systemic lupus erythematosus.

▶Connective Tissue Disorders, Musculoskeletal System

Cyclopia And Synophthalmia

▶Congenital Malformations, Orbit

Cyst, Breast

Luis Pina
Department of Radiology,
Clínica Universitaria de Navarra, Spain
ljpina@unav.es

Definition

Cysts are local dilatations of terminal duct lobular units filled with fluid (1, 2).

Pathology

Cysts are lined by an epithelium that consists of two layers: an inner epithelial layer and an outer myoepithelial layer. Occasionally they have no epithelial lining (1, 2). The fluid shows a variety of colors, such as clear, green, gray, brown, or almost black, and chemical substances, including pigmented secretions, lipofuscin, hemoglobin-derived products, and even secretory substances related to the diet. Some cysts show apocrine metaplasia, with low proportion of sodium and high proportion of potassium in the fluid, indicating a more active cellular secretion and more frequent recurrence. Other cysts have a transudate-like fluid, with high concentration of sodium and low concentration of potassium. Papillary tumors in the wall of a cyst are rare. Both papilloma and ▶papillary carcinoma may be found.

Clinical Findings

Cysts are very frequent lesions, affecting more than half of the female perimenopausal population, although they may be found in women under the age of 30 and also in postmenopausal women. Most cysts are multiple and bilateral and tend to disappear in older women, but hormonal replacement therapy may induce cyst formation.

Usually cysts are asymptomatic lesions detected on routine imaging techniques. However, cysts may be palpable and discovered by the patient, who may be concerned about a lump in her breast. Usually these cysts are mobile, smooth-contoured masses, although they may be hard and indistinguishable from breast cancer. Palpation may suggest the presence of a cyst, but ultrasound is required because some carcinomas can simulate benign lesions as cysts.

▶Simple cysts are benign lesions with no significative risk to develop into breast cancer. Whether the concurrence of family breast cancer history and cysts increases that risk is debatable.

Imaging

Mammography

Cysts present as round to oval well-circumscribed masses if they are surrounded by fat. If cysts are surrounded by fibroglandular tissue, they show obscured margins or may not even be detected on mammography (Fig.1). Curvilinear calcifications in the cyst wall or calcifications inside the cyst cavity (milk of calcium) may be found (3, 4). Cysts usually are multiple and bilateral, but they may also be single.

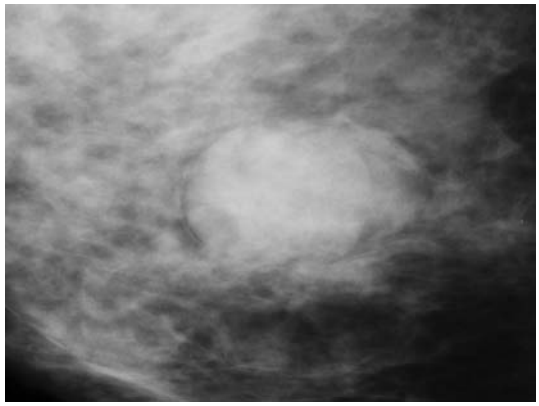

Cyst, Breast. Figure 1 Mammographic appearance of a breast cyst. An oval mass with circumscribed and obscured margins is seen.

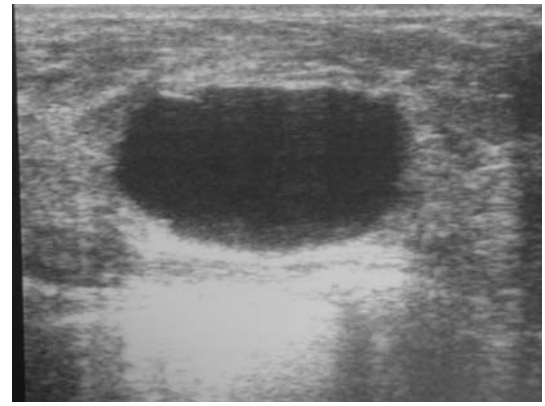

Cyst, Breast. Figure 2 Simple cyst on ultrasonography. An oval, anechoic lesion with posterior acoustic enhancement is seen. A few reverberation echoes are visible peripherally.

In some cases, a cyst is aspirated and filled with air to evaluate the cyst wall on mammography (pneumocystography). This technique allows a good evaluation of the cyst wall, especially for detecting intracystic masses. Nevertheless, the high accuracy of ultrasonography has largely eliminated the use of pneumocystography.

Ultrasound

Simple cysts are thin-walled, anechoic, round to oval lesions with posterior enhancement (Fig. 2). Acoustic shadows are seen at the margins. Sometimes a reverberation artifact may produce internal echoes (3–5). These lesions are soft and may be compressed with the transducer, changing their shape. If the lesions are too deep or small (<5 mm), the acoustic enhancement may not be seen. New ultrasonographic techniques, such as spatial compound imaging or tissue harmonic imaging, may be useful for characterizing a lesion as a cyst (5). Simple cysts are classified as BI-RADS category 2 (benign finding). Occasionally thin septa are seen inside the cyst. Clusters of small cysts may also be observed (Fig. 2).

►Complicated cysts have many of the features of simple cysts but show diffuse and mobile internal echoes (5). These cysts may contain proteinaceous material, blood, cellular debris, infection, or cholesterol crystals. The positive predictive value for carcinoma in these cysts is 0.3%, and therefore they are classified as BI-RADS category 3 (probably benign finding).

►Complex cysts include cysts with internal masses, thick septations, or thick or irregular wall (5). These lesions are suspicious and should be classified as BI-RADS category 4 (suspicious finding). Papilloma, papillary carcinoma, necrotic tumors, abscesses, and hematomas may correlate with these findings (Fig. 3).

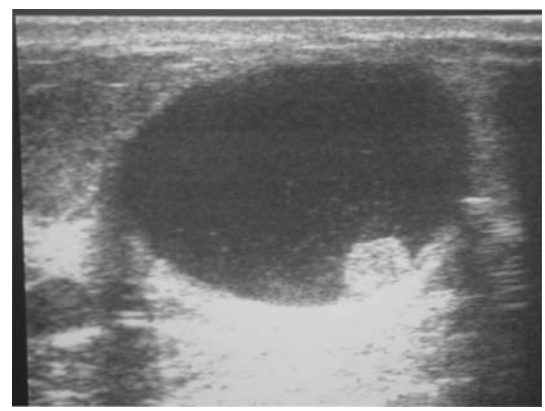

Cyst, Breast. Figure 3 Complex cyst. Ultrasonography reveals a solid lesion within the cyst. Biopsy revealed ►intracystic papilloma.

Magnetic Resonance Imaging

Cysts are smooth-contoured hypointense lesions on T1-weighted sequences and hyperintense on T2-weighted sequences. Typically, cysts do not enhance after contrast medium administration, except if there is wall inflammation or an intracystic mass (3).

Nuclear Medicine

Cysts are not an indication for a nuclear medicine study.

Diagnosis

Ultrasonography is the technique of choice for diagnosing breast cysts (5).

Asymptomatic simple cysts detected on ultrasonography do not need further diagnostic procedures. A 6-month follow-up may be proposed for asymptomatic complicated cysts showing diffuse and mobile internal echoes, as an alternative to fine-needle aspiration.

Symptomatic cysts (palpable, painful) may be aspirated after an ultrasound examination. If the fluid is green or yellow, there is no need for cytologic examination. However, if the fluid is hemorrhagic or if the cyst is complicated, a cytologic study is recommended.

Complex cysts are suspicious lesions that need to be carefully studied. If a negative cytology result is obtained after aspiration of a complex cyst, a biopsy should be performed. Cytology, and even core needle biopsy, may be unable to differentiate between benign papilloma and papillary carcinoma. Sometimes the cytologic examination result of the fluid of a cyst with a carcinoma may be negative (3).

Bibliography

1. Hughes LE (2000) Cysts of the breast. In: Hughes LE, Mansel RE, Webster DJT (eds) Benign Disorders and Diseases of the Breast. Concepts and Clinical Management, Saunders, London, pp 123–135
2. Schnitt S, Connolly JL (2004) Pathology of benign breast disorders. In: Harris JR, Lippman ME, Morrow M et al (eds) Diseases of the Breast. Lippincott Williams & Wilkins, Philadelphia, pp 77–99
3. Heywang-Köbrunner SH, Schreer I, Dershaw DD (1997) Cysts. In: Heywang-Köbrunner SH, Schreer I, Dershaw DD (eds) Diagnostic Breast Imaging. Thieme, Stuttgart, pp 156–165
4. Cardeñosa G (2001) Lobules. In: Cardeñosa G (ed) Breast Imaging Companion. Lippincott Williams & Wilkins, Philadelphia, pp 272–279
5. Mehta TS (2003) Current uses of ultrasound in the evaluation of the breast. Radiol Clin North Am 41:841–856

Cysts, Cerebral and Cervical, Childhood

Huisman T. A.
Johns Hopkins University, Baltimore, USA
thierry.huisman@kispi.unizh.ch

Synonyms

Arachnoid cyst; Cystic hygroma; Branchial cleft cyst; Leptomeningeal cyst; Lymphangioma; Neuroepithelial cyst; Thyroglossal duct cyst

Definition

Epithelial-lined, fluid-filled, well-circumscribed, nonneoplastic benign lesions.

Pathology and Histopathology

Most cerebral and cervical cysts are benign disorders of development. Cysts can also develop as complications of surgery or trauma. Next to esthetic concerns, head and neck cysts can be symptomatic due to compression of vital structures. Intracranial cysts may be incidental findings on imaging or the leading cause of focal neurological deficits. Cysts within the neck may compress neurovascular structures as well as the upper airways. Hemorrhages within these cysts may result in a rapid increase in size, aggravating displacement, and compression of adjacent structures. Finally, secondary infection may complicate the spontaneous course of head and neck cysts (1, 2).

Arachnoid cysts are benign, fluid-filled lesions that are lined by a thin layer of arachnoidea. Arachnoid cysts are believed to result from a duplication or splitting of the arachnoidea. They are located in the space between the dura and pia mater. These cysts are filled with a clear fluid that resembles cerebro-spinal fluid (CSF). The protein content may be elevated compared to CSF. Intralesional hemorrhages are frequently complicated by the development of fibrous membranes dividing the cyst in multiple compartments. Cysts are isolated from and consequently do not communicate with the subarachnoid space or ventricular system. Arachnoid cysts may remodel the adjacent skull (thinning and scalloping) by chronic compression.

Leptomeningeal cysts are complications of skull fractures due to an entrapment of lacerated meninges within the fracture. Chronic CSF-pulsations may prevent fracture consolidation, the fracture may even be widened (growing fracture). Meninges and underlying brain tissue can protrude through the growing skull defect into the subcutaneous tissues. Surgical repair with a dural patch covering the skull defect may be necessary (3).

Neuroepithelial cysts are benign, nonneoplastic malformative fluid-filled cysts lined by a single layer of ependymal like cells. The exact etiology is not yet fully understood. These cysts occur at multiple locations and are named accordingly: intraventricular ependymal cysts, choroid plexus cysts, and choroid fissure cysts. Large cysts may compress adjacent structures. Intraventricular cysts may lead to an entrapment of parts of the ventricular system depending on their location.

Lymphangioma or cystic hygroma is a congenital malformation of the lymphatic channels within the neck.

Lymphangiomas can show multiple small cystic components (capillary lymphangioma), multiple medium-sized cysts (cavernous lymphangioma), or large fluid-filled compartments (cystic lymphangioma or hygroma). They can occur in combination with hemangiomas (lymphhemangioma). Lymphangiomas may involve multiple anatomical spaces within the neck simultaneously. Cysts are lined by a thin endothelial cell layer. Connective tissue stroma may be intermixed.

Branchial cleft anomalies include cysts, sinus tracts, and fistula that result from an anomalous development of the branchial apparatus. Depending on the involved branchial component, different locations of the branchial cleft anomalies are encountered. Anomalies of the first and especially the second branchial apparatus are most frequent. Anomalies of the third and fourth branchial apparatus are rare. Because the branchial apparatus is ectodermal in origin, the branchial cleft anomalies are lined by stratified squamous epithelium. Occasionally, respiratory epithelium is incorporated. Cysts result from a failure to obliterate parts of the branchial apparatus. In sinuses, a residual opening exists into the deep cervical spaces or skin while in fistulas two openings are seen connecting the skin with the deep cervical compartments. Secondary infection may complicate branchial cleft anomalies.

Thyroglossal duct cysts are developmental anomalies that result from a failure of a segment of the thyroglossal duct to obliterate. The thyroglossal duct is the "path" that the thyroid gland follows during its descent from the foramen cecum at the tongue base to its final position in the infrahyoid neck. Cysts may occur at any location along the thyroglossal duct and are lined by squamous or respiratory epithelium. Cysts are usually filled with a serous/mucinous fluid. Small, "lost" thyroid gland components may accompany the cysts.

Clinical Presentation

Arachnoid, leptomeningeal and neuroepithelial cysts are symptomatic due to compression or displacement of functional center of the central nervous system (CNS). Depending on the location, focal neurological deficits, seizures or CSF-circulation disturbances (hydrocephalus) are observed. In many instances however, these cysts are clinically silent and only found incidentally on imaging that is performed for other reasons.

Lymphangioma or cystic hygroma are primarily symptomatic due to a displacement and/or compression of adjacent neuro-vascular structures or upper respiratory tract. In addition, large lesions may interfere with the normal development of the viscerocranium. This may require a more aggressive treatment. On the occasion of viral infections, lymphangiomas may show an intermittent increase in size. Accompanying hemangiomas with involvement of the skin are easily identified on visual inspection.

Branchial cleft and thyroglossal duct cysts usually present as a soft, compressible, painless mass in the neck. Depending on the embryological origin, lesions are in the median or lateral neck. Cysts may enlarge during viral infections. In rare cases, bacterial infection complicates

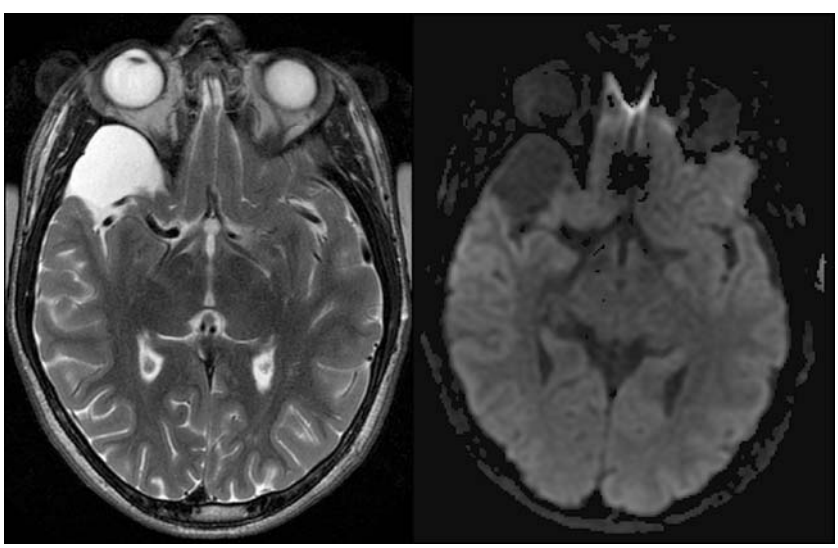

Cysts, Cerebral and Cervical, Childhood. Figure 1 Axial T2-FSE and DWI of a middle cranial fossa arachnoid cyst. The arachnoid cyst is CSF isointense on both sequences. The adjacent temporal lobe is hypoplastic. The dorsal border of the orbit is displaced anteriorly.

the cyst requiring incision or resection of the cyst including fistula and/or sinus tract. Life-threatening compression or displacement of vital structures is rare.

Imaging

Ultrasound is the first line imaging modality in the evaluation of cystic head and neck lesions. Ultrasound usually allows to differentiate between cystic and solid lesions/tumors. Cystic lesions are hypoechoic on ultrasound and may display an accompanying dorsal signal enhancement. Calcifications are equally well delineated with a dorsal signal loss or shadowing. Compared to CT and MRI, ultrasound is more sensitive in identifying intracystic membranes or septae (e.g., in lymphangioma). The real time imaging technique is also very helpful to delineate the exact boundaries of lesions and their relation to neighboring structures. This may be especially helpful in e.g., complex branchial cleft cysts. Duplex sonography allows to evaluate the vascularity of the lesions as well as the relation to adjacent vascular structures. CT and MRI may be used as second line imaging tool. The high spatial resolution and the high tissue contrast as well as the large field-of-view are especially helpful in complex anatomical malformations or lesions. Intracranial cystic lesions can also be examined by ultrasound as long as the fontanelles are not yet closed and may serve as an acoustic window. Transcranial sonography is usually limited because the spatial resolution does not allow to identify accompanying smaller intracerebral lesions.

Arachnoid cysts are sharply marginated extraaxial fluid collections (Fig. 1). On computer tomography (CT) the fluid is isodense with the CSF, on magnetic resonance imaging (MRI) isointense with CSF on all sequences. Acute intralesional hemorrhages increase the density on CT and intensity on T1-weighted imaging. Fluid-sedimentation levels may be identified. Increased protein contents may alter the density and signal intensity of arachnoid cysts. This is especially obvious on FLAIR-imaging. The cyst wall should not enhance. Adjacent brain tissue will be compressed and displaced. The interface between cyst and brain tissue is smooth. Occasionally, an intraparenchymal FLAIR and T2-hyperintense gliosis may be observed. There is no direct communication between the arachnoid cyst and subarachnoid space or ventricular system. The overlying skull or adjacent skull base can be remodeled with outpouching of the skull away from the arachnoid cyst. The internal tabula may be thinned but remains intact. On diffusion weighted imaging (DWI) signal intensity parallels CSF (no restricted diffusion). DWI is especially helpful in differentiating arachnoid cysts from subarachnoidal epidermoids (restricted diffusion). Cisternography can be used to study the exact location and possible communication with additional lesions. This is especially helpful in complex postoperative cases in which recurrent arachnoid cysts developed. Ultrasonography can be helpful in neonates. Uncomplicated arachnoid cysts rarely increase in size. Arachnoid cysts may increase in size after an intralesional hemorrhage or postoperative due to adhesions.

Leptomeningeal cysts may be located next to a skull fracture or extend through a widened fracture into the subcutaneous tissues. Fracture margins are usually smooth. The chronic pulsations may enlarge the fracture (growing fracture) preventing consolidation (Fig. 2). The adjacent subarachnoid space may be widened, brain tissue may protrude through the fracture. On ultrasonography

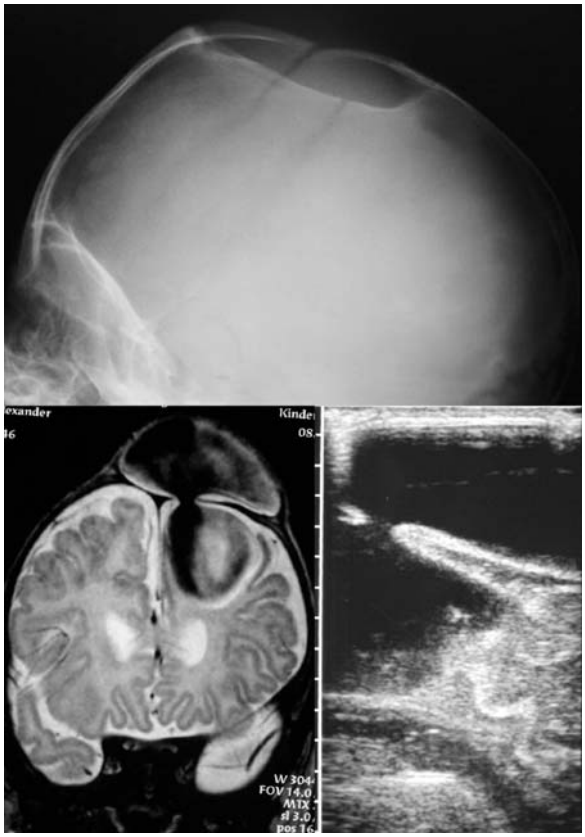

Cysts, Cerebral and Cervical, Childhood. Figure 2 Lateral skull X-ray shows a widened anterior fontanel with smooth osseous borders. Coronal T2-FSE (second row, first image) reveals a large cystic defect within the superior frontal gyrus that communicates across a dural tear with an extracranial cystic component. A T2-hypointense CSF-flow void is seen across the dural tear and within both cystic components. High resolution ultrasonography (second row, second image) confirms MRI findings.

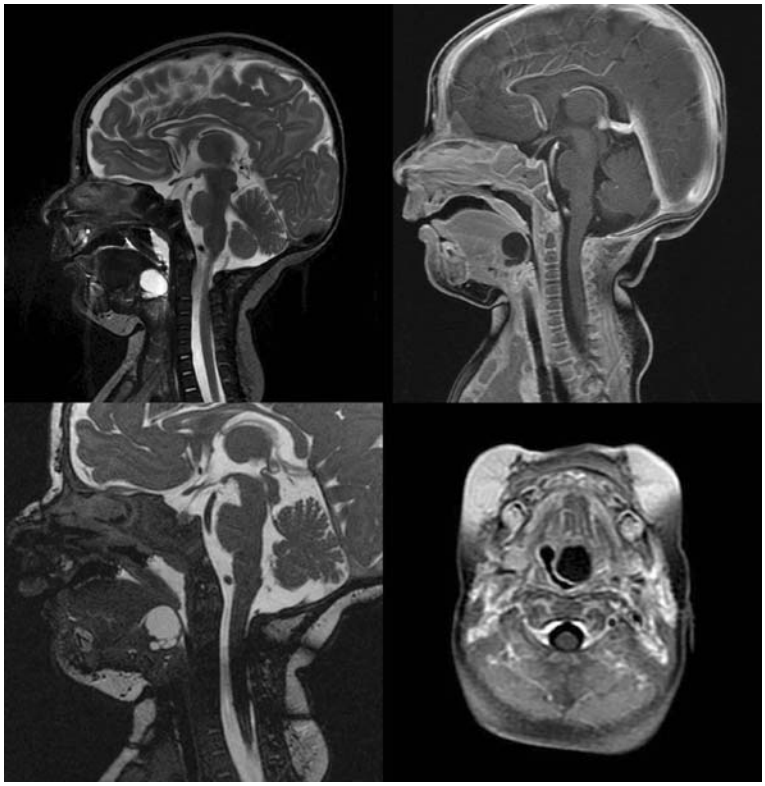

Cysts, Cerebral and Cervical, Childhood. Figure 3 Sagittal T2-FSE, contrast enhanced T1-SE (upper row), sagittal thin slice strongly T2-weighted and contrast enhanced axial T1-SE MR image. A large T2-hyperintense, nonenhancing thyroglossal duct cyst is seen within the floor of the posterior tongue, caudally to the foramen cecum. Several smaller, additional cysts are seen along the lower border of the large cyst.

and MRI, CSF-flow and pulsation artifacts may be seen across the fracture (3). T2*-weighted sequences can be helpful to identify hemorrhagic lacerations within the adjacent cortex. CT is especially helpful to examine the margins of the fracture line. Leptomeningeal cysts can also occur within the skull base after skull base fractures.

Neuroepithelial cysts have similar imaging characteristics as arachnoid cysts. *Lymphangioma or cystic hygroma* appear as hypodense cystic masses on CT. On MRI the cysts are strongly T2-hyperintense and moderately T1-hypointense. Depending on the category of lymphangioma, the lesion may be uniloculated or multiloculated. Cyst walls are usually thin and do not enhance after contrast medium injection unless there is associated infection or hemorrhage. Lymphangiomas often cross the borders of the neck compartments and may displace or wrap neuro-vascular bundles. Fluid–fluid levels may occur spontaneously but are more frequently seen after trauma or punctures. Intralesional hemorrhage changes the density (CT) and intensity (MRI) of the cyst contents. Similar to intracranial arachnoid cysts, elevated protein contents increase density/signal intensity on imaging. Frequently, lymphangiomas show additional contrast enhancing hemangiomatous components. Ultrasonography is the primary imaging modality. The high sensitivity for intralesional septa is especially helpful. In large lymphangiomas the limited field-of-view and penetration depth of ultrasound waves are however disadvantageous to determine the exact extent of large lesions. CT and MRI are used for preoperative planning.

All *branchial cleft (1st to 4th branchial apparatus) and thyroglossal duct cysts* have similar imaging appearances. The cysts are fluid-filled (CT-hypodense, T1-hypointense, T2-hyperintense), well-marginated round or ovoid structures lined by thin walls. Calcifications are rare. The wall of the cysts may show an enhancement if there has been associated recurrent infection. The location and relation to adjacent neck structures allow differentiation between the different cysts. First branchial cleft cysts are located in the area between the external auditory canal and submandibular triangle or in the parotid area. Second branchial cleft cysts are along the anterior border of the sternocleidomastoid muscle, lateral to the carotid arteries and posterior to the submandibular gland. Third branchial cleft cysts are posterior to the carotid arteries and superior to the superior laryngeal nerve while the fourth branchial

cleft cysts are located between the left pyriform sinus apex and thyroid gland, inferior to the superior laryngeal nerve. Thyroglossal duct cysts are midline cysts located somewhere between the foramen cecum and the pyramidal lobe of the thyroid gland (Fig. 3).

Nuclear Medicine

Nuclear medicine studies are used to identify ectopic thyroid gland components.

Diagnosis

Diagnosis relies on the combination of a good clinical examination and high resolution imaging. The differentiation between the different cystic neck masses is based on the proper identification of the anatomical landmarks. Ultrasonography can be especially valuable to differentiate between a uniloculated and multiloculated cystic neck lesion. Thin septa can be missed on CT or MRI. Finally, necrotic neoplastic lesions may mimic cystic lesions and should be considered and consequently be out ruled.

Bibliography

1. Osborn AG (2005) Diagnostic Imaging: Brain. Amirsys, Inc, Salt Lake City, Utah, pp I-7-4-41
2. Harnsberger HR Diagnostic Imaging: Head and Neck. Amirsys, Inc, Salt Lake City, Utah, pp I-7-4-41
3. Huisman TA, Fischer J, Willi UV et al (1999) "Growing fontanelle": a serious complication of difficult vacuum extraction. Neuroradiology 41(5):381–383

Cyst, Posttraumatic

Intramedullary cavity normally of one vertebral segment extension, well marginated. On MRI images cyst shows isointensity with the CSF in all pulse sequence and does not grow.

▶Spinal Trauma

Cystadenoma

Cystadenoma is the most common type of cystic benign ovarian tumor. It accounts for up to 50% of benign ovarian tumors in the reproductive age, and for up to 80% in the postmenopausal age. Cystadenomas are thin-walled unilocular or multilocular cystic lesions filled with serous, mucinous, and sometimes hemorrhagic contents.

▶Masses, ovarian

Cystic Dilatation of the Renal Tubules (1–3)

▶Medullary Sponge Kidney

Cystic Disease of the Renal Pyramids

▶Medullary Sponge Kidney

Cystic Disease, Renal Childhood (MCDK, PCKD)

M. Riccabona[1], R. Fotter[2]
[1]Division of Pediatric Radiology, University Hospital Medical University of Graz, Austria
michael.riccabona@meduni-graz.at
[2]Division of Pediatric Radiology, University Hospital Medical University of Graz, Austria
richard.fotter@meduni-graz.at

Synonyms

Cystic kidney disease; Renal cysts

Definition

Fluid- or urine-filled compartments/cysts replacing a varying amount of renal parenchyma. There are a variety of renal cystic diseases that need to be considered and often can be classified on imaging based on their position, size and appearance: besides the simple renal cyst and rare acquired cystic renal diseases (e.g., in renal failure, posttraumatic), the polycystic kidney disease (PKD, i.e., autosomal recessive or autosomal dominant PKD, medullary cystic disease complex and juvenile nephronophthisis, and glomerulocystic kidney disease), syndromal cystic

kidney disease (hereditary and non-hereditary), ►multicystic dysplastic kidney (MCDK) and dysplastic cysts, ►medullary sponge kidney, as well as complicated renal cysts (haemorrhaged or infected cysts, multiloculated cysts including segmental MCD and ►cystic nephroma), as well as cystic renal tumours have to be considered.

Embryology and Pathogenesis

Cystic renal disease is far less common in childhood than in adults. Inherited diseases as well as a disturbed renal embryogenesis and renal development create a wide spectrum of manifestations that spans from diffuse severe bilateral congenital disease to simple single renal cysts. One of the main mechanism is a disturbance at the junction between metanephrogenic tissue and the ureteral bud, other mechanism in differentiation of the renal parenchyma/genetic origin are also discussed, furthermore degenerative and hyperproliferative changes as well as neoplasms and injuries to the renal parenchyma can lead to cyst formation. Depending on its pathogenesis and the individual entity more or less regular imaging is indicated. Secondary cysts develop after trauma, after infections, in tumours, in chronic renal insufficiency and in inherited cystic kidney disorders.

Clinical Presentation

Presentation and symptoms vary with the underlying condition, from completely asymptomatic in incidental findings to haematuria, hypertension, palpable mass and pain in cystic tumours.

Imaging

Imaging usually relies on ultrasound (US), sometimes (for differentiation of complex cysts, e.g. suspected caliceal diverticula, differential diagnosis against abscesses or tumours, post-traumatic cysts) sectional imaging (usually magnetic resonance imaging (MRI), if unavailable contrast-enhanced computed tomography (CT)) and for rare indications intravenous urography (IVU, e.g. medullary sponge kidney) may be become indicated.

Imaging Strategy

Renal cysts in paediatric patients are generally detected by US. As simple renal cysts are far less common in children than in adults, at least follow-up exams and a detailed family history with nephrourological workup should be considered. If these are just simple cysts, US is sufficient as the single imaging modality. If these cysts grow and cause symptoms, an image-guided drainage and sclerotherapy may become a therapeutic option. If there is a congenital or hereditary (poly-)cystic kidney disease, additional scintigraphy may be valuable for the assessment of (split) renal function during the course of the disease. If the cysts appear to be complicated and do not match any congenital PKD, they should be studied by IVU (for DD against calyceal cysts or detection of a medullary sponge

Cystic Disease, Renal Childhood (MCDK, PCKD).
Figure 1 Schematic drawing of renal cyst and cystic renal diseases. Typical cyst forms and locations in various cystic kidney diseases, with typical features. (Adapted from Riccabona M, Ring E (2001) In: Fotter R (ed) Pediatric Uroradiology. Springer, Berlin-Heidelberg, p 236.) ARPKD, multiple small cysts, situated mostly cortical or at the cortico-medullary border, ADPKD, some big cysts, in all parenchymal areas, GCKD (glomerulocystic kidney disease), predominantly small cortical or subcapsular cysts, MCD medullary cystic disease complex is the medullary microcysts, centered close to the cortico-medullary junction, MSK (medullary sponge kidney) medullary cystic changes, in a radial pattern, centered towards the papilla. Dysplastic cysts may resemble renal cysts, acquired cysts, cysts in ADPKD and MCDK, or complicated cysts.

kidney) and/or MRI or contrast-enhanced CT. If there are still equivocal findings, they should be monitored or—particularly when showing growth or atypically shaped and vascularised areas—should undergo biopsy or surgery.

Diagnosis

Diagnosis is made by imaging, with sometimes only histology revealing the final entity (Fig. 1). Imaging criteria for the simple *uncomplicated renal cysts* on US are small, echo-free, fluid-filled defects, with a regular border and without regional parenchymal abnormalities or solid components. *Dysplastic cysts* look similar and may occur in any form of either primary or secondary dysplastic kidneys, the latter potentially due to a congenital urinary tract malformation such as high-degree vesicoureteral reflux (VUR, reflux nephropathy) or high-grade obstruction (Fig. 2a). The cysts usually are small, may be situated in all renal compartments, and on US the kidneys exhibit some degree of other parenchymal changes such as reduced cortico-medullary differentiation or increased parenchymal echogenicity. In some cases, one can also find a diffuse vascular rarefaction on (amplitude-coded) colour Doppler sonography. As dysplastic cysts may not only grow in size and number, but potentially may undergo malignant transformation (e.g., during renal

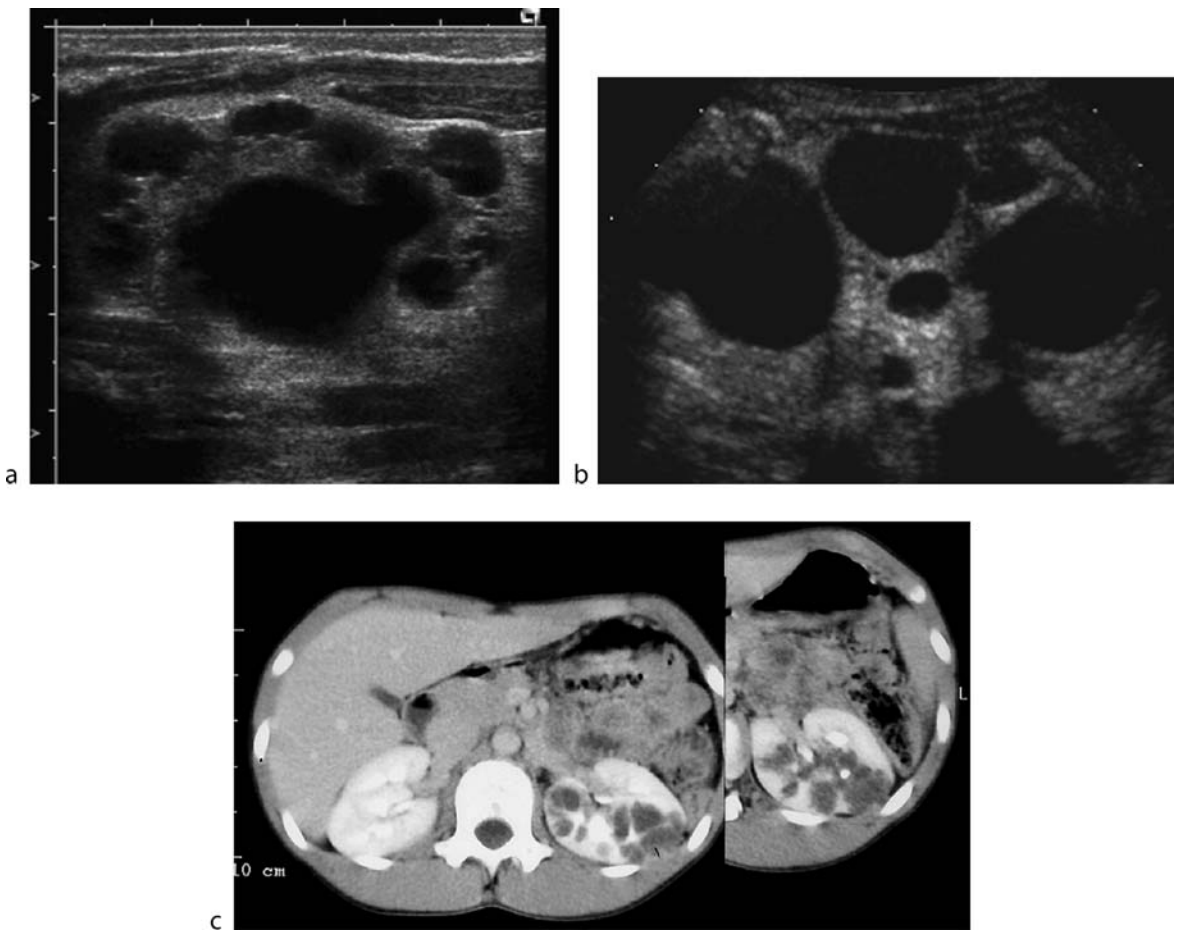

Cystic Disease, Renal Childhood (MCDK, PCKD). Figure 2 DD of renal cysts—imaging examples. (a) Cystic renal dysplasia. US of a hydronephrotic and dysplastic kidney with echogenic and undifferentiated parenchyma and multiple dysplastic cortical cysts. (b) Longitudinal US view of a multicystic dysplastic kidney. Note the missing connection between the cysts of varying size that have no parenchymal outer rim, the lack of a normal collecting system, but some central echogenic-dysplastic residual renal parenchyma, enabling a clear sonographic differentiation from a severe ureteropelvic junction obstruction (UPJO). (c) Contrast-enhanced CT (late phase) of a segmental cystic nephroma. (Adapted from Riccabona M, Ring E (2001) In: Fotter R (ed) Pediatric Uroradiology. Springer, Berlin-Heidelberg, p 246.)

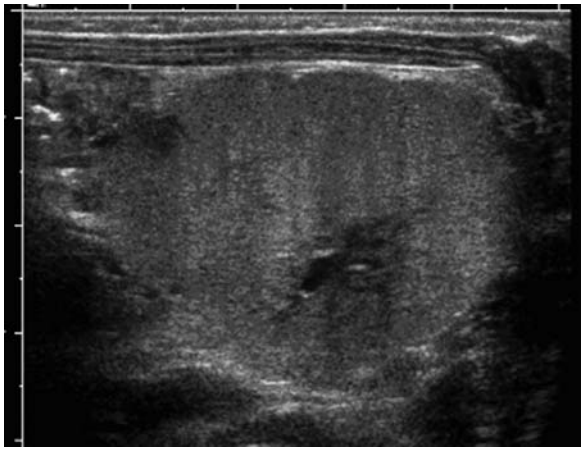

Cystic Disease, Renal Childhood (MCDK, PCKD).
Figure 3 Axial view of a neonate with ARPKD. Not the increased echogenicity, the tiny hyperechic parenchymal dots with some shadowing causing the 'salt and pepper' appearance, and that the microcysts may not or hardly be visible in spit of high-resolution US.

insufficiency), a regular follow-up—not only of the cysts, but also of the entire urinary tract for following the primary condition—is recommended. For this, US is substituted by static renal scintigraphy (Tc99m dimercaptosuccinic acid, DMSA) for the assessment of split renal function, which in future may be replaced by MR-urography.

The most severe form of cystic dysplasia is the *MCDK* (bilateral MCDK is called ▶Potter syndrome or Potter sequence, incompatible with extra-uterine life due to complete renal insufficiency and pulmonary hypoplasia), where the renal parenchyma is nearly entirely replaced by huge cysts, that can more or less resemble a collecting system (Fig. 2b). There may be some (central) residual parenchyma, usually echogenic and undifferentiated on US; sometimes residual perfusion may be depicted on Doppler sonography. Usually there is no renal function. As MCDK has a tendency to regress and vanish spontaneously, nephrectomy is usually postponed and only indicated in those kidneys that cause compression of adjacent structures or grow monstrously, or cause clinical symptoms such as hypertension, infection or malignant transformation. For initial diagnosis US is used, then voiding cystourethrogram (VCUG), MR-urography or DMSA-scintigraphy are performed additionally for the confirmation of the diagnosis and complete work-up which includes assessment of potential residual renal function (i.e. duplex system or segmental MCDK, severe ureteropelvic junction obstruction) and differentiation from severe reflux-nephropathy. Further more, a thorough work-up of the entire genitourinary tract is advocated, as a higher incidence of other urinary tract malformations and ipsilateral genital malformations is reported. Regular US follow-ups are recommended after establishing the initial diagnosis.

The so-called *multicystic nephroma* or multilocular nephroma or multiloculated renal cyst is another rare entity that is a cystic 'malformation' of (parts of) the kidney. On US (as well as on CT or MRI), it is characterised by a conglomeration of small cysts of similar size, with thin membranes and straight borders, without renal tissue involved in the tumour-like formation; usually no or only minimal contrast enhancement or perfusion is seen in the walls of the cysts (Fig. 2c). It is basically a benign tumour that may grow, but usually does not cause destruction or metastasis. Therefore, once imaging (and biopsy, as metanephric tissue making it a potential tumour can only be detected on histology) has established the diagnosis, a conservative approach can be considered. However, in cases with abnormal growth or other indecisive features such as irregular borders of the cysts, destructive behaviour or atypical parenchyma these need to be resected.

Polycystic kidney disease is an inherited familial condition of either autosomal dominant (ADPKD) or autosomal recessive promotion (ARPKD). Different types are established and the age of manifestation varies. On US, the recessive form usually manifests with diffuse parenchymal changes in a diffusely enlarged kidney due to microcysts not depictable by imaging. It may present already neonatally with renal insufficiency (infantile form), or in any other age (juvenile and adult forms). The cysts can be seen unilateral or bilateral, and often they initially are too small to be detected, creating a bilaterally speckled appearance of the kidneys with increased echogenicity of the renal tissue, with inhomogeneously reduced tissue differentiation, also called the 'pepper-salt kidney' (Fig. 3). During the course of the disease, the cysts constantly increase mainly in number, but also in size, eventually leading to an end-stage kidney and chronic renal insufficiency. Additional imaging of the other parenchymal abdominal organs for extra-renal manifestation such as liver fibrosis or pancreatic cysts is recommended. ADPKD is one of the most common inherited diseases that may be detected during childhood, but usually manifests only in adulthood (adult PKD) and exhibits some isolated, uncomplicated (macro-)cysts that tend to grow in size and number, then gradually replacing renal parenchyma—in childhood, this rarely needs treatment and usually is only followed up by US, once the diagnosis is established by family history and US

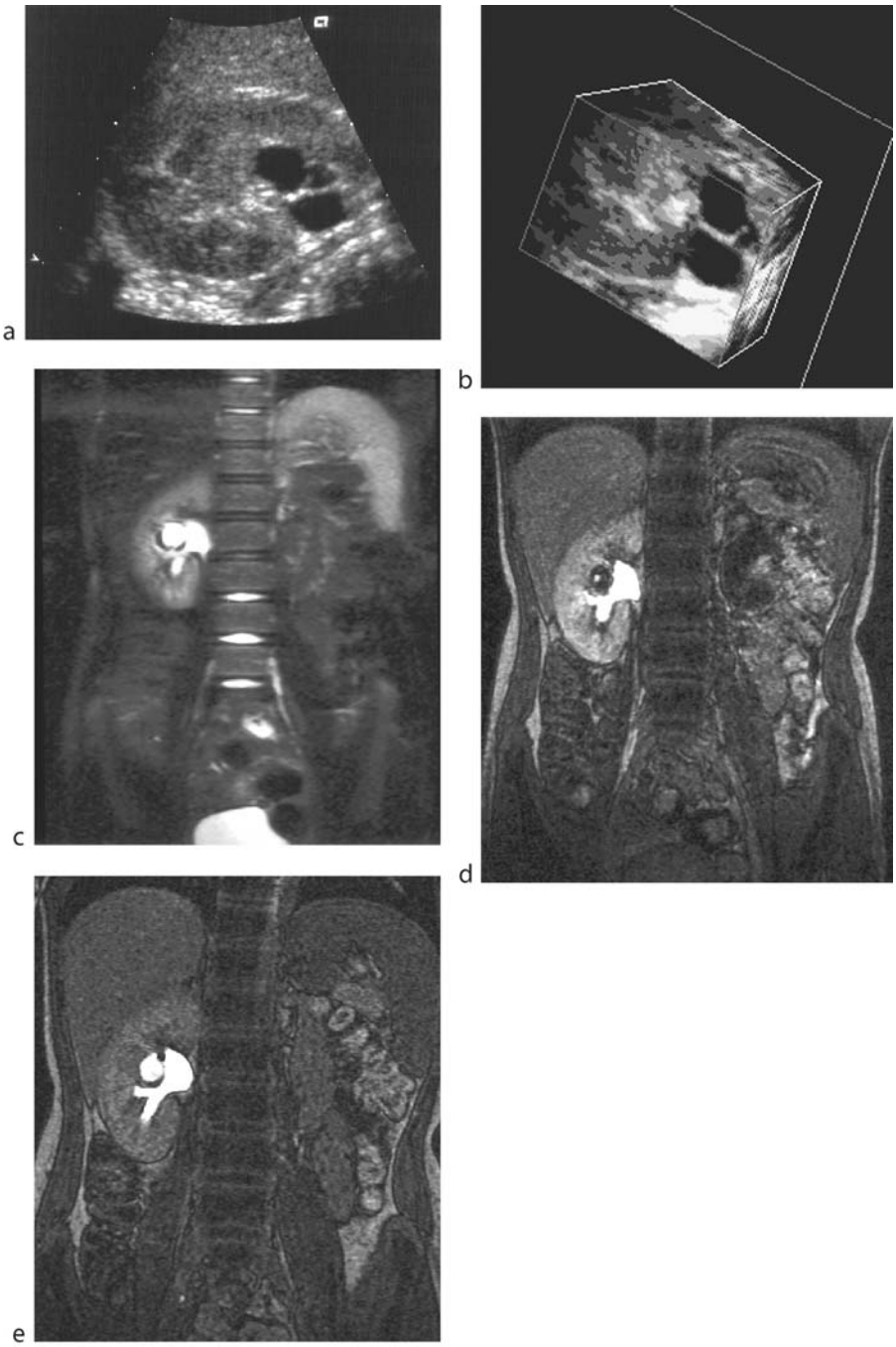

Cystic Disease, Renal Childhood (MCDK, PCKD). Figure 4 Imaging and diagnostic criterial in caliceal diverticulum A: axial conventional to the ultrasound image, demonstrating a cystic lesion located centrally in the kidney close to the renal pelvis. B: 3D-US of the same cyst, suggesting a connection of the cyst to the urinary collecting system (diverticula neck, see arrows and description). C–E: dynamic MR-urography images demonstrate initially the topographic anatomic situation of the "cyst" in a T2-weighted coronal unenhanced image (D), then the contrast enhancement dynamics with a well contrasted collecting system and no contrast within the "cyst" (arrow) in the early phase (E), and the filling of the "cyst" (arrow) in the delayed phase of a gadolinium enhanced T1-weighted 3D-gradient echo sequence proving the connection of the cyst with the collecting system, enabling the diagnoses of a caliceal diverticula.

assessment of the family. Note that ADPKD has a high coincidence with cerebral vessel malformations (particularly cerebral artery aneurysm), thus potentially indicating an active search for them. As PKD has typical US appearances, no other imaging is needed in childhood usually; rarely cysts may haemorrhage or get infected, needing contrast-enhanced CT or MRI for establishing the diagnosis. As we must consider coexisting conditions of the spleen, the liver and the pancreas, all other abdominal parenchymal organs should be included in the regular US follow-up studies.

Glomerulocystic kidney disease is a rare congenital condition with small cystic degeneration of the glomeruli. These tiny cysts are often situated subcapsularly in the renal cortex and—particularly in neonates—may be missed or only be depicted by high-resolution imaging. The kidneys usually are large, with an increased echogenicity of a widened cortex. As diagnosis is made by histology and family history, only US is performed.

Medullary cystic disease (complex) is an autosomal dominant inherited disease with a late onset of chronic renal failure. Histology shows glomerular cysts with thickening of the multilayered membrane, accompanied by some tubular cysts. Depending on the disease state, a growing amount of interstitial fibrosis, chronic inflammation and tubular atrophy with consecutive chronic sclerosing tubulo-interstitial nephropathy is observed. No specific imaging or US features are known.

Medullary sponge kidneys usually exhibit a cyst-like dilatation of the tubules with congestive sludge and calcification in the ectatic tubuli, which easily may be missed during early stages on US. The imaging modality of choice particularly in early stages of a suspected medullary sponge kidney still is IVU.

There are a number of hereditary and non-hereditary *syndromal cysts* as well as cysts in aneuploidies, with partially autosomal recessive, partially autosomal dominant transmission. They usually are part of a complex systemic disease with disturbance of nephrogenesis, combined with dysplastic features. They can present as multiple renal cysts as GCKD, MCDC or ►ARPKD and ADPKD. The pediatric radiologist needs to consider these entities for differential diagnosis and further diagnostic imaging of associated malformations or abnormalities, otherwise the presentation and imaging of syndromal renal cysts does not differ from the imaging of the other cystic renal entities.

(Post-)traumatic, post-surgery and (post-)inflammatory cysts may be tricky. Particularly if infected or after haemorrhage, sedimentations may be present, with a more or less distinguished wall and local parenchymal structural abnormalities. The may also be difficult to differentiate from an urinoma (particularly on US). When the suspicion is raised clinically or sonographically, MR-urography or contrast-enhanced CT may help to distinguish these entities or rare malformations such as a *tertiary calix* or a *calyceal diverticula*, with delayed excretory phase acquisition of either CT- or MR-images being mandatory to differentiate these entities. Note that post-infectious cysts should be considered particularly after uncommon infections such as tuberculosis or after renal abscesses.

Most renal tumours can exhibit cysts, either as part of their entity (e.g. multicystic nephroma) or as regressive or necrotic parts of the tumour (e.g. renal cell carcinoma). Even Wilm's tumour may present in a rare cystic form. Therefore all unusual cysts should be monitored by US and—at least when they grow, develop other signs, or present with a 'complicated' unusual appearance—additional sectional imaging with MRI (or—if unavailable—contrast-enhanced CT) should be considered. Surgery or biopsy with histology remains the ultimate possibility to define the entity in an unclear or equivocal cystic lesion.

Bibliography

1. Babut JM, Bawab F, Jouan H et al (1993) Cystic renal tumours in children—a diagnostic challenge. Europ J Pediatr Surg 3:157–160
2. Kaplan BS, Kaplan P, Rosenberg HK et al (1989) Polycystic kidney diseases in childhood. J Pediatr 115:867–880
3. Kissane JM (1990) Renal cysts in pediatric patients: a classification and overview. Pediatr Nephrol 4:69–70
4. Riccabona M, Ring E (2001) Renal agenesis, dysplasia, hypoplasia and cystic diseases of the kidney. In Fotter R (ed) Pediatric Uroradiology. Springer, Berlin-Heidelberg, pp 229–252
5. Wood BP (1992) Renal cystic disease in infants and children. Urol Radiol 14:284–295

Cystic Duct Anomalies

These anomalies include the congenital variations in the course and site of the cystic duct.

►Congenital Malformations, Liver and Biliary Tract

Cystic Duct Cyst

Saccular cystic dilatation of the cystic duct.

►Congenital Malformations, Liver and Biliary Tract

Cystic Fibrosis

Gundula Staatz
Department of Radiology, Division of Pediatric Radiology, University of Erlangen-Nürnberg, Erlangen
gu.stz.uni-erlangen@t-online.de

Synonym

Mucoviscidosis

Definitions

►Cystic fibrosis is an autosomal recessive inherited disease, caused by a defect in the gene for cystic fibrosis transmembrane conductance regulator (CFTR) on chromosome 7. The incidence in Europe is approximately 1:2500. The disease is characterised by viscous mucous production of exocrine glands resulting in airway plugging and obstruction, bronchiectasis and bacterial infection.

Pathology/Histopathology

The lungs of patients with cystic fibrosis show a variety of abnormalities such as atelectasis, ►mucoid impactions, acute and chronic inflammation, ►bronchiectasis, cyst formation, and fibrosis. Airway mucosal oedema and inflammation, respiratory muscle weakness and fatigue, contribute to the development of respiratory failure.

Histologically luminal neutrophils, neutrophilic and lymphocytic mural inflammation of the bronchial walls, squamous metaplasia of large and small airways, peribronchial and peribronchiolar fibrosis, obliterating fibroproliferative bronchiolitis and prominent hypertrophy of peribronchiolar smooth muscle are found (1). The alveoli adjacent to the bronchi show collapse and epithelialisation, the adjacent intra-alveolar septa are cellular infiltrated. The terminal bronchiole is often completely destroyed due to peripheral abscesses.

Clinical Presentation

Infants with cystic fibrosis have normal lungs at birth and present often initially with gastrointestinal problems like meconium ileus. With the onset of recurrent pulmonary infection, coughing (chronic), wheezing, dyspnoea on exertion, respiratory distress with retractions, chest pain, pneumothorax and haemoptysis occur. The sputum may be purulent, and on physical examination, clubbing, cyanosis and crackles during auscultation are found. Pulmonary infections are predominantly caused by *Staphylococcus aureus*, *Pseudomonas*, *Haemophilus influenza* and fungi. Other symptoms are caused by the involvement of the nose and sinuses, the gastrointestinal system, liver, pancreas, hepatobiliary system, urogenital tract, skin and skeletal system. Severe intra-abdominal manifestations of cystic fibrosis include neonatal meconium ileus, distal intestinal obstruction syndrome (DIOS), biliary cirrhosis, pancreatic cysts, pancreatic fibrosis and atrophy. Cor pulmonale and pulmonary hypertension are late-stage complications, but death is predominantly caused by chronic respiratory failure at a mean age of 33 years (2).

Imaging

Plain chest radiography is performed routinely in almost all patients. Several scoring tests have been established for the assessment of the disease severity, but image findings on chest X-rays may be subtle especially in mild disease and in early stages. High-resolution CT (HRCT) reflects most accurately the morphologic changes in patients with cystic fibrosis with excellent spatial resolution. CT-scoring systems provide a sensitive method for monitoring disease status and progression. MRI is useful for the assessment of mediastinal and vascular anatomy. In recent times, new MRI techniques for functional ventilation imaging with use of inhaled contrast aerosols, oxygen, hyper-polarised noble gases (Helium-3, Xenon-129) and fluorinated gases (sulphur-hexafluoride) have been developed (3). A higher sensitivity in the detection of ventilation defects compared to ventilation scintigraphy, CT or standard pulmonary function tests with lack of radiation is expected for this new MRI technique (3).

The abdominal manifestations of cystic fibrosis are efficiently imaged by ultrasound. Routine sonographic follow-up examinations of the liver, the biliary system, the pancreas and the bowel tract should be performed in each patient. In case of severe abdominal disease, such as liver cirrhosis with ascites or DIOS, CT may be necessary for further evaluation.

Nuclear Medicine

Ventilation perfusion scintigraphy may provide useful information in demonstrating marked functional impairment and abnormal matched ventilation and perfusion defects (1).

Diagnosis

In most children the diagnosis is based on clinical findings, positive newborn screening tests and sweat tests with measurement of sweat chloride concentrations. The chest radiographs of newborns are normal. Early findings on chest radiographs are hyperinflation of the lungs with flattening of the diaphragm and bronchial wall thickening (1). In later stages, peribronchial interstitial thickening, mucoid impactions, bronchiectasis, ring shadows (empty cavities of bronchiectasis), atelectasis, bulla, interstitial emphysema, pneumothorax, hilar lymphadenopathy and cor pulmonale occur (Fig. 1). The disease has a predilection for the upper and middle lung zones.

In HRCT bronchiectasis, peribronchial wall thickening, mosaic perfusion pattern and mucous plugging are the most frequently observed morphologic CT abnormalities in patients with cystic fibrosis. Less frequent are emphysema, collapse, sacculations and bullae observed (4) (Fig. 2). The disease is often accompanied by hilar and mediastinal lymph node enlargement (Fig. 3). The most common morphologic CT abnormalities increase in extent and severity with increasing patient age and correlate significantly with worsening of non-morphologic parameters of pulmonary status (4).

There are only a few studies using ►functional ventilation imaging with MRI in children with cystic fibrosis. Donelly et al. examined 4 children with cystic fibrosis using H-1 and ^{3}He MRI. In all subjects, areas of absent lung ventilation were depicted on the hyperpolarised ^{3}He MR images. These areas of absent ventilation ranged from wedge-shaped peripheral defects to signal voids in entire lung zones. Ventilation was most severely impaired in the upper posterior lung zones, and normal in the lower lung zones (3, 5).

Interventional Radiological Treatment

In patients with long-standing cystic fibrosis, haemoptysis may occur as a complication. Abnormal thin walled and tortuous bronchial arteries, commonly found in areas of bronchiectasis, are eroded secondary to chronic infection. In case of severe haemoptysis, arteriography of the bronchial arteries with subsequent embolisation may be

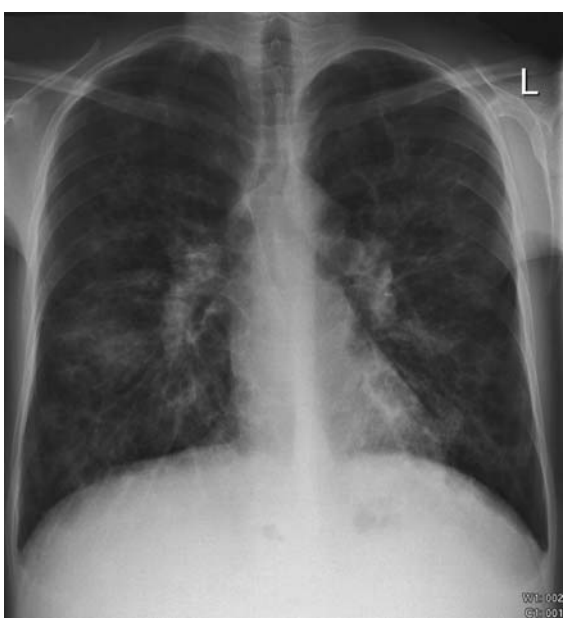

Cystic Fibrosis. Figure 1 A 17-year-old boy with cystic fibrosis. The chest radiograph demonstrates marked hyper-aerated lungs, bronchial wall thickening, bronchiectasis, peribronchial fibrosis, mucoid impactions and bilateral hilar lymphadenopathy.

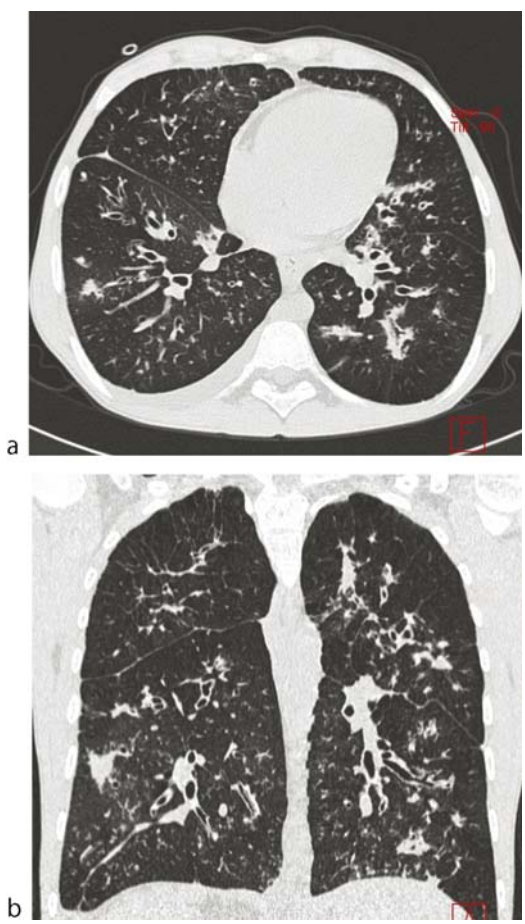

Cystic Fibrosis. Figure 2 Axial HRCT image (a) of cystic fibrosis in a 17-year-old boy and coronal multiplanar reconstruction (b) show emphysema, bronchiectasis, peribronchial wall thickening, mucous plugging and peribronchial fibrosis.

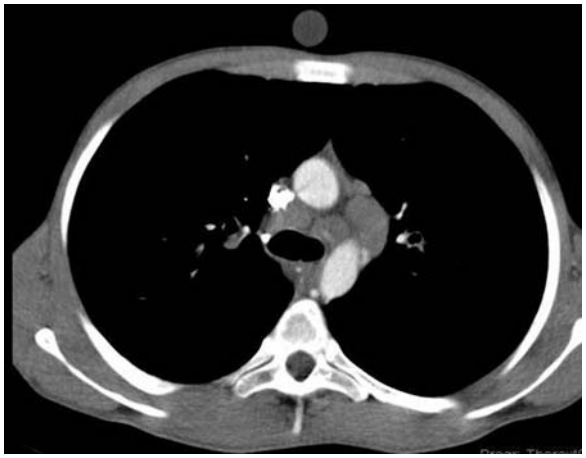

Cystic Fibrosis. Figure 3 Contrast-enhanced CT in a 21-year-old patient with cystic fibrosis. Bilateral hilar and mediastinal lymphadenopathy are identified.

necessary. As embolic materials, polyvinyl alcohol particles, gelatine sponge particles or coils are usually used. Bronchial artery embolisation has shown good results in controlling acute and chronic haemoptysis but in up to 50% of cases repeated embolisation procedures have to be performed due to a high incidence of bleeding from non-bronchial systemic collateral vessels. As major complications of bronchial artery embolisation transverse myelitis, bronchial infarction, oesophago-bronchial fistula, ischaemic colitis and—most feared—spinal infarction and paraplegia due to embolisation of a spinal artery have been described.

Bibliography

1. Rossi UG, Owens CM (2005) The radiology of chronic lung disease in children. Arch Dis Child 90:601–607
2. Moskowitz SM, Gibson RL, Effmann EL (2005) Cystic fibrosis lung disease: genetic influences, microbial interactions, and radiological assessment. Pediatr Radiol 35:739–757. Epub 2005 May 3
3. Kauczor HU, Chen XJ, van Beek EJ et al (2001) Pulmonary ventilation imaged by magnetic resonance: at the doorstep of clinical application. Eur Respir J 17:1008–1823
4. Helbich TH, Heinz- Peer G, Eichler I et al (1999) Cystic fibrosis: CT assessment of lung involvement in children and adults. Radiology 213:537–544
5. Donnelly LF, Mac Fall JR, McAdams HP et al (1999) Cystic fibrosis: combined hyperpolarized ^{3}He-enhanced and conventional proton MR imaging in the lung: preliminary observations. Radiology 212:885–889

Cystic Fibrosis

▶Meconium Ileus

Cystic Hygroma

Multiple cystic structures in neck region, showing lack ofcommunication between cervical lymphatics and venous system.

▶Lymphangioma

Cystic Hygroma, Branchial Cleft Cyst

▶Cysts, Cerebral and Cervical, Childhood

Cystic Hyperplasia

▶Fibrocystic Disease, Breast

Cystic Kidney Disease

▶Cystic Renal Disease, Childhood (MCDK, PCKD)

Cystic-Like Lesions, Hepatic

Chiara Franchini, Riccardo Lencioni
Department of Diagnostic and Interventional Radiology, University of Pisa, Italy
lencioni@med.unipi.it

Definition

Cysts and cystic-like lesions are any focal lesions that contain fluid (liquid or semisolid) material.

True cysts are closed cavities lined by epithelium, while cystic-like lesions do not have necessarily an epithelium and are not necessarily closed cavities.

Pathology and Histopathology

Cysts and cystic-like lesions of the liver in the adult can be classified as developmental, inflammatory, neoplastic, and miscellaneous. Developmental cystic lesions include simple cyst, autosomal dominant polycystic liver disease, ►biliary hamartoma, ►Caroli's disease. Inflammatory cystic lesions include pyogenic, amoebic and tubercular abscesses, and intrahepatic hydatid cyst. Neoplastic cystic lesions include biliary cystadenoma and cystadenocarcinoma, cystic subtypes of primary liver neoplasms, and cystic metastases. Other cystic lesions are intrahepatic haematoma and biloma (1).

Simple Cysts (Bile Duct Cysts)

Simple or true hepatic cysts are very common benign congenital lesions that do not communicate with the biliary tree (1, 2). They result from the obstruction of congenitally aberrant bile ducts, with subsequent stasis and retention of bile. They can be solitary or multiple and their size is very variable, even though frequently is inferior to 5 cm. They tend to increase in number and size with age. They are more common in women. Cysts are cavities lined by epithelium, with a thin wall and a serous content. Rarely they may present as "complicated" cysts due to the presence of hemorrhage or inflammation (1, 2).

Polycystic Liver Disease

►Polycystic liver disease is an autosomal dominant disorder characterized by the presence of multiple, sometimes innumerable cysts in the liver. In some cases, polycystic liver disease appears to occur sporadically. It is characterized by the presence of cysts ranging in size from less than 1 cm to more than 10–15 cm; the cysts are lined by cuboidal or flattened biliary epithelium and contain straw-colored fluid. They do not contain pigmented bile and appear to be detached from the biliary tree (1, 2–5). Polycystic liver disease is thought to be due to a ductal plate malformation of the small intrahepatic bile ducts, which lose communication with the biliary tree. Spontaneous intracystic hemorrhage, infection, and rupture may occur. Polycystic liver disease is often found in association with adult renal polycystic disease (1). Hepatic cysts are found in 40% of cases of autosomal dominant polycystic disease involving the kidneys; nevertheless, they may be seen without identifiable renal involvement at imaging.

Biliary Hamartoma

Bile duct hamartomas, also called von Meyenburg complexes, originate from a failure in involution of embryonic bile ducts (1, 3). They are small clusters of slightly dilated bile ducts embedded in a fibrous, sometimes hyalinized stroma, close to or within the portal tracts. These bile duct microhamartomas contain bile concrements. At pathologic analysis, they appear as grayish-white nodular lesions 0.1–1.5 cm in diameter scattered throughout the liver parenchyma. The nodules may coalesce into larger masses. They do not communicate with the biliary tree (3).

Caroli's Disease

Caroli's disease was described by Jacques Caroli in 1958 as a congenital communicating cavernous ectasia of the biliary tree. It is a rare, autosomal recessive condition characterized by segmental, nonobstructive saccular, or fusiform dilatation of the intrahepatic bile ducts. Other typical pathologic features are the presence of intraluminal bulbar protrusions, bridges across the dilated lumina, and portal radicles partially or completely surrounded by dilated bile ducts. The abnormality may be segmental or diffuse. The pure form of the disease is quite rare, while a various degree of congenital hepatic fibrosis is usually associated. ►Caroli's syndrome is the condition in which features of both congenital hepatic fibrosis and Caroli's disease are simultaneously present (1, 4).

Both varieties may be associated with cystic renal disease, more often autosomal recessive polycystic kidney disease, but also autosomal dominant polycystic kidney disease, medullary sponge kidney, nephronophtisis. There is also an association with cystic dilatation of extrahepatic bile ducts (1, 4). Caroli's disease is supposed to be due to an insufficient resorption of ductal plates, resulting in large dilated segments of the primitive bile duct surrounding a portal vessel (4). If the large intrahepatic bile ducts are affected, the result is the pure form of Caroli's disease, while abnormal development of the small interlobular bile ducts leads to congenital hepatic fibrosis.

Clinical Presentation

Simple Cysts

Hepatic cysts are a common finding, being found in 1% to 3% of the liver routine examinations. They are more often discovered in women and are usually asymptomatic (1, 2); rarely they may cause symptoms like pain, palpable abdominal mass, hepatomegaly, jaundice. Complications occur rarely and are mainly represented by intracystic hemorrhage, infection, compression of adjacent structures, occasionally torsion of the cyst, and rupture.

Polycystic Liver Disease

Usually, patients with polycystic liver disease are asymptomatic and liver dysfunction is quite unlikely to occur (5). However, advanced disease may cause hepatomegaly, which may results in abdominal discomfort and dyspnea. Symptoms may arise in relation to complications, such as intracystic bleeding, infection, or rupture of a cyst, which are quite frequent due to the great number of cysts (1, 5).

Biliary Hamartoma

Bile duct hamartomas are rather common and usually represent an incidental finding at imaging or laparotomy in asymptomatic patients, or at autopsy. The estimated incidence in autopsy series is 0.69–2.8% (1, 3). Complications such as superinfection with formation of microabscesses and degeneration into cholangiocarcinoma are extremely rare (3).

Caroli's Disease

The clinical onset of Caroli's disease usually occurs during childhood. In the pure form it is related to complications including stone formation, cholangitis, and hepatic abscesses. Clinical symptoms are recurrent attacks of right upper quadrant pain, fever, and, more rarely, jaundice. In Caroli's syndrome the clinical scenario is dominated by hepatic fibrosis and portal hypertension, with splenomegaly, oesophageal varices, hemorrhage of the gastrointestinal tract.

Cholangiocarcinoma complicates Caroli's disease in 7% of cases (5).

Imaging

Simple Cysts

At ultrasound (US) a cyst has the typical appearance of an anechoic, round or ellipsoid structure, with posterior acoustic enhancement, and sharply delineated margins, without an own wall. The solid–liquid interfaces appear as highly hyperechoic lines. Sometimes, subtle lateral acoustic shadows can be seen. Rarely, septa or calcifications may be present. Cysts may behave sometimes as occupying-space masses, displacing intrahepatic vessels or biliary branches, or causing swelling of the hepatic margin. A complicated cyst (intracystic bleeding or infection) presents internal echoes (1). At CT scans an hepatic cyst appears as a round or ovoid well-defined lesion, with no evident wall. The content is homogeneous and hypodense with attenuation values similar to the water (<20 HU). Both the wall and their content do not show any enhancement after contrast media administration. In small lesions, attenuation values can be higher due to partial volume effect; in these cases a thin section thickness should be used in order to avoid misdiagnosis of solid nodule; the absence of contrast enhancement will confirm the cystic nature of the lesion. Any enhancement in the periphery or thickening of the wall suggests an inflammatory or neoplastic nature, rather than a simple cyst. Internal inhomogeneity and higher attenuation values (>20 HU) are present in complicated cysts, in which the differential diagnosis from metastases arising from cystic carcinomas (as pancreatic or ovarian ones) can be difficult (1). The ipointensity on T1-weighted images and homogeneous very high signal intensity on T2-weighted images is due to their high water content. On heavily T2-weighted images an increase in signal intensity is seen. This behavior allows differentiation of these lesions from metastatic disease. The wall is never seen and no enhancement is present at the dynamic study. Intracystic bleeding determines high signal intensity, sometimes with a fluid–fluid level, on both T1- and T2-weighted images; the hemorrhage may be dated on the basis of the different appearance of the different phases of degradation of hemoglobin. Fat-saturation sequences may be helpful in confirming the blood content (1).

Polycystic Liver Disease

At ultrasound polycystic liver disease is characterized by the presence of multiple anechoic lesions of various size, often clustered, which causes a diffuse dishomogeneity of the liver parenchyma. The appearance of cystic lesions does not differ from that of simple cysts (1, 2). At CT the typical finding is the presence of multiple homogeneous water-density lesions with regular borders, without a detectable wall. The lesions do not show peripheral neither internal enhancement after contrast media administration. Hemorrhagic cysts, more frequently encountered than in cases of simple hepatic cysts due to the great number of lesions, have attenuation values higher than water at unenhanced CT scans; calcification of the cyst walls, due to previous hemorrhage, may also be detected (1). At MR, hepatic cysts in polycystic liver disease have a homogenous signal intensity and appear markedly hypointense on T1-weighted images and markedly hyperintense on T2-weighted images. Because of their serous content they become even brighter on heavily T2-weighted images. They do not enhance after administration of gadolinium chelates. The intracystic hemorrhage is characterized by signal intensity inhomogeneity (1). Although the diagnosis of polycystic liver disease is easily made with both CT and MR imaging, MR imaging is more sensitive for the detection of complicated cysts.

Biliary Hamartoma

At ultrasound biliary hamartomas have been described as either hypoechoic or anechoic small nodules with posterior acoustic enhancement. Hyperechoic biliary hamartomas or a combination of hypo- and hyperechoic lesions, however, has also been reported (3). In almost all described cases, unenhanced CT showed hypodense small hepatic nodules, scattered throughout the liver and typically measuring between 0.5 and 1.0 cm in diameter. The latter feature is the most essential one in the differential diagnosis from multiple simple cysts. Furthermore, simple cysts are typically regularly outlined, whereas bile duct hamartomas have a more irregular outline. Although homogeneous enhancement of these lesions has been noted in some cases, in most reports no enhancement was seen after contrast media administration (1, 3). The MR appearance of bile duct hamartomas has been reported sporadically. All lesions were hypointense compared with liver parenchyma on T1-weighted images and markedly hyperintense on T2-weighted images. On heavily T2-weighted images, the signal intensity increases further, nearly reaching the signal intensity of fluid. Biliary hamartomas do not exhibit a characteristic pattern of enhancement after administration of gadolinium chelates; some authors observed homogeneous enhancement of these lesions, some others a thin rim enhancement, whereas others did not find any enhancement. At MR cholangiography, bile duct hamartomas appear as multiple tiny cystic lesions that do not communicate with the biliary tree, helping in the differential diagnosis with Caroli's disease (1, 3).

Caroli's Disease

US reveals localized saccular dilatations of intrahepatic bile ducts which appear as multiple cystic lesions. Besides these findings, peculiar features may be demonstrated such as intraluminal bulbar protrusions, complete or incomplete bridging across the dilated ducts, and small portal branches within the cystic structures. The Doppler mode should be used in order to demonstrate this typical aspect. Inside the dilated segments stones or debris may be present, appearing as hyperechoic deposits with or without shadowing. CT typically shows hypoattenuating water-density structures which communicate with the biliary tree (Fig. 1). The presence of small dots showing strong contrast enhancement during the portal-venous phase within the dilated lumina, also known as "central dot sign," is considered very suggestive of Caroli's disease. Bulbar protrusions and bridge formation may also be depicted. Intraluminal biliary calculi may be demonstrated (Fig. 2) (1, 4).

At MR imaging, the cystic dilatations of the biliary tree appear hypointense on T1-weighted images and strongly hyperintense on T2-weighted images. The intraluminal portal radicles present clear enhancement in the portal phase at the dynamic study. MR can demonstrate internal septa and protrusions inside the dilated lumina. MR cholangiography can be extremely useful in diagnosis of Caroli's disease by demonstrating the communication between the saccular or fusiform dilatations of the intrahepatic bile ducts and the biliary tree (Fig. 3). Furthermore, stones, when present, are evident as signal voids within ducts and cystic spaces. Sludge or debris may be also evident. The use of a hepatobiliary contrast medium by imaging the liver in the biliary phase can more confidently demonstrate the biliary nature of the cystic dilatations, which show contrast enhancement. The cholangiographic features of Caroli's disease are well established as saccular or fusiform

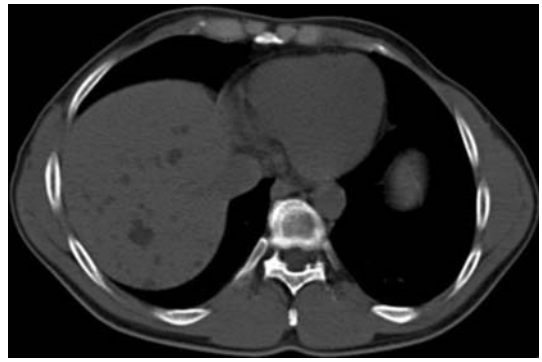

Cystic-Like Lesions, Hepatic. Figure 1 Caroli's disease. Unenhanced CT shows multiple hypoattenuating water-density areas.

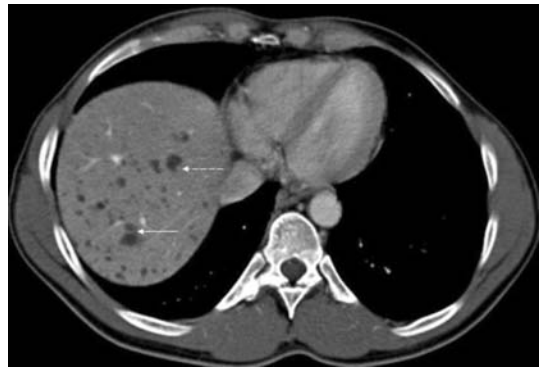

Cystic-Like Lesions, Hepatic. Figure 2 Caroli's disease. Bridging septa within the cystic dilatations may be depicted (*arrow*). The presence of small dots showing strong contrast enhancement during the portal-venous phase within the dilated lumina, also known as "central dot sign," is considered very suggestive of Caroli's disease (*dashed arrow*).

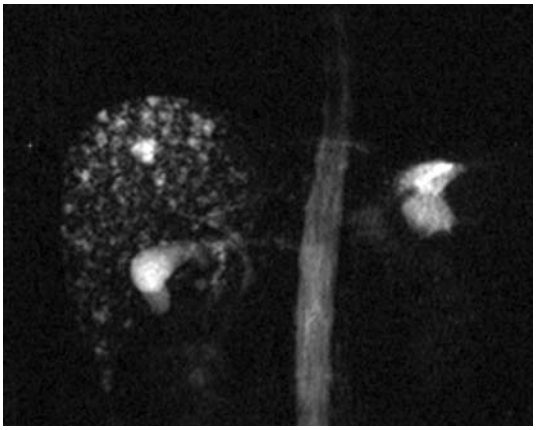

Cystic-Like Lesions, Hepatic. Figure 3 Caroli's disease. MR cholangiography demonstrates the communication between the saccular or fusiform dilatations of the intrahepatic bile ducts and the biliary tree.

dilatation of the intrahepatic bile ducts. Alternating areas of stricture and dilatation are a common observation with cholangiograms (1, 4).

Nuclear Medicine

Hepatobiliary scintigraphy with ^{99m}Tc (IDA iminodiacetic acid) agents reveals large, irregular, multifocal collections of the radiotracer in the liver. These collections correspond to the segmental dilatations, and no extrahepatic obstruction is present, although bile stasis and stone formation may result in atypical obstruction. On early images, if the ducts are dilated enough, they appear as photopenic branching areas within the liver. Overall, scintigraphy is not helpful compared with cross-sectional imaging techniques. Cholangitis can impair hepatic uptake of radiotracers. Obstruction related to stones or debris from the ducts may cause misdiagnosis.

Diagnosis

The diagnosis of a hepatic cystic lesion is based on US, which is the most accurate technique for establishing its cystic nature compared to solid lesions in the liver. At contrast CT or MR, any enhancement in the periphery or thickening of the wall suggests an inflammatory or neoplastic nature, rather than a simple cyst. MR is indicated when cystic lesions have atypical appearance on US. MR allows the distinction between complicated hepatic cysts presenting with hemorrhage inside and other cystic lesions such as underlying metastatic disease with target or halo sign. In the majority of cases, imaging findings in combination with critical clinical information allow an adequate lesion characterization.

Bibliography

1. Mortelé Koenraad J, Ros Pablo R (2001) Cystic focal liver lesions in the adult: differential CT and MR imaging features. Radiographics 21:895–910
2. vanSonnenberg E, Wroblicka JT, D'Agostino HB et al (1994) Symptomatic hepatic cysts: percutaneous drainage and sclerosis. Radiology 190:387–392
3. Wohlgemuth WA, Böttger J, Bohndorf K (1998) MRI, CT, US and ERCP in the evaluation of bile duct hamartomas (von Meyenburg complex): a case report. Eur Radiol 8:1623–1626
4. Choi BI, Yeon KM, Kim SH et al (1990) Caroli disease: central dot sign in CT. Radiology 174:161–163
5. Singh Y, Winick AB, Tabbara SO (1997) Multiloculated cystic liver lesions: radiologic-pathologic differential diagnosis. Radiographics 17:219–224

Cystic Mastopathy

▶ Fibrocystic Disease, Breast

Cystic Neoplasms, Pancreatic

Laura Crocetti[1], Carlo Bartolozzi[1], Piero Boraschi[2], Carla Cappelli[1]
[1]Department of Diagnostic and Interventional Radiology, University of Pisa, Italy
[2]2nd Department of Radiology, University Hospital, Pisa, Italy
l.crocetti@med.unipi.it

Synonyms

Cystic pancreatic tumors; Exocrine cystic neoplasms of the pancreas

Definitions

Cystic tumors of the pancreas are relatively uncommon, accounting for about 10% of cystic lesions of the pancreas and for 1% to 5% of primary pancreatic neoplasms. The incidence is increased in patients with von Hippel–Lindau disease.

According to the AFIP (Armed Forces Institute of Pathology) system, the pancreatic cystic tumors represent primary exocrine lesions and they are distinct into benign,

borderline (with an uncertain malignant potential) and malignant. Serous cystic tumors, mucinous cystic neoplasms and intraductal papillary-mucinous tumors/neoplasms (IPMTs/IMPNs) represent the majority of the cases encountered in practice, accounting for more than 90% of the primary cystic neoplasms of the pancreas; solid pseudopapillary neoplasms represent less than 10%; other cystic neoplasms are represented by other tumors with cystic appearance (e.g. cystic neuroendocrine tumor, acinar cystadenocarcinoma, ►lymphangioma, cystic teratoma) (1).

Pathology and Histopathology

Serous cystic tumors were also known as microcystic adenomas or glycogen-rich cystadenomas. They have an extremely low potential for malignant disease: malignant serous cystadenocarcinomas have been reported, but they are exceedingly rare, accounting for less than 1% of cases. Serous cystadenomas are generally well circumscribed, lobulated tumors, consisting of single (macrocystic or oligocystic adenoma) or multiple (microcystic adenoma) cysts, separated by delicate fibrous septae. The cysts are filled with clear, watery fluid and are often arranged around a central stellate scar, which may be calcified and that lacks in oligocystic adenomas. Cysts are lined by a simple, glycogen-rich cuboidal epithelium. When the cyst is large, it can be difficult to differentiate them from mucinous cystic neoplasms.

The histopathological features of mucinous cystic neoplasms and IPMNs are similar except for a dense mesenchymal ovarian-like stroma which is a requisite feature of mucinous cystic tumors. Moreover characteristically mucinous cystic neoplasms lack a communication with the pancreatic ductal system, whereas a communication is a key feature of IPMN (1).

Mucinous cystic tumors of the pancreas are multiloculated tumors. The inner surface is smooth, but sometimes, especially in large malignant tumors, papillary excrescences and solid nodules can be observed. Microscopically 3 distinct layers can be recognized: the inner epithelial layer producing mucin; the middle layer, which is the densely cellular ovarian-like mesenchymal stroma; the outermost layer, which is the hyalinized connective tissue. The epithelial cells lining the cysts produce abundant mucoid secretion; therefore the cysts contain viscous material, which can also be hemorrhagic. These tumors are classified on the basis of histology as benign, borderline or malignant based on degree of dysplastic changes of the epithelium. According to the model of neoplastic progression, mucinous cystic neoplasms progress through stages of increasing dysplasia from mucinous cystadenoma to borderline mucinous cystic neoplasm to mucinous cystic neoplasm with in situ carcinoma, finally to reach the stage of invasive carcinoma. Cystadenomas contain a single layer of epithelium without significant atypia. In borderline neoplasms the epithelium may form papillae; an in situ carcinoma or invasive carcinoma can arise focally within a mucinous cystic lesion. All these lesions are different from IPMNs, because they are grossly visibile neoplasms that do not involve the duct system of the pancreas (1).

IPMNs are papillary, villous neoplasm that arises within the main pancreatic duct or its branches. They are usually classified into 3 types: main duct, branch duct and mixed, according to the site and extent of involvement. The tumors hypersecrete mucin, which often leads to duct dilatation and/or chronic obstructive pancreatitis. Histologically the involved duct is lined by mucin-producing columnar epithelium which forms papillary proliferations; the tumor can shows varying degrees of atypia and can progress from adenomas without atypia to IPMN borderline with a moderate amount of atypia, to IPMN with carcinoma in situ and finally to infiltrating carcinoma. The tumors generally show intraluminal growth, but they can invade periductal tissues (1).

Clinical Presentation

Many patients with a pancreatic cystic tumor present with no relevant signs or symptoms and such tumors may be discovered incidentally at abdominal ultrasound (US) or computed tomography (CT). Most of the remaining patients present with a variety of non-specific symptoms such as abdominal pain, anorexia, nausea, vomiting, also related to recurrent pancreatitis. If the tumor is large enough, symptoms related to mass effects may predominate, such as a palpable abdominal mass and biliary obstruction. Patients with malignant changes may have a history of weight loss and jaundice.

Imaging

Classically, serous cystic lesions have a lobulated external contour and are composed of a grapelike cluster of cysts. A central stellate scar with calcification is pathognomonic and small septae and internal debris may be seen in individual cysts. Approximately 10% of all serous cystadenomas have cystic components larger than 2 cm and can't be distinguished from mucinous cystic neoplasms. Because the capsule of these tumors is poorly developed, poor distinction of the tumor from the surrounding pancreatic parenchyma is often observed. However, when the cysts are small, it can be difficult to

identify the cystic nature of the neoplasm. The central scar and calcifications may be demonstrated on CT scans, but are not well depicted on US. Endoscopic ultrasonography (EUS) allows better resolution of the honeycomb structure (2). Magnetic resonance (MR) is the modality of choice for the depiction and characterization of cystic pancreatic masses. Serous cystadenomas are usually hyperintense on T2-weighted images and hypointense on T1-weighted images. Occasionally, debris and hemorrhage in the cysts can alter this signal intensity pattern. The septae are well depicted on T2-weighted images, but the central scar is not. Magnetic resonance cholangiopancreatography (MRCP) is helpful in demonstrating the relationship of the mass to the main pancreatic duct. Usually no communication occurs with the pancreatic duct. The main duct is almost never obstructed, but the duct and its branches may be displaced (3,4) (Fig. 1).

Mucinous cystic neoplasms are often larger than 5 cm. US reveals a large, cystic mass sometimes with internal septa, excrescences, mural nodules and debris. The tumor usually has sharply marginated walls and smooth borders. CT shows a well-defined, unilocular or multilocular mass with fluid attenuation. Compared with serous cystic tumors, the cysts are larger (>20 mm in diameter) and less numerous (usually <6). Larger cysts may demonstrate small daughter cysts along their internal surface. Thick internal septae separating the different cystic cavities are typical. Visualization of nodular or papillary excrescences with irregular borders of the septae is possible. If present, calcifications are curvilinear or punctate and confined to the wall or septa. After the contrast medium administration, enhancement of the cyst wall, internal septations, mural nodules and other intracavitary projections is present. The presence of papillary excrescences, mural nodules and other intracavitary projections suggests the differentiation between benign mucinous cystadenoma and cystadenocarcinomas; however, the absence does not indicate that the tumor is benign. At MR, mucinous cystadenoma and cystadenocarcinoma are hypointense or hyperintense on T1-weighted images depending on protein content. T2-weighted images show multiple hyperintense cysts separated by multiple hypointense septa. Intracystic excrescences and mural nodules also have low signal intensity, but they enhance significantly after gadolinium-based contrast agents administration (3,4) (Fig. 2).

Main ductal type of IPMN may be focal or diffuse, the findings of which are reflected on imaging. When there is diffuse involvement of the pancreatic duct, dilatation is present along its whole length. This dilatation is often associated with diffuse and generally uniform pancreatic atrophy. In the early stages of focal or segmental involvement, the features may be difficult to differentiate from focal chronic obstructive pancreatitis. Branch IPMT is most frequently encountered in the region of the uncinate process. It may be microcystic or macrocystic. The microcystic variety may mimic serous cystadenomas on imaging, but communication with the main pancreatic duct (which is frequently dilated) is characteristic. The macrocystic variety may mimic a peripheral mucinous cystic tumor. IPMN can be more confidently diagnosed when imaging reveals a filling defect in the main duct or a branch pancreatic duct. The filling defects are hyperechoic on US (but extremely difficult to visualize), hyperdense on CT and hypointense on T2-weighted MR images. The thickness of the cyst wall and septa is variable with benign tumors; they tend to be thin and regular. In malignant

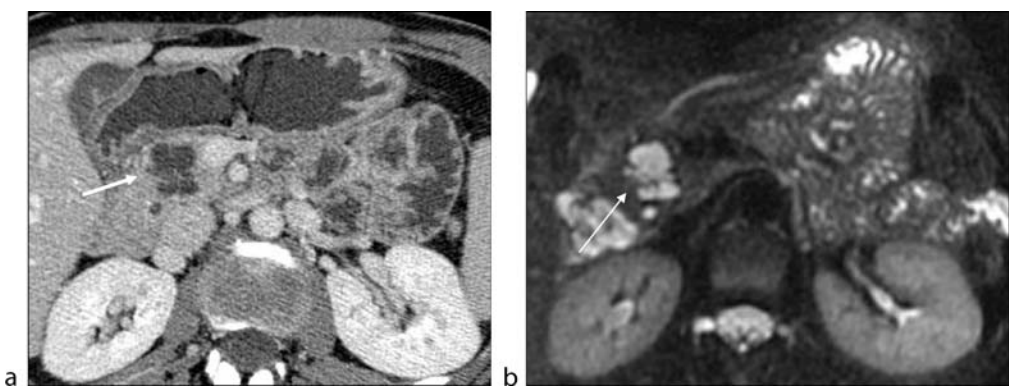

Cystic Neoplasms, Pancreatic. Figure 1 Serous cystoadenoma of the head of the pancreas (arrows). Multidetector CT study (a) and MR study (b). At CT is possible to appreciate a well circumscribed lesion, presenting lobulated borders, constituted by few microcysts. The borders are poorly defined from the normal pancreatic parenchyma and the lesion does not show evidence of contrast enhancement; a thin stellate central scar is also visible but there are no signs of calcifications (a). In an axial fat-suppressed fast spin-echo T2-w, it is possible to appreciate the same lesion as a lobulated hyperintense area with no relationship with pancreatic ducts (b).

tumors, the walls and septa appear irregular and thick, with solid nodules. MRCP study represents the technique of choice for visualizing the typical communication between the IPMN and the ductal system and to evaluate the extent of the tumor. A main pancreatic duct with a maximum diameter of greater than 15 mm, and diffuse dilatation of the duct are suggestive of malignancy in main duct type tumors. Among branch duct-type tumors, malignant tumors tend to be larger than benign tumors (Fig. 3). The intravenous administration of secretin allows the improvement of the pancreatic ducts delineation and therefore the depiction of typical findings of IPMN (5,6).

Because of the anatomical location of the pancreas near to the gastric and duodenal loop, EUS appears to be reliable in distinguishing between solid and cystic lesions. However the features that can be visualized often do not appear to be sufficiently accurate to allow a differentiation between benign and malignant tumors.

Endoscopic retrograde cholangiopancreatography (ERCP) may depict ductal changes in cystic tumors of the pancreas in approximately 80% of patients, allowing also tissue sampling and therapeutic intervention. In particular, in IPMN the communication with the pancreatic duct and an anomalous ampulla of Vater with discharging mucus may be visualized.

Nuclear Medicine

Positron emission tomography (PET) imaging can depict cystic malignant tumors, because it is sensitive to

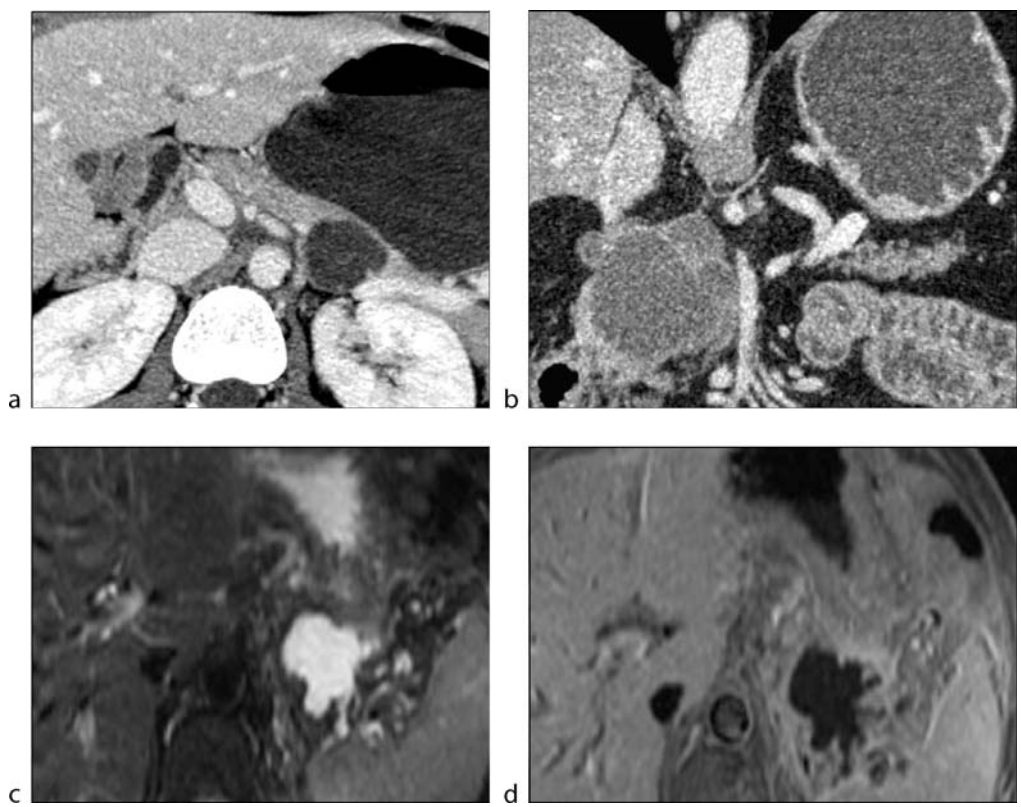

Cystic Neoplasms, Pancreatic. Figure 2 Mucinous tumors of the pancreas at multidetector CT (a,b) and MR (c,d). In (a) a uniloculated, well defined benign mucinous tumor of pancreatic body/tail is depicted. It is possible to appreciate the smooth borders of the lesion, the absence of internal septa and the smooth inner surface. Multiplanar reconstruction (b) on the coronal plane shows a multiloculated malignant mucinous tumor of the pancreatic head: the irregular profile and the thickness of the borders as well as the presence of contrast enhancement are depicted. There is no presence of internal septa or intracavitary projections. The neoplasm infiltrates the fat tissue around the pancreatic head and it is contiguous to the superior mesenteric artery wall, without certain signs of vascular compression. In (c) and (d) a mucinous cystadenocarcinoma of the pancreatic tail is shown by MR images. Axial fat-suppressed fast spin-echo T2-w (c) and gadolinium-enhanced fat-suppressed SPGR T1-w (d) images well exhibit a prevalently cystic lesion at the level of the pancreatic tail. The lesion shows irregularly lobulated, thickened internal walls presenting marked contrast enhancement.

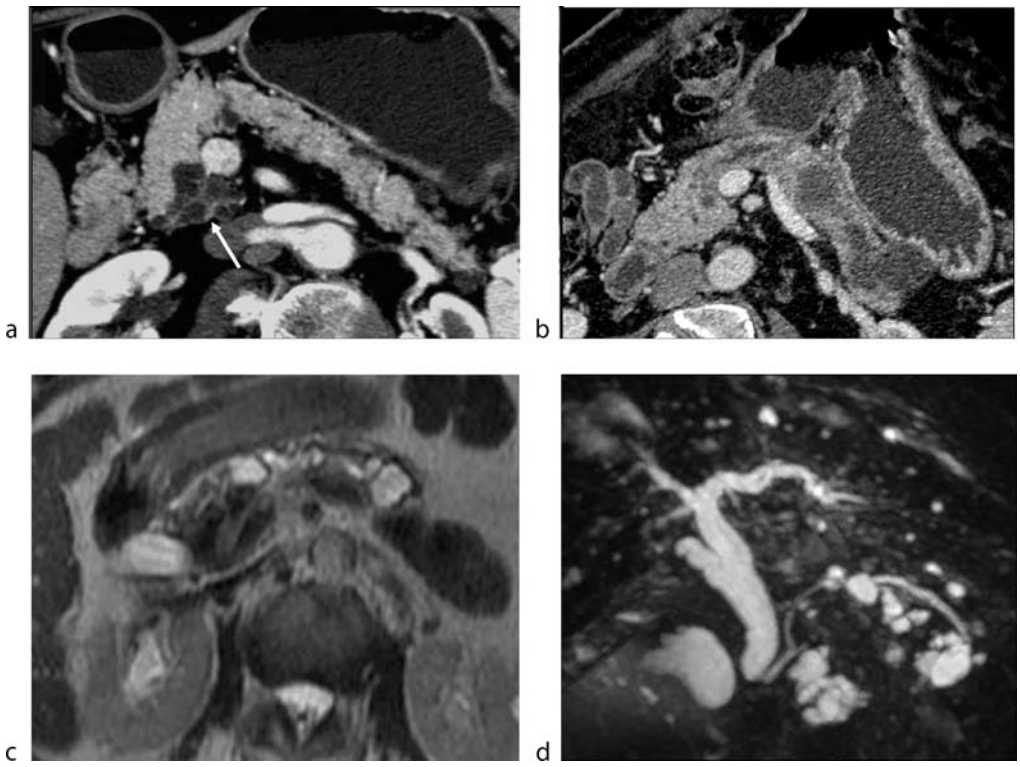

Cystic Neoplasms, Pancreatic. Figure 3 IPMN of the pancreas at multidetector CT (a,b) and MR (c,d). In (a) a IPMN "branch duct-type": a multilobulated lesion constituted by a grape-like cluster of microcysts originating from secondary pancreatic ducts is shown in the uncinate process (a); these microcystic lesions, differently from the serous ones, do not present a central scar. The lesion also shows thin margins and there are no internal septae. The main pancreatic duct is not dilated. In (b) a IPMN "main duct-type": two uniloculated macrocystic lesions, localized in the tail and in the body of the pancreas and originating from the Wirsung duct can be appreciated; the cystic lesions appear filled with an ovarian like stroma fluid and their growth has determined the Wirsung dilatation and the consequent glandular atrophy, due to compression. In (c) and (d) a branch duct-type IPMN can be appreciated at MR. Axial single-shot fast spin-echo T2-w image (c) and coronal oblique MIP reconstruction of MRCP (d) show multiple, diffuse cystic dilatations of secondary pancreatic ducts. The main pancreatic duct appears slightly dilated at the level of the pancreatic tail. Extraepatic biliary tree is also dilated.

hypermetabolic processes. FDG PET is more accurate than CT in identifying malignant lesions and could be used, in combination with CT and tumor markers, in the preoperative evaluation of patients with pancreatic cystic lesions. A positive result on FDG PET strongly suggests malignancy and, therefore, a need for resection. A negative result shows a benign tumor that may be treated with limited resection or follow-up. However, PET is not yet approved for use in the workup of pancreatic lesions.

Diagnosis

With the widespread use of advanced imaging techniques, cystic lesions of the pancreas are now diagnosed relatively frequently. US may aid in the differentiation of solid and cystic lesions, but a complete evaluation of the pancreas is often difficult. CT is excellent not only for the initial detection of the lesion but also for the characterization (by visualization of calcifications, septa, mural nodules) and the staging of malignant lesions (by assessing vascular invasion, infiltration of the adjacent structures and the presence of lymph node metastases, distant metastases or peritoneal carcinosis). MR has the added advantage of providing better characterization of the features of a cyst and its relationship with the pancreatic duct by means of MRCP sequences. Despite advances in imaging, often the differential diagnosis of pancreatic cystic lesion remains difficult; however an accurate diagnosis is imperative for appropriate patient management because the most

important determinant of the prognosis is the identification of malignant or premalignant cysts that require resection. Serous cystadenoma is usually benign, whereas some serous cystadenomas show progressive growth; therefore, surgery is indicated, because complications, such as obstructive jaundice, can result. Surgical removal of the mucinous cystic neoplasms and IPMNs is recommended because of the potential malignant behaviour of these lesions. Therefore obtaining fluid cyst or tissue for histologic confirmation may be essential. A variety of tumor markers that may be present in cyst fluid have been proposed for use in the differentiation among the major types of cystic lesions. Ca 19.9 concentration in cyst fluid has not been confirmed as a useful indicator for discriminating between mucinous and non-mucinous cystic lesions but serum levels of Ca 19.9 are slightly elevated in some patients who have malignant cystic lesions. Levels of cystic carcinoembryonic antigen (CEA) can be increased in the mucin content of the cysts, and they proportionally rises with the degree of malignancy of the tumor. Although amylase is not a tumor marker, its presence in cyst fluid is often used as an indicator of a communication between a cystic lesion and the ductal system, as in cysts that are associated with IPMNs.

The differential diagnosis includes other tumors with cystic appearance and pancreatic lesions with a cystic presentation (including pancreatic pseudocysts or pancreatic fluid collections, ▶congenital pancreatic cysts, retention pancreatic cysts, ▶parasitic cysts, ▶lymphoepithelial cysts).

References

1. Buetow PC, Rao P, Thompson LDR (1998) From the archives of the AFIP. Mucinous cystic neoplasms of the pancreas: radiologic-pathologic correlation. Radiographics 18:433–449
2. Sahani DV, Kadavigere R, Saokar A et al (2005) Cystic Pancreatic Lesions: a simple imaging-based classification system for guiding management. Radiographics 25:1471–1484
3. Demos TC, Posniak HV, Harmath C et al (2002) Cystic lesions of the pancreas. Am J Roentgenol 179:1375–1387
4. Suzuki Y, Atomi Y, Sugiyama M et al (2004) Cystic neoplasm of the pancreas. A Japanese multiinstitutional study of intraductal papillary mucinous tumor and mucinous cystic tumor. Pancreas 28(3):241–246
5. Tanaka M (2004) Intraductal papillary mucinous neoplasm of the pancreas: diagnosis and treatment. Pancreas 28(3):282–288
6. Silas AM, Morrin MM, Raptopoulos V et al (2001) Intraductal papillary mucinous tumors of the pancreas. Am J Roentgenol 176:179–185

Cystic Nephroma

A basically benign, sometimes semi-malignant multicystic renal lesion, usually comprised of multiple small, similar sized cysts that may include some areas of nephroblastomatosous cells (potential malignant transformation), that may replace the entire or parts of the kidney.

▶Cystic Renal Disease, Childhood

Cystic Pancreatic Tumors

▶Cystic Neoplasms, Pancreatic

Cystic Renal Disease, Acquired

JM Correas, O Hélénon
University of Paris V,
Paris, France
jean-michel.correas@nck.ap-hop-paris.fr

Definition

Acquired cystic kidney disease (ACKD) is defined as the development of multiple renal cysts (at least three per kidney) in patients with end-stage renal disease, before or after starting dialysis, without hereditary cystic disease. It can affect the native kidneys in renal transplanted patients, whatever the renal function and the renal graft during chronic rejection.

Pathology/Histopathology

Pathology reveals multiple renal cysts in both atrophic kidneys from the cortex and the medulla. They are typically small, ranging in size from a few millimeters to 30 mm. The presence of hemorrhagic cysts or oxalate crystal deposition in cystic walls and septations as well as within the cysts is common. Atypical cystic walls exhibit multilayered epithelial lining, and papillary proliferations are not unusual (1). Multiple renal tumors are associated with ACKD, including adenomas and carcinomas of various types, with a strong increase in papillary tumor incidence compared with the general population (1). Renal cancer can be detected in approximately 5% of ACKD patients. Tumors are typically multifocal, bilateral, and aggressive, with a rate of metastases of 15% (2). The mean duration of dialysis before development of renal cancer is about 12 ± 7.9 years (2).

Clinical Presentation

The incidence of ACKD increases with the duration of end-stage renal failure. Before patients start dialysis, ACKD is found in about 10% of them. This number increases to 10–20% within the first 3 years of dialysis and can reach 90% after 10 years of dialysis (3), whatever the cause of renal failure. The kidneys regularly increase in size because of the development of cysts in patients undergoing dialysis, whereas they remain small in transplanted patients.

In most cases, ACKD is detected incidentally because the disease is asymptomatic. The recovery of normal renal function after transplantation has no demonstrated impact on the development of ACKD.

Cyst complications, including bleeding and infection, can also appear and reveal the disease. The presence of hemorrhagic cysts is frequent at imaging procedures. Rarely, the hemorrhage is symptomatic and provokes back pain. Severe cyst bleeding can extend to the retroperitoneum or the collecting system and result in reduced hemoglobin serum level, hypotension, and even shock.

Renal tumors are rarely symptomatic and are detected in most cases by incidental imaging studies or systematic follow-up in hemodialyzed or transplanted patients. The incidence of renal cell carcinomas is significantly increased up to seven times in patients undergoing dialysis (2). Seven percent of dialyzed patients can develop small solid renal tumors. In transplanted patients, the prevalence of renal cell carcinoma discovered incidentally is 1.6%.

Imaging

Ultrasonography and Color Doppler Ultrasound

At ▶ultrasound (US), the cysts are detected as sonolucent round lesions with increased posterior acoustical energy. They are typically bilateral, localized within the parenchyma in small kidneys with reduced corticomedullary differentiation. Harmonic tissue imaging is helpful to detect and characterize small hypoechoic lesions (Fig. 1). Almost 50% of hemorrhagic cysts can exhibit a pseudosolid echoic pattern on US. ▶Contrast-enhanced computed tomography (CT) or magnetic resonance imaging (MRI) is then required. Hemorrhagic cysts can remain anechoic, and US can be useful to characterize hyperattenuating cysts at CT in the case of absence of iodinated contrast agent administration or when the enhancement remains equivocal. On color Doppler US (CDUS), typical cysts do not exhibit any signals. Contrast-enhanced US might be useful for diagnosing pseudotumors and to detect vascularity within echoic renal lesions to confirm the presence of a solid renal mass (Fig. 2).

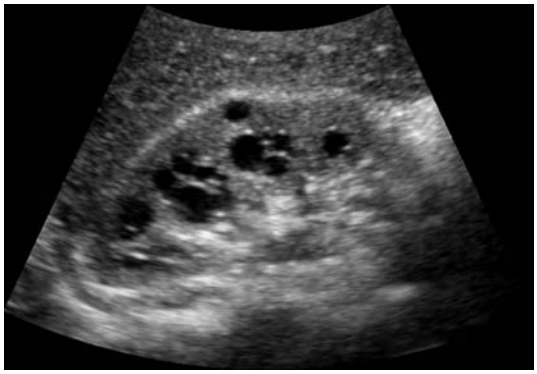

Cystic Renal Disease, Acquired. Figure 1 Harmonic compounding imaging of the native kidney in a renal transplanted patient. Many typical cysts are detected within the cortex and the medulla.

However, US examination in ACKD is difficult due to the reduced size of the kidneys and the hyperechoic parenchyma, making identification of the kidney difficult within the retroperitoneal fat.

CT and MRI

Contrast-enhanced CT remains the gold standard in the diagnosis of ACKD as well as in the characterization of renal masses. Baseline CT is mandatory to detect hyperattenuating cysts and to provide baseline attenuating values. Contrast-enhanced CT improves the detection of numerous small cysts located in both kidneys, predominantly in the cortex (Fig. 3). CT can also detect calcifications in cystic walls or septations.

Hemorrhagic cysts are very common (up to 50% of ACKD patients). They typically exhibit increased attenuation values at baseline (above 50 HU) and no enhancement after iodinated contrast agent administration. Delayed acquisitions during nephrographic and excretory phases are necessary to differentiate these lesions from solid renal tumors. In the case of acute back pain revealing renal bleeding, CT can detect an enlarged hemorrhagic cyst and/or a subcapsular hematoma. The hematoma can extend to the retroperitoneal space. The disappearance of the hematoma should be monitored until disappearance to avoid the misdiagnosis of a bleeding cystic carcinoma.

Solid renal masses are seen as round lesions significantly enhanced after iodinated contrast agent injection. The threshold varies from 15 to 20 HU. In the case of hemorrhagic mass, the enhancement is typically poor and remains below the threshold value. The change in the shape of the lesion that becomes heterogeneous

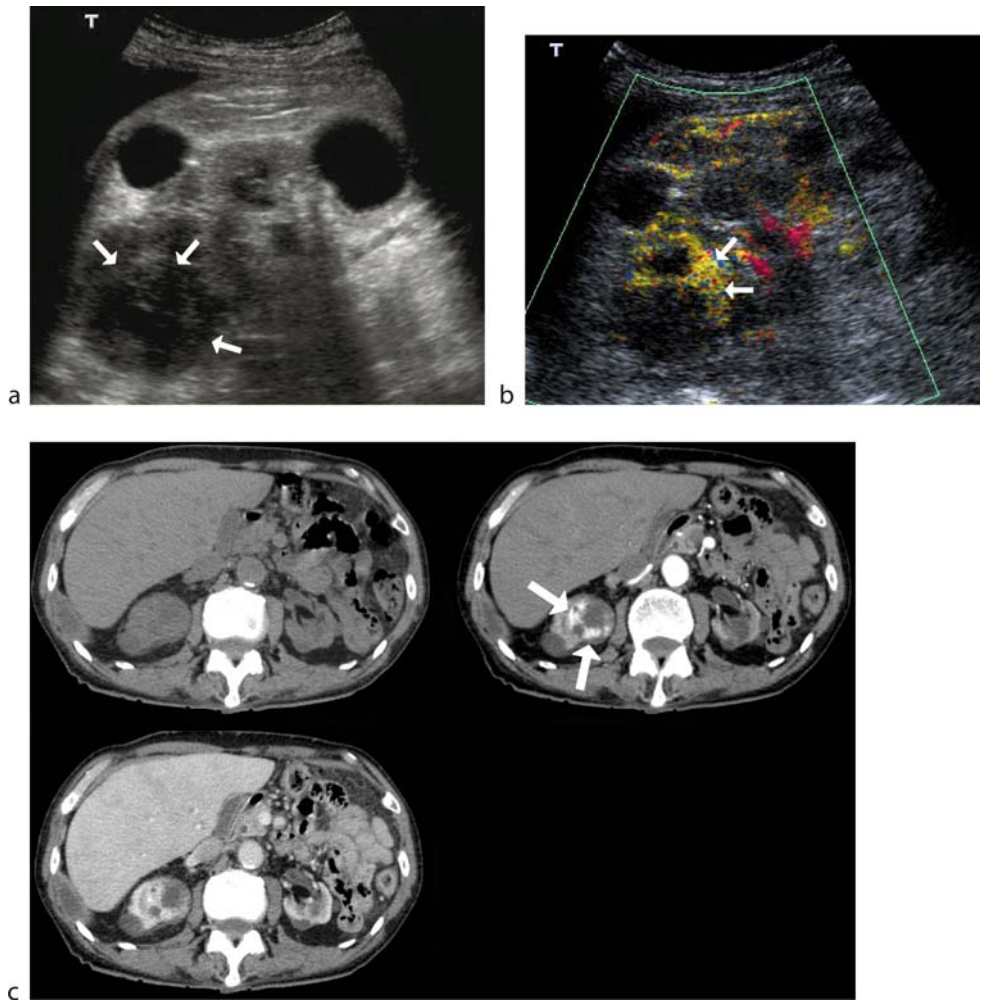

Cystic Renal Disease, Acquired. Figure 2 Ultrasound (US) follow-up of a patient under hemodialysis. (a) At tissue harmonic imaging, a heterogeneous and echogenic mass was detected at the upper pole of the right kidney (*arrows*). (b) Contrast-enhanced US following the administration of SonoVue confirmed the presence of vascularity within the mass, strongly enhancing during arterial phase (*arrows*). (c) Contrast-enhanced computed tomography (CT) with baseline (*top left*), arterial (*top right*), and nephrographic (*bottom left*) acquisitions. CT confirmed the presence of a partially necrotic mass with strong peripheral enhancement. At pathology, the lesion corresponded to a renal cell carcinoma.

indicates the presence of vascularity, and thus is highly suspicious for solid tumors. Solid renal masses should be differentiated from focal renal parenchyma hypertrophy. These pseudotumors exhibit a similar enhancement compared with the normal atrophic parenchyma at all phases of the transit of the iodinated contrast agent, and they remain homogeneous. In the case of equivocal diagnosis, MRI can be useful to confirm the diagnosis of pseudomass.

The staging of a solid renal mass primarily relies on contrast-enhanced CT to detect venous and lymph node extension.

If contrast-enhanced CT can be performed in patients undergoing dialysis, CT cannot be used in patients with persistent renal function. In this case, contrast-enhanced MRI becomes the modality of choice for the diagnosis of ACKD and the characterization of renal masses.

MRI examination should include at least T2-weighted spin-echo sequences with fat suppression and dynamic breath-hold T1-weighted gradient-echo sequences with fat suppression, before and after bolus administration of gadolinium chelate contrast agent. Typical cysts are easily characterized as round lesions of high signal intensity on T2-weighted sequences, of low signal intensity on

T1-weighted sequences at baseline, and with no enhancement after injection of contrast agent (Fig. 4). Hemorrhagic cysts are typically hyperintense on both T1- and T2-weighted sequences and do not exhibit any enhancement. The presence of a fluid iron level indicates the presence of a hemorrhagic cyst.

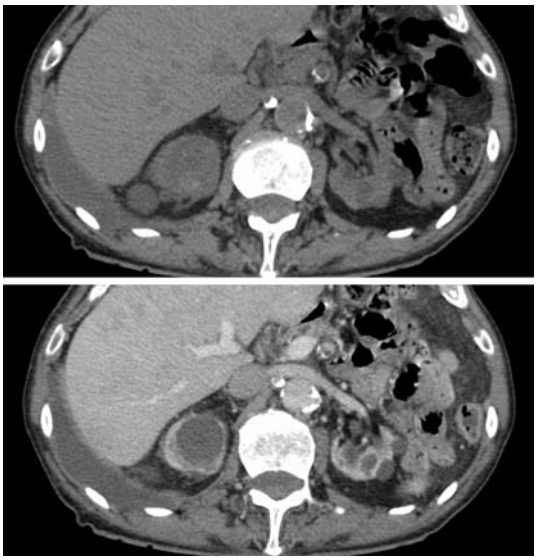

Cystic Renal Disease, Acquired. Figure 3 Computed tomography in ▶acquired cystic kidney disease (*top*: baseline scan; *bottom*: nephrographic phase). Multiple bilateral small cysts are detected within the atrophic parenchyma.

In hemorrhagic cystic tumors, the enhancement can be masked by the baseline hypersignal of the lesion. Follow-up is then necessary to confirm the absence of enhancement when the signal of the lesion will be changed due to metabolism of methemoglobin.

Solid renal masses are typically slightly hyperintense on T2-weighted sequences, and they significantly enhance after contrast agent injection. MRI participates in the staging of renal masses when the administration of iodinated contrast agents is contraindicated or when CT and sonographic findings are inconclusive, particularly regarding tumor extension to the inferior vena cava, the spleen, and the liver.

Angiography

Renal angiography is not done for ACKD diagnosis but for selective embolization in patients with severe active bleeding. To avoid the misdiagnosis of a bleeding tumor, CT needs to be performed until the hematoma disappears.

Nuclear Medicine

Scintigraphy has no value in the diagnosis of ACKD.

Diagnosis

The most difficult ▶differential diagnosis of ACKD is the presence of multiple simple cysts. The size of the cysts and

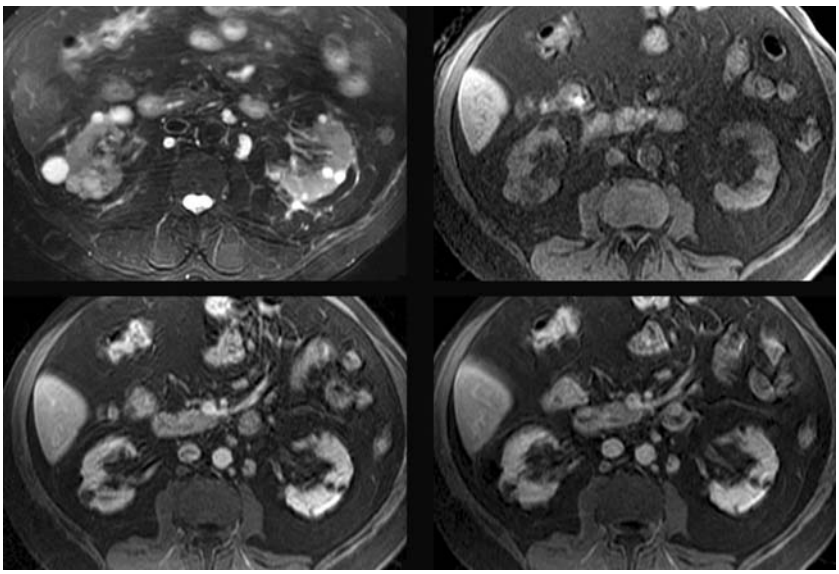

Cystic Renal Disease, Acquired. Figure 4 Typical magnetic resonance imaging (MRI) aspects in acquired cystic kidney disease. *Top left*: T2-weighted acquisition; *top right*: T1-weighted baseline dynamic acquisition; *bottom left*: T1-weighted dynamic acquisition during nephrographic phase; *bottom right*: T1-weighted dynamic acquisition during excretory phase.

their location are not helpful for differentiating the two diseases. When renal function is preserved, the diagnosis is likely to be ACKD, but multiple renal cysts can be found in patients with chronic renal failure.

In medullary cystic disease, the cysts are small and strictly located within the medulla.

At the moment of diagnosis of ACKD, the size of the kidneys is normal or reduced, in contrast to autosomal dominant polycystic kidney disease (ADPKD). In ADPKD, the renal cysts are much bigger than in ACKD, as they typically exceed 5 cm. Cysts can be detected in other locations such as the liver, the spleen, and the pancreas.

Other diseases such as von Hippel Lindau and tuberous sclerosis are easily ruled out with the context (family cases), the presence of associated tumors (hemangioblastoma of the central nervous system, pheochromocytoma, pancreatic cysts, or angiomyolipoma).

There is no definite imaging modality recommended for screening ACKD patients. US offers a clear advantage in terms of cost (Fig. 2). However, the examination is often difficult due to the size and echogenicity of the kidney. CT has the disadvantage of higher cost and secondary effects of iodinated contrast agents (renal toxicity and allergic reactions). However, it is an effective imaging technique and allows comparison when repeated examinations are performed over the years. MRI is probably the most effective modality because it does not have the limitations of iodinated contrast agents. However, its use is limited by restricted access to the machine, the cost of the examination, and some contraindications. The screening test should be repeated once a year, even after successful transplantation.

Still under debate is the efficacy of a screening program for elderly patients undergoing dialysis due to numerous comorbidity factors that reduce the impact of early treatment of renal cancer on the survival rate (4). Minimally invasive treatment of renal tumors such as radio frequency ablation might improve the tolerance of treatment compared with radical nephrectomy in this population at risk for cardiovascular complications. The screening program can be directed at patients at high risk of cancer (male, prolonged dialysis, enlarged kidneys) with good clinical status after 3 years of dialysis (5, 6). The incidence of renal tumors may have been underestimated by imaging techniques. The screening program can also include patients undergoing peritoneal dialysis.

In patients awaiting renal transplantation, the native kidneys should be scanned by either US or CT before the surgical procedure.

After renal transplantation, the native kidneys can be studied by US at the same time as the examination of the renal graft. Despite the lack of published data, transplanted patients, including children, might represent the best population to benefit from a renal tumor screening protocol (7). The decrease in ACKD after successful transplantation should be balanced against the increased aggressive behavior of renal cancers. When an echoic renal mass is detected, contrast-enhanced CT or MRI should be performed, depending on renal function.

Bibliography

1. Ishikawa I, Kovacs G (1993) High incidence of papillary renal cell tumours in patients on chronic haemodialysis. Histopathology 22:135–139
2. Ishikawa I (2004) Present status of renal cell carcinoma in dialysis patients in Japan: questionnaire study in 2002. Nephron Clin Pract 97:c11–c16
3. Levine E (1996) Acquired cystic kidney disease. Radiol Clin North Am 34:947–964
4. Sarasin FP, Wong JB, Levey AS et al (1995) Screening for acquired cystic kidney disease: a decision analytic perspective. Kidney Int 48:207–219
5. Choyke PL (2000) Acquired cystic kidney disease. Eur Radiol 10:1716–1721
6. Peces R, Martinez-Ara J, Miguel JL et al (2004) Renal cell carcinoma co-existent with other renal disease: clinico-pathological features in pre-dialysis patients and those receiving dialysis or renal transplantation. Nephrol Dial Transplant 19:2789–2796
7. Querfeld U, Schneble F, Wradzidlo W et al (1992) Acquired cystic kidney disease before and after renal transplantation. J Pediatr 121:61–64

Cystic Teratoma

▶Teratoma, Ovaries, Mature, Ovalar

Cystitis

Lorenzo E. Derchi, Pietro Pavlica
University of Genova, Largo R. Benzi, 8,
I-16122 Genova, Italy
derchi@unige.it

Definition

The term cystitis indicates the presence of an inflammatory disease of the urinary bladder. Such diseases are a common clinical problem, with more than half of the population experiencing an episode of cystitis during life. They can have a large variety of causes and can be divided, according to their etiology, into two broad categories:

those due to infectious causes, and those of noninfectious origin. In the first group, bacterial lesions are the most frequent, but viral, fungal, and parasitic diseases can also be encountered. Noninfectious inflammations can be congenital, such as the chronic irritative changes of the bladder mucosa in exstrophy of the urinary bladder, or acquired such as lupus erithematosus cystitis, eosinophilic cystitis, pelvic lipomatosis, involvement of the bladder from inflammatory diseases of adjacent organs, and iatrogenic lesions (1, 2).

Pathology/Histopathology

Pathological changes can be limited to the mucosal surface of the bladder or extend to the deep layers of the wall, and vary according to the etiology of the disease process.

Infectious Cystitis

In patients with bacterial cystitis, the main finding is edema of the mucosa, with thickening of the mucosal folds. When severe, edema can cause decreased capacity of the bladder. Bullous edema, that is fluid-filled cystic areas in the lamina propria of the mucosa, can develop, and is often more prominent at the level of the bladder base. The inflammatory process can be focal, and presenting as inflammatory polypoid lesions. In emphysematous cystitis, a condition that is most commonly encountered in patients with poorly controlled diabetes mellitus, bacterial fermentation of excessive glucose causes development of carbon dioxide within the bladder wall. Gas can extend also into the bladder lumen (3). Immunocompromised or debilitated patients can develop, after urologic procedures, infection from urease-producing microorganisms, able to transform urea into ammonia. This causes modification of pH in urine, which becomes alkaline, leading to formation of struvite and calcium phosphate that form stones and encrustations on the bladder wall. The disease, called alkaline-encrustation cystitis may also extend to the ureters and the kidneys. Encrustations are usually thin and regular, covering the urothelial surface, but may be irregular and thick; thickening of the bladder wall and perivesical soft-tissue edema can be associated (4). Mycotic infections of the bladder can cause formation of "fungus balls" within the bladder lumen; these are clusters of pseudomicelia, usually mobile according to patient's decubitus. In diabetic patients with Candida infection, gas can be present in the bladder given the capability of Candida to ferment sugar. If a fungus ball is in the bladder, gas can remain trapped within it. In patients with infestation from schistosomiasis, the disease process is caused by eggs deposited by the female parasite in the small veins of the submucosal layer of the bladder wall, around which a granulomatous reaction and embolic vasculitis develop. The deposited eggs calcify, and this is a macroscopic hallmark of the disease (5). Involvement of the urinary bladder occurs in about one third of patients with urinary tract tuberculosis, usually late in the course of the disease. The mucosa is edematous, with tubercles that coalesce and undergo ulceration. Calcifications can develop.

Noninfectious Cystitis

A large variety of noninfectious conditions can cause inflammatory changes of the bladder mucosa. In lupus erithematosus cystitis, a marked vasculitis of the bladder develops, with immune-complex deposition along small vessels and smooth muscle in the lamina propria of the bladder. Biopsy of the bladder wall in cases of eosinophilic cystitis shows pancystitis, with eosinophils, mast cells, and lymphocytes within the mucosa and tunica propria. Muscle necrosis and fibrosis can be found. Interstial cystitis is a pancystitis of unknown cause, often associated with systemic diseases. Biopsy shows transmural inflammation and fibrosis, submucosal edema and vasodilatation, and presence of mast cells in the submucosa and muscular layers. Cystitis can develop in most patients with pelvic lipomatosis, a condition characterized by benign overgrowth of pelvic fat. The pathogenetic relationship between cystitis and pelvic lipomatosis is not clear; however up to 80% of these patients develop cystitis glandularis. When the bladder is involved by neoplastic or inflammatory disorders arising within surrounding pelvic organs, histology shows an infiltrating inflammatory process, most marked in the outer part of the bladder wall. Perforation into the bladder may occur. Iatrogenic inflammation from foreign bodies, drugs, or radiation can develop in the bladder. The most common one is due to indwelling urethral catheters, in which histology shows vascular dilatation on the mucosa and lamina propria, with bullous edema visible on the surface of the mucosa, especially at the point where the tip of the catheter is in contact with the wall. Such changes can regress very quickly after catheter removal. Drug-induced cystitis may be related to either to direct toxic effect of drug metabolites on the urothelium or to an allergic-type of reaction of the bladder mucosa. Cyclophosphamide cystitis is the typical example of the first type of reaction. Biopsy reveals fibroblastic proliferation with associated atypia; wall fibrosis may develop after several months of therapy. Infiltration of the tunica propria with eosinophils and lymphoreticular cells develops in patients with the allergic-type of induced cystitis. Inflammatory changes of the bladder following pelvic radiotherapy are characterized, in the acute phase, by mucosal ulcerations and

panvesical fibrosis; later effects produce vasculitis and fibrosis with reduced bladder capacity.

Chronic Cystitis

Patients with chronic inflammation of the urinary bladder undergo changes that follow a predictable pathway. Bladder lesions start from Brunn's nests, solid nests of urothelial cells lying in the lamina propria of the wall. Degeneration of the central part of these nests leads to the development of fluid-filled cysts (cystitis cystica). Further chronic irritation leads to the development of these lesions into glandular structures (cystitis glandularis). At last, squamous metaplasia may occur.

Clinical Presentation

Symptoms of cystitis include urgency, frequency, incontinence and suprapubic pain, or discomfort. Hematuria may be the prominent symptom, and in these cases, the term hemorrhagic cystitis is frequently used. Such symptoms, however, are nonspecific, and do not allow to differentiate among the different forms of the disease. Taking into account clinical history can help in the differential.

In bacterial cystitis symptoms vary according to the age of the patient: in neonates, failure to thrive may be observed as a result of poor feeding, vomiting, and diarrhea. In the older child, fever becomes a more prominent symptom. In the adult, the classic symptoms are present. A history of diabetes is commonly found in patients with emphysematous cystitis or in those with mycotic infections. Patients with alkaline encrusting cystitis are usually immunocompromised, with previous urologic procedures. Schistosomiasis is encountered in subtropical Africa, Middle East and in part of southern Europe. A history of tuberculous infection of the upper tract is commonly found in patients with tuberculous cystitis.

For patients with *noninfectious cystitis*, a history of radiation exposure or chemotherapy, or presence of an indwelling catheter allow to address the diagnosis when urinary symptoms develop. Patients with eosinophilic cystitis have predisposing factors such as asthma, bladder trauma, food allergies, and a history of eosinophilic gastroenteritis. Eosinophilia is associated in 50% of cases. When a pelvic inflammatory process extends to the bladder, symptoms are those of the primary process, with the addition of irritative voiding complaints. If a fistula develops, fecaluria and/or pneumaturia are associated.

Interstitial cystitis is a chronic inflammatory disease of the urinary bladder of unknown cause, often associated with systemic diseases such as rheumatoid arthritis, polyarteritis and lupus erithematosus, and/or an allergic condition, predominantly affecting middle-aged women. The diagnosis can be made on presence of chronic unexplained irritative bladder symptoms, sterile urine, and cystoscopic demonstration of urothelial lesions (Hunner's ulcers).

Imaging

Usually, imaging is not needed for the diagnosis of cystitis, which is commonly suspected on clinical grounds and confirmed by urinary cultures. When requested, radiologic studies are chiefly aimed at identifying underlying pathology that may predispose to the development of infection, such as reflux and urinary outlet obstruction. This is especially needed in patients with recurrent episodes of cystitis. Furthermore, it must be remembered that changes affecting the mucosa of the urinary bladder are better analyzed by cystoscopy, and this technique has the capabilities to provide clues for the differential diagnosis of the different forms of the disease and, most important, to allow for biopsy (1, 2).

Imaging is pointed at detecting changes of the wall and content of the bladder. Plain films can show calcifications and gas within the bladder wall, while urography can show irregularities of the mucosal surface. Such findings can be better evaluated when the bladder is not completely full. CT, ultrasonography and MRI can show thickening of the wall, as well as focal lesions. Calcifications are easily seen at CT, but can be appreciated also by ultrasonography.

Nuclear Medicine

Nuclear medicine studies do not offer clues for demonstration of cystitis. Radionuclide retrograde cystography can be used in the pediatric age group to show reflux in children who present with recurrent urinary infections.

Diagnosis

The imaging diagnosis of cystitis is based on demonstration of changes of the bladder wall and content. At urography, thickening and irregularity of the mucosa can be seen, together with decreased capacity of the inflamed, irritated bladder. Such findings are often more prominent at the level of the bladder base, and can be better demonstrated when the bladder is only partially filled in with contrast or in the postvoiding films. Ultrasonography and CT can show diffuse thickening of the wall of the bladder. In patients who develop bullous edema, focal filling defects of rounded shape may be seen, especially near the bladder base. On ultrasonography, bullous edema has been described to cause hypoechoic regions

of wall thickening with smooth transition to normal bladder wall (Fig. 1). Focal forms of cystitis can also present with polypoid lesions that can be difficult to differentiate from malignancies (1).

The diagnosis of emphysematous cystitis is based on demonstration of gas within the bladder wall. Gas within the bladder lumen can be associated. On a plain abdominal film, this can be difficult to distinguish from bowel gas or an adjacent abscess, but can be easily recognized at urography, CT, or ultrasound (Fig. 2). The bladder wall can be thickened, with an irregular outline. Presence of gas in the bladder lumen and not within the bladder wall is usually described as a separate entity (pneumocystis); intraluminal gas has to be differentiated from gas entering from an enteric fistula or following catheterization maneuvers (3).

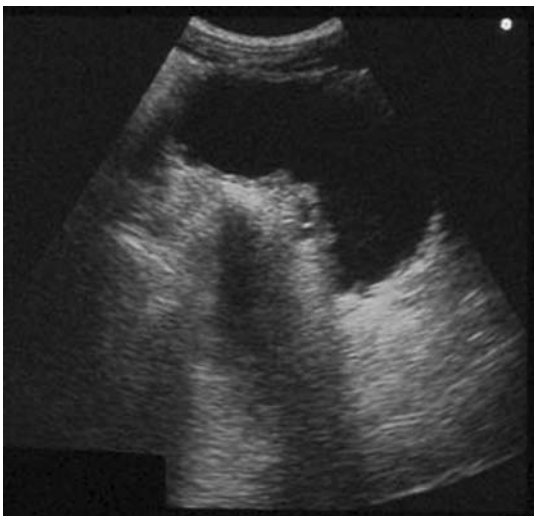

Cystitis. Figure 1 Bullous edema of the posterior wall of the urinary bladder demonstrated by ultrasonography. There is focal thickening of the wall, with smooth transition toward the normal portions; areas of hypoechogenicity are visible within the thickened region.

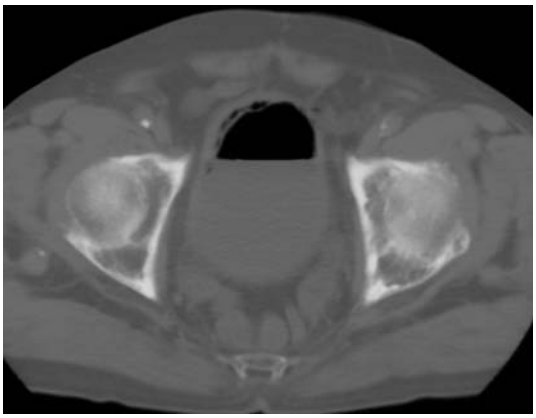

Cystitis. Figure 2 Emphysematous cystitis. CT obtained without i.v. contrast medium shows presence of gas both within the wall and within the bladder lumen.

In patients with alkaline encrusting cystitis, the bladder wall is characterized by presence of encrustations; the disease may also involve the ureters and the kidneys, and calcifications and stones can be seen also at these levels. Detection of wall calcifications in the proper clinical setting on conventional radiographic studies is diagnostic; however, calcifications may be thin, and impossible to recognize. Ultrasonography can detect the encrustations as a linear hyperechogenicities on the mucosal surface of the bladder. Nonenhanced CT is regarded as the best technique to diagnose encrustations. Lesions are usually thin and regular, covering the urothelial surface, but may be irregular and thick; there is also thickening of the bladder wall, and perivesical soft tissue stranding can be associated (4). In mycotic infections, imaging can be normal or show only nonspecific inflammatory changes of the bladder wall; on sonography, echogenic urine can be shown, A "fungus ball," that is a cluster of pseudomicelia, can develop within the bladder, presenting as a nonopaque mass. Such balls are usually mobile within the bladder: on ultrasonography, it is easy to demonstrate changes of position of the fungus ball according to changes in patient decubitus. In diabetic patients with Candida infection, gas can be present in the bladder given the capability of Candida to ferment sugar. In some cases, gas can be seen within the "fungus ball" (1). Schistosomiasis infestation can be imaged at urography as edema of the bladder wall in the early stages. When eggs calcify, they can be seen on plain films or urography; the pattern of calcifications may vary, from thin and regular to thick and irregular, involving the bladder wall completely or only focally (Fig. 3). In the early stages of the disease, contraction capability of the calcified bladder is preserved. Both ultrasonography and CT can detect easily the calcifications in the bladder wall. Involvement of the ureter is the rule, and is early during the disease process. Urography can detect filling defects and stenoses of the distal portions of the ureters, while ultrasound can show thickening of the ureteric walls (5). In patients with tuberculosis of the bladder, diffuse wall thickening, ulcerations of the mucosal surface, fibrous bands, and mural nodules have been described at urography and ultrasound. Calcifications may develop in the wall, and can be seen radiographically.

Patients with pelvic lipomatosis have a typical pear-like appearance of the urinary bladder; when cystitis is associated, imaging can show irregularities of the bladder mucosa. In case of bladder involvement from an adjacent inflammatory process, focal inflammatory changes such as edema, nodularity, or thickening of the wall may be

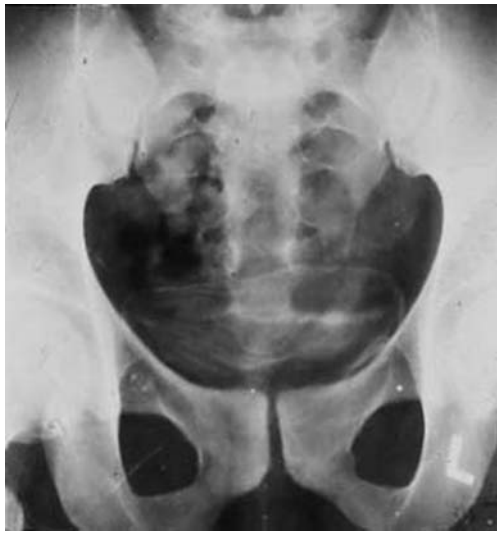

Cystitis. Figure 3 Schistosomiasis of the bladder. Plain radiograph of pelvis shows linear calcifications involving the whole bladder wall.

observed on intravenous urography. CT and ultrasound can show both the primary disease and bladder changes. Fistulous tract may be difficult to demonstrate directly, and can be inferred by presence of air in the bladder. Nonspecific thickening of the bladder mucosa can be detected by urography. Patients with drug-induced and radiation cystitis present with bladder wall edema in the early phases, but late effect of these diseases may cause wall fibrosis and reduction of bladder capacity (1).

Bibliography

1. Saluja S, Lazzarini KM, and Smith RC (2000) Inflammation of the urinary bladder In: Pollak HM and McClennan BM (eds) Clinical Urography. 2nd edn. Philadelphia, WB Saunders, pp 1019–1039
2. Schaeffer AJ (1998) Infections of the urinary tract. In: Walsh PC, Retik AB, Vaughan ED, et al (eds) Campbell's Urology. 7th edn. Philadelphia, WB Saunders, pp 533–614
3. Grayson DE, Abbott RM, Levy AD, et al (2002) Emphysematous infection of the abdomen and pelvis: a pictorial review. Radiographics 22:543–561
4. Thoumas D, Darmallaicq C, Pfister C, et al (2002) Imaging characteristics of alkaline-encrusted cystitis and pyelitis. Am J Roentgenol 178:389–392
5. Palmer PES and Reeder MM (2000) Parasitic diseases involving the urinary tract. In: Pollak HM and McClennan BM (eds) Clinical Urography. 2nd edn. Philadelphia, WB Saunders, pp 1167–1192

Cystocele

Descent of the posterior bladder wall during Valsalva maneuver below the level of the vesico-urethral junction of more than 1 cm is called a cystocele. A cystocele impresses the anterior vaginal wall (grade II) and may evert it to outside the introitus (grade III). A cystocele may persist after relaxation and need manual reposition. ►Pelvic Floor Dysfunction, Genitourinary

Cystosarcoma Phyllodes

►Neoplasms, Phyllodes, Breast

Cyst, Follicular, Ovarium

Rosemarie Forstner
Department of Radiology, Paracelsus Private Medical University, Salzburger Landeskliniken, Salzburg
r.forstner@salk.at

Synonyms

Corpus luteum cysts; Follicle cysts; Follicular cysts; Luteal cysts; Physiologic ovarian cysts; Simple ovarian cysts

Definitions

Physiologic cysts including follicular and luteal cysts constitute the vast majority of cystic ovarian lesions. They typically result from failure during folliculogenesis, most often from rupture or regression of the ovarian follicles. They may also result from continued hemorrhage in a corpus luteum. Follicle cysts are usually larger than the mature ►graafian follicle and range from 3 to 5 cm in size; however, they may attain a diameter of 8–12 cm. ►Physiologic ovarian cysts are an extremely common incidental finding during the reproductive ages. However, they may be found in all age groups, particularly in adolescents and in the early postmenopausal period. Functional ovarian cysts may also develop due to irregularities of pituitary gonadotropin hormone release or due to external hormonal replacement therapy.

Pathology/Histopathology

In women who do not take birth control pills, numerous small, thin-walled cystic follicles and a dominant follicle

are seen within the ovarian peripheral stroma. At midcycle the latter attains a size of 15–25 mm and can be identified partially protruding from the ovarian surface (1). After ovulation the rupture stigma is sealed by a mass of coagulated follicular fluid, fibrin, and connective tissue (1). The normal corpus luteum demonstrates a convoluted yellow lining and usually measures 1.5–2 cm in diameter. If it is larger than 3 cm, it is defined as a corpus luteum cyst (1).

Microscopically, follicle cysts are lined by an inner layer of granulosa cells and an outer layer of theca interna cells (1). They may be luteinized in both layers. ►Corpus luteum cysts demonstrate a convoluted inner lining consisting of large luteinized granulosa cells and an outer lining of luteinized theca interna cells (1). Capillaries from the theca interna penetrate the granulosa layer to reach the central cavity (1). The contents of follicle and luteal cysts vary from serous to serosanguinous to clotted blood.

Follicles may persist for several years after menopause and give rise to sporadic ovulations or cyst development. Solitary ►follicular cysts are a different entity from follicular cysts that occur during the reproductive age (1). They tend to be larger and are most commonly found during menarche and menopause, but may also be seen in the fetus. Cysts related to anomalies in the release of anterior pituitary hormones tend to recur and manifest as multiple large cysts in both ovaries (1).

Clinical Presentation

Most functional cysts are asymptomatic and not hormonally active. Vague abdominal or pelvic pain, pelvic pressure, and lower back pain may be caused by larger functional cysts. Corpus luteum cysts may be hormonally active and become clinically apparent by menstrual disorders and prolonged hemorrhage. Complications of functional cysts include rupture, hemorrhage, and torsion. Intraperitoneal hemorrhage following rupture is characterized by an acute onset of pelvic pain. Similarly, patients with ovarian torsion most commonly experience abrupt onset of severe lower abdominal pain. Follicle cysts in precocious puberty are manifestation of McCune–Albright syndrome (1).

Imaging

Ovarian cysts are a common incidental finding in ovarian imaging.

Transabdominal in combination with *endovaginal sonography* is the primary imaging modality in assessing the ovaries. If physiological cysts do not exceed a size of more than 3 cm they cannot be differentiated from normal follicular derivates in women of reproductive age.

Other imaging modalities for assessing cystic ovarian lesions include *computed tomography (CT) and magnetic resonance imaging (MRI)*. They are infrequently used for further characterization of sonographically detected cystic lesions. More often, functional cysts are incidental findings in pelvic imaging studies for other indications.

Due to partial volume average and proteinaceous contents, follicles are often missed in CT. Furthermore, CT usually does not allow differentiation between ►hemorrhagic functional cysts and hemorrhagic cysts in endometriosis. Hemorrhagic cysts may also mimic solid ovarian lesions in CT. This problem can be overcome by performing a noncontrast series before application of intravenous contrast media. This technique and thin-slice multispiral CT also improve the detection of smaller ovarian cysts. In cystic ovarian lesions, contrast-enhanced images provide better detail of the internal morphology of cystic lesions. They also assist in the differential diagnosis between simple ovarian cysts and other cystic ovarian lesions, for example, cystadenomas, hydrosalpinx, and cystic ovarian cancer.

In MRI imaging, sequences for assessing cystic ovarian lesions include T1-weighted imaging (WI), T2-WI, and contrast-enhanced imaging. If lesions display high signal intensity (SI) on T1-WI, fat saturation techniques are useful to differentiate between proteinaceous or hemorrhagic contents and fat that is pathognomonic for dermoid cysts.

Nuclear Medicine

Nuclear medicine usually does not contribute to the diagnosis of functional ovarian cysts.

Diagnosis

Sonography, particularly endovaginal sonography, is the modality of choice in monitoring follicles and ovarian follicle cysts (Fig. 1).

Ovarian cysts larger than 3 cm in diameter are regarded as follicular cysts (2). Follicle cysts are thin-walled ovarian lesions most commonly filled with watery contents. Compared with follicle cysts, corpus luteum cysts have thicker, well-vascularized walls. The internal echoes depend on the quality of the contents. Bleeding in an unruptured cyst causes a spectrum of sonographic findings related to the temporal sequence of clot formation (3). Corpus luteum cysts often display mildly echogenic echoes, most likely presenting partially solid

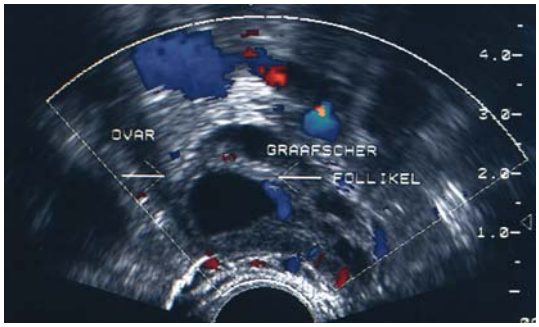

Cyst, Follicular, Ovarium. Figure 1 Color Doppler sonography of a normal ovary at midcycle in a 25-year-old female patient. Transvaginal sonography demonstrates a normal ovary which is located medial of the iliac vessels. Within the ovarian parenchyma, ovarian vessels and small follicles are demonstrated. The graafian follicle presents the largest cystic lesion and measures 15 mm in diameter. (Courtesy of R. Gruber, Salzburg)

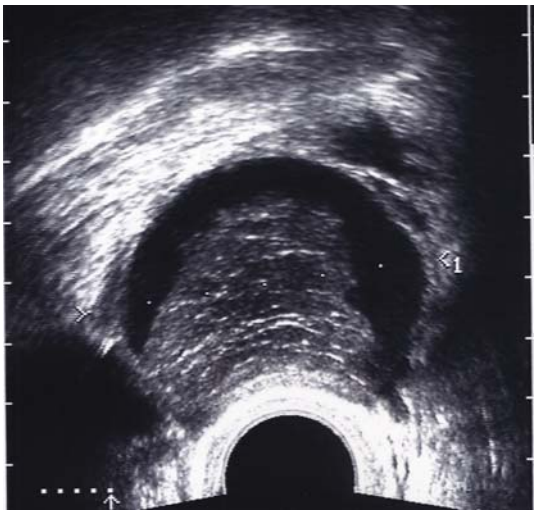

Cyst, Follicular, Ovarium. Figure 2 Hemorrhage in a physiologic cyst. In a 29-year-old female patient with acute pain, a 6-cm right ovarian lesion is demonstrated. It is well delineated and is composed of a solid area with irregular borders surrounded by liquid. The sonographic follow-up showed continuous decrease in size and change in morphology of the internal clot. (Courtesy of R. Gruber, Salzburg)

clots (3). They may also present as cystic lesions with irregular walls due to an adherent clot or may contain internal debris that is not vascularized. Recent hemorrhage frequently appears as an irregular echogenic mass (3) (Fig. 2). A complex mass with internal echoes enhanced through transmission is also a common finding of hemorrhagic functional cysts (3).

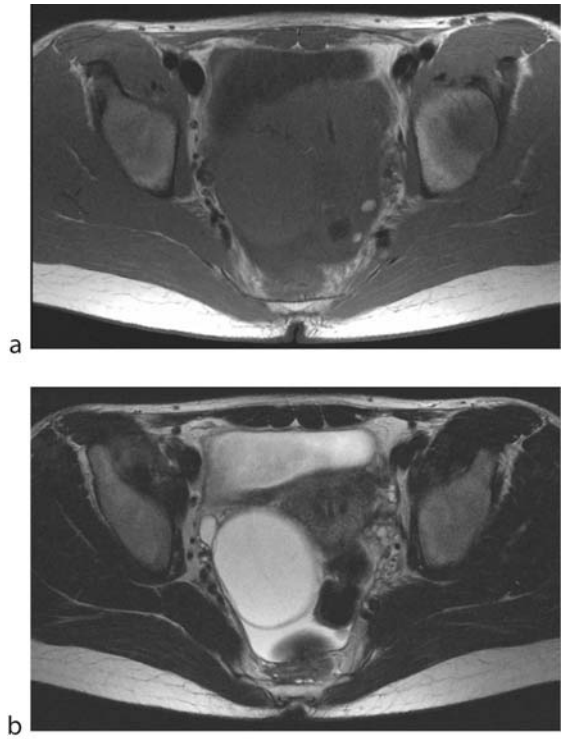

Cyst, Follicular, Ovarium. Figure 3 Follicle cyst in a 31-year-old female patient. Transaxial T1-weighted imaging (WI) (a) and T2-WI (b) show a 6-cm right adnexal lesion. It is cystic and displays higher signal than water on T1-WI (a) due to proteinaceous contents. Thin walls and no evidence of mural thickening or solid areas are demonstrated on T2-WI. Small amounts of ascites in the cul-de-sac are a physiologic finding in this age. The differential diagnosis from unilocular cystoma was only possible by a follow-up.

Echogenic free fluid in the cul-de-sac is a typical finding of cyst rupture into the peritoneal cavity. However, in women of reproductive age, a pregnancy test is mandatory for differentiation of hemorrhagic functional cysts and ▶ectopic pregnancy.

The clue for establishing the diagnosis of functional cysts with watery contents or hemorrhage and for their differentiation from cystadenomas is the decrease in size and change of the internal architecture during a sonographic follow-up. The vast majority of functional cysts will regress within a 2-month observation period (2).

MRI is usually performed complementary to sonography in indeterminate cases. It is particularly helpful for differentiating functional cysts with a complex pattern from hemorrhagic ovarian lesions of other etiologies and teratomas.

Simple ovarian cysts display well-defined, thin walls (<3 mm). Most ovarian cysts have a low to intermediate signal on T1-WI and very high SI on T2-WI due to the presence of simple fluid (2). Cyst walls are usually clearly identified on T2-WI, they display low SI, and enhance mildly following contrast media application. Hemorrhagic and corpus luteum cysts display high to intermediate signal on T1-WI and intermediate to high SI on T2-WI (2). Their appearance varies according to the quantity and age of their hemorrhagic and proteinaceous contents (Fig. 3). Corpus luteum cysts tend to have thicker walls that display smooth distinct contrast enhancement (2). Internal debris is often present, but does not enhance. Enhancement is a sign of solid internal contents, and is highly suggestive of malignancy. Low-signal intensity on T2-WI presenting shading is due to repetitive hemorrhage and allows the diagnosis of endometriomas (2). The diagnostic feature of benign teratomas is demonstration of intralesional fat, which can be diagnosed by fat-suppression techniques.

If an ovarian cyst does not decrease in size, unilocular cystoma, which can present with the same imaging features as functional cysts, is the most important differential diagnosis (2). ►Mesothelial and tubal inclusion cysts occur in the same age group and can also display similar imaging findings to simple ovarian cysts. They can only be differentiated from physiologic ovarian cysts when they are visualized separate from the ipsilateral ovary.

Bibliography

1. Clement PB (2002) Anatomy and histology of the ovary. In: Kurman RJ (ed) Blaustein's Pathology of the Female Genital Tract. Springer, New York, pp 649–674
2. Sala EJS, Atri M (2003) MRI of benign adnexal disease. TMRI 14:305–28
3. Baltarowich OH, Kurtz AB, Pasto ME et al (1987) The spectrum of sonographic findings in hemorrhagic ovarian cysts. Am J Roentgenol 148:901

Cytochrome *c*

A major caspase activation pathway is the cytochrome *c*-initiated pathway. In this pathway, a variety of stimuli cause cytochrome *c* release from mitochondria, which in turn induces a series of biochemical reactions that result in caspase activation and subsequent cell death.
►Apoptosis

Dactylitis

Dactylitis manifests with diffuse swelling and reddening of a digit and occurs in psoriatic arthritis. It may coexist with ray-type distribution of digital arthritis (MCP, PIP, DIP) of one finger or toe.

▶Spondyloarthropathies, Seronegative

DAD

▶Diffuse Alveolar Damage

Dagger Sign

Multisegmental ossification of the interspinal ligaments occurring in the caudad lumbar segments as a facultative feature in long-standing ankylosing spondylitis. It is seen in anteroposterior plain X-ray images of the lumbar spine.

▶Spondyloarthropathies, Seronegative

Dandy–Walker Malformation

Dandy–Walker malformation is nowadays considered one malformation with a variable degree of severity of involvement. The posterior fossa is too large, and there is a variable degree of vermian agenesis and posterior fossa cyst formation.

▶Congenital Malformations, Cerebellar

DCIS

▶Ductal carcinoma in situ (DCIS)

Deformities With Multiple Subluxations

Deformities with multiple subluxations in rheumatic diseases are a late-stage feature and result from ligamen tous support destruction and mutilation. The most frequent sites are the hands and toes, the shoulder, and the craniocervical junction.

▶Rheumatoid Arthritis

Degenerative Conditions of the Spine

Marek J. Sasiadek
Department of General Radiology,
Interventional Radiology and Neuroradiology,
Wroclaw University, Wroclaw, Poland
mareks@rad.am.wroc.pl

Synonyms

Annular Fissures; Degenerative Disease of the Spine; Degenerative Facet Disease; Facet Arthropathy; Spondylarthrosis; Spondylosis

Definitions

Degenerative disease of the spine is a common disorder, which involves the bony and soft tissue structures of the

spine and may result in back pain, radicular pain, and neurological deficits. In spondylosis, all anatomical structures of the so-called "►disco-somatic unit" (intervertebral disk, vertebral bodies, facet joints, ligamenta flava, longitudinal ligaments) are involved in the degenerative process, usually at multiple levels. Other terms associated with spinal degeneration like "spondylarthrosis" and "degenerative disk disease" refer to more specific anatomical locations i.e., facet joints and intervertebral disk, respectively. However, degenerative changes of one structure e.g., intervertebral disk, sooner, or later lead to the involvement of the whole disco-somatic unit.

Degenerative changes of the spine are part of normal aging; they start in late adolescence and progress with age, and may or may not manifest themselves clinically. Many factors can accelerate the development of degenerative changes, e.g., developmental anomalies or infectious disease of the spine. However, the most important factor is trauma, both acute and chronic, including chronic overload.

Degenerative disease is located most frequently in lumbar spine, followed by the cervical spine and the thoracic spine. The lower sections of the lumbar spine (L4-S1 segments) and cervical spine (C4-C7 segments) are most commonly involved.

Pathology/Histopathology

The first stage of disease is usually degenerative dehydration of the nucleus pulposus of the intervertebral disk, combined with fissuring in the adjacent annulus fibrosus (►annular tears) and endplate cartilage microfractures.

These annular tears (concentric, transverse and radial) are present in almost all individuals over forty, however some of them (especially radial tears) can result in disk herniation. Other expressions of disk degeneration are vacuum phenomenon (gas collection, mostly nitrogen within the disc) and calcifications.

Injury of the endplate cartilage causes an aseptic reaction of the subchondral bone, with increase of the water content (discovertebritis, aseptic spondylodiscitis). The further stages of the ►vertebral body degeneration are fatty degeneration and osteosclerosis, as well as formation of marginal osteophytes. The degeneration of the endplates can result in irregularities (erosive osteochondrosis) or intravertebral disk herniations.

►Facet joint degeneration appears as hypertrophy with formation of osteophytes of articular processes, narrowing of the joint space; less commonly as vacuum phenomenon, synovial hypertrophy, or synovial cysts. Facet degeneration together with disk degeneration may lead to ►degenerative spondylolisthesis (anterolisthesis-anterior displacement of the upper vertebra or rethrolisthesis-posterior displacement of the upper vertebra). Involvement of the ligamenta flava results in flaval hypertrophy. All the changes mentioned above can lead to spinal stenosis, either central (narrowing of the central part of the spinal canal) or lateral (narrowing of the lateral recesses of the spinal canal and the intravertebral foramina). This in turn can lead to compression of the spinal cord, (with cord ischemia, edema, myelomalacia or gliosis) or of the cauda equina.

Clinical Presentation

The most common clinical symptom is back pain of variable severity, constant or intermittent, located at the level of the involved spinal segment. Asymmetric disk herniation, lateral spinal stenosis or osteophytes compressing the nerve roots, cause radicular pain or deficit located according to the affected root. Lumbar spinal stenosis may lead to neurologic claudication (pain and numbness of the legs while walking and standing, relieved by sitting) and in cervical or thoracic region to myelopathy with disorders of gait and micturition and reflex abnormalities due to the chronic compression of the spinal cord.

Imaging

Conventional radiography still is usually initial radiological study in these patients, and enables preliminary assessment of bony changes (osteophytes, sclerotic areas in the vertebral bodies, spondylolisthesis, erosive osteochondrosis, scoliosis) as well as direct and indirect signs of disk degeneration (narrowing of an intervertebral space, vacuum phenomenon, disk calcifications), associated congenital anomalies such as transitional vertebrae and in some cases pathology like neoplasms or spondylodiscitis. Lack of direct visualization of soft tissues however severely limits the diagnostic utility of plain films in degenerative, neoplastic, and infectious disease.

Computed tomography (CT) can be applied especially in degenerative bone lesions. It provides good visualization of vertebral body osteophytes and osteosclerotic reaction, facet joint degeneration (Fig. 1) and spinal stenosis, as well as presence of gas (vacuum phenomenon) and calcifications in the degenerated intervertebral disk. However, degenerative bone marrow changes are not detected (see later). CT is also inferior to MRI in evaluating soft tissue lesions such as disk herniation and spinal cord compression. A major disadvantage of CT was formerly the limited coverage of the study in axial plane, now overcome with the introduction of multislice spiral CT units, which also provides excellent multiplanar and 3D reconstructions of bony spinal elements.

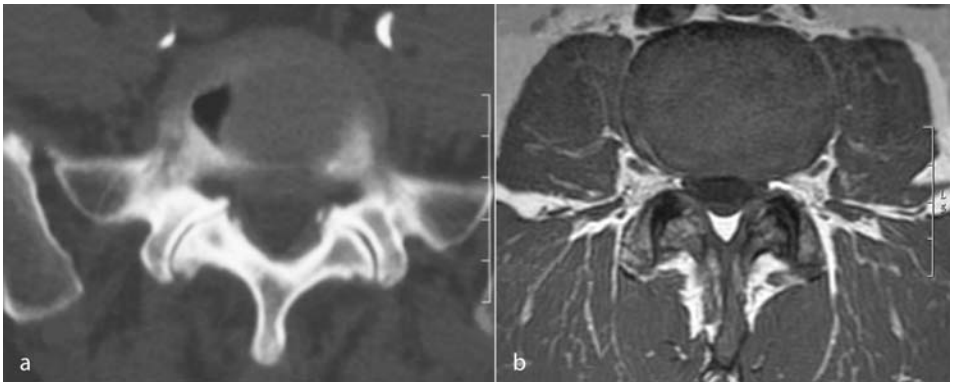

Degenerative Conditions of the Spine. Figure 1 Facet degeneration. (a) CT bone-window image. Degenerative changes in the facet joints, with hypertrophy of the articular processes and osteophytes, narrowing of the lateral recesses of the spinal canal. Note also the vacuum phenomenon in the intervertebral disk. (b) Axial T1-weighted MR image in another patient. Marked degenerative changes of the facet joints, with hypertrophy of the articular processes, narrowing of the intervertebral foramina bilaterally.

Magnetic resonance imaging (MRI) is the method of choice in patients with spondylosis who demonstrate persistent back pain or neurological symptoms. MRI provides excellent visualization of all spinal structures involved in degenerative process (Fig. 2).

The basic MRI protocol includes spin-echo (SE) or fast spin-echo (FSE) T1 and T2-weighted images in the sagittal plane as well as SE/FSE T2-weighted or gradient-echo (GRE) $T2^{*}$-weighted images in axial planes. Fat suppression techniques allow better assessment of the bone lesions and MR myelography a better evaluation of root involvement. Gadolinium enhancement can be used to differentiate scar from recurrent herniation in post-operative cases or degenerative changes from infectious and neoplastic lesions.

Desiccation of the nucleus pulposus is seen as a signal loss on T2-weighted images, annular tears as linear areas of increased signal on T2-weighted and postcontrast T1-weighted images (high intensity zones - HIZ) (Fig. 3). Vacuum phenomenon and calcifications may occasionally be visible on gradient-echo images.

Disc bulging and disc herniation should be evaluated on both sagittal and axial images.

Degenerative bone marrow changes adjacent to vertebral endplates were described by Modic: Type 1 lesions (aseptic spondylodiscitis) exhibit decreased signal on T1-weighted images and increased signal on SE T2-weighted images. Type 2 changes (fatty degeneration) have increased signal on T1-weighted images and intermediate signal on SE T2-weighted images, increasing with FSE T2 weighting. Type 3 (osteosclerosis) have low signal on both T1 and T2-weighted images. MRI also enables diagnosis of vertebral osteophytes (especially with GRE sequence) and erosive osteochondrosis.

Facet joint and ligamenta flava degenerations are well seen on axial images as hypertrophy of the articular processes and thickening of the ligamenta flava, which can contribute to stenosis of the spinal canal and intervertebral foramina (Fig. 1b, Fig. 3).

Degenerative spondylolisthesis and its impact on intraspinal structures can be easily assessed on sagittal images. Stenosis of the spinal canal is best demonstrated on axial images (Fig. 2), and stenosis of the intervertebral foramina on lateral sagittal images.

A major advantage of MRI is the direct visualization of the spinal cord. Compression of the cord and the changes caused by chronic compression can be detected on T2-weighted images.

Postoperative scar tissue enhances homogenously after gadolinium injection and thus can be differentiated from recurrent herniation.

Myelography and radiculography (lumbar myelography) used to be the main method of diagnosing dural sac and nerve root compression due to disk herniation or spinal stenosis. Nowadays, being an invasive study it has been almost completely replaced by CT and MRI, including MR myelography. CT myelography provides more accurate information than conventional myelography/radiculography; however, it is also invasive and was thus abandoned as well.

Discography and CT discography (imaging after injection of contrast medium into the intervertebral disk) are used mainly in centers performing interventional spine procedures. The aim of discography/CT discography is, on one hand, to visualize leakage route of the nucleus pulposus material and, on the other hand, to provoke pain and thus confirm that the examined disk is responsible for the patient's symptoms.

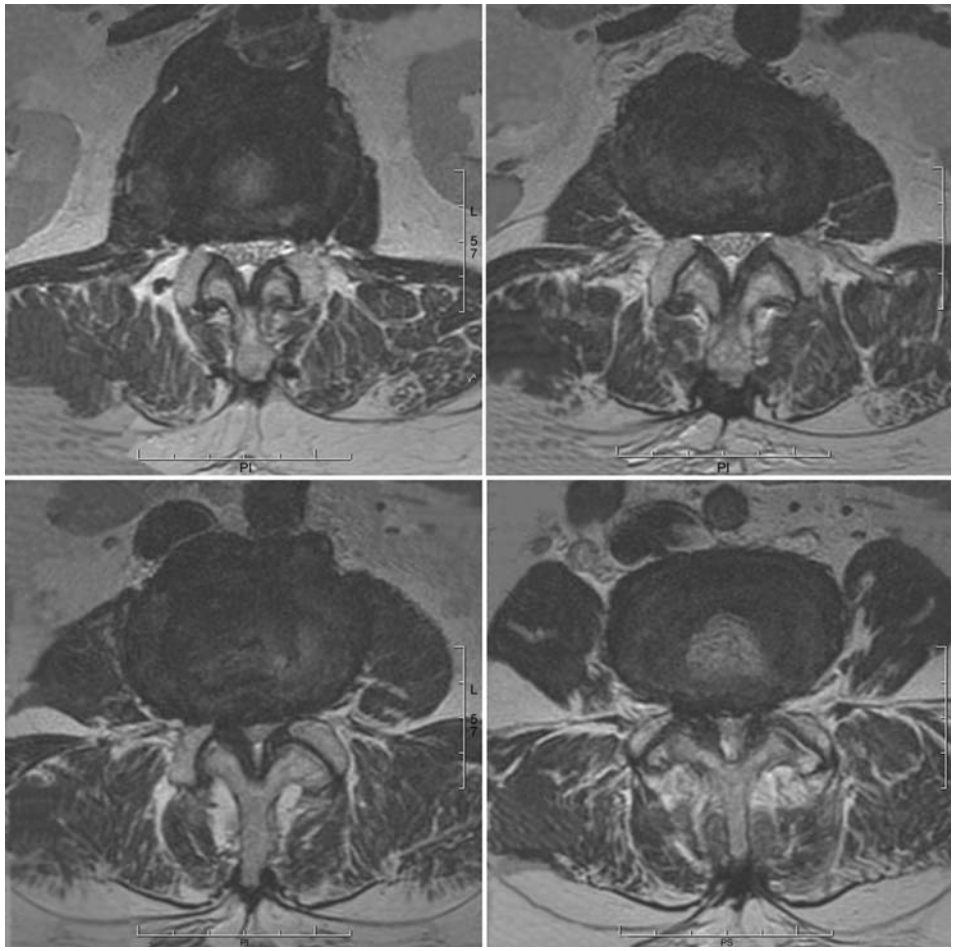

Degenerative Conditions of the Spine. Figure 2 Axial T2-weighted MR images. Degenerative changes in the intervertebral disk (bulging), vertebral bodies (osteophytes), facet joints (hypertrophy of articular processes) and ligamenta flava (hypertrophy) result in severe stenosis of the spinal canal and intervertebral foramina.

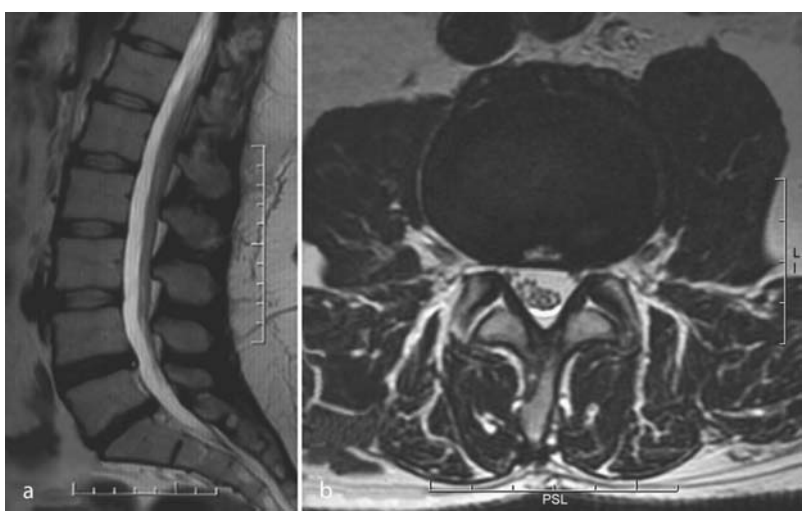

Degenerative Conditions of the Spine. Figure 3 Sagittal (a) and axial (b) T2-weighted MR images in two different patients. High intensity zones (HIZ) in the posterior annulus fibrosus, indicating radial tears. In the sagittal image there are also decreased signal intensities and bulging of L4/L5 and L5/S1 intervertebral disks indicating degeneration.

Vascular studies (Doppler sonography, MR angiography, CT angiography) are advocated in patients with severe cervical spondylosis and cerebellar symptoms, to detect possible compression of the vertebral artery by osteophytes or disk herniation.

Nuclear Medicine

Bone scintigraphy has a limited role in the evaluation of degenerative spine disease. It is usually performed if X-ray/CT/MR images are not clear and do not allow differentiation of vertebral degeneration from neoplastic or infectious lesions of the vertebrae. Usually the latter have markedly increased radiotracer uptake, while degenerative lesions do not show abnormal radioactivity or exhibit a slight, unspecific increase in uptake.

Diagnosis

Diagnosis of degenerative disease of the spine is based on clinical history, physical and neurological examinations as well as imaging studies. In patients with slight or moderate back pain without radicular symptoms and neurological deficit, or "red flags" indicating for example possible neoplastic or infectious disease, imaging can be dispensed with or limited to conventional radiography.

In patients with severe, persistent pain and/or radicular symptoms and/or neurological deficits, MRI or CT is indicated. MRI is the method of choice in such cases, because it provides the best visualization of degenerative changes, soft tissue pathology and nerve root or spinal cord compression (see earlier). CT is performed in patients with the contraindications to MR (e.g., pacemakers) and in cases where detailed assessment of the bone structures is needed (e.g., in central spinal stenosis or facet joint degeneration). Myelography/radiculography and CT myelography are almost completely abandoned. Discography or CT discography is performed in selected groups of patients to confirm the association of clinical symptoms with the imaging findings (see earlier). Vascular studies (Doppler sonography, MR angiography, and CT angiography) are advocated when compression of the vertebral artery by degenerative changes is suspected.

Interventional Radiological Treatment

Interventional procedures in degenerative spinal conditions form a rapidly growing therapeutic field, which have become serious alternatives to surgical procedures and other treatment options. The most frequent interventional procedures are:

- epidural steroid injections
- anesthetic nerve root or facet block
- radiofrequency pulse techniques of denervation of the nerve structures
- injection of spinal cysts (e.g., synovial cysts of the facets) to remove fluid
- transcutaneous discectomy
- electrotherapy of the intervertebral disk

Bibliography

1. Gallucci M, Puglielli E, Splendiani A et al (2005) Degenerative disorders of the spine. Eur Radiol 15:591–598
2. Uhlenbrock D (2004) Degenerative disorders of the spine. In: Uhlenbrock D (ed) MR Imaging of the Spine and Spinal Cord. Thieme Stuttgart, New York, pp 159–268
3. Ross JS, Brant Zawadzki M, Moore KR et al (2004) Diagnostic Imaging Spine Degenerative diseases. Amisys, Salt Lake City, pp. II.2.1–II.2.87
4. Brant-Zawadzki MN, Jensen M (2000) Low back pain. Radiology 217:321–330
5. Vroomen PCAJ, Wilmink JT, de Krom (2002) MCTFM: Prognostic value of MRI findings in sciatica. Neuroradiology 44:59–63

Degenerative Disease of the Spine

▶Degenerative Conditions, Spine

Degenerative Disk Disease

Degenerative disk disease is a clinical syndrome characterized by symptoms related to degeneration of the disk and associate vertebral changes.

▶Herniation, Intervertebral Disk

Degenerative Facet Disease

▶Degenerative Conditions, Spine

Degenerative Joint Disease, Peripheral Joints

Christian Glaser, Sabine Weckbach
Department Clinical Radiology,
Ludwig Maxmillians University, Munich,
Germany
christian.glaser@med.uni-muenchen.de

Definition

OA is a non-inflammatory joint disease characterized by degeneration of the articular cartilage, hypertrophy of bone at joint margins and changes in the synovial membrane. It is best described as a disease of organ failure in which injury to one joint component leads to damage of other components and finally to joint failure ('whole organ disease').

Traditionally, osteoarthrosis was classified as either *primary*, when there is no obvious predisposing cause or underlying abnormality, or *secondary*, when the disease results from anatomic, metabolic or traumatic predisposing factors. However, this classification is misleading as it seems that some mechanical alteration can be found in most of the affected joints so that the term 'primary DJD' seems to merely reflect limited diagnostic capabilities.

OA is common in most populations. It disables about 10% of people older than 60 years with estimated costs of more than $60 billion per year in the US economy (1). More than 75% of individuals over 70 years of age show definite radiographic evidence of osteoarthrosis. OA occurs with equal frequency in men and women with different patterns of joint involvement predominating in each gender. Osteoarthritis of the hands and knees is slightly more common in women while a male preponderance is noted for osteoarthritis of the hip.

Degenerative disease of peripheral joints often affects the joints of the hands, including the proximal and distal interphalangeal joints and the carpometacarpal joint of the thumb, the hip, the knee and the first metatarsophalangeal joint. It is less common in the ankle, wrist, elbow and shoulder which are rarely affected without previous trauma.

Pathology/Histopathology

Although the incidence increases with age, the disease is not solely caused by ageing of articular tissues. Joint trauma, pre-existing articular disease such as rheumatoid arthritis or haemophilia may accelerate the development of OA. Evidence is growing for the role of systemic factors (e.g. genetics, bone density) and of local biomechanical factors (e.g. muscle weakness, obesity) which are particularly important in weight-bearing joints (2). Biochemical forces also play an important part. Cytokines (interleukin-1, tumour necrosis factor-b) and other mediators released from cartilage, synovium or bone affect chondrocyte function and may result in increased enzymatic proteolytic activity. Collagenase 1, 2 and 3 contribute to further breakdown of the cartilage.

Recent findings have re-introduced the potential role of abnormal subchondral bone cell metabolism in the etiopathogenesis of OA. Although the initiating event for cartilage degradation in OA is still unclear one hypothesis is that cartilage breakdown is stimulated by cytokines and growth factors (interleukin-1ß, interleukin-6) locally produced by osteoblasts within the subchondral bone. Considerable evidence indicates that channels and fissures between cartilage and bone provide a route for these biological signals between the compartments. Insulin-like growth factor-1 promotes bone remodelling and proliferation, leading to increased bone stiffness, a situation exacerbating cartilage breakdown; hepatocyte growth factor activates collagenase 3 involved in cartilage degradation and vitamin A derivates induce ectopic collagen type 1 promoting the dedifferentiation of chondrocytes.

In weight-bearing joint areas, progressive thinning of the cartilaginous surface occurs resulting in joint space loss. The involved cartilage develops crevices and cracks which in a later stage progress to large areas of erosions and ulcers of variable depth. Eventually, entire segments of cartilage may be lost. When the cartilage is thinned or absent from the articular surface, the underlying bone is subject to greater local stresses. The weakened subchondral bone shows trabecular fractures, flattening and collapse. Vascular invasion, bone marrow bleeding, infarction and necrosis of subchondral trabeculae account for the bone marrow oedema (BME) like signal pattern in MRI. In addition, bony sclerosis and cyst formation develop. In the less weight-bearing segments at the joint margins, hypervascularity of bone marrow is observed in histologic specimen accounting for remodelling of the bone and the formation of osteophytes. Synovial membrane changes are not as prominent in most patients with DJD as in rheumatoid arthritis. However, synovial inflammation is seen in some phases of the disease and becomes more frequent with increasing disease severity. Osseous or cartilaginous debris leads to local irritation and cause proliferative synovial alterations. This may lead to a vicious circle with release of new mediators of

synovial inflammation that cause progressive cartilage damage, more debris and by this contribute to persistent inflammation.

Clinical Presentation

DJD is characterized by pain and loss of the joint's form and function. Pain is typically insidious in the onset of the disease and gradually progresses, usually for many years. Significant cartilage damage may have occurred before relevant clinical symptoms and radiographic signs appear. Pain is commonly present when the joint is in motion and is—at least in early stages—relieved by rest. Joints often stiffen for short durations after periods of rest, and stiffness tends to abate after a few minutes of motion. Examination of the involved joints may reveal mild tenderness, pain, restricted range of movement, joint effusion and crepitus. In advanced OA, gross deformity, bony enlargement, angulation and marked loss of joint movement may be seen. Frequent complications are misalignment and subluxation of joints. Fibrous or bony ankylosis is rare. Most routine blood tests are normal in patients with uncomplicated OA; however, in inflammatory episodes elevated CRP values and leucocytosis may be noted. Analysis of synovial fluid usually reveals a white cell blood count of less than 2,000/mm^3.

Imaging

Conventional radiographs. There are known inconsistencies between findings on conventional radiographs and clinical symptoms, with only 50% to 60% of subjects with radiographic OA being clinically symptomatic. Clinical symptoms may precede radiographic findings by up to approximately 10 years. The diagnosis of osteoarthrosis in day-to-day practise typically relies on radiographic findings that include joint space loss, cyst formation, subchondral bone sclerosis and osteophytosis (Fig. 1a) findings observed on CT images, too.

MR imaging. MR imaging with high spatial resolution proves to be an important tool in the early detection of OA by identifying cartilage alterations that precede loss of cartilage thickness as identified by joint space narrowing on radiographs. Additionally, MRI is helpful in the follow-up of OA since it directly shows cartilage defects, BME and concomitant internal joint derangement (Fig. 2). Especially meniscal damage and BME are thought to be related to the progression of OA, pathologies that are not visualized by radiographs. Since the development of rapid high resolution 3D gradient echo techniques, such as FLASH or DESS sequences, MRI has been used to diagnose early stages of the disease and to monitor disease progression. Two groups of MR sequences are currently recommended for cartilage imaging: moderately T2-w TSE FS and T1-w 3D GRE FS/WE sequences. In T2-w TSE FS sequences (Fig. 2a, b) the high signal of joint fluid provides an arthrogram-like effect visualizing irregularities and focal defects of the cartilage surface. In addition, these sequences depict internal cartilage signal alterations and allow the assessment of subchondral BME. However, differentiation of deeper cartilage zones from subchondral bone may be difficult. T1-w FS/WE 3D GE sequences (Fig. 2c) profit from high SNR values and spatial resolution for the assessment of gradual cartilage loss. The homogeneous hyperintense signal of cartilage provides a good differentiation of cartilage from subchondral bone. However, there is low sensitivity to internal cartilage matrix changes and differentiation of cartilage from the joint surface can be difficult in (especially proteinaceous) joint effusion.

In addition to clinical diagnosis, more experience has been gained with modern techniques to detect and monitor subtle changes in cartilage structure and metabolism that precede cartilage substance loss. In view of development of disease-modifying drugs or OATS, ACI, microfracture procedures, these tools may alter routine diagnostic in the future. Currently, most data are available from *quantitative volumetric MRI* studies aiming at accurately identifying reduced cartilage volume and ongoing cartilage loss in OA (3). *T2 relaxation time measurements* are related to the collagenous fibre architecture and water content of cartilage. Findings in several studies have indicated that an increase in ►cartilage T2 is a characteristic of cartilage degeneration. (4). ►*Delayed gadolinium enhanced MRI (dGEMRIC)* (5) has been introduced to examine the relative distribution of glycosaminoglycans (GAGs)within the cartilage whose reduction may indicate reversible early damage of cartilage. The dGEMRIC index (longitudinal relaxation time, T_1 (Gd) index) is related to GAG content and differs between asymptomatic and OA joints with a higher index in healthy than in osteoarthritic joints.

Nuclear Medicine

Bone scintigraphy does not play an important role in the diagnostic process of DJD.

Diagnosis

In clinical routine, the diagnosis 'osteoarthrosis' is commonly suspected after physical examination due to pain and loss of joint function. Conventional radiography then confirms the clinical suspicion.

The *American College of Rheumatology* (*ACR*) has developed *diagnostic criteria* for osteoarthritis at various sites (hip, knee and hands). They comprise pain, patient

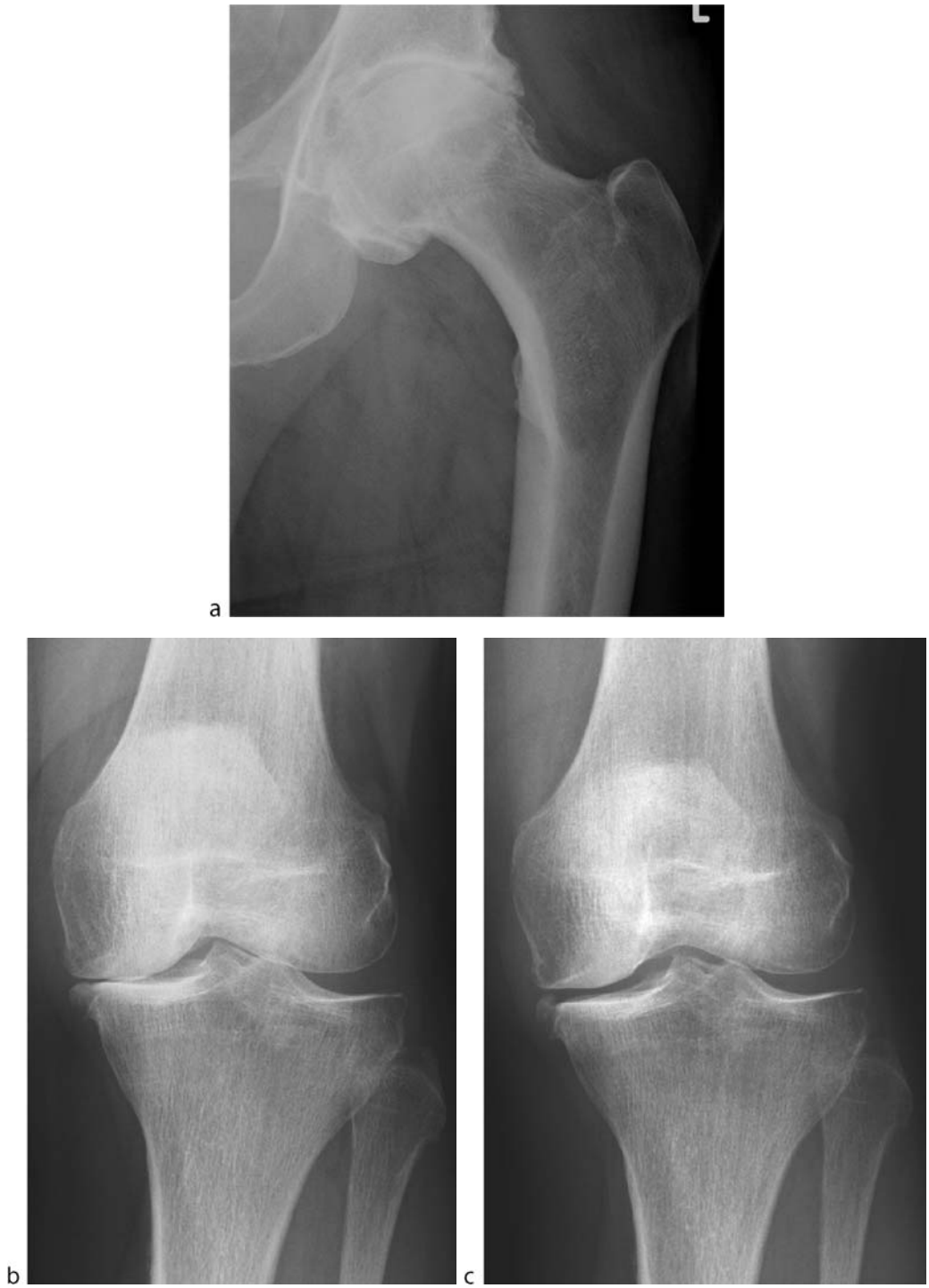

Degenerative Joint Disease, Peripheral Joints. Figure 1 OA in the hip (a) and knee (b, c). There is bony outgrowth, ►joint space narrowing and subchondral sclerosis. Please note the reduction in the apparent joint space width and the more pronounced varus alignment in the weight bearing (b) as compared to the non-weight bearing knee radiograph (c).

age, morning stiffness lasting 30 min or less, deformity of joints, crepitus on motion, erythrocyte sedimentation rate of less than 20 mm/h and osteophytes/joint space narrowing on radiographs.

In daily routine, radiological confirmation is usually made on (whenever possible weight-bearing) conventional radiographs. Imaging under weight-bearing is capable to demonstrate joint space width narrowing to

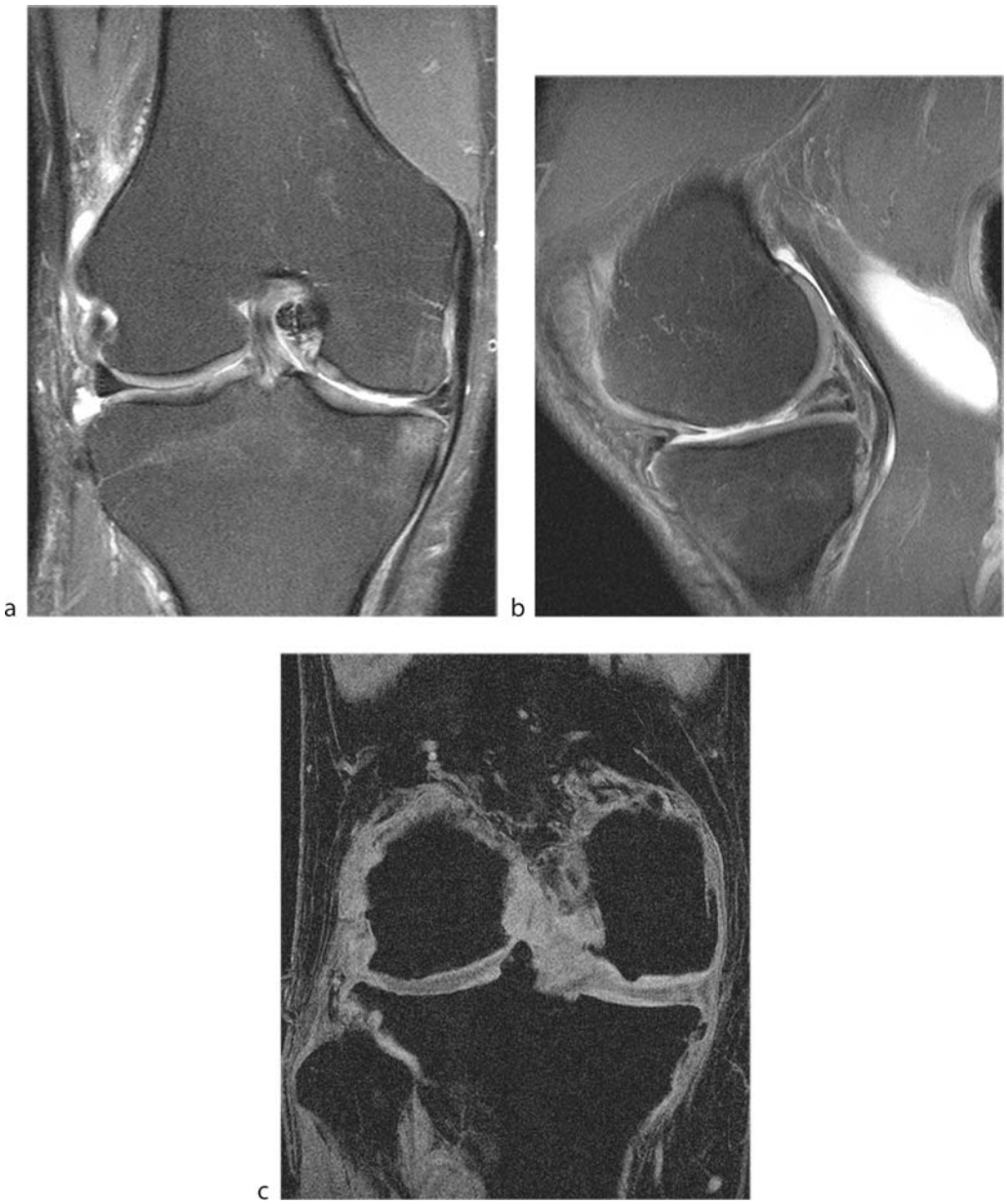

Degenerative Joint Disease, Peripheral Joints. Figure 2 (a, b) Moderately T2-w fs TSE MRI (TE 3000/TR 30) allows excellent differentiation of cartilage from both, joint effusion and subchondral bone. In addition to joint space narrowing, MRI shows bone marrow oedema (BME) of the medial femoral condyle, mild joint effusion and thinning of the cartilage. Please note the associated meniscal pathology, potentially indicating further progression of disease. (c) Coronal 3D-FLASH WE MRI (TE 21/TR 9/FA 25) shows cartilage with uniformly high signal intensity, good differentiation from subchondral bone and (apart from proteinaceous effusion) reasonable differentiation of cartilage from joint effusion. Profiting from the high spatial resolution even more subtle cartilage thinning can be visualized. Please note the intra-articular osteophyte in the medial femoro-tibial compartment and the lateral meniscal extrusion.

a better extent than imaging in the unloaded position (Fig. 1b, c). The semi-quantitative ►*Kellgren–Lawrence Grading System* (developed in 1957) uses joint space narrowing, the formation of osteophytes, subchondral sclerosis and cysts and joint deformity to grade disease severity into four grades, from normal to severe osteoarthrosis (6).

In addition and among others the WOMAC, KOSS and WORMS scores are used for the assessment of osteoarthrosis. Since its development in 1982 the

validated *WOMAC* (*Western Ontario McMasters University*) ▶*Osteoarthritis Index* is used for clinical evaluation (questionnaire) of disease severity. The latest revised version is available in 65 alternate language forms and assesses pain, disability and joint stiffness using 24 questions. For monitoring of disease progression in the knee, the MRI-based semi-quantitative *MR Knee osteoarthritic scoring system* (▶*KOSS-score*) has been described by Kornaat et al (2005). Images are scored for the presence of cartilaginous lesions, osteophytes, subchondral cysts, BME, meniscal abnormalities, effusion, synovitis and Baker's cyst. Similarly, the MRI-based *Whole-organ Magnetic Resonance Imaging Score* (▶*WORMS-score*) described by Peterfy et al (2004) incorporates 14 features among them in addition to the KOSS-score the integrity of cruciate and collateral ligaments and intra-articular loose bodies providing a morphologic 'whole organ' assessment of the knee.

▶Acromegaly

▶Hemochromatosis, Skeletal

Bibliography

1. Buckwalter JA, Saltzman C, Brown T (2004) The impact of osteoarthritis: implications for research. Clin Orthop Rel Res 427:6–15
2. Eckstein F, Glaser C (2004) Measuring cartilage morphology with quantitative magnetic resonance imaging. Semin Musculoskelet Radiol 8(4):329–353
3. Felson DT, Lawrence RC, Dieppe PA et al (2000) Osteoarthritis: new insights. Part 1: the disease and its risk factors. Ann Intern Med 133 (8):635–646
4. Gray ML, Burstein D, Xia Y (2001) Biochemical (and functional) imaging of articular cartilage. Semin Musculoskelet Radiol 5 (4):329–343
5. Kornaat PR, Ceulemans RY, Riyazi HM, Kloppenburg M, Carter WO, Woodworth TG, Bloem JL (2005) MRI assessment of knee osteoarthritis: Knee Osteoarthritis Scoring System (KOSS) inter-observer and intra-observer reproducibility of a compartment-based scoring system. Skeletal Radiol Feb; 34(2):95–102. Epub 2004 Oct. 8
6. Kellgren JH, Lawrence JS (1957) Radiological Assessment of Osteoarthrosis. Ann Rheum Dis 16:494–502
7. Mosher TJ, Dardzinski BJ (2004) Cartilage MRI T2 relaxation time mapping: overview and applications Semin Musculoskelet Radiol 8(4):355–368
8. Peterfy CG, Guermazi A, Zaim S, Tirman PF, Miaux Y, White D, Kothari M, Lu Y, Fye K, Zhao S, Genant HK, (2004) Whole-Organ Magnetic Resonance Imaging Score (WORMS) of the knee in osteoarthritis. Osteoarthritis Cartilage Mar;12(3):177–90

Degenerative Joint Disease (DJD)

▶Degenerative Joint Disease, Peripheral Joints

Degenerative Spondylolisthesis

Displacement of the vertebral body in relation to the one below, in the course of degenerative disease of the spine, mostly due to facet joint arthropathy and ▶intervertebral disk degeneration. Anterior displacement is called anterolisthesis and posterior displacement – retrolisthesis. Spondylolisthesis could be diagnosed on the plain films or CT sagittal reformatted images. MRI provides additional information concerning disk degeneration and degenerative signal changes in adjacent parts of vertebral bodies as well as facet degeneration.

▶Degenerative Conditions of the Spine

Dejerine–Klumpe Paralysis

Injury to the eighth cervical and first thoracic nerve roots or lower trunk.

▶Trauma Birth

Delayed Adverse Reactions to Intravascular Contrast Media

Reactions occurring between 1 h and 1 week after contrast medium injection.

▶Adverse Reactions, Iodinated Contrast Media, Delayed

Delayed Adverse Reactions

▶Adverse Reactions, Iodinated Contrast Media, Delayed

Delayed Gadolinium-enhanced Magnetic Resonance Imaging (dGEMRIC)

A method to examine the relative distribution and content of glycosaminoglycans (GAGs) throughout the cartilage. It contributes to detect early degeneration of cartilage by depicting proteoglycan loss.

▶Degenerative Joint Disease, Peripheral Joints

22q11.2 Deletion

This genetic abnormality (as frequent as 1 in 4,000 live births) often results in several characteristic abnormalities of the upper cervical spine. It encompasses several syndromes including DiGeorge, Shprintzen, and Sedláčkova syndromes. Heart defects and palate defects may be associated.

►Congenital Malformations, Bone

Demineralization, Bone, Childhood

Alan E. Oestreich
Cincinnati Children's Hospital Medical Center, Cincinnati, Ohio, USA
Alan.Oestreich@cchmc.org

Synonym

Osteopenia

Definitions

Decreased bone substance or mass; may be generalized or localized. In childhood, generalized demineralization (i.e., osteopenia) is either due to ►osteoporosis or to ►hyperparathyroidism. After physes have fused, osteomalacia is the third possible cause. The World Health Organisation (WHO) definitions of osteopenia and osteoporosis are not pertinent to pediatrics (1). In general, bone demineralization leads to a lower threshold for fracture; a consequence of immobilization for fracture is disuse osteoporosis, generally a reversible phenomenon. It should be noted that the human eye-and-brain is not a densitometer, but a recognizer of interfaces. Bone density measurement by X-ray densitometry techniques is less accurate in children than adults. Recognition of osteoporosis and hyperparathyroidism by evaluations of interfaces works well in childhood. The amount of bone mass in childhood and adolescence affects quantity of bone mineral later in adulthood.

Pathology/Histopathology

In osteoporosis, a child has less osseous tissue than normal. Eventually, cortical bone is thinner than normal. In acutely and chronically demineralized bone, the trabeculae are thinner than normal, although remaining trabeculae may thicken to buttress the bone. Such bones are more susceptible to fracture. Increased fragility may be caused by osteocytic osteolysis or by decreased bone formation. In hyperparathyroidism, less bone is also present, but cortices are more tunneled than normal, rather than thinned. Since some trabeculae are lost by the process, the remaining trabeculae thicken (possibly an attempt to maintain bony strength). Primary hyperthyroidism is due to parathyroid overactivity from adenoma or hyperplasia. The lamina dura around teeth, the equivalent of tubular bone cortex, becomes washed out and difficult to define on radiographs. In rickets, enchondral growth cartilage remains unmineralized at the ►zone of provisional calcification (ZPC) and continues as osteoid. With initiation of treatment of nutritional rickets, matrix vesicles at the ZPC rapidly ossify, followed by gradual ossification of rickets-affected osteoid between that zone and the already ossified metaphysis. The bony changes of hyperparathyroidism secondary to rickets take longer to heal than treated rickets.

Metaphyseal lucent bands on radiographs during stress represent bone laid down without as much mineral content as otherwise, presumably because the body is expending energy elsewhere during a relative crisis or stress. The lucent bands are known as leukemic lines, but are also seen from intrauterine stress, from adapting to extrauterine life, or from serious illness that lasts for some time. The ZPC remains normally calcified in these situations.

Clinical Presentation

Almost all conditions of generalized bone demineralization are associated with increased incidence of fracture (as do the "overmineralization" conditions of osteopetrosis). Back pain may be related to collapsing vertebrae in osteoporosis. Children under 10 years of age who have a slip of their capital femoral epiphysis usually have an underlying endocrine abnormality, especially hyperparathyroidism or hypothyroidism (some also have Down syndrome). In former times, irradiation of the hip was another cause. Children with scurvy osteoporosis may have a slip the distal femoral epiphysis. Children with rickets may have swollen wrists and knees and knobby anterior rib ends (rachitic rosary) at presentation. The child who walks despite secondary hyperparathyroidism and rickets may develop bowed femurs and tibias.

Imaging

For generalized osteoporosis on plain images, a single lateral image of a calcaneus and nearby bones should be

selected. For rickets, a frontal image of the left knee and one of the left wrist should be obtained. For hyperparathyroidism, a hand and wrist image and, if possible, an oblique image of the mandible to observe for lamina dura around the teeth should be obtained. The hand and wrist image is a good study for all three of the above metabolic demineralization conditions. For fracture search, a full skeletal survey is needed.

Densitometry techniques use computed tomography (CT) images, X-ray transmission technology, and ultrasound techniques. Standards are now available for infants and children. Importantly, they differ from adults, and adult standards should *not* be used. It should be noted that physes are open in children and are of cartilaginous density except for the ZPC, and if included in the sampled region they would lower the value recorded. Similarly, in rickets, unmineralized cartilage extends even further into the expected metaphyseal region. Bone densitometry is valuable in clinical use especially in the evaluation of bone mineralization (see Table 1).

Nuclear Medicine

Bone scanning is useful for detecting or confirming fractures in osteoporosis or hyperparathyroidism. Technetium-99m sestamibi scanning is used to investigate for parathyroid tumors in primary hyperparathyroidism. In oncogenic rickets or osteomalacia, nuclear imaging may identify the responsible benign or malignant causative lesion that is secreting ▶fibroblast growth factor 23 (FGF-23) (2). In hyperparathyroidism, brown tumors may take up radionucleotide. In active hyperparathyroidism, a superscan of generalized increased activity is seen on technetium bone scan. Apparent reflex sympathetic dystrophy in children is almost always pain- or immobilization-induced disuse osteoporosis, and hence not hyperactive on bone scan, except at a fracture.

Diagnosis

Human beings are not densitometers, but are excellent recognizers of interfaces. In osteoporosis, the cartilaginous ZPCs are not demineralized, therefore a greater than normal difference is noted between them and adjacent demineralized bone. The ZPC becomes a sharply seen thin line, for example, at the outer edge of growth centers, tarsal (Fig. 1) and carpal bones, and the nonepiphyseal ends of small tubular bones. In rickets, the ZPCs are not calcified, so that the edges of these bony parts are indistinct. As rickets becomes established, more of what should have been metaphysis is unossified, so that the ▶metaphyseal collar (with its 1–3 mm straight margin) disappears. After successful treatment of the rickets, the ZPC rapidly returns, in less than 10 days, followed by filling in of the metaphyseal collar (Fig. 2). As osteoporosis is established, cortices (from membranous bone)

Demineralization, Bone, Childhood. Table 1 Bone demineralization

1. Osteoporosis	• Immobilization or disuse
	• Idiopathic juvenile osteoporosis
	• Excessive steroids (exogenous or endogenous)
	• Excessive heparin
	• Scurvy
	• Leukemia at presentation, occasionally
	• Various congenital syndromes, including
	  • Geroderma osteodysplastica
	  • Osteogenesis imperfecta
	  • Menkes' syndrome (copper deficiency)
	• Other

2. Hyperparathyroidism	• Primary • Secondary • Renal osteodystrophy
3. Osteomalacia (after physes have fused)	Same causes as rickets in earlier childhood

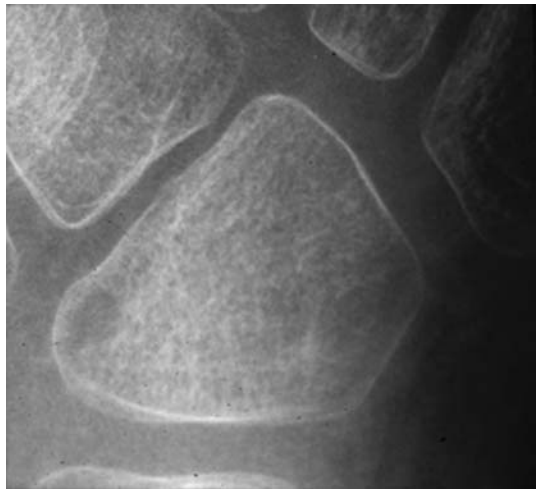

Demineralization, Bone, Childhood. Figure 1 Disuse osteoporosis, after weeks of immobilization. The cuboid and its neighbors show a highly conspicuous difference in density between the thin surrounding zone of provisional calcification and the demineralized bone.

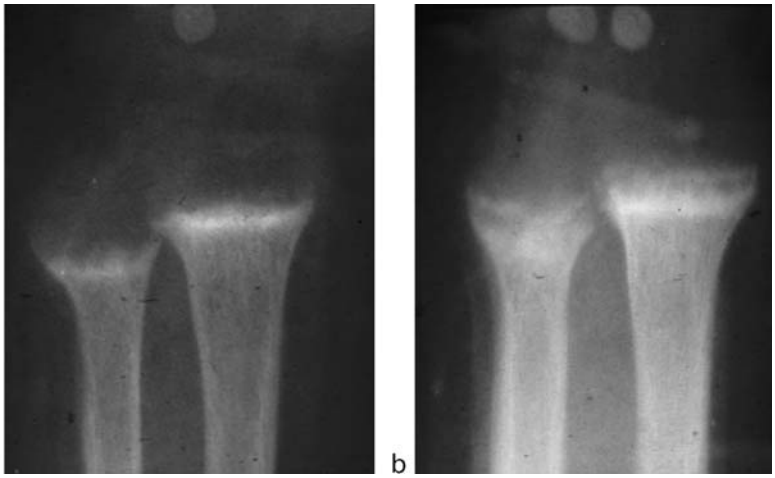

Demineralization, Bone, Childhood. Figure 2 (a) Florid nutritional rickets at age 6 months, with absence of the zone of provisional calcification of distal radius and ulna physes, as well as at the distal radius epiphysis, with lack of a metaphyseal collar; (b) a few days after initiation of vitamin D therapy, the zones of provisional calcification have returned, as have the collars, and unossified osteoid is beginning to fill in within the collar. (*From* Oestreich AE, Crawford AH (1985) Atlas of Pediatric Orthopedic Radiology. Thieme Verlag, Stuttgart p 159)

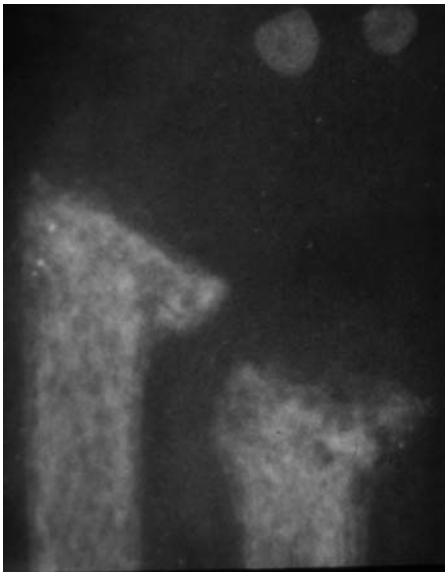

Demineralization, Bone, Childhood. Figure 3 An extraordinarily severe secondary hyperparathyroidism in an infant, with very coarse remaining trabeculae and cortex so washed out as to be barely perceivable. Metaphyseal fracture of at least the radius is one result of the metabolic change.

become thinned in width, but remain well defined. In hyperparathyroidism, cortices have increased tunneling and appear washed out and indistinct (Fig. 3), unlike those of osteoporosis. In hyperparathyroidism, the lamina dura around teeth vanishes by a similar process, and the calvarium may appear demineralized in a salt and pepper pattern. In rickets with hyperparathyroidism, the end plates of vertebral bodies, which are ZPCs in childhood, become indistinct; in osteoporosis, they are more than normally distinct because of demineralized adjacent bone. In both forms of osteopenia, namely, osteoporosis and hyperparathyroidism, fractures are common because of bone of decreased strength. In severe hyperparathyroidism, callus from fracture may, however, not calcify sufficiently to be seen on radiographs after 10 days, a rarity. The margins of the terminal tufts of phalanges may become discontinuous in rickets/hyperparathyroidism. Sharply defined lucent bone lesions, the so-called brown tumors, can appear in advanced hyperparathyroidism. If rickets is clearly evident without hyperparathyroidism, phosphate-losing renal disease, very early rickets, ifosfamide therapy, or FGF-23 fetal growth factor-secreting benign or malignant tumor should be considered as the cause of the rickets.

Densitometry imaging methods usually define a value deviating from an age-matched expected value; the greater the deviation, the less bone substance is judged present.

Metaphyseal and metaphyseal-equivalent (areas adjacent to acrophyseal growth plates) lucent bands are a sign of general stress for some time on the body, be it intrauterine stress, birth, leukemia and other major illness, and occasionally child abuse. If present in the first few days of life, then intrauterine stress is likely. A well-documented cause of lucent bands at birth is infants whose mothers received magnesium therapy late in the

pregnancy. The most common cause of "leukemic lines" is birth, with the lucency appearing after about 10 days of age and lasting for a few months in most infants. Bone-in-bone vertebrae, normally seen in all infants several weeks to months of age, is a manifestation similar to the normal metaphyseal lucencies following the stress of birth and adjustment to extrauterine life: prenatal bone and vertebral end plates (ZPC) are not demineralized, causing the bone-in-bone appearance.

Local demineralization is relatively well defined (termed "geographic") from slow-growing, frequently benign processes. Less-defined margins ("moth-eaten" and more severely "permeated") are signs of aggressiveness or malignancy, as popularized by Gwilym Lodwick (3). Interestingly, the sharpest margins of all are from the most sudden situation, acute fracture. Although Langerhans cell histiocytosis skull lesions tend to have geographic margins, long bone lesions in this condition often have poorly defined margins, although associated periosteal reaction can be quite solid. In general, thick, solid periosteal reaction reflects slower processes than thin, multilayered, or perpendicular hair-on-end periosteal reaction.

Bibliography

1. Griscom NT, Jaramillo D (2000) "Osteoporosis," "osteomalacia," and "osteopenia": proper terminology in childhood. Am J Roentgenol 175:268–269
2. Lodwick GS (1971) Radiologic concepts. The Bones and Joints. American College of Radiology, Chicago, pp 1–82
3. Ward LM, Rauch F et al (2004) Resolution of severe, adolescent-onset hypophosphatemic rickets following resection of an FGF-23-producing tumour of the distal ulna. Bone 34:905–911

Demography, Breast Cancer

The prevalence and characteristics of breast cancer related to geographical location, age, lifestyle and risk factors.

▶Carcinoma, Breast, Demography

Density

The background pattern of breast tissue. This varies according to the proportion of fat and glandular tissue in the breast.

▶Breast, Physiology

Dermoid

▶Teratoma, Ovaries, Mature, Ovalar

Dermoid cyst

▶Teratoma, Ovaries, Mature, Ovalar

Dermoids, MD

Malignant degeneration of dermoids arises from carcinomatous or sarcomatous degeneration of the dermoid plug. It is extremely rare and occurs in postmenopausal women.

▶Teratoma, Ovaries, Mature, Ovalar

DES

▶Di-Ethyl-Stilbestrol

Desmoid Tumor

Benign tumor which may become very aggressive with extensive local invasion. Commonly on MRI decrease in signal intensity occurs on T2 weighting.

▶Neoplasms, Soft Tissues, Benign

Deterministic Risk

This is dependent upon cell death, with the severity of the effects being related to the radiation dose received. Above a threshold dose, the effects of radiation are seen, and the greater the dose, the more severe the effect.

▶Radiation Issues in Childhood

Developmental Cerebral Anomalies

▶Congenital Malformations, Cerebral (neuro view)

Developmental Dysplasia of the Hip (DDH)

▶Hip Dysplasia

Developmental Venous Malformation

Congenital vascular malformation formed by dilated, radially arranged veins draining into an enlarged vein, with normal intervening brain. It is considered an extreme variation of normal venous drainage. Also known as venous angioma.

▶Congenital Malformations, Vascular, Brain

Di-Ethyl-Stilbestrol (DES)

DES invented in 1948, was mainly prescribed for women who experienced recurrent abortions and premature deliveries. DES induced an increased synthesis of placental steroidal hormones. As a major adverse effect, DES was associated with the development of clear cell carcinoma of the vagina and therefore withdrawn in 1971. Further teratogenic changes included structural anomalies of the uterine corpus, cervix, and vagina. The structural changes are highly variable; mainly hypoplasia of the uterocervical portions can be observed (T-shaped uterus). DES exposure is associated with premature delivery, perinatal mortality, and ectopic pregnancy.

▶ Müllerian Duct Anomalies

Diabetes Mellitus

Diabetes mellitus is a chronic metabolic disorder resulting from absolute or relative insulin deficiency. Patients with longstanding diabetes mellitus are especially prone to osteomyelitis of the feet due to contiguous spread of infection from chronic pedal ulcers. Peripheral neuropathy, peripheral arterial occlusive disease and neuropathic osteoarthropathy are important complications of longstanding diabetes mellitus, which all promote chronic pedal infection and subsequent osteomyelitis.

Dialysis Graft

A synthetic vascular graft, which is placed in between a suitable afferent artery and an efferent vein. The graft can have the form of a loop or can be a straight graft. Most commonly, PTFE is used as graft material because of its good tolerance for repeated cannulation and better patency compared to other synthetic graft material.

▶Fistula, Hemodialysis

Diastematomyelia—Split Cord Malformation

▶Congenital Malformations, Spine and Spinal Cord

Diffuse Alveolar Damage (DAD)

A descriptive term for the sequence of events that occurs after acute severe lung injury and results in necrosis of type I pneumocytes and alveolar endothelial cells. During its acute exudative phase, HRCT usually shows scattered or diffuse ground-glass opacities (GGOs), and in the reparative phase HRCT may show findings of fibrosis, such as irregular linear opacities and bronchiectasis.

▶Diffuse Alveolar Pulmonary Damage and Acute Respiratory Distress Syndrome

Diffuse Alveolar Hemorrhage

Bleeding into the lung parenchyma can be secondary to a wide group of disorders. Initially, HRCT features are

widespread lobular GGO with gravity-dependent density gradients through to air-space consolidation often with interspersed areas of GGO. In the process of resorption of intraalveolar blood, parenchymal abnormality is accompanied by inter- and intralobular septal thickening superimposed on areas of GGOs, which may give rise to the appearance of crazy paving.

▶Interstitial Lung Diseases, Known Causes or Association

Diffuse Alveolar Pulmonary Damage and Acute Respiratory Distress Syndrome

Kauczor Hans-Ulrich
Department of Radiology,
German Cancer Research Center, Heidelberg, Germany
hu.kauczor@dkfz-heidelberg.de

Synonyms

Acute lung injury (ALI); Adult respiratory distress syndrome (ARDS); Diffuse alveolar damage (DAD)

Definition

Adult respiratory distress syndrome (ARDS) is defined by an inhomogeneous distribution of ventilation and perfusion followed by low oxygenation [oxygenation index (PaO_2/FiO_2) ≤200 mmHg] without cardiac dysfunction (pulmonary capillary wedge pressure ≤18 mmHg) and bilateral infiltrates at chest radiography (1).

Pathology/Histopathology

Adult respiratory distress syndrome (ARDS) is characterized by a general inflammatory reaction of the lung, which results in severe impairment of the permeability of the pulmonary capillaries with subsequent interstitial and alveolar edema. This ▶diffuse alveolar damage (DAD) is the determining factor for reduced pulmonary compliance, depletion of surfactant, gravity-dependent atelectasis, hyaline membranes, vascular congestion, hemorrhage, and fibrosis. Atelectasis is supposed to be responsible for a pulmonary right-to-left shunt as well as an increase of the pulmonary vascular resistance. Although ARDS may be combined with hydrostatic edema, patients with volume overload or heart failure (left-atrial hypertension) are not considered to have ARDS.

The underlying inflammatory processes of ARDS are reflected by a rather typical time course. In the initial, very early exudative stage of ARDS there is minimal fluid leakage into the interstitium caused by sequestration of neutrophils. Mild hypoxia and pulmonary hypertension are already present. In the following, there is increased leakage of fluid into the interstitial space, which is referred to as permeability edema. It is DAD that permits the proteinaceous permeability edema to leak out into the alveoli and result in alveolar collapse. Microscopic hyaline membranes can be found within respiratory bronchioles and alveolar ducts. Soon the other manifestations of DAD dominate: cellular necrosis, epithelial hyperplasia, inflammation, and eventual fibrosis. The pathological picture is dominated by epithelial damage, which overwhelms any manifestations of capillary endothelial damage. Traditionally, the pathological findings of ARDS are divided in four stages: (1) initial, early exudative phase with swelling and damage of the endothelial cells, microatelectasis and subtle interstitial edema; (2) exudation with massive alveolar edema, accumulation of fibrin, and formation of hyaline membranes; (3) proliferation of alveolar cells, accumulation of collagen, destruction of microvasculature, and hyperplasia of pneumocytes type II; and (4) fibrosis (4).

Clinical Presentation

ARDS is a severe form of respiratory failure and goes along the following symptoms: severe dyspnea, tachypnea, cyanosis refractory to oxygen therapy, decreased pulmonary compliance, and bilateral diffuse alveolar infiltrates on chest radiography. ARDS can be caused by multiple different underlying diseases, either pulmonary, such as pulmonary infection, toxic inhalation, or extrapulmonary, such as trauma, sepsis, renal or hepatic failure. ARDS has a high mortality rate of up to 50%.

Imaging

Since bilateral infiltrates are part of the definition of ARDS, chest radiographs are taken regularly. CT is an important adjunct, since it is much more sensitive showing complications early, surrogates of functional compromise as well as hints that are important for the differential diagnosis. The classical radiographic findings of ARDS include patchy or diffuse airspace disease, combined with normal heart size and normal vascular pedicle. Additional abnormalities are reported with varying frequencies: septal lines, peribronchial cuffing, and thickening of the fissures. The typical clinical course

is reflected by a rather typical time course of radiological patterns, but with fluent transitions. In the *early exudative phase* (1st–24th h), the very first chest radiograph in a patient with acute onset of dyspnea and hypoxemia will not show any abnormalities. There is a time gap of approximately 12 h between onset of respiratory failure and the appearance of radiographic abnormalities characteristic for ARDS. Since CT is much more sensitive, it will demonstrate subtle ground-glass opacities (GGOs) with a predilection in the middle and perihilar or even peripheral subpleural regions. Fluid leakage into the peripheral interstitium is minimal, but occasionally there will be signs of interstitial edema, such as septal lines. Over time, the findings will become more obvious and convert to patchy and ill-defined opacities. They will show a more homogenous appearance throughout both lungs combined with broadening of the peribronchovascular interstitial tissue. These findings indicate the transition to the *exudative phase* (2nd–7th day) with more ill-defined hazy opacities and visible vessels. As alveolar leakage and collapse progress, the opacities become denser and more homogenous, and positive air bronchograms may be a prominent feature (Fig. 1a). At CT, GGOs and consolidations with a patchy, peripheral distribution will be the leading pattern. The patchiness of mild or moderate ARDS at CT reflects the heterogeneous nature of the disease as well as subsequent differences in local compliance and aeration. Often the nondependent lung regions have a normal or ground-glass appearance and the dependent and dorsal lung regions will exhibit some consolidations. Thus, a ventrodorsal and a cephalocaudal gradient of lung attenuation may be observed. These findings are frequently accompanied by CT demonstrated pleural effusions. Depending on the severity of ARDS

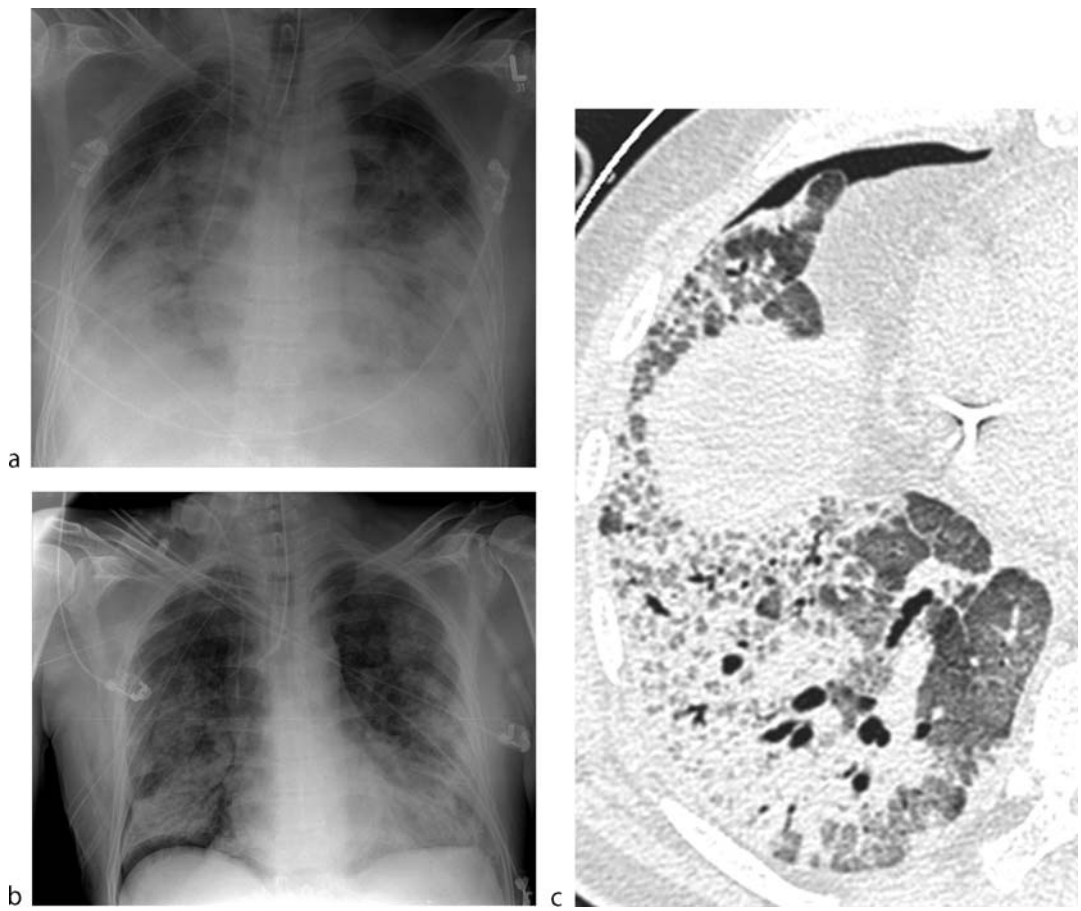

Diffuse Alveolar Pulmonary Damage and Acute Respiratory Distress Syndrome. Figure 1 ARDS chest radiographs in the exudative phase (a) shows bilateral dense infiltrates and positive bronchograms, in the proliferative phase (b) it shows decreased overall lung density with a mixture of ground-glass opacities and a reticular pattern as well as pneumothorax on the right. Close-up CT (c) of the proliferative phase also a mixture of ground-glass opacities and a reticular pattern, dilated bronchi due to positive end expiratory pressure as well as pneumothorax on the right.

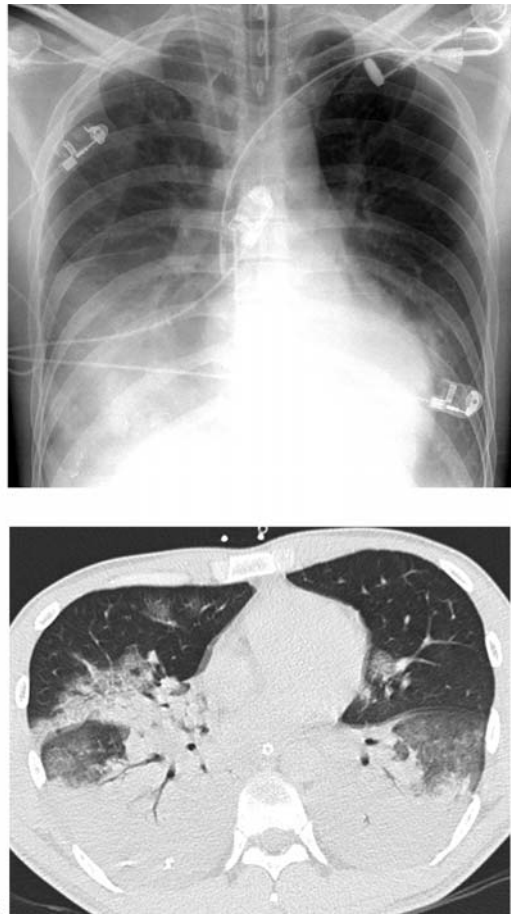

Diffuse Alveolar Pulmonary Damage and Acute Respiratory Distress Syndrome. Figure 2 ARDS chest radiograph (a) and CT (b) in the exudative phase views show large area of atelectasis in both lungs.

massive airspace consolidations and alveolar infiltrations of both lungs will develop which correspond to "full-blown ARDS (Fig. 2)." Later the consolidations become inhomogeneous and change into a reticular pattern. The development of persistent patchy spots may correspond to secondary pneumonia. Artificial respiration may cause typical changes in lung morphology or even complications referred to as ventilator-associated lung injury (VALI), which consists of four major factors: (1) gross air leaks induced by large transpulmonary pressures (barotrauma); (2) overdistention of aerated lung parenchyma which manifests as increased alveolo-capillary permeability (volutrauma); (3) cyclical recruitment and collapse of atelectasis leads to high shear forces between collapsed and aerated alveoli as well as varying shunt fractions during the respiratory cycle (atelectrauma); (4) continuous release of various inflammatory mediators (biotrauma) (3). Typical signs of VALI are abnormal air collections such as interstitial emphysema, cysts, pneumatoceles, pneumothorax, pneumomediastinum, pneumoperitoneum, or pneumoretroperitoneum. For detection and diagnosis, CT is highly superior to supine chest radiographs.

After the exudative phase, ARDS turns into the organizing and *proliferative phase*. The overall lung density decreases as the consolidations give way to a mixture of GGOs and parenchymal distortion (Fig. 1b, c) later turning into a coarser reticular, partly bubbly pattern due to the development of fibrosis (*fibrotic phase*). Cysts may form ranging from a few millimeters to several centimeters in diameter. They can be subpleural or deep in the parenchyma. Rupture of a cyst can cause pneumothorax and/or pneumomediastinum. Not every patient will go through all the mentioned phases in the same way. Although the findings may be decreasing or constant, this scheme gives the basic structure of the development of ARDS over time (2).

In many ARDS survivors, reticular or cystic patterns will prevail. There seems to be a relationship between the preferential site of cyclic recruitment and collapse with the later localization of fibrosis, air cysts, and bronchiectasis.

Diagnosis

The diagnosis of ARDS is made when the definition criteria, including radiology, are met. In the following, radiological examinations play a pivotal role in the clinical management of ARDS patients.

Bibliography

1. Falke K, Hudson L, Lamy M et al (1994) The American–European consensus conference on ARDS. Definitions, mechanisms, relevant outcomes, and clinical trial coordination. Am J Respir Crit Care Med 149:818–824
2. Desai S, Hansell D (1997) Lung imaging in the ARDS: current practice and new insights. Intensive Care Med 23:7–15
3. Slutsky A, Ranieri V (2000) Mechanical ventilation: lessons from the ARDSNet trial. Respir Res 1:73–77
4. Tomashefski J (1990) Pulmonary pathology of the adult respiratory distress syndrome. Clin Chest Med 11:593–619

Diffuse Axonal Injury

Small foci of high signal or hemorrhagic foci in the white matter, corpus callosum, brain stem, or basal ganglia following acceleration–deceleration trauma.

▶Trauma, Head, Non-accidental

Diffuse Axonal Shearing Injury

Focal posttraumatic hemorrhagic lesions resulting from acceleration–deceleration and rotational traumatic forces. They are often located in a parasagittal plane and can be typically observed at the corticomedullary junction, in the brain stem, and in the corpus callosum.
▶Trauma, Head, Accidental

Diffuse Cerebral Edema

Important secondary traumatic brain lesion. Typical signs are the narrowing of ventricles and sulci and the effacement of the basal cisterns.
▶Trauma, Head, Accidental

Diffuse Imaging

▶Optical Tomography

Diffuse Infiltrative Diseases, Hepatic

Massimo Bazzocchi, Giuseppe Como, Chiara Franchini
Università degli Stud, Udine, Udine, Italy
massimo.bazzocchi@med.uniud.it

Synonyms

Liver storage diseases

Definition

Group of hepatic diffuse disorders characterized by anomalous storage of specific substances within the liver, followed by functional and morphological liver abnormalities, which may lead to hepatic dysfunction.

Pathology and Histopathology

The most common hepatic storage diseases are fatty infiltration, ▶hemochromatosis, ▶Wilson disease, and ▶glycogen storage diseases. Rare hepatic storage diseases are ▶Gaucher's disease and ▶amyloidosis.

Iron Overload: Hemochromatosis and Hemosiderosis

▶Iron overload can be separated into two general categories of iron distribution: parenchymal cell iron deposition in hemochromatosis, cirrhosis, intravascular hemolysis, and iron deposition in cell of the reticulo-endothelial system, also called ▶hemosiderosis, which is seen most commonly after multiple transfusions or in diseases with extravascular hemolysis. Iron deposition in hepatocytes causes cellular damage, while iron deposition in reticulo-endothelial cells does not produce a significant organ dysfunction (1). Hereditary hemochromatosis is autosomal recessive disease that is characterized by an anomalous increase in iron absorption from the gastrointestinal tract. This excess of iron is deposited in the form of ferritin and hemosiderin within the parenchymal cells of the liver, pancreas, endocrine glands, heart, skin, and joints. It leads to cellular damage and organ dysfunction. In patients with advanced disease, liver cirrhosis develops (1, 2).

In cirrhosis of various origins, a mild increase in the iron content of the hepatocytes occurs in about 50% of patients, although the exact mechanism responsible for this increase is unknown. It has been suspected that this form of iron overload is a predisposing factor for the development of hepatocellular carcinoma.

In transfusional iron overload, iron is deposited in the reticulo-endothelial cells of the liver, spleen, and bone marrow. When the reticulo-endothelial system is saturated with iron, additional iron deposits are seen in the parenchymal cells of the liver, pancreas, and heart leading to organ dysfunction similar to that seen in primary hemochromatosis (2).

Intravascular hemolysis causes iron deposition in hepatocytes. This is different from extravascular hemolysis, in which senescent native or transfused erythrocytes are removed from the circulation by reticulo-endothelial cells. When red blood cells are destroyed within the circulation, the free hemoglobin binds to plasma haptoglobin and is taken up by hepatocytes, not by reticulo-endothelial cells. In thalassemia major, there is an increased demand for iron in the bone marrow because of ineffective erythropoiesis. This results in increased absorption of iron which accumulates in parenchymal cells. Patients received transfusions may also develop iron deposition in the reticulo-endothelial system (1).

Wilson Disease

Wilson disease, or hepatolenticular degeneration, is a rare autosomal recessive disorder of copper metabolism, due to a deficient synthesis of ceruloplasmin, the copper-binding protein. Copper accumulates in the liver, basal ganglia, and cornea. Copper accumulation in hepatocytes results in cellular necrosis and finally leads to cirrhosis. Kayser–Fleischer rings consist of copper granules in the stromal layer of the eye (1).

Glycogen Storage Diseases

Glycogen storage diseases affecting the metabolism of glycogen, in which an enzyme deficiency results in glycogen accumulation in tissues. Most of these disorders are inherited in an autosomal recessive manner. More than 12 glycogen storage diseases are discussed in the literature (3).

Gaucher's Disease

Gaucher's disease is glycolipid storage disease, characterized by lysosomal storage of glucocerebrosides in pathological macrophages, called Gaucher's cells. It is caused by an autosomal-recessive inherited deficiency of glucocerebrosidase activity. Gaucher's cells infiltrate parenchymal tissues, predominantly the bone marrow, spleen, and liver. There are three clinical forms; type I, or nonneuronopathic Gaucher's disease, is by far the most common (4).

Amyloidosis

Amyloidosis consists in the extracellular deposition of the fibrous protein amyloid in one or more sites in the body. Amyloidosis may be primary or secondary to other conditions, such as chronic inflammatory conditions and multiple myeloma. Familial forms of amyloidosis have also been described. Primary amyloidosis tends to involve peripheral nerves, skin, tongue, joints, heart, and liver while secondary amyloidosis mainly affects parenchymatous organs, such as spleen, kidneys, liver, and adrenals. Although the liver and spleen are frequently involved in primary systemic amyloidosis, the clinical manifestations of hepatic and splenic involvement are usually mild (5).

Clinical Presentation

Hemochromatosis

In hereditary hemochromatosis, the liver is the mainly affected organ, and, if untreated, the hepatic iron overload may lead to cirrhosis. Approximately 20–30% of patients with cirrhosis develop hepatocellular carcinoma. The pancreas is also commonly involved with various degrees of dysfunction, ranging from insulin resistance to insulin-dependent diabetes mellitus. Hyperpigmentation of the skin is often observed. Cardiac involvement includes cardiomyopathy and arrhythmias and is a common cause of death. Arthropathy may occur early in the course of the disease and classically affects the second and third metacarpophalangeal joints. Later in the course of the disease some patients develop pituitary hypogonadism.

Wilson's Disease

Younger patients typically present hepatic manifestations, such as loss of appetite, nausea, jaundice, while the initial symptoms in adults are usually neurologic or psychiatric ones, including dystonia, incoordination, abnormal behavior, depression. Kayser–Fleischer rings are always present. They appear as greenish-yellow or brown rings seen at the limbus of the cornea. Wilson disease is invariably fatal if untreated.

Glycogen Storage Diseases

Patients with Von Gierke disease are at risk for neonatal hypoglycemia. They exhibit hepatomegaly and hypoglycemic seizures at the age of 3–4 months. Long-term complications include short stature, hyperuricemia, renal insufficiency, and hepatic adenoma. In these patients, the adenomas are also more likely to be multiple and to undergo malignant transformation, although the latter is still quite rare (3). In other types of glycogen storage diseases, patients experience muscle symptoms, such as weakness and cramps.

Gaucher's Disease

The principal manifestations are caused by bone marrow infiltration, with consequent skeletal disease including deformities, pathological fractures, and avascular necrosis. These patients develop splenomegaly with hypersplenism. Hepatomegaly is frequently observed in type I Gaucher's disease. For most patients, hepatic involvement has no significant clinical consequences. Nevertheless, in sporadic cases a massive infiltration of the liver by Gaucher's cells is associated to fibrosis and cirrhosis, with development of portal hypertension (4).

Amyloidosis

The liver is frequently involved in primary systemic amyloidosis, but the clinical hepatic manifestations are usually unimportant. Few cases of spontaneous rupture of the liver associated with hepatic amyloidosis have been reported (5).

Imaging

Hemochromatosis

Sometimes, computed tomography (CT) or magnetic resonance (MR) examinations may reveal signs of hemochromatosis in a preclinic stage of disease. At ultrasound (US), iron deposits in the liver do not determine specific findings. The evidences are secondary to chronic liver disease, cirrhosis, or hepatocellular carcinoma. At CT, the increase in hepatic iron content determines diffuse homogeneous hyperdensity of the liver on unenhanced scans. The hepatic vessels appear particularly prominent in contrast with the hepatic parenchyma (Fig. 1). CT demonstrates signs of cirrhosis and a biphasic contrast-enhanced study is required for the detection of hepatocellular carcinoma. MR is more sensitive than CT for detection of hepatic iron deposition, since iron causes inhomogeneity of the magnetic field, leading to spin dephasing and decreasing of signal intensity of liver parenchyma on T2-weighted MR images (Fig. 2). Gradient-echo MR sequences are the most sensitive for mild degrees of iron overload (2). Skeletal muscle does not accumulate iron, so it can be used as a term of comparison. If the liver signal intensity is lower than that of skeletal muscle, increased iron accumulation in the liver can be diagnosed. Iron deposits in parenchymal cells and in reticulo-endothelial cells cause an identical loss of signal intensity; in most patients with hereditary hemochromatosis the spleen is not involved, while in hemosiderosis a splenic involvement coexists. In case of pancreatic involvement, low signal intensity of the pancreas is usually demonstrated. Since several studies have suggested that MR may enable an accurate quantification of hepatic iron concentration, it may be used in assessing the response to treatment in patients with hemochromatosis, avoiding the risks inherent in percutaneous liver biopsy (2). Hepatic iron overload facilitates the detection of focal lesions, namely hepatocellular carcinomas, particularly on T2-weighted sequences, due to the increased natural contrast between the hypointense liver parenchyma and the nodules, which do not contain excess of iron and appear hyperintense (1).

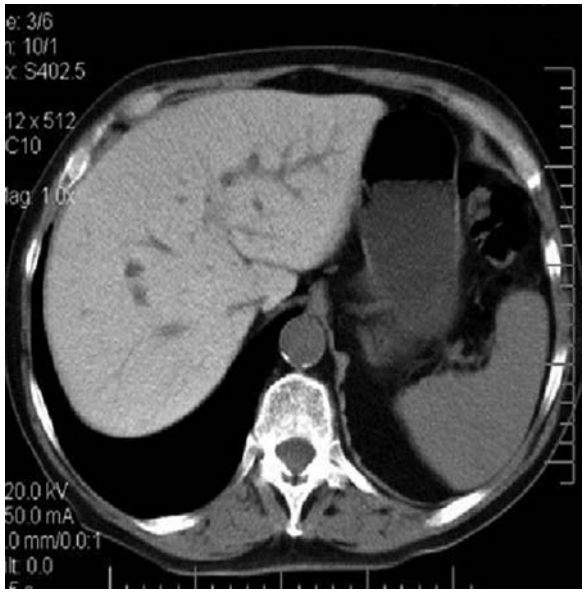

Diffuse Infiltrative Diseases, Hepatic. Figure 1 Liver CT scan: the increase in hepatic iron content determines diffuse homogeneous hyperdensity of the liver on unenhanced scans. The hepatic vessels appear particularly prominent in contrast with the hepatic parenchyma. Hyperdensity of liver is evident compared to the spleen.

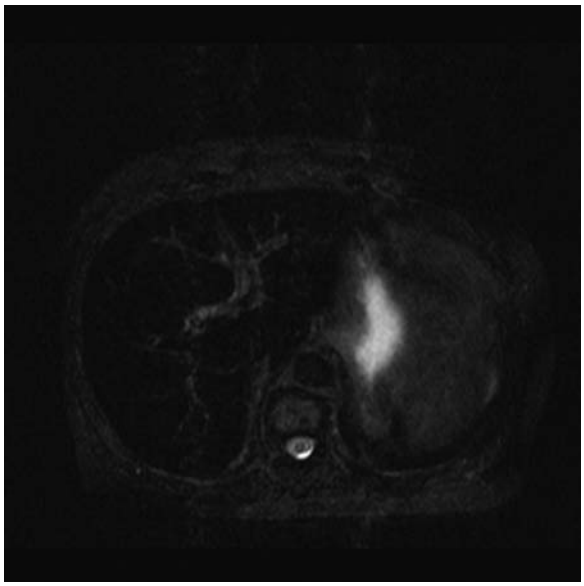

Diffuse Infiltrative Diseases, Hepatic. Figure 2 STIR MR axial acquisition: MR is more sensitive than CT for detection of hepatic iron deposition, since iron causes inhomogeneity of the magnetic field, leading to spin dephasing and decreasing of signal intensity of liver parenchyma on T2-weighted MR images. We can see low signal intensity of liver in this patient with hemochromatosis. Skeletal muscle does not accumulate iron, so it can be used as a term of comparison.

Wilson Disease

US findings in Wilson disease are indistinguishable from those of cirrhosis of other causes. Multiple round foci of decreased echogenicity have also been reported. Hyperechoic nodules are less frequently observed. CT of the liver offers little information. Hepatic attenuation values are usually within normal limits. Concomitant fatty infiltration may hide the increase in density due to copper deposition. Although copper has a paramagnetic effect, substantial changes in liver signal intensity are

not observed. In fact, copper has a slight paramagnetic effect and copper concentration within the liver is relatively low (1).

Glycogen Storage Diseases

Type I glycogen storage diseases generally have more severe US changes than other types. The most frequent US findings are hepatomegaly, hyperechogenicity of the liver, enlarged kidneys. On CT scans, glycogen deposition results in increased hepatic parenchyma density, whereas fatty infiltration causes a decrease in density. Ultimately the density of the liver depends on the relative amounts of each component. Sometimes, the liver may show a geographic pattern. Biphasic contrast-enhanced CT is mandatory in order to detect and characterize hepatocellular adenomas (3). Glycogen is characterized by high signal intensity on T1-weighted MR images.

Gaucher's Disease

Hepatosplenomegaly is a constant finding. US can demonstrate the organomegaly and may be useful in monitoring the reduction in size of liver and spleen in patients undergoing enzyme treatment. In a small number of patients multiple focal lesions, usually hypoechoic, are observed in the spleen and, more rarely, in the liver (4). Very few cases of severe involvement of the liver with massive hepatic fibrosis causing portal hypertension have been described: CT and MR show distortion of liver parenchyma.

Amyloidosis

Imaging findings are not specific. The liver is usually enlarged and shows heterogeneous echogenicity on US. Unenhanced CT scans show diffuse or focal regions of decreased attenuation of hepatic parenchyma, with or without extensive calcification. Postcontrast scans show inhomogeneous enhancement of the liver parenchyma. On T1-weighted MR images, the liver parenchyma has increased signal intensity, while on T2-weighted images the signal intensity is not significantly altered. However, the reason for high signal intensity on T1 is not known (5).

Diagnosis

Hemochromatosis

The standard method of diagnosis is the quantification of hepatic iron concentration by means of liver biopsy with spectrophotometry. A skin biopsy specimen of a hyperpigmented cutaneous area may confirm the diagnosis. MR seems to be a useful tool which may replace liver biopsy, in the follow-up of treated patients (2).

Wilson Disease

Blood copper, ceruloplasmin, urine copper, eye test for Kayser–Fleischer rings, and liver biopsies are used to make the diagnosis. Imaging findings are not specific.

Glycogen Storage Disease

Clinical data, laboratory tests such as creatine kinase levels, muscle biopsy, and liver biopsy are used in the diagnostic work-up. Imaging findings are not specific neither sensitive. Biochemical assay for enzyme activity allows the final diagnosis.

Gaucher's Disease

The final diagnosis is done on the basis of measurement of beta-glucocerebrosidase activity in lymphocytes or in fibroblasts.

Amyloidosis

The combination of imaging findings, particularly liver CT, may suggest the presence of amyloidosis; however, confirmatory diagnosis can usually only be achieved by biopsy (5).

Bibliography

1. Lencioni R, Bartolozzi C (2003) Diffuse liver disease. In: Magnetic Resonance Imaging in Liver Disease, Thieme 2003, pp 93–114
2. Alustiza JM, Artetxe J, Castiella A et al (2004) MR quantification of hepatic iron concentration. Radiology 230(2):479–484
3. Pozzato C, Botta A, Melgara C et al (2001) Sonographic findings in type I glycogen storage disease. J Clin Ultrasound 29(8):456–461
4. Patlas M, Hadas-Halpern I, Abrahamov A et al (2002) Spectrum of abdominal sonographic findings in 103 pediatric patients with Gaucher disease. Eur Radiol 12(2):397–400
5. Kim SH, Han JK, Lee KH et al (2003) Abdominal amyloidosis: spectrum of radiological findings. Clin Radiol 58(8):610–620

Diffuse Interstitial Lung Disease from Unknown Causes

▶Interstitial Lung Diseases, Unknown Etiology

Diffuse Intrinsic Pontine Glioma

Diffuse intrinsic pontine glioma is a highly malignant tumor of the brain stem centered in the pons. It varies

from grades II to IV. Because the histology results in a tumor showing typical MRI features do not influence treatment or prognosis, biopsy is not necessary.
▶Neoplasms, Brain, Posterior Fossa, Pediatric

Diffuse Optical Tomography

▶Optical Tomography

Diffuse Parenchymal Lung Disease From Unknown Causes

▶Interstitial Lung Diseases, Unknown Etiology

Diffuse Parenchymal or Interstitial Lung Disease from Known Causes or Association

▶Interstitial Lung Diseases, Known Causes or Association

Diffusion-Tensor MRI

An MR-based technique which allows to measure water molecular motion in biological tissues. Diffusion is defined as the microscopic random translational motion of molecules in a fluid system. Pathological processes can alter tissue integrity, resulting in a loss or increased permeability of "restricting" barriers, which determines an increase of the apparent diffusion coefficient values. Diffusion measurements can give information about the size, shape and orientation of tissues. A full characterization of diffusion can be obtained in terms of a tensor, a 3×3 matrix that accounts for the correlation existing between molecular displacements along orthogonal directions. From the diffusion tensor, it is possible to derive the mean diffusivity (MD), which is a measure of diffusion that is independent of the orientation of structures, and the fractional anisotropy (FA), which indicates the structural integrity and degree of structural alignment within fiber tracts.
▶Aging Brain

Diffusion-weighted MR Imaging

Diffusion-weighted MR imaging is a technique in which phase-defocusing and phase-refocusing gradients are used to evaluate the rate of microscopic water diffusion within tissues. With the evolution of echo-planar MR imaging with a preparation pulse that is sensitive to diffusion, high-speed imaging has become possible, thus reducing the motion artifacts during image acquisition.
▶Lymphadenopathies, Head and Neck
▶Neoplasms, Salivary Glands

DiGeorge Syndrome

Congenital immunodeficiency syndrome characterised by velofacial abnormalities, congenital heart disease, hypocalcaemia, and increased susceptibility to infections.
▶Congenital Malformations, Thymus

Digital Radiography (DR)

DR uses an X-ray detector made of caesium iodide crystals layered onto an amorphous silicon photodiode panel. No latent image is formed; the photodiode converts the light emitted from the crystals into an electronic signal, from which the image is generated. The image can be viewed on hard-copy film or as soft copy on a workstation.
▶Children, Imaging Techniques

Dilating Uropathy

Dilated collecting and draining system (ureter, renal pelvis, calyxes): any condition of the urinary tract that causes or is associated with dilatation of the urinary system. Note that dilatation does not equal obstruction; obstruction may be one cause for dilatation, other reasons for a dilated urinary tract are laxity, dysplasia, infection or congenital variations such as megacalicosis.
▶Obstructive Uropathy in Childhood

DIN

Ductal intra-epithelial neoplasia.
▶Carcinoma, Ductal, *In Situ*, Breast

Direct Imaging

Carmel T. Chan, Sanjiv Sam Gambhir
Department of Radiology
Molecular Imaging Program at Stanford (MIPS) and Bio-X Program, Stanford University School of Medicine, Stanford, USA
carmelc@stanford.edu
sgambhir@stanford.edu

Synonyms

Targeted Imaging

Definition

Direct imaging generally refers to the imaging of a specific molecular target and/or process (e.g., a receptor protein target imaged with a ligand molecular imaging probe). This is done to determine the location(s), activity, and/or numbers of the target. This is in contrast to indirect imaging where the target is not directly imaged and an indirect readout of that target is performed. Since the target is directly imaged, the direct approach is one of the best ways to determine properties of the target of interest and any changes over time determined through repetitive imaging.

Imaging

Almost any imaging probe can be utilized to image a target directly, including but not limited to radiolabeled probes, optical fluorescence or bioluminescence probes, magnetic resonance imaging (MRI) compatible probes, etc. Direct imaging can be accomplished using two broad categories of molecular imaging probes. The first one involves the use of radiolabeled probes (e.g., labeled with Fluorine-18) that produce signal continuously before and after interacting with their targets through the decay of the radioisotope. Direct imaging of radiolabeled probes can be accomplished by positron emission tomography (PET), single photon emission computed tomography (SPECT), MRI, functional magnetic resonance spectroscopy (fMRS), and autoradiography. A time delay between injection of the probe and imaging will allow the clearance of untrapped/unbound probes and enhance the signal to background ratios, since the scanner cannot distinguish the parent tracer from the bound or metabolized tracer. Another strategy for direct imaging involves the use of activatable or "smart" probes (also referred to as sensors or beacons), which produce signal only when they interact with their targets. Direct imaging of activated probes can be accomplished by optical/fluorescence imaging, but a time delay between the injection and imaging will be required to allow the accumulation of sufficient numbers of activated probe at the target site. Bioluminescence optical imaging has also recently been shown to be able to be used for direct imaging through creation of an imaging probe in which a luciferase protein (not a reporter gene) is attached to an antibody (1). On the other hand, direct imaging of physiological processes and vascular distributions such as changes in blood volume flow can be accomplished with non-specific imaging probes including contrast media, nuclear medicine-based tracers and fluorochrome reporters. Disadvantage of direct imaging: a new substrate must be discovered and labeled to yield a different probe for each new protein to be targeted. Furthermore, each imaging probe must be characterized in lining subjects for optimization of pharmacokinetics and pharmacodynamic properties.

Applications of Direct Imaging

Imaging of Protease Activity in Extracellular Space

Direct imaging utilizing activatable probes have been coupled with near infrared (NIR) imaging to measure protease activity, including cathepsin B, metalloproteinase-2 and metalloproteinase-7 in tumor-bearing nude mice (2). These NIR protease probes (NPP) consist of fluorochromes (with excitation and emission wavelengths in the NIR spectrum) that are covalently coupled to a poly-L-lysine backbone and sterically protected by a methoxy(polyethylene glycol) side chains by means of a synthetic peptide substrate specific for each protease. In the absence of protease activity, the NPPs produce low-fluorescence signals due to the quenching of the proximal fluorochromes. In the presence of active protease activity, the peptide spacer specific for the particular protease is cleaved and fluorochromes in the NPPs are released and become brightly fluorescent. Most recently, the NPP has also been used to image gelatinase activity in macrophages in an inflammatory arthrosclerosis mouse model in combination with fluorescence molecular tomography (3).

Imaging of Cell-Surface Receptors and Ligand Binding

Radiolabeled antibodies have been utilized to image the expression of cell-surface receptors and antigens in tumor xenograft models (4–6). Examples include using iodinated recombinant antibodies for imaging cell surface Human epidermal growth factor receptor 2 (HER2) in breast cancer (7), as well as iodinated and ^{64}Cu-labeled antibodies for imaging carcinoembryonic antigen expression (CEA) in colon cancer using microPET (8). The presence of the large numbers of targets (such as HER2 and CEA) on the cell surface helps to increase the signal to background ratio. MRI has also been used to detect the expression of cell-surface HER2 receptors. HER2-overexpressing cells were imaged in cell culture studies and a murine mammary tumor xenograft model, using biotinylated Her2 antibodies in combination with avidin conjugated gadolinium (9). Dopamine type 2 receptor (D_2R) occupancy has been imaged by a variety of iodinated probes, including ^{123}I-iodobenzamide for imaging hypoxic–ischemic brain injuries in neonates (10, 11) using SPECT. The gastrin-releasing peptide receptor was imaged by microPET in a rat pancreatic cancer model using a ^{68}Ga-labeled bombesin analog (12) and in prostate cancer model using a ^{18}F-labeled bombesin (13) in mice. The somastatin receptor that is highly expressed in neuroendocrine tumors was imaged using ^{111}In-pentetreotide (14–16) whereas the sodium iodide symporter was imaged with ^{123}I or ^{99m} Tc-pertechnetate in metastatic breast cancers (17, 18) and thyroid cancers (19) by SPECT. Most recently, a CEA diabody fused to the Renilla luciferase was used to examine CEA expression in a colorectal cancer xenograft model in nude mice using optical bioluminescence imaging (1). Direct imaging has also been used to image ligands binding to their respective receptors. 6-α-[^{18}F]fluoroestradiol (FES) was used to image the expression of estrogen receptor in breast cancer tumor xenografts in nude mice during tumor progression in response to chemotherapy and hormonal therapy (20).

Imaging of Reporter Gene and Transgene Activities

Although imaging of reporter genes usually is considered indirect imaging (since reporters are often used to infer levels of endogenous proteins), if the goal is to infer levels of reporter protein instead of some other protein, then direct imaging is applicable (4–6). Direct imaging has been utilized for evaluation of transgene and reporter gene expression by mircroPET and optical bioluminescence imaging (6). Herpes Simplex Virus Type I Thymidine kinase gene (HSV-TK) delivered *in vivo* by adenoviral vectors and lentiviral vectors as well as stably expressed in a rat glioma xenograft model was imaged by microPET using radiolabeled HSV-TK substrates such as 8-[^{18}F] fluoropenciclovir, 8-[^{18}F]fluoroganciclovir and -(4-[^{18}F]-fluoro-3 hydroxymethylbutyl) guanine ([^{18}F]-FHBG), and 2-fluoro-5-[^{124}I]iodo-1-beta-D-arabinofuranosyl-uracil (FIAU). The D2R gene was also used an *in vivo* reporter gene in the liver and tumor xenografts for noninvasive, repetitive and quantitative imaging in conjugation with radiolabeled by microPET in living mice. In order to monitor cardiac reporter gene expression noninvasively, a single vector expressing the HSV-TK gene or a bicistronic adenoviral vector carrying the HSV-TK and D2R reporter genes was delivered via intramyocardial injection and HSV-TK and D2R expression were subsequently imaged with [^{18}F]-FHBG and [^{18}F]-FESP respectively by microPET. Likewise, optical reporter genes such as Firefly luciferase and Renilla luciferase have also been used to monitor tumor xenografts, skeletal muscles as well as cardiac gene expression in cell transplantation in living mice and in living rats. Direct monitoring of transgene expression can also be achieved by MRI, in which an engineered transferrin receptor was used to internalize transferrin conjugated monocrystalline iron oxide nanoparticles and superparamagnetic iron particles (21).

Nuclear Medicine

- PET
- SPECT

Diagnosis

- Imaging receptors and cell-surface proteins
- Cancer Imaging
- Cardiology-functional imaging
- Gene delivery
- Monitoring of gene expression

References

1. Venisnik KM, Olafsen T, Loening AM et al (2006) Bifunctional antibody-Renilla luciferase fusion protein for *in vivo* optical detection of tumors. Protein Eng Des Sel 19:453–460
2. Shah, Weissleder (2005) Molecular Optical Imaging: Applications leading to the development of present day therapeutics. NeuroRX 2:215–225
3. Deguchi J-O, Aikawa M, Tung C-H et al (2006) Inflammation in Atherosclerosis. Visualizing matrix metalloproteinase action in macrophages *in vivo*. Circulation 47:1328–1338
4. Ottobrini L, Ciana P, Biserni A et al (2006) Molecular imaging: A new way to study molecular processes *in vivo*. Molecular and Cellular Endocrinology 246:69–75

5. Czernin J, Weber WA, Herschman HR (2006) Molecular imaging in the development of cancer therapeutics. Annu Rev Med 57:99–118
6. Massoud TF, Gambhir SS (2003) Molecular imaging in living subjects: seeing fundamental biological processes in a new light. Genes Dev 17:545–580
7. Herschman HR (2003) Molecular Imaging: Looking at problems, seeing solutions. Science 302:605–608
8. Sundaresan G, Yazaki PJ, Shively JE (2003) 124I-Labeled engineered anti-CEA minibodies and diabodies allow high-contrast, antigen-specific small-animal PET imaging of xenografts in athymic mice. J Nucl Med 44:1962–1969
9. Dmitri Artemov NM, Baasil Okollie, Zaver M. Bhujwalla (2003) MR molecular imaging of the Her-2/neu receptor in breast cancer cells using targeted iron oxide nanoparticles. Magn Reson Med 49:403–408
10. Tranquart F, Saliba E, Barantin L et al (2001) D2 receptor imaging in neonates using I-123 iodobenzamide brain SPECT. Clin Nucl Med 26:36–40
11. Kapucu LO, Koc E, Gucuyener K et al (1703) D2 receptor imaging with iodine-123-iodobenzamide brain SPECT in infants with hypoxic-ischemic brain injury. [see comment]. J Nucl Med 39:1703–1707
12. Schuhmacher J, Zhang H, Doll J et al (2005) GRP receptor-targeted PET of a rat pancreas carcinoma xenograft in nude mice with a 68Ga-labeled bombesin(6–14) analog. J Nucl Med 46:691–699
13. Zhang X, Cai W, Cao F et al (2006) 18F-Labeled bombesin analogs for targeting GRP receptor-expressing prostate cancer. J Nucl Med 47:492–501
14. Schillaci OSA, Scopinaro F, Falchi A et al (2003) Somatostatin receptor scintigraphy with 111In-pentetreotide in non-functioning gastroenteropancreatic neuroendocrine tumors. Int J Oncol 23:1687–1695
15. Schillaci O, Spanu A, Scopinaro F et al (2003) Somatostatin receptor scintigraphy in liver metastasis detection from gastro-enteropancreatic neuroendocrine tumors. J Nucl Med 44:359–368
16. Oberg K (2005) Neuroendocrine tumors of the gastrointestinal tract: recent advances in molecular genetics, diagnosis, and treatment. Curr Opin Oncol 17:386–391
17. Wapnir IL, Goris M, Yudd A et al (2004) The Na+/I- symporter mediates iodide uptake in breast cancer metastases and can be selectively down-regulated in the thyroid. Clin Cancer Res 10:4294–4302
18. Dadachova E, Carrasco, Ekaterina Nancy N (2004) The Na/I symporter (NIS): imaging and therapeutic applications. Semin Nucl Med 34:23–31
19. Estorch M, de Andres L, Camacho V et al (2006) Visualisation of sodium-iodide symporter. Eur J Nucl Med Mol Imaging 33(1):108
20. Aliaga A, Rousseau JA, Ouellette R et al (2004) Breast cancer models to study the expression of estrogen receptors with small animal PET imaging. Nucl Med Biol 31:761–770
21. Moore A, Josephson L, Bhorade RM (2001) Human transferrin receptor gene as a marker gene for MR imaging. Radiology 221:244–250

Disc Herniation

▶Radicular Syndrome of the Spine, Conservative Therapy for

Disco-somatic Unit

The complex of the anatomic structures of a single segment of the spine. It consists of the intervertebral disk, adjacent parts of the vertebral bodies, facet joints, ligamenta flava, and longitudinal ligaments at the given level. All components of disco-somatic unit can be involved to a variable degree by degenerative spine disease.

▶Degenerative Conditions of the Spine

Disease Activity Index

A clinical index widely used for Crohn's disease, usually based on subjective symptoms (abdominal pain, diarrhea, fever etc.), which scores the severity of the disease.

▶Colitis, Ulcerative

Dish

C. Glaser, S. Weckbach
Institut für Klinische Radiologie der LMU München GH, München, Germany
christian.glaser@med.uni-muenchen.de

Definition

According to its pathologic and epidemiologic features, diffuse idiopathic skeletal hyperostosis (DISH) is considered a (systemic) skeletal disorder of unknown etiology described in the elderly and characterized by abundant bone formation/ossification and calcification of connective tissue in spinal and extraspinal sites. The first description of the vertebral findings as "senile vertebral ankylosing hyperostosis" was by Forestier and Rotes-Querol (1950), which was then extended by Resnick et al (1975) including extraspinal manifestations to the more comprehensive concept of DISH (1).

Pathology/Histopathology

Bone formation, ligament ossification, and bony enthesial and periosteal proliferation are characteristic of DISH. Histologically, ossification in DISH is described to exhibit

organized Haversian bone. The new bone formation is attributed to increased proliferation and activity of osteoblasts. An association of metabolic disorders such as dyslipidemia, hyperuricemia, and diabetes mellitus with DISH has been suggested. Elevated levels of insulin-like growth factor and serum growth hormone have been described, peptides recognized to stimulate osteoblastic proliferation and activity. An increased number and size of nutrient foramina in a pathologic study suggested hypervascularity to be involved in the pathogenesis of DISH as a predisposing (local?) factor for onset, progression, and localization in affected ligaments and vertebrae. To date, no clearly accepted association between DISH and HLA-B27 has been demonstrated.

In the spine, linear, mainly craniocaudally oriented, paravertebral and paradiscal bone formation and ►osteophytes are present (Fig. 1). Typically, the anterior longitudinal ligament is affected. Ossification seems to start in the innermost layer of the longitudinal ligament at its junction with the vertebral body and then progresses vertically toward an adjacent vertebra. Alterations in the thickness of bone apposition may create a wave-like or "flowing" appearance. There is anterior vertebral body cortical hyperostosis. At the level of the disc space, a more horizontal extension of bony outgrowth can be found, leading to a bumpy appearance of the anterolateral vertebral aspect. In areas of incomplete ►ankylosis, fibrous tissue extends anteriorly from the level of the disc into the space between the opposing ends of ligament ossification. This feature and incomplete ossification of the deeper portions of the longitudinal ligaments correspond to radiographic lucencies interspersed between the (anterior or posterior) longitudinal ligament and the vertebral body or between struts of ossification in the ligament.

A predilection of the right anterolateral vertebral aspect in the thoracic spine is ascribed to some inhibitory effect of the pulsating descending aorta. This notion is supported by reports on a left-sided predominance in patients with situs inversus.

In 50% of cases, the posterior longitudinal ligament shows ossifications [►ossification of the posterior longitudinal ligament (OPLL)] as well, often found in the cervical spine together with posterior cortical hyperostosis and osteophytosis. Conversely, DISH is found in 20% of patients with OPLL. Less frequent, coexisting ►ossification of the ligamenta flava may be found.

Unlike in seronegative spondylarthropathies, the facet joints are not involved and intra-articular ossification of the sacroiliac join (SI) joint is not found in DISH. However, coexisting DISH and ankylosing spondylitis have been reported in a few cases.

In the extraspinal manifestations, juxta-articular, sometimes bridging (symphysis pubis, SI joint), osteophytes are typical. Prominent bony spur formation is in contrast to the lack of joint space reduction. Bony proliferation at the insertion site of tendons and ligaments may be

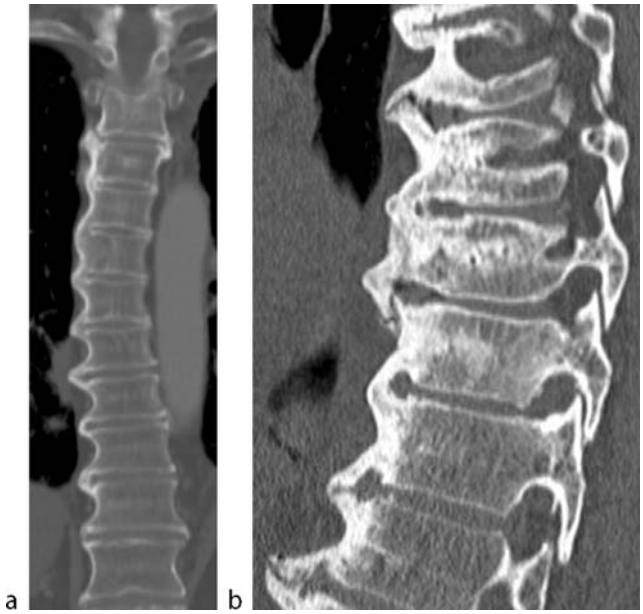

Dish. Figure 1 Coronal (a) and sagittal (b) CT reformations show the characteristic "flowing" aspect of the multisegmental bridging right-sided ossifications. There is increased apparent vertebral body depth (b) and in some of the segments, the fibrous tissue interspersed between the opposing ends of ossified struts is evident. Note the relative sparing of disk height.

prominent. In the pelvis this is along the iliac crest, ischial tuberosity, and trochanters. There is ossification of the iliolumbar and sacrotuberal ligaments. In the heel and foot, the dorsal and plantar aspect of the calcaneus, the dorsal aspect of the talar and navicular bones, as well as the lateral aspect of the cuboid and the base of the fifth metatarsal bones are affected. Anterior patellar hyperostosis and ossification extending into the ligamentous/tendinous portions of the knee extensor mechanism as well as prominent olecranon enthesiophytes are encountered. In the hand, ossification of the phalangeal joint capsules and hyperostosis may be prominent.

An increased rate of postoperative ossification (periarticular and scar tissue) has been described and has led to the recommendation of perioperative prophylactic NSAID administration (2).

Clinical Presentation

DISH is more common in the Caucasian population. The age of patients with a radiographically established diagnosis of DISH is usually 50–75 years and there is a predominance in male (2:1) patients. Prevalence increases with age from 0.3%/0.2% below 50 years to 11.2%/6.9% above 70 years (Scandinavian men/women).

There is a predilection for the spine, but peripheral manifestation occurs in up to two-thirds of documented cases. Most often, the lower thoracic spine (≤100%) is involved, followed by the upper lumbar (68–90%) and the lower cervical (65–78%) spine. In order of decreasing frequency, sites of extraspinal affection are the pelvis (53–66%), heel and foot, elbow, knee (29%), hand, and wrist. Often extraspinal affection is bilateral and symmetric.

Symptoms include (back) stiffness, which is described to be worse in the morning and relieved under mild activity, as well as a restricted range of motion and signs of tendinosis. Usually, symptoms are minor if not absent and some studies fail to demonstrate an increased incidence of back pain attributable to DISH in comparison to spondylosis. Thus, care should be taken to not falsely attribute more severe back pain to DISH instead of investigating other potentially underlying causes. Clinical history may reveal episodes of elbow and ankle pain.

More severe symptoms are usually related to complications in more advanced disease. Dysphagia is attributable to prominent ossifications in the cervical spine. Fused spinal segments are predisposed to fractures, often in the cervical spine, following even minor trauma. This may lead to underestimation of the severity of bony damage and delay in or inadequate treatment. Similar to ankylosing spondylitis, a distraction type of mechanism seems to account for many of the fractures which then follow a horizontal course, either transvertebral or transdiscal. Ultimately, even if no initial neurologic deficit is present, this may result in subsequent quadriplegia and death (3–5). In addition to trauma energy, the severity of injury seems to be related to the extent (number of fused segments) of ankylosis. Awareness of this special situation and meticulous analysis of imaging studies are mandatory, and early computed tomography (CT) studies improving the diagnosis of instability or even magnetic resonance imaging (MRI) is warranted. Advanced OPLL or ligamentum flavum may result in cervical spinal cord compression with eventual myelomalacia or lumbar spinal canal stenosis with concomitant neurological manifestations.

Among rare complications ascribed to DISH are stridor, vocal cord immobilization, compression of the inferior vena cava attributed to local mass effect, and chronic obstructive pneumonia and dyspnea with fibrobullous change related to bronchial obstruction and secondary mechanical thoracic deformity.

Imaging

The diagnosis of DISH is established from radiographic findings of the spine (for criteria, see later). The radiographic morphology of extraspinal affection is also quite characteristic, and is at least strongly suggestive of DISH (1) (Figs 1 and 3).

If visible, linear vertically oriented radiolucencies between the ossified anterior longitudinal ligament and the vertebral body in the (thoracic and cervical) spine are a characteristic feature. Similarly characteristic findings are linear horizontally oriented radiolucencies between the opposing ends of struts of anterior longitudinal ligament ossification.

In contrast to degenerative (osteo)chondrosis, the disk height is preserved in DISH, and end plate sclerosis and vacuum phenomenon are absent. Lack of intradiscal calcification and of vertebral osteoporosis contributes to differentiating DISH from ochronosis. Conversely, marked vertebral sclerosis is characteristic of fluorosis. A history of convulsions and laboratory values help in differentiating DISH from hypoparathyroidism.

Pseudarthrosis subsequent to fracture and marked destructive and reactive end plate changes in the segment immediately adjacent to a fused area of the spine have been described and potential instability in these locations with the risk of development of neurologic deficit has been underlined.

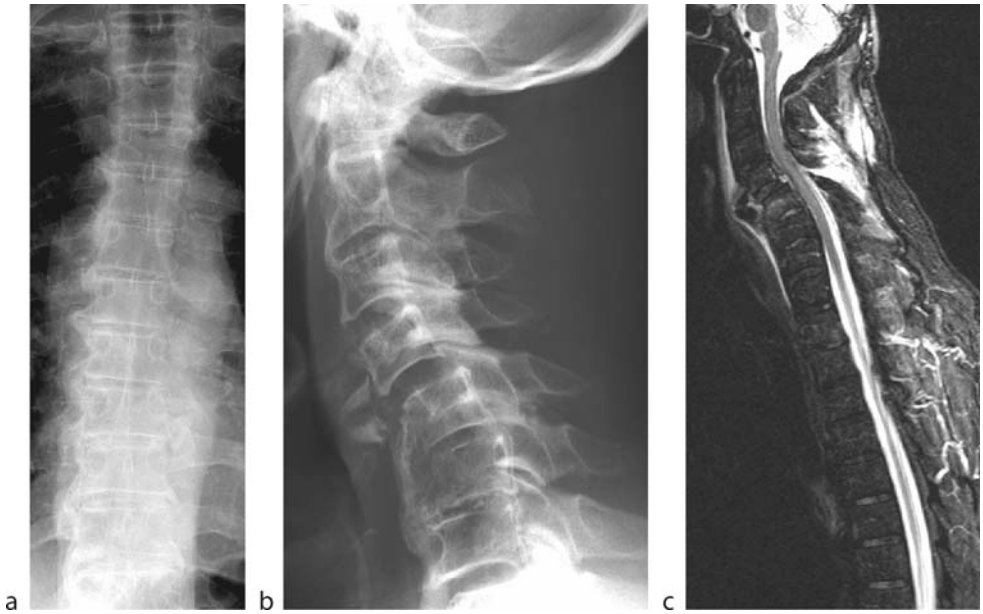

Dish. Figure 2 **This patient presented with persistent pain for several weeks after minor trauma. There is extensive ossification in the thoracic (a) and lower cervical spine (b). In addition, please note the anterior displacement of the fourth against the fifth cervical vertebral body and the two fragments of ossification anterior in this segment consistent with fractured osteophytes (b). MRI (c, sag. T2-weighted TSE) demonstrates high signal intensity anterior and posterior to the affected segment as well as in the prevertebral and nuchal soft tissues. In the lower cervical spine there is ossification in the posterior longitudinal ligament and marked narrowing of the spinal canal, but no signs of myelopathy are present.**

Fluoroscopy may illustrate displacement of the esophagus in patients with cervical affection and—sometimes severe—dysphagia. Bone scan, occasionally performed, usually reveals an increased, diffusely distributed, unspecific tracer uptake.

Although not routinely indicated, CT may demonstrate mass effect on the esophagus or the inferior vena cava. Coronal and sagittal reformations may illustrate the typical distribution pattern and the extent of ossification. CT is helpful in the evaluation of spinal canal affection and in the assessment of vertebral fractures, especially in revealing destruction of the posterior elements and thus pointing out unstable fractures (3, 4). Further, CT may contribute to differentiating para-articular bridging osteophytes in DISH from intra-articular ossification in seronegative spondylarthropathies, for example, in the SI joint.

Similarly, MRI can be of value in cases of spinal canal stenosis or vertebral fractures where it demonstrates mass effects on and affection of the thecal sac and the medulla (Fig. 2). A linearly confined area of fluid-like signal intensity extending through most of the anteroposterior diameter of a vertebra may indicate an instable fracture subsequent to a hyperextension mechanism (5). As an incidental finding in MRI primarily conducted for other purposes, areas of thick bone formation may demonstrate high signal intensity on T1-weighted sequences similar to bone marrow fat.

Diagnosis

The diagnosis of DISH primarily relies on radiographic imaging findings. Three imaging criteria are necessary to establish the diagnosis:

1. Continuous “flowing” calcification and ossification at the anterolateral aspect of four or more consecutive vertebral bodies.
2. Absence of pronounced degenerative changes in the “Bewegungssegment” and gross preservation of disc height.
3. Absence of ankylosis in apophyseal joints as well as absence of changes in the SI joint attributable to seronegative spondylarthropathies (erosions, sclerosis, intra-articular bony bridging).

As these criteria already indicate, DISH should and (by consequent application of the above given criteria) can be differentiated from spondylosis deformans, intervertebral (osteo)chondrosis, and seronegative spondylarthropathies.

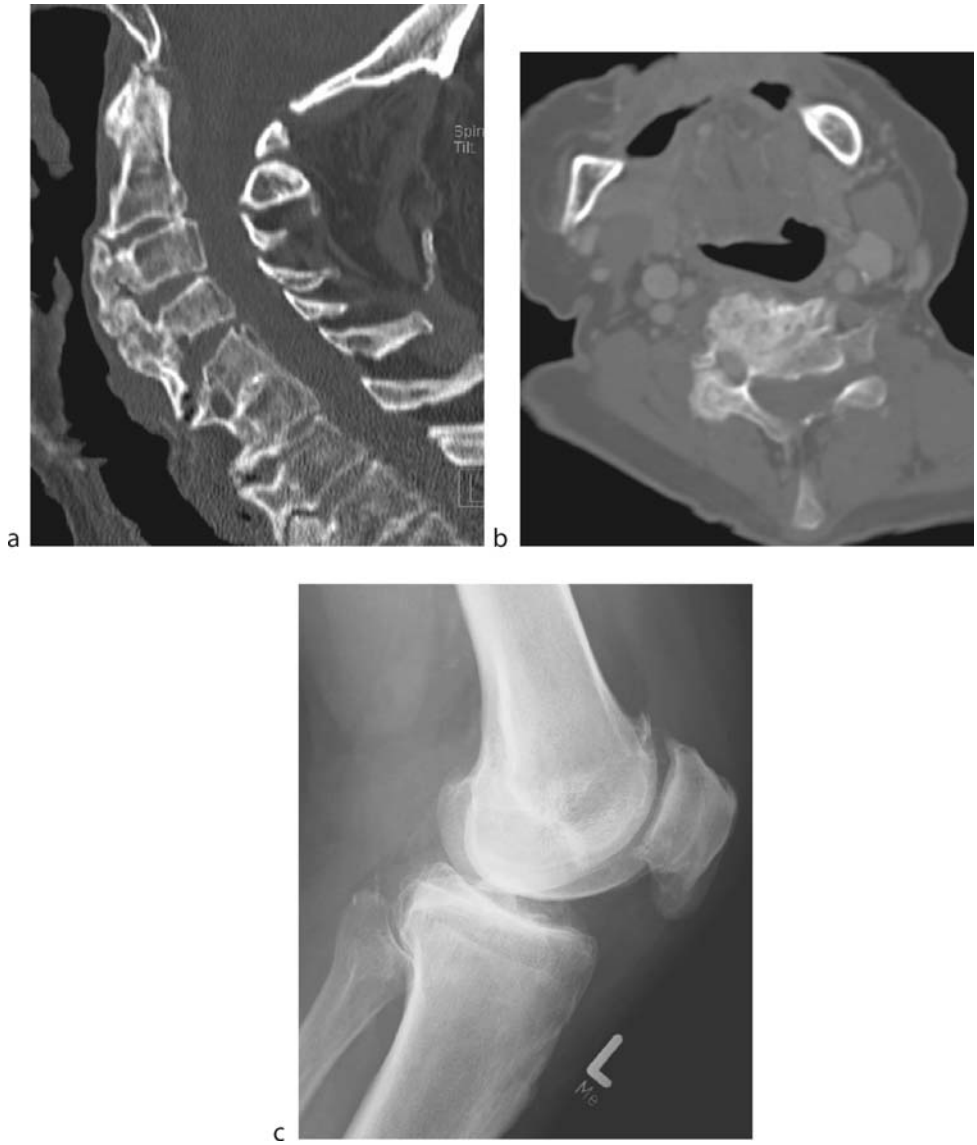

Dish. Figure 3 Sagittal reformations (a) show marked anterior and—to a lesser extent—posterior longitudinal ligament ossification in the cervical spine as well as nuchal ossification. Axial CT (b) underlines the mass effect on the pharynx, presumably explaining dysphagia in this patient. There is marked ossification in proximal portions of the ligamentum patellae (c).

Bibliography

1. Resnick D, Shaul SR, Robins JM (1975) Diffuse idiopathic skeletal hyperostosis (DISH): Forestier's disease with extraspinal manifestations. Radiology Jun 115(3):513–524
2. Belanger TA, Rowe DE (2001) Diffuse idiopathic skeletal hyperostosis: musculoskeletal manifestations. J Am Acad Orthop Surg Jul–Aug 9(4):258–267
3. Burkus JK, Denis F (1994) Hyperextension injuries of the thoracic spine in diffuse idiopathic skeletal hyperostosis. Report of four cases. J Bone Joint Surg Am Feb 76(2):237–243
4. Hendrix RW, Melany M, Miller F et al (1994) Fracture of the spine in patients with ankylosis due to diffuse skeletal hyperostosis: clinical and imaging findings. Am J Roentgenol Apr 162(4):899–904
5. Le Hir PX, Sautet A, Le Gars L et al (1999) Hyperextension vertebral body fractures in diffuse idiopathic skeletal hyperostosis: a cause of intravertebral fluidlike collections on MR imaging. Am J Roentgenol Dec 173(6):1679–1683

Dislocation

Displacement of the femoral head in the hip with no contact remaining with the acetabulum. However, the head may form a pseudoacetabulum higher along the ilium.

▶Dysplasia, Hip, Developmental

Disorders of Neuronal Migration

►Gyration Disorders, Cerebral

Disorders of Neurulation

►Congenital Malformations, Cerebral (neuro view)

Dissection, Aortic, Thoracic

Maria Schoder
Medizinische Universitat Wien, Vienna, Austria
maria.schoder@meduniwien.ac.at

Definition

Etiology of Aortic Wall Dissection

►Aortic dissection is defined as a separation of aortic wall layers. In the majority of cases, an intimal tear through which blood surges into the media is the initial event. Less common is a dissection caused by intramural hemorrhage and an intramural hematoma (IMH) without a detectable intimal tear. Chronic systemic hypertension is the most common factor predisposing the aorta to dissection. Further causes such as inherited connective tissue disorders (i.e., Marfan's syndrome, Ehlers–Danlos syndrome, and annuloaortic ectasia and familial aortic dissection), degenerative, atherosclerotic, inflammatory, or toxic processes, as well as traumatic events, may precede the aortic dissection (Table 1).

Dissection, Aortic, Thoracic. Table 1 Aortic disease etiologies with risk for aortic dissection

Inherited diseases
Marfan's syndrome
Ehlers–Danlos syndrome
Annuloaortic ectasia and familial aortic dissection
Atherosclerosis
Inflammatory diseases
Takayasu's arteritis
Giant cell arteritis
Behcet's disease
Aortitis associated with rheumatoid disease
Ormond's disease
Syphilis
Toxic etiologies
Cocaine
Amphetamine
Traumatic/iatrogenic dissection

Characteristics

Diagnostic Imaging

Aortic dissection may occur anywhere within the aorta. If there are clinical suspicions for aortic dissection, identification of the aortic segments involved is mandatory for further management. It is mandatory to visualize the entire aorta including arch vessels and iliac arteries. The imaging modalities that are highly accurate in diagnosis include multislice computed tomography (MSCT), magnetic resonance imaging (MRI), and transesophageal echocardiography (TEE). Due to technical limitations, such as narrow intercostal spaces, obesity, pulmonary emphysema, and patients on mechanical ventilation, the value of transthoracic echocardiography (TTE) remains limited. Intra-arterial angiography is invasive, and is not the current standard method for initial diagnosis.

MSCT: Multislice scanners allow rapid diagnosis and their accuracy has been improved by the availability of two- and three-dimensional reconstructions. An optimized vascular enhancement is essential for the diagnosis of dissection. Therefore, the use of an automated bolus tracking system for contrast injection in combination with the saline chaser bolus technique is recommended (1). Acquisition parameters depend on the performance of the scanner used.

Diagnostic difficulties might be caused by artifacts such as streak artifacts and aortic motion artifacts. Streak artifacts are caused by sharp contrast interfaces or cardiac motion. These straight lines of low attenuation are usually restricted to a few transverse images. Aortic motion artifacts, which may mimic aortic dissection, are predominantly seen in the ascending aorta (2). They appear as a localized duplication or pseudo-thickening of the aortic wall. These artifacts are caused by pendular movements of the aortic wall between the systolic and diastolic phase. To overcome this diagnostic uncertainty caused by cardiac motion, retrospective or prospective electrocardiography-assisted MSCT has been shown to be relevant in imaging of the ascending aorta. With a 16-slice CT scanner, cardiac gating is limited by a reduced volume coverage; however, 64-slice scanners do not have this limitation.

MRI: A combination of three-dimensional contrast-enhanced MR angiography with cross-sectional MR images provides an overview of the aortic anatomy and details of the dissecting membrane and the aortic wall. Furthermore, flow in the false and true lumen can be quantified with phase contrast cine MRI or tagging techniques. A further advantage is the accurate assessment of aortic regurgitation. Moreover, MRI permits detection of acute and subacute intramural hemorrhage on the basis of methemoglobin which occurs after several days and persists for several months. However, MRI is contraindicated in patients with pacemakers and certain metallic implants, and is inappropriate in hemodynamically unstable patients.

TEE: Besides the ability to identify the entry site of dissection, the presence of an intimal flap, abnormal flow characteristics within the false and true lumen, involvement of coronary and arch vessels, TEE is highly accurate in the diagnosis of aortic valve regurgitation. A disadvantage of TEE is the limited field of view, with inability to visualize the distal extension below the celiac trunk.

Classification and Diagnostic Requirements in Aortic Dissection

Regarding the radiological and pathological variants of aortic dissection, a differentiation of subtypes (Table 2) has been proposed (3, 4). Diagnostic considerations must include extension of the dissection, involvement of aortic side branches, and concomitant complications (Table 3). All dissection subtypes can be seen in their acute and chronic stages. A dissection is classified as acute if it is 2 weeks old or less.

Class 1: Classic aortic dissection. Due to the anatomical location of the dissection, the Stanford classification distinguishes between type A and type B. A type A dissection includes the ascending aorta regardless of the entry site location, whereas a type B dissection presents with the primary intimal tear in the descending thoracic aorta, mostly located just beyond the insertion of the ligamentum arteriosum. The DeBakey classification subdivides the aortic involvement in a type I dissection, involving the entire aorta, a type II dissection that involves the ascending aorta, and a type III dissection that involves the descending aorta.

It is important to differentiate between the true and the false lumen and to visualize the extension of the dissection. The true lumen is usually compressed and is close to the inner curvature of the aortic arch. Intimal calcification indicates the true lumen in acute dissection. The false channel often enhances later than the true lumen. However, the contrast gradient between the aortic channels may reverse during the acquisition.

Malperfusion of abdominal branches and iliac arteries may be caused by the so-called static and dynamic mechanism, as proposed by Williams et al (5). The dynamic narrowing of a branch vessel occurs when the dissection flap is positioned across the vessel origin provoked by the hyper-pressure of the false lumen. In the static mechanism, the intimal flap intersects the vessel origin and in the absence of a peripheral intimal tear, the false lumen constricts the vessel origin.

Class 2: Intramural hematoma/hemorrhage. Intramural hematoma (IMH) and hemorrhage may be the result of ruptured vasa vasorum. There are two types of IMH/hemorrhage. Type I shows a smooth inner aortic lumen and the aortic diameter is usually less than 3.5 cm with a wall thickness greater than 0.5 cm. Type II occurs with atherosclerosis. It demonstrates a rough inner aortic surface and is found more often in the descending than in the ascending thoracic aorta. The aortic diameter is dilated and the wall thickness has a range of 0.6–4 cm. On

Dissection, Aortic, Thoracic. Table 2 Classification of variants of aortic dissection

Class	
1	Classic aortic dissection Separation of intima/media; dual lumen
2	Intramural hematoma/hemorrhage Separation of intima/media; no intraluminal tear or flap imaged
3	Subtle–discrete aortic dissection Intimal tear without hematoma (limited dissection) and eccentric bulge
4	Atherosclerotic penetrating Ulcer penetrating to adventitia with localized hematoma
5	Traumatic/iatrogenic dissection

Dissection, Aortic, Thoracic. Table 3 Diagnostic requirements in aortic dissection

Localization of intimal tears
Communicating versus ▶noncommunicating dissection
Differentiation between true and false lumen
Extension of dissection
Involvement of aortic branches
Coronary arteries
Arch vessels
Visceral and renal arteries
Iliac arteries
Complications
Rupture/contained rupture
Pericardial effusion
Pleural effusion
Perfusion deficit/infarction in organs

unenhanced CT scans, IMH appears as a crescent-shaped area of attenuation in the aortic wall and remains unenhanced after injection of contrast material. IMH tends to maintain a constant circumferential relationship with the aortic wall, differentiating it from a thrombosed false lumen in a classic aortic dissection which usually spirals longitudinally around the aorta.

Class 3: Subtle–discrete aortic dissection. A subtle dissection has been described as a partial intimal tear covered by thrombus. When the tear forms a scar, this constellation is called a discrete dissection.

Class 4: Penetrating atherosclerotic ulcer. A penetrating ulcer occurs from an atherosclerotic plaque that has penetrated the internal elastic lamina into the media. A *penetrating atherosclerotic ulcer* (PAU) can lead to an IMH and aortic dissection, to a ►pseudoaneurysm, and to rupture. Diagnosis is made by demonstrating a focal contrast material-filled outpouching that might be associated with an IMH or an aneurysmal formation.

Class 5: Traumatic/iatrogenic aortic dissection. Blunt chest trauma may cause aortic dissection frequently at the region of the ligamentum botalli at the aortic isthmus. Untreated dissections often lead to pseudoaneurysms and may rupture.

Iatrogenic dissections are mostly catheter-induced and retrograde, and usually they decrease in size as the false lumen thromboses.

Therapy

Alternatively to conventional open repair, less invasive endovascular techniques for the treatment of dissections have gained widespread application, and encouraging results have been reported (6–10).

Acute uncomplicated type B dissections are preferably managed by conservative medical treatment. Complicated type B dissections with signs of rupture or imminent rupture, compromised branch vessels, rapidly expanding aortic diameter, refractory pain, or malignant hypertension require surgical or endovascular therapy. Stent grafts have a self-expanding stent structure covered by polyester or expanded polytetrafluoroethylene (ePTFE). Closure of the entry tear by stent-graft placement may lead to thrombosis of the false lumen with remodeling of the true lumen. Primary closure of the entry tear is reported in 89–100% of cases, with consecutive thrombosis of the false lumen in the descending aorta in 70–100%. Furthermore, lowering the pressure in the false lumen restored the perfusion in branch vessels that were compromised by a dynamic mechanism, as reported by Dake et al (6). However, in vessels with a narrowed origin caused by an intimal flap (dynamic mechanism) additional stenting of the vessel lumen may be required in up to 60% of cases (6). In cases were the branch vessel perfusion is compromised by a hypertensive false lumen, fenestration of the dissection membrane may be necessary (10). The puncture is performed from the true lumen of the infrarenal aorta into the false lumen, which generally tends to have a larger diameter. After placement of a stiff guide wire, the dissection membrane is fenestrated with a balloon until equalization of pressure is achieved.

In traumatic transection, the reported numbers of patients who were treated with stent-graft therapy are still limited. However, perioperative mortality rates in endovascular repair were between 0 and 13%, and were related to comorbid injuries and not associated with the stent-graft procedure (8, 9). Furthermore, paraplegia was not reported after endovascular repair, which compares favorably with surgical results.

Bibliography

1. Haage P, Schmitz-Rode T, Hubner D et al (2000) Reduction of contrast material dose and artefacts by a saline flush using a double power injector in helical CT of the thorax. Am J Roentgenol 174:1049–1053
2. Qanadli SD, El Hajjam M, Mesurolle B et al (1999) Motion artefacts of the aorta simulating aortic dissection on spiral CT. J Comput Assist Tomogr 23:1–6
3. Svensson LG, Labib SB, Eisenhauer AC et al (1999) Intimal tear without hematoma. Circulation 99:1331–1336
4. Erbel R, Alfonso F, Boileau C et al (2001) Diagnosis and management of aortic dissection: recommendations of the task force on aortic dissection, European Society of Cardiology. Eur Heart J 22:1642–1681
5. Williams DM, Lee DY, Hamilton BH et al (1997) The dissected aorta. Part III. Anatomy and radiologic diagnosis of branch-vessel compromise. Radiology 203:37–44
6. Dake MD, Kato N, Mitchell RS et al (1999) Endovascular stent-graft placement for the treatment of acute aortic dissection. N Engl J Med 340:1546–1552
7. Kusagawa H, Shimono T, Ishida M et al (2005) Changes in false lumen after transluminal stent-graft placement in aortic dissection. Circulation 111:2951–2957
8. Rousseau H, Dambrin C, Marcheix B et al (2005) Acute traumatic aortic rupture: a comparison of surgical and stent-graft repair. J Thorac Cardiovasc Surg 129:1050–1055
9. Agostinelli A, Saccani S, Borrello B et al (2006) Immediate endovascular treatment of blunt aortic injury Our therapeutic strategy. J Thorac Cardiovasc Surg 131:1053–1057
10. Hartnell GG, Gates J (2005) Aortic fenestration: a why, when, and how-to guide. Radiographics 25:175–189

Distant Recurrence

Also called systemic recurrence or metastatic disease. In this situation, malignant cells can be demonstrated in a distant organ, such as bone, lungs, liver, brain, or other places. The survival rate is considerably lower than for local or regional recurrences.

►Recurrent Neoplasms, Breast

Diuretic Renogram

Diuretic renal scintigraphy: A nuclear medicine study using medically induced standardized diuresis and Technetium 99m labelled MAG3 as a tracer for assessment of renal function and urinary drainage, which is essential for grading obstruction. MR-urography: A new MR technique that allows for assessment of the urinary tract. Originally this term was only used for heavily T2-weighted sequences that showed the (dilated) urinary system after diuretic stimulation. Now this term is more generously used for all MR techniques applied in assessment of urinary tract malformations, including (diuretic) dynamic assessment of renal function and urinary drainage after Gadolinium application using various fast T1-weigheted sequences.
►Obstructive Uropathy in Childhood

Diverticular Disease

The process defined as thickening of the taenia coli and narrowing of the colonic lumen. Multiple aetiological factors but predominately related to low fibre intake and genetic factors.
►Diverticulitis, Gastrointestinal Tract

Diverticulitis

Inflammation of diverticula often associated with pericolic sepsis and complicated by abscess formation and fistulation.
►Diverticulitis, Gastrointestinal Tract

Diverticulitis, Gastrointestinal Tract

Nicholas R. Carroll
Cambridge University Hospitals,
NHS Foundation Trust, Cambridge, UK
nicholas.carroll@addenbrookes.nhs.uk

Definitions

►Diverticulitis is defined as inflammation of diverticula or small out-pouchings of the colon. The condition depends on pre-existing ►diverticular disease, smooth muscle hypertrophy and narrowing of the colonic lumen, most commonly affecting the left colon, resulting in ►diverticulosis characterised by the formation of diverticula. These are in fact, for the most part, pseudo-diverticula, consisting of mucosa and sub-mucosa only.

The Hinchley classification separates diverticulitis into four stages, (i) ►pericolic abscess or phlegmon, (ii) pelvic, intra-abdominal or retroperitoneal abscess, (iii) generalized purulent peritonitis and (iv) generalized faecal peritonitis.

In about 20% of all people with diverticula, acute or chronic-recurrent diverticulitis develops, often with serious complications as perforation, abscess or fistula formation, obstruction, inflammatory pseudotumor and intestinal bleeding (1).

Pathogenesis

The muscle abnormality in diverticular disease is seen most often in surgically excised specimens in the sigmoid colon, though a pan colonic form of the disease without muscle thickening also exists in the elderly. This is associated with increased colonic wall compliance which is most likely due to collagen failure.

Colonic diverticula therefore results from herniation of the mucosa through weak spots in the muscular wall. The majority of evidence suggests that the morphological changes are the response to a lifelong consumption of a low-residue diet. However, there are complex relations between colonic structure, motility and dietary factors, and it is likely that all of these (and possibly genetic influences) play a role in the pathogenesis to a greater or lesser degree (2).

Clinically manifested diverticulitis has been thought to have its pathologic basis in an abscessed ►diverticulum obstructed by a faecalith, but studies of resected sigmoid colons have failed to produce evidence to support this view. Instead, the outstanding lesion was found to be a perforation in the fundus of a diverticulum, with surrounding peridiverticular or pericolic inflammation. Another surprising finding in pathologic studies was that one out of three sigmoid colons resected for 'diverticulitis' showed no inflammation in or around the diverticula, but the wall of the sigmoid was impressively thickened. This type of diverticulosis, which is frequently symptomatic, has been referred to as painful diverticular disease or spastic colon diverticulosis. Micro perforations of the tip of the diverticula are an important factor leading to inflammation and symptomatic disease (3).

The involvement of diverticula by granulomatous colitis may cause an increased incidence of diverticulitis.

Clinical Presentation

The clinical diagnosis of diverticulitis is suggested by abdominal pain that is most commonly located in the left lower quadrant. The classic clinical features are left lower quadrant pain, tenderness, fever and leukocytosis. Young people often develop severe forms of diverticulitis. Urinary symptoms may occur if the affected colonic segment is close to the bladder. A lower quadrant abdominal or rectal mass may be palpated, but associated rectal bleeding is uncommon and suggests an alternative diagnosis. About 85% of cases of acute diverticulitis involve the descending or sigmoid colon; however, right-sided disease may also occur and is reported more frequently in persons of Asian descent. Sigmoid diverticulitis may mimic acute appendicitis if a redundant colon is in the suprapubic region or lower right quadrant.

Complications

The complications of diverticulitis include

1. Pericolic abscess
2. Perforation.
3. Fistulation, e.g. colovesical fistula
4. Haemorrhage
5. Small bowel obstruction
6. Large bowel obstruction
7. Septic thrombosis of the portal vein
8. Liver abscess

Imaging

The radiological evaluation of patients with acute diverticulitis has a number of objectives: to confirm the clinical findings and rule out other colonic or pelvic disease and to evaluate and stage the degree of inflammatory disease. Direct visualisation of the colon with sigmoidoscopy or colonoscopy has little or no place in evaluation except where bleeding is a major feature or the presence of a significant polyp or carcinoma is suspected.

Plain Radiographs

Plain films may reveal the consequences of complicated diverticulitis such as free air or loculated air within sealed-off collections. In most patients, however plain radiographs are unhelpful except to exclude significant complications on admission to hospital.

Contrast Enema Examination

Contrast enema examination has been the traditional method of imaging patients with suspected diverticulitis whether with water soluble agents or barium.

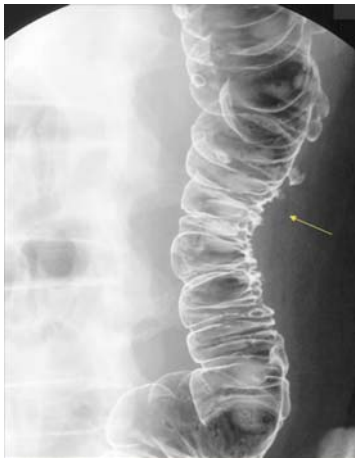

Diverticulitis, Gastroinstestinal Tract. Figure 1 Double contrast barium enema. Some distortion of the diverticula arising from the lateral wall of the descending colon (*arrow*), indicating moderate diverticulitis.

Although the process of diverticular disease and diverticulosis are well-visualised, the changes associated with diverticulitis are less reliably demonstrated. Although distortion and spiculation of the diverticulae may suggest diverticulitis (Fig. 1), contrast studies often underestimate sinus tract and abscess cavity formation and even frank perforation. Although fistulous connection to the bladder and other structures may be visualised, the sensitivity of CE may be as low as 20% in the case of colovesical fistulae.

The main limitation of CE is the inability to assess pericolic inflammatory disease and abscess formation which are the hallmarks of more advanced diverticulitis.

Ultrasound

Ultrasound is the most commonly requested investigation for non-specific abdominal pain. Hypo-echoic wall thickening with associated collection may often be seen in the affected sigmoid segments particularly in a patient with a full bladder as an acoustic window. Some authors claim similar diagnostic accuracy for Ultrasound and CT (4).

Computed Tomography

CT has contributed more to the diagnosis and management of diverticulitis than any other imaging technique. CT clearly visualises not only intramural disease but in particular the mesenteric, peritoneal and retroperitoneal components of diverticulitis. CT is now the examination method of choice for patients with the classic combination of pain, fever, left iliac fossa mass and leukocytosis.

Images are best obtained following prolonged oral preparation, i.e. four doses of 5 mL of diatrizoate meglumine in 100 mL of water over 24 h. Shorter oral preparation up to 1 h prior to imaging or no oral preparation may be appropriate depending on degree of clinical condition. It is however preferable in all cases except where there is absolute contraindication to image during intravenous contrast administration e.g. 100 mL of 300 mg/mL non-ionic iodinated contrast medium at 60 to 70 sec following commencement of injection at 2–3 mL/sec. Multi-detector CT with the facility for coronal and sagittal reformat from isometric voxels improves interpretation of extra-mural disease particularly involvement of other organs such as the bladder.

The findings in acute diverticulitis are listed in Table 1. The most consistent feature is the presence of inflammatory change in the pericoloic fat (Fig. 2). The changes range from very fine linear stranding to large phlegmonous collections or frank abscess formation. Although most collections or abscesses are confined to the sigmoid mesocolon sepsis can spread to involve other spaces and planes such as the psoas muscle. Higher resolution or MDCT can demonstrate fine intramural or extramural fistulae and connections to other organs. (Fig. 3). CT has a high sensitivity and specificity in diagnosis of diverticulitis, up to 97% and 100% respectively (5).

Diagnosis and Staging

CT staging can be correlated with surgical staging methods, see Table 2. Stage 0, the most common, being confined to the serosa of the colon, and represented by CT as moderate mural thickening with little or no extramural inflammation. Conservative management is usually adequate and imaging follow up not required.

Stage 1 is characterised by an abscess or inflammatory mass less than 3 cm in diameter confined to the mesocolon. Antibiotic therapy usually suffices and patients rarely progress to more significant disease. Follow-up CT can be helpful to ensure resolution. Stage 2 disease is signified by CT evidence of spread outside the mesocolon but still confined by pelvic organs. Often at this stage CT drainage can aid in management. Once signs of inflammation are seen throughout the abdomen the disease has become Stage 3 and surgical intervention is invariably required. Faecal peritonitis signifies Stage 4 disease and urgent laparotomy is required.

Diverticulitis, Gastroinstestinal Tract. Table 1 CT findings in patients with diverticulitis

Intramural and extramural diverticula
Induration, thickening or increased vascular markings within sigmoid mesentery
Inflammation, phlegmon or abscess in pericolic fat
Pericolic sinus or fistulae
Associated pelvic abscess or peritonitis
Signs of perforation. Free fluid and peritoneal gas
Faecal peritonitis
Other organ involvement e.g. thickening of bladder mucosa and gas within the urine.

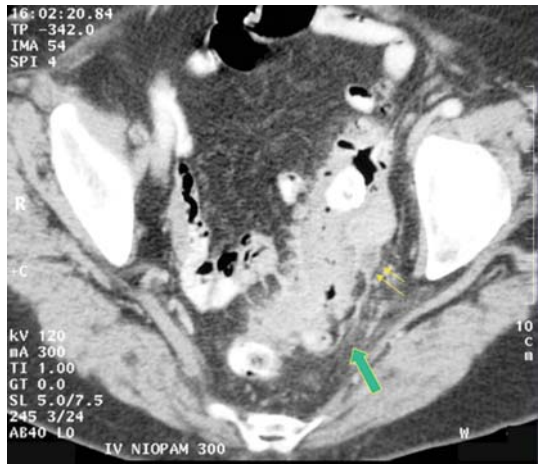

Diverticulitis, Gastroinstestinal Tract. Figure 2 Image from intravenous contrast medium enhanced CT examination of the abdomen and pelvis demonstrating classical features of diverticulitis. Thickened sigmoid loop with intramural and extramural sinus and fistula formation, (solid *arrow*), pericolic inflammation and phlegmon (double *arrow*).

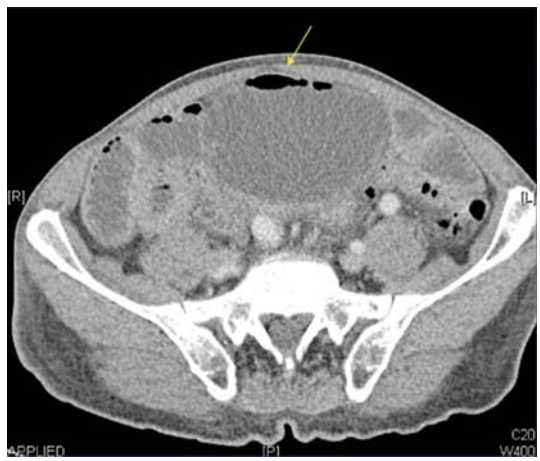

Diverticulitis, Gastroinstestinal Tract. Figure 3 Image from intravenous contrast medium enhanced CT examination of the abdomen and pelvis demonstrating gas in the bladder due to colovesical fistula (*arrow*).

Diverticulitis, Gastroinstestinal Tract. Table 2 Hinchley classification of stages of diverticulitis

Surgical stage	Findings	Management
0	Thickened colon. Some distortion of diverticula and minor pericolic inflammation.	May settle spontaneously or with antibiotic treatment
1	< 3 cm pericolic abscess. Contained within sigmoid mesocolon	Conservative. Antibiotics
2	Pelvic abscess broken out of mesocolon but confined by pelvic organs	Antibiotics aided by percutaneous image guided drainage
3	Peritonitis	Surgery
4	Faecal peritonitis	Surgery

Differential Diagnosis

The most commonly encountered differential dilemma in interpretation of CT of the colon is that between colonic carcinoma and diverticular disease/diverticulitis. Diverticulitis is usually only associated with mild concentric thickening compared to the thickening of carcinoma which is often greater or eccentric but there is considerable overlap. The presence of diverticulosis may suggest diverticulitis but carcinoma may frequently complicate colon affected by diverticular disease. Perforation of a cancer may be particularly difficult to differentiate from diverticulitis. The presence of enlarged nodes may favour the former. Other conditions to differentiate include ischaemic, infectious and inflammatory colitis. Longer segmental involvement and absence of extramural disease may suggest other conditions. Primary epiploic appendagitis is frequently misdiagnosed as either appendicitis or diverticulitis, depending on its location.

Intervention

Patients with pericolic abscess greater than 4 cm in diameter are best managed with a combination of CT guided drainage and intravenous antibiotics. Emergency surgery is reserved for those patients with peritonitis or free perforation. Elective surgery may follow successful conservative management particularly following repeated relapse or bleeding. CT or US guided drainage may also be suitable for draining liver abscess complicating diverticulitis.

Bibliography

1. Paul F, Altaras (1982) J Diverticulosis-diverticulitis. Z Gerontol 15(2):70–8
2. Simpson J, Scholefield JH, Spiller RC (2002). Pathogenesis of colonic diverticula (review). Br J Surg (5):546–554
3. Hoffman P, Layer P (1995) Pathogenesis and pathophysiology of sigmoid diverticulitis (review). Chirurg (12):1169–1172
4. Pradel JA, Adell cJF, Taourel P et al (1997) Acute colonic diverticulitis: prospective comparative evaluation with US and CT. Radiology 205:503–512
5. Cho CK, Morehouse HT, Altermen DD et al (1990) Sigmoid diverticulitis: diagnostic role of CT comparison with barium enema studies. Radiology 176:111–115

Diverticulosis, Colon

Defined as the formation of out pouchings of mucosa and sub mucosa, or diverticula, secondary to the process above. These diverticula form through natural weaknesses where the vasa recta perforate the muscularis propria to penetrate the sub mucosa either side of the mesenteric taenia and on the mesenteric side of the anti-mesenteric taenia.

▶Diverticulitis, Gastrointestinal Tract

Diverticulosis, Gallbladder

This condition of unknown etiology, also termed cholecystitis glandularis proliferans or adenomyomatosis, is characterized by widening of the Rokitansky–Aschoff sinuses, normally represented by small fingerlike invaginations of gallbladder mucosa. These become more evident in the case of diverticulosis and may extend into the muscular or serosal layers as variably cystic spaces.

▶Cholecystoses

Diverticulum(a)

The out pouchings of mucosa and sub mucosa which are therefore pseudo-diverticula rather than true diverticula which contain all layers of the gut and are seen in rare hereditary form arising from the caecum.

▶Diverticulitis

Diverticulum, Oesophagus

Olle Ekberg, MD
Department of Clinical Sciences/Medical Radiology, Lund University, Malmö University Hospital, Malmö, Sweden
olle.ekberg@med.lu.se

Definition

A diverticulum is defined as a circumscribed pouch or sac of variable size created by herniation of the lining mucous membrane through a defect in the muscular coat of the tubular oesophagus. An acquired diverticulum is produced secondarily, mechanically, or by disease. A pseudo-diverticulum is defined as a diverticulum created by an outpouching of the full thickness of the intestinal wall including the muscular layer.

This chapter will deal with three types of diverticula: *Intramural diverticula* that are millimetre-sized diverticula confined to the oesophageal wall. *Pulsion diverticula*, often less than 3–5 cm in size, is located in the midportion of the oesophagus. These are by definition pseudo-diverticula. *Epiphrenal diverticula* that are usually 10–20 cm big diverticula located in the most distal part of the oesophagus.

Pathology/Histopathology

Oesophageal Intramural Pseudo-diverticulosis

In patients with chronic oesophagitis, either due to infection or reflux of gastric content, dilatation of ducts of mucous glands in the oesophagus occurs. These excretory ducts are 2–5 mm in depth and located in the oesophageal wall. Particularly infections of *Candida albicans* has been related to such pseudo-diverticula. There have also been observations that pseudo-diverticulosis is associated with strictures of the oesophagus.

Diverticula of the Oesophagus

These are almost invariably associated with oesophageal motor disorders. This means that a diverticulum has been formed by pulsion due to increased intraluminal oesophageal pressure. Prior hypotheses about a traction mechanism due to fibrosis in adjacent peri-oesophageal tissues, i.e. lymph nodes, have not been verified.

Epiphrenic Diverticula

Also these diverticula are probably due to oesophageal motor disorders. They are located in the distal part of the oesophagus. It is unclear why the diverticula in the distal part of the oesophagus have a tendency to grow to particularly larger size than the mid-oesophageal diverticula.

Clinical Presentation

Oesophageal Intramural Pseudo-diverticulosis

Oesophageal intramural pseudo-diverticulosis usually occurs in elderly. Dysphagia may be present. However, concomitant infections and associated strictures are more symptomatic than the small diverticula *per se*.

Diverticula of the Oesophagus

The symptoms of these diverticula are probably only related to the motor disorders. Patients may experience crampy thoracic pain, regurgitation or even vomiting.

Epiphrenic Diverticula

Also in these patients symptoms from the oesophageal motor disorder predominate. However, these big diverticula also retain food. This food may regurgitate when the patient is recumbent. The retained food may also harbour and grow bacteria. Therefore, a foul smell may be a leading symptom. Patients may also experience pain and this has sometimes been referred to as ischemic.

Imaging

Oesophageal Intramural Pseudo-diverticulosis

The diverticula are best seen when filled with high-density barium contrast medium (Fig. 1). When the

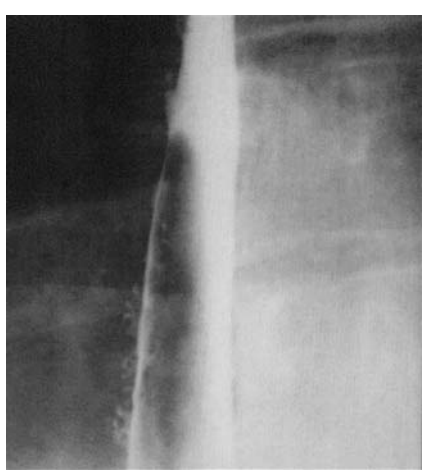

Diverticulum, Oesophagus. Figure 1 Intramural oesophageal diverticulosis. There are several millimetre-sized enlarged mucosal glands on the right side of the oesophagus. The rest of the oesophagus looks normal.

oesophagus is examined with double-contrast technique using effervescent agents the diverticula may be obscured if the oesophagus is dilated and the diverticulum is not particularly demonstrated in profile. On iodine contrast studies, it is an advantage to use 350 mg I/mL in order to enhance visualisation.

Diverticula of the Oesophagus

A diverticulum of the mid-oesophagus is seen as a localised bulge of one up to several centimeters in size (Fig. 2). The contour is smooth and often variable. The diverticulum moves in symmetry with the adjacent oesophagus during the propulsion of the bolus through that particular segment of the oesophagus. The diverticulum may or may not contain air. During double contrast ▶oesophagogram, the diverticulum regularly harbours gas. When the diverticulum does not empty the contrast material, it is likely that it lacks muscular coating indicating that it is a true diverticulum. Usually the diverticula in the mid-oesophagus are of pseudo-diverticular type and contain a muscular layer. Therefore, they empty after the passage of the bolus. However this emptying may be delayed or slow.

Epiphrenic Diverticula

These diverticula are usually diagnosed during radiologic evaluation of dysphagia, regurgitation or thoracic pain. They are often 10 cm or larger in size and often contain

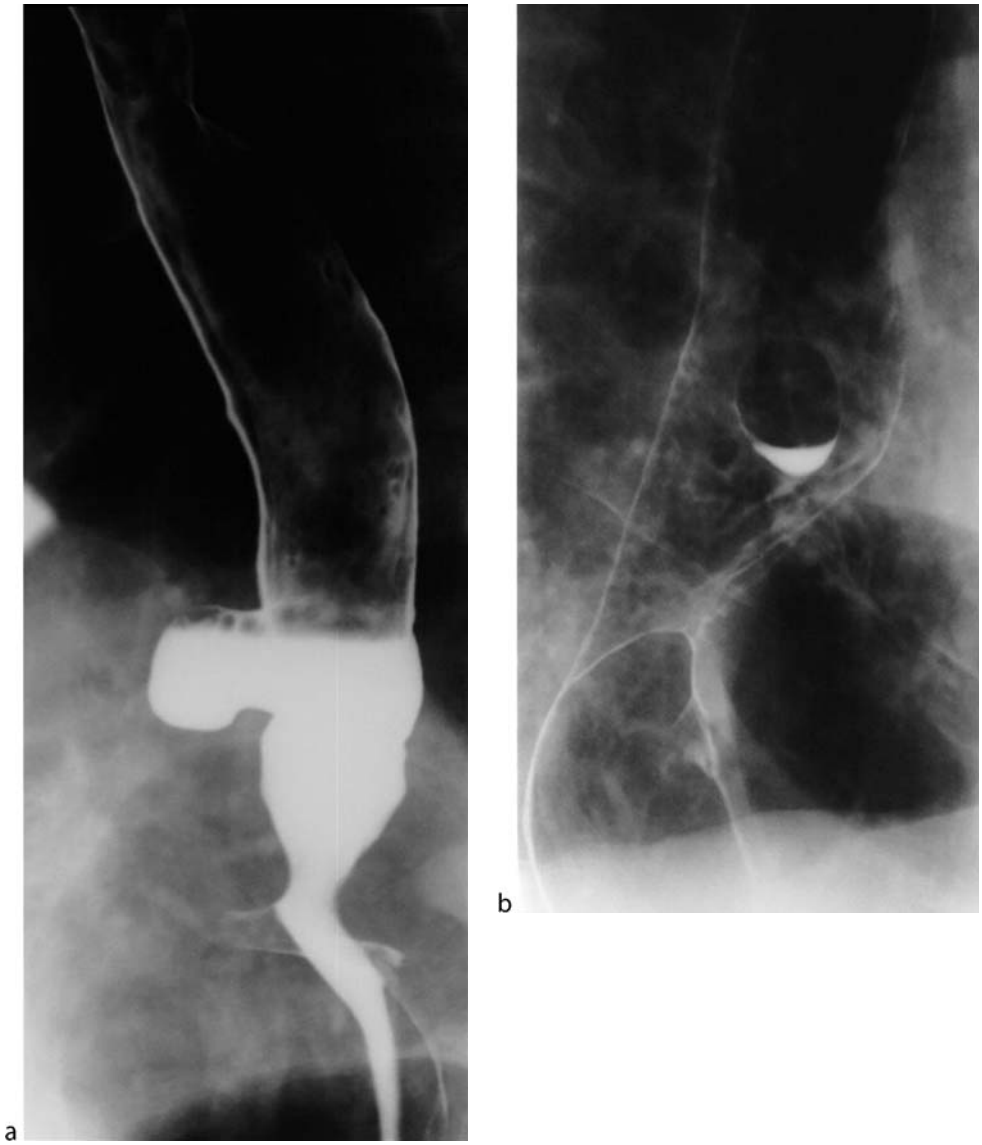

Diverticulum, Oesophagus. Figure 2 A 2-cm sized diverticulum in the mid-oesophagus. The diverticulum contains barium and small amounts of air (a). In (b), the diverticulum contains mostly air.

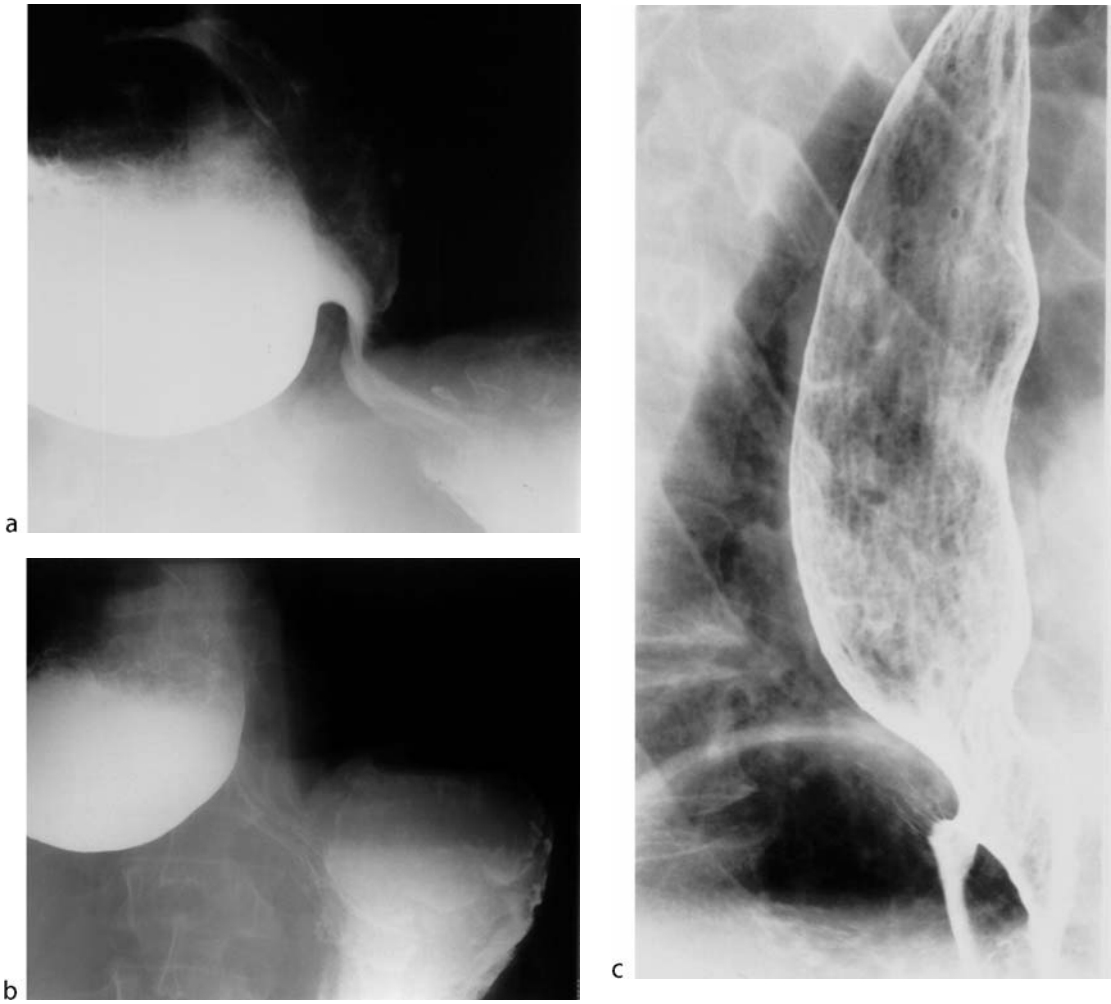

Diverticulum, Oesophagus. Figure 3 A 15-cm sized epiphrenal diverticulum from the right side of the oesophagus. The d is the diverticulum, s is the stomach and e is the distal oesophagus (a–c). The proximal oesophagus is somewhat dilated. Arrow is the opening of the diverticulum.

retained food particles. Endoscopy may also reveal the orifice of the diverticulum but will usually not give any information about the size of the diverticulum (Fig. 3).

Nuclear Medicine

Large diverticula are able to retain isotopes and can thereby be diagnosed.

Diagnosis

Oesophageal Intramural Pseudo-diverticulosis

These diverticula are usually diagnosed on barium contrast oesophagograms. Endoscopically, these diverticula are not discerned due to there very small and narrow openings.

Diverticula of the Oesophagus

The mid-oesophageal diverticula are usually diagnosed during barium oesophagograms performed for evaluation of dysphagia or vomiting. Endoscopy may also reveal these types of diverticula. However, the diagnosis is more difficult.

Bibliography

1. Laufer I (1989) Motor disorders of the esophagus. In: Levine MS (ed) Radiology of the Esophagus. WB Saunders, Philadelphia, pp 229–246
2. Vossough A, Levine MS (2004) Esophageal morphology. In: Ekberg O (ed) Radiology of the Pharynx and the Esophagus. Springer, Berlin, pp 127–147
3. Fulp SR (1992) Esophageal diverticula. In: Castell DO (ed) The Esophagus. Little, Brown & Co, Boston, pp 351–366

Dolichostenomelia

A greater than normal length of the extremities most pronounced in the proximal (humerus and femur) region. An example is Marfan syndrome.
▶Osteodysplasia

Domed Talus

A convex uppermost talus, as seen on AP images, along with concave lowermost tibia and fibula, yielding a ball-in-socket ankle; with a high association with tarsal coalition, fibular hemimelia, reduced number of toe rays, and other features.
▶Congenital Malformations, Bone

Doppler

The frequency shift that results from scatterer motion within the ultrasound beam. It can be used for blood flow or tissue motion applications.
▶Ultrasound Imaging

Doppler Echocardiography

Measures velocities of blood flow based on the change in frequency (or Doppler shift) of the backscattered signal of moving red blood cells.
▶Ischemic Heart Disease
▶Ischemic Heart Disease, Ultrasound

Doppler US

Used for vascular/blood flow studies. US reflected from red blood cells causes a frequency shift related to their velocity, which is recorded as a waveform. Urinary obstruction causes changes in the Doppler waveform. An elevated mean resistive index (RI) over 0.7, although not specific is suggestive for obstruction. An RI difference over 0.4 to 0.6 between the obstructed and normal kidney is more significant for stone obstruction in acute renal colic.
▶Colic, Acute, Renal

Dorsal Induction Anomalies

▶Congenital Malformations, Cerebrum

Dorsiflected Intercalated Segmental Instability

Dorsiflected intercalated segmental instability is a non-specific radiologic feature resulting from scapholunate ligament impairment and also occurring posttrauma in association with sports that place dorsal stress on the carpus, or in rheumatoid arthritis due to ligament or insertional destruction. It is diagnosed with dorsal tilting of the lunate, increased capitolunate angle to >30°, and scapholunate angle >80°.
▶Rheumatoid Arthritis

Double-contrast Barium Study

Imaging study of the upper gastrointestinal tract (pharynx to duodenojejunal flexure) using a small quantity of high-density barium (200–250% w/v) and gas-producing agents. The purpose of this study is to demonstrate fine mucosal detail.
▶Ulcer Peptic

Downhill Varices

Exhibited in patients with SVC obstruction and most commonly involving the upper and mid oesophagus.
▶Varices, Oesophagus

DR

▶Digital Radiography

Drug Delivery Systems

A drug-delivery system consists of microbubble or biopolymer contrast agents containing an active compound (drug) attached or encapsulated in the shell. The active substance is transported with the agent to the target region, inhibiting the extravascular distribution outside of the target region. The local release of the drug is obtained by local destruction of the shell (using high-power ultrasound) or by slow release after binding of the shell to the target region.

▶Contrast Media, Ultrasound, New Clinical Development
▶Local Drug and Gene Delivery with Microbubbles

Drug Discovery and Development

Process which encompasses discovery and acquisition of new agents through pre-clinical and clinical development to drug registration.

▶PET in Drug Discovery Imaging

Drug–Delivery Systems

▶Contrast Media, Ultrasound, New Clinical Development

Drug-induced Hepatitis

A large number of drugs can cause hepatitis. The so-called drug-induced hepatitis or medication-induced hepatitis, is similar to acute viral hepatitis, but hepatocellular destruction is usually more extensive. Halothane (a specific type of anesthetic gas), methyldopa (antihypertensive), isoniazid and rifampicin (tuberculosis-specific antibiotics), oral contraceptives, amiodarone (antiarrhythmic) are only few examples of the innumerable hepatotoxic drugs. The clinical course and severity of drug-induced hepatitis are extremely variable, both dependent on the drug and the individual reaction to the drug. Virtually any drug can be a cause of hepatitis. Manifestations of hepatotoxicity to a medication may occur on the first or second day of use or not until several months later. Usually, the onset is abrupt, with fever, rash, pruritus, anorexia, arthralgia, and nausea. If such symptoms occur after the administration of a drug, its use should be stopped immediately. Laboratory analyses show altered liver tests and eosinophilia.

▶Hepatitis

DSA

Digital subtraction angiography uses a fluoroscopically acquired digital 'mask' image without contrast which is then subtracted from subsequent frames obtained following contrast injection.

Time-consuming, invasive X-ray technique for visualisation of the vascular tree.

▶Cerebral Aneurysms

Dual Modality Iimaging

▶Multi-modality Imaging

Dual-energy X-ray Absorptiometry

Technique to measure areal bone mineral density using radiation with two distinct energies (kVp), most frequently performed at the spine and the proximal femur.

▶Osteoporosis

Duct Disease, Breast

Luis Pina
ljpina@unav.es

Synonyms

Comedomastitis; Duct ectasia; Mastitis obliterans; Periductal mastitis; Plasma cell mastitis; Secretory disease; Varicocele of the breast; Varicocele tumor

Definition

The term "duct disease" includes duct ectasia and periductal mastitis. Both processes may occur independently or, more frequently, in combination. Duct ectasia is defined as the dilatation of the subareolar ducts, usually measuring 1–5 mm. Periductal mastitis is an inflammatory infiltrate surrounding the ducts (1–3).

Pathology

Dilated, thick-walled ducts with thick secretions are seen in the gross specimen (1). On microscopic examination, a leakage of ducts with release of lipid-rich material in the adjacent stroma in seen, inducing periductal inflammation, fibrosis, and fat necrosis. The periductal inflammation may be predominantly composed of plasma cells. Some authors believe that dilatation of the ducts is the primary event, whereas others believe it is secondary to periductal inflammation (1–3).

Clinical Findings

Duct ectasia is found in perimenopausal or postmenopausal women. Microscopically it has been described in up to 40% of autopsies (1).

The first symptom of duct ectasia is spontaneous and intermittent ▶nipple discharge from several ducts. This fluid may be off-white, creamy, brown, gray, or green, and also can be bloody (2). Sometimes the secretions are as thick as toothpaste. The patient usually describes subareolar tenderness. Nipple retraction and a hard retroareolar mass may be found, mimicking breast cancer. Abscess formation and mammary duct fistula can complicate this condition. Cigarette smoking is associated with these complications (2).

Duct disease is a benign condition and does not increase the risk of developing breast cancer.

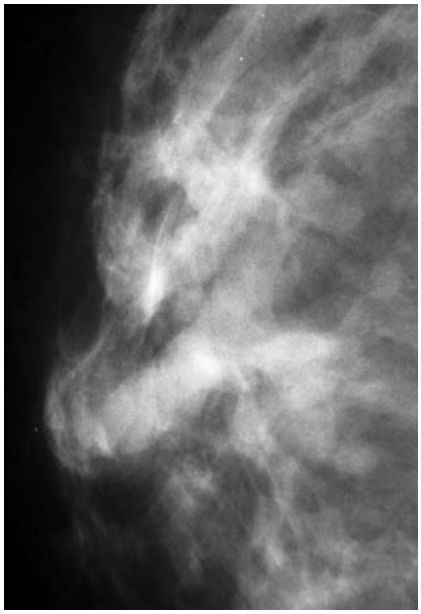

Duct Disease, Breast. Figure 1 Duct ectasia is seen on mammography as dilated tubular structures underneath the nipple. Mediolateral oblique view (detail).

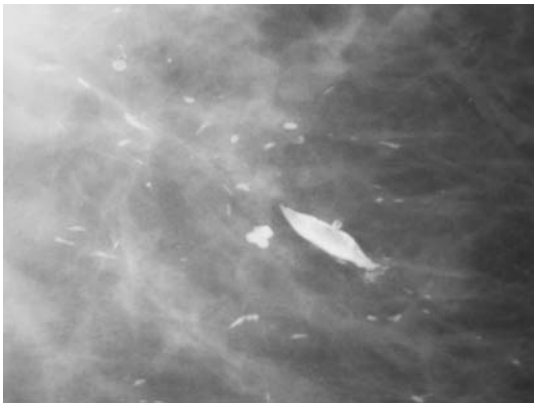

Duct Disease, Breast. Figure 2 Characteristic ▶secretory calcifications. The particles are coarse, dense, smooth-bordered, and pointing toward the nipple.

Imaging

Mammography: Duct ectasia is seen as one or more tubular structures oriented to the nipple (Fig. 1). If the periductal inflammation and fibrosis are predominant, the lesion may be seen as an ill-delimited mass, similar to breast carcinoma (4) (Fig. 2).

Galactography is not indicated for bilateral or pluriorifical nipple discharge. Rarely, the nipple discharge may be unilateral and uniorificial, and galactography is performed. In these cases, a dilated galactophoric tree is seen.

Characteristic calcifications may be found in intraductal, intramural, or periductal locations (5). These calcifications are typically coarse and elongated, pointing toward the nipple (Fig. 2). Other calcifications may be round or elongated with central radiolucency. Most of these calcifications are easily recognized as benign, especially if they are bilateral. However, sometimes the calcifications are very small and similar to the suspicious microcalcifications of intraductal carcinoma. In these cases, a biopsy is warranted (5) (Fig. 3).

Ultrasound: Duct ectasia is seen as fluid-filled tubular structures underneath the nipple (Fig. 3). If a palpable mass is found in the retroareolar space due to

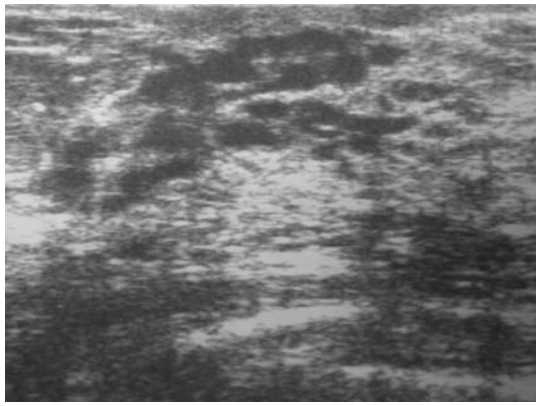

Duct Disease, Breast. Figure 3 Ultrasonography shows subareolar dilated ducts. Ductal ectasia.

inflammation and fibrosis, ultrasonography may detect an irregular hypoechoic mass. In these cases, a biopsy is recommended. The characteristic calcifications are not usually seen on ultrasonography (4).

Magnetic resonance: The periductal inflammation may be responsible for the enhancement after paramagnetic contrast administration.

Nuclear Medicine

There are no indications for nuclear medicine in the diagnosis of duct disease.

Diagnosis

Most ductal ectasias are asymptomatic and are discovered on routine mammographic or ultrasonographic exams. If nipple discharge is absent, there is no need for further diagnostic procedures. However, if the ectasia is palpable or there is nipple discharge, the secretion may be analyzed. The combination of a retroareolar palpable mass and nipple retraction is suspicious, and a biopsy is recommended. The typical calcifications found on mammography are pathognomonic. However, in an initial stage the calcifications may be tiny and simulate breast cancer, especially intraductal carcinoma. In these cases, a biopsy should be performed.

Bibliography

1. Rosen PP (2001) Inflammatory and Reactive Tumors. In: Rosen PP (ed) Rosen's Breast Pathology. Lippincott Williams & Wilkins, Philadelphia, pp 29–63
2. Hughes LE (2000) The duct ectasia/periductal mastitis. In: Hughes LE, Mansel RE, Webster DJT (eds) Benign Disorders and Diseases of the Breast. Concepts and Clinical Management. Saunders, London, pp 143–169
3. Schnitt S, Connolly JL (2004) Pathology of benign breast disorders. In: Harris JR, Lippman ME, Morrow M et al (eds) Diseases of the Breast. Lippincott Williams & Wilkins, Philadelphia, pp 77–99
4. Cardeñosa G (2001) Major subareolar ducts. In: Cardeñosa G (ed) Breast Imaging Companion. Lippincott Williams & Wilkins, Philadelphia, pp 220–223
5. Heywang-Köbrunner SH, Schreer I, Dershaw DD (1997) Inflammatory conditions. In: Heywang-Köbrunner SH, Schreer I, Dershaw DD (eds) Diagnostic Breast Imaging. Thieme, Stuttgart, pp 194–208

Duct Ectasia

▶Duct Disease, Breast

Duct of Santorini

The duct of Santorini is usually the accessory duct of the pancreas that atrophies once the dorsal and ventral glands fuse and once the main duct of Wirsung becomes patent. It is connected to the minor papilla.

▶Congenital Malformations, Bile Ducts

Ductal Carcinoma In Situ

Malignant lesion located in the ductal component and characterized by the fact that the malignant cells do not trespass the basal line of the epithelium.

▶Breast Conserving Therapy

Ductal Intra-Epithelial Neoplasia (DIN) Type 1c to 3

▶Carcinoma, Ductal, *In Situ*, Breast

Ducts

15-20 tubular structures in the breast lined with epithelium which convey secretions from the breast lobules to the nipple.

▶Carcinoma Breast, Imaging Mammography, Secondary Signs

Duodenal Atresia

A congenital abnormality in which there has been failure or canalization of the duodenum in embryological development resulting in complete duodenal obstruction.
▶GI Tract, Paediatric, Congenital Malformations

Duodenal Ulcer

▶Ulcers, Peptic

Duplication Cyst

Duplication of the gastrointestinal tract may occur at any level from the tongue to the anus. It corresponds to a duplicated segment of the gastrointestinal tract. The duplication may or may not communicate with the gastrointestinal tract. It can be round (and cystic) or tubular. At the level of the duodenum, the duplication may communicate with the pancreatic duct.
▶Congenital Malformations, Bile Ducts
▶GI Tract, Paediatric, Congenital Malformations

Duplication of bile ducts

Presence of additional bile ducts. In case of duplication of the common bile duct, both branches may enter into the duodenum or one may empty into the stomach while the other enters into the duodenum. Cases of duplication of the common hepatic and cystic ducts containing ectopic gastric mucosa have been reported.
▶Congenital Malformations, Liver and Biliary Tract

Duplications and Triplications (Kidney, Ureter, Bladder and Urethra) of the Urinary Tract

Increase in number of the ureter, the urethra, the bladder or the kidneys, respectively the pelvo-caliceal system. This embryologically induced condition may lead to impaired urinary drainage, VUR and potentially dysplasia of affected (renal) parenchyma.
▶Urinary Tract

Dural-Based Tumors

Dural-based tumors are benign or malignant tumors involving the dura. Enhanced magnetic resonance imaging is the modality of choice for their diagnosis.
▶Neoplasms, Extraaxial, Brain

DXA

▶Dual-energy X-ray absorptiometry

Dynamic Contrast-enhanced MR Imaging

Dynamic contrast-enhanced MR imaging is performed after the administration of intravenous contrast medium to access vascular characteristics of tumors and normal tissues. T1-shortening from contrast agent is considered a measure of tissue perfusion, capillary permeability, and volume of extracellular space.
▶Neoplasms, Salivary Glands

Dynamic Magnetic Resonance Imaging

MRI technique with very short acquisition time to assess displacement.
▶Incontinence, Urinary

Dysphagia

Difficulty swallowing. The term is properly used to describe some degree of obstruction after swallowing,

but the term is used so loosely by physicians, that the radiologist has to ascertain from the patient the precise nature of the complaint to which the term dysphagia has been applied.

►Gastroesophageal Reflux in Adult Patients: Clinical Presentations, Complications, and Imaging

Dysplasia, Bronchopulmonary

Gundula Staatz
Department of Radiology, Division of Pediatric Radiology, University of Erlangen-Nürnberg Erlangen
gu.stz.uni-erlangen@t-online.de

Synonyms

BPD; Chronic lung disease of prematurity; CLD

Definitions

►Bronchopulmonary dysplasia (BPD) is defined as a chronic lung disease which occurs in premature infants. due to treatment with oxygen and positive pressure ventilation. Pulmonary immaturity, oxygen toxicity, formation of oxygen radicals, volutrauma, and barotrauma as well as additional factors such as pulmonary inflammation contribute to pulmonary damage. BPD is infrequent in infants of more than 1,200 g birth weight and with greater than 30 weeks gestation. Gentler ventilation techniques, antenatal glucocorticoid therapy, and surfactant treatment have minimized severe lung injury in larger and more mature infants (1).

Pathology/Histopathology

Before the surfactant treatment era, airway injury, inflammation, and parenchymal fibrosis were the prominent findings in BPD. Four stages of BPD were identified representing acute lung injury, exudative bronchiolitis, proliferative bronchiolitis, and obliterative fibroproliferative bronchiolitis. Necrotizing bronchiolitis occurs as a result of edema, inflammatory exudate, and necrosis of epithelial cells. Inflammatory cells, exudate, and cellular debris obstruct the terminal airways. Activation and fibroblast proliferation results in peribronchial fibrosis and obliterative fibroproliferative bronchiolitis. Structural changes in the pulmonary arteries were similar to those seen in hypertensive vascular disease and include intimal proliferation, medial hyperplasia, and adventitial thickening (2).

In recent years, due to improved management and treatment, the lungs of infants with BPD showed less fibrosis and more uniform inflation. The large and small airways were remarkably free of epithelial metaplasia, smooth muscle hypertrophy, and fibrosis (3). However, alveoli were found to be less numerous and larger, indicating an interference with septation, despite an increase in elastic tissue that is proportionate to the severity of the respiratory disease before death. Some specimens also had shown decreased pulmonary microvasculature development.

Clinical Presentation

Infants with BPD present with tachypnea, tachycardia, intercostal retractions, nasal flaring, expiratory stridor, poor weight gain, right ventricular hypertrophy, and pulmonary hypertension. A June 2000 National Institute of Child Health and Human Development/National Heart, Lung, and Blood Institute Workshop proposed a severity-based definition of BPD for infants <32 weeks gestational age. Mild BPD was defined as a need for supplemental oxygen (O_2) for 28 days but not at 36 weeks postmenstrual age (PMA) or discharge, moderate BPD as O_2 for 28 days plus treatment with <30% O_2 at 36 weeks PMA, and severe BPD as O_2 for 28 days plus 30% O_2 and/or positive pressure at 36 weeks' PMA (4). Especially during the first two years of life, children with BPD suffer from lung dysfunction, airway hyperactivity, pulmonary hyperaeration, and recurrent respiratory tract infections. The disease may be complicated by right ventricular hypertrophy or pulmonary hypertension. However, in many children the pulmonary function improves over the years with continuing growth and healing of the airways.

Imaging

Imaging of pulmonary diseases in premature infants on intensive care units is based on chest radiography. In recent years, high-resolution computed tomography (HRCT) has been performed for better characterization of pulmonary changes due to BPD, and especially for the evaluation of pulmonary changes as late sequelae (5).

Nuclear Medicine

Scintigraphy is rarely used in infants with BPD. Ventilation and perfusion scans demonstrate a ventilation perfusion mismatch and air trapping with delayed nuclide washout, especially in bullous areas.

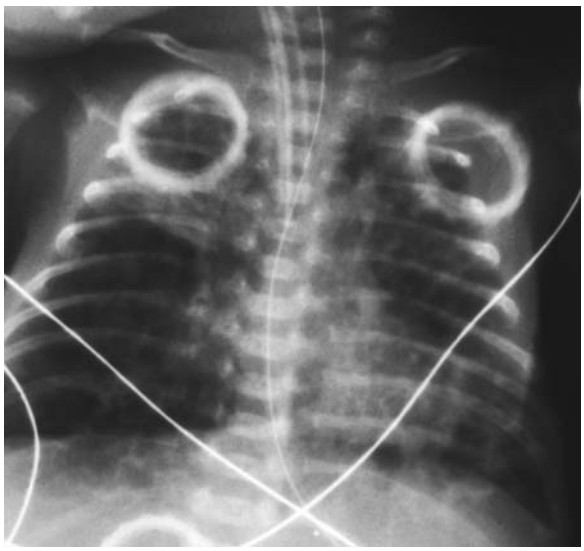

Dysplasia, Bronchopulmonary. Figure 1 Severe bronchopulmonary dysplasia. A coarse reticular pattern associated with pseudocysts (bubbles) especially in the lung bases is demonstrated. Atelectasis in the right upper lobe is also visible.

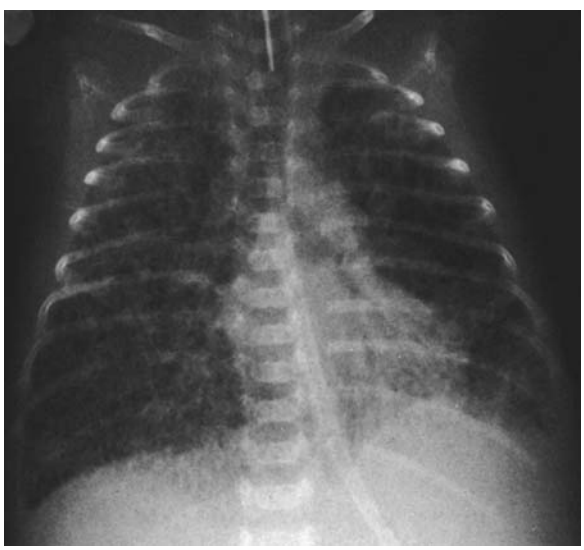

Dysplasia, Bronchopulmonary. Figure 2 Bronchopulmonary dysplasia with hyperinflated lungs, a fine reticular pattern and atelectatic areas in the left lower lobe.

Diagnosis

In 1967, Northway and associates first described four different stages of severity (6). Stage I (2–3 days after birth) is similar to uncomplicated respiratory distress syndrome with fine granular opacities and accentuation of the air bronchograms. In stage II of BPD (4–10 days), nearly complete opacification of the lungs is evident. Chest radiographs in stage III BPD (10–20 days) show small round cystic lucencies alternating with regions of irregular opacity. Stage IV BPD (beyond 1 month) demonstrates further enlargement of lucent regions alternating with thin strands of increased opacity, representing ▶bubbly lungs (2).

The typical radiographic findings with grossly coarse reticular patterns associated with large pseudocysts (bubbles) especially in the lung bases (Fig. 1), are less commonly seen in recent years, due to the changed treatment regimen of respiratory distress syndrome in premature infants. Nowadays, BPD appears typically with a finer reticular pattern, localized hyperlucent areas and generalized hyperaeration (Fig. 2) (5). On HRCT images the late sequelae of bronchopulmonary dysplasia are well-identified, including multifocal areas of hyperaeration, well-defined linear opacities, and triangular subpleural opacities with an external base and an internal apex, vascular attenuation with reduced bronchoarterial diameter ratios, bronchial wall thickening without bronchiectasis and bullae or pneumatoceles (2, 5). The radiological differential diagnosis of BPD includes Wilson-Mikity syndrome, congenital pulmonary lymphangiectasia, neonatal tuberculosis, cystic fibrosis, and Hamman–Rich syndrome.

Bibliography

1. Jobe AH, Bancalari E (2001) Bronchopulmonary dysplasia. Am J Respir Crit Care Med 163:1723–1729
2. Agrons GA, Courtney SE, Stocker JT et al (2005) From the archives of the AFIP: Lung disease in premature neonates: radiologic–pathologic correlation. Radiographics 25:1047–1073
3. Hussain NA, Siddiqui NH, Stocker JR (1998) Pathology of arrested acinar development in postsurfactant bronchopulmonary dysplasia. Hum Pathol 29:710–717
4. Ehrenkranz RA, Walsh MC, Vohr BR et al (2005) National Institutes of Child Health and Human Development Neonatal Research Network Validation of the National Institutes of Health consensus definition of bronchopulmonary dysplasia. Pediatrics 116:1353–1360
5. Oppenheim C, Mamou-Mani T, Sayegh N et al (1994) Bronchopulmonary dysplasia: value of CT in identifying pulmonary sequelae. Am J Roentgenol 163:169–172
6. Northway WH Jr, Rosan RC, Porter DY (1967) Pulmonary disease following respiratory therapy of hyaline membrane disease. N Engl J Med 276:357–368

Dysplasia, Skeletal

Karl Ludwig, Corinna E. E. Nierhoff
Department of Diagnostic Radiology, Orthopedic University Hospital Heidelberg, Heidelberg, Germany
karl.ludwig@ok.uni-heidelberg.de

Synonym

Osteochondrodysplasia

Definition

Skeletal dysplasias are genetic connective tissue disorders affecting skeletal development. They become apparent by the abnormal growth, shape, and composition of bone.

Pathology/Histopathology

Skeletal dysplasias are a heterogeneous group of disorders characterized by systematic development disorders of ossification (1–4).

In recent years, the genetic defect of several dysplasias was discovered. For many conditions the pathogenesis still remains unknown.

Skeletal dysplasias can be divided into osteodysplasias and chondrodysplasias: Osteodysplasias are subgrouped into osteopenic and sclerosing bone dysplasias. The most widely used classification is the International Nomenclature of Constitutional Disorders of Bone. Genetic bone disorders are classified into families of disorders in an attempt to incorporate clinical, radiodiagnostic, and morphological features together with the genetic background (5).

Clinical Presentation

Skeletal dysplasias are a highly heterogenic group comprising more than 200 disorders (1). In general, the appearance is a disproportionate short stature below the mean height of age.

The incidence is about 2–5:10,000 births (6). The inheritance pattern is variable. The most common dysplasias are achondroplasia, osteogenesis imperfecta (OI), and thanatophoric dysplasia.

Achondroplasia

With an incidence of 1:20,000 live births, achondroplasia is the most common osteochondrodysplasia.

Most patients are of normal intelligence and have a normal life expectancy.

The typical features are

- Short stature.
- Hyperkyphosis and lordosis.
- Short limbs.
- Y-shaped growth plates.
- Trident hand with persistent space between the long and ring fingers.
- Short pedicles, which can lead to spinal stenosis.
- Short femoral neck; metaphyseal flaring; dysplastic ileum; narrow sacroiliac groove; and flat-roofed acetabula.
- Prominent calvarial bones in contrast to small cranial base and facial bones.
- Limited elbow extension.
- Genu varum.

Osteogenesis Imperfecta

OI occurs in 1:20,000 to 1:60,000 of live births.

OI results from a defect of type I collagen production that leads to congenital osteopenia with increased bone fragility.

The Sillence classification differentiates four subtypes with different clinical manifestations and different inheritance patterns.

The common feature is a micromelic (short-limbed) dwarfism of variable degree. Bone fragility may cause perinatal death or severe deformities into adulthood.

Common radiological hallmarks include: (Fig. 1)

- Generalized osteoporosis.
- Spinal abnormalities with scoliosis and platyspondyly.
- Deformation of long bones depending on the severity of OI (from overtubulated bone with thin cortex to thickened shortened bone with multiple fractures).
- Hyperplastic callus formation.
- A so-called wormian aspect of skull bone.

An important differential diagnosis in a child with multiple fractures is child abuse.

Thanatophoric dysplasia

Thanatophoric dysplasia is nearly always lethal in the prenatal period.

Typical findings are curved or straight short femurs, symmetric micromelia, narrow thorax with short ribs, and a protuberant abdomen.

Polyhydramnion can be observed.

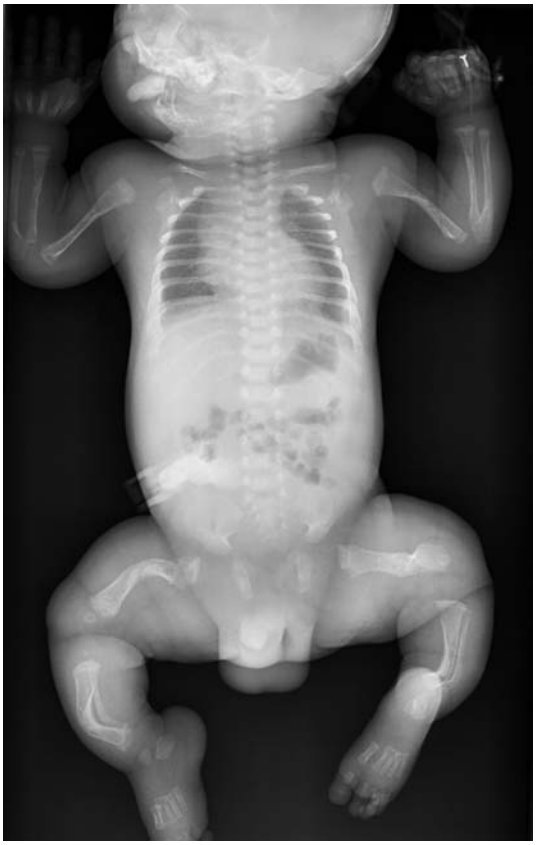

Dysplasias, Skeletal. Figure 1 Babygram shows a reduced bone density, a thinning of cortical bone, and severe deformation of long bones.

Imaging

The radiologic evaluation plays an essential part in establishing the diagnosis.

If the radiologic and clinical identification of a syndrome is not conclusive, further molecular and genetic testing is necessary.

The primary aim of the radiologic work-up is to find out which regions of the skeleton are predominantly affected.

Cardinal information is obtained by analysis of the long bones, the hands, the pelvis, and the spine. Further skeletal imaging—for example, of the skull, feet, and flat bones—is of additional relevance.

The analysis of long bones takes into account their length and shape and determines whether the changes manifest themselves in the epiphyses, metaphyses, or diaphyses. Bone density must be assessed, because increased or decreased bone density is sometimes the clue to specific diagnosis.

Some radiographic features are highly specific for certain pathologies. Examples are the radiographic images of the pelvis of achondroplasia or the hypoplastic scapulae and nonossified thoracic pedicles in campomelic dysplasia.

Timing of ossification should be evaluated because sometimes it gives a diagnostic clue: some dysplasias, for example, achondrogenesis or atelosteogenesis, show a delayed or retarded ossification of skeletal elements. The skeletal survey should be done before puberty to be able to evaluate the growth plate. In many dysplasias specific diagnosis after closure of growth plates is difficult and in certain cases a specific diagnosis cannot be reached.

The radiographic evaluation should include:

- Anteroposterior (AP) and lateral view of the skull and the entire spine.
- AP view of the thorax.
- AP view of the pelvis.
- AP view of the left hand.
- AP view of the long bones (in cases of symmetry it can be limited to one side).
- Lateral view of knee (patella).
- In neonates and children younger than 6 months with suspicion of skeletal dysplasia, a babygram (AP and lateral views of the entire body) is sufficient.

Magnetic resonance imaging (MRI) is used to display associated pathologies of the brain, the brain stem, and the spine.

Myelopathy of the cervicomedullary cord secondary to stenosis of the foramen magnum is best evaluated by MRI.

Helical computed tomography (CT) with multiplanar and three-dimensional reconstructions is useful to show the morphology of complex deformities and allows surgical planning.

Antenatal ultrasound: Prenatal ultrasonography can identify most fetuses with skeletal dysplasia by identification of short limbs and other skeletal and nonskeletal anomalies. The finding of a short femur length (relative to gestational age) on routine prenatal sonographs should alert the examiner and lead to a systematic evaluation of the entire skeleton.

Pathologic ossification and shape of long bones, for example, bowing and angulation of the femur, can be detected by 15–18 weeks' gestation and distinguishes fetuses with skeletal dysplasia from growth-restricted fetuses. Additionally, callus formation in cases of antenatal fractures, thorax hypoplasia, spinal deformities such as platyspondylia, hand deformities, craniofacial malformation, and other associated anomalies can be visualized by ultrasound.

Bone mineral densitometry (BMD) measurements with dual-energy X-ray absorptiometry (DEXA) of the lumbar spine (children >1 year) and femoral neck (children >6 years) or qualitative CT (QCT) of the

lumbar spine in children older than 4 years are accepted techniques with which to confirm osteoporosis in patients with OI.

Nuclear Medicine

Nuclear medicine is not used as a routine method in the evaluation of skeletal dysplasia.

Diagnosis

Because there is a high diversity in clinical and morphological features, the diagnosis of skeletal dysplasia can be very difficult. Typically the diagnosis is based on clinical hallmarks in combination with radiologic and morphologic studies. Biochemical or DNA analysis supports the diagnosis when the gene or the defective gene product is known.

A complete clinical assessment should include the following tests (5):

- Complete personal and family history with pedigree analysis.
- Physical examination with anthropometric measurements of height, weight, head circumference, upper-to-lower segment ratios, sitting height, and arm spans.
- Radiologic work-up.

If not conclusive, the following should be included:

- Biochemical studies to analyze protein defects.
- DNA studies.

Additionally histopathologic evaluation of specimens of chondroosseous tissues can help lead to the correct diagnosis. This requires bone biopsy and it should always be performed if the patient undergoes surgical intervention, for example, because of fracture stabilization.

Bibliography

1. Tahbi H, Lachmann RS (1996) Radiology of Syndromes, Metabolic Disorders und Skeletal Dysplasias. 4th edn. Mosby, St Louis
2. Ornoy A, Borochowitz Z, Lachmann R (1988) Atlas of Fetal Skeletal Radiology, Mosby St Louis
3. Rimoin DL, Krakow D (1999) Diagnosis and Treatment of the Unborn Child. Idelson-Gnocchi, Reddick, Fla, pp 63–65
4. Mortier GR (2001) The diagnosis of skeletal dysplasias: a multidisciplinary approach. Eur J Radiol 40(3):161–167
5. International Working Group on Constitutional Diseases of Bone (1998) International nomenclature and classification of the osteochondrodysplasias (1997). Am J Med Genet Oct 12 79(5):376–382
6. Rasmussen SA, Bieber BR, Benacerraf BR et al (1996) Epidemiology of osteochondrodysplasias: changing trends due to advances in prenatal diagnosis. Am J Med Genet 61:49–58

Dysplastic Nodule, Hepatic

The term dysplastic nodule replaces older terms like adenomatous hyperplasia and macroregenerative nodule and refers to a nodular region of hepatocytes with dysplasia but without definite malignancy, which represent an intermediate step in the pathway of hepatocarcinogenesis in cirrhosis. Dysplastic nodules are considered neoplastic, premalignant nodules. At ultrasound US and unenhanced computed tomography CT it is difficult to distinguish these nodules from regenerative nodules or small hepatocellular carcinomas (HCCs). The signal characteristics at magnetic resonance MR allow to differentiate these nodules from HCC. Usually dysplastic nodules are hyperintense on T1-weighted and hypointense on T2-weighted sequences. Dysplastic nodules may be siderotic, appearing in these cases as hypointense both on T1 and T2-weighted images. The enhancement behaviour at contrast US, CT and MR studies is the most important imaging feature in the differential diagnosis of dysplastic nodule and HCC. The latter is typically hypervascular and shows marked enhancement in the arterial phase, while dysplastic nodules have a prevalent portal blood supply and do not show arterial enhancement. Sometimes a nodule-within-a-nodule appearance may be noted on MR images; this finding consists of one or more hyperintense internal foci within a low signal intensity nodule on T2-weighted images and represents HCC foci developing within a dysplastic nodule. This pattern is particularly evident if a focus of HCC originates within a siderotic regenerative nodule. The central nodule usually also shows enhancement during the arterial phase at dynamic study.

▶Cirrhosis, Hepatic

Dystocia

Prolonged birth, such as due to fetopelvic disproportion.

▶Magnetic Resonance Pelvimetry

Dysuria

Painful or difficult urination. Dysuria is most commonly due to bacterial infection of the urinary tract, causing inflammation of the bladder (cystitis) or kidney (pyelonephritis).

▶Urethra, Stenosis

Echo Enhancers

►Contrast Media, Ultrasound, Commercial Products

Echo Planar Imaging

An MRI technique in which multiple adjacent image slices are acquired in a single acquisition, allowing the acquisition of an entire image volume in a very limited amount of time. This imaging technique is mostly used in fMRI experiments.

►Brain, Functional Imaging

Echo-enhanced Urosonography

US contrast material is instilled into the urinary bladder *via* catheterization to demonstrate VUR. This is achieved by constant scanning of the bladder and the retrovesical space as well as—alternating—the pelvocaliceal system and the proximal ureter for detection of refluxed echo-enhancing material.

►Reflux, Vesicoureteral in Childhood

Echography

►Ultrasound, Imaging

ECMO (Neonate, Pediatric) Imaging

M. Riccabona
Department of Radiology, Division of Pediatric Radiology, Medical University of Graz, University Hospital, Graz, Austria
michael.riccabona@meduni-graz.at

Synonyms

Extracorporeal membrane oxygenation

Definition

Extracorporeal membrane oxygenation (ECMO) is an extracorporeal therapy used in severe respiratory insufficiency that cannot be treated by conventional techniques.

Embryology and Pathogenesis

ECMO depends on the various underlying diseases that necessitate this invasive therapy. The principle of ECMO is to substitute the diseased lung (and partially also heart function). Venous blood is pumped through a filter that uses a membrane for CO_2 elimination and blood oxygenation; this blood is then retuned to the body. Two major approaches are used: (1) Venous ECMO (vv), in which blood is drained from and then infused back into a large vein (i.e., inferior and superior cava vein); (2) Arteriovenous (av) ECMO, in which blood is drained from the right ventricle and infused into the thoracic aorta usually *via* a carotid catheter (this approach additionally allows support of the circulatory system). This therapy needs anticoagulation, putting patients on ECMO at a high risk of hemorrhage.

Clinical Presentation

Severe respiratory and eventually combined cardiac and multiorgan system failure (MOSF) not treatable by conventional means as the common presentation of a variety of congenital or acquired diseases [e.g., diaphragmatic hernia, meconium aspiration syndrome or other severe respiratory distress syndrome (RDS) of various origin, multi-organ system failure multi-organ system failure (MOSF) or severe cardiac conditions, where ECMO may be used as bridging to and after cardiac or thoracic surgery]. Detailed ECMO indications and contraindications vary between different centers and are usually established clinically.

Imaging

There are many imaging methods used in ECMO—most of the imaging needs to be performed at the patients' bedside, as it is difficult and dangerous to transport these critically ill patients to the imaging suite. The *role of imaging* includes:

First, pre-ECMO assessment of disease (see specific chapters and entries); additionally, a detailed assessment of the heart (by echocardiography) and the brain is essential, as well as assessment of potential contraindications (cerebral hemorrhage, brain death, etc.). Subsequently, image-guided catheter placement at onset of ECMO (proper position of the catheter tip) is advocated. Finally, monitoring during ECMO (particularly in case of complications) as well as post-ECMO assessment of potential sequelae are heavily based on imaging.

Imaging Modalities

In *pre-ECMO assessment* mostly *plain film* and *ultrasound* (US) are used [patients are usually too sick to be brought to a computed tomography (CT) or magnetic resonance imaging (MRI) suite]. However, sometimes a *CT* (assessment of the lung or in cerebral hemorrhage) or *MRI* study (hypoxic-ischemic encephalopathy) may become necessary. At *ECMO onset*, US or plain film (and fluoroscopy) studies are used for catheter placement. *Monitoring during ECMO* is mostly performed using plain film and US—in rare cases a CT may become necessary, although bringing the patient on ECMO to the CT suite is quite complicated. *After ECMO* the entire range of imaging modalities may be used, as indicated by the child's specific condition; most commonly US (brain, heart, abdominal parenchymal organs, vessels), plain film (chest, skeletal queries), CT of the chest, and brain MRI are performed for post-ECMO follow-up.

Typical Imaging Findings

Pre-ECMO Assessment

Imaging findings depend on the actual disease, which is usually infant RDS, meconium aspiration syndrome, MOSF (e.g., in severe septicemia), severe cardiac malformation, diaphragmatic hernia and other severe treatable lung malformations, inhalation or aspiration of severely toxic agents with consecutive severe RDS, acute chest syndrome in sickle cell disease, posttransplantation (heart and/or lung) problems. Here, primary diagnosis usually relies on imaging as an essential part of the diagnostic work-up. Furthermore, pre-ECMO assessment for potential ECMO contraindications is necessary and may reveal cerebral hemorrhage, severe brain edema or hypoxic-ischemic encephalopathy, or significant variation of cerebral vessel anatomy with hypoplastic communicant arteries obviating av-ECMO, as does brain death. Finally, a thorough assessment of the patient's cardiac situation is mandatory.

At the Beginning of ECMO

Catheter positioning is one of the most crucial aspects; the catheter tips should be in the aortic arch (arterial line) and in the right atrium (venous line) for av-ECMO, and in the distal inferior cava vein and the right atrium or superior cava vein for vv-ECMO. It is performed differently in various sites. Some centers only measure distances from a chest X-ray and insert the tubes blinded with a postinterventional film to check for and document the position of the catheter tip (Fig. 1a). Some centers use US, which allows for real-time guidance during the procedure and for position correction after having started the extracorporeal circulation (Fig. 1b). The latter may be important, as the consecutive reduction of respirator settings leads to a higher position of the diaphragm, which may cause catheter malposition. For this procedure, the catheters are not fixed initially, but only after repositioning and final adjustment after having started ECMO. Some centers use fluoroscopy to properly position the tips of the large catheters.

Monitoring on ECMO

Most centers have a strict imaging monitoring protocol, which heavily relies on plain film (chest) and US (brain morphology and perfusion, cardiac function, abdominal organ size and perfusion, catheter position and catheter thrombosis or obstruction, other vascular or perfusion disturbances, pleural hemorrhage or effusions, etc.). The appearance of the lung and chest on plain films depends on the underlying condition and the amount of residual mechanical ventilation for respiratory support. Often the

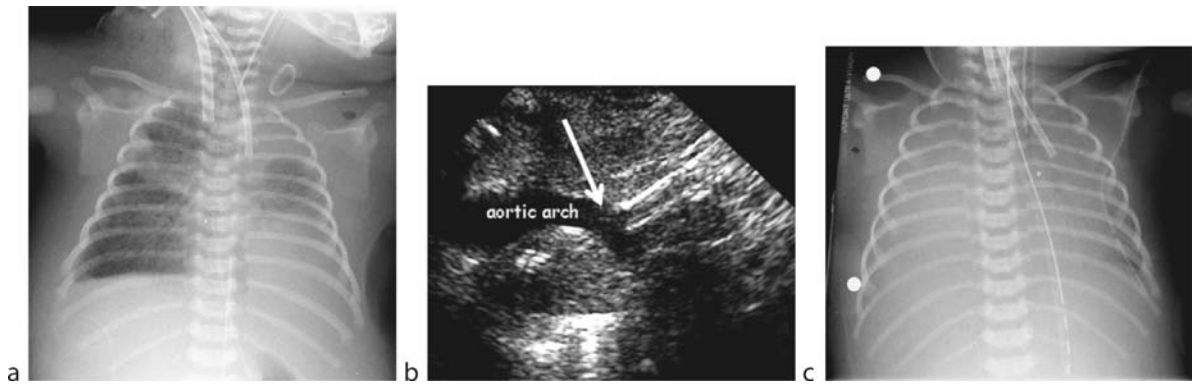

ECMO (Neonate, Pediatric) Imaging. Figure 1 Early imaging in ECMO (a) Chest plain film for catheter positioning at ECMO onset. (b) Sonographically guided catheter positioning of ECMO cannula. The tip of the arterial line (=>, inserted *via* right carotid artery) just reaches the aortic arch. (c) Chest film during ECMO, in the phase of a "resting lung." Note the "white out" of the lung, due to reduced air content (not to be mistaken for pleural effusion), as well as the ECMO lines in place.

lung is virtually put at rest in the early ECMO stages, with hardly any ventilation left. During this "white out" of the lung, hardly any air is left in the lungs, thus creating a soft tissue or fluid-like appearance of the thorax without a visible ventilated lung (Fig. 1c). Later on (when the pulmonary condition improves) or in milder conditions (with an expected short ECMO time of only a few days and avoiding complete lung collapse), high PEEP is applied and high-frequency oscillation or positive pressure ventilation is reassumed, and a better air content of the lung can be seen, with some signs of overinflation, dystelectasis, or structural damage (influenced by the initially underlying condition). During this stage surfactant can be used to support lung recruitment; this can potentially create chest film abnormalities (i.e., in cases of maldistribution). Other lung complications may be noticed during this phase such as pneumothorax, pleural effusion, lung hemorrhage, or edema (e.g., in cardiac insufficiency). Another important aspect in following up patients on ECMO is to regularly check catheter and tube position, as malpositioning or perforation may create a disastrous situation, particularly with the increased risk of hemorrhage (impaired coagulation caused by heparin necessary for performing the extracorporeal circulation).

Typical US findings and tasks during ECMO include: Regular evaluation of the catheter tip position with assessment of possible catheter obstruction, obstruction of corresponding vessels with consecutive congestion, thrombosis, or suboptimal blood flow caused, for example, by malposition of the arterial line in the descending aorta, thus potentially creating hypoperfusion of the supraaortal branches, particularly to the brain and to the coronary arteries. Other sequelae may be caused by venous obstruction such as hypoperfusion or congestion of abdominal organs, renal vein thrombosis, or the commonly observed widening of the cerebrospinal fluid spaces (particularly extracerebral). On arterial Doppler sonography a high diastolic flow may be observed, with little pulsatile undulation (depending on the flow of the ECMO machine) in av-ECMO that should not be mistaken for brain edema or hyperperfusion (Fig. 2a). Furthermore, various complications such as (brain) hemorrhage and other (abdominal organ) pathology (e.g., organomegaly, ascites, infarction, hyper- and hypoperfusion, secondary phenomena in septicemia such as abscess formation etc.) may become visible. Finally, postoperative complications need to be addressed in patients who have been operated on with ECMO and remain on ECMO postoperatively (e.g., after correction of cardiac malformations or diaphragmatic hernia), such as hemorrhage, pleural and pericardial effusion, posthypoxic necrotizing enterocolitis, or bowel perforation.

MRI is hardly applicable in neonates and children on ECMO, as the pump and devices are generally incompatible with the magnet. However, even if difficult, CT may be indicated during ECMO, usually for queries regarding the chest and lungs or in sonographically insufficiently assessable suspected cerebral hemorrhage (Fig. 2b).

Imaging After ECMO

Imaging after ECMO should not be neglected, including monitoring of lung development (chest films, chest CT), assessment of the development of potentially affected parenchymal abdominal organs such as the kidney or the liver (US, scintigraphy, MRI), assessment of cerebral

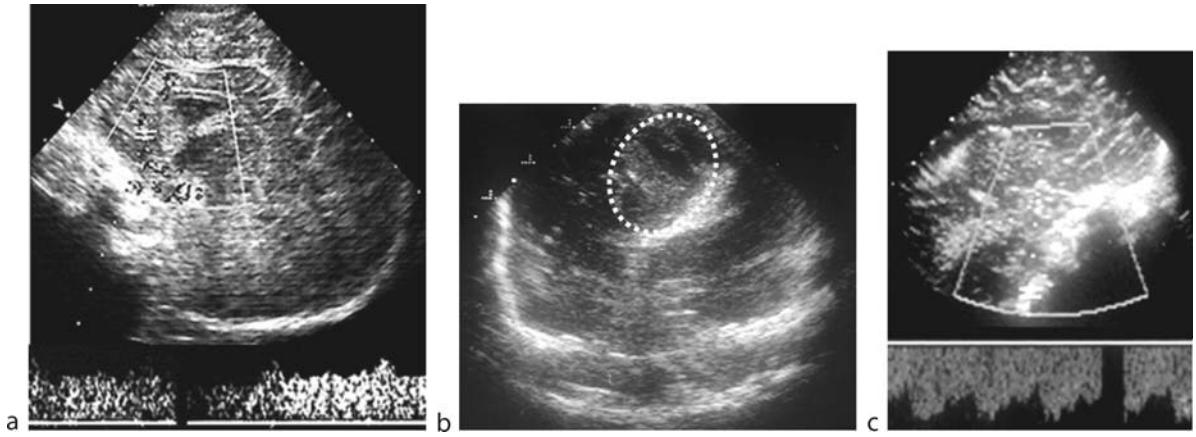

ECMO (Neonate, Pediatric) Imaging. Figure 2 Cerebral US on ECMO (a) Brain duplex Doppler of a newborn on av-ECMO (anterior cerebral artery): note the high diastolic flow velocity due to the ECMO roller pump, with only short systolic flow spikes at normal peak systolic flow velocity still visible. (b) Severe intracranial parenchymal hemorrhage (O) in an infant on av-ECMO for severe RDS after oil inhalation. (c) Additional vertebral steel phenomenon on DDS: reversed flow direction with ECMO-typical flow profile in the (basilar and) vertebral artery due to carotid obstruction by the ECMO cannula.

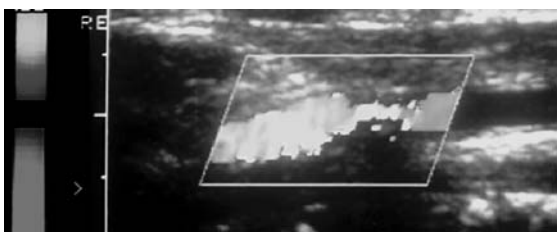

ECMO (Neonate, Pediatric) Imaging. Figure 3 Carotid artery stenosis after av-ECMO. Note the short, narrow concentric stricture at the site of the recanalization procedure, with some aliasing on color Doppler sonography.

outcome (potential hydrocephalus, cerebral atrophy, or hypoxic brain damage) using US and MRI, and assessment of potential vascular complications (stenosis, thrombosis, and occlusion; usually at the site of the catheter). This is performed primarily with US, particularly in vessels that have been recanalized surgically at catheter removal (Fig. 3). In some of these cases, CT or MR angiography or even digital subtraction angiography (DSA) may become necessary for further detailed evaluation of vascular anatomy before deciding on therapy options.

Diagnosis

Imaging diagnosis and diagnostic features depend on the underlying organ, symptom, or condition, as well as on the imaging modality.

Bibliography

1. Canady AI, Fessler RD, Klein MD (1993). Ultrasound abnormalities in term infants on ECMO. Pediatr Neurosurg 19:202–205
2. Hall Jr, Hartenberg MA, Kodroff MB (1985). Chest radiographic findings in neonates on extracorporeal membrane oxygenation. Radiology 157:75–77
3. Lidegran MK, Ringertz HG, Frenckner BP, et al (2005). Chest and abdominal CT during extracorporeal membrane oxygenation: Clinical benefits in diagnosis and treatment. Acad Radiol 12:276–285
4. Riccabona M, Dacar D, Zobel G, et al (1995). Sonographically guided cannula positioning for ECMO. Pediatr Radiol 25:643–645
5. Slovis TL, Sell LL, Bedard MP, et al (1988). Ultrasonographic findings (CNS, thorax, abdomen) in infants undergoing extracorporeal oxygenation therapy. Pediatr Radiol 18:112–117
6. Zobel G, Kuttnig–Haim M, Urlesberger B, et al (1996). Extracorporeal lung support in pediatric patients. Acta Anaesthesiol Scand 109:122–125

ECMO Cannula

An extracorporeal circulation life support technique that replaces ventilation for conditions not treatable by conservative respiration therapy; large catheters are used to drain the blood from the venous system and reinfuse oxygenated blood.

ECST

European Carotid Surgery Trial.
▶Stent, Carotid Artery

Ectopic Kidney

Malposition of the kidney by embryological reasons; these kidneys often are hypo-dysplastic, associated with other genito-urinary tract malformations or dysfunctions, and may be found in the pelvis and mid-abdomen, but even rarely in a thoracic position.

▶Urinary Tract

Ectopic Pancreas

Ectopic pancreas is defined as pancreatic tissue in ectopic anatomical locations, lacking contact with the normal pancreas. Ectopic pancreatic tissue possesses its own ductal system and blood supply.

▶Congenital Anomalies of the Pancreas

Ectopic Pregnancy

Clinically and on imaging, bleeding due to ectopic pregnancy that is most commonly located within the fallopian tube or ovary may be similar to ruptured follicle cysts with hemoperitoneum. A positive pregnancy test allows the definitive diagnosis of ectopic pregnancy.

▶Cyst, Follicular, Ovarium
▶Fetal Imaging

Ectopic Thymus

Aberrant thymic tissue arising from remnants of the thymopharyngeal duct due to migrational defects during thymic embryogenesis.

▶Congenital Malformations, Thymus

Edema

The presence of an abnormal accumulation of fluid in the intercellular spaces of the breast, which may be due to inflammation, vascular or lymphatic obstruction or treatment such as radiotherapy.

▶Carcinoma Breast, Imaging Mammography, Secondary Signs

Embolization, Portal Vein

Gerrit Krupski-Berdien
University Klinik Hamburg-Eppendorf, Hamberg, Germany
krupski@uke.uni-hamburg.de

Synonyms

Liver regeneration, liver hypertrophy, and induced liver growth are used to describe the restoration of destroyed; Lost or removed liver parenchyma; and liver growth following portal vein embolization (PVE)

Definitions

Liver regeneration summarizes both enlargement of a formerly smaller entire liver or liver lobe as well as hepatic cellular and mitochondrial mRNA replication followed by cell division induced by elevated levels of hepatocyte growth factor (HGF).

Pathology/Histopathology

Liver regeneration is a complex process initiated by an increase in portal venous blood pressure. LaBreque and colleagues characterized HGF as the primary cellular signal with secretion from hepatocytes. HGF binds to the c-met receptor (1) at the hepatocyte membrane and causes mitochondrial and nuclear mRNA transcription as well as replication of mitochondria and entire hepatocytes. Apart from HGF, other growth factors include IGF, EGF, and TGF α/β. Proto-oncogenes are also affiliated to c-met regulation and interaction. Fig 1 gives an impression of the interactions of HGF and other growth factors, as well as oncogene products with the hepatocyte c-met receptor.

As result, liver cells divide, and the remaining liver regenerates within 3–6 months. The early volume changes are visible and measurable at 3–4 weeks after PVE; therefore, they do not represent true cell replication but cellular swelling and interstitial edema associated with intercurrent portal hypertension. Nevertheless, the amount

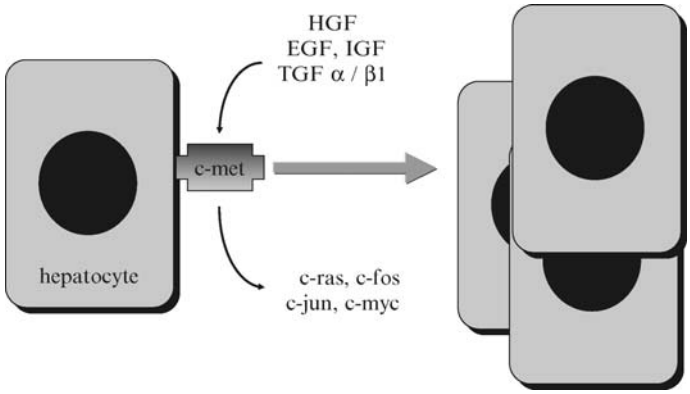

Embolization, Portal Vein. Figure 1 (a, b) Axial multidetector-row computed tomographic image of a 59-year-old man presenting with a Klatskin tumor, bismuth type IIa, proposed for extended right liver lobe resection 3 weeks after percutaneous portal vein embolization of segments IV–VIII (a). The left lateral lobe already looks ballooned. Three months after liver resection, the remaining left lateral lobe has gathered marked size and is almost as large as an entire liver (b).

of early volume increase can be interpreted as an indicator of adequate regeneration induction.

Mitochondria replicate much faster than hepatocytes—within 1–2 weeks. Parallel to this, the liver functional reserve improves markedly, which might be why safe resection can be performed almost 8 weeks after embolization and why PVE enables liver resection in moderate cirrhosis, preventing feared postoperative liver failure.

Potential interactions of proto-oncogenes and excretion of growth factors in a patient with a known tumor always suggests potential collateral tumor growth stimulation. To date, although discussion is ongoing on this topic, there is no clear evidence for tumor growth stimulation (2) after PVE.

Clinical Presentation

Surgical removal remains the method of choice for curative treatment of primary and secondary liver malignancies. Clear resection margins (R0 resection) are the key to cure in liver surgery for metastatic disease. This means extended liver resection in almost 50% of patients (3, 4). To prevent postoperative liver failure, an increase in the future liver remnant and improvement of postoperative liver function are necessary in up to one-third of all patients proposed for extended resection. By definite disruption of the portal venous flow to the right liver lobe using either embolization fluids, particles, coils, combinations of these, or, as formerly done, surgical ligation of the portal venous stem, regeneration of the remaining liver parenchyma is induced, resulting in volume increase and functional reserve improvement (5, 6). After 4–8 weeks, extended hepatic resection is possible, as indicated by volume increase on computed tomographic (CT) volumetry of the future liver remnant.

This two-stage hepatectomy approach facilitates resectability in primarily nonresectable patients. Today this procedure is routinely used in the surgical treatment of central hilar bile duct tumors (Klatskin tumors) as well as in surgery for extended hepatic metastases. In addition, by enhancing the functional reserve (7), PVE can enable resection of hepatocellular carcinoma in cirrhotic liver patients or extended resection in hepatic parenchymal damage associated with chemotherapy (particularly oxaliplatin).

Following PVE, No Specific Signs and Symptoms are Evident.

To prevent tumor growth and spread during liver regeneration and while awaiting resection, particularly in patients with rapidly growing tumor, adjuvant chemotherapy can be performed safely beginning 2 weeks after PVE. This intervals must be adhered to assure adequate regenerative response (which otherwise can be suppressed by antiproliferative drugs or antimetabolites). For chemotherapy, CPT-11 or 5-FU/FA can be used, whereas oxaliplatin should be avoided because of its hepatotoxicity.

Imaging

The regeneration itself cannot be imaged, but liver volume changes (Fig. 2a, b) may be measured using cross-sectional magnetic resonance imaging (MRI) and CT images. CT and MRI volumetry can be performed manually by marking the liver lobe with a variable region of interest and summating the marked areas, or automatically

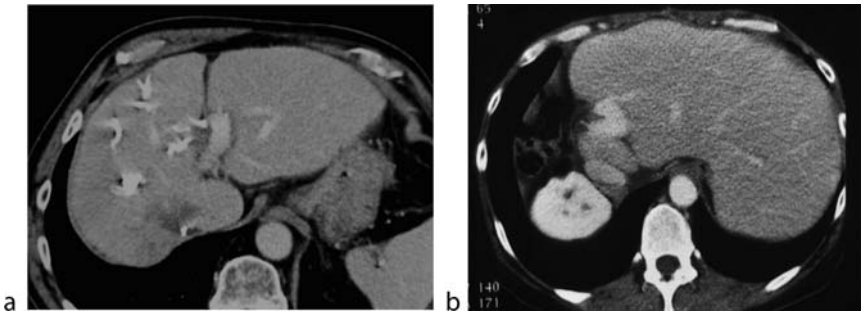

Embolization, Portal Vein. Figure 2 (a, b) Percutaneous direct portogram before (a) and directly after embolization of segments IV–VIII using a mixture of cyanoacrylate and lipiodol.

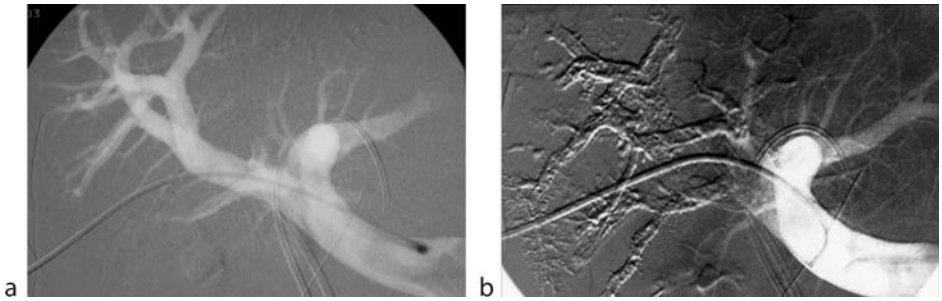

Embolization, Portal Vein. Figure 3 Direct portogram after embolization of segments V–VIII. Segment IV provides two major branches (*, ·) and a few small branches.

using segmentation software (e.g., MeVis, Bremen, Germany) that calculates liver volumes after locating segmental anatomy based on portal venous ramification.

Interventional Radiological Treatment

Before PVE is begun, adequate biliary drainage is obligatory, with a resulting serum bilirubin level at least below 4 mg/dL. Endoscopic or, particularly, multiple percutaneous external drains must be employed in central hilar tumors.

Percutaneous PVE is state-of-the-art for inducing liver regeneration (5). Depending on the indication, one can choose entire right lobar embolization, including segment IV, before extended right resections for maximal regenerative response or limited right lobe embolization in patients with impaired liver function before minor hepatic resections (such as in cirrhotic liver).

An intercostal right-sided puncture comparable with the PTC procedure or a subxiphoidal puncture will give access to the portal venous system. Thereafter, the portal venous system is embolized branch by branch until only the left lateral or left lobe remains perfused.

Both access site and embolization technique or embolization material vary widely among experienced centers, indicating that there is neither a best technique nor a best embolization material. In Japan, right-sided access and pure ethanol as embolization material is preferred, whereas in Europe (6), left-sided ultrasound-guided access and a mixture of cyanoacrylate and lipiodol as embolization material is most frequently used (Fig. 3a, b). The latter technique has three advantages when compared with ethanol and right-sided access: no double-balloon occlusion catheter has to be used; the postintervention clinical course is less eventful (after ethanol use, transaminases will increase up to 1,000 U/L and more because of adjacent liver parenchyma necrosis, contributing to necessary hospitalization time of 2–3 days; on the other hand, in more than 90% of cases patients can be discharged on the day after a procedure using histoacryl-lipiodol embolization); and costs are lower.

Segment IV is technically important and therefore has to be mentioned. Compared with simple right-sided embolization, extended right embolization including segment IV will result in significantly higher resulting volumes of the prospective liver remnant. Unfortunately, regarding the portal venous anatomy, segment IV embolization is rather difficult. In approximately two-thirds of patients, two or more larger portal branches can be seen deriving from the recess of Rex (Fig. 4). The branches to segments II and III are very close, bearing the risk of accidental dislodgement

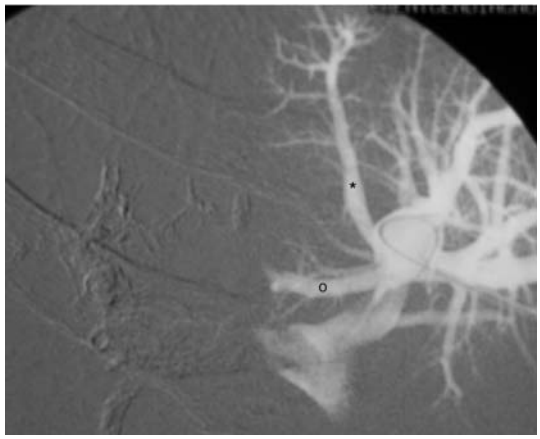

Embolization, Portal Vein. Figure 4

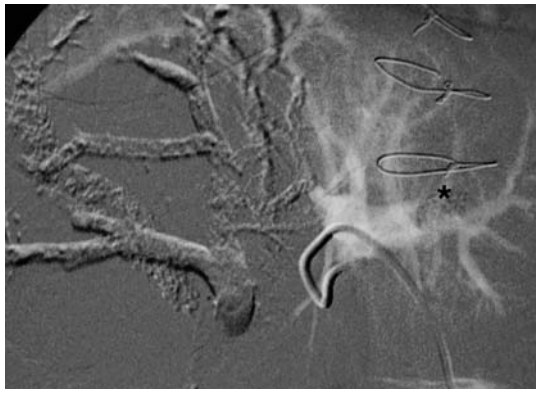

Embolization, Portal Vein. Figure 5 Dislodged embolization material (cyanoacrylate and lipiodol) within the segment II portal vein branch, resulting in a peripheral hypoperfusion.

of embolization material. Therefore, superselective and safe cannulation of these branches is obligatory, often necessitating several SIM-1, Cobra-1 or -2, or even custom-shaped guiding catheters for cannulation attempts. If only subtotal embolization of segment IV can be achieved without overembolization hazard, it is worthwhile to await liver regeneration and perform a second percutaneous embolization in a two-stage procedure within a 4-week interval.

Overall complication rates are low and include dislodgement of embolization material (Fig. 5), hemorrhage (subcapsular), and insufficient regeneration.

Bibliography

1. Bottaro DP, Rubin JS, Faletto DI et al (1991) Identification of the HGF receptor as the c-met oncogene product. Science 251:802–804
2. Elias D, Ouellet JF, de BAere T et al (2002) Preoperative selective portal vein embolization before hepatectomy for liver metastases: long term results and impact on survival. Surgery 131:294–299
3. Jaeck D, Oussoultzolgou E, Rosso E et al (2004) A two-stage hepatectomy procedure combined with portal vein embolization to achieve curative resection for initially unresectable multiple and bilobar colorectal liver metastases. Ann Surg 240:1037–1049
4. Heinemann A, Wischhusen F, Püschel K et al (1999) Standard liver volume in the Caucasian population. Liver Transpl Surg 5 (5):366–368
5. Broering DC, Hillert C, Krupski G et al (2002) Portal vein embolization vs. portal vein ligation for induction of hypertrophy of the future liver remnant. J Gastrointest Surg 6:905–913
6. de Baere T, Roche A, Vavasseur D et al (1993) Portal vein embolization: utility for inducing left hepatic lobe hypertrophy before surgery. Radiology 188:73–77
7. Belghiti J, Ogata S (2005) Assessment of hepatic functional reserve for the indication of hepatic resection. Hepatobiliary Pancreat Surg 12:1–3

Embolization, Transcatheter Embolization

Transcatheter embolization consists in selective occlusion of a systemic or pulmonary vessel through an open-ended catheter using coils, particles or other embolization agents. Embolization is indicated to treat various clinical conditions, including hemorrhage, vascular malformations, AVM or tumors.

▶Pulmonary Arteriovenous Malformations

Emphysema and Bulla

Hans-Ulrich Kauczor
German Cancer Research Center, Heidelberg, Germany
hu.kauczor@dkfz-heidelberg.de

Synonyms

Alpha-1-antitrypsin deficiency; Bullous, bulla hyperinflation; Emphysema (centrilobular, panlobular, paraseptal)

Definition

Emphysema is defined histologically as a constant, irreversible, and abnormal enlargement of the alveolar spaces distal to the terminal bronchioles (3). It corresponds with

destruction of the interstitium within the secondary pulmonary lobule and also the perilobular septae without any increase in soft tissue.

Pathology/Histopathology

According to the site of damage, emphysema may be classified as centrilobular, panlobular, or irregular. In centrilobular emphysema, the damage within the secondary lobule is pronounced along the axial interstitium, especially the respiratory bronchioles, while the peripheral compartment is less or not affected. In panlobular emphysema, the whole lobule is affected, with paraseptal emphysema being a type of panlobular emphysema with a special predilection for a subpleural location at the lung apices. An irregular or paracicatricial emphysema does not respect the normal anatomical architecture of the lung.

The development of emphysema is fostered by an imbalance between proteases and antiproteases. Alpha-1-antitrypsin, which is synthesized in the liver, is the most important pulmonary antiprotease. Its homozygous deficiency leads to panlobular emphysema, which has a basal predominance even in the absence of cigarette smoking. The latter is the single most important cause of emphysema due to an increased release of proteases and elastases, finally resulting in destruction of pulmonary tissue. Emphysema is commonly associated with chronic obstructive pulmonary disease (COPD), which also comprises chronic bronchitis. Emphysema without airway obstruction is infrequent.

A bulla is an air-filled, thin-walled space within the lung with a diameter >1 cm. Its wall is formed by pleura, connective tissue, or compressed lung parenchyma. Two types of bullous disease can be differentiated: bulla with COPD as a particular presentation of otherwise typical emphysema, or primary bulla without other parenchymal disease or airway obstruction.

Clinical Presentation

Cigarette smoking leading to chronic airflow limitation is the major determining factor in the development of emphysema and chronic bronchitis. The patients complain of productive cough and dyspnea. Airflow obstruction and emphysema regularly become apparent after the age of 50 years or after 20–30 pack-years of smoking. According to their presentation, patients with emphysema can be differentiated as "▶pink puffers" or "▶blue bloaters." Pink puffers, or type A patients, are usually thin and complain of severe dyspnea, but they are relatively well oxygenated without hypercapnia and do not suffer from right heart failure (cor pulmonale). Blue bloaters, or type B patients, suffer from severe hypoxemia and hypercapnia and have peripheral edema due to right heart failure but only mild dyspnea.

In emphysema, the thorax becomes fixed in an inspiratory position, the chest is barrel-shaped, thoracic kyphosis is increased, shoulders are raised, and the thorax moves en bloc together with contraction of the accessory respiratory muscles. Complications of emphysema are pulmonary arterial hypertension, right heart failure, recurrent exacerbations of COPD, and polycythemia secondary to hypoxemia.

Primary bullous disease is characteristically asymptomatic with minimal abnormalities at pulmonary function tests, and it can be detected incidentally, such as at chest radiography.

Imaging

Chest Radiography

Chest radiography provides only indirect signs of hyperinflation, which leads to an increase in lung size that can be appreciated in all three orientations (Fig. 1). This increase in size, which is associated with a loss of attenuation, is best seen on the lateral view. The enlargement of the retrosternal space is a very good indicator. It is measured 3 cm below the angulus sterni as the distance between the posterior aspect of the sternum and the anterior aspect of the ascending aorta. More than 2.5 cm is indicative for hyperinflation and emphysema. On the anteroposterior view, two criteria can be applied: First, the enlargement of the intercostal spaces reflects the protrusion of the hyperinflated lung into these spaces. The distance between two ribs can be measured easily. Second, the position of the diaphragm is lowered and its shape flattened. In severe hyperinflation the diaphragm can even be inversed. The changes of the diaphragm are best appreciated by measuring the sternodiaphragmatic angle on the lateral view and the costodiaphragmatic angle on the anteroposterior view, with 90° and 40°, respectively, as thresholds indicating hyperinflation.

The loss of attenuation can be homogeneous or inhomogeneous, such as in localized emphysematous destruction and bulla formation (Fig. 1). Local hyperinflation can induce compression atelectasis of other lung areas. The emphysematous destruction of the pulmonary architecture results in a loss of vascular markings that is best appreciated in the lung periphery. The vascular rarefication and the decreased pulmonary blood volume further enhance the lower attenuation caused by hyperinflation. A nonhomogeneous distribution of emphysema or bullae is associated with displacement of vessels. Rarefication of vessels leads to a substantial reduction of

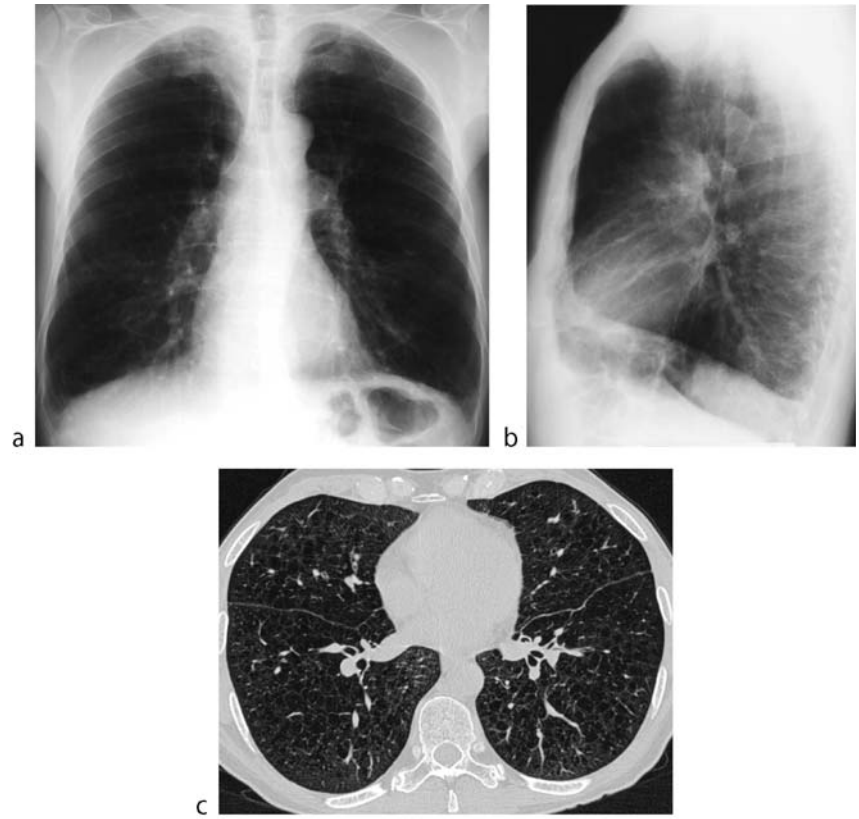

Emphysema and Bulla. Figure 1 Centrilobular emphysema. Chest radiograph postero-anterior (a) and lateral (b) views show hyperinflation with an enlarged retrosternal space and flattened diaphragm as well as a homogeneous loss of attenuation. Computed tomography (c) shows the typical appearance of centrilobular emphysema.

vascular cross-section, ultimately resulting in pulmonary hypertension with its typical radiographic signs: dilation of central pulmonary vessels and abrupt changes of the vascular calibers at the level of the lobar, segmental, or subsegmental branches. Subsequent changes affect the right heart with enlargement and signs of right heart failure, such as pleural effusion.

Bullae are identified as local, thin-walled, sharply delineated areas of avascularity (Fig. 2). They are better seen in the end-expiratory position. Evidence of diffuse emphysema may be present elsewhere in the lung.

Additional Findings on CT

Computed tomography (CT) is capable of directly visualizing the enlargement of the alveolar space and the loss of the connective tissue by a decrease in visible structures and attenuation. Different types of emphysema can be categorized according to location of the low attenuation affecting the central areas of the secondary pulmonary lobule in centrilobular emphysema (Fig. 1) or the whole secondary lobule in panlobular emphysema. Special emphysema types such as paraseptal, paracicatricial, and lobar can also be differentiated (1). Emphysema typically does not show any walls. This is an important criterion for differentiation from other cystic patterns and bullae. Measurements of lung density on CT are generally accepted for quantitation of emphysema. With high-resolution CT, an upper threshold of –950 HU should be used, and the relative fraction of lung area or volume affected by emphysema – called emphysema or pixel index – can be calculated.

CT is much more sensitive than plain radiographs for identifying bulla, and can also reveal concomitant emphysema or compression of adjacent lung (Fig. 2). The latter might be used as an indication for surgical bullectomy.

Nuclear Medicine

Perfusion or ventilation scintigraphy plays only a minor role in the diagnosis of emphysema. On ventilation

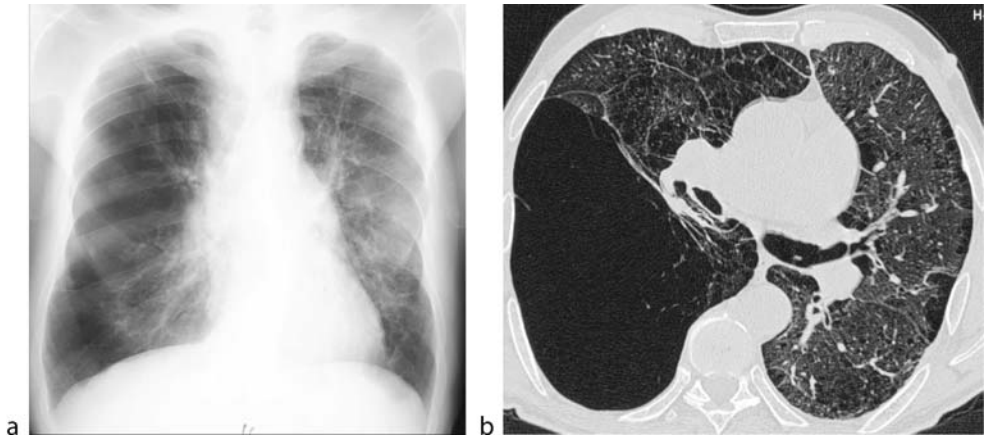

Empyema. Figure 2 Bulla with emphysema. Chest radiograph (a) views show a large area of hyperlucency representing a bulla with compression of the adjacent lung. Computed tomography (b) also shows the large bulla on the right with compression of the adjacent lung and reveals emphysema of centrilobular and paraseptal type in both lungs.

scintigraphy using Technegas, emphysema is associated with a patchy and irregular distribution yielding hot spots and defects. Generally, the distribution of perfusion and ventilation is matched. When using xenon as a tracer for ventilation, single-breath examinations demonstrate a heterogeneous distribution, whereas scans after equilibrium and washout will show retention (trapping) of the tracer in emphysematous areas after a 3 min washout. Bullae are recognized as large perfusion and ventilation defects.

Diagnosis

Although emphysema is defined histologically, it is generally not diagnosed by biopsy and is only an additional finding at surgery for lung cancer. Thus imaging, especially CT, carries the most important role for the morphology-based diagnosis of emphysema (2).

Besides imaging, the diagnosis of emphysema is generally made from the results of lung function tests. A decrease of forced expiratory volume in 1 s (FEV1) indicates airway obstruction as it occurs in COPD and emphysema. A decrease in peak expiratory flow or of FEV1 expressed as a percentage of forced expiratory volume are additional helpful indicators of COPD and emphysema. Hyperinflation relates to an increase in residual volume followed by an increase in functional residual capacity and total lung capacity, which are associated with a decrease in vital capacity. The loss of alveolar surface area due to emphysematous destruction is best assessed by measuring the single-breath diffusion capacity, which will be markedly reduced in emphysema patients. As a result of alveolar hypoventilation and ventilation-perfusion matching, arterial blood gases are commonly disturbed, with hypoxemia frequently associated with hypercapnia (partial and global respiratory failure).

The diagnosis of bulla is usually made on chest radiography or CT.

Bibliography

1. Foster WL Jr, Gimenez EI, Roubidoux MA et al (1993) The emphysemas: radiologic-pathologic correlations. Radiographics 13:311–328
2. Newell JDJ (2002) CT of emphysema. Radiol Clin North Am 40:31–42
3. Snider GL, Kleinerman J, Thurlbeck WA et al (1985) The definition of emphysema. Am Rev Respir Dis 132:182–185

Emphysematous Pyelonephritis

Severe complication of AP that appears in diabetic patients, in which gas is produced within renal tissue.
▶ Pyelonephritis, Acute

Empyema

The presence of gross pus in the pleural cavity; it consists of an effusion containing polymorphonuclear leukocytes and fibrin. The formation of an empyema can be divided into three phases: exudative (pus accumulation),

fibrinopurulent (fibrin deposition and loculation of pleural fluid) and organising (fibroblast proliferation, potentially lung entrapment by scarring).
▶Pleural Effusion
▶Pneumonia in Childhood

Empyema Necessitatis

TB pleural infection that penetrates the chest wall, creating a subcutaneous abscess.
▶Tuberculosis

Empyema, Gallbladder

Suppurative infection associated to cystic duct obstruction in which the gallbladder fills with purulent material.
▶Cholecystitis

En Plaque Meningiomas

En plaque meningiomas are a variant of primary neuraxial meningiomas, which may infiltrate both the dura and the bone cloaking the inner table of the skull.
▶Neoplasms, Extraaxial, Brain

Encephalitis

Encephalitis refers to any diffuse inflammatory process involving the brain that can be caused by a broad spectrum of agents. The most frequent virus responsible for acute viral encephalitis in adulthood is the herpes simplex virus type 1 (HSV-1) and in the neonatal period the herpes simplex virus type 2 (HSV-2). Viral encephalitides in immunocompromised patients are usually caused by human immunodeficiency virus (HIV) and cytomegalovirus (CMV).
▶Encephalitis, Herpes
▶Encephalitis, HIV

Encephalitis, Herpes

E. Turgut Tali, Serap Gultekin
Section of Neuroradiology & MRI Center
Department of Radiology
Gazi University School of Medicine, Besevler,
Ankara 06510 Turkey
turgut.tali@gazi.edu.tr

Definition

Herpes viruses are a large group of double-stranded DNA viruses. Herpes simplex virus type 1 (HSV-1) is the causative agent in 95% of herpetic ▶encephalitis cases and the most common cause of fatal sporadic encephalitis.

Pathology/Histopathology

The gross appearance of the brain in adults with herpes encephalitis initially shows acute inflammation, congestion and/or hemorrhage, and softening. After approximately 2 weeks, these changes proceed to frank necrosis and liquefaction.

Clinical Presentation

Patients with HSV-1 encephalitis may present with fever, headache, nausea and vomiting, and neck stiffness with altered mental status (1).

Imaging

Computed Tomography

Computed tomography (CT) images in the early stage of the disease are frequently normal, despite severe clinical manifestations. Hypodense lesions can be seen in the temporal lobes with or without involvement of the frontal lobes.

Magnetic Resonance Imaging

Magnetic resonance imaging (MRI) is more sensitive and demonstrates the early findings of edematous changes of HSV-1 encephalitis (Fig. 1) (2). These are an increased signal, particularly in the temporal and inferior frontal lobes on fluid attenuation inversion recovery (FLAIR) and T2-weighted images that may be seen as early as 48 h after the onset of symptoms. The signal abnormalities often extend into the contralateral temporal lobe, insular cortex, and cingulate gyri, sparing the basal ganglia (3).

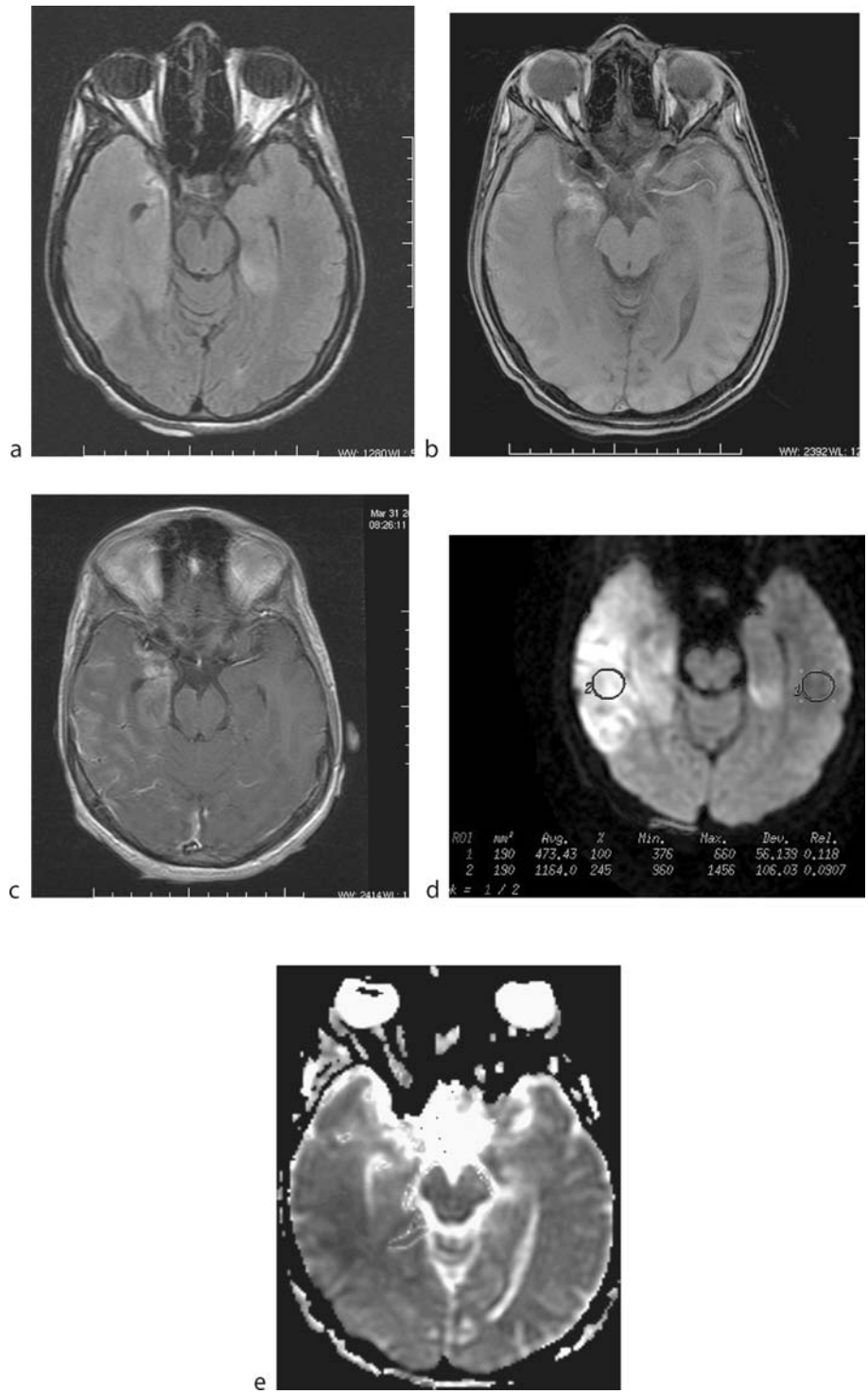

Encephalitis, Herpes. Figure 1 HSV-1 Encephalitis. Axial FLAIR (a) image shows diffuse hyperintense signal with mass effect involving both the gray and white matter primarily in the right temporal lobe together with a small portion of the left temporal lobe. Axial, precontrast (b) T1-weighted image shows hyperintense signal at the anteromedial temporal lobe corresponding to hemorrhage. Mild hyperintensity is also seen along the lateral cortical sulci. There is also effacement of the sulci in the affected area. Postcontrast axial (c) T1-weighted image reveals gyriform enhancement of the right temporal lobe. DWI (d) demonstrates high signal in the affected region where ADC map (e) shows low signal compared to contralateral unaffected area, consistent with cytotoxic edema.

Although HSV-1 results in necrotizing and hemorrhagic encephalitis, frank blood is not commonly seen on imaging studies. Acute hemorrhage on MRI may appear as a focus of moderate to marked hypointensity on GRE images or on T2WI. The late sequelae of HSV-1 are atrophy, encephalomalacia, and dystrophic calcification (4). Two distinct types of diffusion-weighted imaging (DWI) findings have been noted: lesions similar to cytotoxic edema and lesions similar to vasogenic edema. The patients with the former type of lesions have fulminating disease and are in a poor clinical condition. Those with the latter represent early cases and they are in fairly good clinical condition (5). Magnetic resonance spectroscopy (MRS) shows elevated choline, low *N*-acetylaspartate levels, and the presence of lipids and lactate, reflecting necrosis.

Diagnosis

The mainstay in the diagnosis is the detection of HSV DNA in the cerebrospinal fluid by using polymerase chain reaction; however, false-negative results do occur.

Bibliography

1. Castillo M, Thurner M (2004) Imaging viral and prion infections. Seminars in Roentgenol 39:482–494
2. Andreula C (2004) Cranial viral infections in the adult. Eur Radiol 14:E132–E144
3. Steiner I, Budka H, Chaudhuri A, Koskiniemi M, Sainio K, Salonen O, Kennedy PGE (2005) Viral encephalitis: a review of diagnostic methods and guidelines for management. Eur J Neurol 12:331–343
4. Jordan J, Enzamann DR (1991) Encephalitis. Neuroimaging Clin N Amer 1:17–38
5. Sener RN (2001) Herpes Simplex ensefalitis: diffusion MR imaging findings. Comput Med Imaging Graph 25:391–7

Encephalitis, HIV

E. Turgut Tali, Serap Gultekin
Section of Neuroradiology & MRI Center
Department of Radiology
Gazi University School of Medicine, Besevler,
Ankara 06510 Turkey
turgut.tali@gazi.edu.tr
sergultekin@yahoo.com

Definition

Human immunodeficiency virus (HIV) belongs to the retrovirus family of RNA viruses (1). Its most common clinical manifestation is encephalopathy (28% of all AIDS autopsies).

Pathology/Histopathology

The virus is carried to the brain by macrophages and monocytes. The infection damages the blood–brain barrier and induces the production of cytokines. Initially, there is neuronal death leading to atrophy. Afterward, the virus causes astrogliosis, myelin pallor, and the presence of multinucleated cells (2). This gives rise to gradual demyelination and to perivascular nodules of microglial cells, monohistiocytes, and macrophages (1).

Clinical Presentation

The patient presents with progressive subcortical dementia.

Imaging

Computed Tomography

The most common finding is atrophy; however, computed tomography (CT) images are often normal.

Magnetic Resonance Imaging

The most common magnetic resonance imaging (MRI) findings are diffuse brain atrophy and widespread lesions in the periventricular white matter, predominantly the frontal lobes. The gray matter is generally spared and a mass effect is absent. Lesions usually do not enhance following contrast medium administration. The extent of disease roughly parallels the clinical deterioration. The lesions may reduce in size when treated (1, 2). Magnetic resonance spectroscopy (MRS) shows low *N*-acetylaspartate levels. Additionally, elevated levels of choline and myoinositol may be seen in these patients on short-echo time MRS. MRS abnormalities may be detected before the onset of encephalopathy and may be used to monitor the response to treatment (2).

Diagnosis

Clinical findings should guide the imaging studies. Demonstration of the typical imaging findings in an HIV-positive patient with neurological manifestations is very helpful for the diagnosis.

Bibliography

1. Andreula C (2004) Cranial viral infections in the adult. Eur Radiol 14:E132–E144
2. Castillo M, Thurner M (2004) Imaging viral and prion infections. Semin Roentgenol 39:482–484

Encephalopathy of the Newborn

▶Cerebral Neonatal Disease (Neuro View)

Enchondroma

Enchondroma is a benign cartilage-forming tumor arising in the medullary portion of the affected bone.
▶Neoplasms, Bone, Benign

Endoluminal Therapy

Endoluminal therapy refers to treatments that occur from within a blood vessel without the need to open the vessel using conventional surgery.
▶Aneurysm, Aortic and Thoracic

Endometrial Carcinoma

▶Carcinoma, Endometrium Uteri

Endometrium

The endometrium is the central portion of the uterus and undergoes cyclic regeneration due to the hormonal influences of the menstrual cycle. The endometrium is thinnest at time of menstruation and gets thicker throughout the proliferative and secretary phase. After menopause, atrophy of the endometrial lining will occur.

Endoscopic Retrograde Cholangiopancreatography (ERCP)

ERCP is an endoscopical procedure that allows catheterization of the papilla of Vater and radiological evaluation of the biliary tree and pancreatic ducts by means of contrast medium injection. ERCP also offers the possibilities of prompt conversion into a therapeutical procedure such as papillotomy, stone extraction, and biliary and pancreatic stent placement over benign or malignant ductal strictures. The most important complication is the development of acute pancreatitis.
▶Biliary Anatomy

Endoscopic Ultrasound

EUS is the marriage of ultrasound and endoscopy, where ultrasound images of the gut wall and adjacent structures are obtained by passing an ultrasound probe into the gastro-intestinal tract.
▶Neoplasms, Gastroduodenal
▶Neoplasms Oesophagus

Endoscopy of the Oesophagus

Fibre endoscopic examination of the oesophageal mucosa. May also evaluate the distensibility of the oesophagus. It is possible to obtain biopsies during the procedure.
▶Diverticulum, Oesophagus

Endothelium

Endothelium is a single layer of endothelial cells that lines the heart, blood vascular and lymphatic channels.
▶Targeted Microbubbles

Endourologic Surgery

Surgical procedures performed with either endoscopic guidance or fluoroscopic guidance.
▶Ureteropelvic Junction Syndrome

Endovascular Coiling

▶Aneurysm, Intracranial

Endovascular Therapy

All types of treatment with the use of catheters within the venous or arterial system in order to dilate or recanalize arteries and veins or to obstruct vascular malformations or tumor vascularization.

▶Stroke, Interventional Radiology

Endovascular Treatment

▶Aneurysm, Intracranial

Endovascular Treatment of Internal Carotid Artery Stenosis

▶Stent, Carotid Artery

Enhancement

The increase in signal intensity in a vessel or in tissue after the arrival of the contrast agent. The enhancement can be assessed statically (at the time point of maximum concentration in the target region) or dynamically (looking on the time course of contrast agent wash-in and wash-out). The maximum enhancement (peak intensity) is related to the local blood volume, the wash-in time to the local blood flow velocity.

▶Contrast Media, Ultrasound, Application in Folical Splenic Lesions
▶Contrast Media, Ultrasound, Commercial Products

Enlargement of the Spleen

▶Splenomegaly

Enteric-Portal Drainage, Pancreatic

In pancreatic transplantation with enteric-portal drainage technique the arterial graft and the portal vein are anastomosed with the recipient's common iliac artery and superior mesenteric vein, respectively, whereas the exocrine pancreatic secretions are drained by an anastomosis between the donor's duodenum and a small bowel loop. In this technique the insulin is physiologically released in the portal venous system of the recipient.

▶Transplantation, Pancreatic

Enterocele

Descent of the peritoneal sac in between the rectum and the vagina down to the level of the perineum during defecation or Valsalva maneuver is called an enterocele. It may impress the posterior vaginal wall (grade II) and evert it to the outside across the introitus (grade III). An enterocele most often contains the sigmoid colon and mesosigmoid fat, but may also contain small bowel. It may persist after relaxation and need manual reposition.

▶Pelvic Floor Dysfunction, Anovectal Manifestation
▶Pelvic Floor Dysfunction, Genitourinary

Enteroclysis

Small bowel enema by duodenal intubation. The best method of contrast medium examinations. Several techniques exist, e.g., barium monocontrast, double contrast with barium and methylcellulose or air or guarin.

▶Malabsorption

Enterocolitis, Necrotizing

Veronica Donoghue
Radiology Department, Children's University Hospital, Dublin 1, Ireland
veronica.donoghue@cuh.ie

Definition

Necrotizing enterocolitis is due to alteration of the integrity of the intestinal mucosa as a result of ischaemia

and hypoperfusion together with bacterial overgrowth. It is predominantly a disease of premature infants but can also occur in the term infant.

Pathology/Histopathology

The precise aetiology of necrotizing enterocolitis is uncertain and is thought to be multifactorial in origin. Ischaemia and hypoperfusion leading to mucosal damage which often extends through the bowel wall, together with bacterial invasion and inflammatory response are the most likely mechanisms of bowel wall necrosis. The distal ileum and proximal colon are most commonly affected. Bowel perforation occurs in 12–31% of patients. The bacteria involved include *Escherichia coli, Klebsiella and Clostridium*. However, frequently organisms are not isolated in these infants. The hypoperfusion may result from hypoxia-induced spasm of the bowel arterial supply. Other causes include stress, hypothermia and hyperviscosity, hypovolaemia, cardiac left-to-right shunting, decreased ventricular output, cardiopulmonary bypass for cardiac surgery, sepsis, dehydration, shock and cocaine abuse (1). Once ischaemia or hypoperfusion occurs ileus develops. After this initial period the bowel becomes active again and bloody diarrhoea may develop. At this stage there is loss of mucosal integrity and overgrowth of bacteria which leads to the formation of gas in the bowel wall and occasionally in the portal venous system. Pneumoperitoneum may develop following bowel perforation.

Clinical Presentation

Clinically these infants have bile stained aspirates, abdominal distension, tenderness, bloody stools, hypotension and shock. Initial therapy involves nasogastric suction to decompress and rest the bowel and the use of broad spectrum antibiotics and intravenous nutrition. Treatment should be instituted once the diagnosis is suspected clinically without waiting for the development of specific radiological signs.

Imaging

The role of imaging is to confirm the diagnosis and monitor its course. Anteroposterior and cross-table lateral radiographs are performed. A left lateral decubitus view involves unnecessary repositioning if the ill neonate and is less sensitive in the demonstration of free intraperitoneal air (2). The timing of serial radiographs is determined clinically. They are important to determine when to stop therapy and to determine if surgical intervention is required. The earliest and most common radiographic sign is bowel loop distension. This sign however is non-specific but should make one suspicious. Pneumatosis intestinalis is diagnostic (Fig. 1). However inter-observer variability in the diagnosis of pneumatosis is considerable. It maybe cystic (submucosal) or linear (intramuscular or subserosal) in nature. It tends to be an early rather than a late finding and maybe transient. It usually involves the colon or terminal ileum but may occur in other areas of the bowel. There is a poor correlation between the presence and extent of pneumatosis and the severity of the disease. In addition pneumatosis can sometimes be difficult to distinguish from faeces or meconium mixed with air in the bowel lumen.

Bowel wall thickening, a persistently isolated dilated bowel loop, ascites or portal venous gas may develop. Portal venous gas represents dissection of intramural pneumatosis into the lymphatics and mesenteric veins (Fig. 1). This may also be transient (2).

Ultrasonography is useful to detect intraperitoneal fluid and to guide paracentesis. The technique is also useful to detect gas in the portal venous system. Gas in the

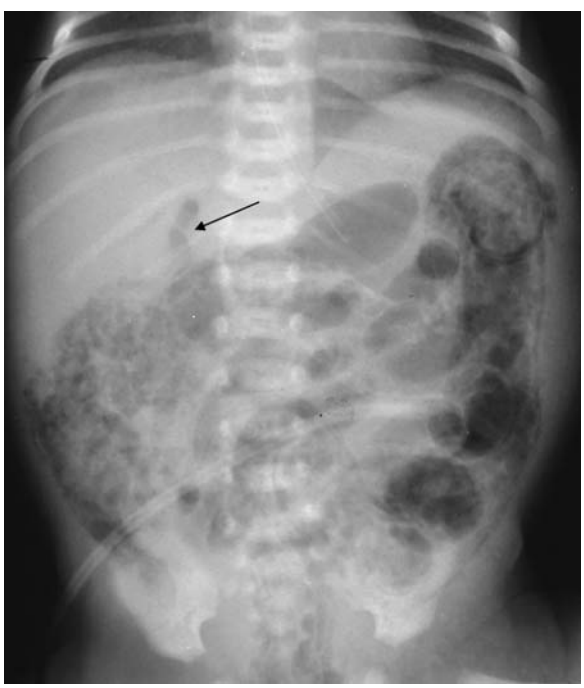

Enterocolitis, Necrotizing. Figure 1 Premature infant with necrotizing enterocolitis. There is diffuse intramural air and portal venous gas (*arrow*). There is also lucency over the liver and central upper abdomen indicating perforation.

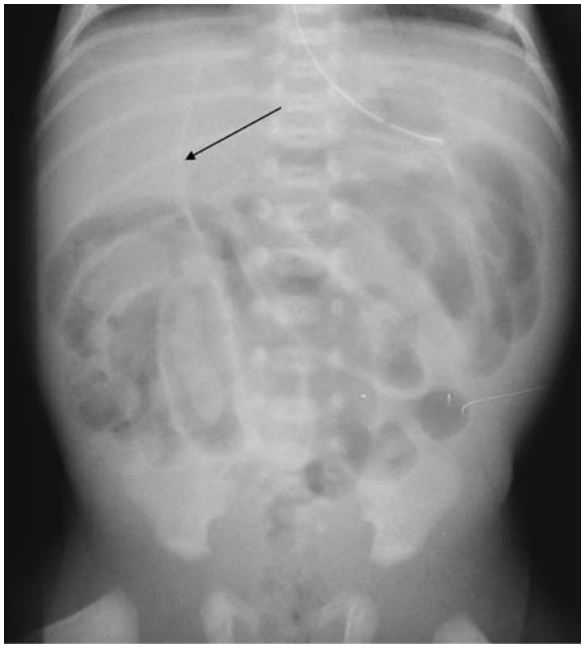

Enterocolitis, Necrotizing. Figure 2 Infant with necrotizing enterocolitis and bowel perforation. There is intramural air in the right flank and both sides of the bowel wall and the falciform ligament (*arrow*) are visible.

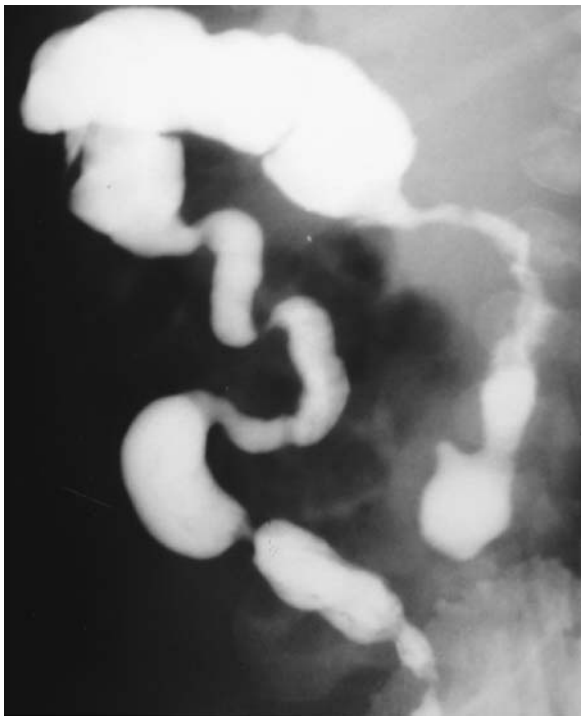

Enterocolitis, Necrotizing. Figure 3 Multiple colonic strictures following necrotizing enterocolitis.

bowel wall and abscess formation are also detected by sonography.

Colour Doppler ultrasound findings of absence of bowel wall perfusion has been shown to be more accurate than clinical examination and plain radiography findings in the prediction of necrosis in neonates with necrotizing enterocolitis and therefore may alter clinical staging and management (3).

The presence of a pneumoperitoneum is an absolute indication for surgical intervention and indicates full thickness bowel wall necrosis and perforation (Fig. 2). When there is a large amount of free air there maybe evidence of a central abdominal lucency, lucency over the liver with air outlining the falciform ligament (Fig. 2). Both sides of the bowel wall may also bee seen. Only 63% of infants with surgically proven perforation however, demonstrate a radiographically detectable pneumoperitoneum.

Other recognized indications for surgery are: clinical deterioration despite aggressive medical management, fixed dilated bowel loops, abdominal mass and ascites. When a neonate is too unwell to undergo surgery a percutaneous drain maybe placed with delayed resection of necrotic bowel.

Patients may go on to develop strictures at previously affected sites (Fig. 3). They maybe solitary or multiple, are usually short and of varying severity. They are suspected in infants with recurrent intermittent obstruction, acute obstruction, low-grade continuing rectal bleeding or constipation. When performing a contrast enema for diagnosis one must take great care to show continuity of the bowel lumen as short strictures maybe obscured by overlapping loops. Strictures may resolve spontaneously particularly if they occur after an acute episode of necrotizing enterocolitis. These latter areas of narrowing are not true fibrotic strictures but more likely areas of inflammatory narrowing.

Diagnosis

The clinical presentation in infants of bile stained aspirates, abdominal distension, tenderness, bloody stools together or in isolation, should make the clinician strongly suspicious of necrotizing enterocolitis and lead to the immediate introduction of medical therapy. The presence of dilated bowel loops together with bowel wall pneumatosis or portal venous air is diagnostic.

Bibliography

1. Swischuk LE (2003) The alimentary tract. In: Swischuk LE (ed) Imaging of the Newborn, Infant and Young Child. 5th edn. Lippincott Williams and Wilkins, Baltimore

2. Donoghue V, Twomey EL (2005) The neonatal gastrointestinal tract. In: Carty H, Brunelle F, Stringer DA, Kao SCS (eds) Imaging Children. 2nd edn. Elsevier, Churchill Livingstone
3. Faingold R, Daneman A, Tomlinson G et al (2005) Necrotizing enterocolitis: assessment of bowel viability with color doppler US Radiology 235:587–594

Enthesitis, Inflammatory Reaction of Tendon and Ligament Insertions

Enthesitis, inflammatory reaction of tendon and ligament insertions is seen in spondyloarthropathies, such as at the iliac crest, tuber ischiadicum, achilles tendon insertion, plantar fascia insertion, and so on, and comprises both destruction and bony proliferation. In magnetic resonance imaging, adjacent bone marrow edema and tendon attenuation, soft tissue edema, and contrast material enhancement in various degrees are present.
▶Spondyloarthropathies, Seronegative

Enzyme-sensing Probes

▶Molecular Probes, Optical Probes

Eosinophilic Granuloma

Eosinophilic granuloma is a bone manifestation of Langerhans cell histiocytosis, which represents an idiopathic, probably nonneoplastic proliferation of Langerhans cells with a localized or systemic clinical expression.
▶Neoplasm-Like Lesions, Bone

Ependymoma

Ependymoma is a tumor originating from the walls of the ventricles in children and young adults. In the posterior fossa, ependymomas often show a characteristic plastic growth, facilitating the differentiation from a medulloblastoma or pilocytic astrocytoma.
▶Neoplasms, Brain, Posterior Fossa, Pediatric

EPI

▶Echo Planar Imaging

Epidermoid Cyst

Cystic tumor of the spleen that accounts for 10% of all nonparasitic splenic cysts. It is a well-defined, thin-walled anechoic lesion. Calcifications and septations may occur.
▶Congenital Malformations, Splenic

Epidural Steroid Injection

The conservative therapy for sciatica
▶Conservative Therapy for Lumbosacral Radicular Syndrome

Epidural/subdural Hematoma

Extracerebral fluid collection with compression and displacement of the brain.
▶Trauma, Head, Accidental

Epiglottitis

Rapidly progressive infection and inflammation of the epiglottis and surrounding tissues that may lead to sudden respiratory obstruction and death.
▶Inflammatory Diseases, Larynx

Epithelial Ovarian Cancer

▶Carcinoma, Ovarium

Epithelial Ovarian Neoplasm

▶Carcinoma, Ovarium

Epithelioid Hemangioendothelioma

▶Hepatic Sarcoma

Epithelioid Hemangioendothelioma, Hepatic

Rare primary hepatic malignancy of vascular origin developing exclusively in adults with a female predominance. This malignancy is typically solid formed of endothelial cells with an epithelioid appearance. Immunohistochemically, these tumoral cells are positive for endothelial markers and negative for epithelial ones. Microscopically, dendritic spindle cells associated with epithelioid round cells within myxoid and fibrous stroma can be seen. Fibrosis and calcifications are described in some cases. Macroscopically, this tumor is formed of multiple solid nodules of variable size located in a peripheral distribution forming large confluent masses composed of a fibrotic central core and a cellular hypervascular periphery. This tumor frequently induces fibrosis causing capsular retraction in the case of peripheral lesions; this capsular retraction is suggestive of epithelioid hemangioendothelioma. Tumoral growth tends to replace hepatic parenchyma and in the case of a protracted course a compensatory enlargement of the uninvolved liver parenchyma can be seen. Extrahepatic involvement includes the peripheral lymph nodes, mesentery, and in some cases the development of calcifications. Metastatic spreading is most commonly confined to the bones and soft tissues.

▶Hepatic Sarcoma

Erb-Duchenne Paralysis

Injury to the fifth and sixth cervical nerve roots with and without involvement of the fourth and seventh roots.

▶Trauma, Birth

ERCP

▶Endoscopic Retrograde Cholangiopancreatography

Erectile Dysfunction (ED)

▶Impotence

Erosions of the Odontoid Process

Erosions of the odontoid process occur in rheumatoid arthritis. They can be located basally laterally, ventrally, and at the tip. These erosions may progress to major destruction of the odontoid process and are part of the inflammatory process of the occiput-C2 area, which may lead to mechanical instability.

▶Rheumatoid Arthritis

Erythropoietic System, Diseases of the

Otmar Schober
Department of Nuclear Medicine, Coordinator Collaborative Research Center, Molecular Cardiovascular Imaging (SFB 656-MoBil), University Hospital Münster
Münster, Germany
schober.otmar@uni-muenster.de

Synonym

Anemia

Definition

Anemia is defined as a low hemoglobin concentration: <13.5 g/dl for men and <11.5 g/dl for women.

Pathology/Histopathology

Anemia may be due to a reduced production (e.g., marrow failure, chronic disease) or an increased loss (e.g., iron deficiency, hemolysis) of erythrocytes.

Clinical Presentation

Fatigue, dyspnea, palpitations, headache, tinnitus, anorexia, dyspepsia, bowel disturbance, pallor, and retinal hemorrhages may occur in anemia. In severe anemia (hemoglobin <8 g/dl), hyperdynamic circulation and heart failure may be present.

Nuclear Medicine

Blood, Erythrocytes and Plasma Volume Determination

Radioactive ^{99m}Tc (short half-life)-labeled erythrocytes are suitable for blood volume determination. The marked erythrocytes must be reinjected within 2 h and the blood samples taken 30 min after injection. Should the erythrocyte kinetics be determined in addition, the labeling must be performed using the long-life ^{51}Cr.

After the radioactively labeled erythrocytes are injected, they distribute themselves in the blood volume. When a blood sample is taken, the concentration of radioactivity in the sample is the same as that in the patient's blood volume. The most important indication for determination of the erythrocyte and the blood volumes is the differential diagnosis of anemias.

Erythrocyte Kinetics

Erythrocytes have an average lifespan of 115 days. The average survival time and the main sequestration site of the mixed-age population can be determined with the patient's particular erythrocytes, following corresponding regulations for ^{51}Cr labeling (1 MBq, $Na_2{}^{51}CrO_2$ in ACD solution) and the measurement of the erythrocyte-bound chromium in the blood (2, 4). In addition, a standard sample is prepared. Blood samples are taken for two weeks without congestion in order to measure their radioactivity and compare them against the standards. From the standardized readings, the half-life of the erythrocyte-bound chromium in the blood is determined. The measured average half-life of the lifespan of the erythrocyte is smaller than the real erythrocyte half-life of 25–40 days; this is called apparent erythrocyte half-life.

The apparent half-life is found to be reduced to 5–20 days in patients with hemolytic anemia. The greatest reductions are seen with acquired autoimmune hemolytic anemia. Further indications are hereditary spherocytosis, nocturnal paroxysmal hemoglobinuria, infections, tumors, and rheumatic diseases; however, the lifespan alone is not pathognomonic.

The sequestration site of the erythrocytes is localized through the uptake measurements (constant measuring times) of the liver, spleen, and heart (as a measure for the blood pool). With acquired hemolytic anemia, the spleen is the main sequestration site. With a considered splenectomy, the contribution of the spleen to erythropoiesis must be taken into account (compare to ferrokinetic). With an intravascular hemolysis, no organ-specific sequestration site is observed. Hereditary spherocytosis (liver-spleen quotient >2) and hereditary nonspherocytic hemolytic anemia (increase from liver and spleen) show characteristic uptake patterns.

Iron Resorption

With the iron isotope ^{59}Fe it is possible to determine intestinal iron resorption (1, 3). Measurement of the whole-body retention from an orally applied $^{59}Fe^{2+}SO_4$ test dose (20 kBq, 2.8 mg) with vitamin C is the most common method. The interindividual (and very different) plasma iron clearance following intravenous injection cannot be applied for determining resorption.

Immediately after the oral application of $^{59}Fe^{2+}SO_4$, the first whole-body measurement is carried out to define the 100% value. Further measurements follow on the third and seventh days. The normal values are considerably varied (10–40%).

The differential diagnosis of iron deficiency anemia is influenced by the results of the iron resorption examination. Reduced iron resorption values point to a disease of the small intestine. Normal values for intestinal iron resorption provide no conclusions to the cause of a proven iron deficiency. If there is an increase in the intestinal iron resorption, the first line of thinking must be blood loss. Heavy blood loss during the examination time can simulate a normal result with an actually increased resorption.

For the diagnosis of hemochromatosis, no crucial significance can be attributed to determination of the intestinal iron resorption. The method promises a differential diagnostic gain for patients with hypersiderinemia and anemia. An increased intestinal iron resorption points to a bone marrow hyperplasia and increased ineffective erythropoiesis (that is, a sideroachrestic or sideroblastic anemia).

Diagnosis

In addition to the hemoglobin concentration, the mean cell volume (76–96 fl) must be determined to discriminate between microcytic, normocytic, and macrocytic anemias.

Bibliography

1. Beshara S, Sorensen J, Lubberink M et al (2003) Pharmacokinetics and red cellg utilization of ^{52}Fe/^{59}Fe-labelled iron polymaltose in anaemic patients using positron emission tomography. Br J Haematol 120:853–859
2. Mock DM, Lankford GL, Widness JA et al (1999) Measurement of red cell survival using biotin-labeled red cells: validation against ^{51}Cr-labelled red cells. Transfusion 39:156–162
3. Nielson P, Kongi R, Buggisch P et al (2005) Bioavailability of oral iron drugs as judged by a ^{59}Fe-whole-body counting technique in patients with iron deficiency anemia. Therapeutic efficacy of iron (II)-glycine sulfate. Arzneimittelforschung 55:376–381
4. Pixberg HU (1975) Isotope methods in the diagnosis of anemia. Med Welt 261349–1353

Esophageal Disease, Childhood

▶Oesophageal Disease, Childhood

Esophageal Foreign Bodies

▶Foreign Bodies, Gastrointestinal

Esophageal Rupture (in Blunt Chest Trauma)

Esophageal rupture is usually due to penetrating trauma. Most patients with esophageal rupture have other significant associated thoracic injuries, which is usually followed by mediastinitis with high mortality (Boerhaave syndrome). Pneumomediastinum, left-sided pneumothorax and hemothorax without rib fractures are indirect signs on chest-X-ray or CT. The method of choice in suspected esophageal perforation is contrast esophagography with water-soluble contrast agents (90% sensitivity), if necessary with additional endoscopy.

▶Chest Trauma

Esophagitis

▶Oesophagitis

Esophagus, Postoperative

Peter Pokieser, Martina Scharitzer, Johannes Zacherl
Medical University of Vienna,
Medical Media Services, Department of Radiology,
Vienna, Austria
peter.pokieser@meduniwien.ac.at

Definition

Imaging of immediate, early, and late complications after surgical procedures of the esophagus has two goals: first, to detect morphological changes, such as leaks, stenoses, or extraesophageal lesions, and second, to evaluate the function of the upper gastrointestinal tract. Morphology and function may interfere in many symptomatic patients after esophageal surgery, and the radiologist has to integrate morphological and functional findings to explain symptoms and to support therapeutic decisions. Fluoroscopy with dynamic recording for the esophageal tube and computed tomography (CT) for extraesophageal complications are the standard tools in these clinical settings.

The diagnoses and surgical operations are numerous. The most common are the following:

- Gastroesophageal reflux disease—Laparoscopic fundoplication or modifications
- Achalasia—Dilatation
- Heller myotomy plus fundoplication
- Esophageal cancer—Total or partial esophagectomy
- Esophageal atresia—Immediate or delayed repair
- Benign tumor—Esophagomyotomy
- Diverticulum—Diverticulectomy.

Pathology/Histopathology

Complications associated with esophageal surgery are generally related to the type of operation performed and the extent of surgery. Complications can be roughly divided into technical complications and those associated with cardiopulmonary aberrations.

Early complications of esophageal surgery include:

- Gastroesophageal reflux
- Recurrent hernia, breakdown of fundoplication, telescope phenomenon
- Aspiration, neuromuscular affection of swallowing
- Anastomotic or staple-line leak
- Leak after dilatation
- Anastomotic edema
- Anastomotic narrowing
- Hypotony or atony of the esophagus or/and stomach
- Pneumothorax
- Mediastinal hematoma, abscess
- Empyema
- Vocal cord paresis
- Chylothorax
- Ischemia
- Extraesophageal injury.

Late complications may include:

- Stricture of anastomosis or after dilatation
- Gastroesophageal reflux and its sequelae
- Recurrent hernia, breakdown of fundoplication, telescope phenomenon
- Aspiration
- Recurrent carcinoma
- Fistula or leaks

Clinical Presentation

Immediate complications are usually managed during or just after the procedure. Perforation of the esophagus during dilatation is an indication for an urgent fluoroscopic work-up (Figs 1 and 2). Postoperative hemorrhage occurs with an incidence of 3–5% and requires urgent reexploration. For many early postoperative complications, radiologic imaging plays the key role in diagnosis.

If the patient aspirates, neuromuscular affection of swallowing can be detected by videofluoroscopy. Neuromuscular swallowing disorders are associated with long-time intubation and risk factors.

Anastomotic or staple-line leaks, conduit ischemia, or perforation due to dilatation are among the most feared postoperative and postintervention complications (Figs 1 and 2). The incidence and seriousness are highly variable, depending on the type of operation, the location of the anastomosis, the experience of the surgeon, and the degree of the complication. A cervical leak is less serious than a thoracic leak, and a small anastomotic leak is less serious than a dehiscence associated with conduit necrosis. Most leaks manifest within 10 days after surgery. The peak of clinical manifestation of anastomotic failure is between days 5 and 7 after surgery. Leaks may be detected at routine radiologic examination 5–7 days after surgery.

The clinical presentation of esophageal leaks can range from completely asymptomatic to all the signs of shock and even death. In some cases, the first signs of an intrathoracic anastomotic leak are chest pain, dyspnea, and the discovery of a pleural effusion on chest radiography or CT. Cervical anastomotic failure characteristically causes saliva effusion *via* drainage and is rarely accompanied by systemic signs of inflammation.

Hypotony or atony of the esophagus or stomach and delayed emptying of the esophageal substitute are typical

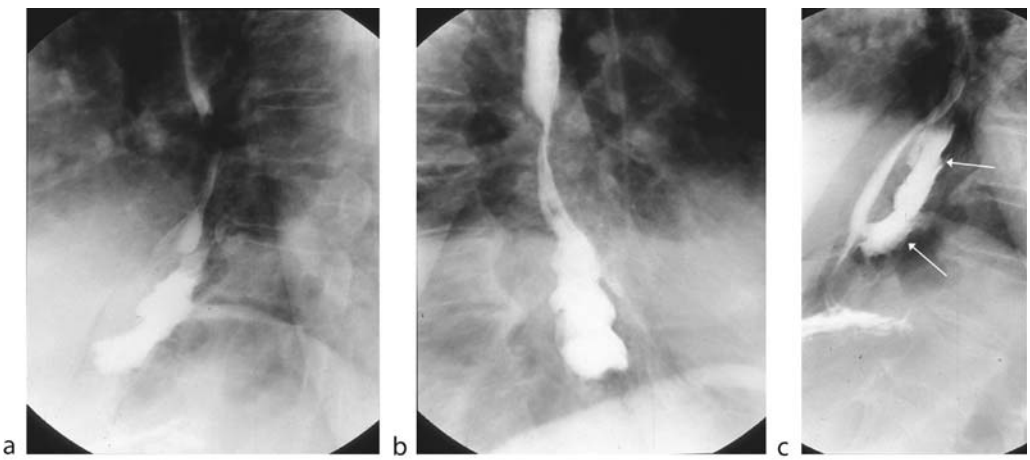

Esophagus, Postoperative. Figure 1 A 75-year-old man after removal of a stent, which was initially inserted endoscopically for treatment of an obstructing squamous cell carcinoma of the distal esophagus. A perforation of the esophagus was suspected. The patient was unstable, and radiologic investigation was limited by difficulties in the patient's positioning. (a, b) The first radiographic examination of the esophagus with water-soluble contrast material in the prone anteroposterior position and slightly rotated to the right side could not definitely reveal perforation. (c) Additional swallows in the strictly prone oblique position revealed a huge retroesophageal extravasation of contrast material (*arrows*).

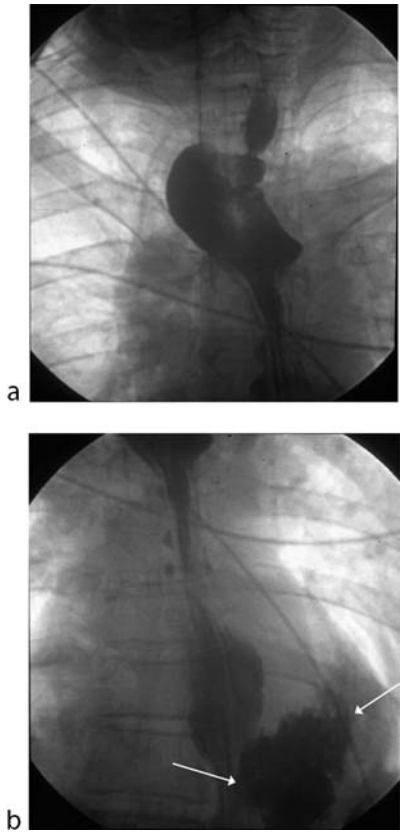

Esophagus, Postoperative. Figure 2
A 45-year-old woman immediately after endoscopic pneumatic dilatation of the lower esophageal sphincter to treat idiopathic achalasia. The surgeon suspected esophageal injury, but the location was unclear, and attempts to locate the perforation site by endoscopy failed. In the operating theater, fluoroscopy was performed by the radiologist, using a catheter carefully introduced below the pharyngoesophageal sphincter. (a) Markedly dilated esophageal lumen of the cervical esophagus, which is characteristic for advanced achalasia. This must not be confused with perforation of the cervical esophagus. (b) Investigation of the lower esophagus revealed an extensive extravasation of contrast material arising from the lower esophagus (*arrows*). Therefore, a thoracic access for surgical repair was chosen.

functional findings of the dynamic radiological investigation. Postoperative motility disorders of the esophagus may lead to regurgitation and dysphagia for solid food and even liquids. After esophagectomy, up to 10% of patients will develop gastric emptying problems due to vagotomy and the anatomical rearrangement. A prophylactic pyloromyotomy or pyloroplasty (dilatation) is done routinely in most centers to avoid this disabling complication.

Uncommon extraesophageal complications, such as pneumothorax, mediastinal hematoma, abscess, empyema, chylothorax, and extraesophageal injury, are diagnosed or suggested by plain chest studies or CT. Ischemia of the gastric pull-up or the interposed colon leads to severe clinical signs of shock. Assuming ischemia, esophagogastroscopy is the appropriate diagnostic approach.

A common late complication of the postoperative esophagus is a stricture of the anastomosis or a restenosis after dilatation of a stenosis. Intermittent or constant dysphagia for solids or accumulated semisolid food (rice, potatoes, and noodles) is the typical clinical presentation.

Imaging

In the immediate period after surgery, pneumothorax, pleural effusion, mediastinal widening, or pneumomediastinum/subcutaneous emphysema on chest X-ray may be highly suggestive of esophageal perforation. To check the patency of an anastomosis and the absence of complications after surgery, a swallowing study is initially done. The use of low-osmolar or isoosmolar water-soluble contrast material is mandatory due to its rapid absorption from the mediastinum in cases of perforation and to avoid lung edema after aspiration. The examination must be performed in two perpendicular planes—in the majority of cases, in the left and right decubitus position. Small collections of extraluminal contrast material may be obscured by the esophagus in the frontal position (Fig. 1). If the examination is not properly done—the rotation of these unstable and critically ill patients is often challenging—a leak cannot be ruled out. Additionally, the investigation of the whole esophagus and the stomach, duodenum, and first loops of the jejunum in patients with complicated operations is important for demonstrating an obstruction, leak, or other possible complication distal to the anastomosis.

Dynamic recording of swallowing facilitates the detection of small perforations because of the possibility of observing the recorded swallow several times in slow motion. Motility disorders of the postoperative esophagus may be evaluated as well.

CT offers some advantages, including evaluation of the pleura, the mediastinum, and the aorta. It is often very difficult to localize the exact site of perforation on a CT scan; on the other hand, CT is excellent for detecting extravasation of contrast material.

Diagnosis

Neuromuscular affection of swallowing can be an early complication after esophageal surgery, especially after

long periods of intubation and in patients with multiple comorbid diseases. A delayed swallowing reflex, pharyngeal weakness, and insufficient closure of the larynx are often found. For swallowing rehabilitation, a therapeutic videofluoroscopic study is helpful, in which the radiologist tries to discover which consistency and amount of contrast material shows the best results, combined with special maneuvers. This is done together with the speech and language pathologist.

Leaks can be very subtle. Videofluoroscopy or digital series must precisely describe the amount of leakage in relation to the ingested volume of the bolus. If a patient can take only 5 mL per swallow, the extravasation of 20% of the bolus is relatively small, measuring 1 mL. If the patient is drinking constantly from a cup, an extravasation of 1 mL seems to demonstrate a small leakage with a good prognosis. After drinking 30 mL or even more contrast material, small leaks of some drops may lead to more or less symptomatic strictures. This example shows how function can be integrated in the evaluation of morphology, without direct visualization of the lesion characteristics. Only huge defects of the anastomosis of massive perforations present a visible disintegration of the gut itself.

Usually a leak after dilatation or other esophageal intervention leads to a severe problem that requires urgent exploration. If such clinical settings are questionable, the radiologic examination is performed in an often difficult situation. When radiography is doubtful, CT can establish extravasation of contrast material in most cases.

Anastomotic edema presents with markedly thickened mucosal folds. The passage of water-soluble contrast material can be hindered and restored completely some days later. Anastomotic narrowing based on technical complications cannot be differentiated from simple edema. However, a regression of edema can be demonstrated by a patent anastomosis in follow-up studies.

Hypotony or atony of the esophagus or stomach is often found in the early postoperative phase. If hypoperistalsis or aperistalsis is not combined with necrosis of the gut, such functional impairments have a good prognosis, but they can affect the patients for some months. It is important to report such findings to avoid numerous endoscopic controls. Vagal denervation may lead to gas bloat of the stomach.

Specific postoperative complications of antireflux procedures consist of recurring hernia and breakdown or malposition of the fundoplication. Esophageal obstruction occurs if the antireflux fundoplication is too tight; esophageal dilatation is usually required. In such cases delayed transit of contrast material through the esophagogastric junction can be detected. But this unspecific functional finding can be found in transient postoperative edema and esophageal motility disorders as well.

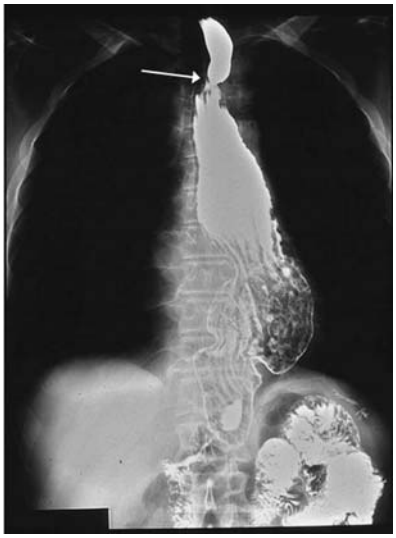

Esophagus, Postoperative. Figure 3
A 55-year-old man after subtotal esophageal resection and gastric tube reconstruction. Double-contrast examination 1 year after surgery showed a typical stenosis at the site of the anastomosis (*arrow*).

Pneumothorax, mediastinal hematoma, abscess, empyema, chylothorax, ischemia of bypass, and iatrogenic extraesophageal injury are relatively uncommon after esophageal surgery.

In cases of stricture of anastomosis or after dilatation, dynamic fluoroscopy of the esophagus can establish the degree and the length of the stenosis and the topographic relationship to the upper or lower aperture of the chest (Fig. 3).

Recurrent carcinoma can mimic a stricture and should be ruled out endoscopically. Late manifestation of a fistula or leak is rare after esophageal surgery. In the presence of an esophagotracheal fistula, laryngeal aspiration can make it difficult to document the penetration of contrast material from the esophagus into the trachea. Careful documentation in such cases is mandatory, and videofluoroscopy can be very helpful.

Bibliography

1. Rubesin SE, Levine MS (1989) Postoperative esophagus. In: Levine MS (ed) Radiology of the Esophagus. Saunders, Philadelphia, p 290
2. Paul S, Bueno R (2003) Section VI: complications following esophagectomy: early detection, treatment, and prevention. Semin Thorac Cardiovasc Surg 15(2):210–215
3. Meloni GB, Feo CF, Profili S et al (2005) Postoperative radiologic evaluation of the esophagus. Eur J Radiol 53:331–340

Essential Thrombocythemia

This chronic myeloproliferative disorder is characterized by an abnormal clonal proliferation of megakaryocytes and a resulting significant increase in platelet count. Clinically it is expressed in the form of abnormal bleeding and an increased risk of thromboembolic events. Splenomegaly is a characteristic finding.

▶Neoplasms, Splenic, Malignant

(Estimation of) skeletal maturation (by imaging)

▶Bone Age

ESWL

▶Extracorporeal Shock Wave Lithotripsy

Ethiodol

▶Contrast Media, Iodinated, Oily

Ewing's Sarcoma

A highly malignant tumor that is found predominantly in the lower extremity, in particular at the diaphysis and metaphysis of the femur followed by the tibia and humerus. Ewing's sarcoma is most common in the first and second decade of life. Typical radiographic findings are permeative bone destruction, lamellar (onion-skin) and spicculated periosteal reactions and soft tissue extension.

▶Neoplasms, Bone, Malignant
▶Neoplasms, Chest, Childhood

Exocrine Carcinoma of the Pancreas

▶Carcinoma, Pancreatic

Exocrine Cystic Neoplasms of the Pancreas

▶Cystic Neoplasms, Pancreatic

Extracorporeal Membrane Oxygenation

▶ECMO (Neonate, Pediatric) Imaging

Extracorporeal Shock Wave Lithotripsy

ESWL is a technique for shattering a kidney/ureter stone or gallstone with a shock wave produced outside the body.

▶Stone Disease, Urinary

Extrahepatic Atresia

▶Congenital Malformations, Bile Ducts

Extramedullary Hematopoiesis

The replacement of hematopoietic cells in the bone marrow by ever-increasing amounts of fibrous tissue leads to the reinstatement of the spleen as a hematopoietic organ. The spleen in such patients may become enormously enlarged, and there is an increased risk of rupture.

▶Splenomegaly

Extruded Disk

An extruded disk is a herniated disk in which, in at least one plane, any one distance between the edges of the disk material beyond the disk space is greater than the distance between the edges of the base in the same plane. Extrusion is distinguished from protrusion by displacement beyond the outer annulus of disk material, with any distance between its edges greater than the distance between the edges of the base.

▶Herniation, Intervertebral Disk

Facet Arthropathy

►Degenerative Conditions, Spine

Facet Joint Degeneration

Degenerative involvement of facet joints, which presents usually as hypertrophy and osteophytes of articular processes with narrowing of the joint space. Less commonly vacuum phenomenon (gas in the joint space), synovial hypertrophy or synovial cysts are observed. Facet joint degeneration is usually accompanied by thickening of the ligamenta flava. The signs mentioned above may be evaluated on axial MR and/or CT images.

Facet disease may be isolated, but usually is associated with degeneration of intervertebral disk, vertebral bodies, and ligamenta flava. It is an important factor in pathogenesis of degenerative spondolisthesis and often contributes to stenosis of spinal canal and intervertebral foramina.

►Degenerative Conditions of the Spine

Facial Nerve Neuralgia

►Facial Nerve Palsy

Facial Nerve Neuropathy

►Facial Nerve Palsy

Facial Nerve Palsy

Alexandra Borges
Instituto Português de oncologia Francisco Gentil, Centro Regional Oncológico de Lisboa, 1093, Lisboa, Portugal
borgesalexandra@clix.pt

Synonyms

Facial nerve neuralgia; Facial nerve neuropathy; Facial nerve paralysis

Definition

Facial nerve palsy (FNP) results from loss of function of the facial nerve. It is characterized by paralysis of the muscles of facial expression which may be associated with loss of other facial nerve functions such as lacrimation, salivation, sound dampening and loss of taste in the two anterior thirds of the tongue.

Pathology/Histopathology

►*Central facial nerve paralysis* (CFNP) results from supra-nuclear lesions and is usually part of a more striking neurological condition that includes symptoms and signs of long tract dysfunction. It results from any lesion affecting the motor tract, most commonly stroke, neoplasm, vascular malformation and infectious/inflammatory conditions (1).

Causes of ►*peripheral facial nerve palsy* (PFNP) include in decreasing order of frequency (Table 1): ►Bell's palsy (57% of cases), temporal bone trauma (17%), herpes zoster oticus (7%), other infectious/inflammatory conditions (4%), neurovascular conflicts (4%), congenital lesions (3%), brainstem lesions (1%) and other miscellaneous conditions (7%) (3).

Lesions involving the brainstem segment (nuclear level) include infarct, vascular malformations, demyelinating

Facial Nerve Palsy. Table 1 Causes of facial nerve palsy (adapted from Roob G) (2)

Central FNP
Any cortical lesion involving the cortical motor area or corticospinal tract (infarct, neoplasm, multiple sclerosis, vascular lesion, etc.)
Peripheral FNP
1) Infection/Inflammation/Demyelination
Bell's or herpetic palsy (HSV)
►Ramsay-Hunt syndrome (herpes zoster oticus and herpes zoster cephalicus)
Otitis media (acute, chronic, cholesteatoma)
MOE (malignant otitis externa or necrotizing otitis externa)
Lyme's disease
HIV infection
Guillain-Barré syndrome
Heerfordt syndrome (sarcoidosis)
2) Trauma
Temporal bone fractures (longitudinal, transverse and complex)
Middle ear and mastoid surgery
Parotid gland surgery
3) Neoplasm
Primary: Facial nerve schwannoma/neuroma, hemangioma, glomus faciale, cylindroma, hamartoma, epidermoid cyst, teratoma
Secondary: Metastasis (hematogenous or leptomeningeal carcinomatosis), perineural spread of parotid gland malignancies, direct invasion from adjacent tumours (meningioma, cholesteatoma, other temporal bone and skull base tumours)
4) ►Neurovascular Conflict (usually with facial dyskinesis)
Vascular loops (AICA, PICA, vertebral artery)
VB dolichoectasia
Aneurysm
5) Brainstem Lesions
Multiple sclerosis
Brainstem neoplasm: Glioma, metastasis
Vascular lesions: infarct, AVM, cavernous angioma
Rhombencephalitis
6) Congenital Lesions
Birth trauma (forceps delivery)
Mobius syndrome
Craniofacial malformations involving the 1st and 2nd branchial arches
7) Others
Paget's disease
Fibrous dysplasia
Ospeoptrosis
Melkersson-Rosenthal syndrome

disease, primary and secondary brainstem neoplasms and rhombencephalitis.

Bell's palsy, a condition for long considered idiopathic is now known to be a viral-induced neuronitis (4). Herpes simplex virus (HSV) is the most commonly implicated agent, thought to be in a dormant state in the geniculate ganglion, being reactivated by non-specific triggering events. The induced inflammatory response, leads to nerve compression against the rigid bony walls of the fallopian canal resulting in ischemia and axonal degeneration. Due to its reduced calibre and blood supply (transitional watershed zone between the vertebral and carotid artery systems), the labyrinthine segment and particularly the meatal portion of the nerve is most susceptible to injury.

Ramsay-Hunt syndrome or herpes zoster oticus is the second most common infectious inflammatory condition afflicting the facial nerve. This condition results from

reactivation of a herpes zoster virus (HZV) lodged in the geniculate ganglion and is characterized by the presence of vesicular eruptions in the ear, face and neck.

Any acute or chronic bacterial infection of the middle ear and mastoid may lead to FNP. In the post-antibiotic era, necrotizing otitis externa became the leading cause of infectious facial palsy. It results from an opportunistic pseudomonas aeruginosa infection often afflicting diabetic and other immuno-compromised patients. The infection begins in the EAC and spreads to the parotid gland, temporal bone and posterior and central skull base. Facial nerve involvement occurs in 38% of cases secondary to spread of infection through the stylomastoid foramen or from direct involvement of the facial nerve canal at the tympanic or mastoid segments.

The widespread use of antibiotics decreased the incidence of FNP secondary to otitis media to 0.16% per year (1). The route of spread to the facial nerve is through small bony dehiscences of the fallopian canal, often seen in the tympanic segment. Facial nerve edema, granulation tissue or even intra-fallopian abscess may ensue and lead to acute FNP.

Lyme's disease, a spirochetal infection, is known to cause FNP in 10% of cases among which, 25% are bilateral (facial diplegia). Prior history of a thick bite is often elicited and associated findings of maculopapular rash, arthritis and meningitis, make the diagnosis straightforward.

HIV infection may course with FNP either due to a direct viral neuronitis or through secondary opportunistic infections.

Trauma is the second leading cause of FNP. It may be secondary to head trauma or to iatrogenic insult, during parotid or temporal bone surgery. Patients with blunt head trauma have a 5% incidence of temporal bone fractures. Longitudinal fractures, the most common, lead to FNP in 10–20% of cases. Facial nerve injury is usually at the level of the geniculate ganglion or tympanic segment and paralysis is typically delayed in onset and transient. Transverse fractures result in FNP in 30 to 50% of cases and paralysis tends to be immediate, complete and irreversible. The most frequent site of injury is the labyrinthine segment and results from nerve impingement or transection by a fractured fragment. Edema from traction and stretching of the nerve or intra-neural haematoma are other possible mechanisms of injury.

Facial nerve tumours are rare, responsible for only 6–10% of cases of FNP. They should be suspected whenever patients present with progressive, longstanding FNP, with ipsilateral recurrent episodes of paralysis or with associated facial twitches. Nevertheless, around 27% of cases present with sudden, acute FNP due to abrupt compromise of vascular supply from mass effect, mimicking Bell's palsy. Facial nerve schwannoma, the most common facial nerve neoplasm, is a benign slow growing tumour, composed of Schwann cells intermingled with a collageneous stroma. Haemangioma, the second most common, is usually small and hard to detect on imaging studies. They can both occur in any segment of the facial nerve, but are more common in the region of the geniculate ganglion (4, 5).

Other tumour histologies have been reported including facial nerve paraganglioma, choristoma, cylindroma, lipoma, teratoma and epidermoid cyst.

Secondary facial nerve involvement by neoplasm results either from direct invasion or from *perineural spread*. The latter is most often associated with parotid malignancies, prone to spread retrogradely along the nerve through the stylomastoid foramen and intratemporal segments. This type of spread is seen in 50% of patients with adenoid cystic carcinoma and early recognition is mandatory, as it should be treated along with the primary tumour (2, 4).

Any tumour of the temporal bone or arising from the posterior and central skull base may lead to FNP by direct extension. These include a variety of pathologic conditions originating within the intra- or extra-cranial compartments. Cholesteatoma, cholesterol granuloma, glomus jugulotympanic and endolymphatic sac neoplasms are among the most commonly implicated. The facial nerve may also be affected by metastatic disease and basilar meningitis (infectious, inflammatory or metastatic in nature).

Neurovascular conflict manifests by hemifacial spasm rather than FNP. This condition results from nerve impingement at the *root entry zone* by an adjacent vessel. The most frequent culprits are loops of the anterior and inferior cerebellar artery (AICA), posterior and inferior cerebellar artery (PICA) and vertebral artery. Vertebrobasilar dolichoectasia and aneurysms may also be implicated (4).

Several bony dysplasias, such as Paget's disease and fibrous dysplasia, may involve the temporal bone, lead to stenosis of the fallopian canal and subsequent FNP.

Clinical Presentation

Facial nerve paralysis manifests by effacement of facial skin folds, smooth forehead, widened palpebral fissure, lower lid sagging with tear dribbling and inferior displacement of the corner of the mouth with drooling of saliva. In the majority of cases, the condition is unilateral and the most obvious feature is facial asymmetry. In mild cases, FNP may only become apparent with voluntary movements. In chronic stages, a continuous diffuse contraction of the facial muscles (hyperkinesis) and facial spasms may ensue. Other facial nerve functions

(lacrimation, acoustic reflex and taste sensation in the anterior tongue) may also be lost.

►*Hemifacial spasm* is characterized by intermittent, involuntary muscle twitches. It is usually secondary to lesions near the *root entry zone* (transitional zone between central and peripheral myelination), often neurovascular conflicts or compression by adjacent mass lesions (4, 5).

Clinical presentation depends on the site of facial nerve injury. Thorough neurological and ENT examinations can establish the topographic diagnosis of facial nerve lesions. Whereas patients with CFNP present with paralysis of the facial muscles sparing the forehead, patients with PFNP present with paralysis of all muscles of facial expression.

Associated deficits of cranial nerves V and VI, locate the lesion at the brainstem where their nuclei and fibres lie close together. The presence of vestibulo-cochlear dysfunction suggests a lesion in the CPA cistern or in the IAC where cranial nerves VII and VIII travel together within the same dural sheath. Lesions in these segments present with VIII nerve symptoms, (sensorineural hearing loss, tinnitus and vertigo), before facial nerve dysfunction can be detected due to higher vulnerability of the tightly packed, thinly myelinated fibres of the vestibulo-cochlear nerve to compression and ischemia.

Mass lesions in the geniculate ganglion and labyrinthine segment may remain clinically silent until growth into the middle cranial fossa, impinge upon the neighbouring trigeminal nerve or lead to Eustachian tube dysfunction. Tympanic segment tumours present with conductive hearing loss due to mechanical interference with the ossicular chain and by a MEC mass on otoscopy. Lesions in the mastoid segment present with sudden or gradual FNP, often mimicking Bell's palsy. Finally, tumours of the parotid segment present as parotid masses and are indistinguishable from other commoner pathologic entities of the parotid space.

Imaging

MR is the modality of choice to image patients with CFNP. Imaging is mandatory to determine the cause and to help planning treatment. In patients with PFNP the role of imaging is controversial as the majority of cases are due to Bell's palsy, usually a benign, self-limited disease, with 80% rate of functional recovery. The main arguments towards imaging include: depiction of prognostic criteria that would identify the 20% of Bell's palsy patients who will do poorly and would benefit from early functional rehabilitation (4, 5), and the early recognition of potentially treatable causes of PFNP other then Bell's palsy. Overall, imaging is mandatory in patients with atypical clinical presentations, with poor clinical prognostic signs and whenever surgical decompression is considered (4, 5).

'Atypical' clinical presentations do not follow the usual course of Bell's palsy and include: sub-acute, slowly progressive or recurrent episodes of PFNP, association with other cranial nerves deficits and presence of facial spasm or twitch. Imaging should also be performed when poor clinical prognostic signs are present such as prolonged course of paralysis, (beyond 3 months), high ►*House-Brackmann grade* from onset (above IV) and in the presence of signs of deinervation on electrophysiologic testing (1, 2).

Whereas the supra-nuclear, brainstem, cisternal, intra-canalicular and parotid segments of the facial nerve are best appreciated using MRI, the temporal bone segments are best evaluated with CT or a combination of CT and MRI (4, 5).

Clinical findings determine the best diagnostic imaging strategy. Patients with FNP and prior history of middle ear infection, temporal bone trauma, prior mastoid surgery or a visible mass on otoscopy should be evaluated primarily with high resolution CT (HRCT). CT is also used as an anatomic roadmap in patients selected for surgical treatment. MRI is the modality of choice in all other clinical presentations. Whenever *hemifacial spasm* or twitch is present CT or MR angiography should be used to rule out neurovascular conflict.

The imaging hallmark of inflammatory conditions is the presence of smooth linear enhancement, without focal mass, depicted on gadolinium-enhanced MRI studies. Enhancement of the intra-canalicular and labyrinthine segments of the nerve is the most typical feature of Bell's palsy (Fig. 1). Contrast-enhancement in other segments

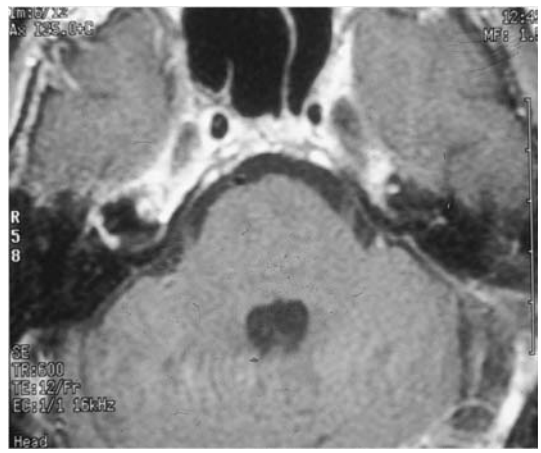

Facial Nerve Palsy. Figure 1 Axial gadolinium-enhanced MR image through the pons shows linear, smooth, segmental enhancement along the intra-canalicular and labyrinthine segments of the facial nerve and enhancement of the geniculate ganglion in a patient with Bell's palsy.

of the nerve is of unclear significance as subtle enhancement can be seen along the tympanic and mastoid segments reflecting the presence of a rich perineural vascular plexus. CT has no role in the evaluation of inflammatory conditions of the facial nerve, except when surgery is considered.

Facial nerve enhancement is not a specific feature for Bell's palsy. It is seen in a variety of other inflammatory and neoplastic conditions. Perineural spread of malignancies along the facial nerve may be a potential pitfall, particularly in the absence of prior history of head and neck neoplasm.

In Ramsay-Hunt syndrome, contrast enhancement along the facial, trigeminal and acoustic nerves and within the membranous labyrinth makes the full-blown picture of this condition on MRI. There is arguable evidence that the facial nerve enhances to a further degree then that seen in Bell's palsy (4, 5).

Infectious conditions of the MEC and EAC coursing with FNP can be adequately evaluated either with CT or MR. CT nicely demonstrates bone changes associated with chronic otitis media, cholesteatoma and necrotizing otitis externa and easily depicts dehiscence and erosion of the facial nerve canal. Contrast-enhanced MRI may be required, to determine the full extent of the inflammatory soft tissue, to detect cranial nerves involvement and access the extent of bone marrow involvement of the skull base.

CT is the modality of choice to assess post-traumatic and post-surgical PFNP. It nicely depicts disruption of the facial nerve canal. MR is reserved for cases of FNP unexplained by CT and may demonstrate FN haematoma (bright lesion on plain T1W images) or FN enhancement due to disruption of the blood–nerve barrier (4).

CT and MR are used complimentarily to achieve a full-blown picture of facial nerve neoplasms. On CT, schwannoma manifests as enlargement and remodelling of the fallopian canal in the segment(s) involved by tumour. It is well suited to determine the relationship between the tumour and other important structures of the MEC and with the petrous apex. On MRI, facial nerve schwannomas present as focal, eccentric, fusiform masses with well-defined margins along the course of the nerve. These tumours are iso-intense to brain on T1W, hyper-intense on T2W and show variable enhancement (Fig. 2).Neoplasms arising from the cisternal and intra-canalicular segments are indistinguishable from the commoner vestibular schwannomas, unless the tumour extends along the labyrinthine segment of the facial nerve (4).

Facial nerve hemangiomas are usually very small, often below the resolution of imaging studies. On CT,

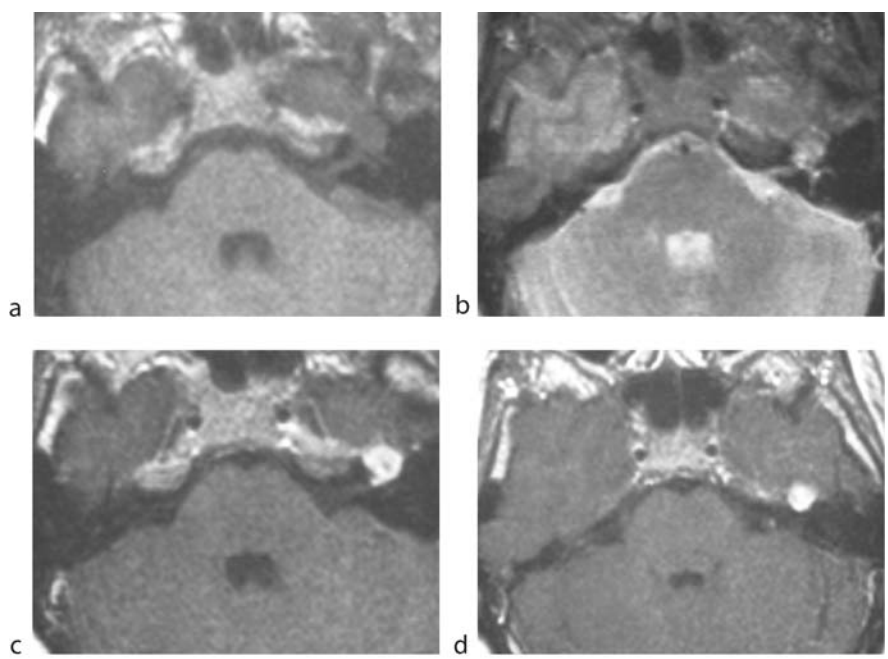

Facial Nerve Palsy. Figure 2 Axial T1W (a), T2W (b), and gadolinium enhanced T1W MR images through the level of the midpons, show a mass in the geniculate fossa extending posteriorly into the middle ear cavity along the tympanic segment of the facial nerve and anteriorly into the middle cranial fossa. The lesion is iso-intense to grey matter on T1W images, heterogeneously hyper-intense on T2W images and enhances vividly on the post-contrast images. Diagnosis: facial nerve schwannoma of the geniculate ganglion and tympanic segment of the facial nerve.

ossifying hemangioma of the facial nerve presents as a lobulated soft tissue mass, with indistinct margins and intra-tumoral bony spicules. On MRI, this tumour tends to be ill-defined, heterogeneous in signal intensity, but otherwise non-specific.

MRI is the modality of choice to depict perineural spread of malignant tumours. It manifests as smooth or nodular thickening and enhancement along the facial nerve; obliteration of the stylomastoid foramen fat pad and atrophy of the muscles of facial expression due to chronic deinervation. PFNP may be the first clinical sign of a parotid malignancy. Therefore, no imaging study is complete without the inclusion of the parotid gland (Fig. 3).

The imaging hallmark of neurovascular conflict is the presence of a vessel crossing the facial nerve perpendicularly at the root entry zone, leading to displacement or indentation of the nerve (4, 5).

Diagnosis

FNP is a clinical diagnosis, based upon signs and symptoms of loss of facial nerve functions. Topographic diagnosis requires a detailed clinical history, neurological and ENT examinations and helps to determine the probable site of nerve injury and to direct further diagnostic testing.

Serologic testing is an important aid in the diagnosis of PFNP secondary to diabetes mellitus, Lyme's disease, HIV, sarcoidosis, Guillain-Barré's syndrome and acute herpes and zoster infections. CSF sampling may also be helpful in cases of viral infection and basilar meningitis. Other diagnostic and prognostic testing includes electroneurography electromyography and evaluation of CN VIII function (audiogram, caloric testing and electronystagmogram).

Because most cases of facial nerve dysfunction are due to Bell's palsy, the major diagnostic challenge is the early recognition of potentially treatable causes aiming for function preservation or rehabilitation.

Interventional Radiological Treatment

Limited to pre-operative embolization of highly vascular lesions mainly facial nerve paragangliomas and glomus jugulo-tympanicum.

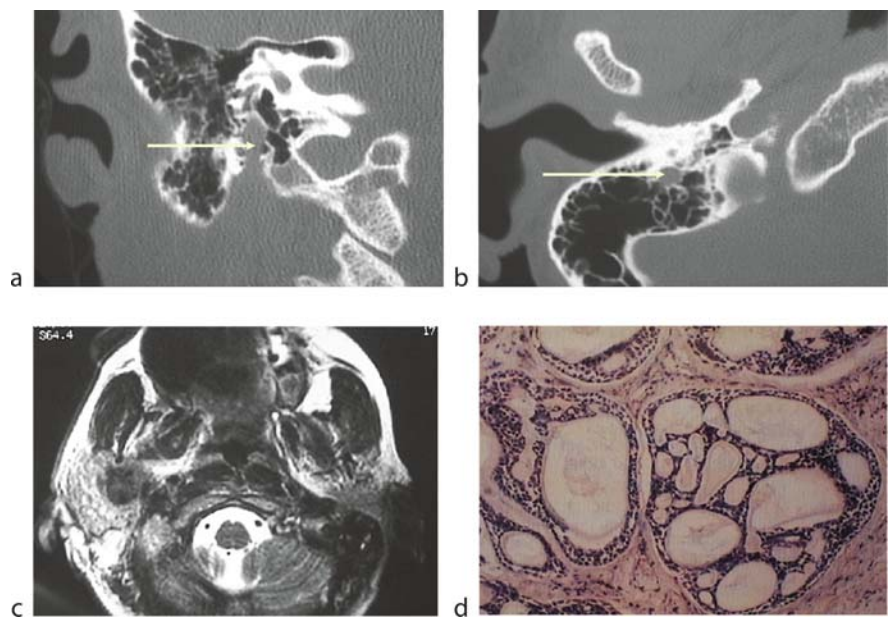

Facial Nerve Palsy. Figure 3 Coronal (a) and axial (b) CT sections through the temporal bone in high resolution bone algorithm show abnormal enlargement and remodelling of the mastoid segment of the facial nerve (*white arrows*). (c) Axial T2W image through the parotid gland shows a mass lesion in the deep lobe of the parotid overlying the expected course of the facial nerve. The lesion is of low-signal intensity on this sequence a feature associated with parotid malignancies. (d) Photomicrograph of the pathologic specimen (hematoxilin and eosin stain; original magnification X 1000), shows multiple microcystic spaces lined by cuboidal epithelial cells with hyperchromatic nuclei, yielding an overall appearance of a Swiss cheese. These are typical features for adenoid cystic carcinoma (cribiform pattern). Diagnosis: Perineural spread of adenoid cystic carcinoma along the mastoid segment of the facial nerve in a patient presenting with peripheral FNP of unknown etiology.

Bibliography

1. Benecke JE (2002) Facial paralysis. Otolaryngol Clin N Am 35(2): 357–365
2. Roob G, Fazekas F, Hartung HP (1999) Peripheral facial nerve palsy: Etiology, diagnosis and treatment. Eur Neurol 41:3–9
3. May M, Klein S (1991) Differential diagnosis of facial nerve palsy. Otolaryngol Clin N Am 24:613–614
4. Borges A (2005) Trigeminal neuralgia and facial nerve palsy. Eur Radiol 15: 511–533
5. Jager L, Reiser M (2001) CT and MR imaging of the normal and pathologic conditions of the facial nerve. Eur J Radiol 40(2): 133–146

Facial Nerve Paralysis

▶Facial Nerve Palsy

False Negatives

Findings that are not detected and/or not disclosed, but ultimately have medical consequences.

▶Incidental Neuroradiological Findings

False Positives

Findings that are detected and disclosed but do not ultimately have medical consequences.

▶Incidental Neuroradiological Findings

Family History

The relevance of one or more female relatives with breast cancer on an individual woman's risk of carrying a genetic mutation responsible for breast cancer.

▶Carcinoma, Breast, Demography

Family of Dysplasias

Concept that several phenotypically different genetic syndromes share a common gene abnormality as their cause.

▶Osteodysplasia

Fascial Weakness and Defects

▶Hernia, Abdominal and Inguinal

Fascioliasis

Hepatobiliary infection caused by flukes of the Trematoda (Fasciola hepatica, Fasciola gigantica), which are common parasites of cattle and sheep. Humans are incidental hosts. These two flukes cause similar diseases in patients, who become infected by ingesting contaminated watercress, raw fish, or raw cattle or sheep liver. The disease is characterized by an acute and a chronic phase that may last for years. From the duodenum, the cercaria and the immature flukes migrate through the bowel wall, the peritoneal cavity, and the Glisson capsule, reaching the bile ducts in which they will mature. Mature flukes migrate toward the larger bile ducts, causing hemorrhage, inflammation, necrosis, and subsequent fibrosis. This disease is reported worldwide, in particular in regions of sheep or cattle production. Clinically, patients may be asymptomatic or may present with fever, eosinophilia, and abdominal pain. US may show hypoechoic areas in the liver, corresponding to the burrow tracks of the larvae. CT shows millimetric lesions or tunnels with a radiating pattern in the liver parenchyma. These hypodense areas (corresponding to necrosis) show enhancing walls resembling abscess features and are mostly located in the periphery. After several months, these cavities decrease in size, and calcifications or granuloma formation can be observed. MR imaging provides findings similar to those in CT. Cholangiography may depict flukes in the biliary tree.

▶Cholangitis

FasL (CD95L)

Ligands of the respective receptors, which trimerize after binding, forming major regulators of apoptosis.

▶Apoptosis

Fat Embolism Syndrome

▶Chest, Thromboembolic Diseases

Fat Necrosis

Traumatic or iatrogenic damage of fat cells of the breast resulting in firm palpable lumps. Clinical, mammographic, and sonographic features may be indistinguishable from malignancy.

▶Trauma, Breast

Fatty Liver

▶Steatosis, Hepatic

FDG

Abbreviation for fluorine-18 desoxyglucose. FDG is used as a radiopharmaceutical for positron emission tomography. The uptake of FDG is considered to represent glucose consumption of tissue. FDG has become the most important radiopharmaceutical for imaging malignant tumors.

▶Proliferation of Neoplasms

18FDG PET

Positron emission tomography using 18F-fluorodeoxyglucose as a radiotracer is a rapidly developing method of staging various cancers and relies on the increased glucose metabolism of malignant cells.

▶Neoplasms Oesophagus

Fecal Incontinence

Fecal, or anal, incontinence is defined as an involuntary loss of rectal content at a socially inappropriate time or place of 1 month or greater in duration, in an individual with a developmental age of at least 4 years.

▶Pelvic Floor Dysfunction, Anorectal Manifestations

Fecal Incontinence - Anal Incontinence

▶Pelvic Floor Dysfunction, Anorectal Manifestations

Femoral Arterial obstruction

▶Occlusion, Artery, Femoral

Femoral Arterial Occlusion

▶Occlusion, Artery, Femoral

Femoroacetabular Impingement

Injury secondary to repetitive trauma of the femoral head upon the acetabulum. Cam-type impingment is characterized by lateral decentering of the femoral head resulting in contact with the acetabulum during flexion. This abnormality is commonly found in young, active patients. Pincer-type impingement is secondary to an abnormal acetabulum contacting the femoral head during normal hip movement. The acetabulum may be unusually deep (coxa profunda) or retroverted. Symptoms occurring in this patient population are of later onset. Both types of impingement lead to labral tears, cartilage abnormalities, and early osteoarthrosis of the hip. Adjacent marrow edema and cystic change is also found on MR imaging.

▶Fractures, Pelvis

Fetal Brain Abnormalities

CNS malformations and brain injury are the primary CNS abnormalities encountered in utero. Isolated ventriculomegaly is still a challenging clinical condition.

▶Fetal Neuroimaging

Fetal Brain MRI

MRI serves as a second imaging tool to confirm or correct ultrasound findings in utero. T1, T2, and diffusion images are routinely used to evaluate the brain parenchyma. Proton spectroscopy is still part of the clinical research protocol.

▶Fetal Neuroimaging

Fetal Imaging

Huisman T. A.
Johns Hopkins University, Baltimore, USA
thierry.huisman@kispi.unizh.ch

Synonyms

Intrauterine MRI; Prenatal MRI

Definition

Fetal magnetic resonance imaging (MRI) is a relatively new, nonionizing imaging modality in which ultrafast MRI sequences allow intrauterine examination of the fetus without the need for fetal sedation. Fetal MRI is advantageous compared to prenatal ultrasonography (US) because it is not obscured by overlying maternal bowel gas, pelvic bone structures, or obesity, is not influenced by the position of the fetus, and is less dependent on the investigator's skills (1, 2, 3).

Pathology/Histopathology

Fetal MRI allows the entire pregnancy to be evaluated, including maternal components, like the ovaries and uterus, as well as the placenta and umbilical cord. In addition, the complete fetus is examined from "tip to toe." If required, the birth canal can also be measured (MR pelvimetry). With progressing diagnostic experience and available data as well as continuous technical improvements (MRI hard- and software), the indications for fetal MRI continue to grow.

Fetal MRI is especially advantageous in the evaluation of the developing fetal central nervous system (CNS) (Figs 1 and 2). The CNS is the most frequently involved "organ" in congenital malformations (1:100 births). In addition, CNS malformations often have a significant impact on the quality of life. Moreover, spontaneous deliveries can be complicated by CNS pathologies and the primary adaptation of the neonate may be influenced. Fetal MRI is progressively applied in pathologies of the fetal thorax and abdomen (Figs 3 and 4); however, it is currently limited in the evaluation of the distal extremities in particular (Table 1).

Congenital lesions can be divided into (a) classic congenital malformations and (b) intrauterine acquired pathologies. In congenital malformations an erroneous development of the CNS has occurred, while in acquired pathologies, initially correctly developed structures have been injured. A significant overlap between both categories can be troublesome for differentiation. An early, minor ischemic event can, for example, result in a migrational disturbance indistinguishable from a primary malformation of cortical development. The most frequent malformations of the CNS include (1) disorders of neural tube closure, (2) disorders of sulcation and migration, and (3) disorders of diverticulation or brain cleavage (Table 1).

Disorders of Neural Tube Closure

Chiari II Malformation: Chiari II malformation is a malformation of the rhombencephalic vesicle characterized by a too-small posterior fossa with coexisting and/or resulting mesencephalic and cerebellar anomalies including a downward displacement of the cerebellum, beaking of the tectal plate, embracement of the brain stem by the cerebellar hemispheres, and frequently a supratentorial hydrocephalus. Chiari II is almost always associated with spinal dysraphism.

Cephaloceles: Cephaloceles comprise varying degrees and/or combinations of protruding brain tissue and meninges through a skull defect. Cephaloceles may occur at multiple anatomical locations and are frequently associated with disorders of neuronal migration and sulcation or commissural malformations.

Dandy-Walker Malformation: Dandy-Walker malformation is characterized by cystic dilatation of the fourth ventricle associated with varying degrees of vermian hypoplasia. In 60% of patients additional CNS malformations are present. The posterior fossa is usually significantly enlarged.

Spinal Dysraphism: Due to a failure of neural tube closure, the meninges and a nonclosed neural tube (neural placode) protrude outside the open bony spinal canal in myelomeningoceles (MMC). MMC is always associated with Chiari II malformation.

Commissural Malformation: The most frequently encountered commissural malformations are anomalies

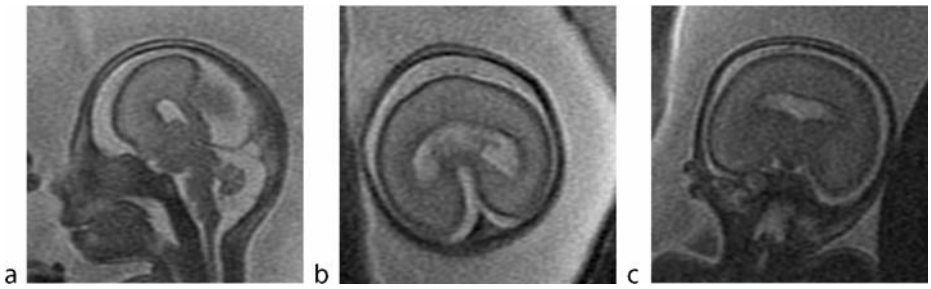

Fetal Imaging. Figure 1 Sagittal, coronal, and axial fetal MRI. Semilobar holoprosencephaly in a fetus, 24th week of gestation.

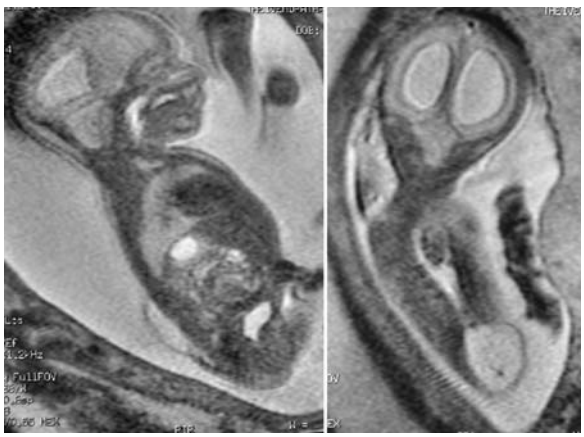

Fetal Imaging. Figure 2 Sagittal and coronal fetal MRI. A lumbar meningomyelocele with an associated Chiari II malformation is seen. In addition, a thoracal diastematomyelia is seen. All findings were confirmed after birth.

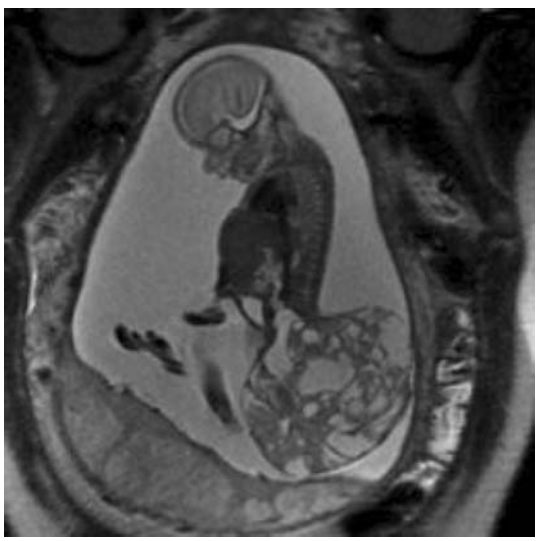

Fetal Imaging. Figure 3 Sagittal fetal MRI. Large, multicystic, partially solid sacrococcygeal teratoma in a fetus, 25th week of gestation. No signs of fetal hydrops.

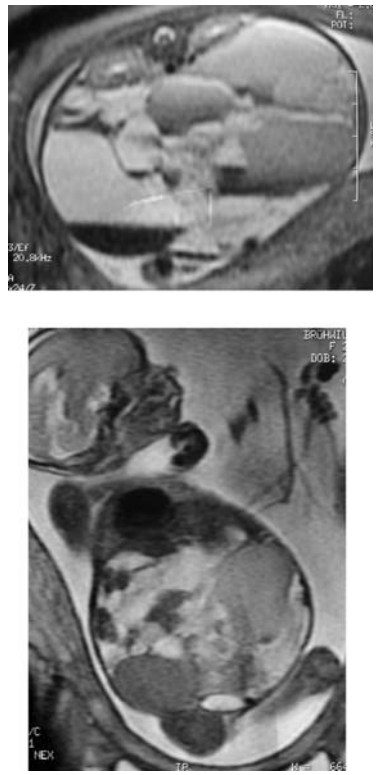

Fetal Imaging. Figure 4 Axial and coronal fetal MRI. A multicystic abdominal lymphangioma with multiple septa and fluid sedimentation levels is seen in a 22-week-old fetus.

of the corpus callosum. Agenesis may be partial or complete. Callosal anomalies are frequently associated with other CNS malformations.

Disorders of Sulcation and Migration

Pachygyria and Polymicrogyria: Pachygyria and polymicrogyria are disorders of neuronal migration and cortical organization. In pachygyria the cortex is thickened, while in polymicrogyria multiple small gyri are seen.

Lissencephaly: Lissencephaly results from an arrested neuronal migration and is characterized by a four-layer

Fetal Imaging. Table 1 Indications for fetal MRI

1. Disorders of neural tube closure
A. Chiari II malformation
B. Cephaloceles
C. Dandy-Walker malformation
D. Spinal dysraphism
E. Commissural malformation
2. Disorders of sulcation and migration
A. Pachygyria and polymicrogyria
B. Lissencephaly
C. Schizencephaly
3. Disorders of diverticulation or brain cleavage
Holoprosencephaly
4. Thoracal and abdominal malformations

cortex with a smooth surface. Bands of neurons are located within the white matter.

Schizencephaly: In schizencephaly, cerebral clefts extend from the brain surface to the ventricle. Most schizencephalies are lined by a malformed/disorganized cortex.

Disorders of Diverticulation or Brain Cleavage

Holoprosencephaly: Failure of the cleavage of the prosencephalon will result in a spectrum of malformations that are characterized by different degrees of fused cerebellar hemispheres. The most severe from is the alobar form, the mildest form is the lobar form.

Thoracal and Abdominal Malformations

Thoracal and abdominal malformations include a wide variety of pathologies such as hemangiomas, diaphragmatic hernias, omphaloceles, renal agenesis, cloacal malformations, hamartomas, etc. A complete list of lesions that can be diagnosed would outgrow this chapter.

Clinical Presentation

Most frequently, intrauterine CNS malformations are encountered on prenatal ultrasonography. Rarely will the mother experience any symptoms. The following description of presentation is consequently related to the child after birth.

Chiari II Malformation

Clinically, it is determined by the associated CNS malformations. The level and extent of spinal dysraphism result in varying degrees of paraplegia and bladder/bowel dysfunctions. The associated cerebral pathology, especially the hydrocephalus, determines the degree of psychomotor retardation.

Cephaloceles

Isolated cephaloceles may present with focal neurological deficits related to the affected functional centers. If associated migrational lesions are present, the child will present with seizures. Depending on the location, the cephalocele can be seen on gross inspection or can, for example, be "hidden" in the nasal cavity in the case of a frontobasal encephalocele.

Dandy-Walker Malformation

Depending on the degree of cystic dilatation of the fourth ventricle, the posterior fossa will be enlarged. Cognitive performance is frequently affected, and 35–50% of children will have normal intelligence. An associated hydrocephalus will result in macrocephaly.

Spinal Dysraphism

Defects of neural tube closure are easily identified on inspection. The neural placode is exposed to the skin surface and cerebrospinal fluid (CSF) leaks out. Frequently, the lower extremities are deformed and/or a hip luxation is present. In lipomeningomyeloceles a subcutaneous lipoma and a hairy tuft can be seen.

Commissural Malformation

Children may present with unspecific symptoms such as seizures, neurodevelopmental delay, microcephaly, hypothalamic–pituitary malfunction, or hypertelorism. Callosal dysgenesis is frequently an incidental finding on postnatal US.

Disorders of Sulcation and Migration

The degree, extent, and location of malformation determine the clinical presentation. Children may present with mental retardation, seizures, and focal neurological deficits. Disorders of migration can occur as part of a syndrome complex.

Disorders of Diverticulation or Brain Cleavage

In the severe forms of holoprosencephalies, a spectrum of symptoms have been described. Hypothalamic–pituitary dysfunction, seizures, mental retardation, dystonia,

microcephaly as well as facial malformations such as cyclopia and fused metopic sutures can be encountered. The face may reflect the brain.

Thoracal and abdominal malformations are usually seen on gross inspection or present with clinical symptoms that are directly related to an impaired function of the affected anatomical regions.

Imaging

MRI relies mainly on T2-weighted single-shot fast spin-echo sequences (slice thickness 3–4 mm). T1-weighted gradient-echo sequences are added to rule out, for example, hemorrhages. Various additional sequences are currently progressively applied including diffusion-weighted sequences, magnetic resonance spectroscopy, as well as thick-slab, strongly T2-weighted sequences that provide a "fetographic" display.

Chiari II Malformation

Chiari II malformation is characterized by a small posterior fossa with herniation of cerebellar structures into the upper cervical spinal canal, deformation of the quadrigeminal plate, varying degrees of callosal dysgenesis, and supratentorial hydrocephalus. Rarely is an associated syringohydromyelia seen.

Cephaloceles

Cephaloceles are protrusions of the meninges and/or brain tissue through a skull defect. Most encephaloceles are occipital. The protruding brain tissue is usually dysplastic. Associated ventriculomegaly may be seen.

Dandy-Walker Malformation

Dandy-Walker malformation is characterized by cystic dilatation of the fourth ventricle, hypoplastic vermis that may be rotated upward, elevated torcula, and varying degrees of posterior fossa enlargement. The cerebellar hemispheres are usually laterally displaced. Associated ventriculomegaly may occur.

Spinal Dysraphism

In MMC a soft tissue defect in combination with a protruding neural placode through a wide open bony spinal canal is seen. The spinal cord is tethered, the dorsal and ventral nerve roots are usually stretched and appear along the ventral surface of the neural placode. Identification of the neural placode can be difficult as the neural placode is ventrally lined by T2-hyperintense CSF and dorsally by equally T2-hyperintense amniotic fluid.

Commissural Malformation

Callosal dysgenesis may be partial or complete. The corpus callosum develops in the following sequence: genu, truncus, splenium, and finally rostrum. If the truncus is missing, the splenium and rostrum will also fail to develop. In callosal agenesis the medial brain surface shows a radiating pattern of gyri and sulci. There is no cingulate gyrus. Both lateral ventricles show a parallel course on axial images, and a mild colpocephaly is frequently seen. On coronal images, the lateral ventricles have a trident shape, the third ventricle may extend interhemispherically. The hippocampi are malrotated.

Pachygyria and Polymicrogyria

In pachygyria the cerebral cortex is thickened, in polymicrogyria multiple small gyri are seen. Combinations of pachygyria and polymicrogyria may be seen.

Lissencephaly

Arrested neurons within the white matter are recognized as T2-hypointense bands that parallel the cerebral surface. In lissencephaly the overlying cortex is smooth, the sulci are shallow.

Schizencephaly

Clefts may extend from the cerebral surface until the lateral ventricles. The clefts are usually lined by thickened, polymicrogyric T2-hypointense cortex. The cleft may be closed (closed lip) or may open to the cerebral surface (open lip). The septum pellucidum is absent in 80% of the cases.

Holoprosencephaly

Depending on the severity of holoprosencephaly, different degrees of fusion of the cerebral hemispheres are seen. In the most severe cases a monoventricle is lined by a fused holosphere. In less severe cases, lobar holoprosencephaly, two hypoplastic frontal lobes are seen with hypoplastic frontal horns and a hypoplastic falx cerebri that extends frontally.

Thoracal and Abdominal Malformations

An exact delineation of the anatomy is essential to identify anatomical malformations. Functional information is very limited, and there are currently no routine intrauterine magnetic resonance angiography sequences available for examining cardiovascular malformations reliably.

Diagnosis

Fetal MRI serves as a second-line imaging tool in combination with prenatal US. Fetal MRI should be considered in complex (cerebral) malformations or pathologies, in those cases where US is limited due to, for example, adipositas or bowel gas and in those cases where the clinicians or parents desire a second imaging modality to confirm, correct, or complete sonographic findings. Diagnosis relies on the best spatial resolution that can be achieved with ultrafast MRI sequences in combination with sensitive phase array surface coils. The ultrafast sequences allow one to "picture freeze" the fetus while it is moving. Fetal MRI should be considered as an examination that evaluates the entire pregnancy, i.e., the uterus, placenta, umbilical cord, as well as the entire fetus. Imaging results should be evaluated by experienced radiologists who are familiar with the anatomy and pathology of fetuses and neonates. In addition, imaging findings should be discussed by an interdisciplinary team of specialists including pediatric (neuro-) radiologists, obstetricians, pediatricians, surgeons, and neonatologists.

Bibliography

1. Huisman TA, Martin E, Kubik-Huch RA et al (2002) Fetal magnetic resonance imaging of the central nervous system. Eur Radiol 12:1941–1951
2. Huisman TA, Wisser J, Martin E et al (2002) Fetal magnetic resonance imaging of the central nervous system: a pictorial essay. Eur Radiol 12:1952–1961
3. Kubik-Huch RA, Huisman TA, Wisser J et al (2000) Ultrafast MR imaging of the fetus. Am J Roentgenol 174:1599–1606

Fetal Neuroimaging

Nadine J Girard, Frederique Chapon, Xavier Combaz
Department of Neuroradiology, Hopital Timone Adultes, France
nadine.girard@mail.ap-hm.fr

Definition

Fetal neuroimaging includes all the imaging methods for examining the fetal central nervous system (CNS). Ultrasound (US) is the main tool for routine examination of the fetal brain. Magnetic resonance imaging (MRI) can serve as a second imaging tool to confirm or correct ultrasound findings. Indications for fetal MRI have increased because of improvements in MR techniques with subsequent ability to detect subtle changes within the fetal brain. Computed tomography (CT) is not used routinely. However, multidetector CT permits helical acquisition with thin slices and volume-rendering reconstructions that may be helpful in assessing spine and cranial vault abnormalities.

Clinical Presentation

MRI is usually performed during the second half of gestation from 18 to 20 weeks onward because US can accurately diagnose severe ▶brain abnormalities before that period of time and is hence usually sufficient for decision making. Moreover, MRI resolution is poor before 18 weeks.

Indications for ▶fetal brain MRI are mainly based on abnormal US findings: Ventricular dilatation is the most frequent indication (40%), followed by suspicion of CNS malformation (31%) and brain injury (1). MRI is of paramount importance in evaluating ventriculomegaly because it has greater sensitivity for detecting associated brain lesions compared with US.

MRI is also performed after normal results of brain US in peculiar contexts: familial (familial history of genetic disorder involving CNS, such as X-linked hydrocephalus and tuberous sclerosis), maternal (coagulation disorders, infections, acute fetal/maternal events), fetal [twin-to-twin transfusion syndrome, fetuses presenting with extracerebral malformations that can be associated with brain lesions, intrauterine growth restriction (IUGR)).

Knowledge of the general rules of fetal maturation is extremely important. Indeed, anatomy and the effects of maturation on the MR signal change according to gestational age. Therefore, the MRI features of a definite pathology will change accordingly (2). Repetition of MR examination is thus necessary when early MR is not conclusive, resulting in illustration of the natural history of a definite pathology. Moreover, the image itself may be confusing because different pathologies can display similar images, especially in young fetuses from 20 to 25 weeks (1).

Imaging

Images are routinely obtained in the sagittal, coronal, and axial planes relative to the fetal head with both T1- and T2-weighted images. The development of fast imaging using multiple phased-array coils is of great benefit and results in good signal homogeneity without necessarily needing to sedate the mother.

T2-weighted single-shot sequences such as HASTE (half-Fourier single-shot turbo-spin echo) provide heavily

T2-weighted images with low-susceptibility weighting and are used to "freeze" the fetus. T2 images of true fast imaging with steady-state precession type (TRUE FISP) are highly accurate for evaluating the face and skull base and in depicting old hemorrhage, calcifications, and lipoma in young fetuses. Thin sections of 1–1.5 mm are obtained with three-dimensional TRUE FISP sequences, which are mainly used in evaluating the midline (i.e., partial corpus callosum agenesis and aqueduct stenosis).

T1-weighted images are required to look for signal changes from normal maturation as well as from hemorrhage, calcifications, leukomalacia, lipoma, and lesions seen in tuberous sclerosis. Gradient echo (GE) or turbo-spin echo (TSE) images can be performed; GE images give an excellent differentiation between the cortical ribbon, the white matter, and the ventricular walls.

Diffusion-weighted images are performed in the postnatal period to detect cytotoxic or vasogenic edema through anisotropic, trace, and apparent diffusion coefficient images. Diffusion-weighted images can show the normal maturation and the premyelinating white matter tracts in which signal changes are seen on diffusion-weighted images before T1- and T2-weighted images do. Therefore, minor abnormalities of the corpus callosum and white matter anomalies may be identified.

Images of the fetal brain are currently obtained with acceptable acquisition time on last-generation magnets: 20–40 sec for T2-weighted images, 45 sec for T1-weighted images, 1 min for three-dimensional T2-weighted images, and 30–50 s for diffusion-weighted images (Fig. 1).

Normal Development of Fetal Brain Anatomy

Developing brain anatomy is characterized by morphological and signal changes along with increasing gestational age (3).

Morphological changes consist of changes in ventricular shape, thickness of the germinal matrix, and volume of the subarachnoid spaces, along with the developing sulcation. From the agyric brain at 18–20 weeks, dramatic changes in sulcus formation can be seen at 24, 28–30, and 34–35 weeks, at which time the gyration appears almost complete. Development of the cerebellum is complex. MRI is able to show the appearance of the fissures of the cerebellum. The lateral ventricles and the subarachnoid space appear relatively enlarged in young fetuses, with a progressing decrease in size along with development of the cerebral mantle. However, the subarachnoid space can remain large throughout gestation, particularly in the parieto-occipital areas, which result from the evolving process of cavitations of the meninx primitiva.

Signal changes result from the maturation process, which includes high cell density, myelination gliosis (the multiplication of glial cells that precedes myelination), formation of myelin proper with accumulation of intracellular lipid myelin precursors, and decreased brain-tissue water content, mainly within the white matter. Signal changes are detected at 20 weeks within the posterior brainstem, germinal matrix, and white matter, in which intermediate layers of migrating cells are present until 30 weeks and give a typical multilayered pattern of the cerebral mantle. Transient intermediate layers within the white matter constitute an important hallmark, and their absence is highly suggestive of white matter damage. Basal ganglia also show similar signal changes, mostly related to high cell density, which are extremely conspicuous at 28–29 weeks and must not be mistaken with cytotoxic lesions. Signal changes are identified in the posterior limb of the internal capsule and optic tracts at 33 weeks as well as in the projecting fibers of the central area of the centrum semiovale at 35 weeks.

Diagnosis

CNS malformations and brain injury are the primary abnormalities encountered in utero (1, 2). Criteria for destruction of the brain include abnormal ventricular morphology (irregular ventricular wall), lack of brain layering, absence of maturation milestones and of normal signals, and the presence of abnormal signals. On the other hand, malformations are characterized by their specific morphological changes. However, these criteria may overlap, such as in cases of vascular malformation with brain damage.

Numerous CNS malformations, from commissural to histogenetic disorders, can be seen in utero with limitations with regard to the accurate assessment of some malformations.

Corpus callosum agenesis (CCA) is the most frequent malformation (Fig. 2). Limitation is seen in cases of partial CCA associated with interhemispheric cyst, which, through its mass effect, can prevent detection of associated cortical malformations (especially micropolygyria) until after delivery and shunting. This condition increases the problem of prognosis in CCA, which is still debated.

Cerebral histogenetic disorders are rarely suspected on US and result from different types of pathogenic disorders: disturbances in cell proliferation (microlissencephalies), cell differentiation (focal cortical dysplasia), cell migration (heterotopia and lissencephalies, or agyria-pachygyria), and organization of the cortex [polymicrogyria (PMG)]. Absence of the multilayered pattern of the cerebral mantle, absence of the normal signal of the cortex, and an abnormal shape of the superficial cerebral hemisphere

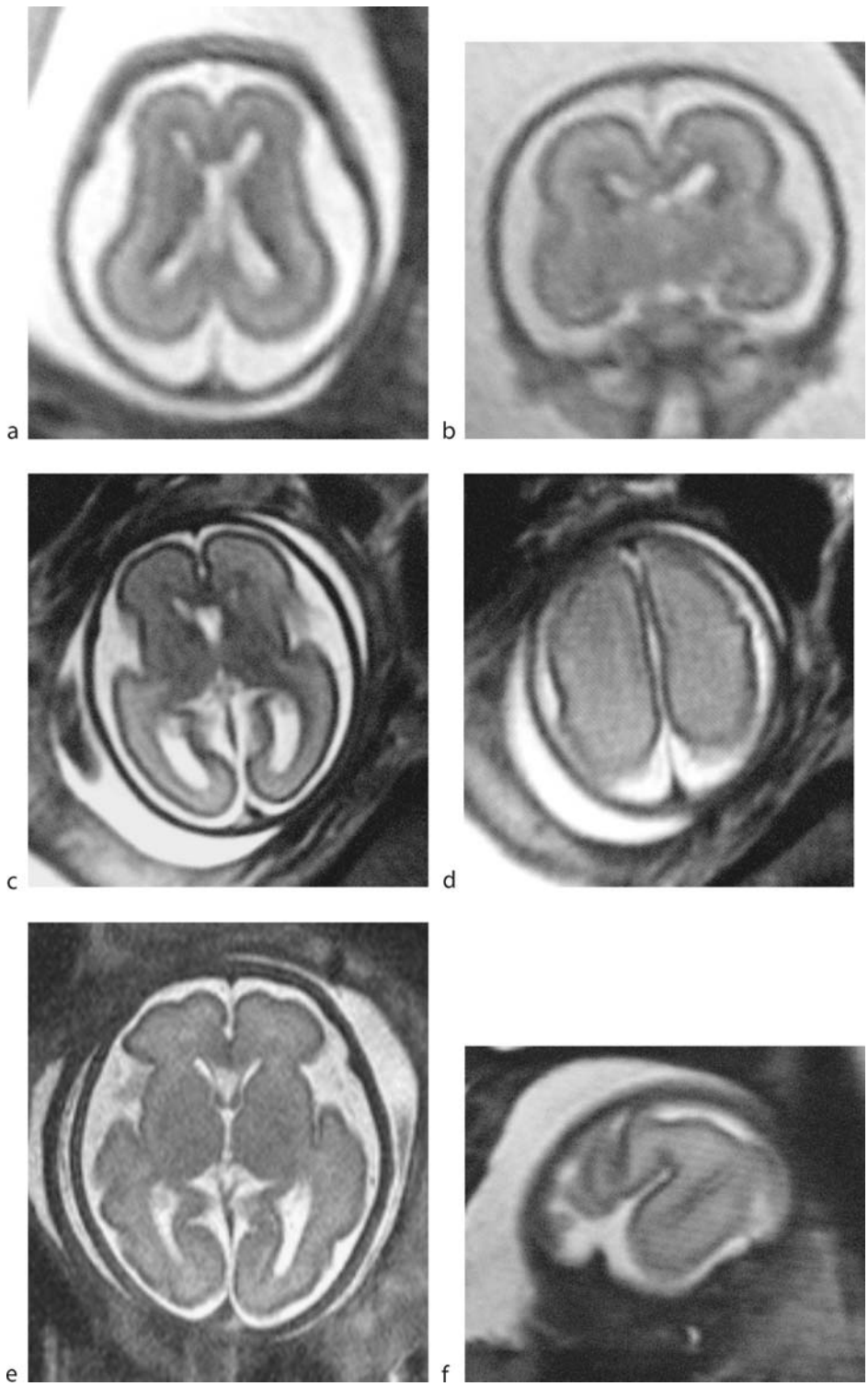

Fetal Neuroimaging. Figure 1 (continued)

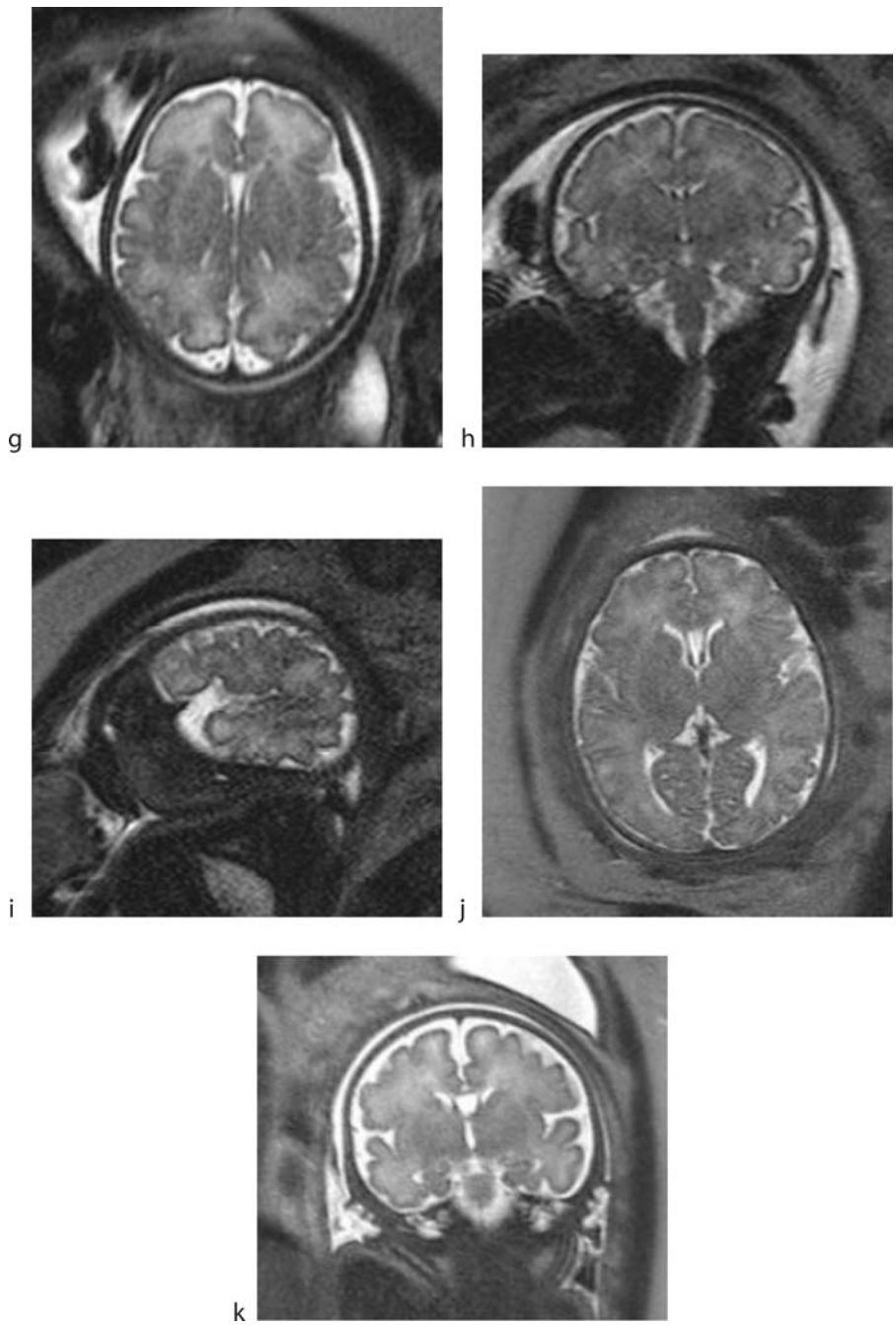

Fetal Neuroimaging. Figure 1 Normal appearance of the fetal brain through T2 images at 20 (a), 24 (b), 28 (c), 32 (d, e), and 37 (f) weeks. The brain is agyric in young fetuses, with prominent lateral ventricles and subarachnoid spaces (a). The central sulcus is seen at the cerebral surface as a depression by 24 weeks (b). By 28 weeks, pre- and postcentral sulci are identified (c) while the superior temporal sulcus is achieved (c). By 32–33 weeks the superior frontal sulcus is depicted at the cerebral surface, while the lateral ventricles and subarachnoid spaces are not as large as in previous stages. Circumvoluted brain is seen at 37 weeks. The germinal matrix is thick in young fetuses and of low signal on T2 images. The cortical ribbon is also of low signal. Intermediate layers are seen within the white matter until 30 weeks, giving a multilayered appearance of the fetal brain. Basal ganglia are also of low signal intensity on T2 due to high cell density.

are suggestive of a cortex/white matter abnormality. Microcephalies are usually diagnosed in the third trimester provided that the head circumference is three standard deviations below the mean.

In posterior fossa malformations, MRI can detect whether the dural structures, especially the tentorium, are normally positioned. Cystic posterior fossa malformations as part of the Dandy–Walker continuum are characterized by an elevated tentorium and bulging of the parieto-occipital vault, whether or not the vermis is partially or totally absent. In contrast, a small posterior fossa is seen in Chiari type 2 malformation related to myelomeningocele. A normally positioned tentorium, usually within a posterior fossa of normal size, is seen in histogenetic disorders such as pontocerebellar hypoplasia, cerebellar dysplasia, rhombencephalosynapsis, and rhombencephaloschisis. Cerebellar hypoplasia is difficult to diagnose because development of the cerebellum is slow, with cellular migration continuing well after birth. Great difficulty is encountered in unilateral cases because the condition may be related to either malformation or a clastic origin. However, severe hypoplasias that have poor prognoses are easy to identify.

Brain injury may result from hypoxia, ischemia, congenital infection (especially toxoplasmosis and cytomegalovirus infection), malformation (cerebral vascular and cardiac malformations), inherited inborn error of metabolism, or tumors.

Different features are encountered in the fetal brain in response to injury. Chronic responses of the brain and the

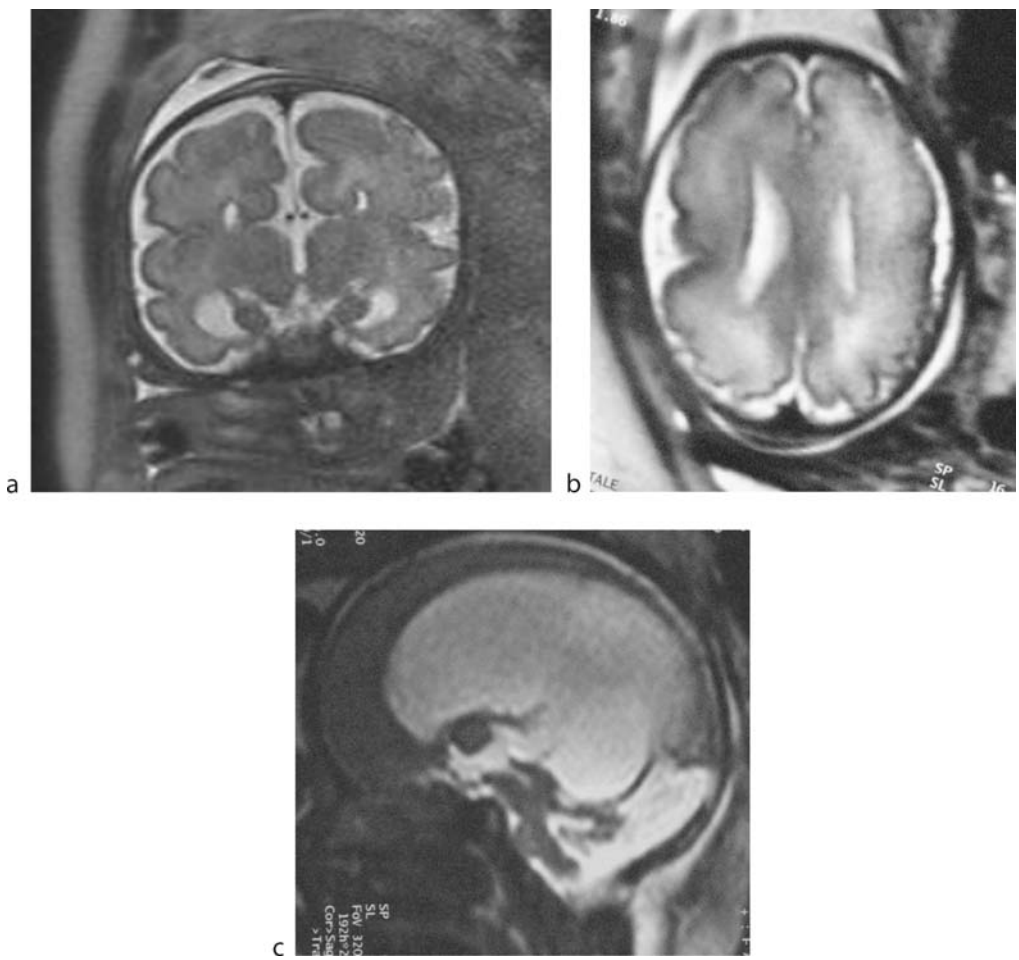

Fetal Neuroimaging. Figure 2 Examples of malformations encountered in utero: corpus callosum agenesis (CCA) at week 31 (a), polymicrogyria (PMG) at week 31 (b), and cerebellar hypoplasia at 26 weeks (c). The corpus callosum is missing between the two cerebral hemispheres. Note the enlarged temporal horns and parallel course of the lateral ventricles, which are widely separated in CCA. In PMG the normal gyration is not identified, with areas of thickened and irregular cortex and enlarged subarachnoid spaces that overlie the cortical abnormality, especially in the right hemisphere. The case with severe cerebellar hypoplasia is associated with ventricular dilatation.

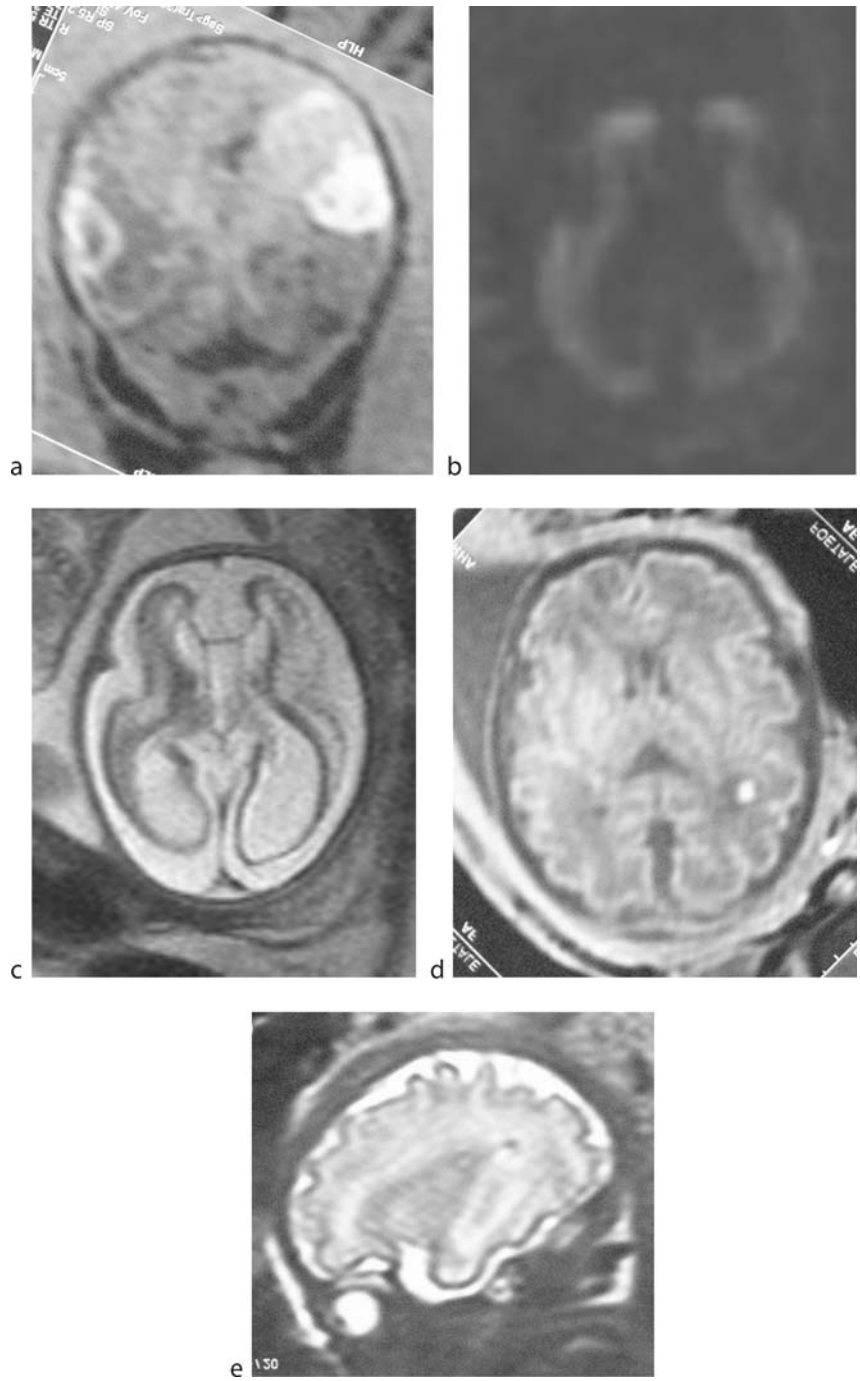

Fetal Neuroimaging. Figure 3 Examples of fetal brain injury: hemorrhage (a), necrosis and cytotoxic edema (b, c), and calcified abscess in toxoplasmosis (d, e). Hemorrhage: coronal T1 image at 34 weeks (a). Large areas of bright signal are seen bilaterally; brain hemorrhage is secondary to thrombocytopenia in this case. Necrosis and cytotoxic edema: axial diffusion (b) and T2 (c) images at 26 weeks in a twin-to-twin transfusion syndrome. Ventricular dilatation is associated with necrosis, seen as areas of bright signal on T2, especially in the left hemisphere with no identification of the normal low signal of the cortex. Cytotoxic lesion of the cortex is also identified as areas of bright signal on diffusion image in the frontal lobes. Toxoplasmosis: axial T1 (d) and parasagittal (e) images at 31 weeks. A nodule of bright signal on T1 and low signal on T2 is identified in the left periventricular area, corresponding to calcification. Note the slight low signal on the T1 image surrounding the bright nodule; this is due to edema.

combination of chronic and acute response are more commonly identified than acute response alone. Acute responses of the fetal brain include hemorrhage (intraventricular, in the germinal matrix, in the cerebral parenchyma, or in the subdural spaces), white matter damage (edema, leukomalacia), focal or diffuse infarction, and venous thrombosis (Fig. 3). Chronic responses of the fetal brain may manifest as ventricular dilatation, thickened or irregular germinal matrix or ventricular wall, white matter gliosis, loss of volume (atrophy), parenchymal cystic cavity (the most severe form being hydranencephaly), ependymal cyst, calcifications, malformations (especially of cortical development, such as PMG), and impaired myelination. Calcifications and cortical malformations are most likely seen in congenital infection, but not exclusively. White matter gliosis is not currently detected on conventional images but is seen at autopsy. Diffusion-weighted images and proton spectroscopy can help detect such cases (4, 5).

Ventriculomegaly may be caused by malformation, destruction of the brain, and, less commonly, by tumors, and is also seen in numerous syndromes in which it involves the frontal horns with a square, sharp shape of their walls. An apparent mechanism for ventricular dilatation is not always found in utero. The prognosis for ventriculomegaly in the fetus is variable. Findings indicative of a more favorable outcome include late diagnosis in the third trimester, slow evolution, a ventricle-hemisphere ratio of no more than 50% of normal and isolated ventriculomegaly. Isolated mild ventriculomegaly (whether unilateral or bilateral) is highly challenging because developmental delay ranges from 19% to 36%. The underlying mechanism of isolated ventriculomegaly can be related to fetal hypoxia (7%), early stages of benign external hydrocephalus (16%), and possible subtle changes of the white matter that are undetectable by conventional MRI.

Inborn errors of metabolism manifesting in utero are rare and extremely challenging in terms of diagnosis and prognostic significance. Metabolic diseases can be suspected because of IUGR, polyhydramnios, or brain malformation. CCA can be seen in pyruvate dehydrogenase deficiency, heterotopia in mitochondrial respiratory chain deficiency, and cortical abnormalities in Zellweger disease. Subependymal cysts are encountered in numerous diseases.

References

1. Brunel H, Girard N, Confort-Gouny S et al (2004) Fetal brain injury. J Neuroradiol 31:123–137
2. Girard N, Gambarelli D (2004) Fetal brain abnormalities. Magnetic resonance imaging. An atlas with anatomic-pathologic correlations. Label production, Marseille, France
3. Girard N, Gambarelli D (2001) Magnetic resonance imaging. Normal fetal brain. An atlas with anatomic correlations. In: Brunelle F, Shaw D, J. Pediatr Fetal Imaging, Rickmansworth, UK
4. Girard N, Fogliarini C, Viola A et al (2006) MRS of normal and impaired fetal brain development. Eur J Radiol. 57:217–225
5. Girard N, Chaumoitre K, Confort-Gouny S et al (2006) Magnetic resonance imaging and the detection of fetal brain anomalies, injury, and physiologic adaptations. Curr Opin Obstet Gynecol 18:164–176

FGF-23

▶Fibroblast Growth Factor 23

Fiberoptic Cholangioscopy

A relatively new and well-established procedure that has found interesting applications in the diagnostic approach and therapeutic management of biliary stones, for the differential diagnosis between benign and malignant lesions, and for the staging of ductal malignancies.

▶Biliary Anatomy

Fibroadenoma

Benign biphasic tumor, with stromal and epithelial proliferation.

▶Neoplasms, Phyllodes, Breast

Fibroadenosis

▶Fibrocystic Disease, Breast

Fibroblast Growth Factor 23

Fibroblast growth factor 23, a gene product that can cause phosphate-losing (oncogenic) rickets or osteomalacia associated with, and arising from, various benign or malignant soft-tissue lesions.

▶Demineralization, Bone

Fibrocystic Changes

A benign disease common in women of the third, fourth, and fifth decades characterised by formation, in one or both breasts, of small cysts containing fluid, associated with stromal fibrosis and with variable degrees of intraductal epithelial hyperplasia and sclerosing adenosis.
▶Breast, Physiology
▶Fibrocystic Disease, Breast

Fibrocystic Disease, Breast

Luis Pina
Department of Radiology
Clínica Universitaria de Navarra, Spain
ljpina@unav.es

Synonyms

Aberrations of normal development and involution (ANDI); Bloodgood's disease; Chronic cystic mastitis; Cystic hyperplasia; Cystic mastopathy; Fibroadenosis; Fibrocystic changes; Hyperplastic cystic disease; Konig's disease; Mammary dysplasia; Mammary dystrophy; Reclus'disease; Schimmelbusch's disease; Sclerocystic disease

Definition

Fibrocystic disease has been a clinical problem for a long time, as it is reflected in the writings of Astley Cooper at the beginning of the nineteenth century. In fact, it is a confusing and inexact term. All clinicians have a concept of what fibrocystic disease is, but it is difficult to define and to differentiate from normal conditions of the breast. Fibrocystic disease is not a distinct entity but a heterogeneous group of abnormalities that include fibrosis, cysts, ▶apocrine metaplasia, ▶adenosis, and ▶hyperplasia (1, 2). Some of these abnormalities cannot be considered as pathologic conditions and do not increase the risk of the individual's developing breast cancer. However, other included conditions, such as some types of hyperplasia, may increase that risk. Nowadays fibrocystic disease is a term that should not be used anymore because it is confusing and does not reflect a real pathology or a risk of developing breast cancer. Fibrocystic disease is in fact a "nondisease."

Pathology/Histopathology

There is no specific pathology of fibrocystic disease. Fibrosis, cysts, apocrine metaplasia, adenosis, and hyperplasia compose the spectrum of fibrocystic disease.

Clinical Findings

Palpation of many normal breasts is difficult and unspecific, especially in young women. Firm, granular, or painful breasts at palpation, with cyclic changes, are frequently found in clinical practice and have for many years been described as "fibrocystic." But again, the term "fibrocystic disease" should not be routinely employed because in most cases it only describes the difficulty of studying these breasts, not a pathologic condition (1, 2).

Imaging

Mammography

The term "fibrocystic disease" should be avoided in mammographic reports, and it is not included in the American College of Radiology (ACR) breast imaging reporting and data system (BI-RADS) lexicon (3). In fact, the ambiguous significance of this term, prolifically used in other times, has made it difficult to standardize mammographic reports. This term has been used to describe dense breasts, usually with multiple round to oval masses, with well-delimited or obscured margins. Dense breasts were initially described as dysplastic by Wolfe. However, this term should also not be used because it is confusing. Nowadays, these types of breasts are classified as ACR class 4 (Fig. 1). The main problem of these breasts is the lower sensitivity to detect carcinoma compared with fatty breasts. Dense breast tissue reduces the sensitivity from 80% in fatty breasts (ACR class 1) to 30% (ACR class 4) (4).

It remains controversial whether dense breast have a higher risk to develop breast cancer than fatty ones. Some studies support this, but additional studies are needed (4).

Ultrasound

Ultrasound is the technique of choice to diagnose ▶breast cysts, a usual component of dense breasts (Fig. 2). It allows accurate characterization of a palpable mass, which is frequently found in these breasts, as cystic or solid. Moreover, ultrasonography may play a role in detecting breast cancers not seen on mammography. Nevertheless, supplemental use of ultrasonography in women with

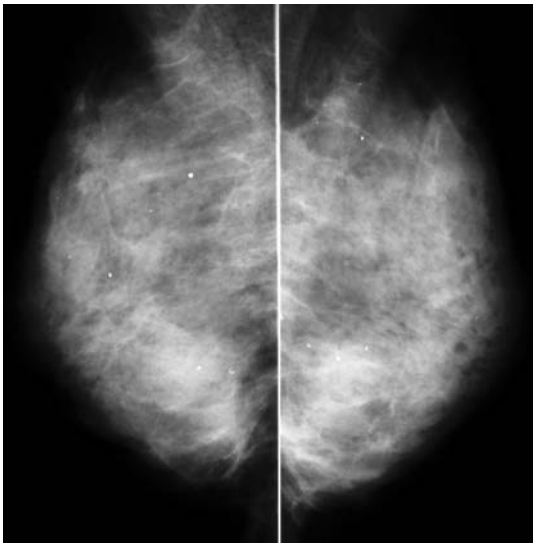

Fibrocystic Disease, Breast. Figure 1 Dense breasts (American College of Radiology class 4). Mediolateral oblique views.

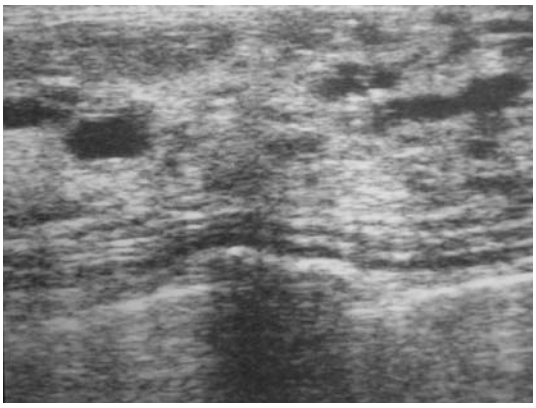

Fibrocystic Disease, Breast. Figure 2 Ultrasonography of dense breasts. Multiple small cysts are seen.

asymptomatic dense breasts is still not accepted as a standard indication (5).

Magnetic Resonance Imaging

Magnetic resonance imaging should not be used to evaluate a breast lump in dense breasts. However, it plays an important role in determining the size of a breast cancer, especially in dense breasts, as well as determining possible multicentricity or bilaterality. Note that dense breasts may cause false positive results on magnetic resonance because the fibroglandular tissue may exhibit enhancement after paramagnetic contrast administration due to hormone stimulation (Fig. 3).

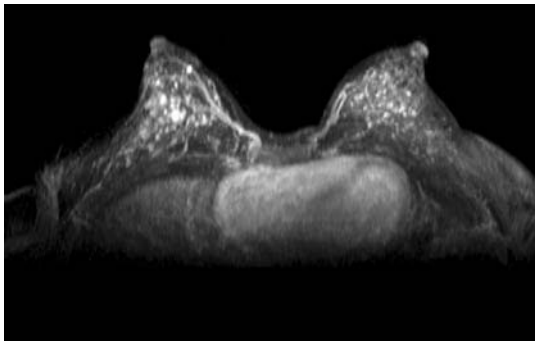

Fibrocystic Disease, Breast. Figure 3 Contrast-enhanced magnetic resonance imaging (Flash3D, MIP) in normal dense breasts. Multiple foci due to spontaneous hormone-induced enhancement are seen.

Nuclear Medicine

Nuclear medicine does not play a role in diagnosing fibrocystic disease. Rarely, dense breasts may uptake the radionuclide, causing false positive results on positron emission tomography scans.

Diagnosis

Cyclic breast pain not associated with a palpable abnormality is not an indication for imaging techniques. Most breast cancers do not present as pain, although in rare cases they may be painful. However, a breast lump always needs to be carefully studied. In spite of the lower sensitivity of mammography in dense breasts, it continues to be the first imaging tool used. If the palpable abnormality is mammographically benign, such as a lipoma, fibroadenolipoma, or an oil cyst, no further diagnostic procedures are required. However, if benignity cannot be ensured, or if the palpable lesion is not identified, an ultrasound exam is needed. Palpable cysts may be easily evacuated, but if a palpable lesion cannot be ensured as benign, a biopsy should be performed.

Bibliography

1. Guinebretière JM, Menet E, Tardivon A et al (2005) Normal and pathological breast, the histological basis. Eur J Radiol 54:6–13
2. Hughes LE (2000) Problems of concept and nomenclature of benign disorders of the breast. In: Hughes LE, Mansel RE, Webster DJT (eds) Benign Disorders and Diseases of the Breast. Concepts and Clinical Management, Saunders, London, pp 1–5
3. American College of Radiology (1995) Breast imaging reporting and data system (BI-RADS). American College of Radiology, Reston, VA
4. Liberman L, Menell JH (2002) Breast imaging reporting and data system (BI-RADS). Radiol Clin North Am 40:409–430
5. Berg WA (2004) Supplemental screening sonography in dense breasts. Radiol Clin North Am 42:845–851

Fibrolamellar Carcinoma (FLHCC)

Rare malignant neoplasm of hepatocellular origin. In the past it was considered a variant of HCC, while it is now seen as an independent entity. Pathologically it is characterised by the presence of abundant fibrous tissue, which is distributed in bands or laminae. The central fibrous scar may show calcifications. Satellite nodules may also be present. This tumour occurs in younger patients, is not associated with hepatic cirrhosis and its histological features are less malignant than those of HCC. Most often it appears as a solitary, large, well-circumscribed mass with lobulated margins. Vascular invasion is rare, while lymphatic metastases are quite common.

Hepatocellular carcinoma (HCC).

▶Hepatocellular Carcinoma

Fibroma

▶Leiomyoma, Uterus

Fibromuscular Dysplasia RAS

RAS secondary to a thickening of one or several layers of the arterial wall; it is of unknown origin.

▶Stenosis, Artery, Renal

Fibro-Osseous Lesions, Facial Skeleton

G Moulin[1], O Monnet[1], J Paris[2], F Facon[2]
C Chossegros[3], MA Chrestian[4]
[1]Department of Radiology, CHU La Timone, Marseille, France
[2]Department of Otorhinolaryngology, CHU La Timone, Marseille, France
[3]Department of Maxillofacial surgery, CHU La Timone, Marseille, France
[4]Department of Pathology, CHU La Timone, Marseille, France
guy.moulin@mail.ap-hm.fr

Synonyms

Benign osseous tumors of the craniofacial region

Definitions

Fibro-osseous lesions (FOLs) of the face are quite rare and consist of lesions with osseous fibrous tissue instead of regular bone matrix. They represent a diverse group of pathologic conditions that includes developmental lesions and reactive or dysplastic diseases. FOLs share overlapping clinical, radiologic, and pathologic features that may lead to diagnostic confusion and possible misdiagnosis.

Because of their resemblances, FOLs are difficult to classify and terminology is unclear in some points. The WHO classification (second edition, 1992) reports three groups (1):

- ▶Fibrous dysplasia
- Benign fibro-osseous tumors: ▶cemento-ossifying fibroma, ▶osteoma, and osteoblastoma
- Cemento-ossifying dysplasia (reactive lesions) includes odontogenic lesions of the mandible: focal cemento-ossifying dysplasia, florid cemento-ossifying dysplasia, and gigantiform cementoma

The main differential diagnoses are ▶Paget's disease that often involves the face or the skull and giant cell tumors.

Pathology/Histopathology

Fibrous dysplasia is an uncommon benign bone disorder of unknown etiology in which normal medullary bone is replaced by fibrotic and osseous tissue. There are two variants of fibrous dysplasia (2): monostotic, which is more common (70%), and polyostotic (30%), which affects many bones and commonly the face.

McCune–Albright syndrome is characterized by polyostotic fibrous dysplasia, "cafe-au-lait" spots, and autonomous hyperfunction of various endocrine organs (precocious puberty). This is a rare disease that exclusively occurs in women. Lesions are usually diagnosed during the third decade of life. Fibrous dysplasia has two periods: an active growth phase until puberty and an adult quiescent phase.

Histopathologically, fibrous dysplasia (Fig. 1) shows irregular-shaped trabeculae of immature bone in a cellular fibrous stroma (3). The anarchic fibrous stroma has a variable cellularity. The bone component has mature and immature bone cells and anarchic trabeculae that are thinned, C- or S-shaped like "Chinese characters." Typically, the trabeculae are embedded in, and blend into, vascularized fibrous tissue lacking the osteoblastic rimming of normal bone.

There is a low but definite rate of malignant transformation (less than 1%) into osteosarcoma. For this reason radiation is generally felt to be contraindicated as a treatment modality for fibrous dysplasia.

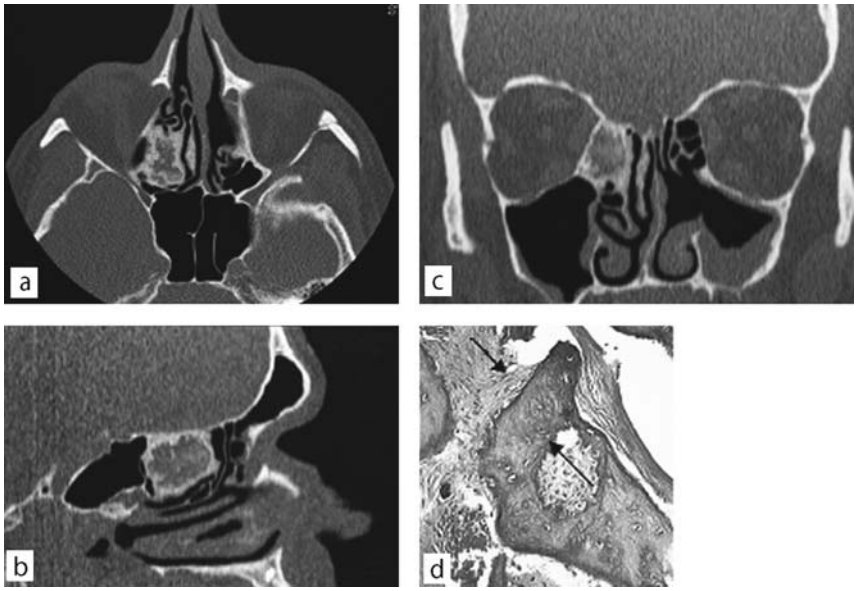

Fibro-Osseous Lesions, Facial Skeleton. Figure1 Fibrous dysplasia: CT scans in (a) axial, (b) coronal, and (c) sagittal axes show an expansile mass of the right ethmoid. The cortices appear intact, the medullary space is composed of ossified and nonossified regions. Histology (d): irregularly shaped trabeculae of osteoid and immature bone, without osteoblastic rimming (arrows).

Cemento-ossifying fibroma belongs to the group of fibro-osseous tumors. Histologically, ossifying fibroma is a benign tumor composed of fibrous tissue with varying amounts of calcified tissue suggestive of bone and/or cement (Fig. 2). Most ossifying fibromas show some degree of bony trabeculae formation. Bone maturation is not achieved and fibrous tissue density is variable. Small hemorrhagic zones can be found, such as local inflammation with giant cells. The most similar entity to ossifying fibromas is fibrous dysplasia.

Juvenile ossifying fibroma is an aggressive variant with the ability to infiltrate. Histologically, juvenile ossifying fibroma arises from the periodontogenic ligament as the cemento-ossifying fibroma. It has a high cellularity.

Also from the fibro-osseous tumor group, osteomas are the most common benign osseous lesion of the sinuses. Although the etiology of these tumors is unknown, they occur most commonly in the frontoethmoid region.

Fitzgerald–Gardner syndrome is an autosomal-dominant disorder characterized by multiple facial osteomas, colic polyposis, and cutaneous lesions (fibromatosis, lipomatosis, leiomyoma). Histologically (3), these lesions are dense, well circumscribed, made of mature lamellar bone, sometimes with fibrous, hematopoietic, or fatty tissue components (Fig. 3).

Osteoblastoma is a rare benign tumor of the face that occurs most commonly in young men (3). Histologically, osteoblastomas are characterized by osteoid trabeculation and loss of fibrovascular connection.

Cemento-ossifying dysplasias are part of the non-neoplastic fibro-osseous tumors of the WHO classification and are periodontogenic reactive lesions. These lesions occur exclusively in the mandible and the maxilla. Many authors do not consider these lesions as genuine facial fibro-osseous tumors.

Clinical Presentation

Fibrous dysplasia presents with facial clinical symptoms such as pains (during active growth phase) and asymmetric deformations, but in adults the diagnosis is often made fortuitously from an x-ray study. Fibrous dysplasia is usually unilateral and most likely involves the frontal, ethmoid, sphenoid, and maxillary bones. Temporal, malar, parietal, occipital, and mandibular bone involvements are rare. Depending of the site of involvement, fibrous dysplasia can yield to headaches, nasal obstruction, mucoceles, and visual disorders (optic nerve compression).

Cherubism is considered as a variant of congenital fibrous dysplasia. It is an autosomal-dominant disorder. Extracranial skeletal involvement is rarely seen in hereditary and nonhereditary forms of the disorder. The mandible is the most severely affected craniofacial component. Bilateral swelling of the cheeks, mandibular enlargement, and maxillary spongious hypertrophy cause orbital manifestations and the tendency of the eyes to look

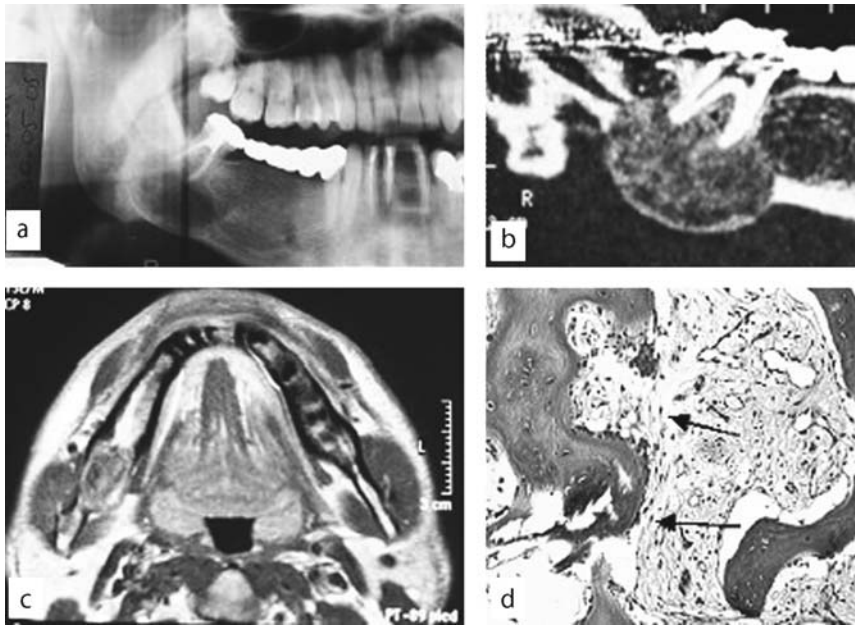

Fibro-Osseous Lesions, Facial Skeleton. Figure 2 Cemento-ossifying fibroma of the mandible. (a) Panoramic radiograph showing a well-circumscribed radiolucency with swelling at the cortices. (b) On sagittal CT scan the lesion is well limited, with high density and bony zones. (c) On axial T1-weighted post-Gd-DTPA MRI, we can see a significant enhancement correlated to the cemento-ossifying fibroma visualization. Histology (d): trabeculae of mature and immature bone in a fibrous stroma, with presence of osteoblastic rimming (→).

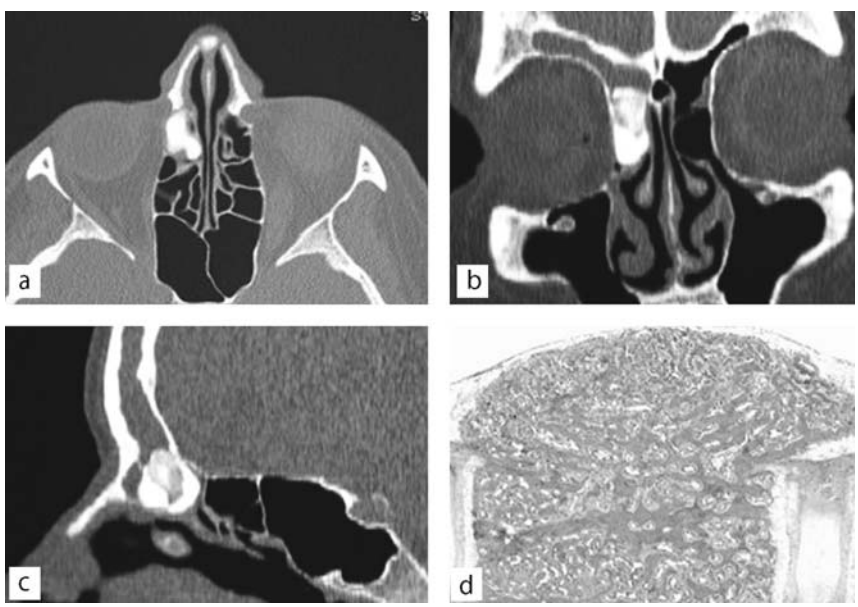

Fibro-Osseous Lesions, Facial Skeleton. Figure 3 Osteoma: (a) axial, (b) coronal, and (c) sagittal CT scans show an osteoma from the right anterior ethmoid cells. It looks like a well-circumscribed dense and calcified mass. For these patients, the osteoma obstructs the right frontal sinus. Histology (d): multiple packed levels of lamellar bone, without fibrous stroma, well circumscribed.

up to the sky. Thus, the pathognomic clinical feature resembles the appearance of "raised to heaven" Renaissance cherubs.

Cemento-ossifying fibromas are more common in women than in men and most often occur in the third and fourth decades of life. They are generally discovered incidentally on an x-ray or present as an asymptomatic mass without pain or swelling. The most common sites of occurrence are the mandible and the maxilla. They can also occur in the orbit and the paraorbital region. The juvenile form occurs most commonly in younger patients in the second decade of life and most likely involves the sinus and para-sinus regions (unifocal or plurifocal).

Osteomas are generally discovered incidentally on an x-ray or present with headache, facial deformation, or visual disorders. They often occur in men in the fifth decade of life but can occur at any age.

Osteoblastomas present with night pains and facial deformation, and teeth may be loosened.

Imaging

Computed tomography (CT) is now the key examination for the diagnosis of these lesions. The radiological appearance of fibrous dysplasia is variable (4). If predominantly fibrous, the lesion will appear radiolucent. If predominantly osseous, the lesion will appear radiodense. An equal mixture of the two will give the characteristic ground-glass appearance.

The radiological diagnosis should be evoked in cases of bone expansion with combined radiodense and radiolucent areas (Pagetoid variant, Fig. 1) or in cases of homogeneous radiodense bone expansion ("ground-glass expansion"). The pseudocystic variant is a radiolucent oval bone tumor with well-defined sclerotic contours.

Cortical bone is usually free of disease and can be deformed but not involved.

T1-weighted magnetic resonance imaging (MRI) reveals intermediate intensity and T2-weighted MRI reveals heterogeneous low intensity. Small hyperintense zones can be seen on T2-weighted images if cystic. Gadolinium enhancement is variable, sometimes intense.

The cemento-ossifying fibroma (Fig. 2) varies with the maturity of the lesion and with the amount of fibrous tissue. These lesions are sharply demarcated and unilocular. At the early stage, the immature lesion is radiolucent with rare calcifications. Later, the mature ossifying fibroma is radiopaque. CT scan shows a bone expansion surrounded by a dense contour. A dense center can be seen in some cases. T1-weighted MRI reveals intermediate intensity and T2-weighted MRI reveals low intensity. Gadolinium enhancement is moderate. The juvenile ossifying fibroma is very similar to ossifying fibromas. However, its aggressiveness yields to bone expansion with possible cortical ruptures without visible periosteal reaction. CT and MRI show calcification and osteoid trabeculation in the surrounding soft tissues. Ossifying fibromas can usually be surgically removed. Tumor recurrence after removal is low.

Radiologically, osteomas have regular contours. These are dense, osseous lesions developed in sinus cavities (Fig. 3). If large, osteomas can be heterogeneous.

For osteoblastomas, CT scans show a round lesion, well circumscribed with regular calcified contours. Osteoblastomas occur in the bone medullary. MRI findings are very similar to those of cemento-ossifying fibroma.

The radiological differential diagnoses are represented by Paget's disease and giant cell tumors.

Although the etiology of Paget's disease is unknown, it is characterized by an increased osteoclastic and osteoblastic activity yielding to the production of a dense and fragile osseous tissue. Paget's disease occurs most commonly in men after 50 years of age with a family history (3). Most often, this is a polyostotic disease (90%) with spinal, pelvic, and cephalic and femorotibial involvement. In cases of cephalic involvement, the most common sites of involvement are the skull vault, the mandible, and the maxilla. Cranial nerve disorders are reported in skull base involvement. Radiologically, the bone can appear flaky or thickened and dense with nonlinear cortical involvement associated with a poor corticomedullary differentiation. Well-circumscribed radiolucent zones can also be seen. T1-weighted and T2-weighted MRI reveal low-intensity zones of bony densification. Gadolinium enhancement is moderate. There is a 5–10% rate of malignant transformation into sarcoma for polyostotic disease. This rate is 2% for monostotic disease.

Giant cell tumors are rare benign lesions, locally aggressive (3). Histologically, these tumors show multinucleated giant cells, arising from osteoclasts, associated with mononucleated epithelial fusiform cells. These tumors most likely occur in the sphenoid, ethmoid, and temporal bone and present with pain and visual disorders. CT scans show lytic lesions, invading surrounding structures. MRI shows a T1 gadolinium enhancement in the early stage.

Nuclear Medicine

Bone scintigraphy is limited to the assessment of extension of the FOL. It is a useful examination for precisely identifying the extrafacial localizations in fibrous dysplasia and Paget's disease.

The role of PET CT has yet to be evaluated.

Diagnosis

FOLs of the face are difficult to diagnose. The radiological resemblance of these tumors requires a good knowledge of the clinical context. The pathologist should also correlate his results with clinicoradiological data for a reliable diagnosis.

In practice, diagnosis is mainly based on imaging; biopsy is very rare for facial lesions.

References

1. Mac Donald-Jankowski DS (2004) Fibro-osseous lesions of the face and jaws. Clin Radiol Jan; 59(1):11–25
2. Mafee MF (2003) Fibro-osseous and giant cell lesions, including brown tumor of the mandible, maxilla, and other craniofacial bones. Neuroimaging Clin N Am 13:525–540
3. Peter M. Som (2003) Head and Neck Imaging fourth edition, vol I, section I, chap 6:261–373, Mosby
4. Fries JW (1957) The roentgen features of the fibrous dysplasia of the 39 pathologically proven cases. Am J Roentgenol 77:71

Fibrosarcoma

One of the malignant tumors having commonly low signal intensity of T2-weighting. May rarely be well circumscribed and mimic a benign tumor with decreased signal intensity on T2-weighting.

▶Neoplasms, Soft Tissues, Malignant
▶Hepatic Sarcoma
▶Neoplasms, Bone, Malignant

Fibrosarcoma, Hepatic

Rare primary malignancy of mesenchymal origin arising from fibroblasts. In some tumors, the development of cellular differentiation allows the presence of collagen. On gross examination, these lesions are grayish white and characterized by a local invasion or a hematogenous metastatic spreading. Clinical and imaging features are common to those of others hepatic sarcomas (leiomyosarcoma).

▶Hepatic Sarcoma

Fibrothecoma

Fibrothecomas are solid ovarian stromal tumors, which may contain dense calcifications or cystic degenerations. They typically occur in postmenopausal women. Due to hormonal effects, women may present with abnormal uterine bleeding.

▶Masses, ovarian

Fibrothorax

▶Postoperative
▶Pleural Thickening, Benign Diffuse

Fibrous Dysplasia

Benign fibro-osseous lesion characterized by replacement of the normal medullary bone by fibrotic and immature bone tissues. There are monostotic or polyostotic forms. The lesions are well circumscribed and more frequently involve the face.

▶Fibro-Osseous Lesions, Facial Skeleton
▶Neoplasm-Like Lesion, Bone

Fibrous Histiocytoma

▶Hepatic Sarcoma

Fibrous Mesothelioma

▶Pleura, Localized Fibrous Tumor

Fibular Deviation of the Toes

Fibular deviation of the toes is a typical deformity in late-stage rheumatoid arthritis with or without subluxation and fibular abduction in the metatarsophalangeal joint as the lower extremity equivalent to ulnar deviation.

▶Rheumatoid Arthritis

Film-Screen (FS) System

Photographic film is sandwiched between two-image intensifier screens. The screens fluoresce when irradiated and produce a latent image on the film. The film requires chemical processing to allow the information it contains to be read by the reporting radiologist.

▶Children, Imaging Techniques

Fine Needle Aspiration, Breast

R. Schulz-Wendtland, K. Anders, W. Bautz
Institute of Radiology, Gynaecological Radiology, University of Erlangen-Nürnberg, Erlangen
ruediger.schulz-wendtland@idr.imed.uni-erlangen.de

According to the "Guidelines for Pathology—Addendum to the European Guidelines for Quality Assurance in Mammography Screening" and according to the recommendations of various pathology societies in Europe, fine-needle aspiration of breast tissue no longer constitutes a significant tool in the diagnostic work-up of breast lesions, because differential diagnosis, for example, lobular *in-situ* carcinoma (LCIS), low- or high-grade ductal *in-situ* carcinoma (DCIS) versus atypical ductal hyperplasia (ADH), is not possible on the basis of aspiration cytology. It has therefore been replaced by interventional methods, providing tissue for histologic assessment. However, two indications for fine-needle aspiration remain.

Indications

Painful cyst

In severely worried patients fearing malignant disease in spite of an unequivocal finding of a cyst (clinical findings, mammography, and ultrasound combined).

Technique

First, the most suitable access should be chosen, taking into account oncological/surgical considerations. Under sonographic guidance, the needle is advanced toward the cyst and pushed forward, until the tip of the needle is visualized within the cyst fluid. The containing liquid is aspirated to achieve complete drainage of the cyst.

Insufflation of the cyst with air and subsequent mammographic pneumocystography are now performed in particular cases only—a negative air contrast test might facilitate the identification of possible microcalcifications (Fig. 1a, b).

Bibliography

1. American College of Radiology (ACR) (Hrsg) (2004) Breast Imaging—Reporting and Data System (BI-RADS™). Reston, Philadelphia
2. Duda VF, Schulz-Wendtland R (Hrsg) (2004) Mammadiagnostik. Springer-Verlag, Berlin, Heidelberg, New York
3. Fischer U (Hrsg) (2003) Mammographiebefund nach BI-RADS™. Thieme-Verlag, Stuttgart
4. Heywang-Köbrunner SH, Schreer J (Hrsg) (2003) Bildgebende Mammadiagnostik. Thieme-Verlag, Stuttgart
5. Lanyi M (Hrsg) (2003) Brustkrankheiten im Mammogramm. Springer-Verlag, Berlin, Heidelberg, New York
6. Parker SH, Jobe WE (Hrsg) (1993) Percutaneous Breast Biopsy. Raven Press, New York

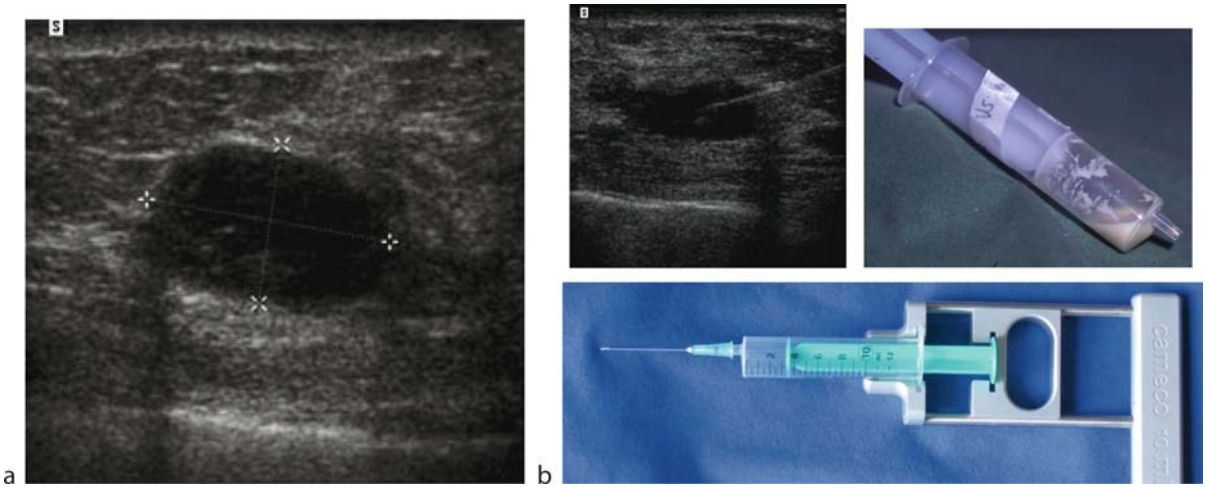

Fine Needle Aspiration, Breast. Figure 1

7. Sickles EA (Hrsg) (2001) Breast Imaging. Lippincott Williams & Wilkins, Baltimore
8. Tabar L, Tot T, Dean PB (Hrsg) (2003) Breast Cancer. Thieme-Verlag, Stuttgart

Fine Needle Biopsy

FNB or FNAB; a histologic specimen is not taken, but cells are aspirated for cytologic diagnosis.
▶Carcinoma, Lobular, *In situ*, Breast

First (Second) Generation Contrast Agent

▶Contrast Media, Ultrasound, High Solubility Gas

Fissure of Annulus

A fissure of annulus is a separation or break between annular fibers, avulsion of fibers from their vertebral body insertions, or breaks through fibers that extend radially, transversely, or concentrically, involving one or more layers of the annular lamellae.
▶Herniation, Intervertebral Disk

Fistula, Arteriovenous, Pulmonary

Pascal Lacombe, Jean-Pierre Pelage
Department of Radiology
Hôpital Ambroise Paré,
Université Paris Ile-de-France Ouest
Boulogne-Billancourt, France
pascal.lacombe@apr.ap-hop-paris.fr

Synonyms

Pulmonary arteriovenous aneurysm; Pulmonary arteriovenous fistula; Pulmonary arteriovenous malformation; Pulmonary telangiectases

Definitions

Pulmonary arteriovenous malformations (PAVMs) are uncommon, abnormal, direct capillary-free communications between pulmonary arteries and pulmonary veins, which are most commonly congenital in nature (1). PAVM results in a ▶right-to-left shunt with single or multiple enlarged feeding arteries and draining veins separated by a thin-walled bulbous-like or serpiginous vascular structure. The loss of normal filtering capillary bed leads to ▶paradoxical systemic embolisms and to impairment of systemic blood oxygenation (2).

Pathology/Histopathology

Etiology

PAVMs are not a common clinical problem (1 PAVM in 5000 autopsies). Approximately 60–90% of the cases of PAVM are associated with hemorrhagic telangiectasia (HHT or Rendu–Osler–Weber syndrome). Conversely, approximately 15–35% of patients with HHT have PAVMs. With the onset of asymptomatic screening programmes in the USA and most European countries, a higher frequency of involvement has been estimated: at least 30% of HHT patients have PAVMs, 30% have hepatic involvement and 10% cerebral involvement.

Abnormal arteriovenous pulmonary communications have been described in a variety of acquired conditions: chronic hepatic disease, thoracic trauma, schistosomiasis, actinomycosis, Fanconi's syndrome, metastatic thyroid carcinoma, mitral stenosis, or congenital cyanotic heart disease after surgery (cavopulmonary anastomoses). We will discuss HHT predominantly as it relates to PAVMs.

HHT is a genetic disorder which is transmitted in an autosomal dominant pattern, and characterized by arteriovenous malformations (AVMs). This disease affects between 1 in 5000 and 1 in 8000 people in Europe and Japan, respectively. There are two classical types of HHT, type 1 and 2, caused by mutations in the endoglin (chromosome 9) and ALK-1 (chromosome 12) genes, respectively. HHT patients without detectable mutations in endoglin or ALK-1 have been recognised by the HHT genetic centres. Some of them are now known to have HHT–juvenile polyposis overlap syndrome caused by Smad4 mutations. More recently, a novel locus for HHT has been identified on chromosome 5.

Classification of PAVMs

A simple PAVM consists in single or multiple feeding arteries originating from a single segmental artery. Conversely, in complex PAVMs, feeding arteries always originate from two or more segmental arteries (3). Multiple lesions

are highly suggestive of an association with HHT. Simple PAVMs usually account for 80–90% of PAVMs but simple and complex PAVMs are frequently seen in the same patient. The majority of PAVMs are located in the lower lobes. In some patients with simple and/or complex PAVMs, a diffuse pattern of PAVMs can be present. Diffuse PAVMs are defined as AVMs involving every subsegmental artery of at least one lobe. They occur in 5% of HHT patients. Bronchial artery hypertrophy or ►systemic supply to PAVM has been described in roughly 5% of PAVM.

Clinical Presentation

To permit a high degree of clinical suspicion of HHT, international consensus clinical criteria have been recently defined (The Curaçao Criteria): spontaneous recurrent epistaxis, mucocutaneous telangiectasia, visceral involvement and an affected first degree relative (4). The HHT diagnosis is definite if three of these criteria are present. It is possible or suspected if two criteria are present, and unlikely if fewer than two criteria are present (4).

Up to 55% of PAVMs are asymptomatic. Most of clinical manifestations can be attributed to right-to-left shunting. Dyspnoea is seen in almost all patients who have associated cyanosis, clubbing, easy fatigability or polycythemia. A concomitant involvement of the liver can induce a high-output cardiac failure. Haemoptysis and haemothorax occur in roughly 10% of patients. Mechanisms of haemoptysis are multiple: rupture of a PAVM into a bronchus, tracheobronchial telangiectases, pulmonary hypertension or bronchial artery supply to PAVM. PAVMs tend to increase in size. A progression of PAVM occurs frequently during the second and third trimesters of pregnancy. Pregnancy predisposes women to worsening of right-to-left shunt and to rupture of PAVMs leading to intrapleural and intrapulmonic haemorrhages.

Since patients with clinically silent PAVMs are still at risk of complications, screening of asymptomatic patients should be performed. Neurological complications in patients with untreated PAVMs are common and the incidence of stroke has been reported to be as high as 40% and that of brain abscess 20% with a mortality of up to 40%. The rate of neurological complications rises to 70% in diffuse PAVMs. These data illustrate the need for aggressive screening and treatment for PAVMs in patients with HHT.

Imaging

Screening imaging methods vary between centers but are based on non-invasive methods to detect the right-to-left shunt or to image the PAVMs.

Chest radiography: Diagnosis of PAVMs may be suspected on chest radiographs. The most common finding is a peripheral circumscribed, noncalcified oval or round lesion connected by blood vessels to the hilum (Fig. 1). However, chest radiography can be normal in 30% of patients with small PAVMs or with PAVMs superimposed on cardiac or diaphragmatic opacities.

►*Contrast echocardiography* (CE) is an excellent tool for detection of small right-to-left shunts. Diagnosis of PAVMs can be made with a high sensitivity (95%). But CE is not correlated with the size, location or number of PAVMs. Overdetection of clinically unimportant PAVMs not requiring embolization may limit the use of CE as the exclusive screening test for PAVM.

Pulmonary angiography: In some centers, a complete diagnostic pulmonary angiography is performed prior to embolotherapy. Selective injections in right and left pulmonary arteries in different projections permit to determine the best projection for occluding the PAVMs and measure the feeding pedicles which help to select the occlusion technique (3).

Computed tomography (CT): When CE is positive indicating a PAVM, thin section spiral chest CT should be performed to confirm the diagnosis and evaluate if treatment is necessary (5). The characteristic appearance of a PAVM on CT scans is the presence of a homogeneous, well-circumscribed, noncalcified nodule measuring up to several centimetres in diameter or the presence of a serpiginous mass connected with blood vessels. Spiral CT and multiplanar reconstructions allow easy identification of the feeding artery, aneurysm sac

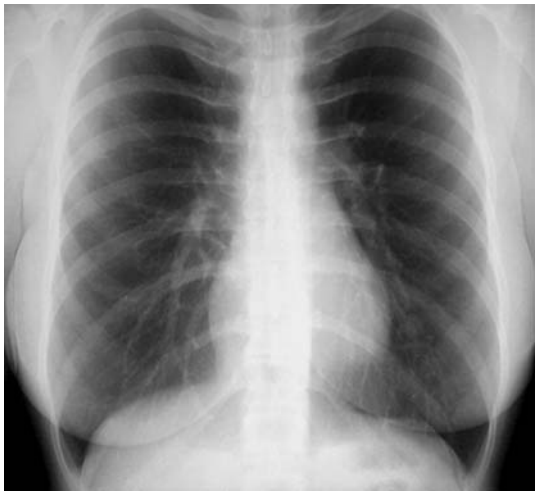

Fistula, Arteriovenous, Pulmonary. Thirty-year old asymptomatic woman with hereditary hemorrhagic telangiectasia. Figure 1 Chest radiography demonstrates a round opacity along the left heart border. Connections with pulmonary vessels are not easily identified.

F

and efferent veins usually without contrast injection (Fig. 2). Multiplanar and three-dimensional reconstructions, potentially useful to obtain precise angioarchitecture of PAVMs before embolization, may replace diagnostic pulmonary angiography (5).

Magnetic resonance imaging (MRI) of PAVMs has been evaluated less than CT. Several techniques have been recently developed to improve sensitivity to flow. The use of gradient-refocused echo MRI technique or MR angiography with venous or arterial signal elimination or contrast injection has been reported with a high sensitivity. The obvious advantage of MRI over CT is the absence of radiation exposure but its main limitations include low sensitivity for detection of small PAVM, expense and limited availability.

Though non-invasive methods have rarely been compared, it seems that CE is the best initial screening tool in patients with suspected PAVMs due to its excellent sensitivity and availability. If the result is negative, the likelihood of significant PAVMs is low. The value of spiral CT in a screening algorithm is still considered low. Conversely, all patients with positive EC should be evaluated using spiral CT in order to identify PAVMs amenable to embolization. In addition, initial CT will be used as a baseline study that can be compared with postembolization examinations (5).

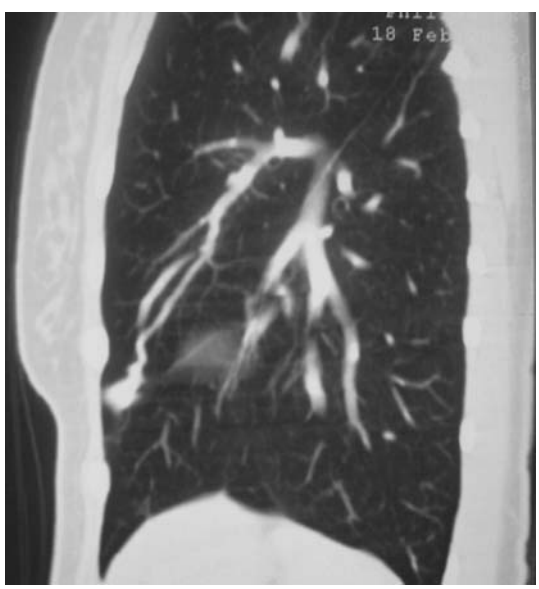

Fistula, Arteriovenous, Pulmonary. Figure 2 Unenhanced spiral CT of the chest with sagittal reconstruction demonstrates the lingular feeding artery and the aneurysm sac. The draining vein of the PAVM lies anteriorly.

Pulmonary Function Tests and Nuclear Medicine

Eighty to 100% of patients with PAVMs had either a PaO_2 <80mm Hg or a SaO_2 <97–98% on room air. Orthodeoxia is the laboratory correlate of platypnea. A decrease in PaO_2 or SaO_2 when going from the recumbent to the upright position is common in patients with PAVMs (most of PAVMs are located in the lower lobes). Oxygen saturation with the patient in upright posture is a better predictor of the presence or absence of PAVMs than the detection of hypoxemia but its sensitivity and specificity are too low (2).

The measurement of right-to-left shunt is performed using the 100% inspired oxygen breathing method, or less frequently using radionuclide scanning. A right-to-left shunt of more than 5% is considered abnormal.

Interventional Radiological Treatment

Medical treatments: These include prophylactic antibiotics to prevent septic embolisms at the time of dental and surgical procedures, medications for high-output heart failure and treatment of hemoptysis.

Surgical techniques: These include vascular ligations or parenchymal resection performed by thoracotomy or thoracoscopy. Properly performed in well-selected patients, surgery carries at least the same risks as any other thoracic surgery. Nowadays, indications for surgery are limited to high-flow PAVM with a short and large feeding artery.

Transcatheter embolization: The current preferred treatment for PAVMs consists of transcatheter embolization using coils or other intravascular devices. Permanent occlusion of PAVMs can be achieved in a vast majority of patients with minimal complications in experienced hands (1). Indications for treatment of PAVMs include prevention of thoracic hemorrhage, improvement of exercise intolerance and, most importantly, prevention of paradoxical embolism. It is usually considered that PAVMs with feeding arteries 3 mm or greater in diameter should be treated to prevent complications (1). In patients with diffuse PAVMs, multiple sessions are usually necessary to treat all the visible PAVMs.

Technique

Embolization is performed after an initial angiographic control (Fig. 3). Catheterization of the feeding pulmonary artery is performed and the catheter tip is positioned immediately proximal to the dilated venous portion. An arterial occlusion is then obtained using pushable coils or

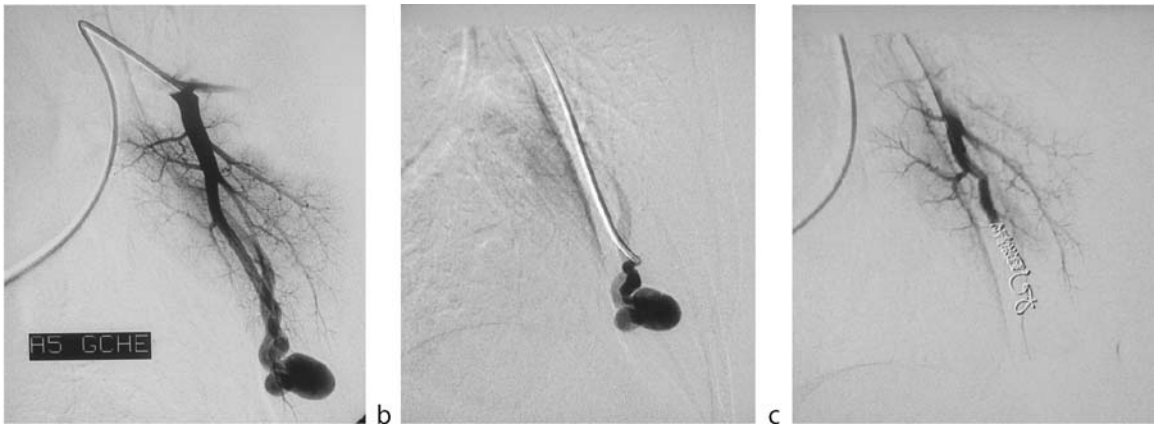

Fistula, Arteriovenous, Pulmonary. Figure 3 Angiography and transcatheter embolization in the same patient. (a) Selective angiography of the medial lingular artery reveals the PAVM with the feeding artery, the aneurysm sac and the draining vein. (b) The catheter is positioned in the feeding artery close to the aneurysmal sac of the PAVM before performing selective embolization. (c) After embolization using four coils, the control angiography demonstrates a complete occlusion of the PAVM.

balloons. Nowadays, most groups favour the use of coils as the primary embolization agent (3).

Results

Long-term follow-up is indicated in all patients with PAVMs even after a successful therapy because of the risks of serial growth of small lesions and reperfusion of embolized PAVMs (1). The long-term clinical outcomes of embolization are successful in 96% of patients. During the follow-up, neurologic complications related to reperfused treated PAVMs have been reported. But the long-term morbidity of reperfused PAVMs is unknown. Repeat treatment is therefore indicated because of recanalization of previously embolized PAVMs or enlargement of untreated PAVMs. In one large study, follow-up with CT scan one or more years after embolization showed that 96% of treated PAVMs were either undetectable or reduced in size (5). CE and MR perfusion imaging are probably too sensitive and remain positive in the majority of patients even after successful occlusion of all angiographically visible PAVMs.

Complications

Complications following embolization of PAVMs are minor and self-limited, most of these only require symptomatic treatment (1). Pleuritic chest pain occurring in the first 24 h after embolization is the most frequent complication (13%). Pleural effusion has been reported in up to 12% of patients. Pulmonary infarction has been observed in 3% of patients. Air embolism during embolization occurs in up to 4% of patients who developed transient symptoms such as angina, bradycardia or perioral paresthesia.

Major complications such as paradoxical embolization of a device and stroke are extremely rare (1%). These migrations may require additional intervention using an intravascular retrieval device.

Pluridisciplinary Management

Embolization of PAVMs requires a specific expertise and should be performed by specially trained interventional radiologists only. Pluridisciplinary management of PAVMs in HHT is mandatory in order to apply the appropriate treatment and to fully educate the patients and their family about the diagnosis, its clinical implications and its hereditary nature.

Thirty-year-old asymptomatic woman with hereditary hemorrhagic telangiectasia.

References

1. Gossage JR, Kanj G (1998) Pulmonary arteriovenous malformations. A state of the art review. Am J Respir Crit Care Med 158:643–661
2. Shovlin CL, Letarte M (1999) Hereditary haemorrhagic telangiectasia and pulmonary arteriovenous malformations: issues in clinical management and review of pathogenic mechanisms. Thorax 54:714–729
3. White RI Jr, Pollak JS, Wirth JA (1996) Pulmonary arteriovenous malformations: diagnosis and transcatheter embolotherapy. J Vasc Interv Radiol 7:787–804
4. Shovlin CL, Guttmacher AE, Buscarini E et al (2000) Diagnostic criteria for hereditary hemorrhagic telangiectasia (Rendu-Osler-Weber syndrome). Am J Med Genet 6(91):66–67
5. Remy J, Remy-Jardin M, Wattinne L et al (1992) Pulmonary arteriovenous malformations: evaluation with CT of the chest before and after treatment. Radiology 182:809–816

Fistula, Hemodialysis

Geert Maleux
Department of Radiology, University Hospitals Leuven, Leuven, Belgium
geert.maleux@uz.kuleuven.ac.be

Definitions

A hemodialysis fistula is defined as a surgically created, direct communication in between an artery and a corresponding superficial vein allowing increased blood flow through the vein in order to provide luminal dilatation and thickening of the vein wall; it is also defined as "arterialisation of the vein". These postoperative changes will induce a flow rate between 200 ml/min and 450 ml/min over the fistula and the corresponding efferent vein, and subsequently will allow easy cannulation of the vein with large-bore needles to perform hemodialysis.

In accordance with the NKF-DOQI (National Kidney Foundation Dialysis Outcome Quality Initiative) guidelines, an autogenous arteriovenous fistula should be the first choice for vascular access because of good clinical performances with regard to patency and infection complications. Within the different types of autogenous arteriovenous fistulas, the radiocephalic fistula at the wrist, as firstly described by Brescia and Cimino in 1966, is the first choice, followed by a radiocephalic or brachiocephalic fistula at or near the elbow. The brachiocephalic fistula has some drawbacks as it might present a higher incidence of distal hand ischemia (steal syndrome), and finally because of potential risk of high output congestive heart failure. A brachiobasilic fistula is less popular as the deep location of the basilic vein makes cannulation more difficult, and therefore the basilic vein is often surgically relocated to a more superficial plane about one month after the fistula creation.

When placement of an autogenous fistula is not possible, a synthetic graft can be placed in between a suitable afferent artery and an efferent vein. Most commonly, polytetrafluoroethylene (PTFE) is used as graft material because of its good tolerance for repeated cannulation and better patency compared to other synthetic graft material. Although grafts can be placed in the forearm, they usually are inserted in the upper arm. In our practice a straight or, less frequently, a loop graft, is placed between the brachial artery and the axillary vein. Finally, when all upper extremity vessels have been exhausted, interposition grafts in the lower limb can be created, but owing to poor patient acceptance, increased incidence of infection (these grafts are mostly placed in the groin) and potential risk of lower extremity deep venous thrombosis, these graft locations are rarely chosen.

Pathology/Histopathology

Dysfunction of a previously well-functioning dialysis fistula is mostly due to the development of a stenosis or even occlusion at the surgically created fistula or, most commonly, at the efferent vein; a stenosis of the afferent artery is rare. Early, postoperative stenoses are mostly due to an error in surgical technique or judgment. Lately developed stenoses can be the result of a progressive anastomotic stenosis, secondary to intimal hyperplasia; other causes of late stenoses are focal fibrosis of the venous wall secondary to chronically high pressure in the venous circulation or to repeated traumatic needle punctures during hemodialysis. Finally, a central ▶venous stenosis is nearly always the result of a previously placed indwelling dialysis catheter or central line. Rather rarely, an atherosclerotic stenosis of the afferent artery can be reason of problems during dialysis.

Other potential pathologies related to a dialysis fistula are infection, aneurysmal dilatation of the vein as a result of high pressure in a vein weakened by repeated cannulation, hand ischemia due to a steal phenomenon and hand edema or arm swelling caused by a venous outflow stenosis or occlusion. In case of hand edema, the venous occlusion is mostly located near the surgically created radiocephalic anastomosis; in case of arm swelling the occlusion will be found at the level of the central veins (axillary, subclavian or innominate vein).

Clinical Presentation

Dysfunction of a dialysis fistula, mostly owing to an underlying venous stenosis, can be diagnosed based on problems during or after a dialysis session: problems of cannulating the vein, high recirculation, increased venous pressure and longer bleeding time after withdrawal of the cannulation needles are classical, but late clinical signs in the course of access failure. Therefore, meticulous physical examination of the vascular access before, and flow measurements during each dialysis session are more sensitive to detect early access failure. A normally functioning arteriovenous fistula has a soft and easily compressible pulse with a low-pitched bruit, continuous with both systolic and diastolic components. In the presence of a venous stenosis, the bruit becomes more forcibly pulsatile and firm proximal to the stenosis, and potentially absent distal to the stenotic segment. Additionally, in case of a central venous stenosis, gross swelling of the entire arm is frequently seen.

Imaging

Digital Subtraction Angiography (DSA): DSA is still the gold standard for evaluating a dysfunctioning fistula. It is not more invasive than cannulation during a dialysis session and, if needed, can be followed immediately by a percutaneous intervention. However, DSA exposes the patient to ionizing radiation and administration of iodinated contrast medium. Although the patient is already in dialysis, the latter still can provoke further deterioration of the residual renal function and finally can induce an allergic reaction to iodine. Technically, a retrograde puncture of the brachial artery is preferred in case of a suspected stenosis of the surgical anastomosis; an antegrade puncture of the efferent vein is made in case of suspected distal outflow stenosis. In the latter case, the fistula itself still can be opacified when contrast is injected after placement of a tourniquet distal to the needle.

Duplex Ultrasound: Duplex ultrasound is a readily available, cheap and completely non-invasive imaging tool (1), but quality of examination largely depends on the operator's skills. Additionally, no clear evaluation can be made of the central veins, neither a complete angiographic mapping of the fistula can be obtained. Therefore, duplex ultrasound only can be used as a first step in the diagnostic work-up of a dysfunctioning dialysis fistula (Fig. 1).

MR Angiography: MR angiography is a relatively new imaging tool in the diagnosis of malfunctioning dialysis fistula, and currently three-dimensional, contrast-enhanced magnetic resonance (3D-Gd-MR) seems to provide most reliable information about the degree and location of stenoses compared to DSA (2). Additionally, MR angiography can provide an angiographic map of the entire fistula and efferent vein up to the superior vena cava, is non-invasive and lacks ionizing radiation and administration of nephrotoxic contrast media. The major drawback today is the fact that MR-guided percutaneous intervention is not yet clinically available.

CT angiography: CT angiography and in particular multi-detector CT (MDCT) is another new diagnostic tool to evaluate a malfunctioning dialysis fistula. Despite the use of ionizing radiation and the mandatory administration of iodinated contrast medium, MDCT has some unique advantages: it is a very fast and highly reliable examination providing a complete vascular map of the fistula (Fig. 2), correct evaluation of the degree of stenosis or of the extent of an aneurysm and MDCT will also depict potential signs of infection of a ▶dialysis graft (3). Finally, in contrast to MR angiography, metallic clips, often located at the arteriovenous anastomosis, will not result in artefacts on CT angiography.

Diagnosis and Interventional Radiological Treatment

Stenosis of a malfunctioning dialysis fistula can occur at any point from the feeding artery to the superior vena

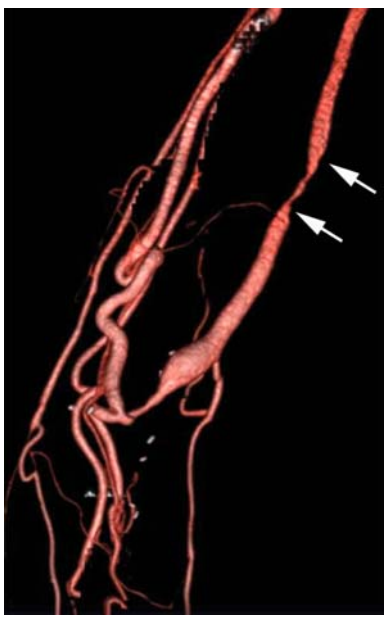

Fistula, Hemodialysis. Figure 2 3D-CT-reconstructions of the same brachiocephalic fistula demonstrating the same significant stenosis (arrows).

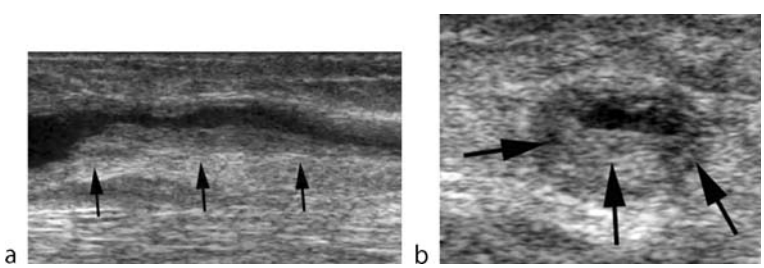

Fistula, Hemodialysis. Figure 1 (a) color-coded US and (b) gray-scale US demonstrate a significant stenosis (arrows) located at the cannulation area of the efferent vein (cephalic vein) of a malfunctioning brachiocephalic fistula.

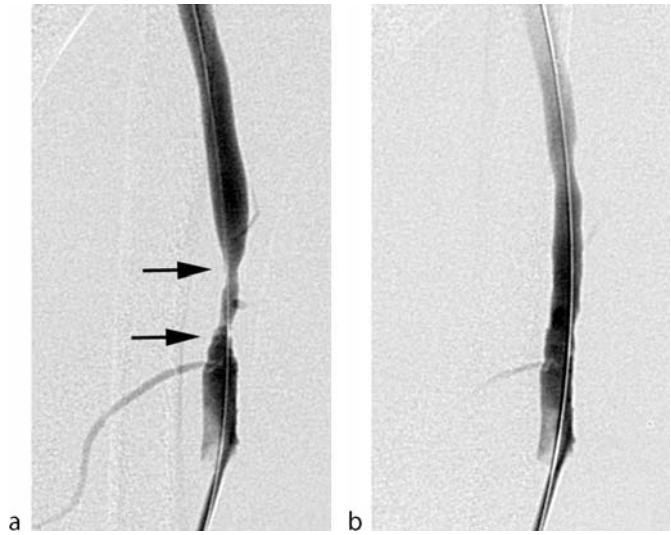

Fistula, Hemodialysis. Figure 3 DSA at the time of percutaneous intervention of the ▶venous stenosis (arrows). (a) No residual stenosis was noted after balloon angioplasty using a high pressure 9 mm diameter balloon.

cava, but the arteriovenous anastomosis and the chronically cannulated venous segments are the most predominant areas of stenosis. The degree of stenosis has to be graded visually, or after comparison with the diameter of the vein proximally and distally to the stenosis. At least, in some rare, doubtful cases, pressure measurements using a pull-back technique can give a more definitive answer about the severity of the stenosis. Indications for treatment (according to the DOQI-guidelines) are: stenosis concomitant with clinical impairment or stenosis threatening access patency. Percutaneous dilatation technique is initiated by placement of a 6 French sheath antegradely or retrogradely in the efferent vein, depending on the location of the stenosis. After administration of 2500 U heparin, the stenosis is crossed by a (hydrophilic) guidewire and the dilatation balloon is placed over the stenosis. As venous stenoses are often very tight, high-pressure balloons with a burst ratio >25 atm are very helpful (4). Cutting balloons can be a valuable alternative to high-pressure balloons in patients presenting with very resistant stenoses. It is also advisable to choose a dilatation balloon with a nominal diameter 1 mm larger than the nominal diameter of the stenosed vein. Finally, a control angiography will show the post-dilatation result (Fig. 3). No stenosis or a residual stenosis of less than 30% is acceptable; if a residual stenosis of more than 30% is present, repeat and prolonged dilatation is mandatory. Persistent stenosis recoil after repeated dilatation is an indication for additional stent placement, especially in cases of central vein stenosis. Self-expandable stents are the preferred type of stent in a dialysis fistula and the nominal diameter should be 1 or 2 mm larger than the vein diameter. Recently, it is found that e-PTFE-covered stents have the potential to prolong the patency of dialysis grafts in case of venous outflow stenosis.

Long-term results of balloon dilatation to save a malfunctioning fistula show a primary patency of 51 and 35% for forearm and upper arm fistulas, respectively. After additional stent placement, the primary patency rates drop to 36 and 20% in the forearm and upper arm, respectively. Global secondary patency rates after both dilatation and/or stent placement can reach 85 and 82% for forearm and upper arm fistulae, respectively (5).

In conclusion, both dialysis fistulae and grafts are prone to stenose or even to occlude owing to both the artificial creation of a direct communication between artery and vein leading to "arterialisation of the vein" and to the repeated cannulation of the vein for each dialysis session. Nevertheless, several, reliable radiological tests are available today to evaluate the fistula and its afferent and efferent vessels; and finally, the interventional radiologist plays a major role in the maintenance of patency of a dialysis fistula and subsequently in the efficacy to dialyse a patient, resulting in a better quality of live and potentially in a longer survival of the dialysed patient.

References

1. Dumars MC, Thompson WE, Bluth EI et al (2002) Management of suspected hemodialysis graft dysfunction: Usefulness of diagnostic US. Radiology 222:103–107
2. Froger CL, Duijm LEM, Liem YS et al (2005) Stenosis detection with MR angiography and digital subtraction angiography in dysfunctional hemodialysis fistulas and grafts. Radiology 234:284–291

3. Ko S-F, Huang C-C, Ng S-H et al (2005) MDCT angiography for evaluation of the complete vascular tree of hemadilaysis fistulas. Am J Roentgenol 185:1268–1274
4. Trerotola SO, Stavropoulos SW, Shlansky-Goldberg R et al (2004) Hemodialysis-related venous stenosis: treatment with ultrahigh-pressure angioplasty-balloon. Radiology 231:259–262
5. Turmel-Rodrigues L, Pengloan J, Baudin S et al (2000) Treatment of stenosis and thrombosis in haemodialysis fistulas and grafts by interventional radiology. Nephrol Dial Transplant 15:2029–2036

Flail Chest

Life threatening condition of multiple rib fractures with paradox movement of the chest wall during respiration and respiratory failure. X-ray signs are serial fractures of at least five neighboring ribs or segmented fractures of at least two ribs. Fractures of the sternum and bilateral rib fractures can be indicative for a flail chest (see Fig. 1, Chest Trauma).

▶Chest Trauma

FLHCC

▶Fibrolamellar Carcinoma

FLT

Abbreviation for 3′-deoxy-3′-[18F]fluorothymidine, a radiopharmaceutical used for positron emission tomography. FLT is a substrate of the cellular thymidine kinase 1 (TK-1), which phosphorylates FLT to FLT-5-phosphate, a precursor of newly formed DNA during cell replication. Preclinical and first clinical studies showed a correlation between cellular FLT accumulation and other tests representing cell proliferation, giving evidence for the possible use of FLT as a proliferation marker.

▶Proliferation of Neoplasms

Fluid Collection, Pancreatic, Acute

Acute fluid collection occur early in the course of acute pancreatitis and it is located in or near the pancreas. It lacks a wall of granulation or fibrous tissue, which characterizes the pancreatic pseudocyst.

▶Pancreatitis, Acute

Fluorescence Imaging

Vasilis Ntziachristos
Harvard Medical School, Harvard University
HMS/MGH, Center for Molecular Imaging Research, Charlestown, USA
vasilis@helix.mgh.harvard.edu

Synonyms

Fluorescence mediated tomography; Fluorescence molecular tomography, FMT; Fluorescence reflectance imaging, FRI; Fluorescence tomography; Fluorescence transillumination imaging

Definition

Fluorescence imaging describes the field of imaging technologies designed to visualize the spatial distribution of substances that emit fluorescence. These techniques incorporate a light source of appropriate wavelength that is used to excite the fluorochromes and a detection system that can perform spectral and spatial separation to differentiate and spatially resolve fluorescence emitted from the fluorescence substances. In its broader sense fluorescence imaging for biomedical applications includes fluorescence microscopy techniques, macroscopic fluorescence imaging of biological specimens and assays, for example in fluorescent gels or plates, and other tissue imaging.

For medical imaging the term attains a narrower definition, that is: a modality that is used to *macroscopically* visualize intrinsic (endogenous) tissue fluorochromes (i.e., collagen, elastin, NADH), endogenously generated fluorescent reporters, that is fluorescent proteins or extrinsically administered fluorescent probes. The technique can be used for *in-vivo* or postmortem imaging on excised organs and it is generally applied for imaging of a field of view of millimeters to several centimeters and similarly, at depths of several millimeters to centimeters. This is in contrast to *in-vivo* fluorescence microscopy that is used for *microscopic* visualization of fluorochromes in tissues at small fields of view (millimeters) and depths of ~200–500 μm.

Fluorescence imaging encompasses several different implementations including photographic methods, advanced planar illumination methods, or tomography methods (1).

Imaging

Fluorescence imaging can be achieved with different implementation strategies, which correspondingly yield different performance characteristics.

The most common approach has been to use photographic methods, that is use a light source to illuminate tissue at a wavelength appropriate for fluorochrome excitation and use a highly sensitive digital camera, for example a charged coupled device (CCD) camera to detect fluorescence emitted back from tissues. A distinguishing feature therefore of this approach is that the light source and the detector reside on the same side of the tissue (see Fig. 1 top). The light source is typically a white light source that is appropriately filtered to select the appropriate wavelength or a laser source. Typically, the fluorescence image acquired is accompanied by a second image which is measured without the fluorescence filter to obtain a photograph of the tissue for image registration purposes (see Fig. 2). This intrinsic light image can also serve as a calibration measurement since it records the exact spatial distribution of the excitation light strength for later correction of excitation field inhomogeneities. This method is very simple and cost-efficient to implement and can be used for a multitude of applications, including intraoperative imaging, skin imaging, and small animal or specimen imaging to enhance the visual inspection and improve the specificity and the identification of disease borders. With appropriate adaptation this same principle of operation can be used with an endoscope, colposcope, in laparoscopy and other conventional optical imaging methods. The technology is well suited for imaging surface activity but its performance and quantification accuracy deteriorates for fluorescent activity coming from deeper in tissues. This is because the technique does not account for light propagation changes and attenuation as a function of depth and of tissue optical properties. The technique is also referred to as *fluorescence reflectance imaging* (FRI) or more accurately as *fluorescence epi-illumination imaging*.

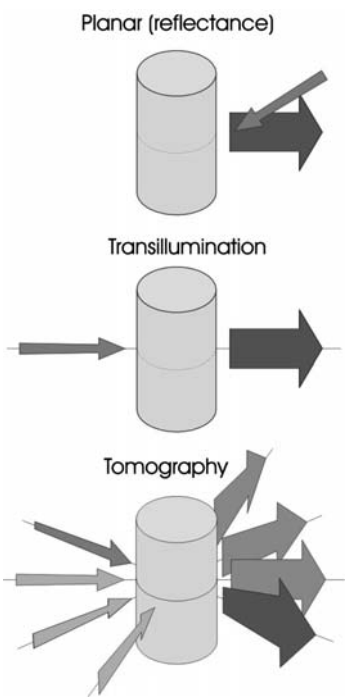

Fluorescence Imaging. Figure 1 Modes of fluorescence imaging.

An alternative fluorescence imaging method uses *transillumination* measurements (Fig. 1 middle). In this case tissue intersects the light beam and signals first propagate in the entire tissue before exciting on the other side and detected by the photon detector (typically also a camera). This approach is particularly interesting when light of near-infrared wavelengths is used. In this spectral region tissue yields low light attenuation and large penetration depths can be achieved (more than 4 cm in muscle and more than 10 cm in lung or breast tissues). Similarly to epi-illumination (reflectance) imaging, the signal recorded depends nonlinearly on activity depth and on optical properties and the method is therefore not well suited for quantitative measurements. Furthermore the resolution drops significantly as tissue thickness increases. The method in fluorescence imaging has found some application in dental or cardiac muscle imaging (invasively) and in small animal imaging.

Epi-illumination and transillumination fluorescence imaging, also referred to as "planar" imaging, offer an easily implemented and sensitive platform for *in-vivo* imaging. Conversely, the application is limited to qualitative observations due to the inability to resolve depth or account for the nonlinear dependence of light on depth and on optical properties.

A third imaging method that has been more recently developed is Fluorescence molecular tomography (FMT) (1). This technology can resolve and quantify fluorochromes deep in tissues through the use of tomographic principles. FMT is based on the general framework of reconstruction techniques that use diffuse light, developed since the early 1990's (2, 3). These approaches employ mathematical models that describe the light propagation in tissue and technological advancements in photon sources and detection techniques for yielding three-dimensional tomography of entire tissues based on diffuse light. Similarly to transillumination most attention has

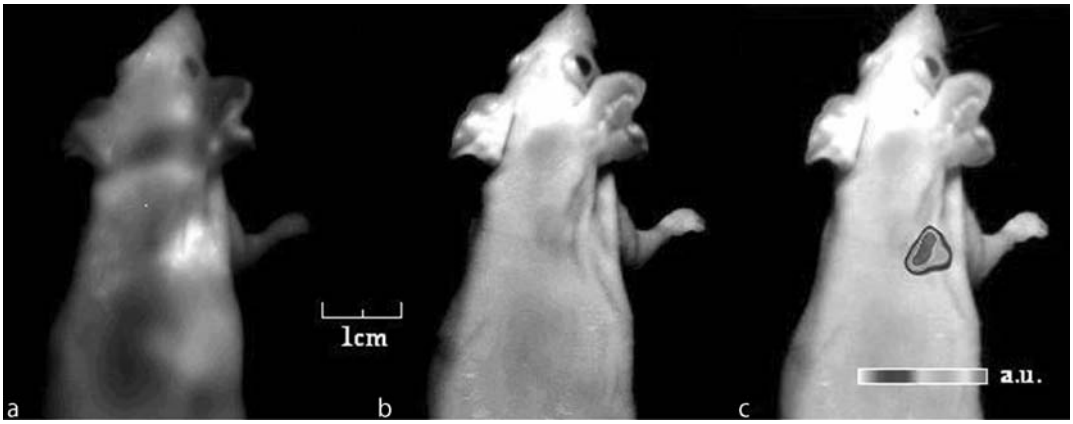

Fluorescence Imaging. Figure 2 Example of fluorescence epi-illumination imaging of an HT1080 tumor implanted at the posterior upper thorax of a nude mouse. (a) A fluorescent image is obtained by a CCD camera by using appropriate band pass filters centred at the emission wavelength. (b) Image obtained at the excitation wavelength (intrinsic image) reveals the tissue surface with higher detail. (c) Superposition of the fluorescence image (after threshold) onto the intrinsic image. Fluorescence here is due to the intravenous injection of a fluorescent probes that is sensitive to major cathepsins and present in higher levels in the malignant tumor. (Image modified from Mol Imag 1(2):82–88 (2002).

been focused on using light in the near-infrared due to the greater penetration depths that can be achieved.

FMT, similarly to other tomographic approaches that use diffuse photons, uses measurements at different projections around the boundary of the illuminated body as shown in Fig. 1 (bottom). It typically obtains measurements at both the excitation and emission wavelengths. It then effectively combines all measurements into an inversion scheme that in its general form takes into account the highly scattering nature of photon propagation and tissue optical heterogeneity and reconstructs fluorochrome distribution with significantly higher resolution and accuracy than the one achieved by planar methods. The resolution achieved in tomographic methods using diffuse photons strongly depends on the depth and overall tissue dimensions and on the tissue optical properties. It further depends on the characteristics of the illumination light employed. Therefore it is complex to define one resolution measure independently of the application. Generally, it has been observed in phantom measurements that submillimeter resolutions can be achieved for the small animal case and resolution worsens to several millimeters for larger tissues.

Originally, several tomographic approaches for *in-vivo* applications used fiber based technology and in some instances matching fluids to simplify experimental and theoretical approaches. More recently however attention has been shifted into developing high performance systems that offer noncontact illumination and using CCD camera measurements, in the absence of fibers and matching fluids, which allow for high spatial sampling of photon fields and experimental simplicity.

Multi-spectral Imaging

Fluorescence imaging can capitalize on the spectral differentiation of different fluorochromes to perform concurrent imaging of multiple targets. Multispectral imaging can be easily achieved using appropriate filters or monochromators although appropriate postprocessing spectral differentiation techniques may be required to reduce cross-talk between fluorochromes that have overlapping spectra. In some applications, multispectral imaging can be similarly used to differentiate specific extrinsically administered fluorescent probes or fluorescent proteins expressed by transgenic cells from background nonspecific tissue fluorescence, typically due to autofluorescence of elastins, collagen, NADH, and other intrinsic tissue fluorochromes. This latter application is more important for imaging application in the visible, since weak autofluorescence is generally observed in the near-infrared.

Optical Domains

There are three distinct domains that optical tomography of tissues operates in, that is the time-domain (TD), the frequency domain (FD), and the continuous wave (CW) domain. Each has distinct advantages and disadvantages and the selection of an appropriate technology largely depends on the specifics of the application. CW methods use light of constant intensity and require simple and low-cost instrumentation and generally yield good signal to noise performance compared to the other two methods.

Time-domain methods illuminate tissue with ultrafast photon pulses (femto-second to pico-second range) and

resolve the arrival of photons as a function of time at different locations around the tissue boundary. Frequency domain technology uses light of modulated intensity at a frequency *f*, which establishes a photon wave of the same frequency in the diffuse medium. In contrast to CW methods, TD and FD methods can differentiate tissue absorption and scattering as well as fluorochrome lifetime. FD methods become more accurate when multiple modulation frequencies are used. They can be further used to improve resolution, for example using early-arriving photons.

In-vivo Applications

Fluorescence imaging can be used in combination with many developed or upcoming fluorescent probes to visualize a multitude of processes in tissues. Examples of imaging protease expression associated with various cancers and inflammation using activatable probes have been demonstrated with epi-illumination or tomographic methods. Imaging of cellular receptors using peptide-near-infrared dye conjugates has been also shown feasible in animal studies. Several other examples have been also demonstrated in applications ranging from imaging apoptosis using annexin-V-fluorochrome conjugates to imaging angiogenesis using fluorescent nanoparticles. Overall, with the increasing technical ability of fluorescence imaging and the growing list of available fluorescent probes and nanoparticles for *in-vivo* use the list of applications is expected to significantly grow.

Clinical Applicability

Much of the *in-vivo* demonstration of fluorescence imaging methods has been so far achieved using small animals. However feasibility to detect fluorochromes from human tissues has been demonstrated in the past for several applications, for example using epi-illumination (endoscopy) in skin, esophageal, cervical, lung, and other accessible epithelial cancers or using tomography through the entire human breast for breast cancer detection (4, 5). As adept new fluorescent probes propagate into the clinic, a significant number of these technologies can be adapted for human imaging, that is intraoperative imaging for tumor margin and metastasis identification, in several endoscopic applications or in the detection of breast cancer.

Diagnosis

Fluorescence molecular imaging is a novel imaging technology that has not been yet evolved as a standard diagnostic procedure. Nevertheless, significant progress has been achieved towards the validation of the technique in transgenic animal models that resemble human disease, for example in spontaneous or induced models of colon, lung, or breast cancer. At the clinical research level, autofluorescence colposcopy has also shown good performance in detecting cervical cancer (6). The following list summarizes areas where fluorescence imaging has strong potential to be used as a diagnostic method:

- Endoscopy
- Colposcopy
- Intraoperative imaging
- Laparoscopy
- Breast cancer
- Oral cancers
- Skin cancers
- Skin diseases (other)
- Arthritis
- Inflammation.

Bibliography

1. Ntziachristos V, Ripoll J, Wang LHV et al (2005) Looking and listening to light: the evolution of whole-body photonic imaging. Nat Biotechnol 23:313–320
2. Gibson AP, Hebden JC, Arridge SR (2005) Recent advances in diffuse optical imaging. Phys Med Biol 50:R1–R43
3. Yodh AG, Chance B (1995) Spectroscopy and imaging with diffusing light. Phys Today 48:34–40
4. Ntziachristos V, Yodh AG, Schnall M et al (2000) Concurrent MRI and diffuse optical tomography of breast after indocyanine green enhancement. Proc Natl Acad Sci USA 97:2767–2772
5. Intes X, Ripoll J, Chen Y et al (2003) *In vivo* continuous-wave optical breast imaging enhanced with indocyanine green. Med Phys 30:1039–1047
6. Drezek RA, Richards-Kortum R, Brewer MA et al (2003) Optical imaging of the cervix. Cancer 98:2015–2027

Fluorescence Imaging

▶Optical Imaging

Fluorescence Mediated Tomography

▶Fluorescence Imaging

Fluorescence Molecular Tomography, FMT

▶Fluorescence Imaging

Fluorescence Reflectance Imaging, FRI

▶Fluorescence Imaging

Fluorescence Tomography

▶Fluorescence Imaging

Fluorescence Transillumination Imaging

▶Fluorescence Imaging

FMRI

▶Functional Magnetic Resonance Imaging

FNB

▶Fine Needle Biopsy

Focal Acute Pyelonephritis with Abscess Formation

▶Abscess, renal

Focal Cortical Dysplasia

Focal cortical dysplasia is often referred to as focal cortical dysplasia of Taylor. It is a cortical malformation that involves the whole cortex and, to a variable extent, the underlying white matter.

▶Congenital Malformations, Cerebrum

Focal Fatty Infiltration

Focal accumulation of fat in tiny sacs within the hepatocytes.

▶Steatosis, Hepatic

Focal Nodular Hyperplasia (FNH) of the Liver is a Completely Benign Lesion Characterized by Nodular Hyperplasia of Hepatic Parenchyma Around a Central Scar Containing an Anomalous Artery

▶Hyperplasia, Focal, Nodular Hepatic

Focal Splenic Lesions

Tumors or other circumscribed abnormalities of the spleen.

▶Contrast Media, Ultrasound, Applications in Focal Splenic Lesions

Follicle Cysts

▶Cysts, Follicular, Ovarium

Follicular Cysts

Follicular cysts present as smooth and thin-walled unilocular cysts within the ovaries. They are most commonly asymptomatic and can only be differentiated from follicles when they exceed a size of 3 cm.
►Cysts, Follicular, Ovarium

Foreign Bodies, Aspiration, Children (Chest View)

Gundula Staatz
Department of Radiology, Division of Pediatric Radiology, University of Erlangen-Nürnberg, Erlangen
gu.stz.uni-erlangen@t-online.de

Definitions

Aspiration of foreign bodies, such as peanuts, carrots or plastic toy pieces, occurs most often in children under the age of 4 years. The worst case is complete airway obstruction with total occlusion of the trachea above the carina. Partial obstruction occurs, when the trachea is partially occluded or when the foreign body obstructs bronchi distal the carina. The majority of foreign bodies lodge in the main bronchi with almost equal incidence on the right and left side.

Pathology/Histopathology

Food particles or organic materials may absorb water from bronchial secretions and tend to increase in size. Oil, salt and vegetable proteins irritate the mucosa, leading to oedema and formation of granulation tissue with subsequent narrowing of the bronchial lumen (1). Non-organic materials are usually inert to the bronchial mucosa, unless they remain in the tracheobronchial tree for a longer time and induce chronic inflammatory changes, such as ulcerations or epithelialisation (1).

Clinical Presentation

Children with foreign body aspiration usually present with the classical triad of choking, coughing and wheezing. Other symptoms are stridor, dyspnoea, haemoptysis or rarely pneumothorax. Crackles, decreased breath sounds in the affected lung and unequal chest expansion may be found on physical examination, but also normal findings are common. Besides acute symptoms of respiratory distress, recurrent pneumonia is observed as late sequelae, especially in patients who aspirated organic material (2).

Imaging

Chest radiography is usually the first imaging technique performed in children with suspected foreign body aspiration. Because most aspirated foreign bodies are radiolucent, the diagnosis is commonly based on indirect signs, such as ►obstructive emphysema, shifting of the mediastinum and unequal movement of the hemidiaphragms. Assessment by inspiratory and expiratory chest X-rays, lateral decubitus radiographs or with the use of fluoroscopy is often necessary additionally to plain chest radiographs. In some instances CT may provide additional information, because of its high sensitivity in demonstrating radiolucent foreign bodies. Low-dose MDCT and virtual bronchoscopy has shown good results in identifying the exact location of a foreign body before bronchoscopy and in ruling out a foreign body in patients with a low level of suspicion and normal or non-specific findings on chest radiography (3). MRI has been used for the diagnosis of peanut inhalation, however the high cost and the need for sedation prevents routine use of MRI in children with foreign body aspiration.

Nuclear Medicine

There are only a few studies dealing with scintigraphy in foreign body aspiration in children. In a European multicentre study many children with foreign body aspiration showed scintigraphic abnormalities 6 months after removal of the foreign body with persistent matched defects of perfusion and ventilation although the chest radiographs were considered normal (4).

Diagnosis

In children with partial airway obstruction, the plain chest X-ray during inspiration often reveals unremarkable findings. Expiratory films are more sensitive by demonstrating air-trapping with over distension of the affected lung distal to the obstruction (obstructive emphysema), deviation of the mediastinum to the contralateral side, a low ipsilateral hemidiaphragm and wide intercostal spaces (Fig. 1). In non-cooperative children lateral decubitus films may replace the inspiratory–expiratory films, showing failure of the affected lung to collapse. A valve-mechanism in foreign body aspiration is easily

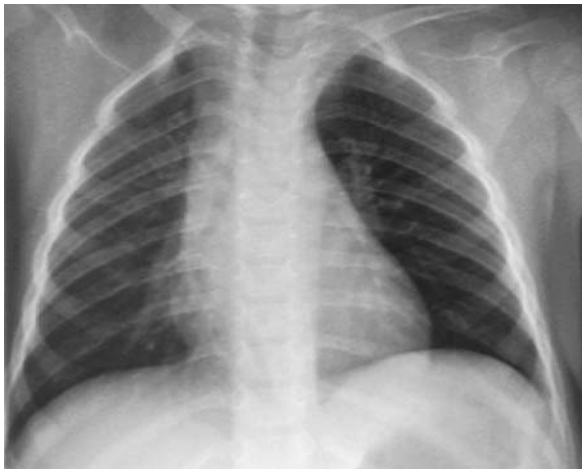

Foreign Bodies, Aspiration, Children (Chest View). Figure 1 Chest radiograph of a 3-year-old infant with aspiration of a peanut into the left main bronchus. Hyperinflation of the left lung with shifting of the mediastinum to the contralateral side is visible.

recognised under fluoroscopy. The mediastinum shifts to the ipsilateral obstructed side during inspiration and to the contralateral side during expiration. Furthermore paradoxical movement of the hemidiaphragms is often visible (Fig. 2). A complete airway obstruction leads to a collapse of the lung distal to the obstruction or to segmental atelectasis. Occasionally a localised pneumothorax may develop peripheral to the collapsed lobe.

The foreign body may be exactly localised on MDCT and virtual bronchoscopy; additional CT findings are hyperaeration of the ipsilateral lung, atelectasis, infiltration and bronchiectasis (3). Chronic bronchitis, bronchiolitis obliterans and bronchiectasis as late sequelae of foreign body aspiration are accurately visualised by CT.

MRI with use of T1-weighted images is helpful for definitive diagnosis and location of peanut fragments in the lower airways because the fatty peanut material appears with a high signal-intensity surrounded by the low signal-intensity lung tissue (5).

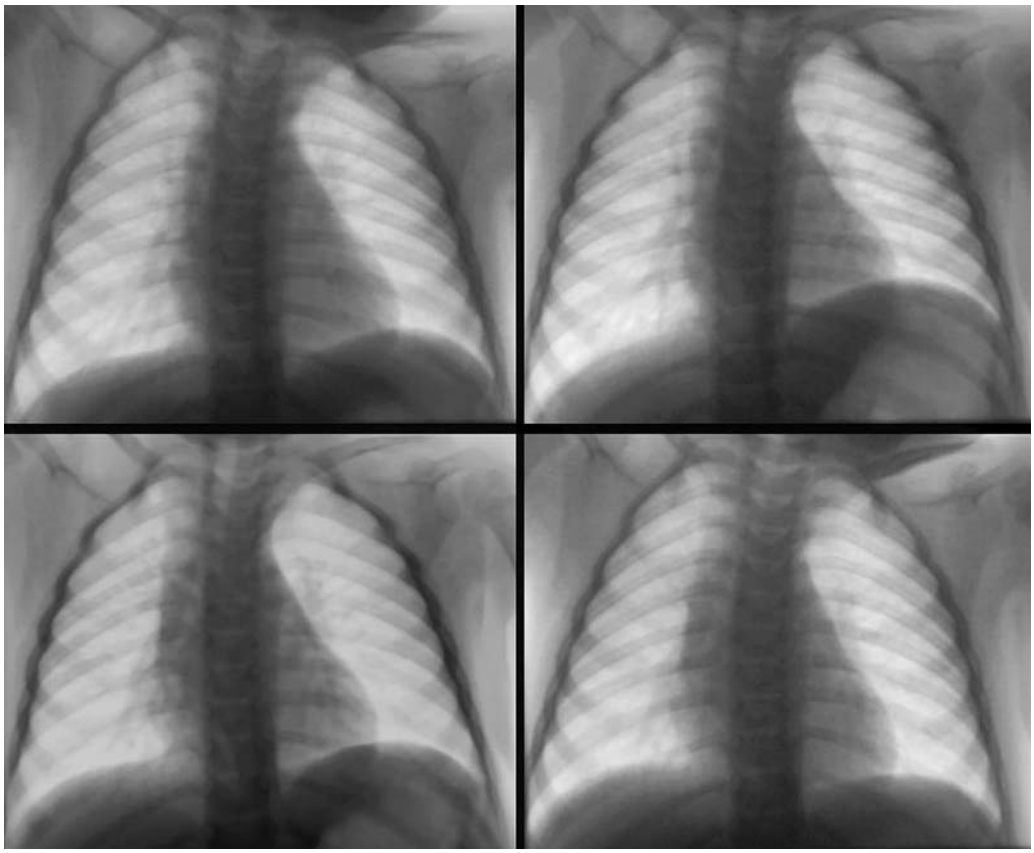

Foreign Bodies, Aspiration, Children (Chest View). Figure 2 Fluoroscopy images of the same patient. Images during inspiration and expiration demonstrate the shifting of the mediastinum and a paradoxical movement of the hemidiaphragms.

Bibliography

1. Bar-Ziv J, Koplewitz BZ, Agid R (2002) Imaging of foreign body aspiration in the respiratory tract. In: Lucaya J, Strife JL (eds) Pediatric Chest Imaging, Chest Imaging In Infants and Children. Medical Radiology, Diagnostic Imaging. Baert Al, Sartor K (eds). Spinger, New York, pp 171–185
2. Oguz F, Citak A, Unuvar E et al (2000) Airway foreign bodies in childhood. Int J Pediatr Otorhinolaryngol 52:11–16
3. Kosucu P, Ahmetoglu A, Koramaz I et al (2004) Low-dose MDCT and virtual bronchoscopy in pediatric patients with foreign body aspiration. Am J Roentgenol 183:1771–1777
4. Piepsz A (1988) Late sequelae of foreign body inhalation. A multicentric scintigraphic study. Eur J Nucl Med 13:578–581
5. Imaizumi H, Kaneko M, Nara S et al (1994) Definitive diagnosis and location of peanuts in the airways using magnetic resonance imaging techniques. Ann Emerg Med 23:1379–1382

Foreign Bodies, Gastrointestinal

Korman Ugur, Selcuk Dogan, Kantarci Fatih, Kurugoglu Sebuh
Istanbul University, Department of Radiology, Istanbul, Turkey
ugurk9@istanbul.edu.tr

Synonyms

Gi Foreign Bodies; Foreign Bodies; Esophageal Foreign Bodies; Swallowed Foreign Bodies; Oropharyngeal Foreign Bodies; Rectal Foreign Bodies

Definition

Foreign bodies (FB) of the gastrointestinal (GI) tract are defined as any external object, introduced voluntarily or accidentally into the digestive system. Foreign bodies may be ingested, inserted into a body cavity, or deposited into the body by a traumatic or iatrogenic injury. In general, foreign bodies in the air and food passages are the sixth most common cause of accidental death in the United States (1). The ingestion of a FB is a relatively common GI emergency that causes significant morbidity. Fortunately, the vast majority of all swallowed objects pass through the GI tract without a problem. Only 1% of involuntary and generally unconsciously ingested FB will perforate the bowel and constitute abdominal emergencies whose diagnosis represents a challenge (2). Those that cause perforation are usually sharp, pointed, or elongated. They are usually fish bones, toothpicks, and chicken bones.

Foreign body ingestions are common in children and mentally handicapped adults. Although exact figures are unavailable, foreign body ingestion is very common among children. In the pediatric population, toddlers aged 2–3 years are most commonly affected because children in this age group are ambulatory and more orally explorative. While children younger than 6 months are rarely able to get a foreign object into the oropharynx, infants can ingest foreign bodies with the assistance of a sibling. Any child can swallow a foreign body; most incidents result in minor annoyance, but a few can lead to major catastrophe.

Pathology/Histopathology

The oropharynx is well-innervated, and patients can typically localize oropharyngeal foreign bodies. Scratches or abrasions to the mucosal surface of the oropharynx can create a foreign body sensation. Chronic foreign bodies or perforations can cause infections in surrounding soft tissues of the throat and neck.

Patients can usually localize foreign bodies in the upper esophagus but localize them poorly in the lower two-thirds of the structure. The esophagus has three areas of narrowing: the upper esophageal sphincter (UES), which consists of the cricopharyngeus muscle; the crossover of the aorta; and the lower esophageal sphincter (LES). These areas are where most esophageal foreign bodies become entrapped. Structural abnormalities of the esophagus, including strictures, webs, diverticula, and malignancies, increase the risk of foreign body entrapment, as do motor disturbances such as scleroderma, diffuse esophageal spasm, or achalasia (3).

Most foreign objects will pass through the pylorus, although on occasion, some objects may remain in the stomach for a long period. Once beyond the pyloric canal most objects, even sharply edged foreign bodies such as pieces of glass or nails, will pass without harm until the terminal ileum which is again a predilection site for obstruction. Ingested objects may occasionally remain fixed in the cecum, ascending colon, or sigmoid. Foreign bodies detected in the rectum have in most instances been introduced transanally.

Clinical Presentation

Nearly one-third of pediatric patients with esophageal foreign bodies are asymptomatic. Symptoms depend on the size, shape, and nature of the FB ingested. Large FB may cause obstruction whereas small and sharp objects may present with symptoms of esophageal irritation. Symptoms related to esophageal foreign bodies are

choking, gagging, coughing, wheezing, dysphagia, dyspnea, fever, hematochezia, or neck, chest, or abdominal pain. Children with chronic esophageal foreign bodies may also present with poor feeding, irritability, fever, or stridor. Most children who have ingested a disk battery remain asymptomatic. Children with a battery lodged in the esophagus typically present with the above mentioned symptoms. Rashes following disk battery ingestion have also been reported and may be a manifestation of nickel hypersensitivity.

It is clear that thin, sharp objects carry a higher risk of perforation; and a safe policy is to treat the patient expectantly unless there are indications for a more aggressive approach. Large foreign bodies are not generally encountered in the small bowel in that rarely pass beyond the pylorus or the duodenojejunal flexure. A perforation of the peritoneal cavity can cause peritonitis whereas a retroperitoneal perforation, at the duodenojejunal flexure for example, can lead to the involvement of the psoas and the formation of an abscess. Nonetheless, the perforation of jejunal or ileal loop is a rare event (<1% of cases) and is usually caused by extremely pointed objects, such as fish bones, chicken bones, and toothpicks (3). Patients with a rectal foreign body may present with abdominal or rectal pain, pruritus, or bleeding.

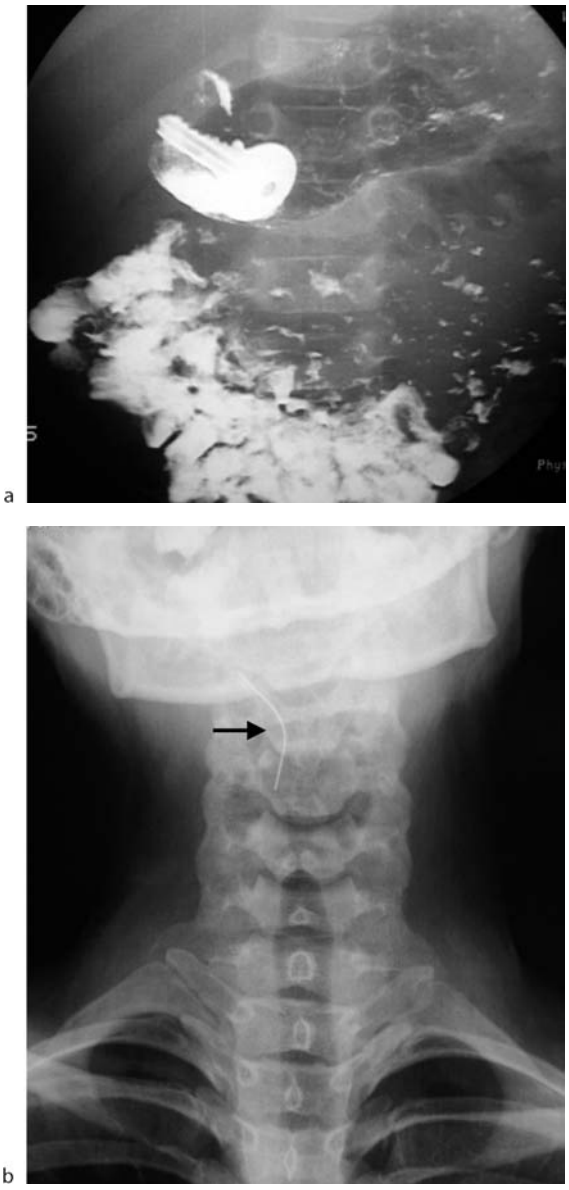

Foreign Bodies, Gastrointestinal. Figure 1 Swallowed metal objects. (a) Key in the stomach. (b) Piriform sinus

Imaging

The relative difficulty in identifying a foreign body varies according to the type of object ingested and its radiopacity. Metal objects with a relatively high atomic weight are readily visible with plain film radiography in that they are intensely radiopaque regardless of their volume (Fig. 1). Radiopaque materials are glass of all types; most metallic objects (except aluminum); most animal bones and some fish bones; some foods; some soil fragments, sand, gravel, and mineral fragments; some medications and poisons (CHIPES: chloral hydrate, heavy metals, iodides, phenothiazines, enteric coated pills, solvents). Nonradiopaque materials at times may not be identifiable as they are composed of material with a relatively low atomic weight and therefore have intrinsically low radiopacity. Nonradiopaque materials are most foods and medicines; most fish bones; most wood, splinters, thorns of all types; most plastics; most aluminum objects (3).

Radiographs

Plain radiographs are indicated for every patient with a known or suspected foreign body in the oropharynx, esophagus, stomach, small and large intestine. Radiopaque objects are easily seen and localized on the radiograph. In cases of nonradiopaque foreign bodies, imaging studies rarely have any influence on management, except in delaying endoscopy or computed tomography (CT) scanning. In small children, a mouth-to-anus radiograph can be obtained. In older children and adults, plain films of the neck, chest, and abdomen should be obtained. A posteroanterior (PA) and lateral chest radiographs provide better localization for foreign bodies within the lumen of the esophagus (Fig. 2). The progress in the bowel, if needed, can be checked periodically with radiographs (Fig. 3).

If the tip of a sharp-edged foreign body has perforated the wall, it may project outside the air-containing lumen.

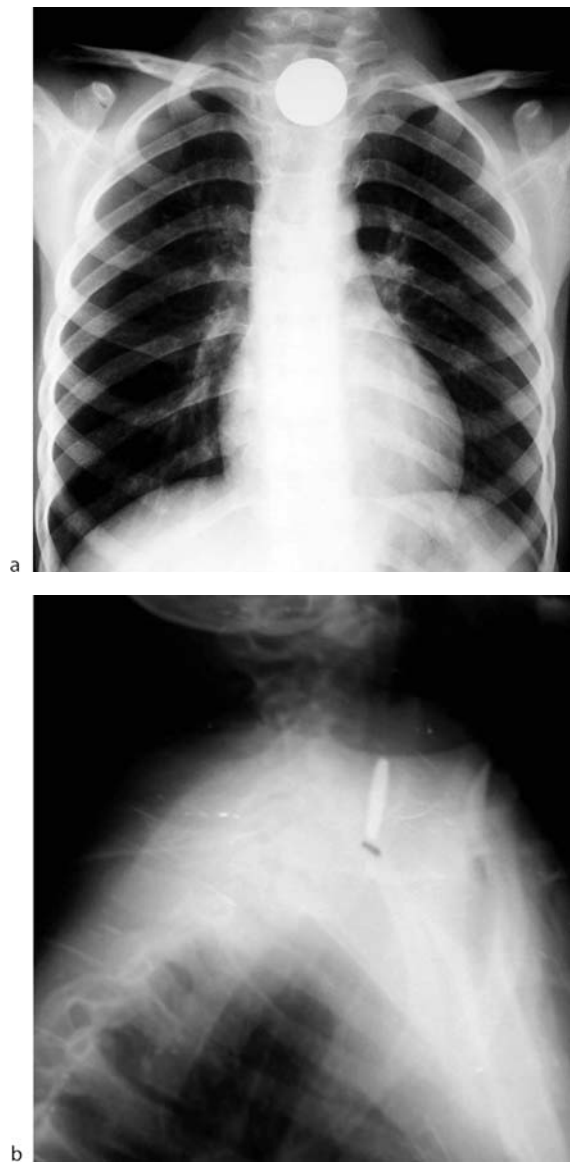

Foreign Bodies, Gastrointestinal. Figure 2 Swallowed coin in cervical/thoracic esophageal junction. (a) PA and

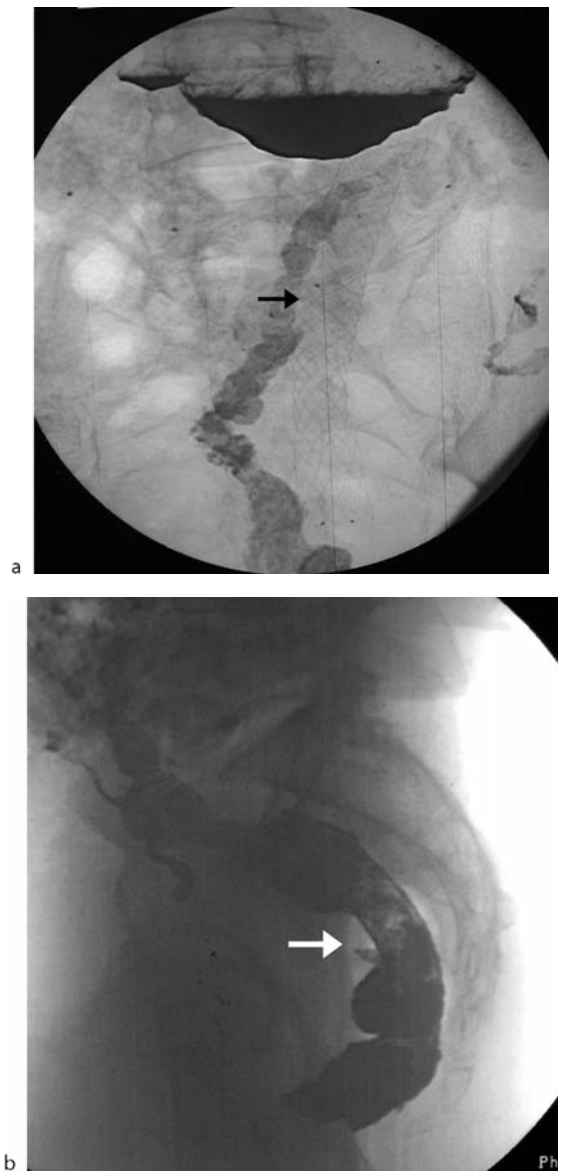

Foreign Bodies, Gastrointestinal. Figure 3 The progress of migrated esophageal metallic stent (arrows) in GI tract. (a) Second day radiograph; stent in small bowels. (b) Third

However, some foreign bodies such as small fish bones or pieces of plastic and wood are only faintly radiopaque and their detection may require CT. Indirect signs, visible on the plain radiograph are soft tissue swelling or air due to edema or hematoma.

Barium or Gastrografin Studies

Barium study may be indicated in cases of ingestion of nonopaque foreign bodies (Fig. 4), such as toothpicks or aluminum soda can tabs, although CT scanning is a much better imaging modality. A barium or gastrografin study, without cotton balls, can sometimes outline the foreign body, but, again, the yield is very low.

Barium swallow can be used for food impactions; however, most authorities believe that it adds nothing to the evaluation and delays definitive treatment. Contrast studies are not useful in detecting foreign bodies in the stomach or small intestine. Barium is contraindicated in cases in which esophageal perforation is suspected. Gastrografin may be used if a study is needed.

Esophagography should first be performed with hydrosoluble contrast medium to exclude perforation

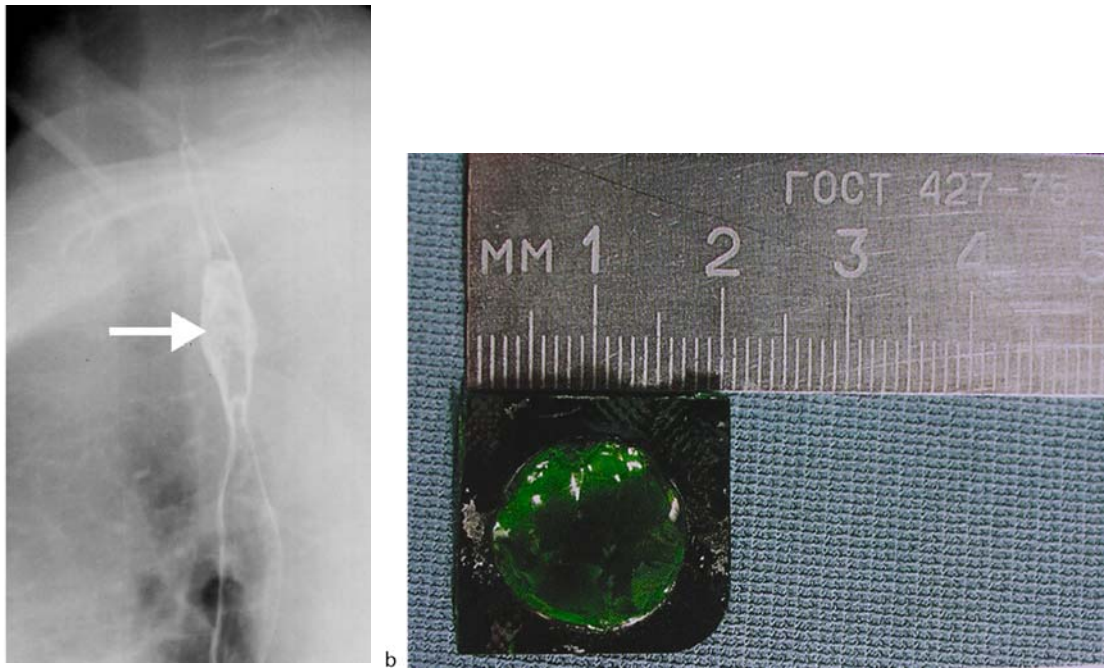

Foreign Bodies, Gastrointestinal. Figure 4 Swallowed pill with its plastic cover in upper thoracic esophagus. (a) Barium

and can then be completed with a barium examination. The contrast medium may impregnate the surface of the foreign body and render it more conspicuous.

Computed Tomography Scanning

Recent technical developments have led CT to be used more frequently in emergency departments and have greatly enhanced CT's ability to accurately discriminate between those patients with a normal or abnormal abdomen, and to further characterize the etiology of the patient's abdominal pain. CT scanning is superior to plain radiographs for localization and identification of foreign bodies. It is now considered the imaging modality of choice to locate nonradiopaque foreign objects in the oropharynx, esophagus, stomach, small intestine, and large intestine. CT scanning is highly reliable in localizing foreign bodies in the esophagus. However, the application is probably unwarranted in every case of acute bone dysphagia, as only a minority of patients who sense foreign bodies after eating chicken or fish have a bone present.

Perforation of intestinal structures by ingested foreign bodies is a challenging diagnosis that should always be invocated in cases of acute abdominal symptoms. The definite diagnosis is based on the demonstration of the responsible foreign body that is optimally achieved by CT. It is also superior to other imaging modalities in demonstration of obstruction caused by a foreign body. Especially, the recent developments in CT (multidetector CT) technology made high-quality multiplanar reconstructions possible (Fig. 5). Conventional CT is able to detect the calcified content of ingested foreign body and the presence of very small quantities of extraluminal gas, but its performance is impaired by a limited spatial resolution, the discontinuity of the sections, and the very poor quality of multiplanar reconstructions (1).

Nuclear Medicine

Scintigraphy has a limited role in the assessment of GI tract foreign bodies.

Diagnosis

Diagnosis of GI tract FB is usually made on the basis radiological imaging. Endoscopic procedures may be required in cases with a history of FB ingestion and subtle radiological findings. Endoscopic procedures are also used for the purpose of treatment besides the diagnostic challenge. Early endoscopic removal from the stomach or

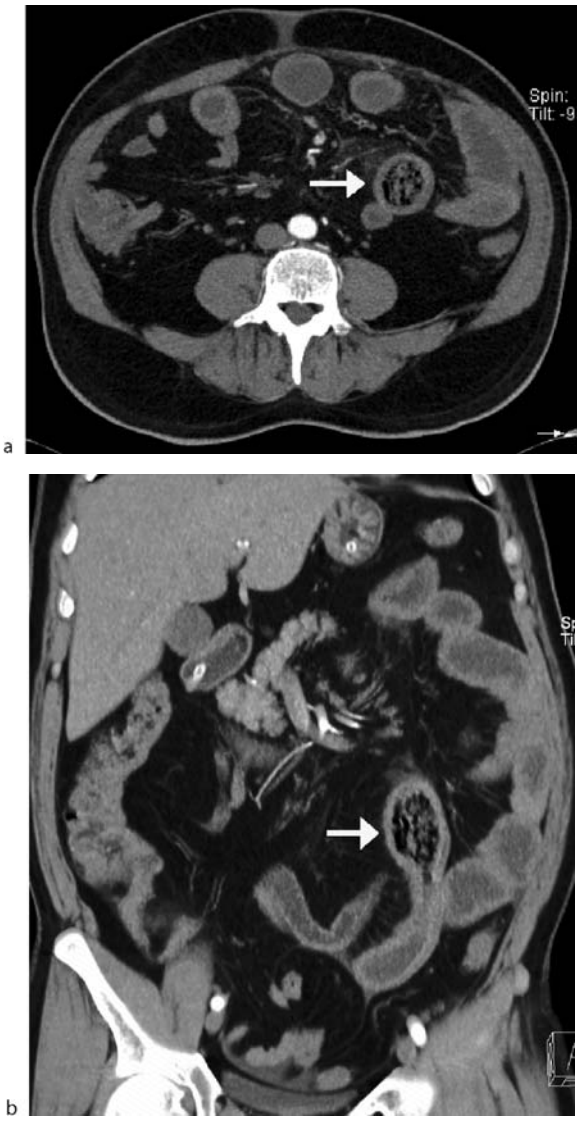

Foreign Bodies, Gastrointestinal. Figure 5 Bezoar; multidetector CT findings. (a) Axial. (b) Coronal CT images demonstrated that heterogeneous and low-density

duodenum is recommended to lessen the morbidity and cost to the health care system. In case of failure, rapid surgical removal of gastric FBs is wise.

Bibliography

1. Cheng W, Tam PK (1999) Foreign-body ingestion in children: experience with 1,265 cases. J Pediatr Surg 34:1472–1476
2. Coulier B, Tancredi MH, Ramboux A (2004) Spiral CT and multidetector-row CT diagnosis of perforation of the small intestine caused by ingested foreign bodies. Eur Radiol 14:1918–1925
3. Hunter TB, Taljanovic MS (2003) Foreign bodies. RadioGraphics 23:731–757

Foreign Body

An object that is inappropriately ingested or inhaled.
▶GI tract, Pediatric, Foreign Bodies

Fracture, Splenic

A splenic fracture is caused by a deep laceration that completely traverses the parenchyma, often extending to the splenic hilum and causing avulsion of a portion of the spleen. It represents a possible severe consequence of splenic trauma.
▶Trauma, Splenic

Fractures, Bone, Childhood

Alan E. Oestreich
Cincinnati Children's Hospital Medical Center, Cincinnati, Ohio, USA
Alan.Oestreich@cchmc.org

Synonym

Broken bones

Definition

A fracture is an acute break in the customary continuity of a bone or its growth cartilage or an acute disturbance of trabeculae, which will result in the formation of callus on follow-up imaging. ▶Avulsion is the discontinuity of a bony or cartilaginous element by traction from muscle, tendon, or ligament. Epiphysiolysis is a Salter I fracture causing discontinuity solely through a physis, most notably through the proximal femoral physis (known as a slipped capital femoral epiphysis, or SCFE). In traumatic dislocations, a shift in relationship occurs between bones that usually articulate with each other so that the articulation is disturbed.

Epiphyseal fractures extend solely through secondary growth centers or their enchondrally-derived equivalents (such as tarsal, carpal, or sesamoid bones or apophyses). In traumatic ▶plastic bowing (1), bones bend but do not break, but do not return to their preinjury shape.

Pathology/Histopathology

Bone is structure that offers support to the body; the characteristics that make it strong also leave it liable to fracture from various forces. Because children's bones are growing as well, their structure has further susceptibility to fracture. The callus of healing has a characteristic histologic pattern that changes through time and space. Typically at a break in a bone, the periosteal reaction begins to calcify at the greater distance from the fracture site and then proceeds inward toward the break under the lifted periosteum. Secondary growth centers, tarsal and carpal bones, and the sesamoids, including the patella, have no periosteum; their healing is by endosteal callus alone: without periosteum, one can have no periosteal reaction.

With SCFE, management is directed at stopping progression of the slip while hoping to avoid interruption of the blood supply (such interruption or impairment of blood supply would cause infarction/avascular necrosis). Chondrolysis of the growth cartilage of the head is sometimes a sequela of SCFE when one or more transphyseal orthopedic pins extend beyond the ossified head into its cartilage. Various epiphyses slip in scurvy in association with osteoporotic weakening of the bone adjacent to the physis.

Clinical Presentation

Pain, swelling, skin discoloration, and loss of function are primary signs of fracture. A child is a "good orthopedist" for about a day, immobilizing a fractured part, but then forgets, and thus casting is still necessary. Symptoms of acute dislocation at the elbow ("nursemaid's elbow") often vanish when positioned by a radiologic technologist for the 90° bent lateral view. Quite frequently after weeks of being in a cast, a child experiences stress fracture in a tarsal or nearby bone by enthusiastic reambulation when the bones are still demineralized from disuse osteoporosis. In acute plastic bowing of the forearm (1), the ability to pronate and supinate is lost; plastic bowing of the fibula occasionally prevents healing of an adjacent tibia fracture.

Repetitive trauma to the back of the ankle, such as from shoes resembling "pumps" of former days, may yield the pump bump (Haglund syndrome) of excessive prominence behind the posterior superior calcaneus, identifiable on plain radiographs as a soft-tissue prominence.

Imaging

Two orthogonal radiographic views at right angles should be obtained for evaluating fracture. At the hips, anteroposterior and frog-leg views are usually adequate instead and are especially pertinent in evaluation for SCFE.

Ultrasound can occasionally reveal occult fractures of cortex if clinical suspicion is high and radiographs unrevealing. Ultrasound may also show nasal bone fractures. Ultrasound is useful in newborns to evaluate for epiphysiolysis of the femur or humerus when those centers are still unossified (2).

Magnetic resonance imaging (MRI) can be helpful for revealing stress fractures of long bones when radiographs show only subtle callus or periosteal reaction, or when much of an elbow fracture traverses unossified cartilage. MRI of the elbow resolves whether a distal humerus fracture is Salter II or IV (3).

Computed tomography (CT) is potentially helpful for more fully describing certain fractures, particularly of the acetabulum about the hip and ▶triplane fractures of the ankle.

When a proximal or midulna is fractured, it is important to show the elbow on two views to rule out associated radius dislocation (Monteggia fracture).

For acute shoulder injury, we recommend the "double-angled trauma oblique" (patient thorax 45° anterior oblique and X-ray beam angled 45° downward), which simultaneously shows glenoid or humeral fractures and possible dislocation. For sternal fracture or sternoclavicular dislocation, which may be difficult to show on plain images, ultrasound can reveal abnormality, but localized CT nicely defines the fractures or dislocations. Multislice CT can rapidly investigate for rib fractures. Tendon tears, including the Achilles, are evaluated well by ultrasound, looking for discontinuity, focal thinning, or hematoma.

In general, for pediatric musculoskeletal imaging, the radiation dose should be as low as reasonably achievable. If film, the images should be high speed. Digital imaging should be optimized for low doses as well. Follow-up bone radiographs need not be of as high resolution as initial diagnostic studies. For some indications, whole-body MRI may soon replace radiographic surveys.

Nuclear Medicine

Bone scanning is sensitive for acute, subacute, and chronic unhealed fractures and is especially helpful for occult fractures, such as in child abuse investigations, positive fat pad signs of fractures, possible pseudarthrosis fracture of orthopedic spinal fusions, sacrum fractures, and suspected stress fracture. Indeed, because in stress fractures no callus is visible on radiographs for 10 days after occurrence, bone scanning can speed the diagnosis as well as look for other sites of involvement. Increased activity compared with the usual physeal uptake may reveal subtle SCFE as well as unossified avulsion of a pelvis apophysis. "Painful normal variant" is a term used by Lawson for symptomatic ossification variants, such as

bipartite patella or accessory navicular of the foot (4). High activity on bone may reveal true injury at those sites. Toddler fractures of tibia, fibula, or tarsal bones may be quite elusive on early radiographs but may be identified by localized activity on bone scanning.

Diagnosis

Fractures specific to childhood are the buckle (also called torus) fracture, traumatic plastic bowing (not a true fracture), toddler fracture, and metaphyseal corner fracture (of abuse, scurvy, and Menkes disease), as well as those fractures through the physis (Salter I–V, classically), including the stubbed toe (or, less commonly, finger) fracture, the Tillaux, the triplane, apophyseal avulsions, and SCFE.

The buckle, or torus, fracture (Fig. 1) appears as a bulge or bend on one or both sides of the normally monotonically curved cortex of a tubular bone (or occasionally a flat bone), most frequently near the wrist. In traumatic plastic bowing, one (or two) long bones bend from trauma but do not break, but also do not return to normal form, remaining bowed. The toddler fracture is a thin oblique or spiral fracture of the tibia or fibula (stress fractures of the toddler tarsal bones are also included in the term). The metaphyseal corner fracture is a Salter II fracture involving a corner of metaphysis plus the physis. Salter I epiphyseolysis goes exclusively through a physis, with a transverse shift of epiphysis relative to the metaphysis. Salter II goes through metaphysis plus epiphysis. Salter III goes through epiphysis plus physis, and Salter IV through epiphysis and metaphysis, crossing the physis. Salter V refers to the rare longitudinal crush of a physis (see Fig. 2). A stubbed toe or finger fracture is a Salter II of the dorsal distal phalanx beneath the nail bed (which has a good chance of being infected). Tillaux is a Salter III sagittal fracture of the distal tibia at a stage when the physis is partially fused. The triplane fracture of the ankle adds a coronal tibial metaphysis fracture to the Tillaux.

Avulsions are traction injuries of ossified, partially ossified, or only-cartilaginous apophyses. If they are only cartilaginous, ultrasound may indeed help diagnosis. When apophyses are at least in part ossified, their avulsion is seen by displacement from the customary position; on follow-up the size of ossification may increase considerably.

SCFE is recognized on plain images earlier on the frog-leg view by a (Klein's) line along the distal outer neck of the femur that does not intersect the capital epiphysis as it is continued upward. The physis also becomes less sharp than normal, and a "blush" of increased density in the neck may be seen, representing an attempt by the

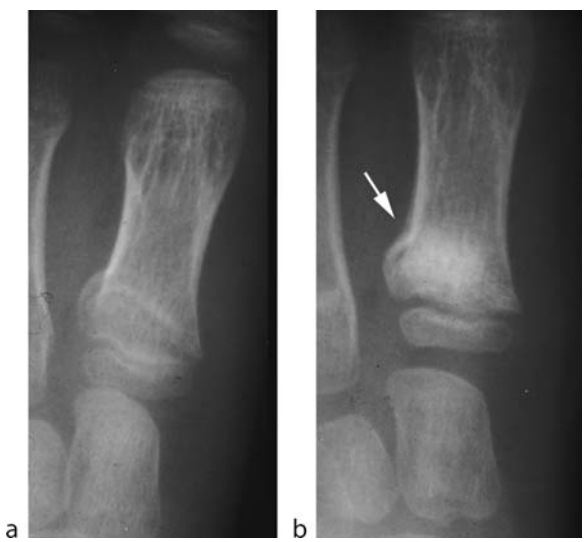

Fractures, Bone, Childhood. Figure 1 "Bunkbed" type buckle fracture of the metaphysis of the first metatarsal of a 4-year-old boy (such fractures often occur upon falling off an upper bunk). (a) The usual smooth curve of the lateral metaphysis and diametaphysis is disturbed by a buckle change in contour. (b) Three and 1/3 weeks later, endosteal and periosteal (*arrow*) callus is evident.

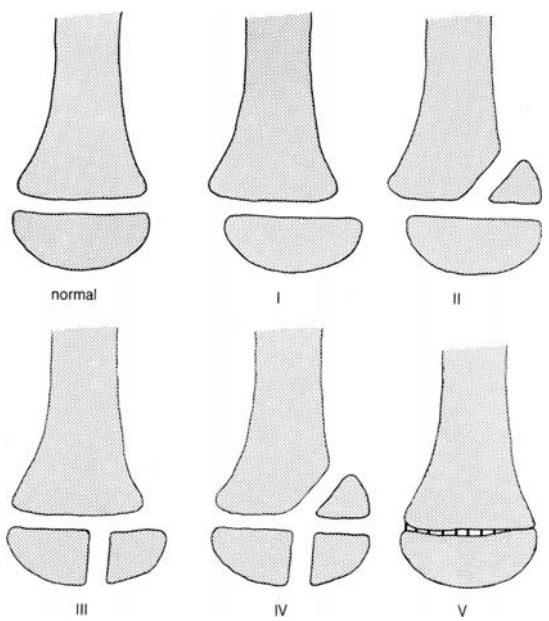

Fractures, Bone, Childhood. Figure 2 Schema of basic Salter (Harris) classification. (From Oestreich AE, Crawford AH (1985) Atlas of Pediatric Orthopedic Radiology. Thieme Verlag, Stuttgart, p 53)

femur to strengthen itself against the deformity. The slipped *distal* femoral epiphysis of scurvy develops vigorous periosteal reaction. Idiopathic chondrolysis of the hip manifests by severe and rapid narrowing of the cartilage space between the femoral head and acetabular roof. However, in SCFE, that cartilage space may become narrow when the slip results in a portion of the head previously not designed to bear weight then becoming the uppermost part.

Stress fractures of bones without periosteum, such as the tarsals, manifest beginning 10 days after the event and only as endosteal callus, often in a linear or curved distribution. Tubular and other membranous-origin bone also show periosteal reaction after 10 days. For fracture of the calcaneus, check the Böhler angle of the two upper surfaces on the lateral image—it normally lies between 28 and 40°. After wrist trauma, be sure to check the lunate-capitate linear alignment on lateral images for possible perilunate dislocation (Fig. 3). Lateral bowing or displacement or obliteration of the fat stripe lateral to the scaphoid may well indicate fracture, especially when the anatomic snuff box is tender after trauma. Fractures of the body of the sacrum and of the sternum may require ultrasound, nuclear scintigraphy, CT, or MRI for identification.

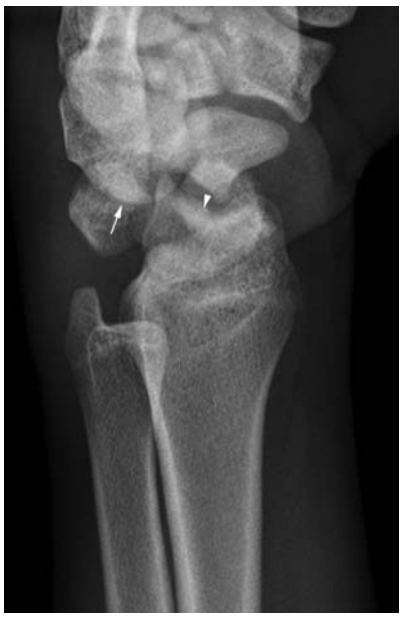

Fractures, Bone, Childhood. Figure 3 Traumatic perilunate dislocation after a 16-year-old boy fell. Note especially that, abnormally, the proximal convex end of the capitate (*arrow*) does not fit into the distal concave end of the lunate (*arrowhead*). The scaphoid is also fractured across its waist.

Bibliography

1. Borden IV (1975) Roentgen recognition of acute plastic bowing of the forearm in children. Am J Roentgenol Radium Ther Nucl Med 125:524–530
2. Bar-On E, Howard CB, Porat S (1995) The use of ultrasound in the diagnosis of atypical pathology in the unossified skeleton. J Pediatr Orthop 15:817–820
3. Anderson SE, Otsuka NY, Steinbach LS (1998) MR imaging of pediatric elbow trauma. Semin Musculoskelet Radiol 2:185–198
4. Lawson JP (1990) Not-so-normal variants. Orthop Clin North Am 21:483–495

Fractures, Pelvis

F

David Malfair
UCSF, San Francisco, USA
dmalfair@hotmail.com

Definitions

Pelvic fractures: osseous disruption of the lower limb girdle comprised of the sacrum and the paired innominate bones.

Pathology/Histopathology

The bony pelvis is a complex osseous structure that provides weight-bearing support and protects the viscera within the pelvic cavity. Enormous stress is generally required to disrupt the osseous and ligamentous structures of the pelvis in patients with normal mineral density. Bone weakened by osteoporosis may be fractured by low-impact injuries such as falls.

Clinical Presentation

Stable Pelvic Fractures

Avulsion Fractures

Osseous disruptions at the sites of muscular insertions are termed avulsion fractures. These fractures occur most commonly at the ischial tuberosity, anterior superior iliac spine and anterior inferior iliac spine as a result of sudden, forceful contraction of the hamstrings, sartorius (Fig. 1) and rectus femorus respectively. Young athletes are most prone to these injuries and present with sudden, focal pain.

The avulsed fragments are variably displaced and usually associated with a focal hematoma and bone marrow edema. The integrity of the involved muscle belly

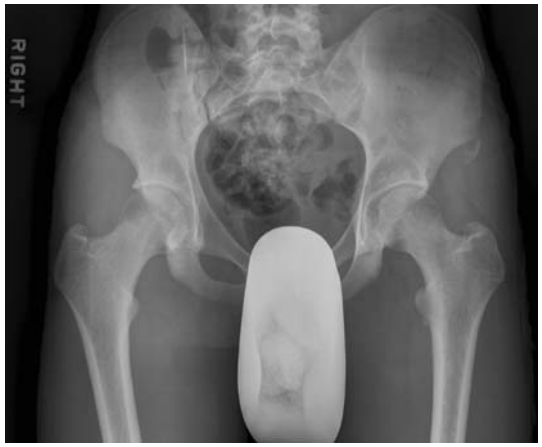

Fractures, Pelvis. Figure 1 AP radiograph of the pelvis demonstrates avulsion fracture of the left anterior superior iliac spine at attachment of sartorius.

and tendon may also be compromised. Sciatic nerve entrapment can occur in the setting of a healing hamstring avulsion fracture.

Sacral Fractures

Isolated acute sacral injuries most often occur after a direct impact from a fall. These fractures are generally oriented in the transverse plane and occur between the third or fourth sacral segment. The distal segment is usually displaced anteriorly. Injury to the lumbosacral plexus is an occasional complication.

Duvernay Fractures

Isolated fractures of the iliac wing are also known as Duvernay fractures. They most commonly occur as a result of direct trauma and seldom pose a diagnostic dilemma. Paralytic ileus and peritonism is not uncommon after this injury, usually due to irritation from a local hematoma.

Unilateral Pubic Rami Fractures

Unilateral pubic rami fractures are rare in high impact injuries. An additional occult bony or ligamentous disruption of the pelvic ring is usually present. Unilateral pubic rami fractures are characteristically associated with mild trauma in osteoporotic patients. Patients present with vague symptoms or inability to weight bear.

Unstable Pelvic Ring Fractures

Unstable pelvic fractures are defined as bony or ligamentous disruption in at least two points of the pelvic ring. These are generally high impact injuries associated with significant trauma to other organ systems. Critical injury to the cardiovascular or central nervous system is an important cause of morbidity and mortality in these patients. The presence and degree of these associated injuries affects the timing of imaging and management of pelvic trauma.

Young and Burgess classified these injuries by their mechanism of injury: lateral compression, AP compression, or vertical shear forces (5). This classification assists the surgeon in external fixation and aids in prognosis and identification of associated injuries.

Lateral Compression Injuries

Type I lateral compression injuries result from direct force on the ilium that internally rotates the ipsilateral hemipelvis causing an impaction injury to the ipsilateral sacrum. Horizontal or coronally orientated fractures of the pubic rami or pubic diastasis are found. Fracture of the ipsilateral sacrum and contralateral pubic rami is known as a bucket handle fracture. Type IIa injuries are similar to type I fractures but with additional disruption of the ipsilateral posterior sacroiliac ligaments. Twenty percent of patients suffer an oblique fracture of the iliac wing rather than a ligamentous injury (Type IIb).

Type III injuries result from internal rotation of the ipsilateral hemipelvis and external rotation of the contralateral hemipelvis. The ipsilateral hemipelvis is similar to a type II lateral compression injury. The contralateral hemipelvis injuries are characteristic of an AP compression injury. This constellation is known as a "windswept pelvis."

Anterior Compression Fractures

Anterior compression injuries result from a force in an anterior–posterior direction that result in external rotation of each hemipelvis. Type I injuries are characterized by diastasis of the pubic symphysis or fractures of the pubic rami. The pubic rami fractures are oriented in the sagittal plane in contradistinction to lateral compression injuries. The posterior ligaments remain intact. Type II AP compression injuries are similar to Type I fractures with additional disruption of the sacrospinous, sacrotuberous, and anterior sacroiliac ligaments. Avulsion fractures at the attachment sites of these ligaments or pubic symphyseal diastasis greater than 2.5 cm suggest this diagnosis.

Type III injuries include the posterior sacroiliac ligaments and result in complete diastasis of at least one SI joint. Sacral fractures are unusual but may occur. Posterior acetabular wall fractures are a common association.

Vertical Shear Fractures

Vertical shear injuries occur most commonly in patients who fall from a height. The classic injury is a Malgaigne fracture; vertical fractures through the sacral ala and ipsilateral pubic rami. However, various combinations of fractures can occur. The most characteristic feature of this very unstable injury is craniocaudal displacement of fracture fragments.

Complications

Internal hemorrhage is the most important local complication of pelvic trauma. Venous bleeding is most common and is effectively treated with fluid resuscitation and early external fixation. Arterial bleeding is frequently refractory to supportive care and percutaneous treatment becomes necessary.

Local organ injury also occurs in the setting of unstable pelvic fractures. Rectal and Lower urinary tract and rectal injuries occur in 2% and 10% of pelvic ring disruptions, respectively. Type II and III AP compression injuries are at highest risk for these injuries.

Acetabular Fractures

The most common mechanism for ►acetabular fractures is motor vehicle accidents. These fractures are often associated with pelvic ring fractures, femoral head fractures, and ►hip dislocations. The most widely used classification system for acetabular fractures is the Judet–Letournel system. This system describes basic injuries to the acetabulum as column, rim, and transverse fractures as elementary fractures (Table 1). Five additional combinations of these elementary fractures are described and are classified as associated injuries.

Column fractures are oriented in the coronal place through the acetabulum. Anterior and posterior column fractures disrupt the ileopectineal and ilioischial lines respectively. Wall fractures involve the lip of the acetabulum without extension into the adjacent columns. Transverse fractures are oriented in the transaxial plane through the anterior and posterior aspects of the acetabulum. They may be slightly oblique and detected as sagittally oriented fractures on transaxial images. Most acetabular fractures require surgery to maintain the congruency of the hip joint. The most common long-term complication is degenerative joint disease.

Fractures, Pelvis. Table 1 Letournel–Judet classification of acetabular fractures

Elementary fractures
• Anterior wall
• Anterior column
• Posterior wall
• Posterior column
• Transverse
Associated
• T-shaped
• Anterior wall/column plus posterior hemitransverse
• Transverse plus posterior
• Posterior Column plus posterior wall
• Both column

Hip Fractures

Minor trauma in a patient with osteoporosis is the characteristic clinical setting of most ►hip fractures. Most hip fractures are subcapital fractures, occurring at the junction of the femoral head and neck. These injuries are intracapsular and often interrupt blood supply to the femoral head. The Garden classification system is a useful way of characterizing these fractures. Stage I is an incomplete impacted fracture occurring at the lateral femoral cortex. Stage II injuries are also impacted but extend completely through the femoral neck. Stage III fractures demonstrate distraction of fracture fragments along the lateral cortical margins. Some bony apposition is seen inferiorly and moderate rotation of fracture fragments is usually present. Stage IV fractures demonstrate no bony apposition. Instability and nonunion are more commonly found in high-grade injuries.

Other intracapsular fractures include transverse cervical and basicervical injuries. Extracapsular hip fractures include intertrochanteric and subtrochanteric fractures. These fractures are usually obliquely oriented and associated fractures of the lesser and greater trochanters are common. Pathologic fractures should be considered in the setting of isolated fractures of the trochanters or transversely oriented subtrochanteric injuries.

Hip fractures are a major source of morbidity and mortality in the elderly. Once bedridden, these patients are deconditioned and at increased risk for comorbid medical problems such as nosocomial infection and deep vein thrombosis. The risk of avascular necrosis often necessitates the placement of a hip prosthesis in intracapsular fractures.

Imaging

Radiographs

The AP radiograph demonstrates 60–70% of acute pelvic fractures in most series (2). The pelvic inlet view is obtained with 45° caudal angulation. It demonstrates anteroposterior displacement of fracture fragments characteristic of AP compression injuries. The pelvic outlet view is obtained at 45° cranial angulation and

demonstrates craniocaudal displacement of fracture fragments characteristic of vertical shear injuries.

Judet views (45° obliques) are helpful to assess the integrity of the columns in acetabular injuries (Fig. 2). Radiographic sensitivity for acetabular fractures is around 70%. Transverse fractures of the sacrum and coccyx are best assessed on lateral views. While most hip fractures are seen on the AP film, lateral views of the hip increase sensitivity for detecting and help further characterize these fractures.

Computed Tomography

The advent of multislice CT technology has revolutionized the role of radiology in trauma. Most trauma centers obtain CT images of the pelvis in serious trauma as a matter of routine. Thin section axial images with coronal, sagittal, and 3D reformats allow excellent accuracy in identifying and characterizing pelvic fractures. Some authors report the addition of CT with multiplanar reformats can alter surgical management in 30% of acute pelvis fractures (1). Pseudoaneurysms or contrast extravasation on contrast enhanced CT is diagnostic of arterial injury and helps guide angiography. Sentinel hematoma can also help localize venous bleeding.

Radiographically occult pelvic fractures are accurately assessed on CT. In the setting of acetabular fractures, CT has a well-established role in the identification of impaction fractures of the femoral head and loose bodies within the joint. CT with multiplanar reformats improves accuracy in the acetabular fracture classification and increases diagnostic certainty.

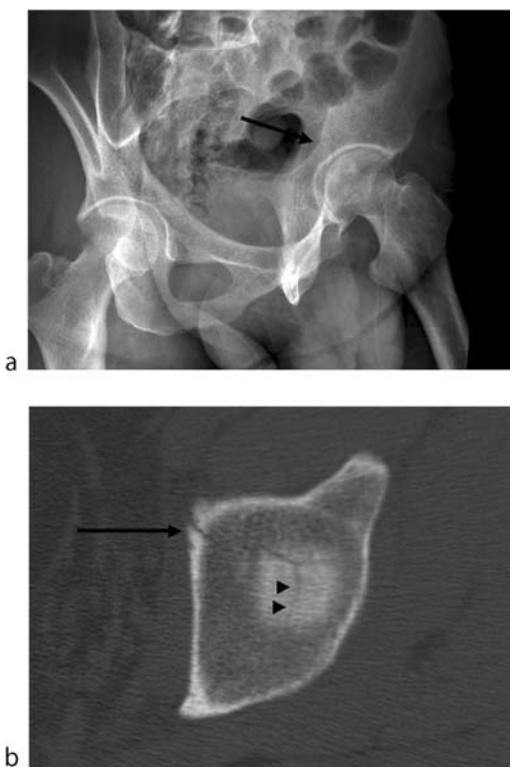

Fractures, Pelvis. Figure 2 (a) Judet view demonstrates a subtle acetabular fracture (*arrow*) that was not apparent on the AP radiograph of the pelvis. Subsequent CT (b) through the region of the superior acetabulum demonstrates an anterior column fracture that is oriented transversely (*arrow*) with a posterior hemitransverse component (*arrowheads*).

Magnetic Resonance Imaging

Magnetic resonance imaging (MRI) is uncommonly used for evaluation of acute pelvic injury. This modality is too time-consuming for these unstable patients and CT is highly accurate is the assessment of acute bony injuries. MR imaging plays an important role in stable patients. It is the most sensitive modality for detecting occult fractures in the pelvis. These fractures present as low-signal linear defects on T1 and T2 images. Surrounding edema is the rule rather than the exception. Sometimes, however, only edema is shown and fracture lines are not visualized. Thus differential diagnosis may include infection and neoplasms, in these cases CT may be helpful.

MR imaging is useful in avulsion injuries as a method of assessing the integrity of the involved muscle and tendon. The actual fracture fragment may be inconspicuous.

MR is the primary imaging method for evaluating pelvic muscle strains and other soft-tissue injuries. Muscle strain is characterized by high-signal edema on fluid-sensitive sequences. In studies evaluating MR in the assessment of occult hip fractures, 40% of the exams diagnosed additional soft-tissue injuries (4).

Nuclear Medicine

Bone scintigraphy is useful in the setting of suspected occult pelvic fractures because of its excellent sensitivity. Weaknesses include its limited specificity and spatial resolution. These weaknesses and the time needed to image the patient limit the usefulness of scintigraphy in the acute trauma setting.

An acute fracture of the pelvis will be hot on all three phases of MDP bone scintigraphy. An acute fracture in the elderly osteoporotic patient may have a normal study in the initial 72 h. After a period of weeks, fracture uptake becomes more linear on scintigraphy and exhibits less

activity on the flow and blood pool phases of the study. The delayed activity at a healing fracture site may persist for 2 to 3 years.

Diagnosis

The increased speed and accuracy of multidetector CT has made it the modality of choice for evaluation of pelvic trauma in most centers. AP radiographs are still useful in hemodynamically unstable patients or when timing of the CT is expected to be delayed. Unstable pelvic fractures can then undergo external fixation and excess bleeding prevented. AP radiographs should also be obtained in suspected hip dislocation to assist immediate reduction.

Radiographs remain the primary imaging modality in patients who suffer low-impact trauma and a hip or pelvis fracture is suspected. Often clinical suspicion persists despite negative radiographs. MR imaging or scintigraphy are very sensitive in detection of these occult fractures.

Intervention

Percutaneous embolization of arterial injury is an effective method of controlling blood loss in unstable pelvic ring fractures. Under what clinical circumstances and at what time that angiography should be performed is a matter of debate. Patients who do not respond to initial resuscitation or have widely diastased fracture fragments have been shown to have a high incidence of arterial injury. Extravasation of contrast or psuedoaneursyms seen on initial contrast enhanced pelvic CT is strong evidence of arterial injury and allows for preprocedure localization of the abnormality. Arterial injury is difficult to predict by the fracture pattern alone, and clinical factors are important in suggesting this diagnosis.

The obturator and pudendal arteries are most commonly injured in anterior disruptions. Posterior disruptions affect the superior gluteal artery most commonly. If an arterial abnormality is identified, subselective vessel catheterization and embolization is performed.

Bibliography

1. Falchi M, Rollandi GH (2004) CT of pelvic fractures. Eur J Radiol 50:96–105
2. Guillamondagut OD, Pryor JP, Gracias VH et al (2002) Pelvic radiology in blunt trauma resuscitation: A diminishing role. J Trauma 53:1043–1047
3. Letournel E, Judet R (1993) Fractures of the acetabulum. 2nd edn. Elson RA translator, (ed) Springer, New York
4. Verbeeten KM, Hermann KL, Hasselqvist M et al (2005) The advantages of MRI in the detection of occult hip fractures. Eur Radiol 15:165–169
5. Young JWR, Burgess AR, Brumback RJ et al (1986) Pelvic fractures: value of plain radiography in early assessment and management. Radiology 160:445

Fractures, Peripheral Skeleton

David Malfair
USCF, San Francisco, USA
dmalfair@hotmail.com

F

Definitions

Fracture: complete or incomplete break in the continuity of bone or cartilage.
Strain: muscular or tendinous injury.
Sprain: soft tissue injury of a ligament.

Pathology/Histopathology

Fractures usually result from a single episode in which excessive force is applied to normal bone. The pattern of osseous disruption depends on the force applied and the underlying mechanical properties of the bone. Most fractures are complete and are described in terms of the location, position, and orientation of fracture fragments. Partial fractures occur commonly in children and include greenstick, bending, and torus fractures.

Injury to the muscular, tendinous, and ligamentous structures is common in acute trauma. Muscular injury from direct impact usually manifests as intramuscular edema or hematoma. Trauma to ligaments and tendons is usually indirect, secondary to an acute distracting force. Mild trauma results in microtears and stretching of these structures. High-grade injuries are characterized by partial or full-thickness tears.

An acute fracture results in a bridging hematoma between fracture fragments. The initial inflammatory and reparative phases result in osseous resorption at the fracture margins. As this hematoma organizes, healing begins with the formation of endosteal and periosteal callus in a process that usually takes 4–16 weeks to complete. Remodeling occurs with replacement of woven with lamellar bone. Prompt healing is promoted by the stability of fracture fragments, close approximation of fragments, intact vascularity, and good nutrition (1).

Acute complications of fractures include neurovascular injury, hypotension, infection, and fat embolism

syndrome. Chronic complications of extremity trauma are common and include venous thrombosis, infection, *nonunion*, *avascular necrosis, complex regional pain syndrome*, degenerative joint disease, and ▶ *myositis ossificans*.

Clinical Presentation

Shoulder

Acromioclavicular (AC) and glenohumeral dislocations are commonly sustained in athletic endeavors as a result of direct impact or falling on an outstretched arm. The normal width of the AC joint is highly variable but usually measures less than 5 mm. It is seldom wider than 3 mm in middle-aged and elderly patients. Disruption of the AC joint is characterized by unilateral widening of the AC joint or vertical displacement of the clavicle in relation to the acromion. Disruption of the coracoclavicular ligament occurs in high-grade AC joint dislocations and its identification may change surgical management (2). Avulsion fractures of the coracoid process, the conoid tubercle of the clavicle, or a coracoclavicular interval greater than 13 mm suggests disruption of this ligament.

The majority of glenohumeral dislocations are anterior and are classified as subcoracoid, subglenoid, subclavicular, and intrathoracic. The subcoracoid position of the humerus is most common and is usually obvious both clinically and on radiology studies. A subglenoid position results in luxatio erecta, persistent nonvoluntary abduction of the humerus. Anterior humeral dislocations are often associated with osseous impaction of the posterolateral humeral head and anteroinferior labral detachment. These lesions are known as Hill-Sachs and Bankart lesions, respectively. Fractures of greater tuberosity are associated with 15% of anterior dislocations. Injuries to the rotator cuff and the articular capsule are also associated with these dislocations. Recurrent dislocations are common in younger patients and those with associated soft tissue and osseous injury. Magnetic resonance imaging (MRI) is helpful for characterizing these abnormalities and assists in surgical planning.

Posterior dislocations usually occur secondary to muscle spasm during seizures. These injuries are difficult to diagnose both clinically and on standard radiographs. Axillary and transcapular radiographs or cross-sectional images are the most reliable methods in the identification of this injury. Reverse Hill-Sachs fractures, injury to the posterior labrum, and lesser tuberosity fractures are associated with posterior dislocations.

Humerus, Elbow, and Forearm

Fractures of the humeral neck most commonly occur in elderly patients with osteoporosis after minor trauma. The surgical neck is usually involved but additional fractures of greater and lesser tuberosity are frequently found. Most humeral neck fractures are minimally displaced as the fragments are held in apposition by partially intact periosteum, joint capsule, and rotator cuff tendons. These injuries are treated by supportive means. A fracture fragment distraction of greater than 1 cm or angulation of greater than 45° indicates high-grade injuries that may require surgical fixation. Fractures of the anatomic neck are less common, but result in disruption of blood supply with high rates of ▶ avascular necrosis of the humeral head. Additional complications of trauma to this region include neurovascular injury and adhesive capsulitis.

Fractures of the humeral shaft occur in high-impact injuries, often in younger patients. Transverse, mid-diaphyseal fractures are most common. Spiral fractures may occur after throwing in healthy young patients. Radial nerve injury occurs in 5–10% of fractures of the humeral diaphysis.

Most fractures of the elbow occur in patients who fall on an outstretched hand. Radial head fractures are most common in adults. These fractures are often minimally displaced and identification of an elbow effusion or displacement of the supinator fat pad may aid in their identification. Imaging of the wrist should be performed in cases of severe comminution of the radial head to rule out a coexisting distal radioulnar joint disruption, an Essex-Lopresti injury. Fractures of the olecranon are the second most common elbow fractures in the adult. Oblique fractures may be subtle but prominence of the olecranon bursa and joint effusion are often present.

The most common elbow fractures in children are supracondylar, lateral condylar, and medial epicondylar in descending order of frequency. Supracondylar fractures may be associated with arterial injury and median nerve palsy. Additionally, suboptimal reduction of supracondylar fractures may result in loss of normal valgus angulation at the elbow. Avulsion fractures of the medial epicondyle may be subtle, especially when the fragment is trapped within the joint. Absence of the medial epicondyle is abnormal if the secondary center of ossification of the trochlea is present.

Transcondylar and intercondylar fractures usually occur as a result of falling on an outstretched hand, often in osteoporotic patients. Displacement and rotation of fracture fragments are common and usually dictate surgical repair. Undisplaced fractures of the lateral condyle are considered stable if they do not extend past the trochlear groove. Similar fractures of the medial condyle are considered stable if they do not extend past the capitellotrochlear sulcus.

Elbow dislocations are usually posterior and secondary to high-impact trauma or falling on an outstretched

arm. Fractures of the coronoid process of the ulna and avulsion of the medial epicondyle are common associated injuries. Fractures of the lateral condyle, radius, olecranon, and capitellum are less frequent.

Numerous combinations of ulnar and radius fracture/dislocations have been described (Table 1). These patterns of injuries underscore the need to image from the elbow to the wrist in the setting of forearm trauma. Surgical reduction is considered in even mildly angulated fractures to preserve an adequate range of motion. Rotational deformity may be subtle on imaging and results in significant impairment.

Wrist and Hand

Most wrist injuries result from a fall on an outstretched hand. Distal radius fractures occur most commonly in patients with osteoporosis. The most common injury is Colles' fracture, which results in dorsal angulation of the distal fragment. The majority of Colles' fractures are intra-articular and a step of greater than 2 mm is an indication for surgical reduction. Closed reduction should attempt to restore the anatomic 15° of ulnar and 10° of dorsal angulation of the distal radial articular surface. Approximately 50% of wrist injuries are associated with triangular fibrocartilage tears and ulnar styloid fractures.

Scaphoid fractures are often radiographically occult and repeat radiography or advanced imaging techniques are often required for correct diagnosis (3). Fractures of the scaphoid are important because of the high risk for ►nonunion and avascular necrosis. These complications occur more commonly in proximal fractures of the scaphoid because of the distal entry points of the nutrient arteries. Ligamentous injuries to the carpus and fractures of the radial styloid, capitate, and triquetrum are associated with scaphoid trauma.

Ligamentous disruption of the scapholunate and radioscaphoid ligament results in scapholunate dissociation. Indirect signs of this injury on radiographs include widening of the scapholunate interval, rotary subluxation of the scaphoid, and an increased volar tilt of the scaphoid on lateral views. Lunotriquetral and triangular fibrocartilage tears are also common ligamentous injuries of the carpus. Diagnosis of these ligament tears is confirmed on arthrography or MRI.

The most common dislocation in the wrist is a dorsal perilunate dislocation in which the lunate continues to articulate with the radius, but the remainder of the carpus is dislocated dorsally. The majority of these dislocations are associated with a scaphoid waist fracture. Lunate dislocations are usually volar and the remainder of the carpus aligns with the radius in a normal position.

Fractures, Peripheral Skeleton. Table 1 Common eponyms for extremity fractures

Arcuate	Fracture of fibular apex associated with posterolateral corner injury
Bony Bankart	Anteroinferior fracture of the glenoid labrum
Barton	Fracture of dorsal rim of radius and dorsal dislocation of carpus
Bennett's	Intra-articular fracture involving the base of the first metacarpal
Boxer's	Fracture of distal fifth metacarpal
Chauffeur's	Fracture of the radial styloid
Chopart	Fracture-dislocation through talonavicular and calcaneocuboid
Colles'	Transverse fracture of distal radius with dorsal angulation of distal fragment
Essex-Lopresti	Comminuted fracture of the proximal radius and disruption of the distal radioulnar joint
Galeazzi's	Fracture of the radius with disruption of the distal radioulnar joint
Hill-Sachs	Impaction fracture of the posterolateral aspect of humeral head
Jones	Transverse fracture at the base of the 5th metatarsal
Lisfranc	Fracture/dislocation involving ligaments between first metatarsal and middle cuneiform
Maisonneuve	Fracture of the proximal fibula associated with ankle injury
Monteggia	Fracture of the ulnar shaft and dislocation of the proximal radius
Nightstick	Isolated ulnar fracture secondary to direct trauma
Rolando	Comminuted fracture of base of the first metacarpal
Segond	Posterolateral flake avulsion fracture of the proximal tibia epiphysis associated with anterior cruciate ligament tears
Smith's	Transverse fracture of the distal radius with volar angulation of distal fragment
Tillaux fracture	Salter 3 fracture of anterolateral aspect of the distal tibial epiphysis

The hand is the most common location of skeletal trauma. The majority of these injuries occur in the phalanges and metacarpals and are due to direct trauma. Injuries to the ulnar collateral ligament of the first digit are important for the radiologist. An MR image can help diagnose a Stenner lesion in these patients where the ulnar collateral ligament is found above the adjacent aponeurosis. The presence of this lesion is an indication for surgery.

Femur, Knee, and Lower Leg

Fractures around the knee are uncommon and usually occur from high-impact trauma. Supracondylar fractures are frequently transverse. Hip fractures and dislocations are associated with this injury, and imaging of the entire femur should be performed. Intercondylar fractures are often comminuted and best characterized by multiplanar computed tomography (CT). Popliteal artery injuries are associated with distal femoral fractures.

Acute injuries to the knee usually involve the ligaments and menisci and are best assessed with MRI. Several fractures of the knee may herald an important soft tissue injury. Segond fractures are a flake avulsion fracture along the posterior lateral tibial epiphysis. These injuries are associated with anterior cruciate ligament and meniscal pathology. In addition, avulsion fractures of the tibial spines and impaction fractures of the lateral condylar sulcus are other osseous findings in anterior cruciate ligament injury. Fractures of the apex of the fibula are important. These may represent avulsion fractures of the arcuate ligament and are the only radiographic evidence of a posterolateral corner injury (Fig. 1). These injuries involve the posterolateral joint capsule, the popliteal tendon, and the cruciate ligaments. These unstable injuries result in accelerated degenerative change and are an indication for urgent orthopedic referral.

Tibial plateau fractures usually occur in older patients with acute injuries, usually twisting injuries in falls but also in direct trauma. Valgus stress is common and 80% of fractures involve the lateral tibial plateau. These fractures may be radiographically occult with the only clue being a lipohemarthrosis. The coexistence of internal derangement in 70–90% of cases makes MRI well suited to their evaluation. Indications for fracture repair include distraction of fracture fragments of greater than 5 mm or depression greater than 10 mm.

Ankle and Foot

Supination-adduction injuries result from an acute varus stress on the foot when weight bearing on the outside of the foot. The initial injury is to the lateral ligaments of the ankle, most commonly the anterior talofibular and calcaneofibular ligaments. Loss of lateral stability results in lateral translation of the tibia on the talus. The shearing forces can lead to an oblique or vertical fracture of the medial malleolus.

Supination-external rotation of the ankle results from inward rotation of the leg while weight bearing on the outside of the foot. The initial injury is disruption of the anteroinferior tibiofibular ligament (AITF). Continued inward rotation of the tibia (external rotation of the planted foot) results in a spiral fracture of the fibula at the level of the ankle mortise followed by disruption of the posteroinferior tibiofibular ligament (PITF). After these injuries, continued force results in tear of the deltoid ligaments. This final stage of injury is unstable. Deltoid ligament injuries may be subtle and stress views are warranted in the setting of a spiral fracture of the fibula at

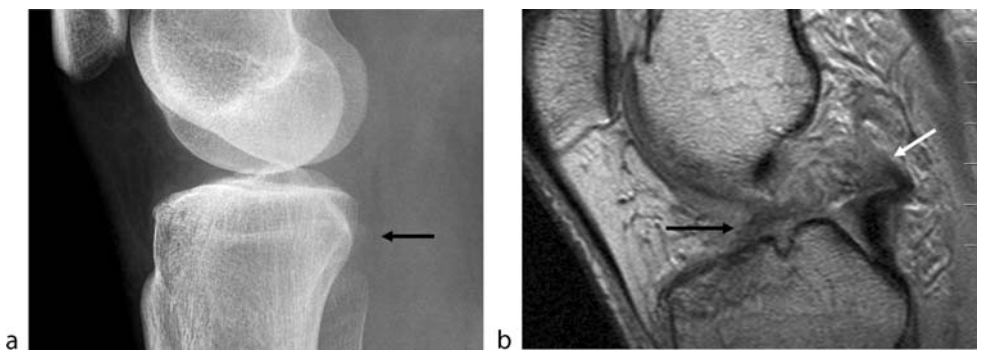

Fractures, Peripheral Skeleton. Figure 1 Coned in lateral view of the knee (a) demonstrates an arcuate fracture (*arrow*) through the apex of the fibula, usually associated with posterolateral corner injury. A sagittal proton density MR (b) demonstrates disruption of the ACL (*black arrow*) and PCL (*white arrow*) in the same patient who suffered a total knee dislocation.

the level of the syndesmosis and soft tissue swelling over the medial malleolus.

Pronation-external rotation occurs when inward rotation of the tibia takes place while weight bearing on the instep of the foot. This force initially places the deltoid ligament under tension and results in a ligamentous sprain or avulsion fracture. Continued motion results in disruption of the AITF ligament and rupture of the interosseous membrane. Fracture of the fibula 10 cm above the mortise usually follows, although fracture of the proximal fibula, a Maisonneuve fracture, may also occur in this setting. Finally, continued rotation results in a posterior malleolar injury at the level of the PITF attachment. Proximal fibular fractures should be sought in the setting of widening of the medial joint space or widening of the distal tibiofibular syndesmoses over 5.5 mm. These injuries may be subtle or temporarily reduce and the only clue to a proximal fibular fracture is medial malleolar swelling and an isolated posterior malleolus fracture.

Pronation-abduction injuries result from a valgus stress on the ankle while weight bearing on the instep of the foot. The initial injury results in a deltoid ligamentous injury or avulsion fracture. The second stage of the injury is disruption of the distal tibiofibular syndesmosis, which may be accompanied by an avulsion fracture of the posterior malleolus. Continued force results in a characteristic oblique fibular fracture above the ankle mortise. The interosseous membrane remains intact.

The calcaneus is the most commonly fractured tarsal bone. Compression fractures of the calcaneus occur in the setting of axial loading and are frequently associated with vertebral compression fractures. Fracture extension into the posterior subtalar facet and depression of this joint should be carefully assessed. Entrapment of the flexor hallicus longus and peroneal tendons may also occur (1). Two common locations for avulsion fractures of the calcaneus include the anterior process and anterolateral aspect of the calcaneus at the attachments of the bifurcate ligament and extensor digitorum brevis muscles, respectively. These injuries are the most commonly seen fractures on ankle radiographs and should be sought on anteroposterior (AP) radiographs.

Osteochondral injuries are the most common fracture of the talus. They are often radiographically occult and are best assessed with cross-sectional imaging. Fractures of the talar neck are predisposed to avascular necrosis. Osteochondral injuries are also common in the tarsal navicular bone.

The most important injury involving the cuneiforms is the Lisfranc fracture-dislocation. The first and second metatarsals are aligned with the medial and middle cuneiforms, respectively. Disruption of this alignment suggests a ligamentous injury. Associated dislocations may follow a homologous (second through fifth metatarsals laterally displaced) or divergent (additional medial displacement of the first metatarsal) pattern. Fractures of the metatarsals and phalanges are common and are often the result of direct trauma.

Imaging

Radiographs

Plain radiographs are sufficient for evaluation of most extremity fractures. As a rule of thumb, two orthogonal views and an oblique view are considered the minimum necessary to assess for the presence or absence of a fracture. Fractures are most commonly seen on radiographs as an abnormal line of radiolucency. Cortical irregularity or disruption is another important sign. Increased sclerosis with bone is found in compression fractures. Joint effusion and displacement of fascial planes are important secondary signs.

Ultrasound

Ultrasound is an excellent modality in acute trauma for assessing the integrity of ligaments and tendons. It is most commonly used in the assessment of the integrity of the rotator cuff and the Achilles and patellar tendons. It also is useful in characterizing hematomas and other muscle injuries and for the detection of nonradiopaque foreign bodies (4).

Computed Tomography

Osseous injury to the extremity is well evaluated by CT. Imaging characteristics of fractures are similar to those in radiography and include abnormal linear lucency, cortical discontinuity, and increased sclerosis. The increased use of multidetector CT (MDCT) with isotropic voxels and advanced PACS systems allows for visualization of fracture fragments in any plane. Therefore, despite inferior spatial resolution compared with radiography, MDCT is better able to fully characterize complex osseous injuries.

MDCT is also able to evaluate the soft tissues in acute trauma. Hematomas demonstrate increased density. Small amounts of air, foreign bodies, and effusions are also frequently found. Tendinous and ligamentous injuries are visualized as focal discontinuity or entrapment within fracture fragments (1).

Magnetic Resonance Imaging

MRI is very sensitive and specific in the identification of osseous trauma. Linear fracture lines are hypointense on T1- and T2-weighted sequences. This low signal abnormality is invariably surrounded by high T2-weighted bone

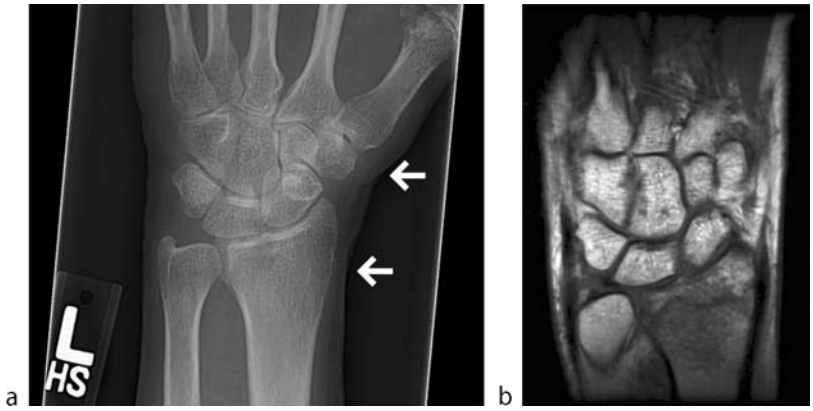

Fractures, Peripheral Skeleton. Figure 2 AP radiograph (a) of the wrist demonstrates no abnormality despite pain (*arrows* placed by technologist) along the radial aspect of the wrist after a fall. A T1-weighted coronal MR of the wrist (b) demonstrates a low signal fracture line in the distal radius.

edema. Enhancement adjacent to the fracture line and periosteum is also noted. Soft tissue trauma to ligaments, tendons, and muscles is also depicted well on MR images. Focal discontinuity and high T2-weighted signal within these structures are the most common signs of injury.

Nuclear Medicine

Bone scintigraphy is useful in the setting of suspected occult fractures because of its excellent sensitivity. Weaknesses include its limited specificity and spatial resolution. These weaknesses and the time needed to image the patient limit the usefulness of scintigraphy in the acute trauma setting.

An acute fracture will be hot on all three phases of MDP bone scintigraphy. An acute fracture in the elderly osteoporotic patient may appear normal in the initial 72 h. After a period of weeks, fracture uptake becomes more linear on scintigraphy and exhibits less activity on the flow and blood pool phases of the study. The delayed activity at a healing fracture site may persist for 2–3 years.

Diagnosis

Most extremity fractures are adequately assessed by radiography. MDCT provides additional information regarding the position of fracture fragments and is helpful in preoperative planning in complex injuries. Occasionally, extremity fractures may be occult on plain radiographs, especially in regions such as the scaphoid and hip. In these cases, scintigraphy, CT, or MRI may be performed to diagnose these injuries (Fig. 2).

Bibliography

1. Choplin RH, Buckwalter KH, Rydberg J et al (2004) CT with 3D rendering of the foot and ankle: technique, normal anatomy and disease. Radiographics 24:343–356
2. Van Fleet TA, Bach B Jr (1994) Injuries to the acromioclavicular joint. Diagnosis and management. Orthop Rev Feb 23(2):123–129
3. Hunter JC, Escobedo EM, Wilson AJ et al (1997) MR imaging of clinically suspected scaphoid fractures. Am J Roentgenol 168 (5):1287–1293
4. Roberts CS, Beck DJ, Heinsen J et al (2002) Review article Diagnostic Ultrasonography: Applications in orthopedic surgery. Clin Orthop Res 401:248–264
5. Rogers LF (2002) Radiology of Skeletal Trauma. 3rd edn. Churchill Livingston, New York
6. Haapamaki V, Kiuru MJ, Koskinen SK (2004) Multidetector CT in shoulder fractures. Emerg Radiol 11:89–94

Fractures, Stress

David Malfair
UCSF, San Francisco, USA
dmalfair@hotmail.com

Synonyms and Definitions

Stress fracture: Injury that occurs secondary to repetitive stress over a period of time. Stress fractures can be further classified as fatigue and insufficiency fractures.

Fatigue fracture: Injury that occurs in normal bones of healthy subjects secondary to an abnormal repetitive stress.

Insufficiency fracture: Injury that occurs when normal repetitive stress is placed on abnormal bone with decreased elasticity.

Pathology/Histopathology

Bone must be strong enough to withstand both acute and repetitive forces. Repetitive stress above a certain threshold induces a reparative response in bone. This remodeling response is initially resorptive in nature with decreased mineral density before an overall increase in cortical thickness and medullary bone strength. During this early reparative phase, bone is more susceptible to trauma. Cyclic forces of sufficient magnitude and periodicity may create microfractures of cancellous bone at this time. With continued activity, the repetitive stress overwhelms the healing response and progresses to macroscopic stress fractures.

This mechanism of injury is similar for both fatigue fractures and insufficiency fractures. In fatigue fractures, the force is large enough to overwhelm the normal healing response of bone. In insufficiency fractures, the bone lacks the strength, elasticity, and capacity for healing to respond to a normal repetitive force.

Clinical Presentation

Epidemiology

Fatigue fractures generally occur in athletes who initiate an intensive training program or change an existing regimen. Females are more prone to stress fractures than men in studies of army recruits (4). Patients with small body-mass index (BMI) ratio and deconditioned athletes are also at higher risk. No racial predilection has been shown.

The majority of fatigue fractures occur in the lower extremity. Runners and new army recruits suffer from the highest incidence of lower extremity fatigue fractures. Upper extremity fatigue fractures are more unusual and tend to occur in specialized athletes (Table 1).

Insufficiency fractures occur in patients with abnormal bone. Risk factors include osteoporosis, rheumatoid arthritis, and renal osteodystrophy. Iatrogenic factors such as radiation and medications such as corticosteroids are other common etiologies. Insufficiency fractures most commonly occur in the pelvic ring and lower extremity.

History

Fatigue fractures can be difficult to diagnose and a delay in appropriate management is not uncommon. In almost every instance, there is an increase in the level of physical activity. The onset of symptoms is gradual over several weeks. Most stress fractures occur between 2 to 8 weeks after increased exercise. Pain is the most common symptom. It occurs with activity and is relieved with rest. With continued activity discomfort is more severe, occurs more quickly and persists at rest. Local tenderness and edema are often noted on exam.

Patients with insufficiency fractures often present with nonspecific pain or difficulty in mobilization. Comorbidities such as arthritis, cancer, medications can also cloud the clinical diagnosis. These fractures are often discovered incidentally on imaging techniques.

Fractures, Stress. Table 1 Common stress fractures and related sports activities

Coracoid of scapula	Trapshooting
Distal humerus	Pitching
Olecranon	Pitching, javelin
Ulnar diaphysis	Wheelchair, crutches
Hook of hamate	Racket sports
Ribs	Rowing, backpack, golf
Sacrum	Marching
Obturator ring	Bowling, gymnastics
Proximal femur	Ballet, marching, gymnastics
Patella	Hurdling
Distal femur	Running
Tibia	Running
Proximal fibula	Jumping, parachuting
Distal fibula	Running
Navicular	Marching, running
Calcaneus	Jumping, prolonged standing
Metatarsal shaft	Marching, running, prolonged standing
Sesamoids of metatarsals	Prolonged standing

Source: Adapted from Resnick D, Goergen T, Pathria MN (1996) In: Resnick D (ed) Bone and Joint Imaging, 2nd edn. WB Saunders, Philadelphia, p 723

Location

Stress fractures occur in almost any bone due to a variety of activities. (Table 1) Several of the most common sites deserve special attention.

Pars Interarticularis

► *Spondylolysis* refers to a spectrum of abnormalities involving the pars interarticularis and occurs with a prevalence of 6%. Stress fractures are the most common etiology of spondylolysis. These injuries usually occur in childhood, most frequently in Caucasian males. The incidence is increased with certain activities such as gymnastics, diving, and weightlifting. Ninety percent of these injuries occur at the L5 vertebral level with most of

the remainder found at L4. The majority of patients are asymptomatic. Some patients present with nonspecific low back pain exacerbated by activity. Frequently, individuals with stress fractures of the pars interarticularis progress to complete fracture and nonunion. The non-united pars defect is known as a spondylolytic defect. A minority of patients with spondylolysis will progress to spondylolysthesis, anterior translation of the vertebral body secondary to bilateral pars defects.

Pelvis

Insufficiency fractures are most commonly found in the pelvis. Women with osteoporosis or radiation treatment are most at risk. Fatigue fractures can also occur in the pelvis in military recruits and female runners. The majority of stress injuries involving the pelvic ring occur in the sacrum and pubic rami. Stress fractures of the sacrum demonstrate a parallel orientation to the sacroiliac joint. They are often bilateral and frequently associated with additional stress fractures in the proximal femora and pubic rami. Delay in diagnosis is common due to insensitivity of radiographs and presentation with nonspecific groin and or back pain.

Proximal Femur

Stress fractures of the femoral neck can be classified as tensile or compressive. The compressive stress fractures occur in the medial aspect of the femoral neck, involving the compressive trabeculae. These injuries are usually stable and are treated conservatively (Fig. 1). Tensile stress fractures occur at the midpoint of the lateral aspect of the femoral neck and are generally treated with internal fixation. Delay in diagnosis or treatment of these fractures can frequently lead to avascular necrosis of the femoral head, nonunion, or varus deformity. Some authors advocate conservative treatment for small or very proximal tensile stress fractures.

Tibia

Stress injuries have many manifestations in the tibia and usually occur in runners or military recruits. Stress fractures most commonly involve the posterior aspect of the proximal tibia. ►Shin splints are defined as a stress reaction of the periosteum of the posteromedial aspect of the tibia. Stress fractures may also occur in the medial aspect of the middiaphysis of the tibia. These types of fractures are treated with conservative management. Atypical stress fractures of the tibia include longitudinal stress fractures and anterior stress fractures of the tibia (Fig. 2). These rare but important subset of tibia fractures are difficult to treat and may progress to complete fracture.

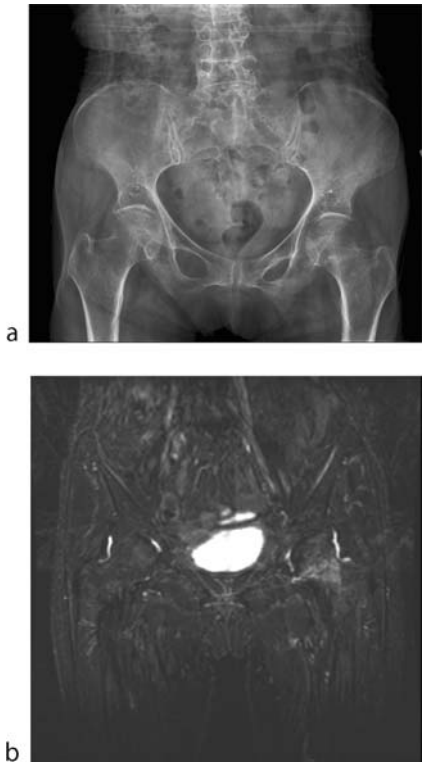

Fractures, Stress. Figure 1 AP radiograph (a) of the pelvis demonstrates subtle sclerosis over left femoral neck. Coronal STIR MR image (b) shows extensive low signal stress fracture through the medial femoral neck surrounded by high signal edema. The severity of this stress injury necessitated percutaneous pinning.

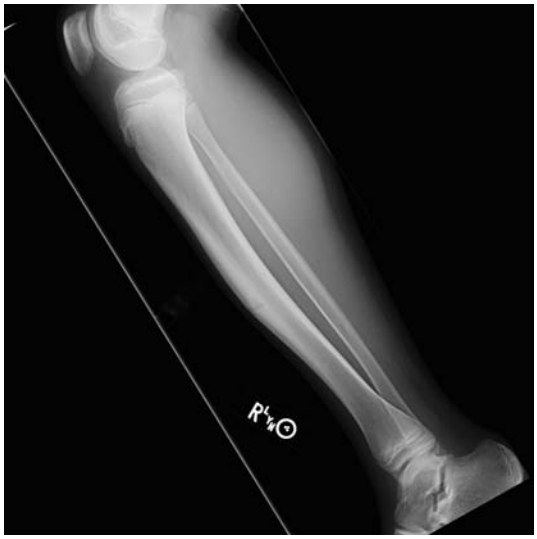

Fractures, Stress. Figure 2 Lateral radiograph of the tibia demonstrates horizontal lucency in the anterior cortex of the tibial diaphysis diagnostic of a stress fracture.

Imaging

Radiography

Overall, the sensitivity of plain films is poor, calculated at 30% in most series. Plain films examination is usually within normal limits with the onset of symptoms. Findings are first seen 2–3 weeks after onset of symptoms (3). The earliest radiographic finding of a cortical stress fracture is diminished radiodensity termed the gray cortex. More commonly, stress fractures are discovered as a transverse/oblique lucency of the cortex with subtle fluffy periosteal reaction. Increased new bone formation may preclude visualization of the fracture and simulate an osteoid osteoma or infection. Stress fractures in cancellous bone are more likely to present with focal sclerosis representing condensation of trabeculae. With healing, sclerosis becomes more prominent in stress fractures of all locations.

Computed Tomography

The evolution of multislice CT with improved spatial resolution and higher quality reformations has increased the accuracy of this modality in the identification and characterization of stress fractures. CT demonstrates excellent sensitivity and specificity for cortical stress fractures. Early stress injuries are characterized by small resorption cavities and osteopenia in the cortex. More advanced stress fractures demonstrate a linear lucency. Periosteal and endosteal bony proliferation is characteristically seen in healing lesions. CT is insensitive for medullary stress injuries, which present as focal areas of sclerosis.

MR

MR is a highly accurate imaging method in the assessment of stress injuries. An early stress response demonstrates high T2-weighted signal within the medullary cavity or cortex. Progression to a stress fracture results in the characteristic appearance of a low signal intensity, transverse linear band on T1- and T2-weighted images. Bone edema surrounding the fracture line demonstrates indistinct margins. Periosteal edema is best identified on STIR sequences and may be the only sign of certain stress injury.

Nuclear Medicine

Bone scintigraphy demonstrates excellent sensitivity but limited specificity in detecting stress fractures. These injuries demonstrate increased activity on the blood flow and blood pool images with increased uptake on the delayed phase. Single photon emission CT (SPECT) increases sensitivity and allows three-dimensional localization of stress fractures.

Diagnosis

In patients with characteristic findings on radiographs and consistent clinical presentation, a stress fracture may be confidently diagnosed. If the radiographs are normal or atypical, MR or bone scintigraphy is recommended. MR imaging is favored by many authors because of its increased specificity and ability to diagnose other soft-tissue ailments (2). CT is increasingly helpful to problem solve and further characterize abnormalities found on MR and nuclear medicine studies.

The imaging differential for stress fractures includes osteoid osteomas, infection, Ewing's sarcoma, and pathological fractures. These entities are best differentiated clinically. The linear lucency of a stress fracture can be differentiated from the oval nidus of an osteoid osteoma on MR and CT imaging. Infection usually demonstrates more widespread uptake on delayed bone scan compared to the focal uptake of a stress fracture. A healing stress fracture can exhibit some features of Ewing's sarcoma. Lack of necrosis, indistinct margins of edema and visualized fracture line on MR favor a diagnosis of stress fracture. In oncology patients, an injury may represent a pathological fracture through a metastasis or an insufficiency fracture from radiation or osteoporosis. T1-weighted MR images are most helpful in demonstrating a low signal mass in the bone marrow of a pathologic fracture (1). The presence of endosteal scalloping and marked muscle edema supports the diagnosis of a pathologic fracture. Sometimes MRI may not show the fracture line but only edema, in particular in the pelvis/sacrum in postmenopausal females with osteoporosis and chronic back pain, and thus a tumor may be suspected. In these cases thin section CT may be useful to show the fracture line and reveal the diagnosis. Alternatively, in difficult cases, interval follow-up studies may also be useful.

Bibliography

1. Fayad L, Kamel I, Kawamoto S et al (2005) Distinguishing stress fractures from pathological fractures: a multimodality approach. Skeletal Radiol 34:245–259
2. Gaeta M, Minutoli F, Scribano E et al (2005) CT and MR imaging in athletes with early stress injuries: Comparison with bone scintigraphy and emphasis on cortical abnormalities. Radiology 235:553–561
3. Lassus J, Tulikoura I, Konttinen Y et al (2002) Bone stress injuries in the lower extremity: a review. Acta Orthop Scand 73(3):359–368

4. Kiura MJ, Pihlajamaki HK, Ahovuo JA (2003) Fatigue stress injuries of the pelvic bones and proximal femur: evaluation with MR imaging. Eur Radiol 13(3):605–611
5. Resnick D, Goergen T, Pathria MN (1996) In: Resnick D (ed) Bone and Joint Imaging. 2nd edn.WB Saunders, Philadelphia, p 723

Free Fragment

A free fragment is a fragment of disk that has separated from the disk of origin.

▶Herniation, Intervertebral Disk

Frequency-Domain Photon Migration

▶Optical Tomography

Fulminant Hepatitis

Submassive to massive hepatic necrosis progressing from onset of symptoms to hepatic encephalopathy within 2 to 3 weeks is called fulminant hepatitis or fulminant hepatic failure. A course extending up to 3 months is called hepatic subfulminant failure. It is quite rare. The most common causes are fulminant viral hepatitis, drug toxicity (acetaminophen, isoniazid, antidepressant), chemical toxicity (mycotoxins of the mushroom *Amanita phalloides*), ischemia or shock. The necrosis may involve the entire liver or only random areas. A lobe may be spared or patchy necrotic areas may be dispersed throughout the liver. Within a week from the onset of necrosis, hepatocellular regeneration occurs. The evolution is variable and depends on the age of the patient and the previous status of the liver. The clinical scenario is dominated by jaundice, encephalopathy, coagulopathy and bleeding, renal failure, cardiovascular failure.

▶Hepatitis

Functional Cysts

An ovarian cysts is a sac filled with fluid or a semisolid material within an ovary. Functional ovarian cysts are the most common type of cysts in the ovary. The represent physiologic, not-disease-related cysts and occur as a normal process of ovulation usually disappearing within 8–12 weeks without treatment. Women who are past menopause almost never have functional ovarian cysts.

Functional Magnetic Resonance Imaging

An MRI technique that is used to visualize neuronal activity indirectly during the performance of specific tasks, using the blood oxygenation level dependent contrast.

▶Brain, Functional Imaging

Functional Renal Imaging

Michel Claudon, Damien Mandry
Department of Radiology, Childrens Hospital, Nancy University Hospital, Vandoeuvre les Nancy, France
m.claudon@chu-nancy.fr

Definition

Functional imaging is intended not only to depict anatomy and morphological anomalies but also to evaluate organ function. It is possible to

- Perform a visual observation
- Calculate some semiquantitative parameters
- Calculate absolute values.

Renal function involves at least two successive physiological processes: glomerular filtration (which depends on the number of nephrons and on blood perfusion) and reabsorption/secretion in the tubules. The functional unit of the kidney is the nephron; each kidney contains about 1.2 million nephrons.

Renal functional imaging has developed for a few reasons. First, the kidney is a paired and symmetric organ. Thus, visual comparison from one side to the other is easy. Second, due to recent technical improvements, the kidneys can be studied with high temporal and spatial resolution, allowing evaluation of blood perfusion, for instance. Other methods have failed to precisely

determine renal function; indeed, they are based on the glomerular clearance of a substance, usually creatinine or inulin. However, because performing this measurement is constraining, creatinine clearance (Cl_{Cr}) is usually roughly estimated by the Cockroft and Gault formula:

$$\left(Cl_{Cr} = \frac{(140 - age) \times BM \times GF}{P_{Cr}}\right),$$

where *BM* is the body mass (kg), *GF* is a gender correction factor (male:1.23, female:1.04), and *P*cr is the plasmatic creatinine rate (μmol/L). For many reasons, this value is underestimated in the elderly, and what is more troublesome is that this value remains normal until at least 50% of the nephrons are inefficient, leading to late diagnosis of renal insufficiency. What emphasizes the role of imaging is that nonspecific contrast media can be used as glomerular filtration rate (GFR) tracers.

Renal Anatomy and Physiology

Two layers compose the renal parenchyma. The cortex, containing the glomerulus, is the more external one and is comprised of the glomerulus, the proximal and distal convoluted tubules, and the beginning of the collecting ducts. Renal blood flow (RBF) represents about 25% of the cardiac blood flow, corresponding to 1.2 L/min. Eighty percent of this RBF is filtrated in the cortex through the glomerulus to form the primary urine, explaining the vascular phase depicted in imaging with high temporal resolution.

The internal layer corresponds to the medulla, which is constituted by the loops of Henle and the distal parts of the collecting ducts. Urine concentration increases as it advances through this layer.

Ultrasonography

Since the development of contrast media, the possibilities of ultrasonography (US) in functional imaging have improved and add to the Doppler techniques that have been used for years in renal imaging. These contrast media are purely intravascular; this means they have no interstitial diffusion and are not filtered through the glomerulus. Therefore, they cannot be used to measure the GFR. But this method allows evaluation of renal perfusion, including regional blood volume and flow, in different pathologic conditions such as renal artery stenosis and chronic obstruction. However, absolute quantification remains complicated because of the numerous parameters and adjustments, and exploration is still limited to a single slice or to a small volume.

Nuclear Medicine

Nuclear medicine (1) remains the reference method for quantifying the GFR or evaluating split function. Different tracers are available, allowing evaluation of the different processes leading to urine formation. First, the most widely used tracer of GFR is DTPA labeled with ^{99m}Tc; 51Cr-EDTA is another GFR tracer, but because of the low energy of the emitted photons, it can be detected only in blood and urine samples. Second, tracers excreted by the tubules help measure RBF because RBF is the ratio between clearance, which is measured, and extraction fraction, which is known. These tracers involve analogs of the hippuric acid—paraaminohippuric acid, orthoiodohipuric acid—labeled with ^{123}I or ^{131}I, which are filtrated by the glomerulus (about 20%), secreted by the tubules (80%), and labeled with mercaptoacetyltriglycine (MAG3). DMSA labeled with ^{99m}Tc is used to measure renal volume by making images in different planes 3 h after the injection, as it is not excreted. This radiopharmaceutical is also useful for measuring split function because the ratio of activity measured in each kidney, after correction for background activity, corresponds to split function.

Dynamic imaging protocols usually involve different phases: acquisition of 60 one-second images to observe the vascular phase, and follow-up of the medullar concentration and excretion during 20–45 min, sensitized by injection of furosemide. Renal perfusion is calculated from the vascular phase by dividing either the upslope of the kidney by that of the aorta (Kirchner index) or the area under the curves (Hilson index). After the vascular peak, activity continues to increase until a peak preceding excretion. From this second part of the curve, split function can also be achieved. Indeed, if correction for background activity and for each kidney volume is applied, it can be derived from the ratio either of the area under the curve or the upslope between 1 and 3 min after injection. Another method is based on the Patlak-Rutland method and is described in the section on computed tomography (CT).

Absolute quantification of the GFR is better achieved by analyzing consecutive blood and urine samples.

Iodinated Contrast Media and Gadolinium Chelates

After intravenous injection, these clinically available contrast media, known as nonspecific agents, have an unrestricted interstitial diffusion and are freely filtered through the glomerulus without secretion or reabsorption by the tubule. Thus, they are suitable for measuring the GFR. Indeed, some authors have used these contrast media to measure GFR by measuring their concentration in blood and urine samples in the same way as measuring

F

clearance of inulin or creatinine. GFR (mL/min) can then be calculated: GFR = $U_t \times V_t/(S_{t-1} + S_t)$, where t is the time of the collected sample, V_t is the urine flow rate (mL/min), and U_t and S_t are, respectively, the urine and serum concentrations of the contrast medium.

Intravenous Urography

Intravenous urography was the first renal functional imaging technique, but it provides only some basic physiological data that add to morphologic data.

Abdominal X-rays are performed before and at various times after intravenous injection of an iodinated contrast medium (usually at the end of injection and at 4, 8, 12, and 20 min).

Two phases of interest about kidneys are distinguished:

1. Nephrographic: This phrase begins with the arrival of the contrast medium in the cortex (vascular nephrogram), which lasts only a few seconds, followed by the concentration of the contrast medium in the medulla, which reaches its maximum between 5 and 10 min after injection in normal kidneys before wash-out.
2. Urographic: This phase begins about 2 min after injection, when the contrast medium is excreted in the renal calyces and pelvis.

Functional evaluation is therefore limited to a visual appreciation of a delayed nephrogram and/or urogram, without any specificity (renal artery stenosis, chronic obstruction).

Computed Tomography

Since the advent of multislice CT and the possibility to repeat the same acquisition in a very short time, the role of intravenous urography has considerably diminished. Indeed, the same observations can be made with CT, and the renal parenchyma can be directly studied (2).

CT also allows quantitative studies because the attenuation of X-ray beams is well correlated with concentration of the contrast medium. Thus, a Patlak-derived method is based on a two-compartmental model. The y-axis corresponds to the comparison between the evolution of the attenuation in regions of interest placed in the aorta (A) and in the kidney (K) (K(t)/A(t)), when a normalized time is on the x-axis $\left(\int_0^t A(t)/A(t)\right)$ (3). The clearance corresponds to the slope of this line, and the fractional vascular volume corresponds to the y-axis intercept.

However, two major drawbacks limit the use of this technique on a routine basis. First, the use of iodinated contrast media may worsen a preexisting renal insufficiency, but this risk is reduced by the small amount of contrast medium injected and the use of nonionic low osmolar contrast media. Second, these measurements are associated with a high radiation dose because of the numerous acquisitions required.

Magnetic Resonance Imaging

Magnetic resonance imaging (MRI) seems to be the most challenging technique for nuclear medicine in renal functional imaging, becoming a one-stop-shop examination by combining this new approach with the high spatial resolution of morphologic imaging provided by MRI (Fig. 1) (4). In fact, it allows achievement of numerous functional parameters, including renal blood volume and flow, GFR, and tubular function (5).

But routine use of MRI is limited by some difficulties. Some are common to all imaging techniques regarding kidneys: their intraabdominal situation results in respiratory motions between two acquisitions in breath-hold or if the acquisition lasts too long, and motion artifacts created by digestive peristalsis. Therefore, many research teams are working on these problems. Other difficulties are specific to MRI: the relationship between signal intensity and the concentration of the contrast medium is very complicated because it depends on the properties of the tissue (T1, T2) and of the contrast medium (relaxivities r1 and r2), which also vary with the temperature and composition of the organ or with the sequence used. Thus, conversion of signal intensities into concentrations based on phantom studies is preferable.

Renal Blood Volume and Flow

Evaluation of renal perfusion is particularly interesting in renal artery stenosis, in diseases with renal microvasculopathy, or in estimation of effects of treatment.

Blood flow in the renal arteries can be measured as in any other artery by using a cine-phase contrast sequence with no contrast agent, but the accuracy of this method is decreased because the vessels are small, and because their course is not a straight line, a partial-volume effect is induced. Signs of renal artery stenosis observed with this method are similar to those noted with Doppler ultrasonography: an early systolic peak decreases in moderate stenosis, and there is a delay in time to maximum systole. Arterial spin labeling is another method without contrast media, but the *in vivo* accuracy of this technique has yet to be demonstrated.

Perfusion parameters can also be evaluated using methods with contrast agents; this is known as dynamic contrast-enhanced imaging. This requires a bolus

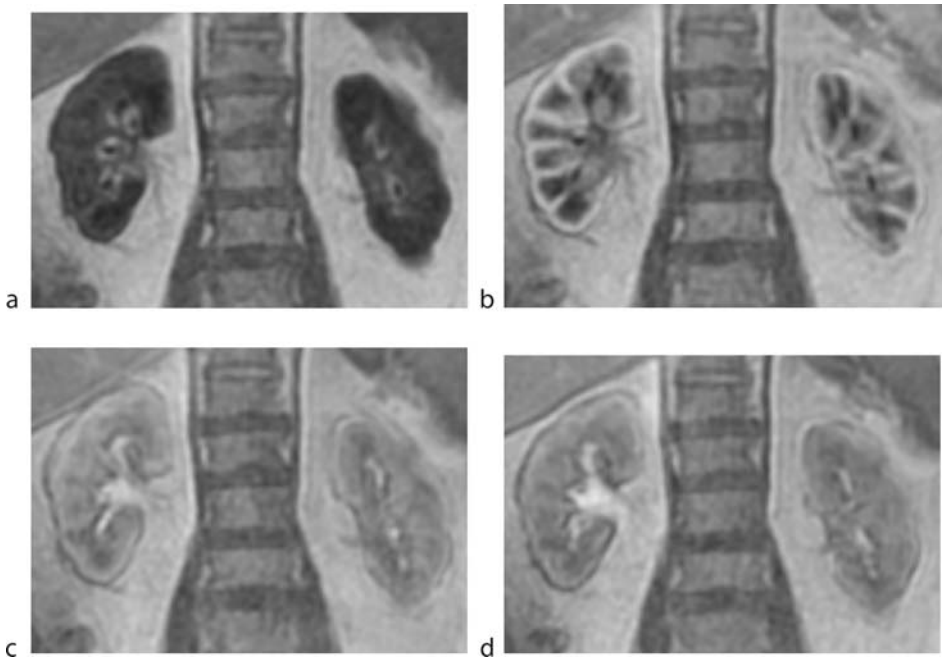

Functional Renal Imaging. Figure 1 Characteristic MR images before (a) and after intra-venous injection of a gadolinium chelate showing the vascular nephrogram (end of vascular phase, b), the nephrogram (urine concentration in the medulla, c) and the urogram (urine excretion in the calyces and pelvis, d). These are similar with CT.

injection and a high temporal resolution, preferably below 1.5 sec, which can be achieved with fast acquisition techniques.

Signal–time curves are derived from regions of interest placed in the aorta and kidney. Various mathematic models have been evaluated; the choice of the appropriate one depends on the contrast agent used. Indeed, clinically available gadolinium compounds have an unlimited interstitial diffusion and are freely filtered through the glomerulus, theoretically requiring resort to a three-compartment model—notwithstanding that this third compartment, representing less than 10% of renal parenchyma, is usually neglected.

Other gadolinium chelates, known as rapid-clearance blood pool agents, have a higher molecular weight that limits their interstitial diffusion without compromising their glomerular filtration; thus, use of a two-compartmental model is possible without making any assumption. Moreover, conversion of signal intensities into concentration is easier because lower doses of gadolinium are injected thanks to their properties. With these gadolinium chelates, T1-weighted sequences are used, such as fast gradient echo with spoiler. T2-weighted sequences are used with ultrasmall particles of iron oxides (USPIO), which have no interstitial diffusion and are not excreted by the kidney. Thus, the central volume principle of Stewart and Hamilton can be applied: RBF = RBV× MTT, where RBF is the renal blood flow (mL/min/100 g), RBV is the renal blood volume, and MTT is the mean transit time. This is the way cerebral perfusion is evaluated.

Glomerular Filtration Rate

Evaluating or measuring GFR requires injecting a contrast medium that is excreted by the kidney. Semiquantitative approaches based on T1-weighted sequences have shown similar results to renal scintigraphy for parameters measured on signal–time curves, such as vascular upslope, time to peak, and area under the curve. Rohrschneider et al demonstrated that similar results could be obtained between dynamic T1-weighted contrast-enhanced MRI and scintigraphy in measuring split function in normal and pathologic conditions (Fig. 2) (6). Parenchymal signal–time curves begin with a vascular upslope corresponding to the arrival of the contrast medium in the vessels and the glomerulus, followed by a brief decrease and then by a second upslope corresponding to glomerular filtration and tubular function, until a peak preceding excretion. Once again, these curves can be converted into concentration–time curves thanks to phantom studies, allowing calculation of the GFR in the same way as is done with CT. However, accurate conversion of

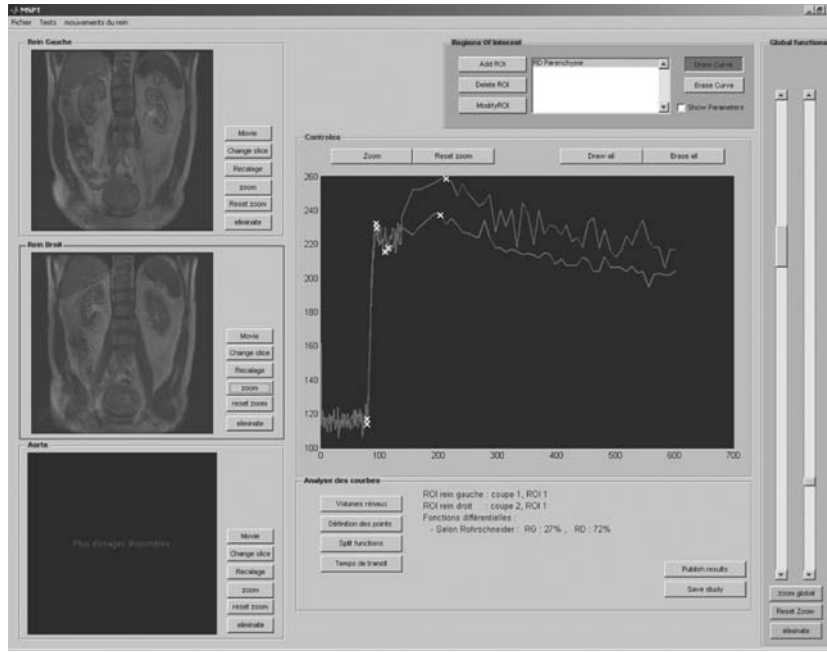

Functional Renal Imaging. Figure 2 Screen capture from dedicated software designed to analyze split renal function using Rohrschneider's technique (From Grenier N, Basseau F, Ries M et al (2003) Functional MRI of the kidney. Abdom Imaging 28:164–175). ROIs are placed on the right (middle row) and left (upper row) kidneys. T (to be suppressed) Signs of nephropathy are more marked on the latter with decreased volume of parenchyma and sinus lipomatosis. Area under each curve during concentration upslope is calculated, and split renal function calculated by taken into account the ROI surface. In that case, area under the curve from the left kidney ROI (lower curve) is much smaller than that of the curve form the right-kidney ROI (upper curve), whereas time-to-peak are similar; indeed, left kidney participates only for 27% of the whole renal function. (Courtesy Pr Felblinger, IADI, INSERM Region Lorraine Universite de Nancy 1, Nancy, France)

signal intensities into gadolinium concentration remains a challenge. Thus, it would be preferable to work on 1/T1 measurements that are better correlated with the concentration than T1, but sequences that are fast enough are not yet available.

Bibliography

1. Hilson AJ (2003) Functional renal imaging with nuclear medicine. Abdom Imaging 28:176–179
2. Blomley MJ, Dawson P (1996) Review article: the quantification of renal function with enhanced computed tomography. Br J Radiol 69:989–995
3. Prigent A Piepsz A (eds) (2005) Functional Imaging in Nephro-Urology. Taylor & Francis, London
4. Bennett HF, Li D (1997) MR imaging of renal function. Magn Reson Imaging Clin N Am 5:107–126
5. Grenier N, Basseau F, Ries M et al (2003) Functional MRI of the kidney. Abdom Imaging 28:164–175
6. Rohrschneider WK, Haufe S, Wiesel M et al (2002) Functional and morphologic evaluation of congenital urinary tract dilatation by using combined static-dynamic MR urography: findings in kidneys with a single collecting system. Radiology 224:683–694

Functional Ventilation MRI

MRI technique for the assessment of lung ventilation with use of inhaled contrast aerosols, oxygen, hyper-polarised noble gases (Helium-3, Xenon-129), and fluorinated gases (sulphur-hexafluoride).

▶Cystic Fibrosis

Fundoplication

This antireflux procedure is indicated in the surgical treatment of gastroesophageal reflux. The fundus is wrapped posteriorly around the distal esophagus and lower esophageal sphincter. The fundus is sutured anteriorly, making a complete 360° wrap (Nissen

fundoplication) or incomplete 270° wrap (Toupet fundoplication) that lies below the level of the diaphragm.
▶Stomach and Duodenum in Adults Postoperative

Fungal, Abscess, Hepatic

Fungal abscesses are most often caused by Candida albicans, and they occur in immunocompromised individuals. They are a manifestation of disseminated fungal disease. Microabscesses often also involve the spleen. Hepatic abscesses caused by Cryptococcus infection and Aspergillus species have also been reported. Hepatic fungal microabscesses in immunosuppressed patients have a miliary distribution and appear as multiple small, often subcentimetric, lesions scattered throughout the liver. At US, four patterns of hepatosplenic candidiasis have been described. The US appearance of hepatic candidiasis in the initial phase is pathognomonic: the "wheel-within-a-wheel" sign consists in a central hypoechoic nidus of necrosis containing fungi surrounded by a hyperechoic zone represented by inflammatory cells and an outer hypoechoic halo corresponding to fibrosis. The second pattern has a "bull's-eye" appearance, due to the presence of a central echogenic area surrounded by a hypoechoic rim. The third pattern is the most commonly encountered at US and consists of uniformly hypoechoic nodules; however, it is the least specific. After therapy the lesions tend to decrease in size and increase in echogenicity, leading to the fourth pattern which consists of echogenic foci with variable degrees of posterior acoustic shadowing. At CT, fungal abscesses appear as multiple small, round lesions distributed in both lobes with low density on unenhanced and enhanced scans, but are better visualized after contrast material administration. These microabscesses usually show central enhancement, although peripheral enhancement may occur. At MRI, fungal abscesses show variable signal intensity. The untreated nodules are minimally hypointense on T1-weighted images before and after administration of contrast material and hyperintense on T2-weighted images. Treated lesions appear mildly hyperintense both on T1- and T2-weighted images and show contrast enhancement. A dark ring is usually seen around these lesions with all sequences.
▶Abscess, Hepatic

Gallbladder Anomalies

Wide spectrum of gallbladder alterations including variation of number, location, size, and shape.

►Congenital Malformations, Liver and Biliary Tract

Gallbladder Cancer

►Neoplasms, Gallbladder

Gallbladder Neoplasms

►Neoplasms, Gallbladder

Gallert Carcinoma

►Carcinoma, Other, Invasive, Breast

Gallstone, Ileus

Mechanical bowel obstruction (either complete or incomplete) caused by impaction of large gallstones. These may erode the gallbladder wall fistulizing and migrating in the adjacent viscus (most frequently duodenum). This condition is observed in patients with recurrent episodes of acute cholecystitis or chronic cholecystitis. Most commonly, the stone impacts at the ligament of Treitz, at the ileal cecal valve, or at any stricture of the small bowel.

►Cholecystitis

Gallstones

Thomas Helmberger[1], Carlo Bartolozzi[2], Chiara Franchini[2]
[1]Clinic of Radiology and Nuclear medicine, University Hospitals Schleswig-Holstein, Campus Luebeck, Germany
[2]Department of Diagnostic and Interventional Radiology, University of Pisa, Italy
thomas.helmberger@uni-luebeck.de
bartolozzi@do.med.unipi.it

Synonyms

Biliary lithiasis; Biliary stones

Definition

Solid particles that form from bile.

Pathology and Histopathology

Gallstones are a relatively common disorder. Women are more frequently affected than men. The prevalence increases with age in both sexes. There are two types of gallstones: cholesterol stones and pigment stones. About 80% of gallstones are mainly composed of cholesterol, with only a small percentage being pure cholesterol. Cholesterol stones often contain alternating layers of cholesterol crystals and mucin glycoproteins. The main component of pigment stones is calcium bilirubinate. Pigment stones are divided into black and brown stones. Black pigment stones consist of polymers of bilirubin, with large amounts of mucin glycoproteins, are hard and are more common in patients with cirrhosis or chronic hemolytic conditions. Brown pigment stones are made up of calcium salts of unconjugated bilirubin, with variable amounts of protein and cholesterol, and are friable; they primarily originate within the intrahepatic bile ducts and are usually associated with infection. They often occur in

Asians (1). Cholesterol is virtually insoluble in aqueous solutions, but in bile it is made soluble by association with bile salts and phospholipids forming mixed micelles and vesicles. The pathogenesis of biliary stones is principally related to supersaturation of bile constituents. Stone formation most often results from increased biliary cholesterol concentration, but may also be due to decreased bile acid synthesis or a combination of both mechanisms (2). Gallbladder dysmotility probably plays a role, too. These factors may be aggravated by a genetic predisposition, diet, and an inactive lifestyle. Additional risk factors for cholelithiasis include obesity, diabetes, use of oral contraceptives, ileal disease, use of certain medications, and total parenteral nutrition (3).

In the majority of the cases, stones develop in the gallbladder (cholelithiasis); afterwards they can migrate into the bile duct. These bile duct stones are called secondary stones. However, more likely they cause bile stasis, which promotes their growth and the formation of additional primary bile duct stones. Biliary stones are also considered to be primary in the rare setting of gallbladder agenesis and in the case of bile duct stones that are diagnosed many years after cholecystectomy.

Gallstones can be of any size and number. Small stones are more likely to migrate and cause symptoms. Extremely tiny sand-like stones form the so-called ►biliary sludge.

The most common complication of cholelithiasis is acute cholecystitis, which occurs when a stone obstructs the cystic duct. Further complications of cholelithiasis include choledocholithiasis, acute pancreatitis, duodenitis, biliary fistula, gallstone ileus, and ►Mirizzi syndrome. Cholelithiasis is found in about two thirds of patients with gallbladder carcinoma and is frequently associated with chronic cholecystitis, suggesting that chronic irritation is a causative factor.

Clinical Aspects

Most patients with gallstones are asymptomatic. Typical symptoms include recurrent right upper quadrant or epigastric pain which can radiate to the angle of the scapula and the right shoulder. Biliary pain generally lasts several hours and is triggered by food intake. Sometimes the pain gets chronic. Patients with acute cholecystitis present with severe abdominal pain, nausea, vomiting, fever, and leukocytosis. Less commonly, gallstones migrate in the common bile duct and may cause pain, cholestasis, and cholangitis. A severe complication of gallstones is acute pancreatitis, due to obstruction of the main pancreatic duct. Sludge and microscopic stones may also cause acute pancreatitis (2).

Patients with intrahepatic stones generally have a prolonged history of recurrent complaints of abdominal pain, fever, chills, and jaundice (1).

Imaging

Gallbladder Stones

Plain radiography does not represent a useful tool in detecting gallstones, because only 15–20% are visible on plain radiographs, due to their calcium content. Oral cholecystography has been the only diagnostic tool for gallbladder lithiasis for decades. Currently, oral cholecystography is obsolete, while ultrasonography (US) is the method most often used to detect cholelithiasis and associated complications, such as acute cholecystitis (2, 3).

Oral cholecystography has a sensitivity close to that of US in detecting gallbladder stones and is even superior in determining the number and size of stones, which appear as filling defects within the opacified gallbladder; it is able to demonstrate cystic duct patency and to provide information about gallbladder contractility, evaluated after a fatty meal. However, US has the advantage of allowing adjacent organs to be explored, providing visualization of the gallbladder and its content, also when it is excluded on the cholecystograph, and being noninvasive. US also allows a functional evaluation of the contractility of the gallbladder after a fatty meal. The nonvisualization of the gallbladder on oral cholecystography may be due to absorption of contrast material through an inflamed gallbladder wall or due to obstruction of the cystic duct. Nevertheless, a normal gallbladder may fail to be visualized in the case of gastric outlet obstruction or poor absorption of the oral contrast agent by the gut (2).

Noninvasive US is the method of choice for the detection of gallstones, providing high sensitivity and accuracy (>95%). US is able to detect stones larger than 1–2 mm in diameter. Typically, gallstones appear as highly echogenic masses with a hypereflective echo from the anterior surface and a marked posterior acoustic shadowing. Usually, the mobility of gallstones can be demonstrated by repositioning the patient, although they may occasionally be adherent to the wall of the gallbladder. The presence of posterior acoustic shadowing is very specific because nonshadowing structures rarely represent gallstones. The finding of the so-called wall-echo-shadow triad is characteristic of a contracted gallbladder filled with stones. The wall of the gallbladder, next to the transducer, is echogenic; below this a thin, anechoic line of bile may be visible; finally, there is a highly echogenic line representing the surface of superficial stones with associated posterior shadowing. The deeper stones and the deeper gallbladder wall are not visible, being obscured by the acoustic shadow (3). In addition, US can rule out

other causes of right upper quadrant pain, can show associated bile duct dilatation, suggesting the presence of common bile duct stones, and can demonstrate signs of acute cholecystitis. US can also detect ▶biliary sludge in the gallbladder, which appears as hypoechoic material usually without acoustic shadowing, forming a layer in the dependent portion of the gallbladder and shifting slowly with positioning (Figs. 1–2) (2).

Computed tomography (CT), endoscopic retrograde cholangiopancreatography (ERCP), and magnetic resonance cholangiopancreatography (MRCP) play a minor role in the primary detection of gallbladder stones. Nevertheless, in studies performed for other reasons cholelithiasis is a common finding. Furthermore, these examinations may be necessary in the assessment of complications such as acute cholecystitis, pancreatitis, choledocholithiasis, and biliary obstruction (3).

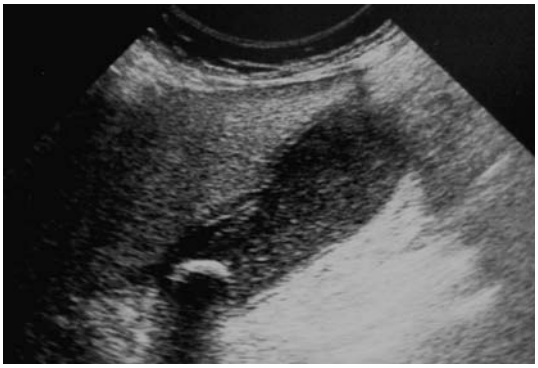

Gallstones. Figure 1 Gallbladder stone, sludge, and cholecystitis. Ultrasound demonstrates a large stone in the infundibulum typically appearing as a highly echogenic mass with a hypereflective echo from the anterior surface and a marked posterior acoustic shadowing. Biliary sludge appears as hypoechoic layer without acoustic shadowing. Inflamed gallbladder wall is thickened and shows a multilayered aspect.

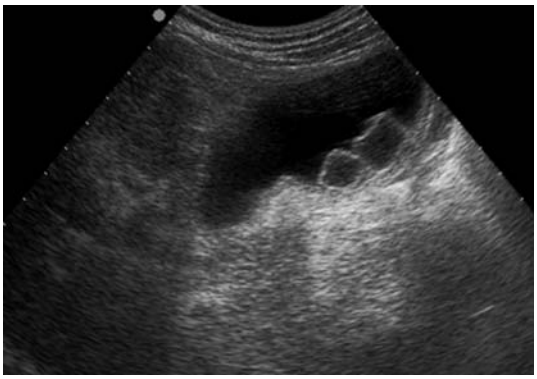

Gallstones. Figure 2 Cholesterol gallstones. At ultrasound, cholesterol stones in the gallbladder appear hypoechoic without posterior shadowing.

Extrahepatic Bile Duct Stones

The recognition of choledochal calculi before and after cholecystectomy for cholelithiasis is a crucial clinical issue. Common bile duct stones can be demonstrated at US, but this technique has low sensitivity. US can demonstrate dilatation of the common bile duct which may suggest choledocholithiasis; however, in patients after cholecystectomy, the biliary duct caliber is not a useful predictor of bile duct lithiasis since the diameter of the extrahepatic duct can rise up to 10 mm overtaking the reservoir function of the former gallbladder (Fig. 3). ERCP allows identification of choledochal stones, appearing as mobile, round, and filling defects, with high accuracy and offers the possibility of interventional removal of calculi. Nevertheless, ERCP is an invasive technique with a relatively high incidence of complications; currently, this procedure is performed solely with an interventional purpose. Purely diagnostic ERCP should be avoided by using less invasive diagnostic imaging modalities, such as MRCP, unenhanced spiral CT, or CT cholangiography with intravenously or orally administered contrast agents. Among these, MRCP is evolving as the most accepted technique, because it is noninvasive, without need for administration of contrast material, and generally provides excellent image quality. The sensitivity of MRCP in the diagnosis of choledocholithiasis is more than 90%. According to numerous studies, the diagnostic accuracy of MRCP for the evaluation of choledocholithiasis is comparable to that of ERCP (1, 3–5).

US has low sensitivity and specificity in demonstrating stones in the main bile duct, since the normal caliber

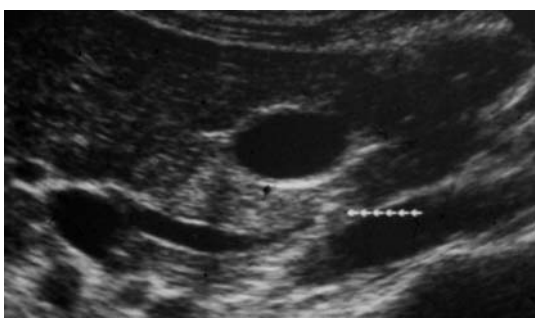

Gallstones. Figure 3 Extrahepatic bile duct stone. Ultrasound is able to detect very small calculi (few millimeters). Small stone (arrow) obstructing the main bile duct, which appears dilated above the level of blockage.

and the presence of meteorism may limit the display of the extrahepatic bile tract.

Spiral CT may be an adequate diagnostic alternative to MRCP in patients in whom MR is contraindicated. Unenhanced thin-section scans may demonstrate choledochal stones, especially if they are calcified. However, the sensitivity of this technique is limited by the high frequency of false-negative results in the case of stones which are isoattenuating to bile. CT cholangiography seems to be as sensitive as MRCP in depicting choledocholithiasis. The high attenuation of bile achieved with cholangiographic contrast agents increases the detection of stones, which appear as filling defects. The maximum intensity projection (MIP) algorithm is routinely used both for MRCP and for CT cholangiography. A limitation of CT cholangiography is the insufficient opacification of bile ducts that may occur in patients with elevated bilirubin levels or liver insufficiency (in general a contraindication for the application of cholangiographic contrast agents) (4).

A possible source of false-positive results at MRCP is the presence of intraductal air, which may be abundant in patients with biliary-enteric anastomoses or after ERCP. On MR images, air is hypointense and may mimic stones on MR cholangiograms acquired in a coronal or oblique plane. In these cases, axial images can solve the diagnostic problem because air is located in nondependent portions of the bile duct, whereas calculi tend to be located in dependent positions. CT in the axial acquisition plane offers advantages in such cases because the negative attenuation of air differs clearly from that of stones. Some limitations are common to both CT cholangiography and MR cholangiography. For example, filling defects such as sludge may be the source of false-positive interpretations and affect the specificity of both techniques (1, 4).

Intrahepatic Bile Duct Stones

US has a limited role in the evaluation of the intrahepatic biliary tree, which can only be visualized when dilated. Intrahepatic calculi may be visualized as strongly hyperechoic lesions with or without shadowing (Fig. 4).

Intrahepatic stones can be depicted on unenhanced CT, but the detection rate is not sufficient because pigmented stones are sometimes not sufficiently hyperattenuating to be visible on CT. Therefore, MRCP is currently the most suitable noninvasive modality in diagnosing intrahepatic biliary stones.

In particular, MRCP seems to be superior to ERCP. Opacification of peripheral intrahepatic bile ducts with ERCP may be difficult in patients with intrahepatic calculi because of the common association of severe ductal strictures. Forced injection of contrast material may be required, but this increases the risk of cholangitis. In addition, an air block may also be a factor in patients with intraductal air hindering adequate contrast injection. In contrast, MRCP is able to depict the entire biliary tract and is very accurate in the identification of intrahepatic stones and associated biliary strictures. MRCP can also detect other associated abnormalities, such as perihepatic biloma or free fluid in the perihepatic spaces. Furthermore, a study of the liver parenchyma with an adequate MR protocol can be performed in the same MRCP session in order to identify malignant processes that can be associated with intrahepatic stone disease (1). Percutaneous transhepatic cholangiography (PTC), performed by injecting contrast material after percutaneous catheterization of an intrahepatic bile duct, allows a good depiction of peripheral bile ducts, but it is an invasive procedure and is used in most centers only as an interventional procedure.

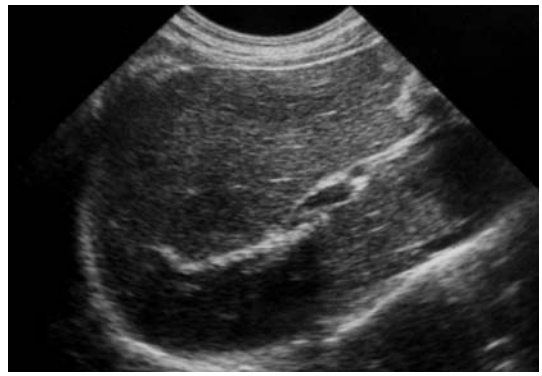

Gallstones. Figure 4 Intrahepatic bile duct stones. Ultrasound shows a line of strongly hyperechoic spots, corresponding to small stones impacted in the intrahepatic bile ducts.

Nuclear Medicine

Cholescintigraphy, performed with 99m-technetium-labeled iminodiacetic acid, which is excreted into the bile, has a high sensitivity and specificity for acute cholecystitis, but it cannot provide anatomical information and cannot identify gallstones (2). Since the diagnosis of acute cholecystitis in general combines clinical and US findings, nuclear medicine studies are no longer necessary.

Interventional Radiology

Cholecystectomy is the standard treatment for gallbladder stones; nevertheless, in selected cases interventional

radiology may be useful in the management of cholelithiasis. Several interventional procedures have been developed for the treatment of gallbladder stones. Among these, percutaneous cholecystostomy and percutaneous contact dissolution currently play a clinical role. Percutaneous cholecystostomy is usually performed in acute cholecystitis in patients at high surgical risk in order to obtain decompression of the gallbladder. Stone extraction may also be performed. US or fluoroscopy after orally administered contrast medium allows visualization of the gallbladder and guides the procedure (3). Cholesterol gallstones can be rapidly dissolved by direct instillation of solvents into the gallbladder through a transhepatic percutaneous catheter. Even if this procedure is usually performed under US guidance, severe complications including death due to systemic effects of the solvent agent are described (2).

Currently, ERCP should be performed only as an interventional procedure for removing common bile duct stones previously detected with noninvasive imaging techniques, mainly MRCP. The first interventional step is papillotomy or sphincterotomy, to widen the opening of the common bile duct into the duodenum by means of an electrocautery cutting instrument inserted into the papilla. Stones can subsequently be removed with balloons or baskets. Sphincterotomy may be complicated with perforation, pancreatitis (ca. 5%), cholangitis, and bleeding. Complications in sphincterotomy are particularly frequent if the common bile duct is not dilated. ERCP is often unsuccessful in removing stones larger than 2 cm in diameter from the common bile duct (2).

Radiological interventions also play a role in the treatment of intrahepatic stones, particularly in patients with clinical manifestations of cholangitis. After percutaneous drainage, stones can be removed by means of a small-caliber endoscope or using baskets under fluoroscopy guidance (1).

In complicated cases, rendezvous maneuvers combining radiological and endoscopic techniques can be helpful.

Diagnosis

US is the method of choice in the diagnosis of cholelithiasis and its associated complications, particularly acute cholecystitis (2, 3). However, among noninvasive techniques, MRCP is gaining wide acceptance and is becoming the modality of choice in the diagnosis of choledocholithiasis (4, 5). Furthermore, MRCP is currently the most suitable modality in diagnosing intrahepatic biliary stones (1).

Therefore, even if ERCP has been the standard of reference for the detection of common bile duct stones, this invasive procedure should currently be performed solely with an interventional purpose.

References

1. Kim TK, Kim BS, Kim JH et al (2002) Diagnosis of intrahepatic stones: superiority of MR cholangiopancreatography over endoscopic retrograde cholangiopancreatography. Am J Roentgenol 179 (2):429–434
2. Vakil N, Everbach EC, Knyrim K (1993) Pathogenesis and treatment of gallstones. N Engl J Med Jun 24; 328(25)1855
3. Bortoff GA, Chen MY, Ott DJ et al (2000) Gallbladder stones: imaging and intervention. Radiographics 20(3):751–766
4. Soto JA, Alvarez O, Munera F et al (2000) Diagnosing bile duct stones: comparison of unenhanced helical CT, oral contrast-enhanced CT cholangiography, and MR cholangiography. Am J Roentgenol 175(4):1127–1134
5. Kim JH, Kim MJ, Park SI et al (2002) MR cholangiography in symptomatic gallstones: diagnostic accuracy according to clinical risk group. Radiology 224(2):410–416

Gamma Camera

A gamma camera is a scintigraphic device that produces an image by simultaneous detection of radiation emitted from the object.

▶Scintigraphy

Gamna–Gandy Bodies

Gamna-Gandy bodies represent siderotic nodules within the spleen and can arise in patients with portal hypertension. They may be detected on T2-weighted images, as tiny hypo-intense nodules scattered throughout the splenic parenchyma. These nodules are pathognomonic of portal hypertension.

▶Portal Hypertension

Ganglion

Cystic soft tissue mass, containing myxoid degenerative fluid, no synovial lining.

▶Neoplasms, Soft Tissues, Benign

Ganglioneuroblastomas

A malignant neoplasm composed of nerve cells and mature ganglion cells. By many regarded as a fully differentiated neuroblastoma.
▶Neuroblastoma

Ganglioneuroma

A tumor containing ganglion cells.
▶Neuroblastoma

Gastric Inlet Patch

A patch of ectopic gastric mucosa in the upper oesophagus
▶Hernia, Hiatus in Adults

Gastric Ulcer

▶Ulcers, Peptic

Gastro-Oesophageal Reflux

The abnormal retrograde passage of stomach contents into the oesophagus.
▶Oesophageal Disease, Childhood
▶Hernia, Hiatus in Adults
▶Reflux, Gastroesophageal in Adults
▶Oesophageal Disease, Childhood

Gastro-oesophageal Reflux Disease

An abnormal frequency or amount of reflux of gastric contents into the oesophagus, accompanied by symptoms.
▶Hernia, Hiatus in Adults

Gastroesophageal Reflux Disease (GERD)

▶Oesophagitis

Gastrografin Enema

An enema performed with the contrast medium 'gastrografin' and almost exclusively performed in neonates with meconium ileus.
▶Occlusion, Bowel in Childhood

Gastrointestinal Stromal Tumor

They are rare soft tissue sarcomas of the GI tract accounting for up to 3% of all GI cancers. These tumors were previously considered to be of smooth muscle origin and labeled as benign leiomyomas or the malignant leiomyosarcoma. More recent studies indicate that only a minority of these tumors have the typical features of smooth muscle and the term gastrointestinal stromal tumor was introduced. Imatinib (a tyrosine kinase inhibitor) has significant impact in a number of these tumors and increases the treatment options either alone or combined with surgery.
▶Neoplasms, Gastroduodenal

Gastrointestinal Tract

Jean Michel Bruel
Service d'Imagerie Médicale Hôpital St. Éloi
CHU de Montpellier, Montpellier, France
jm-bruel@chu-montpellie fr

The radiology of the gastrointestinal (GI) tract is a part of gastrointestinal and abdominal radiology, which is one of the recognized subspecialty areas of radiology where the advances have been and are the greatest and fastest. These advances concern both the diagnostic and the

interventional imaging, and give GI imaging a profound impact on patient management.

In diagnostic imaging, gastrointestinal imaging has been focused for many years on barium studies, performing a highly precise, but indirect evaluation, by moulding (single contrast studies) or coating (double contrast studies) the endoluminal patterns of the bowel wall. Nowadays, if barium studies remain essential for evaluating the function of GI tract, the cross-sectional imaging techniques depict both the GI structures and the digestive tract surroundings; the improvement of 3D techniques results in the virtual endoscopy. In these conditions, the pattern approach of GI imaging has been greatly altered from an indirect analysis (filling defect and narrowing of the digestive lumen, projection of the lumen out of the GI wall, deformation of the lumen, increasing of well-defined peridigestive spaces…) to a direct evaluation of the segments of the alimentary tract (digestive lumen, GI wall itself and the peridigestive fat, vessels, lymph nodes, and organs).

Interventional imaging techniques become pivotal in current clinical conditions: pathological or microbiological studies after image-guided biopsy or sampling, drainage of peridigestive abscesses, digestive stenting.

Through the neck, chest, and abdomen, GI tract includes, in a cranio-caudal way:

- Pharynx and oesophagus
- Stomach and duodenum
- Small bowel including jejunum and ileum
- Colon and rectum

The GI tract surroundings are a main part of the anatomy of the digestive tract, especially within the peritoneal cavity where peritoneal reflections, ligaments, recesses, and mesenteries are basic to an understanding of the GI tract anatomy, inflammatory and neoplastic changes, and the spread and localization of the disease.

Imaging of the Gastrointestinal Tract: A Pattern Approach

The *location and gross morphology* of GI tract segments depend on the normal anatomy and variants. They may be altered by congenital (malrotation, duplication cysts, Meckel's diverticulum) or acquired abnormalities (hernias, bowel obstruction, postoperative appearance of the gut).

The main imaging pattern of GI tract abnormality is the *bowel wall thickening*. The criteria of this thickening need to be analyzed carefully: number, location, transition zones with the normal bowel wall, pattern of attenuation, degree of thickening, symmetric versus asymmetric thickening, focal versus segmental or diffuse involvement, ulcers, and perienteric abnormalities. A focal thickening may expand within the lumen or out of the bowel wall. A filling defect may be caused either by a lesion of the gastrointestinal wall expanding into the lumen or by an intraluminal structure.

A *local defect of the bowel wall* communicating with the lumen could affect only the inner layers of the bowel wall, or spread through all the layers within the mesenteric fat, the peritoneal cavity, or an adjacent organ. These defects may be demonstrated by their content: gas, or positive contrast after opacification either by barium or iodinated contrast media. Such defects could be related to a diverticulum or pseudodiverticulum, an ulcer, a perforation, a sinus tract, or a fistula.

Perienteric abnormalities concern the mesenteric fat, the ligaments and reflections of the peritoneum, the peritoneal cavity and its recesses, the mesenteric lymph nodes. These inflammatory or neoplastic abnormalities may be in reaction to a digestive tract lesion or related to a primitive disease of the peritoneum or mesenteries structures.

Esophageal and gastrointestinal motility disorders may be related to inefficient hypermotility, contractions and spasm, stasis and distention, aperistalsis. Distension may affect bowel loops proximally to an obstruction or be related to a loss of digestive wall contractility (localised ileus and intestinal pseudoobstruction). Abnormal contraction may cause a pseudoneoplastic thickening of the GI wall on nondynamic cross-sectional imaging, and is better evaluated by barium series. Esophageal and gastrointestinal motility disorders concern the swallowing disorders, the oesophageal motility disorders, the gastro-esophageal reflux, the GI tract distension, the colorectal function disorders.

Gastroschisis

A congenital defect of the abdominal wall musculature allowing abdominal contents to herniate outside the abdomen with no peritoneal covering.

▶GI Tract, Paediatric, Congenital Malformations

Gated-SPECT

Gated-single photon emission computed tomography (SPECT) is a technique in which the electrocardiographic signal is used as a trigger during image acquisition, giving the option to provide data with respect to global ejection fraction and regional wall motion and thickening in

addition to perfusion images. The combination of these results gives the clinician better information for optimal risk stratification.

▶Ischemic Heart Disease, Nuclear Medicine

Gaucher Disease

Lysosomal storage disease caused by lack of the enzyme glucocerebrosidase. Glucocerebrosides accumulate in the spleen. Hepatosplenomegaly is usually present, and splenic nodules are described (hyperechoic or hypoechoic).

▶Congenital Malformations, Splenic
▶Diffuse Infiltrative Disease, Hepatic

Gelatinous Carcinoma

▶Carcinoma, Other, Invasive, Breast

Gene Delivery System

▶Local Drug and Gene Delivery with Microbubbles

Gene-delivery System

A gene-delivery system consists of microbubble contrast agents usually with a lipid shell, containing genes in the form of oligodendronucleotides. After local destruction of the microbubbles, the gene fragments are incorporated into the nuclear DNA of the cells. Instead of genes, antisense molecules can be used to block the activity of endogenous genes. The transport of the nucleotides into the cells is facilitated by sonoporation, an effect causing the transient formation of micropores in the capillary vessels.

▶Contrast Media, Ultrasound, New Clinical Development

Gene Therapy

Gene therapy can be defined as the transfer of defined genetic material to specific target cells of a patient for preventing, altering, or treating of diseases.

▶Local Drug and Gene Delivery with Microbubbles

Genital Tract

Paolo Toma*, Claudio Granata, Anna Dell'Acqua
Department of Radiology, Giannina Gaslini Hospital for Sick Children, Genova, Italy
paolotoma@ospedale-gaslini.ge.it

Definitions

Nonneoplastic abnormalities of the male and female genital tract which are not caused by chromosomal conditions.

Pathology

Male Genital Organs

Cryptorchidism. At birth, undescended testes are found in 3% of term infants and in 33% of preterm newborns weighing less than 2,500 g. Testicular migration can stop anywhere along the course from the retroperitoneum to the scrotum. Cryptorchidism is thought to be caused by a disturbance of local factors or an anomaly of the hypothalamic-pituitary-testis axis. About 90% of undescended testes are located in the inguinal canal, with the remaining 10% located in the abdomen. An undescended testis has an increased risk of malignancy and can lead to infertility. Cryptorchidism may be bilateral in about 10% of cases. Very rarely, the missing testis is ectopic and can be found in the perineum, in the contralateral hemiscrotum, or at the base of the penis.

Acute scrotum is secondary to several causes: torsion of the testis, torsion of a testicular appendage, orchitis and epididymitis, idiopathic scrotal edema, and incarcerated hernia.

Torsion of the testis is caused by the testis and the spermatic cord twisting on their axis, causing obstruction of blood flow. Two types are known: intravaginal torsion, most common in adolescents, and extravaginal torsion which is observed in newborns and usually occurs *in utero*. In most cases, intravaginal torsion is associated with an abnormal development of the tunica vaginalis which completely surrounds the testis, epididymis, and caudal part of the spermatic cord (so that there is no posterior attachment to the scrotum) allowing the testis to twist within.

Intravaginal torsion requires surgical detorsion within 6 h of onset of symptoms: after 12–24 h only 20% of testes recover, whereas after 24 h the testis is unsalvageable in most cases. Extravaginal torsion *in utero* usually leads to a necrotic or atrophic testis.

The testicular appendages (appendix testis and appendix epididymis) are remnants of mesonephric tubules. Both appendices are pedunculated and may twist, especially in prepubertal boys.

Acute *orchiepidydimitis* is commonly secondary to infections caused by *Escherichia coli*, and—in sexually active boys—by *Chlamydia trachomatis* and *Neisseria gonorrhoeae*. More rarely, bladder outlet obstruction or genitourinary malformations (ectopic ureter ending in the vas deferens or seminal vesicles) may cause urine reflux leading to orchiepidydimitis.

Idiopathic scrotal edema is characterized by enlargement and thickening of the wall of one of both hemiscrota. Its cause is unclear.

Inguinal incarcerated hernia may compress the spermatic cord and cause infarction of the testis.

Varicocele is the dilatation of the veins of the pampiniform plexus of the testis. Varicocele can be idiopathic—usually on the left side—or secondary to increased intra-abdominal pressure by a retroperitoneal mass. Most varicoceles in adolescents are idiopathic and are usually caused by incompetent valves in the internal spermatic vein causing blood reflux in the pampiniform plexus. Varicocele may cause ipsilateral hypotrophy of the testis and infertility.

Rare conditions. Cystic dysplasia of the rete testis is a rare abnormality often associated with ipsilateral agenesis of the kidney. This malformation is due to a developmental defect of the mesonephric duct which is the cause of both the dilation of the testicular rete testis and renal agenesis. *Cysts of the seminal vesicles* represent another very rare malformation whose etiology is caused by an abnormal development of the mesonephric or wolffian duct, which can be associated with abnormal development of the ipsilateral upper urinary tract.

Female Genital Organs

Embryology. Two pairs of genital ducts develop in both sexes: the mesonephric or wolffian ducts, which connect the mesonephros to the cloaca, and the paramesonephric or müllerian ducts. The ureteric bud originates at 5 weeks of gestational age and reaches the metanephros inducing its differentiation into the kidney. The müllerian ducts are lateral to the mesonephric ducts, develop at 6 weeks' gestational age and at about 7–8 weeks fuse to form the uterovaginal canal that reaches the urogenital sinus at the müllerian tubercle. The urogenital sinus develops from the separation of the cloaca into the urogenital sinus and rectum. At the same time the vagina proliferates and subsequently undergoes canalization, becoming patent (hymen excluded) at about 22 weeks of gestation. Graaf's follicles first appear in the seventh month of gestation. The feminization of both fetal internal and external genitalia is largely a nonhormonal process. As the genital system develops in association with the urinary system, up to 50% of females with abnormalities of the genital tract are also affected by urinary abnormalities (1).

Uterovaginal Malformations

Uterovaginal anomalies can be classified into three groups according to faulty embryological steps.

Müllerian agenesis. The *Mayer–Rokitansky–Küster–Hauser syndrome* (MRKHS) is a condition caused by a developmental defect of the caudal portion of the müllerian duct. Type A (typical form) is characterized by no vagina or uterus and normal external genitalia; the fallopian tubes, ovaries, and kidneys are normal. In type B (more rare), the uterus may be normal except for the lack of a conduit to the *introitus*, or may be rudimentary with aplasia of one or both uterine horns, or asymmetrical horns; however, any of the lateral or vertical fusion abnormalities may be seen. The fallopian tubes are hypoplastic or absent. Absent or streak ovaries, or inguinal hernias containing an ovary, have been reported. Associated malformations are found in the upper urinary tract, skeletal system, and spina. The karyotype is normal.

Disorders of lateral fusion. Failed unilateral development of a müllerian duct causes a unicornis uterus with or without a rudimentary horn uterus. Complete failure of fusion of the müllerian ducts results in a didelphys uterus, whereas partial failure results in a bicornuate or in a bicornis bicollis uterus. Failure of resorption of the midline septum results in a septate uterus.

Disorders of vertical fusion. The interruption of fusion can occur at any level and may be multiple; high transverse vaginal septa are more common, whereas middle and low transverse septa are rarer. Imperforated hymen is not a disorder of vertical fusion and it is caused by the persistence of the central epithelial cells of the urogenital diaphragm; it is not associated with other abnormalities.

From a practical point of view, it is preferable to consider vaginal anomalies according to the presence or absence of obstruction, as the association between anomalies of vertical and lateral fusion is frequent. Obstructive vaginal anomalies are: imperforated hymen, transverse vaginal septum, obstruction of a rudimentary horn, atresia of the uterine cervix, and vagina. Non-obstructive vaginal anomalies are: longitudinal vaginal septum and incomplete transverse vaginal septum (2, 3).

Nonneoplastic Ovarian Masses

Cysts. Follicular cysts account for about 70% of ovarian masses in children. In newborns they are a consequence of maternal hormonal stimulation *in utero*. In postmenarchal girls, cysts are caused by a Graafian follicle which

continues to grow after a failed ovulation or when a corpus luteum does not involute after ovulation: they often have a complete involution within a few menstrual cycles.

Ovarian torsion. Ovary torsion may occur in an adnexum containing a cyst (typically in newborns) or a tumor. In young girls it usually occurs in a normal ovary.

Disorders of Puberty

Precocious puberty. It is defined as the development of secondary sexual characteristics (breast tissue, pubic and axillary hair, external genitalia, and menses) before 8 years of age. Most cases are the result of idiopathic activation of the hypothalamic-pituitary-gonadal axis (central or true isosexual precocity), or increased estrogen levels with low gonadotropin levels, in most cases caused by an autonomous follicular cyst (peripheral pseudosexual precocity), or increased level of androgens (premature adrenarche). The remaining cases are the result of hypothalamic or pituitary gland lesions and adrenal or ovarian tumors.

Amenorrhea. Primary amenorrhea is defined as the failure of menstruation by 16 years of age, or no thelarche nor adrenarche by 14 years of age, or no menarche more than 3 years after adrenarche and thelarche. The causes include hypothalamic and pituitary lesions, androgen-producing tumors, and abnormalities of the ovary (gonadal dysgenesis, polycystic ovary), the uterus (absence or hypoplasia), or the vagina (imperforate hymen, atresia) (2, 3).

Clinical Presentation

Male Genital Organs

Acute scrotum is a condition characterized by scrotal swelling and acute pain. Torsion of the testis, torsion of a testicular appendage, idiopathic scrotal edema, and orchitis and epididymitis show very similar clinical features. However, these conditions require a very different treatment: immediate surgery is needed for testicular torsion, whereas medical treatment is usually adequate for orchitis and epididymitis, torsion of testicular appendages, and idiopathic scrotal edema. The differentiation between these conditions on the basis of clinical findings only may be extremely difficult: therefore, ultrasound (US) with color Doppler sonography (CDS) is mandatory.

Small *varicoceles* can be detected only by palpation, whereas large varicoceles appear as multiple serpiginous structures in the hemiscrotum. A varicocele may become more evident during erect position or Valsalva's maneuver.

Rare conditions. Cystic dysplasia of rete testis may cause an asymptomatic scrotal mass, whereas a cyst of the seminal vesicles usually presents in adulthood with oligozoospermia, hemospermia, and urinary complaints.

Female Genital Organs

Uterovaginal malformations. Patients with MRKHS have normal external genitalia and secondary sexual development and present with primary amenorrhea or cyclic lower abdominal pain. Neonates with vaginal obstruction may present with a palpable pelvic or abdominal mass caused by the accumulation of secretions secondary to maternal hormone stimulation, whereas adolescent girls present with amenorrhea, recurrent lower abdominal pain, or a lower abdominal mass. Most patients with uterine anomalies present with amenorrhea, dysmenorrhea, or hematometra; after the second decade of life, infertility and abortion are common.

Ovarian cysts and ovarian torsion. Lower abdominal pain is a common finding; in a few cases a large cyst may cause excessive estrogen production and be responsible for precocious puberty. Up to 30% of cysts may undergo torsion. Acute abdominal pain is the main symptom in young girls, whereas in newborns torsion may be asymptomatic. Usually, neonatal ovarian cysts are initially detected during pregnancy by routine US and can twist *in utero*.

Imaging

Male Genital Organs

US is the primary imaging method for evaluating the scrotum and its content. The association with CDS studies allows the evaluation of both morphology and perfusion. Scrotal US is performed with a high-frequency linear array transducer (10 MHz and above) to maximize resolution of the scrotal contents. To improve the sensitivity a dedicated CDS setting (high frequency is necessary) is mandatory.

Female Genital Organs

Transabdominal US is the study of choice for girls with suspected anomalies of the genital tract. The urinary bladder should be distended to serve as an acoustic window, but not overfilled: overfilling may compress the uterus modifying the uterine shape and thus the fundus/cervix ratio. US is usually performed with 5–7-MHz sector transducer, although 3.5 MHz can be used in large patients. In newborns, high-resolution linear probes (10 MHz and above) are also very useful. Scans of the uterus and vagina are obtained in both the sagittal and transverse

planes, and then the transducer should be angled to obtain views of all axes of both ovaries. Instillation of fluid into the bladder and rectum can help in detecting absence of the vagina and uterus.

MRI should be performed in cases of congenital malformations to define further the anatomy of the anomaly. MRI examinations should include axial, sagittal, and coronal T1- and T2-weighted sequences using phased array or surface coils to allow the highest resolution possible. Fat saturation sequences are useful in highlighting the anatomic structures.

Diagnosis

Male Genital Organs

Normal findings. On US, the testis is seen as ovoid-shaped and with a medium and uniform echogenicity. Echogenicity tends to increase with age until puberty; at puberty a slightly nonhomogeneous echogenicity can be observed sometimes. The hilum of the testis appears as a linear echogenic structure along the superoinferior axis. The epididymis lies on the upper pole of the testis, it is triangular, and its echogenicity is similar to that of the testis. With current US equipment, flow within testicular arteries is seen in virtually all testes. The normal epididymis shows minimal flow with CDS.

Cryptorchidism. US is the diagnostic tool of choice to detect a nonpalpable testis lying in the inguinal canal (sensitivity about 90%, specificity 100%). The undescended testis may appear hypotrophic in comparison with the contralateral testis. US is restricted to detecting testes located in the abdomen. MRI can be performed in such cases, but usually it is not performed as it requires sedation or anesthesia, and a surgical approach is necessary anyway.

Acute scrotum. In intravaginal testicular torsion, the US examination may show an abnormally enlarged and twisted testicular cord and the testis, which is suspended in the scrotum like "a clapper in a bell." US findings differ in relation to the duration of torsion. After the very first hours from the onset of torsion, on gray-scale US the testicular structure appears normal. After 4–6 h, edema causes testicular swelling and the testis appears hypoechoic. After 24 h, the testicular structure becomes heterogeneous because of hemorrhage and ischemia. Other common findings are an abnormal orientation of the testis within the scrotum, an enlarged epididymis, reactive hydroceles, and scrotal wall thickening. At the onset, an acute torsion can be easily confirmed with CDS if blood low is detected in the contralateral asymptomatic testis and absent in the painful testis. Partial torsion may cause reduced flow in comparison with the asymptomatic testis. Reactive hyperemia—mimicking epididymo-orchitis—may be observed in cases of spontaneous detorsion: however, the combination of spontaneously resolved pain and hyperemia should suggest the right diagnosis. Sometimes the differential diagnosis is not so evident and caution is recommended before excluding torsion. In inveterate torsion (more than 24 h), typical findings on CDS are hyperemia of the scrotal wall and paratesticular tissues with absent testicular flow. In extravaginal torsion, US findings range from an enlarged heterogeneous testis–in cases of recent torsion—to a minimally enlarged or normal sized testis with peripheral echogenicity due to calcifications in the tunica albuginea. Scrotal wall thickening and hydroceles are not uncommon. On CDS, flow is absent.

On US, a twisted testicular appendage, when detectable, appears as a small hypoechoic or hyperechoic mass close to the superior aspect of the testis or epididymis. Epididymal and testicular hypoechogenicity with enlargement, hydroceles, and scrotal wall thickening are commonly associated. CDS imaging often shows epididymal hyperemia and the avascular torsed appendage. Associated testis hyperemia is not uncommon. The differential diagnosis with epidydimo-orchitis may be difficult. Twisted appendages may eventually calcify and break free to become scrotoliths.

On US, epididymitis is characterized by an enlarged hypoechoic or hyperechoic epididymis with increased blood flow. Testicular involvement, which occurs in about 20% of cases, appears as increased size and reduced echogenicity. Rarely, secondary focal orchitis can be observed: focal lesions appear as hypoechoic areas close to the inflamed epididymis (Fig. 1).

In idiopathic scrotal edema there is thickening and often hyperemia of the scrotal wall with a normal testis and epididymis (4).

Varicocele. On US, it is characterized by tortuous and enlarged veins of the pampiniform plexus (range: 3–4 to 7 mm; normal maximum size of an individual vein: 2 mm in prepubertal boys, 3 mm in adolescents). The enlarged veins increase in size during Valsalva's maneuver or in erect position. CDS shows blood reflux into the pampiniform plexus very well; the US probe should also be placed on the ipsilateral groin with the patient standing erect in order to precisely assess blood reflux in the distal spermatic vein. Phleboliths may develop in long-standing varicoceles; ipsilateral testicular hypotrophy is not uncommon.

Other conditions. On US, cystic dysplasia of the rete testis is characterized by multiple tubular and cystic dilatations of the rete testis, often associated with absence of the ipsilateral kidney. On US, cysts of the seminal vesicles may be variable in size and, not unlike cystic dysplasia of the rete testis, ipsilateral kidney agenesis is often present.

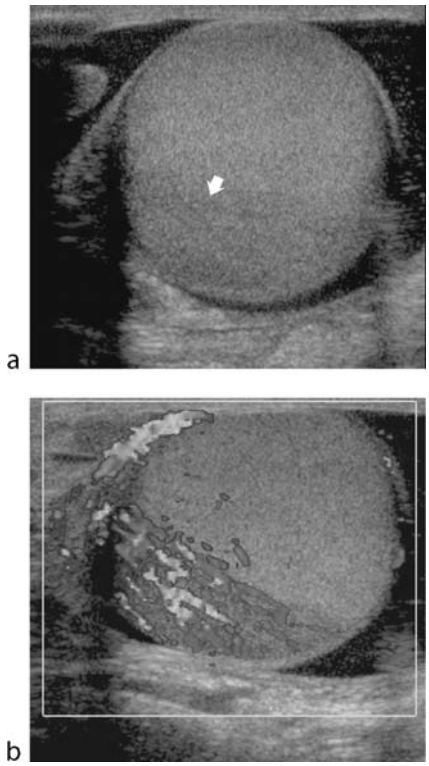

Genital Tract. Figure 1 Focal orchitis. (a) Enlarged testis with a hypoechoic area inside (*thick white arrow*). (b) Color Doppler sonography: hyperemia of the involved area.

Female Genital Organs

US Findings

Normal uterus, vagina, and ovaries: The normal neonatal uterus is a tubular structure with the anteroposterior diameter of the cervix equal or slightly greater that of the fundus. The mean length is 3.4 cm, (range 2.3–4.6 cm), the mean fundal width 1.2 cm (range 0.8–2.1 cm), and the mean cervical width 1.4 cm (range 0.8–2.2 cm). The endometrial lining is often echogenic. In infants the uterus regresses in size, with the width of the fundus equal or slightly smaller than that of the cervix. From infancy until about 7 years of age, uterine length and width do not change: the length range is from 2.5 to 3.5 cm, whereas fundus and cervical width is from 0.5 to 1 cm. The endometrial canal is usually not visualized. After 7 years of age, the uterus increases in length and width, with the corpus growing more than the cervix. Finally, at puberty the uterus becomes pear-shaped with the fundus larger than the cervix; after puberty it measures 5 to 8 cm in length, 1.5 to 3 cm in maximum anteroposterior diameter, and 3.5 cm in width. The endometrial lining is seen and varies according to the phases of the menstrual cycle. The vagina appears as a tubular structure with a hypoechoic wall (5).

Ovarian size is determined by assessment of the volume according to the formula $V = 1/2\ length \times width \times depth$. Volume is slightly grater than 1 cm^3 for the first year of life and 0.67 cm^3 for the second year. The mean ovarian volume is less than or equal to 1 cm^3 in girls under 6 years of age, and then it starts increasing. In prepubertal girls (6–10 years), volume ranges from 1.2 to 2.3 cm^3, in premenarchal girls from 2 to 4 cm^3. In postmenarchal girls, the volume averages 8 cm^3 (range 2.5–20 cm^3). Normal microcystic follicles are easily seen from birth to 12 years of age (3).

Congenital anomalies of the uterus and vagina: At US, patients with MRKHS shows absence of the vagina and an absent or small uterus. Unilateral kidney anomalies can be observed in 50% of cases.

The diagnosis of unicornis uterus can be suggested when there are two horns of different size or when the uterus appears small and laterally located on US images. The US findings of a didelphys uterus are two divergent horns with a deep fundal cleft, two endometrial stripes, two cervices, and two vaginas (Fig. 2); the bicornuate shows two horns, one cervix, and one vagina. The septate uterus presents with two closely apposed endometrial canals surrounded by a common myometrial layer.

The US findings of hydrocolpos or hematocolpos are those of a tubular, fluid-filled midline mass representing the dilated vagina between the bladder and the rectum; the uterine cavity may (hydro- or hematometrocolpos) or may not be distended. Debris can be demonstrated in the fluid.

Precocious puberty. The role of US in this condition is to evaluate the size of the uterus and ovaries, and to differentiate between the fundus and cervix. A fundo-cervical ratio (fundus larger than cervix) greater than 2 with an echogenic endometrium suggests estrogens stimulation. Uterine and bilateral ovarian enlargement are typical of true isosexual precocity, whereas unilateral ovarian enlargement with a stimulated uterus is indicative of pseudosexual precocity. Follicles smaller than 9 mm are not a reliable indicator of precocious puberty. In pseudoisosexual precocity caused by an autonomous follicular cyst, US can demonstrate a unilateral follicular ovarian cyst, which is characterized by the daughter-cyst sign (presence of follicles within the main cyst) (3).

The uterus and ovaries maintain the small prepubertal appearance in cases of adrenarche.

Ovarian cysts and ovarian torsion. Size is the main criterion with which to differentiate a physiological follicle from a pathological cyst, with cysts larger than 3 cm considered pathological. US findings are different, according to the presence or absence of hemorrhage. Non-hemorrhagic cysts appear as a unilocular, thin-walled, and anechoic mass with posterior acoustic enhancement. Hemorrhagic cysts have similar findings when there is

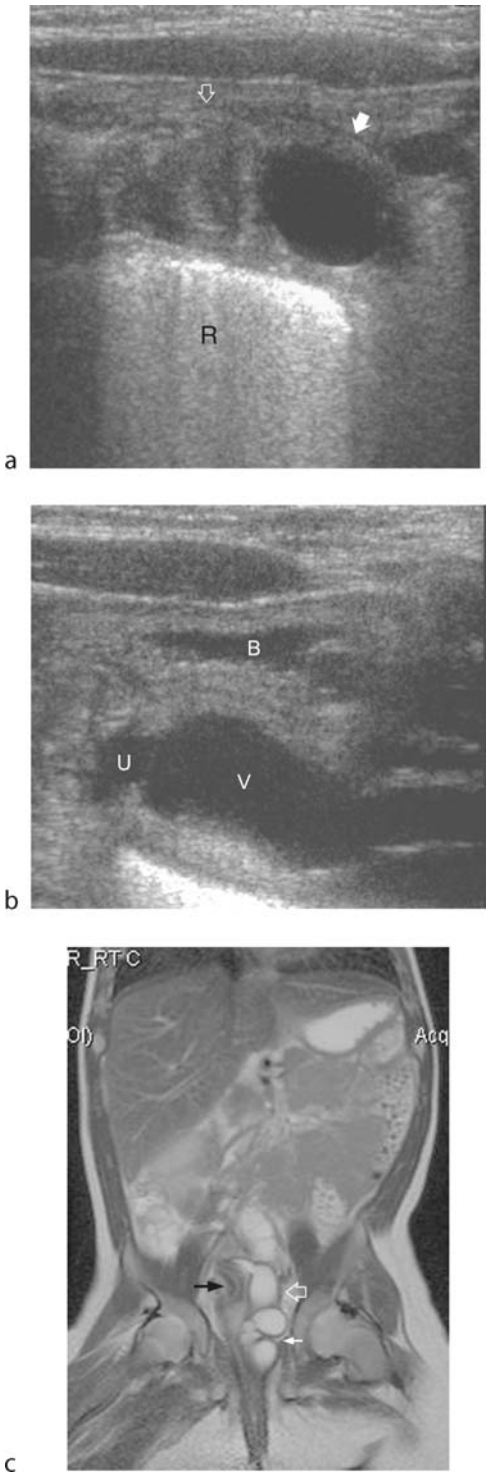

Genital Tract. Figure 2 Uterus didelphys with distal vaginal atresia of one vagina and secondary distension. (a) Transverse section. Right uterus: *open white arrow*; Left dilated vagina: *thick white arrow*; Rectum: R. (b) Sagittal view. Left dilated uterus: U, vagina: V, and Bladder: B. (c) MRI coronal view (T2 sequence). Right uterus and vagina (*black arrow*); left dilated uterus and vagina (*open white arrow*); Left ovary (*white arrow*).

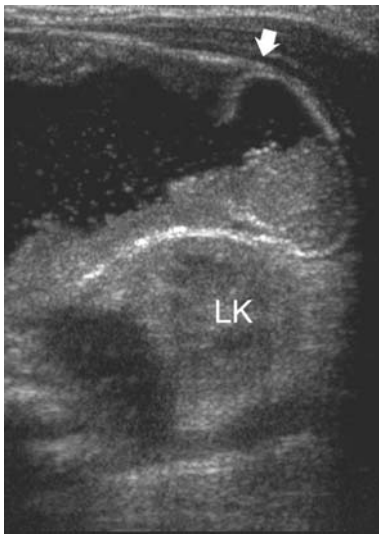

Genital Tract. Figure 3 Complicated ovarian cyst (*thick white arrow*) in a newborn with adnexal torsion. The cyst contains a fluid-debris level and has an echogenic wall. left kidney: LK.

fresh blood, whereas a complex heterogeneous appearance can be observed when clotting occurs (Fig. 3). Finally, the cyst again becomes anechoic with clot lysis.

A torsed ovary usually appears markedly enlarged. The only US finding relatively specific for torsion is the observation of multiple, small (7 to 12 mm in size), peripherally located cysts caused by vascular congestion and transudation of fluid into the follicles (plum-cake sign). The presence or the absence of blood flow on CDS does not exclude or confirm torsion.

In newborns, an ovarian cyst usually appears as an anechoic, easily mobile, thin-walled mass with posterior acoustic enhancement. Occasionally, it may be located far from the pelvis and its side in the abdomen does not determine from which ovary it originates, unless the opposite ovary can be also visualized. A fluid–fluid level is a frequent finding in a torsed ovary, and it is caused by hemorrhage within the cyst. Cysts smaller than 3 cm are considered follicles stimulated by maternal hormones.

Bibliography

1. Wood Gray S, Skandalakis JE, Broecker B (1995) The female reproductive tract. Embryology for Surgeons. 2nd edn. chapter 22, pp 816–847
2. Shatzkes DR, Haller JO, Velcek FT (1991) Imaging of uterovaginal anomalies in the pediatric patient. Urol Radiol 13:58–66
3. Garel L, Dubois J, Grignon A et al (2001) US of the pediatric female pelvis: a clinical perspective. Radiographics 21:1393–1407

4. Siegel MJ (1997) The acute scrotum. Radiol Clin North Am 35:959–976
5. Siegel MJ, Surrat JT (1992) Pediatric gynecologic imaging. Obstet Gynecol Clin North Am 19:103–127

Genitourinary Tract

Marie-France Bellin
Service de Radiologie, Hôpital Paul Brousse, Villejnif, France
marie-france.bellin@pbr.ap-hop-paris.fr

Imaging of the genitourinary (GU) tract is evolving rapidly and, in the past few years, remarkable advances have been made that have modified diagnostic strategies. For decades, intravenous urography (IVU) was the primary means of evaluation of the upper urologic tract. It has now almost completely been replaced by modern cross-sectional imaging techniques: ultrasonography (US), computed tomography (CT), and magnetic resonance imaging (MRI). Few patients with urinary symptoms escape diagnostic imaging and most undergo multiple examinations.

US is frequently used as the first-line imaging modality; the use of US contrast agents for GU imaging is highly promising, but has been less thoroughly studied than in the liver. The application of CT to GU imaging has literally exploded and technical advances, particularly multidetector row CT, have had a major impact on the evaluation of retroperitoneal disorders. With increased speed and quality, CT has made major inroads into vascular imaging and CT urography is developing rapidly. MRI provides unique soft-tissue contrast, and allows for effective evaluation of a wide range of renal and vascular disorders, as well as bladder and prostate cancers. The lack of exposure to ionizing radiation and the safety profile of MR contrast agents are especially attractive for children, women of childbearing age and patients with renal insufficiency. MR urography using heavily T_2-weighted pulse sequences or gadolinium-enhanced T_1-weighted sequences has shown potential to detect, localize, and characterize collecting-system abnormalities. Functional MRI of the kidney is also making rapid progress. The promise of tomorrow's technology is better, faster, safer, and more cost-effective imaging of the GU tract.

Imaging of the GU tract is oriented toward symptoms and disease entities rather than imaging modalities. Thus the radiologist needs to know the main targets of each particular disease, and the respective advantages and limitations of all modalities. It is not enough for the radiologist today to understand technique and interpretation for accurate diagnosis, one must also have some understanding of the basic principles of physiology and the disease process, including pathologic aspects, genetics, as well as treatment options.

Schematically, six major anatomic areas with their different frequencies of involvement, functional aspects, and pathologies are usually defined: kidney, ureter, bladder, urethra, prostate, and scrotum.

Standard anatomic structures and their variants can be visualized by all the different cross-sectional imaging modalities, each with its proper advantages and limitations reflecting its respective intrinsic properties. The accurate analysis of imaging findings includes determination of the size, number, morphology, localization, and extension of pathologic abnormalities. Assessment of their vascularization is crucial not only for their characterization but also for evaluating treatment efficacy. US, CT, and MRI can be used for this evaluation. Functional imaging is mainly based on MRI.

Kidney diseases can be divided into several major groups: acquired renal cystic disease, acute pyelonephritis, acute renal colic, acute renal insufficiency, acute renal obstruction, acute tubular necrosis, anatomic variants of the GU tract, benign solid tumors of the kidney, chronic pyelonephritis, chronic renal insufficiency, chronic renal obstruction, complications of renal transplantation, functional imaging of the kidney (CM structure), glomerulonephritis, hypertension, lymphomatous involvement of the GU tract, medullary sponge kidney, normal transplanted kidney, polycystic kidney disease, renal abscess, renal arteriovenous fistula, renal artery aneurysm, renal artery stenosis, renal cell carcinoma, renal cysts, renal infarction, renal papillary necrosis, renal pseudotumor, renal vein thrombosis, retroperitoneal fibrosis, trauma of the GU tract, urinary incontinence, urinary stone disease, urinary tuberculosis, and urothelial tumors of the kidney and ureter.

Ureteral diseases can be divided into several major groups: acute renal colic, acute renal obstruction, anatomic variants of the GU tract, lymphomatous involvement of the GU tract, retroperitoneal fibrosis, trauma of the GU tract, ureterocele, ureteropelvic junction syndrome, urinary stone disease, urinary tuberculosis, urothelial tumors of the kidney and ureter, and vesicoureteral reflux.

Bladder diseases can be divided into several major groups: anatomic variants of the GU tract, cystitis, lymphomatous involvement of the GU tract, neurogenic bladder, tumors of the bladder, urethra and/or urachus, urinary incontinence, urinary stone disease, urinary tuberculosis, and vesicoureteral reflux.

Urethral diseases can be divided into several major groups: anatomic variants of the GU tract, stenosis of the urethra, trauma of the GU tract, urinary incontinence, and urinary tuberculosis.

Genito-Urinary Tract

M. Riccabona, R. Fotter
Division of Pediatric Radiology, University Hospital, Medical University of Graz, Graz, Austria
michael.riccabona@meduni-graz.at
richard.fotter@meduni-graz.at

Definition

Normal anatomy of the urinary tract may include some more or less frequent variations; the clear differentiation of a "variant" from a "malformation" is difficult and can often only be made in the individual case with regard to the clinical development of the affected urinary tract.

Embryology

The embryologic development of the mesodermal kidney is complex with three successive stages: the pronephros, the mesonephros, and the final metanephros (Fig. 1). The kidneys develop in the pelvic cavity and migrate during the first trimester before they eventually take their normal position in the retroperitoneal space of the upper abdomen, with a simultaneous rotation of the renal pelvis, which eventually in a normal kidney points in an anterior-medial direction. The kidney is initially supplied by sacral branches of the aorta, and during its assent into the abdominal cavity the kidneys acquire successively higher branches with regression of the earlier, more caudal vessels. The differentiation of the renal tissue depends on proper contact between the metanephric tissue and the ureteric bud. Disturbance of this development may lead to variety of variants, dysplasia, and malformations (Table 1). The development of the lower urinary tract and the bladder is also complex and involves both the urinary and the genital tract, with formation of a primary cloaca which eventually differentiates into the urinary bladder (by septation and separation of vagina and rectum), the ureter (from the arising ureteric bud), the urethra, and the genitalia (maturation of the organs arising from the Wolffian and the Müllerian duct) (Fig. 2). Disturbance of this complex development may lead to a number of variants and malformations (Table 2).

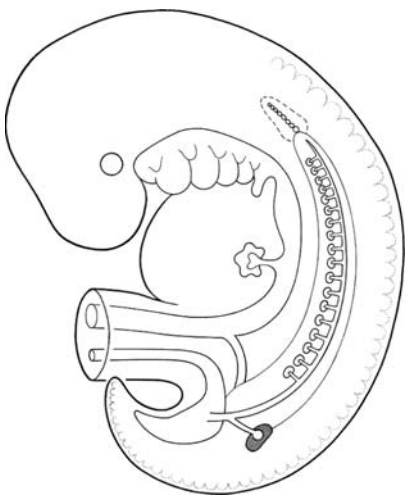

Genito-Urinary Tract: Anatomy and Variants. Figure 1 Kidney development—pronephros, mesonephros, metanephros (from Benz-Bohm (2001) In: Fotter R (ed) Pediatric Uroradiology. Springer, Berlin-Heidelberg, p 44, Figure 2.1).

Clinical Presentation

Normal anatomy and usual variants do not cause any clinical symptoms.

Imaging

All imaging modalities may be applied to visualize the urinary tract.

Radiological anatomy: Anatomically, the kidney consists of the outer cortex, the inner medulla, and the centrally positioned collecting system, with the major supplying and draining vessels running close to the collecting system (Fig. 3a). Kidney position (in relation to other abdominal structures) as well as renal shape, histology, and function change with age; as the kidneys are less protected by the ribs in infancy, they are at higher risk for traumatic injury. These are reflected in age-dependent contrast dynamics and in different tissue appearances on various imaging modalities, particularly on ultrasound (US) (Fig. 3b and c). Physiologically, there is a marked lobar architecture in the infant (persistent fetal lobulation). The kidney usually has three groups of calices (upper, middle, lower), potentially with compound papillae (two papilla draining together into one calyx) particularly in the polar region (these are prone to intrarenal reflux). Usually, there is one main renal artery and renal vein, with the left renal vein crossing in front of the aorta. From this main artery, segmental arteries divide, along with segmental branches, into the arcuate arteries. Furthermore, there is a capsular supply with potential anastomoses between peripheral intralobular arteries and the capsular vessels deriving from the suprarenal, renal, and genital arteries. On US the neonatal kidney is initially quite echogenic, with a marked differentiation between

Genito-Urinary Tract: Anatomy and Variants. Table 1 List of most important kidney variants and "malformations"

Type	Comments, remarks, subtypes
Position and Rotation anomalies*	malrotation, malposition/renal ectopia (abdominal, thoracic)
Renal agenesis*	bilateral agenesis is lethal
Fusion anomalies*	horseshoe kidney (pre-aortal isthmus), crossed fused renal ectopia
Variations of renal vessels*	unusual course, e.g. retro-aortal (left) renal vein persisting or additional/accessory arteries and/or veins
Ureteral variations*	retro-/circumcaval ureter, ureteral folds, ureter fissus
Duplex (triplex) kidney*	caused by two (three) ureteric buds, with the lower ureter draining the upper renal moiety (usually obstructive), and the higher and more laterally inserting ureter (often refluxing) draining the lower moiety
Calyceal abnormalities*	calyceal diverticula, tertiary calyx, megacalicosis
other collecting system abnormalities	bifid collecting system ("incomplete duplication")

* some of these entities may cause symptoms and sequalae and thus may be also considered more a malformation and not just a variant (see *Urinary tract, Entry: Congenital malformations, genito-urinary tract*)

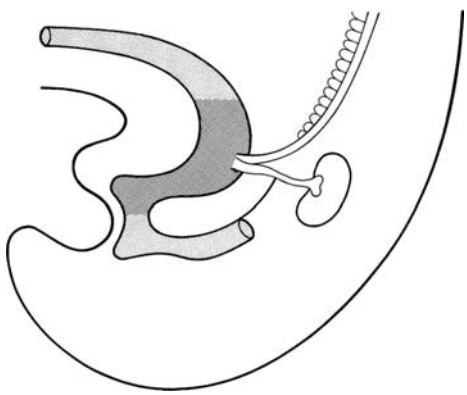

Genito-Urinary Tract: Anatomy and Variants. Figure 2 Development of the lower urinary tract—schematic diagram of the urogenital sinus (from Benz-Bohm (2001) In: Fotter R (ed) Pediatric Uroradiology. Springer, Berlin-Heidelberg, p 44, Figure 2.2).

Genito-Urinary Tract: Anatomy and Variants. Table 2 Most important lower urinary tract variants and malformations

Duplications of bladder, ureter, urethra, ureter fissus*
Megaureter (refluxing and/or dysplastic and/or obstructive)*
Persisting urachus, urachus cyst/-diverticula*
Diverticulum*
Bladder septations*
Megacystis*

There may be numerous associated anomalies of the genital tract (see *Urinary tract, Entry: Congenital malformations, genito-urinary tract*)
*Many of these entities may cause symptoms and sequelae and thus may also be considered as a malformation and not just a variant

the medulla and cortex, which decreases during growth (Table 3).

The renal pelvis varies in size and can be located predominantly intra- or extrarenally, and consecutively the shape of the ureteropelvic junction may vary. In early childhood, some mild tortuosity and elongation of the ureter with widening of the mid-ureter, short kinks, and intraluminal mucosal folds of the proximal ureter are common as a persistent fetal characteristic in the infant. Ureters in children may be highly mobile, and they may be difficult to visualize. The ureter courses down through the bladder muscular wall and then submucosally to its orifice, which usually is to the end/in the corner of the trigonum.

The urinary bladder is divided into a vertex, body, and the fundus, with the trigonum being the posterior aspect of the bladder base. This triangular space is formed by the two ureteral ostia superior-laterally and by the internal urethral meatus inferiorly to the midline. In infants, an incompletely filled bladder may occasionally show a transient herniation of the inferior lateral wall, which then appears like "bladder ears" that disappear when the bladder is full. The fetal urachus arising from the bladder roof coursing toward the umbilicus usually closes around birth and may still be visible in early childhood as a fibrous remnant—failure of this involution may lead to a persisting duct or cysts. Bladder capacity varies with age (Table 4). As the infant's bladder reaches up into the abdomen, there is a higher risk of intraperitoneal bladder rupture in any kind of trauma or nonaccidental injury. Only after 6 years does the bladder begin to be located more and more in the greater pelvis, and it only becomes a purely pelvic organ after puberty. The bladder neck is the poorly delineated junction between the bladder and the urethra at the level of the internal urethral sphincter.

The urethra differs with gender. The male urethra is divided into a posterior and anterior segment, with the prostatic urethra extending from the bladder neck to the urogenital diaphragm. This posterior urethra has a number of anatomical landmarks, e.g., veromontanum, physiologic (semi-)circular folds that may mimic mild posterior ureteral valves, thin anterior wall mucosa folds at the level of the veromontanum called "incisura," the prostate utricle, and numerous openings of prostatic ducts to the wall of the posterior urethra with potential reflux into these (Fig. 4). A final incision is caused circumferentially by the urogenital diaphragm, followed by the membranous part of the anterior and inferior urethra. Important landmarks are the Cowper glands, which may appear as contrast medium-filled structures in projection at the beginning of the membranous urethra. Accumulation of contrast material may be seen physiologically at the glans penis in uncircumcised infants on

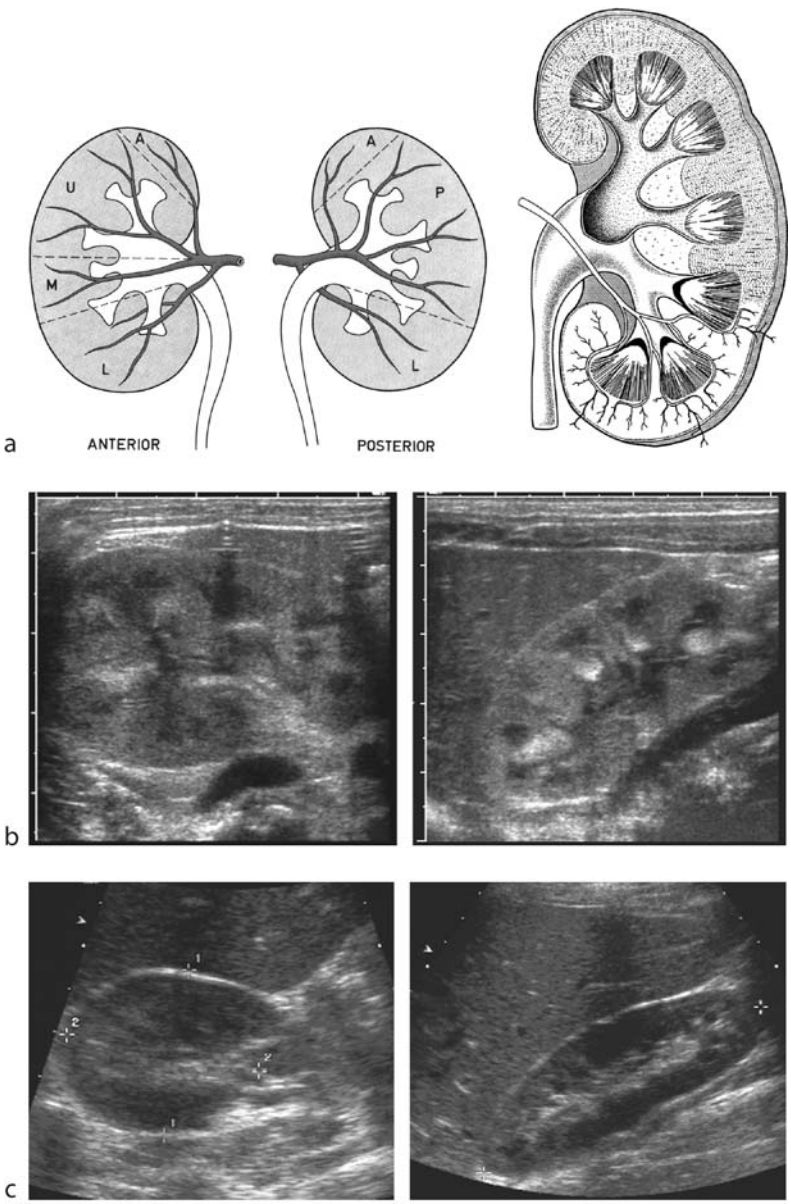

Genito-Urinary Tract: Anatomy and Variants. Figure 3 Renal anatomy. (a) Schematic graph of renal anatomy (adapted from Benz-Bohm (2001) In: Fotter R (ed) Pediatric Uroradiology. Springer, Berlin-Heidelberg, p 49, Figure 2.10 and 2.11). (b) US of a neonatal kidney: more spherical shape, broad corticomedullary complex with echogenic cortex and prominent corticomedullary differentiation, no or minimal central sinus echoes, echogenic papillae, fetal lobulation. (c) US appearance of the kidney in an adolescent for comparison.

Genito-Urinary Tract: Anatomy and Variants. Table 3 Weight-correlated development of renal size

Renal size	Comment
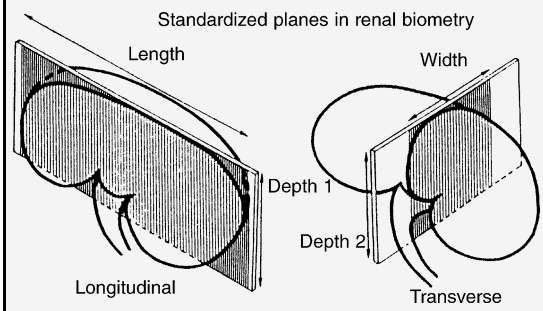 (a) Correct planes for measurement of renal size (Dinkel et al. 1985). See also Fig 3c.	Exact measurement of real maximal length and diameters of the kidneys is of utmost importance. Most inaccuracies derive from measurements taken in a slightly oblique or displaced section
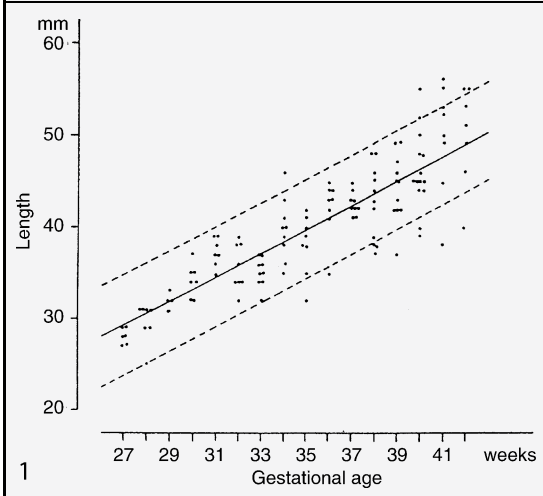	
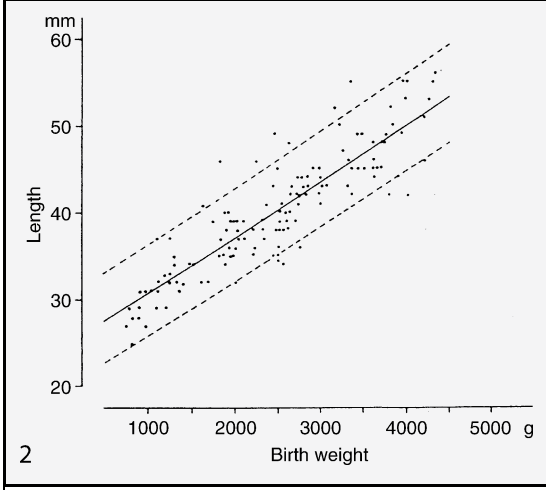	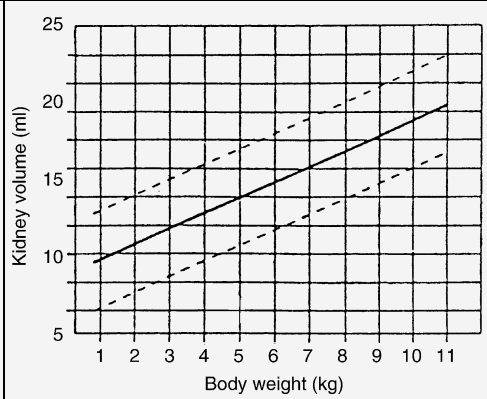 (b) Kidney length related to gestational age and birth weight in-term and preterm neonates (Chiara et al. 1989)

(continued)

voiding cystourethrography (VCUG) studies. The female urethra is much shorter, has a large variation in its normal appearance—depending on the degree of relaxation of the external sphincter and the muscles of the pelvic floor during inspection or voiding. This as well as some reflux of contrast material into the vagina during VCUG is a frequent finding without significance.

The definition of and differentiation between variant, anomaly, or malformation are difficult and cannot be made on the basis of clinical significance only; therefore,

Genito-Urinary Tract. Table 3 (continued)

Renal size	Comment
(c) Growth charts for kidney length and volume (Dinkel et al. 1985)	

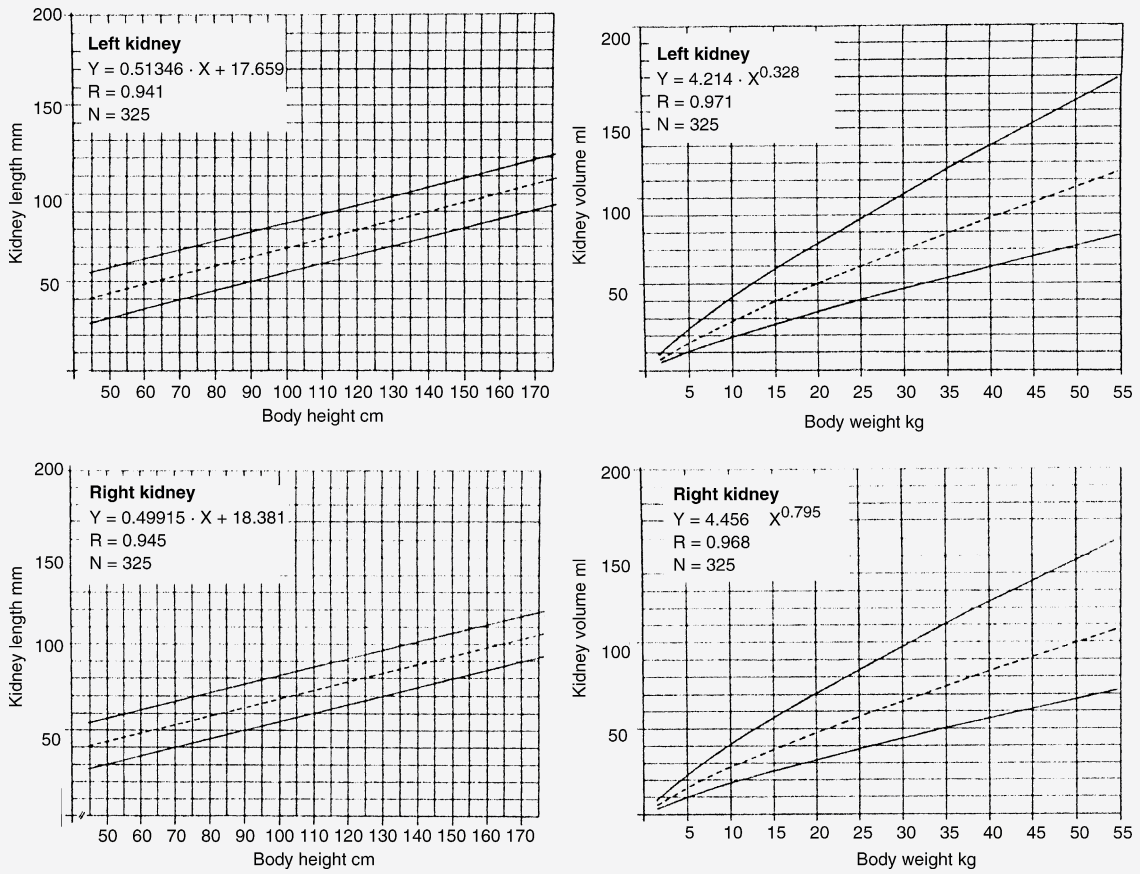

Kidney volume of neonates and infants related to body weight (Mean ± 2 SD are shown) (Peters et al. 1986)

From Ring E, Riccabona M, Fotter R (2001) In: Fotter R (ed) Pediatric Uroradiology, Springer, Berlin-Heidelberg, pp 413–420, Figure 26.3–26.6, pp 416–417; Dinkel E, Ertel M, Dittrich M et al (1985) Pediatr Radiol 5:38–43

most of the variants are described in the entry "Malformation, Congenital, Urinary Tract, Childhood" except for those mentioned earlier.

Imaging modalities: Usually the urinary tract is imaged by US and VCUG; rarely, intravenous urography (IVU) can be performed. On US, a comprehensive study should be performed in a well-hydrated child with full bladder and must include postvoid reassessment. Renal size and bladder capacity should always be assessed using weight-correlated growth charts (Table 3). Standard protocols for performing VCUG and IVU in infants and children exist, with IVU only being recommended in infants older than 4-6 weeks due to the neonatally immature kidney function. In the pediatric age group, (multidetector spiral) computed tomography (CT) is performed only for trauma and complicated stone disease as well as for tumors, applying age-adapted low-dose protocols with weight-related amounts of contrast medium and size or age-adapted delay timing. Additionally, magnetic resonance (MR) urography is becoming a comprehensive imaging tool for most parts of the pediatric urinary tract, with an excellent demonstration of the kidney parenchyma, the collecting system and ureters, the bladder, all surrounding soft tissue structures, and the major vessels; only visualization and evaluation of the urethra may be difficult. New approaches using dynamic diuretic contrast-enhanced MR techniques also allow for functional evaluation. It should be noted that sufficient distension of the collecting and draining system (achievable by proper hydration and administration of diuretic drugs) as well as (often) some sedation—in younger children and infants—is essential for good-quality examinations.

Genito-Urinary Tract: Anatomy and Variants. Table 4 Graph and equations for assessing age related changes of normal bladder capacity in childhood

Bladder capacity (BC)

BC (mL) = (Age in years+2) × 30

BC (mL) = (30 × age in years) + 60 (both formulas are identical)

Bladder capacity in children with myelodysplasia

BC (mL) = (24.5 × age in years) + 62

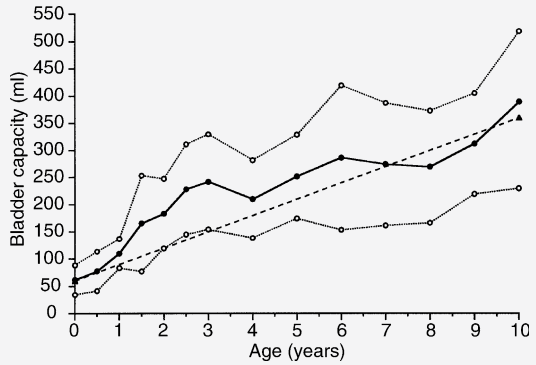

From Ring E, Riccabona M, Fotter R (2001) In: Fotter R (ed) Pediatric Uroradiology, Springer, Berlin-Heidelberg, pp 413–420, Table 26.14, p 419, Figure 26.8, p 419

Bladder capacity (mean ± 1 SD) during childhood. The dotted line represents the formula-derived estimation of BC. Data obtained from Zerin et al. (1993)

Comment: The above-mentioned formula seems to underestimate mean BC during the first few years of life. This may reflect the normal development of BC but could be influenced by bladder training to reach continence. Children with myelodysplasia seem to have a BC? 20–25% less than neurologically intact children (Palmer et al. 1997).

Bibliography

1. Benz-Bohm (2001) Urinary tract: embryology, anatomy and anatomical variants. In: Fotter R (ed) Pediatric Uroradiology. Springer, Berlin-Heidelberg, pp 43–54
2. Chiara A, Chirico G, Barbarini M, et al (1989) Ultrasonic evaluation of kidney length in term and preterm infants. Eur J Pediatr 149:94–95
3. Currarino G, Wood B, Majd M (1993) The genitourinary tract and retroperitoneum. Normal findings and anatomical variants. In: Silverman FN, Kuhn JP (eds) Caffey's Pediatric X-Ray Diagnosis: An Integrad Imaging Approach, Vol 2. 9th edn. Mosby, St. Louis, Baltimore, Boston, Chicago, London, Philadelphia, Sydney, Toronto, pp 1201–1221
4. Moore KL, Persaud TVN (1998) The developing human. Clinically Oriented Embryology. 6th edn. WB Saunders Company, Philadelphia, London, Toronto, Montreal, Sydney, Tokyo
5. Palmer LS, Richards I, Kaplan WE (1997) Age-related bladder capacity and bladder capacity growth in children with myelomeningocele. J Urol 158:1261–1264
6. Peters H, Weitzel D, Humburg C, et al (1986) Sonographische Bestimmung des normalen Nierenvolumens bei Neugeborenen und Säuglingen. Ultraschall Med 7:25–29
7. Ring E, Riccabona M, Fotter R (2001) Normal values. In: Fotter R (ed) Pediatric Uroradiology. Springer, Berlin-Heidelberg, pp 413–420
8. Zerin JM, Chen E, Ritchey ML, et al (1993) Bladder capacity as measured at voiding cystourethrography in children: relationship to toilet training and frequency of micturition. Radiology 187:803–806

GERD

▶Reflux, Gastroesophageal in Adults

GERD

▶Gastro-oesophageal Reflux Disease

GERD/GORD

▶Hernia, Hitatus in Adults

Germ Cell Tumors

Anterior mediastinum, potentially malignant.

▶Neoplasms, Chest, Childhood
▶Teratoma, Childhood

Germinal Matrix Hemorrhage

▶Hemorrhage, Intracranial, Neonates (Neuro View)

Germinomas

▶Neoplasms, Chest, Childhood

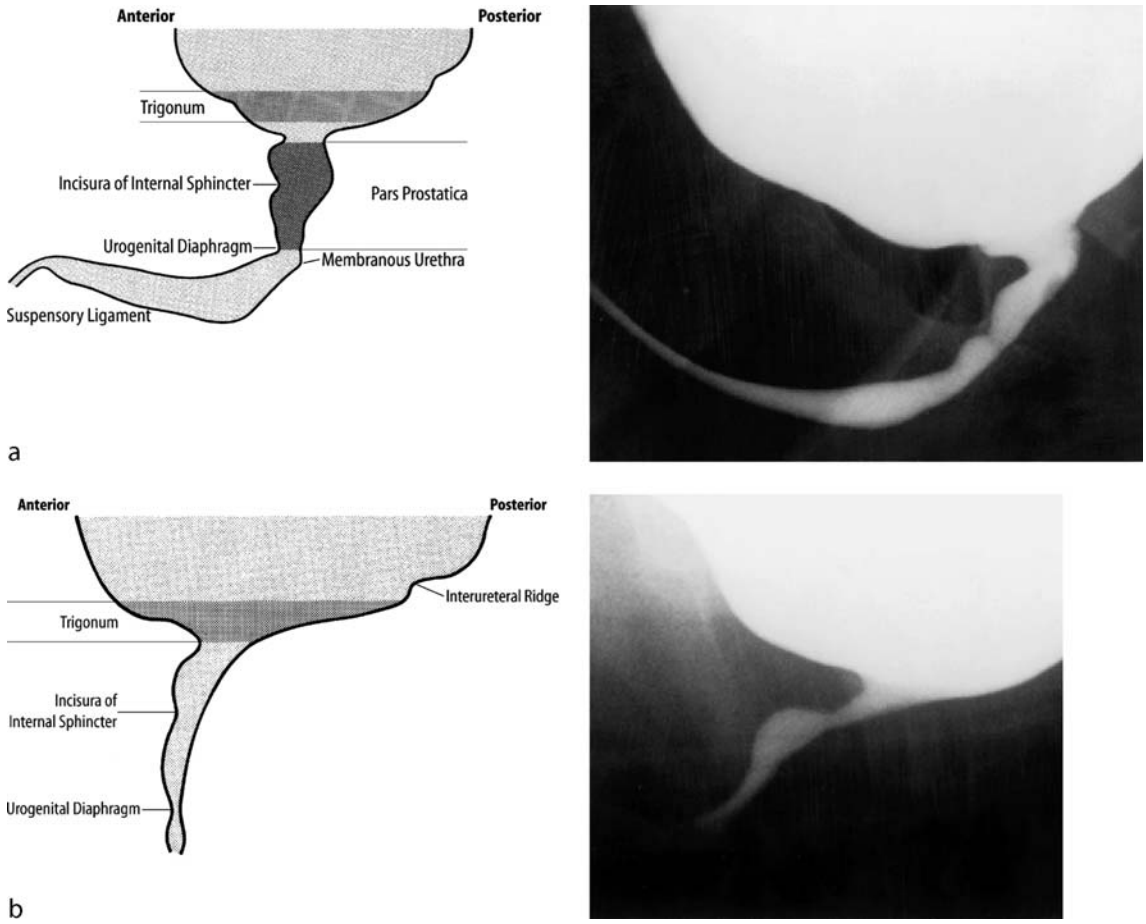

Genito-Urinary Tract: Anatomy and Variants. Figure 4 Schematic drawing of the normal urethra, with corresponding lateral VCUG views (from Benz-Bohm (2001) In: Fotter R (ed) Pediatric Uroradiology. Springer, Berlin-Heidelberg, p 51, Figure 2.12). (a) Male urethra and (b) female urethra. Diagrams of urethrogram and urethrogram showing landmarks of normal structures.

Gestational Trophoblastic Disease

Gestational trophoblastic disease comprises a spectrum of lesions originating from the placental trophoblast. Classic hydatidiform moles are characterized by a diffuse trophoblastic hyperplasia with abundant, villous edema. Macroscopically it looks like a bunch of grapes. Molar pregnancies can invade into the uterine myometrium. Clinically, beta HCG is elevated mimicking pregnancy. The lack of fetal activity and the presence of a hyperechoic polycystic mass within the uterine cavity on US establish the diagnosis.

▶Fetal Imaging

GFR

▶Glomerular Filtration Rate

Gi Foreign Bodies

▶Foreign Bodies, Gastrointestinal

GI Tract, Pediatric, Foreign Bodies

Melanie Hiorns
Radiology Department, Great Ormond Street Hospital for Children, London, UK
HiornM@gosh.nhs.uk

Synonyms

Foreign body (FB); Foreign object; Ingested foreign body; Oesophageal foreign body

Definition

An ingested object in the gastrointestinal (GI) tract.

Pathology/Histopathology

Children of all ages may ingest foreign bodies (FBs) either because they are very young, or by accident, or occasionally intentionally. Children with neurological impairment may be at increased risk. Most ingested objects are radio-opaque and the most common objects include coins, batteries, very small toys or components of toys, nails, pins, beads, marbles, pen tops, etc. Most of these objects pass through the entire GI tract uneventfully but some objects will get stuck at either a physiological narrowing in the gut or will become embedded in the wall of the gut. The main physiological points of obstruction are the cricopharyngeus muscle, aortic knuckle (Fig. 1) and the gastro-oesophageal junction. The ileocaecal valve may also present a point of obstruction. If a patient has had previous surgery to the oesophagus, or elsewhere in the GI tract, the level of the anastamosis may also be a point of hold-up. An FB that becomes impacted may cause erosion of the gut wall at any point along the GI tract. This may occur within 24–48 h, or even sooner in some cases. Of particular concern are lithium batteries which may erode the oesophageal wall in 12 h and therefore need to be removed promptly. The inflammation caused by a lithium battery in the oesophagus may subsequently cause a stricture. Also of recent concern are small, battery-sized magnets found in children's toys and electrical goods. If only one magnet is swallowed it can be allowed to pass through the gut uneventfully but if two are swallowed they may come to lie in adjacent loops of bowel and then become 'fixed' by their magnetic attraction to one another, eventually perforating the bowel wall (1). In this situation they should be removed promptly by laparotomy. FBs may erode through the oesophageal wall leading to an inflammatory response with subsequent granuloma formation. Fistulas have been reported as a complication of this. An FB lodged longer than 24 h poses a greater risk of oesophageal perforation, mediastinal abscess formation, and airway narrowing (2). The method of removal of the object, if it is in the oesophagus, will be determined as much by the history as by the findings on imaging.

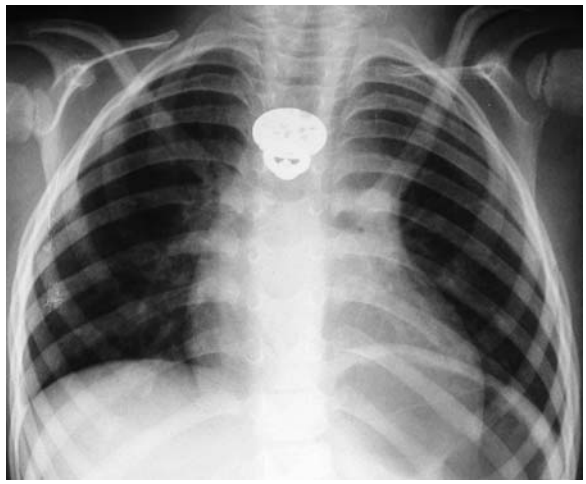

GI Tract, Pediatric, Foreign Bodies. Figure 1 AP chest radiograph showing a radio-opaque ▶foreign body lodged at the level of the aortic knuckle.

Clinical Presentation

The most common age for FB ingestion is in toddlers and young children with the vast majority of patients being under 5 years. Most patients will present to an emergency department and the carer will usually give a history of what they believe has been swallowed. When an object has been swallowed without the carer being aware the presentation may be significantly delayed. Most foreign bodies that are stuck in the oesophagus will lead to dysphagia but some may lead to stridor. Other symptoms may include drooling, gagging, vomiting, retrosternal pain, haemoptysis and acute respiratory distress. When the young or non-verbal patient is experiencing dysphagia he may suddenly express a preference for liquids and liquid or soft foods and this may provide a clue to the underlying pathology of a foreign body. Occasionally a FB may get stuck very high in the oesophagus or in the hypopharynx and may alternatively present with chronic respiratory distress, recurrent pneumonia (due to over-spill of foods into the airway) or, rarely, failure to thrive. Sometimes an ingested FB may be an incidental finding on a chest or abdominal radiograph performed for another reason.

Imaging

No imaging of any kind is necessary in the majority of cases. If the object is believed clinically to be stuck in the oesophagus, imaging is recommended and if the ingested object is radio-opaque its position can be determined by a chest X-ray (AP and lateral views) with a slightly extended field to include the cervical region. If it is non radio-opaque either a contrast study or endoscopy can be performed. Endoscopy is usually preferable as the object can then also be removed. If the patient is believed to have ingested, a battery imaging should always be performed because of the risk of erosion and this will then also require a supine abdominal X-ray. If there is clinical concern regarding associated mediastinitis or paraoesophageal abscess CT may be required.

On an AP chest X-ray, an object stuck at the thoracic inlet will be projected in the midline at the level of the clavicles, and will usually appear en face i.e. as a complete disc. A coin stuck in the trachea at this level will usually appear to be on edge, i.e., sagittally orientated due to the configuration of the cartilaginous rings in the trachea (Fig. 2). Objects stuck in the oesophagus at the aortic arch will lie at the impression of the aortic arch and objects stuck at the gastro-oesophageal junction will be seen approximately 3 vertebral bodies above the gastric air bubble in the midline.

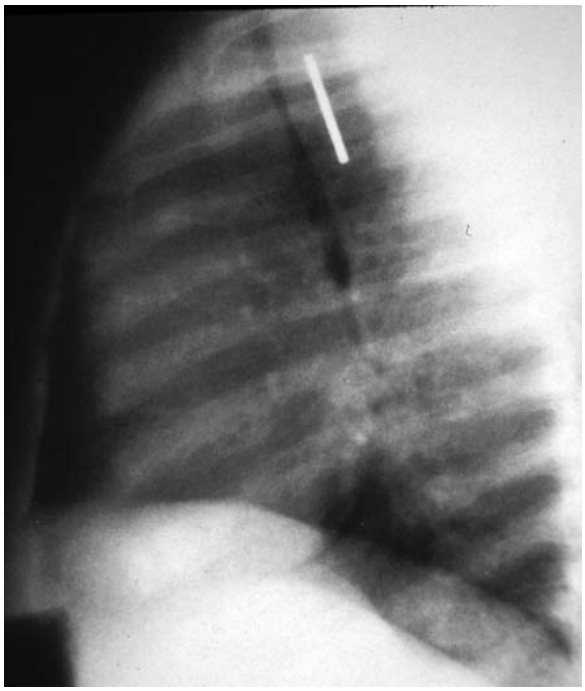

GI tract, Pediatric, Foreign Bodies. Figure 2 Lateral chest radiograph showing a coin in the oesophagus. Note the air-filled trachea anteriorly and that the coin is lying in a coronal plane and is therefore seen edgeways on this lateral view. These two features locate it to the oesophagus.

Nuclear Medicine

No role to play.

Diagnosis

By imaging as above, primarily plain films, rarely by (pre- or post-endoscopy) contrast study, CT or MRI for complication such as mediastinitis.

Interventional Radiological Treatment

Fluoroscopic balloon catheter extraction of the foreign body is performed in some centres and involves passing a deflated Foley catheter beyond the FB under fluoroscopic guidance with the patient in a head down position on a steeply tilted fluoroscopy table. Once the balloon part of the catheter is past, the FB is then inflated and the whole catheter is slowly withdrawn thereby pulling the FB out ahead of it (3). This technique has recently been criticised by some operators due to the risk of aspiration of the FB as it exits the pharynx and is therefore not so widely practised. Endoscopic removal of oesophageal FBs is now the treatment of choice in many centres.

Bibliography

1. Uchida K, Otake K, Iwata T et al (2006) Ingestion of multiple magnets: hazardous foreign bodies for children. Pediatr Radiol 36(3):263–264
2. Gilchrist BF, Valerie EP, Nguyen M et al (1997) Pearls and perils in the management of prolonged, peculiar, penetrating esophageal foreign bodies in children. J Pediatr Surg 32(10):1429–1431
3. Morrow SE, Bickler SW, Kennedy AP et al (1998) Balloon extraction of esophageal foreign bodies in children. J Pediatr Surg 33(2): 266–270

GI Tract, Paediatric, Congenital Malformations

Melanie Hiorns
Radiology Department, Great Ormond Street Hospital for Children, London, UK
HiornM@gosh.nhs.uk

Synonyms

Anorectal malformation; Colonic atresia; Duodenal atresia; Duplication cysts; Gastroschisis; Jejunal atresia;

malrotation (with or without volvulus); Oesophageal atresia; Omphalocele; Rectal atresia; Stenosis; Tracheo–oesophageal fistula.

Definition

Congenital malformations of the gastrointestinal (GI) tract are those, which have developed in utero. They may be genetically determined, due to a developmental 'accident' or have been acquired in utero secondary to an insult such as ischaemia. Some of these conditions are now detected on antenatal ultrasound scanning but if not they usually present in the first few hours of life, and occasionally later.

Pathology/Histopathology

Congenital malformations of the GI tract arise from a wide spectrum of abnormalities and the pathology/histopathology is specific to the type of malformation.

Clinical Presentation

Oesophageal atresia (OA) is discussed in the section on 'Oesophageal disease, childhood'.

Duodenal atresia is sometimes detected antenatally on ultrasound as fluid can be seen in a distended stomach and proximal duodenum. As the atresia is usually at or below the level of the ampulla of Vater (insertion of the common bile duct) the infant will present after birth with vomiting or severe reflux which is characteristically bile stained. The abdomen will be distended and no gas or fluid will pass beyond the atresia. Duodenal stenosis will present in a similar way depending on the severity of the stenosis, although in these patients some gas and fluid will pass on through the rest of the GI tract.

Jejunal atresia presents in a similar way to duodenal atresia as above, although the abdomen may be more dilated and the vomiting less pronounced. The vomitus will still be bile stained.

Malrotation is the abnormal positioning and fixation of the midgut within the abdomen after it is withdrawn back into the abdomen during the tenth week of embryological life. It is discussed in greater detail in the section on 'GI tract, paediatric, specific problems'.

Ileal atresia: The neonate will present with obstruction, and usually associated vomiting which will be bile stained. The patient may fail to pass meconium in the first 24 h of life.

Colonic and rectal atresia: The infant will not pass meconium in the first 24 h of life and the abdomen will become increasingly distended.

Anorectal malformation: The first check at birth may show that the anus is not present and/or male infants may pass bits of meconium per urethra and females may show meconium on the labia or vaginal introitus.

Duplications of the intestine may occur anywhere along the GI tract but are most common in the small bowel, and may be cystic or tubular. Cystic duplications are more common and do not usually communicate with the lumen of the bowel. Tubular duplications usually communicate with the lumen. Either of these may present incidentally but often present as an abdominal mass and are at risk of bleeding, ulceration, and perforation if they contain gastric mucosa.

Omphalocele is persistence of the herniation of the abdominal contents into the umbilical cord. It is frequently detected antenatally but will otherwise be immediately visible at birth. It has a high association with small bowel malrotation and volvulus.

Gastroschisis: This abdominal wall defect will present at birth with a non-midline defect of the abdominal musculature (more common on the right) and this allow the extrusion of the abdominal viscera without involving the umbilical cord. It may or may not be detected antenatally.

Meckel's diverticulum: This is a small bowel diverticulum that often contains gastric mucosa. Clinical presentation may be with bleeding, anaemia, abdominal pain, or perforation.

Imaging

Oesophageal atresia (OA): See the section on 'Oesophageal disease, childhood'.

Duodenal atresia: The characteristic X-ray appearance is that of a distended gas filled stomach and a proximal duodenum; the so-called 'double bubble' sign. This may have been detected antenatally on ultrasound examination. A water soluble contrast study will show hold-up of contrast in the 2nd part of the duodenum. The remainder of the abdomen will be gasless in complete duodenal atresia. Imaging is not always necessary and some centres proceed straight to surgery on the basis of the abdominal X-ray.

Jejunal atresia may have a similar appearance to duodenal atresia on abdominal X-ray although further gas filled distended loops are usually seen (see Fig. 1 entry: Occlusion, bowel, childhood). A contrast study may or may not be necessary, but if an upper GI series is performed, then it will show several dilated loops of bowel with no contrast or air distally.

Malrotation: The normal position of the duodenal jejunal flexure is to the left of left pedicle of the superimposed vertebral body (2). The DJ flexure should also be at the height of the pylorus, thereby completing

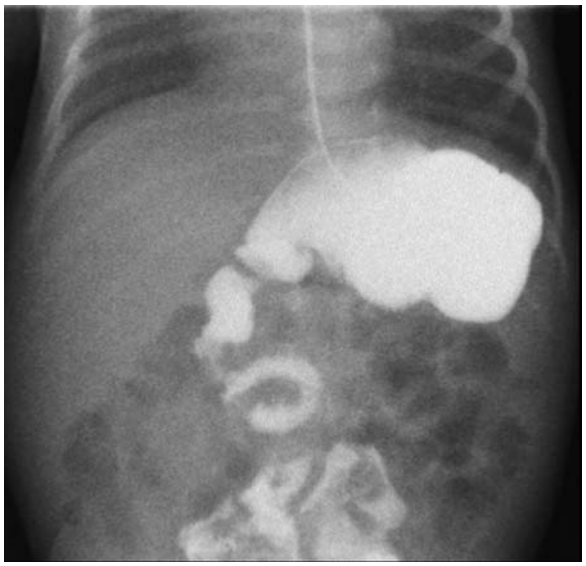

GI Tract, Paediatric, Congenital Malformations. Figure 1 Malrotation on an upper GI series. The DJ flexure is too low and is too medial. The jejunum then loops to the right and inferiorly. This patient is not volved. See (Fig. 4) in the section on 'GI tract, paediatric, specific problems'.

the normal 'C' shape of the duodenum. If the layout of the bowel does not fulfil these two criteria on an upper GI series then malrotation must be suspected (Fig. 1). Ultrasound may be useful in demonstrating the normal relative positions of the SMA and SMV, with the SMV normally lying to the right of the SMA. If this relationship is reversed malrotation may be present. See the section on 'GI tract, paediatric, specific problems' for malrotation with acute volvulus.

Ileal atresia: The plain abdominal film will show multiple dilated loops of gas filled bowel. A contrast enema will demonstrate a microcolon and if contrast refluxes into the distal ileum it may be possible to show the exact position of the most distal atresia, this being the limit to which contrast will pass. There may be several atresias higher in the ileum or jejunum that will therefore not be demonstrated by contrast enema.

Colonic and rectal atresia: If the infant has failed to pass meconium a contrast enema may be performed. This will demonstrate an abrupt ending of the lower part of the large bowel and the exact level will determine if this is colonic or rectal. Imaging may also be performed by abdominal radiograph in conjunction with ultrasound, saline being instilled in the rectum; this technique is particularly useful for the lower anomalies including anal atresia.

Anorectal malformation: Imaging is usually by loopogram and micturating cystogram for high anomalies and by abdominal radiograph, possibly augmented by ultrasound for low anomalies. Please see the relevant section.

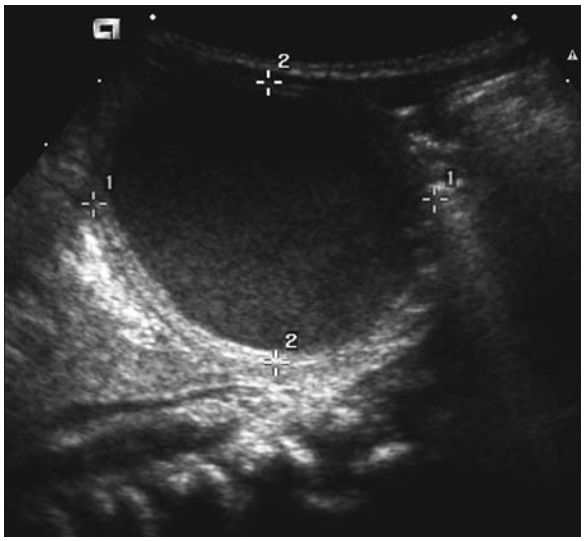

GI Tract, Paediatric, Congenital Malformations. Figure 2 Ultrasound showing a duplication cyst of the bowel. Note the visible layers of the bowel wall.

Duplications of the intestine: Ultrasound is the first investigation of choice and this may show one or several cystic structures closely related to the bowel. Typically the lining of a duplication cyst shows three layers of mucosa consistent with bowel wall although this is not always demonstrated (Fig. 2). The cysts may contain debris and may therefore be either anechoic or of mixed echogenicity. Tubular duplications may be detected on ultrasound but may also be shown on a contrast study. Cystic duplications may appear as filling defects on a contrast study.

Omphalocele does not usually require any immediate imaging and the infant will proceed directly to surgery although due to the high incidence of malrotation and UGI may be requested prior to surgery or soon after.

Gastroschisis: Imaging is not usually required.

Meckel's diverticulum: Nuclear scintigraphy remains the mainstay of imaging (technetium-99 m) with an area of increased uptake being identified in the lower abdomen (3). Occasionally a Meckel's diverticulum can be shown on contrast studies as a filling defect in the distal small bowel but this is unreliable. Ultrasound may also be used and can detect the diverticulum if it becomes obstructed and is therefore distended by fluid, in which case care must be taken to differentiate it from an obstructed appendix. It is a helpful adjunct in centres without ready access to nuclear medicine facilities.

Nuclear Medicine

Nuclear medicine has a limited role in the assessment of congenital malformations of the GI tract. It may be used in

the search for a Meckel's diverticulum (technetium-99 m) and occasionally for ectopic gastric mucosa in duplications elsewhere in the GI tract.

Diagnosis

The diagnosis in all of these conditions is usually either made clinically or on the basis of the imaging as outlined above as these are all structural abnormalities. Subsequent histopathology of resected specimens may demonstrate bowel layers in a duplication cyst and gastric mucosa in a Meckel's diverticulum.

Interventional Radiological Treatment

A significant complication of oesophageal atresia repair is stricture formation and image guided balloon dilatation is the preferred technique for dilatation of these strictures.

Bibliography

1. Berrocal T, Madrid C, Novo S et al (2004) Congenital anomalies of the tracheobronchial tree, lung, and mediastinum: embryology, radiology, and pathology. Radiographics 24(1): e17. Epub 2003 November 10
2. Strouse PJ (2004) Disorders of intestinal rotation and fixation ('malrotation'). Pediatr Radiol 34(11):837–851
3. Kumar R, Tripathi M, Chandrashekar N et al (2005) Diagnosis of ectopic gastric mucosa using 99 T cm-pertechnetate: spectrum of scintigraphic findings. Br J Radiol 78(932):714–720

GI Tract, Pediatric, Specific Problems

Melanie Hiorns
Radiology Department, Great Ormond Street Hospital for Children, London, UK
HiornM@gosh.nhs.uk

Synonyms

Hypertrophic pyloric stenosis (HPS); Intussusception; Malrotation; Midgut volvulus; Pyloric stenosis; Small bowel volvulus

Definition

Intussusception is the prolapsing and invagination (or "telescoping") of a length of bowel, the "intussusceptum," into an adjacent segment, the "intussuscipiens." Four types of intussusception are described: ileocolic, ileo-ileocolic, colocolic, and ileoileal. Ileocolic is the most frequent and occurs in 90% of the cases.

HPS is the idiopathic hypertrophy and hyperplasia of circular muscle fibers of pylorus with proximal extension into gastric antrum. HPS may be inherited as a dominant polygenic trait and has an increased incidence in firstborn boys. It is considered an acquired rather than congenital condition.

Malrotation is the abnormal positioning and fixation of the midgut within the abdomen after it is withdrawn back into the abdomen during the tenth week of the embryological life. As a result twisting (or "►volvulus") of the midgut (third part of duodenum and beyond) can occur around the vascular pedicle of the superior mesenteric artery and superior mesenteric vein. This volvulus and compromise of the arterial and venous supply to the gut results in ischemia. The infant will present with bile stained vomiting due to the duodenal obstruction. The small bowel twists in a corkscrew pattern and depending on the degree of volving vascular compromise may ensue eventually resulting in necrosis, perforation, and gangrene.

Pathology/Histopathology

Intussusceptions most symptomatic intussusceptions in children arise in the ileum and are due to mucosal oedema and lymphoid hyperplasia of Peyer's patches following viral gastroenteritis or upper respiratory tract infection. These are termed "idiopathic intussusceptions" and occur predominantly at the ileocaecal valve (95%). In a small proportion of cases (5%) a "lead point" may initiate the intussusception. Typical lead points include a Meckel's diverticulum, polyps, duplication cysts, suture granulomas, appendiceal inflammation, Henoch Schonlein purpura, and occasionally inspissated meconium. Symptomatic ileocolic and ileo-ileocolic intussusceptions are generally idiopathic, rather than secondary to a lead point.

HPS is due to hypertrophy of the circular muscle layer in the pylorus eventually leading to a functional stenosis/gastric outlet obstruction. Histological examination shows that the muscle layer is deficient in the quantity of a variety of nerve terminals, and it is postulated that this abnormal innervation leads to the failure of relaxation of the pyloric muscle and increased synthesis of growth factors that lead to hypertrophy and hyperplasia resulting in obstruction (1). Prostaglandin E_2 has been reported in association with the development of HPS. Prostaglandin E_2 generation in the gastric mucosa and its concentration in the gastric secretions of patients with HPS have been reported to be significantly greater than in normal controls.

Prostaglandin E_1 and E_2 induce proliferation of the gastric mucosa and are related to muscle contraction in the human gastrointestinal tract. Prostaglandin drug therapy may have a similar effect.

Volvulus: During embryological life (6 to 10 weeks) the midgut is contained outside the fetal abdomen by a physiological umbilical herniation. The mid gut is then withdrawn back into the fetal abdomen at approximately week 10 and in this process normally undergoes physiological rotation so that the small bowel comes to lie centrally and the large bowel to lie peripherally. If this process does not happen correctly the bowel is described as malrotated or nonrotated and the bowel is not properly fixed by its mesentery. This poor fixation allows the small bowel to twist on its mesentery resulting in volvulus and vascular compromise. The caecum lies inferior to the pylorus and is fixed to the posterior abdominal wall by peritoneal bands (Ladd's bands) that pass over the duodenum and may cause obstruction in addition to the risk of volvulus.

Clinical Presentation

Idiopathic intussusception most commonly occurs between the ages of 3 and 9 months (40%) with a range between 3 months and 2 years. Seventy five percent of the cases are in children under 2 years of age, and in children older than 2 years a cause for a secondary lead point should be sought either at the time of the acute presentation or in the recovery period. Idiopathic intussusception is more common in boys (male:female = 2:1). The incidence of idiopathic intussusception is reported to be seasonal, being commonest in the late spring and the autumn. The clinical diagnosis of ileocolic and ileo-ileocolic intussusception can be difficult and there may be a delay in making the diagnosis. The classical clinical triad is of abdominal pain, red current jelly stool, and a palpable abdominal mass but these combined findings are only present in less than 50% of children with the condition. The child will typically draw up his legs to the abdomen during bouts of colic and this may be associated with facial pallor and the passage of red current jelly stools. Clinical examination of the abdomen is often difficult in a distressed child. The child may be shocked and peripherally shut down at the time of presentation. However, conversely, some children may be pain free at the time of presentation with only a history of bloody stools to suggest the diagnosis.

Infants with HPS usually present 2–8 weeks after birth (but may present in the first week) with classic "projectile" nonbilious vomiting, regurgitation, difficulty in feeding and, if severe, weight loss. There is sometimes a history of progression over a period of several weeks after birth (15–20%). Clear, or milky, nasogastric aspirates >10 mL are often present (92% sensitive, 86% specific). HPS occurs mainly in males but is also seen in females with an incidence of 3 cases per 1000 (male:female = 4–5:1) and sometimes with a positive family history. On examination there may be a palpable mass in the epigastrium, sometimes described as "olive-shaped", (80% sensitive in experienced hands, 14% false positive) and this combined with the clinical presentation may be enough to reassure the surgeon to proceed to operation without the need for further imaging.

Malrotation with volvulus usually presents within the first few days of life; there may be delayed presentation in chronic volvulus with only partial compromise to the intestine and its blood supply resulting in a protein loosing enteropathy. The cardinal sign is bilious vomiting or nasogastric aspirates indicating obstruction of the duodenum beyond the ampulla of Vater. If the volvulus has been present for some time (more than 12–24 h) the infant may present in shock and with sepsis from bowel ischemia or infarction.

Imaging

Intussusception: The abdominal radiograph has traditionally been the first investigation in children presenting with suspected intussusception. The most frequent plain film findings are those of reduced large bowel gas and the presence of a mass. However, the AXR is unreliable in confirming or refuting the presence of an intussusception and further imaging is always required. Ultrasound is the investigation of choice (2). If intussusception is suspected clinically ultrasound may be used as the first line investigation. A linear high-frequency transducer is used and whilst the whole abdomen should be scanned the intussusception is most frequently demonstrated in the right flank. Other common sites for demonstration of the intussusception are the left flank and the epigastrium. The intussusceptum is usually seen as a 3–5 cm diameter soft tissue concentric mass in transverse section (Fig. 1), and a sausage-like mass in longitudinal section. The characteristic appearances are of the circular wall of the intussuscipiens, and the central echogenic mucosa of the intussusceptum, with the appearance on transverse scans of the eccentric, semilunar, hyperechoic mesenteric fat that is pulled with vessels and lymph nodes into the intussusception by the intussusceptum: the "crescent and donut" sign.

HPS: If imaging is required ultrasound is the modality of choice. Barium studies are no longer appropriate as the first line investigation. A linear high-frequency transducer is used and is placed slightly obliquely on the epigastrium with the patient supine. The hypertrophied pylorus is

identified in longitudinal section as a tubular structure with echogenic mucosa seen centrally with the thickened muscle layer encasing it. The double-track sign of the echogenic mucosa and the echo poor fluid trapped between the fold of mucosa is typical in HPS but may also be seen in pyloric spasm and should not be considered pathognomic (3). In transverse section the hypertrophied pylorus appears as a midechogenic donut. The pyloric canal is elongated (>12 mm) and there is persistent spasm of the pyloric canal with little if any fluid passing into the duodenum, with a hyperperistalsing stomach (4). There is persistent thickening of the circular muscle in the elongated canal (>4 mm) which is fixed in the spasm (Fig. 2). It is important to distinguish HPS from pyloric spasm which can have a similar appearance and therefore the ultrasound examination must be continued over a reasonable period of time to see if the pylorus relaxes and opens. If doubt still remains the patient should be re-examined after a delay. A pyloric web would not be expected to result in such a degree of muscle hypertrophy but must be included in the differential diagnosis.

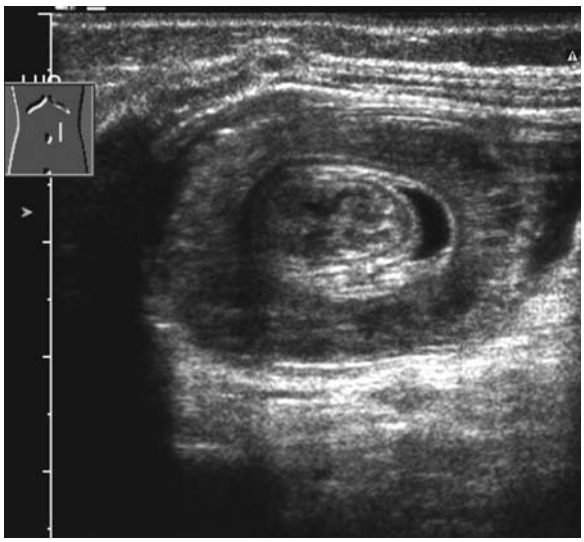

GI Tract, Pediatric, Specific Problems. Figure 1 Ultrasound performed with a high-frequency linear transducer showing the characteristic donut appearance of an intussusception in transverse section.

Volvulus: An infant with bilious vomiting requires immediate investigation. The abdominal radiograph may show a high gastrointestinal obstruction but equally may be nonspecific. The bowel gas pattern will partly be determined by the duration of the volvulus and whether the volvulus is intermittent. The presence of free air within the abdomen is a poor prognostic sign implying that perforation has already occurred.

An upper gastrointestinal series is the investigation of choice in most centers but ultrasound can elegantly demonstrate the volved bowel which is identified by a whirlpool appearance of the twisted small bowel and an absence of color flow on Doppler (Fig. 3). For the upper GI series either barium or water-soluble contrast can be used although water-soluble contrast is preferred in the neonate. In this particular clinical situation it is helpful to start with the patient in a right lateral position as the contrast is instilled so that it immediately passes into the

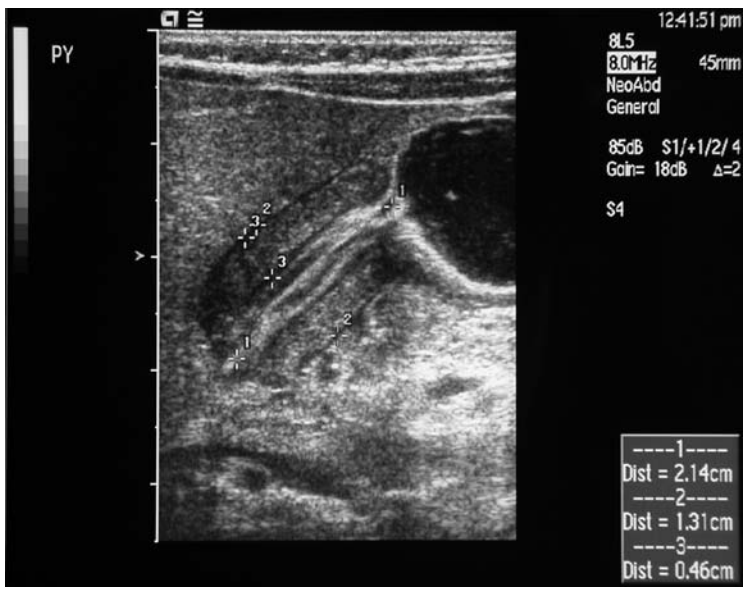

GI Tract, Pediatric, Specific Problems. Figure 2 Ultrasound appearances in ▶hypertrophic pyloric stenosis. The muscle layer is thickened and the pylorus is elongated.

duodenum. The child can then, quickly, be positioned supine so that the position of the DJ flexure can be accurately assessed without excess contrast in the stomach obscuring the DJ flexure. In normality the DJ flexure should lie to the left (5), of the superimposed pedicle of the vertebral body and the height of the DJ flexure should be at approximately the level of the pylorus thereby completing the normal "C" shape of the duodenum. An acute volvulus will show a spiralling or corkscrew appearance of the upper small bowel, typically from the third or fourth part of the duodenum and including the upper jejunum (Fig. 4). If the volvulus is especially tight there may be a complete obstruction at the level of the duodenum and in this case it is difficult to distinguish malrotation with volvulus from other causes of duodenal obstruction, such as a duodenal web (6), but volvulus must be presumed till proven otherwise. Emergency surgery is required before the bowel becomes ischemic or infarcts.

Ultrasound can be used to demonstrate the relationship between the superior mesenteric artery and the superior mesenteric vein which is often reversed in malrotation. However, most centers find that whilst this may be helpful as an adjunct it is not secure enough to exclude the diagnosis of malrotation (7) and an upper GI series is still required.

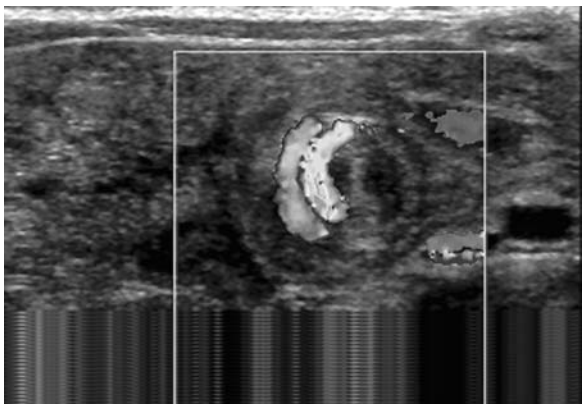

GI Tract, Pediatric, Specific Problems. Figure 3 CDS demonstrating the "whirl pool sign" in a baby with acute volvulus (Courtesy of M. Riccabona, Graz).

Nuclear Medicine

Not applicable to any of these entities.

Diagnosis

The diagnosis of intussusception is made by ultrasound as described above, rarely an enema may be performed for confirming the diagnosis before reduction, or it may be incidentally be picked up by an abdominal CT performed for unclear abdominal symptoms.

Diagnostic criteria of HPS are detailed above.

The diagnosis of volvulus is sometimes made by plain film and surgery, sometimes by US, or an upper GI series

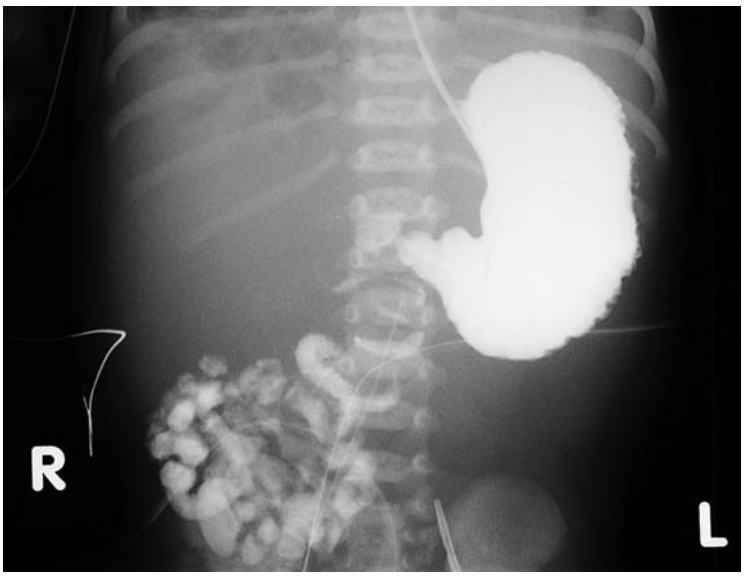

GI Tract, Pediatric, Specific Problems. Figure 4 An upper GI series in a neonate with malrotation and volvulus. Note the spiral, or corkscrew, of contrast in the volved small intestine. The duodenojejunal flexure lies medial to the left pedicle of the superimposed vertebral body and most of the small bowel lies to the right side of the abdomen.

may be performed. Asymptomatic malrotation is diagnosed by an upper GI series and confirmed at surgery, US can only offer indirect signs and neither prove nor rule out malrotation unless there is an acute volvulus.

Interventional Radiological Treatment

Nonsurgical reduction is the treatment of choice in ileocolic intussusception. Barium or water-soluble contrast media have been used for the hydrostatic reduction of intussusception in the past but these techniques have largely been replaced by the use of the ▶air enema under fluoroscopic guidance, or ultrasound guided hydrostatic or air reduction (8). The fluoroscopic guided air enema is currently the most universal procedure but as experience grows ultrasound guided reduction is likely to become the method of choice, avoiding the need to use ionizing radiation. The principle of reduction is to raise the intraluminal pressure in the distal colon to push the intussusceptum retrogradely along the colon, thereby reducing the intussusception, until it is completely resolved, usually through the ileocaecal valve. Complete reduction is achieved when either air or contrast media flood back into multiple loops of terminal ileum. Success rates of between 70% and 90% are reported. Pneumatic reduction can occasionally be successful in ileo-ileal intussusception but this is more commonly treated by surgery; but note that ileo-ileal intussusceptions often resolve spontaneously without treatment.

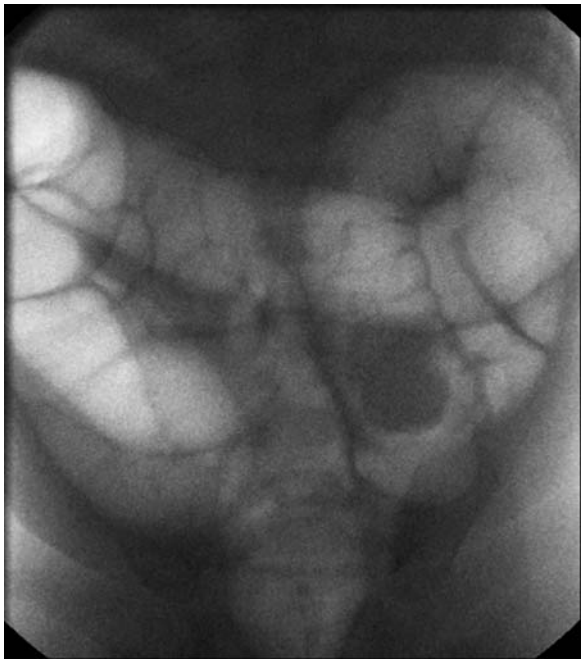

GI Tract, Pediatric, Specific Problems. Figure 5 Air enema shows the soft tissue filling defect of the intussusception in the mid abdomen outlined by air that has been introduced per rectum.

The procedure is performed by passing a catheter per rectum and insufflating the bowel under fluoroscopic or ultrasound guidance. Air will outline the intussusceptum as a "mass" and it will then be seen to pass retrogradely back along the colon as the air pressure is maintained (Fig. 5). Initially pressures of typically 80 mm of mercury (equivalent) are used, rising to a maximum of 120 mm of mercury. A risk of the procedure is of bowel perforation. This may be due to the bowel already being perforated but the perforation being undetected until the air is introduced, or be secondary to the bowel being ischemic and fragile, and perforating under the pressure of air being used to insufflate the bowel. The risk of perforation is approximately 1% overall (2), but is higher in patients presenting late. Hence air reduction should only be attempted in centers with pediatric surgery available.

No interventional approaches are available in HPS and malrotation with volvulus.

Bibliography

1. Hernanz-Schulman M (2003) Infantile hypertrophic pyloric stenosis. Radiology 227(2):319–331
2. Daneman A, Navarro O (2003 and 2004) Intussusception. Part 1: a review of diagnostic approaches. And Part 2: An update on the evolution of management. Pediatr Radiol 33(2):79–85 and 34(2):97–108
3. Cohen HL, Blumer SL, Zucconi WB (2004) The sonographic double-track sign: not pathognomonic for hypertrophic pyloric stenosis; can be seen in pylorospasm. J Ultrasound Med 23(5): 641–646
4. Rohrschneider WK, Mittnacht H, Darge K et al (1998) Pyloric muscle in asymptomatic infants: sonographic evaluation and discrimination from idiopathic hypertrophic pyloric stenosis. Pediatr Radiol 28(6):429–434
5. Strouse PJ (2004) Disorders of intestinal rotation and fixation ("malrotation"). Pediatr Radiol 34(11):837–851
6. Berrocal T, Torres I, Gutierrez J et al (1999) Congenital anomalies of the upper gastrointestinal tract. Radiographics 19(4):855–872
7. Millar AJ, Rode H, Cywes S (2003) Malrotation and volvulus in infancy and childhood. Semin Pediatr Surg 12(4):229–236
8. Yoon CH, Kim HJ, Goo HW (2001) Intussusception in children: US-guided pneumatic reduction–initial experience. Radiology 218(1):85–88

Giant Cell Tumor

Giant cell tumor of bone is a benign osseous lesion with a tendency for aggressive growth and local recurrence.
▶Neoplasms, Bone, Benign

Giant Shining Corners

Giant shining corners exhibit a large triangular-shaped sclerosis of the anterior vertebral corner and refer to an osteitic focus in SAPHO.

▶Spondyloarthropathies, Seronegative

Giant Ulcer

A giant ulcer is a gastric or duodenal ulcer greater than 2 cm.

▶Ulcer Peptic

Gigantism

▶Acromegaly

Globus

A sensation of a lump in the throat that is usually an indication of the presence of gastro-oesophageal reflux.

▶Hernia, Hiatus in Adults

Glomerular Disease

▶Glomerulonephritis

Glomerular Filtration Rate

The quantity of glomerular filtrate produced each minute by all nephrons in both kidneys. Average GFR is about 125 mL/min (10% less for women). About 99% of this is reabsorbed; the rest is excreted as urine.

▶Tubular Necrosis, Kidney, Acute

Glomerulonephritis

Fulvio Stacul, Michele Bertolotto, Cristiana Gasparini, Manuel Belgrano, Elena Trincia
Department of Radiology, University of Trieste, Trieste, Italy
fulvio.stacul@aots.sanita.fvg.it

Synonyms

Glomerular disease; Glomerulopathy; GN; Nephritis

Definitions

Glomerular diseases are classified as primary and secondary. Primary glomerulopathies are those disorders that affect glomerular structure, function, or both in the absence of a multisystem disorder. The clinical manifestations are predominately the consequence of the glomerular lesion, and lead to a variety of clinical syndromes.

The terms glomerulonephritis, glomerulopathy, and glomerular disease are usually used interchangeably to denote glomerular injury, although some authors reserve the former term for injury with evidence of inflammation such as leukocyte infiltration, antibody deposition, and complement activation.

Pathology/Histopathology

The glomerular tuft is composed of four major components: the endothelial cells, the podocytes, the mesangium, and the capillary loop basement membrane. The capillary wall carries a net negative charge, and acts as both a charge-selective and size-selective filter. The filtration of albumin, a negatively charged molecule, is restricted to a greater extent than is the filtration of neutral molecules of an equivalent size. In patients with glomerulonephritis, the negative charge of the glomerular capillary wall is lost resulting in enhanced filtration of negatively charged molecules. ▶Proteinuria is often the first indication of glomerular disease.

Antibody-mediated and cellular immune responses have been implicated in the pathogenesis of the majority of glomerulonephritis. Final diagnosis of the different forms is based on findings at renal biopsy. In particular, minimal change disease is characterized at electron microscopy by diffuse effacement of the podocyte foot processes. At light microscopy, the appearance of glomeruli, tubules, and interstitium is normal. No immune deposits are detected.

Membranous glomerulonephritis is an antibody-mediated disease in which the immune complexes localize to the subepithelial aspect of the capillary loop. Focal segmental glomerulosclerosis presents with capillary loop collapse, hyaline and lipid deposition and often adhesion to Bowman's capsule. The remainder of the glomerular tuft is normal in appearance. Ultrastructurally, the glomeruli show effacement of podocyte foot processes. Poststreptococcal glomerulonephritis is the most common form of acute postinfectious glomerulonephritis and occurs following a skin or pharyngeal infection with Group A beta-hemolytic streptococci. These glomerulonephritis are immune complex mediated. The glomeruli show diffuse mesangial proliferation and endocapillary proliferation accompanied by infiltration of neutrophils and mononuclear inflammatory cells. The main pathologic finding in rapidly progressive glomerulonephritis is fibrinoid necrosis. Extensive crescent formation is present in at least 50% of glomeruli. IgA nephropathy is an antibody-mediated glomerular disease in which the immune deposits localize to the mesangium. Membranoproliferative glomerulonephritis presents with proliferation of mesangial and endothelial cells and expansion of the mesangial matrix, thickening of the peripheral capillary walls by subendothelial immune deposits and mesangial interposition beneath the endothelium.

Clinical Presentation

Several clinical syndromes related to glomerulonephritis have been described. Nephrotic syndrome consists of massive proteinuria, hypoalbuminemia with edema, lipiduria, and hyperlipidemia. Acute nephritis, or nephritic syndrome, consists of the abrupt onset of hematuria, proteinuria, ►azotemia, and hypertension. Rapidly progressive glomerulonephritis is characterized by features of nephritis and progressive renal insufficiency. Although much overlap exists, glomerular diseases may be classified by their predominant clinical manifestations. Indeed, minimal change disease, membranous glomerulonephritis, and focal segmental sclerosis often present clinically as a nephrotic syndrome, while acute postinfectious glomerulonephritis and rapidly progressive glomerulonephritis usually present as a nephritic syndrome. IgA nephropathy and membranoproliferative glomerulonephritis can present both clinical manifestations.

Virtually all forms of acute glomerulonephritis can progress to chronic glomerulonephritis. This condition is characterized by irreversible and progressive glomerular and tubulointerstitial fibrosis, ultimately leading to a reduction in the ►glomerular filtration rate, increased ►serum creatinine, and progressive ►renal failure.

Imaging

Urography and angiography are not indicated to evaluate glomerular disease, but they have been used in the past in these patients as well to rule out obstruction and renal artery stenosis. In patients with acute glomerulonephritis and slight to moderate decrease in glomerular filtration rate renal size is normal or symmetrically increased. Enhancement is normal, or slightly reduced. Angiography shows no significant changes. Severe and rapidly progressive forms of acute glomerulonephritis present with markedly reduced enhancement. Opacification of small peripheral intrarenal vessels is reduced at angiography, and the nephrographic phase is poor.

In chronic glomerulonephritis, renal size is usually reduced. Angiography demonstrates reduced opacification of peripheral branches, delayed wash out of the interlobar arteries, and heterogeneous appearance of the nephrographic phase.

Color Doppler US is the imaging modality of choice in patients with renal disease; however, in patients with glomerulonephritis no specific features are found. In acute glomerulonephritis, the kidneys appear normal or with a variety of pathologic changes that can be observed also in patients with other renal pathologies. The most typical appearance is diffusely increased echogenicity of both kidneys. Renal sinus may appear inhomogeneous at US for fibrosis, atrophy and loss of adipose tissue with a progressive reduction of the differentiation between the renal sinus and the renal parenchyma.

In glomerulonephritides with a prevalent mesangial matrix and basement membrane involvement, such as IgA nephropathy, minimal change disease, membranous glomerulonephritis, cortical echogenicity is usually normal (Fig. 1a). Positive correlation has been observed between renal enlargement and extent of glomerular hypercellularity and crescent formation, and between cortical echogenicity and severity of glomerular sclerosis, crescent formation, interstitial inflammatory cell infiltration, tubular atrophy and interstitial fibrosis (1). Renal cortical echogenicity is closely related to histologically measured average glomerular diameters, which is increased in glomerulonephritis (2), but in the clinical practice quantification of the US signal intensity does not provide useful information. Increased cortical echogenicity is more common in patients with advanced disease and associated vascular or tubulointerstitial involvement such as rapidly progressive glomerulonephritis, and diabetic glomerulosclerosis (Fig. 2a). As results from anatomical correlation studies, most patients with acute glomerulonephritis present with normal appearance of the renal vasculature at color Doppler US (Fig. 1b). Waveform Doppler analysis can be useful to differentiate acute glomerular from

acute tubulointerstitial nephropathies. Indeed, renal RI is usually normal in glomerulonephritis (Fig. 1c) except for rapidly progressive and proliferative forms (Fig. 2b) in which RI may be increased (3). RIs are significantly correlated to the amount of pathologic changes in arteriolosclerosis, glomerular sclerosis, edema and interstitial fibrosis. These findings are nonspecific, and RIs analysis does not distinguish different forms of renal medical disorders.

In chronic glomerulonephritis the kidneys usually appear small, with reduced vascularity, and high RI at Doppler interrogation of the parenchymal vessels (Fig. 3). These changes reflect the anatomical changes of the kidney in which the process has involved also the tubulointerstitial compartment.

CT is not suited to patients with glomerulonephritis because no clinically useful information is obtained and iodinated contrast agents are nephrotoxic.

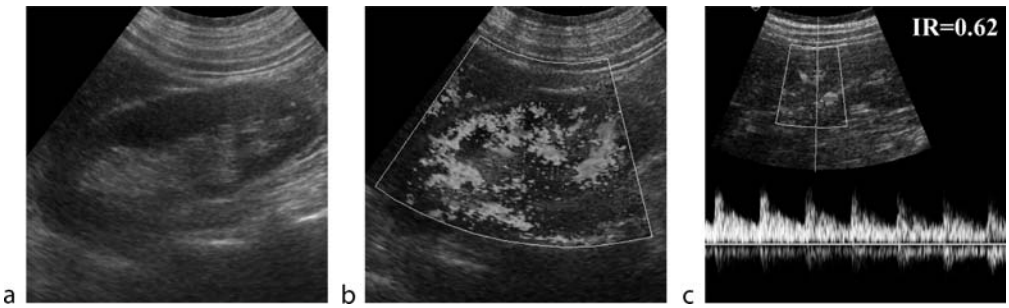

Glomerulonephritis. Figure 1 IgA nephropathy. Kidneys (a) present normal morphological appearance at US. Color Doppler US (b) shows normal vascularization of the renal parenchyma. Normal resistive index (RI) values of 0.62 (c) are recorded at duplex Doppler interrogation of the parenchymal vessels.

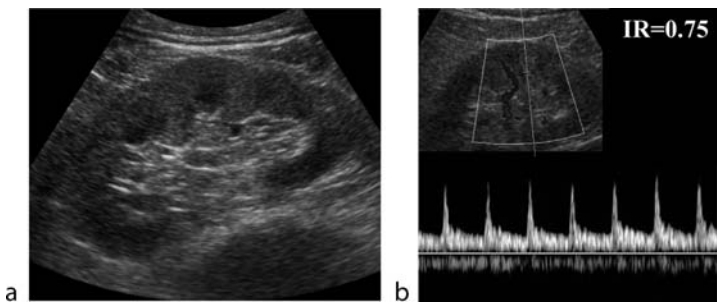

Glomerulonephritis. Figure 2 Rapidly progressive glomerulonephritis. Kidneys reveal a slight increase in cortical echogenicity (a) with an increased cortico-medullary differentiation and at duplex Doppler interrogation (b) increased resistive index (RI) values of 0.75 are recorded.

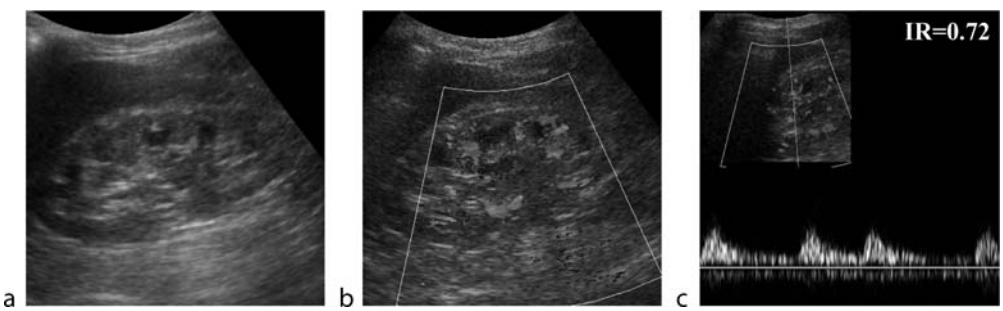

Glomerulonephritis. Figure 3 Chronic glomerulonephritis. Increased cortical echogenicity and cortico-medullary differentiation (a) Renal length is reduced. Color Doppler US (b) shows reduced vascularization of the renal parenchyma. Duplex Doppler interrogation (c) shows increased resistive index (RI) value of 0.72.

Magnetic Resonance Imaging (MRI) is under investigation in animal models to evaluate nephropathies by imaging the macrophages that migrate in the site of renal damage (4). Although these results are promising, however, their value must be demonstrated in human native and transplanted kidneys. Macrophages are usually virtually absent in normal kidneys; however, migration into renal tissues occurs frequently in specific nephropathies such as acute proliferative types of glomerulonephritis, renal graft rejection, and in nonspecific conditions such as hydronephrosis. The macrophagic activity may vary, depending on the type of renal disease and its severity; in glomerulonephritis it predominates in the cortex, whereas in interstitial nephritis or hydronephrosis it is diffused in all kidney compartments. Ultra-small superparamagnetic iron oxide (►USPIO) particles are taken up by phagocytic cells, and could be used as a magnetic resonance contrast agent for exploration of the mononuclear phagocytic activity. Recent experimental studies have demonstrated that USPIO enhanced MRI could have a role in evaluation and differentiation of nephropathies in rat and, in particular, to differentiate glomerular versus interstitial macrophagic infiltration. Since in glomerulonephritis macrophages migrate selectively in the glomeruli, T2*-weighted gradient-echo sequences obtained 24 h after USPIO administration show a significant decrease in signal intensity of the renal cortex, whereas in other nephropathies signal intensity decreases in all renal compartments. Moreover, a strong correlation was observed between the degree of signal intensity variation and the estimate of glomerular damage which may have important implications in clinical practice for the follow-up of patients.

Nuclear Medicine

Radionuclide assessment of GFR is the standard criterion for measuring renal function. However, because it is expensive and not widely available, serum creatinine concentration and creatinine clearance are commonly used. Gallium-67 citrate has an affinity for inflammatory lesions and, clinically, has been used to detect and monitor inflammation. In particular, gallium scan may be useful for evaluation of active or acute lesions and to predict response to therapy in patients with lupus nephritis (5).

Diagnosis

Diagnosis of glomerulonephritis is based on clinics and laboratory findings and usually requires renal biopsy. Imaging findings are not specific, but can provide useful additional information in selected cases and guide biopsy.

Bibliography

1. Page JE, Morgan SH, Eastwood JB, et al (1994) Ultrasound findings in renal parenchymal disease: comparison with histological appearances. Clin Radiol 49:867–870
2. Garra BS, Insana MF, Sesterhenn IA, et al (1994) Quantitative ultrasonic detection of parenchymal structural change in diffuse renal disease. Invest Radiol 29:134–140
3. Platt JF, Ellis JH, Rubin JM, et al (1990) Intrarenal arterial Doppler sonography in patients with nonobstructive renal disease: correlation of resistive index with biopsy findings. Am J Roentgenol 154:1223–1272
4. Hauger O, Delalande C, Deminiere C, et al (2000) Nephrotoxic nephritis and obstructive nephropathy: evaluation with MR imaging enhanced with ultrasmall superparamagnetic iron oxide-preliminary findings in a rat model. Radiology 217:819–826
5. Lin WY, Lan JL, Wang SJ (1998) Gallium-67 scintigraphy to predict response to therapy in active lupus nephritis. J Nucl Med 39:2137–2141

Glomerulopathy

►Glomerulonephritis

Glycogen Storage Diseases

Glycogen storage diseases are inherited metabolic disorders, characterized by glycogen accumulation in tissues. More than 12 glycogen storage diseases are discussed in the literature and most of them have an autosomal recessive transmission. The most common ones include von Gierke disease (glycogen storage disease type Ia), Pompe disease (glycogen storage disease type II), Cori disease (glycogen storage disease type III). Liver and muscles are the most commonly and seriously affected tissues. In type I glycogen storage disease, liver and kidneys are the most severely involved organs. Long-term complications include short stature, hyperuricemia, renal insufficiency, and hepatic adenoma. The most frequent US findings are hepatomegaly, hyperechogenicity of the liver, enlarged kidneys. On CT scans, glycogen deposition results in increased hepatic parenchyma density, whereas fatty infiltration causes a decrease in density. Ultimately, the density of the liver depends on the relative amounts of each component. Biphasic contrast-enhanced CT is mandatory in order to detect and characterize hepatocellular adenomas. Glycogen is characterized by high signal intensity on T1-weighted MR images. Imaging findings are not specific neither sensitive. Biochemical assay for enzyme activity allows the definitive diagnosis.

►Diffuse Infiltrative Diseases, Hepatic

GN

▶Glomerulonephritis

Goitre

term applied to general enlargement of the thyroid gland.
▶Congenital malformations, Thyroid, and Functional Disorders

Golden S-sign

A right upper lobe atelectasis caused by a central obstructing neoplasm, which itself causes the characteristic perihilar bulging of the collapsed lobe.
▶Atelectasis

GORD

▶Reflux, Gastroesophageal in Adults
▶Gastro-oesophageal Reflux Disease

Gout

Giuseppe Guglielmi
Professor of Radiology, University of Foggia, Foggia, Italy,
Department of Radiology, Scientific Institute Hospital San Giovanni Rotondo, Italy
g.guglielmi@unifg.it

Synonyms

Gouty arthritis; King's foot; Podagra; Primary gout; Secondary gout; Tophi

Definition

Gout is a monosodium urate crystal-induced arthritis that results from a systemic metabolic disease. Other typical characteristics include an increased uric acid pool, hyperuricemia, acute (episodic) and chronic arthritis, and deposits of monosodium urate crystals in connective tissue (tophi) and kidneys (1). The classic presentation of gout is podagra or pain in the first metatarsophalangeal joint.

Pathology/Histopathology

Homo sapiens possess a mutated uricase gene, which results in the inactivation of the enzyme. Excess urate leads to extracellular deposition of urate crystals and, since urate solubility decreases with lower temperatures, the deposition favors peripheral joints. Gout then follows when the inflammatory response is triggered.

The difference between uric acid production and disposal determines the total-body pool. The latter is the result of xanthine oxidase on purine bases (dietary purines, nucleic acids of senescent cells, and metabolic turnover of cellular purine nucleotides). Most urate is eliminated by urinary excretion, whereas approximately one-third is eliminated by bacterial degradation in the gut.

Approximately 10% of patients have an overproduction of urate and the vast majority has a reduced clearance of filtered urate despite normal renal function. Both hyperuricemia and idiopathic gout are associated with obesity and hypertriglyceridemia. Other risk factors include: exposure to lead, a high dietary intake of purine rich foods (red meat, liver, and fish), medications which impair renal excretion (aspirin, diuretics, levodopa, and cyclosporine), diabetes, kidney disease, family history, age, and gender.

Neutrophils play an important role in acute inflammation in gout. They ingest monosodium urate crystals and then release leukotrienes, interleukin-1, and glycoproteins which amplify neutrophil infiltration. Activated neutrophils produce superoxide and release lysosomal enzymes that induce pain, vasodilation, and vascular permeability and contribute to chronic articular destruction and tissue necrosis. Gout develops in less than 5% of individuals with hyperuricemia. Differences in protein modulators between gouty and non-gouty individuals account for the variability in inflammatory response to urate crystals.

Clinical Presentation

One of the oldest known diseases, gout was first described more than 2,000 years ago. In the past, it was often called

"the disease of kings" because it was associated with the wealthy who overindulged in food and drink. Today, it affects approximately 0.5–0.7% of men and approximately 0.1% of women (2). The incidence in families with individuals with gout ranges from 6 to 80%. Gout most often occurs in middle-aged men and postmenopausal women.

The most frequent early manifestation of gout is fulminating arthritis affecting only one joint (75% of the initial attacks), often the metatarsophalangeal joint of the first toe (50%, called podagra), but the tarsal joint, ankle, heel, knee, wrist, and elbow (in descending order of frequency) can also be affected. The first episode frequently begins at night with intense pain and swelling. The joint rapidly becomes warm, red, and tender with a clinical appearance that is similar to cellulites. The initial attacks spontaneously subside with complete recovery within hours for mild attacks and days for severe attacks. The patient then reenters an asymptomatic phase ("intercritical" or "interval" gout) (2). Very severe attacks may be associated with fever, leukocytosis, and an increased erythrocyte sedimentation rate (2). Polyarticular acute gout may be seen in hypertensive male patients with an ethanol abuse problem or postmenopausal women. Inflamed Heberden's or Bouchard's nodes may be a first manifestation of gouty arthritis (1).

Repeated acute attacks cause chronic nonsymmetric synovitis in a portion of gouty patients. This condition may be confused with ►rheumatoid arthritis. Less frequently, these attacks will be the only manifestations and even less frequently, inflamed or noninflamed periarticular tophaceous deposits without chronic synovitis are the only manifestation (1).

Imaging

Early findings in gout are limited to soft tissue modifications, typically an asymmetrical swelling around the affected joint. Edema of the surrounding soft tissue may be present. After repeated episodes, a cloudy area of increased opacity may be seen on plain film radiographs. The first bony changes usually appear in the first metatarsophalangeal joint and occur during the intermediate phase. These cystic changes are located outside the joint or in the juxta-articular area and are described as punched-out lytic lesions that can progress becoming sclerotic with an increase in size. Fractures can be present in severe cases. Hallmark findings in the later stages are numerous interosseous tophi and severe symptomatic joint space narrowing. Marked deformities, subluxation, and calcification in soft tissue may also be present. Sometimes, in earlier stages or less progressive disease only degenerative changes of the first metatarsophalangeal joint may be found (Fig. 1).

Computed tomography is useful for the visualization of findings that cannot be clearly visualized on plain film radiology.

Magnetic resonance (MR) imaging is not routinely used as an imaging examination of gout. It may be a useful

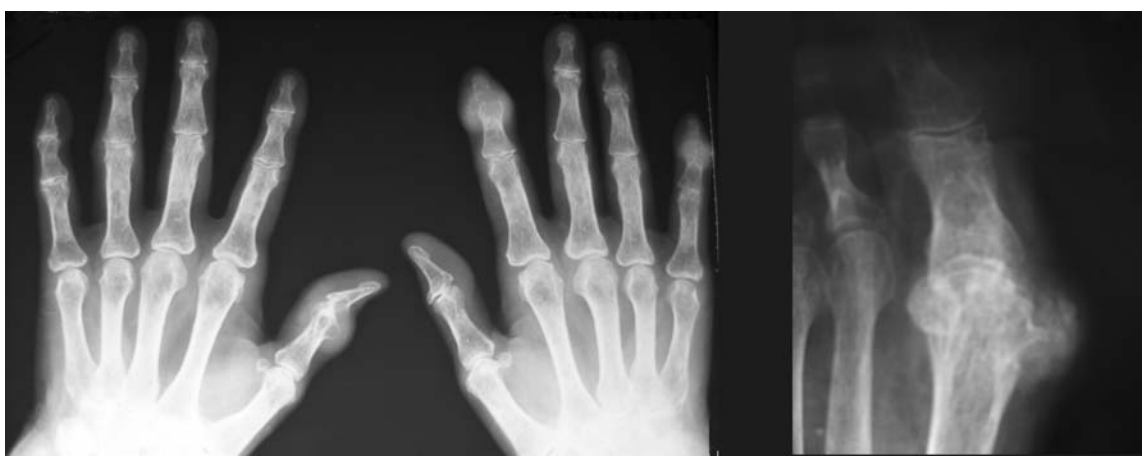

Gout. Figure 1 Anteroposterior radiographs of the hands and feet of an 84-year-old woman presenting with pain and swelling of the first finger of the left hand and the second and fifth fingers of the right hand. Peripheral erosion of the distal interphalangeal joint of the first digit of the left hand and the second and fifth digits of the right hand can be observed. Subchondral cysts and thickening of the periarticular soft tissue are also present. A reduction of the joint space of the metatarsophalangeal joint of the first toe associated with calcification of the articular cartilage and a partially calcified bursitis can be observed. Erosive changes of the medial surface of the metatarsal head are also visualized.

imaging technique for the differentiation of a gouty tophus from an infectious or neoplastic process (3). On MR images, gouty tophi can sometimes present as tumor-like lesions both in the bones and the soft tissues, and without a clinical history it may be difficult to separate these entities.

Nuclear Medicine

Nuclear medicine studies can be a useful tool for confirming the presence of the disease when a suspicion arises and for measuring the extent of gouty arthritis. The characteristic findings in a triple-phase bone scan include increased activity seen in the affected area in all three phases.

Diagnosis

Gout should be suspected in cases of severe inflammatory arthritis with a sudden onset, especially if only a single joint of a lower extremity is affected and if there is a history of repeated attacks with asymptomatic periods in between (1). Suspicion of gout can be confirmed by needle aspiration of the tophaceous deposits, if present, or the synovial fluid of acutely or chronically inflamed joints. The effusion may have an abnormal appearance due to the presence of leukocytes (cloudy) and large amounts of crystals (thick pasty or chalky) (2). Negatively birefringent, needle-shaped sodium urate crystals under polarized light microscopy confirm the diagnosis. The leukocyte count can range from 500 to over 50,000 depending on the acuteness of the inflammation (2). Cell culture and gram staining procedures should always be performed to evaluate the presence of an infection. The underlying metabolic disease can be evaluated by arthrocentesis of the first metatarsophalangeal joint and knees, which often present crystals even between gout attacks.

Serum uric acid levels can be normal but are almost always elevated at some point of the disease. Analysis of the uric acid content of a 24-h urine collection can indicate an elevated excretion (>800 mg/24 h) suggesting overproduction. Elevated urinary uric acid excretion, a risk factor for renal stones, indicates allopurinol as treatment rather than uricosuric drug therapy.

Other pathologies that must be considered in the differential diagnosis of gout include: ▶pseudogout, ▶acute rheumatic fever (▶Rheumatic Fever, Acute), rheumatoid arthritis, traumatic arthritis, ▶osteoarthritis, ▶pyogenic arthritis, sarcoid arthritis, ▶cellulitis, bursitis, tendinitis, and thrombophlebitis (2). Many of these conditions can coexist with gout.

Bibliography

1. Reginato AJ (2004) Gout and Other Crystal Arthropathies. In: Kasper DL, Braunwald E, Fauci A et al (eds) Harrison's Principles of Internal Medicine. 16th edn. McGraw-Hill Professional New York, USA, pp 2046–2049
2. Hershfield MS (2003) Gout and Uric Acid Metabolism. In: Goldman L, Ausiello D (eds) Cecil Textbook of Medicine. W. B. Saunders Company, pp 1703–1708
3. Yu JS, Chung C, Recht M et al (1997) MR imaging of tophaceous gout. Am J Roentgenol London, UK 168:523–527

Gouty Arthritis

▶Gout

Graafian Follicle

The largest ovarian follicle that attains a size of 15–25 mm at midcycle in women of reproductive age. It displays thin walls and can be identified partially protruding from the ovarian surface.

▶Cyst, Follicular, Ovarium

Gradenigo's Syndrome

A syndrome characterized by ipsilateral abducens nerve (sixth cranial nerve) paralysis, severe pain in the area supplied by the ophthalmic branch of the trigeminal nerve (fifth cranial nerve), and an intercurrent inflammatory diseases of the inner ear, mastoid sinus, or both. Other symptoms are photophobia, excessive lacrimation, fever, and reduced corneal sensitivity.

▶Temporal Bone, Inflammatory Diseases, Acute, Chronic

Graf Classification

An ultrasound classification based on hip morphology (1) that characterizes normal, immature, and frankly dislocated hips in infancy.

▶Dysplasia, Hip, Developmental

Granular Cell Tumour

Benign tumour derived from Schwann cells with prominent granularity in the cytoplasm.
▶Breast, Benign Tumours

Granulocytic Sarcoma

▶Hepatic Sarcoma

Granulocytic Sarcoma, Hepatic

Extramedullary tumor composed of immature precursors of myeloid cells. Usually this tumor appears before, during, or after an acute myeloid leukemia, chronic myeloproliferative disorders, or myelodysplastic syndromes. Histologically, it may resemble hepatic infiltration due to acute myeloid leukemia.
▶Hepatic Sarcoma

Granuloma

Rounded conglomerate of epithelioid cells, multinucleated giant cells, and lymphocytes. "Caseating versus noncaseating" is a gross descriptor. Necrotizing and nonnecrotizing granulomata are the appropriate histologic descriptors, although these are not mutually exclusive.
▶Sarcoidosis, Musculoskeletal System

Granulomatous Disease in Childhood, Chronic

An error of body defense in which white cells can ingest, but not kill, organisms that do not contain hydrogen peroxide. Also known as Landing-Shirkey disease, it is a dysfunction of the phagocytic oxidative mechanism secondary to a genetic defect in the phagocytic oxidase enzyme.
▶Osteomyelitis, Neonates, Infants, Childhood: Including Septic Arthritis and Other Important Soft Tissue Infections/Abscesses

Granulomatous Enteritis

▶Crohn Disease

Granulomatous Enterocolitis

▶Crohn Disease

Granulomatous Lobular Mastitis

Affection of the breast lobule with noncaseating granulomata and microabscesses.
▶Inflammation, Breast

Granulosa Cell Tumors

Granulosa cell tumors are sex cord stromal neoplasms and comprise less than 5% of ovarian malignancies. However, they account for the majority of hormonally active ovarian tumors. Estrogen effects may induce precocious pseudopuberty or postmenopausal bleeding.
▶Masses, ovarian

Granzyme B, Perforin

Proteins released by an effector cell (cytotoxic T cell), inducing apoptosis in target cells by forming transmembrane pores and through cleavage of effector caspases such as caspase 3.
▶Apoptosis

Graves' Disease

An autoimmune disease of the thyroid gland, usually presenting with hyperthyroidism.
▶Thyroid Autoimmune Diseases
▶Congenital malformations, Thyroid, and Functional Disorders

Grawitz Tumor

▶Carcinoma, Renal Cell

Greulich–Pyle Bone Age

Bone age estimation by overall visual comparison to gender specific standard images from the atlas of Greulich and Pyle, with number of months deviated from the mean also stated.
▶Bone Age

Gynecomastia

Karin Bock, Volker Duda
University of Marburg, Germany
bock@med.uni-marburg.de
duda@med.uni-marburg.de

Synonyms

Medical subject headings (MeSH)

- Male breast enlargement
- Breast enlargement, male
- Enlargement, male breast

Definition

Nonneoplastic enlargement of the male breast, characterized by hyperplasia of ductal and stromal elements.

Physiological gynecomastia is normally observed in newborns, adolescents, and aging males, that is, in periods of hormonal instability. Thus, gynecomastia can affect approximately 30% of healthy men, as shown in autopsy studies (1).

In contrast, enlargement of the breast almost entirely due to fat deposition is termed pseudogynecomastia or adiposomastia.

Pathology/Histopathology

Histologically, the normal male breast contains subareolar ducts comparable to those in prepubertal girls. Due to hormonal stimulation, these ducts can increase in number, elongate, and branch. Proliferation of epithelial and myoepithelial elements appears, causing increased vascularity and cellularity of the surrounding stroma, with edema being a common component. Because lobule formation is very rare in men, fibroadenoma or cysts seldom develop.

Gynecomastia is not only associated with endogenous hormonal instability, but also with exogenous factors influencing hormonal levels, such as hepatic and renal disease, thyroid dysfunction, hormone-producing tumors, and numerous drugs (e.g., cardiac glycosides, diuretics, antacids, antiretroviral therapy for HIV, marijuana, anabolics).

Whether gynecomastia is a risk factor for male breast cancer is unclear, although it has been reported in association with male breast cancer.

Clinical Presentation

Gynecomastia has a range of manifestations. The condition can occurs bilaterally or unilaterally as a diffuse thickening or a disk-like formation under the nipple. Associated pain, tenderness, and soreness are common complaints. Axillary nodal enlargement may occur despite the benign etiology.

Imaging

Mammography

In gynecomastia, stimulated subareolar ducts and periductal fibrous tissue appear as triangular areas of more or less water-dense tissue radiating form behind the nipple into the periphery of the breast. Right behind the nipple, ducts and periductal fibrosis appear as nearly homogeneous as they are packed closely. The size of the water-dense tissue equals the degree of stimulation and is most prominent in the proliferative phase (2).

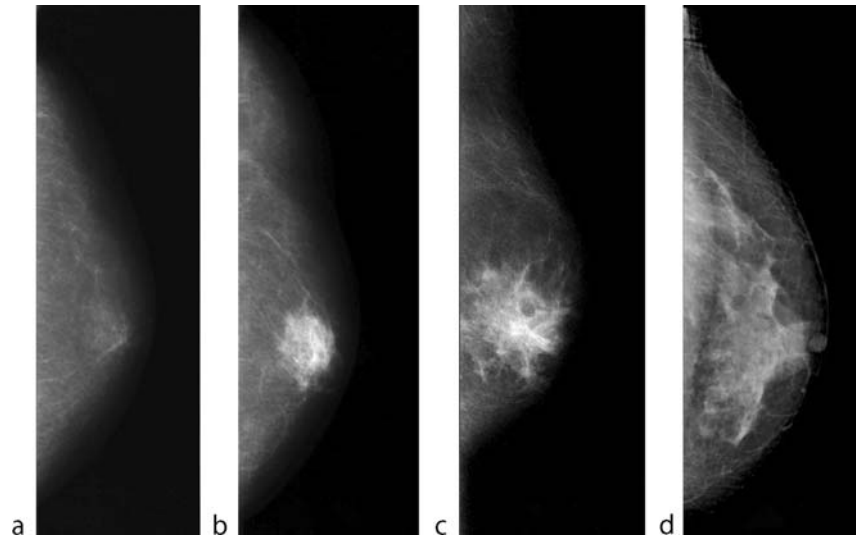

Gynecomastia. Figure 1(a–d) Mammographic imaging of male breast enlargement (cc views). (a) Adiposomastia, i.e., fatty tissue only. (b) Gynecomastia nodularis, that is, convex margins of water-dense region behind nipple. (c) Gynecomastia dendritica; that is, serrated margins of water-dense region behind nipple. (d) Gynecomastia diffusa; i.e., concave margins, widely spread water-dense tissue.

Enlargement of the male breast lacking prominent water density in the subareolar region is a sign of adiposomastia or so-called pseudogynecomastia (Fig. 1a).

Mammographically, three different types of true gynecomastia can be distinguished:

- Gynecomastia nodularis with convex margins, which makes it difficult to clearly distinguish between gynecomastia and subareolar masses (Fig. 1b).
- Gynecomastia dendritica with serrated margins, especially prominent in the deep margins, caused by widely diverging ducts with insatuated fatty tissue (Fig. 1c).
- Gynecomastia diffusa, displaying mostly concave margins, comparable to the distribution of regular female breast tissue (Fig. 1d).

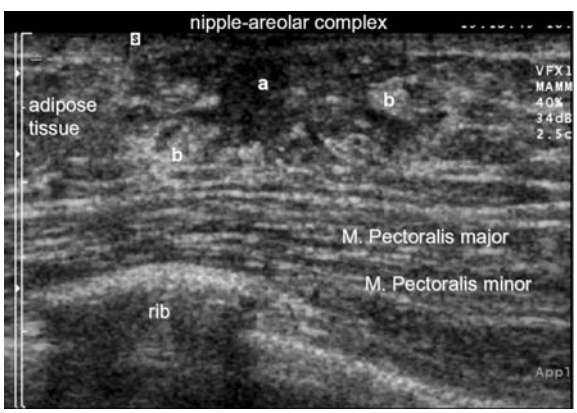

Gynecomastia. Figure 2 B-mode sonography 10 MHz (Siemens, Sonoline Elegra®) of mixed-phase gynecomastia; prominent hypoechoic ducts (a) embedded in hyperechoic dense fibrous tissue (b).

Ultrasound

The sonographic appearance of gynecomastia varies depending on the proliferative activity.

The typical appearance of proliferative-phase gynecomastia is dominated by stimulated, hypoechoic, and markedly enlarged subareolar ducts. These individual ducts are poorly defined and cannot be demonstrated sonographically as separate structures, but appear mass-like, which makes it difficult to distinguish them from nodular masses. Proliferating gynecomastia can display angular margins and a branch pattern and sometimes microlobulation. An increased metabolic activity is often associated with visibly increased color flow.

The quiescent phase of gynecomastia is dominated by hyperechoic periductal stromal fibrosis; residual small ducts might be seen.

A third, mixed phase reflects the presence of both prominent hypoechoic ducts and markedly hyperechoic dense periductal fibrosis (3), (compare Fig. 2).

Multimodal Diagnosis

The combination of clinical findings, mammography, and breast ultrasound improves the diagnostic confidence. Nevertheless, a normal imaging evaluation should never overrule a strongly suspicious finding on physical examination.

Diagnosis

Physiological gynecomastia, diagnosed by the patient's history including illness, medication, nutrition, and drug abuse, does not require imaging testing. When an underlying etiology for breast enlargement cannot be identified from history and physical examination, imaging is warranted to exclude primary or metastatic breast cancer or paraneoplastic estrogen production.

The imaging modality should be chosen in accordance to the patient's age. In boys and young men, the method of first choice should be ultrasound. In older men mammography is recommended, applying the same standards as for women. So far, there is no place for other imaging techniques in the diagnosis of clinical findings of the male breast.

Minimal invasive biopsy, i.e., core needle biopsy, can help in the diagnosis in cases of nodular gynecomastia, where malignancy cannot be excluded after clinical and imaging examinations.

Bibliography

1. Williams MJ (1963) Gynecomastia. Its incidence, recognition and host characterization in 447 autopsy cases. Am J Med 34:103–112
2. Copans DB (1998) The male breast, Chapter 18. In: Kopans DB Breast Imaging. 2nd edn. Lippincott-Raven Publishers, Philadelphia
3. Stavros AT (2004) Evaluation of the male breast, Chapter 16. In: Stavros AT Breast Ultrasound. Lippincott Williams & Wilkins, Philadelphia

Gyration Disorders, Cerebral

Huisman T.A.
Johns Hopkins University, Baltimore, USA
thierry.huisman@kispi.unizh.ch

Synonyms

Anomalies of cortical development; Disorders of neuronal migration

Definition

Spectrum of inherited or acquired congenital malformations characterized by a disruption of the normal architecture of the cerebral cortex.

Pathology and Histopathology

Cortical development results from a complex, programmed sequence of neuronal *proliferation*, *migration*, and cortical *organization* (1–3). Sulcation refers to the infolding of the cerebral surface resulting in multiple, complex branching sulci. The pattern and complexity of the cerebral sulci is tightly related to cortical development.

Subependymal germinal matrix cells begin to *proliferate* into premigratory neurons by the 7th week of gestation. Within the following weeks, these neurons start to *migrate* toward the cortical plate along radial glial cell processes that extend from the germinal matrix to the surface of the brain. Once these neurons have reached the cortical plate, *organization* processes will result in a complex layering of the neurons. The architecture and width of the cortical layers varies between functionally differing cortices.

Cortical malformations or gyration disorders result from a disturbance of the sequence of neuronal proliferation, migration and cortical organization. The etiology is manifold and includes genetic disorders, metabolic diseases, infections, ischemic, or hemorrhagic injuries to the germinal matrix or radial glial fibers or toxic substances ingested by the mother as well as exposure of the fetus to radiation. The timing of interaction with cortical development is essential and may determine severity and extent of cortical malformation.

Anomalies of cortical development can be divided into (A) neuronal migration anomalies and (B) cortical organization anomalies. Neuronal migration anomalies include (a) generalized lissencephalies (Type I and II) and generalized heterotopias as well as (b) focal/multifocal partial lissencephalies and focal/multifocal subependymal/subcortical heterotopias. Cortical organization anomalies include (a) generalized polymicrogyria and (b) focal/multifocal polymicrogyria, schizencephalies and focal cortical dysplasia (FCD) without or with balloon cells (1–3).

In Type I lissencephaly areas of agyria (absence of gyri) and pachygyria (broad gyri with thickened cortex) may coexist. The cortex is composed of a thin outer layer of neurons, an underlying "cell sparse zone" and an inner thick layer of arrested neurons. On gross inspection, the brain surface appears smooth. In Type II lissencephaly, a

thickened cortex with shallow sulci is seen in combination with a characteristic irregular white–gray matter junction (cobblestone appearance). Type II lissencephaly is frequently seen in Walker–Warburg syndrome and Fukuyama's congenital muscular dystrophy.

Heterotopias are collections of normal neurons in abnormal anatomical locations, that is, distant to the cerebral cortex. Heterotopias result from an arrest of neuronal migration along the glial fiber tracts. This may result from infections, ischemia, hemorrhage, or may be genetically determined (X-linked band heterotopia).

In cortical organization anomalies (cortical dysplasias) like polymicrogyria the migrating neurons reach the cortex but the intracortical arrangement is disturbed resulting in multiple small gyri. The width of the cortex may be normal or widened. In FCD, a localized cortical dyslamination occurs. Neurons are frequently enlarged and malorientated throughout both the gray and white matter. In FCD Type II (Taylor), balloon cells accompany the enlarged neurons. The cortex is frequently thickened.

Schizencephaly refers to a cerebral cleft that extends from the brain surface to the ventricular system. The cleft is lined by dysplastic gray matter. The cleft walls may be separated by cerebrospinal fluid (open lip schizencephaly) or adhere to each other (closed lip schizencephaly). The etiology is the focus of ongoing investigation.

Clinical Presentation

Children with lissencephaly are usually severely disabled with psycho-motor retardation. Initial hypotonia frequently evolves into spasticity. Refractory seizures may develop at a very early age. Microcephaly is frequent. In focal heterotopias and in cortical organization anomalies, especially in focal cortical dysplasia, severe therapy refractory seizures may interfere with normal development. In schizencephaly, focal neurological deficits may accompany seizures. The degree of mental retardation is related to the extent of cerebral clefting/malformation. Vision may be limited because of a coexisting hypoplasia of the optic nerves and absence of the septi pellucidi in schizencephaly (1–3).

Imaging

Triplanar MRI combining T1, T2, and FLAIR sequences is essential in evaluating disorders of cortical development. High resolution, thin sliced T2-weighted images are especially helpful in delineating cortical anatomy. FLAIR images may be helpful due to its high lesion conspicuity (e.g., gliosis). Contrast injection is rarely necessary as in disorders of cortical development the blood brain barrier is intact (1–3). Functional MRI techniques like diffusion weighted imaging can be helpful.

Neuronal Migration Anomalies

Lissencephaly

Type I: Also known as agyria–pachygyria complex (Fig. 1a), the brain surface is smooth with shallow sulci. The cortex is significantly thickened with a characteristic T2-hypointense thin outer layer that is separated from a wide deeper layer of arrested neurons by a T2-hyperintense "cell-sparse zone." The junction zone between the deeper layer of neurons and the adjacent white matter is smooth. On axial images, the brain resembles the figure "eight." The sylvian fissures are wide open and vertically orientated. The ventricular system is enlarged.

Type II: The cortex is thickened (pachygyric) with shallow sulci. The gray–white matter interface displays a characteristic irregular junction zone resembling "cobblestones." Hypomyelination of the white matter and hydrocephalus may be observed.

Heterotopia

Generalized heterotopia: This is also known as band heterotopia, laminar heterotopia, or double cortex. The ectopically located neurons are arranged in bands that parallel the surface of the brain or the ventricular contour (Fig. 1b). The width of these bands may vary. The ectopic neurons are T1/T2-isointense with gray matter or cortex. In X-linked band heterotopia, the bands of neurons are usually symmetrically arranged within the white matter of the cerebral hemispheres. The overlying cortical ribbon may be normal or pachygyric.

Focal/multifocal heterotopia: Focal collections of heterotopic neurons may be located anywhere between the cerebral cortex and ventricular system. They are accordingly described as subcortical or subependymal/periventricular heterotopias. On MRI, these focal heterotopias are isointense with the cortex on all imaging sequences. According to their histology, the blood brain barrier is intact and no adjacent white matter edema occurs.

Cortical Organization Anomalies

Generalized Polymicrogyria

Polymicrogyria is characterized by multiple small gyri. The gyri may be too small to be detected on routine imaging or may mimic pachygyria. Thin slices with a

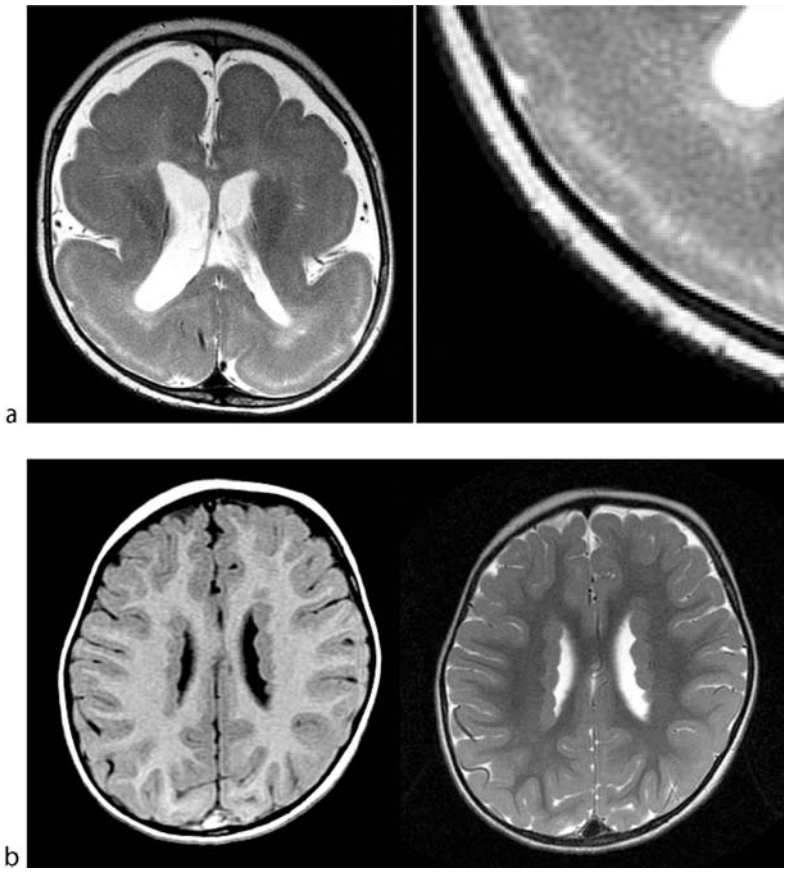

Gyration Disorders, Cerebral. Figure 1 (a) Axial T2-FSE MRI. Type II lissencephaly with a T2-hypointense thin outer layer that is separated from a wide deeper layer of arrested neurons by a T2-hyperintense "cell-sparse zone." The junction zone between the deeper layer of neurons and the adjacent white matter is smooth. The sylvian fissures are wide open and vertically orientated, the ventricular system is enlarged. (b) Axial T1-SE and T2-FSE MRI. Symmetrical, subependymal heterotopia. The heterotopic collection of neurons is isointense to the cortex and result in an undulated lateral border of the ventricles.

good signal-to-noise ratio and a good gray–white matter differentiation are mandatory (Fig. 2a). Symmetrical, bilateral polymicrogyria can be seen in syndromes (e.g., Aicardi) as well as in metabolic diseases (e.g., Zellweger). In addition, polymicrogyria may be seen in congenital cytomegalovirus infection. Depending on the underlying etiology, MRI may reveal additional focal lesions.

Focal Cortical Dysplasia

Focal cortical dysplasia refers to a localized cortical organization anomaly in which the cortex is dyslaminated. In focal cortical dysplasia the involved cortex may have a variable appearance. Pachygyria and polymicrogyria may be seen (Fig. 2b). The dysplastic cortex is usually isointense to normal gray matter. Calcification may occur.

In focal cortical dysplasia Type II (Taylor), the balloon cells may increase the signal intensity of the dysplastic cortex on T2-weighted images. The adjacent white matter may show a T2- and FLAIR hyperintense streak extending into the subependymal region.

Schizencephaly

Closed lip schizencephaly can be identified by the dysplastic gray matter lining the cleft. Open lip schizencephalies are easier to recognize as the opening cerebral cleft is filled with T2-hyperintense cerebrospinal fluid. The clefts connect the ventricles directly with the subarachnoid space. Gray matter may extend to the subependymal zone, mimicking subependymal heterotopia. In closed lip schizencephaly a dimple or focal outpouching of the ventricular wall is frequently identified. Prominent pial

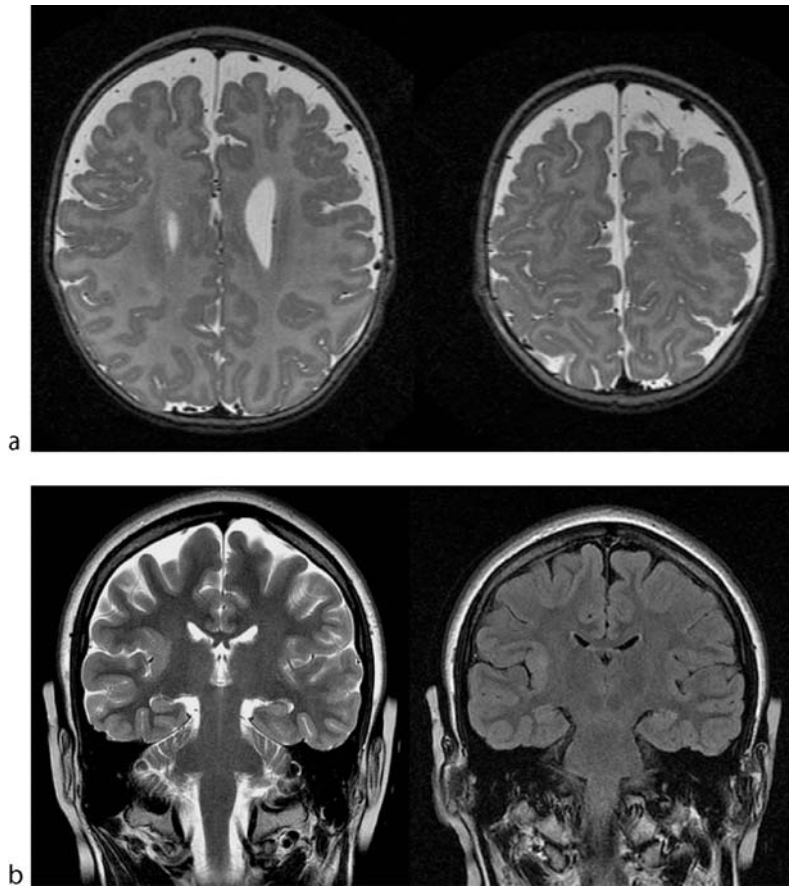

Gyration Disorders, Cerebral. Figure 2 **(a) Axial, high resolution (0.8 mm slice thickness) T2-FSE MRI. Asymmetrical, multifocal polymicrogyria (left > right) of both frontal and central cortices. The multiple small, tightly packed gyri efface the sulcal pattern of the affected areas. (b) Coronal T2-FSE and FLAIR MRI. Focal cortical dysplasia with a pachygyric insular cortex. No additional lesions were seen. The signal intensity of the affected cortex is isointense to the normal cortex.**

vessels are seen along the lateral opening of the cleft. Schizencephaly may be bilateral and the perisylvian area is most frequently affected (Fig. 3). The septum pellucidum is absent in up to 80% of cases, the optic nerves may be hypoplastic.

Nuclear Medicine

Nuclear medicine studies may be helpful to identify small areas of cortical dysplasia. Between seizure activities these lesions are usually hypometabolic/hypoperfused while they may be hypermetabolic/hyperperfused during seizure activity or shortly thereafter (2). PET and SPECT studies are nonspecific and suffer from a limited spatial resolution; the high lesion conspicuity is however very helpful in guiding imaging studies with a high spatial resolution like MRI. Nuclear medicine studies show you where to look; MRI uses this information for highly detailed focused studies.

Diagnosis

Diagnosis relies on a proper neurological examination and electro-encephalography (EEG). High resolution MRI examinations should identify underlying disorders of cortical development. A thorough knowledge about neuronal proliferation, migration, and cortical organization is mandatory to identify and understand the encountered lesions. However, in many cases of refractory seizures no morphological correlate is seen. In those cases, functional MRI techniques including diffusion weighted sequences, perfusion weighted sequences,

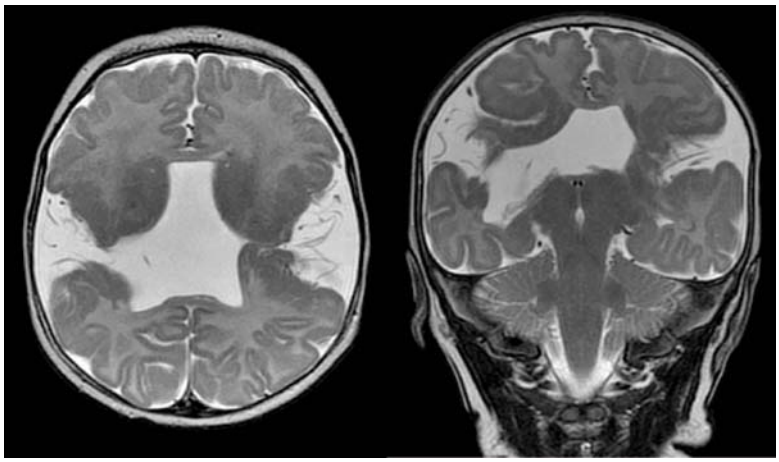

Gyration Disorders, Cerebral. Figure 3 Axial and coronal T2-FSE MRI. Right sided open lip schizencephaly in combination with a left sided closed lip schizencephaly. The septum pellucidum is missing, the ventricles appear "box-shaped." Prominent pial vessels are seen within the lateral aspects of the clefts. Both clefts are within the perisylvian region. The clefts are lined by a dysplastic, pachygyric-polymicrogyric cortex.

MR-spectroscopy and functional MRI (fMRI) with simultaneous EEG-monitoring inside the MRI-scanner should be considered. The simultaneous EEG–MRI–fMRI examination combines the strengths of each individual modality: excellent resolution in time (EEG), high resolution in space (MRI), and event related functional information. These combined examinations are however not yet widely available and time consuming.

Bibliography

1. Osborn AG, Tong KA (1996) Sulcation and cellular migration disorders. In: Handbook of Neuroradiology: Brain and Skull. 2nd edn. Mosby-Year Book, St. Louis, Missouri, pp 146–152
2. Barkovich AJ (2000) Congenital malformations of the brain and skull. In: Pediatric Neuroimaging. 3rd edn. Lippincott Williams and Wilkins, Philadelphia-New York, pp 254–382
3. Ball WS (ed) (1997) Pediatric Neuroradiology. Philadelphia-New York, Lippincott-Raven, 5:146–160

H&E Staining

Haematoxylin and eosin-staining.
►Calcifractions, Breast
►Carcinoma, Ductal, *In Situ*, Breast

H-Fistula

A descriptive term for the configuration of a tracheo-oesophageal fistula that occurs in the absence of oesophageal atresia.
►Oesophageal Disease, Childhood

HADD

Lynne Steinbach
Department of Radiology, University of California, San Francisco, USA
lynne.steinbach@radiology.ucsf.edu

Synonyms

Calcific tendinitis; Calcific tendinosis; Calcium hydroxyapatite deposition disease; Hydroxyapatite rheumatism; Peritendinitis and bursitis; Peritendinitis calcarea

Definitions

Calcium hydroxyapatite deposition disease (HADD) is characterized by periarticular calcifications, usually in tendons near their osseous attachments. Bursae, ligaments and peritendinous tissues may also be affected. This disorder is usually monoarticular and most commonly presents between the ages of 40 and 70 years. Although the etiology is not known, it is thought to be related to either repetitive microtrauma that results in necrotic tissue that takes up the HADD crystals or to a metabolic disorder.

Rarely, HADD can present with intra-articular deposition of crystals, producing an acute arthritis. A milky white effusion may be seen on radiographs. There is also a controversial form of arthropathy that has been called "chronic apatite arthropathy," "apatite-associated destructive arthropathy" (AADA), or "idiopathic destructive arthropathy." It is not known whether this is caused by HADD, but some believe that there is an association. This disorder is common in elderly patients, mostly women (90%) in their seventies. It has a predilection for large joints, including shoulders, hips, and knees. The patients present with joint swelling, reduced range of movement, instability, and loss of function of the affected joint but relatively mild pain and little evidence of inflammation. Large, "cool" synovial effusions are often hemorrhagic and noninflammatory. Radiographically, one sees a rapidly progressive course with evidence of accelerated osteoarthritis, extensive bone destruction, and intra-articular osteochondral bodies.

Pathology/Histopathology

Deposition of hydroxyapatite crystals in fibrous connective tissues, in a typically granular way, can cause an inflammatory synovitis and tendonitis; this may be associated with necrosis and loss of fibrous structure. The deposits appear milky or cheesy in consistency and are chalk-like in quality.

Clinical Presentation

Almost half of the patients present with pain, erythema, swelling, and limitation of motion of the neighboring joint. This is thought to result from rupture of a calcific deposit into an adjacent soft tissue space or bursa causing an acute, self-limited inflammatory reaction. Phagocytosis of hydroxyapatite crystals by neutrophils and macrophages results in the release of lysosomal enzymes and other inflammatory mediators. This is known as acute

►calcific periarthritis. Clinically, HADD can also be accompanied by fever and mimic an infection. A characteristic that distinguishes HADD from infection is that the ESR and leukocyte count are normal.

Treatment is often symptomatic with most symptoms subsiding in less than 2–3 weeks. Nonsteroidal antiinflammatory medication (NSAID) is the treatment of choice. Local corticosteroid injections and oral or parenteral steroids can be used for those who do not tolerate NSAIDs. Symptomatic deposits can also be removed surgically as well as by image-guided needle puncture, aspiration and lavage, and steroid injection if symptoms do not resolve quickly.

Imaging

HADD initially presents on *radiographs* and *CT* as a thin, cloud-like, poorly defined clump of calcification in periarticular soft tissues such as tendons, ligaments, bursas, or synovium. With time, the calcifications become more dense and homogeneous with sharp definition. Deposits may remain static over the years. They can also enlarge, change shape, or disappear. Rarely, the crystal can deposit in the joint. The calcification of HADD is difficult to identify on *MRI* due to the low signal intensity of the calcification and often presents with an aggressive appearance on MRI with marrow and soft tissue edema that simulates infection, injury, or neoplasm. HADD may cause bone erosion (1).

Nuclear Medicine

Skeletal scintigraphy may show increased radiotracer uptake in or around the joints, but these findings are not specific.

Diagnosis

Imaging characteristics and typical diagnostic features of HADD may vary from joint to joint. The most typical and common affected site is the shoulder joint.

Shoulder

The shoulder accounts for 60% of cases of acute calcific periarthritis (2). Periarticular calcifications in one or both shoulders occur in up to 7.5% of adults. Calcifications can be seen in any of the rotator cuff tendons, with the supraspinatus tendon being the most common tendon in the body for HADD deposition. This calcification can be seen near the greater tuberosity on the AP external rotation views of the shoulder. Calcifications of the infraspinatus and teres minor tendons are best seen in profile on internal rotation AP views, lateral to the humeral head (Fig. 1). Subscapularis tendons calcification occurs close to the lesser tuberosity of the humerus. HADD is also seen in the origin of the long head of the biceps above the glenoid fossa, and below the coracoid at the origin of the short head of the biceps and coracobrachialis tendons. Calcification adjacent to the inferior margin of the glenoid indicates HADD at the origin of the triceps tendon. Subacromial subdeltoid bursa calcification appears as a teardrop-shaped radiodense area below the acromion and deltoid muscle. The pectoralis major tendon calcifications are seen along the anterior aspect of the humeral shaft.

Hip

The hip is the second most common site to see HADD. The calcifications usually collect in the gluteus medius tendon near the greater trochanter (Fig. 2) or at the acetabulum. Further down, calcifications are commonly seen at the gluteus maximus attachment along the posterolateral femoral shaft of the femur, best seen on the frog-leg view. Calcifications can also be observed at other tendinous attachments along the femur, including the iliopsoas tendon attachment to the lesser trochanter, and at the hamstring origins along the ischium.

Elbow

HADD is seen in flexor and extensor tendon attachments adjacent to the epicondyles as well as in the collateral

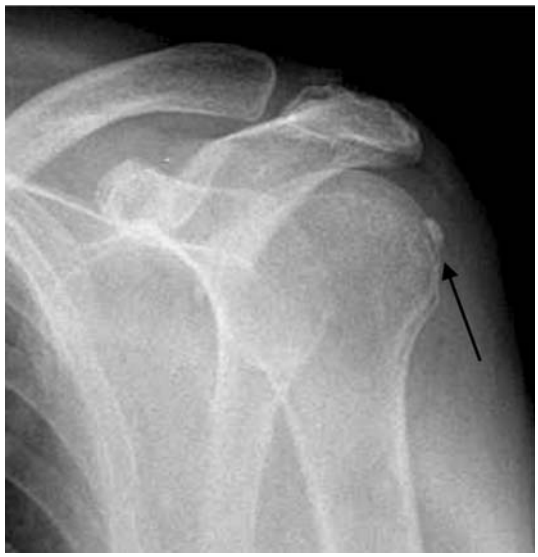

HADD. Figure 1 HADD is identified in the region of the infraspinatus tendon on this AP radiograph of the left shoulder taken in internal rotation (*arrow*).

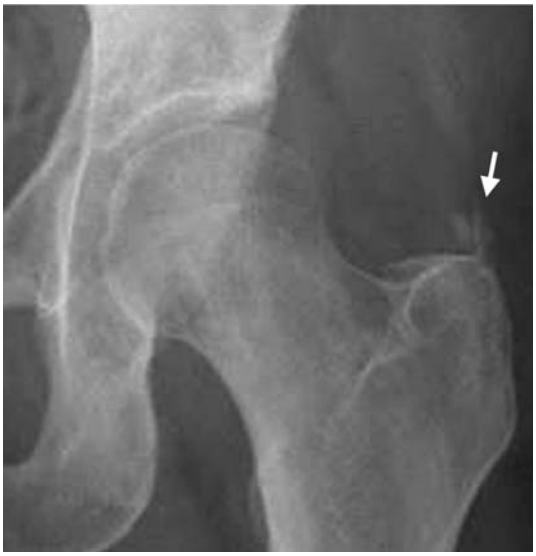

HADD. Figure 2 Calcification consistent with HADD is seen adjacent to the greater trochanter on this AP view of the left hip (*arrow*).

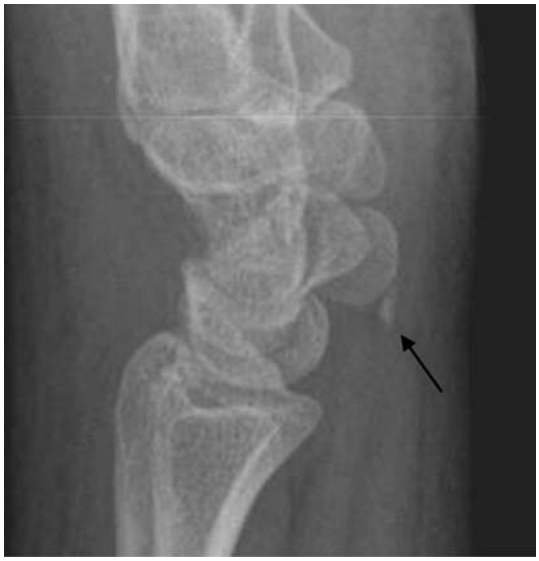

HADD. Figure 3 Just below the pisiform is a homogenous calcification consistent with HADD in the flexor carpi ulnaris tendon on this lateral view of the wrist (*arrow*).

ligaments. It may also be seen at the triceps, brachialis, and biceps tendon attachments on the olecranon, ulnar, and radial tuberosities, respectively. Olecranon bursal calcification has also been described.

Wrist and Hand

Calcifications of tendons and ligaments of the wrist and hand are seen with the wrist involved more frequently than the hand. The most common site of deposition is in the flexor carpi ulnaris tendon near its attachment to the pisiform (Fig. 3). HADD can lead to carpal tunnel syndrome. Calcifications are also common around the metacarpophalangeal and interphalangeal joints.

Knee

In the knee, HADD tends to occur near tendon attachments. Calcifications are most common adjacent to the femoral condyles, fibular head, and prepatellar region. The popliteus tendon and lateral collateral ligament are sites of involvement with HADD that have been recently described in the literature (3).

Ankle and Foot

Calcific deposits may occasionally be identified in the ankle and foot. HADD has been described in the tendons of the flexor hallucis longus and brevis, and the peroneal tendons. In the first metatarsophalangeal joint, hydroxyapatite pseudopodagra as this HADD is known, occurs predominantly in young, premenopausal women. Unlike most other locations, HADD is more common in young, premenopausal women in this latter site (4).

Spine

HADD in the tendon of the longus coli muscle and tendon was first described by Hartley in 1964 (5). This muscle originates from the anterior surfaces of the upper three thoracic and lower three cervical vertebral bodies and inserts into the anterior tubercle of the atlas and the second, third, and fourth cervical vertebrae. The calcification has a predilection for the superolateral portion of the muscle. Patients present with sudden onset of severe pain in the neck and throat exacerbated by swallowing and head movement. Radiographs and CT demonstrate calcification anterior to the upper cervical spine, particularly C2. Soft-tissue swelling accompanies an acute episode and may extend to the thoracic area. A differential diagnosis for calcification in this region includes an ossicle beneath the anterior arch of C1, a calcified stylohyoid ligament, and a horizontal fracture of the anterior arch of C1. Calcifications can also occur elsewhere in the spine including the ligamentum flavum, infraoccipital region, and interspinous bursae, around the odontoid process and in the apophyseal joints.

Differential Diagnosis

A very characteristic homogeneous, cloud-like appearance distinguishes HADD from most other disorders. Finding

the calcifications in the specific sites favored by HADD without an underlying disorder should separate this entity from others in the differential diagnosis. HADD should not be confused with the more linear and diffuse CPPD crystal calcifications described in this article. Gouty tophi are more faintly calcified and are associated with elevated urate levels. Heterotopic bone and myositis ossificans has a trabecular pattern with a cortical rim, which can be distinguished from HADD and CPPD calcifications. ▶Tumoral calcinosis, either primary idiopathic or secondary to renal disease, may mimic HADD if in small amounts. One would look for a metabolic disorder in the latter to try to distinguish this. Collagen vascular disease such as scleroderma or dermatomyositis can also produce calcifications that mimic HADD. These calcifications are usually more widespread, can involve the subcutaneous tissues, and have a known underlying disease to go along with them. Periarticular metastatic calcification may also be seen with metastatic calcification due to sarcoidosis, hypervitaminosis D, hypoparathyroidism, and milk-alkali syndrome.

Bibliography

1. Hayes CW, Rosenthal DI, Plata MJ et al (1987) Calcific tendinitis in unusual site associated with cortical bone erosions. Am J Roentgenol 149:967–970
2. Faure G and Daculsi G (1983) Calcific tendinitis: a review. Ann Rheum Dis 42:49–53
3. Garcia GM, McCord GC, and Kumar R (2003) Hydroxyapatite crystal deposition disease. Semin Musculoskelet Radiol 7:187–193
4. Fleming DJ, Murphey MD, Shekitka KM et al (2003) Osseous involvement in calcific tendinitis: a retrospective review of 50 cases. Am J Roentgenol 18:965–972
5. Hartley J (1964) Acute cervical pain associated with retropharyngeal calcium deposit: a case report. J Bone Joint Surg 46-A:1753–1754

Haemangioma and Haemangioendothelioma in Childhood

Johan G. Blickman[1], Dewi Ashi[2]
[1]Department of Radiology, UMC, Nijmegen, Netherlands
[2]Department of Radiology, Faculty of Medicine, University of Indonesia, Cipto Mangunkusumo General Hospital, Salemba, Jakarta Pusat, Indonesia
j.blickman@rad.umcn.nl

Definition

Hemangioma is a benign vascular tumor with endothelial proliferation. This tumor typically shows a rapid proliferative stage followed by a slower involutional stage. It is the most common benign soft tissue tumor in infancy, occurring in approximately 10% of full-term babies. The female-to-male ratio is 3:1.

Hemangioendothelioma is a benign vascular tumor that occurs in the liver in young infants. It undergoes a rapid proliferative phase and regression. It is the third most common hepatic tumor in children after hepatoblastoma and hepatocellular carcinoma. It may be isolated or diffusely involve the liver. Approximately 85% of affected patients present by 6 months of age, and 50% of patients also have cutaneous hemangiomas. The tumor has a 2:1 female predilection.

Pathology/Histopathology

In hemangioma the tissue reveals proliferating endothelial cells and may also contain other elements such as fat, smooth muscle tissue, myxoid stroma, hemosiderin, thrombus, and even bone.

Infantile hemangioendothelioma manifests as a mesenchymal tumor composed of a connecting network of predominantly small diameter vascular channels lined by endothelial cells. Unlike hemangiomas that contain larger blood-filled spaces with endothelial cell lining, infantile hemangioendothelioma is not an obviously vascular tumor at gross examination of the cut surface. Areas of varying degrees of hemorrhage, necrosis, calcification, thrombosis, or fibrosis are often present in large tumors.

Two types of infantile hemangioendothelioma based on tumor size and vascularity exist: Type I lesions are often calcified and consist of multiple small vascular channels with an immature endothelial cell lining and a fibrous stromal separation containing bile ductules between the channels. Type II lesions have a more disorganized appearance, with an endothelial cell lining and no stromal bile ductules.

Clinical Presentation

Hemangioma

The clinical presentation of hemangioma depends on the depth, location, and stage of evolution. The typical appearance is a slightly raised bluish-red plaque that resembles the surface of a strawberry. Visceral hemangiomas occurring in the liver can present with jaundice, while visceral hemangiomas located in the intestines can result in bloody stool. Hemangiomas located in the airway can produce stridor or dyspnea.

Syndromes associated with hemangioma include *Klippel–Trenaunay syndrome*, characterized by limb

hypertrophy with subcutaneous hemangiomas; *Kasabac–Merritt syndrome,* the association of hemangiomas with disseminated intravascular coagulation; and *PHACE syndrome* (posterior fossa abnormalities, hemangioma of the face, arterial abnormalities, coarctation of the aorta, cardiac defects, and eye abnormalities), which may involve extensive facial lesions.

Multiple cutaneous hemangiomas are associated with concomitant visceral lesions.

Hemangioendothelioma

The clinical presentation of hemangioendothelioma may include a palpable abdominal mass, hepatomegaly, diffuse abdominal distention, and congestive heart failure due to secondary arteriovenous (AV) shunting (less common than in giant hemangioma or AV malformation). These tumors are usually benign, but malignant sarcomas have been reported to arise in existing hemangioendotheliomas.

Imaging

Hemangioma: Plain films may show increased soft tissue density and, rarely, skeletal abnormality. Ultrasound during the proliferative phase shows a variably echogenic mass (Fig. 1). Doppler sonography has shown high vessel density (>5 vessels/cm^2) and peak arterial Doppler shift (>2 kHz) in hemangiomas, which is useful in distinguishing hemangiomas from other vascular malformations.

In the involutional phase, the lesion decreases in size and has a reduced number of vessels.

Computed tomography (CT) and magnetic resonance imaging (MRI) in the proliferative phase demonstrate a homogeneous mass with an intense, persistent, and usually lobular enhancement pattern. Involuting hemangiomas are more heterogeneous with less enhancement.

MRI often demonstrates heterogeneous intermediate signal intensity on T1-weighted images. On T2-weighted images, high signal intensity is seen with a flow void in and around the mass. Hemorrhage or fat deposition is seen as high signal intensity on T1- and T2-weighted images.

Angiography reveals a well-circumscribed mass with intense, persistent tissue staining in a lobular pattern and enlargement of feeding arteries. Angiography is required only if endovascular intervention is contemplated.

Hemangioendothelioma: Plain abdominal radiography may show hepatomegaly and a nonspecific mass effect in the upper abdomen, with displacement of intestinal structures and occasional calcifications within the mass.

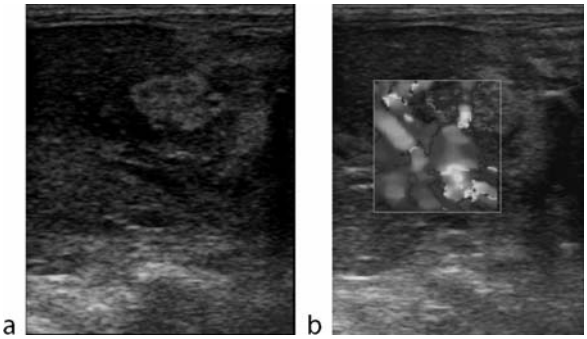

Haemangioma and Haemangioendothelioma in Childhood. Figure 1 Doppler ultrasound shows a highly vascularized lesion in the liver. (cited from Fletcher, 2004)

The appearance of hemangioendothelioma on ultrasound is variable and nonspecific. It may be either hyperechoic or hypoechoic. Most of the tumors have well-defined borders toward the surrounding liver parenchyma. The caliber of the aorta may abruptly decrease below the level of the celiac axis because of increased hepatic arterial flow secondary to intrahepatic AV shunting.

CT shows a well-defined homogeneous or heterogeneous mass, hypoattenuating relative to the normal liver parenchyma. In about 40% of cases there may be calcifications. The postcontrast enhancement pattern resembles that of an adult giant hemangioma (peripheral enhancement in the early phase and central enhancement in the delayed phase). In larger tumors this central enhancement may not occur because of fibrosis, hemorrhage, or necrosis.

On MRI, low signal intensity on T1-weighted images and high signal intensity on T2-weighted images are seen. Flow voids may be observed on T2-weighted images in a tumor with AV shunting and high blood flow. The presence of hemorrhage, necrosis, and fibrosis make the tumor appear heterogeneous both on T1- and T2-weighted images. Postcontrast enhancement is similar to that on CT (Figs 2 and 3).

Angiography is performed only if embolization is considered either as definitive therapy or as a temporizing method prior to transplantation. Characteristically, there is prolonged pooling of contrast within the mass. Internal AV shunting with large draining veins may be seen.

Nuclear Medicine

Hemangioma: Radiolabeled red cell scintigraphy.

Hemangioendothelioma: Nonspecific, early uptake may be seen. Blood pool studies may show increased activity.

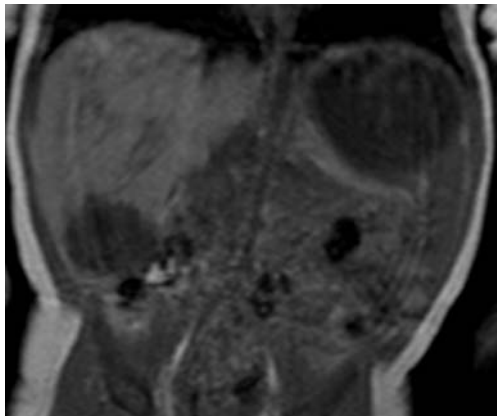

Haemangioma and Haemangioendothelioma in Childhood. Figure 2 On T1-weighted image, a hypointense lesion is seen in the right lobe of the liver.

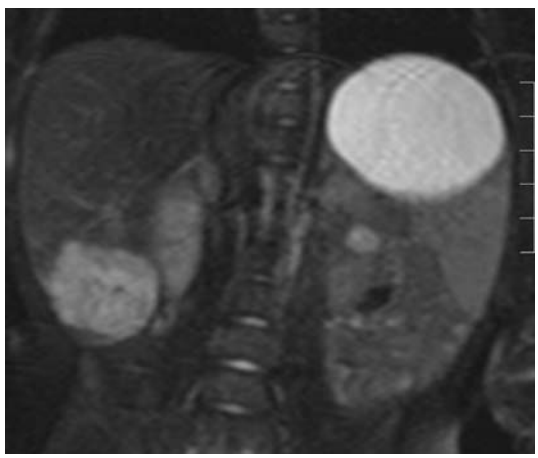

Haemangioma and Haemangioendothelioma in Childhood. Figure 3 On T2-weighted image, the le-

Diagnosis

Most hemangiomas are recognized clinically and do not require imaging. Imaging is required for atypical soft tissue masses, for deep hemangiomas with normal overlying skin, and for evaluation of deep extension of obvious hemangiomas. It is also required for hemangiomas that compromise important structures (subglottic hemangioma, periorbital lesions) or that cause high-output cardiac failure or thrombocytopenia (Kasabach–Merritt syndrome).

Differential diagnosis (Fig. 4):

Vascular malformation:

- Abnormal size and/or number of vascular structures
- Usually manifests as cutaneous birthmarks
- No regression.

The clinical manifestations of infantile hemangioendothelioma are variable. The tumor may be asymptomatic and discovered incidentally, but more often the tumor is large and manifests as hepatomegaly, abdominal distention, and/or a palpable upper abdominal mass. High-output failure and platelet consumption due to significant AV shunting can be present. Hematologic abnormality may be seen, including anemia and thrombocytopenia. The serum -fetoprotein level is usually normal, in contrast to hepatoblastoma. Ultrasound shows one or more solid masses with high flow in color Doppler. MRI shows a well-defined mass with an enhancement pattern resembling that of adult giant hemangioma.

Differential diagnosis:

Hepatoblastoma:

- α fetoprotein level is elevated.

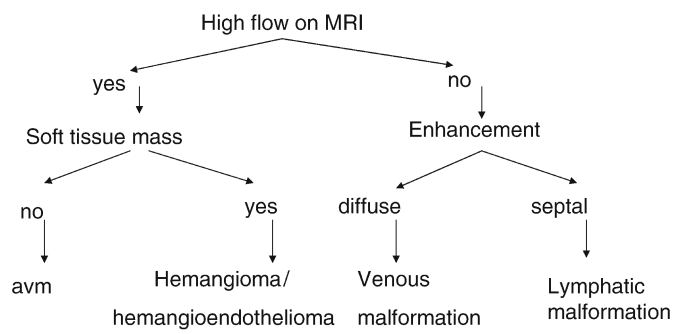

Cited from Fletcher BD. EI: Caffey's pediatric diagnostic imaging

Haemangioma and Haemangioendothelioma in Childhood. Figure 4 Differential diagnosis of hemangioma: algorithm for diagnosing hemangioma versus vascular malformation.

Hepatocellular carcinoma:

- Most common hepatic malignancy in children over 5 years of age
- Rarely occurs under 3 years of age.

Bibliography

1. Pediatric Radiology, 2nd edition, The Requisites. Hans Blickman, MD, PhD, Boston University School of Medicine, Boston, MA. Mosby, 1998
2. Oslo (2001) Paediatric Imaging, edited by Helen Carty, Volume 7, in The Encyclopaedia of Medical Imaging. Edited by Holger Pettersson, MD, PhD, and David Allison, MD, FRCR Lund, Sweden: NICER Institute/ISIS Medical Media
3. Fletcher BD (2004) Soft tissue neoplasms. In: Kuhn JP, Slovis TL, and Haller JO (eds) Caffey's Pediatric Diagnostic Imaging. 10th edn. Mosby, Philadelphia, pp 2017–2018
4. Schlesinger AE, Parker B (2004) Tumor and tumor-like condition. In: Kuhn JP, Slovis TL, and Haller JO (eds) Caffey's Pediatric Diagnostic Imaging. 10th edn. Mosby, Philadelphia, pp 1494–1495
5. ▶http://www.emedicine.com/ped. Arterial Vascular Malformations including Hemangiomas and lymphangiomas. Last updated: October 8, 2004
6. Roos JE, Pfiffner R, Stallmach T et al (2003) Infantile Hemangioendothelioma. Radiographics 23:1649–55

Haemangioma, Hepatic

Marzio Perri, Riccardo Lencioni
Department of Diagnostic and Interventional Radiology University of Pisa, Italy
lencioni@med.unipi.it

Definition

Hepatic hemangiomas are benign, vascular tumors of the liver.

Epidemiology

The prevalence of hemangiomas ranges from 1% to 2% in the general population, the tumor being typically discovered incidentally during evaluation of nonspecific abdominal complaints. The prevalence of hemangiomas has been overestimated in autopsy series (from 2% to as high as 20%), because of overrepresentation of elderly patients with comorbid illnesses. The majority of hemangiomas are small (<4 cm). Liver nodes greater than 4 cm in size are defined cavernous hemangiomas. The reported female:male gender ratios range from 1.6:1 to 6:1.

Pathogenesis

The pathogenesis of hemangioma is unknown. Congenital hamartoma is a likely candidate. A pathogenic role of sex hormones has been postulated, because of consistent female predominance in larger tumors, and tumor enlargement/recurrence in hysterectomized women under estrogen replacement therapy and in patients with a long use of oral contraceptives. Cavernous hemangiomas may have accelerated growth during pregnancy and often display estrogen receptors. However, tumor growth was also induced or influenced by such drugs as metaclopramide.

Pathology and Histopathology

Macroscopically, the tumors are ovoid, soft, reddish-purple or blue masses separated from the surrounding parenchyma by a fibrous pseudocapsule. Varying degrees of fibrosis, hyalinization, calcification, thrombosis, and shrinking are seen. Extensive fibrosis and hyalinization, with narrowing or obliteration of vessels, are typical for sclerosed hemangiomas. Microscopically, hemangiomas are vascular abnormalities characterized by multiple blood-filled sinusoidal spaces and vascular lakes lined by endothelial cells. Vascular channels are separated by a fibrous tissue. They are fed by hepatic artery branches and their internal circulation is slow. Blood vessels and arteriovenous shunting may be seen in large septa. The tumor seems to grow by ectasia rather than by hyperplasia or hypertrophy.

Clinical Presentation

The most common clinical presentation of a hemangioma is an incidental finding on hepatic imaging and the majority of patients will have a single tumor node. A few patients may present with isolated diffuse hemangiomatosis in association with Rendu-Osler-Weber's disease or skeletal hemangiomatosis. Cavernous hemangiomas are typically silent, benign clinically and rarely expanding or symptomatic tumors. The few patients with symptoms complain one of the following: abdominal swelling, abdominal pain, early satiety, anorexia, abdominal mass, and hepatomegaly. There seems to be no correlation between symptoms and number of tumors, as well. Atypical hemangiomas exist that form arteriovenous shunts causing severe symptoms including heart failure. Other unusual clinical presentations of an hepatic hemangioma include hemobilia, inflammatory pseudotumor caused by recurrent intranodal thrombosis, caval thrombosis, portal hypertension, and torsion of a pedunculated tumor.

Imaging

Ultrasound and Contrast-Enhanced Ultrasound

The most common ultrasound (US) appearance of hemangioma is that of a sharply demarcated lesion with uniformly increased echogenicity relative to normal liver. This pattern is observed in about 70% of hemangiomas detected by US. The remaining cases show atypical US patterns, and appear either as hypoechoic lesions with a hyperechoic border or as lesions with heterogeneous internal structure. Heterogeneity is commonly observed in large hemangiomas. While there are no vascular patterns that can be used to reliably diagnose hemangioma with conventional color or power Doppler US, early clinical experience with US contrast agents has suggested that contrast-enhanced ultrasound (CEUS) can provide useful information (1, 2). Most liver hemangiomas (78–93%) show peripheral nodular enhancement during the early phase of the contrast-enhanced study, with progressive centripetal fill-in (Fig. 1)(1, 2). Diffuse contrast enhancement with homogeneous fill-in or persistent hypoechoic appearance due to absent contrast enhancement can be observed in small, high-flow hemangiomas or thrombosed hemangiomas, respectively (1).

Computed Tomography

The standard spiral computed tomography (CT) protocol for suspected hemangioma includes baseline and contrast-enhanced scanning in the arterial, the portal venous, and the delayed phase. Most hemangiomas are hypoattenuating on baseline scans, show peripheral nodular enhancement of vascular attenuation on arterial and portal phase imaging, and are hyperattenuating with possible central hypoattenuation or isoattenuation to vascular space in the delayed phase (Fig. 2). This pattern has a sensitivity of 67–86% and a specificity of 99–100% for the diagnosis of hemangioma. Atypical CT features are observed in hemangiomas with either high flow or very

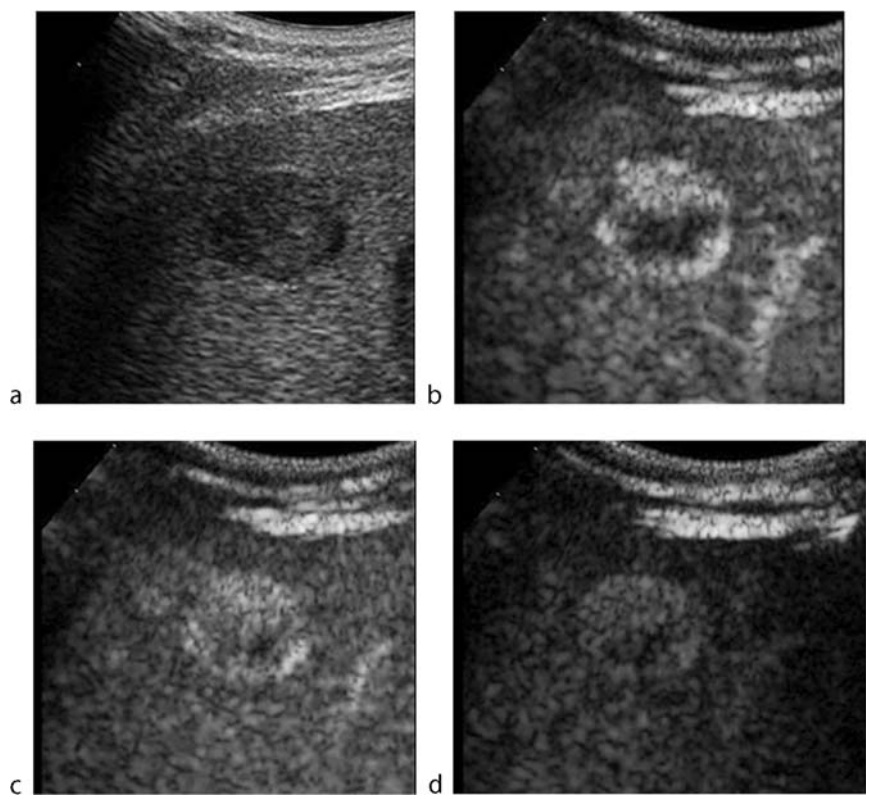

Haemangioma, Hepatic. Figure 1 Typical hemangioma at contrast-enhanced US. Baseline US (a) shows a hypoechoic, well-defined lesion in the right liver. In the arterial phase (b) (25 sec after SonoVue injection), the lesion shows peripheral globular enhancement while in the portal venous (c) and delayed phases (d) (60 sec and 120 sec after SonoVue injection, respectively) a progressive but incomplete centripetal fill-in is observed.

slow flow. High-flow hemangiomas show rapid filling after contrast administration, resulting in homogeneous enhancement during the hepatic arterial or portal venous phase (3). This feature is relatively common in small hemangiomas. Differentiation of high-flow hemangioma from hypervascular malignant tumors may be difficult, and relies on attenuation equivalent to that of the aorta during all phases of CT imaging, including the delayed phase. Very slow-flow hemangiomas appear either as nonenhancing lesions or as lesions with weak peripheral enhancement without centripetal progression. These features may be related to thrombosis or abundant fibrosis, and mimic a hypovascular malignant tumor.

Magnetic Resonance Imaging

Magnetic resonance (MR) imaging protocol for characterizing suspected hemangioma includes gradient-echo T1-weighted sequences, fast spin-echo T2-weighted sequences with short and long (>200 msec) echo times, and serial dynamic gadolinium-enhanced gradient-echo T1-weighted sequences. Hemangioma appears as a homogeneous focal lesion with smooth, well-defined margins. The lesion is hypointense to liver parenchyma on T1-weighted MR images and strongly hyperintense to liver parenchyma on T2-weighted MR images (Fig. 3). The high signal intensity on heavily T2-weighted (long echo time) MR images gives to hemangiomas a consistent "light-bulb" pattern with 100% sensitivity and 92% diagnostic specificity. Dynamic contrast-enhanced MR imaging shows quite a typical perfusion pattern in hemangioma, that is, peripheral nodular enhancement in the early phase with centripetal progression to uniform or almost uniform enhancement during the portal venous and the delayed phase. Such a characteristic enhancement pattern has a sensitivity of 77–91% and a specificity of 100% for the diagnosis of hemangioma (4). However, very small (<1.5 cm), high-flow hemangiomas frequently

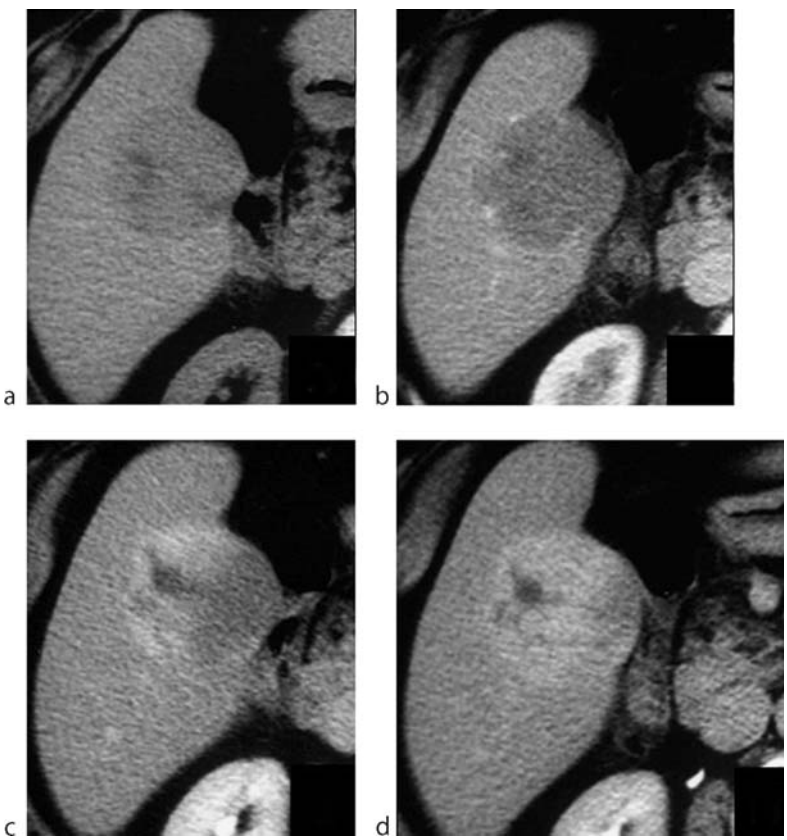

Haemangioma, Hepatic. Figure 2 Typical hemangioma at multiphase contrast-enhanced spiral CT. On unenhanced CT scan (a) the lesion is hypodense with well-defined margins. A peripheral, globular enhancement of the lesion that progress centrally is observed during the arterial (b) and portal venous (c) phase. Delayed scan (d) shows hemangioma almost completely filled with contrast material.

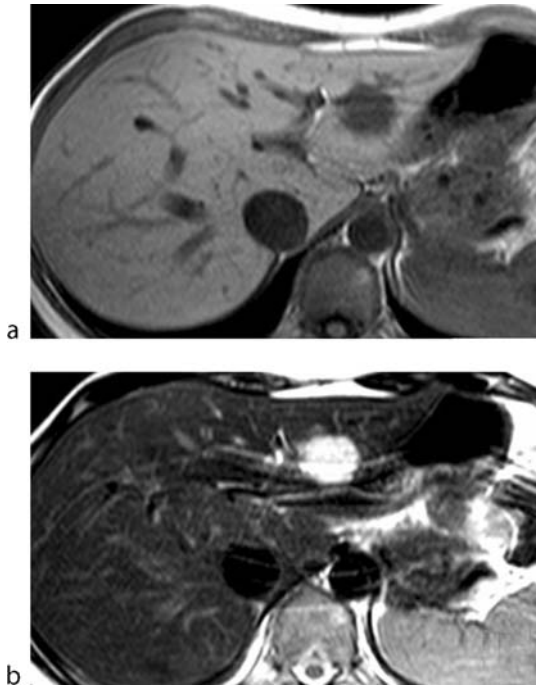

Haemangioma, Hepatic. Figure 3 Typical hemangioma at MR. T1-weighted MR image (a) shows hepatic hemangioma in the left lobe as a well-defined hypointense mass. Conversely, on the T2-weighted fast spin-echo MR image (b) the lesion appears markedly hyperintense.

exhibit an hypervascular pattern, with uniform enhancement in the arterial phase, that may persist in the portal venous and delayed phases (4). In these cases, diagnostic assessment may be difficult, and requires careful analysis of baseline and contrast-enhanced images. Hemangioma shows a peculiar feature after the injection of reticuloendothelial system-targeted MR agents, that is lesion hyperintensity on T1-weighted postcontrast MR images. This is due to the T1 effect of superparamagnetic iron oxide particles trapped within the slow-flow vascular channels of the lesion.

Nuclear Medicine

^{99m}Tc-pertechnetate-labeled red blood cell scintigraphy is a relatively specific examination for characterizing hemangioma. Using this method, there is a decreased activity on early dynamic images and increased activity on delayed blood pool images. Comparison between ^{99m}Tc-pertechnetate-labeled red blood cell single-photon emission CT (SPECT) and MR imaging has shown that MR imaging had higher sensitivity and specificity than SPECT, especially for lesions smaller than 2 cm in diameter.

Diagnosis

The recommended diagnostic work-up for suspected hemangioma is dependent on the clinical scenario. If an hemangioma with typical US features is incidentally detected in a patient with neither history of malignancy nor chronic liver disease, no additional investigation may be required. It has been shown that in this clinical setting the risk of misinterpreting a malignant tumor for an hemangioma is negligible (0.5%). Conversely, in incidental lesions with atypical US features for hepatic hemangioma, further diagnostic work-up is recommended. Additional investigation is also mandatory—regardless of the US features—for any lesion detected in a patient at increased risk for malignancy. MR imaging is currently the most accurate technique for diagnostic confirmation of suspected hemangioma. Despite promising results obtained in recent investigations, contrast-enhanced US is at an early stage of clinical application. On the other hand, spiral CT has limitations in achieving a reliable diagnosis of small lesions, especially in the setting of liver cirrhosis. High-flow hemangiomas that enhance homogeneously in arterial phase CT scans may not be confidently distinguished from small hypervascular hepatocellular carcinoma. Because MR imaging has greater sensitivity to small differences in contrast enhancement and because several fast MR sequences can be used to track the passage of a small, tight bolus of contrast material, MR images may show the characteristic enhancement patterns of hemangioma and hepatocellular carcinoma better than CT images. In addition, MR imaging—besides the information provided by the dynamic gadolinium-enhanced study—can offer improved capability in lesion characterization through the analysis of lesion signal intensity on baseline sequences, especially heavily T2-weighted sequences. In the setting of cirrhosis, diagnosis of hemangiomas should meet strict CT or MR imaging criteria whereas percutaneous biopsy can be used to solve uncertain diagnosis.

Bibliography

1. Quaia E, Calliada F, Bertolotto M et al (2004) Characterization of focal liver lesions with contrast-specific US modes and a sulfur hexafluoride-filled microbubble contrast agent: diagnostic performance and confidence. Radiology 232:420–430
2. Wen YL, Kudo M, Zheng RQ et al (2004) Characterization of hepatic tumors: value of contrast-enhanced coded phase-inversion harmonic angio. Am J Roentgenol 182:1019–1026

3. Kim T, Federle MP, Baron RL et al (2001) Discrimination of small hepatic haemangiomas from hypervascular malignant tumors smaller than 3 cm with three-phase helical CT. Radiology 219:699–706
4. Semelka RC, Brown ED, Ascher SM et al (1994) Hepatic haemangiomas: a multi-institutional study of appearance on T2-weighted and serial gadolinium-enhanced gradient-echo MR images. Radiology 192:401–406

Halo Sign

A rim of ground glass opacity surrounding the circumference of a nodule or mass in CT. It is pathologically based on intraparenchymal hemorrhage around the lesion. It is seen in invasive aspergillosis but also in other infections (candidiasis, herpes, CMV, etc.), in malignoma (adenocarcinoma, broncho-alveolar carcinoma, Kaposi sarcoma, metastases), Wegener's granulomatosis or other processes.

▶Nodules, Pulmonary, Solitary

Hamartoma

Tumor-like nonneoplastic overgrowth of tissue of disordered structure.

▶Lymphangioma

Hamartoma, Biliary

This entity also named microhamartoma or von Meyenburgh complex is a benign malformation of intrahepatic bile ducts. Histologically characterized by a focal disarray of dilated tortuous bile ducts, set in a dense fibrocollagenous stroma. Macroscopically these malformations are multiple millimetric grayish nodules. They are frequently associated with congenital hepatic fibrosis and polycystic liver disease but their pathogenesis remain unknown.

▶Congenital Malformations, Liver and Biliary Tract

Hampton Hump

Pleural-based shallow consolidation in the form of a truncated cone with the base against the pleural surface

▶Thromboembolic Pulmonary Arterial Diseases

Hampton's Line

A radiolucent line that separates barium in the ulcer crater from barium in the gastric lumen, created by the undermining of mucosa with minimal edema. It is considered one of the pathognomonic features of benign ulcer.

▶Ulcer Peptic

Hand Held Gamma Probe Detectors

Gamma probe detectors are imaging detectors. A wide range of probe systems are available with different detector materials, detector sizes, and collimation. They are used for preoperative and intraoperative detection of SLNs.

▶Sentinel Node, Scintigraphy

Hand–foot Syndrome

Infarction of small tubular bones in hands and/or feet in early childhood sickle cell anemia.

▶Osteonecrosis in Childhood

Harmonic Imaging

Ultrasound maging approach in which the non-linear harmonic components of the echoes from microbubble contrast agents is detected.

▶Specific Imaging Techniques (Contrast Media, Ultrasound)

Hashimoto's Thyroiditis

Hashimoto's thyroiditis is an autoimmune disease presenting as a chronic lymphocytic inflammation of the thyroid gland.

▶Thyroid Autoimmune Diseases

HCC

▶Hepatocellular Carcinoma

Head and Neck

Alfredo Blandino, Ignazio Pandolfo
Department of Radiological Science, University of Messina, Italy
ablandino@unime.it

The introduction of the newer imaging modalities such as computed tomography (CT), magnetic resonance (MR), and ultrasonography has dramatically changed the way imaging methods are used to diagnose diseases of the head and neck region.

In particular, the latest advances in the field of CT (multislice CT with the introduction of the isotropic pixel) and consequent improvements in the postprocessing of the images (three-dimensional imaging, VRT, SSD, and virtual endoscopy) has led to the increased quality and quantity of the diagnostic information in certain anatomic areas such as the paranasal sinuses, larynx, and temporal bone (Wang 2001, Rodt 2002).

On the other hand, progress in the field of MRI with the introduction of thin sections, high-resolution imaging, and fast T1- and T2-weighted sequences has made MRI the procedure of choice in the study of some anatomic regions of the head and neck, particularly in the suprahyoid area. Moreover, improvements in the gradient echo and fast spin-echo T2-weighted techniques have meant that MRI may now be used to evaluate the membranous labyrinth and its fluid content, structures never seen before (Casselman 2002).

The goal of providing anatomic information that accurately maps a lesion is met very well by all these imaging methods.

Recently, the areas of new investigation have involved metabolic and functional imaging techniques that may be more successful than cross-sectional imaging in the diagnosis as well as in the follow-up of neoplastic diseases (Shah 2003). These techniques include dynamic contrast-enhanced MR imaging for evaluating soft tissue masses and cervical lymph nodes, the use of ultrasmall superparamagnetic iron oxide contrast agents, and functional techniques such as *in vivo* and *in vitro* MR spectroscopy of head and neck cancer and lymph nodes and apparent diffusion coefficient mapping of parotid glands (Star-Lack 2000, Mack 2002, Sumi 2002).

Positron emission tomography (PET) and thallium-201 single photon emission tomography (Tl-201 SPECT) are other innovative techniques that may be helpful in providing functional and metabolic information about abnormalities of the head and neck region, with the aim not only of differentiating between benign and malignant diseases but also of providing information that helps assess the response to nonsurgical organ preservation treatment protocols (Fischbein 1999, Hanasono 1999, Mukherji 2000).

From the anatomic point of view, the head and neck region is encompassed between the skull base and the inlet of the mediastinum. The skull and its contents, in fact, are usually considered as pertaining to the field of neuroradiology. All of the remaining anatomic structures except the cervical spine and vessels (which are dealt with by neuroradiology and vascular radiology, respectively) are usually covered by head and neck radiology. The base of the skull represents the boundary between the head and skull contents and is generally considered under the scope of head and neck radiology.

From the topographic point of view, we can distinguish the face, which is located anteriorly and superiorly, and the neck, which runs more posteriorly from the base of the skull to the inlet of the mediastinum. The face includes the:

1. Orbits and their contents
2. Nose and paranasal sinuses
3. Oral cavity with the oral tongue
4. Jaws and temporomandibular joint
5. Salivary glands

The neck is composed of muscles, fat, vessels, nerves, lymphatic tissue, fascial planes, and a visceral compartment, including the aerodigestive tract (pharynx and larynx) and the thyroid and parathyroid glands.

After a brief description of the neck anatomy, we will consider key points of the several anatomic components of the head and neck with a short summary of their most frequent abnormalities.

Finally, lymphatic metastasis and perineural spread are two typical means by which malignancy spreads in the head and neck region and should be considered separately.

Anatomy of the Neck

Muscles and Triangles (Som 2003)

The most important anatomic landmark of the neck is the sternocleidomastoid muscle, which runs in the lateral neck, from the mastoid process to the sternum and clavicle. In its oblique course, the muscle divides the neck into anterior and posterior triangles.

The anterior triangle is limited posteriorly by the sternocleidomastoid muscle and anteriorly by the anterior belly of the omohyoid muscle. Its superior boundary is traditionally considered to be the undersurface of the body of the mandible.

Another fundamental anatomic structure is the hyoid bone, which divides the anterior triangle into suprahyoid and infrahyoid compartments.

In the anterior and more superficial part of the neck, close to the midline on each side, there are two triangles called muscular triangles that containing the infrahyoid strap muscles (thyrohyoid muscle and sternohyoid muscle). The strap muscles are very superficial and cover the thyroid gland and the thyroid cartilage.

Finally, the posterior triangle, encompassed between the sternocleidomastoid muscle anteriorly and the trapezius muscle posteriorly, is divided by the inferior belly of the omohyoid muscle into a larger occipital triangle and a smaller one, called the subclavian triangle.

The Fascia and Spaces of the Neck (Som 2003)

Classically, the neck is divided into spaces delimited by fasciae, which may limit to a varying extent the spread of infection and neoplastic diseases. The fasciae of the neck are traditionally classified as superficial cervical fascia (SCF) and deep cervical fascia (DCF). The SCF covers the face and neck and lies on the platysma and mimic muscles.

The DCF, conversely, is characterized by a more complex structure and is divided into three layers: the superficial layer of the DCF (SLDCF), the middle layer of the DCF (MLDCF), and the deep layer of the DCF (DLDCF). The SLDCF represents an outer layer that completely encircles the neck. The MLDCF, with its deep division, covers the surface of the esophagus and pharynx and at this level is termed "visceral fascia." Ventrally, the DLDCF covers the anterior surface of the cervical vertebrae. This fascia is termed prevertebral fascia and is divided into two layers, which are separated by a thin connective plane and are fused at the level of the fourth thoracic vertebra.

For this reason, this virtual space is a potential route for the spread of infection into the mediastinum and is known as the "danger space."

Finally, the expansion of the three layers of the DCF contributes to the formation of the carotid sheath, an anatomic compartment containing the internal carotid artery and part of the external carotid artery; the jugular vein; cranial nerves IX, X, XI, and XII; and lymph nodes.

According to most authors, the suprahyoid part of the carotid sheath can be considered part of the parapharyngeal space (the retrostyloid compartment).

The Lymphatic System of the Neck

The lymphatic system of the head and neck consists of lymphatic tissue associated with the mucosa, forming the Waldeyer's ring, and of about 300 lymph nodes embedded in fat tissue. The traditionally used classification for identifying the lymph nodes was that of the French anatomist Rouvière. More recently, the Rouvière system was replaced by a simpler system based on levels.

Base of the Skull

The base of the skull can be divided into three regions: anterior, posterior, and central. The anterior skull base consists of the roof of the orbits, the cribriform plate of the ethmoid bone, the frontal sinus, and the lesser wing of the sphenoid; this topic is covered in the section on paranasal cavities.

The posterior skull base is the temporal bone, and this topic is covered in the section on temporal bone.

The central skull base is formed of the sphenoid bone with a smaller contribution from the basiooccput. Since the foramina of the sphenoid bone open in the bordering soft tissue, the latter must be considered an integral part of the skull base (Curtin 2003). The most important extracranial soft tissues are the pterygolopalatine fossa and the masticator space, whereas the cavernous sinus and Meckel's cave are the landmarks of the intracranial soft tissue bordering the skull base.

In general, lesions of the central skull base can be divided into three categories:

- Intracranial lesions involving the skull base (this topic will be covered separately).
- Primary or secondary osseous lesions.
- Extracranial lesions involving the skull base (this topic will be covered separately).

Globes and Orbits

The orbits are two recesses containing the globes, lacrimal glands, muscles, blood vessels, nerves, and adipose and connective tissue.

For descriptive purposes, the orbit has been divided into the extraperiosteal, subperiosteal, extraconal, conal, and intraconal spaces (Mafee 1995). The intraconal space is separated from the other spaces by the rectum muscles and their intermuscular septa and contains the optic nerve.

The subdivision of the orbit into different spaces has great value both for radiological diagnosis as well as for surgical planning, as some lesions have a predilection for a specific space.

CT and MRI are the two most common techniques used for imaging this complex anatomic region.

CT is the technique of choice for bony details, for detecting calcification, and for evaluating foreign, especially metallic, bodies in or around the globe and orbit (Lakits 1999). The radiation dose to the lens is one of the major disadvantages of CT.

Conversely, MRI, because of its ability to detect different soft tissues and fluids, has become the method of choice for imaging eye disorders.

From a schematic point of view, it is possible to distinguish ocular from orbital diseases.
Ocular diseases include:

- Congenital ocular diseases
- Ocular detachments
- Retinoblastoma
- Persistent hyperplastic primary vitreous

Orbital diseases include:

- Congenital diseases
- Inflammatory and granulomatous
- Benign and malignant tumours
- Trauma
- Optic nerve diseases

Teeth, Mandible, Maxilla, and Temporomandibolar Joint (TMJ)

Panoramic radiography still remains the basic X-ray evaluation of the mandible--maxillary region, giving a survey of the entire mandible, the maxilla (including the lower part of the nasal cavity and maxillary sinuses), and the teeth. This single examination can be supplemented by other techniques such as intraoral radiography, CT, and MRI.

CT has become an important diagnostic tool in the assessment of this anatomic region, especially with the development of a dental reformatting program (i.e., the Dentascan) (Au-Yeung 2001, Gahleitner 2003).

Dental caries and periodontal disease are generally evaluated with panoramic and intraoral radiographs, whereas space-occupying lesions of the mandible and maxilla are better studied using CT and, rarely, MRI.

It should be remarked that despite the application of all the radiological methods, a definitive diagnosis of space-occupying masses is difficult to obtain, and surgical and histological examination are mandatory. The most important features that should be considered in order to obtain a tentative radiological diagnosis are (1) the location of the lesion within the mandible or the maxilla, (2) the size, shape, and demarcation of the lesion, (3) the relationship of the lesion to the adjacent tooth structures, and (4) the degree of lucency and the presence of intralesional calciossification. The analysis of these criteria forms the basis for the final radiological diagnosis.

It should also be stressed that the dental reformatting program has opened up new horizons in the field of dental implants and has introduced a new era of cooperation between the radiologist and the dentist or oral surgeon (Mupparapu 2004).

Moreover, the ability of MR imaging to visualize soft tissue structures in and around the temporomandibular joint (TMJ) make this the primary imaging technique for most clinical presentations, especially for internal derangement related to displacement of disk (Rudisch 2001).
Teeth, mandible, and maxillary diseases include:

- Caries and periodontal diseases
- Benign and malignant odontogenic and nonodontogenic tumours
- Trauma
- Infectious diseases
- Fibro-osseous lesions

TMJ disease includes:

- Internal derangement of the TMJ
- Tumours and tumour-like conditions
- Trauma

The Nose and Paranasal Sinuses

The paranasal sinuses include the frontal, ethmoid, sphenoid, and maxillary sinuses. They are air-filled cavities that develop in the facial bones and in the base of the skull.

From the embryological point of view, all of the sinuses originate as evaginations of the nasal fossae. The paranasal sinuses contribute to humidifying and warming the inspired air, to improving the resonance of the voice, to increasing the olfactory area, and to absorbing shock to the face and head in trauma.

The nasal fossa is divided by the turbinates (superior, middle, and inferior) into three distinct air passages, called the superior, middle, and inferior meati.

The posterior ethmoid cells and the sphenoid sinus drain into the superior meatus. Into the middle meatus drain the frontal sinus (*via* the frontal recess), the maxillary sinus (*via* the maxillary ostium and infundibulum), and the anterior ethmoid cells. Finally, the inferior meatus receives the nasolacrimal duct.

An understanding of the anatomy of the lateral wall of the nasal fossa and particularly of the osteomeatal unity (middle turbinatus, bullae ethmoidalis, infundibulum, ostia, and uncinate process) is the key for guiding

functional endoscopic surgery in chronic inflammatory rhinosinusal diseases (Harnsberger 1990).

For this reason, CT study has become the most requested imaging procedure for examining the paranasal sinuses. High-resolution CT with three-dimensional and SSD reconstruction is also the first-line evaluation in traumatic and congenital lesions of the face and paranasal sinuses.

Finally, both CT and MRI can be used to evaluate benign and malignant lesions of the nose and paranasal sinuses in order to study local extension, with particular regard to involvement of some critical areas such as the pterygoid fossa or orbit (Som 2003).

Diseases of the nose and paranasal sinuses include:

- Congenital diseases
- Chronic inflammatory diseases
- Granulomatosis
- Benign and malignant diseases
- Trauma

Oral Cavity

The oral cavity is the most ventral portion of the aerodigestive tract, separated from the oropharynx by the anterior tonsillar pillar and the soft palate. The oral cavity includes the mobile or anterior two-thirds of the tongue, the hard palate, the flour of the mouth, the lips, and the gingivobuccal and buccomasseteric regions, including the retromolar trigone. The base of the tongue and soft palate belong to the oropharynx.

The primary reason for imaging the oral cavity is to evaluate and stage squamous cell carcinomas, which account for 90–95% of all malignant neoplasms of this head and neck region. Alterations of normal anatomy or abnormal regions of density on CT or signal intensity on MR are the key features in the diagnosis (Sigal 1996). Smoking and alcohol use are considered the most relevant risk factors for developing the carcinoma, which arises more frequently in the lips.

Congenital, vascular, and inflammatory lesions are by far the most frequent pathologies among the benign disorders.

Diseases of the oral cavity include:

- Congenital diseases
- Inflammatory diseases
- Benign and malignant tumours

Salivary Glands

The salivary glands are divided into major and minor salivary glands. The paired parotid, submandibular and sublingual glands are referred to as the major salivary glands. The minor salivary glands are clusters of salivary tissue present throughout the submucosa of the oral cavity, particularly concentrated in the buccal, labial, palatal, and lingual regions, but also found in the paranasal sinuses, pharynx, and upper respiratory tract.

Major and minor salivary glands produce the saliva, a clear, viscid fluid that moistens the mouth, lubricates food, and converts starch into maltose with the enzyme ptyalin.

Imaging studies of major salivary glands have evolved from conventional X-ray to sialography, ultrasound, radionuclide studies, contrast-enhanced CT, and MRI.

Despite the diagnostic effectiveness of all of these techniques, we must take into account the fundamental role still played by fine-needle aspiration in the diagnostic approach to benign and malignant lesions of the parotid and submandibular glands.

Stones of the submandibular or parotid ducts causing obstruction and salivary colic pain are a frequent disease. Acute and chronic infections, autoimmune disease (such as Sjogren's syndrome), and benign and malignant tumours are the others common salivary gland diseases.

Salivary gland diseases include:

- Benign and malignant lesions
- Acute and chronic inflammations
- Salivary stones

Pharynx

The pharynx is a musculomembranous tube extending from the skull base to the level of the caudal cricoid cartilage; anatomically it has been subdivided into three sections: cranially, the nasopharynx, which extends from the skull base to the hard palate; at an intermediate level, the oropharynx, which extends from the hard palate to the level of hyoid bone; and caudally, the hypopharynx, which extends from the hyoid bone to the caudal cricoid cartilage (Mukherji 2003).

Nasopharynx

The nasopharynx, the most cranial cavity of the pharynx, is roughly tubular or cuboidal in shape. The roof is formed by the floor of the sphenoid sinus and upper clivus; inferiorly the nasopharynx is continuous with the oropharynx at the level of the soft palate, and anteriorly it communicates with the choanae, through which it is continuous with the nasal cavities. Posteriorly this airway space is limited by the lower clivus and upper cervical spine along with the prevertebral musculature.

Very important superficial anatomic landmarks of the nasopharynx are the torus tubarius, the Eustachian tube orifices, and the lateral pharyngeal recesses (i.e., the fossa of Rosenmuller).

The submucosa contains minor salivary glands as well as a prominent lymphoid component, the most important of which are the adenoids or nasopharyngeal tonsils, situated in the roof of the nasopharynx.

Oropharynx

The oropharynx is posterior to the oral cavity and originates at the level of the soft palate. It includes the tongue base, the soft palate, the palatine tonsils and the pharyngeal constrictor muscles.

The palatine tonsils reach maximal size at puberty, whereas the lingual tonsils lie at the tongue base.

Hypopharynx

The hypopharynx will be described in the sections dealing with the larynx.

Carcinomas accounts for the vast majority of malignant diseases of the nasopharynx and oropharynx. Tobacco and alcohol use as well as prior irradiation, poor oral hygiene, and Epstein–Barr virus infection are the most important epidemiological factors in the development of upper aerodigestive tract cancers (Mendenhall 1994).

CT and MRI provide images with noteworthy information and striking anatomic details, which are very helpful in evaluating the presence and extension of neoplastic disease.

Anatomically closely correlated to the upper pharynx are some spaces and fossae that can be secondarily involved in neoplastic and infectious diseases but can also be the primary source of pathologic process.

The parapharyngeal space is a predominantly fat-filled space with an inverted pyramid shape that extends from the base of the skull to the level of the greater cornu of the hyoid bone. This space is subdivided into an anterior, or prestyloid, and a posterior, or retrostyloid, compartment, which is also known as the carotid space.

The masticator space is situated lateral to the parapharyngeal space and contains the masticator muscles and the upper part of the mandible. It is generally affected by vasculogenic tumours and inflammatory lesions.

The pterygopalatine and infratemporal fossa are two important crossway regions, containing vascular, nervous, and muscular structures.

The pathology of the rhinopharynx and oropharynx and related spaces includes

- Benign and malignant tumours
- Infections
- Primary and secondary lesions of the parapharyngeal space

Temporal Bone

Temporal bone consists of five parts: the squamous, mastoid, petrous, and tympanic portions and the styloid process.

The petrous and mastoid portions are the most important parts of the temporal bone because of their significant role in head and neck diseases. The petrous bone represents the posterior part of the base of the skull and contains the outer, middle, and inner ear. The outer ear consists of the external auditory canal, which is separated from the middle ear by the tympanic membrane. The tympanic cavity communicates with the nasopharynx by means of the Eustachian tubes and is crossed by the ossicular chain. In the middle ear is also part of the course of the facial nerve.

More laterally, the petrous bone contains the inner ear, which consists of the bony labyrinth (vestibule, semicircular canals, and cochlea) containing the membranous labyrinth (cochlear duct, vestibular sense organs, and endolymphatic duct and sac). The space between the bony and membranous labyrinth is filled by a small amount of fluid (perilympha), and the membranous labyrinth is filled by the endolympha.

In the more lateral part of the petrous bone runs the internal auditory canal, which contains cranial nerves VII and VIII, the intermediary nerve, and the internal auditory artery.

The diagnostic imaging technique and the algorithmic approach to temporal bone diseases depend on the symptom complex and clinical presentation (Swartz 1998). High-resolution CT is the method of choice when detection of the finest bony details is necessary, as in the suspicion of chronic otomastoiditis, in trauma, in otosclerosis, and in evaluation of postsurgical middle ear.

But in adult patients complaining of retrocochlear sensorineural hearing loss, contrast-enhanced MRI is mandatory to detect an acoustic tumour.

Vertigo should be studied both with CT and MRI. In the presence of peripheral facial nerve palsy, both CT and MRI can be employed, and the choice is related to clinical presentation.

Diseases of the temporal bone include

- Congenital conditions
- Trauma
- Acute and chronic inflammatory diseases
- Benign and malignant tumours
- Otosclerosis and dysplasias
- Facial nerve palsy

Larynx and Hypopharynx

Larynx

The larynx is a very complex structure composed of cartilage, fibrous membranes, ligaments, mucosa, fat, and muscles (Hermans 2001).

The laryngeal framework consists of the epiglottis, thyroid, cricoid, and arytenoid cartilages. The thyroid cartilage is suspended from the hyoid bone by the thyrohyoid membrane. The thyroid and cricoid cartilages are connected by the cricothyroid membrane. The epiglottis and arytenoids are connected by the aryepiglottic folds, which contain the aryepiglottic muscles and quadrangular membrane.

The muscles of the larynx can be divided into intrinsic and extrinsic. The intrinsic muscles connect the different cartilages and enable their coordinated movements. All of the intrinsic muscles except the posterior cricoarytenoid are adductor muscles (closing).

The larynx can be subdivided from cranial to caudal into three regions: supraglottis, glottis, and subglottis. The supraglottis region includes the epiglottis, the aryepiglottic folds, the false vocal cords, the ventricle, and the upper part of the arytenoids. The glottis includes the true vocal cords, the anterior and posterior commissure, and the lower part of arytenoids. The subglottis region includes the lower part of the cricoid.
The three main functions of the larynx are:

- Protection of the airway during deglutition, by constricting the supraglottis and glottis structures
- Provision of the overpressure of the air in the lungs
- Production of the voice due to passive vibration of the true vocal cords and modulation of the air column

The main role of diagnostic imaging of the larynx is to supply additional information to establish pretherapeutic staging and correct treatment of laryngeal cancer (radiation therapy versus surgery or total laryngectomy versus conservative surgery). The paralaryngeal space and cartilages are the critical areas in defining the pretreatment planning. Both state-of-the-art CT and MRI can give all the information needed by the surgeon, but most authors prefer CT as the first-line technique because it is more available and shorter in duration, resulting in less motion degradation of the images. Moreover, multislice CT gives high-quality coronal and sagittal reconstruction images and enables dynamic study during phonation.

Hypopharynx

The hypopharynx is the lower part of the pharynx and extends from the level of the hyoid bone to the inferior margin of the cricoid. The hypopharynx can be divided into three subsites: the pyriform sinus (paired), the posterior hypopharyngeal wall, and the postcricoid region.

The pyriform sinuses are grooves created by the impression of the larynx on the anterior wall of the pharynx. The aryepiglottic folds separate the pyriform sinus from the laryngeal lumen. The apex of the pyriform sinus is located at the level of the cricoarytenoid joint.

The posterior wall of the hypopharynx is continuous with the posterior wall of the oropharynx, is 6–7 mm high, and laterally is in direct continuity with the pyriform sinuses.

The postcricoid region extends from the level of the arytenoid cartilages to the lower border of the cricoid and is composed of the mucosa covering the posterior aspect of the cricoid cartilage.

Over 90% of hypopharyngeal carcinomas are squamous cell carcinomas. In 80–90% of cases, the hypopharyngeal carcinoma originates in the pyriform sinus, whereas tumours of the posterior wall and retrocricoid area are rarer. About 75% of the patients have lymph node metastasis at the time of the initial diagnosis.

Submucosal diffusion and invasion of the laryngeal framework are very frequent events and are well detected by CT as well as by MRI.
Diseases of the larynx and hypopharynx include:

- Laryngeal and hypopharyngeal carcinoma
- Inflammatory disease
- Benign tumours
- Laryngeal trauma

Thyroid and Parathyroid Glands

The thyroid gland has two lobes connected by an isthmus and is situated anteriorly to the first three tracheal rings; each lobe has a superior and inferior pole. The size of the gland varies with patient age, gender, and weight. It is generally situated in the neck above the level of the clavicle, but sometimes, extension in the superior mediastinum can occur.

The thyroid gland synthesizes hormones that play a fundamental role in regulating several metabolic functions, including lipid catabolism, cardiac rate and output, and skeletal growth.

Cross-sectional imaging, mainly ultrasound but also CT and MR imaging, provides anatomic and morphologic information, which needs to be integrated with functional information obtained using nuclear medicine (Loevener 2003).

The number of parathyroid glands range from 1 to 12, although most individuals (about 80%) have four. In 75% of patients, the upper parathyroid gland lies posterior to the middle one-third of the thyroid gland, whereas the

most common anatomic location of the lower parathyroid glands is lateral to the lower pole of the thyroid gland.

Imaging of the parathyroid glands basically focuses on detecting adenomas in patients with primary hyperparathyroidism, and the role of imaging is debated regarding the primary method to be used to recognize such adenomas (Loevener 2003). Not infrequently, surgical exploration of the neck is requested to discover the diseased gland in patients with clinical signs of primary hyperparathyroidism.

Moreover, the close anatomic relationship with the thyroid gland can be the cause for accidental removal of the glands during thyroid surgery.

Diseases of the thyroid and parathyroid glands include:

- Congenital thyroid anomalies
- Autoimmune diseases
- Thyroid goiter
- Benign and malignant lesions of the thyroid and parathyroid gland

Lymphadenopathies

The detection of metastatic nodal disease is a critical event because it is one of the greatest prognosticators in the natural history of head and neck cancer. In fact, in patients with upper aerodigestive tract tumours, survival is reduced by nearly 50% in the presence of metastatic disease at the time of diagnosis.

Unfortunately, the imaging diagnosis suffers from lack of specificity because a wide variety of diseases may cause confusion and/or mimic metastatic nodal involvement. These include bacterial and viral diseases, lymphomatous, tuberculosis, and other granulomatosis diseases such as sarcoidosis.

However, only gross metastatic disease can be identified because microscopic neoplastic deposits escape current detection methods. Nevertheless, it is possible that in the near future, the newer diagnostic modalities like MR spectroscopy, PET, and thallium-201 SPECT might improve the specificity and sensitivity in the diagnosis of nodal metastasis (Star-Lack 2000, Hanasono 1999).

The current diagnostic criteria of lymphadenopathy are based on the following:

1. Size evaluation
2. Morphology evaluation
3. Central necrosis
4. Extranodal tumour extension

Congenital Neck Lesions

There is a wide range of congenital neck lesions that must be considered in the differential diagnosis with lymphadenopathies. They include anomalies of the branchial apparatus, vascular and lymphatic lesions, and thyroid anomalies (Som PM 2003).

Perineural Spreading

Perineural spreading is due to macroscopic neoplastic diffusion along the neural sheath and is a highly typical event in head and neck malignancies (Parker 1991, Chong 1996). The perineural spread can occur in a retrograde or anterograde direction and is characterized by relevant therapeutic and prognostic implications. Virtually any head and neck malignancy (squamous cell carcinoma, adenoid-cystic carcinoma, lymphoma, melanoma, etc.) may spread along the perineural route. The trigeminal and facial nerves are the most common routes of perineural spread.

Bibliography

1. Au-Yeung KM, Ahuja AT, Ching AS et al (2001) Dentascan in oral imaging. Clin Radiol 56:700–713
2. Casselman JW (2002) Diagnostic imaging in clinical neuro-otology. Curr Opin Neurol 15:23–30
3. Chong VFH, Fan YF, Khoo JBK (1996) Nasopharyngeal carcinoma with intracranial spread: CT and MR characteristic. J Comput Assist Tomogr 20:563–569
4. Curtin HD, Rabinov JD, Som PM (2003) Central skull base: embryology, anatomy, and pathology. In: Som PM, Curtin HD (eds) Head and Neck Imaging. 4th edn. Mosby Year Book, St Louis, pp 785–863
5. Fischbein N, Anzai Y, Murkherje SK (1999) Application of new imaging techniques for the evaluation of squamous cell carcinoma of the head and neck. Semin Comput Tomogr Ultrasound Magn Reson Imag 20:187–212
6. Gahleitner A, Watzek G, Imhof H (2003) Dental CT: imaging technique, anatomy and pathologic conditions of the jaws. Eur Radiol 13:366–376
7. Hanasono MM, Kunda LD, Segall GM et al (1999) Uses and limitations of FDG positron emission tomography in patients with head and neck cancer. Laryngoscope 109:880–885
8. Harnsberger R (1990) Imaging for the sinus and nose. In: Harnsberger r (ed) Head and Neck Imaging Handbook. Mosby Year Book, St Louis, p 387–419
9. Hermans R (ed) (2001) Imaging of the larynx. Berlin Heidelberg New York, Springer-Verlag
10. Lakits A, Prokesch R, Scholda C et al (1999) Multiplanar imaging in the preoperative assessment of metallic intra-ocular foreign bodies. Helical computed tomography versus conventional computed tomography. Ophthalmology 106:1232–1234
11. Loevener LA (2003) Thyroid and parathyroid glands: anatomy and pathology. In: Som PM, Curtin HD (eds) Head and Neck imaging. 4th edn. Mosby Year Book, St Louis, pp 2134–2172
12. Mack MG, Balzer JO, Straub R et al (2002) Superparamagnetic iron oxide-enhanced MR imaging of head and neck lymph nodes. Radiology 222:239–244
13. Mafee MH (1995) Orbit and globe. In: Valvassori GE, Mafee MF, Carter BL (eds) Imaging of the head and neck. Thieme Medical Publishers ed., p 158–215
14. Mendenhall WM, Million RR, Mancuso AA et al (1994) Nasopharinx. In: Million RR, Cassisi NJ (eds) Management of head and neck cancer: a multidisciplinary approach. J.B.Lippincot, Philadelphia, pp 599–626

15. Mupparapu M, Singer SR (2004) Implant imaging for dentist. J Can Dent Assoc 70:32
16. Mukherji SK (2003) Pharinx. In: Som PM, Curtin HD (eds) Head and Neck Imaging. 4th edn. Mosby Year Book, St Louis, p 1465–1520
17. Mukherji SK, Gapany M, Neelon B et al (2000) Evaluation of thallium-201 single photon emission computed tomography for predicting early treatment response in patients with squamous cell carcinoma of the extracranial head and neck treated with non-surgical organ preservation therapy: initials results. J Comput Assist Tomogr 24:146–151
18. Parker GD, Harnsberger HR (1991) Clinical radiologic issues in perineural spread of malignant diseases of the extra cranial head and neck. Radiographics 11:383–399
19. Rodt T, Ratiu P, Becker H et al (2002) 3D visualisation of the middle ear and adjacent structures using reconstructed multi-slice CT datasets, correlating 3D images and virtual endoscopy to 2D cross-sectional images. Neuroradiology 44:783–790
20. Rudisch A, Innerhofer K, Bertram S et al (2001) Magnetic resonance imaging findings of internal derangment end effusion in patients with unilateral temporomandibular joint pain. Oral Surg Oral Med Oral Pathol Oral Radiol Endod 95:556–571
21. Shah GV, Fischbein NJ, Patel R et al (2003) Newer MR imaging techniques for head and neck. Magn Reson Imaging Clin N Am 11:449–469
22. Sigal R, Zagdansky A, Schwaab G et al (1996) CT and MR imaging of squamous cell carcinoma of the tongue and floor of the mouth. Radiographics 16:787–810
23. Som PM, Brandwein MS (2003) Tumors and tumorlike conditions. In: Som PM, Curtin HD (eds) Head and Neck Imaging. 4th edn. Mosby Year Book, St Louis, pp 261–373
24. Som PM, Curtin HD (2003) Fascia and spaces of the neck. In: Som PM, Curtin HD (eds) Head and Neck Imaging. 4th edn. Mosby Year Book, St Louis, pp 1805–1827
25. Som PM, Smoker WRK, Curtin HD et al (2003) Congenital lesions. In: Som PM, Curtin HD (eds) Head and Neck Imaging. 4th edn. Mosby Year Book, St Louis, pp 1828–1864
26. Som PM, Smoker WRK, Balboni A et al (2003) Embryology and anatomy of the neck. In: Som PM, Curtin HD (eds) Head and Neck Imaging. 4th edn.: Mosby Year Book, St Louis, p 1757–1804
27. Star-Lack JM, Adalsteinsson S, Adam MF et al (2000) *In vivo* ^{1}H MR spectroscopy of human head and neck lymph node metastases and comparison with oxygen tension measurements. AJNR 21:183–193
28. Sumi M, Takagi Y, Uetani M et al (2002) Diffusion-weighted echoplanar MR imaging of the salivary glands. Am J Roentgenol 178:959–965
29. Swartz JD, Harnsberger HR (eds) (1998) Imaging of the Temporal bone. 3rd edn. Thieme Medical Publishers, NY
30. Wang D, Zhang W, Xiong M et al (2001) Laryngeal and hypopharyngeal carcinoma: comparison of helical CT multiplanar reformation, three-dimensional reconstruction and virtual laryngoscope. Chin Med J 114:54–58

Head and Neck Cancer

Malignant or benignant cellular growth caused by abnormal and uncontrolled cell division at level of head and neck.

▶Carcinoma, Hypopharynx
▶Neoplasms, Benign and Malignant, Larynx

Head, Injury

▶Trauma, Head, Accidental

Heartburn

A burning retrosternal sensation associated with reflux of gastric acid into the oesophagus.

▶Reflux, Gastroesphageal in Adults

Helicobacter Pylori

A bacillus that colonizes the stomach and predisposes to peptic ulceration both by acid hypersecretion and by compromising mucosal defense mechanisms.

▶Ulcers, Peptic

Hemangioma

Vascular malformation, benign. Several types depend on pathology—venous, capillary, arterial, or combination.

▶Neoplasms, Bone, Benign
▶Neoplasms, Soft Tissues, Benign

Hemangiomas

Benign tumors or malformations of mature vessels.

▶Breast, Benign Tumours

Hematoma

Collection of extravasated blood in a traumatic tear or surgical cavity.

▶Trauma, Breast

Hematoma, Epidural

▶Trauma, Head, Accidental

Hematoma, Hepatic

Hepatic hematoma is an encapsulated, intraparenchymal blood collection. It is usually located between the capsule of the liver and the parenchyma in the anterolateral aspect of right lobe; however, a hematoma can exist anywhere within the liver parenchyma. Hematoma of the liver usually results from trauma and is caused by bleeding into a tissue laceration. Iatrogenic causes, such as percutaneous needle biopsy, interventional radiology procedures involving catheters or wires, and biliary lithotripsy, are often involved. Hepatic hematomas arising from spontaneous bleeding are rare. Hepatic hematoma appears as a well-defined, round (intraparenchymal hematomas), or curvilinear (subcapsular hematomas) mass.

The Ultrasound Appearance of Hepatic Hematoma Changes with Time. It is usually hyperechoic in the acute phase, whereas it appears inhomogeneously hypoechoic, with internal echoes due to septation and debris, in a more chronic stage.

In an acute or subacute setting, computed tomography (CT) features of hematoma are hyperdense areas on baseline CT scan not enhanced after contrast medium administration, whereas chronic hematoma is hypoattenuating on the precontrast scan and can display rim enhancement following intravenous contrast medium administration.

The magnetic resonance characteristics of hepatic hematoma depend mainly on the age of the hemorrhagic lesion. Acute hematoma shows an intermediate signal intensity on T1-weighted images and a low signal intensity on T2-weighted images due to the high-intracellular concentration of deoxyhemoglobin in red blood cells, whereas subacute hepatic hematoma, because of the presence of extracellular methemoglobin, appears as a heterogeneous mass with pathognomonic high signal intensity on T1-weighted images and intermediate signal intensity on T2-weighted images.

▶Trauma Hepatobiliary

Hematoma, Subdural

▶Trauma, Head, Accidental

Hematomyelia

Hemorragic collection inside traumatized spinal cord, best visible on GRE T2* MR images some hours after trauma, normally at the site of impact.

▶Spinal Trauma

Hematopoiesis Disorders in Childhood

Johan G. Blickman[1], Dewi Ashi[2]
[1]Department of Radiology, UMC, Nijmegen, Netherlands
[2]Department of Radiology, University of Indonesia, Cipto Mangunkusumo General Hospital, Jakarta Pusat, Indonesia
j.blickman@rad.umcn.nl

Definition

▶Leukemia is a malignant proliferation of white blood cells. Responsible for 35% of pediatric oncological disease, it is divided into acute lymphatic leukemia (▶ALL; 85%) and acute myeloid leukemia (▶AML; 15%). ALL is slightly more common in males than females, with a peak incidence at 3 years of age. There is no difference in incidence of AML between males and females.

Pathology/Histopathology

Laboratory findings are immature leukemic blast cells and pancytopenia.

Clinical Presentation

The clinical presentation includes anemia, lethargy, dyspnea, anorexia, fever, bone pain, hepatosplenomegaly, and petechiae and epistaxis due to thrombocytopenia.

Imaging

Plain radiographic findings include the following:

Skeletal: Metaphyseal lucent band, local rarefied lesions, general osteoporosis. Periosteal bone formation may simulate a primary bone tumor. A soft tissue mass or

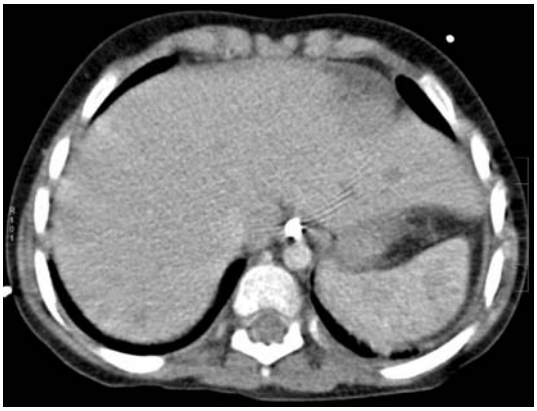

Hematopoiesis Disorders in Childhood. Figure 1 Multiple hypodense lesions are visible on both spleen and liver.

chloroma is a rare presentation. Spinal involvement may produce vertebral collapse.

Chest: Mediastinal enlargement due to hilar lymphadenopathy (10% of patients)

Abdomen: May reveal a sentinel loop of dilated terminal ileum in patients with neutropenic colitis, as the disease most often affects the cecum (typhlitis).

Ultrasound (US) may demonstrate a thickened bowel wall and small bowel, as well as hepatosplenomegaly with heterogeneous echogenicity due to infiltration of leukemic cells. Infiltration of the kidney usually consists of diffuse involvement that distorts the calyceal system, associated with focal hypoechoic areas. Testicular involvement may show hypoechoic diffuse or localized focal lesions.

Computed tomography (CT) shows hepatosplenomegaly with low attenuation lesions and periportal hypodense lesions that do not enhance after contrast injection. Renal images on CT are similar to those seen on US (Fig. 1).

Magnetic resonance imaging (MRI) can detect bone marrow infiltration as a patchy or diffuse decrease in signal in fatty marrow. Leptomeningeal disease shows as mass lesions.

Nuclear Medicine

Nuclear medicine techniques are used to rule out nonleukemic disorders in patients who complain of bone pain. These are not used for patients who have already been diagnosed with leukemia.

Diagnosis

The diagnosis of leukemia is made not on imaging modalities but on laboratory findings such as peripheral blood and bone marrow aspiration.

The *differential diagnosis* includes Langerhans cell histiocytosis, infection, and malignant lymphoma.

References

1. Barnes PD (1998) Accessory organs of Digestion. In: Hans Blickman (ed) Pediatric Radiology: The Requisites. 2nd edn. Mosby St. Louis, pp 143
2. Carty H (2001) Paediatric Imaging: In: The Encyclopaedia of Medical Imaging, Vol. 7. Published by The NICER Institute, Oslo, pp 311–312
3. Kottamasu SR (2004) Bone changes in diseases of the blood and blood-forming organs. In: Kuhn JP, Slovis TL, and Haller JO (eds), Caffey's Pediatric Diagnostic Imaging. 10th edn. Philadelphia, Mosby, pp 2425–2426
4. http://www.onkologychannel.com./leukemias. Last update February 8, 2005

Hematopoietic Bone Marrow

Differential diagnosis of hematopoietic bone marrow and malignant disease may be difficult. Usually, a higher amount of hematopoietic bone marrow is found in younger patients, but reconversion of bone marrow from fatty marrow, in particular after chemotherapy, is not infrequent.

▶Myeloproliferative Disorders

Hematuria

Whether it be microscopic or gross should be further investigated. It may or may not be accompanied by pain. Painful hematuria can be caused by a number of disorders including infections and stones in the urinary tract. Painless hematuria can also be due to a large number of causes, including cancer.

▶Neoplasms, Bladder

Hemifacial Microsomia

Hemifacial microsomia is the second most common facial birth defect after cleft lip and palate; it is characterised by facial asymmetry with unilateral hypoplasia of the face. Zygoma and the lateral maxilla, in the upper face, and mandible, in the lower face, are most affected; the nose and columella deviate toward the hypoplastic side.

Anomalies of mouth (micro- or macrostomia), ears, eyes and central nervous system and/or plagiocephaly may coexist.
▶Congenital Malformations, Nose and Paranasal Sinus

Hemifacial Spasm/Hyperkinesia

Unilateral, intermittent, involuntary muscle twitches in the facial nerve territory. It is more prevalent in women and most commonly results from nerve compression at the root entry zone.
▶Facial Nerve Palsy

Hemihypertropy

Abnormal enlargement of one side of the body.
▶Neoplasms, Kidney, Childhood

Hemobilia

Hemobilia is a hemorrhage in the biliary tree due to an abnormal communication between the high-pressure hepatic artery system and the lower-pressure biliary tree. Causes include liver trauma (blunt or penetrating), iatrogenic injuries (percutaneous liver biopsy, bile duct interventions, intraarterial procedures), liver and bile duct tumors, aneurysms or pseudoaneurysms of the hepatic artery, infectious cholangitis, and gallstones. Hemobilia may be asymptomatic or give rise to biliary colic or obstruction if clot formation occurs in the bile duct. Most bleedings in the biliary tree are characterized by occult blood loss, but hypotension and shock are rarely observed. The computed tomography scan findings are often characteristic, with intrahepatic artery pseudoaneurysm formation. The diagnosis is usually confirmed by selective hepatic arteriography, and if a bleeding point is found, embolization may be considered.
▶Trauma Hepatobiliary

Hemochromatosis

Hereditary hemochromatosis (also called primary or idiopathic hemochromatosis) is an autosomal recessive disease characterized by an anomalous increase in iron absorption from the gastrointestinal tract. This excess of iron accumulates within the parenchymal cells of the liver, pancreas, endocrine glands, heart, skin, and joints. If left untreated, it leads to cellular damage and organ dysfunction. In patients with advanced disease, liver cirrhosis develops. At ultrasound (US), iron deposits in the liver do not determine specific findings. At computed tomography (CT), a diffuse homogeneous hyperdensity of the liver parenchyma can be appreciated on unenhanced scans. Biphasic contrast-enhanced CT study is required for the detection of hepatocellular carcinoma. A decrease of signal intensity of liver parenchyma is observed on T2-weighted magnetic resonance (MR) images. Since several studies have suggested that MR may enable an accurate quantification of hepatic iron concentration, it may be used in assessing the response to treatment in patients with hemochromatosis, avoiding the risks inherent in percutaneous liver biopsy.
▶Diffuse Infiltrative Diseases, Hepatic

Hemochromatosis, Arthropathy

Typically degenerative morphology, showing subchondral cyst formation, sclerosis, and thinning of cartilage. Chondrocalcinosis involving both fibrous and hyaline cartilage is frequently seen, particularly in the large joints. The distribution is characteristic with selective degenerative changes of the second and third metacarpophalangeal joints while abnormalities in the intercarpal joints are variable and the interphalangeal joints are spared.
▶CPPD

Hemochromatosis, Skeletal

Giuseppe Guglielmi
University of Foggia, Foggia,
Department of Radiology,
Scientific Institute Hospital San Giovanni Rotondo,
Italy
guglielmi_g@hotmail.com

Synonyms

Acquired or secondary hemochromatosis; Hereditary or genetic hemochromatosis; Iron overload

Definitions

Hemochromatosis is a condition of iron overload which results in parenchymal tissue damage (1). In European descendents, the disorder is most often hereditary (primary) hemochromatosis. Acquired (secondary) hemochromatosis occurs in a variety of chronic anemias that are caused by ineffective erythropoiesis (for example, thalassemia major or sideroblastic anemia), as the result of multiple transfusions or as the result of one of the following less frequent conditions: chronic oral iron ingestion (in absence of iron deficiency), African (Bantu) hemochromatosis, porphyria cutanea tarda, portacaval shunt, juvenile hemochromatosis, neonatal hemochromatosis, and congenital atransferrinemia. In acquired iron-loading disorders, massive iron deposits in parenchymal tissues can lead to the same clinical and pathologic features as in hemochromatosis.

Pathology/Histopathology

Hereditary or genetic hemochromatosis is an autosomal recessive disease most often caused by inheritance of a mutant HFE gene. The HFE gene is tightly linked to the HLA-A locus on chromosome 6p and encodes a 343-amino-acid complex class-1-type molecule that is structurally related to MHC class I proteins. Two missense mutations have been identified: C282Y resulting in a substitution of cysteine at position 282 with tyrosine and H63D resulting in a substitution of histidine at position 3 with aspartate. Hereditary hemochromatosis not associated with this mutation is termed non-HFE-related hemochromatosis (juvenile hemochromatosis, a rare disorder effecting males and females equally, is the most common example). Other forms of hemochromatosis are known to have a genetic basis which must still be defined (2).

Only the normal (wild type) HFE protein forms a normal complex with β_2-microglobulin and transferring therefore the mutant HFE protein remains trapped intracellularly, reducing transferring receptor mediated iron uptake by the crypt cells of the intestines. This upregulates the divalent metal transporter (DMT-1) on the brush border of the villous cells, leading to an inappropriate increase of intestinal iron absorption (1).

Hemochromatosis is a common genetic disease and is most common among northern European populations where approximately 1 in 10 persons are heterozygous carriers and 0.3 to 0.5% are homozygotes. Disease expression is variable and influenced by several factors including dietary iron intake and blood loss (menstruation and blood donation). The clinical expression of the disease is 5 to 10 times more frequent in men than in women.

The inappropriately high intestinal absorption of iron steadily increases from birth. While the normal content of iron is approximately 3–4 g, in advanced disease, the body may contain 20 g or more of iron that is deposited mainly in parenchymal cells of the liver, pancreas, and heart. Iron may be increased 50- to 100-fold in the liver and pancreas and 5- to 25-fold in the heart (1). Iron deposition in the pituitary causes hypogonadotropic hypogonadism in both men and women. Tissue injury may result from disruption of iron-laden lysosomes, from lipid peroxidation of subcellular organelles by excess iron, or from stimulation of collagen synthesis by activated stellate cells.

Clinical Presentation

Most individuals with hemochromatosis are asymptomatic. Initial symptoms include weakness, lassitude, weight loss, change in skin color, abdominal pain, loss of libido, and symptoms of diabetes mellitus (1). Hepatomegaly, suntan-like hyperpigmentation of exposed and nonexposed areas of the skin, spider angiomas, splenomegaly, arthropathy, ascites, atrial, or ventricular arrhythmias, congestive heart failure, loss of body hair, testicular atrophy, and jaundice are prominent in advanced disease. In non-treated advanced cases, the skin may become slate gray, and hepatosplenomegaly, ascites, pleural effusion, and arthritis can develop. The arthritis may affect any joint but usually involves the second and third metacarpophalangeal joints, knees, and hips. These joints may be deformed with or without inflammatory signs.

The liver is usually the first organ to be affected, and hepatomegaly is present in more than 95% of symptomatic patients (1). Hepatic enlargement may exist in the absence of symptoms or of abnormal liver function tests. Hepatocellular carcinoma develops in approximately 30% of patients with cirrhosis, and it is the most common cause of death in treated patients. Excessive skin pigmentation is present in over 90% of symptomatic patients at the time of diagnosis. Diabetes mellitus occurs in approximately 65% of patients and is more likely to develop in those with a family history of diabetes. Arthropathy is present in 20–70% of patients and may be the presenting feature (3). It usually starts in the metacarpophalangeal joints, but the wrists, knees, and hips may also be affected. Cardiac involvement is the presenting manifestation in approximately 15% of patients. The most common manifestation is congestive heart failure, which occurs in approximately 10% of young adults with the disease, especially those with juvenile hemochromatosis. Hypogonadism occurs in both sexes and may antedate other clinical features. Manifestations include loss of libido, impotence,

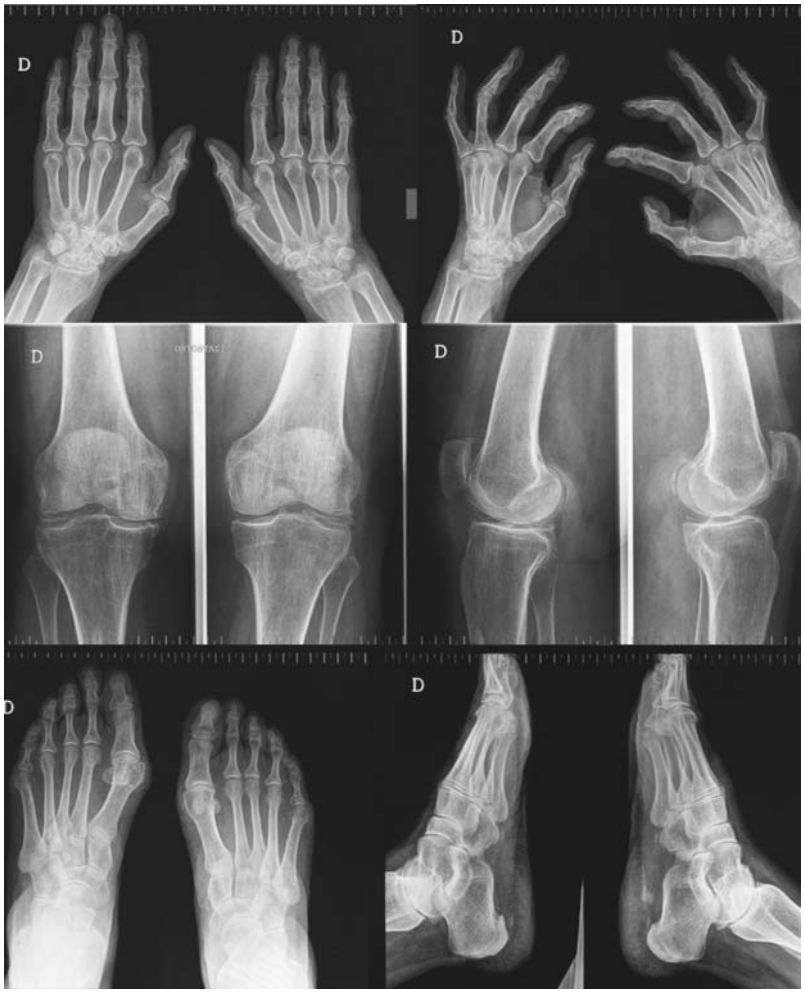

Hemochromatosis, Skeletal. Figure 1 Digital radiographs of the hands, knees, and feet of a 73-year-old woman with symptomatic diffuse arthralgia. Antero-posterior and oblique projections of the hands show a reduction of the articular space of the metacarpophalangeal and proximal and distal interphalangeal joints. Bilateral periarticular calcification, especially of the metacarpophalangeal joints and the triangular cartilage of the wrist requiring a differential diagnosis with ►calcium pyrophosphate dehydrate crystals deposition disease. Erosion is not observed. The osteochondral degenerative disease is associated with calcification of the menisci and hyaline cartilage of the knee. At the feet bilateral thickening and partial calcification of the plantar aponeurosis and of the first metatarsophalangeal bursa as well as bilateral calcified tendinopathy are present.

amenorrhea, testicular atrophy, gynecomastia, and sparse body hair.

The primary treatment is the removal of excess iron from the system by phlebotomy (500mL of whole blood once a week).

Imaging

Radiologic manifestations of hemochromatosis arthropathy are identical to degenerative osteoarthritis and chondrocalcinosis (4). Approximately half of the patients with hemochromatosis have radiographic evidence of osteoarthritis and 30% of chondrocalcinosis even in the absence of osteoarthritis (4). Other radiological features include cystic changes of the subchondral bones (typically of 1–5 mm and appear in the metacarpal heads), loss of articular cartilage with concentric narrowing of the joint space, diffuse demineralization, hypertrophic bone proliferation, and calcification of the synovium (3) (Fig. 1). Joint lesions will improve in 30% of the cases with therapy, but 20% will worsen symptomatically. Destructive arthropathy is an unusual finding (3).

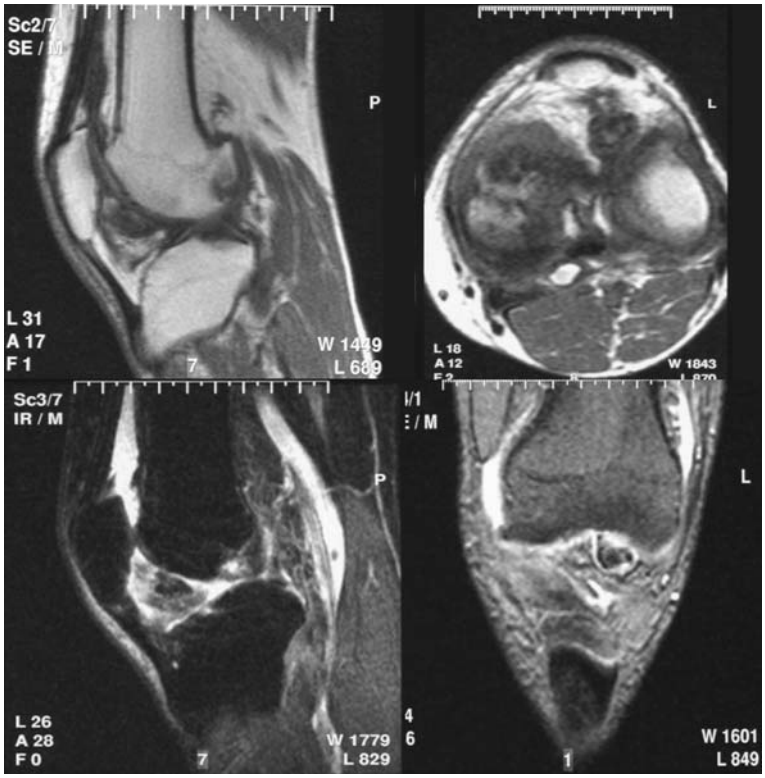

Hemochromatosis, Skeletal. Figure 2 Multiplanar magnetic resonance study with SE, GE, and FSE sequences of a 30-year-old man with knee pain (predominately right). A hypointense signal in the T1 and T2 sequences is located predominately in Hoffa's fat pad at the margins of the hyaline cartilage of the femoral trochlea. The cartilage shows signs of erosion and fissures indicating an advanced stage of degeneration.

The onset of arthropathy favors the second and third metacarpophalangeal joints while the other metacarpophalangeal joints and proximal interphalangeal joints are involved less frequently and to a lesser extent (4). The carpal joints, larger joints and the spine may also be involved and show changes similar to those seen in the hand (4).

Differential diagnosis of hemochromatosis arthropathy of the hand includes calcium pyrophosphate dehydrate crystals deposition disease, ▶degenerative joint disease and rheumatoid arthritis (4). Hemochromatosis arthropathy is more widespread and presents characteristic beak-like osteophytes of the metacarpal heads (4). Degenerative joint disease is more extensive in the interphalangeal joints and less severe in the metacarpophalangeal joints (4). While rheumatoid arthritis presents predominately erosive changes (4).

The excess iron in the liver parenchyma results in an attenuation in CT ("white liver" in unenhanced scans with a density above 70 HU) (4). The sensitivity varies with the amount of excess iron and reaches 100% with a fivefold increase (4). Similar results are obtained with magnetic resonance imaging using spin-echo sequences. The excess iron in other affected organs can also be seen with these imaging modalities.

A loss of signal intensity may be seen in the articular cartilage in T1- and T2-weighted magnetic resonance images of involved joints. This may be due to the presence of excess iron in the cartilage, synovium and/or synovial fluid (4) (Fig. 2).

Nuclear Medicine

Nuclear medicine techniques have limited use in this disease.

Diagnosis

Diagnosis of hemochromatosis is supported by the association of hepatomegaly, skin pigmentation, diabetes mellitus, heart disease, arthritis, and hypoganodism (1). Early diagnosis before permanent organ damage occurs is important because it increases the life expectancy from

Hemochromatosis, Skeletal. Table 1 Iron panel results indicating hemochromatosis

Serum iron	Above normal
Serum ferritin	Above normal
Transferring iron saturation percentage	Above normal
Total iron bonding capacity	Below normal
Transferrin	Below normal
Serum transferring receptor	Normal to below normal

2 years to that of a normal individual. A detailed family history can play a key role in diagnosis. Laboratory tests should exclude the possibility that the iron deposition is due to a hematological disease. Total-body iron store increase, especially parenchymal iron concentrations, should be assessed (see Table 1). Genetic testing for the two known mutations is negative in approximately 10% of the cases, indicating the presence of other, not yet identified, mutations.

The characteristic radiological features of hemochromatosis suggest that imaging techniques, especially computed tomography and magnetic resonance imaging, can be diagnostic but their elevated cost exclude their use for screening.

Bibliography

1. Powell LW (2004) Hemochromatosis. Dennis L. Kasper, Eugene Braunwold, Anthony Fauci et al (eds) Harrison's Principles of Internal Medicine. 16 th edn. McGraw-Hill Professional, Philadelphia, pp 1991–1997
2. Limdi JK, Crampton JR (2004) Hereditary haemochromatosis. Q J Med 97:315–324
3. Powell LW, Yapp TR (2000) Hemochromatosis. Clin Liver Dis 4:211–228
4. Jager HJ, Mehring U, Gotz GF et al (1997) Radiological features of the visceral and skeletal involvement of hemochromatosis. Eur Radiol 7(8):1199–1206

Hemoglobin Disorders

▶Hemoglobinopathies, Skeletal Manifestations

Hemoglobin S Disease

▶Hemoglobinopathies, Skeletal Manifestations

Hemoglobinopathies, Skeletal Manifestations

Remide Arkun
Department of Radiology, Ege University, School of Medicine, Izmir, Turkey
rarkun@yahoo.com

Synonyms

Blood diseases; Hemoglobin disorders; Hemoglobin S disease

Definitions

The hemoglobinopathies are a group of diseases resulting from molecular abnormalities of hemoglobin and associated with anemia and characteristic abnormalities of the skeleton.

Thalassemia is a genetically determined disorder of hemoglobin synthesis resulting in chronic hemolytic anemia, and also inadequate production or total absence of normal alpha or beta globin chains. Thalassemia may exist in a homozygous form, called thalassemia major, or a heterozygous form, termed thalassemia minor. Thalassemia intermedia represents a poorly defined intermediate variety of the disease.

Sickle cell disease is a term that describes all conditions characterized by the presence of S hemoglobin (Hb S).The presence of sickle cell erythrocytes is a hereditary transmitted as a Mendelian dominant. In the genetic analysis of families with the sickle cell trait, both parents must transmit the sickling character for an offspring to show the clinical picture of the sickle cell anemia (homozygous due to S-S hemoglobin). If one parent has normal A hemoglobin and the other S hemoglobin, the offspring will show the sickled trait (S-A hemoglobin) but not anemia. Hemoglobin S in combination with abnormal hemoglobin C (sickle cell S-C disease), a less severe form. The combination of hemoglobin S-thalassemia rarely occurs (1, 2).

Pathology/Histopathology

The hypoxia of anemia represents a stimulus for increased erythropoiesis and bone marrow hyperplasia, through the action of the hormone erythropoietin (1). In infants all bones are involved, whereas in older children and

adults only bone with active marrow are affected (2). Erythropoiesis also occurs at extra-medullary sites, most commonly resulting in a paraspinal mass but occasionally affecting organs containing pluripotential stem cells.

A hypertransfusion regimen reduces the extent of marrow expansion. However, iron overload and hyperuricemia are potential consequences of repeated blood transfusions. High serum iron levels are associated with abnormalities of the synovium and articular cartilage.

In sickle cell anemia, precipitating factors that promote deoxygenation of red blood cells enhance sickling and responsible for the painful crises. The formation of the rigid sickled red cell is due to polymerization of the abnormal hemoglobin. These changes result in increased viscosity and stasis. Ischemia is the clinical (as well as radiologic and pathologic) consequence of these cellular characteristics. The bone marrow is a prime target of ischemia and infarction because of high oxygen utilization. Pain and tenderness frequently are related to infarction of bone marrow. In patients with sickle cell trait, painful crises usually are not apparent unless the patient is exposed to an atmosphere low in oxygen (1, 2).

Other skeletal abnormalities of the hemoglobinopathies are; vascular occlusion, bone infarction, epiphyseal osteonecrosis, growth disturbances, generalized osteoporosis and fractures, osteomyelitis, and septic arthritis (3).

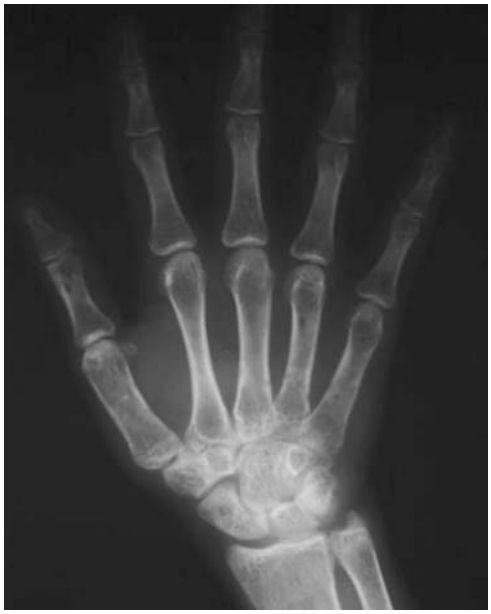

Hemoglobinopathies, Skeletal Manifestations.
Figure 1 Anteroposterior plain film of hand shows decreased bone density, round small radiolucent areas on both first and fourth metacarpal bone. There is loss of cortical concavity on first metacarpal bone.

Imaging

Skeletal Manifestations of Untreated Thalassemia

Radiographic features of thalassemia derive from erythroid hyperplasia of bone marrow, more marked than in other hereditary anemias. Medullary spaces are widened, resulting in the thinning of cortices by pressure atrophy. Many trabeculae are resorbed and those remaining are coarsened, which may result in the appearance of "cob-webbing" in the pelvis. Skeletal manifestations are rare before 6 months of age and seen after end of first year of life. Initially both the axial and the appendicular skeleton are altered, but as the patient reaches puberty, the appendicular skeletal changes diminish, owing the normal regression of the marrow from the peripheral skeleton (1, 2).

The earliest changes are in the small bones of the hands and feet. Marrow expansion also causes a loss of the normal concave outline of long bones. These changes are most commonly seen in the humerus and femur, the tubular bones in the hands and feet (Figs 1 and 2).

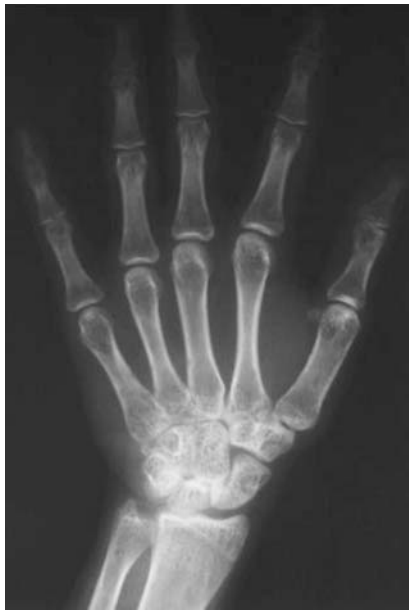

Hemoglobinopathies, Skeletal Manifestations.
Figure 2 Anteroposterior plain film of hand, demonstrating a coarse trabeculations due to bone marrow expansion on the carpal bones.

In severe cases, the femur may develop a flask-like shape. Widening of the metaphyses and epiphyses resembles an Erlenmeyer flask (3).

Skull changes consist of the widening of diploic spaces and displacement and thinning of the outer table (Fig. 3). The diploic trabeculae orient themselves perpendicularly to the tables, producing the radial pattern called "hair-standing-on-end" (Fig 4). The frontal bones reveal the earliest and most severe changes, and the inferior aspect of the occiput is usually unaltered. Overgrowth of marrow in the frontal, temporal, and facial bones consistently impedes pneumatization of paranasal and mastoid sinuses (4) (Fig. 5). Maxillary alterations can produce lateral displacement of the orbits, leading to hypertelorism, malocclusion of the jaws, and displacement of dental structures, resulting in "rodent facies." These changes are unusual in other anemias.

There is an initial increase in the height-to-width ratio of the vertebral bodies, in untreated thalassemic patients. The vertebrae may eventually become biconcave and lose height, secondary to multiple compression fractures. Rarely, central squared-off vertebral depressions or H vertebrae, characteristic of sickle cell anemia, are noted in thalassemia major. A "bone-within-bone" appearance occurs in the spine and ribs (Fig. 6). Generalized osteoporosis and osteopenia are features of thalassemia. Growth retardation and premature fusion of growth plates in the tubular bones occur commonly, and is in part, due to the disease process but may also result from desferrioxamine (DFX) therapy. On plain radiographs, obliteration of the epiphyseal line is usually asymmetrical resulting in both growth retardation and deformity. Shortening and deformity of the extremity may be apparent. In the humerus, varus deformity is characteristic (1, 3).

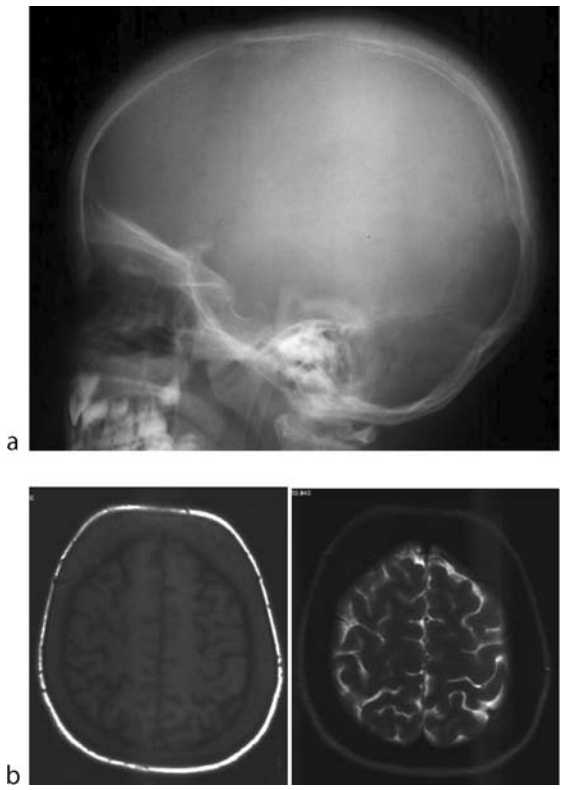

Hemoglobinopathies, Skeletal Manifestations.
Figure 3 Lateral plain film and MRI exam of cranium, showing increased density at diploic space and decreased signal intensity on both T1-weighted and T2-weighted axial images.

Skeletal Changes Secondary to Hypertransfusion (Crystal Deposition) and Iron-Chelation Therapy

Iron overload and hyperuricemia are potential consequences of repeated blood transfusions. Secondary hemochromatosis resulting from repeated transfusions. Articular abnormalities are seen less frequently, and affect the large joints more commonly than primary hemochromatosis. Radiological features include symmetrical loss of articular space, cystic lesions, collapse and flattening of the subchondral bone, and osteophyte formation (3). Calcium pyrophosphate dihydrate crystal deposition may lead to chondrocalcinosis (1).

Initially, iron-chelation therapy was first used to reduce iron overload in hypertransfused thalassemic patients. Over the following years a new pattern of skeletal changes emerged. The radiological changes were attributed to the

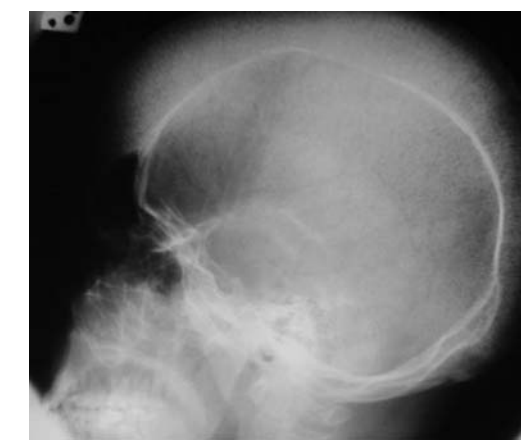

Hemoglobinopathies, Skeletal Manifestations.
Figure 4 Hair-standing-on-end appearance in an untreated thalassemic patient.

effect of DFX on the growth plates of young thalassemic patients. Although, the exact mechanism of production of the skeletal lesions remains unclear, a common pattern of dysplastic changes affecting the spine and long bones, as

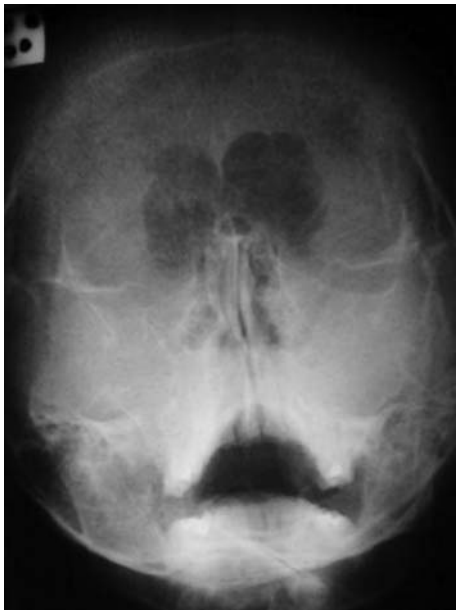

Hemoglobinopathies, Skeletal Manifestations.
Figure 5 In an untreated thalassemic patient, resulting in obliteration of maxillary sinuses due to bone marrow expansion.

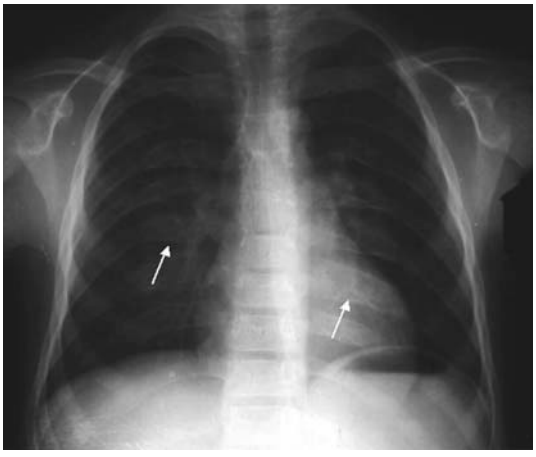

Hemoglobinopathies, Skeletal Manifestations.
Figure 6 Chest radiograph of untreated thalassemic patient, demonstrating bone-within-bone appearance (*white arrows*).

well as growth retardation, has been observed even with optimal transfusion regimens (3).

Repeated hypertransfusion can result in hemosiderosis. Iron deposition occurs at bone marrow, other solid organs, and breast tissue. Iron deposition is evident as areas of reduced signal intensity on spin-echo sequences both on T1-weighted and T2-weighted sequences on MRI (1, 3) (Fig. 7).

Extra-Skeletal Manifestations of Thalassemia

Extra-medullary hematopoiesis occasionally arises in organs containing pluripotential stem cells. The marrow has accelerated activity, extraosseous herniation of medullary tissue is observed. Posterior paravertebral mediastinal masses, representing sites of extra-medullary hematopoiesis, result from extraosseous extensions of medullary tissue derived from vertebral bodies and ribs (1, 3) (Fig. 8).

Skeletal Manifestations of Sickle Cell Anemia

The presence of a chronic hemolytic anemia results in bone marrow hyperplasia. Sickle cell anemia is most likely to produce marrow hyperplasia and deossification; the variants are more often associated with bone infarction. In the spine, a step-like end-plate depression is frequently present (Fig. 9). Although this has been considered pathognomonic of sickle cell anemia, it may also appear in Gaucher disease, thalassemia major and congenital hereditary spherocytosis (2).

Marrow hyperplasia produces widening of the medullary cavities and rarefaction of remaining trabeculae in the spongiosa and cortex. In the skull, diffuse widening of the diploic space is associated with thinning of inner and outer tables of the skull. Focal radiolucent areas simulate metastasis or myeloma. Radial trabeculation causing a "hair-on-end" appearance may be seen, but not as commonly as with thalassemia. Mandibular involvement is common. Increased radiolucency and a coarsened trabecular pattern are characteristic. The base of the occiput is spared (1). Osteoporosis in the long bones tends to disappear in adolescence. The flat bones, especially ribs, will also present a thickened trabecular pattern with a cortical narrowing. There may be rib notching, "bone-within-bone" and a "spatula" appearance (2).

The major orthopedic complications of the sickle cell disease are bone infarct, osteomyelitis, and avascular necrosis of the femoral and humeral heads. Osteonecrosis is the sequela of the sickling phenomenon in which sequestration of cells occurs. In infants and children, bone infarcts most frequently occur in the diaphyseal portions of small tubular bones; in adult in the metaphyseal and subchondral portions of long bones. In children, osteonecrosis may involve the small tubular bones of the hand and feet, leading to the "hand-foot" syndrome or dactylitis. Infraction is often preceded by a painful soft-tissue swelling of finger or toe, then within 10 days, varying degrees of periostitis. Focal osteosclerosis is also seen. The findings resemble those of osteomyelitis. Infarction of vertebral bodies also occur, and massive infarction may cause collapse of the centra and has been

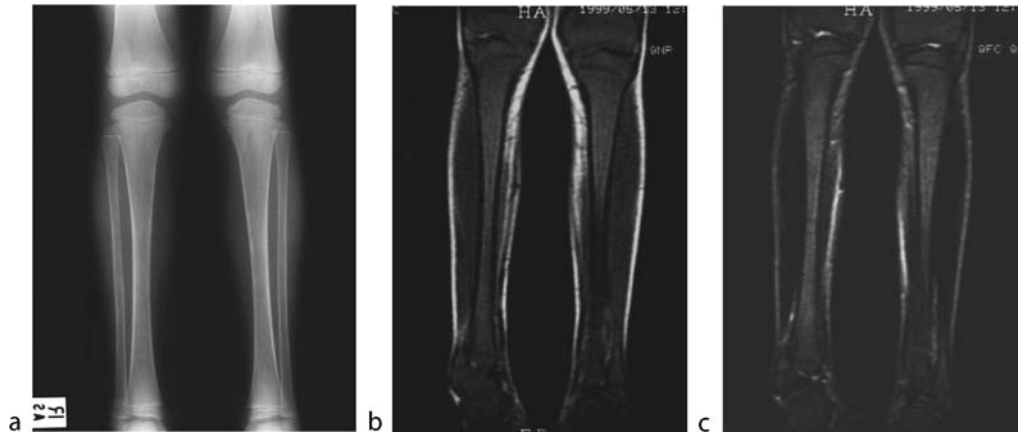

Hemoglobinopathies, Skeletal Manifestations. Figure 7 Fourteen years thalassemic patient, received by iron-chelation therapy showed no abnormality on plain radiography of both cruris (a), MRI showed decreased signal intensity on both T1-weighted and T2-weighted coronal images due to iron deposition on bone marrow (b).

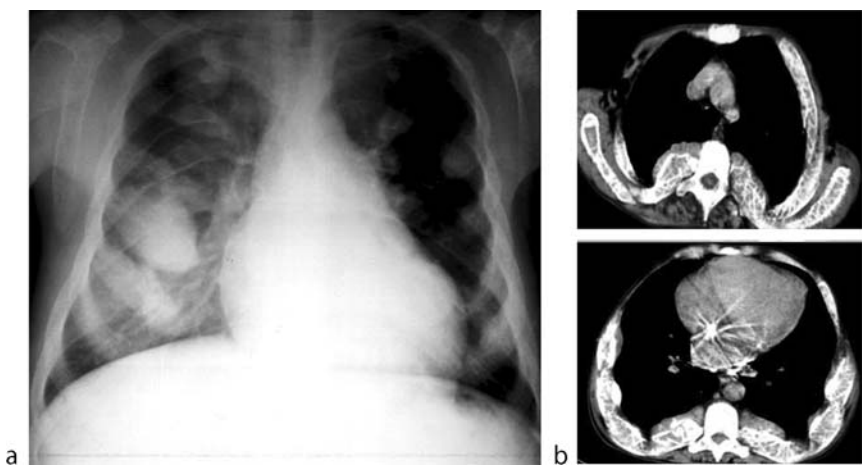

Hemoglobinopathies, Skeletal Manifestations. Figure 8 Chest radiograph of untreated thalassemic patient, demonstrating expansion at the costochondral junction (a), chest CT showed expansion and coarse trabeculation on both costae and bilateral scapulas. There is also soft-tissue density at bilateral paravertebral area (b) (extra-medullary hematopoiesis).

termed the "fish vertebral" sign. Occasionally in older children, infarction of the capital femoral epiphysis leads to an appearance simulating that of Legg-Calvé-Perthes disease. In children with sickle cell anemia, the distal femur is a common site for acute long-bone diaphyseal infarcts.

Pathologic fractures are often a complication in patients with sickle cell anemia, perhaps because of the thin cortices due to marrow hyperplasia. Underlying factors could also be bone infarcts and/or osteomyelitis.

Patients of sickle cell anemia are prone to bacterial infection. The ischemic zones are appropriate foci for the settling of organism during the bacteremia. Bone and joint infections in sickle cell anemia are caused by salmonellae in over 50% of cases. Staphylococci represent a second common cause of osteomyelitis in sickle cell anemia. Osteomyelitis in most frequent in the long tubular bones. Roentgenographic changes are usually those of periostitis, with single or double layering of periosteal new bone reaction, and may progress to bone destruction with massive involucrum formation. Septic arthritis complicating sickle cell anemia is less frequent than osteomyelitis. Joint effusions in sickle cell anemia that are not associated with infection are relatively

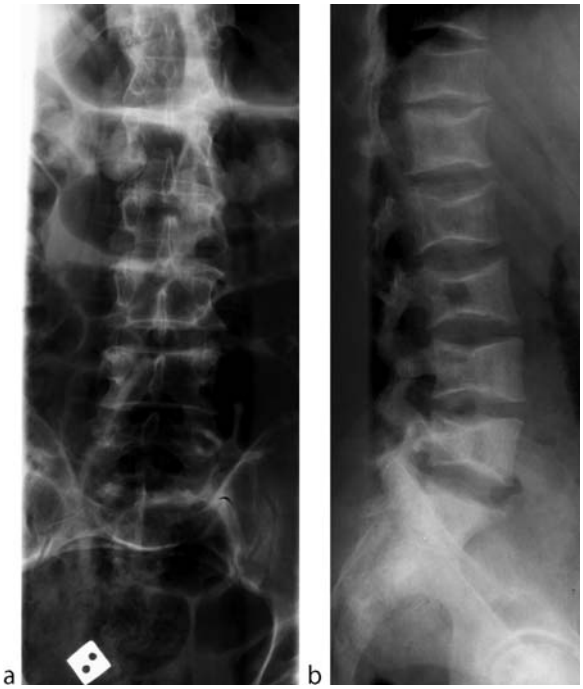

Hemoglobinopathies, Skeletal Manifestations.
Figure 9 Anteroposterior (a) and lateral (b) radiography of lumbar vertebrae showed increased density, step-like end-plate depression on vertebral bodies.

common. These effusions, which most frequently involve the knee and elbow, are associated with clinical manifestations of crises and presumably relate to synovial ischemia (1, 2).

Bibliography

1. Resnick D (1989) Bone and Joint Imaging. W.B.Saunders Company, Philadelphia, PA, pp 662–674
2. Edeiken J, Dalinka M, Karasick D et al (1990) Edeiken's Roentgen Diagnosis of Diseases of Bone. 4th edn. Williams & Wilkins, Baltimore, MD, pp 1315–1339
3. Tyler PA, Madani G, Chaudhuri R et al (2006) The radiological appearances of thalassaemia. Pictorial review. Clin Radiol 61:40–52
4. Caffey J (1957) Cooley's anemia: a review of the roentgenographic findings in the skeleton. Am J Roentgenol Radium Ther Nucl Med Sep;78(3):381–391
5. Barton JC, Cockshott WP (1962) Bone changes in hemoglobin SC disease. Am J Roentgenol Radium Ther Nucl Med Sep;88:523–532

Hemoperitoneum

Hemoperitoneum consists of the presence of blood in the peritoneum, usually resulting from abdominal trauma with laceration of liver, spleen, or other intraabdominal organs. Intraaddominal spontaneous bleeding caused by coagulation disorders and ulcer or neoplasm perforation is rare. Intraperitoneal blood tends to collect in the pouch of Douglas. However, smaller quantities of blood may commonly be contained in the right subhepatic and the right paracolic space and may provide an indication for the origin of the bleeding. In abdominal trauma patients, hemoperitoneum represents an important prognostic factor, and a timely diagnosis is mandatory.

Because diagnostic peritoneal lavage and ultrasound (US) are simple, inexpensive, and sensitive investigations for the detection of hemoperitoneum, they are widely employed for the first-line abdominal evaluation in trauma patients. Hemoperitoneum is commonly the only indication of injury on US, and it appears as a hypoechoic–anechoic collection located in the subhepatic space or in the pouch of Douglas. On unenhanced computed tomography scans, acute hemoperitoneum appears as a intraperitoneal fluid collection homogeneously or heterogeneously hyperattenuating.

▶Trauma Hepatobiliary

Hemophilic Arthropathy

Hemophilic arthropathy is a chronic joint disease caused by repeated hemarthroses in patients with bleeding disorders (most commonly severe hemophilia A and B).

▶Bleeding Disorders, Osteoarticular

Hemophilic Osteoarthropathy

▶Bleeding Disorders, Osteoarticular

Hemophilic Pseudotumor

A rare tumor-like lesion of bone and/or soft tissues that can develop in hemophilic patients following intraosseous, subperiosteal, and/or intramuscular bleeding.

▶Bleeding Disorders, Osteoarticular

Hemoptysis

Jean-Pierre Pelage, Pascal Lacombe
Department of Radiology
Hôpital Ambroise Paré,
Université Paris Ile-de-France Ouest,
Boulogne-Billancourt, France
jean-pierre.pelage@apr.ap-hop-paris.fr

Definitions

Hemoptysis is the expectoration of blood or blood-stained sputum from the lungs or airways (bronchi, larynx, trachea). The word hemoptysis comes from the greek "haima" meaning blood and "ptysis" which means spitting. When blood originates from outside the respiratory tract, the spitting is commonly described as pseudohemoptysis. For instance, differentiating between hemoptysis and hematemesis is an integral part of diagnosis.

Hemoptysis may be either self-limiting or recurrent. Hemoptysis can range from small quantities of bloody sputum to life-threatening amounts of blood. Classifying hemoptysis as mild or massive is somewhat arbitrary since it is difficult to accurately quantify the amount of blood. Thus, massive hemoptysis is variably defined as hemoptysis exceeding 200–600 mL within a period of 24 h or less. Massive hemoptysis, encountered in approximately 10% of cases, is a medical emergency since the reported mortality rate can be as high as 75%. Mild hemoptysis must be carefully investigated to prevent recurrence that could be life-threatening. In addition, in patients with already compromised lung function, even a small amount of blood in the bronchial tree may lead to acute airway obstruction and asphyxiation.

Pathology/Histopathology

Blood traversing the lungs can originate from low pressure and low resistance ▶pulmonary arteries accounting for 99% of the cardiac output and high pressure and high resistance ▶bronchial arteries accounting for 1% of the cardiac output. The pulmonary arteries supply exclusively the pulmonary capillary bed whereas the bronchial arteries provide the nutritive blood supply to the airways, the lymph nodes, visceral pleura and other portions of the mediastinum. There are normal anastomoses between both circulations but any abnormal process creating obstruction, compression of pulmonary artery branches or destruction of the pulmonary capillary bed may induce a compensatory development of these anastomoses. Thus, despite the quantitatively smaller contribution of the bronchial circulation to the normal pulmonary blood flow, the bronchial arteries are generally a more important source of bleeding than the pulmonary circulation (90% versus 10% approximatively) in lung disease. In addition to being perfused at a high pressure, the bronchial arteries supply blood to lesions within the airways and may become hyperplastic and tortuous, potentially causing massive hemoptysis. In the presence of pleural thickening, non-bronchial systemic arteries may develop through the pleural surface and become enlarged as a result of the inflammatory pulmonary process.

Clinical Presentation

There are many underlying disorders that can cause hemoptysis. In the past, tuberculosis, bronchiectasis and lung abscess accounted for 90% of cases. Recent reports suggest that nowadays the most common causes of hemoptysis are airway diseases including bronchitis in long-term smoking patients with or without bronchiectasis, which may account for up to 30% of cases and neoplasms. Pulmonary parenchymal diseases including infection (tuberculosis, aspergilloma and lung abscess) and inflammatory disorders, pulmonary vascular disorders (pulmonary embolism, pulmonary arteriovenous malformations, etc) may also cause hemoptysis. Immunologic lung disease, pulmonary hemorrhage in patients undergoing chemotherapy or bone marrow transplant and acquired cardiac disease are usually not amenable to interventional radiological treatment because specific treatments should be applied. Depending upon the study, up to 30% of patients with hemoptysis have no cause identified even after careful evaluation. These patients are classified as having idiopathic hemoptysis.

In patients presenting with hemoptysis, the initial approach is dictated by the clinical presentation. In case of massive hemoptysis and severe functional decompensation, the first priorities are to maintain the airway, optimize oxygenation and stabilize the hemodynamic status. The major question to be answered is whether or not the patient should be intubated for better gas exchange, suctioning and protection from sudden cardiorespiratory arrest. Once stabilization is accomplished, diagnostic (i.e. determine the site and cause of bleeding) and therapeutic interventions should be promptly performed because recurrent bleeding occurs unpredictably. History and physical examination are helpful in diagnosing some etiologies of hemoptysis. The precise timing and nature of the further evaluation are dictated by the suspected underlying pathologic process and the clinical condition of the patient.

Arteriography and embolization should be used immediately for both diagnosis and therapy in those patients who continue to bleed despite vasoconstrictive drugs and endobronchial therapy. Bronchial artery embolization should be attempted when bleeding is refractory to medical therapy, and surgery may be needed in severe hemorrhage. Emergent surgical intervention should be considered in operative candidates with unilateral or localized bleeding when embolization is not available or not feasible, when bleeding continues despite embolization or when bleeding is associated with persistent respiratory compromise.

Imaging

Diagnostic studies for hemoptysis include chest radiography, bronchoscopy and spiral computed tomography (CT) of the chest. Bronchoscopy and chest radiography have been considered the primary methods for the diagnosis and localization of hemoptysis. More recently, many researchers currently suggest that spiral CT should be performed prior to bronchoscopy particularly in case of massive hemoptysis. Arteriography has both a diagnostic, by demonstrating occasionally the site and the cause of bleeding, and a therapeutic value with selective embolization of bronchial or non-bronchial systemic arteries.

Chest Radiography

A good quality chest radiography should always be obtained. Localized pulmonary infiltration or condensation, atelectasis, cavitation, mass or signs of chronic bronchitis or bronchiectasis may indicate the source of bleeding. However, hemoptysis may occur from an area that appears normal by routine chest radiography.

Bronchoscopy

Fiberoptic bronchoscopy performed early in the evaluation, while the patient is actively bleeding, provides an important yield for lateralizing the bleeding side, localizing the specific site and identifying the cause of the bleeding. Identification of the bleeding site requires visualization of regions with continued fresh bleeding. Small volume lavage may sometimes help suggest the bleeding site. Flexible bronchoscopy can be performed at the bedside at the time of intensive care unit admission. In those patients with lateralized or localized persistent bleeding, immediate control of the airway may be obtained during the procedure with topical therapy, endobronchial tamponade or unilateral intubation of the nonbleeding lung. If the bleeding cannot be localized because the rate of hemorrhage makes it impossible to visualize the airway, emergent rigid bronchoscopy or emergent arteriography is indicated depending on their availability.

Spiral CT

Over the past 5 years, early use of multi-detector row computed tomography (MDCT) has been advocated to help localize the bleeding site as well as the cause of hemoptysis. CT may also serve as a guide for other diagnostic or therapeutic procedures such as bronchoscopy or transcatheter embolization. MDCT allows rapid scanning throughout the thorax, multiplanar reconstructions without loss of z-axis information owing to near isotropic voxel size and acquisition of various three-dimensional images. Analysis of both lung parenchyma and visualization of the bronchial and non-bronchial systemic feeder vessels and pulmonary artery branches can be achieved simultaneously when iodinated-contrast material is administered (Fig. 1). Multiplanar (parallel to the axis of the bronchial arteries) and maximum intensity projection reconstructions are helpful to identify the origin and course of the bronchial and non-bronchial enlarged systemic arteries (Fig. 1). The sensitivity and accuracy of MDCT in the depiction of ▶non-bronchial arteries is as high as 80% and may be particularly helpful before embolization. Multiple parenchymal abnormalities are consistent with direct or indirect signs of bleeding. These include ground-glass opacities, consolidation, atelectasia, etc. MDCT may identify the cause of bleeding by demonstrating bronchiectasis, aspergillosis, lung abscess or neoplasm (Figs. 1 and 2).

Arteriography

Arteriography has been a major addition to the diagnostic and therapeutic armamentarium for the management of hemoptysis. Since the majority of massive bleeds arise from the bronchial circulation, bronchial arteriography has a higher yield than pulmonary angiography. The pulmonary arterial circulation is the source of bleeding in fewer than 10% of patients with hemoptysis. When the pulmonary arterial circulation is involved, the most common underlying conditions are necrotizing pneumonia, tumoral ulceration, Rasmussen's aneurysms (due to tuberculosis) or iatrogenic pulmonary artery tear, as occurs with perforation from Swan–Ganz catheters (Fig. 3). Systemic arteriography is performed with a digital substraction technique by using a transfemoral approach and with the Seldinger technique. The most commonly used catheters to select the bronchial arteries are Cobra, Mikaelson, Simmons or Judkins right catheters. The usual angiographic criteria for arteries causing hemoptysis include

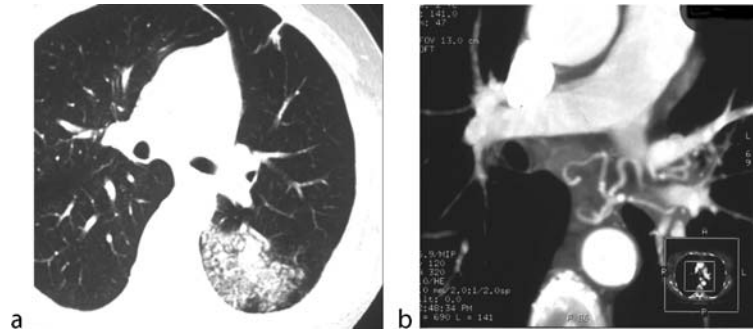

Hemoptysis. Figure 1 (a), MDCT (lung window settings) in a patient with massive hemoptysis demonstrates parenchymal consolidation of left lung base. (b) MDCT with iodinated-contrast administration in the same patient shows enlarged and tortuous bronchial arteries.

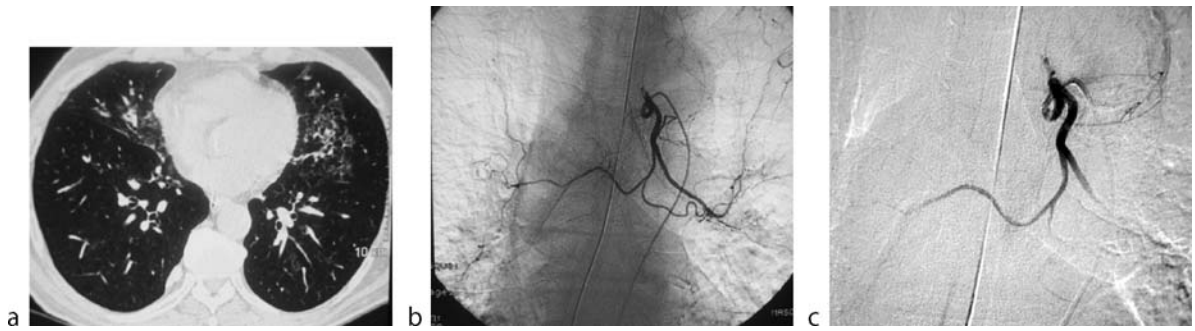

Hemoptysis. Figure 2 (a) MDCT (lung window settings) in a patient with hemoptysis demonstrates bilateral bronchiectasis. (b) Systemic arteriography in the same patient shows an enlarged and tortuous right–left bronchial artery. (c) Arteriogram obtained after selective embolization using 500–700 μm tris-acryl microspheres shows distal devascularization.

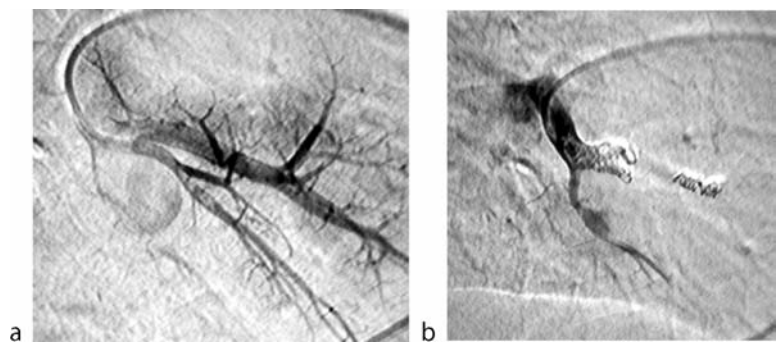

Hemoptysis. Figure 3 (a) Pulmonary angiogram (lingular branch) performed in a patient with massive hemoptysis after the use of a Swan–Ganz catheter shows a large extravasation of contrast material consistent with a pseudoaneurysm. (b) Angiogram obtained after selective embolization of two subsegmental pulmonary artery branches with coils shows satisfactory devascularization.

enlarged and tortuous bronchial or non-bronchial arteries, neovascularity or hypervascularity, antegrade or retrograde shunting to the pulmonary artery, extravasation of contrast material or bronchial artery aneurysm (Fig. 2). Both bronchial and non-bronchial transpleural systemic arteries may be causing hemoptysis and should be investigated. Non-bronchial arteries frequently involved in hemoptysis or recurrent bleeding include intercostal, inferior phrenic,

subclavian, axillary and internal mammary arteries. There is also a high incidence of bleeding from non-bronchial systemic collateral vessels among patients who have undergone a previous bronchial artery embolization procedure. Therefore, persistence of bleeding after a technically good embolization suggests an origin other than those previously occluded. Bronchial arteries of anomalous origin or non-bronchial arteries initially not evaluated or missed and the pulmonary circulation should then be studied (Fig. 3).

Interventional Radiological Treatment

Jacques Remy and coworkers reported for the first time successful bronchial artery embolization in four patients with massive or repeated hemoptysis in 1973. Remy et al subsequently reported a study of 104 patients presenting either with massive or repeated hemoptysis treated with bronchial artery embolization using gelatin sponge pledgets. In 90% of cases, the source of hemoptysis is the bronchial circulation. However, non-bronchial systemic arteries can be a significant source of massive hemoptysis and a cause of recurrence after successful bronchial artery embolization. Knowledge of the bronchial artery anatomy, together with an understanding of the pathophysiologic features of massive hemoptysis, are essential for planning and performing arterial embolization in affected patients. According to Cauldwell et al, the bronchial arteries originate with a few exceptions from the proximal portion of the descending thoracic aorta. The right bronchial artery arises from the lateral or dorsolateral aspect of the aorta, most frequently in a common trunk with an intercostal artery (intercostobronchial artery). The left bronchial artery usually originates from the anterior aspect of the thoracic aorta or the concavity of the aortic arch. A left–right bronchial artery may also be seen (Fig. 2). Radiologists should be alerted to the possible presence of anomalous bronchial arteries, especially when significant bronchial artery supply to areas of abnormal pulmonary parenchyma is not demonstrated at a catheter search or aortography of the descending aorta. Thus, bronchial arteries of anomalous origin may arise from the convex surface of the aortic arch or from the supra-aortic arteries. Non-bronchial systemic circulation of the lung and the arteries of the pulmonary ligament may also cause hemoptysis.

Various embolization materials have been used to perform bronchial artery embolization. The use of resorbable pledgets of gelatin sponge, non-spherical (larger than 355 μm) or spherical polyvinyl alcohol particles (larger than 700–900 μm), tris-acryl gelatin microspheres (larger than 500–700 μm), acrylic glue and steel-coils are recommended (Fig. 2).

Coils are usually the most common embolization agents to perform embolization of pulmonary artery branches (Fig. 3).

Results Associated with Embolization

Technical failure of attempted embolization can be observed in about 10–20% of cases because of catheterization failure, catheter instability or visualization of dangerous branches such as the anterior spinal artery. Embolization is able to achieve an immediate control of hemoptysis in 70–95% of cases, confirming that systemic circulation is the primary source of bleeding in hemoptysis. Regarding mid-term and long-term results, embolization is sometimes considered as a palliative treatment with a relapse of bleeding occurring in up to 30% of patients. However, recurrence is influenced by the etiology of hemoptysis. For instance, in patients with aspergilloma or cystic fibrosis, the recurrence rate is higher than in patients with tuberculosis or bronchitis. Complications are rare in experienced hands but major complications have already been reported. Spinal cord injury related to invisible anastomotic connections between the bronchial circulation and the anterior spinal artery have been reported. Careful analysis of the angiographic images particularly to identify a spinal artery when injecting into a right intercostobronchial artery and the systematic use of microcatheters may reduce the rate of this complication. Subintimal dissection of the aorta and transient thoracic pain have also been reported in several studies.

References

1. Cahill BC, Ingbar DH (1994) Massive hemoptysis: assessment and management. Clin Chest Med 15:147–167
2. Cauldwell E, Siekert R, Lininger et al (1948) The bronchial arteries: an anatomic study in 150 human cadavers. Surg Gynecol Obstet 86:395–412
3. Remy J, Voisin C, Ribet M et al (1973) Treatment, by embolization, of severe or repeated hemoptysis associated with systemic hypervascularization [in French]. Presse Med 2:2060
4. Mal H, Rullon I, Mellot F et al (1999) Immediate and long-term results of bronchial artery embolization for life-threatening hemoptysis. Chest 115:996–1001
5. Revel MP, Fournier LS, Hennebicque AS et al (2002) Can CT replace bronchoscopy in the detection of the site and cause of bleeding in patients with large or massive hemoptysis. AJR Am J Roentgenol 179:1217–1224
6. Remy-Jardin M, Bouaziz N, Dumont P et al (2004) Bronchial and nonbronchial systemic arteries at multi-detector row CT angiography: comparison with conventional angiography. Radiology 233:741–749

Hemorrhage, Intracranial, Neonates (Neuro View)

Huisman T.A.[1], Veronica Donoghue[2]
[1]Johns Hopkins University, Baltimore, USA
[2]Children's University Hospital, Dublin, Ireland
thierry.huisman@kispi.unizh.ch
veronica.donoghue@tsch.ie

Synonyms

Germinal matrix hemorrhage; Subependymal hemorrhage

Definition

Rupture of arterial or venous vessels with extravasation of blood into the germinal matrix, brain parenchyma, ventricular system, or subarachnoid space.

Pathology and Histopathology

Intracranial hemorrhage is one of the most common causes of acute focal neurological symptoms (e.g., seizures). Multiple factors including location, extension and etiology determine morbidity and mortality. Germinal matrix hemorrhages (GMH) are the most frequent intracranial hemorrhages in premature and term neonates though it is rare in the term infants (1, 2). The germinal matrix is a highly perfused transient zone along the lateral ventricles composed of postmitotic, premigratory cells. These cells migrate toward the cortical plate along radial glial cell processes that extend to the surface of the brain. The thickness of the germinal matrix correlates with gestational age; the germinal matrix regresses as cells migrate. The germinal matrix is in a close anatomical relation to the subependymal deep venous system. GMH results from rupture of the fragile venous capillaries in and along the germinal matrix. Hemorrhage may compress neighboring, initially patent veins with can thrombose on follow-up. Larger hemorrhages may compromise the venous drainage of the adjacent white matter with resulting venous ischemia of the hemispheric white matter and/or intraparenchymal hemorrhage. The relationship between GMH and prematurity is well known and has been confirmed by many autopsy studies. Many other factors have also been considered including coagulation disorders, hypercarbia, hypernatremia, hyperosmolarity, and metabolic acidosis. GMH occur postnatally in the vast majority of cases supporting the theory that hemorrhages are associated with phases of neonatal distress.

Less frequently, intracranial hemorrhages may occur due to neonatal tumors, intracerebral arteriovenous malformations (e.g., vein of Galen malformation), trauma, dural sinus thrombosis, or coagulation disorders. Subarachnoidal, subdural, and epidural hematomas may result from a traumatic birth.

Clinical Presentation

Small GMH may be asymptomatic. Larger GMH present with various combinations and degrees of impaired consciousness, hypotonia, seizures, increased irritability, poor feeding, and respiratory insufficiency or even coma. A rapid drop in hematocrit may signal massive intraventricular bleeding. A complicating posthemorrhagic hydrocephalus should be suspected if signs of increased intracranial pressure become apparent. The increased intracranial pressure may lead to a bulging of the fontanelle in combination with an increase of the head circumference. In most severe cases a compression of the brain stem leads to loss of pupil and oculomotor reflexes, decerebrate posture, and respiratory arrest. Venous infarctions may result in varying focal neurological deficits depending on the involved functional center.

Imaging

GMH are classified into three grades. Grade I: subependymal hemorrhage limited to the GM, grade II: intraventricular hemorrhage in which less than 50% of the ventricular volume is affected, and grade III: intraventricular hemorrhage in which more than 50% of the ventricular volume is affected. In previous classifications, a grade IV hemorrhage was defined as a GMH with extension into the adjacent cerebral hemispheres. This kind of neonatal hemorrhage is nowadays classified as "hemorrhagic venous infarction." This descriptive terminology takes the etiology better into account (3).

On imaging, the location and size of the hemorrhages should be described. Hemorrhages are typically described as small (<1 cm in diameter), medium (>1 cm, <2 cm in diameter), or large (>2 cm in diameter). In addition, the degree of complicating hydrocephalus should be estimated. Serial measurements of the diameter of the anterior horns of the lateral ventricles at the level of the foramen Monroi can be used to determine the evolution of a hydrocephalus on follow-up.

Ultrasonography (US) uses the anterior fontanelle as an acoustic window to perform high resolution imaging of the brain in neonates and babies. Typically, coronal

and sagittal images covering the brain from anterior to posterior and left to right are acquired. Additional acoustic windows include the posterior and temporal fontanelle. Suboccipital views through the foramen magnum are used to image the posterior fossa. In addition, power Doppler US is used to assess patency of the major arterial and venous intracranial vessels. The profile of the arterial blood flow may give important information about the intracranial pressure and degree of brain swelling.

US has become the primary modality to examine the neonatal brain because it is a high resolution imaging modality, lacks ionizing radiation, can be performed at the bed side is widely available and is relatively cheap. In addition, serial examinations can easily be performed giving us the fourth dimension of time in the evaluation of cerebral pathologies.

In the acute and subacute phases GMH are hyperechoic (Fig. 1). On follow-up, hemorrhages become isoechoic and finally hypoechoic in the chronic phase. This process parallels the spontaneous evolution and resorption of hemorrhages. Finally, small hypoechoic cysts may be the sole remnant of GMH. In the case of an intraventricular extension (grade II and III), blood clots can be seen within the ventricles (Fig. 2). In addition, a hyperechoic lining of the ventricles can be seen, most probably reflecting a reactive chemical ependymal inflammation in reaction to the intraventricular blood products. In rare cases, an enlarged hyperechoic choroid plexus may indicate extension of the hemorrhage into the choroid plexus. Small grade I hemorrhages are typically seen at the foramen of Monro (Fig. 1), larger hemorrhages may be seen anywhere along the germinal matrix.

Venous infarction is characterized by a fan shaped hyperechonic injury of the cerebral white matter (Fig. 3). This signal change matches the course and distribution of the intramedullary veins that converge and drain into the subependymal, deep venous system. Two-third of the cerebral white matter drains into the deep venous system while the superficial one-third drains into the superficial venous system. Consequently, venous ischemia involves predominantly the periventricular white matter as GMH compromises drainage into the deep venous system. On US a corresponding signal alteration of the deep, periventricular white matter is seen. Venous ischemia is frequently complicated by hemorrhages on follow-up examination. Color Doppler sonography may be able to demonstrate compression or thrombosis of the subependymal veins. Follow-up examinations will show a progressive, hypoechoic cystic resorption of the infarcted brain.

Complicating hydrocephalus is easily identified by US. Follow-up examinations are necessary to monitor ventricular dilatation and to determine if a ventricle drainage should be considered. Duplex Doppler of the intracranial vessels during anterior fontanelle compression has been reported as a useful indicator of altered cranial compliance in infants with hydrocephalus and may be helpful in predicting the need for shunt placement (5). The addition of views of the thoracolumbar spine may identify an echogenic subarachnoid space due to the presence of high protein and red blood cell contents. This may help identify which infants are likely to benefit from lumbar puncture for therapy for progressive ventricular dilatation (6).

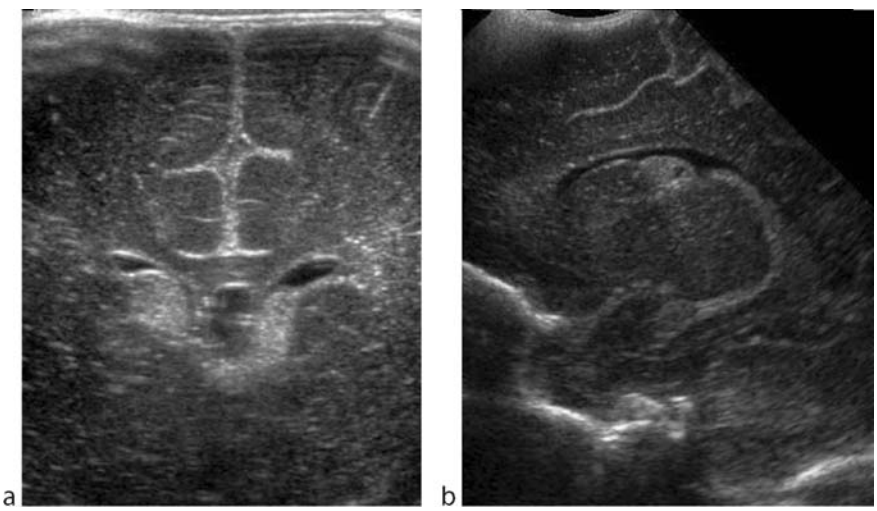

Hemorrhage, Intracranial, Neonates (Neuro View). Figure 1 Four weeks old premature girl (31 weeks of gestation). Coronal (a) and sagittal (b) ultrasonography reveal a bilateral hyperechoic grade I germinal matrix hemorrhage near the foramen Monroi. No ventricular dilatation is seen.

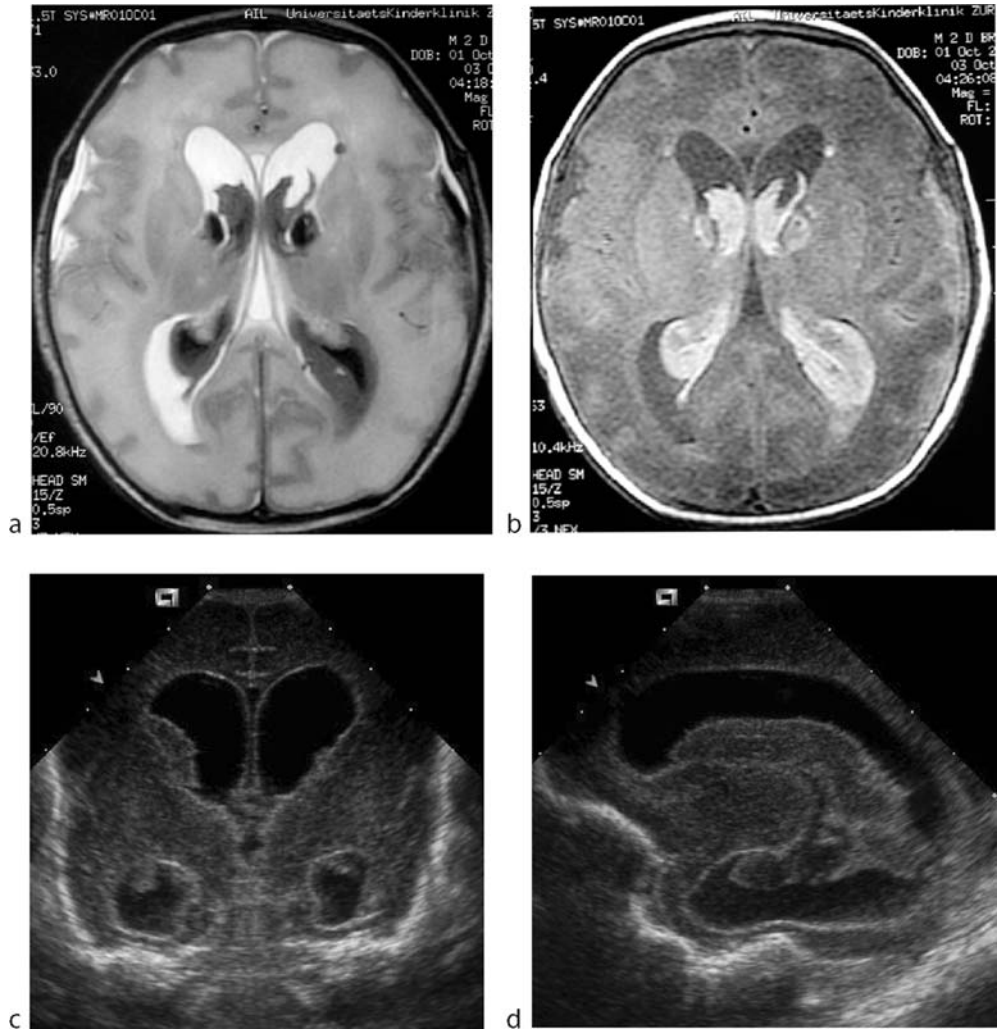

Hemorrhage, Intracranial, Neonates (Neuro View). Figure 2 Three days old premature boy (29 weeks of gestation) axial T2-weighted (a) and T1-weighted (b) MRI show a bilateral T2-hypointense and T1-hyperintense grade III hemorrhage. A mild hydrocephalus is seen. One week later coronal (c) and sagittal (d) ultrasonography reveal a partial resorption of the hemorrhage, the hydrocephalus is however slightly progressive.

Computer tomography (CT) is sensitive for identifying GMH and their complications. Hyperacute hemorrhages are isodense to normal brain tissue. Progressive blood clot retraction increases hemorrhage density during the acute and early subacute phases, while progressive red blood cell lysis during the late subacute phase will decrease the attenuation of the hematoma. Progressive resorption in the chronic phase will result in a hypodense, cyst filled with cerebrospinal fluid (CSF) (4). Several studies have shown that US is as sensitive as CT in the diagnosis of GMH. Major disadvantage of CT is the use of ionizing radiation and the need to transport the neonate to a CT-suite. CT is indicated in those cases where the findings on US do not explain neurological symptoms. In addition, CT should be considered in suspected pathology within the posterior fossa (brainstem and cerebellum). Finally, in cases where the acoustic windows are too small for an adequate evaluation of the cranial vault, CT should be considered.

Magnetic resonance imaging (MRI) is widely accepted as the most sensitive imaging modality for intracranial hemorrhage and its sequelae. T2*-weighted sequences, that are exquisitely sensitive for blood products, are especially helpful (Fig. 3). In the hyperacute stage the hemorrhage is T1-iso or hypointense and T2-hyperintense; in the acute stage T1-iso or hypointense and T2-hypointense (Fig. 3), in the early subacute stage T1-hyperintense and T2-hypointense, in the late subacute stage T1 and T2-hyperintense and finally in the chronic phase T1-hypointense and T2-centrally hyperintense surrounded

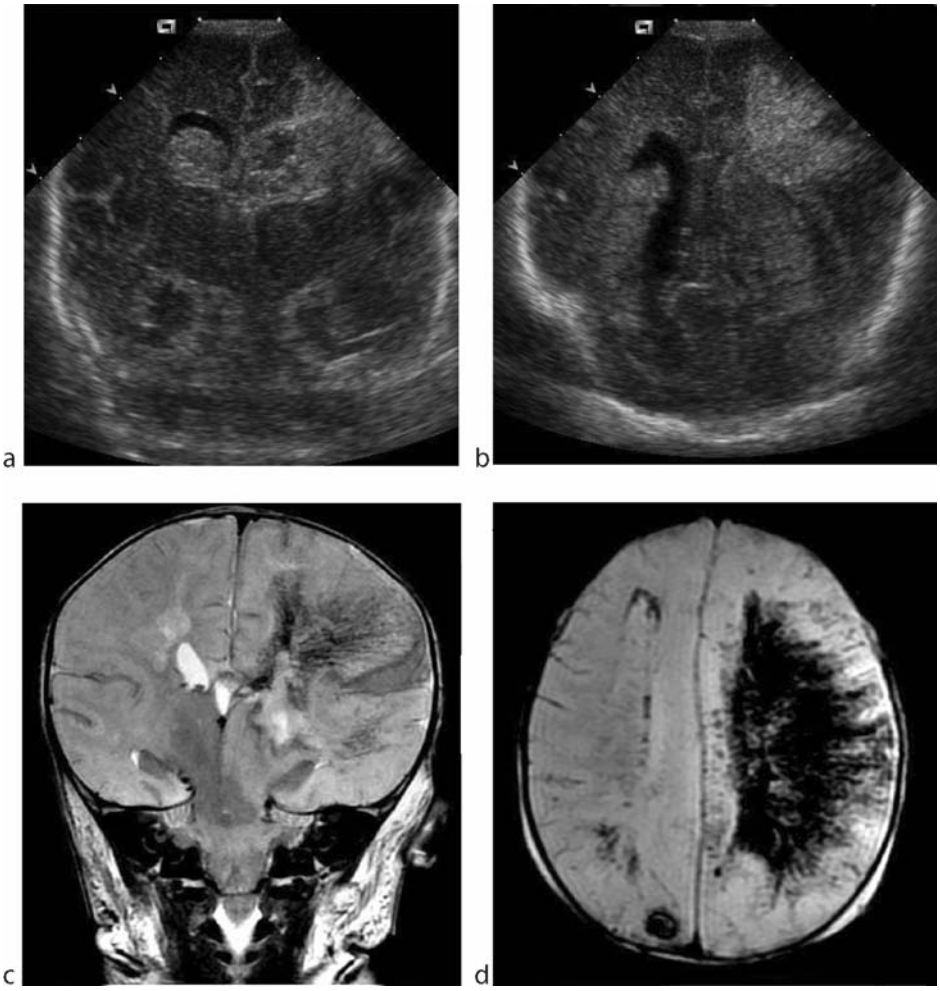

Hemorrhage, Intracranial, Neonates (Neuro View). Figure 3 Five days old premature boy (28 weeks of gestation) coronal (a, b) ultrasonography shows a hemorrhagic venous ischemia within the left hemisphere next to a bilateral GMH. Follow-up coronal T2-weighted (c) and axial T2*-weighted (d) MRI confirms the fan shaped hypointense venous hemorrhagic infarction of the left hemisphere. The degree of hemorrhage is better seen on T2*-weighted images. The GMH is already partially resolved.

by a rim of hypointensity (hemosiderin) (4). Similar to CT, MRI should be considered in cases where US does not explain neurological symptoms. Major disadvantage of MRI is the complexity of examining a neonate inside the MRI scanner and the limited availability.

Diagnosis

Clinically, GMH should be suspected and ruled out in preterm and term neonates who present with seizures, altered consciousness, bulging fontanelle, progressive head circumference, or other acute focal neurological deficit. GMH is easily identified on US, CT, or MRI. Imaging should identify secondary complications including hydrocephalus and hemorrhagic venous infarction. US remains the primary imaging modality of choice. CT and MRI should be considered if US-findings do not explain neurology. CT and MRI are indicated in neonatal hemorrhages other than GMH.

Bibliography

1. Ramenghi LA, Mosca F, Counsell S et al (2005) Magnetic resonance imaging of the brain in preterm infants. In: Tortori-Donati P (ed) Pediatric Neuroradiology. Springer, Berlin, Heidelberg, New York, pp 217–222
2. Barkovich AJ (2000) Pediatric Neuroimaging. 3rd edn. Lippincott Williams & Wilkens, Philadelphia pp 174–176
3. Deeg KH, Staudt F, van Rohden L (1999) Classification of intracranial hemorrhage in premature infants. Ultraschall Med 20:165–170

4. Huisman TA (2005) Intracranial hemorrhage: ultrasound, CT and MRI findings. Eur Radiol 15:434–440
5. Taylor GA (2001) Sonographic assessment of posthemorrhagic ventricular dilatation. Radiol Clin North Am 39:541–551
6. Rudas G Almassy Z Papp B et al (1998) Echodense spinal subarachnoid space in neonates with progressive ventricular dilatation: a marker of non-communicating hydrocephalus. Am J Roentgenol; 171:1119–1121

Hemorrhagic Functional Cysts

Bleeding may complicate corpus luteum cysts. Bleeding into the cyst or rupture within the peritoneal cavity manifests as acute abdominal pain and is the leading cause of gynecologic emergencies.

▶Cyst, Follicular, Ovarium

Hemosiderosis

In transfusional iron overload, iron is deposited in the reticulo-endothelial cells of the liver, spleen, and bone marrow. At ultrasound, iron deposits in the liver do not determine specific findings. At computed tomography, a diffuse homogeneous hyperdensity of the liver parenchyma can be appreciated on unenhanced scans. Biphasic contrast-enhanced CT study is required for the detection of hepatocellular carcinoma. A decrease of signal intensity of liver parenchyma is observed on T2-weighted magnetic resonance images. A splenic involvement is also present.

▶Diffuse Infiltrative Diseases, Hepatic

Hemothorax

Pleural effusion predominantly contains blood. It is frequently found in patients with lacerations or tears of intercostal vessels, lung, diaphragm, mediastinum, large vessels, and heart. Hemothorax due to lung contusion and venous lesions tends to be self-limiting, while it is often massive when due to lung laceration or mediastinal and arterial lesions. Pleural fluid of more than 200–300 mL can be detected on the "supine" radiograph. The diagnosis of acute hemothorax is generally based on ultrasound or CT. A rare differential diagnosis is chylothorax due to rupture of the thoracic duct.

▶Chest Trauma

Hepatic Benign Tumor in Children

▶Hepatic Pediatric Tumors, Benign

Hepatic Fibrosis Congenital

Autosomal disorder that may be associated with biliary duct ectasia and infantile or adult polycystic kidney disease.

▶Congenital Malformations, Liver and Biliary Tract

Hepatic Injury

▶Trauma, Hepatobiliary

Hepatic Lymphoproliferative Disease

▶Lymphoma, Hepatic

Hepatic Mesenchymal Malignant Tumors

▶Hepatic Sarcoma

Hepatic Obstruction

▶Budd-Chiari Syndrome

Hepatic Pediatric Tumors, Benign

Huisman T.A.[1], Paola Vagli[2]
[1]Johns Hopkins University, Baltimore, USA
[2]Department of Diagnostic and Interventional Radiology University of Pisa, Italy
bartolozzi@do.med.unipi.it

Synonyms

Hepatic benign tumor in children; Liver tumors in infancy; Pediatric neoplasms of the liver

Definition

Benign hepatic neoplasms of childhood include a variety of lesions that are predominantly of mesenchymal origin. Most lesions present as a right upper quadrant palpable mass or with abdominal distension. Many of the lesions are initially asymptomatic and may be an incidental finding on cross-sectional imaging. Benign lesions include cavernous hemangioma, ►infantile hemangioendothelioma, ►mesenchymal hamartoma, focal nodular hyperplasia, ►nodular regenerative hyperplasia, and hepatocellular adenoma. The distribution and incidence of lesions differ from adults.

Pathology and Histopathology

Cavernous Hemangioma

Children are less frequently involved than adults, the exact incidence is however unknown. In children, hemangiomas frequently resolve spontaneously. Lesions are often small (<2 cm), single, red-purple, and spongy. Microscopically, hemangiomas are composed of well-marginated, dilated, large vascular channels lined by a thin layer of endothelial cells. Fibrosis, thrombosis, and calcifications may be present. Occasionally, cardiac failure results from arteriovenous shunting in large hemangiomas. Multiple lesions are considered a part of the syndrome of systemic hemangiomatosis.

Infantile Hemangioendothelioma

Most common liver tumor in the first year of life. Benign, single, multifocal, or diffuse infiltrating lesion composed of thin vascular channels lined by endothelial cells. The lesion is nonencapsulated well circumscribed, soft, and spongy with occasionally areas of hemorrhage, fibrosis, and dystrophic calcifications. Spontaneous regression has been reported. Congestive heart failure may occur. Histologically it is considered a variant of cavernous hemangioma. Differentiation between these two lesions is difficult. In hemangioendothelioma, the size of the vascular spaces is smaller (i.e., capillary) compared with hemangiomas.

Mesenchymal Hamartoma

Benign, usually multicystic mesenchymal lesion originating from primitive connective tissue in the portal tracts. It accounts for 22% of the benign liver tumors in children with a male predominance. The lesion is composed of loose mesenchymal tissue containing small bile ducts, cystic remnants of portal triads and cysts filled with serous fluid. About 80% of the lesions are seen in children younger than 2 years.

Focal Nodular Hyperplasia

Circumscribed, usually asymptomatic lesion of epithelial origin. Histologically, the lesion consists of hyperplastic hepatocytes with small bile ducts and intralesional arteries and veins. The lesion is sharply demarcated from the surrounding liver. A central fibrous scar or septa with prominent vessels can be observed. The lesion is usually firm and irregular. Focal nodular hyperplasia is rare in children compared to adults occurring most frequently between 6–10 years.

Nodular Regenerative Hyperplasia

Benign proliferation of hepatocellular nodules. Histologically, the nodules are composed of hyperplastic hepatocytes. Cause is unknown, it is associated with a variety of systemic diseases including myelo-lymphoproliferative diseases, metabolic diseases and cardiovascular diseases. There is usually no preexisting liver cirrhosis (1–4).

Hepatocellular Adenoma

Rarely diagnosed in children. Adenomas are primarily seen in teenage girls taking oral contraceptives. Usually, adenomas are solitary well-circumscribed lesions, partially or completely encapsulated and composed of sheets of hepatocytes. Tumor hemorrhage and rupture present with acute abdominal pain.

Clinical Presentation

Cavernous Hemangioma

Cavernous hemangiomas are usually asymptomatic and often diagnosed incidentally on ultrasound (US)

examinations. Large lesions may present as asymptomatic palpable masses or with congestive heart failure secondary to arteriovenous shunting within the tumor. Rarely tumor rupture with hemoperitoneum occurs. ►Kasabach–Merrit syndrome may occur. Hemangiomas may be discovered in the prenatal period because of hemorrhage into the amniotic fluid causing severe anemia and congestive heart failure or hydrops fetalis. Alpha fetoprotein may be highly elevated in preterm infants with hemangiomas.

Infantile Hemangioendothelioma

Clinical presentation strictly depends on the size of the lesions. Presenting symptoms include hepatomegaly, abdominal enlargement, or congestive heart failure due to multiple arteriovenous shunts within the tumor. Associated hemangiomas of the skin are reported in 20% of cases. The systemic administration of steroids, interferon alpha, and vincristine may reduce size and number of lesions.

Mesenchymal Hamartoma

Mesenchymal hamartomas are usually asymptomatic lesions presenting with an enlarging abdomen. The lesion may grow slowly over months or enlarge rapidly over a period of days due to intralesional accumulation of serum. The large size of the lesion may result in respiratory distress or compression of the inferior caval vein. Transformation into malignant sarcomas have been reported and surgical resection is recommended.

Focal Nodular Hyperplasia

Most children are asymptomatic, lesions can be found incidentally on cross-sectional imaging for another condition. Less than 10% of children may complain of episodic abdominal pain, vomiting, or diarrhea.

Nodular Regenerative Hyperplasia

Children are usually asymptomatic, the lesion is frequently misdiagnosed as focal nodular hyperplasia or metastatic disease. Hepatomegaly, abdominal mass, or portal hypertension are infrequently diagnosed. Malignant transformation into hepatocellular carcinoma has been reported (1–4).

Hepatocellular Adenoma

Most adenomas are asymptomatic. Episodic or acute abdominal pain is usually related to a hemorrhage within the adenoma.

Imaging

Cavernous Hemangioma

US: Hemangiomas are hyperechoic, well-circumscribed solid lesions. Large hemangiomas may show a central hypoechoity due to necrosis or fibrosis. The vascular etiology is confirmed by Doppler US.

Computed tomography (CT): Hemangiomas are typically hypodense with an irregular peripheral enhancement and progressive filling-in on delayed scans. In larger lesions, the necrotic or fibrotic center will show a limited enhancement. Calcifications may be seen.

Magnetic resonance imaging (MR): Hemangiomas are T1-hypointense and strongly T2-hyperintense (light-bulb). Dynamic contrast-enhanced sequences show an enhancement pattern similar to the CT enhancement.

Infantile Hemangioendothelioma

US: Findings are nonspecific. Lesions can be hypo-, hyper-, or mixed hypo-hyperechoic. Doppler US will confirm the vascular nature of the lesion. Lesions are usually well defined.

CT: Hemangioendotheliomas display the same hypodense pattern as hemangiomas; a progressive centripetal enhancement is observed with a delayed wash out and decrease of the attenuation values within the periphery of the lesion (Fig. 1). Central nonenhancing areas correspond to necrotic or hemorrhagic areas.

MR: Lesions are T1-hypointense and T2-hyperintense (Fig. 2). The peripheral areas are usually less T2-hyperintense than the central components. After contrast injection, a peripheral enhancement with subsequent centrifugal fill-in is seen with a prolonged and homogeneous enhancement on late phase images.

Mesenchymal Hamartoma

US: Appearance is variable and nonspecific. The solid mass may be hyperechoic while the cysts are hypoechoic. Occasionally, echogenic material is seen within the cyst secondary to hemorrhage.

CT: Hamartomas are homo- or heterogeneous hypodense with possible calcifications. After contrast injection, a strong peripheral enhancement is seen, the center of the lesion is usually less enhancing (Fig. 3). On delayed images, a washout of the periphery in combination with a progressive enhancement of the center reverses the contrast enhancement pattern.

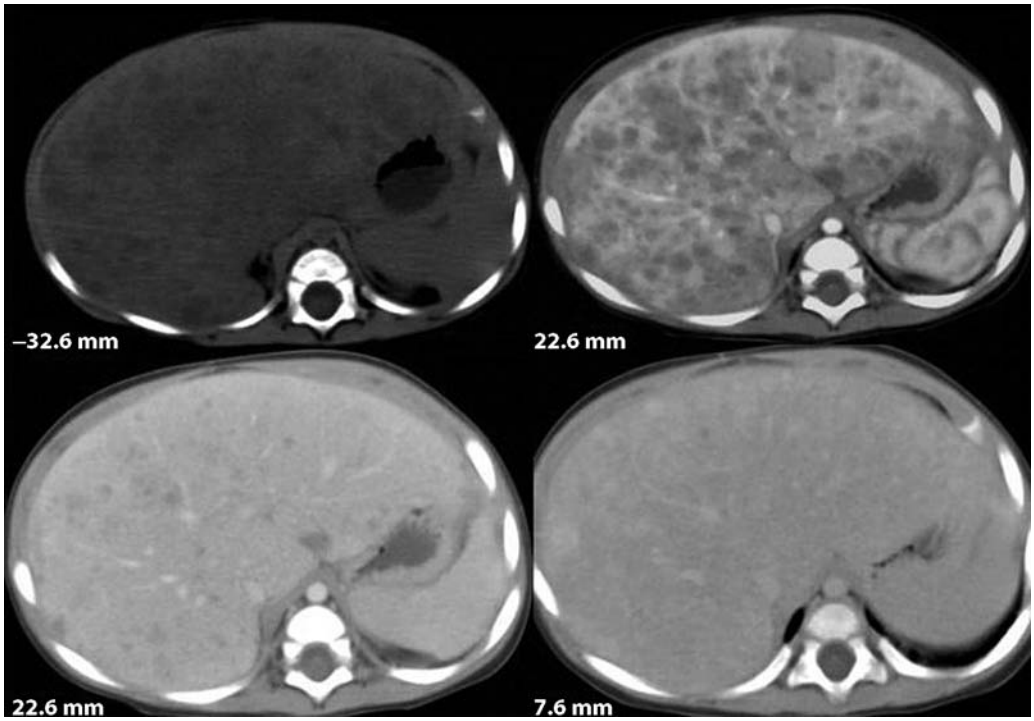

Hepatic Pediatric Tumors, Benign. Figure 1 CT scans show a diffuse involvement of both hepatic lobes in a patient with infantile hemangioendothelioma. Basal scan (*up left*) displays multiple hypodense nodules with a progressive centripetal enhancement in the arterial (*up right*) and venous (*down left*) phases. Delayed scan (*down right*) shows a delayed wash out of the lesions.

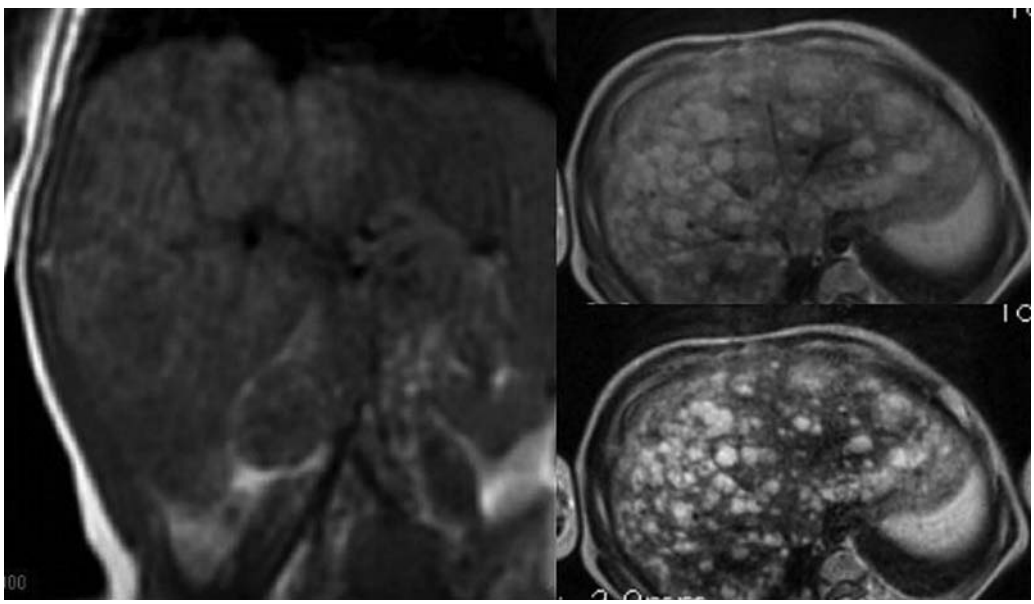

Hepatic Pediatric Tumors, Benign. Figure 2 Infantile hemangioendothelioma (same case of Fig. 1). Coronal T1-weighted image (*left*) shows multiple hypointense nodules. Increasing the echo time nodules appear progressively hyperintense on axial T2-weighted images (echo time 50 up right and echo time 100 down right).

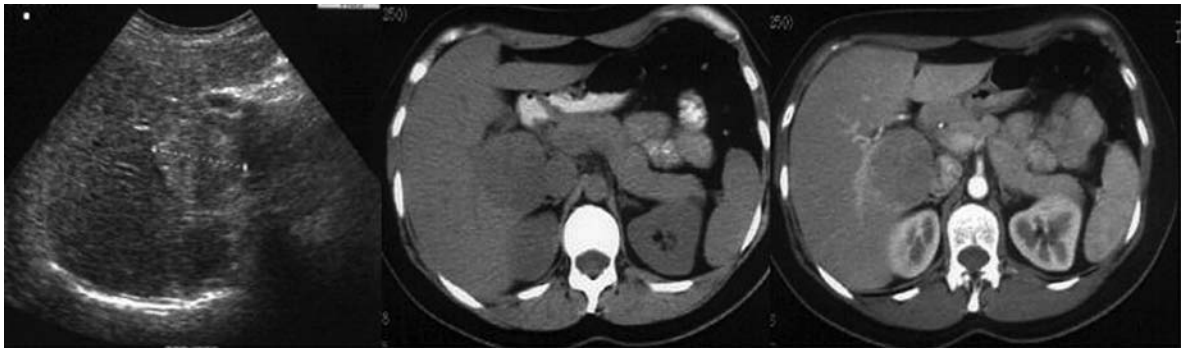

Hepatic Pediatric Tumors, Benign. Figure 3 Mesenchymal hamartoma. US shows an hepatic hyperechoic solid mass (*left*); the same lesion appears homogeneously hypodense on basal CT scan (*middle*). After contrast administration peripheral enhancement with a less-enhancing center is shown on CT (*right*).

MR: MR appearance depends on whether the hamartoma is predominantly mesenchymal (stromal) or cystic. Stromal lesions are T1- and T2-hypointense while the cystic types are T1-hypo- and T2-hyperintense. Cystic types may show a variable T1-hyperintensity according to its proteinaceous contain.

Focal Nodular Hyperplasia

US: Hypo-, iso-, or hyperechoic, well-circumscribed lesions. A central scar with small bile ducts can be seen in about one-third of the cases.

CT: Lesions are often difficult to identify on precontrast scans. After the injection of contrast media, an early enhancement with rapid washout is observed. The central scar may have a delayed, persisting enhancement.

MR: Lesions are homogeneous isointense to normal liver, the central scar may be T1-hypo-, and T2-hyperintense. Contrast enhancement is similar to CT.

Nodular Regenerative Hyperplasia

US: Nodules may be hyper-, iso-, or hypoechoic mimicking metastatic disease. The liver may be enlarged. Intralesional hemorrhages have been described.

CT: Lesions are hypodense without a significative enhancement.

MR: Nodules may be T1- and T2- hypo-, or hyperintense. Signal and enhancement pattern is nonspecific (1–4).

Hepatocellular Adenoma

US: Adenomas may be hypo-, iso-, or hyperechoic focal lesions. A peripheral hypoechoic rim is occasionally seen.

CT: Hypodense, homogeneously enhancing focal lesion with occasionally hemorrhagic components. On delayed images, the adenoma is usually isodense.

MR: T1-hypo- and T2-hyperintense lesions. Fat inclusions as well as hemorrhages may alter the signal intensities. Contrast enhancement is similar to CT.

Nuclear Medicine

Cavernous Hemangioma and Infantile Hemangioendothelioma

^{99m}Tc labeled sulfur colloid scans are usually unrevealing or nonspecific, although by means of blood pool studies an increased activity corresponding to the hypervascularity may be seen. Conversely SPECT (single photon emission tomography) scans using ^{99m}Tc labeled red blood cells show a typical early blush of this lesions.

Focal Nodular Hyperplasia and Nodular Regenerative Hyperplasia

^{99m}Tc labeled sulfur colloid scans are helpful as the majority of lesions show an uptake of tracer by the Kuppfer's cells within the nodules.

Diagnosis

Cavernous Hemangioma and Infantile Hemangioendothelioma

Differential diagnosis includes metastatic neuroblastoma and regenerative nodules in case of multiple lesions or hepatoblastoma in case of a solitary lesion. The peripheral nodular enhancement after contrast medium administration and filling in on delayed scans is characteristic for hemangioma and hemangioendothelioma. The persistent and markedly elevated alpha-fetoprotein levels in case of hepatoblastoma help to differentiate.

Mesenchymal Hamartoma

Differentiation from cystic sarcomas can be difficult for large hamartomas. Solid hamartomas may show vascular enhancement patterns mimicking other mesenchymal derived masses such as hemangioma and hemangioendothelioma.

Focal Nodular Hyperplasia and Nodular Regenerative Hyperplasia

Most lesions are discovered as a palpable mass and/or hepatomegaly. Imaging, especially enhancement pattern may suggest correct diagnosis. Biomarkers are not yet available.

Hepatocellular Adenoma

Hepatocellular adenoma should be suspected in teenage girls taking oral contraceptives who present with acute abdominal pain (hemorrhage within the adenoma) in combination with a focal finding on imaging.

Bibliography

1. Silverman FN, Kuhn JP (1993) Tumors and tumorlike conditions. In: Silverman FN (ed) Caffey's Pediatric X-ray Diagnosis: An Integrated Imaging Approach. Mosby, St. Louis, pp 954–965
2. Donnelly LF, Bisset GS 3rd (2002) Unique imaging issues in pediatric liver disease. Clin Liver Dis 6(1):227–246
3. Tomà P, Lucigrai G, Oddone M (1999) Pediatric tumors of the liver. In: Bartolozzi C, Lencioni R (eds) Liver Malignancies. Springer, Berlin Heidelberg, pp 403–422
4. Donnelly LF, Bisset GS 3rd (1998) Pediatric hepatic imaging. Radiol Clin North Am 36(2):413–427

Hepatic, Pediatric Tumors, Malignant

Huisman TA[1], Paola Vagli[2]
[1]Johns Hopkins University, Baltimore, USA
[2]Department of Diagnostic and Interventional Radiology, University of Pisa, Italy
thierry.huismann@kispi.unizh.ch
bartolozzi@do.med.unipi.it

Synonyms

Pediatric hepatic neoplasms; pediatric liver tumors

Definition

Primary hepatic neoplasms are rare in children. Less than 2% of all childhood tumors originate within the liver, 64% of the primary liver tumors are malignant. Hepatic tumors are the third most common abdominal malignancies after Wilms' tumor and neuroblastoma.

Pathology and Histopathology

Hepatoblastoma

►Hepatoblastoma is the most frequently occurring primary hepatic malignancy of childhood. The median age of diagnosis is 1 year. An increased risk for hepatoblastomas is known in Beckwith–Wiedemann syndrome, hemihypertrophy, fetal alcohol syndrome, Gardner's syndrome. The majority of hepatoblastomas are solitary solid tumors. Hepatoblastomas can also be multicentric, diffuse, or multicystic. The tumor is usually coarsely nodular or lobulated may be diffuse infiltrative and tends to be hypervascularized. Areas of necrosis, hemorrhage and calcifications are frequently present. Thrombosis of the porto-venous system may occur (1–3).

Hepatocellular Carcinoma

HCC is the second most common primary hepatic malignancy in children. HCC has two age peaks: 2–4 years and 12–14 years. HCC is associated with biliary atresia, familial polyposis, hereditary ►tyrosinemia, ►Byler's disease, neonatal hemochromatosis and chronic hepatitis B infection. The association with cirrhosis is less common than in adults although also in children, HCC is frequently seen in conjunction with preexisting liver disease. HCCs are single or multicentric solid masses, with or without tumor capsule. Areas of central necrosis and hemorrhage are frequent. Invasion of the porto-venous system may occur. Fibrolamellar HCC is a histologic variant of HCC with a more favorable survival rate (2–3).

►Undifferentiated Embryonal Sarcoma

Highly malignant hepatic tumor occurrs throughout the entire pediatric age group but most frequently in older children. They represent the malignant form of mesenchymal hamartoma. Tumors are typically large on presentation, can be solid and/or cystic, are usually well defined and hypovascular. A pseudocapsule of dense fibrous connective tissue may separate the lesion from normal liver tissue. Hemorrhage and necrosis are frequently seen.

Rhabdomyosarcoma of the Biliary Tree

►Rhabdomyosarcoma of the biliary tree and gallbladder is rare (>1% of all rhabdomyosarcomas) and affects

almost exclusively children under 5 years. The tumor typically extends along the biliary tree with resulting obstruction of the biliary ducts (jaundice). Infiltration of the porta hepatis is frequent. Metastatic spreading may involve the liver, lungs, peritoneal cavity, and retroperitoneal lymph nodes (1–3).

Hepatic Metastases

Virtually any malignant neoplasm may metastasize into the liver. The most common abdominal tumors that metastasize into the liver are neuroblastoma, Wilms' tumor, and rhabdomyosarcoma. Depending on the histology of the primary tumor, liver metastases have different characteristics. The liver may show multiple small, subcapsular located lesions without significant enlargement or may have multiple large lesions with resulting hepatomegaly.

Clinical Presentation

Hepatoblastoma

The majority of children present with an enlarging abdomen and a palpable nontender hepatic mass. In advanced stages of disease, anorexia, weight loss, nausea, vomiting, and abdominal discomfort may occur. Jaundice is seen only in a minority of children or in advanced stages. Symptoms of an acute abdomen may result from tumor rupture. The production of cytokines may result in an extramedullary hematopoiesis. In addition, paraneoplastic syndromes including precocious puberty, hypercalcemia and hypoglycemia occur. Serum alpha-fetoprotein is elevated in 75–96% of patients. Survival is determined by tumor resectability.

Hepatocellular Carcinoma

Children with a HCC usually present with an enlarging abdomen and a palpable hepatic mass. Symptoms include abdominal pain, discomfort and less frequently, fever, nausea, weight loss, and jaundice. Alpha-fetoprotein is elevated in 40–50% of children. Prognosis is poor with low survival rates. Treatment is surgical resection or liver transplantation. Chemotherapy has limited value.

Undifferentiated Embryonal Sarcoma

In the majority of children, presenting clinical symptoms is an abdominal mass with or without abdominal pain. Fever and jaundice may occur. Serum alpha-fetoprotein is rarely elevated. In half of cases, extramedullary hematopoiesis is seen. About 15% of children survive if radical surgical resection is achieved.

Rhabdomyosarcoma of the Biliary Tree

Symptoms are related to the close relation between tumor and biliary tree in which biliary obstruction results in jaundice (60–80% of children). Fever, abdominal distension, nausea, and vomiting occur. Bilirubin and alkaline phosphatase are usually elevated. Surgical resection and/or chemotherapy are treatment options; the proximity to the porta hepatis usually prevents radical surgery.

Hepatic Metastases

Abdominal distension due to a hepatomegaly and a progressive hepatic failure is the leading sign. Paraneoplastic symptoms are related to the histology of the primary tumor. In patients younger than 4 weeks, severe hepatomegaly may result in hypoventilation.

Imaging

Hepatoblastoma

Ultrasound (US): The solid tumor component is heterogeneous hyperechoic while the necrotic areas are hypoechoic or anechoic. Intratumoral hemorrhages and calcifications appear hyperechoic. Color Doppler US may show infiltration or compression of the hepatic venous vessels.

Computed tomography (CT): Hepatoblastomas are usually hypodense, well marginated with heterogeneous contrast enhancement that is slightly less accentuated compared to normal liver. A peripheral enhancing rim or septa may be evident in the delayed phases. Calcifications appear hyperdense, while areas of necrosis are hypodense and do not enhance. Tumor thrombus within the portovenous system is evident as filling defects.

Magnetic resonance imaging (MR): T1-hypo-, T2-heterogeneous hyperintense with a moderate, inhomogeneous contrast enhancement. Calcifications and hemorrhages are easily identified. To rule out tumor thrombus or cavernous transformation of the portovenous system, MR angiography is recommended.

Hepatocellular Carcinoma

US: HCC mimic hepatoblastoma, calcifications are less frequent. Doppler US may show intratumoral arteriovenous shunting as well as tumor thrombus within the porto-venous vessels.

CT: Typically hypodense, infrequently isodense with a strong, heterogeneous enhancement. Calcifications are seen in 10% of children. The presence of arterial-portal shunts may prolong enhancement of unaffected liver lobes and portal vein enhancement.

MR: T1-hypo- and T2-hyperintense with central areas of T1-hyperintensity corresponding to intralesional hemorrhages or fat inclusions. Contrast enhancement is similar to CT. A fibrous pseudocapsule may be seen.

Undifferentiated Embryonal Sarcoma

Typically, this neoplasm appears solid on US while cystic on CT and MR.

US: Iso- or hyperechoic solid tumor with small anechoic multiseptated cystic areas. The variable echogenicity depends on the prevalence of myxoid, solid, necrotic, or hemorrhagic components and calcium depositions.

CT: Hypodense on CT mimicking a cystic nature. Intralesional septa as well as a peripheral pseudocapsule may enhance. Intralesional hemorrhages are hyperdense.

MR: T1-hypo- and T2-hyperintense with an enhancement pattern similar to CT. Intralesional hemorrhages appear T1-hyperintense.

Rhabdomyosarcoma of the Biliary Tree

US: Rhabdomyosarcomas are typically hyperechoic. Depending on the size and rate of growth, cystic degeneration and hemorrhage will result in a heterogeneous hypoechoic appearance. The presence of portal venous displacement without thrombosis is common.

CT: Inhomogeneous hypodense mass with a variable contrast enhancement. An enhancing peripheral pseudocapsule is seen in some cases. A grape-like tumor cluster may be revealed.

MR: T1-hypo- and T2-hyperintense, contrast enhancement is usually intense but inhomogeneous. MR cholangiography (MRCP) is useful to depict the biliary tree showing the presence of filling defects related to the ductal tumor.

Hepatic Metastases

US: Most metastases are hypoechoic, multiple and located within the periphery of the liver. Presentation depends on the nature of the primary tumor. Hyperechoic metastases may be calcified or hemorrhagic. A diffuse involvement, e.g., neuroblastoma may simulate a large heterogeneous mass.

CT: Variable appearance. Most frequently, metastases appear as hypodense lesions on pre- and postcontrast scans. Calcifications are evident in neuroblastoma. In rare cases, liver metastases can be isodense or may have a target-like aspect with a central hypodensity (necrosis) in combination with an enhancing peripheral rim (Fig. 1). Hepatic involvement in lymphoma is characterized by a poorly defined, low attenuation mass with irregular margins.

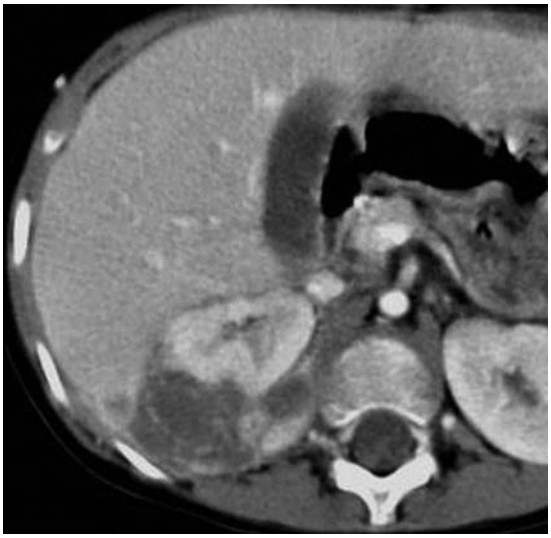

Hepatic, Pediatric Tumors, Malignant. Figure 1 CT image displays the presence of a small metastasis with target-like aspect in the VI hepatic segment in a child with right suprarenal neuroblastoma.

MR: Signal intensities of liver metastases are related to the signal intensities of the primary tumor. Most frequently, lesions are T1-hypo- and T2-hyperintense (Fig. 2). In case of lymphoma, MR shows areas associated to T1 and T2 relaxation times equal to those of the spleen (1–4).

Nuclear Medicine

Hepatoblastoma

^{99m}Tc sulfur colloid liver scintigraphy shows prominent early tracer uptake at the site of the tumor persisting into the venous phase. Delayed images typically demonstrate a photopenic defect because the Kupffer's cells are replaced by tumor cells. Photopenic defects also correlate to foci of necrosis. Lesion must be at least 2 cm to be detected by planar scintigraphy. Smaller lesions can be detected by single photon emission computed tomography (SPECT).

Rhabdomyosarcoma of the Biliary Tree

Scintigraphy using gallium or tallium may be employed to assess the metastatic spreading especially in case of skeletal involvement.

Hepatic Metastases

Radionuclide liver scans will show multiple photopenic areas or a generalized decrease of the liver activity. Sensitivity of nuclear medicine is lower than US, CT, or MR.

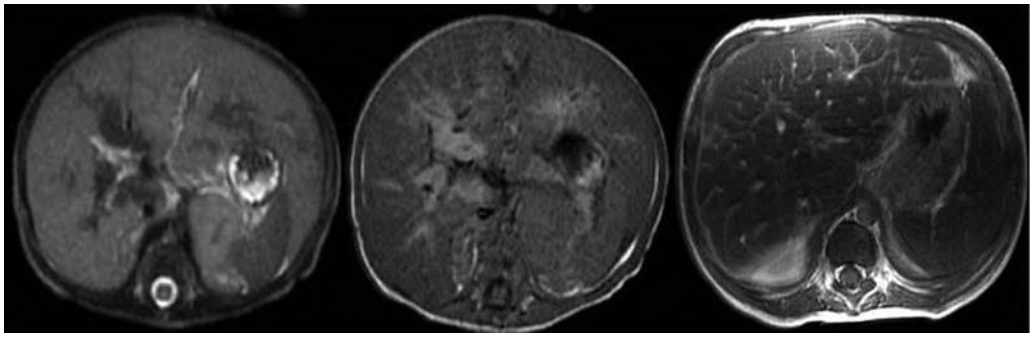

Hepatic, Pediatric Tumors, Malignant. Figure 2 Boy, 4 days old, axial T2-FSE (*left*) and T1-SE MR images (*middle*). Follow-up axial T2-FSE (*right*). Severe hepatomegaly due to diffuse liver metastasis in suprarenal left-sided neuroblastoma. Follow-up imaging 10 months later shows a spontaneous regression of the metastases and primary tumor.

Diagnosis

Hepatoblastoma

Large, inhomogeneous hepatic masses in child less than 5 years and elevated serum alpha-fetoprotein indicate hepatoblastoma. Imaging features are similar to those of HCC, the absence of an underlying chronic liver disease may help to differentiate hepatoblastoma from HCC.

Hepatocellular Carcinoma

The presence of liver cirrhosis increases the likelihood of HCC although the differentiation from regenerating nodules may be difficult. Serum alpha-fetoprotein is frequently elevated.

Undifferentiated Embryonal Sarcoma

Differentiation from hepatoblastoma or HCC can be difficult. The differential appearance on US versus CT and MR may help establish diagnosis. The lesion should be differentiated from benign mesenchymal hamartoma.

Rhabdomyosarcoma of the Biliary Tree

Biliary duct dilatation in combination with a small tumor in a central location is suggestive for rhabdomyosarcoma of the biliary tree. Initially, clinical symptoms are often misdiagnosed as infectious hepatitis. The US aspect of a solid hilar mass within the porta hepatis surrounded by a hypoechoic area (intraluminal rhabdomyosarcoma) may be mistaken for a choledochal cyst.

Hepatic Metastases

Clinical history and a known history of malignant disease help diagnose hepatic metastases. In addition, the multiplicity, location, enhancement pattern, and size will help diagnose metastases.

Bibliography

1. Schneider G, Grazioli L, Saini S (2003) Imaging of malignant focal liver lesions. In: Schneider G, Grazioli L, Saini S (eds) MRI of the Liver. Springer-Verlag Italia, Milano, pp 207–220
2. Tomà P, Lucigrai G, Oddone M (1999) Pediatric tumors of the liver. In: Bartolozzi C, Lencioni R (eds) Liver Malignancies. Springer, Berlin Heidelberg, pp 403–422
3. Silverman FN, Kuhn JP (1993) Tumors and tumorlike conditions. In: Silverman FN (ed) Caffey's pediatric X-ray Diagnosis: An Integrated Imaging Approach. Mosby, St. Louis, pp 954–965
4. Donnelly LF, Bisset GS 3rd (1998) Pediatric hepatic imaging. Radiol Clin North Am 36(2):413–427

Hepatic Sarcoma

Carlo Bartolozzi, Davide Caramella, Paola Vagli
Department of Diagnostic and Interventional Radiology, University of Pisa, Italy
bartolozzi@do.med.unipi.it

Synonyms

Angiosarcoma; Chloroma; Epithelioid hemangioendothelioma; Fibrosarcoma; Fibrous histiocytoma; Granulocytic sarcoma; Hepatic mesenchymal malignant tumors; Histiocytoma fibrous malignant; Leiomyosarcoma hepatic; Primary malignancies of the liver of mesenchymal origin

Definition

Hepatic sarcomas are primary malignancies originating from the different types of mesenchymal supportive

tissue of the liver. Hepatic sarcomas, with the exception of angiosarcoma and the undifferentiated embryonal sarcoma (found in children and also in adults), are particularly rare.

Pathology and Histopathology

Angiosarcoma, Hepatic

Primary malignancy of the liver occurs in adults (60–70 years mean age) with a relevant male predominance, arising from vascular endothelial cells of the liver. This form, although rare (2% of all primary liver tumors), represents the most common primary mesenchymal malignancy of the liver. Tumor onset seems to be related to chronic exposure to toxic agents such as inorganic arsenic, and vinyl chloride, or to long-term irradiation with thorium oxide (thorotrast) used in the past (1930–1940) as angiographic contrast medium. In some cases, association with hemochromatosis, von Recklingausen's disease, alcoholic cirrhosis, and anabolic steroids intake has been described. However, most of these tumors occur in the absence of known risk factors. On gross examination, four forms have been described: multifocal nodules, large solitary masses, mixed patterns of a dominant mass with nodules, and, rarely, a diffusely infiltrating micronodular tumor. Tumor size may vary from a few millimeters to several centimeters. The presence of internal hemorrhage determines the red-brown appearance of the nodules. Larger tumors are usually ill defined, not capsulated, with a sponge appearance and may contain cystic areas with blood debris filling. This tumor is composed of malignant endothelial spindle-shaped cells organized to form vessels that may range from abortive or cavernous forms to structured, frequently dilated sinusoids. Neoplastic cells develop along vascular channels forming solid nodules or cavitary spaces. Fibrosis and hemosiderin are frequently encountered in the solid portions of the tumor. In cases of thorotrast-induced sarcomas, particles of this substance may be found inside neoplastic cells. Liver cell hyperplasia with dilatation of the sinusoids and increased fibrosis leading to portal hypertension are typical early stages of tumor growth. Early metastatic spreading to the lungs and spleen is common (1).

Epithelioid Hemangioendothelioma, Hepatic

It is a rare primary hepatic malignancy of vascular origin developing exclusively in adults (with a peak in the third to fourth decade of life), with a female predominance. It was originally described as a soft tissue tumor, but recently (1982) it has been recognized as a distinct entity reported exclusively at the level of the liver and lungs. This tumor also should not be confused with the benign infantile hemangioendothelioma occurring in pediatric patients. At the present time, the etiology and pathogenesis of this tumor remain unclear and no risk factors have emerged. This malignancy is typically solid, consisting of endothelial cells with an epithelioid appearance. Immunohistochemically, these tumoral cells are positive for endothelial markers and negative for epithelial ones. Microscopically, dendritic spindle cells associated to epithelioid round cells within myxoid and fibrous stroma can be seen. Fibrosis and calcifications are described in some cases. Tumoral cells tend to invade small vessels (sinusoids, small branches of the Hepatic and portal veins). Macroscopically, two forms have been described: a multifocal nodular pattern of infiltration in the early stages that increases in size and coalesces forming a diffuse pattern. Large lesions are composed of multiple solid nodules of variable size located in a peripheral subcapsular region forming large (more than 4 cm) confluent masses with a fibrotic central core and a cellular hypervascular periphery. An avascular rim may be seen around the lesion due to the presence of tumoral compression and obliteration onto sinusoids and tributaries of the portal and Hepatic veins. Neoplastic cells invasion of these venous vessels may also occur. Intratumoral calcifications, necrosis, and hemorrhage are common findings. This tumor frequently induces fibrosis causing capsular retraction in the case of peripheral lesions; this capsular retraction is suggestive of ▶epithelioid hemangioendothelioma. Tumoral growth tends to replace hepatic parenchyma and in the case of a protracted course, a compensatory enlargement of the uninvolved liver parenchyma can be seen. Extrahepatic involvement includes the peripheral lymph nodes and mesentery with the development of calcifications in some cases. Metastatic spreading is most commonly confined to the bones and soft tissues (2, 3).

Leiomyosarcoma, Hepatic

Although very rare, this primary mesenchymal tumor of the liver shows a slightly higher incidence with respect to other sarcomas such as ▶malignant fibrous histiocytoma and ▶fibrosarcoma. Most frequently, this tumor occurs in adult patients (mean age 40–60 years). This is a very rare pediatric hepatic malignancy occurring mostly in immunocompromised patients. Some cases have been described in HIV-infected children or in hepatic allografts in pediatric liver recipients. Gender predilection has not been described. The lesions are composed of large spindle cells immunohistochemically positive to smooth muscle proteins. The distinction between primary ▶hepatic leiomyoma and ▶leiomyosarcoma is not always easy because the histological criteria for malignancy are not well defined. Usually, differentiation between benign and

malignant tumors of the smooth muscle is made considering some factors such as tumor size, cellularity, nuclear atypia, number of mitoses, and presence of necrosis. In addition, the mitotic rate, if more than ten mitoses for HPF, is considered the most reliable factor for predicting prognosis. Macroscopically, this sarcoma appears as large, solid, solitary masses located in a normal noncirrhotic liver. The lesions are often polylobulated containing a variable amount of internal hemorrhage or necrosis (4).

Histiocytoma Fibrous Malignant, Hepatic

Rare sarcomatous neoplasm most commonly affects limbs and rarely the abdominal organs such as the stomach, intestine, peritoneal wall, pancreas, and liver. The number of described cases have increased since 1970 when this tumor was definitively classified as a separate pathologic and nosologic entity. This tumor occurs mostly in elderly patients, without gender prevalence. Histologically, it appears as sarcomatous changes in normal components of the mesenchymal stroma resembling a reticulosarcoma. Macroscopically, it is a rapidly growing bulky mass with polylobulated shapes.

Clinical Presentation

Angiosarcoma, Hepatic

This tumor is very aggressive and consequently associated with a poor prognosis (median survival after diagnosis is 1 year). The surgical approach may play a role only in cases of lesions confined to one hepatic lobe without metastases. The clinical presentation is nonspecific including weight loss, weakness, abdominal pain, hepatomegaly, and intraperitoneal bleeding. Thrombocytopenia, disseminated intravascular coagulation, and hemolytic anemia have been described. The pathogenesis of all these hematologic abnormalities is probably related to the traumatism created inside the poorly organized tumoral vessels (1).

Epithelioid Hemangioendothelioma, Hepatic

The clinical course is related to a highly variable malignant potential, which is intermediate between that of benign endothelial tumors (hemangioma) and malignant angiosarcoma with a median patient survival of 5–10 years after diagnosis. Clinical signs and symptoms are not specific such as jaundice, upper quadrant pain, and liver failure. In rare cases, associated hemoperitoneum and Budd-Chiari syndrome have been described. It may happen also that this tumor is incidentally discovered (2, 3).

Leiomyosarcoma, Hepatic

The clinical presentation is not specific. A variable range of signs and symptoms such as abdominal pain, hepatomegaly, jaundice, and liver failure may occur. In some cases, daughter nodules and large tumoral lesions rupture may develop. Metastases are mainly hematogenous and the biological behavior of the tumor determines the precocity of the metastatic spreading (4).

Histiocytoma Fibrous Malignant, Hepatic

Symptoms are mainly due to compression of this large, rapidly growing mass on the neighboring organs.

Imaging

Angiosarcoma, Hepatic

Ultrasound (US) shows sarcomatous nodules as hyperechoic masses (that can be either single or multiple) with an inhomogeneous echo structure in the case of internal areas of hemorrhage and necrosis. Computed tomography (CT) depicts hepatic angiosarcoma on unenhanced scans as a hypodense area with unshaped borders, in some cases containing foci of higher attenuation due to fresh hemorrhage or areas of lower attenuation (near water density) related to old hemorrhage. In cases of thorotrast-induced tumors, neoplastic nodules as well as involved lymph nodes and the spleen show an inhomogeneous hyperdensity due to thorotrast storage. The enhancement pattern is similar to that of cavernous hemangiomas (angiosarcoma may also contain cavernous vessels) with peripheral enhancement followed by progressive centripetal opacification (Fig. 1). Therefore, these areas of enhancement frequently show a lower attenuation than the aorta and bizarre shapes or peripheral ring-shaped enhancement. Magnetic resonance (MR) features of angiosarcoma resemble those of hemangiomas. The presence in both of blood-filled vascular spaces determines the high signal intensity on T2-weighted images. After gadolinium injection, a peripheral centripetal enhancement may be seen (Fig. 2). In some cases, the presence of proteinaceous material shows an inhomogeneous signal intensity on T2-weighted images, while hypointense areas suggest the presence of hemosiderin, fibrous solid portions, or fresh hemorrhage. High signal intensity areas on T1-weighted images suggest subacute hemorrhage.

The main role of angiography in the case of hepatic angiosarcoma is interventional with a palliative purpose by means of intratumoral injection of chemotherapeutic agents or chemoembolization. Angiography may also depict the hypervascular nature of this lesion showing the presence of a peripheral spot, late in the arterial phase, with

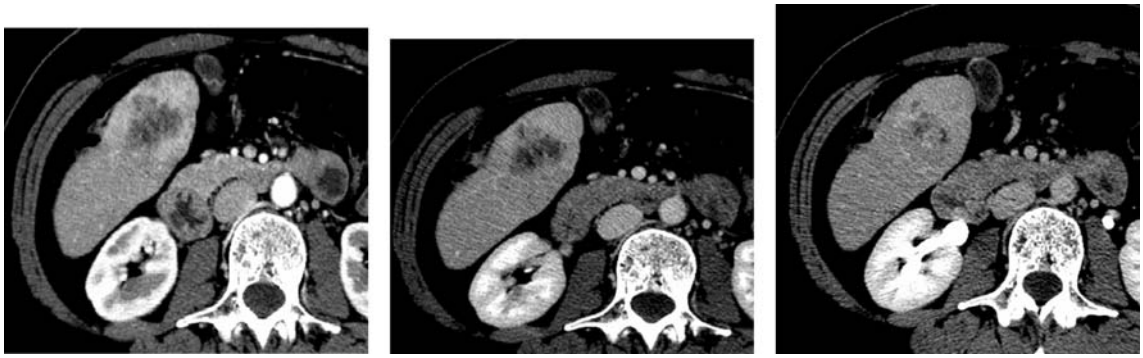

Hepatic Sarcoma. Figure 1 Angiosarcoma. Enhanced CT scans show a large focal liver lesion with hyperdense areas predominantly at the periphery of the mass; a progressive, but incomplete centripetal fill in with contrast medium is observed during the portal venous (*middle*) and delayed phases (*right*).

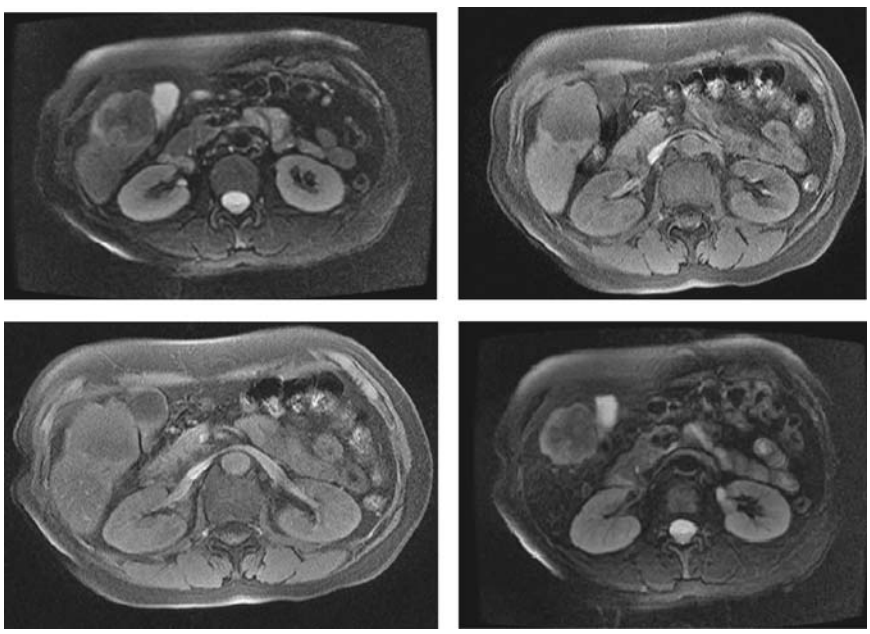

Hepatic Sarcoma. Figure 2 MR: T2-weighted image of the same lesion (*up left*). The nodule appears slightly hyperintense. On dynamic acquisition the lesion shows a progressive, persistent, peripheral enhancement without the discontinuous and globular pattern typical of hemangiomas (*up right, down left*).Delayed T2-weighted image obtained 10 min after RES targeted contrast medium administration shows the hyperintensity of the lesion respect to the surrounding parenchyma demonstrating the absence of mature reticulo endothelial cells content (*down right*).

intralesional accumulation of contrast material from the mid arterial phase to the late venous phase. The presence of the described peripheral spot should help to distinguish hepatic angiosarcomas from hemangiomas (1).

Epithelioid Hemangioendothelioma, Hepatic

The pathologic anatomy of epithelioid hemangioendothelioma explains its appearance on diagnostic images. US depicts multiple well-defined solid coalescing nodules forming large confluent masses, predominantly hypoechoic; although in some cases iso- or hyperechoic nodules have been described associated with a hypoechoic peripheral rim or central area. In addition, in regions of massive involvement a diffusely heterogeneous echo texture may appear.

Unenhanced CT scans depict tumoral conspicuity well as a hypodense area with associated calcifications in some cases. The hypodense pattern is mostly due to the presence of the myxoid stroma. Enhanced scans may show a target

appearance of the lesions due to the presence of a central unenhancing area associated with a hypervascular hyperdense peripheral proliferating rim surrounded by an unenhanced area due to the avascular outer zone if present. In the late venous phase the lesion tends to become isodense. The absence of the avascular outer zone determines the isodensity of the peripheral vascular rim with respect to the enhancing normal surrounding hepatic parenchyma and makes it difficult to delineate the tumoral contours (Fig. 3). Other findings include capsular retraction (although the liver capsula is not usually affected) and compensatory hypertrophy of the unaffected liver segments.

MR features are similar of those of CT. Both T1- and T2-weighted images, especially after gadolinium enhancement, show concentric changes of signal corresponding to regions of different histology. The overall signal tends to be low on T1-weighted images and heterogeneously high on T2-weighted images. Delayed phases after gadolinium administration may show a peripheral wash out which is useful for characterization. On delayed images acquired after hepatobiliary contrast medium administration, these lesions appear hypointense. Central areas of reduced signal may correspond to coagulation, necrosis, hemorrhage, or calcifications (2, 3).

Leiomyosarcoma, Hepatic

US usually depicts a large mass with a variable echo pattern according to the presence of central necrosis and hemorrhage. Satellite nodules may also be seen. Unenhanced CT shows hypodense, homogeneous masses without calcifications. Heterogeneous peripheral enhancement due to viable tissue may be observed after contrast medium administration.

The MR signal is not characteristic. Usually, these lesions appear hypointense both on T1- and T2-weighted images. Gadolinium administration shows a peripheral rim of enhancement similar to that shown by CT (4).

Histiocytoma Fibrous Malignant, Hepatic

The US pattern is extremely variable, ranging from hypo- to hyperechoic patterns. In some cases, calcifications may be present and may be depicted on unenhanced CT scans. CT has an important role in tumoral staging and presurgical planning. CT depicts the tumor as a hypodense lesion, in some cases heterogeneous for the presence of areas of internal necrosis. Well-vascularized areas (usually peripheral) tend to enhance after contrast medium administration.

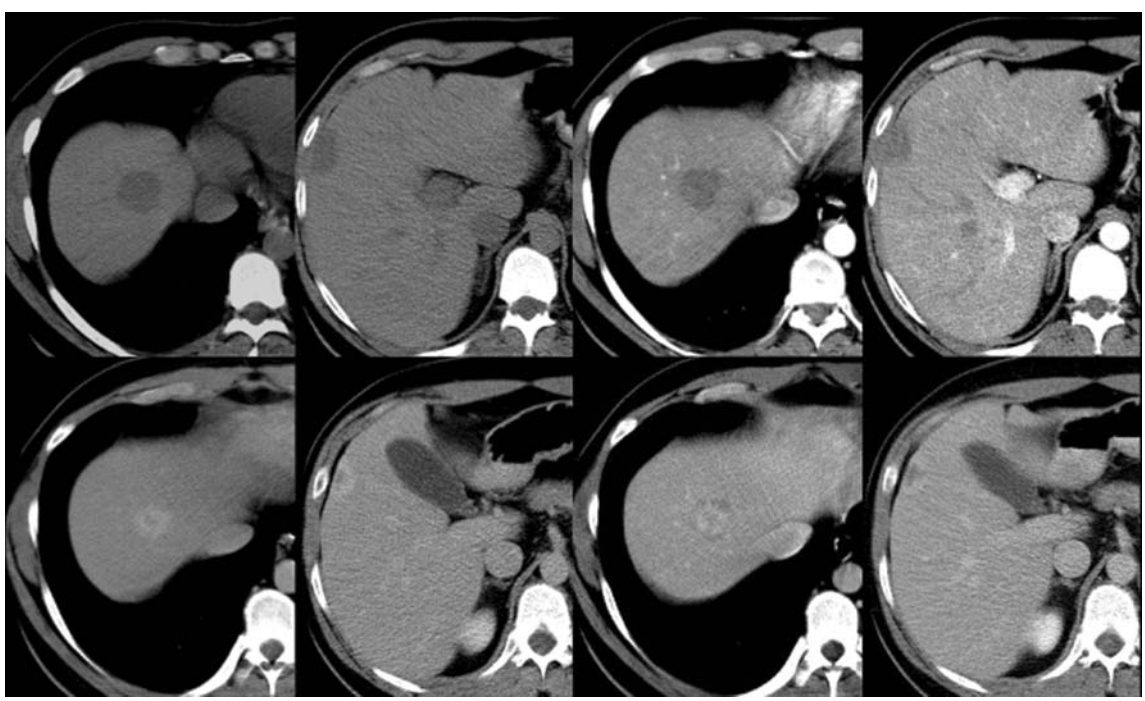

Hepatic Sarcoma. Figure 3 Hepithelioid hemangioendothelioma.Basal CT scans obtained at two different levels in the same patient show the presence of two uniformly hypodense lesions (*up left*) in the right lobe. A peripheral enhancement is progressively appreciated after contrast administration, delineating a central unenhancing area (*up right, down left*). The hypodense outer zone is shown in the major lesion on delayed phase (*down right*).

Diagnosis

Angiosarcoma, Hepatic

The differential diagnosis must include large hemangiomas, even though both angiosarcoma and hemangioma are composed of blood-filled vessels or cavernous spaces explaining their common features on CT and MR images. A differential criterion is the centripetal enhancement after contrast medium administration that in the case of hemangiomas is denser and typically globular. Angiosarcomas with central hemorrhage or necrosis show an incomplete opacification after contrast medium administration simulating large hemangiomas, which commonly do not fill in completely with contrast material. Some authors believe that it is extremely difficult to distinguish hepatic sarcomas from other hypervascular tumors of the liver such as hypervascular metastases (neuroendocrine tumors) or hepatocellular carcinoma. In addition, these lesions may demonstrate internal hemorrhage and heterogeneity associated with an early and heterogeneous enhancement. The presence of a delayed enhancement in the case of angiosarcoma helps to differentiate it from hepatocellular carcinoma. The presence of splenic involvement and hematologic disorders associated with the absence of background cirrhosis and alpha fetoprotein elevation may also help to diversify it from hepatocellular carcinoma (1).

Epithelioid Hemangioendothelioma, Hepatic

The multiple concentric rim pattern may suggest the feature of one abscess, although the clinical setting allows the diagnosis to be made.

MR hyperintensity of the lesion on T2-weighted images is similar to other malignancies but not as intense as the characteristic high signal of hepatic hemangiomas.

Multiple confluent peripheral solid masses, associated with capsular retraction depicted by the different diagnostic imaging techniques (US, CT, MR), are suggestive of epithelioid hemangioendothelioma.

Leiomyosarcoma, Hepatic

Imaging features of leiomyosarcoma are not peculiar, resembling those of other hepatic mesenchymal malignancies, so that a definitive diagnosis is achieved by means of histology.

Histiocytoma Fibrous Malignant, Hepatic

The imaging pattern resembles that of other hepatic sarcomas. The presence of calcifications may help to differentiate it from leiomyosarcoma.

Bibliography

1. Koyama T, Fletcher JG, Johnson CD et al (2002) Primary hepatic angiosarcoma: findings at CT and MR imaging. Radiology 222:667–673
2. Schneider G, Grazioli L, Saini S (2003) Imaging of malignant focal liver lesions. In: Schneider G, Grazioli L, Saini S (eds) MRI of the Liver. Springer-Verlag Italia, Milano, pp 212–215
3. Manfredi R, Maresca G, Cotroneo AR et al (1999) Rare primary malignancies of the liver. In: Bartolozzi C, Lencioni R (eds) Liver Malignancies. Springer, Berlin Heidelberg, pp 153–167
4. Tsuji M, Takenaka R, Kashihara T et al (2000) Primary hepatic leiomyosarcoma in a patient with hepatitis C virus-related liver cirrhosis. Pathol Int 50(1):41–47

Hepatic Transplantation

▶Transplantation, Liver

Hepatic Vascular Pathologies

▶Vascular Disorders, Hepatic

Hepatic Vascularization

Hypervascular liver tumors receive their blood supply from the hepatic artery, in contrast to normal liver tissue, that receives approximately 70% of its blood supply from the portal vein.

▶Chemoembolization

Hepatitis

Bartolozzi Carlo, Massimo Bazzocchi, Giuseppe Como, Chiara Franchini
Department of Diagnostic and Interventional Radiology, University of Pisa, Italy
bartolozzi@med.unifi.it
massimo.bazzocchi@med.uniud.it

Synonym

Diffuse inflammatory disease of the liver

Definition

Hepatitis is any disease featuring diffuse inflammation of the liver, characterized by partial or extensive necrosis involving all hepatic lobules. Acute hepatitis is a diffuse inflammation of the liver usually due to hepatotropic viruses and causing necrosis and acute inflammatory infiltrates. In chronic hepatitis, the hepatic inflammation and necrosis continue for at least 6 months. ►Fulminant hepatitis is characterized by submassive to massive hepatic necrosis, progressing from onset of symptoms to hepatic failure within 2 to 3 weeks.

Pathology and Histopathology

Acute Hepatitis

Various possible viral agents may cause acute hepatitis. Unless otherwise, the specified term "viral hepatitis" is reserved for infections that are caused by a group of viruses which shows a particular affinity for the liver. The main hepatotropic viruses are hepatitis A virus (HAV), hepatitis B virus (HBV), hepatitis C virus (HCV), hepatitis D virus (HDV), also called delta agent (which requires the presence of the hepatitis B virus), and hepatitis E virus (HEV). A vast array of other viruses may also produce hepatitis, including cytomegalovirus, Epstein-Barr virus (EBV, the agent responsible for mononucleosis), herpes viruses, yellow fever virus, rubella virus, Coxsackie virus, and adenovirus. Nonviral infectious acute hepatitis may be related to severe bacterial infections and amoebic infection. ►Toxic hepatitis usually has an acute onset and it can be due to drugs, hepatotoxic substances such as fungal toxins and alcohol. The morphologic changes in acute viral hepatitis and in drug-related hepatitis are virtually the same. Grossly, the liver is enlarged and more or less green depending on the degree of jaundice. Histologically, the major findings are necrosis of isolated or clustered hepatocytes, diffuse liver cell injury, reactive changes in Kupffer cells and sinusoidal lining cells, consisting in hypertrophy and hyperplasia, inflammatory infiltrate in portal tracts, hepatocytic regeneration during the recovery phase. In more severe acute inflammation, confluent necrosis may lead to bridging necrosis connecting portal-to-portal, central-to-portal, or central-to-central regions of adjacent lobules.

Fulminant Hepatitis

Submassive to massive hepatic necrosis progressing from onset of symptoms to hepatic encephalopathy within 2 to 3 weeks is called fulminant hepatitis or fulminant hepatic failure. The most common causes are fulminant viral hepatitis, drug toxicity (acetaminophen, isoniazid, antidepressant), chemical toxicity (mycotoxins of the mushroom *Amanita phalloides*), ischemia or shock.

Chronic Hepatitis

Chronic hepatitis is a process present for at least 6 months and has a number of different causes, including viral hepatitis (HBV, which leads to chronicization in more than 90% of infected neonates and in 5% of adults, of whom one-fourth progress to cirrhosis; HCV, with a risk of chronicization greater than 50% of infected patients, of whom half progresses to cirrhosis; superinfection by HDV in patients infected by HBV, whose outcome is a more severe chronic hepatitis), chronic alcoholism, drugs (isoniazid, alpha-methyldopa, methotrexate), autoimmunity, metabolic disorders (Wilson's disease and hemochromatosis), alpha 1-antitrypsin deficiency. Chronic hepatitis is classified, on the basis of the extent of inflammation, in chronic persistent hepatitis (in which inflammation is confined to the portal tracts), chronic active hepatitis (in which inflammation spreads from the portal tracts into the parenchyma and surrounds regions of necrotic hepatocytes), chronic lobular hepatitis (in which persistent inflammation is confined to the lobule). Most histological features are common to all forms of chronic hepatitis. In the mildest forms of chronic hepatitis, the inflammatory infiltrate is limited to the portal tracts; this consists of lymphocytes, macrophages, and occasional plasma cells. Liver architecture is usually preserved. The histological mark of progressive disease is the so-called "piecemeal necrosis," consisting of necrosis of hepatocytes of the lining plate associated to spilling of chronic inflammatory infiltrate out of the portal tracts. Lobular inflammation with focal hepatocellular necrosis may be present. Bridging necrosis may connect adjacent portal–portal, central–central, and portal–central zones. Continued loss of hepatocytes results in fibrous septum formation, which, accompanied by hepatocellular regeneration, results in cirrhosis. Some histological features are specific of chronic hepatitis of different etiology. In chronic HCV hepatitis, lymphoid aggregates in portal tracts and mild fatty change are seen in about one-half of cases and bile duct damage is observed in most cases. "Ground glass" hepatocytes are sometimes present in chronic HBV hepatitis.

Clinical Aspects

Acute Hepatitis

The symptoms of acute hepatitis are considerably variable. Sometimes acute hepatitis is completely asymptomatic. Children usually show mild symptoms. The early stage is characterized by aspecific manifestations such as weakness, low fever, nausea, loss of appetite, changes in taste perception, headache. This syndrome is followed by the jaundice phase, in which the scleral

and cutaneous jaundice is associated to dark urine and light-colored stools. Weakness may last for weeks during the recovery phase.

Fulminant Hepatitis

The clinical scenario is dominated by jaundice, encephalopathy, coagulopathy and bleeding, renal failure, cardiovascular failure. The evolution is variable and depends on the age of the patient and the previous status of the liver.

Chronic Hepatitis

Many patients with chronic hepatitis have no symptoms. The most common manifestations are weakness, muscles, and joints pains. Mild right-upper-quadrant discomfort may occur. Jaundice may appear in the later stages of chronic hepatitis.

Imaging

Imaging has a limited role in the diagnosis of hepatitis, especially in acute hepatitis. It may be helpful in the evaluation of chronic hepatitis, especially in assessing complications. Probably the most important role of imaging in suspected hepatitis is to help exclude the presence of other hepatic diseases, such as cholestasis, diffuse metastatic disease, and cirrhosis (1).

Acute Hepatitis

Specific sonographic signs of acute hepatitis have not been described. Ultrasound (US) is performed in order to exclude biliary obstruction in patients with jaundice, but does not allow a definite diagnosis of acute hepatitis. Usually the liver is uniformly enlarged and the hepatic margins are regular. In the large majority of cases, the echo structure does not show any modification. Sometimes, US demonstrates a diffuse decrease in parenchymal echogenicity, which causes a relative increase in the echogenicity of the portal vein walls ("starry night" pattern) (1–3). Transient changes in morphology and motility of gallbladder may occur in acute hepatitis. In early stages, the gallbladder may be contracted with thickened wall whereas in advanced stages it may be enlarged with normal wall and shows a reduced response to cholecystokinetic stimula (4). Enlarged inflammatory periportal, hilar, and coeliac lymph nodes may be present (Fig. 1).

In acute hepatitis, the computed tomographic (CT) findings are aspecific and inconstant and may vary from normal liver to hepatomegaly with homogeneous parenchymal hypodensity, to diffuse inhomogeneity with alternating hypodense and hyperdense areas. Periportal edema may be appreciable as a hypodense halo along intrahepatic portal vessels. This CT sign is called "periportal tracking" and can involve both minor and major branches, sometimes being visible also around the inferior vena cava. The use of contrast media allows a better depiction of the periportal tracking, which becomes more

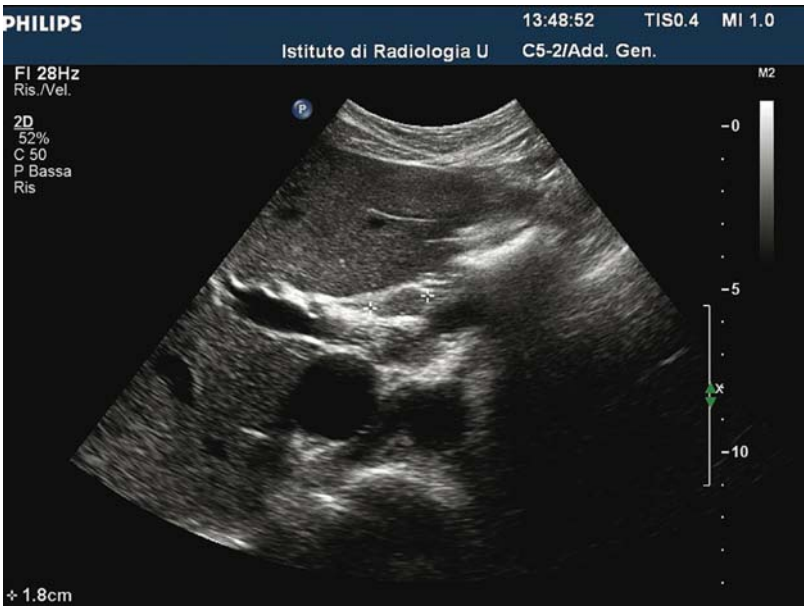

Hepatitis. Figure 1 US scan of porta hepatis: enlarged lymph nodes of the porta hepatis and of the coeliac trunk may be demonstrated. These inflammatory lymphadenopathies have an elongated morphology.

easily distinguishable from the vessel lumen during the portal-venous phase. Sometimes in the early stage, multiple-regenerating nodules may be detected.

Fulminant hepatitis is characterized by the presence of multiple confluent necrotic areas. Necrosis appears as a hypodense area with a hyperdense border due to concomitant fibrosis and regeneration. After contrast medium administration, necrosis remains unenhanced whereas fibrosis and regenerative nodules show variable contrast enhancement.

On magnetic resonance (MR) images acute inflammation of the liver determines a specific increase of T1 and T2 relaxation times, due to the increased content in water protons. Nevertheless, variations of signal intensity are rarely appreciable. On T2-weighted images, it is sometimes depicted a hyperintense band along the portal vessels, related to inflammatory phenomena with edema. A common finding is the presence of inflammed enlarged lymph nodes (5).

Chronic Hepatitis

In patients with chronic hepatitis, imaging studies are used to evaluate the development of cirrhosis and ascites and to exclude hepatocellular carcinoma. US does not show peculiar findings in chronic hepatitis. The liver is usually increased in size and has regular margins. The echo structure may be normal or have a coarsened texture and increased parenchymal echogenicity, when fibrotic or fibrosteatotic phenomena are associated. This causes portal vein radicles to be less conspicuous. The appearance of the liver is essentially identical to that seen with diffuse fatty change. In some cases, the sonographic appearance is indistinguishable from cirrhosis. Enlarged lymph nodes of the porta hepatis and of the coeliac trunk may be demonstrated. These inflammatory lymphadenopathies have an elongated morphology and a central hyperechoic line may be depicted (1–3). In patients with chronic hepatitis, the CT and MR imaging features resemble those of early-stage liver cirrhosis.

In chronic active hepatitis, the "periportal tracking," appearing as a hypodense band on CT and hyperintense band on T2-weighted MR images may be depicted, due to inflammation and edema. Geographic zones of reduced density at CT and increased signal intensity on T2-weighted MR scans correspond to edema and indicate active disease (3, 5) (Fig. 2).

Diagnosis

In acute hepatitis, the diagnosis is done on the basis of clinical and laboratory data. The laboratory data allows establishing the presence of liver inflammation and its cause. In chronic hepatitis, biopsy is needed in order to assess the stage and the grade of the disease. Laboratory data provide information about the cause of the disease and the degree of liver function impairment. HCV-related hepatitis is suspected when serum aminotransferases are elevated and anti-HCV is present in serum (indicative of past and current infection). The diagnosis is confirmed by the finding of HCV RNA in serum (indicative of active viral replication). In HBV infection, HBsAg is a marker of acute and chronic disease; HBeAg and HBV-DNA indicate active viral replication. Anti-HBs is indicative of serum immunity after vaccination, anti-HBc IgG is marker of past or recent HBV contact whereas anti-HBc IgM is a marker of acute infection if the titer is high and chronic infection if the titer is low.

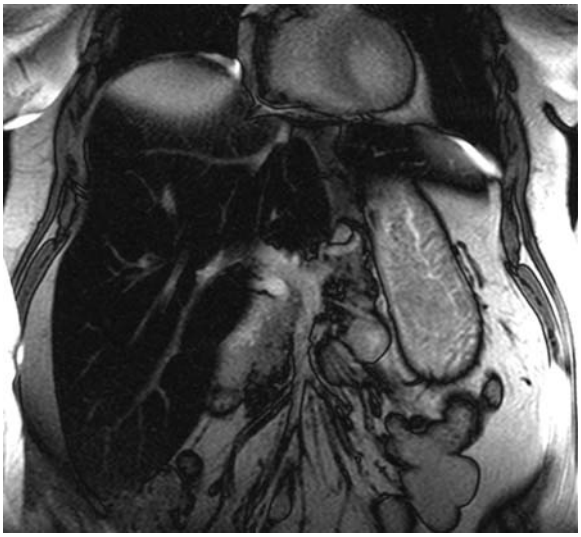

Hepatitis. Figure 2 Coronal MR scan of the liver, true-FISP sequence: ►nonalcoholic steatohepatitis (NASH), also called nonalcoholic fatty liver disease (NAFLD) is a liver inflammation with fatty degeneration not due to abuse of alcohol. This condition is more common in women and it is associated with obesity, diabetes mellitus type II, and insulin resistance as in this patient. Liver is enlarged. In this out-of-phase condition, liver has low signal for high grade of steatosis.

Bibliography

1. Mortele KJ, Segatto E, Ros PR (2004) The infected liver: radiologic–pathologic correlation. Radiographics 24(4):937–955
2. Tchelepi H, Ralls PW, Radin R et al (2002) Sonography of diffuse liver disease. J Ultrasound Med 21(9):1023–1032
3. Mortele KJ, Ros PR (2001) Imaging of diffuse liver disease. Semin Liver Dis 21(2):195–212
4. Ferin P, Lerner RM (1985). Contracted gallbladder: a finding in hepatic dysfunction. Radiology 154(3):769–770
5. Lencioni R, Bartolozzi C (2003) Diffuse liver disease. In: Magnetic Resonance Imaging in Liver Disease. Thieme, New York, pp 93–114

Hepato-Biliary Malformations

▶Congenital Malformations, Liver and Biliary Tract

Hepatobiliary System

Carlo Bartolozzi
Division of Diagnostic and Interventional Radiology, University of Pisa, Pisa, Italy
bartolozzi@med.unipi.it

Recent advances in imaging techniques have determined a radical change in the radiological approach to the diagnosis and treatment of hepatobiliary, pancreatic, and splenic diseases. Particularly, improvements in ultrasound (US), computed tomography (CT), magnetic resonance (MR), and nuclear medicine allow an accurate noninvasive evaluation of parenchymal, vascular, and biliary structures.

This section presents an overview of the hepatobiliary system (liver, pancreas, spleen), providing an accurate description of the anatomy (normal and radiological) and pathology, emphasizing the most relevant diagnostic tools. Special emphasis has been put on focal and diffuse disease detection and characterization, which may enable definitive diagnosis without the need for histological specimens. Pediatric diseases and congenital malformations are covered separately. Finally, radiological interventional procedures and organ transplantation imaging are discussed.

The liver enables multiple vital functions (metabolic, storage, and digestive) that are reflected in its peculiar complex anatomy (**Anatomy, Normal and Radiological, Biliary System**) consisting of parenchyma, biliary ducts, and a double vascular supply. The liver occupies much of the right hypochondrial region of the abdomen. It has two major surfaces, a superior or diaphragmatic surface and an inferior or visceral one. It can be divided in two different ways, by external lobation and by segmentation. The classical anatomic subdivision into four externally defined lobes is based on approximately H-shaped indentations on the visceral surface. In contrast, the internal lobation and segmentation are based on the branching pattern of the portal vein, hepatic artery, and hepatic ducts, with the major hepatic veins occupying and helping to demarcate the planes between the lobes and segments.

The choice of the most appropriate liver imaging approach, tailored on the clinical request, is mandatory as it is now possible to electively depict the hepatic parenchyma or vascular and biliary anatomy.

Since the introduction of fast imaging and new contrast agents an extremely accurate evaluation of liver parenchyma has been obtained. Cross-sectional imaging techniques, including US, CT, and MR, are well-established modalities enabling diagnosis of focal and diffuse liver disease in most cases. The use of contrast agents increases both sensitivity and specificity of liver lesion detection and characterization.

Extracellular contrast agents are largely employed in CT and MR (vascular interstitial agents) and, recently, in US (blood pool agents), increasing lesion detection and providing crucial additional information about the dynamic contrast behavior for lesion characterization. However, the vascular pattern may not be specific for each focal lesion, and the diagnostic accuracy of dynamic phase imaging alone can be unsatisfactory. Therefore, the advent of novel MR contrast agents with liver-specific properties may increase tissue characterization, enabling an accurate evaluation both of diffuse and focal liver disease.

Diffuse liver diseases comprise many different pathological conditions, including metabolic disorders, infections, and chronic toxic injury. Imaging techniques are increasingly becoming involved in the study of such affections. Because several diffuse liver diseases predispose to the development of primary hepatic neoplasms, the aim of imaging is to characterize some of these conditions and to detect neoplasms at an early stage.

Particularly, hepatitis (**Hepatitis**) and hepatic cirrhosis (**Cirrhosis, Hepatic**) have a high prevalence, representing a major health problem. In such conditions, as well as in several rare diffuse infiltrative diseases of the liver (**Diffuse Infiltrative Diseases, Hepatic**), imaging techniques are largely employed to screen for neoplastic changes.

Finally, structural and morphological changes induced by several diffuse liver diseases, such as fatty infiltration (**Steatosis, Hepatic**) and diffuse infiltrative disease, especially in cases of heterogeneous distribution, must be distinguished from tumors.

However, imaging techniques are used mainly for differentiating benign and malignant focal liver lesions. Benign lesions are currently classified according to their cellular origin into hepatocellular, cholangiocellular, and mesenchymal types. Benign proliferation of hepatocytes leads to hepatic adenoma (**Adenoma, Hepatic**) and focal nodular hyperplasia (**Hyperplasia, Focal, Nodular Hepatic**). Hepatic hemangioma (**Hemangioma, Hepatic**) is the most common benign tumor affecting the liver and develops from endothelial cells. Hepatic cysts and cystic like lesions (**Cystic-like Lesions, Hepatic; Abdominal**) are of congenital or developmental origin arising from biliary

epithelial cells in most cases. Finally, other rare benign lesions may originate from mesenchymal tissue (**Lipomatous Tumors, Hepatic**), and biliary duct epithelium such as biliary cystoadenoma (**Neoplasms, Bile Duct**).

Most benign tumors are incidental findings and do not produce clinical symptoms. They must be diagnosed noninvasively and differentiated from malignancies. However, because of the possibility of malignant degeneration, as in the case of hepatic adenoma, the benign tumors must also be differentiated from one another. Benign focal liver lesions include inflammatory/infectious diseases (**Hydatid Disease; Abscess, Hepatic**) and traumatic lesions such as hepatic hematoma and biloma (**Trauma, Hepatobiliary**).

The liver is an important organ from an oncologic perspective. Primary hepatic neoplasms are common, especially in the presence of several diffuse liver diseases. Histologically, primary hepatic malignancies can be divided on the basis of their origin from hepatocytes (**Hepatocellular Carcinoma**), bile duct epithelium (**Neoplasms, Bile Duct**), and mesenchymal tissue (**Lymphoma, Hepatic; Sarcoma, Hepatic; Lipomatous Tumors, Hepatic**). Hepatocellular carcinoma is the most common primary malignancy of the liver, representing the main complication of chronic hepatitis and cirrhosis. Because surgical and percutaneous procedures (**Interventional Hepatic Tumors, Procedures**) are well-established therapeutic options for hepatocellular carcinoma treatment, early diagnosis is a crucial point, nowadays possible for radiologists.

The liver provides fertile soil for metastases (**Metastases, Hepatic**), not only due to its dual blood supply from both the systemic and splanchnic circulation, but also for sinusoid vascular architecture and a rich biochemical environment favoring rapid growth of metastatic cells. It is the most common site of metastases from a variety of cancers, particularly gastrointestinal tumors. The radiologist's challenge in liver malignancies is not only diagnosis and staging but also treatment (**Interventional Radiological Procedures, Hepatic**) and evaluation of the response to therapy.

Moreover, the assessment of the vascular branches' course and segmental and subsegmental anatomy has become of utmost importance, particularly because of the increasing necessity of accurate localization of liver lesions and preoperative demarcation of resection planes.

Volumetric techniques, such as CT and MR, implemented by three-dimensional reformation allow investigation of the variability in anatomic relationships between external landmarks and hepatic vascular structures, clarifying segmental and subsegmental anatomy and offering the possibility to obtain images at the peak of vascular enhancement. This allows precise depiction of hepatic vessels and generation of angiographic images, particularly useful in the imaging of focal liver lesions as well as in pre- and posttransplant liver imaging evaluation (**Transplantation, Hepatic**) and in **Vascular Disorder Hepatic** assessment.

Vascular imaging with Doppler US has expanded the role of US to permit rapid assessment of vessel patency and blood flow direction, allowing not only a morphologic but also a dynamic and functional approach, particularly useful for portal vein evaluation in **Portal Hypertension**.

Vascular hepatic disorders (**Vascular Disorders, Hepatic**), representing a miscellaneous group of pathological conditions affecting the visceral vessels, can be accurately depicted by means of CT and MR technologies, allowing angiographic applications and restricting angiography to a therapeutic role.

Diagnosis of biliary affections, especially several benign conditions affecting the gallbladder (**Gallstone; Cholecystosis; Cholecystitis**), represents an everyday challenge for radiology. US is routinely employed for the first assessment of such diseases, while CT may be used to implement the role of US, especially when evaluation of the distal portion of the biliary duct is required or to assess the tumoral spreading in cases of malignancy (**Gallbladder Tumors**). However, when a more accurate evaluation of the biliary tree is required (**Cholangitis; Occlusion, Bile Ducts**), cholangiographic techniques must be employed. Since the advent of MR cholangiography, an accurate evaluation of the biliary branches can be obtained noninvasively, while direct cholangiography (transhepatic or retrograde) is used for treatment only.

Pediatric conditions (**Pediatric Tumors, Hepatic, Benign; Pediatric Tumors, Hepatic, Malignant**) and congenital malformations (**Congenital Malformations, Liver and Biliary Tract**) are covered separately.

The pancreas is a gland consisting of two different components: The exocrine pancreas secretes digestive enzymes (amylase, lipase, etc.), which are collected in the pancreatic ductal tree and, *via* the main pancreatic ducts of Wirsung and Santorini, flow into the duodenum. The endocrine pancreatic insulae produce various hormonal substances (insulin, glucagon, gastrin, VIP, etc.), which are released in the portal venous system.

The pancreas is located in the retroperitoneum. Its deep position, posteriorly to the stomach and intestinal loops, has in the past limited its radiological explorability; it was possible to obtain only indirect signs of pancreatic disease with conventional radiology. The advent of tomographic techniques has permitted direct visualization of the gland, and consequently, imaging has assumed a fundamental role in diagnosis, staging, and pre- and posttherapeutic evaluation of pancreatic disorders. Nowadays, the radiologist has a complete and detailed view of the normal anatomy of the pancreas and its ductal and vascular systems, and can thus easily identify congenital

abnormalities (**Congenital Abnormalities, Pancreatic**) and precisely define postsurgical anatomy in patients having pancreas transplantation.

US usually represents the first examination performed when a pancreatic disease is suspected. The sonographic study of the pancreas has some limitations because of its anatomic location; particularly, the pancreatic tail can be difficult to visualize. Nevertheless, it often displays indirect signs of pancreatic disease, such as dilatation of biliary and pancreatic ducts, abdominal fluid collections, ascitis, peritoneal carcinosis, and hepatic metastases.

Doppler US can integrate the US exam; a recent application of Doppler US is the follow-up of the transplanted pancreas. Thanks to the possibility of assessing the patency of vascular anastomoses and of identifying abnormalities in parenchymal vascularization, abdominal US and Doppler US enable correct assessment of the transplanted pancreas and therefore represent an effective diagnostic technique for first recognition of parenchymal and vascular complications (**Transplantation, Pancreatic**).

US contrast media have been employed in experimental studies in the evaluation of focal pancreatic lesions. The usefulness of contrast-enhanced US in demonstrating pancreatic malignancies is still not evident. However, indirect signs of pancreatic cancer, such as ductal dilatation and vascular involvement, seem to become clearer after contrast administration.

Spiral CT is the standard imaging modality for evaluating the pancreatic gland because it allows visualization of the entire organ and accurate assessment of the relationships with adjacent anatomic structures. Furthermore, the use of iodinate contrast medium allows study of the pancreas in different phases of contrast distribution; this is crucial in characterizing focal lesions and evaluating the vascular structures, especially in malignancies (**Carcinoma, Pancreatic**; **Cystic Neoplasms, Pancreatic; Islet Cells Tumors, Pancreatic**). Image processing can improve depiction of the vessels and, in cases of neoplastic disease, increase the accuracy of assessing the vascular involvement. CT represents the imaging technique of choice for the detection of pancreatic neoplasms and for local and distant staging; furthermore, on the basis of CT findings it is possible to establish the resectability of the lesion.

In transplanted patients, the CT examination, performed in selective arterial, pancreatic, and venous phases, enables detailed visualisation of the transplanted pancreas, including the anastomoses for exocrine pancreatic drainage and those of the afferent and efferent vessels, thus allowing accurate identification of possible complications.

In acute inflammatory disease of the pancreas (**Pancreatitis, Acute**), CT allows complete visualization of the pancreas and retroperitoneum, thus demonstrating the typical pancreatic findings, fluid collections, and possible complications. CT is also used to assess the severity and estimate the prognosis of acute pancreatitis, by means of the well-established CT criteria.

In the early stage of chronic pancreatitis (**Pancreatitis, Chronic**), the diagnosis is based mainly on clinical and laboratory data, due to the absence of the typical morphologic changes detectable by means of imaging. In advanced disease, imaging plays a key role in diagnosis, demonstrating characteristic findings (calcifications, ductal dilatation, etc). The major limitation of imaging modalities concerns differentiation of focal chronic pancreatitis and cancer. In general, differentiation between cancer and focal pancreatitis is difficult with a single imaging modality and may sometimes require the use of contrast-enhanced CT, MR, positron emission tomography (PET) imaging, and, in selected cases, histological evaluation.

Technical advances in MR have promoted the application of this technique in the study of the pancreas; in fact, MR is able to provide a paramount view of the pancreatic region, including the parenchyma, the ductal system, and the vascular structures. Hence, a comprehensive assessment of most pancreatic diseases can be achieved with a single examination.

Unenhanced MR sequences provide additional information about the pancreatic parenchyma and pancreatic lesions with respect to CT examination, for example in characterization of cystic lesions.

The current major areas of investigation are dynamic contrast-enhanced imaging techniques, use of tissue-specific contrast agents, and magnetic resonance cholangiopancreatography (MRCP).

The use of contrast media, both vascular interstitial (gadolinium chelates) and tissue specific (Mn-DPDP), can improve the depiction and the characterization of focal lesions.

Mn-DPDP contrast-enhanced MR has proven to be very helpful in the detection of small tumors, thanks to the very little uptake of the agent into tumors with respect to normal parenchyma, which results in a reliable increase of pancreas-tumor contrast, thus improving the detectability of neoplastic lesions.

Mn-DPDP may also improve the staging of pancreatic cancer by increasing the sensitivity of MR imaging in detecting liver metastases during the same examination.

The pancreatic ductal system can be visualized with high diagnostic accuracy either by means of heavily T2-weighted scans, which highlight the signal intensity from static fluids, o by using hepatobiliary contrast media. MRCP allows depiction of pancreatic ductal tree abnormalities with an accuracy similar to that of endoscopic retrograde cholangiopancreatography (ERCP).

The MRCP sequences can also be applied to perform pharmacodynamic studies; for instance, it is possible to evaluate the pancreatic ductal system after intravenous secretin administration to enhance the delineation of the main pancreatic duct and its side branches, and to obtain additional information concerning signal voids and strictures.

Locoregional vessels can be accurately assessed in the same session by using MR angiography techniques and image reformations.

Finally, nuclear medicine, by using somatostatin receptor analog, may be useful in evaluating pancreatic endocrine tumors.

The spleen is formed by reticular and lymphatic tissue and is the largest lymphatic organ. It is located in the left hypochondriac region of the abdominal cavity between the fundus of the stomach and the diaphragm. The spleen has two main functions: It represents an important site for the immunological response, and it is the principal site of destruction of senescent erythrocytes or abnormal blood elements. During fetal life, the spleen also works as a hematopoietic organ.

The spleen is an uncommon site of primary disease; however, it is secondarily involved in various different pathological conditions.

Modern imaging modalities such as US, CT, and MR offer an easy examination of the spleen and show high sensitivity in demonstrating focal or diffuse abnormalities, but low specificity in characterizing the different diseases. US and CT are screening modalities for the spleen, while MR is performed for problem solving in selected clinical settings. Use of organ-specific contrast agents, such as superparamagnetic iron oxide particles, represents a promising tool to improve the detection of splenic disorders.

Currently, splenic angiography is not used as a diagnostic tool and is almost exclusively performed for interventional procedures, while conventional nuclear medicine techniques have been widely replaced by radiological modalities. However, the advent of PET imaging seems to improve splenic lesion detection, particularly in malignancies.

Enlargement of the spleen (**Splenomegaly**) is the most common, but quite nonspecific, manifestation of disease in this organ, including hematologic, neoplastic, infectious, and immunologic disorders, as well as storage diseases and portal hypertension.

Focal splenic lesions are uncommon. The most frequent are cysts; both benign and malignant primary tumors are rare. Benign neoplasms (**Neoplasms, Splenic, Benign**) include hemangiomas, hamartomas, and lymphangiomas, while lymphoma and hemangiosarcoma represent the most common primary splenic malignancies (**Neoplasms, Splenic, Malignant**). Splenic metastases are usually correlated with widespread malignant disease.

The spleen is the most frequently injured organ in cases of blunt abdominal trauma. US and CT are able to accurately depict direct and indirect signs of traumatic splenic injuries (**Trauma, Splenic**).

The spleen may be a target for various infectious agents that can lead to formation of splenic abscesses (**Spleen, Infections, Disease; Hydatid Disease, Abdominal**).

The most common congenital anomalies (**Congenital Abnormalities, Splenic**) of the spleen are accessory spleens, lobulations, and notches (**Splenic Anomalies**).

Hepatoblastoma

It is the most common primary hepatic malignancy in children and represents the most frequent malignant tumor in pediatric patients after neuroblastoma and Wilms' tumor. This tumor originates from hepatocytes but may also contain mesenchymal elements. Hepatoblastoma frequently presents as a large mass, mostly located in the right hepatic lobe but multicentric, diffuse, and multicystic lesions can also be seen. These tumors are frequently hypervascular with neovascularity and encased vessels.

▶Hepatic, Pediatric Tumors, Malignant

Hepatocellular Carcinoma

Carlo Bartolozzi, Chiara Franchini
Division of Diagnostic and Interventional Radiology, University of Pisa, Pisa, Italy
bartolozzi@do.med.unipi.it

Synonyms

HCC; Primary malignant hepatocellular tumour

Definition

Hepatocellular carcinoma (HCC) is a primary malignant neoplasm that originates from hepatocytes.

Pathology/Histopathology

HCC is a common malignancy worldwide, with an estimated incidence of up to 1,000,000 new cases per year.

The highest incidence rates are found in sub-Saharian Africa and the Far East. Areas of low incidence include North America and Northern Europe, while Mediterranean countries have an intermediate to high incidence. The geographic distribution of HCC is related to the etiology of the disease: in Western countries and in the Far East, most cases occur in patients with liver cirrhosis, mainly due to hepatitis B or C virus infection and alcohol abuse (1). Cirrhosis is a premalignant condition: the development of HCC represents a common long-term complication of cirrhosis. HCC may rarely occur in non-cirrhotic livers.

On gross pathology, HCC may show three different patterns: in the nodular form, most commonly associated with liver cirrhosis, it presents as single or multiple nodular lesions, with or without a capsule. The true fibrous capsule may be surrounded by the so-called 'pseudocapsule', which consists in compressed liver tissue at the periphery of the nodule, containing small vessels and bile ducts. The massive form, most frequently encountered in non-cirrhotic livers, appears as an infiltrative mass. The diffuse form is quite rare and consists in a miliary infiltration of the liver parenchyma (1).

From a histologic point of view, there are four different types of HCC: the most frequent variant is the trabecular type. The other forms are the pseudo-glandular type, the solid type, the scirrhous or sclerosing type. On the basis of Edmondson and Steiner' s classification these tumours can be described as well differentiated, moderately differentiated, poorly differentiated, or undifferentiated (anaplastic). Occasionally the malignant liver cells may contain glycogen or fat.

The large majority of overt HCC have an arterial blood supply. Only a few, well-differentiated HCCs have a portal blood supply. Haemorrhage and necrosis may occur in advanced HCC (1).

A tendency to grow into the portal veins, producing tumour thrombi, is a peculiar feature of HCC. Satellite or 'daughter' lesions located near the main tumour represent intrahepatic metastases developed *via* the portal branches. Lymphatic metastases are not common; they usually involve hepatic hilar lymph nodes. Extrahepatic haematogenous metastases, usually associated with advanced-stage tumours, are most commonly encountered in lung, followed by bone and adrenal gland (2).

Different types of hepatocellular nodules can be found in the cirrhotic liver: regenerative nodule, low-grade and high-grade dysplastic nodule, HCC. A stepwise carcinogenesis for HCC has been proposed in which these lesions represent the sequence of events. Dysplastic nodules are considered premalignant nodules. Foci of HCC can be found in dysplastic nodules (3). According to the *de novo* pathway, a single cell or a group of hepatocytes may give rise to a focus of HCC (3).

In the progression from regenerative nodule to overt HCC, there is a reduction in portal blood supply and development of new arterial anomalous vessels, called non-triadal arteries, which become the dominant blood supply in overt HCC lesions.

►Fibrolamellar carcinoma (FLHCC) is a rare malignant neoplasm of hepatocellular origin. In the past, it was considered a variant of HCC, whereas it is now seen as an independent entity. Pathologically, it is characterized by the presence of abundant fibrous tissue. The central fibrous scar may show faint calcifications. Satellite nodules may also be present. This tumour occurs in younger patients, is not associated with hepatic cirrhosis and its histological features are less malignant than those of HCC. Most often, it appears as a solitary, large, well-circumscribed mass with lobulated margins (1, 2). Vascular invasion is rare, whereas lymphatic metastases are quite common (3).

Clinical Presentation

HCC is usually poorly symptomatic until it has reached an advanced stage.

In the low and intermediate-incidence geographic areas the tumour typically develops as a complication of a long-standing cirrhosis in elderly patients (>50–60 years). Symptoms due to a small tumour are indistinguishable from those of the underlying liver disease. The most common manifestations are right hypochondrial or epigastric pain, weight loss, ascitis, hepatic failure, jaundice.

In the high-incidence geographical areas the tumour often develops in absence of cirrhosis in younger individuals (<40 years); when the patients become symptomatic, the neoplasm has already a large size. The most common manifestations are severe, often diffuse abdominal pain, weakness, weight loss, lack of appetite, constipation.

Rarely HCC may present with acute abdomen due to haemoperitoneum caused by the rupture of the tumoral mass. Late symptoms can be due to extra-abdominal metastases, mainly bone and pulmonary lesions. In patients without cirrhosis or other underlying liver disease, HCC is usually diagnosed at a very advanced stage (3). FLHCC usually becomes symptomatic when the tumoural mass has reached a large size, causing palpable mass, abdominal pain, nausea.

Imaging

Ultrasound

At ultrasound (US) the small, classical, nodular type HCC appears as a well demarcated round lesion. The

demonstration of a hypoechoic halo can be due to the presence of the fibrous capsule or the so-called 'pseudocapsule' (compressed liver tissue at the periphery of the nodule); the capsule is more often seen in larger tumours. The infiltrative nodular HCC shows irregular and poorly demarcated margins, without a peripheric halo. Most commonly, HCC has a hypoechoic pattern, but it may also be hyperechoic. A minority of lesions have an isoechoic pattern, frequently with a peripheral hypoechoic halo. Small HCC usually have a homogeneous appearance, whereas large HCC often show a heterogeneous echostructure due to internal mosaic architecture, characterized by components of different echogenicity separated by thin septa. Spontaneous massive necrosis may be present in large HCC lesions and is shown as an internal hypoanechoic area. The infiltrative type HCC is depicted as an uneven area with ill-defined margins. In the diffuse form, a large part of the parenchyma is replaced by tumoural tissue. At US, the rare diffuse type appears as multiple small hypoechoic nodules scattered throughout the liver (4).

At colour Doppler and power Doppler studies, HCC usually shows intratumoral vascular signals, due to its hypervascularity. The two characteristic findings of HCC are the 'basket pattern', which is a fine blood-flow network surrounding the tumour, and the 'vessel within the tumour', which is the presence of vessels flowing into the nodule and branching within it. These findings are almost always depicted in large HCC lesions, more rarely in small nodules. On Doppler, spectral analysis of intratumoral vessels an arterial waveform with high resistive indices is demonstrated (4).

At contrast-enhanced US HCC appears hyperenhancing in the arterial phase, hypoenhancing or isoenhancing in the portal phase and hypoenhancing in the delayed phase. Necrotic phenomena, when present, are appreciable as non-enhancing intratumoral areas.

US associated to Doppler studies are also very useful in evaluating thrombosis of the main portal veins. As patients with cirrhosis are at high risk of developing portal thrombosis, a differential diagnosis between neoplastic and non-neoplastic thrombosis is required. At conventional US portal thrombosis is depicted as echoic material within the portal veins, which obliterates partially or completely the vascular lumen. Malignant thrombosis appears as solid mass in a portal vessel often in contiguity with the main tumour; Doppler study may show the presence of arterial flow within the neoplastic thrombus (4), while US contrast, agents may demonstrate a clear enhancement in the arterial phase (Fig. 1).

FLHCC appears as a large solitary mass, with clear margins and iso- or hyperechoic pattern. A central hyperechoic scar with microcalcifications may be detected (4).

Computed Tomography

The majority of HCC lesions are hypervascular tumours. Therefore, the best vascular phase to depict HCC is the arterial phase. The use of a spiral scanner is mandatory to perform a complete covering of the hepatic parenchyma during the arterial phase. The standardized computed tomography (CT) protocol for the study of patients with known or suspected HCC consists in unenhanced acquisition followed by dual-phase contrast-enhanced examination, in which an arterial phase and a portal-venous phase are obtained. Delayed phase images may also be useful, particularly to evaluate the presence of a capsule (2).

On unenhanced scans, HCC usually appears isodense or slightly hypodense; in the case of severe fatty metamorphosis, CT shows areas of negative attenuation values. When

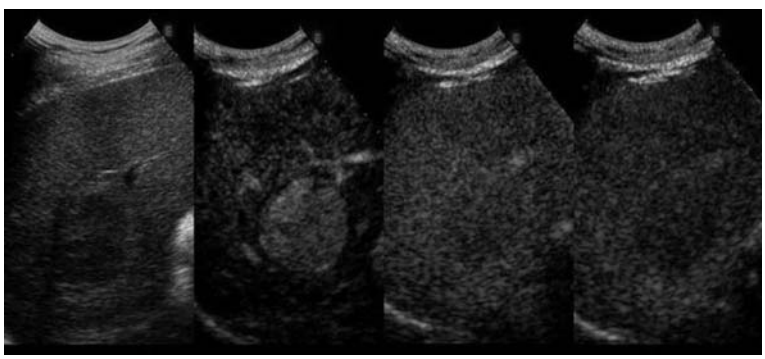

Hepatocellular Carcinoma. Figure 1 US. A hypoechoic nodule in a cirrhotic liver is appreciable at US examination. Contrast-enhanced US shows strong enhancement in the arterial phase and wash out in the following phases. This pattern is typical of HCC.

the degree of fat deposition differs among internal portions of the tumour, the characteristic mosaic architecture is visualized. Spontaneous necrosis is shown as a clear isodense area within the tumour. Deposition of haemosiderin may occur in regenerative and dysplastic nodules, resulting in increased attenuation on precontrast scans.

Classical nodular type HCC appears as a sharply demarcated lesion which may or may not be encapsulated. The capsule is more often seen in larger tumours and is depicted as a peripheral rim that is hypodense on unenhanced and arterial-phase images and hyperdense on delayed phase.

The infiltrative type HCC is characterized by an irregular and indistinct tumour-non-tumour boundary and is demonstrated as an uneven area with unclear margins.

In the diffuse form there is a massive involvement of a large part of the hepatic parenchyma. This type is characterized by numerous small hypodense nodules diffusely distributed in the liver (2).

The large majority of overt HCC lesions are fed from the hepatic artery. These lesions show homogeneous or inhomogeneous contrast-enhancement during the arterial phase, thus appearing markedly hyperdense. Therefore, even small nodules can be depicted. Early-stage HCCs with immature vasculature fail to enhance and cannot be distinguished on the arterial phase.

Almost no overt HCC tumours are fed by the portal vein, so the lesions show wash out in the portal-venous phase and appear as hypodense defects. Early-stage HCCs maintain a portal blood supply, so they appear slightly hypodense or even isodense in the portal-venous phase, being hardly detectable (Fig. 2) (2).

CT is an ideal technique for the staging of HCC, because it allows a reliable assessment of number, size, location and features of the nodules, tumoural vascular invasion, extrahepatic metastases. Satellite lesions are hypervascular like the main tumour and appear as tiny foci of enhancement in the arterial phase. Tumour thrombi in the main portal branches appear as solid masses within the vessel with a marked hypervascularity in the arterial phase (2).

FLHCC usually appears as a solitary, large mass, with well-defined and lobulated margins (2).

Magnetic Resonance

HCC demonstrates variable signal intensities on magnetic resonance (MR) images.

On unenhanced T1-weighted scans nodular HCC is usually seen as a well-defined mass showing a moderate hypointensity. Patterns of isointensity are often observed in well-differentiated HCC. Hyperintensity on T1-weighted images may be due to fatty metamorphosis, haemorrhagic necrosis, glycogen or copper deposition. Fat and glycogen are more common in well-differentiated HCC. On unenhanced T2-weighted scans nodular HCC usually shows moderate hyperintensity. The high intensity on T2-weighted images correlates with the degree of malignancy: well-differentiated lesions may appear isointense, while regenerative nodules are never hyperintense; dysplastic nodules and early HCCs show similar MR features, although the latter may be hyperintense, while dysplastic nodules are almost never hyperintense on T2-weighted images (3). Using T2-weighted scans HCC nodules are depicted more evidently than with T1-weighted scans, due to the higher contrast between the tumour and the surrounding parenchyma (1). HCC may arise within a high-grade dysplastic nodule. These lesions have a nodule-within-a-nodule appearance on MR images, consisting of one or more hyperintense internal foci within a low signal intensity nodule on T2-weighted images (3). The tumour capsule is more likely to be seen on T1-weighted images, detected as a thin hypointense rim. T2-weighted images delineate a single hypointense rim or a double ring with inner hypointensity, corresponding to the fibrous capsule, and outer hyperintensity, corresponding to the pseudocapsule. The typical mosaic pattern of large HCC lesions is well demonstrated on MR: intratumoral hypointense septa are detected on T1-weighted scans, while inhomogeneity is seen on T2-weighted scans (1).

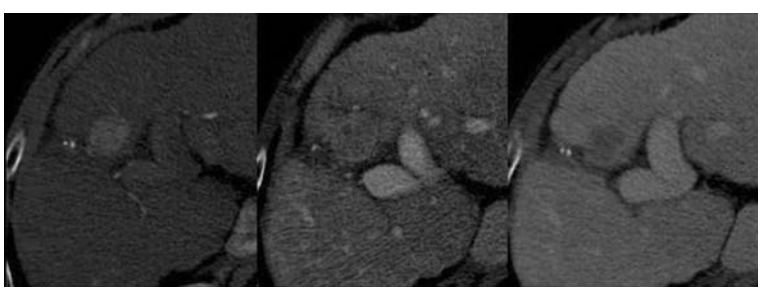

Hepatocellular Carcinoma. Figure 2 CT. Classical nodular HCC has a clear enhancement in arterial phase and wash out in the portal-venous and delayed phases. The capsule is optimally depicted on delayed phase as a peripheral hyperdense rim.

Dynamic study after bolus administration of gadolinium-chelates using fast T1-weighted sequences can demonstrate the typical arterial supply of overt HCC. The enhancement in the early arterial phase may show different patterns: peripheral, central, mixed, complete or absent. More often, the arterial enhancement appears inhomogeneous. A nodule-within-nodule pattern can be observed. A minority of HCC nodules, usually well differentiated, do not show any arterial enhancement. Tumour enhancement decreases in the middle phase leading to isointensity. The pseudocapsule shows delayed enhancement. This is due to the large extracellular spaces of the capsular region, which include vascular lakes within the compressed liver parenchyma (Fig. 3) (1).

Hepatobiliary contrast agents pass from blood through the hepatobiliary system with partial excretion through the kidneys and bile ducts. Many of them can be used both as vascular contrast agents in dynamic studies and as hepato-specific agents in delayed T1-weighted scans. In the hepatobiliary phase, the normally functioning parenchyma shows a clear enhancement. Lesions that do not have hepatobiliary function, such as non-hepatocellular lesions or undifferentiated hepatocellular lesions, fail to enhance, appearing as clearly contrasted defects. The conspicuity and the detection rate of lesions are increased. The degree of tumour enhancement of HCC correlates with its histologic differentiation and preservation of hepatobiliary function. Therefore, HCC may become hyperintense, hypointense or isointense, depending on the amount of uptake relative to the surrounding parenchyma, which correlates with its differentiation. Cirrhotic livers show a decreased uptake of hepatobiliary agents in comparison with normal livers, due to a decreased hepato-biliary function (1).

RES-targeted agents consist of suspensions of iron particles, which are removed directly from the blood by the reticuloendothelial cells of the liver and spleen. The presence of iron particles, captured in the Kupffer cells of the normal liver, produces a significant signal loss on T2-weighted images during the hepato-specific phase. Focal lesions usually do not contain Kupffer cells, thus-appearing hyperintense in the hepato-specific phase. Lesion demarcation and visualization are improved and the detection rate is increased. HCC usually cannot adsorb these agents because Kupffer cells are lacking, but this is variable and depends on the grade of the tumours (1).

FLHCC appears as a solitary capsulated mass with well-defined lobulated margins. In general tumours are iso- or hypointense on T1-weighted scans and iso- or hyperintense on T2-weighted scans. Typically, the scar has low signal intensity both on T1 and T2-weighted images (1).

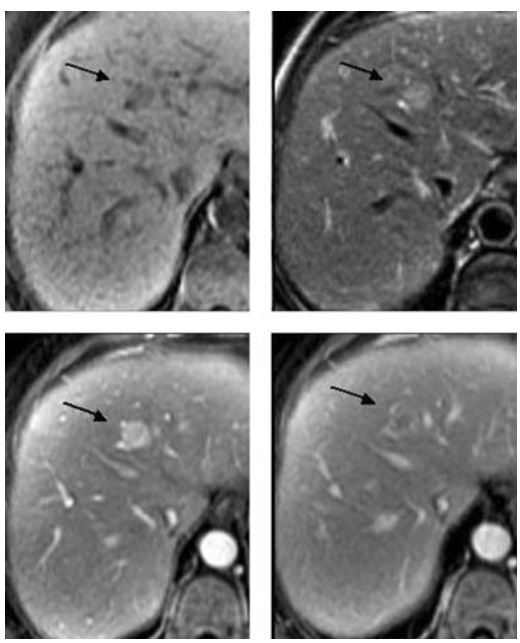

Hepatocellular Carcinoma. Figure 3 MR. Classical nodular HCC (*arrows*) appears moderately hypointense on unenhanced T1-weighted scans and moderately hyperintense on unenhanced T2-weighted scans.Dynamic study after bolus administration of gadolinium-chelates using fast T1-weighted sequences demonstrates the typical enhancement in the arterial phase with wash out in the following phases. The pseudocapsule shows delayed enhancement.

Diagnosis

The detection of a nodule at US in a cirrhotic patient should raise the suspicion of HCC. In case the nodule is less than 1 cm in size the recommended protocol is to repeat US every three months; lack of growth over a period of more than 1–2 years suggests the nodule is not a HCC. If the nodule size ranges from 1 to 2 cm, the finding should be investigated with two dynamic imaging techniques (CT, MR, contrast US); the coincident demonstration of the typical enhancement pattern (hypervascular nodule with washout in the portal-venous phase) at two modalities allows the diagnosis of HCC; otherwise, biopsy of the nodule is recommended. For nodules above 2 cm in size, imaging techniques are usually able to establish a confident diagnosis without needing confirmation with a positive biopsy. In cirrhotic livers, a nodule greater than 2 cm showing the typical features of HCC (hypervascular nodule with washout in the portal-venous phase) at one dynamic imaging technique (US, CT, or MR) and/or with a concomitant increase of alpha fetoprotein serum level above 200 ng/mL must be considered a HCC and should not be biopsied. The EASL conference recommended that

the diagnosis of HCC can be made in nodules greater then 2 cm in cirrhotic livers by demonstrating characteristic arterial vascularization on two dynamic imaging modalities (5, 6).

Interventional Radiology

Several interventional radiologic procedures, including percutaneous and intraarterial techniques, can be employed in treatment of HCC. Percutaneous treatments are considered a curative treatment for small HCC in patients who cannot undergo resection or in patients listed for transplantation. Percutaneous ethanol injection (PEI) is the most commonly used technique in nodules up to 3 cm in size, while radiofrequency (RF) ablation represents a valid alternative and its efficacy is clearly superior to that of PEI in larger lesions (7). Trans-arterial chemoembolization (TACE) is widely performed for palliative treatment of large/multifocal vascularized HCC. The best candidates are patients who have preserved liver function and without vascular invasion or extrahepatic disease.

Single large HCC tumours can be profitably treated with the combination of TACE and PEI. Treatment response is usually evaluated by dual-phase spiral CT or dynamic MR 1 month after the procedure. On CT, the necrotic lesion obtained after ablative treatments appears as a hypodense non-enhancing area. On MR, the ablated tissue shows slight hyperintensity on T1-weighted images and strong hypointensity on T2-images, while viable tumoural tissue maintains a clear hyperintensity on T2-weighted scans. Both on dual-phase spiral CT and dynamic MR, residual viable neoplastic tissue can be easily demonstrated as enhancing areas in the arterial phase within or at the periphery of the treated nodule. On CT, lesions treated with TACE appear as highly hyperdense areas, due to the retention of lipiodol; this may not allow a confident interpretation of contrast-enhanced images. On the contrary, MR signal intensity is minimally influenced by the presence of iodized oil, so areas of enhancing tissue can be easily recognised. Contrast-enhanced ultrasonography might become a real-time alternative to assess therapeutic response (7).

Bibliography

1. Lencioni R, Bartolozzi C (2003) Primary malignant tumors. In: Vogl, Lencioni, Hammerstingl, Bartolozzi Eds Magnetic Resonance Imaging in Liver Disease. Thieme, 163–197
2. Bartolozzi C, Donati F, Cioni D et al (1999) Computed tomography of hepatocellular carcinoma In: Bartolozzi, Lencioni Eds. Liver Malignancies. Springer-Verlag pp 71–94.
3. Hussain SM, Zondervan PE, IJzermans JNM et al (2002) Benign versus malignant hepatic nodules: MR imaging findings with pathologic correlation. Radiographics 22:1023–1036
4. Lencioni R, Menu Y (1999) Ultrasound and Doppler ultrasound of hepatocellular carcinoma. Liver Malignancies. Springer
5. Bruix J, Sherman M, Llovet JM et al (2001) EASL panel of experts on HCC. Clinical management of hepatocellular carcinoma. Conclusions of the Barcelona-2000 EASL conference. European Association for the study of the liver. J Hepatol September 35 (3):421–430
6. Bruix J, Sherman M (2005) AASLD practice guideline: management of hepatocellular carcinoma. Hepatology November 42 (5):1208–1236
7. Lencioni R, Cioni D, Crocetti L et al (2005) Early-stage hepatocellular carcinoma in patients with cirrhosis: long-term results of percutaneous image-guided radiofrequency ablation. Radiology March 234(3):961–967. Epub 2005 Jan 21

Hepatocystic Duct

Accessory duct draining the liver parenchyma into the gallbladder.

▶Congenital Malformations, Liver and Biliary Tract

Hepatomegaly

Abnormal increase of the liver size. When the growing involves the left lobe, it could cause displacement of the right anterior wall of the gastric body.

▶Compression, Extrinsic, Stomach and Duodenum

Hereditary or Genetic Hemochromatosis

▶Hemochromatosis, Skeletal

Hereditary Spherocytosis

Hereditary spherocytosis is the most common disorder of the red blood cell membrane, the bag that contains the hemoglobin molecules that carry oxygen through the bloodstream. Most cases of spherocytosis are hereditary, with autosomal dominant inheritance. The abnormal cells pass with greater difficulty through the spleen and are consequently destroyed abnormally quickly.

▶Splenomegaly

Hernia nuclei Pulposi

▶Hernia, Disk, Intervertebral

Hernia, Abdominal and Inguinal

Sat Somers
Department of Radiology, McMaster University,
1200, Main Street West
Hamilton, Ontario, Canada L8N 3Z5
somers@mcmaster.ca

Synonyms

Abdominal wall defects; Fascial weakness and defects

Definition

The protrusion of a viscus through an orifice or a defect in the wall of a cavity in which it is confined is defined as a hernia.

Pathology

Hernias may occur in several locations in the abdomen. They may contain bowel, omentum, bladder, and, on occasion, other abdominal organs such as liver and gall bladder. Generally, the herniation occurs through openings or potential spaces that already exist. However, weaknesses may occur in muscle tissue or fascia, encouraging the passage of a viscus. Muscle weakness may occur with wasting or previous surgery. Occasionally, hernias may be secondary to trauma. As the development of each of the abdominal hernias may be unique to its location, they are discussed under the respective subheading. The two most common sites of herniation in the abdomen are the diaphragm and inguinal areas.

Clinical Presentation

The clinical presentation depends on the location and type of hernia. Complications of a hernia, such as obstruction, may be the first clinical presentation in a significant number.

Hiatal Hernia

The oesophageal hiatal hernia is the most common. In this hernia, a portion of the stomach herniates through the oesophageal hiatus. Though often considered synonymous with reflux, there is really very poor correlation between a hiatal hernia and reflux oesophagitis. The function of the lower oesophageal sphincter and the presence of reflux are the factors that produce symptoms and cause complications. There are two types of hiatus hernia. The sliding hiatus hernia is the more common type. In this hernia, the gastro-oesophageal junction is displaced more than 1 cm above the diaphragmatic hiatus. Small hiatal hernias often reduce in the upright position. The para-oesophageal hiatus hernia is the less common type. It represents about 1% of the total diaphragmatic hernias. Here the gastro-oesophageal junction remains in the normal location but a portion of the stomach, usually the fundus, herniates above the diaphragm. If the hernia is large, the herniated stomach can volvulate and become strangulated. These patients will experience severe pain. If there is no strangulation present, which is most often, the patient may complain of intermittent symptoms of proximal obstruction (vomiting), or early satiety. The hernia may include stomach or omentum. When there is gross ascites present, the hernia may include fluid.

Bochdalek Hernia

If the embryonic pleuroperitoneal canal persists, a defect is present in the diaphragm, and herniation can occur through this opening. This defect is the foramen of Bochdalek. The secondary effects of a Bochdalek hernia depend on its size. The larger hernias are often seen in the neonatal period and can contain omentum, spleen, kidney, and retroperitoneal fat. It is usually seen as a posterior lateral mass above the left hemidiaphragm. When present in the neonatal period, the infant may have an ipsilateral hypoplastic lung and respiratory distress. These hernias are more often seen on the left. This is presumably because of the protective effect of the liver on the right, though herniation can also occur through the pleuroperitoneal canal on the right. Bochdalek hernias when seen in the adult are usually small.

Morgagni Hernia

This is the least common type of diaphragmatic hernia. It is due to a defect in the para-sternal portion of the diaphragm and is invariably right-sided. It may contain omentum, transverse colon, or liver. It is usually seen as a right-sided asymptomatic cardiophrenic angle mass. Most often, it is asymptomatic but like most hernias it can obstruct.

Traumatic Hernia

Rupture of the hemidiaphragm allows herniation of abdominal contents through the tear. The tear that is usually in the central or posterior aspect of the diaphragm may follow penetrating injury or blunt thoracoabdominal trauma. Again, the left side is affected in over 90% of cases as the liver dissipates the traumatic forces and protects the right hemidiaphragm. Traumatic hernia is suspected when gas-filled loops of bowel or stomach are seen in left lower thorax following severe trauma. The left lobe of the liver may herniate, in addition to the stomach, small bowel, colon, kidney and spleen. The contour of the left hemidiaphragm may also be indistinct or elevated on radiographs.

Inguinal Hernia

In inguinal hernias, bowel, omentum or bladder may herniate into the inguinal canal. This may present as a scrotal or labial mass. In the majority, the hernia contains bowel. The hernia may reduce spontaneously or can often be reduced manually. When it cannot be reduced, it is said to be incarcerated. Incarcerated hernias can strangulate (Fig. 1). Inguinal hernias are often asymptomatic but may cause obstruction (1). The hernias may be classified as direct or indirect (2). The inferior epigastric artery gives off the cremasteric artery at the deep inguinal ring. The hernia passing lateral to the artery (that is through the deep ring) is an indirect hernia and that passing medial to the artery is a direct hernia.

Umbilical Hernias

In infants, they result from an abdominal wall defect at the umbilicus. Umbilical hernias may be seen in up to 20% of newborns. They are more evident with prematurity and in situations associated with raised intra-abdominal pressure. Almost all hernias have a fascial defect of 5 mm or less closer by the first year of life. Larger hernias close over a longer period of time. In adults, they may occur through the umbilical cicatrix or through the linea alba either just above or below the umbilicus. Ten percent of adults with umbilical hernias have a history of childhood umbilical hernia. Other associated causes are ascites associated with congestive heart failure, nephrosis or cirrhosis. They may also occur with multiparity, obesity, intra-abdominal malignant tumours, and advanced age. Most of the patients with umbilical hernias are women in a ratio of 3:1 women to men. The aetiology of a weak umbilical cicatrix is not clear. It may be related to an abnormality of decussation of the aponeurotic fibres in the midline. The hernial contents in adults and infants are similar. They may contain omentum or small bowel. In adults, the hernia may also contain metastatic deposits or be the site of collateral pathways in portal hypertension.

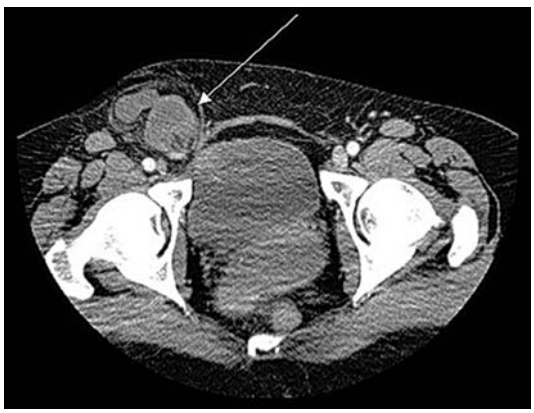

Hernia, Abdominal and Inguinal. Figure 1 Inguinal hernia causing obstruction. Dilated bowel within hernia shown by arrow.

Exomphalos (Omphalocele) and Gastroschisis

These two herniations are often confused. An omphalocele is a congenital defect of the abdominal wall in which there is herniation of abdominal viscera into the base of the umbilical cord. The viscera is covered by a translucent avascular membrane made up mostly of peritoneum on the inside and amniotic membrane on the outside. The umbilical cord inserts into the sac with the vessels running radially within its wall. The sac may contain a single loop of bowel, or the entire liver and numerous other viscera. They are differentiated from umbilical hernias by the size of the fascial defect. In umbilical hernias, the defect is always small and is usually less than 4 cm in diameter. The abdominal musculature is usually well developed. The omphalocele likely represents persistence of a portion of the extra-embryonic coelom and failure of the intestine to return into the abdominal cavity.

In gastroschisis, the defect in the abdominal wall is in the extra-umbilical location and there is therefore an absence of a membraneous sac. There are other differences as well. This includes (a) the herniated intestine is covered by a thick gelatinous material and is foreshortened, (b) the umbilicus is situated to the left of the herniated bowel and separated from the fascial defect by a bridge of skin, (c) the abdominal cavity is well developed in contrast to an omphalocele and the midgut is invariably malrotated with the caecum being located on the left side of the abdomen and (d) other congenital abnormalities are evident.

Obturator Hernias

These hernias pass through the obturator foramen in the pelvic bone. They have been found to be the cause of between 0.4% and 0.8% of mechanical obstruction. There is a preponderance in females with the ratio being 5 or 6 to 1. Therefore, males are affected in only 15% of these hernias. The greater incidence in women is related to the anatomic differences in the obturator foramen. In women, the foramen is smaller and more triangular yet its transverse diameter is greater. Pregnancy has also been incriminated. Most of these hernias occur in the seventh to eighth decades of life. In addition to aging, the other predisposing factors are chronic lung disease, associated with wasting and emaciation. The protective layer of fat around the obturator foramen is lost in these patients, predisposing to herniation. Bilateral obturator hernias are rare. It tends to be more common on the left in men and on the right in women. The hernia usually contains small intestine, in most instances, the ileum. Rarely a Richter-type hernia occurs. Occasionally the sac is empty. It may also contain omentum, appendix and fallopian tubes.

The obturator canal is a fibro-osseous structure about 2 to 3 cm in length. It passes downward and obliquely ends in the obturator region of the thigh. It readily admits the tip of a finger but its walls are firm and unyielding. Therefore, strangulation occurs easily.

Perineal Hernias

Perineal hernias are protrusions of abdominal contents through the fascia and muscles that form the pelvic floor. Perineal hernias can affect any part of the pelvic floor. There is a weakness between the iliococcygeus and pubococcygeus muscles and many hernias pass through this gap. Perineal hernias can be subdivided into anterior and posterior, based on their relationship of the transverse perineal muscle. Anterior perineal hernias may be evident in the labia majora where they are known as labial or pudendal hernias. Anterior perineal hernias almost never occur in men. Posterior perineal hernias occur in both men and women but with far greater frequency in women.

Spigelian Hernias

These are rare and seen in males and females equally. Persons of any age may be affected. Predisposing conditions include obesity, increased abdominal pressure brought on by episodes of coughing or sudden lifting of a heavy weight. Aging is also a predisposing factor as most spigelian hernias occur in elderly individuals. These hernias are protrusions through the linea semilunaris (3), a line that marks the outer border of the rectus muscle and extends from the tip of the ninth costal cartilage to the pubic tubercle. This line has also been described as the point of division of the internal oblique into anterior and posterior layers to enclose the rectus muscle. A spigelian hernia has also been defined as a spontaneous abdominal defect situated lateral to the rectus muscle, with the protrusion passing through the spigelian fascia, which is limited laterally by the muscular fibres of the internal oblique and medially by the insertion of external oblique aponeurosis to form the anterior rectus sheath. Most of these hernias are small in size but be up to 14 cm in diameter. They may contain omentum or bowel. The neck is often narrow and the hernial ring rigid, therefore, incarceration and strangulation (Fig. 2) are the very present dangers.

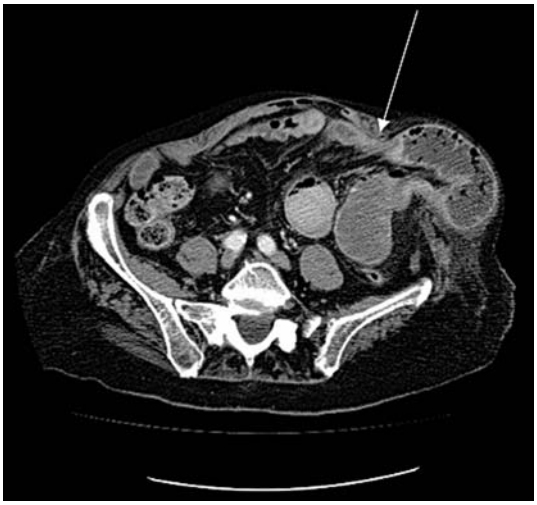

Hernia, Abdominal and Inguinal. Figure 2 CT of Spigelian hernia with obstruction. The distal limb is collapsed (arrow).

Lumbar hernias

They are defects of the parietal abdominal wall that can occur anywhere in the lumbar region. The area is bounded above by the 12th rib, below by the iliac crest, behind by the erector spinae muscle and vertebral column and anteriorly by a line from the 12th rib straight downward to the iliac crest. They are also known as Petit hernias.

Incisional Hernias

This hernia develops in the scar of a surgical incision. The defect in the fascia varies in size, but may be as large as 12 to 15 cm. The hernia itself may be extremely large despite of a small fascial defect. Incisional hernias usually contain omentum and small bowel. Rarely, the hernia may contain other viscera. The only covering is skin and

subcutaneous tissue. They occur in 1% to 14% of patients who have had transparietal abdominal operations. Incisional hernias do not usually cause serious problems.

Imaging

Imaging of hernias includes plain films, barium studies, ultrasound, CT and MRI. The imaging modality used depends on the location of the hernia.

Diagnosis

Hiatal hernia on chest radiographs, are seen as an air fluid level, or a mass, in the immediate supra-diaphragmatic retrocardiac area. The hernia can be confirmed with a barium swallow or CT. On CT, there is a usual widening of the oesophageal hiatus in the diaphragm and the hernia is seen above it (Fig. 3). The upper limit of a normal hiatal opening is 1.5 cm and when a hernia is present, it is often widened to 3–4 cm. This is easily measured on a CT scan.

A Morgagni hernia may be distinguished from partial eventration by demonstrating the diaphragmatic defect on coronal magnetic resonance imaging (MRI) or CT.

Inguinal hernias can be difficult to diagnose in obese patients on clinical examination. They are easily seen with multidetector CT (MDCT), especially if it is the cause of an obstruction.

Traumatic hernias may be diagnosed by an upper or lower barium study of the bowel but MDCT with coronal and sagittal reconstruction, or, sometimes ultrasound, is often more useful. Diagnosis of a traumatic hernia may be delayed because these patients often have associated thoracic and abdominal injuries that may obscure the clinical and radiographic findings. The diagnosis is therefore often made later with symptoms caused by intestinal obstruction and strangulation, or compression of the left lung. These symptoms include pain, vomiting, fever, dyspnea and cough.

All the others are best seen on MDCT, but MRI is also useful in the diagnosis of obturator, perineal, incisional, sciatic hernias. Ultrasound may also diagnose 'lumps' that turn out to be hernias.

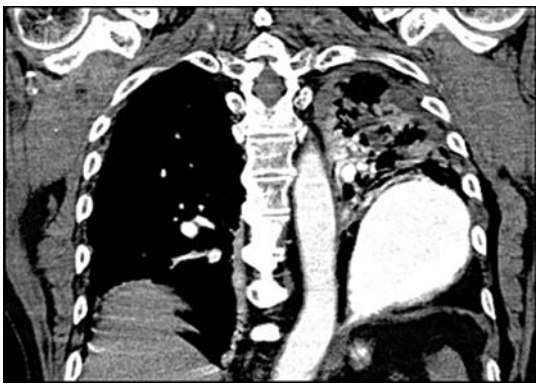

Hernia, Abdominal and Inguinal. Figure 3 Coronal reconstruction showing hiatal hernia with stomach above left hemidiaphragm. There is partial collapse/consolidation of the left lung.

Bibliography

1. Perrott Charles A (2004) Inguinal hernias: room for a better understanding. Am J Emergency Med 22(1):48–50
2. Cervantes, J (2004) Editorial update. Inguinal hernia in the new Millennium. World J Surg 28:342–347
3. Koksal N, Altinli E, Celik A et al (2004) Extraperitoneal laparoscopic approach to spigelian hernia combined with groin hernias. Surg Laparasc Endosc Percutan Tech 14(4):204–206

Hernia, Diaphragm, Congenital

Melanie Hiorns
Radiology Department, Great Ormond Street Hospital for Children, London, UK
HiornM@gosh.nhs.uk

Synonyms

Bochdalek hernia; Congenital diaphragmatic hernia (CDH); Hiatus hernia; Morgagni hernia; Para-oesophageal hernia; Sliding hernia; Traumatic hernia

Definition

A ►hiatus hernia is the herniation of part of the stomach through the diaphragmatic hiatus into the chest. If the part of the stomach that has herniated lies alongside the lower oesophagus but the main body of the stomach remains below the diaphragm, and therefore the gastro-oesophageal junction also remains below the diaphragm, it is termed a para-oesophageal hernia. This type of hernia is uncommon in children unless they have had surgery such as a Nissen's fundoplication. If the cardia of the stomach has moved cranially though the diaphragm such that the diaphragmatic hiatus forms a waist around the upper part of the stomach and the GOJ is within the chest this is termed a sliding hiatus hernia. The sliding type is more common in children, particularly in infants.

Other defects in the diaphragm result in either a Bochdalek or a ►Morgagni hernia, and these are not related to herniation of the oesophagus. These may be large defects of the diaphragm that allow herniation of bowel and/or abdominal organs into the chest. These are termed ►congenital diaphragmatic hernias (CDH) as opposed to a 'hiatus' hernia. A Morgagni hernia is secondary to an anteromedial parasternal defect of the diaphragm. The Morgagni hernia lies anterior and in a central location, with herniated structures more commonly seen on the right, it usually presents in older children and is usually small. The herniated structures may include liver, omental fat, or part of the transverse colon. A ►Bochdalek hernia is a posterolateral defect of the diaphragm and results in a posteriorly located herniation. It is left sided, more commonly seen in newborns and infants, and is usually large. It accounts for 90% of congenital diaphragmatic hernias and may contain part of the bowel, spleen, left lobe of liver, kidney or part of the pancreas. Herniation can also occur following trauma.

Pathology/Histopathology

In infants a hiatal hernia is thought to occur secondary to immaturity of the lower oesophageal sphincter (LES) and reflux may also occur as a result of this. In older children it is due to the LES sliding through the diaphragmatic hiatus as a result of incompetence of the phrenicoesophageal membrane. Morgagni and Bochdalek hernias are secondary to maldevelopments of the diaphragm. These congenital diaphragmatic hernias may allow herniation of abdominal structures such as bowel and solid organs of the upper abdomen into the chest can result in hypoplasia of the lung on the affected side. This hypoplasia is characterised by a reduction in cross-sectional area of the pulmonary vasculature. The lungs have a reduced alveolar capillary membrane for gas exchange, which may be further decreased by surfactant dysfunction. In addition to parenchymal disease, there may be increased muscularisation of the intra-acinar pulmonary arteries.

Traumatic hernias through the diaphragm are usually following blunt trauma to the abdomen with an associated sudden rise in intra-abdominal pressure causing abdominal contents to push up into the chest, usually secondary to a rupture of the diaphragm rather than passing through an existing hiatus.

Clinical Presentation

The child with a hiatal hernia may present with reflux and intermittent vomiting, with repeated chest infections (1) or with epigastric pain. However, vomiting and reflux are very common in infancy and the incidence of hiatus hernia is low, typically only 0.5% of children undergoing UGI (2, 3) so the imaging of the vomiting but otherwise healthy infant may not be justified. Sometimes a hernia may be an incidental finding on an upper GI series performed for another reason. Hiatal hernias are more common in children who have undergone a Nissen's fundoplication, in which case they may be either para-oesophageal or of the rolling type.

Children with significant congenital diaphragmatic hernias usually present with cyanosis and respiratory distress in the first minutes or hours of life, although a later presentation is possible in the first few months of life. Only rarely do patients present outside infancy. Congenital diaphragmatic hernias may also be detected in utero, either on a routine antenatal ultrasound or if the mother presents with poly-hydramnios.

Traumatic hernias may present acutely at the time of injury but may present months or years later. They may be detected incidentally with bowel, liver or spleen being shown on an incidental chest X-ray; or may present with discomfort or obstruction from compromised bowel or solid organs in the chest. If a large volume of the chest is filled with abdominal contents the patient will present with dyspnoea.

Imaging

Sometimes indirect signs of particularly large hiatal hernias that contain air may be detected on chest radiographs as a radiolucent viscus seen behind the cardiac silhouette. The definite and detailed imaging diagnosis of a hiatus hernia is achieved by an upper gastrointestinal series and barium is used. In a sliding hiatus hernia gastric folds will be seen extending up through the diaphragmatic hiatus (Fig. 1a); in a rolling hernia, part of the cardia will be demonstrated as an outpouching parallel to the lower oesophagus but in continuity with the remainder of the stomach that is below the diaphragm.

Imaging for congenital diaphragmatic hernias may be initiated in the antenatal period on the basis of an antenatal ultrasound which may demonstrate bowel loops peristalsing in the chest. Other antenatal sonographic findings include poly-hydramnios, an absent or intra-thoracic stomach bubble, and mediastinal and cardiac shift away from the side of the herniation. Ultrasound will also show which organs may have herniated into the chest. This antenatal work-up allows plans to be made expectantly for the management of the child at the time of delivery. Both 3D ultrasound and MRI may also be used in the antenatal period to give an estimation of lung

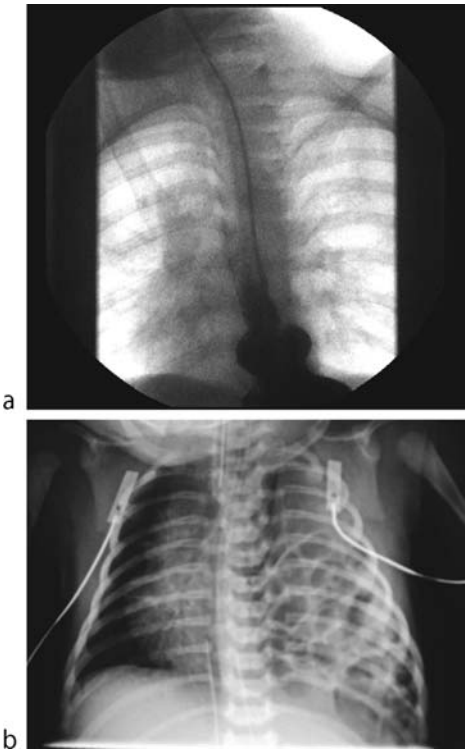

Hernia, Diaphragm, Congenital. Figure 1 (a) An upper GI series in a child with persistent vomiting show a small hiatus hernia above the diaphragm and associated reflux. (b) Chest radiograph of a newborn infant with congenital diaphragmatic hernia showing gas filled loops of bowel in the left hemithorax and mediastinal shift to the right.

volume and are potential predictors of pulmonary hypoplasia and postnatal outcome.

A chest X-ray taken shortly after birth will classically show cyst-like structures in the left hemithorax representing the herniated bowel in the chest (Fig. 1b). If the chest X-ray is taken very early after birth the loops of bowel may still be exclusively fluid filled and will appear as a radiopaque mass. There will be a reduced number of bowel loops in the abdomen which will be relatively gasless; additionally the liver and/or spleen may be in the chest.

Subsequent imaging of CDH is by ultrasound and MRI or CT, which will demonstrate the extent of the hernia and what its contents are.

Traumatic hernias are usually imaged in the acute situation by CT, but ultrasound and MRI may also be used.

Nuclear Medicine

No role in this condition.

Diagnosis

Achieved by imaging as described above.

Interventional Radiological Treatment

No role in this condition.

Bibliography

1. Imamoglu M, Cay A, Kosucu P et al (2005) Congenital paraesophageal hiatal hernia: pitfalls in the diagnosis and treatment. J Pediatr Surg 40(7):1128–1133
2. Riggs Jr (1976) The incidence of hiatal hernia in infants and children. Results of a survey of members of the Society for Pediatric Radiology. Radiology 120(2):451
3. Simanovsky N, Buonomo C, Nurko S (2002) The infant with chronic vomiting: the value of the upper GI series. Pediatr Radiol 32(8): 549–550

H

Hernia, Disk, Intervertebral

Massimo Gallucci, Amalia Paonessa, Nicola Limbucci
Department of Neuroradiology, University of L'Aquila, Italy
massimo.gallucci@cc.univaq.it

Synonyms

Hernia nuclei pulposi; Lumbar or cervical disk hernia; Protruded or extruded intervertebral disk; Ruptured intervertebral disk

Definitions

Intervertebral ►disk herniation and other ►degenerative disk changes can be grouped under a broader category of degenerative spinal manifestations that also include pathologic changes affecting the vertebral body (spondylosis) as well as the articular processes and associated ligaments (spondylarthrosis); these are discussed in detail elsewhere. Disk herniation has been separated from these other spinal degenerative changes because of the specific diagnostic and therapeutic interests involving this condition. Degenerative disk changes affect the disk itself as well as the adjacent end plates and are due to trauma, normal aging, and chronic overload. The difference

between changes due to normal aging on the one hand and true pathologic changes on the other hand is confusing, and the separation is often arbitrary.

Pathology/Histopathology

Three main pathogenetic mechanisms are involved in degenerative disk disease:

1. Acute trauma leading to spinal instability with alterations in spinal alignment and anatomy, which may accelerate degenerative changes.
2. Chronic static and dynamic overload, causing chronic traumatisms. The integrity of the spinal curves is also involved in the process because loss of alignment decreases the load-absorbing function of these curves. L5 and S1 are maximally involved by overload. For this reason, lumbar disk herniation is located between the L4 and S1 levels in 90% of cases, at L3–L4 in 7%, and at L1–L3 in only 3% of cases.
3. Decreased permeability of the end plates, leading to loss of function of disk fibroblasts and chondrocytes, with subsequent alteration of the keratin/chondroitin sulfate ratio. Matrix degeneration determines the loss of water in the nucleus pulposus and the consequent rigidity.

Degenerative changes of the annulus fibrosus may result in two lesions: (i) breakdown of bridges among annular fibers, with annular weakness and diffuse or focal bulging, or (ii) radial tears of the annular fibers, producing herniation of the nucleus through the annulus. ►Fissures can progress to more severe disruption and consequent herniations. Herniated material may include nucleus, cartilage, fragmented bone, or annular tissue. Dehydration and progression of annular fissures can result in dramatic destruction of the disk, with collapse of the disk space and gas formation (1).

Natural history: Unequivocal and generally applied treatment protocols do not exist, but long-term follow-up results of surgically and nonsurgically treated patients indicate that after 5–10 years, the success rate is similar. After 1 year, a good clinical outcome is registered in up to 95% of untreated patients. Up to 63% of disk herniations may show a spontaneous volume reduction on magnetic resonance imaging follow-up 6–12 months after the diagnosis (2). The causes of spontaneous reduction of herniated disk material are shrinkage due to dehydration, fragmentation, and phagocytosis of the material.

Classification: The most accepted nomenclature for disk herniation was published in 2001 (3) (Fig. 1):

1. ►Bulging disk: A disk in which the contour of the outer annulus extends in the axial plane beyond the edges of the disk space, over greater than 50% of the circumference of the disk and usually less than 3 mm beyond the edges of the vertebral body.
2. Asymmetric bulge: a bulging more evident in one section of the periphery of the disk, but not so focal as to be characterized as a protrusion.
3. Disk herniation: Localized displacement of disk material beyond the normal margins of the intervertebral disk space.

Disk herniation may take the form of protrusion or extrusion:

1. ►Protruded disk: A herniated disk in which the greatest distance, in any plane, between the edges of the disk material beyond the disk space is less than the distance between the edges at the base in the same plane.
2. Contained disk herniation: Displaced disk tissue that is wholly within an outer perimeter of uninterrupted outer annulus or capsule.
3. ►Extruded disk herniation: A herniated disk in which any one distance between the edges of the disk material beyond the disk space is greater than the distance between the edges of the base in the same plane.
4. Migrated disk: A herniated disk in which a portion of extruded disk material is displaced away from the tear in the outer annulus through which it has extruded.
5. Sequester or free fragment: A fragment of disk that has separated from the disk of origin and has no continuous bridge of disk tissue to the disk of origin.

Relative to the axial plane the herniation may be (i) central, (ii) right-left central, (iii) right-left subarticular, (iv) right–left foraminal, and (v) right-left extraforaminal (Fig. 2).

Clinical Presentation

Disk herniation can present clinical symptoms by two mechanisms: diskogenic pain and compression of nervous structures. In the first condition, local pain is due to stimulation of receptors in the outer annulus fibrosus *via* the recurrent spinal nerve of Luschka.

The second condition is more complex and depends on the level and location of the herniation, its extension, and its relationship with neural structures. In the case of herniation located at the cervical or dorsal levels, compression of the spinal cord can occur, with abnormal reflexes and progressive disturbance of gait and micturition. More commonly, disk herniations can compress nerve roots, causing radicular pain that also depends on the release of inflammatory molecules causing chemical radiculitis. In late stages, sensory or motor deficits are also possible.

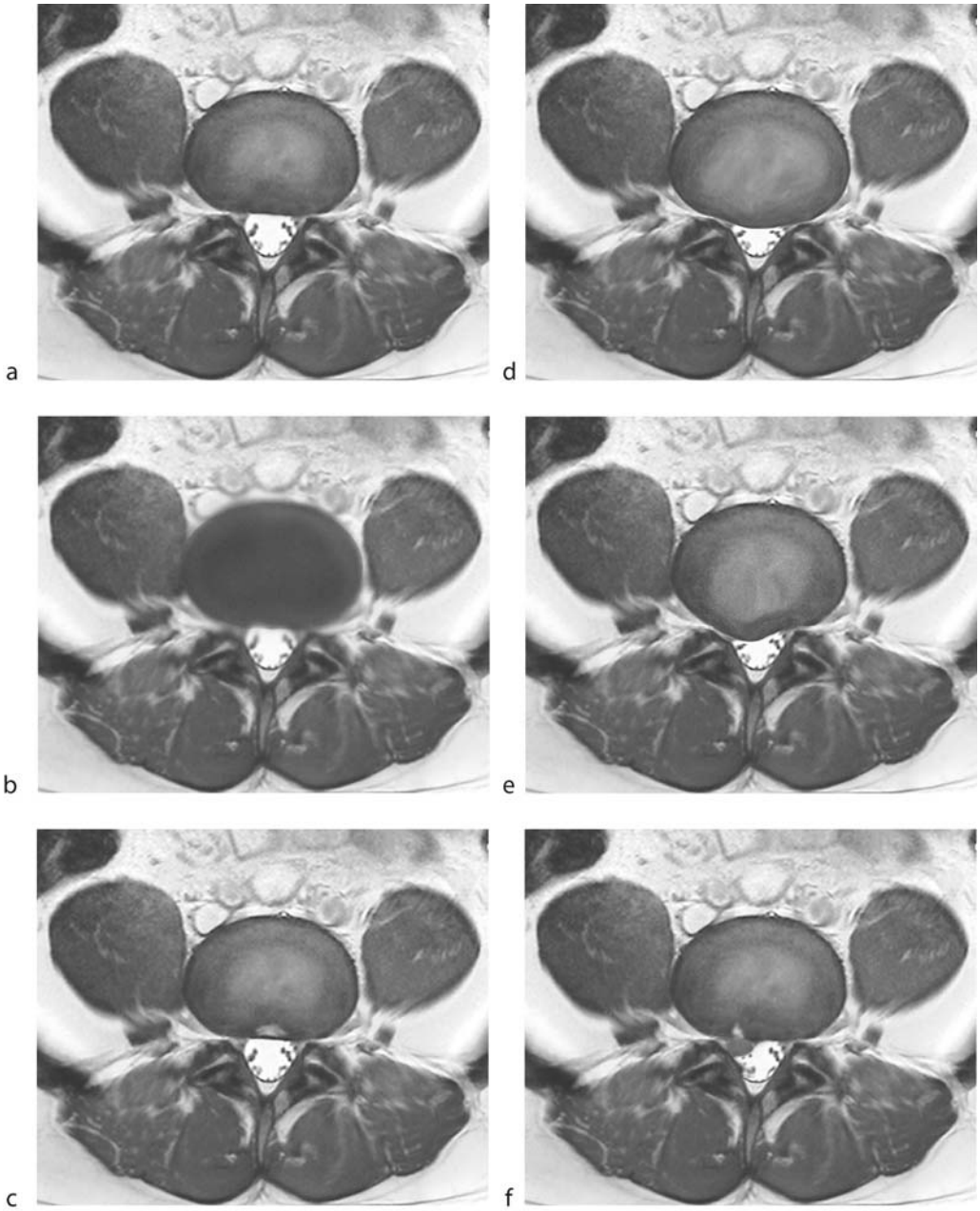

Hernia, Disk, Intervertebral. Figure 1 Axial morphology of normal and pathologic lumbar disk (fast spin-echo T2-weighted). (a) Normal disk with regular profile and hyperintense nucleus pulposus. (b) Dehydrated disk with hypointense nucleus. (c) Annular fissure. (d) Bulging disk. (e) Right-central protrusion. (f) Right-central ▶free fragment with associated annular fissure. For disk extrusion, see Fig. 2. Note: Simulation with Adobe Photoshop 6.

Imaging

Conventional radiographs of the spine are useful to diagnose degenerative disk disease and exclude other causes of pain. In acute disk herniation, plain films can be normal, especially in young patients. When disk herniation is associated with degenerative changes, the most evident sign is reduction of the intervertebral space due to loss of disk height. Sclerosis of the end plates is common. Radiography is limited by the inability to directly visualize the disk and the herniation. This is possible with diskography, which is invasive and is now used only in selected cases to confirm the diskogenic origin of pain.

X-ray myelography shows deformations of the dural sac and root sleeves caused by disk herniations and other lesions. The examination is accurate for demonstrating

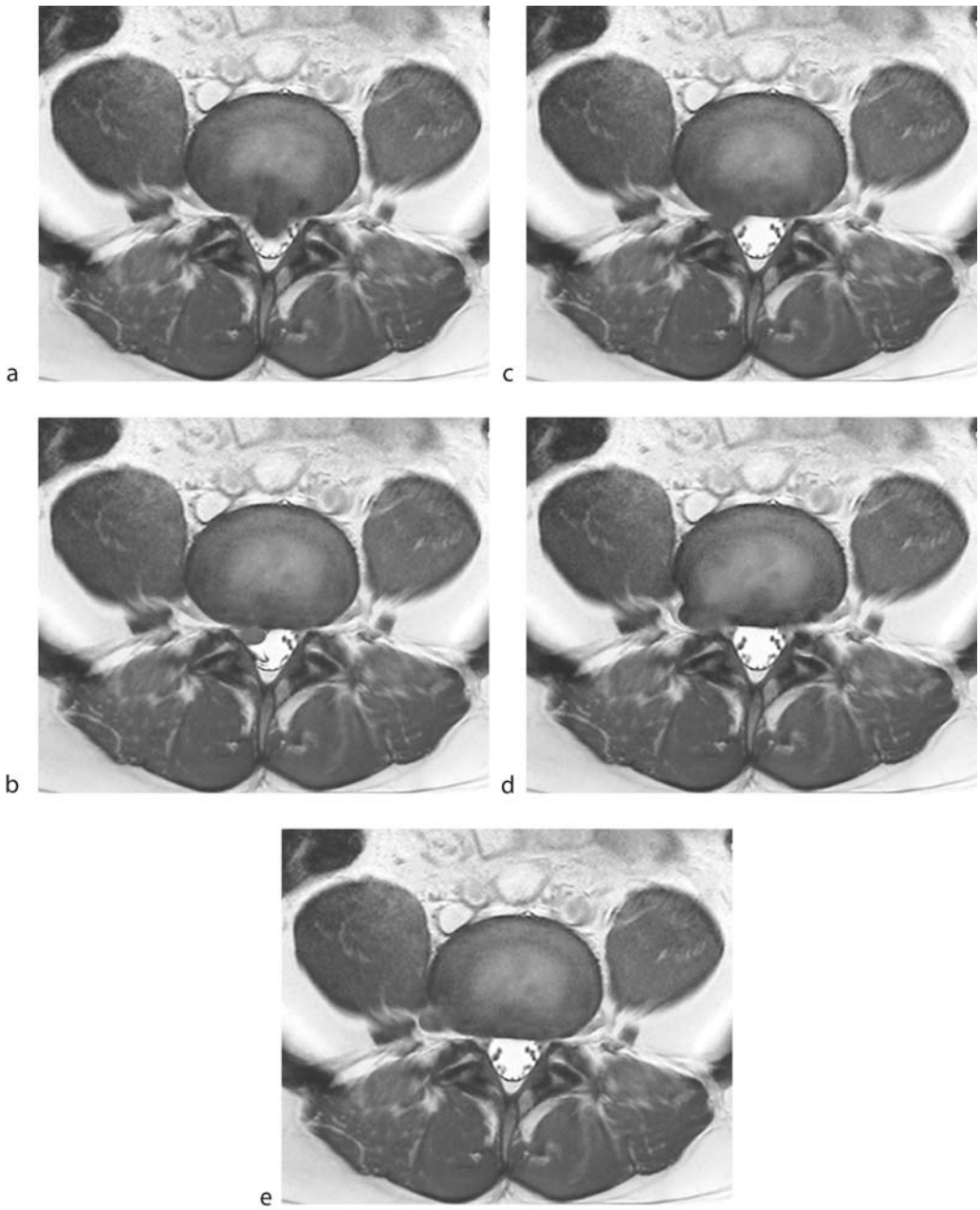

Hernia, Disk, Intervertebral. Figure 2 (continued)

root compression, but it is invasive and rarely used at present.

Computed tomography (CT) allows the differential diagnosis between bulging and herniation, evaluation of dimensions and location of the herniated disk, and detection of free fragments. The disk is hypodense, and the nucleus pulposus cannot be exactly identified. CT allows easy identification of calcified herniations and associated spondylotic changes and can determine stenoses of the foramina, the lateral recesses, and the vertebral canal. CT sensitivity can be improved by combining CT and myelography (myelo-CT).

Magnetic resonance imaging (MRI) is the technique used most often for evaluating disk herniation. The examination should comprise sagittal T1- and T2-weighted sequences and axial T1- and/or T2-weighted sequences. MRI myelographic images may help to clarify root compression, and intravenous gadolinium injection may be useful when postoperative scarring obscures recurrent disk herniation.

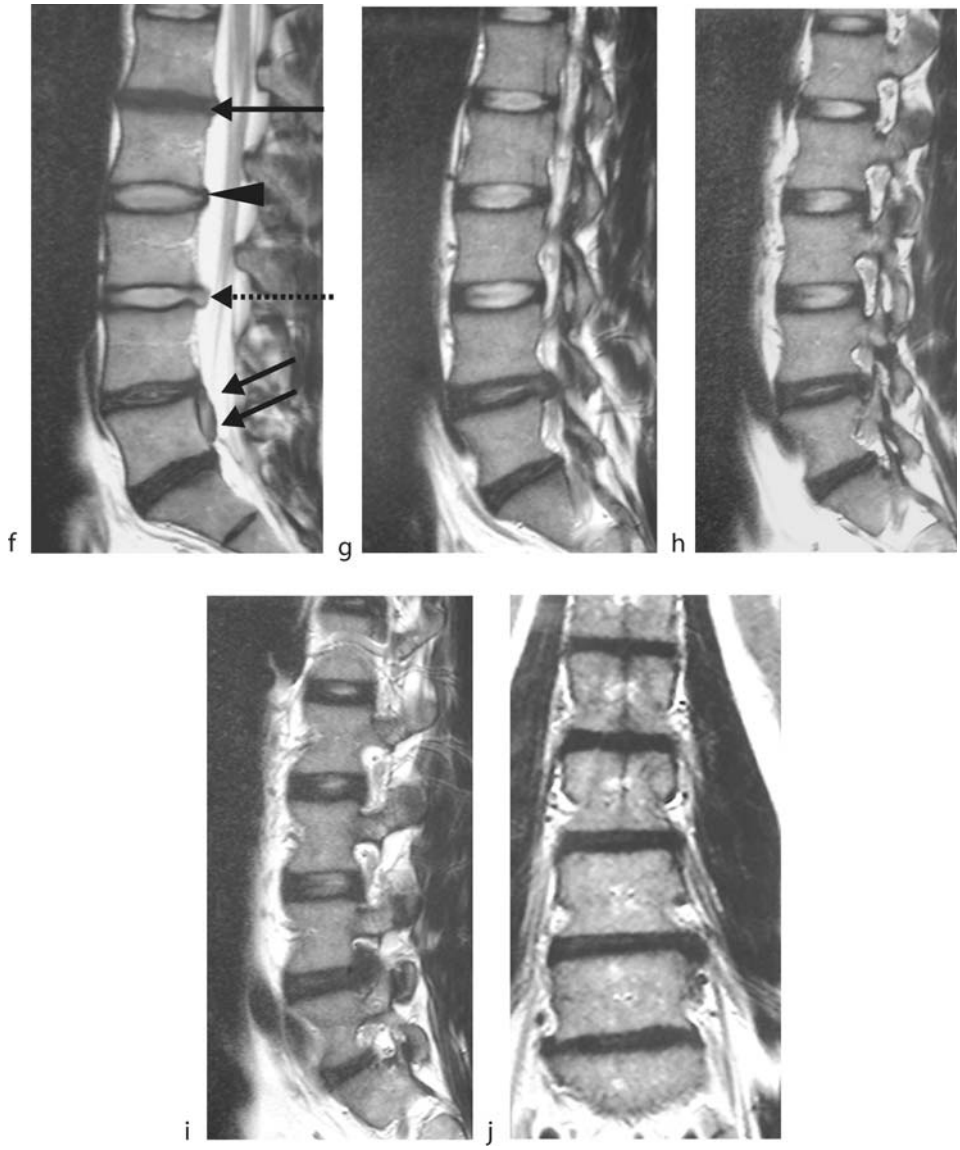

Hernia, Disk, Intervertebral. Figure 2 Location of lumbar disk extrusions relative to axial plane. Central (a axial, f sagittal). Right-central (f) (b axial, g sagittal). Subarticular (c axial, h sagittal). Intraforaminal (d axial, i sagittal). Extraforaminal (e axial, j coronal). (e) Various kinds of disk degenerative diseases with central location: bulging of dehydrated disk (*black arrow*), protrusion (*black arrowhead*), extrusion (*dotted arrow*), extrusion with free fragment (*double arrow*). Note: Simulation with Adobe Photoshop 6.

Disk degeneration is evident as loss of disk height and signal intensity on all sequences due to dehydration of the nucleus pulposus. The presence of a radial tear of the annulus is demonstrated by a band of high signal intensity on T2-weighted images, sometimes showing enhancement on T1-weighted postgadolinium images.

MRI is more sensitive than CT for detecting disk herniation at all levels and is preferred over CT thanks to the superior multiplanar imaging and the intrinsic better soft-tissue contrast. The herniation is usually associated with disk degeneration, and its signal is usually low but is higher than that for the rest of the disk. Acute herniations can be hyperintense on T2-weighted fast spin-echo images. The hyperintensity of the herniated fragment is thought to be due to the high hydration of the nucleus compared with the annulus (1). A hyperintense signal has been reported in up to 80% of sequestered disks.

At cervical and thoracic levels, the diagnosis of disk herniation can be more difficult than at the lumbar spine because these herniations are usually smaller.

Gradient-echo (GRE) sequences can be useful because there is little epidural fat at this level, while the epidural venous plexus is well represented. This venous structure has high signal on GRE sequences; therefore, small herniations can be seen.

Diagnosis

MRI is the optimal diagnostic tool, comparable in sensitivity to myelo-CT, for diagnosing disk herniation. The principle of disk herniation diagnosis is the same with CT and MRI. The herniation is seen as a focal contour abnormality along the posterior disk margin with a soft-tissue mass displacing the epidural fat and, sometimes, the thecal sac and the nerve roots. The herniation is usually contiguous with the rest of the disk.

MRI can be used for follow-up of untreated disk herniation. Spontaneous reduction or disappearance of the herniation is frequently possible. The main predictive MRI signs are hyperintense signal of the herniation on T2-weighted images and enhancement after gadolinium administration. In our experience, free fragments regress spontaneously by 6 months in 100% of cases, while extruded and T2-weighted hyperintense disk herniations regress spontaneously in 80% (4).

The high sensitivity of MRI in detecting even very mild changes of the disk anatomy may sometimes lead to overinterpretation of the findings, giving pathologic meaning to paraphysiological features and vice versa. Abnormal MRI findings are not in themselves necessarily pathologic, nor do they necessarily constitute an indication for surgery or other invasive treatment; they always need to be compared with the clinical evaluation, with treatment tailored to the individual patient.

Interventional Radiological Treatment

The first techniques employed were chemonucleolysis and aspiration diskectomy, both presently done only rarely. A widely performed intervention is intraforaminal/epidural steroid injections, but the success rate is only 40–60% after 6 months. Newer procedures are annuloplasty in bulging disks, percutaneous laser disk decompression, and intradiskal ozone injections, and the reader is referred to separate essays dealing with operative and nonoperative therapeutic procedures (5).

Bibliography

1. Galluci M, Limbucci N, Paonessa A, and Splendiani A (2007) Degenerative disease of the spine. Neuroimaging Clin N Am 17:87–107
2. Bozzao A, Gallucci M, Masciocchi C et al (1992) Lumbar disk herniation: MR imaging assessment of natural history in patients treated without surgery. Radiology 185:135–141
3. Fardon DF and Milette PC (2001) Combined task forces of the North American Spine Society, American Society of Spine Radiology, and American Society of Neuroradiology nomenclature and classification of lumbar disk pathology. Recommendations of the combined task forces of the North American Spine Society, American Society of Spine Radiology, and American Society of Neuroradiology. Spine 26:E93–E113
4. Splendiani A, Puglielli E, De Amicis R et al (2004) Spontaneous resolution of lumbar disk herniation: predictive signs for prognostic evaluation. Neuroradiology 46:916–922
5. Galluci M, Limbucci N, Zugaro L et al (2007) Sciatica treatment with intraadiscal and intraforaminal injection of steroid and O2-O3 vs Steroid only. Radiology 242:907–13

Hernia, Hiatus in Adults

Giles Stevenson[1], Phil Shorvon[2]
[1]Cowichan Hospital, McMaster University' Duncan' British Columbia, Canada
[2]Central Middlesex Hospital, London, England
gilse@shaw.ca

Synonyms

Gastro-oesophageal reflux; GERD/GORD; Hiatus hernia

Definition

►Hiatus hernia is defined as loss of the intra-abdominal portion of the oesophagus, with the gastro-oesophageal junction coming to lie above the diaphragmatic hiatus.

►Gastro-oesophageal reflux disease (GERD) is defined as an abnormal frequency of reflux of gastric acid into the oesophagus. GERD has become one of the most common gastrointestinal complaints in industrialized nations, but for the majority of people it is only a minor inconvenience. For a minority it may become a major health problem, and its complications of stricture, choking and adenocarcinoma may be fatal. Since 1980, advances in understanding of the underlying mechanisms of reflux and its control have allowed a more rational approach to treatment of the symptoms. However, elimination of the disease requires modification of the life style choices that usually, but not always, underline the disease and this is much more difficult to achieve. Hiatus hernia and gastro-oesophageal reflux are commonly, but not necessarily, associated.

Pathology

Anatomy

There is normally about 2.5 cm of intra-abdominal oesophagus which includes most of the 3–4 cm long lower oesophageal sphincter (►LES). With respiration the sphincter slides up and down within the diaphragmatic hiatus, but gastric rugal folds are not seen above the hiatus. If they are, then a hiatus hernia is present. The stages of sliding hiatus hernia development range being present on inspiration only with abdominal compression, present at all phases of respiration with the patient lying down, or finally may be present with the patient erect in all phases of respiration in which case the oesophagus may also be shortened.

In some older patients with long standing hiatus hernia more of the stomach rolls up into the chest until the stomach is largely intra-thoracic. In this case the fundus usually remains inferiorly in the chest while the greater curve of the body rotates superiorly and the antrum passes down through the diaphragmatic hiatus anterior and to the right of the lower oesophagus.

Physiology and Pathogenesis

In the 1960s, reflux was thought to be controlled by the intra-abdominal portion of the oesophagus which acted as a flutter valve. The key breakthrough in understanding came from the laboratory of Wylie J Dodds who was working with the Dent sleeve, a multi-channel catheter whose long separate compartments allowed measurement of pressure over a length rather than at a fixed point. This allowed the lower oesophageal sphincter pressure (►LESP) to be measured even if it slid up and down with respiration. Multiple such measuring stations along the catheter as well as pH measuring points allowed the observation in normal subjects that the lower oesophageal sphincter undergoes transient collapse of pressure from its normal of about 40 mm Hg to zero with swallowing, but that in addition, transient inappropriate total collapses of sphincter pressure occurred two or three times a night. These spontaneous inappropriate collapses of sphincter pressure may be accompanied by acid reflux and a drop in pH that recovers with swallowing while the subject is in light REM sleep. It was soon established that individuals with reflux disease have dozens of such LESP collapses every night, and during the daytime. If the stomach is full when these occur then there is frequent acid reflux. In normal subjects, there are usually less than three or four such episodes of LESP collapse in 24 h, and they are more frequent in the day than at night and last for less than 5 min. It seemed therefore that the acid reflux disease was due to a neuromuscular abnormality of frequent LES relaxations.

However, subsequent work has shown that there is more to reflux than simply the LES pressure. The competence of the sphincter is dependant on position, pressure and length. An intra-abdominal position of the LES bolsters effective sphincter pressure, as intra-abdominal pressure is applied equally to stomach and to the LES, and contraction of the gastric sling fibres maintains the acute angle between stomach and oesophagus. When the abdominal oesophagus is short, as in the presence of a sliding hiatus hernia, intra-abdominal pressure is applied mainly to the stomach, and LESP is more readily overcome. Pressure and length are related in that the longer the sphincter, the lower the pressure required to maintain competence, and conversely a shorter sphincter needs a higher pressure for competence.

Thus it is highly relevant that overdistension of the stomach opens the lower part of the contiguous sphincter causing shortening (Fig. 1), and this shortening of the sphincter can be demonstrated to initiate a transient collapse of sphincter pressure, more in hiatus hernia patients than in those with a long segment of intra-abdominal oesophagus.

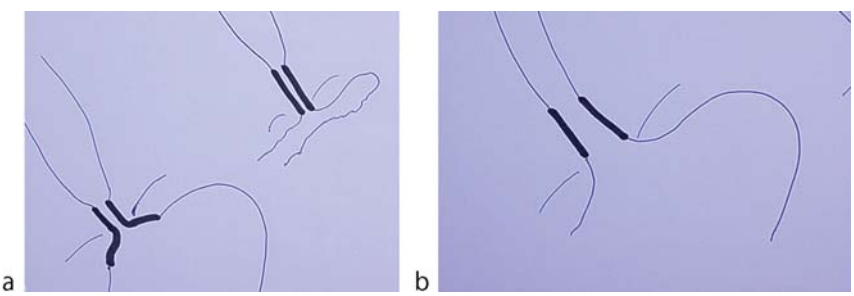

Hernia, Hiatus in Adults. Figure 1 (a) Diagram illustrates a normally closed LES with the stomach empty, and shows how as the fundus distends the sphincter is partially taken up, with opening of the lower portion. This shortens the effective sphincter, and precipitates episodes of transient LESP collapse. (b) This shows the final stage with a permanently defective sphincter that is lax and open, and has migrated up into the chest with some shortening of the oesophagus.

This suggests that shortening of the sphincter is the key in determining frequency of collapse and subsequent reflux. Even in normal individuals, overeating has been shown to shorten the LES sufficiently to cause intermittent LES collapse and gastro-oesphageal reflux. In addition instillation of fat into the gastric antrum causes tonic contraction of the pylorus and delayed gastric emptying in dogs and humans, prolonging fundal distension.

The present understanding can therefore be summarized, as described by DeMeester and Karilas (1, 2). Overeating and delayed gastric emptying (the latter enhanced by fat in the diet), cause prolonged fundal distension with opening of the lower end of the LES shortening its effective length. This leads to repetitive LESP collapse, reflux with mucosal inflammation, and the many symptoms of GERD. Reflux is more likely to occur when the stomach is full and the lower end of the sphincter is distended, which explains the common experience that night heartburn is exacerbated by going to bed shortly after eating.

In the majority of patients reflux is due to frequent inappropriate sphincter relaxations. In a minority of patients (perhaps 10%) prolonged reflux with no relief of the underlying causes will lead to a permanently defective sphincter which is defined as a pressure less than 6 mm Hg, a length of less than 2 cm, and in intra-abdominal length of less than 1 cm. It is part of the role of the radiologist to identify these patients and distinguish them from those with early GERD with or without complications.

Upper Sphincter

If acid is dripped experimentally into the oesophagus while the pressure of the sphincter at the cricopharyngeus is being measured, an abrupt increase in pressure will be observed. If the acid is instilled into the lower sphincter the reflex pressure increase is modest, but if into the upper oesophagus, it is a greater increase. The reason for this is unknown, but it may serve to protect the airway and larynx to some extent when the oesophagus floods with acid, though this is not totally successful and laryngeal oedema and symptoms are seen in severe reflux disease. Repeated reflux leads to a chronic increase in cricopharyngeal sphincter pressure and to thickening of the muscle. This is associated with restriction in the degree of relaxation of the sphincter in some patients with sometimes a permanent posterior bar remaining throughout the swallow. These bars occasionally act as a functional stricture causing dysphagia, and may make endoscopy difficult. However, if a small cannula is passed through the cricopharyngeus under direct vision with an endoscope, the endoscope can then easily be passed into the oesophagus over the cannula which acts as a guide wire, indicating that this is no true fibrous stricture, but merely a bar of hypertrophied non-relaxing muscle.

The increased tone of the sphincter leads to delayed opening of the sphincter, and to premature contraction at the end of the swallow so that a little barium at the tail end of the bolus is trapped above the closing sphincter. Sometimes the increased pressure caused in the pharynx leads to transient herniation of mucosa posteriorly through the small triangular defect between the horizontal and oblique fibres of the cricopharyngeus as a brief transient mini ▶Zenker's diverticulum. This little herniation is a reliable radiological sign of gastro-oesophageal reflux disease (Fig. 2). In a small number of patients, the herniation slowly enlarges and becomes permanent, and such patients may present in later life with regurgitation of food swallowed some hours previously, that has been trapped in a Zenker's diverticulum. As with the bar described above, endoscopy may be difficult in these patients as the endoscope tends to pass posteriorly into the diverticulum. As with the bars, a cannula can be used to intubate the cricopharyngeus in patients with a large Zenker's diverticulum, and this may best be done with radiographic guidance as the guide wire often preferentially enters the diverticulum rather than the lumen and this is not always easy to detect endoscopically.

The ▶Gastric Inlet Patch (Gip)

An island of ectopic gastric mucosa is present at the upper end of the oesophagus in from 0.3% to 5% of subjects, with a figure of 2.4 in one prospective radiological study. The patch, a salmon pink area of mucosa just below the cricopharyngeus, is best seen during slow withdrawal of the endoscope through the upper oesophagus. Its detection on barium study requires views of the well-distended upper oesophagus in two projections which explains why it is rarely seen unless specifically looked for. It is usually asymptomatic, but may contain parietal cells and produce acid, undergo dysplasia, cause strictures or webs, and invasive adenocarcinoma. With acid production it may cause sleep disturbance with coughing and globus.

When patients have pharyngeal, laryngeal or respiratory symptoms of GERD but no apparent hiatus hernia or detectable reflux, an acid producing gastric inlet patch will occasionally be the cause.

Oesophageal Motility

There are five types of oesophageal contractions that may be recognized by the radiologist. Peristaltic contractions may be primary (initiated by swallowing) or secondary (initiated either spontaneously in mid oesophagus or by mid oesophageal distension). Non-peristaltic contractions may be of low amplitude and not obliterate the lumen (less than 25 mm Hg pressure) and are called tertiary contractions by radiologists. Sometimes these

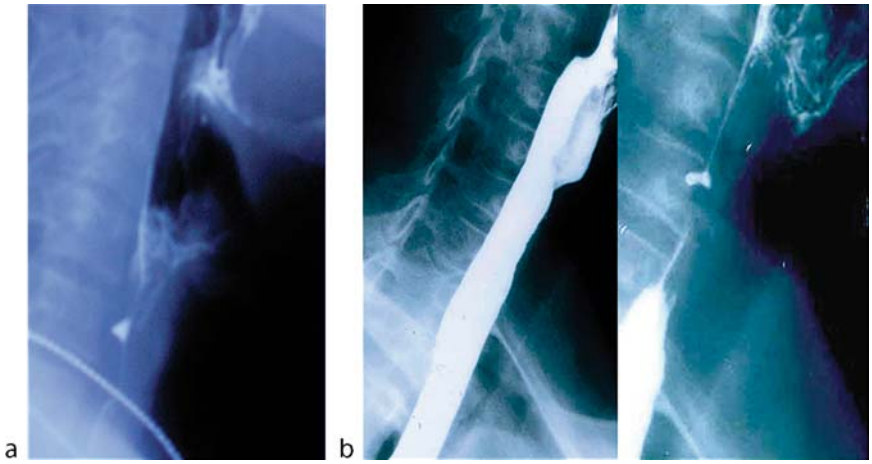

Hernia, Hiatus in Adults. Figure 2 (a) This shows the most common cricopharyngeal abnormality seen in patients with GERD. There is slight premature contraction of the upper sphincter which traps a few drops of barium from the tail of the swallowed bolus. (b) This shows how, although the posterior wall of the sphincter is smooth when it is distended, the premature contraction is producing increased pressure which transiently forces some mucosa through Killian's dehiscence, producing a momentary Zenker's diverticulum that is only present for less than a second. This is not an uncommon finding in patients with GERD and ►globus.

non-peristaltic contractions are of high amplitude and completely obliterate the lumen either segmentally, or as corkscrew (Presby) oesophagus. In some conditions such as nutcracker oesophagus and diffuse spasm, these high amplitude non-peristaltic contractions may reach 600 mm Hg, and be associated with severe chest pain, mimicking a myocardial infarct. Much more commonly, non-cardiac chest pain that mimics an infarct is due to gastro-oesophageal reflux disease. The final type of oesophageal contraction is called the feline oesophagus and is often observed radiologically and occasionally endoscopically, usually as a transient transverse fine ridging of the oesophageal mucosa that occurs immediately after an episode of reflux. It may be thought of as an oesophageal shiver, and is almost certainly caused by a transient contraction of the longitudinally orientated muscularis mucosae in response to contact with acid.

Assessment of the Relationship Between Oesophageal Motility and Gastro-Oesophageal Reflux

The most frequent motility disorder associated with GERD is ineffective primary and secondary peristalsis, at least as measured by manometry (It has for many years been obvious to radiologists that far more common are the low amplitude non-peristaltic tertiary contractions, of such low amplitude that they may not be noticeable on manometry.). However only a minority, 30–40% of patients with reflux disease, have impaired peristalsis and it is more common in advanced GERD such as those with associated respiratory symptoms, oesophagitis and ►Barrett's oesophagus. Disappointingly, most studies have shown that optimal medical control of reflux does not produce improvement in peristaltic amplitude, and nor does fundoplication. Barium video fluoroscopy has been shown to be excellent in ruling out ineffective primary peristalsis, (and thus in excluding achalasia and scleroderma).

Oesophageal peristalsis may be defective as part of a primary motility disorder, but may also deteriorate secondary to long standing GERD. In patients with heartburn the most important primary disorder to detect is scleroderma which is an uncommon but not rare cause of GERD. Its particular significance is that because of the lack of propulsive power in the oesophagus, these patients do very badly with fundoplication surgery which is contraindicated. The weakest part of the normal stripping wave is around the level of the aortic arch where the striated muscle of the upper portion blends with the smooth muscle of the lower oesophagus. In the earliest stage therefore of scleroderma, or of diminished motility secondary to reflux, examination of a single swallow of barium will reveal that the primary wave is inefficient at the level of the arch leaving some barium behind at this point, a phenomenon called proximal escape. By the time scleroderma presents with reflux symptoms however, the motility disorder has progressed and the radiologist will see that the peristalsis that starts in the pharynx fades out around the arch of the aorta, and that there is no visible

peristalsis in the lower two thirds of the oesophagus. Whenever severely diminished peristalsis is seen in the oesophagus in a patient with reflux, especially if the oesophagus is more distensible than usual, enquiry should be made for Raynaud's phenomenon and the possibility of scleroderma should be mentioned in the report. In patients with chest pain in whom reflux is being assessed, occasionally vigorous achalasia, diffuse spasm and rarely nutcracker oesophagus will be encountered. Assessment of oesophageal motility is therefore a necessary part of the examination in suspected reflux disease and it is best carried out with the patient prone oblique making single swallows of barium at least 30 sec apart. Many patients routinely double swallow, and the second swallow interrupts and aborts the first primary wave, so it is essential that the leading edge of the peristaltic wave (the upper end of the barium bolus) be kept at the bottom of the screen so that any second peristalsis coming down from above can be detected, and the result of those swallows discarded.

Any cause of severe oesophagitis will impair peristalsis including Herpes, Candida, Cytomegalovirus and irradiation. In most of these motility may recover with healing, though less foten following radiation because of fibrosis.

Effect on Lower Oesophageal Sphincter Pressure and Cardia

There is usually an acute angle between the intra-abdominal portion of the oesophagus and the stomach. In the presence of a lax taken up sphincter this acute angle is lost, as it is when a hiatus hernia is present. It may sometimes be possible to assess the length of the sphincter, especially in those patients with severe reflux, when it may be apparent that between the barium in the lower oesophagus, and the barium in the hernia, there are only a few millimetres of closed lumen. In more advanced disease the LES is permanently wide open with continual free reflux. In some patients with hiatus hernia, one of the rugal folds may have at its upper end a swelling, looking like a polyp and usually called a sentinel fold. Herlinger has shown that these swellings at the top of a rugal fold are usually oedema, but in a minority of cases (4/23 in one series) the finding was due to a small gastric adenocarcinoma. For this reason, the finding of one of these nodules at the oesophagogastric junction should always lead to endoscopy for biopsy, although endoscopists do not always find a correlating nodule—oedema is a reversible finding.

Effect of Gastric Emptying Changes

There is an association between GERD and impaired gastric emptying. It is not clear whether this is usually cause and effect or merely an association. If gastric emptying is impaired, gastro-oesophageal reflux will often follow, and respond to treatment of the cause (Fig. 3). Gastric emptying is impaired in diabetes and by a high fat meal. This is difficult to assess on barium examination, but will be implied if there are gastric distention, food residue in the stomach, poor antral peristalsis and poor flow of barium to the duodenum. Obesity, diabetes and high-fat diet are commonly associated and are associated with GERD.

Mucosal Damage

Acid reflux leads to oesophagitis though only a minority of patients with symptomatic GERD have endoscopic evidence

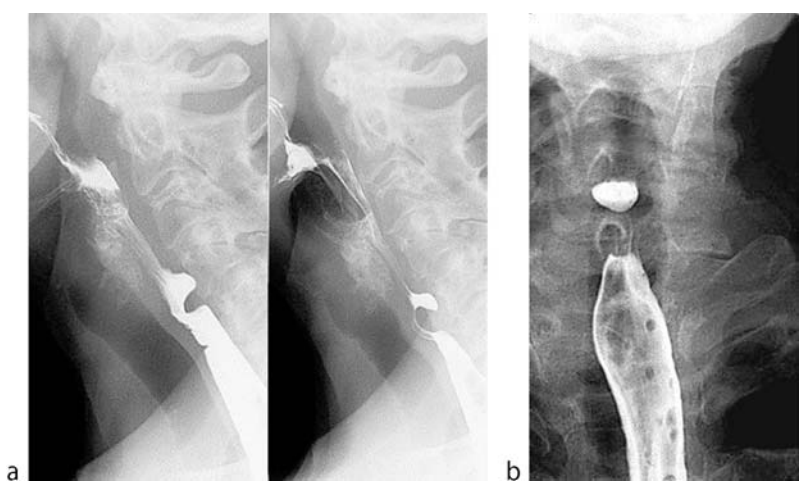

Hernia, Hiatus in Adults. Figure 3 (a) This patient with GERD shows a cricopharyngeal bar due to incomplete relaxation of the upper sphincter, and a slightly later stage in the progression to Zenker's diverticulum. Barium persists for a while in the herniated mucosa (b).

of oesophagitis, which has been graded endoscopically into four stages, under the Los Angeles classification. Grade 1 is a mucosal break <5 mm in length, and grade 4 a mucosal break >75% of the circumference of the oesophagus. This classification is not helpful radiologically as it does not distinguish between erythema and ulceration. The two earliest stages which are loss of the vessel pattern due to oedema, and linear erythema are not detectable on barium meal study. Once there is a mucosal break with surface white slough endoscopically, this is potentially detectable as barium adheres to the slough and a small linear irregular longitudinal barium shadow may be seen. This is reliable when it is seen, and especially when there are multiple such linear ulcers with oedema such that longitudinal folds do not efface with distension. However there is no published correlation between the endoscopic grading and the barium finding. It is sufficient to say that good quality double contrast barium studies can often demonstrate moderate and severe ulcerative oesophagitis, and are useless in showing mild or minimal reflux oesophagitis.

Strictures, Rings and Pseudo-Diverticulosis

A peptic stricture does occur with long standing oesphagitis but is not the most common cause of dysphagia in reflux disease. Much more common is the Schatzki ring which is a short ring narrowing at the gastro-oesophageal mucosal junction (Fig. 4). The ring is only apparent when the oesophagus above and the hiatus hernia below are distended more than the ring itself. A symptomatic ring (causing meat bolus dysphagia for example) may have a calibre of 12 or even 15 mm, so that good distention is essential to demonstrate the ring and this may not always be achievable with erect double contrast views. The prone oblique view with a deeply held inspiration as the barium bolus passes through the LES is the best view with liquid swallows. If the history is of dysphagia, and the liquid swallows are normal, a solid marshmallow bolus should be given for the patient to swallow, unchewed, with a few sips of barium. This will often reveal the presence of a Schatzki ring missed on the liquid study. One half of a standard large North American or European marshmallow, kept fresh in a sealed container, is suitable. Alternatively, if the consistency of the local marshmallow is unsatisfactory, as it is for example in Australia (it is too soft and squeezes out into a long string that can not show a mild stricture) a recipe for a home mode gelatin barium bolus has been published). Ott et al. have shown that properly conducted barium studies are more sensitive than endoscopy in detecting Schatzki rings. Longer peptic strictures are usually obvious, but when mild or long can be overlooked, and any suspicion should be confirmed with a solid bolus. In patients with long standing chronic oesophagitis, and mild stricturing, pseudo-diverticula may form due to enlargement of goblet cells, and produce a striking appearance of multiple small barium collection alongside the margins of the thickened oesophageal wall. Oesophageal pseudo-diverticulosis is easily missed at endoscopy although its clinical relevance is uncertain. The pseudo-diverticula can be at, above or below the strictures, and may even rarely occur without strictures. They are often associated with candida colonization.

Barrett's Oesophagus and Adenocarcinoma

Prolonged gastro-oesophageal reflux may lead to a change in the lower oesophageal mucosa whereby the squamous epithelium becomes replaced by a fundic type of gastric mucosa in which dysplasia is prone to occur, followed in some cases by the development of adenocarcinoma. Most

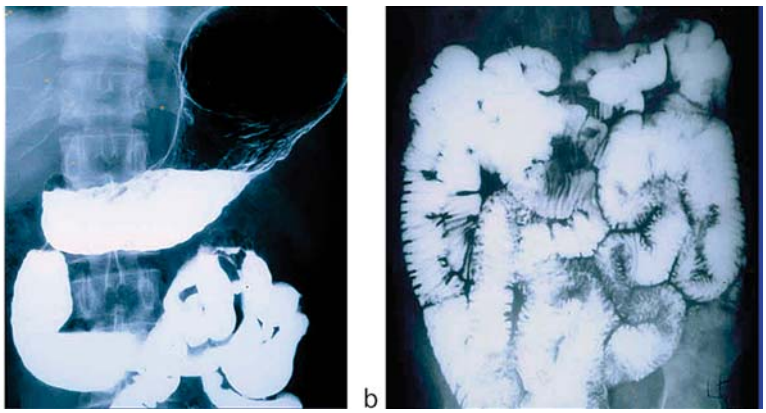

Hernia, Hiatus in Adults. Figure 4 (a) This 27 year old medical student presented with heartburn, and the image shows retained food in the stomach due to delayed gastric emptying. This is due to the severe duodenal and jejunal changes from Coeliac disease. (b). His heartburn resolved on gluten free diet as his gastric emptying returned to normal.

often the gastric metaplasia is limited to the lower oesophagus as short fingers of salmon coloured mucosa spreading up from the gastro-oesophageal junction, and carcinoma in this short segment Barrett's is uncommon, but can occur. Sometimes the zone of transition may spread most of the way up the oesophagus. This new gastric mucosa in the oesophagus is immune to oesophagitis, and remains smooth on barium study, though sometimes with a velvety surface of small polygonal islands resembling areae gastricae—rarely seen but permitting a definitive diagnosis when they are noticed.

The finger like projections can occasionally be seen on good double contrast views but this is unreliable. Oesophagitis in such patients occurs in the lower end of the remaining squamous mucosa. Therefore, the finding of a segment of smooth oesophagus above the gastro-oesophageal junction (as defined by the cessation of rugal folds), above which the changes of oesophagitis can be seen, such as ulceration, spasm or scarring, allows a confident diagnosis of Barrett's oesophagus at barium meal study. Only a minority of patients with Barrett's can be diagnosed in this way. The gastric mucosa in the lower oesophagus is however liable to undergo peptic ulceration, with a substantial discrete ulcer of some depth and with defined margins. Such a discrete ulcer does not occur in peptic oesophagitis, and the differential diagnosis is rather of ulcerated squamous carcinoma, or a discrete ulcer from unusual infection such as cytomegalovirus or herpes. Finally, the oesophagus in long segment Barrett's tends to be more distensible than usual, and there is usually a permanently defective sphincter with a hiatus hernia and free reflux. The high risk patient in whom endoscopy may be recommended, even when Barrett's oesophagus can not be diagnosed radiologically, are middle aged men, overweight, with a long history of reflux whose heartburn symptoms may have typically diminished in recent years, and who have a lax sphincter and rather distensible oesophagus (Fig. 5).

Dysphagia from cancer may be the presenting symptom in these patients, as the heartburn often diminishes as the gastric mucosa extends up the oesophagus. The cancers may arise at the cardia or anywhere in the metaplastic gastric mucosa. Cancer is less common in short segment Barrett's but does occur.

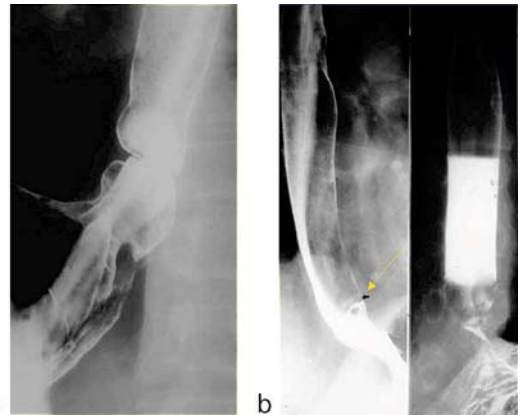

Hernia, Hiatus in Adults. Figure 5 **(a) A prone oblique film on deep inspiration as the patient swallowed showed this Schatzki ring above a hiatus hernia, which was not visible on the erect double contrast views. (b) This patient has a minimal Schatzki ring (*arrow*), barely detectable on the erect double contrast views, but nevertheless it is sufficient to obstruct a half large marshmallow, support a column of barium and reproduce the patient's symptoms of Dysphagia.**

Hiatus Hernia and Short Oesophagus

Hiatus hernia often accompanies GERD, but is neither necessary nor sufficient for its diagnosis. It is more readily seen with abdominal pressure, i.e. prone, and therefore a small hiatus hernia may be reported from a barium meal study when it is not apparent endoscopically. A hiatus hernia is most significant when the gastro-oesophageal junction is permanently above the hiatus, as this may indicate oesophageal shortening. This is critical in advanced disease in which surgery may be considered, since if the intra-abdominal position of the LES cannot be restored without undue tension, a different operation will be required (4). However there is disagreement on how common this is, and how reliably it may be recognized by the radiologist. Some surgeons find that 23% of patients requiring surgery for GERD have a ►short oesophagus and require some form of Collis gastroplasty (3). Other surgeons regard this as rare, occurring in less than 5% of surgical patients. In some elderly patients, although the GE junction may be well above the hiatus with the patient erect, the oesophagus is elongated and tortuous and the LES can readily be pulled down at surgery. In other cases the oesophagus is straight and a high GE junction probably does mean a short oesophagus with irreducible hernia (Fig. 6). The radiologist must recognize the position of the gastro-oesophageal junction and report when the oesophagus appears to be short, while acknowledging that this does not necessarily mean that a gastroplasty will be needed at operation. The radiologist examining the patient erect is in a good position, with the double contrast films, to identify the position of the gastro-oesophageal junction by identifying the top of the rugal folds, and thus alert the surgeon to the potential problem.

Most patients with sliding hiatus hernia do not have a short oesophagus, and the hernia is often only present when the patient is horizontal, and when the stomach is

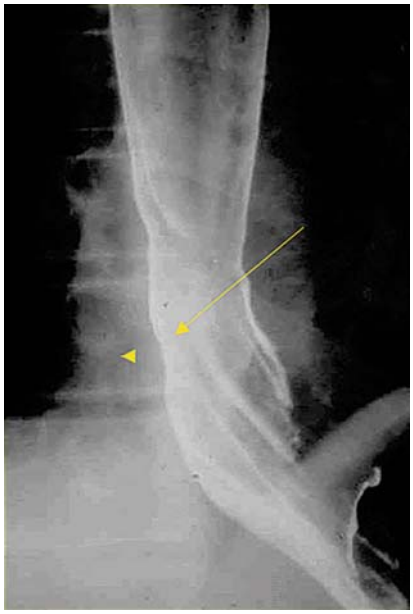

Hernia, Hiatus in Adults. Figure 6 **This patient with very mild bolus Dysphagia has a mild stricture from peptic oesophagitis. The erect double contrast view of the gastro-oesophageal junction also shows that there is a hiatus hernia with the patient in the erect position, (the *arrow* indicates the top of a gastric rugal fold), and this appearance suggests that there may well be a short oesophagus. The surgeon should be alerted to the likelihood that a Collis gastroplasty may be required instead of a routine fundoplication.**

distended. In old age a hiatus hernia may enlarge progressively. In this case the enlargement may occur with the LES always above the hiatus, or instead the lateral part of the fundus and greater curve of the body may roll up into the thorax through the lax diaphragmatic hiatus, and lie above the LES. This is very rarely associated with volvulus and necrosis, and many of these patients are too frail for surgery for what are often quite minor symptoms. Some surgeons grade hiatus hernias into four types, and if your surgeon does, then it will be helpful to indicate the type in the report. Type I is the common sliding hernia. In Type II the GE junction remains at or below the hiatus with superior herniation of the gastric fundus. Type III has features of both Types I and II, and is more common than II. Type IV is used to describe herniation of most or all of the stomach into the chest usually with rotation of the greater curve of the body up above the fundus.

Bibliography

1. De Meester TR (2002) The Evolving concepts of reflux: The ups and downs of the LES. Can J Gasroenterol 16:327–331
2. Kahrilas PJ, Shi G, Manka M et al (2000) Increased frequency of transient lower esophageal sphincter relaxation induced by gastric distention in reflux patients with hiatal hernia. Gastroenterology 118:688–696
3. Mattioli S, Lugaresi ML, Di Simone MP et al (2004) The surgical treatment of intrathoracic migration of the gastro-oesophageal junction and of short oesophagus in gastro-oesophageal reflux disease. Eur J Cardiothorac Surg 25:1079–1088
4. Canon CL, Morgan DE, Einstein DM et al (2005) Surgical approach to gastroesophageal reflux disease: What the radiologist needs to know. Radiographics 25:1485–1499

Heterotaxia Syndrome or Situs Ambiguous

This syndrome implies a disordered organ arrangement in the chest and/or abdomen. The anatomy is unpredictable. The visceral malformation is associated with indeterminate atrial arrangement. Asplenia is associated with right isomerism or bilateral right-sidedness. Polysplenia is associated with left isomerism or bilateral left-sidedness.

▶Congenital Malformations, Splenic

Heterotaxia Syndromes, Ambiguous Situs Abdomen

▶Congenital Malformations, Splenic

Heterotopia

Heterotopia gray matter in an abnormal location, between the germinal matrix and the final destination, the cortex.

▶Congenital Malformations, Cerebrum

Hiatal Hernia

▶Reflux, Gastroesophageal in Adults

Hiatus Hernia

Herniation of part of the stomach upwards through the diaphragmatic hiatus and into the chest; 'sliding' and 'rolling' types are described.

▶Hernia, Hiatus in Adults
▶Hernia, Diaphragm, Congenital
▶Reflux, Gastroesophageal in Adults

Hibernoma

Benign mesenchymal tumor developing from vestiges or fat storage organs. These tumors, originating from both brown and white fat tissues, are considered a variant of lipoma. Hibernomas are usually capsulated, highly vascularized with a slow growth. Imaging features show inhomogeneous masses with relatively well-defined margins.

▶Lipomatous Neoplasms, Hepatic

HIE

▶Hypoxic-Ischaemic Encephalopathy

High ARM

ARM where the blind pouch ends above the sling of the hypotrophic puborectalis muscle. There can be associated rectobulbar fistulas in males or rectovaginal fistulas in females.

▶Anorectal Malformation

High Osmolality Contrast Media

A high osmolality contrast medium is a water-soluble imaging contrast agent that has osmolality (a measure of the number of particles in solution) much higher than human blood. For radiographic iodinated contrast media, this is typically around four times the osmolality of human blood. Certain adverse effects of contrast media are attributed, at least in part, to elevated osmolality. See also iso-osmolality contrast media and low osmolality contrast media.

▶Adverse Reactions, Iodinated Contrast Media, Acute Renal

High Pressure Balloon

Balloon catheter with nominal burst ratio of more than 25 atm.

▶Fistula, Hemodialysis

High-Resolution MR Imaging

High-resolution MR imaging using a small surface coil (e.g., a 47-mm microscopy coil) offers images with high signal-to-noise ratios of the superficial organs and tissues.

▶Neoplasms, Salivary Glands

Hilgenreiner Lines

Horizontal and vertical lines constructed on frontal radiographs of the hips for evaluation of possible dysplasia, subluxation, or dislocation.

▶Dysplasia, Hip, Developmental

Hilum

The normal lymph node contains fat-filled hilum, through which almost all vessels enter the lymph node. The hilum is depicted by sonography and CT as an echogenic central structure and a fat-density structure, respectively, and is identified by T1-weighted MR imaging as a hyperintense area. The presence of intact hilum on sonographic, CT, and MR images is a hallmark of the normal lymph node.

▶Lymphadenopathies, Head and Neck

Hip Dislocation

Most commonly occurs posteriorly in the setting of major trauma with resultant posterior displacement and internal rotation of the femur. Diaphyseal fractures of the femoral shaft are not infrequently seen and may obscure the clinical diagnosis of hip dislocation sciatic nerve injury occurs in 10% of these injuries. Posterior labral tears and posterior acetabular fractures are commonly associated. Compression fractures of the femoral head may also occur, usually on its inferomedial aspect. Approximately 10% of hip dislocations are anterior. Impaction fractures of the superolateral femoral head and fractures of the anterior acetabular rim are associated with these injuries. Hip dislocations are best assessed by CT after urgent reduction. MR is also useful in assessing the integrity of the labrum and the cartilage.

▶Fractures, Pelvis

Hip Dysplasia

Karl Ludwig
Department of Diagnostic Radiology, Orthopedic University Hospital Heidelberg, Heidelberg, Germany
karl.ludwig@ok.uni-heidelberg.de

Synonym

Developmental dysplasia of the hip (DDH)

Definition

Developmental dysplasia of the hip (DDH) is defined as a deformity of the acetabulum of varying degree in which the femoral head may be located correctly or displaced in relation to the acetabulum.

Pathology/Histopathology

For its correct development the acetabulum needs a sufficient pressure of the femoral head. DDH develops *in utero* if the contact between the femoral head and the acetabulum is too loose. Different factors have been discussed concerning the development of DDH (1): mechanical reasons can be responsible for DDH if intrauterine space is limited, such as in oligohydramnios. DDH is more frequent in primiparous mothers. Increased levels of estrogens have been shown to cause a delayed maturation of collagen and therefore present a functional factor for the development of DDH. Genetic factors are reported to contribute to the development of DDH. Furthermore, environmental factors may contribute to the development of DDH; in particular, the way newborns are held by their mothers is different in various cultural settings and is reported to influence the risk of DDH.

In the majority of cases, DDH develops in the late phase of pregnancy based on the risk factors described earlier but without underlying disease. In a minority of cases, DDH develops in the early phase of pregnancy due to an underlying neuromuscular disorder such as spina bifida or arthrogryposis multiplex.

Clinical Presentation

The incidence of DDH is reported to be in the range of 2–6 newborns per 1,000. It is 4–8 times more frequent in females than in males (1). The clinical presentation varies greatly and ranges from near normal findings that are found on screening examinations to complete dislocation of the hip.

DDH should be diagnosed as early as possible. Clinical diagnosis is mainly based on specific tests including the Ortolani's and Barlow's maneuver, but sonography is more accurate. In some centers sonography is used as a routine screening for DDH in newborns, or sonography is routinely performed in newborns at risk (2). Radiography becomes most useful from the age of 3–6 months, when the relevant structures of the acetabulum and femoral head are sufficiently ossified.

Imaging

Sonography

Sonography plays a major role in DDH in the newborn and infant. The technique of hip joint sonography for diagnosing DDH was described by Graf in the early 1980s (2). Within the sonographic examination, the acetabular angle and the acetabular coverage are measured by a standardized technique and can be compared to age-related reference values. Based on this comparison, four grades of hip dysplasia have been defined. Sonography is reported to detect one-third more pathologic cases than clinical examination alone. Though sonography is most useful in very young age groups, sonographic methods have also been described in patients older than 2 years, with the intention of preventing patients from radiation exposure (2).

Radiography

Radiography is most useful from the age of 3–6 months, when the ossification of the relevant joint structures is sufficient. In patients younger than 6 weeks, radiography shows no changes of DDH (1). Usually, anteroposterior views of the pelvis are obtained, with optional frog-leg views or, in older patients, faux-profile views.

There are typical measurements indicating deformity of the acetabulum, the proximal femur, and the relationship between both structures. These include the acetabular index (AI), the center-edge (CE) angle, and the percentage of coverage of the femoral head (1, 3). The acetabular index is the angle of the acetabular roof to the Hilgenreiner's line, a line through the two triradiate cartilages (Fig. 1). The CE angle is the angle between the center of the femoral head on one hand and a line perpendicular to a line through both femoral head centers on the other hand. It is used in older children in whom the femoral heads are completely ossified. The percentage of coverage of the femoral head is measured using three lines perpendicular to the Hilgenreiner's line and cutting the medial and lateral aspects of the femoral head and the lateral corner of the acetabulum. Dividing the distances between these lines leads to the percentage of coverage of the femoral head.

The frog-leg view projection is used for determining antetorsion and the center-collum-diaphysis angle. Faux-profile projections serve for measuring the vertical-center-anterior angle.

All these and further measurements indicate whether and to what degree there is a deformity of the acetabulum or the proximal femur (3). These results can be compared with age-related normal values.

Computed Tomography

Computed tomography can be performed as an additional method to measure the anterior and posterior acetabular sector angle in patients being evaluated for surgical correction (3).

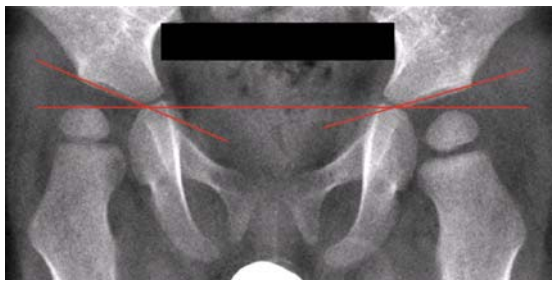

Hip Dysplasia. Figure 1 Anteroposterior radiograph of the pelvis. *Lines* indicate the measurement of the acetabular index, which is pathologically high on the right side and indicates the presence of developmental dysplasia of the hip.

Nuclear Medicine

Nuclear medicine does not play a role in the diagnosis of DDH.

Diagnosis

A complete evaluation includes a physical examination and either a sonographic or radiographic examination. Whether sonographic or radiographic imaging is used depends mostly on the patient's age. Diagnosis can usually be made very accurately on the basis of measurements performed with both methods.

Bibliography

1. Gerscovich EO (1997) A radiologist's guide to the imaging in the diagnosis and treatment of developmental dysplasia of the hip. Skeletal Radiol (Part I) 26:386–397
2. Gerscovich EO (1997) A radiologist's guide to the imaging in the diagnosis and treatment of developmental dysplasia of the hip. Skeletal Radiol (Part II) 26:447–456
3. Delaunay S, Dussault RG, Kaplan PA et al (1997) Radiographic measurements of dysplastic adult hips. Skeletal Radiol 26:75–81

Hip Dysplasia

Abnormal growth or development of the acetabulum, femoral head, and associated ligaments and soft tissues.
▶Congenital Malformations of the Musculoskeletal System

Hip, Dysplasia, Developmental

Alan E. Oestreich
Cincinnati Children's Hospital, Medical Center, Cincinnati, , Ohio, USA
Alan.Oestreich@cchmc.org

Synonym

Formerly known as "congenital hip dislocation"

Definitions

Abnormal configuration, motion, or position of the hip apparent in the first days of life or discovered on follow-up later in childhood. The location of the femoral head with respect to the acetabulum, the steepness of the roof of the acetabulum, the shape of the outer corner of the roof, and abnormal clinical (or sonographic) testing for subluxability of the hip are major features at presentation. The findings may either ameliorate or progress if not treated.

Pathology/Histopathology

The anatomy of hip bone and cartilage on ultrasound images closely follows what is seen on gross dissection at autopsy. In dislocations, one question is interposition of the fatty pulvinar between the acetabulum and femoral head, which may prevent reduction.

Clinical Presentation

A hip click, asymmetric buttocks, and eventually an abnormal gait are signs of developmental dysplasia of the hip. Asymmetry will not be found, however, in bilateral disease.

Neuromuscular weakness, especially of the hip abductors, is typically a risk for acquired dislocation/►subluxation of valgus hips, a different entity from developmental dysplasia of the hip.

Imaging

Until about 3 months of age in girls, perhaps somewhat later in male infants, evaluation for the usual developmental dysplasia of the hip is by ultrasound. A coronal approach from the side is used, with evaluation and any angle measurements from images that simulate the frontal radiographs, but also show cartilage as separate from other soft-tissue structures. Subluxability (resembling the Barlow test) may be dynamically viewed while imaged by ultrasound.

In infancy, plain films for developmental dysplasia usually require only one frontal image, thus sparing the radiation of a second (frog leg) view. A straight pelvis (nonoblique) position should be sought. A computed tomography (CT) reconstructed image could also be used if available. Magnetic resonance imaging (MRI) is generally not needed, but nicely shows any trapped pulvinar (also evident on CT) in irreducible dislocation, as well as the musculotendinous structures of the region.

In preparation for corrective surgery for hip dislocation, a three-dimensional rotatable presentation from CT slices may help to guide the surgeon.

Diagnosis

Before the femoral head ossifies, ultrasound is the preferred imaging modality. A subluxed or dislocated femoral head is not 50% covered by the cartilage of the acetabular roof. The cartilaginous head is indeed well visualized early in infancy on ultrasound (including the channels of blood vessels within it). The ultrasound findings are graded according to Graf (1), in part using the α-angle between the extension of the vertical lateral edge of the ilium and the acetabular roof line (see Table 1). Normal, or Graf I, has an α-angle of at least 60°, and a well-formed lateral margin of the acetabular roof. In Graf I and most cases of Graf II, the femoral head is seen to be at least 50% covered by the roof. In Graf II (Fig. 1), the α-angle lies between 50 and 59°, and the

Hip, Dysplasia, Developmental. Table 1 ►Graf classification

Graf	Sonographic type	Acetabular outer corner	α-angle (degrees)
I	Mature	Sharp or slightly rounded	>60
IIA	Immature hip <3 months of age	Rounded	50–60
IIB	Immature hip >3 months of age	Rounded	50–60
IIC	Dysplasia, stable	Rounded	43–49
IID	Dysplasia, unstable (decentering)	Rounded or slightly flattened	43–49
III	subluxed (eccentric)	Flattened	<43
IV	Dislocated	Deformed	Not measurable

Modified from Keats TE, Sistrom C (2001) Atlas of Radiologic Measurement. 7th edn. Mosby, St. Louis, p 216.
In I–IIC, cartilage roof of acetabulum covers the femoral head
In IID, cartilage roof is displaced upward
In III, cartilage roof is displaced, either devoid of echoes or echogenic
In IV, cartilage rood is trapped between femoral head and ilium.

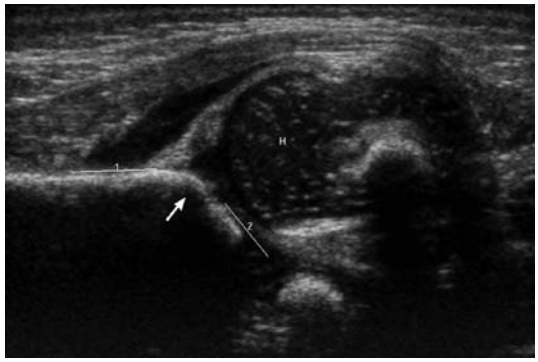

Hip, Dysplasia, Developmental. Figure 1 Example of a Graf II hip in a 9-day-old infant. The head (H) of the femur is 50% covered; the α-angle (between lines 1 and 2) is 53°, and the outer corner of the acetabulum (*arrow*) is more rounded than angular (we presume the head is 50% covered).

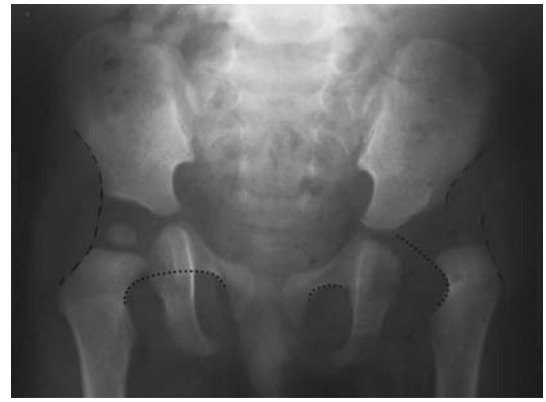

Hip, Dysplasia, Developmental. Figure 2 A 15-month-old girl with left developmental dysplasia of the hip leading to subluxation. The Shenton line (*dots*) on the left is disturbed, as is the "outside Shenton" curve (*dashes*), which is normal on the right in comparison (From Oestreich AE, Crawford AH (1985) Atlas of Pediatric Orthopedic Radiology. Thieme Verlag, Stuttgart, p 184).

lateral roof is rounded. This is an immature hip. In Graf III, the angle is between 43 and 49° and the head is subluxed whereas in Graf IV the hip is dislocated and the angle is below 43°. As the hip is subluxed, one looks for a trapped pulvinar between the head and acetabulum. During ultrasound visualization of the hip, subluxability can be dynamically demonstrated.

The ▶Hilgenreiner horizontal line on plain images connects the lowest ossified points of the two acetabular roofs; the Hilgenreiner vertical line perpendicular to it is constructed at the lateral corner of the roof. The proximal femoral shaft should be at least partly medial to the vertical line on the anteroposterior (AP) image. The acetabular angle is constructed between the horizontal line and the line connecting the lowest and outermost points of the roof. The higher the angle, especially above 45°, the more dysplastic the acetabulum. In some cases of complete dislocation, no acetabular roof has formed at all.

After the femoral head ossifies, the ossification tends to be greater on the nondysplastic hip in unilateral disease. The femoral head is displaced lateral to the vertical line in subluxation or dislocation. The inner curve of the femoral neck should be able to be smoothly continued to the lower surface of the superior pubic bone, the normal Shenton line (Fig. 2). An "outer Shenton" line is also present in normal cases on AP, with the curve of the lateral surface of the neck of the femur continuing with the lateral outer curve of the iliac bone (Fig. 2).

The acetabular angle is relatively low in Down syndrome, achondroplasia, Rubinstein–Taybi syndrome, and often in long-standing neuromuscular disease.

Hip dislocation in early infancy is also a manifestation of several dysostoses/dysplasias, including Larsen syndrome (knees are also dislocated at birth) and geroderma osteodysplastica congenita (osteoporosis, Walt Disney dwarf facies) (2).

Bibliography

1. Graf R (1987) Guide to Sonography of the Infant Hip. Thieme Verlag, Stuttgart and New York City
2. Lisker R, Hernandez A et al (1979) Gerodermia osteodysplastica hereditaria: report of three affected brothers and literature review. Am J Med Genet 3:389–395

Hip Fractures

Minor trauma in a patient with osteoporosis is the characteristic clinical setting of most hip fractures. Most injuries are subcapital fractures, occurring at the junction of the femoral head and neck. These injuries are intracapsular and often interrupt blood supply to the femoral head. Other intracapsular fractures include transverse cervical and basicervical injuries. Extracapsular hip fractures include intertrochanteric and subtrochanteric fractures. These fractures are usually obliquely oriented and associated fractures of the lesser and greater trochanters are common. Pathologic fractures should be considered in the setting of isolated fractures of the trochanters or transversely oriented subtrochanteric injuries.

▶Fractures, Pelvis

Hirschsprung Disease and Related Disorders

Melanie Hiorns
Radiology Department, Great Ormond Street Hospital for Children, London, UK
HiornM@gosh.nhs.uk

Synonyms

Aganglionosis of the colon; Chronic intestinal pseudo obstruction; Congenital megacolon. Related disorders include Hypoperistalsis syndrome; Hypoganglionosis; Neuronal intestinal dysplasia (NID); Total colonic aganglionosis; Ultra short segment Hirschsprung's disease

Definition

This group of disorders is known collectively as the dysganglionoses and they are all characterised by abnormalities in innervation of the bowel. ►Hirschsprung's disease is defined as ►aganglionosis of part or, occasionally, the entire large bowel. The most distal part of the rectum is always affected but the proximal extent of the disease is variable.

Hirschsprung's disease is a dominantly inherited multigenic disorder with incomplete penetrance and variable expressivity. Of the genes identified so far, the RET proto-oncogene is the major susceptibility gene and accounts for most cases.

Pathology/Histopathology

Hirschsprung's disease is characterised histologically as the congenital absence or deficiency of the ganglion cells in the myenteric and submucosal plexuses (1) of the rectum and the distal, non-dilated part of the colon, together with a hyperplasia of cholinergic nerve fibres in the circular muscle layer, muscularis mucosae and mucosa with a high activity of acetylcholinesterase.

Hypoganglionosis is described histologically as a variable length of gut with abnormal numbers of ganglion cells. It is believed to be the primary cause of intestinal pseudo-obstruction and may represent a forme-fruste of Hirschsprung's disease.

Hyperganglionosis is described as having two distinct patterns: ganglioneuromas (nodular proliferations of ganglion cells often associated with multiple endocrine neoplasia type 2B and not seen in children) and NID. NID is a controversial entity but a consistently described feature is of increased density of the submucosal ganglia (2).

Chronic intestinal pseudo-obstruction is a rare clinical condition also known as chronic adynamic ileus, pseudo Hirschsprung's disease and adynamic bowel syndrome. ►Megacystis-microcolon-intestinal hypoperistalsis syndrome is the most severe form of chronic intestinal pseudo-obstruction. Histologically abnormalities are either seen in the myenteric plexus with an associated visceral myopathy, or show argyrophobic cells or argyrophilic cells on silver stains.

Clinical Presentation

Hirschsprung's disease is the most common cause of neonatal obstruction of the colon and accounts for 33% of all neonatal obstructions. Overall there is an incidence of approximately 1 in 5,000 to 1 in 8,000 live births. Occurrence is usually sporadic but it is reported to be familial in 4%. In classic Hirschsprung's disease and in 'ultra short segment disease' there is a male to female ratio of 3:1 and in total colonic aganglionosis the ratio is 1.8:1.

The absence of the intramural ganglion cells interferes with normal relaxation and peristalsis of the bowel wall and the internal anal sphincter. The abnormally innervated segment of colon becomes hypertonic and behaves as a functional stenosis leading to partial or complete colonic obstruction. Immediately proximal to the aganglionic segment the intestine becomes markedly dilated with faeces and gas. Presentation is most common in the full term infant during the first six weeks of life (70–80%) and is extremely rare in premature infants. Failure to pass meconium in the first 24 h of life is common and Hirschsprung's disease must be considered in the differential diagnosis until proven otherwise. However, in some cases obstruction may not be the predominant feature and the infant may present with diarrhoea or an enterocolitis. In a small proportion of cases presentation will be delayed until the child is older and presents with intractable constipation.

Hyper- and hypoganglionosis will also present a similar and overlapping clinical picture and need to be considered in the differential diagnosis until histology is available.

Chronic intestinal pseudo obstruction (also known as chronic adynamic ileus, pseudo Hirschsprung's disease and adynamic bowel syndrome) tends to be more severe in cases with an earlier presentation. In the neonatal period, symptoms include failure to pass meconium, abdominal distension or bilious vomiting. Constipation may subsequently develop. In older children presentation may be abrupt or slowly progressive. Urinary tract involvement occurs in up to 50% of patients.

Imaging

After Hirschsprung's disease is suspected clinically, a water-soluble contrast enema should be performed. If the patient is beyond the neonatal period dilute barium can be used (3). The imaging should begin with the patient in a lateral position to best demonstrate the rectum and sigmoid and their relative sizes. The classic appearance is that of a short segment of normal appearing distal rectum with a 'transition zone' (an abrupt increase of calibre of the rectum or sigmoid colon) to distended gas and stool filled colon (Figs. 1 and 2). The recto-sigmoid index may be used to assess the comparative size of the rectum and sigmoid: the rectum is normally of larger diameter than the sigmoid and if this relationship is reversed an abnormality of bowel innervation is likely.

The affected part of the bowel is the distal part that is of small calibre. However it is frequently the case that the transition zone may not be so clearly demarcated as the colon proximal to the aganglionic section may be not be entirely normal but may be hypoganglionic and in these cases there may only be subtle cone-shaped tapering towards the rectum. In the neonate, the distal (affected) rectum may show a serrated (or 'saw-tooth') appearance representing abnormal (spastic) contractions.

Enterocolitis may be a complication of Hirschsprung's disease and presents with abdominal pain and profound, often bloody, diarrhoea. The enema findings are those of spasm, mucosal oedema, cobblestoning and ulceration and are indistinguishable from the appearances of any other acute colitis.

Imaging in megacystis-microcolon-intestinal hypoperistalsis syndrome usually shows a very large volume bladder on ultrasound that may empty poorly and a microcolon on the first contrast enema at birth.

Nuclear Medicine

It has no role to play in these conditions

Diagnosis

The diagnosis is confirmed by biopsy. It is usually the case that a suction biopsy is performed initially. If this shows ganglion cells the diagnosis of Hirschsprung's disease is excluded, but if no ganglion cells are identified a full thickness biopsy is then performed for full histological assessment. Hirschsprung's disease is characterised by congenital absence or deficiency of the ganglion cells in the myenteric and submucosal plexuses of the rectum and the distal, non-dilated part of the colon, together with a hyperplasia of cholinergic nerve fibres in the circular muscle layer, muscularis mucosae and mucosa with a high activity of acetylcholinesterase. Therefore Hirschsprung's disease is a histological and not an imaging diagnosis.

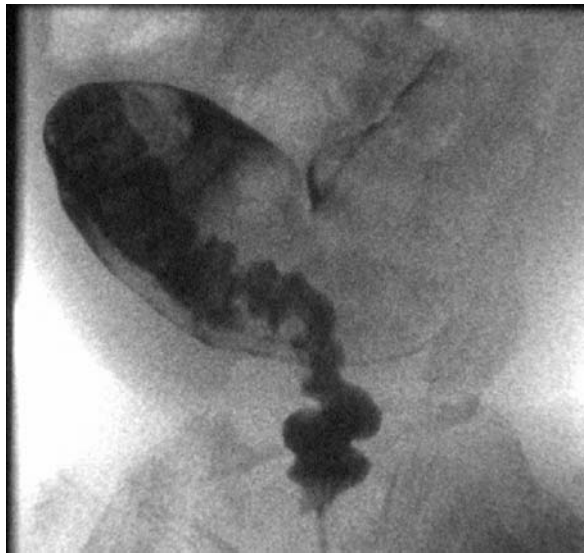

Hirschsprung Disease and Related Disorders.
Figure 1 Contrast enema in an infant in a lateral position showing a normal calibre rectum and then an abrupt change in calibre to a grossly distended sigmoid colon that is filled with stool.

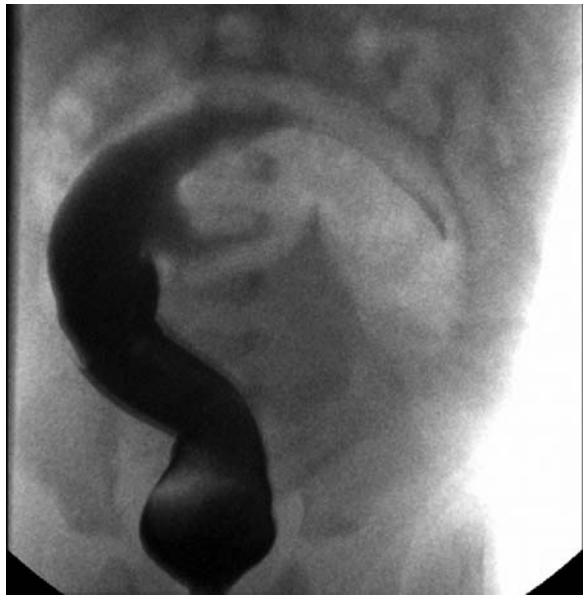

Hirschsprung Disease and Related Disorders.
Figure 2 Contrast enema in a neonate showing a dilated, air filled, sigmoid loop and an abrupt change of calibre at the recto–sigmoid junction.

Interventional Radiological Treatment

It is not applicable.

Bibliography

1. Kapur RP (2000) Developmental disorders of the enteric nervous system. Gut 47:iv81–iv83
2. Puri P (2003) Intestinal neuronal dysplasia. Semin Pediatr Surg 12(4):259–264
3. Fotter R (1998) Imaging of constipation in infants and children. Eur Radiol 8:248–258

Hirschsprung's Disease

An absence or deficiency of the ganglion cells of the myenteric plexus in the wall of the colon resulting in abnormal innervation and function of the colon.
▶Hirschsprung Disease and Related Disorders

Histiocytoma Fibrous Malignant

▶Hepatic Sarcoma

Histiocytoma Fibrous Malignant, Hepatic

Rare sarcomatous neoplasm that most commonly affects limbs and rarely the abdominal organs such as the stomach, intestine, peritoneal wall, pancreas, and liver. This tumor occurs mostly in elderly patients. Histologically, this tumor appears as sarcomatous changes in normal components of the mesenchymal stroma resembling a reticulosarcoma. Macroscopically, it is a rapidly growing bulky mass with polylobulated shapes.
▶Hepatic Sarcoma

Histiocytosis

Contains granulomatous lesions with characteristic Langerhans' cells.
▶Neoplasms, Chest, Childhood

Histopathology

Microscopic examination, immunohistochemistry and genetic studies after percutaneous or open biopsy, mostly performed under imaging guidance.
▶Tumors, Spine

HN

▶Hydronephrosis

HOCM

▶High Osmolality Contrast Media

Hodgkin-lymphoma

Malignant lymphoma from B-cell origin, microscopically characterized by the presence of so-called Reed-Sternberg cells. Rarely involves the breast.
▶Lymphoma, Breast

Holoprosencephaly

Group of cerebral malformations characterised by 'the tendency for the prosencephalon to remain as a whole, as a simple vesicle incompletely transformed into a complex di- and telencephalon with lobes and hemispheres'. On the basis of the severity of brain anomalies, three different forms of holoprosencephaly, alobar, semilobar and lobar, can be recognised. However, by definition, all forms exhibit continuity of the frontal cortex across the midline. Patients with severe forms of holoprosencephaly manifest a spectrum of orbital, ocular, nasal and aural anomalies, including an elongated tube-like nasal analog termed the proboscis. Holoprosencephalic facies are characterised by hypotelorism.
▶Congenital Malformations, Nose and Paranasal Sinus

Honda Sign

Honda sign is a feature of bone scan and describes an H-shaped hot spot in the os sacrum, typical for insufficiency fracture.
▶Rheumatoid Arthritis

Hormone Replacement Therapy

This is medication containing one or more female hormones, commonly estrogen plus progestin (synthetic progesterone). Some women receive estrogen-only therapy (usually women who have had the uterus removed). HRT is most often used to treat symptoms of menopause such as hot flashes, vaginal dryness, mood swings, sleep disorders, and decreased sexual desire. This medication may be taken in the form of a pill, a patch, or vaginal cream.
▶Breast, Physiology
▶Breast, Therapy Effects
▶Carcinoma, Breast, Demography

Horner's Syndrome

Consists of enophthalmos, miosis, ptosis and ipsilateral facial anhidrosis. Lung cancer invading the cervical thoracic sympathetic nerves is a common cause.
▶Neoplasms Pulmonary

House-Brackmann Grading

A clinical grading system that stratifies the degree of facial nerve paralysis from I (normal) to VI (complete paralysis) with a good correlation with the degree of neuronal injury demonstrated by electrophysiologic testing. It is used as a clinical prognostic indicator, in patients follow-up and to evaluate response to therapy.
▶Facial Nerve Palsy

Hox Genes

Homeobox (hox) genes control many factors of intrauterine development including direction, segmentation, and number of repetitive structures such as sclerotomes.
▶Congenital Malformations, Bone

HRCT

High-resolution computed tomography (HRCT) has a significant impact in studies of small parts because it can resolve an object of 0.5 mm diameter. With HRCT, a combination of section thickness and the unique reconstruction algorithm of a particular CT scanner is possible, which determines the final appearance of the ear image.
▶Temporal Bone, Inflammatory Diseases, Acute, Chronic

HRT

▶Hormone Replacement Therapy

HSG

▶Hysterosalpingography

Hyaline Membrane Disease

This condition, encountered in premature infants, is due to a deficiency of the lipoprotein pulmonary surfactant superimposed on structural immaturity of the lungs.
▶Chest, Neonatal

Hydatid Disease, Abdominal

Riccardo Lencioni, Chiara Franchini
Department of Diagnostic and Interventional Radiology, University of Pisa, Pisa, Italy
lencioni@med.unipi.it

Definition

Hydatid disease is a zoonosis produced by the larval stage of the *Echinococcus* tapeworm.

Pathology and Histopathology

Echinococcus granulosus and *Echinococcus multilocularis* are the two most common causes of hydatid disease. The most frequently encountered type in humans is *E. granulosus* and is commonly seen in the great grazing regions of the world (the Mediterranean region, Africa, South America, the Middle East, Australia, and New Zealand). *E. multilocularis* is less common but more invasive, mimicking a malignancy.

The definitive host is usually a dog but may be some other carnivore. The adult worm of the parasite lives in the proximal small bowel of the definitive host and releases eggs which are excreted in the feces. Sheep are the most common intermediate hosts. They are infected grazing on contaminated ground. Humans may become intermediate hosts through contact with a definitive host (usually a domesticated dog) or ingestion of contaminated water or vegetables. The egg loses its layer in the duodenum and an embryo, called oncosphere, is released. The embryo passes through the intestinal wall into the portal circulation and reaches the liver, where it may die or develop into a cyst. The right lobe is the most frequently involved portion of the liver (1, 2). In humans, hydatid disease involves the liver in approximately 75% of cases.

The hydatid cyst has three layers: the outer layer, or pericyst, is composed of modified host cells that form a fibrous protective zone; the middle laminated membrane is acellular and allows the passage of nutrients; the rupture of the laminated membrane predisposes to infection; the inner germinal layer produces the scolices (the larval stage of the parasite) and the laminated membrane. The middle and the inner layers form the true wall of the cyst, called endocyst. Daughter vesicles are small spheres that contain the protoscolices and are formed from an outpouching of the germinal layer. Scolices and vesicles form a white sediment known as hydatid sand. Daughter cysts may grow through the wall of the mother cyst, particularly in bone disease. The thickness of these layers depends on the tissue in which the cyst is located. The layers tend to be thick in the liver, less developed in muscle, absent in bone, and sometimes visible in the brain. Peripheral calcifications are common in both viable and nonviable cysts. Cyst fluid is clear or pale yellow, has a neutral pH, and contains sodium chloride, proteins, glucose, ions, lipids, and polysaccharides. The fluid is antigenic and may also contain scolices and hooklets (1–3).

Complications of hydatid cysts include local complications and hematogenous dissemination.

Local complications comprise cyst rupture, cyst infection, exophytic growth, transdiaphragmatic thoracic involvement, perforation into hollow viscera, peritoneal seeding, biliary communication, portal vein involvement, abdominal wall invasion. Intrahepatic complications are cyst rupture and infection. Rupture is usually a step of the natural history of hepatic hydatid cysts. There are three different types of cyst rupture; contained rupture involves the endocyst, while the pericyst remains intact; communicating rupture implies passage of the cyst contents into the biliary radicles incorporated into the pericyst; direct rupture, usually complicating superficially located cysts, involves both the pericyst and endocyst, allowing free spillage of hydatid material. Infection occurs only after rupture of both the pericyst and endocyst (communicating and direct rupture), which allows bacteria to pass easily into the cyst. Exophytic growth usually occurs through the bare area of the liver and the gastrohepatic ligament. Transdiaphragmatic migration usually occurs *via* the bare area of the liver. The involvement varies from simple adherence to the diaphragm to rupture into the pleural cavity, seeding in the pulmonary parenchyma, and chronic bronchial fistula. Spontaneous rupture of the cyst into hollow viscera is an extremely rare complication. Peritoneal seeding is almost always secondary to hepatic disease and is usually related to previous surgery, but sometimes it occurs spontaneously. Hydatid cysts communicate with the biliary tree *via* small biliary radicles incorporated into the pericyst. However, frank rupture into the biliary tree may occur. Compression of the portal vein and thrombosis is a rare event. Cysts may invade the abdominal wall, usually passing through a small orifice.

The most common sites of hematogenous dissemination are the lungs, involved in about 15% of cases in humans. Other possible anatomic locations are spleen, brain, bone, kidneys.

Involvement of the spleen is quite uncommon and isolated splenic involvement is even more uncommon. In some series, the spleen is the third most common location of hydatid disease after the liver and lungs. Splenic involvement may be due to hematogenous dissemination or intraperitoneal spread from a ruptured liver cyst. Splenic hydatid cysts are usually solitary (1).

In rare cases, retroperitoneal localization has been described. Hydatid disease of the pancreas is extremely rare and is usually associated to other localizations. The pancreas may also be involved in acute inflammation secondary to liver hydatid disease when intracystic debris is eliminated through the biliary tree (1).

E. multilocularis is responsible for the rare multilocular or alveolar form of hydatid disease. Definitive hosts are foxes and, less commonly, cats and dogs. Humans are infected either by direct contact with a definitive host or indirectly by ingestion of contaminated water or vegetables. This type of *Echinococcus* produces multilocular cysts which grow by exogenous proliferation. The cyst wall is composed of an inner germinal layer, a syncytial tegument, and an outer acellular laminated layer. These lesions

show a strong tendency to develop central liquefactive necrosis, which may be surrounded by vital vesicles. The liver is the most commonly involved organ (3).

Clinical Presentation

Echinococcal lesions are often asymptomatic for many years and are discovered incidentally on imaging examinations. When symptomatic, hepatic hydatid cysts classically produce upper abdominal pain and hepatomegaly. In case of ruptured cyst, the passage of the cyst contents into the blood circulation can produce anaphylaxia due to the antigenic nature of the cyst fluid, although cyst rupture may be clinically silent. Infection usually manifests as a hepatic abscess.

Direct rupture into hollow viscera may present with hydatidemesis or hydatidorrhea.

If the rupture is followed by biliary communication, with subsequent biliary obstruction and cholangitis, jaundice, fever, and chills may occur.

The most frequent clinical manifestations of splenic involvement are abdominal pain, splenomegaly, and fever (1).

Imaging

E. granulosus Cysts

Hydatid cysts have been classified into four types on the basis of their appearance, reflecting the natural history of echinococcal disease (4).

Type I cyst appears as a simple cyst without internal architecture.

At ultrasound (US) it appears as an anechoic lesion with regular margins, and may contain hydatid sand and tiny septa. Rolling the patient during the examination disperses the sand and creates a "falling snowflakes" pattern, consisting in small fluctuant echoes. At computed tomography (CT), a type I hydatid cyst appears as a well-defined lesion, with a water-like density. The cyst wall and, when visible, the septa, usually show contrast enhancement after contrast medium injection. Magnetic resonance (MR) images show similar features to those of a simple liver cyst, including hypointensity on T1-weighted images and marked hyperintensity on T2-weighted images. A hypointense rim, particularly evident on T2-weighted scans, may be appreciable. This finding corresponds to the pericyst which is rich in collagen (1–3).

Type II cyst is a lesion containing daughter cysts and matrix, also referred to as multivescicular hydatid cyst.

Type II lesions have a US appearance that is generally specific and diagnostic of echinococcal disease. US is the most sensitive modality for the detection of membranes, septa, and hydatid sand. Daughter cysts are seen inside the mother cyst. Floating membranes or vesicles may also be seen in the cyst. Detachment of the endocyst from the pericyst is probably related to decreasing intracystic pressure, degeneration, host response, trauma, or response to therapy. When most of the cyst is filled with matrix, it may appear as an echogenic lesion mimicking a solid mass. At CT, viable daughter cysts have a consistently lower density than that of mother cyst. This finding is useful in differentiating multivescicular hydatid cyst from various septated cystic lesions. On the basis of CT appearance, multivescicular hydatid cysts have been classified into three types. Type IIA lesions contain small round daughter cysts at the periphery. Type IIB lesions contain larger, irregularly shaped daughter cysts that occupy almost the entire volume of the mother cyst. The high-attenuation fluid that surrounds the daughter cysts gives the appearance of septa, and creates a "rosette" appearance. Type IIC lesions, representing the degeneration of old cysts filled with matrix, appear as relatively high-attenuation round or oval masses with scattered calcifications and occasional daughter cysts. The hydatid matrix appears hypointense on T1-weighted MR images and markedly hyperintense on T2-weighted MR images; daughter cysts may appear hypointense or isointense relative to the maternal matrix both on T1- and T2-weighted images. The "snake sign" represents the presence of floating parasitic membranes within the cysts. These membranes have low signal intensity both in T1- and T2-weighted scans (1–3).

Type III cysts represent dead cysts with total calcification (Figs. 1–3).

At US, they demonstrate strong posterior acoustic shadowing. At CT, they appear as round, completely calcified lesions. At MR, they manifest as hypointense areas in all sequences (1–3).

Type IV cysts represent complicated hydatid lesions.

Intrahepatic complications of hydatid cysts include cyst rupture and infection and may occur in both type I and type II cysts. Rupture occurs in 50–90% of cases in the natural history of hepatic hydatid cyst, being due to the degeneration of parasitic membranes as a result of age, therapy, or host defense response. Sometimes it may be related to minor trauma. Rupture of a hydatid cyst may be contained, communicating, or direct. Contained ruptures involve the endocyst, while the pericyst remains intact. In these cases, endocyst detachment is seen at US, CT, and MR as undulating floating membranes within the cyst. The parasitic membranes appear as hypointense linear images on T2-weighted MR scans. In communicating rupture, the cyst content passes into the biliary radicles. In these cases, the cyst has a higher echogenicity than in contained rupture. US can demonstrate the presence of hydatid sand in the biliary channels. Direct rupture involves both the pericyst and endocyst, with

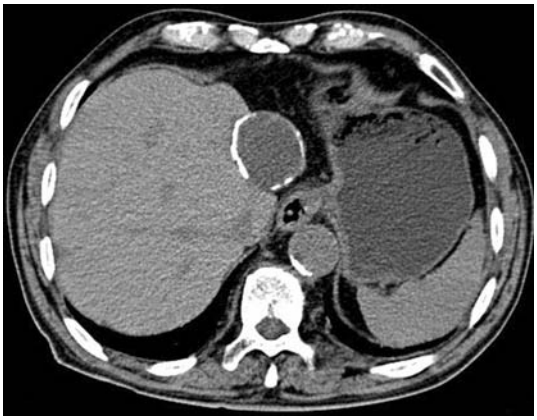

Hydatid Disease, Abdominal. Figure 1 Hydatid cyst of the liver (type III). Unenhanced CT shows a round cystic lesion with water-density content and peripheral calcifications.

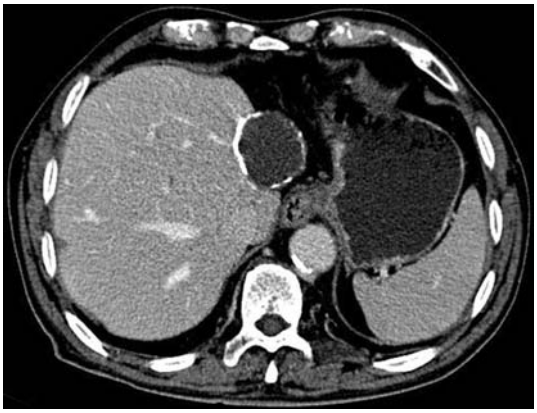

Hydatid Disease, Abdominal. Figure 3 Hydatid cyst of the liver (type III) same case of Fig 1. Enhanced CT portal-venous phase. The cyst dose not show any contrast enchancement both in the arterial and portal-venous phase.

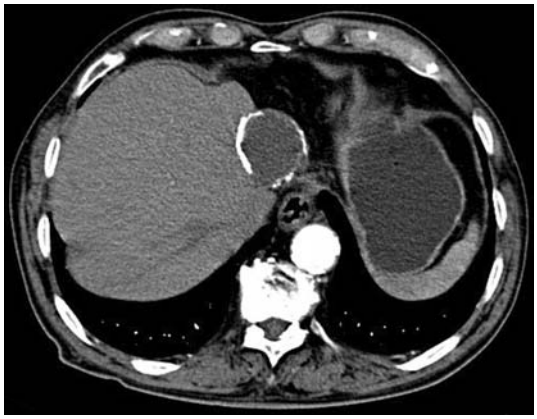

Hydatid Disease, Abdominal. Figure 2 Hydatid cyst of the liver (type III) same case of Fig 1. Enhanced CT arterial phase. The cyst does not show any contrast enhancement both in the arterial and portal-venous phase.

consequent leakage of hydatid material into the peritoneal cavity, pleural cavity, hollow viscera, abdominal wall. Direct rupture is more frequent in superficially located lesions. In communicating and direct ruptures, the cyst empties and may became smaller and less spherical; US, CT, and MR may demonstrate a cyst wall fissure and leakage of the cyst contents.

Infection may complicate communicating and direct rupture, which allows the passage of bacteria into the cyst. US and CT findings are similar to those in other hepatic abscesses. US findings that suggest infection include a solid appearance, mixed echogenicity with solid and fluid components, internal echogenic foci, air–fluid or fluid–fluid levels, poor delimitation. All these US findings are nonspecific and may be observed in uninfected ruptured cysts. CT is the standard modality in the study of infected cysts. Infected cysts usually have ill-defined margins. After contrast administration, the typical hyperdense peripheral rim of abscesses is depicted. Patchy enhancing areas, corresponding to inflammatory changes, near the lesion may occasionally be seen. CT also most clearly depicts gas or air–fluid levels within the cyst (1–3).

In case of transdiaphragmatic migration of hydatid disease from the liver, chest radiography may show pleural effusion, elevation of the diaphragm, lung consolidation, or laminated atelectasis at the lung base. US can confirm the presence of hepatic hydatid disease and demonstrate pleural effusion. CT is very useful in demonstrating migration of hydatid disease and assessing the thoracic component. MR, thanks to the possibility of obtaining sagittal and coronal scans, allows an optimal depiction of the diaphragmatic defect and of the migration of the cyst through the diaphragm, giving an accurate presurgical evaluation. Rarely the cyst may perforate into hollow viscera. CT may demonstrate the presence of orally administered contrast material inside the cyst cavity. Changing the patient position may demonstrate filling or emptying of the cyst cavity. Barium study can be used to depict the fistula between the cyst and the hollow viscus. CT is the modality of choice in identifying peritoneal localization because it allows imaging of the whole abdomen and pelvis. Cysts may be multiple and located anywhere in the peritoneal cavity. In some cases they may occupy the entire peritoneal cavity, simulating a multiloculated mass. This condition is called encysted peritoneal

hydatidosis. Communication of ruptured hydatid cyst with the biliary tree may be suspected on the basis of both direct and indirect imaging signs. Direct visualization of the cyst wall defect or of a communication between the cyst and a biliary radicle is possible with US and CT, especially in cases of wide communication. The presence of hydatid material in the biliary branches may sometimes be observed; in these instances, US demonstrates anechoic or echoic material filling the biliary radicles or the main bile duct, while CT depicts hyperdense material within the biliary tree. Endoscopic retrograde cholangiopancreatography and percutaneous transhepatic cholangiography can demonstrate the communication in more detail.

Indirect signs of biliary communication include increased echogenicity at US and fluid levels and signal intensity changes at MR imaging. An air–fluid level within the cyst may indicate infection, as well as rupture into the biliary tree or into a hollow viscus or development of a bronchopleural fistula. A fat–fluid level within the cyst has also been described as an indirect sign of biliary communication. Dilatation of the biliary tree may be the only, but aspecific imaging sign of hydatid cyst communicating with the biliary tree. Compression of the portal vein occurs rarely and may lead to thrombosis followed by cavernous transformation. Doppler US, CT, and MR can demonstrate the lack of flow in the portal vein and the presence of multiple small vessels with venous flow at the hepatic hilum, indicating portal cavernomatosis. Hydatid cysts may invade the abdominal wall. Imaging reveals a cystic mass within the abdominal wall that is similar to and in communication with the hepatic component of the hydatid cyst (1).

Splenic hydatid cysts have imaging features which are very similar to those of hepatic hydatid cysts. Any type of hydatid cyst can be seen in the spleen. Cyst wall calcification may occur and is better depicted at CT than at radiography or US. Splenic echinococcal lesions are usually solitary (1, 2).

Information about the appearance and location of hydatid cysts of the pancreas is inadequate due to their rarity (2). US and CT show a cystic lesion of the pancreas which may or not have some characteristics of hydatid cysts. Dilatation of the pancreatic duct due to compression may be associated.

E. multilocularis Cysts

At US, the typical presentation of echinococcal *multilocularis* is the so called "hailstorm" pattern, characterized by multiple echogenic nodules with indistinct margins. Larger lesions with central liquefactive necrosis have a hypoechoic structure, with some internal echoes and present irregular hyperechoic margins. CT demonstrates multiple irregular, ill-defined lesions which are usually hypodense. At MR, these lesions appear hyperintense on T2-weighted scans. This pattern may mimic either metastases or pyogenic abscesses. However, the enhancement after administration of contrast medium is absent or minimal. In advanced stages, the lesions are larger and irregularly shaped, and present central hypodensity with irregular tiny calcifications, corresponding to liquefactive necrosis. Hilar infiltration is a common event, resulting in biliary obstruction with dilatation of the intrahepatic bile ducts and invasion of the portal and hepatic veins, with subsequent atrophy of the affected liver segments due to hypoperfusion (3).

Interventional Radiology

Although previously thought to be contraindicated, percutaneous drainage of uncomplicated hydatid cysts is gaining wider acceptance as an effective and safe alternative to surgery. Generally, percutaneous drainage is combined with instillation of a sclerosing scolicidal agent after pretreatment with mebendazole (5).

Diagnosis

Echinococcal lesions are often asymptomatic for many years and are discovered incidentally on imaging examinations. Clinical data, imaging findings, and serology usually give useful and complementary information on the nature of the cyst and allow a definite diagnosis. Biochemical analysis usually demonstrates eosinophilia, while serologic tests for the parasite are positive in only 25% of patients.

However, hydatid disease in the pancreas may be a disturbing diagnostic problem and must be distinguished from cystic neoplasms. Usually the definite diagnosis is achieved at surgery.

Imaging is also a useful tool in monitoring treatment response.

Bibliography

1. Pedrosa I, Saiz A, Arrazola J et al (2000) Hydatid disease: radiologic and pathologic features and complications. Radiographics May–Jun; 20(3):795–817
2. Polat P, Kantarci M, Alper F et al (2003) Hydatid disease from head to toe. Radiographics Mar–Apr; 23(2):475–494
3. Mortele KJ, Segatto E, Ros PR (2004) The infected liver: radiologic-pathologic correlation. Radiographics Jul–Aug; 24(4):937–955
4. Lewall DB, McCorkell SJ (1985) Hepatic echinococcal cysts: sonographic appearance and classification. Radiology Jun; 155 (3):773–775
5. Khuroo MS, Wani NA, Javid G et al (1997) Percutaneous drainage compared with surgery for hepatic hydatid cysts. N Engl J Med Sep 25; 337(13):881–887

Hydrocele

Pathologic fluid accumulation located between the layers of the tunica vaginalis testis. Inflammatory diseases such as epididymitis and orchitis, as well as testicular cancer or a posttraumatic condition, may cause hydrocele.
►Scrotal Disorders

Hydronephrosis

Dilatation of the renal collecting system (pelvo-caliceal system).
►Hydronephrosis in childhood

Hydronephrosis in Childhood

M. Riccabona, R. Fotter
Department of Radiology, Division of Pediatric Radiology, University Hospital Graz, Graz, Austria
richard.fotter@meduni-graz.at
michael.riccabona@meduni-graz.at

Synonyms

(Dilating)uropathy; Hydronephrosis; Nephro-ureteral dilatation; Pyeloectasia

Definition

The term ►hydronephrosis (HN) was derived from earlier times in imaging, when any detectable dilatation of the renal collecting system was considered a potential obstructive and dilative uropathy. With the improved resolution of modern ultrasound (US) techniques, 'physiological' distension of the normal renal calyces and pelvis as well as of the ureter became visible and we learned that this phenomenon does exist without any pathological meaning. Though often done, describing such a renal unit as a hydronephrotic kidney and ureter may be misleading, as this condition may still represent a physiological transient phenomenon mostly without clinical implications. Various grading and scoring suggestions have been introduced. The most commonly used grading system of HN in paediatrics has been derived from the Society for Fetal Urology (SFU), after birth applicable only to neonates and infants (Fig. 1). This grading scale is defined as follows:

- HN 0 = no collecting system visible
- HN I = just the renal pelvis with an axial diameter less than 5–7 mm visible
- HN II = axial renal pelvis diameter less than 5/7–10 mm, some non-dilated calyces with normal forniceal shape visible
- HN III = marked dilatation of the renal calyces and pelvis larger than 10 mm with loss of forniceal and papillar differentiation without parenchymal narrowing
- HN IV = gross dilatation of the collecting system with narrowing of the parenchyma
- In some places HN V is used additionally to communicate an extreme HN with only a membrane-like residuum of the renal parenchyma

Embryology

Embryology varies with the underlying disease.

Clinical Presentation

HN itself has no typical clinical presentation: clinical symptoms depend on degree of HN, patient age, potential underlying causes (e.g. secondary HN in tumour conditions), whether HN is uni- or bilateral, and additional complications such as urinary tract infection.

Imaging

HN is usually detected during foetal US, in screening situations, or—far less commonly—in a focussed US examination of the urinary tract or the abdomen based on clinical symptoms. The degree of dilatation may vary with patient hydration and bladder filling, therefore a standardised assessment is recommended. As a variety of conditions can lead to some degree of dilatation, the purpose of imaging is not only to detect HN, but also to help to differentiate the various entities such as physiological distension due to diuresis or (neonatal) system laxity, reactive laxity in infection, refluxing uropathy with consecutive dilatation of the ureter and renal pelvis, or obstructive uropathy due to an obstruction at any level of the urinary tract. Finally, non-obstructive and non-refluxive, purely dilative uropathy with macro-/mega-/hydrocalyces, calyceal diverticula or just a physiologically

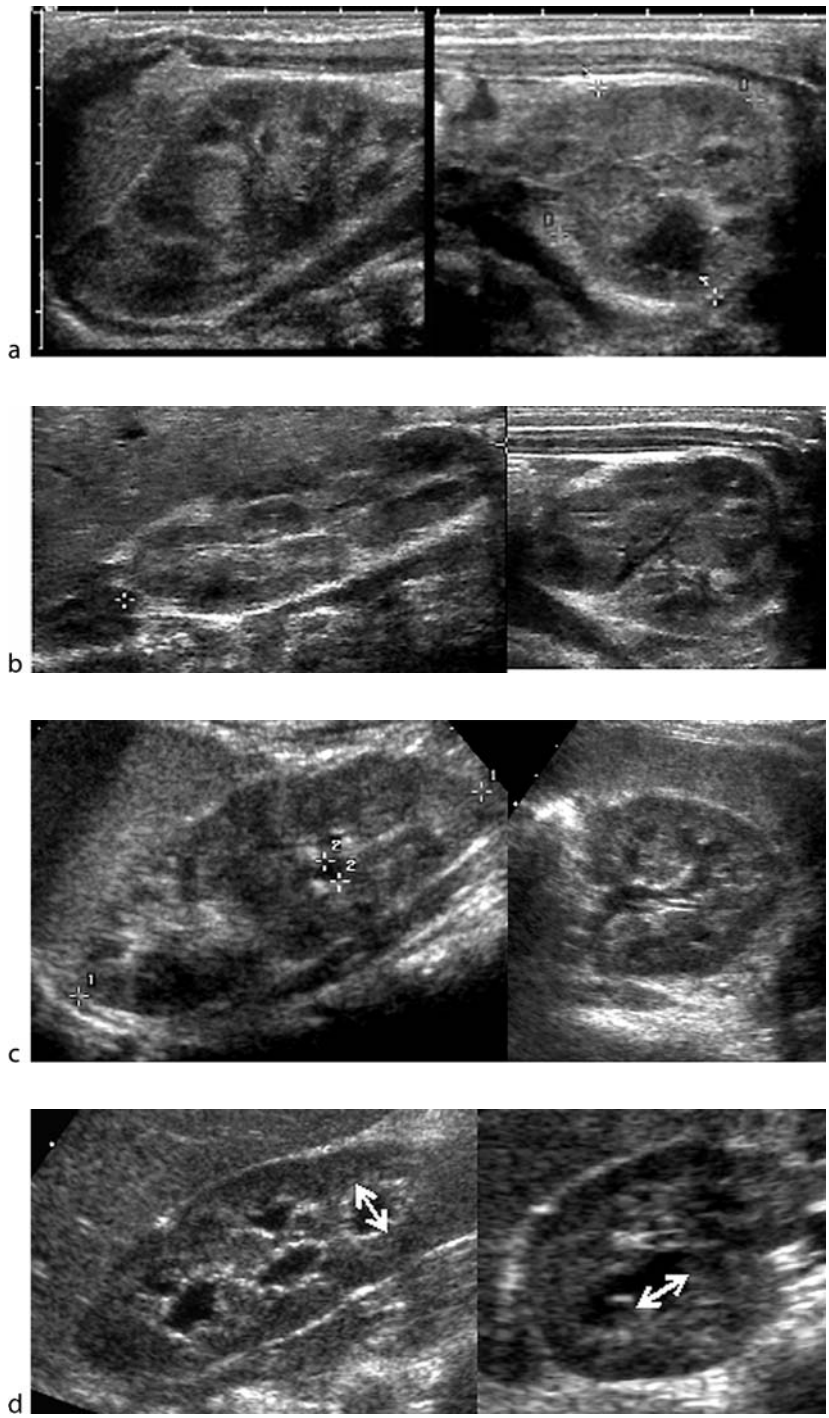

Hydronephrosis in Childhood. Figure 1 (continued)

ectatic renal pelvis should be considered. Standardised imaging algorithms may be helpful for a thorough and economic work-up of these babies with particularly prenatally diagnosed HN (Table 1).

Imaging Modalities

Basically, ultrasound (US) in a standardised fashion and a well-hydrated child is the primary imaging tool. It allows for adequate initial assessment of dilatation of the ureter,

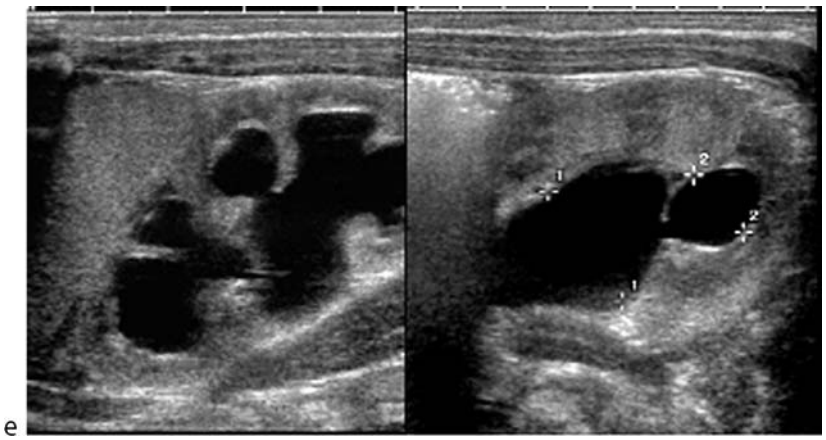

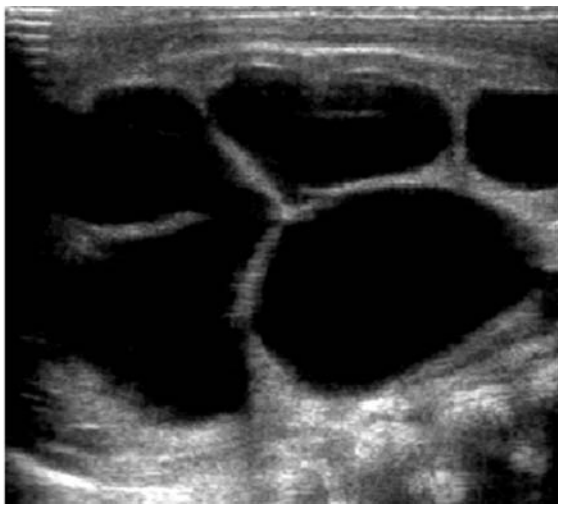

Hydronephrosis in Childhood. Figure 1 Neonatal grading of hydronephrosis on US, adapted according to the 'SFU' grading system, in longitudinal (left) and axial (right) display. HN 0° = no visualization of any fluid within the collecting system HN 1° = only renal pelvis filled with fluid and thus visible HN 2° = some calyces visible, but normal shape of calyces and normal parenchyma HN 3° = dilated calyces (⇔) with flattened fornices, rounded papillas, without parenchymal narrowing HN 4° = gross dilatation of the entire collecting system (++) with narrowing of the parenchyma HN 5° = extreme dilatation of the distorted collecting system with only a residual rim of parenchyma (only used in a few centres to describe a monstrous HN 4°).

the renal pelvis and the calyces with simultaneous comprehensive assessment of the renal parenchyma, and for follow-up. The use of extended US criteria based on indirect signs such as bladder wall morphology, changing degree of calyceal dilatation, thickened urothelium (►urothelial sign), parenchymal structure analysis or calyceal shape, or of colour Doppler sonography (i.e. accessory renal vessel causing uretero-pelvic junction obstruction, retrocaval ureter, etc.) often allows to narrow the differential diagnosis and to set up the consecutive imaging pathway (Fig. 2). Note that age-dependent normal values for renal size and age-dependent appearance of the renal parenchyma should be considered, as well as correlation of the findings with the state of hydration and bladder filling (see entry 'Urinary Tract, Anatomy'). A post-void evaluation may help to differentiate various conditions and should be part of any compulsory urinary tract US examination. Depending on the initial findings and the suspected diagnosis, only US follow-up (in low-degree HN without any other clinical symptoms, e.g. in screening conditions or after foetal US), a thorough work-up for vesico-ureteric reflux (VCUG and/or echo-enhanced cystosonography, as well as radionuclide cystography and renal scintigraphy—see entry 'VUR'),

Hydronephrosis in Childhood. Table 1 Imaging algorithm for prenatally detected hydronephrosis (based on prenatal classification). A potential imaging algorithm for neonates with prenatally diagnosed 'hydronephrosis' based on the SFU classification

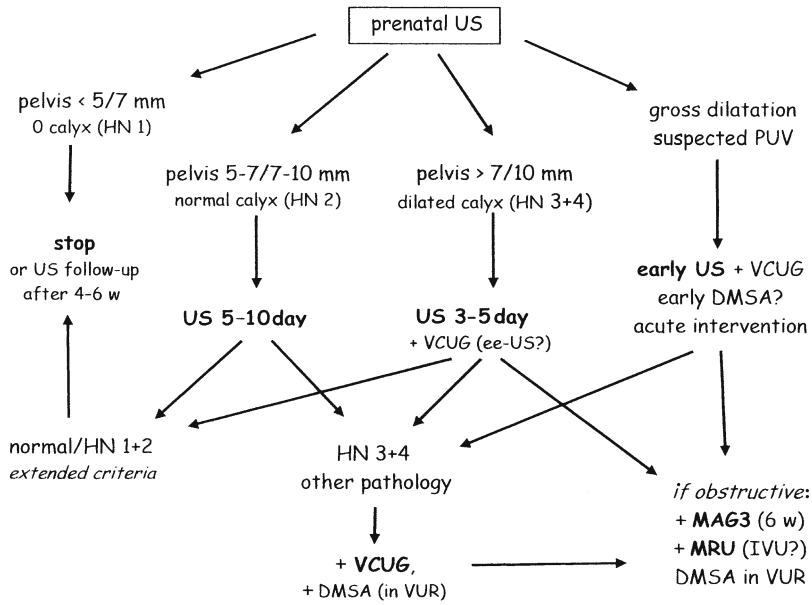

Abbreviations: DMSA, static renal scintigraphy; HN, hydronephrosis; MAG3, dynamic renography; MRU, MR-urography; US, ultrasound; UT, urinary tract; VCUG, voiding cystourethrography.
Source: Adapted from Riccabona M, Fotter R (2004) Pediatr Radiol 34:295–301.

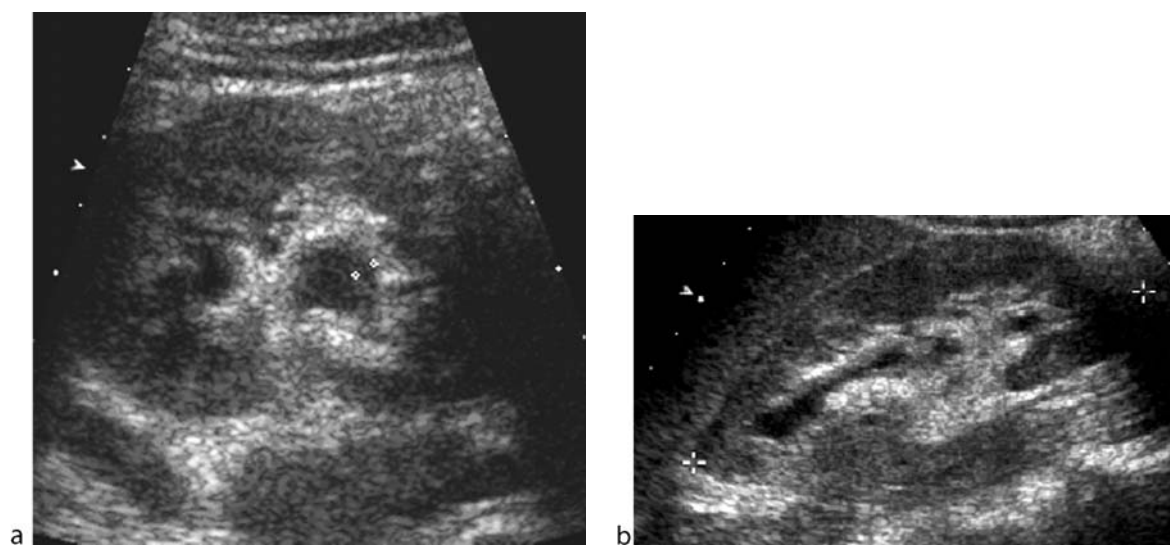

Hydronephrosis in Childhood. Figure 2 Example for 'extended US criteria': the urothelial sign. US of the right kidney at the level of the renal pelvis: note the thickened pelvic wall known as the 'urothelial sign' (marked ++ in the axial view) that is reported in urinary tract infection and ▶obstructing or refluxing uropathy.

or an imaging protocol for the assessment of obstructive uropathy (see entry 'Obstructive Uropathy', using diuretic renography and MR-urography/IVU) will become indicated.

Imaging Algorithms (Table 1)

As the knowledge on pathogenesis and physiological development of various conditions is constantly deepening, the imaging algorithms for working-up neonates and

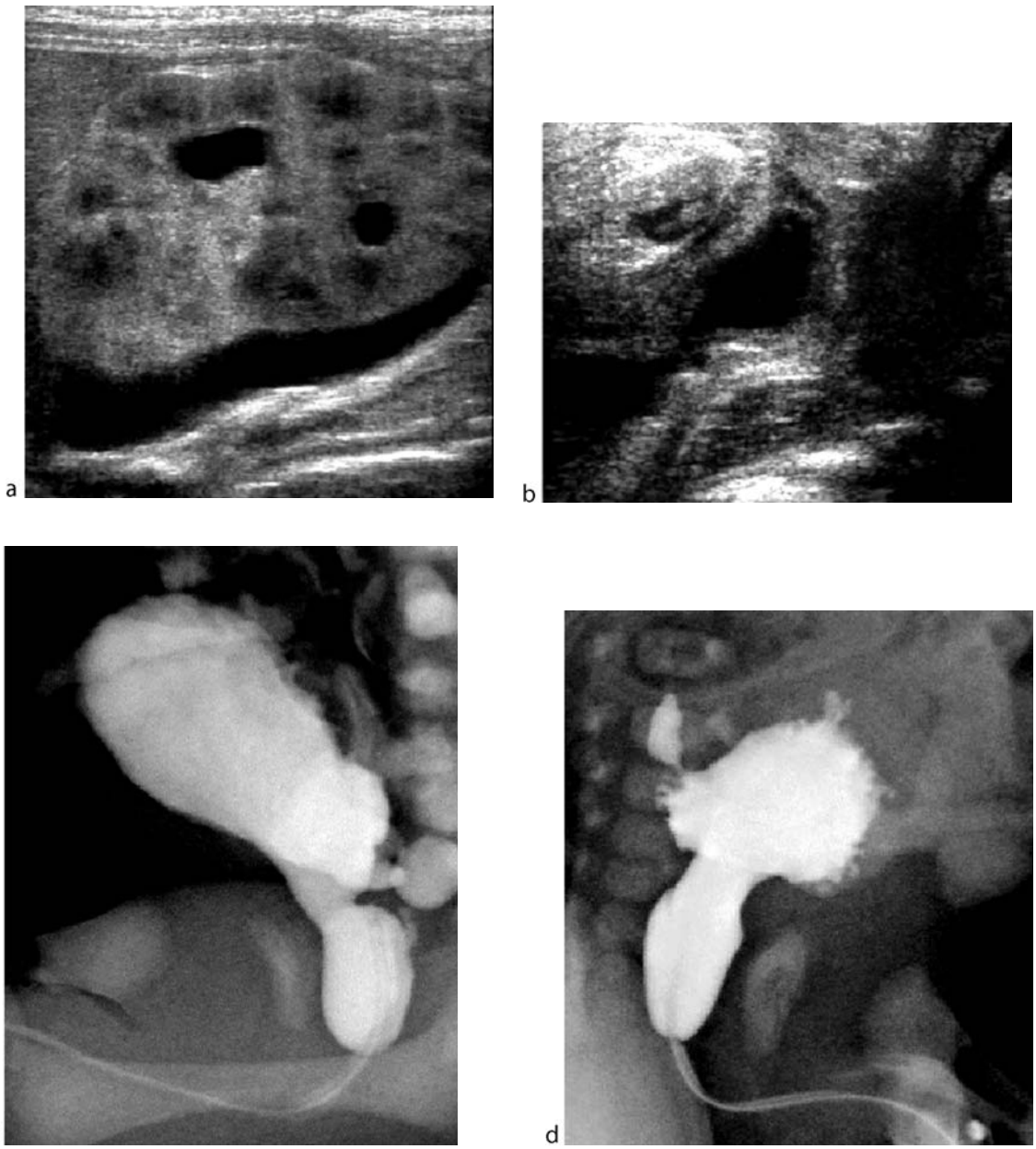

Hydronephrosis in Childhood. Figure 3 Imaging findings in PUV–US (a and b) and VCUG (c and d). (a) Longitudinal US section of the right kidney with perirenal urinoma (due to intra-uterine calyceal rupture) shows mild dilatation of the collecting system with some parenchymal inhomogeneity as well as a parenchymal cyst as a sign for dysplasia. (b) Perineal US (sagittal plane) demonstrates a posterior urethral valve (PUV) in the same neonate; note the thickening of the bladder wall with some irregularity of the inner urinary bladder wall contour. (c and d) VCUG demonstrates PUV with bladder diverticula and VUR on spot films in lateral (c) and anterior–posterior projection (d).

infants with HN are constantly undergoing changes—however, at present, usually US follow-up is recommended in low-degree HN; VCUG or echo-enhanced urosonography is suggested for mid-grade HN (for differentiation of refluxing versus obstructive uropathy), and an additional diuretic renal scintigraphy or diuretic MR-urography (or IVU, if MR-urography is unavailable) are suggested for cases with persisting high-grade HN or deterioration of mid-grade HN. There is one additional aspect that needs to be considered: Neonatal boys with huge bladders, bladder wall thickening and particularly gross HN may suffer from ▶posterior urethral valves; furthermore

the 'Prune belly syndrome' should be considered. In these conditions early imaging and intervention (US, VCUG, cystostomy or/and nephrostomy) may become indicated during the earlier days of life for obstructive renal insufficiency (Fig. 3).

Diagnosis

Diagnostic features depend on the underlying cause and HN grade. Diagnosis is made based on imaging that depicts dilatation of the collecting urinary system. On MRU, scintigraphy and IVU, missing or delayed contrast excretion and delayed drainage of the contrast material or radiotracer indicate significant obstruction. In severe unilateral acute obstruction DDS may exhibit asymmetrically elevated resistive indices of the affected kidney.

Bibliography

1. Fred E, Avni FE, Hall M et al (2001) Postnatal imaging of fetal uropathies. In: Fotter R (ed) Pediatric Uroradiology. Springer, Berlin-Heidelberg, pp 321–337
2. Gordon I, Riccabona M (2003) Investigating the newborn kidney—update on imaging techniques. Seminar Neonatal 8:269–278
3. Owen RJT, Lamont AC, Brookes J (1996) Early management and postnatal investigation of prenatally diagnosed hydronephrosis. Clin Radiol 51:173–176
4. Pope JC, Brock JW, Adams MC et al (1999) How they begin and how they end: classic and new theories for the development and deterioration of congenital anomalies of the kidney and the urinary tract. J Am Soc Nephrol 10:2018–2028
5. Riccabona M, Fotter R (2004) Reorientation and future trends in paediatric radiology. Minutes of a symposium. Pediatr Radiol 34:295–301

Hydrops, Gallbladder

This condition, also called "mucocele of the gallbladder," is characterized by the massive distension (more than 5 cm in the transverse section) of the gallbladder lumen as a result of prolonged obstruction of the cystic duct usually caused by an impacted stone. The distended gallbladder contains clear mucus (white bile) produced by the mucosal epithelial cells. This condition may be either asymptomatic or symptomatic with right upper quadrant discomfort or pain. A palpable mass is usually appreciable in the right upper quadrant. US shows an enlarged gallbladder of biconvex shape with an anechoic content, although sludge or stones can be present. The gallbladder wall usually shows a normal thickness.

▶Cholecystitis

Hydroureter (= Megaureter)

Idiopathic/congenital or secondary dilated ureter, e.g. due to obstruction at the uretero-vesical junction.

▶Hydronephrosis in childhood

Hydroxyapatite Rheumatism

▶HADD

Hypernephroma

▶Carcinoma, Renal Cell

Hyperparathyroidism

Thomas M. Link
Clinical Director MQIR, Department of Radiology, San Francisco, USA
tmlink@radiology.ucsf.edu

Synonyms and Definitions

▶Primary hyperparathyroidism is due to an increased secretion of parathyroid hormone (PTH) induced by overactive parathyroid glands. In ▶secondary hyperparathyroidism, a metabolic disorder such as kidney failure with decreased calcium levels in the blood leads to increased PTH levels. ▶Tertiary hyperparathyroidism is defined as an autonomous production of PTH by the parathyroid glands, which was originally induced by a metabolic disorder with secondary hyperparathyroidism. ▶Renal osteodystrophy due to chronic renal failure encompasses a bone disease that is characterized by secondary hyperparathyroidism, osteomalacia, and osteoporosis.

Pathology/Histopathology

PTH maintains appropriate serum calcium concentrations, regulates bone metabolism, and is essential for bone

remodeling. It affects osteoclasts and osteoblasts, but osteoclastic activity is more pronounced with pathological serum concentrations of PTH. As bone is resorbed, fibrous tissue replaces it; microfractures and hemorrhage may occur, and subsequent growth of fibrous tissue may cause ►brown tumors.

Primary hyperparathyroidism is due to an adenoma of the parathyroid gland in 50–80% of cases, to diffuse hyperplasia in 10–40%, and to multiple adenomas in 10%. Rarely, it is due to a carcinoma of the parathyroid gland. The differential diagnosis should always include multiple endocrine neoplasia (types I or IIA).

Secondary hyperparathyroidism is caused by chronic hypocalcemia, either due to chronic renal failure or intestinal malabsorption. Chronic renal failure is accompanied by other changes with elevated phosphate levels and reduced renal production of 1,25-dihydroxycholecalciferol or vitamin D3. Alkaline phosphatase is frequently increased. In patients on long-term hemodialysis, an accumulation of aluminum prevents mineralization of osteoid. All of this may lead to osteopenia, osteomalacia, and insufficiency fractures. Renal osteodystrophy is a complex disease that has features of secondary hyperparathyroidism, osteomalacia, and osteoporosis but also a varying degree of osteosclerosis. Bone resorption goes along with fibrous replacement of the bone marrow, and brown tumors may develop if osteoclastic activity is substantial. Osteosclerosis is also a typical finding and may be due to the anabolic activity of PTH, an increase in woven bone, or accompanying oxalate deposition. In addition, certain proteins such as beta-2-microglobulin are no longer eliminated by the kidneys, resulting in deposition of amyloid.

Tertiary hyperparathyroidism develops in patients with chronic secondary hyperparathyroidism with stimulated growth of the parathyroid glands, causing an autonomous adenoma. This goes along with hypercalcemia and inability to control osteomalacia despite vitamin D therapy.

Clinical Presentation

Primary hyperparathyroidism typically presents with hypercalcemia after routine laboratory testing. Symptomatic bone disease is found in 10–25% of the patients, and one of the earliest findings may be nonspecific back pain. Other important clinical findings include nephrolithiasis (in 10–20%), pancreatitis, and peptic ulcer disease as well as neuromuscular, neuropsychiatric, and cardiovascular disease.

In secondary hyperparathyroidism features of renal failure are usually present, and bone and joint pain may develop; this pain is usually vague and commonly located in the lower back, hips, knees, and legs. More severe pain may be due to insufficiency fractures or to periarticular deposition of hydroxyapatite, which typically occurs with marked hyperphosphatemia. In addition, muscular weakness or bowing deformities of the weight-bearing long bones may be found.

Imaging

Conventional Radiographs

Conventional radiography is the standard imaging procedure in the diagnosis of bone changes induced by hyperparathyroidism. In primary hyperparathyroidism radiographs of the hands may show subperiosteal resorption, in particular at the tufts of the distal phalanges and the radial side of the middle phalanges II and III. These findings are pathognomic (Fig. 1). Other typical findings include resorption of the lamina dura around the teeth, the distal clavicle, and the sacroiliac joints with widening of the joint spaces. Resorptive changes at the sternoclavicular and acromioclavicular joints, the symphysis, and the ribs are also demonstrated. In skull radiographs, a salt-and-pepper appearance is described that consists of intermingled areas of decreased density with small sclerotic areas (1).

Radiographs of the skeleton may show osteopenia, which may be generalized or asymmetric. Fine trabeculations are lost, and the bone structure may appear coarse or thickened. In later stages a ground-glass pattern may be found. However, it should be noted that on conventional radiographs bone loss must be in the order of more than 30% in order to be diagnosed. In addition to subperiosteal resorption, intracortical, endosteal, subligamentous, and subtendinous bone resorption may be found in hyperparathyroidism.

In more advanced disease, brown tumors are demonstrated, which are well-circumscribed lytic lesions of bone due to focal osteoclastic resorption and subsequent fibrous replacement. These lesions may be single or multiple, with expansion of the overlying bone. Typical locations are the pelvis and femur, clavicle, ribs, and mandible. After treatment of the hyperparathyroidism, these tumors usually calcify.

Calcium pyrophosphate deposition disease (CPPD) may also be observed with calcification of the menisci of the knee and triangular fibrocartilage. It is more common in primary than in secondary hyperparathyroidism.

Findings in secondary hyperparathyroidism are very similar to those in primary hyperparathyroidism. In a previous study by Mayet et al that analyzed radiographic findings in patients with secondary hyperparathyroidism, pathological changes were found in hand radiographs of 56% of the patients, in 45% at the acromioclavicular joints, in 31% at the shoulders, and in 27% at the pelvis (2).

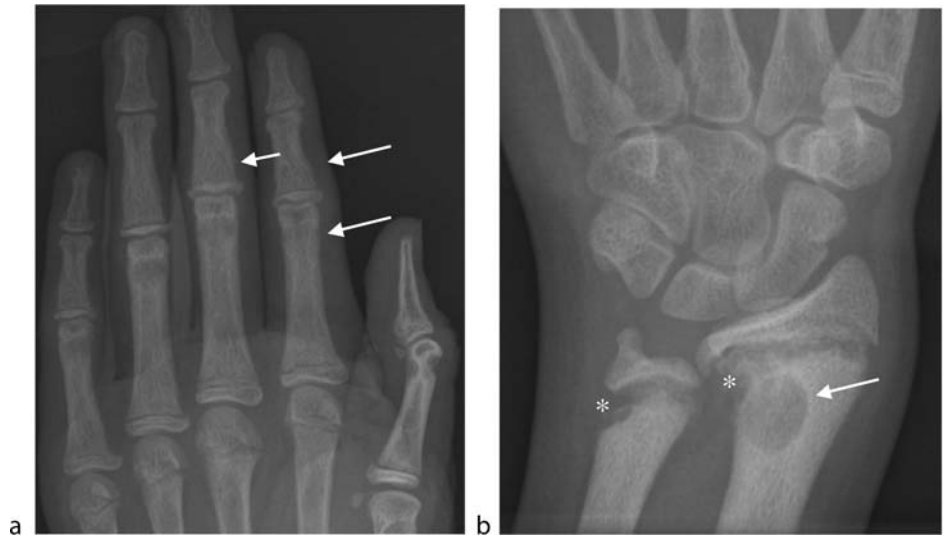

Hyperparathyroidism. Figure 1 Hand radiograph in an adolescent with end-stage renal failure and resorptive bony changes at the diaphyses, in particular of the middle and proximal phalanges II and III at the radial aspect (*arrows* in a). In addition, a brown tumor (*arrow* in b) and widening of the growth plates (*asterisk* in b) are demonstrated, the latter being a finding consistent with rickets.

In renal osteodystrophy additional features of osteomalacia and sclerotic bony changes are shown. These sclerotic changes occur in approximately 20% of patients and may be found at the spine, pelvis, ribs, and extremities, more frequently at the metaphyses and sometimes at the epiphyses, which may mimic aseptic necrosis of the bone. One of the most typical findings is the rugger-jersey spine with bands of increased bone density adjacent to the endplates.

Extraosseous calcification is also a characteristic finding in secondary hyperparathyroidism, in particular in long-standing disease. These calcifications include tumoral calcifications around the joints (hip, shoulder, and knee), with or without bony erosion, vascular, corneal, subcutaneous, and visceral calcifications. More rare findings include periosteal reactions around the metatarsals, femora, and pelvis.

Osteomalacia may sometimes be predominant in patients with renal osteodystrophy with Looser zones and pathologic fractures, bone deformities, and osteopenia. In children, typical changes of the growth plate with widening and disorganization as well as irregularities of the metaphyseal margins may be found; these findings are consistent with rickets (3).

In patients on long-term hemodialysis, additional findings are shown that may be due to aluminum intoxication or deposition of amyloid: (i) Aluminum intoxication may cause osteomalacia and rickets with insufficiency fractures, and (ii) amyloid depositions may be found in the bone appearing as lytic, sharply demarcated, juxta-articular lesions. In addition, (iii) destructive spondylarthropathies, (iv) osteonecrosis, (v) articular rheumatologic manifestations, and (vi) tendonitis and tendon rupture as well as (vii) an increased incidence of musculoskeletal infections may be found (3).

DXA and QCT

Dual X-ray absorptiometry (DXA) and quantitative computed tomography (QCT) are used to assess loss of bone mass and are more sensitive to these changes than conventional radiographs. However, loss of bone mineral density (BMD) is a nonspecific finding for hyperparathyroidism. Also note that due to sclerotic bony changes in renal osteodystrophy, BMD may be falsely increased and not correctly reflect actual fracture risk.

CT

Findings that may be better visualized with computed tomography (CT) than with conventional radiography are brown tumors and insufficiency fractures, particularly of the pelvis. Erosive changes of the sacroiliac joints may also be better characterized with CT imaging. The axial CT image of the pelvis presented in Fig. 2 shows, in addition to a brown tumor in the right iliac wing and erosive changes of the sacroiliac joints, a coarse, ground-glass-like trabecular bone structure. Soft tissue calcifications are

also better depicted with CT, and extensive Schmorl's nodes may be well visualized.

MRI

Magnetic resonance imaging (MRI) is useful to detect insufficiency fractures or reactions. It also may show osteonecrosis and slipped capital femoral epiphyses. More important, however, is that in the absence of conventional radiographs and CT images, MRI findings may be confused with those found in neoplastic disease such as diffuse nonspecific bone marrow changes, brown tumors, and tumorlike metastatic calcifications. The MR signal in these latter calcifications may be variable, and contrast enhancement may also be found. Fig. 3 shows metastatic calcifications in the second digit of the left hand in a patient with secondary hyperparathyroidism, which were interpreted as tumors at first, as they show contrast enhancement in the coronal fat-saturated T1-weighted images, but the conventional radiograph clearly shows the extensive soft tissue calcifications. Brown tumors can sometimes show intraosseous and extraosseous components with cystic changes, which can easily be mistaken for primary bone tumors or metastatic disease in the absence of findings indicating end-stage renal disease.

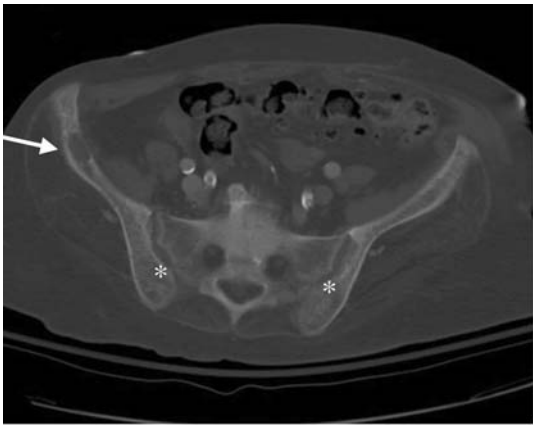

Hyperparathyroidism. Figure 2 Computed tomography of the pelvis in a patient with secondary hyperparathyroidism shows resorptive changes at both SI joints (*asterisk*) and a brown tumor within the right iliac bone (*arrow*).

Nuclear Medicine

Skeletal scintigraphy may present pathological findings that may help in differentiating hyperparathyroidism from malignant disease in the presence of increased

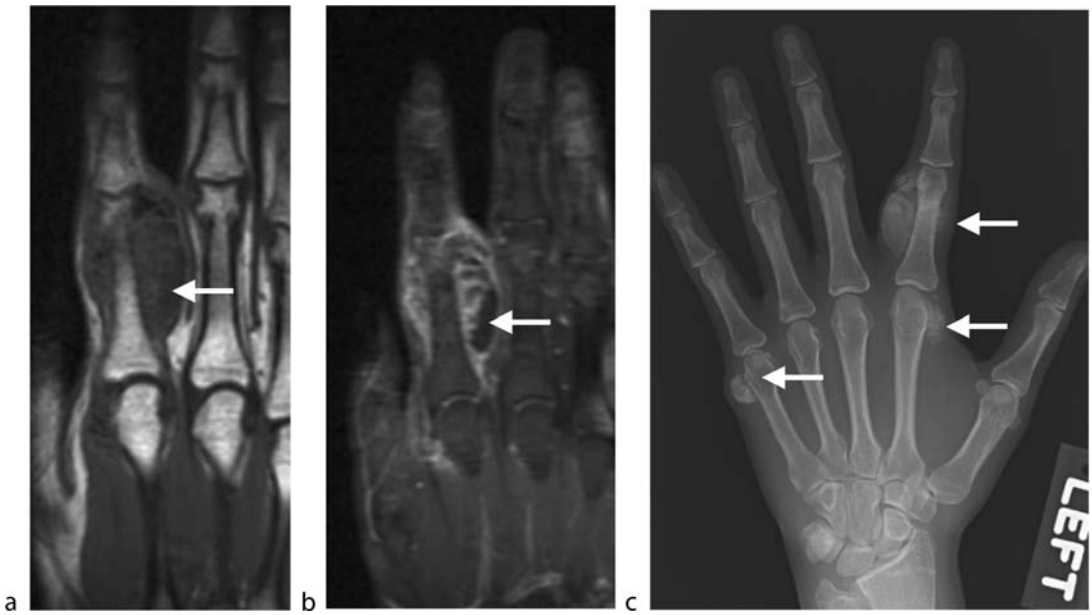

Hyperparathyroidism. Figure 3 Coronal T1-weighted magnetic resonance imaging without (a) and with contrast enhancement and fat saturation (b) of the left hand, showing partially enhancing tumorlike lesions with low signal intensity areas (*arrows*) at the second digit. Radiograph of the left hand (c) clearly shows calcifications at the second and fifth digits (*arrows*).

calcium levels. Typical findings include increased uptake of technetium throughout the skeleton; sometimes a so-called super-scan is found. Typically increased uptake is most apparent at the axial skeleton, the calvarium, the mandible, the long bones, and the sternum. In secondary hyperparathyroidism due to renal failure, kidney and bladder may not be well visualized on technetium scans.

Diagnosis

To diagnose primary or secondary hyperparathyroidism, the history and clinical findings are extremely important (4). Increased calcium levels in primary hyperparathyroidism and a history of end-stage renal failure in secondary hyperparathyroidism are key findings required to correctly assess imaging findings. Although pathology on conventional radiographs and CT images is usually fairly straightforward, it may be more difficult to interpret this pathology on MR studies.

The differential diagnosis of intracortical bone resorption includes hyperthyroidism and acromegaly, while subchondral resorptions and deformities may be similar to those found in inflammatory arthropathies (rheumatoid and psoriasis arthritis), osteonecrosis, and chondrocalcinosis. Resorptions at the sacroiliac joints may sometimes appear as in ankylosing spondylitis. Brown tumors can be difficult to differentiate from primary or secondary bone tumors. Bony sclerosis is also found in myelofibrosis, mastocytosis, Paget's disease, neoplastic disorders, and sarcoidosis, and after radiation therapy. Soft-tissue calcifications have to be differentiated from calcium–pyrophosphate deposition disease.

Bibliography

1. Resnick D, Niwayama G (1988) Parathyroid disorders and renal osteodystrophy. In: Resnick D Diagnosis of bone and joint disorders, 2nd edn. WB Saunders, Philadelphia, pp 2219–2249
2. Mayet W, Hermann E, Wandel E et al (1991) Rheumatologische und radiologische Symptome bei sekundärem Hyperparathyreoidismus: Retrospektive Langzeit-Studie bei 175 chronischen Dialysepatienten. Z Rheumatol 50:313–319
3. Jevtic V (2003) Imaging of renal osteodystrophy. Eur J Radiol 46:85–95
4. Tigges S, Nance E, Carpenter W et al (1995) Renal osteodystrophy: imaging findings that mimic those of other diseases. Am J Roentgenol 165:143–150

Hyperplasia

Proliferation of epithelial cells lining the walls of ducts and lobules.

▶ Fibrocystic Disease, Breast

Hyperplasia, Benign, Prostate

Jurgen J. Fütterer
Department of Radiology, Radboud University Medical Centre Nijmegen, Nijmegen, The Netherlands
j.futterer@rad.umcn.nl

Synonym

Benign prostatic hypertrophy

Definition

Benign prostatic hypertrophy (BPH) is a noncancerous enlargement of the prostate gland that may restrict the flow of urine from the bladder consisting of nodular hypertrophy of the fibrous, muscular, and glandular tissue within transition zone and periurethral areas.

Epidemiology

Thirty million men worldwide have symptoms related to benign enlargement of the prostate. BPH is first detectable around the fourth decade of life (1). The prevalence of BPH is only 8% in males in their 40s (2). According to the National Institutes of Health (NIH), BPH affects more than 50% of men over age 60 and as many as 90% of men over the age of 70.

Pathophysiology

The cause of BPH of the prostate gland is unknown. It is possible that the condition is associated with hormonal changes that occur as men age. The testes produce the hormone testosterone, which is converted to dihydrotestosterone and estradiol. High levels of dihydrotestosterone, a testosterone derivative involved in prostate growth, may accumulate and cause hyperplasia. How and why levels of dihydrotestosterone increase remains a subject of research (3, 4). BPH is a proliferative process of the cellular elements of the prostate (i.e. an enlarged prostate). BPH involves both the stromal and epithelial elements of the prostate arising in the periurethral and transition zones of the prostate gland (for the distribution of BPH, see Table 1). The pathogenesis of BPH is still largely unresolved, but multiple partially overlapping and complementary theories have been proposed, all of which seem to be

Hyperplasia, Benign, Prostate. Table 1 Distribution of BPH in the prostate

BPH love distribution
Lateral lobe prostatic enlargement (70%)
Middle and lateral lobe enlargement (20%)
Middle lobe prostatic enlargement (10%)

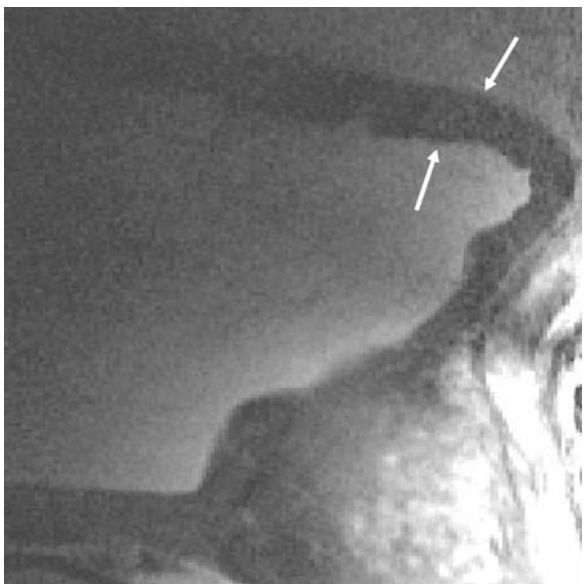

Hyperplasia, Benign, Prostate. Figure 1 T2-weighted saggital view demonstrates a thick trabeculated bladder wall (white arrows).

operative at least to some extent. At the moment two theories are hypothesized, namely the neoplastic and hormonal theory. The first theory assumes that the enlargement is a benign neoplasm. The latter theory, hypothesize that with advancing years, the balance between androgenic and estrogenic stimulation of the prostate is deregulated. As aging occurs, estrogenic stimulation becomes more active with concomitant decline in androgenic activity. Hypertrophic changes first commence in the region of the inner group of prostatic glands in the lateral lobes of the prostate. Progressive enlargement causes indentations of the urethra and atrophy of the outer glands with compression of the stroma to form a false capsule around the enlarging fibroadenomyoma. The enlarged prostate will therefore have a true and false capsule with the main blood supply, between these two capsules. The hypertrophied tissue is relative avascular. The prostate grows in two different ways. In one type of growth, cells multiply around the urethra and compress it. Which may result in that the bladder becomes hypertrophied with trabeculation (Fig. 1), sacculation, and, occasionally, diverticulum formation. The second type of growth is middle lobe prostate growth in which cells grow into the urethra and the bladder outlet area. Castrated males do not develop BPH.

Symptoms

Many symptoms of BPH stem from obstruction of the urethra and gradual loss of bladder function, which results in incomplete emptying of the bladder. Common symptoms of BPH include hematuria (caused by straining to void), dribbling after voiding, frequent urination (nocturia), feeling that the bladder has not emptied completely after urination, weak urine stream, leakage of urine, and sudden urgent need to urinate (5). Acute urinary retention can result from holding urine for a long time in severe cases of BPH (6). Acute urinary retention causes severe pain and discomfort. Catheterization may be necessary to drain urine from the bladder and obtain relief.

Diagnostic Tests and Imaging Techniques in Benign Prostatic Hypertrophy

Digital rectal examination—This examination gives a general idea of the size and condition of the prostate gland.

Prostate-specific antigen—A prostate-specific antigen (PSA) test can be taken to rule out cancer as a cause of urinary symptoms. However, much remains unknown about the interpretation of PSA levels, the test's ability to discriminate cancer from benign prostate conditions, and the best course of action following a finding of elevated PSA.

Urine flow study—A reduced flow often suggests BPH (7).

Cystoscopy—This examination allows to identify the location and degree of the obstruction and determine the size of the gland.

Transrectal ultrasound—Transrectal ultrasound (TRUS) is useful for determining prostate size in patients with lower urinary tract symptoms. TRUS can assess the prostate anatomy, zonal anatomy, and internal changes (Fig. 2). Prostatic volume can easily be assessed with TRUS. Generally, TRUS is not indicated for the initial evaluation of BPH. Imaging of the prostate using TRUS is recommended in selective patients. Ruling out prostate cancer in patients with elevated PSA (>4 ng/mL) is a strong indication to proceed imaging studies and TRUS-guided biopsies.

Computed tomography—With computed tomography (CT), BPH appears as a homogeneous-enhancing area with well-defined borders (Fig. 3). CT has no

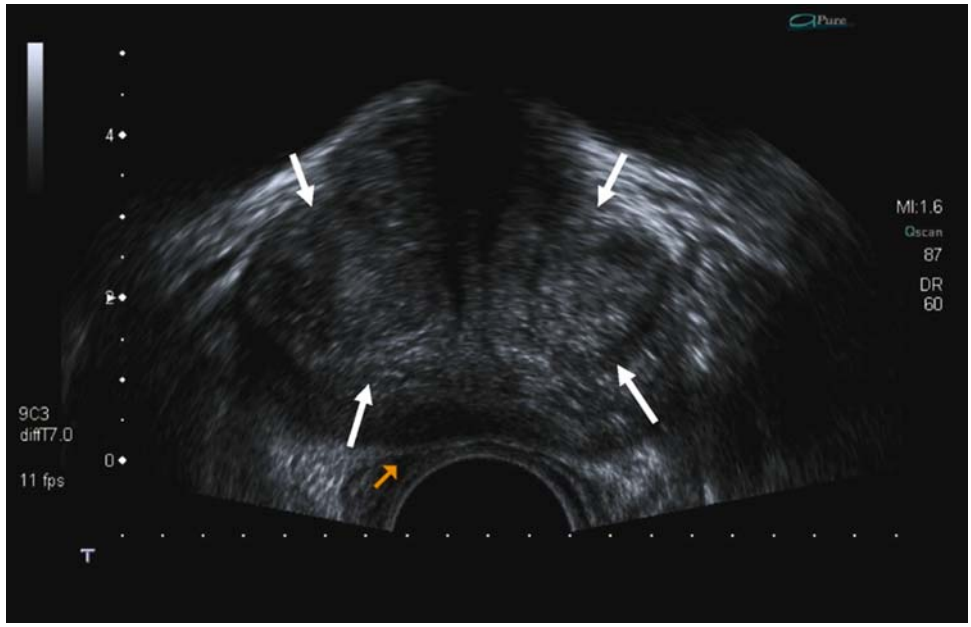

Hyperplasia, Benign, Prostate. Figure 2 Transrectal ultrasound image of the prostate in the axial plane in a 64-year-old patient. In the central gland, two large benign prostatic hyperplasia nodules are present (white arrows).

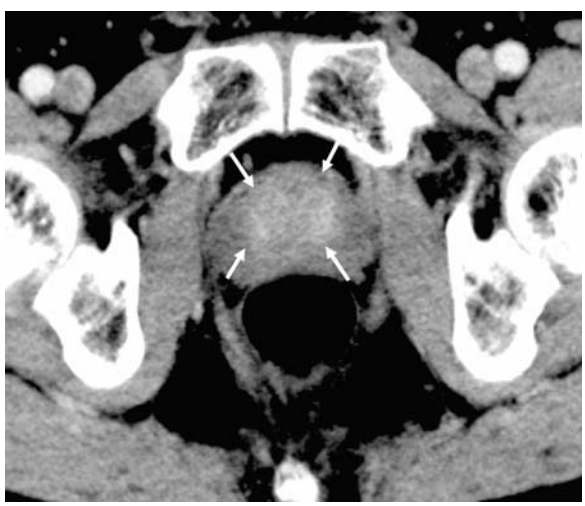

Hyperplasia, Benign, Prostate. Figure 3 Axial CT plane after intravenous contrast agent demonstrates homogeneous enhancing benign prostatic hyperplasia nodules in the central gland of the prostate (white arrows).

place in the evaluation of BPH because of low intraprostatic tissue contrast/resolution, which consequently does not allow the evaluation of the ratio of glandular to stromal tissue in the prostate. Prostate volumes can be estimated with this imaging modality. However, this imaging method is costly and has limited availability.

Magnetic resonance imaging—Magnetic resonance (MR) imaging allows high intraprostatic tissue contrast/resolution, which can be used to estimate prostate volume and glandular to stromal ratio. MR imaging has high accuracy for determining the histologic type (8). BPH nodules appear as nodular heterogeneous (iso- to high) signal intensities lesions with a small rim of low signal intensity in the central gland (9) (Fig. 4).

Positron emission tomography—Positron emission tomography (PET), using [^{11}C]acetate, has been reported to be of clinical relevance for the diagnosis of prostate cancer (10). Normal prostate tissue or BPH can show enhanced accumulation of [^{11}C]acetate, especially in younger men. Preliminary results indicate that careful interpretation of [^{11}C]acetate PET images of prostate cancer is necessary because of the standardized uptake value (SUV) and the early-to-late activity ratio of the SUV for the normal prostate and for BPH overlap significantly with those for prostate cancer (11).

Currently, indication for the treatment in BPH patients is based on subjective measurements of symptoms. Thus, imaging does not play a major role in the evaluation of such patients. However, the primary imaging investigation of choice is TRUS of the prostate, which may be performed either by an urologist or by a radiologist, depending on the local availability of expertise. Also TRUS is a noninvasive, cost-efficient, quick and easily available modality.

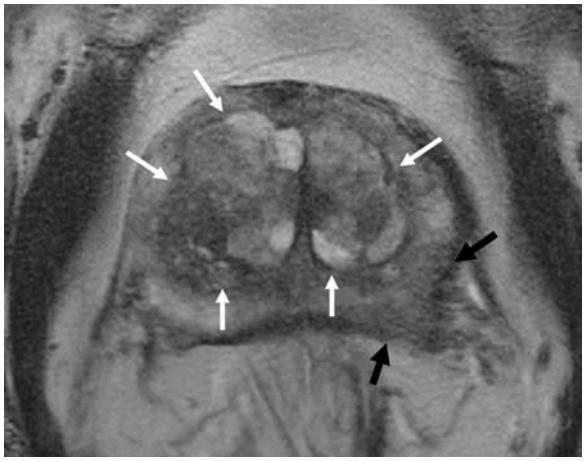

Hyperplasia, Benign, Prostate. Figure 4 T2-weighted transverse plane of the prostate in a 63-year-old male. In the central gland of the prostate, two large benign prostatic hyperplasia nodules with low to high signal intensities are present (white arrows). Note the low signal intensity area in the left peripheral zone representing prostate carcinoma (black arrow).

International Prostate Symptom Score—Alternative to imaging modalities, the International Prostate Symptom Score (IPSS) was introduced. This score was developed to quantify and validate responses to the questions asked. A set of seven questions has been adopted worldwide and yields reproducible and quantifiable information, regarding symptoms and response to treatment. Each question allows the patient to choose one of six answers indicating increasing severity of symptoms on a scale of 0–5; the total score ranges from 0 to 35. Questions concern incomplete emptying, frequency, intermittency, urgency, weak stream, straining, and nocturia. The eighth question is known as the bother score and pertains to the patient's perceived quality of life (QOL). Scores can range from 0 (delighted) to 6 (terrible). After calculating the total score for all eight questions, patients are classified as 0–7 (mildly symptomatic), 8–19 (moderately symptomatic), or 20–35 (severely symptomatic).

Treatment

Patients with (mild) symptoms are initially treated with medical therapy. Management with hormone substitutes emerged from the discovery of a congenital form of pseudohermaphroditism secondary to dihydrotestosterone deficiency. This deficiency produced a hypoplastic prostate. Type II 5-alpha reductase is an enzyme responsible for the conversion of testosterone to dihydrotestosterone. The 5-alpha reductase inhibitors block the conversion of testosterone to dihydrotestosterone, causing lower intraprostatic levels of dihydrotestosterone. This leads to inhibition of prostatic growth, apoptosis, and involution. Transurethral resection of the prostate (TURP) has long been the most common method by which obstructing prostate tissue is removed through the urethra. The indications for surgical intervention include acute urinary retention, failed voiding trials, recurrent gross hematuria, urinary tract infection, and renal insufficiency secondary to obstruction. TURP has a significant risk of morbidity (18%) and mortality (0.23%). Prostatic stents are flexible devices that can expand when put in place to improve the flow of urine past the prostate. However, their use has been associated with encrustation, pain, incontinence, and overgrowth of tissue through the stent, possibly making their removal quite difficult. Their full role and long-term effects are not fully known yet. Radical prostatectomy is now reserved for patients with very large prostates, patients with concomitant bladder stones or bladder diverticula, and patients who cannot be positioned for transurethral surgery.

Bibliography

1. McConnell JD (1998) Epidemiology, etiology, pathophysiology and diagnosis of benign prostatic hyperplasia. In: Campbell's Urology. 7th edn. WB Saunders, Philadelphia, pp 1429–1452
2. Berry SJ, Coffey DS, Walsh PC et al (1984) The development of human benign prostatic hyperplasia with age. J Urol 132:474–479
3. Bartsch G, Rittmaster RS, Klocker H (2002) Dihydrotestosterone and the concept of 5alpha-reductase inhibition in human benign prostatic hyperplasia. World J Urol 19:413–425
4. McNeal JE (1978) Origin and evolution of benign prostatic enlargement. Invest Urol 15:340–345
5. Barry MJ, Cockett AT, Holtgrewe HL et al (1993) Relationship of symptoms of prostatism to commonly used physiological and anatomical measures of the severity of benign prostatic hyperplasia. J Urol 150:351–358
6. Jacobsen SJ, Jacobson DJ, Girman CJ et al (1997) Natural history of prostatism: risk factors for acute urinary retention. J Urol 158:481–487
7. Joorgensen JB, Jensen KME, Bille-Brahe NE et al (1986) Uroflowmetry in asymptomatic elderly males. Brit J Urol 58:390–395
8. Schiebler ML, Tomaszewski JE, Bezzi M et al (1989) Prostatic carcinoma and benign prostatic hyperplasia: correlation of high-resolution MR and histopathologic findings. Radiology 172:111–137
9. Kahn T, Burrig K, Schmitz-Drager B et al (1989) Prostatic carcinoma and benign prostatic hyperplasia: MR imaging with histopathologic correlation. Radiology 173:847–851
10. Oyama N, Akino H, Kanamaru H et al (2002) ^{11}C-acetate PET imaging of prostate cancer. J Nucl Med 43:181–186
11. Kato T, Tsukamoto E, Kuge Y et al (2002) Accumulation of [^{11}C]acetate in normal prostate and benign prostatic hyperplasia: comparison with prostate cancer. Eur J Nucl Med 11:1492–1495

Hyperplasia, Breast

Luis Pina
Department of Radiology, Clínica Universitaria de Navarra, Spain
ljpina@unav.es

Definition

Hyperplasia is the proliferation of epithelial cells lining the wall of ducts and lobules. It may involve the ducts (ductal hyperplasia) or the lobules (lobular hyperplasia). Three categories of ductal hyperplasia have been reported: ►mild ductal hyperplasia, moderate or florid ductal hyperplasia, and atypical ductal hyperplasia (1).

Pathology/Histopathology

Hyperplasia shows no specific features on gross examination (2). Mild ductal hyperplasia consists of a proliferation of more than two but less than four cell layers between basement layer and lumen, without cellular atypia (1). Moderate or florid ductal hyperplasia is defined as an intraductal epithelial proliferation greater than four cell layers, usually enough to distend the ductule and bridge the lumen. Some cellular atypia is seen (1).

Atypical ductal hyperplasia is characterized by the proliferation of evenly distributed monomorphic cells with ovoid to round nuclei. Structures such as micropapillae, arcades, bridges, and others may be found, mimicking ductal carcinoma *in situ*. Differentiating between the two entities may be difficult. The criteria used include the involvement of only one duct or a size equal or less than 2 mm. Nevertheless, an important variability may be found between pathologists (1, 2).

►Atypical lobular hyperplasia is composed of cells similar to those found in lobular carcinoma *in situ*. The differentiation may be difficult. If less than half of the acini are filled, distorted, or distended by the proliferation, the lesion is considered atypical lobular hyperplasia. If there are luminal spaces free of cells and if different types of cells are intermixed, the lesion is also considered atypical lobular hyperplasia instead of lobular carcinoma *in situ* (1).

Clinical Findings

Hyperplasia can affect females at virtually any age, although most women are between 35 and 60 years of age (1).

Hyperplasia is an alteration associated with no specific clinical features. Most cases are microscopic in dimension and thus nonpalpable and asymptomatic (2). However, hyperplasia may be associated with other coexisting lesions, such as radial scar-complex sclerosing lesion, pseudoangiomatous stromal hyperplasia, papilloma, sclerosing adenosis, and duct ectasia. The clinical findings may be due to the accompanying lesion and present as pain, nipple discharge, or a palpable mass, usually referred to as breast thickening.

Mild hyperplasia does not increase the risk of developing breast cancer. Moderate or florid hyperplasia carries a small risk (relative risk about 1.5). However, atypical ductal hyperplasia and atypical lobular hyperplasia are well-recognized risk factors for breast cancer, with a fourfold and even tenfold increased risk if there is a marked family history (1). It is controversial whether ductal hyperplasia may evolve into atypical ductal hyperplasia or low nuclear-grade ductal carcinoma *in situ*.

Imaging

Mammography

There are no characteristic findings on mammography to diagnose hyperplasia. The diagnosis is made based on biopsy of suspicious calcifications, masses, or architectural distortions (Figs. 1, 2 & 3), but the former are the most frequent (3). The calcifications associated with ductal hyperplasia, atypical ductal hyperplasia, and low nuclear-grade ductal carcinoma *in situ* are similar, being usually round, punctate, or irregular. No linear calcifications are found due to the lack of necrotic debris.

Ultrasound

There are no conclusive ultrasonographic features for diagnosing hyperplasia. If hyperplasia is associated with other lesions, the ultrasonographic appearance is usually that of the accompanying alteration (3).

Magnetic Resonance

Both atypical ductal hyperplasia and atypical lobular hyperplasia may enhance after paramagnetic contrast administration.

Nuclear Medicine

Nuclear medicine does not play a role in the diagnosis of hyperplasia.

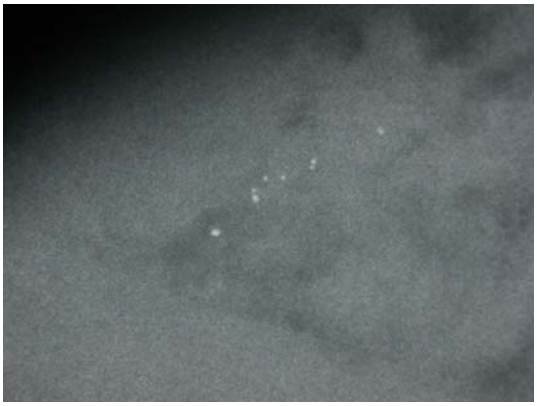

Hyperplasia, Breast. Figure 1 Round calcifications in a linear distribution. Pathology: florid ductal hyperplasia.

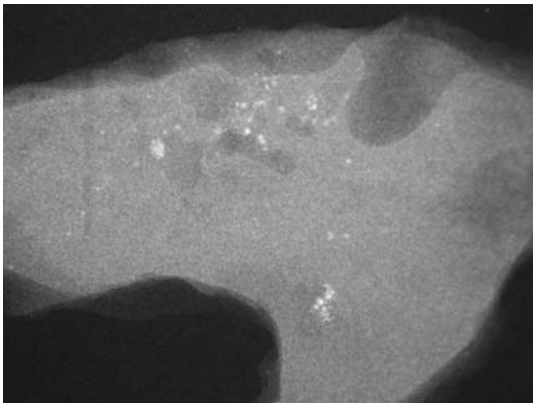

Hyperplasia, Breast. Figure 2 Surgical specimen of calcifications of intermediate concern, rounded and flaky. Pathology: atypical ductal hyperplasia.

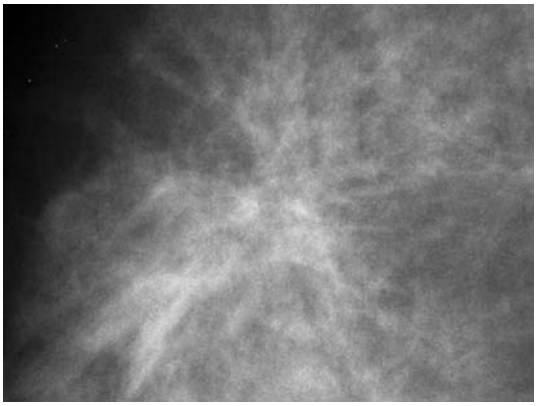

Hyperplasia, Breast. Figure 3 Architectural distortion. The lesion was a complex sclerosing lesion with atypical ductal hyperplasia. In this case, the complex sclerosing lesion was the cause for the mammographic image, and the atypical hyperplasia was not visible.

Diagnosis

Hyperplasia is a histopathologic term, usually diagnosed as the result of biopsy of nonpalpable lesions such as breast calcifications. The widespread use of mammography and percutaneous biopsy techniques has led to a increasing number of cases. The management after percutaneous breast biopsy is important. A result of atypical ductal hyperplasia at 14-gauge core biopsy underestimates carcinoma in 20–50% of cases (4, 5). Vacuum-assisted devices decrease this underestimation, but underestimation persists in up to 38% of cases (4, 5). Even the complete removal of the mammographic lesion does not ensure the absence of carcinoma. Thus, a diagnosis of atypical ductal hyperplasia at percutaneous biopsy warrants surgical excision. Atypical lobular hyperplasia at percutaneous biopsy is also an indication for surgical excision. However, mild or ▶moderate ductal hyperplasia diagnosed at core needle biopsy does not need further intervention.

Bibliography

1. Hughes LE (2000) The relationship between clinician and pathologist in benign breast disorders. In: Hughes LE, Mansel RE, Webster DJT (eds) Benign Disorders and Diseases of the Breast. Concepts and Clinical Management. Saunders, London, pp 49–59
2. Rosen PP (2001) Ductal hyperplasia. Ordinary and atypical. In: Rosen PP (ed) Rosen's Breast Pathology. Lippincott Williams & Wilkins, Philadelphia, pp 201–228
3. Cardeñosa G (2001) Terminal duct. Ductal hyperplasia. In: Cardeñosa G (ed) Breast Imaging Companion. Lippincott Williams & Wilkins, Philadelphia, pp 239–241
4. Berg WA (2004) Image-guided breast biopsy and management of high risk lesions. Radiol Clin North Am 42:935–946
5. Liberman L (2000) Clinical management issues in percutaneous core breast biopsy. Radiol Clin North Am 38:791–807

Hyperplasia, Focal, Nodular Hepatic

Riccardo Lencioni, Marzio Perri
Department of Diagnostic and Interventional Radiology University of Pisa, Pisa, Italy
lencioni@med.unipi.it

Definition

Focal nodular hyperplasia (FNH) of the liver is a completely benign lesion characterized by nodular hyperplasia of hepatic parenchyma around a central scar containing an anomalous artery.

Epidemiology

FNH is the second most common benign tumor of the liver, with an estimated prevalence of 0.4–0.8% in unselected autopsy series. The tumor has a female:male ratio of between 2 and 26:1 and the average age at presentation is between the ages of 35 and 50 years.

Pathogenesis

FNH appears to be the result of a hyperplastic response of the hepatic parenchyma to an arterial lesion and/or portal venous ischemia. A congenital vascular malformation is suggested by the presence of a central fibrous scar containing abundant arteries with spider-like malformations and the association with other vascular abnormalities such as hepatic hemangioma and hereditary hemorrhagic telangiectasia. The finding of unbalanced expression of angiopoietin1 and angiopoietin2 genes coupled with expression of angiopoietin1 protein by the endothelial cells of dystrophic vessels, suggests a role of angiopoietin genes in FNH. Clonality studies and overexpression of important genes, involved in cell omeostasis such as Bcl-2 and transforming growth-factor alpha, support the important role for hepatocellular proliferation, in FNH. Conversely, the role of oral contraceptives in FNH is disputed. Their use has been associated with increase in size and vascularity of FNH nodes and tumor regression was observed after drug withdrawal.

Pathology and Histopathology

Macroscopically, the vast majority of the patients have a single, pale tan to light brown lesion causing a central scar radiating into the liver tissue. FNH may present with classical and nonclassical forms. The latter include telangiectatic, mixed hyperplastic/adenomatous, with cytologic atypia and multiple FNH syndrome forms. Eighty percent of the patients present with the classical form, which is characterized by abnormal nodular architecture, malformed-appearing vessels, and bile duct proliferation. The majority of classical forms contain one to three macroscopic scars. Microscopically, classical FNH lesion shows nodular hyperplastic parenchyma, the nodules being completely or incompletely surrounded by fibrous septa. The central scar contains malformed vessels of various caliber, mostly large and tortuous arteries showing intimal or muscular fibrohyperplasia. Dense bile ductular proliferation accompanies the vascular structures both in the central scars and in the radiating septa with histologic cholestasis. A mild degree of macrovascular steatosis is often present. Nonclassical forms of FNH show atypical histology and bile ductular proliferation, but lack either nodular architecture or malformed vessels.

Clinical Presentation

FNH is usually an incidental finding but a few patients may have symptoms as a palpable mass or hepatomegaly. Liver chemistry is usually unaltered. In a few patients, FNH may cause slight elevations in serum GGTP levels. Serum tumor markers AFP, Ca 19.9, and CEA are invariably negative.

Imaging

Ultrasound and Contrast-Enhanced Ultrasound

FNH may have variable ultrasound (US) features. It usually appears as a round mass that is slightly hypoechoic or slightly hyperechoic with respect to liver parenchyma. Some lesions may be isoechoic to liver and be detected only because of vascular displacement. The lesion is frequently homogeneous. In fact, the detection of the central scar at baseline US is uncommon. Typical findings at color or power Doppler US include the presence of a central feeding artery with a stellate or spoke-wheel pattern determined by vessels running into radiating fibrous septa originating from the central scar. Doppler spectral analysis can show an intralesional pulsatile waveform with high diastolic flow and low resistive index (1). The specificity of US in the diagnosis of FNH has improved following the introduction of US contrast agents. At contrast-enhanced ultrasound (CEUS), FNH shows central vascular supply with centrifugal filling in the early arterial phase, followed by homogeneous enhancement in the late arterial phase. In the portal phase the lesion remains hyperechoic relative normal liver tissue, and becomes isoechoic in the late phase. This pattern has been observed in 85–100% of FNH (2). The central scar becomes detectable as a hypoechoic area in the portal phase of the contrast-enhanced study.

Computed Tomography

FNH is usually isoattenuating or slightly hypoattenuating to surrounding liver at baseline computed tomography (CT) scanning. The detection rate of the central scar, that appears as a hypoattenuating structure, is related to the size of the lesion. It may be identified in 35% of lesions

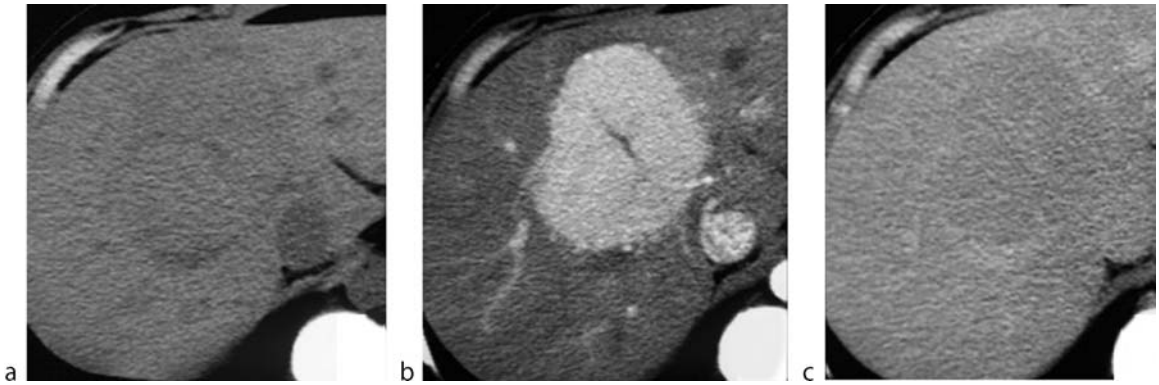

Hyperplasia, Focal, Nodular Hepatic. Figure 1 Typical FNH on multiphasic spiral-CT. On unenhanced CT scan (a) a slightly hypodense nodule is depicted. At the dynamic enhanced-CT study the nodule shows homogeneous enhancement except for the central scar in the arterial phase (b) becoming isoattenuating with the surrounding liver in the portal venous phase (c).

smaller than 3 cm in diameter and in 65% of those exceeding 3 cm (3). FNH shows strong homogeneous enhancement during the arterial phase of the contrast-enhanced CT study. The central scar is typically hypoattenuating during the arterial phase. In the portal venous and delayed phases, FNH becomes isoattenuating to the hepatic parenchyma (Fig. 1). On delayed images, the central scar may become hyperattenuating because of contrast distribution within its fibrous stroma.

Magnetic Resonance

Magnetic resonance (MR) imaging is the most accurate imaging method to characterize FNH. Owing to the affinity of its cells with normal hepatocytes, FNH is usually slightly hypointense or isointense with respect to normal liver parenchyma on T1-weighted images and slightly hyperintense or isointense on T2-weighted images (4). The hallmark of the lesion, the central stellate scar, is usually depicted because of its hypointensity on T1-weighted images and hyperintensity on T2-weighted images, reflecting its pathologic substratum of a vascularized connective tissue (4). At baseline MR imaging, however, the mentioned typical features, that are, homogeneous structure, isointensity to liver, and presence of the central scar, are observed in only 20–25% of the cases. Diagnostic confirmation requires a contrast-enhanced MR study. This is usually performed through serial dynamic imaging following the administration of a Gadolinium chelate (5). FNH shows strong, homogeneous enhancement in the arterial phase sparing the central scar, while it becomes isointense to liver parenchyma in the portal venous and delayed phases. The central scar may show contrast uptake in the delayed phase owing to the interstitial distribution of the contrast agent. These features have a specificity of more than 95% for the diagnosis of FNH (5). However, even with the administration of Gadolinium chelates, the central scar may not be detectable as many as 22% of the FNHs, including 80% of those smaller than 3 cm (5). Liver-specific MR contrast agent provides an alternate strategy to diagnose FNH. Owing to the affinity of its cells with the hepatocytes, FNH takes up hepatocyte-targeted agents, like normal parenchyma. These agents are then trapped within the lesion, since FNH is unable to effectively eliminate the compound *via* biliary excretion. Hence, it appears hyperintense to normal parenchyma on T1-weighted images (Fig. 2). Also, the central scar, that does not take up the hepatocyte-targeted agent—becomes well delineated in up to 90% of cases. This approach may enable diagnosis of 90% of the FNHs with atypical features at the baseline and conventional contrast-enhanced dynamic study (5). The diagnosis of FNH has also been achieved with the use of RES-targeted agents. Because of its rich Kupffer cell population, FNH takes up iron oxide particles, and shows marked signal intensity decrease on T2-weighted images. The central scar is usually well delineated on postcontrast images as it does not contain RES cells and therefore keeps a high signal intensity.

Nuclear Medicine

^{99m}Tc sulfur colloid scintigraphy has long been used to characterize FNH. In fact, up to 80% of these lesions show uptake owing to their Kupffer cell population. Unfortunately, the uptake of sulfur colloid is not highly specific. In one series, sulfur colloid studies were diagnostic in only about 20% of FNHs.

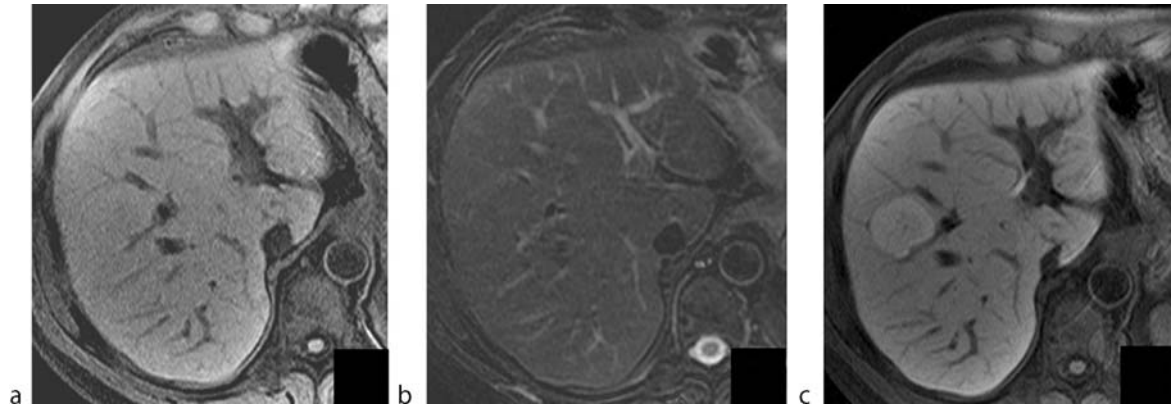

Hyperplasia, Focal, Nodular Hepatic. Figure 2 Focal nodular hyperplasia after Mn-DPDP. On baseline T1 (a) and T2-weighted (b) images the hepatic nodule is not clearly appreciable. Conversely, on the delayed T1-weighted image after Mn-DPDP administration (c) a hyperintense, well-defined lesion is depicted in the right hepatic lobe.

Diagnosis

FNH is usually incidentally detected. Diagnostic confirmation can rely solely on imaging findings, when the typical features are detected in the proper clinical setting. CT can be used to characterize lesions of medium-to-large size, but has limitations in the diagnosis of small lesions. Although promising results have been recently reported with the use of CEUS, MR imaging is the most accurate technique to diagnose FNH. MR imaging, by means of liver-specific contrast agents, enhances the informations provided by the baseline and dynamic gadolinium-enhanced study, improving the capability in lesion characterization, especially in case of small lesions. The use of percutaneous biopsy should be restricted to cases with questionable findings. In patients with atypical FNH, a scoring system has been proposed to categorize lesions into definite FNH, possible FNH, and negative for FNH.

Bibliography

1. Gaiani S, Piscaglia F, Serra C et al (1999) Hemodynamics in focal nodular hyperplasia. J Hepatol 31:576
2. Kim MJ, Lim HK, Kim SH et al (2004) Evaluation of hepatic focal nodular hyperplasia with contrast-enhanced gray scale harmonic sonography: initial experience. J Ultrasound Med 23:297–305
3. Brancatelli G, Federle MP, Grazioli L et al (2001) Focal nodular hyperplasia: CT findings with emphasis on multiphasic helical CT in 78 patients. Radiology 219:61–68
4. Bartolozzi C, Cioni D, Donati F et al (2001) Focal liver lesions: MR imaging-pathologic correlation. Eur Radiol 11:1374–1388
5. Grazioli L, Morana G, Federle MP et al (2001) Focal nodular hyperplasia: morphologic and functional information from MR imaging with gadobenate dimeglumine. Radiology 221:731–739

Hyperplastic Cystic Disease

▶Fibrocystic Disease, Breast

Hyperprostaglandin E

Hyperostosis and symptoms similar to Caffey disease, but as a known sequela of high doses of prostaglandin E1 or E2, usually given to maintain patency of the ductus arteriosus.

▶Caffey Disease

Hypersensitivity Contrast Reactions

▶Adverse Reactions, Iodinated Contrast Media, Acute, Non renal

Hypertelorism

Lateral shift of the orbits.

▶Congenital Malformations, Musculoskeletal System

Hypertension, Arterial

Michael Uder
Universitätklinikum Erlangen, Erlangen, Germany
michael.uder@idr.imed.uni-erlangen.de

Definition

Individuals with a systolic blood pressure (BP) of 140 mmHg or more or a diastolic BP of 90 mmHg or more have to be considered as hypertensive. A systolic BP of 120–139 mmHg or a diastolic BP of 80–89 mmHg has recently been defined as prehypertension, which indicates an increased risk for progression to hypertension (1).

Pathology/Pathophysiology

Hypertension can be classified as either essential or secondary. Essential hypertension is the term used when no specific medical cause can be found to explain a patient's condition. Secondary hypertension means that the high BP is secondary to other conditions, such as kidney disease or hormone-producing tumors.

Renovascular hypertension (RVH) is one of the most frequent types of secondary hypertension. It results from stenosis of the main renal artery or one of its major branches. The true prevalence of RVH is unknown but it may account for 1–5% of all cases in hypertensive adults. The pathophysiology of hypertension in renal artery stenosis (RAS) was first described by Goldblatt. Reduction of arterial perfusion pressure in the stenosed kidney leads to activation of the renin-angiotensin-aldosterone system (RAA) causing systemic angiotensin II-dependent vasoconstriction and aldosterone-mediated volume expansion (Fig. 1). Local RAA activation, arterial wall remodeling, and oxidative stress are responsible for maintaining the hypertension. These local paracrine and structural changes may also contribute directly to renal injury (2). In the majority of cases, RVH is caused by either atherosclerotic RAS or fibromuscular dysplasia (FMD). Atherosclerosis accounts for 70–90% of cases of RAS and usually involves the ostium and proximal one-third of the main renal artery (Fig. 2). FMD is a collection of vascular diseases that affects the intima, media, and adventitia of the middle and distal portion of the main renal artery and its major branches. It is responsible for 10–30% of cases of RAS (Fig. 3). Neurofibromatosis, Takayasu's arteritis, and radiation are rare causes of RVH.

Imaging

Intra-arterial digital subtraction angiography (*IA-DSA*) is traditionally regarded as the 'gold standard' in assessing renal artery anatomy. Due to its high spatial resolution, DSA is particularly useful in the early detection of FMD, in the diagnosis of intrarenal branch artery stenoses, and in kidneys with complex anatomy, including multiple accessory arteries. Disadvantages of this technique include significant interobserver variation in assessing the degree of stenosis, the absence of functional information, and the risks of contrast agent nephropathy and cholesterol emboli syndrome. Contrast arteriography is used routinely before angioplasty or surgical intervention.

Ultrasonography can be used to measure renal size and detects renal asymmetry that may be due to RAS. Importantly, kidneys less than 7 cm long are unlikely to benefit from revascularization procedures. Color-coded Doppler ultrasonography can identify RAS using either peak systolic velocity in a stenosis or by poststenotic flow phenomena. Velocities of 180–200 cm/sec at the point of maximum stenosis are widely used as the cut-off point to establish at least 50% stenosis. However, this test is unsuccessful in about 10–20% of the examinations. RASs can be detected indirectly by measuring acceleration and the waveform in intrarenal arteries distal to a stenosis. Combining direct and indirect measurements may increase the diagnostic yield. The reported sensitivity and specificity of color-coded Doppler ultrasonography for diagnosis of RAS ranges from 80 to 90% in the hands of experienced investigators. A recent meta-analysis showed that the accuracy is significantly lower than that of contrast-enhanced magnetic resonance angiography (CE-MRA) and multidetector computed tomography angiography (MD-CTA). It has been proposed to use the resistance index calculated from the Doppler spectrum as a predictor of therapeutic outcome. However, there are conflicting data about the value of this parameter.

Three-dimensional *CE-MRA* is widely accepted to be the best MR imaging technique for investigation of narrowed renal arteries. CE-MRA is typically performed using a spoiled gradient echo sequence acquiring the entire 3D data set in 20–30 sec with a spatial resolution of $1.5 \times 1.5 \times 1.5$ mm^3 or better. To get information of the dynamics of blood flow, time-resolved MRA such as multiphasic MRA or time-resolved imaging of contrast kinetics has been proposed. Although these techniques are valuable for the detection of delayed flow, they suffer from relatively poor spatial resolution. Besides anatomical abnormalities, MR imaging can determine the functional significance of narrowed renal arteries. Multiple functional parameters such as renal perfusion, glomerular

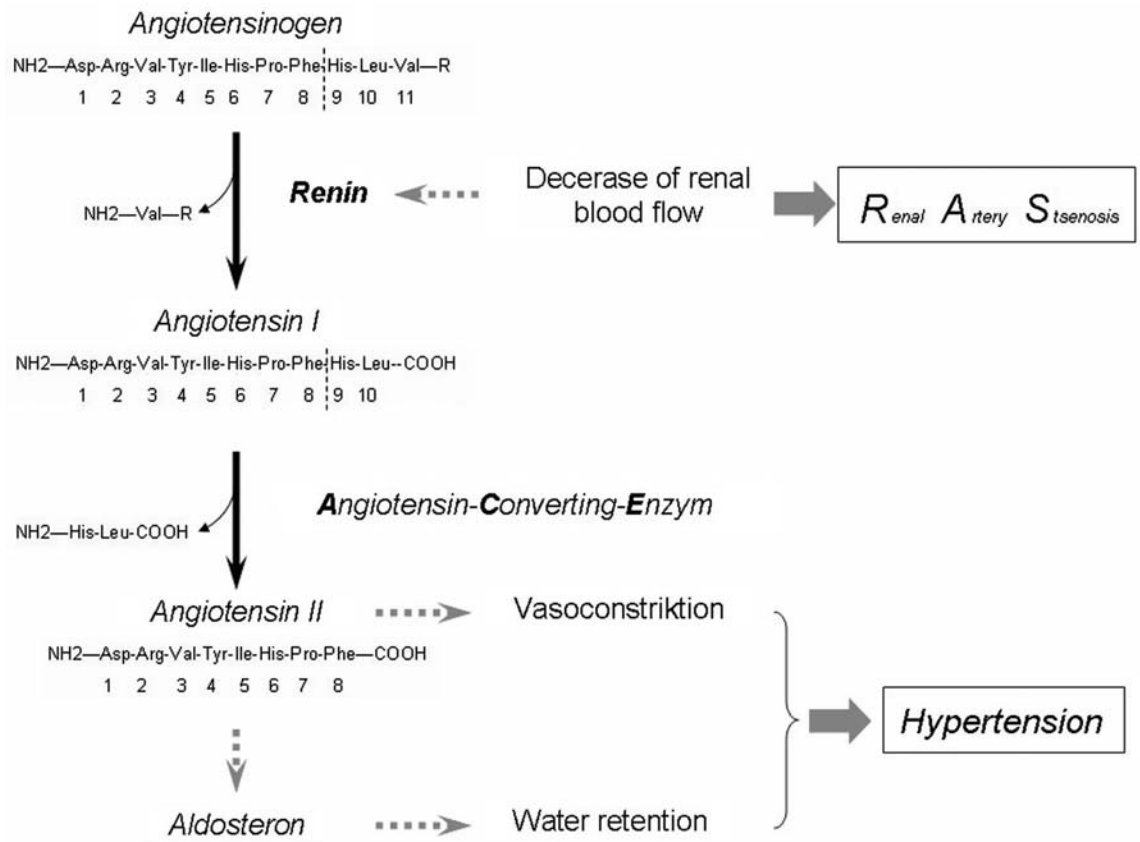

Hypertension, Arterial. Figure 1 Classic Goldblatt mechanism. A stenosis of the renal artery leads to the formation of renin *via* a reduction in renal circulation. This renin is released *via* the renal vein into the systemic circulation. It converts angiotensinogen into angiotensin I. This occurs after the splitting of two amino acids to angiotensin II by angiotensin-converting enzyme. Angiotensin II leads to constriction of peripheral resistance vessels and to water retention *via* the release of aldosterone. Together they cause systemic arterial hypertension (according to: Uder M, Humke U (2005) Endovascular Therapy of Renal artery stenosis—Where do we stand today? Cardio Vasc Intervent Radiol 28:139–47).

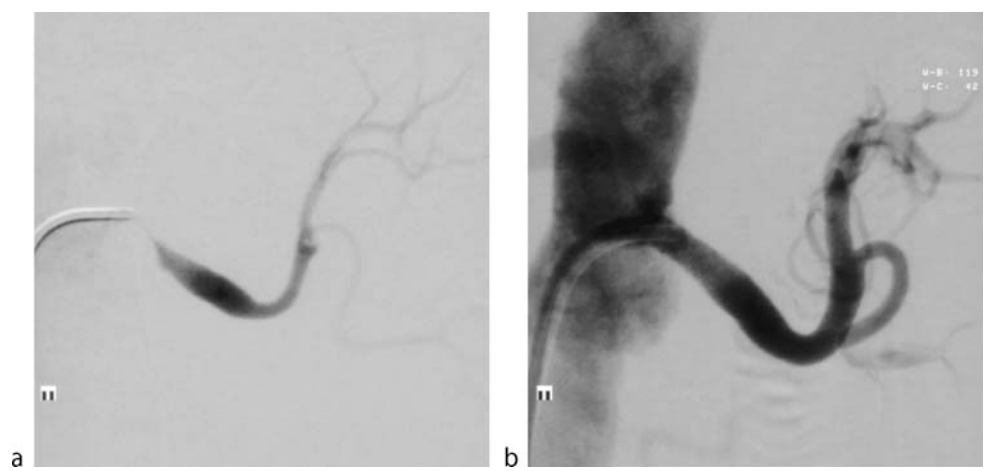

Hypertension, Arterial. Figure 2 High-grade atherosclerotic stenosis of the ostium of the left main renal artery in a 53-year-old man who had severe hypertension before and after deployment of a balloon-expandable stent (according to: Uder M, Humke U (2005) Endovascular Therapy of Renal artery stenosis—Where do we stand today? Cardio Vasc Intervent Radiol 28:139–47).

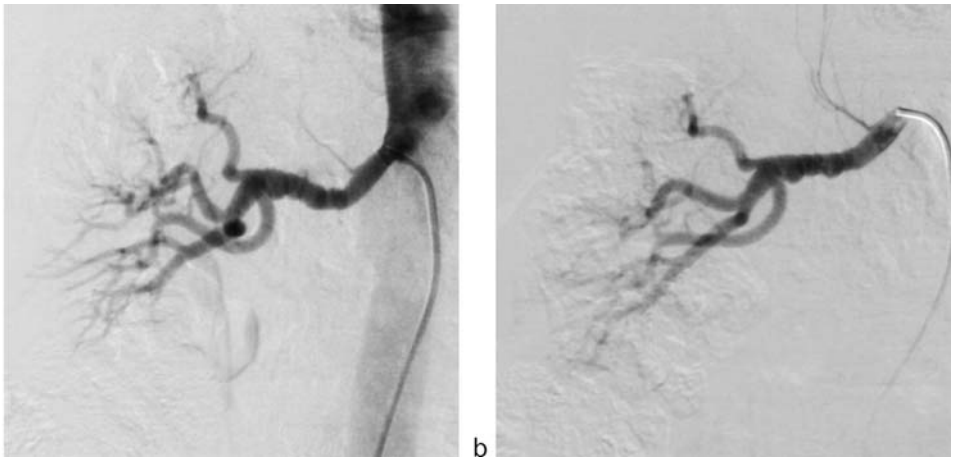

Hypertension, Arterial. Figure 3 Fibromuscular dysplasia of the renal artery in a 43-year-old man with severe hypertension. (a) Typical changes in the distal main artery. (b) After PTA with a 6-mm balloon catheter, irregularities of the vessel still appear. However, the patient became normotonic within 3 days, because the web-like stenoses were torn apart (according to: Uder M, Humke U (2005) Endovascular Therapy of Renal artery stenosis—Where do we stand today? Cardio Vasc Intervent Radiol 28:139–47).

filtration rate (GFR), tubular concentration, and transit and oxygenation can be assessed using MRI. Although there are promising results with the new techniques, today they are not yet used in clinical routine.

With the introduction of multidetector row (MD) scanners, *CTA* has become an alternative for evaluation of renal arteries. Sixty-four-row scanners can cover the abdominal aorta and its side branches in a few seconds with submillimeter *z*-axis resolution, which allows near-isotropic imaging. To provide sufficient vessel-to-background contrast, 80–150 mL of 300–400 mg I/mL nonionic contrast medium is needed. Injection speeds range from 2–6 mL/sec. CTA data sets have to be acquired in breath-hold with individualized timing of contrast material bolus. The spatial resolution of MD-CTA is superior to that of CE-MRA, and has reached $0.6 \times 0.6 \times 0.6$ m^3.

The method has been successfully used for the assessment of atherosclerotic RAS. Broad experience in patients with FMD is still missing. CTA is as accurate as MRA but has the disadvantage of radiation dose and radio-contrast volume.

Nuclear Medicine

Captopril renography is a functional test used to detect the angiotensin II dependence of GFR. In patients with activation of the RAA system, the preadministration of 25–50 mg oral captopril delays the uptake of tracer, reduces peak uptake, prolongs parenchymal transit, and slows excretion. The result of the test can be affected by factors such as volume depletion, concurrent medication, underlying renal dysfunction, and bilateral RAS. Therefore careful preparation of the patient is mandatory. It is widely used as a screening test for RAS, but in reality it provides little additional information than an assessment of plasma creatinine level 3–5 days after introducing the drug. However, its most useful role is probably in predicting the benefit from revascularization of a stenosed kidney. Most data are from studies of patients with RAS due to FMD, and there are few available data from patients with atherosclerotic RAS.

Diagnosis

The low prevalence of renovascular disease in patients with arterial hypertension makes universal screening for RAS in all hypertensive patients inappropriate. Therefore, imaging studies should be limited to groups with a higher clinical index of suspicion. Clinical indicators for RVH are abrupt onset of hypertension before age 30 or after age 55, accelerated or malignant hypertension, hypertension refractory to multiple drugs, hypertension in the presence of diffuse atherosclerosis, presence of a systolic/diastolic epigastric bruit, hypertension with unexplained renal insufficiency, azotemia induced by an ACE inhibitor or angiotensin receptor blocker, asymmetry of kidney size, and flash pulmonary edema. In these patients a secondary screening is mandatory to exclude RAS. Although there is no general consensus on which is the best imaging method, for

the initial screening noninvasive methods such as ultrasound, MRA or CTA, or scintigraphy are widely preferred. A meta-analysis showed the superiority of both CTA and MRA over both captopril renography and ultrasonography for noninvasive detection of RAS (3). In contrast, a recent prospective multicenter comparative study including more than 400 patients casts doubts on the usefulness of CTA and MRA in patients with suspected RAS (4). The study showed that neither CTA nor MRA were able to rule out RAS in patients with a high pretest probability of the disorder.

A major problem with RAS is determining whether such lesions are functionally significant. Based on animal experiments, a reduction of lumen diameter of 70% is seen as relevant. In newer studies motivated by an analogous conclusion for the evaluation of stenoses of the coronary arteries or the leg vessels, stenosis of the renal artery of more than 50% has already been used as cut-off for hemodynamical significance. However, for stenoses between 50 and 70%, data that persuasively demonstrate their relevance are missing. An angiographically proven stenosis is highly suggestive of being hemodynamically effective, if collateral vessels become visible or when arterial phase, parenchymogram, and excretion into the collecting system are delayed in comparison to the contralateral side.

For stenoses based on a fibromuscular dysplasia, proof of the typical changes in the presence of renal insufficiency or hypertension is sufficient as a treatment indication. Estimation of the angiographic stenosis grade does not play a role here, because the web-like stenoses cannot be reliably evaluated angiographically for their relevance to renal blood flow.

Interventional Radiological Treatment

Many studies show that removal of hemodynamically relevant stenoses of the renal artery can lead to an improvement in or cure of arterial hypertension (5). The success of the treatment is not dependent solely on the degree of the stenosis but also on its etiology, on the age of the patient, and the duration of hypertension, for instance. Treatment of stenoses in fibromuscular dysplasia shows cure of the hypertension in 40% of patients and improvement in 51% of patients, with cumulative success rates up to 90% over 10 years. The results for atherosclerotic RAS are less favorable. An improvement of hypertension by PTA or stenting of the renal artery can be reached in a maximum of two-third of patients. In total, 30–50% of the treated patients get a relapse of hypertension within short to midterm follow-up. Three randomized controlled trials showed no benefit of PTA over antihypertensive medication in terms of changes in BP. However, meta-analyses of 210 patients from the randomized trials showed a moderate but significant advantage for the angioplasty as opposed to pure pharmacological therapy in change of both systolic and diastolic BP. However, the value of angioplasty or stenting in RAS for treating arterial hypertension cannot yet be definitely rated with the available data.

Angioplasty has become the primary treatment for fibromuscular dysplasia of the renal arteries, with a technical success in nearly all patients and excellent long-term results. In approximately 10–20% of the patients, the procedure has to be repeated due to a relapse of hypertension by restenoses.

Atherosclerotic RAS does not respond as well to PTA therapy as do dysplastic stenoses. In atherosclerotic stenoses distant to the aortic wall, PTA is the first treatment option, with success rates of 70–90%. Stents should only be used if angioplasty fails. In ostial stenoses secondary to aortic plaque, a stent is needed to achieve technical success in most cases. Of the stented patients, 20% were faced with a restenosis within 6–12 months, whereby the risk increases with smaller stent diameters.

The endovascular therapy of atherosclerotic renal artery stenoses is afflicted by a complication rate of 5–36% with periprocedural deaths reported in less than 2% of cases. Most frequently observed complications are hematoma formation and puncture trauma. Cholesterol embolism was identified as a main reason for the loss of kidney function after angioplasty and stent placement.

Bibliography

1. Chobanian AV, Bakris GL, Black HR et al (2003) National Heart, Lung, and Blood Institute Joint National Committee on Prevention, Detection, Evaluation, and Treatment of High Blood Pressure; National High Blood Pressure Education Program Coordinating Committee; The Seventh Report of the Joint National Committee on Prevention, Detection, Evaluation, and Treatment of High Blood Pressure: the JNC 7 report. JAMA 289:2560–2572
2. Dzau VJ (2001) Tissue angiotensin and pathobiology of vascular disease: a unifying hypothesis. Hypertension 37:1047–1052
3. Vasbinder GB, Nelemans PJ, Kessels AG et al (2001) Diagnostic tests for renal artery stenosis in patients suspected of having renovascular hypertension: a meta-analysis. Ann Intern Med 135:401–411
4. Vasbinder GB, Nelemans PJ, Kessels AG et al (2004) Renal Artery Diagnostic Imaging Study in Hypertension (RADISH) Study Group Accuracy of computed tomographic angiography and magnetic resonance angiography for diagnosing renal artery stenosis. Ann Intern Med 141:674–682
5. White CJ (2006) Catheter-based therapy for atherosclerotic renal artery stenosis. Circulation 113:1464–1473
6. Uder M, Humke U (2005) Endovascular Therapy of Renal artery stenosis–where do we stand today? Cardio Vasc Intervent Radiol 28:139–47

Hypertension, Pulmonary

Edwin J. R. van Beek
Department of Radiology, Carver College of Medicine, C-751 GH, Iowa City, USA
edwin-vanbeek@uiowa.edu

Definition

Pulmonary hypertension is defined as a mean pulmonary arterial pressure of greater than 25 mm Hg causing excessive loading of the right heart. The etiology of pulmonary hypertension is manifold. It may be caused at the precapillary level (pulmonary arterial obstruction, such as chronic thromboembolic pulmonary embolism), capillary level (often labeled as idiopathic) and postcapillary level (usually due to left heart diseases, such as mitral valve stenosis or insufficiency). The most important differentiation should be focused on eliminating thromboembolic disease and shunts, as these are treatable through medication, interventional radiological procedures or surgery (1).

Pathology/Histopathology

Due to the heterogeneity of this group of disorders, the pathology and histopathology may differ considerably. A classification of pulmonary hypertension has been widely adopted, and the main causes are presented in the Table 1.

Several of the main types are

1. Precapillary pulmonary hypertension, with its main cause of (recurrent) pulmonary embolism.

Hypertension, Pulmonary. Table 1 The revised World Health Organization classification of pulmonary hypertension

Group I Pulmonary arterial hypertension
Idiopathic (primary)
Familial
Related conditions: collagen vascular disease, congenital systemic-to-pulmonary shunts, portal hypertension, HIV infection, Drugs and toxins (e.g., anorexigens, rapeseed oil, L-tryptophan, methamphetamine, and cocaine); other conditions: thyroid disorders, glycogen storage disease, Gaucher's disease, hereditary hemorrhagic telangiectasia, hemoglobinopathies, myeloproliferative disorders, splenectomy
Associated with significant venous or capillary involvement
Pulmonary veno-occlusive disease
Pulmonary-capillary hemangiomatosis
Persistent pulmonary hypertension of the newborn
Group II Pulmonary venous hypertension
Left-sided atrial or ventricular hear disease
Left-sided valvular heart disease
Group III Pulmonary hypertension associated with hypoxemia
Chronic obstructive pulmonary disease
Interstitial lung disease
Sleep-disordered breathing
Alveolar hypoventilation disorders
Chronic exposure to high altitudes
Developmental abnormalities
Group IV Pulmonary hypertension due to chronic thrombotic disease, embolic disease, or both
Thromboembolic obstruction of proximal pulmonary arteries
Thromboembolic obstruction of distal pulmonary arteries
Pulmonary embolism (tumor, parasites, foreign material)
Group V Miscellaneous
Sarcoidosis, pulmonary Langerhans'—cell histiocytosis, lymphangiomatosis, compression of pulmonary vessels (adenopathy, tumor, fibrosing mediastinitis)

Source: Simonneau G, Galie N, Rubin LJ et al (2004) Clinical classification of pulmonary hypertension. J Am Coll Cardiol 43:5S–12S

2. Capillary pulmonary hypertension, which includes media hyperplasia and the so-called idiopathic forms of pulmonary hypertension.
3. Postcapillary pulmonary hypertension, which is related to diseases that give rise to pulmonary venous hypertension. These may be primarily associated with pulmonary venous occlusive disease or with cardiac disorders, including mitral valve regurgitation, left-to-right shunts and increased back-up pressures in the presence of left-sided heart failure.

In all instances, pulmonary hypertension will increase the preload as well as the after-load on the right ventricle. Given sufficient time, the heart will respond by developing right ventricular hypertrophy (cor pulmonale), while the central pulmonary arteries will become dilated (a main pulmonary artery diameter of >3 cm should be considered pathological).

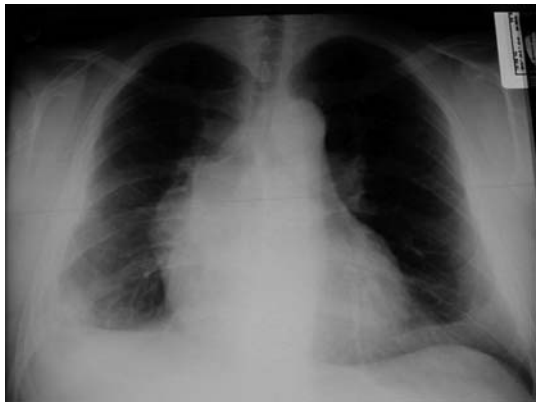

Hypertension, Pulmonary. Figure 1 PA chest radiography, demonstrating enlargement of the right heart with double contour due to enlargement of right atrium and large central pulmonary arteries.

Clinical Presentation

The clinical presentation of pulmonary hypertension depends on the underlying etiology. Gradual onset of symptoms is typical, and these often consist of (a combination of) progressive shortness of breath, palpitations, and episodes of syncope. Most patients will demonstrate a gradual decline in walking distance or inability to perform exercise. Acute presentation is rare, occurring in 5% of cases, whereas the vast majority will have experienced symptoms in excess of 6 months following onset of symptoms (2).

With progressive pulmonary hypertension, the right heart will ultimately fail and right heart failure signs and symptoms will develop, including pitting edema, ascites, raised jugular vein pressure, tachycardia, enlarged pulsating liver, loud P2 sound and/or pansystolic murmur, right ventricular heave and pleural effusions. Sudden death may occur.

Imaging

Chest radiography will help distinguish disorders that may mimic symptoms, such as pneumonia, tuberculosis, and heart failure. In patients with established pulmonary hypertension, the heart configuration and the main pulmonary arteries are usually (but not always!) enlarged (Fig. 1). Vascular pruning may be evident, resulting in hyperlucent areas in the lungs.

Right heart catheterization is currently the reference method for measurements of pressures, pressure gradients and combination with stress tests helps to assess the potential response to treatment.

Echocardiography will reveal right ventricular overload, consisting of right ventricular hypertrophy, wall motion abnormalities, bowing of the interventricular septum to the left and tricuspid valve regurgitation. Echocardiography is capable of giving an estimate of the pulmonary artery pressure.

CT pulmonary angiography is a very useful technology for the comprehensive assessment of the pulmonary vascular system, and is also capable of evaluating the consequences of pulmonary hypertension, such as right heart dilatation and hypertrophy, bronchial artery hypertrophy and perfusion anomalies (Fig. 2).

Magnetic resonance imaging (MRI) has many different techniques, which may be employed for the diagnosis of pulmonary hypertension and its etiologies. These techniques include vascular assessment, including MR perfusion and MR angiography, quantification of blood flow across the pulmonary valve and anatomical and cine imaging of the heart (Fig. 3). Although it is currently not possible to determine the exact measurement of pulmonary arterial pressure, MRI is a useful test to give an overall impression of the severity of the disease and may help to determine the precise etiology of pulmonary hypertension (3).

Nuclear Medicine

Traditionally, perfusion (-ventilation) lung scintigraphy was the main diagnostic test for pulmonary vascular

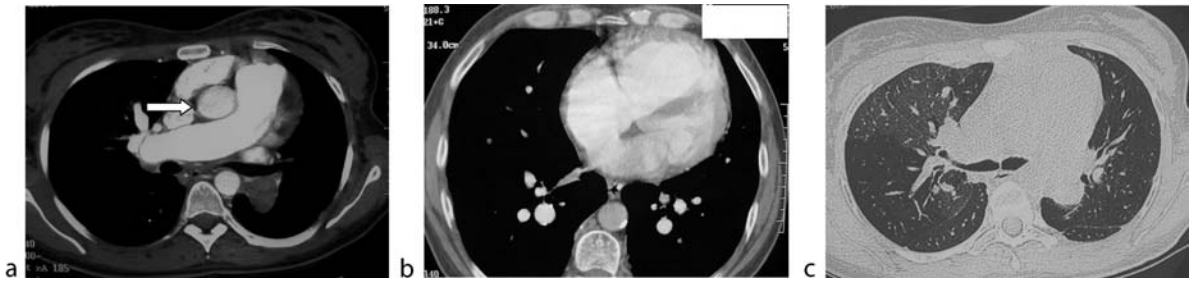

Hypertension, Pulmonary. Figure 2 CT findings in pulmonary hypertension. (a) Pulmonary artery dilatation (notice the size of the corresponding aorta, *arrow*). (b) Right ventricular hypertrophy, as demonstrated by anterior wall thickening (compare this to the left ventricular wall). (c) Mosaic perfusion, as indicated by areas of high attenuation (this is where the lung is receiving increased/shunted blood flow) versus areas of low attenuation which are hypoperfused.

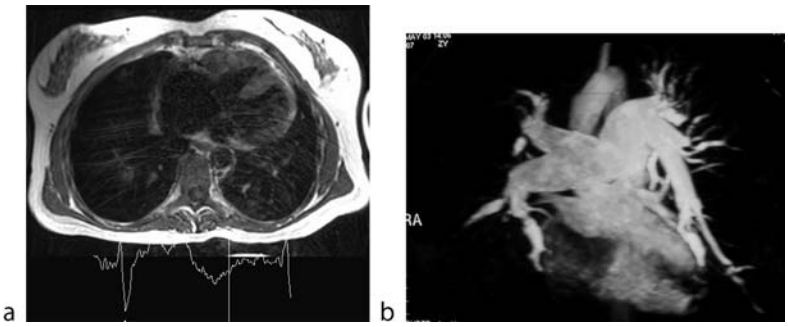

Hypertension, Pulmonary. Figure 3 MRI findings in pulmonary hypertension. (a) Patient with ventricular septal defect and Eisenmenger syndrome. Notice the high septal defect, the distended right atrium and the right ventricular hypertrophy. The perfusion scintigram of this patient is demonstrated in Figure 5. (b) Patient with chronic thromboembolic pulmonary hypertension. Notice large central pulmonary arteries, multiple caliber changes in the segmental branches, consistent with webs and stenoses after recanalization of pulmonary emboli.

disease. With the advent of CT and MRI, this technology has been largely omitted from the diagnostic work-up. Nevertheless, perfusion scintigraphy is still considered a useful adjunct to assess the severity of pulmonary hypertension and to monitor disease progression and response to therapy. Furthermore, it is exquisitely sensitive to the development or presence of left-to-right shunts and capable of determining the actual severity of these shunts (Fig. 4).

Diagnosis

The diagnosis of pulmonary hypertension is often delayed due to the insidious onset of symptoms. Once the diagnosis is considered, chest radiography and ECG findings will be abnormal in 80% of patients (2). Echocardiography is a first line investigation, and will raise further suspicion of increased pressures and may demonstrate right ventricular dysfunction. The final diagnosis will be made by right heart catheterization, while non-invasive tools, such as perfusion scintigraphy, CT and MRI will assist in determining the etiology and extent of the disease process. These tools are also increasingly being developed to help monitoring disease progression and response to treatment.

Interventional Radiological Treatment

There is an, albeit limited, role for interventional radiological treatment. First, inferior vena cava filters may be inserted in patients who undergo surgical corrections. Second, left-to-right shunts may be treated through

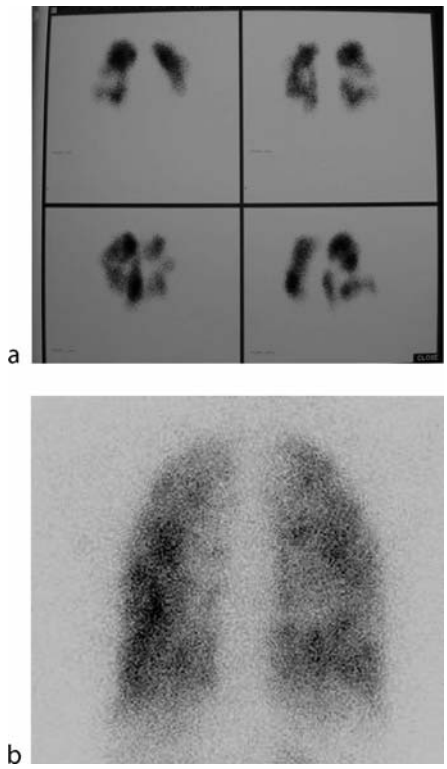

Hypertension, Pulmonary. Figure 4 Perfusion scintigraphic findings in different etiologies of pulmonary hypertension. (a) Patient with chronic thromboembolic pulmonary hypertension. Notice that there are multiple wedge-shaped defects, similar to that seen in acute pulmonary embolism. (b) Patient with ventricular septal defect, Eisenmenger syndrome, and right-to-left shunt. The lungs show inhomogeneous tracer uptake, with photopenic central hilar areas due to pulmonary artery dilatation. Notice that the kidneys are visible; quantification of the shunt can be performed by calculating the actual uptake as a percentage of the total injected dose.

invasive radiological procedures, including coil occlusion of arteriovenous fistulas and placement of umbrellas to cover patent foramen ovale, persistent ductus arteriosus, or small ventricular septal defects.

Bibliography

1. Simonneau G, Galie N, Rubin LJ et al (2004) Clinical classification of pulmonary hypertension. J Am Coll Cardiol 43:5S–12S
2. Elliot C, Kiely DG (2004) Pulmonary hypertension: diagnosis and treatment. Clin Med 4:211–215
3. Roeleveld RJ, Marcus JT, Boonstra A et al (2005) A comparison of noninvasive MRI-based methods of estimating pulmonary artery pressure in pulmonary hypertension. J Magn Reson Imaging 22:67–72

Hypertension, Renal

Nicolas Grenier
Service d'Imagerie Diagnostique et Thérapeutique de l'Adulte, Groupe Hospitalier Pellegrin, Bordeaux, France
nicolas.grenier@chu-bordeaux.fr

Synonyms

Renovascular disease; Renovascular hypertension

Definitions

►*Renovascular disease* (RVD) is a complex entity involving renal arterial lesions, renal disease, and hypertension. The relationships between these three entities are variable from patient to patient and difficult to assess, but their severity and their association increase the patient's cardiovascular and renal risks.

►*Renovascular hypertension* (RVH) is a reversible cause of hypertension secondary to a decrease in renal perfusion pressure, which activates the renin–angiotensin system and leads to the release of renin and the production of angiotensin II (angiotensin II increases sodium reabsorption and induces postglomerular and systemic arterial vasoconstriction, causing renovascular hypertension). The prevalence of RVH is around 1% among hypertensive patients.

►*Renal artery stenosis* (RAS) is the main cause of RVH, but small-vessel intrarenal vascular disease can also be responsible for it. Its prevalence is unknown. Only the stenoses that reduce the internal diameter by >60% produce a significant decrease in renal blood flow. They can be atherosclerotic (90% of cases) or dysplastic (fibromuscular dysplasia, 10% of cases), ostial or not, and be located on main or accessory arteries. Small-vessel intrarenal vascular lesions are almost exclusively atherosclerotic.

The relationship between hypertension and RAS is also difficult to assess, the best test being the reversibility of hypertension after revascularization. In fact, the majority of patients with atherosclerotic RAS and hypertension have essential hypertension as suggested by the absence of benefit of revascularization.

Atherosclerotic, or ischemic, nephropathy is a complex entity. It is an important cause of end-stage renal failure (ESRF), causing up to 14% of ESRF over the age of 50 years. It is a consequence of the association of multiple factors, including decreased renal blood flow (secondary to bilateral RAS or to unilateral stenosis plus contralateral occlusion or to unilateral stenosis in a solitary kidney), intrarenal

atherosclerotic arterial disease, atheroembolism, diabetes, increased oxidative stress, medullary hypoxia, endothelial dysfunction, inflammatory response, and proteinuria. This multiplicity of causal factors explains the great heterogeneity of renal damage. There are several arguments in favor of nonischemic factors being responsible for ▶atherosclerotic nephropathy: (i) the presence of atheroembolic disease and focal segmental glomerulosclerosis at histology; (ii) a variable functional response to revascularization, with evolutive processes independent of a reduction of renal blood flow; and (iii) the possible observation of patients with two equal-sized kidneys, unilateral RAS, and impaired renal function, or of patients with severe bilateral RAS and relatively preserved renal function.

Characteristics

Clinical distinction between renovascular and essential hypertension is difficult and based on classical criteria such as, among others, the onset of hypertension before or after the age of 50 years, the absence of a family history of essential hypertension, an abdominal bruit, duration of hypertension of less than 1 year, hypokalemia, and decreased renal function (Table 1).

Atherosclerotic RAS is the most common cause of RAS. The prevalence increases with age, particularly in patients with diabetes, aorto-iliac occlusive disease, coronary artery disease, or hypertension. Progression of the degree of stenosis occurs in approximately 51% of renal arteries 5 years after diagnosis, and 3–16% of renal arteries progress toward occlusion. But in many cases, these arterial lesions are never detected because they are asymptomatic. Most of these stenoses are located at the ostium of the renal arteries and are in fact perirenal aortic plaques extending into the ostia.

Hypertension, Renal. Table 1 Clinical features suggestive of atherosclerotic renal artery stenosis

1. Hypertension
• Abrupt onset before the age of 50 year or after the age of 55 year
• Accelerated or malignant hypertension
• Refractory to treatment with ≥3 drugs
2. Renal abnormalities
• Progressive or otherwise unexplained renal insufficiency in the setting of hypertension in elderly patients
• Abrupt rise in serum creatinine after ACE inhibition
• Low grade proteinuria and unremarkable urinary sediment
• Significant discrepancy in size between the two kidneys
• Unexplained hypokalemia
3. Other findings
• Abdominal or flank bruit
• The presence of various atherosclerotic manifestations and/or abdominal aortic aneurysm
• Unexplained left ventricular hypertrophy
• Flash pulmonary edema
• Severe retinopathy

Fibromuscular dysplasia (FMD) is the second cause of RAS, occurring preferentially in females between 15 and 50 years of age. It is usually located more distally than atherosclerotic RAS, on the distal two-thirds of the renal artery and its branches, and may affect the intima, media (90% of cases), or adventitia. Depending on its type, FMD is characterized by long or short (diaphragm-like) stenoses and aneurysmal dilatations. Intimal and periarterial FMD are commonly associated with progressive dissection and thrombosis, whereas medial FMD progresses in 30% of patients and is rarely associated with dissection or thrombosis.

When atherosclerotic disease progresses unilaterally, the size of the ipsilateral kidney, its cortical thickness, and its blood flow decrease, whereas the serum creatinine concentration and glomerular filtration rate remain normal because of compensatory changes within the contralateral kidney. When the disease progresses bilaterally, both kidneys present with progressive shrinkage and cortical thinning and irregularities. Usually, serum creatinine concentration increases and GFR decreases when more than 50% of renal mass is lost. Renal atrophy develops in approximately 21% of patients with RAS of more than 60%.

The radiological imaging techniques available today have to reach four objectives: (i) to detect and characterize the RAS in terms of nature and anatomical and hemodynamic severity, (ii) to assess the anatomical consequences of the RAS on the artery itself and on the renal parenchyma, (iii) to assess the functional and cellular consequences of the RAS on the kidney, and (iv) to identify criteria of associated renal impairment related to RVD.

Because the cardiovascular risk mainly depends on the degree of hypertension, improving blood pressure control has been a major task. Today, we know that medical treatment can achieve this control without renal revascularization in many cases. Therefore, management of these patients does not always require, as before, an early diagnosis of RAS, even though recent improvements in radiological techniques allow an accurate diagnosis of RAS noninvasively.

Imaging of RAS

Intraarterial digital subtraction angiography is considered the gold standard for diagnosing RAS, but it is limited

now to characterizing the stenosis before transluminal angioplasty during the same procedure.

Doppler ultrasound has gained a major place in the detection of RAS. The examination includes measurement of both kidneys, spectral sampling of two or three interlobar or segmental arteries of each kidney, and spectral sampling of both renal arteries. Diagnosis is based on direct proximal criteria (Fig. 1a) using both focal changes of color related to acceleration (aliasing) and turbulence (perivascular artifact) and spectral waveform changes at the site of stenosis (spectral broadening and increased velocity). Once detected, stenoses are considered significant (≥60%) when the renoaortic velocity ratio (RAR) is higher than 3.5 and/or when the peak systolic velocity is ≥180 cm/sec. Intrarenal wave forms may present changes distally to severe (>75%) RAS: slowed systolic acceleration, defined by an acceleration time of systolic peak >0.07 sec and a decreased resistive index (RI). Ultrasound contrast agents may improve the feasibility of the test in patients with a high body mass index or with decreased renal function.

Multislice computed tomography (CT) angiography provides high-resolution images of renal arteries with 1 mm (or less) slice thickness. Using an 80–100 mL bolus of iodinated contrast agent and maximum intensity projections (MIP) of reformatted slices, delineation of the true lumen and its separation from calcification are enhanced. Drawbacks of CT angiography are the ionizing radiation and the need for iodinated contrast media, a problem when renal function is impaired. Sensitivity (92%) and specificity (99%) in detecting significant stenoses are high. FMD stenoses, which are more distal than atherosclerotic stenoses, can also be better characterized using multislice CT (Fig. 1b).

Magnetic resonance (MR) angiography has moved from flow-enhanced (time-of-flight or phase-contrast) sequences to 3D breath-hold T1-weighted and contrast-enhanced acquisitions (Fig. 1c). Fluoroscopic guidance of arrival of the bolus in the aorta improves the reproducibility of the technique. Parallel acquisition techniques allow improved spatial resolution without increasing the acquisition time and yield an isotropic resolution of 1 mm^3 in a single breath-hold. These improvements are responsible for an improved grading of stenoses, which has the same interobserver variability as conventional angiography, and better detection of accessory arteries. Its performance is excellent, with sensitivity and specificity for diagnosis of significant RAS of 88–100% and 71–99%, respectively.

Comparison of techniques: A recent meta-analysis compared the validity of CT angiography, MR angiography, and ultrasound for diagnosing RAS in patients suspected of having RVH. Receiver-operating characteristic curves found that CTA and gadolinium-enhanced 3D MR angiography were significantly better than the other diagnostic tests and seemed to be preferred in patients referred for evaluation of RVH.

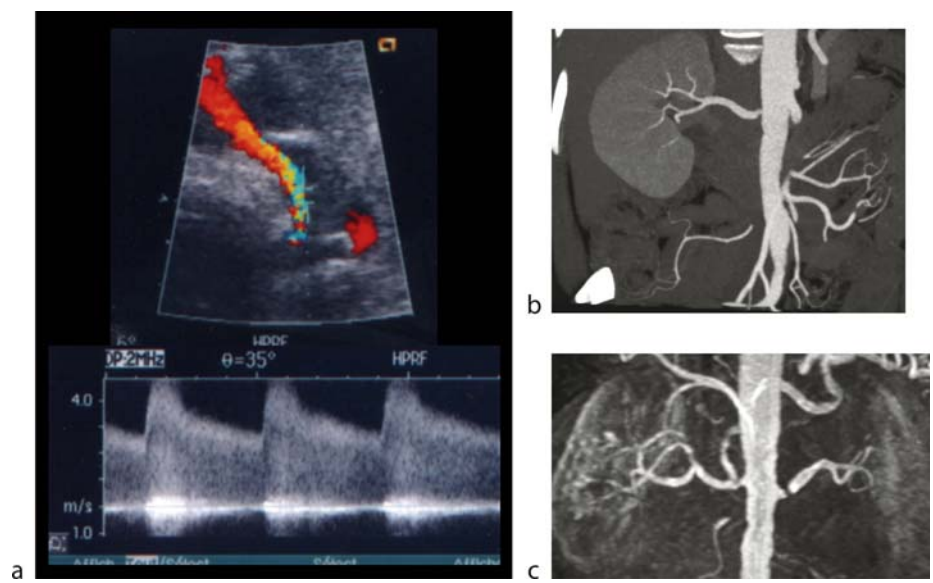

Hypertension, Renal. Figure 1 Diagnosis of renal artery stenosis. (a) Color flow sonography showing an aliasing phenomenon on the proximal segment of right renal artery and flow changes evocative for significant stenosis: severe spectral broadening and increased peak systolic velocity around 5 m/sec. (b) CT angiography showing an ostial stenosis of the right renal artery. (c) MR angiography showing a post-ostial stenosis of the left renal artery.

Anatomic and Hemodynamic Consequences of RAS

Detection of RAS further requires evaluating the severity of narrowing and its consequences on renal flow, renal parenchyma, and renal function, to improve the inter-observer variability and to define predictive factors of improvement after revascularization.

Renal Anatomy changes

The *renal anatomy* changes when the renal blood flow is significantly decreased. Two parameters have been proposed to evaluate this effect in RAS:

- *Measurement of renal length*: To be significant, a length difference of 1 cm should be considered, attesting to a hemodynamically significant RAS (Fig. 2a). If the renal length is <8 cm, revascularization is contra-indicated because the patient is less likely to get benefit from it.
- *Measurement of cortical thickness and cortical area*: A threshold of 8 mm for cortical thickness and 800 mm^2 for cortical area allows one to distinguish control kidneys from poststenotic kidneys. Its prognostic value has still to be evaluated.

Renal Arterial Flow Below the Stenosis

3D phase-contrast MR sequences, with flow encoding in the three directions, is sensitive to flow velocity, and velocity–time curves can be obtained. It is possible to separate normal velocity–time curves and abnormal curves evocative for moderate or high grade stenoses (Fig. 2b). This combined approach has revealed the best interobserver variability and almost perfect intermodality agreement with digital subtraction angiography. A renal flow index—renal flow (mL/min) divided by renal volume (cm^3)—less than 1.5 mL/min/cm^3 seems predictive of a successful outcome of revascularization.

Intrarenal Hemodynamics

By sampling distal intrarenal vessels with Doppler ultrasound, two types of flow curve changes can be observed: A decreased RI is related to a compensatory vasodilatation due to severe RAS upstream, but an increased RI is compatible, in this context, with the diagnosis of atherosclerotic nephropathy. Radermacher et al showed that an RI > 0.8 was associated with a poor prognosis in patients with RAS shown by an absence of improvement of hypertension, renal function or kidney survival after revascularization.

Consequences of RAS on Renal Function

Glomerular Filtration

Baseline semiquantitative evaluation or quantification of glomerular filtration is neither sensitive nor specific enough to detect renal dysfunction due to RAS. Blockade of the renin–angiotensin system by angiotensin-converting enzyme (ACE) inhibitors, such as captopril, is mandatory for this purpose. Administration of ACE inhibitors decreases the vasoconstrictor-stimulating effect of angiotensin II, which produces a drop in glomerular filtration on the side of the stenosis. A positive test, defined as a functional change induced by the ACE inhibitor, demonstrates the diagnosis of "functional stenoses" producing renovascular hypertension, which means a real link between

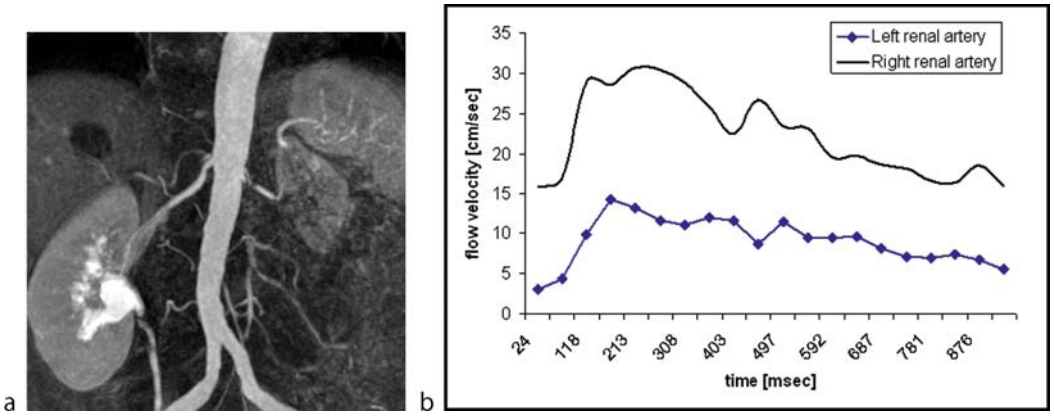

Hypertension, Renal. Figure 2 Anatomical and hemodynamical consequences of renal artery stenosis. (a) MR Angiography shows a left renal astery stenosis showing a decreased of size of the kidney. (b) The MR phase-contrast acquisition shows flow velocity–time curves on each renal artery, with a normal curve on the right and an altered flow within left renal artery. (Courtesy of Dr Stephan Schoenberg, Muenchen, Germany)

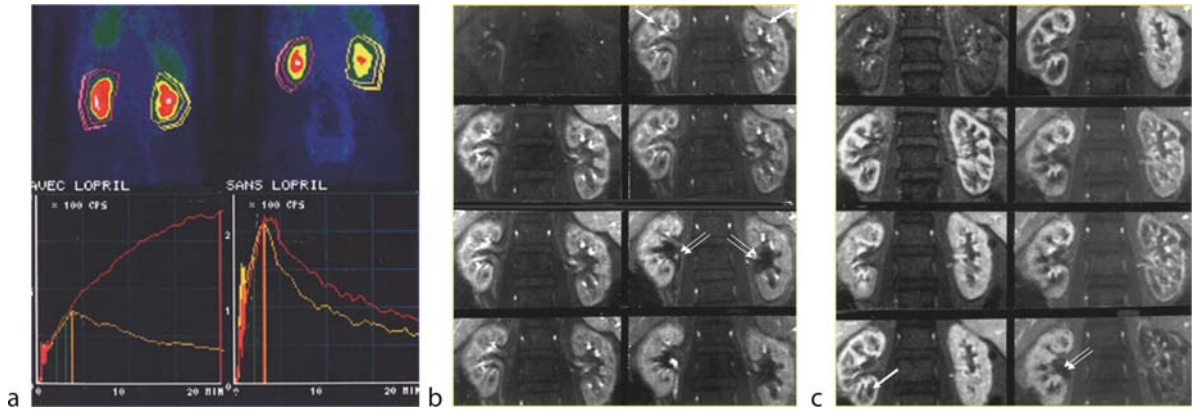

Hypertension, Renal. Figure 3 Functional renal consequences of renal artery stenosis. (a) Positive captopril MAG3-Tc99 scintigraphy obtained in a patient with stenosis of the left renal artery: the baseline study shows symmetrical elimination of the tracer (right of the image). After captopril (*left* of the image), there is an accumulation of the tracer within the left kidney whereas it remains unchanged in the right. (b, c) Dynamic Gd-enhanced MR imaging of the kidneys before (a) and after (b) captopril administration in the same patient (from *top-to-bottom* then *left-to-right*): before captopril, the tubular phase with low signal intensity within medulla (*arrows*) and excretion of contrast medium within renal collecting system (*double arrows*) are symmetrical. After captopril, the right kidney shows a normal tubular phase (*arrow*) and normal excretion (*double arrow*) whereas tubular phase is delayed on the left but then enhances with time, extending within the cortex and providing a complete low signal intensity of the left kidney; this effect is related to a severe retention of the contrast agent within the entire left kidney induced by captopril.

RAS and hypertension. This test has traditionally been coupled with scintigraphy but more recently with dynamic MR imaging (Fig. 3).

Renal Perfusion

Absolute quantification of parenchymal perfusion can be assessed with diffusible (as gadolinium chelates) or purely intravascular contrast agents (as iron oxide particles). A 50% decrease in cortical perfusion (from 400 to 200 mL/min/100 g) has been observed below tight (80%) stenoses. However, its potential role in prognosis has not been demonstrated to date.

Bibliography

1. Safian RD, Textor SC (2001) Renal artery stenosis. N Engl J Med 344:431–442
2. Scoble JE (1999) Atherosclerotic nephropathy. Kidney Int 56: S106–S109
3. Vasbinder GB, Nelemans PJ, Kessels AG et al (2001) Diagnostic tests for renal artery stenosis in patients suspected of having renovascular hypertension: a meta-analysis. Ann Intern Med 135:401–411
4. Radermacher J, Chavan A, Bleck J et al (2001) Use of Doppler ultrasonography to predict the outcome of therapy for renal artery stenosis. N Engl J Med 344:410–417
5. Taylor AT, Fletcher JW, Nally JV et al (2001–2002) Society of Nuclear Medicine Procedure Guideline for Diagnosis of Renovascular Hypertension 2.0. Society of Nuclear Medicine Procedure Guidelines Manual. 82–86

Hyperthyroidism

The physiological manifestation of increased thyroid function, hormone production or insensitivity of the end organs to thyroid hormone.

▶Congenital malformations, Thyroid, and Functional Disorders
▶Thyroid Autoimmune Diseases

Hypertrophic Arthropathy, Secondary

Secondary hypertrophic arthropathy is one of the more common and specific paraneoplastic diseases that may present as an oligoarthritis or polyarthritis of the distal joints with clubbing, painful periostitis of the distal long bones, and noninflammatory synovial effusions. Linear ossification of the distal long bones separated by a radiolucent zone from the underlying cortex can be seen in radiographs. Usually acromegaly induced bone changes are not as painful and linear ossifications along the bones are not found.

▶Acromegaly

Hypertrophic Pyloric Stenosis

Thickening of the muscle wall and mucosa in the pylorus of the stomach resulting in gastric outlet obstruction and typically occurring in young infants and resulting in classic projectile vomiting.

►GI Tract, Pediatric, Specific Problems

Hypertrophic Pyloric Stenosis (HPS)

►GI Tract, Pediatric, Specific Problems

Hypertrophic, Osteoarthropathy

Bauer Jan S
Institut für Röntgendiagnostik, Technical University Munich, Germany
jsb@roe.med.tum.de

Definition

Hypertrophic osteoarthropathy is characterized by ►periostitis, arthritis, and bilateral clubbing of the digits on the hands and feet. Hypertrophic osteoarthropathy may be divided into primary and secondary forms. ►Primary hypertrophic osteoarthropathy can be hereditary or idiopathic and is very rare (3–5% of all cases of hypertrophic osteoarthropathy). ►Secondary hypertrophic osteoarthropathy is often associated with intrathoracic neoplastic or inflammatory conditions.

Pathology/Histopathology

Periostitis with new periosteal deposition of bone is the hallmark of the disease. While the new surface is rough in primary hypertrophic osteoarthropathy, it has a more linear appearance in secondary hypertrophic osteoarthropathy (Fig. 1). In histologic cross sections, the delineation between the old and new periosteal bone is less distinct in primary compared to secondary hypertrophic osteoarthropathy, where the new bone is often less dense than the original cortex. However, if

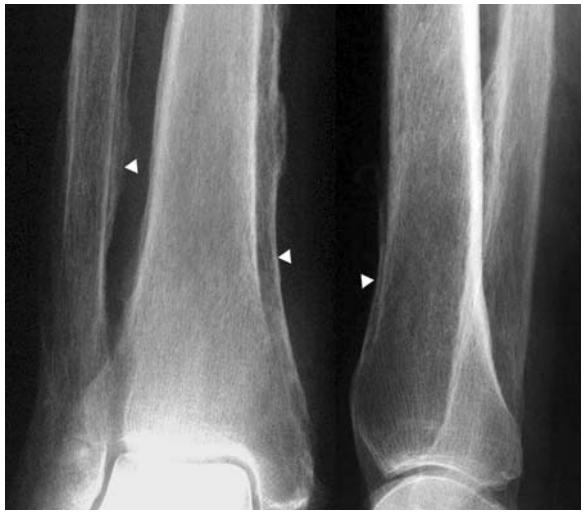

Hypertrophic, Osteoarthropathy. Figure 1 Radiograph of the right distal tibia and fibula in an anteroposterior and lateral view. The patient suffered from lung cancer and severe, burning pain in both distal legs. The periosteal appositions (white ►) have a linear appearance typically found in secondary hypertrophic osteoarthropathy. (Courtesy of Prof. Thomas M. Link, San Francisco.)

secondary hypertrophic osteoarthropathy has a longer history, e.g. in congenital cyanotic heart disease, the findings are more similar to that of primary hypertrophic osteoarthropathy. As in primary hypertrophic osteoarthropathy, osteolysis of the digits can also be found.

Articular inflammation with joint effusion is found more commonly in secondary than in primary hypertrophic osteoarthropathy. The synovial membrane presents with a mild cellular hyperplasia and a thickening of the subsynovial blood vessels. The synovial fluid is viscous and noninflammatory.

The ►clubbed digits are not a result of the periostitis, but due to an internal soft tissue edema with collagen and fiber deposition. Arterio-venous anastomosis can develop in the nail bed. Thickening of vessel walls is seen with a lymphocyte infiltration. In electron microscopy, Weibel–Palade bodies and Golgi complexes can be found indicating cellular damage.

Clinical Presentation

Hypertrophic osteoarthropathy is a syndrome characterized by digital clubbing, arthritis, periostitis, swelling and thickening of the skin of distal extremities and the head (pachydermia), as well as local nervous dysfunctions like hyperhidrosis (1). Digital clubbing was first described by

Hippocrates in the 5th century BC (2). A first description of hypertrophic osteoarthropathy was given by Friedreich in 1868. Primary hypertrophic osteoarthropathy is a hereditary autosomal dominant disease with variable penetrance. It affects males about seven times more often, is more severe in males, and is more common in African Americans than in Caucasians. The onset of primary hypertrophic osteoarthropathy is typically during adolescence. The disease often starts with enlargement of the hands and feet, producing a paw-like appearance. Digital clubbing is a frequent, though not invariable feature of hypertrophic osteoarthropathy. Its presence should not be equated with the syndrome, as several other disorders show clubbing without any other features of hypertrophic osteoarthropathy. Coarsening of the skin of the face and scalp, known as cutis verticis gyrata, may be observed as well as seborrheic dermatitis and palmoplantar hyperhidrosis. The clinical manifestation patterns are variable, ranging from the full syndrome (periostitis, pachydermia, and cutis verticis gyrata) or a partial expression (no involvement of the head) to a "forme fruste" (pachydermia without periostitis) (3). Primary hypertrophic osteoarthropathy usually shows a progression of about 10 years, when it arrests spontaneously. The life expectancy is normal, but disabling can occur if the axial skeleton is involved with stiffness, kyphosis, and neurological manifestations as spinal nerve roots get compressed by new bone formations.

In 1890, Bamberger and Marie independently described secondary hypertrophic osteoarthropathy as a syndrome of digital clubbing and periostitis in patients suffering from chronic heart and lung diseases (4, 5). Secondary hypertrophic osteoarthropathy shows an even distribution between males and females with no racial preference. Life expectancy is not changed by secondary hypertrophic osteoarthropathy, but it is often limited by the underlying disease. Symptoms are somewhat different from primary hypertrophic osteoarthropathy. In secondary hypertrophic osteoarthropathy, the periostitis is often associated with a deep, burning pain. Arthritis is more frequent (up to 40% of patients) and can mimic symptoms of rheumatoid arthritis when affecting small joints. Cutis verticis gyrata is observed much less frequently. However, with a long duration of secondary hypertrophic osteoarthropathy, like in congenital cyanotic heart disease, symptoms and findings can fully correlate with those observed in primary hypertrophic osteoarthropathy.

Imaging

Periostitis is the characteristic feature of the disease (6). Bones most affected are tibia, fibula, radius, and ulna. Periosteal appositions usually start developing at the distal end of the diaphysis. In case of primary hypertrophic osteoarthropathy, the periosteal appositions extend to the epiphyseal regions and appear irregular and exuberant. The cranium and pelvis can be affected as well. In more advanced stages, osteolysis can appear at the distal phalanges and ossification of ligaments can be observed. Joint capsules, menisci, and discs can also ossify. Synostosis can develop, particularly between carpal and tarsal bones, as well as at the symphysis pubis. In an advanced stage of primary hypertrophic osteoarthropathy, synovialitis may affect joints causing limited motion due to periosteal appositions near the joint.

In secondary hypertrophic osteoarthropathy, the appositions are linear thin lines separated from the cortical bone. They also can have an "onion-skin"-like appearance, but are usually not as irregular as in primary hypertrophic osteoarthropathy. In a later stage of the disease, the new periosteal bone fuses with the original cortex. The epiphysis is usually not involved. Besides the tibia, fibula, radius, and ulna, periosteal appositions can also appear at the femur, humerus, metacarpalia, metatarsalia, and the phalanges. Rarely an involvement of the scapula, the clavicle, rips, spine, or skull is found. As in rheumatoid arthritis, joint effusion can be found as well as osteoporosis near the joint. In contrast to arthritis, no joint space narrowing or erosive bony lesions are seen. The digital clubbing leads to radiographically evident soft tissue swelling.

Nuclear Medicine

Radionuclide bone scanning using technetium Tc99m polyphosphate can reveal the disease in an early stage, where plain films are still negative. It shows increased uptake of the tracer in the cortex of diaphysis and metaphysis. In primary hypertrophic osteoarthropathy, the epiphysis is also involved. The activity usually increases bilaterally in a linear fashion. Clubbed digits and associated synovitis can both show increased activity, particularly in an early phase of the scan.

Diagnosis and Differential Diagnosis

Differential diagnosis between primary and secondary hypertrophic osteoarthropathy can be achieved based on radiographic findings (irregular, with epiphyseal involvement in primary hypertrophic osteoarthropathy), clinical presentation (e.g. painful periostitis in secondary hypertrophic osteoarthropathy), and the patient's family history (positive in 1/3 cases of primary hypertrophic osteoarthropathy).

Other differential diagnoses to consider are ▶thyroid acropachy, ▶venous stasis, hypervitaminosis A, infantile cortical hyperostosis, acromegaly, and endosteal hyperostosis. In thyroid acropachy, pretibial myxedema and a

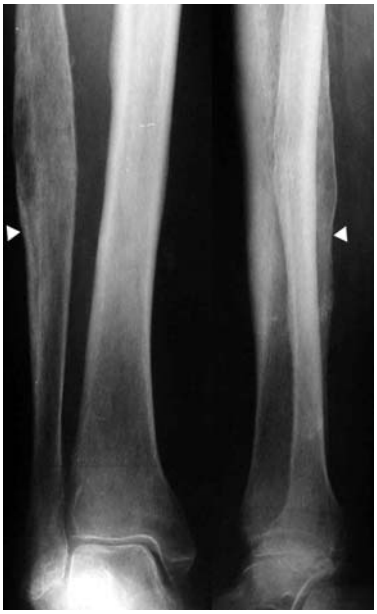

Hypertrophic, Osteoarthropathy. Figure 2 Radiograph of the right distal tibia and fibula in an anteroposterior and lateral view. The patient suffered from venous stasis with ulceration in both lower limbs. The periosteal appositions are more pronounced in the fibula (white ►). They have an irregular appearance and are not separated from the original cortex. (Courtesy of Prof. Thomas M. Link, San Francisco.)

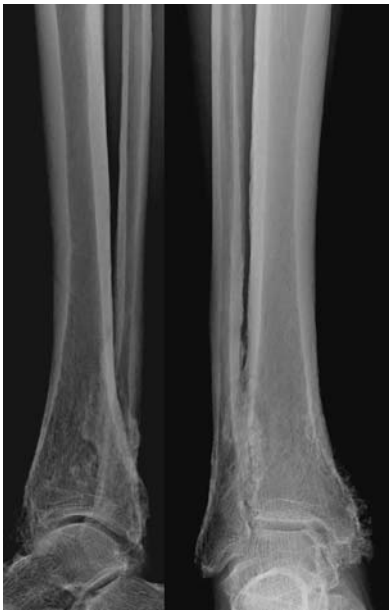

Hypertrophic, Osteoarthropathy. Figure 3 Radiograph of the right distal tibia and fibula in a lateral and anteroposterior view of a 59-year-old patient with pachydermoperiostitis. Multiple regions of periosteal reaction are identified involving the diaphysis, metadiaphysis, metaphysis, and epiphysis of the tibia and fibula. (Courtesy of Prof. Kenneth E. Sack, San Francisco.)

history of thyroid dysfunction are present; the typical speculated periosteal appositions have a predilection for small tubular bones. Venous stasis shows a predilection for the lower extremity with signs of phlebolitis, soft tissue swelling, and ulceration. The periosteal appositions have an undulated osseous contour and cortical thickening appears as the appositions are not well separated from the original cortex (Fig 2). In hypervitaminosis A, soft tissue nodules may be present with epiphyseal deformities. Infantile cortical hyperostosis is characterized by cranial destructions and skeletal deformities. A differentiation from acromegaly is clinically possible. In endosteal hyperostosis, digital clubbing is not evident. Other diseases, like fibrous dysplasia, Paget's disease, fluorosis, diffuse idiopathic skeletal hyperostosis are usually easily differentiated from hypertrophic osteoarthropathy (Fig. 3).

Bibliography

1. Martinez-Lavin M, Matucci-Cerinic M, Jajic I et al (1993) Hypertrophic osteoarthropathy: consensus on its definition, classification, assessment and diagnostic criteria. J Rheumatol 20(8):1386–1387
2. Hippocrates (1849) Hippocrene Books: Prognostic: Regimen in Acute Diseases, Sacred Disease, Art, Breaths, Law, Decorum, Physician, Dentition. Harvard University Press, London, UK
3. Touraine A, Solente G, Gole L (1935) Un syndrome ostéodermopathique: La pachydermie plicaturée avec pachypériostose des extrémités. Presse Méd 43:1820–1824
4. Bamberger E (1891) Über Knochenveranderugen bei chronishen Lungen und Herzkrankheiten. Z Klin Med 18:193–217
5. Marie P (1890) De l'ostéo-arthropathie hypertrophiante pneumique. Rev Méd 4:146–148
6. Resnick D (1995) Diagnosis of Bone and Joint Disorders. 3rd edn. W.B. Saunders, Philadelphia

Hypervascular Liver Lesions

HCC is the most common hypervascular malignant liver lesions. Other lesions prone to chemoembolization derive from neuroendocrine tumors.

►Chemoembolization

Hypopharynx

A musculomembranous conduit that lies behind the larynx.

►Carcinoma, Hypopharynx

Hypophysis

▶Pituitary Gland

Hypoplasia, Pancreatic

In pancreatic hypoplasia the exocrine elements, or more rarely also the endocrine elements, are underdeveloped.
▶Congenital Abnormalities, Pancreatic

Hypotelorism

Narrowed intercanthal area.
▶Congenital Malformations, Musculoskeletal System

Hypothenar Hammer Syndrome

Symptoms occurring in patients who use the palm of the hand for pushing, pounding, or twisting (mechanics, carpenters, etc.). Typical symptoms are more or less similar to those of Raynaud's syndrome.
▶Ischemia, Brachial

Hypothyroidism

The physiological manifestation of increased thyroid function, hormone production or insensitivity of the end organs to thyroid hormone.
▶Congenital malformations, Thyroid, and Functional Disorders

Hypoxic-Ischaemic Encephalopathy (HIE)

Diagnosis made in a neonate who develops neurological signs such as seizures, altered tone and poor feeding following resuscitation at a birth usually complicated by foetal distress.
▶Hypoxic, Ischaemic Brain Injury

Hypoxic, Ischaemic Brain Injury

Mary Rutherford
Robert Steiner MR Unit
Imaging Science Dept, MRC Clinical Sciences Centre
Imperial College
Hammersmith Campus, London, USA
m.rutherford@imperial.ac.uk

Synonyms

Birth asphyxia; Hypoxic-ischaemic encephalopathy; Neonatal; Perinatal; Seizures

Definitions

Perinatal hypoxic-ischaemic (HI) brain injury is defined here as an injury arising from a lack of blood and oxygen, birth asphyxia, occurring during labour or delivery. There may be a clear sentinel event such as a cord prolapse or uterine rupture that precedes signs of foetal distress detected as abnormalities in foetal heart rate seen on cardiotocograph with or without meconium stained liquor. These signs are usually accompanied by a low cord pH < 7.1. The diagnosis of ▶hypoxic-ischaemic encephalopathy is made when such neonates require resuscitation at birth, having low Apgar scores <5 at 1 min and often <5 at 5 min, and then develop abnormal neurological signs such as seizures, abnormal tone, irritability and poor feeding. The pattern of injury sustained in the brain depends on the length and nature of the hypoxic-ischaemic insult.

Aetiology

Following a significant HI event to the brain there is a period of primary energy failure, which initiates a cascade of reactions leading to secondary energy or mitochondrial failure. These reactions include increased glutamate, NMDA receptor activation, intracellular calcium accumulation, free radical formation and mitochondrial failure. Cellular swelling is followed by necrosis and is associated with acute changes on diffusion weighted imaging with a decreased apparent diffusion coefficient (ADC). In some regions of the brain, cells will die from apoptosis. In acute HI, tissues with a high metabolic rate are most susceptible to injury. In the neonatal brain this involves all areas that are actively myelinating, e.g. corticospinal tracts, basal ganglia and thalami (BGT), hippocampal region, brainstem. White matter is often relatively spared if there is an isolated acute event but will show secondary atrophy in

the presence of severe BGT injury. The dentate nucleus of the cerebellum is considered to be very susceptible to hypoxic-ischaemic injury but the cerebellum rarely demonstrates abnormal MR signal intensity acutely.

Middle cerebral artery infarction may occur as the result of spasm or embolus. There is an increased incidence of thrombophilic disorders in neonates with perinatal infarction. Factor V Leiden has been associated with more extensive infarction and poorer outcomes. The cause of focal haemorrhagic lesions is often not ascertained.

Clinical Presentation

Neonates with global HI brain injury may present with a full encephalopathy; altered tone, poor feeding and altered conscious level with or without seizures. With focal injuries the only presenting feature may be seizures. Neonates may require assisted ventilation because of respiratory depression secondary to the injury or to anti-convulsant medication administered to control seizures. An early EEG recording is useful for assessing the severity of the insult and will relate to the likelihood of abnormal outcome: the presence of depressed background activity is more worrying than the presence of seizures. The incidence of hypoxic-ischaemic encephalopathy is approximately 1.66/1,000 in the UK.

In infants with marked basal ganglia lesions feeding remains difficult for weeks or months. Infants with mainly ►white matter lesions usually have no feeding problems and neurologically may examine quite normally. The white matter, however, atrophies and they develop a secondary microcephaly.

Imaging

MR imaging is the modality of choice for assessing the brain in infants with suspected perinatal brain injury at term. Ultrasound is complimentary but needs to be performed serially for at least the first week to detect lesions. It may still be difficult to identify peripheral infarction and subtle but clinically significant basal ganglia lesions. CT is unable to detect many lesions within the basal ganglia and thalami, to determine their severity or to visualise the signal intensity within the posterior limb of the internal capsule. It may add little to a good cranial ultrasound. Optimal MR imaging can identify the pattern of injury in great detail providing information that can then be used to predict outcome. The timing is important whilst early imaging may be required so that decisions about continuing intensive care can be made the severity of injury may not be obvious unless diffusion weighted sequences are used. The ideal imaging window is from 1–4 weeks.

An optimum MR examination should include T1 and T2 weighted images in the transverse plane and T1 weighted images in sagittal plane should be obtained. Sequences may need to be adapted to the neonatal brain with its higher water content and longer T1 and T2 values. Diffusion weighted imaging should be used in the first week from delivery as it may identify areas of ischaemia that are not yet obvious on conventional imaging. T1 transverse images are the most useful for assessing the posterior limb of the internal capsule (PLIC) (1).

There is not usually any need for contrast. A venogram is helpful in delineating associated thrombosis from subdural haemorrhage within the major sinuses. By the time most neonates are imaged, haemorrhage is evident on conventional T1 and T2 weighted sequences. It is usually necessary to sedate neonates for MR examination; anaesthesia however is not justified. Feeding and wrapping neonates can occasionally produce a natural sleep for long enough to image.

Imaging Patterns in HIE

A brain with a clinically significant HI injury will show abnormalities on MR imaging but expertise is required in interpretation. If the MR images are normal or show mild changes only in a neonate who is encephalopathic or having on going seizures then an alternative diagnosis is likely. These neonates always warrant a full metabolic screen as certain metabolic disorders may coexist or masquerade as hypoxic-ischemic encephalopathy (HIE) e.g. non-ketotic hyperglycinaemia.

The most common sites of injury in the neonate with HI injury are the basal ganglia and thalami. The severity of these lesions can be graded as mild, moderate or severe (Fig. 1) (2). They are related to the development of cerebral palsy. The intervening PLIC is normally partly myelinated in the term neonate but in BGT injury it loses its normal signal intensity. This single sign can be used to predict an abnormal motor outcome (1). In association with lesions within the BGT there may be abnormalities within the cortex, usually around the central sulcus, insula and interhemispheric fissure. The subcortical white matter adjacent to these areas of "cortical highlighting" develops a long T1 and long T2 consistent with ischaemic change (Fig. 2) . This tissue usually atrophies and appears gliotic at follow up after 1 year of age. The medial temporal lobe may also show obvious cortical and subcortical abnormalities. In infants with severe BGT lesions WM that initially has a normal appearance develops a long T1 and long T2 over the first month of life. It subsequently atrophies resulting in poor head growth and a secondary microcephaly.

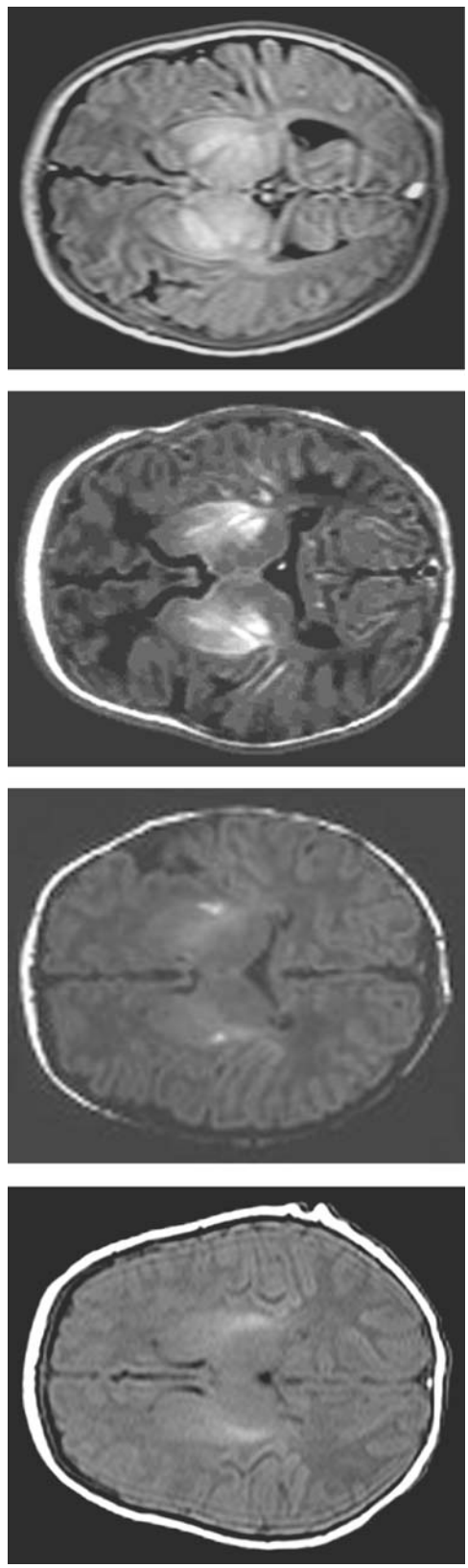

Hypoxic, Ischaemic Brain Injury. Figure 1 Classification of basal ganglia and thalamic lesions. T1 weighted images showing a normal appearance, mild, moderate and severe basal ganglia lesions in neonates presenting with hypoxic-ischaemic encephalopathy.

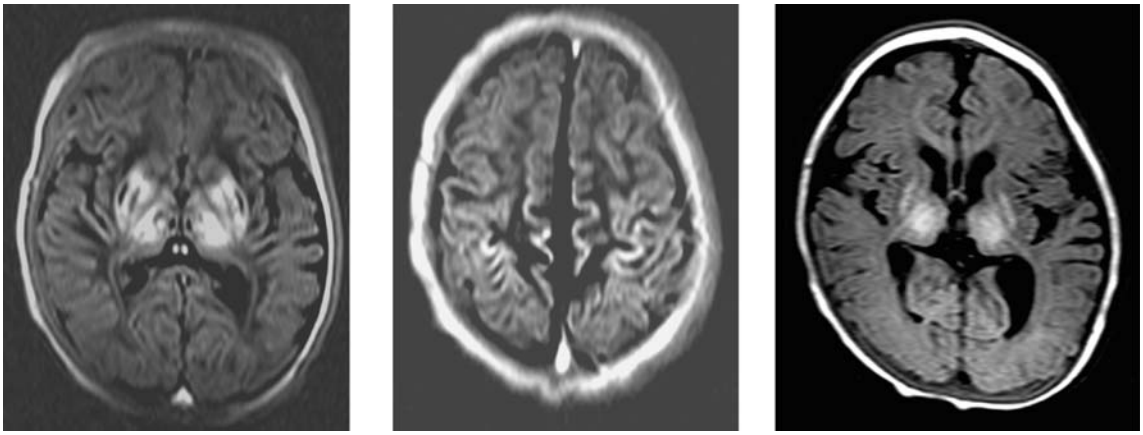

Hypoxic, Ischaemic Brain Injury. Figure 2 Cortical and subcortical WM abnormalities. Infant with established severe basal ganglia lesions showing cystic breakdown and some atrophy. There is abnormal cortical highlighting along the interhemispheric fissure and the central sulcus. There is abnormal low signal intensity in the subcortical white matter. At 5 months of age there is persisting abnormal signal intensity with the atrophied basal ganglia and thalami and white matter atrophy.

In approximately 40% of infants with a global HI injury there is additional more significant WM injury involving periventricular and deep white matter (Fig. 3). Occasionally infants with signs of HIE show only white matter involvement with no BGT lesions. This can be graded as mild, moderate or severe (3). These infants do not develop cerebral palsy unless the WM involvement is very extensive. They do however develop cognitive impairment the severity of which is related to the severity of white matter abnormality. Severe WM injury may be associated with haemorrhage. On later imaging the findings can be identical to late findings in periventricular leucomalacia.

Infants with early seizures, but no encephalopathy, usually show focal infarction or haemorrhagic lesions. The infarction is usually in the region of the middle cerebral artery more often on the left side. If extensive there is involvement of hemisphere, BGT and PLIC. This combination of three sites predicts later hemiplegia (Fig. 4) (4, 5). Infants with extensive middle cerebral artery infarction may have a genetic disorder such as Factor V Leiden. Focal haemorrhage may occur at any site within the brain and be seen in association with apparent germinal matrix involvement or subdural haemorrhage (Fig. 5). There may be additional non-haemorrhagic WM abnormalities.

Prediction of Outcome

1. ►Basal ganglia and thalamic lesions are associated with later motor impairments in the form of cerebral palsy.
2. The signal intensity within the posterior limb of the internal capsule is a good predictor of abnormal motor outcome.
3. White matter lesions are associated with cognitive impairments. Motor impairments are only seen with very extensive WM injury.

Infants with only mild basal ganglia and thalamic lesions and a normal PLIC (Fig. 1) may have a normal outcome. They may however have transient abnormalities in tone during the first year with some delay in motor milestones. They may occasionally develop a tremor in early childhood. Imaging later in childhood may be unremarkable.

Infants with moderate BGT lesions have an abnormal SI in the PLIC (Fig. 2). They usually maintain their head circumference because they have no additional WM atrophy. They show a dystonic or athetoid form of cerebral palsy. They may or may not gain independent walking. Imaging later in childhood may show atrophy of the lateral lentiform, with focal areas of long T1 and long T2 within the posterior aspect of the putamen and the lateral thalami.

Infants with severe BGT show involvement of caudate head, lentiform nuclei and thalami with abnormal signal intensity within the PLIC. The BGT atrophy sometimes with associated cystic change. There is associated secondary WM atrophy and poor head growth (Fig. 1). These infants develop severe forms of spastic cerebral palsy. They often show little development and may develop life threatening chest infections secondary to aspiration. Seizures may develop later in infancy and may be difficult to control.

Infants with severe BGT and severe early WM lesions have a similar poor developmental outcome (Fig. 3).

Infants with only WM involvement develop secondary microcephaly and cognitive impairments (Fig. 4). There is usually only mild motor impairment unless the WM injury is extensive with or without additional

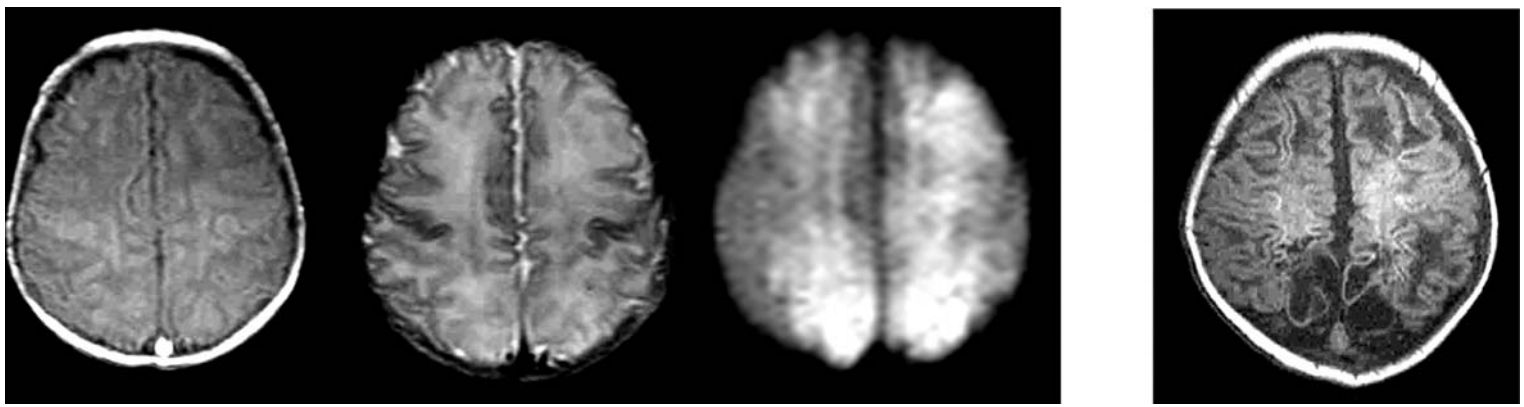

Hypoxic, Ischaemic Brain Injury. Figure 3 White matter infarction in a neonate presenting with HIE. Aged 5 days. There is some loss of grey white matter differentiation on the conventional scans, most obvious on the T2 weighted images. Diffusion weighted imaging show widespread abnormal signal intensity consistent with restricted diffusion and impending infarction. At 3 weeks of age there has been extensive infarction of the white matter (*right*). This may have been difficult to predict with T1 weighted images alone.

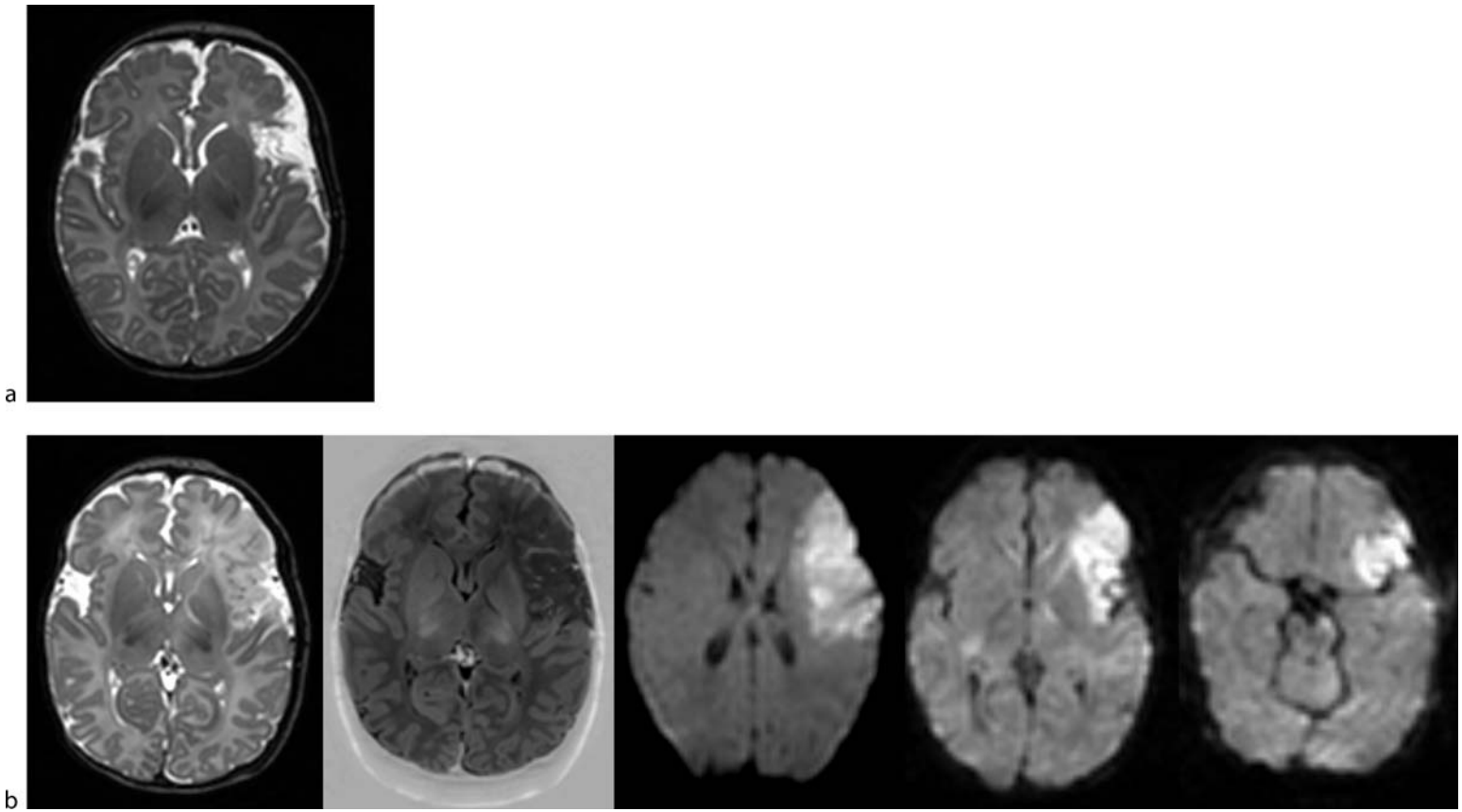

Hypoxic, Ischaemic Brain Injury. Figure 4 Middle cerebral artery infarction. (a) T2 weighted image showing small infarct in frontal lobe on left. There is a symmetrical appearance to the BGT and PLIC. This infant would be very unlikely to develop a motor impairment. (b) Left middle cerebral artery infarct at 5 days from delivery. There is a symmetrical appearance to the myelinated part of the PLIC. However there is some abnormal signal intensity within the more anterio part of the PLIC and the anterior internal on all sequences. There is additional abnormal signal intensity within the brainstem on the diffusion tensor images. This combination would put this infant at increased risk of a later hemiplegia.

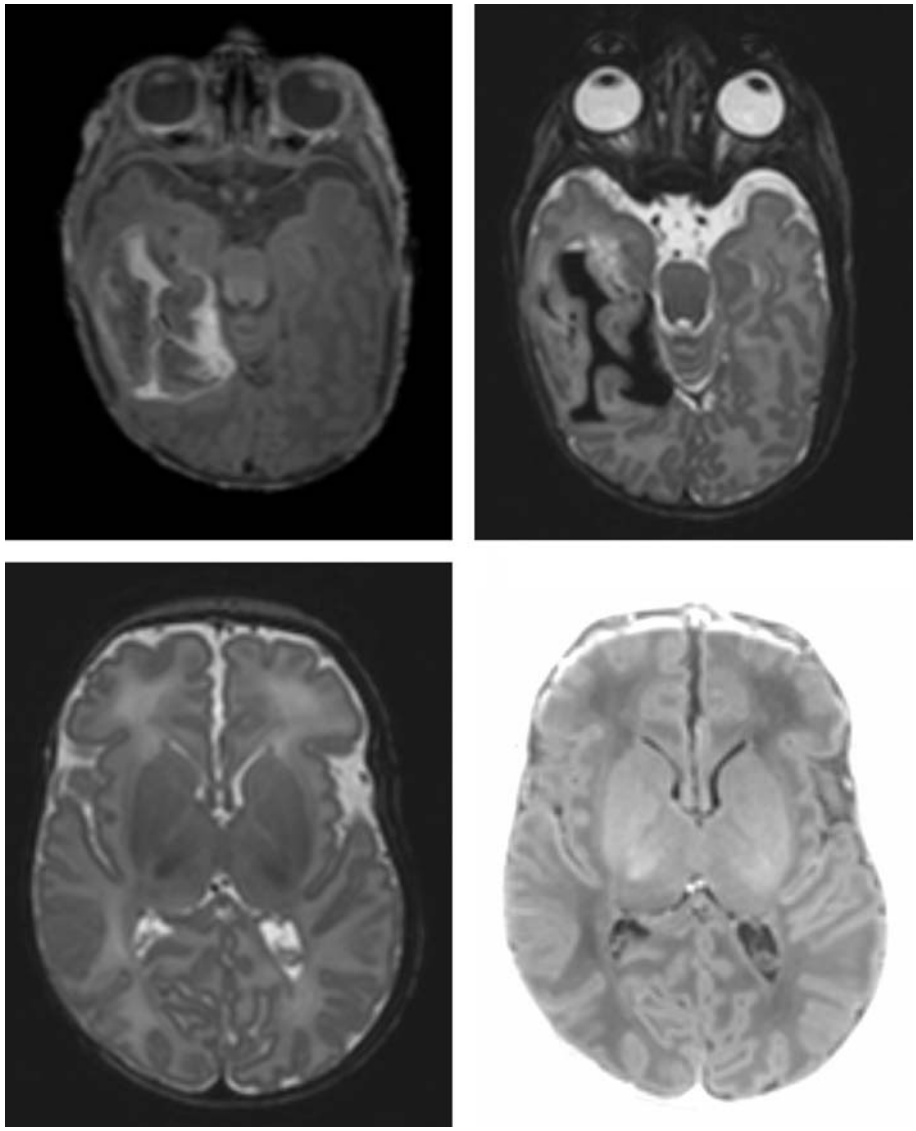

Hypoxic, Ischaemic Brain Injury. Figure 5 Focal haemorrhage Term born neonate presenting with seizures. There is a large haemorrhage involving the right temporal lobe. The appearances of the BGT and posterior limb of the internal capsule are symmetrical and within normal limits. This child is highly unlikely to develop any motor impairment.

haemorrhage. Motor impairment in these severe cases usually takes the form of a diplegic cerebral palsy (3).

Focal infarction or haemorrhage site of lesions determines outcome (Fig. 5). White matter lesions or haemorrhagic lesions that do not involve the corticospinal tracts particularly the PLIC usually show a normal motor outcome (Fig. 5).

References

1. Rutherford MA, Pennock JM, Counsell SJ et al (1998) Abnormal magnetic resonance signal in the internal capsule predicts poor neurodevelopmental outcome in infants with hypoxic-ischemic encephalopathy. Pediatrics 102:323–328
2. Rutherford MA (2002) MR imaging of the neonatal brain. W B Saunders ISBN 0 7020 2534 8
3. Cowan F Dubowitz L, Mercuri E, Counsell S, Barnett A et al (2003) Cognitive deficits without major motor difficulties following perinatal asphyxia and early encephalopathy: a consequence of white matter injury 2003 Early Hum Dev 73:113–114
4. Mercuri E, Cowan FM, Rutherford MA et al (1995) Ischaemic and haemorrhagic brain lesions in infants with seizures and normal Apgar scores. Arch Dis Child 73:F67–74
5. Rutherford M, Srinivasan L, Dyet L et al (2006) Magnetic resonance imaging in perinatal brain injury: clinical presentation, lesions and outcome. Pediatr Radiol 36(7):582–592

Hysterosalpingography

HSG is an X-ray technique to visualize the inside of the uterus and tubes after administration of contrast agent into the endometrial cavity. It provides a morphological assessment of the endometrium cavity and supplies information regarding tubal patency. Typically, the question of müllerian duct anomaly arises during HSG examination if the typical trigone configuration of the cavity is not demonstrated. Because only the internal contour of the uterus can be assessed and the outer contour remains unclear, the characterization of uterine anomalies is somehow difficult, especially in the common case of differentiation between bicornuate and septate uterus.

▶ Müllerian Duct Anomalies

IDC

►Carcinoma, Ductal, Invasive

Idiopathic Interstitial Lung Diseases

►Interstitial Lung Diseases, Unknown Etiology

Idiopathic Respiratory Distress Syndrome

►Chest, Neonatal

Ileus

Dilated small bowel.
►Occlusion and Subocclusion, Small bowel in adults

Iliac Artery Obstruction

►Stenosis, Artery, Iliac

Iliac Artery Occlusion

►Occlusion, Artery, Iliac

Iliac Artery Stenosis Artery

►Occlusion, Artery, Iliac

Iliac Vein Obstruction

►Thrombosis, Vein, Ilia

Iliac Vein Occlusion

►Thrombosis, Vein, Ilia

Immature Teratomas

Immature teratomas are malignant germ cell tumors that occur in children. They are solid tumors with fast growth that may contain small foci of fat and scattered calcification.
►Teratoma, Ovaries, Mature, Ovalar

Immune Thyroiditis Type Basedow

►Thyroid Autoimmune Disease

Immunoproliferative Small Intestinal Disease

Also known as alpha-chain disease or Mediterranean lymphoma, IPSID is associated with microbial or parasitic colonization of the small bowel.
►Neoplasms, Small Bowel

Imperforate Anus

▶Anorectal Malformation

Imperforated Hymen

Caused by the persistence of the central epithelial cells of the urogenital diaphragm; it is not associated with other abnormalities. It may cause hydro- or hematometrocolpos.

▶Genital Tract

Impotence

Räto T. Strebel[1], Hubert John[2]
[1]Department of Urology, University Hospital Zurich, Zurich, Switzerland
[2]Klinik Hirslanden, Leiter Zentrum für Urologie, Zurich, Switzerland
raeto.strebel@usz.ch

Synonym

Erectile dysfunction (ED); Impotentia coeundi

Definition

Impotence is defined as "male erectile dysfunction, that is, the inability to achieve or maintain an erection sufficient for satisfactory sexual performance" (1).

Imaging

Prescription of a PDE-5-inhibitor is the recommended primary treatment in most men, irrespective of the etiology. Therefore, imaging studies in the field of erectile dysfunction will rarely influence the treatment of these patients. Imaging in the field of erectile dysfunction is warranted in men with a presumed vasculogenic erectile disorder that may be amenable to surgical or interventional treatment. A Doppler ultrasound examination of the penile arteries after pharmacologically inducing an erection (intracavernosal injection of prostaglandin E1, e.g., 10 µg Alprostadil) is the preferred technique to assess an arteriogenic ED (depending on peak systolic arterial flow rates). Moreover, a veno-occlusive ED can be suspected when high end-diastolic arterial flow rates are recorded. The index of vascular resistance (RI) can be calculated and adds further information when considering a veno-occlusive ED. Several investigator and patient dependent factors make this examination subject to artifacts. Patient's anxiety and a cold and busy examination room are not helpful to facilitate relaxation of smooth muscle cells within the corpus cavernosum after pharmacostimulation.

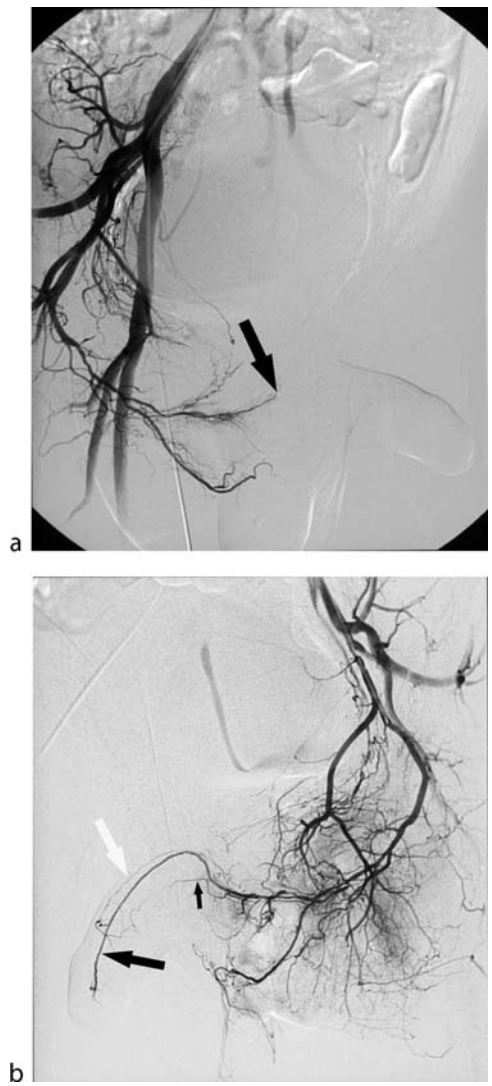

Impotence. Figure 1 **(a) Selective arteriography of the anterior trunk of the right internal hypogastric artery depicting an occlusion of the right common penile artery (black arrow). (b) Selective arteriography of the left internal pudendal artery depicting normal dorsal penile (fat black arrow) and cavernosal artery (small black arrow). The right dorsal penile artery is filled through collaterals from the left side (white arrow) (With courtesy of the department of radiology, University Hospital Zurich, Switzerland.).**

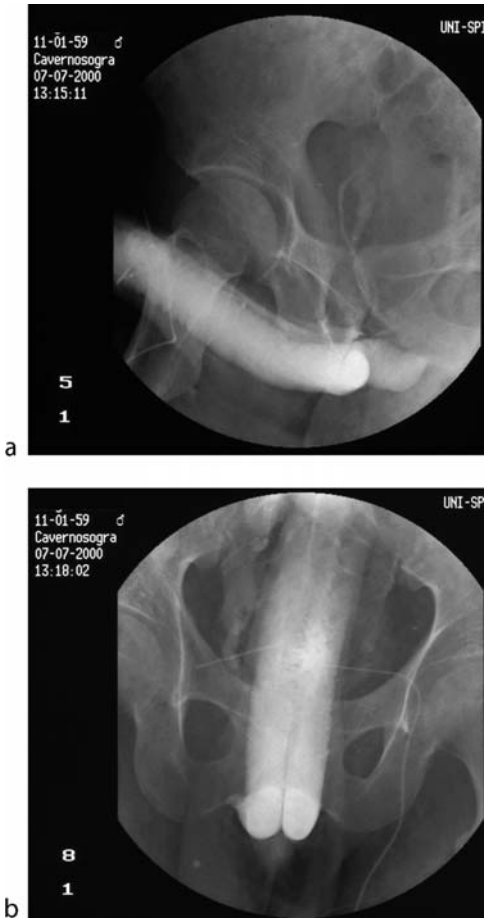

Impotence. Figure 2 (a and b) Cavernosography depicting early venous outflow in superficial dorsal and pelvic veins.

Selective penile arteriography is advisable before planning surgery when Doppler ultrasound examination results are abnormal (Fig. 1a, b). Arteriography offers the best anatomical information concerning the pelvic arterial inflow. Additionally, a dynamic infusion cavernosometry and cavernosography can help to confirm the diagnosis of a veno-occlusive ED (Fig. 2a, b). However, the clinical consequences and diagnostic yield of this study, in the light of color Doppler flow studies, remain limited.

Bibliography

1. Montague DK, Jarow JP, Broderick GA et al (2005) Chapter 1: The management of erectile dysfunction: an AUA update. J Urol 174(1):230–239

Impotentia Coeundi

▶Impotence

In vivo Receptor Imaging

Visualization of receptors mainly by means of nuclear medicine. Radiolabeled vectors are administered to patients. After a distribution phase, the radiopharmaceutical binds stably to the receptors and can be visualized with gamma cameras, including positron emission tomography (PET) scanners.

▶Receptor Studies, Neoplasms

Inborn Errors of Metabolism

Refers to a number of rare genetic defects that result in (a) abnormalities in the synthesis of enzymes and transportation proteins that result in the normal metabolic pathways and (b) accumulation of abnormal metabolites.

▶Congenital Malformations, Adrenals
▶Neurometabolic Disorders

Inborn Splenic Abnormalities

▶Congenital Anomalies, Splenic

Incidental Findings

Incidental findings are defined as observations of potential clinical significance made unexpectedly in healthy subjects or in patients recruited to research and that are unrelated to the purpose or variables of a study.

▶Incidental Neuroradiological Findings

Incidental Neuroradiological Findings

Judy Illes[1,2], Matthew P. Kirschen[1,2,3]
[1]Stanford Center for Biomedical Ethics, Stanford University, Stanford, USA
[2]Department of Radiology, Stanford University, Stanford, USA
[3]Program in Neurosciences, Stanford University, Stanford, USA
illes@stanford.edu

Synonyms

Accidental clinical findings; Incidentalomas; Lesions of unknown etiology; Unexpected clinical findings

Definitions

►Incidental findings are defined as observations of potential clinical significance made unexpectedly in healthy subjects or in patients recruited to research that are unrelated to the purpose or variables of a study. Clinically significant incidental findings in research, such as that of a tumor or arteriovenous malformation (Fig. 1), are distinguished from discovery of significant findings in clinical situations because they are not prompted by a complaint or an individual's medical history. This entry will focus on the complex issues surrounding the discovery of incidental findings primarily in the domain of neuroimaging research in which tens of thousands of human subjects are scanned each year as healthy volunteers.

A decade of empirical work on incidental findings in brain imaging, genomics, and other areas of research has yielded new knowledge about the frequency, investigator responsibility, and risks and benefits of disclosure. Early guidance on how such unexpected findings might be handled, especially given the variation in clinical significance with which they occur, is offered by the genetics literature. The 1999 National Bioethics Advisory Commission (NBAC) and the 2004 *Working Group on Reporting Genetic Results of NIH's National Heart Lung and Blood Institute*, for example, recommended that research results should be given to subjects if (a) the findings are scientifically valid and confirmed, (b) the findings have significant implications for the subject's health, and (c) a course of action to ameliorate or treat the concerns is readily available. However, the genetics guidelines and discussion address, as intended, data that might predict a health condition rather than reveal the presence of a potentially clinically significant medical condition.

Characteristics

Although case reports and retrospective studies of incidental findings in clinical medicine have been published in the past with some frequency, there were only a few reports of incidental neuroradiological findings in healthy control subjects recruited to brain imaging for research purposes until recently. Early data suggest anomalies in as many as 18–20% of research subjects (1). In 2–8% of the subjects, findings were clinically significant and required clinical evaluation with various degrees of urgency, from routine to immediate, depending on the nature of the finding. In another retrospective study, three of four findings in adults aged 18–59 years were found to require urgent referral (e.g., arteriovenous malformations, extra-axial lesions) (2). In the same study, incidental findings were discovered in 47% of older adults (≥60 years), although most required only routine follow-up such as for nonspecific white matter lesions. In

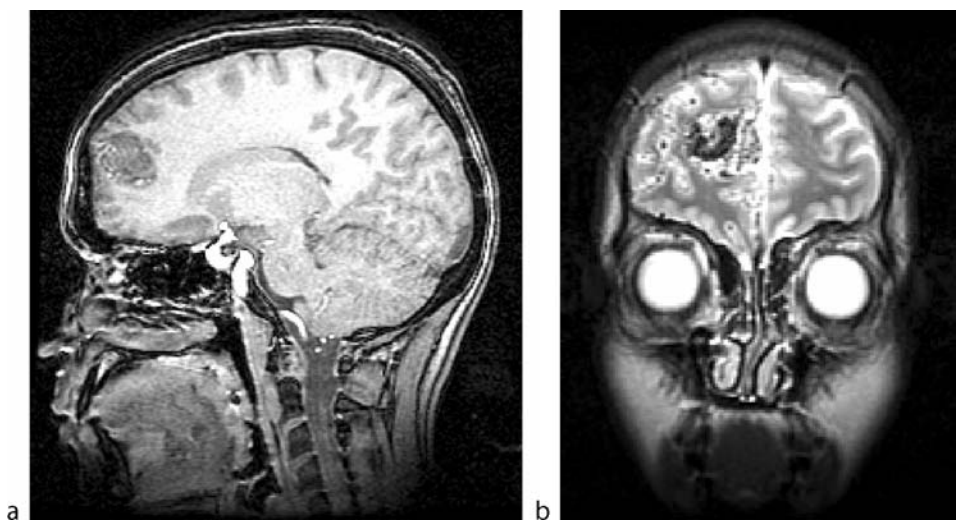

Incidental Neuroradiological Findings. Figure 1 Sagittal T1-weighted (a) and coronal T2-weighted (b) research MRI scans collected at 3T showing an arteriovenous malformation in the right frontal cortex of a 25-year-old woman. The image is displayed in radiological convention. (Courtesy of the Richard M. Lucas MRI Center, Stanford University.)

another study based on a sample of ultra healthy air force pilots, incidence was only a fraction of a percent (3). In a study of 225 pediatric subjects, incidental findings were found in 21%. In 5% of the cohort, the findings were clinically significant (4).

Management

Protocols

Wide variability exists in the way that incidental findings are handled. One group worked for more than a year to develop practical guidelines for managing incidental findings. This group of leaders in neuroscience, bioethics, policy, and law reached consensus that investigators engaged in brain imaging research must anticipate incidental findings in their experimental protocols and establish a pathway for handling them (5). A majority of this group felt that an individual with medical training should review any suspicious brain finding. If there is sufficient reason to think that the finding may be significant, the principal investigator or designate should inform the subject or the subject's surrogate in the case of children or subjects with limited decisional capacity. A minority of the group felt that given continuing uncertainty about true incidence and risks of ▶false positive findings, subjects should be given the option to decline to be told (i.e., right to not know). In addition, they maintained that investigators should have the option not to pursue findings beyond clearly articulating a management plan both to the Institutional Review Board (IRB) and to participants when obtaining informed consent (see also "Disclosure" below). Principal investigators bear primary responsibility for handling all findings in their research and for managing them appropriately.

A variable element in research protocols is the extent and immediacy of the involvement of medically trained staff. Physicians may be involved as principal investigators of a study, as collaborators, or as ad hoc consultants. One obvious impact of physician involvement in a research protocol is in the cost of conducting the research. Another is in the accessibility of medically trained personnel. Beyond the issues of cost and availability is the level of responsibility of a clinician in a research setting. A limited clinical relationship is established that may confer responsibility beyond the researcher–subject relationship when a clinician provides a clinical read of a research scan even for the sole purpose of assessing whether a clinical work-up is mandated, and even with the inherent limitations of the scan given research acquisition parameters.

Disclosure

One of the greatest risks to participants, just as to patients in the clinical setting, is the communication of a suspicious finding that ultimately has no clinical significance. The major consequences involve personal and psychological cost, financial cost, and cost to privacy.

1. Psychological cost: Awaiting clinical work-up for a finding detected in the context of research participation may cause significant anxiety for an individual who, by all measures, is asymptomatic and has contributed altruistically to the research enterprise.

   While mortality of follow-up tests such as routine MRI or CT scans is certainly slight, morbidity may be greater with the administration of contrast or the use of radiation. For certain types of findings (e.g., vascular malformation or tumors) further more risky diagnostic tests such as angiography or biopsy might be indicated. Anxiety may be exacerbated for patients for whom MRI is contraindicated because of claustrophobia.
2. Financial cost: The financial cost of clinical follow-up of an incidental finding is borne by the participant or a third party insurance carrier since such coverage is not a usual part of the funding for research. This is different at a small number of imaging centers in the United States, such as at the National Institutes of Health, where every research subject is required to be a patient and undergoes a complete clinical examination before being entered into a protocol.
3. Cost to privacy: Discovery and follow-up of an incidental finding may have implications for a participant's future medical insurability, even if the result is negative, and possibly to employability in cases where fitness is partly assessed by medical history.

Subject Selection

Challenges to subject selection arise in designing research protocols when incidental findings are a possibility. These include proper inclusion/exclusion criteria based on the risk of incidental findings occurring, subjects' ability to obtain follow-up health care, researchers' ability to track or contact subjects for follow up, and the inclusion of populations that may be vulnerable. Ethical considerations play an important role when thinking about special populations such as pediatric subjects, pregnant subjects, and subjects with limited access to health care and health insurance.

Good neuroimaging studies providing baseline images of "normal" pediatric brains in various developmental stages are lacking and make predictions about the possible clinical significance of a pediatric incidental finding particularly difficult.

Involvement of subjects such as university students and employees of imaging laboratories must be carefully considered given risks to privacy, such as the discovery of an incidental finding and other broader ethics risks such as the possibility of coercion in recruitment. The sense of

subjects' rights in research, such as that of the right to withdraw, maybe also be compromised in a setting in which a power relationship exists.

In the case of adults with diminished decision-making capacity, it is important to clarify who is empowered to make research decisions for the participant. Inclusion of disadvantaged or disenfranchised subjects who do not have ready access to health care, either through a lack of insurance or the availability of medical facilities, is essential to much research involving mental illness and addiction disorders. Protocols should have a safety net for these subjects and for the real costs that may directly stem from the discovery of a finding requiring work up. Requiring contact information is justifiable because of potential for the discovery of life-saving information.

Overall, ensuring the protection of human subjects in neuroimaging, and trust in and integrity of the scientific process are of paramount importance.

References

1. Katzman GL, Dagher Azar P, Patronas Nicholas J (1999) Incidental findings on brain magnetic resonance imaging from 1000 asymptomatic volunteers. JAMA 281:36–39
2. Illes J Rosen AC, Huang L et al (2004) Ethical consideration of incidental findings on adult brain MRI in research. Neurology 62:888–890
3. Weber F, Knopf H (2006) Incidental findings in magnetic resonance imaging of the brain of healthy young men. J Neurol Sci 240:81–84
4. Kim BS, Illes J, Kaplan RT, et al (2002) Incidental findings on pediatric MR images of the brain. Am J Neuroradiol 23:1674–1677
5. Illes J, Kirschen MP, Edwards E et al (2006) Incidental findings in brain imaging research. Science 311:783–784. For further information please visit http://www.ninds.nih.gov/news_and_events/proceedings/ifexecsummary.htm

Incidentalomas

►Incidental Neuroradiological Findings

Incomplete Border Sign

A radiographic finding commonly seen with a pleurally based mass. The inferior border of the mass is well defined as it is imaged tangential to the X-ray beam, whereas the superior border is imaged en-face and therefore appears ill defined.

►Pleural Mesothelioma, Malignant

Incontinence, Urinary

Catherine Roy
Department of Radiology B, University Hospital of Strasbourg, Hôpital Civil 1, Strasbourg, France
catherine.roy@chru-strasbourg.fr

Definition

Dysfunction of the bladder, caused by various abnormalities, is a rather common clinical symptom, especially in women. ►Incontinence, Urinary is defined as any involuntary urine loss that is a social or a hygienic problem. Stress urinary incontinence is defined as urine loss during daily or physical activities that increase abdominal pressure (in the absence of detrusor contraction or overdistended bladder). Perineal descent, cystoceles, and prolapses are often associated with urinary incontinence. Cystoptosis corresponds to the descent of any part of the bladder below the horizontal line drawn at the inferior edge of the pubic bone symphysis. When the neck and the bladder base fall, the result is cervicocystoptosis. When, rarely, the isolated neck falls, it is called cervicoptosis.

Pathology

Urinary incontinence requires integrity of both the nervous system and overall pelvic anatomical support structures, including muscular and fascial components. If the intravesical pressure exceeds the intraurethral pressure, incontinence results. Alternatively, it has been suggested that urethral compression against the endopelvic fascia and vagina is responsible for closure, as stated in the "hammock theory" (1). The most important risk factor for urinary incontinence is obstetric injury first with vaginal delivery, second with prolonged labor, and then forceps delivery. The mechanism of urinary incontinence in pregnancy remains unclear, but it may be due to a combination of endocrine and mechanical factors. Less common causes of urinary incontinence include urethral diverticula, overflow incontinence secondary to pharmacologic or neurologic causes, and very rarely in women bladder outlet obstruction.

Urinary incontinence is divided into two main etiologic groups (1).

Urge Urinary Incontinence (or Vesical Incontinence)

Urge incontinence is the involuntary loss of urine associated with an abrupt and strong desire to void. It is the occurrence

of involuntary contractions during filling or provoked by coughing or postural changes which the patient is unable to inhibit. The diagnosis is made by urodynamic testing. The role of imaging techniques is limited to searching for a rare cause such as a morphologic abnormality, an adjacent pathology, or a neurological disease.

Stress Urinary Incontinence (or Urethral Incontinence)

Stress Urinary incontinence is defined as urine loss during current daily or physical activities that increase abdominal pressure (in the absence of detrusor contraction or overdistended bladder). It may result from two distinct mechanisms: hypermobility of the bladder neck in 75% of cases (HBN) or intrinsic sphincter deficiency (ISD) in the others 25% of cases.

- With HBN, the basic anatomy and function of the bladder neck and urethra are intact. It is primarily caused by weakened pelvic floor support caused by denervation, musculofascial defects, or both secondary to aging, obesity, pregnancy, and vaginal delivery. The bladder neck and proximal urethra descend below their normal pelvic positions during straining, owing to weak musculofascial bladder and urethra attachments to the pelvic wall. When this normal anatomic position is altered, the urethra is no longer able to respond to the increase in abdominal pressure.
- In the case of ISD, the urethral sphincter is defective. It is unable to generate adequate urethral pressure to collapse the urethral lumen, and the bladder neck remains open even at rest. The bladder neck and urethra are well supported in their pelvic position. ISD can be caused by sympathetic nerve injury (surgery, trauma) or by degenerative processes (myelodysplasia, spinal cord lesions at the conus medullaris). Indeed, in most cases, it remains idiopathic.

Clinical presentation

It occurs in 38% of women over the age of 60 years and 59% of women after 75 years. The problem is seen even in the young, occurring episodically in as many as 45% of women over 18 years of age. The initial and essential step for the diagnosis of Urinary incontinence is a clinical examination and urodynamic testing with voiding speed evaluation. Voiding speed, the simplest urodynamic study, is performed particularly on patients with no obvious neurological lesion or those who may have an obstructed bladder outlet.

Imaging

Over the past decade, the most widely used imaging studies were voiding bead chain cystourethrograms and dynamic retrograde urethrograms, in addition to the minimally invasive colpocystodefecography, developed by Bethoux in France (2), and transabdominal ultrasound. These studies are designed to analyze and quantify the mechanisms of incontinence, whereas transabdominal ultrasound is used to assess overall urinary status and postvoiding bladder volume. Alternative advanced ultrasound techniques and ►magnetic resonance imaging (MRI) are now emerging as new tools for imaging pelviperineal defects.

Ultrasound: Ultrasound offers major advantages over X-rays for imaging the bladder and urethra. It provides good soft-tissue morphologic analysis of the urethrovesical junction and dynamic bladder neck imaging with quantified movements. Examinations are easy, relatively quick (10–15 min), and inexpensive. Evaluation is limited, however, to the anterior pelvic compartment, and requires operators to have experience and knowledge of urodynamics (3).

Three different approaches to ultrasound are available today: external ultrasound (transabdominal, perineal, and introital); endosonography (transvaginal and transrectal); and endoluminal (intraurethral) sonography. Transabdominal ultrasound gives an overall evaluation of the urinary tract, but misses the perineal floor.

In perineal scanning, a narrow curved array linear probe (3–5 MHz) or a common sectorial vaginal or transrectal probe (5–7.5 MHz) is applied to the perineum, whereas for introital sonography only the second one can be used, placed under the distal part of the urethra at the introïtus. Image quality depends partly on the probe's proximity to the target area, meaning that endosonography produces the clearest images. However, route choice requires a compromise between image quality and degree of interference in normal lower urinary tract function. Probe placement in endosonography displaces the bladder neck and compresses the urethra. Dynamic studies can consequently be limited, inhibiting normal voiding. Thus, perineal or introïtal US seems to be the pertinent technique using a common endoluminal probe. The sagittal plane is used to obtain a cross-sectional view through the bladder and urethra. The best image quality is obtained with a bladder filled with approximately 300 mL of urine (Fig. 1). Evaluation is first performed at rest in lateral decubitus with knee flexion and in standing position. Dynamic studies are then carried out during pelvic floor contraction and maximum straining in each position.

The normal aspect is a closed bladder neck in all positions or situations (Fig. 2). Correct identification of

I

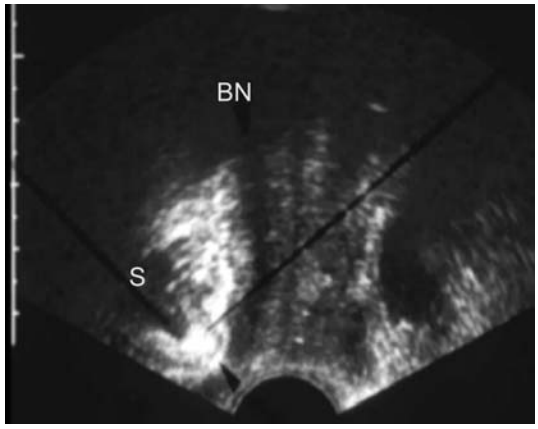

Incontinence, Urinary. Figure 1 ***Ultrasound*** **perineal technique. Sagittal view. Lateral decubitus. Rest. Normal aspect. The probe is located just behind the urethral meatus. The bladder neck (BN) is clearly above the reference line. It is closed. The urethra has a hypoechoic pattern. (S): symphysis pubic bone.**

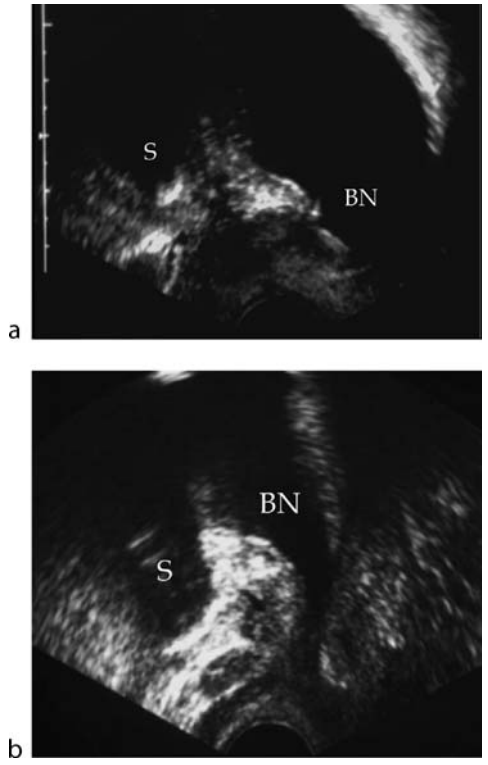

Incontinence, Urinary. Figure 2 ***Perineal ultrasound technique*****. Sagittal view. Lateral decubitus. (a) Hypermobility of bladder neck (HBN). Maximum straining. The bladder neck is under the reference line. It appears slightly funneled. The urethra has moved down and horizontally. Cystocele is associated with enlargment of the angle between the urethra and bladder base. (b) Rest. Intrinsic sphincter insufficiency (ISD). The bladder neck (BN) is opened at rest with a clear funneled aspect. It is located at the level of the inferior border of the symphysis pubic bone (S). There was no abnormal displacement during straining.**

the bladder neck, which should remain closed, can be problematic with external techniques. In certain orientations, notably a strict sagittal view, an anechoic posterior shadow artifact caused by the urethra's fibrous normal component hides the bladder neck. This is easily avoided by tilting the probe slightly.

The long axis of the symphysis and the lower border of the symphysis pubic bone are used as fixed landmarks. The position of the bladder neck and displacements are calculated using a horizontal line as reference perpendicular to the axis of the symphysis (Fig. 1). At rest, the normal position of the bladder neck is above or at the level of the reference line and the angle is around 50°.

The diagnosis of HBN (Fig. 2) can be made with a displacement up to 1 cm associated or not with a low position of the bladder neck at rest under the reference line.

Isolated ISD is suggested by bladder neck funneling or a clearly opened urethra at rest and vesicalization of the urethra or opened urethra with voiding during maximum straining (Fig. 2). However, the position of the bladder inside the pelvic cavity remains within normal limits.In the recommendations of the First International Consultation on Incontinence held in Monaco in 1998 (4), bladder neck and pelvic floor ultrasound were considered only as a complementary investigational imaging technique in the evaluation of female incontinence and pelvic floor disorders and not as diagnostic for stress Urinary incontinence. They also recommended that only residual urine measurement by transabdominal ultrasound should be included in the routine initial evaluation of incontinent patients. However, ultrasound evaluation of the bladder neck can help to document the pelvic floor anatomy and discover mixed abnormalities, which is a rather common finding. Ultrasound can also be used to evaluate postsurgical slings or other medical devices and complications.

Magnetic Resonance Imaging

Pelvic floor weakness is a global abnormality, affecting all three compartments. Noninvasive dynamic imaging of the whole pelvic cavity may also be possible.

Morphologic analysis of muscles is made by T1-weighted spin-echo imaging, whereas T2-weighted fast spin-echo imaging is used for pelvic organs. Highly detailed morphologic evaluation of soft tissues, especially the urethra and bladder neck, is provided by addition of an endoluminal coil, located endovaginally or endorectally. This may be used in combination with a phased array multicoil to assess the

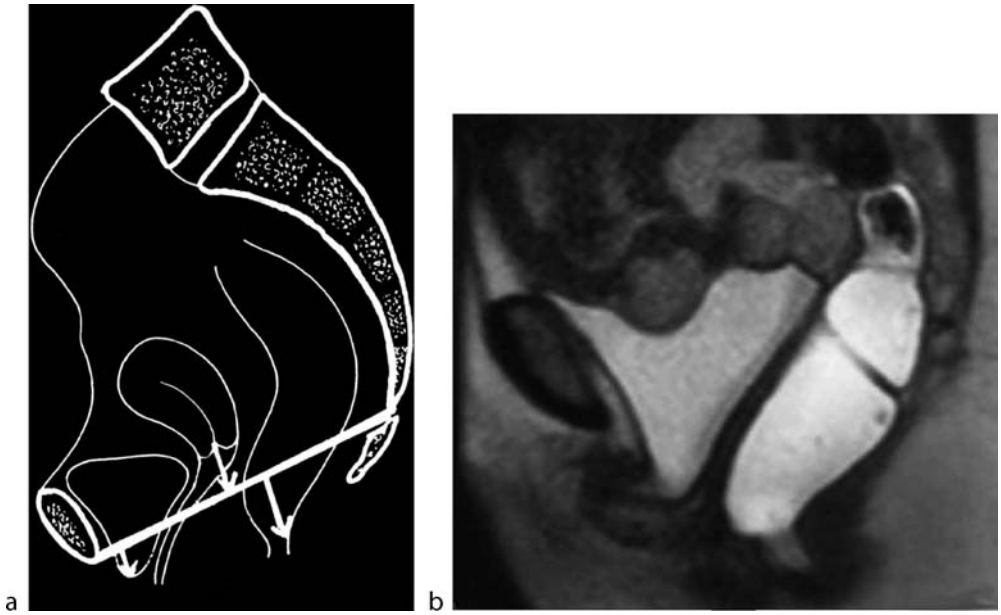

Incontinence, urinary. Figure 3 ***MRI. Sagittal view*****. (a) Drawing of reference line. The pubococcygeal line is commonly used. At normal aspect during rest, the bladder neck is slightly above or at the level of this line. Displacements are easily calculated as shown. This figure demonstrates hypermobility of the bladder neck with normal middle and posterior compartments. (b) Maximum straining. Hysterectomy. Hypermobility with opened bladder neck. Note the associated posterior descent.**

entire pelvic cavity. Fast T2-weighted imaging allows dynamic imaging of the mobility of pelvic floor structures during straining, without any kind of opacification except for the rectum filled with 120 cc of sonographic gel to obtain homogeneous hypersignal inside. Imaging is performed sagittally, to assess displacement, and coronally, to assess levator ani muscles curves. Pelvic prolapse can be imaged in all three compartments simultaneously. Dynamic MRI is used to determine the frequency of associated urinary, genital, and anorectal abnormalities in women with pelvic floor dysfunction.

Pelvic organ descent is measured in relation to a reference line drawn from the inferior border of the symphysis pubic bone to the last coccygeal joint (pubococcygeal or pubosacral lines) on a sagittal plane (Fig. 3). At rest, the normal bladder neck is located between 1 and 2 cm above the reference line or at its level. During straining, the bladder neck goes back and down but remains at the level or slightly below the line. While not as accurate as ultrasound in finding tiny details on the bladder neck or urethra during movement, dynamic MRI can demonstrate an open or funneled bladder neck (Fig. 3). Endoluminal MRI demonstrates the characteristic "target" appearance of the urethra. It is useful in identifying urethral abnormalities (including diverticula) and periurethral tissues (congenital abnormalities, fistulae, tumors).

References

1. De Lancey JO (1994) Structural support of the urethra as it relates to stress urinary incontinence:the hammock hypothesis. Am J Obstet Gynecol 170:1713–1723
2. Béthoux A, Bory S, Huguier M et al (1965) Le colpocystogrramme. Son application à l'étude des prolapsus vaginaux et des incontinences d'urine. J Chir 90:51–62
3. Khullar V, Abbott D, Cardozo LD et al (1994) Perineal ultrasound measurement of the urethral sphincter in women with urinary incontinence:an aid to diagnosis. Br J Radiol 67:713–718
4. Artibani W, Andersen JT, Ostergard DR et al (1998) Imaging and other investigations. In Incontinence. Report of the Ist International Consultation on Incontinence, Monaco
5. Kirschner-Hermanns R, Wein B, Niehaus S et al (1993) The contribution of MRI of the pelvic floor to the understanding of urinary incontinence. Br J Urol 72:715–718

Indirect Imaging

Carmel T. Chan, Sanjiv Sam Gambhir
Department of Radiology, Molecular Imaging Program at Stanford (MIPS) and Bio-X Program, Stanford University School of Medicine, Stanford, USA
carmelc@stanford.edu
sgambhir@stanford.edu

Definition

Indirect imaging refers to imaging a process or molecular target indirectly. For example, if one is imaging a protein target and using that information to infer location(s), activity, or numbers of a different molecular target, which would be considered indirect imaging. The target is often considered a surrogate for the true target of interest. The indirect imaging approach is in distinction to direct imaging in which the target of interest is directly imaged.

Imaging

Indirect imaging is useful when production of an imaging probe specific for a target of interest is difficult/impossible, or when the target of interest is present in relatively low amount and cannot be imaged directly using standard techniques such as labeled antibodies and ligands. For the latter, higher levels of imaging signal per unit level of target and probe interaction can be achieved with indirect imaging through different signal amplification strategies that will be described below (1). Indirect imaging can be accomplished by both radiolabeled probes and optical probes in conjugation with micropositron emission tomography (microPET), bioluminescence/fluorescence imaging respectively, as well as magnetic resonance imaging (MRI). As in the case for direct imaging, a time delay between injection of the probe and imaging is required for clearance of untrapped/unbound probes and enhancement of signal to background ratios, since the scanner cannot distinguish the parent tracer from the bound or metabolized tracer.

Applications Indirect Imaging

Indirect Imaging of Endogenous Gene Expression

In order to monitor endogenous gene expression noninvasively, one would need to develop specific probes that will recognize the gene product(s). For example, labeled antibodies or ligands are needed to detect cell surface proteins and those secreted into the extracellular space whereas another set of probes that can penetrate the cells will be needed to image intracellular targets. Ideally, specific probes can be made to allow direct imaging of targets of interest (See Applications of Direct Imaging in "Direct Imaging".). However, when such probes are not readily available, the expression of an endogenous gene can still be imaged indirectly by fusing the promoter of that gene to drive the expression an imaging reporter gene (Fig. 1). In order to study the regulation of vascular endothelial growth factor (VEGF) noninvasively during wound healing in skin, the express of VEGF protein was indirectly imaged using the Firefly Luciferase (FL) (2, 3)

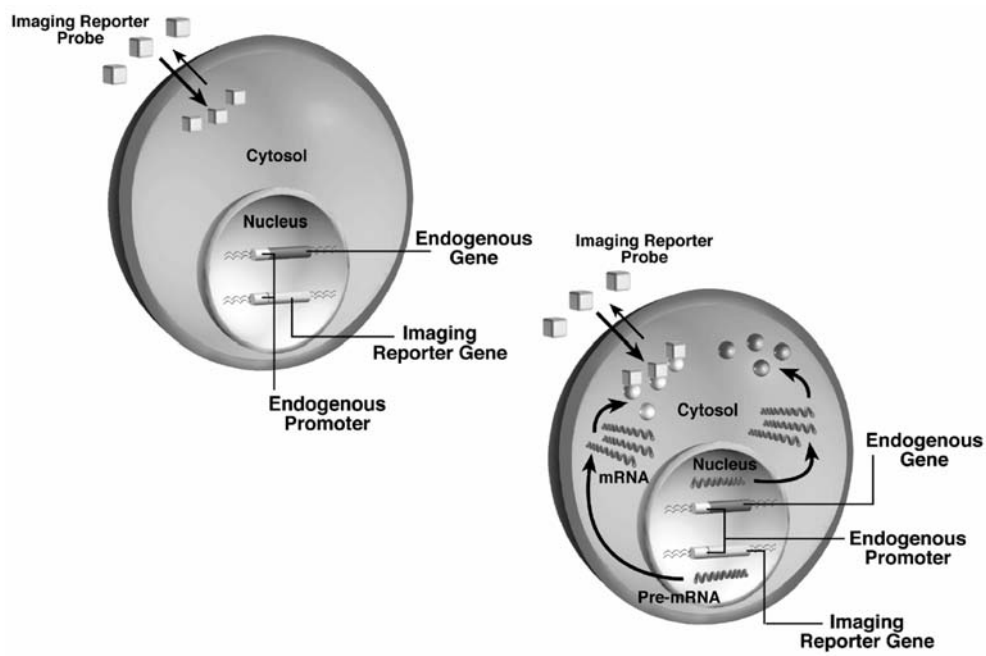

Indirect Imaging. Figure 1 Concept of indirect imaging to monitor endogenous gene expression. An endogenous promoter is fused to an imaging reporter gene of interest. Transcription of the endogenous gene and imaging reporter genes are regulated by the same endogenous promoter. Expression of the endogenous gene can then be indirectly inferred from that of the imaging reporter gene.

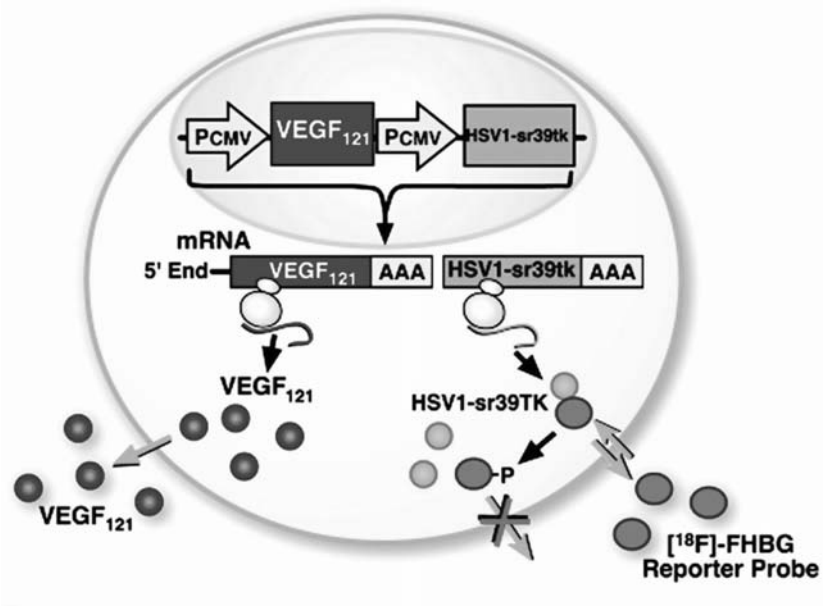

Indirect Imaging. Figure 2 Schematic diagram for indirect imaging of vascular endothelial growth factor (VEGF) expression in a rat myocardium infarction model. An adenovirus carry the gene cassettes expressing the therapeutic $VEGF_{121}$ and HSV1-sr39tk reporter gene was used to infect the rat myocardium. The production of VEGF protein was indirectly imaged by microPET using HSV1-sr39tk as the reporter gene and [^{18}F]-FHBG as the substrate. Reproduced with permission from Wu JC et al (2004) Circulation 110:685–691.

as the optical reporter gene for bioluminescence imaging. The kinetics of VEGF production in the ischemic rat myocardium infected with an adenovirus carrying both VEGF and the Herpes Simplex Virus Type 1 thymidine kinase (HSV-tk) was indirectly imaged by microPET using the HSV-Tk as the reporter gene (1) (Fig. 2). The promoter activity of the prostate-specific antigen (PSA) in a prostate cancer xenograft models was also indirectly imaged using the same approach, in which FL and the mutant HSV-TK (HSV1-sr39tk) were used the reporter gene for optical bioluminescence and microPET imaging respectively. To noninvasively determine the influence of protein diets on endogenous albumin gene expression, a transgenic mouse model in which the endogenous albumin promoter was used to drive the expression of the Mutant HSV-TK reporter gene was utilized. The expression of the albumin gene was indirectly monitored from HSV-tk activity, using microPET in conjunction with 9-[4-[^{18}F]fluoro-3-(hydroxymethyl) butyl]guanine (FHBG) as the HSV-TK substrate. Even though endogenous promoters are highly specific for the genes of interest, they are relatively weak compared to other constitutively active viral promoters such as the cytomegalovirus (CMV) promoter. As a result, direct fusion of an endogenous promoter to the reporter gene(s) often leads to very low levels of reporter mRNA/protein and hence low sensitivity for imaging in living subjects. To circumvent this issue of high specificity but poor sensitivity, the two-step transcriptional amplification (TSTA) system was developed to monitor transcription of a weak/endogenous promoter noninvasively in living animals. The TSTA system is based on the use of a weak/tissue-specific promoter to drive the expression of a strong transcriptional activator (effector), which in turns binds to a strong promoter (e.g. CMV) that drives the expression of the reporter gene (Fig. 3). A bidirectional TSTA system has also been developed that allows simultaneous amplification of two different reporter genes driven by the same promoter, as well as possible replacement of one of the reporter gene with a therapeutic gene of interest. Most recently, transgenic mice models utilizing TSTA system have also been developed to image the tissue-specific and temporal regulation of the PSA promoter and VEGF promoter activity using FL as the reporter gene.

Indirect Imaging of Protein–Protein Interactions

Protein–protein interactions play an important role in all aspects of cell function, including biosynthesis and degradation of macromolecules (DNA, RNA, and proteins), as well as cellular responses to proliferation, differentiation, survival and apoptosis signals. Despite of the rapid increase in number of molecularly targeted agents, the technologies available for studying protein–protein have been limited to *in vitro* analyses such as co-

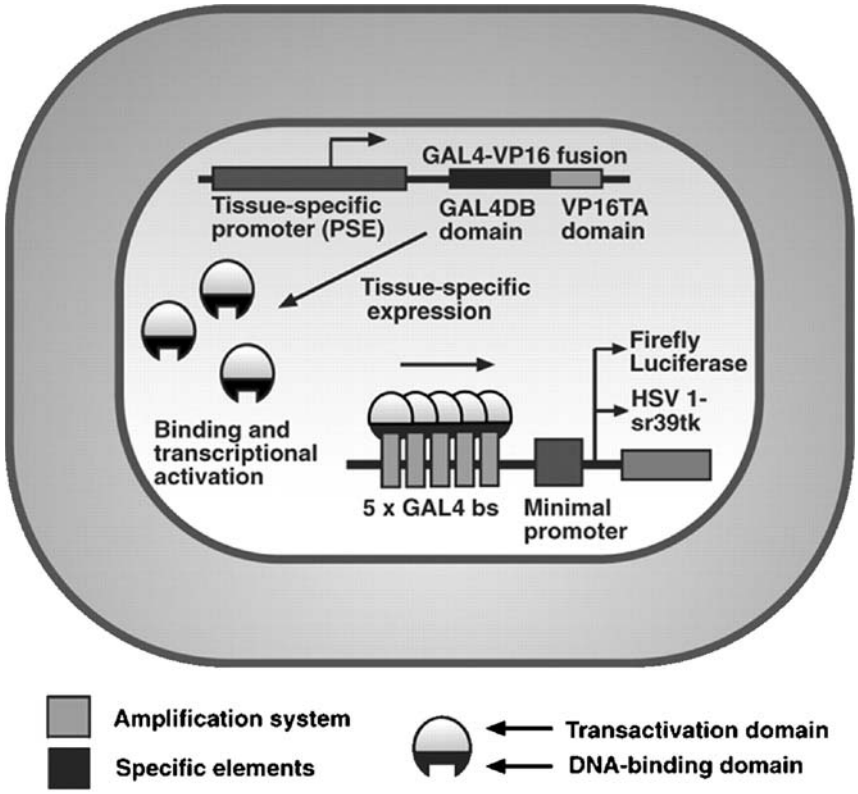

Indirect Imaging. Figure 3 Schematic diagram for indirect imaging of endogenous promoter activity using the two-step transcriptional amplification (TSTA) system. In the first step, the expression of the GAL4-VP16 transactivator is driven by a tissue-specific promoter (e.g., PSE). In the second step, GAL4-VP16 transactivator binds to the GAL4 response elements in a minimal promoter to drive the expression of reporter genes (either *fl* or HSV1-sr39tk), leads to reporter protein, which in turn leads to a detectable signal in the presence of the appropriate reporter probe (D-Luciferin for FL and FHBG for HSV-sr39tk). The TSTA system thus allows amplification of the imaging signals without sacrificing tissue specificity. Reproduced with permission from Iyer M et al (2001) PNAS 25:14595–14600).

immunoprecipitation (co-I.P.)/western blotting and cell binding and cytotoxicity assays, which are labor intensive and invasive in nature. To overcome limitations in studying protein–protein interactions intact cells in their native environment, the split Renilla Luciferase (RL)–Protein-Fragment-Assisted-Complementation (SRL–PFAC) technology and other split reporter protein strategies were developed and validated for noninvasive, indirect imaging of protein–protein interactions, both in cell culture and in living animals (4). The SRL–PFAC is based on the complementation of N-terminal (amino acids (aa) 1–229) and C-terminal fragments (aa 230–311) of full length RL mediated by two interacting proteins. As proof-of-principle, interaction between the transcription factors MyoD and Id was imaged noninvasively in tumor cells, both in cell culture and in living animals. The SRL–PFAC has also been adapted to monitor homodimerization of HSV1-TK (5) as well as rapamycin-mediated interaction between mTOR kinase and immunophilin FKBP12. In addition to the split RL, split firefly luciferase, split β-galactosidase and split β-lactamase PFAC have also been developed to monitor protein–protein interactions and protein translocation in intact cells. Advantages of using split enzyme fragment-assisted-complementation technologies for indirect imaging of protein–protein interactions include signal amplification through the enzymatic reaction in the presence of the substrates, the ability to study protein–protein interactions in intact cells in their native environment and repetitively image the same animal for dynamic monitoring of protein–protein interaction in response to therapies. See "Protein–Protein Interactions, Applications." for a more detailed description of molecular imaging of protein–protein interactions.

Indirect Imaging of Pharmacokinetics and Pharmacodynamics of Drug Treatment

Indirect imaging has also been utilized to monitor the pharmacokinetics and pharmacodynamics of drug treatment. For example, contrast enhanced ^{1}H MRI and

functional magnetic resonance spectroscopy (fMRS) have been used to indirectly monitor the release of the antimetabolite fludarabine monophosphate and gadolinium (Gd)-DTPA from an interstitial liposome depot in rats, respectively (6). The effect of tamoxifen in a murine breast cancer xenograft model in rats was indirectly imaged by dynamic contrast-enhanced MRI to monitor vascular permeability (7). Most recently, the stomach acidity (pH) in rats treated with different nitroxide compounds were monitored using low-field electron paramagnetic resonance techniques that can be extended for monitoring of drug pharmacology and different biological processes such as wound healing and tumor acidosis (8). Indirect imaging has also been used for evaluation of the pharmacodynamics of response to therapy. Heat shock protein 90 (HSP90) is involved in protein folding and is overexpressed in cancer cells. 17-allylamino-demethoxy geldanamycin (17-AAG) is a HSP90 inhibitor known to degrade HSP90 client proteins such as HER2. The efficacy of 17-AAG in a mouse tumor xenograft models was determined using cell-surface HER2 receptor as a surrogate marker (9). The expression of cell-surface HER2 before and after treatment with 17-AAG was determined by microPET imaging. 17-AAG was found to decrease the level of cell-surface HER2. However, since 17-AAG inhibits the chaperone activity of HSP90 and subsequently lead to degradation of multiple client proteins, down-regulation of cell-surface HER2 alone may not be the sole determinant for response to 17-AAG treatment.

Indirect Imaging Tumor Grades and Responses to Treatment Using Radiolabeled Metabolic Tracers and MRI Contrast Agents

Chemotherapy and radiation treatment can lead to decrease in tumor size, proliferation as well as metabolism and these events can be imaged indirectly using metabolic tracers (10). For example, ^{18}F-2-fluoro-2-deoxyglucose [^{18}F-FDG] is a biochemical mimic of glucose that can be transported into the cells by the glucose transporter and phosphorylated by hexokinase and retained inside the metabolically (glycolytic) active cells. FDG can be considered a direct imaging technique if one is interested in determining glucose transporter levels and/or hexokinase activity, but if instead FDG uptake/accumulation is being used to infer levels of other proteins or a cellular process than this should be considered indirect imaging. FDG has been used for diagnosis, staging and evaluation of response to chemotherapy in different cancers in human. Another metabolic tracer that has been used for cancer imaging is 3′-deoxy-3′-[^{18}F] fluorothymidine (FLT). FLT is transported into cells by the nucleoside transporter and subsequently phosphorylated by human thymidine kinase, which is upregulated before and after DNA proliferation. FLT has also been used as a marker for cell proliferation in staging as well as evaluation of response to chemotherapy in tumor xenograft models as well as in human clinical trials. In addition to being indirect imaging agents for evaluation of a drug/treatment that is targeted to an upstream or downstream effects of proliferation, FLT and FDG can also be used for direct imaging for mammalian thymidine kinase activity and hexokinase activity respectively. In addition to PET, MRI has also been used for screening, staging of tumor grades and responses to treatment in conjunction with different contrast agents such as gadolinium and superparamagnetic iron oxide particles.

Nuclear Medicine

- PET

Diagnosis

- Oncology-tumor staging and diagnosis
- Cardiology-indirect imaging of promoter activity and gene expression
- Pharmacokinetics and pharmacodynamic of chemotherapy agents and tracers

References

1. Massoud TF et al (2003) Molecular imaging in living subjects: seeing fundamental biological processes in a new light. Genes Dev 17 (5):545–580
2. Zhang N et al (2004) Tracking angiogenesis induced by skin wounding and contact hypersensitivity using a Vegfr2-luciferase transgenic mouse. Blood 103(2):617–626
3. Ryan PL et al (2005) Photonic monitoring in real time of vascular endothelial growth factor receptor 2 gene expression under relaxin-induced conditions in a novel murine wound model. Ann NY Acad Sci 1041(1):398–414
4. Paulmurugan R et al (2005) Imaging protein-protein interactions in living subjects. TrAC Trend Anal Chem 24(5):446–458
5. Massoud TF et al (2004) Molecular imaging of homodimeric protein-protein interactions in living subjects. FASEB J 18(10): 1105–1107
6. Port R et al (2006) Simultaneous sustained release of fludarabine monophosphate and Gd-DTPA from an interstitial liposome depot in rats: potential for indirect monitoring of drug release by magnetic resonance imaging. Cancer Chemother Pharmacol 1–11
7. Marzola PP et al (2005) Effect of tamoxifen in an experimental model of breast tumor studied by dynamic contrast-enhanced magnetic resonance imaging and different contrast agents. Invest Radiol 40(7):421–429
8. Potapenko DI et al (2006) Real-time monitoring of drug-induced changes in the stomach acidity of living rats using improved pH-sensitive nitroxides and low-field EPR techniques. J Magnetic Resonance, 182(1):1–11
9. Smith-Jones PM et al (2004) Imaging the pharmacodynamics of HER2 degradation in response to Hsp90 inhibitors 22(6):701–706
10. Barentsz J et al (2006) Commonly used imaging techniques for diagnosis and staging. J Clin Oncol 24:3234–3244

Induratio Penis Plastica (IPP)

▶Peyronie's Disease

Indurative Mastopathy

▶Radial Scar, Breast

Infantile Choriocarcinoma

Rare tumor developing from the mother's placenta and spreading to the child. Hypervascularized lesion with infant anemia. Usually rapid tumor progression with deathly outcome. High levels of beta-HCG are diagnostic.
▶Hepatic Pediatric Tumors, Malignant

Infantile Cortical Hyperostosis

▶Caffey Disease

Infantile Hemangioendothelioma, Hepatic

Variant of cavernous hemangioma. Lesion presents often in the first 6 months of life and the majority of the patients are less than 1 month of age. Infantile hemangioendothelioma is most commonly a diffuse alteration with typical histological findings. The vascular channels in hemangioendothelioma are thinner compared to the vascular channels in hemangioma.
▶Hepatic Pediatric Tumors, Benign

Infarction, Renal

O Hélénon, E Dekeiser, JM Correas
Necker Hôpital, Service de Radiologie
Paris, France
olivier.helenon@nck.aphp.fr

Synonyms

Infarct; Ischemic necrosis; Necrotic area

Definition

Renal infarction is defined as a coagulated necrotic area of renal parenchyma that results from renal arterial occlusion.

Pathology/Histopathology

The loss of blood supply results in a wedge-shaped area of coagulative necrosis that affects mostly the renal cortex but can extend into the medulla. It produces a pale area of ischemic renal tissue. Some blood supply from capsular vessels is responsible for the presence of a viable subcapsular band of cortex. The size of parenchymal loss depends on both the distribution of the occluded artery and the development of collateral arterial supply arising from the pelvicalyceal arterial network and transcapsular perforating arteries. After several weeks the infarcted parenchyma starts to shrink and will leave a cortical scar.

Renal infarction can result from various causes including embolism mechanism in patients with cardiovascular diseases, renal artery spontaneous dissection, vasculitis, shock, and trauma. In renal transplant, it is mostly due to renal arterial branch injuries occurring during surgery including kidney removal in donor and transplantation.

Clinical Presentation

Acute renal infarction produces acute symptoms including sudden onset of flank pain and tenderness or upper abdominal pain, fever, hypertension, hematuria, proteinuria and leukocytosis. Patient also can be asymptomatic.

Imaging

Color-Doppler Ultrasound

At color-Doppler ultrasound (CDUS), segmental infarct appears as hypoechoic area with complete loss of Doppler signals showing color flow defects with sharp edges (1) (Fig. 1). Appropriate settings (low pulse repetition frequency, PRF and optimal gain) are mandatory to obtain optimal sensitivity of the technique. Although CDUS is a valuable method in the detection of renal allograft necrosis, it is less accurate for the diagnosis of perfusion defects in native kidneys because of their deeper location. Perfusion assessment at the level of the upper and lower poles is limited by the direction of the vessels perpendicular

to the US beam. The diagnosis of small perfusion defects in native and transplanted kidneys also remains difficult despite the improvement of the Doppler technique, particularly in small hypoperfused kidneys.

Ultrasound contrast agents are helpful to improve the performance of CDUS in case of technical problems and/or the small infarct size. When the renal function is compromised, they provide critical information without any renal toxicity even at the bedside of the patients. Postcontrast studies using nonlinear gray-scale imaging provide the highest resolution and sensitivity in the detection of cortical defects at an early arterial phase following contrast injection (2, 3) (Fig. 2). In renal transplants, contrast-enhanced US plays a critical role to differentiate ischemia due to medical complications, such as acute tubular necrosis and acute rejection, from true infarction.

CT and MRI

►Contrast-enhanced CT remains the gold standard in the diagnosis of renal infarction. It easily demonstrates the presence of a perfusion defect, as a wedge-shaped nonenhancing area triangular in shape and cortically based, typically associated with a subcapsular enhanced rim of cortex supplied by capsular arteries (called "rim sign") (4) (Fig. 3). Such a cortical rim helps differentiate defects of ischemic origin from hypoattenuating infiltrative lesions such as acute pyelonephritis. Focal renal swelling can also be seen at an acute phase. Follow-up CT examinations show progressive reduction of the size of the cortical defect that lead to a cortical scare after several months (Fig. 4).

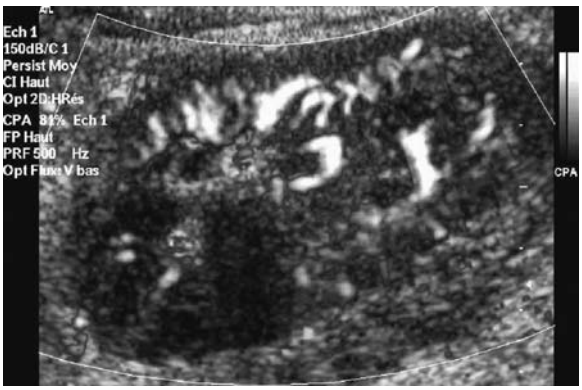

Infarction, Renal. Figure 1 Power Doppler US of a renal infarction. Longitudinal scan of the left kidney shows hypoechoic area of the upper pole with loss of color Doppler signal.

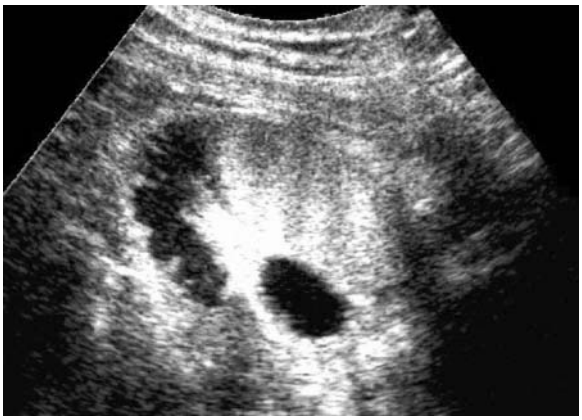

Infarction, Renal. Figure 2 Contrast-enhanced gray-scale US of a renal infarction. Transverse scan following contrast injection shows a wedge-shaped nonenhancing area related to arterial perfusion defect.

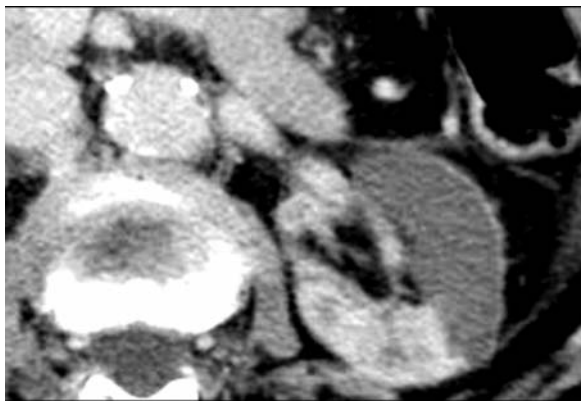

Infarction, Renal. Figure 3 Acute segmental infarction of the left kidney. Contrast-enhanced CT scan shows the presence of a large wedge-shaped nonenhancing perfusion defect associated with a subcapsular enhanced rim of cortex.

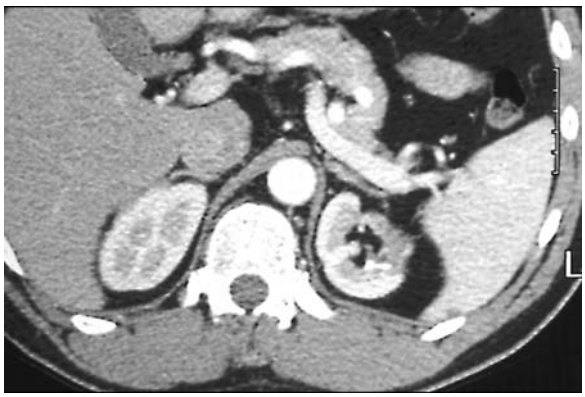

Infarction, Renal. Figure 4 Follow-up CT scan 6 months after infarction of the left kidney. Segmental infarction has lead to a cortical scare.

I

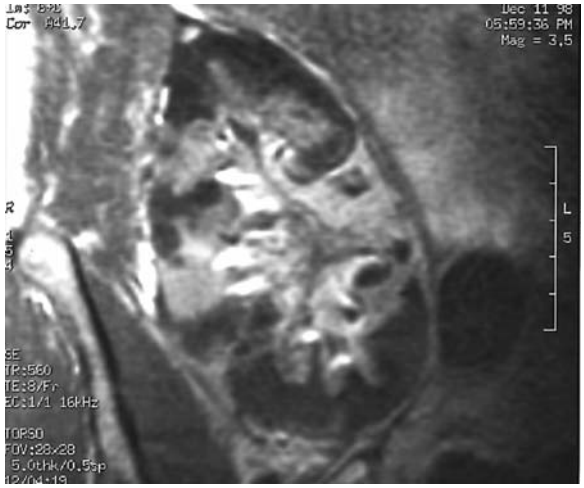

Infarction, Renal. Figure 5 Multifocal cortical infarction after renal transplantation. Contrast-enhanced MR imaging shows multiple perfusion defects. Note the presence of a typical rim sign at lower pole.

Gadolinium-enhanced MR imaging, especially in patients with critical renal failure, is also a modality of choice particularly when early accurate diagnosis is clinically required. The infarcted area exhibits a slight increase in signal intensity on T2-weighted images and is hypointense on T1-weighted images (5). Postcontrast features are similar to that of CT findings (Fig. 5).

Nuclear Medicine

Scintigraphy is of limited value in the diagnosis of renal of renal infarction. It can however demonstrate a focal loss of tracer uptake corresponding to the region of parenchymal infarction.

Diagnosis

Clinical history and findings are often confusing since it can mimic acute pyelonephritis or renal colic. While CDUS can strongly suggest the diagnosis at initial screening, accurate diagnosis relies on contrast-enhanced cross-sectional techniques (CT or MRI) or even contrast-enhanced US in skill hands.

Bibliography

1. Hélénon O, El Rody F, Correas JM, et al (1995). Color Doppler US of renovascular disease in native kidneys. Radiographics 15: 833–854
2. Taylor GA, Barnewolt CE, Claudon M, et al (1999). Depiction of renal perfusion defects with contrast-enhanced harmonic sonography in a porcine model. Am J Roentgenol 173:757–760
3. Correas JM, Hélénon O, Moreau JF (1999). Contrast-enhanced ultrasonography of native and transplanted kidney diseases. Eur Radiol S3:394–400
4. Wong WS, Moss AA, Federle MP, et al (1984). Renal infarction: CT diagnosis and correlation between CT findings and etiologies. Radiology 150:201–205
5. Hélénon O, Attlan E, Legendre C, et al (1992). Gd-Dota-enhanced MR imaging and color Doppler US of renal allograft necrosis. Radiographics 12:21–33

Infarction, Spleen

Splenic infarction is a relatively rare disease. It is the result of arterial or venous compromise and is associated with a heterogeneous group of diseases, including embolic and autologic disorders, splenic vascular diseases, and anatomic abnormalities. Splenic infarction may be segmental or global, involving the entire organ.

▶Spleen, Infectious Diseases

Infected Necrosis, Pancreatic

Pancreatic necrosis is a diffuse or focal area of nonviable pancreatic parenchyma, which is typically associated to acute pancreatitis with peripancreatic fat necrosis. Secondary infection of the pancreatic necrosis is a possible complications and leads to clinical findings of infection. Distinction between sterile and infected necrosis is critical, since development of infection increases the mortality risk. Often cultures obtained by needle aspiration are necessary and surgical drainage is needed.

▶Pancreatitis, Acute

Infection

An inflammation resulting from the invasion of the body by pathogenic microorganisms.

▶Oral Cavity, Inflammatory Diseases
▶Infection Imaging

Infection of Skeletal Muscle

▶Infection, Soft Tissue

Infection of the Breast

►Breast, Infection

Infection, Opportunistic, Brain

Majda M. Thurnher
Universitätsklinik für Radiodiagnostik, Medizinische Universität Wien, Vienna, Austria
majda.thurnher@meduniwien.ac.at

Synonyms

Cerebral infections; Immunsuppression

Definition

►Opportunistic infections are infections caused by organisms that usually do not affect persons with a healthy immune system, but can affect people with a poorly functioning immune system.

Pathology/Histopathology

Viral Infections

Cytomegalovirus

Cytomegalovirus (CMV) is the member of the herpesvirus family, the infection in adults is a result of the reativation of a latent infection. Small microglial nodules and inclusion-bearing cytomegalic cells are widely distributed in the cortex, basal ganglia, brain stem, and cerebellum in CMV diffuse micronodular encephalitis (1).

Progressive Multifocal Leukoencephalopathy

►Progressive multifocal leukoencephalopathy (PML) is a subacute opportunistic infection caused by JC *Polyomavirus* (JCV) with increased incidence due to the acquired immunodeficiency syndrome (AIDS) epidemic (0.7–11% of HIV patients will develop PML during the course of their illness) (2). The histopathological hallmark of PML is demyelination with enlarged oligodendroglial nuclei and bizzare astrocytes. The disease is usually multifocal, and the lesions may occur in any location in the white matter.

Fungal Infections

Cryptococcosis

Approximately 5–10% of patients with AIDS develop CNS ►cryptococcosis caused by *Cryptococcus neoformans*. The infection is a result of a newly acquired infection with hematogenous dissemination of the infection from the lung to the CNS. Cryptococcal meningitis is the most common manifestation, where the subarachnoid spaces are thickened and filled with multiple organisms and their material. From the subarachnoid space, cryptococcus extends along the Virchow-Robin perivascular spaces into the basal ganglia, thalami, midbrain, and cerebellum. The Virchow-Robin spaces become dilated. With disease progression, dilated perivascular spaces become confluent and cystic lesions develop called "gelatinous pseudocysts." Cryptococcoma is the only parenchymal form of the cryptococcal CNS infection. The lesions result from the direct invasion of the brain by the fungus with the development of a granulomatous reaction.

Aspergillosis

Aspergillusis accounts for 18–28% of all fungal brain abscesses, and it is the most common CNS complication following bone marrow transplantation. Meningitis, abscess or granuloma, vascular invasion with thrombosis and infarction, and hemorrhage and aneurysm formation are manifestations of cerebral ►aspergillosis. Pathologically, hyphal elements invade cerebral vessels, resulting in thrombosis and infarctions. Sterile infarctions become septic when the fungus erodes the wall of the vessel with extension into the brain parenchyma with inflammatory reactions and necrosis.

Parasitic Infections

Toxoplasmosis

Cerebral ►toxoplasmosis results from infection by an intracellular protozoan, *Toxoplasma gondii*.

After the acute infection, the latent form, called encysted bradyzoites, remains in the tissues until a decline in immunity. Rupture of the cysts releases the free tachyzoite, which causes acute illness. In AIDS patients, toxoplasma causes necrotizing encephalitis.

Clinical Presentation

Viral Infections

Cytomegalovirus

In immunocompromised patients, CMV can produce a variety of clinical syndromes. Five distinct neurological

syndromes due to the CMV infection have been described: retinitis, myelitis/polyradiculopathy, diffuse micronodular encephalitis, ventriculoencephalitis, and mononeuritis multiplex.

Progressive Multifocal Leukoencephalopathy

Pyramidal signs, gait disturbances, hemiparesis, extrapyramidal and cerebellar signs, sensory deficits, cognitive dysfunctions are parts of the "multifocal" clinical picture of PML. Without treatment, the prognosis for PML is usually poor, with death occurring after 2.5 to 4 months. Only a small number of cases will have a more benign clinical course (only 7 to 9% of patients demonstrate prolonged survival without therapy). Recent studies have shown clinical and radiological improvements in patients with PML who underwent highly active antiretroviral therapy (HAART).

Fungal Infections

Aspergillosis

Clinical presentation of cerebral aspergillosis includes fever, alterations of mental status, seizures, depression. In some cases stroke-like symptoms will develop.

Parasitic Infections

Toxoplasmosis

The clinical symptoms in cerebral toxoplasmosis are nonspecific; usually patients have fever, seizures, headaches, or altered mental status.

Imaging

Viral Infections

Cytomegalovirus

The most common imaging findings in patients with CMV encephalitis are: cortical atrophy, periventricular enhancement, and diffuse white matter abnormalities. Generalized atrophy is the most commonly reported CT abnomality, but it is a nonspecific finding. Periventricular enhancement is also not diagnostic; it has been described in cases of lymphoma, toxoplasmosis, and other infections. Rarely, cerebral mass lesions due to CMV or choroids plexitis were observed.

Progressive Multifocal Leukoencephalopathy

The findings on MR imaging correlate very well with macroscopic changes. PML lesions are patchy, scalloped, high signal intensity lesions on T2-WI MR images located in the white matter with extension along the white fibers (2). Subcortical arcuate fibers are involved, mass effect is mild or absent, and peripheral, faint enhancement is a rare feature. On T1-WI images, the PML lesions are marked hypointense (Fig. 1).

Fungal Infections

Cryptococcosis

In cases of cryptococcal meningitis CT scans rarely show meningeal enhancement, whereas enhanced T1-WI MR

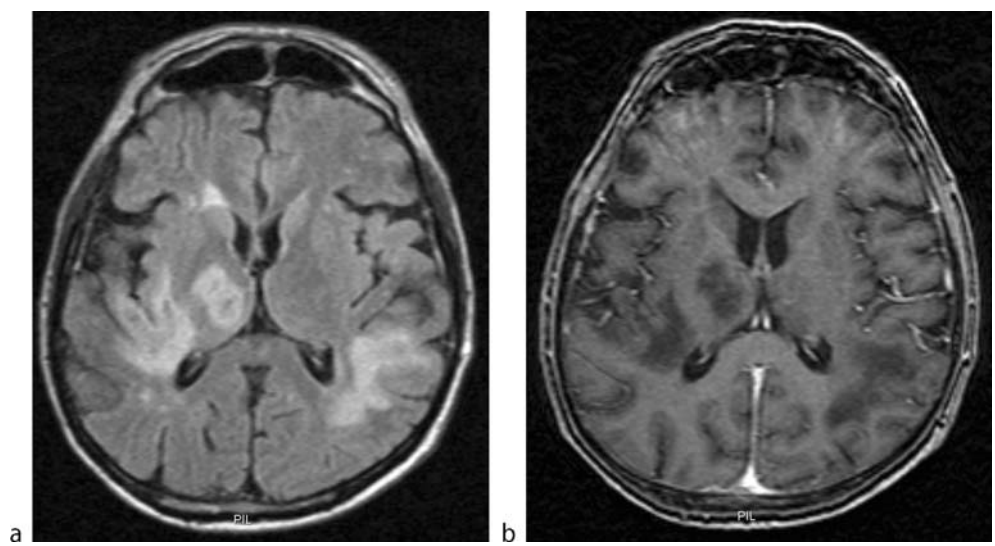

Infection, Opportunistic, Brain. Figure 1 PML in an 35-year-old male HIV positive patient. On axial fluid-attenuated inversion-recovery (FLAIR) MR image (a) high signal intensity lesions located bilateral in the white matter, without involvement of the subcortical fibers are observed. The lesions are hypointense on T2-WI MR image (not shown) and do not show enhancement on postcontrast images (b). Mass effect is also not present.

images may demonstrate meningeal disease. Dilated perivascular spaces will be recognized on MR images as multiple, bilateral, small round- or oval-shaped lesions, located usually in the basal ganglia, which show high signal on T2-WI images, and have signal slightly higher than the CSF on T1-WI MR images. Enhancement is not present. Gelatinous cysts do not differ from the dilated Virchow-Robin spaces on MR images. Enhancement and mass effect are also absent. On CT, cryptococcomas are hypodense with high signal on T2-WI images, and low signal on T1-WI MR images. On enhanced images, the lesions usually demonstrate a ring-like or nodular enhancement, and cannot be distinguished from granulomas of other origin.

Aspergillosis

On MR imaging, brain lesions in aspergillosis usually have low signal centrally or peripherally on T2-WI images, probably due to accumulation of fungi containing iron, magnesium, and manganese, as well as blood breakdown products (Fig. 2). Contrast enhancement is rarely present, depending on the severity of the immunocompetence (3).

Parasitic Infections

Toxoplasmosis

On nonenhanced CT scans, toxoplasma lesions are hypodense with edema and mass effect. Solid, nodular- or ring-enhancing lesions are typically observed on postcontrast scans. On T1-WI MR images, toxoplasma lesions have iso-to-low signal centrally. Signal intensity on T2-WI images depends on the stage of the lesion, which could be iso, hypo, or hyperintense (4). Enhanced T1-WI images reveal ring or nodular enhancement. Approximately 10 days after the initiation of therapy, a decrease in the number and size of the lesions with reduction in edema and mass effect should be observed on follow-up MR examinations (Fig. 3). Calcifications are often seen in healed foci. The MR spectroscopic pattern of toxoplasma lesions is nonspecific, consistent with anaerobic inflammation within the abscess.

Nuclear Medicine

Viral Infections

Progressive Multifocal Leukoencephalopathy

Patients with PML had two different patterns on thalium and gallium scans: patients with positive gallium and negative thallium scans, and a second group with negative thallium and gallium scans. Demyelination and destruction explain negative thallium and gallium scans. Positive gallium and negative thallium scans may be a result of coexisting pathology.

Parasitic Infections

Toxoplasmosis

Based on conventional MR imaging, cerebral toxoplasmosis cannot be distinguished from primary cerebral lymphoma.

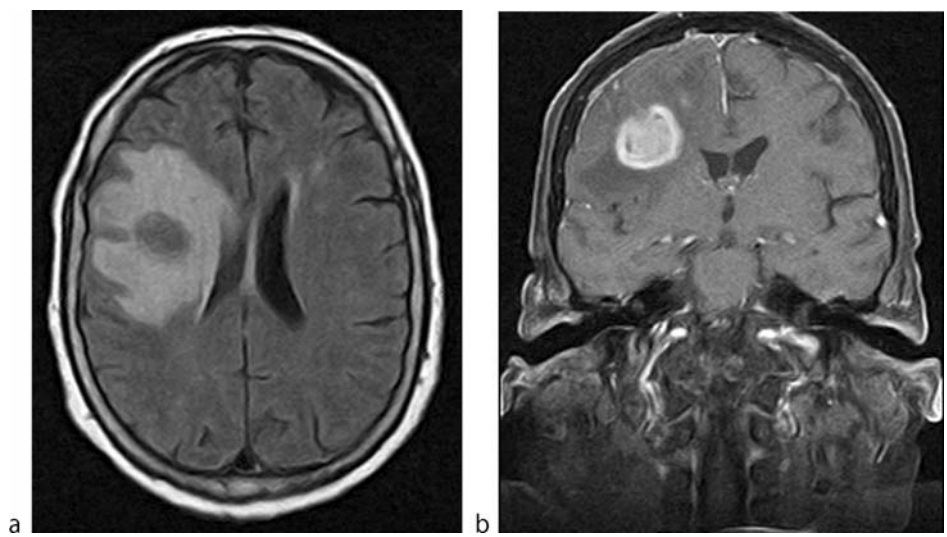

Infection, Opportunistic, Brain. Figure 2 Cerebral aspergillosis in a female patient 2 months after bone marrow transplantation. Low signal intensity lesion with extensive perifocal edema located in the white matter of the right frontal lobe is shown on axial FLAIR MR image. (a) Marked enhancement of the lesion is demonstrated on coronal postcontrast T1-weighted MR image with fat suppression (b).

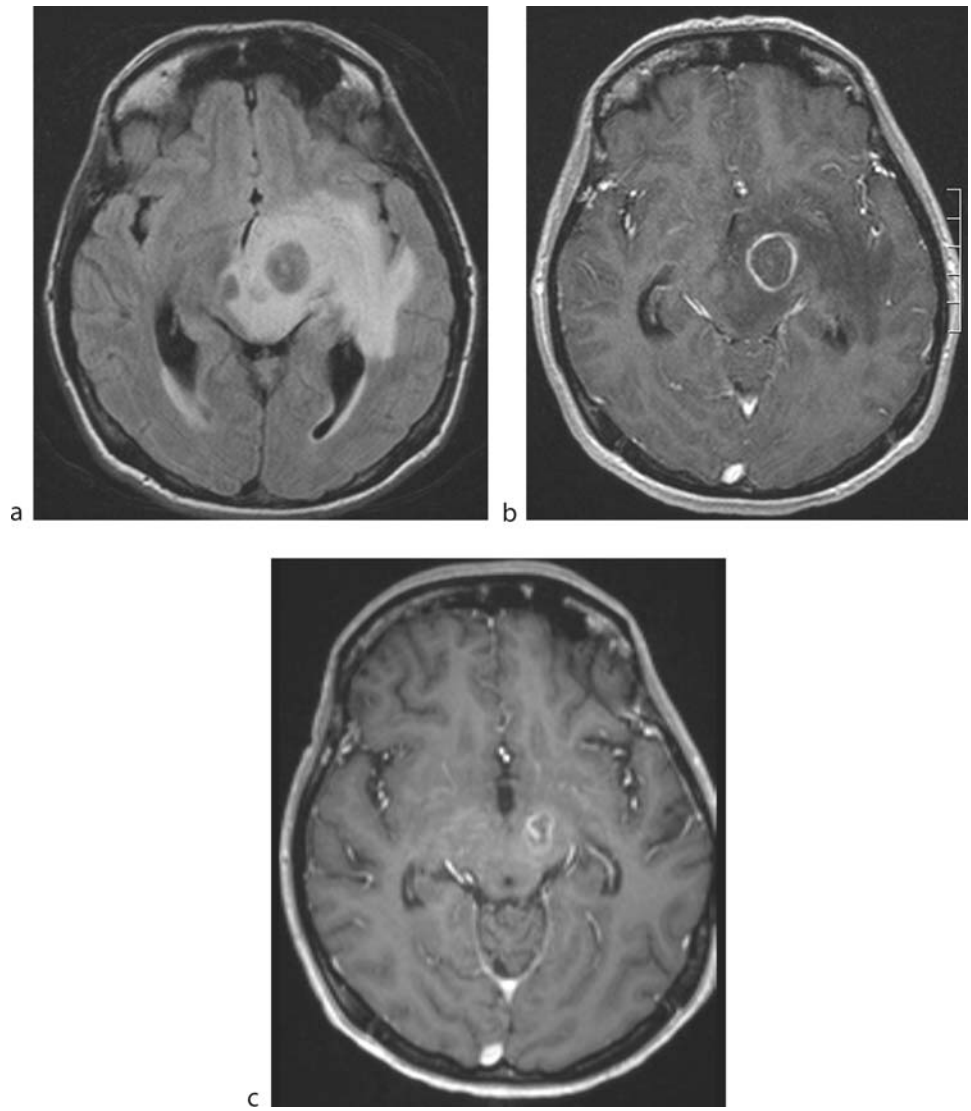

Infection, Opportunistic, Brain. Figure 3 Cerebral toxoplasmosis in an AIDS patient. On axial FLAIR MR image (a) hypointense lesion with perifocal edema located in the left basal ganglia region is hown. On axial postcontrast T1-weighted MR image (b) ring-like enhancement of the lesion is demonstrated. Decrease in size and enhancement is shown on follow-up MR examination (c) 1 month after the initiation of antitoxoplasmosis treatment.

The use of Thallium-201 (^{201}TI) brain SPECT in AIDS patients has been proven to be very helpful in distingushing toxoplasmosis from lymphoma (Ruiz). Positive ^{201}TI brain SPECT is suggesstive of CNS lymphoma, and negative uptake suggests infection in AIDS patients.

The potential use of F-18 fluorodeoxyglucose (FDG)-positron emission tomography (PET) in differentiating lymphoma from toxoplasmosis in AIDS patients has been also examined (5). The standardized uptake values (SUVs) over cerebral lesions were much higher in lymphomas than in toxoplasma lesions.

Diagnosis

Viral Infections

Cytomegalovirus

The infection of the CNS due to CMV is difficult to diagnose while the patient is alive because the virus is difficult to culture from cerebrospinal fluid (CSF). The recent development of the polymerase chain reaction (PCR) technique has allowed isolation of CMV based on the presence of DNA within the CSF.

Progressive Multifocal Leukoencephalopathy

A rapid onset of symptoms in an HIV positive patient with multifocal clinical picture, typical MR imaging findings, and positive JCV PCR in CSF are sufficient evidence for clinical diagnosis of PML. However, a negative result of JCV DNA PCR of the CSF does not rule out PML.

Fungal Infections

Aspergillosis

Because of the high mortality rate of 85–100% early suspicion of aspergillosis is essential. The diagnosis is usually based on a combination of clinical findings in a patient with risk factors and isolation of the microorganism, radiological data, serological detection of antibodies or antigens, or histopathological evidence of invasion.

Parasitic Infections

Toxoplasmosis

Differentiation between lymphoma and toxoplasmosis in AIDS patients remains a diagnostic dilemma. The combination of a neuroradiological examination, a compatible radionuclide study (^{201}TI SPECT, PET), and CSF analysis (Epstein–Barr virus DNA) is a current approach in those patients.

Bibliography

1. Morgello S, Cho E, Nielsen S et al (1987) Cytomegalovirus encephalitis in patients with acquired immunodeficiency syndrome: an autopsy study of 30 cases and a review of the literature. Hum Pathol 18:289–297
2. Thurnher MM, Thurnher SA, Mühlbauer B et al (1997) Progressive multifocal leukoencephalopathy in AIDS: initial and follow-up CT and MRI. Neuroradiology 39:611–618
3. Dietrich U, Hettmann M, Maschke M et al (2001) Cerebral aspergillosis: comparison of radiological and neuropathologic findings in patients with bone marrow transplantation. Eur Radiol 11:1242–1249
4. Brightbill TC, Ihmeidan ICH, Donovan Post MJ et al (1995) Neurosyphilis in HIV-positive and HIV-negative patients: neuroimaging findings. Am J Nuroradiol 16:703–711
5. Villringer K, Jager H, Dichgans M et al (1995) Differential diagnosis of CNS lesions in AIDS patients by FDG-PET. J Comput Assist Tomogr 19:532–536

Infection, Soft Tissue

Catherine M Phan, Thomas M Link
Hôpital de Bicêtre, Service de Radiologie BROCA, Le Kremlin-Bicêtre, France
catherine.phan@bct.aphp.fr

Synonyms

Infectious myositis; Infection of skeletal muscle; Primary muscle abscess; Pyomyositis

Definition

Soft tissue infections can develop separately, but frequently they are associated with musculoskeletal infections involving joints and bones. Infection is often considered as a therapeutic emergency requiring the radiologist's assessment of the presence or absence of infectious disease and its extent. Soft tissue infections can be focal (►abscess) or diffuse (►cellulitis) and are subdivided according to the compartment involved. The specific entities discussed are cellulitis, pyomyositis, abscess, ►necrotizing fasciitis, tenosynovitis, and septic bursitis. They could be the primary event (cellulitis, muscle abscess) possibly leading to infective periostitis, osteitis, and osteomyelitis, or the consequence of spread of infection from adjacent structures (spondylodiskitis, osteomyelitis, and arthritis).

Pathophysiology

Soft tissue infections cause considerable morbidity with variable degrees of severity. Predisposing factors are open fracture, foreign bodies, and prosthetic material, as well as impaired immunity affecting drug abusers, diabetics, patients with immunodeficiency virus or leukemia, and patients taking immunosuppressive medication. Patients with human immunodeficiency virus infection are susceptible to bacterial and fungal infections (1). They are predisposed to osteomyelitis, septic arthritis, and pyomyositis.

Isolated soft tissue infections are less common than those involving bone and joint at the same time. The principal routes by which soft tissue can be contaminated are hematogenous spread of infection, spread from a contiguous source of infection, direct implantation, and postoperative infection (2). Isolated soft tissue infections arise from direct implantation (skin breaches, penetrating wounds, foreign bodies, decubitus ulcers, open fracture, and surgery) and less frequently from hematogenous spread from distant sites of infection. Human bites (*Staphylococcus aureus, Bacillus fusiformis*) and animal bites (*Pasteurella multocida, S. aureus*, and *Staphylococcus epidermidis*) are also common causes of infection from direct implantation. Infection could extend to adjacent soft tissue by progressing from osteomyelitis to osteitis to periostitis or from the vertebral body endplate to the disk to the closest adjacent vertebral body to soft tissue

I

(subligamentous, paraspinous phlegmon, or abscess) in the case of spondylodiskitis.

Pyomyositis consists of a primary muscle abscess, and is prevalent in tropical countries, in immunocompromised patients, and in drug abusers. Bacteria, mycobacteria, fungi, viruses, and parasitic agents may be responsible.

Clinical Presentation

Clinical features of soft tissue infection are not specific to the compartment involved and initially include pain, rigor, fever, and soft tissue enlargement.

Clinical diagnosis is based on the appearance of lesions, degree of pain, and systemic toxicity. Knowledge of the organisms involved does not always help define the tissue depth of disease, but aids in choosing antimicrobial therapy.

Cellulitis represents acute, febrile, and diffuse inflammation of subcutaneous fat and skin. Stiffness may precede visible signs of skin involvement or lymphangitis by 24 h. Tender regional lymphadenitis often develops. The involved area may show blistering and local necrosis. Desquamation may occur on recovery.

Myositis—Muscular Abscess

Nonspecific clinical features of myositis are fever, localized myalgia and stiffness, swelling, and tenderness. In certain instances, it is the anatomic location rather than the morphologic characteristics of the lesion or the etiologic infecting agent that distinguishes the particular type of infection. Clinical manifestations of psoas abscess include fever, lower abdominal or back pain, or pain referred to the hip or knee.

Necrotizing fasciitis **(NF)** usually afflicts patients with impaired immunity. It is characterized by rapidly extensive infection of superficial and deep soft tissue. The overlying skin is classically warm, indurated with a mottled appearance and purple patches. Crepitus due to superficial fascial emphysema is rarely palpable. Extreme pain followed by anesthesia suggests the diagnosis. At the late stages, there is local coagulopathy and thrombosis of the blood vessels with necrosis of the deep soft tissues. NF is differentiated from the other soft tissue infections by a rapid progression to multisystem failure and death without early recognition and treatment.

Imaging

Conventional Radiographs

In the case of a suspected musculoskeletal infection, plain radiographs (XR) are normal until soft tissue infections are advanced; however, they allow assessment of associated bony destruction or joint erosion. They are of little value, showing a nonspecific thickening of soft tissue. They can reveal the presence of gas in subcutaneous fascial planes (necrotizing fasciitis) or in muscle (a minority of muscle abscess). The presence of subcutaneous gas on a radiograph does not necessarily indicate a clostridial infection, because *Escherichia coli, Peptostreptococcus* species, and *Bacteroides* species may produce gas under appropriate conditions.

Ultrasonography

Ultrasonography (US) is an important modality for evaluation of musculoskeletal infections especially in children because it is nonionizing and very sensitive for fluid collection and joint effusions (3). It allows detection of clinically occult collections providing guidance for diagnostic aspiration and could change the management of patients with initially diagnosed cellulitis. It should be performed in conjunction with radiography and could help to differentiate abscess from necrotic or cystic tumors, hematoma, and joint fluid. With the development of high-frequency and color Doppler sonography, US remains an accessible and inexpensive technique for studying infectious tenosynovitis and bursitis.

Computed Tomography

Computed tomography (CT) provides high spatial resolution and allows a precise visualization of the anatomic structures involved by infection. After contrast medium administration, enhancement of abscess walls, internal septa, and inflammation of deep fascia are well visualized. CT may also be used to guide interventional procedures to drain abscesses.

MRI

Magnetic resonance (MR) imaging is the ideal technique for assessing the soft tissue abnormalities produced by infectious processes. On MR images, soft tissue alterations consist of signal intensity changes that reflect the increased water content of the inflammatory soft tissues. These changes are nonspecific; however, they are helpful in detecting the presence and extent of the infection, which is suspected clinically on the basis of physical and laboratory findings and predefined by other imaging studies.

Intravenously administered gadolinium allows differentiation of an abscess from cellulitis or phlegmon in the soft tissues, or an abscess from bone marrow edema in the marrow space; Gadolinium also increases the visualization of sinus tracts and sequestra, and plays an important role in the diagnosis of fascia abnormalities in necrotizing fasciitis, if readily available at an early stage.

Diagnosis

Cellulitis

The diagnosis is usually clinical, but imaging excludes underlying abscess formation or other complication. *Plain radiographs* depict nonspecific findings: soft tissue swelling, displacement of fat planes, and the presence or absence of radiolucent gas foci (streaks, bubbles by gas-forming organisms) and radiopaque foreign bodies (needle, tips).

US typically shows edema as diffuse thickening of skin and subcutaneous fat, dissected by a reticular pattern of anechoic strands (Fig. 1a) with progressive transition to normal tissue. CT provides similar information with a precise depiction of the infectious focus and the presence of gas (Fig. 1b). MR findings show diffuse areas of low signal intensity on T1-weighted and high signal intensity on T2-weighted images, with a reticulated pattern in the subcutaneous fat and skin thickening without abnormality of deep fascial planes. The signal intensity in the same pathological areas is increased by gadolinium contrast.

Abscess

Abscesses, even sizeable ones, are difficult to discern on plain radiographs, but their visualization is facilitated by signs such as periosteal reaction or joint effusions. US detects abscesses as a fluid collection, totally or partially anechoic with well-marginated hyperechoic rim in the acute and subacute phases (Fig. 2). Echogenicity can vary by the presence of internal debris, hemorrhage, or septum. The abscess content could be hyperechoic, isoechoic, or appears as diffuse homogeneous low-level echoes, mimicking a solid mass. Color Doppler imaging, dynamic compression of the fluid collection, and motion of the purulent material within the collection may help differentiate echogenic fluid from a solid tumor or hematoma.

CT and MRI are the best imaging modalities for the extent of abscess formation. On CT scans, abscess walls and internal septa typically enhance after contrast administration (Fig. 3).

On MR scans, muscle abscesses are fluid-filled cavities that are bright on T2-weighted images, with a rim that shows postcontrast enhancement (Fig. 4). Such a pattern is typical for an abscess, but it may be seen in other entities including ischemic foci in muscle and necrotic soft tissue tumors.

Infectious Myositis—Pyomyositis

MR findings are not specific in pyomyositis. There is diffuse muscle enlargement with intermediate signal intensity on T1-weighted images, and diffuse high signal intensity on T2-weighted images sometimes with abscesses (4). The precise diagnosis is made after aspiration or biopsy and the culture of the abnormal muscle.

Necrotizing Fasciitis

CT and MRI are used to distinguish cellulitis from necrotizing fasciitis (Fig. 5) (1). With necrotizing fasciitis, the abnormalities are seen in the subcutaneous fat, as for cellulitis, with an extension in the deep fasciae between muscles and into muscles. The abnormalities are best demonstrated with MRI on short T1 inversion recovery (STIR) images. Muscle involvement is not required for making the diagnosis of necrotizing fasciitis but fascial involvement is. Linear high signal intensity is seen in both superficial and deep fasciae representing the fascial necrosis. The associated muscle involvement, when present, is seen as areas of high signal intensity within the muscles on T2-weighted or STIR images with or without hyperintense fluid collections from abscesses. Postcontrast T1-weighted images show linear enhancement of the fascia, focal enhancement of the affected muscles, and peripheral enhancement of the abscesses. Contrast administration is not necessary for making the diagnosis of necrotizing fasciitis. During the surgical debridement,

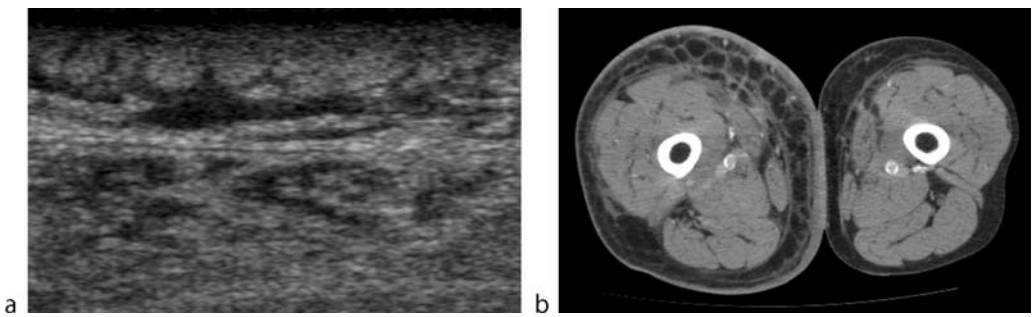

Infection, Soft Tissue. Figure 1 Infectious cellulitis of the right thigh. Ultrasonography (a) shows diffuse thickening of the skin and subcutaneous tissues characterized by a reticular pattern of anechoic strands. The CT image (b) also demonstrates findings of cellulitis (e.g., skin thickening, stranding of the subcutaneous fat, and blurring of the fat).

tissue biopsies are performed to obtain proper cultures for microorganisms.

Septic Tenosynovitis/Septic Bursitis

Septic or aseptic causes of tenosynovitis and bursitis cannot be distinguished by imaging features. They are often described with adjacent cellulitis. Septic cases result from tuberculosis or usually from penetrating trauma. The most common pathogen is *S. aureus* or *Staphylococcus pyogenes* (2). US findings for septic tenosynovitis are accumulation of fluid within the tendon sheath, tendon enlargement compared with the contralateral size, and hyperemia seen with Doppler. US may help to exclude other diagnoses such as septic arthritis, cellulitis, or foreign bodies. Septic bursitis most frequently involves the olecranon or prepatellar bursa. US demonstrates a fluid collection within the bursa with possible thickened wall, hyperemia in the walls, and debris or septae within the collection. Fluid surrounding a tendon or within a bursa is well depicted with US and will be seen as low signal intensity on T1-weighted and high signal intensity on T2-weighted images, with enhancement of the synovial lining after intravenous injection of gadolinium contrast.

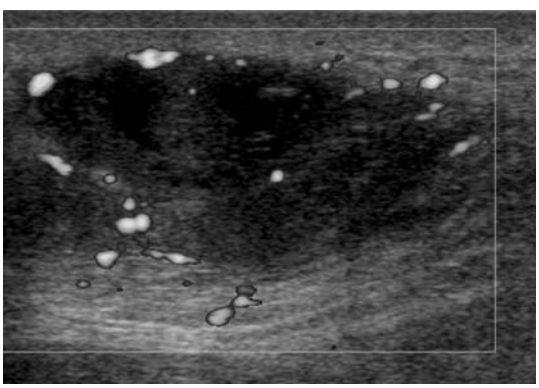

Infection, Soft Tissue. Figure 2 Fifty-year-old diabetic woman with erythema, edema, and firm mass on the thigh. Transverse sonogram with 7.5-MHz linear-array transducer shows well-defined, subcutaneous, anechoic mass with few internal echoes. Thick, hyperemic rim of the soft tissue abscess is seen at the periphery with color Doppler sonogram. *Staphylococcus* was cultured from abscess fluid after aspiration.

Diabetic Foot Infection

Foot disease in diabetics is a common problem and results frequently in one or more of the following: vascular disease, infection, and neuroarthropathy. Infection in diabetics is usually related to a soft tissue injury, followed by cellulitis; the infection may remain limited to the soft tissues or extend to the bones and the joints. CT scans and XR offer useful bony anatomic information, in particular for sequestrum. However, soft tissue details are limited and sensitivity and specificity for determining infection are low, especially in the early stages of infection. MRI remains the optimal imaging modality for soft tissue infection. Combined indium-111-labeled leukocyte technetium phosphate bone scintigraphy is the radionuclide procedure of choice for determining infection in neuropathic joints. Soft tissue ulcerations account for more than 90% of diabetic pedal osteomyelitis cases. They usually occur under pressure areas of the foot, such as the plantar soft tissues beneath or adjacent to the first and fifth metatarsal heads, the calcaneal tuberosity, the distal phalanges, and the malleoli. Ulcers can be identified on MRI as soft tissue defects of low signal intensity on both T1-weighted and T2-weighted images. Findings that suggest infection instead of diabetic neuropathy include osteomyelitis with bone marrow areas of low signal on T1-weighted and high signal on T2-weighted or STIR images associated with soft tissue ulcer or sinus tract overlying the abnormal bone and located as

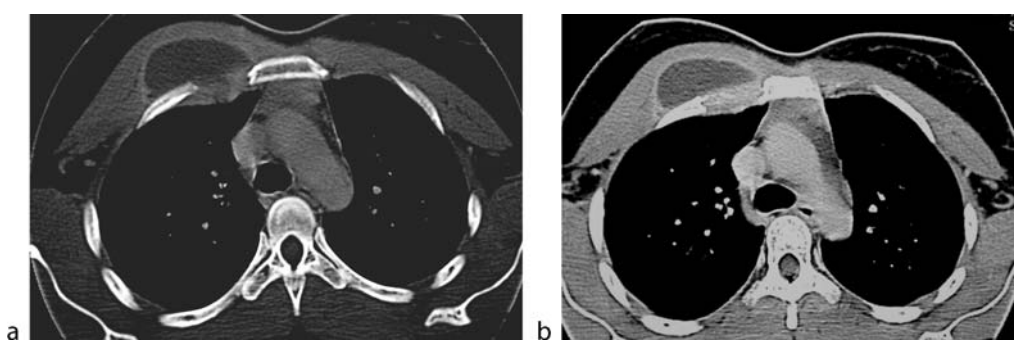

Infection, Soft Tissue. Figure 3 Chest wall tuberculosis arising from costochondral infection in a 65-year-old woman with active pulmonary tuberculosis. Thoracic axial CT images (a, b) show a soft tissue lesion of homogeneous low density in the right chest wall with a rim enhancement by iodine contrast. Aspirated fluid revealed *Mycobacterium tuberculosis*.

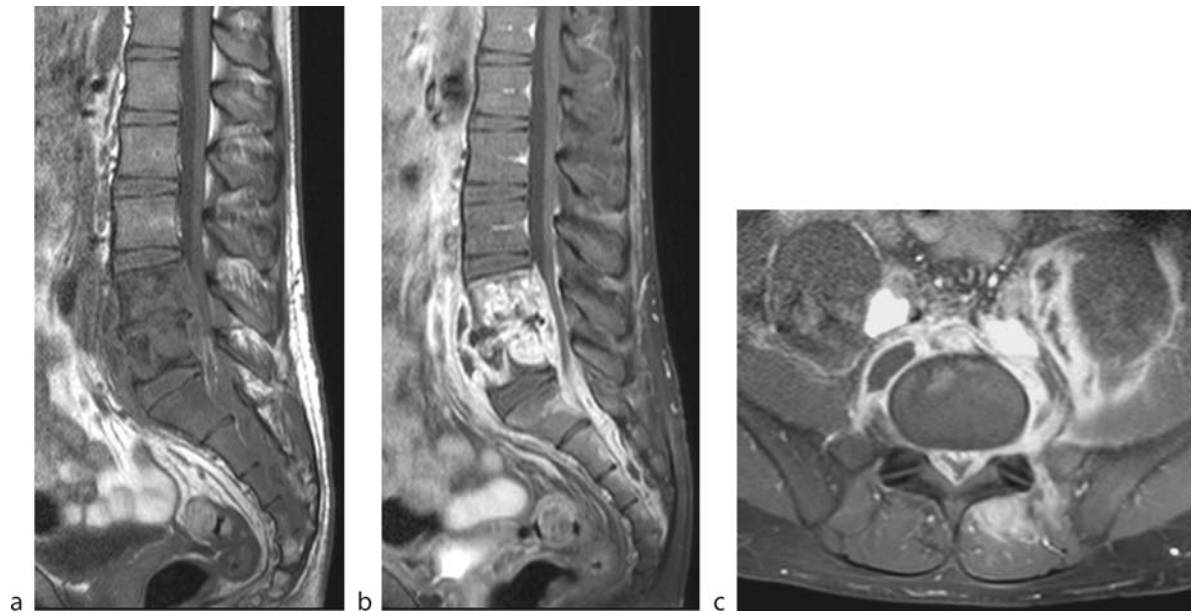

Infection, Soft Tissue. Figure 4 MRI depicts well a paraspinal and subligamentous abscess associated with lumbar spondylodiskitis in a 29-year-old North African man. T1 sagittal image (a) shows abnormal, low signal in two adjacent vertebral bodies with endplate destruction. There are soft tissue masses extending anteriorly and posteriorly to the vertebral bodies. Fat-saturated T1 sagittal (b) and axial (c) contrast-enhanced axial images show the anterior subligamentous, epidural, and paraspinal abscesses.

previously described. Abnormalities suggesting diabetic neuroarthropathy are joint misalignment and destruction and fragmentation of bone at the intertarsal and tarsometatarsal joints.

Foreign Bodies

Foreign bodies are most often wood, thorns, or glass. Their sites of predilection are the feet and hands. Foreign bodies in the soft tissue create an inflammatory reaction and may lead to the occurrence of an abscess, a sinus tract, or osteomyelitis. The identification of particles of glass or wood is difficult and can be done using XR combined with US or CT. On MR images, foreign bodies usually have a linear form with low signal intensity on all sequences surrounded by high signal intensity on T2-weighted images corresponding to granulation tissue, cellulitis, or abscess.

Nuclear Medicine

Nuclear medicine plays an important role in the assessment of periprosthetic infection and osteomyelitis in children, including early detection of infectious disease, differentiation of osteomyelitis from cellulitis, and identification of renewed activity in cases of chronic osteomyelitis. However, radionuclide studies are currently less widely used in the evaluation of infectious diseases due to the development of CT and MRI. Three main radionuclide studies including technetium phosphate bone scintigraphy, indium-111-labeled leukocyte scintigraphy, and fluorodeoxyglucose-PET (FDG-PET) can be performed for diagnosing soft tissue or bony infection (5).

Technetium phosphate bone scintigraphy with three phases is commonly used if bone infection is suspected: serial images are obtained at the angiographic phase (first minute just after intravenous technetium compound bolus), a postinjection image is obtained at the blood pool phase (end of the first minute), and further images are obtained at a delayed phase (2 or 3 h later). Osteomyelitis shows increased accumulation of the radionuclide within the bone during all three phases. In the case of cellulitis, early scans show increased uptake of soft tissue corresponding to hyperemia and later scans are normal.

Indium-111-labeled leukocyte scintigraphy based on leukocyte accumulation within the abscess is more sensitive in detecting peripheral than axial disease, and soft tissue infections than bone infections and chronic ones.

FDG-PET with CT has the advantage of high-resolution anatomical depiction of infectious sites, higher sensitivity in the uptake, and reliable diagnosis of axial infection compared to other radiotracers tested (gallium, radio-labeled serum albumin, thymidine) (5) (6). FDG-PET may be limited in differentiating between malignant and infectious processes as well as in postoperative patients.

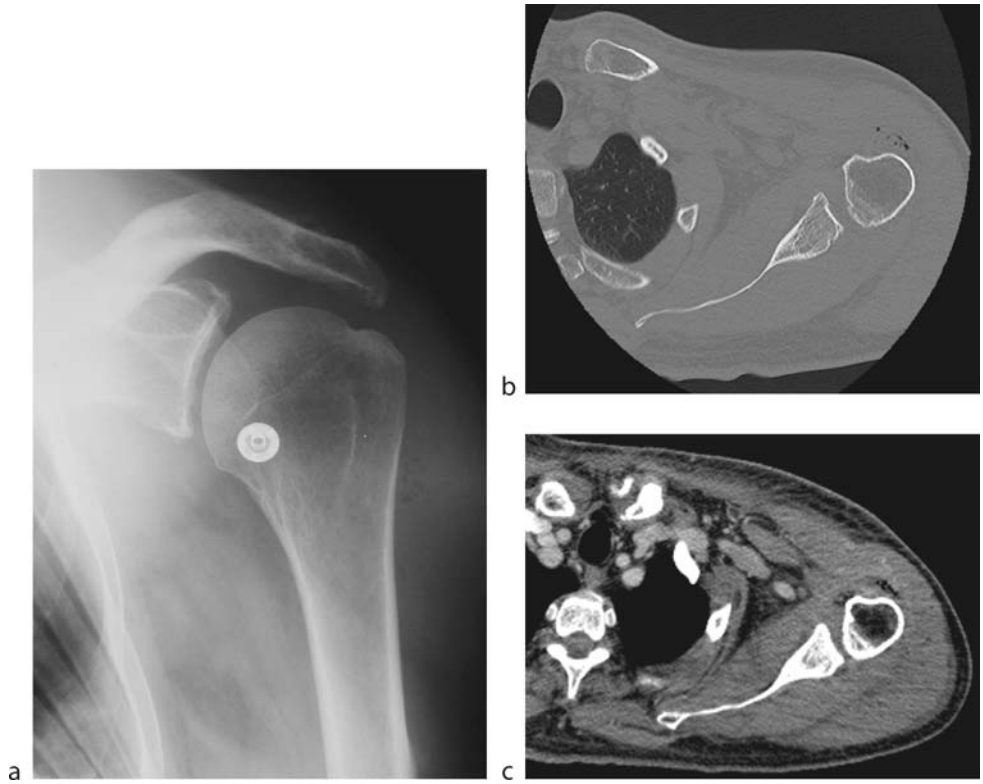

Infectious Diseases. Figure 5 **Anterioposterior radiograph (a) of the left shoulder demonstrates gas bubbles in the deep soft tissue in a splenectomized, diabetic, 80-year-old man. CT scan (b) obtained after ultrasonography confirms gas bubbles under the deep fascia of the deltoid, and shows an abscess within the deltoid associated with fluid collection and thickening of subcutaneous fat. After iodine injection (c), typical enhancement of the fascia associated with abscess in the deltoid muscle are well depicted suggesting the diagnosis of an early necrotizing fasciitis, which was surgically confirmed.**

Bibliography

1. Restrepo CS, Lemos D, Gordillo H et al (2004) Imaging findings in musculoskeletal complications of AIDS. Radiographics 24:1029–1049
2. Resnick D (1989) Osteomyelitis, septic arthritis, and soft tissue infection: mechanisms and situation. In Bone and Joint Imaging. 3rd edn. Philadelphia, PA 19106, Saunders pp 729–755
3. Loyer EM, DuBrow RA, David CL et al (1996) Imaging of superficial soft-tissue infections: sonographic findings in cases of cellulites and abscess. Am J Roentgenol 166:149–152
4. Soler R, Rodriguez E, Aguilera C et al (2000) Magnetic resonance imaging of pyomyositis in 43 cases. Eur J Radiol 35:59–64
5. Love C, Tomas MB, Tronco GG et al (2005) FDG PET of infection and inflammation. Radiographics 25:1357–1368
6. Zhuang H, Yu J, Alavi A (2005) Application of fluorodeoxyglucose-PET imaging in the detection of infection and inflammation and other benign disorders. Radiol Clin North Am 45:121–134

Infections of the Spleen

▶Spleen, Infectious Diseases

Infectious Diseases

Heinrich K. Geiss
Qualitätsmanagement-Hygiene-Konzern,
Bad Neustadt/Saale, Germany
h.geiss.qm@rhoen-klinikum-ag.com

In 1969 the US federal government's principal spokesperson on matters of public health, Surgeon General William H. Stewart, testified to the US Congress: "The time has come to close the book on infectious diseases." In fact, infections are still the most frequent diseases, and prospects of improving the situation in the near future are dismal. According to the World Health Organization, infections account for about one-third of all deaths worldwide, second only to cardiovascular diseases (Table 1).

Additionally, within the last 30 years a plethora of new and reemerging infections were recognized and face

Infectious Diseases. Table 1 Deaths by cause worldwide, estimates for 2002 (Source: The World Health Report 2003)

Cause	Number of deaths	%
Total deaths	57,027,000	
Cardiovascular diseases	16,655,000	29.2
Infectious diseases	14,967,000	26.3
Neoplasms	7,254,000	12.8
Injuries	5,188,000	9.1
Respiratory diseases	3,696,000	6.5
Perinatal diseases	2,464,000	4.3
Digestive diseases	1,963,000	3.4
All other causes	4,840,000	9.2

mankind with almost insurmountable problems. Not only are new epidemics like AIDS and SARS of significant concern, but the resurgence of diseases like malaria and tuberculosis are also ominous developments. At the same time, the underdeveloped world has to bear the brunt; in these areas of the world—with poor sanitation, overcrowding, uncontrolled urbanization, poverty, and little or no access to medical care—infectious diseases continue to cause significant morbidity and mortality. So as long as this part of the world cannot provide its inhabitants with the basic needs of clean water, sufficient and healthy food, shelter, and adequate medical care, the fight against infections can never be won.

In contrast, in developed countries, mortality from infectious diseases has been reduced significantly by improvements in sanitation, widespread vaccination, and access to medical care. However, new problems have evolved. So-called infections of leisure or diseases that complicate exposure to vacation climates, pets, recreational activities, and exotic cuisine pose problems of diagnosing and adequately treating these infections. Also, we have to pay a high price for medical progress: organ transplantation, invasive surgery, implantation of prosthetic devices, and immunosuppressive therapies have prolonged survival for some diseases but also resulted in compromised immunity and render previously normal individuals susceptible to microbes formerly considered to be pure saprophytes.

Even more intriguing is the steadily increasing resistance of bacteria, fungi, and viruses against anti-infective agents. The stunning success of the pharmaceutical industry in the western world in creating new antibiotics over the past four decades has caused the society and the scientific community to become complacent about the potential of bacterial resistance. Despite the warning in renowned textbooks that "it requires but a moment's reflection to realize that the substitution of a prescription for a broad-spectrum antibiotic or a quick injection of penicillin for the systematic collection of facts and thoughtful consideration of diagnostic possibilities is a fallacious, unwise, and dangerous practice….They should never be prescribed as placebos, antipyretics, or substitutes for diagnosis" (1), the misuse and overuse of these originally termed "miracle drugs" became more or less general practice and finally led to the situation that is described as the postantimicrobial era. The increasing frequency of drug resistance has been attributed to combinations of microbial characteristics, selective pressures of antimicrobial use, and societal and technologic changes that enhance the transmission of drug-resistant microorganisms. Antimicrobial resistance is resulting in increased morbidity, mortality, and health-care costs. In fact, this problem is dramatic not only because microorganisms "invent" new mechanisms of drug resistance but also because most pharmaceutical companies withdraw from research on new antiinfectives because their profit margin is too small in the long run.

The relationship between the human host and the microbial world represents the interaction of two very complex systems. Microbial forms are ubiquitous on the Earth's surface, on plants, and in water and constitute more than half of our planet's biomass. Bacteria and archaea, the two domains of the prokaryotic world, were the first forms of life to appear on Earth about 3.8 billion years ago. They were the absolute sovereigns of the world for about 1 billion years and created the global geochemical cycles that allowed other forms of life to develop. It is obvious that in the course of their long records, bacteria developed an abundant variety of metabolic capabilities that allowed them to survive even under unfavorable conditions. Bacteria acquired knowledge of how to maximize the plasticity of their genomes, constantly acquiring new genetic information and mutating or rearranging existing genes. These ever-changing capabilities enable bacteria to colonize all the niches the Earth provides. When warm-blooded animals and humans appeared on the evolutionary scene, of course bacteria immediately took advantage of these new niches for colonization. Taking into consideration that the human body is an almost infinite source of nutrients and offers shelter under constant temperature and humidity conditions, humans are an optimal habitat for continuous colonization, creating a biosphere of their own. Colonization begins when the primarily germ-free fetus leaves the protective amniotic sac. Within a very short period, the normal flora is constituted, forming a dense bacterial covering mainly of the skin, the oropharynx, and the intestinal and vaginal tracts. In fact, reduced to pure numbers, the human body consists of 10% mammalian cells and at least 90% prokaryotic cells, which form our normal flora. The human host is also surrounded by an abundant number of environmental microorganisms, some of which

may interact transiently with the human body. Therefore, it is clear that the ability of bacteria to grow and damage human tissue has an effect on human evolution.

Under normal conditions, this microbe–human interaction is in equilibrium based on the microbes' capability to harm and the host's defense system. This equilibrium is just one aspect of the human–microbe interaction. At the other end of the scale is the ultimate damage by microorganisms: death. However, infection and disease, like everything else in life, are continuous processes. Nevertheless, as with other complex continuous processes, it is convenient and, perhaps because of the limitations of our imagination, necessary to describe and define the dynamics of an infection as a sequence of more or less discrete steps.

In scientific terms, "infection" is defined as the process of microorganisms that are capable of causing disease to occupy and multiply in a particular area of the human body. An infection that produces symptoms is called an infectious disease. Thus, infection does not inevitably result in disease. Because common speech usually associates the term "infection" with disease, it seems rational to replace the scientific meaning by the term "colonization" because its understanding is more neutral. This proposal seems justified with regard to the fact that microorganisms forming the body's normal flora, which are usually regarded as noninfecting or benign, nevertheless may cause infectious disease depending on the immune status of the host involved. Healthy people colonized with obvious pathogens, such as *Salmonella typhi*, are called asymptomatic carriers, but they may serve as sources of infectious diseases when they transmit their "bug" to other people. Another example is the asymptomatic carriage of highly antibiotic-resistant bacteria, like methicillin-resistant *Staphylococcus aureus* (MRSA), which is a much feared and epidemically spreading hospital pathogen.

Although a specific infectious disease will not occur in the absence of the causative organism, the mere presence of the organism in the body does not invariably lead to clinical illness. Indeed, the production of symptoms in humans by many microorganisms is the exception rather than the rule. The occurrence of disease depends on the contributions of both host and pathogen to this process that is based on a microbe's ability to cause damage as a function of the host's immune response. In fact, the host may experience damage during the state of colonization by a given microorganism, the damage being part of a continuum spanning from "none" to "significant." Progressive damage that results from the host's inability to contain or eliminate the inflicting microorganism may lead to disease or death. However, damage may be mediated not only by the pathogen but also by the host's immune response (e.g., aberrant immune responses such as those associated with rheumatic fever or poststreptococcal glomerulonephritis). In this respect, damage is an inclusive term that encompasses cell, tissue, and organ damage. Damage at the cellular level includes necrosis, apoptosis, and malignant transformation. Damage at the organ and tissue levels includes granulomatous inflammation, fibrosis resulting from chronic inflammation, and tumor.

The transition from colonization to an infectious disease is defined by characteristic symptoms that have been well known since antiquity: fever (calor), pain (dolor), inflammation (rubor), swelling (tumor), and impaired function (functio laesa), of which fever has been recognized as a cardinal manifestation of disease. However, in clinical practice the variability of the disorders attributable to infection of humans by microorganisms is so variable that generalizations about them are difficult. The clinical manifestations of infection can duplicate those of diseases of any other etiology. It is obvious that the presence of one, several, or all of the so-called characteristic features of infection does not constitute proof of the microbial origin of illness in a given patient. Conversely, serious, even fatal, infectious disease may exist in the absence of fever or other signs and symptoms.

Nevertheless, the majority of acute infectious diseases are accompanied by fever, and its occurrence accounts for a large proportion of visits to physicians worldwide. In evaluating patients with elevated body temperature it is important to distinguish between disorders that lead to hyperthermia—an imbalance between heat-generating and heat-dissipating mechanisms—and fever, defined as a controlled elevation of body temperature in response to a control setpoint change in the hypothalamus mediated by endogenous pyrogens. But even when hyperthermia is excluded, a wide variety of diseases causing fever have to be considered: Besides infection, other causes include inflammatory, immune, granulomatous, neoplastic, vascular, and metabolic disorders; trauma; and tissue infarction.

This diagnostic dilemma is best exemplified with the case of sepsis, the most severe and life-threatening form of a febrile state. The clinical situation of a physician confronted with a patient in whom sepsis is suspected is best described using the statement of the US Supreme Court Justice P. Stewart: "I can't define obscenity, but I know it when I see it." However, in contrast to this theoretical problem, modern medicine needs clear definitions to provide a sound basis for diagnostic and therapeutic approaches in critically ill patients.

In the late 1980s and early 1990s it was recognized that the original definition of sepsis by Schottmüller (continuous or intermittent release of pathogenic microorganisms into the bloodstream from a focus within the body, leading to subjective and objective signs of disease) focusing on bacteria recovered from blood cultures was

far too narrow because a variety of overlapping clinical conditions may mimic an acute infectious process and be equally catastrophic. Progress in medical knowledge and expanding therapeutic modalities made clear that the clinical picture of sepsis falls within a more general inflammatory response of the organism, which is triggered not only by localized or generalized infection but also by trauma, thermal injury, or sterile inflammatory processes such as acute pancreatitis.

This was the background for a consensus conference of the American College of Chest Physicians and the Society of Critical Medicine, leading to the concept of systemic inflammatory response syndrome, or SIRS (2), which was updated in 2001 (3). The term "sepsis" is now divided into four different disease entities:

- SIRS
- Sepsis
- Severe sepsis
- Septic shock

The common denominator is the occurrence of a systemic inflammation, and differentiation is based on the fact that signs of systemic inflammation can and do occur in the absence of infection among patients with a variety of disease states in which clinical manifestations are protean and even distinct biochemical features (such as interleukin 6, procalcitonin, or C-reactive protein) are not consistently present.

The distinction of infectious from noninfectious SIRS is based on the definition of infection as "a pathological process caused by invasion of normally sterile tissue or fluid or body cavity by pathogenic or potentially pathogenic micro-organisms" (3). However, as mentioned earlier, this definition does not encompass the so-called toxi-infections that may be induced by members of the normal body flora (enterocolitis by *Clostridium difficile* enterotoxin). Because of these limitations, the systemic response to infection is designated "sepsis," which includes a wide set of diagnostic criteria. Besides general parameters such as fever, tachycardia, tachypnea, and altered mental status, the criteria include a set of inflammatory, hemodynamic, and tissue perfusion parameters. Again, it is emphasized that in clinical reality, none of these findings is specific for sepsis.

This example illustrates how the definition of a certain infection may change over time depending on our ever-increasing knowledge in pathophysiology and the ongoing improvement and progress in diagnostic methods or single diagnostic parameters. Similar to the complexity in the diagnosis of sepsis, an increasing number of patients present with nonspecific signs of infection, especially immunocompromised patients or patients in intensive care units. In these patients a single diagnostic step almost never suffices to unequivocally confirm the diagnosis of an infection. It is always the combination of different tests, the interpretation of which with respect to the clinical picture should enable the clinician to establish a diagnosis.

Diagnostic procedures are usually divided into laboratory and imaging studies. Laboratory tests obtained in patients with suspected infectious diseases fall into three categories: (i) those that assess the degree and severity of the inflammatory response to infection, (ii) those that help determine the site and complication of organ involvement by the process, and (iii) those that are employed to determine the etiology of the infectious agent, either by culture or histology or by a specific immune response. In addition, imaging technologies are categorized into traditional and conventional techniques (such as X-ray and ultrasound), more advanced techniques (such as computed tomography and magnetic resonance imaging), and finally, specific nuclear imaging techniques. In contrast to the first two methodologies, the latter techniques allow, for the first time, detection of infection-related abnormalities based on physiological or biochemical tissue changes. A dazzling array of changes within the different body compartments can be visualized by diagnostic imaging, including features of the following—probably incomplete—list:

Central Nervous System

- Intracerebral abscess
  i. Ring-enhancing mass
  ii. Vasogenic edema
  iii. Mass effect
  iv. Hypodense area
- Cerebritis
- Encephalitis
- Subdural abscess
- Epidural abscess
- Calcification
- Ventricular compression
- Sulcal effacement
- Midline shift
- Granulomatous disease
- Cysticercosis
- Toxoplasmosis
- Mycotic aneurysma
- Postinfectious vasculitis
- White matter disease

Spine

- Osteomyelitis
- Discitis
- Intervertebral discitis

- Bone erosion
- End-plate erosion
- Sclerosis
- Pott's disease

Head and neck

- Sinusitis
  i. Mucosal thickening
  ii. Sinus opacification
- Periorbital infection
- Mastoiditis
- Soft tissue neck infection

Chest

- Pneumonia
- Necrotizing pneumonia
- Bronchopneumonia
- Aspiration pneumonia
- Localized empyema
- Pulmonary emboli
- Lung abscess
- Atypical pneumonia
- Interstitial inflammation
- Interstitial infiltrate
- Pneumocystis jiroveci pneumonia (PCP)
- Fungal pneumonia
- Aspergillosis
- Tuberculosis
- Parapneumonic effusion
- Pleural thickening
- Pleural effusion
- Lobar consolidation
- Segmental consolidation
- Apical fibrosis
- Air–Crescent sign
- Halo sign
- Diffuse pulmonary infiltrate
- Pulmonary nodules
- Cavitation
- Ground-glass attenuation
- Mediastinitis
- Adenopathy

Abdomen

- Solid organ abscess
  i. Hepatic abscess
  ii. Splenic abscess
  iii. Pancreatic abscess
  iv. Renal abscess
- Perinephritic abscess
- Subphrenic abscess
- Peritoneal abscess
- Pyelophlebitis
- Appendicitis
- Cholecystitis
- Diverticulitis
- Inflammatory bowel disease
- Necrotic pancreatitis
- Gas formation
- Bowel wall thickening
  i. Colitis
  ii. Enteritis
- Gallbladder wall thickening
- Fistula

Soft tissue and osteoarticular infection

- Gas edema
- Gas formation
- Osteopenia
- Scalloping of the cortical bone
- Sequestration
- Periostal deviation
- Reactive bone formation
- Osteoblastic change
- Bone demineralization
- Periarticular soft-tissue swelling
- Widening of the joint space
- Vascular graft infection

General

- Whole body scan
- White blood cell scan
- Cellular labeling
- Antigranulocyte monoclonal antibodies
- Inflammatory response imaging
  i. Increased blood flow
  ii. Increased capillary permeability
  iii. Recruitment of white blood cells

Bibliography

1. Petersdorf RP (1980) Important consideration in infectious disease. In: Isselbacher KJ, Adams RD, Braunwald E et al Harrison's principles of internal medicine. 9th edn. McGraw-Hill, Auckland, p 541
2. Bone RC, Sprung CL, Sibbald WJ (1992) Definitions for sepsis and organ failure. Crit Care Med 20:724–726
3. Levy MM, Fink MP, Marshall JC et al (2003) 2001 SCCM/ESICM/ACCP/ATS/SIS international sepsis definition conference. Intensiv Care Med 29:530–538
4. World Health Report 2003 ▶http://www.who.int/whr/2003/en/

Infectious Myositis

►Infection, Soft Tissue

Infiltrating Ductal Carcinoma

►Carcinoma, Ductal, Invasive

Infiltrating Epitheliosis

►Radial Scar, Breast

Infiltrating Lobular Carcinoma (ILC)

►Carcinoma, Lobular, Invasive

Infiltrating Papillary Carcinoma

►Carcinoma, Other, Invasive, Breast

Inflammation

►Oral Cavity, Inflammatory Diseases

Inflammation, Chronic, Nose, and Paranasal Sinus

Silvio Mazziotti
Department of Radiological Sciences, University of Messina, Messina, Italy
smazziotti@unime.it

Definitions

Rhinosinusitis is defined as the inflammation of the nasal cavity and the adjacent paranasal sinuses and is most often the result of a viral infection (typically a cold) that causes the mucous membrane of the nose to become inflamed, blocking the drainage from the sinuses into the nose and throat. It may develop as a result of nasal allergies or other conditions that obstruct the nasal passages. However, any factor that causes the mucous membrane to become inflamed may lead to ►sinusitis. Bacteria and fungi are more likely to grow in sinuses that are unable to drain properly. Bacterial or fungal infections in the sinuses often cause more phlogosis and are more likely to last longer and worsen with time.

The terms acute, recurrent acute, subacute, and chronic rhinosinusitis have been used to define the illness by its duration (1).

Acute rhinosinusitis has a relatively rapid onset and is normally of 4 weeks duration or less and symptoms totally resolve. Resolution of symptoms usually occurs within 5 to 7 days, and patients usually recover without medical intervention.

Recurrent acute rhinosinusitis is defined as four or more episodes of acute disease within a 12-month period, with resolution of symptoms between each episode.

Subacute rhinosinusitis is basically a low-grade continuum of acute infection of more than 4 but less than 12-weeks duration.

Chronic rhinosinusitis is distinguished by symptoms that persist for 12 weeks or more or occurs more than four times a year with symptoms persisting for more than 20 days. The most frequent complications of inflammatory rhinosinusitis are ►Polyps Nasal and cysts. Chronically obstructed sinus secretions can accumulate and a ►mucocele can develop.

Pathology/Histopathology

Rhinosinusitis is inflammation or infection of the mucous membranes that line the inside of the nose and sinuses. The evoked completely reversible inflammatory changes in acute disease are swelling of the turbinates, thickening of mucosae in the nasal fossae and sinuses due to submucosal edema, and variable amount of sinus secretions. In acute sinusitis, fluid often collects in the sinus cavity, giving rise to an air-fluid level.

The chronic disease can result in an atrophic, sclerosing, or hypertrophic polypoid mucosa. These different mucosal alterations often coexist with one another and with areas of acute inflammations of either an allergic or an infectious etiology. The bony sinus walls surrounding a chronically infected sinus frequently

become thickened and sclerotic with reactive new bone formations. Epithelial hyperplasia and mucosal infiltration of leukocytes are common features of chronic rhinosinusitis.

Nasal polyps are outgrowths of nasal mucosa made up of edema fluid with sparse fibrous cells, a few mucus glands and a surface epithelium invaded by some inflammatory cells. Inflammatory polyps may be present in the nose and/or paranasal sinuses. Polyps are gelatinous in appearance, rarely bleeding, mobile, and insensitive to manipulation. They have a characteristic gray color that allows to distinguish them from the normal pink nasal mucous membrane.

A ▶retention cyst is a spherical mucoid-filled cyst that forms when a mucous gland of the sinus mucosa becomes obstructed; its walls are thus defined by the epithelium of a mucous gland and duct itself, not by the walls of the sinus. There is almost always air still surrounding the retention cyst, while bony expansion and remodeling of the sinus do not often occur.

A sinus mucocele is defined as a mucous collection of mucoid secretions lined by the mucus-secreting epithelium of a paranasal sinus. It occurs when a sinus ostium or a compartment of a septated sinus becomes obstructed, thus causing the sinus cavity to be mucous-filled and airless. The obstruction is often inflammatory in nature, but may also be due to tumor, trauma, or surgical manipulation. It is the most common expansile lesion of the paranasal sinuses and leads to outward expansion with bony remodeling. Initially, the bony structures remain intact, but with further expansion deossification may occur.

Clinical Presentations

In acute sinusitis, nasal congestion and discharge are almost always present. The discharge is typically thick and contains pus that is yellowish to yellow–green. Severe headache occurs and there is pain or pressure in specific areas in the face. The symptoms of recurrent acute and chronic sinusitis tend to be vague and generalized, last longer than 8 weeks, and occur throughout the year, even during nonallergic seasons. Nasal congestion and obstruction are common. Chronic cough, yellowish discharge, bad breath, and postnasal drip may occur. Sufferers do not usually experience facial pain unless the infection is in the frontal sinuses: in this case, it usually results in a dull, constant ache. Facial tenderness or pressure, however, may be present. Sinusitis complicated by the presence of polyps will not resolve until the polyps have been reduced in size, either medically or surgically. Signs and symptoms of a mucocele may last from a few days to years and are most often due to mass effect. A mucocele in the frontal sinuses typically leads to frontal headaches and inferolateral proptosis with diplopia. Additionally, a superomedial orbit mass may develop, and the voice may be nasal in quality. A mucocele in the ethmoidal sinuses frequently presents as lateral proptosis as well as nasal congestion. A mucocele in the maxillary sinuses causes upward displacement of the eye, a cheek mass, and nasal congestion. A mucocele in the sphenoid sinuses can lead to suboccipital headaches and visual loss.

Imaging

Conventional Sinus Radiographs

The plain radiographic examination for rhinosinusitis can include Caldwell (antero-posterior view), Waters (occipito-dental view), and lateral view. The Caldwell and Waters views best demonstrate the frontal and maxillary sinuses. The lateral view is the best choice for visualization of the sphenoid sinus and adenoidal tissue in children. Nevertheless, these views do not allow a good evaluation of ethmoidal cells (2, 3). Opacification, moderate-to severe mucosal thickening, or air-fluid levels in patients with persistent symptoms are generally considered suggestive of sinusitis. Such abnormalities are easily detected in maxillary and frontal sinuses by standard radiographs. Isolated polyps may be visualized by plain radiography but their precise localization often requires further imaging procedures. Although standard sinus radiographs are often considered useful in the diagnosis and monitoring of acute sinusitis, they are of limited value in the evaluation of chronic unremitting disease (2, 3). Low cost and small radiation dosage are advantages of this technique, and the possibility of portable examination can be helpful in the intensive care setting. The major drawback of plain radiography is its low sensitivity in the diagnosis of rhinosinusitis; in fact, interpretation of standard radiographs may be controversial: overlay of anatomical structures may mimic mucosal thickening or air-fluid levels and a hypoplastic sinus may be misinterpreted as pathologic opacification. Standard radiographs are inadequate for determination of the need for, or guidance of, endoscopic sinus surgery in both children and adults.

Computed Tomography

CT is currently the modality of choice for the evaluation of the regional anatomy of the nasal cavity and the paranasal sinuses (4). In contrast with plain radiographs, CT excellently demonstrates the anterior ethmoid cells, the upper two-thirds of the nasal cavity and the frontal recess. There is also strong evidence that CT is the gold standard for precise delineation of inflammatory sinus

disease secondary to obstruction of the ostiomeatal complex. Axial views parallel to the hard palate can provide important anatomical data. Optimal demonstration of the anterior ethmoid sinuses and ostiomeatal channels requires CT imaging in coronal planes that, in addition, closely correlate with the surgical approach. Ideally, coronal and axial 1.5 mm slices are performed with a helicoidal CT scan, which allows for a 3D reconstruction. Highly contrasting densities identify air within the bony sinuses, fat within the orbit and soft tissues outlined by air in the nasal cavity.

The primary role of CT scans is to aid in the diagnosis and management of recurrent and chronic sinusitis, or to define the anatomy of the sinuses prior to surgery. The characteristics of chronic inflammatory disease on CT are mucoperiosteal thickening, soft tissue mass, and osteitis of the ethmoid bony architecture. Bony erosion is unusual and is more frequently associated with more invasive processes such as mucocele, polyposis, or a neoplastic lesion. The region most frequently involved with inflammatory disease is the middle meatus. Associated maxillary sinus mucoperiosteal disease and, to a lesser extent, frontal sinus disease are frequently found.

It is well known that sinusitis may originate from or be perpetuated by local factors predisposing to sinus ostial obstruction. Current surgical strategy aims to remove the causative disease and reestablish ventilation and mucus clearance. In this respect, coronal CT offers an optimal view of the components of the ostiomeatal complex and enables the detection of significant anatomical variants: Haller's cells, agger nasi cells, paradoxical curvature of the middle turbinate, bulla ethmoidalis, deformities of the uncinate process, or concha bullosa. In terms of preoperative assessment, coronal CT serves as an anatomical map for the surgeon and it has been demonstrated that it greatly improves the planning and the safety of functional endoscopic surgery.

CT scan is the preferred imaging technique for the diagnosis of polyps and the evaluation of the extent of polyposis. Solitary polyps can be detected by CT imaging, although they cannot be differentiated from mucous retention cysts as both entities are shown as homogeneous soft-tissue masses with smooth and outwardly convex borders (Fig. 1). However, this is of little consequence, as any treatment for these common benign entities is the same.

In more severe polyposis, the major CT features are polypoid masses associated with complete pansinus opacification and infundibular widening; bony changes assume a destructive appearance that, in more advanced cases, suggests malignant tumors or granulomas (Fig. 2).

The CT finding of an expanded, airless sinus cavity filled with secretions characterized by rather homogeneous mucoid attenuation is characteristic of a mucocele (Fig. 3).

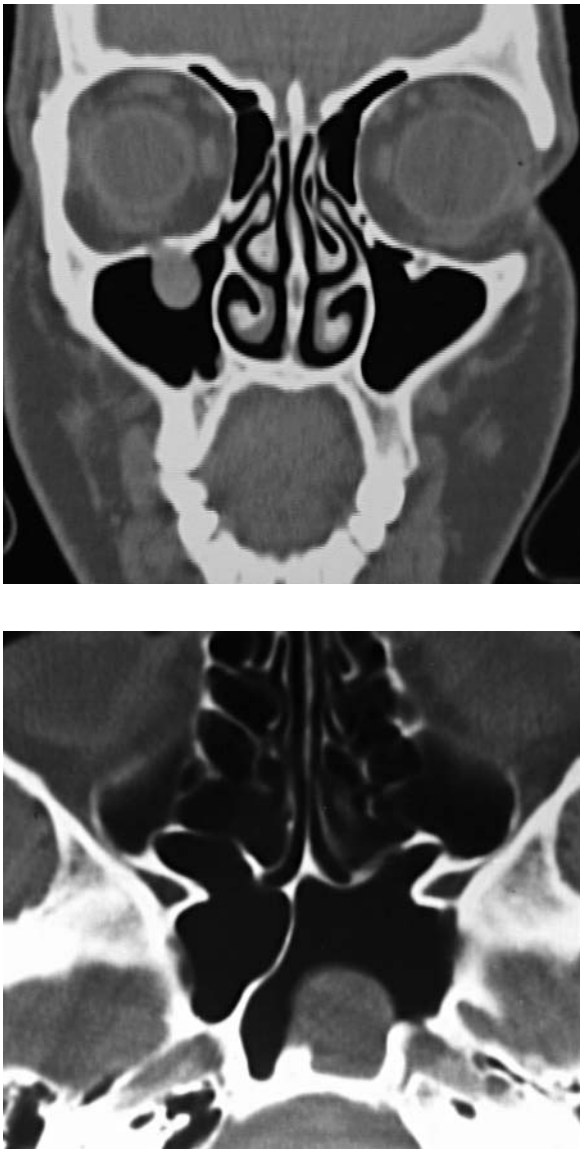

Inflammation, Chronic, Nose, and Paranasal Sinus. Figure 1 Coronal (a) and axial (b) CT scans. In (a) there is a solitary retention cyst or polyp in the right maxillary sinus. In (b) there is a retention cyst or polyp in the left sphenoid sinus. The sinuses are otherwise normal.

Magnetic Resonance Imaging

MR provides better imaging of soft tissues than CT, but it is less suited to imaging the bony anatomy of this region, and more particularly that of the ostiomeatal complex (4, 5). Because bone and air yield similar signal intensities on MRI, resolution of bony structures is poor and it is difficult to perceive anatomical characteristics critical for the surgeon. Furthermore, in the patient with extensive inflammatory disease mainly involving the ethmoid sinuses, the signal intensity on T2-weighted images of

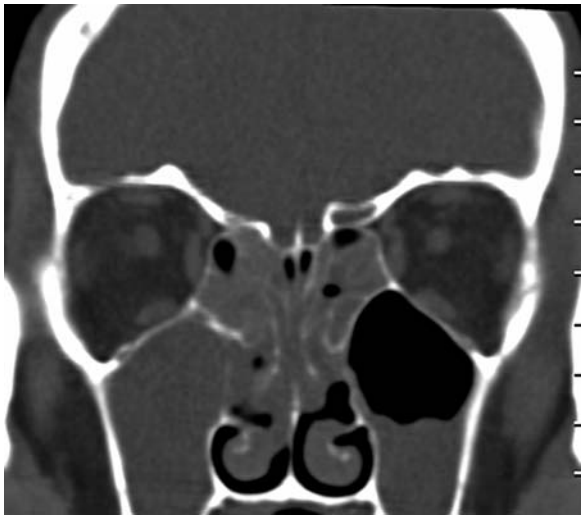

Inflammation, Chronic, Nose, and Paranasal Sinus. Figure 2 Coronal CT scan shows diffuse pansinusitis with the evidence of mucosal thickening and polyposis. Bony changes with a destructive appearance are also evident.

the pathologic process is indistinguishable from the appearance of the normal mucosa in the edematous phase of the nasal cycle. Although MRI has significant limitations in the definition of anatomy, it is extremely sensitive in evaluation of paranasal sinus mucosal disease in the frontal, maxillary, and sphenoid sinuses because the mucosa in these sinuses does not suffer the cyclic edema.

The etiology of certain disease processes and other sinus lesions may be better differentiated by MR. MR is often useful in the differential diagnosis between inflammatory diseases and malignant tumors. Bacterial and viral inflammations have high signal intensity on T2-weighted images, whereas neoplastic processes demonstrate an intermediate bright signal on T2-weighted images. Fungal concretions have very low signal intensity on T2-weighted images similar to that of air. MRI with Gadolinium contrast is useful for cases complicated by orbital or intracranial extension.

Nuclear Medicine

Nuclear medicine has a limited role in the assessment of rhinosinusitis. Rhinoscintigraphy may be a quick and reliable imaging method for evaluating the ciliary activity of nasal mucosa and the nasal mucociliary clearance function in patients with sinusitis.

Diagnosis

Clinical judgment with a careful history and physical examination should generally suffice in the diagnosis of

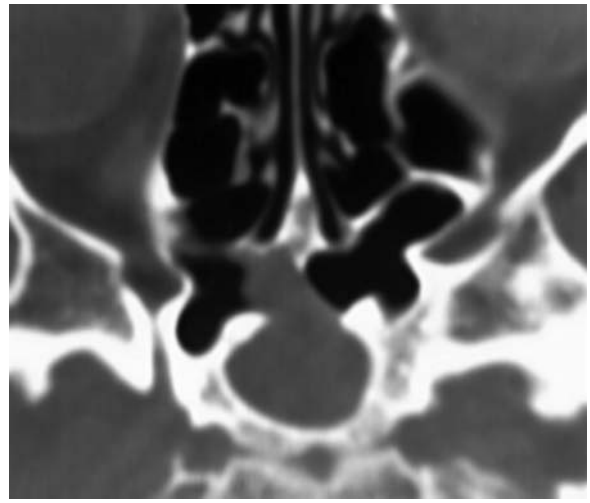

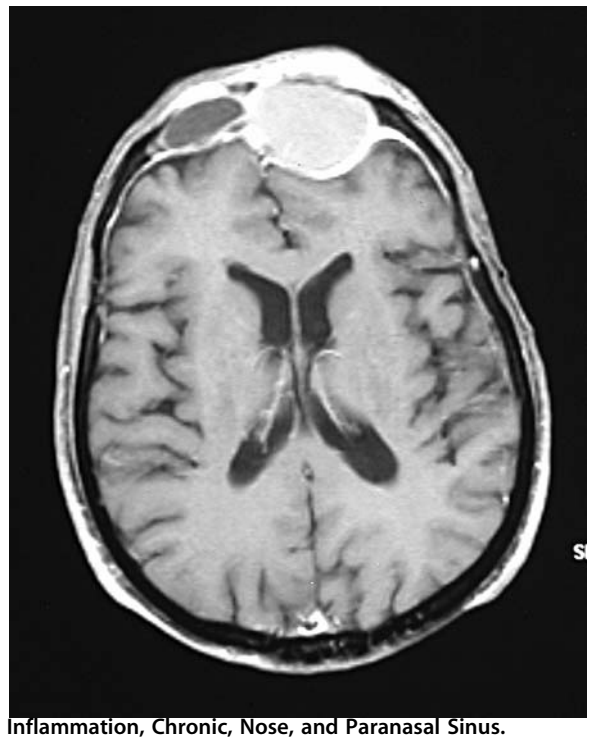

Inflammation, Chronic, Nose, and Paranasal Sinus. Figure 3 Mucocele. Axial CT scan (a) shows an expanded airless sphenoid sinus cavity filled with fairly homogeneous mucoid attenuation secretions. The sinus walls are remodeled. Axial T1-weighted MR image (b) shows bilateral expansive frontal sinus masses. On the right side has low signal intensity, on the left one it is hyperintense due to the high protein content of the entrapped secretions.

uncomplicated acute or subacute rhinosinusitis. Therefore, in these cases confirmatory plain radiography, given its low sensitivity, is rarely necessary.

However, when symptoms are recurrent or refractory despite adequate treatment, further diagnostic

evaluations may be indicated. In patients requiring confirmation of sinusitis, simple axial and coronal CT images can be adequate for screening purposes. In clinical practice, diagnosis of sinonasal polyposis is usually assessed by endoscopy but CT scan is frequently performed to help evaluate the disease.

Given the cost, the longer acquisition time, and the poor delineation of bony anatomy by MRI, it should only be used in rare cases of suspected sinonasal neoplasia, fungal sinusitis, or supposed intracranial or orbital complications of rhinosinusitis.

CT and MR should not be used in the initial diagnostic stages of patients with uncomplicated rhinosinusitis.

Bibliography

1. Willett LR, Carson JL, Williams JW Jr (1994) Current diagnosis and management of sinusitis. J Gen Intern Med 9:38–45
2. Kuhn JP (1986) Imaging of the paranasal sinuses: current status. J Allergy Clin Immunol 77:6–8
3. Skinner DW, Richards SH (1991) A comparison between sinus radiographic findings and the macroscopic appearances of the paranasal sinus mucosa. Ear Nose Throat J 70:169–172
4. Jorissen M (1996) Recent trends in the diagnosis and treatment of sinusitis. Eur Radiol 6(2):170–176
5. Rao VM, El-Noueam KI (1998) Sinonasal imaging. Radiol Clin North Am 36:921–939

Inflammatory Carcinoma

▶Carcinoma, Other, Invasive, Breast

Inflammatory Lesion

▶Oral Cavity, Inflammatory Diseases

Inflammatory Mass of Ovaries and Fallopian Tubes

▶Abscess TuboOvarian

Inflammatory Pseudotumor

Most common mass lesion of the lung with unclear origin.

▶Neoplasms, Chest, Childhood

Infrainguinal Arterial Obstruction

▶Occlusion, Artery, Popliteal
▶Occlusion, Artery, Femoral

Infrainguinal Arterial Occlusion

▶Occlusion, Artery, Femoral

Inframesocolic Peritoneal Compartment

This extends between the transverse mesocolon and the pelvis and between the anterior abdominal wall and the anterior perirenal space. It is subdivided into left-right paracolic gutters and left-right inframesocolic cavities by the descending-ascending mesocolon and the small bowel mesentery, respectively.

▶Peritoneal Collections

Insufficiency, Acute, Renal

Patrice Taourel
Service d'Imagerie Médicale, Hôpital Lapeyronie,
371 avenue du Doyen Gaston Giraud,
34295 Montpellier, Cedex 5
p-taourel@chu-montpellier.fr

Definition

Acute renal insufficiency is the sudden rapid deterioration in renal function. There is no clearly defined set of biochemical criteria that characterize renal insufficiency. In some forms of renal insufficiency, known as renal failure, the renal function is insufficient to maintain homeostasis.

Pathology

The causes of acute renal insufficiency can be divided into three main categories: prerenal or functional causes, renal causes, and postrenal causes.

Prerenal causes constitute the most common causes of acute renal insufficiency and are associated with renal hypoperfusion. Such conditions include congestive heart failure, diuretic use, sepsis, dehydration due to gastrointestinal causes (diarrhea, vomiting), renal or respiratory loss, hemorrhage, burns, cirrhosis with ascites, and diabetic ketoacidosis. Renal artery stenosis, when treated by angiotensin-converting enzyme inhibitor, represents a rare but interesting model of functional cause of renal failure due to a decrease of the glomerular filtration pressure by an excessive vasodilatation of the postglomerular arteriole.

Renal causes may result from damage to any portion of the kidney: the tubule, the glomerulus, the blood supply, or the interstitium. Tubular nephropathy includes acute obstruction of the tubules mainly due to precipitation of urate in patients receiving chemotherapy or to precipitation of Bence Jones proteins, and acute tubular necrosis, which constitutes the most common renal cause of acute renal insufficiency. Acute tubular necrosis is due to two mechanisms: hypoperfusion of the kidney with decreased glomerular filtration and increased pressure in the tubules. The renal involvement is reversible with treatment of the cause. A large number of conditions are reported in relation to acute tubular necrosis, including burns, sepsis, snake bites, toxins, transfusion, incompatible transfusion, dehydration, peritonitis, and pancreatitis; some of these are the same as for functional renal failure, explaining why these two conditions may be associated and that their differential diagnosis is difficult.

The vascular nephropathy responsible for acute renal insufficiency includes acute renal vein thrombosis, renal artery occlusion, and disease of the intrarenal arteries, such as collagen vascular diseases (polyarteritis nodosa, Wegener's granulomatosis, and systemic lupus erythematous), scleroderma, and intravenous drug abuse.

Acute interstitial nephritis is underestimated in frequency, and diagnosis is difficult because it is not revealed by any clinical finding such as edema or hypertension and because the diuresis is preserved for a long time. It may occur in association with a variety of drugs, such as penicillin, sulfonamide derivatives, or nonsteroidal anti-inflammatory agents, or with a number of nonrenal infectious processes; it may be due to tumoral infiltration of the two kidneys in lymphoma, for instance; or it may arise in an idiopathic form. Glomerular damage constitutes less than 5% of acute renal insufficiency as a result of acute glomerulonephritis, drug toxicity, Goodpasture's syndrome, or systemic lupus erythematosus.

Postrenal causes refer to the onset of acute renal insufficiency due to acute obstruction. Although acute obstruction accounts for only 15% of acute renal insufficiency, it is the most commonly sought cause because it is the one most easily reversed under appropriate treatment.

Clinical Presentation

Uremia may result in symptoms related to a number of different organ systems including the gastrointestinal tract (nausea, vomiting), the cardiovascular system (hypertension, cardiac arrhythmias, pericarditis), the nervous system (personality changes, seizures, somnolence), and the hematopoietic system (anemia, bleeding diathesis). However, clinical findings are more often due to the cause of the acute renal failure and to the hydroelectrolytic changes than to the consequences of uremia.

Imaging

Ultrasound

Ultrasound (US) is the best available imaging study for patients with renal failure. It permits clinicians to know the size of the kidney as evaluated by its maximum length, which has become the standard parameter because it is simple and correlates well with renal volume. (The average renal length is 11 cm in adults.) US also allows measurement of the cortical thickness from the outer border of the medullary pyramids to the renal capsule (which normally measures about 10 mm) and analysis of the outline of the kidney, which may be rounded, lobulated, or dented.

US permits study of the cortical echogenicity, which is most often inferior to the liver echogenicity. Although the echogenicity of the renal cortex and liver may be the same in a minority of healthy subjects, a renal cortex more echogenic than the liver is clearly abnormal past the age of 6 months and indicates renal disease.

Corticomedullary differentiation must be analyzed. Prominently hypoechoic medullary pyramids usually indicate increased cortical echogenicity (Fig. 1), whereas

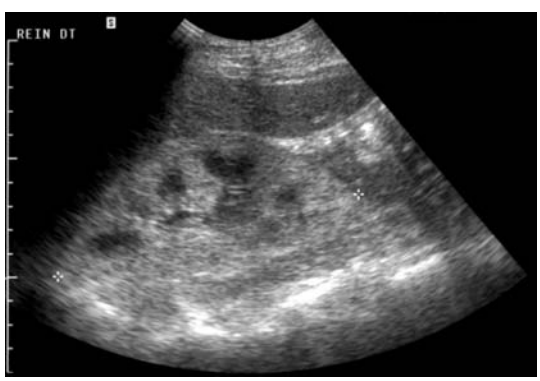

Insufficiency, Acute, Renal. Figure 1 Acute renal insufficiency due to glomerulopathy. The cortex of the kidney is hyperechoic, making the medulla appear very hypoechoic.

hyperechoic pyramids indicate medullary disease. But the main use of US is to seek dilated fluid-filled calyces in the renal sinus that may be differentiated from venous engorgement and peripelvic cysts.

US is an useful tool to differentiate acute from chronic renal insufficiency because in acute renal insufficiency, the kidneys have a normal size or are enlarged whereas in chronic insufficiency, they are more often decreased in size with decreased thickness of the renal cortex, which is considered the most sensitive finding. However, renal size is conserved or increased in glomerulopathy and diabetic nephropathy. Consequently, in the clinical context of renal insufficiency, normal kidney size does not affirm the acute character of the affliction, whereas a decrease in kidney size, as well as in the thickness of the cortex, rules it out.

The main task of US is to look for an obstruction. However, in the clinical setting of two native kidneys, acute obstructive renal failure is rare except in patients with bilateral iatrogenic postoperative obstruction. The lack of calyceal dilatation effectively rules out obstruction as a cause of acute renal failure. For diagnosing non-obstructive causes of acute renal insufficiency, US may provide limited but interesting information regarding the nature of the underlying renal disease and must be integrated to the clinical setting. Swelling of the renal cortex in conjunction with a history of an inciting event or the presence of granular casts in the urine indicates acute tubular necrosis, whereas enlarged, echogenic kidneys in conjunction with hematuria are indicative of nephritis. In a patient with nephrotic syndrome and acute renal failure, swollen, echogenic kidneys may instead indicate renal vein thrombosis, particularly if there is new-onset hematuria or the renal vein is prominent with luminal echoes. Unilateral cortical atrophy with hypertension and unremarkable urinary sediment should raise suspicion for renovascular disease.

Doppler

Doppler improves the sonographic assessment of renal dysfunction. In the setting of acute renal failure, its principal use is to demonstrate the patency of the renal arteries and veins and to look for thrombosis.

Arterial thrombosis may lead to acute renal failure in patients with a single kidney. In other cases, it may decompensate a chronic renal insufficiency in acute failure in patients with nephroangiosclerosis and severe atherosclerosis. Thrombosis of the renal artery occurs most commonly as a complication of severe atherosclerosis or transluminal angioplasty. The most common Doppler finding is absence of an intrarenal arterial signal. If there is incomplete occlusion or if collateral vessels are present, a severe tardus-parvus abnormality is detected. In some patients, US may demonstrate a proximal renal artery stump.

Thrombosis of the renal vein is usually caused by an underlying abnormality of hydration, the clotting system, or the kidney itself. In infants it is mainly due to dehydration, whereas in adults the most common cause is membranous glomerulonephritis. Color Doppler may image the renal vein thrombosis, and spectral analysis may show abnormality of the arterial wave with a shift in the anterograde frequency and reversal of flow during diastole.

The clinical role of Doppler for differentiating renal disease by the resistive index (RI) is more controversial. Classically, patients with isolated glomerular disease have normal RI values, whereas subjects with vascular or arterial disease have markedly elevated RI values. However, these data indicate rather a trend, and there is no cut off to differentiate disease in a given patient.

Computed Tomography

Computed tomography (CT) is not recommended for exploring the cause of renal insufficiency because such exploration needs intravenous contrast except for the search for a ureteral stone. However, it may sometimes be performed when the renal function is unknown or when dialysis is scheduled. Analysis of the CT nephrogram gives some information. When bilateral, global absence means a total lack of renal function; when unilateral, it is most often seen with blunt abdominal trauma with renal pedicle injury. Segmental absence is attributable to focal renal infarction (Fig. 2), most likely due to arterial emboli. Global persistence may be unilateral, caused by renal artery stenosis, renal vein thrombosis, urinary tract obstruction, systemic hypotension, intratubular obstruction, or abnormalities in tubular function. A striated nephrogram is caused by ureteric obstruction, acute pyelonephritis, contusion, renal vein

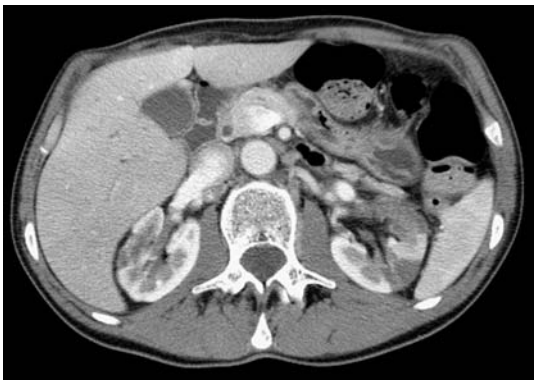

Insufficiency, Acute, Renal. Figure 2 Bilateral renal infarcts complicating a spontaneous dissection of the renal arteries

thrombosis, tubular obstruction, hypotension, or autosomal recessive polycystic disease. The rim pattern is most often associated with renal infarction and occasionally with acute tubular necrosis and renal vein thrombosis.

Magnetic Resonance Imaging

Magnetic resonance imaging (MRI) has great potential in the noninvasive evaluation of important functional renal parameters such as glomerular filtration, renal perfusion, tubular concentration, renal diffusion, and the oxygenation state of the kidneys. To date, however, MRI is used more in research than in clinical practice.

Nuclear Medicine

Because the excretion of radiopharmaceuticals depends on renal function, they cannot be used to evaluate all patients with renal failure. This is particularly true concerning products excreted primarily by glomerular filtration (technetium). Products excreted by tubular secretion may demonstrate the kidneys even when renal dysfunction is relatively advanced. In clinical practice, radionuclide studies usually only help exclude arterial occlusion because images are difficult to interpret when renal function is markedly impaired.

Diagnosis

An acute renal insufficiency may be diagnosed in a clinical setting that makes obvious the cause of the renal failure, or it may be discovered by clinical findings of hyperuremia or by biochemical results. The goals of imaging are the following:

1. To differentiate acute renal failure from chronic failure
2. To understand the mechanism of the renal failure: functional, postobstructive, or due to nephropathy
3. To seek the cause of the nephropathy: tubular, glomerular, interstitial, or vascular

Most often, the diagnosis of the causes of the renal failure is obvious in the clinical context because several causes may be involved; for instance, in the clinical setting of shock, functional insufficiency and acute tubular necrosis may explain the renal failure and may be related. In the lack of clinical orientation, the imaging strategy is based on US rather than on Doppler. US is used to look for a dilatation of the calyces and seek for findings of chronic renal insufficiency by showing kidneys with decreased size. Doppler is used to look for a thrombosis of the renal artery or veins or a bilateral stenosis of the renal arteries. Other parameters, including kidney echogenicity and the RI, have only an orientation value and do not substitute for renal biopsy.

Insufficiency, Chronic, Renal

Patrice Taourel
Service d'Imagerie Médicale, Hôpital Lapeyronie,
371 avenue du Doyen Gaston Giraud,
34295 Montpellier, Cedex 5
p-taourel@chu-montpellier.fr

Definition

Chronic renal insufficiency is the gradual progressive loss of renal function. The renal dysfunction is attributable to the loss of functioning renal parenchyma and, as such, is irreversible. Consequently, in most cases, the process of chronic renal insufficiency results in the need for dialysis or renal transplantation

Pathology

The causes of chronic renal insufficiency may be divided into three main categories: prerenal causes, renal causes, and postrenal causes:

Prerenal chronic renal insufficiency is due to medical conditions that cause continuous hypoperfusion of the kidneys, leading to kidney atrophy (shrinking), loss of nephron function, and chronic renal failure. These conditions include poor cardiac function, chronic liver failure, and atherosclerosis of the renal arteries.

Renal chronic renal insufficiency may result from damage to any portion of the kidney: the gomerulus, the tubule, the blood supply, or the interstitium.

- The main cause of glomerulopathy that is responsible for renal failure is diabetes, and diabetic nephropathy is the most common cause of chronic renal failure in industrialized countries. It occurs as a result of glomerular hyperperfusion that leads to glomerular hypertension, which results in glomerular sclerosis. Other causes of secondary glomerulopathies include amyloidosis, systemic lupus erythematosus, or primary glomerulopathies when there is no extrarenal finding. Theoretically, glomerulopathies are slowly evolutive; however, in some cases the evolution to terminal renal failure may be fast, in particular in the context of HIV nephropathy.
- The tubulo-interstitial involvement in nephropathy may be due to drugs, infection, tumoral infiltration by lymphoma or leukemia, or precipitation of urate or calcium in the metabolic causes of nephropathies.
- The vascular nephropathies represent a cause of chronic renal failure increasing in frequency. The disease may be a

result of three mechanisms: nephrosclerosis due to hypertension which constitutes the second leading cause of chronic renal failure, distal renal infarct due to emboli, or ischemia of the kidneys by bilateral stenosis of the renal arteries.

- Constitutional diseases, such as polycystic disease or Alport's syndrome, are responsible for about 10–15% of cases of chronic renal failure.

Postrenal chronic renal insufficiency is due to obstruction of the normal flow of urine, leading to obstructive uropathy, progressively reduced renal blood flow, and glomerular filtration and damage to the nephrons. Abnormalities that may hamper urine flow and cause postrenal chronic renal insufficiency include bladder outlet obstruction due to an enlarged prostate gland or bladder stone, neurogenic bladder, kidney stones in both ureters, obstruction of the tubules, retroperitoneal fibrosis of any cause, and vesicoureteral reflux.

Clinical Presentation

Patients with mildly diminished renal reserve are asymptomatic, and renal dysfunction can be detected by laboratory testing. A patient with mild to moderate renal insufficiency may have only vague symptoms. Nocturia is noted, principally due to a failure to concentrate the urine during the night. Lassitude, fatigue, and decreased mental acuity are often the first manifestations of uremia. Neuromuscular features then follow including twitches, peripheral neuropathies, muscle cramps, and convulsions. Anorexia, nausea, vomiting, stomatitis, and an unpleasant taste in the mouth are almost uniformly present. The skin may appear yellow–brown and there are bony lesions of renal osteodystrophy. Malnutrition is very common. In advanced renal failure, gastrointestinal ulcerations and bleeding are common. Hypertension related to hypervolemia is present in 80% of patients, and cardiomyopathy and pericarditis are not rare.

Imaging

Ultrasound

Ultrasound (US) is the best available imaging study for patients with renal failure. The size of the kidney can be evaluated using its maximum length, which has become the standard parameter because it is simple and correlates well with renal volume. Average renal length is 11 cm in adults. US also allows measurement of the cortical thickness from the outer border of the medullary pyramids to the renal capsule, which normally measures about 10 mm, and it allows analysis of the outline of the kidney that may be rounded, lobulated, or dented. The cortical echogenicity can be studied with US, which is most often inferior to the echogenicity of the liver. Although the echogenicity of the renal cortex and the liver is the same in minority of healthy subjects, a renal cortex more echogenic than the liver is clearly abnormal past the age of 6 months and indicates renal disease. The corticomedullary differentiation must be analyzed. Prominently hypoechoic medullary pyramids usually indicate increased cortical echogenicity, whereas hyperechoic pyramids indicate medullary disease and particularly medullary nephrocalcinosis for which the most common causes are medullary sponge kidney (Fig. 1), renal tubular acidosis type 1, and hypercalcemic states. With US, one can search for dilated fluid-filled calyces in the renal sinus (Fig. 2) that may be differentiated from venous engorgement and from peripelvic cysts.

US is a useful tool with which to differentiate acute from chronic renal insufficiency, since in acute renal insufficiency the kidneys have a normal size or are enlarged, whereas they are more often decreased in size

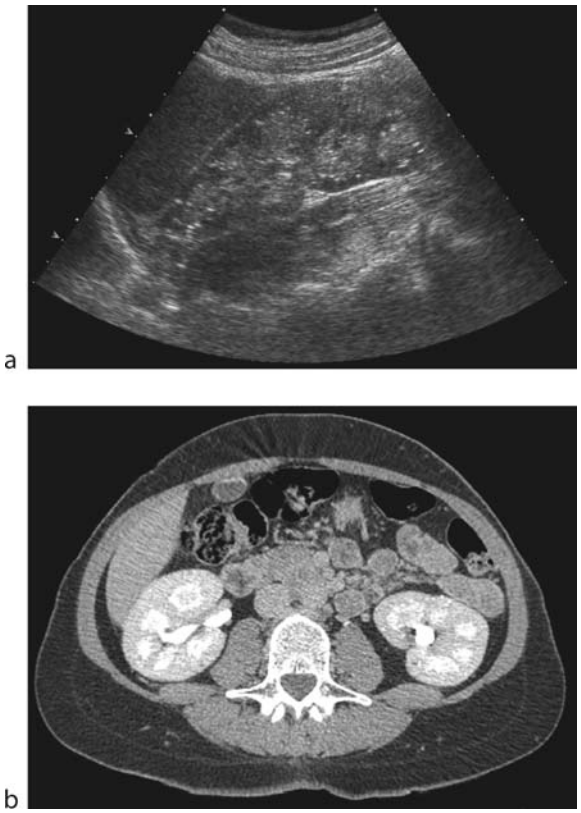

Insufficiency, Chronic, Renal. Figure 1 Medullary nephrocalcinosis due to medullary sponge kidney. (a) US shows hyperechoic renal pyramids without obvious shadowing; (b) CT at the excretory phase shows stasis of urine in the dilated distal collecting tubes.

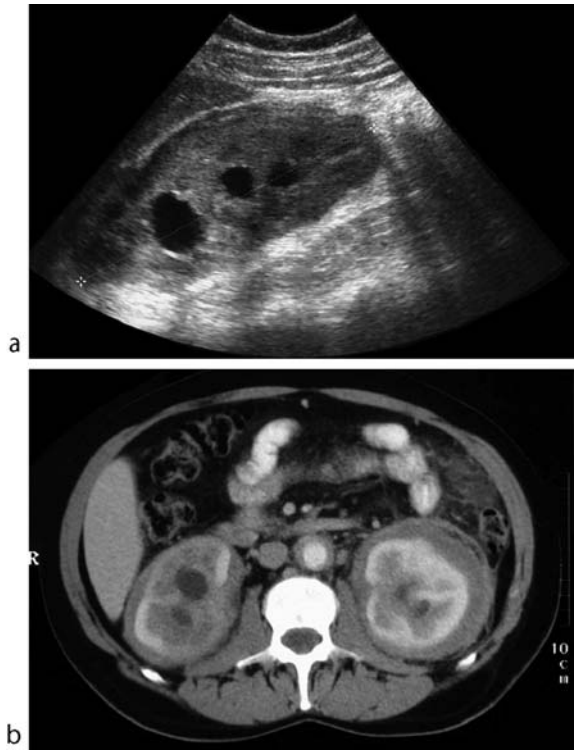

Insufficiency, Chronic, Renal. Figure 2 Bilateral perirenal fibrosis. (a) US shows dilatation of the calices; (b) CT clearly shows the perirenal fibrosis responsible for the obstruction.

with a decreased renal cortex thickness that is considered the most sensitive finding. However, renal size is conserved or increased in glomerulopathy or in diabetic nephropathy. Consequently, in the clinical context of renal insufficiency, a decrease in the size of the kidney, as well as in the thickness of the cortex, may confirm chronic disease, although a normal-sized kidney does not rule it out.

US is mainly used to look for an obstruction. Chronic obstruction produces increasing dilatation of the ureter and the collecting system proximal to the obstruction lesion. The amount of dilatation varies from case to case. In general, the dilatation increases both with the duration of obstruction and as a direct function of the intraluminal pressure. The most severe dilatation therefore does not occur with very mild obstruction or with complete obstruction after which urine formation tends to cease, but rather at an intermediate state in which the degree of obstruction increases intraluminal pressure but does not cause immediate severe oliguria.

In chronic renal failure, the size of the kidney and the thickness of the cortex are most often decreased. A very thin cortex indicates severe, irreversible renal disease. However, enlarged, very echogenic kidneys suggest amyloidosis, HIV nephropathy, or nephritis. Normal-sized or moderately enlarged kidneys that are echogenic are suggestive of glomerulopathies, such as diabetic nephropathy, immunoglobulin A nephropathy, or membranous nephropathy. Renal size is preserved even in advanced diabetic nephropathy, often with only a modest increase in cortical echogenicity, an appearance that is distinctly unusual in advanced renal failure from other causes. Cortical irregularity with a history of multiple urinary tract infections suggests the diagnosis of chronic pyelonephritis, particularly if dilatation of the calyces is present. In the absence of such a history, cortical scarring could represent vascular disease with previous infarcts. In polycystic kidney disease, US easily shows a huge and bilateral renal enlargement due to numerous cysts of variable size.

Doppler

Doppler improves the sonographic assessment of renal dysfunction. In the setting of chronic renal failure without cause, the principal interest is to look for a stenosis of the renal arteries by showing an increased peak systolic frequency shift at stenosis and a poststenotic spectral broadening with a decrease of the resistive index within the intrarenal arteries.

The clinical role of Doppler for differentiating renal disease using the resistive index (RI) is controversial. Some studies suggest that an increased RI of the renal arteries is associated with the severity of systemic atherosclerosis and that the intrarenal vascular resistance differs depending on the underlying renal disease, with a greater increase in diabetic nephropathy than in chronic glomerulonephritis and nephrosclerosis. However, these data indicate a trend, and there is no cut-off for differentiating disease in a given patient.

Computed Tomography

Computed tomography (CT) is not recommended in the exploration of the cause of renal insufficiency, because such exploration needs intravenous contrast agents, except when searching for a ureteral stone. However, in cases where the renal function is not known or because dialysis is scheduled CT can be performed. The analysis of the CT nephrogram gives some information. A global absence when bilateral means a total lack of renal function. Segmental absence is attributable to focal renal infarction, most likely due to arterial emboli. Global persistence may be unilateral, caused by renal artery stenosis, renal vein thrombosis, or urinary tract obstruction, or due to systemic hypotension, intratubular obstruction, or abnormalities in tubular function. Striated nephrograms are caused by ureteric obstruction, acute pyelonephritis, contusion, renal vein thrombosis, tubular obstruction, hypotension, and autosomal recessive polycystic disease.

Magnetic Resonance Imaging

Magnetic resonance imaging (MRI) has a great potential in the noninvasive evaluation of important functional renal parameters such as glomerular filtration, renal perfusion, tubular concentration, the oxygenation state of the kidneys, and renal diffusion. However, to date, the evaluation of these parameters is more in the field of research than in clinical practice. The main clinical interest of MRI in the daily clinical evaluation of patients with renal failure is to permit the morphological evaluation of the kidneys and the urinary tree after noniodinated contrast enhancement.

Nuclear Medicine

Because the excretion of radiopharmaceuticals depends on renal function, they cannot be used to evaluate all patients with renal failure. This is particularly true for products (Technetium) excreted primarily by glomerular filtration, whereas products excreted by tubular secretion may demonstrate the kidneys even when renal dysfunction is relatively advanced. In clinical practice, radionuclide studies usually only help exclude arterial occlusion, because images are difficult to interpret when renal function is markedly impaired.

Diagnosis

In most cases, the cause of the renal failure is known (diabetic nephropathy, uropathy, polycystic kidney disease) and the goals of imaging will be to look for an aggravating factor (obstacle, stenosis of the renal artery).

In some cases, the renal failure is discovered after clinical findings of hyperuremia or is more often revealed by biochemical test results. In these cases the goals of imaging are

- To differentiate acute renal failure from chronic failure;
- To seek the cause of the nephropathy: tubular, glomerular, interstitial, or vascular. This diagnostic step is crucial because (a) some diagnoses are obvious on imaging (polycystic kidney disease, bladder outlet obstruction), (b) in some cases it may be possible to treat the cause (surgery of a uropathy, dilatation of a stenosis of the renal artery), (c) the prognosis depends on the cause, (d) some renal diseases (glomerulopathy) may recur on the renal transplant;
- To look for factors worsening the renal failure (obstacle).

The imaging strategy is based on US. US will provide some clues of the cause of nephropathy, based on the size of the kidney, the presence of cysts, the outline of the kidneys, their symmetry, and the corticomedullary differentiation. In patients with a suspicion of vascular nephropathy, Doppler will look for findings of stenosis of the renal artery. Renal biopsy, often guided by imaging, is used to discover the cause of the renal failure when the size of the kidney is preserved and when the calyces are not dilated.

Intermediate ARM

ARM where the rectal pouch enters the sling of the puborectalis muscle; depending on the gender, either rectobulbar or rectovaginal fistulas can exist.

▶Anorectal Malformation

Intermittent Imaging

Imaging of ultrasound contrast media at a low frame rate (typically one image every second or every few seconds) to minimize bubble destruction caused by the ultrasound itself.

▶Time Intensity Curves

Internal Derangement, Temporomandibular Joint

Bodo Kress[1], Marc Schmitter[2]
[1]Department of Neurology, University of Heidelberg Medical Section, Heidelberg, Germany
[2]Department of Prosthodontic, Department of Neurology, University of Heidelberg Medical Section, Heidelberg, Germany
bodo_kress@med.uni-heidelberg.de

Synonyms

Temporomandibular arthropathy; Temporomandibular joint disorders

Definition

Internal derangement is caused by an abnormal movement and/or position of the disc. Naturally, the disc with its posterior attachment is located in closed-mouth position on the zenith of the condyle. During the opening of the mouth, the condyle and the disc slide on the tuberculum articulare. In joints presenting a disc displacement, the disc is located in front of the condyle. If the patient opens

the mouth, the condyle might slide on the disc and consequently, the condyle–disc relation normalises during mouth opening (anterior disc displacement with reduction). This action is clinically associated with a click during opening and closing.

In other cases, the condyle might not slide on the disc during mouth opening (anterior disc displacement without reduction). Thus, the disc–condyle relation remains pathological in the opened-mouth position. Consequently, there is often a limitation of the mouth opening in combination with pain as the disc closes the condyle in its movement. However, many subjects present an anterior disc displacement without suffering from any clinical signs or symptoms (the data vary between 7% and 35%).

Anatomy

The main components of the temporomandibular joint (TMJ) are the head of the mandible, the tubercle, the mandibular fossa and the articular disc. The disc has a posterior attachment to the ligamentous apparatus (the superior and inferior strata of the bilaminar zone). The articular disc plays a major role in TMJ function. It consists of an avascular anterior part, which is composed of fibrocartilage and a vascularised posterior part. The anterior part includes an anterior band, an intermediary zone and a posterior band. Under physiological conditions, the biconcave disc separates the TMJ into two compartments, which coordinate rotational movements (lower portion) and translational movements (upper portion). The face of a clock can be used for describing the anatomical location of the disc in relation to the condyle with the head of the mandible in the middle. When the mouth is closed, the posterior attachment of the disc is located at a position between 11 and 12 o'clock in the sagittal plane (Fig. 1a) (3).

When the mouth is open, the disc is interposed between the head of the mandible and the tubercle in the sagittal plane (Fig. 1b). Portions of the articular disc are not infrequently located medial to the head of the mandible in the coronal plane (Fig. 2a–c).

The head of the mandible is homogeneously structured without bony attachments and/or conspicuous flat areas. Under physiological conditions there is (almost) no fluid within the joint.

Pathology/Histopathology

Internal Derangement (Sagittal View)

Partial anterior displacement is diagnosed if the posterior attachment of the disc is located at a position between 10 and 11 o'clock or if anterior displacement cannot be seen on all slices.

Complete anterior displacement is diagnosed if the posterior attachment of the disc cartilage is located at a position below 10 o'clock on all slices or if it has no contact with the condyle (Fig. 3a). Anterior displacement is the most common type of internal derangement. The distinction between partial and complete anterior displacement in the closed-mouth position has no clinical relevance. What is clinically important is whether the disc resumes its normal position relative to the condyle when patients open their mouths (anterior disc displacement with reposition) or whether the disc remains anterior to the condyle on mouth opening (anterior disc displacement without reposition, Fig. 3b). Whereas anterior disc displacement with reposition is often accompanied by clicking sounds on opening and closing the mouth, anterior disc displacement without reposition is char-

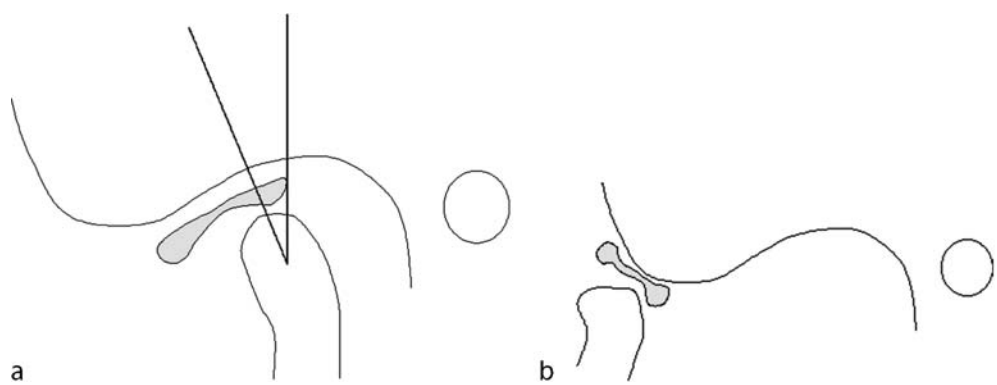

Internal Derangement, Temporomandibular Joint. Figure 1 Schematic drawing of a normal disc in the closed mouth (a) and opened mouth position, sagittal view (b). In the closed-mouth position the posterior attachment of the disc is located at a position between 11 and 12 o'clock, in the opened mouth position at a position between the condyle and the tubercle.

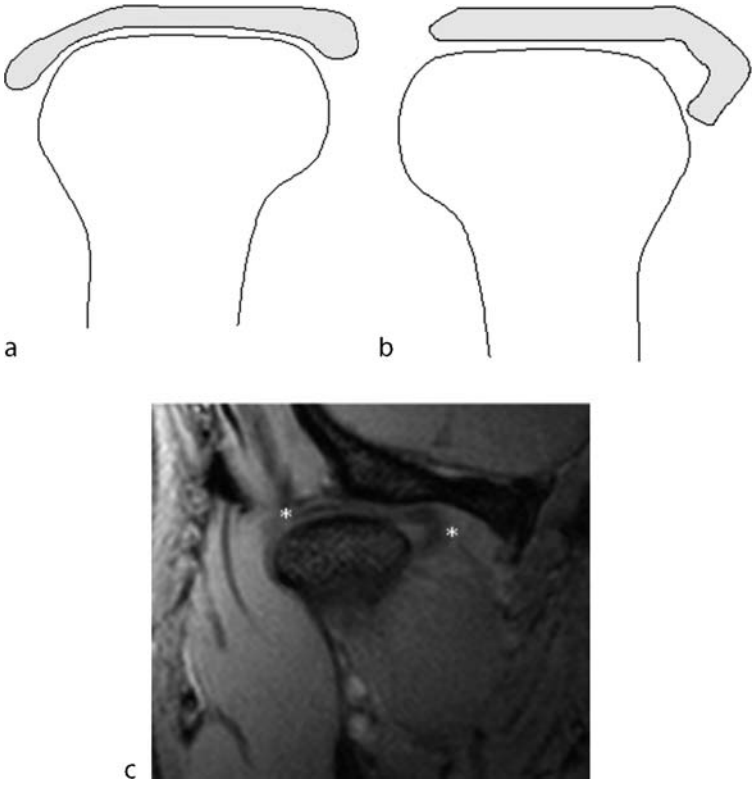

Internal Derangement, Temporomandibular Joint. Figure 2 MR image and schematic drawing of a normal disc (coronal view). Coronal T1-weighted FLASH 2D sequence with the mouth closed (a) and opened (b, c).

acterised by a limitation of mouth opening. Posterior disc displacement is relatively rare.

Internal Derangement (Coronal View)

While there is an extensive literature on the pathology of internal derangement in the sagittal plane, very few studies have focused on the coronal view. Normal and abnormal disc positions in the coronal plane, for example, have not yet been sufficiently defined. A review of the literature shows that there is only one prospective study that describes disc positions in a population of symptom-free subjects (Fig. 2a–c) (5). Medial displacement of the disc on mouth opening has been described as a pathological condition in many publications but appears to be within the range of normal variation. By contrast, the absence of a medial orientation seems to be a pathological finding. In addition, the coronal view can help avoid false-negative results in patients evaluated for disc position in the sagittal plane. A further systematic scientific analysis of coronal disc positions (especially in association with the clinical presence of clicking sounds and unremarkable sagittal MR images) might in the future offer useful diagnostic information (Table 1).

Clinical Presentation and Examination

The main clinical symptom is unilateral arthrogenous pain and/or a limited mandibular range of motion. For the clinical examination of the stomatognathic system, standardised criteria should be used and applied by calibrated examiners to obtain a higher reliability (1). A basic distinction should be made between arthrogenic and myogenic changes, which is often difficult, especially in patients with limited mouth opening. The importance of this distinction and the associated difficulties are explainable when the proximity of the TMJ to the surrounding muscles is taken into consideration. Diagnosis is facilitated by detailed information about clinical findings and their diagnostic significance.

Functional disorders are multi-factorial in origin. For this reason, the approach to the patient should include an assessment of psychosocial factors, although arthrogenic disorders are less commonly associated with psychosocial findings than myogenic disorders. The research diagnostic criteria for temporomandibular disorders (RDC/TMD) (1) is an examination protocol that meets all relevant requirements and is used worldwide for the assessment of functional disorders.

The clinical examination for patients suffering from TMD (e.g. the RDC/TMD) includes palpation of muscles (e.g. the masseter and temporal muscles) and portions of the TMJ (e.g. the lateral and posterior poles of the condyle) and documentation of sites painful to palpation. In addition, the range of motion of the mandible is assessed by measuring (maximum) mouth opening as well as lateral and protrusive movements. An additional clinical item to be considered is the assessment of joint sounds since grinding sounds, for example, may be indicative of changes in the shape of the condyle. The fluctuating character of TMJ sounds, however, must be considered in the examination.

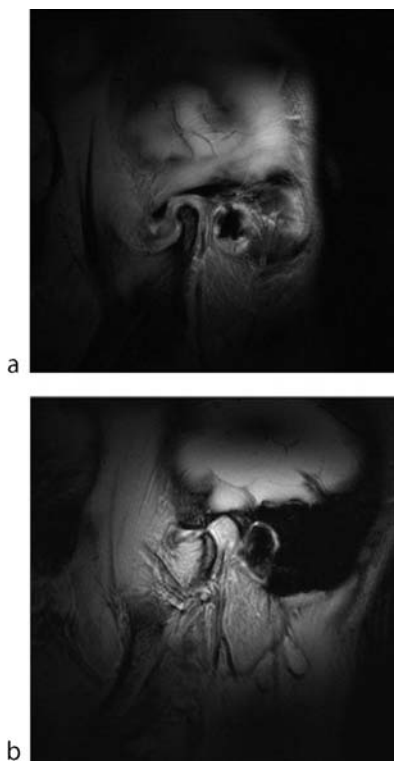

Internal Derangement, Temporomandibular Joint.
Figure 3 MR image and schematic drawing of complete anterior disc displacement (a) without reposition (b). Sagittal T1-weighted FLASH 2D sequence with the mouth closed (a) and opened (b).

Imaging of the Temporomandibular Joint

As the clinical assessment of the TMJ condition is sometimes unreliable because of fluctuating joint sounds, psychosocial aspects and the overlap of muscular and arthrogenous findings, imaging of the TMJ is necessary in some cases.

Magnetic resonance imaging offers high soft-tissue contrast and is therefore ideally suited for visualising tumourous, inflammatory and degenerative conditions of the TMJ. CT and X-ray only show bony structure and have a role in trauma (2).

The critical structures of the TMJ, such as the posterior attachment of the disc are very small. In addition, the accuracy of MRI findings depends not only on image resolution and quality but also on the anatomical knowledge of the radiologist. The higher the image quality, the higher will be inter-rater reliability or in other words, the level of agreement between the examiners with regard to disc position (4). For this reason, high image resolution and a good signal-to-noise ratio are important. Further factors that make image acquisition difficult are the pain that most patients feel when opening their mouth and the movements of the mandible that are associated with swallowing. This limits the examination time and requires the use of magnetic resonance systems with a field strength of 1.5 T and bilateral surface coils. These surface coils should have a diameter not exceeding 10 cm and should be placed over the TMJ. When MRI is used for evaluating patients suspected of having internal derangement, a TMJ positioning device that can be adjusted steplessly to each patient should be used in order to achieve a maximal opening of the mouth. This helps minimise mandibular movements during imaging.

Magnetic Resonance Imaging Protocol

The advantages and disadvantages of the various types of sequences must be carefully considered in selecting the most appropriate sequences. Spin echo sequences offer high soft-tissue contrast but are associated with a long imaging time at a relatively low resolution. The

Internal Derangement, Temporomandibular Joint. Table 1 MRI protocol for diagnosing internal derangement

		TE (msec)	TR (msec)	Field of view	Matrix	Slice thickness (mm)	Acquisition time (min)
Coronal oblique	PD FLASH 2D	10.2	208	120×120	256×256	3	3.32
Sagittal oblique	PD FLASH 2D	10.2	208	120×120	256×256	3	3.32
Coronal oblique	T2 TSE	112	5290	120×120	256×256	3	3.41

advantages of gradient-echo sequences are a short imaging time, high resolution and small slices. Although these sequences offer less contrast, they are widely used for functional MRI. We use a modified FLASH 2D sequence. PD-weighted sequences have proved to be effective in diagnostic imaging of other joints. With a reduced flip angle, the modified FLASH 2D sequence allows us to obtain images similar to PD-weighted scans. This sequence makes it possible to delineate the head of the mandible, the disc and the dorsal ligamentous apparatus. For this reason, we use it in object-oriented coronal and sagittal planes in the closed-mouth and open-mouth positions. Cine mode MRI at different openings of the mouth is not required since it does not provide additional information of clinical relevance and offers images of poor quality. The protocol also includes a coronal T2-weighted sequence that is used for imaging joint effusion and bone oedema.

The administration of an intravenous contrast agent is not necessary when internal derangement is suspected but may be required for diagnostic imaging of patients with tumours. In these cases, a T1-weighted fat-saturated sequence should be used.

Joint Effusion

An abnormal fluid collection within the TMJ is always a pathological condition that is not necessarily accompanied by pain. By contrast, minimal amounts of fluid in the lateral and medial recesses serve as physiological conditions.

Joint Contour

The head of the mandible usually has a smooth surface. Arthrotic osteophytes of the head of the mandible may be indicative of degeneration. It should be noted, however, that healthy joints can also show minimal shape changes within the range of normal variation. Depending on their extent, these changes can cause deformation of the condyle. They must be distinguished from mutilating abnormalities of the TMJ, which can be a sign of arthritis especially in young patients and should not be diagnosed as arthrotic changes. The administration of a contrast agent is not necessary since contrast enhancement of the synovial membrane must be expected in the presence of such marked joint lesions. Instead, patients should be advised to consult a rheumatologist and undergo serological testing.

In addition, cartilage lesions are found in the TMJ as in other joints. Cortical or osteochondral defects with loose fragments can occur.

Under normal physiological conditions, the disc has a biconcave shape but often adopts a different shape in the course of disc displacement, for example, it becomes biconvex. In the late stage of disc degeneration it is no longer possible to delineate the contours of the disc.

Range of Motion

Range of motion in the anterior–posterior direction depends on mouth opening capacity and thus shows individual differences. Asymmetries, where one mandibular head moves further in the ventral direction than the other one, are pathological conditions. In healthy test subjects, the condyle not infrequently (in more than 40% of cases) slides over the tubercle. Hypomobility is a pathological condition that is associated with the limitation of mouth opening and is characterised by a limited range of motion of the condyle in relation to the tubercle. It is often accompanied by an asymmetric opening of the mouth and occurs together with anterior disc displacement without reduction.

Diagnosis

Anterior displacement: Posterior attachment is below 10 o'clock position in closed mouth,
With reposition: Disc is in the normal position on mouth opening,
Without reposition: Disc is in front of the condyle on mouth opening,
Posterior displacement (very rare): Posterior attachment is dorsal to 1 o'clock position in closed mouth,
Hypomobility: Limitation of mouth opening and is characterised by a limited range of motion of the condyle in relation to the tubercle,
Joint effusion: An abnormal fluid collection within the TMJ.

Bibliography

1. Dworkin SF, LeResche L (1992) Research diagnostic criteria for temporomandibular disorders. J Craniomandib Disord 6:301–355
2. Katzberg R (1989) Temporomandibular joint imaging. Radiology 170:297–307
3. Rammelsberg P, Pospiech P, Jäger L et al (1997) Variability of disk position in asymptomatic volunteers and patients with internal derangements of the TMJ. Oral Surg Oral Med Oral Pathol Oral Radiol Endod 83:393–399
4. Schmitter M, Kress B, Hahnel S et al (2004) The effect of quality of temporomandibular joint MR images on interrater agreement. Dentomaxillofac Radiol 33:253–258
5. Schmitter M, Kress B, Ludwig C et al (2005) Temporomandibular joint disk position in the coronal MRI plane in symptom-free subjects. Radiology 236:559–564

Internal Hernia

The protrusion of bowel through a defect in its mesentery, but where the abnormally positioned bowel lies within the abdominal cavity.

▶Small Bowel, Postoperative

Internal Rectal Prolapse – Intussusception

▶Pelvic Floor Dysfunction, Anorectal Manifestations

Internal Urethrotomy

Surgical procedure that involves incising a urethral stricture transurethrally using endoscopic equipment. The incision is made under direct vision with an urethrotome and allows release of scar tissue. Care must be taken not to injure the corpora cavernosa because this could lead to erectile dysfunction.

▶Urethra, Stenosis

Intersex

▶Ambiguous Genitalia

Intersexuality

▶Ambiguous Genitalia

Interspinous Distance

Narrowest distance on an axial section between the ischial spines.

▶Pelvimetry, Magnetic Resonance

Interstitial Lung Diseases, Known Causes or Association

David M Hansell[1], Nicola Sverzellati[2]
[2]Department of Radiology, Royal Brompton Hospital, London, UK
[1]Department of Clinical Sciences, Section of Radiology, University of Parma, Italy
d.hansell@rbh.nthames.nhs.uk
nicolasve@tiscali.it

Synonyms

Diffuse parenchymal or interstitial lung disease from known causes or association

Definition

Many factors may produce diffuse predominantly interstitial infiltration of the lung. These entities comprise: hypersensitivity pneumonitis (HP), smoking-related interstitial lung disease, collagen vascular diseases, pulmonary vasculitis, drug toxicity, and radiation induced lung fibrosis.

Pathology/Histopathology

Hypersensitivity Pneumonitis

Hypersensitivity pneumonitis is an immunologically induced inflammatory disease of the lung parenchyma and terminal airways as a consequence of repeated inhalation of a variety of organic dusts and other agents in a sensitized host. The classic histopathology of HP features the triad of cellular bronchiolitis, a lymphoplasmocytic interstitial infiltrate, and poorly formed nonnecrotizing granulomas. However, pathologic features may vary with disease stage and a fibrotic pattern very similar to usual interstitial pneumonia (UIP) or nonspecific interstitial pneumonia (NSIP) is frequently seen in chronic, fibrotic HP.

Smoking-Related Interstitial Lung Disease

The increasing recognition that Langerhans cell histiocytosis (LCH), respiratory bronchiolitis-interstitial lung disease (RB-ILD), and desquamative interstitial pneumonia (DIP) form a spectrum of interstitial patterns in response to smoking-related lung injury has led to the proposal of the term "smoking-related interstitial lung

disease" to cover these entities. The variety of interstitial lung diseases associated with cigarette smoking is wider than generally appreciated and these often coexist (1). Respiratory bronchiolitis (RB) is a histopathologic lesion, characterized by the presence of pigmented intraluminal macrophages within respiratory bronchioles, whereas RB-ILD disease occurs when RB is extensive enough to cause symptoms and physiologic evidence of interstitial lung disease. LCH in adults results from the accumulation of specific histiocytic cells known as Langerhans cells in the lung, and is strongly associated with cigarette smoking.

Collagen Vascular Diseases

The collagen vascular disorders can affect many parts of the lung: the pleura, alveoli, interstitium, vasculature, lymphatic tissue, or airways. Most of the parenchymal manifestations of collagen vascular diseases are similar to those found in lone idiopathic interstitial pneumonias (IIPs).

Pulmonary Vasculitis

Pulmonary vasculitis may occur in the context of a systemic vasculitis or may be associated with other underlying diseases such as collagen or drug induced lung diseases. Principally small-vessel primary vasculitis, which causes alveolar hemorrhage and/or inflammatory infiltrates more reminiscent of diffuse interstitial lung disease (2).

Miscellaneous Causes of Pulmonary Fibrosis

Drug Toxicity

Numerous agents including cytotoxic (such as bleomycin, methotrexate, and cyclophosphamide) and noncytotoxic drugs (such as nitrofurantoin, sulfasalazine, and amiodarone) have the potential to cause pulmonary toxicity damage. The spectrum of the abnormalities includes mainly diffuse alveolar damage (DAD), nonspecific interstitial pneumonia, organizing pneumonia (OP), eosinophilic pneumonia, and pulmonary hemorrhage (3). Granulomatosis-like reactions as well as pulmonary vasculitis may also be caused by drug toxicity.

Radiation Induced Lung Fibrosis

Radiation effects on the lung are commonly seen within 6–8 weeks of starting treatment, and peak 3–4 months after completing treatment. After the early transient radiation, pneumonitis fibrosis progresses, consolidates, and contracts over the following months.

Clinical Presentation

Hypersensitivity Pneumonitis

The clinical features of HP are classically divided into three stages, based on the duration of the patient's symptoms: acute, subacute, and chronic. However, significant clinical and radiological overlap can often occur between these nominal phases.

Smoking-Related Interstitial Lung Disease

Patients with RB are usually asymptomatic whereas most patients with RB-ILD have mild symptoms that are not disabling. Cough and dyspnea are the most common presenting symptoms, though pneumothorax may be the presenting complaint in patients affected by LCH.

Collagen Vascular Diseases

The lung disease associated with collagen vascular disease may precede the clinical presentation of the collagen disease by 5 years or more. The pulmonary symptoms resemble mainly those of patients with other interstitial lung diseases.

Pulmonary Vasculitis

Wegener's Granulomatosis

At presentation, upper airway involvement with sinusitis and rhinitis is the most common clinical feature in patients affected by Wegener's granulomatosis. The pulmonary symptoms include hemoptysis, cough, chest pain, and dyspnea.

Churg-Strauss Syndrome

The diagnosis of Churg-Strauss syndrome is made in the presence of the following findings: (1) asthma, (2) eosinophilia greater than 10%, (3) neuropathy, (4) transient or migratory pulmonary opacities.

Microscopic Polyangitiis

A nongranulomatous necrotizing systemic vasculitis is usually responsible for the pulmonary–renal syndrome. Hence, important features that distinguish it clinically from any other vasculitis are the presence of glomerulonephritis and the frequency of pulmonary hemorrhage.

Miscellaneous Causes of Pulmonary Fibrosis

Drug Toxicity

Recognition of drug-induced lung disease can be difficult because the clinical manifestations are often nonspecific, and may be attributed to infection, radiation pneumonitis, or recurrence of the underlying disease.

Radiation Induced Lung Fibrosis

If any symptoms (dyspnea, cough, and fever) related to pulmonary irradiation occur, they are mainly seen in the acute phase. In chronic phase, if fibrosis is not severe and extensive, patients are usually asymptomatic.

Imaging

Hypersensitivity Pneumonitis

Chest radiography, in the acute or subacute phase, is often nonspecific; ground-glass opacification (GGO) or a nodular/reticulonodular pattern may be present. In chronic HP reticular opacities and volume loss occur.

A variety of high resolution computed tomography (HRCT) patterns have been described in HP. GGOs, mosaic attenuation, nodules, and reticular abnormalities may all be found in acute or subacute or chronic forms of the disease since significant clinical and radiological overlap can often occur between these nominal phases. Diffuse or patchy GGO with a geographic distribution is the most common finding in the acute phase, although HRCT is rarely obtained at this stage. The nodules are the most distinctive HRCT feature, and they are often seen in the subacute stage; they are centrilobular, poorly defined, of GG attenuation in contrast to the nodules of most other inhalational diseases. A mosaic pattern, due to small airways involvement with expiratory air-trapping, provides supportive evidence for the diagnosis, especially when it occurs in association with GGOs and nodules (Fig. 1) (4). Findings of fibrosis, such as reticular opacities, honeycombing, and traction bronchiectasis are only present in the chronic phase; at this stage, the predominant mid-lung distribution of the abnormalities in association with areas of air-trapping may help to differentiate chronic HP from other fibrotic lung diseases such as nonspecific interstitial pneumonia and usual interstitial pneumonia.

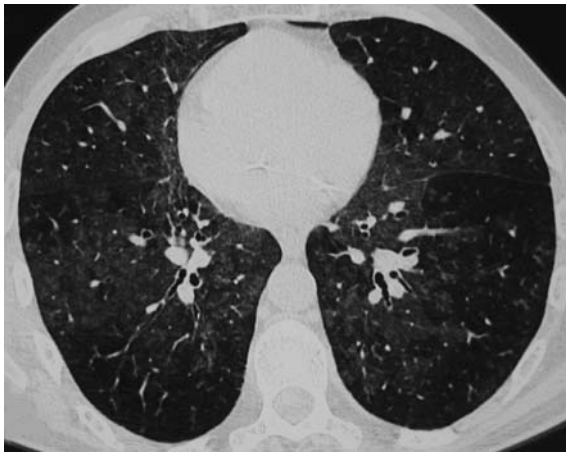

Interstitial Lung Diseases, Known Causes or Association. Figure 1 Subacute hypersensitivity pneumonitis (farmer's lung). Inspiratory HRCT shows mosaic attenuation, with areas of poorly defined ground-glass nodular opacities superimposed on a background of decreased attenuation.

Smoking-Related Interstitial Lung Disease

It is unusual to be able to diagnose RB-ILD by chest radiography alone. The HRCT features of both RB and RB-ILD are essentially represented by hazy centrilobular nodules predominating in the upper lobes and small patches of GG attenuation; in RB-ILD these abnormalities are more widespread and often associated with a background of emphysema and bronchial wall thickening. Interlobular septal thickening due to interstitial fibrosis may be seen in RB-ILD, but is rarely a prominent feature. Knowledge of a smoking history is clearly important, and may help to distinguish RB/RB-ILD from subacute HP which is usually not associated with this habit. RB-ILD differs from DIP in that GG attenuation of RB-ILD is usually less extensive, patchier, and more poorly defined.

Chest radiography in LCH shows nodular, cystic, reticular, or reticulonodular lesions, almost invariably involving the middle and upper lung zones, and frequently sparing the costophrenic sulci. Pneumothorax is a recognized feature of Langerhans cell histiocytosis. The HRCT appearance is a cystic-nodular pattern involving mostly the upper lobes. Nodules are usually <5 mm in diameter, have a peribronchiolar and centrilobular distribution, and may cavitate. Cysts are usually <10 mm in diameter but may coalesce becoming >20mm and leading to bizarre-shaped spaces with a bilobed, clover-leaf, or branching appearance. Nodules and cysts can occur independently of each other, but in the majority of patients they are found concomitantly. Occasionally, patchy or diffuse GGOs may be seen, probably related to areas of RB and DIP (1).

Collagen Vascular Diseases

Rheumatoid Arthritis

The chest radiograph of a patient affected by RA is usually normal but may show hyperinflation, reticulonodular

pattern, or pleural effusions. The "rheumatoid lung," interstitial inflammatory, and fibrotic pulmonary disease occur in a minority of patients; however; such term seems to be of little use as a descriptor, since lung biopsies show a wide range of abnormalities, including interstitial pneumonia, lymphoid hyperplasia, OP, and DAD, and HRCT more accurately reflects these changes than chest radiography. Although UIP and less frequently NSIP are the most frequent by encountered patterns, airway diseases including bronchiectasis and bronchiolectasis (even away from the fibrotic areas) and obliterative bronchiolitis (which causes a mosaic pattern) are not uncommon. It should be kept in mind that patients with rheumatoid arthritis often receive chronic drug therapy so that there may be coexistent drug-induced disease.

Systemic Sclerosis

As with other fibrosing lung diseases, the initial radiographic abnormalities may be subtle and consist of fine reticulation; as the disease progresses, the lower zone reticulation become coarser and more extensive.

The HRCT features of lung disease in patients with systemic sclerosis closely resemble those in patients with idiopathic nonspecific interstitial pneumonia. The finding of pulmonary arterial enlargement out of proportion to the severity of the lung fibrosis may indicate an independent vasculopathy akin to primary pulmonary hypertension. The presence of a dilated esophagus may also suggest of systemic sclerosis (Fig. 2).

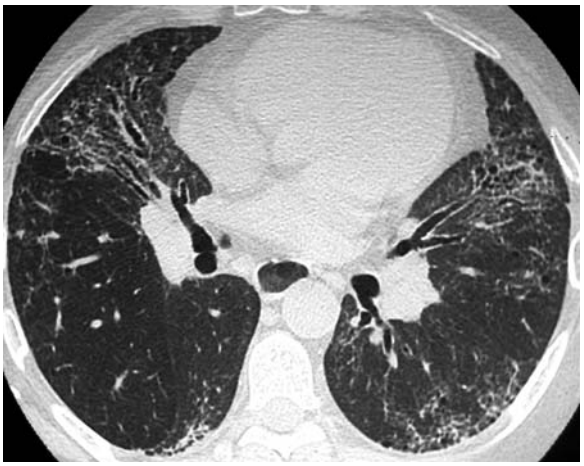

Interstitial Lung Diseases, Known Causes or Association. Figure 2 A 55-year-old patient with systemic sclerosis. HRCT through the lung bases shows fine reticulation and ground-glass opacity with a patchy distribution, consistent with a nonspecific interstitial pneumonia (NSIP) pattern (note the esophageal dilatation).

Systemic Lupus Erythematosus

Pleuropulmonary involvement of some sort occurs in approximately one-half of patients with systemic lupus erythematosus (SLE). The most common radiographic findings (not usually coexistent) consist of pleural effusion, cardiovascular changes, elevation of the diaphragm associated with basal atelectasis, and parenchymal consolidations and/or GGO pattern. The latter may reflect infection, pulmonary hemorrhage, lymphoproliferative infiltrate, or rarely of acute lupus pneumonitis characterized histologically by changes of DAD; moreover, fibrotic interstitial lung disease (NSIP, UIP, and OP subtypes) is generally regarded as an unusual manifestation of SLE.

Polymyosistis/Dermatomyositis

Radiographic changes in the lungs usually consist of symmetric reticulonodular opacity; more acute cases may show areas of airspace opacity. The HRCT changes are consistent with the pathologic findings, and represent OP and/or NSIP. Bilateral multifocal consolidation tends to occur in the lower zones with a subpleural and bronchovascular predilection, usually accompanied by linear opacities or GGO. In time, a fine honeycombing pattern equivalent to usual interstitial pneumonia may develop.

Pulmonary Vasculitis

Wegener's Granulomatosis

Chest radiographs typically show bilateral, multiple rounded opacities which may cavitate. The CT findings, although variable, consist mainly of subpleural or peribronchovascular nodules or masses; central cavitation usually occurs in nodules measuring greater than 2 cm in diameter, and the walls of cavitated lesions are often thick and irregular. Predominant bilateral air-space consolidation due to pulmonary hemorrhage is an infrequent but serious complication. Bronchial abnormalities, including bronchiectasis and bronchial wall thickening, have been reported in about 40% of cases. Tracheal narrowing is an important and relatively common manifestation of Wegener's granulomatosis.

Churg-Strauss Syndrome

The main HRCT features of Churg-Strauss syndrome consist of air-space consolidation or GGOs, nodules, and septal lines: these findings reflect the presence of air-space eosinophilic infiltrates as well as OP, and interstitial edema (which may be secondary to cardiac dysfunction) (5). Airway changes, in particular bronchial wall thickening, may be ascribed to the underlying asthma (Fig. 3).

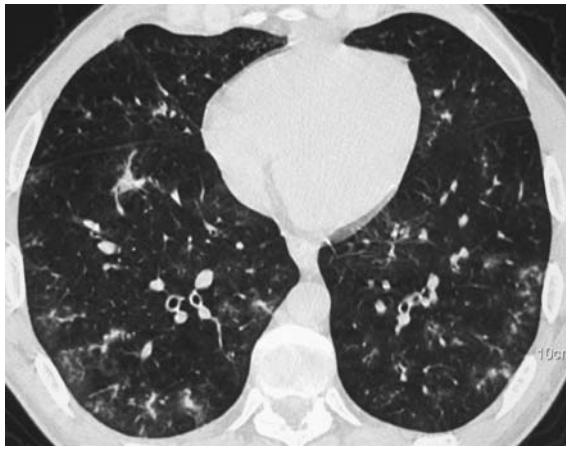

Interstitial Lung Diseases, Known Causes or Association. Figure 3 A 28-year-old man with Churg-Strauss syndrome. HRCT shows patchy ground-glass attenuation and poorly defined nodules with a peripheral distribution. Areas of decreased attenuation and bronchial wall thickening are also present, reflecting the underlying asthma.

Microscopic Polyangitiis

The HRCT findings are mostly related to ▶diffuse alveolar hemorrhage caused by capillaritis. Thus, consolidation as well as patchy GGO may be seen.

Miscellaneous Causes of Pulmonary Fibrosis

Drug Toxicity

The spectrum of abnormalities seen on HRCT in patients with drug-induced lung disease reflects the underlying histopathological findings including mainly DAD, NSIP, OP, eosinophilic pneumonia, and pulmonary hemorrhage (3). Some drugs can produce more than one pattern of histopathological involvement, and amiodarone toxicity is arguably the only condition in which CT can be used to make a definitive diagnosis by virtue of the high-attenuation values of amiodarone deposits in the lung.

Radiation Induced Lung Fibrosis

The earliest radiographic finding is a diffuse haze in the irradiated region with obscuration of vascular margins; scattered consolidations appear, and these areas may coalesce into a geometric area of pulmonary opacity. At this stage, CT findings are GGO and consolidation with a geographic distribution. With time the opacities become more linear or reticular and distort adjacent structures. 3D conformal radiotherapy can produce atypical findings, sometimes suggesting residual tumor or relapse.

Nuclear Medicine

Radiation Induced Lung Fibrosis

Fluoro-deoxyglucose positron emission tomography (FDG PET) imaging is more accurate than chest radiographs, and CT for distinguishing persistent or recurrent tumor from posttreatment scarring or fibrosis.

Diagnosis

Hypersensitivity Pneumonitis

Clinical and HRCT features often are characteristic enough to make the diagnosis. If the diagnosis remains equivocal, bronchoscopy may be helpful by demonstrating lymphocytosis on bronchoalveolar lavage or granulomas on transbronchial biopsy.

Smoking-Related Interstitial Lung Disease

A firm histological confirmation generally requires an open or thoracoscopic lung biopsy. However, the identification of Birbeck granules on electron microscopic evaluation of the cell pellet from a bronchoalveolar lavage can be diagnostic for LCH.

Collagen Vascular Diseases

Many of these diseases are characterized by the presence of a specific type of autoantibody, which may greatly assist specific diagnosis. Careful evaluation of the chest radiograph and CT can yield some useful clues to the presence of collagen vascular disease.

Pulmonary Vasculitis

Their diagnosis is based on clinical, radiographic, and histopathalogic findings. Although this group of diseases eludes a precise clinical or histological diagnosis, an increasing array of HRCT features can be used to corroborate pulmonary vasculitis as the dominant pathologic process.

Miscellaneous Causes of Pulmonary Fibrosis

Drug Toxicity

Diagnosis of drug-induced lung disease requires careful correlation of the history of drug exposure, compatible radiological findings, exclusion of alternative diagnoses, and improvement after withdrawal of offending agent.

Radiation Induced Lung Fibrosis

Radiological manifestations typically have a characteristic temporal relationship to the completion of therapy. Knowledge of this temporal relationship and an understanding of the expected patterns of radiation fibrosis associated with different radiation therapy techniques is needed to suggest a diagnosis of radiation induced lung fibrosis and to differentiate it from recurrent tumor or superimposed infection (6).

Bibliography

1. Hansell DM, Nicholson AG (2003) Smoking-related diffuse parenchymal lung disease: HRCT-pathologic correlation. Semin Respir Crit Care Med 24:377–392
2. Marten K, Schnyder P, Schirg E et al (2005) Pattern-based differential diagnosis in pulmonary vasculitis using volumetric CT. AJR Am J Roentgenol 184:720–733
3. Erasmus JJ, McAdams HP, Rossi SE (2002) High-resolution CT of drug-induced lung disease. Radiol Clin North Am 40:61–72
4. Patel RA, Sellami D, Gotway MB et al (2000) Hypersensitivity pneumonitis: patterns on high-resolution CT. J Comput Assist Tomogr 24:965–970
5. Silva CI, Muller NL, Fujimoto K et al (2005) Churg-Strauss syndrome: high resolution CT and pathologic findings. J Thorac Imaging 20:74–80
6. Choi YW, Munden RF, Erasmus JJ et al (2004) Effects of radiation therapy on the lung: radiologic appearances and differential diagnosis. Radiographics 24:985–997

Interstitial Lung Diseases, Unknown Etiology

Nicola Sverzellati[1], David M Hansell[2]
[1]Department of Clinical Sciences, Section of Radiology, University of Parma, Parma, Italy
[2]Department of Radiology, Royal Brompton Hospital, London, UK
nicolasve@tiscali.it

Synonyms

Diffuse interstitial lung disease from unknown causes; Diffuse parenchymal lung disease from unknown causes; Idiopathic interstitial lung diseases

Definition

The term "idiopathic interstitial lung diseases" is applied to a group of disorders with distinct histological and radiological appearances and without a known cause. These disorders essentially include sarcoidosis, ►lymphangioleiomyomatosis, ►pulmonary alveolar proteinosis, eosinophilic pneumonia, and idiopathic interstitial pneumonias (IIPs).

Idiopathic Interstitial Pneumonias

Pathology/Histopathology

The evolution of the classification of the IIPs over time has culminated in seven entities: idiopathic pulmonary fibrosis (IPF), corresponding to the pathology of usual interstitial pneumonia (UIP); nonspecific interstitial pneumonia (NSIP); desquamative interstitial pneumonia (DIP); respiratory bronchiolitis-associated interstitial lung disease (RBILD); cryptogenic organizing pneumonia (COP), formerly known as bronchiolitis obliterans organizing pneumonia; acute interstitial pneumonia (AIP); and lymphocytic interstitial pneumonia (LIP) (1).

The histological diagnosis of UIP is based on temporal and spatial heterogeneity of the fibrotic lesions (variegated appearance with scattered areas of normal lung, fibroblastic foci, honeycombing, etc.) with patchy involvement and normal lung adjacent to severely fibrotic lung. In contrast to UIP, the pathologic findings of NSIP are spatially and temporally uniform and consist primarily of interstitial inflammation or fibrosis. The main pathologic finding of COP consists of polypoid masses of granulation tissue within peripheral airways, extending into the alveoli and associated with interstitial and peribronchial cellular infiltration. Although DIP is currently classified as an IIP (1), its usual association with cigarette smoking has led it to be considered part of a spectrum of smoking-related lung diseases. DIP is characterized by spatially homogeneous thickening of alveolar septa, associated with intraalveolar accumulation of macrophages. AIP is a rapidly progressive form of interstitial pneumonia that is histologically identical to acute respiratory distress syndrome (ARDS). LIP occurs almost exclusively in patients who either have a connective tissue disorder (particularly Sjögren syndrome), immunodeficiency or Castleman disease. Though not usually idiopathic, it was included in the classification of IIPs (1) largely because it is important in the histological differential diagnosis of the IIPs. LIP is characterized by marked infiltration of the interstitial space by a monotonous sheet of lymphocytes.

Clinical Presentation

The most frequent presenting symptoms of patients affected by IIPs are progressive dyspnea, nonproductive cough, and (more commonly in COP) an influenza-like illness. Less common symptoms include nonspecific chest pain and constitutional symptoms such as weight loss and

fatigue, whereas patients with AIP and dyspnea progress rapidly to respiratory failure.

Imaging

Almost all patients affected by IIPs have abnormal chest radiographs characterized mostly by a variety of nonspecific patterns, most frequently a reticular pattern; however, consolidations and patchy abnormalities may predominate, especially in COP and AIP.

UIP. Abnormalities are predominantly basal, often patchy, with a strikingly peripheral distribution. The typical high-resolution computed tomography (HRCT) image is characterized by the presence of reticular opacities, within which are cystic airspaces (honeycombing), and traction bronchiectasis (Fig. 1). Ground-glass opacity (GGO) is usually present but is less extensive than the reticular pattern. Mediastinal adenopathy is a frequent accompaniment.

A rapid development of new areas of GGO and/or consolidation raises the possibility of an accelerated phase of the disease, an opportunistic infection, or pulmonary edema. Other complications include pneumothorax, pneumomediastinum, lung neoplasms, pulmonary hypertension, and cardiac failure.

NSIP. The CT features of NSIP consist mainly of GGO and reticular opacities involving the lower zones, with a peripheral and/or a peribronchovascular distribution. GGO occurs as an isolated finding in about one-third of patients but is more commonly associated with reticular abnormality or consolidation, which may represent foci of organizing pneumonia. Honeycombing, if present, is limited in extent compared with UIP.

Even though no single feature or combination of CT features can be identified as being entirely specific for a histological diagnosis of NSIP, a summary of the CT findings, particularly the extent of the disease, is very important for the evaluation of patients with NSIP. There is a better correlation between response in terms of disease extent on CT than the absolute histopathological subtype of disease, presumably due to the global assessment of the lung provided by CT in contrast to the inherent sampling of lung biopsy (2).

COP. CT shows consolidations that are usually bilateral, patchy, asymmetric, peripheral, and migrating; the lower lung zones are more frequently affected (Fig. 2). GGOs are present in about 60% of cases (3). Other CT findings include small centrilobular nodules, irregular lines, and ill-defined perilobular densities. COP in its usual radiological manifestation may spontaneously resolve or respond to steroid therapy, but some cases associated with reticular opacities may progress to irreversible fibrosis. When considering the dominant feature of COP on CT – namely consolidation – other entities, such as infections, bronchioalveolar carcinoma, lymphoma, and vasculitis, should be excluded.

DIP. The main feature on CT is the presence of GGO, which is usually bilateral and symmetrical. The distribution is basal and peripheral. Small thin-walled cysts may occur within the areas of GGO, whereas signs indicating architectural distortion (irregular linear opacities, honeycombing) are seen in about one-third of cases.

AIP. The earliest CT appearances are bilateral and patchy GGOs, often associated with consolidation in the

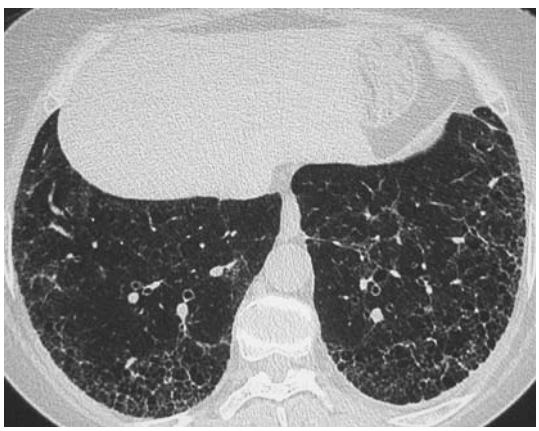

Interstitial Lung Diseases, Unknown Etiology. Figure 1
A 63-year-old man with usual interstitial pneumonia. High-resolution computed tomography shows peripheral honeycomb lung destruction and reticular abnormality in the lower lobes.

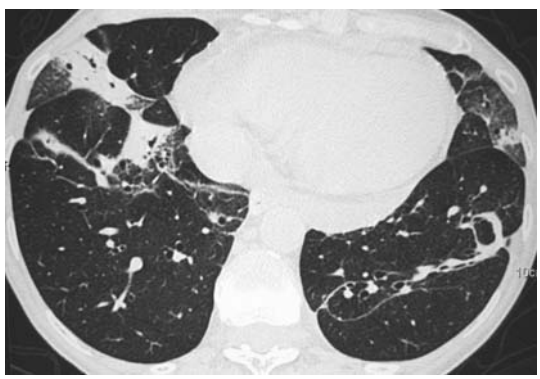

Interstitial Lung Diseases, Unknown Etiology. Figure 2
A 52-year-old man with recurrent migratory consolidation due to cryptogenic organizing pneumonia. The consolidation has a predominant peribronchovascular distribution.

dependent lung. In surviving patients, CT shows a progressive change from GG attenuation to traction bronchiectasis, cystic lesions, and reticular opacities, predominantly in the nondependent lung.

Patients with AIP are more likely to have a symmetric bilateral distribution of the lesions with lower lung predominance compared with patients with ARDS (1). Other differential diagnoses include acute exacerbation of an underlying chronic idiopathic fibrosis or systemic disease (connective tissue diseases and vasculitis), infections, pulmonary edema, and pulmonary hemorrhage.

LIP. The concomitant presence of GGOs, poorly defined nodules (centrilobular or subpleural) and scattered thin-walled cysts can help differentiate LIP from other IIPs on HRCT but the range of CT appearances of the rare IIP is wide, and a confident HRCT diagnosis is unusual. Other common findings are lymphadenopathy and interlobular septal thickening.

Nuclear Medicine

To date, nuclear medicine techniques such as positron emission tomography (PET) and lung scanning have no well-documented clinical role in the diagnosis, management, or prognosis of most diffuse lung processes.

Diagnosis

HRCT assumes a central role in defining the morphologic pattern of the IIPs, particularly in distinguishing between UIP from the other IIPs. Because UIP has a worse prognosis than the other forms of IIPs, it is important to clearly separate those patients who have the pattern of UIP on HRCT from those with other patterns. However, the HRCT features of each IIP may not be characteristic, and there is overlapping as well as coexistence of these entities.

When the HRCT pattern is typical, UIP can be confidently diagnosed in more than half of cases. Nevertheless, a confident diagnosis of UIP on HRCT is not straightforward in about one-third of patients with biopsy-confirmed UIP; in such cases, the honeycombing is less pronounced and the GGO may predominate, resembling an HRCT appearance of NSIP.

In all the other cases of IIPs, surgical biopsy is usually warranted to secure a definite diagnosis.

Sarcoidosis

Pathology/Histopathology

Sarcoidosis is a systemic disease of unknown etiology characterized by noncaseating granulomatous inflammation. Although known to affect any organ system, the lungs and its associated lymph nodes are involved in 90% of patients. Pathologic findings in sarcoidosis consist of noncaseating granulomas with epithelioid cells and large, multinucleated giant cells. In the lungs, granulomas are predominantly distributed along lymphatic pathways, being characteristically found along bronchovascular bundles, interlobular septa, and pleura. Although granulomas may remain stable for a long time or resolve spontaneously (or in response to treatment), in a minority of cases a centripetal fibrosis tends to obliterate the granulomas, leading to an extensive interstitial fibrosis with destruction and distortion of the lung architecture.

Clinical Presentation

Sarcoidosis most commonly presents between 20 and 40 years of age. Presentation as an incidental radiographic finding occurs in about 50% of cases. Respiratory illness, erythema nodosum, and ocular symptoms represent the other common presentations. Acute onset with erythema nodosum or asymptomatic bilateral hilar lymphadenopathy usually heralds a self-limiting course with spontaneous resolution, whereas insidious onset, especially with lung involvement or multiple extrapulmonary lesions, may be followed by progressive fibrosis of the lung and other organs (4). Sarcoidosis occurring in blacks is later in onset, is more likely to involve peripheral nodes, and to become chronic and disseminated; in general, the prognosis of sarcoidosis is worse in blacks than in whites. Although patients with sarcoidosis usually have a restrictive defect, an obstructive impairment can be surprisingly related to the extent of the reticular pattern depicted on HRCT or to small airway involvement and air trapping.

Imaging

Frequently, the diagnosis is first brought to attention by incidental findings on chest radiography, and staging of the disease is traditionally based on chest radiograph findings: stage O = no demonstrable abnormality; stage I = nodal enlargement only; stage II = nodal enlargement associated with parenchymal abnormality; stage III = pulmonary opacity not associated with node enlargement or evidence of fibrosis; stage IV = lung fibrosis (parenchymal distortion, lobar volume loss, etc.). Generally, the abnormalities on chest radiography mostly consist in hilar (typically symmetric) and mediastinal adenopathy, profuse bilateral small nodules, rounded or irregular, associated with linear and irregular opacities in the middle and upper zones. Symmetry is an important diagnostic feature of the hilar adenopathy associated with sarcoidosis because symmetric adenopathy is unusual in lymphoma, tuberculosis, and metastatic disease.

Hilar and mediastinal lymphadenopathy is seen more frequently on CT, which can also allow a more detailed analysis of nodal calcification. Because of their typical "perilymphatic" distribution, the nodules depicted on HRCT are clustered along the bronchovascular bundles, interlobular septa, interlobar fissures, adjacent to the costal pleural (sometimes mimicking small pleural plaques), and also in the centrilobular regions (Fig. 3) (5). Nodules tend to predominate in perihilar regions with relative sparing of the lung periphery and may be grouped unilaterally or bilaterally in small areas. Nodules of sarcoidosis typically measure 1–5 mm, but rarely, multiple ill-defined large nodules (ranging in diameter from 1 to 4 cm) can be observed on chest radiography. In approximately 10% of patients with sarcoidosis, a confluence of granulomas may cause compression of the alveoli and result in poorly defined bilateral parenchymal consolidations containing an air bronchogram; both parenchymal consolidations or large nodules can, although rarely, cavitate. Innumerable small interstitial granulomas (beyond the resolution of CT) may cause patchy GGOs on HRCT.

Although the parenchymal abnormalities are often reversible, pulmonary fibrosis occurs in approximately 20–25% of cases. Classic changes include linear opacities (radiating laterally from the hilum), fissural displacement, bronchovascular distortion (bronchiectasis), and honeycombing concentrated in the upper zones of the lungs. Finally, HRCT can also help demonstrate other specific complications (pulmonary hypertension, bronchial stenosis, etc.) and comorbidities (such as aspergilloma colonization of the cavities).

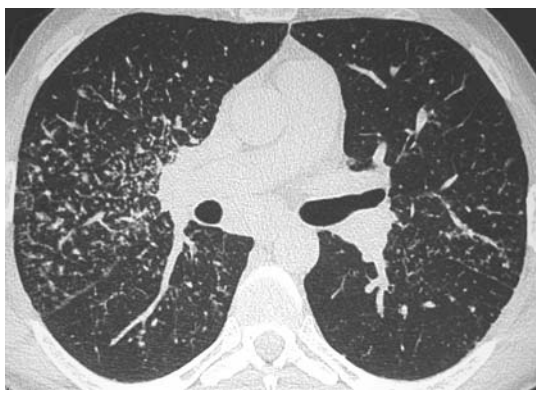

Interstitial Lung Diseases, Unknown Etiology.
Figure 3 Sarcoidosis. High-resolution computed tomography shows small nodules along interlobular septa, pulmonary vessels, and visceral pleura (e.g., the left oblique fissure).

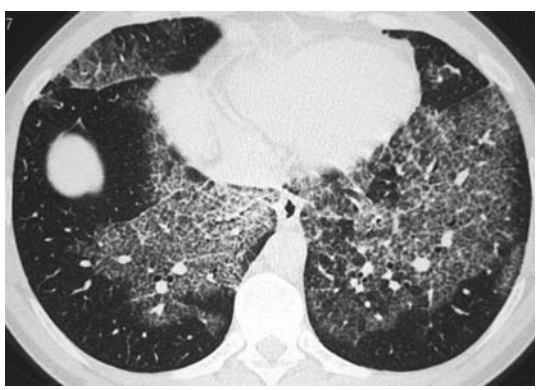

Interstitial Lung Diseases, Unknown Etiology.
Figure 4 Pulmonary alveolar proteinosis. High-resolution computed tomography shows extensive bilateral ground-glass opacity with a geographic distribution and a fine reticular pattern with interlobular as well as intralobular septal thickening superimposed (crazy-paving pattern).

Nuclear Medicine

Only PET scanning with various markers has shown utility in detecting occult disease activity in patients affected by sarcoidosis.

Diagnosis

The definitive diagnosis of sarcoidosis requires clinical and imaging features compatible with the diagnosis, as well as confirmation of the presence of noncaseating granulomas. Laboratory investigations may show various nonspecific derangements such as high serum levels of angiotensin converting enzyme (ACE), hypercalcemia, and a decreased CD4:CD8 ratio in the blood serum. Chest radiography still plays an important role in diagnosis of sarcoidosis, while CT is superior for demonstrating subtle mediastinal lymphadenopathy and associated parenchymal involvement. Histological confirmation of the presence of granulomas is critical in the diagnosis of sarcoidosis; transbronchial biopsy has a high diagnostic yield because of the predominantly peribronchovascular distribution of the granulomas.

Bibliography

1. American Thoracic Society/European Respiratory Society (2002) International multidisciplinary consensus classification of the idiopathic interstitial pneumonias. Am J Respir Crit Care Med 165:277–304
2. Screaton NJ, Hiorns MP, Lee KS et al (2005) Serial high resolution CT in non-specific interstitial pneumonia: prognostic value of the initial pattern. Clin Radiol 60:96–104
3. Lynch DA, Travis WD, Muller NL et al (2005) Idiopathic interstitial pneumonias: CT features. Radiology 236:10–21
4. Koyama T, Ueda H, Togashi K et al (2004) Radiologic manifestations of sarcoidosis in various organs. Radiographics 24:87–104
5. Nishimura K, Itoh H, Kitaichi M et al (1993) Pulmonary sarcoidosis: correlation of CT and histopathologic findings. Radiology 189:105–109

Intertuberous Distance

Narrowest distance on an axial section between the ischial tuberosities.

►Pelvimetry, Magnetic Resonance

Interval Cancer

An interval cancer is a malignant tumor that presents clinically during the interval between routine screenings and that was not visible or not suspected on review. This type must be distinguished from missed cancers that were overlooked on prospective initial studies, but were visible on review.

►Carcinoma, Ductal, Invasive

Interventional Hepatic Procedures

Riccardo Lencioni, Marzio Perri
Department of Diagnostic and Interventional Radiology University of Pisa, Pisa, Italy
lencioni@med.unipi.it

Several image-guided interventional procedures, including percutaneous and intra-arterial therapies, have been developed to treat primary and secondary liver malignancies. Percutaneous techniques of tumour ablation consist in the direct application of chemical agents (ethanol or acetic acid) or thermal agents, including heating (radiofrequency, laser and microwaves) and freezing (cryoablation) to a focal tumour (1). In intra-arterial therapies, chemotherapeutic and/or embolizing agents are delivered into the hepatic arterial system.

Techniques

Ethanol Injection

►Percutaneous ethanol injection (PEI) has been the most widely used tumour ablation technique (2, 3). PEI induces local tumour necrosis as a result of cellular dehydratation, protein denaturation and chemical occlusion of tumour vessels. Since it allows a real-time control, US guidance is the best option for PEI administration enabling a faster procedure time, precise centring of the needle in the target, and continuous monitoring of the injection. Fine non-cutting needles, with either a single end hole or multiple side holes, are commonly used for PEI. PEI may be performed under local anaesthesia and patient hospitalization is not required. The treatment schedule typically includes four to eight session performed once or twice weekly. However, number of session and amount of ethanol to inject may vary according to the size of the lesion, intra-tumour ethanol distribution and patient's compliance.

Radiofrequency Ablation

Percutaneous ► radiofrequency (RF) ablation works on the principle that alternating current operated within the radiofrequency range can produce focal thermal injury in tissues (2, 3). The thermal damage caused by RF heating is dependent on both the tissue temperature and the duration of heating and when a 90–105°C temperature throughout the entire target volume is achieved and maintained for at lest 4–6 min, a large area of coagulative necrosis can be obtained. In RF ablation, the patient is part of a closed-loop circuit that includes an RF generator, an electrode needle, and a large dispersive electrode (ground pads). In each treatment session the electrode needle is placed within the liver tumour under US, CT or MR, guidance. Grounding is achieved by attaching large ground pads and the electrode is then attached to the RF generator. Since the dimension of RF thermal lesions is related not only to tissue-anatomic characteristics (heat conduction and heat lost *via* circulation) but also to technical elements (current intensity and size of the needle electrode), several technological improvements have been introduced in order to optimize RF results. Particularly, modified electrodes, such as cooled-tip electrode needles and expandable electrode with multiple retractable lateral-exit prongs on the tip, allow to obtain a larger volume necrosis and to make the procedure more effective. With any technology, each insertion lasts 10–20 min, since after this time the impedance rise induced by coagulative necrosis not allow further heat diffusion in the tumour. RF treatment may be performed by using local anaesthesia or conscious sedation.

Laser Ablation

►Laser ablation uses laser light produced by a neodymium yttrium albuminium garnet (Nd:YAG; wavelength 1,064 nm) delivered through a quartz fibre optic with a diameter of 400 μm with diffuse light emission. Laser light is converted into heat in the target area with an ensuing coagulative necrosis, secondary degeneration and

atrophy, and tumour shrinkage with minimal damage to surrounding structures. The dimension of the coagulative necrosis laser induced depends on laser power, laser irradiation time and the optical and thermal tissue characteristics (4).

Microwave Ablation

►Microwave ablation is an electromagnetic method of inducing tumour destruction by using devices with frequencies greater than or equal to 900 kHz (5). In microwave ablation a microwave generator and needle electrodes are employed. The microwave energy is transmitted *via* a flexible cable and delivered by the electrodes. Microwaves cause vibration and rotation of molecular dipoles, predominantly water, resulting in a thermal coagulation of tissues.

Cryoablation

►Cryotherapy is defined as local tumour destruction *in situ* by freezing. The resulting freeze process causes irreversible cellular damage and tissue necrosis is obtained (3–5). Different methods, including repeated freeze cycles, temporary hepatic inflow occlusion and multi-needle probe systems, have been developed to increase the size of cryolesion.

Transcatheter Arterial Embolization and Chemoembolization

►Transcatheter arterial embolization (TAE) consists in a temporary or permanent peripheral occlusion of the hepatic artery. It requires catheterization of the segmental hepatic artery supplying the liver tumour following by intra-arterial injection of embolic materials. ►Transcatheter arterial chemoembolization (TACE) combines peripheral occlusion and local deposition of chemotherapeutic agents, consisting in intra-hepatic arterial injection of chemotherapeutic agents followed by embolic agents. The anti-tumour effect depends on the synergy between the actions of chemotherapy and ischemia, since the occlusion of the tumour arterial supply advantageously follows the controlled infusion of the chemotherapeutic drug. TACE can be performed by using several different techniques, including conventional and segmental catheterism. Conventional TACE is performed by injecting an anticancer-in-oil emulsion followed by embolic material at the level of the proper hepatic artery while in segmental and subsegmental technique a microcatheter is inserted into the more distal branches of the hepatic artery, and the drug as well as the embolic material are injected solely in the feeding artery of the tumour. This allows a more strong anticancer effect, sparing at the same time the non-cancerous liver parenchyma (3). A large variety of chemotherapeutic drugs and embolic agents have been used.

Clinical Applications

Radiological interventional procedures have been employed in the treatment of either primary or secondary unresectable hepatic malignancies. A robust evidence concerning the clinical value of these techniques is currently available for the use of ethanol injection, radiofrequency ablation and TACE. An appropriate use of each treatment technique can only be done when the therapeutic strategy is decided by a multidisciplinary team and is tailored to the individual patient and to the features of the disease (2, 3).

Ethanol Injection

PEI is cheap, easy to perform, repeatable and has been the most widely used ablation technique in HCC patients. It is a well-tolerated treatment, with a high anti-tumoural efficacy in small solitary, nodular-type HCC (3 cm or less). Since HCC nodules have a soft consistency and are surrounded by a firm cirrhotic liver, injected ethanol diffuses within tumour tissue easily and selectively, leading to complete tumour necrosis in a great number of small lesions (2). The injected ethanol does not always accomplish complete necrosis in HCC nodules because of its inhomogeneous distribution within the lesion, especially in the presence of intra-tumoural septa, and repeated treatment session are usually required. In hepatic metastases the hard consistency of the neoplastic tissue impairs an adequate diffusion of ethanol resulting in a poor tumour control.

Radiofrequency Ablation

RF ablation is an effective treatment both in primary and metastatic liver tumour and represents the most widely used method for percutaneous thermal ablation. RF ablation seems to be more effective than PEI in the treatment of small HCC. Particularly, RF can achieve a more effective local tumour control than PEI with fewer treatment sessions. However, despite RF may provide marginal anti-tumour benefits also in lesions larger than 3 cm in diameter, where PEI is unable to disrupt the intra-tumoural septa, the treatment of large HCC is still problematic (2). RF is also effective in the treatment of hepatic metastases and to date it represents a valuable option in unresectable, solitary and small hepatic metastases arising from colorectal adenocarcinoma (3, 4). Although more invasive than PEI, RF ablation is considered to be safe, with a relatively low complication rate. Particularly, RF treatment of lesion adjacent to the gallbladder or to the hepatic hilum as well as

of lesions located along the surface of the liver is associated with a higher risk of complications.

Transcatheter Arterial Chemoembolization

TACE may be an effective method of controlling hepatic disease in many patients with liver-dominant neoplasms, such as HCC, colorectal metastases and neuroendocrine tumours (3). Particularly, TACE remains a valuable approach for HCCs in the intermediate stage.

Moreover, TACE can also be used as an adjuvant to other forms of therapy and, since the absence of tumour seeding risk, it represents the first therapeutic option in HCC patients waiting for liver transplantation.

TACE has also been proved to be effective in the treatment of hepatic metastases arising from neuroendocrine tumours and colorectal cancer.

Bibliography

1. Goldberg SN, Charboneau JW, Dodd GD III et al (2003) International Working Group on Image-Guided Tumor Ablation Image-guided tumor ablation: proposal for standardization of terms and reporting criteria. Radiology 228(2):335–345
2. Lencioni R, Cioni D, Crocetti L et al (2004) Percutaneous ablation of hepatocellular carcinoma: state-of-the-art. Liver Transpl 10(2):S91–97
3. Bartolozzi C, Lencioni R (eds) (1999) Liver Malignancies. Springer-Verlag, Berlin Heidelberg, New York
4. Vogl TJ, Muller PK, Mack MG et al (1999) Liver metastases: interventional therapeutic techniques and results, state of the art. Eur Radiol 9(4):675–684
5. Ng KK, Lam CM, Poon RT et al (2003) Thermal ablative therapy for malignant liver tumors: a critical appraisal. J Gastroenterol Hepatol 18(6):616–629

Interventional Procedures

Procedures which treat disease states by open surgery or minimally invasive methods.

▶Aneurysm, Aortic and Thoracic

Intervertebral Disk Degeneration

Degenerative changes in the intervertebral disk usually begin with dehydration of the nucleus pulposus and annular tears. Dehydration is easily diagnosed on sagittal T2-weighted MR images as decreased signal of the disc. This can be accompanied by narrowing the intervertebral space due to the decreased height of the intervertebral disk, which may be seen on plain films, sagittal reformatted CT images and sagittal T2-weighted MR images. Other features of disk degeneration are vacuum phenomenon (the presence of the gas in the disk due to the production of the nitrogen during the degenerative process) and calcifications; both are excellently visible on CT examination, may be also seen on plain films and MR gradient-echo images. Degeneration of the intervertebral disk is often associated with disk bulging and may lead to disk herniation. On the other hand it is almost always combined with degenerative changes of the adjacent vertebral endplates and very often-with degeneration of the other structures of the disco-somatic unit.

▶Degenerative Conditions, Spine

Intestinal Angina

Abdominal pain related to transient intestinal ischemia, appearing 20–30 min after a meal.

▶Vascular Disorders, the Gastrointestinal Tract

Intra-Axial Brain Tumors

▶Neoplasms, Brain, Intraaxial

Intra- and extracranial, (cervical) cysts

Intra- and extracranial, (cervical) cysts are epithelial lined, well circumscribed, fluid filled non-neoplastic benign lesions. Depending on their location, adjacent stuctures may be displaced or compressed. Clinical symptoms vary with cyst location.

▶Cyst, Cerebral and Cervical, Childhood

Intra-dural Extra-medullary Space

This space is limited by the surface of the cord and the dura and is filled by cerebrospinal fluid. The cord is covered by pia matter and arachnoid membrane. In the spinal canal the arachnoid and pia matter form separate layers. The subarachnoid space separates them everywhere except where it is traversed by the nerve roots and the spinal

ligaments. The dura is separated from the vertebral canal by a layer of tissue that contains the internal vertebral venous plexus and a deposit of adipose tissue that lies in a dorsal recess between the ligamenta flava.
▶Tumors, Spine, Intradural, Extramedullary

Intracellular Reporter System

Intracellular reporter systems utilize gene products that are present within the cells
▶Reporter Systems

Intracystic Papillary Carcinoma

Variant of intraductal papillary carcinoma, located within a cyst.
▶Cyst, Breast

Intracystic Papillary Carcinoma with Invasion

▶Carcinoma, Other, Invasive, Breast

Intracystic Papilloma

Benign papillary tumor inside a cyst.
▶Cyst, Breast

Intrahepatic Suppuration

▶Abscess, Hepatic

Intralesional Tumor Resection

When the surgical margins are within the tumor margins, thus making residual tumor and recurrent tumor more common and associated with a poorer prognosis.
▶Neoplasms, Soft Tissues, Malignant

Intraosseous Lipoma

Intraosseous lipoma is a benign bone lesion composed of mature adipose tissue, which in most cases originates from the medullary portion of bone. Rarely, lipomas can develop in cortical or periosteal locations.
▶Neoplasms, Bone, Benign

Intraparenchymal Hematoma, Splenic

A collection of clotted blood within the disrupted splenic parenchyma. It represents a possible finding in cases of splenic parenchymal or vascular lesion.
▶Trauma, Splenic

Intraperitoneal Chemohyperthermia

In addition to surgery, local chemotherapy is applied in the peritoneal cavity with optimal biological effects in a hyperthermic stage. Arterial vascularization of a neoplasm is used as a route for locoregional application of chemotherapeutic agents.
▶Chemoperfusion

Intrarenal Abscess

▶Abscess, Renal

Intrauterine MRI

▶Fetal Imaging

Intravascular Contrast Media

▶Contrast Media, MRI, Blood Pool Agents

Intravenous Urography

Recently nonionic contrast agents are administered intravenously, which are excreted by the kidney into the renal pelvis, ureters, bladder, and urethra (at miction). IVU is useful for the diagnosis of obstruction, trauma, tumors, congenital malformation, and infection. It can assess kidney function, intra- and extraluminal pathology, and differentiate stones from other abdominal calcifications. It can differentiate nonmalignant from malignant causes of obstruction, haematuria, and pain. Radiopaque calculi projecting inside the collecting system, independent of the patient's position, can be less, equal or more opaque as surrounding contrast, while radiolucent calculi present as a filling defect. IVU confirms the diagnosis of acute stone obstruction also if KUB is inconclusive by assessing secondary signs of obstructing calculi: delayed excretion, persisting nephrographic effect, extravasations in spontaneous forniceal rupture, mild and local dilatation. After obtaining a KUB, 20 min postcontrast films are proposed in obstruction. In carefully conducted IVU, stones or other pathology can be assessed within the time of examination in the majority of cases using solely four images. The application of prone or slightly oblique standing projections, when necessary to opacify the collecting system to the level of obstruction, under fluoroscopic control, reduces the examination time and number of films. Rarely delayed films are required.

▶Colic, Acute, Renal
▶Medullary Sponge Kidney

Intrinsic Brain Tumor

▶Neoplasms, Brain, Supratentorial, Pediatric

Intussusception

The invagination or "telescoping" of a loop of bowel within itself, most commonly occurring as an ileo-colic intussusception but also including ileo-ileal and ileo-ileo-colic.

▶GI Tract, Pediatric, Specific Problems

Intussusception

▶GI Tract, Pediatric, Specific Problems

Invasive Ductal Carcinoma

An invasive carcinoma is a tumor with extension of tumor cells through the ductal basement membrane. A spiculated mass with irregular margins, sometimes with amorphous or pleomorphic microcalcifications, is a typical sign of invasive ductal carcinomas.

▶Carcinoma, Ductal, Invasive

Involucrum

An involucrum is a layer of reactive, vital bone that has been formed around dead bone in chronic osteoneyelitis in an attempt to confine the ongoing infection.

▶Osteomyelitis

Involucrum, Sequestrum, Cloaca

When bone infection has been untreated or inadequately treated for weeks, the periosteal reaction forms a sheath, the involucrum, around the devitalized shaft, the sequestrum, with pus from the marrow discharging through a hole in the sequestrum, the cloaca (from the Latin word for sewer).

▶Osteomyelitis, Neonates, Childhood

IOCM

▶Iso-Osmolality Contrast Media

IPSID

▶Immunoproliferative Small Intestinal Disease

Ipsilateral Breast Tumor Recurrence

▶Recurrent Neoplasms, Breast

Iron Overload

Iron overload can be subdivided into two types: parenchymal cell iron deposition in hemochromatosis, cirrhosis, intravascular hemolysis, and iron deposition in cell of the reticulo-endothelial system, also called hemosiderosis, which is seen most commonly after multiple transfusions or in diseases with extravascular hemolysis. Iron deposition in hepatocytes causes cellular damage, while iron deposition in reticulo-endothelial cells (Kupffer cells in the liver) does not produce a significant organ dysfunction.

▶Diffuse Infiltrative Diseases, Hepatic
▶Hemochromatosis, Skeletal

Ischemia

In ischemia, oxygen deprivation is accompanied by an inadequate removal of metabolites due to reduced perfusion. During the ischemic condition, an imbalance occurs between oxygen supply and demand, which may manifest as anginal discomfort, deviation of the ST segment on electrocardiography, or impairment of the regional or global left ventricular function.

▶Ischemic Heart Disease, Nuclear Medicine

Ischemia, Brachial

Elias N. Brountzos
Department of Radiology,
Athens University, Medical School, Greece
ebrountz@cc.uoa.gr

Synonyms

Acute upper extremity ischemia

Definition

Acute arterial insufficiency of the upper extremity

Pathology

Embolization is the most common cause of acute upper-limb ischemia. Embolization of the upper-limb arterial bed represents 15–32% of all peripheral emboli (3). The heart is the source of emboli in 90% of the cases. Other sources of emboli are shown in Table 1. The brachial artery is more frequently embolized (60%), followed by the axillary artery (23%), the subclavian artery (12%), and the forearm and digital arteries (5%). Iatrogenic trauma to the upper extremity arteries occurs during arterial cannulation for angiography or monitoring. Thrombosis of the brachial artery is common after arteriotomy for cardiac catherization (0.3–28%). Percutaneous brachial artery catheterization is more often complicated with local complications compared to femoral catheterization. Because of the collateral supply, many patients remain asymptomatic. Nevertheless immediate surgical intervention with thrombectomy is recommended because many initially asymptomatic patients develop symptoms of ischemia later. Axillary artery thrombosis complicates transaxillary arteriography in 0.8% of the patients. Immediate thrombectomy is required. Radial artery thrombosis occurs in 40% of the patients undergoing radial artery cannulation for monitoring, but ischemic symptoms develop in only 0.5%. Other iatrogenic injuries are encountered during blind placement of central venous catheters.

Non-iatrogenic arterial trauma of upper extremities is not rare. Of all arterial injuries in civilian experience, the axillary artery is injured in 5–9%, the brachial artery in 30%, and the forearm arteries in 7–20%. The causative agents are missiles or sharp objects. Other mechanisms include stretch injuries from falls or those occurring during shoulder dislocation. Brachial artery injury is a complication of fractures and dislocations of the elbow.

Clinical presentation: The presentation is similar to that of the lower extremity acute ischemia with pulseness, palor, pain, paresthesias, and paralysis. Usually it involves the hand and the fingers. Mild symptoms are not rare with the patient complaining of only a cold hand (1). The clinical picture of embolization maybe dramatic or symptoms may develop over the course of several hours. Physical examination is essential to access the level of obstruction.

Ischemia, Brachial. Table 1 Acute upper extremity ischemia. Etiology

1. Iatrogenic injury (axillary, brachial, radial artery cannulation)
2. Non iatrogenic trauma
3. Embolization
a. Cardiac origin
b. Proximal artery ulcerated plaque
c. Aneurysms (ascending aorta, innominate, subclavian, axillary, brachial, ulnar)
d. Thoracic outlet syndrome
e. Fibromuscular disease
4. Steal phenomenon after arteriovenous fistula formation
5. Aortic dissection

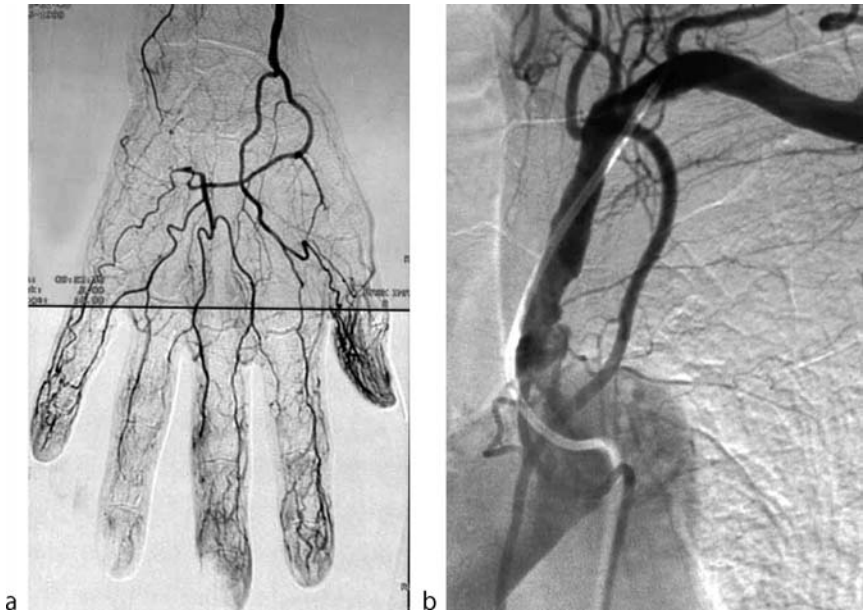

Ischemia, Brachial. Figure 1 (a) Hand DSA in a patient with acute onset of left-hand ischemia depicts atherosclerotic disease of the hand arteries, absence of the ulnar artery and the deep palmar arch, and filling defects of the digital arteries suggestive of peripheral embolization. (b) Selective DSA of the left subclavian artery depicts ulcerated occlusive lesion of the left subclavian artery.

Imaging and Diagnosis

If embolization is suspected, color Doppler sonography or other noninvasive imaging modalities can evaluate large arteries, but may fail to provide detailed information on the hand arterial pathology. Angiography is recommended to rule out proximal arterial embolic source. Imaging from the arch to the digits should be performed. The proximal arteries should be evaluated for aneurysm containing thrombus or atherosclerotic lesions. With digital embolization, luminal defects are depicted in the involved vessels (Fig. 1). In non-iatrogenic trauma the diagnosis is obvious in the presence of active arterial hemorrhage, expanding hematoma, ischemia, or absence of pulses. Sometimes the patient has to go immediately to surgery. Imaging is mandatory to rule out subclinical vascular injury. Angiography is the recommended imaging modality as it can be used in the same session for interventional treatment. Findings include spasm, intimal flaps, thrombosis, laceration, frank exsanguination, and pseudoaneurysm.

Interventional treatment

Surgical exploration with thrombo-embolectomy is the treatment of choice for acute ischemia of the upper limb. Intra-arterial thrombolysis has promising results. When the source of emboli is a proximal ulcerated plaque, stent placement can be used as an alternative to surgical reconstruction. Following arterial trauma, extravasation or pseudoaneurysms can be treated by embolization.

References

1. Kaufman JA (2004) Upper-extremity arteries. In: Kaufman JA and Lee MJ (eds) The Requisites. Vascular and Interventional Radiology. Philadelphia, Mosby, pp 142–162
2. Porter JM, Edwards JM (2000) Occlusive and vasospastic diseases involving distal upper extremity arteries—Raynaud's syndrome. In: Rutherford RB (ed) Vascular Surgery, Denver Colorado, WB Saunders, pp 1170–1183
3. Whitehouse WM, Jr (2000) Upper extremity revascularization. In: Rutherford RB (ed) Vascular Surgery, Denver Colorado, WB Saunders, pp 1162–1170
4. Connell DA, Koulouris G, Thorn DA et al (2002) Contrast-enhanced MR angiography of the hand. Radiographics 22:583–599
5. Brountzos EN, Petersen B, Binkert CA et al (2004) Primary stenting of subclavian and innominate artery occlusive disease: a single center experience. Cardiovasc Inter Rad 27:616–623

Ischemia, Limb, Acute

Dierk Vorwerk
Klinikum Ingolstadt, GmbH, Direktor des Institues für diagnostische und interventionelle Radiologie, Krumenauerstraße 25, 85049 Ingolstadt
dierk.vorwerk@klinikum-ingolstadlt.de

Synonyms

Acute arterial occlusion; Acute ischemic limb

Definition

Acute leg ischemia is mainly a result of embolic disease either from the heart or from ulcerating atherosclerotic lesions that may induce thrombus formation and consecutive thrombus induction. It may also be of iatrogenic origin due to invasive studies or percutaneous interventions such as vascular recanalization.

True thrombosis may occur in the case of a thrombophilic state or due to physical rest such as long-distance flights or long car driving. If thrombosis occurs in an artery that allows sufficient collateral flow onto a preexisting lesion, a sufficient collateralization, symptoms may be less severe. Thus, diagnosis may be made late leading to the state of subacute or chronic thrombosis.

Pathology/Histopathology

Acute ischemia of a peripheral limb is caused by acute embolic embolization of clot material of mainly cardiac origin, acute thrombosis from preexisting arterial lesions, or, rarely, coagulation problems.

Clinical Presentation

In general, the duration of symptoms of up to 4 weeks is classified as acute, between 1 and 3 months as subacute, and longer than 3 months as chronic thrombosis of the artery. This classification is of practical importance since treatment – both surgically and percutaneously – is influenced by the age of the occlusion. A simple mechanical removal of the embolus/thrombus becomes more difficult the longer an occlusion exists.

Clinically, acute ischemia is classified into four different states: stage I, with mild symptoms and no tissue or nervous deficits representing acute limb threatening; stage IIa, with minimal sensory loss, no muscle weakness but inaudible arterial Doppler signals; stage IIb, with extended sensory loss, mild to moderate muscle weakness, and inaudible arterial signal; and stage III, with profound anesthesia of the limb, muscular paralysis, and inaudible venous and arterial signals (1).

Clinical examination, pulse status, and duplex sonography are valuable tools for making the diagnosis of an acute leg ischemia. The patient's history is important for analyzing potential risk factors such as arrhythmias or heart valve disease.

Imaging

Duplex sonography and angiography are the principle imaging modalities that are used to make the diagnosis. Magnetic resonance (MR) angiography and computed tomography (CT) angiography may play a role in the future, but the painful state and the acuteness of the event lead to agitation of the patient, preventing lengthy imaging protocols which require full cooperation.

Angiographic imaging is frequently required to analyze the extent and the location of thrombotic occlusions (Fig. 1a–f). An ipsilateral antegrade approach is recommended if the ipsilateral femoral pulse is present and normal. An antegrade puncture is preferred so as to continue with a percutaneous intervention if possible. A contralateral retrograde approach is performed if the ipsilateral femoral pulse is abnormal. The diagnostic catheter is introduced into the iliac artery *via* a cross-over maneuver if the proximal iliac artery is patent. If involvement of the common or profound femoral arteries is suspected, sonography or duplex sonography may be added as a simple diagnostic tool.

Hand injection of dye and a 4 to 5 F access are usually sufficient to establish the diagnosis.

To date, other imaging modalities such as MR angiography or CT angiography do not play a major role in the diagnosis of acute ischemia as the potential combination of the diagnostic and interventional procedure in one step favors direct transarterial imaging.

In the case of renal insufficiency or contrast media intolerance, carbon dioxide or MR contrast agents may be used as alternative contrast media for catheter-directed angiography. Carbon dioxide is, however, frequently very painful in acute ischemic limbs limiting the imaging quality by movement artifacts.

Nuclear Medicine

Nuclear medicine plays no particular role in the diagnosis of acute ischemia.

Diagnosis

Diagnosis based on the clinical and angiographic findings is usually easy to make. It is more difficult to detect the underlying source of acute occlusion, the extent of the thrombosed arterial segment, and the best appropriate therapeutic approach.

Interventional Radiological Treatment

According to the TASC document (1), treatment of acute ischemia depends on the clinical stage. In stage I and IIa, surgical treatment with open embolectomy or thrombectomy by use of Fogarty embolectomy balloons and its

derivatives as well as thrombolysis by use of thrombolytic agents including rtPA and urokinase are accepted concepts. In stage IIb, Fogarty embolectomy is the treatment of choice, while thrombolysis is not recommended due to potential complications that may result from bleeding into revascularized tissue, resulting in a compartment syndrome. In early stage III, surgical thrombectomy may be tried; however, in advanced stage III cases, only amputation remains the principal option.

As usual, a correct diagnosis in time and rapid onset of treatment are mandatory for limb salvage and they need to be implemented in each center dealing with acute disease. It is, however, true that acute ischemic states are frequently overseen or neglected also by the patient. The

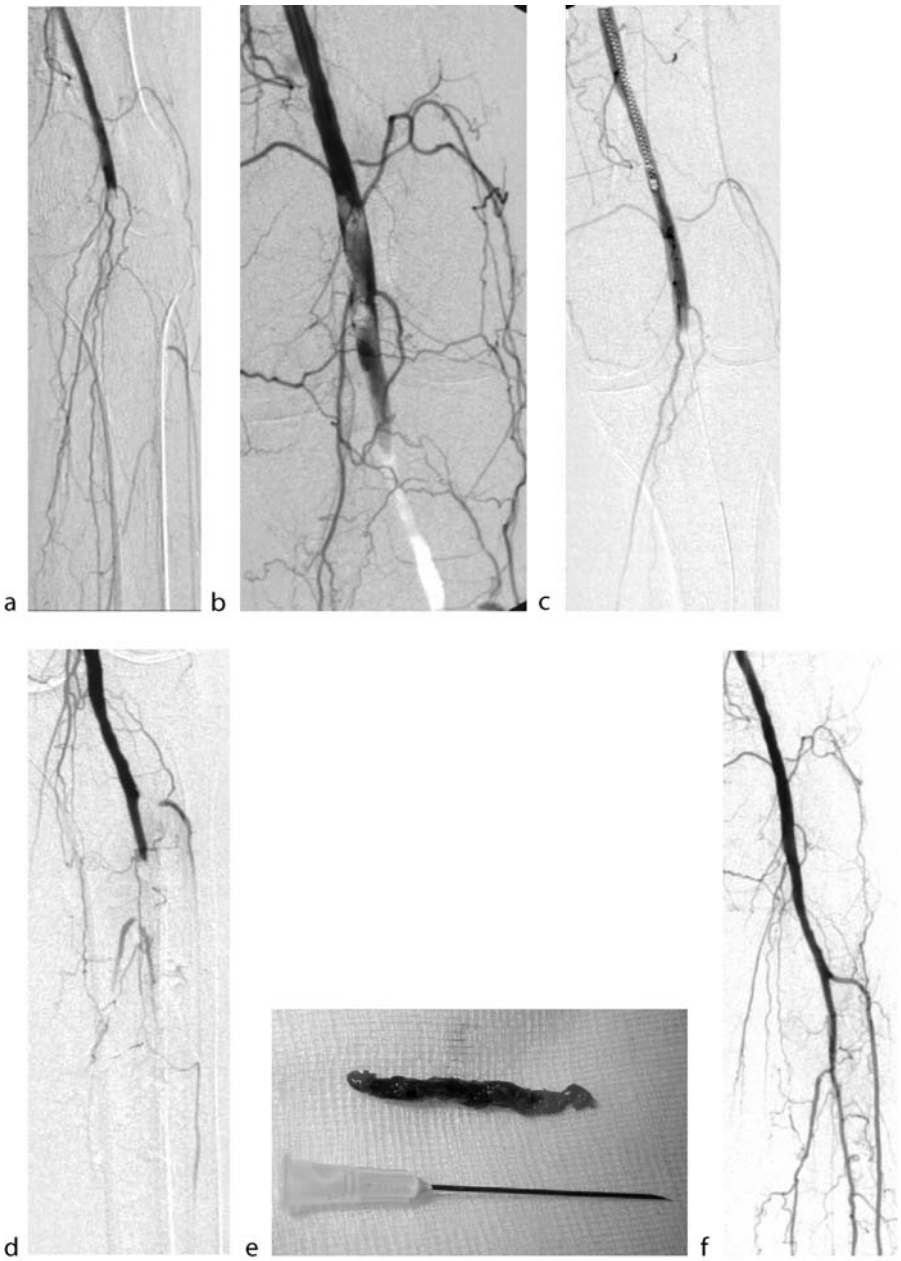

Ischemia, Brachial. Figure 1a–f Acute ischemia of the lower left leg. (a) Acute embolic occlusion of the poplietal artery at the level of the joint. (b) Aspiration fails to clear the popliteal artery but demasks a large thrombus. (c/d) After rotational thrombectomy by a Rotarex catheter, the popliteal lumen has ben reopened but there is still occulsion of the distal popliteal artery and the trifurcation. (e) Aspiration removes a larger clot from the distal popliteal artery. Trifurcation is now reperfused.

time factor is crucial for the success of a surgical approach as well as for percutaneous interventions.

To achieve a successful and enduring result, at least one lower limb artery or a major collateral has to be reopened down to the foot in order to establish a sufficient outflow situation and to avoid early rethrombosis. Follow-up medication is an important part of the treatment concept.

Thrombolysis has some drawbacks that prevent its widespread use in subacute and acute thrombosis and embolic disease. It is relatively time consuming and a rapid revascularization is rare. In particular, in advanced stages a treatment duration of up to 24 h may worsen the clinical situation with an unpredictable outcome. Local bleeding may occur at the entry site, complicating an adjunctive surgical approach – if required. Reduced clotting abilities after thrombolysis also interfere with surgery. Furthermore, the subset of patients with acute ischemia are frequently of older age and their comorbidities often contraindicate the use of thrombolytic agents.

Two different trials – the STILE and TOPAS trials – have advocated thrombolysis to be equivalent to surgery. The TOPAS trial found a limb salvage rate of 72% after 6 months for the urokinase group vs. 75% in the surgical group. The STILE trial found a similar outcome at 30 days for both treatments. Earnshaw et al., however, found that patients with a neurosensory deficit and acute ischemia had a significantly lower limb salvage rate (31%) compared to those treated by surgery (59%) (2). Berridge et al., performing an analysis of randomized data available on thrombolysis vs. surgery in acute ischemia, found no significant difference with regard to limb salvage for up to 1 year and with regard to overall survival, but found a significant increase in stroke rate, major hemorrhage, and distal embolization at 30 days in patients undergoing initial thrombolysis (Berridge).

Fogarty embolectomy *via* a femoral or popliteal approach is a quick method in the case of circumscribed thrombi, but it may become difficult in concomitant atherosclerotic stenoses or extensive thromboses including the lower limb arteries.

In older thrombi, wall adhesion of the occluding clots can complicate removal of clots by use of Fogarty embolectomy balloons and sometimes additional instruments are required.

Instruments for Mechanical Thrombectomy

Mechanical removal of thrombosis *via* a percutaneous approach is an old dream of interventional radiologists who – like surgeons – prefer a quick, elegant, and effective solution to the problem instead of going through lengthy procedures, which thrombolysis certainly can turn out to be. Many different mechanical devices were developed with enthusiasm, introduced into clinical practice, tested as insufficient and have disappeared from the market. The Kensey catheter is an early example of this not-too-small family of disappointed hopes.

In the meantime, however, some valid instruments and techniques are available which allow successful and relatively safe and timely removal of clot material.

They include:

- Manual aspiration
- Hydrodynamic thrombectomy
- Rotational thrombectomy
- Atherectomy
- Stent placement

In addition, a number of other devices or treatment options are under development and evaluation and their number is still growing.

References

1. TASC working group TASC: (2000) Management of peripheral arterial disease. Transatlantic intersociety consensus. Int Angiol 19 (Suppl. 1) 152:161–163
2. Ouriel K, Veith FJ, Sasahara AA (1998) A comparison of recombinant urokinase with vascular surgery as initial treatment for acute arterial occlusion of the legs. Thrombolysis or Peripheral Arterial Surgery (TOPAS) Investigators. N Engl J Med. Apr 16;338 (16): 1105–1111
3. [No authors listed] (1994) Results of a prospective randomized trial evaluating surgery versus thrombolysis for ischemia of the lower extremity. The STILE trial. Ann Surg Sep;220(3):251–266
4. Earnshaw JJ, Gregson RH, Makin GS et al (1989) Acute peripheral arterial ischemia: a prospective evaluation of differential management with surgery or thrombolysis. Ann Vasc Surg. Oct;3(4):374–379
5. Berridge DC, Kessel D, Robertson I (2002) Surgery versus thrombolysis for acute limb ischaemia: initial management. Cochrane Database Syst Rev (3):CD002784. Review
6. Starck EE, McDermott JC, Crummy AB et al (1985) Percutaneous aspiration thromboembolectomy. Radiology Jul;156(1):61–66
7. Sniderman KW, Bodner L, Saddekni S et al (1984) Percutaneous embolectomy by transcatheter aspiration. Work in progress. Radiology Feb;150(2):357–361
8. Wagner HJ, Starck EE, Reuter P (1994) Long-term results of percutaneous aspiration embolectomy. Cardiovasc Intervent Radiol Sep–Oct;17(5):241–246
9. Canova CR, Schneider E, Fischer L et al (2001) Long-term results of percutaneous thrombo-embolectomy in patients with infrainguinal embolic occlusions. Int Angiol Mar;20(1):66–73
10. Henry M, Amor M, Henry I et al (1998) The Hydrolyser thrombectomy catheter: a single-center experience. Endovasc Surg Feb;5(1):24–31
11. Kasirajan K, Gray B, Beavers FP et al (2001) Rheolytic thrombectomy in the management of acute and subacute limb-threatening ischemia. J Vasc Interv Radiol Apr;12(4):413–421
12. Görich J, Rilinger N, Sokiranski R et al (1998) Mechanical thrombolysis of acute occlusion of both the superficial and the deep femoral arteries using a thrombectomy device. AJR Am J Roentgenol May;170(5):1177–1180

13. Hopfner W, Bohndorf K, Vicol C et al (2001) Percutaneous hydromechanical thrombectomy in acute and subacute lower limb ischemia. Rofo Mar;173(3):229–235. German
14. Zeller T, Frank U, Burgelin K et al (2002) Long-term results after recanalization of acute and subacute thrombotic occlusions of the infra-aortic arteries and bypass-grafts using a rotational thrombectomy device. Rofo Fortschr Geb Rontgenstr Neuen Bildgeb Verfahr Dec;174(12):1559–1565
15. Reekers JA (1998) A balloon protection sheath to prevent peripheral embolization during aortoiliac endovascular procedures. Cardiovasc Intervent Radiol Sep–Oct;21(5):431–433

Ischemia, Mesenteric, Acute

Stefan Müller-Hülsbeck
Department of Radiology, University Hospital Schleswig-Holstein, Campus Kiel, Kiel, Germany
muehue@rad.uni-kiel.de

Synonyms

Acute mesenteric arterial embolus (AMAE); Acute mesenteric arterial thrombosis (AMAT); Acute mesenteric infarction; Acute mesenteric ischemia; Acute mesenteric occlusive disease; Acute mesenteric venous thrombosis; Mesenteric vascular occlusion; Nonocclusive mesenteric ischemia (NOMI); Occlusive mesenteric arterial ischemia (OMAI)

Definitions

Acute mesenteric ischemia is the acute interruption of blood flow to the small or large intestine. The word "ischemia" means decrease in oxygen supply. Mesenteric ischemia is a condition in which the mesenteric arteries do not deliver enough blood and oxygen to the small and large intestines. This makes it difficult for the intestines to digest food and can cause segments of the intestine to die. "Occlusion of the mesenteric vessels is apt to be regarded as one of those conditions of which the diagnosis is impossible, the prognosis hopeless, and the treatment almost useless" (1). Antonio Beniviene first described mesenteric ischemia in the fifteenth century. It was studied more intensively in the mid-nineteenth century after case reports by Virchow and others.

Pathology/Histopathology

In practice, acute mesenteric ischemia (AMI) is divided into four different primary clinical entities: (1) acute mesenteric arterial embolus (AMAE), (2) acute mesenteric arterial thrombosis (AMAT), (3) nonocclusive mesenteric ischemia (NOMI), and (4) mesenteric venous thrombosis (MVT). Occlusive mesenteric arterial ischemia (OMAI) includes both AMAE and AMAT.

Typically, the celiac artery trunk (CAT) supplies the foregut, hepatobiliary system, and spleen; the superior mesenteric artery (SMA) supplies the midgut (i.e., small intestine and proximal mid-colon); and the inferior mesenteric artery (IMA) supplies the hindgut (i.e., distal colon and rectum). However, multiple anatomic variants are observed. Venous drainage is through the superior mesenteric vein (SMV), which joins the portal vein.

AMI arises primarily from problems in the SMA circulation or its venous outflow. Collateral circulation from the CA and IMA may allow sufficient perfusion if flow in the SMA is reduced because of occlusion, low-flow state (NOMI), or venous occlusion. The inferior mesenteric artery is seldom the site of lodgment of an embolus. Only small emboli can enter this vessel because of its smaller lumen. When lodgment occurs, the embolus lodges at the site of division of the inferior mesenteric artery into the left colic, sigmoidal, and superior hemorrhoidal arteries. In such instances, collateral flow from the middle colic and middle hemorrhoidal arteries (through the vascular arcades of the inferior mesenteric artery distal to the embolus) may sustain the perfusion of the left colon (2).

Insufficient blood perfusion to the small bowel and colon may result from arterial occlusion by embolus or thrombosis (AMAE or AMAT), thrombosis of the venous system (MVT), or nonocclusive processes such as vasospasm or low cardiac output (NOMI). Embolic phenomena account for approximately 50% of all cases, arterial thrombosis for about 25%, NOMI for roughly 20%, and MVT for less than 10% (3). Hemorrhagic infarction is the common pathologic pathway, whether the occlusion is arterial or venous.

Embolic AMI is usually caused by an embolus of cardiac origin. Typical causes include mural thrombi after myocardial infarction, atrial thrombi associated with mitral stenosis and atrial fibrillation, vegetative endocarditis, mycotic aneurysm, and thrombi formed at the site of atheromatous plaques within the aorta or at the sites of vascular aortic prosthetic grafts interposed between the heart and the origin of the SMA. Most often, emboli lodge about 6–8 cm beyond the SMA origin, at a narrowing near the emergence of the middle colic artery.

Damage to the affected bowel portion may range from reversible ischemia to transmural infarction with necrosis and perforation.

The mucosal barrier becomes disrupted as the ischemia persists, and bacteria, toxins, and vasoactive substances are released into the systemic circulation. This can cause death from septic shock, cardiac failure, or multisystem organ failure before bowel necrosis actually occurs. As hypoxic

damage worsens, the bowel wall becomes edematous and cyanotic. Fluid is released into the peritoneal cavity, explaining the serosanguinous fluid sometimes recovered by diagnostic peritoneal lavage. Bowel necrosis can occur in 8–12 h from the onset of symptoms.

Thrombotic AMI is a late complication of preexisting visceral atherosclerosis. Symptoms do not develop until two of the three arteries (usually the CA and SMA) are stenosed or completely blocked (4, 5).

Clinical Presentation

Symptoms are initially nonspecific, before evidence of peritonitis is found (6–8). Thus, diagnosis and treatment are often delayed until the disease is far advanced; the key to diagnosis lies in a high index of suspicion. Patients with advanced ischemia present with diffuse peritonitis, shock, and severe metabolic derangements. The diagnosis will become obvious at the time of surgery. Often these patients cannot be salvaged; the mortality is reported to be between 70 and 90%. While the prognosis is grave for patients in whom the diagnosis is delayed until bowel infarction has already occurred, patients who receive the appropriate treatment in a timely manner are much more likely to recover. In the early stage of ischemia the patient complains of severe abdominal pain (due to vasospasm) in the absence of peritoneal findings. This scenario has been described by clinicians as "pain out of proportion to the physical findings." Symptoms often found are: severe abdominal pain out of proportion to physical examination findings, pain initially of a visceral nature and poorly localized, nausea, vomiting, diarrhea, gastrointestinal bleeding may be present.

Imaging

A flow-chart for the diagnosis and treatment of patients at risk of AMI is given in Fig. 1(9).

- Plain abdominal films (abnormal in 20–60% of cases)

Findings on plain films of the abdomen are often normal in the presence of AMI. However, plain films are warranted to exclude identifiable causes of abdominal pain such as perforated viscus with free intraperitoneal air. Therefore, all patients should have an upright and supine plain film of the abdomen in order to rule out visceral perforation or bowel obstruction.

Positive findings are usually late and nonspecific (ileus, small bowel obstruction, edematous/thickened bowel walls, and paucity of gas in the intestines). More specific signs, such as pneumatosis intestinalis—i.e., submucosal gas, thumbprinting of bowel wall, and portal vein gas—are late findings.

- Computed tomography scan

Computed tomography (CT) scan helps to evaluate AMI and to exclude other causes of abdominal pain. CT angiography has a sensitivity of 71–96% and a specificity of 92–94% (10). Although still not considered the gold standard compared with classic angiography, CT angiography is noninvasive, readily available, and the preferred modality for MVT (90% sensitivity). Moreover, with recent multidetector CT scanners, accuracy is expected to be much higher, close to 100%.

CT scan may also show pneumatosis intestinalis, portal vein gas, bowel wall, and/or mesenteric edema, abnormal gas patterns, thumbprinting, streaking of mesentery, and solid organ infarction. Bowel wall edema is the most common finding on CT scan. Arterial occlusion may show nonenhancement of the vessels (Fig. 2). MVT usually shows a thrombus in the SMV or portal vein. Finally, intraluminal thrombus in involved vessel is well detected (11).

- Angiography

This was the gold standard for diagnosis and presurgical planning and is often an important part of treatment. To promptly diagnose patients with true AMI, a low threshold for obtaining early angiographs should be adopted for patients at risk. Sensitivity is reported to be 88% for AMI. Nowadays, multidetector CT is equal or even more adequate in presenting vascular anatomy and surrounding tissue, such as in the bowel.

- Ultrasonography

Duplex sonography studies are highly specific (92–100%) but not as sensitive (70–89%) as angiography (12). The examination cannot detect clots beyond the proximal main vessels nor can it be used to diagnose NOMI. Ultrasound is considered a second-line study for AMI. It is often less useful in the presence of dilated fluid-filled loops of bowel.

Some studies show that the usefulness of duplex scanning is similar to that of CT scanning if it is performed for MVT. It may show a thrombus or absent flow in the involved arteries or veins. Other possible findings include portal vein gas, biliary disease, free peritoneal fluid, thickened bowel wall, and intramural gas.

- Magnetic resonance imaging/magnetic resonance angiography

Magnetic resonance imaging (MRI) and magnetic resonance angiography (MRA) provide findings similar to CT scan in AMI. Sensitivity of MRA is 100% and specificity is 91%. MRA is particularly effective for evaluating MVT; however, in emergency situations MR should not be the first choice.

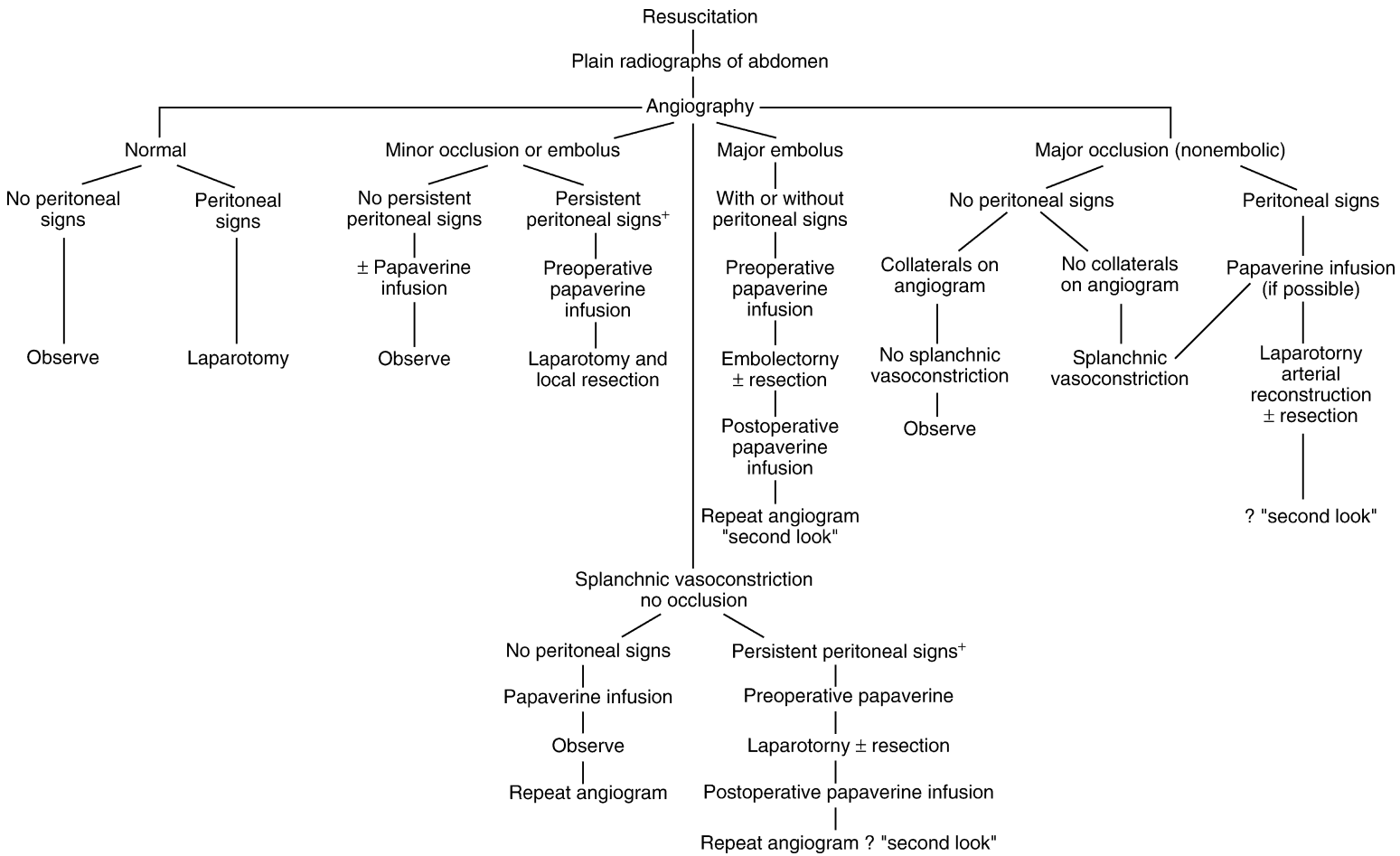

Ischemia, Mesenteric, Acute. Figure 1 A flow-chart for the diagnosis and treatment of patients at risk of AMI (modified from Oldenburg WA, Lau LL, Rodenberg TJ et al (2004) Acute mesenteric ischemia—A clinical review. Arch Int Med 164:1054–1062.

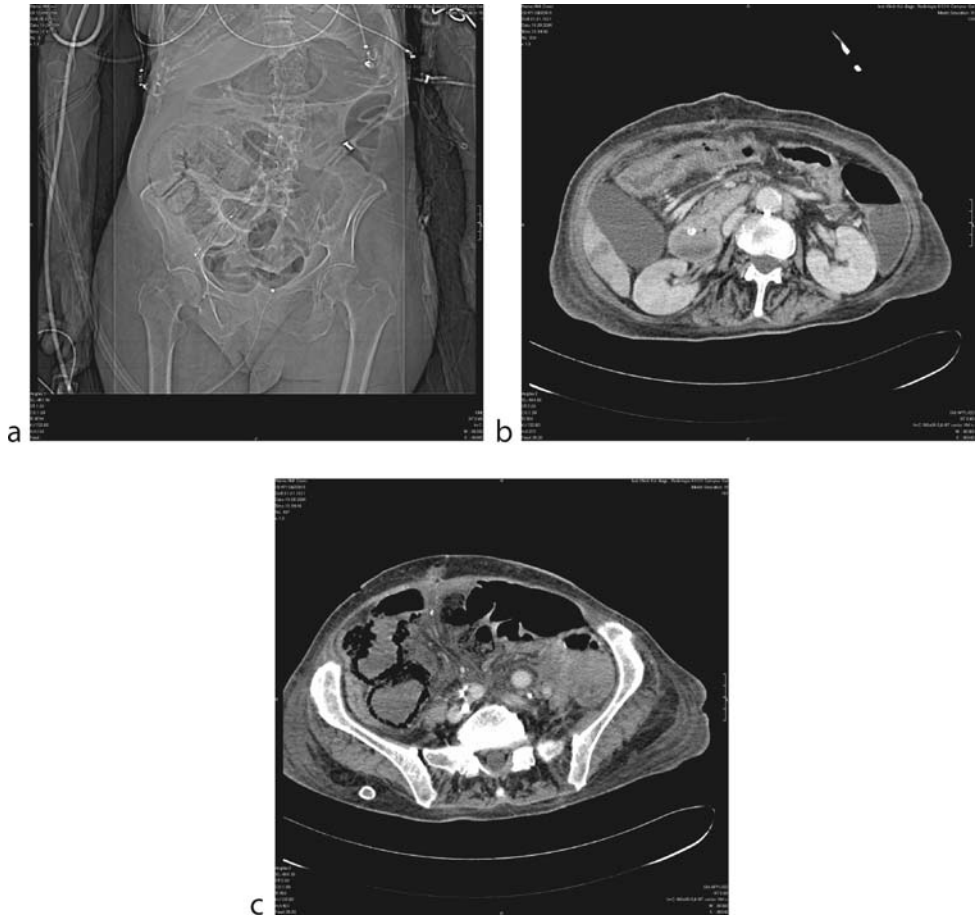

Ischemia, Mesenteric, Acute. Figure 2 CT scan of a patient suffering from AMI. Celiac trunk is severely stenosed and SMA is partially occluded by calcified plaque material. On CT scout view, pneumatosis intestinalis is visible (a). The bowel is edematous and thickened (b), clear signs of pneumatosis intestinalis are often seen in advanced acute mesenteric ischemia (AMI) with gangrenous bowel proven by surgery (c).

Nuclear Medicine

It is not of importance for the diagnosis of AMI.

Diagnosis

Clinical sequelae in combination with typical imaging findings make the diagnosis clear.

Interventional Radiological Treatment

- Angiographically infused papaverine (Vasodilator therapy)

Catheter-directed papaverine infusion in the affected vessel following angiography is useful for all arterial forms of AMI. It relieves reactive vasospasm in occluded arterial vessels and is the only treatment for NOMI other than resection of gangrenous bowel.

After angiography, an infusion of 30 mg/h should be started, and the dose should be adjusted up to 60 mg/h for a clinical response. This is continued for at least 24 h for a maximum of 5 days. If the catheter slips into the aorta, significant hypotension can occur (13). Papaverine is incompatible with heparin (crystallization)

- Angiographically infused thrombolytics

Thrombolytics infused through the angiogram catheter can be a life-saving therapy for selected patients with embolic AMI (14).

Bleeding is the main complication. Thrombolytic administration is risky and should only be undertaken if peritonitis or other signs of bowel necrosis are absent. It must be started within 8 h of symptom onset. If symptoms do not improve within 4 h or if peritonitis develops, the

perfusion should be stopped and surgery should be performed.

- Angioplasty after thrombolysis

A very select group of patients who have atherosclerotic plaques at the origin of the SMA after thrombolysis are eligible for angioplasty. Angioplasty can be technically difficult because of the anatomy of the SMA. The use of low-profile Monorail devices (0.014 or 0.0018 in. compatible) might enhance technical success rates. Restenosis rates are 20–50% (15).

- Heparin for MVT

Heparin anticoagulation is the main treatment for MVT. If no signs of bowel necrosis exist, the patient may not even need an operation. Heparin may increase the chance of bleeding complications. An avenue of study for possible future clinical trials may be the use of enoxaparin (Lovenox) or other low-molecular-weight heparins as a potential substitute for heparin in the treatment of MVT.

Heparin should be administered as a bolus of 80 U/kg, not to exceed 5,000 U, and then as an infusion at 18 U/kg/h until full conversion to oral warfarin. Appropriate monitoring of anticoagulation using activated partial thromboplastin time (aPTT) is mandatory.

Surgery

Thrombectomy/embolectomy, arterial bypass, and resection of necrotic bowel are typical procedures (16–18).

- Complications: Sepsis/septic shock, multiple system organ failure, death
- Mortality: 70–90% overall; from arterial embolism: 60–80%, from arterial thrombosis: 70–100%, from nonocclusive mesenteric ischemia: 40%, from mesenteric venous thrombosis: 25–30%

Bibliography

1. Cokkinis AJ (1961) Intestinal ischaemia. Proc R Soc Lond B Biol Sci 54:354–356
2. Rosenblum JD, Boyle CM, Schwartz LB (1997) The mesenteric circulation. Anatomy and physiology. Surg Clin North Am 77:289–306
3. Bassiouny HS (1997) Nonocclusive mesenteric ischemia. Surg Clin North Am 77:319–326
4. Cognet F, Ben Salem D, Dranssart M et al (2002) Chronic mesenteric ischemia: imaging and percutaneous treatment. Radiographics 22:863–879
5. AbuRahma AF, Stone PA, Bates MC et al (2003) Angioplasty/stenting of the superior mesenteric artery and celiac trunk: early and late outcomes. J Endovasc Ther 10:1046–1053
6. Fink S, Chaudhuri TK, Davis HH (2000) Acute mesenteric ischemia and malpractice claims. South Med J 93:210–214
7. Boley SJ, Brandt LJ, Sammartano RJ (1997) History of mesenteric ischemia. The evolution of a diagnosis and management. Surg Clin North Am 77:275–288
8. Mansour MA (1999) Management of acute mesenteric ischemia. Arch Surg 134328–330; discussion 331
9. Oldenburg WA, Lau LL, Rodenberg TJ et al (2004) Acute mesenteric ischemia—A clinical review. Arch Int Med 164:1054–1062
10. Kirkpatrick ID, Kroeker MA, Greenberg HM et al (2003t), Biphasic CT with mesenteric CT angiography in the evaluation of acute mesenteric ischemia: initial experience. Radiology 229: 91–98
11. Kumar S, Sarr MG, Kamath PS (2001) Mesenteric venous thrombosis. N Engl J Med 345:1683–1688
12. Nicoloff AD, Williamson WK, Moneta GL et al (1997) Duplex ultrasonography in evaluation of splanchnic artery stenosis. Surg Clin North Am 77:339–355
13. Kozuch PL, Brandt LJ (2005) Review article: diagnosis and management of mesenteric ischaemia with an emphasis on pharmacotherapy. Aliment Pharmacol Ther 21:201–215
14. Yamaguchi T, Saeki M, Iwasaki Y et al (1999) Local thrombolytic therapy for superior mesenteric artery embolism: complications and long-term clinical follow-up. Radiat Med 17:27–33
15. Mohammed A, Teo NB, Pickford IR (2000) Percutaneous transluminal angioplasty and stenting of coeliac artery stenosis in the treatment of mesenteric angina: a case report and review of therapeutic options. J R Coll Surg Edinb 45:403–407
16. Hansen KJ, Deitch JS (1997) Transaortic mesenteric endarterectomy. Surg Clin North Am 77:397–407
17. Hladak P, Raupach J, Lojak M et al (2005) Treatment of acute mesenteric thrombosis/ischemia by transcatheter thromboaspiration. Surgery 137:122–123
18. Klempnauer J, Grothues F, Bektas H (1997) Long-term results after surgery for acute mesenteric ischemia. Surgery 121:239–243

Ischemia, Mesenteric, Chronic

Stefan Müller-Hülsbeck
Department of Radiology, University Hospital Schleswig-Holstein, Kiel, Germany
muehue@rad.uni-kiel.de

Definitions

Chronic mesenteric ischemia (CMI), first described as "abdominal angina" by Councilman in 1894 (1), Goodman in 1918 (2) and as entity by Dunphy in 1936 (3), is a rare disorder that is often diagnosed late. CMI is a condition caused by narrowing of the arteries to the intestines. There are three main arteries to the intestines and, in general, two of them must be narrowed to cause symptoms.

Pathology/Histopathology

Because of the extensive collateral arterial network of the gut, chronic mesenteric ischemia is relatively uncommon. The incidence of CMI is estimated to be at 1 in 100,000 (4), although autopsy studies of an unselected population demonstrated mesenteric atherosclerosis in 35% to 70% of the cases (5). It is usually related to extensive mesenteric atherosclerosis. In more than 95% of patients, the

cause of mesenteric ischemia is diffuse atherosclerotic disease, which decreases the flow of blood to the bowel. Symptoms of CMI arise when transient episodes of inadequate, usually postprandial blood flow in the mesenteric arteries are not able to assuage the physiological demand in the intestines. Stenoses in visceral arteries commonly are caused by atheroma, mainly in the proximal segments of the vessels. Fatty infiltration in the arterial wall results in stenosis or finally occlusion of one or more visceral arteries. As the atherosclerotic disease progresses, symptoms worsen. The number of involved arteries before symptoms occur is still debated. So, at least two vessels of the celiac trunk, the superior mesenteric artery and the inferior mesenteric artery, should be stenosed or occluded for the diagnosis of CMI with abdominal angina (6, 7). The presence of a stenosis in a single visceral vessel collateral flow may allow patients to be asymptomatic. Usually, all three major mesenteric arteries are occluded or narrowed.

The pathophysiologic mechanism by which ischemia produces pain is still not completely understood.

Chronic mesenteric ischemia is a rare diagnosis. No reports of the actual incidence have been published. Moawad searched 20 years of literature and found only 330 cases. Because many cases are not reported, the true prevalence could be much higher. Autopsy studies support this theory, with findings of stenosis in up to 30% of selected patients with a history of abdominal pain.

Clinical Presentation

Patients classically present with chronic postprandial pain, nausea, diarrhea and obvious weight loss, which often results in "food fear" in patients. CMI is caused by intermitting transient episodes of inadequate intestinal blood supply, usually concurring with the increased metabolic demand at digestion (7). As no sensitive and specific tests are available to diagnose CMI, accurate acquisition of medical history and exclusion of other conditioning gastrointestinal causes are essential (8). Patients with the diagnose of CMI are usually over 60-year-old. However, most patients do not present with "classic" symptomatology and are frequently misdiagnosed for other diseases. In some patients, if untreated, the narrowing in the arteries leads to clotting causing severe abdominal pain and death.

Imaging

- Ultrasound

Ultrasonography (US) uses sound waves to generate images of internal organs on a monitor. A special ultrasound (Doppler) of the celiac, superior mesenteric and inferior mesenteric arteries can help your doctor determine if there is decreased blood flow, which indicates a likelihood of chronic mesenteric ischemia.

Mesenteric duplex ultrasonography is a non-invasive method of analyzing flow through the vessels. Unfortunately, intraperitoneal gas, respiratory movements, obesity and any previous abdominal surgeries limit results.

Besides duplex sonography as an accurate non-invasive technique of detecting significant stenoses in mesenteric vessels (9), computed tomography angiography and magnetic resonance angiography have been established for pretreatment evaluation of the celiac artery and superior mesenteric artery. With duplex sonography as the easiest to perform screening and follow-up tool, intraarterial digital subtraction angiography (DSA) remains the most precise technique for the evaluation of the degree of the stenosis.

Based on currently available literature, MRI and computerized tomography (CT) should be performed as second step for diagnostic imaging; if anything remains open, DSA should be performed in order to start interventional treatment during the same session.

We currently perform multi-detector CT with 3D reformatting in all patients with suspected acute or chronic mesenteric ischemia. In our experience, CT has eliminated the need for additional imaging studies such as Doppler US or diagnostic angiography. However, further investigation is necessary to determine the scope of utility of multi-detector row CT in this clinical setting (10).

Nuclear Medicine

Not of importance for the diagnosis of AMI.

Diagnosis

Clinical sequelae in combination with typical imaging findings makes the diagnosis clearer.

Interventional Radiological Treatment

Until the 1990s, open surgery was considered the treatment of choice; percutaneous transluminal angioplasty (PTA) was reserved for patients for whom surgery carried a high risk. Many surgical procedures have been described with various results. The blockage in the involved arteries is removed, and the arteries reconnected to the aorta. Alternatively, a bypass around the blockage, usually with a prosthetic plastic tube graft, is performed. Endarterectomy and aortovisceral bypass have been employed. Until today, surgical revascularisation has been the method

of choice for treatment of patients with CMI (7). Surgical procedures such as endarterectomy and aortoceliac and aortomesenteric bypass grafting are associated with relatively high peri-operative major complications (15–33%) and mortality (0–17%) (11–13). Thus, there has been a demand for a less invasive technique. As an alternative method, PTA and stenting was established in the early 1980s. However, only few studies have been performed since then to prove the safety and durability of percutaneous angioplasty and stenting with results for periprocedural major complications of up to 25% and mortality of up to 13%, most of them with inhomogeneous collectives of both PTA and stenting in one study (6, 11–19).

More recently, balloon angioplasty has appeared to provide good results with a less invasive approach. In order to obtain good long-term results with acceptable recurrence rate, we gather minimal invasive PTA, and stent procedures should only be performed by experienced physicians.

Therefore, we recommend after diagnosing CMI to plan interdisciplinarily (gastroenterologist, surgeon and interventionalist/radiologist) the optimal therapeutic approach towards the management of the stenosed arteries for each affected individual. However, there are no definite recommendations for the planning of the right procedure, since only descriptive studies, blind experience and case reports and no type I data (i.e., randomized trials) or type II data (i.e., nonrandomized controlled trials) have been available so far (7, 12). In general, open vascular surgery was the method of choice for patients with CMI, whereas

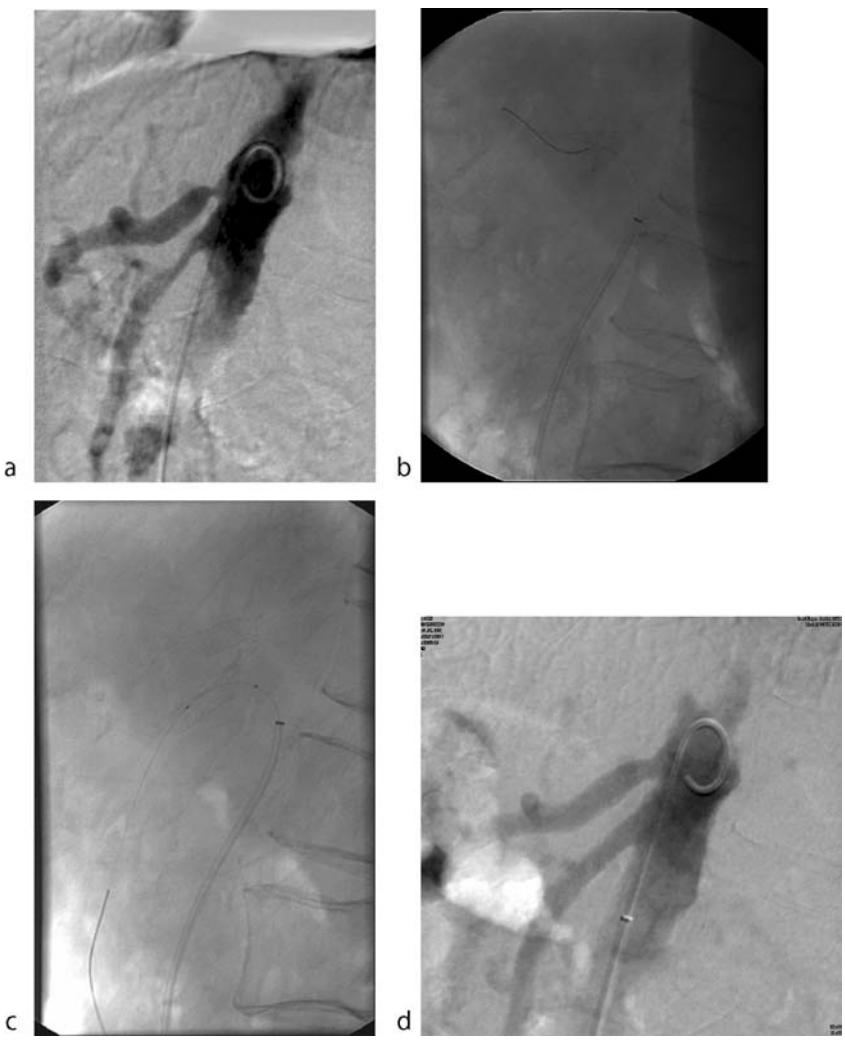

Ischemia, Mesenteric, Chronic. Figure 1 (a) DSA presenting a severe stenosis involving the origin of the celiac artery and the superior mesenteric artery. (b) In order to treat symptoms of CMI in the 62-year-old patient stent placement was performed in the celiac artery (6 × 18 mm) and the superior mesenteric artery (5 × 18 mm) during the same approach, so-called rapid-exchange/monorail devices were used. (c) The fluoroscopic view shows unfolded stents in a proper position. (d) The final angiography reveals patent arteries, with a remaining light luminal narrowing of the celiac artery.

endovascular therapy with or without stent implacement was reserved for patients with multi-morbidity and at high operative risk. For surgical revascularization, excellent long-term patency ranges from 70 to 93% (mean 84%), but an overall perioperative morbidity rate of 29% and mortality rate of 7% gives rise to concern (12, 18). Endovascular therapy with a mean primary patency rate of 76%, at 15 months, a peri-inervent ional complication rate close to 0%, an initial technical success rate of 96% and a mean mortality rate of 4% seems to be effective as well (20; Fig. 1). Despite visceral PTA being a safe and effective alternative to open surgery, it still seems to offer inferior patency and durability rates (15). However, due to the absence of comparative trials of open revascularization versus endovascular therapy and due to different evaluation criteria with a tendency of referring multimorbid patients to endovascular therapy, it is undoubtedly problematic to easily compare those numbers.

It has to be ruled out that in case of median arcuate ligament syndrome, it should be treated in symptomatic cases by surgery (21). It is discussed that it arises from celiac plexus compression and consequently is not an indication for PTA or stent placement (12, 18, 19).

Unfortunately, there is no specific diagnostic test for CMI. A high index of suspicion should be maintained in patients with post-prandial pain and weight loss. If imaging presents in these patients focal stenoses, the very promising and safe technique of PTA and stent placement should be performed immediately as the initial treatment for patients with CMI.

References

1. Councilman WT (1884) Three cases of occlusion of the superior mesenteric artery. Boston Med Surg J 130:410–411
2. Goodman GH (1918) Angina abdominis. Am J Med Sci 155:524–528
3. Dunphy JF (1936) Abdominal pain of vascular origin. Am J Med Sci 192:109–112
4. van Wanroij JL, van Petersen AS, Huisman AB et al (2004) Endovascular treatment of chronic splanchnic syndrome. Eur J Vasc Endovasc Surg 28:193–200
5. Taylor LM Jr, Moneta GL (1991) Intestinal ischemia. Ann Vasc Surg 5:403–406
6. Cognet F, Ben Salem D, Dranssart M et al (2002) Chronic mesenteric ischemia: imaging and percutaneous treatment. Radiographics 22:863–879
7. Abu Rahma AF, Stone PA, Bates MC et al (2003) Angioplasty/stenting of the superior mesenteric artery and celiac trunk: early and late outcomes. J Endovasc Ther 10:1046–1053
8. Brandt LJ, Boley SJ (2000) AGA technical review on intestinal ischemia. American Gastrointestinal Association. Gastroenterology 118:954–968
9. McShane MD, Proctor A, Spencer P et al (1992) Mesenteric angioplasty for chronic intestinal ischaemia. Eur J Vasc Surg 6:333–336
10. Horton KM, Fishman EK (2001) Multi-detector row CT of mesenteric ischemia: can it be done? Radiographics 21:1463–1473
11. Moneta GL, Lee RW, Yeager RA et al (1993) Mesenteric duplex scanning: a blinded prospective study. J Vasc Surg 17:79–84
12. Allen RC, Martin GH, Rees CR et al (1996) Mesenteric angioplasty in the treatment of chronic intestinal ischemia. J Vasc Surg 24:415–421
13. Kasirajan K, O'Hara PJ, Gray BH et al (2001) Chronic mesenteric ischemia: open surgery versus percutaneous angioplasty and stenting. J Vasc Surg 33:63–71
14. Rose SC, Quigley TM, Raker EJ (1995) Revascularization for chronic mesenteric ischemia: comparison of operative arterial bypass grafting and percutaneous transluminal angioplasty. J Vasc Interv Radiol 6:339–349
15. Maspes F, Mazzetti di Pietralata G, Gandini R et al (1998) Percutaneous transluminal angioplasty in the treatment of chronic mesenteric ischemia: results and 3 years of follow-up in 23 patients. Abdom Imaging 23:358–363
16. Sheeran SR, Murphy TP, Khwaja A et al (1999) Stent placement for treatment of mesenteric artery stenoses or occlusions. J Vasc Interv Radiol 10:861–867
17. Hallisey MJ, Deschaine J, Illescas FF et al (1995) Angioplasty for the treatment of visceral ischemia. J Vasc Interv Radiol 6:785–791
18. Matsumoto AH, Tegtmeyer CJ, Fitzcharles EK et al (1995) Percutaneous transluminal angioplasty of visceral arterial stenoses: results and long-term clinical follow-up. J Vasc Interv Radiol 6:165–174
19. Nyman U, Ivancev K, Lindh M et al (1998) Endovascular treatment of chronic mesenteric ischemia: report of five cases. Cardiovasc Intervent Radiol 21:305–313
20. Schaefer PJ, Schaefer FK, Hinrichsen H, Jahnke T, Charalambous N, Heller m, Muller-Huelsbeck S. Stent placement with the monorail techinque for treatment of mesenteric artery stenosis. J Vasc Interv Radiol. 2006 Apr; 17(4); 637–643
21. Reuter SR, Bernstein EF (1973) The anatomic basis for respiratory variation in median arcuate ligament compression of the celiac artery. Surgery. 73:381–385

Ischemic Heart Disease, CT

Gabriel P Krestin, Filippo Cademartiri, Ludovico La Grutta, Alessandro Palumbo, Giuseppe Runza, Patrizia Malagutti, Francesca Pugliese, W Bob Meijboom, Nico R Mollet, Pim J de Feyter
Department of Radiology, Erasmus Medical Center, Rotterdam, The Netherlands
filippocademartiri@hotmail.com

Short Description

Ischemic heart disease (IHD) remains the leading cause of death in the Western world, and early detection of disease allows optimal therapeutic management. Consequently, substantial effort has been invested to develop techniques that can detect coronary artery disease (CAD).

Noninvasive coronary artery imaging challenges any diagnostic modality because the coronary arteries are small and tortuous, and they course in multiple

planes around the heart, while cardiac contraction and respiration cause motion artifacts. Therefore, noninvasive coronary imaging requires high spatial and temporal resolution. In addition, anatomic coverage should be fast to allow scanning within one breath-hold. One of the most recent noninvasive coronary imaging modalities is multislice spiral computed tomography (CT) or multidetector row helical CT. The literature on four-slice CT and 16-slice CT as applied to the imaging of coronary arteries shows a progressive improvement in detecting coronary stenosis (1). The results of 64-slice-generation scanners show further improvement in diagnostic performance (2). CT of the coronary arteries promises to be the diagnostic modality in the clinical field for assessing the coronary lumen and wall. Preliminary experiences also show potential in assessing left ventricular function, volumes, and delayed-enhancement viability (3, 4).

Characteristics

CT Criteria for Eligibility

Coronary CT angiography (CTA) can be performed with reliable results in a selected patient population with sinus rhythm, heart rate below 70 bpm, and the ability to hold their breath for 20 s (16-slice CT technology) or for less than 12 s (64-slice CT technology). Patients with contraindications to intravenous iodinated contrast material should be excluded or treated accordingly. A high-calcium burden impairs the diagnostic accuracy and, in particular, reduces specificity, but sensitivity generally remains preserved.

CT Technology

Coronary CTA requires retrospective electrocardiographic gating of the image reconstruction. This allows a flexible approach to image reconstruction in virtually any phase of the cardiac cycle. Optimization of the reconstruction windows allows the generation of datasets with the least residual motion artifacts.

A high-temporal resolution of the CT scanner has been achieved by combining a fast gantry rotation speed (down to 330 ms for 64-slice CT) that provides a temporal resolution of half the rotation time (i.e., down to 165 ms for 64-slice CT). For angiographic contrast enhancement, a bolus of 80–100 mL contrast material with high-iodine concentration should be administered through an antecubital vein with a flow rate of 4–5 mL/s. The use of a saline bolus chaser administered after the main bolus of contrast material improves the vascular attenuation and allows a reduction in contrast volume.

The heart rate should be reduced below 70 bpm in order to preserve a diagnostic image quality. For this purpose, β-blockers can be administered before the scan (for instance, 100 mg of metoprolol 1 h in advance).

Routine reconstruction should be performed in the end-diastolic and end-systolic phases. Images should be reconstructed with thin slices and 50% overlap between the slices.

The reconstructed contiguous axial slices are stacked in a volume to generate a three-dimensional dataset from which any paraxial, coronal, sagittal, or oblique plane can be created. Other display modalities are useful for performing the evaluation, such as multiplanar reconstruction (MPR) or curved MPR, thin-slab maximum intensity projections (MIPs), and or volume rendering (VR).

Diagnostic Performance of Coronary CT Angiography

Initial results with four-slice CT were promising, and high sensitivity and specificity to detect IHD were reported. However, 20–30% of coronary segments had to be excluded from analysis due to nondiagnostic quality. Substantial improvement was achieved by the introduction of 16-slice scanners with submillimeter collimation as well as faster rotation times. Pooled analysis of available data (11 studies, 681 patients) has demonstrated a sensitivity of 88% with a specificity of 96%, with a concomitant increase in the number of assessable segments (5). For both, four-slice and 16-slice studies, vessel diameter thresholds for assessment were adopted (i.e., vessels of 1.5–2 mm or more).

Recently the diagnostic performance of the latest 64-slice CT scanner, with increased temporal (165 ms) and spatial (0.4 mm^3) resolution, was evaluated (2). Sensitivity and specificity for assessment of significant stenoses were 99 and 95%, respectively, with no exclusion of segments and with no threshold in vessel size for image evaluation (2).

Clinical Applications

Given the current literature and evidence, there are few clinical applications for coronary CTA. What can be said is based on speculation referring to validation series. The most important feature of coronary CTA is the high-negative predictive value, which indicates a reliable capability of ruling out the presence of significant IHD. Accordingly, CT should be used as a first-line imaging technique to exclude the presence or recurrence of IHD in eligible patients (Fig. 1).

The applications that appear to be feasible, based on current validation literature, are evaluation of patients with a low-pretest likelihood of the presence of a significant coronary stenosis (Figs. 2 and 3), evaluation of patients with recurrent angina, follow-up of proximal

coronary stents (Fig. 4), follow-up of patients with previous coronary artery bypass graft (CABG; Fig. 5), and evaluation of coronary artery anomalies.

Coronary CTA can exclude the presence of significant coronary stenosis in patients with low-intermediate pretest probability because of the high-negative predictive value, and it may be properly used after an inconclusive stress test or in patients with atypical chest pain.

The high density of stent struts limits the reliability of in-stent lumens. However, preliminary data indicate that 16- and 64-slice CT scanners can detect in-stent restenosis. The presence of stent occlusion or in-stent restenosis may be assessed in proximal segments.

The assessment of CABG is reported as being reliable with CT. However, the presence of metallic surgical clips around arterial grafts, extensive atherosclerosis, and previous stenting of native coronary arteries are some of the limitations that have been encountered.

Coronary CTA can show coronary anomalies because of its three-dimensional and volumetric capabilities.

The introduction in clinical practice of 64-slice CT, and most probably the next generation of CT scanners with multiple tube-detector units, will allow the triage of acute chest pain. CT is the noninvasive gold standard for diagnosing pulmonary embolism and aortic dissection. The possibility to include the assessment of coronary arteries in a thoracic scan will provide a totally new approach in assessing acute chest pain.

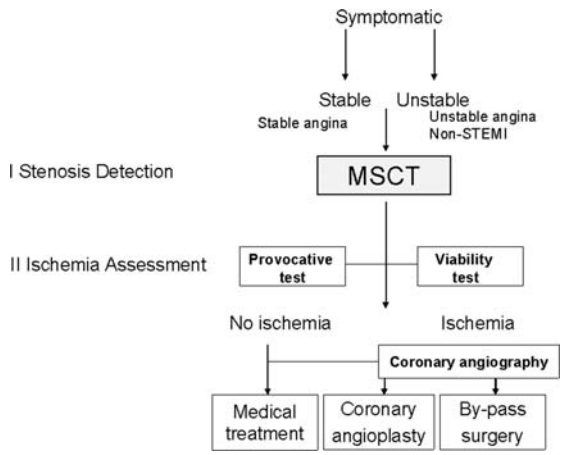

Ischemic Heart Disease, CT. Figure 1 Proposed diagnostic algorithm of suspected coronary ischemia. The first-line imaging modality could be computed tomography, providing two important pieces of information: detection of any atherosclerotic involvement of coronary arteries, and stratification of patients based on the presence of significant stenosis (>50% lumen reduction). The second stage would be evaluation of patients for stress ischemia. Provocative performance is likely to improve when patients are referred after tests that ensure the presence of significant coronary atherosclerosis. In the final stage, morphology and functional information are covered, and a decision for the need for conventional/interventional coronary angiography can be made.

Plaque Imaging with CT

The newer information available since the introduction of coronary CTA is coronary artery wall evaluation. CT can show the presence of plaques and their tissue features (i.e., predominantly calcified, mixed, or predominantly noncalcified). Regarding noncalcified plaque components, it has been suggested that the attenuation measured could indicate the predominant composition as fibrous or lipid.

Other important information that can be derived from CT is the extent of vessel wall remodeling. This information is of great value because the risk of acute coronary syndromes caused by plaque disruption and

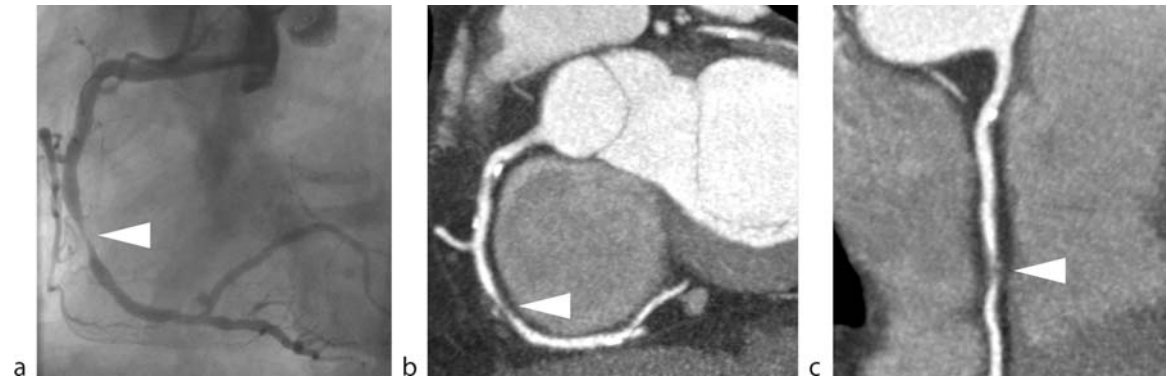

Ischemic Heart Disease, CT. Figure 2 Diagnosis of a patient with stable angina. Conventional coronary angiography displays a significant stenosis (*arrowhead*) in the distal right coronary artery (a). The 64-slice computed tomography maximum intensity projections depict the same lesion (*arrowhead*) in an angiography-like way (b, c).

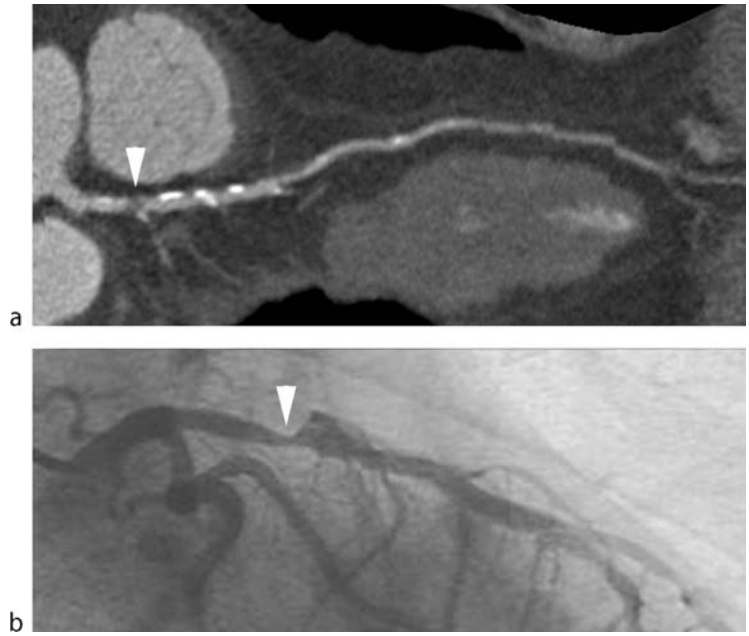

Ischemic Heart Disease, CT. Figure 3 Diagnosis of patient with atypical chest pain. Significant coronary artery stenosis (*arrowhead*) is detected by 64-slice computed tomography (a) and confirmed by conventional coronary angiography (b).

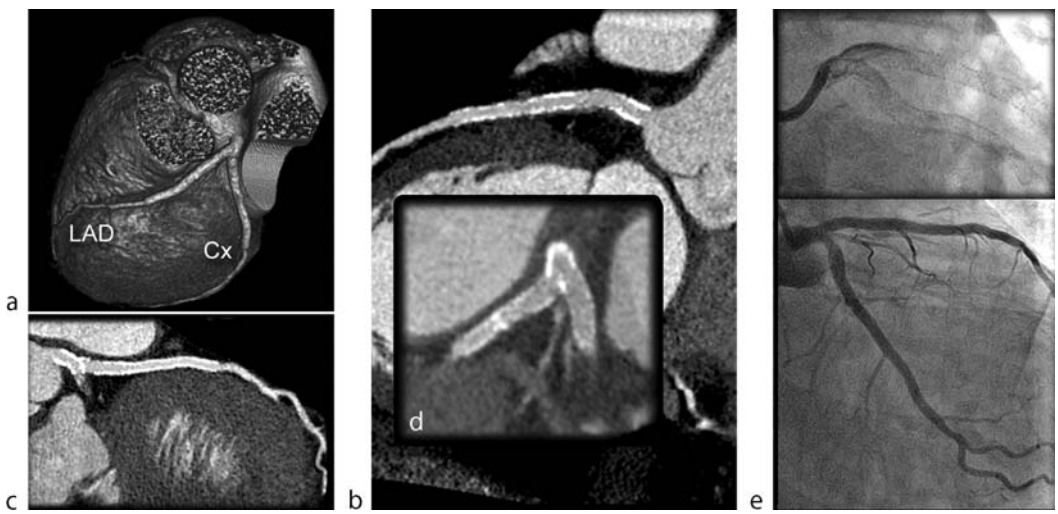

Ischemic Heart Disease, CT. Figure 4 Follow-up of bifurcation stenting of the left main coronary artery using 64-slice computed tomography angiography. The volume-rendered image (a) shows the anatomical configuration of the left coronary artery and the stents. The curved multiplanar reconstructions along the vessels show the lumen in one single plane (b, c). A dedicated plane can be used to display the bifurcation of the stent, which is the main site of restenosis (d). The stent is patent in the proximal region (left main) and in the two main branches (left anterior descending [LAD] and circumflex [Cx]) as confirmed by the conventional coronary angiogram (e).

thrombosis depends on plaque composition (i.e., non-calcified, predominantly lipid plaques with positive remodeling) rather than on stenosis severity. For this reason, reliable noninvasive assessment of plaque constitution could be important in risk stratification of patients with IHD.

Limitations

CT has several limitations in terms of spatial and temporal resolution and contrast-to-noise ratio, which are the reasons for the tight selection of patients for its clinical application. Coronary calcifications limit the

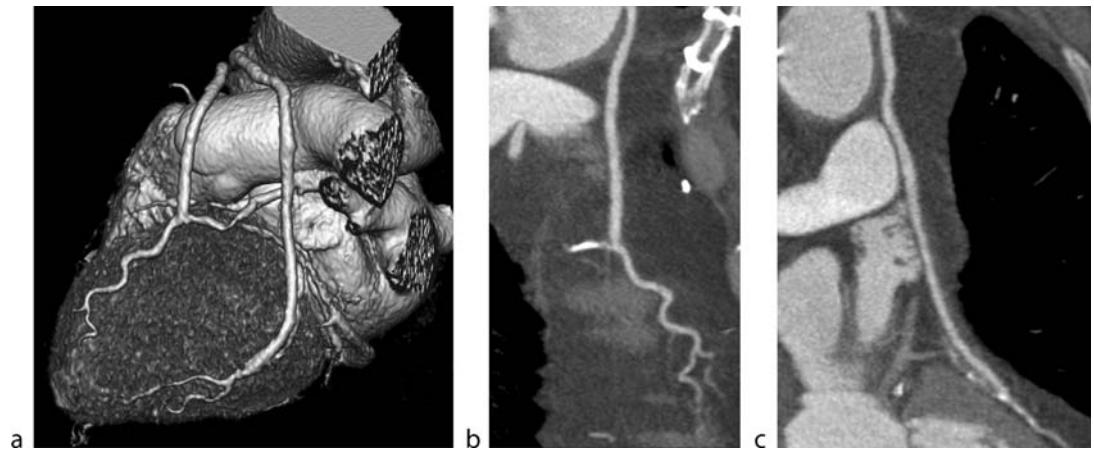

Ischemic Heart Disease, MRI. Figure 5 Follow-up of a coronary artery bypass graft using 64-slice computed tomography angiography. The volume-rendered image displays two venous bypass grafts (a). The first graft runs from the aorta to the first diagonal branch; the second graft runs from the aorta to the second marginal branch. The maximum intensity projections show that both grafts are patent (b, c).

reliability of the assessment of stenosis. Nonsinus heart rhythm, such as atrial fibrillation, prevents diagnostic coronary CTA. Heart rates >70 bpm result in progressively poorer image quality, and a drop out of assessable segments limits the diagnostic accuracy.

Coronary CTA is also a technique that requires highly specific and long training. For this reason it remains a severely operator-dependent modality.

The main concern, though, remains the radiation exposure associated with CT. The effective x-ray doses of 64-slice coronary CTA are reported to be 15.2 mSv and 21.4 m Sv for men and women, respectively, without prospective tube current modulation. This is to allow end-systolic reconstruction for diagnostic purposes. The application of prospective tube current modulation algorithms may reduce the x-ray dose down to 50% of the nominal one, depending on the heart rate.

Conclusion

Coronary CTA is at present the only clinical noninvasive modality for assessing the coronary arteries. The field of application is still restricted by technical limitations and the lack of large clinical trials. This information will become available soon as new generation scanners progressively extend the spectrum of indications.

References

1. Mollet NR, Cademartiri F, Krestin GP et al (2005) Improved diagnostic accuracy with 16-row multi-slice computed tomography coronary angiography. J Am Coll Cardiol 45:128–132
2. Mollet NR, Cademartiri F, van Mieghem CA et al (2005) High-resolution spiral computed tomography coronary angiography in patients referred for diagnostic conventional coronary angiography. Circulation 112:2318–2323
3. Salm LP, Schuijf JD, de Roos A et al (2005) Global and regional left ventricular function assessment with 16-detector row CT: Comparison with echocardiography and cardiovascular magnetic resonance. Eur J Echocardiogr 2006 Aug; 7(4): 308–314
4. Mahnken AH, Koos R, Katoh M et al (2005) Assessment of myocardial viability in reperfused acute myocardial infarction using 16-slice computed tomography in comparison to magnetic resonance imaging. J Am Coll Cardiol 45:2042–2047
5. Schuijf JD, Bax JJ, Shaw LJ et al (2005) Meta-analysis of comparative diagnostic performance of magnetic resonance imaging and multislice computed tomography for noninvasive coronary angiography. Am Heart J 2006 Feb; 151(2): 404–411

Ischemic Heart Disease, MRI

Jörg Barkhausen
Department of Diagnostic and Interventional Radiology and Neuroradiology, University Hospital Essen, Essen, Germany
joerg.barkhausen@uni-essen.de

Short Description

Magnetic resonance imaging (MRI) has emerged as a non-invasive cardiac imaging technique and plays an increasingly important role in the assessment of coronary artery disease (CAD). Its superb spatial and temporal

resolution combined with excellent soft tissue contrast currently allows accurate assessment of cardiac morphology, global cardiac function, regional wall motion and the extent of myocardial infarction. Regional myocardial perfusion can be assessed by first-pass techniques using ultrafast T1-weighted sequences. MR coronary angiography has become feasible and high-resolution imaging with or without contrast-enhancement may allow for characterization of atherosclerotic plaque. Some of the techniques are currently used in clinical routine whereas others must be considered a field of active research (Fig. 1).

There are two common clinical scenarios in which MRI is frequently applied in patients with CAD:

1. To detect CAD and myocardial ischemia
2. To define the extent of myocardial infarction and to distinguish different causes of wall motion abnormalities including scar, myocardial stunning and myocardial hibernation

This review discusses the diagnostic accuracy and the impact of different MRI techniques on management of CAD patients.

Detection of Coronary Artery Disease and Myocardial Ischemia

Several non-invasive tests including stress ECG, stress echocardiography, nuclear techniques, cardiac computed tomography are used in clinical routine for the detection of CAD. However, due to limited sensitivity and specificity of all non-invasive techniques, the final diagnosis as well as the exclusion of CAD is established by catheter angiography in the majority of patients. MRI offers different morphologic and functional techniques including wall motion analysis at stress, first-pass stress perfusion, MR coronary angiography and coronary vessel wall imaging for the detection of CAD.

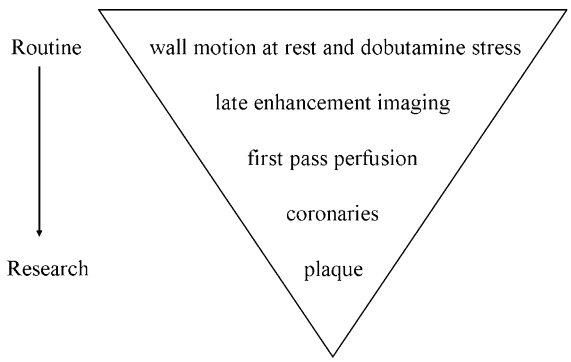

Ischemic Heart Disease, MRI. Figure 1 Status of different MR techniques for the assessment of ischemic heart disease.

Wall Motion Analysis at Stress

CAD may result in global or regional wall motion abnormalities of the left ventricle and lead to heart failure. The MR analysis of the global left ventricular function at rest, expressed as left ventricular ejection fraction, has impact on patient management and predicts patients' prognosis. Regional wall motion abnormalities are classified as hypo-, a- or dyskinesia of the left ventricular myocardium, but the different pathophysiological causes of wall motion abnormalities (scar, stunning, hibernation) cannot be differentiated by analysis of rest function.

The assessment of regional wall motion at pharmacological stress provides additional information to the rest examination. Low-dose dobutamine stress MRI can be used to assess myocardial viability. Dysfunctional myocardium that improves at low-dose dobutamine can be characterized as ischemic myocardium (hibernation), with a high probability of recovery of function after revascularization.

High-dose dobutamine stress MRI can identify myocardial ischemia non-invasively. The positive inotrope and chronotrope effects of dobutamine increase the myocardial oxygen demand and new or worsened wall motion abnormalities at stress are sensitive signs of hemodynamically significant CAD. High-dose dobutamine MRI can be performed with a standard dobutamine/atropine stress protocol, which was introduced for stress echocardiography. However, compared to stress echocardiography, detection of wall motion abnormalities by stress MRI provides a significantly higher accuracy for the diagnosis of significant CAD.

Stress Perfusion

Contrast enhanced first-pass myocardial perfusion imaging uses fast T1-weighted sequences during injection of a contrast bolus. The T1-shortening effect of the contrast agent results in a successive increase of the signal intensity in the right ventricle, the left ventricle and the myocardium. To be well suited for first pass imaging MR pulse sequences have to fulfil several, to some degree contradictory requirements. Most sequences provided for the assessment of myocardial first pass perfusion make use of a saturation-recovery pre-pulse to achieve heavily T1-weighted images followed by a fast data read out by means of gradient echo, echo planar imaging or steady-state free precession techniques. However, sequence optimization must be considered an area of active research and no general recommendations can be given.

Contrast dose varies between 0.025 and 0.15 mmol/kg of extra-cellular Gd-chelates in different studies. As different sequences are more or less sensitive to susceptibility artefacts, the optimum total amount of contrast depends

on the applied MR sequence and on the employed post-processing methods. Myocardial first-pass perfusion studies can be analyzed in different ways including qualitative approaches, semi-quantitative methods and finally a fully quantitative analysis. Visual assessment is operator-dependent whereas semi-quantitative and quantitative methods are time consuming, and approved post-processing tools are not available for clinical applications.

Since the early 1990s, several groups have evaluated the diagnostic potential of first-pass perfusion MRI for the non-invasive detection of CAD against coronary angiography and nuclear techniques in a number of smaller studies. Although coronary angiography must be considered as an imperfect standard of reference, because a morphologic and a functional approach for the detection of significant stenoses are compared, the sensitivity and specificity of perfusion MRI ranged from 65 to 92% and from 76 to 100%, respectively.

However, large clinical trials defining the impact of first pass perfusion MR imaging onto patient management are still lacking, and a consensus on optimal imaging protocols and post-processing techniques has not been achieved so far. Therefore, MR first pass perfusion imaging must still be considered an area of active research, and the technique is not ready for clinical use.

MR Coronary Angiography

Invasive coronary artery angiography still serves as the gold standard for the diagnosis of CAD. However, limitations inherent to catheter coronary angiography include a major complication rate of approximately 0.3–1.1% considerable radiation exposure as well as excessive cost to the health care systems. These drawbacks have promoted alternative imaging strategies. With the development of ultrafast imaging sequences, magnetic resonance angiography of the coronary arteries (MRCA) has recently become possible.

Magnetic resonance angiography has replaced diagnostic catheter angiography for most vascular territories in clinical routine, but magnetic resonance coronary angiography is still an area of active research. The major challenges for MRCA include spatial resolution and coverage, compensation of cardiac and respiratory motion and signal-to-noise issues. Initial studies using two-dimensional (2D) time-of-flight MR angiography techniques suffered from poor through-plane resolution, but these shortcomings were compensated by the introduction of nearly isotropic fast three-dimensional (3D) techniques. Advantageous features of 3D imaging techniques are the acquisition of thinner slices, superior signal-to-noise ratio (SNR) and the total coverage of tortuous coronary arteries.

In order to prevent vessel blurring, compensation of cardiac motion using ECG triggering is mandatory. All data for image reconstruction are collected in an acquisition window of 80–150 msec in mid to late diastole where displacement of the coronaries is minimized. To suppress the effects of respiration MRCA scan can either be performed in a single breath-hold or using respiratory gating. For breath-hold MRCA the scan time must be adapted to the patients' breath-hold capabilities, limiting the number of slices and the spatial resolution. For free-breathing MRCA using the navigator approach can be performed with high spatial resolution, however, image quality may be reduced by navigator failure depending on the patients breathing pattern.

MRCA using standard 3D-gradient echo sequences leads to rather poor contrast between blood and myocardium. To overcome this limitation T2 preparation has been introduced to suppress myocardial signal. Recently, steady-state free precession sequences have become clinically available, improving contrast between blood and myocardial tissue. Another approach for improving the quality of 3D-MRCA is to use T1-shortening contrast agents. Extra-cellular contrast agents are of limited value because they only permit data acquisition directly after intravenous application during the first arterial pass of the agent. Recently, blood pool MR contrast agents have been introduced for MRCA, which are characterized by higher T1-relaxivities and an intravascular distribution. These new intravascular MR contrast agents have recently been shown to improve breath-hold and navigator MRCA.

Until now, only two larger studies have compared free-breathing MRCA with X-ray angiography and reported high sensitivities and specificities for the detection of relevant CAD. Nevertheless, approximately one third of all examinations were not assessable due to impaired image quality. It can be concluded that MRCA is still challenging and the technique is not ready for clinical use in CAD patients.

Plaque Imaging

All luminographic techniques including conventional, computed tomography and magnetic resonance angiography, frequently underestimate the true burden of atherosclerosis because early stage atherosclerotic plaques, which do not compromise the arterial lumen cannot be detected. However, these non-stenotic plaques are of great clinical interest, because about one third of all myocardial infarctions occur due to plaque rupture in a vascular segment without stenoses.

Furthermore, it is well established that the risk of an acute event mediated by plaque rupture is predicted by

the composition of the plaque rather than the degree of luminal narrowing. Plaques with a large necrotic lipid core and a thin fibrous cap are associated with a high risk of rupture.

Due to its ability to distinguish different plaque components like lipids, the fibrous tissue, calcium and thrombi, high-resolution multi-contrast MRI is considered the most promising technique for imaging of the vessel wall. Recently, compounds that accumulate in atherosclerotic plaques or that bind to plaque components have shown promising results in animal studies.

Assessment of Myocardial Infarction and Myocardial Viability

The concept of myocardial 'late enhancement' (LE) or 'delayed enhancement' in contrast-enhanced cardiac MRI is currently being established for the assessment of myocardial viability. Animal studies have demonstrated that myocardial areas accumulating extra-cellular gadolinium-based contrast agents in the equilibrium phase after intravenous administration reliably reflect irreversible myocardial damage after myocardial infarction.

For the detection of late enhancement inversion-recovery gradient echo sequences should be performed 10 to 20 min after injection of 0.1–0.2 mmol/kg Gd-based contrast. The inversion time (TI) has to be adjusted manually between 180 and about 300 msec to null the signal of normal myocardium. These sequences optimize the image contrast and allow a reliable differentiation between infarcted tissue and normal myocardium.

Cardiac MR combining contrast-enhanced imaging (ceMRI) and cine sequences has shown potential characterizing myocardial tissue in patients with ischemic heart disease. Regional myocardial wall motion abnormalities can be caused by irreversible (scar tissue) or reversible myocardial damage, the latter of which can be differentiated in myocardial hibernation and myocardial stunning. MRI allows the discrimination of myocardial infarction (dysfunction with hyper-enhancement), myocardial stunning (dysfunction, normal perfusion, no hyper-enhancement), myocardial hibernation (dysfunction, hypo-perfusion, no hyper-enhancement) and normal myocardium (normal function without hyper-enhancement (Fig. 2).

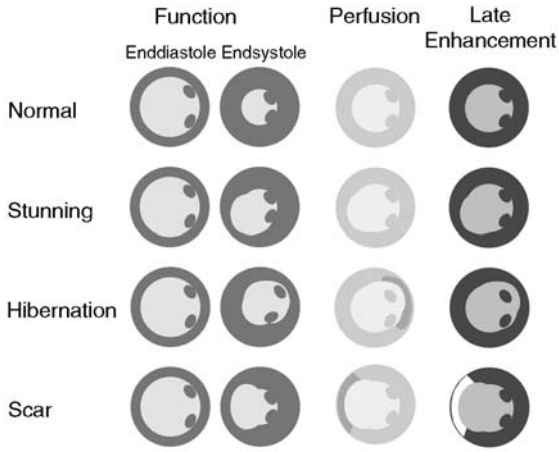

Ischemic Heart Disease, MRI. Figure 2 MR characterization of normal and dysfunctional myocardium.

Acute Myocardial Infarction

Acute myocardial infarctions (MI) are characterized by a loss of the cell membrane integrity. Therefore, standard extra-cellular contrast agent can enter the space formerly occupied by the cells resulting in an increased fractional distribution volume. However, a dark zone in the centre of the enhancing area can frequently be detected in acute MI. Although, the great epicardial coronary arteries are patent after acute percutanenous coronary interventions (PCI) or thrombolysis, there might be areas without early contrast uptake, because the small vessels and capillaries are occluded. This no-reflow phenomenon for MR has been described more than 10 years ago and can now be visualized *in vivo* using MRI.

Within the first week after acute MI wall motion abnormalities can either be caused by infarcted or stunned myocardium. Stunning is defined as dysfunctional but viable myocardium due to a temporary severe ischemia. The differentiation between stunned and infarcted segments in patients with recent myocardial infarction is clinically important and can easily be made by MRI because irreversible damaged myocardium shows late enhancement whereas stunned myocardium does not (Fig. 2). Based on this criterion, contrast-enhanced MR reliably distinguishes stunning from infarction and allows predicting the functional improvement of stunned myocardium.

The true extent of irreversible myocardial injury defined by MRI using the late enhancement approach is a strong predictor of patients' outcome. Furthermore, no-reflow areas detected within the area of late enhancement are an additional independent risk factor and are associated with an increased number of cardiac events and poor prognosis.

Acute myocardial infarction can reliably be distinguished from chronic scar tissue using T2-weighted images. While acute MI appears bright due to myocardial oedema, chronic MI is isointense to myocardium on

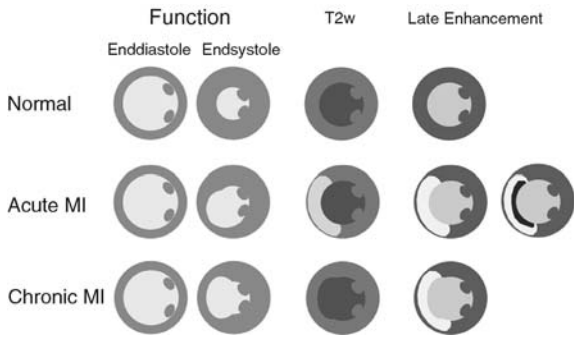

Ischemic Heart Disease, Nuclear Medicine. Figure 3 MR appearance of acute and chronic myocardial infarction.

T2-weighted images (Fig. 3). Additionally, chronic myocardial infarctions frequently show wall thinning due to scar formation, whereas in acute MI the end-diastolic wall thickness is not different from normal myocardium. Another criterion to distinguish acute and chronic myocardial infarctions is the no reflow phenomenon, which can only be detected within the first 4 to 6 weeks after an acute myocardial infarction.

Chronic Myocardial Infarction

Chronic myocardial infarctions show a homogenously increased signal intensity compared to normal myocardium 5 to 30 min after contrast injection (Fig. 3). Whereas the contrast agent is rapidly washed out from normal myocardium, the contrast agent accumulates in the increased interstitial space of non-viable myocardium. Additionally, the reduced perfusion of scar tissue results in a delayed wash out of the contrast agent. Chronic myocardial infarction shows homogenous enhancement after contrast application (Fig. 3).

In patients with a history of myocardial infarction, myocardial dysfunction can be caused by scar tissue or myocardial hibernation. Hibernation is defined as dysfunctional but viable myocardium due to chronic ischemia. The differentiation between hibernating and infarcted segments in patients with a history of myocardial infarction is clinically important and can easily be made by MRI because irreversible damaged myocardium shows late enhancement whereas hibernating myocardium does not.

This differentiation is clinically important because patients with hibernation benefit from re-vascularization whereas patients with scar tissue do not. The delayed enhancement technique has recently been introduced into clinical routine for the assessment of myocardial viability. Contrast-enhanced MRI can reliably discriminate between reversible (hibernation) and irreversible ischemic injury and predicts functional recovery after re-vascularization with high sensitivity and specificity.

Comparing MRI with positron emission tomography (PET) as the reference standard for the detection and quantification of myocardial scar tissue, several studies demonstrated a higher sensitivity of MRI for the detection of small scars, reflecting the higher spatial resolution of the LE images. Furthermore, MRI is superior defining the transmural extent of infarcted myocardium which is a strong predictor of functional recovery after revascularization. Analyzing regional contractility before and after re-vascularization, function improved in about 3/4 of segments without hyper-enhancement, whereas almost none of the segments with hyper-enhancement of more than 75% of the left ventricular wall showed a recovery of function.

However, although LE is very sensitive in detecting and localizing myocardial scarring, it is, on the other hand, not specific for ischemic damage. Pathologically controlled studies have shown that extra-cellular contrast agents accumulate not only in infarction scars, but generally in tissues with increased water content. Thus, the presence of LE has been described in myocardial areas of fibrosis, inflammation and edema where the extra-cellular volume is enlarged. Different entities of myocardial diseases or disorders are accompanied by fibrosis and acute or chronic inflammation and might, therefore, be diagnosed based on the pattern and localization of LE in contrast-enhanced MRI. Whereas myocardial infarctions always involve the sub-endocardial layer of the myocardium and the area of late enhancement is related to the territories of the coronary arteries, non-ischemic entities frequently show a more patchy and sub-epicardial distribution.

Ischemic Heart Disease, Nuclear Medicine

M. P. M. Stokkel
Department of Nuclear Medicine, LUMC, Leiden, The Netherlands
m.p.m.stokkel@lumc.nl

Synonyms

Myocardial perfusion scintigraphy

Definition

Many pathological conditions with respect to the coronary blood flow have been described. Hypoxia is the condition in which the oxygen supply is diminished despite an adequate perfusion of the myocardium. Anoxia

is regarded as the absence of oxygen supply, whereas in ►ischemia the oxygen deprivation is accompanied by inadequate removal of metabolites due to a reduced perfusion. During the ischemic condition an imbalance occurs between oxygen supply and demand, which may manifest as anginal discomfort, deviation of the ST segment on electrocardiography, or impairment of the regional or global left ventricular function. In the presence of coronary obstruction, an increase in myocardial oxygen requirement leads to a transitory imbalance or the so-called demand ischemia. This condition may be caused by exercise, tachycardia, or emotion and is responsible for most episodes of chronic stable angina. On the other hand, imbalance caused by a reduction of the oxygen supply related to increased vascular tone or the presence of thrombi is termed supply ischemia. This form of ischemia is responsible for episodes of unstable angina and myocardial infarction.

Nuclear medicine dedicated to imaging procedures of the heart using radiopharmaceuticals—so-called nuclear cardiology—has been an active clinical specialty for at least three decades. Major advances have occurred over the past years in both radiopharmaceutical development and instrumentation. Nuclear cardiology gives insight into many functional aspects of the heart and thus into risk stratification and prognosis (1). The clinical applications of nuclear cardiology include ►*myocardial perfusion scintigraphy*, measurement of the left ventricular ejection fraction, assessment of myocardial viability, assessment of myocardial fatty acid metabolism, and assessment of receptor integrity.

Pathology/Histopathology

A strong correlation between ischemic heart disease and prognostic factors, such as smoking, hypertension, diabetes, and hypercholesterolemia has been established. Other contributory factors may be lack of exercise and physiological characteristics. These factors lead to initiation and progression of a process of reduction in the lumen of the coronary artery. This process is characterized by the formation of an atheroma affecting the intima, fibrin, and platelet deposition on the intima, hemorrhage under the intima, thrombosis, or a combination of these factors. The anterior descending coronary artery is especially vulnerable to atheroma, and sudden occlusion of this vessel is particularly dangerous. In myocardial infarction, there is usually an occlusion due either to a platelet thrombus or to rupture of an atheromatous plaque, which may result in subendocardial or transmural infarction. During an acute infarction an inflammatory reaction occurs, and if the epicardial surface is affected, it may lead to overlying pericarditis.

Clinical Presentation

►*Angina pectoris* is the name for a clinical syndrome due to myocardial ischemia. The symptoms are commonly provoked by exertion, particularly out of doors, or by anxiety. It is usually experienced as a sense of oppression or tightness in the middle of the chest, and the patient commonly places his or her hand on the sternum. Angina pectoris is likely to be worse on a cold day or when walking against a wind or uphill and it commonly occurs after meals. In all of these circumstances, a greater coronary blood flow is demanded to fulfill the increased oxygen requirement. The pain is commonly accompanied by discomfort in the arms (most often the left), wrists, and hands. Angina may more rarely be epigastric or interscapular or may radiate to the neck and jaw. There may be accompanying breathlessness or even syncope.

Imaging

The acquisition and display of nuclear medicine images depends on detecting photons emitted during the decay process of a radionuclide. These radionuclides are intravenously administered to a patient and are either labeled to specific tracers or are unlabeled. The photons are detected with a scintillation (gamma) camera interfaced with a computer. The photomultiplier tubes translate the scintillations that occur in a large sodium iodide crystal into voltage pulses, which are finally measured as an electrical signal. The computer is a principal component of all nuclear imaging systems as it uses software containing reconstruction algorithms and functionality for quantifying static and dynamic images.

Over the past years, single photon emission computed tomography (SPECT) has been used more commonly in cardiovascular imaging. A series of planar images is acquired over a 180–360° arc around the patient's thorax, which gives the option of three-dimensional imaging of the heart. The transaxial images are reconstructed into short-axis and horizontal and vertical long-axis orientations. The overall result is an improvement in anatomical resolution and contrast in relation to planar imaging, but it requires more stringent quality control measures of the whole imaging device. Finally, by using the electrocardiogram (ECG) signal as a trigger for image acquisition, the so-called ►*gated-SPECT* method, perfusion imaging is combined with functional imaging to reveal data with respect to perfusion, global ejection fraction, and regional wall motion and thickening. As a result, it provides the clinician better information with respect to risk stratification and prognosis.

I

Nuclear Medicine

Radiopharmaceuticals for Myocardial Perfusion Imaging

The regional distribution of myocardial perfusion can be visualized with radiopharmaceuticals that accumulate proportional to the regional blood flow. In 1874, Thallous chloride-201 (Tl-201) became available, which has the advantage of viability assessment in addition to perfusion evaluation. Over the past decade, however, Technetium-99m (^{99m}Tc)-labeled compounds became available. These latter radiopharmaceuticals have better imaging characteristics and novel biological properties. Although worldwide ^{99m}Tc-labeled compounds are most commonly used, combinations with both radiopharmaceuticals are still in use (2).

Thallium-201

Thallium-201 is a cyclotron-produced radiopharmaceutical that emits mercury X-rays at 69–83 keV and photons with an energy of 135, 165, and 167 keV. Its physical half-life is 74 h, but its biological half-life is 58 h. Because of the relative long half-life and the rather high whole body doses, only a small amount of radioactivity can be administered. The first-pass extraction fraction is approximately 85%, whereas the overall uptake is about 4% of the injected dose. The initial accumulation is proportional to the blood flow, and once it has entered the cell it continuously exchanges across the cell membrane. This process involves the Na^+, K^+-ATP-ase pump. Consequently, with one single injection, this radiopharmaceutical may provide images related not only to the initial blood flow but also to a redistribution process. The latter images reflect the distribution of the potassium pool and hence myocardial viability. A disadvantage of this compound is that because of this redistribution process, acquisition should start very shortly after administration, whereas the acquisition time is limited.

Technetium-99m-Labeled Compounds

Over the past years, a number of ^{99m}Tc-labeled compounds have been introduced in clinical practice. The most commonly used agent is ^{99m}Tc-sestamibi, a lipophilic monovalent cation, which later on came to be used for tumor scintigraphy. The production of these compounds is on site. The advantage of ^{99m}Tc over Tl-201 is the optimal energy of photons emitted, 140 keV, which can be easily detected by sodium iodide crystals in the gamma camera. Consequently, better image quality can be achieved using these compounds. The half-life of ^{99m}Tc is approximately 6 h, whereas the radiation exposure for patients is less than obtained with Tl-201. Because of the favorable dosimetry, up to 1,000 MBq of these agents can be administered per day.

The initial myocardial uptake is similar to Tl-201 and is proportional to the regional blood flow. In contrast to Tl-201, however, there is rapid accumulation in the liver as well as excretion into the biliary tract. Consequently, extracardiac activity may be observed, which may interfere especially with interpretation of the inferior wall. Uptake in the myocardium is by passive diffusion followed by binding to intracellular membranes. The myocardial distribution remains stable over time and can be imaged for several hours after administration. There is no significant redistribution. The most commonly used ^{99m}Tc-labeled compounds are ^{99m}Tc-sestamibi and ^{99m}Tc-tetrofosmin (3).

Stress-Rest Imaging Protocols

To assess myocardial perfusion, different study protocols have become available. The aim of these imaging protocols is to differentiate, on one hand, normal from abnormal perfusion studies. On the other hand, the aim is to differentiate persistent perfusion abnormalities from reversible ischemia and, in the case of the use of Tl-201, to assess the presence of viable tissue. In this respect, different protocols have become available over the past years (3).

Stress Protocols

To assess myocardial perfusion, different stress protocols are available. The choice of protocol depends on the condition, comorbidity, medication, abnormalities on ECG, and so on. In most nuclear cardiology centers, a stress test is followed by a rest study, but it has been stated that in the case of a normal stress study, the performance of a rest study is questionable.

Physical exercise: Several treadmill protocols exist. Endpoints for physical exercise are severe symptoms as dyspnea and angina, hypotension, exhaustion, and ST-segment depression on electrocardiography. During peak exercise, the radiopharmaceutical is administered intravenously in an antecubital line, after which time the patient is encouraged to exercise for another 1 or 2 min.

Pharmacological vasodilatation: If disabilities or contraindications to physical exercise exist, pharmacological alternatives are available. The most commonly used are adenosine infusion and dobutamine stress. Adenosine is a vasodilator with minimal side effects. The only contraindications are chronic obstructive pulmonary disease and AV block. Maximum dilatation is achieved after 4–4.5 min, at which time the radiopharmaceutical is administered, and the infusion continues for 1.5–2 min. Side effects include transient headache, abdominal

discomfort, and nausea. The advantage of adenosine over other techniques is its rapid clearance and, consequently, the instantaneous reversibility of symptoms.

Dobutamine stress increases myocardial oxygen demand by increasing contractility, heart rate, and blood pressure. The increase in flow is comparable to that of physical exercise but less than that with adenosine. The infusion protocol takes about 15 min, with administration of the radiopharmaceutical in the 12th min. The most commonly reported side effects include ventricular ectopy, headache, dyspnea, paresthesia, and flushing; however, their reversibility is less rapid than in adenosine protocols.

One-day stress–rest study: Several study protocols can be used during a one-day stop-and-shop imaging strategy:

1. Tl-201 (100 MBq) injected at peak exercise, delayed imaging after 2–4 h to assess redistribution, followed by reinjection of Tl-201 (75 MBq) to assess the perfusion at rest.
2. ^{99m}Tc-labeled compounds (250–500 MBq) injected at rest, followed by a stress study 2 h later using 750–1,000 MBq of a ^{99m}Tc-labeled compound.
3. Dual isotope imaging, which is based on the injection of Tl-201 at rest and a ^{99m}Tc-labeled compound during stress.

Two-day stress-rest study: This is the most commonly used strategy. The major advantage over a one-day stress-rest study protocol is the fact that the amount of activity is comparable under both circumstances (500–1,000 MBq), revealing better image quality and the option of optimal gating during stress as well as rest. Although Tl-201 can be used in this protocol, the use of ^{99m}Tc-labeled compounds is advised because they give a better option of gating during both studies and, again, better image quality.

Interpretation of Images

Myocardial perfusion studies are reconstructed and presented in short-axis and horizontal and vertical long-axis projections. The initial interpretation is visual, in which the heart is subdivided into segments (e.g., 9, 17, or 20 segments). For each segment, the perfusion is scored as normal (0), slightly to moderately diminished uptake (1), moderately to severely diminished uptake (2), or no uptake (3). It is important to assess the size of the left ventricle and the distribution pattern of the radiopharmaceutical, either homogeneous or irregular. An irregular pattern may indicate microangiopathy caused by diabetes or cardiomyopathy. The visual analysis is done for the stress as well as for the rest study, and the results are combined with a semiautomatic analysis method developed by Germano and Berman (4). This software package gives the option to measure the left ventricular ejection fraction, the regional wall motion, and wall thickening. Furthermore, a polar map, or bull's eye display is used to compare the stress–rest images semiautomatically. The purpose of this map is to generate one single image that encompasses the relative distribution of the radiopharmaceutical. Relative uptake on short-axis images is compressed to a color-coded concentric ring with the apical slice in the center and the basal slices on the periphery of the map. The combination of all data finally results in the following interpretations:

1. Normal intensity, homogeneous distribution, normal function of the myocardium (Fig. 1)
2. Defect in one or more segments, abnormal function in these segments, which may be indicative for infarction (Fig. 2)
3. Reversible defect, which is a defect present on initial stress images and no longer present on the resting or delayed images. This pattern indicates ischemia (Fig. 2). Functional abnormalities may be seen, which commonly correspond to the severity of the perfusion abnormalities.

It must be realized that artifacts may occur, leading to possible misinterpretation of the reconstructed images. Motion artifacts may show up as reversible defects, which can be assessed on the raw data images. A typical motion artifact is the so-called upward creep of the heart, which is caused while the patient recovers from stress and the heart consequently moves into the horizontal position. Other common artifacts are caused by attenuation. Acquisition is normally performed with the patient in the prone position, because in this position the overall attenuation by the camera table at one side is comparable with the attenuation of photons passing through the chest at the other side. When acquisition is done in the supine position, it may cause artifacts in the inferior wall. Attenuation by large and/or dense breast tissue will result in abnormalities in the anteroseptal region.

Diagnosis

Myocardial perfusion scintigraphy is an extremely sensitive and reliable method for the assessment of perfusion abnormalities and prognostic stratification (5, 6). Indications for perfusion scintigraphy are visualization of ischemia (site, extent, and severity), stratification of risk for cardiac death (low, intermediate, or high), identification of the culprit artery, determination of viability of dysfunctioning myocardium, and, in certain cases, recommendation for the type of therapy as medical, coronary artery bypass graft (CABG), or transplantation. In most of the studies published over the past year, myocardial perfusion

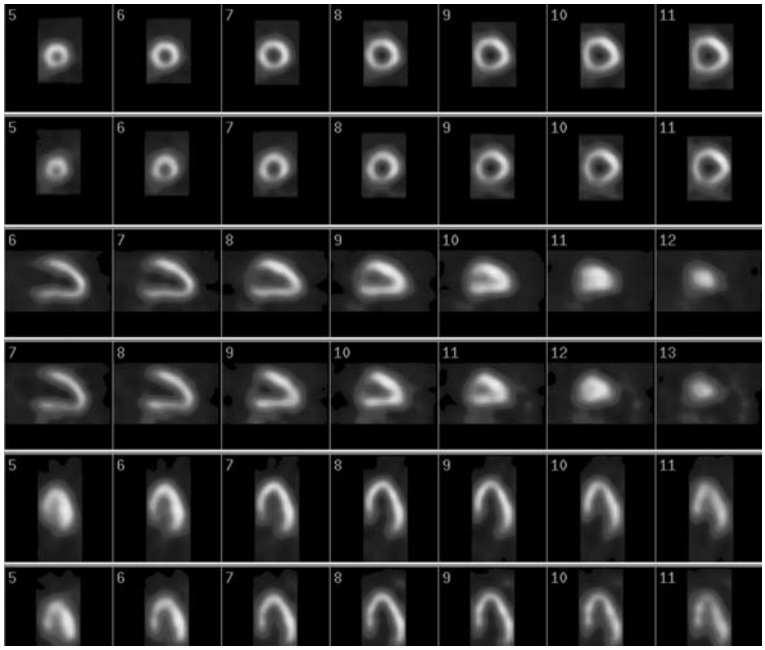

Ischemic Heart Disease, Nuclear Medicine. Figure 1 Standard short-axis and horizontal and vertical long-axis reconstructions of a stress–rest myocardial perfusion study with ^{99m}Tc-tetrofosmin. The first, third, and fifth rows demonstrate stress images, and the second, fourth, and sixth rows demonstrate rest images. A normal distribution pattern is seen without perfusion defects. This patient, who presented with atypical chest pain was categorized into the very-low-probability risk group for cardiac events.

scintigraphy has revealed a sensitivity and specificity of 80–100% and 80–90%, respectively, for detecting ischemia or infarction, whereas the negative predictive value is up to 99%. It has been concluded from these studies that gated-SPECT myocardial perfusion scintigraphy has significant incremental prognostic value regarding individual parameters such as age and gender, risk factors such as hypercholesterolemia and hypertension, and ECG changes. Following perfusion scintigraphy, patients can be stratified into the following risk groups for a major cardiac event:

1. Low risk (<1%)
   a. Normal or near normal perfusion
   b. Normal left ventricular ejection fraction with normal or near normal perfusion
2. Intermediate risk (<1% for cardiac death, but 1% for nonfatal myocardial infarction)
   a. Small perfusion defect (15% of left ventricle volume) with normal left ventricular ejection fraction and absence of nonperfusion markers of left ventricular decompensation with exercise
3. High risk (>3% for cardiac death)
   a. Severe left ventricular dysfunction at rest
   b. Severe left ventricular dysfunction with exercise
   c. Large stress-induced perfusion defect
   d. Moderate stress-induced perfusion defect with abnormal Tl-201 lung uptake
   e. Multiple moderate stress-induced perfusion defects
   f. Large fixed perfusion defect with left ventricular dilatation.

Low-risk patients can be followed medically, whereas high-risk patients are ideal candidates for revascularization. An intermediate-risk patient can be followed medically except for special circumstances such as intolerability of symptoms or other reasons.

In patients who do undergo interventions, follow-up is indicated based on the technique used, the presence of symptoms, the relative risk for subsequent problems, and, finally, the time that has passed since the intervention. For example, the time to assess for restenosis after percutaneous transluminal coronary angioplasty is approximately 3–6 months. The majority of restenoses occur by this time interval regardless of recurrent symptoms. In the published studies, nuclear perfusion imaging demonstrated a superior sensitivity of 87% and a specificity of 78% compared with 46 and 77%, respectively, for the treadmill test. Assessment of perfusion after CABG by gated-SPECT studies definitely provides better insight into the site and extent of ischemia compared with treadmill tests. To understand abnormalities seen on the scans, however, knowledge of pre-CABG anatomy, vessels that were bypassed, and operative reports should be

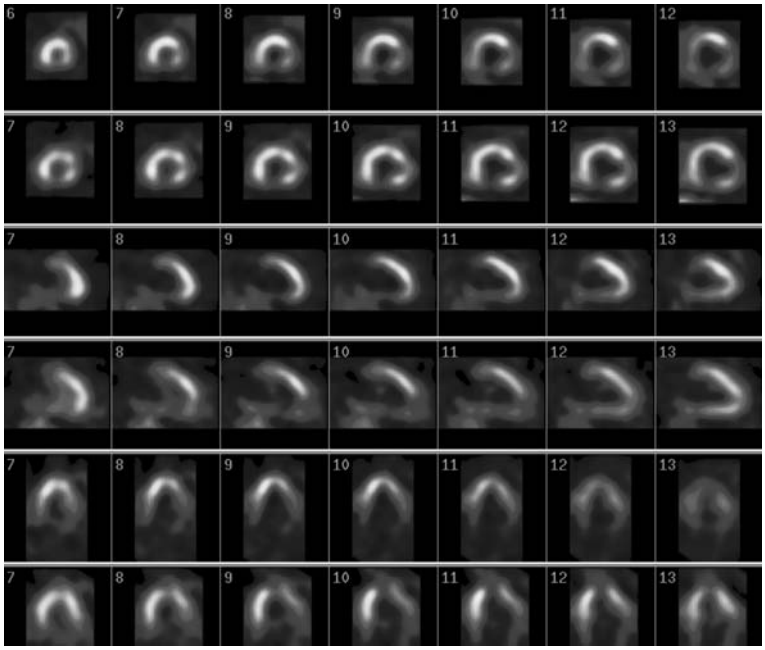

Ischemic Heart Disease, Nuclear Medicine. Figure 2 Myocardial perfusion scintigraphy with ^{99m}Tc-tetrofosmin in a patient with typical angina 1 year after myocardial infarction. The short axis and vertical long axis demonstrate persistent perfusion defects in the inferior and lateral wall in an enlarged left ventricle, consistent with myocardial infarction. Reversibility is seen in the septal and inferolateral wall, categorizing this patient into the high-risk group.

available, as these post-CABG scans may demonstrate a combination of nonrevascularized but diseased vessels, entrapped vessels, new disease, disease beyond anastomotic sites, or pathology of the grafts themselves.

Hibernation and Stunning

Hibernation refers to a condition of chronic sustained abnormal contraction due to chronic underperfusion in patients with coronary artery disease. In these patients, revascularization may cause recovery of function, even more than a year after intervention. In addition to this chronic underperfusion phenomenon, stunning is defined as repeated ischemic attacks, which may also result in chronic dysfunction with flow remaining normal or mildly reduced. The term "jeopardized myocardium" includes the entire spectrum ranging from stunning to hibernation. It is beyond the scope of this essay to describe in detail the principles and applications of jeopardized viable myocardium assessment. In summary, under such conditions glucose metabolism remains preserved in viable tissue. Regional glucose metabolism can be assessed with fluorodeoxyglucose (FDG), a radiolabeled glucose analog, and SPECT imaging. Dysfunctional segments with both preserved perfusion and glucose metabolism are thought to represent stunned myocardium, whereas segments with preserved glucose metabolism but reduced perfusion are considered hibernating myocardium. In contrast, segments with reduced perfusion and concordantly reduced FDG uptake are considered scar tissue. In this respect, myocardial perfusion studies performed at rest are a prerequisite for an optimal viability assessment and, consequently, for the prediction of functional recovery and long-term prognosis.

Bibliography

1. Faber TL, Cooke CD, Folks RC et al (1999) Left ventricular function and perfusion from gated SPECT perfusion images: an integrated method. J Nucl Med 40:650–659
2. Berman B, Germano G, Lewin H et al (1998) Comparison of post-stress ejection fraction and relative left ventricular volumes by automatic analysis of gated myocardial perfusion single photon emission computed tomography acquired in supine and prone positions. J Nucl Cardiol 5:40–47
3. Shridhara B, Sochor H, Rigo P et al (1994) Myocardial single-photon emission computed tomographic imaging with technetium 99m tetrofosmin: stress-rest imaging with same-day and separate-day rest imaging. J Nucl Cardiol 1:138–143
4. Germano G, Berman DS (2005) Quantitative single-photon emission computed tomography imaging. Curr Cardiol Rep 7:136–142
5. Shaw LJ, Iskandrian AE, Hachamatovitch R et al (2001) Evidence-based risk assessment0 in noninvasive imaging. J Nucl Med 42:1424–1436
6. Shaw L, Hachamovitch R, Heller GV et al (2000) Noninvasive strategies for the estimation of cardiac risk in stable chest pain patients. The Economics of Noninvasive Diagnosis (END) Study Group. Am J Cardiol 86:1–7

Ischemic Heart Disease, Ultrasound

Bernard P. Paelinck
University Hospital Antwerp, Antwerp, Belgium
bernard.paelinck@ua.ac.be

Synonyms

Coronary artery disease; Doppler echocardiography

Definitions

Ischemic heart disease results from stenosis and/or occlusion of one or more coronary arteries. When ►myocardial perfusion is reduced, ischemia develops with resulting impairment of myocardial function. Reversible myocardial dysfunction due to transient and chronic ischemia is defined as stunned and hibernating myocardium, respectively (1). Irreversible myocardial dysfunction or myocardial infarction occurs when prolonged ischemia results in myocyte death (2).

Pathology/Histopathology

In ►myocardial stunning, myocardial function is temporarily impaired, which may result from reperfusion injury with generation of free radicals and calcium overload. With maintenance of normal perfusion, myocardial function returns to normal. In hibernating myocardium, a mixture of normal, atrophied, and hypertrophied myocytes is found. Prolonged hypoperfusion leads to reversible downregulation of myocardial function and to variable structural changes, ultimately including loss of myocytes.

Myocardial infarction is characterized by myocardial muscle necrosis. Acute or evolving myocardial infarction is characterized by infiltration of polymorphonuclear leukocytes (after 6 h) in addition to cell death. Acute myocardial necrosis can be recognized by the release of myocardial proteins in the blood (e.g., myoglobin, troponins T and I, creatine kinase) and by the loss of electrically functioning cardiac tissue (Q waves on electrocardiograms). Healed myocardial infarction is manifested as scar tissue without cellular infiltration and requires about 6 weeks or more to develop after the acute event (2).

Clinical Presentation

Ischemic heart disease remains one of the leading causes of morbidity and mortality. Angina pectoris is a typical symptom of ischemia. Dyspnea can occur as a result of extensive ischemic reversible myocardial dysfunction and is referred as "angina equivalent." Acute myocardial infarction is usually accompanied by typical chest pain, lasting for at least 20 min, but may also present without symptoms.

Ultrasound Imaging

Ischemia

Ischemia results in a sequence of events referred to as "the ischemic cascade": initially diastolic dysfunction, at a later stage systolic dysfunction, eventually followed by electrocardiographic changes, and finally by angina pectoris.

The initial diastolic abnormality is prolonged and delayed myocardial relaxation. This is apparent from decreased early left ventricular filling (E) and a decreased early atrial (A) to mitral filling ratio (or E/A) assessed by ►Doppler echocardiography. With worsening diastolic function, the left ventricular compliance is decreased and left ventricular filling becomes dependent on increased left atrial pressure, causing an increased E/A ratio. As the underlying impaired relaxation is masked and because the left ventricular filling pattern resembles the normal filling pattern, it is called pseudonormalization. Combining E peak velocity, which is dependent on both left atrial pressure and myocardial relaxation, with tissue Doppler-assessed early diastolic mitral annulus velocity (Ea), which is mainly dependent on myocardial relaxation, allows differentiation ("unmasking") of a normal from a pseudonormal signal. With ongoing decrease in compliance, the mitral filling pattern becomes restrictive (Fig. 1).

With prolonged ischemia, regional myocardial thickening and motion are decreased (less than 30% = hypokinesia, or absent = akinesia) or systolic outward motion occurs (dyskinesia). Regional wall motion of the left ventricle is assessed in 17 segments (American Heart Association) and analyzed in different views (apical and parasternal ultrasound windows). Each segment is assigned a wall motion score: normal: 1, hypokinesia: 2, akinesia: 3, and dyskinesia: 4. A wall motion score index is calculated as the sum of segmental scores divided by the number of segments. The segmental wall motion abnormalities in ischemia correspond to coronary perfusion territories. Left anterior descending artery disease results in abnormalities of the anterior, anteroseptal, and apical segments, while right coronary artery disease results in abnormalities of the inferior and basal posteroseptal

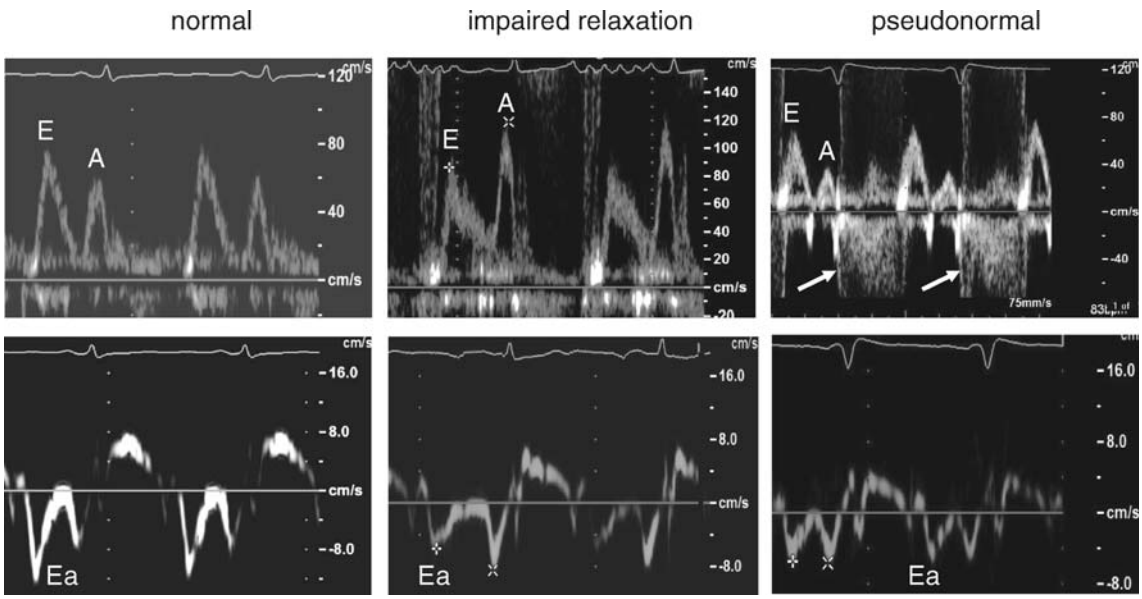

Ischemic Heart Disease, Ultrasound. Figure 1 Doppler echocardiography of mitral filling pattern (upper panel) together with tissue Doppler-assessed mitral annular velocities (lower panel) showing representative traces of normal, impaired relaxation and pseudonormal mitral filling pattern. Note decreased Ea in impaired relaxation and pseudonormal mitral filling pattern. Arrows indicate reverse flow due to mitral regurgitation. E; early left ventricular filling, A; atrial or late ventricular filling, Ea; early diastolic mitral annulus velocity.

segments. Circumflex artery disease affects motion of the lateral and posterior segments. These patterns of segmental dysfunction may vary depending on the coronary dominance pattern and the site of ►coronary artery disease.

Patients with ►coronary artery disease frequently have normal left ventricular function at rest. Diagnosis of coronary artery disease using stress echocardiography is based on the induction of a decreased myocardial oxygen supply/demand ratio resulting in new or worsening segmental systolic wall motion abnormalities. Depending on patient characteristics (capability of exercise) and echolab logistics, physical exercise (treadmill or bicycle) or pharmacological (inotropic stress: dobutamine; vasodilator stress: adenosine, dipyridamole) stress testing can be performed. Exercise echocardiography has a mean sensitivity and specificity of 84 and 82%, respectively, while dobutamine echocardiography has a mean sensitivity and specificity of 80 and 84%, respectively, to detect coronary artery disease (3). The accuracy of stress echocardiography is highly dependent on endocardial border definition. In the case of a suboptimal acoustic window, improved endocardial border delineation can be obtained by using ►Second harmonic imaging. and (optionally) administration of intravenous contrast agents to assess myocardial perfusion.

Besides diagnosis and assessment of the location and extent of myocardial ischemia, stress echocardiography is used for the preoperative risk evaluation in major noncardiac surgery and for the assessment of myocardial viability. Identification of dysfunctional but viable myocardium (as opposed to necrotic myocardium) has important prognostic value and is predictive of the recovery of function after revascularization. Indicators of myocardial viability include contractile reserve to inotropic stimulation (augmentation of regional myocardial function) and preserved myocardial thickness (>6 mm).

Myocardial Infarction

In the emergency department, echocardiography is essential in the bedside evaluation of a patient with chest pain (but a nondiagnostic electrocardiogram). In the acute phase of myocardial infarction, the affected myocardium is dysfunctional (akinetic, hypokinetic, or dyskinetic) but wall thickness is still preserved. Two-dimensional echocardiography has, in addition, prognostic implications and the amount of myocardial dysfunction allows estimation of the amount of myocardium at risk. If wall motion during chest pain is normal, the likelihood of acute myocardial infarction remains low. Echocardiography is also useful in detecting other causes of chest pain such as: pericarditis, pulmonary embolism, and aortic dissection.

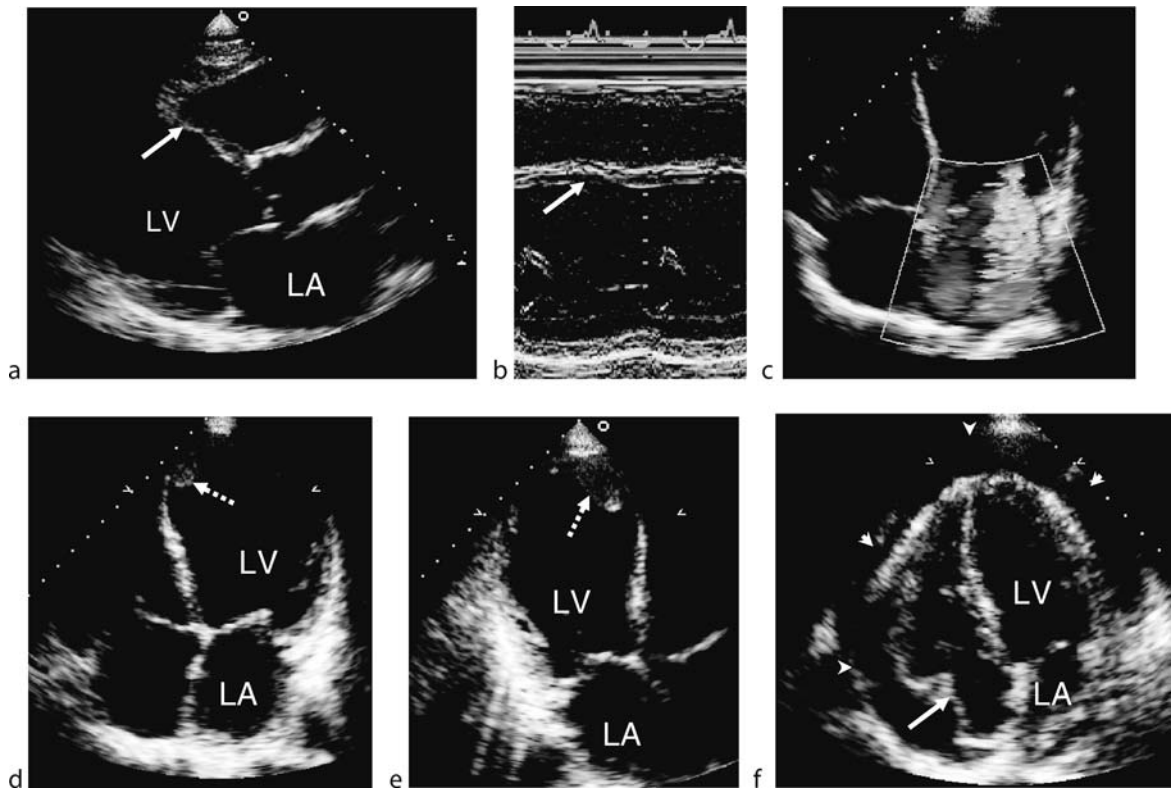

Ischemic Necrosis. Figure 2 **(a) Parasternal long-axis view and (b) ►M-mode echocardiogram. showing dilatation of the left ventricle and thin-walled infarcted anteroseptal wall (arrow). Note absence of thickening in infarcted myocardial wall. (c) Two-dimensional echocardiogram of ischemic mitral regurgitation, (d) apical four-chamber, and (e) three-chamber view showing mid and apicoseptal thin-walled aneurysm with intracavitary thrombus (dashed arrow). (f) Large pericardial effusion (arrowheads) with partial collapse of the right atrial wall (arrow). LA; left atrium, LV; left ventricle.**

Besides assessment of left ventricular dysfunction, two-dimensional echocardiography with Doppler is the primary imaging technique for the initial evaluation of postmyocardial infarction complications: right ventricular involvement, free wall rupture, ventricular septal rupture, papillary muscle rupture causing acute flail mitral leaflet, pericardial effusion and tamponade, intraventricular thrombus, and false and true ventricular aneurysm (Fig. 2). Transesophageal imaging is often necessary to visualize mechanical complications such as muscular rupture.

After several weeks, myocardial infarction results in thinning and increased intensity of the involved segments. A nontransmural myocardial infarction may result in hypokinesia rather than akinesia. Expansion of the infarction zone, global left ventricular dilatation and distortion, together with segmental compensatory hypertrophy, is referred to as postinfarction remodeling. Due to left ventricular dilatation and/or ischemia, mitral regurgitation is often present in ischemic cardiomyopathy. Doppler interrogation of the mitral filling pattern helps guide therapy, including diuretics. Depressed left ventricular ejection fraction, mitral regurgitation, and restrictive mitral filling pattern are associated with a poor prognosis and cardiac death.

References

1. Underwood SR, Bax JJ, vom Dahl J et al (2004) Imaging techniques for the assessment of myocardial hibernation. Report of a Study Group of the European Society of Cardiology. Eur Heart J 25:815–836
2. Myocardial infarction redefined – A consus document of The Joint European Society of Cardiology/American College of Cardiology Committee for the redefinition of myocardial infarction. (2000) J Am Coll Cardiol 36:959–69
3. Schuijf JD, Shaw LJ, Wijns W et al (2005) Cardiac imaging in coronary artery disease: differing modalities. Heart 91:1110–1117
4. Ommen SR, Nishimura RA (2003) A clinical approach to the assessment of left ventricular diastolic function by Doppler echocardiography: update 2003. Heart 89(Suppl III):iii18–iii23

Ischemic Necrosis

►Infarction, Renal

Ischemic Nephropathy

Renal insufficiency secondary to RAS; it can be stabilized, improved, or cured after revascularization.
▶Stenosis, Artery, Renal

Islet Cells Transplantation

In pancreatic islet transplantation, pancreatic cells are taken from a donor and transferred into the recipient. In this procedure, islet is removed from pancreas of a deceased donor by means of specialized enzymes. A typical transplant requires about 1 million islets, equal to two donor organs. Because the islets are extremely fragile, transplantation occurs immediately after they are removed. The surgeon uses ultrasound to guide placement of a catheter through the upper abdomen and into the liver; the islets are then injected through the catheter into the liver. Then cells attach to new blood vessels and begin releasing insulin. Nowadays the procedure is still experimental and more research is needed to answer questions about how long the islets will survive and how often the transplantation procedure will be successful.
▶Transplantation, Pancreas

Islet Cells Tumors, Pancreatic

Laura Crocetti, Carlo Bartolozzi, Carla Cappelli
Department of Diagnostic and Interventional Radiology University of Pisa, Pisa, Italy
l.crocetti@med.unipi.it

Synonyms

Neuroendocrine tumors of the pancreas

Definitions

Neuroendocrine tumors of the pancreas, or islet cell tumors, are rare pancreatic tumors. Among clinically functioning islet cell tumors of the pancreas, insulinoma is the most frequent; others, such as glucagonomas, VIPomas (tumors producing vasoactive intestinal peptide, VIP), somatostatinomas, PPomas (tumors producing pancreatic polypeptide), GFRomas (growth factor releasing hormone tumors), and others, are very rare. Some neuroendocrine tumors secrete more than one hormone, whereas approximately 15–20% of islet cell tumors do not secrete any hormones and are called nonsecreting tumors. They may be single or multiple and benign or malignant. Islet cell tumors may appear multiple, especially in case of multiple endocrine neoplasia (MEN), and are most often found in the pancreas. An extrapancreatic location is reported with a frequency of 10% for gastrinomas; extrapancreatic insulinomas are very rare. ▶Pancreatic carcinoid tumors, producing serotonin, are exceedingly rare. Patients with von Hippel–Lindau's disease are more prone to the development of tumors such as pheochromocytoma and neuroendocrine pancreatic tumors (1, 2).

Pathology/Histopathology

The most common islet cell tumor is insulinoma. About 70% are solitary adenomas, 10% are multiple adenomas, and 10% are carcinomas, whereas the remainder are a mixed group of diffuse hyperplasia of the islet and adenomas occurring in ectopic pancreatic tissue. Adenomas are usually encapsulated and histologically composed of cords of well-differentiated beta cells with typical granules. Malignant tumors show anaplasia; local invasion and spread to the local lymph nodes occur. Other islet cell tumors are similar in histology and differ in content of granules, which may be identified by means of immunohistochemistry (1, 2).

Clinical Presentation

Insulinomas are most common between the fifth and seventh decades of life. The typical clinical feature is hypoglycemia due to uncontrolled insulin secretion. Symptoms related to recurrent hypoglycemia are headache, slurred speech, psychological alterations, visual disturbances, confusion, and, eventually, coma and death. The body tries to compensate for the hypoglycemia by secreting catecholamines, which can result in tremulousness, diaphoresis, palpitations, cardiac arrhythmias, and irritability. Because symptoms due to hyperinsulinism develop early, insulinomas are usually <15 mm in size and solitary at the time of diagnosis; however, multiple tumors are found in 10% of cases, especially in patients with Wermer syndrome or MEN type I (1, 2).

Gastrinomas are the second most common hormone-secreting tumor of the pancreas. They occur more frequently in men than in women. In 30–50%, gastrinomas are associated with other disorders as a part of the

MEN I syndrome. Approximately 90% of all gastrinomas are found in the "gastrinoma triangle," an area limited by the junction of the cystic and common bile duct, the junction of the body and neck of the pancreas, and the second and third portions of the duodenum. Gastrinomas can also be found outside the pancreas, which has never been described for insulinomas. Approximately 60% of all gastrinomas are malignant. Gastric and/or duodenal ulcers develop in the majority of patients due to uncontrolled secretion of gastrin, which is called the Zollinger–Ellison syndrome. Patients with gastrinoma commonly complain about midgastric pain; and diarrhea and weight loss are present in at least 40% of patients. In approximately one-third of the patients, esophagitis is found (1, 2).

The glucagonoma syndrome is a combination of diabetes mellitus and necrolytic migratory erythema. Glucagonomas are single and slow-growing tumors, with metastatic spreading in more than 75% of cases at the time of the diagnosis, most commonly to the liver and the bones. Glucagonomas have been reported in patients suffering from MEN I. A fasting plasma level of glucagon of more than 1,000 ng/L establishes the diagnosis. An erythematous, raised, sometimes psoriatic, and ultimately crusted skin rash has been described in association with glucagonoma. The face, abdomen, perineum, and distal extremities are often the affected portions of the body. After resolution, the regions of acute eruption usually remain indurate and hyperpigmented. Others symptoms, such as glossitis, stomatitis, angular cheilitis, dystrophic nails, and hair thinning, have also been described. The diabetes is mostly mild or even asymptomatic and may manifest only as an abnormality on an oral glucose tolerance test. Weight loss, hypoaminoacidemia, anemia, and thromboembolic disease can also occur in association with this syndrome. Due to the unspecific and often very mild symptoms, these tumors usually are large at the time of diagnosis (1, 2).

Verner and Morrison described a syndrome of watery diarrhea, hypokalemia, hypochlorhydria, and renal failure in association with non-beta-cell tumors of the pancreatic islets. The clinical features are caused by the high levels of VIP secreted by the tumors. The typical manifestations of VIPoma include secretory diarrhea, profound weakness, hypokalemia, and hypochlorhydria. High plasma VIP levels in combination with a stool volume of least 1 L/day are indicative for a VIPoma. The majority of VIPomas are located in the pancreas. In contrast to insulinomas and gastrinomas, they grow to a considerable size before becoming clinically apparent. Although slow-growing, VIPomas usually are malignant and accompanied by metastases in approximately 60% of cases (1, 2).

Somatostatinomas are extremely rare endocrine tumors. The classic triad of somatostatinoma syndrome includes diabetes mellitus, steatorrhea, and cholelithiasis. These symptoms derive from the inhibitory actions of somatostatin, including inhibition of insulin release, pancreatic enzyme and bicarbonate secretion, and gallbladder motility. Like glucagonomas and VIPomas, somatostatinomas are usually single, large, and malignant (1, 2).

No specific syndrome has been associated with pancreatic polypeptide (PP)-secreting tumors. Possible clinical symptoms of PPomas include rash-like efflorescences, weight loss, jaundice, and abdominal pain. The lack of specific symptoms is the reason such tumors are often diagnosed at a stage when they have a mass effect (size >5 cm). The diagnosis can be established by measuring fasting circulation levels of PP (1, 2).

Nonsecreting islet cell tumors are often considerably large at the time of diagnosis compared to hormone-secreting tumors. Because of their mass effect, they cause symptoms such as abdominal pain, jaundice, bowel obstruction, and weight loss. In most cases, nonsecreting islet cell tumors are solitary lesions, being malignant in more than 80% (1, 2).

Imaging

On ultrasound (US), most of the endocrine pancreatic tumors appear as small, round, hypoechoic lesions compared with the pancreatic parenchyma. Larger tumors, which usually do not secrete any hormones and thus do not cause any symptoms at an early stage, may present with a heterogeneous pattern due to necrosis, calcifications, or hemorrhage. Invasion of the peripancreatic structures, hepatic and lymph nodes metastases, and peritoneal carcinosis are more common in nonsecreting malignant tumors. Due to the low specificity of US, other imaging techniques are a necessity in cases of any positive findings in the US examination. However, the use of harmonic imaging and US contrast agents may improve sensitivity. Endoscopic ultrasound (EUS) imaging of small islet cells tumors of the pancreas is more sensitive than transabdominal US. At intraoperative ultrasound (IOUS), the sonographic appearance of islet cell tumors is identical to that of transabdominal US. With high-frequency scanners, the sensitivity of IOUS is very high (3, 4).

Computed tomography (CT) is widely used to identify and localize islet cell tumors. Single or multislice spiral CT scanners represent the standard equipment. The typical scanning protocol consists of several phases (at least three), including a precontrast phase for detecting hypodense lesions, cystic lesions or calcifications; early arterial and pancreatic phases for detecting hypervascular lesions; and a portal-venous phase for detecting hypovascular lesions, being isodense at the precontrast scan or arterial phase

scan. In some cases, a further scan in the delayed phase may demonstrate a late enhancement, particularly in malignant tumors. For examination of the pancreas, slice thickness may vary between 1 and 3 mm. Typically, 120 mL of highly concentrated contrast agent is administered intravenously at an injection rate of 3–5 mL/sec. Additionally, the previous administration of 1,000 mL of water as a "negative" oral contrast as well as the administration of intravenous butyl scopolamine or glucagon may help detect small lesions in the pancreatic head and define their relationship with the duodenum. Islet cell tumors typically appear hyperdense compared with the surrounding tissue at the early arterial and pancreatic phases (Fig. 1). Large, mostly nonsecreting tumors may be centrally hypointense at the arterial and portal-venous phases due to a central necrosis. Sometimes, tumors can be detected even at the precontrast phase because of microcalcifications. Malignant islet cells tumors may require a scan in the delayed phase to demonstrate a late enhancement (Fig. 2). Rarely, an islet cell tumor may present as a cystic lesion. Without a specific clinical syndrome (and/or elevation of a specific hormone), the typical hyperdense appearance may be not sufficient for differentiating an islet cell tumor from other pancreatic lesions. The main advantage of CT is the possibility to stage malignant lesions by identifying local spread and distant metastases (3, 4).

At magnetic resonance (MR), islet cell tumors appear to be hypointense on T1-weighted images and hyperintense on heavily weighted T2-weighted images. Using intravenous gadolinium-DTPA may help differentiate hyperintense islet cell tumors from the normal-enhancing pancreatic tissue. The use of mangafodipir trisodium (MnDPDP) also may help to increase diagnostic sensitivity. Additionally, MR cholangiopancreatography (MRCP) can be used to depict an obstruction of the common bile duct or the main pancreatic duct as an indirect sign for a malignant tumor; however, it does not help differentiate islet cell tumors from other pancreatic neoplasms (3, 4).

Nuclear Medicine

Nuclear medicine is useful for tumor imaging and staging because neuroendocrine tumors express peptide hormone receptors on their membranes, and radiolabeled compounds can bind to such receptors. Over the last decade, a

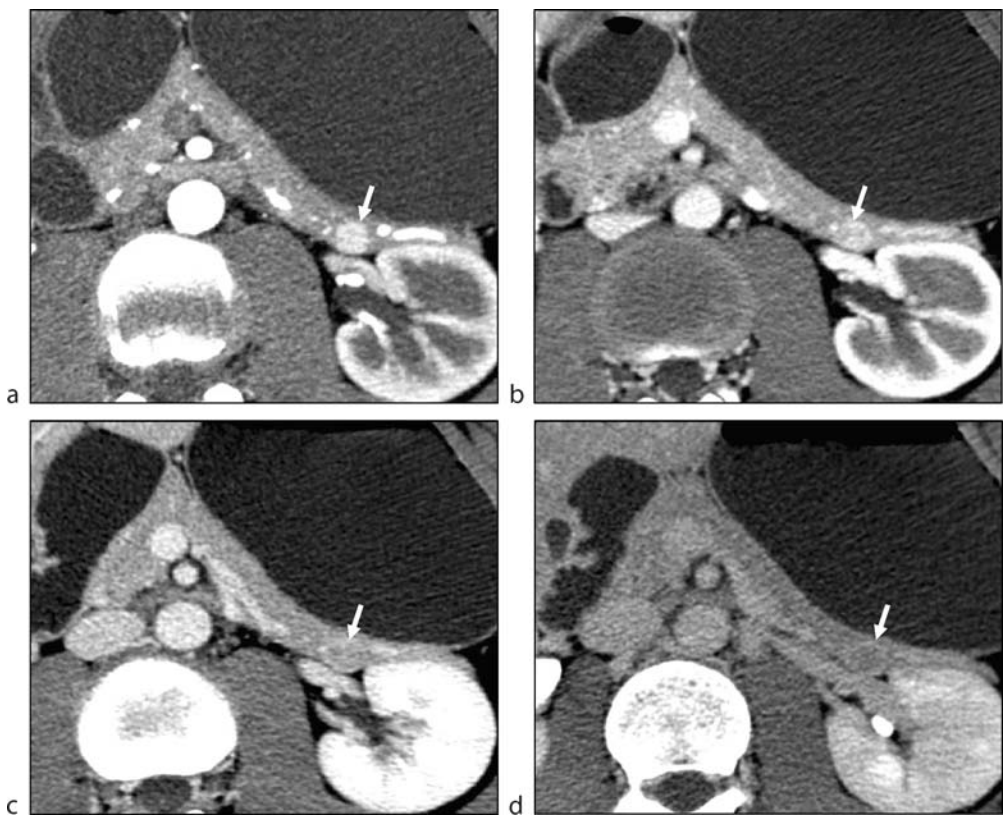

Islet Cells Tumors, Pancreatic. Figure 1 Multidetector computed tomographic study of typical insulinoma of the pancreatic tail. The nodule (*arrows*) appears hyperdense in the early arterial (a) and pancreatic (b) phases, with wash-out and a hypodense appearance in the venous (c) and delayed (d) phases.

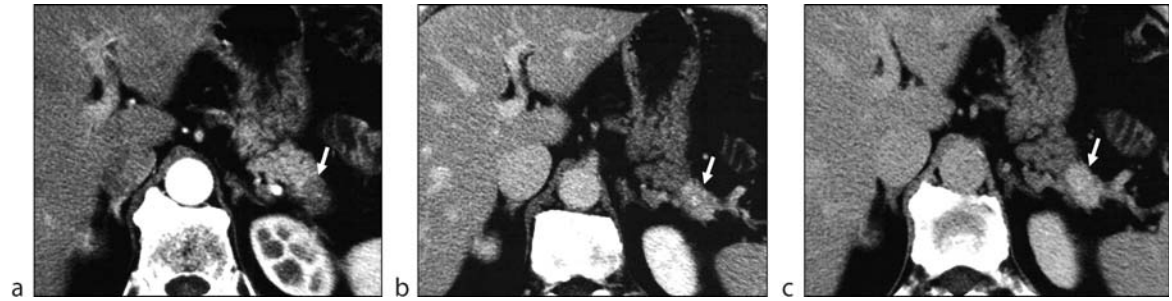

Islet Cells Tumors, Pancreatic. Figure 2 Multidetector computed tomographic study of malignant islet cells tumor of the pancreatic tail. The nodule (*arrows*) appears hypodense in the arterial phase (a) with a late enhancement in the venous (b) and delayed (c) phases.

somatostatin analog labeled with indium-111, ^{111}In-DTPA-D-Phe^{1}-octreotide, has been made available, exhibiting efficient uptake at tissues with high-density receptors for somatostatin. Scintigraphy with ^{111}In-DTPA-D-Phe^{1}-octreotide has been used for evaluating several types of cancer, especially neuroendocrine tumors, as well as medullar thyroid carcinomas, small cell lung cancer, and a certain fraction of breast cancers. In terms of diagnostic accuracy, scintigraphy with ^{111}In-DTPA-D-Phe^{1}-octreotide has shown satisfactory results only in the study of neuroendocrine tumors. Scintigraphic investigation envisages the intravenous administration of 111–148 MBq (3–4 mCi) of ^{111}In-DTPA-D-Phe^{1}-octreotide and "total body" acquisition after 4 and 24 h postinjection. Single photon emission computed tomography (SPECT) should be performed in all patients, preferably at 24 h. In some patients, a 48-h acquisition may be necessary to evaluate unclear accumulation in the abdomen. All images should be obtained with a large-field-of-view gamma camera equipped with a medium-energy parallel-hole collimator (3, 4).

Diagnosis

History taking, clinical examination, and laboratory tests are the basic tools to make up the diagnosis, especially in hormone-producing tumors causing typical symptoms.

Inactive endocrine tumors are generally at an advanced stage of disease at the time of their diagnosis because they become symptomatic only due to their mass effect or, in malignant cases, due to their metastases.

The role of imaging is to localize, demonstrate the extent of, and stage the lesion. Most islet cell tumors are easily identifiable by modern cross-sectional imaging techniques.

Bibliography

1. Pereira PL, Wiskirchen J (2003) Morphological and functional investigations of neuroendocrine tumors of the pancreas. Eur Radiol Sep 3(9):2133–2146
2. Roche A, Baert AL, Therasse E et al (1994) Endocrine tumours of the pancreas. In: Baert AL (ed) Medical Radiology: Radiology of the Pancreas. Springer, Berlin Heidelberg, New York
3. Gouya H, Vignaux O, Augui J et al (2003) CT, endoscopic sonography, and a combined protocol for preoperative evaluation of pancreatic insulinomas. Am J Roentgenol Oct 181(4):987–992
4. Fidler JL, Fletcher JG, Reading CC et al (2003) Preoperative detection of pancreatic insulinomas on multiphasic helical CT. AJR Am J Roentgenol Sep 181(3):775–780

Iso-Osmolality Contrast Media (IOCM)

An iso-osmolality contrast medium is a water-soluble imaging contrast agent that has osmolality (a measure of the number of particles in solution) equal or very close to the osmolality of human blood. See also high osmolality contrast media and low osmolality contrast media.

▶Adverse Reactions, Iodinated Contrast Media, Acute Renal

IVU

▶Intravenous Urography

Jejunal Atresia

A congenital abnormality, usually due to an ischaemic insult in embryological development resulting in complete occlusion of the lumen of jejunum.
►GI Tract, Paediatric, Congenital Malformations

Johansson Blizzard Syndrome

Autosomal recessive syndrome associating motor, somatic, and mental retardation. There are severe oligodentia, migrograthia, and sensorineural defects as well. There are several endocrinal deficits including hypothyroidism, hypopituitarism, pancreatic insufficiency, and lipomatosis.
►Congenital Anomalies of the Pancreas

Joint Infections

►Osteomyelitis, Neonates, Childhood

Joint Space Narrowing

Joint space narrowing reflecting cartilage loss and to a certain extent meniscal extrusion is one of the radiographic imaging criteria for the diagnosis of degenerative joint disease together with formation of osteophytes, presence of subchondral sclerosis and subchondral cysts.
►Degenerative Joint Disease, Peripheral Joints

Juvenile Aseptic Bone Necroses

►Juvenile Osteonecroses

Juvenile Avascular Necroses

►Juvenile Osteonecroses

Juvenile Osteonecroses

Christian R. Krestan
Department of Radiology, Medical University of Vienna, Vienna General Hospital, Waehringer Guertel 18–20, A–1090 Vienna, Austria
christian.krestan@meduniwien.ac.at

Synonyms

Juvenile aseptic bone necroses; Juvenile avascular necroses

Definitions

In principle, the same definition applies to juvenile osteonecrosis as is used for adult osteonecrosis. The prevalence of these osteonecroses is limited to childhood and adolescence. It is an avascular, ischemic necrosis found at the epiphyseal and subarticular region.

Pathology/Histopathology

The anatomy and histology of the articular and subarticular region are important for understanding the pathophysiology of osteonecrosis. The adult pattern of vascular supply usually becomes established at the age of 18 years with the closure of the endplate (1). The number of subchondral vessels (arterial vessels, capillaries, sinusoids, and venous vessels) at the base of the articular hyaline cartilage reaches their highest level with adolescence and decline by approximately 20% until the seventh decade of life. This vascular bed of the subchondral

regions is very important for the nourishment of the base of the articular cartilage.

Special vascular supplies, different from adult vascularization, have a great impact on the development of osteonecrosis. For example, the growth plate represents an effective barrier preventing anastomoses between the femoral head and femoral neck.

Necrosis of the trabeculae and marrow is found histologically, which can lead to flattening and collapse of bones. In this case compression of trabeculae and intertrabecular detritus is observed. In the case of healing, viable bone is deposited on dead trabeculae with reconstitution of intertrabecular marrow.

Clinical Presentation

The clinical symptoms depend on the anatomic location of the osteonecrosis. One of the most important juvenile osteonecroses is Perthes' disease. The clinical manifestation is characterized by limping, pain and limitation of joint motion, particularly on abduction and internal rotation of the hip. Even atrophy of the soft tissues of the thigh, muscle spasm, and contractures can be found. The differential diagnosis can be acute irritable hip syndrome with transient synovitis, which is, however, a self-limiting disease. The cause of transient synovitis of the hip and the relationship to Perthes' disease are not clear. Patients with Freiberg's infarction may present with local pain, soft tissue swelling, and limitation of motion of the affected metatarsophalangeal joint. In Köhler's disease the foot may be held in a slight varus position and the patient walks on the outer side of the foot. Again, localized pain and swelling are the main clinical features.

Imaging

Basically, standard radiographs still have to be used in the diagnosis of juvenile osteonecrosis. Soft tissue swelling on the lateral side of articulation is characteristic. Every second patient may present with smallness of the femoral ossification nucleus in Perthes' disease. Lateral displacement and even flattening and sclerosis of the femoral ossification nucleus are further findings. Ultrasound can be used for the detection of a joint effusion and joint space widening, which is, however, unspecific and can be found in a variety of clinical conditions. Radiographs are not suitable for early diagnosis because in the initial stages usually no radiographic abnormalities are found. Due to its unbeatable sensitivity for bone marrow changes including visualization of necrotic tissue, magnetic resonance imaging ►(MRI) is the imaging modality of choice for early diagnosis (2) (Fig. 1a, b). Signal intensities of the femoral epiphysis in Perthes' disease are usually reduced on T1- and T2-weighted MR images (3). MRI may reveal findings consistent with transient bone marrow edema, which may be a precursor for Perthes' disease. Further findings are a thickening of both the femoral and acetabular articular cartilage with subsequent lateralization of the hip. In patients with Freiberg's infarction a serpentine region of lowered signal intensity can be found in the head of the second metatarsal bone on T1-weighted images, with surrounding bone marrow edema on T2-weighted sequences and an associated joint effusion. In Panner's disease a low-signal intensity demarcation of the capitulum humeri is characteristic on T1-weighted images with a hyperintense edema on short T1 inversion recovery (STIR) images representing bone marrow edema in early phases of the disease.

Nuclear Medicine

Reduction of blood flow appears as a "cold" spot on radionuclide studies in patients with osteonecrosis. Comparative studies with MRI using a dynamic gadolinium-enhanced subtraction technique and bone scintigraphy demonstrated good agreement between both techniques in the depiction of epiphyseal necrosis in Legg-Calvé-Perthes disease (4). MRI is nowadays widely accepted as a nonionizing substitute for bone scintigraphy, which is especially relevant in juvenile patients.

Diagnosis

The most common sites for juvenile osteonecrosis are the femoral head, the navicular bone, the head of the second metatarsal bone, and the capitulum of the humerus.

Legg-Calvé-Perthes disease affects children, particularly those between the ages of 4 and 8 years. The disorder is more frequent in boys than girls with a ratio of approximately 6:1. Bilateral abnormalities are detected in about 10–20% of cases. In cases in which both hips are involved, the two hips are usually affected sequentially, not simultaneously.

The early radiographic signs include soft tissue swelling due to an effusion, diminutive femoral head ossification center with lateral displacement, fissuring/fracture, flattening, and sclerosis (Fig. 1c).

The pathologic basis of the above-mentioned radiographic signs is osteonecrosis. Necrosis of the marrow and trabeculae is observed with a resulting collapse and compression of the trabeculae and flattening of the joint surface. Healing is characterized by revascularization of the marrow starting from the periosteal and ligamentum teres vessels. Reconstitution of intratrabecular marrow

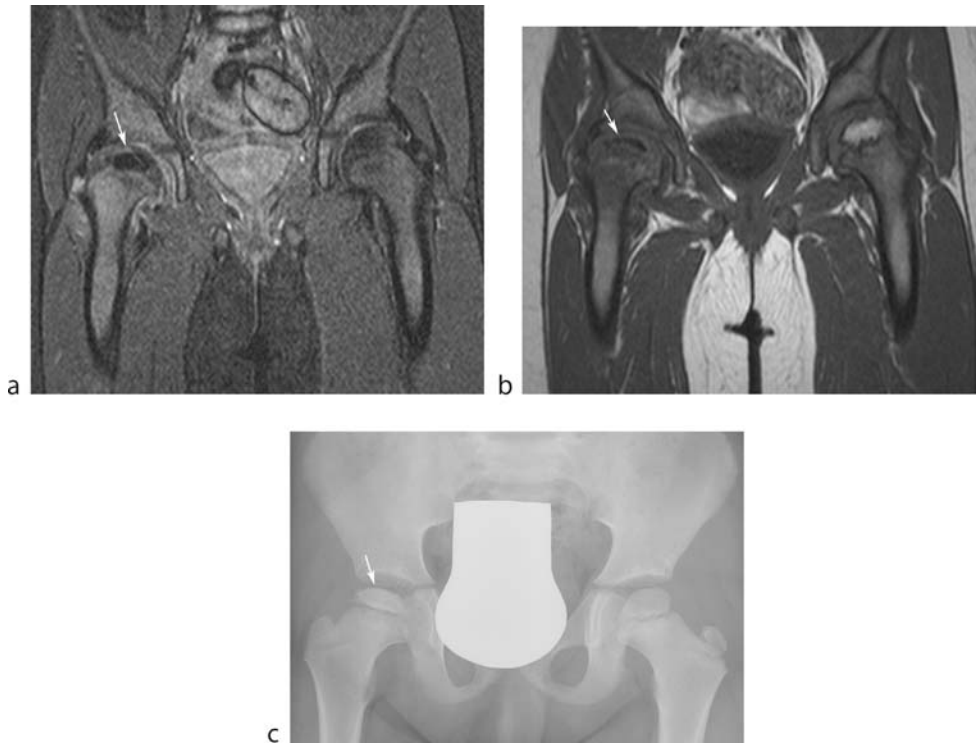

Juvenile Osteonecroses. Figure 1 (a) Coronal MRI (STIR) demonstrates marked signal reduction of the right femoral head in ►Legg-Calvé-Perthes disease. (b) Coronal MRI (T1-SE) demonstrates marked signal reduction of the right femoral head in Legg-Calvé-Perthes disease. (c) Anteroposterior view of the pelvis shows flattening of the right femoral head with sclerosis in Legg-Calvé-Perthes disease in a 5-year-old girl.

and the trabeculae is almost always complete, but some degree of flattening of the head and shortening and broadening of the femoral neck is not unusual. The synovialis may show reactive inflammatory changes in the acute phase.

The etiology of the osteonecrosis is based on vascular insufficiency. The factors leading to the deficient blood supply have not been precisely identified. One explanation is the change of vascular supply in this age group. Before the age of 4 years, two groups of vessels are left (superior and inferior retinacular arteries). Between the ages of 4 and 7 years, the importance of the lateral epiphyseal vessels is established as the metaphyseal and fovea vessels decrease. After the age of 8 years, the importance of the ligamentum teres vessels increases again. The open growth plate prevents anastomosis between the vessels of the neck and the head. This vessel reorganization during the period of 4–7 years and possible failures in this reorganization do not explain the male prevalence of the disease. A second theory stresses the posttraumatic etiology. Direct repetitive compression leads to subchondral fractures. Traumatic synovitis with effusion could lead to compression of the adjacent vasculature with infarctions leading to osteonecrosis.

Finally, a genetic cause has been discussed. This genetic and developmental factor may lead to alterations in the blood vessels or (and) to a localized abnormal maturation of epiphyseal cartilage that is responsible for the delay in the skeletal maturation, which is also a very typical feature in Legg-Calvé-Perthes disease.

A better prognosis is observed in boys and younger patients, perhaps indicating that a longer elapsed time before skeletal maturity allows more extensive remodeling and healing of the femoral head.

Grading and classification systems try to stage the different disease phases, the extent, and the end result of the disease.

The four stages are characterized by: 1. epiphyseal irregularity, dislocation, and increased density, 2. epiphyseal fragmentation, 3. increasing homogeneity, and 4. normal ossification or deficient healing.

The extent of disease is graded according to Caterall in four groups:

Patients in groups 3 and 4 have a poorer prognosis, in general. It is, however, evident that no simple radiologic observation is indicative of a good or poor result, and that a combination of clinical and radiologic findings must be used for prognostic accuracy.

Besides standard radiographs, MRI is applied for early diagnosis and follow-up of the disease. With bone scintigraphy the reduced or missing uptake of the radioisotope in the head of the femur is indicative of the onset of the disease. The increasing radioisotope uptake parallels the healing process; however, bone scintigraphy has been largely replaced, as stated above.

As in the adult type of osteonecrosis, MRI is ideally fitted for the early detection and follow-up of Legg-Calvé-Perthes disease. The missing ionizing radiation is another important advantage of this modality. Moreover, it allows direct visualization of neighboring bone marrow changes. One important feature is thickening of cartilage and loss of containment of the femoral head within the acetabulum (5). Thickening and contrast enhancement of the synovial structures with effusion are other typical MRI findings.

In dislocations of the femoral head and slipped epiphysis, the ligamentum teres vessel and the retinaculum vessels may be torn, resulting in diminished blood flow.

Dislocation of the hip joint is a common complication of acetabular fractures, too. Osteonecrosis has been reported in as many as 10–20% of patients with hip dislocation. Reposition has to be done within 6 h after the trauma to minimize the risk of osteonecrosis development.

Freiberg's Disease

Women are predominantly affected by a factor of 5:1. Most commonly it is found in the age group of 13–18 years. Typically, the head of the second metatarsal bone is involved, but it may also be found in any other metatarsal heads. The disease is unilateral. MRI reveals a localized subchondral marrow edema with flattening of the cortical endplate and fragmentation. Radiographic abnormalities include subtle flattening, increased radiodensity, and cystic lucent areas. The process ends with deformity, defect healing, and collapse of the bone. Complete healing can be seen, even after many years (Fig. 2).

Köhler's Disease

The relationship between Köhler's disease of the tarsal navicular bone and osteonecrosis has not been defined. Its etiology could go back to an altered ossification or a vascular insufficiency. It affects more boys than girls (5:1) and is found in the age between 3 and 7 years. Unilateral involvement is seen in 80% of all cases. In one-third of all cases an additional trauma can be elicited. Some authors believe it is not a disease at all, but only an altered sequence of tarsal ossification. The "disease" is self-limiting and reversible. The imaging findings are the same as those described in the other bones (Fig. 3).

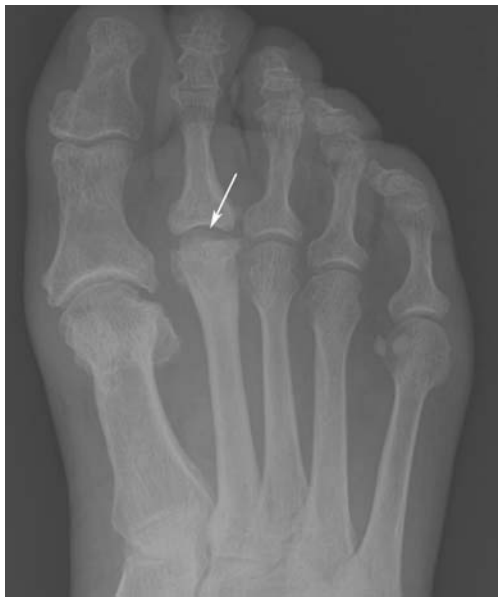

Juvenile Osteonecroses. Figure 2 Anteroposterior view of the right foot with flattening of the head of the second metatarsal bone (Freiberg's disease).

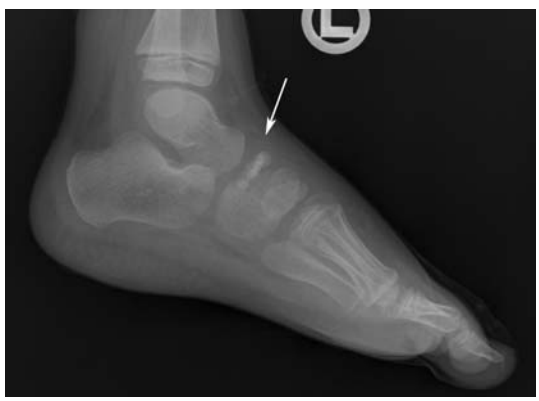

Juvenile Osteonecroses. Figure 3 Lateral view of the left foot with collapse of the navicular bone (Köhler's disease) in a 5-year-old boy.

Panner's Disease

It is a rare disease involving the capitulum of the humerus. It appears usually between the age of 5 and 10 years. Boys are almost exclusively affected. It may be found in patients with chronic trauma. Bilateral involvement is rare; it is most likely that, similar to Legg-Calvé-Perthes disease, a change in the vascularization because of maturation makes the capitulum especially vulnerable to mechanical trauma.

Bibliography

1. Resnick D (2002) Diagnosis of Bone and Joint Disorders, vol 4, 4rd edn. W.B. Saunders Company. Philadelphia, pp 3495–3558
2. Kramer J et al (2002) [Perthes disease]. Radiologe 42(6): 432–439
3. Mahnken AH et al (2002) MR signal intensity characteristics in Legg-Calve-Perthes disease. Value of fat-suppressed (STIR) images and contrast-enhanced T1-weighted images. Acta Radiol 43(3):329–335
4. Lamer S et al (2002) Femoral head vascularisation in Legg-Calve-Perthes disease: comparison of dynamic gadolinium-enhanced subtraction MRI with bone scintigraphy. Pediatr Radiol 32(8):580–585
5. Rush BH, Bramson RT, Ogden JA (1988) Legg-Calve-Perthes disease: detection of cartilaginous and synovial change with MR imaging. Radiology 167(2):473–476

Karyotype

The complete chromosomal complement of the individual.
►Ambiguous Genitalia

Kasabach–Merrit Syndrome

Condition characterized by thrombocytopenia, anemia, and coagulopathy. It may occur from sequestration of hematopoietic cells in large hemangiomas.
►Neoplasms, Splenic, Benign
►Hepatic Pediatric Tumors, Benign

Kasai Procedure

Bilio-digestive anastomose. Surgical intervention performed to obtain a biliary drainage in which the porta hepatis is dissected and a loop of small intestine is anastomosed to the exposed draining biliary radicles.
►Congenital Malformations, Liver and Biliary Tract

Kashin–Beck Disease

An acquired disease in which various sites of enchondral growth are impaired; at a physis, involvement leads to local fusion.
►Osteonecrosis in Childhood

Kellgren–Lawrence-scale

Developed in 1957 this radiography based scoring system semi-quantitatively grades OA in four severity grades from normal to severe using the criteria joint space narrowing, osteophytes, cysts and subchondral sclerosis.
►Degenerative Joint Disease, Peripheral Joints

Kidney cancer

►Carcinoma, Renal Cell

Kidney Fusion Anomalies

Congenital variations and malformations of the kidneys that have embryological reasons and lead to fusion of two kidneys, usually at the lower pole, that then form a joined organ in atypical position and rotation, and thus may be accompanied by urinary tract diversion or obstruction. Typical examples are the cross fused- or horse shoe kidney.
►Urinary Tract

Kidney Stones

►Colic, Acute, Renal

Kidney, Ureter, Bladder Plain Film

KUB can be diagnostic of urinary stones, since 90% are radiopaque. It is necessary for the follow-up of stone passage or for lithotripsy planning and survey. It can miss small stones, radiolucent urate stones, or stones overlying bone. Sometimes phleboliths, vascular calcifications, calcified lymph nodes, appendicoliths, granulomas, various calcified masses, and even bowel contents can be confused with urinary tract stones. KUB taken prior to conventional contrast studies is necessary for their detection.
►Colic, Acute, Renal

King's Foot

▶Gout

Klatskin Tumors

The Klatskin tumor is a type of cholangiocellular carcinoma arising from the bile duct epithelium at the convergence of the right and left hepatic ducts. According to the Bismuth classification, four different types of Klatskin tumors are distinguished: type I involves the main hepatic duct below the bifurcation, type II affects the main hepatic duct bifurcation, type III involves segmental ducts beyond the primary hepatic duct bifurcation in one liver lobe (type IIIa: right lobe, type IIIb: left lobe), and type IV involves segmental ducts in both liver lobes.

▶Neoplasms, Bile Ducts

Klippel–Trenaunay–Weber Syndrome

Rare congenital malformation that may include large cutaneous hemangiomas, soft tissue and bony hypertrophy, venous malformations, and lymphatic abnormalities.

▶Neoplasms, Splenic, Benign

Konig's Disease

▶Fibrocystic Disease, Breast

Koss-score

This semi-quantitative MRI based knee osteoarthritic scoring system is used to monitor disease progression of osteoarthritis. MR images are scored for the presence of cartilaginous lesions, osteophytes, subchondral cysts, bone marrow oedema, meniscal abnormalities, presence and size of an effusion, synovitis and Baker's cyst.

▶Degenerative Joint Disease, Peripheral Joints

KUB

▶Kidney, Ureter, Bladder Plain Film

Kulchitsky Cell

Or synonym *enteroendocrine cell* contains granules that may be either argentaffinic or argyrophilic. They are scattered throughout the digestive tract, are of several varieties and are believed to produce more than 20 gastrointestinal hormones and neurotransmitters.

▶Neoplasms of the Chest in Childhood

Kyphoscoliosis

A curvature of the spine that is backward and lateral.

▶Neurofibromatosis, Musculoskeletal Manifestations

Laceration, Hepatic

Hepatic lacerations represent the most common form of hepatic injury. These lesions can be single or multiple and tend to involve hepatic parenchymal areas contiguous to intrahepatic portal vascular branches and suprahepatic veins; in particular, typical lacerations are parallel to hepatic veins or the posterior segmental right branch of portal vein. The cause of injury is the "shaking" forces that operate near the central vascular structures.

A large range of severity must be distinguished in lacerative lesions of the liver, including small and superficial lesions of the hepatic capsule (capsule tears), lacerations involving the central portal triad (deep lacerations), and major deep lacerations extending between two margins of the organ (hepatic fracture). Hepatic lacerations can, occasionally, slightly increase in size within the first week, also becoming less sharply defined; however, they usually disappear within 4–6 months.

Hepatic laceration is a typical lesion appearing as a nonenhancing linear streaking area on contrast-enhanced computed tomography. Appearances on ultrasound of hepatic laceration change with time: it initially appears slightly echogenic, becoming hypoechoic or cystic after several days.

►Trauma, Hepatobiliary

Laceration, Splenic

A splenic parenchymal lesion with a linear or branching appearance that may reach the splenic margins without completely traversing the parenchyma.

►Trauma, Splenic

Lactating Adenoma

Benign tumor that occurs during pregnancy or the puerperal period. It is composed of compact aggregates of lobules with secretory hyperplasia.

►Adenoma, Breast

Laennec's Cirrhosis

Hepatic cirrhosis in which increased connective tissue spreads out from the portal spaces compressing and distorting the lobules, causing impairment of liver function, and ultimately producing the typical hobnail liver.

►Cirrhosis, Hepatic

Lamina Dura

The radiographic dense line that surrounds roots of erupted teeth and all of not yet erupted teeth is washed out in hyperparathyroidism and several other conditions, including Langerhans cell histiocytosis and local periapical infection.

►Battered Child Syndrome

Laminectomy

►Radicular Syndrome of the Spine, Surgical Therapy for

Langerhans Cell

Langerhans cell histiocystosis (LCH) contain granulomatous lesions containing characteristic Langerhans cells.
▶Neoplasms, Chest Childhood

Laparoscopy

▶Optical Imaging

Large Bowel Obstruction

▶Occlusion, Bowel in Childhood

Large Core Needle Biopsy

Percutaneous puncture technique used to remove cylinders of tissue from suspicious lesions for histological study. For breast lesions, 14-gauge needles are the most commonly used. Each specimen to be obtained requires a new insertion of the needle.
▶Breast Conserving Therapy

Large Joints

Large joints comprise the shoulder, hip, and knee. In rheumatic diseases such as rheumatoid arthritis and spondyloarthropathies, (primary) manifestations of the large and small joints, respectively, are considered as (indistinct) subsets.
▶Spondyloarthropathies, Seronegative

Laryngeal Tuberculosis

Bronchogenic or lymphogenic infection of the larynx with mycobacterium tuberculosis with increasing incidence in immunocompromised population, may be indistinguishable from laryngeal carcinoma on imaging studies.
▶Larynx, Inflammatory Diseases

Laryngitis, Acute

Acute, predominantly viral infection causing dysphonia and a dry cough.
▶Larynx, Inflammatory Diseases

Laryngitis, Chronic

Gradual development of hoarseness and pain caused by inflammation due to exogen factors, granulomatous or fungal disease.
▶Larynx, Inflammatory Diseases

Laryngotracheitis

An acute viral inflammation of the upper and lower respiratory tracts, characterized by inspiratory stridor, subglottic swelling, and respiratory distress that is most pronounced on inspiration.
▶Larynx, Inflammatory Diseases

Larynx

A cartilaginous structure at the top of the trachea that contains elastic vocal cords.
▶Neoplasms, Benign and Malignant, Larynx

Larynx, Inflammatory Diseases

Michael Lell[1], Johannes Zenk[2], Holger Greess[1]
[1]Department of Radiology, University Erlangen-Nürnberg, Erlangen, Germany
[2]Department of Head and Neck Surgery, University Erlangen-Nürnberg, Erlangen, Germany
michael.lell@idr.imed.uni-erlangen.de

Definition

Inflammatory diseases of the larynx may be of infectious or noninfectious origin. Acute infections present with a sudden onset and develop symptoms like fever and respiratory distress. Chronic infections develop over a longer period and present with hoarseness and pain.

Acute infections of the larynx are predominately relatively harmless viral infections but hazardous infections like ►laryngotracheitis (croup), ►epiglottitis, and diphtheria must be taken into consideration, because the latter can be lethal especially for children. Angioneurotic edema causing inspiratory stridor affects adolescents and adults more commonly than children.

►Chronic laryngitis develops over weeks to month and the dominant symptoms are hoarseness and pain caused by exogen factors (cigarette smoking, occupational contact with toxic fumes, voice abuse, gastroesophageal reflux disease), granulomatous and fungal infections. Systemic diseases involving the larynx are rheumatoid arthritis, sarcoidosis, Wegener's granulomatosis, and ►amyloidosis. Radiation therapy induces inflammatory changes of the laryngeal mucosa and submucosal tissue, which usually decrease within the first 6 months after completion of the therapy but may persist for years.

Pathology and Histopathology

►*Acute unspecific laryngitis* is usually caused by viruses (rhinovirus, influenza and parainfluenza virus, coxsackie virus, adenovirus, and respiratory syncytial (RS) virus), which can be associated with group A streptococcus, *Staphylococcus*, hemophilus influenzae, or *Moraxella catarrhalis*. Less common causes are thermal, allergic, or chemical inhalative substances. Serous–mucous, purulent–catarrhal, or fibrinous–purulent inflammatory changes may be observed. Pseudomembranous-necrotizing inflammation is characteristic for diphtheria.

Laryngotracheitis or croup is an infection of the subglottic larynx in the age group of 3 months to 3 years and usually is caused by a parainfluenza virus (type 1), less common are RS virus and type A influenza virus. Rapid onset of inflammatory edema of the cricovocal membrane and cranial trachea cause severe airway narrowing. *Epiglottitis* or supraglottitis occurs in an older age group (2–4 years), but can also occur in the adult population and is commonly caused by hemophilus influenza type B (HIB). In the adult population, hemophilus parainfluenzae, *Streptococcus pneumoniae*, group A streptococcus, or *Staphylococcus aureus* is also common, but there is also a high rate of negative blood cultures. Epiglottitis causes inflammation and swelling of the epiglottis, vallecula, arytenoids, and aryepiglottic folds.

Angioneurotic edema is characterized by episodes of increased capillary permeability with extravasation of intravascular fluid and subsequent edema of the cutis or mucosa of the upper airways or gastrointestinal tract. Hereditary angioneurotic edema is caused by a C1-esterase inhibitor deficiency. Allergic edema is caused by drugs (amongst others angiotensin-converting enzyme inhibitors and ionic contrast material) and food.

Tuberculosis of the larynx is rare but gained increasing importance in immunocompromised patients. The larynx is most often infected through bronchogenic spread from active lung disease but may also be affected lymphogenic or hematogenous. Mucosal hyperemia and thickening, nodules and ulcerations can be found at laryngoscopy and deep biopsy is required to exclude carcinoma. Biopsy reveals acid-fast bacilli and cultures should be performed to confirm diagnosis.

Other granulomatous diseases include Wegener's granulomatosis, sarcoid, pemphigus, leprosy, and numerous mycotic infections. Wegener's granulomatosis is characterized by necrotizing granuloma affecting the upper respiratory tract, lung, and kidneys. Laryngeal involvement is rare, mucosa ulceration and bone destruction as well as glottic and subglottic stenosis can result. Sarcoid usually affects the supraglottis, less commonly the glottis and subglottis. It may present as an isolated submucosal mass, indistinguishable from tumor.

Rheumatoid arthritis can affect the cricoarytenoid and cricothyroid joints as well as other synovial joints in the body.

Relapsing perichondritis is a rare inflammatory disease of unknown etiology. The cartilages of the ear, nose, larynx, trachea, and joints can be affected. Initially, edematous soft tissue around the cartilage is found with progression to cartilage destruction and collapse.

Amyloidosis is not a single entity but rather a group of diseases characterized by the presence of extracellular

deposition of amyloid in tissues. Less than 1% of all benign tumors in the larynx are amyloidomas. The supraglottic larynx is the most commonly involved region, amyloid deposits are located in the submucosa. Yellow-reddish tumorlike lesions with vitreous consistency can be found at inspection.

Gastroesophageal reflux disease (GERD)-related laryngitis or reflux laryngitis is common, but the prevalence varies considerably in the literature. The presence of gastric acid in the larynx can cause inflammation in the posterior larynx, especially in the interarytenoid region, aryepiglottic folds, and posterior cord area. In laryngoscopy, edema and erythema can be found as well as mucosal ulcerations in the posterior larynx.

Radiotherapy (RT) frequently induces edema and chronic inflammatory disease. Histologic findings are an acute inflammatory reaction with leukocytic infiltration, histiocyte formation, necrosis, and hemorrhage. Smaller vessels demonstrate detachment of the lining endothelial cells causing increased permeability resulting in interstitial edema. Deposition of collagenous fibers is found in the following 1–4 months, leading to sclerosis and hyalinosis of connective tissues. This inflammatory process eventually results in obstruction in the small arteries, veins, and lymphatics. By 8 months, there is advanced sclerosis, hyalinosis, and fragmentation of the collagen fibers. The formation of collateral capillary and lymphatic channels may reduce interstitial fluid.

Clinical Presentation

Acute unspecific laryngitis is characterized by dysphonia and dry cough. In advanced cases, pain and dysphagia may occur.

Laryngotracheitis has a gradual onset and typical symptoms are stridor and barking cough.

Epiglottitis or supraglottitis typically present with a sore throat and painful dysphagia/inability to swallow, along with stridor and dyspnoea. The onset is sudden with a rapid progression. Epiglottitis is a life-threatening condition because total airway obstruction may occur very rapidly.

Angioneurotic edema is characterized by recurrent edema of the face, respiratory, and gastrointestinal tract. The episodes occur spontaneous without concomitant symptoms and last for 2–3 days causing inspiratory stridor.

Tuberculosis present with dysphonia, dysphagia, and sore throat.

Wegener's granulomatosis, sarcoid, pemphigus, leprosy, mycotic infections and *rheumatoid arthritis* can present with hoarseness and dyspnoea but other organ manifestations usually cause the leading symptoms.

Relapsing perichondritis shows a prolonged course, increased subjective discomfort and typical pain on palpation.

Amyloidosis rarely affects the larynx. Symptoms are hoarseness and dyspnoea. *Gastroesophageal reflux disease* (GERD)-related laryngitis or reflux laryngitis present with chronic hoarseness, sore throat, chronic cough, dysphagia, or globus.

Radiotherapy (*RT*) frequently induces edema and mucositis leading to dyspnoea, dysphonia, and dysphagia. Delayed complications include soft tissue necrosis, osteochondronecrosis, fistula formation, pharyngeal motility dysfunction and strictures, and recurrent laryngeal nerve paralysis.

Imaging

Imaging is only occasionally performed in patients with inflammatory disease of the larynx, most patients are diagnosed clinically. Imaging may be done to exclude foreign bodies, recurrent tumor, and to localize the site of biopsy before performing laryngoscopy. Assessment of complications like abscess formation is another indication for cross-sectional imaging.

Conventional radiographs may be used in the diagnosis of laryngotracheitis (croup) or epiglottitis (supraglottitis).

CT and MRI are helpful to assess the submucosal extent of disease and to detect cartilage involvement. Imaging should be performed prior to biopsy in order to avoid misinterpretation of biopsy trauma and underlying disease.

High-resolution MRI is more sensitive to soft tissue changes than CT, but suffers from motion artefacts related to prolonged acquisition time. Fast gradient echo imaging can be performed in patients short of breath, but these patients are preferentially imaged with multislice spiral CT (MSCT) scanners.

The entire larynx can be examined with submillimeter collimation in less than 10 sec, minimizing motion artefacts and allowing phonation scans with MSCT.

Acute unspecific laryngitis is diagnosed clinically.

Laryngotracheitis causes mucosal swelling in the subglottic area and can be appreciated on a frontal radiograph as the "wine-bottle" or "steeple" sign. Paradoxical dilatation of the hypopharynx during inspiration should alert the clinician to the diagnosis.

Epiglottitis or supraglottitis is a life-threatening condition because total airway obstruction may occur very rapidly. Therefore the patient must never be out of an environment where emergency tracheostomy can be performed. If imaging is performed, thickening of the epiglottis and supraglottic larynx can be seen on lateral

plain films. The thin curvilinear shape is lost ("thumb print sign"), the epiglottis bends into the enlarged aryepiglottic folds and the vallecula looses definition ("vallecula sign"). In severe cases, the arytenoids prominence may be swollen. CT or MRI can be employed in selected cases to exclude abscess formation.

Angioneurotic edema: CT or MRI demonstrates edema of the laryngeal mucosa.

Tuberculosis of the larynx: Imaging features are nonspecific and may be indistinguishable from squamous cell carcinoma. Diffuse or nodular soft tissue thickening with or without infiltration of the paraglottic and preepiglottic spaces and perichondritis can be found (1) (Fig. 1). Diffuse bilateral thickening without destruction of the laryngeal skeleton is common. The cricoarytenoid joint can be involved, causing fixation.

Wegener's granulomatosis, sarcoid, pemphigus leprosy, and mycotic infections: Radiographic findings in granulomatous disease are nonspecific soft tissue thickening and biopsy is required to establish the correct diagnosis.

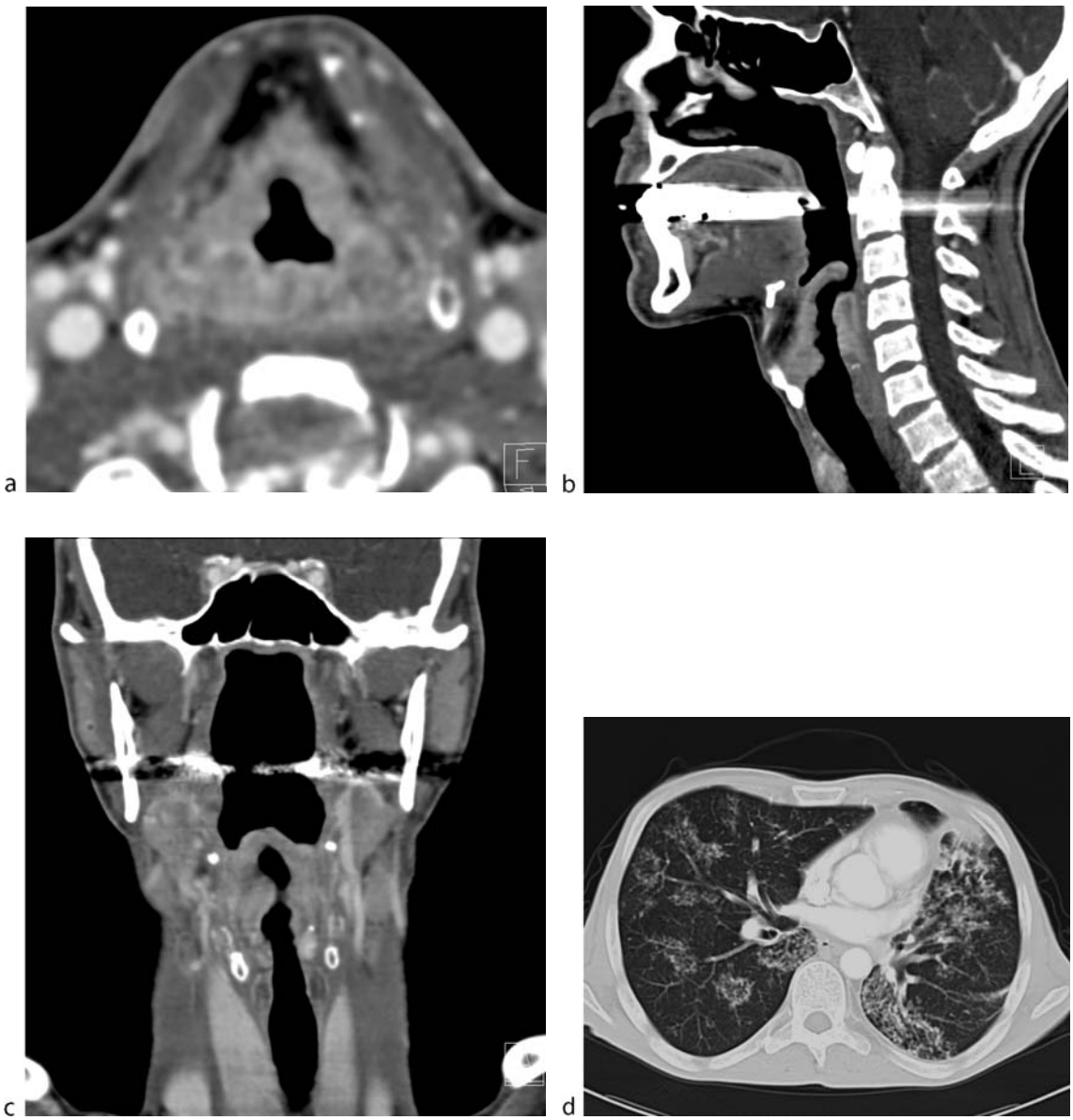

Larynx, Inflammatory Diseases. Figure 1 ▶**Laryngeal tuberculosis: diffuse bilateral thickening of the glottic and supraglottic larynx. (a) Axial section at the level of the false cords demonstrates nodular mucosal thickening with peripheral contrast enhancement. The extent of laryngeal involvement can be appreciated on sagittal (b) and coronal (c) images. Active pulmonary tuberculosis was present (d).**

Rheumatoid arthritis: On CT irregular sclerosis or erosion of the joints can be identified.

Relapsing perichondritis: Initially, edematous soft tissue around the cartilage is found with progression to cartilage destruction and collapse. Edema and inflammation can present with high signal intensity (SI) on T2-weighted images along the margins of the cartilage. Other imaging findings are cartilage expansion, sclerosis or destruction, and soft tissue calcification.

Amyloidosis: The supraglottic larynx is the most commonly involved region, amyloid deposits are submucosal. The lesions may appear as a well-defined homogeneous mass or diffuse soft tissue infiltration (Fig. 2). Although bone erosion has been described in skull base and spine lesions, cartilage or bone destructions are uncommon in the larynx. Although the amyloid itself does not enhance with contrast material administration, peripheral enhancement can be found with CT or MRI. Enhancement may be caused by the foreign body giant-cell reaction that is evoked by amyloid deposition. Calcification has been described and is best appreciated on high-resolution CT scans. Amyloidosis is isointense to muscle on T1-weighted images and can be hypointense (2) or iso- to slightly hyperintense on T2-weighted images. This may help to differentiate calcified focal amyloidoma from chondrosarcoma, which is markedly hyperintense on T2-weighted images (3).

Gastroesophageal reflux disease (GERD): Imaging findings are nonspecific, demonstrating edematous soft tissue swelling in the posterior larynx.

RT results in radiologic changes that involve both the exolaryngeal and endolaryngeal regions. In the larynx, RT

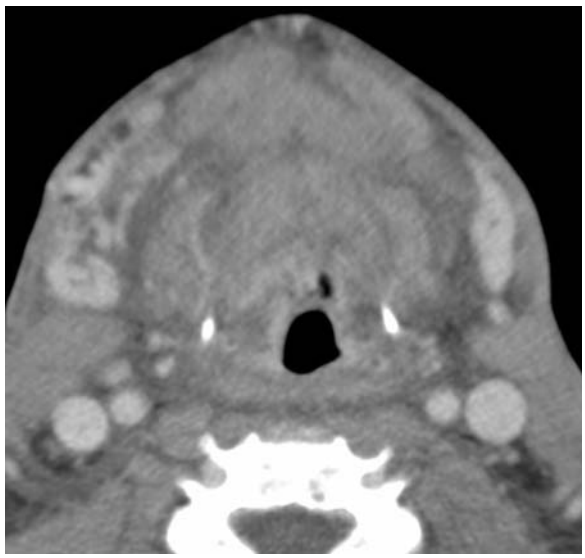

Larynx, Inflammatory Diseases. Figure 2 Amyloidosis in a patient with multiple myeloma. Extensive amyloid deposition in the supraglottic larynx.

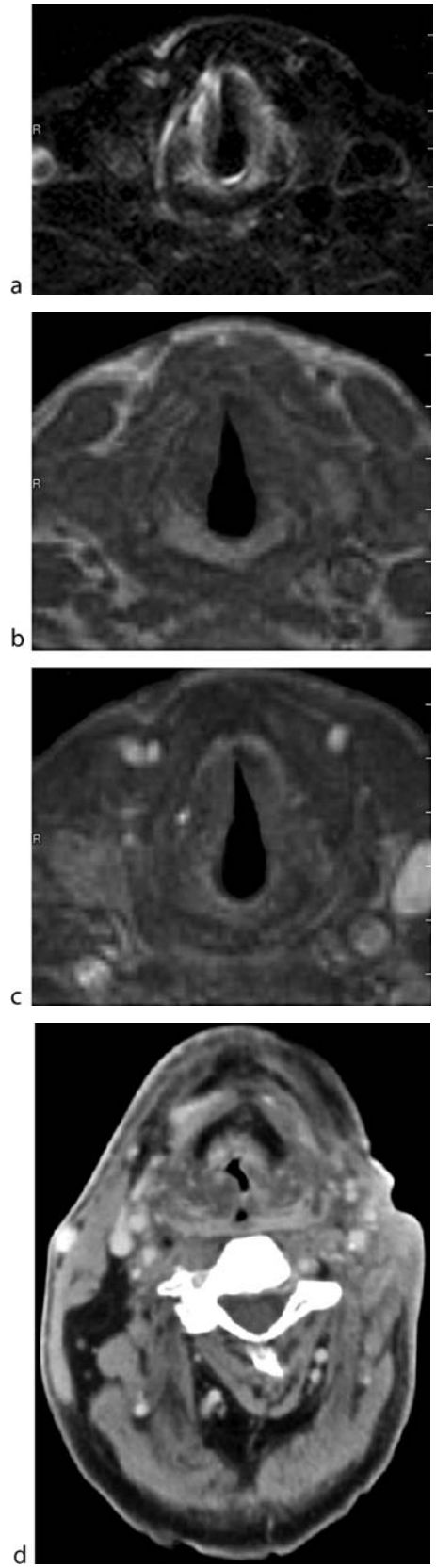

Larynx, Inflammatory Diseases. Figure 3 (continued)

results in thickening of the epiglottis and is typically seen on CT and MRI within 3 months after RT (4). Almost all patients will show increased attenuation in the fat layers, thickening of the aryepiglottic folds and the false vocal cords (Fig. 3). Early changes at the glottic level include increased attenuation of the paraglottic fat planes, typically identified within 2 months following RT. Symmetric subglottic thickening occurs in about 80% of patients. Late changes at the glottic level include thickening of the anterior and posterior commissure. These changes occur within 7 and 14 months, respectively, and are irreversible (5). Unilateral paramedian position of the vocal cord, anteriomedial displacement of the arytenoids cartilage, ipsilateral dilatation of the pyriform sinus, laryngeal ventricle and vallecula, as well as thickening and anteromedial displacement of the aryepiglottic fold indicates recurrent laryngeal nerve paralysis. Soft tissue necrosis and chronic inflammatory disease most often observed within the first two years after RT can be focal and mimic recurrent tumor. Follow-up examinations or biopsy may be required for diagnosis.

Nuclear Medicine

Nuclear scans have a limited role in the assessment of inflammatory lesions of the larynx. Radionuclide bone scans in patients with rheumatoid and collagen vascular disease can be positive over affected joints as well as over the larynx and may be used for primary diagnosis as well as therapy follow-up.

Diagnosis

Diagnosis of inflammatory disease of the larynx is done clinically (including laryngoscopy) and imaging is rarely performed. MRI is more sensitive to inflammatory changes than CT due to better soft tissue resolution. The purpose of imaging is to exclude other causes of stridor such as foreign body aspiration or tumor and to diagnose complications like abscess formation. If abscess is suspected, CT-guided intervention can be performed in the same session. High-resolution CT is recommended in the diagnosis of perichondritis, demonstrating chondral sequestration.

Larynx, Inflammatory Diseases. Figure 3 (a–c) Patient with mild edema of the glottis 12 months after RT [(a) T2-weighted, (b) T1-weighted, and (c) T1-weighted + Gd fat suppression]. (d) Different patient with extensive supraglottic edema 6 months after postoperative radiochemotherapy and neck dissection.

Bibliography

1. Moon WK, Han MH, Chang KH et al (1996) Laryngeal tuberculosis: CT findings. Am J Roentgenol 166:445–449
2. De Foer B, Hermans R, Feenstra L (1993) CT and MRI of laryngeal amyloidosis. Rofo 159:492–494
3. Rodriguez- Romero R, Vargas- Serrano B, Cortina-Moreno B et al (1996) Calcified amyloidoma of the larynx. Am J Neuroradiol 17:1491–1493
4. Nomayr A, Lell M, Sweeney R (2001) MRI appearance of radiation-induced changes of normal cervical tissues. Eur Radiol 11:1807–1817
5. Mukherji SK, Weadock WJ (2002) Imaging of the post-treatment larynx. Eur J Radiol 44:108–119

Laser Ablation, Hepatic Tumors

Percutaneous image-guided technique in which laser light is used to induce thermal ablation of hepatic malignancies.

▶Interventional Hepatic Procedures

Late Adverse Reactions

▶Adverse Reactions, Iodinated Contrast Media, Delayed

LCH

▶Langerhans' Cell Histiocytosis

LCIS

▶Lobular Carcinoma *In Situ*

Lead

Lead (Pb, atomic number 82) is an elemental heavy metal which was used until recently as an additive in paints and gasoline. Though incidence of lead poisoning is declining, it remains a problem in urban areas where older homes still exist. Neurological symptoms of chronic lead poisoning include lethargy, irritability, headaches, behavioral changes and developmental delay. In severe cases,

encephalopathy, seizures, coma and death can occur. On imaging, acute lead encephalopathy presents with lesions in the thalami, putamina, claustra and insulae.
▶Toxic Disorders, Brain

Legg-Calvé-Perthes Disease

First described in 1910, it is an osteonecrosis of the femoral head occurring in young children (4–7 years). The juvenile vascular architecture with a tendency toward critical ischemia plays a major role in this disease.
▶Juvenile Osteonecroses

Leiomyoma, Hepatic

It is a very rare, well-circumscribed, smooth muscle tumor of the liver in some cases associated with human immunodeficiency virus infection. Hepatic leiomyoma does not show peculiar radiological features. On US, it appears as a solid hypoechoic lesion with internal echoes. Unenhanced CT depicts a hypodense lesion with an early peripheral or a delayed homogeneous enhancement. This lesion usually shows a low signal on T1-weighted images and high signal on T2-weighted images with an enhancement pattern that resembles that seen on CT scans.
▶Hepatic Sarcoma

Leiomyoma, Uterus

Martin Unterweger
Institute of Radiology, Kantonsspital, Baden, Switzerland
Martin.Unterweger@ksb.ch

Synonyms

Uterine fibroid; Myoma; Fibroma; Uterus myomatosus

Definition

Leiomyomas are the most common benign tumors of the uterus. They have been described in up to 40% of woman by the fifth decade of life and are the most common cause for uterine enlargement after pregnancy. Leiomyomas arise from the smooth muscle cells. Over 90% of leiomyomas are located in the corpus uteri and only about 5% are in the cervix. They can rapidly increase in size during pregnancy. After menopause, they normally regress in size and may calcify. A single lesion may be found, but leiomyomas are more commonly multiple and usually variable in size.

Pathology/Histopathology

Leiomyomas present macropathologically as well-circumscribed tumors containing muscle and some parts of fibrous tissue. Leiomyomas have a pseudo capsule of areolar tissue. Rarely leiomyomas become cancerous (<0.1%). They are classified according to their location in relation to the uterine wall as intramural, submucosal, subserosal, or in the broad ligament. The intramural location is most commonly seen.

Clinical Presentation

Symptoms usually come from pressure effects due to the large pelvic mass. Leiomyomas can result in pelvic pain, dysmenorrhea, and abnormal uterine bleeding. Submucosal leiomyomas in the uterine cavity can cause infertility, abortion, or hypermenorrhea. Intramural leiomyomas are also associated with infertility. The majority of women with fibroids (up to 80%) has no symptoms. They may grow during the pregnancy and decrease in size after menopause. Subserosal leiomyomas can grow exophytic from the uterus and may undergo a torsion and in this specific situation present as acute abdomen.

Imaging

Transvaginal-ultrasonography (TV-US) remains the primary imaging modality for clinically suspected leiomyomas and normally no further imaging techniques are required. MRI is indicated when sonography results are inconclusive. Sonography is especially limited, if the uterus is retroflexed, with a 20% amount of incorrect diagnosis. MRI is especially useful for diagnosing leiomyomas in patients undergoing work-up for infertility. Furthermore, it is possible to differentiate between leiomyomas and adenomyosis using MR imaging. Prior to myomectomy or embolization, MRI may also be useful to evaluate the location and precise size of leiomyomas. On MRI, leiomyomas present as well-circumscribed masses of similar or slightly low T1 and low T2 signal intensity

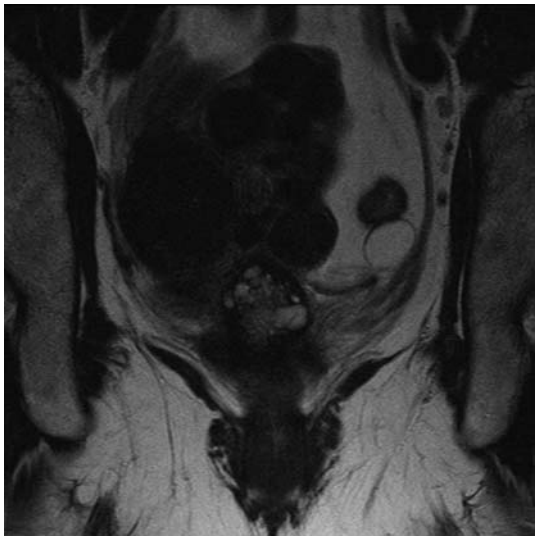

Leiomyoma, Uterus. Figure 1 Coronal T2 weighted MR image of uterus with multiple low intense leiomyomas.

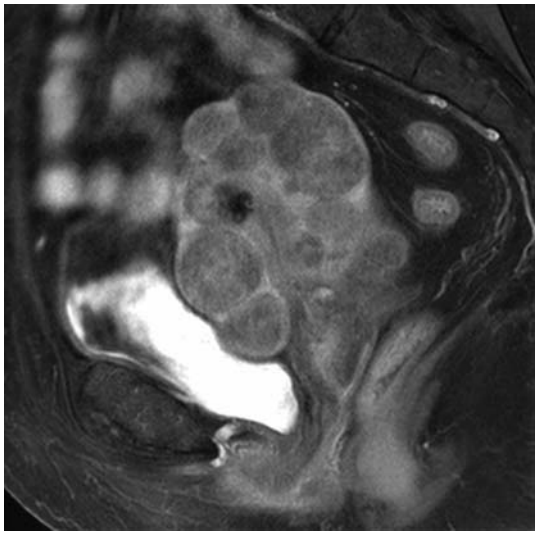

Leiomyoma, Uterus. Figure 2 Sagittal contrast enhanced MR image demonstrate the relative homogenous enhancement of the uterine myomas.

relative to the myometrium (Fig. 1). They show as a diffuse homogeneous enhancement after intravenous gadolinium administration (Fig. 2). The enhancement is less pronounced than that of the adjacent normal myometrium. Degenerative leiomyomas present in MRI as inhomogeneous on T2 weighted images and often with areas of T2 weighted hyperintense signal alterations (Fig. 3).

CT is not the imaging technique of choice for searching leiomyomas, because the differentiation between leiomyomas as solid lobulated masses and the normal myometrium of the uterus is difficult on CT images. Signs like focal calcifications and irregular low-density areas in a mass are also suggestive for leiomyomas.

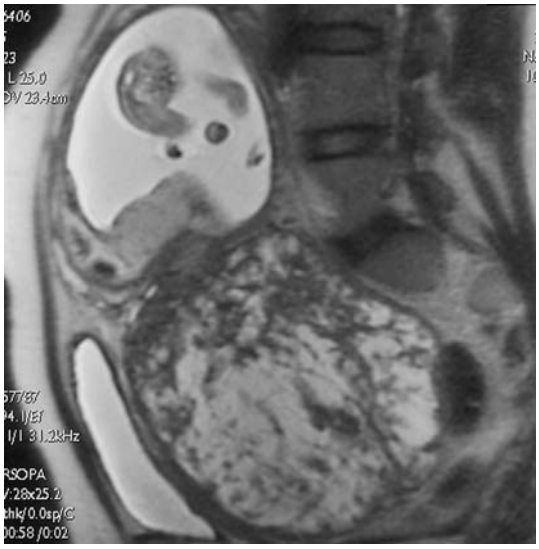

Leiomyoma, Uterus. Figure 3 Sagittal T2 weighted MRI in a pregnant woman demonstrates a large leiomyoma with necrosis.

Diagnosis

Symptoms, pelvic exam, and imaging (TV-US and MRI) are the basis for diagnosing leiomyomas. They often present as incidental findings. In asymptomatic patient, further work-up is necessary as long as the leiomyomas show the classic features as described earlier. In symptomatic patients and in cases with indeterminate imaging findings (e.g., necrosis, strong contrast-enhancement, and increase in size) histological exploration is necessary.

Interventional Radiological Treatment

An interventional radiological treatment of uterine leiomyomas is possible with the embolization of the uterine artery (5).

Bibliography

1. Hricak H, Finck S, Honda G et al (1992) MR imaging in the evaluation of benign uterine masses: value of gadopentetate dimeglumine-enhanced T1 weighted images. AJR 158:1043–1050
2. Mittl RL, Yeh IT, Kressel HY (1991) High-signal intensity rim surrounding uterine leiomyomas on MR images: pathologic correlation. Radiology 180:81–83

3. Hamm B, Kubik-Huch RA, Fleige B (2001) MRI and CT of the female pelvis. Eur Radiol 11 (Supl. 2). S233–S224
4. Gabriel H, Pinto CM, M Kumar et al (2004) MRI detection of uterine necrosis after uterine artery embolization for fibroids. AJR Am J Roentgenol 183:733–736
5. Torigian DA, Siegelman ES, KP Terhune et al (2005) MRI of uterine necrosis after uterine artery embolization for treatment of uterine leiomyomata. AJR Am J Rontgenol 184:555–559

Leiomyosarcoma

Relatively commoner sarcoma, after MFH and liposarcoma, subtypes associated with vessels, guarded prognosis.
▶Neoplasms, Soft Tissues, Malignant

Leiomyosarcoma, Hepatic

Rare primary mesenchymal tumor of the liver occurring in adult patients. The lesions are composed of large spindle cells immunohistochemically positive to smooth muscle proteins. Macroscopically, this sarcoma appears as large, solid, solitary masses located in a normal noncirrhotic liver. The lesions are often polylobulated containing a variable amount of internal hemorrhage or necrosis.
▶Hepatic Sarcoma

Leptomeningeal Cyst

▶Cysts, Cerebral and Cervical, Childhood

LES

A functional sphincter involving the lower 3–4 cm of the oesophagus called the lower oesophageal sphincter.
▶Hernia, Hiatus in Adults

Lesions of Unknown Etiology

▶Incidental Neuroradiological Findings

LESP

The hydrostatic pressure measured in the lower oesophageal sphincter.
▶Hernia, Hiatus in Adults

Leukemia

An acute or chronic disease of unknown cause involving the blood forming organs. It is characterized by an abnormal proliferation of leucocytes (white cells) in tissue, with or without a corresponding count in the circulating blood. The type leucocyte most prominently involved determines the classification.
▶Leukemia

Leukemia, Acute

Acute lymphoblastic and myeloblastic leukemia are usually diagnosed by blood tests, but typical diffuse bone marrow infiltration can be demonstrated with MRI, showing low signal in T1-weighted sequences, enhancement after contrast administration, and bright signal on T2-weighted sequences.
▶Myeloproliferative Disorders

Levovist (SHU 508A)

Galactose-based microbubble US contrast agent used with high mechanical index. The bubbles consist of air and are stabilized by a palmitic acid shell. The agent has a liver-specific late phase. Commercially available in Europe and many other countries (not in the USA). Manufacturer: Schering AG, Germany.
▶Contrast Media, Ultrasound, Hepatic

Leyomioma

Benign tumour composed of smooth muscle cells.
▶Breast, Benign Tumours

LFT

▶Lymph Flow Transport

Ligand (Synonym Vector)

Generic term for molecules with specific activity for a receptor, which carry the radionuclide to the target receptor.
▶Receptor Studies, Neoplasms

LIN

▶Lobular Intraepithelial Neoplasia

Linear, No-threshold Risk Model

This theory assumes that any radiation dose, however small, has the potential to cause cancer.
▶Radiation Issues in Childhood

Lingual Developmental Disorders

Congenital abnormalities of the tongue most frequently include processes that diffusely enlarge the tongue (macroglossia) and processes that cause focal masses. Ectopic thyroid tissue or persistent thyroglossal duct cysts may be present in the tongue.
▶Congenital Malformations, Oral Cavity

Lipiodol

▶Contrast Media, Iodinated, Oily

Lipoma

Mature, uniform fat cells in mass form, benign fatty soft tissue tumor, may be subcutaneous, intramuscular, or interseptal.
▶Neoplasms, Soft Tissues, Benign
▶Lipomatous Neoplasms, Hepatic

Lipoma, Hepatic

Extremely rare benign mesenchymal tumor, composed uniformly of mature adipocytes with a variable degree of fibrous stroma. Macroscopically, hepatic lipomas are usually solitary, yellowish masses, well circumscribed, and round. The presence of pure fat determines the characteristic imaging features of these lesions.
▶Lipomatous Neoplasms, Hepatic

Lipomatous Neoplasms, Hepatic

Davide Caramella, Paola Vagli
Department of Diagnostic and Interventional Radiology, University of Pisa, Pisa, Italy
caramella@do.med.unipi.it

Synonyms

Angiomyolipoma; Benign lipomatous tumors; Fatty tumors hepatic; Hibernoma; Lipoma; Liposarcoma; Malignant lipomatous tumors; Myelolipoma hepatic

Definition

Liver tumors (both benign and malignant) composed mainly or partially of adipocytes. The presence of mature adipocytes characterizes benign lesions. Benign hepatic

tumors made up of fat include ►lipoma, ►hibernoma, and combined tumors such as angiomyolipoma (blood vessels, muscle, and fat), ►myelolipoma (hematopoietic tissue and fat), angiomyelolipoma (blood vessels, hematopoietic tissue, and fat). The terms myelolipoma and angiomyelolipoma are suggested in the case of prominent hematopoietic foci.

Malignant forms include ►liposarcoma with its histological subtypes.

Pathology And Histopathology

Lipoma, Hepatic

Hepatic lipomas are extremely rare, benign mesenchymal tumors composed of mature adipocytes. A variable amount of fat content is present in all liver tumors; however, pure lipomas are uniformly composed of fat, whereas the other lesions have fat mixed with other components such as blood vessels, muscles, or hematopoietic tissue (angiomyolipoma, myelolipoma, angiomyelolipoma). Therefore, these lipomatous combined tumors have intermediate imaging features. ►Hepatic lipoma commonly occurs in a noncirrhotic liver and ranges from a few millimeters to more than 10 cm in diameter. Macroscopically, hepatic lipomas are usually solitary, yellowish masses, well circumscribed, and round. Histologically, they are composed of mature adipocytes with a variable degree of fibrous stroma.

The risk of malignant degeneration is not documented (1).

Angiomyolipoma, Hepatic

►Hepatic angiomyolipoma is a very uncommon, benign mesenchymal tumor composed of a variable amount of fat, proliferating blood vessels, and muscle elements (smooth muscle with thick-walled blood vessels). This lesion has also been considered a hamartoma and its benign nature is confirmed by the DNA diploid pattern shown by flow cytometry. It can occur as a solitary mass or as multiple lesions in the case of tuberous sclerosis or Bourneville–Pringle syndrome. These tumors are well circumscribed, ranging in size, and predominantly occurring in women. When these tumors reach large sizes, intratumoral large vessels (called macroaneurysms) and areas of hemorrhage may appear.

Liposarcoma, Hepatic

Liposarcoma is a rare mesenchymal malignancy originating from lipoblasts, which is usually described in the retroperitoneum and extremities and only in very few cases in the liver. Liposarcomas account for 15% of all sarcomas and are most frequent in the fifth decade of life, although primary liposarcomas of the liver have also been described in children. Classification of liposarcomas into five major histological types (myxoid, round cell, well-differentiated, dedifferentiated, pleomorphic) reflects a combination of the two basic histological aspects of this tumor: the differentiation stage of lipoblasts and the overall degree of cellularity and cellular pleomorphism. This tumor, like other primary sarcomas of the liver, presents as an isolated, usually infiltrating, large mass developing in a noncirrhotic liver. Metastatic spread is mainly hematogenous.

Clinical Presentation

Lipoma, Hepatic

These lesions usually do not cause symptoms and are discovered incidentally. An association with any underlying disease has not been described (1).

Angiomyolipoma, Hepatic

Commonly hepatic angiomyolipomas do not produce symptoms and consequently are discovered incidentally. In some cases, they can reach large sizes showing an increased propensity for hemorrhage. However, unlike renal angiomyolipomas, no cases of rupture have been reported. In some cases, association with abdominal pain may result from intratumoral hemorrhage (1). When associated with the Bourneville–Pringle syndrome the lesions are generally multiple, progressive, and symptomatic.

Liposarcoma, Hepatic

Clinical symptoms are aspecific and may appear in the case of compression determined by large masses. Reported signs and symptoms include: abdominal pain, nausea, vomiting, abdominal distension, and weight loss. In some cases, massive ascites and pleural effusion have been described.

Imaging

Lipoma, Hepatic

Ultrasound (US) shows lipomas as homogeneous echogenic masses. Features of intrahepatic lipomas on computed tomography (CT) images include the presence of a well-marginated, homogeneous, low-density mass with attenuation values similar to those of subcutaneous fat (less than −20UH). Pure lipomas do not enhance after contrast medium administration, but a variable enhancement occurs in lesions containing angiomatous elements.

Magnetic resonance imaging (MR) presents intrahepatic lipomas as homogeneous, well-demarcated lesions with signal intensity equal to that of subcutaneous or retroperitoneal fat in all pulse sequences. On MRI, lipomas appear as masses with high signal intensity on T1-weighted images with only a slight signal increase on T2-weighted images. On fat-suppressed protocols the lesions appear hypointense; therefore, a distinction from other cases of hyperdensities on T1-weighted sequences such as areas of hemorrhage, copper overload, or peliotic changes is possible. MRI is also important in demonstrating the presence of a homogeneous fat content. These tumors do not show signal changes in contrast-enhanced sequences (1, 2).

Angiomyolipoma, Hepatic

This tumor usually presents as a combination of fat tissue and other tissue types. Imaging features of angiomyolipoma are related to the distribution and amount of fat and to the relative proportion of its three histological components. On US, typical lesions appear hyperechoic, making the differentiation from hemangiomas difficult. Frequently, they present a mixed hyper-hypoechoic pattern. In the case of very homogeneous predominantly lipomatous tumors, the presence of a posterior acoustic enhancement may be shown. All fat-containing tumors of the liver (angiomyolipoma, lipoma, myelolipoma), show common features on CT, related to the presence of fatty areas, typically hypodense on unenhanced scans. After contrast medium administration, both on CT and MR images, these lesions usually appear heterogeneously enhancing according to the soft tissue contrast uptake. Enhancement of the vascular components is clearly depicted, while the lipomatous areas show little or no enhancement.

MRI is the modality of choice for demonstrating the fatty nature of these lesions. Angiomyolipomas typically appear as well-circumscribed masses on MR images. On MRI, the high signal intensity on T1-weighted images and the hyper- to isointensity on T2-weighted images associated with a heterogeneous pattern is considered a specific feature. The hyperintensity is mostly related to the fat content, disappearing with fat-saturated sequences. In addition, MRI allows fatty areas to be distinguished from hemorrhage. This tumor is not capsulated, and therefore the peripheral rim depicted on MR images corresponds to surrounding compressed liver parenchyma. Atypical lesions without fat content show mixed signal with heterogeneous enhancement on MR imaging. When employing dynamic MRI or MR angiography, the large intratumoral vessels occurring in large angiomyolipomas are well depicted (2, 3).

Liposarcoma, Hepatic

Imaging findings are not specific and resemble those of other liver sarcomas. US usually shows a poorly defined, lobulated, infiltrating, echogenic tumor associated with shadowing. Internal hyperechoic and hypoechoic areas related to hemorrhage and necrosis have been described (4, 5).

CT features include the presence of a large solid mass containing hypodense foci due to the presence of fat, old hemorrhage, or necrosis. Contrast enhancement is limited, because of the poor vascularity of these lesions. On MR images, the lesions appear inhomogeneous reflecting the presence of areas with fat signal intensity.

Diagnosis

Lipoma, Hepatic

The imaging appearance of lipomas is characteristic, and consequently percutaneous biopsy or surgery is usually unnecessary. The differential diagnosis includes other neoplastic lesions of the liver with fatty degeneration, such as ▶angiomyolipoma, hepatic adenoma, or hepatocellular carcinoma. The overall structure of lipoma consisting of fat is revealed by means of specific MR sequences such as fat-suppressed or in-phase and out-of-phase techniques. Fatty hepatocellular carcinoma is usually discovered in cirrhotic patients and it shows a different behavior after contrast medium administration compared with lipoma. Fatty hepatocellular carcinoma is characterized by heterogeneous enhancement (both on CT and MRI) due to the absence of contrast uptake by the fatty areas (1, 2).

Angiomyolipoma, Hepatic

Successful imaging diagnosis relies on the identification of intratumoral fat, although it can be difficult to distinguish this tumor from other fat-containing hepatic tumors. The enhancement of the soft tissue on both CT and MR images after intravenous injection of contrast medium allows distinction between pure lipomas and angiomyolipomas. However, this criterion is not sufficient to allow a clear-cut distinction between angiomyolipoma and angiomyelolipoma. Early enhancement phases of both CT and MRI are helpful in differentiating between angiomyolipomas and fatty hepatocellular carcinoma. The enhancement of the vascularized fatty areas is typical of angiomyolipoma, while the areas of fatty change in hepatocellular carcinoma are almost avascular. The diagnosis of hepatic angiomyolipoma is easy when a fatty lesion is discovered in a patient with known tuberous sclerosis. Moreover, when the diagnosis of tuberous sclerosis is not known, other lesions, both benign and

malignant containing areas of fatty density, may mimic angiomyolipoma. Seldom, hepatic angiomyolipomas do not contain fat and then the diagnosis remains unclear requiring fine-needle aspiration biopsy (2).

Liposarcoma, Hepatic

Primary liposarcoma of the liver, although extremely rare, must be considered in the differential diagnosis of a hepatic mass that develops in a noncirrhotic liver. Imaging features are not specific, resembling those of other sarcomas. The presence of fatty areas in the case of differentiated lesions is highly suggestive of liposarcoma. However, the final diagnosis is only possible on histological specimens (4).

Bibliography

1. Horton KM, Bluemke DA, Hruban RH et al (1999) CT and MR imaging of benign hepatic and biliary tumours. Radiographics 19 (2):431–451
2. Hammerstingl RM, Marquardt F, Schwarz W et al (2003) Benign liver tumours. In: Vogl TJ, Lencioni R, Hammerstingl RM, Bartolozzi C (eds) et al Magnetic Resonance Imaging in Liver Disease. Georg Thieme Verlag, Stuttgart, New York, pp 154–155
3. De Bruecker Y, Ballaux F, Allewaert S et al (2004) A solitary hepatic lesion: MRI-pathological correlation of an hepatic angiomyolipoma (2004:4b). Eur Radiol 14(7):1324–1326
4. Nelson V, Fernandes NF, Woolf GM et al (2001) Primary liposarcoma of the liver: a case report and review of literature. Arch Pathol Lab Med 125(3):410–412
5. Khan A, Sherlock DJ, Wilson G et al (2001) Sonographic appearance of primary liver liposarcoma. J Clin Ultrasound 29(1):44–47

Lipomyelocele—Lipomyeloschisis

▶Congenital Malformations, Spine and Spinal Cord

Lipophagic Granuloma

Nonsuppurative inflammation in an area of fat necrosis, gradually evolving to a scar. Clinical, mammographic, and sonographic features may be indistinguishable from malignancy.

▶Trauma, Breast

Liposarcoma

Fat density or signal intensity may be evident in some low-grade liposarcoma, commonly with irregular nodular tumor septae or variable amounts of solid nonfatty tissue; however, this is increasingly sparse in higher grade lesions.

▶Neoplasms, Soft Tissues, Malignant
▶Lipomatous Neoplasms, Hepatic

Liposarcoma, Hepatic

Rare mesenchymal malignancy originating from lipoblasts, which usually has been described in the retroperitoneum and extremities, and only in very few cases in the liver. This tumor presents as an isolated usually infiltrating and large mass developing in a noncirrhotic liver. Imaging findings are not specific and resemble those of other liver sarcomas. The presence of fatty areas may suggest the final diagnosis.

▶Lipomatous Neoplasms, Hepatic

Liver Allografting

▶Transplantation, Hepatic

Liver Cirrhosis

▶Cirrhosis, Hepatic

Liver Embolization

▶Chemoembolization

Liver Injury

▶Trauma, Hepatobiliary

Liver Metastases

▶Metastases, Hepatic

Liver Replacement

▶Transplantation, Liver

Liver Storage Diseases

▶Diffuse Infiltrative Diseases, Hepatic

Liver Trauma

▶Trauma, Hepatobiliary

Liver Tumors in Infancy

▶Hepatic Pediatric Tumors, Benign

Living Donor Liver Transplant

▶Transplantation, Hepatic

Living Donor Liver Transplantation

Liver transplantation procedure consisting in a partial hepatectomy in living donors for donation to a recipient. Left liver segments and the right lobe are used for donation in pediatric and adult recipients, respectively.
▶Transplantation, Hepatic

Living Related Liver Transplant

▶Transplantation, Liver

LN

▶Lobular Neoplasia

Lobar Nephritis

▶Pyelonephritis, Acute

Lobar Nephronia

Localized inflammatory renal masses due to ascending bacterial infection. It can produce focal scarring.
▶Pyelonephritis, Acute

Lobectomy

▶Postoperative

Lobular Intraepithelial Neoplasia (LIN)

Synonym for lobular carcinoma *in situ*.
►Carcinoma, Lobular, *In situ*, Breast

Lobular Neoplasia (LN)

Synonym for lobular carcinoma either invasive lobular carcinoma or lobular carcinoma *in situ*.
►Carcinoma, Lobular, *In situ*, Breast

Local Drug and Gene Delivery with Microbubbles

Peter Hauff
Global Drug Discovery, Bayer Schering Pharma AG, Berlin, Germany
peter.hauff@bayerhealthcare.com

Synonyms

Drug delivery system; Gene delivery system; Nonviral vector; Targeted delivery

Definition

Local drug or gene delivery with ultrasound comprises the transport of microbubbles containing bioactive substances, their ultrasound controlled release in the region of interest and ultrasound-induced enhancement of substance penetration (►sonoporation) into the surrounding tissue or cells. It provides a technique for noninvasive ►gene therapy and organ-specific ►drug delivery.

Mode of Action

Ultrasound contrast agents (USCAs) for the delivery of bioactive substances such as drugs or genes consist of shell stabilized gas-filled microbubbles whereby the substances can be attached to the microbubble shell surface, or incorporated into the microbubble shell or lumen. A further approach is the coadministration of microbubbles and bioactive substances. Following injection, the substance-loaded microbubbles can be destroyed in the region of interest with ultrasound of a certain frequency and intensity. After intravenous injection, substance release can currently only be performed from microbubbles which are targeted passive in the region of interest (e.g., after phagocytosis) or passing through the ultrasound beam during blood circulation. However, a higher level of substance release may be achieved by using substance-loaded specific microbubbles (active targeting) which would lead to their higher target accumulation. The ultrasound-triggered substance release allows spatially and temporally controlled and precisely targeted therapies. In addition, ultrasound can promote and enhance released substance uptake by targeted tissues or cells, and this capability is called sonoporation. The ultrasound-induced sonoporation effect, which works as well without microbubbles, can be amplified by the additional use of microbubbles (1). Further advantages of this approach are seen for instance in the protection of encapsulated bioactive substances (e.g., protection of DNA from nucleases) within the blood; low level of invasiveness; ►nonviral vector system for gene therapy and the possibility to visualize the breakup of the microbubbles on the screen of the ultrasound device through the color pixels that are produced when the bubbles are destroyed (SAE, stimulated acoustic emission effect) by using the color Doppler mode (Fig. 1).

Indication

Although local drug and gene delivery with ultrasound is currently at an experimental preclinical stage, researchers were able to demonstrate their feasibility *in vitro* and in animal models. In the majority of the published *in vivo* cases, the microbubbles have been tested for their use as nonviral ►vector system for the genetic treatment of ischemic diseases, mainly by intramuscular injection, or of tumors after systemic administration. Most of the investigators used so-called marker genes for their feasibility studies, such as β-galactosidase and luciferase, in order to identify the optimum experimental settings. Only few investigations have been performed with microbubbles containing therapeutic agents. A successful genetic treatment of tumors could be shown more recently by using microbubbles containing the tumor suppressor gene *p16* (2). Another group was able to show *in vivo* the potential of microbubbles loaded with the

Local Drug and Gene Delivery with Microbubbles. Figure 1 Principle of ultrasound-induced substance release from microbubbles (MBs) and their monitoring. *Left*, transmission electron micrograph of macrophages containing intact MBs (before sonication). *Middle*, ultrasound image of the liver of a rat after administration of MBs in color Doppler mode. *Yellow dots* are visible caused by the ultrasound-induced disruption of MBs during sonication which is called ►stimulated acoustic emission (SAE). Each *yellow dot* represents one MB. *Right*, a transmission electron micrograph of a macrophage containing shell fragments of destroyed MBs (after sonication). Hence, the gas core (and possible encapsulated substances) has been released.

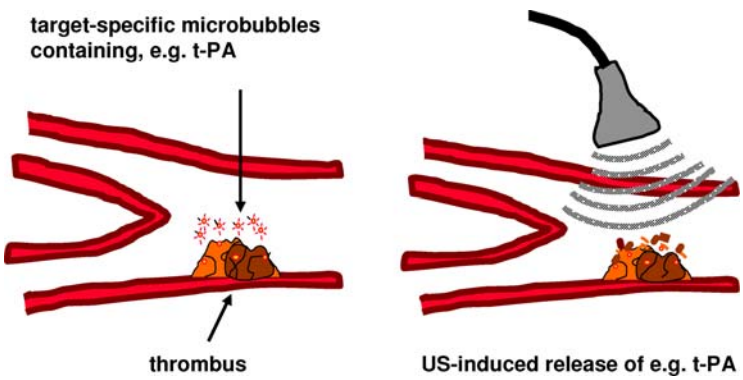

Local Drug and Gene Delivery with Microbubbles. Figure 2 Ultrasound-induced thrombolysis (principle). *Left*, thrombus-specific microbubbles containing a fibrinolytic agent accumulate at the thrombus. *Right*, the fibrinolytic agent is released from ultrasound-induced disrupting MBs.

Smad7 gene as a useful therapeutic strategy for the prevention of renal fibrosis in association with hypertension. Finally, it could be shown already in humans that the coadministration of microbubbles and a fibrinolytic agent lead to a significant acceleration of thrombolysis by ultrasound treatment of the thrombus which is also referred to as "sonothrombolysis" (4) (Fig. 2).

Bibliography

1. Li T, Tachibana K, Kuroki M et al (2003) Gene transfer with echo-enhanced contrast agents: comparison between Albunex, Optison, and Levovist in mice—initial results. Radiology 229:423–428
2. Hauff P, Seemann S, Reszka R et al (2005) Evaluation of gas-filled microparticles and sonoporation as gene delivery system. Feasibility study in rodent tumor models. Radiology 236:572–578

3. Hou CC, Wang W, Huand XR et al (2005) Ultrasound-microbubble-mediated gene transfer of inducible Smad7 blocks transforming growth factor-β signaling and fibrosis in rat remnant kidney. Am J Pathol 166:761–771
4. Brekendeld C, Remonda L, Nedeltchev K et al (2005) Endovascular neuroradiological treatment of acute ischemic stroke: techniques and results in 350 patients. Neurol Res 27 Suppl 1:29–35

Local Recurrence

The most frequent breast recurrence, which occurs either in the scar margins or near the place where the primary neoplasm was removed.
▶Recurrent Neoplasms, Breast

LOCM

▶Low Osmolality Contrast Media

Log-roll Test

Rolling a femur like a log on physical exam. Pain or resistance is elicited when the hip contains more than the normal minimal fluid.
▶Transient Synovitis

Longitudinal Relaxation Time

Relates to the T1 time constant, which determines the rate at which excited protons return to equilibrium within the lattice.
▶Contrast Media, MRI, Oral Agents

Looser's Zone

Radiolucent bands of unmineralized osteoid on radiographic images which are typical for osteomalacia.
▶Osteomalacia

LORA

Late onset (LO) (>65 years) rheumatoid arthritis (RA) is frequently atypical concerning the affection of larger joints. It is said that LORA patients are more likely to go into remission. However, LORA can be as damaging as classical RA, and joint erosions are often observed at presentation. Disease compounded by age-associated factors may in fact have a worse prognosis later, rather than early, in life.
▶Rheumatoid Arthritis

Low ARM

ARM where the rectum passes through a well-developed puborectalis muscle sling. The aboral ending is an anocutaneous fistula in males, whereas in females this is represented by an anocutaneous or anovestibular fistula.
▶Anorectal Malformation

Low Osmolality Contrast Media (LOCM)

A low osmolality contrast medium is a water-soluble imaging contrast agent that has osmolality (a measure of the number of particles in solution) higher than human blood. For radiographic iodinated contrast media, this is typically twice the osmolality of human blood. See also high osmolality contrast media and iso-osmolality contrast media.
▶Adverse Reactions, Iodinated Contrast Media, Acute Renal

LR

▶Local Reccurrence

LRS

▶Lumbar Radicular Syndrome

LT

▶Transplantation, Liver

Lumbar or Cervical Disk Hernia

▶Hernia, Disk, Intervertebral

Lumbar Radicular Syndrome

A complex of signs and symptoms indicating lumbosacral nerve root involvement.
▶Radicular Syndrome of the Spine, Conservation Therapy for

Lumpectomy

Breast surgical technique that consists of the surgical removal of a tumor along with a small margin of the surrounding normal breast tissue.
▶Breast Conserving Therapy

Lung Abscess

Thick-walled cavity within the lung filled with pus.
▶Pneumonia in Childhood

Lung Contusion

Typically induced by blunt chest trauma and presents as edema and hemorrhage with intact histological structure of the lung. The corresponding patchy or confluent radio opacities develop within 6 h and start to decrease after 2–3 days with restitution after 3–10 days. CT is superior to chest X-ray in defining their extent. Infection and ARDS are life threatening complications of ▶lung contusion which are associated with progressive radio opacities after 48 h.
▶Chest Trauma

Lung Laceration

The local rupture of lung parenchyma with round or oval shaped accumulations of blood and air following direct perforation or indirect deceleration forces due to blunt trauma. On chest X-ray, areas of laceration are often masked by surrounding contusions. Pneumothorax and superinfection are quite frequent complications, whereas cerebral air embolism is rare. If uncomplicated, the corresponding radio opacities vanish after 3–7 weeks, sometimes with remaining scars (see Fig. 2, Page 000).
▶Chest Trauma

Lung Resection

▶Postoperative

Lung Scintigraphy

Refers to two different examinations: the ventilation (V) and the perfusion (Q) scan. Normal V/Q studies show homogeneous patterns of evenly matched ventilation (V) and perfusion (Q). Pulmonary diseases are frequently associated with scintigraphically detectable perturbations of the ventilation and/or perfusion. Two types of perturbations are differentiated: match defects that are typical for pulmonary embolism and mismatch defects that are commonly caused by nonembolic pulmonary diseases.
▶Pulmonary Function, Nuclear Medicine Methods

Lung Transplantation

▶Postoperative

Lung Volume Reduction

▶Postoperative

Luteal Cysts

▶Cyst, Follicular, Ovarium

Lymph Flow Transport

LFT comprises the use of lymph for the transport of substances. For indirect lympho-sonography, interstitial injected microbubbles enter the lymph vessels through gaps between lymphatic endothelial cells or by transcellular endo- or exocytosis and is transported by the lymph flow to the respective regional lymph node.
▶Targeted Microbubbles

Lymph Node Metastasis

▶Lymphopoietic System, Diseases of the

Lymphadenopathies, Head and Neck

Misa Sumi, Takashi Nakamura
Department of Radiology and Cancer Biology, Nagasaki University School of Dentistry, Nagasaki, Japan
misa@nagasaki-u.ac.jp

Synonyms

Benign and malignant nodes in the neck

Definition

The term lymphadenopathy indicates inflammatory, granulomatous, or neoplastic involvement of nodes with or without increasing the volume. The whole neck contains approximately 300 nodes. Several classification systems have been used for the regional categorization of the nodes in the neck. However, recent advances in CT and MR imaging have enabled the use of an image-based classification with the aid of anatomical landmarks that are identified on CT and MR images (1). This classification system categorizes the cervical nodes into seven groups; the nodes at levels I to VII. Supraclavicular, retropharyngeal, parotid, facial, occipital, postauricular, and the other superficial nodes are referred by their anatomic names. Metastasis to one or more of these nodes has not been reported to have a high impact on the patients' prognosis. However, such metastasis may influence the local control and surgical plan and should be carefully followed-up.

Pathology/Histopathology

Cervical lymph node metastases originate most frequently from squamous cell carcinomas of the mucosal lining of the upper aerodigestive tract and uncommonly originate from the salivary and thyroid glands and skin. Malignant melanoma of the head and neck skin is a possible origin of nodal metastasis in the neck. Nodal metastasis is considered to occur after cancer cells that had migrated into the lymphatic vessels travel *via* the afferent lymphatic vessels and settle into the nodal cortex; here, metastatic cancer cells continue to proliferate and form cancer foci in the node. Cancer growth in the nodes requires angiogenesis for the tumor blood supplies. Growing cancer cell foci gradually displace and destroy the surrounding nodal lymphatic tissues and may obliterate the nodal ▶hilum. Large cancer foci are frequently associated with liquefaction or coagulation necrosis (central nodal necrosis) and keratinization (cancer pearl).

Malignant lymphomas are classified into Hodgkin's and non-Hodgkin's lymphomas. Non-Hodgkin's lymphomas are subclassified into B-cell neoplasm (precursor B-cell neoplasm and peripheral B-cell neoplasm), and T-cell and natural killer (NK)-cell neoplasms (precursor T-cell neoplasm and peripheral T-cell and NK-cell neoplasm). Hodgkin's tumors are subclassified into five types (lymphocyte-rich, nodular sclerosis, mixed cellularity, lymphocyte depletion, and nodular lymphocyte-predominant). In the head and neck region, Hodgkin's lymphomas occur predominantly in the nodes, while about two-thirds of non-Hodgkin's lymphomas arise in the nodes.

The lymph nodes are also enlarged because of nodal abscesses secondary to bacterial (mycobacterial) infections or

cat scratch disease in the head and neck region. Tuberculosis is a rare case but should be considered for differential diagnosis when enlargement of multiple lymph nodes is associated with irregular contrast medium enhancement on CT or MR images. Viral infections such as mononucleosis, herpes, cytomegalovirus, and HIV are common causes of single and multiple lymph node enlargements. Sarcoidosis, Castleman's disease, and Kimura's disease are also rare causes of enlargement of cervical lymph nodes.

Clinical Presentation

Metastatic nodes in patients with head and neck cancer are painless and firm masses in the neck. A single metastatic node will increase in size with the growth of metastatic cancer cells in the node. Further spread of metastatic cancer along the lymphatics may involve the down stream nodes, and may be eventually fixed to adjacent tissues. Nodal lymphomas are painless, single large or multiple small rubbery masses, are often bilateral, and are sometimes complicated with recurrent fevers. Inflammatory adenopathy such as bacterial adenitis and cat scratch disease presents as painful masses. Kimura's disease and sarcoidosis cause painless multiple masses in the neck, basically unilaterally in the former and bilaterally in the latter. Castleman's disease is usually associated with a solitary asymptomatic enlarged node.

In patients with head and neck cancer, the presence or absence of nodal metastasis is the most important predictive factor. Therefore, early detection of metastatic nodes and their effective differentiation of them from nonmetastatic nodes is a very critical step for the staging of patients with head and neck cancer and for planning treatment with surgery, radiotherapy, and chemotherapy.

Nodes at levels I and II of the neck receive lymphatic drainage from the anterior facial structures and skin, oral floor, and anterior oral cavity. Nodes at levels II–IV receive lymphatic drainage from the parotid and retropharyngeal regions and the nodes at level IB. The nodal chain at levels II–IV serves as a common pathway for all the lymphatics of the upper aerodigestive tract and neck. Thus, these drainage patterns result in different incidences of metastatic nodes at different levels of the neck. The incidence of adenopathy or enlarged nodes is higher in patients with pharyngeal cancer than in those with oral cancer. Metastasis from the oral cavity occurs predominantly to nodes at levels IB and IIA. Level IA is a common site for metastasis from cancers of the lower gingiva, oral floor, and tongue. Cancers of the oral floor and tongue can metastasize to nodes in levels III and IV, but metastatic nodes from other oral cancers are uncommon at this level. In contrast, laryngeal and esophageal cancers rarely metastasize to nodes at levels IA and IB. Levels VA, VB, and VI are uncommon sites for metastasis from head and neck cancers.

The sentinel node is the first node to receive lymphatic drainage from a primary cancer. The presence of metastatic cancer in the sentinel node indicates possible involvement of the downstream nodes in that chain. On the contrary, if the sentinel node does not contain cancer, the downstream nodes are not likely to harbor metastasis.

Imaging

Computed Tomography

CT imaging is most commonly used for screening metastatic nodes in patients with head and neck cancer, because CT provides excellent information about their location, size, and even internal architectures of the node.

Increase in size of the node, a rounder shape, and rim enhancement (central nodal necrosis) or irregular enhancement after contrast enhancement due to tumor necrosis are the hallmarks for the metastatic nodes. The minimal axial diameter is a better criterion than the maximal axial diameter (2). A minimal axial diameter of 10 mm has been reported to be the most effective size criterion. ►Nodal necrosis is considered a pathognomonic feature of metastatic nodes from head and neck squamous cell carcinomas. It occurs as cancer cells infiltrate into the medullary portion of the nodes and surpass the blood supply. Nodal necrosis has been reported to occur in 56–63% of metastatic nodes larger than 1.5 cm in diameter.

The general features of nodal lymphoma are multiple, bilateral, nonnecrotic enlarged nodes. However, nodal necrosis has been reported in 27% of non-Hodgkin's lymphomas (most commonly in the diffuse large cell lymphomas in the palatine tonsil).

Application of the multidetector-row CT can improve the diagnostic performance for the detection of malignant nodes in the neck. It allows displaying coronal, sagittal, axial, and paraxial images of the node without increasing the examination time. Therefore, the multidetector-row CT technique could permit more precise assessment of the topographical relationships of the node to vessels as well as the volumetric assessment of enlarged nodes in the neck.

Magnetic Resonance Imaging

The performance of MR imaging in diagnosing metastatic nodes in the neck has not been highly ranked. However, recent advances in MR imaging technology have enabled fast, ►high-resolution MR imaging and functional imaging of the cervical nodes, thereby greatly improving

the diagnostic ability. Lymph node metastases lead to drastic changes in the components and structure of the nodes and are associated with proliferation and necrosis of the cancer cells, angiogenesis, and obliteration of the hilar fat. Application of a small-sized surface coil allows the evaluation of the detailed architecture of metastatic nodes (Fig. 1), for example, liquefaction necrosis, cancer cell nests, keratinization, and extranodal spread. The combined use of some of these high-resolution MR features has greatly improved the diagnostic ability of MR imaging for the detection of metastatic cervical nodes (3).

In addition, the ►apparent diffusion coefficients (ADCs) obtained by ►diffusion-weighted MR imaging of lymphadenopathy may provide additional information that is distinct from the morphological features. Among metastatic nodes, nodal lymphomas and benign nodes, the ADCs are lowest in nodal lymphomas and highest in metastatic nodes. The presence of necrosis in the metastatic cancer increases the ADC levels of the lesion. In contrast, nodal lymphomas are usually displayed as nonnecrotic masses (Fig. 2). High cellularity in lymphomas leads to restricted water diffusion, which,

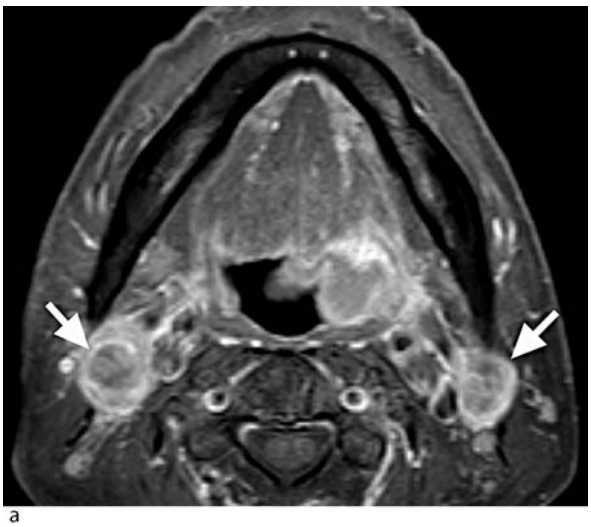

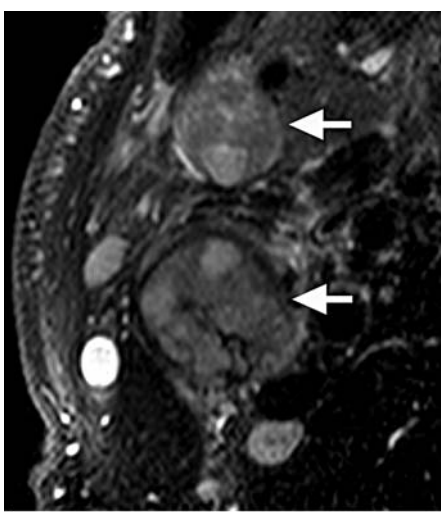

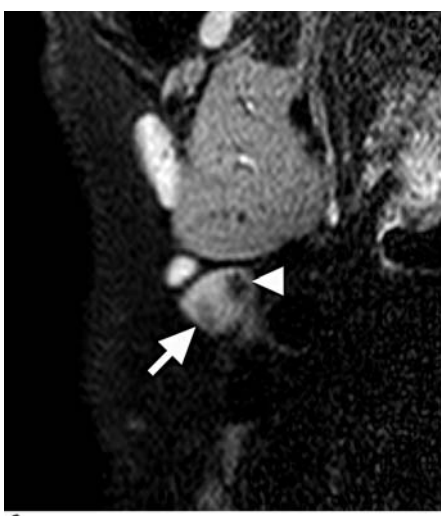

Lymphadenopathies, Head and Neck. Figure 1 MR imaging of metastatic lymph nodes. Gadolinium-enhanced, fat-suppressed T1-weighted image (a), high-resolution, fat-suppressed T2-weighted image using a 47-mm microscopy coil (b, c) show cervical nodes (arrows) metastatic from squamous cell carcinomas of tonsil (a), oropharynx (b), and tongue (c). Metastatic nodes exhibit central nodal necrosis with rim enhancement (a), concomitant presence of cancer cell nests with intermediate to low signal intensity, and liquefaction necrosis with hyperintense signals (b), and hypointense keratinization areas (arrowhead) (c).

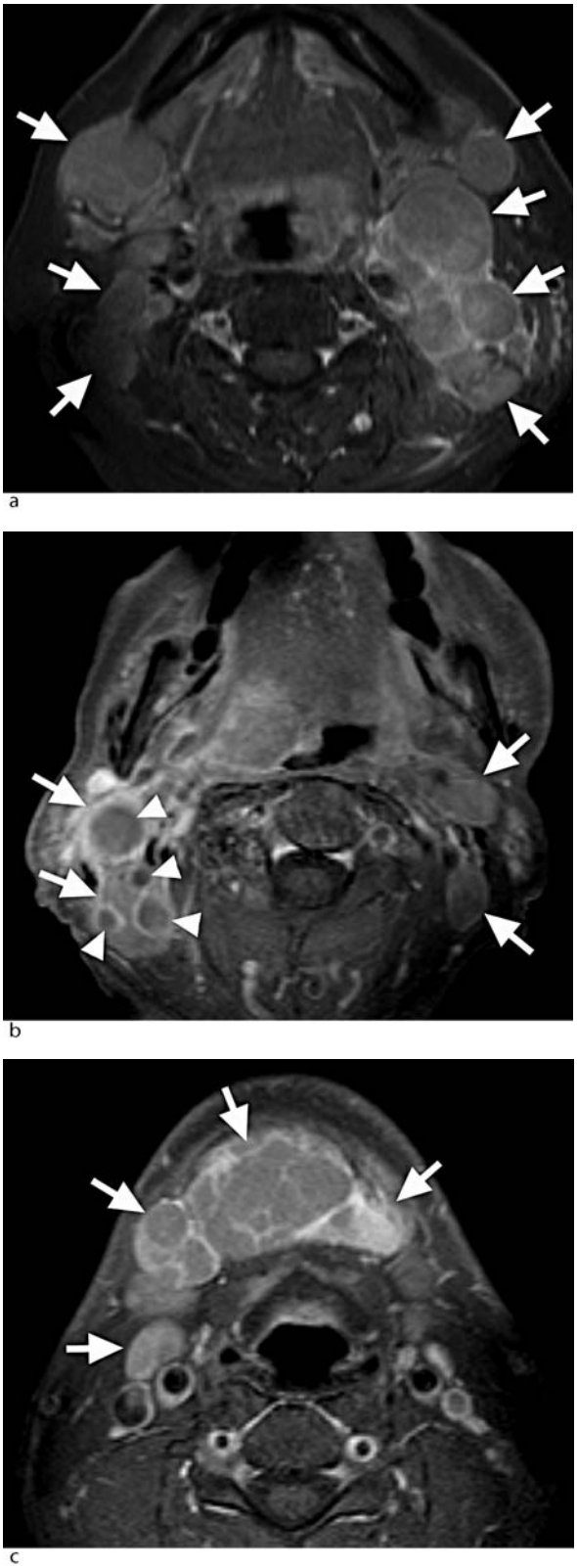

Lymphadenopathies, Head and Neck. Figure 2 MR imaging of nodal lymphomas. Gadolinium-enhanced, fat-suppressed T1-weighted MR images of non-Hodgkin's lymphomas (arrows) (a, b), and Hodgkin's lymphoma (arrows) (c). Necrosis (arrowheads) may be associated with diffuse large B-cell lymphoma as in (b). Enhanced blood flow signals are characteristic features of Hodgkin's lymphomas as in (c).

in turn, results in low ADC levels. The ADC measurements could significantly and independently contribute to the discrimination of metastatic cervical nodes and nodal lymphomas (3).

Sonography

The evaluation of metastatic nodes by a high-resolution sonography is also based on the assessment of their internal architecture and determination of their size. Abnormalities in the metastatic nodes may be reflected by the increased parenchymal echogenicity or loss of hilar echogenicity. In addition, the recent development of Doppler sonography has highlighted the diagnostic significance of changes in the nodal blood flow while differentiating metastatic nodes from reactive nodes.

The minimal axial diameter is the most accurate size criterion. The best size criterion for metastatic nodes differed among the different neck levels; a recent report postulated that in the palpably N0 necks, a minimal axial diameter of 7 mm for level II and 6 mm for the other neck levels provide the optimal diagnostic ability (4).

Power Doppler sonography has a greater dynamic range than conventional color Doppler sonography, thus providing enhanced visualization of the microvascularity of the lymph nodes (Fig. 3). The detection of abnormal blood flow signals is considered important in differentiating metastatic nodes from reactive nodes. Nodal blood flow signals are usually classified as follows: (1) hilar (reactive), (2) parenchymal (metastatic), or (3) no blood flow signals (metastatic) (5).

Nodal lymphomas are usually displayed as round areas with a pseudocystic appearance and posterior acoustic enhancement. The sonographic features result from the uniform cellular arrangement in lymphomas. Hilum in lymphomas is narrowed or absent and may be associated with hilar blood flow signals; otherwise, lymphomas are poor in blood flow signals.

Nuclear Medicine

Lastly, we should comment on the recent advances in positron emission CT (PET) for the detection of metastatic nodes. PET with 2-[18F] fluoro-2-deoxy-D-glucose (FDG) could be used as another functional imaging modality for the detection of metastatic nodes. Malignant nodes have higher glucose utilization than

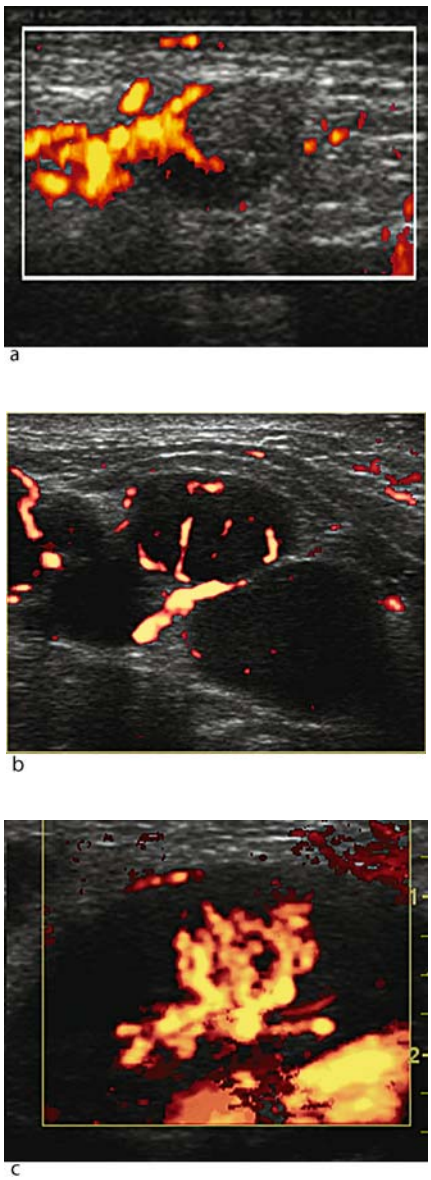

Lymphadenopathies, Head and Neck. Figure 3
Sonographic imaging of lymphadenopathies. Power Doppler sonography shows changes in hilar echogenicity and blood flow signals in lymphadenopathy. Lost hilar echogenicity and hyperechoic tumor areas associated with displaced blood flow signals in metastatic node (a), homogeneously hypoechoic tumor associated with varying amounts of sparse blood flow signals in nodal lymphomas (b), and, rich vascularity radiating from hilar region in lymphadenitis (c).

normal nodes. Accordingly, FDG-PET might detect metastatic nodes that are negative by the size criteria on MR imaging. However, metastatic nodes that contain large necrotic areas are negative by the FDG-PET criteria due to the low glycolytic activity of the necrotic material. The FDG-PET criteria have not been well established, and the poor accuracy of FDG-PET in the visual interpretation of a lesion is a frequent problem. Other disadvantages of FDG-PET are limited clinical availability, low spatial resolution, and high cost. Further studies are necessary to facilitate the clinical application of FDG-PET for head and neck imaging.

Diagnosis

In general, sonography performed better than CT in detecting benign and malignant lymphadenopathies, particularly for metastatic nodes in patients with head and neck squamous cell carcinomas (2). Nevertheless, the fact that sonographic examination requires considerably greater amount of time than CT may greatly diminish the value of sonography. In addition, sonography is not suitable for the detection of deep cervical nodes such as those in the retropharyngeal space. Fine-needle aspiration cytology has become the standard procedure in the diagnosis of lymphadenopathies in the neck. This technique could be performed more accurately under sonographic guidance. On the other hand, MR imaging with high tissue contrast can provide useful information regarding the changes in nodal structures and components in lymphadenopathy. Furthermore, some MR imaging techniques such as coronal short inversion time inversion recovery (STIR) turbo spin-echo imaging, allow rapid MR imaging for screening with high sensitivity and negative predictive value. Therefore, CT or rapid MR imaging should be the first choice for the diagnosis of cervical lymphadenopathy, and it may be reasonable to perform sonographic examination or functional (e.g., diffusion-weighted MR imaging) and high-resolution MR imaging using a small surface coil for the detailed study of suspected cervical nodes, following CT or MR screening.

Bibliography

1. Som P, Curtin HD, Mancuso AA (2000) Imaging-based nodal classification for evaluation of neck metastatic adenopathy. Am J Roentgenol 174:837–844
2. Sumi M, Ohki M, Nakamura T (2001) Comparison of sonography and CT for differentiating benign from malignant cervical lymph nodes in patients with head and neck squamous cell carcinomas. Am J Roentgenol 176:1019–1024
3. Sumi M, Van Cauteren M, Nakamura T (2006) MR microimaging of benign and malignant nodes in the neck. Am J Roentgenol 186:749–757
4. van den Brekel MWM, Castelijins JA, Snow GB (1998) The size of lymph nodes in the neck on sonograms as a radiologic criterion for metastasis: How reliable is it? Am J Neuroradiol 19:695–700
5. Ariji Y, Kimura Y, Hayashi N et al (1998) Power Doppler sonography of cervical lymph nodes in head and neck cancer patients. Am J Neuroradiol 19:303–307

Lymphadenopathy

Pinar Balci, MD
Dokuz Eylül University School of Medicine, Department of Radiology, Izmir, Turkey
pinar.balci@den.edu.tr

Synonym

Adenomegaly

Definitions

Lymphadenopathy is the term used to indicate enlargement of lymph nodes. It involves swelling of one or more lymph nodes and is a recognized symptom of many diseases, including acute infection (bacterial or viral) or chronic infection (tuberculous lymphadenitis, cat-scratch disease). Lymphadenopathy may be tumoral (Hodgkin's lymphoma, non-Hodgkin's lymphoma, metastasis) or be of unknown etiology (sarcoidosis).

In the breast, subdermal and intramammary lymphatics anastomose at the subareolar plexus; their path is centrifugal toward the axillary, internal mammary, and intercostal chains. The axillary chains form the main drainage. The associated nodes are subdivided into six groups: external mammary, scapular, axillary, central, subclavicular, and interpectoral (Rotter). A small amount of the lymphatic flow from the breast crosses to the opposite side, and some passes to the upper abdominal nodes *via* diaphragmatic lymphatics. Furthermore, some lymph nodes may occur within the breast; these are intramammary lymph nodes. Although they may occur in any location within the breast, they are usually situated on the posterior half of the upper outer quadrant (1).

For surgical purposes, the lymph nodes in the axilla are divided into three levels according to their relationship with the pectoralis minor muscle. Nodes lying lateral to this muscle are termed level I, those deep to the pectoralis minor are level II, and those lying medial to it are level III. Additionally, a small percentage of breast cancers drain medially into the internal mammary chain. These nodes follow the internal mammary vessels and are usually present in the first three intercostal spaces.

The most common cause of axillary lymph node enlargement is nonspecific benign adenopathy (29%) (2). Causes of this change can include skin and nail infections or inflammatory processes in the arm, breast infections, or inflammation and breast surgery. It is generally known and accepted that involvement of regional nodes is an important prognostic parameter in breast cancer. A large number of nonmalignant diseases have been reported to cause axillary lymphadenopathy. These include tuberculosis, human immunodeficiency virus (HIV) and acquired immunodeficiency syndrome (AIDS), sarcoidosis, rheumatoid arthritis, psoriasis, and other collagen vascular diseases.

Although lymphadenopathy is the most common cause of axillary masses, other abnormalities, including epidermal cysts, silicone granuloma, abscesses, cysts, lipomas, primary breast carcinoma, and other benign breast tissue lesions, have been reported. Some lesions probably arise from accessory breast tissue in the axilla. Hence, the differential diagnosis of axillary masses should be similar to that for breast masses (3).

Pathology/Histopathology

Lymphatic capillaries drain close to 10% of all interstitial fluid back to the venous circulation. The lymph circulates first through capillaries, and then lymph vessels, converges toward the cysterna chili located between the T11 and L2 levels and then through the thoracic ducts, and then merges before draining into the venous angle between the internal left jugular vein and the left subclavian vein. Lymph nodes thus form barriers to the lymphatic drainage. Afferent lymphatics converge toward the outer nodal cortical surface before exiting the nodes *via* centrally located medullary sinuses. As such, they can be seen as barriers to the lymphatic extension of cancer cells. Additionally, nodes receive a specific blood supply *via* both arterial and venous branches (4).

Axillary lymphadenopathies play an important role in staging of tumor and metastasis of breast carcinoma in cases of breast masses, particularly in women. Clinically palpable lymph nodes of the axilla do not always indicate metastasis. In histopathologic examination, huge lymph nodes may be reactive; on the other hand, nonpalpable nodes may have metastasis microscopically, as in invasive lobular carcinoma. Of lymphoid tissue neoplasms, Hodgkin's and non-Hodgkin's malignant lymphomas and plasmocytic tumors are among the causes of axillary lymphadenopathies. Both primary and metastatic breast lymphoma may accompany such cases, or the breast may even be uninvolved. Lymphadenopathy may be due to systematic or regional skin and soft tissue non-neoplastic diseases. Miscellaneous systematic infections may occasionally lead to lymphadenopathy, with specific findings of infection or reactive hyperplasia. In addition, malignant tumors of tissues and organs may result in metastasis of axillary lymph nodes, as in malignant melanoma and lung and other organ malignant tumors.

The frequency with which a primary tumor is detected pathologically in the ipsilateral breast varies from 55 to 82%. Most cases in which lymphadenopathy is associated with a visible breast cancer represent metastatic breast disease. In those where there is no visible breast disease, causes include connective tissue disease (commonly rheumatoid arthritis), hematological malignancies, occult carcinomas, dermal infection, and benign reactive nodes.

Clinical Presentation

The first step in clinical examination of the breast is palpation of regional lymph nodes (axillary and supraclavicular nodes). In cases of palpable lymphadenopathy of superficial lymph node sites, the following features of such adenopathy must be taken into consideration:

- Site or sites of adenopathies
- Number of palpable ganglions
- Size of ganglions
- Consistency of adenopathy (tough as stone, soft as rubber, fluctuating): Although not a rule, adenopathies due to cancer metastasis frequently have a tough consistency; adenopathies due to lymphoma have a rubbery consistency; and adenopathies having pus are soft. Metastatic ganglions may also be painful. Although ganglions due to lymphoma are generally not painful, ganglions showing enlargement in a short time may be painful.
- Mobility: Enlarged ganglions having single localizations can be easily mobilized. On the other hand, lymphadenopathies showing package formations and adherent to surrounding tissue are likely to be immobile. In cases of tough and immobile lymphadenopathies, cancer metastasis is the strongest possibility.
- Condition of the skin over the lymphadenopathy: Erythema, warmth, and fistulization (in some cases) may indicate inflammatory adenopathies such as tuberculous adenitis.

Imaging

The normal mammographic pattern of lymph nodes is reniform or coffee-bean-shaped with a fatty hilum. The size of normal nodes is variable. If only the parenchyma excluding the fatty hilum of the small axis is determined, this measurement allows some correlation with the presence of malignant involvement (accuracy 70–80%). Lymphadenopathy on mammography underestimates the extent of disease as demonstrated by the current series. This may be partly due to the fact that most axillary nodes are not included in the oblique mammogram. In addition, a deposit that does not enlarge the node or replace the fatty hilum is unlikely to appear pathological even if it is included on the mammogram. When mammographic imaging of axilla is desired, this can be optimized using the axillary view. This view is performed using a small rectangular compression paddle over the axilla and angling the view 40°. Even with this optimized view, only about the lower half of level I can be imaged mammographically (1).

Sonographically, lymph nodes are also coffee-bean-shaped and smoothly marginated, with an echo-poor cortex and a central echogenic fatty hilum. Ultrasound, while able to accurately determine size and morphology, presents technical difficulties in imaging all axillary nodes, and small subcapsular metastatic deposits may not be visualized. Unlike mammography, ▶sonography is capable of imaging the entire axilla. Conventional ultrasound has a high sensitivity for detecting enlarged lymph nodes, whereas its specificity is moderate. Tumor-associated alterations of intranodal angioarchitecture are not specific enough to allow reliable differential diagnosis of lymphadenopathy by color-coded Doppler ultrasound. Power Doppler ultrasound has improved the distinction among inflamed, reactive, and metastatic nodes (5).

Lymph node imaging has not played a significant role in staging of patients with breast cancer because of the inability of imaging to detect microscopic nodal metastases. Axillary dissection is more accurate in this situation. But to decrease the morbidity associated with axillary dissection, sentinel node sampling is increasingly being used as an alternative procedure for histopathologic staging. The technique involves injecting blue dye or isotope in the breast and locating the first node or nodes to which it travels, this node being the "sentinel node." This node is then removed. If it does not contain metastatic disease, no further axillary dissection is performed (1, 4).

▶Magnetic resonance imaging (MRI) using gadolinium chelate as the contrast agent has a high positive predictive value for axillary nodal metastases. The use of ultrasmall particles of iron oxide (USPIO) as a so-called specific contrast agent is presently being investigated. USPIO accumulates in the reticuloendothelial system of normal lymph node tissue and causes a decrease of signal intensity on T2-weighted images by its ferromagnetic properties. In metastatic nodes, USPIO does not accumulate; therefore, signal intensity does not change. However, in the patient who presents with axillary adenopathy or supraclavicular adenopathy and occult carcinoma, MRI of the breast may be the diagnostic test of choice because of its high sensitivity and high negative predictive value. In women with axillary lymph node metastasis, breast MRI should be included as part of the work-up when conventional imaging and clinical breast examinations are negative. MRI has proved to be valuable in identifying the breast as the primary source, with

localization ranging from 75 to 100%. Breast MRI can eliminate uncertainty about the primary site and offer the opportunity for optimal treatment (4).

Nuclear Medicine

Positron emission tomography (PET) using (fluorine 18) 2-deoxy-2-fluoro-D-glucose (FDG) may also be useful in assessing axillary lymph nodes. It is reported that the sensitivity, negative predictive value, specificity, and accuracy of PET are 95, 95, 66, and 77%, respectively.

Detection of small microscopic malignant foci in lymph node may not be possible with PET. But the major advantage of PET appears to be its capability to image distant metastases simultaneously. Thus, in selected patients its use may be cost-effective (1). However, FDG is not specific for tumor imaging; macrophages involved in inflammatory and infectious diseases can accumulate the tracer in large amounts as well, making the characterization of mediastinal nodes particularly challenging. In addition, lymph nodes involved with several types of tumors, such as bronchioloalveolar cell carcinoma and carcinoid tumor, are often false-negative with FDG-PET. False-negative outcomes may also arise in lymph nodes that are smaller than 1 cm or that contain micrometastases. In melanoma and breast cancer, for example, surgical sentinel node biopsy remains the method of choice for detecting metastatic spread in the draining lymph nodes. In fact, spatial resolution of PET is relatively low, compared with cross-sectional imaging, and deep foci of uptake are attenuated by the surrounding tissues. The implementation of PET-computed tomography (CT) fusion, either by computer coregistration or, more recently, by dedicated dual-modality scanners, have partly overcome these obstacles (4).

Diagnosis

Axillary lymph nodes are frequently visualized on routine *mammography* as a well-defined mass that is isodense or hypodense compared with breast parenchyma and contains a central fatty hilum(3). Oblique view mammography, now routine in breast cancer screening, permits visualization of the low anterior axilla. Normal axillary lymph nodes are frequently identified and are typically small and oval with a lucent center due to hilar fat. Enlarged but otherwise normal axillary lymph nodes may be seen in older patients due to fatty replacement of normal lymphoid parenchyma (6). Size is not significant because a large central fatty hilum may cause nodes to be >2.5 cm. Abnormality of axillary lymph nodes is suggested by an increase in nodal density and loss of the fatty hilum. Although nodal size and margins are variable in both benign and malignant lesions, a pattern of spiculated nodes has been reported to result from perinodal extension from a biologically aggressive carcinoma. Microcalcifications are commonly present in the primary breast carcinoma but are rarely seen in axillary node metastases. Axillary node calcifications are usually pleomorphic and faint. Similar calcifications may also be seen with metastatic ovarian and thyroid carcinoma. Coarse calcifications may be seen in granulomatous disease such as tuberculosis and fat necrosis (Fig. 1). Tuberculosis of the breast is rare, and tuberculous axillary lymphadenitis without evidence of tuberculous mastitis is even rarer. The HIV epidemic has resulted in a higher percentage of extrapulmonary tuberculosis, and more cases of tuberculous lymphadenitis can be expected because peripheral lymph node tuberculosis is one of the more common manifestations of extrapulmonary tuberculosis.

If silicone drains from breast augmentation prostheses into the axillary nodes, it may be observed as extremely dense. Mammographically, intramammary lymph nodes appear in the typical morphology of a lymph node (1, 3) and are recognized as typical morphology of lymph nodes in imaging modalities.

Sonographically, asymmetric thickening and focal lobulations in the cortex, partial or complete replacement of the echogenic fatty hilum, focal or diffuse decrease of echogenity within the nodal cortex, and marginal irregularity in some metastatic cases or increased transverse diameter of the lymph node parenchyma can occur. Overall size does not have clinical significance. Several series have reported *color Doppler ultrasound* (US) findings that indicated malignancy: displacement of hilar vessels, focal absence of perfusion, aberrant vessels, and subcapsular vessels. The longitudinal-transverse axis ratio and the presence of a peripheral versus central flow pattern were shown in recent publications on ▶color Doppler US (Fig. 2) Different flow patterns can be depicted on US; metastatic nodes tend to show a more peripheral vasculature than benign or reactive nodes. The usual figures for accuracy and specificity range between 85 and 88%. However, inherent limitations of US are well known, including the poor accessibility of deeply located nodes, in contrast to the use of MRI or CT. Combining Doppler US with microbubble contrast agents could overcome this drawback, and contrast-enhanced US lymphography following the interstitial injection of submicron-diameter bubbles could even compete with isotope sentinel node detection, as suggested by a recent animal study (1, 4).

Lymph nodes located within the breast or lower axilla may be visualized on imaging studies of the breast. Unfortunately, imaging methods are often unable to differentiate inflammatory and neoplastic nodes.

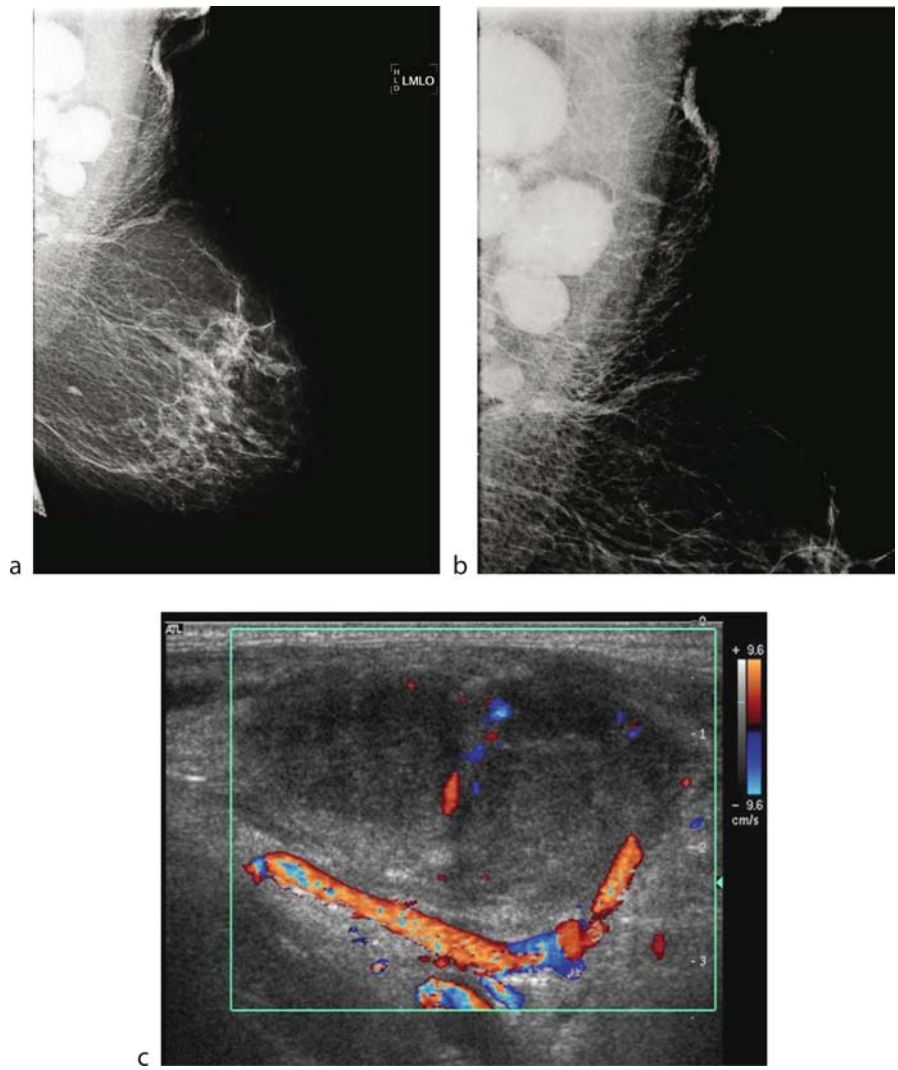

Lymphadenopathy. Figure 1 **(a) Mammogram in MLO position shows large lymph nodes with coarse calcifications due to tuberculosis lymphadenitis in the axillary region. Its magnification is seen in (b). (c) Doppler view of the same patient**

Owing to their low invasiveness and availability, *cross-sectional imaging techniques* have gained widespread acceptance for lymph node imaging. However, whether with CT or MRI, criteria for lymph node metastases remain limited to size assessment. Maximum short axis diameters of normal-sized nodes usually do not exceed 1 cm. However, this value may vary depending on the node's location. Additional morphologic features suggestive of normal nodes include the presence of a fatty hilum, regular contours, and homogeneous signal or density on MRI and CT. Nevertheless, micrometastases, such as in breast cancer, are commonly reported in normal-sized nodes. Improving the spatial resolution of cross-sectional imaging and, especially, being able to identify morphologic alterations of either lymph node cortex and sinus could allow better distinction of the involved tumor and normal nodes. Several studies have assessed whether dynamic enhancement of lymph nodes following intravenous injection of extracellular contrast agents (gadolinium-based contrast agents on MRI) could improve the identification accuracy of nodal metastases. In contrast to extracellular contrast agents, iron oxide-based contrast agents reach lymph nodes indirectly (USPIO). Benign and reactive nodes share the presence of phagocytic or mononuclear cells in contrast to massively involved metastatic nodes, which fail to show a decreased signal intensity after USPIO injection: therefore, benign nodes can be distinguished from tumor-involved nodes regardless of size criteria. USPIO thus behave as "negative" contrast agents (4).

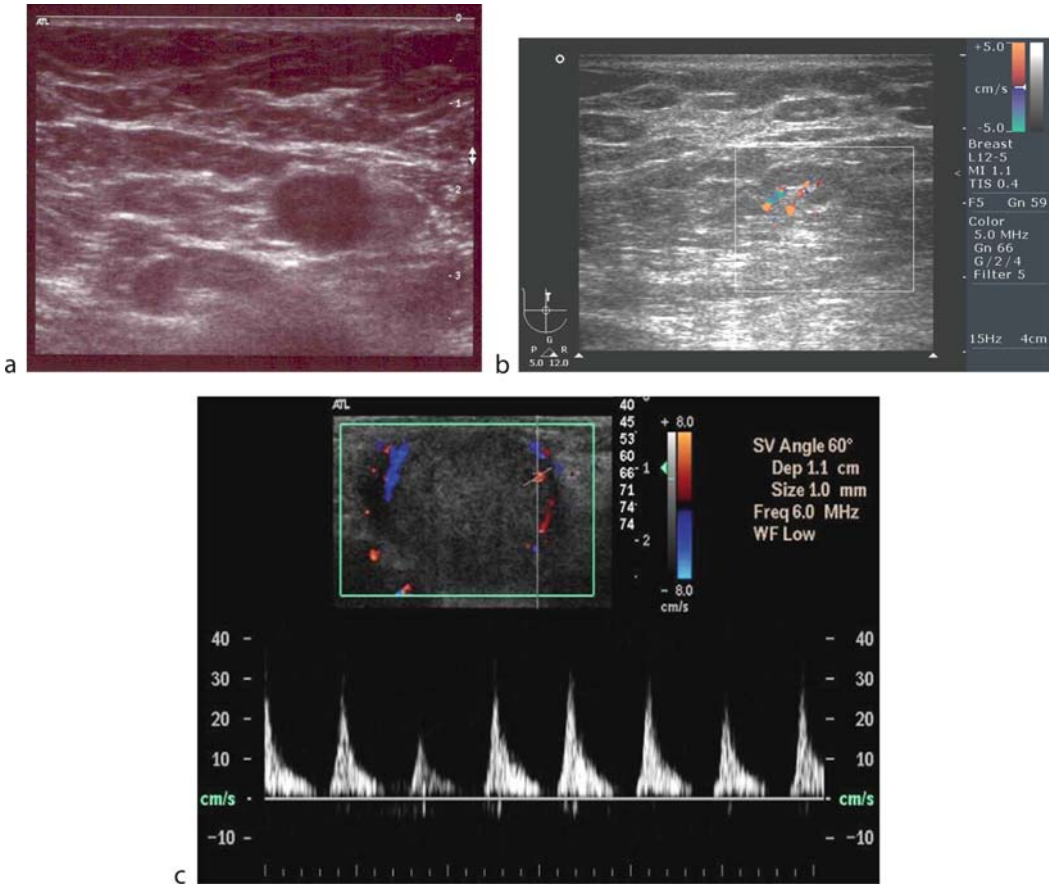

Lymphadenopathy. Figure 2 **(a) Benign and malignant lymph nodes in the same image. B-mode scan shows loss of the echogenic fatty hilum, focal lobulations in the cortex, and diffuse decrease of echogenicity within the nodal cortex in metastatic lymph node on the right and a typical benign node on the left side of the figure. (b) Benign reactive lymph nodes on color Doppler ultrasound with smooth cortex, small size, and central vascularization. (c) Malignant lymph nodes on color Doppler ultrasound reflecting large size, loss of echogenic hilus, and peripheral**

Lymphoscintigraphy has recently regained interest in oncology for the surgical evaluation of the sentinel node, which is defined as the first lymphatic relay in the drainage territory of a primary tumor and is thought to be the first site of metastases in cases of lymphatic spread. The technique has evolved with the use of patent blue dye and ^{99m}Tc-labeled nanocolloids, both of which make it easier to identify the sentinel node intraoperatively. As initially demonstrated for both melanoma and breast cancer, lymphoscintigraphy allows avoidance of unnecessary invasive lymph node dissection procedures by identifying the sentinel node with the guidance of a gamma probe intraoperatively. In addition, it warrants better nodal staging because skip metastases during lymph node extension of a cancer are rare. Based on several reports, the success rate of sentinel node resection exceeds 90%, and the overall accuracy exceeds 95% (4) (Fig. 3). This technique may help decrease the extent of axillary surgery and reduce the postoperative sequelae of axillary dissection, including lymphedema.

Indirect Interstitial CT and MR Lymphography

The concept of indirect interstitial CT and MR lymphography closely matches that of sentinel node mapping. Small-sized contrast agents injected intradermally can reach lymphatic vessels owing to the increased permeability of the fenestrated endothelial lining of distal lymphatic capillaries. Similarly to radio-isotopes, such agents then follow the lymphatic flow and progressively converge toward afferent nodes. However, the literature remains limited to animal studies, and clinical trials on humans still have to be conducted. Similar results can be obtained with MR following interstitial administration of iron-oxide-based contrast agents or macromolecular gadolinium-based contrast agents (4).

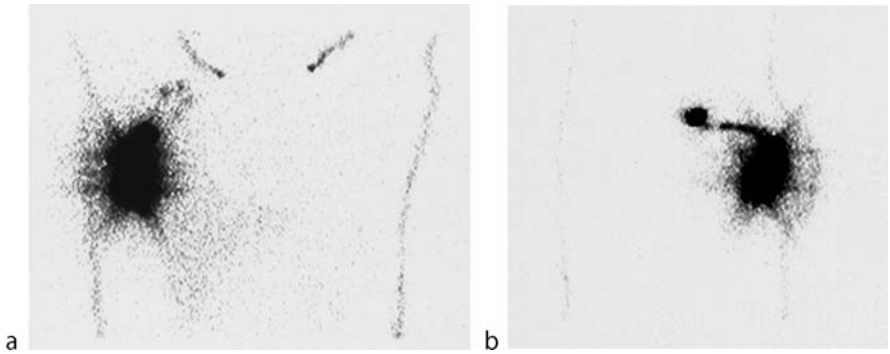

Lymphangioma. Figure 3 Sentinel lymph node imaging shows increased accumulation of tumor site and mapping of sentinel node. (a) Anterior view. (b) Lateral view.

Intervention

Female patients presenting with unilateral axillary masses and normal breast on physical examination can be a diagnostic and therapeutic challenge because there are many causes of axillary masses, including benign and malignant diseases. Mammographically detected enlarged axillary lymph nodes that show any abnormal radiological features or are clinically palpable merit further investigation, including biopsy (6). For those whose diagnosis of axillary adenopathy remains a mystery, fine-needle aspiration or excisional biopsy of the axillary node is necessary to determine the cause (3). Fine-needle aspiration biopsy is very useful in this setting. Although a negative diagnosis cannot definitely exclude malignant involvement, a possible diagnosis is quite reliable and can be used to influence treatment decisions (1).

Bibliography

1. Heywang-Köbrunner SH, Dershaw D, Schreer I (2001) Diagnostic Breast Imaging. 2nd edn. Thieme, Stuttgart, pp 313–324
2. Walsh R, Kornguth PJ, Soo MS et al (1997) Axillary lymph nodes: mammographic, pathologic and clinical correlation. Am J Roentgenol 168:33–36
3. Muttarak M, Chaiwun B, Peh WCG (2004) Role of mammography in diagnosis of axillary abnormalities in women with normal breast examination. *Australas Radiol* 48(3):306–310
4. Luciani A, Itti E, Rahmouni A et al (2006) Lymph node imaging: basic principles. Eur J Radiol 2006 Feb 10; (Epub ahead of print)
5. Golder WA (2004) Lymph node diagnosis in oncologic imaging: a dilemma still waiting to be solved. Onkologie Apr 27(2):194–199
6. Lim ET, O'Doherty A, Hill AD et al (2004) Pathological axillary lymph nodes detected at mammographic screening. Clin Radiol 59(1):86–91

Lymphangioleiomyomatosis

A rare idiopathic disease characterized by smooth muscle cell proliferation occurring both in the lungs and in the mediastinum and retroperitoneum. In the thorax it manifests as numerous lung cysts, recurrent pneumothorax, chylous effusion, and lymphadenopathy. Lymphangioleiomyomatosis predominantly affects the lungs of women of childbearing age and individuals affected by tuberous sclerosis. On chest radiography the unusual combination of a reticular pattern and hyperexpansion of the lungs is typical, and pneumothorax or pleural effusion are commonly present. Widespread cysts are the characteristic feature on computed tomography. They are multiple, thin-walled, and rounded; vessels are seen at the periphery of the cysts and generally are not displaced, as is often the case in centrilobular and bullous emphysema. The cysts do not show preferential distribution, unlike the cysts in Langerhans cell histiocytosis, which typically spare the costophrenic regions.

▶Interstitial Lung Diseases, Unknown Etiology

Lymphangioma

Johan G. Blickman[1,*], Dewi Ashi[2]
[1,*]Department of Radiology, UMC, Nijmegen, Netherlands
[2]Department of Radiology, Faculty of Medicine, University of Indonesia, Cipto Mangunkusumo General Hospital, Salemba, Jakarta Pusat, Indonesia
j.blickman@rad.umcn.nl

Synonym

Congenital lymphatic malformation

Definition

Lymphangiomas are uncommon hamartomatous congenital malformations of the lymphatic system that

involve both the skin and subcutaneous tissues. Two major groups based on depth and size of abnormal lymph vessels are defined: Group I consists of lesions located superficially, and group II consists of lesions more deeply located (such as cavernous lymphangioma and ►cystic hygroma). The female-to-male ratio is equal. About 50% of lymphangiomas are seen at birth, and most are evident by the time the patient is 5 years old.

Pathology/Histopathology

Dilated lymph channels cause the papillary dermis to expand. These channels are more numerous in the upper dermis and often extend into the subcutis. These vessels contain smooth muscle. The lumen is filled with lymphatic fluid and often contains lymphocytes, red blood cells, and neutrophils.

Clinical Presentation

Lymphangiomas can occur anywhere in the skin and mucous membranes. The most common sites are the head and neck, followed by the proximal extremities, the buttocks, and the trunk. Sometimes they can be found in the bowel wall, pancreas, and mesentery.

Lymphangioma circumscriptum (group I) involves small clusters of vesicles measuring about 2–4 mm on the skin. These clear vesicles can vary from pink to red to black secondary to hemorrhage. This lesion can have a warty appearance and as a result can be confused with warts.

Cavernous lymphangiomas typically appear as subcutaneous nodules with a rubbery consistency. The overlying skin has no lesions or changes. The area of involvement varies, ranging from lesions smaller than 1 cm in diameter to larger lesions that involve an entire limb.

Cystic hygroma commonly occurs in the neck and parotid gland. It is a soft and translucent mass, with diameters larger than those of cavernous lymphangiomas.

Imaging

Plain films may show a large mass displacing adjacent structures.

Ultrasound (US) reveals an anechoic mass that is multilocular with fine septations. Sometimes the loculated space may be hypoechoic or hyperechoic depending on the chyle or blood content (Fig. 1).

Computed tomography (CT) also demonstrates septae and loculation. The attenuation value ranges from near fat to near water, depending on the fluid content. Postcontrast, the septa may enhance.

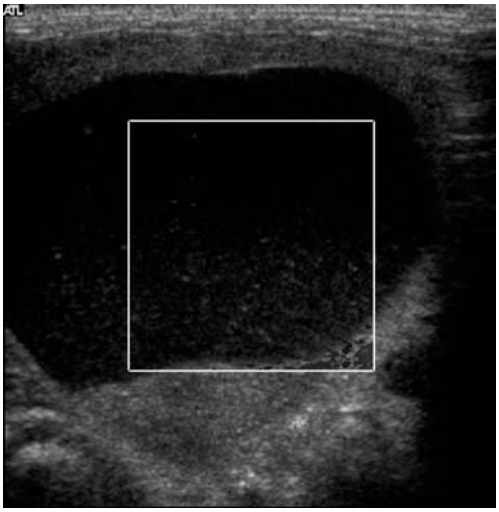

Lymphangioma. Figure 1 US shows hypoechoic mass without vascular flow.

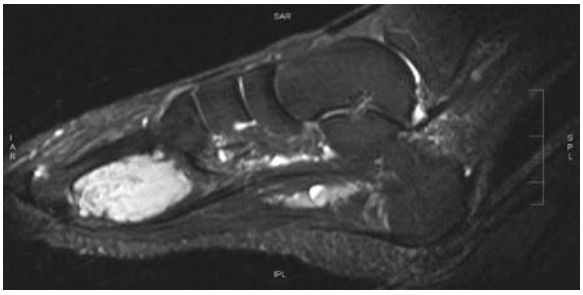

Lymphangioma. Figure 2 On T2WI a hyperintense lesion is seen on the plantar side of the foot.

Magnetic resonance imaging (MRI) shows cyst characteristics ranging from fluid (hypointense on T1-weighted images) to fat (hyperintense on T2-weighted images; Fig. 2).

Nuclear Medicine

Nuclear medicine has no place in lymphangioma evaluation.

Diagnosis

The diagnosis of lymphangioma is based mainly on clinical history, physical examination, US, and conventional light microscopy.

US and CT can delineate septae and cysts. Both CT and MRI can define the extension of the lesion and involvement in surrounding tissues. If the lesions contain

large cystic structures, they are treated with percutaneous sclerosing.

Immunohistochemical investigation for difficult cases is useful for differentiating between lymphangioma and hemangioma. Test results with factor VIII-related antigen are positive for hemangioma and negative for lymphangioma. Immunohistochemical studies for laminin show the typical multilayered basal lamina blood vessels in the case of hemangioma and discontinuous basal lamina in lymphangioma.

▶Congenital Malformations, Oral Cavity
▶Cystic Neoplasms, Pancreatic

Bibliography

1. Barnes PD (1998) Neuroimaging. In: Hans Blickman (ed) Paediatric Radiology: The Requisites. 2nd edn. Mosby St. Louis, pp 265–266
2. Oslo (2001)Paediatric Imaging. In: Carty H (ed) The Encyclopedia of Medical Imaging, vol 7, Publisahed by The NICER Institute, Oslo, p 317
3. Schlesinger AE, Parker B (2004) Tumor and tumor-like condition, In: Kuhn JP, Slovis TL, and Haller JO (eds) Caffey's Pediatric Diagnostic Imaging. 10th edn. Mosby, Philadelphia, pp 1628–1629, p 1913
4. http://www.emedicine.com/derm. Lymphangioma last update November 8, 2005

Lymphangioma

▶Cysts, Cerebral and Cervical, Childhood

Lymphangioma, Hepatic

Convolute of dilated lymphatic channels that may contain proteinaceous material or blood. Usually solitary hepatic lesion, if multiple lesions are seen in multiple organs the condition is referred to as lymphangiomatosis.

▶Hepatic Pediatric Tumors, Benign

Lymphangiomatosis, Splenic

Diffuse involvement of the spleen by multiple lymphangiomas. It can be part of a generalized multisystem syndrome involving the liver, bone, lung, and/or brain, and it presents during infancy, childhood, or adolescence.

▶Neoplasms, Splenic, Benign

Lymphedema

Lymphatic edema of the arm, which affects 10–20% of patients who have suffered some kind of axillary surgery, especially if the patient also underwent radiation therapy and/or the lymph nodes contained cancer cells. Early signs of lymphedema are a feeling of tightness, pain, heaviness, swelling, redness, and less movement or flexibility.

▶Breast Conserving Therapy
▶Lymphopoietic System, Diseases of the

Lymphoepithelial Cyst

Lymphoepithelial cyst of the pancreas is extremely rare. It is a well-defined cystic lesion lined by mature keratinizing squamous epithelium surrounded by a rim of lymphoid tissue. They present predominantly in middle-aged or elderly males with non-specific symptoms. At imaging lymphoepithelial cysts show mainly a cystic appearance, but they may contain some debris as a result of their keratin content. The differential diagnosis includes all cystic lesions, but particularly dermoid cysts.

▶Cystic Neoplasms, Pancreatic

Lymphoma

▶Neoplasms, Chest, Childhood

Lymphoma Hepatic, Primary

Malignancy limited to the hepatic parenchyma with no evidence of further nodal or extranodal involvement.

▶Lymphoma, Hepatic

Lymphoma Hepatic, Secondary

Hepatic involvement in patients with systemic lymphoma.

▶Lymphoma, Hepatic

Lymphoma, Breast

Els M. Vanherreweghe, Geert M. Villeirs
Department of Radiology, Ghent University Hospital
Ghent, Belgium
geert.villeirs@ugent.be

Definition

Breast lymphoma is an uncommon haematologic malignancy of the breast, representing about 0.5% of all malignant lymphomas and 2% of extranodal lymphomas. In most cases, the breast is involved as part of disseminated extranodal disease, usually ►non-Hodgkin lymphoma and very rarely Hodgkin lymphoma. Primary lymphoma of the breast, with or without axillary nodal involvement, is unusual.

Pathology/Histopathology

The majority of mammary lymphomas are of the ►B-cell type, with rare occurrences of T-cell lymphoma. Microscopically, they appear similar to extramammary lymphoma and consist of diffuse or focal (single or multiple) infiltration of the breast parenchyma with dense populations of lymphoma cells. They are fairly well circumscribed from the surrounding tissue, but usually show some marginal irregularities or indistinctness, because of their peripheral reactive lymphoid infiltrate. In contrast to primary breast carcinomas, however, they show no spiculations, since they do not elicit a desmoplastic reaction.

Clinical Presentation

Most breast lymphomas present as a rapidly growing painless palpable lump that is fairly mobile and relatively soft and elastic. Skin thickening, enlargement of the breast, and systemic symptoms such as fever, weight loss and night sweats may also be present. At the time of diagnosis, bilateral disease is present in about 10% of patients and enlarged axillary lymph nodes may be associated.

Mammography

The mammographic instance of breast lymphomas is non-specific and there is no correlation between the different subtypes of lymphoma and their mammographic features. Breast lymphomas can present as solitary or multiple, round or lobulated, fairly well-circumscribed nodules with smooth or indistinct borders, but without spiculations or calcifications (Fig. 1). In diffuse involvement, an asymmetric density with skin thickening and coarsening of the trabecular framework of the breast may be observed.

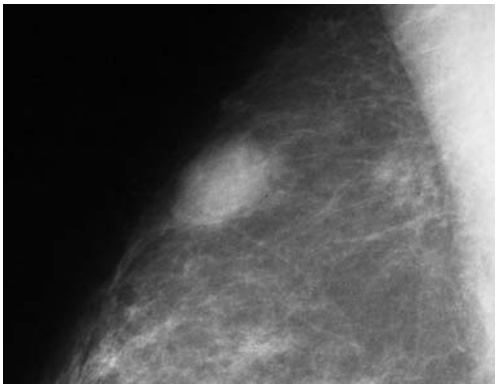

Lymphoma, Breast. Figure 1 Breast lymphoma presenting as an oval fairly well-circumscribed mass in the upeer outer quadrant. Note that no spiculations or calcifications are present.

Axillary nodal involvement is mammographically indistinguishable from nodal metastases of primary breast carcinoma.

Sonography

Breast lymphomas may be recognized as single or multiple, round or lobulated, heterogeneously hypoechoic masses with variable through-transmission and fairly well-circumscribed margins (Fig. 2). When there is peripheral reactive lymphoid infiltration, an ill-defined echogenic rim may surround the lesion. The skin may also be thickened and the lymphomatous tissue may show decreased echogenicity (Fig. 3).

Magnetic Resonance Mammography

The magnetic resonance instance of breast lymphoma is non-specific. On T1-weighted images, fairly well circumscribed hypointense masses that enhance rapidly, sometimes in a ringlike fashion, have been reported. On T2-weighted images, the masses may be ill defined or show a hyperintense halo. Magnetic resonance mammography can be helpful in determining the extent of involvement, but differentiation from primary breast carcinoma is not possible.

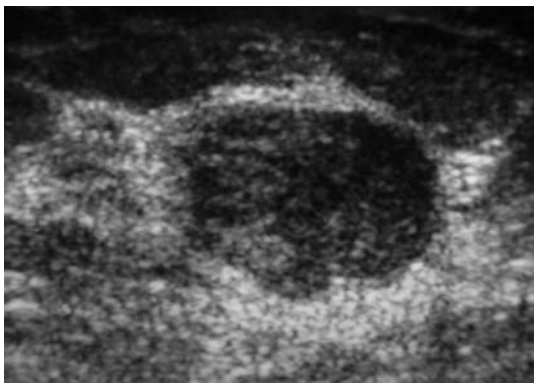

Lymphoma, Breast. Figure 2 Sonogram of a lobulated well-circumscribed heterogeneously hypoechoic breast lymphoma.

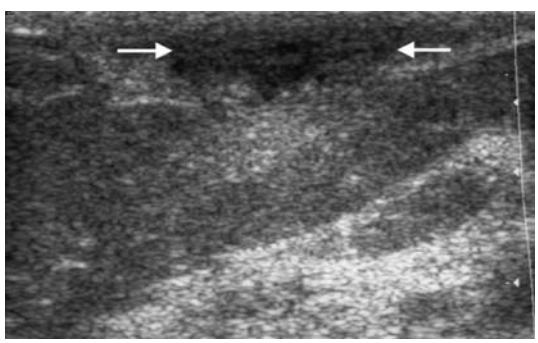

Lymphoma, Breast. Figure 3 Cutaneous B-cell lymphoma of the breast presenting as a lobulated fairly well-circumscribed hypoechoic mass adherent to the skin.

Nuclear Medicine

PET/CT scan may be useful to detect extramammary localizations of lymphoma and to distinguish between breast involvement in extranodal lymphoma or primary mammary lymphoma.

Diagnosis

Since most mammary lymphomas are part of a disseminated extranodal disease, any palpable abnormality in the breast in a patient with known lymphoma should raise the suspicion of mammary involvement. The diagnosis of primary breast carcinoma is limited to those patients without evidence of extramammary lymphoma at the time of diagnosis. Since the clinical and imaging presentation of both primary and secondary lymphoma are generally non-specific, the diagnosis should be obtained through cytological smear, core biopsy or excisional biopsy.

Bibliography

1. Meyer JE, Kopans DB, Long JC (1980) Mammographic appearance of malignant lymphoma of the breast. Radiology 135:623–626
2. Hugh JC, Jackson FI, Hanson J et al (1990) Primary breast lymphoma. An immunohistologic study of 20 new cases. Cancer 66:2602–2611
3. Giardini R, Piccolo C, Rilke F (1992) Primary non-Hodgkin's lymphomas of the female breast. Cancer 69:725–735
4. Bobrow LG, Richards MA, Happerfield LC et al (1993) Breast lymphomas: a clinicopathologic review. Hum Pathol 24:274–278
5. Brogi E, Harris NL (1999) Lymphomas of the breast: pathology and clinical behaviour. Semin Oncol 26:357–364

Lymphoma, Genito Urinary Tract

Eric de Kerviler[1], Olivier Mathieu[1], Cédric de Bazelaire[1], Pauline Brice[2], Jacques Frija[1]
[1]Service de Radiologie, Hôpital Saint-Louis, Paris, France
[2]Hôpital de jour d'Hématologie, Hôpital Saint-Louis, Paris, France
eric.de-kerviler@sls.ap-hop-paris.fr

Synonyms

Lymphomas of the male genital tract; Lymphomas of the urinary tract

Definition

Lymphomas are tumors of the lymphatic tissue and account for 5% of all cancers. Although, lymphomas mainly involve lymphatic organs (lymph nodes, bone marrow, thymus, spleen, and mucosa-associated lymphoid tissue), they can also involve organs systems not containing lymphoid tissue. The most frequent extranodal localizations are digestive tract, skin, bone marrow, and head and neck. Genitourinary (GU) lymphomas represent 2 to 10% of all lymphomas. The GU tract may be affected either primarily or much more frequently secondarily in disseminated lymphomas or at recurrence.

Pathology/Histopathology

Most of lymphomas involving the GU tract are aggressive non-Hodgkin's lymphoma (mainly of B-cell origin), but low-grade lymphomas may be also seen. The appearance of a renal lesion in a patient followed up for a low-grade

lymphoma suggests a transformation into a high-grade lymphoma. Usually, GU involvement is observed in patients with disseminated lymphoma, having other extranodal lesions. Primary renal lymphoma is a discussed entity, which has been reported in less than 0.7% of extranodal lymphoma series in the literature. Indeed, lymphoid tissue is not present in normal kidneys, and extrarenal lesions are frequently diagnosed at autopsy.

Clinical Presentation

Patients with lymphomas of the GU tract long remain asymptomatic and the diagnosis is usually made at CT. Clinical symptoms are usually nonspecific: pain, palpable mass, or less commonly, hematuria, edema, and hypertension. Serum creatinine level is increased in 10–40% of cases. In aggressive lymphomas, B symptoms such as night sweats, fever, or weight loss may be present.

Imaging

Urinary Lymphomas

Lymphomas of the urinary tract mainly involve kidneys, and may exhibit different patterns, depending on the mechanism of spread (1). The hematogenous spread usually results in tumor foci in the renal cortex, with progressive infiltration and formation of expansile masses displacing the collecting system, ultimately leading to complete replacement of kidney parenchyma. Infiltrative growth from retroperitoneal or perirenal preserve renal contours but invades kidney hilum and may compress excretory cavities.

Masses/Nodules

Masses are one of the most common patterns of renal lymphomas. They consist of multiple *bilateral nodules* seen within kidney parenchyma, and usually reflect advanced disease in patients presenting for staging evaluation (Fig. 1). In some cases, lymphomas manifest as a *solitary tumor* simulating a renal cell carcinoma. Unique or multiple, lymphomatous nodules appear as round solid lesions in the renal parenchyma, hypoattenuating at CT, with little enhancement after contrast administration. At sonography, nodules appear hypoechoic with little vascularity. Nodules may displace calices and modify renal contours.

Contiguous Retroperitoneal Extension

Contiguous retroperitoneal involvement is also a common pattern, observed in 25–30% of patients (2). Initially, lymphoma is confined to retroperitoneal lymph nodes.

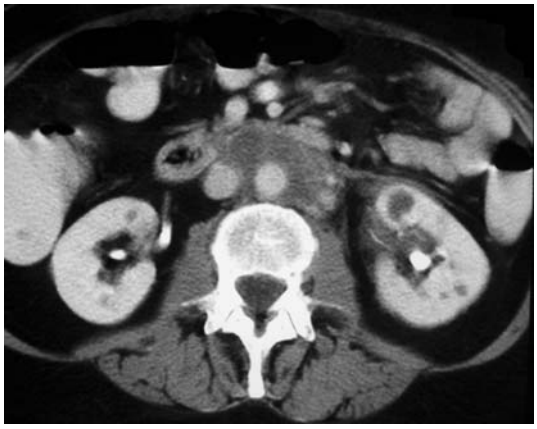

Lymphoma, Genito Urinary Tract. Figure 1 Contrast-enhanced CT examination in a patient with diffuse large B-cell lymphoma shows bilateral hypoattenuating nodules and retroperitoneal lymph nodes.

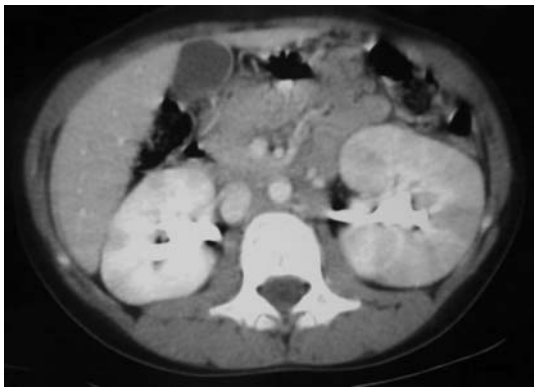

Lymphoma, Genito Urinary Tract. Figure 2 Contrast-enhanced CT examination in a young patient with lymphoblastic lymphoma shows lymphomatous infiltration of both kidneys, which causes nephromegaly and heterogeneous pattern of enhancement.

Then, lymph nodes grow up and typically result in a bulky retroperitoneal mass that invades the renal hilum, and secondarily spreads toward the parenchyma (Fig. 2). As a result, the renal collecting system may be obstructed, leading to renal failure. Before initiating therapy, placing a double-J ureteral catheter allows decreasing serum creatinine level and protecting kidneys from chemotherapy toxicity.

Infiltrative Disease

The infiltrative form of the disease is due to lymphomatous proliferation within the interstitium of the kidney. It is observed in 20% of patients, is almost always bilateral,

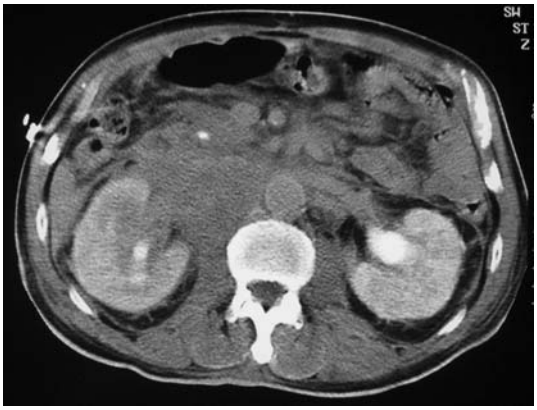

Lymphoma, Genito Urinary Tract. Figure 3 Contrast-enhanced CT examination in a patient with diffuse large B-cell lymphoma shows a large mass in the right retroperitoneum with extension into the right kidney. The heterogeneous pattern of enhancement in the kidneys suggests also an infiltrative pattern.

but may induce subtle changes, which may be misdiagnosed in the early stages of the disease. The main pattern of lymphomatous infiltration is enlarged kidneys with preserved contours (Fig. 3). Kidneys enhance only slightly after contrast injection due to impaired renal function. In some cases, contrast injection delineates more focal areas of infiltrations presenting as poorly defined hypoattenuating foci (3).

Perirenal Infiltration

Perirenal infiltration is rare in an isolated form without parenchymal involvement or retroperitoneal lymph nodes. It may appear as a thickening of the Gerota fascia, a renal sinus infiltration, or perirenal masses (2). The diagnosis may be difficult if the patient does not receive contrast material. However, after contrast, a sharp delineation between tumor and normal kidney is clearly seen since lesions usually enhance much less than normal kidney parenchyma. When present, this pattern is highly suggestive of lymphoma.

Excretory Cavities Involvement

Lymphomas involving the excretory cavities alone are very rare. They are more frequently seen at relapse than at initial diagnosis.

The diagnosis ureteral lymphomas can be made on a follow-up CT, or in a patient presenting with hydronephrosis. The typical pattern is a circumferential thickening of the ureteric wall, either segmental or total, sometimes associated with an infiltration of the surrounding fat.

Lymphomas involving the bladder are exceptional. They usually result from a contiguous pelvic extension in patients with aggressive lymphomas and bulky iliac lymph nodes or pelvic masses. They usually appear as a defect into the bladder resulting from the tumor bulging. Few reports of lymphoma involving the urethra have been published.

Genital Lymphomas

Genital lymphomas in male patients are mainly represented by testicle lymphoma. Lymphomas involving the prostate, the epididymis and the seminal vesicles are much less frequent.

Testicles

Primary testicular lymphomas are rare and represent 0.5–2% of all lymphomas. They are more frequently observed in elderly patients. Testicular lymphomas are usually aggressive lymphomas of diffuse large B-cell type. In the largest published series, the diagnosis was obtained by orchidectomy in 95% of cases, and the disease was at a localized stage in 79% of cases (4). Lesions are unilateral in 90% of cases, bilateral in 10%, and are best seen by sonography. Testicular lymphomas are hypoechoic relative to the surrounding parenchyma in about 95% of cases. The frequency of disseminated lymphomas in patients with testicular lymphomas depends on the examinations performed, and ranges between 13 and 66% in the literature. This kind of lymphoma is usually considered as a lymphoma having a pejorative outcome, with 50% extranodal relapse at 2 years, mainly in the central nervous system.

Prostate

Prostate lymphomas are very rare, and represent less than 0.1% of all lymphomas. They are usually diagnosed in elderly patients or on prostatectomy specimens. As opposed to prostate cancer, any part of the prostate may be involved. Clinical symptoms are the same as those seen in adenomas. Imaging studies detect a mass but the prostate specific antigen remains normal. Diagnosis relies on biopsy.

Lymphoma in Immunocompromised Patients

Immunocompromised patients may develop lymphoma more often than healthy subjects.

Acquired Immunodeficiency Syndrome

It is estimated that 10% of HIV positive patients will develop lymphoma. Lymphomas in AIDS patients are

usually high-grade lymphomas (diffuse large B-cell lymphomas, B-cell immunoblastic lymphomas, and Burkitt lymphomas), presenting at stage IV with multiple extranodal lesions. Among these, kidney is frequently involved. The clinical course is more aggressive, and the disease is both more extensive and less responsive to chemotherapy than in general population.

Kidney Transplant Recipient

Lymphoma is a serious complication following solid organ transplantation. The risk for lymphoma during the first posttransplant year is 20- and 120-fold higher after kidney or heart transplantation, respectively, than that in the general population. Approximately 2% of renal transplant recipient will develop lymphoma. Whereas literature reports agree that the majority of lymphomas occur during the first few months after transplantation, little is known about the long-term risk for lymphoma development. Posttransplant non-Hodgkin lymphomas differ from lymphomas in the general population in histopathologic findings, higher extranodal involvement, a more aggressive clinical course, poorer response to conventional therapies, and poorer outcomes like AIDS-related lymphomas. The renal transplant itself may be involved, mainly in the nodular form.

Diagnosis

Apart from the testicular lymphoma, which is often localized, the diagnosis of lymphoma in general is evoked on a suggestive distribution of lesions at CT that is multiple lymph nodes associated with extranodal lesions. However, in patients with one renal nodule and sentinel retroperitoneal lymph nodes, the question of a renal cancer raises. The final diagnosis of lymphoma with appropriate subtyping is based on histopathology only. The progresses made in image-guided needle biopsy techniques and immunochemistry studies make possible to obtain a definite diagnosis of lymphoma in up to 93% of cases (5). This minimally invasive procedure is safe, easy to perform in the kidneys and reliable. In order to optimize tissue sampling and allow immunochemistry and cytogenetic studies, a coaxial technique is highly recommended. The use of large-cutting needles is possible since lesions are usually hypovascularized. Therefore, open surgery may be avoided as first diagnostic procedure in the management of patients with urinary lymphoma, and should now be fortuitous in case of an equivocal mass or a complication. In patients with testicular masses, the diagnostic approach still remains surgical biopsy or orchidectomy.

Bibliography

1. Hartman DS, David CJ, Goldman Jr et al (1982) Renal lymphoma: radiologic-pathologic correlation of 21 cases. Radiology 144:759–766
2. Cohan RH, Dunnick NR, Leder RA et al (1990) Computed tomography of renal lymphoma. J Comput Assist Tomogr 14:933–938
3. Urban BA, Fishman EK (2000) Renal lymphoma: CT patterns with emphasis on helical CT. Radiographics 20:197–212
4. Zucca E, Conconi A, Mughal TI et al (2003) Patterns of outcome and prognostic factors in primary large-cell lymphoma of the testis in a survey by the International extranodal lymphoma study group. J Clin Oncol 21:20–27
5. de Kerviler E, Guermazi A, Zagdanski AM et al (2000) Image-guided core-needle biopsy in patients with suspected or recurrent lymphomas. Cancer 89:647–652

Lymphoma, Hepatic

Carlo Bartolozzi, Davide Caramella, Paola Vagli
Department of Diagnostic and Interventional Radiology, University of Pisa, Pisa, Italy
bartolozzi@med.unipi.it

Synonyms

Hepatic lymphoproliferative disease

Definition

Hepatic lymphoma is considered to be primary when the malignancy is limited to the hepatic parenchyma and there is no evidence of further nodal or extranodal involvement. Hepatic involvement in patients with systemic lymphoma is defined as ►secondary hepatic lymphoma.

Pathology/Histopathology

Primary lymphoma of the liver, first documented in 1965, is extremely rare, representing only 0.4% of all extranodal lymphomas. However, the liver is often a secondary site of lymphomatous involvement, occurring in approximately half of the patients with non-Hodgkin's lymphoma and in 60% of patients with Hodgkin's disease at autopsy (1, 2).

►Primary hepatic lymphoma typically occurs during the fifth decade of life and has a male predominance. It is more common among immunocompromised patients, and a strong association has been identified with chronic hepatitis C.

►AIDS-related lymphomas represent a nosological entity whose characteristic features resemble those of lymphomas seen in organ transplant recipients. Extranodal disease is more frequent, with marked predilection for the brain and the gastrointestinal tract. The liver is the second most common site of abdominal involvement after the bowel. AIDS-related lymphomas are highly aggressive tumors with poorly differentiated histological subtypes, most frequently non-Hodgkin's types, and are associated with a poor prognosis. Patients are typically diagnosed with advanced stages of disease (3).

The interrelationship between chronic hepatitis C and primary hepatic lymphoma remains unclear, although an increased incidence of hepatic lymphomas has been reported in patients affected by chronic hepatitis C. It has been documented that the hepatitis C virus may promote the clonal expansion of B-cells as occurs in associated cryoglobulinemia; additionally, viral cRNA has been detected within extrahepatic lymphoma tissue.

While Hodgkin's disease, non-Hodgkin's lymphoma, and various leukemias may secondarily involve the liver, virtually all primary hepatic lymphomas are non-Hodgkin's types. Most cases of primary lymphoma of the liver are of intermediate or high grade according to the classification of the working formulation for clinical usage. Diffuse large cell lymphoma is the most commonly encountered histological subtype, and most cases are B-cell lymphomas. The rare Hodgkin's lymphoma is generally of Reed–Stemberg cell type. Macroscopically the primary hepatic lymphoma usually occurs as a single large lobulated mass involving both hepatic lobes, and less often as multiple lesions. Conversely, Hodgkin's disease occurs more frequently as miliary lesions than masses. In both Hodgkin's and non-Hodgkin's lymphoma, initial involvement is seen in the portal areas, where the lymphoid tissue is mostly localized.

A few cases of primary hepatic mucosa-associated lymphoid tissue (MALT) lymphomas have been described in the literature. These lymphomas have a good prognosis and are low-grade B-cell lymphomas, occurring in a variety of extranodal sites but rarely as primary hepatic lymphomas. Different from other MALT lymphomas, these are not associated with autoimmune disorders. Typically, primary ►hepatic MALT lymphomas appear as lymphoid infiltrates invading the liver in a serpiginous fashion, with nodular entrapment of normal liver (4).

Secondary hepatic involvement by malignant lymphoma (both Hodgkin's and non-Hodgkin's types) often appears diffusely infiltrative. Distinct nodular lesions are exceedingly uncommon in Hodgkin's disease but occur in half of the patients with non-Hodgkin's lymphoma. However, the nodule size is usually small, less than 1 cm (5).

Clinical Presentation

The most common early signs and symptoms are epigastric and right upper quadrant pain or discomfort and hepatomegaly without splenomegaly.

Fever, weight loss, and night sweats may be present. Jaundice and ascites are uncommon.

Liver function tests are usually normal except for elevated lactic dehydrogenase and alkaline phosphatase levels. Alpha-fetoprotein and carcinoembryonic antigen levels are invariably normal.

In immunocompromised patients the disease demonstrates an aggressive course.

Imaging

Ultrasound (US) displays primary liver lymphoma as a large hypoechoic mass, sometimes anechoic with a cystic-like appearance and typically with homogeneous echo structure and regular margins. In the diffuse forms, the echogenicity and architecture may be both normal and subverted.

Computed tomography (CT) findings of hepatic lymphoma consist of a large, lobulated, usually homogeneous, sharply marginated, solitary mass that is hypodense on nonenhanced scan and appears demarcated and lightly enhancing after contrast medium administration (Fig. 1). Low enhancement is due to tumoral hypovascularity. The degree of necrosis and the presence of calcifications can be variable. Typically, lymphomas do not infiltrate surrounding structures such as the vascular vessels, which are dislocated instead by mass effect (2).

On magnetic resonance imaging (MR) the tumor usually appears homogeneously hypointense on T1-weighted images, isointense to the spleen in T2-weighted images (because of its rich cellularity), and minimally enhanced on early postgadolinium spoiled gradient echo images (Fig. 2).

AIDS-related lymphomas may show atypical imaging patterns such as a rim enhancement or an inhomogeneous appearance, simulating a complex mass.

The appearance of primary liver lymphoma is in contrast to secondary involvement, which is diffusely infiltrative or micronodular (Fig. 3) in most cases and is frequently associated with the presence of retroperitoneal lymphadenopathy. When discrete lesions are present, they appear similar to those of primary hepatic lymphoma (5).

Nuclear Medicine

Imaging using radionuclide ^{67}Ga has proved useful for evaluating posttreatment lymphoma residual masses,

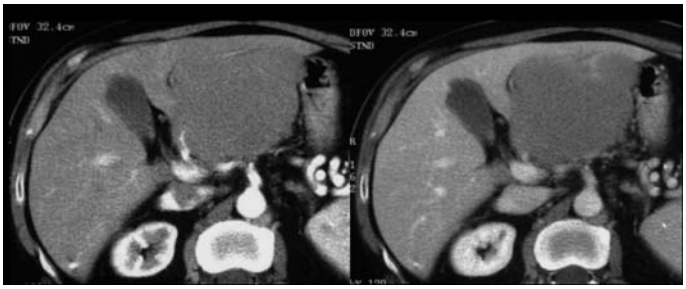

Lymphoma, Hepatic. Figure 1 Primary hepatic lymphoma. Computed tomography scans shows a large mass involving most of the left hepatic lobe, causing compression but not infiltration of the surrounding structures (hepatic vessels). The lesion appears hypodense both in the arterial (*left*) and portal (*right*) venous phases.

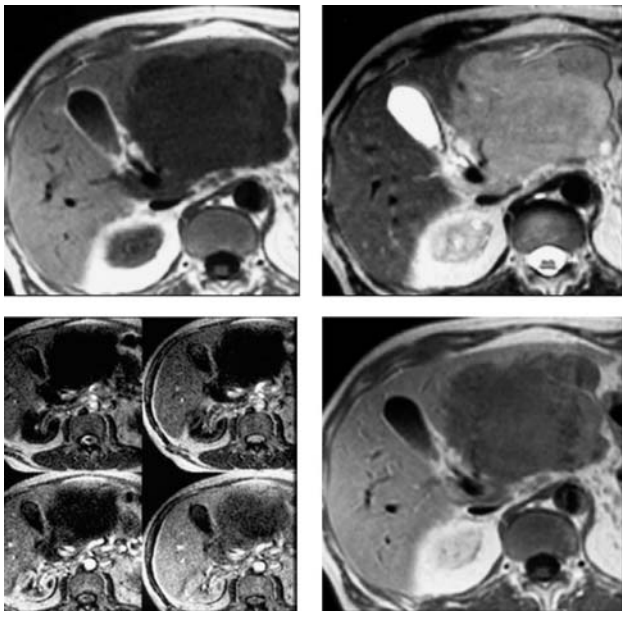

Lymphoma, Hepatic. Figure 2 Magnetic resonance study of the same lesion of in Fig. 1: T1-weighted image shows a homogeneous hypointense mass (upper left). T2-weighted image at the same level shows hyperintensity of the mass that is almost isointense to fat (upper right). After Gd–DTPA administration, the nodule reveals moderate enhancement in the arterial phase (*lower left*), with a hypointense pattern in the delayed phase (*lower right*).

although the presence of normal bowel mucosal uptake and a relatively poor spatial resolution reduce the diagnostic accuracy of this technique. Fluorodeoxyglucose positron emission tomography (FDG-PET) imaging is a tomographic technique that allows precise localization of active glucose metabolism, suggesting potential sites of active disease.

Diagnosis

Imaging features of primary liver lymphoma are not specific when using a single modality. On the contrary, the integration of findings obtained with different imaging techniques may suggest the diagnosis. In the differential diagnosis, a solitary metastasis must be considered; however, a unique large metastasis is very unusual in the absence of a known primary tumor. Classic hypervascular hepatocellular carcinoma, focal nodular hyperplasia, and hepatic hemangioma can be excluded by contrast-enhanced CT if the typical hypodensity of lymphoma is demonstrated. The combination of clinical history, liver findings, and the presence of other supportive findings such as retroperitoneal lymphadenopathy can lead to the correct differentiation between primary hepatic lymphoma and other liver diseases.

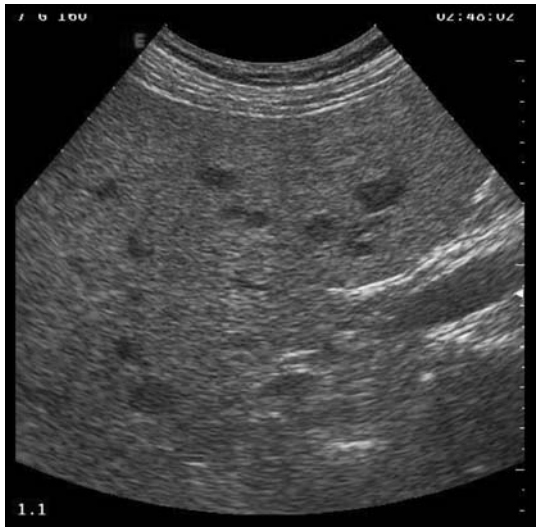

Lymphoma, Hepatic. Figure 3 Secondary lymphomatous hepatic involvement. Ultrasound image shows an aspecific pattern consisting of multiple hypoechoic nodular areas of infiltration of the liver parenchyma.

Finally, the appearance of a normal biliary tree and the absence of a late enhancement on dynamic MRI allows the diagnosis of cholangiocarcinoma to be ruled out (2).

Bibliography

1. Ryan J, Straus DJ, Lange C et al (1988) Primary lymphoma of the liver. Cancer 61(2):370–375
2. Sanders LM, Botet JF, Straus DJ et al (1989) CT of primary lymphoma of the liver. Am J Roentgenol 152(5):973–976
3. Rizzi EB, Schinina V, Cristofaro M et al (2001) Non-Hodgkin's lymphoma of the liver in patients with AIDS: sonographic, CT, and MRI findings. J Clin Ultrasound 29(3):125–129
4. Kirk CM, Lewin D, Lazarchick J (1999) Primary hepatic B-cell lymphoma of mucosa-associated lymphoid tissue. Arch Pathol Lab Med 123(8):716–719
5. Gazelle GS, Lee MJ, Hahn PF et al (1994) US, CT, and MRI of primary and secondary liver lymphoma. J Comput Assist Tomogr 18(3):412–415

Lymphoma, Pancreatic

Lymphoma (predominantly the non-Hodgkin B cell type) involves the pancreas secondarily in approximately 30% of patients with widespread disease. Primary lymphoma of the pancreas is uncommon, representing 1–5% of cases of extranodal lymphomas. The most common clinical findings are abdominal pain and weight loss. Although representing classic symptoms of nodal non-Hodgkin's lymphoma, fever and night sweats are rare in patients with primary pancreatic involvement. Jaundice represents an infrequent finding, even with large lesions involving the pancreatic head.

On sonography, primary ▶pancreatic lymphoma usually appears as a homogeneous hypoechoic mass with enlarged peripancreatic lymph-nodes. At CT, pancreatic lymphoma generally appears as a larger, bulky tumor and is often seen as a homogeneous mass. Enhancement after administration of contrast medium is usually poor. Two distinct CT patterns have been described, including focal and circumscribed masses and diffuse enlargement of the gland. The diffuse infiltrating pattern may mimic the imaging findings of pancreatitis with gland enlargement and irregular infiltration of the peripancreatic fat. Dilatation of Wirsung's duct is usually mild. Encasement of the peripancreatic vessels may occur, but vascular obstruction is uncommon despite the presence of a large tumor, a helpful distinguishing feature from other malignant tumors. The presence of associated enlarged peripancreatic lymph nodes also favors the diagnosis of lymphoma. At MR examination, lymphoma appears as a low-signal-intensity homogeneous mass within the pancreas on T1-weighted images with poor enhancement after gadolinium administration. On T2-weighted images, the lesion shows a more heterogeneous appearance. Only mild pancreatic ductal dilatation is usually visible on MRCP. Despite the rarity of primary pancreatic lymphoma, it is important to differentiate this entity from adenocarcinoma as the management of these two conditions is different. If the imaging findings are suggestive of lymphoma, a definitive diagnosis must be achieved by percutaneous or endoscopic biopsy averting unnecessary surgery, because lymphomas are generally treated by chemotherapy.

▶Carcinoma, Pancreatic

Lymphomas of the Male Genital Tract

▶Lymphoma, Genito Urinary Tract

Lymphomas of the Urinary Tract

▶Lymphoma, Genito Urinary Tract

Lymphopoietic System, Diseases of the

Otmar Schober
Department of Nuclear Medicine, Coordinator Collaborative Research Center, Molecular Cardiovascular Imaging (SFB 656-MoBil), University Hospital Münster, Albert-Schweitzer-Str. 33, D48149 Münster, Germany
schober.otmar@uni-muenster.de

Synonyms

Lymphedema; Lymph node metastasis

Definition

1. Lymphedema is defined as an increased accumulation of lymphatic fluid in the extravascular compartment.
2. Lymph node metastasis is defined as regional or distant lymphogenic spread of malignant solid tumors.

Pathology/Histopathology

1. Lymphedema may be due to an injury or insufficiency of lymph vessels, an increased venous pressure (e.g., deep vein thrombosis, right heart failure) or a decreased intravascular oncotic pressure (e.g., albumin deficiency).
2. Infiltration and/or destruction of lymph nodes by malignant solid tumor cells.

Clinical Presentation

1. Lymphedema initially presents with swelling of the legs which is often painful and extends above the legs in severe cases.
2. Lymph node metastasis may often show painless, hardened, and immobile lymph node enlargement.

Imaging

The procedure of lymphoscintigraphy using indirect interstitial injections offers advantages compared with the radiological procedures of lymphatic angiography and lymphadenography with contrast medium for the visualization of the lymphatic drainage system as well as the lymph node stations. Admittedly, the latter techniques stand out for their more detailed representation, but they are more complicated and more invasive, because the lymphatic vessels must be cannulated directly. The nodi lymphatici iliacae internae and mammariae internae are not amenable to radiological imaging but only to scintigraphic visualization after interstitial injection of the tracer in the surrounding connective tissue.

In the case of suspected lymph node metastasis, ultrasound and computed tomography or combined ^{18}F-FDG-PET-CT should be performed in order to determine the size, shape, and metabolic activity of the lymph nodes (cf. oncology).

Nuclear Medicine

Using lymphoscintigraphy, the first priority is to visualize the lymphatic drainage system in the surroundings of malignant tumors. In this way the possible metastasizing routes of the particular tumor can be determined (1, 2). As a rule, colloidal particles are used in lymphoscintigraphy, for example, denaturated albumin. Owing to their size, from 20 to 30 nm, these particles are removed *via* the lymphatic drainage system and retained and phagocyted in the reticuloendothelial system (RES) of the lymph nodes. The colloidal particles are labeled with 20–40 MBq ^{99m}Tc and injected intra- or subcutaneously, mostly in several smaller portions, into the surrounding tissue of the tumor. Direct injection into the tumor should be avoided so as not to risk a transfer of tumor cells into healthy tissues.

Acquisitions are performed immediately after injection in order to visualize the primary lymphatic routes. Preoperatively, it may be necessary to draw these routes on the skin of the patient. Static late acquisitions, mostly after several hours, serve to register the lymph node stations, whose knowledge is necessary for the surgical planning. The primary lymph node or the primary lymph node stations, which are a first filter station in the lymphatic drainage system of the tumor, are called the "sentinel lymph nodes" (SLNs). In patients with malignant melanoma, breast cancer, and tumors in the small pelvis—like the cervix, vagina, prostate, bladder, and rectum—for the preoperative visualization of the draining lymph vessels and the regional lymph nodes, the SLN should be visualized scintigraphically, because the surgical procedure of lymphadenectomy is particularly dependent on the histology of this lymph node (Fig. 1). The reliability of the detection of the SLN is further increased through the intraoperative application of a gamma detector. Therefore, unnecessary radical lymphadenectomies can be prevented. The targeted removal of the primary lymph node means that the therapeutic

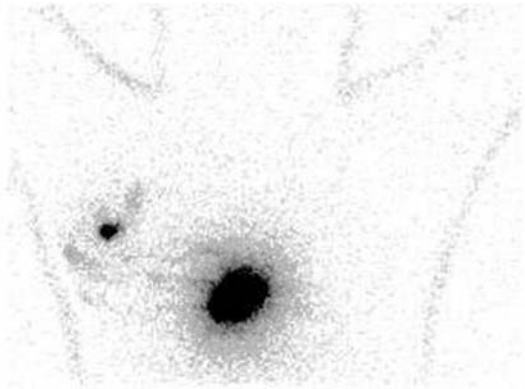

Lymphopoietic system, diseases of the. Figure 1 ***Malignant melanoma*****. After intradermal injection of ^{99m}Tc-nanocolloid in the area of a median thoracic malignant melanoma, a sentinel lymph node (SLN) is detected in the right axilla. For improved localization, the body contours are delineated using a cobalt marker.**

perspectives remain preserved for many patients in an early tumor stage, despite the fact that lymphogenic metastatic spread has already occurred.

Lymphedema

Lymphoscintigraphy is also applied for the assessment of a primary or secondary lymphedema (3–5). In the case of an injury to the lymph vessels or a valve insufficiency, a diffuse outflow of lymphatic fluid occurs in the surrounding tissue ("dermal backflow"). As an indication of a proximal lymphatic vessel obstruction, collaterals between the distal lymphatic vessels can be detected. A subcutaneous injection of 20 to 40 MBq of a ^{99m}Tc-labeled microcolloid is made in the first or second interdigital space of the hands or feet. The removal of the tracer can be increased by mobilization of the extremities. During the first 2 h after the injection, planar scintigrams of the extremities are acquired and further acquisitions are made after an endurance test (e.g., 20 min climbing stairs).

Diagnosis

1. Lymphedema can be diagnosed by inspection and palpation. In order to determine the cause of the lymphedema, venous insufficiency, right heart failure, and albumin deficiency have to be excluded. An injury or insufficiency of lymph vessels can be determined by lymphoscintigraphy.
2. Lymph node metastasis is often diagnosed by inspection, palpation, and primarily morphologic imaging procedures. The exact anatomical position of the sentinal lymph node (SLN) can be determined using lymphoscintigraphy.

Bibliography

1. Belhocine TZ, Scott AM, Even-Sapir E et al (2006) Role of nuclear medicine in the management of cutaneous malignant melanoma. J Nucl Med 47:957–967
2. Thompson JF, Uren RF (2005) Lymphatic mapping in management of patients with primary cutaneous melanoma. Lancet Oncol 6:877–885
3. Moshiri M, Katz DS, Boris M et al (2002) Using lymphoscintigraphy to evaluate suspected lymphedema of the extremities. Am J Roentgenol 187:405–412
4. Szuba A, Shin WS, Strauss HW et al (2003) The third circulation: radionuclide lymphoscinitgraphy in the evaluation of lymphedema. J Nucl Med 44:43–57
5. Weissleder H, Weissleder R (1988) Lymphedema: evaluation of qualitative and quantitative lymphoscintigraphy in 238 patients. Radiology 167:729–735

M-mode Echocardiography

Motion (M) mode display displays the grey-scale level along the length of the ultrasound beam during time.
►Ischemic Heart Disease, Ultrasound

Macklin Effect

The pathophysiology of pneumomediastinum in severe blunt trauma is a three-step process: blunt traumatic alveolar ruptures, air dissection along bronchovascular sheaths, and spread of this blunt pulmonary interstitial emphysema into the mediastinum. A pneumomediastinum is therefore not necessarily related to direct rupture of the tracheobronchial tree.
►Chest Trauma

MacMahon–Tannhauser Syndrome

Pericholangiolitic biliary cirrhosis, xanthomatous biliary cirrhosis. Congenital hypoplasia of intralobular bile duct resulting in intrahepatic cholestasis and primary biliary cirrhosis associated with peculiar features such as hepatic ostheoartropathy.
►Congenital Malformations, Liver and Biliary Tract

Macroadenoma

Pituitary gland tumor of at least 1 cm located in the sella turcica with a variable suprasellar extension and occasional invasion of the skull base. The patient presents either with endocrine disease or with neurological/ophthalmologic signs. On magnetic resonance imaging these tumors can be solid or cystic, and they may contain hemorrhagic or necrotic areas.
►Pituitary Gland

Magnetic Resonance Imaging

Technique characterized by high contrast resolution using the signals generated in the tissues in response to a magnetic field, produced by the instrument and converted by a computer into images of body structures: the acquisition is possible on different planes.
►Carcinoma, Hypopharynx
►Neoplasms, Benign and Malignant, Larynx
►Osteonecrosis, Adults
►Lymphadenopathy

Magnetic Resonance Cholangiopancreatography

A noninvasive technique for the evaluation of the biliary tract. It is performed with the use of heavily T2-weighted images obtained with different pulse sequences without the injection of contrast medium that demonstrates stationary fluids, including bile and pancreatic secretions, as having high signal intensity whereas solid organs show a low signal intensity. This technique also allows the visualization of the pancreatic ducts generally after the administration of a secretive agent (secretin).
►Biliary Anatomy
►Congenital Malformations, Bile Ducts

Magnetic Resonance Imaging, Activatable Imaging Agents

Ralph Weissleder, Alexander R. Guimaraes
Center for Molecular Imaging Research, Massachusetts General Hospital, Charlestown, USA
weissleder@helix.mgh.harvard.edu

Magnetic resonance imaging (MRI) continues to be one of the diagnostic modalities of choice of producing noninvasive, high spatial resolution, multiplanar imaging of various disease states. It has recently become possible to expand MRI to obtain molecular information using genetic reporter systems (1) (see Chapter on genetic reporters). An alternative strategy has been to use targeted (see Chapter on targeted imaging agents) and activatable imaging agents. The different forms of activation strategies include: (i) imaging agents that change magnetic properties after specific enzymatic reactions (i.e., through cleavage of sugars or other molecules affecting water diffusion to paramagnetic metals [e.g., LacZ (2)]; (ii) imaging agents that amplify their signals due to oligomerization and protein binding [e.g., MPO (3)]; and (iii) nanoparticle-based magnetic relaxation switches (MRSW) capable of sensing DNA–DNA, protein–protein, and small molecule interactions (4).

Agents Based on Cleavage

Louie and Meade et al have recently demonstrated an example of a novel "smart" contrast probe that remains silent until activated by a specific transgene product (2). By using bacterial β-galactosidase (LacZ), because it is easily assayed, and not expressed in most mammals, they developed a contrast agent that was associated with a substrate for LacZ, galactopyranose. They covalently linked galactopyranose to a chelated paramagnetic Gd^{3+}, in a way that precluded access of water protons to the Gd^{3+} atom. This interaction with the LacZ substrate cleaved the galactopyranose, and thus allowed access of water protons to Gd^{3+} which shortened T1 and thus produced contrast. With intravenous mRNA to allow β-galactosidase activity within organisms, injection of this novel smart probe, produced visualization of those cells involved with LacZ activity. Using this technique, the authors measured an approximate 50% drop in T1, 100% increase in relaxivity with cleavage of the galactopyranose (2). Similar strategies have been employed using calcium activation, pH sensitive strategies, and through changes in viscosity through protein binding.

Agents Based on Oligomerization

Chen et al have recently synthesized an activatable paramagnetic MR imaging agent that targets the enzyme myeloperoxidase (MPO), which is an enzyme that is a marker of inflammation (3). This class of contrast imaging agents is highly sensitive to MPO activity, and have been shown to image *in vivo* sites of MPO activity that reflect inflammation. The imaging agent based on a covalent conjugate of Gd-DOTA and serotonin (3-(2-aminoethyl)-5-hydroxyindole). When the imaging agent was exposed to MPO, there was a resultant increase in molecular mass, and consequently increase in MR signal, with concomitant delayed clearance from tissue. Furthermore, MPO-mediated oxidation products bind to and cross-link with plasma proteins causing more local accumulation. The association with proteins also further contributes to the increase in MR signal due to R1 increase. The summation of these factors causes an approximate fivefold increase in R1, and thus increased contrast-to-noise (3).

MPO is implicated in multiple disease states including Alzheimer's disease, multiple sclerosis, lung cancer, and leukemia, and this class of agent, because of its capability of detecting sites of active inflammation in infection or injury, may lend further insight into these disease processes. One exciting possibility is in vulnerable plaque imaging, given the role that inflammation plays in atherosclerosis and plaque vulnerability. Furthermore, there is now an accumulating body of evidence that MPO plays a central role in this process, because MPO is found in high abundance in vulnerable plaques and in culprit lesions. Recent clinical trials have found that serum MPO levels predict cardiovascular risk in patients with acute coronary syndrome and chest pain. Furthermore, MPO-deficient humans appear to have decreased risk for cardiovascular diseases. Additional agents using this principle include dopa-DOTA and DPTA-bis-amide based agents.

Superparamagnetic-Based Activatable Reporter Systems

Magnetic nanoparticles (MNP) offer another means of achieving signal amplification through exploitation of their spatial arrangement. Through specific molecular interaction (e.g., DNA–DNA or small molecule–protein interactions) they can be induced to assemble into larger nanoassemblies and the superparamagnetic iron-oxide cores of the nanoparticles become more efficient at dephasing the spins of water protons, that is, at enhancing the spin–spin relaxation rate ($1/T_2$). Both dispersed (~40 nm) and clustered or nanoassembled state (~200 nm) remain in

Magnetic Resonance Imaging, Activatable Imaging Agents. Table 1 Summary of MRSW sensors developed to date

Target	Target	MRSW sensor
DNA	Telomeres	$(CCCTAA)_3$-CLIO
mRNA	GFP	CLIO-ATTTGCCGGTGT; TCAAGTCGCACA-CLIO
Protein	GFP	Anti-GFP-av-CLIO
	CA-125	Anti-CA125-av-CLIO
	Avidin	Biotin-CLIO
	Anti-avidin-Ab	Avidin-CLIO
Enzyme activity	BamH1	CLIO-TTA-CGC-CTAGG-ATC-CTC; AAT-GCG-GGATCC-TAC-GAG-CLIO
	Dam-methylase	Methylated BamH1 MRSW sensor
	MboI	Methylated BamH1 MRSW sensor
	DpnI	Methylated BamH1 MRSW sensor
	Caspase-3	Av-CLIO; Biotin-GDEVDG-CLIO
	Renin	RK(Btn)IHPFHLVIHTK(Btn)R; av-CLIO
	Trypsin	Btn-$(G)_4$RRRR$(G)_3$K(Btn) or Btn-GPARLAIK(Btn); av-CLIO
	MMP-2	Btn-GGPLGVRGK(Btn); av-CLIO
	AKT	CLIO-CGGKGSGSGRPRTSSFAEG; CLIO-antiphosphopeptide
	Telomerase	CLIO-AATCCCAATCCC; AATCCCAATCCC-CLIO
	Peroxidases	CLIO-phenol; CLIO-tyrosines
Small molecule detection	Enantiomeric	CLIO-D-Phenylalanine
	Impurity	
Organism	Phage	Anti-fd bacteriophage-av-CLIO
	Herpes simplex virus (HSV)	Anti-glycoproteinD(HSV-1)-av-CLIO; anti-HSV1-av-CLIO
	Adenovirus-5	Anti-adenovirus-5-av-CLIO
	Bacterial mRNA	CLIO-GTCGTCAACTAC; CACTGAACAACA-CLIO

solution and the conversion between the two states can be induced repeatedly (4). It has also been shown that this is a reversible process, and thus these nanoassemblies can be disassembled and returned to their original dispersed state by methods including heat, enzyme cleavage, pH alteration, and disulfide bond reduction (4). This reversibility provides a powerful medium of distinguishing subtle changes in the environment for which they are applied, and have thus been termed MRSW (4). This technology has been used to measure multiple different molecular reversible molecular interactions at extremely low contrast agent concentration (fM). Concentrations as low as 0.5 fM have been observed for DNA and proteins, whereas targets like viruses, with large, high multivalence, allow for detection of as few as five viral particles per 10 μL of herpes simplex virus-1 and adenovirus-5 (4).

We have exploited this observation and demonstrated MRSW assays are homogenous assays that can sense a wide variety of molecular interactions with high sensitivity and specificity with no sample preparation (Table 1). At the concentrations used (<20 μg Fe/mL) the nanoassemblies have not been noted to precipitate and are thus stable, and since these MNP are being used in clinical trials, there is a strong possibility of *in vivo* application in the near future.

Bibliography

1. Weissleder R, Mahmood U (2001) Molecular imaging. Radiology 219(2):316–333
2. Louie AY et al (2000) In vivo visualization of gene expression using magnetic resonance imaging. Nat Biotechnol 18(3):321–325
3. Chen JW et al (2004) Human myeloperoxidase: a potential target for molecular MR imaging in atherosclerosis. Magn Reson Med 52 (5):1021–1028
4. Perez JM et al (2002) Magnetic relaxation switches capable of sensing molecular interactions. Nat Biotechnol 20(8):816–820

Magnetic Resonance Imaging, Genetic Reporter Systems

Ralph Weissleder, Alexander R. Guimaraes
Center for Molecular Imaging Research, Massachusetts General Hospital, Charlestown, USA
weissleder@helix.mgh.harvard.edu

Magnetic resonance imaging (MRI) continues to be the diagnostic modality of choice of producing noninvasive, high spatial resolution, multiplanar imaging of various

disease states. Only recently have technological advances in MRI systems and molecular biologic techniques advanced to such a degree to allow imaging of gene expression, *in vivo* (1). Imaging of gene expression using MRI may be achieved by two approaches: (i) imaging of introduced reporters or enzymes, which bind or metabolize (super) paramagnetic substrates; or (ii) imaging of a unique spectroscopic signature (2).

MR Imaging Strategies

Imaging gene expression by the use of receptors expressed on the cell surface, can be achieved by endocytotic internalization of supraparamagnetic nanoparticles (e.g., MION) (1). Tumor cells have a higher rate of endocytosis than normal cells and thus can be labeled selectively. For example, the human transferrin receptor (TfR) is expressed at higher levels on a variety of tumor cell types and can be imaged using transferrin (Tf) bound supramagnetic particles. Further, a genetically engineered form of the human transferrin receptor (ETR), lacking the negative feed back mechanism that results in the down-regulation of endogenous TfR expression, was expressed in 9L glioma tumors (1). At 24 h after perfusion of supraparamagnetic Tf particles into tumor-bearing mice, ETR tumors *in vivo* showed considerably enhanced MR signal intensity as compared to the same tumors lacking the ETR. HSV-based amplicon vectors have also been used to deliver ETR as a reporter, the expression of which can be probed with a dextran cross-linked iron-oxide (CLIO)Tf superparamagnetic nanoparticles, with ETR gene expression correlating with expression of therapeutic genes carried by the same amplicon. Thus, MRI of ETR expression can serve as a surrogate for measuring therapeutic transgene expression.

Another related example of the above is the use of ferritin transgenes. Following transfection of a metalloprotein from the ferritin family, into specific host tissues, the protein is made superparamagnetic as the cell sequesters endogenous iron from the organism. In this approach, the cells construct the MRI contrast agent *in situ* using genetic instructions introduced by the vector. No exogenous metal-complexed contrast agent is required, thereby simplifying intracellular delivery.

An alternative method with further amplification (and hence sensitivity) is the use of metabolically biotinylated reporter proteins (BAP) on the cell surface and imaging this with detectable versions of (strept)avidin (e.g., CLIO-streptavidin). One model recombinant reporter protein incorporates the prokaryotic *Propionibacterium shermanii* 1.3S transcarboxylase domain (PSTCD) biotin acceptor peptide (BAP) between an N-terminal signal sequence and the PDGF receptor transmembrane domain (TM). Western blot analysis of cell homogenates, immunocytochemistry of nonpermeablized cells and FACS analysis demonstrated that this BAP-TM reporter protein is efficiently biotinylated by endogenous biotin ligase in mammalian cells with the biotin displayed on the cell surface. Magnetic resonance (MR) imaging of subcutaneous tumors *in vivo* showed a significant difference in T2 values of BAP-TM-reporter-expressing tumors over control tumors following intravascular injection of streptavidin-CLIO. This BAP-TM reporter can allow noninvasive real time imaging of any cell type transduced to express it in culture and *in vivo,* and should be compatible with use in humans since (strept)avidin-biotin interactions are being used in clinical trials. In our hands it also represents the most efficient reporter gene developed so far.

Another way to monitor gene expression *in vivo* by MRI is to use biocatalysts to generate MR probes *in situ.* Several enzymatic systems have come forth based on single enzymes, such as tyrosinase, to catalyze the conversion of low-relaxivity substrates into high-relaxivity products. Tyrosinase, an enzyme normally involved in melanogenesis, has a remarkably high metal-binding capacity (up to 35% by weight), particularly of iron, that results in the high signal intensity in melanomas on T1-weighted images. Tyrosinase catalyzes two major reactions that occur primarily in lysosomes or premelanosomes: (i) the hydroxylation of L-tyrosine with the formation of L-DOPA (3,4-dehydroxy-L-phenylalanine) and (ii) the subsequent oxidation of DOPA with the formation of DOPA quinone. Several COOH-terminally truncated mutant forms of tyrosinase were engineered based on the hypothesis that in the absence of sorting signals, tyrosinase would not be sequestered exclusively in lysosomes/premelanosomes and tyrosinase-generated quinones could then cause toxicity to tumor cells. The expression efficiency, enzyme activity, and toxicity of these mutant tyrosinases were compared in several transformed cell lines. The mutant tyrosinases were able to convert certain model prodrugs into cytotoxic agents with resultant cell death and antiproliferative effects. Thus, tyrosinase mutants can serve for both antitumor gene therapy, as well as imaging marker gene expression.

The use of novel MRI contrast agents that can indicate reporter gene expression for commonly used marker enzymes, like β-galactosidase, offer the promise of *in vivo* mapping of gene expression in transgenic animals. One approach is the use of paramagnetic chelates that have the capacity to change their magnetic properties upon enzymatic hydrolysis (3). A paramagnetic galactopyranose chelator substrate for β-galactosidase has been developed based on the observation that the relaxivity of chelated gadolinium can be modulated by conjugating into β-galactose *via* a spacer. The removal of β-galactose from the paramagnetic conjugate by β-galactosidase mediated hydrolysis results in an increase in relaxivity

by about 40%, which is detectable by MR imaging. This phenomenon has been used to image β-galactosidase activity in Xenopus laevis embryo (3).

Other recent examples of imaging transgene expression include the utililzation HeLa cells, transfected to express a truncated form of the $H2K^K$ antigen, $tH2K^K$. When exposed to $tH2K^K$ antibodies conjugated to a superparamagnetic iron-oxide particle and imaged with MRI, there was a marked decrease in the $tH2K^K$ expressing cells (4).

MR Spectroscopy

MR spectroscopy (MRS) shares the same principle as MRI. In MRS, the signal obtained from a single element is further separated into its different chemical forms. It is thus possible to define a spectrum of nuclear magnetic resonance signals, in which the several chemical forms of an element give peaks in specific positions and thus offer the potential to measure gene expression. MRS has been used for quantitative noninvasive imaging of tumors (5). Animals bearing tumors expressing the cDNA encoding for cytosine deaminase from yeast (yCD) were treated with nontoxic 5-fluorocytosine (5-FC) prodrug. The yCD catalyzed conversion of 5-FC to the chemotherapeutic agent 5-fluorouracil (5-FU) was quantitated *in vivo* using 19F MRS. This study demonstrated the local conversion of 5-FC to 5-FU, validating the concept of localized chemotherapy by enzyme prodrug activation. The ability of MRS to follow prodrug conversion dynamically and to distinguish between individual metabolites is a significant advantage over PET methods, which would require measurement of plasma metabolite levels.

Gemacitabine (dFdCyd) is a cytotoxic deoxycytidine (dCyd) analog that has demonstrated significant antitumor activity in a variety of human tumor models. dFdCyd is converted to an active metabolite by phosphorylation to a triphosphate derivative, dFdCTP, which is then incorporated into DNA. This reaction is catalyzed by a rate-limiting enzyme, deoxycytidine kinase (dCK). 19F MRS has been recently used to detect increased incorporation of dFdCTP in human colon carcinoma xenografts in mice infected with a retroviral vector containing the dCK gene. This finding has potential clinical relevance in dCK gene-directed therapy through enhancing cytotoxic effects of dFdCyd chemotherapy and allows use of 19F MRS as a noninvasive tool to determine efficacy of prodrug conversion.

Recent advances in the development of magnetic nanoparticles and their use in cell tracking heralds high potential for MRI in the future. Magnetic nanoparticles have been used to track and recover as few as 100 cells after a specific population of cells was specifically labeled and followed using MRI. Also, magnetic nanosensors (see Chapter—activatable imaging agents) have recently been developed with the capacity to detect specific DNA or mRNA sequences. Following hybridization of superparamagnetic nanoparticles bound to DNA to cellular nucleotide sequences, these probes exert sensitive and reversible effects on spin–spin relaxation of water protons.

Bibliography

1. Weissleder R et al (2000) In vivo magnetic resonance imaging of transgene expression. Nat Med 6(3):351–355
2. Allport JR, Weissleder R (2001) In vivo imaging of gene and cell therapies. Exp Hematol 29(11):1237–1246
3. Louie AY et al (2000) In vivo visualization of gene expression using magnetic resonance imaging. Nat Biotechnol 18(3):321–325
4. So PW et al (2005) Generic method for imaging transgene expression. Magn Reson Med 54(1):218–221
5. Stegman LD et al (1999) Noninvasive quantitation of cytosine deaminase transgene expression in human tumor xenografts with in vivo magnetic resonance spectroscopy. Proc Natl Acad Sci USA 96 (17):9821–9826

Magnetic Resonance Imaging, Molecular MR Imaging

M

Ralph Weissleder, Alexander R. Guimaraes
Center for Molecular Imaging Research, Massachusetts General Hospital, Charlestown, USA
weissleder@helix.mgh.harvard.edu

Magnetic resonance imaging (MRI) is a noninvasive, multiplanar imaging modality based on the manipulation of the inherent nuclear magnetic moment of endogenous nuclei (most commonly ^1H in H_2O) within subjects, or after exogenous administration of agents which alter the natural relaxation mechanisms of these nuclei. By exposing nuclei to a static magnetic field, and within that static field, perturbing a steady-state equilibrium with time and space varying magnetic fields, one can obtain images with exquisite spatial resolution and soft-tissue contrast of disease states such as cancer, stroke, neurodegenerative diseases, autoimmune diseases, and trauma. After perturbation, all nuclei relax by two unique and codependent relaxation mechanisms: T1 (spin–lattice relaxation), and T2 (spin–spin relaxation). By exploiting these relaxation mechanisms, contrast agents and pulse sequence algorithms can be designed to further specify the imaging patterns of many diseases. This can be achieved by spectroscopic methods, the use of unique pulse sequence strategies [e.g., diffusion-weighted imaging

(DWI), functional MRI (fMRI)], MR detectable reporter transgenes (see Chapter on genetic reporter systems), activatable MR imaging agents (see Chapter on activable reporter systems), or targeted MR imaging agents (see Chapter on targeted imaging agents). Molecular MR imaging aims to provide detailed, specific molecular and cellular information in diagnostic imaging studies.

Intrinsic MR Contrast Mechanisms

Magnetic Resonance Spectroscopy

Magnetic resonance spectroscopy (MRS) has been used for some time to analyze the metabolic properties of cells and tissues in organs and in living systems. Multiple nuclei possess a nuclear magnetic moment, and can thus be probed using nuclear magnetic resonance. The nuclei most often investigated with MRS can be divided between their capability of being inherently monitored using extant MR technology (e.g., ^{1}H,^{31}P, and ^{23}Na), or by whether they need to be exogenously administered (e.g., ^{19}F, ^{13}C,^{7}Li). Either through single-voxel localized techniques (e.g., STEAM, PRESS), or through multiphase encoding spectroscopic imaging, MRS has advanced the study of cellular and organ physiology, *in vivo* and *in vitro* in normal and diseased systems.

Using the administration of exogenous metabolites, MRS has shown the capability of monitoring and quantifying *in vivo* concentrations in many normal and diseased states. A few examples include the following: (i)^{19}F MRS has been used to rapidly monitor the pharmacokinetics of fluorinated chemotherapeutic agents (e.g., 5-flurouracil); (ii) ^{13}C label has been used on multiple carbon atoms of the glucose molecule to study metabolism in disease states such as cancer and cardiac; (iii) ^{7}Li is an uncommonly interrogated nucleus, but has been used to better understand and correlate the uptake and brain concentration of ^{7}Li to therapeutic efficacy in patients suffering from manic depression and other psychiatric illnesses routinely treated with lithium.

Although exogenously administered metabolites continue to be used, it is the endogenous nuclei, ^{1}H and ^{31}P, that have most impacted *in vivo* study of human disease (1). In summary, although inherently an insensitive technique, ^{31}P MRS has been used to study energy, phospholipids, and carbohydrate metabolism *in vivo* and *in vitro* noninvasively in human disease states including neuromuscular diseases (e.g., muscular dystrophy, neurologic diseases, psychiatric disease, hepatobiliary disease, and cardiovascular disease).

As ^{31}P MRS continues to evolve in development and application to many disease states, the application of ^{1}H MRS to human disease states has made a significant impact on extant, quotidian clinical care. The following metabolites in the ^{1}H MR spectrum have played a role in the study of disease states: (i) lactate—resonating at approximately 1.5 ppm, is a metabolic end-product of anaerobic glucose metabolism, and has been shown to correlate to degree of ischemia in neurologic and cardiovascular disease states, and has demonstrated a role in cancer prognosis, monitoring and therapeutic efficacy of anticancer medications that reduce intracellular pH[1]; (ii) N-acetyl aspartate—resonating at 2 ppm relative to tetramethylsilane (TMS), is only seen in functional neurons and easily quantified because of its relative isolation with the ^{1}H MR spectrum. Its loss has been correlated in many neurologic disease states (e.g., stroke, multiple sclerosis, cancer, and Alzheimer's disease); (iii) citrate, which resonates at approximately 2.3 ppm, although a normal intermediate within the Kreb's citric acid cycle, is not usually visualized within the ^{1}H MR spectrum of normal tissues, but has played an important role in prostate cancer, where it is thought to play a role as a carbon source for sperm and seminal fluid in distinguishing normal prostate gland from prostate gland involved with malignancy; (iv) creatine, which resonates at approximately 3.0 ppm, is a direct measure of cell energy viability, and its ^{1}H MRS quantification has been correlated to cell viability, and as such, is routinely used as an internal standard when quantifying other more specific markers of disease within the ^{1}H MR spectrum (i.e., choline and citrate)(1); (v) choline, which resonates at approximately 3.2 ppm, has been shown to be a sensitive and specific marker for cancer diagnosis and staging, has been shown to be elevated in cancers of the breast, prostate, colon, cervix and brain, as well as metastatic disease, and has been used in quantifying and distinguishing efficacy of treatment in chemo and radiation treatment strategies (1).

Diffusion-Weighted Imaging

A second intrinsic contrast mechanism in MRI exploits the dependency of water mobility on the directionality of the extracellular matrix, molecular viscosity and membrane permeability to probe water diffusion directly, and indirectly tissue cellularity in disease states (stroke, malignancy). Diffusion-weighted MR imaging (DWI) is performed by imparting two field gradients of equal strength, surrounding the 180° pulse of a spin echo sequence, which makes the MR signal intensity dependent on the phase shift imparted in water molecules. Varying the symmetric gradient strengths, thus probing different diffusion sensitivities, can facilitate calculation of the apparent diffusion coefficient (ADC) (2). Raw diffusion-weighted images are in routine clinical utility in the study of acute ischemic disease in humans. As a result of water mobility being impaired by areas of increased cellular

density, it has been proposed that the ADC value is inversely related to cellularity of brain tumors.

Early results from using the ADC in both pre-clinical and clinical treatment trials in various malignancies (e.g., breast, brain) indicate that changes in the ADC may predict later changes in tumor volume, and may be an early surrogate marker of treatment efficacy (2). Preliminary results suggest with decreases in contrast enhancement were increases in water mobility as measured by increased ADC, which suggests tumor necrosis in both animal models and clinical trials. (2)

Contrast Agents

Gadolinium-Based Agents

This section provides a brief overview of commonly used MR contrast agents. See also chapters on targeted (MR-targeted imaging agents) and activatable (MR-activatable agents) for additional compounds. Targeted contrast agents characterize the extrinsic contrast mechanisms of MR molecular imaging. Those contrast agents that use Gd (III) can be categorized as low molecular weight or high molecular weight (macromolecular) contrast agents (3, 4). The low molecular weight contrast agents, which Gd(III) with a diethylenetriaminepentaacetic acid (DTPA) chelate is the most ubiquitous, have been used for molecular imaging because their chemical structure lends itself well to coupling with other molecules or targets (3). Gd-DTPA allows the evaluation of physiological parameters such as the status of the blood–brain barrier, perfusion, with mathematical modeling, tumor enhancement, and renal function. Because of the relative nonspecificity of Gd-DTPA, the relatively poor relaxivity, as well as short intravascular half-life, there has been increased interest in gadolinium-based macromolecular contrast agents to attach more Gd(III) groups to each molecule (3, 4).

Macromolecular contrast agents that use Gd(III) have been developed with varying protein based conjugates including the following: (i) albumin, which has been demonstrated to have long lived intravascular components, and as a result continues to be used both as a conjugate for other biomolecules, as well as a primary imaging agent for angiogenesis; (ii) avidin, which binds to streptavidin, the combination of which has been used as a prelabeling mechanism to bind to the biotin ligands; (iii) poly-L-lysine; (iv) polyamidoamine (PAMAM) dendrimers; and (v) direct conjugation to monoclonal antibodies (mab). Another approach that has been attempted to increase delivery of number of gadolinium groups to the target is by cross-linking liposomes labeled with a large concentration of gadolinium, thus increasing the relaxivity of the target. In all cases, the goal is to increase the contrast to noise after delivery of target to background. Although of significant preclinical and biomedical research interest, these strategies have not reached the clinical arena.

Superparamagnetic Magnetic Nanoparticles

An alternative contrast agent strategy is based on the superparamagnetic iron oxide containing nanoparticles [a.k.a magnetic nanoparticles (MNP)]. These materials typically consist of a 3–5 nm core of superparamagnetic iron-oxide and polymer coatings, to which biomolecules can be attached (5). Iron-oxide MNP have R2 relaxivities between 50 and 400 $(\text{mM sec})^{-1}$ and typically contain multiple thousands of iron atoms per nanoparticle. When clustered R2 relaxivities can reach as high as 300,000 $(\text{mM sec})^{-1}$ (5). Because these MNP are superparamagnetic their R2 relaxivity dominates over the R1 relaxivity and is thus most sensitive on T2- and T2*-weighted pulse sequences.

Historically, polymer-coated iron-oxide molecules have been used in the treatment of anemias, and because of the relaxivity properties multiple variants of iron-oxide MNP with polymer coating have been developed. The first iron-oxide MNP, because of size heterogeneity, were rapidly phagocytosed by macrophage, and served as excellent imaging agents for the liver and spleen, demonstrating good sensitivity for distinguishing metastases from normal liver and splenic parenchyma. By refining the chemical structure and making the molecule smaller (25–30 nm) and homogeneous in size (termed monodisperse—one crystal per nanoparticle), these MNP were found to have increased vascular half lives (>10 h in mice, and >24 h in humans) as well as lymphotrophic components (6).

Other derivatives of iron-oxide MNP involve iron-oxide crystals (3–10 nm in diameter) coated with lipid and polyethylene glycol (PEG), which can reduce binding of plasma proteins and phagocytosis and clearance by macrophage. The most ubiquitous, and widely clinically used MNP offer a superparamagnetic iron-oxide core with a dextran or dextran derivative coating (Feredex®, Resovist®, Combidex®, and ferumoxytol) (5). Depending on the size and surface characteristics of these surface coats, different clearance mechanisms exist (5, 7).

Clinical Applications of Molecular MR Imaging

Using these techniques, advances have been made in contrast agent development in clinical and preclinical

Magnetic Resonance Imaging, Molecular MR Imaging. Table 1 List of targeted and nonspecific MRI based contrast agents and their specific clinical or preclinical application

Disease	Imaging agent	Application
Cancer	Iron oxide (ferumoxide)	Liver cancer
	Iron oxide (ferumoxtran, ferumoxytol)	Nodal staging/angiogenesis
	Integrin a_vB_3	Angiogenesis
Infection	Iron oxide	Inflammation
Inflammatory diseases (e.g., arthritis)	Iron oxide	Inflammation
Neurological	Beta-amyloid targeted iron oxide	Alzheimer's disease
Thrombosis	Fibrin (Gd-labeled)	Acute/subacute thrombi
Atherosclerosis	Iron oxide (ferumoxtran)	Macrophages/inflammation
	Integrin a_vB_3/VCAM	Angiogenesis
	Gadofluorine	Lipid-rich plaques

models including earlier detection of disease, drug discovery and development, and biomedical research, including the elucidation of enzymatic and cellular events in inflammation, angiogenesis, apoptosis, stem cell trafficking, and atherosclerotic disease. Table 1 illustrates various targeted, and nonspecific MRI based contrast agents and their specific clinical or preclinical application (8). Although a detailed listing of all applications of MR molecular imaging is beyond the scope of this chapter, we highlight the application of MRI within cancer and atherosclerotic disease.

Molecular Imaging of Cancer

Cancer Staging

MR molecular imaging has made marked strides in cancer staging, in specific, lymph node metastases (6). As with cancer detection, extant imaging approaches rely on computed tomography (CT), conventional radiography, and MRI for cancer staging, and these imaging approaches, in their conventional form, lack the sensitivity and specificity to distinguish potential metastatic involvement of lymph nodes that are less than 1 cm. in short axis. In addition, small lymph nodes (<1 cm) remain beyond the detection threshold of this technique as well.

The development and clinical introduction of lymph node targeted MNP has been shown to significantly improve diagnostic accuracies of MR imaging for nodal staging in prostate cancer (6). Within this technique, images are performed before and 24 h after the administration of magnetic nanoparticles, in particular Ferumoxtran-10 [Combidex—Advanced Magnetics, Inc., Cambridge, MA]. Secondary to their iron-oxide core, T2*-weighted imaging is performed. There is reliable accumulation within normal lymph nodes, and the lack of contrast uptake, as determined by a lack of T2* decrease in signal, has been shown to correlate to the presence of metastatic deposits (6). Preliminary studies in patients with prostate cancer show that MNP are highly accurate reporters for detecting tumor burden even in clinically occult disease. This methodological approach has increased the sensitivity of MRI detection of metastatic involvement of lymph nodes from values as low as 43% to >90%, with specificities approaching 100% (6).

In later more recent work, Weissleder and Harisinghani have expanded upon this work to semiautomate data analysis routines in lymphotropic magnetic resonance imaging (LMRI). With this semiautomated approach, the combination of two variables was determined to increase the sensitivity and specificity of LMRI with MNP to 94.3% and 93.5%, respectively, with positive and negative predictive values 93.5% and 98%.

Although, gadolinium-based approaches have been applied to lymph node imaging, these have not reached clinical utility.

Angiogenesis Imaging

The imaging of neovascular content is currently one of the most intensely studied tumor pathways because of the rapid development of novel strategies to inhibit neovascular growth in cancer. Angiogenesis is a prominent feature of invasive cancers and is associated with adverse prognosis (9). Toward that end, recent increased interest has focused upon the rapid development and implementation of drugs to inhibit neovascular growth (angiogenesis inhibitors). Multiple variants of these inhibitors continue to be developed and are in various phases of ongoing clinical trials. Documentation of the degree of angiogenesis in primary and metastatic tumors is also important for treatment planning and assessing the efficacy of angiogenesis inhibitors, including low-dose cytostatic therapies.

Current biomarkers of angiogenesis include serum markers (e.g., VEGF, FGF), microvessel density (MVD) quantification, tissue markers (e.g., histologic staining for CD31, FVIII, Ulex lectin) and imaging (e.g., nuclear imaging, CT imaging with dynamic contrast or MR imaging). MVD is a correlative, surrogate marker of angiogenesis, and has been shown to be of prognostic significance in various malignant therapies. Concurrent with recent advances in the development of angiogenic inhibitors, has been technological improvements in imaging angiogenesis, so as to provide a noninvasive, surrogate marker of anti-angiogenic efficacy.

Imaging angiogenesis with MRI has been focused into three different arenas: (i) functional imaging using dynamic tracking of contrast administration; (ii) steady state blood volume determinations of neovascular density; and (iii) specific molecular markers of angiogenesis.

Functional dynamic contrast enhanced MRI (DCE-MRI) approaches rely on the "leaky" nature of angiogenic blood vessels associated with malignancy. By using a small contrast agent, dynamic imaging is used and with the aid of compartmental modeling, various parameters are derived including permeability surface area product (a.k.a Ktrans), and fractional plasma volume. DCE-MRI has been applied clinically to many cancer systems including breast, brain, prostate, and renal cell, with interesting results, but confounded by high variance.

By imaging primary neoplasms, before and following the administration of MNP, a parametric map of tumor blood volume can be calculated by the change in T2* within the primary neoplasm. By correlating tumor blood volume to known blood volume of muscle, one can derive a vascular volume fraction (VVF). We refer you to the original description of this technique for further elaboration of the mathematical details of the technique (10).

In animal models it has been shown to have high accuracy when compared to other surrogate markers of angiogenesis (e.g., microvessel density, radiolabeled blood volume measurements). In recent xenograft treatment trials, results suggested that VVF measurements are earlier and more reliable indicators of successful antiangiogenic treatment regimen than is tumor volume.

MR Molecular Imaging of Atherosclerosis

The noninvasive assessment and identification of high-risk atherosclerotic lesions and thus, those patients deemed "high-risk" for a cardiovascular, or cerebrovascular events, remains an important focus of clinical research. One goal of molecular imaging has been to provide functional information about those biologic processes specific to atherosclerosis (8), and the pathophysiology of vulnerable plaque including inflammation, apoptosis and angiogenesis.

Activated macrophages have been found to play a key role in the pathophysiology of atherosclerosis and their presence is specific for high-risk lesions. Imaging of macrophages may offer a window into separating and identifying those patients and plaques at high risk for disruption. Iron-oxide MNP accumulate within macrophages, have been found to accumulate within human atherosclerotic macrophages and are therefore preferentially found in macrophage-rich carotid plaques. After intravenous injection of magnetic nanoparticles, there was uptake and enhancement of carotid plaques on T2* sensitive gradient echo techniques as compared to baseline MRI. Histopathologic analyses of carotid endarterectomy specimens confirmed iron localized within these regions.

Specific targets have been exploited as well. An example is VCAM-1, which is a critical component of the leukocyte-endothelial adhesion cascade. By using this protein and binding to a CLIO—Cy5.5 backbone (a cross-linked iron-oxide nanoparticle that provides a platform for novel magneto-fluoro MR contrast agent development in animals), MRI and fluorescent imaging demonstrated high affinity for endothelial cells expressing VCAM-1 but low affinity for macrophages *in vitro* and *in vivo* in both neoplastic and atherosclerotic models. In addition to VCAM-1, the CLIO platform has been used to image selectively E-selectin in mouse xenograft models of Lewis lung carcinoma by attaching E-selectin-binding peptide to CLIO (Cy5.5) nanoparticle, as well as apoptosis through attachment of CLIO (Cy5.5) to Annexin V.

Bibliography

1. Gillies RJ, Morse DL (2005) In vivo magnetic resonance spectroscopy in cancer. Annu Rev Biomed Eng 7:287–326
2. Ross BD et al (2003) Evaluation of cancer therapy using diffusion magnetic resonance imaging. Mol Cancer Ther 2(6):581–587
3. Aime S et al (2002) Insights into the use of paramagnetic Gd(III) complexes in MR-molecular imaging investigations. J Magn Reson Imaging 16(4):394–406
4. Artemov D (2003) Molecular magnetic resonance imaging with targeted contrast agents. J Cell Biochem 90(3):518–524
5. Weissleder R et al (1990) Ultrasmall superparamagnetic iron oxide: characterization of a new class of contrast agents for MR imaging. Radiology 175(2):489–493
6. Harisinghani M et al (2003) Noninvasive detection of clinically occult lymph-node metastases in prostate cancer. N Engl J Med 348 (25):2491–2499
7. Libby P (2002) Inflammation in atherosclerosis. Nature 420 (6917):868–874
8. Jaffer FA, Weissleder R (2005) Molecular imaging in the clinical arena. JAMA 293(7):855–862
9. Folkman J, Cole P, Zimmerman S (1966) Tumors behavior in isolated perfused organs: in vitro growth and metastasis of biopsy material in rabbit thyroid and canine intestinal segment. Ann Surg 164:491–502
10. Bremer C et al (2003) Steady-state blood volume measurements in experimental tumors with different angiogenic burdens a study in mice. Radiology 226(1):214–220

Magnetic Resonance Imaging, MR-Targeted Imaging Agents

Ralph Weissleder, Alexander R. Guimaraes
Center for Molecular Imaging Research, Massachusetts General Hospital, Charlestown, USA
weissleder@helix.mgh.harvard.edu

Exploiting T1 and T2 contrast mechanisms have dominated the design of novel magnetic resonance imaging (MRI) agents targeted for various clinical and preclinical molecular imaging applications. Multiple such targets have been exploited using paramagnetic [e.g., Gd (T1-based)] and superparamagnetic [e.g., iron oxide magnetic nanoparticles (MNP)]. For nontargeted MR contrast agents see Chapter (MRI—molecular imaging). Table 1 is a list of many targets for which imaging agents have been developed.

Paramagnetic-Targeted Imaging Agents

Targeted paramagnetic imaging agent strategies can be categorized based on the size of the molecule being developed. Examples of small molecule (<1,000 Da) approaches to contrast agent development include: (i) MnDPDP, which binds to a vitamin B6 analog, and is a commonly used hepatobiliary agent and (ii) MS-325, a small contrast Gd-based contrast agent that binds to

Magnetic Resonance Imaging, MR-Targeted Imaging Agents. Table 1 List of Various Targeted Imaging Agents, their respective sizes, and targets

Type	Size	Imaging agent	Targets
Paramagnetic (Gd)			
	Small molecule		
		MS-325	Albumin
		Mn-DPDP	Hepatocytes
	Peptides		
		Gd(DTPA)	Nonspecific
	Macromolecules		
		Mab	Antibodies
		Streptavidin	Biotin + antibodies
		Polylysine	Antibodies
		Dendrimers	Receptors (folate)
		MPEG-polylysine	
	Nanoparticles		
		Micelles	Cell internalization
		Liposomes	Cell internalization
		Nanoshells	Cell internalization
Superparamagnetic (MNP)			
	Nanoparticles		
		MION-36-antimyosin	Myosin
		CLIO-Tf, MION-Tf	TfR
		CLIO-Cy5.5-VHS	VCAM-1
		CLIO-Cy5.5-BCDSDSDITWDQLWDLMK	E-selectin
		CLIO-L-R-Cy.5.5	Cathepsin-B
		CLIO-Bombesin	GRPR
		CLIO-Cy5.5-RGD	AvB3
		CLIO-Cy5.5-YCAREPPTRTFAYWG	Muc-1
		CLIO-Mab	CD40 ligand
		CLIO-annexin	Phosphatidyl serine
		CLIO-Tat(FITC)	Cell labeling
		MION-46, MION-47, CLIO-Cy5.5	Macrophages
		CLIO-annexin	Annexin V

albumin, which increases its intravascular half-life, making it suitable for angiographic studies.

A number of targeted approaches using direct peptides bound to Gd-DTPA have been investigated but remain low in sensitivity (1).

Macromolecular contrast agents that use Gd(III) have also been developed for MR imaging using the following platforms: (i) albumin has a long lived intravascular component and as a result continues to be used both as a conjugate for other biomolecules, as well as a primary imaging agent for angiogenesis (1); (ii) avidin, which binds to streptavidin, the combination of which has been used as a prelabeling mechanism to bind to the biotin ligands (1); (iii) poly-L-lysine; (iv) polyamidoamine (PAMAM) dendrimers; and (iv) direct conjugation to monoclonal antibodies (mab). Specific examples of targeted gadolinium contrast agents using some of these approaches include a dendrimer (PAMAM) conjugated to Gd-DTPA which demonstrated affinity to the folate receptor in folate expressing ovarian tumor xenografts. In an alternative approach, breast cancer xenografts expressing HER-2/neu receptors were imaged with a two-step labeling protocol using biotinylated Herceptin mab and avidin-Gd-DTPA conjugates (1).

Nanoparticle-Based Targeted MR Imaging Agents

Nanoparticles with magnetic properties have been developed to further amplify MR signal (2). Nanoparticle imaging agents can be divided into those that are paramagnetic and those based on superparamagnetic agents.

Paramagnetic Magnetic Nanoparticle–Based Targeted Agents

Paramagnetic nanoparticles using Gd(III) have been developed using micelles liposomes, and nanoshells (1). These methods improve cell internalization and serve as an amplification strategy for targeted MR paramagnetic imaging contrast agent development. One example that has been targeted for angiogenesis imaging with a paramagnetic substrate is the $\alpha_v\beta_3$ ligand. This receptor integrin has been shown to be selective for angiogenic endothelium and tumor cells and was therefore chosen as a potential, specific marker for directed molecular target–specific agent development both for diagnostic imaging as well as therapeutic efforts, possibly. This has been exploited in a variety of different avenues including other MRI-targeted approaches either using antibodies conjugated to liposome nanoparticles sequestering Gd, or other direct antibody conjugations to nanoparticles. These approaches open up a novel means of addressing specific angiogenesis targets, and also demonstrate novel means of addressing the benefits of soft-tissue contrast, and superior spatial resolution inherent to MRI, while solving some of the inherent low sensitivity associated with MRI.

Magnetic Nanoparticles

An alternative approach for molecular targeting of contrast agents is based on superparamagnetic nanoparticles (MNP). This is an attractive platform for targeted agents for the following reasons: (i) the use of long-circulating nanoparticles improves the bioavailability of imaging ligands and avoids rapid renal clearance; (ii) nanoparticles can be used to attach small molecules in multivalent form, resulting in binding affinities that vastly surpass those of single molecules; and (iii) fluorescent nanoparticle platforms can be used as screening techniques to identify "binders."

Almost all *clinical* preparations to date have relied on dextran or carbohydrate derivatives as coating materials because of their prior use as a plasma expander and because of their affinity for iron oxides. The most widely used polymer-coated magnetic nanoparticles (Feridex, Resovist, Combidex, AMI-228/ferumoxytol) all contain dextran or dextran-derivatized coating. An important distinction between first generation polydisperse and second generation monodisperse preparations is the much longer half-life of the latter. For this reason, polydisperse materials are only useful for liver imaging, whereas monodisperse materials have a wider range of applications.

One of the earliest approaches at direct targeting includes direct conjugation of magnetic iron oxide nanoparticles (MNP) to monoclonal antibodies. These agents, however, demonstrated low sensitivity and specificity for the target. In order to make iron oxide MNP more target-specific, multiple strategies have been employed. By formation of Schiff bases between the amine of the biomolecule of attachment and aldehyde of the dextran coating of MNP, we devised a reproducible scheme based on earlier work by Molday to conjugate biomolecules to MNP's (3). Early examples include asialoglycoprotein receptors for liver imaging, antimyosin-labeled MNP for detection of myocardial infarcts, and labeled secretin for imaging of pancreatic acinar cells. More recent examples include conjugating MNP to the C2 domain of the protein synaptotagmin, which binds to phosphatidylserine, a protein present on the plasma membrane of apoptotic cells.

While second generation MNP are useful for lymph node and angiogenesis imaging, these materials have the disadvantage that the dextran coating is not tightly associated with the iron oxide core, yielding inefficient starting materials for targeted agents. An alternative approach for targeted synthesis using superparamagnetic MNP cross-links and aminates the dextran of dextran-coated MNP's to therefore provide an amino group for

binding biomolecules. One experimental agent that has been used widely is amino-CLIO (cross-linked iron oxide). Each amino-CLIO bears approximately 40 amino groups for attachment of biomolecules, and is approximately 40–50 nm in size. An example targeted human endothelial cells, by using the F(ab)2 fragment of human E-selectin mab, conjugated to CLIO. The CLIO-based platform has been used to synthesize target-specific agents for specific receptors, enzymes, integrins, and specific cells. Using phage display technology and high-throughput screening approaches, this technology has been used to synthesize agents specific for targets such as E-selectin and activated macrophage specific agents.

One specific target that has been exploited is the VCAM-1, which is a critical component of the leukocyte-endothelial adhesion cascade. By using phage display, a specific sequence was found that showed high binding specificity for VCAM-1, while blocking leukocyte–endothelial interactions. By using this protein and binding to a CLIO—Cy5.5 backbone, MRI and fluorescent imaging demonstrated high affinity for endothelial cells expressing VCAM-1 but low affinity for macrophages *in vitro*. *In vivo*, this contrast agent successfully identified VCAM-1 expressing endothelial cells in a murine tumor necrosis factor-α induced inflammatory model and colocalized with VCAM-1 expressing cells in atherosclerotic lesions present in cholesterol-fed apolipoprotein E apoE$^{-/-}$ mice.

Utilizing the CLIO backbone has used other combined MRI and fluorescent imaging probes. In addition to VCAM-1, this technology has been used to image selectively E-selectin in mouse xenograft models of Lewis lung carcinoma by attaching E-selectin-binding peptide to CLIO (Cy5.5) nanoparticle, as well as apoptosis through attachment of CLIO (Cy5.5) to Annexin V.

Other nanoparticles used for imaging include methylmethacrylate, zeolite doped GdNaY nanoparticles, ferrofluids, and synthetic magnetic nanoparticles, which obviate the need for dextrans, having much tighter polymer coatings (a *sine qua non* for small molecule conjugation), and yet be biodegradable. This family of compounds offers a very promising platform for targeting applications in MR imaging, and because the synthetic polymer coatings are biodegradable, may be soon applicable to patients.

Cell-Targeted Imaging

To track cells *in vivo* and visualize by MRI, they must be tagged magnetically. Previous attempts at tagging cells with magnetic beads proved efficient for *in vitro* separation of cells, but because beads were recognized as foreign by macrophage and the reticuloendothelial system, they were rapidly eliminated from the blood when injected intravenously *in vivo*. Labeling lymphocytes with magnetic nanoparticles demonstrates a possible solution to this problem, but the low labeling efficiency exacerbates the inherently low sensitivity of MRI in cell trafficking studies as compared to fluorescence and nuclear medicine. Unmodified magnetic nanoparticles have been used at high concentrations *in vitro* to label monocytes, T-cells, glioma cells and macrophage, and oligodendrocyte progenitors.

Multiple methodological approaches have been used to induce internalization of MNP into nonphagocytic cells. In specific, by linking amino-CLIO to the human immunodeficiency virus (HIV) tat peptide, which contains a membrane translocating protein, Lewin et al, developed a cell labeling approach that internalized MNP with high specificity into hematopoietic and neural progenitor cells with very low concentration of MNP (10–30 pg) per cell (4). High spatial three-dimensional imaging demonstrated the heterogeneity of T-cell recruitment within this model, and more significantly, the data indicate that serial administration of CD8 + T-cells appear to home to different intratumoral locations, which suggested that dose division may enhance the potency of T-cell based immunopotentiation therapies clinically.

Other approaches that have been used for cell labeling and include the following: (i) dendritic cells using MD-100; (ii) genetically engineered anti-Her-2/neu directed NK cells; and (iii) labeled Sca1 + bone marrow cells with superparamagnetic iron oxide MNP (ferumoxides-poly-L-lysine complexes). In summary, these cell-based approaches offer an exciting potential to advance multiple areas of cell-based therapy including stem cell therapy, cell implantation therapy, and immunopotentiation therapies.

Although efficacious, these strategies often require high levels of receptor expression and illustrate the problem of sensitivity facing contrast agent design. In considering novel targeted agents, sensitivity is of utmost import and various techniques need to be considered to overcome these obstacles. Some of these include receptor overexpression, and the presence of activatable or "smart" agents (those agents that undergo a physiochemical process to "activate" their contrast mechanisms). Please refer to Chapter (MRI—genetic reporter systems), for a detailed discussion on various amplification strategies used for transgene expression imaging, that may also be used in the synthesis of targeted agents.

Bibliography

1. Artemov D (2003) Molecular magnetic resonance imaging with targeted contrast agents. J Cell Biochem 90(3):518–524
2. Weissleder R et al (1990) Ultrasmall superparamagnetic iron oxide: characterization of a new class of contrast agents for MR imaging. Radiology 175(2):489–493

3. Molday RS, MacKenzie D (1982) Immunospecific ferromagnetic iron-dextran reagents for the labeling and magnetic separation of cells. J Immunol Methods 52(3):353–367
4. Lewin M et al (2000) Tat peptide-derivatized magnetic nanoparticles allow in vivo tracking and recovery of progenitor cells. Nat Biotechnol 18(4):410–414

Magnetic Resonance Mammography

▶MR Mammography

Magnetization Transfer MRI

An MR-based technique which provides estimates of tissue integrity. MT-MRI is based on the interactions between protons in free fluid and protons bound to macromolecules. When off-resonance irradiation is applied, the magnetization of bound protons becomes saturated. Magnetization is then transferred from these protons to more mobile protons, which causes a reduction of the tissue signal. A low-MT ratio reflects a reduced capacity of macromolecules in tissue to exchange magnetization with surrounding water molecules, and is interpreted as an indication of damage to myelin and to other cellular structures, such as the axonal membranes.
▶Aging Brain

Malabsorption

Günther Antes
Department of Radiology, Klinikum Kempton-Oberallgäu, Kempton, Germany
gantes@gmx.de

Synonyms

Malabsorption; Malassimilation; Maldigestion

Definition

Deficient delivery of nutrients into the body can be a result of malfunction at several levels. This results into the classification of *malabsorption*, ▶*maldigestion*, and ▶*malassimilation*. In clinical practice these three terms are applied liberally.

Pathology/Histopathology

The causes of malabsorption can be congenital or acquired (Table 1).

Malabsorption. Table 1 Classification of malabsorption

Malabsorption
▶Sprue (celiac disease)
Ischemia
Hypogammaglobulinemia
Radiation enteropathy
Lymphoma
Short bowel syndrome
Whipple's disease
Amyloidosis
Mastocytosis
Eosinophilic gastroenteritis
Parasitosis
Tropical sprue
Crohn's disease (extensive)
Maldigestion
Chronic pancreatitis
Pancreatic resection
Cholestasis
Ileal resection
Zollinger-Ellison syndrome
Lactose (disaccharidase) deficiency
Malassimilation
Lymphangiectasia
Abetalipoproteinemia
Bacterial overgrowth
Pseudoobstruction (idiopathic)
Systemic sclerosis
Diverticulosis
Obstructive lesions
Fistulae
Surgical blind loop
Immune deficiencies
Miscellaneous
Drugs
Alcohol
Gastric surgery
Endocrinopathy
Malnutrition

1. Malabsorption proper refers to a deficient intake and metabolism by the columnar cells that line the mucosa of the small intestine.
2. Maldigestion within the small bowel lumen may follow the deficient secretion of enzymes, especially those derived from the pancreas, or the diminished delivery of bile with its effect on the solubilization of fat. Maldigestion also can occur at the brush border of the epithelium where enzymes normally aid in the digestion of carbohydrates and peptides.
3. Malassimilation refers to malfunction in the transport of absorbed and metabolized nutrients from the intestinal mucosa into the body.

Other entities of malabsorption are bacterial overgrowth and miscellaneous causes.

Clinical Presentation and Diagnosis

The leading symptoms of malabsorption are chronic diarrhea and weight loss. The diagnosis of malabsorption is made clinically and not radiologically. However, imaging may play an important role.

Imaging

►Enteroclysis is the best contrast medium examination of the small bowel for the exploration of malabsorption. Terms like "*flocculation*" or others used in follow-up small intestinal examinations are often based on artifacts. However, even with proper technique, one can observe a reduction of the mucosal coating, which can be interpreted as a nonspecific sign of mucosal irritation or enteritis.

CT and MRI can be helpful in detecting causes of maldigestion like chronic pancreatitis, cholestasis, tumors, and Crohn's disease. Ultrasonography can detect changes of the intestinal wall e.g., Crohn's disease, amyloidosis, or lymphoma.

Nuclear Medicine

Scintigraphy plays no major role in the assessment of malabsorption, except in hormone producing tumors, e.g., Zollinger-Ellison syndrome (ZES) and carcinoid. There are two *in vivo* tests that can be applied. This is the ^{14}C-breath test for fat malabsorption and the vitamin B12 absorption test (Schilling test) to diagnose pernicious anemia and malabsorption syndrome.

Lactose Intolerance

Lactose intolerance is world wide the most common cause of malabsorption. In Europe, 10–15% and in many parts of the world over 95% of the population are unable to ferment and resorb lactose because of an enzyme deficiency in the small intestinal mucosa. In lactose intolerance, enteroclysis is usually normal. The same is true also for other intestinal allergies if the patient is asymptomatic at the time of the examination.

Sprue (Celiac Disease)

In a normal small bowel, the number of folds in the jejunum (≥5/2.5 cm) is greater than in the ileum. In sprue, there is a loss of folds in the duodenum and jejunum (Fig. 1). This is caused by the damage of the mucosa and deeper intestinal wall by the influence of gluten on the proximal small bowel. The lumen of the jejunum becomes more or less dilated and a reduction of contractions is observed. This leads to a regional hypoperistalsis. Thus, the jejunum resembles a colon like appearance ("colonization"). In the ileum, there is a resulting increase of folds combined with a regional hyperperistalsis. The ileum takes the form of a jejunum ("jejunization"). The process can be conceived as a

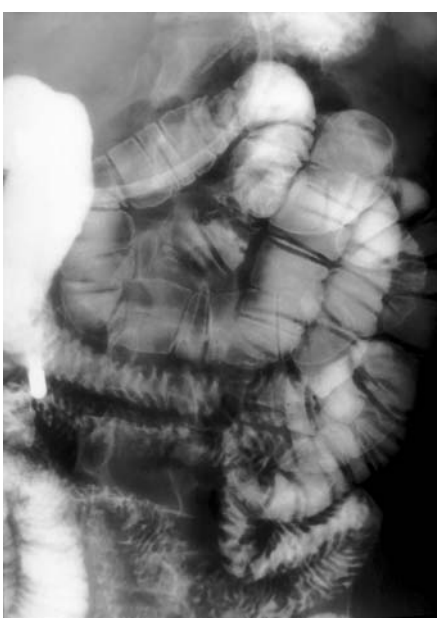

Malabsorption. Figure 1 Sprue. Typical fold pattern showing loss of valvulae conniventes and some dilatation in the jejunum ("colonization") and an increase of folds associated with an increase of contraction in the ileum ("jejunization").

compensatory response to the loss of mucosal surface in the jejunum.

Complications of long standing celiac disease are lymphoma and adenocarcinoma and rarely ulcerative jejunoileitis.

Bacterial Overgrowth

An overgrowth of the normal flora of the small intestine by pathogenic bacteria can be caused by diverticula (Fig. 2), fistulae, strictures, postoperative changes, and in immune deficiencies, but also in disturbed motility, e.g., diabetic neuropathy, scleroderma or idiopathic intestinal pseudoobstruction. Apart from morphologic changes, a poor mucosal coating and early flocculation and fluid retention as signs of a nonspecific enteritis are often observed.

Short Bowel Syndrome

Up to 50% of the middle part of the small intestine can be removed without serious consequences. An intact duodenum, at least 50 cm of the jejunum, and the preserved colon are necessary for the survival without parenteral nutrition. In case of resection of the colon, 150 cm of small bowel has to be preserved.

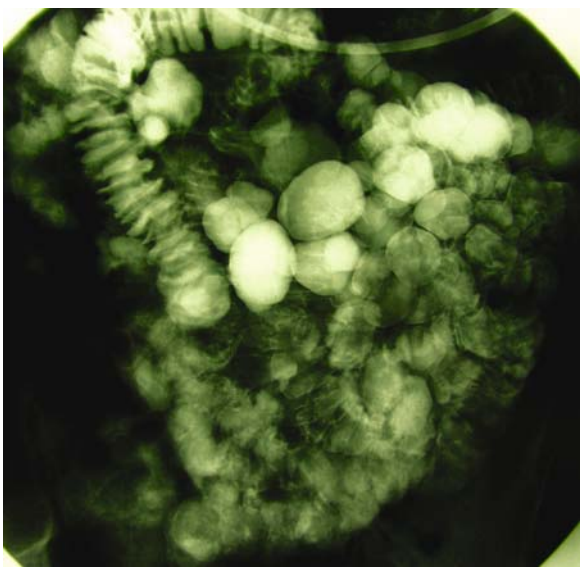

Malabsorption. Figure 2 Bacterial overgrowth in diverticulosis. Apart from the multiple diverticula there are thickened folds and a reduced mucosal coating as a sign of a nonspecific enteritis.

Intestinal Lymphangiectasia and Protein Loosing Enteropathy

A primary and a secondary form exist. Primary lymphangiectasia is a congenital malformation of the lymphatics that manifests between birth and early adulthood. Secondary intestinal lymphangiectasia can be caused by several conditions that obstruct the lymph flow, such as retroperitoneal fibrosis, malignant infiltration of the retroperitoneum or severe congestive heart disease. As a result of both forms, the removal of nutrients from the intestine into the portal and systemic circulation is impaired leading to protein loosing enteropathy and malabsorption.

The radiological findings are nonspecific and include thickened and distorted folds with numerous small or larger nodules. The bowel wall may be thickened. Ultrasonography, CT, and MRI can detect lymphoma, tumors, and inflammatory conditions causing secondary lymphangiectasia.

Zollinger-Ellison Syndrome

Gastrinomas are endocrine tumors secreting excessive amounts of gastrins that may cause ZES. This is characterized by severe ulcer disease in the stomach, duodenum and small bowel and watery diarrhea. This leads to protein loosing enteropathy, steatorrhea, and malabsorption. Gastrinomas are usually located in the pancreas or duodenum. More than 50% of the tumors are malignant and have set metastases in most cases at the time of detection. Gastrinomas may be part of the multiple endocrine neoplasia type I (MEN I) syndrome.

CT, MRI, angiography, and endoscopic ultrasonography help to detect gastrinomas. The somatostatin receptor scintigraphy with 111 indium octreotide is often the most sensitive test for detecting these lesions.

Amyloidosis

A primary and a secondary form exist. In primary amyloidosis, the gastrointestinal tract is involved in 70% of patients. Secondary amyloidosis is rarely associated with chronic inflammatory conditions such as rheumatoid arthritis, Crohn's disease, and familial Mediterranean fever. Radiological findings include nonspecific diffuse of localized nodular changes of the intestinal surface and wall thickening that can resemble Crohn's disease. This can be also seen on CT or ultrasonography (Fig. 3).

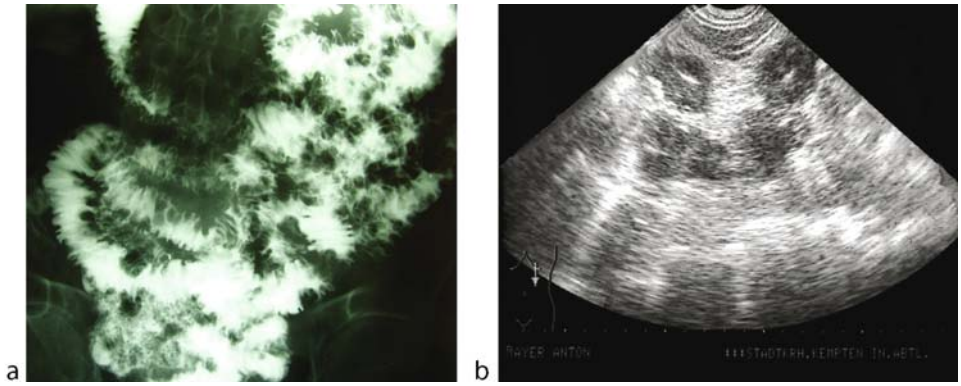

Malabsorption. Figure 3 Amyloidosis. (a) There is a thickening and distortion of the folds and intestinal wall. A nonpropulsive, pendular peristalsis can be observed that is caused by amyloid deposits in the vessel walls leading to a chronic ischemia and occult blood loss. (b) Ultrasonography shows the wall thickening.

Whipple's Disease

This disease is caused by the organism *Tropheryma whippelii*. The disease is characterized by fever, cachexia, malabsorption, and systemic manifestations. The radiologic findings include thickening of the small bowel folds and a diffuse micronodular pattern. CT may reveal lymph nodes in the mesentery and retroperitoneum.

Eosinophilic Gastroenteritis

Eosinophilic infiltration of the mucosa and intestinal wall may affect the entire GI-tract. Symptoms include malabsorption, especially protein loss, resulting in hypoalbuminemia. Radiologic findings may include thickening of small bowel folds and of the intestinal wall, simulating Crohn's disease, carcinoma, or lymphoma. The distribution may be regional or general.

Bibliography

1. Ekberg O, Florén C-H (2002) Radiology of malabsorption. In: Gourtsoyiannis NC (ed) Radiological Imaging of the Small Intestine. Springer-Verlag, Berlin, Heidelberg
2. Herlinger H (2000) Malabsorption. In: Gore RM, Levine MS (eds) Textbook of Gastrointestinal Radiology. 2nd edn. Saunders, Philadelphia
3. Herlinger H, Maglinte DDT (1989) Malabsorption and immune deficiencies. In: Herlinger H, Maglinte DDT (eds) Clinical Radiology of the Small Intestine. Saunders, Philadelphia
4. Antes G (1998) Bildgebende Dünndarmdiagnostik. Spinger-Verlag, Berlin, Heidelberg

Malabsorption

▶Malabsorption

Malassez Epithelial Rests

The remaining cells of the root sheath in the periodontal ligament.

▶Neoplasms, Odontogenic

Malassimilation

Malabsorption because of malfunction in the transport of absorbed nutrients.

▶Malabsorption

Maldigestion

Malabsorption because of deficient secretion of enzymes.

▶Malabsorption

Malignant Angioendotheliomatosis

Malignant Angioendothelimatosis is a rare pulmonary lymphoma characterized by proliferation of malignant

endothelial cells within small blood vessels with makroscopic appearance of pulmonary nodules. Its origin is usually within pulmonary arterial branches, and it is classically associated with pulmonary arterial hypertension.
▶Neoplasms Pulmonary

Malignant Fibrous Histiocytoma

More prevalent aggressive tumor in older age groups, commonly in the thigh. May be associated with hemorrhage and variable signal intensities on MRI. Up to 20% is reported as having some radiographically evident soft tissue calcification.
▶Neoplasms, Soft Tissues, Malignant

Malignant Lesions of the Nasopharynx

▶Neoplasms, Nasopharynx

Malignant Mesenchymoma

▶Neoplasms, Soft Tissue, Malignant

Malignant Oropharyngeal Tumors

▶Neoplasms, Oropharynx

Malignant Ovarian Neoplasm

▶Carcinoma, Ovarium

Malignant Peripheral Nerve Sheath Tumor

Large nerve sheath tumors, commonly over 5 cm in size, variable signal intensity with cystic regions presenting with neurological systems.
▶Neoplasms, Soft Tissues, Malignant

Malignant Pleural Thickening

CT criteria for malignant pleural thickening include pleural thickening greater than 1cm, pleural thickening that is either circumferential or involves the mediastinal pleural surface, or nodular pleural thickening.
▶Pleural Mesothelioma, Malignant

Malrotation

A congenital abnormality in which the midgut is abnormally positioned and fixed within the abdomen. This may allow the midgut to twist or "volve" on its mesentery leading to vascular compromise of the gut.
▶GI Tract, Pediatric, Specific Problems

Malrotation (with or without volvulus)

▶GI Tract, Pediatric, Congenital Malformations

MALT Lymphoma, Hepatic

Mucosa-associated lymphoid tissue lymphoma. This is a nosological entity characterized by a good prognosis. Histologically, this is a low-grade B-cell lymphoma that may primarily involve the liver.
▶Lymphoma, Hepatic

Mammary Dysplasia

▶Fibrocystic Disease, Breast

Mammary Dystrophy

▶Fibrocystic Disease, Breast

Mandibulofacial Dysostosis

Mandibulofacial dysostosis, also known as Treacher Collins syndrome, is characterised by all or most of the following: hypoplastic or agenetic zygomatic arches, maxillary narrowing or overprojection, small mandible, broad or protruded nose, microstomia, anomalous development of eyelids and/or ears.

▶Congenital Malformations, Nose and Paranasal Sinus

Manubriosternal Junction

Synchondritis of the symphysis or manubriosternal junction is characterized by adjacent sclerosis and bony destruction. Symphyseal involvement is typically seen in ankylosing spondylitis. Sternal manifestations are seen in ankylosing spondylitis, psoriatic arthritis, and SAPHO syndrome.

▶Spondyloarthropathies, Seronegative

Marchiafava–Bignami Disease

Marchiafava–Bignami disease is a rare disorder associated with chronic alcohol abuse. First described by Italian pathologists performing autopsies in chronic alcoholics, the disease is characterized by cystic, layered necrosis and demyelination of the genu and body of the corpus callosum, with occasional splenial involvement. Clinically, patients present with cognitive impairment, gait disturbance, hypertonia, dysarthria, and signs of interhemispheric disconnection. Occasionally, the disease is fatal. MRI demonstrates signal changes in the corpus callosum without mass effect.

▶Toxic Disorders, Brain

Marshmallow

The soft gelatin based commercial product which is useful as a solid bolus for assessment of dysphagia.

▶Gastroesophageal Reflux in Adult Patients: Clinical Presentations, Complications, and Imaging

Mass

A localized rounded space occupying lesion seen on two different mammographic views. Masses account for 15-20% of cancers detected by screening mammography.

▶Carcinoma, Breast, Imaging Mammography, Primary Signs

Mass Lesion of Soft Tissues

▶Neoplasms, Soft Tissue, Benign

Masses, Ovarian

Rosemarie Forstner
Department of Radiology, Paracelsus Private Medical University, Salzburger Landeskliniken, Salzburg, Austria
r.forstner@salk.at

Synonyms

Benign and malignant ovarian tumors; Ovarian neoplasm

Definition

The ovaries consist of three functional and anatomical components that may give rise to tumors. They include

the surface epithelium, germinal tissue, and ovarian stroma consisting of sex cord and mesenchymal cells. Epithelial neoplasms comprise up to 75% of ovarian tumors and 85% of ovarian malignancies (1).

Histopathology

Epithelial neoplasms are classified into benign, borderline, and malignant on the basis of histologic and clinical features (1). Dermoid cysts derive from germ cells and are the most common benign tumors in females younger than 45 years (2). ►Cystadenomas account for the majority of benign ovarian tumors in postmenopausal age.

Imaging

Differential Criteria for Benign and Malignant Lesions

Discrimination between benign and malignant ovarian tumors is one of the most important issues in ovarian imaging. Based on these findings, surgical management may be directly affected, including the adequate therapeutic approach, surgical technique, and need of subspecialty cooperation.

Sonography including endovaginal sonography and Doppler analysis is the primary imaging modality for assessing ovarian masses (1, 3). Contrast-enhanced computed tomography (CT) and particularly magnetic resonance imaging (MRI) are currently performed in indeterminate cases to further characterize lesions as benign or malignant (4).

In CT and MRI, fat is the pathognomonic finding in dermoids, and fibroids can be reliably diagnosed with MRI. For all other ovarian tumors, features suggesting that a lesion is benign include: lesion size less than 4 cm, entirely cystic architecture, wall thickness less than 3 mm, lack of internal structures, lack of ascites, lack of peritoneal disease or lymphadenopathy. Using these criteria preoperative characterization of ovarian lesions by MRI studies yields an accuracy of 91–95% (4).

Diagnosis

Differential Diagnoses of Ovarian Masses According to Imaging Features

Adnexal masses may be characterized according to their predominant morphologic appearance at imaging. As imaging findings often overlap, for differential diagnostic purposes neoplastic and nonneoplastic ovarian masses are included in the list. The latter can only be used as a general approach based on the most common appearance at imaging. If ovarian masses display a spectrum of imaging findings, they are enlisted in more than one category.

Completely cystic: Physiologic ovarian cyst, cystadenoma, hydrosalpinx, paraovarian cyst.

Cystic with proteinaceous or hemorrhagic contents: Cystadenoma, endometrioma, hydropyosalpinx.

Cystic with Septations: Cystadenoma, ►granulosa cell tumors, carcinoma.

Cystic with papillary excrescences or mural nodules: ►Borderline tumor, ovarian cancer, clear cell cancer, cystadenoma, dermoid.

Fat Containing: Dermoid, malignant teratoma.

Mixed Solid and Cystic: Carcinoma, tubo-ovarian abscess, cystadenofibroma, Brenner tumor.

Predominantly Cystic: Cystadenoma, tubo-ovarian abscess, cystic dermoid, carcinoma.

Solid with Necrosis: Metastases, ovarian cancer, dysgerminoma, sclerosing cell tumor of the ovary.

Predominantly Solid: Fibroma, dysgerminoma, lymphoma, metastases, ovarian cancer.

Solid with Calcifications: Fibroma, Brenner tumor, dysgerminoma, malignant teratoma.

Benign Ovarian Neoplasm

Benign ovarian neoplasms account for the majority (60–80%) of ovarian tumors. Although there is a large spectrum of ovarian tumors, the majority is encompassed by only a few different histologic types. In a larger series of benign ovarian lesions, 58% were teratomas, followed by 37% cystadenomas (25% serous and 12% mucinous), 4% fibromas/►fibrothecomas, and 1% Brenner tumors (2).

Benign Ovarian Teratomas: See cross-reference Benign Teratoma.

Cystadenoma

Cystadenomas are the most common type of cystic ovarian tumors. Cystadenomas account for 37–50% of benign ovarian tumors in the reproductive age. Their frequency increases with age, and after menopause cystadenomas account for up to 80% of the benign ovarian tumors. Cystadenomas are thin-walled, unilocular or multilocular cystic lesions filled with serous, mucinous, and sometimes hemorrhagic contents (1, 3) (Fig. 1). Rarely, small papillary projections may be found within the cyst walls.

Serous cystadenomas are bilateral in up to 20% of cases, whereas mucinous cystadenomas are bilateral in only 2–3% of cases. Mucinous cystadenomas may be filled with sticky gelatinous fluid and tend to be large (<10 cm) at the time of presentation. In contrast to serous

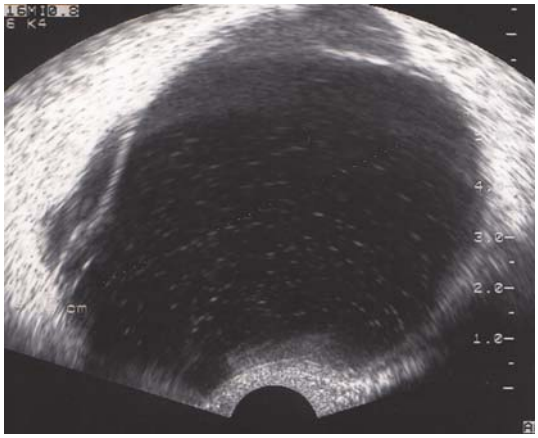

Masses, Ovarian. Figure 1 Mucinous cystadenoma in a 40-year-old female patient. Transvaginal sonography demonstrates a 9-cm cystic lesion that contains thin septations. Multiple fine echoes are seen within the cyst presenting proteinaceous or mucinous contents. There was no evidence of mural thickening, papillary projections, or solid areas within the lesion.

cystadenomas, mucinous cystadenomas are typically multilocular with different locular contents (1, 3). Rupture of a mucinous cystadenoma can result in pseudomyxoma peritonei.

Fibromas/Fibrothecomas

Fibromas and fibrothecomas are solid ovarian tumors which resemble uterine fibroids on imaging. However, they tend to show mild or delayed contrast enhancement (3). They occur unilaterally (90%), and are typically found in peri- and postmenopausal women.

Fibromas are composed of mostly fibroblasts and spindle cells and abundant collagen contents. Fibromas are not hormonally active. Fifteen percent of fibromas are associated with ascites, and in 1% pleural fluid is also found. This triad of an ovarian fibroma, ascites, and pleural effusion constitutes the benign ►Meig's syndrome.

Fibrothecomas consist of thecal cells with abundant and varying amounts of fibrosis, and rarely contain dense calcifications or cystic degenerations (1) (Fig. 2). Sixty percent of thecomas are hormonally active. Women may present with abnormal uterine bleeding. Furthermore, thecomas are associated with endometrial carcinomas in 20% of cases.

Brenner Tumors

Brenner tumors are rare ovarian tumors that occur at a mean age of 50 years. The vast majority is benign, less

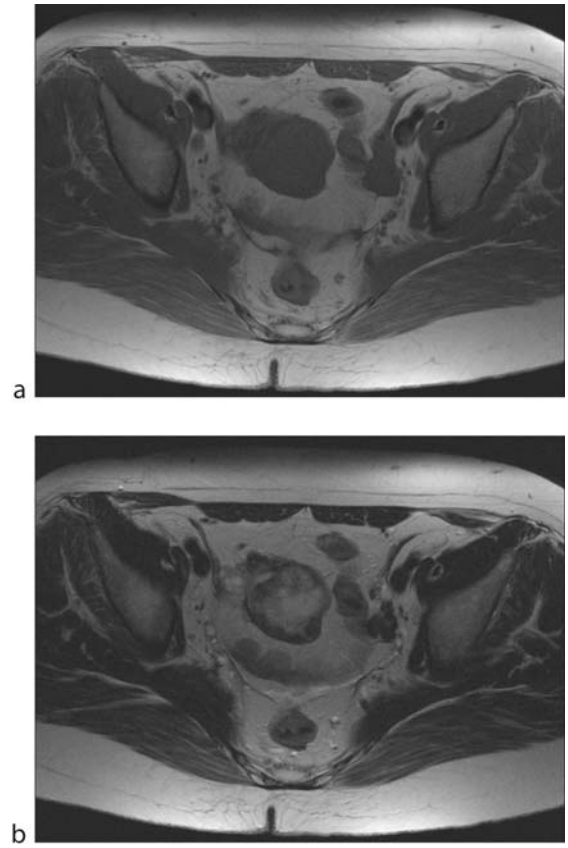

Masses, Ovarian. Figure 2 Fibrothecoma in a postmenopausal patient. In a 56-year-old woman with history of hysterectomy for benign disease, a solid right adnexal mass is demonstrated, which shows intermediate signal intensity (SI) on T1-weighted imaging (WI) (a) and inhomogeneous peripherally very low SI on T2-WI (b) with areas of high SI. Contrast uptake was very low (not shown). Histopathology revealed fibrothecoma with central areas of degeneration.

than 2% demonstrate borderline or malignant transformation. They are typically small, solid, unilateral ovarian tumors, which may show extensive calcifications (1). Sixty percent of Brenner tumors measure less than 2 cm in size. If cystic components are found, Brenner tumors may be associated with cystadenomas or other epithelial neoplasms (collision tumors).

Malignant Ovarian Tumors

Malignant tumors of the ovary and borderline tumors comprise 21 and 4%, respectively, of primary ovarian tumors (2). Epithelial ovarian cancer constitutes 85% of ovarian cancers, among which serous epithelial and mucinous ovarian tumor types account for the majority

of cancers (2). Unfortunately, there is poor correlation between the gross appearance on pathology and the histologic subtypes of ovarian cancer, and the aggressiveness cannot be determined on the basis of imaging studies. Cancer dissemination most commonly occurs peritoneally and by direct extension. Lymphatic and hematogenous seeding is less commonly found. Large amounts of free fluid in ovarian cancer are highly associated with peritoneal metastases.

Malignant germ cell tumors that represent two-thirds of malignancies in females less than 20 years of age and malignant stromal neoplasm are responsible for 7% of primary ovarian neoplasm each (1).

►Ovarian metastases account for 5–15% of ovarian malignancies.

Ovarian Cancer: see cross-reference Carcinoma Ovarian.

Borderline Tumors

Borderline tumors are epithelial ovarian cancers with low malignant potential. They tend to present as often large, bilateral, cystic ovarian tumors with mural nodules or papillary projections (1). At imaging they cannot be differentiated from invasive ovarian cancer; however, they represent a different entity. Compared to epithelial ovarian cancer, the survival rate stage for stage is much better. In a 7-year follow-up, the survival rate of stage I disease was 99% and for stage II and III disease it was 92%. Borderline tumors account for approximately 4–14% of all ovarian malignancies and are diagnosed at a median age of 40 years.

Dysgerminomas

Dysgerminomas present as multilobulated, well-delineated, solid uni- or bilateral ovarian tumors. Speckled calcifications, central areas with necrosis or hemorrhage, and strongly enhancing fibrovascular septations are other imaging features (1, 3). Seventy-five percent of dysgerminomas occur in early reproductive age, 10% are found in prepubertal girls, and 15–20% are diagnosed during pregnancy or postpartum. The vast majority of patients with dysgerminomas are diagnosed in early stage disease.

Malignant Teratomas

Immature teratomas or malignant teratomas are the second most common germ cell malignancies after dysgerminomas. They are extremely rare malignant tumors which are typically encountered in females between 10 and 20 years of age. In postmenopausal women they are an extremely rare finding and arise from secondary malignant transformation of the dermoid plug in dermoids. Immature teratomas are typically large at the time of diagnosis and present as solid or predominantly solid tumors with cystic elements and areas of fat and calcifications. They may be associated with dermoid cysts, more commonly in the ipsilateral (26%) than in the contralateral ovary. Rarely, they may produce steroids and cause pseudoprecosity in prepubertal girls.

Granulosa Cell Tumors

Granulosa cell tumors are classified as neoplasms of a low-grade malignancy. They typically present as unilateral, often large ovarian tumors that display a broad spectrum from entirely cystic to sponge-like multicystic to completely solid ovarian lesions (3). Granulosa cell tumors account for less than 5% of ovarian malignancies, and are the most common ovarian tumors with estrogen production. Two subgroups of granulosa cell tumors, the juvenile and the adult subtype, can be differentiated. Estrogen effects may induce precocious pseudopuberty or postmenopausal bleeding. Adult granulosa cell tumors

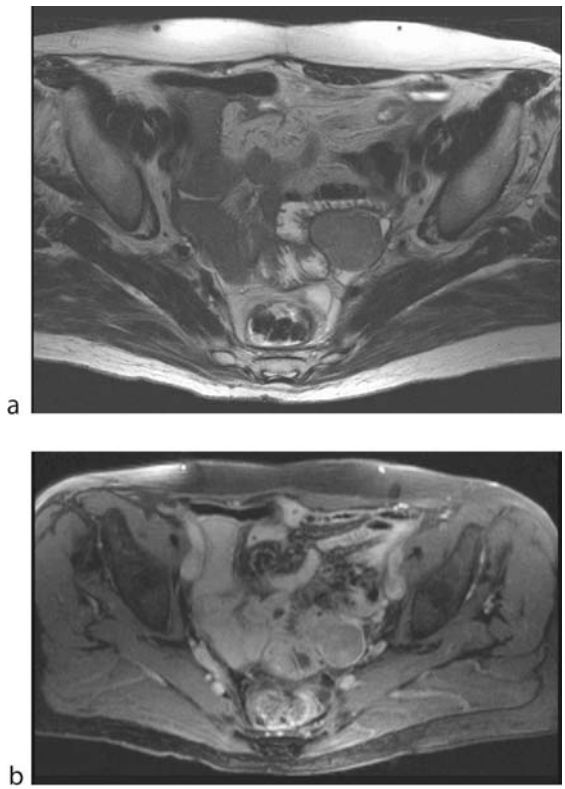

Masses, Ovarian. Figure 3 Ovarian metastasis of breast cancer. In a postmenopausal female, transaxial T2-WI (a) and contrast-enhanced T1-WI with fat suppression (b) demonstrate a 4-cm solid lesion of the left adnexal lesion. It can be discriminated by adjacent bowel loops as it is surrounded by small amounts of ascites. SI on T2-WI is intermediate and higher than expected in fibromas, contrast enhancement is slightly inhomogeneous.

usually occur after 30 years of age and peak in the perimenopausal age. In this tumor type, late recurrence may be seen several years after the initial therapy for tumor manifestation.

Ovarian Metastases

Ovarian metastases present as bilateral ovarian masses in 75% of cases. They account for approximately 5–15% of malignant ovarian tumors and originate most commonly from colon, stomach, breast, and melanomas as primaries. Ovarian metastases seem more common in premenopausal women due to the higher vascularity of the ovaries in this age, and they may be associated with hormonal activity. Approximately 50% of ovarian metastases consist of Krukenberg tumors which contain mucin-secreting signet ring cells surrounded by ovarian stroma. Krukenberg tumors display characteristic imaging features that include bilateral, oval or kidney-shaped solid ovarian tumors, often with central necrosis (5). Metastatic cancers different from Krukenberg tumors may have a variable often mixed cystic and solid or predominantly cystic or solid appearance (Fig. 3) and tend to resemble ovarian cancer (5).

Bibliography

1. Jeong YY, Outwater EK, Kang HK (2000) Imaging evaluation of ovarian masses. Radiographics 20:1445–1470
2. Koonings PP, Campbell K, Mishell DR et al (1989) Relative frequency of primary ovarian neoplasm: a 10-year review. Obstet Gynecol 74:921–926
3. Jung SE, Lee JM, Rha SE et al (2002) CT and MRI of ovarian tumors with emphasis on the differential diagnosis. Radiographics 22:1305–1325
4. Stevens SK, Hricak H, Stern JL (1991) Ovarian lesions: detection and characterization with gadolinium-enhanced MRI at 1.5 T. Radiology 181:481–488
5. Togashi K (2003) Ovarian cancer: the role of US, CT and MRI. Eur Radiol 13 (Suppl 4):L87–104

Mastitis

▶Breast, Infection

Mastitis Obliterans

▶Duct Disease, Breast

Mastitis, Puerperal, Acute

Bacterial infection of lactiferous ducts occurring during pregnancy and lactation, usually due to *Staphylococcus aureus*.

▶Infection, Breast

Match Defect

Most of the nonembolic pulmonary diseases lead to match defects in ventilation/perfusion lung scintigraphy which are defined as regions affected by a severe reduction or complete loss of perfusion, while the ventilation in the same region is likewise distinctly reduced.

▶Pulmonary Function, Nuclear Medicine Methods

Mature Teratomas

Mature teratomas or dermoid cysts or dermoids are the most common benign ovarian tumors in woman of reproductive age. They typically present as a cystic ovarian lesion that contains fat or sebaceous material, most commonly associated with calcifications or bone and hair. More than 90% of dermoids display pathognomonic findings in CT and MRI.

▶Teratoma, Ovaries, Mature, Ovalar

Maximum Intensity Projection

A relatively simple post-processing technique for CT and MR angiograms. Parallel rays are traced through a volume of data and only the voxels with the highest attenuation or signal along is ray is displayed. Images lack depth information.

▶Carotid and Vertebral Artery Pathology

Mayer–Rokitansky–Küster–Hauser Syndrome

This is caused by a developmental defect of the caudal portion of the müllerian duct. Type A is characterized by

no vagina or uterus and normal external genitalia; tubes, ovaries, and kidneys are normal. In type B, the uterus may be normal except for the lack of a conduit to the introitus, or may be rudimentary with aplasia of one or both uterine horns, or asymmetry of the horns; however, any of the lateral or vertical fusion abnormalities may be seen. The tubes are hypoplastic or absent. Associated malformations are found in the upper urinary tract, skeletal system, and spina.

▶Genital Tract

Mazabraud's Syndrome

Multiple soft tissue myxomas associated with multiple fibrous dysplasia of bone and endocrinopathies.

▶Neoplasms, Soft Tissues, Benign

MCDK

▶Multicystic Dysplastic Kidney

MDA

▶Müllerian Duct Anomalies

MDCT

▶Multidetector Computed Tomography

Mechanical Index

Estimate of the acoustic energy of an ultrasound field used in clinical sonography. The mechanical index (MI) is displayed on the screen of modern US scanners. It is defined as the estimated peak rarefractional pressure in vivo, divided by the square root of the center frequency of the beam. The MI was developed to quantify the likelihood that exposure to diagnostic ultrasound will produce an adverse biological effect by a nonthermal mechanism. It is also used to control the amplitude of the US during contrast-enhanced sonography, since the amplitude used determines the nature and degree of nonlinear bubble behavior (cross reference) and thus the echo response obtained from the microbubble contrast agent.

▶Contrast Media, Ultrasound, Hepatic

Meconium Aspiration Syndrome

Respiratory distress in an infant born through meconium-stained amniotic fluid where symptoms cannot otherwise be explained. It usually occurs in term or post-term infants.

▶Neonatal Chest

Meconium Aspiration Syndrome

▶Chest, Neonatal

Meconium Ileus

Veronica Donoghue
Radiology Department, Children's University Hospital, Dublin, Ireland
veronica.donoghue@cuh.ie

Synonyms

Cystic fibrosis; Microcolon

Definition

Meconium ileus is due to bowel obstruction as a result of impaction of thick tenacious meconium in the distal ileum. It is usually considered an early manifestation of cystic fibrosis. About 10–12% of patients with cystic fibrosis present with meconium ileus. It can rarely occur with other rare pancreatic abnormalities such as pancreatic atresia or stenosis of the pancreatic duct.

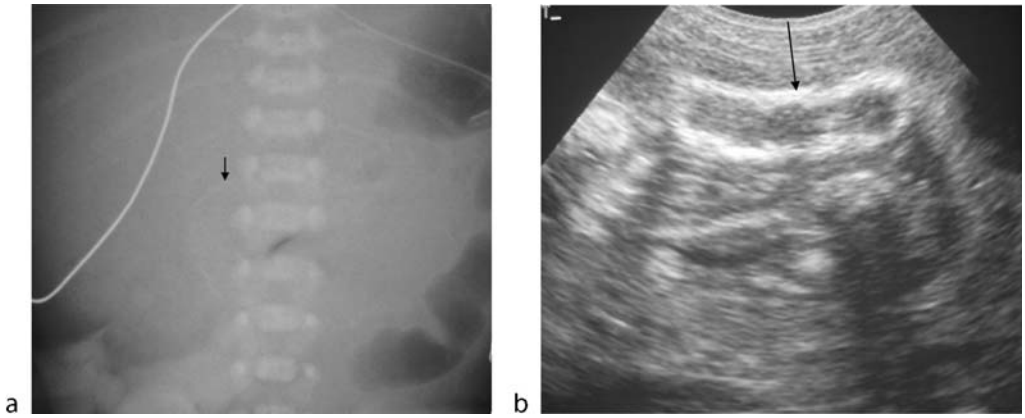

Meconium Ileus. Figure 1 (a) Plain abdominal radiograph with curvilinear calcification (short arrow) secondary to bowel perforation in an infant with meconium ileus. (b) This is also well seen on sonography (long arrow).

Pathology/Histopathology

Analysis of the enzyme activity of disaccharidases such as lactase, sucrase, maltase, and palatinase has shown to be increased in the meconium of infants with cystic fibrosis compared to meconium from normal infants. Normal meconium contains ~50% protein-bound carbohydrate as opposed to ~10% in the meconium from cystic fibrosis specimens.

Clinical Presentation

Clinically, infants with meconium usually present with bilious vomiting, abdominal distension and failure to pass meconium in the first 24 h of life. Pulmonary manifestations of cystic fibrosis are not usually present at birth but may develop shortly after with a bronchiolitis type picture (1).

Imaging

Abdominal radiographs show multiple dilated air filled bowel loops indicating low intestinal obstruction. In general these infants have fewer air–fluid levels than those with small bowel atresias. This however is a nonspecific finding. A "soap-bubble" appearance maybe seen in the right lower quadrant due to a mixture of air and meconium. Meconium ileus maybe complicated by volvulus, intestinal atresia, and perforation with meconium peritonitis or pseudocyst formation. There maybe evidence of a pneumoperitoneum or ascites. If meconium peritonitis is present there may be associated peritoneal calcification which maybe seen to extend into the scrotum. A localized perforation may form a meconium pseudocyst which may have curvilinear peripheral calcification (Fig. 1a).

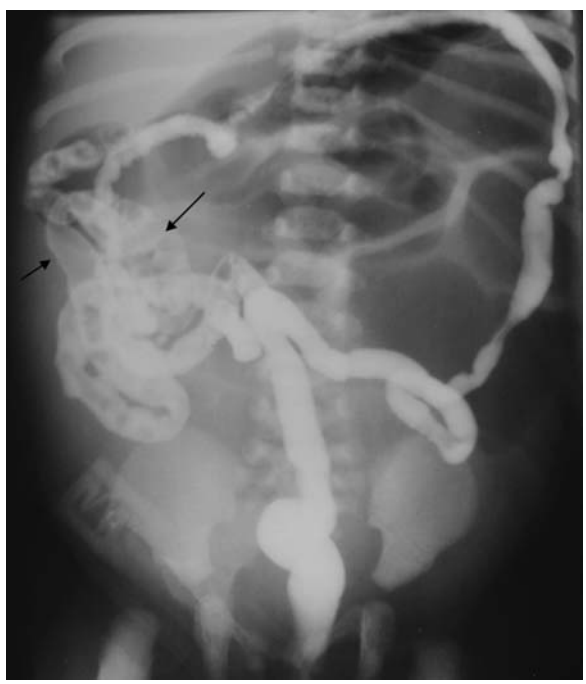

Meconium Ileus. Figure 2 Contrast enema outlining a microcolon and inspissated meconium in the distal ileum (arrows). There are dilated air filled bowel loops proximal to the obstruction.

Peritoneal calcification may also be well seen on sonography (Fig. 1b). Volvulus is caused by the weight of a meconium filled bowel. A contrast enema clinically demonstrates a microcolon with inspissated meconium identified in the distal ileum and dilated small bowel proximal to the obstruction (2) (Fig. 2).

Older infants may suffer from chronic constipation and intestinal obstruction due to fecal impaction. This is

referred to as ►meconium ileus equivalent. These patients may also present with intussusception. Mucosal thickening of the small and large bowel also occurs in the older patients with cystic fibrosis, probably due to mucous accumulation in the submucosal glands. Other findings in older children include benign pneumatosis intestinalis as a result of chronic constipation, poorly functioning gallbladder, biliary sludge, liver cirrhosis, and portal hypertension. In later childhood a severe colitis can be seen as a result of the pancreatic enzyme replacement therapy used in these infants (1).

►Meconium plug syndrome is a condition unrelated to meconium ileus and usually presents very early in life with failure to pass meconium and abdominal distension. It is the result of delayed peristaltic activity in an otherwise normal colon. The etiology is uncertain. It is associated with maternal drug ingestion, eclampsia, diabetes, and prematurity. In meconium plug syndrome the colon has a normal caliber. The plug is in the rectosigmoid region but may extend proximally throughout the entire colon. The infant usually passes the plug following a contrast enema or rectal examination.

Diagnosis

The diagnosis of meconium ileus is made by demonstrating a microcolon with the identification of meconium in the distal small bowel causing proximal obstruction in an infant with abdominal distension and failure to pass meconium in the first 24 h of life. Ultrasonography has been shown to be useful in distinguishing infants with meconium ileus from ileal atresia, both of whom have a microcolon. Infants with meconium ileus have multiple loops filled with echogenic thick meconium whereas those with atresia have dilated loops filled with fluid and air.

Interventional Radiological Treatment

Once the diagnosis is established a therapeutic enema should be performed to relieve the obstruction (3). The choice of contrast medium is controversial but we use dilute gastrografin (diatrizoate meglumine) (2) (see also chapter Gastrointestinal, children, bowel obstruction). It is hyperosmolar and causes fluid shift into the bowel lumen even when diluted. Extreme care must be taken with fluid and electrolyte balance to avoid hypotension and circulatory collapse in the newborn infant. The aim is to introduce contrast medium into the distal small bowel proximal to the obstructing inspissated meconium but care must be taken to avoid over distension of the microcolon. Several attempts maybe made (1–2 per 24 h) provided there is progressive clinical improvement in terms of abdominal distension and passage of meconium. The infants' fluid and electrolyte balance must be closely monitored during and after each procedure.

Overall the therapeutic enema success rate is 50–60% with a perforation rate of 3–10%. In unsuccessful cases surgery often reveals complications. This procedure can also be performed in the older children with meconium ileus equivalent to help relieve bowel obstruction.

Bibliography

1. Swischuk LE (2003) The alimentary tract. In: Swischuk LE (ed) Imaging of the Newborn, Infant and Young Child. 5th edn. Lippincott Williams and Wilkins, Baltimore
2. Donoghue V, Twomey EL (2005) The neonatal gastrointestinal tract. In: Carty H, Brunelle F, Stringer DA, Kao SCS (eds) Imaging Children. 2nd edn. Elsevier Churchill Livingstone, Edinburgh London New York Philadelphia St. Louis Sydney Toranto
3. Kao SCS, EA Jr (1995) Nonoperative treatment of simple meconium ileus: a survey of the Society for Pediatric Radiology. Pediatr Radiol 25: 97–100

Meconium Ileus Equivalent

This condition is due to fecal impaction leading to intestinal obstruction in infants with cystic fibrosis.
►Meconium Ileus

Meconium Plug Syndrome

The result of delayed peristaltic activity in an otherwise normal colon of uncertain etiology.
►Meconium Ileus

Mediastinal Cystic Masses

Koji Takahashi
Department of Radiology, Asahikawa Medical College, Asahikawa, Japan
taka1019@asahikawa-med.ac.jp

Definition

Cystic masses of the mediastinum are encapsulated lesions that contain fluid and are lined with epithelium. Most cystic masses are congenital and include foregut

duplication cysts (i.e., bronchial, neurenteric, and esophageal duplication cysts), pericardial cysts, and thymic cysts. Meningoceles, pancreatic pseudocysts, hematoma, abscess, and cystic schwannoma also appear as cystic mediastinal masses.

Pathology

Bronchogenic cysts are considered to result from defective development of the lung bud during the fetal period (1). The cyst wall often contains cartilage, smooth muscle, and mucous glands and is typically lined with respiratory epithelium. Cyst fluid is usually serous but can be hemorrhagic and contain variable amounts of protein or calcium.

Pericardial cysts are outpouchings of the parietal pericardium, which has no communication with the pericardial space, and result from aberrations in the embryogenesis of the coelomic cavity. These cysts are commonly round or spherical in shape, thin walled, unilocular, and contain clear or straw-colored fluid (2). Cyst walls consist of connective tissue and a single layer of mesothelial cells.

Esophageal duplication cysts may result from either abnormal budding of the foregut or a failure of complete vacuolation of the originally solid esophagus (3). The cysts are lined by gastrointestinal tract mucosa and have a double layer of smooth muscle. The cysts are commonly located adjacent to the esophagus.

Congenital thymic cysts are quite rare and are derived from a remnant of the thymopharyngeal duct. Multilocular thymic cysts may be the sequela of various inflammatory processes (4, 5).

Clinical Presentation

In most clinical situations, mediastinal cystic masses are incidentally detected on imaging. Symptoms might include chest pain, cough, dyspnea, and dysphagia, especially in esophageal duplication cysts. Symptomatic patients are likely to undergo surgery.

Imaging

On the radiographs, focal deformity of mediastinal contours and lines and/or displacement of normal structures must be present so as to identify a mass. On CT, typical features of mediastinal cystic masses include (1) an encapsulated smooth round or oval masses, (2) homogeneous water attenuation, (3) no enhancement of cystic contents with/without minimal enhancement of its wall, and (4) no infiltration of adjacent mediastinal structures. Some mediastinal cysts may reveal high attenuation similar to solid lesions due to a high level of protein and calcium oxalate in the cystic contents. In such situations, magnetic resonance imaging (MRI) can be useful in the differentiation of cystic masses from solid lesions. High signal intensity corresponding to cerebrospinal fluid (CSF) on

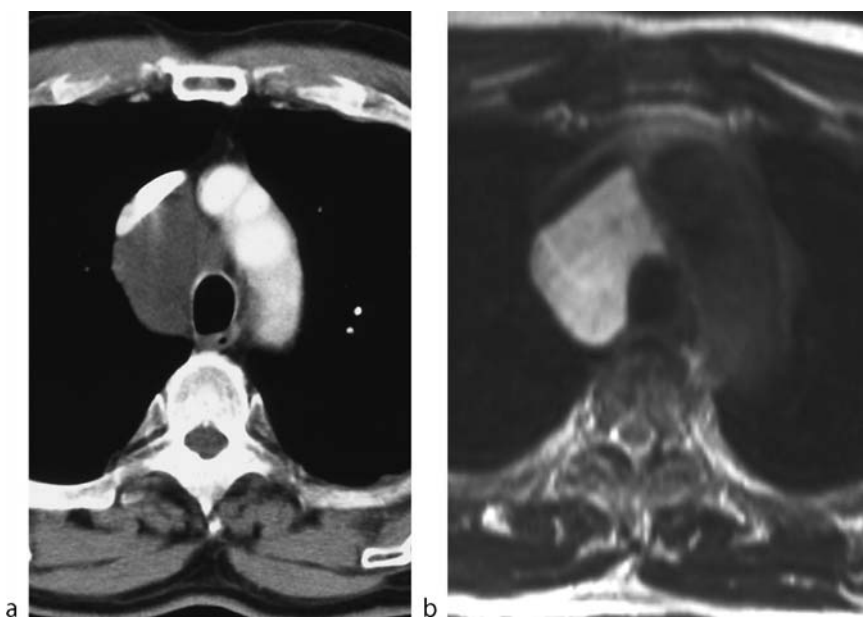

Mediastinal Cystic Masses. Figure 1 **Bronchogenic cyst. (a) Contrast-enhanced CT scan shows a thin-walled cystic mass abutting the trachea. (b) On axial T2-weighted MR image, the mass reveals homogeneous high signal intensity consistent with serous fluid.**

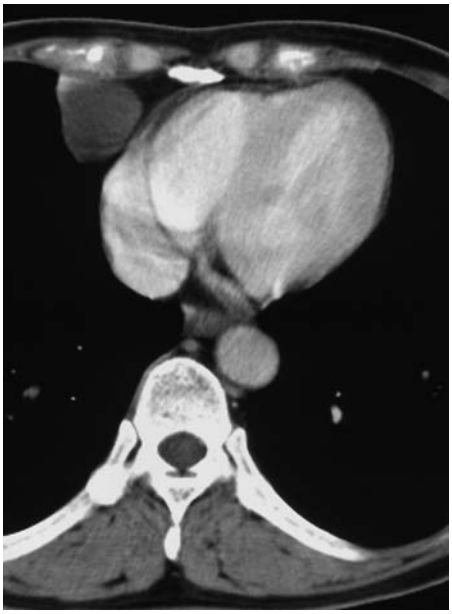

Mediastinal Cystic Masses. Figure 2 Pericardial cyst. Axial contrast-enhanced CT scan shows a well-defined cystic mass in the right cardiophrenic angle.

T2-weighted sequences, a fluid–fluid level, and lack of contrast enhancement are highly suggestive of the cystic nature of the lesions.

The majority of bronchogenic cysts are located in the paratracheal or subcarinal region. Rarely, they are seen in the anterior mediastinum or the inferior aspect of the posterior mediastinum. On chest radiographs, bronchogenic cysts usually present as a well-defined mass of homogeneous density in the subcarinal or right paratracheal regions. Computed tomography (CT) is very useful for making a specific diagnosis of bronchogenic cyst. Bronchogenic cysts typically appear as a well-defined, round or elliptical mass with a uniformly thin wall (Fig. 1). Cyst contents reveal homogeneous low attenuation consistent with fluid. In nearly 50% of patients, the cysts have higher attenuation and may be indistinguishable from soft tissue lesions.

The majority of pericardial cysts are located in the cardiophrenic angles and they are more frequent on the right side. On CT, the cysts characteristically appear as a round or oval lesion of water attenuation abutting the pericardium (Fig. 2). Occasionally, cyst contents show soft tissue attenuation.

The vast majority of esophageal duplication cysts are indistinguishable from other mediastinal congenital cysts. However, the cyst walls may be thicker (Fig. 3) and the lesions may be more tubular in shape and be in more intimate contact with the esophagus.

Thymic cysts appear as smoothly marginated thin-walled mass lesions of water attenuation in the anterior mediastinum (Fig. 4).

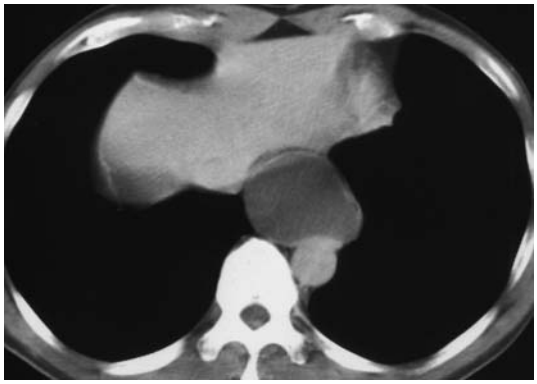

Mediastinal Cystic Masses. Figure 3 Esophageal cyst. Axial contrast-enhanced CT scan shows a well-defined cystic mass which abuts and displaces the esophagus. The mass has a relatively thick wall.

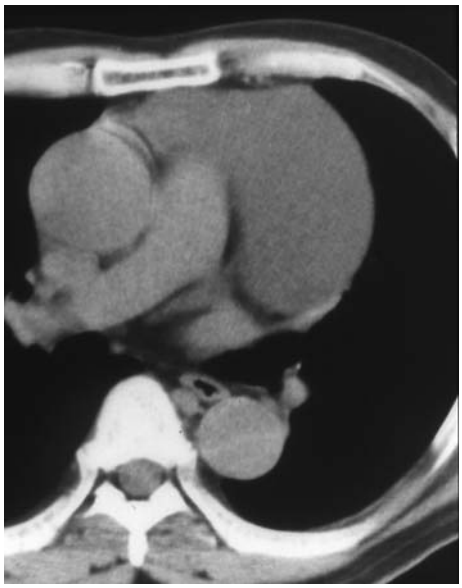

Mediastinal Cystic Masses. Figure 4 Thymic cyst. Axial contrast-enhanced CT scan shows a mass of homogeneous fluid attenuation in the anterior mediastinum.

References

1. Ribet ME, Copin MC, Gossclin B et al (1995) Bronchogenic cysts of the mediastinum. J Thorac Cardiovasc Surg 109:1003–1010
2. Wychulis AR, Connolly DC, McGoon DC et al (1971) Pericardial cysts, tumors, and fat necrosis. J Thorac Cardiovasc Surg 62:294–300
3. Salo JA, Ala-Kulju K (1987) Congenital esophageal cysts in adults. Ann Thorac Surg 44:135–138
4. Lindfors KK, Meyer JE, Dedrick CG et al (1985) Thymic cysts in mediastinal Hodgkin's disease. Radiology 156:37–41
5. Avila NA, Mueller BU, Carrasquillo JA (1996) Multilocular thymic cysts: imaging features in children with human immunodeficiency virus infection. Radiology 201:130–134

Mediastinal Germ Cell Tumors

Koji Takahashi
Department of Radiology, Asahikawa Medical College, Asahikawa, Japan
taka1019@asahikawa-med.ac.jp

Definition

Germ cell tumors are believed to develop from a germ cell during the process of maturation of a primordial germ cell into a gamete. The mediastinum is the most common site of extragonadal germ cell tumors (1). The vast majority of mediastinal germ cell tumors arise within the anterior mediastinum or in the proximity of the thymus, and only 3% of them arise within the posterior mediastinum (2).

Pathology/Histopathology

Germ cell tumors include teratoma, seminoma, embryonal carcinoma, yolk sac tumor (endodermal sinus tumor), choriocarcinoma, and mixed germ cell tumor. Mature teratoma is the most common histologic type. Seminoma is the most common malignant subtype.

Teratoma

Teratoma usually derives from more than two embryonic layers: ectoderm, endoderm, and mesoderm. Dermoid cyst refers to a tumor composed solely of ectodermal elements. Histologically, teratoma can be divided into mature teratoma, immature teratoma, and teratoma with malignant transformation. Mature teratomas are usually unilocular or multilocular cystic lesions and consist predominantly of ectoderm elements including skin and its appendages followed, in order of frequency, by bronchial tissue, gastrointestinal mucosa, smooth muscle, fat, bone, cartilage, and pancreatic tissue (1). Immature teratomas show various adult tissues derived from three germinal layers but in addition contain immature tissue, most commonly primitive neuroepithelial tissue. Teratomas with malignant transformation contain foci of frankly malignant neoplasms such as angiosarcoma, rhabdomyosarcoma, adenocarcinoma, and squamous cell carcinoma.

Seminoma

Seminoma is a well-demarcated, large, soft, and usually homogeneous mass with small foci of hemorrhage and necrosis (1).

Clinical Presentation

Mediastinum germ cell tumors most commonly occur during the period from the second to the fourth decades of life, and they are much more common in men than women. Most mediastinal germ cell tumors arise within the anterior mediastinum (2). Mature teratomas are often clinically silent. Symptoms might be due to local compression, rupture, or infection and include chest pain, cough, dyspnea, and fever. Most patients with immature teratoma and other malignant germ cell tumors are symptomatic, presenting with fatigue, weight loss, chest pain, cough, or dyspnea.

Teratoma

Mature teratomas are often clinically silent. Symptoms are due to local compression, rupture, or infection. Most patients with immature teratoma and other malignant germ cell tumors are symptomatic, presenting with fatigue, weight loss, chest pain, cough, or dyspnea.

Seminoma

Seminoma occurs almost exclusively in males during the period from the second to the fourth decades of life. Symptoms are usually derived from the presence of invasion to the adjacent mediastinal structures (airways and vessels) and include chest pain, shortness of breath, and superior vena cava syndrome.

Nonseminomatous Malignant Germ Cell Tumor

Nonseminomatous malignant germ cell tumors are rare, highly malignant tumors that usually occur in young adults and are much more common in men than women. Tumors are usually associated with symptoms including chest pain, cough, fever, and dyspnea and occasional elevation of tumor markers: alpha-fetoprotein from yolk sac tumor and embryonal carcinoma components and the beta fraction of human chorionic gonadotropin from the choriocarcinoma component.

Imaging

Teratoma

The typical radiographic appearance of a mature teratoma is a well-demarcated, occasionally lobulated anterior mediastinal mass. On computed tomography (CT), a mediastinal mature teratoma is a well-defined cystic lesion containing fluid, soft tissue, and fat attenuation. Calcifications of various morphological configurations may also be present within the lesion (Fig. 1) (3). A fat-fluid level is diagnostic of mature teratoma. Rarely, a tooth or a part of bone is seen within the lesions. Mediastinal mature teratomas may be associated with

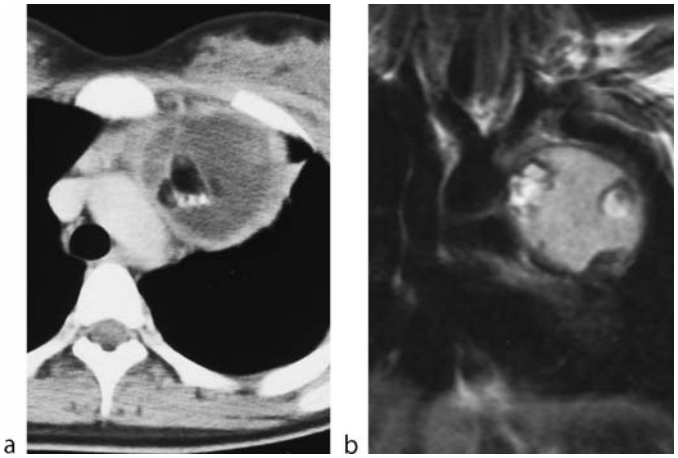

Mediastinal Germ Cell Tumors. Figure 1 Mature teratoma. (a) Contrast-enhanced computed tomography shows a thick-walled cystic mass in the anterior mediastinum, which consists of areas of water, fat, and calcification. (b) On coronal T1-weighted magnetic resonance image, the mass shows various signal intensities.

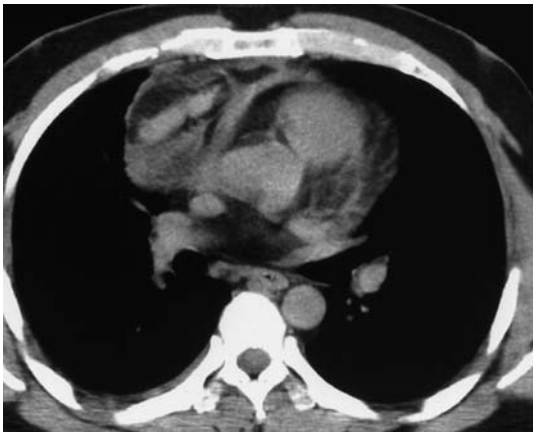

Mediastinal Germ Cell Tumors. Figure 2 Ruptured mature teratoma. Axial computed tomography shows a cystic mass consisting of fat, water, and soft tissue in the anterior mediastinum. Pericardial effusion suggests rupture of the tumor into the pericardial space.

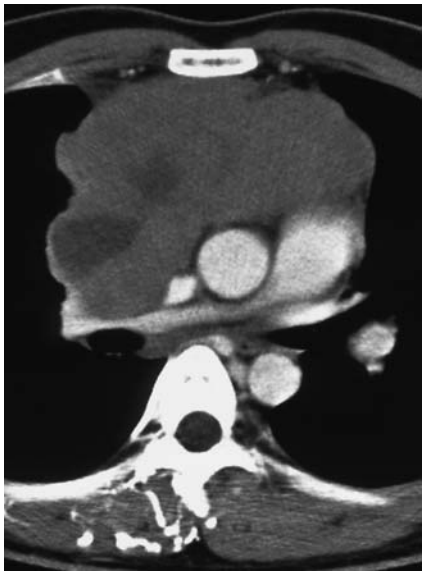

Mediastinal Germ Cell Tumors. Figure 3 Seminoma. Contrast-enhanced computed tomography shows a lobulated mass in the anterior mediastinum that displaces the superior vena cava and right pulmonary artery. The tumor includes limited areas of cystic change.

complications such as atelectasis or obstructive pneumonitis due to airway compression, pneumonitis due to rupture into the lung, and effusion due to rupture into the pleural space or pericardium (Fig. 2) (4).

Seminoma

Seminoma appears as a large, well-demarcated anterior mediastinal mass. On CT, seminoma has a homogeneous internal attenuation that shows only slight enhancement. A low-attenuation area due to degenerative change may appear but is usually limited (Fig. 3) (5, 6). Radiological evidence of invasion to the adjacent structures and collections of pleural or pericardial effusion are uncommon.

Nonseminomatous Malignant Germ Cell Tumor

Nonseminomatous malignant germ cell tumors usually appear as a large anterior mediastinal mass on radiographs. On CT and magnetic resonance imaging (MRI), the tumors consist of irregular soft tissue and multiple areas of low attenuation due to cystic necrosis and hemorrhage (Fig. 4) (5, 6). Obliteration of the adjacent fat planes and invasion to the surrounding structures may occasionally be seen.

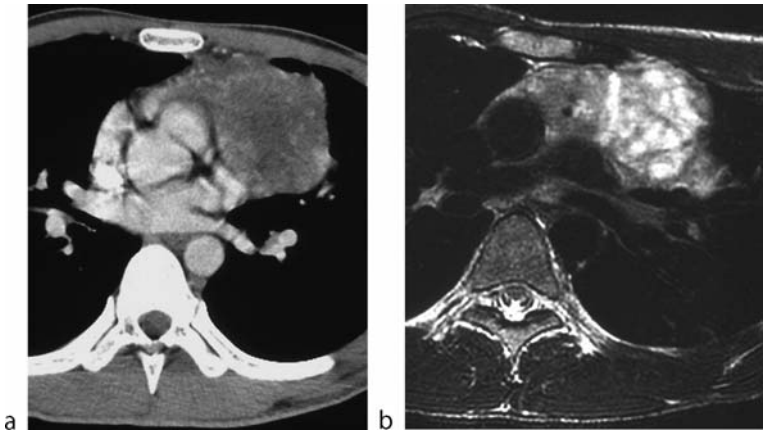

Mediastinal Germ Cell Tumors. Figure 4 Nonseminomatous malignant germ cell tumor. (a) Contrast-enhanced computed tomography shows an irregularly shaped mass in the anterior mediastinum. The tumor reveals fluid attenuation, representing widespread necrosis. (b) Axial T2-weighted magnetic resonance image shows prominent cystic changes within the tumor.

Bibliography

1. Shimosato Y, Mukai K (1997) Germ cell tumors. In: Rosai J (ed) Tumors of the Mediastinum. 3rd edn. Armed Forces Institute of Pathology, Washington DC, pp 183–206
2. Dehner LP (1983) Gonadal and extragonadal germ cell neoplasia of childhood. Hum Pathol 14:493–511
3. Moeller KH, Rosado-de-Christenson ML, Templeton PA (1997) Mediastinal mature teratoma: imaging features. Am J Roentgenol 169:985–990
4. Sasaka K, Kurihara Y, Nakajima Y (1998) Spontaneous rupture: a complication of benign mature teratomas of the mediastinum. Am J Roentgenol 170:323–328
5. Drevelegas A, Palladas P, Scordalaki A (2001) Mediastinal germ cell tumors: a radiologic-pathologic review. Eur Radiol 11:1925–1932
6. Lee KS, Gilm J, Han CH et al (1989) Malignant primary germ cell tumors of the mediastinum: CT features. Am J Roentgenol 153:947–951

Mediastinal Malignant Lymphoma

Koji Takahashi
Department of Radiology, Asahikawa Medical College, Asahikawa, Japan
taka1019@asahikawa-med.ac.jp

Definition

Malignant lymphoma accounts for nearly 20% of all mediastinum neoplasms in adults and 50% in children (1). Most often lymphoma involves the mediastinum secondary to generalized disease, while a mediastinal disease can also be a primary lesion. Hodgkin's disease is the most common primary mediastinal lymphoma.

Pathology

Hodgkin's Disease

Hodgkin's disease is the most common lymphoma to manifest in the mediastinum and may involve mediastinal lymph nodes, thymus or both. Nodular sclerosis, which is characterized by orderly bands of interconnecting collagenous connective tissue subdividing abnormal lymphoid tissue into isolated cellular nodules, is by far the most common histologic subtype. The cellular proliferation within the nodules is polymorphic, with small and large lymphocytes, plasma cells, eosinophils, and histiocytes. The distinctive feature is the presence of Reed–Sternberg cells.

Non-Hodgkin's Lymphoma

In non-Hodgkin lymphoma, the two most common forms of primary mediastinal lymphoma are lymphoblastic lymphoma and diffuse large cell lymphoma, while virtually any histologic type of lymphoma may be identified. Most lymphoblastic lymphomas have features of thymic T cells and exhibit a diffuse infiltrative pattern growth. Diffuse large cell lymphoma mostly shows to be of B-cell origin.

Clinical Presentation

Common symptoms of patients with large mediastinal lymphomas include dyspnea, cough, chest pain, malaise, fever, and superior vena cava syndrome

Diffuse large cell lymphoma tends to occur in young to middle-aged adults.

Imaging

Hodgkin's Disease

Mediastinal adenopathies most commonly involve prevascular and paratracheal regions (Fig. 1a). Other sites include subcarinal, hilar, paracardiac, internal mammary, and posterior mediastinal nodes. Most patients are young female adults. On CT, involved nodes usually are well defined and discrete and reveal homogeneous soft-tissue attenuation (Fig. 1b). While involved nodes with cystic and necrotic changes are identified in up to 21% of cases. Thymic involvement is another common manifestation and thymic enlargement is seen in 40% of adult patients.

Non-Hodgkin's lymphoma

Lymphoblastic lymphoma

Bulky disease is easily appreciated on the chest radiograph by mediastinal widening due to mass effect (Fig. 2a). On CT, low-attenuation areas reflecting necrosis are commonly seen after contrast enhancement (Fig. 2b). Pleural and pericardial effusions are also frequent. In extensive disease, tumor may spread to extrathoracic lymph nodes and central nervous system.

Diffuse Large Cell Lymphoma

The most commonly involved lymph nodes in the mediastinum are anterior mediastinum and paratracheal nodes followed by the subcarinal, hilar, internal mammary, pericardial, and posterior mediastinal nodes in decreasing order of frequency. On CT, involved nodes typically show homogeneous soft-tissue attenuation while, less commonly, reveal internal low-attenuation area or rim enhancement (Fig. 3). Pulmonary parenchymal involvement is seen on CT in approximately one third of the patients and commonly appears as nodules, masses, and focal air-space consolidation.

Overall, MRI shows the same morphological features as CT. Advantages of MRI might be detection of chest wall involvement and pleural disease, evaluation of viability of residual mass.

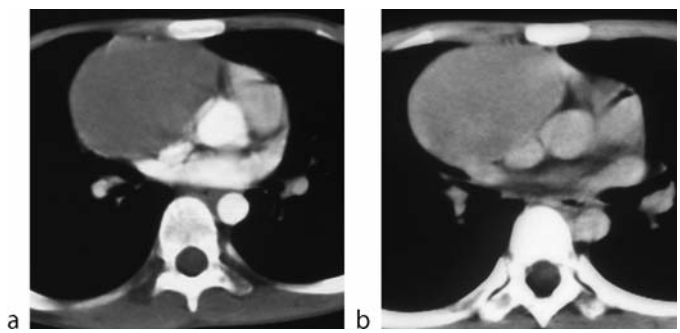

Mediastinal Malignant Lymphoma. Figure 1 Hodgkin's disease. (a) Early phase of contrast-enhanced CT scan shows a mass lesion of low attenuation in the anterior mediastinum. (b) On equilibrium phase of contrast-enhanced CT, the tumor shows moderate homogeneous enhancement.

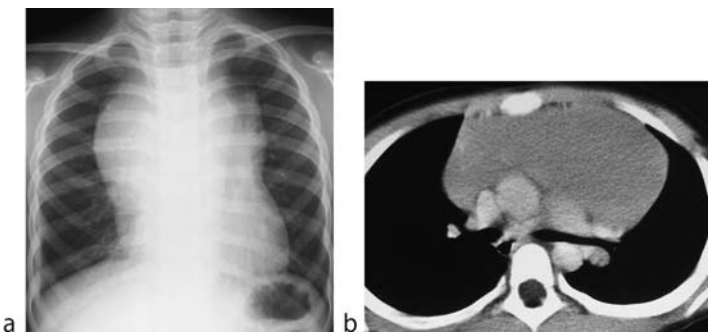

Mediastinal Malignant Lymphoma. Figure 2 Lymphoblastic lymphoma. (a) Chest radiograph shows prominent widening of the upper mediastinum. (b) Axial contrast-enhanced CT shows a huge mediastinal mass of soft-tissue attenuation displacing the great vessels and bilateral main bronchi.

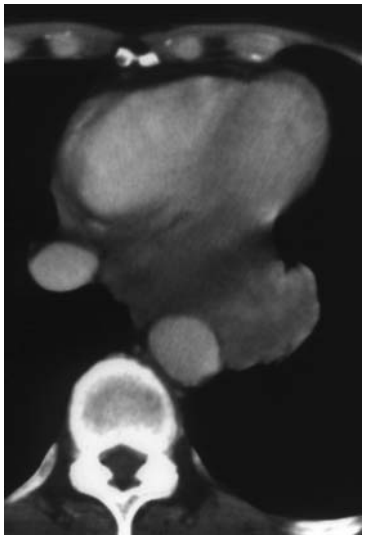

Mediastinal Malignant Lymphoma. Figure 3 Diffuse large cell lymphoma. Contrast-enhanced CT scan shows an irregular shaped mass lesion of inhomogeneous attenuation adjacent to the descending aorta.

Nuclear Medicine

Lymphoma usually shows prominent FDG uptake at initial staging. PET/CT is more sensitive and specific than contrast-enhanced CT for evaluation of Hodgkin's disease and high-grade non-Hodgkin lymphoma.

Bibliography

1. Shimosato Y, Mukai K (1997) Malignant lymphoma. In: Rosai J (ed) Tumors of the Mediastinum. 3rd edn. Armed Forces Institute of Pathology, Washington DC, pp 207–226
2. Pombo F, Rodriquez E, Caruncho MV (1994) CT attenuation values and enhancing characteristics of thoracoabdominal lymphomatous adenopathy. J Comput Assist Tomogr 18:59–64
3. Picozzi VJ, Coleman CN (1990) Lymphoblastic lymphoma. Semin Oncol 17:96–103
4. Castellino RA, Hilton S, O'Brien JP et al (1996) Non-Hodgkin lymphoma: contribution of chest CT in the initial staging evaluation. Radiology 199:129–132
5. Carlsen SE, Bergn CJ, Hoppe RT et al (1993) MR imaging to detect chest wall and pleural involvement in patients with lymphoma: effect on radiation therapy planning. Am J Roentgenol 160:1191–1195
6. Rahmouni A, Divine M, Lepage E et al (2001) Mediastinal lymphoma: quantitative changes in Gadolinium enhancement at MR imaging after treatment. Radiology 219:621–628
7. Moog F, Bangerter M, Diederichs CG et al (1997) Lymphoma: role of whole-body 2-deoxy-2-fluoro-D-glucose PET in nodal staging. Radiology 203:795–800
8. Schaefer NG, Hany TF, Taverna C et al (2004)Non-Hodgkin lymphoma and Hodgkin's disease: coregistered FDG PET and CT at staging and restaging—Do we need contrast-enhanced CT? Radiology 232:823–829

Mediastinitis

Koji Takahashi
Department of Radiology, Asahikawa Medical College, Asahikawa, Japan
taka1019@asahikawa-med.ac.jp

Definition

Mediastinitis can be divided into acute and chronic or fibrosing mediastinitis. Acute mediastinitis usually is bacterial and most commonly results from esophageal perforation. Chronic mediastinitis typically is fungal or tuberculous infection. Other causes of chronic disease include autoimmune disease, drug, radiation therapy, and syphilis.

Pathology

Acute mediastinitis is relatively uncommon bacterial infection and most commonly associated with esophageal perforation. Other causes include esophageal or cardiac surgery, spread of infection from adjacent regions, including retropharyngeal space, bone, and joints, tracheal or bronchial perforation, penetrating trauma, or necrosis of neoplasm (1). Esophageal perforation is usually related to endoscopic procedures. Spontaneous perforation may occur after forceful vomiting (Boerhaave's syndrome). The usual site of tear is adjacent to the gastroesophageal junction.

Fibrosing mediastinitis is a rare disease manifested by chronic inflammation and fibrosis, which focally or diffusely involves the mediastinum. The most common causes of fibrosing mediastinitis are histoplasmosis and tuberculosis, but it can also be related to autoimmune disease, radiation therapy, retroperitoneal fibrosis, methysergide therapy, or may be idiopathic (2). Histoplasmosis infection typically results in focal disease, whereas idiopathic disease is usually diffuse. Chronic mediastinitis leads to obstruction of various mediastinal structures, most commonly the superior vena cava (39%), followed by decreasing in order bronchi (33%), pulmonary artery (18%), and esophagus (9%) (3).

Clinical Presentation

The patients with acute mediastinitis are often very ill and associated with retrosternal pain, chills, and high fever. Acute mediastinitis especially from esophageal perforation has a high mortality rate.

The most common clinical symptoms of chronic mediastinitis are related to the superior vena cava syndrome: headache, cyanosis, and puffiness of the face, neck, and arms.

Imaging

The main radiographic features of acute mediastinitis are widening of the mediastinum, pneumomediastinum, pneumothorax, hydropneumothorax, and pleural effusions. Esophagography can be performed safely to confirm the presence and precise location of esophageal perforation. CT findings of acute mediastinitis are mediastinal widening, diffuse or streaky infiltration of mediastinal fat, pleural or pericardial effusion, and air bubbles and fluid collection in the mediastinum (Fig. 1). In cases with abscess formation, which can be single or multiple, localized fluid collections with or without air bubbles or air fluid level are present. In patients after median sternotomy, it is important to consider the normal postoperative appearance of the mediastinum, which can mimic the features of mediastinitis. Air bubbles and fluid collections are normal in the first week or two after sternotomy.

Fibrosing mediastinitis due to histoplasmosis or tuberculosis typically shows adenopathy and/or calcification most commonly in the upper mediastinum. The diffuse form may be manifested by extensive widening of the upper mediastinum, narrowing of the lower trachea or main bronchi. But chest radiographs may be normal in appearance in either focal or diffuse disease. CT is a good diagnostic modality for assessing and diagnosing the extent and site of the disease by soft tissue infiltration and enhancement (Fig. 2). In patients with focal disease by

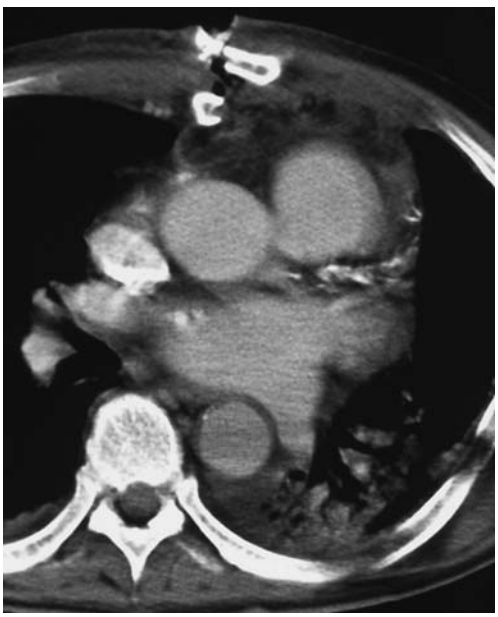

Mediastinitis. Figure 1 Acute mediastinitis after cardiac surgery. Contrast-enhanced CT scan shows dehiscence of the sternum and multiple irregular strands and small fluid collection in the anterior mediastinum.

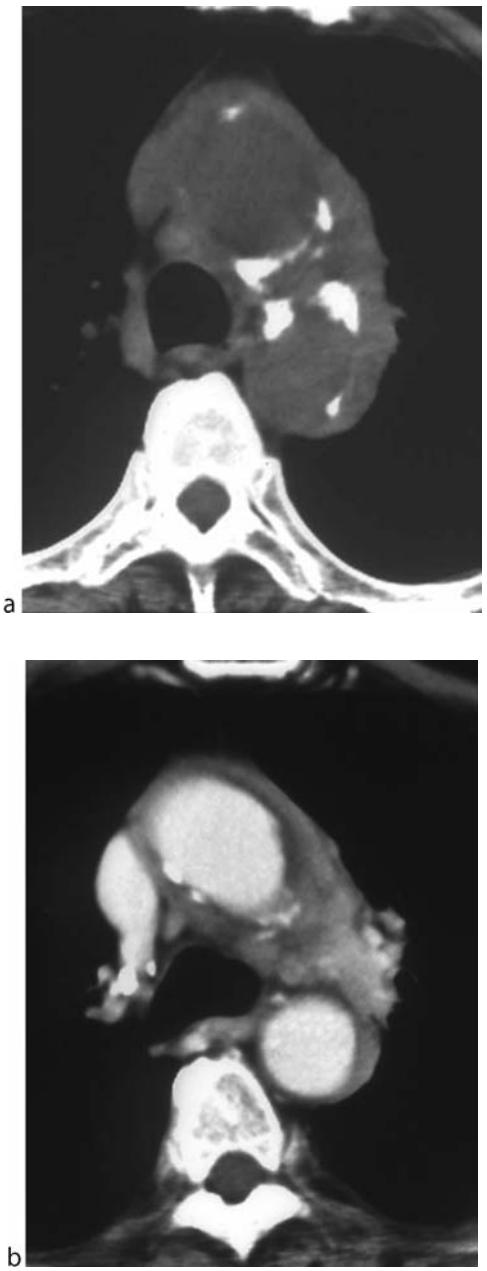

Mediastinitis. Figure 2 Idiopathic fibrosing mediastinitis. (a) Axial CT scan shows diffuse soft tissue infiltration in the mediastinum. (b) Contrast-enhanced CT scan shows moderate enhancement of the soft tissue in the mediastinum.

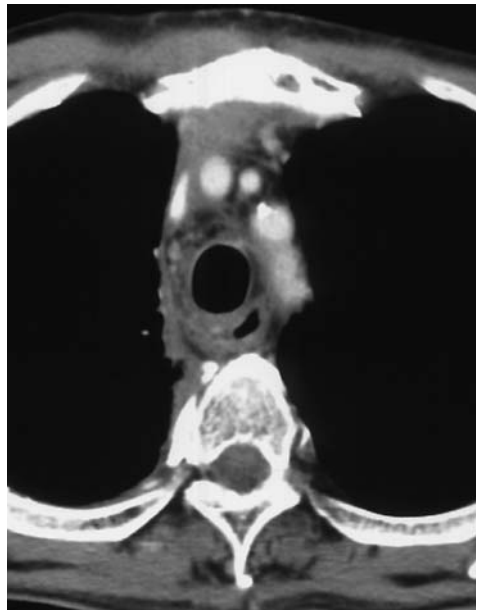

Mediastinitis. Figure 3 Fibrosing mediastinitis due to irradiation. Axial contrast-enhanced CT scan at the level of upper mediastinum shows an area and strands of soft tissue attenuation limited to the mediastinum. The right brachiocephalic vein is narrowed.

histoplasmosis, CT shows the enlarged calcified nodes most commonly in the right paratracheal region, whereas other regions: the left paratracheal, subcarinal, or posterior mediastinal regions may also be involved (4). Calcification is rare in the diffuse form which typically shows diffuse increase in attenuation of the mediastinal fat tissue. CT is useful for assessing involvement of mediastinal structures: narrowing and compression of superior vena cava, airway, pulmonary arteries, and veins (Fig. 3). Although MR imaging and CT are equivalent in assessing the extent of adenopathy or fibrosis, MR allows assessment of vascular involvement without contrast material. On MR imaging, fibrosing mediastinitis shows low intensity on T2-weighted images due to its fibrous content. The major disadvantage of MR is that it cannot confidently identify calcification.

Bibliography

1. Carrol CL, Jeffrey RB, Federle MP et al (1987) CT evaluation of mediastinal infections. J Comput Assist Tomogr 11:449–454
2. Mole TM, Glover J, Sheppard MN (1995) Sclerosing mediastinitis: a report on 18 cases. Thorax 50:280–283
3. Sherrick AD, Brown LR, Harms GF et al (1994) Radiologic findings of fibrosing mediastinitis. Chest 106:484–489
4. Schowengerdt CG, Suyemoto R, Main FB (1969) Granulomatous and fibrous mediastinitis—a review and analysis of 180 cases. J Thorac Cardiovasc Surg 57:365–379

Medullary Carcinoma

▶Carcinoma, Other, Invasive, Breast

Medullary Sponge Kidney

R. H. Oyen
Department of Radiology, University Hospitals Gasthuisberg, Leuven, Belgium
raymond.oyen@uz.kuleuven.ac.be

Synonyms

Cacchi-Ricci disease; Cystic dilatation of the renal tubules (1–3); Cystic disease of the renal pyramids; Precalyceal canalicular ectasia; Renal tubular ectasia

Definition

Medullary sponge kidney is characterized by dilated collecting tubules within one or more renal pyramids of one or both kidneys (1–3). Renal size is usually normal. Cysts in other organs are not found. The pathogenesis of medullary sponge kidney is unknown. Medullary sponge kidney has been reported in 0.5% of excretory urograms (2).

Pathology

On cut section there are multiple cyst-like cavities ranging from 1 mm to several millimeters in diameter in one or more pyramids (1, 3). These cysts represent dilatation of the terminal portion of the collecting ducts, the ducts of Bellini. The abnormalities are confined to the papillary portions of the pyramids. Cysts usually communicate proximally with collecting tubules and distally with papillary ducts or the calyx.

Calculi frequently form within the dilated spaces. The most commonly documented change with time is an increase in the number and size of renal calcifications. Less commonly, new cavities develop in previously uninvolved papillae. Interstitial fibrosis and inflammation occur in more advanced forms (1–3).

Clinical Presentation

While medullary sponge kidney has been described in patients of all ages, it is most often encountered in patients in the third and fourth decades of life (1–3). A few cases have suggested a hereditary pattern with abnormalities documented in siblings or several generations. It also has been associated with hemihypertrophy, Ehlers–Danlos syndrome, congenital hypertrophic pyloric stenosis, and hyperparathyroidism (3).

Uncomplicated medullary sponge kidney usually causes neither symptoms nor impaired renal function, although there have been reports of impaired concentration or acidification of urine. Calculi may cause renal colic, hematuria, fever, dysuria, or flank pain.

Imaging

The urographic criterion for the diagnosis of medullary sponge kidney is the demonstration of discrete linear densities in one or more papillae (1–4). Cystic dilatations of the collecting ducts appear as clusters of small rounded spaces in the papillae. The papillae may be enlarged. Precalyceal calculi become surrounded by contrast material.

Advanced stages of medullary sponge kidney cause severe deformity of the papillae with marked distortion of the calyces. Calcifications are numerous and large.

The sonographic findings of medullary sponge kidney are nonspecific and include subtle anechoic spaces and echogenic deposits in the pyramids (1, 2). Increased echogenicity is most evident in the periphery of each pyramid near the septal cortex. When complicated with lithiasis, a typical acoustic shadow is observed.

Unenhanced computed tomography (CT) scans are either normal or demonstrate medullary nephrocalcinosis (precalyceal calculi) (1, 2, 5). Enhanced CT scans and contrast-enhanced magnetic resonance imaging (MRI) during the excretory phase may show accumulation of contrast material in the dilated spaces of the pyramid. MRI is insensitive in detecting calcification.

Differential Diagnosis

The differential diagnosis includes papillary blush, papillary necrosis, tuberculosis, and calyceal diverticulum (2).

Bibliography

1. Hartman DS (1989) Renal cystic disease. In: Davidson AJ (ed) AFIP Atlas of radiologic-pathologic correlation. W.B. Saunders Company, 1989, A.J. Davidson, Ed. Fascicle 1. pp 108–119
2. Kawashima A, Goldman SM (2000) Medullary sponge kidney. In: Pollack HM, McClennan BL (eds) Clinical Urography. W.B. Saunders Company, 2000, H.M. Pollack and B. McClennan, Eds. pp 1384–1397
3. Gambaro G, feltrin GP, Lupo A et al (2006) Medullary sponge kidney (Lenarduzzi-cacchi-Ricci disease): a Padua Medical School discovery in the 1930s. Kidney Int 69(4):663–670
4. Saxton HM (1989) Opacification of collecting ducts at urography. Radiology 170(1):16–17
5. Boag GS, Nolan R (1988) CT visualization of medullary sponge kidney. Urol Radiol 9(4):220–221

Medulloblastoma

Medulloblastoma is the most frequent malignant tumor in the posterior fossa in children. The main varieties are the classic and desmoplastic types, which vary according to histology, localization, age of the patient, and prognosis.

▶Neoplasms, Brain, Posterior Fossa, Pediatric

Megacystis-microcolon-intestinal Hypoperistalsis Syndrome

The most severe form of chronic intestinal pseudo obstruction associated with very large bladder volume and a microcolon.

▶Hirschsprung's Disease and Related Disorders

Meig's Syndrome

A benign condition that is characterized as a triad of ovarian fibroma, ascites, and pleural effusion, which typically resolve after fibroid resection.

▶Masses, ovarian

Melhem Hyperostosis and Hyperphosphatasemia

Hyperostosis from periosteal reaction associated with hyperphosphatemia, as described by Melhem and colleagues.

▶Caffey Disease

Meninges

The meninges consist of three membranes covering the brain and spinal cord. From without inward: the dura mater, the arachnoid, and the pia mater.

▶Neoplasms, Extraaxial, Brain

Meningiomas

Meningeal tumours may take origin from any of the covering membranes of the neuraxis: pia matter, arachnoid membrane and dura mater. They will be found to be attached to any of these three meninges or to their extension to the central neuroaxis.

▶Neoplasms, Extraaxial, Brain Tumors, Spine, Intradural, Extramedullary

Meningitis

E. Turgut Tali, Serap Gultekin
Section of Neuroradiology & MRI Center,
Department of Radiology,
Gazi University School of Medicine, Besevler
Ankara 06510, Turkey
turgut.tali@gazi.edu.tr
sergultekin@yahoo.com

Definition

Meningitis is a pathological process involving diffuse inflammation of the membranes (pia-arachnoid mater and cerebrospinal fluid, or dura-arachnoid mater, or both) surrounding the brain and spinal cord. Meningitis is the most common form of central nervous system (CNS) infection. The etiology varies according to the age of the patients and the status of their immune system. In adults, the most common agents for bacterial meningitis include streptococci and *Neisseria meningitidis*. Aseptic meningitis is usually caused by viral pathogens. Meningeal tuberculosis (TB) is the most common presentation, and is most frequently seen in children and adolescents.

Pathology/Histopathology

Bacteria that reach into the subarachnoid space stimulate the production of cytokines and other inflammatory products. The inflammation may extend to the walls of arteries and veins resulting in vasculitis and thrombosis. Accumulation of the exudate may cause the obstruction of the cerebrospinal fluid (CSF) flow and lead to communicating or obstructive hydrocephalus (1).

Clinical Presentation

Meningitis classically manifests as a febrile illness accompanied by meningismus. The patients most commonly present with headache, neck stiffness, fever, and chills.

Imaging

Computed Tomography

The computed tomography (CT) findings are mostly normal in the early phase of meningitis. On noncontrast studies, meningeal inflammation is seen as a subtle "loss of sulci," mild ventricular dilatation, and subarachnoid enlargement. Contrast-enhanced CT may show meningeal enhancement.

Magnetic Resonance Imaging

Unenhanced magnetic resonance (MR) scans of patients with uncomplicated acute bacterial meningitis may be unremarkable. Only 50% of patients with meningitis show subarachnoid space obliteration (1). Postcontrast MR studies can demonstrate leptomeningeal enhancement (Fig. 1). Fluid attenuation inversion recovery (FLAIR) images show the CSF within the subarachnoid space to be of higher signal intensity than expected in meningitis. Magnetization transfer techniques may also help in the visualization of enhancing meninges. On MR spectroscopy, elevation of lactate, large amounts of amino acids, acetoacetate, and reduced glucose with normal NAA, Cr, and Cho levels have been reported.

Imaging findings in patients with viral meningitis are frequently normal. The common triad of imaging findings in TB meningitis is basal meningeal enhancement, hydrocephalus, and infarctions in the supratentorial brain parenchyma and brain stem.

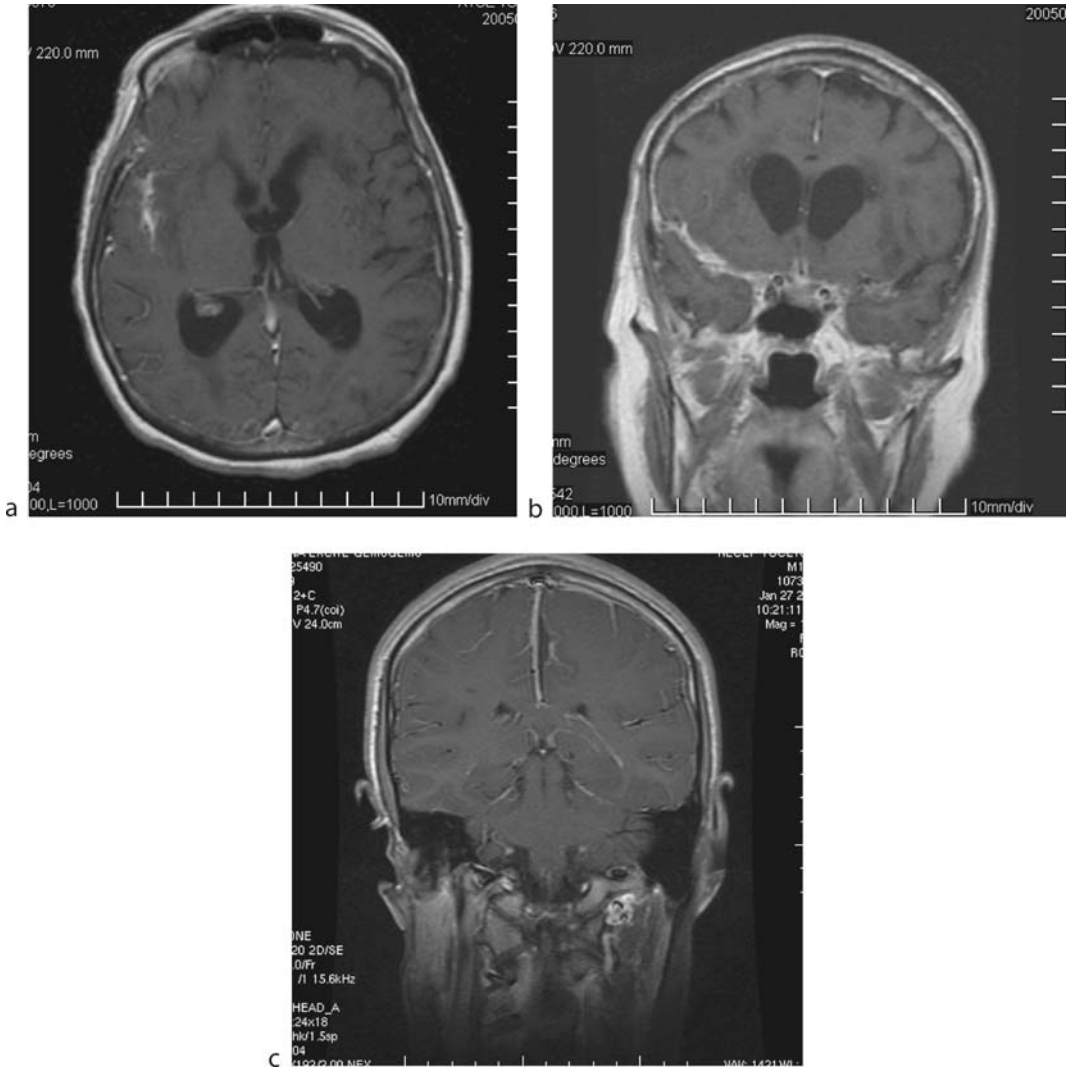

Meningitis. Figure 1 Meningitis. Axial (a) and coronal (b) postcontrast T1-weighted images show nodular and diffuse pia-subarachnoid type enhancement of meningitis on the right temporal lobe along the sylvian fissure. Coronal (c) postcontrast T1-weighted images from another patient exhibit diffuse pia-subarachnoid type enhancement along the cortical sulci. Thickened and enhanced falx corresponding to dura-subarachnoid type meningitis together with parafalcine subdural effusion are also seen in the same patient.

Diagnosis

Lumbar puncture with examination of the CSF represents the cornerstone of the diagnosis in suspected cases. Peripheral blood studies are nonspecific. Blood cultures are positive in up to 75% of patients. Polymerase chain reaction for TB can confirm the diagnosis rapidly.

References

1. Castillo M (2004) Imaging of meningitis. Semin Roentgenol 39: 458–464

Menstrual Cycle

Martin Unterweger, Rahel A. Kubik
Institute of Radiology, Kantonsspital Badan, Switzerland
Martin.Unterweger@ksb.ch

Definition

The menstrual cycle is defined as a recurring cycle of physiological changes in females that is associated with

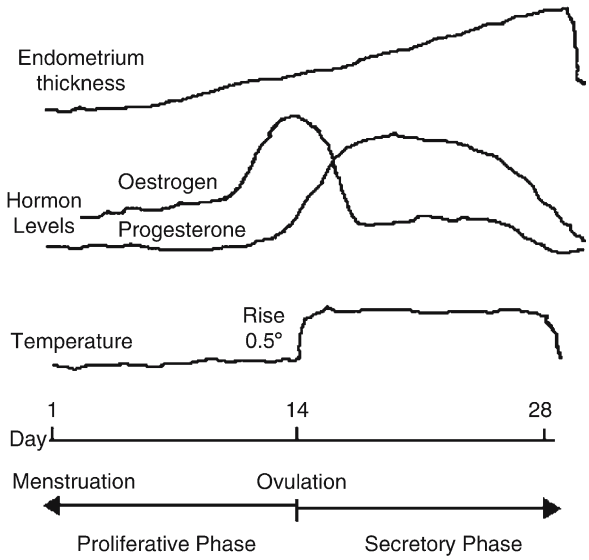

Menstrual Cycle. Figure 1 Endometrial thickness, temperature, and hormone levels during the menstrual cycle.

fertility. In women of reproductive age, the time of imaging during the menstrual cycle influences the imaging appearance of the female genital organs, i.e., uterus and ovaries.

The menstrual cycle of hormonal changes is measured from the beginning of the first day of menstruation. The average menstrual cycle is 28 days with a wide individual range. The hormones (estrogen and progesterone) control the menstrual cycle. At the beginning of the menstrual cycle from days 1–4 is the menstruation. Then the pituitary gland releases FSH, which makes the immature follicles to grow in the ovaries. Estrogen level rises, since the developing follicle secretes the hormone in the proliferative phase (days 5–12). During the ovulation, estrogen is at the maximum level and the follicle on the ovary's wall bursts releasing the egg. After ovulation, the secretory phase begins (days 12–28). Both estrogen and progesterone are secreted by the corpus luteum, which is developed from the burst follicle and remains in the ovary. With the disappearance of the corpus luteum, hormone levels fall, which causes the rejection of the endometrium though menstruation (Fig. 1). The principle rule is that morphologic changes during the menstrual cycle of the uterus and ovaries are similar to radiological changes.

Normal Anatomy of the Female Genital Organs and Changes During the Menstrual Cycle

The uterus is divided into three parts: fundus, corpus, and cervix. Normal size of the uterus for women of the reproductive age is 6–9 cm in length and 4–6 cm in transversal dimension. The cervix uteri is smaller and measures normally around 2.5–3.5 cm. Cross sectionally, the uterus has three different layers: (1) Serosa (2) Myometrium (3) Endometrium.

During the menstrual cycle, endometrial thickness varies. The endometrium, as the central portion of the uterus, is thinnest at time of menstruation, being normally thinner than 4 mm. Endometrium gets thicker during the proliferative phase, in the secretory phase endometrium thickness slowly further increases. The thickness of the endometrium varies widely normally the maximal thickness is 3–6 mm in the proliferative phase and 5–13 mm in the secretory phase. In the area of the cervix, the endometrium is normally thinner.

The endometrium stripe does not vary in women with oral contraception. The postmenopausal endometrium is normally thinner than 3 mm, unless the postmenopausal woman takes hormonal replacements therapy. On imaging, a thickened endometrium has a broad differential diagnosis, including endometrial hyperplasia, endometrial polyp, and endometrial carcinoma.

The myometrium also varies slightly in size during the menstrual cycle and becomes thicker in the proliferative and secretory phase. The ovaries vary in size with the female age. Ovarian size in neonates is approximately $3 \times 2.5 \times 1.5$ mm. Mean ovarian volume in premenopausal women is 4.9 cm^3 with an upper limit of 20 cm^3. In postmenopausal women, the mean volume of the ovary is 2.2 cm^3 with an upper limit of 10 cm^3. The ovaries consist of different types of follicles, e.g., primary, secondary, primordial. During the menstrual cycle, the so-called secondary "Graafian" follicle matures. Maturation can be suppressed by hormonal contraception. Without contraception, the Graafian follicle after releasing an egg becomes the corpus luteum. If no pregnancy follows, the corpus luteum changes in the corpus albicans, which normally degenerates completely. Follicles will be seen as functional cysts on the different imaging techniques.

Imaging

On sonography, the endometrium appears hyperechogenic, while myometrium occurs hypoechogenic. Therefore, the thickness of the endometrium can be measured with sonography. A focal thickening of the endometrium must be recognized as pathologic and needs further examination, because is could also be a sign for an endometrial carcinoma or another pathology as described earlier.

Functional cysts can be sonographically detected as anechogenic well-defined lesions in the ovaries. The greatest number will be found at birth with a significant decrease in number after menopause (Fig. 2).

A small amount of free pelvic fluid is physiologic in women at the time of ovulation. On MRI, the uterus is best evaluated on T2-weighted sagittal imaging. Three zones can be recognized: The innermost hyperintense zone is the endometrium, followed by the myometrium that consists of two different signal intensities on MRI. While the inner layer of the myometrium, the "junctional zone" is hypointense, the outer layer of the myometrium is isointense relating to skeletal muscle (Fig. 3). The junctional zone does not correlate to a real anatomic structure, but it is described as the innermost, less water-containing layer of myometrium. Another hypothesis explains the low signal intensity of the junctional zone by the presence of compact smooth muscle bundles and the increase in percentage of nuclear area in comparison to the subserosal myometrium.

At the end of the menstrual cycle, the myometrium appears with a higher signal intensity caused by increased vascularization, so that the contrast to the "junctional zone" and endometrium is more pronounced and the zonal anatomy of the uterus is best differentiated at this time of the menstrual cycle. Therefore, if possible, patients with congenital uterine malformations should be scheduled for MRI toward the end of their menstrual cycle. During menstruation, a common MR finding is an irregular thickening of the junctional zone due to uterine contraction. This is also a finding in diffuse uterine adenomyosis and a pitfall for false positive diagnosis of this entity on MRI.

On MRI, the ovaries can be best seen on transversal or coronar T2-weighted images. They are normally isointense to the uterus on precontrast T1-weighted images and enhance after contrast media is applied. In the proliferative phase about 10–20 follicles start developing in the ovaries. Functional cysts are normally sharp defined with a high signal intensity on T2-weighted MRI images (Fig. 4). The corpus luteum and albicans (Fig. 5), however, may show an irregular cyst wall and demonstrate variable enhancement. The corpus luteum after releasing the egg could also cause a hemorrhage, which will be seen as high signal intensity on T1-weighted images.

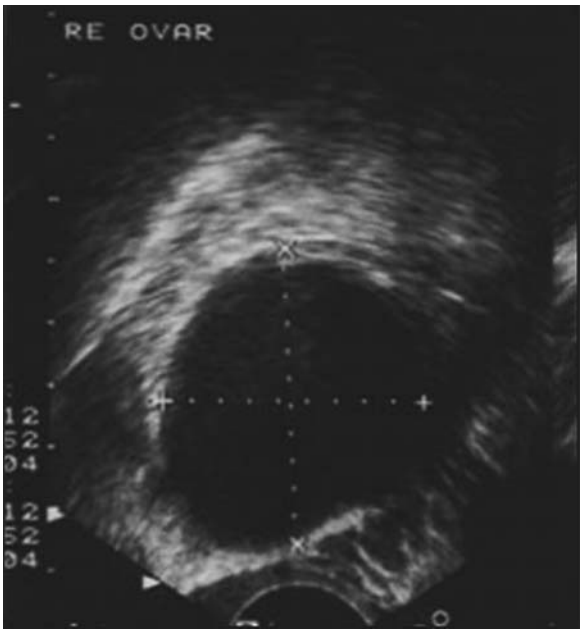

Menstrual Cycle. Figure 2 Sonography demonstrates a large functional cyst in the right ovary.

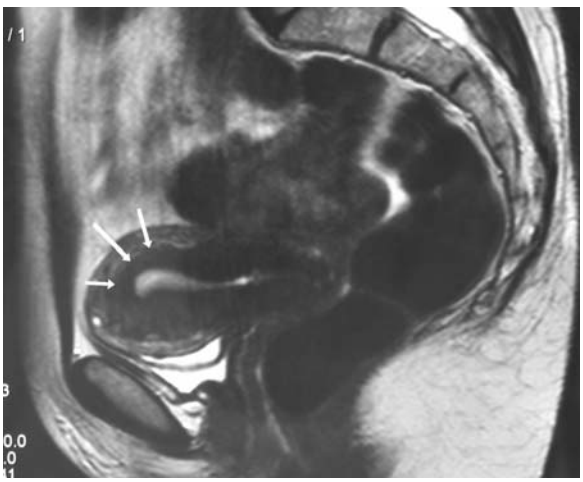

Menstrual Cycle. Figure 3 Zonal anatomy of the uterus, sagittal T2-weighted MRI: Endometrium, junctional zone of the myometrium (arrows) and the outer myometrium.

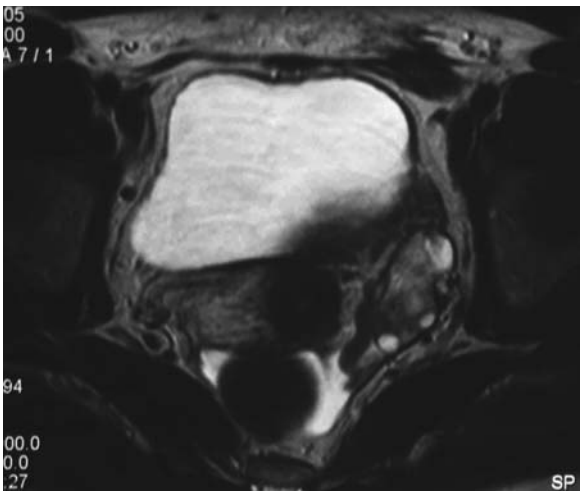

Menstrual Cycle. Figure 4 Axial T2-weighted MRI of 44-years-old woman with multiple cysts in the left ovary (large arrows). Physiologically a small amount of free fluid (small arrows) is seen in the pouch of Douglas.

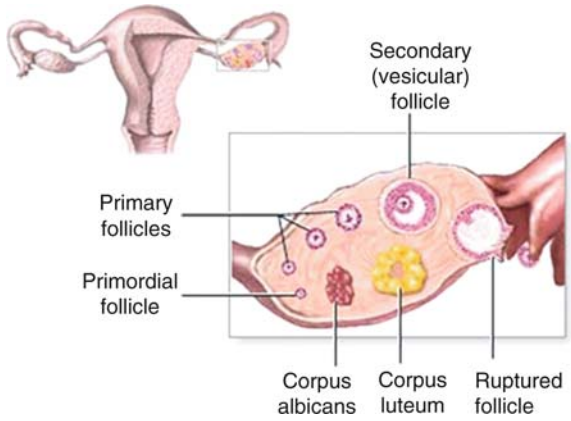

Menstrual Cycle. Figure 5 Different kinds of follicular

As mentioned above, small amount of free pelvic fluid is a physiological finding, seen in many women at ovulation, but can be present during the entire phase of the menstrual cycle. Especially, T2-weighted MRI is very sensitive for free fluid in the pouch of Douglas. Therefore, without any underlying pathology, some amount of fluid in the female pelvis is a physiological finding in most cases and should not be termed ascites (Fig. 4).

Bibliography

1. Haynor DR, Mack LA, Moss et al (1986) Changing appearance of the normal uterus during the menstrual cycle: MR studies. Radiology 161:459–462
2. Semelka R (2002) Abdominal Pelvic MRI. Wiley Liss Inc., New York pp 1052–1054
3. Baerwald AR, Adams GP, Pierson RA (2005) Form and function of the corpus luteum during the human menstrual cycle. Ultrasound Obstet Gynecol May 25(5):498–507.
4. Bartoni JM, Moulin G, Delannoy L et al (1991) The normal uterus on magnetic resonance imaging and variation associated with the hormonal state. Surg Radiol Anat 13:213–220
5. Pavlik EJ, DePriest PD, Gallion HH et al (2001) Ovarian volume related to age. Gynecol Oncol Feb 80(2):333–334

Mercury

Mercury (Hg, atomic number 80) is an elemental heavy metal found in both its elemental form and in organic compounds. Elemental mercury is a liquid at room temperature and is highly volatile. Organic mercury is most frequently encountered in contaminated fish. Elemental mercury fumes and organic mercury are highly toxic to the central nervous system. Elemental mercury toxicity was common in the hat-making industry in the early nineteenth century, manifesting as tremors, hallucinations, and psychosis. Chronic organic mercury exposure results in an entity known as Minamata disease, which is characterized by visual field defects, sensory abnormalities, and ataxia.

▶Toxic Disorders, Brain

Mesenchymal Hamartoma, Hepatic

Rare congenital mesenchymal solid/cystic lesion originating from the primitive connective tissue in the portal tracts. It accounts for 22% of the benign liver tumors in children with a marked male predominance. Lesions may be large, usually well demarcated without capsule and formed by a mixture of cysts, bile ducts, vessels, and connective tissue.

▶Hepatic Pediatric Tumors, Benign

Mesenchymal Tumors, Pancreatic

Mesenchymal or soft tissue tumors of the pancreas are nonepithelial tumors arising from the connective, vascular, and neuronal tissue in the pancreas and are classified according to their main histologic component. All these neoplasms are exceedingly rare, representing 1–2% of pancreatic neoplasms and do not differ in structure and imaging findings from those seen in other organs. Benign soft tissue neoplasms that have been reported include benign fibrous histiocytoma, hemangioendothelioma, lymphangioma, lipoma, schwannoma, and neurofibromas (in patients with von Recklinghausen syndrome). Malignant mesenchymal tumors reported in the literature include leiomyosarcoma, fibrosarcoma, malignant fibrous histiocytoma, liposarcoma, rhabdomyosarcoma, hemangiopericytoma, and malignant schwannoma. However, some of these tumors probably represent undifferentiated carcinomas or secondary involvement of the pancreas by primarily retroperitoneal sarcomas. Moreover, sarcomas are often difficult to distinguish from undifferentiated carcinomas also at histology.

▶Carcinoma, Pancreatic

Mesenteric Vascular Occlusion

▶Ischemia, Mesenteric, Acute

Mesomelic

A shortness of the extremities most pronounced in the intermediate (radius and ulna, and tibia and fibula) region. An example is Ellis–van Creveld syndrome.
▶Osteodysplasia

Mesorectal Fascia

Fascia enveloping rectum and its surrounding mesorectal fat. This mesorectal fat contains lymph nodes and blood vessels.
▶Rectal Carcinoma

Mesothelial and Tubal Inclusion Cysts

Inclusion cysts are cystic, thin-walled lesions which range between 1 and 12 cm in size. Like ovarian cysts, they are most commonly an incidental finding. Although they can occur at any age, they are most commonly encountered in middle-aged women. At imaging, they can only be differentiated from ovarian cysts if they are found separate from the ipsilateral ovary.
▶Cyst, Follicular, Ovarium

Mesothelial Fibroma

▶Pleura, Localized Fibrous Tumor

Metabolic Diseases

▶Neurometabolic Disorders

Metabolic Encephalopathies

▶Neurometabolic Disorders

Metaphyseal Collar

As a part of normal growth at the metaphysis of long bones, a one-cell-layer thick collar of membranous-origin "bone bark" that surrounds part of the enchondral physeal cartilage as well as the newest metaphyseal bone, giving 1–3 mm straight margins to that portion of the metaphysis; described by Laval-Jeantet.
▶Caffey Disease

Metastases, Breast

Geert M. Villeirs
Genitourinary Radiology, Ghent University Hospital, Ghent, Belgium
geert.villeirs@ugent.be

Definition

Breast metastases are relatively rare. The most common primary tumors that can metastasize to the breast are contralateral breast cancers and extramammary tumors such as melanomas, lung cancer (especially oat-cell tumors), ovarian cancer, sarcomas, and gastrointestinal carcinoid tumors. In addition, virtually any primary site has been reported to occasionally metastasize to the breast, for example, thyroid, stomach, colon, rectum, kidney, bladder, cervix, uterus, and so on. In male patients, breast masses can be found to be metastatic from prostate cancer. Hematologic tumors, such as lymphomas, can also affect the breast, but should be regarded as part of a systemic disease and are discussed elsewhere in this volume.

Pathology/Histopathology

Many metastases are found in the subcutaneous fat rather than in the breast parenchyma. If they are large enough, they can be palpated as a solitary nodule. Multiple and bilateral lesions are generally found only later in the

course of the disease. The nodules tend to be rounded and well demarcated. Diffuse infiltration may occur in ovarian carcinomas, but it is uncommon in other primary extramammary malignancies. Rarely, metastases may induce an intense inflammatory reaction resembling an inflammatory breast carcinoma.

Microscopically, breast metastases usually reflect the primary cells of origin well, but the diagnosis may be less obvious when the lesion originates from an undifferentiated primary tumor or from a contralateral breast tumor, in which the metastatic cells may closely resemble those of a primary breast tumor. Some clues may help the pathologist to differentiate a metastatic form a primary malignancy. With few exceptions, metastatic lesions are highly cellular and do not present with an intraductal (DCIS) component. Estrogen and progesterone receptors are rarely present in metastatic lesions, except when arising from ovarian or prostatic tumors. Unlike primary breast tumors, metastases are not usually located within an area of proliferative change (with or without atypia). They tend to displace the surrounding normal breast tissue without eliciting a desmoplastic reaction and therefore are fairly well circumscribed with no spiculations.

Clinical Presentation

On average, the interval between the treatment of a primary cancer and the development of breast metastases is approximately 2 years. Metastases at sites other than the breast usually have already occurred before a breast metastasis is detected or they occur coincidentally.

Breast metastases may present as solitary or multiple palpable masses. They are usually painless, fairly mobile, smoothly outlined, and rounded. In the absence of a desmoplastic reaction, their palpable size usually closely approximates their mammographic size. In rare cases of diffuse infiltration or inflammatory reaction, skin thickening, peau d'orange, and diffuse swelling of the breast can be observed.

On the basis of clinical examination, however, breast metastases can rarely be distinguished from other breast lesions, although a history of rapid growth and of a known primary malignancy may be suggestive.

Mammography

There are no reliable mammographic criteria that distinguish breast metastases from other breast lesions. Most breast metastases present as solitary round, oval, or lobulated masses with well-defined margins (Fig. 1). Sometimes the margins may be partly indistinct or angular, but spiculation is exceedingly rare. Later in the course of the disease, multiple or bilateral equally sized masses may be observed. In the case of diffuse infiltration or inflammatory reaction, the density of the involved side may increase, along with skin thickening and diffuse trabecular thickening.

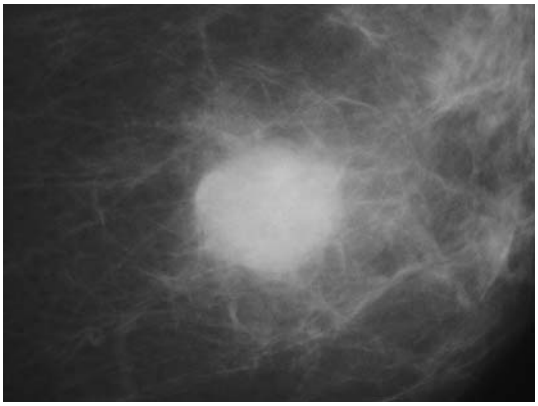

Metastases, Breast. Figure 1 Breast metastasis from ovarian cancer, presenting as fairly well-defined lobulated mammographic mass.

Calcifications are rarely present, except for coarse calcifications involving necrotic areas or calcifications in metastases from ovarian carcinoma or thyroid medullary carcinoma.

Sonography

Although sonography can identify a simple cyst as the cause of a palpable or mammographic abnormality, it does not allow a reliable differentiation of breast metastases from other abnormalities. Breast metastases are usually round, oval, or lobulated, and they have a well-circumscribed margin (Fig. 2). Sometimes the margins may be partly indistinct or angular, but spiculation or an echogenic halo due to surrounding desmoplastic reaction is usually absent. The lesions are hypoechoic, with fairly homogeneous internal structure, except when central necrosis occurs. They show normal or enhanced through-transmission, but acoustic shadowing may occur in the presence of intense fibrosis. The compressibility under varying scan pressures depends on the type of the primary tumor, and on Doppler interrogation, many breast metastases appear hypervascular (Fig. 3).

Magnetic Resonance Mammography

There are only few reports on magnetic resonance imaging (MRI) of breast metastases. Most reported cases show a round or oval, well-circumscribed lesion with low signal intensity on T1-weighted images and intermediate to high signal intensity on T2-weighted images. Following

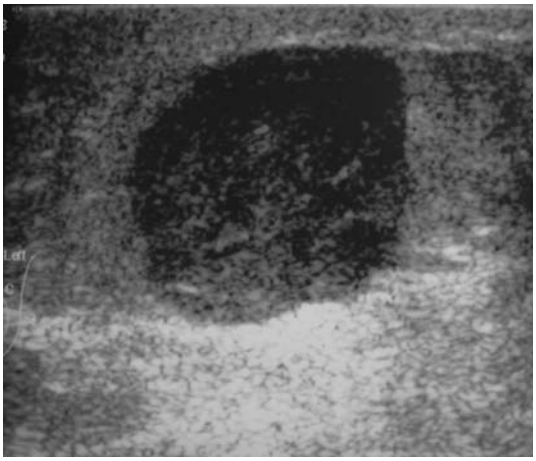

Metastases, Breast. Figure 2 Sonogram of breast metasis from ovarian cancer, presenting as a well-defined lobulated hypoechoic mass with enhanced through-transmission.

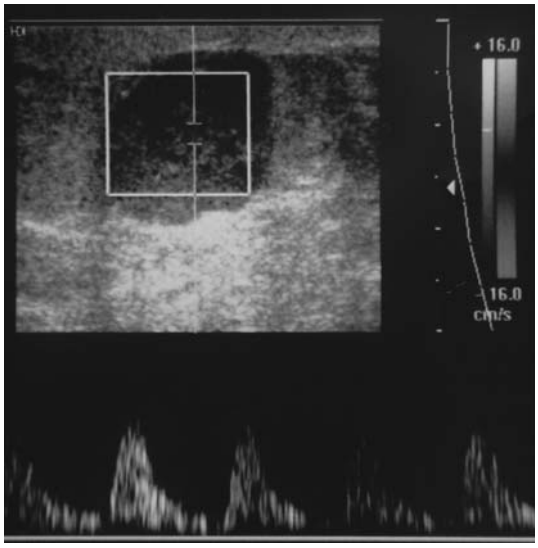

Metastases, Breast. Figure 3 Hypervascular appearance of breast metastasis on Doppler-interrogation.

intravenous contrast administration, most lesions exhibit a fast ring-like enhancement with wash-out pattern, indistinguishable from other breast malignancies.

Percutaneous Biopsy

Since breast metastases cannot reliably be diagnosed clinically, mammographically, sonographically, or on MRI, biopsy is the only way to confirm the presence of a metastasis. Information about a prior tumor and a tissue sample large enough to contain all necessary information for accurate diagnosis are of utmost importance for the pathologist.

Bibliography

1. Hajdu S, Urban J (1972) Cancers metastatic to the breast. Cancer 29:1691–1696
2. Bohman L, Bassett L, Gold R et al (1982) Breast metastases from extramammary malignancies. Radiology 144:309–312
3. Paulus D, Libshitz H (1982) Metastasis to the breast. Radiol Clin North Am 20:561–568
4. Yang W, Metreweli C (1999) Sonography of nonmammary malignancies of the breast. Am J Roentgenol 172:343–348
5. Wurdinger S, Schutz K, Fuchs D et al (2001) Two cases of metastases to the breast on MR mammography. Eur Radiol 11:802–806

Metastases, Hepatic

Laura Crocetti, Carlo Bartolozzi, Marzio Perri
Department of Diagnostic and Interventional Radiology, University of Pisa, Italy
l.crocetti@med.unipi.it

Synonyms

Liver metastases

Definition

A malignant tumor of the liver following hepatic migration of tumor cells originating from a primary malignant tumor in another organ.

Epidemiology

The liver is second only to regional lymph nodes as a site of metastatic disease and hepatic metastases represent the most common malignancy of the liver. The true prevalence of liver metastases is unknown; however, between 25 and 50% of patients with known nonhematological malignancies have liver metastases at the time of diagnosis (1, 2).

The liver may be the site of metastasis from virtually any primary malignant neoplasm. The frequency of metastasis to the liver varies considerably with the cell type and the location of the primary tumor, but the most common primary tumor sites are the colon, stomach, pancreas, breast, and lung. Lymphoma may involve the liver as well.

Most metastases to the liver are bloodborne *via* the hepatic artery or portal vein, but lymphatic spread of tumors from the stomach, pancreas, ovary, or uterus may also occur. Particularly, the portal circulation provides

direct access to the liver for tumor cells arising from the gastrointestinal tract and accounts for the high frequency of liver metastases from organs drained by the portal vein.

Pathology/Histopathology

The gross features of liver metastases are variable. Lesions are multiple in most cases and depending on the origin of the primary tumor, may be expansive, infiltrative, surface spreading, or miliary (1, 2).

Metastases from colon carcinoma often appear as a few large nodules with central umbilication. Nodules from breast and lung carcinoma are usually medium in size and often show an early central umbilication, whereas a central necrosis is typical for small cell carcinoma, seminoma, sarcoma, and melanoma. Metastatic lesions of miliary type may be observed in breast, prostate, and stomach metastatic cancer. In contrast to the liver parenchyma, hepatic metastases get their blood supply almost exclusively from the hepatic artery.

Most metastases maintain the microscopic features of the primary tumor, including the degree of stroma growth, particularly conspicuous in neoplasms arising from the breast, pancreas, and stomach (1, 2). Other metastases, such as lesions arising from small cell carcinomas and melanomas, do not usually evoke a local reaction and may grow in the sinusoids.

Clinical Presentation

Symptoms due to hepatic metastases may be few and the extent of liver involvement on images may be surprising in the absence of clinical or laboratory signs suggestive of hepatic functional insufficiency. Hepatomegaly is the most common finding, followed by ascites and jaundice. Liver function tests tend to be insensitive and nonspecific (1, 2).

Imaging

The ultrasound (US) appearance of liver metastases is extremely variable, including hypoechoic, isoechoic, hyperechoic, calcified, cystic, and diffuse-infiltrative patterns (1–3).

Depending on tumor vascularity, cellular composition, the degree of tissue invasion, and the presence or absence of necrosis, the echogenicity of the lesions can vary.

A hypoechoic appearance, corresponding to hypovascular and uniform neoplastic tissue, is usually observed in metastases originating from melanoma, lymphoma, and breast, lung, and cervical cancer, while hyperechoic metastases can be observed in tumors arising from colon, renal, breast, and islet cell carcinomas. Particularly, metastases from gastrointestinal or pancreatic tumors exhibit a central hyperechoic area surrounded by a hypoechoic halo. This characteristic target pattern is highly suggestive for malignancy and is often secondary. A calcified pattern is commonly due to mucinous adenocarcinomas of the colon or ovary. Cystic metastases, including those from sarcomas and ovarian, pancreatic, and colon cancers, are rare. In rare cases, metastases may cause diffuse parenchymal changes because of the confluence of areas of focal spread, infiltrating tumors, or miliary metastatic deposits, and the liver may appear diffusely heterogeneous. According to this extremely variable, usually nonspecific US appearance of liver metastases, characterization of such lesions with conventional US is not possible in most cases.

Despite Doppler US modalities that allow the addition of information concerning tumor vascularity and enabling improved US characterization of focal liver lesions in some cases, US suffers a relatively poor sensitivity and specificity compared with other imaging techniques, such as spiral computed tomography (CT) and magnetic resonance (MR) imaging. However, with the advent of US contrast agents and new contrast-specific imaging techniques, lesion detection and characterization have significantly improved.

Contrast-enhanced ultrasound (CEUS) provides crucial additional information about the dynamic contrast behavior for lesion characterization, and after US contrast agent injection, metastases show characteristic features. Most metastases are hypovascular and show a typical pattern consisting of absent or peripheral enhancement in the arterial, portal–venous, and delayed phases. Hypervascular lesions (metastases arising from renal cell carcinoma, breast carcinoma, islet cell tumors, carcinoids, melanoma, and sarcoma) exhibit an early, intense, and homogeneous enhancement compared with the surrounding liver during the arterial phase, becoming hypoenhancing in the portal–venous and delayed phases (3). More important, the use of contrast agents substantially improves the ability of US to detect liver metastases. Both portal–venous and delayed-phase imaging markedly increase the contrast between the enhancing normal liver and the nonenhancing metastases, improving the lesion detection rate, especially for very small lesions (<1 cm) and for lesions appearing isoechoic on baseline scan.

Finally, intraoperative ultrasound (IOUS) of the liver can be used in the operative setting before hepatic resection because of its extremely high sensitivity for detecting small hepatic metastases. With a sensitivity of 98% and a specificity of 95%, IOUS is generally considered the gold-standard imaging technique for detecting liver lesions. It is used to evaluate the extent of malignant liver disease and to plan resections by assessing the relationship of a tumor to large vessels.

Spiral CT is the most commonly used imaging modality for both detection and characterization of hepatic metastases. Hepatic metastases usually appear as low attenuating or isoattenuating masses on nonenhanced CT scans. Depending on lesion size, the margins tend to be irregular, and necrosis may be present. Central low attenuation may be the result of necrosis or cystic change. Calcification can be observed within metastases arising from mucinous adenocarcinomas of the colon, pancreas, or ovary. Most metastases, including those arising from the colon, stomach, pancreas, and lung, are usually hypovascular because they receive only minimal arterial and portal venous blood supply due to confluent dense cellularity, fibrosis, or necrosis. On contrast-enhanced spiral CT, a hyperdense rim may be observed during the arterial phase, particularly in colon carcinoma metastases, due to viable tumor in the periphery of the lesion, which appears against a hypodense (necrotic) center. However, the optimal scanning time for detecting hypovascular metastases is the portal–venous phase, when the normal liver parenchyma is maximally enhanced, revealing the relatively hypoattenuating lesions (Fig. 1). In the equilibrium phase, metastases can be isoattenuating. Hypervascular metastases are relatively rare and are often secondary to renal cell carcinoma, breast carcinoma, islet cell tumors, carcinoid tumors, melanoma, and sarcomas. When hypervascular metastases are suspected, a multiphase contrast-enhanced spiral CT evaluation, including at least arterial and portal–venous scans, should be performed. The best phase for detecting hypervascular metastases is the arterial phase. Small hypervascular metastases usually show a strong and homogeneous enhancement with respect to the liver parenchyma, whereas larger lesions appear heterogeneous or show an enhancing peripheral rim surrounding the necrosis. In the portal–venous phase, most hypervascular metastases become isodense and difficult to detect because the tumor still receives some contrast *via* the hepatic artery, and the liver parenchyma also receives contrast *via* the portal vein (1, 2, 4).

Finally, CT arterioportography (►CTAP) currently represents the most sensitive nonsurgical imaging technique for detecting hepatic metastases, with an overall detection rate of 81–94%. However, CTAP is invasive and has a high false-positive rate (5).

Magnetic Resonance (MR) imaging is commonly used as the definitive imaging modality for the detection and characterization of focal liver lesions. The standard MR imaging protocol should always include nonenhanced T1- and T2-weighted and contrast-enhanced pulse sequences by using high-field-strength MR scanners (≥1.0 T) with fast gradients and phased-array surface coils.

Liver metastases usually appear as hypointense lesions on T1-weighted images and as hyperintense lesions on T2-weighted images compared with normal liver parenchyma, according to the higher content of free water molecules. However, depending on the degree of vascularity, necrosis, and hemorrhage, the MR appearance of metastases is variable. The presence of coagulative necrosis, fibrous tissue, or calcification may result in decreasing signal intensity on T2-weighted images, whereas colliquative necrosis, edema, and cystic components lead

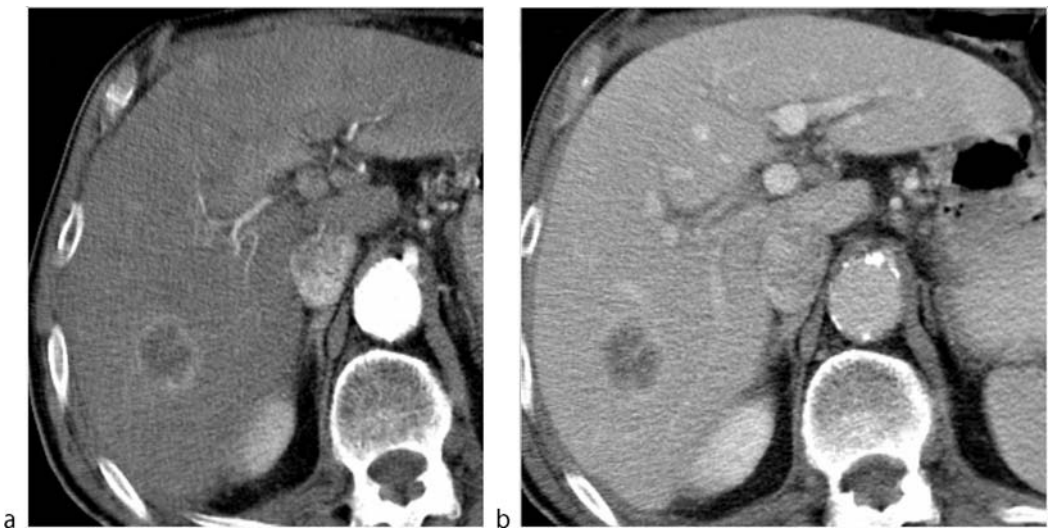

Metastases, Hepatic. Figure 1 Hypovascular metastases on contrast-enhanced multidetector spiral computed tomography (CT), with a characteristic appearance of hepatic metastases arising from colon cancer on dual-phase contrast-enhanced spiral CT. Arterial-phase spiral CT (a) shows a hypodense lesion with slight peripheral enhancement in the right liver, which becomes more evident during the portal–venous phase (b).

to higher signal intensity. Particularly, on T2-weighted images approximately 20% of all metastases (50% of colorectal metastases) show a peripheral hyperintense halo consisting of central necrosis surrounded by viable tumor (halo pattern), whereas another 5–20% may exhibit a central increase in signal intensity due to colliquative necrosis with an outer ring of lower signal intensity (target pattern).

Another characteristic feature of solid metastases is that they demonstrate a considerable signal intensity drop on heavily T2-weighted images using dual or multiecho T2-weighted pulse sequences. Finally, high signal intensity on T1-weighted images can be observed in rare metastatic lesions containing melanin (metastases from melanoma) or mucin (metastases from mucinous carcinoma of the pancreas or ovary), and in metastases complicated by intralesional hemorrhage (4, 5).

On dynamic gadolinium-enhanced MR imaging, the enhancement pattern of hepatic metastases is identical to that observed on contrast-enhanced spiral CT. Hypovascular metastases appear typically hypointense with respect to the surrounding normal liver tissue after intravenous bolus administration of gadolinium chelates, and higher lesion-to-liver contrast is observed during the portal–venous phase. Hypervascular lesions exhibit intense and homogeneous enhancement in the arterial phase, followed by isointensity or slight hypointensity during the portal and equilibrium phases (1, 2, 4, 5) (Fig. 2).

The availability of MR contrast agents with liver-specific properties further increases the potential for detecting hepatic metastases. After administration of Gd-BOPTA, Gd-EOB-DTPA, or Mn-DPDP, liver metastases appear clearly hypointense against a strongly enhanced normal liver during the delayed T1-weighted ►hepatobiliary phase, with a significant improvement in lesion conspicuity, particularly for metastases <1 cm in diameter. However, metastases from neuroendocrine tumors may rarely show a variable uptake of hepatobiliary contrast agents. Of interest, Gd-BOPTA and Gd-EOB-DTPA have both ►extracellular and hepatobiliary properties, allowing more accurate lesion characterization, which can be especially useful when benign and malignant lesions coexist in the same patient.

Detection and characterization of focal liver lesions can also be improved by administration of ►reticuloendothelial system (RES)-targeted agents consisting of superparamagnetic iron oxide (SPIO) particles or ultrasmall superparamagnetic iron oxide (USPIO) particles. Because of the absence of Kupffer's cells, metastases generally do not show a significant signal drop on T2-weighted images after SPIO injection, appearing as hyperintense nodules against a darkened normal liver (Fig. 3). Improved lesion resolution from suppression of peritumoral edema makes these agents particularly useful in preoperative evaluation of hepatic metastases from primary colorectal cancer. Moreover, SPIO agents are also useful in differentiating metastases from focal liver lesions with phagocytic elements, including focal nodular hyperplasia, adenomas, and well-differentiated hepatocellular carcinomas that result in contrast uptake and show decreased signal intensity on T2-weighted images (2).

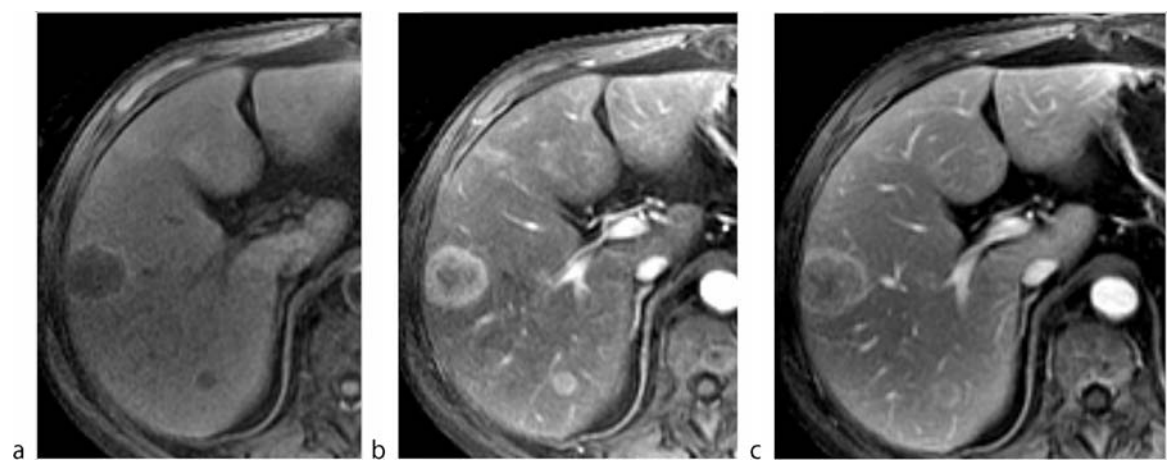

Metastases, Hepatic. Figure 2 Hypervascular metastases on dynamic magnetic resonance imaging (MRI), with a characteristic appearance of hepatic metastases arising from carcinoid. Baseline T1-weighted MRI (a) demonstrates two well-defined hypointense nodular lesions in the right hepatic lobe. On gadolinium-enhanced dynamic MRI, both lesions show an early and intense enhancement during the arterial phase (b). The larger lesions appear heterogeneous in the portal-venous phase with an isointense appearance of the peripheral zone, whereas the smaller lesion becomes isointense and difficult to detect (c).

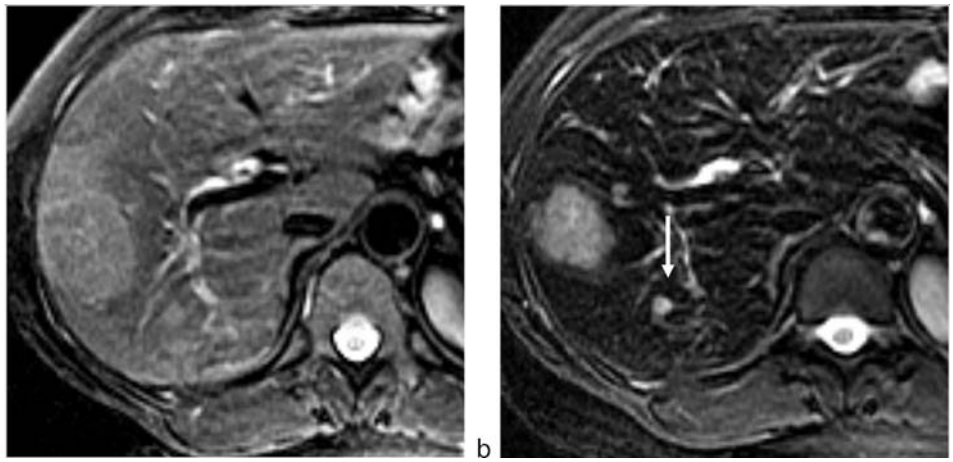

Metastases, Hepatic. Figure 3 Liver metastases on reticuloendothelial system-targeted enhanced magnetic resonance imaging. Two hyperintense lesions are depicted on baseline T2-weighted image (a). In the liver-specific phase, a third small lesion can be appreciated (b).

Nuclear Medicine

^{99m}Tc-sulphur colloid scintigraphy, although quite sensitive in lesion detection, is almost nonspecific and is rarely used as an imaging test for liver metastases. However, scintigraphy with a somatostatin receptor analog (such as ^{111}In-octeotride) may be useful for evaluating suspected hepatic metastases arising from carcinoids and other neuroendocrine tumors.

Recently, positron emission tomography (PET) has emerged as an important diagnostic tool in the evaluation of metastatic liver disease. Particularly, fluorine-18-fluorodeoxyglucose PET (^{18}F-FDG-PET) has been shown to be highly sensitive for detecting hepatic metastases arising from different primaries (6).

Diagnosis

The noninvasive diagnosis of liver metastasis at an early stage is almost entirely dependent of imaging. US is usually the first-line imaging investigation for hepatic screening of oncologic patients. Because of its noninvasive character, low cost, and widespread availability, US can be used to help distinguish patients with diffuse disease who are not eligible for curative treatment, patients with no liver metastases, and patients with a limited number of metastases. The patients in the latter group should undergo CEUS, CT, MR imaging, or FDG PET for the selection of appropriate therapeutic approaches (6).

Contrast-enhanced spiral CT offers a comprehensive evaluation, allowing a simultaneous examination of the extrahepatic abdomen and even the pelvis and chest (2, 4, 6). Since the recent advances in hardware and software and the introduction of tissue-specific contrast agents, MR imaging has also gained an important role in the diagnosis of liver metastatic disease. Particularly, the use of hepatobiliary and RES-targeted MR contrast media seem to have significantly improved the detection of hepatic colorectal metastasis, especially in lesions smaller than 1 cm (4, 5).

Interventional Radiology

Surgical treatment is currently considered the best therapeutic option for liver metastatic disease, but only 20% of patients are suitable for surgical resection. Therefore, alternative local or locoregional interventional radiological procedures, including percutaneous tumor thermal ablation (cryoablation and radiofrequency, laser, and microwave ablation) have been largely used in an attempt to obtain large tumor necrosis and improve survival data in patients with unresectable liver metastases (1, 2).

Because the biology and characteristics of metastatic disease may limit the applicability of a local or systemic therapy, the choice of the most appropriate interventional radiological procedures depends mainly on the biology of the primary tumor and, in the case of disease being confined to the liver, by the number and topographic location of the metastases.

Colorectal liver metastasis is the most frequent indication for the use of regional treatment concepts for the liver, but metastases from other primary tumors such as metastases from breast and neuroendocrine tumors (carcinoids) may also benefit from local therapies.

Local ablative thermal therapies, particularly radiofrequency thermal and laser ablation, seem to be able to obtain a remarkable local tumor control rate with improved survival results in solitary or fewer than three hepatic lesions that do not exceed 3 cm in their greatest dimension and that arise from colorectal adenocarcinoma. Transcatheter arterial chemoembolization represents a valid therapeutic option in hypervascularized metastases originating from neuroendocrine tumors.

Percutaneous ethanol injection, because of a nonhomogeneous distribution of the ethanol within the lesion and poor tumor control has limited use in treating liver metastases.

References

1. Bartolozzi C, Lencioni R (1999) Liver Malignancies. Springer-Verlag, Berlin Heidelberg New York
2. Lencioni R, Cioni D, Bartolozzi C (2005) Focal Liver Lesions: Detection, Characterization, Ablation. Springer-Verlag, Berlin Heidelberg New York
3. Albrecht T, Oldenburg A, Hohmann J, et al (2003) Imaging of liver metastases with contrast-specific low-MI real-time ultrasound and SonoVue. Eur Radiol 13(3):79–86
4. Sica GT, Ji H, Ros PR (2000) CT and MR imaging of hepatic metastases. AJR 174:691–698
5. Bartolozzi C, Donati F, Cioni D, et al (2004) Detection of colorectal liver metastases: a prospective multicenter trial comparing unenhanced MRI, MnDPDP-enhanced MRI, and spiral CT. Eur Radiol 14:14–20
6. Bipat S, van Leeuwen MS, Comans EFI, et al (2005) Colorectal liver metastases: CT, MR imaging, and PET for diagnosis—meta-analysis. Radiology 237:123–131

Metastases, Pancreatic

The prevalence of metastatic involvement of the pancreas is not well known. Although pancreatic metastases are commonly considered infrequent, the occurrence at autopsy ranges from 3 to 12% of patients with advanced malignancy, and they account for 2–5% of pancreatic malignant tumors. A wide variety of primary tumors may metastasize to the pancreas, but the most frequently reported primary are kidney, breast, lung, and thyroid tumors and melanoma. Metastases may occur many years after the initial diagnosis, and treatment of the primary tumor or may be discovered before the primary site is known. Patients may have few or no symptoms referable to the pancreas. Concomitant intra-abdominal metastases to the liver, lymph nodes, and adrenals can be discovered at the time of diagnosis of pancreatic metastases. Metastases do not show any predilection for a specific area of the pancreas. Possible imaging patterns include multifocal lesions or large solitary masses with well-defined margins in the majority of cases, but diffuse infiltration and enlargement of the gland can be observed. Dilatation of the pancreatic duct can occur in up to one-third of cases; obstruction of the biliary tree is less common; and encasement of the major peripancreatic vascular structure is rare. The enhancement pattern is variable and often mimics the enhancement characteristic of the primary tumor. Many lesions, as they grow to a significant size, tend to exhibit heterogeneous enhancement. The suspicion of pancreatic metastases is based mainly on the history of a previously known cancer; however, the metastases may, rarely, be discovered before the primary site is known. The imaging appearance of the secondary lesions usually repeats the appearance of the primary tumor and consequently may suggest the diagnosis, particularly when multiple lesions are demonstrated or other metastatic localizations are present. Solitary hypovascular or hypervascular pancreatic metastases may mimic primary pancreatic ductal carcinomas or lymphomas and islet cell tumors, respectively. In these cases, histological confirmation is always requested.

▶Islet Cells Tumors, Pancreatic

Metastases, Skeletal

Catherine M. Phan, Thomas Link
Hôpital de Bicêtre, Service de Radiologie BROCA, Le Kremlin-Bicêtre, France
catherine.phan@bct.aphp.fr

Synonyms

Bone metastases; Metastatic disease of the skeleton; Skeletal metastases

Definitions

Malignant neoplasms infiltrate the skeleton from the primary site either by direct extension or by lymphatic or hematogenous dissemination. Different imaging techniques, including conventional radiographs (XR), skeletal scintigraphy, computed tomography (CT), magnetic resonance imaging (MRI), and positron emission tomography (PET), can be used for the detection, diagnosis, monitoring of the treatment, and follow-up of ▶bone metastases.

Pathology/Histopathology

General Mechanisms of Tumor Dissemination

Metastases may reach the skeleton by means of four main mechanisms:

1. *Hematogenous dissemination* (arterial and venous system) is the main mechanism for neoplastic cells to infiltrate the skeleton. Especially in prostate, breast, and colorectal cancer, tumor cells spread through the venous system into the skeleton. For spinal spread, Batson's paravertebral plexus plays a major role, since it is valveless and allows caudal or cranial blood flow depending on abdominal and pelvic pressure. Increased abdominal pressure causes blood to be diverted from the systemic caval system to the valveless vertebral venous system. Retrograde venous blood flow in Batson's plexus may explain the location of 70% of bone metastases in prostate cancer at the pelvis, sacrum, and inferior lumbar spine.
2. *Lymphatic spread* is a relatively infrequent route for the transportation of tumor cells to the bone. After metastatic invasion of lymph nodes, the adjacent skeleton may be secondarily involved with paravertebral soft tissue masses and scalloped erosions of the vertebral bodies. The left side of the vertebral bodies is more frequently affected by direct invasion from local lymph nodes because of the closer location of left-sided lymph nodes to the spine.
3. *Direct invasion* from the primary tumor or by extension from a secondary site (lymph node) is rare and usually associated with a detectable tumoral soft tissue mass.
4. *Intraspinal spread* may occur in patients with intracranial neoplasms and leads to subarachnoid deposit by means of cerebrospinal fluid.

Pathophysiology

The osseous response to tumor cells consists of bone resorption or bone formation, or both (1). Tumor cells arising in bone may produce factors that can stimulate osteoclast formation and bone resorption. Alternatively, tumor cells can also produce factors that stimulate osteoblast recruitment and differentiation, and new bone synthesis. The balance between osteoclastic and osteoblastic remodeling processes determines whether a predominant osteolytic, osteosclerotic, or mixed pattern is identified on radiographs.

Frequency and Distribution of Skeletal Metastasis

Bone metastases are much more common than primary skeletal neoplasms. They may be the first sign of the primary tumor in 20–25% of cases. Solitary bone metastases are frequently seen with renal, thyroid carcinoma, or hepatocellular carcinoma. In 3–4% of cases, the primary tumor remains unknown. In adults, the most common cancers causing bone metastases are breast carcinoma (70% in women), prostate cancer (60% in men), and lung and renal cancers in both genders. In children, bone metastases are much less common and include neuroblastoma, Ewing's sarcoma, osteosarcoma, and malignant tumor of soft tissue.

Axial Skeleton

Two main causes explain the predominant distribution of bone metastases to the axial skeleton and the proximal long bones:

1. Batson's venous plexus distribution, as well as the overall skeletal vascularity, results in a predilection for hematogenous spread to the axial skeleton and the proximal long bones.
2. In adults, bone metastases generally occur in the axial skeletal and the proximal part of long tubular bone corresponding to the distribution of residual red marrow, although they may be found anywhere in the skeletal system.

Axial sites are the following, in decreasing order of frequency: spine (lumbar, thoracic, cervical), pelvis, ribs, sternum, femur, humerus, and skull.

Long Tubular Bones

The long tubular bones, femur and humerus, are involved most frequently in cases of skeletal metastases with metaphyseal, diaphyseal, or epiphyseal location.

Short Tubular or Irregular Bones

Metastatic lesions at the bones of hands, wrists, and feet are infrequent. Imaging findings of acrometastases are an osteolytic appearance with frequent soft tissue mass and rarely periosteal reaction. Bronchogenic, renal, and colonic carcinoma are the main causes of such metastases.

Cortical Metastatic Lesion

Eccentrically located, scalloped erosions of the external surface of the cortex may be observed in cases of bronchogenic carcinoma ("cookie bite metastasis"). They may also arise from kidney cancer, and less frequently from breast, pancreas, larynx, and uterine malignancies.

Clinical Presentation

Bone pain is a common clinical sign that is due to increased medullary pressure and stretching of the periosteal membrane. Metastases that involve joints or periarticular bones may produce symptoms similar to arthritis. Complications of bone metastases include the occurrence of hypercalcemia, pathologic fracture (incidence: [16–60%]), and compression of adjacent neurologic structures such as the spinal cord or cranial nerves. A soft tissue mass and deformity are additional possible manifestations. Infiltration of the bone marrow by metastatic cells results in impaired hematopoiesis and the development of leukoerythroblastic anemia. The associated thrombocytopenia and leukopenia predispose to hemorrhage and infection.

Imaging

Imaging is an essential part of the management of bone metastases. However, no consensus has been reached concerning the optimal imaging modality because the evolution of bone metastases depends of the primary tumor and its aggressivity. When assessing bone tumor response in clinical practice, most oncologists do not use the criteria either developed by the International Union Against Cancer (UICC) (2), the World Health Organization (WHO) (3), or the Response Evaluation Criteria in Solid Tumors (RECIST) group, which consider bone lesions to be nonmeasurable.

Criteria for assessment of bone response are based on plain radiography for the UICC and on plain film or scan for the WHO. Four types of tumor response are defined: (i) complete response: disappearance of all lesions (recalcification of lytic lesion for the UICC; follow-up of at least 4 weeks for the WHO); (ii) partial response: partial decrease in size of measurable lesions (at least 50% and no new or progressive lesions for the UICC; recalcification of lytic lesions or decreased density of osteoblastic lesions for at least 4 weeks for the WHO); (iii) no change: unchanged lesions or limited increase (25%) and decrease (50%) in size of measurable lesions according to the UICC (the WHO requires at least an 8-week interval between the therapy onset and the assessment of stable lesion); and (iv) progressive disease: some or all lesions persist, progress and/or new lesions appear.

Conventional Radiographs

XR remains the most accessible practical method for characterizing symptomatic bone metastases. Bone lesions appear as areas of decreased or absent density (osteolytic), with disrupted or absent trabecular structure, or as sclerotic lesions with rim (osteoblastic).

XR is relatively insensitive in detecting bone metastases. Skeletal metastases become apparent on XR only after a loss of 30–75% of normal bone mineral content. Lesions in trabecular bone (medullary lesions) are more difficult to detect by XR than are lesions in cortical bone because of the limited contrast within trabecular bone. This is even more important in elderly patients with osteopenic bones. Advanced osteolytic lesions of the cancellous bone could be missed in the absence of reactive new bone or cortical involvement. Therefore, XR is less sensitive than bone scintigraphy for detecting and screening initial bone metastases. Combining XR and bone scintigraphy is recommended for diagnosing suspicious or symptomatic lesions.

The response of osteolytic lesions to treatment may be visible as lesion sclerosis on XR, corresponding to active bone formation, and reappearance and normalization of trabecular structure. Sclerosis tends to progress from the periphery of the lesion to its center and may make subtle areas of bone involvement more visible, contributing to a false interpretation of a new sclerotic lesion. Tumor dimensions are not easy to measure on conventional radiographs and cannot reflect only by themselves the response to therapy. For osteoblastic lesions, an increase in density may be visualized in both responding and progressing disease. Combined analyses of findings on radiographs (number, density, size of lesion) and Technetium–99m (^{99m}tc) bone scintigraphy improve the diagnostic accuracy, not only in detecting bone metastases but also in assessing the response to therapy.

Computed Tomography

Computed tomography (CT) offers superior skeletal visualization (sensitivity: [71–100%]) (4). Early detection of metastases in bone marrow is possible with CT before the detection of bone destruction. Metastases in bone marrow appear as an area with higher attenuation than the normal bone marrow. CT is useful for the evaluation of focal abnormalities seen on bone scintigraphy that cannot be confirmed by using radiographs. After therapy, sclerosis of an osteolytic lesion on CT also suggests a response to treatment. Progressive lysis or new areas of lysis within a sclerotic or mixed region represent disease progression. However, considering ionizing radiation exposure, CT is not the most suitable technique for the diagnosis and the follow-up of bone metastases.

MRI—Whole-Body MRI

MRI has evolved as the preeminent imaging technique in detection of changes in bone marrow constituency and in soft tissue. The diagnostic sensitivity of MRI in diagnosing bone metastases ranges from 82% to 100%, and its

specificity from 73% to 100%. Use of gadolinium with MRI allows one to distinguish viable tumor from necrotic tissue. Additionally, many studies have shown that MRI depicts early hematogenous dissemination of tumor cells to bone marrow before reactions in adjacent bone are detectable with bone scintigraphy. With the use of new techniques such as contiguous, coronal short T1 inversion recovery (STIR) and T1-weighted sequences, ►whole-body MRI provides a high sensitivity and specificity equal to or greater than those obtained with PET, and it could become the standard of practice in the future (5).

Diagnosis

Conventional Radiographs

The radiological findings of Skeletal metastases vary according to the patterns of bone response, their number, and their location. The radiographic appearance of skeletal metastases may help to identify the primary tumor (Table 1) and can be classified as purely osteolytic, purely osteosclerotic, or mixed osteolytic–osteosclerotic. Osteolytic lesions may be well circumscribed (geographic bone destruction) or poorly defined (moth eaten or permeative bone destruction). Osteosclerotic lesions may be focal or diffuse in distribution.

A few other radiographic features can help to identify the primary tumor. Their depiction and differential diagnosis are given in Table 2. Destruction of one or both pedicles of a vertebra is a typical radiographic finding of Skeletal metastases (Fig. 1) that is rarely present in multiple myeloma.

Destruction and Collapse of Vertebral Body

Radiological findings suggesting malignant vertebral body collapse (Fig. 2) include involvement of the upper thoracic spine (>T7), fracture of the posterior part of the vertebral body, pedicle destruction or soft tissue mass (asymmetrical paravertebral and >1cm), angular or irregular deformity of the vertebral endplates, convex posterior wall instead of angled posterior wall in benign vertebral collapse, and preservation of discal height. Fracture lines related to osteoporotic fractures are well visualized with CT and MRI. With the axial plane, CT and MRI can also define the risk of spinal cord compression.

MRI

The typical MRI appearance of bone metastatic disease is characterized by low signal intensity on T1-weighted images (equal or lower than muscle and disk). On fat-saturated T2-weighted or STIR sequences, a higher signal intensity than surrounding marrow is found. On nonfat-saturated T2-weighted images, however, metastases may not be well differentiated from the surrounding bone marrow, and the same applies to nonfat-saturated T1-weighted sequences. Fat-saturated contrast-enhanced images, however, clearly show the lesions most of the time. Sclerotic metastases usually show low signal intensity on all sequences. Marrow and soft tissue edema surrounding a metastatic lesion may be extensive or nonexistent. Benign lesions such as Paget's disease and hemangiomas could have similar signal to metastases on

Metastases, Skeletal. Table 1 Radiographic features of various primary tumors

Osteolytic metastases	Osteosclerotic metastases	Mixed metastases
Frequently	Frequently	Frequently
Lung	Prostate	Lung cancer
Breast	Breast	Breast cancer
Thyroid	Malignant carcinoid (bronchial, abdominal)	Uterine cervix
Kidney	Less common cause	Less common cause
Colon	Lymphoma	Ovarian tumor
Less common cause	Medulloblastoma	Testicular tumor
Urinary bladder	Mucinous adenocarcinoma of GI tract	GI tract
Adrenal	TCC of bladder	
Uterine cervix	Medullar thyroid carcinoma	
Testicular tumor	Chest cancer	
GI tract	Neuroblastoma	
Upper respiratory an digestive tract	Osteosarcoma	
Ewing's sarcoma		
Melanoma		
Prostate		

GI: gastrointestinal.

Metastases, Skeletal. Table 2 Radiographic features that are helpful in the differential diagnosis

Feature	Metastases	Differential diagnosis
Sclerosis of vertebral body	Common	Paget's disease (enlargement, coarsened trabecular pattern, "picture frame" appearance)
		Lymphoma, chordoma, mastocytosis
		Hemangioma (accentuated vertebral striation)
		Renal osteodystrophy
		Osteopetrosis (sandwich vertebral body)
Periosteal reaction	Rare	Primary tumors
	Prostate carcinoma	Osteosarcoma
	GI malignancies	Ewing's sarcoma
	Retinoblastoma	
	Neuroblastoma	
Bone expansion	Occasionally	Paget's disease
	Thyroid carcinoma	
	Kidney carcinoma	
	Hepatoma	
Acral location	Rare	Infection
	Lung	Primary tumor (very rare)
	Kidney	
Soft tissue mass	Rare	Infection (swelling rather than mass)
Soft tissue ossification	Rare	Osteosarcoma of soft tissue
	GI carcinomas	Posttraumatic heterotopic ossification
	TCC of bladder	Pseudomalignant osseous tumor of soft tissue
	Breast carcinoma	Ossification after burn and neurologic injuries
	Bronchogenic carcinoma	

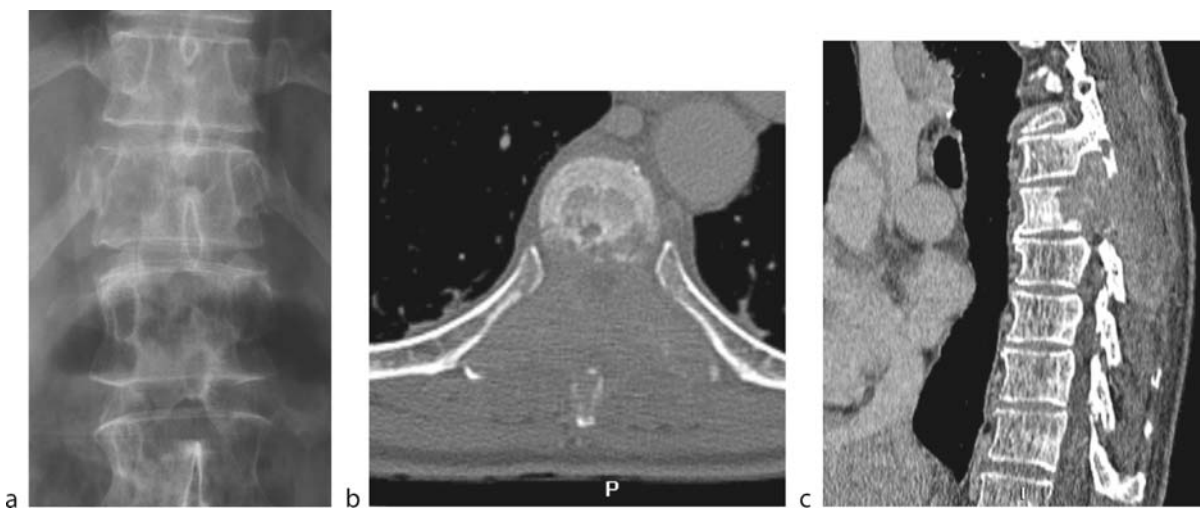

Metastases, Skeletal. Figure 1 Metastatic lung adenocarcinoma. Anteroposterior radiograph of the thoracic spine shows a pedicle destruction (a). Axial CT (b) and sagittal reconstruction (c) allow one to establish the destruction of the vertebral bodies and its epidural extension with spinal cord compression and paravertebral soft tissue extension.

T1- and T2-weighted images, and MRI findings should be correlated with other imaging findings to avoid errors. Although most metastatic lesions are focal, metastases may show a diffuse homogeneous or heterogeneous pattern in the marrow. MRI can monitor the response of metastases to therapy by showing metastatic lesion changes in size and signal. A resolving metastatic lesion appears with a rim of high signal intensity of yellow

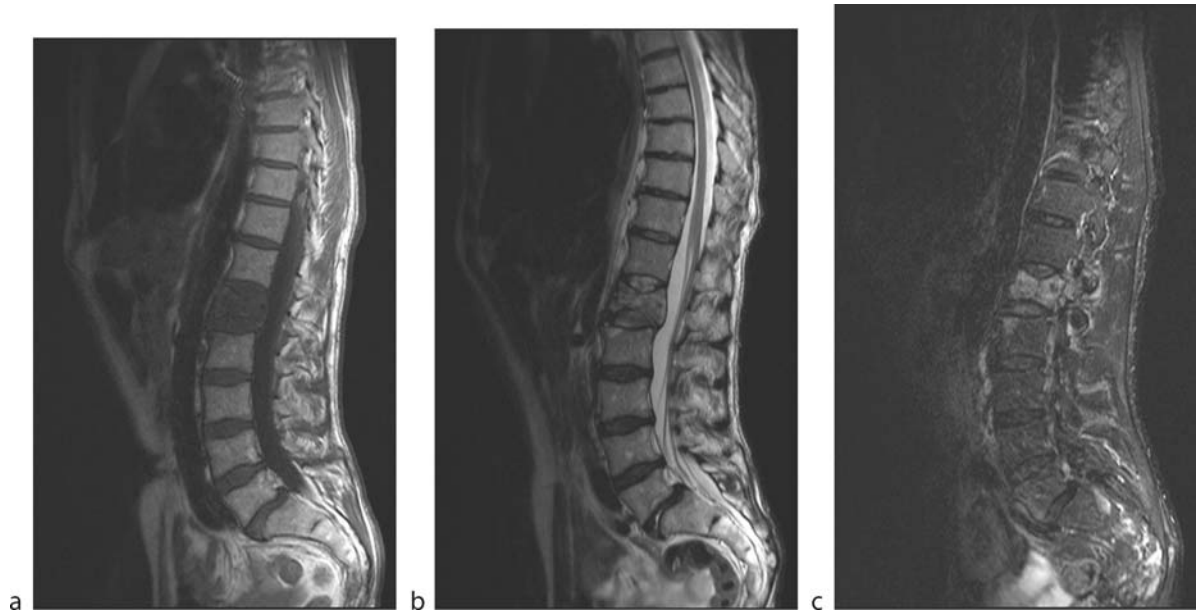

Metastases, Skeletal. Figure 2 Malignant vertebral collapse is demonstrated by the low signal on T1-weighted images with pedicle involvement and convexity of the posterior wall (a), heterogeneous bright signal on T2-weighted images (b), and destruction of the vertebral body on CT images (c).

marrow surrounding a focal shrinking marrow lesion on T1-weighted images. A focal lesion surrounded by a halo of high signal intensity edema on T2-weighted images indicates an active lesion. Complete fatty replacement of marrow where lesions once existed can occur after treatment. However, the MRI appearance of metastases within the bone marrow may also be quite similar before and after treatment and may not indicate treatment failure, since granulation tissue may substitute tumor and show similar imaging characteristics.

Nuclear Medicine

Bone Scintigraphy

Radioisotope bone scintigraphy is the standard whole-body imaging technique for screening bone metastases (6). The typical finding for bone metastases is a focus or foci of increased accumulation of the tracer in osteoblastic activity areas ("hot spots") modulated by skeletal vascularity (Fig. 3). Many radiopharmaceuticals (radionuclides) have been used including ^{99m}Tc bound to hydroxyethylene diphosphonate, hydroxymethyl enedi-phosphonate, or dicarboxy propane diphosphonate. Although bone scintigraphy is more sensitive than radiographs, bone scintigraphy has lower specificity (78% to 100%) and higher false-positive rates because it reflects an elevated rate of bone turnover as seen in neoplasia, trauma, arthropathy, or inflammation. In a patient with a known primary malignant tumor, the presence of multiple "hot spots" or a "superscan" on the bone scan is suggestive of metastases; however, osteomalacia, mastocytosis, and myelofibrosis may have a similar pattern. In many cases, further imaging (radiographs, CT, MRI) is required to characterize a solitary region or disseminated foci of radionuclide uptake. There are a number of other limitations to this technique, including difficulty in visualizing the spine because of the overlying hepatic and splenic activity, false-negative findings in cases of very aggressive pure osteolytic metastases, slow bone turnover, or an avascular site ("cold spots"). This may be seen in plasma cell myeloma, leukemia, and highly aggressive anaplastic carcinomas. After radiation therapy, patients could have a false-negative bone scans.

The appropriate intervals between screening bone metastases have not been defined. Three issues should be considered for assessing the response of bone metastases: the lack of specificity, the reduction in isotope uptake in cases of a fast progressive disease, and the flare phenomenon. This phenomenon corresponds to an increase of radionuclide uptake in a lesion during the first 6 months after therapy relating to an increase in regional blood flow or an increase in the bone turnover at the site of metastases or both. This may be indistinguishable from truly progressive disease. A healing bone tumor response usually appears as a decrease in the intensity of the nuclide uptake by metastatic foci. The discovery of new lesions on serial bone scintigraphy is a more reliable sign of tumor progression than an increase in radionuclide uptake at the sites of old lesions.

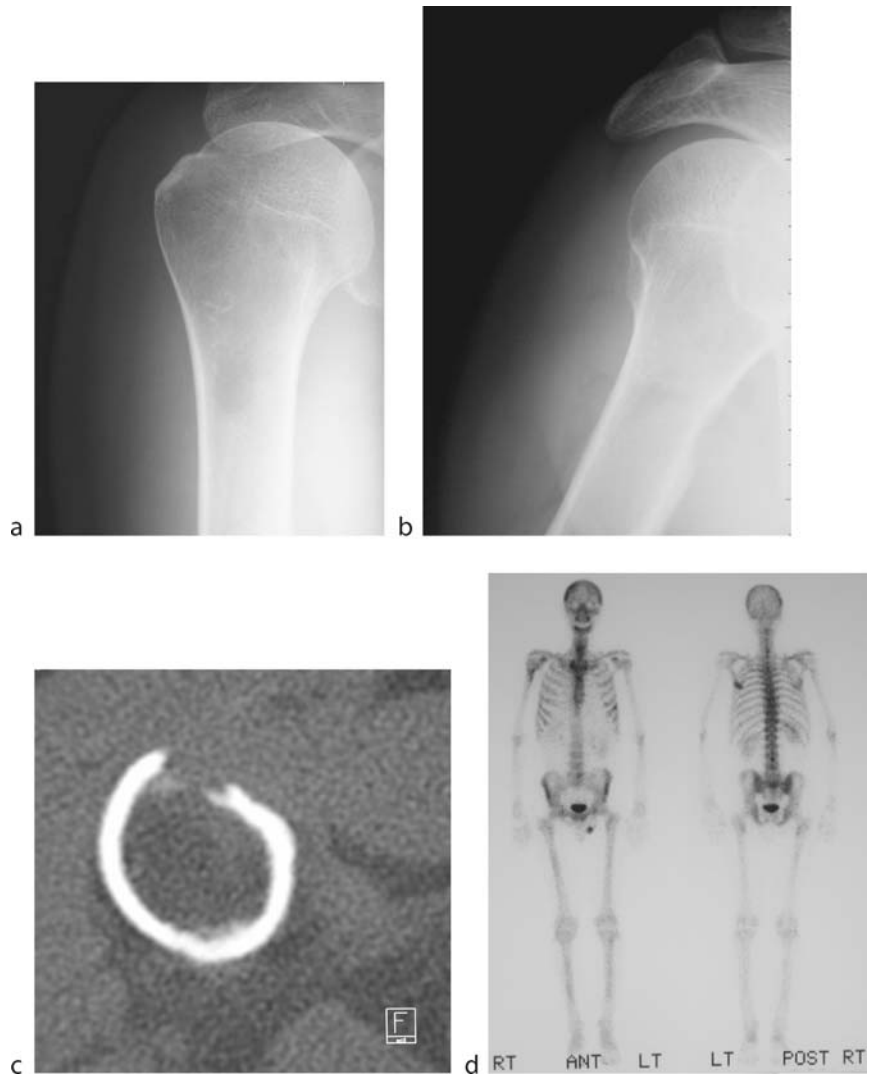

Metastases, Skeletal. Figure 3 Radiographs (a, b) of the right shoulder show a diaphyseal lucency corresponding to an osteolytic lesion with cortical destruction and anterior soft tissue extension (b) in a 50-year-old patient with hepatocarcinoma. (c) CT scan well depicts the cortical destruction of the proximal humerus and intramedullary involvement. (d) Anterior (*left*) and posterior (*right*) ^{99m}Tc MDP bone scans confirm bone metastasis of the proximal humerus and demonstrate metastases at other locations (left scapula, 8 and 9 left ribs).

Bone scintigraphy associated with conventional radiographs of areas with abnormal findings on bone scans remains a good technique for bone metastases screening in cases of osteophilic neoplasia (breast (useless if stages I or II), prostate (useless if PSA level <10 ng/mL, Gleason score: 2–5), kidney, thyroid, osteosarcoma, neuroblastoma, and epidermoid carcinoma).

With ameliorated gamma camera design, single-photon emission computed tomography (SPECT) sensitivity and specificity of bone scintigraphy are improved. However, it should be considered that with new technical developments whole-body CT and MRI may be considered as viable alternatives to skeletal scintigraphy.

Positron Emission Tomography

PET was previously considered as a research tool, but there has been substantial increase in its clinical applications in recent years (6). For Skeletal metastases, two radiopharmaceuticals are currently used: 18F-fluoride and 2-deoxy-2-[18F]-fluoro-D-glucose (18FDG). The mechanism of 18F-fluoride uptake is similar to that of ^{99m}Tc-methylene diphosphonate. 18FDG PET is used to measure glucose metabolism in many types of cancer and may distinguish benign from malignant bone lesions. The sensitivity of 18FDG PET dependent on the intensity of primary tumor glucose metabolism ranges from 62% to 100%, and its specificity from 96% to 100%. (Its variable

sensitivity is explained by the variable intensity of the glucose metabolism of the primary tumor.) The best results are obtained for pulmonary cancer and lymphomas. The performance of PET in assessing bone metastases is superior to that of bone scintigraphy in breast cancer but lower in prostate cancer.

18FDG PET is more sensitive for detecting osteolytic metastases than osteoblastic lesions. PET can help in identifying bone metastases at early stages of growth before a host reaction of osteoblasts occurs. It depicts, for instance, early malignant bone marrow infiltration due to the increased glucose metabolism in neoplastic cells.

The disadvantages of PET are high cost, limited availability, and false-positive findings observed with inflammatory, infectious diseases, traumas, or benign diseases (Paget's disease).

The fusion of PET and CT technology (PET–CT) increases the potential of an accurate detection of bone metastases. An accurate clinical role for PET in monitoring the response of bone metastases, however, requires further studies.

Interventional Radiological Treatment

Initially limited to preoperative embolization of vascular masses, new endovascular and percutaneous techniques have been developed for bone metastases. Endovascular embolization is used to induce tumor necrosis, reduce tumor size, and relieve tumor pain. Local infusion of antimitotic drugs (intra-arterial chemotherapy) and chemoembolization combining intra-arterial chemotherapy and selective embolization has been developed.

Vertebroplasty is a technique in which polymethylmethacrylate is percutaneously injected into a collapsed vertebral body under imaging guidance. Its primary aim is pain relief, and to a lesser extent reinforcement and stabilization of the malignant collapse of vertebrae. Cementoplasty is a variation of vertebroplasty for osteolytic metastases in bones other than vertebrae.

Radiofrequency (RF) ablation is a percutaneous technique recently used for *in-situ* destruction of bone metastases. RF thermoablation uses long waves of electromagnetic radiation to produce thermal coagulation and necrosis.

Bibliography

1. Resnick D (1995) Tumor and tumor-like lesions of bone: imaging and pathology of specific lesions. In Diagnosis of Bone and Joint Disorders. 3rd edn. Saunders, Philadelphia, PA 19106, OS, pp 3628–3928
2. Therasse P, Arbruck SG, Eisenhauer EA et al (2000) New guidelines to evaluate the response to treatment in solid tumor: European Organization for Research and Treatment of Cancer, National Cancer Institute of the United States, National Cancer Institute of Canada. J Natl Cancer Inst 92:205–216
3. WHO (1979) Handbook for Reporting Results of Cancer Treatment. World Health Organization. Geneva, Switzerland
4. Hamaoka T, Madewell JE, Donald A et al (2004) Bone imaging in metastatic breast cancer. J Clin Oncol 22:2942–2952
5. Engelhard K, Hollenbach HP, Wohlfart K et al (2004) Comparison of whole-body MRI with automatic moving table technique and bone scintigraphy for screening for bone metastases in patients with breast cancer. Eur Radiol 14(1):99–105
6. Cook G, Fogelman I (2005) Radioisotope and PET imaging of bone metastases. In Textbook of Bone Metastases. Wiley, Chichester, West Sussex p019 850, England, pp 77–90

Metastatic Disease of the Skeleton

▶ Metastases, Skeletal

Methanol

Methanol (CH_3OH), also known as wood alcohol, is a clear, colorless liquid, found in solvents and antifreeze, which smells and tastes similar to ethanol (CH_3CH_2OH). Methanol and its breakdown products, formaldehyde and formic acid, are toxic to the central nervous system. Ingestion of methanol can result in blindness, obtundation, and death.

▶ Toxic Disorders, Brain

MFH

▶ Malignant Fibrous Histiocytoma

MI, Mechanical Index

Estimate of the intensity of the transmitted pulses in diagnostic ultrasound, which is displayed by ultrasound machines. The MI calculations are based on peak rarefactional pressure and center frequency. It provides only a relatively inaccurate approximation of the true acoustic intensity in tissue. The MI is a critical variable in contrast

enhanced ultrasound and can be adapted by changing the acoustic output of the scanner. It determines the type and degree of interaction between the ultrasound pulse and a contrast microbubble.
▶Contrast Media, Ultrasound, Safety and Adverse Reactions

Microadenoma

Pituitary gland tumor of less than 1 cm. Because of its size it can be difficult to detect, and high-precision magnetic resonance imaging is needed. Most patients present with hyperprolactinemia. Treatment can consist of surgery, but most patients are treated medically.
▶Pituitary Gland

microbubble Imaging Techniques

▶Specific Imaging Techniques, Contrast Media, Ultrasound

Microbubble Oscillation

A specific response of ultrasound contrast agent micro-bubbles during insonation with adequate acoustic pressure (insonation power). If the acoustic pressure is becoming too high, the oscillation of the micro-bubbles is getting so strong that the membrane ruptures and the gas is escaping from the bubble shell within a few milliseconds, resulting in the disappearance of the contrast agent signal.
▶Contrast Media, Ultrasound, Commercial Products

Microbubble-Enhanced Ultrasound of the Spleen

▶Contrast Media, Ultrasound, Applications in Focal Splenic Lesions

Microbubble-specific Imaging Modes

Ultrasound imaging modes which are specifically tuned to detect harmonic signals emitted from resonating microbubbles in response to insonating ultrasound waves.
▶Contrast Media, Ultrasound, Applications in Focal Splenic Lesions

Microbubbles

Nico de Jong
ErasmusMC,
Rotterdam, The Netherlands
n.dejong@erasmusmc.nl

Synonyms

Bubbles; Contrast microbubbles; Ultrasound contrast agents; Ultrasound contrast media

Definition

A microbubble is a gas cavity in liquid. The gas can be air, nitrogen, or a high molecular weight gas such as SF_6 or C_3F_8. The liquid is typically water. Microbubbles have a mean size of 3 μm, and in general 95% of the bubbles are smaller than 10 μm. The microbubbles are stabilized by means of encapsulation by a shell that consists of biocompatible material such as protein, lipid, or polymer. In medical ultrasound, microbubbles are used as contrast agents.

Characteristics

The bubbles are smaller than red blood cells and are therefore appropriate for intravenous injection. Unencapsulated free gas bubbles were first used as ultrasound contrast agents as early as 1968 but proved to be unsatisfactory because their size was uncontrolled, inappropriate, and unstable. Once injected, they did not persist long enough in the circulation to permit an adequate ultrasound examination of the left side of the heart.

Because these agents are intended to image the left heart chambers and ultimately to assess the perfusion of the myocardium, they must fulfill certain requirements.

The contrast microbubbles should be administered intravenously, either by bolus or infusion. The microbubbles must be small enough and stable enough to ensure pulmonary passage. In addition, they must be injected in a sufficient concentration to opacify the left heart. Furthermore, the injected microbubbles should remain in the blood pool and be safe and nontoxic. The duration and persistence of the microbubbles should be comparable to that of imaging conditions to enable acquisition of echo images, which is in the order of 1 to a few minutes. To behave as a perfect blood pool, the microbubbles should display the same flow dynamics as the blood itself and ultimately be metabolized from the blood pool. To comply with these requirements, several bubble physical properties must be elaborated carefully. These properties include the size, the gas, and the shell.

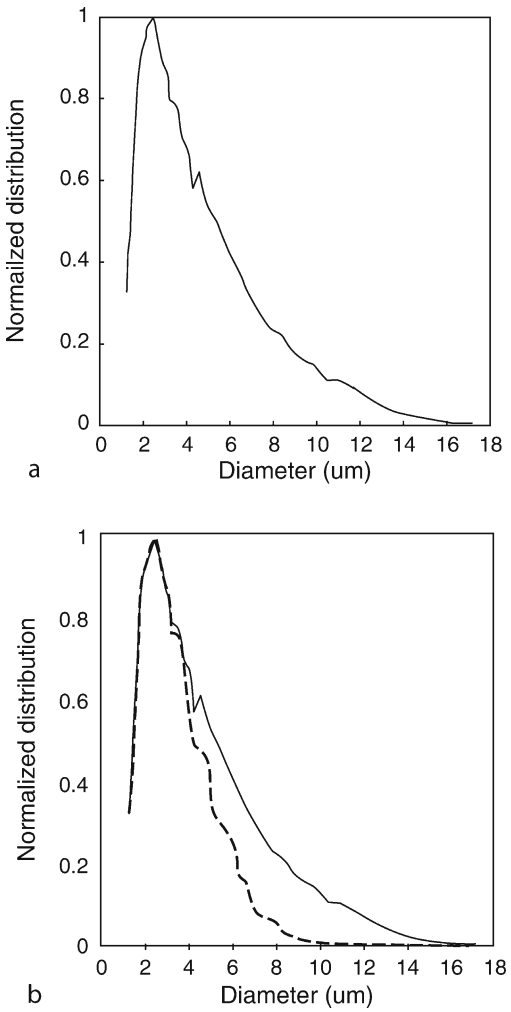

Microbubbles. Figure 1 Size distribution of Albunex. (a) Measured distribution. (b) The *solid line* indicates measured size distribution, and the *dashed line* indicates simulated distribution after lung passage.

Below the resonance frequency the scattering of a gas bubble increases with the sixth power of the bubble radius, while this is the second power for frequencies above the resonance frequency. Therefore, larger microbubbles scatter more ultrasound energy than smaller ones. Because ultrasound scattering of a cross-section of a gas bubble, which represents its scattering capabilities, increases with the sixth power of the bubble radius, larger microbubbles scatter more ultrasound energy than smaller ones. Moreover, the mean bubbles size in current commercial available agents is between 3 and 4 μm corresponding to a resonance frequency around 2 MHz. This is equal to the frequency used in precordial diagnostic ultrasound.

Fig. 1a shows a typical size distribution of a commercially available contrast agent, Albunex, which is a first-generation contrast agent. The size distribution was measured with a Coulter Multisizer. The mean diameter of this distribution is 3.8 μm, and less than 4% of the microbubbles are larger than 10 μm, whereas fewer bubbles with a diameter greater than 15 μm are present in the distribution. The size distribution of a contrast agent will however, change when crossing the lungs. Due to the sieving action of the lungs, larger bubbles are eliminated. Fig. 1b demonstrates this effect using simulations. The lung capillaries (1) with a mean diameter between 4.5 and 5.5 μm will filter larger microbubbles, whereas the number of smaller microbubbles remains unaffected.

Bibliography

1. Hogg JC (1987)Neutrophil kinetics and lung injury. Physiol Rev67(4)

Microbubbles

▶Contrast Media, Ultrasound, New Clinical Development

Microcalcification

Impalpable small calcified particles 1-2 mm in diameter which are visible in the breast on mammography. Microcalcifications are common and seen in about 1/3 of all mammograms. The majority are benign and do not require further investigation.

▶Carcinoma, Breast, Imaging Mammography, Primary Signs

Microcalcifications

▶Calcifications, Breast

Microcolon

▶Meconium Ileus

Microphthalmos

▶Congenital Malformations, Orbit

Microscopy

▶Optical Imaging

Microwaves Ablation, Hepatic Tumours

Electromagnetic method of inducing thermal tumour ablation by using devices with frequencies greater than or equal to 900 kHz.

▶Interventional Hepatic Procedures

Midgut Volvulus

▶GI Tract, Pediatric, Specific Problems

Mirizzi Syndrome

Mirizzi syndrome is the presence of a large gallstone or multiple small gallstones impacted in the cystic duct or in the gallbladder neck, causing obstruction of the common hepatic duct. There are two types of Mirizzi syndrome: in type I, inflammatory changes of gallbladder wall lead to fusion with the common hepatic duct and its secondary stenosis, whereas in type II, direct pressure necrosis of the duct walls determined by stones leads to cholecystocholedochal fistula formation. Predisposing factors are a low cystic duct insertion and a cystic duct which runs parallel to the common bile duct.

Clinical features of Mirizzi syndrome are those of biliary obstruction and imaging is necessary to make a diagnosis. US is the first examination. CT may also be used as a second-step examination. Imaging findings include impacted stone in the cystic duct or in the gallbladder neck, thickening of the gallbladder wall due to chronic phlogosis, dilatation of the common hepatic duct above the level of the impacted stone, narrowing of the common hepatic duct at the level of impaction, and normal caliber of the common hepatic duct below the impaction. ERCP or PTC may be required to confirm the diagnosis, but MRCP usually represents a valid non-invasive alternative to ERCP and PTC.

▶Gallstones
▶Occlusion, Bile Ducts

Mismatch Defect

A mismatch defect in the ventilation/perfusion lung scan is the scintigraphic manifestation of pulmonary embolism. It is defined as a pulmonary region with regular ventilation but severely reduced or no perfusion. Apart from embolism, mismatch defects are induced by only a few and, more importantly, rare nonembolic diseases.

▶Pulmonary Function, Nuclear Medicine Methods

Moderate Ductal Hyperplasia

Proliferation of ductal epithelium of more than four cell layers, distending the ductule.

▶Hyperplasia, breast

Molecular Beacons

▶Molecular Probes, Optical Probes

Molecular Imaging

Vasilis Ntziachristos
Harvard Medical School, Center for Molecular Imaging Research, Charlestown, USA
vasilis@helix.mgh.harvard.edu

Molecular imaging is a shift in the radiological paradigm that has gradually evolved over the past decade and intensified as a separate imaging entity over the past few years. The term encompasses all non-invasive medical imaging aiming at visualizing molecular activity in living tissues. A commonly used definition identifies Molecular Imaging as: "*the visual representation, characterization, and quantification of biological processes at the cellular, subcellular and molecular levels within intact living organisms*".

Molecular imaging has come to practice in recent years due to key advancements in i) developing new or transferring existing molecular and cell biology techniques to reporting technologies for in-vivo imaging, ii) the use of transgenic animal models, iii) the development of advanced reporter probes for high specificity and detection sensitivity and iv) the development or improvement of appropriate imaging technology. In contrast to conventional radiological approaches visualizing anatomy or function, the key principle of molecular imaging follows the paradigm of nuclear medicine in which an appropriate *molecular imaging probe* (for example a radiolabeled probe targeted to a cellular receptor) is non-invasively imaged through the body. However, this key principle has exploded to several different imaging strategies employing several distinct imaging and probe technologies appropriate for imaging an increasing number of complex gene-expression and molecular function patterns. This is a highly interdisciplinary science that can be seen as an addition to standard Radiology, which typically entails only imaging systems and methods and a smaller set of imaging probes. Molecular Imaging can work synergistically with more conventional radiology practices and promises to significantly improve healthcare and drug discovery by identifying disease at an earlier stage and quantifying treatment responses in-vivo and over time.

Molecular imaging has two distinct entities that must work synergistically to achieve successful imaging, that is i) imaging technology, ii) reporting strategies of imaging targets. Those broad areas can be further classified as follows:

Imaging technology

Molecular Imaging is accomplished with different modalities including 1) Scintigraphy and Single Photon Emission Computed Tomography (SPECT), 2) Positron Emission Tomography (PET), 3) Magnetic Resonance Imaging (MRI), 4) Optical Imaging, including Fluorescence Planar Imaging, Bioluminescence Imaging and Fluorescence Molecular Tomography (FMT) and 5) Ultrasound. These approaches are further complemented by X-ray computed tomography (CT) for high resolution anatomical imaging.

An emerging field in radiology is this of ***multi-modality imaging*** where typically two (or more) complementary imaging methods are combined, i.e. one yielding high resolution anatomical information with one yielding high molecular specificity. It is important to note here the recent emergence of hybrid systems that combine CT with SPECT for small animal imaging and novel clinical CT/PET scanners that are gaining ground as they allow for the accurate co-registration of molecular and anatomical contrast.

A secondary classification of molecular imaging systems can group nuclear imaging methods, i.e. imaging techniques that use ionizing radiation and isotopes (i.e. Scintigraphy, SPECT and PET) and techniques using non-ionizing radiation such as optical imaging, MRI and ultrasound. Some more detailed description of these modalities is given in the third section of this hyper-essay.

Reporting strategies

Reporting strategies can be separated in 1) *Direct imaging methods*, i.e. via the use of probes that report on specific molecular process (e.g. a receptor target imaged with a ligand molecular imaging probe) and 2) *Indirect imaging methods* (e.g. expression of an imaging reporter gene indirectly measuring expression of an endogenous gene). Several different approaches have been developed for optimal designs that address these categories as addressed in more detail in the following:

Direct imaging

This strategy uses imaging probes that are generally externally administered. Imaging probes are an essential part of molecular imaging and their development generally considers four distinct issues, i.e.

1. A *reporting mechanism* that reports on the position and accumulation of the probe to the imaging technology selected.
2. A *delivery technology* to ensure favorable probe kinetics in crossing of biological barriers such as

vascular and cellular membranes and synergistic clearance of non-bound or non-delivered probe.
3. *Bio-compatibility* so that responses of the immune system and toxicity are minimized.
4. An *amplification strategy* to maximize contrast and signal to noise ratio's so that highly sensitive detection is achieved.

Imaging probes are divided in two major categories, namely *active probes*, i.e. probes that carry an active reporting component and *activatable probes* i.e. probes that carry an inactive reporting component which is activated through interaction with a molecular target. The latter are also known as *molecular beacons, switches* or *smart probes*. Active probes are generally used to image proteins and receptors via direct interaction with the receptor or other protein (e.g. binding) or preferred accumulation into cells. Activatable probes include molecules that change some physical parameter after interaction with a specific target. They are generally found as optical or MR probes. Several fluorescent probes have been developed to exploit quenching and energy transfer mechanisms to change light emission characteristics that can be detected with high sensitivity. MR probes have also shown capable to change relaxation times after modification from a molecular target.

Another paradigm of direct imaging methods is the use of aptamers for in vitro specific protein-binding studies. Aptamers are DNA or RNA oligonucleotides isolated to bind to various biomolecules with high specificity. Cellular targets can be assessed making this a potentially useful technology for in-vivo imaging. A similar approach using antisense and aptamer oligonucleotide probes has been developed for hybridization to target mRNA thus imaging direct gene expression at the transcriptional level. Radiolabeled antisense nucleotides are called RASON's although fluorochromes or magnetic nano-particles could be used in principle as well. However the low number of target copies coupled with delivery issues and high, non-specific background limits the application of the latter approach to in-vivo imaging applications.

Indirect imaging

This imaging strategy as evolved from corresponding in-vitro reporting assays. Most indirect imaging schemes involve the use of a *reporter-gene* that is used in conjunction with a *reporter probe*. Contrast is generated by the reporter probe after transcription of the reporter gene. Generally, the reporter gene is introduced into the cells of interest via delivery vectors and placed under control of a promoter/enhancer element. The promoter can lead to continuous reporter gene transcription (constitutive promoter) or it can be activated by specific transcription factors (TF) (inducible promoter). When the reporter gene is transcribed it results in translation of mRNA to a gene product, which could be an enzyme, receptor or other protein. This gene product can be a reporter molecule itself (for example a fluorescent protein) or it can lead to trapping of a molecular probe or to increasing the density of appropriate molecular targets that a molecular probe can attach to.

Reporter gene imaging is a generalizable platform that in contrast to the direct imaging method, only one or few well validated reporter-gene and reporter probe pairs can be used to image many different molecular and genetic processes. On the downside is the introduction of foreign proteins and genes which limits applicability to animals and perhaps gene therapy protocols.

Applications of reporter gene imaging include marking of cells for cell-trafficking imaging, monitoring of endogenous gene expression or of externally transfected genes, imaging in gene therapy protocols and imaging of proteins and protein-protein interactions, but this platform is highly versatile to be applied to many other applications as well.

Examples of Molecular Imaging

In the following, some common examples of molecular imaging are given, for different imaging modalities. This is a highly emerging field and the following are given to impart some flavor of the diversity that exists in this field of imaging sciences, and not as an exhaustive list of the technology or the application.

Positron emission tomography (PET)

Positron emission tomography images the bio-distribution of positron emitting radio-nuclides by reconstructing the origin of γ-rays exiting the tissue of investigation. The positron, emitted during the radionuclide decay, travels a short distance in tissue ($\sim$1 mm) until it encounters an electron. The two particles "annihilate" resulting in the emission of two gamma rays of 511 keV each, traveling at opposite directions. Common positron emitting isotopes include ^{15}O, ^{13}N, ^{11}C, and ^{18}F although ^{14}O, ^{64}Cu, ^{6}2Cu, ^{124}I, ^{76}Br, ^{82}Rb, and ^{68}Ga can be occasionally used as well. Production of isotopes is typically performed in a cyclotron.

Detection of γ-rays is typically achieved through an array of scintillation crystals to convert -ray energy into visible light, suitable light sensors, readout electronics, and image processing units. The coincidence detection of both -rays in PET within nanoseconds of each other defines the line of response in space and thus the direction of flight. In contrast to SPECT, attenuation (quantifiable reduction

in events present at the face of the detector due to absorption or scatter through tissues) of the emitted radiation in PET can be corrected precisely because the total length through the body determines the attenuation factor along a coincidence line. By doing so, quantitative information about the tracer distribution can be obtained. The reconstruction software then takes the coincidence events measured at all angular and linear positions to reconstruct an image that depicts the localization and concentration of the positron-emitting radioisotope within a plane of the organ that was scanned.

PET-Advantages: One of the advantages of PET is that drugs or existing molecules involved in a process if interest or known to interact with a specific target can be modified with a radiolabel while minimally perturbing the parent molecule. Therefore many diverse biological and molecular processes can be followed. The sensitivity of PET is relatively high in the range of 10^{-11}–10^{-12} mole/L, and is independent of the location depth of the reporter probe of interest. Typically, several million cells accumulating reporter probe have to be in relative close proximity for a PET scanner to record them as a distinct entity relative to the background. Development of molecular imaging assays with PET is particularly advantageous because of the ability to validate them in cell culture and small animal models prior to using the same reporter probe in established clinical PET centers around the world. The ability to perform translational research from a cell culture setting to preclinical animal models to clinical applications is one of the most unique and powerful features of PET technology.

PET-Disadvantages: Many of the positron-emitting isotopes used have relatively short half-lives (e.g. ^{18}F has $t_{1/2}$ = 110 min), so that the chemical reactions leading to incorporation of the isotope into the parent molecule and subsequent introduction into the subject must take place relatively quickly. Moreover PET cannot distinguish between two or more different isotopes if injected simultaneously. Therefore for studying multiple molecular events, subsequent injection of molecular probes at times allowing for the decay of one isotope prior to administration of the other. This complicates experimental procedures in such studies. Furthermore the spatial resolution of most clinical PET scanners is $\sim(6–8)^3$ mm^3, and $\sim 3^3$ mm^3 in brain scanners. Small animal imaging can be currently achieved with resolutions of less than 2^3 mm^3.

Enabling molecular-imaging technologies for PET: The most common reporter gene imaging strategy for PET is the introduction of the wild-type HSV1-*tk* reporter gene or a mutant HSV1-*sr39tk* gene encoding. These genes encode for thymide kinase 1 (TK1) that can phosphorylate radiolabeled probes with higher efficiency than mammalian TK enzymes. This results in reporter probe entrapment and accumulation in tranduced cells yielding contrast in PET images. Reporter gene imaging via up-regulation of membrane receptors is also a common strategy for PET labeling and is exploited as a contrast mechanism.

Optical Imaging

Optical imaging encompasses a series of photonic technologies that may study complex molecular processes in whole animals and human tissues. Optical observations are overwhelmingly used in the bio-medical field through microscopy and histology and through the availability of several optical sensing in-vitro assays for molecular detection. The transfer of several of these technologies to in-vivo applications has been enabled primarily by 1) the development of bio-compatible probes and reporter systems that preferentially fluoresce in the near-infrared and 2) the development of appropriate imaging systems and method that offer low light detection with high sensitivity. Red shifting of the reporter probes is essential for achieving high penetration due to the low light absorption from tissue in the near-infrared. An important emerging technology is the use of tomographic methods that account for photon propagation in tissues in order to provide accurate three-dimensional images of photon propagation in tissues.

Optical Imaging advantages The major advantage of optical methods is the high versatility owing to the existence of a variety of fluorescent probes and reporter gene imaging strategies including expression of fluorescent proteins and bioluminescence. The technology is economic and can be made portable and of small form factors, therefore it is ideally suited for small animal imaging, endoscopy and some large organ applications (i.e. breast). Other advantages include high detection sensitivity, especially in small animals, the use of non-ionizing radiation and the capacity to resolve multiple targets simultaneously using fluorescent reporters emitting at different wavelengths.

Optical Imaging disadvantages Major disadvantages include the compromised resolution and non-linear dependence of photon intensity with the depth, due to the highly photon scattering nature of tissue. This reduces the detection sensitivity at larger tissues and worsens resolution.

Enabling Technologies: A variety of targeted and activatable imaging probes have been developed. In addition fluorescent proteins and bioluminescence approaches have revolutionized modern biology and are increasingly used in molecular imaging applications. Transfection of cells with the firefly luciferase gene (Fluc) encodes Firefly luciferase, an enzyme that oxidizes its substrate Dluciferin to result in light emission (bioluminescence). This chemiluminescent reaction can only take place under physiological conditions within living cells

expressing Fluc. Another luciferin–luciferase system used in molecular imaging is based on the sea pansy Renilla luciferase, which uses a different substrate (coelenterazine) that is not ATP-dependent. Other bioluminescence reporter systems have been demonstrated as well. Bioluminescent light emitted from cells can be detected through the animal with highly sensitive, low-noise detection CCD cameras, while offering very low background activity from naturally occurring tissue bioluminescence. In this way a highly versatile molecular activity can be tagged and detected when the reporter gene is expressed. A similar approach, in the fluorescence mode, involves fluorescence proteins (FP's). FPs have become essential reporter molecules for different biomedical applications as they offer a generalized platform for imaging cellular and sub-cellular processes. Mutants of the original green fluorescent protein (GFP) from the jellyfish Aequorea offer bright emission and recent red-shifting of the emission spectrum of different FP offer multi-target visualization capacity and increased detection sensitivity. Finally several active and activatable probes have been developed for targeting cellular receptors, proteins or enzymes. An attractive example is the use of biocompatible probes loaded with many fluorochromes that are dark in their inert state due to close proximity to each other leading to self-quenching. Upon interaction with specific enzymes the fluorochromes loose proximity and can fluoresce, resulting in an on/off light switching mechanism. Fluorescent probes are also appropriate for clinical translation for endoscopic, intra-operative and other application.

Magnetic resonance imaging (MRI)

MRI spatially resolves the relaxations of magnetic dipoles (i.e. atoms with unpaired spins such as hydrogen, phosphorus or carbon) placed in high strength magnetic field and subsequently perturbed from equilibrium using appropriate radio-frequency pulses in the presence of magnetic gradients. MRI can optimally differentiate soft-tissue differences with high detail and offers rich contrast information since dipole relaxation depends on the biophysical environment and interactions between them. Elegant technologies such spin-tagging or diffusion-weighted MRI can be used to further assess functional tissue characteristics such as flow, tissue perfusion and membrane permeability. In addition, the use of appropriate nano-particles that change the MR signal intensity can further improve contrast and in the context of molecular imaging to probe cellular and subcellular activity. More common MRI contrast agents include paramagnetic metal cations such as chelated gadolinium or dysprosium, or super-paramagnetic nano-particles that can be used as compartmental, targeted, or smart probes.

MRI advantages The major advantage of MRI is the high spatial resolution that can be achieved and that anatomical, functional and molecular information can be extracted simultaneously.

MRI disadvantages The major MRI drawback is the reduced sensitivity, which directs the use of relatively large amounts of metal cations.

Enabling molecular-imaging technologies for MRI. Examples of MR molecular imaging includes the Galactopyranoside/Galactosidase System where cell transfection with marker gene LacZ leads to production of b-galactosidase that can cleave a cap of specially engineered MR probes. This process can change the relaxation parameters of the agent resulting in up to 50% decrease in T1. Other examples have shown that transfection with cDNA inset coding for human tyrosinase leads to upregulation of tyrosinase after transcription, which catalyses the hydroxylation of tyrosine to dioxyphenyl alanine (DOPA) which is then oxidized to DOPA-quinone. DOPA-quinone yields melanins through spontaneous cyclization and polymerization, which have high iron-binding capacity. This can significantly increase the MR contrast of transfected cells, similarly to naturally occurring contrast seen in some melanomas on T1-weighted images. Direct targeting of endothelial markers such as the integrin $a_v\beta_3$ has also been demonstrated using paramagnetic liposomes or targeted nanoparticles.

MR Spectral Imaging A special category of magnetic resonance technology is the use of spectroscopic imaging, i.e. localized spectroscopy from spatially resolved voxels within tissue. MR spectra depend on the biochemical composition of each voxel. Therefore localized Magnetic Resonance Spectroscopic imaging is often referred to as a special method of molecular imaging that does not require the use of exogenous reporter probes. Typical molecules targeted by MR spectral imaging are choline, creatine, N-acetyl aspartate (NAA), lactate, myoinositol, glutamine and glutamate, lipids, leucine, and alanine.

Scintigraphy and SPECT

The use of gamma cameras combined with the use of radiolabeled traces has been considered the precursor to molecular imaging as it has evolved today. Injected and targeted γ-emitting isotopes (e.g. ^{99m}Tc, ^{111}In, ^{123}I, ^{131}I) can be detected through tissue using gamma cameras. Planar images can be obtained for two-dimensional observations. A more elegant technique obtains high energy photons at different view angles by rotation around the sample and combines these projections tomographically to obtain three-dimensional images through the body. A characteristic of gamma camera detection is the use of lead collimators, necessary to define the angle of incidence of photons collected. The use of collimators is

the main reason of the reduced sensitivity seen in SPECT as compared to PET. In SPECT, collimator design is always a compromise between spatial resolution and sensitivity: reducing the size of the holes or using longer septae improves spatial resolution but reduces sensitivity. Examples of enabling technologies include imaging apoptosis with radio-labeled annexin V, imaging of antisense oligonucleotides and several radiolabeled receptor-binding molecules, antibodies etc.

Ultrasound

Ultrasound imaging is based on interaction of tissue with high frequency pressure waves. Most clinical ultrasound typically uses frequencies at the 2–10 MHz but higher frequency ultrasound is used for intravascular studies or small animal imaging with frequencies reaching 30–50 MHz. As frequency increases resolution increases as well but penetration depth decreases. Ultrasound has also been considered for molecular imaging with the use of targeted ultrasound contrast agents, i.e. targeted micro-bubbles.

Molecular Imaging

▶Targeted Microbubbles

Molecular Probes, Delivery

Alexei Bogdanov
Departments of Radiology and Cell Biology, University of Massachusetts Medical School, Worcester, USA
alexei.bogdanov@umassmed.edu

Synonyms

Administration of molecular imaging agents

Definition

Manipulations and procedures for the administration of imaging agents (drugs). After the distribution in the body these imaging agents generate signals specific for a given target molecule and could be detected by using biomedical imaging modalities. In the above context the delivery is, as a rule, an invasive procedure designed to penetrate physical barriers existing in the body and is regulated by corresponding institutional or government committees.

A system of measures that increase the probability of a given imaging agent to localize in the compartment of the body that harbor the target molecule. In the latter context the delivery of molecular probes is related to imaging agent (drug) targeting *in vivo*.

Characteristics

Molecular Probe Administration

Depending on whether molecular probe is exogenous or endogenous, delivery modes may differ. In the case of *exogenous probe* (agent) delivery procedures are used to ensure that sufficiently high concentration of imaging probes will be achieved in the target organ (i.e. blood stream, brain, liver etc.) during the time window required for imaging. The manual, semi- or fully automated devices (injection systems and pumps) are used for this purpose and are similar to those used for delivery of any other contrast agent. *Endogenous probes* (i.e. molecules that are detectable with imaging modalities) are synthesized by the cells of the host due to exogenous gene (or cDNA) expression which includes transcription, translation and posttranslational processing of the corresponding expression product. Expression of these probes is induced by delivery of exogenous genetic material which includes: (i) a compaction of nonviral expression vectors with polycations or packaging DNA or RNA encoding imaging marker genes into virions in cell culture; (ii) transfection or transduction of cells *in vivo*. The latter stage includes delivery of genetic material *in vivo* and is, essentially, a gene therapy procedure. If labeled with radioisotopes or fluorescent proteins, nonviral or viral delivery step could be monitored by using imaging. In above case both delivery and the subsequent gene expression could be imaged *in vivo*.

Molecular Probe Delivery to the Target Tissue (Organ)

The efficacy of molecular probe delivery depends on: (i) chemical and physical characteristics of the probe molecule or nanoparticle, i.e. molecular mass or hydrodynamic radius, electrochemical or surface charge, hydrophobicity and reactivity of chemical groups comprising the probe; (ii) the presence of anatomic or physiological barriers in the body. Transporter-specific small molecules (positron-emitting isotope-labeled for PET) are usually delivered into cells through plasma membrane glucose transporters (for example, Glut-1 glucose transporter in the case of ^{18}F-labeled 2-fluoro-2-deoxy-D-glucose, FDG). Glut-1 and Glut-3 are usually

M

overexpressed in cancer cells thereby enabling imaging of the probe "trapped" inside the cell due to hexokinase activity which mediates phosphorylation of FDG. The role of Glut-1 has been also confirmed in endothelial uptake of FDG. Other PET tracer molecular probes include ^{18}F-α-methyl-tyrosine (FMT), ^{18}F-DOPA for dopaminergic neuronal uptake imaging in Parkinson's disease and others. Unlike non-charged polar FDG molecule, positively charged drugs intended for imaging (or polyplexes for gene delivery) usually bind to α1-acid glycoprotein and lipoproteins whereas negatively charged imaging drugs bind to albumin. In addition, many imaging drugs and probes, especially nanoparticles with multiple hydroxyl groups on the surface bind C3b as a result of C3 complement component activation which could lead to toxicity and anaphylactoid reactions in some species. "Decoration" of nanoparticles and some polymers with plasma proteins increases non-specific uptake in phagocytes thereby promoting a more rapid elimination from circulation. The existing tissue barriers dramatically affect probe delivery. In general, distribution of any drug after systemic administration (usually intravenous) is not uniform due to the local differences in blood supply, binding to blood components, as well as local acidity, and transcellular (membrane) transport. To reach the target molecule (i.e. cell surface receptor or carbohydrate, cytoplasmic protein, mRNA or nuclear target), imaging molecules are required to pass through one or more tissue barriers. The only exception is the class of imaging probes specific for vessel-lining and circulating (hematopoietic) cells. The common tissue and cellular barriers are: (i) endothelial cells and basal membrane (basal lamina, consisting of laminin, fibronectin, tenascin, collagens, and proteoglycans), (ii) connective tissue cells, (iii) parenchymal cell membrane, (iv) nuclear membrane (if delivery of the probe to the cell nucleus is the goal) (Fig. 1). Endothelial cells represent the continuous thin barrier in most normal tissues that controls the exchange of nutrients and cells between the blood and the interstitial compartments. In the liver endothelial cells have multiple pores and fenestrae. Trans-endothelial delivery is usually enabled by targeting to calveolae components which accelerates transcytosis. This is accomplished by using targeting specific plasma membrane proteins present in calveolae. Transcytosis of albumin-bound imaging probes is mediated with specific protein shuttling protein gp 60 (albondin). However, albumins with high degree of amino group modification (for example, albumins highly modified at available amino groups with imaging drugs, i.e. fluorochromes or chelates) are not transported by transcytosis but are endocytosed, stored and degraded in lysosomes. Paracellular delivery from apical to basolateral side of endothelium can be accelerated by selective opening of tight junctions which consist of complexes formed by nectins, claudins, occludins, and junctional adhesion molecules. Tight junctional permeability and drug delivery can be increased by nitric oxide (sodium nitroprusside) or mannitol treatments. The latter is effective in transient opening of the blood–brain barrier. Subsequent steps of delivery could be complicated by the following negatively acting factors: (i) most of the "large" transcytosed imaging probes, including nanoparticles, are accumulated in basal membrane and extracellular matrix components that limit the accessibility of parenchymal cells to these probes; (ii) probes based on high-affinity ligands (antibodies and some library-derived peptides) labeled with imaging molecules or nanoparticles (fluorochromes, isotopes or bound to a MRI agent) are usually bound to superficial layers (cells) of the target organ/tissue and do not permeate into deep layers. This may result in partial imaging artifacts. To allow better permeation through membrane barriers several synthetic peptides (known as "cell penetrating peptides" (CPP) or "protein transduction domains" (PTD) have been tested. Many arginine rich

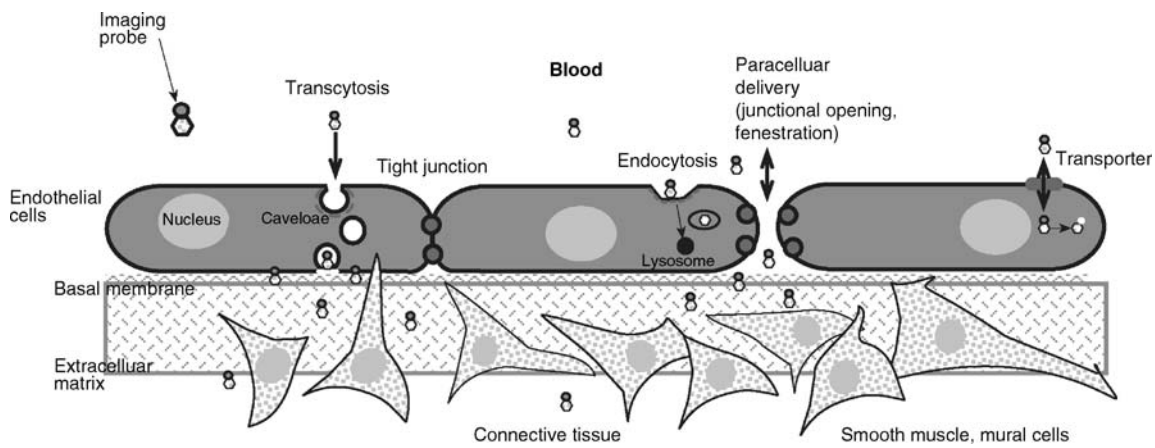

Molecular Probes, Delivery. Figure 1 Schema showing various mechanisms of drug delivery to and across endothelial barriers (blood–tissue): (i) transcytosis; (ii) endocytosis; (iii) paracellular transport; (iv) transporter-mediated transport.

peptides (including HIV Tat-derived peptide 47–57) were initially shown to assist in translocating large proteins, particles (including superparamagnetic nanoparticles and fluorescent liposomes) into cells *via* energy-independent mechanism suggesting unique translocating mechanisms. The CPP/PTD approach has been used successfully to load isolated cells *ex vivo* with superparamagnetic nanoparticles for tracking stem/progenitor cells administered locally *in vivo* using MRI. Later studies have not confirmed the energy dependent translocation and suggested endocytosis as the major route of CPP/PTD-conjugated imaging probes into the cell interior. However, if Tat or other CPP/PTD peptide-conjugated imaging probes escape endosomes due to rupture or artificial endosomal pH neutralization (e.g. with ammonium chloride treatment), the probe accumulates in the nucleus since cell penetrating peptides often include nuclear translocation sequences (RKRRQRRR sequence in the case of Tat peptide). Amino acids of above sequences interact strongly with proteins of nuclear membrane (importins/karyopherins) and the resultant complex docks and translocates through nuclear pore complex. The lack of any targeting ligands in imaging probes in some cases also can be used for increasing delivery of larger molecules with the diameter of several nm—200 nm in the interstitium. The use of polymer coatings (e.g. covalently bound methoxy polyethylene glycol) enables the probe to escape recognition of the reticuloendothelial system resulting in longer times in circulation. Long circulating probes extravasate slowly due to transcytosis or leakage through the endothelial fenestrations, defects in endothelial lining and specialized endothelium (high endothelial venules in lymph nodes) and accumulate in the interstitium. In pathology (cancer, inflammation) the transfer occurs through abnormally permeable endothelial lining. Interstitial delivery allows molecular imaging of proteinases expressed by fibroblasts by using self-quenched macromolecular optical imaging probes. In the presence of normal lymphatic drainage interstitially accumulated probes are carried with lymph flow to lymph nodes (dextran-coated nanoparticles, some PEGylated particles) where, if recognized by macrophages and dendritic cells, such particles are retained. This effect underlies lymph node specific delivery and imaging. Special mechanisms of probe retention in the target organ include solubility and molecular mass changes in response to enzymatic activity present in the target: the increase in solubility (hydrophilicity) and size would result, for example, in the increase of longitudinal relaxivity which is important for MR imaging.

A Distinction between Therapeutic and Imaging (Diagnostic) Drug Delivery

The combination of size, charge, hydrophobicity and surface chemistry (for nanoparticles) are the main factors that determine the fate of imaging probes in the body. It is critical to underline the difference between therapeutic drugs and imaging probes (drugs). Therapeutic effect of the former usually outweighs poor specificity for any given diseased organ under treatment if toxicity profile of the drug is acceptable. The imaging drug, however, should have a very specific distribution to target organs and relatively low non-specific delivery to other tissues/compartments since low specificity of the imaging probe would result in low target/background imaging ratio and poor imaging contrast.

Bibliography

1. Mader K (2005) Non-invasive spectroscopic and imaging techniques in drug delivery. Adv Drug Deliv Rev 57:1083–1084
2. Muzykantov V (2003) Biological barriers for drug targeting. In: Muzykantov VR, Torchilin VP (eds) Biomedical Aspects of Drug Rargeting. Kluwer Academic Pubs, Boston, pp 27–44
3. Licha K, Olbrich C (2005) Optical imaging in drug discovery and diagnostic applications. Adv Drug Deliv Rev 57:1087–1108
4. Schnitzer J (1998) Vascular targeting as a strategy for cancer therapy. New Engl J Med 339:472–474
5. Jain RK (2001) Delivery of molecular medicine to solid tumors: lessons from in vivo imaging of gene expression and function. J Control Release 74:7–25

Molecular Probes, Optical Probes

M

Christoph Bremer
Department of Clinical Radiology & Interdisciplinary, Center for Clinical Research (1ZKF), University of Muenster, Muenster, Germany
bremerc@uni-muenster.de

Synonyms

Activatable probe; Enzyme-sensing probes; Molecular beacons; Nonspecific fluorochromes; Nonspecific probes; Optical contrast agents; Optical probes; Optical tracers; Perfusion type optical contrast agents; Smart probes; Targeted probes; Targeted optical contrast agents; Target-specific probe.

Definition

Optical contrast agents for *in vivo* imaging are ideally fluorochromes with excitation and emission maxima in the near infrared range (NIR; 650–950 nm) since absorption of the photons by water, oxy- and deoxy-hemoglobin are minimal in this spectral range ("diagnostic window"). Cyanine dyes represent one of the most prominent classes of optical contrast agents for *in vivo* imaging (1). More recently, inorganic quantum dots

(QDs, fluorescent semiconductor nanocrystals) have been introduced as a novel class of optical contrast agents which can be exactly tuned to a specific wavelength by size variation. The unique property of QDs is a broad absorption band, relatively narrow and symmetrical luminescence band and high resistance to photo degeneration. Biological applications of these novel contrast agents are currently under investigation.

As outlined above, optical probes can be classified as "nonspecific", "targeted," and "smart" probes (Fig. 1) (2).

Nonspecific contrast agents such as indocyanine green (ICG) show distribution patterns which depend solely on their pharmacological formulation (i.e., molecular weight, hydrophilicity, lipophilicity, protein binding etc.). These agents can help to measure surrogate parameters for tissue perfusion, vascular permeability or vascular volume. However, true molecular targets cannot be imaged using this approach.

Targeted contrast agents are linked to specific affinity ligands such as peptides, antibody-fragments or small molecules imparting molecular specificity to the probe. In the early phase after injection, high levels of unbound circulating contrast media contribute to the background signal resulting in a slight decrease of the signal-to-noise ratio (SNR). After clearing of the unbound probe, the fluorochromes are ideally retained at the target structure allowing for the detection, for example of cell surface proteins (Fig. 1).

"*Smart*" *contrast agents* can be "activated" upon enzymatic conversion of the probe ideally resulting in an "off" and "on" status. A prominent example was first described by Weissleder and consisted of a large 450 kD carrier molecule coupled to several fluorochromes emitting photons in the NIR; (1). In the native state, mutual energy transfer occurs amongst the fluorochromes, resulting in a quench of the signal. After enzymatic release of the fluorochromes an up to several 100-fold, signal increase can be observed. "Smart" optical probes thus provide a high SNR which is desirable for molecular target identification.

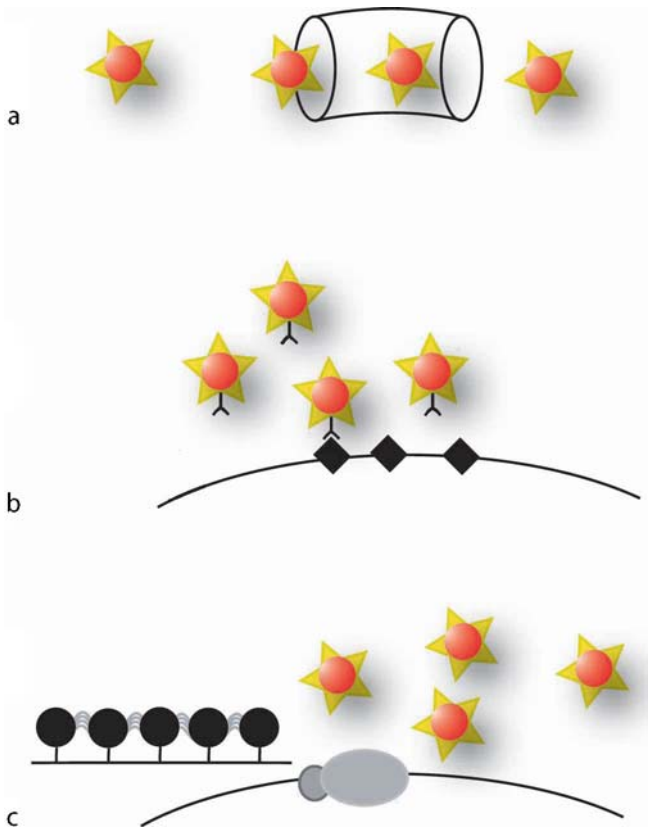

Molecular Probes, Optical Probes. Figure 1 ***Design of different optical contrast agents*. Nonspecific optical contrast agents (a) show simple perfusion and/or permeability properties of the tissue. Targeted probes (b) bind *via* specific ligands to protein structures on the cell surface (e.g., tumor associated receptors). "Smart probes" (c) are activated by an enzymatic conversion from their native (little to no signal) to become brightly fluorescent after enzymatic cleavage (c, *right*; reprinted with permission from Bremer C, Ntziachristos V, Weissleder R (2003) Optical-based molecular imaging: contrast agents and potential medical applications. Eur Radiol 13:231–243).**

Indications

Nonspecific optical contrast agents are in part clinically available (e.g., ICG, cardio green). ICG is clinically approved and applied for liver function tests, for studying cardiac output, and for ophthalmic angiography. With respect to noninvasive optical imaging, ICG has been successfully applied in an off label use for the detection of breast cancer lesions using diffuse optical tomography (DOT) techniques combined with conventional Gd-enhanced MRI (3).

In experimental investigations, xenograft tumors could be clearly differentiated regarding their levels of angiogenic activity. The underlying contrasting mechanism is thought to be based on vessel permeability leading to an accumulation of fluorescent dyes in the tumor interstitium and is thus comparable to other clinically applied imaging modalities (e.g., contrast enhanced MRI). Currently novel nonspecific fluorochromes are being systematically evaluated in phase I clinical trials for breast cancer lesion detection in combination with DOT.

Targeted optical contrast agents have been designed using different affinity ligands such as peptides, proteins, antibodies or antibody fragments (Figs. 1 and 2).

By conjugation of flourescein and carbocyanine dyes to various peptide motifs, tumor associated cell receptors such as the somatostatin-, bombesin-, vasointestinal peptide- folate and the epidermal growth factor (EGF)-receptor could be selectively targeted in experimental studies. Molecular markers of endothelial proliferation such as the $\alpha v\beta_3$ integrin could be successfully visualized by linking 'RGD' peptide sequences to cyanine dyes. Moreover the conjugation of a cyanine dye to more complex proteins such as annexin-V allowed to fluorescently label apoptotic or necrotic cell types and tissues facilitating an early assessment of treatment response to chemotherapy. Antibody based targeted fluorochromes have been designed to visualize E-selectin expression as an early proinflammatory marker. A bisphononate-NIR dye-conjugate showed distinct binding affinity to hydroxylapatite (HA) allowing for the detection of osteoblastic activity *in vivo*.

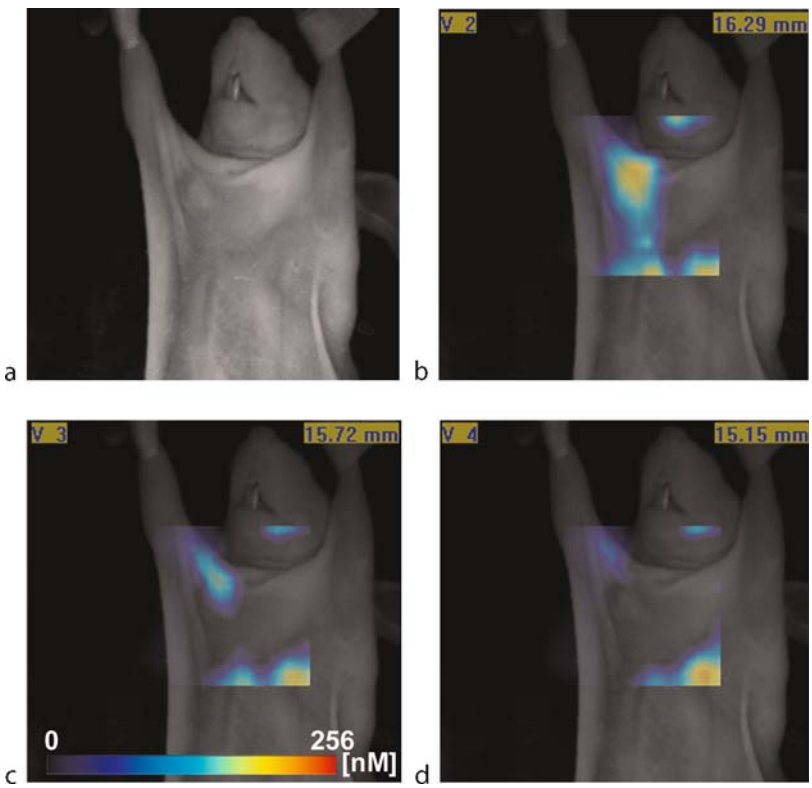

Molecular Probes, Optical Probes. Figure 2 ***FMT imaging of $\alpha v\beta_3$-expression using a target-specific optical probe.*** **Fluorescence-mediated tomography was acquired 24 h after injection of a target-specific optical probe recognizing the integrin $\alpha v\beta_3$, which is a sensitive marker of angiogenesis (a—*white light* image, b–d coronal sections of FMT data superimposed on a; fluorochrome concentration is color encoded). Target affinity was achieved by coupling a cyclic "RGD" peptide to the dye.**

M

More recently, small non-peptidic molecules (i.e., drug precursors) could be labeled with cyanine dyes through polyethylene glycol (PEG) linkers and still preserve binding affinity of the ligands.

Besides the affinity of the single ligand, steric composition can greatly influence the target affinity of a probe. In this respect, multimeric affinity ligands may substantially increase the ability of the optical probe to bind to the target structure.

Generally speaking, potential clinical indications for the application of targeted optical probes arise from the specific molecular structure which can be displayed by the fluorochrome. Imaging of certain tumor cell receptors (e.g., EGF-receptor) may potentially allow (i) detection of disease at an early stage, (ii) stratification of tumor types for novel molecular targeted therapies and (iii) assessment of treatment effects by targeting cellular apoptosis substantially earlier than is the case with conventional response markers (e.g., tumor size regression).

"*Smart*" *optical contrast agents* significantly change their fluorescence emission upon enzymatic conversion (Figs. 1 and 3). These probes therefore show little background fluorescence in their native state while brightly fluoresce after cleavage by the target enzyme. Thus the signal to noise yield is substantially higher compared to the targeted probes.

The first autoquenched fluorescent probe was developed by Weissleder et al consisting of a long circulating carrier molecule conjugated to 12–14 cyanine dyes. The proximity of the dyes in the native molecule results in a signal quench due to fluorescence resonance energy transfer (FRET) while a strong fluorescence signal increase can be detected after probe is cleaved (Fig. 1). The first generation of these protease sensing optical probes is activated by lysosomal cysteine or serine proteases such as cathepsin-B. Meanwhile, probe specificity could be tailored to other enzyme systems by insertion of enzyme-specific peptide stalks between the carrier and the fluorochromes. Thus cathepsin-D, matrix-metalloproteinase-2 (MMP-2) or thrombin and other enzyme systems could be visualized using this approach (1, 4). "Smart" optical probes have been applied to study cancer progression, tumor metastasis, atherosclerosis, myocardial infarction, thrombosis, and inflammation. Since these molecules consist of a large backbone carrier molecule (approximately 400 kD) with several dyes attached to it the overall molecular weight is relatively high. Thus these probes tend to be retained systemically for a long time which is not desirable for diagnostic purposes. More recently, however, smaller activatable optical probes could be designed by attaching NIR fluorescence absorber (e.g., NIRQ820) through a peptide stalk to a NIR dye.

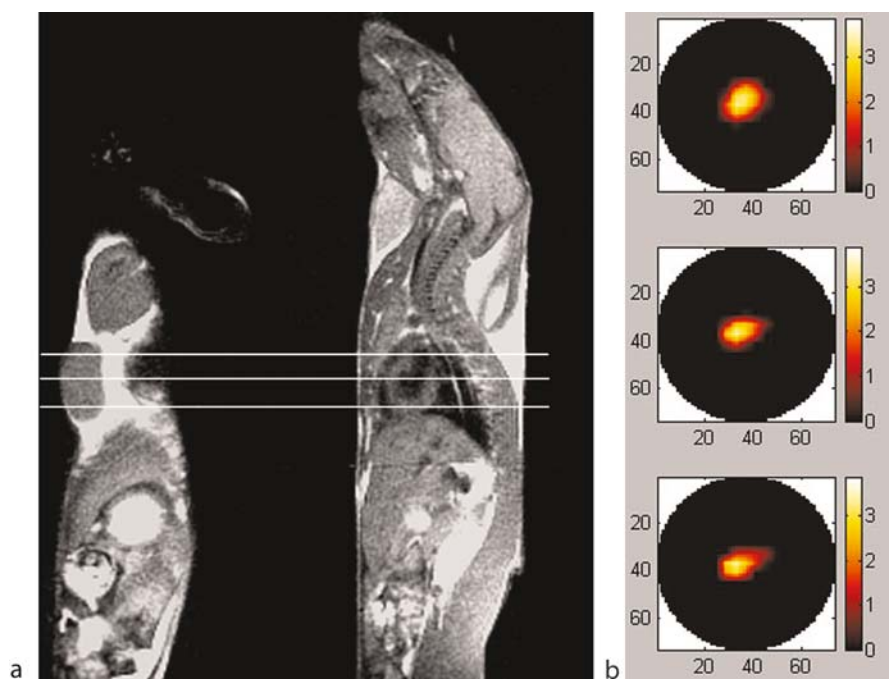

Molecular Probes, Optical Probes. Figure 3 ***Imaging of tumor protease expression by FMT using a "smart" optical probe.*** **In a transgenic mouse model, spontaneous breast cancer lesions were examined anatomically by MRI (sagittal T1w SE sequence) and optical molecular imaging was performed using a "smart" protease sensing probe (b, axial FMT images). Note the strong tissue fluorescence in the tumor nodule representing the expression of cysteine proteases, a molecular marker that is correlated with tumor aggressiveness (reprinted with permission from Bremer et al Inv Radiol 2005).**

Potential clinical applications of these probes are numerous. Various proteases are known to be key players in oncology, allowing the tumor to invade locally the tissue, form new vascular supply (i.e., perform angiogenesis) and induce distant metastasis. Moreover, proteases such as MMP-2 play a significant role in cardiovascular disease. For instance, it is well established that MMPs contribute to plaque instability in atherosclerotic disease. Other inflammatory diseases are linked to a high degree of protease over expression. Cysteine proteases have, for example, been shown to be upregulated in arthritis and to be a sensitive maker for anti-inflammatory treatment.

Use And Dosage

The potential clinical use of the optical probes presented here is necessarily co-defined by the technical constraints of detecting optical signatures in the tissue. Thus the application of noninvasive optical techniques is limited by the depth penetration of the modalities. However, a variety of clinical issues can be addressed using planar and tomographic imaging techniques. Surface weighted reflection techniques can easily be integrated into endoscopic, laparoscopic, or handheld devices. Combining these sensors with specific (molecular) optical contrast agents would greatly enhance the diagnostic possibilities for endoluminal diagnostics as well as intraoperative imaging. Thus, for example, real time, intraoperative guidance of tumor resection can be envisioned by combining a "tumor selective" optical probe with intraoperative planar imaging devices. Dual labeled probes (i.e., labeled with an MR and optical contrast agents) can be exploited for preoperative tumor localization and for intraoperative guidance by fluorescence reflectance imaging.

Different targets relevant to various aspects of disease have been imaged successfully in an experimental setting including (tumor) cell receptors, endothelial proliferation markers, cancer related or inflammatory proteases and apoptosis associated membrane structures.

Depending on the type of probe applied, optical probes with molecular specificity should significantly enhance the detection and characterization of pathology. Moreover, treatment response should be monitored more sensitively for example by apoptosis-avid agents.

Besides detecting a single reporter molecule multiwavelength, imaging approaches targeting several molecular targets simultaneously can be envisioned using fluorochromes with distinct excitation and emission spectra.

Since optical imaging is a highly sensitive imaging modality, low amounts of fluorochrome suffice for imaging specific molecular structures. The sensitivity of the imaging approach is currently thought to be in the range of (or even higher than) scintigraphic techniques. Based on experimental data generated for targeted and "smart" optical probes, 10–100 nmol/kg bw of the optical probe may provide sufficient optical signal for target detection. This, however, is 3–4 orders of magnitude lower than compared to clinically applied doses of Gd-DTPA for example (5).

Bibliography

1. Weissleder R, Ntziachristos V (2003) Shedding light onto live molecular targets. Nat Med 9:123–128
2. Bremer C, Ntziachristos V, Weissleder R (2003) Optical-based molecular imaging: contrast agents and potential medical applications. Eur Radiol 13:231–243
3. Ntziachristos V, Yodh AG, Schnall M et al (2000) Concurrent MRI and diffuse optical tomography of breast after indocyanine green enhancement. Proc Natl Acad Sci USA 97:2767–2772
4. Bremer C, Tung CH, Weissleder R (2001) In vivo molecular target assessment of matrix metalloproteinase inhibition. Nat Med 7:743–748
5. Persigehl T, Heindel W, Bremer C (2005) MR and optical approaches to molecular imaging. Abdom Imaging 30:342–354

Molecular Probes, Ultrasound Probes

M

Katherine Ferrara
Department of Biomedical Engineering, Center for Molecular and Genomic Imaging, University of California, Davis, USA

Synonyms

Molecularly-targeted ultrasound contrast agents

Definition

Active and passive targeting mechanisms allow ultrasound contrast agents to accumulate in sites of interest. Active targeting uses ligands attached to the contrast agent shell surrounding each micron or nanometer diameter agent, where these ligands are optimized to adhere to endothelial cell targets (Fig. 1). Passive targeting relies on the size of the contrast agents to restrict their location to the vascular space, or to allow accumulation of the agents in leaky tumors. Agents currently approved for human use as ultrasound contrast agents are microndiameter bubbles,

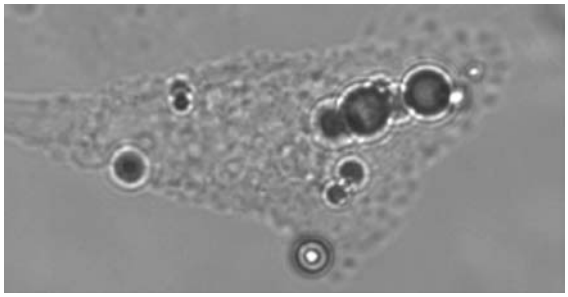

Molecular Probes, Ultrasound Probes. Figure 1 Targeted ultrasound contrast agents adherent to an endothelial cell *in vitro*.

which produce passive targeting of the vascular space. *Ultrasound molecular agents* include molecularly targeted microbubbles, liposomes, and nanoparticles all of which are currently under development (1–4).

Following transmission of a brief ultrasound pulse, targeted ultrasound imaging techniques measure differences in the returned echo amplitude, spectrum, or pulse-to-pulse correlation to detect the presence of localized agents.

Approaches

There are three major types of agents proposed for targeted ultrasound imaging:

- *Microbubble agents* (2, 3) are small gas bubbles (typically a gaseous perfluorocarbon) with a stabilizing shell (albumin, lipid, or polymer) and most frequently used as the basis for molecularly targeted agents.
- *Perfluorocarbon emulsion nanoparticles* (1), with a mean diameter of hundreds of nanometers, are composed of a liquid perfluorocarbon and can include a lipid coating and a diluent for drug delivery.
- *Echogenic liposomal agents* (4) use a formulation involving lyophilization that entraps air in the lipid bilayers when rehydrated.

Requirements

Targeted ultrasound imaging should produce diagnostically significant localization of a receptor or of variations in vascular permeability with a high contrast to noise ratio. Echoes from bound or localized agents should ideally be differentiable both from circulating agents and from tissue. A small number of agents bind at a site of increased receptor density, and this small number can produce a detectable change in the echo. Quantitative estimation of receptor density may be difficult with targeted ultrasound imaging due to the relatively small number of agents, which bind to a large number of active receptors, however, accurate and consistent differentiation of normal and diseased tissue has been shown to be feasible.

Shell Characteristics

Most of the current work with targeted ultrasound contrast agents has involved the attachment of a peptide or antibody to a lipid shell either before or after the creation of the microbubble. Small molecule ligands can be directly attached to the lipids and the ligand–lipid conjugate is then purified. Large proteins (including antibodies) are often attached through covalent or noncovalent chemistry after the contrast agent is formed due to the harsh conditions that accompany microbubble creation. It is more difficult to purify the resulting targeted vehicle following this approach. Chemistries used to attach the ligand to the lipid membrane include:

- Biotin–streptavidin approaches, in which biotin is attached to the lipid or polyethylene glycols (PEG) molecule (2, 3),
- Carboxylic acid–amine approaches, in which a carboxylated lipid derivative is incorporated into the microbubble shell and reacts with an amine on the ligand (2),
- Maleimide–thiol approaches, in which a maleimide–PEG–lipid is incorporated in the monolayer shell and reacts with a thiol-containing targeting ligand (1, 2, 4).

Microbubble Agents

The major advantage to the use of microbubble contrast agents for targeted imaging is that the great difference in material properties between these agents and plasma produce very strong echoes, with properties that can be easily distinguished from the surrounding tissue. Due to the very high contrast-to-noise ratio, an echo from a single microbubble may be detected by a clinical ultrasound instrument.

Possible disadvantages of current targeted microbubbles include the relatively large size and the low circulation time (minutes to tens of minutes). Micron-diameter agents may not be able to bind to the desired site in the presence of high levels of shear stress *in vivo*. The diameter of the agents may be reduced using polymeric shells, which can be stable at an initial diameter of

hundreds of nanometers and may circulate for an extended time interval.

Lipid-shelled microbubbles, used in currently published targeted ultrasound imaging research, incorporate a combination of lipids and an emulsifier at a ratio of the order of nine to one. The monolayer shell includes longer chain saturated lipid molecules such as distearoyl phosphatidylcholine, in addition to the emulsifier, typically incorporated as either PEG40-sterate or a PEGylated lipid. Microbubble formation is accomplished through agitation using a sonicator or modified dental amalgamator, and high temperatures typically occur during this process. The resulting microbubbles can then be purified (removing the excess lipid, streptavidin, biotintylated ligand) by centrifugation using a low speed over several minutes.

Both *in vitro* and *in vivo*, the binding efficiency of targeted has not yet been shown to vary greatly with the affinity of the ligands. Probably due to multivalency, the number of agents bound under similar conditions has not been greatly altered by the use of peptide or antibody-based ligands. Some improvement in efficiency has been noted with the presence of excess lipid in loose folds near a microbubble or the use of combined ligand strategies, such as targeting both integrins and selectins.

Detection of Microbubbles

Microbubbles with an initial diameter of the order of a few microns have a resonance frequency in the low megahertz frequency range, the same range of frequencies employed by clinical ultrasound instruments. When excited by an ultrasound wave with a low to moderate intensity (hundreds of kilopascals), their oscillation results in echo components at the transmission frequency and multiples and submultiples of this frequency. The harmonic multiple and submultiple components can usually be easily differentiated from tissue echoes. Alternative multipulse sequences use varied transmission amplitude, phase, and frequency to further improve the contrast to noise ratio, which can be as high as 30 dB. Oscillation of the microbubbles is altered when the agents bind to a receptor, and these small changes in the resulting echo may be used to estimate their density in future studies.

Microbubble contrast agents are destroyed by an ultrasound pulse of sufficient amplitude (amplitude depends upon initial radius and frequency), typically by fragmentation of the bubble into a set of smaller microbubbles where the resulting small gas fragments diffuse more rapidly. Comparison of images before and after microbubbles are fragmented provides a source of contrast to distinguish microbubble and tissue echoes.

Perfluorocarbon Emulsion Nanoparticles

The liquid composition of perfluorocarbon emulsion nanoparticles makes them resistant to pressure and mechanical stress, greatly increasing their circulation time as compared with microbubbles. In addition, with a diameter in the hundreds of nanometers, these particles should bind over a greater range of physiologically relevant shear stress than microbubbles. Peptide or antibody-based targeting ligands can be attached to an outer lipid membrane. An additional diluent may be added to solubilize a drug.

Imaging perfluorocarbon nanoparticles with ultrasound is more challenging than microbubbles, in which nonlinear echo components are not typically produced and therefore tissue and agent echoes have similar spectra. Their echogenicity is not as great as that of a gas-filled agent of similar size, however, the summed echo amplitude of a fixed number of particles increases when they are deposited in a layer.

Liposomal Agents

Liposomal agents, like perfluorocarbon emulsion nanoparticles, can circulate for extended periods, providing the opportunity for larger numbers of agents to bind to a site of interest. Echogenicity, on a per agent basis, is expected to be lower than a microbubble based agents, but should increase when the agents bind in a coherent layer. Liposomal agents also allow for the incorporation of hydrophobic or hydrophilic drugs, and can therefore function both as imaging and drug delivery agents.

Applications

Of the many molecular markers that could be used for active targeting, ultrasound research applications have so far been limited to those which are accessible through the vasculature, including inflammation, thrombus, and angiogenesis (Fig. 2). Due to their relatively large size, targeting of microbubbles to capillaries or postcapillary venules has shown the greatest success.

Microbubbles targeted to integrins (incorporating either monoclonal antibodies or RGD-containing disintegrins or peptide) have been shown to be retained in tumors and models of angiogenesis. Perfluorocarbon nanoparticles and liposomal agents have been shown to target atherosclerotic plaques as well as angiogenesis.

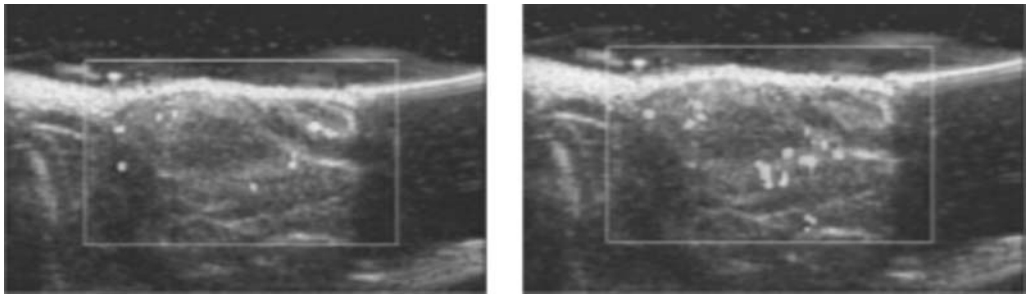

Molecular Probes, Ultrasound Probes. Figure 2 Control and targeted ultrasound contrast agents within a model of angiogenesis. A matrigel plug infused with basic fibroblast growth factor to stimulate angiogenesis was implanted within a rat model. Contrast agents were injected and allowed to circulate for 15 min. Overlaid B-mode (10.3 MHz) and power Doppler images (7.2 MHz, PRF 868 Hz) were then acquired. Left image shows the remaining control agents, right image shows targeted agents which were bound to the site (Image courtesy of Paul Dayton and Susanne Stieger, University of California, Davis).

Drug Delivery

Targeted ultrasound particles have the potential to be used for both imaging and drug delivery (3, 5). Several architectures for microbubble-based drug-delivery particles have been described and are under test, including particles with a drug covalently attached to the lipid shell, a thick drug-carrying oil shell encapsulating a microbubble, and a lipid shell carrying nanoparticles or liposomes. With a gas bubble at the center of the particle, low ultrasound pressure levels can be used to deflect the particle using a Bjerknes force and enhance targeting efficiency and the gas particle can be fragmented at the site of interest with a high-pressure pulse.

Nanoparticles and liposomal particles can also be used to carry a drug, as well as to create an image. Perfluorocarbon nanoparticles, have an impedance difference in comparison with plasma, and therefore their biodistribution and properties may be affected by ultrasound.

Bibliography

1. Lanza GM and Wickline SA (2001) Targeted ultrasonic contrast agents for molecular imaging and therapy. Prog Cardiovasc Dis 44(1):13–31
2. Klibanov AL (2005) Ligand-carrying gas-filled microbubbles: ultrasound contrast agents for targeted molecular imaging. Bioconjug Chem January–February 16(1):9–17
3. Bloch SH, Dayton PA, and Ferrara KW (2004) Targeted imaging using ultrasound contrast agents. Progress and opportunities for clinical and research applications. IEEE Eng Med Biol Mag September–October 23(5):18–29
4. Hamilton AJ, Huang SL, Warnick D et al (2004) Intravascular ultrasound molecular imaging of atheroma components *in vivo*. J Am Coll Cardiol February 4 43(3):453–460
5. Shortencarier MJ, Dayton PA, Bloch SH et al (2004) A method for radiation-force localized drug delivery using gas-filled lipospheres. IEEE Trans Ultrason Ferroelectr Freq Control July 51(7):822–831

Molecular Targets

Christoph Bremer
Dept. of Clinical Radiology and Interdisciplinary Center for Clinical Research (IZKF), University of Muenster, Muenster, Germany
bremerc@uni-muenster.de

Definition

Molecular targets are cellular or tissue structures that are intended to be visualized by means of molecular imaging. Different biological structures can potentially serve as imaging targets, ranging from proteins to DNA and RNA.

Characteristics

From sequencing of the human genome, it became clear that the whole human genome consists of approximately 34,000 genes. Therefore, numerous structures could potentially serve as novel tissue-specific markers for *in vivo* imaging. High-throughput analysis tools in genomics and proteomics help to identify new specific target molecules that are upregulated in various disease processes. Profiling-mediated discovery of novel disease-specific markers will spur the development of more specific imaging agents [Feindegen, 2003 #93]. Based on this knowledge, new types of receptor/target ligands (see later) can form the basis for new imaging and therapeutic agents.

Targets for molecular imaging should generally be (i) clinically relevant (i.e., linked to a certain type of disease

or be predictive of disease outcome), (ii) abundantly overexpressed compared with healthy tissue, and (iii) easily accessible (e.g., extracellular). Typically, specific proteins (e.g., cell receptors) are chosen as molecular targets since the "natural amplification" mechanism from gene to protein (i.e., one gene translates to several copies of proteins) can be exploited, and—depending on the site of expression—proteins may be more easily accessible.

Targeting interstitially localized or extracellular proteins is the most promising approach to *in vivo* molecular diagnostics, as pharmacological barriers are minimal. Enzymes can be exceptionally interesting targets when combined with enzymatically activatable fluorophores because one target structure (e.g., matrix metalloproteinase, cathepsin) can process several hundreds of reporter probes and thus vastly amplify the signal for molecular imaging.

However, even intracellular structures (e.g., caspases, RNA, DNA) can theoretically be targeted by different imaging approaches. For this purpose, membrane translocation signals can facilitate entry of the probe into the intracellular space. Different approaches have been described to achieve improved transmembrane migration of reporter probes, including the HIV-derived tat-peptide, dendrimers, and polyamine residues.

Molecularly-Targeted Ultrasound Contrast Agents

▶Molecular Probes, Ultrasound Probes

Mondor's Disease

Band-like painful skin thickening and erythema due to thrombosis of a subcutaneous vein, often associated with preceding trauma or surgery to the breast.

▶Cutaneous Lesions, Breast

Morbus Basedow

▶Thyroid Autoimmune Disease

Morbus basedow, Autoimmune disease

An autoimmune disease of the thyroid gland, usually presenting with hyperthyroidism.

▶Thyroid Autoimmune Diseases

Morbus Paget

Geert M. Villeirs
Division of Genitourinary Radiology
Ghent University Hospital, Ghent, Belgium
geert.villeirs@ugent.be

Definition

Paget's disease of the nipple–areolar complex occurs in association with about 1–5% of all breast carcinomas. The presence of malignant cells in the nipple and/or areola causes eczematoid changes that may be the first sign of the underlying malignancy. Carcinomas presenting with only this sign are usually diagnosed early in their course and therefore have a rather favourable prognosis.

Pathology/Histopathology

Paget's disease is characterized by permeation of the nipple–areolar epidermis by large malignant cells containing large nuclei and abundant pale cytoplasm. They cause chronic inflammation of the dermis and may be so numerous that they completely destroy the epidermis, causing frank ulceration and erosion of the nipple and/or areola.

The permeating cells originate from a retroareolar carcinoma or from a carcinoma anywhere in the breast, virtually always of ductal type (either *in situ* or a combination of *in situ* and infiltrating carcinoma), and migrate through the ductal system towards the nipple and areola.

Clinical Presentation

The clinical presentation of Paget's disease is a unilateral itchy erythema of the nipple and/or areola, progressing to eczematous changes with moisture and scaling, and ultimately effacement, ulceration and erosion of the nipple. Bloody nipple discharge may be present.

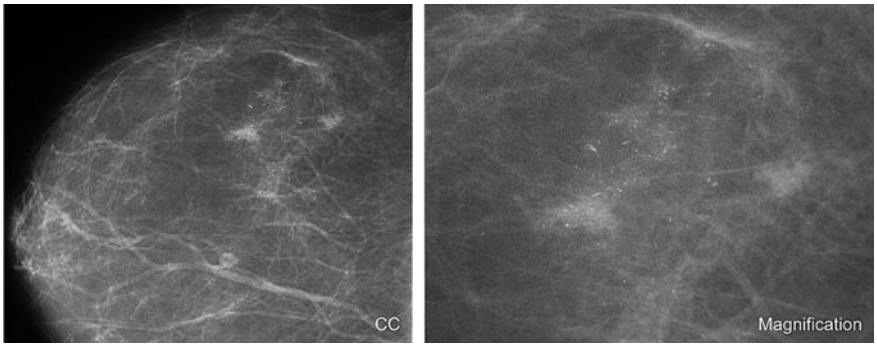

Morbus Paget. Figure 1 Casting-type calcifications of intraductal carcinoma in a patient with Paget's disease of the nipple.

Mammography

On mammography, the nipple/areolar involvement usually is not apparent, although nipple retraction, skin thickening or calcifications have been reported. When Paget's disease is suspected clinically, the mammogram is rather performed to detect an underlying carcinoma by the presence of a mass or suspicious microcalcifications (Fig. 1).

Sonography

Sonography is of limited use in Paget's disease, except to detect or exclude an underlying carcinoma.

Magnetic Resonance Mammography

In addition to the demonstration of an underlying carcinoma, magnetic resonance mammography may show non-specific enhancement of the thickened nipple–areolar complex.

Percutaneous Biopsy

The clinical diagnosis of Paget's disease can be confirmed by a cytologic smear or excisional biopsy of the eczematous nipple–areolar complex.

Bibliography

1. Ikeda DM, Helvie MA, Frank TS et al (1993) Paget disease of the nipple: radiologic–pathologic correlation. Radiology 189:89–94
2. Burke ET, Braeuning MP, McLelland R et al (1998) Paget disease of the breast: a pictorial essay. Radiographics 18:1459–1464
3. Kollmorgen DR, Varanasi JS, Edge SB 3rd et al (1998) Paget's disease of the breast: a 33-year experience. J Am Coll Surg 187:171–177
4. Frei KA, Bonel HM, Pelte MF et al (2005) Paget disease of the breast: findings at magnetic resonance imaging and histopathologic correlation. Invest Radiol 40:363–367

Morgagni Hernia

Maldevelopment of the diaphragm resulting in a defect that is characteristically central and anterior.

▶Hernia, Diaphragm, Congenital: Including 'Hiatus Hernia, Childhood'

Morgagni Hernia

▶Contrast Media, Ultrasound, Influence of Shell on Pharmacology and Acoustic Properties

Morphometry, MR, Brain

Frederik Maes
Universitaire Ziekenhuizen, Lenven, Belgium
Frederik.Maes@uz.kuleuven.ac.be

Definition

Magnetic resonance (MR) brain morphometry refers to the characterization of morphological, that is, structure- or shape-related features of the brain or its substructures from MR image data, using suitable, computer-aided image analysis methodologies. Current MR imaging technology provides the ability to generate three-dimensional (3D) image volumes of the entire brain with near-isotropic spatial resolution of about $1 \times 1 \times 1$ mm per volume element or voxel. Such 3D image volumes can be sliced and visualized on a computer display along

multiple arbitrarily oriented two-dimensional (2D) planes through the brain (MPR or multiplanar reformat), providing a more comprehensive understanding of the 3D anatomy. While visual inspection of the image data is subjective and merely provides a qualitative assessment of morphological characteristics of the brain's anatomy, often objective, quantitative measures, which are obtained by image-based measurements, are of interest. This is typically the case when brain images of different subjects have to be compared in order to detect and characterize subtle morphological differences between them (e.g., a population of normal controls versus patients) or when morphological changes over time have to be assessed in a single individual by comparing images acquired at different time points (e.g., lesion evolution in response to therapy). Morphometric parameters of interest are, for instance, distances between anatomical landmarks, volumes of structures of interest, regional distribution of white and gray matter, location and size of possible lesions, and description of object shape (using suitable mathematical representations) and its deviation from the expected, normal shape.

Characteristics

A prerequisite for the quantification of shape-related parameters of an anatomical structure of interest from image data is that this structure has been defined in the images, that is, its contour (in 2D) or surface (in 3D) has been delineated with sufficient accuracy in order to discriminate this structure from other surrounding structures and background. The process of object delineation in images is termed image segmentation. While in principle the surface of the objects of interest can be delineated manually by an expert in several 2D images displayed on screen, such manual segmentation is tedious and time-consuming and typically subject to significant intra- and interobserver variability. In the field of medical image analysis, more efficient and robust (semi-) automated image processing approaches for segmentation of anatomical objects in medical image data are therefore being investigated.

These methods can be broadly classified as being low-level or model-based. Low-level approaches make use of the intensity information only in the images and they segment the object of interest based on heuristic and often simplistic rules, such as assumed object intensity homogeneity (e.g., thresholding, region growing strategies), object boundary contrast (e.g., edge detection strategies), or combinations thereof. For complex-shaped anatomical objects such as the brain, with significant biological shape variability and possible pathological deviations, in complex image data such as MR images, including noise, intensity inhomogeneity, partial volume effects, and other imaging artifacts, such low-level approaches are usually insufficient to generate accurate delineations of the brain or its substructures and often require tedious, manual postprocessing to correct for segmentation errors. Model-based approaches, on the other hand, incorporate prior knowledge about the appearance of the object of interest in the images, that is, information about the expected intensity and/or shape of the object, as well as contextual information such as its spatial relation to other objects. Model-based approaches apply an optimization strategy to find the parameters of the model that best fit the image data. They are generally more robust than low-level approaches, because the model used imposes constraints on the segmentation result that can compensate for ambiguities in the image data. A typical example of such model-based segmentation is the classification of MR brain image voxels in different tissue classes (usually "white matter," "gray matter," and "cerebrospinal fluid") using a Gaussian mixture model for the image intensity (one or more Gaussian distributions per tissue class), while also incorporating models to correct for MR bias field intensity inhomogeneity and to impose local regularity of the segmented tissue maps (1).

Many applications of MR brain morphometry involve the analysis of multiple MR image volumes for the assessment of morphological differences between different subjects or within a single subject over time. While in principle the morphometric parameters of interest can be obtained from each volume separately and subsequently compared, the analysis is much facilitated if the image volumes are spatially aligned and normalized first, such that corresponding voxels in each image also correspond anatomically. When the images have been segmented in different tissue maps, a voxel-by-voxel statistical analysis can be performed to detect local anatomical differences between different (groups of) subjects (so-called voxel-based morphometry (3)). Image alignment or registration is a fundamental problem in image analysis. Affine registration only compensates for global differences in pose (3D translation and rotation) and size between different images (12 parameters or degrees of freedom), while nonrigid registration also compensates for local shape differences (using a deformation field with many more degrees of freedom, up to three per voxel). Voxel-based nonrigid registration requires a suitable similarity measure to assess the geometric correspondence between different images based on their intensities, as well as an appropriate regularization strategy to ensure that the resulting deformation field is well-behaved and physically realistic (2). The latter is typically achieved by representing the deformation field using smooth basis functions (e.g., B-splines) or by

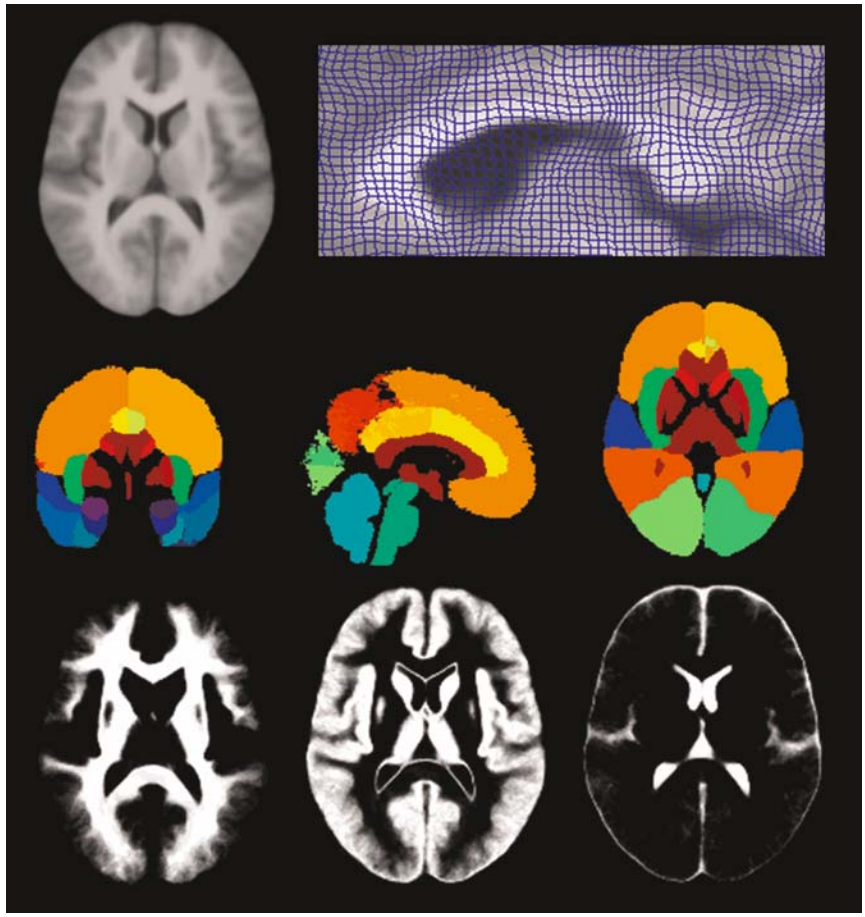

Morphometry, MR, Brain. Figure 1 Brain atlas constructed by averaging a set of segmented MR brain images of different subjects after spatial normalization by nonrigid image registration. *Top*: averaged brain image template and typical deformation pattern near the corpus callosum; *middle*: coronal, sagittal, and axial slices with averaged segmentations of different subcortical structures; bottom: averaged tissue maps, showing the expected spatial distribution of white matter, gray matter, and cerebrospinal fluid.

imposing smoothness penalties or physics-based constraints (e.g., elastic or viscous fluid model). An often-used similarity measure is maximization of mutual information of corresponding voxel intensities. This approach assesses the statistical dependence of the intensities in both images based on their joint histogram, without making assumptions about the nature of the data, which makes the method applicable to multimodal data (e.g., MR/PET or MR-T1/MR-T2 registration) as well.

Spatial normalization by (nonrigid) registration of a set of similar MR brain images of different subjects allows one to average all images voxel by voxel such that a brain image template or atlas is obtained with "average" shape. By also averaging the segmented tissue maps of all subjects, an atlas of the expected spatial distribution of different tissue types (or of other brain structures of interest) can be constructed (Fig. 1). This atlas can then be used for atlas-based segmentation and morphometry of new brain images by (nonrigid) registration of the atlas to the images under study. In addition, shape differences between a set of images of different subjects can be assessed by statistical analysis of the deformation fields that spatially align all images.

Bibliography

1. Van Leemput K, Maes F, Vandermeulen D et al (1999) Automated model-based tissue classification of MR images of the brain. IEEE Trans. Medical Imaging 18(10): 897–908
2. Maes F, Vandermeulen D, Suetens P (2003) Medical image registration using mutual information. Proc. IEEE 91(10): 1699–1722
3. Good CD, Johnsrude I, Ashburner J et al (2001) Cerebral asymmetry and the effects of sex and handedness on brain structure: A voxel-based morphometric analysis of 465 normal adult human brains. NeuroImage 14(3): 685–700

Morris Syndrome

Rare association of testicular feminization and multiple liver hemangiomas.
▶Hepatic Pediatric Tumors, Benign

Mosaic Perfusion

The redistribution of blood flow from hypoventilated lung to the normally ventilated areas by the reflex of hypoxic vasoconstriction (Euler-Liljestrand) or from hypoperfused areas due to pulmonary artery obstruction to non-obstructed lung areas. This redistribution causes increased attenuation of lung parenchyma in these areas and larger calibres of the respective pulmonary artery branches when compared to the hypoventilated areas. These differences are readily appreciated on inspiratory scans and do not change much on expiratory scans.
▶Airway Disease

Mosaic Perfusion Pattern

Patchy attenuation of lung parenchyma due to regional differences in perfusion.
▶Bronchitis and Bronchiolitis in Childhood

Motor Dysfunction of the Oesophagus

Abnormal contraction of the musculature of the oesophageal wall leading to slow and irregular transportation of bolus through the oesophagus. However, transportation may be normal while the contraction pressure is too high which may lead to ischemic pain.
▶Diverticulum, Oesophagus

MOTSA

Three-dimensional–time-of-flight MRA technique in which the imaging volume is acquired as multiple overlapping thin slabs. This reduces the problem of progressive saturation of protons as they progress deeper into a 3D imaging volume, which would otherwise reduce signal from flowing blood.
▶Carotid and Vertebral Artery Pathology

Mounier–Kuhn Disease

A congenital condition characterized by tracheobronchomegaly. Clinical findings kare recurrent pneumonia, loud cough, hoarseness, dyspnea, copious purulent sputum production. The findings at conventional chest radiography include tracheobronchomegaly, increase in lumen of the trachea with Valsalva and narrowing with Muller maneuver, and sac-like recesses.
▶Airway Disease

MPI

▶Myocardial Perfusion Imaging

MPNST

▶Malignant Peripheral Nerve Sheath Tumor

MPR

Multiplanar reformatted CT produces three basic images: axial images with a superimposed curve, cross-sectional images, and panoramic images.
▶Temporal Bone, Inflammatory Diseases, Acute, Chronic

MR Contrast Agents, Extracellular

Extracellular MR contrast agents consist of a variety of gadolinium chelates that after intravenous administration are rapidly redistributed from the vascular compartment into the extracellular space and then undergo renal excretion.
▶Metastases, Hepatic

MR Contrast Agents, Hepatobiliary

Hepatobiliary agents represent a heterogeneous group of paramagnetic molecules designed for greater hepatobiliary uptake and excretion than that of conventional MR contrast agents. They exhibit very high T1 relaxivity in the liver parenchyma, producing significant enhancement of normal liver tissue.

▶Metastases, Hepatic

MR Contrast Agents, Reticuloendothelial System (RES)-Targeted

The RES-specific contrast agents consist of a suspension of superparamagnetic iron oxide (SPIO) particles or ultrasmall superparamagnetic iron oxide (USPIO) particles. These contrast media are taken up by RES cells and produce distortions of the local magnetic field, resulting in signal loss on T2-weighted images.

▶Metastases, Hepatic

MR Mammography

Silvia Obenauer
Department of Radiology, Georg-August-University of Goettingen, Robert-koch-str. 40, Goettingen, Germany
obenauerheuser@yahoo.de

Synonyms

Magnetic resonance mammography; MR mammography (MRM); MRI mammography

Definition

Over the last few years, tremendous advances have been made in the field of magnetic resonance (MR) imaging of the breast. Developments have been made in surface coil technology, resulting in improved spatial resolution, as well as in imaging protocols, resulting in improved temporal resolution. MR mammography (MRM) has a high sensitivity of 88–100% with a relatively low specificity. Therefore, differentiation between benign and malignant lesions is often not possible. In these cases, the patient can be followed up 6 months later or they may undergo MR-guided breast biopsy. MR-guided breast biopsy techniques continue to develop.

Technique

To date, most of the breast MR imaging studies that have been reported in the literature have been performed with high-field-strength MR imaging systems (1–1.5 T). Because of the open architecture and low cost of the lower field strength, open MR systems are widely used to perform contrast-enhanced breast MR imaging at lower field strength. One concern is the signal-to-noise ratio per unit time of sampling data. The need to compromise spatial or temporal resolution is exacerbated at lower field strengths. A second issue is fat suppression, and a third aspect is the difference in contrast characteristics.

Breast Coils

Breast MR imaging is typically performed with the patient in prone position, lying on a platform placed in the MR imager, allowing the breast to extend independently of the patient. Prone patient positioning minimizes the effects of respiratory motion and is preferred to supine imaging, which results in lower image quality.

A dedicated breast surface coil should be used when performing breast MR imaging. These normally include phased-array, bilateral breast coils. The acquisition should be performed in the coronal transverse plane, with a rectangular field of view oriented with the long axis in the medial-to-lateral direction. Imaging of the transverse plane is advantageous, compared with imaging in the coronal plane, because a finding on a transverse MR image can then be correlated with a similarly positioned craniocaudal mammographic view.

Use of paramagnetic contrast agents at a dose of 0.1 mmol per kilogram of body weight is the method of choice. The contrast agent is given as bolus followed by a saline flush.

Imaging Protocols

The protocols for breast MR imaging vary dramatically. Although the hallmark of breast MR imaging is contrast-enhanced imaging, T2-weighted images can be valuable in establishing the diagnosis of a cyst or fibroadenoma. Therefore it is recommended that a fast spin-echo T2-weighted sequence through the breast be acquired

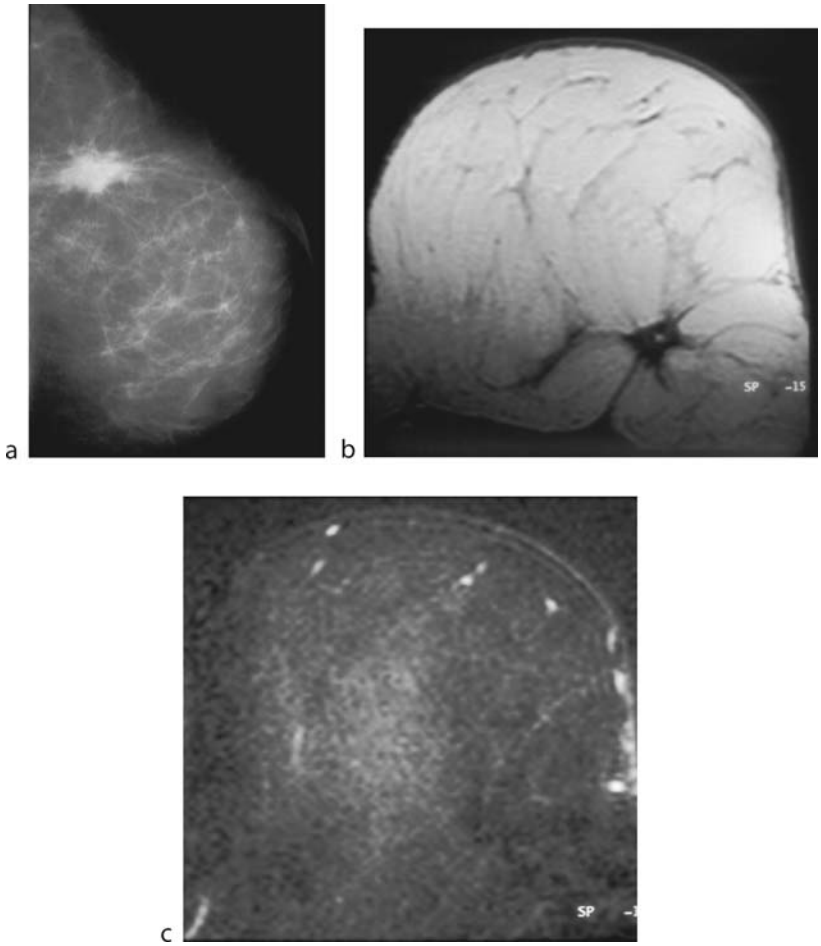

MR Mammography. Figure 1 Patient with previous tumorectomy. Focal mass on postoperative mammography (a). T1-weighted MR mammography showing a mass (b), no enhancement in subtraction image revealing a scar, and no tumor (c).

routinely before administration of contrast material. The T2-weighted sequence should be performed with fat suppression and at a section thickness of approximately 3 mm.

T1-weighted images are acquired before and after intravenous administration of contrast material. Gradient-echo sequences, two- or three-dimensional, are performed, which are much more sensitive to the T1-shortening effects of gadolinium chelates than are spin-echo sequences.

Fat Suppression

Standard presaturation of fat during every repetition time can be used. Fat suppression can also be achieved by means of postprocessing image subtraction. Identical imaging parameters before and after contrast agent administration are required. Subtracted images will yield the difference in signal intensity between the unenhanced and enhanced images, directly proportional to the degree of enhancement.

When evaluating breast MR imaging examinations, morphologic and dynamic criteria should be taken into account as classified by the ►MRM-BI-RADS.

MRM-BI-RADS

Features in MRM according to the BI-RADS classification are summarized in the chapter on the BI-RADS lexicon.

Indications for MR Mammography

In routine practice, MRM can be used to detect local recurrence in a treated breast and breast cancer in patients with axillary lymph node metastasis and no radiographic or clinical evidence of a primary breast cancer (cancer of unknown origin = CUP syndrome). MRM should be done for the detection of ruptures of silicone implants. MRM is

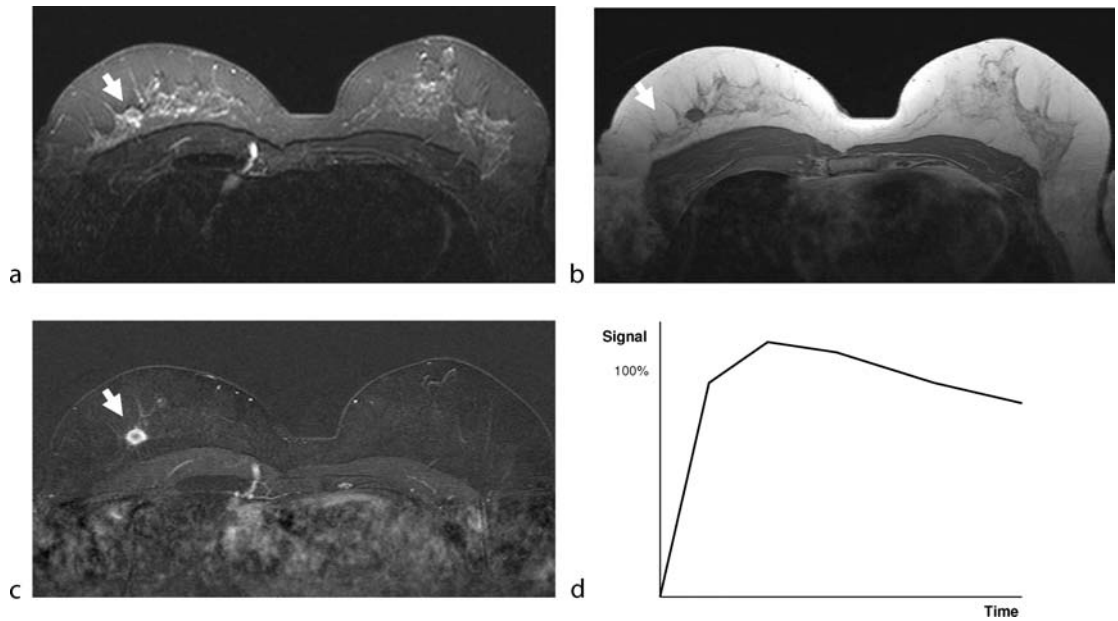

MR Mammography. Figure 2 Typical example of an invasive tumor in the right breast. T2-weighted image with intermediate signal (a), T1-weighted sequence with hypointensity of the tumor (b), and rim enhancement in the subtraction image of the irregular mass (c). In the signal intensity curve, there is initial enhancement >100% and postinitial wash-out (d).

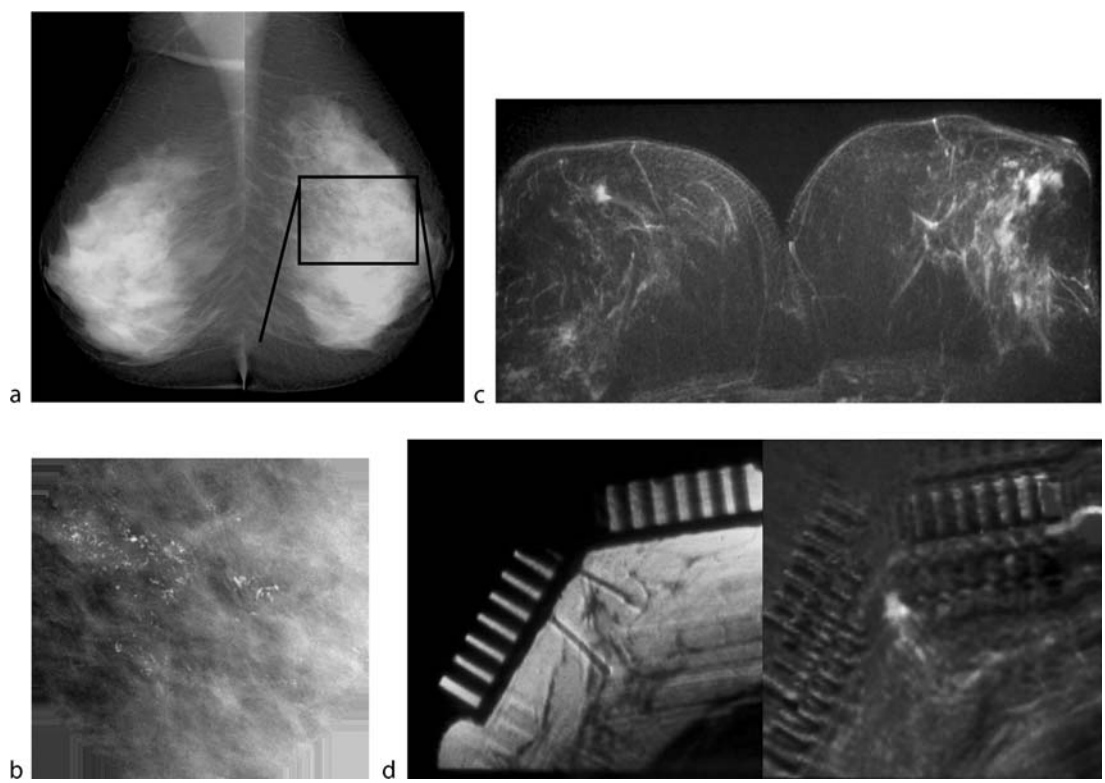

MR Mammography. Figure 3 Suspicious segmental pleomorphic microcalcification on mammography (a) of the left breast with magnification view (b). Maximum intensity image in MRM with typical diffuse enhancement in left breast directed to the nipple and with a suspicious mass in the right breast (c). Preoperative wire localization of the mass in the right breast on T1-weighted and subtraction image (d). Histology revealed a ductal carcinoma *in situ* in the left side

capable of detecting, diagnosing, and staging breast cancer preoperatively. The extent of the cancer can be determined more accurately than with conventional imaging, for example, multifocal or multicentric cancer (examples in Figs. 1–3). At present, screening MRM has not been validated and has only been evaluated in high-risk patients. Because of its high negative predictive value, MRM may be a useful adjunct for further evaluation of a dubious mammographic abnormality, such as architectural distortion. MR imaging is also used to evaluate response to neoadjuvant chemotherapy in locally advanced breast cancers.

Six months are recommended between open breast biopsy and MRM, and 12 months between surgery/radiation (lumpectomy, tumorectomy) and MRM. MRM should be done in the second phase of the menstruation cycle (Figs 1–3).

MR-guided Breast Biopsy and Localization

Different potential solutions for MR-guided breast biopsies and localizations have been used, from single breast coils to dedicated double breast coils.

Except in open magnets, the patient must be removed from the magnet for the radiologist to gain access to the breast in order to perform the localization or biopsy procedure. Because MR imaging is usually performed with the patient prone, the lateral breast is accessible, but access to the medial breast may be more difficult. After contrast medium injection, lesion conspicuity diminishes over time because of the transient nature of contrast enhancement. For MR imaging-guided surgical biopsy, confirmation of lesion retrieval is difficult because the lesion does not enhance *ex vivo*.

Bibliography

1. Orel SG (2000) MR imaging of the breast. Radiol Clin North Am 4:899–913
2. Fischer U (2000) Lehratlas der MR-Mammographie. Thieme Verlag
3. Kaiser WA (1994) False positive results in dynamic MR mammography. Causes, frequency and methods to avoid. Magn Reson Imaging Clin N Am 2:539–555, MR Mammography, Springer, Berlin 1993
4. Heywang SH, Wolf A, Pruss E et al (1989) MR imaging of the breast with Gd-DTPA: use and limitations. Radiology 171:95–103
5. Orel SG, Schnall MD (2001) MR imaging of the breast for the detection, diagnosis, and staging of breast cancer. Radiology 220:13–30
6. Ikeda DM, Hylton NM, Kinkel K et al (2001) Development, standardization, and testing of a lexicon for reporting contrast-enhanced breast magnetic resonance imaging studies. J Magn Reson Imaging 13:889–895

MR Mammography (MRM)

▶MR Mammography

MRA

Magnetic resonance angiography uses the magnetic resonance principle with radiofrequency pulse manipulations.

Rapid, relatively cheap, non-invasive technique for visualisation of the vascular tree.

▶Cerebral Aneurysms

MRCP

▶Magnetic Resonance Cholangiopancreatography

MRI Mammography

▶MR Mammography

Mucinous Carcinoma

▶Carcinoma, Other, Invasive, Breast

Mucocele

Mucoceles are defined as chronic, cystic lesions in the paranasal sinuses. They are lined by respiratory epithelium, the normal lining of the paranasal sinus, but are the result of obstruction of the sinus ostium, causing the accumulation of secretions into an expanding mass. Expansion and inflammation lead to remodeling and erosion of bone, which changes the bony architecture significantly.

▶Inflammation, Chronic, Nose, and Paranasal Sinus

Mucocele-like Tumors

Tumors composed of cysts distended with mucin that extrudes into the surrounding stroma.
▶Breast, Benign Tumours

Mucoid Impaction

Inspissated secretion in segmental bronchial obstruction.
▶Cystic Fibrosis

Mucoviscidosis

▶Cystic Fibrosis

Müllerian Duct Anomalies

MDA are an uncommon but often treatable cause of infertility. Patients with MDA are known to have a higher incidence of infertility, repeated first trimester spontaneous abortions, fetal intrauterine growth retardation, fetal malposition, preterm labor, and retained placenta. The role of imaging is to help detect, diagnose, and distinguish surgically correctable forms of MDA from inoperable forms. In some correctable lesions, the surgical approach is altered based on imaging findings.
▶ Müllerian Duct Anomalies

Multicentricity

One or more tumors are more than 2 cm away from the main tumor, often in different quadrants. Mastectomy is usually performed.
▶Carcinoma, Multiple, Breast

Multicystic Dysplastic Kidney

A congenital type of renal dysplasia, where the kidney is entirely replaced by cysts of varying sizes, with only minimal residual non-functioning dysplastic parenchyma.
▶Cystic Renal Disease, Childhood

Multidetector Computed Tomography

New generation of CT scanners where a 2D array of detector elements replaces the linear array detector elements used in typical conventional and helical CT scanners. The two-dimensional detector array allows acquisition of multiple scans simultaneously and greatly increases the speed of CT image acquisition. With MDCT thin collimation and thus the acquisition of near isotropic imaging of the urinary tract is possible. Isotropic datasets are the basis of high quality multiplanar reformations and 3D reconstructions of the organs including virtual cystoscopic views.
▶Neoplasms, Bladder

Multidetector Row CT

By using multiple rows of CT detectors, scan times can be considerably shortened and smaller slice thicknesses are possible. Improved speed enables the coverage of large volumes of anatomy in a single breath-hold whereas thinner slices produce high-quality axial and multiplanar images.
▶Neoplasms, Gastroduodenal

Multifocality

One or more masses are found in one quadrant, at a maximum of 2 cm away from the main tumor. The therapy of choice is quadrantectomy.
▶Carcinoma, Multiple, Breast

Multi-modality Imaging

Simon R. Cherry
Department of Biomedical Engineering, Center for Molecular and Genomic Imaging, University of California—Davis, Davis, USA
srcherry@ucdavis.edu

Synonym

Dual modality imaging

Definition

Each imaging modality provides specific types of information regarding the morphology, physiology, metabolism, molecular composition, or molecular pathways within biological tissue, and provides that information on a certain spatial and temporal scale and with a particular sensitivity for detection. No one imaging modality can address all measurements of interest related to a biological system; therefore, it can be advantageous to acquire images of the same subject using different modalities. *Multimodality imaging* involves the simultaneous or sequential acquisition of imaging data using two or more imaging modalities. A common example would be functional/structural imaging using nuclear medicine techniques (*PET* or *SPECT*) to measure some aspect of biologic or molecular function, combined with X-ray computed tomography (*CT*) or magnetic resonance imaging (*MRI*) to measure structure (1, 2).

Characteristics

Approaches

There are three major approaches to acquiring multimodality imaging datasets:

- *Software registration* of images acquired on two independent imaging systems. The subject is imaged on two different imaging systems at two different times. Image registration algorithms are used to co-register the imaging data from the two modalities.
- *Combined modality imaging systems* in which two separate imaging instruments are placed in close proximity (usually with a fixed geometric relationship to each other) with a common imaging stage/bed and a common software platform. The subject is moved in rapid succession through the two imaging modalities and the image data are automatically registered because of the known spatial relationship of the two systems.
- *Integrated modality imaging systems* in which the hardware of the two imaging modalities are integrated in such a way that simultaneous acquisition of the same tissue volume with the two imaging modalities is possible, with automatic registration of the datasets.

Requirements

Multimodality imaging should provide diagnostically or scientifically significant information not available from a single imaging modality. To the extent possible, the image quality of each modality employed in multimodality imaging should not be compromised to obtain multimodality datasets.

Software Approaches

Image registration algorithms have been developed for co-registering image datasets from a wide range of modalities. Approaches include the use of intensity information within the images themselves, the identification of common points within the two image datasets, matching of surface features between two imaging, and the application of external fiducial markers, affixed to the skin or bone, that can be visualized in each modality (3). Two major categories of image registration algorithms have been developed:

- *Rigid-body registration algorithms* are suited to situations in which there is no deformation of the objects to be registered between the two scans, and where the images themselves do not contain any spatial distortions. In this case, the image datasets can be matched by a simple combination of three translations and three rotations. Six parameters completely define the transformation. This approach is well suited for registering images of the human brain using modalities such as *PET*, *SPECT*, *CT*, and *MRI*.
- *Elastic or nonrigid body transformations* are used when there is spatial distortion between the two datasets. This can be caused by relative motion and changes in shape of the internal organs, for example due to differences in the exact body position on the scanner bed for each individual imaging session. Registration becomes far more complicated and can involve both globally and locally elastic parameters. The robustness of the algorithm depends on the degree of deformation that exists between the two datasets, and the

information content of the image characteristics used for co-registration. Elastic transformation algorithms are usually required for registration of images originating from the thorax or abdomen, and have been widely applied to registering *SPECT* or *PET* images with *MRI* or *CT* images.

Hardware Approaches

The most common approach to multimodality imaging systems is to combine two independent scanners with a common subject platform/bed, common control and acquisition systems, and a common display system. With careful design, each scanner operates just as well as part of such a multimodality system as it would on its own, and therefore this approach generally involves little to no compromise in image quality or performance. The advantage is that multimodality data are acquired quickly and efficiently, compared with using individual scanners. If images from the two modalities are acquired in rapid succession, then, assuming the subject does not move between the scans, and that the geometric relationship of the two instruments is known, the two image sets are registered to each other without the need for the software registration algorithms described earlier. One common form of multimodality imaging system is the PET/CT scanner. Typically, PET and CT scanners are located back-to-back, with a single patient bed that traverses both imaging systems. The PET and the CT data are acquired in rapid succession. Both SPECT/CT and PET/CT systems are now widely employed in clinical practice (1, 2), primarily for *oncology applications* (Fig. 1). They are also being developed for preclinical imaging in animal models for *molecular imaging* applications (Fig. 2).

A greater challenge is to integrate two imaging systems to enable simultaneous or rapidly interleaved acquisition of the two modalities over the same part of the body. This is important in applications where there is the desire to correlate in time, the signals from two separate modalities. An example of this would be measurements with *fMRI* and *EEG* imaging to study neuronal activation patterns and circuitry, or measurements with *PET* and *MR spectroscopic imaging* to study metabolic pathways. This type of multimodality imaging places stringent requirements on the instrumentation, as they must be able to operate at the same time, and without significant interference. It is therefore not uncommon that in these studies, the image quality of one or both modalities may be compromised compared to the results that would be obtained using each modality on its own. For successful use of such integrated modality systems, the additional information gained by the temporal correlation of the two datasets must outweigh any deterioration in image quality.

Applications

The integration of structural imaging with functional or *molecular imaging* has been by far the largest source of applications for multimodality imaging. The development of multimodality imaging, whether *via* hardware or

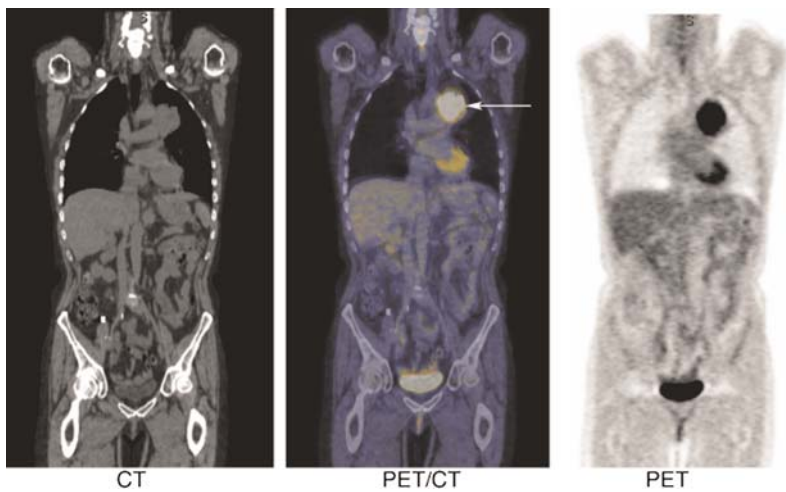

Multi-modality Imaging. Figure 1 Multimodality images from a PET/CT scanner showing high accumulation of the metabolic tracer ^{18}F-fluorodeoxyglucose in a lung tumor (*arrow*). (Images courtesy of Dr. Cameron Foster and Dr. Ramsey Badawi, UC Davis Medical Center, and reprinted with permission from the Annual Review of Biomedical Engineering, Volume 8, copyright 2006 by Annual Reviews, ►www.annualreviews.org.)

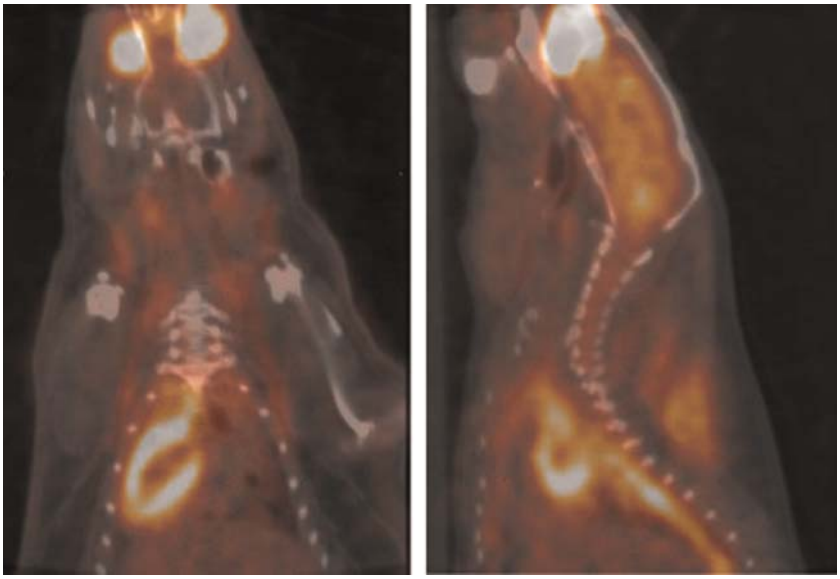

Multi-modality Imaging. Figure 2 Coronal (*left*) and sagittal (*right*) images from a multimodality PET/CT scanner showing images of a mouse. Metabolic activity imaged by PET following injection of ^{18}F-fluorodeoxyglucose (*hot wire color scale*) is fused with anatomic CT imaging (*grayscale*). (Images courtesy of Hongjie Liang, UC Davis)

software approaches, has been driven by the need to correlate function (defined in its broadest sense and including metabolism, molecular targets and pathways, immunological homing, gene expression, etc.) with its anatomic localization in the subject. Some examples of specific questions that can be addressed *via* structural–functional multimodality imaging include:

- Correlation of radiotracer uptake in suspicious lesions with CT findings to improve diagnosis and staging of cancer patients (PET/CT and SPECT/CT).
- Studying neuronal circuitry following task-specific activation (MRI/EEG).
- Surgical planning with the goal of preserving vital functions in patients with brain tumors and intractable seizures (combinations of PET, MRI, fMRI, and intraoperative optical imaging).
- Radiotherapy planning using functional imaging to better define target volume (PET/CT).
- Imaging of cell trafficking and engraftment using radiolabeled, magnetically or fluorescently labeled cells (combinations of SPECT, PET, MRI, and optical imaging).
- Imaging location and extent of gene expression in genetically engineered animal models and in monitoring of therapeutic gene delivery (combinations of PET, SPECT, optical imaging, MRI, CT).

Multimodality imaging is being used for all the applications described earlier and has become a widely accepted approach to problems ranging from molecular imaging basic science investigations in small animal models through to advanced diagnostics in the clinic.

In addition to the obvious advantages of correlating structure and function through multimodality imaging, there often are additional benefits in which the two modalities can be used in a synergistic fashion to actually improve image quality or image quantification. For example, in SPECT/CT and PET/CT imaging, the CT scan can be used to correct for tissue attenuation of the photons emitted in the PET or SPECT scans, thus improving quantification of radiotracer uptake. It may also be possible to incorporate anatomical information from MRI or CT into the reconstruction of PET, SPECT, and optical imaging datasets to improve quantification of the distribution of radiotracer or fluorescent probes *in vivo*.

A new class of multimodality applications involves the use of two functional imaging modalities to measure two different biological parameters at the same time. Combinations of modalities that are in the early stages of being explored include PET/optical, PET/ultrasound, ultrasound/optical, and PET/MR spectroscopy. Multimodal contrast agents, imaging probes, and imaging reporter gene systems are also being developed. These will open up new opportunities for studying interactions within biological systems, for example the interaction of a drug with its target and its effect on the function of that target, or the flux through two competing pathways following a targeted intervention on one of the pathways.

Bibliography

1. Townsend DW, Cherry SR (2001) Combining anatomy and function: a path to true image fusion. Eur Radiol 11:1968–1974
2. Hasegawa BH, Iwata K, Wong KH et al (2001) Dual modality imaging of function and physiology. Acad Radiol 9:1305–1321
3. Hill DLG, Batchelor PG, Holden M et al (2001) Medical image registration. Phys Med Biol 46:R1–45

Multiphase Bone Scintigraphy

Literally, the bone scintigraphy is the investigation approximately 3 h after intravenous injection of the radiotracer, when a good bone/soft tissue ratio is reached. For certain indications, early phases are added to the investigation using the same radioactivity, which is applied anyway. The radionuclide angiography is performed immediately after injection and reflects arterial perfusion. Early static images acquired a few minutes later display the blood pool.

▶Bone Scintigraphy

Multiple Endocrine Neoplasia (MEN) Syndrome

MEN syndrome is a hereditary disorder that involves many glands. There are three forms: MEN 1, MEN 2a, and MEN 2b. MEN 1 is characterized by development of excessive normal tissue (hyperplasia) or an adenoma (tumor) of the parathyroid, pancreas, pituitary, adrenals (rarely), or thyroid gland (rarely). MEN 2a is characterized by medullary thyroid cancer, unilateral or bilateral pheochromocytoma, and primary parathyroid hyperplasia. MEN 2b is characterized by medullary thyroid cancer and pheochromocytoma, but not hyperparathyroidism.

▶Neoplasms, Thyroid, Benign and Malignant

Multiple Myeloma

Most frequent primary malignant neoplasm of the bone marrow (proliferation of B-lymphocytes) in older patients. MRI is more sensitive than radiographs and CT to stage disease. May have a focal, variegated, or diffuse pattern in the MR images.

▶Myeloproliferative Disorders

Multiple Sclerosis

M. A. Sahraian[1], E. W. Radue[2]
[1]Department of Neurology, Sina Hospital, Hassan abad Square, Tehran, Iran
[2]Department of Neuroradiology, University Hospital, Petersgraben 4, 4031 Basel, Switzerland
eradue@uhbs.ch

Definition

Multiple Sclerosis (MS) is an inflammatory demyelinating disease of the central nervous system (CNS) with various degrees of axonal loss. MS most commonly affects young adults between the age of 20 and 40 years and leads to significant neurological disability after 10 to 15 years. The disease favors women over men by a ratio of nearly 2 to 1 and is clinically defined as a predominantly white matter disease distributed in both time and space. There could be a relationship between environmental factors and genetic predisposition. Genetic studies have convincingly shown that multiple genes are involved. The mechanism of these genetic factors and their interactions with the environmental agents in establishing the disease are largely unknown.

In general, the first-degree relatives of probands have a higher risk for developing the disease than the general population. Migrational studies stressed the importance of environmental factors.

There is also a geographic preference for people living in Northern latitudes and Caucasians are considerably more susceptible than Asians or Blacks (1, 2).

Pathology/Histopathology

MS is considered an autoimmune disorder in which autoreactive T-cells drive an inflammatory process leading to myelin oligodendrocyte destruction and axonal loss. The external appearance of the brain is usually normal but slight atrophy with widening of the sulci and enlargement of the ventricles may be seen in some chronic cases.

In sectioning, lesions of varying size become apparent in the white matter of the CNS. The major characteristic of these lesions is focal demyelination.

Different mechanisms are involved in myelin destruction. T-cell, macrophage-mediated myelin damage and precipitation of immunoglobulin with complement fixation are two major phenomenons leading to myelin destruction in MS plaques.

The following four patterns of demyelination have been identified:

Patter I: T-cell/macrophage-mediated demyelination
Patter II: Antibody/complement-mediated demyelination
Patter III: Oligodendrocyte dystrophy with oligodendrocyte apoptosis
Patter IV: Primary oligodendrocyte degeneration with features similar to viral infection or toxic oligodendrocyte damage but not to autoimmunity.

It has been convincingly demonstrated that axonal injury occurs during lesion formation, even in the early stage of MS. Axonal loss is probably the principle determinant of irreversible neurological disability and progressive course (2, 3).

Clinical Presentation

The symptoms of MS vary depending, in part, upon the location of the plaques within the CNS. Weakness in one or more limbs, optic neuritis, paresthesia, and diplopia are the most common presenting symptoms. Other common manifestations include bladder and bowl dysfunction, sexual problems and ataxia. Fatigue is one of the most common complaints reported by the patients and signs of cognitive dysfunction can be detected in about half of the patients using neuropsychological investigations (1).

Four different clinical courses have been described for Multiple Sclerosis:

The first, "relapsing-remitting" MS is characterized by self-limited attacks of neurological dysfunction followed by remission over the next several days or weeks. Most of these patients will evolve into a "secondary progressive" type characterized by a chronic and steady increase of disability. If the patients have a steady neurological decline from the onset, without relapse, they are described as "primary progressive" type of MS.

"Progressive-relapsing" are the patients who have a progressive course from the beginning although they also experience occasional attacks. It should be noted that a small group of patients will remain clinically stable and fully functional for 15 years after the onset of symptoms (benign MS), however, most patients develop moderate to severe disability in this period of time (1, 3).

Imaging

Computer tomography is now rarely used in the diagnosis and follow-up of MS. With CT, it was possible to visualize just some of the MS lesions. In longstanding and severe cases, ventricular dilatation and cortical atrophy can be observed.

MRI has a far better sensitivity for identifying MS plaques and now plays an essential role in initial evaluation of MS patients, predicting prognosis in patients presenting with symptoms highly suggestive of acute inflammatory CNS demyelination and in providing primary outcome measures in phase I and II trials of MS therapeutics.

Three main groups of lesions can be identified with conventional MR imaging. These include acute lesions demonstrating blood-brain-barrier leakage on contrast-enhanced MR images (enhancing lesions), chronic severely damaged areas that are hypointense on T1 images with contrast (chronic black holes), and hyperintense T2 lesions.

MS Lesions in T2-Weighted Images

Focal white matter areas of increased signal intensity in T2 WI images are the characteristic appearance of multiple sclerosis. They are usually round or oval in appearance with a variable size and with the major axis perpendicular to the corpus callosum (Dawson's fingers). They tend to be located in periventricular areas but other common sites are subcortical and infratentorial regions.

Inflammation, demyelination, gliosis, edema, and axonal loss will increase the signal intensity on T2 WI images without any specific pattern. This lack of pathological specificity is one of the possible reasons for poor correlation between T2 WI lesions and disability in MS.

Lesions in the cerebrum are much more likely to be clinically silent compared with those in the brain stem or spinal cord.

The increase in lesion-brain contrast of fluid attenuated inversion recovery (FLAIR) images results in better lesion detection particularly in the subcortical region. Signal suppression from bulk water in CSF also increases depiction of lesions in periventricular area. Flow artifacts and lower sensitivity for posterior fossa are two disadvantages of this technique (Fig. 1).

Enhancing Lesions

Enhancing lesions are the lesions that appear hyperintense after the administration of contrast agent in T1 WI images due to impairment of the blood-brain-barrier.

In MS, most new lesions go through a phase of enhancement usually persisting for 2 to 6 weeks and rarely for 3 to 4 months. Once contrast enhancement ends, the hypointense lesions may become isointense or develop into persistent black holes. In fact, less than 40% of gadolinium-enhancing lesions develop into chronic black holes (Fig. 2).

MS Lesions in T1-Weighted Without Contrast

A black hole (BH) is defined as any hypointense region visible on T1 WI sequences correlating with a region of

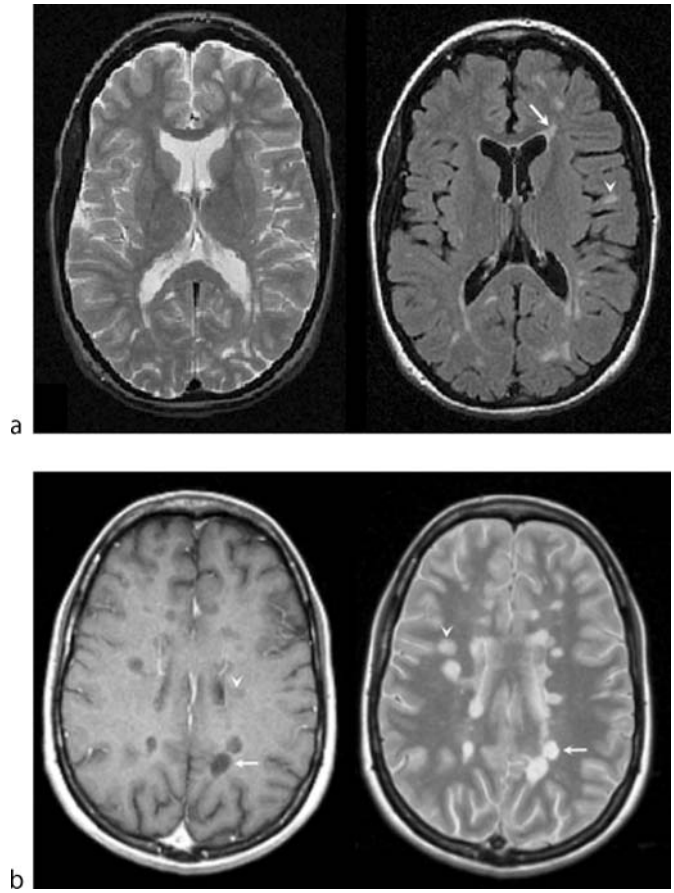

Multiple Sclerosis. Figure 1 (a) T2 WI left and FLAIR right sequence of a patient with RRMS, show hyperintense white matter lesions. Note that FLAIR is superior in demonstrating periventricular (*arrow*) and subcortical lesions (*arrow head*). (b) Axial T2 WI (*right side*) demonstrate multiple hyperintense lesions typical for MS (*arrow*) in periventricular and subcortical area (*arrow head*). T1 WI with contrast (*left side*) demonstrate multiple hypointense lesions (*black holes*) with different degrees of hypointensity.

high signal intensity on T2 WI images. Black holes are considered to be acute when they coincide with a contrast-enhancing lesion (CEL) and to be persistent when no corresponding CEL exists.

There are several different reports about the correlation of T1 WI black holes and disability. In some studies, T1 lesion load showed a higher correlation with the expanded disability status scale (EDSS) for patients with RRMS or secondary progressive in cross sectional studies.

T1 hypointensity is in principle caused by an expansion of the extracellular space either by an increase in water content or the loss of structural components. In fact the pathological correlates of T1 hypointense lesions are dependent, in part, on the lesion age.

T1 black holes typically begin as contrast-enhanced lesions and evolve differently from patient to patient and also within the same patient. Their intensities are different from black like cerebrospinal fluid to light gray like cerebral cortex. The enhancing lesions that appear hypointense in noncontrast images may become isointense to the normal appearing white matter or develop into chronic black holes. The longevity of persistent BHs may vary after contrast enhancement. Some lesions may be visible for a relatively short period of time, some enlarge or shrink and some others may eventually become permanent.

Volumetric Changes

Brain atrophy is another imaging hallmark of multiple sclerosis. It usually appears as enlarged ventricles and a reduced size of corpus callosum. Atrophy is seen in all stages in a progressive manner, including patients with early MS. The exact mechanism is not clear but demyelination and axonal loss seem to be the main causes. The quantitative measure of atrophy has been studied and sometimes included as an outcome measure in clinical trials.

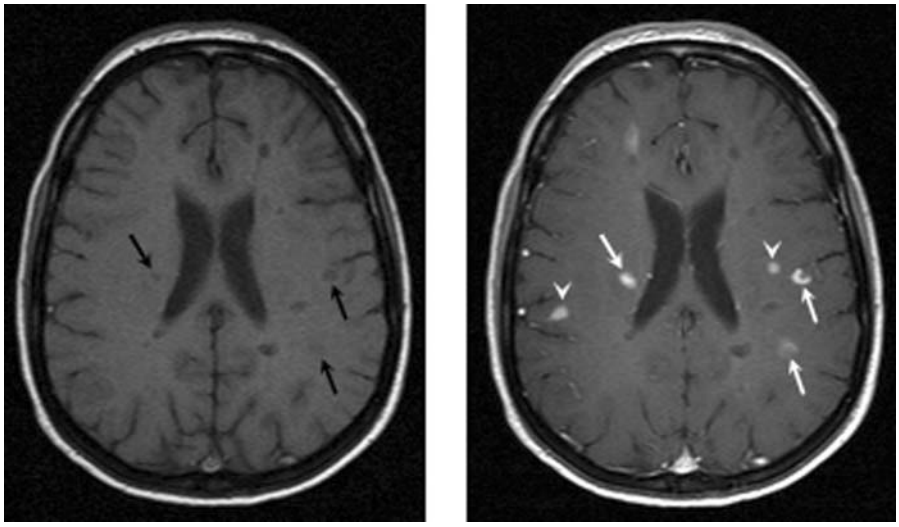

Multiple Sclerosis. Figure 2 T1W images with left and without right contrast in a patient with RRMS demonstrate Several enhancing lesions. Some of these lesions have corresponding hypointensity on TWI without contrast (*arrows*).

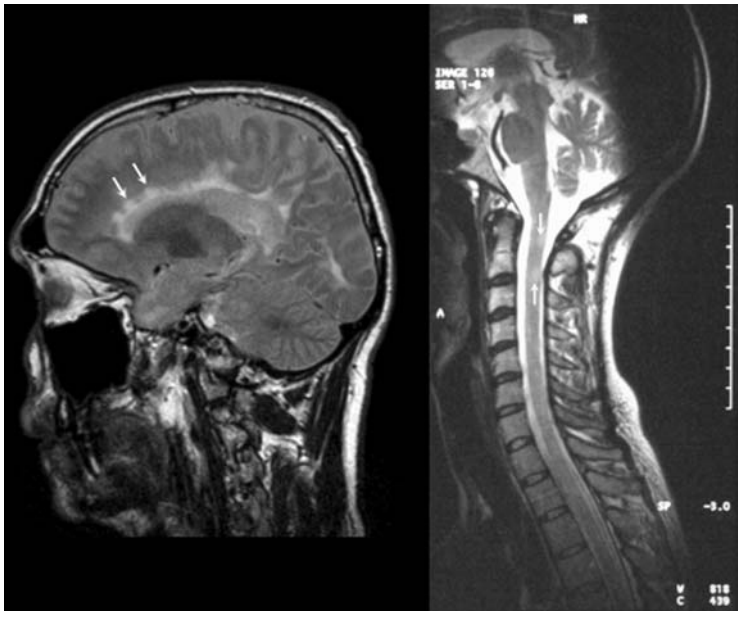

Multiple Sclerosis. Figure 3 Sagittal T2 WI of patient with MS demonstrates typical spinal cord lesions (*right side*) most commonly seen in cervical part (*arrows*). Sagittal T2 WI of another MS patient (*left side*) with multiple hyperintense lesions typical for MS (*arrows*).

Diagnosis

MS is a clinical diagnosis, dependent on a detailed history, neurologic examination and supportive paraclinical investigations. In fact, the diagnosis is based on the principle of dissemination in time and space of a disease compatible with MS in the absence of better explanations.

The previous diagnostic criteria for MS was codified by Poser for use in clinical trials of MS and included clinically definite MS, laboratory (cerebrospinal fluid) supported definite, probable, and possible MS.

As MRI was relatively new at that time, it was included as paraclinical element to support the diagnosis.

In the new McDonald criteria, the diagnosis of MS also requires evidence of lesions disseminated in time and

Multiple Sclerosis. Table 1 The 2005 revisions to the McDonald diagnostic criteria for multiple sclerosis

Clinical presentation	Additional data needed for diagnosing MS
Two or more attacks[a]; objective clinical evidence of two or more lesions	None[b]
Two or more attacks[a]; objective clinical evidence of one lesion	Dissemination in space demonstrated by: MRI[c] *or* Two or more MRI-detected lesions consistent with MS plus positive CSF[d] *or* Await further clinical attack[a] implicating a different site
One attack[a]; objective clinical evidence of two or more lesions	Dissemination in time demonstrated by: MRI[e] *or* Second clinical attack[a]
One attack[a]; objective clinical evidence of one lesion (monosymptomatic presentation; clinically isolated syndrome)	Dissemination in space demonstrated by: MRI[c] *or* Two or more MRI-detected lesions consistent with MS plus positive CSF[d] *and* Dissemination in time demonstrated by: MRI[e] *or* Second clinical attack[a]
Insidious neurological progression suggestive of MS	One year of disease progression (retrospectively or prospectively determined) *and* Two of the following: positive brain MRI (nine T2 lesions or four or more T2 lesions with positive VEP)[f] Positive spinal cord MRI (two focal T2 lesions) Positive CSF[d]

If criteria indicated are fulfilled and there is no better explanation for the clinical presentation, the diagnosis is MS; if suspicious, but criteria are not completely met, the diagnosis is "possible MS"; if another diagnosis arises during the evaluation that better explains the entire clinical presentation, then the diagnosis is "not MS."

[a]An attack is defined as an episode of neurological disturbance for which causative lesions are likely to be inflammatory and demyelinating in nature. There should be subjective report (back up by objective findings) or objective observation that the event lasts for at least 24 h.

[b]No additional tests are required; however, if tests (MRI, CSF) are undertaken and are negative, extreme caution needs to be taken before making a diagnosis of MS. Alternative diagnosis must be considered. There must be no better explanation for clinical picture and some objective evidence to support a diagnosis of MS.

[c]MRI demonstration of space dissemination must fulfill the criteria derived from Barkhof and colleagues and Tintore and coworkers as presented in the text.

[d]Positive CSF determined by oligoclonal bands detected by established methods (isoelectric focusing) different from any such bands in serum, or by an increased IgG index.

[e]MRI demonstration of time dissemination must fulfill the criteria explained in the text.

[f]Abormal VEP of type seen in MS (5).

space but MRI findings have a major impact in this regard.

Dissemination in space can be demonstrated by the Barkhof MRI criteria which requires 3 out of the following 4 elements

- At least one Gd-enhancing lesion or nine T2 hyperintense lesions
- At least one infratentorial lesion
- At least one juxtacortical lesion
- At least three periventricular lesions.

In this criteria spinal cord imaging can be helpful in fulfilling the criteria for dissemination in space. A spinal cord lesion is equivalent to, and can substitute, for a brain infratentorial lesion, but not for a periventricular or juxtacortical lesion; an enhancing spinal cord lesion is equivalent to an enhancing brain lesion and an enhancing spinal cord lesion can count doubly in fulfilling the criteria (e.g., a single enhancing spinal cord lesion can "count" for an enhancing lesion and an infratentorial lesion and individual spinal cord lesions can contribute together with individual brain lesions to reach the required lesions to satisfy Barkhof criteria.

MRI can also assist in demonstrating dissemination in time. According to revised McDonald criteria any new T2 lesion if it appears at any time compared with a reference scan done at least 30 days after the onset of initial clinical event or detecting a new Gd-enhancing lesion at least 3 months after the onset of the initial clinical event, if not at the site corresponding to the initial event can demonstrate dissemination in time (Fig. 3).

Table 1 shows the 2005 revision to the McDonald diagnostic criteria for MS (1, 5).

Bibliography

1. Inglese M (2006) Multiple sclerosis: new insights and trends. Am J Neuroradiol 27:954–957
2. Hafler DA (2004) Multiple sclerosis. J Clin Invest 113:788–794
3. Ge Y (2006) Multiple sclerosis: the role of MR imaging. Am J Neuroradiol 27:1165–1176
4. Bakshi R, Minagar A, Jaisani Z et al (2005) Imaging of multiple sclerosis: role in neurotherapeutics. NeuroRx 2:227–303
5. Polman CH, Reigold SC, Eden G et al (2005) Diagnostic criteria for multiple sclerosis: 2005 revision to the "McDonald Criteria". Ann Neurol 58:840–846

Multi-pulse Techniques, Contrast Media, Ultrasound

Multi-pulse techniques are used in microbubble specific imaging for two key purposes. Firstly, a phase and/or amplitude modulated pulse train can be used to preferentially detect the non-linear response of the microbubbles to differing acoustic stimuli against the linear tissue background. Secondly multiple pulses can be used to provide information on the motion of the microbubbles within the circulation, in the same way that multiple pulses are processed for colour or power Doppler imaging.

See under Contrast media, ultrasound, specific imaging techniques, phase modulation, amplitude modulation for further details.

Multislice Computed Tomography

▶Ischemic Heart Disease, CT

Musculoskeletal Radiology

Thomas M. Link
Department of Radiology, University of California, San Francisco, CA, USA
tmlink@radiology.ucsf.edu

Introduction

Musculoskeletal radiology has emerged as an important subspecialty in radiology and currently gains increasing significance due to sports- and age-related diseases of the musculoskeletal system. A number of imaging modalities are available, the most important being conventional radiography and magnetic resonance imaging (MRI). *Conventional radiography* (CR) is the basic technique to image bones and calcified soft tissue changes; it should be performed before more advanced imaging modalities are applied. CR is very useful to characterize focal and generalized bony disorders but also calcified soft tissue lesions. In the last 20 years, MRI has gained a tremendous importance in the depiction of bone, bone marrow, joints, and soft tissue structures. It is the most sensitive technique to depict (1) bone marrow morphology and pathology, (2) joint disorders including ligamentous and cartilage lesions, and (3) soft tissue pathology. MRI is extremely sensitive but sometimes not very specific in diagnosing specific disease entities. *Computed tomography* (CT) is used less frequently for the assessment of musculoskeletal disease but has a number of important indications such as the assessment of fractures, in particular in the spine and pelvis, and the stability of these fractures. CT may also be very useful in characterizing focal bony and calcified soft tissue pathology, not well-accessible with plain radiographs such as in the pelvis and shoulder. In addition, CT is used for image guided procedures such as bone biopsies and osteoid osteoma ablations. *Ultrasound* is less suited for bone pathology but may be used to depict soft tissues such as tendons and the rotator cuff of the shoulder. With Doppler ultrasound, vascularized lesions may be better characterized.

Musculoskeletal radiology can be structured according to disease entities in general or according to anatomy associated pathology. In this hyperessay, we are focusing on the different pathological entities that will subsequently be presented in the individual essays.

Trauma

Fractures usually are diagnosed on conventional radiographs, which should be obtained at least in two different projections. CT is useful in depicting the true extent of fracture, in particular in complex injuries. MRI, the imaging modality of choice for many musculoskeletal injuries, shows occult osseous (such as bone contusions) and osteochondral injury as well as tendon, ligament, and muscle injuries (15).

Among the *peripheral fractures* those of the distal radius are one of the most frequent fracture types (Fig. 1). In the wrist, CT and MRI accurately depict radiographically occult carpal bone fractures especially those of the scaphoid. In the preoperative planning of complex wrist fractures CT is of value, while MRI is very sensitive in the detection of posttraumatic complications such as avascular necrosis. Proximal humerus fractures, frequently seen in older patients, may require surgery if significant segment displacement is present, i.e., more than 45°C of angulation or more than 10 mm separation between fracture fragments according to Neer. True extent of these fractures is frequently underestimated in radiographs and requires CT for further assessment. Joint luxation is seen most frequently in the shoulder; associated lesions include Hill–Sachs defect and Bankart lesions. Fractures of the proximal femur are a frequent

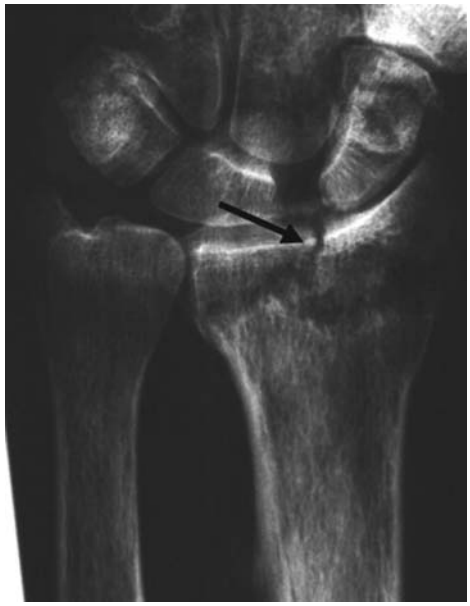

Musculoskeletal Radiology. Figure 1
Dorso-palmar radiograph of the wrist showing a distal radius fracture with intraarticular extension (arrow).

complication of osteoporosis and may be divided into femur neck and intertrochanteric fractures. Imaging of tibial plateau fractures in the knee is particularly crucial for good postoperative results, requiring CT and MR imaging. Fractures with a depression of less than 5 mm may be treated operatively. Segond fractures are avulsion injuries of the lateral tibia due to excessive tension on the lateral capsular ligament of the knee. These fractures usually herald extensive damage of the knee such as anterior cruciate ligament fractures. Supination injuries in the ankle are frequently found and may result in fractures of the distal fibula. In the foot, the calcaneus is the most commonly fractured tarsal bone.

In *spine and pelvic fractures*, CT is usually required to assess whether fractures are stable and to plan operative interventions. 2D-reformations of these images and 3D-renderings are required and may be easily obtained with modern Multislice-CT scanners (18).

In children, *growth plate fractures* are particularly important since they may result in growth disturbances, and these are usually categorized according to the Salter–Harris classification.

Stress fractures may be divided into fatigue fractures, which are due to repetitive abnormal stress to a bone with normal elastic resistance and insufficiency fractures that occur when the elastic or mineral resistance of the bone is inadequate to withstand the stresses of normal activity (Fig. 2). The latter fractures are typically found in osteoporosis.

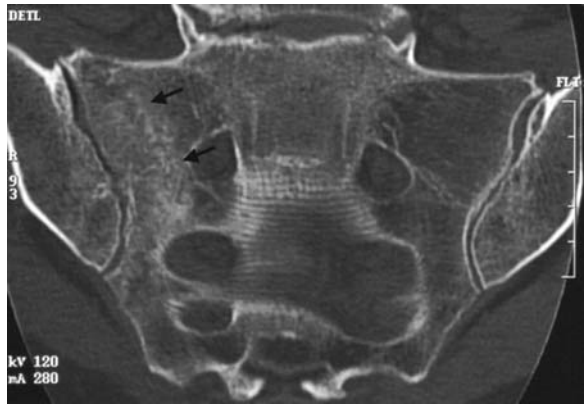

Musculoskeletal Radiology. Figure 2 CT of the sacrum with coronal reformation depicting a right-sided insufficiency fracture of the sacrum (arrow).

Inflammatory Diseases

Infectious Diseases

Septic osteomyelitis or arthritis may be due to bacteria such as *Staphylococcus aureus* or less frequently due to gram negative, mycobacterial, and fungal organisms. Four principal routes of contamination are observed: (1) hematogenous spread via the bloodstream, (2) spread from a contiguous source of infection such as infected sinus, cutaneous abscesses or dental infections, (3) direct implantation due to trauma, or (4) postoperative infection. Depending on the virulence of the organism osteomyelitis may have a more acute, subacute or chronic course. Conventional radiographs show associated pathology relatively late. At the earliest 3 days after bacterial contamination, subtle changes of the soft tissues may be observed. Typical signs after 1 to 2 weeks are lucent lesions, which may be focal or more diffuse, periosteal changes, and cortical resorption. In less aggressive lesions or a more chronic course of disease, sclerosis may be a more predominant finding (Fig. 3) and lesions may be well-defined. These lesions include Brodie's abscess and Garre's sclerosing osteomyelitis. Early diagnosis in bone infection may be best achieved with MRI, which shows focal lesions and reactive edema (low in signal in T1, high in signal in T2, and contrast enhancement in T1-weighted sequences) very sensitively (14). However, differential diagnosis to neoplastic lesions may be sometimes be difficult.

Rheumatoid Arthritis and Related Diseases

Rheumatoid diseases affecting the joints and spine include rheumatoid arthritis but also seronegative spondyloarthropathies such as psoriatic arthritis, ankylosing spondylitis, and Reiter's disease. Rheumatoid arthritis is a fairly

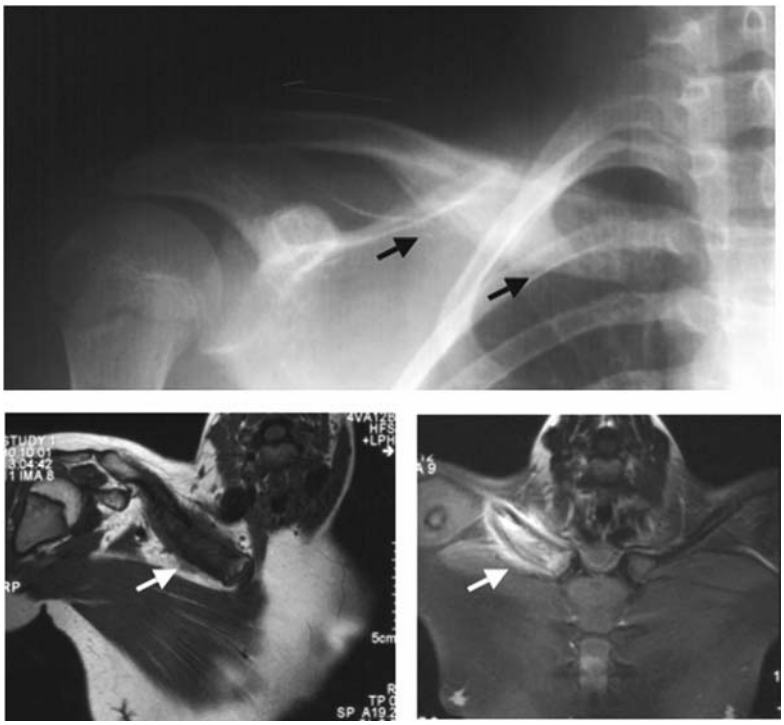

Musculoskeletal Radiology. Figure 3 Conventional radiographs, T1-weighted and fat saturated T1-weighted contrast-enhanced spinecho MR images of the right clavicula. The radiograph shows sclerosis and increased diameter due to periostitis of the clavicula (black arrows). The MR images depict low signal of the clavicula on the T1-weighted images while the contrast-enhanced images show contrast uptake with high signal in the clavicula (white arrows). These findings are consistent with osteomyelitis.

common disease, most commonly affecting middle-aged women. The joints most commonly involved are the hands and feet (Fig. 4). In radiographs, soft tissue swelling, juxtaarticular osteopenia, and later joint erosions are shown. In the hands, the most frequently affected joints are metacarpo-phalangeal joints as well as the intercarpal, radio-carpal, and ulno-carpal joints. At later stages of disease erosive changes of the upper cervical spine may occur with instability at the level of C0–C2. Ankylosing spondylitis usually affects younger males and has an insidious onset with low back pain. Most commonly the sacroiliac joints are affected first and show erosive and proliferative changes as well as sclerosis. Ankylosis is found in advanced stages. Conventional radiographs usually show these changes at a relatively advanced stage while MRI is more suited to detect early changes (17). Typical changes at the spine are shining corners (Romanus lesions), squaring, syndesmophytes, and discovertebral destructions. Psoriatic arthritis is found in 2–6% of patients with psoriasis (13). Typical features of psoriasis arthritis are erosive and proliferative changes at the joints with less pronounced osteoporosis. In the hands, individual fingers or/and the distal interphalangeal joints are affected typically. Retrocalcaneal bursitis, sacroiliac arthritis, and paravertebral ossifications are other typical changes found in this disease. Reiter's syndrome, enteropathic arthropathies, Behcet's syndrome are rare diseases that may also cause arthritis, sacroiliitis and spine changes.

Other diseases that cause polyarthritis and arthropathies are systemic lupus erythematosus, progressive systemic sclerosis, dermatomyositis and polymyositis, mixed connective tissue disease, rheumatic fever, and vasculitides such as polyarteritis nodosa.

Degenerative Diseases

Degenerative joint disease is found in the aging individual and is nowadays considered as one of the most important joint diseases and a major cause of disability. Osteoarthritis has typical imaging features on radiographs including osteophytes, subchondral sclerosis, and cyst formation (Fig. 5). Enthesophytes at the osseous sites of tendon attachment are also frequent findings in degenerative disease. Sometimes degenerative joint disease shows an erosive pattern, which may be difficult to differentiate from inflammatory, rheumatoid joint disease.

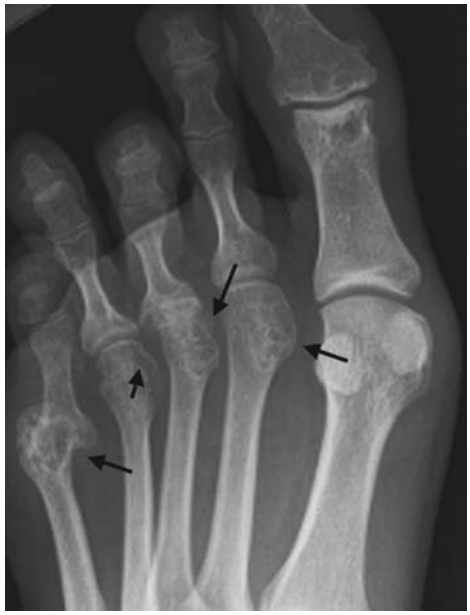

Musculoskeletal Radiology. Figure 4
Conventional dorsoplantar radiograph of the left foot with erosions of the second to fifth metatarsal heads and the first intertarsal joint as well as subluxation in the fifth and third metatarsophalangeal joint consistent with rheumatoid arthritis (black arrows).

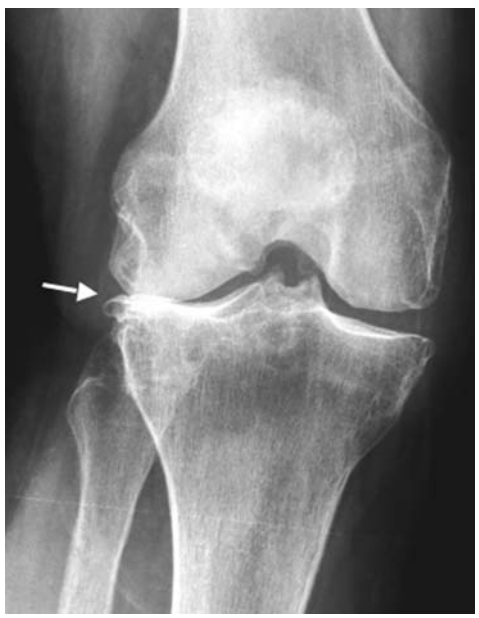

Musculoskeletal Radiology. Figure 5
Conventional anteroposterior radiograph of the right knee joint with medial joint space narrowing, subchondral sclerosis, and osteophytes (arrow) consistent with osteoarthritis of the knee.

Degenerative disease of the spine shows a typical pattern on conventional radiographs with a variety of morphologic signs such as osteochondrosis with disc space narrowing and reactive sclerosis, spondylosis deformans, and osteoarthritis of the facet joints. During the course of disease degenerative spondylolisthesis, retrolisthesis, vertebral alignment disorders, spinal stenosis, and segmental instability may occur. Another important entity is posterior disc displacement due to degenerative disk disease (11). This may manifest as anular bulge, discal protrusion (displaced nucleus pulposus extends through some fibers of the annulus fibrosus but is still confined by the intact outmost fibers), discal extrusion (nucleus penetrates all of the fibers of the annulus and lies under the posterior longitudinal ligmanent), and discal sequestration (displaced nucleus penetrates or extends around posterior longitudinal ligament and lies within epidural space or the displaced nucleus migrates a considerable distance in a cranial or caudal direction).

In *diffuse idiopathic skeletal hyperostosis* (*DISH*) abnormal bone formation is found where tendons and ligaments attach to bone, predominantly in the spine. Diagnostic criteria for spinal involvement in DISH are (1) flowing ossification or calcification along the anterolateral aspect of at least 4 contiguous vertebrae, (2) preserved intervertebral disc height and absence of extensive degenerative disc disease, and (3) absence of apophyseal joint ankylosis and sacroiliitis (13).

Crystal-Induced and Related Diseases

Calcium pyrophosphate deposition disease (*CPDD*) is observed in middle-aged and elderly patients and may mimic a variety of other conditions such as rheumatoid arthritis, gout and degenerative joint disease. A variety of names have been used to describe CPPD including pseudogout, chondrocalcinosis, articular and periarticular calcification, and pyrophosphate arthropathy. Radiologic features include (1) calcification of the hyaline cartilage and fibrocartilage such as the menisci (Fig. 6) and the triangular cartilage of the wrist, (2) synovial calcification, (3) capsular calcification as well as (4) tendon, bursa and ligament calcification (1). Calcium hydroxyapatite crystal deposition and CPDD may occur both in the same patient, even the same joint.

Calcium hydroxyapatite crystal deposition disease (*HADD*) results in granular periarticular accumulations of calcium hydroxyapatite most commonly found in the shoulder. These deposits may appear thin, cloud-like and poorly defined but with time they get denser, more homogeneous and more sharply delineated. In these

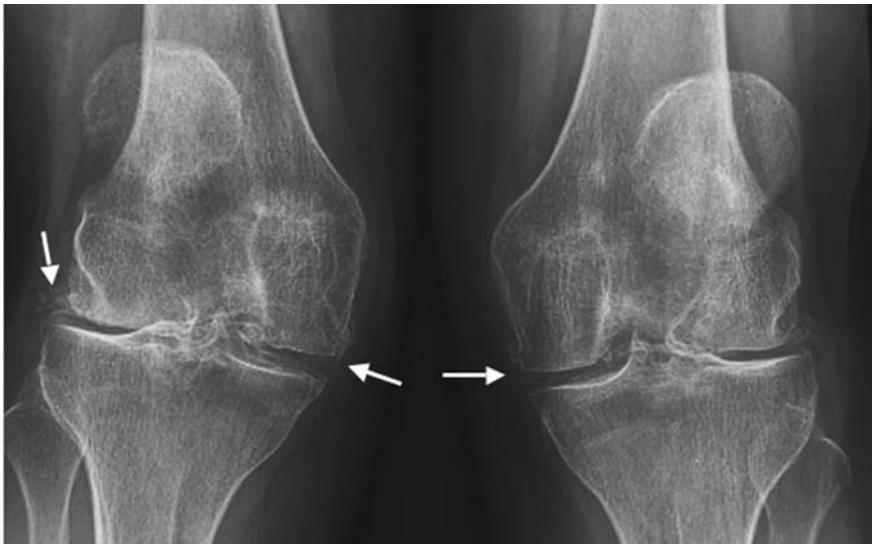

Musculoskeletal Radiology. Figure 6 Conventional anteroposterior radiograph of both knee joints with calcification of the menisci, the hyaline cartilage and synovial, and capsular calcifications (arrows) consistent with CPDD.

patients, acute or chronic symptoms may be found, including pain, tenderness, swelling, and restricted motion of the joint.

Gout (*monosodium urate crystal deposition disease*) may lead to an arthritis that has an asymmetric polyarticular involvement and predominantly affects feet, hands, wrists, elbows, and knees. Radiographic signs of gout are usually found late in the course of the disease and may only show those of degenerative disease or (1) lobulated eccentric soft tissue masses, (2) intraarticular or extraarticular bone erosions with relative preservation of the interosseous joint space, (3) subperiosteal apposition of bone, and (4) intraosseous calcification. Idiopathic gout is far more frequently in males than in females and occurs most frequently during the fifth decade of life.

Neuropathic Joint Disease

Neuroarthropathy may be caused by central or peripheral neuronal lesions, such as syringomyelia, meningomyelocele, trauma, diabetes mellitus, alcoholism, amyloidosis, and administration of corticosteroids. The deprivation of sensory feedback in the joints leads to continuous stress and progressive deterioration. Radiographic signs include (1) joint space narrowing, (2) fragmentation, (3) sclerosis of bone, (4) osteophytosis, and (5) subluxation (Fig. 7) (6).

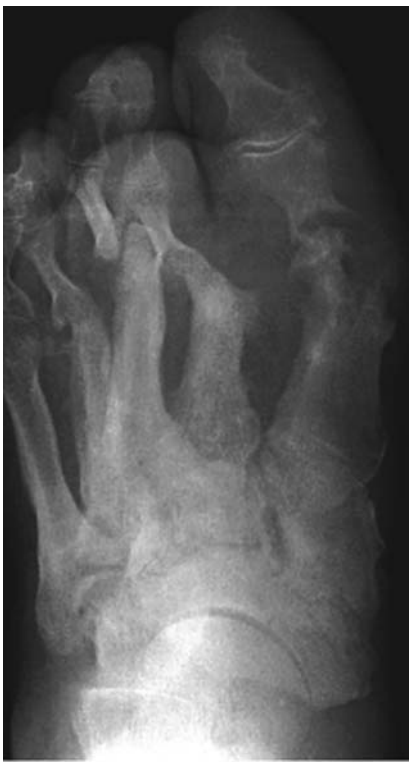

Musculoskeletal Radiology. Figure 7 Conventional dorsoplantar radiograph of the left foot with extensive destructions of the metatarsophalangeal joints corresponding with neuropathic joint disease.

Metabolic and Endocrinological Diseases

Osteoporosis is the most frequent metabolic disease and is defined as a disease, which is associated with a loss of bone mass and a deterioration of bone structure, both resulting in an increased bone fragility and susceptibility to fracture (Consensus, 1993 #363). Since the bone density, the parameter which can be determined best *in vivo*, has a high precision and correlates well with the biomechanically determined bone strength the WHO defined osteoporosis in postmenopausal females on the basis of the individual's bone mineral density compared to a young normal reference population (WHO, 1994 #362).

As populations age the incidence of osteoporosis and subsequent fractures is increasing. According to the international Osteoporosis Foundation, more than 40% of middle-aged women will suffer one or more osteoporotic fractures during their remaining lifetime. The most important fracture sites are the proximal femur, the spine and the distal radius. Hip fractures are the worst complication of osteoporosis with substantial morbidity and high one-year mortality. Vertebral fractures occur with a higher incidence earlier in life than other types of osteoporotic fractures (Fig. 8). However, it is difficult to determine the exact number of fractures that occur annually as a substantial proportion are clinically undetected.

Diagnostic techniques to determine bone mineral density include dual X-ray absorptiometry (DXA) and quantitative CT (QCT) (9). DXA of the spine and the hip (Fig. 9) in an anterior–posterior projection are the most frequently used examinations. The areal bone mineral density values obtained from these examinations are compared to a young normal and to an age-matched population (Fig. 9).

Rickets and osteomalcia are due to abnormalities in vitamin D metabolism and syndromes resulting from renal tubular phosphate loss. Rickets occurs during growth in children and adolescents and results from an interruption of the development and mineralization of the growth plate while osteomalacia is found in adults and results from inadequate or delayed mineralization of osteoid in mature cortical and spongious bone. Typical radiological findings in rickets include widening of the growth plate and disorganization and fraying of the spongy bone in the metaphyseal region, while in osteomalacia osteopenia and a coarsened, unsharp pattern of the trabecular bone is found (13).

Hemochromatosis and Wilson's disease are rare diseases of iron and copper metabolism, which show a similar

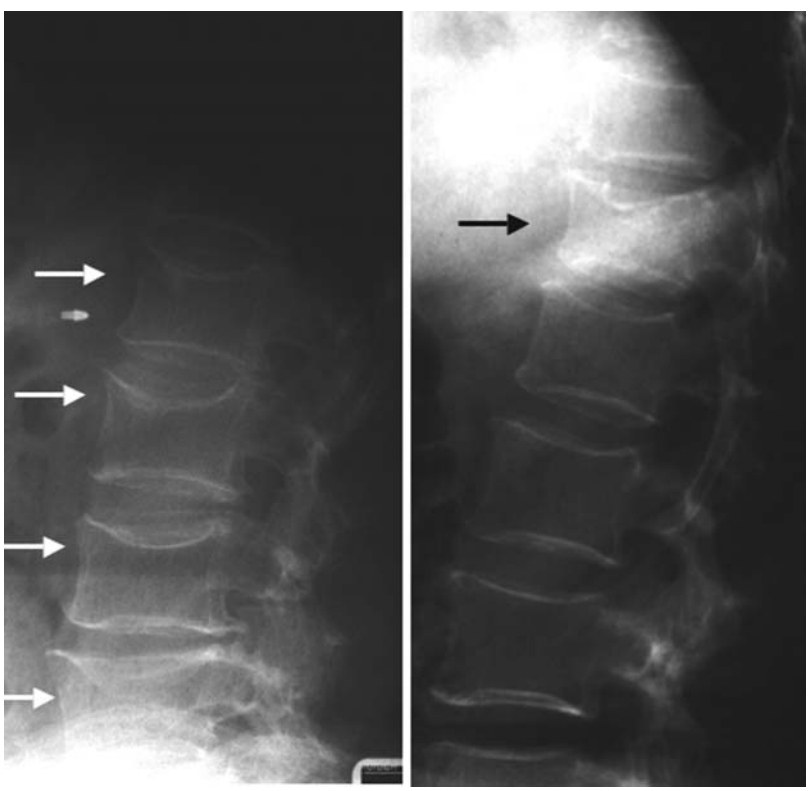

Musculoskeletal Radiology. Figure 8 Lateral radiographs of the thoracic and lumbar spine showing multiple osteoporotic compression fractures of the vertebrae (arrows).

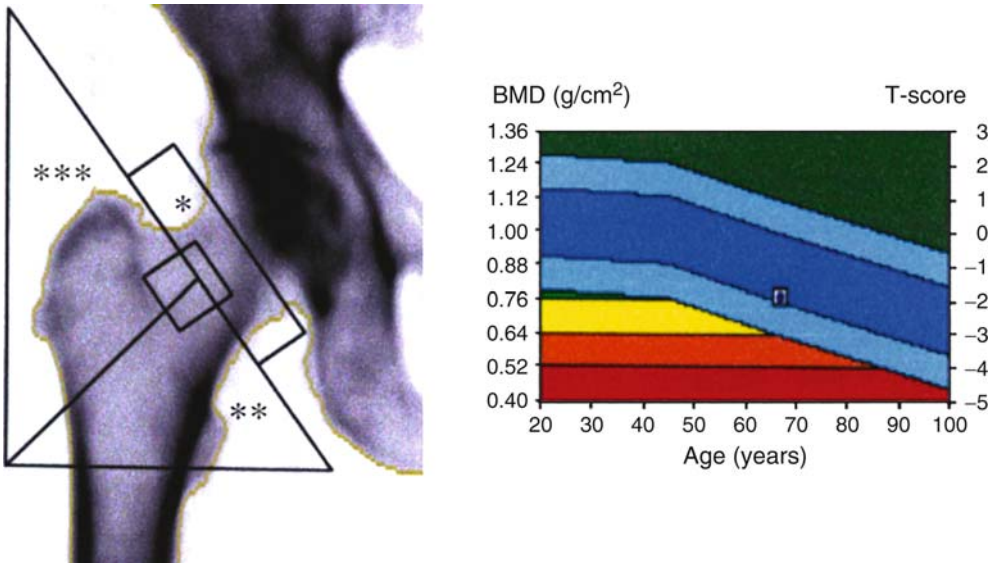

Musculoskeletal Radiology. Figure 9 DXA image of the right hip with regions of interest (ROI) including neck (*), intertrochanteric (**), and trochanteric (***) ROI. The right image shows neck BMD value in relation to young normal BMD

pattern as CPDD. In hemochromatosis chondrocalcinosis, joint space narrowing, subchondral cyst formation, and osteophytes are found, most typically located in the metacarpophalangeal joints of the second and third digit.

Alkaptonuria is another rare disorder resulting from an inability to metabolize homogentisic acid, which is oxidized to an ochronotic pigment. This ochronotic pigment is stored in cartilage and connective tissues and leads to discal calcification, disc space narrowing and a severe extraspinal "degenerative" arthropathy.

Hormonal disorders that affect the musculoskeletal system include pituitary disorders (e.g., acromegaly), hyperparathyroidism, thyroid disorders, and Cushing's disease. Acromegaly results from elevated levels of growth hormones resulting in activation of enchondral and periosteal bone formation with soft tissue proliferation. Primary hyperparathyroidism is most commonly due to adenomas and less commonly due to diffuse hyperplasia and carcinoma. Secondary hyperparathyroidism is frequently linked to chronic renal failure and in common with osteomalacia, osteoporosis and soft tissue calcifications are found in *renal osteodystrophy*. Typical radiologic signs in hyperparathyroidism include subperiosteal, subchondral, trabecular, and intracortical bone resorption as well as brown tumors.

Paget's disease is a relatively frequent disease (up to 3% of the population over the age of 40 years) characterized by excessive abnormal remodeling of bone. Typical radiographic features include an initial osteolytic stage and subsequent osteosclerotic stages with increased radiodensity, an accentuated trabecular pattern and picture frame vertebrae (Fig. 10). Complications include fractures, deformities, articular alterations, and neoplasms (10).

Osteonecroses

Osteonecrosis may be due to a number of disease processes such as trauma, hypercortisolism, hemoglobinopathy, alcoholism, irradiation, and pancreatitis. But it may also occur spontaneously, most commonly in the hip and the knee. In conventional radiographs signs of osteonecrosis are usually found fairly late; these include subchondral lucency, patchy areas of lucency and sclerosis and finally bone collapse with deformity and secondary degenerative changes. MRI can show these changes at a substantially earlier stage before collapse of the bone has occurred (Fig. 11). Infarction in the bone marrow shows shell-like calcifications in radiographs and central fatty necrosis with surrounding granulation tissue that is low in signal in T1-weighted images and high in signal in fat saturated T2-weighted images. The most frequent sites of osteonecrosis are the hip, knee, talus, humeral head, scaphoid, and the vertebrae (Kuemmel's disease). Complications include degenerative changes, intraarticular bodies, cysts, and rarely malignant degeneration.

The entity osteochondroses encompasses (1) *juvenile osteonecroses*, (2) conditions related to trauma and abnormal stress, and (3) variations of the normal pattern of ossification. These are characterized by fragmentation and sclerosis of an epiphyseal or apophyseal center. Diseases characterized by osteonecrosis include Legg–Calve–Perthes

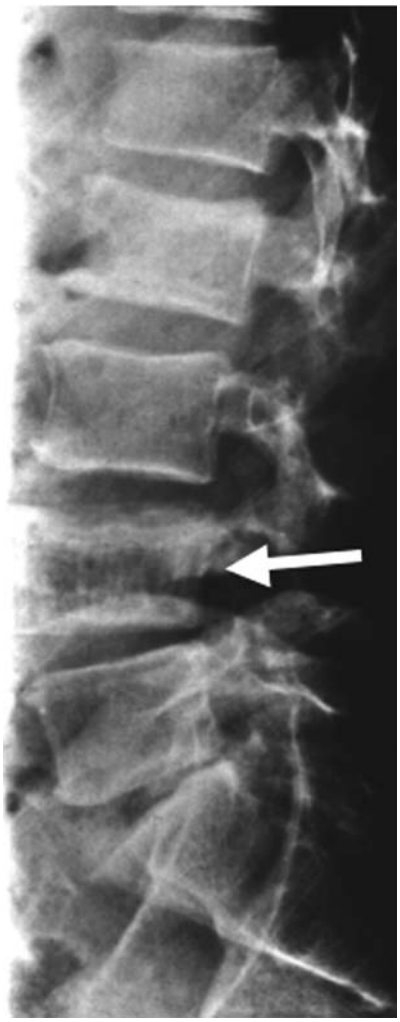

Musculoskeletal Radiology. Figure 10 Lateral radiographs of the lumbar spine showing an L4 vertebrae that is larger in diameter but lower in height compared to the other vertebrae (arrow). This vertebra also has a frame-like structure, all findings being consistent with Paget's disease.

disease (femoral head), Koehler's disease (tarsal navicular), Freiberg's infraction (metatarsal head), Panners's disease (capitulum of humerus), Kienboeck's disease (carpal lunate), and Thiemann's disease (phalanges of hand). Blount's disease (proximal tibial epiphysis), Osgood–Schlatter disease (tibial tuberosity), Sinding–Larsen–Johansson disease (patella), and Scheuermann's disease (discovertebral junction) were attributed to a more trauma related etiology.

Bone and Soft Tissue Tumors

Primary bone tumors are frequently found in younger patients, the substantially more common secondary bone tumors (mostly metastases) are found in patients older

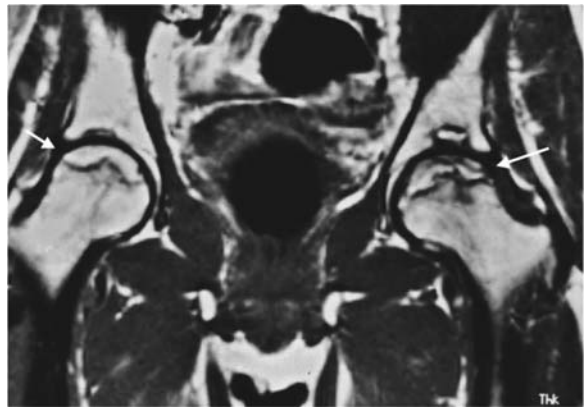

Musculoskeletal Radiology. Figure 11
Coronal T1-weighted spinecho image of the pelvis. Avascular necrosis (AVN) of both hips with low signal intensity lines demarcating the necrosis (arrows), but no deformity of the femoral head.

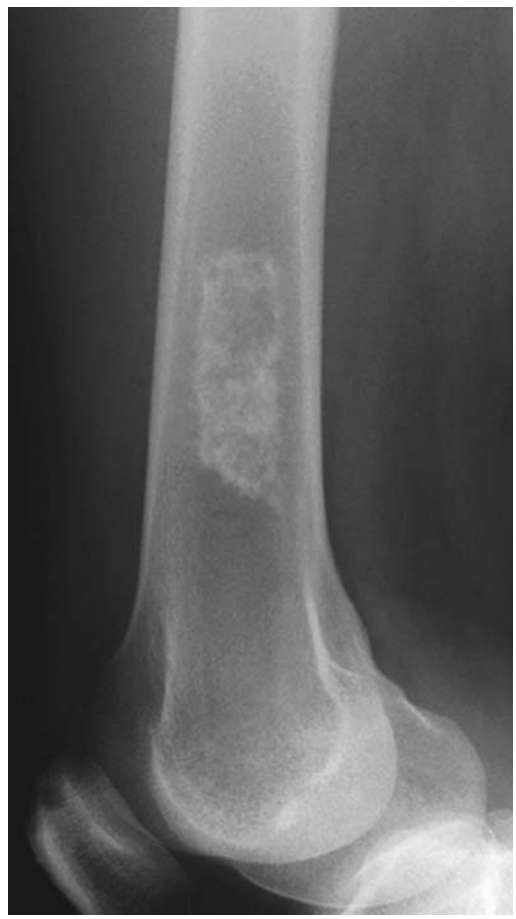

Musculoskeletal Radiology. Figure 12 Lateral radiograph of the distal femur bone showing ring- and arc-like calcifications consistent with enchondroma. No cortical destruction or scalloping that would suggest malignant transformation.

than 50 years. In bone tumors, an intimate cooperation between radiology and pathology is required to obtain correct diagnoses. The primary imaging technique for bone tumors is CR. Using specific criteria focusing on matrix, periosteal reactions, and tumor border approximately 70–80% of diagnoses can be made with conventional radiographs. In the spine, pelvis, and shoulder region CT may give additional information. In the last years we learned a number of new criteria for assessing MR images of bone tumors, however, up to now the most important role of MRI is to show the tumor extent preoperatively, i.e., to show joint invasion and invasion of the neuromuscular bundle and to monitor tumor size following chemotherapy.

Primary bone tumors can be divided into benign and malignant lesions and also be classified according to the tissue of origin, such as osseous and cartilage-forming tumors.

Osseous tumors include osteoma, osteoidosteoma, osteoblastoma (all benign), and osteosarcoma (Fig. 13) (malignant). Cartilage-forming tumors are enchondroma (Fig. 12), osteochondroma (the most frequent bone tumors), chondroblastoma, chondromyxoid fibroma (all benign), and chondrosarcoma (malignant). Tumors arising from fibrous tissues are nonossifying fibroma, desmoplastic fibroma (benign), and fibrosarcoma (malignant). Other important tumor entities are locally aggressive lesions such as giant cell tumors and chordoma. An important malignant entity are Ewing's sarcomas.

Tumorlike lesions are defined as nonneoplastic bone lesions that may simulate tumors. These include simple bone cysts, aneurysmal bone cysts, eosinophilic granuloma, intraosseous ganglion, and epidermoid cysts as well as fibrous dysplasia (4).

Skeletal metastases can develop due to hematogenous dissemination, direct extension, and lymphatic spread. They can either be osteolytic or osteoplastic. The most common carcinomas that metastasize to the bone arise from the breast, prostate, and lung. Kidney and thyroid carcinoma metastases show a high affinity to the skeleton. Skeletal scintigraphy, whole body MRI and positron emission tomography (PET) are well-suited diagnostic techniques to assess skeletal metastases.

Soft tissue tumors are relatively frequent lesions but commonly the preoperative radiological diagnosis is challenging. Conventional radiographs are of limited usefulness. Calcifications may sometimes be found and the morphology may be helpful in the differential diagnosis. Ultrasound and MRI are the best techniques for soft tissue lesions. Ultrasound is useful to image cystic lesions and with Doppler ultrasound vascularization of a lesion may be characterized. MRI is a sensitive tool to depict soft tissue lesions but a specific tumor diagnosis is only possible in less than 60% of cases (8, 12). Tumors that may be diagnosed with a relatively high confidence are hemangiomas, lipomas, pigmented villonodular synovitis, and cysts.

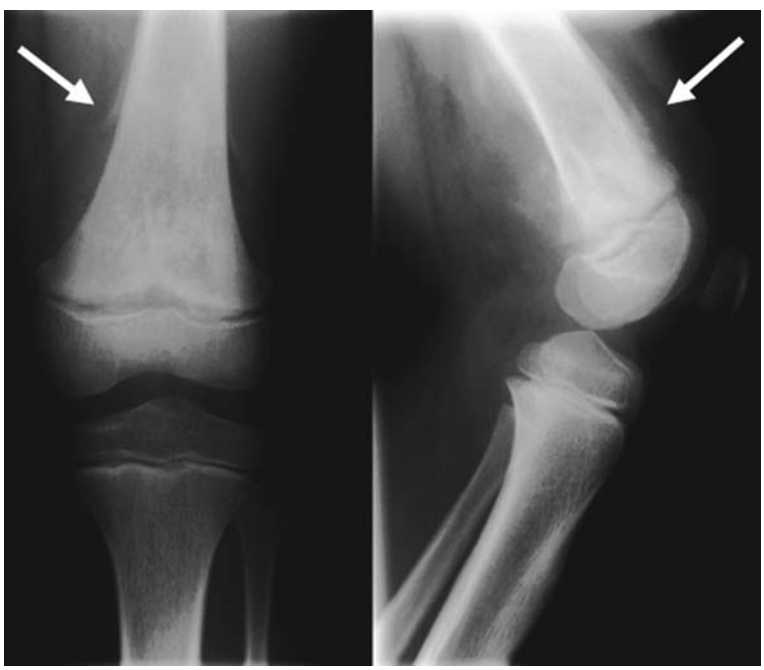

Musculoskeletal Radiology. Figure 13 Lateral and anteroposterior radiographs of the left knee joint. Complex periostal reactions (arrows), sclerosis, and lytic areas in the distal femur metaphysis consistent with osteosarcoma.

Diseases of the Hematologic and Hematopoetic Systems

Hemoglobinopathies include sickle cell anemia, hereditary spherocytosis, and thalassemia. These diseases are associated with characteristic abnormalities of the skeleton related to marrow hyperplasia and vascular occlusion and encompass fracture, infection, osteonecrosis, and growth disturbances.

Multiple myeloma or plasma cell myeloma is a malignant disease of plasma cells that originates in the bone marrow but may involve other tissues as well. This disease representing 10–15% of malignancies of the hematologic system usually occurs in 40–80-year-old patients and demonstrates typically an increase in the globulin serum protein fraction. Most often multiple osteolytic lesions are noted in the spine, ribs, skull, pelvis, and femur but solitary lesions, i.e., plasmocytoma, may be found for longer periods of time. Diffuse skeletal osteopenia is also a frequent finding, while sclerosis in multiple myeloma is rarely found and more frequently related to complications of the disease or to fracture (13).

Myeloproliferative disorders include leukemia, lymphoma, systemic mastocytosis, and polycythemia vera. Each of these entities has relatively typical musculoskeletal findings ranging from diffuse or focal synovial and osseous infiltration (in leukemia and lymphoma) to sclerotic or lytic osseous lesions (mastocytosis and lymphoma) to osteonecrosis (polycythemia vera).

Bleeding disorders are most frequently related to hemophilia and show a number of relatively typical skeletal abnormalities resulting from hemorrhage in soft tissues or subperiosteal, intraosseous or intraarticular location. Typical findings in the joints include joint effusion, soft tissue swelling, epiphyseal overgrowth, subchondral cysts, osseous erosion, and secondary degenerative changes. MRI is the most accurate imaging modality for assessing hemophilic arthropathy and may have a significant impact on patient management. MRI is anticipated to be useful in documenting early joint changes when treatment may be most effective (7).

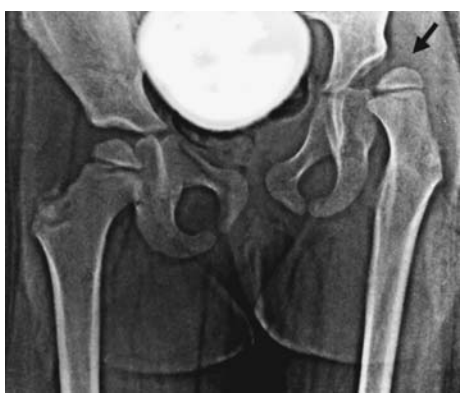

Musculoskeletal Radiology. Figure 14
Anteroposterior radiograph of the pelvis showing left-sided hip dysplasia with enlarged acetabular angle, partial uncovering of the femoral head, and coxa valga (arrow).

Congenital Disorders

Congenital dysplasia of the hip is a relatively frequent deformity that affects females more frequently than males

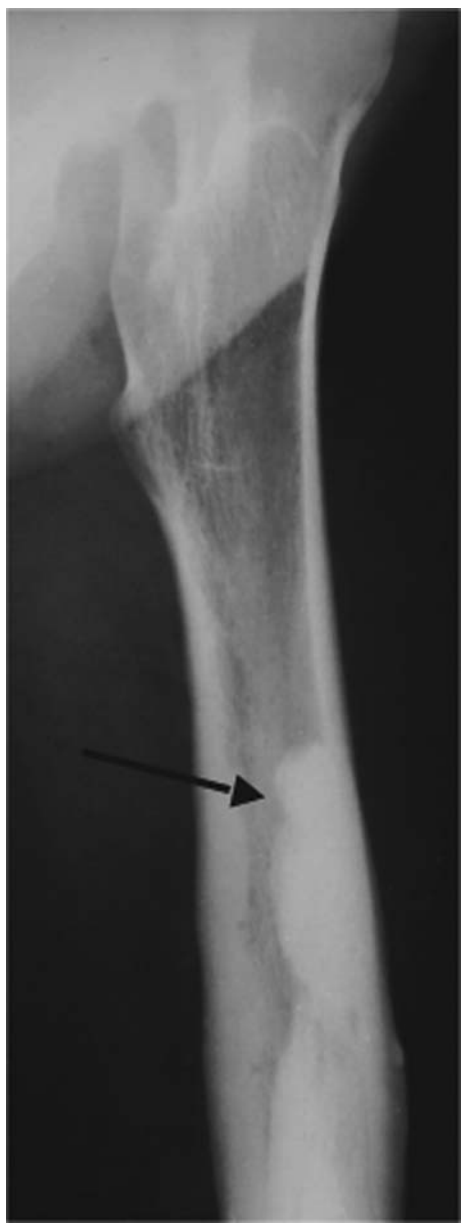

Musculoskeletal Radiology. Figure 15 Lateral radiograph of the proximal femur with areas of well defined sclerosis consistent with melorheostosis.

(Fig. 14) hip dysplasia. Early diagnosis is crucial and variety of radiologic techniques are used (5). *Scoliosis* is the most frequent spinal anomaly and etiology ranges from idiopathic to vertebral dsyplasias and tumors. Other relatively common *congenital* or *heritable anomalies* include foot deformites such as club foot deformity, tarsal coalition, proximal femoral focal deficiencies, Klippel–Feil syndrome, and Madelung's deformity.

Inborn *disorders of the connective tissue* that show typical radiological signs include Marfan's syndrome, Ehlers–Danlos syndrome, osteogenesis imperfecta, homocystinuria, and multiple epiphyseal dysplasias (13).

Skeletal dysplasias are numerous, have a large number of different etiologies, and may show a broad variety of radiological findings (16). The most important dysplasias are (1) Osteochondrodysplasias (e.g., achondrogenesis, spondyloepiphyseal dysplasia, and achondrodysplasia), (2) dysostoses (e.g., Crouzon's syndrome), (3) dysplasias due to chromosomal aberrations (e.g., Trisomy 8, 13, 18, and 21), and (4) dysplasias due to primary metabolic abnormalities (e.g., mucopolysaccharidoses).

Various Diseases

Skeletal disorders that show enostosis and hyperostosis are osteopoikilosis, osteopathia striata, and melorheostosis (Fig. 15) (2, 3). Primary and secondary hypertrophic osteoarthropathy as well as vascular insufficiency show a pattern of periosteal new bone formation. Systemic diseases that may also show skeletal abnormalities include sarcoidosis, neurofibromatosis, and tuberous sclerosis.

Bibliography

1. Bencardino JT, Hassankhani A (2003) Calcium pyrophosphate dihydrate crystal deposition disease. Semin Musculoskelet Radiol 7: 175–185
2. Benli I, Akalin S et al (1992) Epidemiological, clinical and radiological aspects of osteopoikilosis. J Bone Joint Surg Br 74:504–506
3. Freyschmidt J (2001) Melorheostosis: a review of 23 cases. Eur Radiol 11:474–479
4. Freyschmidt J, Ostertag H et al (1998) Knochentumoren—Klinik, Radiologie, Pathologie. Springer, Berlin, Heidelberg, New York
5. Gerscovich E (1997) A radiologist's guide to the imaging in the diagnosis and treatment of developmental dysplasia of the hip. I. General considerations, physical examination as applied to real-time sonography and radiography. Skeletal Radiol 26:386–397
6. Jones E, Manaster B et al (2000) Neuropathic osteoarthropathy: diagnostic dilemmas and differential diagnosis. Radiographics 20: S279–S293
7. Kerr R (2003) Imaging of musculoskeletal complications of hemophilia. Semin Musculoskelet Radiol 7:127–136
8. Kransdorf M, Murphey M et al (1999) Imaging of soft tissue neoplasms in the adult: benign tumors. Semin Musculoskelet Radiol 3:21–38
9. Link T, Majumdar S (2003) Osteoporosis imaging. Radiol Clin North Am 41:813–839
10. Lopez C, Thomas D et al (2003) Neoplastic transformation and tumor-like lesions in Paget's disease of bone: a pictorial review. Eur Radiol 13(Suppl):L151–L163
11. Modic M (1999) Degenerative disc disease and back pain. Magn Reson Imaging Clin North Am 7:481–491
12. Murphey M, Kransdorf M et al (1999) Imaging of soft tissue neoplasms in the adult: malignant tumors. Semin Musculoskelet Radiol 3:39–58
13. Resnick D (1989) Bone and Joint Imaging. WB Saunders Company, Philadelphia, London, Toronto
14. Santiago Restrepo C, Gimenez C et al (2003) Imaging of osteomyelitis and musculoskeletal soft tissue infections: current concepts. Rheum Dis Clin North Am 29:89–109
15. Sofka C, Pavlov H (2001) Sports injury update: imaging features. Curr Probl Diagn Radiol 30:174–187
16. Spranger J, Langer L et al (1974) Bone Dysplasias: An Atlas of Constitutional Disorders of Skeletal Development. WB Saunders, Philadelphia
17. Vinson E Major N (2003) MR imaging of ankylosing spondylitis. Semin Musculoskelet Radiol 7:103–113
18. Wedegartner U, Gatzka C et al (2003) Multislice CT (MSCT) in the detection and classification of pelvic and acetabular fractures. Rofo Fortschr Geb Rontgenstr Neuen Bildgeb Verfahr 175:105–111

Myelocele—Myeloschisis

▶Congenital Malformations, Spine and Spinal Cord

Myelofibrosis

Malignant disease due to polyclonal activation of fibroblasts, which secrete collagen and cause fibrosis of the bone marrow. Sclerotic changes may be shown in radiographs. MRI demonstrates relatively characteristic bone marrow changes with low signal intensity infiltration of the bone marrow in both T1- and T2-weighted sequences.

▶Myeloproliferative Disorders

Myelofibrosis, Idiopathic, Chronic

Chronic idiopathic myelofibrosis, one of a group of diseases called chronic myeloproliferative disorders, involves hematopoietic stem cells and is associated with marrow fibrosis. The principal biochemical change in myelofibrosis reflects increased turnover of the hematopoietic cell population. The most common presentation is with symptoms referable to anemia or the characteristic massive splenomegaly.

▶Neoplasms, Splenic, Malignant

Myelolipoma Hepatic

►Lipomatous Neoplasms, Hepatic

Myelolipoma, Hepatic

Very uncommon mesenchymal tumors composed of adipose tissue associated to hematopoietic tissue elements. The presence of lipoblasts in the adipose tissue components requires great attention in order to avoid an erroneous diagnosis of sarcoma. Diagnostic imaging features reflect its complex structure.

►Lipomatous Neoplasms, Hepatic

Myelomalacia, Posttraumatic

Diffuse damage of the spinal cord visible in the chronic stage, normally as evolution of cord contusion. Micro and macrocyst are present.

►Spinal Trauma

Myeloproliferative Disorders

Thomas M. Link
Clinical Director MQIR
Department of Radiology, San Francisco,
USA
tmlink@radiology.ucsf.edu

Synonyms and Definitions

Myeloproliferative disorders are a group of diseases that cause an overproduction of blood cells, platelets, white blood cells, and red blood cells in the bone marrow. These disorders include ►myelofibrosis, polycythemia vera, chronic and ►acute leukemias, (►Luekemia, Acute) and primary thrombocythemia. In this review we will also include ►multiple myeloma and other neoplastic diseases of the bone marrow, but not secondary neoplasias such as metastases of the bone marrow.

Pathology/Histopathology

Myeloproliferative disorders arise from an overproduction of one or more types of cells. The reason for this abnormal increase in cells is largely unknown, but there are a number of associated findings, including the Philadelphia chromosome in chronic myelogenous leukemia (CML) and overexposure to radiation, electrical wiring, or chemicals in a number of myeloproliferative diseases. Characteristically, basophilia and teardrop cells are found in myeloproliferative disorders.

In *myelofibrosis* polyclonal activation of fibroblasts occurs, leading to secretion of collagen and then fibrosis. This results in extramedullary hematopoiesis in the liver and spleen and immature blood cells in the peripheral blood. In *polycythemia vera* an increase in all three cell types is found, which results in pancytosis with normal differential and high hematocrit. In *CML* substantial leukocytosis (>20,000/mL) with too many myelocytes is found, and leukocyte alkaline phosphatase is decreased. *Acute myelogenous leukemia* (AML) is the most frequent leukemia found in adulthood and has a number of different subtypes. Auer rods and discrete tumor masses infiltrating the soft tissues are typical findings. *Acute lymphoblastic leukemia* (ALL) is the most common childhood malignancy; B-cell, T-cell, and null cell ALL are differentiated, with B-cell ALL having a better prognosis. Positive staining for periodic acid Schiff's (PAS) and negative myeloperoxidase staining are typically found in ALL. Idiopathic *thrombocythemia* is a rare malignant disease with megakaryocytes that have a bizarre morphology and platelet counts of more than 1 million/mL.

Multiple myeloma (*MM*) is a clonal B-lymphocyte neoplasm and the most frequent primary malignancy of the bone marrow, accounting for 10% of hematologic malignancies. It is usually systemic, but solitary osseous myeloma is found in approximately 5% of the cases, and frequently these tumors progress to MM. Serum protein electrophoresis reveals monoclonal spikes due to gammopathy, and Bence-Jones proteins are a typical finding in the urine. Lytic lesions found in the bone are due to an osteoclast-activating factor produced by the tumor cells. Amyloidosis and light-chain cast nephropathy are additional characteristic findings. Histologically, sheets of plasma cells are found in the bone marrow.

Mastocytosis, or respectively mast cell disease, is characterized by the abnormal growth and accumulation of mast cells within the bone or other organs. The diagnosis of ►systemic mastocytosis is most commonly established by a thorough histological and immunohistochemical examination of a bone marrow trephine specimen.

Clinical Presentation

Patients with myeloproliferative disorders frequently have no clinical symptoms when their physicians first make the diagnosis. A sign that is common for myeloproliferative disorders is an enlarged spleen, which can lead to abdominal pain and a feeling of fullness. In addition, since the bone marrow is infiltrated by pathological cells, anemia, decreased functional white blood cells and thus more frequent infections, and decreased thrombocytes and thus higher incidence of bleeding may occur. Other relatively common signs and symptoms include fatigue, general malaise, weight loss, fever and night sweats, nosebleeds, blood in the urine, bruising, dyspnea, and bone or joint pain.

More specific symptoms may be found in individual disease entities, such as intense itching after bathing in warm water, burning pain in the skin and emboli in *polycythemia vera*, substantial anemia in *myelofibrosis*, and substantial increase in spleen size in *CML*. In *MM* typical clinical findings include back pain, hypercalcemic symptoms (weakness, weight loss, altered mental status, constipation), pathological fractures, frequent infections, and findings related to nephropathy. Symptoms in systemic *mastocytosis* are flushing, itching, abdominal cramping, and shock. In addition, musculoskeletal pain, abdominal discomfort, nausea, vomiting, ulcers, diarrhea, and skin lesions may also be found.

Imaging

Conventional Radiographs

Conventional radiographs are not very sensitive in visualizing early disease because a substantial amount of bone (up to 50%) has to be lost before increased lucency is found. Still, skeletal radiography is the primary diagnostic study and also gives substantial information on fracture risk, which may be more difficult to evaluate with magnetic resonance imaging (MRI). Infiltration of the bone marrow can be either diffuse or focal with accompanying osteopenia, but sclerotic changes may be found such as in myelofibrosis, mastocytosis, and, rarely, MM. Pathological fractures may be found at later stages and are a typical finding in MM.

In *MM* the skeletal radiographic survey still has an important role in the Durie–Salmon clinical staging criteria for newly diagnosed MM with the presence of two clearly defined lytic lesions indicating a high tumor burden and stage III disease. The skeletal survey is also used to judge progression of disease. Four distinct forms are found in myeloma: (i) solitary lesions (plasmocytoma), (ii) diffuse skeletal involvement (myelomatosis), (iii) diffuse skeletal osteopenia, and (iv) sclerosing myeloma (1). Plasmocytomas are typically lytic lesions that affect the spine, pelvis, skull, ribs, and proximal extremities. Diffuse myelomatosis is characterized by multiple lytic lesions with discrete margins and uniform size. Diffuse skeletal osteopenia does not show focal lytic lesions and is difficult to differentiate from severe osteoporosis, particularly since this form of disease is frequently associated with multiple vertebral compression fractures. Sclerotic changes in MM are frequently associated with polyneuropathy, organomegaly, endocrinopathy, monoclonal gammopathy, and skin changes, which is also described as POEMS syndrome (1).

CT

Computed tomography (CT) is more sensitive in depicting focal osteolytic changes than conventional radiography but less sensitive than MRI in visualizing bone marrow pathology. The main roles of CT are to better assess fracture risk and fracture, to guide biopsy, and to better characterize focal pathology in the bone marrow.

In multiple myeloma osteolytic lesions, expansile masses, diffuse osteopenia, fractures, and, rarely, osteosclerosis may be found (1). Multidetector row whole-body CT may be useful to optimize staging of MM as it is faster, better tolerated by patients, and more sensitive than skeletal survey.

MRI

MRI is very sensitive for detecting bone marrow pathology; however, it should be noted that problems may occur if bone marrow infiltration is diffuse, and differentiation of ▶hematopoietic bone marrow and neoplastic infiltration may sometimes be difficult. MR techniques have evolved substantially, and extensive coverage of the skeleton is possible with good image quality and within a reasonable acquisition time. Standard sequences for bone marrow pathology include T1-weighted spin-echo, STIR, and T2-weighted fat-saturated fast spin-echo sequences. Contrast-enhanced sequences may add information, for example to better assess intraspinal pathology or soft tissue extension of lesions, but such applications are controversial.

In evaluating MR images, one has to be aware of signal characteristics of normal bone marrow: In young patients, substantial amounts of hematopoietic bone marrow are found, and below the age of 10 years in T1-weighted images the bone marrow may be lower in signal intensity than surrounding muscle or intervertebral disc (2). Above the age of 10 years, lower signal intensity is considered

pathological. Conversion from hematopoietic to fatty bone marrow starts in the periphery and the distal part of the long bones. By the age of 20 years, most of the appendicular skeleton contains fatty bone marrow, while the central skeleton including proximal femur and the humerus contains largely hematopoietic bone marrow. In the sixth decade of life, a substantial amount of fatty bone marrow is also found in the axial skeleton. Note also that reconversion of fatty to hematopoietic bone marrow may be observed, associated, for example, with status postchemotherapy, obesity, pulmonary pathology, smoking, and marathon running.

There are four pathological MR patterns in myeloproliferative disorders:

1. A focal pattern with localized areas of abnormal marrow is low in signal in T1-weighted images, bright in fat-saturated T2-weighted images, and showing contrast enhancement; this pattern is found in multiple myeloma and lymphoma but is most typical for metastatic disease from solid primary malignancies.
2. The diffuse pattern shows replacement of the normal marrow with intervertebral discs and muscle appearing in T1-weighted sequences similar or higher in signal than the bone marrow (Fig. 1). The bone marrow is bright in fat-saturated T2-weighted or STIR sequences and shows substantial contrast enhancement (Fig. 1). Depending on the degree of diffuse bone marrow infiltration, however, diagnosis may be difficult, and if less than 20% of the bone marrow is diffusely infiltrated, it is not possible to differentiate malignant infiltration with confidence from hematopoietic bone marrow. The diffuse pattern of disease is found in acute leukemias but may also be found in multiple myeloma and other myeloproliferative diseases.
3. The variegated pattern consists of multiple, innumerable, small foci of disease on a background of normal bone marrow (Fig. 2). These foci are low in signal intensity in T1-weighted images, bright in T2-weighted images, and enhance after contrast administration. If no fat saturation is used, the lesions may be masked by contrast medium in T1-weighted images. The variegated pattern is typically found in MM.
4. Predominantly fibrotic lesions such as myelofibrosis cause diffuse low signal intensity changes both in T1- and T2-weighted images (Fig. 3). Differentiation may be difficult from osteoblastic metastatic disease if no radiographs are available.

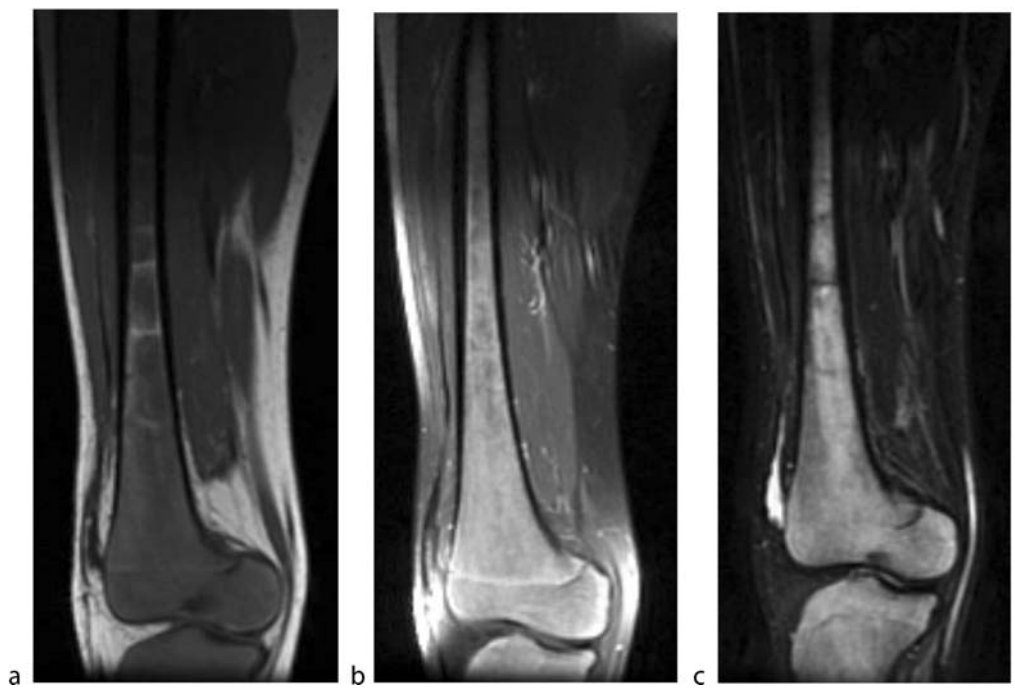

Myeloproliferative Disorders. Figure 1 Coronal magnetic resonance images of the distal femur and the knee demonstrating diffuse bone marrow infiltration in a 17-year-old patient with acute lymphatic leukemia. (a) T1-weighted image with low signal intensity in bone marrow, similar to signal intensity of the surrounding muscle. (b) Substantial enhancement of the bone marrow is shown after gadolinium administration. (c) STIR sequence demonstrates bright signal in the bone marrow.

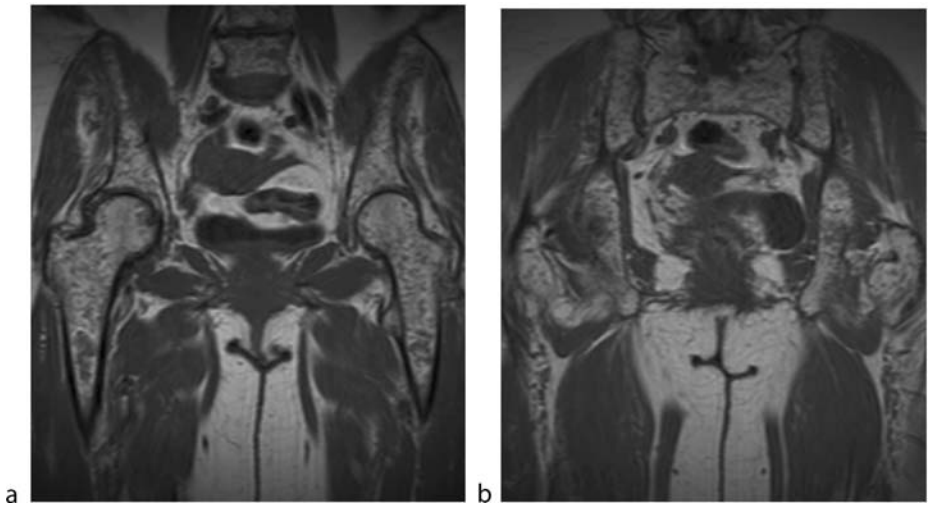

Myeloproliferative Disorders. Figure 2 Coronal T1-weighted images of the pelvis and the proximal femur demonstrating multiple myeloma with variegated pattern of bone marrow infiltration.

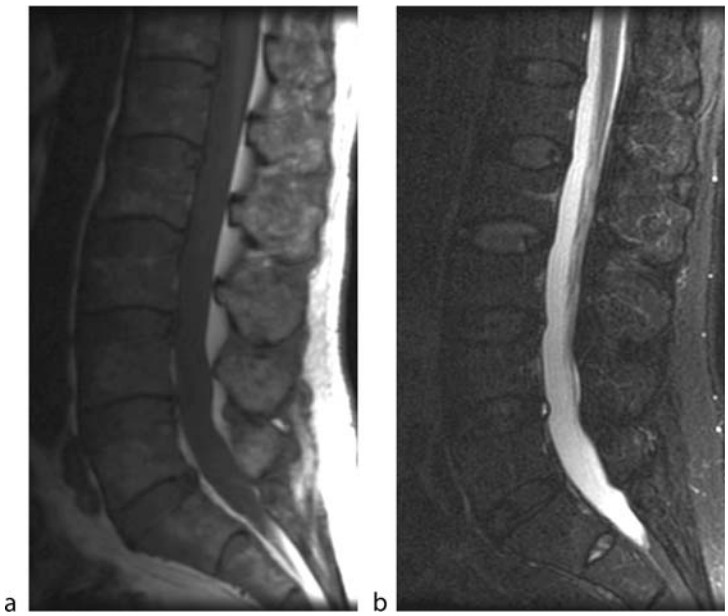

Myeloproliferative Disorders. Figure 3 Sagittal magnetic resonance images of the lumbar spine obtained in a patient with myelofibrosis. (a) T1-weighted image with low signal intensity bone marrow, similar in signal intensity to the intervertebral discs. (b) In fat-saturated T2-weighted image, bone marrow also appears low in signal intensity.

Nuclear Medicine

Standard nuclear medicine scans have a limited role in assessing bone marrow pathology.

Standard technetium 99m bone scintigraphy frequently does not show increased uptake in MM because it is primarily an osteolytic neoplasm. Increased uptake may reflect complications of the disease such as pathologic fracture. More favorable results have been found with radiotracers such as gallium 67 and ^{99m}Tc sestamibi.

FDG PET may be a suitable technique to evaluate bone marrow pathology sensitively, and good results have been found for MM in focal, diffuse, and mixed diffuse and focal disease.

Diagnosis

A diagnosis of myeloproliferative disorders is usually not made with radiographic techniques. Usually, blood tests detecting abnormal types or numbers of red or white blood cells with anemia and leukemia, or bone marrow biopsies directly showing histopathology of the bone marrow lead to the diagnosis. However, radiographic techniques can visualize the extent of bone marrow infiltration and can demonstrate complications of the disease. Some myeloproliferative disorders also have fairly typical radiographic findings.

In *myelofibrosis* the predominant radiographic feature is osteosclerosis, which may be found in 30–70% of the patients and is most evident in the bones of the axial skeleton, in particular the spine and pelvis (3). There may be small areas of relative radiolucency, and cortical thickening due to endosteal sclerosis is also found. Rarely, periosteal bone formation, specifically at the distal femur and proximal tibia, may be found. MRI is more sensitive in assessing the extent of the disease; low signal intensity changes both in T1- and T2-weighted images are shown due to replacement of marrow fat by collagen and reticulin fibers. Note, however, that these signal changes may also be found in children with leukemia and Gaucher's disease as well as in iron overload (chronic hemolysis, thalassemia) and AIDS (3). Other findings related to myelofibrosis are hemarthrosis due to impaired coagulation, secondary gout (5–20% of patients), polyarthralgias, and polyarthritis, as well as extramedullary hematopoiesis with tumor like masses that may be found in different locations, including the spinal canal (3).

In *acute leukemias* radiographic findings include metaphyseal banding, periosteal reactions, osteolysis, osteosclerosis, and osteopenia. Advanced disease may present with a higher rate of severe radiographic abnormalities such as geographic destructive osteolysis and periosteal reactions. A diffuse MR pattern (Fig. 1) is typical but not very specific. MRI is sensitive in depicting bone marrow infiltration but has a poor specificity in differentiating active disease from posttreatment changes in AML, yet may better predict response in ALL (4). MRI may also help in differentiating tumor involvement (such as chloromas) from complications of the disease (such as osteomyelitis).

Other myeloproliferative disorders such as *CML*, *polycythemia vera*, and *thrombocythemia* may have similar imaging findings, which are nonspecific and may have only a limited role in staging the disease or determining prognostic outcome.

MM is one of the most frequent hematological malignancies. Typical findings in MM have been described previously in the text. Conventional radiographs may show diffuse demineralization or variegated or focal patterns. Osteosclerosis is shown rarely. It should be noted that in diffuse infiltration, MRI is only reliable if more than 20% of the bone marrow is infiltrated (5). Compared with the variegated pattern (Fig. 2), diffuse or focal marrow involvement tends to have a higher tumor burden (6). The focal pattern is most frequently seen, while a diffuse pattern is seen in 25% of the patients. After treatment, bone marrow changes may resolve but may also be unchanged, even if patients achieve complete remission. Sometimes changes in the enhancement pattern may be shown, or transformation of a diffuse into variegated or focal pattern may be found (4). Progression of vertebral compression fractures also does not necessarily suggest disease progression but may be due to collapse of the unsupported vertebrae. MRI has an important role in assessing extraosseous masses and neurologic involvement of the disease, such as infiltration of the spinal canal.

Lymphoproliferative disorders are divided into Hodgkin's and non-Hodgkin's lymphomas, and infiltration of the bone marrow is found in 5–15% of patients with Hodgkin's and in 20–40% of patients with non-Hodgkin's disease (4). MRI may show the infiltration more sensitively than bone marrow scintigraphy but may be less accurate than FDG PET in assessing therapy response. On T1-weighted MR images, involvement is usually more diffuse or heterogeneous and less frequently focal. These MR findings are not specific for this disease entity and may be found in other myeloproliferative disease too. A soft tissue mass around an apparent intact cortical bone, however, raises concern for lymphoma, though it may be found in small cell malignancies too.

Systemic mastocytosis is a rare disorder that shows skeletal abnormalities in 70%, with 28% of the patients having pain. Conventional radiographs may show osteoblastic or, less frequently, osteolytic changes, which are nonspecific. MRI is substantially more sensitive in showing bone marrow pathology. Depending on the extension of the cell infiltration, bone marrow involvement may be either nonhomogeneous or homogeneous. In a previous study, nonhomogeneous involvement was more frequent, especially in the pelvis and humerus, while in the spine it was homogeneous in 50% and nonhomogeneous in 50%. There was no correlation between percentage of mast cells in bone marrow biopsy and extent or pattern of bone marrow involvement (7).

Important MRI *differential diagnoses* in myeloproliferative disorders include hematopoietic bone marrow, which sometimes is very difficult to differentiate from neoplastic disease, metastatic disease due to primary carcinomas or sarcomas, and osteoporotic compression fractures in patients with MM. In MR images hematopoietic bone marrow is usually not geographic and is

more vague in appearance; it is frequently symmetric and located in the metaphyses, the signal is brighter than that of muscle in T1-weighted sequences. Bone scan is negative while FDb PET may be positive. Metastases are frequently more focal and rarely diffuse. In patients with osteoporotic compression fractures, the bone marrow signal may be normal if fractures are old. In subacute and acute fracture the bone marrow signal may be abnormal but usually extends parallel to the endplate and does not involve the whole vertebra. The posterior border of fractured vertebrae in osteoporosis is usually concave and not convex, and signal abnormalities do not typically extend into the pedicles.

Bibliography

1. Angtuaco EJ, Fassas AB, Walker R et al (2004) Multiple myeloma: clinical review and diagnostic imaging. Radiology 231:11–23
2. Carroll KW, Feller JF, Tirman PF (1997) Useful internal standards for distinguishing infiltrative marrow pathology from hematopoietic marrow at MRI. J Magn Reson Imaging 7:394–398
3. Guermazi A, de Kerviler E, Cazals-Hatem D et al (1999) Imaging findings in patients with myelofibrosis. Eur Radiol 9:1366–1375
4. Moulopoulos LA, Dimopoulos MA (1997) Magnetic resonance imaging of the bone marrow in hematologic malignancies. Blood 90:2127–2147
5. Wasser K, Moehler T, Nosas-Garcia S et al (2005) [Correlation of MRI and histopathology of bone marrow in patients with multiple myeloma.]. Rofo 177:1116–1122
6. Vande Berg BC, Lecouvet FE, Michaux L et al (1998) Magnetic resonance imaging of the bone marrow in hematological malignancies. Eur Radiol 8:1335–1344
7. Roca M, Mota J, Giraldo P et al (1999) Systemic mastocytosis: MRI of bone marrow involvement. Eur Radiol 9:1094–1097

Myocardial Hibernation

Chronic reversible myocardial dysfunction secondary to coronary artery disease.

▶Ischemic Heart Disease, Ultrasound

Myocardial Perfusion Imaging

MPI is an established technique for the diagnosis and prognosis of CAD that provides information about the physiologic significance of CAD.

▶Single Photon Emission Computed Tomography

Myocardial Perfusion Scintigraphy

Myocardial perfusion scintigraphy is a nuclear medicine technique that can be used to visualize and assess myocardial perfusion. This technique is based on detecting photons emitted from radiopharmaceuticals, of which the uptake in the myocardium is proportional to the regional blood flow. It is used to prognostically stratify patients into low-, intermediate-, and high-risk groups for cardiac events.

▶Ischemic Heart Disease, Nuclear Medicine

Myocardial Perfusion Scintigraphy

▶Ischemic Heart Disease, Nuclear Medicine

Myocardial Stunning

Reversible myocardial dysfunction secondary to transient ischemia.

▶Ischemic Heart Disease, Ultrasound

Myofibroblastoma

Benign spindle cell tumour of the mammary stroma composed of myofibroblasts.

▶Breast, Benign Tumours

Myoma

▶Leiomyoma, Uterus

Myometrium

The muscular and thickest layer of the Uterus. It consists mostly smooth muscle. The most inner layer of the myometrium is known as junctional zone.

Myositis

Myositis is one feature of connective tissue diseases such as SLE, Sharp's syndrome, dermato-/polymyositis. Leading clinical symptoms are muscle weakness and exercise-related pain. MR imaging is employed for localization of inflammatory affected muscles if biopsy is required. In the acute stage excessive edema and contrast material enhancement of the affected muscles are seen. Fasciitis in the neighborhood is common. Muscle atrophy with fat interposition and fascial undulation develops.

▶Connective Tissue Disorders, Musculoskeletal System

Myositis Ossificans

Heterotopic formation of bone and cartilage in soft tissues, most commonly within muscles. The majority of these lesions occur secondary to trauma. Burns, paralysis, and idiopathic causes are also common. The lesion presents as a soft tissue mass with calcification. Maturation to heterotopic bone with an internal trabecular pattern occurs in the next few months. Regression is common and usually begins between 6 and 12 months. Myositis ossificans may appear very aggressive on MR images. It is better assessed with radiographs and CT, which demonstrate a characteristic peripheral rim of calcification/ossification. It is this feature that helps differentiate it from an osteosarcoma, which is generally characterized by central ossification. Delayed bone scan demonstrates marked uptake in early lesions and decreased uptake in mature lesions. The decreased activity on delayed imaging correlates with lower recurrence rates after surgery.

▶Fractures, Peripheral Skeleton
▶Neoplasms, Soft Tissue, Benign

Myxoedema

▶Congenital malformations, Thyroid and Functional Disorders

Myxoma

Benign soft tissue mass containing gelatinous myxomatous material, often with a small region of visible fat within the wall, when multiple myxoma may be associated with Mazabraud's syndrome.

▶Neoplasms, Soft Tissues, Benign

NASCET

North American Symptomatic Carotid Endarterectomy Trial.

►Stent, Carotid Artery

N-regional Lymph Node Metastases

M-distant metastases.

►Neoplasms, Oral Cavity

Nash and Moe Classification

For evaluation of the scoliotic rotation of the vertebrae, the method of Nash and Moe is widely used. There are 5 grades of rotation. Grade 0 rotation means the pedicle outlines are symmetric and with equal distance to the lateral borders of the vertebral body. Grade 4 is the maximum rotation.

►Scoliosis

Near-Infrared Imaging

►Optical Tomography

Near-Infrared Tomography

►Optical Tomography

Necrosis, Papillary, Renal

Henrik S. Thomsen[1], Marie-France Bellin[2]
[1]Department of Diagnostic Radiology, Copenhagen University Hospital at Herlev, Herlev, Denmark
[2]Université Paris-Sud 11, AP-HP, Service de Radiologie, Hôpital Paul Brousse, Villejuif, France
hentho01@heh.regionh.dk

Definition

Renal papillary necrosis is not a pathologic entity but a descriptive term for the disorders causing necrosis of the renal papillae. Renal papillary necrosis develops in a variety of diseases that cause chronic tubulointerstitial nephropathy. The lesion is predominant in the inner medulla. Major underlying causes of renal papillary necrosis are: pyelonephritis, obstructive uropathy, sickle cell disease, tuberculosis, calculi, analgesics, renal vein thrombosis and diabetes mellitus. Other causes include acute tubular necrosis, chronic alcoholism and severe infantile diarrhea. Transplanted kidneys, particularly cadaveric allografts, appear to be susceptible to renal papillary necrosis.

Pathology/Histopathology

The basic lesion in renal papillary necrosis is an impairment of the vascular supply and subsequent focal or diffuse ischemic necrosis of the distal segments of the renal pyramids. In the affected papilla, the sharp demarcation of the lesion and coagulative necrosis seen in the early stages of the disease closely resemble those of infarction.

In diabetes the kidneys are enlarged in earlier stages and become small and scarred in later stages. Acute bacterial infection within the renal pyramids may impair the circulation to the papilla causing vascular sclerosis and secondly induce an infarct like necrosis of the distal segment of the renal pyramid.

Histologically analgesic nephropathy is characterized by chronic tubulointerstitial nephropathy and renal papillary necrosis. In milder cases the disease may be limited to one or

several papillae and the kidneys are usually normal sized. In advanced cases however the kidneys eventually become shrunken due to diffuse fibrosis and atrophy.

Calcifications in the renal papillae or cortex and perinephric hematoma can be accompanying features. Even though histologic damage may be present in all papillae, radiological detectable lesions may be spotty or unilateral.

Clinical Presentation

There are no direct signs or symptoms of papillary necrosis. The most common symptoms are nonspecific: uremia, infection and flank pain. In many cases the cause is multifactorial.

Diabetes mellitus is the most common condition associated with renal papillary necrosis, accounting for more than 50% of all cases and renal papillary necrosis has been reported in about 25% of patients with insulin dependent diabetes mellitus. It is often associated with urinary tract infection and impaired renal function but can also be seen in patients without evidence of apparent diabetic nephropathy.

Analgesic nephropathy is caused by excessive intake of analgesics, usually more than 1 kg. It is most common in middle-aged women. Urinary tract infection accompanies in about 50% of patients and pyuria and urinary tract obstruction due to sloughed papillae are also common.

Pyelonephritis can result in papillary necrosis and infection is present in most cases of renal papillary necrosis. However, its exact prevalence as the cause of renal papillary necrosis is difficult to determine because infection may develop secondary to obstruction or diabetes.

In *S*-hemoglobinopathy medullary ischemia caused by sickling is the main cause of the disease. Papillary necrosis can be seen in both homozygous and heterozygous-*S* hemoglobinopathies but is more common in heterozygous-*S* disease. Homozygous-*S* disease is commonly associated with occlusion of small vessels, resulting in lobar infarcts, tubular obliteration and fibrosis but heterozygous-*S* hemoglobinopathies often manifest as papillary necrosis without association with renal failure.

Imaging

Most radiological information is from the time of intravenous urography. The use of contrast medium is mandatory. It must be given either intravenously or retrogradely. No significant difference with regard to diagnosis has been reported between intravenous urography and the now common CT-urography, but the experience is still limited. Ultrasonography may overlook papillary lesions, especially the early stages. Whether the spatial resolution of MR-urography is adequate is unknown. With regard to obstruction the value of all four modalities seems equivalent.

The radiographic appearance of papillary necrosis depends on the degree of disease. The renal size is normal in most patients, although the kidneys may shrink as the disease progresses. The contour remains smooth except in some advanced cases in which a 'wavy' appearance develops owing to the prominence of septal cortex surrounding atrophic areas of centrilobar cortex. In an early stage of the disease, papillary swelling may be the only abnormality. Necrosis of the papilla and disruption of its uroepithelial lining takes several forms. One may find faint streaks of density oriented parallel to the long axis of the papilla, usually extending from the fornix, after intravenous injection of a contrast agent.

Papillary necrosis is readily detectable when there is cavitation of the central portion of the papilla or complete sloughing of the papillary tip. Medullary cavitation is often central but may also be eccentric. The long axis of the cavity parallels the long axis of the papilla. The shape of the cavity varies from long and thin to short and bulbous.

With complete separation, the sloughed tissue is seen as a triangular radiolucent filling defect in the opacified calyx. Margins at the point of separation are initially rough but later become smooth. Necrotic tissue may pass into the renal pelvis and beyond causing obstruction. The remaining calyx has a round or saccular shape and smooth margins.

Calcification in papillary tissue is common in analgesic nephropathy. Nephrocalcinosis may be seen either in papillae that have no other radiological abnormality or in those that have cavitated. In most instances, foci of calcification are round, homogeneous and are arranged in a semilunar arc. Necrotic tissue passing down the pelvocalyceal system and the ureter produces obstruction.

Nuclear Medicine

Renography is useful for the diagnosis of obstruction in particular when the renal function is reduced and the risk of contrast medium induced nephropathy is increased. The papillary necrosis itself is not seen by nuclear medical methods.

Diagnosis

Typical changes of papilla demonstrated by an imaging modality, most typically intravenous urography or CT-urography.

Interventional Radiological Treatment

None

Bibliography

1. Brix AE (2002) Renal papillary necrosis. Toxicol Pathol 30:672–674
2. Davidson AJ, Hartman DS (1994) Radiology of the Kidney and Urinary Tract. WB Saunders Co, Philadelphia

Necrotizing Fasciitis

Necrotizing fasciitis is a surgical emergency needing prompt recognition and radical debridement of devitalized tissue. It consists of rapidly progressing infection and necrosis of fascia associated with superficial and deep soft tissue involvement.

►Infection, Soft Tissue

Negative Magnetic Resonance Contrast Agents

This term refers to substances that exhibit a low signal intensity on both T1-weighted and T2-weighted images. Superparamagnetic particles can be considered a typical negative magnetic resonance contrast agent.

►Contrast Media, MRI, Oral Agents

Neonatal Cholestasis

Neonatal cholestasis is a state of improper metabolism of the bilirubin due to hepatic failure or obstruction in the neonatal period. Clinically, jaundice develops within the 24 h of life. Biologically, the rate of rise of serum bilirubin is greater than 5 mg/dL in 24 h, and the direct bilirubin is greater than 1 mg/dL. Also abnormal is the persistence of neonatal jaundice beyond 2 weeks of age. In this condition, the stools become acholic.

►Congenital Malformations, Bile Ducts

Neonatal Diseases of the Central Nervous System

►Cerebral Neonatal Disease (Neuro View)

Neonatal Pneumonia

This is caused by transplacentally transmitted infections, perinatal infections acquired via ascending infection from the vagina or transvaginally during the birth process and those acquired nosocomially in the postnatal period.

►Neonatal Chest

Neoplasm, Renal Solid Benign

►Tumors, Renal Parenchymal
►Tumors, Renal Mesenchymal

Neoplasm-Like Lesions, Bone

Klaus Woertler
Technical University Munich
Munich, Germany
woertler@roe.med.tum.de

Synonyms

Tumorlike lesions of bone

Definition

The term tumorlike lesions of bone summarizes various nonneoplastic conditions which originate from or affect the bone and present as solitary or multiple bone lesions.

Pathology/Histopathology

The most important tumorlike lesions of bone are ►nonossifying fibroma, ►fibrous dysplasia, ►simple bone cyst, ►aneurysmal bone cyst, and ►eosinophilic granuloma (Langerhans cell histiocytosis), which are also included in the WHO classification of bone tumors, although many other nonneoplastic alterations of bone can arise in a tumorlike fashion and therefore could be added to this selection. The lesions mentioned above all demonstrate distinct histopathologic features which

usually allow for a specific diagnosis. However, a detailed description of the histologic characteristics of every single lesion would go far beyond the scope of this essay.

Clinical Presentation

Nonossifying fibroma, monostotic fibrous dysplasia, ►osteofibrous dysplasia, and simple bone cyst are clinically asymptomatic in the majority of cases and are often detected incidentally on radiographs obtained for some other reason. Particularly larger lesions can give rise to pain, swelling, and stiffness of nearby joints or can lead to pathologic fracture. Aneurysmal bone cysts are mostly painful and, if located in the spine, are often associated with neurologic symptoms due to spinal cord or nerve compression. Patients with eosinophilic granuloma usually experience local pain and swelling not infrequently accompanied by fever, leucocytosis, and an elevated blood sedimentation rate. Neurologic deficiencies in patients with spinal manifestations of Langerhans cell histiocytosis are relatively rare.

For the tumorlike lesions mentioned above Table 1 gives an overview on the typical patient ages, the sex ratios, and the most common sites of involvement within the skeleton and within bone.

Imaging

Nonossifying fibroma (Fig. 1) demonstrates characteristic features on conventional radiographs. The lytic lesions that arise within the cortex have a lobulated contour often associated with a sclerotic border, a shell-like periosteal reaction, and, especially in larger lesions, trabeculations. These abnormalities are virtually diagnostic and usually obviate the need for further imaging or biopsy.

Fibrous dysplasia (Fig. 1) occurs as a monostotic manifestation more often than as a polyostotic disease. Solitary lesions typically present as well-defined intramedullary radiolucencies with "ground glass"-like density and sclerotic margins that might be associated with thickening of the adjacent cortex and variable degrees of bone expansion. In areas of complex anatomy, such as the skull, the spine, and the pelvis, CT can add valuable information with a view to differential diagnosis of fibrous dysplasia as well as the extent of bone involvement. CT images are particularly advantageous in demonstration of well-demarcated borders, osseous expansion, and "ground glass" matrix as typical features (Fig. 2). Compared with CT, MR imaging findings are less specific in differential diagnosis of fibrous dysplasia. However, MR imaging (whole body MR imaging) can demonstrate the full extent of the disease in young patients with polyostotic manifestations without unnecessary radiation exposure.

Osteofibrous dysplasia (ossifying fibroma, Kempson–Campanacci lesion) in the majority of cases affects the anterior cortex of the tibial shaft. Radiographically, it shows similar features as fibrous dysplasia, nonossifying fibroma, or adamantinoma (Fig. 1). Bowing of the tibia of various degrees is apparent in approximately 80% of patients with osteofibrous dysplasia. In most cases, cross-sectional imaging can add only little information to conventional radiography.

Simple bone cyst (solitary bone cyst, unicameral bone cyst) has a relatively typical radiographic appearance particularly if involving a long tubular bone (Fig. 1). Most lesions are centrally located and cause well-defined geographic bone destruction with thinning of the cortex and moderate expansion. Pathologic fracture is not uncommon and can give rise to a "fallen fragment", an osseous fragment that migrates to the dependent portion of the lesion thereby proving that it has a liquid content. CT and MR imaging both can verify the cystic character of

Neoplasm-Like Lesions, Bone. Table 1 Tumorlike lesions of bone: clinical data and skeletal distribution (LTB = long tubular bones)

Lesion	Typical age of patients and sex ratio	Typical sites within skeleton	Typical locations within bone
Nonossifying fibroma	2 Decade M:F = 2:1	LTB (femur, tibia) > others	LTB: Meta(dia)physis
Fibrous dysplasia (solitary lesion)	2–4 Decade M:F = 1:1	LTB (femur, tibia), ribs, skull > others	LTB: Metaphysis, diaphysis
Osteofibrous dysplasia	1–2 Decade M:F = 2:1	Tibia, fibula (occasionally)	Diaphysis
Simple bone cyst	1–2 Decade M:F = 3:1	LTB (humerus, femur), calcaneus, pelvis > others	LTB: Metaphysis, diaphysis
Aneurysmal bone cyst	1–2 Decade M:F = 1:1	LTB, spine > others	LTB: Metaphysis spine: posterior elements
Eosinophilic granuloma (LCH)	1 Decade M:F = 3:4	Skull, femur, spine, pelvis, ribs > others	LTB: Diaphysis, metaphysis

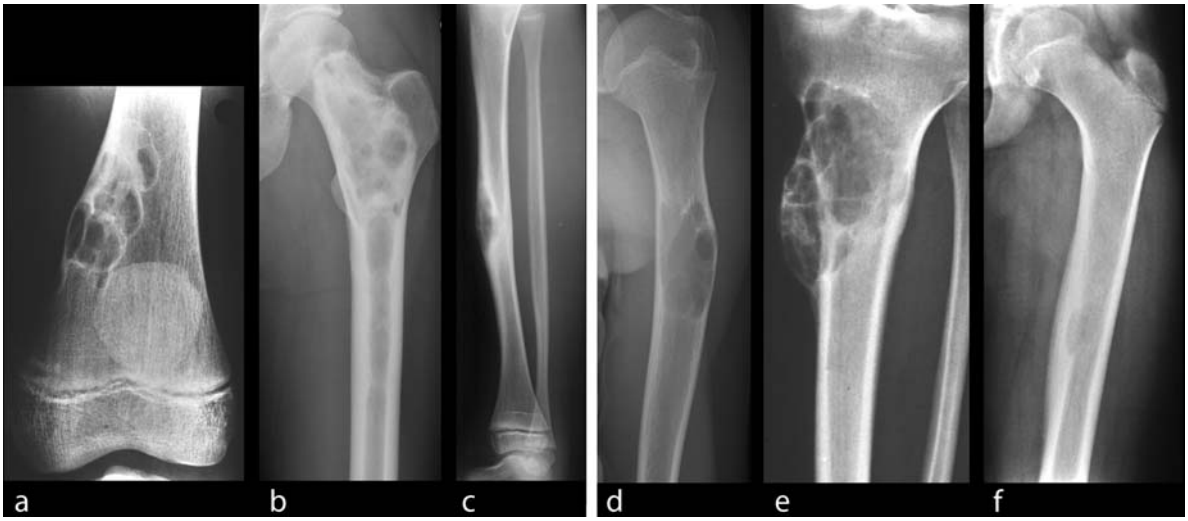

Neoplasm-Like Lesions, Bone. Figure 1 Tumorlike lesions of bone: radiographic findings. (a) Nonossifying fibroma of the femur: anteroposterior radiograph shows a lobulated, cortically based lesion with sclerotic margins, trabeculations, and a shell-like periosteal reaction. (b) Monostotic fibrous dysplasia of the femur: anteroposterior radiograph shows a large, well-defined lesion of ground glass density bordered by a thick sclerotic rim and extending from the femoral neck into the proximal diaphysis. (c) Osteofibrous dysplasia of the tibia: lateral radiograph shows a well-defined lucency with sclerotic borders and trabeculations at the typical site of involvement within the anterior cortex of the midshaft of the tibia. Note the slightly increased tibial bowing. (d) Simple bone cyst of the humerus: anteroposterior radiograph demonstrates a centrally located, well-defined lytic lesion with a delicate sclerotic margin and slight expansion of the lateral cortex. (e) Aneurysmal bone cyst of the tibia: anteroposterior radiograph shows an eccentrically located lytic lesion exhibiting well-defined borders, trabeculations, and marked expansion with formation of a thin neocortex. (f) Eosinophilic granuloma (Langerhans cell histiocytosis) of the femur: anteroposterior radiograph reveals a medullary osteolytic lesion within the diaphysis that causes endosteal erosion of the medial cortex and a lamellated periosteal reaction.

the lesion and therefore can help to establish the diagnosis in anatomically complex areas such as the pelvis.

Aneurysmal bone cyst (ABC) on radiographs usually appears as an expansile osteolytic lesion regardless of its location within the skeleton. In long tubular bones, the most common features are well-defined margins with or without a sclerotic rim, eccentric location, marked expansion with formation of a thin neocortex, and trabeculations: the so-called "soap bubble appearance" (Fig. 1). However, the lesion might also present with more aggressive findings and therefore can not always confidently be diagnosed with radiography alone. Because MR imaging has the potential to reflect the pathologic anatomy of ABC independent from its location, it represents the most informative additional imaging modality with a view to differential diagnosis (Fig. 3). Primary ABCs are exclusively composed of multiple cystic spaces which contain noncoagulated blood and blood breakdown products which due to sedimentation effects often cause fluid levels particularly on T2-weighted images. Most lesions are surrounded by a rim of low signal intensity and typically demonstrate marked enhancement of cyst walls and internal septations with intravenous contrast administration. The presence of solid components does not generally exclude the diagnosis of primary ABC, but should alert to the most important differential diagnoses, teleangiectatic osteosarcoma, and ABC secondary to

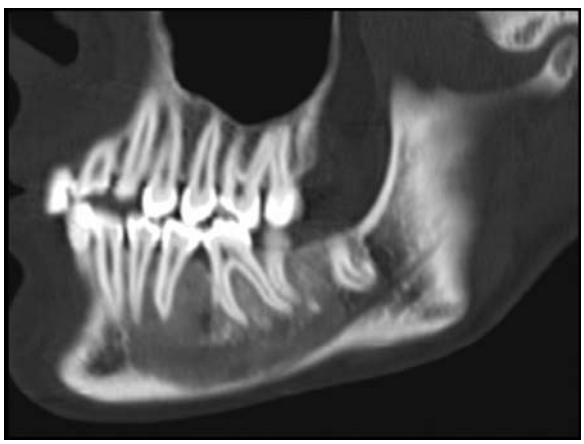

Neoplasm-Like Lesions, Bone. Figure 2 Fibrous dysplasia of the mandible: CT. Sagittal CT reformation image shows a well-demarcated, slightly expansile lesion with ground glass density and some irregular ossifications. Note the distortion of adjacent teeth.

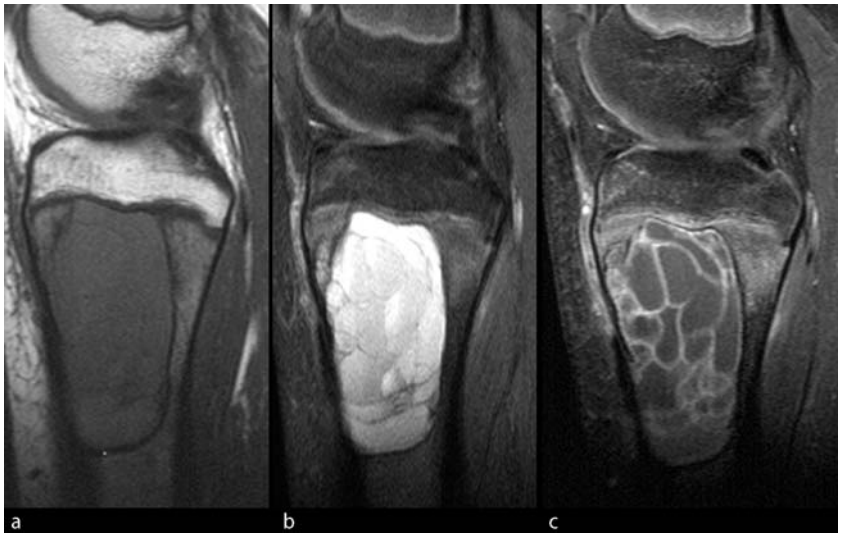

Neoplasm-Like Lesions, Bone. Figure 3 Aneurysmal bone cyst of the tibia: MR imaging. (a) Sagittal T1-weighted SE, (b) fat-suppressed T2-weighted TSE, and (c) contrast-enhanced fat-suppressed T1-weighted SE images show and internally septated lesion with multiple cystic cavities bordered by a rim of low signal intensity. Note the hyperintense cystic compartments at the bottom of the lesion on T1-weighted image, fluid levels on T2-weighted image, and enhancement of cyst walls and septations with contrast administration. Edema of adjacent bone marrow and soft tissue, as seen in this case, is not an unusual finding in aneurysmal bone cysts.

another bone lesion, such as giant cell tumor or osteoblastoma.

Eosinophilic granuloma as a solitary lesion represents the most common manifestation of *Langerhans cell histiocytosis* (60–80% of cases). Further osseous lesions are detected in only 10–20% of patients who initially present with a solitary granuloma. The radiographic features of eosinophilic granuloma vary with its skeletal location. Lesions of the skull and those located in flat bones often appear purely osteolytic and sharply delineated. The presence of a radiodense focus within a lytic lesion of the cranium has been described as a "button sequestrum." In long tubular bones, eosinophilic granuloma in most cases arises as a medullary radiolucency with central location and various degrees of endosteal erosion of the cortex (Fig. 1). Active lesions are often accompanied by a simple lamellar or an "onion skin"-like periosteal reaction. Spinal lesions typically cause destruction of vertebral bodies with consecutive collapse and flattening ("vertebra plana"), most often observed in the thoracic and lumbar spine. MR imaging usually shows an intramedullary lesion of low T1- and high T2-weighted signal intensity which is associated with more or less extensive edema of bone marrow, periosteum, and adjacent soft tissues. A rim of low signal intensity at the periphery of the main lesion seen on STIR images has been reported to represent a possible indicator of initial healing. In general, the imaging appearance of eosinophilic granuloma is rather unspecific with subacute osteomyelitis, osteoblastoma, and Ewing's sarcoma representing the main differential diagnoses. Whole body MR imaging is more sensitive than skeletal scintigraphy and radiography in detection of osseous manifestations of Langerhans cell histiocytosis and therefore, should be used as the screening method of choice for documentation of the presence and extent of skeletal involvement.

Nuclear Medicine

Skeletal scintigraphy is not very helpful in the specific diagnosis of solitary tumorlike lesions of bone, but can add information in cases of polyostotic involvement (e.g., in fibrous dysplasia).

Diagnosis

Nonossifying fibroma, fibrous dysplasia and simple bone cyst in most cases can sufficiently be diagnosed by means of radiography and do not require biopsy. The diagnosis of osteofibrous dysplasia should be verified by histology in order to exclude adamantinoma. With a view to their possible differential diagnoses histologic verification is also necessary in ABC and eosinophilic granuloma. The final diagnosis should be established by a combination of radiographic and histologic findings.

Bibliography

1. Fletcher CDM, Unni KK, Mertens F (eds) (2002) Pathology and genetics of tumours of soft tissue and bone. In: World Health Organization Classification of Tumours. IARC Press, Lyon
2. Forest M, Amouroux J (1997) Pathology of pseudotumoral lesions. In: Forest M, Tomeno B, Vanel D (eds) Orthopedic Surgical Pathology: Diagnosis of Tumors and Pseudotumoral Lesions of Bone and Joints. Churchill Livingstone, Edinburgh, pp 519–670
3. Resnick D (1995) Tumors and tumor-like diseases: imaging and pathology of specific lesions. In: Resnick D (ed) Diagnosis of Bone and Joint Disorders. 3rd edn. WB Saunders, Philadelphia, pp 3628–3938
4. Conway WF, Hayes CW (1993) Miscellaneous lesions of bone. Radiol Clin North Am 31:339–358
5. Woertler K (2003) Benign bone tumors and tumor-like lesions: value of cross-sectional imaging. Eur Radiol 13:1820–1835

Neoplasms of the Nasopharynx

►Neoplasms, Nasopharynx

Neoplasms of the Rhinopharynx

►Neoplasms, Nasopharynx

Neoplasms, Benign and Malignant, Larynx

Stefano Cirillo
Institute for Cancer Research and Treatment, Turin, Italy
stefano.cirillo@ircc.it

Definitions

Laryngeal neoplasms, either benign or malignant, originate from the mucosa and surrounding cartilaginous or connective structures of any part of the ►larynx.

The larynx is shaped like a pyramidal frustum joining the upper aerodigestive tract with the trachea. Its upper base faces the tongue and its lower base continues with the trachea. It is primarily an organ of phonation, but also an important regulator of respiration, and it prevents aspiration during swallowing.

The larynx lies in the visceral space of the neck, in front of the esophagus, is lined by prismatic epithelium, and is suspended by muscular and cartilaginous structures (thyroid cartilage, cricoid cartilage, and arytenoids).

The organ is divided into three anatomical regions: supraglottis, glottis, and subglottis.

An important anatomical structure is the prelaryngeal space, the deepest space of the larynx, which is mainly occupied by fat tissue, and extends vertically between the thyroid cartilage and the laryngeal lumen; at the level of the vocal folds this space is named paraglottic. The supraglottic portion of the prelaryngeal space is in communication with the pre-epiglottic space.

Neoplasms can be benign, such as polyps, papillomas, hemangioma, paragangliomas, and chondromas, or malignant, including squamocellular or nonsquamocellular carcinoma.

Pathology/Histopathology

The following rare varieties of benign tumors can arise in the larynx.

Chondroma: Usually 2 cm or less, it arises posteriorly from the cricoid cartilage and projects anteriorly, often causing partial airway obstruction. This benign tumor may evolve into a chondrosarcoma.

Hemangioma: In infants it is a sessile, poorly circumscribed subglottic mass, often associated with obstructive symptoms. In adults, it is uncommon and usually supraglottic.

Paraganglioma: It commonly involves the aryepiglottic fold. It is more frequent (70%) in males and has a malignant behavior in 3–25% of cases.

Papilloma: It is a warty outgrowth of the laryngeal surface epithelium; in children it is usually multiple, most commonly located on true vocal cords, false cords, epiglottis, subglottic area, and rarely within the tracheobronchial tree. Recurrence is common, at times years after excision or destruction, and may be massive and rapidly growing, leading to airway compromise. In adults, mostly male, it is often solitary and recurrences frequently exhibit dysplasia.

Vocal cord polyp: It is more common in heavy smokers or singers, due to inflammation, allergy, or immunologic causes. It almost never evolves into malignancy. It appears as a smooth, round, 1–3-mm growth on the true vocal cords, often on their anterior third.

Nonsquamous cell carcinomas: They are malignant carcinomas including adenoid cystic carcinoma, angiosarcoma, chondrosarcoma, liposarcoma, lymphoma, melanoma, and rhabdomyosarcoma. These nonsquamous tumors typically grow beneath the laryngeal mucosa and are therefore more difficult to diagnose clinically than squa-

mous cell carcinomas. Cross-sectional imaging findings are important in defining the disease extent and in directing the clinician to the optimal transmucosal biopsy site.

Squamous cell carcinoma: This malignant carcinoma is the most common laryngeal neoplasm accounting for more than 90% of all malignant lesions; the most frequent histopathological type is the nondifferentiated type, while other varieties such as basaloid, papillary, spindle cell, and verrucous types are very rare.

Squamous cell carcinomas originate in 30% of cases from the supraglottic larynx. Most frequently, in 30–40% of the cases, they arise from the junction between the false cord and the epiglottis.

Epilaryngeal cancers spread to the pharynx (base of the tongue, pyriform sinus, hypopharynx wall); vestibular cancers spread both along the surface and deeply in the pre-epiglottic and paraglottic spaces (Table 1).

The true vocal cords are the most common site of origin of laryngeal carcinomas. The anterior portion of the true vocal cord is the most common location of squamous cell carcinoma. Anteriorly, the tumor may extend to the anterior commissure, where it may involve the contralateral true vocal cord. Advanced lesions arising from the posterior third of the cord may extend posteriorly to involve the cricoarytenoid joint and the interarytenoid region. Tumors may extend inferiorly to involve the subglottic region (Table 2).

Neoplasms, Benign and Malignant, Larynx. Table 1
T staging for supraglottic carcinoma

T1	Tumor in one supraglottic subsite with normal cord mobility
T2	Tumor invading the mucosa in more than one supraglottic subsite without laryngeal fixation
T3	Endolaryngeal tumor with fixed vocal cord ± invasion of the postcricoid area or pre-epiglottic tissues
T4a	Tumor invading through to the thyroid cartilage ± other extra laryngeal tissues (resectable), e.g., trachea, cervical soft tissues, strap muscles, thyroid, esophagus
T4b	Tumor invading the prevertebral space, encasing the carotid artery, or invading the mediastinal structures (unresectable)

Neoplasms, Benign and Malignant, Larynx. Table 2
T staging for carcinoma of true vocal cords

T1	Limited to cords with normal mobility
T2	Spreading (supra ± subglottis) with impaired vocal cord mobility
T3	Endolaryngeal tumor with fixed vocal cord ± invasion of the postcricoid area or pre-epiglottic tissues
T4	Limited to larynx with fixed vocal cord

Subglottic carcinomas are rare and account for only 5% of all laryngeal carcinomas. The subglottic region is more commonly involved by the direct extension of a glottic or supraglottic carcinoma than by tumors elsewhere. When present, these lesions are characteristically circumferential and often extend to involve the undersurface of the true vocal cords. They have a tendency to early invasion of the cricoid cartilage and to extension through the cricothyroid membrane (Table 3).

The most important prognostic factors for laryngeal cancers include tumor volume and T stage and N stage. The presence of adenopathy at the time of diagnosis is the most important factor for predicting lymph nodal recurrence (3). The survival rate for ▶head and neck squamocellular carcinomas decreases to 50% in patients with homolateral adenopathy, 75% in those with contralateral adenopathy, and even further when capsular rupture of the lymph nodes is present.

The first station of lymph drainage from the supraglottic larynx is at the level of the subdigastric and the middle anterior cervical nodes; the second station is at the level of the lower anterior cervical nodes. The glottic larynx contains only a few nodes, and nodal spread occurs only when the primary tumor extends to the supraglottis or subglottis. The first station of lymph drainage from the subglottic larynx is at the level of the lower anterior cervical nodes, the paratracheal nodes, and the supraclavicular nodes. Glottic and subglottic tumors metastasize to the ipsilateral lymph nodes, but supraglottic tumors often spread to nodes on both sides of the neck.

Clinical Presentation

Laryngeal cancer is the most common cancer of the upper aerodigestive tract (25% of the cases) and represents 4–5% of all neoplasms. The incidence of laryngeal tumors is correlated with smoking, alcohol, and poor oral hygiene.

Laryngeal cancers account for approximately 1.2% of all newly diagnosed cancers; their incidence ranges from

Neoplasms, Benign and Malignant, Larynx. Table 3
T staging for subglottic carcinomas

T1	Tumor limited to the subglottis
T2	Tumor extending to the vocal cords with normal or impaired mobility
T3	Tumor limited to the larynx with fixed vocal cord
T4a	Tumor invading through to the thyroid cartilage ± other extra laryngeal tissues (resectable), e.g., trachea, cervical soft tissues, strap muscles, thyroid, esophagus
T4b	Tumor invading the prevertebral space, encasing the carotid artery, or invading the mediastinal structures (unresectable)

2.5 to 17.1 per 100,000 inhabitants in males, and from 0.1 to 1.3 per 100,000 in females in European countries; the peak incidence occurs at 50–60 years of age (1)(2).

The symptoms of laryngeal tumors largely depend on their size and location. Common symptoms for supraglottic tumors include mild odynophagia, mild dysphagia, and mass sensation. Uncommon symptoms include severe dysphagia and ear pain. For glottic and subglottic tumors, the most common presenting symptom is hoarseness of the voice. Uncommon symptoms include odynophagia, ear pain, thyroid cartilage pain, and airways obstruction. All the above symptoms are, however, not specific for a malignant lesion.

Diagnosis

The physical examination must include a systematic assessment of the patient's general health condition, searching for signs of associated conditions and metastatic disease. The neck and supraclavicular fossa are palpated to search for cervical adenopathy, other masses, and laryngeal crepitus. The oral cavity and oropharynx are examined under direct endoscopic vision. The larynx should also be examined by indirect laryngoscopy after anesthetic spray administration.

If there is a suspicion of cancer, biopsy is usually performed during direct laryngoscopy with the patient under general anesthesia; vital coloring is used to better identify the lesion. The examination should be extended to the whole upper aerodigestive tract and to the esophagus to exclude a second neoplastic lesion.

In cases where cancer is confirmed histologically it is very important that extension be evaluated accurately, in order to plan the most appropriate treatment. Laryngeal tumors arise from the mucosa, thus they are usually visible on the surface, but their submucosal spread may not be accurately evaluated by endoscopic examination alone. Indeed, clinical and endoscopic examinations underestimate tumor extension in 45–50% of cases. Integration between clinical data, endoscopic data, and imaging [computed tomography (CT)/►magnetic resonance imaging (MR)] is necessary for correct staging. Clinical staging is sufficient only for glottic cancer without involvement of the anterior commissure or with preserved vocal cordal motility, or exophytic cancer of the epiglottis and false vocal cord.

Imaging

The possibility that patients may benefit from conservative surgery or radiotherapy depends on the accuracy of the pretreatment assessment of cancer extension. CT and MRI can both assess the depth of invasion extension, which must be accurately evaluated in the following regions:

a. For supraglottic cancers:
   - Infiltration of the base of the tongue
   - Diffusion to the pre-epiglottic space
   - Diffusion to the superior prelaryngeal space
   - Extension to the pyriform sinus
   - Extension to the glottis plane
   - Involvement of the cartilage

b. For glottic cancers:
   - Diffusion to the paraglottic space
   - Diffusion to the cartilage
   - Involvement of the anterior commissure
   - Vertical diffusion (supraglottic or subglottic)

The imaging criteria used for tumor involvement are abnormal contrast medium enhancement, soft tissue thickening, presence of a bulky mass, infiltration of fatty tissue even without distortion of the surrounding soft tissues, or a combination of these signs. Imaging can underestimate the mucosal extension and overestimate the deep extension in the presence of edema, which may not be differentiated from neoplastic tissue.

►Multidetector CT (MDCT) is the first-choice examination for staging laryngeal neoplasms. The short scanning time of this technique limits the possibility of motion artifacts caused by swallowing and makes it possible to perform scans during functional and dynamic maneuvers, such as phonation or Valsalva, useful for identifying the tumor, and evaluating the degree of extension of the malignant tissue (Figs 1 and 2).

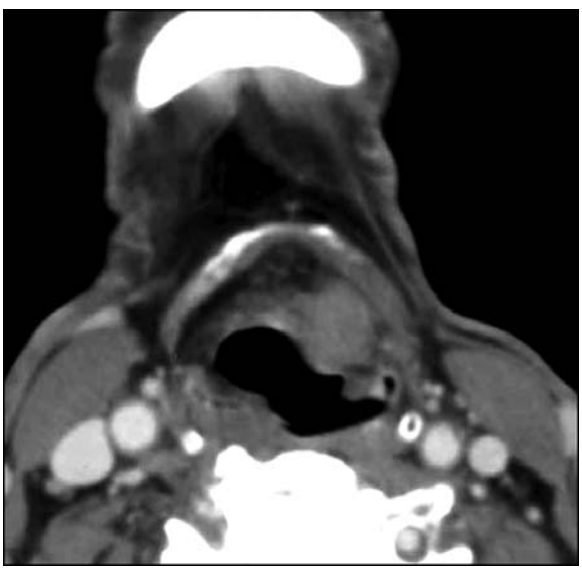

Neoplasms, Benign and Malignant, Larynx. Figure 1 Epiglottic cancer, MDCT – nodular mass in paraglottic superior space.

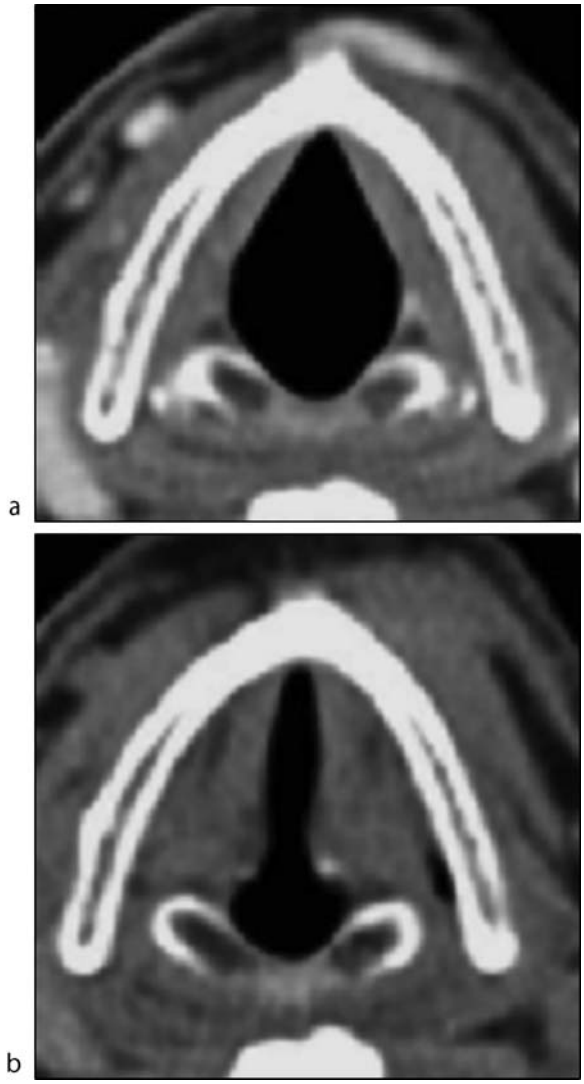

Neoplasms, Benign and Malignant, Larynx. Figure 2 Dynamic maneuver during laryngeal scans, MDCT: (a) abduction and (b) adduction of vocal folds.

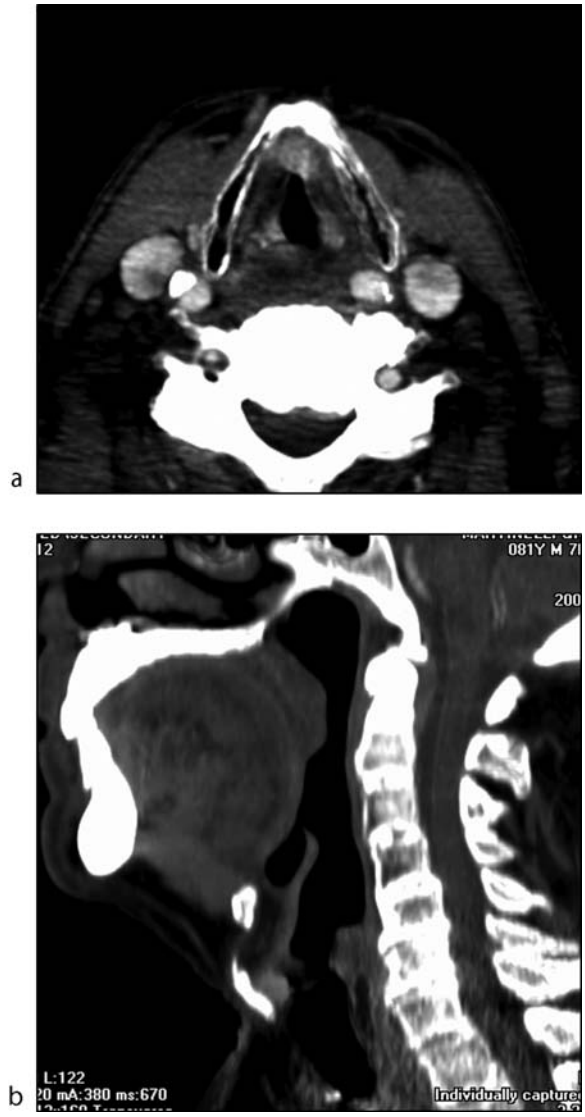

Neoplasms, Benign and Malignant, Larynx. Figure 3 Anterior commissure cancer, MDCT – lesion on (a) axial plane and on (b) sagittal reconstruction.

MDCT allows one to obtain excellent multiplanar reconstructions, with optimal tumor visualization and accurate measurement of its volume and adenopathy diameter (Fig. 3).

With MRI, a high contrast resolution can be obtained between the various anatomical structures, but images are often deteriorated by motion artifact caused by the long acquisition time, especially in patients in advanced stages who have dyspnea, cough, and large respiratory excursions.

If conservative surgery is planned, MRI is a complementary test to MDCT when the latter cannot exclude with certainty infiltration of the base of the tongue and of the cartilage.

False-positive results, however, are inevitable with both imaging modalities, due to inflammation.

MDCT and MRI have the same accuracy in the evaluation of diffusion to the epiglottic space (90–95%) and to the glottis plane. Sensitivity for assessing involvement of the paraglottic space is 93% for MRI and 97% for MDCT, while specificity is lower, being 50–76% for either test due to the difficulty in differentiating edema from neoplastic tissue.

MDCT and MRI may not provide sufficient diagnostic accuracy in evaluating involvement of the pyriform sinus: this may help explain the high rate of hypopharyngeal recurrences.

Involvement of the anterior commissure is considered if a soft tissue with a thickness of more than 1 mm is present (4,5).

Nuclear Medicine Tests

Nuclear medicine tests are useful in the follow-up of patients who underwent surgery or radiotherapy, for whom there is a clinical suspicion of local recurrence. In this setting, FDG-positron emission tomography (PET) provides a high sensitivity (86–100%) and specificity (69–87%) (5).

PET has some limitations due to its low spatial resolution and to the absence of anatomic reference points, which is of particular relevance considering the complexity of the head and neck region. Moreover, uptake is at times present in physiological conditions generating possible false-positive findings. Anatomic limitations can be partially overcome by the combination of CT-PET, which permits simultaneous acquisitions of morphological and metabolic data.

References

1. Sturgis EM, Wei Q, Spitz MR (2004) Descriptive epidemiology and risk factors for head and neck cancer. Semin Oncol Dec; 31(6):726–733
2. American Cancer Society: Cancer Facts and Figures 2006. Atlanta, Ga: American Cancer Society, 2006.
3. Thawley SE, Panje WR, Batsakis JG et al (1999) Comprehensive Management of Head and Neck Tumors. 2nd edn. Philadelphia, Pa: WB Saunders
4. Becker M, Hasso AN (1996) Imaging of malignant neoplasms of the pharynx and larynx. In: Taveras JM, Ferruci JT (eds) Radiology: Diagnosis—Imaging—Intervention. Lippincott, Philadelphia, PA, pp 1–16
5. Zbären P, Becker M, Laeng H (1997) Staging of laryngeal cancer: endoscopy, computed tomography and magnetic resonance imaging versus histopathology. Eur Arch Otolaryngol 254(1):117–122

Neoplasms, Benign, Large Bowel

Andrea Laghi, Franco Iafrate
Unit of CT and MR University of Rome "La Sapienza", Polo Pontino, I.C.O.T. Latina, Italy
andrea.laghi@uniroma1.it
francoiafrate@tin.it

Definitions

A ▶*polyp* is any circumscribed protrusion of normal mucosa into the colonic lumen, whether originating from the mucosa or situated submucosally.

According to Morson (1) there are two main groups of polyps projecting into colonic lumen:

- Nonneoplastic polyps (including hyperplastic, inflammatory, juvenile, or hamartomatous lesions).
- Neoplastic (or adenomatous) polyps.

Since most of the colorectal tumors (90–95%) arise from sporadic adenomas (polyps) and most of the remaining are accounted for by several hereditary cancer syndrome, a quick and right diagnosis as well as an appropriate treatment is extremely important in the prevention of colonic cancer.

Pathology/Histopathology

Nonneoplastic polyps include hyperplastic, inflammatory, juvenile, or hamartomatous lesions, which lack dysplastic features.

Hamartomatous polyps are the most common form of polyps in children. They are usually seen in the 4th to 6th year of life in many syndromic forms. The incidence in adulthood is 0.5–3.3% of all endoscopically removed polyps. More than 80% are usually found in the rectum. These polyps can vary in size between 0.3 and 0.5 cm and they are usually pedunculated, even if occasionally can be sessile.

Peutz–Jeghers Syndrome is an autosomally inherited syndrome due to mutations in LKB1 gene, identified in 50–60% of cases. This condition is characterized by hamartomatous polyps of smooth muscle through the GI tract and mucocutaneous pigmentation. Affected individuals have hamartomatous polyps in the small and large bowel and characteristic mucocutaneous brown to black melanin spots most commonly observed in the perioral area. The size of the polyp is 0.3 to 5 cm; they are commonly pedunculated, but occasionally they can be sessile. They cannot be distinguished from adenomas during endoscopy, and should be removed if possible. Risk of gastrointestinal and other malignancies is slightly increased.

Juvenile Polyp Syndrome (JPS) is cystic dilationsof glandular structures in the lamina propria without malignant potential. This syndrome is an uncommon condition that tends to be sporadic although 20–50% has a family history showing autosomal dominant inheritance (2). JPS grows from the lining of the bowel and originates in the tissues supporting that lining. It does not arise from the colonocytes (colonic lining cells) but from the tissues underneath the lining cells. Juvenile polyps are relatively common in children even if by adulthood 50–200 polyps may be present, commonly in the rectosigmoid junction. Juvenile polyposis may or may not be familial. Familial juvenile polyposis has been associated with mutations in two genes: *SMAD4* on chromosome 18 and *PTEN* on chromosome 10. There is a small but significant risk of cancer in patients with juvenile polyposis, mostly due to development of adenomatous tissue in juvenile polyps.

Hyperplastic polyps are lesions characterized by an epithelial dismaturityand hyperplasia caused either by a disturbed maturation process of cell in crypts without a known cause or either by hypertrophy of the crypts due to excessive epithelial cells. These polyps can be seen very

frequently in 75% of subjects aged over 40 years and are usually multiple. Most are often tiny lesions ranging in size between 2 and 5 mm. They are the most common colorectal neoplasms (10 times > adenomas). They have no malignant potential and they are often so small that may be missed even on endoscopic examination.

►*Colorectal adenomas* are benign neoplasms, pedunculated or sessile arising from the epithelial cells of the colorectum, with varying degrees of cellular atypia. Although benign, they are the direct precursors of adenocarcinomas and follow a predictable cancerous temporal course unless interrupted by treatment. There are three histological types:

- tubular adenomas
- villous adenomas
- tubulo-villous adenomas

According to world health organization (WHO) criteria, villous adenomas are composed of greater than 80% villous architecture. Tubular adenomas are encountered most frequently (80–86%). Tubulovillous adenomas are encountered less frequently (8–16%), and villous adenomas are encountered least frequently (5%). It has been shown that the removal of polyps by ►colonoscopy reduces the risk of getting colon cancer significantly. Malignant potential is determined by the size with 1% risk of adenocarcinoma if lesser than 1 cm in diameter; 10–50% risk if greater than 2 cm as well as by histologic type—greatest malignant potential for villous adenoma; least for tubular. This distribution of adenomatous polyps is paralleled by the distribution of colonic cancer. They may look like a wart when small and when they grow they may appear like a cherry on a stem or fig. There may be single or multiple polyps. The incidence of polyps increases with age, particularly above 40 years of age (M:F = 2:1). The cumulative risk of cancer developing in an unremoved polyp is 2.5% at 5 years, 8% at 10 years, and 24% at 20 years after the diagnosis.

The probability of any singular polyp becoming cancerous is dependent on its gross appearance, histologic features, and size. The risk of cancer is much higher in sessile villous adenomas than in pedunculated tubular adenomas (3). Cancer is found in 40% of villous adenomas, as compared to 15% in tubular adenomas. The good news is that 65% of adenomas are tubular, with villous adenomas accounting for only 10% of adenomatous polyps.

Adenomas are believed to have an abnormal process of cell proliferation and apoptosis. Clinical, autoptical, and epidemiological studies provide evidence of adenoma-to-carcinoma progression. The mean age of adenoma diagnosis is 10 years earlier than with carcinoma, and progression to carcinoma takes a minimum of 4 years.

Molecular genetic studies also describe an adenoma-to-carcinoma sequence through accumulation of lesions in a variety of genes, with activation of oncogenes and inactivation of tumor suppressor genes. The K-ras oncogene is described in 9% of small adenomas, 58% of adenomas larger than 1 cm, and 46% of colorectal carcinomas. Inactivation of tumor suppressor genes on arms 5q, 18q, and 17p is thought to be essential in tumorigenesis. As mutated in 30–60% of persons with sporadic adenomas and adenocarcinomas, the APC gene, on 5q, has an important role in adenoma formation.

Clinical Presentations

They may present with bleeding, prolapse, and rarely intussusception, but most commonly they are asymptomatic. Colonic polypectomy has simplified the management of this condition.

They may, however, cause painless rectal bleeding or bleeding not apparent to the naked eye. Obstruction can occur if they are large.

Usually the colorectal polyps are the ones causing symptoms, such as bleeding, diarrhea, abdominal cramps, and anemia. In such cases surgery is performed, choosing between the same operations offered to patients with familial adenomatous polyposis: colectomy and ileorectal anastomosis, proctocolectomy and pouch, or proctocolectomy and ileostomy.

Imaging

A *double contrast barium enema* (DCBE) is given in order to perform an X-ray examination of the large intestines. Pictures are taken after rectal instillation of barium sulfate (a radiopaque contrast medium) (Fig. 1).

DCBE is generally accepted as less sensitive than colonoscopy for detecting polyps or CRC. Enthusiasm for the double contrast barium enema has declined in recent years in favor of colonoscopy, despite its lower cost and more recently in favor of ►computed tomographic colonography (CTC).

The reason for this decrease in use as a diagnostic tool lies in the reduced sensitivity of this test in detecting polyps of lesser than 1 cm, in detecting polyps in areas where a single lumen is not detectable (i.e., sigmoid, rectosigmoid, hepatic, and splenic flexures) and patient comfort and compliance issues.

If a polyp is greater than 1 cm, the diagnostic accuracy of this technique has been reported as up to 95%; for polyps smaller than 1 cm well-performed air-contrast barium enema has a sensitivity of 61%.

A false-positive rate of 5–10% is found because of improper cleaning of the bowel. Diverticulosis or redundant bowel can result in a false-negative rate of 10%, especially in the rectosigmoid. The accuracy

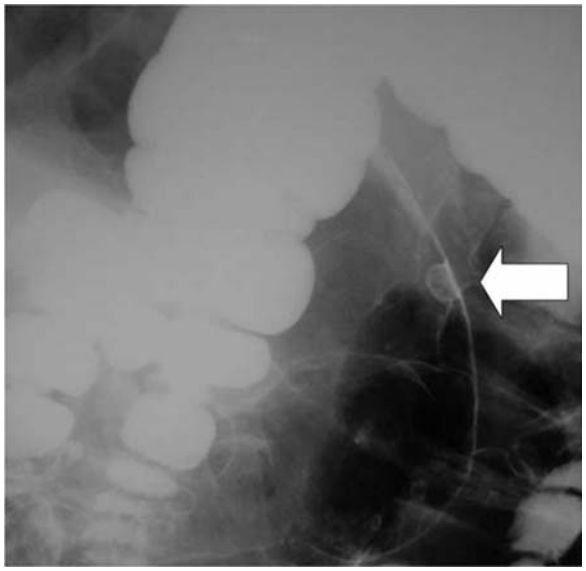

Neoplasms, Benign, Large Bowel. Figure 1 Polypoid lesion in a 56 year old female with familial history of adenomatous polyposis. Close-up view of an overhead image from a double-contrast enema examination shows a 1.5 cm well-defined polypoid lesion (arrow) of the colon.

of the procedure also can have an element of operator dependence.

CTC well known even as *Virtual Colonoscopy* (VC) is a novel imaging modality for the evaluation of the colonic mucosa in which thin-section spiral CT provides high resolution two-dimensional (2D) axial images; (Fig. 2a) CT data sets are edited off-line in order to produce multiplanar reconstructions (coronal and sagittal images) as well as three-dimensional (3D) modeling, including endoscopic-like views (Fig. 2b).

Reported diagnostic accuracy for polyps >5 mm exceeds that of barium enema and approaches that of conventional colonoscopy.

CT colonography requires no sedation—a major factor if dealing with old, unstable patients—or screening of asymptomatic subjects who would like to be able to return to work immediately after the procedure. In contrast, colonoscopy is associated with appreciable morbidity and even mortality including significant cardiovascular effects related to sedation.

The success rate of CT colonography approximates 100%, if bowel preparation and distension are optimal, whereas up to 6% of conventional colonoscopy cannot reach the caecum. CT colonography has been investigated as a technique for colon cancer screening. Although it requires a full bowel cleansing similar to that required for conventional colonoscopy, the procedure requires no sedation or analgesia, and is faster to perform than conventional colonoscopy. When a colonoscopy is not

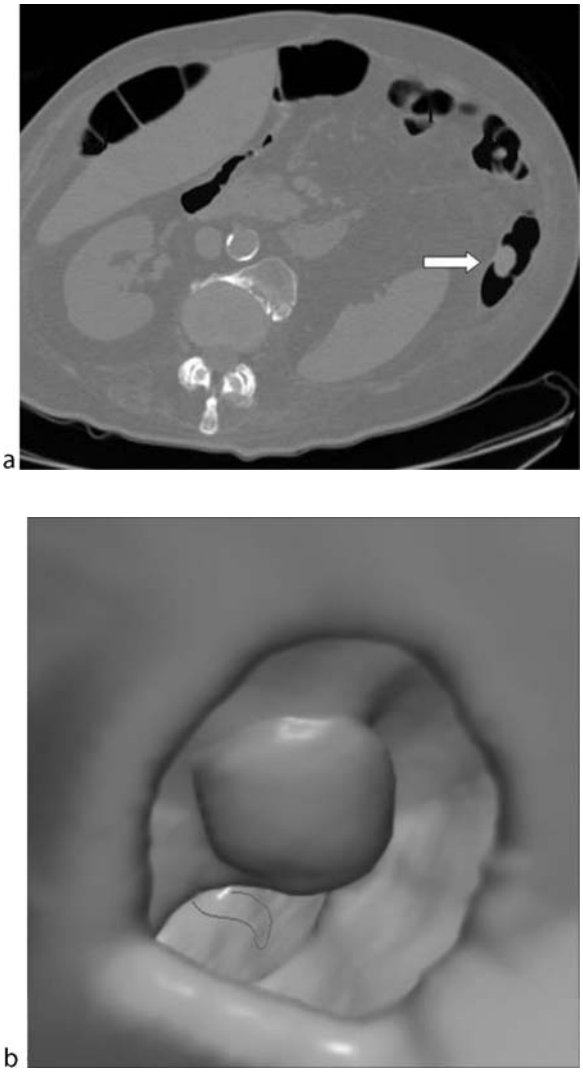

Neoplasms, Benign, Large Bowel. Figure 2 (a) Polypoid lesion in a 65 year old frail and uncooperative patient with rectal bleeding. Axial CT image obtained after colonic distension with air during CT colonography exam shows a 2 cm sessile polyp (arrow) of the descending colon. (b) Endoscopic like view of the same lesion where the polypoid lesion is easily appreciated (axial image obained using Lightspeed VCT 64 detector row, GE, USA; and endoluminal image obtained using VIATRONIX, V3D, USA).

possible CTC is an acceptable alternative. However, since it is only a screening procedure, patients with positive findings require conventional colonoscopy afterward. For this reason CT colonography is generally not being offered in a diagnostic setting (i.e., in symptomatic patients) because these patients have a high probability of having an abnormality that will require a colonoscopy.

CT colonography can detect overt cancers, but these are rare in asymptomatic patients. The major benefit from

CT colonography and other colon cancer screening techniques results from identification and removal of cancer precursors called adenomatous polyps. This assessment reviews evidence on the effectiveness of CT colonography as an alternative to colonoscopy for the purpose of colon cancer screening.

MR Colonography

High performance gradient systems together with fast MRI scanning techniques allow the acquisition of complex 3D data sets within comfortable breath hold.

Whereas MR has not been able to provide the necessary spatial and temporal resolution, this technique provides some advantages as optimal soft-tissue contrast and lack of radiation exposure. Fecal tagging to obviate the need for bowel preparation can be used in MR as well as in CTC. Compared to CTC, MR colonography is still under development and promises to reach the accuracy of CTC (4).

Diagnosis

Diagnosis relies on good history and physical examination of patients at risk. Rectal examination can identify cancers up to 8 cm above the dentate line that represent 20% of colorectal cancer.

Fecal occult blood testing (FOBT): is a test that detects the presence of occult (detectable only by chemical means and not visible) blood in the stool. This test has been suggested as a possible adjunct to other screening modalities. Only 20–40% of patients with adenomas have positive test findings, usually resulting from distal and larger polyps. On the other hand, the estimated 30–50% sensitivity is too low to consider FOBT as an effective single screening modality in high risk individuals, particularly since a positive FOBT is unlikely to occur as a result of adenomas before malignant transformation.

Flexible sigmoidoscopy: Flexible sigmoidoscopy can reach as high as the descending colon and can be done by a trained primary care physician. Sigmoidoscopy has been proven to reduce the incidence and mortality of colon cancer through early detection, however, is not an adequate method of screening in hereditary colon cancer as 2/3 of the lesions develop proximal to the splenic flexure. In these cases colonoscopy should be used. Flexible sigmoidoscopy can detect about 65–75% of polyps and 40–65% of colorectal cancers. This test, for an investment of 3–5 min, can with little discomfort reduce the likelihood of your developing colon cancer and if colon cancer is present detecting it at an early, highly curable stage.

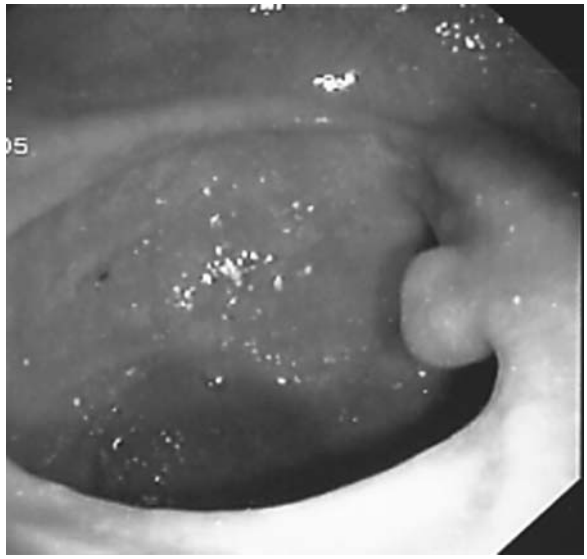

Neoplasms, Benign, Large Bowel. Figure 3 Conventional colonoscopy of 53-year old female with familial history of adenomatous polyposis showing a 1 cm lesion of the ascending colon.

Colonoscopy: Colonoscopy remains the gold standard for visualization, biopsy, and removal of colonic polyps (Fig. 3).

The removal of all polyps by colonoscopy has been demonstrated to reduce the risk of colon cancer by 76–90%.

Colonoscopy is the "gold standard" for the detection of colonic neoplasms and the preferred colorectal cancer screening strategy. The incidence rate of colorectal cancer has been shown to be reduced up to 90% in subjects who had polypectomy versus patients in three reference groups, including two cohorts in which colonic polyps were not removed and one general-population registry. It can be completed in more than 95% of examinations with negligible risk. Colonoscopic screening in individuals with average risk has been found to be cost effective, and similar to cervical or breast cancer screening techniques in cost-effectiveness per life-year saved. Medicare has approved the use of screening colonoscopy in average-risk beneficiaries.

The evidence to support colonoscopy is derived from data showing a decreased incidence of colorectal cancer mortality in subjects who have undergone colonoscopic adenoma removal. Additionally, colonoscopic screening has been shown to have favorable cost effectiveness when compared to other screening strategies.

Bibliography

1. Morson B (1974) The polyp-cancer sequence in the large bowel. Proc R Soc Med 67:451–457
2. Desai DC, Neale KF, Talbot IC et al (1995) Juvenile polyposis. Br J Surg 82:14–17

3. Jass JR, Sobin LH (eds) (1989) WHO International Histological Classification of Tumors. Hystological Typing of Intestinal Tumours. 2nd edn. Springer, Berlin Heidelberg, New York
4. Lauenstein T, Goehde S, Rueheme S et al (2002) MR Colonography with barium-based fecal tagging: initial clinical experience. Radiology 223:248–254

Neoplasms, Bile Ducts

Thomas Helmberger[1], Carlo Bartolozzi[2], Marzio Perri[2], Gabriele Caproni[2]
[1]Clinic of Radiology and Nuclearmedicine, University Hospitals Schleswig-Holstein, Campus Luebeck, Luebeck, Germany
[2]Department of Diagnostic and Interventional Radiology, University of Pisa, Pisa, Italy
thomas.helmberger@uni-luebeck.de
bartolozzi@do.med.unipi.it

Synonyms

Cholangiocarcinoma, CC; Cholangiocellular carcinoma, CCC; Klatskin tumor

Definition and Classification

Cholangiocellular carcinoma (CCC) is a malignant tumor arising from the bile duct epithelium and comprises 15–25% of all liver and biliary tract malignancies. The tumors may arise at any part and from any component of the bile duct epithelium, ranging from the terminal ductules (canals of Hering) to the ampulla of Vater as well as at the peribiliary glands (intramural and extramural). According to the site of origin, cholangiocarcinoma can be differentiated into intrahepatic/peripheral, hilar (Klatskin tumor), and extrahepatic.

Intrahepatic CCC includes tumors originating from small biliary intrahepatic ductules and is considered as a peripheral, mass-forming tumor.

Hilar CCCs arise from one of the hepatic ducts or the bifurcation of the common hepatic duct and are classified, according to the Bismuth classification, into four different types: type I involves the main hepatic duct below the bifurcation, type II affects the main hepatic duct bifurcation, type III involves segmental ducts beyond the primary hepatic duct bifurcation in one liver lobe (type IIIa: right lobe, type IIIb: left lobe), and type IV involves segmental ducts in both liver lobes.

Finally, CCCs originating from the bile duct below the bifurcation of the right and left hepatic ducts are classified as extrahepatic (1).

Pathology

The gross appearance of intrahepatic CCC is of a gray-white mass with irregular margins. The mass may be solitary or multiple with satellite nodules in its periphery. Size varies, from a few millimeters to more than 15 cm in diameter. The tumor consists typically of a huge amount of whitish fibrous tissue at cut section, especially in large lesions with central necroses. Calcifications and hemorrhages are rare. Finger-like extensions along the portal triads are frequent. Similar to HCC, intrahepatic CCC has the propensity to invade small portal vessels, resulting in portal vein thrombosis. Metastases to regional lymph nodes and pulmonary and peritoneal spreading are common.

Different histological forms of hilar and extrahepatic CCC (such as infiltrative, nodular, and papillary) have been described.

The infiltrative type is the most common (over 70% of cases) and it appears as a sclerotic lesion with abundant fibrous tissue growing along the bile duct wall. It results in a diffuse, firm, gray-white annular thickening of the bile with complete or nearly complete obstruction of the lumen. The extent of the tumor may vary, ranging from few millimeters to several centimeters in length. A dense fibroblastic reaction may compress or encase the adjacent vascular structures.

The nodular form usually consists of a small (1–2 cm in diameter), gray-white nodule causing biliary obstruction. The tumor arises within the mucosa, invades the bile duct wall, and grows outward to form a nodular, exophytic mass.

The papillary CCC is a distinctive pathologic entity characterized by the presence of an intraluminal polypoid or sessile mass of the hepatic bile duct associated with partial biliary obstruction and dilatation. The tumor is usually small and is a low-grade malignancy (2).

Histopathology

Irrespectively of the primary localization of the tumor, whether it is intra- or extrahepatic, more than 90% of CCCs are well to moderately differentiated adenocarcinomas that exhibit glandular or acinar structures with intracytoplasmic mucinous components. Characteristically, the malignant cells are of cuboidal or low columnar type resembling biliary epithelium. In more poorly differentiated tumors, solid cords of cells without biliary ducts may be present. The dense fibrous stroma is characteristic and may dominate the histological architecture. The tumor tends to invade lymphatics, blood vessels, perineural and periductal spaces, and portal tracts, which might be responsible for the secondary atrophy of the dependent hepatic segments particularly in peripheral CCC. Spread along the lumen of large bile ducts can be seen, especially in hilar tumors (2).

Clinical Presentation

CCC occurs more frequently in patients in the sixth decade of life. It is associated with primary sclerosing cholangitis, intrahepatic stone disease, choledochal cyst, congenital hepatic fibrosis, clonorchiasis, and exposure to Thorotrast.

Clinical signs and symptoms, including jaundice, itching, clay-colored stools, dark urine, weight loss, and abdominal pain, may vary according to the various sites of origin of the tumor (1, 3).

Jaundice is usually the leading sign in tumors located in the common bile duct or common hepatic duct as a sign of biliary obstruction.

Abdominal pain and weight loss are the most common symptoms in intrahepatic CCC, whereas painless jaundice occurs later and is often a marker of advanced disease.

Extrahepatic cholestasis is reflected in elevated levels of direct bilirubin. Levels of alkaline phosphatase and gamma-glutamyltransferase (GGT) usually rise in conjunction with bilirubin.

There are no specific tumor markers for CCC, although elevation of serum carcinoembryonic antigen (CEA) and CA 19–9 is often found.

Imaging

Intrahepatic CCC

The most common appearance of intrahepatic CCC on ultrasound (US) is as an ill-defined, predominantly hypoechoic mass; however, US patterns may vary from homo- or heterogeneous hypo-, iso-, or hyperechogenicity. Hyperechoic foci with acoustic shadowing, suggesting calcifications, and segmental bile duct dilation in the presence of normal extrahepatic ducts may be observed. The presence of satellite nodules is frequent and contributes to a poor prognosis of CCC.

Color Doppler US allows definition of portal vein involvement, without significant usefulness in characterizing the primary tumor mass (3).

On unenhanced computed tomography (CT) scans, intrahepatic CCC usually appears as a large and irregular mass hypodense or isodense relative to the normal hepatic parenchyma. The mass is round or oval, more or less well demarcated, and may demonstrate segmental biliary ductal dilatation peripheral to the tumor. After contrast medium administration, parenchymal CCC usually demonstrates a thin and incomplete rim-like enhancement during both the arterial and portal venous phases (Fig. 1). The central part of the tumor usually does not enhance during these phases, whereas there may be delayed enhancement based on the interstitial transition of extracellular iodinated contrast agents. This pattern of enhancement reflects the hypovascular, desmoplastic composition of most CCCs. Satellite nodules are frequent and variable in size. Additional ancillary CT findings include capsular retraction, intratumoral calcification, invasion of portal or hepatic veins more commonly than in HCC, and dilatation and thickening of peripheral intrahepatic biliary ducts (especially when associated with clonorchiasis). Extrahepatic spread is common and lymph node metastasis with involvement of the celiac and left gastric areas or direct invasion of the omentum is frequently detected (1, 4).

The magnetic resonance (MR) appearance of intrahepatic CCC is that of a noncapsulated tumor, hypointense on T1-weighted images and slightly hyperintense on T2-weighted images. However, the signal intensity of the tumor is variable according to the amount of fibrosis, necrosis, and mucinous components within the tumor.

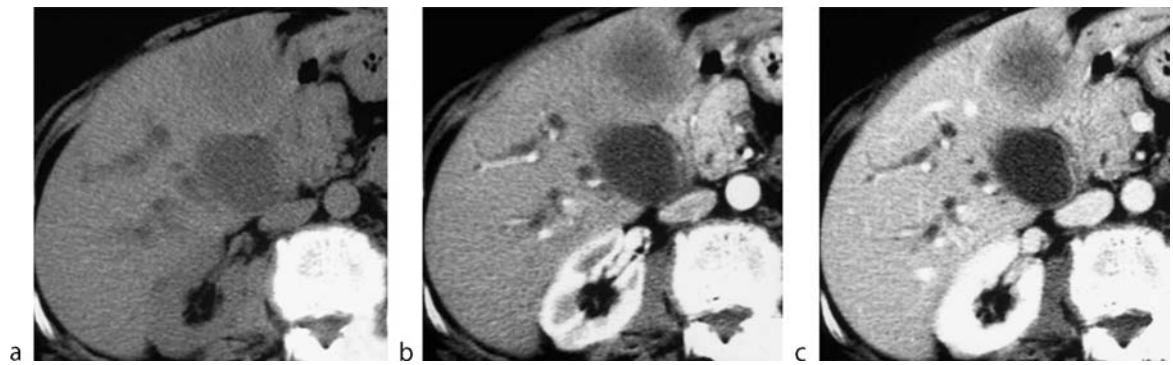

Neoplasms, Bile Ducts. Figure 1 Peripheral cholangiocellular carcinoma. On unenhanced CT scans (a) the lesion appears as an ill-defined and slightly hypodense mass. After contrast medium administration the lesion shows minimal peripheral enhancement during the arterial (b) and portal venous (c) phases. Peripheral biliary ducts dilatation, distal to the mass, is also evident.

A central hypointensity, corresponding to fibrosis, is usually best appreciated on T2-weighted images. Dilatation of peripheral portions of the intrahepatic biliary ducts may be present and can easily be displayed with standard MR cholangiopancreatography (MRCP) sequences (heavily T2-weighted sequences) which is rarely seen in HCC.

On dynamic contrast-enhanced MR studies, minimal to moderate peripheral enhancement is usually observed followed by moderate progressive, delayed filling. Pooling of contrast within the tumor, reflecting the large amount of fibrous tissue, is typically seen on delayed MR images corresponding to the known CT findings (5).

Hilar and Extrahepatic CCC

The US appearance of hilar and extrahepatic CCC includes biliary duct dilatation, mass or bile duct wall thickening, and lobar atrophy with crowded, dilated ducts.

Biliary duct dilatation is almost invariably present in hilar and extrahepatic CCC, and can be a useful sign in the differential diagnosis with other hepatic tumors. Typically, ►Klatskin tumors manifest as segmental dilatation and nonunion of the right and left ducts at the porta hepatis.

Although US is accurate for revealing the level of bile duct obstruction, visualization of the tumor mass is difficult and, therefore, characterization of a hilar or extrahepatic cholangiocarcinoma requires meticulous evaluation of the exact localization of the luminal alteration or ductal occlusion. The papillary and nodular forms of cholangiocarcinoma are relatively easy to see on US, appearing as a poorly defined, usually isoechogenic, nodular lesion with associated mural thickening. In contrast, infiltrating CCCs, the most common subtype, are difficult to appreciate on US, appearing only as a focal or diffuse thickening of the bile duct wall.

Lobar atrophy is often extremely subtle on US images. In this case, US scans demonstrate crowded, dilated ducts within the atrophic lobe. The dilated ducts will often almost reach the liver surface, which is pathognomonic. The associated cholangiocarcinoma is often at a hilar localization with a predominant involvement of the duct which drains the dependent segment (3, 4).

Hilar and extrahepatic CCCs usually appear as a focally thickened ductal wall obliterating the lumen on thin-section spiral CT scans. Following intravenous contrast medium administration, enhancement of the lesion is poor to moderate (Fig. 2). The degree of contrast enhancement probably depends on the presence of the fibroid components of the lesion. An enhancing border or pseudocapsule may be visible in well-delineated tumors. In a minority of cases there is early marked contrast uptake in the tumor, but often contrast enhancement is only noted on delayed scans (1, 4).

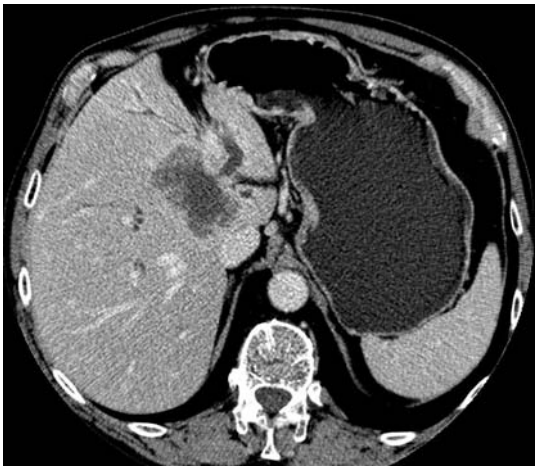

Neoplasms, Bile Ducts. Figure 2 Hilar cholangiocellular carcinoma. Portal venous phase spiral CT shows a large and hypodense mass with lobulated margins at the hepatic hilum, mainly in segment IV. The contrast enhancement of the tumor is peripheral and irregular. Dilatation of the left hepatic duct and peripheral biliary ducts is present.

Lobar hepatic atrophy with marked dilatation and crowding of bile ducts is usually observed on CT scans in patients with hilar CCC in addition to fuzzy invasion of adjacent liver parenchyma and of the hepatoduodenal ligament.

In contrast, satellite nodules are less commonly seen in hilar CCC compared to intrahepatic CCC according to the earlier clinical manifestation of lesions situated at the hilum.

Lymphatic metastases usually involve the portacaval, superior and posterior pancreatoduodenal lymph nodes. Retroperitoneal lymphadenopathy, peritoneal spread, and proximal intestinal obstruction occur in advanced stages.

On MR images, hilar and extrahepatic CCCs appear hypointense to the liver on T1-weighted and moderately hyperintense on T2-weighted images, while on dynamic T1-weighted MR images acquired after gadolinium injection, minimal to moderate incomplete enhancement may be present at the tumor periphery on delayed images. In addition, the combined use of dynamic MR and MRCP depicts the primary tumor in a vast majority of cases and allows evaluation of the overall extent of the biliary tree involvement. The morphology of bile duct stricture detectable on high-resolution MRCP closely reflects the gross morphologic changes along the biliary ductal walls: papillary lesions appear as protuberant, as sessile flat or polypoid-like intraluminal lesions, while diffusely infiltrating tumors may be visualized as a diffuse narrowing of the ductal lumen (5).

Percutaneous transhepatic cholangiography is indicated in any patient who is cholestatic with nondilated bile ducts when there is doubt about the diagnosis and in whom an endoscopic intervention is not possible.

Nuclear Medicine

^{99m} Tc imminodiacetic acid (HIDA) and ^{99m} Tc sulfur scans are the classic nuclear medicine techniques used to display hepatic tumors such as CCCs, but they are of significance only in comparison to contrast-enhanced CT and MRI.

^{99m} Tc HIDA is excreted into the biliary ducts and may reveal the site of biliary obstruction. After injection, the common bile duct and cystic duct are usually visualized within 15 min. However, the ducts might not be visualized, even in healthy patients.

^{99m} Tc sulfur colloid helps in localizing lesions larger than 2 cm. However, the appearances on sulfur colloid and HIDA scans are nonspecific and false-positive findings may occur as a result of the misinterpretation of benign tumors and other malignant tumors.

Positron emission tomography (PET) can be used to assess the metabolism with the administration of positron-emitting radiolabel tracers such as 18F-FDG.

Recent studies have demonstrated the potential role of PET. In particular, 18F-FDG-PET seems to improve the depiction of CCC superimposed on primary sclerosing cholangitis due to the additional inflammatory component and allows the detection of metastatic lymph nodes or peritoneal seeding that other modalities fail to demonstrate.

Diagnosis

Intrahepatic CCC

Intrahepatic CCC classically manifests as a large, well-defined hepatic mass with lobulated margins and peripheral rim enhancement on both contrast-enhanced spiral CT and dynamic MR images. Both modalities are equally effective in the detection and characterization of the tumor, enabling a correct diagnosis and staging of intrahepatic CCCs in a great number of cases (1).

The differential diagnosis includes some bulky hepatic tumors of either primary or secondary origin. Due to a histologically similar appearance in metastatic adenocarcinomas, the differential diagnosis can be difficult for the pathologist. However, absence of a known primary malignancy, a relatively large size, and other ancillary findings such as bile duct dilatation and capsular retraction may support the diagnosis of CCC (4).

The vast majority of HCCs are hypervascularized and therefore easily differentiated from CCCs. Nevertheless, some variants of HCC such as sclerosing, fibrolamellar, and cholangiohepatocellular carcinoma may mimic intrahepatic CCCs. Especially in the latter cases, even biopsy may be unable to resolve the diagnostic dilemma.

Hilar and Extrahepatic CCC

Whenever extrahepatic CCC is suspected, the following aspects should be assessed: biliary dilatation, level of obstruction, presence of mass, focal or diffuse thickening of the bile duct wall, presence of a hepatic tumor, local lymph nodes involvement, and portal vein thrombosis.

US is the primary diagnostic procedure in most cases. US is accurate in revealing the level of bile duct obstruction, but the tumor mass is detected in a few cases only (3–5). In contrast, thin-section contrast-enhanced spiral CT and MR (dynamic MR and MRCP) depict the lesion and allow correct evaluation of the tumor extent in a great number of cases. In addition, dynamic CT and MR provide an accurate evaluation of vascular involvement, of secondary liver atrophy, and of lymphadenopathy of the peripancreatic, periduodenal, periportal, celiac, and mesenteric nodes.

The differential diagnosis of ductal CCC depends on its location. Lesions at the ductal confluence may be mimicked by inflammatory cholangitis (acquired immunodeficiency syndrome, sclerosing cholangitis), oriental cholangitis, benign biliary tumors, HCC, or gallbladder cancer, while ampullary or pancreatic cancer, nonshadowing stones, biliary adenomas or papillomas, blood clots, and benign strictures may simulate lesions of the distal common bile duct. Moreover, metastatic tumoral tissue in the bile ducts or adjacent nodes may mimic CCC at any anatomical level.

Lobar hepatic atrophy with marked dilatation and crowding of bile ducts is highly suggestive of hilar and peripheral CCC, although long-standing biliary obstruction from surgical trauma or focal biliary obstruction can cause similar findings.

Extrahepatic bile duct adenoma is a rare benign lesion of the biliary duct appearing as a polypoid filling defect within the bile duct at direct MRI or MR cholangiography. It is usually located at the common bile duct or at the common hepatic duct and is difficult to differentiate from small nodular extrahepatic or hilar CCC. However, additional findings of hepatoduodenal ligament adenopathy and tumor extension into adjacent structures are helpful diagnostic features supporting a malignant differential diagnosis (4).

Moreover, since intraductal papillary CCC produces single or multiple intraductal masses, the differential diagnosis from a bile duct stone may be difficult. Furthermore, the clinical manifestations of both diseases are similar. On

US a papillary tumor does not cast a shadow like some nonshadowing stones, and on precontrast CT the tumor appears as a high- or low-attenuation soft tissue mass.

Interventional Radiology

Although the prognosis of patients with CCC after surgical resection is poor, complete resection of the tumor is currently considered the best therapeutic option.

Since only 20–40% of patients are suitable for surgical treatment, palliative interventional radiological and gastroenterological procedures, such as percutaneous biliary drainage and stenting, may be employed in an attempt to improve survival and life quality.

Percutaneous transhepatic biliary drainage (PTBD) represents a useful palliative treatment for resolving jaundice. It is indicated as a preoperative or preinterventional decompression procedure, particularly when endoscopic treatment has failed or is not indicated. Preoperative PTBD helps to reduce the incidence of postoperative sepsis, abscess, bleeding, and renal failure. Obviously, urgent PTBD is mandatory in cases of neoplastic biliary obstruction complicated by acute cholangitis (6).

Expandable metallic stents are often used in cases of biliary obstruction caused by an unresectable hilar CCC. Several studies show that the use of metallic stents is able to shorten hospitalization and to improve the quality of survival by lowering significantly the obstruction-related serum bilirubin levels. However, several early (fever, sepsis, bilioma, hemobilia, bile peritonitis, pancreatitis, cholecystitis) or late complications may occur. Late complications such as recurrent symptoms of cholangitis, cholangiohepatic abscess, or jaundice are usually related to stent occlusion by tumor ingrowth, overgrowth, and stent migration. In an attempt to prevent or to delay stent occlusion by tumor ingrowth, covered stents have been used. However, although covered devices impair tumor ingrowth, they cannot prevent neoplastic outgrowth. In addition, the long-term durability of the covered membrane is problematic.

Bibliography

1. Han JK, Choi BI, Kim AY et al (2002) Cholangiocarcinoma: pictorial essay of CT and cholangiographic findings. Radiographics 22 (1):173–187
2. Lim JH, Park CK (2004) Pathology of cholangiocarcinoma. Abdom Imaging 29(5):540–547
3. Bloom CM, Langer B, Wilson SR (1999) Role of US in the detection, characterization, and staging of cholangiocarcinoma. Radiographics 19:1199–1218
4. Lee WJ, Lim HK, Jang KM et al (2001) Radiologic spectrum of cholangiocarcinoma: emphasis on unusual manifestations and differential diagnoses. Radiographics 21Spec No:S97–S116
5. Schneider G, Grazioli L, Saini S (2002) MRI of the Liver. Springer, Berlin, Heidelberg
6. Lencioni R, Cioni D, Bartolozzi C (2005) Focal Liver Lesions: Detection, Characterization, Ablation. Springer-Verlag, Berlin, Heidelberg, New York

Neoplasms, Bladder

G. Heinz-Peer
Department of Radiology, Medical University, Vienna, Austria
gertraud.heinz-peer@akhwien.at

Definition

Carcinoma of the urinary bladder is one of the most common malignant tumors of the urinary tract and represents 2% of all malignancies. It is a disease of later life with a peak incidence during the seventh decade. Bladder cancer is three times more common in men than women and it affects twice as many Whites as Blacks (1). The most well documented risk factor of bladder cancer is cigarette smoking, to which has been attributed up to 45% of urothelial cancers (1). Although difficult to prove with certainty, occupational exposure to β-naphtylamine, paints, oils, gasoline, zinc, chromium, and rubber has been associated with 18–40% of bladder cancer cases. Other risk factors include chronic bladder infection or inflammation, pelvic irradiation, and treatment with cyclophosphamide (1). A genetic propensity to develop bladder cancer has also been observed (1).

Other primary tumors, such as non-Hodgkin's lymphoma and pheochromocytoma are very rare and may arise in the bladder wall. Secondary involvement of the bladder by lymphoma may occur, representing direct spread from grossly involved pelvic lymph nodes. Metastases may also develop within the bladder wall, the extraluminal component being more obvious than the intraluminal mass, providing a clue to the diagnosis in patients with known disseminated disease due to cancers such as malignant melanoma and breast cancer.

Pathology

Most bladder tumors arise from the urothelium. Transitional cell tumors account for 95% of all primary malignant bladder lesions (2). The rest are squamous cell carcinomas, mixed transitional and squamous cell tumors, adenocarcinomas, and undifferentiated lesions

(2). Most bladder cancers arise on the lateral walls (47%) or in the region of the trigone (21%). Adenocarcinomas, which account for 3% of all bladder tumors, usually arise in the region of the trigone, but are occasionally seen as exophytic growths arising at the bladder dome and originating from a persistent urachus.

About one-third of cancers are multifocal at the time of diagnosis, and the whole bladder epithelium may undergo malignant change. Recurrences and new tumors are frequent (2). Bladder tumors show a variable pattern of growth and are classified as papillary, infiltrative, papillary and infiltrative, or nonpapillary and noninfiltrative (carcinoma *in situ*). Grade I lesions are well-differentiated tumors and are usually papillary, whereas grade III lesions are poorly differentiated and frequently show an infiltrating pattern of growth. Tumor grade correlates with the natural history of the disease, as those with grade III tumors invading muscle have a significantly worse prognosis than those with grade I or II superficial lesions (1). Approximately one-third of patients present with muscle invasive disease at the time of initial diagnosis (1).

Tumor stage refers to the depth of invasion. The tumor/nodes/metastasis (TNM) staging system is most widely used. Historically, tumors confined to the mucosa (Ta) and lamina propria (T1) have been classified as superficial; muscle invasive tumors are classified as T2-T3. In general, there is a correlation between T-stage and the risk of recurrence, progression, and metastasis.

Once the tumor has penetrated the basement membrane (T1) or muscle (T2-T4), there is an increased likelihood of distant metastases, depending on the depth of penetration (Fig. 1). The tumor may involve adjacent organs (prostate, uterus, vagina, rectum, small intestine) and extend to the pelvic side wall. Transitional cell carcinoma (TCC) of the prostate is present in approximately 40% of men with invasive bladder cancer (1). Coexistent adenocarcinoma of the prostate is present in 40% of men undergoing cystoprostatectomy for invasive TCC (1).

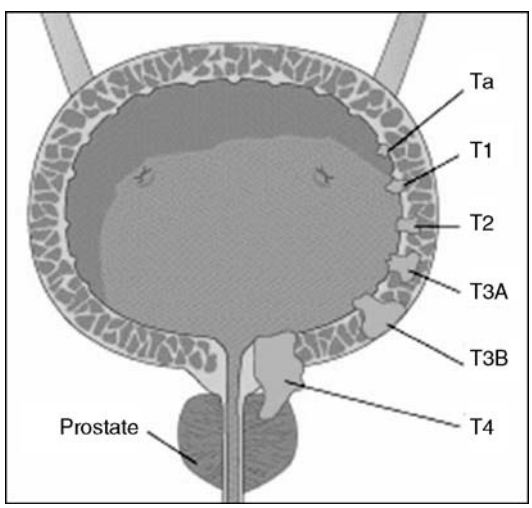

Neoplasms, Bladder. Figure 1 Depth of tumor penetration according to TNM system of staging bladder carcinoma.

Synchronous upper urinary tract urothelial tumors occur in 2–5% of patients (2).

Distant metastasis may occur *via* the lymphatic or vascular systems. The regional lymphatics include the paravesical, obturator, and external iliac lymph nodes. The most common sites of distant metastasis are liver, lung, and bone.

Clinical Presentation

Patients most commonly present with painless ►hematuria, either gross or microscopic. The bleeding may be intermittent, so one should not be lured into a sense of false security by the spontaneous disappearance of bleeding. Irritative voiding symptoms, including frequency, urgency, and dysuria, occur and are often associated with CIS. This constellation of symptoms, however, may also occur with benign entities, such as urinary tract infection, prostatism, and prostatits.

Locally advanced tumors may lead to ureteric obstruction, pelvic side wall muscle invasion, or invasion of adjacent organs. These advanced tumors present with pelvic or abdominal pain and symptoms related to the urinary tract.

Imaging

Excretory Urography

In the past, routine imaging surveillance consisted of periodic excretory urography. In addition, excretory urography was generally performed to examine the upper urinary tract for synchronous tumors, which occur in 2.3% of patients with TCC of the urinary bladder. Excretory urography can also be used to detect other abnormalities such as stones or masses that could account for the patients' hematuria. However, negative findings in excretory urography cannot exclude urothelial cancer.

Computed Tomography

Bladder tumors appear on CT as soft tissue density lesions arising from the bladder wall. The tumor may be sessile or pedunculated, but in some cases the only abnormality seen is thickening of the bladder wall. Tumors enhance following injection of intravenous contrast medium, often to a greater degree than the normal bladder wall.

In the pre-MDCT era, several limitations and difficulties associated with CT staging of bladder cancer

have been reported. Review of the literature shows that the accuracy of CT study in the staging of bladder neoplasm has varied between 68 and 85%, and it has been shown that CT has failed in staging early tumors (TIS-T3a). In patients with suspected perivesical spread and more advanced disease, however the usefulness of CT has been reported.

CT has been regarded as inferior to MRI for staging bladder cancer, but as similar in evaluation of extravesical disease.

Multidetector CT offers new possibilities for imaging of the urinary bladder and urinary tract. Using thin collimation, near isotropic imaging of the urinary tract is possible and provides high quality multiplanar reformations and 3D reconstructions of the organ including virtual cystoscopic views.

Since the initial report of Vining et al (3), a growing number of articles on detection of bladder lesions with ►virtual cystoscopy have been published. In general, results of these studies indicated that virtual cystoscopy allows accurate assessment of localization and morphology (pedunculated or sessile) of bladder masses. Additionally, the decrease of post processing time from 6–8 h to a few minutes allows its routine use in the clinical praxis.

Song et al (4) showed that transverse and virtual views are complementary in lesion detection and characterization, and thus should always be used for accurate lesion detection. These authors also recommend that imaging in both positions is necessary for visualization of the entire mucosal surface without obscurity caused by residual urine (4).

Preliminary results of various studies show excellent detection rates, including lesions <5 mm (Fig. 2) and also accurate staging of bladder tumors by combined evaluation of source data and virtual cystoscopy (Figs. 3–5).

At present, virtual cystoscopy based on volumetric data obtained with thin section multislice CT and the use of perspective volume-rendering technique seems to be the most accurate method regarding lesion detection in the urinary bladder.

For virtual ureterorenoscopy i.v. application of contrast media is the only possibility to get sufficient contrast of the excretory system. Negative contrast agents like room air or CO_2 cannot be used in this particular procedure.

Stenzl et al (5) described the usefulness of VE based on CT datasets in imaging of the reconstructed lower urinary tract. 3D reconstruction aided in the interpretation of intraluminal changes, indentations of the pouch wall, voiding problems resulting from a descent of the pouch floor ("pouchocele"), and incisional hernias. Additionally, this series also added to the authors understanding of the postoperative evolution of orthotopic intestinal bladder substitutions (5).

There are still some limitations of virtual cystoscopy. A major limitation is that it is unable to depict flat lesions (carcinoma *in situ*) which appear as subtle mucosal color changes at conventional cystoscopy. In addition, mucosal thickening secondary to fibrosis cannot be distinguished from a neoplasm. Virtual cystoscopy lacks the ability to provide tissue for histologic evaluation.

Magnetic Resonance Imaging

Tumors of the urinary bladder, whether infiltrative, sessile, or pedunculated, can be detected with MR imaging if they exceed 7–8 mm in diameter. Disruption of the muscle layer suggests deep tumor invasion. Immediately after intravenous administration of contrast agent containing gadolinium, tumor, mucosa, and lamina propria show earlier and greater enhancement compared with the muscle layer of the bladder wall or other tissues.

A limitation of MR imaging is the determination of extent of tumor growth in the muscle layer of the bladder wall (differentiation between stages T2 and T3a). However, the use of endorectal surface coils or phased array multicoils in combination with i.v. contrast agents is

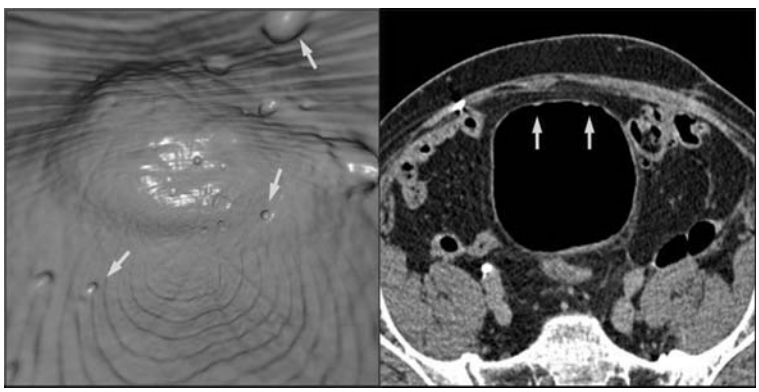

Neoplasms, Bladder. Figure 2 Multiple Ta Lesions: VE view (left image) shows multiple, tiny, polypoid lesions < 5 mm (*arrow*), presenting as focal mural thickening on the corresponding 2D image (right image).

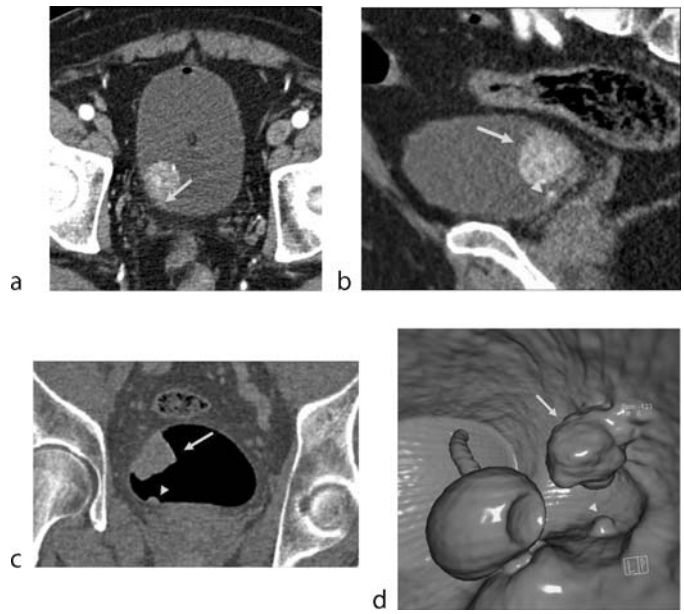

Neoplasms, Bladder. Figure 3 Stage Ta-T1: Contrast enhancing tumor (*arrow*) spreading along the posterior-lateral surface of the bladder wall with no signs of transmural growth. Synchronous small Ta-T1 lesion on the floor of the bladder (*arrowhead*) (upper left and right and lower left images). VE showing the large lobulated (*arrow*) and the tiny, polypoid lesion (*arrowhead*). The Foley catheter balloon is seen in the foreground (lower right image).

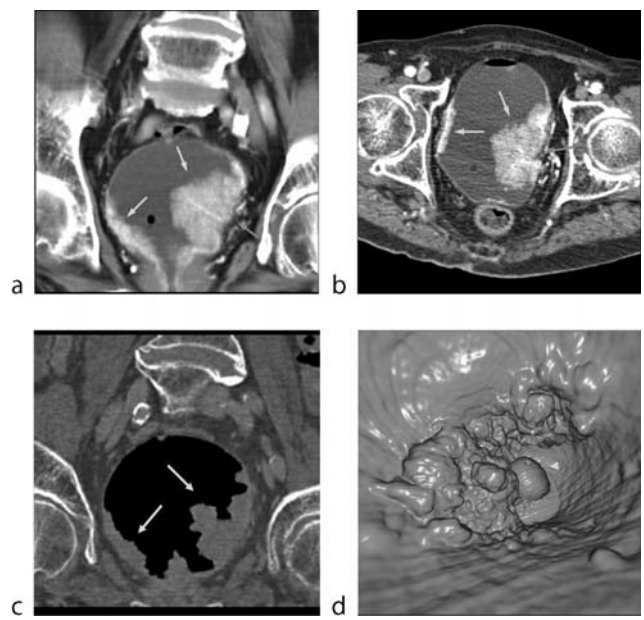

Neoplasms, Bladder. Figure 4 Stage T2-T3a: Carpet-like spreading bladder tumor infiltrating into the outer layer of the bladder wall (left and right upper and left lower images). Retraction effect due to mural invasion (a, b). VE (right lower image) shows an overview. Foley catheter (*arrow*).

continuing to evolve the role of MR in imaging bladder tumors.

Lämmle et al (6) showed high reliability in the diagnosis of urinary bladder cancer by MR-imaging based virtual cystoscopy. In this study, overall detection rate for bladder tumors was 91%, the detection rate for tumors >1 cm was 100%. Utilizing T2-weighted and Gd-enhanced T1-weighted MR-urography, Beer et al (7) evaluated maximum intensity projection (MIP) and virtual endoscopy in patients with suspected urogenital disease. Results of this study showed that both datasets were equal regarding virtual ureterorenoscopy. For virtual

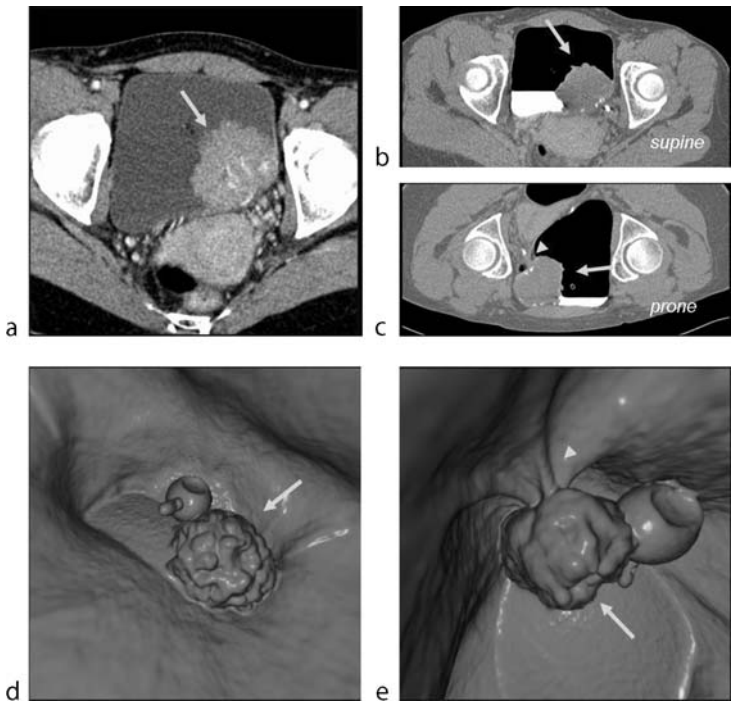

Neoplasms, Bladder. Figure 5 Pedunculated bladder carcinoma (*arrow*): Mobility while dual positioning. Stalk (*arrowhead*). No signs of bladder wall infiltration—T1 tumor.

cystoscopy, T2-weighted datasets were superior to the Gd-enhanced T1-weighted sequences. In addition, 86% of endoluminal diseases were revealed on virtual endoscopy (VE) compared to 15% on MIP images. In renal pelvis evaluation MIP images were superior to VE. Negative contrast agents do not have any role in this setting (7).

Diagnosis

When a clinical diagnosis of bladder tumor is suspected, the initial investigation consists of urine cytology and lower urinary tract endoscopy. The development of flexible cystourethroscopy has allowed diagnostic endoscopy to be performed safely in an office setting with improved patient comfort. It allows thorough endoscopic assessment of the entire urethra, including the prostatic urethra in men, and the entire urinary bladder. Papillary and well-circumscribed bladder tumors are easily recognized. Areas of CIS may appear only as red areas on the mucosa. After endoscopic visualization of a bladder tumor, the histopathologic diagnosis and initial treatment are achieved by transurethral resection (TUR) of the tumor. Complete endoscopic resection of the tumor using a loop diathermy electrode is attempted, unless there is obvious extravesical extension. Areas of abnormal appearing mucosa are biopsied (1).

However, conventional cystoscopy may be limited by diminished visualization of areas such as the mucosa of the bladder neck and within diverticula. In addition, conventional endoscopy proves to be technically very difficult in patients with urinary diversion, and some structures may not even be visualized. Conventional cystoscopy may be invasive, uncomfortable, time consuming, and expensive. In addition, rare complications like iatrogenic injury to the urethra and bladder as well as urinary sepsis may occur. In patients with bacteriuria, acute cystitis, urethritis, prostatitis, obstructive prostatic hypertrophy, and stricture or rupture of the urethra conventional cystoscopy may be contraindicated.

The treatment and prognosis of urinary bladder carcinoma is largely determined by the depth of tumor growth and the extent of tumor metastases (1). Bladder saving treatment is used for superficial tumors (stages Ta-T1), whereas for stage T2-T3b tumors, radical cystectomy is performed. The treatment for stage T4a and T4b tumors and for metastatic disease is usually palliative radiation and chemotherapy, respectively.

The accuracy of the UICC clinical staging which includes deep fractioned TUR is sufficient for superficial tumors. However, the accuracy of clinical staging for stage T2-T4b tumors is poor.

In conclusion, CT- and MR-imaging including virtual endoscopy techniques of the urogenital tract have enormously improved over the past few years. Contributing to this progress is the continuing improvement of MR hard- and software as well as the advent of ►Multidetector computed tomography (MDCT) and the ability

to acquire near isotropic datasets. Commercially available 3D workstations and the rapid evolution of supporting software also fasten the improvement.

Considering the limitations and contraindications of conventional cystoscopy, CT- or MR-imaging including virtual cystoscopy seems to be an alternative in a patient suspected or known to have bladder cancer who is not a candidate for conventional cystoscopy. In addition, these techniques seem to be most appropriate in evaluation of the upper urinary tract. The high accuracy in detection of lesions <5 mm as well as short postprocessing times have tremendously improved the clinical utility of thin section MDCT and virtual cystoscopy and may justify its incorporation into imaging algorithm for evaluation of hematuria. The high degree of accuracy in the depiction of the topographical anatomy of the transposed structures in patients with urinary diversion makes MDCT- and MR-virtual endoscopy unambiguous in this setting.

Bibliography

1. Dunnick NR, Sandler CM, Newhouse JH, (2001) The urinary bladder. In: Dunnick NR et al (eds) Textbook of Uroradiology. Lippincott Williams & Wilkins, pp 352–393
2. WongYou-Cheong JJ, Wagner BJ, and Davis CJ (1998) Transitional cell carcinoma of the urinary tract: radiologic-pathologic correlation. Radiographics 18:123–142
3. Vining DJ, Zagoria RJ, Liu K, et al (1996) CT cystoscopy: an innovation in bladder imaging. Am J Roentgenol 166:409–410
4. Song JH, Francis IR, Plat JF, et al (2001) Bladder tumor detection at virtual cystoscopy. Radiology 218:95–100
5. Stenzl A, Frank R, Eder R, et al (1998) 3-dimensional computerized tomography and virtual reality endoscopy of the reconstructed lower urinary tract. J Urol 159:741–746
6. Lämmle M, Beer A, Settles M, et al (2002) Reliability of MR imaging based virtual cystoscopy in the diagnosis of cancer of the urinary bladder. Am J Roentgenol 178:1483–1488
7. Beer A, Saar B, Link TM, et al (2001) Virtuelle endoskopie des urogenitaltraktes auf der basis T2-gewichteter und kontrastmittelunterstützter T1 gewichteter datensätze. Fortschr Röntgenstr 173:997–1005

Neoplasms, Bone, Benign

Klaus Woertler
Technical University Munich, Munich, Germany
woertler@roe.med.tum.de

Synonyms

Benign bone tumors

Definition

Benign bone tumors are true neoplasms that originate from bone.

Pathology/Histopathology

Bone tumors can histologically be classified according to their matrix production and/or predominant cell type. The World Health Organization (WHO) classification of bone tumors includes benign neoplasms categorized as osteogenic tumors (►osteoid osteoma and ►osteoblastoma), cartilage tumors (►osteochondroma, ►enchondroma, periosteal chondroma, ►chondroblastoma, and chondromyxoid fibroma), fibrogenic/fibrohistiocytic tumors (desmoplastic fibroma and benign fibrous histiocytoma), vascular tumors (►hemangioma), lipogenic tumors (►intraosseous lipoma), and ►giant cell tumor. Osteoid osteomas, osteochondromas, and enchondromas together account for approximately 20% and giant cell tumors for up to 10% of all primary bone tumors. With the exception of the relatively frequent hemangiomas of the spine, all other benign bone neoplasms are very rare.

A detailed description of the specific histologic features of all lesions mentioned above would go far beyond the scope of this essay.

Clinical Presentation

With the exception of enchondroma, intraosseous lipoma, hemangioma, and giant cell tumor, most benign bone tumors occur in children and young adults. Whereas enchondroma, osteochondroma, lipoma, and hemangioma usually are asymptomatic and therefore are often detected incidentally, osteoid osteoma, osteoblastoma, chondroblastoma, and giant cell tumor cause clinical symptoms in the majority of cases. Pain and swelling are the most common but unspecific complaints. Patients with osteoid osteoma can exhibit more typical clinical features, with pain that becomes more severe at night and promptly responds to analgesics. Pathologic fracture overall represents a rare finding in benign bone tumors, but is relatively frequent in enchondromas of the hand. Osteochondromas can become symptomatic due to compression of adjacent soft tissues, nerves, and vessels.

Table 1 gives an overview on the typical ages of patients, the gender ratios, and the skeletal distribution of the most common benign bone neoplasms.

Neoplasms, Bone, Benign. Table 1 Benign bone tumors: clinical data and skeletal distribution (*LTB* long tubular bones, *STB* short tubular bones)

Tumor	Typical age of patients and gender ratio	Typical sites within skeleton	Typical locations within bone
Osteoid osteoma	1st–3rd decades M:F = 2–4:1	LTB (femur, tibia) > spine > others	LTB: diaphysis > meta-/epiphysis Spine: posterior elements
Osteoblastoma	1st–3rd decades M:F = 2:1	Spine, flat bones, LTB > others	Spine: posterior elements LTB: diaphysis > metaphysis
Enchondroma	3rd–4th decades M:F = 1:1	STB of the hand, LTB (femur, humerus, tibia)	LTB: (dia)metaphyses
Osteochondroma	1st–3rd decades M:F = 2:1	LTB (femur, humerus, tibia) > others	LTB: metaphysis spine: posterior elements
Chondroblastoma	2nd decade M:F = 2–3:1	LTB (humerus, femur, tibia) > others	LTB: epiphysis (epimetaphysis), apophysis
Intraosseous lipoma	3rd–5th decades M:F = 1:1	LTB, calcaneus > others	LTB: metaphysis
Hemangioma	3rd–4th decades M:F = 1:2	Spine, skull > others	Spine: vertebral body
Giant cell tumor	3rd–4th decades M:F = 1:2	LTB > others	LTB: epi/metaphysis spine: vertebral body

Imaging

Osteoid osteoma (Fig. 1) in cortical locations typically has the radiographic appearance of a round or oval radiolucency of <1.5 cm in diameter (nidus) accompanied by reactive bone sclerosis and a solid periosteal reaction. However, the nidus, which consists of highly vascularized connective tissue with a variable amount of mineralized osteoid, might also be invisible on radiographs. Osteoid osteomas located in the axial skeleton or in small bones and those with a medullary, subperiosteal, or intraarticular localization in long bones are often accompanied by less sclerosis and can present with uncharacteristic or misleading radiographic features. Computed tomography (CT) represents the method of choice in depiction of the nidus and thus in establishing the diagnosis. On magnetic resonance (MR) imaging, the nidus tissue can show various signal intensities depending on its amount of matrix production and mineralization. T2-weighted, STIR, and contrast-enhanced pulse sequences usually show edema of bone marrow and periosteum in the surrounding area of the nidus, which might also extend into adjacent soft tissues. Hypervascularity was demonstrated by angiography in the past, but today can easily be visualized by dynamic CT or MR imaging. The typical arterial enhancement pattern of osteoid osteoma can be used to differentiate the lesion from subacute osteomyelitis.

Osteoblastoma (Fig. 1) differs from osteoid osteoma in having a nidus >1.5 cm in diameter and showing a variety of radiographic features. Most lesions originating from the medullary canal or cortex of long tubular bones display a geographic lytic pattern delineated by a sclerotic rim, often in association with expansion of bone and periosteal reactions. However, in most cases the radiographic findings are nondiagnostic. Osteoblastomas of the spine can present as expansile lesions that arise from the posterior elements, most commonly of a thoracic or lumbar vertebra, but they can also be invisible on conventional radiographs. As in osteoid osteoma, CT is therefore the preferred imaging modality for detecting the nidus, assessing the patterns of bone destruction and periosteal reaction, depicting osteogenic matrix mineralizations, and defining tumor extent before surgical resection. MR imaging usually offers more unspecific findings with various signal intensities within the nidus and prominent edema of nearby bone marrow and soft tissues.

Osteochondroma (osteocartilaginous exostosis; Fig. 2) can occur as a solitary lesion or as part of a familial skeletal syndrome with autosomal dominant inheritance, termed hereditary multiple exostoses. Radiographs are usually pathognomonic, as they show one single or multiple sessile or pedunculated osseous excrescenses in continuity with the marrow and cortex of the host bone. The osseous stalk is covered by a cap of hyaline cartilage that might demonstrate calcifications on radiography and that usually ossifies with skeletal maturity.

Malignant transformation into a (low-grade) chondrosarcoma is rare in patients with solitary osteochondroma, but has been reported to occur in 5–25% of patients with multiple lesions. Malignancy should be suspected if the thickness of the cartilage cap exceeds 2 cm

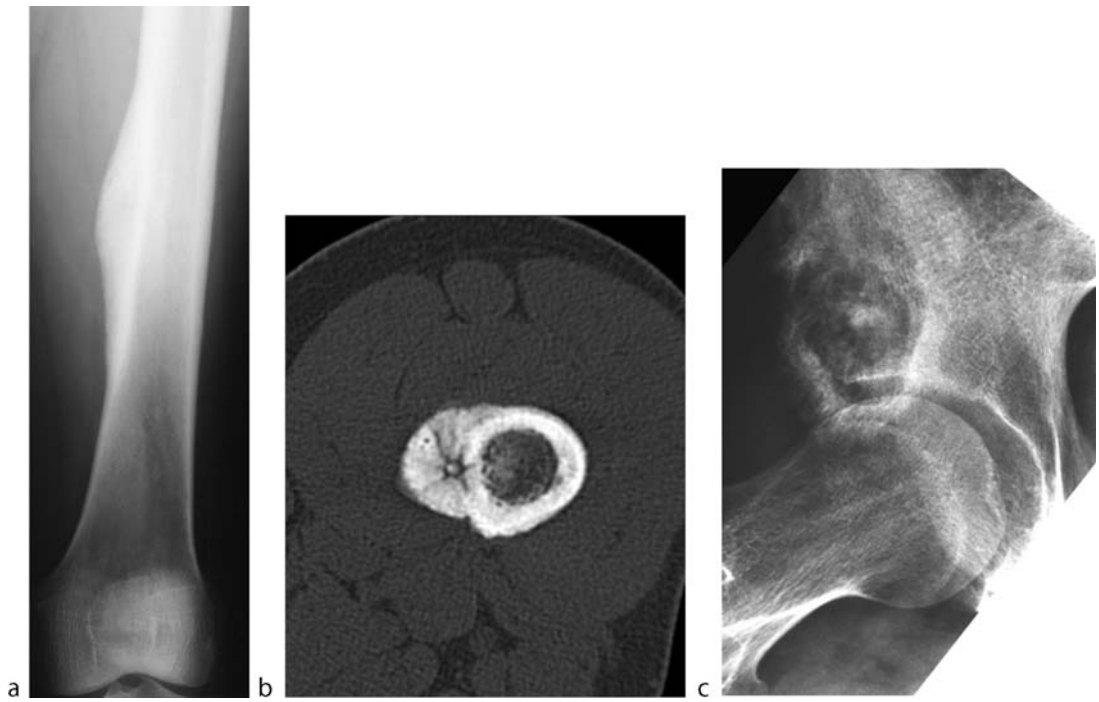

Neoplasms, Bone, Benign. Figure 1 Benign bone neoplasms: osteogenic tumors. (a) and (b) Osteoid osteoma. (a) Anteroposterior radiograph shows circumscribed cortical hyperostosis at the midshaft of the femur. The nidus is hardly visible on radiography. (b) Corresponding computed tomography scan demonstrates centrally mineralized nidus within extensive periosteal new bone formation. Note associated sclerosis of adjacent medullary bone. (c) Osteoblastoma of the ilium. Radiograph shows geographic bone destruction with relatively well-defined margins, incomplete sclerotic rim, and central mineralizations. The cortex is partially destroyed.

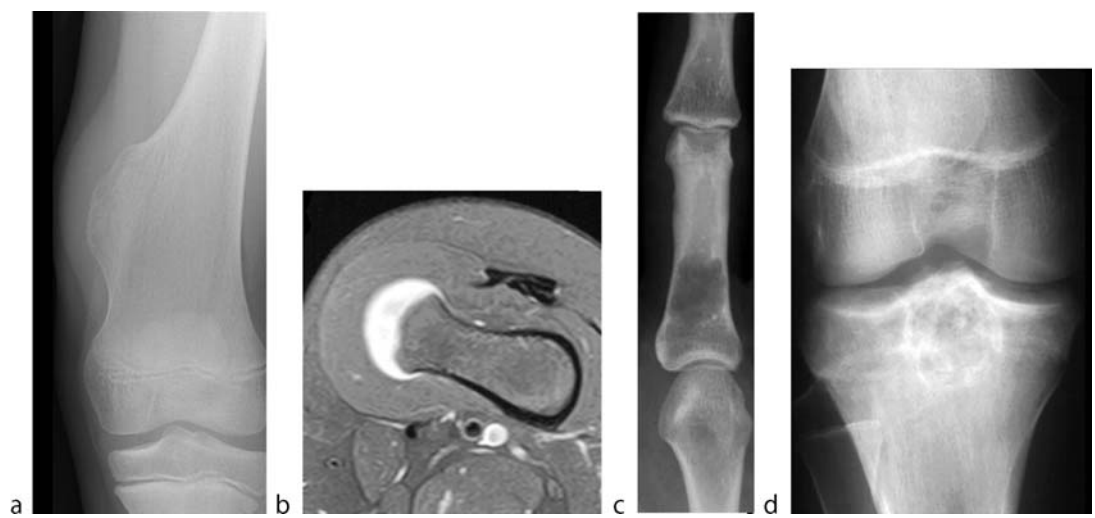

Neoplasms, Bone, Benign. Figure 2 Benign bone neoplasms: chondrogenic tumors. (a) and (b) Osteochondroma. (a) Anteroposterior radiograph of the femur shows sessile bony outgrowth arising from the distal metadiaphysis. Note continuity of the cortex and marrow with those of tumor-bearing bone. (b) Corresponding transverse T2-weighted magnetic resonance image with fat suppression demonstrates hyperintense cartilage cap covering the osseous stalk. (c) Enchondroma. Radiograph of the third finger shows centrally located, lobulated lucency with endosteal scalloping of the cortex within the proximal phalanx. (d) Chondroblastoma. Anteroposterior radiograph demonstrates round osteolytic lesion with sclerotic rim and central mineralizations in the proximal epimetaphysis of the tibia.

in adults and 3 cm in children. MR imaging with the use of T2-weighted pulse sequences represents the most reliable method to assess cartilage cap thickness, whereas CT shows a tendency for underestimation, and ultrasound can be limited by the anatomic localization and orientation of the osteochondroma.

Enchondroma (Fig. 2) of long tubular bones typically presents as a centrally located oval radiolucency with a sharply delineated and lobulated contour, various degrees of endosteal scalloping, and cartilaginous matrix mineralizations. Punctate, flocculent, or rings-and-arcs-like calicifications/ossifications represent characteristic mineralization patterns that usually allow for the radiographic diagnosis. Lesions located in the short tubular bones of the hand more often appear purely osteolytic, with more pronounced endosteal erosion or even expansion of bone. Epiphyseal or axial location, a lesion size >5–6 cm, periosteal reactions, cortical thickening, deep endosteal erosion (more than two-thirds of cortical thickness) or expansion of a major bone, cortical penetration, and enlargement of a radiolucency over time are findings that should alert to the differential diagnosis of chondrosarcoma. In this regard, CT represents the most valuable imaging method because it is best suited to assess the integrity of the cortex. On MR imaging, enchondromas reveal the typical morphology of a well-differentiated cartilaginous lesion with low signal intensity on T1-weighted images, very high signal intensity on T2-weighted images, and peripheral/septal enhancement following contrast administration ("rings and arcs"). However, compared with CT, MR imaging is less reliable in depicting cortical alterations.

Chondroblastoma (Fig. 2) in typical cases shows the radiographic appearance of a round osteolytic lesion with thin sclerotic borders, which is eccentrically positioned within the epiphysis of the affected bone. Approximately 50% of chondroblastomas show matrix mineralizations that are detectable on conventional radiographs. Solid or lamellated periosteal reactions might be visible at the metaphysis or the diametaphyseal shaft. On MR images, chondroblastomas often show more inhomogeneous signal and a less typical enhancement pattern than other benign cartilaginous lesions. Furthermore, the lesions often cause edema of adjacent bone marrow and reactive synovitis.

Intraosseous lipoma (Fig. 3) usually presents as a nonaggressive radiolucent lesion surrounded by a thin sclerotic margin. Trabeculations and osseous expansion might be evident. Central calcifications or ossifications due to liponecrosis are seen in many cases. Particularly in the proximal femur and the calcaneus, this radiographic appearance is virtually pathognomonic. CT and MR imaging can both be used to verify the lipomatous character of the lesion. Cystic areas, calcifications, and new bone formation are additional findings in lesions with partial or extensive fat necrosis (stages 2 and 3 lipomas).

Hemangiomas (Fig. 3) of the spine usually involve the vertebral body and produce a coarse, vertically oriented trabecular pattern on radiography. On transverse CT or MR images, these thickened trabeculae are seen as

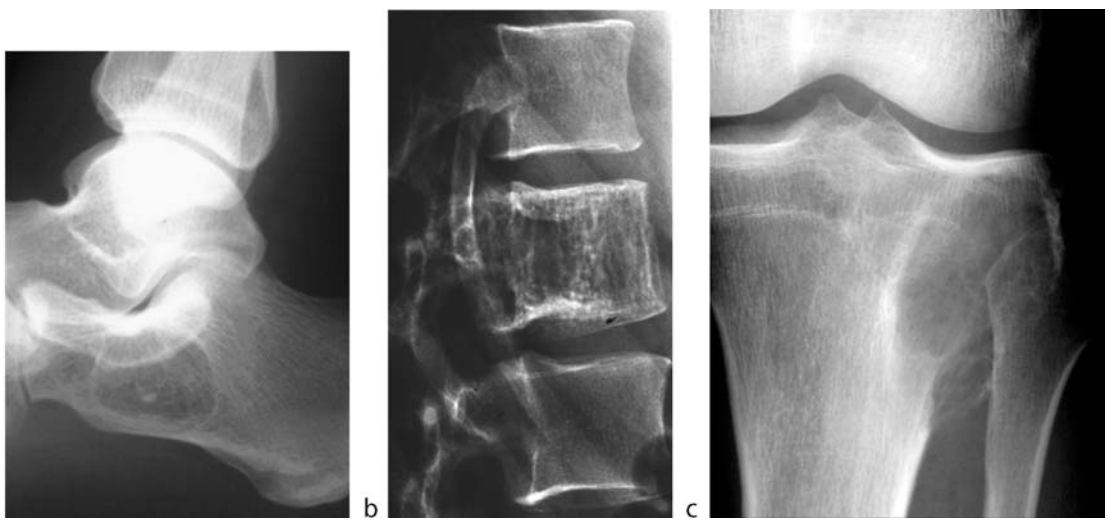

Neoplasms, Bone, Benign. Figure 3 Benign bone neoplasms; miscellaneous lesions. (a) Intraosseous lipoma: lateral radiograph shows the pathognomonic appearance of a calcaneal lipoma with delicate sclerotic margin and central mineralization. (b) Hemangioma: lateral radiograph shows rarefication the of bone structure of the first lumbar vertebra with a vertical trabecular pattern. Note extension into the pedicles. (c) Giant cell tumor: anteroposterior radiograph demonstrates a purely osteolytic lesion with eccentric localization in the proximal epimetaphysis of the tibia. The tumor shows well-defined intraosseous borders and destruction of the cortex with formation of a slightly expanded, incomplete neocortex.

multiple punctate areas within the matrix of the hemangioma, termed polka-dot appearance. At extraspinal sites, hemangiomas show more variable radiographic features, although lytic lesions with slight expansion and a radiating, lattice-like or honeycomb trabecular pattern a highly suggestive of the diagnosis. Particularly in anatomically complex areas, CT can be helpful in identifying these features. The MR imaging appearance of hemangiomas varies with its composition of vascular and nonvascular components. Lesions with a predominantly fatty matrix show high signal intensity on T1-weighted images, intermediate to high signal intensity on T2-weighted images, and a loss of signal on STIR or fat-suppressed T2-weighted images. Predominance of the vascular component results in hypointensity on T1-weighted images, hyperintensity on STIR and T2-weighted images, and marked contrast enhancement.

Giant cell tumor (Fig. 3) typically arises as a purely osteolytic lesion with relatively well-defined margins, which in most cases lack a sclerotic rim. In long tubular bone, the majority of lesions show eccentric location within the epimetaphysel region and variable degrees of cortical violation without a significant periosteal reaction. MR imaging is best suited to demonstrate the true extent of giant cell tumors, particularly with a view to extraosseous growth, which is observed in more than 30% of cases. Many giant cell tumors arise with more or less low signal intensity on T1- as well as T2-weighted MR images, a feature that has been attributed to the presence of hemosiderin deposits and/or high collagen content. Contrast enhancement is usually marked and diffuse, except in cystic areas that might develop following hemorrhage or due to formation of a secondary aneurysmal bone cyst.

Nuclear Medicine

In general, skeletal scintigraphy does not play a major role in the diagnosis of benign bone tumors. Enchondroma, intraosseous lipoma, and hemangioma can represent incidental findings on examinations with bone-seeking agents. The double-density sign is a relatively typical scintigraphic finding in patients with osteoid osteoma. The term describes a hot spot representing the nidus surrounded by an area of less increased uptake, which corresponds with the reactive zone of sclerosis.

Diagnosis

Osteoid osteoma, osteochondroma, enchondroma, intraosseous lipoma, and hemangioma can usually be sufficiently diagnosed by imaging and require histologic verification only in doubtful cases. Osteoblastoma, chondroblastoma, and giant cell tumor should undergo biopsy, and both radiologic and histologic findings have to be considered together to establish the final diagnosis.

Bibliography

1. Fletcher CDM, Unni KK, Mertens F (eds) (2002) Pathology and genetics of tumours of soft tissue and bone. In: World Health Organization Classification of Tumours. IARC Press, Lyon
2. Resnick D (1995) Tumors and tumor-like diseases: Imaging and pathology of specific lesions. In: Resnick D (ed) Diagnosis of Bone and Joint Disorders. 3rd edn. Saunders, Philadelphia, pp 3628–3938
3. Giudici MA, Moser RP, Kransdorf MJ (1993) Cartilaginous bone tumors. Radiol Clin North Am 31:237–259
4. Bloem JL, Kroon M (1993) Osseous lesions. Radiol Clin North Am 31:261–278
5. Woertler K (2003) Benign bone tumors and tumor-like lesions: value of cross-sectional imaging. Eur Radiol 13:1820–1835

Neoplasms, Bone, Malignant

Mark Davies
MRI Centre, Royal Orthopaedic Hospital, Northfield, Birmingham, UK
wendy.turner@roh.nhs.uk

Synonyms

Chondrosarcoma; Fibrosarcoma; Osteo sarcoma

Definition

Primary malignant bone neoplasms/tumours arise from the osseous tissues (e.g. ►osteosarcoma) or the bone marrow tissues (e.g. myeloma). They tend to be locally aggressive causing bone destruction and have the propensity to develop metastases to distant organs—typically the lungs.

Pathology/Histopathology

Bone tumours are classified according to their tissue of origin and then into benign (see Neoplasms, bone, benign) and malignant subtypes (Table 1) (1). The incidence is less than one new case per 100,000 population per year. This compares with an incidence for tuberculosis in the developed world of approximately one per 10,000 population per year. The management and prognosis for a sarcoma depends on the histological grade. The higher the

Neoplasms, Bone, Malignant. Table 1 Classification of the most common malignant primary bone tumours by tissue of origin. Percentages show relative frequency (excluding myeloma)

Osteogenic tumours	
Osteosarcoma	35%
• Conventional high grade	
• Telangiectatic	
• Low grade central	
• Secondary (radiation-induced/Paget's disease)	
• Surface (parosteal/periosteal/high grade surface)	
Cartilage tumours	
Chondrosarcoma	26%
• Central (primary and secondary)	
• Peripheral (primary and secondary)	
• Dedifferentiated	
• Mesenchymal	
• Clear cell	
Fibrogenic and Fibrohistiocytic tumours	
Fibrosarcoma	
Malignant fibrous histiocytoma	6%
Ewing's sarcoma/Primitive neuroectodermal tumour	16%
Ewing's sarcoma	
Hematopoietic tumours	
Myeloma	
Lymphoma	
Notochordal tumours	
Chordoma	8%
Vascular tumours	
Angiosarcoma	1%

grade, the increased likelihood after surgery of developing local recurrence and metastatic disease. In general, higher grade lesions show increased cellularity, nuclear enlargement and hyperchromasia, mitotic figures and necrosis. It is important to stress that bone tumour pathology is far from straightforward. Close radiological–histological correlation is important as a small biopsy may not show representative tissue (sampling error) or fail to reveal the highest grade component of the lesion. A multi-disciplinary approach to diagnosis is recommended and both biopsy and pathological assessment is best carried out in specialist centres (2).

Clinical Presentation

Primary bone malignancies, with the exception of chondrosarcoma and myeloma, develop in children, adolescents or young adults. Pain and swelling in an otherwise fit individual are the cardinal signs. Frequently, tumours, particularly around the knee, may be mistaken for athletic injuries. The pain generally increases in severity and is typically non-mechanical in nature. Central lesions developing from the pelvis or shoulder girdle tend to present later than extremity lesions due to the relative size of the normal to neoplastic tissues. Occasionally, the tumour may present with a pathological fracture although this is more commonly seen with benign lytic bone tumours such as the simple bone cyst. Ewing's sarcoma may present with fever, fatigue and a raised serum white cell count suggestive of osteomyelitis.

Imaging

Despite newer imaging techniques, the radiograph is the preliminary and single most important imaging investigation. Early signs of a bone sarcoma and/or osteomyelitis include areas of ill-defined lysis of sclerosis of bone, periosteal new bone formation and soft tissue swelling (Fig. 1). In time, cortical destruction will occur with evidence of a soft tissue mass. The pathological process may be well established even in the presence of a normal radiograph. Up to 50% of trabecular bone must be destroyed before a discrete area of lucency can be seen radiographically. Erosion or destruction of the cortex is more readily seen. Once a bony abnormality has been detected, the next objective of imaging is to attempt to characterize the lesion and, in doing so, indicate an appropriate differential diagnosis. Subsequent imaging is directed at surgical staging if the lesion is considered likely to be a sarcoma (see later).

Diagnosis

When faced with a radiograph of a potential bone sarcoma it is essential to know the age of the patient and whether there is an evidence of pre-existing bone lesions which might pre-dispose to malignant transformation (Table 2). The next important factor to note is the site of origin in the skeleton and which part of the bone is involved. Most bone tumours, benign and malignant, occur around the knee and as such little diagnostic information can be deduced by noting the affected bone in these cases. There are exceptions. Cartilage tumours of the hands and feet are common and usually benign. Adamantinoma, a low-grade sarcoma, classically involves the diaphysis of the tibia and is extremely rare at any other site. Chordoma characteristically arises from the clivus or sacrum. Both the longitudinal and transverse origin of the tumour should be noted. Malignancy is particularly rare in the epiphysis pre-skeletal fusion. Most osteosarcomas

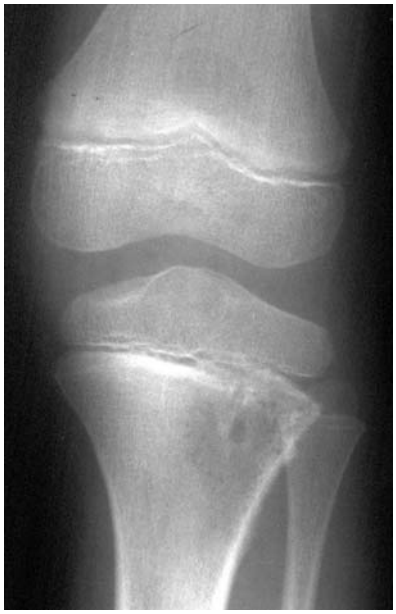

Neoplasms, Bone, Malignant. Figure 1 Child with early osteosarcoma. There is lysis of the lateral tibial metaphysis with minor cortical erosion.

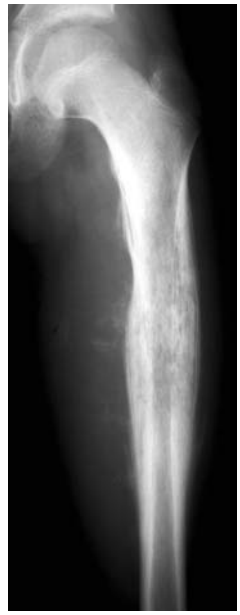

Neoplasms, Bone, Malignant. Figure 2 Adolescent with Ewing's sarcoma femoral diaphysis. There is permeative bone destruction, lamellar (onion skin) and spiculated periosteal reactions and soft tissue extension.

Neoplasms, Bone, Malignant. Table 2 Bone lesions associated with an increased risk of sarcomatous degeneration (modified from reference 1)

High Risk	
Ollier's disease and Maffucci's syndrome	
Familial retinoblastoma syndrome	
Rothmund-Thomson syndrome	
Moderate Risk	
Hereditary multiple exostoses (diaphyseal aclasis)	(<5%)
Paget's disease	(<1%)
Irradiated bone	(<0.5%)
Low Risk (rare but recognized association)	
Fibrous dysplasia	
Bone infarct	
Chronic osteomyelitis	
Osteogenesis imperfecta	
Giant cell tumour	

are metaphyseal in origin whereas Ewing's sarcoma may be metaphyseal or diaphyseal (Figs 1 and 2). Most of the malignant tumours arising on the surface of bone are the rarer forms of osteosarcoma, for example, parosteal, periosteal and high-grade surface osteosarcoma. Approximately 50% of parosteal osteosarcoma arises on the posterior surface of the distal femoral metaphysis (Fig. 3).

The radiographs of the tumour should then be analyzed to assess the biological activity of the lesion.

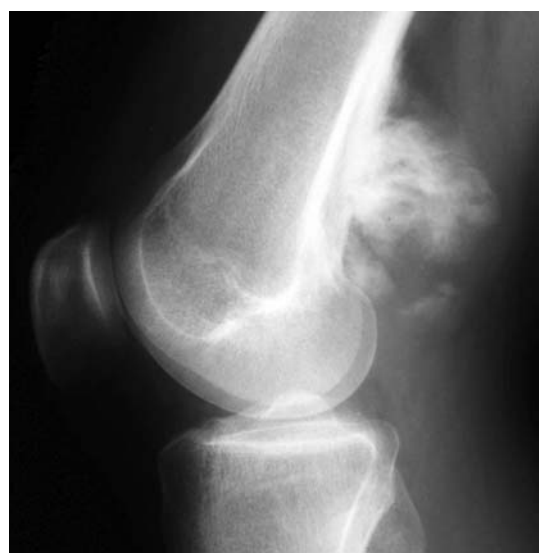

Neoplasms, Bone, Malignant. Figure 3 Parosteal osteosarcoma arising at the classic site on the posterior aspect of the distal femur. The tumour osteoid is indicated by the density of the lesion.

Aggressive features such as permeative or motheaten bone destruction and a complex ▶periosteal reaction (Codman angle, hair-on-end/spicculated+/−interrupted) will suggest in a young patient a sarcoma (Figs 1 and 2). Matrix minetralization, if present may help indicate whether the

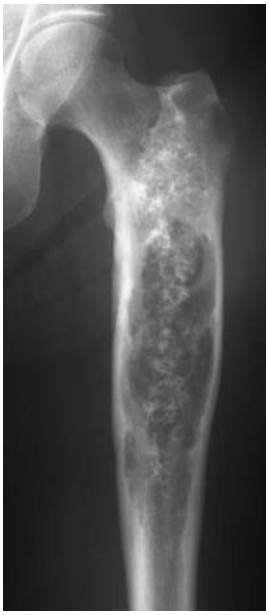

Neoplasms, Bone, Malignant. Figure 4 Central chondrosarcoma femur. The cartilage matrix is indicated by the stippled/popcorn calcification.

lesion is bone-forming (osteogenic) or cartilage-forming. Tumor osteoid is typified by solid (sharp-edged) or cloud to ivory-like (ill-defined edge) patterns (Fig. 3). Tumour cartilage is variously described as stippled, flocculent, ring-and-arc and popcorn in appearance (Fig. 4). Identifying the pattern of matrix calcification will significantly reduce the differential diagnosis, but matrix *per se* has no influence as to whether the lesion is benign or malignant. It is necessary to combine the analysis of the aggressive features and the matrix mineralization to deduce the likely nature of the sarcoma. In a minority of cases both CT and MRI may contribute to establishing the imaging diagnosis. Both are sensitive to subtle cortical breaching and soft tissue extension that are early signs of a sarcoma. Faint mineralization is also more readily appreciated on CT. Fluid–fluid levels are well demonstrated on both CT and MRI and are seen in a large number of different bone lesions. In the immature skeleton with the appropriate radiographic appearances, fluid–fluid levels are most commonly seen in aneurysmal bone cysts. The most important differential diagnosis in this situation is telangiectatic osteosarcoma, which frequently contains fluid–fluid levels.

Staging, Biopsy and Follow-Up

The surgical staging system most commonly used for bone sarcomas is that adopted by the Musculoskeletal Tumor Society (3). This assigns one of three grades according to the local extent of the tumour (assessed using MRI), presence or absence of metastases (assessed using whole-body bone scintigraphy and chest CT) and the histological grade (assessed on the biopsy and re-evaluated following surgical excision). The MRI scan will accurately identify the extent of the tumour in the bone, confirming or excluding skip metastases, extent in soft tissue and relationship to the adjacent neurovascular bundle and joint (Fig. 5). The sensitivity of chest CT has been improved with the introduction of multi-slice technology. Overstaging is a potential hazard as up to 70% of solitary nodules less than 5mm in diameter at initial presentation in children with solid extra-thoracic tumours are benign (4). Bone scintigraphy, or alternatively whole-body MRI is used to exclude skeletal metastases. Both osteosarcoma and Ewing's sarcoma may present with multi-focal bone lesions. Staging studies are preferably performed before biopsy as they may indicate the optimum site to biopsy and the trauma of the procedure may exaggerate the apparent extent of the lesion. Needle biopsy under fluoroscopic control will usually suffice in most cases. CT-guided biopsy may be helpful when the lesion is small or relatively inaccessible e.g. pelvic or spinal tumours. Most patients with a biopsy-proven bone sarcoma will undergo adjuvant chemotherapy before undergoing definitive surgery. The exception is chondrosarcoma that is not sensitive to chemotherapy or radiotherapy. Staging studies are repeated prior to surgery to assess the effect of chemotherapy. The preferred technique to assess response is MRI. In Ewing's sarcoma, obliteration of the extra-osseous component usually indicates a good response. In osteosarcoma, a dynamic contrast-enhanced sequence is required with a scan temporal resolution of no greater than 3 sec. Comparison of time intensity curves obtained pre- and post-chemotherapy gives a reliable indication of tumour response. As a general rule in bone sarcomas a good response to chemotherapy (as indicated by >90% tumour necrosis) is associated with an improved prognosis. Definitive surgery requires wide excision of the sarcoma and replacement of the affected bone with a prosthesis or an allograft. After surgery, follow-up imaging protocols concentrate on identifying development of local recurrence and distant metastases. This involves chest radiographs at regular intervals (3 monthly for 2 years, 6 monthly for the next 3 years and thereafter annually). If the chest radiograph is suspicious of metastatic disease a chest CT is performed. There is some evidence that resection of one or several pulmonary metastases are associated with prolonged survival. Clearly, multiple bilateral pulmonary metastases are not amenable to surgery. If there is clinical suspicion of local recurrence then an MRI scan should be performed. A gadolinium chelate may have to be administered to help distinguish an enhancing local recurrence from a post-operative seroma.

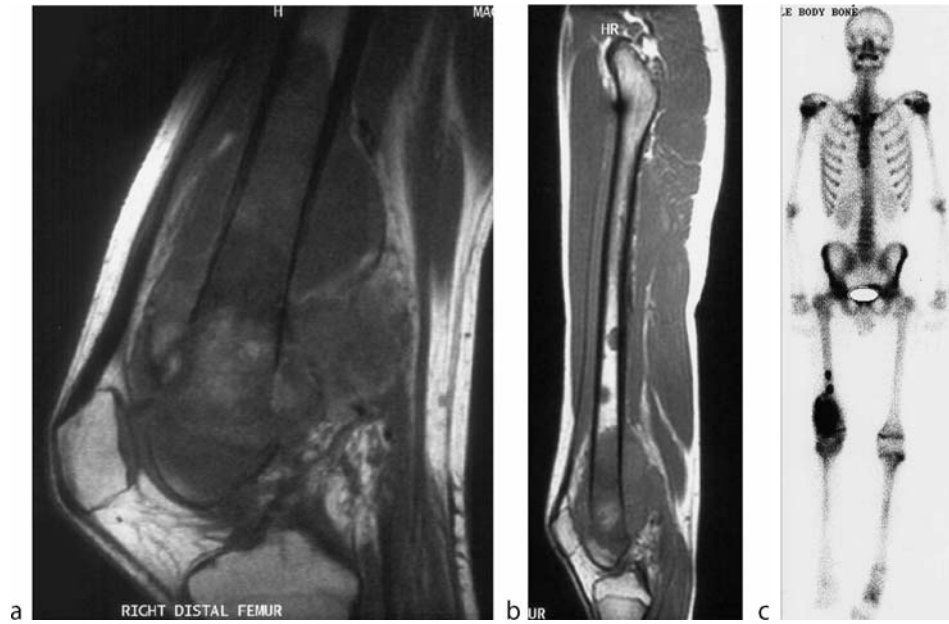

Neoplasms, Bone, Malignant. Figure 5 Osteosarcoma distal femur. (a) The small field of view sagittal T1-weighted image fails to show the two proximally located skip metastases evident on (b) large field of view sagittal T1-weighted image of the femur and (c) the bone scintigraphy.

Bibliography

1. Fletcher CDM, Unni KK, and Mertens F (2002) WHO Classification of Tumors: Pathology and Genetics of Tumors of Soft Tissue and Bone. IARC Press, Lyon, pp 226–232
2. Mankin HJ, Mankin CJ, and Simon MA (1996) The hazards of biopsy revisited. J Bone Joint Surg (Am) 78A:656–663
3. Enneking WB, Spanier SS, and Goodman MA (1980) A system for the surgical staging of musculoskeletal sarcoma. Clin Orthop 153:106–123
4. Grampp S, Bankier AA, Zoubek A et al (2000) Spiral CT of the lung in children with malignant extra-thoracic tumors: distribution of benign vs. malignant pulmonary nodules. Eur Radiol 10:1318–1322

Neoplasms, Brain, Extraaxial

Antonios Drevelegas
Radiology Department, Aristoteles University of Thessaloniki, Thessaloniki, Greece
adrev@med.auth.gr

Definition

These extracerebral tumors are usually benign. The location of a brain tumor affects treatment planning and predicts the tumor's prognosis. ►Meningiomas are the most common extraaxial neoplasms in the supratentorial compartment. Other extraaxial neoplasms are schwannomas, metastatic lesions, arachnoid cysts, epidermoids, dermoids, and bone neoplasms.

Pathology/Histopathology

Meningiomas are well-circumscribed globular or lobulated ►dural-based tumors, clearly demarcated from the brain. Histologically, meningothelial, fibrous, and transitional meningiomas are the most commonly found forms. Although psammoma bodies are often found in meningiomas, when abundant, they characterize the tumor as ►psammomatous meningioma. Less commonly found subtypes are angiomatous, microcystic, and secretory meningiomas. The above-described subtypes are grade I by World Health Organization (WHO) classification. In contrast, the WHO grade II (chordoid, clear cell, and atypical) meningiomas and especially the WHO grade III (papillary, rhabdoid, and anaplastic) meningiomas are more aggressive, with a higher risk for recurrence.

Schwannomas are benign slow-growing tumors that can arise from any nerve containing Schwann cells, including distal portions of the cranial nerves. Macroscopically these

are encapsulated, well-circumscribed tumors and are more often globular than fusiform in configuration. Microscopically, two patterns can be distinguished, according to the morphology of the tumor cells and their spatial arrangements: Antoni A, with a compact texture, and Antoni B, with intratumoral cysts.

Metastases on macroscopic examination often appear discolored, rounded, firm, and well demarcated. Certain metastatic tumors such as melanomas tend to bleed, forming frank hematomas. Calcifications appear rarely in metastatic brain tumors. Edema is commonly found in the brain parenchyma adjacent to the tumor. Metastatic lesions to the leptomeninges appear as focal areas of abnormal meningeal thickening on the surface of the brain. Microscopically, metastatic tumors tend to exhibit histologic features similar to those in their primary sites. In poorly differentiated tumors, specific immunohistochemical markers are used to characterize them.

Arachnoid cysts are congenital cysts filled with cerebrospinal fluid (CSF) and are produced by splitting of the arachnoid membrane. *Epidermoids* and *dermoids* are considered by some to represent a continuum of ectodermally derived cystic epithelial congenital lesions. Both types of cysts are lined with stratified squamous epithelium, with dermoids adding mesodermal elements such as hair and sebaceous and sweat glands.

The most common of the *primary bone tumors* of the skull are chordoma, chondrosarcoma, eosinophilic granuloma, and plasma cell myeloma. *Chordoma* is a benign, slow-growing neoplasm arising from notochordal remnants. About one-third of all chordomas occur in the sphenooccipital region. They involve the clivus and extend through the dura into the middle or posterior cranial fossa. *Chondrosarcoma* is a malignant tumor arising from cartilage or embryonal rest of the skull. *Eosinophilic granuloma* belongs to the Langerhans cell histiocytosis. The skull is one of the most common sites of involvement. This tumor is a destructive osseous lesion characterized by a vast number of eosinophils and histiocytes. *Plasma cell myeloma* is a malignant disease of plasma cells that usually originates in the bone marrow of the skull.

Clinical Presentation

The presenting signs and symptoms of the extraaxial brain tumors are related to the tumor's type, location, and size. They are often nonspecific and vague and are primarily related to brain compression and edema from the adjacent neoplasm.

Meningiomas produce signs of increased intracranial pressure (nausea, headache, vomiting) in 50% of patients. Confusion, focal weakness, and seizures are the most common symptoms, while paresis is the most frequently found physical sign. Normal physical examination has been reported in 26% of patients.

In *schwannomas*, the symptoms depend on which cranial nerve is involved. Tinnitus, sensorineural hearing loss, and disequilibrium are the most common symptoms of acoustic schwannomas. In trigeminal schwannomas, pain, paresthesias, and masticatory muscle weakness are the most common symptoms, while paresis is the most common symptom in facial nerve schwannomas.

Metastases during the early stages of the disease are usually asymptomatic. As the tumor enlarges, edema develops, and neurological symptoms appear.

Arachnoid cysts are usually asymptomatic. In *epidermoids* and *dermoids*, the symptomatic onset is generally slow, lasting years or more. Rupture of these lesions can produce aseptic meningitis, which can be lethal.

Primary bone tumors may cause pain, cranial nerve deficits, and compression of the brain stem.

Imaging

Meningiomas. On plain radiographs, hyperostosis and, rarely, bone erosion may be seen (en plaque).

On noncontrast computed tomography (NCCT), meningioma appears as a unilobular, homogeneous, high-density mass in association with brain parenchyma (Fig. 1a). The hyperdensity on NCCT has been attributed to compact and dense cellularity with a relatively small amount of intercellular water and in part to the presence of calcified psammoma bodies within the tumor. Calcification is seen on CT in 20–27% of meningiomas. It is usually microscopic or punctuated but may be large, conglomerate, peripheral, or central. Among the histological subtypes, transitional and fibroblastic meningiomas most frequently show visible calcium deposits on CT, with an incidence of 39%. After administration of contrast material, approximately 72–80% show intense and homogeneous contrast enhancement (Fig. 1b).

On magnetic resonance imaging (MRI), meningiomas are seen as peripheral unilobular masses with broad-based dural attachments and smooth, well-defined borders. On T1-weighted images, meningiomas are usually isointense or mildly hypointense to normal gray matter (Fig. 1c).

Although the signal intensity on T2-weighted images varies, most tumors are reported to be isointense to mildly hyper- or hypointense compared with gray matter (Fig. 1d).

Nearly all meningiomas enhance rapidly and intensely following contrast administration (Fig. 1e). The wide variation of signal intensity among meningiomas reflects the diversity of their histopathology. Meningiomas hyperintense to the cortex on T2-weighted images are more frequently of syncytial or angiomatous subtype. Tumors

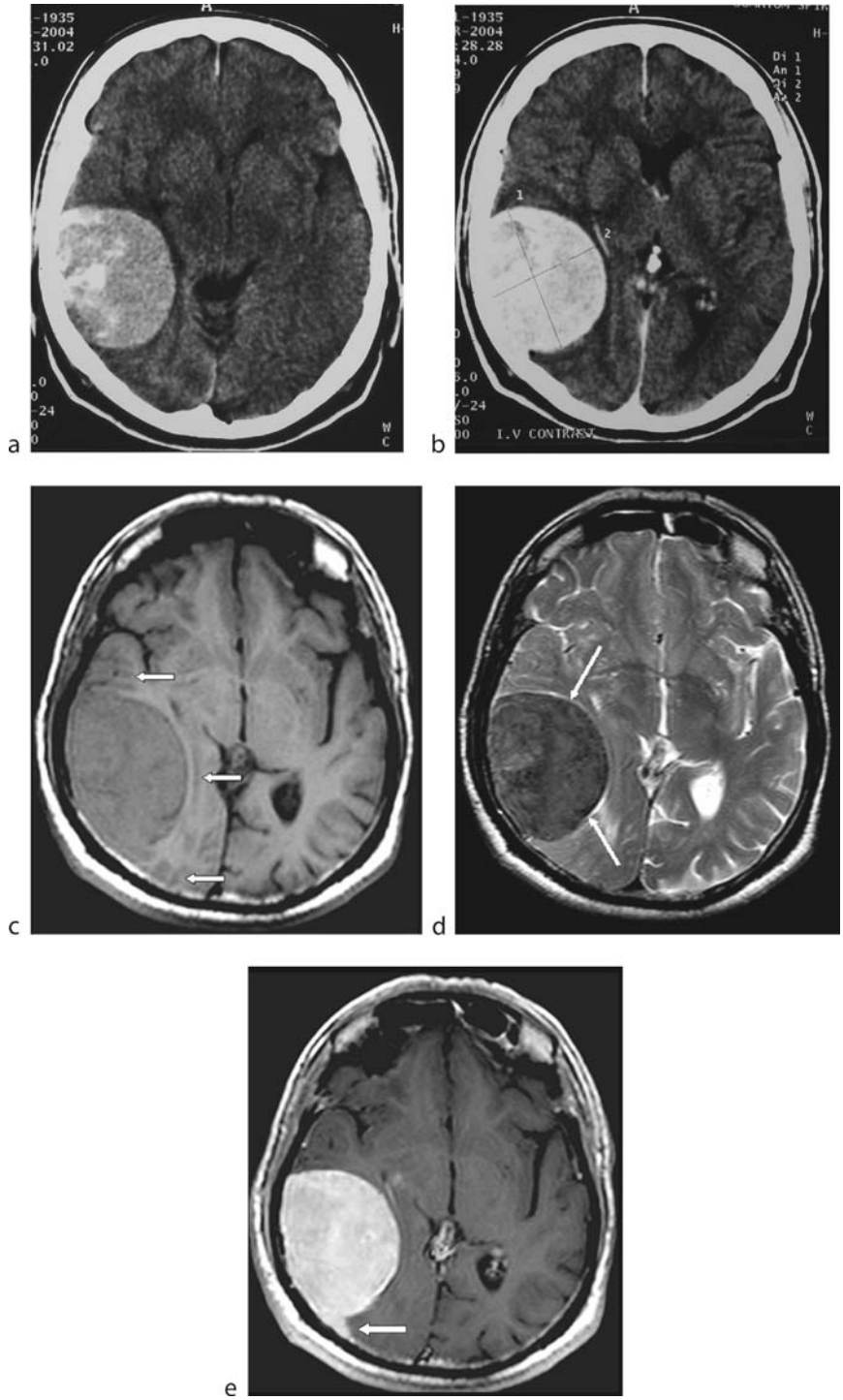

Neoplasms, Brain, Extraaxial. Figure 1 Right inferior temporoparietal meningioma. (a) Axial noncontrast computed tomography (CT) shows a hyperdense mass with dense calcified foci. (b) Postcontrast CT shows intense and homogeneous enhancement. (c) Axial T1-weighted image shows an isointense mass to the gray matter compressing the adjacent cortical convolutions (*arrows*). (d) Axial T2-weighted image demonstrates a slightly hypointense mass. Note the cerebrospinal fluid cleft between the tumor and the brain parenchyma (*arrows*). (e) The tumor enhances strongly and homogeneously after the administration of contrast medium. Note the enhanced dura (dural tail sign, *arrow*).

hypointense on T2-weighted images are more frequently of fibroblastic or transitional subtype.

Once a tumor is suspected, the intraaxial or extraaxial location should be confirmed. Useful MRI features confirming the extraaxial location of a tumor are white matter buckling, the dural tail sign, presence of the signal void pseudocapsule, and a CSF cleft.

White matter buckling is the inward bowing of the gray-white junction of the adjacent brain parenchyma (Fig. 1c). The dural tail sign is a linear enhancement along the dura mater on either side of the meningioma on contrast-enhanced MRI and is considered an important finding in the diagnosis of meningioma (Fig. 1e). This sign is not specific to meningioma but is observed in other conditions, including glioma, brain metastasis, acoustic neuroma, lymphoma, adenoid cystic carcinoma, sarcoidosis, and aneurysm. The signal void pseudocapsule consists of a linear signal void representing the dura itself, interposed between the tumor and the brain parenchyma. A CSF cleft represents CSF trapped between the cortex and the meningioma, which demonstrates low-signal intensity on T1-weighted images and high-signal intensity on T2-weighted images (Fig. 1d).

Other MRI features seen in meningiomas are peritumoral edema, cystic changes, lipomatous transformation, intracranial hemorrhage, poorly defined margins, cavernous sinus involvement, and focal or diffuse irregular contour. Venous sinus invasion may be seen in parasagittal meningiomas that are better depicted on MR venous angiography.

On diffusion-weighted imaging, meningiomas may show variable appearance, while the apparent diffusion coefficient was not indicative of malignancy, grade, or histologic subtype. On perfusion MRI, the meningiomas are hyperperfused. In MR spectroscopy, they are characterized by the presence of alanine, low creatine and N-acetyl-aspartate, high choline and glutamine, and the absence or low quantities of lipids.

Angiography shows a vascular tumor, usually supplied from meningeal branches arising from the external carotid artery with dense homogeneous tumor blush in the late arterial and capillary phase.

Schwannomas on CT appear isodense or slightly hypodense, and on MRI they are isointense to hypointense on T1-weighted images and hyperintense on T2-weighted images (Fig. 2). After the administration of contrast medium, they show intense enhancement. Cystic degenerations are common. The main differential diagnosis of acoustic schwannoma is cerebellopontine angle meningioma (Table 1).

Metastases in the calvarium appear on plain radiographs as osteolytic or osteosclerotic lesions. CT is very sensitive in detecting calvarial metastases. Contrast-enhanced MRI is used to detect subtle intradiploic lesions and to determine extension of the metastatic lesion of the calvarium into the epidural space with involvement of the underlying dura or brain. Dural metastases usually occur as an extension of the tumor to the dura from the adjacent calvarial metastases. Occasionally, dural metastases may occur without associated bony involvement. The most common primary tumors associated with dural metastases are those of breast, lung, and prostate; melanoma; and neuroblastoma. Lymphoma and leukemia are other common tumors. Postcontrast T1-weighted MRI is more sensitive in depicting meningeal involvement (Fig. 3a). Leptomeningeal metastases or meningeal carcinomatosis is usually the result of hematogenous spread from extracranial malignancies. Leptomeningeal metastases present on postcontrast T1-weighted and fluid-attenuated inversion recovery (FLAIR) studies with increased enhancement in the subarachnoid spaces of the cortical sulci, the fissures, and the cisterns (Fig. 3b). A major drawback in the diagnosis of meningeal carcinomatosis by either CT or MRI is that the changes described above lack specificity and may also be seen in inflammatory or infectious pathology.

Arachnoid cysts show density on CT similar to that of CSF. Scalloping of the adjacent calvarium is often present. They are well defined, with no calcification and no enhancement. On MRI, arachnoid cysts show CSF signal intensity on all pulse sequences.

Epidermoids appear on CT as hypodense masses with irregular borders and rare contrast enhancement. Dense lesions have been reported, and calcification is occasionally seen. On MRI, they typically have low signal on T1-weighted images and increased signal on T2-weighted images, following that of CSF on all pulsing sequences. They can demonstrate increased signal on T1-weighted images because of a high lipid content. Epidermoid and arachnoid cysts can also be discriminated on the basis of diffusion-weighted images. Conventional spin echo imaging shows both long T1 and T2 images. On diffusion-weighted images, epidermoid cysts show high signal intensity because of restricted motion of protons by the presence of membranes of densely layered epithelium.

The CT appearance of *dermoids* is similar to that of epidermoids. Their MR appearance depends on the amount of fat present, although they generally have increased signal on both T1- and T2-weighted images. CT and MRI can both allow the diagnosis of rupture.

CT of *bone tumors* clearly demonstrates the mass and the bony component of the tumor. MRI better depicts the extent of the lesion and its relationship to adjacent structures.

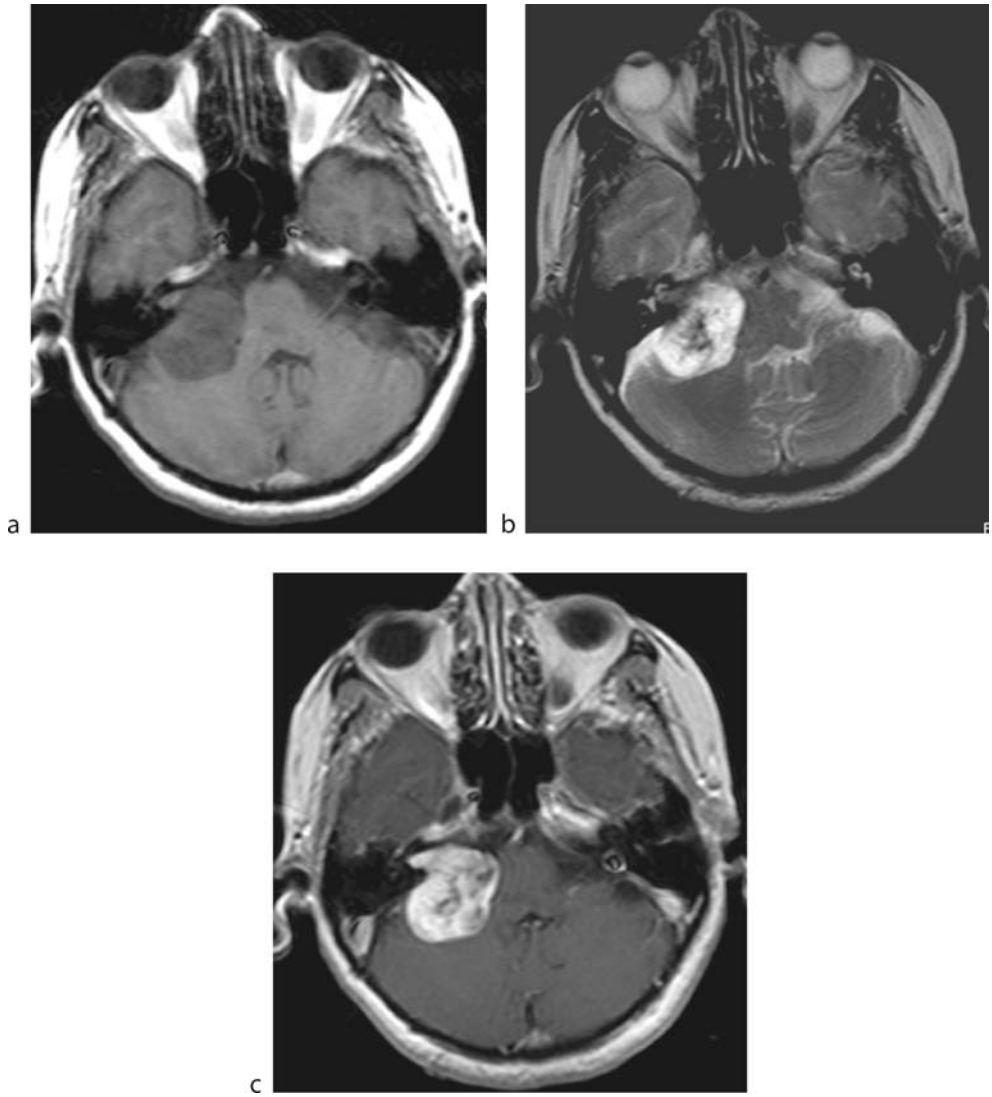

Neoplasms, Brain, Extraaxial. Figure 2 Right vestibulocochlear schwannoma. (a) Axial T1-weighted image shows a hypointense mass compressing the adjacent cerebellum. (b) Axial T2-weighted image shows a well-demarcated, heterogeneously hyperintense mass. (c) Postcontrast T1-weighted image shows intense heterogeneous enhancement of the mass extending into the right internal auditory canal.

Neoplasms, Brain, Extraaxial. Table 1 Radiological differential diagnosis between schwannoma and meningioma in the cerebellopontine angle (internal auditory canal, *IAC*)

	Schwannoma	Meningioma
Intracanalicular component	Almost always (95%)	Rare
Centered around the IAC	Yes	No, eccentric
Calcifications	No	Possible
Necrotic/cystic parts	Frequent	Rare
Dural tail sign	Possible	Possible
Secondary arachnoid cyst	Possible in large tumors	No
Influence on the bone	Enlargement of the IAC	Hyperostosis, enostosis, invasion
Supratentorial extension	No	Possible
Contact with facies posterior	Sharp angle	Broad-based contact

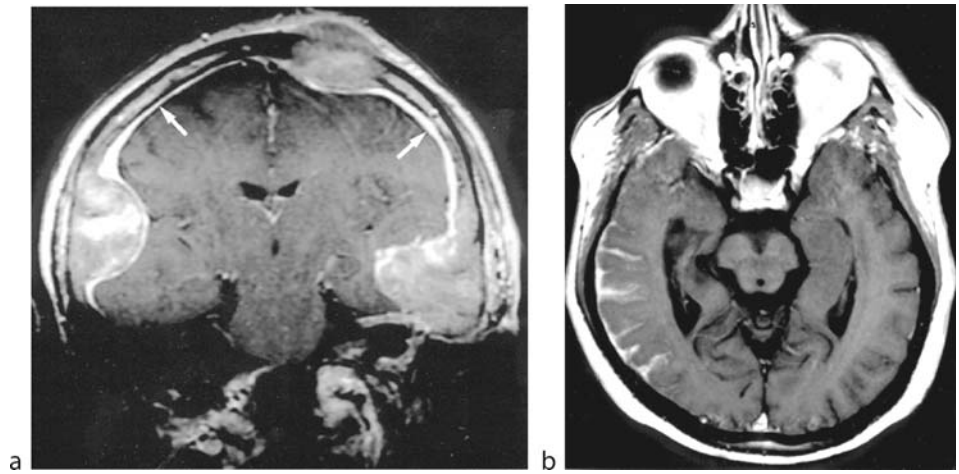

Neoplasms, Brain, Extraaxial. Figure 3 **Meningeal carcinomatosis. (a) Coronal postcontrast T1-weighted magnetic resonance imaging (MRI) of the brain in a patient with metastatic prostate carcinoma. Three destructive metastatic lesions are seen in the skull. Associated soft tissue tumors are also present extending into the epidural space and compressing the brain parenchyma. The abnormal enhancement of the dura (*arrows*) represents tumor invasion. (b) Postcontrast T1-weighted MRI of the brain in a patient with metastatic breast carcinoma. There is evidence of meningeal carcinomatosis manifested by abnormal enhancement of the leptomeninges over the convexity of the right cerebral hemisphere.**

Bibliography

1. Drevelegas A, Karkavelas G, Chourmouzi D et al (2003) Meningeal tumors. In: Drevelegas A (ed) Imaging of Brain Tumors with Histological Correlations. Springer-Verlag, Berlin, Heidelberg, New York, pp 177–214
2. Drevelegas A (2005) Extraaxial brain tumors. Eur Radiol Mar; 15(3):453–467
3. Hakyemez B, Yildirim N, Gokalp G et al (2006) The contribution of diffusion-weighted MR imaging to distinguishing typical from atypical meningiomas. Neuroradiology 48(8):513–520

Neoplasms, Brain, Intraaxial

Guido Wilms
Universitaire Ziekenhuizen Leuven, Leuven, Belgium
Guido.Wilms@uz.kuleuven.ac.be

Synonym

Intra-axial brain tumors

Definition

Intra-axial brain tumors are intracranial tumors arising from the neurons, supporting glial cells (astrocytes, oligodendrocytes, ependymal cells), lymphatic tissue, or blood vessels of the brain or from spread of cancers primarily located in other organs (metastases). Intra-axial neoplasms account for more then 75% of all intracranial tumors.

Pathology/Histopathology

The histological classification of brain tumors was defined by the World Health Organization in 1993 and revised in 2000. Primary neuronal tumors (e.g., gangliocytoma, central neurocytoma) are extremely rare. Most primary brain tumors originate from glia and are called gliomas with reference to their cell of origin: astrocytes (astrocytomas), oligodendrocytes (oligodendrogliomas), or ependymal cells (ependymoma). There are also mixed forms, called mixed gliomas or oligoastrocytomas. Additionally, mixed glioneuronal tumors can also be encountered (tumors displaying a neuronal as well as a glial component, for example, gangliogliomas, dysembryoplastic neuroepithelial tumors).

Other varieties of primary brain tumors include: primitive neuroectodermal tumors (PNET, for example, medulloblastoma, medulloepithelioma, neuroblastoma, retinoblastoma, ependymoblastoma), tumors of the pineal parenchyma (e.g., pineocytoma, pineoblastoma), choroid plexus tumors, and others.

From a histological perspective, astrocytomas, oligodendrogliomas, and oligoastrocytomas are benign but are diffusely infiltrating so that neurosurgical removal is not possible. They have a high tendency for anaplastic transformation. Glioblastoma multiforme represents the

most aggressive variety of malignant glioma. At the opposite end of the spectrum are the more circumscribed astrocytomas, the pilocytic astrocytomas. The majority are located in the posterior cranial fossa, affect mainly children and young adults, and have a clinically favorable course and prognosis.

Another type of primary intracranial tumor is primary cerebral lymphoma, also known as primary central nervous system lymphoma, which is a type of non-Hodgkin's lymphoma that is much more prevalent in those with severe immunosuppression, for example, AIDS.

Primary brain tumors rarely metastasize, but rather they spread in the spinal canal through the cerebrospinal fluid.

The most frequent types of metastatic brain tumors originate in the lung, skin (malignant melanoma), kidney (hypernephroma), breast (breast carcinoma), and colon (colon carcinoma).

Clinical Presentation

The most frequent general signs and symptoms are seizures, headache, or behavioral changes. Other symptoms relate to the location of the tumor: progressive loss of power or sensation in a limb, imbalance, visual problems, and cranial nerve deficits. Large tumors can cause hydrocephalus with signs of intracranial hypertension.

Imaging

Imaging of brain tumors is done with computed tomography (CT) or magnetic resonance imaging (MRI) before and after intravenous injection of contrast media. Contrast enhancement reflects breakdown of the blood–brain barrier (BBB) rather than an estimation of the vascularity. Advantages of MRI are the absence of ionizing radiation, a higher sensitivity for pathology, easy multiplanar imaging without repositioning of the patient, fewer contrast media reactions, and less toxicity. Moreover, MRI includes more advanced imaging techniques, such as diffusion imaging, diffusion tensor imaging, perfusion imaging, and spectroscopy.

The goals for imaging are: detection (is there a mass lesion?), diagnosis, and differential diagnosis (which kind of tumor is it? is it a tumor, an abscess, a cavernoma, an MS plaque?), grading (is the lesion benign or malignant?), preoperative set-up (extension of the lesion?), and follow-up (is there residual or relapsing tumor? is there radionecrosis?).

Based on published series, some images are almost pathognomonic: pilocytic astrocytoma (a cyst with an enhancing mural nodule), subependymal giant-cell astrocytoma (a calcified strongly enhancing nodular lesion in Monro's foramen in patients with tuberous sclerosis), cystic ganglioglioma (a cystic or nodular enhancing lesion in the temporal lobe in young patients with temporal epilepsy), and central neurocytoma (a tumor in the lateral ventricle with broad base on the septum pellucidum).

Diagnosis

The diagnosis and differential diagnosis of gliomas are challenging with routine imaging. Classically, a benign diffusely infiltrating astrocytoma is homogeneous, with minimal edema and absent contrast enhancement. Anaplastic tumor or anaplastic transformation is characterized by necrosis, edema, hemorrhage, and irregular contrast enhancement. Contrast enhancement is considered essential for diagnosing malignancy or malignant transformation of a previously benign tumor.

However, a significant amount of nonenhancing lesions appear to be anaplastic gliomas at biopsy, while 50% of enhancing oligodendrogliomas are benign. Malignant cells are found outside the margins of contrast enhancement, and areas of maximal enhancement do not necessarily correspond to areas of maximal malignancy. Finally, enhancement reflects breakdown of the BBB, as in tumors but also in (radio)necrosis.

Further problems concern the differentiation of "ring-enhancing necrotic" lesions (metastasis, glioma, abscess), the differentiation of multifocal lesions (lymphoma, malignant glioma, and metastasis), and the differentiation between radionecrosis and tumor recurrence.

Diffusion-weighted imaging (DWI) can solve some of these problems. Due to hypercellularity, there is low diffusion in cerebral lymphomas leading to a strong hypersignal on DWI allowing one to differentiate them from glioma or metastasis. Pus in the center of the abscess is a viscous fluid that consists of bacteria, inflammatory cells, mucoid proteins, and cellular debris. This again leads to strong hypersignal on DWI, allowing one to differentiate necrotic glioma or metastasis from an abscess (Fig. 1).

Apparent diffusion coefficient (ADC) values, which are a quantitative expression of diffusivity, can help in the grading of malignant gliomas. Lower ADC values are present in the solid portions of anaplastic gliomas (Fig. 2a-c). Nonenhancing brain gliomas with low ADC are anaplastic.

Perfusion-weighted imaging (PWI) is another powerful tool in the differential diagnosis. By measuring the drop of signal on T*-weighted imaging during the first pass of a bolus of contrast agent "passing through" the brain, the relative cerebral blood volume (rCBV) and flow

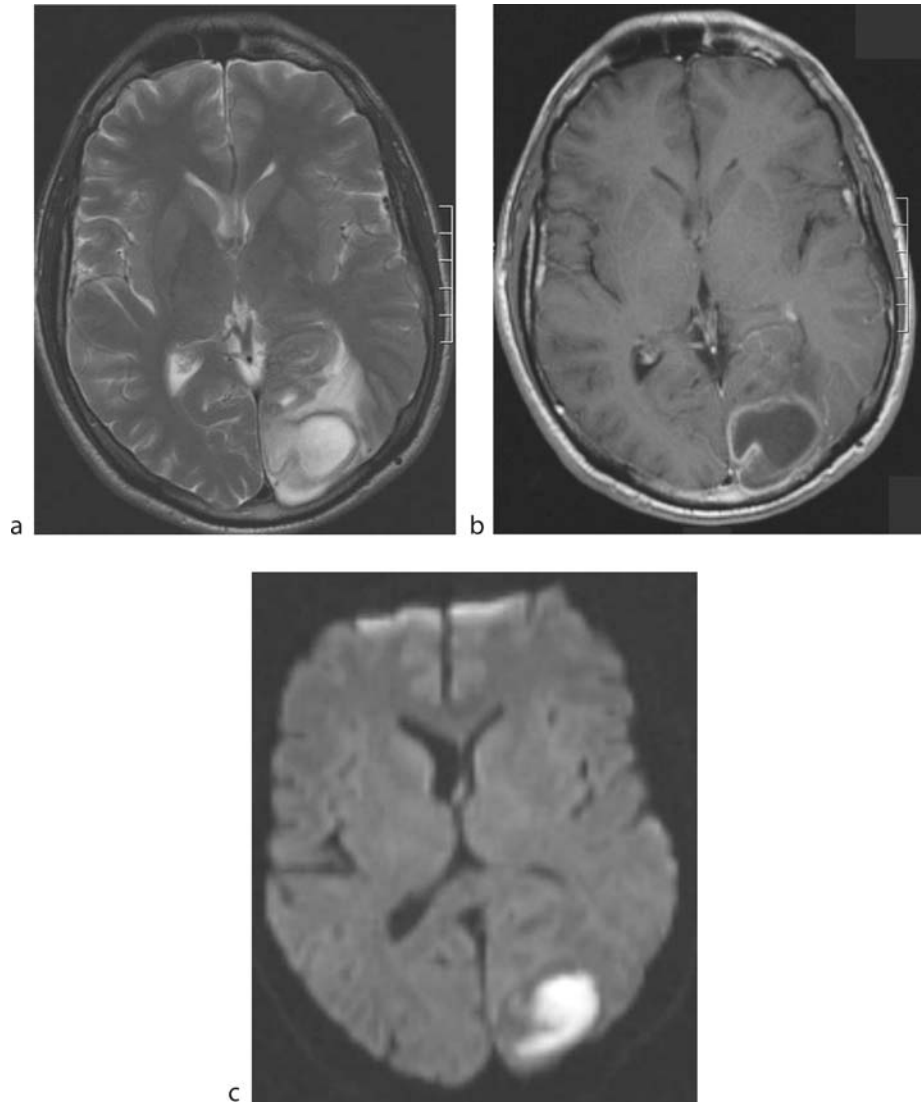

Neoplasms, Brain, Intraaxial. Figure 1 Brain abscess simulating glioblastoma. (a) Transverse T2-weighted sequence: evidence of rounded hyperintense lesion in the left occipital lobe. Note surrounding edema. (b) Transverse gadolinium-enhanced T1-weighted image at the same level: the ring-like enhancement of the lesion can be seen in glioblastoma, metastasis, abscess, and so on. (c) Transverse diffusion-weighted sequence (*b* = 1,000): the lesion is strongly hyperintense pointing to diffusion restriction. This is due to the presence of pus and cellular debris in the center of the lesion.

through the tumor can be measured. Since tumor aggressiveness is correlated with endothelial neovascularization ("angiogenesis"), a high correlation exists between tumor grade and rCBV as measured with PWI (Fig. 2d). In this way, malignancy is detected in nonenhancing lesions, the optimal site for biopsy can be determined based on higher angiogenesis rather than the breakdown of the BBB, and less vascular lymphoma is differentiated from hypervascular malignant glioma. Finally, by definition, avascular radionecrosis is differentiated from glioma recurrence.

Metabolic information can be obtained from tumoral tissues with MR spectroscopy. The widely used "single-voxel proton MR spectroscopy" examines NAA (*N*-acetylaspartate), tCr (total creatine), and tCho (total choline) in particular. Typically, there is an increase in tCho (cellular proliferation), a decrease in NAA (replacement of normal neurons by tumor cells), and in some lesions decreased tCr (energy metabolism). With better techniques (shorter echo time), other components such as myoinositol, glutamate, glutamine, and lipids can be studied. This allows further differentiation between

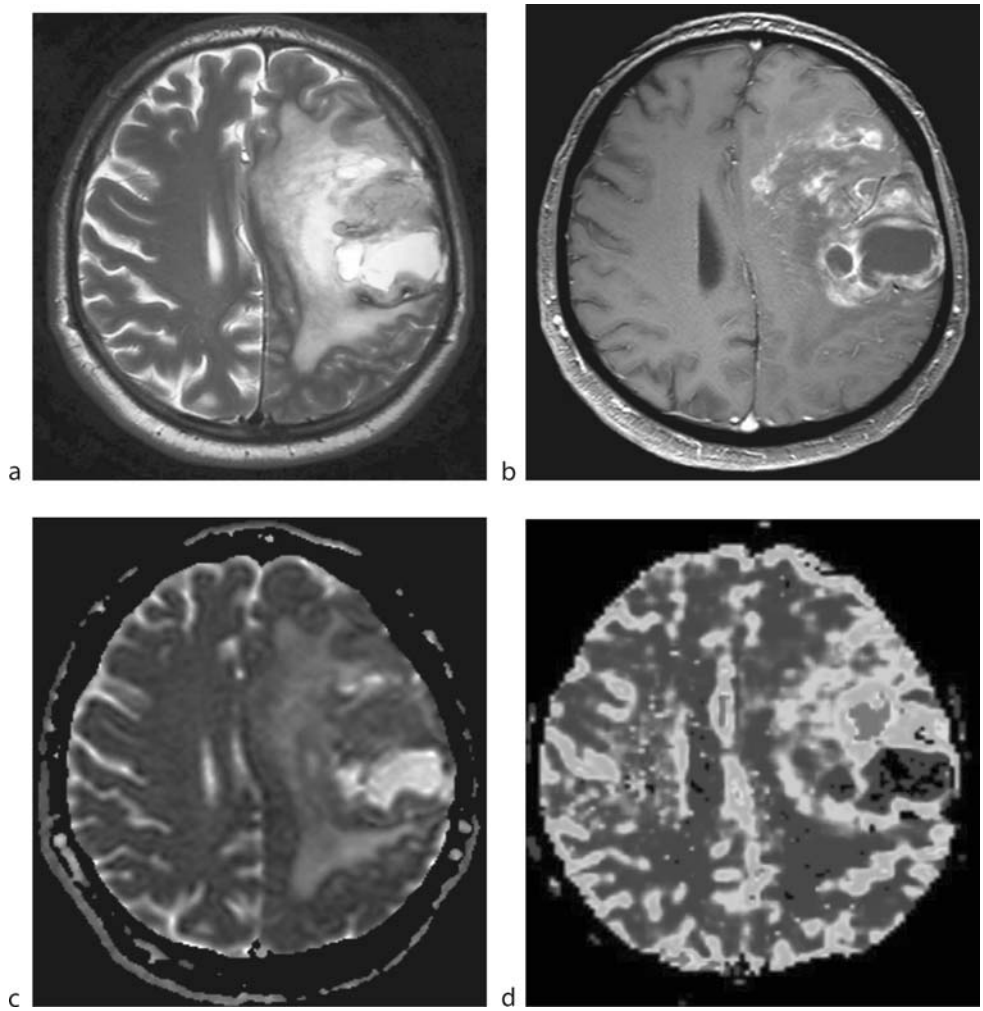

Neoplasms, Brain, Intraaxial. Figure 2 Glioblastoma multiforme. (a) Transverse T2-weighted sequence: evidence of huge lesion in the left hemisphere. The aspect of the lesion is very inhomogeneous. The anterior hypointense nodule corresponds to the "core" of the tumor. The more posterior hyperintense part represents a necrotic part. The lesion is surrounded by edema. (b) Transverse gadolinium-enhanced T1-weighted image at the same level: the lesion shows inhomogeneous enhancement with patch areas of enhancement in the anterior part and more ring-like enhancement in the posterior part. (c) Transverse ADC map at the same level: the ADC values in the "core" of the tumor are low, due to high cellularity. The surrounding edema has higher ADC values. Perfusion rCBV map of the lesion: the center of the lesion has high rCBV, pointing to extensive neoangiogenesis typical of a malignant tumor. Please note that the site of maximal neoangiogenesis does not correspond to the areas of maximal enhancement.

low- and high-grade glioma, oligodendroglioma and astrocytoma, schwannoma, hemangioblastoma, and meningioma. Diagnosis of radionecrosis is easy.

Functional MRI shows the "brain at work." Performance of a specific task in the magnet, such as finger tapping, the (inarticulate) pronunciation of words, or watching visual stimuli, "lights up" the motor cortex, the speech areas of Broca and Wernicke, and the visual cortex, respectively. This allows localization of these functional areas. It has also been demonstrated that a tumor can only be safely removed without a risk of functional deficit if the distance to an eloquent zone is less than 2 cm. If the distance is smaller than 1 cm, the risk of a severe functional deficit is 50%. A disadvantage of the method is that the test relies on the capacity of patients to perform certain tasks that can be hampered by the patient's symptoms, for example, paralysis. Nevertheless, it has been shown that on the basis of data obtained from functional MRI, the removal of a brain tumor is safer and more complete.

With diffusion-tensor imaging (DTI) it is possible, based on the anisotropic diffusion in white matter tracts, to actually visualize the different white matter tracts and

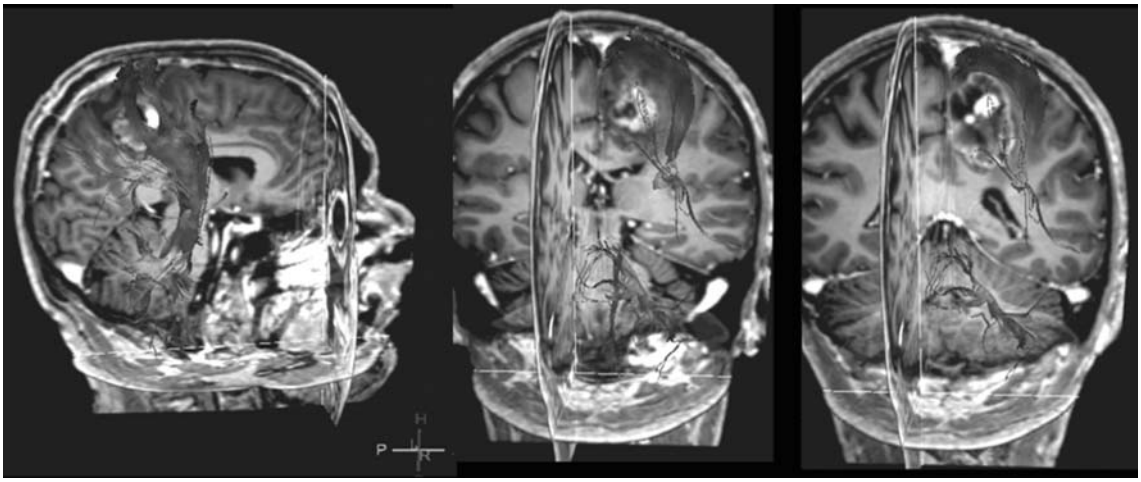

Neoplasms, Brain, Intraaxial. Figure 3 Diffusion-tensor imaging (DTI) in brain metastasis fused with the contrast-enhanced T1-weighted images. The enhancing metastasis of an esophageal cancer is located in the right pre- and postcentral gyri. Functional MRI confirmed the location of the lesion within the primary motor cortex strip. DTI fiber-tractography of the right corticospinal tract (colored areas) reveals that it runs laterally and cranially along the lesion. The DTI suggests that it is feasible to remove the metastasis using a medial wall approach, which would spare fibers of the corticospinal tract. The lesion was totally removed with this medial approach. Postoperatively, neurological (motor) status was unchanged.

to determine their relationship with the tumor. Since this technique is independent of the patient's functional capacity, it allows even better determination of the operability than functional MRI (Fig. 3).

Bibliography

1. Wilms G, Demaerel P, Sunaert S (2005) Intra-axial brain tumours. Eur Radiol 15(3):468–484
2. Al- Okaili RN, Krejza J, Wang S et al (2006) Advanced MR imaging techniques in the diagnosis of intraaxial brain tumors in adults. Radiographics 26:S173–189S
3. Osborn AG, Blaser S, Salzman K (2004) Diagnostic Imaging: Brain, Chapter 6: Neoplasms. Amirsys, Inc, Salt Lake City, UT

Neoplasms, Brain, Posterior Fossa, Pediatric

M. Warmuth-Metz
Department of Neuroradiology
University of Würzburg, Germany
warmuth@neuroradiologie.uni-wuerzburg.de

Definition

Tumors of the central nervous system (CNS) account for 20.3% of all tumor diseases in children in Germany up to the age of 15 years at the time of diagnosis. The incidence is 2.8 per 100,000. About 42% of CNS tumors in children are localized in the posterior fossa, comprising about 15% of tumors in the brain stem. The most frequent pathologies are cerebellar and pontine astrocytomas, ▶medulloblastomas (infratentorial primitive neuroectodermal tumors, or PNET), ▶ependymomas, and—increasingly often diagnosed—atypical teratoid rhabdoid tumors (ATRTs). Hemangioblastomas, choroid plexus tumors of the 4th ventricle subependymomas, cerebellar liponeurocytomas, and dysplastic cerebellar gangliocytomas (Lhermitte–Duclos disease) are tumors found in adolescence and adulthood.

Pathology/Histopathology

Astrocytomas belong to the tumors of glial origin. The most frequent ▶pilocytic astrocytoma corresponds to a grade I tumor. Diffuse astrocytomas vary in the degree of malignancy from grade II to grade IV (glioblastoma multiforme). While mitotic activity, necrosis, and vascular proliferation are absent in grade II, grade III is characterized by a marked increase in mitoses, and grade IV shows necrosis and vascular proliferations (1).

Medulloblastomas are highly cellular grade IV tumors of embryonal origin. The classic type (about 75%) arises in the vermis. The desmoplastic subtype shows a nodular pattern involving the hemispheres and has a better prognosis than the classic type. A more benign variant is the medulloblastoma with extensive nodularity, while

large cell medulloblastomas behave more aggressively than the classic type.

Ependymomas can be divided into grades II and III (anaplastic) variants. While grade II tumors show moderate cellularity, cell density and the number of mitoses increase in grade III. Key histological features are perivascular pseudorosettes and ependymal rosettes, which are absent in grade III tumors. The high grades show microvascular proliferation and pseudopalisading necrosis.

ATRTs are highly malignant embryonal tumors that occur most often in very young children. Data on their localization differ, but the most recent clinical studies show a slight predominance in the supratentorial compartment. Until recently, the tumors have been misdiagnosed as PNET. The histological hallmark is the presence of rhabdoid cells together with variable components of PNET, mesenchymal, and epithelial cells.

Clinical Presentation

Tumors arising from the cerebellum may lead to specific cerebellar symptoms such as ataxia or neck pain, especially during inclination of the head. If the 4th ventricle or parts of the cerebrospinal fluid (CSF) pathways are compressed, the resulting hydrocephalus leads to signs of increased intracranial pressure, including headache, vomiting, and visual disturbances. Tumors within the pons or medulla oblongata may result in cranial nerve disturbances, hemisyndromes, or signs of increased intracranial pressure. Periaqueductal tumors lead to the signs of long-standing increased intracranial pressure because of hydrocephalus. Multiple nerve palsies and crossed spastic paresis are typical signs of pontine tumors. Whereas low-grade astrocytomas may have long-standing and astonishing mild or even missing clinical symptoms, the duration of symptoms in high-grade tumors rarely exceeds some weeks.

Imaging

Magnetic resonance imaging (MRI) is the imaging modality of choice. However, computed tomography (CT) still seems to be the most frequent type of examination for the initial diagnosis of brain tumors, even in children. Some specific features that might be of important differential diagnostic impact, including calcifications and an estimation of a tumor's cellular density, are better identified by CT (2). MR spectroscopy (MRS) is useful for estimating cellular proliferation or tumor composition, such as the demonstration of tumor necrosis. A possible advantage of MRS is the monitoring of tumor response to treatment or the differentiation between a recurrence and a treatment-related necrosis. The differential diagnosis between the tumors of the cerebellum is, to some extent, possible by their localization, growth patterns, and CT density or signal intensities on MRI (3). Tumors in the brain stem can be differentiated concerning their histology mainly by their localization (2).

Medulloblastoma

Two different types of medulloblastomas show different behavior on imaging. The most frequent, classic type expresses markers of primitive periventricular precursor cells, which are found in the vermis of the cerebellum. The desmoplastic type of medulloblastoma expresses markers of the outer granular cells of the cerebellar cortex and is found in roughly 25% of patients. According to these histogenetic differences, classic medulloblastomas usually arise in the vermis of the cerebellum and then extend into the 4th ventricle. Desmoplastic medulloblastomas are most often found in the surface of the cerebellar hemispheres, often invading the overlying dural structures. Medulloblastomas are highly cellular tumors with rather low signal intensity on T2-weighted MRI compared with cortex. But due to the coexistence of necrotic areas or bleeding residue, the low T2 signal is sometimes hard to depict. More accurate is a high density on CT, leading most often to hyperdense and, rarely, isodense CT values in the solid parts of the tumor. CT density can be used in the differentiation from cerebellar pilocytic astrocytomas, which can be found in the same location. Medulloblastomas already show a high rate of leptomeningeal dissemination at the time of diagnosis. Because meningeal dissemination is one of the most important prognostic factors, staging consisting of CSF examination and complete cranial and spinal MRI are essential for adequate treatment. Enhancement can be uniform and strong but is more often patchy and mild, partial, or completely missing (2–4). This leads to considerable problems in defining ▶residual tumor after surgical resection (5). The residual tumor definition should be performed within 72 h after surgery because nonspecific postoperative cerebral enhancement begins after this time (Fig. 1).

Ependymoma

Ependymomas (grades II and III) arise from the ependymal layer of the 4th ventricle; therefore, they do not show such a strict relationship to a definite structure around the ventricle. Usually they arise from the lower part of the 4th ventricle, but they may also be isolated in the cerebellopontine angle. They are so-called plastic tumors and grow out of the openings of the 4th ventricle surrounding the cranial and spinal nerves and vessels (4). Meningeal dissemination is rare at the time of initial diagnosis. More often, a local recurrence or the progression of a residual tumor is observed. MRI signal intensities and CT density are similar to those of medulloblastomas (Fig. 2).

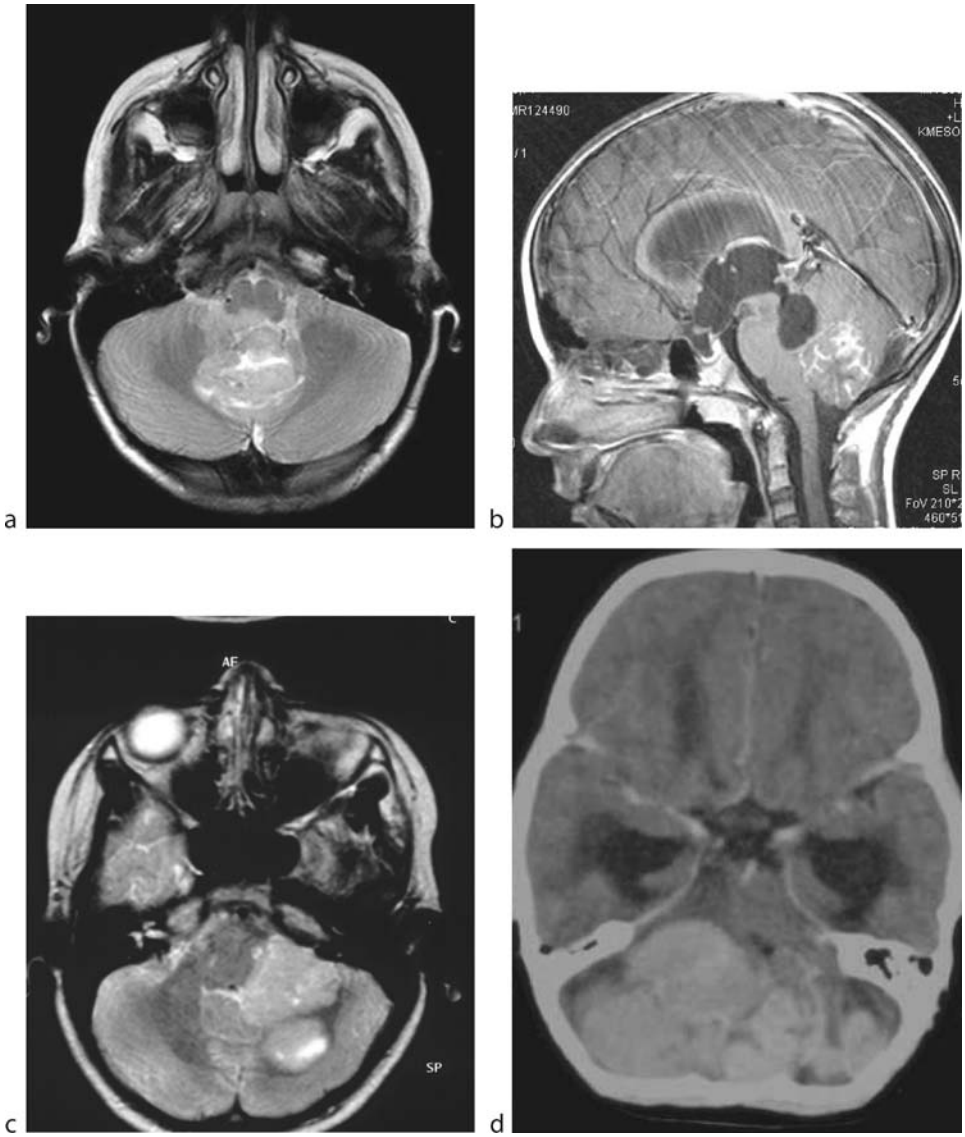

Neoplasms, Brain, Posterior Fossa, Pediatric. Figure 1 Medulloblastoma. (a) On T2-weighted axial magnetic resonance imaging (MRI), the typical relationship of a classical medulloblastoma to the vermis cerebelli is clearly visible. Signal intensity near isointensity to the gray matter gives an impression of cell density within the tumor. An infiltration of the lower parts of the floor of the 4th ventricle on the right-hand side cannot be excluded. (b) Sagittal T1-weighted enhanced MRI of the same patient shows some enhancement and also the origin of the tumor from the lower part of the vermis. (c) The typical localization of a desmoplastic medulloblastoma within the left hemisphere is seen on the axial T2-weighted image. (d) Typical medulloblastoma with extensive nodularity on postcontrast computed tomography. This type of tumor has a better prognosis.

Atypical Teratoid Rhabdoid Tumors

The highly malignant ATRTs primarily affect very young children. The supratentorial (mostly frontal) localization is more frequent than the infratentorial. Quite often, huge tumors, often not differentiable from medulloblastomas, involve both compartments. In about 40% of cases, a seemingly typical pattern of enhancement with a bandlike peripheral character can be seen. Meningeal dissemination and tumor bleeding are quite frequent.

Cerebellar Astrocytoma

Low-grade astrocytomas are the most frequent tumors in children. The most common location is within the cerebellum. The histologically benign tumor usually enhances and can be solid or at least partly cystic. Cyst walls containing tumor usually enhance and can be differentiated from cystic hemangioblastomas without enhancement of the cyst walls. Cellular density is low; therefore, T2 signal is usually very high, and CT density is

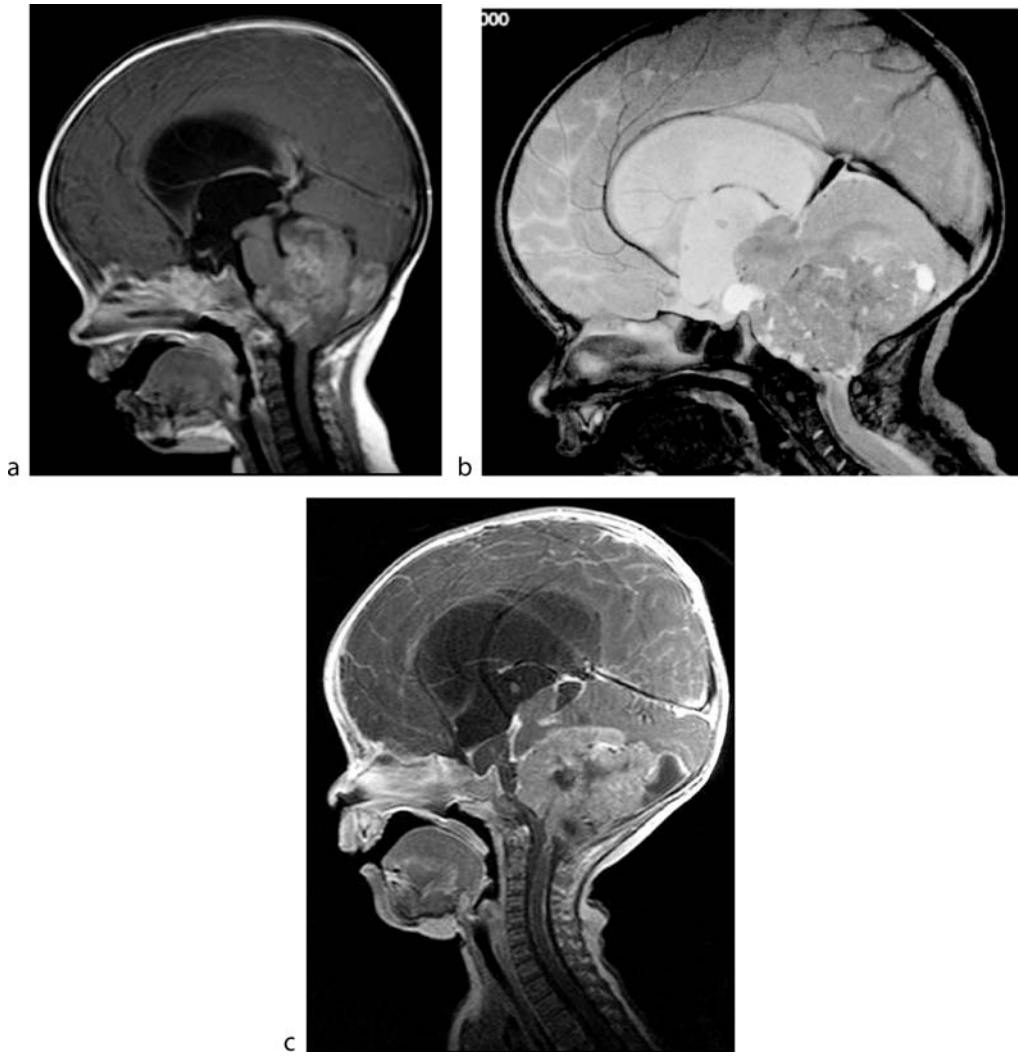

Neoplasms, Brain, Posterior Fossa, Pediatric. Figure 2 Ependymoma and atypical teratoid rhabdoid tumor (ATRT). (a) The typical growth pattern of an ependymoma arising from the lower parts of the 4th ventricle, growing within the cisterns, and surrounding the brain stem is demonstrated on sagittal postcontrast T1-weighted magnetic resonance imaging (MRI). (b) A very low signal on T2-weighted sagittal MRI correlates with very high cellularity in this baby with an infratentorial ATRT. (c) Besides the large moderately enhancing ATRT seen on postcontrast T1-weighted sagittal MRI in another very young child, meningeal dissemination is best seen within the cervical spinal canal.

either hypodense or isodense in the solid tumor parts. Calcification is possible in all sorts of infratentorial tumors and does not enable differential diagnosis. Up to about 7% of low-grade astrocytomas are complicated by asymptomatic meningeal dissemination.

Quadrigeminal Plate Tumors

Quadrigeminal plate tumors are of astrocytic origin in most cases. The typical tectal glioma leads to a long-standing hydrocephalus on the basis of compression of the aqueduct. Tumors are small without enhancement and usually do not require specific treatment after CSF diversion. Follow-up is mandatory because some tumors may develop atypical characteristics such as contrast enhancement or growth into the thalami and may eventually require treatment.

Pontine Tumors

Diffuse and focal tumors must be differentiated. Focal tumors may have a benign course, show prominent exophytic components, and represent pilocytic astrocytomas. Diffuse tumors in children older than 2 years are associated with an extremely bad prognosis. Biopsy may reveal grade II–IV astrocytoma with no predictive value for treatment

or prognosis; therefore, biopsy or even resection is usually followed by the risk of further neurological damage. The differentiation between focal and diffuse tumors is most reliable on the basis of an estimation of the percentage of cross-sectional area of the pons infiltrated by tumor, with a cut-off point of 50%. The tumor margins in so-called diffuse pontine gliomas are very often sharp, so we do not believe this is a reliable criterion. Enhancement may be seen but is often absent in the beginning. Meningeal dissemination is rare but possible. Typical features are splitting of the pontine fibers by tumor infiltration and encasement of the basilar artery. Hydrocephalus is usually not present despite sometimes large tumor masses in the posterior fossa (Fig. 3).

Tumors of the Medulla Oblongata

Diffuse tumors of the medulla oblongata may behave similarly to diffuse pontine gliomas, but histological verification should be attempted because the differential diagnosis cannot be made with similar accuracy on the basis of MRI. Many tumors in the medulla oblongata lead to a pronounced and typical exophytic growth of its dorsal part and are therefore called dorsal exophytic

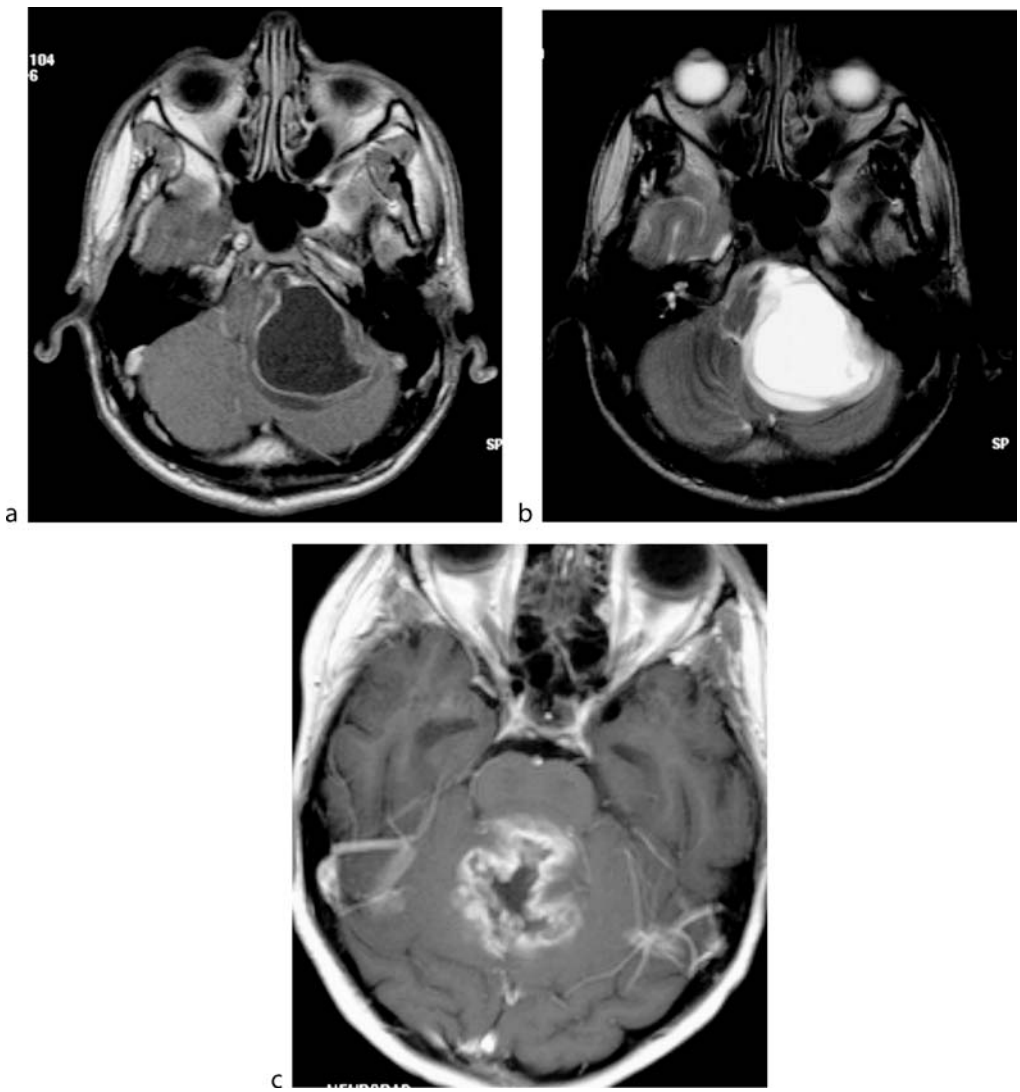

Neoplasms, Brain, Posterior Fossa, Pediatric. Figure 3 Pilocytic astrocytoma. (a) Pilocytic astrocytoma in the left cerebellar hemisphere with a typical large cyst. (b) The same tumor on T2-weighted magnetic resonance imaging (MRI) shows a very high signal not only within the cyst but also within the solid margin. (c) On postcontrast T1-weighted MRI, the differentiation between a pilocytic astrocytoma seemingly arising from the vermis cannot be reliably differentiated from a classical medulloblastoma.

tumors of the medulla oblongata. Histologically, these tumors are most often of astrocytic origin, either grade I or II. Rarely, gangliogliomas are found in this location. As in all low-grade tumors, neurosurgical resection or debulking should be attempted as often as possible before any other form of treatment. Histological diagnosis of the tumor *via* biopsy before an attempt at resection is usually not necessary. Independent of the tumor grade, enhancement may be present. CT density of the solid part shows hypodensity or isodensity, and calcifications do not allow further differentiation (Fig. 4).

Diagnosis

Although CT and MRI features of tumors of the posterior fossa are sometimes very characteristic only in cases of diffuse pontine glioma or typical tectal glioma, histological verification by biopsy or resection is dispensable. Cytological examination of the CSF in cases of meningeal dissemination can clarify tumor histology.

Imaging should always aim not only at the diagnosis of the tumor itself but also at the staging of disease dissemination. Therefore, imaging must include a spinal

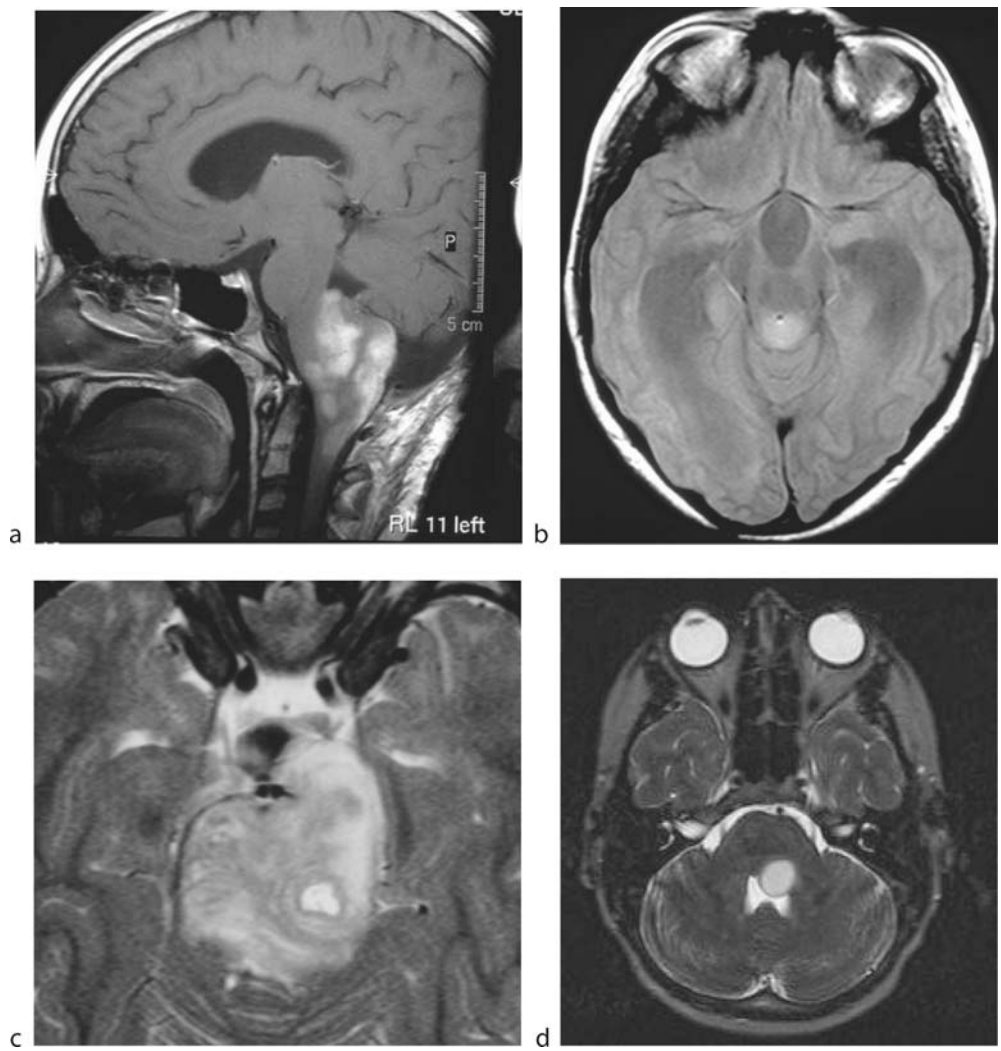

Neoplasms, Brain, Posterior Fossa, Pediatric. Figure 4 Brain stem tumors. (a) The dorsal exophytic part is typical in this low-grade tumor restricted to the medulla oblongata and the upper cervical cord. Histology demonstrated a pilocytic astrocytoma. (b) A fairly sharply delineated small tumor on proton density-weighted magnetic resonance imaging (MRI) within the tectal plate has led to a long-standing hydrocephalus occlusus. In this typical tectal plate glioma, only third ventriculostomy was necessary. (c) Diffuse infiltration of the pontine fibers and encasement of the basilar artery are typical features of a ►diffuse intrinsic pontine glioma. (d) Focal tumor of the left dorsal pons. Despite the unequivocal enhancement on T1-weighted MRI (not shown), histology revealed a grade II astrocytoma.

staging MRI in tumors with a known propensity for meningeal dissemination.

The correct identification of residual tumor after resection on the basis of early postoperative MRI or CT (within 72 h) facilitates subsequent treatment decisions and is therefore absolutely necessary as the basis of further evaluations (5).

Bibliography

1. (2000) Pathology and genetics of tumors of the nervous system. In: Kleihues P, Cavenee WK (eds) WHO Classification of Tumors. IARC Press, Lyon
2. Barkovich JA (2000) Intracranial, orbital and neck tumors of childhood. In: Barkovich JA (ed) Pediatric Neuroimaging. Lippincott Williams and Wilkins, Philadelphia
3. Warmuth-Metz M, Kühl J, Rutkowski S et al (2003) Differenzialdiagnose infratentorieller Hirntumoren bei Kindern. Radiologe 43:977–985
4. Osborn AG (2004) Neoplasms and tumorlike lesions. Diagnostic Imaging. Brain. Salt Lake CityAmirsys, Section 6.
5. Warmuth-Metz M (2003) Postoperative imaging after brain tumor resection. Acta Neurochir (Suppl) 88:13–20

Neoplasms, Brain, Supratentorial, Pediatric

Huisman TAMD[1], Ulrike Brehmer[2]
[1]Director and Chairman of Paediatric Radiology, Johns Hopkins University, Baltimore
[2]Department of Diagnostic Imaging, University Children's Hospital, Zürich, Switzerland
thierry.huisman@kispi.unizh.ch
ulrike.brehmer@kispi.unizh.ch

Synonyms

Cerebral tumors in childhood; Intrinsic brain tumor

Definition

Neuroepithelial tumors are primary neoplasms of embryonic neural tube origin. Gliomas originate from astrocytes, oligodendrocytes, or ependymal cells.

Central nervous system (CNS) tumors are the second most common tumor in children after leukemia. Low-grade tumors are more frequent in children than in adults. In children, 25% of CNS tumors are located supratentorially, 17% are suprasellar, and 35% are infratentorial. During the first 2 years of life, cerebral tumors are more common in girls than in boys. At older ages, boys are affected twice as frequently as girls. The peak incidence of brain tumors in children is below the age of 5 years.

Different tumors present at different ages. In children younger than 1 year of age, two-thirds of the CNS tumors are located supratentorially. Astrocytomas are most frequent (40–50%), followed by primitive neuroectodermal tumors (PNETs; 20%), and 20% are of various other histologies. Astrocytomas, choroid plexus papillomas, teratomas, and embryonal tumors typically occur in the first 2 years. Ependymomas and medulloblastomas usually present before age 4 years. The peak age for pilocytic astrocytomas is between 5 and 9 years.

Astrocytomas are the most frequent pediatric brain tumors in general and may arise at any location within the CNS, including the spinal cord. Prognosis depends on the tumor grade, tumor site, and invasion of the functional center. Outcome is usually excellent, with a 5-year survival of 85–95%.

Meningiomas and metastases are rare in children. Children may develop CNS neoplasms after treatment of non-CNS malignancies.

Pathology/Histopathology

Brain tumors are classified according to the dominant cell type within the tumor and are graded according to the World Health Organization (WHO) classification. Grades I and II are considered *low grade* and grades III and IV are considered *high grade*.

Neuroepithelial Tumors

Astrocytomas are the most common neoplasm in children. Fifty percent are located supratentorially.

1. *Pilocytic astrocytomas* (WHO grade I) are the most frequent astrocytomas in children (Fig. 1a). They may present in the cerebellum, hypothalamus, thalamus, anterior visual pathway, or cerebral hemispheres. A solid tumor nodule is frequently seen in combination with cysts of various sizes. Microscopically, loose spongy areas are intermixed with compact cellular regions. Spontaneous evolution into higher-grade malignancy may occur.
2. *Fibrillary astrocytomas* (WHO grade II) are the second most common astrocytomas in children. Occasionally they are seen in the cerebellum, but they are more frequent in the brain stem, spinal cord, and cerebral hemispheres. Microscopically there is moderately increased cellularity. Histologically, well-differentiated fibrillary or gemistocytic astrocytes are seen within a loosely structured and commonly microcystic matrix. Progression to higher-grade malignancy over time is frequent.

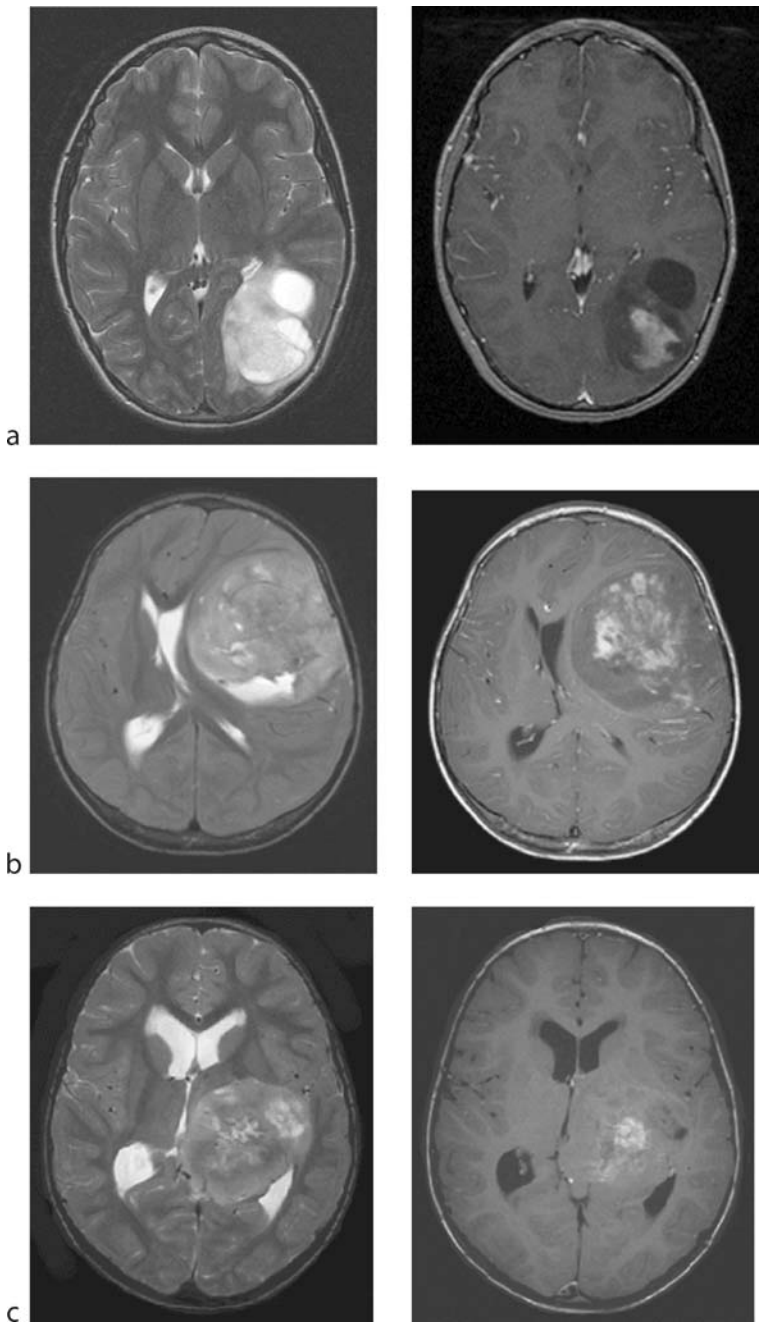

Neoplasms, Brain, Supratentorial, Pediatric. Figure 1 (a) Axial T2 fast spin echo (FSE) and contrast-enhanced T1 spin echo (SE) magnetic resonance image of a pilocytic astrocytoma; partially solid, partially cystic tumor of the left hemisphere in a 12-year-old boy (*left*). After contrast administration, the axial T1-weighted image shows partial enhancement of the solid component. The left lateral ventricle is compressed. (b) Axial T2 FSE and contrast-enhanced T1 SE magnetic resonance image of a primitive neuroectodermal tumor; left-sided insular mass in a 2-year-old child. The tumor reaches the cortex. There is significant midline shift with compression of the left lateral ventricle. The tumor reveals an irregular enhancement of solid components. An eccentric necrosis is seen along the dorsal border (*right*). (c) Axial T2 FSE and contrast-enhanced T1 SE magnetic resonance image of an ependymoma; heterogeneous tumor in the left cerebral hemisphere in a 3-year-old girl with epicenter adjacent to the posterior horn of the lateral ventricle. No significant edema is seen. Compression of the foramen of Monroe and the Sylvian aqueduct results in an obstructive hydrocephalus. The tumor shows sparse contrast enhancement on T1-weighted images (*right*).

3. High-grade astrocytomas, including *anaplastic astrocytoma* (WHO grade III) and *glioblastoma multiforme* (GBM; WHO grade IV), are usually located within the cerebral hemispheres and brain stem. These tumors are predominantly seen in adults.
4. *Subependymal giant cell astrocytomas* (WHO grade I) are seen in tuberous sclerosis and are typically located at the foramina of Monroe. Microscopically, large multinucleated cells are seen mixed with abundant hyalinized blood vessels.

Neuronal and Mixed Neuronal/Glial Tumors

1. *Gangliogliomas* may occur at any age but are more frequent in children. They typically present in the temporal lobes. Microscopically, clusters of large neurons are mixed with astrocytes and perivascular lymphocytes.
2. *Dysembryoplastic neuroepithelial tumor* (DNET) is a benign cortical tumor with a multilobulated "bubbly" appearance. DNETs are commonly temporal located. The overlying skull may be scalloped. Microscopically, DNETs contain glial cells and neurons. At the junction to normal brain, areas of cortical dysplasia may be apparent.
3. *PNETs* are embryonal tumors and represent the second most common CNS neoplasm in childhood (20%; Fig. 1b). Microscopically they consist of undifferentiated small round cells with divergent patterns of differentiation along astrocytic, neuronal, ependymal, or melanocytic lines. The histogenesis of this tumor type is still discussed in the literature.
4. *Atypical teratoid rhabdoid tumor* is an embryonal tumor that is equally frequent supratentorial and infratentorial and may involve the pineal gland. This tumor occurs in children younger than 2 years. Microscopically it consists of areas of varying differentiation, such as neuroglial, epithelial, or mesenchymal cells and the characteristic rhabdoid cells. The latter is a medium-sized cell with a prominent nucleolus in an eccentric nucleus and granular cytoplasm. Immunocytochemically there exists a broad phenotype with positivity for multiple antisera.
5. *Ependymomas* are the fifth most frequent CNS tumor in childhood (Fig. 1c). Of these, 65% are located infratentorially, 25% supratentorially, and 10% in the spinal cord. Cerebral hemispheric tumors occur near the ventricles and grow either into the hemispheric parenchyma or into the ventricles. Cysts and calcifications are frequent. Microscopically, ependymomas present glial and epithelial properties. In most cases they have characteristic perivascular pseudorosettes around blood vessels, and 25% show anaplasia with a high mitotic rate, pleomorphism, and necrosis.

Suprasellar Tumors

Seventy-five percent of suprasellar tumors are craniopharyngiomas, 15% are germ cell tumors, and 10–15% are of various histology. Craniopharyngiomas comprise up to 10% of all CNS tumors in children and represent the fourth most common intracranial neoplasm. Germinomas are the most frequent germ cell tumor. Optic nerve gliomas are pilocytic astrocytomas (WHO grade I) and present predominantly in the first decade of life (75%). Up to one-third of these tumors are associated with neurofibromatosis type 1.

Intraventricular Tumors

Ependymoma and choroid plexus papilloma/carcinoma are the most common frequent intraventricular tumors. Papillomas may produce excessive amounts of cerebrospinal fluid, resulting in a hydrocephalus. They occur in infancy or early childhood and are predominantly located in the lateral ventricles. Macroscopically, papillomas are soft, cauliflower-like, grayish-pink vascular masses. Choroid plexus carcinomas show a high degree of mitosis and cell atypia. Immunocytochemistry and electron microscopy help distinguish these tumors from other malignancies, including ependymomas.

Differential Diagnosis

A careful analysis of the clinical history, neurological symptoms, and laboratory and imaging findings allows differentiation of lesions. Differentiation between an abscess and a necrotic GBM remains difficult. Advanced imaging techniques, including diffusion-weighted imaging, are helpful.

Clinical Presentation

Clinical presentation depends on many factors, including the age of the child, the location and extent of the lesion, the rate of tumor progression, and complicating factors such as vasogenic edema, intralesional hemorrhage, or necrosis. Histology and tumor grade determine prognosis.

In neonates the open fontanelles prevent a significant increase in the intracranial pressure. This may delay diagnosis. Consequently, tumors are frequently large on initial diagnosis. As soon as the fontanelles are closed, the symptoms of raised intracranial pressure in children are similar to those in adults and include headache, vomiting, and altered consciousness. Depending on the tumor's location, various neurological symptoms may occur, including focal neurological deficits and seizures.

Neoplasms, Brain, Supratentorial, Pediatric. Table 1 Computed tomographic (CT) and magnetic resonance (MR) features of supratentorial childhood tumors (*CECT*, contrast-enhanced computed tomography; *GM* gray matter; *CSF* cerebrospinal fluid; *WM* white matter)

Supratentorial tumors	Imaging characteristics	CT	MR imaging		MR + CT with contrast
			T1-weighted	**T2-weighted**	**T1-weighted + CECT**
Astrocytoma:	Well-circumscribed cystic +/− solid mass	Solid parts: hypodense to isodense	Solid: isointense/ hypointense to GM	Solid: hyperintense to GM	95% enhance:
Pilocytic	Cysts with mural nodule	Cysts: hypodense	Cysts: isointense to CSF	Cysts: hyperintense to CSF	−10% solid + homogeneous
	Little or no surrounding edema	Ca^{2+}: 20%			−40% solid with necrosis + heterogeneous enhancement
	Hemorrhage rare				−50% nonenhancing cyst + enhancing nodule
					Cyst wall sometimes enhances
Fibrillary	Ill-defined	Hypodense to iso-dense	Infiltration of adjacent brain	Homogeneous	Usually no enhancement unless focal differentiation
	Homogeneous	Ca^{2+}: 20%	Homogeneous	Hyperintense	
	Rarely cysts +hemorrhage		Hypointense		
Anaplastic	Ill-defined	Hypodense	Isointense to hypointense	Heterogeneous Hyperintense	Usually no enhancement unless focal differentiation, then focal heterogeneous
	Hemorrhage	Ca^{2+}	Infiltration of WM + possibly GM		
	Rarely cysts				
Glioblastoma multiforme	Irregular margins	Isodense or hypo-dense	WM mass	Heterogeneous Hyperintense	95% irregular rim enhancement around central necrosis
	Mass + surrounding edema	Ca^{2+} rare		Hypointense blood products	*or*
	Central necrosis				Solid or patchy enhancement
	Hemorrhage				
Subependymal giant cell tumor	Well-circumscribed, often lobulated	Heterogeneous	Hypointense to isointense to GM	Ca^{2+}: hypointense	Heterogeneous enhancing mass near foramen of Monroe
	Intraventricular mass in tuberous sclerosis	Hypodense to iso-dense	Ca^{2+}: hyperintense to hypointense		
	Near foramen of Monroe	Variable Ca^{2+}			
	Hydrocephalus				

Ganglioglioma	Cortically based circumscribed cyst + mural nodule or solid tumor	Variable density, mostly hypodense	Solid: hypointense to isointense	Hyperintense mass	50% enhance: solid, rim, or nodular
	Remodeling of bone	Ca^{2+}: 35–50%		Possibly heterogeneous	Heterogeneous
					Rarely, meningeal enhancement
Primitive neuroectodermal tumor	Large complex mass + surrounding edema	Hypodense to isodense	Hypointense to isointense to GM	Solid: isointense to hyperintense to GM	Heterogeneous enhancement
	Homogeneous or heterogeneous mass	Ca^{2+}: 50–70%		Hyperintense Surrounding edema	CSF seeding
	Often hemorrhage + necrosis				
Atypical teratoid rhabdoid tumor	Heterogeneous	Hypodense to isodense	Isointense	Hyperintense cysts	Heterogeneous enhancement
	50%: infratentorial	Cysts + Ca^{2+} common	Hyperintense Hemorrhage	Hypointense blood products	Meningeal spread + CSF seeding
	40%: hemispheric or suprasellar		Hyperintense cysts to CSF		
	10–20%: disseminated hydrocephalus				
Ependymoma	Intra-/periventricular large soft mass growing out of foramina	Variable density	Heterogeneous	Heterogeneous	Variable heterogeneous mild to moderate enhancement
	Small cysts + hemorrhage	Ca^{2+}: 50%	Isointense to hypointense	Isointense to hyperintense	
				Hyperintense cysts	
				Hypointense blood products	
Choroid plexus tumor (papilloma or carcinoma)	Lobulated cauliflower-like intraventricular mass	75%: isodense to hyperdense	Isointense to hypointense	Isointense to hypointense	Strong homogeneous enhancement
	50%: lateral ventricle, left >> right	Ca^{2+}: 25%:	CSF entrapment	Flow voids in tumor	Occasional cysts +small necrotic foci
	10%:3rd ventricle			Ca^{2+}: hypointense	CSF seeding
Germinoma	80–90%: midline infiltrating mass near 3rd ventricle	Hyperdense to GM	Isointense to hypointense to GM	Isointense to hyperintense to GM	Strong homogenous enhancement
	Well-circumscribed	Large mass:		Hyperintense: cysts + necrosis	CSF seeding
	May engulf pineal gland	cysts + necrosis + hemorrhage		Hypointense blood products	
	Hydrocephalus				

Nuchal rigidity, back pain, and radicular symptoms may indicate intracranial or intraspinal cerebrospinal fluid dissemination.

Imaging

Various imaging techniques can be used to examine the cranial vault, including transfontanellar ultrasonography (US), computed tomography (CT), magnetic resonance imaging (MRI), and digital subtraction angiography (DSA; Table 1).

US is primarily used in neonates. Sagittal and coronal images can be acquired at the bedside without the use of ionizing radiation. Midline shifts and obvious tumors may be diagnosed, but a detailed study of the neuroanatomy is limited. CT is a first-line imaging tool in children who have acute onset of neurological symptoms. MRI's high spatial resolution, multiplanar imaging capability, ability to generate different tissue contrasts, use of contrast media, functional techniques—including diffusion-weighted imaging, perfusion-weighted imaging, and MR spectroscopy—and the lack of ionizing radiation make it ideally suited to image the child with a brain tumor (Fig. 1a, c). Because of the long acquisition times, the examination is often performed under general anesthesia, especially in young children. DSA is rarely indicated. Advanced functional MRI techniques have replaced most scintigraphy indications.

It goes without saying that currently no imaging modality is capable of making a histological diagnosis. But by combining the anatomical and functional imaging information with the child's age, the neurological symptoms, and the tumor's location and progress over time, the histology of the lesion may be speculated with varying degrees of certainty.

Diagnosis

Diagnosis relies on an accurate neurological examination. The radiologist should guide the neurologist in choosing the appropriate imaging modality and should localize the tumor with regard to the different anatomical and functional regions within the CNS. In addition, displacement, encasement, or infiltration of important, potentially threatened fiber tracts or vessels should be studied. By combining the age, location, and biological behavior of the tumor, the radiologist should be able to make the most likely diagnosis. In addition, he or she should differentiate the lesion from nonneoplastic lesions that can mimic tumors. Furthermore, before surgery, tumor seeding within the cerebrospinal canal or ventricular system should be ruled out. Postoperative imaging should be performed as soon as possible, preferably within 24 h of surgery, because this allows discrimination between residual tumor and postoperative blood–brain barrier disruption.

Bibliography

1. Barkovich AJ (2005) Pediatric Neuroimaging. 4th edn. Lippincott Williams & Wilkins, Philadelphia, pp 506–614
2. Osborn AG (2004) Diagnostic Imaging Brain. 1st edn. Amirsys Inc., Salt Lake City, pp I–6–4–104
3. Tortori-Donati P (2005) Pediatric Neuroradiology: Brain. Springer, Berlin, Heidelberg, pp 329–411

Neoplasms, Chest, Childhood

Johan G. Blickman[1], Dewi Ashi[2], Yvonne L. Hoogeveen[2], Carla Boetes[2]
[1]Department of Radiology, UMC St Radboud, Nijmegen, The Netherlands
[2]Department of Radiology, Faculty of Medicine, University of Indonesia, Cipto Mangunkusumo General Hospital, Jakarta Pusat, Indonesia
j.blickman@rad.umcn.nl

Synonyms

Bronchial adenocarcinoma; Ewing's sarcoma; Germ cell tumors; Germinomas; Histiocytosis; Inflammatory pseudotumor; Lymphoma; Neuroblastoma; Plasma cell granuloma; Primitive neuroectodermal tumors; Teratocarcinomas; Teratomas; Thymoma;

Definition

The ►*thymus* is a gland situated in the ►anterior mediastinum. It is the source of T lymphocytes and plays an important role in cell-mediated immune responses (see Pediatric Imaging Case Review Ward, Robert J. Blackman, Hans. 2005. Elsevier health sciences).

Bronchial adenocarcinomas are rare neoplasms of the tracheal bronchial tree commonly referred to as adenomas, which are low-grade malignant lesions that can metastasize. Benign ►bronchial adenomas are extremely rare. More then half of these lesions are bronchial cancerous tumors that arise from ►Kulchitsky's cells of the respiratory epithelium, part of the amine precursor uptake and decarboxylation (►APUD) system. Mucoepidermoid carcinomas account for 80% of bronchial adenomas.

Chest wall ►*Ewing's sarcoma* and *primitive neuroectodermal tumors* are biologically related lesions. The peak incidence is between 10 and 15 years of life, and they are more common in males.

►*Germ cell tumors* include teratomas, teratocarcinomas, germinomas, and embryonal cell carcinomas, among others.

Histiocytosis is a group of disorders characterized by granulomatous lesions in various organs. It occurs in all ages and there is no difference between boys and girls.

The etiology of *inflammatory pseudotumor of the lung* is multifactorial and probably a repair phenomenon. It is the most common mass lesion of the lung in children, comprising approximately 50% of benign lung lesions in childhood. They can occur at any age; the youngest case reported is of a 12-month-old patient. Sometimes these lesions are difficult to differentiate from embryonic *pulmoblastoma* (pulmonary blastoma), which may have a malignant and semimalignant course.

Lymphoma: In the first years of life, these lymphatic tumors are known as non-Hodgkin's lymphoma (NHL). In the teenage years, these tumors predominantly represent Hodgkin's lymphoma/disease (HD) and are almost always associated with lymphadenopathy (supradiaphragmatic). In the younger age group, the cells can be difficult to distinguish from acute lymphoblastic leukemia and are therefore known as "leukemia lymphoma complex." Of all mediastinal tumors, approximately 20% consist of malignant lymphomas of the mediastinum. Together with germ cell tumors they account for 80–85% of anterior mediastinal masses. There is a male preponderance in the pediatric population.

Neuroblastoma is a neurogenic tumor originating from the paravertebral sympathetic chain. *Ganglioneuromas* usually occur in older children and adolescents; neuroblastoma and ganglioneuroblastoma occur in the first decade of life. Thoracic neuroblastoma comprises about 15% of all cases of neuroblastoma. There is less dissemination than in the abdominal variant, with about 20% of cases presenting with metastatic disease.

Additionally, there are other entities such as metastasis or the rare pulmonary or pleural sarcoma.

Pathology/Histology

The thymus consists of lymphoid tissue containing dense accumulations of lymphocytes. It is surrounded by a thin, connective tissue capsula.

Bronchial adenocarcinomas are histologically similar to salivary gland tumors. They can be of high- or low-grade malignancy. Rarely, they metastasize to regional lymph nodes and their clinical history is usually one of respiratory infections, low bar consolidation, and a central or nodal mass.

Ewing's sarcoma of the chest and *primitive neuroectodermal tumors* are histologically different entities, but they both consist of malignant, small, round cells.

Germ cell tumors can be malignant (10%) and can be associated with elevated levels of human chorionic gonadotropin or alpha-fetoprotein. Most often they are located in the anterior mediastinum. Germ cell tumors are asymptomatic in more than half of patients and they seldom occur before the second decade of life. *Teratomas* are the most common type, with varying degrees of differentiation. The immature types can be potentially malignant. If located in the thymus, it may be seen as an anterior mediastinal mass, sometimes with calcifications.

Histiocytosis is characterized by granulomatous lesions with infiltration of large histiocytes and monocytes in varying degrees. ►Langerhans' cells are seen in the cytoplasm of histiocytes.

Inflammatory pseudotumor is a benign tumor typically characterized by localized proliferation of mononuclear inflammatory cells, plasma cells, lymphocytes, and eosinophils.

Pulmoblastoma is a mostly benign embryologic tumor that rarely turns malignant.

Lymphoma varies with age and cell type. Histology determines the diagnosis of NHL, HD, and leukemia lymphoma complex.

Neuroblastoma is derived from primitive ganglion cells. These may partially differentiate into cells having the appearance of immature neurons.

Presentation

Thymoma can be seen in childhood in combination with myasthenia gravis.

Children with *bronchial adenocarcinoma* present with wheezing, hemoptysis, or lobar collapse. Very seldom are they asymptomatic. Adenoid cystic carcinoma or cylindroma, a slow-growing lesion, may also present with respiratory symptoms and persistent atelectasis.

The child with *Ewing's sarcoma* of the chest or *primitive neuroectodermal tumors* presents in most cases with chest pain and/or a palpable mass and, often, pleural effusion.

Patients with *germ cell tumors* may present with chest pain, hemoptysis, and possibly even a ruptured tumor. A minority of the patients is asymptomatic.

If *histiocytosis* is located in the thymus, it may be seen as an anterior mediastinal mass, sometimes with calcifications. If the disease is located in the lungs, the child presents with coughing and/or dyspnea.

Inflammatory pseudotumor: It is unclear whether there is a relationship with malignancy. In children without a known underlying malignancy, an ►inflammatory pseudotumor is more likely than a malignant lesion. There is seldom a history of trauma or preceding infection, although some of these lesions begin as a radiologically designated "pneumonia."

Pulmoblastoma has a similar presentation.

In *lymphoma*, clinical presentation varies with the extent of disease, particularly in its systemic manifestations. It can be silent or present with fatigue, swollen nodes, and malaise.

The presentation of *neuroblastoma* depends on its anatomic site of origin. In the posterior mediastinum, neurogenic tumors make up the majority of the differential diagnosis in the abdomen. Fifty percent of children with intraspinal extension of a neuroblastoma are symptomatic when they present.

Imaging

The normal *thymus* is seen in infancy as a low radiopaque structure that usually allows the pulmonary vessels to be seen through it. The so-called sail sign is due to a prominent thymus with straight borders. On conventional thorax images, the thymus becomes less noticeable after the age of 4 years; however, it is still easily seen on computed tomography (CT) and magnetic resonance (MR) images until after puberty (Fig. 1a and b). Under the age of 10 years, the thymus has an intermediate signal on T1-weighted images and is hyperintense on T2-weighted MR images. *Ectopic thymus* is in most cases positioned in the neck. Cervical thymus may contain cysts and cross-sectional imaging may be necessary, with a preference for MRI. It may show a mass effect on surrounding organs, contrary to the normal thymus. *Thymolipoma* is seen in children and young adults and is mostly discovered as an incidental finding. On CT and MR images, it is seen as a fatty mass containing solid, thymic tissue elements. The solid tissue elements enhance after administration of intravenous contrast medium. There is no invasion of adjacent structures.

On CT images, *bronchial adenocarcinomas* are generally ovoid, soft tissue masses. Calcification is seen in about 50% of cases.

Ewing's sarcoma of the chest or *primitive neuroectodermal tumor* is, on CT, a solid heterogeneous mass with, especially in larger lesions, necrotic centers. In most cases there are no calcifications in the tumor (Fig. 2). There may be cortical rib destruction. On T2-weighted MR images the tumor is hyperintense and in most cases these lesions are of intermediate signal on T1-weighted images. Contrast enhancement is variable. Ultrasound (US) is sometimes superior to CT and MRI in delineating the diaphragm.

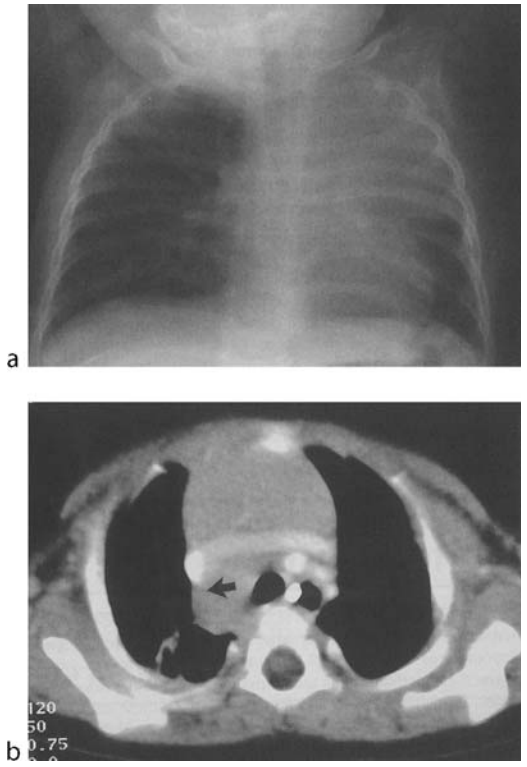

Neoplasms, Chest, Childhood. Figure 1 (a) Chest radiograph showing the thymus as a density that looks like a right, upper lobe consolidation. (b) CT of the thorax showing a normal homogeneous thymus with extension posterior to the superior vena cava (*arrow*).

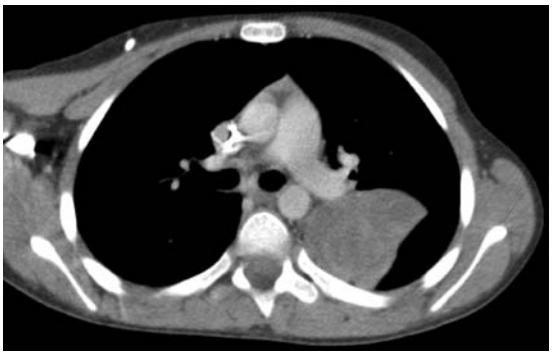

Neoplasms, Chest, Childhood. Figure 2 Ewing's sarcoma, extraosseous, situated in the posterior mediastinum. Large, solid lesion with a few low-attenuation lesions.

Most of the *germ cell tumors* can be diagnosed on CT (Fig. 3). Attenuation values are indicative of the germ cell layers and MR signal intensity may mirror this. They are usually well demarcated and have thick walls.

Histiocytosis (Fig. 4): On a conventional thorax image, interstitial and nodular changes can be seen. Upper lobe

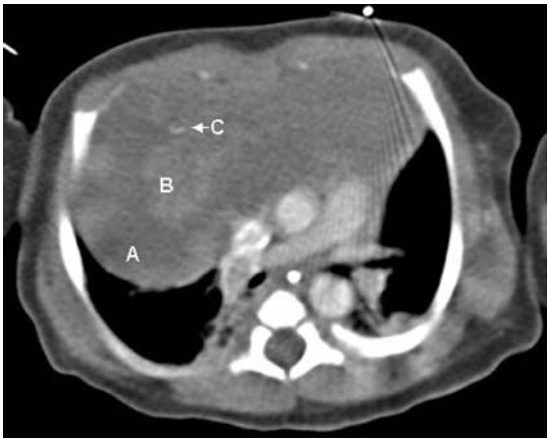

Neoplasms, Chest, Childhood. Figure 3 Germinoma: a large lesion situated in the anterior mediastinum in a newborn child containing the three germ layers: fat (A), soft tissue (B), and bone (C).

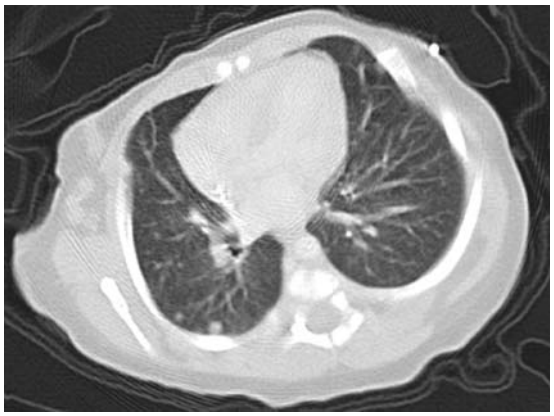

Neoplasms, Chest, Childhood. Figure 4 CT of histiocytosis of the lung. Bilateral increased interstitial markings with small nodules.

involvement is at least equal to lower lobe involvement. CT scanning in an early stage of the disease may show a ground glass appearance, resulting in the typical honeycomb lung in the later phase. If the thymus is also involved, the organ is enlarged and shows cysts and calcifications on CT images. Mediastinal and hilar lymphadenopathy can also be present. The thoracic bone structures should also be evaluated for bony lesions on CT scanning. There is no role for MRI.

Inflammatory pseudotumor/pulmoblastoma: A majority of the lesions occur in the lower lobe; they are approximately 3–4 cm in diameter and can about the pleura (Fig. 5a). CT is the major modality used in the evaluation of these lesions, and these masses are usually well circumscribed. If they reach the lung surface, they can

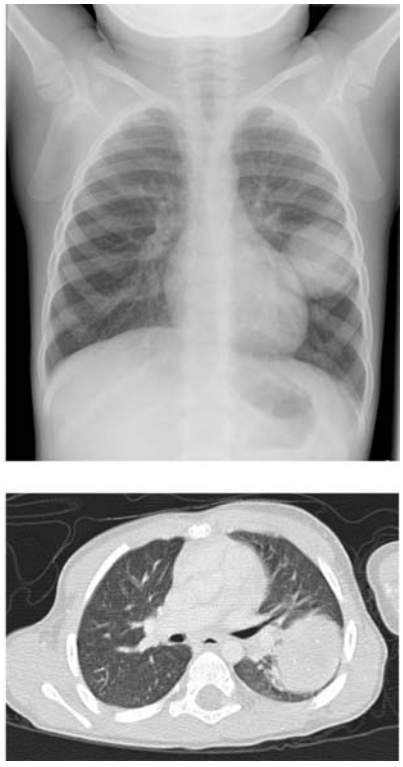

Neoplasms, Chest, Childhood. Figure 5 (a) Chest radiograph of inflammatory pseudotumor with round mass in left lower lobe of the lung. (b) CT of the same inflammatory pseudotumor.

be visualized with US (Fig. 5b). They can resemble a coin lesion, possibly with calcification, an endobronchial mass, and a spicular mass with necrosis. There is varied enhancement following intravenous administration of contrast medium. Lymphadenopathy and plural effusion are rare. MRI is of no additional value.

Lymphoma

NHL: Typically, an anterior mediastinal mass is noted on chest radiographs (Fig. 6a). Pleural effusions are frequently noted. In addition, there may also be pericardial effusion. Airway compression may be noted, which might be important when subsequent CT imaging is contemplated. CT can be omitted as there is seldom any additional staging information. On the other hand, staging in the abdomen, and sometimes in the neck region, make CT the most efficient modality.

HD: In contrast to NHL, HD is usually nodal (Fig. 6b). It is rare before 5 years of age and is characterized by the so-called Reed-Sternberg cell. The nodular sclerosing type accounts for 70% of all cases, with 20% having mixed cellularity. Painless adenopathy is the usual presentation; 30% of cases have hilar adenopathy. CT will demonstrate

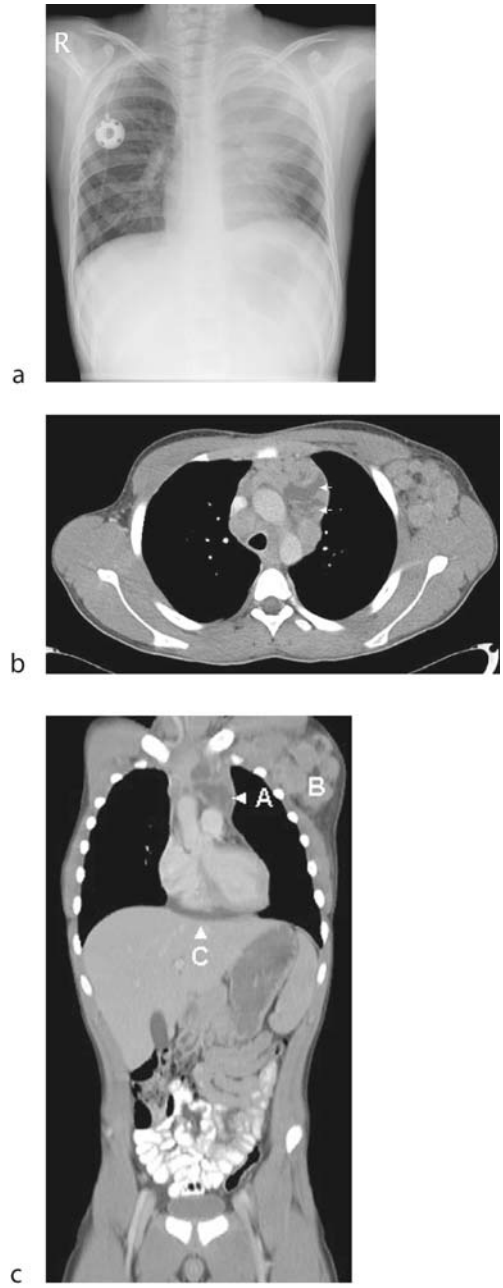

Neoplasms, Chest, Childhood. Figure 6 (a) NHL: chest radiograph of lesion situated in the anterior mediastinum, no effusion, normal ribs. (b) CT of Hodgkin's lymphoma in the anterior mediastinum with necrotic areas (*arrows*). Large lymph nodes in left axillary tail. (c) Coronal thorax and abdomen image of a patient with Hodgkin's lymphoma showing the mediastinal tumor (A), left axillary involvement (B), and pericardial effusion (C).

abnormalities in about 50% of patients with a normal chest radiograph. Pleural effusions as well as pericardial effusions occur frequently (Fig. 6c). Calcification is seldom present before treatment has been initiated.

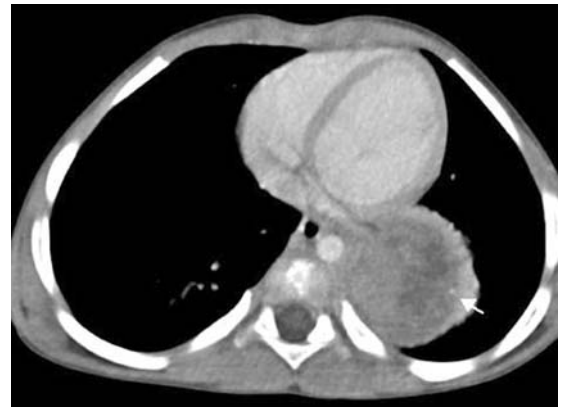

Neoplasms, Chest, Childhood. Figure 7 CT image of neuroblastoma. *Arrow* indicates calcification.

Neuroblastoma: Usually the chest radiograph shows a mass, possibly with calcifications, that may erode the posterior rib and vertebral body. This is then often verified by US; however, cross-sectional imaging is needed to detect nodal enlargement and intraspinal extension. Approximately 80% contain calcification on CT images (Fig. 7). Assessment of the enlargement of intervertebral neural foramina is best shown with MRI. To exclude or identify metastatic disease, sonography, nuclear medicine bone scan, or MIBG scintigraphy should also be performed.

Interventional Radiology

There is no place for interventional radiologic treatment in these conditions; sometimes imaging my help by offering a safe, image-guided biopsy option or may enable uncomplicated drainage of secondary collections (usually using US, CT, or rarely fluoroscopy).

Bibliography

1. Kim OH, Kim WS, Kim MJ et al (2000) Ultrasound in the diagnosis of pediatric chest disease. Radiographics 20:653–671
2. Curtis JM, Lacey D, Smyth R et al (1998) Endobronchial tumours in childhood. Eur J Radiol 29(1):11–20
3. Maziak DE, Todd TR, Keshavjee SH et al (1996) Adenoid cystic carcinoma of the airway: thirty-two-year experience. J Thorac Cardiovasc Surg 112(6):1522–1531; discussion 1531–1532
4. Dick EA, McHugh K, Kimber C et al (2000) Radiology of non-central nervous system primitive neuroectodermal tumors: diagnostic feature and correlation with outcome. Clinical Radiology 56:206–215
5. Dulmet EM, Macchiarini P, Suc B et al (1993) Germ cell tumors of the mediastinum. A 30-year experience. Cancer 72(6):1894–1901
6. Smets A, Mortele K, de Praeter G et al (1997) Pulmonary and mediastinal lesions in children with Langerhans cell histiocytosis. Pediatr Radiol 27(11):873–876
7. Agrons, Rosado-de-Christenson ML, Kirejczyk WM et al (1998) Pulmonary inflammatory pseudotumor: radiologic features. Radiology 206(2):511–518

8. Hedlund GL, Navoy JF, Galliani CA et al (1999) Aggressive manifestations of inflammatory pulmonary pseudotumor in children. Pediatr Radiol 29(2):112–116
9. White KS (2001) Thoracic imaging of pediatric lymphomas. J Thoracic Imaging 16(4):224–237. Review
10. Thoracic neuroblastoma: a Pediatric Oncology Group study. GA, Adams SJ, Shochat Smith EI (1993) 28(3):372–377; discussion 377–378

Neoplasms, Gallbladder

Thomas Helmberger[1], Carlo Bartolozzi[2], Paola Vagli[2]
[1]Clinic of Radiology and Nuclear Medicine, University Hospitals Schleswig-Holstein, Campus Luebeck, Germany
[2]Department of Diagnostic and Interventional Radiology, University of Pisa, Pisa, Italy
thomas.helmberger@uni-luebeck.de
bartolozzi@do.med.unipi.it

Synonyms

Benign and malignant tumors of the gallbladder; Gallbladder cancer; Gallbladder neoplasms

Definition

Gallbladder tumors are defined as primary tumors, both benign and malignant, arising from the gallbladder wall.

Pathology/Histopathology

Adenoma, Gallbladder

In the majority of cases, benign tumors originating from the epithelium of the gallbladder are associated with cholelithiasis. The overall incidence is low (0.5% of cholecystectomy specimens), with a female predominance.

Adenomas of the gallbladder are less common with respect to other benign lesions such as cholesterol polyps and adenomyoma. An increased prevalence of adenomas of the gallbladder and the biliary tract can be associated with both adenomatous polyposis and Peutz-Jeghers syndrome.

Histologically, adenomas are subdivided into tubular (the most frequent variant), papillary, and tubulopapillary types. On gross specimen, the tumors appear as polypoid structures projecting into the gallbladder lumen, with a broad base or pedunculated with a well-defined stalk. Tubular adenomas present a typically lobular contour, whereas papillary types may have a cauliflower-like appearance. The lesion size is variable usually <2 cm in diameter. In about 10% of cases there are multiple adenomas. Malignant progression is reported rarely (1).

Carcinoma, Gallbladder

Although uncommon, carcinoma of the gallbladder represents the most frequent malignant tumor of the biliary tree and the sixth most common malignancy of the gastrointestinal tract, accounting for 3% of all gastrointestinal tumors. The reported incidence in patients undergoing cholecystectomy is about 1%, whereas in autopsy studies it ranges from 0.5 to 24%. Peak incidence is in the seventh decade of life with a female predominance (3:1). An increased incidence is reported in Native Americans.

Even if a multifactorial etiology is considered in most cases, gallbladder carcinoma seems to be related to long-standing (more than 15 years) cholecystolithiasis. More than 80% of patients have cholesterol gallstones. Theoretically, malignant transformation may be related to a peculiar bile composition causing gallstone formation, associated chronic inflammation, and repetitive epithelial repair, followed by dysplasia. In animal studies, chronic inflammation has been confirmed as the most important pathogenetic factor. This theory may also explain the higher incidence in women.

Also, porcelain gallbladder, an advanced stage of chronic cholecystitis, is closely associated with gallbladder cancer. The presence of an anomalous pancreaticobiliary junction as well as congenital cystic disorders of the biliary tree have been suspected as other predisposing factors, as well as a genetic mutation on gene p53 and K-ras. Previous infection by *Salmonella typhi* and exposure to some environmental carcinogens (methylcholantrene) have been reported as potential risk factors. Although lacking proof, an association with lifestyle factors such as cigarette smoke, coffee, alcohol abuse, and obesity has been suggested. An increased risk of developing carcinomas of the extrahepatic biliary tract in patients with chronic inflammatory bowel disease (ulcerative colitis, Crohn's disease) and primary sclerosing cholangitis has also been reported, indicating an association with an autoimmune distortion. In rare cases, an adenoma–carcinoma sequence has been histologically documented.

Histologically, this malignant tumor arises from the gallbladder epithelium. The most common primary form is ►adenocarcinoma (►Adenocarcinoma, Gallbladder) (90% of cases) originating from the columnar cells with a pattern similar to other bile duct carcinomas. Several subtypes with slightly different biological behavior can be

differentiated: papillary, nodular, and tubular tumors with or without mucin production. The papillary type seems to be more often localized and less infiltrative, whereas the nodular type shows early spread to regional lymph nodes and, *via* venous drainage, the liver bed.

Less frequent epithelial tumors include ►squamous cell carcinoma (Squamous Carcinoma, Gallbladder), ►adenosquamous carcinoma (►Adenosquamous Carcinoma, Gallbladder) (►adenoacanthoma (►Adenocanthoma, Gallbladder)), ►small cell carcinoma (►Small Cell Carcinoma, Gallbladder) (oat cell), and anaplastic carcinoma. While well-differentiated tumors with metaplasia are typically less invasive, undifferentiated tumors are associated with a poorer prognosis.

In most cases (60%) the tumors involve the fundus of the gallbladder; location in the body and neck occurs in 30 and 10% of cases, respectively. Macroscopically the tumors are usually diffusely infiltrating, whereas an intraluminal polypoid growth is less common.

At the time of diagnosis, an extensive tumoral involvement of the gallbladder can be observed with metastatic lymph nodes in half the cases. Early metastatic involvement includes hepatoduodenal and pancreaticoduodenal lymph nodes; right celiac and retroperitoneal lymph nodes may be involved as well. Local spread through the gallbladder wall leads to direct invasion of the liver bed, extrahepatic biliary ducts, duodenum, and, less commonly, the colon. Spread to the organ wall may determine intraperitoneal seeding with implants on the liver surface, bowel, and pelvis. Hematogenous metastases are most commonly seen in the liver.

Staging of the tumoral extent is a prerequisite for establishing appropriate treatment and the patient's prognosis. Tumoral staging is performed according to the TNM classification. Another classification commonly used and more strictly related to the clinical presentation is the Nevin–Moran staging system (Table 1).

Other exceedingly rare malignant tumors of the gallbladder include malignant mesenchymal tumors (embryonal rhabdomyosarcoma, leiomyosarcoma, and malignant fibrous histiocytoma), ►carcinosarcoma, carcinoid, lymphoma, and melanoma (2, 3).

Neoplasms, Gallbladder. Table 1 Nevin–Moran staging system for gallbladder carcinoma

Stage	Tumor location
I	Intramucosal tumor
II	Mucosa and muscolaris involved
III	All three layers involved
IV	All three layers and cystic duct lymph nodes involved
V	Liver or distant metastases

Clinical Presentation

Adenoma, Gallbladder

Gallbladder adenomas are usually asymptomatic lesions that are occasionally discovered. Chronic or intermittent right upper quadrant pain may occur in patients with large adenomas or adenomas obstructing the cystic duct.

Carcinoma, Gallbladder

Due to its natural history, the clinical presentation of gallbladder carcinoma is more common in advanced stages of disease. Clinical symptoms are not specific. Patients may present at early stages with symptoms attributable to gallstones or cholecystitis, such as abdominal pain, nausea, and vomiting. Constitutional symptoms, including fatigue, weight loss, anorexia, hepatomegaly, and ascites, occur late and are considered poor prognostic signs. Jaundice and Courvoisier gallbladder (i.e., painful hydrops) occur in cases of invasion of the extrahepatic biliary tree and are not specific. Clinical signs may include a palpable mass in the right upper quadrant, supraclavicular lymphadenopathy, and rectal shelf in cases of pelvic spreading. Duodenal or colonic obstruction and cholecystoenteric fistulae are signs highly indicative of very advanced stages.

Laboratory tests may reflect the presence of extrahepatic cholestasis (increased levels of conjugated bilirubin, alkaline phosphatase, and gamma glutamyl transpeptidase). Tumor markers such as CA19-9, CA125, and carcinoembryonic antigen can be elevated but are not specific.

Patients with gallbladder carcinoma have an overall mean survival of 6 months, and the 5-year survival rate is about 5%. Surgery is the therapy of choice; however, because most gallbladder carcinomas are quite advanced when detected, surgical treatment is often not amenable. Only one-fourth of patients are eligible for curative resection (tumors incidentally diagnosed at cholecystectomy). Radiation therapy with or without concurrent chemotherapy is the therapeutic approach for surgically nontreatable patients (3).

Imaging

Adenoma, Gallbladder

Ultrasound (US) displays gallbladder adenomas as nonmobile structures protruding into the gallbladder lumen, with smooth margins. A lobulated or cauliflower appearance is infrequent. In cases of pedunculated adenomas, visualization of the stalk with the patient in lateral decubitus is helpful. The thickness of the adjacent gallbladder wall is usually normal (<3 mm). Adenomas present moderately hyperechoic without acoustic shadowing and may be

heterogeneous or hypoechoic with increasing size. On contrast-enhanced computed tomography (CT), gallbladder adenomas appear as intraluminal soft-tissue masses that are isodense or hypodense in comparison with hepatic parenchyma. In CT the differentiation of noncalcified gallstones can be crucial, whereas in magnetic resonance cholangiopancreatography (MRCP), small, nonmobile, filling defects inside the gallbladder lumen can be the only finding (1).

Carcinoma, Gallbladder

The role of conventional radiology is very limited and reveals suspicious signs only incidentally. A systematic work-up by conventional imaging is not appropriate anymore. Plain abdominal films may demonstrate calcifications of the gallbladder wall (porcelain gallbladder) or calcified gallstones. Punctate calcifications of the primary tumor or metastases may be seen with mucinous tumors. Biliary gas resulting from a cholecystoenteric fistula is uncommon. In further advanced tumors, barium studies can show invasion or displacement of the duodenum or transverse colon.

US is used mostly as a diagnostic modality. Features on US range from a relatively normal or distended gallbladder with only an intraluminal polyp or focal wall thickening, to the presence of a large, ill-defined mass associated with invasion into the surrounding structures. In contrast to the fine-lined normal gallbladder wall, neoplastic mural thickening appears heterogeneous. Advanced gallbladder carcinoma typically presents as a large, single or multinodulated, hyperechoic, inhomogeneous mass associated with strong echoes and acoustic shadowing due to gallstones or tumoral calcifications. The presence of an extraluminal complex mass extending to the liver that is indistinguishable from the surrounding parenchyma, with multiple hypoechoic areas due to necrosis, is a sign of advanced disease. US can also show signs of tumoral spread such as hilar lymphadenopathy and bile duct dilatation but is inferior to CT or magnetic resonance (MR) imaging for further staging in terms of intraperitoneal disease and distant metastases.

In CT, gallbladder carcinoma is determined by a focal or diffuse wall thickening up to an isoattenuating or hypoattenuating soft-tissue mass filling and/or replacing the gallbladder in more advanced cases. Fuzzy borders and heterogeneous enhancement (due to the combination of both necrotic and viable tissues) of the mass is common. While a bright enhancement is often present in cases of isolate tumoral wall thickening, the less common polypoid tumors may show well-defined round borders and may be isoattenuating or hypoattenuating after contrast medium administration (Fig. 1)(3, 4).

Metastatic lymphadenopathy may be seen as well-defined nodular masses in the hepatoduodenal ligament or the presence of an infiltrating, soft-tissue enhancing mass, obscuring portal vein margins. Other frequent sites of lymphatic spread, well depicted by CT, are the peripancreatic lymph nodes. Associated biliary dilatation due to obstruction at the level of the hepatic hilum or soft-tissue invasion into the liver bed is usually well visualized. Peritoneal and distant hematogenous metastases (mostly in the liver and less frequently in lungs, skeleton, pancreas, and brain) may be detected.

MR does not represent a primary imaging modality for gallbladder cancer but may be helpful to distinguish benign from malignant mural thickening. MR findings in gallbladder carcinoma resemble those known from CT.

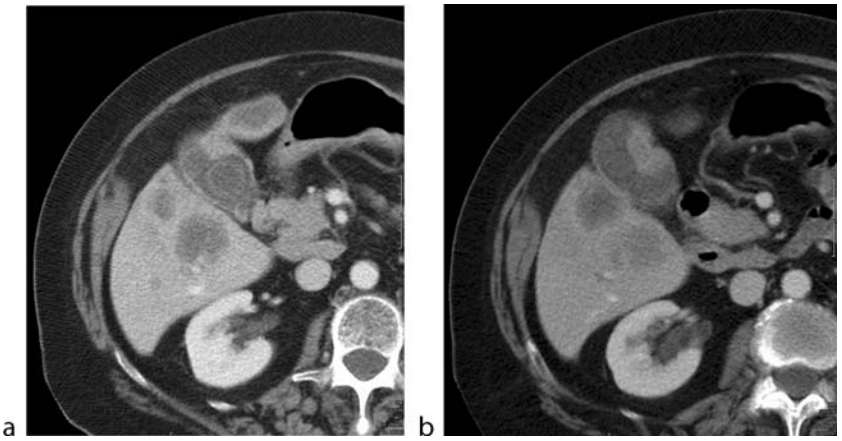

Neoplasms, Gallbladder. Figure 1 (a, b) Gallbladder carcinoma, polypoid form. Computed tomography scans at two different levels show a focal thickening extending beyond the gallbladder wall and protruding into the lumen, with lobulated contours, and isoattenuating with respect to the adjacent wall. Metastatic spread to the liver parenchyma and intraluminal stones are also displayed.

Gallbladder carcinoma is associated with prolonged T1 and T2 relaxation times, appearing hyperintense and poorly marginated on T2-weighted images, and isointense to hypointense on T1-weighted images. Ill-defined early enhancement is the typical aspect of gallbladder carcinoma at dynamic gadolinium-enhanced MR imaging (5).

MRCP may complete the study of the biliary tree, showing filling defects in the gallbladder lumen or also in the biliary tree and providing an excellent, noninvasive overview of potential biliary obstruction.

Direct cholangiography (percutaneous transhepatic cholangiography, or PTC) or endoscopic retrograde cholangiopancreatography (ERCP) may be indicated if cytology is desired or an intervention (such as drainage or stent placement) in cases of jaundice is recommended.

Angiography is of no additional value in the diagnosis of gallbladder carcinoma whenever tumoral neovascularization, arterial, and/or venous encasement/invasion can be displayed by angiography.

Nuclear Medicine

Carcinoma, Gallbladder

FDG-positron emission tomography (PET) and biliary scintigraphy with ^{99m}Tc iminodiacetic acid analogs are not specific and are not indicated in gallbladder carcinoma. Whether CT–PET will gain some importance in this disease is not yet defined.

Diagnosis

Adenoma, Gallbladder

Differentiation of gallbladder malignancies is crucial, especially in case of lesions >1 cm and/or associated with focal gallbladder thickening. Adenomas usually tend to be more homogeneous than malignant lesions.

Carcinoma, Gallbladder

Despite advances in diagnostic imaging, early-stage carcinoma is usually diagnosed only incidentally. Many benign conditions may resemble imaging features of gallbladder carcinoma. Gallbladder wall thickening may be appreciated in cholecystitis (acute and chronic), heart failure, hypoalbuminemia, and liver cirrhosis. The presence of a diffuse mural thickening instead of a focal involvement (more typical of gallbladder carcinoma) associated with specific clinical features may help differentiate benign from malignant processes. Pronounced wall thickening (>1 cm) when associated with irregularity and lymphadenopathy should suggest malignancy. However, adenomyomatosis can cause focal gallbladder thickening and mimic carcinoma. The presence of hyperechoic areas creating "comet-tail" reverberation artifacts in the Rokitansky-Ashoff sinuses may lead to diagnosis. Polypoid lesions are difficult to distinguish from polypoid carcinoma. Larger polyps with cauliflower appearance suggest malignancy, whereas polyps <5 mm are unlikely to be malignant. Polyps ranging between 5 and 10 mm must be followed up.

Metastases of melanoma may also cause polypoid gallbladder lesions. Tumefactive sludge may mimic an intraluminal mass; nevertheless, a tumor can usually be excluded in cases of dislodgement of the sludge and the absence of vascularization on Doppler US. Xanthogranulomatous cholecystitis—an inflammatory process with mural thickening and involvement of the surrounding tissue, including lymph nodes—may cause difficulties in differentiation from gallbladder carcinoma. In ambiguous cases MR may be helpful for differentiating focal or diffuse mural thickening from gallbladder carcinoma, adenomyomatosis, and chronic cholecystitis (3).

Bibliography

1. Levy AD, Murakata LA, Abbott RM et al (2002) From the archives of the AFIP. Benign tumors and tumorlike lesions of the gallbladder and extrahepatic bile ducts: radiologic-pathologic correlation. Radiographics 22(2):387–413
2. Henson DE, Albores-Saavedra J, Corle D (1992) Carcinoma of the gallbladder. Histologic types, stage of disease, grade, and survival rates. Cancer 70(6):1493–1497
3. Levy AD, Murakata LA, Rohrmann Jr (2001) Gallbladder carcinoma: radiologic-pathologic correlation. Radiographics 21(2):295–314
4. Yoshimitsu K, Honda H, Shinozaki K et al (2002) Helical CT of the local spread of carcinoma of the gallbladder: evaluation according to the TNM system in patients who underwent surgical resection. Am J Roentgenol 179(2):423–428
5. Yoshimitsu K, Honda H, Jimi M et al (1999) MR diagnosis of adenomyomatosis of the gallbladder and differentiation from gallbladder carcinoma: importance of showing Rokitansky-Aschoff sinuses. Am J Roentgenol 172(6):1535–1540

Neoplasms, Gastroduodenal

K. M. Harris[1], A. G. Chalmers[1]
Consultant Radiologists, Leeds General Infirmary, Leeds, UK
keith.harris@leedsth.nhs.uk
Alan.Chalmers@leedsth.nhs.uk

Imaging of gastroduodenal neoplasms relies on the complimentary roles of computed tomography (CT) and ▶endoscopic ultrasound (EUS). Multidetector row technology has established CT as the primary technique for the overall evaluation and ▶staging of gastroduodenal tumours (1). For the specific detail of local staging, EUS is the most accurate tool currently available.

Stomach

Benign Tumours

Approximately 85–90% of all gastric neoplasms are benign.

Polyps

Gastric polyps can be demonstrated by a good quality double contrast barium meal. Most of them that are less than 1 cm diameter, arise in the gastric fundus and body, are hyperplastic and have no premalignant potential. Adenomas account for up to 10% of gastric polyps. Dysplastic adenomas have a malignant potential; the risk of malignancy increasing with increasing polyp size (>2 cm). Any sizable or unusual polyp must be evaluated with endoscopy and biopsy.

Submucosal Tumours

Benign submucosal tumours include lipomas, haemangiomas, neural tumours and small ▶gastrointestinal stromal tumours (GISTs). These tumours may be demonstrated by contrast radiology and have no discriminating features. A fatty mass on CT will represent a lipoma but otherwise evaluation of submucosal lesions requires EUS to establish the exact layer of origin within the bowel wall. By assessing position and morphology, EUS can indicate the probable aetiology (2) as well as categorising lesions as highly likely to be benign and safe to ignore, indeterminate and worthy of follow-up, or of concern and requiring biopsy or resection.

Malignant Tumours

Gastric Cancer

Gastric cancer (3) is the second commonest cancer worldwide with adenocarcinoma, accounting for more than 90% of all of malignant tumours of the stomach. Gastric cancer presents with a wide range of symptoms including dyspepsia, anorexia and weight loss. Diagnosis is usually made by upper gastrointestinal endoscopy and biopsy. On barium, certain features suggest malignancy such as thickened irregular folds and shallow eccentric ulceration but it is essential that any suspicion is confirmed with endoscopy and biopsy. Prognosis is related to tumour stage and accuracy is essential to plan the most appropriate management, predict prognosis, and reduce unnecessary surgical interventions.

Tumour staging is based upon the widely accepted tumour-node-metastasis (TNM) classification:

Primary tumour (T)

T1: Tumour invades lamina propria or submucosa
T2: Tumour invades the muscularis propria or the subserosa
T2a: Tumour invades muscularis propria
T2b: Tumour invades subserosa
T3: Tumour penetrates the serosa (visceral peritoneum) without invading adjacent structures
T4: Tumour invades adjacent structures (e.g. spleen, pancreas, transverse colon, etc.)

CT has clear advantages when evaluating spread of disease outside the stomach but despite optimised multidetector techniques is inferior to EUS when assessing the layers of the gastric wall. EUS is the only imaging technique that can reliably discriminate the component layers allowing accurate prediction of T stage (Fig. 1a–d). The omental reflections around the stomach are not clearly seen with EUS, making it impossible to determine whether tumour has penetrated through the muscularis propria into the greater or lesser omenta to breach the visceral peritoneum, i.e. T2b or T3.

Multiplanar and 3D techniques are considered a routine component of any multidetector CT assessment of gastroduodenal pathology and its potential spread. Coronal reformats are particularly suited for the study of gastric pathologies, both from improved staging accuracy and the improved overview afforded to the surgeons and medical oncologists. 3D-rendering techniques (virtual gastroscopy) have been advocated for gastric fold assessment. Direct invasion into adjacent structures (T4) can be difficult to establish on both CT and EUS. CT relies upon tumour contact with the contiguous organ and loss of intervening fat plane. EUS can exclude direct invasion if free movement is shown between tumour and adjacent organ.

Regional lymph nodes (N)

N0: No regional lymph node metastasis
N1: Metastasis in 1 to 6 regional lymph nodes
N2: Metastasis in 7 to 15 regional lymph nodes
N3: Metastasis in more than 15 regional lymph nodes

The regional lymph nodes are the perigastric nodes along the lesser and greater curvatures, and the nodes located along the left gastric, common hepatic, splenic and coeliac arteries. Involvement of other intra-abdominal lymph nodes, such as the hepatoduodenal, retropancreatic, mesenteric, and para-aortic, is classified as distant metastasis (M1). The CT assessment of nodal involvement relies almost entirely on size with upper limits of normal chosen to achieve a best compromise between sensitivity and specificity. Currently >6 mm maximum diameter short axis is advocated for regional nodes, rising to >8 mm for non-regional nodes. Certain morphological features such as nodal enhancement or a rounded margin suggest infiltration whereas clusters of smaller nodes should raise concern. Reported CT accuracy rates are no better than 50–70%. Lymph nodes are well seen on EUS and several morphological features correlate well with malignant

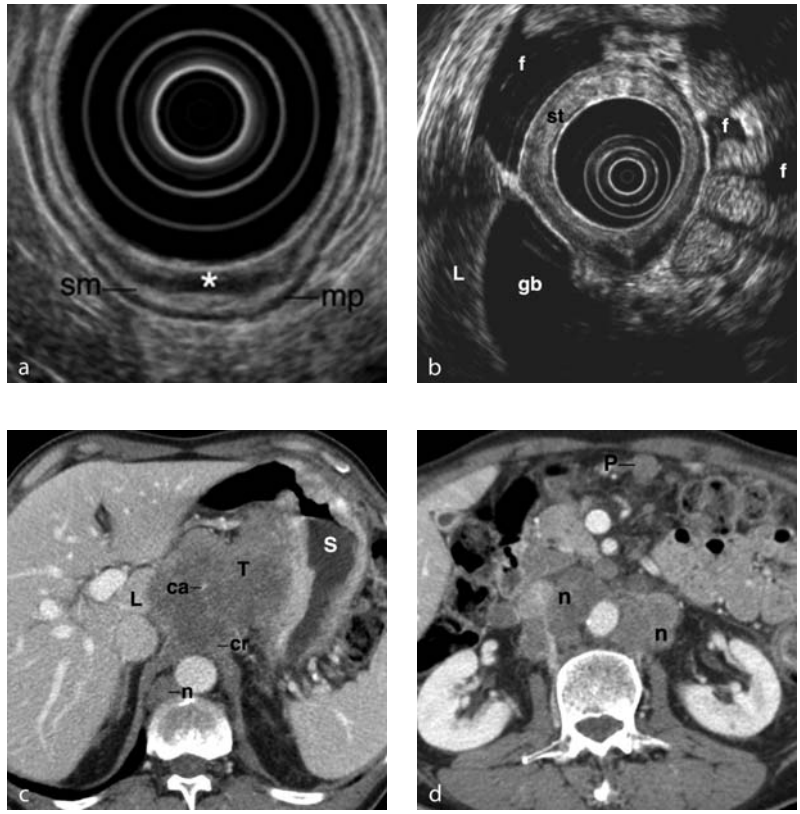

Neoplasms, Gastroduodenal. Figure 1 Gastric cancer. 1a: EUS image of a T1 gastric cancer (*) demonstrating preservation of a normal layer of submucosa (sm) deep to the tumour, mp = muscularis propria. 1b: EUS demonstrating small volume ascites (f), thick-walled stomach (st) due to tumour infiltration, L = liver, gb = gallbladder. 1c: CT of an advanced gastric cancer (T) extending from the posterior wall of stomach (S) to liver (L) and abut the diaphragmatic crura (cr). Encasement of the coeliac axis (ca) and a retrocrural node (n) also noted. 1d: Same patient as 1c demonstrating further non-regional lymphadenopathy (n) and peritoneal tumour deposits (P).

infiltration. Hypoechoic nodes greater than 1 cm with well-defined rounded margins are likely to be malignant.

Distant metastasis (M)

M0: No distant metastasis
M1: Distant metastasis

CT provides an excellent whole body survey for the common sites of metastatic disease namely lung, liver, adrenals, ovaries, peritoneum and bone. EUS can detect low volume ascites, which may be the first indication of peritoneal spread. Magnetic resonance imaging (MRI) and positron emission tomography (PET) are not part of routine staging but have roles to play in problem-solving equivocal CT or EUS findings. PET may be helpful in detecting distant metastases and reports suggest that PET is more sensitive than CT for the detection of peritoneal disease. However, some gastric tumours such as mucinous or signet ring types typically take up fluorodeoxyglucose (FDG) poorly. For recurrent disease, PET may be useful when CT is negative or equivocal.

Lymphoma

The commonest site of extranodal non-Hodgkin's lymphoma is the stomach (approximately 25%) but lymphoma only accounts for 2–8% of all gastric malignancies. Morphology ranges from ulcers, nodules and polyps to fold enlargement and diffuse infiltration. The CT appearances of lymphoma and carcinoma can be similar. Lymphoma is often advanced at presentation with an average tumour size of 10 cm. Mural thickening is characteristically more marked and lymph nodes are larger. Mucosa-associated lymphoid tissue (MALT) lymphoma is most frequently found in the gastrointestinal tract, particularly the stomach. Gastric MALT lymphoma may regress completely after *Helicobacter pylori* eradication and EUS has been shown to be more sensitive than endoscopy and CT for staging and predicting tumour response. EUS can differentiate superficial from infiltrative variants which are of prognostic significance and can confirm remission or persistence of the disease during follow-up (4). Continuing gastric wall thickening, even

with negative histology, requires repeated biopsies as persistent disease is likely.

Metastases

Metastases to the stomach are uncommon being found at post-mortem in only 2% of patients dying from malignancy. They may present as focal lesions (e.g. melanoma, lung, Kaposi's sarcoma), or as diffuse linitis type infiltration (e.g. breast). Direct or transperitoneal spread from other abdomino–pelvic tumours can occur.

Gastrointestinal Stromal Tumours

Most GISTs arise in the stomach (60–70%). About 10–30% of all GISTs are malignant and the risk of malignancy increases with size (>5 cm). Liver and the peritoneal cavity are the commonest sites for metastatic disease but lymph node and bony metastases are rare. Gastrointestinal bleeding is the commonest symptom but most small gastric GISTs are asymptomatic and detected incidentally. Barium studies show features of a submucosal mass—a smooth well-defined filling defect with either intact mucosa or central umbilication. Smaller GISTs are typically intramural and EUS will show them usually arising from the fourth hypoechoic layer, the muscularis propria (Fig. 2a). The vast majority have very low malignant potential but EUS can predict malignant change by identifying irregular margins, cystic spaces, and malignant-looking lymph nodes (5).

With increasing size, a more exophytic morphology is seen and patients typically present with abdominal pain or a palpable mass. The CT features of larger GISTs are variable and range from uniformly solid to marked heterogeneity with solid and frankly cystic change mimicking lymphoma or sarcoma (Fig. 2b and 2c). GISTs can appear aggressive with involvement of multiple adjacent organs but in contrast to adenocarcinoma, they tend to abut and displace rather than infiltrate. Peritoneal spread can be extensive.

After imatinib, both the primary mass and the peritoneal changes can display a rapid reduction in size and density with cystic changes mimicking a pseudomyxoma appearance (Fig. 2d). As most GISTs and their metastases take up ^{18}FDG, a preoperative PET study is highly sensitive in demonstrating metastatic disease not visible on other imaging. PET can also be used to assess response to non-surgical treatment.

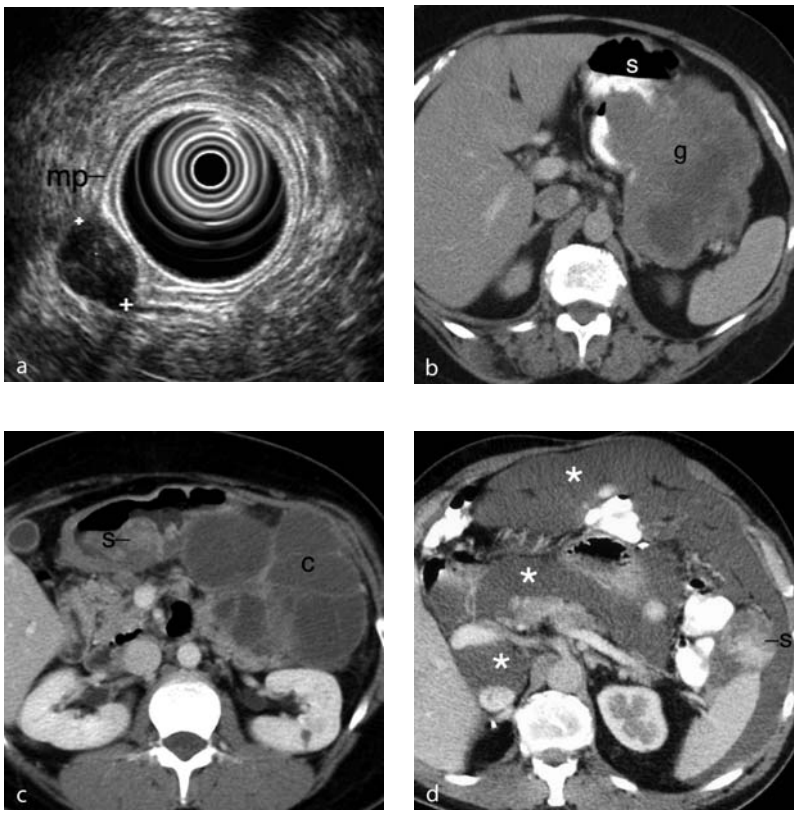

Neoplasms, Gastroduodenal. Figure 2 Gastrointestinal stromal tumours (GIST). 2a: EUS of a small gastric GIST (12 mm between +) arising within the muscularis propria (mp). 2b: CT demonstrating a large GIST (g) arising from the posterior wall of the stomach (S). 2c: CT of a gastric GIST with both solid (S) and cystic components (C). 2d: GIST following imatinib therapy. Low density peritoneal tumour mimicking pseudomyoma peritonei (*) along with a persisting solid component (S).

Carcinoid

Approximately 30% of gastrointestinal carcinoid tumours arise in stomach. The lesions can be small and submucosal, large and ulcerated, focal or multicentric. Benign and malignant variants occur. Small carcinoid tumours are best demonstrated by EUS or on CT during the arterial phase of contrast enhancement.

Duodenum

Tumours arising in the duodenum include carcinoma, GIST, neuroendocrine pathologies such as carcinoid and glucagonoma, schwannomas and paragangliomas. They account for 20% of all small bowel neoplasms.

Benign Tumour

Adenoma

Duodenal polyps are less common than gastric and are usually hyperplastic or adenomatous. Adenomas are the commonest symptomatic small bowel tumour, most frequently encountered in the duodenum, and present with bleeding, obstruction, or intussusception. If multiple polyps are seen, a polyposis syndrome should be considered when 60–70% of symptomatic lesions will be malignant.

Brunner's Gland Hamartomas

These are rare tumours of the duodenum, usually benign with only rare incidences of malignancy. Smaller lesions present as incidental findings during barium examination or endoscopy whereas larger lesions present with bleeding or obstruction. EUS may help characterise the lesion but histology is crucial and endoscopic snare excision or surgery is required depending on the size.

Lipoma

Can be polypoidal or submucosal.

Haemangioma

These are frequently symptomatic with bleeding a common presentation. Imaging features include calcified intraluminal phleboliths and the demonstration of feeding vessels.

Carcinoid

The majority of duodenal carcinoids are located in the proximal duodenum, can be single or multiple, intraluminal and polypoidal, or intramural. In contrast to jejunal and ileal carcinoids, duodenal carcinoid rarely produces symptoms of carcinoid syndrome. The majority are gastrin cell tumours with one-third of these leading to Zollinger–Ellison syndrome.

Malignant Tumour

The majority of small bowel carcinomas arise in the duodenum or proximal jejunum. They are often advanced at presentation and symptoms include anaemia due to chronic bleeding or vomiting due to obstruction. Duodenal carcinomas are rare but show an increased incidence in patients with familial adenomatous polyposis and long-standing coeliac disease. Early tumours can be polypoidal and may be detected by barium or endoscopy. More advanced tumours show shouldered irregular stricturing. Biopsy of any suspicious lesion is essential to detect malignant change and CT is required for tumour staging.

Lymphoma

Secondary involvement of the small bowel is more common than primary disease with approximately 40% of gastric lymphoma showing duodenal extension.

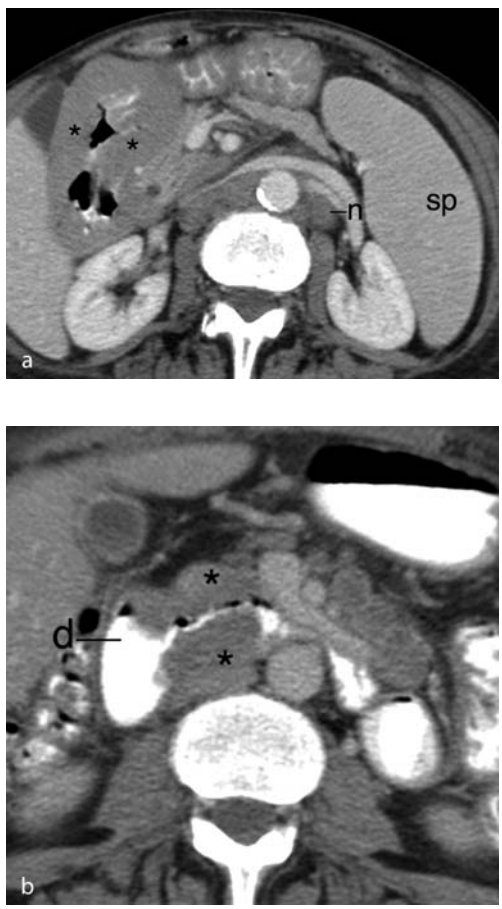

Neoplasms, Gastroduodenal. Figure 3 Duodenal tumours. 3a: CT of a patient with duodenal lymphoma—note the gross wall thickening (*), splenomegaly (sp) and para-aortic lymphadenopathy (n). 3b: CT demonstrating a duodenal stricture (*) due to metastases from a squamous cell lung cancer, d = duodenum.

Imaging may demonstrate nodular wall thickening of various degrees or an eccentric mass (Fig. 3a).

Secondary Spread to Duodenum

Metastases to small bowel are found more frequently than primary neoplasms with lung and melanoma among the commoner primaries (Fig. 3b). The duodenum may be directly invaded by tumours originating in pancreas, gall bladder, bile ducts or colon, or from other tumours of the retroperitoneum such as sarcomas. High resolution curved planar reformats provided by ►multidetector row CT can provide useful diagnostic information with respect to adjacent organ involvement.

Ampullary tumours are discussed elsewhere.

Bibliography

1. Ba-Ssalamah A, Prokop M, Uffmann M et al (2003) Dedicated multidetector CT of the stomach: spectrum of diseases. Radiographics 23:625–644
2. Kawamoto K, Yamada Y, Utsunomiya T et al (1997) Gastrointestinal submucosal tumours: evaluation with endoscopic ultrasound. Radiology 205:733–740
3. Kumano S, Murakami T, Kim T et al (2005) T Staging of gastric cancer: role of multi-detector row CT. Radiology 237:961–966
4. Lévy M, Hammel P, Lamarque D et al (1997) Endoscopic ultrasonography for the initial staging and follow-up in patients with low-grade gastric lymphoma of mucosa-associated lymphoid tissue treated medically. Gastrointest Endosc 46:328–333
5. Palazzo L, Landi B, Cellier C et al (2000) Endosonographic features predictive of benign and malignant gastrointestinal stromal cell tumours. Gut 46:88–92

Neoplasms, Kidney, Childhood

Johan G. Blickman[1], Dewi Ashi[2]
[1]Department of Radiology, Nijmegen, The Netherlands
[2]Department of Radiology, Faculty of Medicine, University of Indonesia, Cipto Mangunkusumo General Hospital, Jakarta Pusat, Indonesia
j.blickman@rad.umcn.nl

Synonym

Nephroblastoma

Definition

Malignant tumor of the kidney usually arises from ►nephroblasts. It is the most common genitourinary malignancy in children (95%).

Predisposing anomalies may consist of ►aniridia, ►hemihypertrophy, ►Beckwith–Wiedemann syndrome, and Drash syndrome as well as congenital genitourinary anomalies (horseshoe kidney).

Incidence

1. The peak incidence is between 1 and 3 years of age.
2. The female:male ratio is equal.
3. It is rare in the neonatal period.
4. The incidence of bilateral tumor is up to 10%.

Pathology/Histopathology

The classical triphasic Wilms' tumor consists of blastemic, stromal, and epithelial elements.

Tumors with favorable histology do not contain any anaplastic changes. In the National Wilms' Tumor Study Group 5 (NWTS 5), the tumor stage is determined operatively in five stages.

The 4-year survival rate is 94% for those patients whose most advanced lesion is stage I or stage II, and 76% for those whose most advanced lesion is stage III.

In Europe, the staging system is based on the radiologic findings.

Clinical Presentation

1. Abdominal mass, occasionally with pain
2. Hematuria
3. Nonspecific sign such as fever, or hypertension

Imaging

Ultrasonography (US) reveals an intrarenal mass of heterogeneous echogenicity and may contain cystic components, either portions of obstructed and entrapped pyelocaliceal systems or hemorrhagic and necrotic tumor (Fig. 1). Extensions into the inferior vena cava and right atrium are characteristic routes of tumor growth and can be well visualized with sonography, computed tomography (CT), and magnetic resonance imaging (MRI). The tumor typically forms a pseudocapsule, but may invade the renal capsule spreading into the retroperitoneal space, or may grow directly into mesentery and omentum.

On CT, Wilms' tumor is generally spherical and intrarenal and contains small amounts of fat or fine calcifications. Calcifications are seen in about 9% of Wilms' tumor.

After contrast medium injection, the tumor shows heterogeneous enhancement and less enhancement than the

Stage	Description
I (43% of patients)	Tumor is limited to the kidney and is completely resected
II (23% of patients)	The tumor is completely resected, but there is regional extension of the tumor (penetration of the renal sinus capsule, or extensive invasion of the soft tissue of the renal sinus). The blood vessels within the nephrectomy specimen outside the renal parenchyma, including those of the renal sinus, contain tumor
III (23% of patients)	Residual nonhematogenous tumor is present after surgery, and is confined to the abdomen

(*continued*)

renal parenchyma. Low attenuation representing necrosis, cystic degeneration, or hemorrhage is seen (Fig. 2).

On MRI, the tumor is intense on T1-weighted images (WI) and hyperintense on T2-WI. After contrast administration, Wilms' tumor is hypointense in relation to normal renal parenchyma and may define the borders more clearly.

Nuclear Medicine

Depicts bone metastasis.

Diagnosis

Most often, Wilms' tumor presents as an abdominal mass, and sometimes there is hematuria.

Imaging findings can differentiate Wilms' tumor from neuroblastoma.

Rarely, Wilms' tumor will invade surrounding tissues and even more rarely extend into the spinal canal, this being much more frequent with neuroblastoma. Clear cell sarcoma and rhabdoid tumor of the kidney are more aggressive than Wilms' tumor, but they cannot be differentiated on imaging.

A definite diagnosis of Wilms' tumor is based on histopathology.

Differential Diagnosis

1. Neuroblastoma: The imaging hallmark is distortion of the renal parenchyma in Wilms' tumor and renal displacement by neuroblastoma.

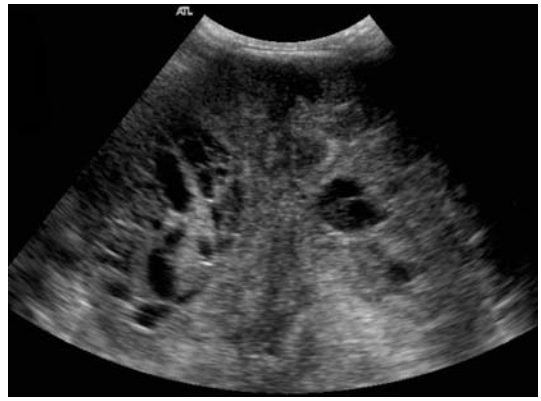

Neoplasms, Kidney, Childhood. Figure 1 Wilms' tumor: US shows intrarenal mass with pelviocaliceal distortion.

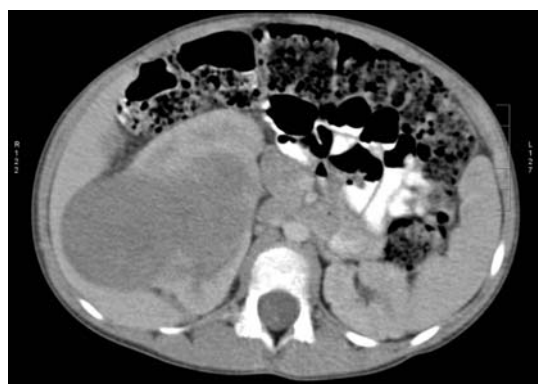

Neoplasms, Kidney, Childhood. Figure 2 CT shows a mass originating from the right kidney with distortion of the parenchyma.

2. Clear cell sarcoma of the kidney: This tumor is not a Wilms' tumor variant, but it is an important primary renal tumor associated with a significantly higher rate of relapse and death than Wilms' tumor of favorable histology findings.
3. Rhabdoid tumor of the kidney: This tumor tends to metastasize not only to the lungs, but also to the brain (10–15%). There is a distinct clinical presentation with fever, hematuria, and young age (mean 11 months) (see Table 1, Neuroblastoma).

Bibliography

1. Barnes PD (1998) Neuroimaging. In: Hans Blickman (ed) Pediatric Radiology: The Requisites. 2nd edn. Mosby St. Louis, pp 294–295
2. Carty H (2001) Paediatric Imaging. In: The Encyclopedia of Medical Imaging, Vol 7. Published by The NICER Institute, Oslo, pp 565–566
3. Feintein KA (2004) Renal neoplasms. In: Kuhn JP, Slovis TL, Haller JO (eds) Caffey's Pediatric Diagnostic Imaging. 10th edn. Mosby, Philadelphia, pp 1787–1790
4. http://www.emedicine.com/med. Wilms' Tumor. Last update June 2, 2005

Neoplasm, Large Bowel, Malignant

Andrea Laghi, Franco Iafrate
Director of Unit of CT and MR, University of Rome "La Sapienza", Polo Pontino, I.C.O.T. Latina, Italy
andrea.laghi@uniromal.it
francoiafrate@tin.it

Definitions

►Colorectal cancer (CRC) is the second leading cause of cancer related deaths in the United States and the most common cancer of gastrointestinal tract with approximately 150,000 new cases every year (1).

It is the second most lethal cancer in men after bronchial carcinoma and in women after breast cancer, with a slight female predominance in colon cancer and male predominance in rectal cancer. Despite these statistics, mortality from colon cancer has decreased over the past 30 years, possibly because of earlier diagnosis through screening and better treatment modalities.

When detected at an early stage, this type of cancer has great potential for cure, with a 5-year survival rate of 90% when the cancer is localized versus a survival rate of less than 10% when it has metastasized. Unfortunately, while incidence rates have stabilized since the mid-1990s, only 38% of colorectal carcinomas are localized at initial diagnosis, whereas almost 20% of newly diagnosed cases have distant metastases (2).

Most of colorectal tumors (90–95%) arise from sporadic adenomatous polyps and most of the remaining are accounted for by several hereditary cancer syndromes.

Prognosis is closely related to the stage at presentation and this underlies the importance of early detection. The strongest risk factor for colon cancer is age (Table 1). Incidence rates rise from 10 per 100,000 at age 40–45 to 300 per 100,000 at age 75–80. The cumulative life time risk for the disease is 1 in 20.

Neoplasm, Large Bowel, Malignant. Table 1 Risk factors for colorectal cancer

Personal history of adenomas or colorectal cancer
First-degree relative age <60 years with adenoma or colorectal cancer, or two first-degree relatives of any age with colorectal cancer
Inherited colorectal cancer syndromes
Hereditary nonpolyposis colorectal cancer
Familial adenomatous polyposis
Ulcerative colitis and Crohn's colitis

Pathology and Histopathology

The most common colon cancer cell type is adenocarcinoma which accounts for 95% of cases. Other rarer types include lymphoma and squamous cell carcinoma.

Adenocarcinoma is a malignant epithelial tumor, originating from glandular epithelium of the colorectal mucosa. This tumor invades the wall, infiltrating the muscularis mucosae, the submucosa, and the muscularis propria. Tumor cells describe irregular tubular structures, harboring pluristratification, multiple lumens, reduced stroma ("back to back" aspect). Sometimes, tumor cells are discohesive and secrete mucus which invades the interstitium producing large pools of mucus/colloid (optically "empty" spaces)—mucinous (colloid) adenocarcinoma, poorly differentiated. If the mucus remains inside the tumor cell, it pushes the nucleus at the periphery "signet-ring cell". Depending on glandular architecture, cellular pleomorphism and mucosecretion of the predominant pattern, adenocarcinoma may present three degrees of differentiation: well, moderate, and poorly differentiate. Histologically, most colon carcinomas arise from the mucosal lining and are adenocarcinomas.

The mucinous adenocarcinoma subtype occurs in about 10% of patients. It is found more frequently in men and is generally more aggressive. Thus, these patients will more often present with an advanced stage of cancer. Flat lesions, defined as masses with a height no more than one-half their width, are potentially problematic because their morphologic characteristics can result in a false-negative diagnosis at conventional ►colonoscopy as well as other imaging modalities. Lymph node involvement is not possible until the muscularis mucosa has been invaded; at first, regional lymph nodes are involved; later the more centrally located nodes.

Lymph node metastases may affect the paracolic, paraortic, iliac, and even inguinal nodes (in case of rectal cancer).

Clinical Presentation

CRC can have a subacute or acute presentation that is strictly related to the location of the primary lesion. Morphologically, colorectal carcinomas initially arise *in situ*, then slowly progress into a sessile mass. Their subsequent appearance and clinical behavior depend on where they originate.

Left colon lesions more often cause abdominal pain, changing in bowel habits, melena or hematochezia and tend to be diagnosed earlier because they cause obstruction, and are susceptible to ulceration due to vascular encroachment.

In the right colon, neoplastic lesions occasionally cause hematochezia, but more often bleeding is occult, causing anemia with correlated symptoms such as tiredness, malaise, and pallor. Right-sided lesions are generally diagnosed later because of the relatively larger caliber of the right colon, and they tend to grow into polypoid fungating masses with a propensity for necrosis. Approximately 50% of patients can present an unexplained weight loss, even if this symptom is almost never the sole manifestation of CRC.

Acute presentation with large bowel obstruction with impossibility to pass for air or fecal material, abdominal pain, and distention accounts for less than 10% of patients.

Rarely colon cancer presents itself as perforation with focal or diffuse peritonitis. Metastatic disease may present acutely with jaundice, pruritus, ascites, and hepatomegaly due to spreading of the tumor.

It is also possible that there will be no symptoms at all. This is the reason why periodical screening for the disease is recommended.

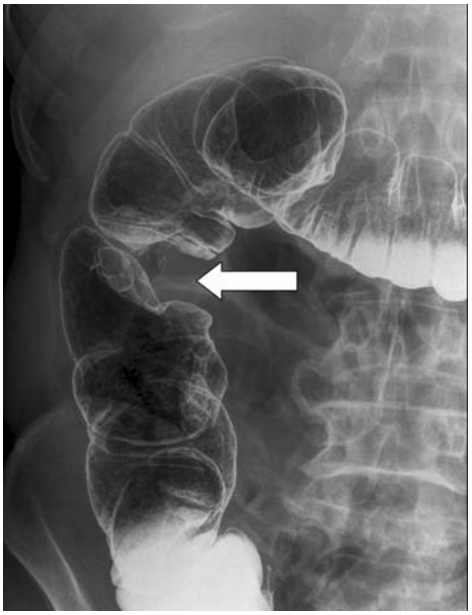

Neoplasm, Large Bowel, Malignant. Figure 1 Adenocarcinoma of the colon with typical "apple core" appearance in 75 year old male with rectal bleeding and anemia. DCBE shows a constant annular lesion (arrow) in the ascending colon, close to hepatic flexture, proved to be a carcinoma as expected.

Imaging

Plain Film: In patients with obstructing symptoms diagnosis, the abdominal plain film can demonstrate some dilations of the colon proximal to the obstructing colonic carcinoma. Free intraabdominal air can be seen in case of perforation.

Double Contrast Barium Enema (*DCBE*) is generally accepted as less sensitive than colonoscopy and CT Colonography for detecting CRC (Fig. 1). DCBE has the advantage of imaging the entire colon. However, recent evidence suggests it is inaccurate for the detection of polyps and early cancers and suboptimal for colorectal cancer screening or surveillance. In a prospective study comparing the use of DCBE and colonoscopy, the miss rate of barium enema for polyps larger than 1 cm was 52% (3). If DCBE is the only option for screening or surveillance, it should be coupled with flexible sigmoidoscopy. The use of flexible sigmoidoscopy allows visualization of the rectosigmoid, which may not be well seen on barium enema because of the overlapping loops of bowel. Lesions detected on DCBE warrant colonoscopic evaluation.

Computed Tomography (*CT*): Colorectal carcinomas are clinically staged by using the modified Astler-Coller-Dukes staging system or the TNM staging system established by the American Joint Committee on Cancer. Accurate staging is necessary for determining patient prognosis and therapeutic management. In contrast to most other tumors, the staging for colorectal tumors depends more on the depth of invasion than on the size of the primary mass. However, conventional CT has not been accurate in determining the depth of invasion or in evaluating tumor foci in nonenlarged lymph nodes. Therefore, routine preoperative assessment for local disease is generally not performed. In patients suspected to have distant metastases or adjacent organ invasion, conventional CT has been shown to be accurate in determining the appropriate surgical procedure and neoadjuvant therapy.

►*Computed Tomographic Colonography (CTC) or Virtual Colonoscopy* (*VC*) is a noninvasive, rapidly evolving technique that has been shown in some studies to be comparable with conventional colonoscopy for the screening of colorectal cancer.

The role of CT colonography in staging has yet to be defined. A recent study reported that multidetector CT colonography with contrast media has an 83% accuracy for identifying tumor wall invasion by colorectal carcinoma and an 80% accuracy for identifying regional lymph node involvement with a combined transverse and multiplanar reformation image evaluation (4) (Fig. 2).

In addition, a preoperative CT colonography examination is increasingly being performed after incomplete colonoscopy to assess for Synchronous lesion. In all these cases as well as in the follow-up of those patients who underwent surgical hemicolectomy, the use of intravenous contrast agent is required. Concerning the use of VC as screening tool, current uses of VC generally do not

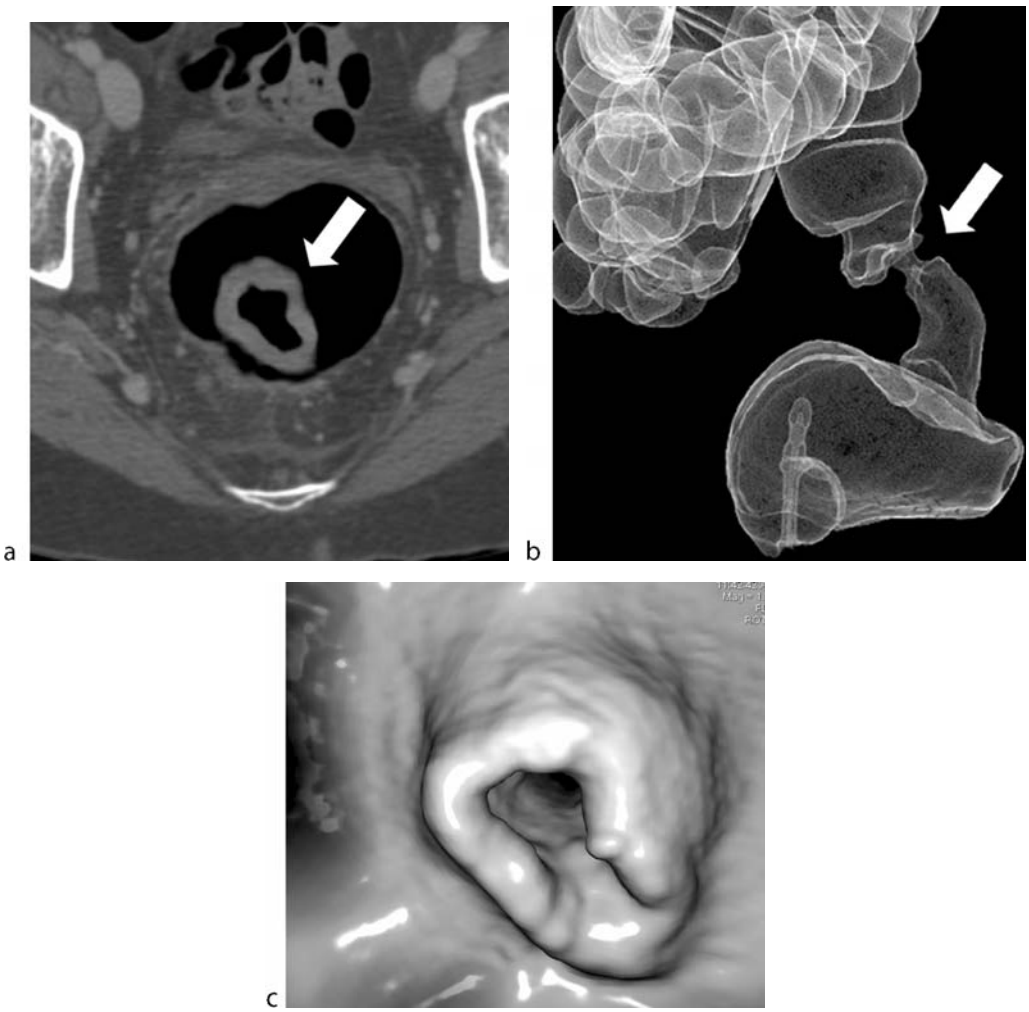

Neoplasm, Large Bowel, Malignant. Figure 2 Stenosing carcinoma of the rectum in a 47 year old female with malaise and rectal bleeding; (a) Axial 2D slice shows annular thickening (arrow) of the colonic rectal wall; (b) Virtual double contrast enema view demonstrates typical "apple-core" lesion (arrow), and (c) Endoluminal view of the stricture, with annular, irregular lesion, and eccentric stenotic lumen (images obtained using Lightspeed VCT 64 detector row, GE and ADW 4.3, GE, USA).

include the screening of asymptomatic persons, as also suggested by the American Cancer Society and the American Gastroenterological Association both of which decided that it should not yet be used for colorectal cancer screening, because data on true screening populations are missing. A practical approach is to consider VC as a currently credible alternative screening method and as a reasonable alternative to the other colorectal cancer screening tests when a patient is unable or unwilling to undergo conventional colonoscopy (Fig. 3).

At present, *magnetic resonance imaging* (*MRI*) is the best imaging modality for completely fulfilling the clinical requirements for preoperative staging of rectal cancer, where CT has limitations in differentiating the different layers of the rectal wall, demonstrating mesorectal fascia and depicting tumor invasion in surrounding pelvic structures.

Diagnosis

The diagnosis of colorectal polyps and cancer is most often made during a colonic evaluation performed for gastrointestinal symptoms, colorectal cancer screening, or as part of endoscopic surveillance.

Once the diagnosis is suspected based on history, physical examination, or screening tests, every attempt should be made to obtain biopsy of the primary lesion and rule out synchronous cancer (3–5%).

Fecal Occult Blood Test (*FOBT*): This test has been suggested as possible adjunct to other screening modalities. Randomized trials have found that the use of annual FOBTs have decreased the mortality from colorectal cancer by up to 33%, but the estimated 30–50% sensitivity is considered too low as an effective single

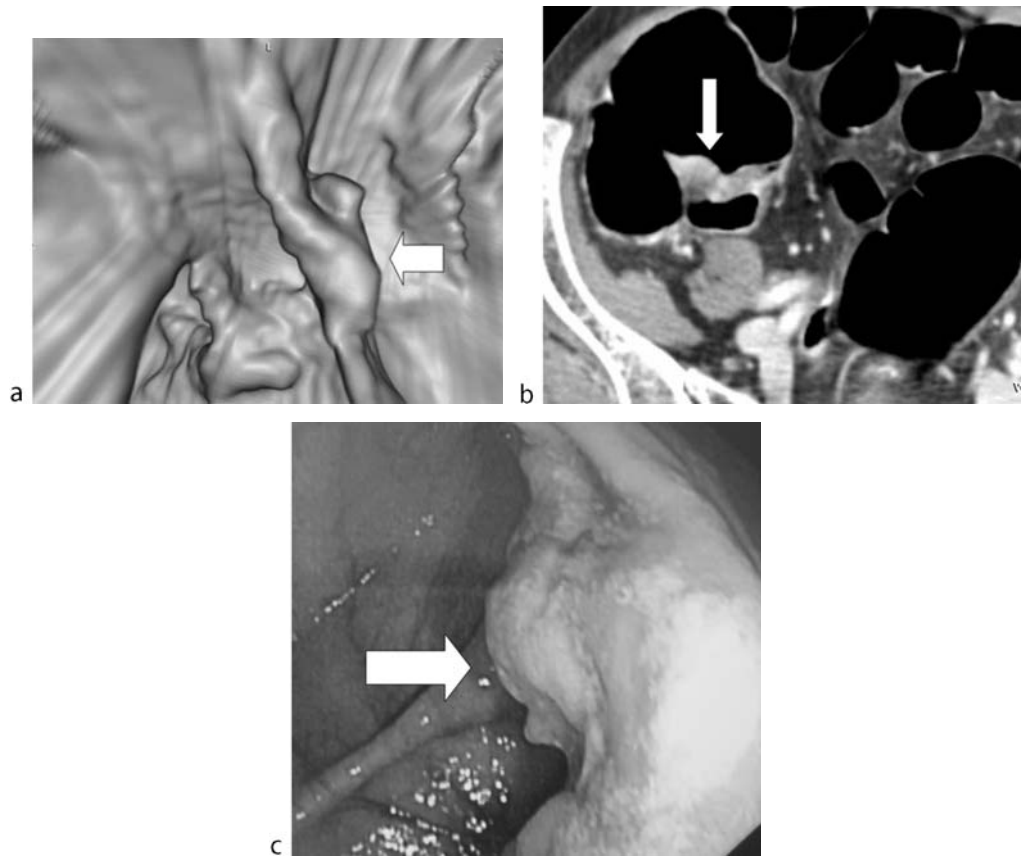

Neoplasm, Large Bowel, Malignant. Figure 3 A 72 year old women with adenocarcinoma of ileocecal valve who underwent incomplete colonoscopy due to severe diverticular disease; (a) Three-dimensional threshold-rendered endoluminal CT colonograph of ascending colon shows an ileocecal valve characterized by irregular surface (arrow); (b) Axial CT scan using abdominal window at same level as (a) reveals a vegetating sessile lesions with a large base of implant (arrow) that enhanced following intravenous administration of contrast agent, and (c) Endoscopic examination reveals an engorged mass on ileocecal valve (arrow) representing an adenocarcinoma of ileocecal valve (axial image obtained using Lightspeed VCT 64 detector row, GE, USA; amd endoluminal image obtained using Vitrea 3.7 Vital Images, USA).

screening modality in high-risk population. The reductions in mortality are associated with a shift to detection of earlier-stage cancer. In addition, one study found the incidence of colorectal cancer was reduced by 20% in an annually screened group. This is likely due to polypectomy in patients whose positive FOBT was evaluated by colonoscopy. Since large polyps and cancers intermittently bleed, the peroxidase activity of hemoglobin in the stool can be detected by a color change when it catalyzes the oxidation of guaiac by a peroxide reagent. A special diet (e.g., a meat-free, high-residue diet without vegetables having peroxidase activity, such as turnips and horseradish) is recommended for at least 24 h before three separate stool specimens are collected at least 1 day apart. Unrehydrated test sensitivity is low at approximately 80%, with a specificity of up to 98%. Any positive FOBT should be evaluated by colonoscopy.

Sigmoidoscopy: Results of several case–control studies show a reduction in deaths from colorectal cancer in subjects who undergo sigmoidoscopic examinations. The reported reduction in mortality varies between 59% and 80%. The most well-known study compared the use of rigid sigmoidoscopic screening in 261 patients who died from cancer of the distal colon or rectum to 868 control subjects. Screening reduced the rectosigmoid cancer mortality rate by 60%, and the protective effect of sigmoidoscopy was noted to last for up to 10 years. This reduction in mortality may have resulted from earlier detection of cancer and removal of premalignant polyps. Sigmoidoscopic screening allows the lower third of the colorectal mucosa to be visualized directly and diagnostic biopsy to be performed at the time of examination. Both the sensitivity and the specificity are high for detection of polyps and cancer in the segment of the bowel examined.

Unfortunately, however, nearly 50% of polyps and cancers are beyond the limits of detection of the longest (e.g., 60 cm) flexible sigmoidoscope.

Opinions vary regarding the need for colonoscopy for patients in whom a single, small adenoma (<1 cm) is found on flexible sigmoidoscopy. Many studies have shown that the prevalence of advanced proximal neoplasms in patients with distal adenomas is up to 9%. Therefore, the use of colonoscopy to detect proximal neoplasia in patients with distal adenomas is strongly recommended. Additionally, colonoscopic screening has been shown to have favorable cost effectiveness when compared to other screening strategies.

Colonoscopy: Colonoscopy is the "gold standard" for the detection of colonic neoplasms and the preferred colorectal cancer screening strategy. The incidence rate of colorectal cancer has been shown to be reduced up to 90% in subjects who had polypectomy versus patients in three reference groups, including two cohorts in which colonic polyps were not removed and one general-population registry. It can be completed in more than 95% of examinations with negligible risk. Colonoscopic screening in individuals with average risk has been found to be cost effective, and similar to cervical or breast cancer screening techniques in cost-effectiveness per life-year saved.

Bibliography

1. Wingo PA, Tong T, Bolden S (1995) Cancer statistics, 1995. CA Cancer J Clin 45:8–30
2. Jemal A, Tiwari RC, Murray T et al (2004) Cancer statistics, 2004. CA Cancer J Clin 54:8–29
3. Winawer SJ, Stewart ET, Zauber AG et al (2000). A comparison of colonoscopy and double-contrast barium enema for surveillance after polypectomy. National Polyp Study Work Group. N Engl J Med 342:1766–1772
4. Rex D, Johnson D, Lieberman D et al (2000) Colorectal cancer prevention 2000: screening recommendations of the American College of Gastroenterology. Am J Gastro 95:868–877

Neoplasms, Nasopharynx

Alfredo Blandino, Ignazio Pandolfo
Department of Radiological Science
University of Messina, Messina, Italy
ablandino@unime.it

Synonyms

Malignant lesions of the nasopharynx; Neoplasms of the nasopharynx; Neoplasms of the rhinopharynx; Tumors of the nasopharynx

Definition

Neoplasms of the nasopharynx include all the malignant lesions originating from the nasopharyngeal mucosa.

Pathology/Histopathology

The mucosa covering the walls of the nasopharynx is composed of squamous pseudostratified epithelium associated with a submucosal lymphoid stroma and seromucinous glands. It is the reason why a wide variety of malignant neoplasms can originate in the nasopharynx.

The most frequent malignant lesion arising in the nasopharynx is squamous cell carcinoma, which accounts for about 70% of cases. Lymphomas account for approximately 20%. The remaining 10% of malignant tumors include neoplasms stemming from seromucinous minor salivary glands (adenoid cystic carcinoma, mucoepidermoid carcinoma, adenocarcinoma, malignant mixed tumors, acinic cell carcinoma).

Squamous cell carcinoma of the nasopharynx is a worldwide diffuse tumor and one of the most common malignancies in adults in China, where it is characterized by an epidemic incidence. The etiology is related to environmental, genetic, and infectious factors. There is, in fact, a very close correlation between such tumors and the Epstein–Barr virus, the DNA of which can be found in the tumoral cells.

The World Health Organization's histopathological classification of nasopharyngeal carcinoma includes three types: (i) squamous cell carcinoma (type 1), (ii) non-keratinizing carcinoma (type 2), and (iii) undifferentiated carcinoma (type 3).

The latter is very similar to a large cell lymphoma and includes some subtypes of malignancies such as lymphoepithelioma, spindle cell carcinoma, clear cell carcinoma, and anaplastic carcinoma.

Hodgkin's and non-Hodgkin's lymphoma originating in the rhinopharynx as an isolated primary site of involvement is considered a rare event. More common is the involvement of the nasopharynx in the presence of systemic and advanced disease.

Hodgkin's lymphoma is more frequent in young adults, and the diagnosis is suggested by the presence of Reed-Stemberg cells in the biopsied material. In contrast, non-Hodgkin's lymphoma is more often found in older patients and is frequently related to immunodeficiency states. The histopathologic classification of non-Hodgkin's lymphoma is actually based on evaluation of immunologic markers, which allows differentiation of the disease into T-cell, B-cell, and histiocytic lymphomas.

Localization in the nasopharynx of tumors derived by seromucinous glands is a rare event because the minor

salivary glands are represented more in different areas of the head and neck, such as the soft palate, oral cavity, and nasal fossa. Such tumors are typically characterized by submucosal spreading, perineural diffusion, and low propensity to give nodal metastasis.

Finally, plasma cell tumors of the nasopharynx are mainly represented by extramedullary plasmocytoma, which accounts for 20% of all plasma cell neoplasms.

Clinical Presentation

The clinical presentation of malignant tumors of the nasopharynx is closely related to their localization, size, and pattern of spreading. In most cases, the neoplasm is represented by a mass centered in the posterolateral recess of the nasopharynx because of its origin in the Rosenmuller fossa. Nodal metastasis can be found in 75–90% of cases of squamous cell carcinoma at presentation.

Patterns of spread include:

1. Anterior diffusion toward the nasal and pterygopalatine fossa (PFF).
2. Antero-inferior diffusion with involvement of the soft palate and oropharynx.
3. Lateral diffusion with involvement of the parapharyngeal and masticator spaces.
4. Posterior spreading with infiltration of the prevertebral muscles.
5. Superior diffusion toward the base of the skull, which can be involved by direct bony invasion and/or by perivascular diffusion (along the internal carotid artery or middle meningeal artery) and perineural diffusion (along the mandibular nerve). Invasion of the base of the skull can lead to intracranial progression of the disease with involvement of the cavernous sinus.

On the basis of the above features, patients with nasopharyngeal tumors can be described in the following manner:

1. Asymptomatic patients with neck masses due to metastatic lymphadenopathy.
2. Patients with serous otitis media due to Eustachian tube obstruction; in many cases, symptoms of a chronic otitis are the only signs of the presence of a nasopharyngeal malignancy.
3. Patients with neurological symptoms due to involvement of the posterior cranial nerves (IX, X, XI, XII) in the case of posterolateral tumoral spread. Conversely, lateral (toward the parapharyngeal and masticator spaces) and superior (toward the base of the skull and cavernous sinus) diffusion of the tumor can determine the involvement of the trigeminal and/or the oculomotor nerves (III, IV, V, VI). Obviously, the neurological symptoms are peculiar to more advanced disease.

Ancillary and nonspecific symptoms include nasal obstruction, epistaxis, headaches, sore throat, proptosis, and trismus.

Finally, nasopharyngeal carcinoma, compared with other malignancies of the head and neck, is characterized by a higher frequency of distant metastasis (5–41%). The most common sites are the bones (20%), liver (9%), and lungs (13%).

Imaging

Conventional radiographs are no longer performed for diagnosing nasopharyngeal neoplasms. Computed tomography (CT) and magnetic resonance imaging (MRI) have been proved to be valuable in the modern diagnosis of tumors in this deep anatomical region. Both techniques have dramatically improved the accuracy in defining the tumor extent as well as the presence of regional nodal metastasis.

Due to the better soft-tissue contrast resolution, MRI is more suitable for delineating neoplastic lesions from surrounding normal structures compared with CT; moreover, MRI is more sensitive than CT in detecting subtle skull base involvement as well as perineural tumor spread.

Because a CT examination can be performed within a few seconds with modern techniques, CT remains the most commonly used technique for detecting and staging nasopharyngeal carcinoma, as access to MRI is still limited. However, MRI is the recommended modality in the assessment of recurrence.

Liver ultrasound and chest X-ray are generally routinely performed as part of the overall staging procedure, whereas bone scans are reserved for clinical suspicion of osseous metastasis.

General features of nasopharyngeal tumors are similar on CT and MRI. In typical cases, a huge, poorly marginated soft-tissue mass, centered in the lateral pharyngeal recess with occupation of the nasopharyngeal lumen, is seen, with a variable degree of deep extension and infiltration (Fig. 1). On MRI, most tumors appear isointense to muscles on nonenhanced T1-weighted images and moderate to strong hyperintense on T2-weighted images. On contrast-enhanced imaging, the tumor shows mild inhomogeneous uptake, which reflects the degree of vascularization as well as the intratumoral necrosis (Fig. 2).

The most common direction of tumoral spreading is lateral, where the soft-tissue tumoral mass obliterates and/or infiltrates the fat of the parapharyngeal space with displacement of the pterygoid muscles; further lateral spread involves the masticatory and infratemporal spaces with infiltration of the muscles of mastication. In such cases, the presence of fluid within the middle ear and mastoid cells due to serous otomastoiditis is often demonstrated (Fig. 3).

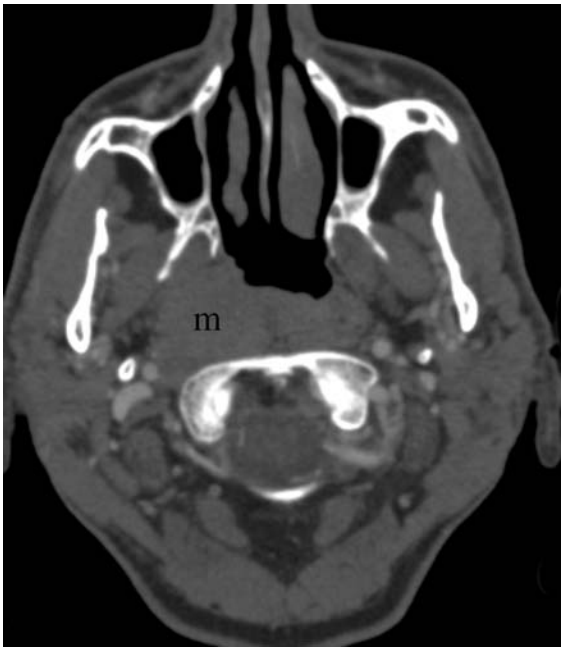

Neoplasms, Nasopharynx. Figure 1 Axial contrast-enhanced computed tomography scan. A huge mass (m) centered on the right lateral wall and Rosenmuller fossa is shown. Note also the involvement of the ipsilateral parapharyngeal space and posterior infiltration of the prevertebral muscles.

In anterior spreading, the tumor can reach the nasal fossa inferiorly and the pterygoid plate superiorly with secondary involvement of the PFF. The obliteration of the fat content of this fundamental anatomical landmark is the hallmark of involvement. From the PFF the tumors often show a tendency to spread along the maxillary nerve (perineural diffusion or spreading) to reach the cavernous sinus, Meckel's cave, the trigeminal nerve, or the skin in the infraorbitary region.

Enlargement or remodeling of bony walls of the cranial nerves are the CT features suggesting perineural spreading, whereas direct enlargement of the nerves is well appreciable with MRI.

Inferior spread can occasionally occur, with a subtle submucosal soft tissue causing oropharyngeal wall thickening.

Posterior spread is characterized by obliteration of the retropharyngeal space and infiltration of the prevertebral muscles; posterosuperior neoplastic extension may involve the jugular foramen and the adjacent hypoglossal canal.

Finally, but not infrequently, carcinoma of the nasopharynx can spread superiorly involving the skull base. Subtle erosion with a mottled appearance of the clivus or the basisphenoid is the key finding in CT imaging; on MRI, infiltration with replacement of high signal intensity of bone marrow on T1-weighted images is very suggestive of skull base neoplastic involvement.

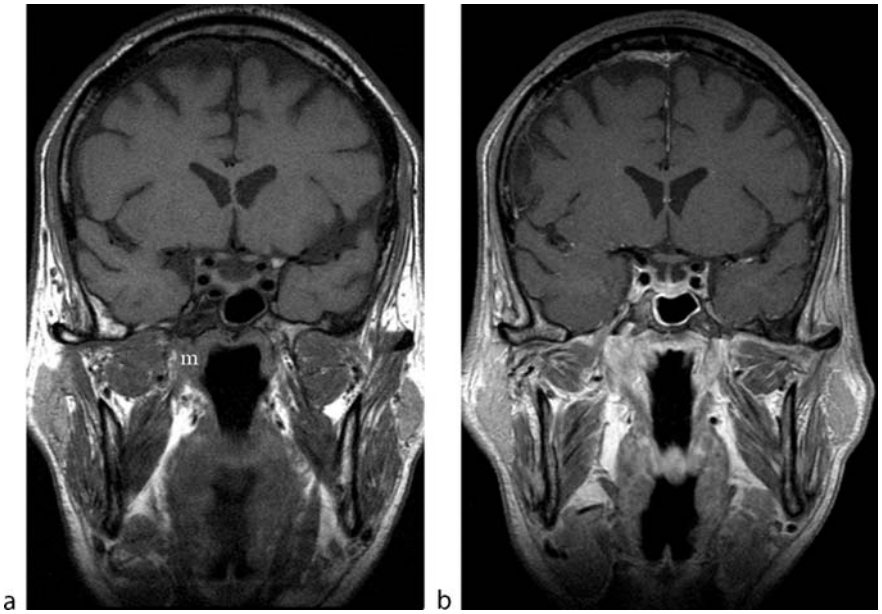

Neoplasms, Nasopharynx. Figure 2 (a) On coronal T1-weighted magnetic resonance image, a soft-tissue mass (m) abutting right superior-lateral wall of the nasopharynx is well demonstrated. The lesion effaces the upper part of the parapharyngeal space. (b) Coronal contrast-enhanced T1-weighted image shows mild enhancement of pathological tissue.

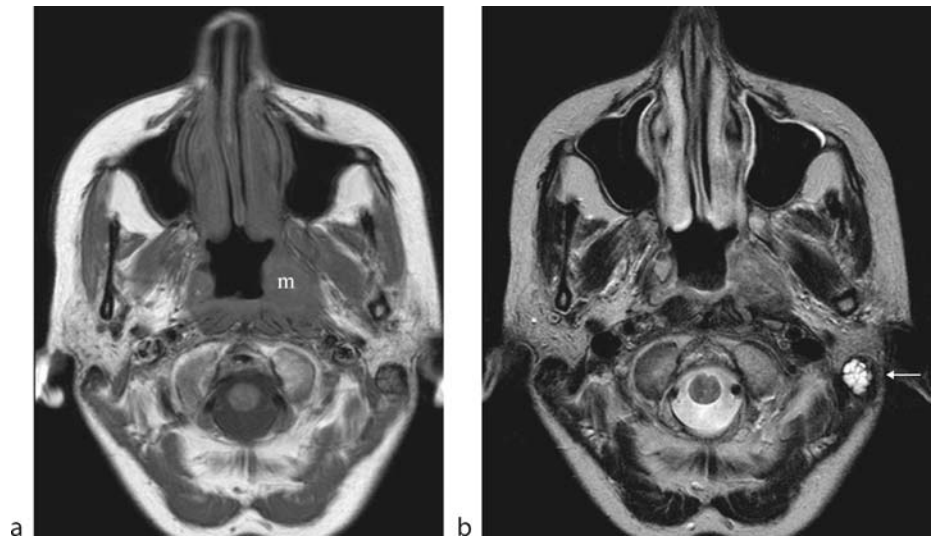

Neoplasms, Nasopharynx. Figure 3 (a) Axial T1-weighted magnetic resonance image shows a mass (m) involving the left wall of the nasopharynx with infiltration of the elevator and tensor veli palatine muscles and partial obliteration of the fat in the anterior parapharyngeal space. (b) T2-weighted image shows fluid into the mastoid cells (*arrow*) due to a serous otomastoiditis.

The third cranial branch of the trigeminal nerve (mandibular nerve) is a common preformed route of intracranial diffusion of nasopharyngeal neoplasms.

Cervical nodal metastases are better studied with CT, which is also useful in depicting nodal necrosis and extracapsular spread.

Nevertheless, MRI is also well suited in clinical practice.

Nuclear Medicine

Nuclear medicine techniques are not routinely employed in nasopharyngeal neoplasms, but they can provide relevant information in certain cases.

18-fluoro-2-deoxyglucose positron emission tomography (18-FDG PET) is the newest and leading nuclear medicine procedure, giving information about the degree of glucose metabolism in different tissues. A certain level of increased uptake of FDG is considered to indicate malignancy. However, routine use of PET in pretherapeutic staging of nasopharyngeal carcinoma cannot be recommended. Sometimes an 18-FDG PET scan can be considered in nasopharyngeal cancer to search for occult distant metastases.

Nevertheless, the major role of this nuclear medicine technique is its high value in detecting residual or recurrent neoplastic tissue following radiotherapy.

The advent of CT–PET and MRI–PET can provide even more information by coregistering tracer uptake with anatomic information. CT–PET scanning is recently being evaluated for the identification of the most active tumor regions, which will allow biological radiotherapy planning using intensity-modulated radiotherapy techniques.

Diagnosis

The diagnosis of nasopharyngeal neoplasms is based on histopathology obtained by biopsy during rhinoscopy. Staging and full extension of tumors are of the utmost importance for therapeutic decisions and the patient's prognosis.

CT and MRI are nowadays the fundamental modalities used to obtain all of this information, whereas 18-FDG PET, CT–PET, and MRI–PET should be used in selective cases, especially for detecting tumoral recurrence after chemotherapy and radiotherapy.

Bibliography

1. Chong VFH (2006) Neoplasms of the nasopharynx. In: Hermans R (ed) Head and Neck Cancer Imaging, Springer-Verlag, Berlin
2. Chong VFH, Fan YF, Mukherji SK (1998) Nasopharyngeal carcinoma. Semin Ultrasound CT MR 19:449–462
3. Manavis J, Sivridis L, Koukorakis MI (2005) Nasopharyngeal carcinoma: the impact of CT-scan and of MRI on staging, radiotherapy treatment planning, and outcome of the disease. Clin Imaging 29:128133
4. Ng SH, Chang TC, Ko SF et al (1997) Nasopharyngeal carcinoma: MRI and CT assessment. Neuroradiology 39:741–746
5. Tsai MH, Shiau YC, Kao CH et al (2002) Detection of recurrent nasopharyngeal carcinoma with positron tomography using 18-fluoro-2-deoxyglucose in patients with indeterminate magnetic resonance imaging findings after radiotherapy. J Cancer Res Clin Oncol 128:279–282

Neoplasms, Nose and Paranasal Sinus

Akif Sirikci[1], Enver Ozer[2]
[1]Radiology Department, Gaziantep University, School of Medicine, Gaziantep, Turkey
[2]Department of Otolaryngology, Head and Neck Surgery, University Medical Center, The Ohio State University, Columbus, USA
sirikci@yahoo.com

Definition

Neoplasms of the nose and paranasal sinuses include all the malignant and benign tumors stemming from mucosa that covers the rhinosinusal apparatus.

Although tumors of the nose and paranasal sinuses are uncommon, accounting for only 0.3% of all cancers and 4% of all head and neck malignancies, the disease is occasionally confined to sinuses (1). The tumor behaves like a benign infectious disease in the beginning, with the actual diagnosis only being made in the advanced stage thereby explaining the overall poor prognosis of malignancies in this region.

Pathology/Histopathology

The most commonly encountered sinonasal malignancy (SNM) is squamous cell carcinoma (80%), with 25–60% of these carcinomas originating from the maxillary antrum, followed by the nasal cavity (30%), ethmoids (10%), and sphenoid and frontal sinuses (2%). An increased risk is observed in those exposed to nickel, chromium pigment, bantu snuff, thorotrast, mustard gas, polycyclic hydrocarbons, and cigarette smoke, as well as in wooden furniture, isopropyl alcohol, and radium production workers (2, 3). Cervical lymph node involvement which occurs in 25–35% of SNMs is associated with a poor prognosis.

Adenoid cystic carcinoma and adenocarcinomas are next in frequency (10%) (2). Adenoid cystic carcinoma is the most common minor salivary gland tumor, accounting for one-third of these malignancies, and more than 80% originate from the maxillary sinus and nasal cavity (3). Perineural invasion with secondary invasion of the orbit and intracranial compartments is common. Approximately one-half of the patients have distant metastasis to the lungs, brain, and bones (3).

Adenocarcinomas are more commonly found in the upper nasal cavity and ethmoid sinuses. The prognosis depends on the differentiation of the tumor and is comparable with that of adenoid cystic carcinoma (2, 3).

Less than 4% of melanomas arise from the sinonasal cavity. It is believed that nasal melanomas originate from melanocytes that migrated from the neural crest to the mucosa of the sinonasal cavity during embryological development. Prognosis is poor with a mean survival of 2 years. The cervical nodal metastasis rate is 40% and local recurrence is seen in two-thirds of patients. Nasal melanomas have a better prognosis than those originating in the paranasal sinuses (3).

Olfactory neuroblastomas (esthesioneuroblastomas) are rare neoplasms of the cribriform region and arise from the olfactory nerves. When intracranial extension is present, craniofacial resection is necessary. Subarachnoid seeding occurs because of direct extension of the tumor or after surgery (3).

A variety of benign neoplasms such as osteoma, chondroma, schwannoma, neurofibroma, ossifying fibroma, cementoma, and odontogenic tumors can arise from the sinonasal cavity. Some are classified as intermediate neoplasms, such as inverted papilloma, meningioma, hemangioma, and hemangiopericytoma.

Juvenile fibroangioma can be considered as a rare, benign, highly vascularized tumor of the nasosinusal region because of its particular growth. It occurs exclusively in young male patients.

Finally, one should recall that malignant transformation occurs in about one of eight patients with multiple neurofibromatosis (von Recklinghausen's disease) and in 10% of inverted papilloma patients. Recurrence is likely due to the locally aggressive behavior of hemangiopericytoma (3).

Clinical Presentation

The clinical presentation of sinonasal tumors depends on the site of origin, size, vascularization, and pathway of tumor diffusion.

The main symptoms can be summarized as follows: nasal obstruction, epistaxis and nasal discharge, exophthalmos due to orbital involvement, and cranial nerve impairment due to involvement of the skull base with secondary perineural extension.

Over the last 30 years, the morbidity and mortality rates of ACB surgeries for sinonasal tumors have improved significantly with the availability of new imaging technologies such as computed tomography (CT) and magnetic resonance imaging (MRI), intraoperative navigation systems together with a multidisciplinary team approach, and a variety of craniofacial resection techniques (2). Parallel to technical developments, a variety of ACB reconstruction methods such as microvascular

free-flap reconstructions and oto- and homografts are widely used, and thus postoperative complication rates have decreased.

Diagnosis

The diagnosis is based on endoscopy, biopsy, and radiological imaging, namely, CT and MRI.

To distinguish the clinical and radiological appearance of neoplasms in the paranasal sinuses and nasal cavity from coexistent inflammatory changes that usually occur with such tumors, it is necessary to be familiar with the normal anatomy or anatomical variations and the drainage pattern of sinus secretions.

Basically, the paranasal sinuses are composed of four pairs of sinuses: frontal, maxillary, ethmoidal, and sphenoid sinuses. The most prognostically significant structures are above and behind the maxillary antrum. Superiorly the orbit, ethmoid sinuses, and the ACB and the posterior border approach the pterygoid plates, the pterygoid space, and the infratemporal fossa (4). The sphenoid sinus is in the center of the head and is related to very complex structures: the optic nerve and pituitary gland are superior to it and the internal carotid artery and cavernous sinuses sit laterally. Thus, the complete resection of a malignancy involving the sphenoid is occasionally possible (2).

The pattern of spread of SNMs is mostly *via* direct invasion or perineural extension as in cases of adenoid cystic carcinoma. Detailed knowledge about the anatomical boundaries of the paranasal sinuses is essential to map the extent of the disease and to plan the surgical resection and reconstruction preoperatively (2).

The American Joint Committee on Cancer (AJCC, 2002) staging criteria of primary tumors (T) for SNMs are shown in Table 1.

Imaging

It is often difficult for the radiologist to hone down on a particular histological diagnosis because of the marked overlap of the imaging appearance of different tumors on CT and MR images (4) (Figs. 1–3).

CT and MR are complementary and together can provide adequate information of both bony and soft

Neoplasms, Nose and Paranasal Sinus. Table 1 Staging of the paranasal sinus carcinoma

Maxillary sinus
Primary tumor (T)
• TX: Primary tumor cannot be assessed
• T0: No evidence of primary tumor
• Tis: Carcinoma *in situ*
• T1: Tumor limited to maxillary sinus mucosa with no erosion or destruction of bone
• T2: Tumor causing bone erosion or destruction including extension into the hard palate and/or the middle of the nasal meatus, except extension to the posterior wall of maxillary sinus and pterygoid plates
• T3: Tumor invades any of the following: bone of the posterior wall of maxillary sinus, subcutaneous tissues, floor or medial wall of orbit, pterygoid fossa, ethmoid sinuses
• T4a: Tumor invades anterior orbital contents, skin of cheek, pterygoid plates, infratemporal fossa, cribriform plate, sphenoid or frontal sinuses
• T4b: Tumor invades any of the following: orbital apex, dura, brain, middle cranial fossa, cranial nerves other than maxillary division of trigeminal nerve (V_2), nasopharynx, or clivus
Nasal cavity and ethmoid sinus
Primary tumor (T)
• TX: Primary tumor cannot be assessed
• T0: No evidence of primary tumor
• Tis: Carcinoma *in situ*
• T1: Tumor restricted to any one subsite, with or without bony invasion
• T2: Tumor invading two subsites in a single region or extending to involve an adjacent region within the nasoethmoidal complex, with or without bony invasion
• T3: Tumor extends to invade the medial wall or floor of the orbit, maxillary sinus, palate, or cribriform plate
• T4a: Tumor invades any of the following: anterior orbital contents, skin of nose or cheek, minimal extension to anterior cranial fossa, pterygoid plates, sphenoid or frontal sinuses
• T4b: Tumor invades any of the following: orbital apex, dura, brain, middle cranial fossa, cranial nerves other than (V_2), nasopharynx, or clivus.

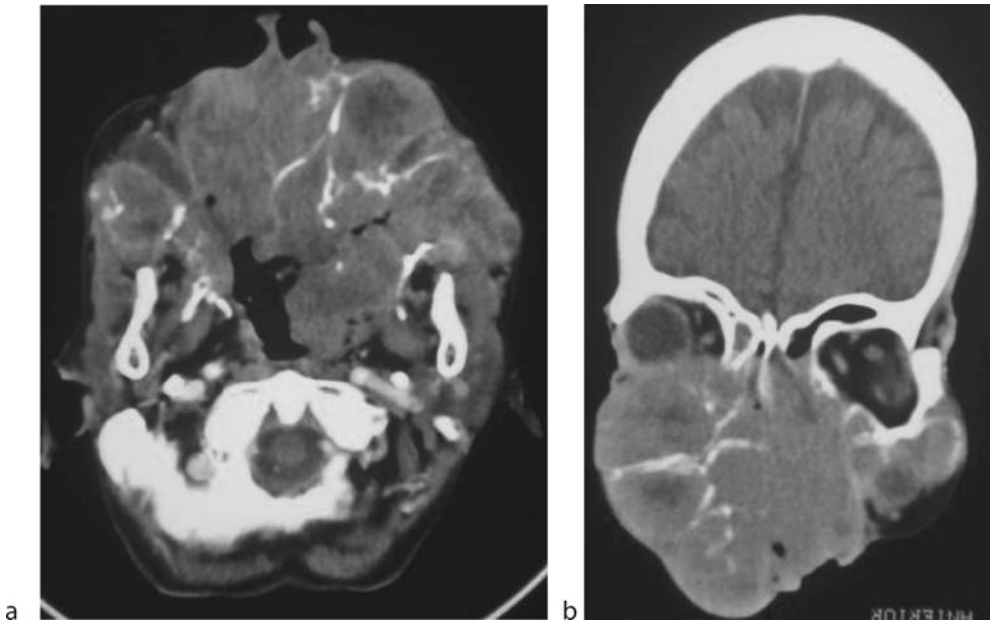

Neoplasms, Nose and Paranasal Sinus. Figure 1 Axial (a) and coronal (b) CT scan show a giant squamous cell carcinoma of the nasal cavity and paranasal sinuses. Note the extensive destruction of the bones and invasion into the paranasal soft tissues.

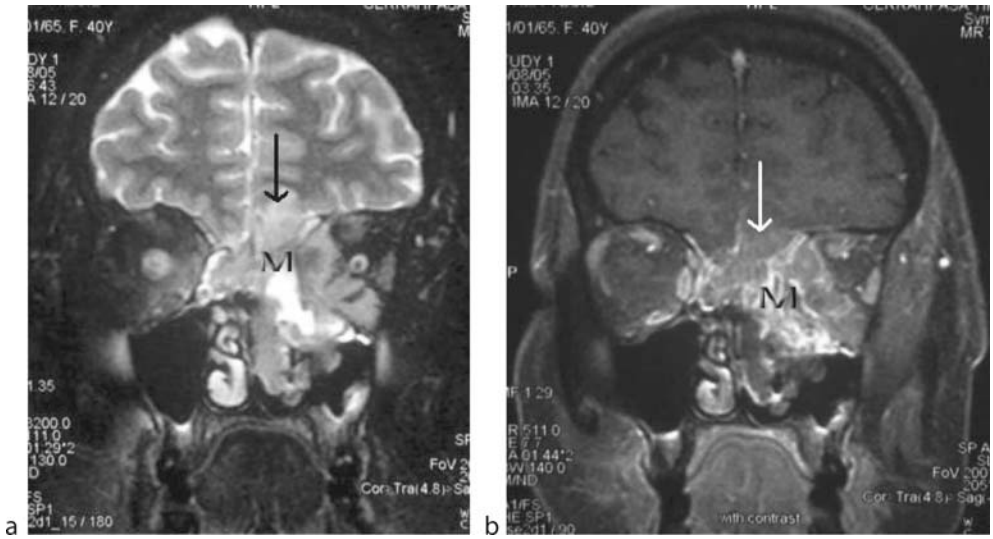

Neoplasms, Nose and Paranasal Sinus. Figure 2 Olfactory neuroblastoma, a rare neoplasm arising from the olfactory epithelium and found in the upper nasal cavity. (a) T2-weighted coronal MR scan, showing a large mass (M) in the left nasal cavity and left ethmoid air cells. (b) Corresponding enhanced fat-suppressed coronal T1-weighted MR image shows enhancement of the tissue consistent with the tumor. Note tumor extension into the orbit and cribriform plate/skull base (*arrow*).

tissue involvement. In the appropriate clinical setting, the CT and MR appearance of the nasal tumors will allow the radiologist to provide the differential diagnosis.

Extension of the neoplasm outside of the sinonasal cavity to the adjacent anatomic locations has significant impact on the patient's operability, the type of resection, the surgical approach, the necessity for radiation therapy, the placement of radiation portals, and the prognosis (3).

The role of the radiologist is to provide accurate information about the tumor location and mapping, and to detect critical areas of involvement, which may alter surgical approach and treatment planning.

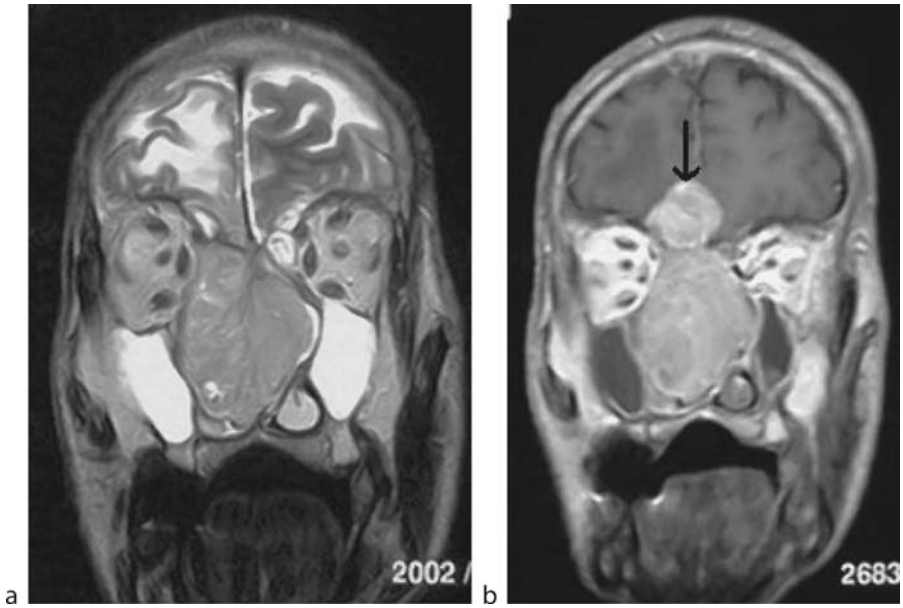

Neoplasms, Nose and Paranasal Sinus. Figure 3 Angiosarcoma of the nasal cavity. (a) T2-weighted coronal MR image reveals centrally located tumoral mass occupying the nasal cavity. (b) Coronal postcontrast T1-weighted MR image shows extension of the tumor centered at the cribriform plate into the anterior cranial fossa (*arrow*). The lesion enhances diffusely. Note the postobstructive inflammatory fluid retention in the maxillary sinuses.

CT is helpful in evaluating soft tissue details and its relationship to bone and air-containing space of the sinuses (5).

A benign soft tissue mass may cause a gradual pressure atrophy and erosion of the adjacent bone, which can easily be seen on CT images (Fig. 1).

The hallmark of malignancies involving the sinonasal cavity is the presence of osseous destruction (4). CT is an excellent modality for detecting bone erosion or destruction.

Skull base invasion is more commonly seen in malignant lesions such as carcinomas, lymphomas, and sarcomas. The pattern of osseous destruction of benign and malignant lesions is similar at the skull base, because osseous remodeling in this location is unusual (3) (Figs. 2 and 3).

Osseous destruction with the involvement of orbital fat suggests orbital invasion. Presence of nodularity at the interface between the tumor and periorbita, assessment of the extraocular muscles (enlargement, displacement, and signal abnormalities), and evaluation of the integrity of the osseous structures including the orbital walls adjacent to the tumor are further criteria for orbital invasion. However, none of these criteria is very accurate (3, 5).

It may be difficult to differentiate the neoplasm from postobstructive inflammatory changes on CT images. MR imaging provides excellent delineation of tumor from surrounding soft tissue, inflammatory tissue, and retained secretions within the sinuses (5).

SNMs tend to have lower T2 signal with respect to fluid collections within the paranasal sinuses on MR imaging (Fig. 3). Tumors tend to have more homogeneous contrast enhancement as opposed to rim enhancement seen with the inflammatory mucosa, which is seen better on contrast-enhanced MR imaging.

Carcinomas of the nasal cavity and paranasal sinuses share similar gross and microscopic pathological characteristics. They are highly cellular tumors with little free water and, as such, are represented by a homogeneous MR appearance, with low to intermediate signal intensity on T1- and T2-weighted images (5) (Fig. 3).

In postoperative patients, differentiating the residue and the recurrent tumor from the granulation tissue is also a problem. In this regard CT has limited utility because these tissues frequently have overlapping densities, making their distinction difficult. MR imaging can be more sensitive and specific in this distinction (3).

In conclusion, paranasal sinus neoplasms are difficult to diagnose in early stages of the disease. A high index of clinical suspicion leading to more detailed studies is therefore necessary. Use of different imaging technologies is essential and crucial for planning a treatment strategy.

Nuclear Medicine

Nuclear medicine plays a fundamental role in the evaluation of recurrent disease or in the evaluation of nodal metastasis from SNMs by means of PET-FDG.

Interventional Radiological Treatment

Embolization of juvenile angiofibroma is the only application of radiological interventional procedures.

Bibliography

1. Goldenberg D, Golz A, Fradis M et al (2001) Malignant tumors of the nose and paranasal sinuses: a retrospective reveiw of 291 cases. Ear Nose Throat J 80:272–277
2. Cummings CW (ed) (2005) Cummings Otolaryngology Head and Neck Surgery. Vol 2. Mosby, Philadelphia pp 1197–1214
3. Loevner LA, Sonner AI (2002) Imaging of neoplasms of the paranasal sinuses. Magn Reson Imaging Clin N Am 10:467–493
4. Philips CD, Futterer SF, Lipper MH et al (1997) Sinonasal undifferentiated carcinoma: CT and MR imaging of an uncommon neoplasm of the nasal cavity. Radiology 202:477–80
5. Chow JM, Leonetti JP, Mafee MF (1993) Epithelial tumors of the paranasal sinuses and nasal cavity. Radiologic clinic of North America 31:61–73

Neoplasms, Odontogenic

Fabio Minutoli
Department of Radiological Sciences
University of Messina, Messina, Italy
fminutoli@unime.it

Synonyms

Benign and malignant odontogenic tumors

Definitions

Odontogenic lesions arise from the cells and tissues that are part of the tooth-forming apparatus.

They can be found in the mandible, maxilla, and gingiva. Odontogenic lesions include odontogenic cysts and tumors (1). Odontogenic cysts are epithelial-lined structures derived from odontogenic epithelium containing fluid or semisolid material (2). They can be classified as inflammatory or developmental cysts (1). Odontogenic tumors may arise from epithelial or mesodermal elements, or both, involved in odontogenesis (3). They are in the majority of cases benign although some malignant odontogenic tumors have been reported. Odontogenic carcinoma is a carcinoma arising within the jawbone without a lesion of the mucosa (1). It can be subcategorized in: malignant ameloblastoma, when it represents a malignant transformation of a benign ameloblastoma; primary intraosseous carcinoma; carcinoma arising in preexisting odontogenic cyst.

Pathology/Histopathology

Cysts

The most common odontogenic cyst is *periapical (radicular) cyst*, an inflammatory cyst that results from a periapical granuloma. It arises by ►Malassez epithelial rests stimulation by chronic apical periodontitis due to periapical diffusion of a pulp infection in carious teeth. The cyst wall, lined by stratified nonkeratinizing squamous epithelium, may show inflammatory changes.

Dentigerous (*follicular*) *cyst*, the second most common odontogenic cyst, forms within the normal dental follicle. It is lined by stratified squamous nonkeratinizing epithelium and is usually larger than the normal dental follicle. It surrounds the crown of an unerupted tooth, most frequently mandibular or maxillary third molars or maxillary canines and may become quite large leading the risk for pathologic jaw fracture. Tumoral lesions like ameloblastoma, mucoepidermoid carcinoma, and squamous cell carcinoma may occasionally develop within the cyst wall.

The third most common odontogenic cyst is *odontogenic keratocyst* (*primordial cyst*). It is lined by stratified keratinizing squamous epithelium and is often filled by degenerating keratin, appearing as a foul-smelling cheese-like material. This cyst is aggressive, can be difficult to remove and frequently recurs. It more often grows in the mandible and may be in conjunction with an impacted tooth. Multiple odontogenic keratocysts may develop as part of the genetic disorder known as "►basal cell nevus syndrome."

Uncommon odontogenic cysts are represented by: calcifying odontogenic cyst (Gorlin cyst), a developmental lesion with both cyst and solid neoplasm features (1) also identified with the term "odontogenic ghost cell tumor," because of the presence of a characteristic cell with eosinophilic cytoplasm an no nucleus in the cyst wall; lateral periodontal cyst, a developmental cyst arising from epithelial remnants in the periodontal ligament that grows along the lateral aspect of the tooth, most commonly in the mandibular premolar area.

Residual cyst is a term of convenience used to identify a retained cyst (most frequently a periapical cyst) from a

tooth that have been removed. It should be differentiated by primordial cyst that develops instead of a tooth, since it derives from cystic degeneration of a dental follicle which formed without ever-completing odontogenesis.

Benign Neoplasms

Ameloblastoma (18% of odontogenic tumors) is a slow-growing, cystic, epithelial tumor thought to arise from ►ameloblasts. It has not a capsule, is locally aggressive and infiltrative and tends to recur after surgical excision. It has a wide spectrum of histological varieties including follicular, plexiform, acanthomatous, keratinizing, granular cell, basal cell, clear cell types, and a desmoplastic variant (3). It is located more commonly in the mandible, preferentially in the molar regions. About 1% of ameloblastomas are malignant.

Other epithelial tumors include adenomatoid odontogenic tumor (adenoameloblastoma), an uncommon well-circumscribed tumor with ductlike structures and calcifications that usually occurs around the crows of anterior teeth of young patients and is usually associated with impacted tooth; *calcifying epithelial odontogenic tumor (Pindborg tumor)*, a locally aggressive tumor composed of polyhedral epithelial cells in a fibrous stroma, often accompanied by spherical calcifications and hyaline deposits that usually occurs in posterior mandible in association with impacted tooth; squamous odontogenic tumor, a rare, potentially aggressive tumor made by islands of stratified epithelium containing microcysts and calcifications in a dense fibrous background.

Tumors deriving from connective tissue include odontogenic myxoma (3–6% of odontogenic tumors), a noncapsulated tumor consisting of a mucoid ground substance with scattered rounded and angular cells, characterized by rapid and locally aggressive growing with propensity to invade local soft tissues; cementoblastoma, a rare, well-circumscribed neoplasm of functional cementoblasts, usually observed in patients younger than 25 years, growing in association with the apical cemental layer of a molar or premolar tooth with the mandibular first molar being most frequently involved; and odontogenic fibroma.

Tumors derived from mixed epithelial and connective tissue include odontoma, the most common odontogenic tumor, commonly found on unerupted teeth, made up of various components of teeth (enamel, dentin, cementum, and pulp) arranged in a disorderly pattern and bearing no morphologic similarity to normal or rudimentary teeth (complex odontoma) or approaching normal tooth structure (compound odontoma), and located more frequently in the premolar and molar regions of the mandible and in the incisor-canine region of the maxilla, respectively; ameloblastic fibroma, a circumscribed lesion usually located over unerupted molars in young patients; ameloblastic fibro-odontoma, a mixture of soft tissue components of ameloblastic fibroma and the hard tissue elements of complex odontoma, always associated with developing teeth; ameloblastic odontoma, a very rare tumor containing an ameloblastomatous component and odontoma-like elements.

Malignant Neoplasms

Odontogenic malignancies are rare and most commonly located in the mandible. Malignant ameloblastoma is "a neoplasm in which the pattern of an ameloblastoma and cytological features of malignancy are shown by the primary growth in the jaws and/or by any metastatic growth" (1). Primary intraosseous carcinoma may develop from epithelial components that participate in the development of the teeth or from epithelial cells that become enclosed within the deeper structures of the jaw during embryonic development. Carcinomatous transformation of the epithelium in odontogenic cysts is a rare event although it has been reported in dentigerous cysts, radicular cysts, residual cysts, and keratocysts.

Other rare malignant epithelial lesions are clear cell odontogenic carcinoma and malignant odontogenic ghost cell tumor (odontogenic ghost cell carcinoma), a histologically malignant solid tumor related to calcifying odontogenic cyst.

Odontogenic sarcomas include ameloblastic fibrosarcoma, ameloblastic fibrodentinosarcoma and ameloblastic fibroodontosarcoma, odontogenic carcinosarcoma (1).

Clinical Presentation

Odontogenic lesions are frequently asymptomatic. When clinically evident, swelling is the most common presenting symptom. Lesions, that usually grow slowly, may reach a considerable size determining facial deformities or pathologic fractures. Pain is infrequent and often associated with cementoblastoma or secondary cysts infection. Lesions may determine displacement of teeth or may prevent or delay their eruption.

Imaging

Plain X-rays and ►pantomography are the main imaging tools in investigating odontogenic lesions. Radiographic approach is highly effective in detecting odontogenic lesions and permits evaluation of lesion size and margins, location, radiological pattern (radiolucent, mixed radiolucent–radiopaque, or radiopaque lesion), and relationships between lesion and tooth (periapical, pericoronal,

no relationship with tooth). Small lesions (less than 2 cm) can be evaluated by radiography alone, whereas larger lesions may require further radiological examinations (4).

Computed tomography permits an excellent assessment of the topography and extent of the lesions and better demonstrates the degree of bone resorption, ►osteosclerosis, cortical bone swelling, destruction, and calcification. CT dentascan also provides cross-sectional as well as panoramic sectional imaging.

Magnetic resonance imaging is effective in differentiating between tumors and cysts, in evaluating the appearance of fluid in cystic lesions and the infiltration of malignant tumors in the jawbone (especially permeative extension) and surrounding soft tissues (4).

Cysts appear as well-demarcated radiolucencies (Figs. 1 and 2), calcifying odontogenic cyst often contains scattered calcifications. Cysts show different relationships with tooth: radicular and lateral periodontal cysts have

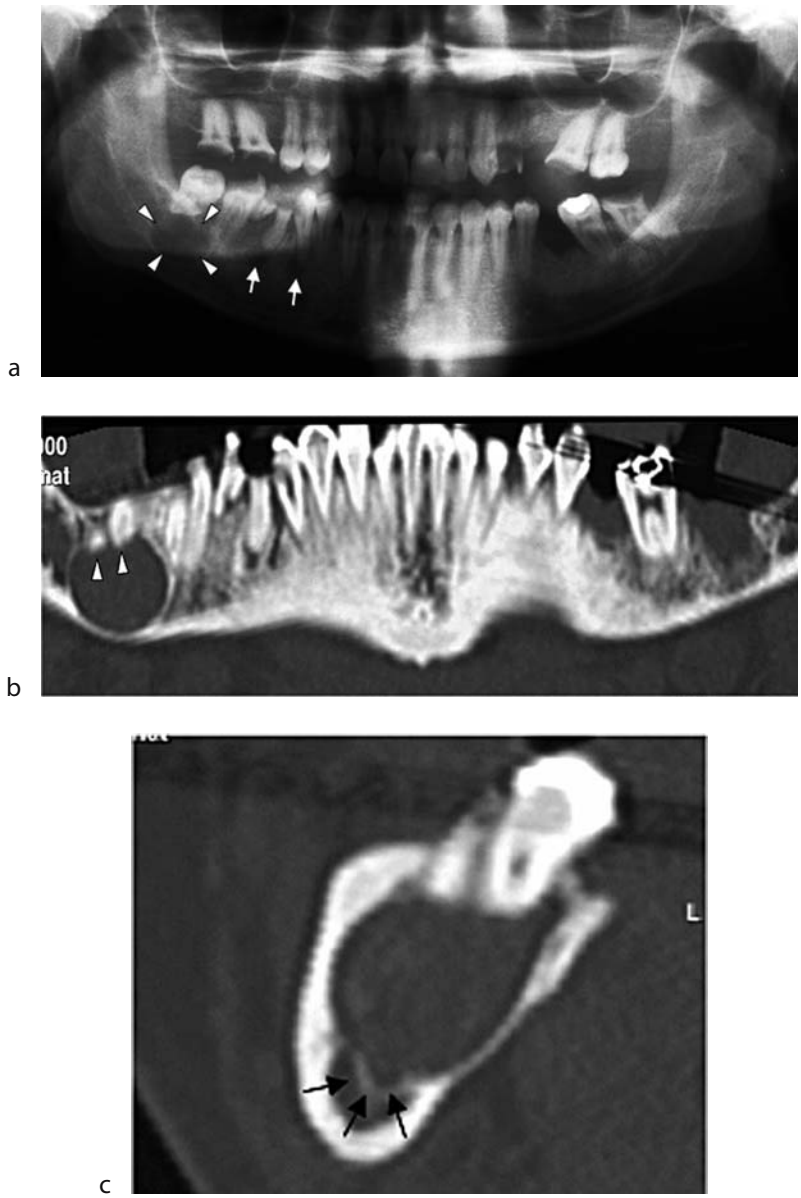

Neoplasms, Odontogenic. Figure 1 Radicular cysts. Pantomogram (a) reveals a radiolucent, well-defined lesion (arrowheads) around the apices of the mandibular third molar tooth associated with defect of the upper cortical margin of the mandibular canal. Similar smaller lesions can be seen around the apices of the mandibular first molar tooth and the second premolar tooth (arrows). Panoramic reformat (b) and cross-section oblique view (c) from spiral CT better show the relationships between the larger cyst, the slightly resorped tooth roots (arrowheads) and the mandibular canal (arrows).

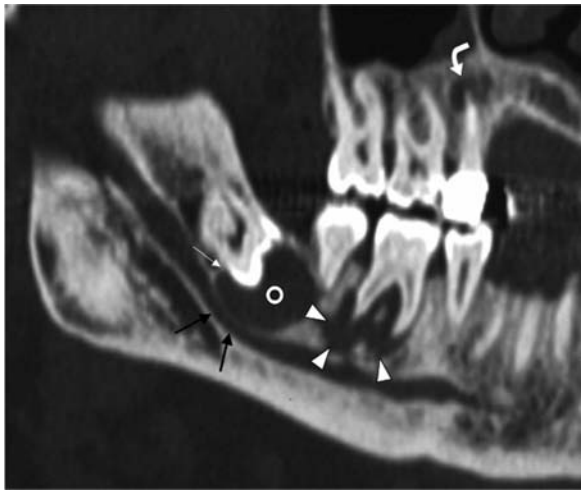

Neoplasms, Odontogenic. Figure 2 Panoramic reformat from multidetector spiral CT demonstrates an expansive, well-defined, unilocular area of osteolysis (circle) in the mandible incorporating the crown of the unerupted third molar tooth. The lesion wall converges to the cementoenamel junction (white arrow) strongly suggesting the diagnosis of dentigerous cyst. The lesion determines remodeling of the mandibular canal (black arrows). Also note well-circumscribed radiolucency arising from the apex of the upper second premolar tooth (curved arrow) compatible with periapical granuloma. Irregular periapical radiolucencies (arrowheads) and widening of the periodontal lucency separating the roots of the mandibular first molar tooth from the lamina dura, due to periapical abscesses, are also appreciable.

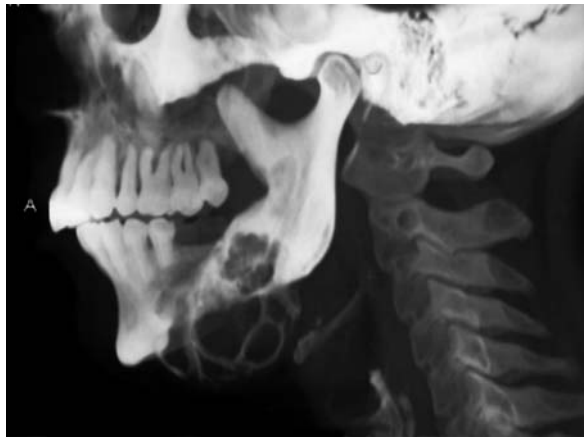

Neoplasms, Odontogenic. Figure 3 MIP reconstruction from multidetector spiral CT shows a huge multilocular lesion in the body of the mandible determining swelling and bone resorption. The lesion was a recurrent ameloblastoma.

a periapical location; dentigerous cyst, odontogenic keratocyst and calcifying odontogenic cyst are usually pericoronal; primordial and residual cysts are associated with missing tooth. Larger lesions may expand the cortex, extent into the maxillary sinuses or nasal cavity and displace teeth. Periapical cyst and calcifying odontogenic cyst may determine tooth root resorption. Radiographically, radicular cysts cannot be differentiated from periapical granulomas, which are usually less than 1.6 cm in diameter (4). On MR imaging, cysts show high signal intensity on T2-weighted images and regular walls with slight to strong enhancement. Odontogenic keratocyst characteristically presents with inhomogeneous cyst content (5).

Ameloblastoma appears as a unilocular or multilocular radiolucency (Fig. 3), commonly with a pericoronal location or without any contact with tooth. In multilocular lesions, loculi can vary in size and shape and may confer a honeycombed or bubble-like appearance to the lesion. Ameloblastoma can reach a considerable size causing bony expansion or extensive destruction of the mandible or maxilla and loss of the lamina dura, erosion of the tooth apex and displacement of the teeth. It sometimes break the cortex extending into the adjacent soft tissues. Ameloblastoma can be differentiated from a cyst by demonstrating enhancing irregularly thick walls and septa or papillary projections on contrast-enhanced T1-weighted images at MR imaging (5). Unusual radiographic findings (mixed radiolucent–radiopaque appearance with poorly defined margins) can be related to the desmoplastic variant.

Odontogenic fibroma, ameloblastic fibroma, squamous odontogenic tumor, and odontogenic myxoma also appear as radiolucencies. The last two show tendency to cause extensive destruction of bone and to extend into the adjacent soft tissues.

A mixed radiolucent–radiopaque appearance is usually associated with adenomatoid odontogenic tumor, calcifying epithelial odontogenic tumor and ameloblastic fibroodontoma. The formers appear as a radiolucent lesion with many calcifications, usually associated with the crown of an impacted tooth; the latter usually presents as a solitary mass or several small radiopaque masses with lucent well-defined margins that may resemble miniature teeth.

Odontoma, at first appearing as a radiolucent area, undergoes progressive calcification during its development that initially results in small, speckled calcific densities and eventually forms a radiopaque mass surrounded by a lucent ring due to fibrous capsule. The tumor is situated between the roots of teeth and is frequently associated with unerupted teeth. The teeth contained in a compound odontoma are dwarfed and usually distorted, with simple roots.

Benign cementoblastoma appears as a radiopaque mass surrounded by a radiolucent zone of uniform width associated with the tooth root, sometimes expanding the cortical bone.

Malignant lesions usually present as a radiolucent lesion with ill-defined, irregular, or moth-eaten margins showing inhomogeneous enhancement on gadolinium-enhanced T1-weighted images (4).

Nuclear Medicine

Bone scintigraphy has a limited role in the assessment of odontogenic lesions. It could be of support in evaluating whether a soft-tissue mass is a recurrence or fibrous healing and in evaluating patients with suspected ►osteomyelitis.

Diagnosis

Diagnosis of odontogenic lesions is mainly based on imaging, although an exact definition of the lesion is often impossible because of considerable overlapping of the imaging features. Furthermore, many nonodontogenic jaw lesions (dysplastic and inflammatory lesions, non-odontogenic cysts, and tumors) have similar appearance.

Final diagnosis is obtained histopathologically, after biopsy or surgical treatment.

Bibliography

1. Kramer IRH, Pindborg JJ, Shar M (1992) Histological Typing of Odontogenic Tumours: World Health Organization: International Histological Classification of Tumours. Springer-Verlag, Berlin, pp 1–42
2. Weber AL (1993) Imaging of cysts and odontogenic tumors of the jaw. Definition and classification. Radiol Clin North Am 31:101–120
3. White SC, Pharoah MJ (2004) Oral Radiology: Principles and Interpretation. CV Mosby, St. Louis
4. Weber AL, Kaneda T, Scrivani SJ et al (2003) Jaw: cysts, tumors, and non tumorous lesions. In: Som PM, Curtin HD (eds) Head and Neck Imaging. Mosby Inc, St. Louis, pp 930–994
5. Minami M, Kaneda T, Ozawa K et al (1996) Cystic lesions of the maxillomandibular region: MR imaging distinction of odontogenic keratocysts and ameloblastoma from other cysts. Am J Roentgenol 166:943–949

Neoplasms Oesophagus

Ashley Roberts[1], Brinder Mahon[2]
[1]University Hospital of Wales, Cardiff, UK
ashley.roberts@cardiffandvale.wales.nhs.uk
[2]Queen Elizabeth Hospital, Birmingham, UK

Synonyms

Oesophageal cancer; Oesophageal malignancy; Oesophageal tumour

Definition

Oesophageal neoplasms may be benign or malignant. While benign oesophageal neoplasms are rare, oesophageal cancer (OC) is increasingly common and responsible for 1–1.5% of all cancers in the western world and 4–10% of all gastrointestinal tract malignancies. Despite advances in imaging and treatment 5-year survival is lesser than 10%. OC is predominantly of two types—squamous cell carcinoma (SCC) and adenocarcinoma (AC).

Worldwide SCC accounts for 70% of OC and has a very wide variation in geographical incidence. It is endemic in northern China, parts of South Africa, Northern Iran and Northwest France. In non-endemic areas, smoking and alcohol are risk factors with heavy use causing a 44-fold increase. Other risk factors include achalasia, caustic injury, human papilloma virus, head and neck tumours, Plummer–Vinson syndrome, sprue and tylosis.

The incidence of AC of the oesophagus and gastro-oesophageal junction (GOJ) has rapidly increased over the last 20 years, and is now the commonest OC in white men in the USA. The single most important risk factor is ►Barrett's oesophagus. Prospective studies indicate the annual incidence of malignant transformation in Barrett's oesophagus is 1–2%. Overall risk of adenocarcinoma is 125 times greater than in the general population (1).

Less common forms of OC include mucoepidermoid carcinoma, spindle cell carcinoma, small cell carcinoma, leiomyosarcoma and lymphoma.

Pathology/Histopathology

Squamous Cell Carcinoma

About 20% of SCC involves the upper third (<24 cm from the incisors or above the aortic arch), 50% mid-oesophagus (25–32 cm) to the level of the pulmonary vein and 30% the lower oesophagus. They may be fungating (60%), ulcerated (25%) or infiltrative (15%).

Adenocarcinoma

About 90% occur in the distal oesophagus. About 20–50% of all AC arise from Barrett's oesophagus and dysplasia predicts malignant transformation. Low grade dysplasia has variable progression or regression, whereas 33% of patients with high grade dysplasia will have unsuspected foci of AC and oesophagectomy is usually indicated. AC is macroscopically similar to SCC.

SCC and AC may spread directly, *via* lymphatics or through the haematogenous route. Direct extension occurs into aorta, heart, lungs, airway, thoracic duct, azygous vein and diaphragm. Sub-mucosal extension may

be a feature. The oesophageal wall lacks serosa, allowing easier spread to the adventitia and adjacent structures. AC commonly (35–60%) directly invades the GOJ and proximal stomach, and the degree of involvement influences surgical planning. Complex lymphatic drainage of the oesophagus can lead to skip metastases in the absence of segmental lymph node involvement e.g. gastric and hepato-duodenal ligaments drain the lower third of the oesophagus but may be involved in 44% of middle third and up to 10% of upper third tumours.

Haematogenous metastases are more common with locally advanced disease. Lungs and liver are the most likely sites but metastases may be seen in the adrenals, kidneys, pancreas, peritoneum and bone.

Clinical Presentation

Dysphagia occurs in 90% and weight loss in 70%. These alarm symptoms should prompt urgent investigation. Unfortunately, when they are present the disease is often advanced with a poor prognosis. Other symptoms include retro-sternal pain and regurgitation, which may lead to aspiration. Tumour friability may cause bleeding with haematemesis or anaemia. Anorexia and satiety may occur if the tumour involves the stomach. Other symptoms include odynophagia and pneumonia secondary to tracheo-oesophageal fistula.

Imaging

Imaging has a role in the diagnosis, staging and follow-up of OC. Barium studies are still used for diagnosis but this has generally been superseded by endoscopy and biopsy. Computed tomography (CT) has a role following neo-adjuvant chemotherapy +/-radiotherapy to exclude disease progression prior to surgery, and in the detection of recurrence. However, the greatest modern impact of imaging is in pre-treatment staging.

Staging

Pre-operative ►TNM classification provided by imaging governs treatment strategy and predicts prognosis.

The primary tumour is classified from Tis to T4 depending on the degree of oesophageal wall involvement.

Tis-carcinoma *in situ*

T1—invades lamina propria or sub-mucosa
T2—invades muscularis propria (MP)
T3—through the muscularis propria into adventitia
T4—adjacent structures
N1—regional lymph node metastases
M1—distant metastases

Lower thoracic oesophagus—M1a coeliac nodes, M1b other distant metastases
Upper thoracic oesophagus—M1a cervical nodes, M1b other
Mid-thoracic oesophagus—M1b non-regional lymph nodes or other

GOJ tumours have no separate TNM classification, which is unfortunate. However, the Siewert I, II and III classification describes whether the tumour arises above, at or below the GOJ, and can assist surgical planning.

A reasonable staging strategy is to exclude metastatic disease with CT, and then assess local disease extent with Endoscopic Ultrasound (EUS). ►FDG-PET is increasingly used as it becomes more widely available.

Computed Tomography

Following gastric distension with water (if not limited by dysphagia) post-contrast CT of the chest and abdomen is performed and reviewed with reformatted images as required. T1 OC may not be visible, and as the oesophageal wall layers cannot be seen clearly with CT the distinction between T2 and T3 tumours can be difficult. It is reasonable to assume 100% circumferential tumours are T3 or greater. CT has reported sensitivity of 58%, and specificity of 80% for estimating T staging with better accuracy with advancing T stage (2).

Aortic invasion is found in only 3% at autopsy and is probably less frequent at initial staging. Loss of fat planes is a poor predictor as they are often absent. Aortic invasion is unlikely if the mass involves the aortic circumference by <45 degrees, intermediate between 45 and 90 degrees and highly suggestive if >90 degrees, particularly when the small triangle of fat between oesophagus, aorta and spine is obliterated. However, distinguishing between primary tumour and lymph nodes can be difficult (Fig. 1a and b).

The likelihood of airway invasion increases with respiratory symptoms, tumour length and EUS T stage. The posterior wall of the normal cervical trachea often has a concave appearance as opposed to the convex lower trachea. Disruption of this appearance or asymmetry/nodularity suggests tracheobronchial invasion. However, overall accuracy for diagnosis of tracheobronchial invasion on bronchoscopy, bronchoscopic ultrasonography, EUS and CT are reported as 78%, 91%, 85% and 58%, respectively (3). CT is poor in the assessment of pleural and pericardial invasion but thickening adjacent to the tumour, local effusions, and inward deformity are suggestive. Diaphragmatic invasion can also be difficult to assess, particularly if there is a hiatus hernia. However this is of limited significance, as it would not preclude resection.

There is a 60–80% prevalence of lymph node disease at diagnosis. If lymph nodes are enlarged, metastases are suspected (5 mm supra-clavicular; >6 mm retrocrural;

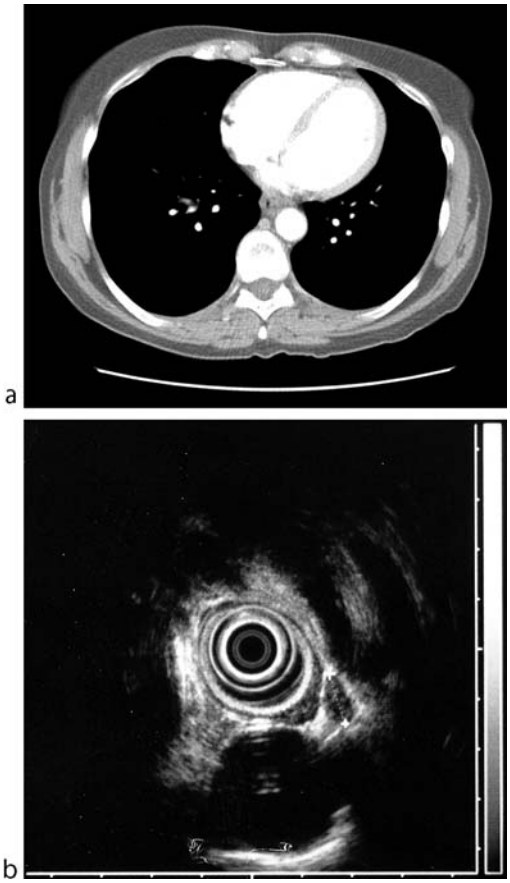

Neoplasms Oesophagus. Figure 1 (a) Post-contrast CT through the lower oesophageal SCC. Abnormal soft tissue contiguous with the oesophagus abuts almost 25% of the aortic circumference raising the possibility of T4 disease. (b) EUS at 7.5 MHz at the same level as Fig. 1a illustrates the CT appearance is due to a lymph node (between calipers). T2 N1 disease was confirmed at resection.

>8 mm gastrohepatic ligament; >10 mm in the remainder). Reported N staging sensitivity is 79%, and specificity is 84% (2).

Distant metastases from oesophageal cancer at presentation are seen in the liver in 35% and lungs in 20%. Ascites, pleural effusions or nodules in the omentum or pleura are suspicious for metastases and should be further investigated, e.g. laparoscopy. Indeed in AC, laparoscopy when performed routinely identifies metastases in up to 10%. Non-regional lymph nodes are considered to be M1 disease, particularly coeliac and cervical nodes.

EUS

EUS performed at 5–12 MHz depicts the gastrointestinal wall as a five-layered structure of alternating hyper and hypoechoic bands, which correlates well with histology. The fourth (hypoechoic) layer represents the MP. By defining the relationship of the primary tumour to the MP, a pre-operative T stage can be established. EUS is almost unique in providing this detailed pre-operative information (Figs 2 and 3).

Lymph node metastases are defined by EUS using the following criteria: hypoechoic structure, sharp borders, round contour and size greater than 10 mm. Reactive nodes may have an echogenic centre representing the fatty hilum and this feature is usually considered a benign characteristic. However, we have described central echogenic areas, presumed to be due to necrosis, as an additional sign of malignant lymphadenopathy. The site and number of malignant looking lymph nodes seen pre-operatively is closely related to prognosis. However, even when the EUS features described earlier are present, accuracy for predicting malignant invasion may be only 80%. It is therefore important to establish if a distant lymph node is malignant as its presence may deny a patient potentially curative surgery. We therefore perform EUS guided biopsy of lymph nodes considered to be M1.

Comparative studies with CT consistently demonstrate superior T and N staging accuracy with EUS. In a systematic review by Harris et al., the T & N staging accuracy of EUS approaches 90% and 80%, respectively (4). While helical CT has had little impact on the role of EUS in this disease, we have reported a complementary role for the locoregional staging of OC in the setting of a multidisciplinary team (2).

EUS has its greatest impact with advanced, non-resectable tumours by preventing open and closed thoracotomy. In patients with T4 disease on pre-operative EUS, surgery has no impact on survival compared to non-surgical groups. Patients who have unnecessary surgery have been shown to have poor quality of life.

Transcutaneous Ultrasound

Some centres, particularly in the Far East, use neck US to exclude lymph node metastases in SCC. US may help characterise liver lesions, and guide biopsy.

Magnetic Resonance Imaging

Magnetic resonance imaging (MRI) has a limited role in the assessment of oesophageal neoplasms. Endoluminal MRI offers no advantage over EUS. MRI is occasionally used to clarify the nature of liver lesions.

Nuclear Medicine

The preceding staging strategy assumes FDG-PET is unavailable, but it is increasingly used for staging

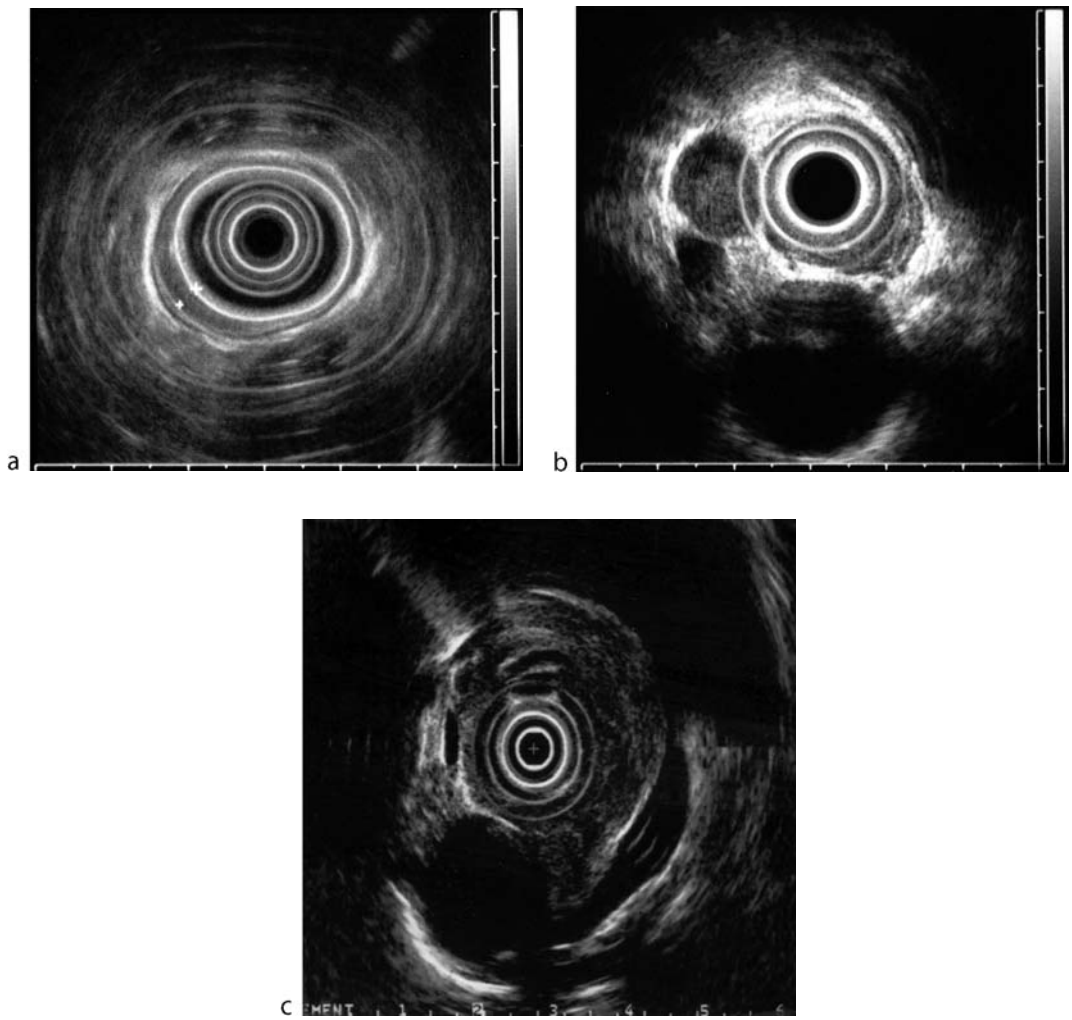

Neoplasms Oesophagus. Figure 2 EUS of various stages of OC in three different patients. (a) EUS of the distal oesophagus (12 MHz) with mucosal thickening (between calipers). The hyperechoic sub-mucosa and hypoechoic MP deep to this are intact. AC confined to the mucosa was confirmed on resection. (b) The MP is absent between 5 and 8 o'clock but the tumour is separate from aorta at 6 o'clock. Malignant looking lymph node at 9 o'clock. T3 N1 confirmed at resection. (c) EUS of T4 OC invading the aortic wall at 6 o'clock. Treated with a stent.

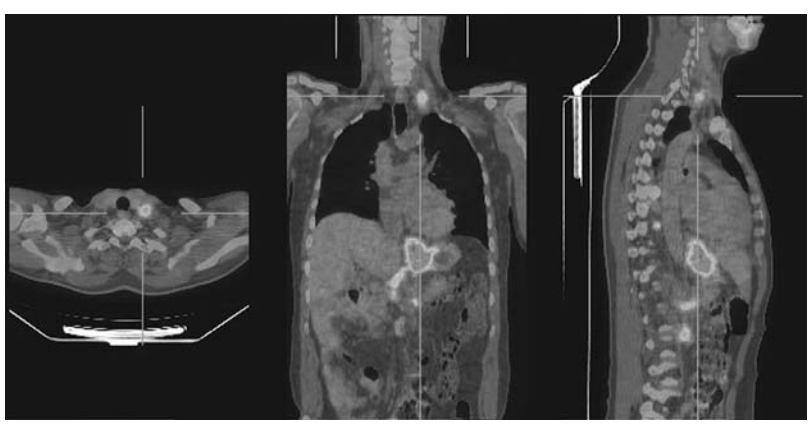

Neoplasms Oesophagus. Figure 3 PET CT demonstrating ^{18}FDG uptake in a junctional oesophageal tumour and a supra-clavicular node rendering this patient inoperable.

oesophageal cancer. In the detection of hepatic metastases in gastrointestinal tumours in general, FDG-PET is more sensitive (90%) than CT (72%) or MRI (76%). In a meta-analysis of the staging performance of FDG-PET in oesophageal cancer only, sensitivity and specificity was 67% and 97% for M1 disease and 51% and 84% for N1 disease (5). There is therefore an argument for performing FDG-PET first to exclude M1 disease, but this is limited by cost and availability. While ^{18}FDG accumulates in over 92% of primary tumours, only limited T stage information is obtained.

If surgery is to be denied on the basis of M1a disease on FDG-PET, then ideally histological confirmation should be obtained as false positives do occur.

Diagnosis

Histological diagnosis of oesophageal cancer is made by endoscopic mucosal biopsies.

Interventional Radiological Treatment

Self expanding, metal mesh oesophageal stents are used to palliate dysphagia in patients with inoperable oesophageal cancer. Other indications include recurrence, tracheo-oesophageal fistulae, anastamotic leaks and perforation. Placement can be performed with endoscopic or fluoroscopic control or in combination. Recent technical advances include anti-reflux, anti-migration and retrievable devices. Most patients (75–90%) resume a near normal diet after stent placement, but further intervention is required in up to 60%. Survival may be increased by the use of concurrent chemoradiotherapy or endoluminal brachytherapy, although this may lead to more stent-related complications.

Bibliography

1. Shaheen N, Ransohoff DF (2002) Gastroesophageal reflux, Barrett oesophagus, and oesophageal cancer: clinical applications. J Am Med Assoc 287:1982–1986
2. Weaver SR, Blackshaw GR, Lewis WG et al (2004) Comparison of special interest computed tomography, endosonography and histopathological stage of oesophageal cancer. Clin Radiol 59:499–504
3. Nishimura Y, Osugi H, Inoue K et al (2002) Bronchoscopic ultrasonography in the diagnosis of tracheobronchial invasion of esophageal cancer. J Ultrasound Med 21:49–58
4. Harris KM, Kelly S, Berry E et al (1998) Systematic review of endoscopic ultrasound in gastro-oesophageal cancer. Health Technol Assess 2(18):I–iv, 1–134
5. van Westreenen HL, Westerterp M, Bossuyt PMM, et al (2004). Systematic review of the staging performance of ^{18}F-fluorodeoxyglucose positron emission tomography in esophageal cancer. J Clin Oncol 22:3805–3812

Neoplasms, Oral Cavity

Sabrina Kösling
Martin-Luther-Universität Halle-Wittenberg,
Klinik für Diagnostische Radiologie, Halle, Germany
sabrina.koesling@medizin.uni-halle.de

Definition

Neoplasms are characterised by an abnormal growth of tissue, which occur within structures of the oral cavity. Malignant neoplasms show a greater degree of anaplasia and have the properties of invasion and metastasis. Neoplasms of the oral cavity are soft tissue tumours arising from the mucosal surfaces or deeper structures.

Typical benign tumours of the oral cavity are papillomas and fibromas. Other benign soft tissue neoplasms as fibromatosis, lipoma, leiomyoma, rhabdomyoma or neurogenic tumours (granular cell tumour, schwannoma, neurofibroma) are less frequent at this site.

Haemangiomas and lymphangiomas as congenital vascular lesions are presented in another chapter. Cysts and dermoids are developmental cystic degenerations and not true neoplasms. The known salivary gland neoplasms may arise from minor salivary glands in the oral cavity. They are discussed in the salivary gland chapter.

Compared to other lesions, malignant lesions are found seldom (7%) in the oral cavity; 90% of them are squamous cell carcinomas (1). Adenocarcinomas may occur; melanomas and sarcomas are exceedingly rare.

Pathology/Histopathology

Papillomas are characterised by a growth of keratinised or non-keratinised squamous epithelium with normal maturation pattern. They contain fibrovascular connective tissue and chronic inflammatory cells. In fibromas—hyperplasias of fibrous connective tissue—there is a proliferation of fibroblasts and collagen fibres. Several patterns that reflect progressive stages of fibroblastic differentiation are identified microscopically in fibromatosis. Dense or moderately dense, rather vascular, bland collagenic connective tissue with scattered chronic inflammatory cells can be observed. In lipomas, superficial or deeper adipose tissue proliferates; in leiomyomas smooth muscle—in the oral cavity usually of the blood vessels—and in rhabdomyomas skeletal muscle. The submucosal granular cell tumours are composed of diffuse sheets of large cells of either nerve or muscle origin with a cytoplasm of densely packed eosinophilic granules. In schwannomas (synonym:

neurilemoma) there is a fibroblastic proliferation of the nerve sheath cells (Schwann's cell). Neurofibromas consist of diffuse proliferations of perineural fibroblasts that are orientated in either a random or nodular pattern (2).

Squamous cell carcinomas develop from the stratified squamous epithelium of the mucosa. Histologically, they show large polygonal or fusiform cells with atypical nuclei and increased mitotic activity. They may contain keratinised and inflammatory cells. Depending on the differentiation four degree (G1–G4) are distinguished: high, moderate, poor, undifferentiated or anaplastic. Adenocarcinomas (G1–G4) are epithelial tumours with glandular components, which may produce mucus. Carcinomas of the oral cavity are classified according to the ►TNM criteria of ►UICC (Tables 1 and 2).

At first presentation about 60% of the patients with carcinomas of the oral cavity have nodal metastases, even if the tumours are small. The first order drainage of oral cavity carcinomas is the submental and submandibular lymph node group for anterior processes, and the jugulodigastric node for posterior lesions. From there the drainage of both regions goes mostly down into the deep cervical and spinal accessory chain. Especially carcinomas of the tongue are predisposed to bilateral affection.

Melanomas are malignant neoplasms deriving from cells that are capable of forming melanin, which may occur in the mucosa of the oral cavity. The usually high malignant sarcomas are formed by the proliferation of mesodermal cells.

Clinical Presentation

Neoplasms are usually painless. Benign tumours, but also adenoid cystic carcinomas grow slowly—malignant more rapidly. Due to slow growing, benign tumours are often asymptomatic and will be detected incidentally. A criterion of benignancy is that the lesion is movable against the undersurface. Depending on the localisation and size, neoplasms can cause dysphagia, dyspnoea and difficulties in speaking; if the tumour is injured bleedings might occur. Malignant epithelial tumours are often accompanied by foetor ex ore.

Some tumours have a characteristic optical appearance. Papillomas are white or pink, sessile or pedunculated exophytic nodules of cauliflower-like appearance; they may occur anywhere on the oral mucosa. The firm and often exophytic fibromas, located on the buccal mucosa, tongue, lips or gingiva, are usually smaller than 2 cm. Lipomas are soft on palpation and of yellow colour. A nodular, possibly exophytic, ulcerous, hard, easily bleeding mass, which is more or less fixed and sometimes painful on palpation, is suspicious to be a carcinoma; otalgia may occur due to connection of the lingual to the facial nerve. Often enlarged lymph nodes can be palpated. Clinical signs of infiltration are a fixed tongue and trismus. Mesenchymal and neurogenic neoplasms lie submucosally without typical clinical signs.

Imaging

Conventional radiographs are performed in tumour diagnostics of the dental apparatus. They do not play a role in tumour imaging of the oral cavity. CT and MRI have been proved to be valuable in the modern diagnostics of neoplasms in this region. Ultrasound is of secondary importance (4).

Neoplasms, Oral Cavity. Table 1 T-categories of oral cavity tumours (UICC)

T0: No evidence of tumour
TIS: Carcinoma *in situ*
T1: Tumour ≤20 mm
T2: Tumour >20 mm, ≤40 mm
T3: Tumour >40 mm
T4a: Infiltration through cortical bone, in external tongue muscles, maxillary sinus or skin
T4b: Infiltration of the masticator space, pterygoid process or skull base, or encasement of internal carotid artery

Neoplasms, Oral Cavity. Table 2 N-Categories of oral cavity tumours (UICC)

NX: Regional lymph nodes are not assessable
N0: No regional lymph node metastases
N1: Metastasis(es) in solitary ipsilateral lymph node—≤30 mm
N2a: Metastasis(es) in solitary ipsilateral lymph node—>30 mm, but ≤60 mm
N2b: Metastasis(es) in multiple ipsilateral lymph nodes—none of them >60 mm in its largest dimension
N2c: Metastasis(es) in bilateral or contralateral lymph nodes—none of them >60 mm in its largest dimension
N3: Metastasis(es) in lymph nodes >60 mm in its largest dimension

Computed Tomography and Magnetic Resonance Imaging

Neoplasms of the oral cavity are detected by clinical investigation. Imaging is performed to depict the full extension in larger benign tumours and especially in malignancies, first of all in carcinomas. Very small tumours with mucosal spread can be undetectable on CT and MRI. Due to the better soft tissue contrast, MRI is more suited in the delineation of tumourous lesions from surrounding structures compared to CT. Beam-hardening artefacts caused by dense bones and teeth, or by dental fillings may seriously disturb the visibility of tumours on CT. On the other side, a CT examination is performed within a few seconds with modern technique whereas a complete MRI study lasts about 30 min. In the case of less co-operative patients CT should be preferred.

The general signs of tumours on CT are similar to those on MRI. Tumours show a space-occupying growth, larger ones an obliteration of fat planes. An infiltration of muscle and bone are hints for a malignancy. Cortical erosion is seen better on CT (Fig. 1a), the extent of medullary invasion better on MRI (Fig. 1b). Many tumours show a ►contrast enhancement, which is different to surrounding structures. Larger tumours have sometimes inhomogeneities. On MRI, most tumours appear isointense to muscles on unenhanced T1-weighted images, and moderate to strong hyperintense on T2-weighted images. Except of lipomas and cystic lesions, there are no characteristic densities or signal intensities for a single neoplasm on CT or MRI (Fig. 2).

In general, cancer has several modes of spread. Firstly, most tumours grow superficially within the mucosa. Mucosal spread is best evaluated by inspection. Before invasion of muscles and bones tumour spreads within spaces, along the muscular fasciae and the periosteum. Cancer may show a ►perineural spread and lymph node metastases. Both have a negative impact on prognosis.

The deep spread of a neoplasm cannot be exactly assessed by clinical examination; this is where imaging plays a role. In dependence of the primary site (floor of the mouth, tongue, oral mucosa with different sub-sites, upper and lower gingiva, hard palate), carcinomas show preferential ways of extension with increasing growth, which can be best visualised by MRI: Tongue carcinomas grow first along the intrinsic muscles deeper into the tongue, along extrinsic lingual muscles into the sublingual and submandibular space; they can reach the base of the tongue and the muscles of the floor of the mouth. Cancers in the floor of the mouth (Fig. 3) spread along the muscles, periosteum of the mandible, within the lingual septum and submandibular space; the tongue and tongue base may be involved; relative early the mandible is invaded; the Warton's duct can be occluded resulting in an adenitis of the sub-mandibular gland. Carcinomas of the oral mucosa and gingiva spread first into the buccal space; later they may invade the masticator space; a retromolar localisation is endangered for a perineural spread along the inferior alveolar nerve. Cancers of the hard palate break early through into the maxillary sinus, a perineural spread along the palatine nerves to the pterygopalatine ganglion may occur.

In lymph node judgment, morphological criteria—size larger than 10 mm, central necrosis, indistinct nodal margin as a sign of extra-capsular spread—are used for

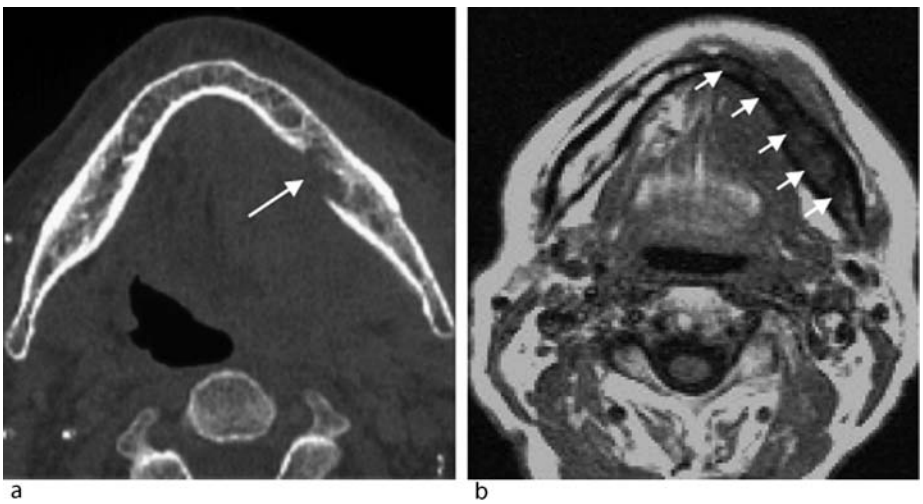

Neoplasms, Oral Cavity. Figure 1 T4-stage squamous cell carcinoma of the floor of the mouth in two different patients. (a) Axial high-resolution CT in bone window shows a cortical defect in the mandible (arrow). The extent within the bone marrow is not quite clear. (b) Axial T1-weighted image demonstrates a wide medullary invasion of the mandible (arrows).

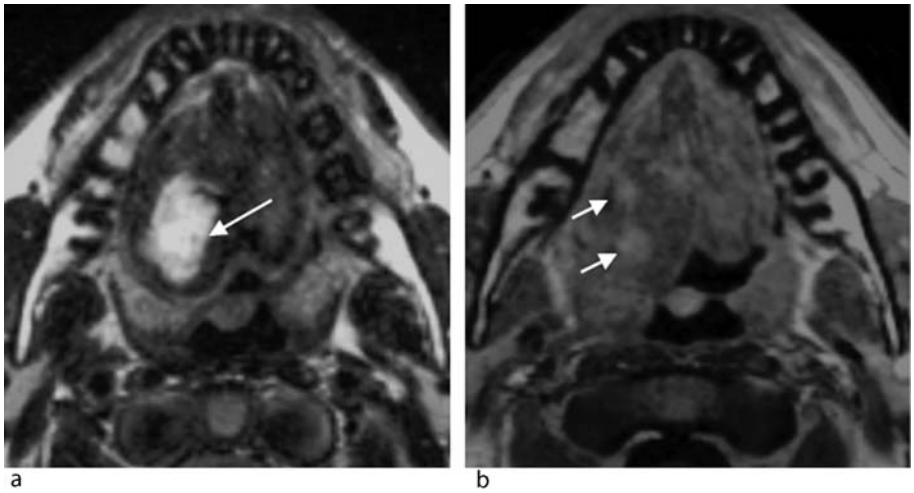

Neoplasms, Oral Cavity. Figure 2 Axial MRI of a patient in whom clinicians found an unclear mass in the tongue. (a) On T2-weighted image the lesion can be demonstrated best (arrow) and estimated in size. It is relatively sharp demarked. (b) On contrast-enhanced T1-weighted image, the tumour showed a described enhancement (arrows) and is less well demarcated. The imaging diagnosis was 'probably benign neoplasm'. Histology revealed a regressively changed fibroma.

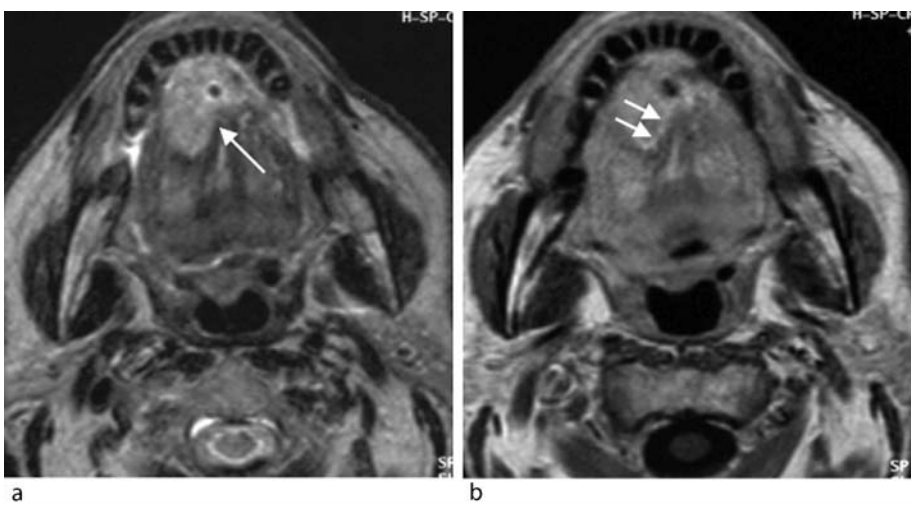

Neoplasms, Oral Cavity. Figure 3 Bioptically proven squamous cell carcinoma of the floor of the mouth. (a) Axial T2-weighted images visualise a hyperintense mass in the anterior part of the oral cavity, which crosses the midline (arrow). (b) On axial contrast-enhanced T1-weighted image, there is a blurred margin of the tumour (arrows), which is suspicious of infiltration of the genioglossal muscle as T4 criteria. The patient underwent radiochemotherapy.

the distinction between normal and metastatic lymph nodes in CT and MRI, but the number of false-negative and false-positive findings is still high with this approach. If enlarged lymph nodes are related to the primary disease and the corresponding lymph node drainage, the results can be improved. The major problem of both methods is the high false-negative number in normal sized lymph nodes with micro-metastases. Despite of technical improvements in CT and MRI, this problem is not sufficiently solved at present.

Imaging is part of the clinical staging. Tumour size in its greatest dimension can be determined for T1 to T3 categories and for the T4 category invasion of skeletal muscles and/or bone (Table 1). If a tumour is accompanied by inflammatory changes, imaging tends to overestimate the tumour size because both processes

cannot be differentiated exactly. Criteria for the single N categories are the number of affected lymph nodes, their size and if they are ipsilateral or bilateral (Table 2).

Ultrasound

In the hand of experts, ultrasound examination can deliver a lot of information. It provides access to most structures of the oral cavity. Usually, tumours appear as hypoechoic space-demanding structures. Especially in the tongue, a tumour and its spread within the internal muscles can sometimes be better delineated than on CT or MRI. The method is of special relevance in the examination of major salivary glands and as duplex-high-resolution-sonography in the assessment of lymph nodes, where malignant lymph nodes show irregular central vessels. If ultrasound is combined with fine-needle aspiration cytology, the specificity of lymph node findings can be increased significantly. A larger tumour extension into deeper spaces, bone invasion and retropharyngeal lymph node metastases cannot be diagnosed sufficiently. Therefore, sonography is not suitable as a solitary method in tumour imaging.

Nuclear Medicine

In the diagnostics of the oral cavity carcinomas, nuclear medicine techniques can provide relevant information in certain cases. Due to the lack of anatomic details, they have to be supplemented by CT or MRI in shape of co-registration or comparative investigation. Nowadays, ►^{18}FDG PET is the leading procedure, which gives information about the degree of glucose metabolism in different tissues. A certain level of increased uptake of FDG is considered as malignancy. Several reports confirmed an increased ^{18}FDG uptake in primary tumours, lymph node and distant metastases of head and neck squamous cell carcinomas. However, the clinical use of ^{18}FDG PET is discussed controversially. Higher accuracy compared to CT and MRI have been reported in lymph node assessment, detection of unknown sites in patients with cancer of unknown primary (CUP) and in differentiation of recurrent cancer from post-therapeutic changes. Nevertheless, a routine use of PET in pre-therapeutic staging of oral cavity squamous cell carcinomas cannot be recommended; in this situation PET is reserved for cases with equivocal findings by CT or MRI (5).

Diagnosis

The diagnosis of oral cavity tumours is based on histopathology. The dignity of mucosal lesions and their superficial spread can be better judged by clinical methods compared to imaging. Submucosal tumours cannot be assessed clinically with the same safety. Small, superficial and benign appearing neoplasms are excised without imaging. Imaging is needed in larger and/or malignant appearing neoplasms.

Beside of histology, the knowledge about the full tumour extension is important for the therapeutic decision and patient's prognosis: extension into deep soft tissue structures and spaces; infiltration of skeletal muscles, bone, neighbouring spaces and skin; crossing the midline of the tongue or floor of the mouth; perineural spread; relation to the common or internal carotid artery; and metastatic involvement of lymph nodes. The imaging method of first choice to get this information is MRI nowadays (5). In contraindications for MRI or non-compliant patients, CT is the alternative method. PET and sonography can provide relevant diagnostic information as complementary techniques.

Bibliography

1. Parker SL, Tong T, Bolden S et al (1996) Cancer statistics. CA Cancer J Clin 46:5–27
2. http://www.dental.mu.edu/oralpath.htm
3. Sobin LH, Wittekind Ch (eds) (2002) International Union Against Cancer. TNM Classification of Malignant Tumours. 6th edn. Wiley-Liss, Baltimore, MD
4. Lenz M, Hermans R (1996) Imaging of the orapharynx and oral cavity. Eur Radiol 6:536–549
5. Dammann F, Horger M, Mueller-Berg M et al (2005) Rational diagnosis of squamous cell carcinoma of the head and neck region: comparative evaluation of CT, MRI, and ^{18}FDG PET. Am J Roentgenol 185:1326–1331

Neoplasm, Oropharynx

Francesca Granata
University of Messina, Messina, Italy
longomar@tin.it

Synonyms

Malignant oropharyngeal tumours

Definitions

Neoplasm of the oropharynx means a primary malignancy arising from the mucosa of this anatomic region.

The oral portion of the upper aerodigestive tract is formed by two regions: the oral cavity and the oropharynx. The oropharynx communicates, in addition to the oral cavity, with nasopharynx, hypofarynx and larynx (1).

The boundaries of this anatomical region is the soft palate superiorly and the hyoid bone inferiorly (2). The anterior part of oropharynx includes the posterior one-third of the tongue (posteriorly to the circumvallate papilla); the upper part is formed by the soft palate and uvula. Laterally, there are two facial arches, the anterior (palatoglossus muscle) and the posterior arch (palatopharyngeal muscle) and between them is the tonsillar fossa which harbours the palatine tonsil (1). The posterior oropharyngeal wall is bounded by upper pharyngeal constrictor muscles and is related to the second and third cervical vertebrae.

Moreover, the oropharyngeal region includes the lingual tonsil which lies at the base of the tongue, more concentrated on the lateral surfaces. The lingual tonsil and the palatine tonsils jointly, as well as other collection of lymph tissue in this area, form the Waldeyer's ring.

Pathology/Histopathology

The majority of tumours involving the oropharynx are squamous cell carcinomas antigen (SCCA) which represent about 90% of the total. They arise from oropharyngeal mucosa. The incidence of SCCA of oropharynx increases in patients with a history of tobacco or alcohol abuse (1, 2).

Other histological types of tumours are less common such as lymphoma, minor salivary gland tumours and other rare mesenchymal lesions (1, 2).

The mesenchymal neoplasms of oropharynx are rare and include: rhabdomyoma and rhabdomyosarcoma (most common in childhood), granular cells tumours, fibromatoses, schwannomas, neurofibromas, and hemangiomas (2).

In most cases, imaging techniques have little specificity and histologic diagnosis is needed.

Clinical Presentation

Oropharyngeal tumours can be clinically silent. Sometimes, the symptomatology can be represented by dysphagia or slight pain even if latero-cervical lymphadenopathy is often the only finding.

Imaging

The goal of modern diagnostic imaging is to establish the location, the size and the extent of oropharyngeal tumour. Moreover, it is important the pre-therapeutic evaluation of the relationship between tumoural mass and some critical structures like lingual artery and vein, carotid artery, internal jugular vein, muscles, connective tissue spaces and bone.

Computed tomography (CT) scan and magnetic resonance imaging (MRI) are the techniques of choice in the evaluation of oropharyngeal tumours.

Computed Tomography Scan Method

The oropharynx should be studied during suspended respiration (2).

The region of interest should be extended from the base of the skull to the upper mediastinum (aortic arch). Contrast-medium injection is mandatory to define the tumoural boundaries and metastatic lymphoadenopathies (2, 3).

The axial plane is obligatory for the evaluation of oropharyngeal region.

With modern multislice CT scanners, coronal and sagittal scans can be reconstructed from the volume data set (multiplanar reformation, MPR) or 3D images can be calculated with volume-rendering techniques. Coronal and sagittal images are useful to define the anatomical spread of the tumour and to reduce artefacts due to dental fillings (amalgam, gold or ceramics) (3).

Bone algorithms are essential to evaluate any pathologic bone involvement.

Magnetic Resonance Imaging Method

The advantages of MRI in comparison with CT scan are better tissue contrast and the absence of degradation due to dental fillings. The disadvantages are the long imaging time (20–30 min MRI versus 20–30 sec CT scan) and the subsequent difficulty for the patient to remain motionless (3).

The MRI study of oropharynx is performed primarily in the axial plane. It is essential to obtain axial T1- and T2-weighted images. These images are usually obtained by FSE sequences. Scanning with contrast-medium (Gd-DTPA) is mandatory; the dosage is 0.2 mmol/kg body weight. Optional coronal and sagittal T1-weighted images before and after Gd-DTPA can be obtained, respectively to study lateral and midline tumours. To overcome the problems due to the high fat signal in FSE images, fat suppression techniques are used on both T2-weighted images and T1-weighted images after gadolinium injection (3).

Alternative fat-suppressed technique is short-tau inversion recovery (STIR) without contrast-medium injection. This technique is very sensitive in tumour location.

Moreover, dynamic T1-weighted GE sequences can be used after gadolinium injection to study tumour vascularisation because of their high temporal resolution (3).

Disadvantages of GE sequences are represented by susceptibility artefacts at the air-bone-tissue borders and near dental fillings.

Diagnosis

Imaging techniques play an essential role in the diagnosis and stadiation of oropharyngeal tumours.

The location and the size of the neoplasm, the degree and direction of infiltration into neighbouring structures and the degree of regional lymph node involvement significantly orientate prognosis and therapy (2, 4).

According to the TNM criteria, oropharyngeal tumours are classified:

- Stage T1: <2 cm in maximum diameter
- Stage T2: >2 cm–<4 cm
- Stage T3: >4 cm
- Stage T4: Tumour involving bony structures (mandible or jaws), soft tissues of the neck or extrinsic muscles of the tongue.

Tumour Detection

A malignant oropharyngeal neoplasm appears like a space-occupying growth associated with obliteration of fat planes. Direct sign of an advanced neoplasm is the infiltration of muscle and of bone structures (4).

After contrast-medium injection, squamous cell carcinomas enhance in 85% of cases (4).

The tumoural tissue has a density between 80 and 90 HU, different from the muscle (70 HU) and the fat tissue (100/200 HU).

Moreover, the tumoural mass often shows structural inhomogeneities with intralesional necrosis.

Some oropharyngeal tumours (15%) can be isodense to the muscle on CT scan.

MRI presents an excellent tissue contrast which allows easily differentiation between tumour and normal structures (2–4).

This peculiarity is useful in detection of small neoplasm in the oropharynx (4).

In addition to general diagnostic signs, analogous to CT scan, MRI evaluation offers specific findings.

In T1-weighted images, neoplastic tissue is significantly hypointense in comparison with fat tissue. Also, tumours are slightly hypontense or isointense than muscles.

In T2-weighted images, tumours have high signal intensity. Peritumourous oedema may also produce high signal leading to over-estimation of tumour size.

Therefore, MRI sensitivity can be improved using fat suppression techniques (FS-T2 FSE or STIR sequences). (Fig. 1).

After gadolinium injection, all neoplasms show contrast-enhancement, better depicted using fat suppression techniques on T1-weighted sequences.

Spread Patterns and Lymphatic Drainage

Oropharyngeal tumours present different spread patterns in relation to the site of origin (1, 2, 4).

Carcinomas arising on the anterior tonsillar pillar (ATP) tend to spread along the palatoglossus muscle and its fascial attachments as far as to the tongue base.

The neoplasm may spread superiorly to the soft palate and to nasopharynx. Nasopharyngeal infiltration is usually unilateral. The lymphatic drainage of ATP tumours is primarily to the submandibular and internal jugular nodes (2, 4).

Isolated carcinomas of posterior tonsillar pillar (PTP) are rare and usually small.

Carcinomas of the tonsil can spread anteriorly to involve the tongue base, the floor of the mouth and retromolar trigone; laterally, neoplasm can involve

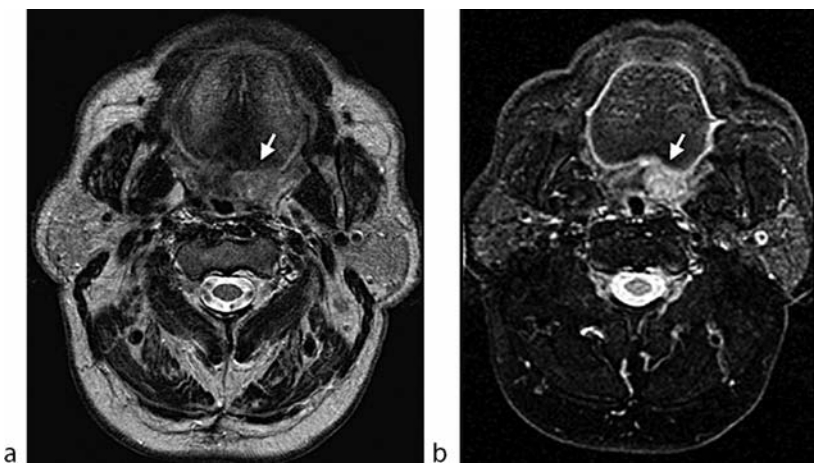

Neoplasm, Oropharynx. Figure 1 SCCA of palatine tonsil. Axial FSE T2-weighted image. A small tonsillar tumour is visible on the left side (arrow). The neoplasm is substantially isointense to contiguous normal tissues. Axial fat suppression T2-weighted image. The fat saturation technique allows easier the tumour detection (arrow).

parapharyngeal, masticator and carotid spaces; superiorly, the soft palate and the nasopharynx. (Fig. 2)

Lymph node metastasis occurs primarily in the upper internal jugular or retropharyngeal nodes (2, 4).

SCCA of tongue base may extend laterally to involve the mandible and medial pterygoid muscles; superiorly, to tonsillar fossae and soft palate; anteriorly to the oral tongue and floor of the mouth; inferiorly, to the vallecula, pre-epiglottic space, epiglottis or hypopharynx. (Fig. 3) Lymphatic drainage is often to internal jugular and submandibular nodes (2, 4).

Tumours arising from the soft palate can spread in any direction. The tonsillar pillars and hard palate are usually involved first. Deeply, these neoplasms can involve parapharyngeal space, the nasopharynx and the skull base. Palatal carcinomas drain first to upper internal jugular and subdigastric nodes, with subsequent involvement of lower internal jugular or retropharyngeal nodes.

SCCA of the posterior oropharyngeal wall spread inferiorly into the hypopharynx and cranially into nasopharynx. They commonly spread submucosally invading the retropharyngeal fat. Lymphatic drainage is to submandibular and jugulo-digastric nodes (2, 4).

For depiction of tumour spreading, sagittal and coronal images on both CT scan and MRI are well-suited. On MRI, T2-weighted FSE with fat suppression, FS T1-weighted FSE or T1-weighted GE after gadolinium injection are very sensitive in lymphadenopathy detection.

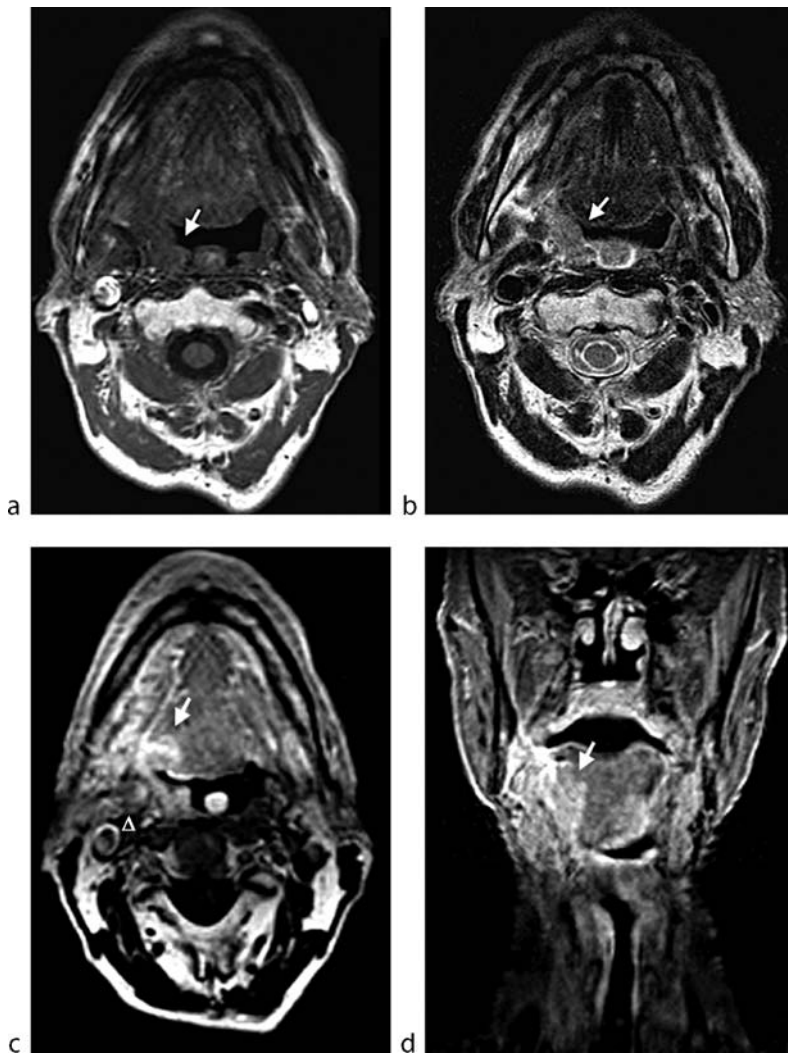

Neoplasm, Oropharynx. Figure 2 SCCA of palatine tonsil. (a, b) Axial T1 and T2-weighted images show a tonsillar tumour on the right side (arrows). The lesion is about 2 cm in diameter. (c, d) Axial and coronal Gd-DTPA fat suppression T1-weighted images. The tumoural tissue shows intense enhancement. Note the tumoural spreading to the tongue base, anteriorly (arrows), and to parapharyngeal space, laterally (arrowhead).

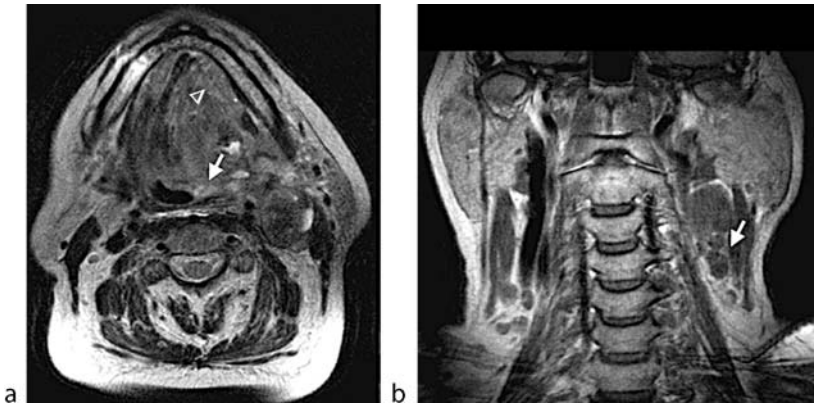

Neoplasm, Oropharynx. Figure 3 SCCA of tongue base. Axial T2-weighted image. A neoplastic mass is visible on the left side of the tongue. Note the bulging of the free edge of the tongue (arrow) and the infiltration of the mylohyoid muscle (arrowhead). Coronal T1-weighted image shows ipsilateral lymphadenopathies along the course of the internal jugular chain (arrow).

Nuclear Medicine

18-FDG positron emission tomography (PET) and PET/CT scan fusion have useful role in the follow-up of patients with head and neck cancers to localise tumour remnants or relapses and to define radiotherapic planning of treatment.

Bibliography

1. Yates CB, Phillips CD (2001) Oral cavity and oropharynx. Curr Probl Diagn Radiol 30(2):38–59
2. Mukherji SK, Holliday RA (1996) Pharynx, chapter 8. In: Som PM, Curtin H (eds) Head and Neck Imaging. Mosby, St. Louis
3. Lenz M, Grees H, Dobritz M (2000) Kersting-Sommerhoff B. Methods: MRT. Eur J Radiol 33:178–184
4. Lenz M, Grees H, Baum U, et al (2000) Oropharynx, oral cavity, floor of the mouth: CT and MRI. Eur J Radiol 33:203–215

Neoplasms, Parathyroid

Emanuele Neri, Salvatore Mazzeo, Valentina Battaglia
Diagnostic and Interventional Radiology, University of Pisa, Italy
neri@med.unipi.it

Synonyms

Parathyroid adenoma; Parathyroid cancer

Definitions

Parathyroid glands are four small endocrine glands, exceptionally five or six, located behind the thyroid lobes; 80% of superior parathyroid glands are located at the cricothyroid junction, while inferior parathyroid glands are variably located (61% near the lower pole of the thyroid lobes and 26% in thyrothymic ligament). Incidence of ectopic parathyroid glands reported is variable (2 to 8%).

Parathyroid glands regulate the calcium level through the secretion of the parathyroid hormone (PTH).

Primary parathyroid gland carcinoma is extremely rare, with an estimated annual prevalence of about 0.005%, i.e. five cases of primary carcinoma/100,000 cases of primary hyperparathyroidism (HPT) or less than 1% of all cases of HPT.

Parathyroid adenomas (PA), that are benign tumors, account for 85% of all cases of this disease. Most are functional and cause excessive secretion of PTH, resulting in HPT.

In addition to the solitary or sporadic PA tumors, approximately 5% are associated with hereditary cancer syndromes such as multiple endocrine neoplasia (MEN).

Pathology/Histopathology

Parathyroid glands are composed of chief cells, oxyphilic cells and intermediate cells. Histologically, primary HPT can be attributed to a single adenoma in 80 to 85% of cases, hyperplasia in 15 to 20% of cases and carcinoma in 1% of cases. Double or multiple adenomas have been reported in patients with primary HPT including MEN.

Hyperplasia is defined as an enlargement of more than two glands, whereas adenoma is traditionally considered to be a single gland disorder. The parathyroid adenoma consists of hypercellular parathyroid tissue arranged in solid sheets or cords with a trabecular pattern. Occasionally, interspersed adipocytes are seen with the adenoma. Nuclear pleomorphism may be present; however, mitoses, capsular invasion, or vascular invasion mitigate against a benign lesion. Parathyroid adenomas include the following subtypes: oncocytic adenoma, lipoadenoma, large clear cell adenoma, water-clear cell adenoma and atypical adenoma.

Clinical Presentation

Most PTG tumors are functional and cause excessive secretion of PTH, resulting in HPT.

HPT may be classified as a primary, secondary, or tertiary disorder.

Primary HPT is caused by PA.

Secondary HPT (hyperplasia) develops in response to chronic depression of serum calcium levels, generally due to renal impairment. In a minority of patients, this parathyroid hyperactivity becomes autonomous, resulting in tertiary HPT.

Widespread testing of calcium in blood using automated analyzers in the clinical laboratory has led to the detection of hypercalcemia early in the course of HPT and in the majority of cases before other signs of HPT are apparent. Symptoms of HPT can be variably, aches and pains, depression, abdominal pain, nausea, vomiting, fatigue, excessive urination, confusion, muscle weakness.

The excess calcium released by the bones leads to osteoporosis, osteomalacia and kidney stones, because of high levels of calcium excreted into the urine by the kidneys.

Imaging

Diagnostic imaging of parathyroid is not essentially aimed to diagnose HPT, but to detect hyperplasia or neoplasms in the parathyroids or in ectopic glands. It is still controversial the use of imaging in preoperative evaluation; surgical series shows that the success rate of the intervention is excellent (95%) even if a preoperative imaging is missed. However, there is general agreement that imaging is required in cases with persistent or recurrent HPT after surgery.

At present, ultrasound (US) and SPECT scanning with Tc-99m Sestamibi are the first imaging steps and the preferred methods to identify a pathologic parathyroid gland before surgery. US has a high sensitivity in detecting parathyroid adenomas in patients without thyroid diseases associated (90%) and lower in presence of thyreopaties (70%). Sensitivity reported of SPECT ranges between 70 and 100%. US can be useful mainly in localizing parathyroid cervical adenomas and in perithyroidal region, but it frequently fails in identifying ectopic lesions such as for parathyroid adenomas localized in the mediastinum and retro or paratracheoesophageal compartment (Fig. 1). US must be performed with high resolution linear transducers (at least 10MHz), and a critical factor influencing the accuracy of the technique is the experience of the examiner; this explains the variance of sensitivity among different authors. Therefore, the use of US can be suggested only if an experienced operator is performing the exam.

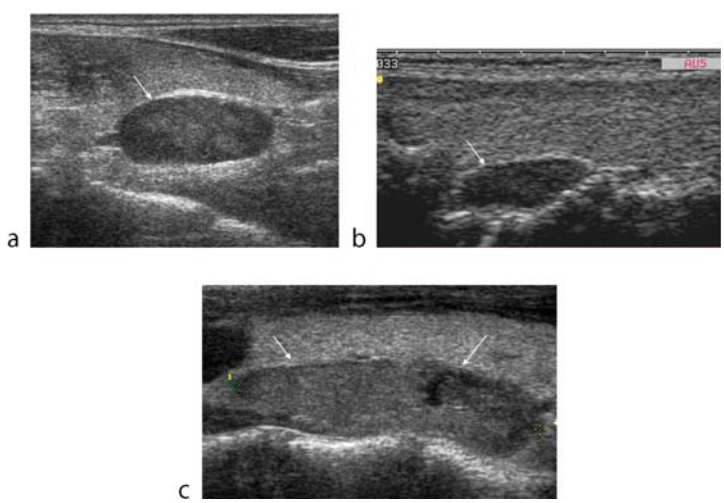

Neoplasms, Parathyroid. Figure 1 US: Typical hypoechoic pattern and shape of the lower (a) or upper (b, c) parathyroid lesions (*arrows*).

In case of thyroid goiter, the detection of parathyroid lesion can be more difficult.

The use of color-Doppler US examination is frequently helpful to differentiate parathyroid from thyroid nodules or cervical lymphnodes on the basis of the different vascular pattern.

SPECT is performed by injecting 20 to 25 mCu of technetium-99m sestamibi; images are obtained at 10–15 min then 2–3 h after the injection. Late phase is preferable for detecting parathyroid adenomas, as thyroid nodules clear uptake faster than do parathyroid neoplasms.

Sestamibi is taken up by the high mitochondrial content of adenomatous parathyroid cells, greater than surrounding parenchyma. False positive cases can be caused by solid thyroid nodules (adenomas), Hurthle cell carcinoma, malignant thyroid lymph node metastases.

It is proven that a combination of US and SPECT results in improved diagnostic accuracy before surgery in pre-operative diagnosis of parathyroid disease.

MRI can be extremely valuable for localizing a parathyroid adenoma although the sestamibi has decreased the need for it dramatically. At best, an MRI will find less than 10% of diseased parathyroid glands; therefore the indications for getting this scan are very few.

A renewed interest has received CT, with the advent of the multidetector technology. Multidetector CT allows to

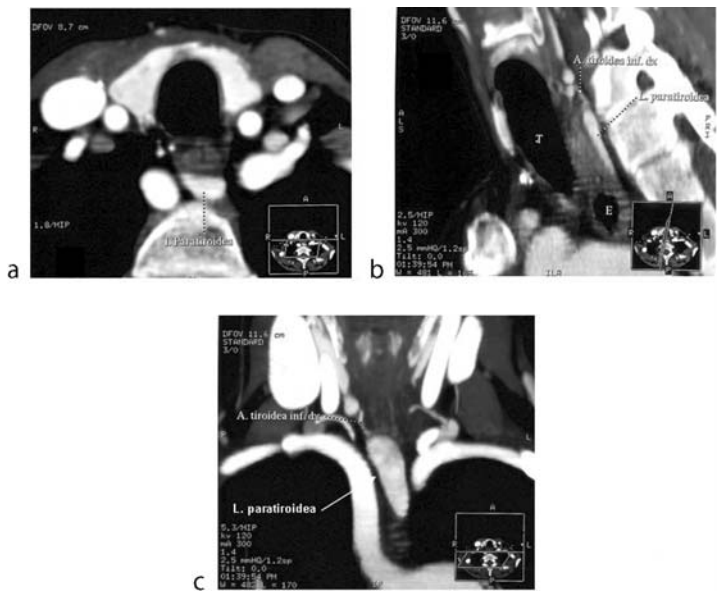

Neoplasms, Parathyroid. Figure 2 Multidetector CT: Retroesophageal parathyroid lesion (ectopic site). Axial (a), sagittal (b) and coronal scan (c).

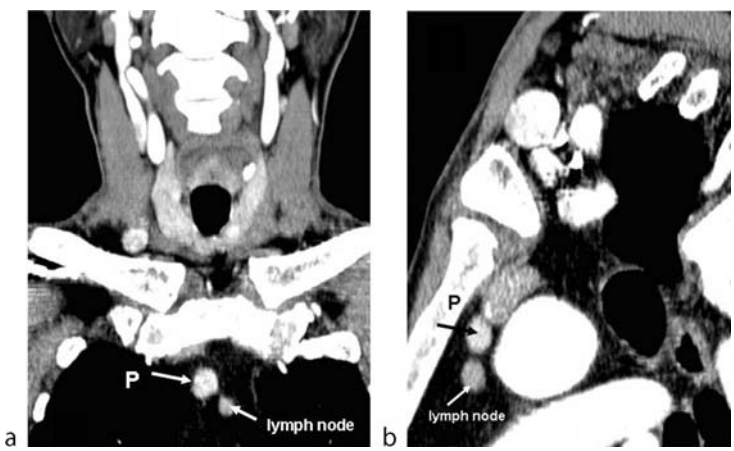

Neoplasms, Parathyroid. Figure 3 Multidetector CT: The scan distinguishes hypervascular retrosternal parathyroid nodule (P) from hypodense lymph-node. Axial (a) and sagittal (b) scan.

study at very high resolution and with optimal contrast enhancement the mediastinal area. Ectopic parathyroids can be detected as hypervascular nodules and well differentiate from lymph nodes (hypovascular) (Figs 2 and 3).

Diagnosis

Diagnosis of HPT is based on two laboratory evidences, elevated serum Ca and elevated PTH (suppressed in PTH-rp induced hypercalcemia). The 2002 National Institutes of Health (NIH) consensus panel on the management of asymptomatic primary HPT (2002 NIH Panel) classified primary HPT into two categories: asymptomatic and symptomatic. Asymptomatic primary HPT accounts for 75 to 80% of all HPT cases. In both asymptomatic and symptomatic HPT, hypercalcemia in concert with an increased serum PTH concentration is the biochemical hallmark for the diagnosis of primary HPT. Other useful tests can be the dosage of albumin, phosphorous, BUN/Cr, 24-h urine Ca (r/o FHH) and bone mineral density.

Imaging is essentially used for pre-operative planning or in case of recurrent HPT after surgery.

Bibliography

1. Adami S, Marcocci C, Gatti D (2002) Epidemiology of primary hyperparathyroidism in Europe. J Bone Miner Res 17 Suppl 2:N18–N23
2. Mazzeo S, Caramella D, Lencioni R et al (1995) [Preoperative imaging in the detection of parathyroid tumefaction in patients with primary hyperparathyroidism. The authors' own experience] Radiol Med (Torino) Dec 90(6):747–755. Italian
3. Mazzeo S, Caramella D, Marcocci C et al (2000) Contrast-enhanced color Doppler ultrasonography in suspected parathyroid lesions. Acta Radiol Sep 41(5):412–416
4. Mazzeo S, Caramella D, Lencioni R et al (1996) Comparison among sonography, double-tracer subtraction scintigraphy, and double-phase scintigraphy in the detection of parathyroid lesions. Am J Roentgenol Jun 166(6):1465–1470
5. Adams BK, Devi RT, Al-Haider ZY (2004) Tc-99m sestamibi localization of an ectopic mediastinal parathyroid tumor in a patient with primary hyperparathyroidism. Clin Nucl Med Jun 29(6):388–389

Neoplasms, Phyllodes, Breast

Luis Pina
Department of Radiology, Clínica Universitaria de Navarra, Navarra, Spain
ljpina@unav.es

Synonyms

Cystosarcoma phyllodes; Phyllodes tumor

Definition

Phyllodes tumor is a fibroepithelial tumor of the breast that exhibits a diverse range of biologic behavior (1).

Pathology

The gross appearance is a round to oval well-circumscribed mass without a true capsule. Microscopically, this tumor shows a variety of appearances from those resembling ►fibroadenomas to others like sarcomatous tumors. Many phyllodes tumors show a characteristic leaf-like architecture. The epithelial component is usually single layered, but other changes, such as hyperplasia, atypical hyperplasia, or *in situ* carcinoma, may be seen. However, the stromal component determines their clinical behavior. Four histologic features are important for classifying this lesion (1): (i) stromal cellular atypia, (ii) mitotic activity per 10 high-power fields, (iii) stromal overgrowth, and (iv) tumor margins. Phyllodes tumors can be classified into three categories: benign, borderline, and malignant. The first type shows increased stromal cellularity with mild to moderate atypia, low mitotic rates (<4/10), no stromal overgrowth, and well-circumscribed margins. ►Borderline phyllodes tumors have stromal atypia, mitotic rates between 4/10 to 9/10, no stromal overgrowth, and they can have microscopically infiltrative margins. Malignant cases are characterized by severe stromal cellularity and atypia, high mitotic rates (10/10), infiltrative borders, and stromal overgrowth (Fig. 1).

Clinical Findings

Phyllodes tumors are rare lesions, accounting for no more than 0.3–1% of all primary breast tumors (2). Patients are typically one decade or more older than women with fibroadenomas. Malignant cases still affect older patients (1).

Usually, these lesions present as smoothly marginated, round or polylobulated palpable masses resembling fibroadenomas. An important feature is a rapid growth, sometimes from a previously stable nodule. Very large tumors may cause visible bulging and skin ulceration (1, 2).

Recurrence may be found in 21% of cases (2). A surgical excision with wide margins (>10 mm) is associated with a low risk of recurrence.

Axillary dissection is not routinely performed since nodal involvement is very rare.

Hematogenous metastases of malignant cases are uncommon, accounting for 10% of all phyllodes tumors (2). The lung is the most commonly affected organ.

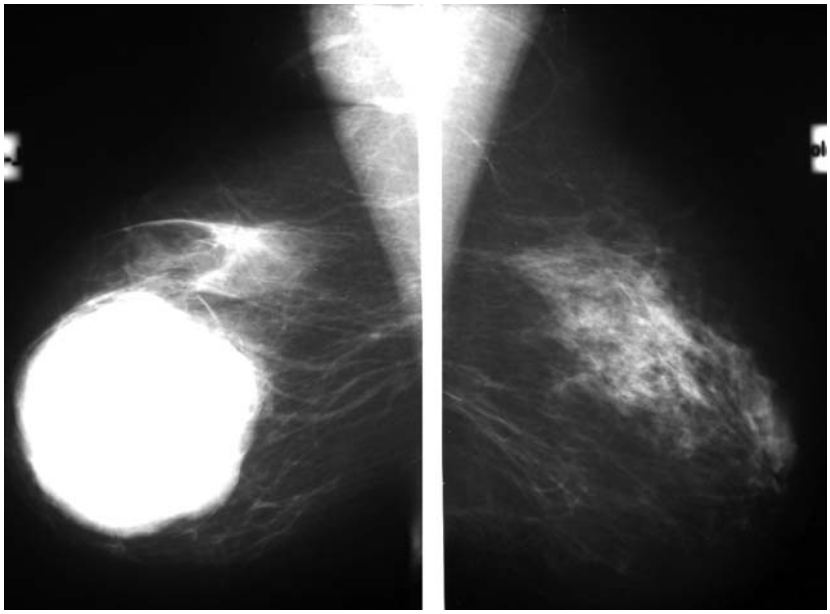

Neoplasms, Phyllodes, Breast. Figure 1 Well-circumscribed round mass. Notice the high density of the lesion. The patient, a 59-year-old woman, reported a rapid growth in the last 3 months. Pathology: ▶malignant phyllodes tumor.

Imaging

Mammography

Mammographic features are similar to those of fibroadenomas showing as oval, round or lobulated masses with well-circumscribed margins, but occasionally indistinct margins may be seen (Figs. 1 and 2). However, adjacent fibroglandular tissue may occult the lesion. Sometimes mammography may detect coarse calcifications inside a phyllodes tumor, similar to fibroadenomas. Lesions greater than 30 mm are more likely to be malignant.

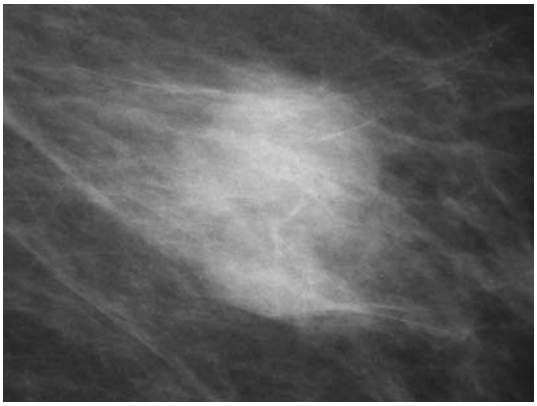

Neoplasms, Phyllodes, Breast. Figure 2 A lobulated mass with indistinct margins. Craniocaudal view, (detail). Biopsy revealed a ▶benign phyllodes tumor.

Ultrasound

Phyllodes tumors appear as oval, round, or lobulated masses with well-delimited margins and acoustic enhancement, resembling fibroadenomas. However, ultrasound may detect internal cysts and heterogeneous echostructure (Fig. 3). Both findings are not specific, but very often they lead to a biopsy (3, 4).

Magnetic Resonance

Phyllodes tumors present as oval, round, or lobulated well-circumscribed masses, usually hyperintense on T2-weighted images. After contrast medium administration, these lesions enhance rapidly. The role of magnetic resonance is not well established, but it may be useful for planning conservative surgery or evaluating thoracic wall involvement (4).

Nuclear Medicine

There are no indications for the diagnosis of phyllodes tumor.

Diagnosis

The rapid growth of a palpable, round to oval smoothly marginated mass is the main symptom to raise the suspicion of a phyllodes tumor. However, the widespread use of mammography has led to the detection of nonpalpable

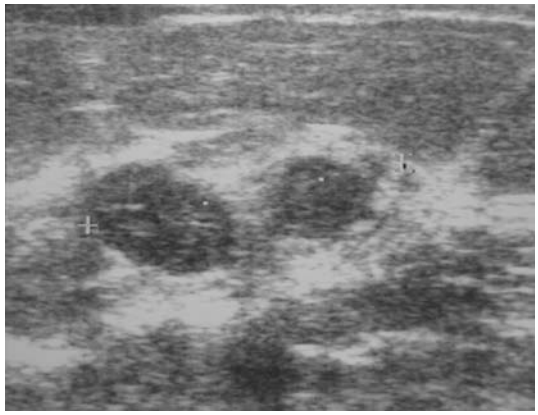

Neoplasms, Phyllodes, Breast. Figure 3 Ultrasonography of the case presented in Fig. 2. Lobulated hypoechoic solid mass.

phyllodes tumors. The main goal is to differentiate them from other benign lesions, such as fibroadenomas (1). This differentiation is usually difficult without a biopsy.

The fibroepithelial composition of phyllodes tumors is similar to fibroadenomas, and this feature makes the differentiation between both lesions difficult. Furthermore, the wide spectrum of benign to malignant cases increases this difficulty. Fine-needle aspiration usually fails to distinguish fibroadenoma and phyllodes. The cystic component may be misinterpreted as "fibrocystic change." Core needle biopsy may suggest the diagnosis, but the differentiation with a fibroadenoma may be impossible. In most cases excisional biopsy is needed for diagnosis, especially if a rapid growth of a solid mass is detected (1, 5).

Bibliography

1. Anderson BO, Lawton TJ, Lehman CD et al (2004) Phyllodes tumors. In: Harris JR, Lippman ME, Morrow (eds) M et al Diseases of the Breast. Lippincott Williams & Wilkins, Philadelphia, pp 991–1006
2. Bellocq JP, Magro G (2003) Fibroepithelial tumours. In: Tavassoli FA, Devilee P (eds) Pathology and Genetics of Tumours of the Breast and Female Genital Organs. International Agency for Cancer, Lyon, pp 99–103
3. Cardeñosa G (2001) Lobules. In: Cardeñosa G (ed) Breast Imaging Companion. Lippincott Williams & Wilkins, Philadelphia, pp 269–306
4. Heywang-Köbrunner SH, Schreer I, Dershaw DD (eds) (1997) Other semi-malignant and malignant tumors. Diagnostic Breast Imaging. Stuttgart, Thieme, pp 265–279
5. Hughes LE (2000) Fibroadenoma and related tumors. In: Hughes LE, Mansel RE, Webster DJT (eds) Benign Disorders and Diseases of the Breast. Concepts and Clinical Management. Saunders, London, pp 73–94

Neoplasms Pulmonary

Katharina Marten, Christoph Engelke
Department of Radiology, Klinikum rechts der Isar, Technical University Munich, Munich, Germany
katharina.marten@roe.med.tu-muenchen.de

Synonym

Pulmonary neoplasms

Definition

Primary neoplasms of the lung encompass numerous distinct histological entities that arise from various pulmonary tissues and are best categorised according to the classification scheme proposed by the world health organisation (WHO). These tumours include pulmonary carcinoma, neuroendocrine neoplasms, neoplasms of the tracheobronchial glands, tracheobronchial papillomas and rarely among others, primary pulmonary lymphoma, primary pulmonary sarcoma, ►pulmonary haemangiopericytoma and ►malignant angioendotheliomatosis.

Pathology/Histopathology

The term pulmonary carcinoma refers to tumours arising from the epithelial surface of the bronchi and alveoli, and embraces four main histological subtypes: adenocarcinoma, squamous cell carcinoma, small cell carcinoma and large cell carcinoma.

Adenocarcinoma (Figs. 1, 2) is the most common pulmonary carcinoma in the United States, accounting for about 30–35% of all cases, and can be subdivided into four histological subtypes: acinar carcinoma, papillary carcinoma, solid carcinoma with mucin formation and ►bronchioloalveolar carcinoma (BAC). Most adenocarcinomas (except BAC) are peripherally located and well circumscribed. BAC may present as solitary nodule or as parenchymal consolidation. Non-destructive growth is a characteristic feature, as tumour cells spread along the pulmonary framework, commonly forming a single layer. The surrounding interstitium is thickened by fibrous tissue or a chronic inflammatory infiltrate. Focal fibrosis and necrosis occur frequently, while cavitation is relatively rare (1–3).

Squamous cell carcinomas (Fig. 3) account for about 30% of all pulmonary carcinomas. Most frequently they arise from the segmental or lobar bronchial epithelium. Early lesions may expand within the bronchial mucosa

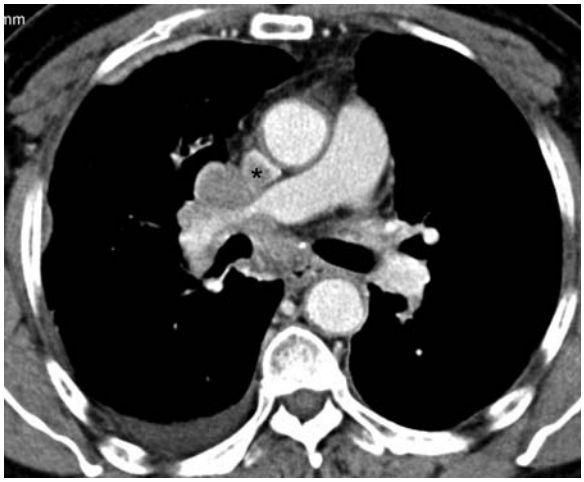

Neoplasms Pulmonary. Figure 1 Sixty-nine year-old woman with stage IV inoperable non-small-cell Lung cancer of the right upper lobe. Note the tumour compression of the right pulmonary artery, the invasion into the ▶superior vena cava (*) and the infracarinal mediastinum. There is right-sided pleural effusion containing malignant cells due to pleural invasion.

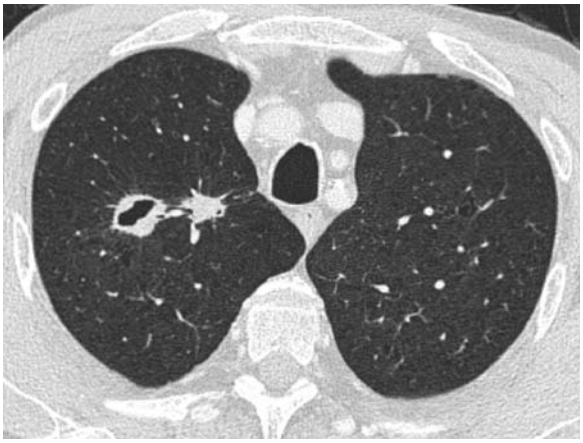

Neoplasms Pulmonary. Figure 3 Fifty-three year-old male smoker with cavitating nodule and solid satellite nodule in the apical right upper lobe segment displaying extensive marginal spiculations and feeding bronchus. Note the moderate centrilobular bilateral emphysema of the upper lobes. The lesions were bioptically confirmed as non-small-cell lung cancers.

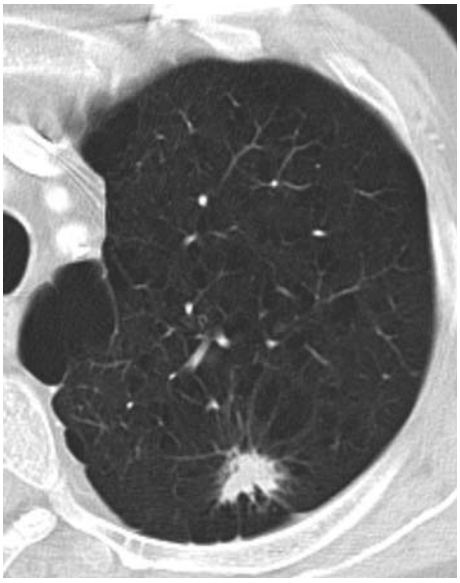

Neoplasms Pulmonary. Figure 2 Seventy-one year-old male smoker with incidental finding of a 1.8 cm solid nodule in the posterior left upper lobe segment displaying spiculated margins and pleural tags. Note the advanced centrilobular emphysema of the right upper lobe. The lesion was bioptically confirmed as non-small-cell lung cancer.

without invasion into the airway lumen or the peribronchial tissue. At a later stage, however, most lesions invade and obliterate the bronchial lumen as polypoid or papillary tumours with subsequent airway obstruction expressed by distal atelectasis and obstructive pneumonitis. Large tumours often display central necrosis and erosion into a local bronchus with drainage of necrotic parts and resulting cavitation. Histologically, invasive squamous cell carcinoma is characterised by inter-cellular bridges and/or keratinisation. Tumours may be well differentiated, displaying obvious keratinisation, or are poorly differentiated, rendering differentiation from large cell or small cell carcinoma difficult. Histological variants of squamous cell carcinoma include small cell, papillary, clear cell and basaloid tumours (1, 2).

Small cell carcinoma (Fig. 4) contributes to about 15–25% of all pulmonary carcinomas. Evidence suggests that it is a neuroendocrine tumour, most likely derived from undifferentiated airway epithelial cells capable of neuroendocrine differentiation. Small cell carcinoma is typically located in the vicinity of proximal airways, most commonly of lobar and main bronchi. Rarely, tumours are located in the lung periphery without obvious airway association. Early, centrally located small cell carcinoma is frequently poorly defined and spreads along submucosal and peribronchovascular connective tissues. Advanced lesions invade the adjacent lung parenchyma and obliterate underlying bronchi and vascular structures. Endobronchial growth occurs much less frequently than in squamous cell carcinoma. Histologically, tumour cells may be round or fusiform and may be grouped in clusters, sheets or rosettes; stroma is normally scanty. Necrosis is frequent; a desmoplastic reaction is commonly minimal or absent (1, 2).

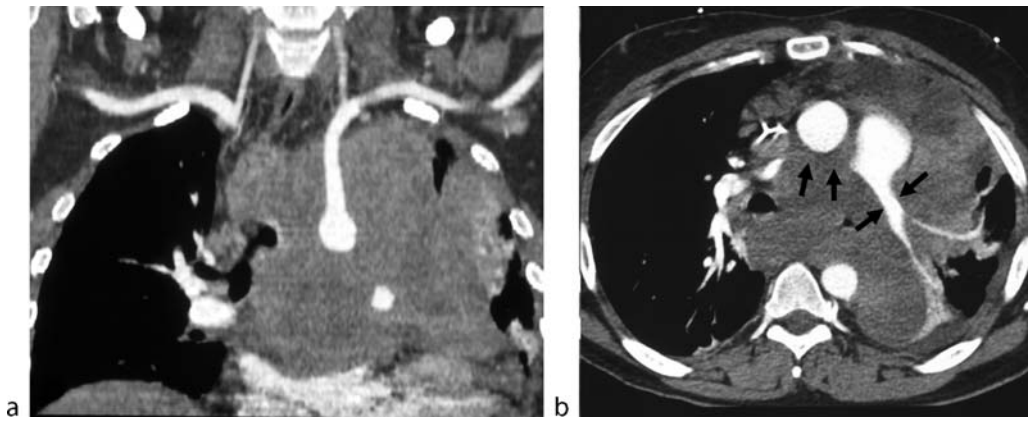

Neoplasms Pulmonary. Figure 4 Forty-nine year-old male smoker with extensive disease from small-cell lung cancer. (a) There is complete mediastinal encasement by tumour masses. (b) The patient had massive secondary pulmonary hypertension with dilated pulmonary artery trunk due to compression of the main pulmonary arteries (arrows).

Large cell carcinoma is diagnosed in 15–20% of pulmonary carcinoma cases. Most frequently it occurs in the lung periphery and often has a bulky appearance. Cavitation is rare, but focal necrosis is a common feature. Large cell carcinoma consists of sheets of large cells containing abundant eosinophilic cytoplasm. Inter-cellular bridges, keratinisation, acinar or papillary structures are absent. A number of histological subtypes exist, e.g. large cell neuroendocrine carcinoma, clear cell carcinoma, basaloid carcinoma and lymphoepithelioma-like carcinoma, among others (1, 2).

Neuroendocrine neoplasms encompass carcinoid tumours, pulmonary tumorlets and neuroendocrine cell hyperplasia. These tumours display common ultrastructural and immunohistochemical features resembling neuroendocrine cells, i.e. cells that contain neurosecretory granules and polypeptide hormones that occur in the normal tracheobronchial epithelium. Carcinoid tumours are low-grade malignancies, which are derived from the glandular or surface epithelium of the airways. Clinicopathologically, they are subdivided into typical and atypical forms. About 80–90% of cases are typical carcinoids that most frequently arise within lobar, segmental or proximal subsegmental bronchi (1). Occasionally, multiple tumours occur. Typical carcinoids are histologically well-defined tumours, which may be separated from the adjacent airway epithelium by a thin layer of connective tissue. If there is association to an airway, the epithelium is commonly intact and may display squamous metaplasia or ulceration. The overall histological pattern of atypical carcinoids closely resembles that of typical carcinoids. However, atypical carcinoids display increased mitotic activity, nuclear pleomorphism and hyperchromasia, areas of increased cellularity or necrosis.

The term *neoplasms of the tracheobronchial glands* refers to a group of tumours with the histological appearance of tracheobronchial mucous glands, with close resemblance of oropharyngeal salivary glands. The most common histological types are adenoid cystic carcinoma and mucoepidermoid carcinoma. Adenoid cystic carcinoma most commonly arises within the tracheal and main bronchial lumen and in about 10–15% in the lung periphery. Mucoepidermoid carcinoma develops in the trachea and bronchi (1, 2).

Clinical Presentation

The clinical presentation of lung neoplasms is non-specific, and symptoms commonly occur only at an advanced tumour stage. They may reflect local disease, particularly tracheal or bronchial obstruction (e.g. wheeze, cough, haemoptysis or obstructive pneumonitis), or originate from tumour invasion into neighbouring anatomic structures such as the mediastinum or the chest wall. At late stages distant hepatic, osseous or cerebral metastases may cause symptoms specific to their locations. ▶Paraneoplastic syndromes (see keywords) may result from hormone secretion by the tumour or from immunologic reactions. Non-specific symptoms further include fatigue and weight loss.

Imaging

On chest radiography (CXR) and CT, *pulmonary carcinomas* commonly present as a lung nodule (lesser than 3 cm in size) or a pulmonary mass. This is particularly the case in squamous cell and adenocarcinomas, whereas small cell carcinomas may present with

isolated hilar or mediastinal lymphadenopathy. Occasionally, obstructive pneumonitis or atelectasis may occur as isolated findings, predominantly in squamous cell and small cell carcinomas. Differentiation of the obstructing tumour from post-obstructive atelectasis may be challenging. On CXR, segmental or lobar atelectasis, consolidation and mucous plugging of bronchi distal to the obstruction are common. A specific feature is 'Golden's S sign' which refers to a focal convexity of the tumour with the concave shape of the inter-lobar fissure resulting from distal atelectasis with a characteristic S-shaped configuration. On CT, the tumour displays moderate contrast enhancement (15–30 Hounsfield units (HU) for most lesions on dynamic contrast-enhanced scans), whereas areas of atelectasis enhance conspicuously (>50 HU).

Peripheral carcinomas presenting as a pulmonary nodule may rarely display calcifications that are typically eccentric and result from tumoural engulfment of a pre-existing granuloma. Calcifications are more common in mass lesions larger than 3 cm in size. Carcinomas commonly display irregular, spiculated margins. Smooth or lobulated margins occur less frequently. Air bronchograms or bronchiolograms may be detected after engulfment of these structures by the tumour. Cavitation of peripheral carcinomas occurs most frequently with squamous cell carcinoma and is associated with hilar or mediastinal lymphadenopathy. A very important CT feature is the air-space pattern which almost exclusively occurs in BAC, reflecting the non-destructive growth of these tumours. This pattern may be localised or diffuse ranging from ground-glass opacification to frank air-space consolidation without displacement of normal lung structures. In mixed subtype adenocarcinomas with BAC component, a prominent BAC component is likely to have a ground glass appearance, while adenocarcinomas with invasive component are likely to be solid on thin section CT. This differentiation is important because lesions with large ground glass components are less likely to have vascular invasion or lymph node metastases. Mixed subtype adenocarcinomas with BAC component may occur as solitary or multiple unilateral or bilateral nodules, or a large mass with satellite nodules within the same lobe. The lobar consolidation pattern in BAC which is commonly combined with the 'CT angiogram sign' in BAC refers to well-opacified vessels surrounded by low-density pulmonary parenchyma following contrast administration; however, it is difficult to distinguish from pneumonia and may also occur in other disorders (1, 3).

Carcinoid tumours most commonly present with evidence of airway obstruction on CXR, as a large majority of these tumours (80–85%) are located within lobar or segmental bronchi (1). Complete obstruction will induce peripheral atelectasis, reflected by increased attenuation with loss of volume or precipitate obstructive pneumonitis with features of pneumonia commonly without volume loss. Recurrent infections distal to the obstruction site may result in bronchiectasis and lung abscesses formation. In cases of partial proximal airway obstruction, hypoxic vasoconstriction and volume loss of the dependent lung may suggest the presence of an endobronchial lesion and should prompt bronchoscopy. Peripherally located carcinoid tumours present as pulmonary nodules that are well-defined, homogeneous, often lobulated, round or oval in shape. Most lesions measure 1–3 cm in diameter; however, large lesions also occur, particularly in atypical carcinoid tumours. Intratumoural calcification is frequently detected on CT and may display variable patterns (1).

Adenoid cystic carcinoma presents as a lobulated, polypoid or smooth endotracheal or endobronchial mass on CXR which encroaches onto the airway lumen. CT is an excellent tool for the assessment of extraluminal growth and mediastinal invasion. The radiographic features of *mucoepidermoid carcinoma* are variable, ranging from a solitary nodule or mass to consolidation, atelectasis or a central mass with obstructive pneumonitis. The CT findings include a mass, which is oval or lobulated in shape, and may display punctuate calcifications. With involvement of the trachea there may be an evidence of an intra-luminal nodule on CT and with larger lesions also on CXR.

Tracheobronchial papillomas may be solitary or multiple and are seen on CXR and CT as nodules within the airway lumen. On CT the presence of multiple papillomas may be evident by the detection of diffuse nodular thickening of the tracheal wall. Chronic bronchial obstruction is bound to induce atelectasis, obstructive pneumonitis or bronchiectasis, while partial obstruction may as well cause the decreased perfusion and decreased attenuation pattern of the affected parenchyma. With tumour involvement of the distal airways and lung parenchyma, a nodular pattern may be evident with predilection for the perihilar and posterior lung regions. Cavitation of such nodules, with occasional air–fluid level formation, is more frequent with larger lesions (2).

Primary pulmonary lymphoma may present as single or more commonly multiple pulmonary nodules or masses 2 mm to 8 cm in size, as well as unilateral or bilateral areas of consolidation. Distribution is frequently peribronchial, air bronchograms commonly occur. Less common findings on CT are thickening of the bronchovascular bundles, ground-glass opacification and septal lines (1).

Nuclear Medicine

Positron-emission tomography (PET) using intravenous administration of 2-(fluorine-18)-fluoro-2-deoxy-D-

gluocose (^{18}FDG) is likely to become more important for the diagnosis of lung neoplasms in the future, particularly for the differentiation of benign from malignant pulmonary nodules larger than 8–10 mm in size. ^{18}FDG-PET imaging relies on physiologic glucose metabolism to diagnose lung cancer and has a high sensitivity and specificity for malignant nodules of at least 0.8 cm in diameter. However, false-positive diagnoses occur in active granulomatous infections, whereas false-negative diagnoses are commonly encountered in BAC and carcinoid tumours. Single-photon emission computed tomography (SPECT) imaging is clearly inferior to PET imaging in the differentiation of benign and malignant pulmonary nodules. Both PET and SPECT, however, play important roles in lymph node staging of lung cancer, with their sensitivities and specificities for diagnosis of malignant lymphadenopathy reaching 80%. Imaging of distant metastasis of lung cancer has also become a domain of PET-imaging, particularly in combination with CT. Octreotide-PET imaging holds promise in the diagnosis of small peripheral carcinoid tumours with ectopic ACTH production, that are difficult to detect on CT (4, 5).

Diagnosis

The capacity of CXR to reveal early stage lung neoplasms is limited. Recent technologic advances with application of computer-aided diagnosis and dual-energy subtraction methods on digital CXR data may offer certain improvements on this. Latest technologies in CT, particularly thin-collimation multislice CT (MSCT) possess a very high sensitivity for the detection of pulmonary nodules, but have a limited specificity for diagnosis of lung cancer (6). Advances in scanning technique such as dynamic contrast-enhanced CT for perfusion imaging, as well as recognition and metric assessment by computer-aided diagnosis with automated nodule volumetry may enhance its ability to determine nodule growth and therefore help to diagnose malignancy at an early stage. Sputum analysis encompasses sputum cytology, sputum immunostaining and newer methods such as sputum polymerase chain reaction based assays for detecting oncogene mutations. Sputum cytology has a relatively low overall sensitivity for detection of lung cancer of 20–30%, showing moderate variation with the employed technique. The sensitivity is highest for squamous cell carcinoma and lowest for adenocarcinoma. Centrally located lesions, lesions larger than 2 cm and lower lobe lesions are best detected with sputum cytology. The false-positive rate is very low (<2%). *Conventional bronchoscopy* is valuable for detection of nodular or polypoid lesions larger than 2 mm and flat or superficially spreading lesions greater than 2 cm. *Autofluorescence bronchoscopy* is an optical imaging method used for localisation of small pre-invasive lesions that are not visible by conventional white light bronchoscopy. *Percutaneous transthoracic needle core biopsy* (PTNB) under CT guidance is performed for histological diagnosis of lung nodules, masses and infiltrates, particularly if malignancy is suspected. A specific benign diagnosis is infrequently made using PTNB, but when obtained, can obviate surgery. CT fluoroscopy offers advantages in needle guidance and permits more rapid and accurate biopsy procedures in pre-selected cases. *Video-assisted thoracoscopy* permits visualisation of the entire hemithorax and lung and allows minimally invasive sampling of pulmonary lesions through a very small access. In many cases it constitutes a viable alternative to exploratory thoracotomy and has largely replaced open lung biopsy in the diagnosis of peripheral lung nodules, including subpleural nodules as small as 3 mm. In few cases *thoracotomy and open lung biopsy* may be required for diagnosis of solitary pulmonary nodules, which can be converted to curative surgery after mediastinal staging in cases with of frozen section diagnosis of lung cancer.

Bibliography

1. Hansell DM, Armstrong P (2004) Imaging of Diseases of the Chest. Hanoncourt Publishers Limited, Mosby
2. Muller NL, Coleman NC, Fraser RS et al (2001) Radiologic Diagnosis of Diseases of the Chest. WB Saunders Philadelphia
3. Travis WD, Garg K, Franklin WA et al (2005) Evolving concepts in the pathology and computed tomography imaging of lung adenocarcinoma and bronchioloalveolar carcinoma. J Clin Oncol 23:3279–3287
4. Lowe VJ, Naunheim KS (1998) Positron emission tomography in lung cancer. Ann Thorac Surg 65:1821–1829
5. Westlin JE, Janson ET, Arnberg H et al (1993) Somatostatin receptor scintigraphy of carcinoid tumors using the [111In-DTPA-D-Phe1]-octreotide. Acta Oncol 32:783–786
6. Swensen SJ, Jett JR, Hartman TE, et al (2005) CT screening for lung cancer: five-year prospective experience. Radiology 235:259–265

Neoplasms, Small Bowel

J-N. Bruneton, P. Chevallier
Service d'Imagerie Médicale Diagnostique et Interventionelle, Hopital de l'Archet, Nice, France

Pathology/Histopathology

Although the small intestine accounts for approximately 75% of the entire length of the gastrointestinal tract and

more than 90% of the mucosal surface, it is rarely the site of malignant tumors (less than 2% of all gastrointestinal malignancies). Approximately 40 different histologic tumor types have been described in the small bowel. While symptomatic tumors are nearly always malignant, three-quarters of all neoplasms discovered at autopsy are benign.

The small bowel sites at greatest risk for malignant tumors are the duodenum for adenocarcinomas and the ileum for ►carcinoid tumors and lymphomas. Adenocarcinomas are the most common malignant tumors of the small intestine (30–50%), followed by carcinoids (25–30%), and lymphomas (15–20%). Leiomyomas are the most frequent benign tumor, followed by adenomas, lipomas, and hamartomas.

The low susceptibility of the small bowel to malignant change has been attributed to numerous pathogenetic mechanisms, including the relatively rapid transit of intestinal contents (comparatively short exposure of the intestinal mucosa to carcinogens), moderation of mucosal irritation by the liquid nature of small bowel contents, low bacterial load, and the relatively high concentration of lymphoid tissue with a high level of immunoglobulin A.

A number of small bowel inflammatory disorders predispose to malignancy: celiac disease (lymphoma), Crohn's disease (adenocarcinoma), immunoproliferative disease [►immunoproliferative small intestinal disease (IPSID)], and diffuse intestinal lymphoma.

Various genetic disorders are also associated with an increased incidence of small intestinal tumors: ►Peutz–Jeghers syndrome (hamartomatous polyps), Gardner's syndrome and familial adenomatous polyposis coli (adenoma, adenocarcinoma), von Recklinghausen's disease (paraganglioma). Juvenile polyposis and Cowden disease are less common.

Clinical Preservation

Aside from those rare acute cases necessitating surgical treatment (for example intussusception of a lipoma or a metastasis of melanoma), small intestinal tumors most often run an insidious course with nonspecific symptoms that include intermittent abdominal pain, anemia, bleeding, and intestinal obstruction (1).

Benign small intestinal tumors are often asymptomatic, although complaints may include bleeding (leiomyoma, hemangioma), intestinal obstruction (desmoid tumor), or intussusception (lipoma).

Adenocarcinoma associates the following presenting symptoms, in decreasing order of frequency: pain, weight loss, vomiting, hemorrhage, obstruction. An average of 5 months generally elapses between the initial clinical complaint and diagnosis. Carcinoid tumors tend to occur in the terminal ileum. After an initial phase with nonspecific clinical symptoms, a carcinoid syndrome (cutaneous flushing, diarrhea) may occur in case of hepatic metastases.

Imaging

Gastric and colonic endoscopy, ultrasound, and small bowel barium examinations are the first-line studies for all nonspecific clinical gastrointestinal symptoms. Lesions demonstrated by small bowel evaluation are usually already advanced (for example infiltrating adenocarcinoma, lymphomatous mass, hepatic metastases of carcinoid tumors). Barium studies are insensitive for the detection of small, and thus resectable, lesions (1).

CT (oral intake of 1 L of water and intravenous administration of an iodinated contrast agent) can visualize smaller lesions with features that may suggest the etiology (hypervascularity of a ►stromal tumor, fat density of a lipoma). MRI does not provide any supplementary information compared to CT.

Double-contrast barium air enteroclysis performed after duodenal intubation allows visualization of the mucosal surface; the sensitivity of the procedure is markedly better than that of conventional barium follow-through examinations. CT enteroclysis combining the infusion of water through a nasojejunal tube and iv iodinated contrast administration is currently the most sensitive technique and has replaced enteroclysis for most imaging teams (2–4). The procedure does have two major drawbacks, however: its invasive nature that means it is reserved as a second-line technique, and its failure to detect certain small lesions (hemangioma).

Endoscopic ultrasonography (EUS) allows high-resolution imaging of the ampullary region and is more effective than CT or MRI for the work-up of neoplasms in this location. In case of hemorrhage or a negative CT enteroclysis examination, angiography may demonstrate the site of bleeding and the responsible lesion.

Enteroscopy is rarely indicated. The development of swallowable video capsules that transmit images of the small bowel lumen has facilitated early diagnosis of small bowel tumors, but the technique is hampered by the scarcity of available machines, the relatively long operator time, and obstructive phenomena, which constitute a contra-indication.

Nuclear Medicine

Scintigraphy with technetium-labeled red blood cells can identify sites of bleeding even when blood loss is as low as 0.1 mL/min.

Various markers have been tested to improve the detection of carcinoids by nuclear medicine techniques: 131 I-metaiodobenzylguanidine (MIBG), somatostatin, octreotide. The potential role of PET CT for small bowel tumors remains unclear owing to the insufficient number of studies conducted to date.

Diagnosis

Benign Small Intestinal Tumors

Leiomyoma is the most frequent benign small bowel tumor, the peak incidence occurring at approximately 60 year of age. The jejunum is the site of predilection, followed by the duodenum and the ileum. These stromal tumors exhibit a variety of growth patterns: intramural, intraluminal, subserosal, or dumbbell-shape. The ulceration of these hypervascular tumors explains the frequency of hemorrhage (60% of cases). Presence of a palpable mass is correlated with subserosal growth (20%). Obstructive phenomena are observed in cases of intraluminal growth. Prior to the development of CT, angiography allowed the diagnosis by revealing a hypervascular lesion, regardless of location (subserosal tumors in particular are well visualized). MRI and CT enteroclysis can demonstrate lesions as small as 1 cm and obviate the need for angiography (Fig. 1).

Adenoma is nearly always asymptomatic and thus most often a discovery on imaging studies. These tumors are generally solitary, except in cases of familial adenomatous polyposis. As for colonic adenomas, a villous component and size greater than 1 cm are risk factors for malignancy. This risk can exceed 40% in the duodenum, which explains the necessity for resection.

Lipomas are the third most common type of small intestinal neoplasm. More than two-thirds are asymptomatic and these tumors are thus increasingly discovered at CT examination. Less frequently, intestinal obstruction (often intermittent) is the clinical complaint. CT allows pathognomonic diagnosis by revealing a homogeneous mass with low (fat) attenuation. The only risk of lipomas is obstruction; malignant transformation is inexistent.

Relatively rare tumors that are sometimes multiple, *hemangiomas* are occasionally visualized by angiography.

Intestinal nodular lymphoid hyperplasia is usually asymptomatic. Characterized by the presence of submucosal masses (enlarged lymphoid follicles), it is encountered in cases of IgA deficiency and involves the distal portion of the small bowel. The risk of transformation to lymphoma is low (5).

Hamartomas are typically asymptomatic and have no potential for malignant change.

Malignant Small Intestinal Tumors

Adenocarcinoma is the most frequent malignant neoplasm of the small intestine and usually occurs in the duodenum, associated or not with stenosis, tumor infiltration, or ulceration (Figs 2). The ampulla of Vater

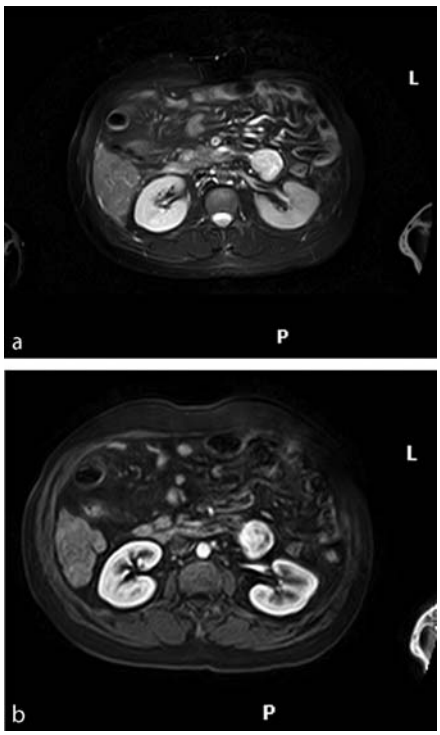

Neoplasms, Small Bowel. Figure 1 MRI of a duodenal leiomyoma discovered incidentally. Axial T2-weighted scan with fat suppression (a) revealing a homogeneous, hyperintense tumor; T1-weighted sequence after intravenous gadolinium administration (b) demonstrating tumor hypervascularity.

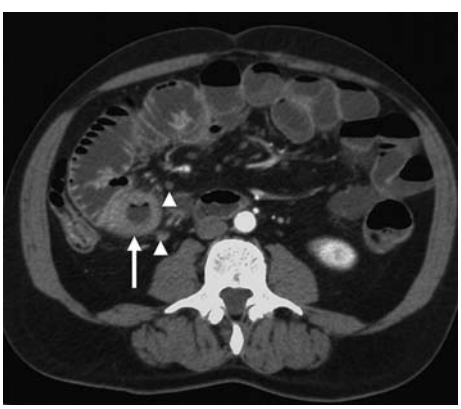

Neoplasms, Small Bowel. Figure 2 CT examination of the small bowel for unexplained anemia. Thickened jejunal loop (arrow) with enlarged satellite nodes (arrowheads) corresponding to an adenocarcinoma with nodal extension.

is the most common site of small bowel adenocarcinomas. It is also the most common site of degeneration of familial adenomatous polyposis after the colon. Diagnosis of ampullary adenomas is often prompted by symptoms of bile duct obstruction. Adenomas have a better prognosis than other malignant tumors that invade the main bile duct. Diagnosis is made by endoscopy and disease extension work-up is best performed by EUS and MRI.

Leiomyosarcoma occurs predominantly in the jejunum, followed by sites in the ileum and the duodenum. Like leiomyomas, leiomyosarcomas can reach large dimensions before any symptoms appear owing to the frequency of subserosal growth. The frequency of ulceration explains the incidence of bleeding. Differentiation of a leiomyoma from a leiomyosarcoma can be difficult, and molecular determination of the malignant potential of stromal tumors appears to be an effective aide for identification of malignancy. The only effective therapy for these tumors is surgery, even though hypervascular hepatic metastases are already often present at diagnosis.

Primary small bowel lymphoma is a non-Hodgkin's lymphoma, and the small bowel is the second most common gastrointestinal location after the stomach. The majority are B-cell lymphomas of intermediate or high grade malignancy. Clinical symptoms are often minimal, contrasting with the extensive nature of these lesions, and this disparity is a diagnostic factor. Abdominal pain, asthenia, diarrhea, and weight loss are possible, as is regional lymph node involvement. The most characteristic imaging appearance is aneurysmal dilatation of a segment of the small bowel and destruction of the mucosal folds owing to the absence of desmoplastic reaction. Infiltrating polypoid involvement or sprue is less suggestive of the diagnosis. In less than 7% of cases, a complication such as perforation leads to diagnosis. Small bowel sites of Hodgkin's disease and secondary lesions are usually associated with advanced stages of the lymphomatous process (1, 5).

Neuroendocrine Tumors

The most frequent examples are *carcinoids*; other etiologies such as *paragangliomas*, *somatostatinomas*, and *vipomas* are less common. Small bowel carcinoids secrete serotonin or serotonin precursors. Imaging permits early detection of lesions smaller than 1 cm but not etiologic diagnosis. The development of nodal metastases and the presence of retractile mesenteritis, often with calcification, allow presurgery etiologic diagnosis. Patients with hypervascular hepatic metastases may develop a clinical carcinoid syndrome that regresses after surgical resection, associated or not with endovascular treatment of any residual lesions (chemoembolization). Somatostatin scintigraphy allows early detection of carcinoid lesions and characterization of small lesions demonstrated by CT.

Systemic Diseases Associated with Small Bowel Neoplasms

Peutz–Jeghers syndrome is a rare autosomal dominant disease characterized by hamartomatous polyposes of the gastrointestinal tract (in particular the small intestine) and focal melanin pigmentation of the skin and mucous membranes. The intestinal polyps tend to be multiple and vary in form and size. Barium follow-through examination suffices to demonstrate these lesions that involve risks of intussusception and bleeding.

Celiac disease may be complicated by a T-cell lymphoma that is difficult to diagnose by imaging when it manifests as a nonspecific mucosal ulceration in the jejunum.

Immunoproliferative small intestinal disease (Mediterranean lymphoma or diffuse small intestinal lymphoma) is associated with endemic parasitic and microbial colonization that explains why it is seen almost exclusively in underdeveloped countries. This immunoblastic type of lymphoma causes chronic diarrhea and a malabsorption syndrome that may last months or even years. Involvement of the distal duodenum and the initial portion of the jejunum can be demonstrated by a barium contrast examination that shows thickened mucosal folds and ulcerations.

Individuals with *Crohn's disease* have a 5 to 20-fold higher risk of developing an ileal adenocarcinoma than the normal population.

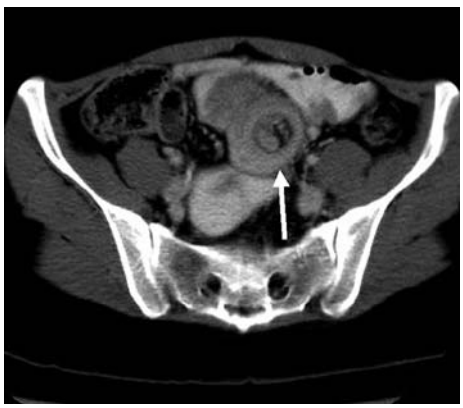

Neoplasms Small Bowel. Figure 3 CT enteroclysis with iv administration of iodinated contrast material and upper GI tract opacification revealing small bowel–small bowel intussusception (arrow) due to metastasis of melanoma to the small bowel.

Metastases

Secondary involvement of the intestine is more common than primary tumors, and may occur by hematogenous spread, local extension, or intraperitoneal seeding. Primaries in the stomach, colon, or genitourinary tract may spread by local extension or seeding to the serosal surface of the intestine, where rounded, centimeter-sized nodules may be demonstrated by enteroclysis (Fig. 3). Malignant cells may implant along the mesenteric border of the small bowel loops and induce fibrosis. Hematogenous spread usually produces a multinodular, polypoid appearance along the antimesenteric border.

Bibliography

1. Bruneton JN (1990) Imaging of gastrointestinal tract tumors. Springer Verlag, Heidelberg.
2. Horton KM, Fishman EK (2004) Multidetector-row computed tomography and 3 dimensional computed tomography of small bowel neoplasms: current concept in diagnosis. J Comput Assist Tomogr 28:106–116
3. Korman MU (2002) Radiologic evaluation and staging of small intestine neoplasms. Eur J Radiol 42:193–205
4. Maglinte DD, Bender GN, Heitkamp DE et al (2003) Multidetector-raw helical CT enteroclysis. Radiol Clin North Am 41:249–262
5. Gill S, Heuman DM, Mihas AA (2001) Small intestinal neoplasms. J Clin Gastroenterol 33:267–282

Neoplasms, Soft Tissues, Benign

Suzanne E. Anderson
University Hospital of Bern, Inselspital Bern, Switzerland
suzanne.anderson@bluewin.ch

Synonyms

Mass lesion of soft tissues

Definition

Benign mass lesion or architectural disturbance not associated with metastatic potential.

Pathology/Histology

The World Health Organization has classified the histological types and names of benign soft tissue tumors (1, 2) (summarized in Table 1). The incidence is 300 per 100,000 population (1). Benign soft tissue tumors are far more common than their malignant counterparts, which have an incidence of 2 to 3 per 100,000 population (1). There are six main benign soft tissue tumors (3): ▶lipoma and variants, benign fibrotic histiocytoma, nodular fasciitis, neurogenic tumors, fibromatosis, and ▶pigmented villonodular synovitis or giant cell tumor of tendon sheath (summarized in Table 2). If ▶ganglion is added to the commonest soft tissue tumor benign list, this makes up some 70% of all benign lesions (2). This percentage is increased if vascular and lymphangioma lesions are included. The age at presentation of the tumor is important as certain tumors are more likely to occur within particular age groups. For example, lymphangioma of the newborn is shown in Fig. 1.

Clinical Presentation

Presentation is usually due to an increasing mass, often accompanied by discomfort or pain. If tumor occurs near a joint, there may be associated joint pain and if it occurs near the essential structures such as a neurovascular bundle, there may be secondary features such as nerve compression (Fig. 2a).

Treatment

If a tumor appears benign and classical in imaging appearances, such as a subcutaneous lipoma or a ganglion cyst associated with a joint, some patients may elect to have conservative nonoperative treatment. More commonly, after biopsy for confirmation of the imaging diagnosis and exclusion of other diagnoses, the tumor is surgically resected. Detailed anatomical review is required before resection for appropriate and complete tumor resection, to identify normal vascularity and tumor vessels, for safety of possible adjacent neurovascular bundle structures, to ascertain if vascular grafting is required, and for cosmetic aspects. Many hemangiomas may not require any further therapy but may need preventative support if a young patient wishes to continue sport. Rarely endocrine manipulation therapy or radiotherapy may be used for benign aggressive desmoid tumors.

Prognosis

As the diagnosis of these tumors is benign, the prognosis is usually excellent. Rarely some benign tumors will reoccur, such as hemangiomas, or more commonly the aggressive desmoid. In the latter, the prognosis may often be guarded, though fortunately these cases are rare.

Neoplasms, Soft Tissues, Benign. Table 1 Modified WHO classification: histological of benign soft tissue tomers

Tumor group	Tumor type
Lipomatous tumors benign	Lipoma and variations
(Myo)fibroblastic tumors	
Benign	Nodular fasciitis
	Proliferative fasciitis
	Proliferative myositis
	►Myositis ossificans
	Ischemic fasciitis
	Elastofibroma
	Fibrotic hamartoma
	Fibromatosis (and subgroups)
	Fibroma/fibroblastoma (and subtypes)
Intermediate	Superficial fibromatosis
	Desmoid
	Lipofibromatosis
Fibrohistiocytic tumors	
Benign	Giant cell tumor of tendon sheath (GCTTS)
	Diffuse giant cell tumor/pigmented villonodular synovitis (PVNS)
Intermediate	Plexiform histiocytic tumor
	Giant cell tumor of soft tissues
Neurogenic tumors	
Benign	Neuroma and variants
	Neurofibroma and variants
	Benign schwannoma (neurinoma) and variants
	Perineurioma and variants
Tumors of smooth muscle	
Benign	(Angio)leiomyoma and variants
Pericytic tumors	
Benign	Glomus tumor and variants
	Myopericytoma
Tumors skeletal muscle	
Benign	Rhabdomyoma and variants
Vascular tumors	
Benign	►Hemangioma and variants
	Angiomatosis
	Lymphangioma
Chondroid/osseous tumors	
Benign	Chondroma of soft tissues
Tumors of unknown differentiation	
Benign	►Myxoma and variants
	Pleomorphic hyalinizing angioectatic tumor
	Ectopic hamartomatosis Thymoma
Intermediate	Angiomatoid fibrotic histiocytoma
	Ossifying fibromyxoid tumor
	Mixed/myoepithelial/parachordoma

Neoplasms, Soft Tissues, Benign. Table 2 Commonest benign soft tissue tumors

Lipoma and variants	16%
Benign fibrotic histiocytoma	13%
Nodular fascitis	11%
Neurogenic tumors	10%
Fibromatosis	7%
Pigmented villodular synovitis (PVNS/GCTTS)	4%

Imaging

Role of imaging in benign soft tissue lesions is to provide a specific or provisional diagnosis, to anatomically locate the lesion, to describe relevant secondary features, and to exclude other diagnoses. The use of at least two imaging modalities in combination is considered best practice. Imaging allows for the diagnosis of a solid versus cystic tumor or components, with either computed tomography

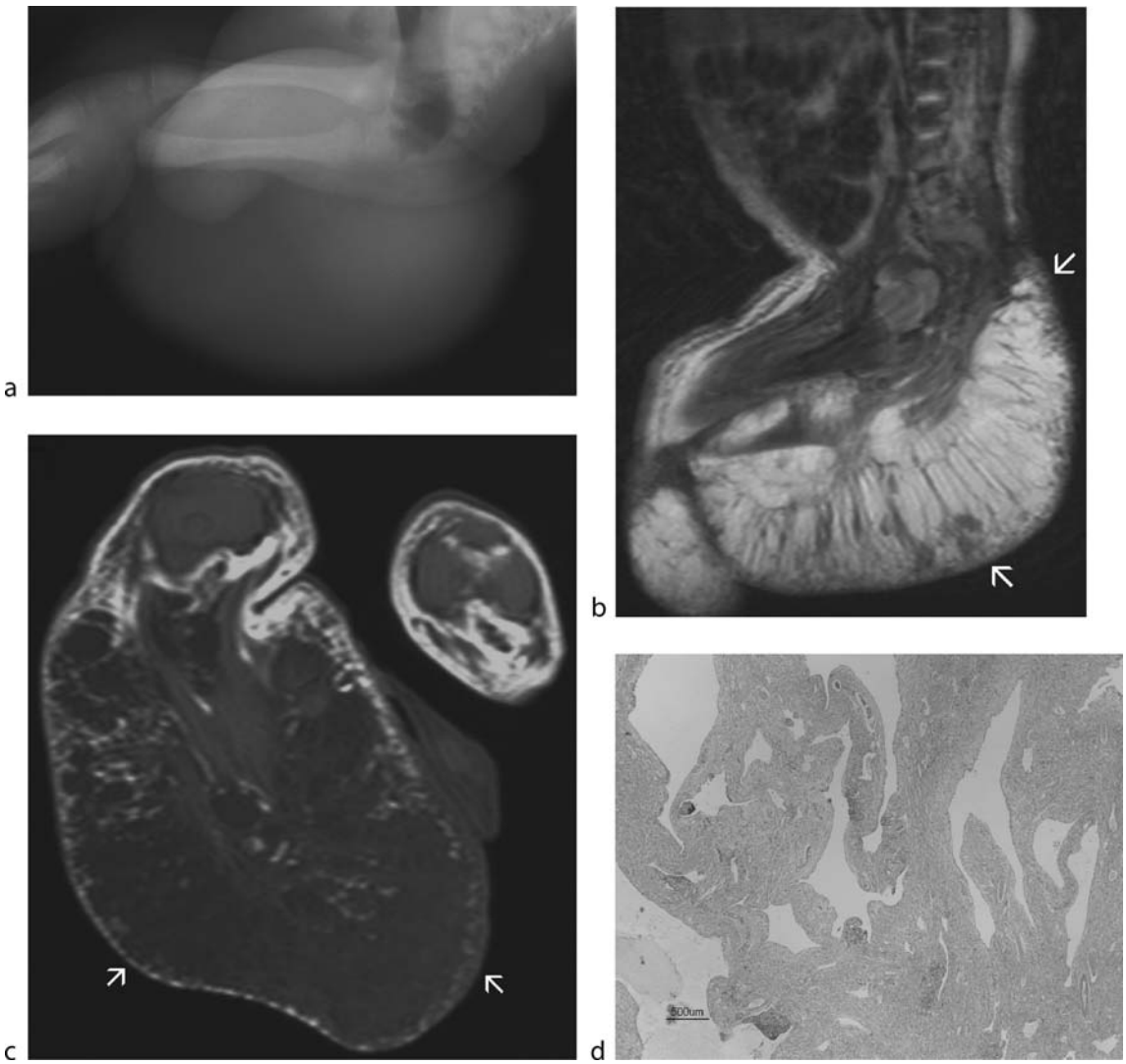

Neoplasms, Soft Tissues, Benign. Figure 1 Eight day old baby with a large benign right thigh soft tissue tumor, a lymphangiohemangioma. (a) Lateral radiograph of thigh showing large benign soft tissue tumor, lymphangiohemangioma. No calcifications are seen. (b) MRI sagittal STIR (short tau inversion recovery) image shows the large high signal intensity mass at the posterior aspect of the thigh (arrows). (c) MRI axial image just below the level of the knee shows the low signal intensity of the mass. (d) Histopathology of the lesion, hematoxylin and eosin staining, magnification factor 2 demonstrates large dilated lymphatic channels. Some areas of hemangioma formation were also found. (Courtesy of Edouard Stauffer, Institute of Pathology, University Hospital of Bern, Inselspital, Switzerland.)

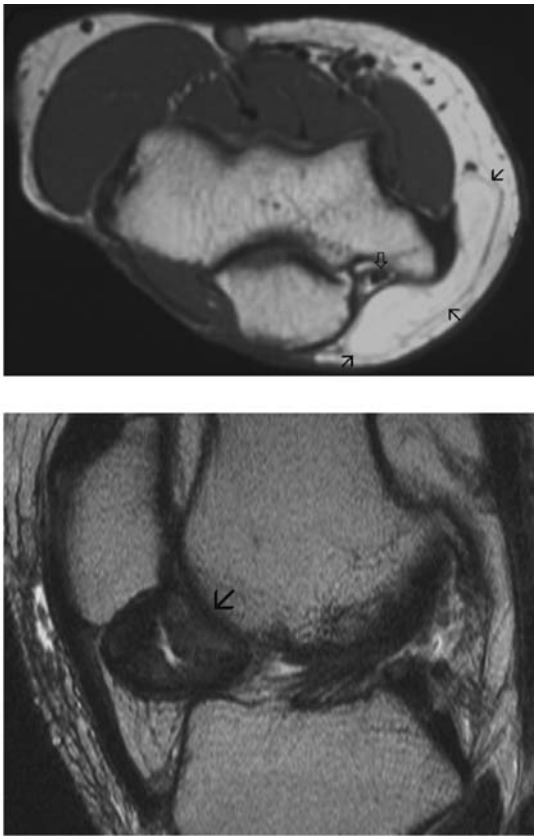

Neoplasms, Soft Tissues, Benign. Figure 2 Importance of MRI signal intensity of soft tissue mass. (a) Axial T1-weighted image of the elbow of a 56-year-old male with ►cubital tunnel syndrome, due to a mass with an increased signal intensity, paralleling that of fat, and consistent with a subcutaneous lipoma (arrows), compressing the ulnar nerve (open arrow). This was confirmed at surgery and with pathology. (b) Sagittal T2-weighted image of the knee of a 51-year-old male with a decreased signal intensity mass (arrow) within the anterior aspect of the knee, within Hoffa's fat pad. Decreased signal intensity within the mass on T2 weighting and an intraarticular knee location, made pigmented villonodular synovitis (PVNS) the most likely diagnosis. Prepatellar bursitis is also evident. The tumor diagnosis was confirmed at surgery and pathology.

(CT) or magnetic resonance imaging (MRI), particularly imaging after contrast administration or with ultrasound (color Doppler imaging has a role here). The demonstration of solid portions of a tumor allows for appropriate selection of a biopsy site. A cystic tumor or one with cystic components may be due to, for example, a myxoma, ganglion of soft tissue, or due to hemorrhage or necrosis within the tumor itself. Clear anatomical delineation of the tumor site is important preoperatively for surgical planning and also for assisting with the diagnosis. Imaging is also important for follow-up after surgical resection, to review for complications or residual tumor, and to follow-up after nonsurgical therapies such as endocrine and radiotherapy treatment for some desmoid tumors.

Radiographs

Are usually performed in two planes to review local anatomy for any bone or joint involvement, presence of calcification or ossification (suggesting myositis ossificans) phlebolith formation (suggesting hemangiomas), or fat density (implying often a benign diagnosis). They may also be used for preoperative review of the thorax.

Computed tomography

Computed tomography depicts the anatomical site, the mass features, and secondary features, such as neurovascular displacement. With multislice technique availability, CT angiography technique for preoperative normal and tumor vascularity is increasing. This technique also allows for excellent depiction of calcification and ossification.

Magnetic Resonance Imaging

MRI is the recognized gold standard for tumor imaging. It should be performed and read out in a combination with radiographs or CT. This is due to the fact that the detection of calcifications on MRI may be obscured and the presence of this feature may alter the differential diagnosis. MRI allows for multiplanar imaging and in site into the appearance of all structures including bone and joint and soft tissues. MRI signal intensity may influence the diagnosis as the signal intensities of some tumors are more commonly associated with a particular appearance on T1 and T2 weighting (Tables 3 and 4). An increased signal intensity mass on T1 weighting in a superficial location is characteristic for a lipoma (see Fig. 2a). A decreased signal intensity mass within a joint on T2 weighting is highly suggestive for a diagnosis of pigmented villonodular synovitis (see Fig. 2b). Other specific signs and features may help with the diagnosis on MRI such as the presence of high vascular flow voids or vascular pooling in tumors consistent with hemangiomas or arteriovascular malformations. *MRI angiography*: An additional sequence may help confirm or further characterize a lesion (4) or give preoperative vascular and tumor anatomy.

Ultrasound

High-resolution ultrasound alone or in combination with color Doppler imaging has been shown to be helpful with tumor imaging allowing solid versus cystic differentiation, vascularity features, and anatomical delineation. However, MRI remains the reported gold standard.

Neoplasms, Soft Tissues, Benign. Table 3 List of benign soft tissue tumors commonly associated with an increased signal intensity on T1 weighting on MRI

Lipoma and variants
Vascular tumors and variants (lymphangioma)
Elastofibroma dorsi
Subacute hemorrhage

Neoplasms, Soft Tissues, Benign. Table 4 List of benign soft tissue tumors commonly associated with a decreased signal intensity on T2 weighting on MRI

Desmoid tumor
Fibromatosis
PVNS/GCTTS
Morton's neuroma
Hyperacute and chronic hemorrhage
Xanthoma
Amyloidosis
Scar tissue
High flow vascular malformations
Calfication, tumoral calcinosis

Nuclear Medicine

Bone Scan and Positron Emission Tomography Scan

These techniques of imaging are commonly used to determine any bone involvement or to exclude metastatic tumor in a soft tissue mass initial workup. Their role is more significant in the imaging of malignant soft tissue lesions.

Diagnosis

Initial Radiological Diagnosis

Primary signs of a benign lesion include the presence of a dominant mass, often with well-defined borders, architectural distortion with altered density (on computed tomography), or altered signal intensity (on MRI). The diagnosis is influenced by the appearance of the mass, for example, whether there is evidence of fat or vessels on the location of the mass, on the age of the patient, and whether the lesion is single or multiple.

Secondary signs are usually less than with malignant lesions, however due to the mass effect there may be evidence of neurovascular displacement.

The presence of multiple soft tissue lesions versus a solitary lesion may help with the differential diagnosis. Lipomas and hemangiomas may occur at multiple sites. Some of these multiple lesions may be related to syndromes such as ►Mazabraud's syndrome, ►neurofibromatosis NF1, and angiomatous syndromes such as Maffucci, Olser–Weber–Rendu, Klippel–Trenaunay, or Kasabach–Merritt syndromes.

Body location and local anatomical site can be helpful. Lipomas commonly occur in a subcutaneous location. The anatomical center of a lesion may assist in suggesting the cell or tissue origin of the tumor (see Table 1). Some tumors are more likely to occur at specific anatomical sites, such as the synovial hemangioma, though rare, it has a predilection for the anterior knee, or elastofibroma dorsi of the posterior chest wall inferior to the scapula. Intraarticular masses have a relatively specific differential list including pigmented villonodular synovitis (PVNS), synovial hemangioma or synovial chondro/osteomatosis, lipoma arborescens, and intraarticular lipoma.

Differential Diagnosis

Pseudotumors are not uncommon and their imaging may mimic a benign soft tissue. They can be categorized into posttraumatic, sports or occupationally related, associated with aging and degeneration, or congenital or developmental abnormalities or relate to overuse of normal anatomical variants. Some common examples include muscular hematomas after sports injuries associated with various degrees of muscle tears and myositis ossificans (Fig. 3), infection or abscess formation, and foreign body reaction.

Pitfalls

Pitfalls include the differential diagnostic list described earlier. A well-circumscribed, apparently benign-appearing mass may rarely be malignant, such as a small well-defined focal synovial cell sarcoma, 2 cm in size. Due to this issue, good clinical practice supports the use of biopsy preoperatively to achieve histological confirmation of a benign lesion, before final surgery.

Follow-up after Therapy

Imaging after therapy allows for clarification of treatment and response, review of any residual tumor, and any complications.

Interventional Radiology

In relation to benign tumors, the role of interventional radiology may be diagnostic, to delineate tumor vessels and normal vascular anatomy preoperatively or

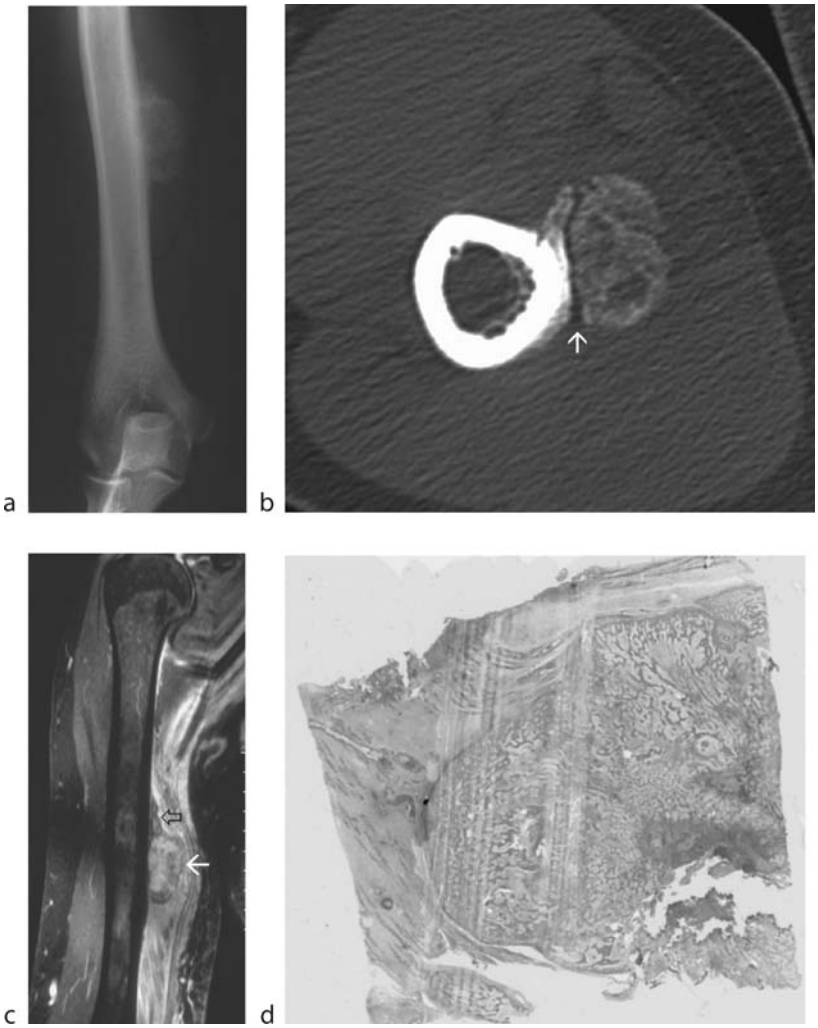

Neoplasms, Soft Tissues, Benign. Figure 3 Twenty-four year old female with the history of minor trauma with upper limb mass, myositis ossificans. (a) Radiograph shows characteristic peripheral calcification within the lesion, and some periosteal new bone reaction. (b) Axial computed tomography shows that the calcified mass is separated from the adjacent bone and periosteal reaction (arrow), which is another characteristic feature of myositis ossificans. (c) MRI sagittal STIR image shows the partially calcified mass (arrow) with adjacent periosteal reaction (open arrow) and marked soft tissue increased signal intensity within adjacent soft tissues, which is another characteristic feature of myositis ossificans. This marked adjacent soft tissue reaction would be the most unusual in a malignant soft tissue tumor unless it had undergone trauma or biopsy. (d) Hematoxylin and eosin-stained macrosection demonstrating the presence of osteoid bone formation. (Courtesy of Edouard Stauffer, Institute of Pathology, University Hospital of Bern, Inselspital, Switzerland.)

therapeutic for specific treatment such as embolization with hemorrhage.

References

1. Fletcher CDM, Unni KK, Mertens F (eds) (2002) Pathology and genetics of soft tissues and bone. In: World Health Organization Classification of Tumors. IARC Press, Lyon
2. Kransdorf MJ, Murphey MD (1997) Imaging of Soft Tissues. WB Saunders Company, Philadelphia
3. Kransdorf MJ (1995) Benign soft tissue tumors in a large referral population: distribution of diagnosis by age, sex and location. Am J Roentgenol 164:395–402
4. Anderson SE, De Monaco D, Buechler U et al (2003) Imaging features of pseudoaneurysms of the hand in children and adults. Am J Roentgenol 180:659–664

Neoplasms, Soft Tissues, Malignant

Suzanne E. Anderson
University Hospital of Bern, Inselspital Bern, Switzerland
suzanne.anderson@insel.ch

Synonyms

Malignant mesenchymoma; Sarcoma

Definition

Soft tissue mass characteristically able to invade adjacent structures and to form metastases at distant sites.

Pathology/Histology

Malignant soft tissue tumors are relatively rare, though occur approximately as commonly as multiple myeloma of bone, and twice as common as sarcoma of bone (1–3). There is an incidence of some 2 to 3 per 100,000 population for malignant soft tissue tumors (1, 2). The mortality rate remains relatively high on average at 50%, dependant on tumor stage and histology grade at time of presentation.

The world health organization classified and cataloged the malignant soft tissue tumors (1, 2) (summarized in Table 1). Some seven malignant tumor types are the commonest, being ►malignant fibrous histiocytoma (MFH), ►fibrosarcoma, ►liposarcoma, ►synovial sarcoma, ►malignant peripheral nerve sheath tumor (MPNST), ►rhabdomyosarcoma, and ►leiomyosarcoma (3) (summarized in Table 2).

Clinical Presentation

Commonly patients present with a slowly enlarging soft tissue mass, which is often painless. It may be associated with pain if the mass undergoes tumor necrosis or hemorrhage, traumatized, or if there is a sudden rapid growth phase. Some patients may present at the change of seasons when they alter their clothing habits and only then notice anatomical asymmetry. The commonest site is that of the lower limb, in particular the thigh, due to the presence of a large muscle and soft tissue bulk.

Prognosis

Primary predictors of ►prognostic outcome are initial compartment staging and histological grade and also response to initial therapy.

Neoplasms, Soft Tissues, Malignant. Table 1 Soft Tissue tumors, malignant simplified WHO classification of soft tissue tumors

Tumor group	Tumor type
Lipomatous tumors malignant	Liposacoma (and subtypes)
(Myo)fibroblastic tumors intermediate (seldom metastasize) malignant	Solitary fibrotic tumor and hemangiopericytoma inflammatory myofibroblastic sarcoma low-grade myofibroblastic sarcoma myxoinflammatory fibroblastic sarcoma Infantile fibrosarcoma Fibrosarcoma (and subtypes)
Fibrohistiocytic tumors malignant	Malignant fibrotic histiocytoma (and subgroups)
Neurogenic tumors malignant	Malignant peripheral nerve sheath tumor (MPNST) and variants
Tumors of smooth muscle malignant	Leiomyosarcoma
Pericytic tumors malignant	Malignant glomus tumor
Tumors of skeletal muscle malignant	Rhabdomyosarcoma (and subtypes)
Vascular tumors intermediate malignant	Hemangioendothelioma and variants Kaposi sarcoma Epitheloid hemangioendothelioma Angiosarcoma of soft tissues
Chondro/osseous tumors	Mesenchymal chondrosarcoma extraskeletal osteosarcoma
Tumors of unknown differentiation malignant	Synovialsarcoma epitheloid sarcoma alveolar soft tissue sarcoma clear cell sarcoma extraskeletal myxoid chondrosarcoma Extraskeletal Ewing sarcoma/PNET Desmoplastic small round cell tumor Extrarenal rhabdoid tumor malignant mesenchymoma intimal sarcoma

Source: Fletcher CDM, Unni KK, Mertens F (eds) (2002) Pathology and genetics of soft tissues and bone. In: World Health Organization Classification of Tumors. Lyon, IARC Press.

Kransdorf MJ, Murphey MD (1997) Imaging of Soft Tissues, WB Saunders Company.

Neoplasms, Soft Tissues, Malignant. Table 2 Most common malignant soft tissue tumors (3)

Malignant fibrous histiocytoma	22%
Fibrosarcoma	18%
Liposarcoma	17.5%
Synovial sarcoma	17%
Malignant peripheral nerve sheath tumor(MPNST)	5%
Rhabdomyosarcoma	5%
Leiomyosarcoma	4%

Imaging

Role of Imaging

Is central in the diagnosis and staging of malignant soft tissue tumors. Best clinical practice supports histological confirmation of the tumor prior to definitive surgery. Poorly imaged or nondocumented cases prior to surgery have a vastly poorer outcome due to intralesional surgical technique with increased local tumor recurrence and metastatic rates (4). Larger tumor nodules are easily recognized with magnetic resonance imaging (MRI); however, residual microscopic tumor cell groups remain difficult to determine with current imaging modalities (4).

The initial role of imaging for malignant soft tissue tumors is that of anatomical delineation for local staging for ▶compartment anatomy and for ascertaining a diagnosis or provisional diagnosis (Figs 1 and 2). Central to the role of imaging in malignant soft tissues tumors is the concept of compartment anatomy.

Imaging with Staging and Clinical Follow-Up

After initial imaging diagnosis and histological confirmation, imaging is used to follow posttherapy changes prior to surgery. It is also useful in reviewing for complications such as postoperative seromas/hematomas and local tumor recurrence (Fig. 3).

Radiographs

High-quality radiographs of the mass in two planes, including nearby joints are standard requirements. Specific features that are reviewed include the presence of soft tissue calcification, bone erosion or destruction, and joint involvement.

Computer Tomography

High-resolution computer tomography (CT) is useful for anatomical local staging and may be used to delineate the morphology including the internal structure of the tumor to aid in the diagnosis. It delineates the presence of subtle calcification, which may affect the diagnosis, and be less obvious on MRI. It is commonly used for whole body staging, of chest, abdomen, and pelvis to exclude metastatic disease prior to surgery and in follow-up imaging. CT angiography multislice technique allows for depiction of normal and tumor vascularity. CT is also an important technique to guide biopsy. Especially in this setting compartment anatomy is extremely important and the route to access the lesion should be discussed with the tumor surgeon before the intervention as contamination of compartments that will not be removed during surgery has to be avoided.

Magnetic Resonance Imaging

MRI is the best diagnostic technique for malignant soft tissue tumor diagnosis and local staging. With its multiplanar capabilities, excellent depiction of anatomical detail for bone and joint and soft tissues MRI in combination with radiographs and/or CT is the main stay in imaging. However, MRI is less well suited to diagnose specific tumor entities. Calcification, for example, which may be very influential in the differential diagnostic list, such as with synovial sarcoma in some 30%, may be not obvious or visible on routine MRI, therefore radiographs performed in conjunction with the MRI or CT are essential for making a good diagnosis. Some malignant soft tissue sarcomas have specific or suggestive MRI signal characteristics on T1- and T2-weighting (see Tables 3 and 4) (Fig. 3). *MRI angiography,* an additional sequence, may allow for depiction of normal and tumor vascularity prior to surgery. Both T1- and T2-weighting are important for tumor characterization, with STIR (Short Tau Inversion Recovery) being important for review of adjacent bone structures. Certain tumors may have specific or suggestive signal characteristics (see Tables 3 and 4) which may be helpful in making the diagnosis or the provisional diagnosis. The vast majority of tumors remain nonspecific in their pattern. The correct histological diagnosis based on imaging alone, has been reported as low as 25% (2). However, it may rapidly increase in some tumor subtypes, for example in low-grade liposarcoma where the presence of some regions of relatively normal appearing fat signal make the diagnosis specific. Also increase in experience with imaging readout and working in teams supervised by a senior experienced tumor radiologist can greatly increase the diagnostic accuracy. The delineation of cystic (hemorrhage, tumor necrosis, or tumor mucin production) versus solid lesions or tumor components is important to allow for the optimal planning and biopsy placement. Contrast administration is reported as being very useful in this regard.

Ultrasound

High-resolution ultrasound either alone or used with color Doppler ultrasound is largely used as an adjunct to

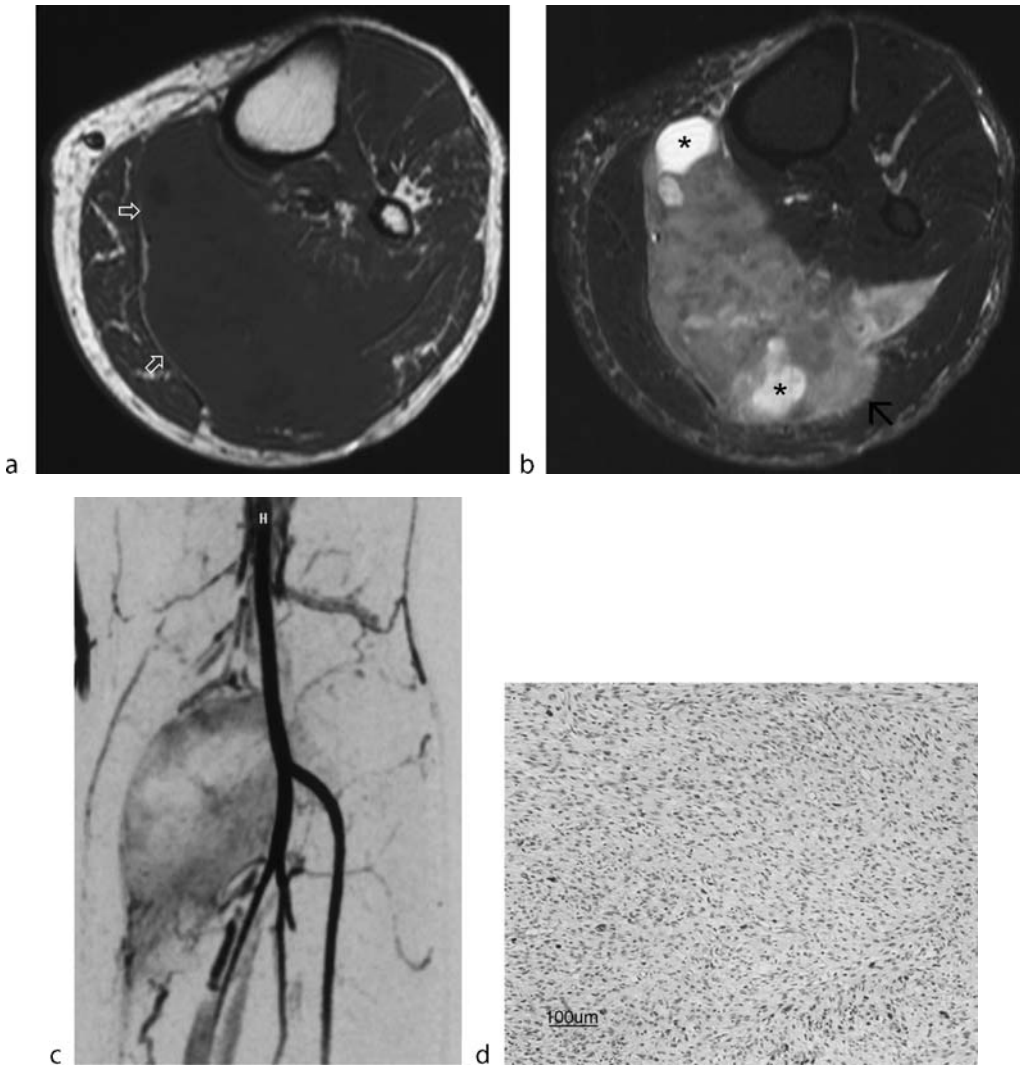

Neoplasms, Soft Tissues, Malignant. Figure 1 Fifty-eight year male with increasingly painful calf mass of lower limb. (a) Axial T1-weighted image shows mass (*arrows*) within soleus muscle with some heterogenous signal intensity. (b) Corresponding axial STIR image shows the tumor to have increased signal intensity (*arrows*) with multiple heterogenous higher signal intensity regions (*) consistent with hemorrhage. There is evidence of tumor extension into adjacent muscle into the lateral head of gastrocnemius muscle (*arrow*). (c) Contrast-enhanced 3D MR angiography shows a very vascular tumor blush of contrast, tumor vascularity and normal vascular structures only displaced by the tumor of the lower limb. (d) Hematoxylin and eosin stained histopathology at a magnification of 10× shows a characteristic dense cellular tumor, Grade II leiomyosarcoma. Image courtesy of Edouard Stauffer, MD, Institute of Pathology, University

CT and MRI for biopsy, cystic versus solid differentiation, and for specific enquiries, also for metastatic staging of the abdomen.

Differential Diagnosis

These include benign soft tissue lesions and pseudotumors such as myositis ossificans (see previous chapter: neoplasms, soft tissue, benign), abscess or infection, postsports or occupational injury or symptomatic normal variants. However, usually with these entities, there is no true mass at the center of the area of abnormality on imaging.

Pitfalls

The tumors' border may be difficult to ascertain with imaging and in particular there may be difficulty in

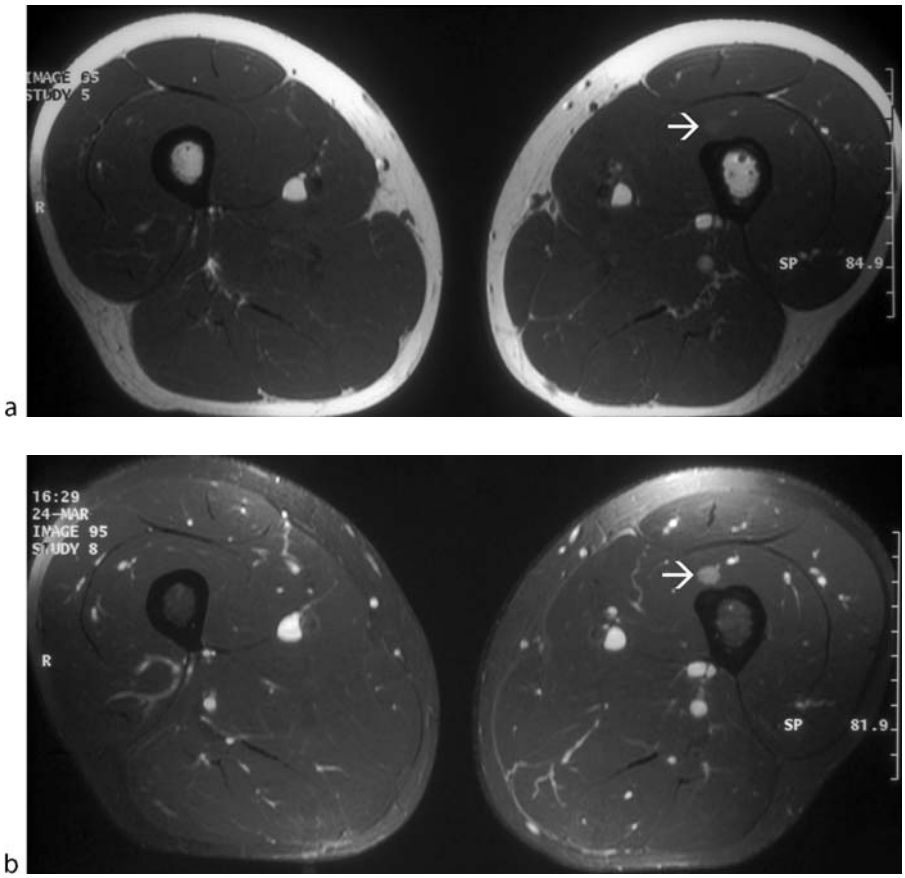

Neoplasms, Soft Tissues, Malignant. Figure 2 Forty-year old male with minor thigh discomfort and history of previous malignant melanoma of the skin. (a) Axial T1-weighted image through the thigh shows a focal mass with high signal intensity (*arrow*), suspicious for a melanoma metastasis. (b) Corresponding T1-weighted fat saturated postcontrast administration image showing prominent contrast within the lesion, confirmed at biopsy to be a melanoma.

determining whether an adjacent joint is involved or not. The ▶pseudocapsule of the malignant tumor may mimic a well-defined benign appearing lesion. A very dense cellular homogeneous lesion with decreased signal intensity of T2-weighting may mimic a benign lesion such as a desmoid or a giant cell tumor of tendon sheath. Pseudocystic lesions are a pitfall as they may appear as a fluid-contained benign lesion such as a ganglion or myxoma. These lesions include synovial sarcomas, chondrosarcomas of soft tissue (mesenchymal or myxoid types), and soft tissue metastases. Aspiration of fluid from these lesions notoriously may lack malignant cells, giving false and misleading information supporting a benign diagnosis. Metastatic disease, such as from an esophageal adenocarcinoma primary first presenting in soft tissues may mimic a primary malignant sarcoma. Large hemorrhage into a malignant sarcoma may mask the tumor. This may occur in MFH or with synovial sarcomas, making the diagnosis very difficult; however, short-term follow-up usually shows some evidence of tumor formation.

Nuclear Medicine

Bone Scan, PET Scan

Are largely for staging for bone and soft tissue metastases, with an increase in use with positron emission tomography combined with computer tomography (PET-CT) allowing correlation with spurious or dubious findings.

Diagnosis

Malignant soft tissue diagnosis is dependant on the patients' age, clinical history of presentation, presence of solitary or multiple lesions, anatomical site (intracompartmental vs. extracompartmental or multiple compartments), localization within regional anatomy (superficial soft tissue vs. interseptal), and the morphology of the tumor. The sensitivity and specificity of tumor imaging diagnosis have been shown to improve if experienced

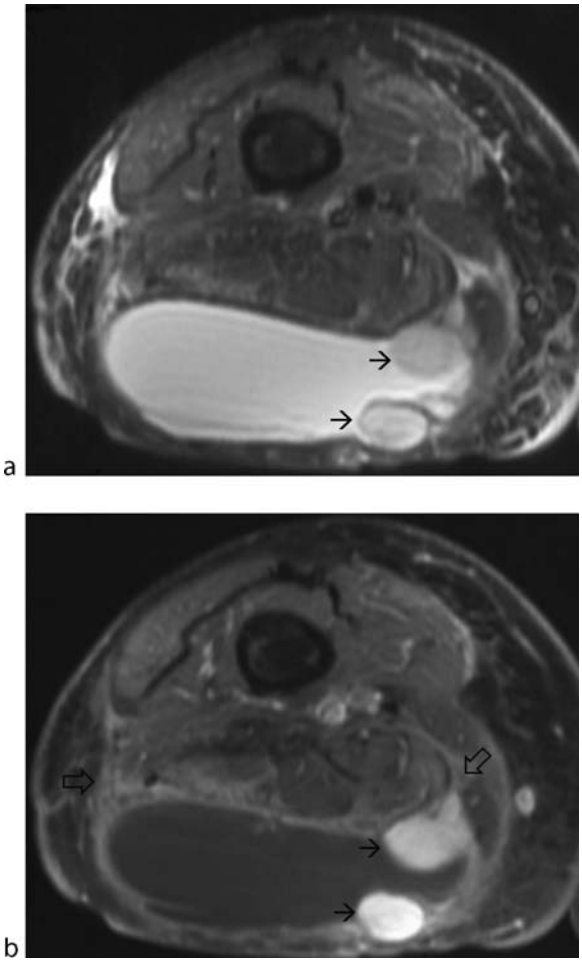

Neoplasms, Soft Tissues, Malignant. Figure 3 Seventy-five year female with a history of intralesional surgery for liposarcoma and increasing painless mass of the thigh. (a) Axial STIR image shows a large postoperative high signal intensity fluid collection (*arrow*) with two focal tumor nodules extending from the wall of the lesion (*arrows*). These are consistent with malignant tumor nodules. (b) Corresponding axial T1-weighted fat saturated image after the administration of contrast shows contrast enhancement within the tumor nodules (*arrows*) and extension of contrast-enhancing tumor into adjacent structures (open arrows) consistent with compartment contamination.

radiologists are involved with imaging interpretation and with supervision of juniors in training.

Characteristic Imaging Features

Primary signs are a dominant mass with commonly irregular and ill-defined borders with invasion of adjacent structures, presence of irregular calcifications, anatomical distortion, presence of focally altered density (on CT) and signal intensity (on MRI). *Secondary features* include distortion, asymmetry or evidence of invasion of adjacent anatomy (e.g., secondary bone destruction), lymphadenopathy, or metastatic disease. Secondary involvement of bone with destruction is often a sign of a higher grade lesion, associated with a poorer prognosis. Neurovascular bundle encasement is also a poor feature. Vascular grafting may be possible; however, limb function may be markedly inferior if nerve sacrifice against amputation is performed. Case by case management is required.

Neoplasms, Soft Tissues, Malignant. Table 3 List of malignant tumors commonly associated with an increased signal intensity on T1-weighting on MRI

Liposarcoma and subgroups
Melanoma and metastases (Melanin)
Clear cell sarcoma (Melanin)
Subacute hemorrhage
Calcification
Myxoid material

Neoplasms, Soft Tissues, Malignant. Table 4 List of malignant tumors commonly associated with a decreased signal intensity on T2-weighting on MRI

Fibrosarcoma
High-grade sarcoma (compact and cellular)
Hyperacute and chronic hemorrhage
Scar tissue
High-flow vascular tumors
Calcification or products within tumor

Benign Versus Malignant

A tumor is more likely to be malignant if it has an irregular MRI signal intensity on both T1- and T2-weighting, a high-signal intensity on T2-weighting, surrounding tissues with altered signal intensity, a size greater than 5 cm and located deep in soft tissues. Further criteria include, extension beyond the compartment, i.e., tumor invasion of the fascia, neurovascular incasement, secondary bone involvement, and early and marked contrast enhancement within the tumor. However, if a lesion does not have specific features then a conservative diagnosis or indeterminate diagnosis should be given and followed by biopsy for histological typing of the mass.

Multiple versus solitary lesions. The more common malignant soft tissue tumors are listed in Table 2. The differential list for multiple lesions of soft tissue includes malignant melanoma, Merkel Cell tumor and other skin tumors, and metastatic disease. Some syndromes such as

NFI, neurofibromatosis, with multiple nerve sheath tumors may be at an increased risk of multiple malignant soft tissue tumors.

Interventional Radiological Treatment

Interventional radiology is largely for potential intervention with intraarterial chemotherapy in specific cases or embolization prior to surgery to decrease blood loss.

Bibliography

1. Fletcher CDM, Unni KK, Mertens F (eds) (2002) Pathology and genetics of soft tissues and bone. In: World Health Organization Classification of Tumors. Lyon, IARC Press
2. Kransdorf MJ, Murphey MD (1997) Imaging of Soft Tissues, WB Saunders Company, Philadelphia
3. Campanacci M (1999) Bone and Soft Tissue Tumors. 2nd edn. Padua: Piccin Nuova Libraria. Vienna, New York, Heidelberg: Springer Verlag
4. Davies AM, Mehr A, Parsonage S et al (2004) MR imaging in the assessment of residual tumour following inadequate primary excision of soft tissue sarcomas. Eur Radiol 14(3):506–513

Neoplasms, Splenic, Benign

Piero Boraschi[1], Francescamaria Donati[1], Alessio Auci[2], Simonetta Salemi[2], Marzio Perri[2], Carla Cappelli[2]
[1]2nd Department of Radiology, University Hospital of Pisa, Pisa, Italy
[2]Department of Diagnostic and Interventional Radiology, University of Pisa, Pisa, Italy
p.boraschi@do.med.unipi.it
bartolozzi@do.med.unipi.it

Synonyms

Benign neoplasms of the spleen; Benign tumors of the spleen; Splenic benign tumors

Definition

Benign focal lesions of the spleen include benign vascular splenic tumors (hemangioma, hamartoma, lymphangioma, littoral cell angioma, hemangioendothelioma, hemangiopericytoma), and splenic cysts (primary or secondary).

Pathology and Histopathology

Hemangioma

Hemangioma is the most common benign primary neoplasm of the spleen. It arises from the sinusoidal epithelium, usually appearing on gross examination as a small, encapsulated, intraparenchymal bluish-red spongy tumor. Histopathologic evaluation reveals a nonencapsulated proliferation of vascular channels of variable size, ranging from capillary to cavernous, which are lined with a single layer of endothelium filled with red blood cells. Areas of infarction, hemorrhage, thrombosis, and fibrosis may be observed within the lesion (1, 2).

Hamartoma

Hamartoma is a rare benign lesion consisting of an anomalous mixture of normal splenic red pulp elements. It is usually a solitary, well-circumscribed, solid nodular lesion. Microscopically it appears as a mixture of unorganized vascular channels lined by endothelial cells and surrounded by fibrotic cords of predominant splenic red pulp. Focal necrosis, cystic components, and minute calcifications may be observed within the lesion (1, 2).

Lymphangioma

Splenic lymphangiomas are rare, benign lesions of vascular origin that show lymphatic differentiation. They may occur in isolation or as a manifestation of systemic lymphangiomatosis. These lesions tend to occur in subcapsular locations, reflecting the anatomic distribution of splenic lymphatics. On cut section, lymphangiomas vary in appearance and may contain large macroscopic interconnecting cysts (cystic lymphangioma) or microscopic cysts (cavernous lymphangioma). The cysts may contain chylous, serous, hemorrhagic, or mixed fluid. Mural or septal calcifications may be present. Histologically, lymphangioma is composed of multiple endothelium-lined vascular channels filled with eosinophilic proteinaceous material. The supporting stroma is composed of collagen and may contain lymphocytes and lymphoid aggregates (1, 3).

Littoral Cell Angioma

Littoral cell angioma is a tumor of vascular proliferation that is unique to the spleen. This very rare neoplasm has characteristic morphologic and immunophenotypic features (vascular and histiocytic antigens) that distinguish it from other vascular splenic tumors. Morphologically it consists of multiple nodules composed of vascular channels

of red pulp and usually involves the spleen in a diffuse manner, although a focal form has been described (4).

Hemangiopericytoma

Hemangiopericytoma is a rare neoplasm with a relatively high-malignant potential. Gross examination reveals a well-defined, solid tumor with a pseudocapsule, which has a rich vascularization. Intratumoral hemorrhagic or necrotic areas may be present. At histopathologic evaluation, pericytes proliferating around vascular channels lined with endothelium are observed (1).

Hemangioendothelioma

Hemangioendothelioma is a very rare primary vascular tumor of the spleen and has variable malignant potential. Hemangioendotheliomas are well-circumscribed and nonencapsulated solid splenic masses. Microscopically, hemangioendothelioma is composed of vascular and stromal elements, and several histologic patterns, ranging from well differentiated to highly undifferentiated, have been described (1).

Splenic Cysts

Cysts are relatively common benign splenic lesions and can be divided into primary or true cysts and secondary or false cysts according to their etiology and pathophysiology. Primary cysts have a cellular lining and can be caused by either a congenital event (epithelial cyst) or parasitic infestations (hydatid cyst). Secondary cysts have no cellular lining and may be of posttraumatic, inflammatory, or degenerative origin (2, 5).

Clinical Presentation

Most benign splenic lesions are incidental findings and do not produce clinical symptoms.

However, larger and multiple lesions may manifest with splenomegaly and abdominal pain. Spontaneous rupture and massive hemoperitoneum represent rare complications.

Thrombocytopenia, anemia, and coagulopathy may occur from sequestration of hematopoietic cells either in large hemangiomas (Kasabach-Merritt syndrome) or hamartomas, while malignant degeneration has been reported in splenic hemangiopericytoma and hemangioendothelioma.

Associations between several benign splenic tumors and generalized multisystem disorders such as tuberous sclerosis, Wiskott–Aldrich syndrome, lymphangiomatosis and Klippel–Trenaunay–Weber syndrome, have been rarely reported (1, 2, 3).

Imaging

Hemangioma

On ultrasound (US), splenic hemangiomas are either well-defined hyperechoic solid tumors (capillary hemangioma) or more complex lesions (cavernous hemangioma). Most capillary hemangiomas are well-defined hypoattenuating or isoattenuating masses on nonenhanced computed tomography (CT) scans, showing a homogeneous and marked enhancement after contrast medium administration, while the cavernous type usually appears as a complex cystic-solid mass with a inhomogeneous nodular centripetal enhancement. Splenic hemangiomas appear as hypointense or isointense lesions on T1-weighted magnetic resonance imaging (MR) and strongly hyperintense on T2-weighted images; however, central areas of low intensity on T2-weighted images corresponding to regions of fibrosis or thrombosis are often observed in large hemangiomas (1). After administration of MR extracellular contrast agents, early nodular centripetal enhancement with uniform enhancement at delayed imaging is the most common pattern (Fig. 1).

Hamartoma

On US images the splenic hamartoma appears as a solid mass with variable, heterogeneous echogenicity. Most hamartomas show high blood flow on color Doppler US, reflecting the hypervascularity of the red pulp within the lesion (1). Most splenic hamartomas are hypoattenuating or isoattenuating on nonenhanced CT scans. On MR imaging, hamartomas are usually isointense on T1-weighted images and heterogeneously hyperintense on T2-weighted images due to the presence of hypointense fibrotic and necrotic areas. After contrast administration, a diffuse, early, and heterogeneous enhancement is usually observed on both CT and MR dynamic contrast enhancement imaging (Fig. 2).

Lymphangioma

US, CT, and MR typically show large, septated, subcapsular cystic lesions. Curvilinear peripheral mural calcifications may be seen on CT, and significant enhancement is usually not observed after contrast medium administration. The cyst contents have high signal intensity on T2-weighted MR images, usually resulting in hypointensity on T1-weighted images. However, high T1 signal intensity due to internal bleeding or to the proteinaceous nature of the intracystic fluid may also be observed. The fibrous septa appear as hypointense bands on both T1- and T2-weighted images (1).

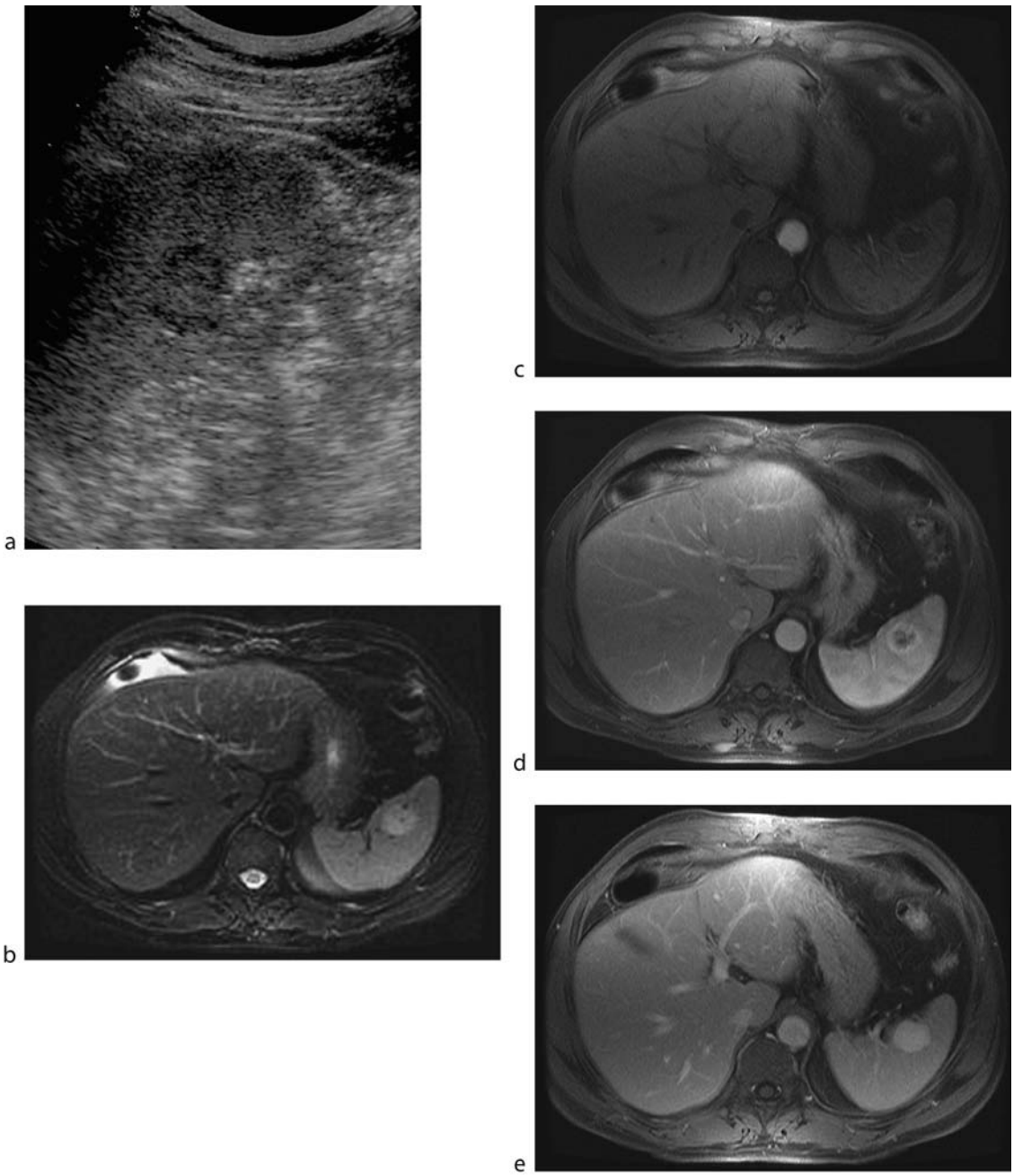

Neoplasms, Splenic, Benign. Figure 1 Hemangioma. On ultrasound, splenic hemangioma appears as a well-defined hyperechoic nodule (a). On T2-weighted magnetic resonance (MR) image, the lesion is slightly hyperintense (b). After administration of MR extracellular contrast agents, the early nodular centripetal enhancement with uniform enhancement at delayed imaging is appreciable (c–e).

Littoral Cell Angioma

Sonographic characteristics of littoral cell angioma include splenomegaly with a diffuse heterogeneous echo texture of the spleen. On early-phase postcontrast CT scan, the spleen presents multiple small areas of low attenuation; delayed filling of the nodules makes the areas isodense with the surrounding enhancing splenic tissue. On MR, littoral cell angioma appears as multiple hypointense nodules on both T1- and T2-weighted images, due to the presence of hemosiderin (4).

Hemangiopericytoma

Hemangiopericytomas appear as hypoechoic nodules on US, and speckled calcifications may be observed on CT scans. They have low signal intensity on T1-weighted MR and are usually hyperintense on T2-weighted images.

Hemangioendothelioma

On US, hemangioendothelioma is usually a hypoechoic mass with intratumoral necrotic areas. Color Doppler US shows an abnormal vascularization characterized by the presence of arterial flow and low resistive index in the solid areas of the tumor (1, 3). On CT scan, hemangioendothelioma usually appears as a low-attenuating mass with enhancement of the solid tumoral portions. On MR, splenic hemangioendothelioma is a heterogeneous solid lesion that, because of the presence of hemosiderin, may show low signal intensity on both T1- and T2-weighted images (1).

Splenic Cysts

On US examination, the typical splenic cyst appears as a homogeneous anechoic area with marked echo enhancement. However, complex cysts are frequently observed. At CT, splenic cysts are typically hypoattenuating, with a thin or imperceptible wall and no rim enhancement. Cystic wall calcification and septations are well demonstrated (Fig. 3). On both T1- and T2-weighted MR images, splenic cysts have a signal intensity equal to that of water; however, in cysts that are complicated by protein or hemorrhage, an increased T1 signal intensity may be

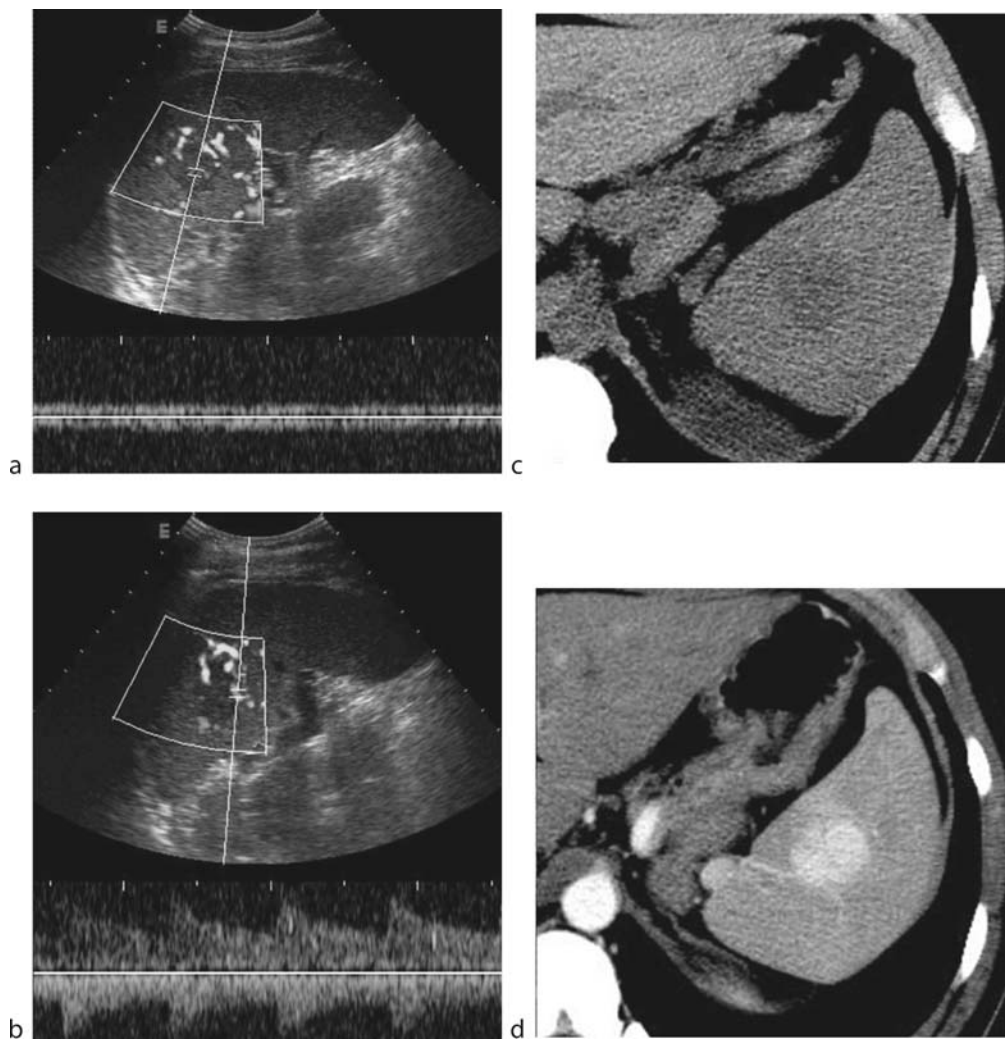

Neoplasms, Splenic, Benign. Figure 2 (continued)

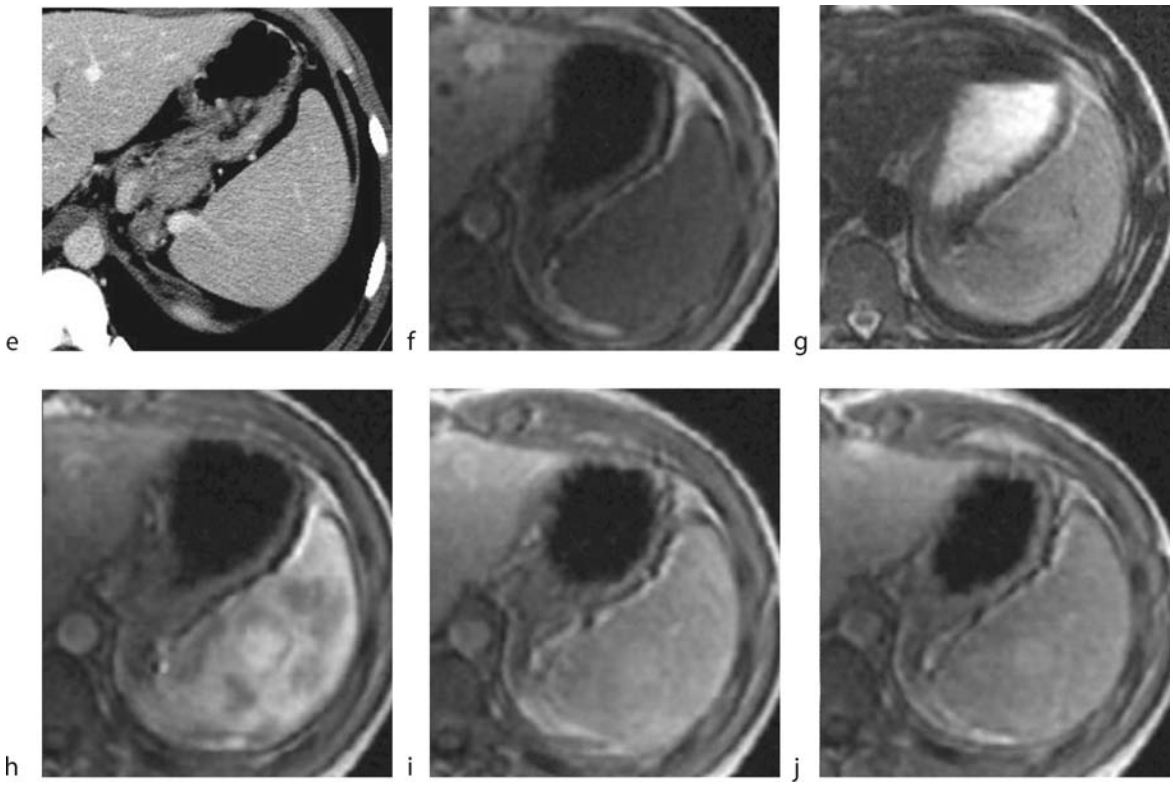

Neoplasms, Splenic, Benign. Figure 2 Hamartoma. This focal lesion shows high blood flow on color Doppler ultrasound (a, b), reflecting the hypervascularity of the red pulp within the hamartoma. On nonenhanced computed tomography (CT) scanning (c), hamartoma appears hypoattenuating. After contrast administration, a diffuse enhancement is observed on early and delayed CT scans (d, e). At magnetic resonance imaging (MR), hamartoma is isointense relative to normal splenic tissue on both T1- and T2-weighted images (f, g). On postcontrast MR dynamic imaging (h–j), a diffuse and early enhancement is demonstrated.

observed. On MR, cystic septations and endoluminal debris, which are typically present on parasitic cysts, are easily identified (2, 3, 5).

Nuclear Medicine

Nuclear medicine is not useful for evaluating benign focal lesions of the spleen because hypervascular lesions do not show radiotracer uptake on 99m-technetium sulfur colloid scintigrams (3).

Diagnosis

Although benign focal lesions of the spleen are relatively uncommon, they must be correctly characterized and differentiated from malignancies. A cystic lesion usually exhibits a fluid content and a well-defined outline without solid components, but reliable differentiation between primary and secondary cysts is usually not possible at imaging. The characterization of the other benign lesions, including splenic hemangioma, hamartoma, and several rare vascular tumors, is usually difficult. Although the most common hypervascular mass in an asymptomatic patient is splenic hemangioma, the imaging appearance of that lesion is often complex, and differentiation from hamartoma or malignancies, particularly angiosarcoma, may not be possible. Large subcapsular solitary lobulated cystic abnormalities discovered incidentally in pediatric patients are typical for lymphangioma; however, differential diagnosis may also include echinococcal or other splenic cysts.

In conclusion, several imaging modalities are necessary to improve focal splenic lesion characterization and role out malignancies. However, splenectomy is necessary for definitive evaluation of a splenic mass with atypical imaging features (1).

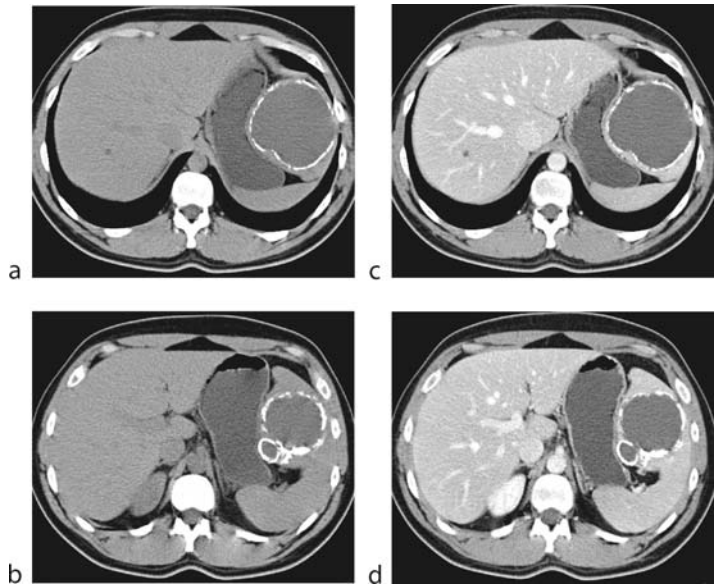

Neoplasms, Splenic, Benign. Figure 3 Hydatid cyst. Nonenhanced computed tomography scans (a, b) show a round, low-attenuating cystic splenic lesion with multiple daughter cysts and peripheral calcifications. No enhancement is seen in the lesion after intravenous contrast material administration (c, d).

Bibliography

1. Abbott RM, Levy AD, Aguilera NS et al (2004) From the archives of the AFIP: primary vascular neoplasms of the spleen: radiologic-pathologic correlation. Radiographics 24:1137–1163
2. Robertson F, Leander P, Ekberg O (2001) Radiology of the spleen. Eur Radiol 11:80–95
3. Paterson A, Frush DP, Donnelly LF et al (1999) A pattern-oriented approach to splenic imaging in infants and children. Radiographics 19:1465–1485
4. Kinoshita LL, Yee J, Nash SR (2000) Littoral cell angioma of the spleen: imaging features. Am J Roentgenol 174:467–469
5. Urrutia M, Mergo PJ, Ros LH et al (1996) Cystic masses of the spleen: radiologic-pathologic correlation. Radiographics 16:107–129

Neoplasms, Splenic, Malignant

Piero Boraschi[1], Francescamaria Donati[1], Alessio Auci[2], Simonetta Salemi[2], Marzio Perri[2], Carla Cappelli[2]
[1]2nd Department of Radiology, University Hospital of Pisa, Pisa, Italy
[2]Department of Diagnostic and Interventional Radiology, University of Pisa, Pisa, Italy
p.boraschi@do.med.unipi.it
bartolozzi@do.med.unipi.it

Synonyms

Malignant neoplasms of the spleen; Malignant tumors of the spleen; Splenic malignancies; Splenic malignant tumors

Definition

Malignant neoplasms of the spleen include primary lymphoreticular tumors (lymphomas and chronic myeloproliferative disorders), primary nonlymphoreticular tumors (hemangiosarcoma, leiomyosarcoma, and fibrosarcoma), and splenic metastases.

Pathology and Histopathology

Lymphoma

Splenic lymphoma is the most common malignant tumor of the spleen and can be primary (when limited to the spleen and hilar lymph nodes) or secondary (when the spleen is involved as a part of a disseminated disease).

Primary lymphoma of the spleen is an extremely rare entity, with a reported incidence of less than 1%; most of these are low-grade B-cell non-Hodgkin's lymphomas. In contrast, the spleen is commonly involved in systemic lymphoma (approximately 25–40% of patients with Hodgkin's or non-Hodgkin's lymphoma at the time of initial diagnosis).

Grossly, an enlarged spleen with one or more intraparenchymal tumor nodules, often less than 1 cm in diameter, is usually observed; however, a diffuse, infiltrative tumor growth and single large lesions have also been described. Generally, malignant lymphomas show a homogeneous, highly cellulated histologic structure lacking fibrous septa (1).

Chronic Myeloproliferative Disorders

The chronic myeloproliferative disorders consist of *chronic idiopathic myelofibrosis*, *essential thrombocythemia*, and *polycythemia rubra vera*. All of these disorders are thought to result from a hematopoietic stem cell lesion. In many cases these proliferations are clonal and neoplastic (2).

Hemangiosarcoma

Although very rare, splenic hemangiosarcoma is the most common nonlymphoreticular malignant tumor of the spleen. It arises from splenic sinus endothelial cells, and at gross examination it usually appears as a large, poorly defined, nodular red mass diffusely involving the spleen. Areas of hemorrhage and necrosis are usually seen within the tumor. Microscopically the tumor consists of abnormal anastomosing vascular channels lined by malignant endothelial cells. Papillary formations and solid areas within the tumor are common (3).

Leiomyosarcoma

Splenic leiomyosarcoma is an extremely rare nonlymphoreticular malignant tumor that originates from muscular cells. Lesions are hypercellular. Even in poorly differentiated examples, actin and myosin are present in the tumor cells (3).

Fibrosarcoma

Fibrosarcoma of the spleen is another extremely rare nonlymphoreticular malignant tumor. This is a fibroblastic malignant lesion that consists of bundles of spindle-shaped cells arranged at angles to one another (3).

Metastases

Metastases of the spleen are rare and usually associated with disseminated disease. Splenic metastases usually occur as a result of hematogenous spread from lung, breast, prostate, stomach, or ovarian cancer or from malignant melanoma. The gross features of splenic metastases are variable, including either single or multiple lesions with cystic, solid, or complex structure. Microscopically, metastases resemble the primary tumors (4).

Clinical Presentation

Lymphoma

Clinically, patients with primary non-Hodgkin's splenic lymphoma most often present with a palpable mass, splenomegaly, and abdominal pain. In contrast, splenic involvement by systemic Hodgkin's disease is relatively frequent, and splenomegaly is the typical clinical finding. However, nonspecific signs (fever, weight loss, and night sweats) due to the systemic disease are usually also observed (1, 2).

Chronic Myeloproliferative Disorders

The chronic myeloproliferative disorders are chronic diseases that sometimes convert to an acute myeloid leukemic phase. Most patients are over 60 years of age at diagnosis, and one-third of patients are asymptomatic at presentation. Massive splenomegaly is a characteristic finding (2).

Hemangiosarcoma

Unlikely hepatic hemangiosarcomas, no associations with exposure to thorium, vinyl chloride, or arsenic have been observed. The most frequent clinical findings are splenomegaly, abdominal pain, fever, fatigue, weight loss, anemia, and consumptive coagulopathy. Major complications include rupture of the spleen, which often leads to fatal hemoperitoneum. The lymphatic system, liver, lungs, and bone are the most frequent metastatic sites. Hemangiosarcomas are highly aggressive neoplasms, and the prognosis is poor (3).

Leiomyosarcoma and Fibrosarcoma

Leiomyosarcoma and fibrosarcoma, extremely rare primary nonlymphoreticular malignant tumors of the spleen, present clinical findings like those of splenic hemangiosarcoma. These lesions are aggressive with high rates of both local recurrence and metastatic disease.

Metastases

Metastatic disease involving the spleen is uncommon, and isolated metastasis to the spleen is extremely rare. Most patients with splenic metastases have widely disseminated metastatic disease usually arising from lung, colorectal, endometrial, ovarian, thyroid, pancreatic, or gastric cancers or, most commonly, melanoma. Although most patients with splenic metastases are clinically asymptomatic, painful splenomegaly, splenic vein thrombosis, and splenic rupture have been rarely reported (4).

Imaging

Lymphoma

The lymphomatous nodule is typically hypoechoic, and an inhomogeneous hypoechoic mass or multiple hypoechoic lesions less than 1 cm in size are the most common

features on ultrasound (US) (2). Computed tomography (CT) findings include a homogeneous enlarged spleen without masses, a solitary mass, multifocal lesions, or diffuse infiltration (Figs. 1, 2). The focal lesions are typically hypodense on nonenhanced scanning and appear demarcated and lightly enhancing after contrast medium administration, while the infiltrative pattern and tumor foci smaller than 1 cm may be difficult to detect on CT (1). On magnetic resonance imaging (MR), splenic lymphoma is usually isointense both on T1- and T2-weighted sequences, with light and heterogeneous enhancement after injection of gadolinium. Reticuloendothelial system (RES)-specific MR contrast agents can improve the accuracy of diagnosis of splenic lymphoma.

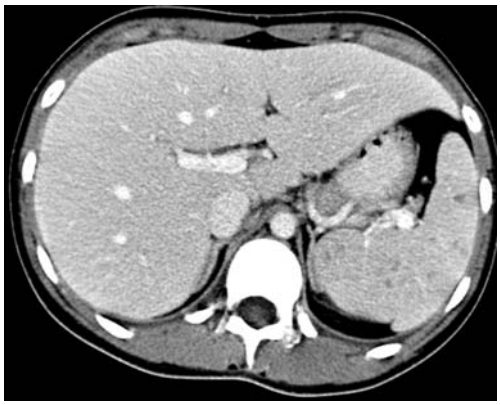

Neoplasms, Splenic, Malignant. Figure 1 Splenic lymphoma in Hodgkin's disease. Postcontrast-enhanced computed tomography shows an enlarged spleen with numerous hypodense lesions, smaller than 1 cm, corresponding to foci of lymphoma.

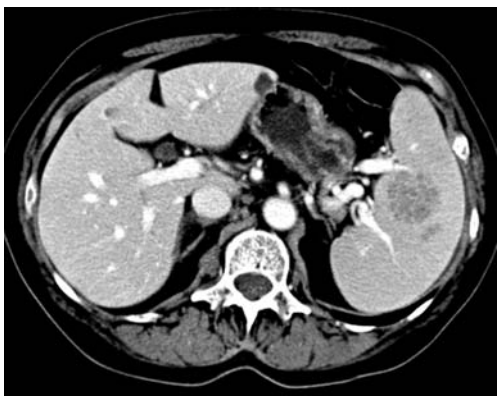

Neoplasms, Splenic, Malignant. Figure 2 Primary splenic non-Hodgkin's lymphoma. Postcontrast-enhanced computed tomography demonstrates splenomegaly with a typical low-attenuating mass; a second small lesion is also appreciable.

This contrast is selectively taken up by the normal spleen and not by malignant cells, thus improving the tumor/spleen contrast on T2-weighted images (1, 2).

Chronic Myeloproliferative Disorders

Imaging findings of chronic myeloproliferative disorders are similar to those of lymphoma (Fig. 3).

Hemangiosarcoma

Sonographically, splenic hemangiosarcoma appears as a complex, poorly defined mass with a heterogeneous echostructure. Increased Doppler flow may be seen in the more solid echogenic portions of the tumor. On CT scans, a heterogeneous low-density and poorly defined mass with peripheral enhancement and areas of necrotic degeneration is usually observed. Calcifications and areas of high CT attenuation due to acute hemorrhage may be present. Hypervascular metastasis to the liver, lungs, bones, and lymphatic system are well identified on CT. The tumor usually demonstrates low signal intensity on both T1- and T2-weighted MR images. However, areas of increased and decreased signal intensity due to the intratumoral presence of blood products and necrosis are often observed. Contrast-enhanced MR reveals heterogeneous enhancement within the tumor, corresponding to the pathologic findings of solid tumor with necrotic tissues (3).

Leiomyosarcoma and Fibrosarcoma

Imaging findings of leiomyosarcoma and fibrosarcoma are similar to those of hemangiosarcoma.

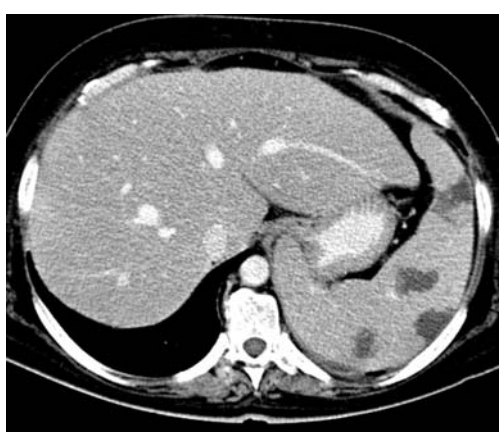

Neoplasms, Splenic, Malignant. Figure 3 Acute myeloid leukemia in a patient affected by polycythemia rubra vera. Postcontrast-enhanced computed tomography demonstrates splenomegaly with multiple ischemic areas.

Metastasis

Several different US patterns of the splenic metastases have been described, including multifocal or diffuse hypoechoic lesions, hyperechoic nodules, and cystic tumors. On CT, splenic metastases usually appear as hypoattenuating solid or cystic masses with inhomogeneous contrast enhancement. Intratumoral calcifications or necrotic areas may be present.

Metastases are usually minimally hypointense to isointense with spleen on T1-weighted MR and slightly hyperintense on T2-weighted sequences. Because metastases show a lack of Kupffer cells, no significant loss of signal intensity on T2-weighted superparamagnetic iron oxide (SPIO)-enhanced images is observed, with a significant improvement in detection of secondary involvement of the spleen in oncology patients (1, 4).

Nuclear Medicine

Metabolic imaging allows the recognition of active tumor mass because of its fixed tracer. In patients with Hodgkin's disease and non-Hodgkin's lymphoma, gallium-67 scintigraphy and fluorine-18-fluorodeoxyglucose positron emission tomography (18F-FDG-PET) have been widely employed. Gallium-67 scintigraphy has played an important role in monitoring response to therapy and follow-up of patients with lymphoma; however, recent studies suggest the use of 18F-FDG-PET in place of gallium scanning for staging Hodgkin's disease and non-Hodgkin's lymphoma. Particularly, 18-FDG-PET offers several advantages, including improved spatial resolution, reduced nonspecific abdominal uptake, and a shorter imaging time (5).

Diagnosis

Imaging modalities can delineate focal splenic lesions, but their accurate diagnosis is often difficult, and both incidentally discovered lesions and masses in patients with known malignancies represent diagnostic dilemmas. On imaging, the malignant lesions are more likely to be multifocal due to metastases, or they tend to be diffuse and ill defined due to rapid growth (4). They may present different structures, including a homogeneous composition in lymphoma, variable patterns in metastases, and, usually, a complex cystic appearance in hemangiosarcoma. Irregular borders, signs of infiltration of the surrounding splenic parenchyma, lymphonodal masses, and extrasplenic metastases are highly suggestive for malignancy. Moreover, functional imaging, including both nuclear medicine (18F-FDG-PET and gallium scintigraphy) and MR-SPIO imaging, has the potential to improve the accuracy of tumor diagnosis by exploiting biological and histopathologic differences between malignant and benign tissue (1, 4, 5).

In conclusion, although accurate evaluation with cross-sectional imaging may be helpful in differentiating between benign and malignant splenic lesions, percutaneous biopsy or splenectomy should be performed in doubtful cases.

Bibliography

1. Robertson F, Leander P, Ekberg O (2001) Radiology of the spleen. Eur Radiol 11:80–95
2. Brunning RD, Bennett JM, Flandrin G et al (2001) Myelodysplastic syndromes. In: Jaffe ES, Harris NL, and Stein H (eds) Pathology and Genetics of Tumors of Hematopoietic and Lymphoid Tissues. IARC Press, Lyon, France. World Health Organization Classification of Tumors, vol 3, pp 61–73
3. Abbott RM, Levy AD, Aguilera NS et al (2004) From the archives of the AFIP: Primary vascular neoplasms of the spleen: radiologic-pathologic correlation. Radiographics 24:1137–1163
4. Lam KY, Tang V (2000) Metastatic tumors to the spleen: a 25-year clinicopathologic study. Arch Path Lab Med 124:526–530
5. Wirth A, Seymour JF, Hicks RJ et al (2002) Fluorine-18 fluorodeoxyglucose positron emission tomography, gallium-67 scintigraphy, and conventional staging for Hodgkin's disease and non-Hodgkin's lymphoma. Am J Med 112(4):262–268

Neoplasms, Temporal Bone

Gabriele A. Krombach
Department of Radiology, University Hospital, Aachen, Germany
krombach@rad.rwth-aachen.de

Definition

Tumors arising in the temporal bone can originate from all the different types of tissue that occur in the temporal bone, such as bone, nerves, the meninges, and soft-tissue components (skin, fat, lymph nodes, muscle). The tumors can be benign or malignant. Most tumors are acquired, but congenital tumors such as congenital cholesteatoma also occur. Most tumors of the temporal bone have a typical age peak and characteristic symptoms.

Pathology/Histopathology

Exostosis

Exostosis is a broa-based overgrowth of compact bone in the medial osseous part of the external auditory canal. It occurs in ocean swimmers, divers, and surfers and is

known as a response to cold water exposure. Thus, it usually occurs bilaterally. Histology shows concentric layers of subperiosteal bone.

Osteoma

Osteoma is a benign bony tumor that can arise in the external auditory canal, the mastoid, or the petrous pyramid. It has all layers of normal bone and occurs unilaterally. It is usually located lateral to the isthmus of the external auditory canal.

Malignant Neoplasm of the External Auditory Canal

Squamous cell carcinoma is a malignant epithelial tumor that may arise from the external auditory canal, pinna, or middle ear.

Basal cell carcinoma is a slowly growing local aggressive tumor that can occur at the outer ear. It is also caused by chronic exposure to sunlight. It arises from the basal cells, which represent the deepest layer of the skin. The tumor consists of basophilic cells of high mitotic activity. Basal cell carcinoma does not metastasize.

Ceruminal gland adenocarcinoma is a malignant tumor of modified apocrine glands, located in the external auditory canal. Ceruminal gland carcinomas are characterized by a loss of the normal glandular double cell layer and presence of pleomorphic luminal epithelial cells.

Squamous cell carcinoma arises from keratinocytes. It is predominantly located at areas that are exposed to sunlight or at which chronic inflammation is present. It represents the most common malignant tumor of the external ear.

Other malignant tumors, such as malignant melanoma and sarcomas, can also occur within the outer auditory canal or ear.

Acquired Cholesteatoma

Cholesteatoma is a sac lined by keratinizing stratified squamous epithelium, trapped and growing in the middle ear space, mastoid, or other pneumatized spaces of the temporal bone. It can arise from the pars flaccida or the pars tensa of the tympanic membrane. It may develop following retraction of the tympanic membrane due to negative middle ear pressure associated with Eustachian tube dysfunction. Cholesteatoma can also develop after invasion of keratinized stratified squamous epithelium from the surface of the tympanic membrane into the middle ear after (small) perforation of the tympanic membrane.

Glomus Tympanicum

Glomus tympanicum is a benign paraganglioma of the middle ear. It arises in the glomus bodies situated along the tympanic branch of the glossopharyngeal nerve (Jacobson's nerve), as it bends around the cochlea. This tumor is strongly vascularized.

Middle Ear Adenoma

Middle ear adenoma is a benign tumor of glandular origin, originating from the mucosa and growing slowly. It can occur at any part of the middle ear.

Schwannoma

Schwannomas are benign neural neoplasms. Possible localizations in the temporal bone are the middle ear (tumors arising from the facial nerve, chorda tympani, or Jacobson's nerve), inner ear (cochlear nerve or vestibular nerve), or the cerebellopontine angle (vestibulocochlear nerve), where it is the most common tumor. Schwannomas arise from the Schwann cells wrapping the nerves. Acoustic schwannomas always arise from the vestibular portion of the cranial nerve VIII. Bilateral acoustic schwannomas are associated with neurofibromatosis type II. Intralabyrinthine schwannomas originate from the Schwann cells surrounding the peripheral fibers of the cochlear nerve or the cristae or maculae of the vestibule.

Meningioma

This benign tumor represents the second most common tumor in the cerebellopontine angle and originates from the dura. This strongly vascularized tumor develops from the arachnoid villi component of the leptomeninges. It may contain calcifications. In larger tumors, areas of cystic degeneration can be present. Meningiomas may express estrogen receptors.

Lipoma

Lipomas of the cerebellopontine angle are congenital benign fatty lesions. They originate from maldevelopment of mesoderm or of meningeal precursor tissue, namely the meninx primitive. Generally, the VII and VIII cranial nerves pass through the mass.

Endolymphatic Sac Tumor

Endolymphatic sac tumor is an adenomatous tumor arising from the pars rugosa (middle third) of the endolymphatic sac. This tumor arises from the cells lining the endolymphatic sac. It is hypervascularized and has been reported to contain a speculated calcified matrix in almost all known cases.

Rhabdomyosarcoma

Rhabdomyosarcoma is a malignant tumor of skeletal muscle origin. It is a highly aggressive neoplasm arising from rhabdomyoblasts, which are embryonal cells that usually differentiate into striated muscle cells. In the temporal bone it is supposed to originate from the muscle cells in the vicinity of the Eustachian tube in the middle ear.

Clinical Presentation

Exostosis

Exostosis is usually asymptomatic. If the tumor is large, it can lead to retention of debris, external otitis, and/or hearing loss. The latter depends on the degree of canal obstruction. Pain and tinnitus are other possible symptoms. Exostosis should be surgically removed if symptomatic.

Osteoma

Osteoma is usually asymptomatic. If the tumor obstructs the outer auditory canal, debris can accumulate and cholesteatoma may result in the long run.

Malignant Neoplasm of the External Auditory Canal and Ear

Basal cell carcinomas are asymptomatic. At the beginning they appear as small erosions. Suspicion should be raised if erosions at sunlight-exposed areas persist over 3 weeks. Squamous cell carcinomas appear crusty and bleed easily.

Ceruminal gland adenocarcinomas cause local pain.

Malignant neoplasms of the external auditory canal and ear have a peak at higher ages (>70 years).

Acquired Cholesteatoma

Individuals of all ages may develop cholesteatoma. The leading symptom is chronic otorrhea and conductive hearing loss. In more advanced stages, symptoms are due to progressing bone erosion and may include vertigo (erosion of the lateral semicircular canal) or facial palsy (erosion of the facial nerve canal). Meningitis, abscess in the temporal lobe, and lateral sinus thrombosis are possible late-stage complications.

Glomus Tympanicum

Due to the vascular nature of the tumor, pulsatile tinnitus is the most common symptom at initial presentation (90%). Conductive hearing loss occurs in 50% of patients and is due to blocked movement of the tympanic membrane.

Middle Ear Adenoma

Dizziness, tinnitus, and conductive hearing loss are the most common symptoms. The age peak is 40–50 years.

Schwannoma

Middle ear schwannoma may cause conductive hearing loss. Intralabyrinthine schwannoma causes vertigo or sensorineural hearing loss. Patients with acoustic schwannoma classically present with sensorineural hearing loss, tinnitus, and disequilibrium. The age peak is 40–60 years.

Meningioma

Symptoms depend on the exact location and size of the tumor and may include dysfunction of cranial nerves V, VII, and VIII. There is a female predominance (2–3:1). The age peak is >60 years.

Lipoma

Most lipomas are asymptomatic. Dizziness and sensorineural hearing loss are the most common symptoms. Only in cases unresponsive to medical therapy is surgical decompression done. Because nerve fibers run through the lipoma, surgical therapy is extremely difficult.

Endolymphatic Sac Tumor

Sensorineural hearing loss and tinnitus are common symptoms. The tumor occurs in patients between 20 and 80 years. Endolymphatic sac tumors have a higher incidence in patients with von Hippel–Lindau disease.

Rhabdomyosarcoma

This tumor is the second most common head and neck malignancy in children and has an age peak at 4–6 years. Otalgia, bloody otorrhea, facial nerve palsy, and sensorineural hearing loss are common symptoms.

Imaging

Exostosis

High-resolution computed tomography (HRCT) with bone algorithm shows a circumscribed tumor that consists of dense compact bone. It has a broad base and begins deep to the isthmus within the medial aspect of the osseous internal auditory canal in the close vicinity of the annulus.

Osteoma

HRCT demonstrates a pedunculated tumor with both layers of normal bone (cortical shell and trabecular bone).

Malignant Neoplasm of the External Auditory Canal and Ear

HRCT and MRI usually do not allow for a specific diagnosis of malignant tumors in adults. However, erosion of the underlying bone and infiltration of neighboring structures are signs of malignancy of a mass. The main role of imaging is to assess the extent of the neoplasm and infiltration of vital structures and determine the presence of metastasis. The periparotid lymph nodes represent the primary lymphatic drainage of the ear. Thus, the parotid gland and upper neck must be included in imaging studies.

Acquired Cholesteatoma

HRCT shows the extent of the soft-tissue mass. Erosion of bone is usually present (Fig. 1) and allows differentiation of cholesteatoma from middle ear adenoma. On MRI, the mass is isointense to cerebrospinal fluid on T1- and T2-weighted images. Cholesteatoma does not enhance after administration of contrast medium, but due to granulation tissue, there is enhancement at the rim of the tumor.

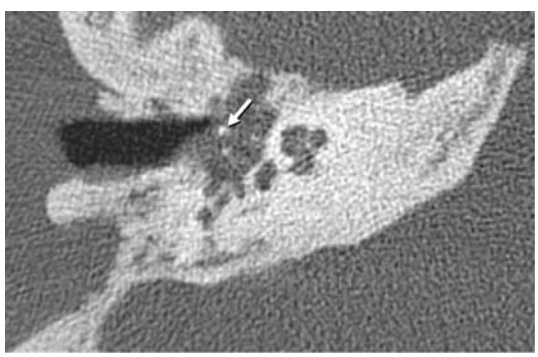

Neoplasms, Temporal Bone. Figure 1 Acquired cholesteatoma. The axial high-resolution computed tomographic image shows a middle ear cavity opacification. The ossicles are eroded (*arrow*).

Glomus Tympanicum

MRI is the modality of choice and demonstrates a hyperintense middle ear mass on T2-weighted images. After intravenous administration of contrast medium, the tumor strongly enhances on T1-weighted images. CT does not demonstrate erosion of the bone. The ossicles are usually spared.

Middle Ear Adenoma

CT shows a mass behind the intact tympanic membrane. The mastoid is usually well pneumatized. The ossicles are encased by the tumor, but usually no bony erosion is present.

Schwannoma

The CT appearance of middle ear schwannoma is nonspecific, and differentiation from paraganglioma is usually not possible. On MRI, schwannomas strongly enhance on T1-weighted images after the administration of contrast medium (Fig. 2). T2-weighted high-resolution images also show the tumor (Fig. 3).

Meningioma

Meningiomas enhance strongly on CT and MRI after intravenous injection of contrast medium. The dural tail sign—linear enhancement along the adjacent dura—is a typical finding on MRI. Brain edema in the vicinity of the tumor is a sign of infiltration of the arachnoid. In these cases the tumor is difficult to remove, and a higher rate of recurrence must be expected.

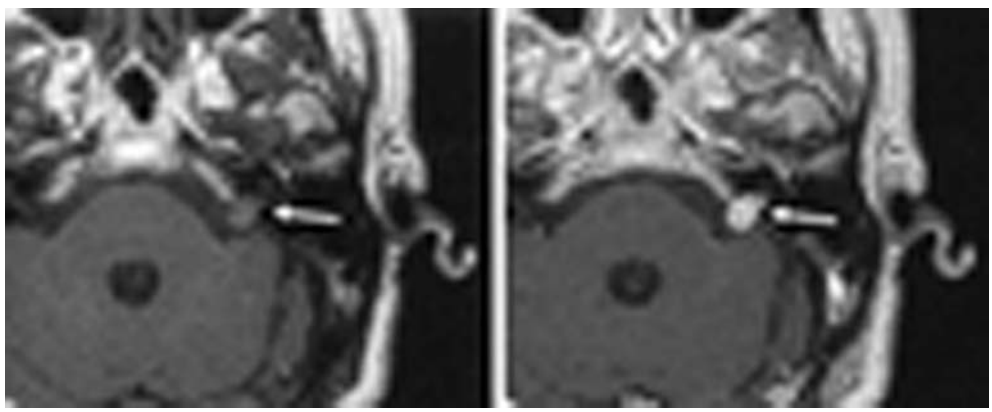

Neoplasms, Temporal Bone. Figure 2 Acoustic schwannoma. Axial T1-weighted magnetic resonance image before (*left*) and after intravenous administration of contrast medium (*right*). The tumor is isointense to the brain before administration of contrast medium (*arrow* in the *left* image). It strongly enhances after administration of contrast medium (*arrow* in the *right* image).

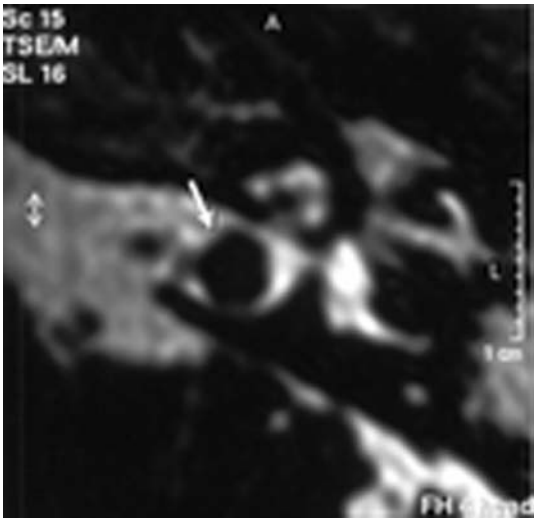

Neoplasms, Temporal Bone. Figure 3 Acoustic schwannoma. The T2-weighted magnetic resonance image shows a small tumor (*arrow*) in the internal auditory canal.

Lipoma

On T1-weighted MR images, the tumor has the typical high signal intensity of fatty tissue. It loses signal if fat saturation techniques area applied.

Endolymphatic Sac Tumor

HRCT shows a soft-tissue mass located at the posterior wall of the temporal bone, eroding the bone. The tumor matrix contains speculated calcifications. MRI shows foci of enormous enhancement within the mass after intravenous injection of contrast medium.

Rhabdomyosarcoma

HRCT demonstrates a mass that causes extensive bony destruction. On T2-weighted MR images, rhabdomyosarcoma is hyperintense. On T1-weighted images, the mass is hypointense and enhances after intravenous administration of contrast medium.

Nuclear Medicine

In patients with neoplasm of the temporal bone, nuclear medicine has only a limited role.

Bone scintigraphy with technetium 99 m methylene diphosphonate may lead to detection of metastasis to the temporal bone at an early stage or show metastasis from a temporal bone neoplasm to other parts of the body.

Diagnosis

Several tumors, such as schwannoma and lipoma, have a pathognomonic appearance on imaging. In all tumors without such a pathognomonic imaging appearance, biopsy or surgical removal and histology are essential for correct diagnosis.

In patients with exostosis, otoscopy shows a circumferential stenosis of the external auditory canal. In cholesteatoma, otoscopy shows a retraction pocket or perforation of the tympanic membrane and a white mass behind the tympanic membrane.

If otoscopy shows a reddish mass behind the posteroinferior part of the tympanic membrane, glomus tympanicum tumor must be considered. Before biopsy can be performed, imaging is required to rule out an aberrant internal carotid artery. This developmental anomaly causes similar clinical symptoms (pulsatile tinnitus and conductive hearing loss) and has the same appearance at otoscopy. Furthermore, glomus tympanicum must be differentiated from glomus jugulare, which arises from the jugular foramen and may extend through the posterior floor of the middle ear cavity into the middle ear, because the two tumors require different surgical approaches.

Bibliography

1. Vogl T, Bruning R, Schedel H et al (1989) Paragangliomas of the jugular bulb and carotid body: MR imaging with short sequences and Gd-DTPA enhancement. Am J Roentgenol 153(3):583–587
2. Salzman KL, Davidson HC, Harnsberger HR et al (2001) Dumbbell schwannomas of the internal auditory canal. Am J Neuroradiol 22(7):1368–1376
3. Dahlen RT, Johnson CE, Harnsberger HR et al (2002) CT and MR imaging characteristics of intravestibular lipoma. Am J Neuroradiol 23(8):1413–1417
4. Gaeta M, Blandino A, Minutoli F et al (1999) Sudden unilateral deafness with endolymphatic sac adenocarcinoma: MRI. Neuroradiology 41(10):799–801

Neoplasms, Thyroid, Benign and Malignant

Carmela Visalli
Department of Radiologic Sciences,
University of Messina, Messina, Italy
cvisalli@unime.it

Synonyms

Benign and malignant neoplasm; Thyroid nodules; Thyroid tumors

Definition

Thyroid neoplasms include all lesions caused by abnormal thyroid tissue growth due to excessive cellular division and proliferation. They are comprehensive, including benign and malignant nodules. Nodules are palpable masses in the thyroid gland, often found incidentally on ultrasound examination. They occur in 4–7% of the population and can be solitary lesions or occur in a context of multinodular enlargement of the gland. This pathological condition is four times more common in women than in men and occurs more often in people who live in geographic areas with iodine deficiency or who are exposed to ionizing radiation.

Pathology/Histopathology

In general, nodular disease of the thyroid is common; however, malignancy of the thyroid is rare. Approximately 5–10% of thyroid nodules are malignant, whereas the remainders represent a variety of benign diagnoses, including colloid nodules, degenerative cysts, hyperplasia, thyroiditis, and benign neoplasms (Table 1). A rational approach focal to management of a thyroid nodule is based on the clinician's ability to distinguish the more common benign entities from malignancy in a highly reliable and economic way.

Colloid nodules are the most common and do not have an increased risk of malignancy. Most follicular adenomas are benign; however, some may share morphological aspects with follicular carcinoma. Although carcinoma of the thyroid gland is rare, it is the most common malignancy of the endocrine system.

Neoplasms, Thyroid, Benign and Malignant.
Table 1 Types of thyroid nodules

Adenoma	• Macrofollicular adenoma
	• Microfollicular adenoma
	• Atypical adenoma
	• Papillary adenoma
Liquid nodule	• Simple cyst
	• Colloid nodule
Inflammatory nodule	• Focal thyroiditis
Carcinoma	• Papillary (60–80%)
	• Follicular (10–20%)
	• Medullary (5–10%)
	• Anaplastic (5%)
Other malignancy	• Lymphoma (4%)
	• Sarcoma
	• Teratoma
	• Metastases (2–17%)

Thyroid carcinoma usually presents as a solitary nodule. There are four forms: papillary, follicular, medullary, and anaplastic (1). Differentiated tumors (papillary or follicular) are highly treatable and usually curable. Poorly differentiated tumors (medullary and anaplastic) are aggressive, metastasize early, and have a much poorer prognosis. ▶Thyroglobulin can be used as a tumor marker for well-differentiated forms.

Women are affected more often than men, and any age group can be affected, although thyroid cancer usually occurs in people between the ages of 25 and 65 years.

Papillary Thyroid Cancer

Papillary thyroid cancer is the most common type of thyroid cancer, accounting for 60–80% of all thyroid malignancies. It occurs more frequently in women and presents in the 30–40-year-old age group. It is also the predominant cancer type in children with thyroid cancer and in patients who have had radiation to the head and neck. In this group the cancer tends to be multifocal, with early lymphatic spread and a poor prognosis.

Papillary carcinoma is a nonencapsulated lesion that histologically consists of a stromal core and packed papillae with a small amount of colloid within follicles. Small calcified bodies, known as psammoma bodies, may be found in the stroma.

Follicular Thyroid Cancer

Follicular thyroid cancer occurs in approximately 20% of patients with thyroid cancer and is more common in women above 50 years of age. A particular form of follicular cancer is Hürthle cell carcinoma, characterized by large polygonal thyroid follicular cells.

Follicular carcinoma is an encapsulated lesion, generally solitary and characterized by angioinvasive behavior with a consequently high frequency of distant metastases. Regional lymph node involvement has been reported to be less than 13%. When lymph nodes are involved, the prognosis is usually poor. Because this cancer is usually very well differentiated, it is difficult to distinguish from follicular adenoma. For the definitive diagnosis, demonstration of capsular or surrounding thyroid tissue invasion is necessary.

Medullary Thyroid Cancer

Medullary thyroid cancer originates from the parafollicular cells (C cells), which produce the hormone calcitonin. Carcinoembryogenic antigen (CEA) is a tumoral marker produced by medullary thyroid cancer. Its prognosis is poorer than that for follicular or papillary

thyroid cancer, especially when it has metastasized beyond the thyroid gland. This cancer can develop as a "sporadic form" or as a part of the complex syndrome of ►multiple endocrine neoplasias, type 2 (MEN 2a and MEN 2b).

Medullary thyroid cancer can cause diarrhea and flushing episodes. The main sites of spread of this cancer are local lymph nodes in the neck and mediastinum, as well as liver, lung, and bone.

Anaplastic Thyroid Cancer

This form of neoplasm has a very poor prognosis, with a high mortality (near 100%) due to its aggressive behavior, rapidly invading surrounding tissue and the trachea.

Other Tumors

The thyroid gland may also be the site of other tumors, including sarcoma, lymphoma, teratoma, and metastasis from other cancers, such as lung, breast, and kidney neoplasms.

Clinical Presentation

At physical examination, thyroid nodules may be diffuse or localized, soft or hard, mobile or fixed, and painful or painless (2). If nodules are less than 1 cm in diameter, they are usually not palpable unless they are located in the anterior portion of the gland. Physical characters indicative of malignancy are a hard, fixed lesion; nodules greater than 4 cm; or hoarseness.

After clinical examination, the diagnostic algorithm for evaluating a thyroid nodule includes the following:

- Laboratory tests: thyroid stimulating hormone (TSH), triiodothyronine (T3), thyroxine (T4), antithyroid peroxidase antibodies, thyroglobulin, calcitonin
- Ultrasonography
- Nuclear medicine imaging (scintigraphy and positron emission tomography)
- Fine-needle aspiration (FNA)
- Computed tomography (CT)
- Magnetic resonance imaging (MRI)

Laboratory Tests

Laboratory tests are important for distinguishing different thyroid diseases, but thyroid function tests should not be used to determine whether a nodule is benign or malignant, even if the presence of clinical and laboratory signs of hyperthyroidism or hypothyroidism is most likely related to a benign nodule.

The serum TSH level allows assessment for thyrotoxicosis (<TSH) or hypothyroidism (>TSH).

Thyrotoxicosis may be due to a diffuse toxic goiter (Graves' disease), toxic multinodular goiter, or single toxic nodule (Plummer's disease).

The most common cause of hypothyroidism is Hashimoto's thyroiditis.

When the TSH level is normal, nodular aspiration should be considered.

Thyroglobulin levels are useful tumor markers once the diagnosis of malignancy has been assessed, but they are nonspecific with regard to differentiating a benign from a cancerous thyroid nodule (2).

Imaging

After physical examination, ultrasound is the first imaging modality for assessing thyroid disorders. CT and MRI have a small role, but specific indications include staging of cancer or evaluation of the extension of mediastinal goiter (3).

Ultrasonography

Ultrasonography with high-resolution probes is used to confirm the presence of a nodule, to determine whether it is a solitary nodule, and to assess any cystic component. It can also differentiate thyroid from adjacent nonthyroidal masses.

Ultrasonography is sensitive for identifying a focal lesion. In fact, it detects more nodules than palpation. It is suitable for evaluating the size, location, and structure of a nodule (solid or cystic, hypoechoic, hyperechoic, with or without halo sign, microcalcifications) (Fig. 1). In a solid hypoechoic nodule, irregular borders, central microcalcifications, prevalent, intranodular vascularity, and cervical adenopathies are the main signs suggesting malingnance.

Conversely, findings of hyperechoic texture, comet-tail artifacts from colloid, lack of blood flow in the nodule, a peripheric halo, and a smooth border.

Because ultrasonography cannot confidently distinguish benign from malignant nodules, FNA is necessary for this (4). Ultrasonography can guide the biopsy and be used to determine changes in the size of nodules over time, either in the follow-up of a lesion thought to be benign or in detecting recurrent lesions in patients with thyroid cancer (3, 4).

The predictive value of ultrasonography may significantly increase if the ultrasonographic parameters of thyroid nodules, such as microcalcifications, echogenicity, and halo sign, are combined with their vascular pattern. In fact, color Doppler and spectral analysis can demonstrate different vascular patterns as prevalent perinodular or central vascularization (Fig. 2). Many studies have shown that nodules with perinodular vascularization have a lower risk of malignancy than nodules with central vascularization.

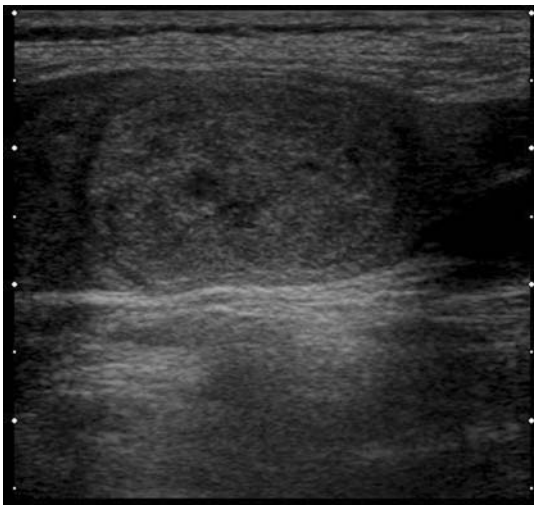

Neoplasms, Thyroid, Benign and Malignant. Figure 1 Longitudinal section of the right lobe of the thyroid. Nodule with hypoechoic and dishomogeneous structure, regular borders with halo sign.

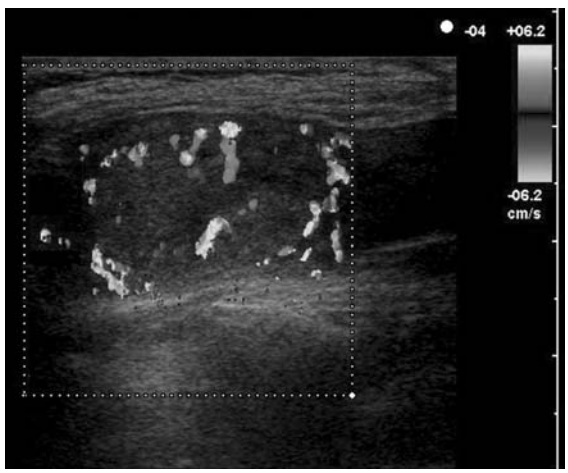

Neoplasms, Thyroid, Benign and Malignant. Figure 2 The nodule shows a rich periferic and intranodular vascularization at the evaluation with color Doppler.

CT and MRI

CT and MRI usually have no place in the assessment of patients with thyroid nodules, but nodules may be found incidentally during examination of the neck for reasons not relating to the thyroid gland. CT and MRI do play an important role in evaluating the mediastinal extension of thyroid masses and also in assessing the spread of cancer (3).

Nuclear Medicine

Scintigraphy

Scintigraphy is still the standard method for functional imaging of the thyroid (3). The two isotopes most commonly used are ^{123} I and ^{99m} Tc-pertechnetate.

Thyroid scanning measures the amount of iodine (usually ^{99m} technetium isotope) trapped within the nodule. A normal scan indicates that the iodine uptake is similar in both lobes of gland. A nodule is classified as "cold" (decreased uptake), "warm" (uptake similar to that of surrounding tissue), or "hot" (increased uptake). A large number of thyroid nodules may be cold on radionuclide scan, but only 5–15% of these are malignant. A "hot" nodule is hyperfunctional and is almost always benign.

Nuclear imaging cannot reliably distinguish between benign and malignant nodules and is not required if nodules are present.

FNA biopsy has replaced nuclear imaging as the initial evaluation procedure. However, in patients with a suppressed TSH level, thyroid scanning determines regional uptake or function and can be used as a secondary study (4).

Positron Emission Tomography

Positron emission tomography (PET) with 18F-fluorodeoxyglucose (FDG) is an imaging technique that might improve the diagnostic accuracy, allowing identification of metabolic alterations in tumors. At present it plays only a small role in thyroid imaging but can be particularly useful to evaluate metastatic disease. FDG PET measures the body's metabolic activity, and areas in which cancer is present will show up as brighter on the scan because the disease is more metabolically active than noncancerous cells.

Radiometabolic Therapy

Nuclear medicine plays a specific role in the ablative treatment of differentiated thyroid neoplasms. Ablation

therapy is performed with ^{131}I and for the following indications:

- To destroy the small amount of thyroid tissue remaining in the neck after surgery
- To treat functional metastases
- To treat patients with elevated thyroglobulin levels

Before and after ablation therapy, a whole-body ^{131}I scan is necessary to identify metastatic disease and treatment response, respectively.

Diagnosis

For a diagnosis of thyroid neoplasm, evaluation of the patient should start with anamnesis, physical examination, and laboratory tests (TSH, T3, T4, autoantibodies). Ultrasonography should then be done to confirm the presence of a nodule or multiple nodules and their structural characteristics. If a solitary thyroid nodule is found, FNA biopsy should be performed to determine whether the nodule is malignant.

FNA biopsy is believed to be the most effective method available for distinguishing between benign and malignant lesions. This modality has a sensitivity of 68–98% and a specificity of 72–100%. The accuracy of FNA biopsy in diagnosing thyroid conditions depends highly on the expertise and experience of the cytopathologist and the technical skill of the physician performing the biopsy. The results of FNA are interpreted as benign, malignant, suspicious, or indeterminate. False-negative or false-positive cases may occur when nodules are very large or very small; these errors can be minimized by using ultrasound-guided biopsy.

To confirm a thyroid nodule or to obtain functional information, thyroid scintigraphy can be used. Although thyroid scanning may give a probability that a nodule is benign or malignant, it cannot truly differentiate benign from malignant nodules (5).

References

1. Baloch ZW, Li Volsi VA (2000) Mini-symposium: endocrine pathology. Newly described tumors of the thyroid. Current Diagnostic Pathology 6:151–164
2. Bennedbaeck FN, Perrild H (1999) Diagnosis and treatment of the solitary thyroid nodule. Results of a European survey. Clinical Endocrinology 50:357–363
3. Naik KS, Bury RF (1998) Imaging the thyroid. Clinical Imaging 53:630–639
4. Iannuccilli JD, Cronan JJ, Monchik JM (2004) Risk for malignancy of thyroid nodules as assessed by sonographic criteria. The need for biopsy. J Ultrasound Med 23:1455–1464
5. McHenry CR, Slusarczyk SJ, Askari AT et al (1998) Refined use of scintigraphy in the evaluation of nodular thyroid disease. Surgery 124:656–662

Neoplasms, Urethra

Franck Koskas[1], Olivier Hélénon[2], Marie-France Bellin[1]
[1]Department of Radiology, University Paris-Sud 11, Paul Brousse Hospital, Villejuif, France
[2]Department of Radiology, University Paris, Necker Hospital, Paris, France
franckkoskas@hotmail.com
marie-france.bellin@pbr.ap-hop-paris.fr

Synonyms

Proliferative disorders of the urethra; Tumors of the urethra

Definition

Urethral neoplasms include benign and malignant tumors, the latter being either primary tumors of the urethra or metastatic tumors. They are rare entities.

The urethra represents the distal part of the urinary tract. It extends from the bladder neck to the external urethral meatus.

Characteristics

Urethral neoplasms are rare entities with only a few reported series in the radiology literature. Herein, we review the anatomy and histology specific to male and female urethras. We also describe the imaging features of urethral tumors.

Normal Anatomy and Histology of the Male Urethra

The male urethra has a mean length of 18 cm and is subdivided into anterior and posterior portions, each of which is subdivided into two parts:

1. The posterior urethra stretches from the bladder neck to the lower edge of the urogenital triangle and includes:
   a. The prostatic urethra, which is 3 cm long in the young male, is the widest part of the canal. It is spindle-shaped and narrowest at its junction with the membranous urethra.

   On the floor of the canal is a narrow longitudinal ridge, the seminal colliculus. On each side of the ridge lies the prostatic sinus, a depressed fossa into

which the periurethral prostate ducts empty. At the summit of the seminal colliculus (verumontanum), lies the blind pouch of the prostatic utricle surrounded by the slit-like openings of the ejaculator ducts of the seminal vesicles.

b. The membranous urethra, approximately 1.5 cm long, passes through the urogenital triangle, which contains the Cowper glands embedded in the external urethral sphincter. In this tract, the urethra is surrounded by the compressor muscle of the urethra and the perineal muscles.

2. The anterior urethra, 14–15 cm long is subdivided into:
   a. The bulbar urethra, which is of larger diameter (1.5–2 cm), is surrounded by the bulb of the corpus spongiosum, does not have stiff fascia, and extends from the perineal area to the suspensor ligament of the penis. Many small mucous glands of Littré are located at its inner surface.
   b. The penile or pendulous urethra, has a relative uniform diameter approximately 1 cm, stretching from the penile ligament to the external urethral meatus. Before its emergence at the meatus, there is an ampullar dilatation called fossa navicularis. Glands of Littré are also located near the fossa navicularis but fewer than in the bulbar urethra.

Because of its complex embryological origin, the urethral epithelial lining has several histological characteristics: transitional epithelium, from the bladder neck to the seminal verumontanum; then cylindrical, to the fossa navicularis, and, finally squamous epithelium, to the external meatus. These differences explain the histological diversity of urethral tumors.

Normal Anatomy and Histology of the Female Urethra

The female urethra is about 3–4 cm long, nearly equivalent to the length of the male posterior urethra. It extends from the internal urethral meatus at the bladder neck through the urogenital triangle to the external urethral meatus, anterior to the vaginal opening. A sit courses obliquely downward and forward, it is slightly curved with the concavity directed forward and upward. Multiple tiny urethral mucous glands, called the para-urethral glands of Skene, open into the urethral canal.

The same histological diversity as in males is found with transitional, cylindrical, and squamous epithelia.

The outer portion of the urethra is composed of striated muscle, which, in the upper two thirds of the urethra, is primarily circular and extends proximally to blend with the bladder base. The lower portion of the urethra is located close to the anterior vaginal wall and enveloped by common musculature (the compressor muscle of the urethra).

Pathological, Clinical, and Imaging Features

Clinically, these tumors are often heralded by obstructive voiding symptoms and hematuria, which clears near the end of micturition. On urethrograms, urethral tumors appear as filling defects and only the localization provides a clue to determine the origin. Biopsy is mandatory to establish the correct diagnosis.

Benign Tumors

For both men and women, condylomata are found on the anterior urethra: it is the most common abnormality.

Benign tumors of the urethra are very rare: they may be of epithelial or mesenchymal origin. In women, leiomyoma of the urethra is extremely rare.

In men, a fibroepithelial polyp is of embryonic origin, usually originating in the prostate and projecting into the urethra. The polyp is connected to the verumontanum *via* a stalk, which maintains the polyp in the prostatic urethra or, sometimes, with extension through the bladder neck into the bladder (Fig. 1). MRI cannot differentiate between benign and malignant tumors.

Malignant Tumors of the Male Urethra

Carcinoma of the male urethra is rare, representing less than 1% of all urological cancers, and predominantly concerns men over 50 years old.

Tumors of the male urethra are classified according to their location and histological diversity.

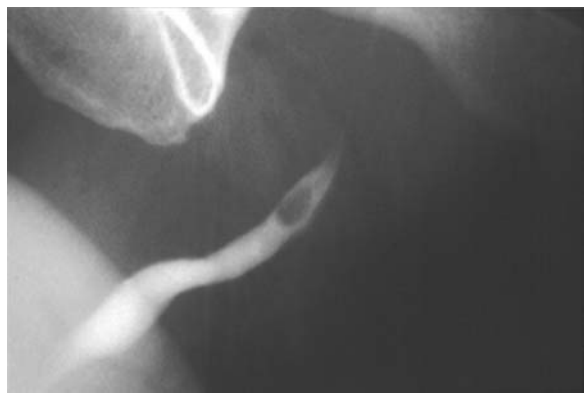

Neoplasms, Urethra. Figure 1 Voiding ►urethrography. Polyp arising from the anterior urethra. (Reprinted with permission from Helenon et al, 2005)

The bulbomembranous urethra is the most frequent site (around 60% of cases), followed by the penile urethra (30%) and the prostatic urethra (10%).

Histologically, 80% of male urethral carcinomas are squamous cell carcinomas, 15% are transitional cell carcinomas, and 5% are adenocarcinomas or undifferentiated carcinomas. The histological subtype of urethral cancers also varies according to the anatomical location. The prostatic urethra gives rise to transitional cell carcinomas in 90% of patients and squamous cell carcinomas in 10%. In the bulbomembranous, squamous cell carcinomas develop in 80% of patients, transitional cell carcinomas in 10%, and adenocarcinomas or undifferentiated carcinomas in 10%. In the penile urethra, squamous cell carcinomas represent 90% of the patients and transitional cell carcinomas the remaining 10%. Adenocarcinomas arise from the Littré or Cowper glands (Fig. 2).

►Urethritis secondary to sexually transmitted infectious disease can cause urethral stricture and is considered a risk factor for malignancy. In fact, more than 50% of patients with a carcinoma of the urethra have a history of urethral stricture, which is always symptomatic and the stricture is most frequently located in the bulbomembranous urethra (most common site of urethral carcinomas).

Urethral Cancer Staging System

1. Ta—Noninvasive carcinoma
2. Tis—Carcinoma *in situ*
3. T1—Tumor is confined to the subepithelial connective tissue
4. T2—Tumor invades the prostate, periurethral muscle or the corpus spongiosum
5. T3—Tumor invades the corpus cavernosum, the bladder neck or beyond the prostatic capsule
6. T4—Tumor invades other adjacent organs
7. N0—No regional lymph node metastasis
8. N+—Evidence of regional lymph node involvement
9. M0—No evidence of distant spread of disease
10. M+—Evidence for distant spread of disease.

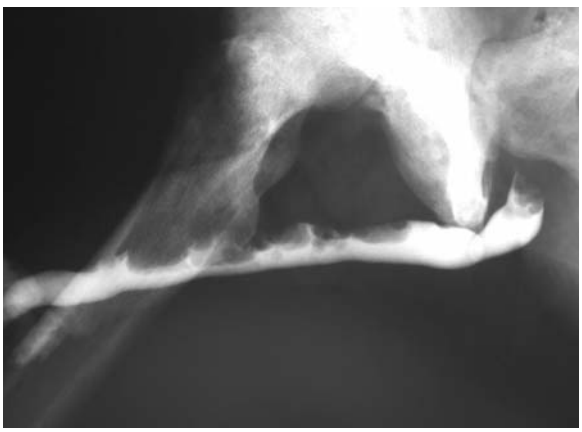

Neoplasms, Urethra. Figure 2 Retrograde urethrography. Multiple recurrent tumors of a transitional cell carcinoma. (Reprinted with permission from Helenon et al, 2005)

Male urethral carcinomas can disseminate directly to adjacent structures or metastasize to regional lymph nodes. The lymphatic vessels from the anterior urethra drain into the superficial and deep inguinal lymph nodes and, occasionally, into the external iliac lymph nodes. Tumors of the posterior urethra most commonly spread to the pelvic lymph nodes.

On MR images, urethral tumors have signal intensity similar to or lower than that of the surrounding the corpus cavernosum on T1-weighted images and intermediate to low signal intensity on T2-weighted images. On contrast-enhanced MR images, the tumor usually shows mild enhancement. Sometimes, it has very high signal intensity on T2-weighted images due to associated inflammation.

MRI can be especially useful for local staging (extension into the tunica albuginea or septa of the corpus cavernosum) and for detection of tumors that invade the root of the penis when physical examination is poorly accessible.

Surgical excision is the primary treatment of choice: anterior urethral carcinoma usually has a better prognosis than posterior urethral carcinoma, which is often associated with extensive local invasion and distant metastases.

Malignant Tumors of Female Urethra

Carcinoma of the female urethra is four times more frequent than that of the male urethra but still remains an uncommon pathology (less than 0.01% of all carcinomas in women). It predominantly affects women over 50 years old with risk factors, such as chronic irritation, urinary tract infection, and proliferative lesions, such as caruncles, papillomas, adenomas, polyps, and leukoplakia of the urethra.

Anterior (40% of cases) and posterior urethral cancers (60% of cases) can be distinguished.

Anterior tumors are located in the distal third of the urethra and the lymphatic drainage empties into the superficial and deep inguinal nodes. Local surgical excision is the treatment of choice for these lesions.

Because the posterior urethra lymphatic vessels drain into the external iliac, hypogastric and obturator nodes, local spread to the bladder neck and trigone explain

the poor prognosis: fewer than 10% of women are still alive at 5 years with a 4 cm tumor. For such advanced lesions, combined surgery, radiation therapy, and, possibly, chemotherapy is necessary.

Two thirds of urethral carcinomas are squamous cell carcinomas, followed by transitional cell carcinomas (20%), adenocarcinomas (10%), undifferentiated tumors and sarcomas (8%), and melanomas (2%).

Urethral Cancer Staging System

1. Ta—Noninvasive carcinoma
2. Tis—Carcinoma *in situ*
3. T1—Tumor is confined to the subepithelial connective tissue
4. T2—Tumor invades periurethral muscle
5. T3—Tumor invades the anterior part of vagina or bladder neck
6. T4—Tumor invades other adjacent organs
7. N0—No regional lymph node metastases
8. N+—Evidence of regional lymph node involvement
9. M0—No evidence of distant spread of disease
10. M+—Evidence of distant dissemination.

On MR images, the tumor has low signal intensity on T1-weighted images and relatively high signal intensity on T2-weighted images. The size of the tumor is best evaluated on sagittal T2-weighted images. Tumors in the distal urethra may extend into the adjacent perineum and the target-like appearance of the normal urethra on axial T2-weighted images may be disrupted. MR is helpful in evaluating the size, location, and local extension of urethral tumors. Its accuracy to assess local tumor extension has been reported to be 90%.

Metastatic Tumors of the Urethra

Metastatic tumors are uncommon and mainly concern the male urethra. Bladder carcinomas may spread to the anterior urethra by means of seeding during urethral instrumentation or at cystectomy. The corpus spongiosum can become involved by carcinoma spread from the spermatic cord, testis, prostate and rectum, and can be responsible for extensive urethral narrowing and irregularity. Hematogenous metastases of malignant melanoma and primary prostate, bladder, colonic, testicle or kidney cancer to the corpora cavernosa and corpus spongiosum have been reported.

In conclusion, the diagnosis is based on urethrography detecting a nonspecific filling defect. MRI is unable to differentiate between benign and malignant tumors, making biopsy mandatory. The aim of MRI is to help stage the malignant tumor to determine the best strategy of treatment.

Bibliography

1. Pavlica P, Barozzi L, Menchi I (2003) Imaging of male urethra. Eur Radiol 13:1583–1596
2. Ryu JA, Kim B (2001) MR Imaging of the male and female urethra. Radiographics 21:169–1185
3. Helenon O, Ramella G, Lapray JF, et al (2005) Urètre. In: Imagerie de l'appareil urinaire. Flammarion (ed) 2:898–930
4. Kawashima A, Sandler CM, Wasserman NF, et al (2004) Imaging of urethral disease: a pictorial review. Radiographics 24:S195–S216

Neovascularization

The process of formation of new vessels, such as in tumors.

▶Contrast Media, Ultrasound, Applications in Kidney Tumor

Nephritis

▶Glomerulonephritis

Nephritis, Bacterial, Acute

Severe renal infection, term initially applied to diabetic or immunocompromised patients, with prolonged clinical course and parenchymal loss.

▶Pyelonephritis, Acute

Nephritis, Interstitial, Chronic

Kidney disease that primarily affects the renal interstition and tabules, characterized by tubulointerstitial fibrosis and atrophy, associated with a mononuclear cellular infiltrate.

▶Chronic Pyelonephritis

Nephro- and Urolithiasis

►Nephrocalcinosis and Urolithiasis in Childhood

Nephroblastoma

Alternative name for Wilms' tumor, which is a cancerous tumor of the kidney in children.
►Neoplasms, Kidney, Childhood

Nephrocalcinosis

Renal lithiasis in which calcium deposits form in the renal parenchyma and result in reduced kidney function and blood in the urine.
►Stone Disease, Urinary

Nephrocalcinosis and Urolithiasis in Childhood

M. Riccabona, R. Fotter
Department of Radiology, Division of Pediatric Radiology, Universiy Hospital Graz, Graz, Austria
michael.riccabona@meduni-graz.at

Synonyms

Nephro- and urolithiasis; Urinary tract calculus; Urinary tract stone

Definition

Nephrocalcinosis (NC) is a microscopic renal tubular or interstitial calcification. Depending on the location a medullary, a cortical or a diffuse type can be differentiated. Note that in a variety of diseases urolithiasis and NC may occur simultaneously, with urolithiasis being a sequelae of the underlying disease that causes NC. Urolithiasis is defined as macroscopic calcification in the urinary collecting system. Urinary stones are composed of crystal agglomerations, sometimes mixed with proteins that form at the papillae, the epithelium or in the collecting system.

Embryology and Pathogenesis

Causes are infection (particularly in children), hypercalciuria, cystinuria or oxaluria (potentially familial), as well as impaired inhibitor function such as low citrate excretion, some (diuretic) drugs and various metabolic disorders (e.g. Bartter's syndrome). Incidence varies widely with a large geographic distribution (more common in the far and middle east), with some age (typical medullary changes in pre-term newborns), gender (boys affected more often than girls), composition (uric acid stones are extremely rare in children) and race variation (less often in black people). Urinary calculi can occur in the kidney, the ureter and the urinary bladder, the latter—as a primary condition—becoming rare. NC and urolithiasis is less common in children than in adults. They should always give reason for a thorough investigation (metabolic causes, familial disease, underlying renal or urinary tract condition) (Table 1).

Clinical Presentation

Nephrolithiasis and urinary tract calculi as well as NC may be clinically asymptomatic; if stones cause obstruction they present with pain, colic, (micro-) haematuria, (secondary) urinary tract infection. In nephrolithiasis clinical presentation depends on the underlying condition and the stage of the disease, ranging from asymptomatic patients to renal insufficiency and urolithiasis with all its potential symptoms.

Imaging

Imaging usually relies on detailed ultrasound (US) as the initial study. There NC is seen as an increased echogenicity of the affected structure that may start with just an increased echogenicity of the cortico-medullary junction, with an inversion of the normal renal parenchymal pattern in medullary NC, an increased cortico-medullary differentiation with a very echogenic cortex in cortical NC, or a diffusely increased echogenicity with loss of differentiation in the diffuse type (Fig. 1). Using the location and amount of echogenicity changes (that correspond with the degree of the disease) US offers a grading possibility (Table 2). In long-standing disease, these areas may eventually become very echogenic and exhibit a stone-like appearance, obviating analysis of the deep renal structures.

Stones—if calcified—sonographically are echogenic and cause posterior acoustic shadowing as well as (often) a twinkling artefact on colour Doppler sonography (CDS) (Fig. 2). Note that for visualisation of a calculus in the

Nephrocalcinosis and Urolithiasis in Childhood.
Table 1a Causes for ▶nephrocalcinosis and urolithiasis. Common causes of nephrocalcinosis and important differential diagnosis

Nephrocalcinosis	Common causes
Medullary	ACTH therapy
	Adrenal insufficiency
	Bartter's syndrome
	Bone metastases
	Cushing syndrome
	Hypercalciuria
	Hyperoxaluria
	Hyperparathyroidism
	Hyper-, Hypothyroidism
	Idiopathic hypercalcaemia
	Lipoidnecrosis
	Lesch-Nyhan syndrome
	Lowe's syndrome
	Malignant neoplasm
	Medication: furosemide, dexamethasone
	Medullary sponge kidney
	long time parenteral nutrition, ascorbic acid supplementation
	d-RTA
	Tyrosinaemia
	Sarcoidosis, other granulomatous diseases
	Sickle cell disease
	Vitamin D, A intoxication
	William's syndrome, Wilson's disease
Cortical	Chronic hypercalcaemia
	Lipoidnecrosis
	Ethylene glycol intoxication
	Primary hyperoxaluria
	Sickle cell disease
	Acute cortical necrosis
Differential diagnosis	Alport syndrome
	Chronic glomerulonephritis
	Kidney transplant rejection
	Pyelonephritis
	Renal tuberculosis
	Renal vein thrombosis
	Tamm-Horsfall depositions

Nephrocalcinosis and Urolithiasis in Childhood.
Table 1b Metabolic disturbances associated with urolithiasis and/or nephrocalcinosis

Hypercalciuria	
Normocalcemic hypercalciuria	Idiopathic hypercalciuria
	d-RTA
	Diuretics—Furosemide
	Bartter's syndrome
	Wilson's disease, Lowe's syndrome
Hypercalcemic hypercalciuria	Primary hyperparathyroidism
	Immobilisation
	Hyperthyroidism
	Hypothyroidism
	Cushing syndrome—ACTH therapy
	Adrenal insufficiency
	Hypervitaminosis D, A
	Idiopathic hypercalcaemia of childhood
Hyperoxaluria	Primary hyperoxaluria type I, II, III
	Secondary hyperoxaluria:
	Malabsorption syndromes
	Lack of intestinal *Oxalobacter formigenes*
	Short bowel syndrome
	Dietary
Cystinuria	Type I, II, III
Hyperuricosuria	Inborn errors of metabolism
	Lesch–Nyhan syndrome
	Glycogen-storage diseases, type I, III, V, VII
	Overproduction in
	Leukaemia
	Non-Hodgkin's lymphoma
	High-protein diet
Hypocitraturia	d-RTA
	Idiopathic

Source: Adapted from Benz-Bohm G, Hoppe D (2001) In: Fotter R (ed) Pediatric Uroradiology, Springer Berlin–Heidelberg–New York, pp 281–286, Table 17.2, p 283 and Table 17.5, p 287.

distal ureter a sufficiently extended urinary bladder is mandatory. Assessment of the ureteric bladder inflow jet (by CDS) can be helpful for differentiating complete from partial obstruction (Fig. 3). In a significant acute obstruction, the resistance index is asymmetrically elevated in the parenchymal arteries of the affected kidney, despite of an often only minimally dilated collecting system of a swollen, enlarged, slightly hyperechoic and hazy differentiated kidney. Non-calcified calculi may appear less echogenic and cause no or little dorsal shadowing—particularly infectious and uric acid 'stones', which in children are seen more commonly in combination with other pre-existing urinary tract malformations or systemic/metabolic disease.

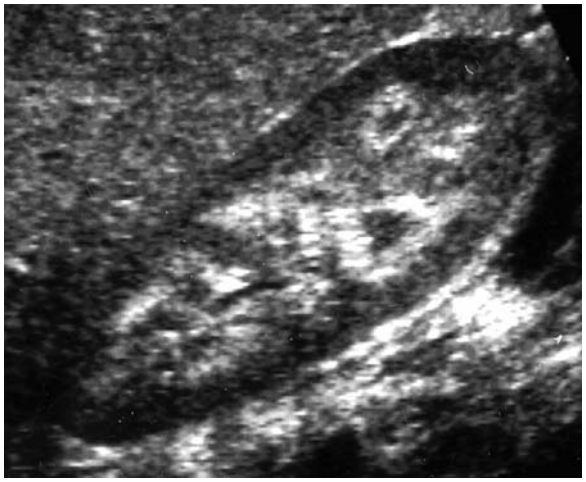

Nephrocalcinosis and Urolithiasis in Childhood.
Figure 1 Nephrocalcinosis (NC)—ultrasound (US) appearance. Note the echogenic papilla and (outer) medulla, particularly the rim-like hyperechoic appearance of the cortico-medullary junction.

Nephrocalcinosis and Urolithiasis in Childhood.
Table 2 Sonographic grading of medullary nephrocalcinosis (Dick et al. 1999)

Grade I	Mild increase in echogenicity around the border of the medullary pyramids
Grade II	Mild diffuse increase in echogenicity of the entire medullary pyramids
Grade III	Greater, more homogeneous increase in the echogenicity of the entire medullary pyramid

Source: Adapted from Benz-Bohm G, Hoppe D (2001). In: Fotter R (ed) Pediatric Uroradiology, Springer Berlin–Heidelberg–New York, pp 281–286, Table 17.3, p. 284

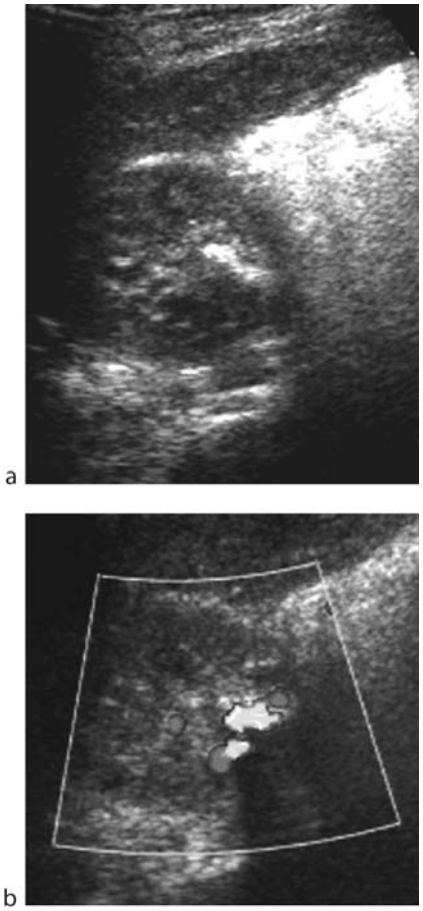

Nephrocalcinosis and Urolithiasis in Childhood.
Figure 2 Twinkling artefact in urolithiasis. (a) Axial view of grey scale US depicts the echogenic calculus in the renal pelvis (but only little shadowing). (b) Twinkling colour signals on colour Doppler sonography (CDS) in the same view caused by the calculus.

US is usually supplemented by an abdominal *plain film* focused at the kidney, ureter and bladder region ('KUB'). Age-adapted exposure and film-screen combinations should be chosen. It demonstrates calcification projecting on the urinary tract structures.

Intravenous urography (IVU) is hardly necessary in children, only in some rare cases, where US and KUB cannot sufficiently diagnose the condition it may become indicated. If applied, age-adapted contrast dose and selected number of individually timed exposures should be used for a tailored investigation to reduce radiation burden.

In difficult cases or complex disease, spiral (multislice) CT is the best method for looking at urolithiasis and particularly ureteral stones. Usually un-enhanced low dose protocols suffice. Only for differentiation of tumour-like lesions with calcifications (e.g. xanthogranulomatous pyelonephritis, tuberculosis) intravenous iodinated contrast is recommended. MR has currently no role in investigating nephrolithiasis and NC in children.

Diagnosis

Diagnosis is made by imaging, with functional information important for clinical decision making, particularly in urolithiasis with colic and acute obstruction. Usually a detailed US study of a properly hydrated urinary tract at sufficiently extended bladder supplemented by a KUB-film—together with clinical and laboratory information—suffices for making the diagnosis in

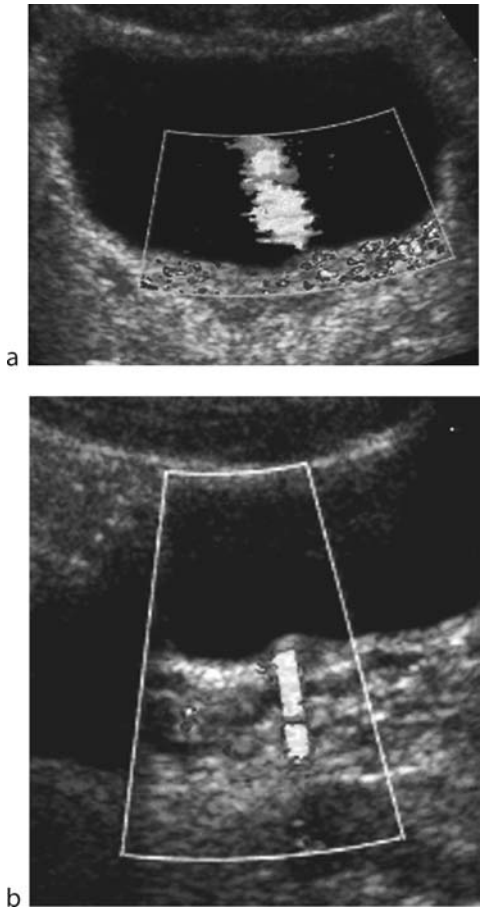

Nephrocalcinosis and Urolithiasis in Childhood.
Figure 3 Colour Doppler sonography (CDS) of the bladder in urolithiasis. (a) Normal ureteral bladder inflow jet from the left side demonstrated on CDS in an infant with an obstructing distal ureteral calculus of the right ureter, with no depictable urine inflow from right side. (b) Note the twinkling pre-ostial ureteral calculus in the distal right ureter just at the ostium.

infants and children and reveals all treatment relevant information (Table 3). Rarely IVU or CT may become necessary.

Follow-up—particularly in NC—is usually performed by US; and often US appearance persists even when the underlying disease is treated and has diminished or ceased.

Nephrocalcinosis and Urolithiasis in Childhood.
Table 3 Diagnostics in urolithiasis and nephrocalcinosis

Patient history	Familial stone disposition, stone recurrence
Stone localisation	US, abdominal X-ray, IVU, Spiral-CT
Lab	Electrolytes, uric acid, creatinine, urea, Mg, PO4, plasma oxalate, acid base status, AP
Urine	Culture, sediment
	24 h urine ⇒ Promotors and Inhibitors
Renal function	Clearance
Diet	Daily fluid intake ⇓, meat ⇑, milk ⇑⇑
Ask for	Diuretics, ACTH
Drugs	Vitamin D, A, C overdose
	Allopurinol
	Chemotherapy
Inherited	Cystinuria
Metabolic	Primary hyperoxaluria
Disorders	Xanthinuria
	2,8-Dihydroxyadeninuria
	D-RTA
	Dent's disease
	Lesch–Nyhan syndrome
	Wilson's disease
	Bartter's syndrome
	William's syndrome
	Lowe's syndrome
Chronic	Malabsorption syndromes (e.g. Cystic fibrosis)
Diseases	Steatorrhoea
	Celiac disease
	Short bowel syndrome
Immobilisation	Hypercalciuria
Stone analyses	Infrared-spectroscopy, X-ray diffraction
Differential diagnosis	e.g. Appendicitis
Imaging	Primarily: US
	Supplemented by KUB
	Selected cases: IVU, CT
	e.g. complicated, unclear, XPN
	DD Tumour, pre-operative
	Rare cases: Nephrostomy + Pelography
	e.g. complete obstruction, bridging
	infected(pyonephrosis), urosepsis

Source: Adapted from Benz-Bohm G, Hoppe D (2001). In: Fotter R (ed) Pediatric Uroradiology, Springer Berlin–Heidelberg–New York, pp 281–286, Table 17.4, p 286

Bibliography

1. Alon US (1997) Nephrocalcinosis. Pediatrics 9:160–165
2. Benz-Bohm G, Hoppe D (2001) Urolthiasis and nephrocalcinosis. In: Fotter R (ed) Pediatric Uroradiology, Springer Berlin–Heidelberg–New York, pp 281–286, Table17.2, p 283, Table 17.5, p 287, Causes for nephrocalcinosis and Urolithiasis
3. Cremin B, Wiggelinkhuizen J, Bonnici F (1982) Nephrocalcinosis in children. Br J Radiol 55:413–418
4. Dyer RB, Chen MYM, Zagoria RJ (1998) Abnormal calcifications in the urinary tract. Radiographics 18:1405–1424
5. Riccabona M, Lindbichler F, Sinzig M (2002) Conventional imaging in paediatric uroradiology. Eur J Radiol 43:100–109

Nephrolithiasis (Renal Lithiasis)

The presence of calculi in the kidney.

▶Stone Disease, Urinary

Nerves, Cranial

Tarek A. Yousry, Indra Yousry
Institute of Neurology, London, UK
t.yousry@ion.ucl.ac.uk

Definitions

Cranial nerves are the means by which the brain receives information from, and controls the activities of the head, neck and to a lesser extent the thoracic and abdominal viscera. The cranial nerves (CN) consist of 12 pairs of which the CN III–XII are genuine peripheral nerves.

The olfactory tract and the optic nerve are parts of the brain, because their fibres are medullated by oligodendrocytes (central glial cells). The other cranial nerves (CN III–XII) have segments of variable length covered by central glia. These segments are considered to be part of the brain and are known as the root entry or exit zones. These zones are important as symptomatic neurovascular contacts only occur at their site. The central segments of the motor nerves are shorter than those of the sensory nerves; the longest central segment however, is found in CN VIII.

The *olfactory nerve*s (CN I) are the only sensory cranial nerves that project directly to the cerebral cortex rather than *via* the thalamus. They arise from nerve cells within the olfactory mucosa that coats the superior part of the middle and lateral walls of the nasal cavity. They pass through the cribriform plate of the ethmoid bone and terminate in the olfactory bulbs (Fig. 1a). From here the olfactory tract passes posteriorly and terminates by forming three striae: the lateral, the intermediate and the medial olfactory striae.

The *optic nerve* (CN II) is constituted by a great number of nervous fibres arising from cells in the retina which converge towards the optic disc and, pass through the sclera and choroid membranes, and as they emerge from the eyeball form the optic nerve. CN II passes through the orbital cavity, optic canal and ends at the optic chiasm (Fig. 1a).

The *oculomotor nerve* (CN III) is a motor nerve. Its nuclei are situated at the level of the superior colliculus. The nerve emerges along the internal margin of the cerebral peduncle, passes through the interpeduncular fossa to enter the lateral wall of the cavernous sinus (Fig. 1b). It then passes through the superior orbital fissure into the orbit. It innervates the superior, inferior and medial recti as well as the levator palpebrae. CN III also carries parasympathetic fibres to the sphincter ciliary muscles of the pupil.

The *trochlear nerve* (CN IV) is a motor nerve. Its nucleus is situated at the level of the inferior colliculus. It crosses the midline and exits at the posterior surface of the mesencephalon below the inferior colliculus (Fig. 1c). It then travels around the mesencephalon, enters the lateral wall of the cavernous sinus, passes through the superior orbital fissure into the orbit where it innervates the superior oblique muscle.

The *trigeminal nerve* (CN V) has motor and sensory nuclei. The motor nucleus is located in the pons, the sensory nuclei extend in the brainstem from the mesencephalon to the cervical spinal cord. CN V emerges from the pons with a large sensory root and small superior and inferior motor roots (Fig. 2a). All roots enter the trigeminal cavity (Meckel's cave) where the sensory root continues into the trigeminal ganglion and then provides three main branches. The ophthalmic nerve (V1) enters the lateral wall of the cavernous sinus, and passes through the superior orbital fissure into the orbit. The maxillary nerve (V2) enters the lateral wall of the cavernous sinus, and passes through the foramen rotundum into the pterygopalatine fossa. The mandibular nerve (V3) carries in addition to the sensory fibres the motor fibres of the trigeminal cavity. It passes through the foramen ovale.

The *abducens nerve* (CN VI) is a motor nerve. Its nucleus is situated at the lower level of the pons. CN VI exits the brainstem at the pontomedullary junction (Fig. 2b). It then travels through the pontine cistern, enters the cavernous sinus through Dorello's canal, and passes through the superior orbital fissure into the orbit where it innervates the lateral rectus muscle.

The *facial nerve* (CN VII) has motor and sensory nuclei. The motor nucleus is located at the floor of the 4th ventricle. The motor fibres for the viscera (parasympathetic) arise from the superior salivatory nucleus and the lacrimal nucleus. The visceral sensory fibres terminate in the nucleus solitarius in the dorsal medulla oblongata.

The motor (CN VII) and the sensory (CN VIIb, intermediate) nerve roots exit the brainstem at the pontomedullary junction and enter the internal auditory meatus (Fig. 2c). CN VII then enters the facial canal and exits the skull through the stylomastoid foramen. The parasympathetic fibres of the lacrimal nucleus and visceral sensory fibres pass as the greater petrosal nerve through the Vidian canal.

The *vestibulocochlear nerve* (CN VIII) is a sensory nerve which consists of the cochlear and the (superior and

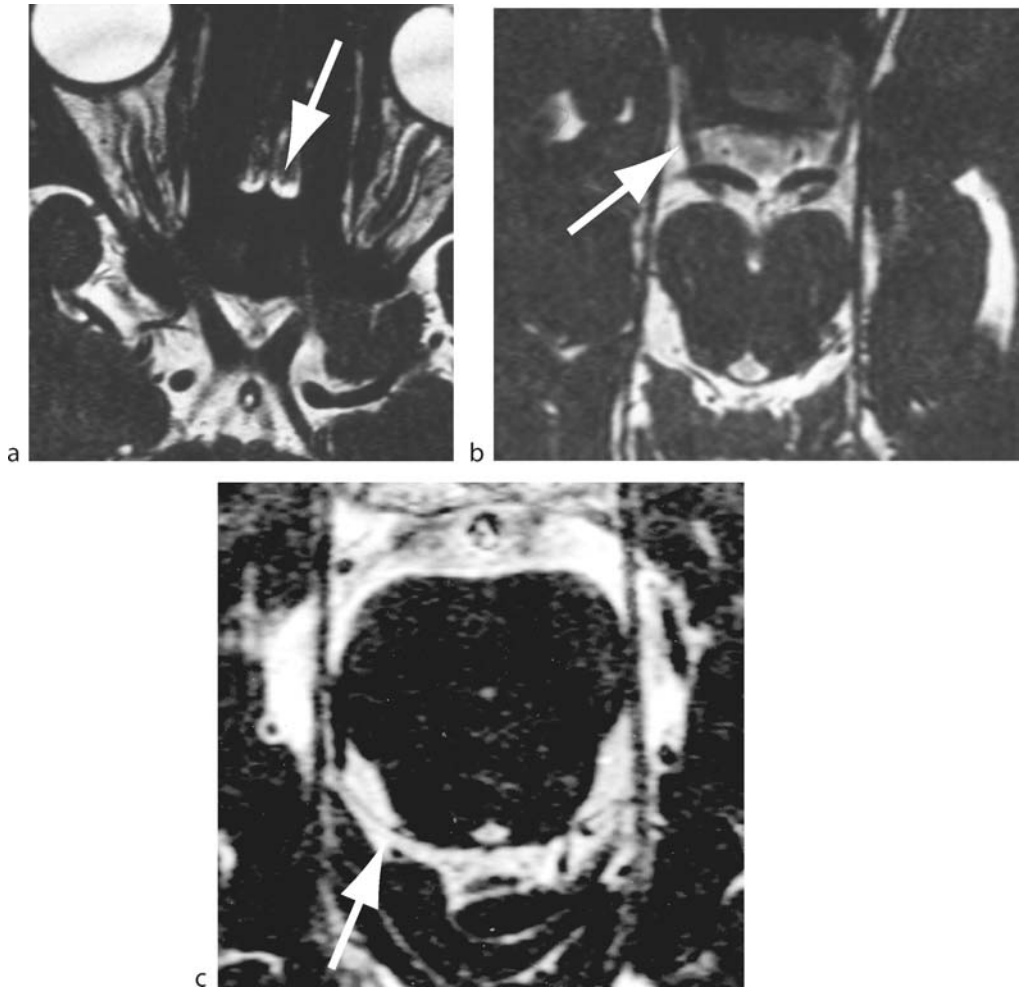

Nerves, Cranial. Figure 1 CISS images showing the olfactory nerve (*arrow*, a), optic nerve (*arrowhead*, a), oculomotor nerve (*arrow*, b) and trochlear nerve (*arrow*, c).

inferior) vestibular nerves (Fig. 2c, d). The cochlear as well as the vestibular nuclear complex are located in the dorsolateral side of the brainstem at the level of the pontomedullary junction. The medial vestibular nucleus bulges into the 4th ventricle as the 'vestibular area'. The nerve enters the pons at this level coming from the internal auditory canal.

The *glossopharyngeal nerve* (CN IX) is a mixed nerve. The motor fibres arise from the ambiguous nucleus located in the medulla oblongata. The motor fibres for the viscera (parasympathetic) arise from the inferior salivatory nucleus. The visceral sensory fibres terminate in the nucleus solitarius in the dorsal medulla oblongata. CN IX emerges from the posterolateral sulcus of the medulla oblongata, traverses the premedullary cisterns and exits the skull through the anterior compartment of the foramen jugulare.

The *vagus nerve* (CN X) is a mixed nerve. The motor fibres arise from the ambiguous nucleus in the lateral medulla oblongata. The motor fibres for the viscera arise from the dorsal nucleus of the vagus nerve, which bulges into the 4th ventricle as the vagal trigone. The visceral sensory fibres terminate in the nucleus solitarius in the dorsal medulla oblongata. CN X emerges from the posterolateral sulcus of the medulla oblongata and exits the skull together with the nervus accessorius through the intermediate space of the foramen jugulare (Fig. 3a).

The *accessorius nerve* (CN XI) is a motor nerve with two roots. The cranial root arises from the nucleus ambiguous and exits the medulla oblongata anterior to the posterolateral sulcus (Fig. 3b). The spinal root arises from the spinal accessory nucleus in the lower medulla and the upper five spinal cord segments. It courses between the dorsal and ventral roots of the upper cervical nerves, enters the foramen magnum and joins the cervical root in the intermediate portion of the jugular foramen.

The *hypoglossal nerve*. (CN XII) is a motor nerve. Its nucleus is located in the posterior medulla oblongata,

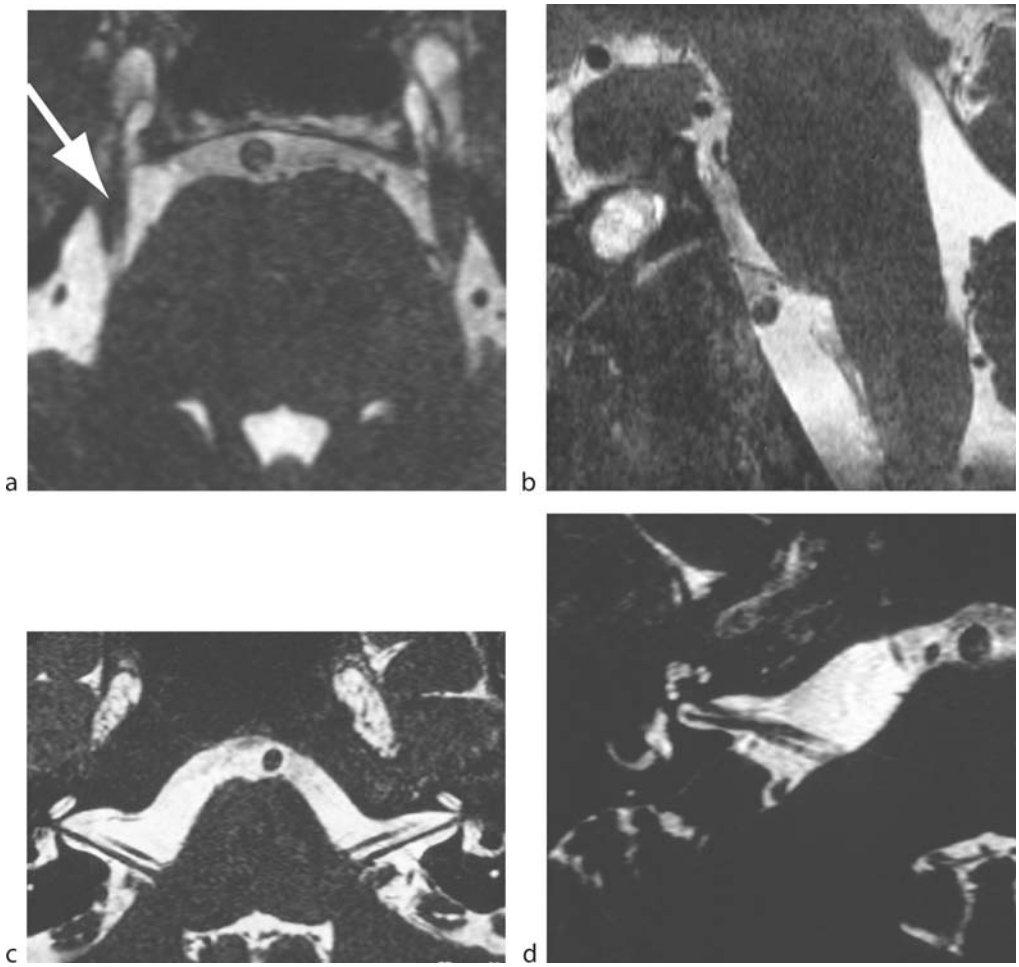

Nerves, Cranial. Figure 2 CISS images showing the trigeminal nerve (*arrow*, a), abducens nerve (*arrow*, b), facial nerve (*arrow*, c) and superior vestibular nerve (*arrowhead*, c) and cochlear nerve (*arrow*, d) and inferior vestibular nerve (*arrowhead*, d).

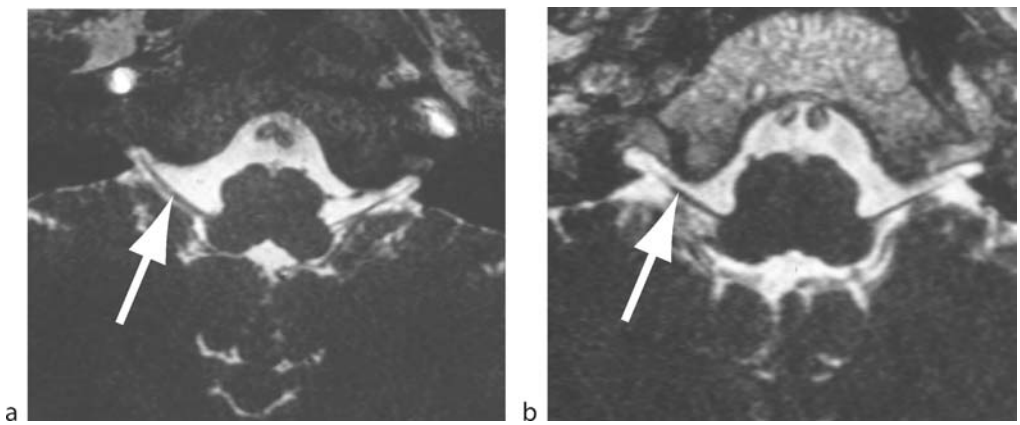

Nerves, Cranial. Figure 3 CISS images showing the vagus nerve (*arrow*, a) and accessory nerve (*arrow*, b).

causing a bulging of the floor of the 4th ventricle, the hypoglossal trigone. The nerve rootlets emerge from the preolivary sulcus, pass through the premedullary cistern, and pass through the hypoglossal canal as one trunk.

Imaging

The visualisation of the cranial nerves is a function of the thickness of the nerves and of anatomic properties of the segment that is to be identified.

Anatomically the cranial nerves III–XII can be divided into the following segments: (i) intramedullary,(ii) cisternal, (iii) foraminal and (iv) extracranial segments.

Nuclei. The cranial nerve nuclei are currently not accessible to conventional *in-vivo* MR imaging. Some nuclei however, can be identified through the bulges they cause in the floor of the 4th ventricle. These are the nuclei of CN VI (facial colliculus), CN VIII (vestibular area), CN X (vagal trigone) and CN XII (hypoglossal trigone). These bulges are important landmarks for the identification of the corresponding nuclei.

Intramedullary segments. The intramedullary segments are currently not accessible to conventional *in-vivo* MR imaging. However, tractography has the potential to visualise those segments in the future.

Cisternal segments. The visualisation of the various cranial nerves in their cisternal course is determined by, among other factors, the anatomic properties of each individual nerve such as the nerve's diameter, the course and the amount of surrounding cerebrospinal fluid (CSF). The small diameter of some of these nerves is in many instances the main reason for the difficulties encountered in visualising them.

The larger nerves can be well visualised with the regularly used T2 FSE sequences. The smaller nerves can be usually identified with that sequence, though the reliability increases with the use of sequences with a cisternographic effect (3D CISS, 3D DRIVE and FIESTA). Some nerves, for example the trochlear nerve, can only be identified when using these sequences.

A problem encountered when using the CISS, 3D DRIVE and FIESTA sequences is the differentiation of nerves and vessels. This can be achieved by combining the 3D CISS sequence with a plain and an enhanced TOF sequence. The comparison of the source images with the 3D CISS images in the appropriate plane will allow the differentiation of nerves, arteries and veins. It is this combination that enabled the reliable identification of the smallest cranial nerves, CN IV. This combination of sequences also enabled for the first time the reliable identification of an arterial neurovascular contact at the root exit zone of the trochlear nerve in patients with 'superior oblique myokymia', thus supporting the neurovascular compression hypothesis.

The 3D CISS, 3D DRIVE and FIESTA sequences, are therefore the standard sequences to be used in the evaluation of cranial nerves. A further improvement in imaging resolution can be achieved at higher field strength such as 3T.

Foraminal segments. The foraminal segments of CN V1, V2, V3, IX–XII as well as the cavernous segments of CN III, IV, V1 and VI are best visualised on MR using contrast-enhanced 3D CISS, MPRAGE or TOF sequences. The evaluation of the bony structures, however, is best performed by high resolution computed tomography (HRCT).

Bibliography

1. Leblanc A (2001) Encephalo-peripheral nervous system: anatomy, imaging, vascularisation. Springer Verlag, Berlin, Heidelberg
2. Yousry I, Camelio S, Schmid UD et al (2000) Visualization of cranial nerves I–XII: value of 3D CISS and T2-weighted sequences. Eur Radiol 10:1061–1067
3. Yousry I, Dieterich M, Naidich TP et al (2002) Superior oblique myokymia magnetic resonance imaging support for the neurovascular compression hypothesis. Ann Neurol 51:361–368

Neuralgia

▶Spinal Nerve Roots, Clinical Syndromes

Neuroarthropathy

▶Neuropathic Joint Disease

Neuroblastoma

Johan G. Blickman[1], Dewi Ashi[2]
[1]Department of Radiology, UMC St Radboud, Nijmegen, Netherlands
j.blickman@rad.umcn.nl
[2]Department of Radiology, University of Indonesia, Jakarta Pusat, Indonesia

Definition

Malignant round cell tumor arising from the ▶adrenal medulla (commonest), premature neuroblasts of the embryonic neural crest and sympathetic ganglia.

Incidence

The third most common malignancy of childhood after leukemia and primary brain neoplasm.

Neuroblastoma accounts for about 10% of all pediatric neoplasms and is the commonest extracranial solid tumor.

In the majority of cases, it presents between 2 months and 2 years of age, but the lesion may also present in the neonatal period. The tumor is slightly more common in boys than girls, with familial incidence reported.

Pathology/Histopathology

Neuroblastoma is composed of small round cell that characteristically arranged in rosettes. ►Ganglioneuroma represents the most differentiated end of the spectrum and is benign. ►Ganglioneuroblastomas represents an intermediate mixed group.

Approximately two-thirds of the tumors are located in the abdomen, followed by tumors arising in the paravertebral sympathetic chain or the presacral soft tissue region. It can spontaneously transform into more benign ganglioneuroma(blasto)ma.

The International neuroblastoma staging system (INSS) defines the significance of tumor resectability, anatomic "midline," and lymph node involvement (Table 1).

Clinical Presentation

Neuroblastoma is clinically silent until it invades adjacent structures. Symptoms may include bone pain, fever, weight loss, anemia, and hypertension (10%). Two-thirds demonstrate excess of urinary catecholamine excretion and present with flushing, sweating, and irritability. Leg edema due to tumor compression of veins may occur.

Paraneoplastic syndromes may occur and present with myoclonus and watery diarrhea. Horner syndrome can be a clinical presentation of a cervical tumor location. Syndromes associated with neuroblastoma include Beckwith-Wiedemann, Klippel–Feil, and fetal alcohol.

Neuroblastoma. Table 1 The international neuroblastoma staging system (INSS)

Stage	Description
I	Localized tumor confined to the area of origin complete gross excision
IIA	With or without microscopic residual
IIB	Unilateral tumor with incomplete gross excision; ipsilateral and
III	Contralateral lymph node negative microscopically
IV	Unilateral tumor with complete or incomplete gross excision with
IVS	positive ipsilateral regional lymph node identifiable, but the contralateral lymph nodes are negative microscopically.
	Tumor crosses the midline
	Distant metastases
	Metastatic disease confined to liver, skin, and bone marrow, with the primary tumor stage 1 or 2. (Age <1 year)

Imaging

Conventional radiographs may reveal a mass that in two-third of the cases contains calcification (stippled, diffuse, amorphous). Widening of the interpedicular distance and paravertebral mass may be seen on plain abdominal X-ray.

Ultrasound (US) is used as the screening modality for suspected abdominal pathology and shows the organ of origin, liver metastases, and identifies tumor encasement of vessels. The tumor is inhomogeneous on US. It has hypoechoic regions due to hemorrhage, necrosis, or cyst formation and hyperechoic regions due to calcification (Fig. 1). Mainly cystic lesions may be present particularly in neonates.

CT is superior to US in defining the extent and retroperitoneal spread of the primary tumor (Fig. 2). It reveals tumor calcification in about 85% of the patients. The lesions have an attenuation equal to or less than that of the muscle. Enhancement is heterogeneous after contrast injection.

MRI has advantages over CT in that extension to the vertebrae canal, bone marrow involvement, encasement of the superior mesentery artery (SMA) and other vessels can be better evaluated.

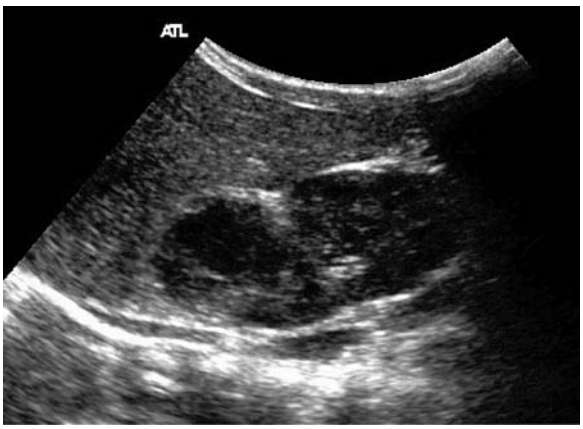

Neuroblastoma. Figure 1 Neuroblastoma shows inhomogeneous tumor originating from the adrenal gland indenting the renal upper pole.

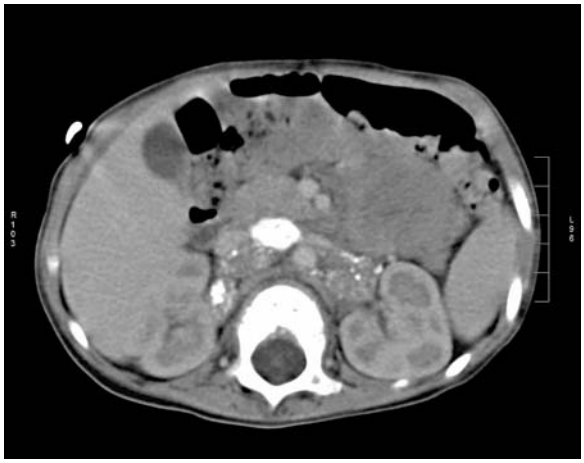

Neuroblastoma. Figure 2 CT image shows masses containing calcifications originating from both adrenal glands highly suggestive for bilateral neuroblastoma.

The lesion shows a low signal on T1 and high signal on T2 weighted images (WI). Inhomogeneous intensity is a result of necrosis. Neuroblastoma rarely invades into major veins, which occurs more frequently in the case of Wilms' tumor.

Nuclear

Tc 99mMDP identifies bone metastases, commonly located in the metaphyseal regions of long bones and the cranium. I123MIBG uptake occurs in the metabolically active neural crest tumor and this agent can detect primary, recurrent, and metastatic disease.

Diagnosis

Bone marrow aspirate is performed for bone marrow invasion. Increase of urinary catecholamine metabolites (vanillylmandelic acid, homovallic acid, and 3-methoxy-4-hydroxyphenylglycol) is very sensitive sign for the diagnosis.

Differential diagnosis: Suprarenal mass include.

Wilms tumor:
–calcification uncommon
–pelvocliceal distortion (arise from kidney)
–lung metastasis in 20% (neuroblastoma uncommon)
–mean age 3 years (neuroblastoma less than 2 years)
–more frequently invades into major veins

Neonatal adrenal hemorrhage
–avascular
–low signal in T2WI
–resorption in follow up examination

Pheochromocytoma
–mostly occur above 6 years of age
–US: hypoechoic, partly solid mass with small cyst.

Bibliography

1. The Requisites. Pediatr Radiol :177–179
2. Carty H (ed) (2001) Paediatric imaging. The Encyclopedia of Medical Imaging, Vol. 7, Oslo, The NICER Institute, pp 364–366
3. Daneman A (2004) Adrenal gland. In: Kuhn JP, Slovis TL, Haller JO (eds) Caffey's Pediatric Diagnostic Imaging. 10th edn. Philadelphia, Mosby, pp 1894–1908
4. Stark DD, Moss AA, Brasch RC et al (1983) Neuroblastoma: diagnostic imaging and staging. Radiology 48:101–105

Neuroblastoma

▶Neoplasms, Chest, Childhood

Neurocutaneous Syndromes

Philippe Demaerel
Department of Radiology, University Hospitals, Leuven, Belgium
philippe.demaerel@uz.kuleuven.ac.be

Synonyms

Congenital malformation; Ectodermal; Phakomatoses

Definitions

Neurocutaneous syndromes are multisystem disorders affecting mainly structures of ectodermal origin, for example, the skin, the eye, and the nervous system. Although there is a long list of hereditary phakomatoses, the most common include ▶neurofibromatosis type 1 (NF1), ▶tuberous sclerosis, ▶Sturge–Weber syndrome, and von Hippel–Lindau disease (1). The central nervous system is usually involved early during antenatal brain maturation.

Pathology/Histopathology

Although various organs can be involved in neurocutaneous syndromes, the focus of this section is only on central

nervous system abnormalities. NF1 involves intracranial as well as cutaneous tumors. While the cutaneous lesions are neurofibromata, the intracranial tumors are often gliomata, involving the anterior visual pathway in particular. In addition, dysplastic lesions can be observed, for example, dural ectasia and skull base bone dysplasia.

Tuberous sclerosis is an autosomal dominant disorder and as a result of the abnormal expression of the genes in the stem cells of the germinal matrix, a maldevelopment occurs. This results in cortical malformations, subependymal abnormalities, as well as white matter abnormalities and the development of tumors at the foramen of Monro.

The pathology in Sturge–Weber syndrome is different and represents a vascular malformation. The abnormality affects multiple meningeal capillaries and small veins. This probably results from a persistence of embryonic vascularization that is present between the fourth and the eighth week of gestation. Often, cortical calcifications are seen in the brain adjacent to this meningeal angiomatosis and these may reflect chronic ischemia due to an ineffective venous drainage.

von Hippel–Lindau disease is another autosomal dominant disorder known as central nervous system angiomatosis. Apart from the occurrence of tumors in various organs, more than one hemangioblastoma is found in the central nervous system.

Clinical Presentation

The observation of café-au-lait spots is often the first manifestation of NF1. The most important central nervous system manifestation is glioma of the anterior visual pathway (2). These may be asymptomatic or may present with loss of vision. Occasionally these gliomas may regress spontaneously. Specific diagnostic criteria exist for NF1. These include, apart from the two already-mentioned abnormalities, plexiform neurofibromata, dysplastic bone lesions, axillary or inguinal freckling, and hamartomata of the iris.

The typical clinical presentation of tuberous sclerosis consists of at least one of the following primary features: adenoma sebaceum (peri)ungual fibroma, cerebral hamartoma (calcified), subependymal tubers, and a fibrous plaque of the forehead; in addition, there should be at least two of the following secondary features: cutaneous lesions, infantile spasms, ocular hamartomata, angiomyolipoma, cardiac rhabdomyoma, and a first-degree relative with tuberous sclerosis.

The typical clinical feature of Sturge–Weber syndrome is the facial port-wine nevus involving the distribution of the trigeminal nerve branches on the same side as the intracranial angiomatosis. Seizures and developmental delay are often present. The characteristic occipital involvement of meningeal angiomatosis can cause homonymous hemianopia.

The clinical presentation of von Hippel–Lindau disease is related to the presence of a neoplasm in the central nervous system or elsewhere. It has been suggested that to diagnose this autosomal dominant disorder one must have at least one cerebellar or retinal hemangioblastoma in addition to a renal tumor, a pheochromocytoma, or a cyst (in the kidney, liver, or pancreas).

Diagnosis

The imaging aspects of the four common neurocutaneous syndromes will be briefly reviewed.

Gliomata involving the anterior visual pathway are common in NF1 and they may extend into the optic radiation. They may show a variable degree of enhancement (Fig. 1). There have been reports on spontaneous regression, but most are slowly progressive tumors. Occasionally, brain stem gliomas can be seen and plexiform neurofibromas involving the skull base. A typical finding in NF1 is the occurrence of bright lesions in the cerebral and cerebellar gray nuclei (Fig. 1). These abnormalities do not enhance and are asymptomatic. The underlying pathogenesis remains unknown. They are often referred to as hamartomata. They appear during the first year of life and tend to disappear in the second decade.

Intracranial manifestations of tuberous sclerosis include subependymal (calcified) hamartomata, subependymal giant cell tumors, cortical tubers, and (linear) white matter abnormalities (3).

Generally, subependymal hamartomata do not enhance and are commonly located in the region of the foramen of Monro. In the first 2 years of life, they are not yet calcified and may be difficult to recognize on computed tomography (CT) images (Fig. 2). It has been demonstrated that these subependymal lesions can show a variable degree of enhancement without any suspicion of development of a giant cell astrocytoma. However, when there is evidence of progressive growth with obstruction at the foramen of Monro, the lesion should be considered a giant cell astrocytoma warranting further treatment (Fig. 2).

Cortical tubers are the most characteristic from a pathological point of view. They are related to the abnormal process of proliferation, migration, and organization of the cortex. They may be difficult to depict on CT, but are clearly seen on magnetic resonance imaging (MRI), particularly on fluid-attenuated inversion-recovery (FLAIR) images (Fig. 2). Occasionally, they may calcify. These lesions are histologically identical to the focal cortical dysplasia with balloon cells. Their

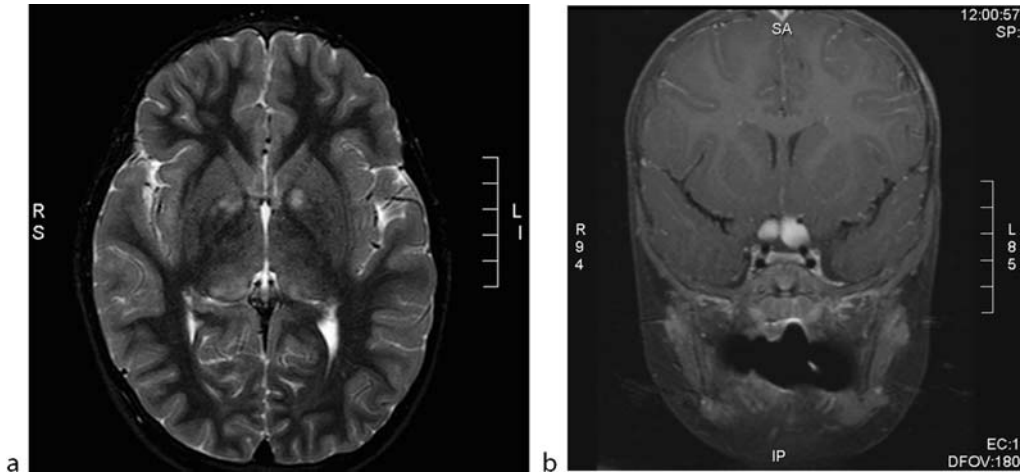

Neurocutaneous Syndromes. Figure 1 Neurofibromatosis type 1. MRI shows the presence of hamartomata in the globus pallidus on both sides (a). Coronal contrast-enhanced images demonstrate a chiasmatic glioma (b).

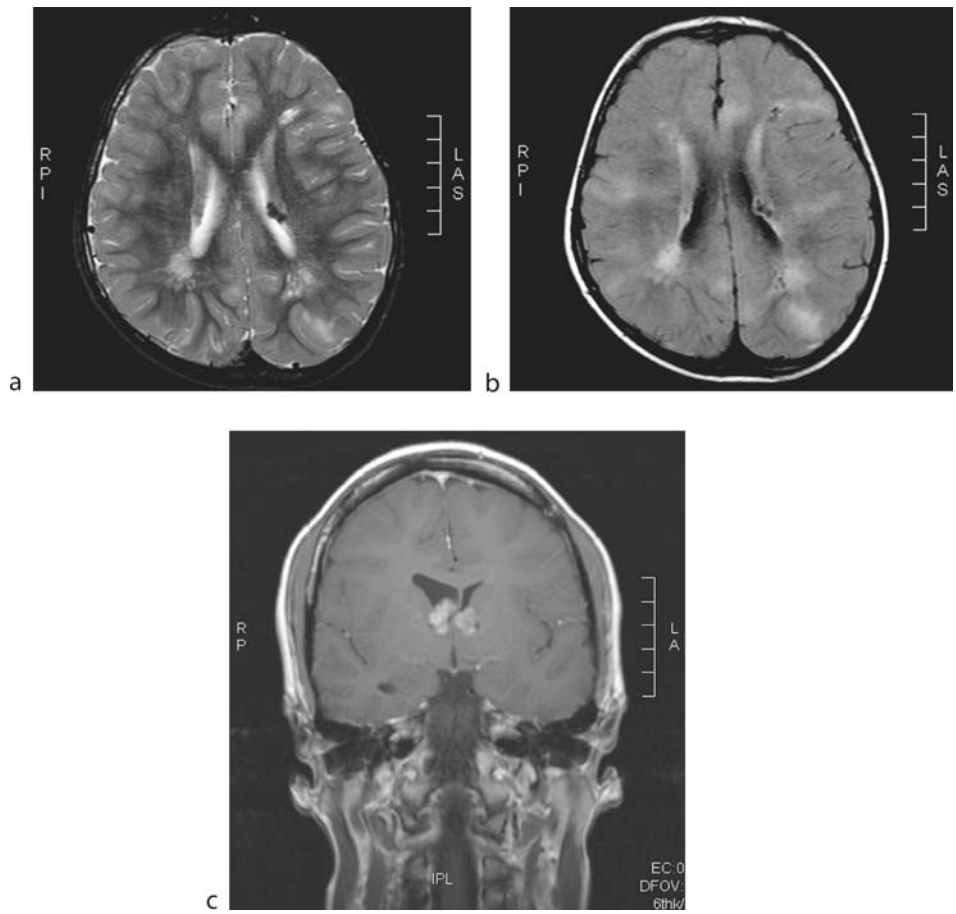

Neurocutaneous Syndromes. Figure 2 Tuberous sclerosis. T2-weighted (a) and FLAIR (b) images show the different characteristic features: subependymal hamartomata, cortical tubers, and linear white matter lesions. Note that these lesions are seen better on the FLAIR image (b). The enhancing mass at the foramen of Monro is the typical presentation of a giant cell astrocytoma (c).

appearance changes as myelination progresses from a low signal to a high signal on T2-weighted images. The high signal of the "mature" cortical tuber results from the presence of astrogliosis, seen on histology sections.

Finally, white matter abnormalities can be observed in tuberous sclerosis (Fig. 2). Histologically, they contain giant neurons and dysplastic balloon cells. Although calcification is rare, it can be seen. One of the particularities of these lesions is the fact that they can be seen to extend in a curvilinear or linear way from the ependymal surface toward the cortex.

Although CT is accurate in demonstrating the cortical calcification in Sturge–Weber syndrome, MRI is more sensitive for imaging pial angiomas (Fig. 3). The changes on the T2-weighted images can be subtle and may be limited to a mild decrease in the signal intensity of the white matter or a mild degree of cortical atrophy (Fig. 3). On contrast-enhanced images, a pial or meningeal enhancement will be seen (Fig. 3). The angioma will compromise the superficial venous flow. Usually, the parietal and occipital lobes will be involved. Enlarged vascular structures may be seen in the periventricular region, most likely representing hypertrophic venous drainage. The ipsilateral choroid plexus is frequently enlarged (Fig. 3). This phenomenon is thought to reflect the increased venous drainage through the deep venous system.

In the later stage, atrophy will develop in the ipsilateral hemisphere and due to a lack of brain growth there will be cranial asymmetry.

von Hippel–Lindau disease is characterized by the presence of hemangioblastomata. The cerebellum and the spinal cord are the most common locations. The typical appearance consists of a fluid-filled cyst with a tumoral vascular nodule within the wall of the cyst (Fig. 4). The small hemangioblastomata appear solid, but when they enlarge, they will become cystic.

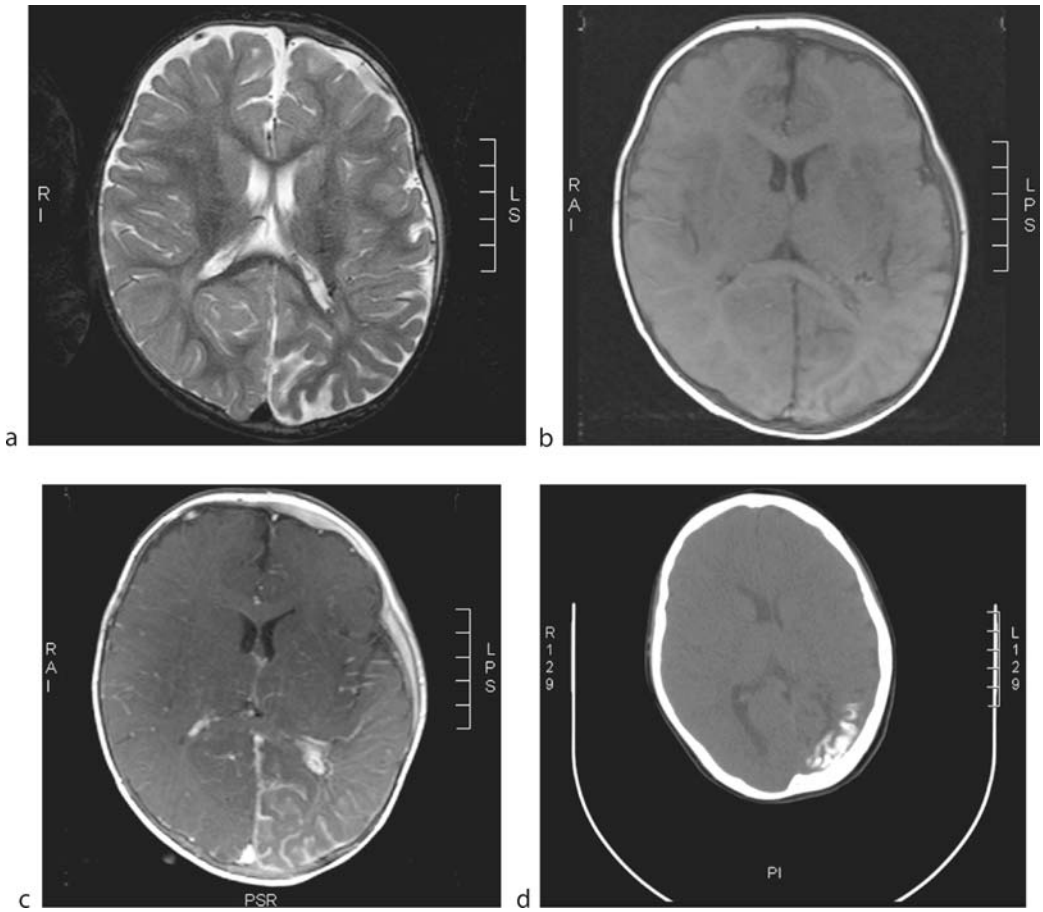

Neurocutaneous Syndromes. Figure 3 Sturge–Weber syndrome. On a T2-weighted image, only a subtle focal atrophy is seen in the left parietal and occipital lobe with an abnormal deep venous drainage (a). The T1-weighted images before (b) and after contrast (c) show leptomeningeal angiomatosis in this area and hypertrophy of the choroidal plexus. CT shows the gyral calcification (d) better.

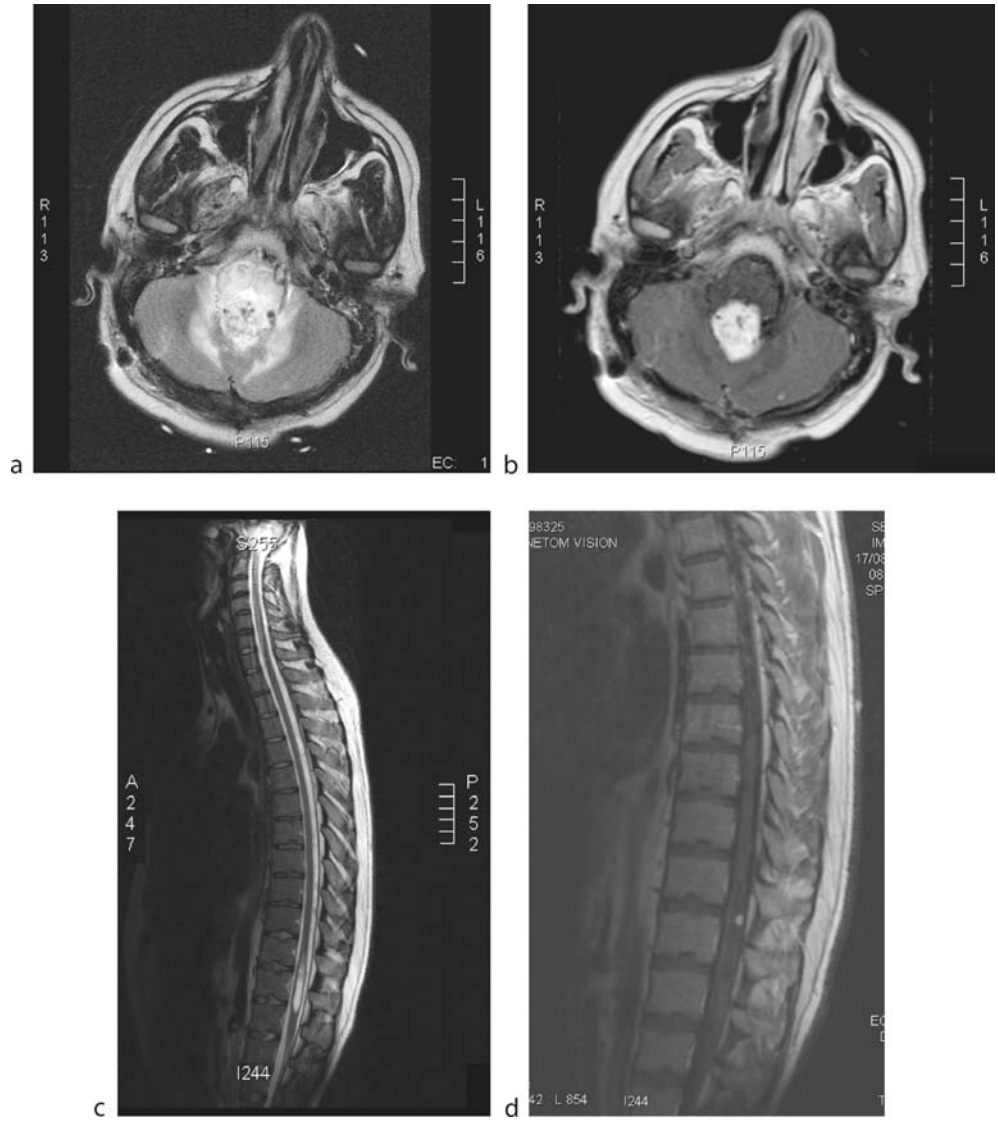

Neurocutaneous Syndromes. Figure 4 von Hippel–Lindau disease. On the axial T2-weighted image the hemangioblastoma can be seen with surrounding edema in the vermis (a). Following the administration of contrast medium, the hemangioblastoma in the vermis as well as a second smaller cerebellar hemangioblastoma are visible (b). There is a hemangioblastoma in the thoracic spinal cord with a cystic component (c) and an enhancing mural nodule (d).

The cystic component of spinal cord hemangioblastoma can sometimes be difficult to differentiate from edema. On T2-weighted images, the cyst has a higher signal and is more sharply delineated than cord edema (Fig. 4). The mural nodule is best seen on enhanced T1-weighted images.

The presence of more than one hemangioblastoma is highly suggestive of von Hippel–Lindau disease.

Bibliography

1. Barkovich AJ (2005) Pediatric Neuroimaging. 4th edn. Philadelphia: Lippincott Williams & Wilkins. ISBN 0-7817-5766-5, pp 440–505
2. Mukonoweshuro W, Griffiths PD, Blaser S (1999) Neurofibromatosis type 1: role of neuroradiology. Neuropediatrics 30:111–119
3. Evans JC, Curtis J (2000) The radiological appearances of tuberous sclerosis. Br J Radiol 73:91–98

Neuroectoderm

Ectoderm of the dorsal surface of the early vertebrate embryo that gives rise to neurons and glia of the nervous system.

▶Neoplasms of the Chest in Childhood

Neuroendocrine Tumors of the Pancreas

▶Islet Cells Tumors, Pancreatic

Neuroepithelial Cyst

▶Cyst, Cerebral and Cervical, Childhood

Neurofibroma

A benign neurogenic soft tissue tumor that may exist as a solitary tumor or as part of Neurofibromatosis. NF type I
▶Neurofibromatosis, Musculoskeletal Manifestations

Neurofibromas

These tumours are of Schwann cell origin but they can be distinguished from schwannomas by their morphologic features, especially those relating to the arrangement and form of the neoplastic cells and the character of the interstitial stroma (5).
▶Tumors, Spine, Intradural, Extramedullary

Neurofibromatosis

Neurofibromatosis (NF) is an autosomal dominant disease which manifest as a neurocutaneous syndrome. There are two principal types: neurofibromatosis 1 (NF-1 or von Recklinghausen disease) and neurofibromatosis 2 (NF-2). Approximately 90% of neurofibromatosis patients are NF-1 and the optic glioma is the most common intra-cranial tumour arising in these patients. NF-2 is much less common, and is associated with intra-cranial tumours originating from Schwann cells and meninges, which are typically multiple. The classic presentation of NF-2 is with bilateral acoustic neuromas. Both NF-1 and NF-2 are associated with spinal tumours, but of different types and frequencies
▶Neoplasms, Soft Tissue, Benign
▶Tumors, Spine, Intradural, Extramedullary

Neurofibromatosis Type 1 (NF1)

One of the more common autosomal dominant disorders, initially described by von Recklinghausen. The NF1 gene, located on chromosome 17, appears to be a tumor suppressor gene that is inactivated in patients with NF1. The most common neuroradiological abnormality is glioma of the anterior visual pathway.
▶Neurocutaneous Syndromes

Neurofibromatosis, Musculoskeletal Manifestations

Filip M. Vanhoenacker
Department of Radiology, University Hospital Antwerp, Belgium
filip.vanhoenacker@pandora.be

Synonyms

Central neurofibromatosis; Peripheral neurofibromatosis or Von Recklinghausen's disease

Definition

Neurofibromatosis (NF) is an autosomal dominant inherited disorder, involving multiple organ systems. The gene expression is variable.

Eight subtypes of the disease have been described, but generally two clinical subtypes account for 99% of cases: NF type I (peripheral NF or Von Recklinghausen's disease) and NF type II (central neurofibromatosis). A rigorous distinction between central and peripheral types is not completely accurate because NF-1 often has central features.

NF-1 is much more frequent than NF-2. Because skeletal involvement is exclusively seen in NF-1, affecting 50% of patients, further discussion will be focused on NF-1.

NF type I is a neuroectodermal and mesodermal dysplasia, characterized by a triad of pigmented cutaneous lesions, multiple soft elevated, cutaneous tumors, and various osseous manifestations of the axial and appendicular skeleton (1). The long arm of chromosome 17 is abnormal. Its incidence is estimated as 1:3000.

Pathology/Histopathology

The hallmark of the disease is the presence of peripheral neurofibromas. Three subtypes of ►neurofibroma exist: cutaneous, subcutaneous, and plexiform. Both cutaneous and subcutaneous neurofibroma are nonspecific for NF-1, whereas a plexiform neurofibroma is highly specific for the disease.

Grossly, a neurofibroma consists of a grayish brown or gray, firm rubbery mass. Histologically, interlacing strands of elongated foam cells and pigment are arranged in a characteristic palisading pattern.

Malignant degeneration may be seen in approximately 5% of cases (malignant peripheral nerve sheath tumor, previously designated as a neurofibrosarcoma). Other neurogenic tumor types are less frequent.

Clinical Presentation

Cutaneous Manifestations

Cutaneous abnormalities include café au lait spots, fibroma molluscum, and elephantiasis neuromatosa.

Café au lait spots in NF-1 are well marginated macules (in contrast to *café au lait* spots in fibrous dysplasia which are geographically jagged), and develop in 50% of patients with NF-1.

Fibroma molluscum are multiple, asymptomatic cutaneous nodules, which are elevated above the skin's surface. Fibroma molluscum is the most frequent lesion of NF-1.

Elephantiasis neuromatosa is a term designated for thick large soft tissue masses that create skin folds. The histological counterpart of this lesion is a plexiform neurofibroma.

Ocular Manifestations and Intracranial Manifestations

Optic glioma may produce blurred vision, scotoma and transient blindness (1). A defect in the superior orbital wall may result in drooping of the upper eyelid, dislocation of the eyeball, or pulsating exophthalmos, due to temporal lobe herniation with transmission of cerebrovascular pulsation to the globe (1).

Macrocephalus, facial asymmetry, iris hamartomas (Lisch nodules), learning disabilities, neuropsychological abnormalities, and neuroradiological findings (brain gliomas, areas of high signal intensity on T2-weighted images, plexiform neurofibroma in the head and neck area) are other characteristics.

Spinal Involvement

►Kyphoscoliosis and atlantoaxial subluxation may be complicated by paraplegia.

Gastrointestinal tract manifestations.

Location of neurofibromas in the gastrointestinal tract may result in pain, intestinal bleeding, and obstruction (2).

Vascular Manifestations

Vasculopathy may cause occlusive cerebrovascular disease, hypertension due to proximal renal artery stenosis, mesenteric artery insufficiency, congenital heart disease, major branch arterial stenosis and coarctations of the thoracic and abdominal aorta, and aneurysms (2, 3).

Other Extraskeletal Manifestations

Endocrine abnormalities include MEA IIb syndrome (medullary thyroid carcinoma, pheochromocytoma, and multiple mucosal neuromas), osteomalacia, hyperparathyroidism, and small bowel carcinoid tumors (2, 3).

Imaging

Spine

The vertebral column is very frequently affected in NF-1. The most common radiographic feature is the presence of kyphoscoliosis, occurring in 50% of patients (1, 3, 4). Kyphosis predominates usually over scoliosis. Typically, the kyphoscoliosis involves a short segment of 5–7 vertebrae and is acutely angular in presentation. Although the lower thoracic spine is most frequently involved, cervical kyphosis causing reversal of the normal lordosis is another common finding of NF I.

►Scalloping of the posterior vertebral body margins is also very characteristic. There exist two types of scalloping: the posterocentral and the eccentric unilateral type. The posterocentral scalloping affects multiple levels and is secondary to dural ectasia (Fig. 1), whereas the eccentric unilateral type occurs at one level and is due to pressure erosion of a dumbbell neurofibroma, causing enlargement of the neuroforamen.

Erosion of the posterior surface of the vertebral body, pedicles and enlargement of the intervertebral neuroforamen may also be caused by an *intrathoracic meningocele*, which represents a focal protrusion of the

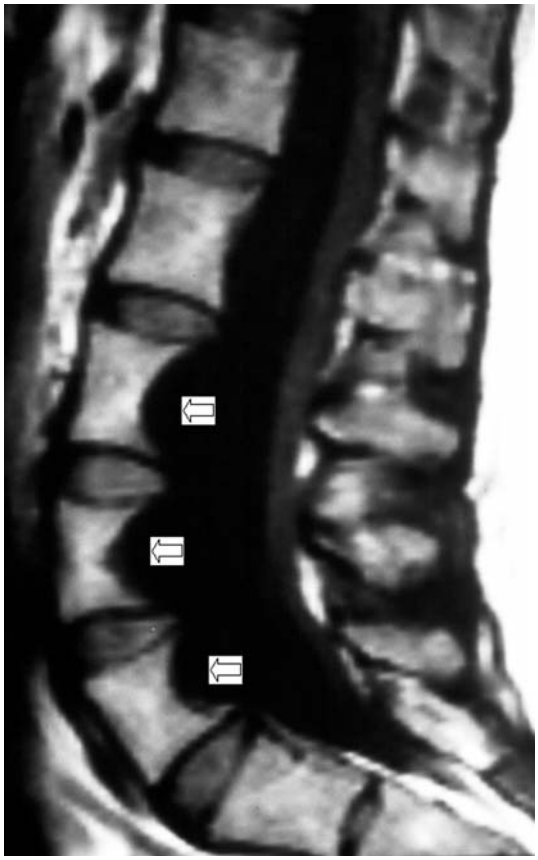

Neurofibromatosis, Musculoskeletal Manifestations. Figure 1 Sagittal T1-weighted spin-echo MR image of the lumbar spine demonstrating posterior vertebral scalloping associated with dural ectasia (white arrows).

dura and the arachnoid. Extension of these meningoceles along the adjacent posterior ribs and transverse processes may cause pencilling and spindling.

Skull

Agenesis of the posterosuperior wall of the *orbit*, the sphenoid wing and the orbital plate of the frontal bone may allow direct contact of the middle cranial fossa contents with the orbital soft tissues (Fig. 2).

Radiographically, the bony abnormalities may result in a harlequin appearance of the orbit. Often there is an associated deformity and/or decreased size of the ipsilateral ethmoid and maxillary sinus. Enlargement of the optic foramen and superior orbital fissure may be caused by an optic nerve glioma or plexiform neurofibroma respectively.

A *lambdoidal defect* is a typical bone defect occurring in the lambdoid suture just posterior to the junction of the parietomastoid and occipitomastoid sutures.

Macrocrania (increased skull size) may be due to associated macroencephaly (increased brain size). Aggregated granular *calcifications* are rarely seen in the area of the temporal lobe (3).

Chest and Ribs

A twisted ribbon appearance of the ribs may be due to both pressure erosion of intercostal neurofibromas or by a mesodermal dysplasia not related to the presence of neurofibromas (Fig. 3).

Appendicular Skeleton

Bowing, *pathologic fracture*, and ▶pseudarthrosis of the long bones may occur. The tibia in its lower two-thirds is the most commonly affected bone. Anterolateral bowing is usually present in the first decade and may be associated with a gracile, abnormally formed or hypoplastic fibula. Bone deformity may cause pathologic fracture, which fails to heal (pseudarthrosis). There is no evidence of neural hypertrophy as primary causative factor in the pathogenesis of pseudarthrosis, as neural tissue has never been demonstrated in or near the site of the defective bone healing (1, 3).

Other sites for pseudarthrosis are the radius and the clavicle. A twisted *ribbon like* appearance—similar as seen at the ribs may also occur at the long bones.

Focal gigantism or local overgrowth or hypertrophy of both the skeletal and soft tissues is the result of chronic hyperemia owing to hemangiomas and lymphangiomas associated with NF.

Hypertrophy may involve a single bone or the entire extremity. The bones are usually normal in shape, and the associated muscles and joints are proportionately enlarged along with the soft tissues (1).

Cystic Lesions Within the Bone

NF-1 may occasionally present with cystic osseous lesions. The term "cystic" is a pure descriptive one, as biopsy has never been performed in these lesions (3).

Two types of cystic lesions have been described, subperiosteal and intraosseous. The subperiosteal type, described as caves, pits, or notches along the external cortex, has been attributed to mechanical pressure from adjacent neurogenic tissue and to focal hemorrhage from poorly adherent, dysplastic periosteum, which then proliferates over the lesion (3).

The pathogenesis of intraosseous cystic lesions is still a matter of debate. Several hypotheses have been proposed. Some authors ascribe them to direct invasion of the periosteum, cortex, and haversian canals by neurofibromatous tissue. Other investigators thought that they represent nonossifying fibromas or fibrous cortical defects

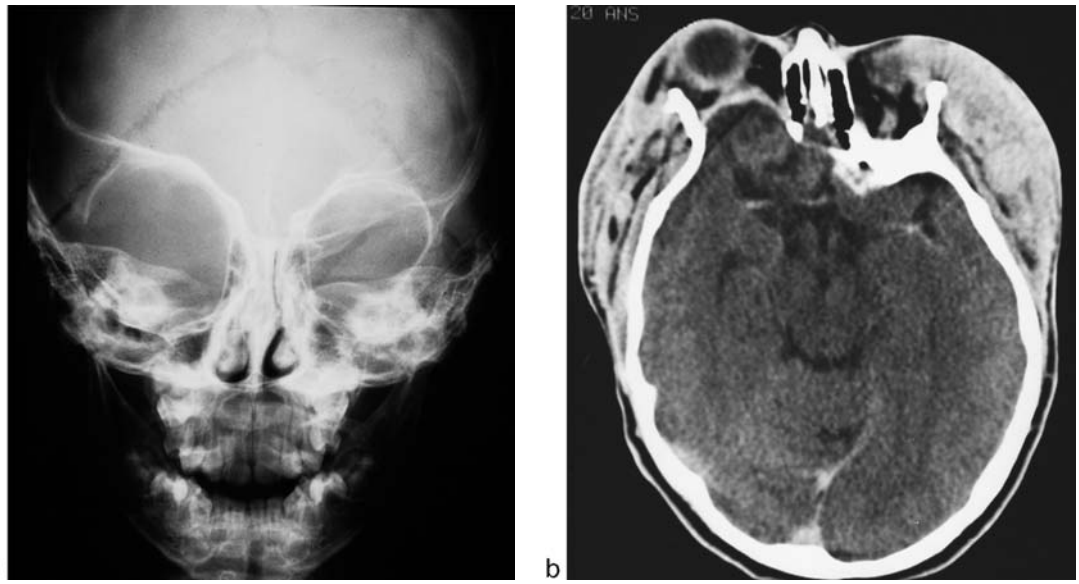

Neurofibromatosis, Musculoskeletal Manifestations. Figure 2 (a) Plain radiograph of the skull showing hypoplasia of the posterosuperior wall of the right orbit, distortion of the greater and lesser wings of the sphenoid bone and the orbital plate of the frontal bone. (b) CT scan of another patient showing hypoplasia of the right orbit, with protrusion of the temporal lobe into the right orbit. Note also the presence of subcutaneous plexiform neurofibromas on the ipsilateral and contralateral side.

(1, 3). However, histological proof of the true nature of these lesions was never evident.

Other radiographic manifestations within the appendicular skeleton are *intramedullary longitudinal streaks of increased density. Polydactyly* is also more frequent in NF-1 as compared with the general population (3).

Soft Tissues Tumors

Peripheral nerve tumors in NF-I most frequently involve neural supporting tissue. The two most common benign tumor types are solitary or multiple neurofibromas and neurilemomas (►schwannomas).

Neurofibromas may appear as soft-tissue opacities on standard radiographs. On ultrasonography these lesions appear as a well-demarcated fusiform, hypoechogenic structures, in close relation to the native nerve.

On CT, the lesions have a low density. Magnetic resonance imaging (MRI) is the imaging technique of choice for detection and characterization tumors of the peripheral nerves.

The most important imaging feature that should suggest the diagnosis of a neurogenic tumor is the presence of a fusiform mass, representing the tubular entering and exiting nerve in a typical nerve distribution. Other imaging features suggestive for a neurogenic tumor are the target sign, the fascicular sign, and the split fat sign and associated muscle atrophy. The fascicular sign represents multiple small ringlike structures (with peripheral higher signal intensity) on T2-weighted images, corresponding to fascicular bundles seen in neurogenic neoplasms. The split fat sign represents a rim of fat surrounding the lesion, due to the fact that the normal neurovascular bundle is normally surrounded by fat.

On MRI, neurogenic tumors are of low to intermediate signal intensity on T1-weighted images and of variably increased signal intensity on T2-weighted MR images.

Although the presence of a so-called target sign, consisting of a peripheral hyperintense rim and central hypointensity on T2-weighted images maybe in favor of a neurofibroma rather than a schwannomas, there is substantial overlap, rendering MRI not useful technique to distinguish peripheral located schwannomas from neurofibromas.

Contrast uptake is variable, but strong central zone enhancement and weak peripheral contrast uptake suggest the neurogenic origin.

Malignant degeneration occurs almost exclusively in preexisting (plexiform) neurofibroma, whereas, this is very rare in schwannoma (3). The mean age of appearance is 42 years. The criteria suggestive of MPNST are a large mass (more than 5 cm in diameter), with compression of the adjacent structures, a more nonhomogeneous appearance (due to hemorrhage and necrosis), invasion of fat planes, the presence of associated lymph nodes, adjacent bone destruction, and perilesional edema.

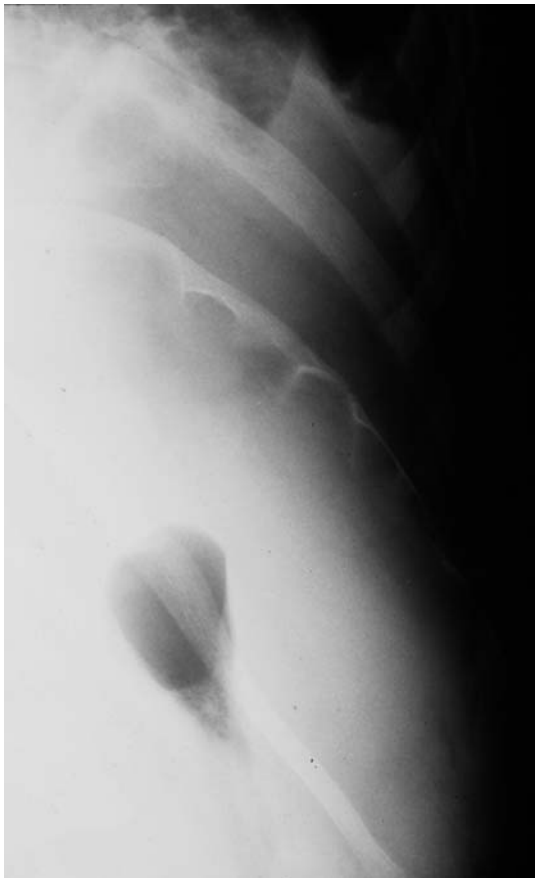

Neurofibromatosis, Musculoskeletal Manifestations. Figure 3 Plain radiograph of the left lower ribs demonstrating a ribbon-like appearance of the inferior aspect of rib 11, due to pressure erosion of an adjacent neurofibroma. Note also widening of the intercostal space between rib 11 and 12.

Osteomalacia

Osteomalacia may be seen in longstanding NF-I, owing to renal tubular dysfunction.

Diagnosis

Diagnostic criteria are based on the presence of the National Institutes of Health criteria. At least two criteria must be present (2, 5).

1. More than six café-au-lait spots (of more than 5 mm in diameter in prepubertal individuals and more than 15 mm in postpubertal individuals).
2. At least two neurofibromas of any type or one plexiform neurofibroma.
3. Freckling in the axilla (Crowe sign) or inguinal region.
4. Optic glioma.
5. More than two Lisch nodules.
6. Distinctive osseous lesions, such as sphenoid dysplasia or thinning of the long bone cortex, with or without pseudarthrosis.
7. First-degree relative (parent, sibling, child) with NF-I.

Bibliography

1. Yohum TR, Rowe LJ (2005) Tumors and tumor-like processes. In: Yochum TR, Rowe LS (eds) Essentials of Skeletal Radiology. 3rd edn. Lippincott Williams & Wilkins, Philadelphia, pp 1137–1372
2. Dähnert W (1999) Differential diagnosis of brain disorders. In: Dähnert W (ed) Radiology Review Manual. 4th edn. Williams & Wilkins, Baltimore, pp 181–277
3. Feldman F (2002) Tuberous sclerosis, neurofibromatosis, and fibrous dsyplasia. In: Resnick D (ed) Diagnosis of Bone and Joint Disorders. W.B. Saunders Company, Philadelphia, pp 4792–4843
4. Tsirikos AI, Ramachandran M, Lee L et al (2004). Assessment of vertebral scalloping in neurofibromatosis type 1 with plain radiography and MRI. Clin Radiol 59: 1009–1017
5. National Institutes of Health Consensus Development Conference (1988). Neurofibromatosis. Conference statement. Arch Neurol 45:575–578

Neurometabolic Disorders

Zoltan Patay
Department of Radiological Sciences, St. Jude Children's Research Hospital, Memphis, USA
zoltan.patay@stjude.org

N

Synonyms

Congenital metabolic disorders; Inborn errors of metabolism; Metabolic diseases; Metabolic encephalopathies

Definitions

Metabolic disorders are generally divided into two categories: inborn errors of metabolism and acquired metabolic diseases.

Inborn errors of metabolism represent a vast group of genetically determined pathologies. Classification of disease entities may be based on organ system involvement, cellular organelle involvement, dominant biochemical abnormality, or even age of onset. Those with central nervous system (CNS) involvement may be further broken down according to substance involvement (exclusive white matter or gray matter involvement or both), resulting in subcategories referred to as leukodystrophies, poliodystrophies, or pandystrophies (Table 1).

Neurometabolic Disorders. Table 1 Various classification schemes for metabolic diseases

Classification Schemes				
Organ system involvement	Substance involvement	Cellular organelle involvement	Biochemical abnormality	Age of onset
Exclusive involvement of nervous system	Leukodystrophies	Mitochondrial disorders	Organic acidopathies	Neonatal
Exclusive systemic involvement	Poliodystrophies	Lysosomal (storage) disorders	Amino acidopathies	Infantile (early, late)
Mixed system involvement	Pandystrophies	Peroxisomal diseases	Disorders of carbohydrate metabolism	Juvenile (early, late)
		Golgi complex abnormalities	Disorders of metal metabolism	Adult

Strictly speaking, the term "neurometabolic disorders" refers to metabolic diseases with exclusive involvement of the nervous system, but in everyday practice it is used to encompass all inborn errors of metabolism with any degree of nervous system involvement (with or without systemic or other organ system involvement).

Acquired metabolic diseases usually occur in specific clinical (or social) settings, such as hypovitaminoses in malnutrition (Wernicke's encephalopathy, subacute combined degeneration of the spinal cord), ketoacidosis in diabetes mellitus, or neonatal hypoglycemia in premature infants. Severe forms of hyperbilirubinemia may lead to lesions within the deep gray matter structures (kernicterus). Toxic encephalopathies (alcohol, lead, drug, chemotherapy induced) are exogenous sometimes iatrogenic forms of acquired metabolic diseases.

Characteristics

Magnetic resonance (MR) imaging has contributed significantly to early diagnosis and/or characterization of inborn errors of metabolism.

Basic Concepts

The inherently high sensitivity of conventional MR imaging in detecting lesions within brain and/or spinal cord parenchyma is usually not coupled with the desirable degree of specificity. However, the increasing acceptance of the concept of the selective vulnerability of different structures of the CNS to various noxious metabolic insults and the subsequent development of the principles and implementation of the methodology of pattern recognition have significantly enhanced the value of MRI in the diagnostic work-up of neurometabolic diseases. The concepts of selective vulnerability and pattern recognition constitute the foundations of mainstream clinical diagnostic imaging in such conditions. The individual lesions represent the imaging substrates of selective vulnerability and the sum of lesions with resultant lesion patterns defines the imaging phenotypes of various disease entities.

Imaging Techniques

Prerequisites of diagnostically adequate MRI examination in clinically suspected or confirmed metabolic disorders include selection of an optimal plane for all potentially vulnerable structures (e.g., sagittal for cerebellar vermis, coronal for subthalamic nuclei), high spatial resolution (typically 512 matrix or better), and optimized sequences for lesion detection (e.g., myelin sensitive sequences for demonstration of normal or abnormal myelin).

Image Analysis

In order to obtain the most complete data set for pattern recognition, a systematic evaluation of the brain structures is mandatory.

Recognition of various structure involvement and progression patterns has a differential diagnostic value in leukodystrophies (Fig. 1). The cerebral white matter is assessed in different lobes (frontal, parietal, occipital, and temporal) separately. Depending on the magnitude of involvement in different lobes or central and peripheral white matter structures, anteroposterior or posteroanterior as well as centripetal or centrifugal progression gradients of the disease process may be identified. Sparing or involvement of subcortical U-fibers may be characteristic to specific disease entities (metachromatic leukodystrophy vs. Canavan's disease). The corpus callosum should be assessed for signal abnormalities and volume changes (swelling or atrophy); it usually reflects the magnitude and the possible progression gradient of hemispheric white matter abnormalities. The central tegmental structures of the pons are frequent lesion sites in metabolic and neurodegenerative processes. These are nonspecific, but still useful in raising the possibility of a metabolic

disorder. In metabolic diseases, the cerebellar hemispheric white matter is perhaps less frequently involved than the cerebral white matter, but the presence of signal abnormalities and their distribution can be of great value in pattern recognition.

The cerebral cortex is quite difficult to assess for atrophic changes; nevertheless, in some diseases (GM2 gangliosidosis, megalencephalic leukoencephalopathy with subcortical cysts, Canavan's disease) thinning of the cortex may be obvious on MR images. Occasionally, cortical dysplasia may be associated with inborn errors of metabolism (Zellweger's disease, fumaric aciduria). In the acute phase of organic acidopathies, swelling of the basal ganglia is a typical finding, whereas in the chronic stage, atrophy is characteristic. These changes are associated with abnormal signal intensities best appreciated on T2-weighted images (Fig. 2). Other gray matter structures, such as thalami, claustra, are less frequently abnormal. The red nuclei are often spared in metabolic disorders, but involvement of the surrounding white matter structures and of the substantia nigra with a resultant hypersignal on T2-weighted images results in the so-called giant panda face appearance, which may be seen in Wilson's disease or glutaric aciduria type 1. The dentate nuclei of the cerebellum may be involved in all kinds of organic acidopathies and mitochondrial diseases.

Published data on the MR imaging findings of spinal cord and cauda equina lesions in neurometabolic diseases are sparse. Histopathological data suggest that

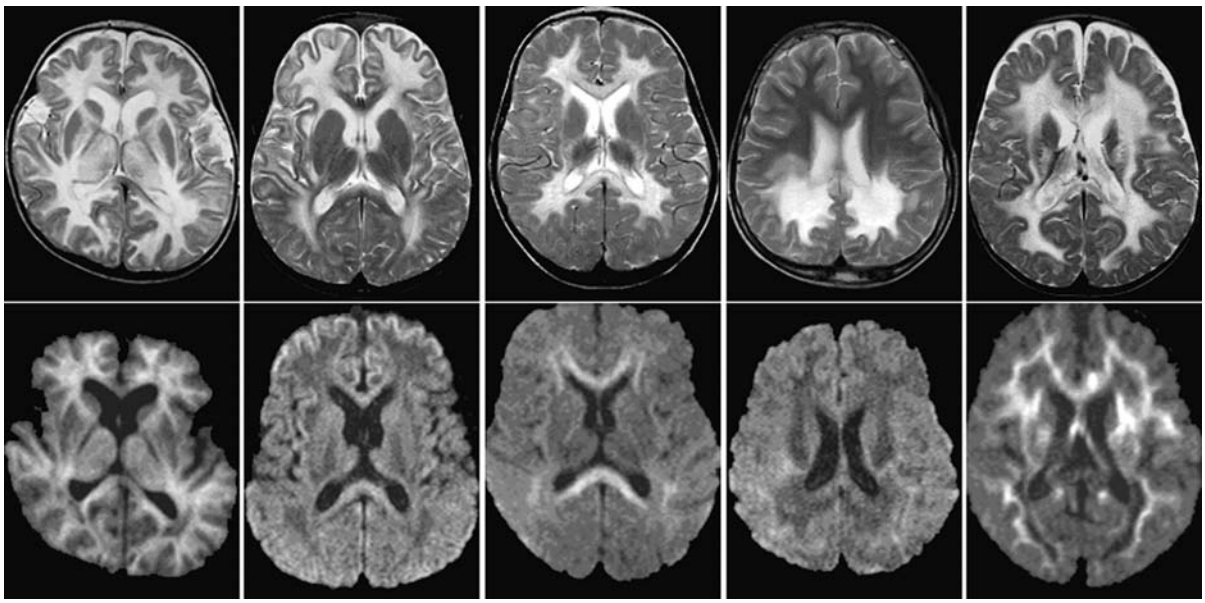

Neurometabolic Disorders. Figure 1 Different imaging patterns in leukodystrophies (from *left* to *right*: Canavan's disease, megalencephalic leukoencephalopathy with subcortical cysts, metachromatic leukodystrophy, X-linked adrenoleukodystrophy, Krabbe's disease) with corresponding diffusion-weighted images.

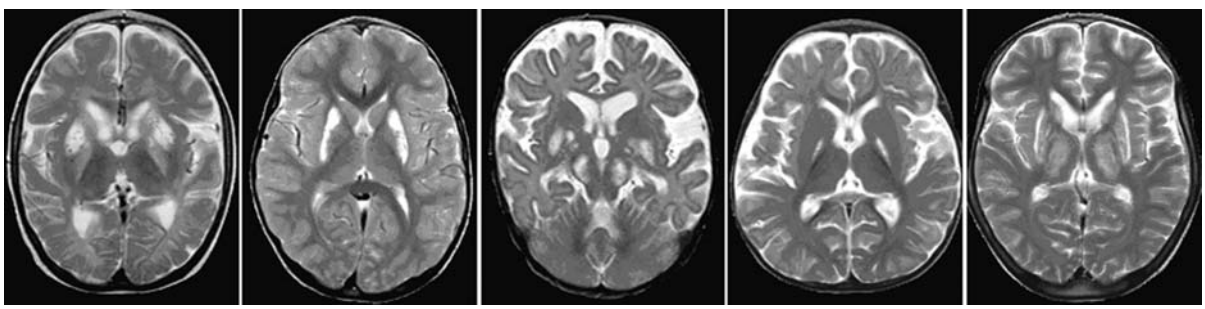

Neurometabolic Disorders. Figure 2 Patterns of deep gray matter involvement in metabolic diseases (from *left* to *right*: 3-methylglutaconic aciduria, biotin-dependent encephalopathy, Leigh's disease, methylmalonic acidemia, Wilson's disease).

both white matter tracts and gray matter structures are prone to damage in a series of diseases, including Canavan's disease, Cockayne's disease, Krabbe's disease, GM2 gangliosidosis, non-ketotic hyperglycinemia, cerebrotendinous xanthomatosis, carbohydrate-deficient glycoprotein syndrome, glutaric aciduria type 2, and cobalamin and methyltetrahydrofolate deficiency (hyperhomocystinemia).

Identification of additional gross morphological abnormalities may also be useful in the process of pattern recognition. Macrocephaly, for example, in some leukodystrophies (megalencephalic leukoencephalopathy with subcortical cysts, Canavan's disease, Alexander's disease), in type 1 glutaric aciduria, GM2 gangliosidosis, and L-2-hydroxyglutaric aciduria is an important pattern element. Other metabolic disorders present with microcephaly (Zellweger's disease, Aicardi-Goutière syndrome, Cockayne's disease, Pelizaeus–Merzbacher disease). Bony abnormalities affecting the skull and spine are typical and very characteristic in some forms of mucopolysaccharidoses.

Common and Uncommon Imaging Findings

Atrophy of different brain structures is common in metabolic diseases. It may be diffuse or focal, affecting specific structures (basal ganglia, cerebellar vermis, corpus callosum). Cerebellar atrophy is consistently associated with some of the metabolic disease entities (neuronal ceroid lipofuscinosis, 3-methylglutaconic aciduria, carbohydrate-deficient glycoprotein syndrome, many lysosomal storage disorders, Menke's disease, mitochondrial diseases). Atrophy is often progressive and may be the sole indicator of an insidious metabolic disorder.

Symmetry of the lesions is a characteristic, although inconsistent, feature. Gray matter structures (basal ganglia, dentate nuclei) are almost always symmetrically involved, but rarely asymmetrical involvement of the basal ganglia may be present in metabolic diseases, especially during early stages of the disease. White matter lesions in metabolic diseases may be patchy, but in extensive leukodystrophies white matter involvement typically shows a strong tendency to symmetry.

Delayed and/or hypomyelination is frequently associated with metabolic disorders, especially in infants during the most active period of myelination. In some diseases (Zellweger's disease, non-ketotic hyperglycinemia) it can be severe; in others, such as Pelizaeus–Merzbacher disease, the imaging findings suggest arrest of the myelination process.

Intravenous contrast injection is usually not indicated in inborn errors of metabolism, since pathological contrast uptake is uncommon and rarely increases specificity. Exceptions exist, however. In X-linked adrenoleukodystrophy, contrast enhancement in the actively demyelinating zone is practically pathognomonic. Contrast enhancement in the brain is a hallmark diagnostic feature in Alexander's disease, and patchy enhancement may occasionally be present within the periventricular white matter in Krabbe's disease.

The incidence of true brain malformations is low in metabolic diseases. This may be explained by the typically postnatal onset of most diseases. In metabolic disease with intrauterine onset (especially if energy metabolism is affected, as in peroxisomal, fatty acid oxidation, and respiratory chain defects), malformations or disturbed development of the CNS (and of other organs) is more frequently encountered (e.g., characteristic bilateral perisylvian polymicrogyria in Zellweger's disease). Documented malformations in various other metabolic disorders include diffuse polymicrogyria, pachygyria, open opercula, callosal abnormalities (hypo- or dysplasia, dysgenesis), cerebellar dysgenesis, Chiari type 1 malformation, and tethered cord.

Imaging Patterns in Metabolic Disorders

Individual parenchymal lesions in metabolic diseases are usually nonspecific. Conversely, compiling positive and negative structure-specific findings during the process of image analysis may yield lesion patterns, many of which are nonspecific; nevertheless, these are still important since they may be useful in raising the possibility of a metabolic disorder along with other differential diagnostic alternatives. In some instances, the lesion pattern may be suggestive of a specific disease entity or group of diseases, whereas occasionally the imaging pattern is actually pathognomonic.

Pathognomonic MR Imaging Patterns

This category includes L-2-hydroxyglutaric aciduria, glutaric aciduria type 1, neonatal maple syrup urine disease, Zellweger's disease, X-linked adrenoleukodystrophy, Canavan's disease, Alexander's disease, megalencephalic leukoencephalopathy with subcortical cysts, leukodystrophy with brainstem and spinal cord involvement, and high lactate, as well as some of the mucopolysaccharidoses presenting with perivascular depositions.

Suggestive MR Imaging Patterns

The best known of these metabolic diseases are methylmalonic aciduria (mut0, mut-, CblA and CblB forms), 3-methylglutaconic aciduria (type 1 and 4), beta-ketothiolase deficiency, late-onset forms of maple syrup urine disease, homocystinuria, biotin-responsive basal ganglia disease, non-ketotic hyperglycinemia, Krabbe's disease, metachromatic leukodystrophy, GM2 gangliosidosis, fucosidosis, mucolipidosis type 4, Pelizaeus–Merzbacher

disease, vanishing white matter disease, many of the "mitochondrial diseases" (Leigh's disease, MELAS, Kearns-Sayre disease), cerebrotendinous xanthomatosis, Menke's disease, and Wilson's disease.

Nonspecific MR Imaging Patterns

All other metabolic disorders fall into this group. It comprises many relatively frequent disorders, notably propionic acidemia, ethylmalonic acidemia, HMG-coenzyme A lyase deficiency, biotinidase deficiency, phenylketonuria, homocystinuria, and the so-called urea cycle defects.

Bibliography

1. van der Knaap MS, Valk J (2005) Magnetic Resonance of Myelination and Myelin Disorders. 3rd edn. Springer, Berlin, Heidelberg, New York
2. Patay Z (2005) Metabolic disorders. In: Tortori-Donati P (ed) Pediatric Neuroradiology Vol. 1 (Brain). Springer, Berlin, Heidelberg, New York, pp 543–722
3. van der Knaap MS, Valk J (1991) Pattern recognition in magnetic resonance imaging of white matter disorders in children and young adults. Neuroradiology 33:478–493

Neuronal Migration Disorders

▶Congenital Malformations, Cerebrum

Neuropathic Joint Disease

H. P. Ledermann[1], W. B. Morrison[2]
[1]Department of Radiology, University Hospital Basel, Institute of diagnostic Radiology, Basel, Switzerland
[2]Department of Radiology, Thomas Jefferson University Hospital, Philadelphia, USA
Ledermannhp@uhbs.ch

Synonyms

Charcot neuroarthropathy; Neuroarthropathy; Neuropathic or neurotrophic joint disease

Definition

Charcot neuroarthropathy is a chronic and progressive disease of bone and joints, characterized by either painful or painless bone and joint destruction on limbs that have lost sensory innervation. Affected joints exhibit synovitis, instability, subluxation, and destruction. Central (upper neuron) and peripheral (lower motor neuron) lesions can lead to neuropathic osteoarthropathy. Central lesions that may produce neuropathic osteoarthropathy include syphilis, syringomyelia, meningomyelocele, trauma, multiple sclerosis, Charcot Marie-Tooth disease, congenital vascular anomalies, and other causes of cord compression, injury, or degeneration. Peripheral causes include diabetes mellitus, alcoholism, amyloidosis, infection, pernicious anemia, and trauma.

Pathology/Histology

The pathogenesis of Charcot neuroarthropathy has been explained by two theories: the neurovascular theory and the neurotraumatic theory. The neurovascular theory suggests that an increase in the blood supply to bone due to damage to tropic nerves causes bone resorption and weakening, leading to fractures and deformities. The neurotraumatic theory, on the other hand, suggests that insensate joints undergo repetitive trauma, resulting in fractures and progressive destruction. This latter theory is supported by several animal experiments and currently thought to best explain the destruction of insensate joints.

Typical sites of joint involvement can be observed (Table 1) depending on the concomitant disease leading to sensory deprivation (1). Early alterations of neuropathic osteoarthropathy include an enlarging and persistent effusion, minimal subluxation, fracture, and fragmentation. These early changes may rapidly progress, and acute subluxations or dislocations may be encountered. More advanced abnormalities consist of depression, absorption, and shattering of subchondral bone, significant sclerosis and osteophytosis, intraarticular osseous fragments, subluxation, massive soft tissue enlargement with effusion, and fracture of neighboring bones. Pathologically, the capsule is thickened, the synovial membrane is indurated and embedded, and metaplastic osteocartilaginous bodies in the synovium produce ossific lesions, which eventually may become far removed from the joint itself (1). Considerable amounts of cartilaginous and osseous debris (detritic synovitis) should suggest to the pathologist that the changes may represent neuropathic joint disease.

Clinical Presentation

The following discussion focuses on diabetic neuroarthropathy of the foot, which is by far the most frequent cause of neuropathic bone disease in the developed world. The majority of patients with pedal neuropathic joint disease present between the fifth and sixth decades of life, and most will have had diabetes mellitus for at least 10 years.

Neuropathic Joint Disease. Table 1 Typical sites of involvement in neuropathic joint disease

Disease	Site of Involvement
Tabes dorsalis	Knee, hip, ankle, spine
Syringomyelia	Glenohumeral joint, elbow, wrist, spine
Diabetes mellitus	Metatarsophalangeal, tarsometatarsal, intertarsal joints
Alcoholism	Metatarsophalangeal, interphalangeal joints
Amyloidosis	Knee, ankle
Meningomyelocele	Ankle, intertarsal joints
Congenital sensory neuropathy, hereditary sensory radicular neuropathy	Knee, ankle, intertarsal, metatarsophalangeal, interphalangeal joints
Idiopathic	Elbow, shoulder

Source: From Resnick D (2002) Neuropathic osteoarthropathy. Diagnosis of Bone and Joint Disorders. 4th edn. vol 3, chapter 72, pp 3564–3595.

Acute presentation: In acute pedal neuroarthropathy, there is usually moderate pain and edematous swelling, although the foot might be completely insensate (2). On examination, the foot is swollen, warm, and tender and can be markedly erythematous. At this stage, the differential diagnosis includes cellulitis, acute gout, deep venous thrombosis, and osteomyelitis, and it can be a considerable challenge to make an accurate diagnosis on clinical examination.

Chronic presentation: Chronic neuropathic pedal arthropathy is characterized by established deformity without symptoms of inflammation (2).

Imaging

Radiographic Changes

The radiographic changes of neuropathic joint disease are often summarized using the mnemonic of the "6 Ds": dense subchondral bone (sclerosis), degeneration (repair by osteophytes), destruction of articular cortex, deformity, debris, and dislocation.

In acute pedal neuroarthropathy, radiographs may reveal only soft-tissue swelling and joint effusion. Radiographic findings of early neuropathic osteoarthropathy manifested by subluxation or malalignment may be very subtle; for example, at the Lisfranc joint, the medial margin of the second metatarsal shaft should align precisely with the medial margin of the second cuneiform. Computed tomography (CT) or contralateral comparison radiographs may be helpful to confirm early malalignment. In subacute stages of the disease, radiographs may demonstrate collapse and fragmentation of the articular surface, subchondral cysts, and marginal erosions. However, bone density is generally preserved; in fact, the bones may demonstrate proliferation manifested by increased density.

Chronic neuropathic osteoarthropathy results in joint subluxation and dislocation as well as destruction and fragmentation of juxtaarticular bone. In later stages of disease, adjacent bones can become necrotic and collapse (Fig. 1a). The degree of sclerosis, osteophytosis, and fragmentation is greater than in any other process. Collapse, sclerosis, and fragmentation of the metatarsal heads may resemble changes of Freiberg's infraction but can be more aggressive and extensive. Broadening of the bases of phalanges may lead to a cupped appearance. Occasionally, shortening and resorption of the ends of the metatarsals and phalanges occurs. Bony ankylosis represents the end stage of joint destruction but is uncommon. Asymptomatic fractures can be discovered in 22% of diabetic patients with neuropathy. Calcaneal fractures are common, and avulsion by the Achilles tendon may be the first radiographic abnormality at the time of presentation. Neuropathic disease of the Lisfranc joint typically results in superior and lateral subluxation of the metatarsals, leading to a "rocker-bottom" type of deformity (Fig. 1b) with increased weight-bearing stress on the cuboid. In this setting, callus and ulcer formation beneath the cuboid is common. Spinal neuropathic arthropathy affects the disc space, the adjoining vertebral bodies, and the facet joints. The lower thoracic and lumbar spine are most commonly affected. Radiographic changes include loss of disc space, vacuum disc, bone sclerosis, debris, disorganization, osteophyte formation, abrupt curvature, and extensive paravertebral soft-tissue calcification. Involvement of the three vertebral columns, including destruction of the facet joints, is an important sign, distinguishing neuropathic arthropathy of the spine from spondylodiscitis (3).

Magnetic Resonance Imaging

Acute neuropathic osteoarthropathy: The involved joints in this early stage of disease often show little deformity or malalignment. Joint effusion is common, with prominent subchondral edema that may extend far into the medullary cavity (Fig. 2). Signal intensity changes in the bone marrow consisting of low signal intensity on T1-weighted images and high signal on T2-weighted images may be identical

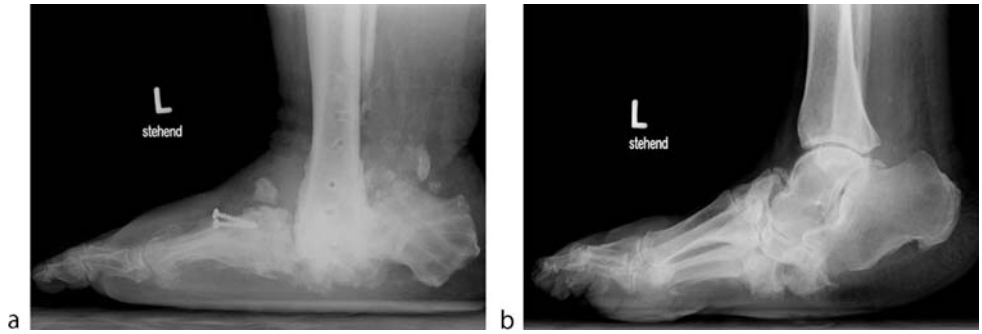

Neuropathic Joint Disease. Figure 1 (a) Lateral view in standing position, revealing extensive destruction of the upper and lower ankle joint in a diabetic patient with long-standing neuropathic arthropathy. All typical radiographic findings of neuropathic joint disease are displayed: dense subchondral bone (sclerosis), degeneration (repair by osteophytes), destruction of articular cortex, deformity, debris, and dislocation. (b) Lateral view of the left foot in standing position of a diabetic patient with subacute neuropathic arthropathy in the midfoot affecting the Chopart, intertarsal, and Lisfranc joints. Note the plantar subluxation of the hindfoot with typical rocker-bottom deformity and dorsal subluxation of the metatarsal bases.

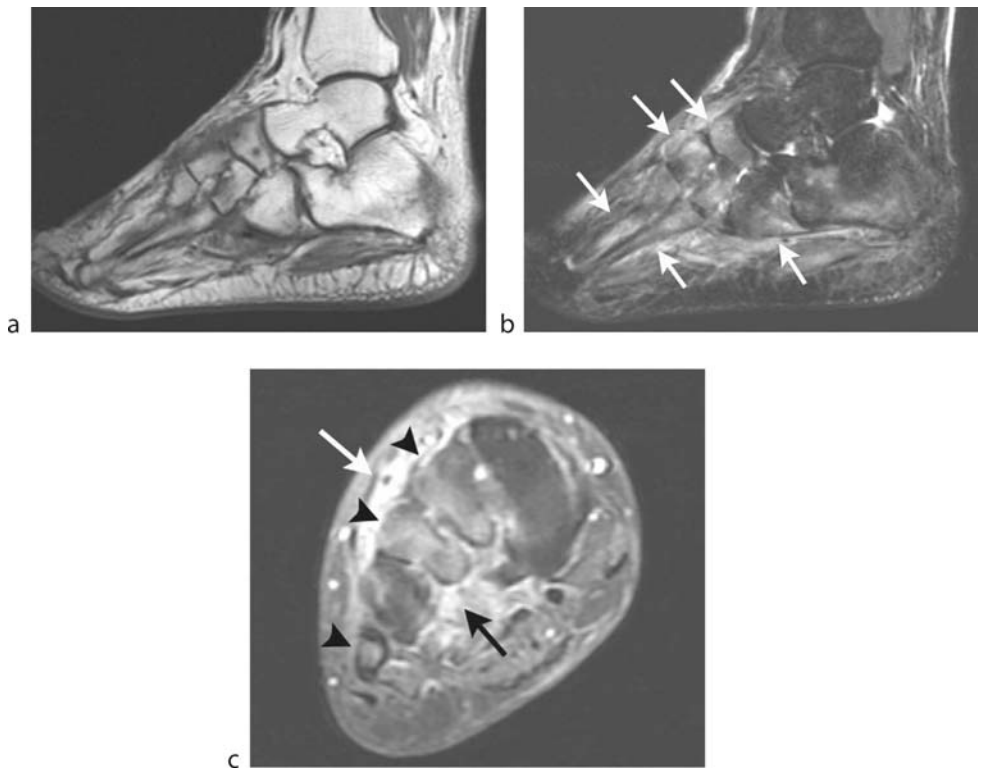

Neuropathic Joint Disease. Figure 2 Acute neuropathic arthropathy in a 37-year-old diabetic patient. (a) T1-weighted sagittal image reveals patchy hypointensity in the bone marrow, affecting all bones around the Lisfranc joint and the navicular and cuboid bone. (b) T2-weighted, fat-suppressed image with corresponding diffuse bone marrow hyperintensity (*arrows*). (c) Coronal contrast-enhanced, fat-suppressed T1-weighted image shows diffuse contrast enhancement in the bone marrow of the second, third, and fifth rays (*arrowheads*) with periarticular soft-tissue enhancement (*arrows*).

to those observed in osteomyelitis (Fig. 2). Erosions may be seen at the joint margins. On gadolinium-enhanced images, marrow enhancement is typically present, with predominantly subchondral distribution. Periarticular soft-tissue enhancement may also be seen. Recent fractures related to neuropathic osteoarthropathy may contribute to signal intensity changes in the marrow and cortex of bones, which leads to potential diagnostic pitfalls.

Bone destruction and deformation may be less conspicuous on magnetic resonance (MR) exams, and radiographic correlation often helps in understanding the extent of these findings. MR imaging findings of spinal neuropathic joint disease are similar to those of spondylodiscitis. The following findings are, however, indicative of neuropathic joint disease: identification of gas in the affected intervertebral disc, spondylolisthesis, involvement of the facet joints, diffuse abnormalities of signal intensity in the vertebral bodies, and rim enhancement of intervertebral discs (3).

Chronic neuropathic osteoarthropathy typically appears as decreased signal intensity on all sequences, consistent with osteosclerosis. Joint deformity is common, with subluxation or dislocation. Subchondral cysts present as well-marginated foci of low signal intensity on T1-weighted images and high signal intensity on T2-weighted images. Bone proliferation is present, with "debris" or intra-articular bodies.

Differential Diagnosis Between Pedal Neuropathic and Osteomyelitis

Radiologic distinction between neuropathic osteoarthropathy and osteomyelitis on MR imaging may be facilitated considering the following general principles (summarized in Table 2): First, the vast majority of cases of osteomyelitis in diabetic feet occur *via* contiguous spread related to ulceration and cellulitis. Therefore, a bone marrow abnormality without contiguous soft-tissue infection or nearby skin ulceration favors diagnoses other than infection. In addition, neuropathic osteoarthropathy is primarily an articular disease; marrow abnormalities centered in a subarticular location favor such an articular disorder. Distribution of osteomyelitis mirrors that of ulceration, which is most common at the toes, metatarsal heads, calcaneus, and malleoli, whereas neuropathic arthropathy is most common at the Lisfranc and Chopart joints. Finally, neuropathic arthropathy tends to involve a number of joints in a region, whereas infection tends to remain localized or spread contiguously.

Differential Diagnosis Between Noninfected and Infected Neuropathic Joint Disease

It is often clinically impossible to diagnose infection in acute or subacute neuroarthropathy since both entities present with symptoms such as swelling, redness, and tenderness. As stated earlier, MR imaging findings of infection and neuropathic disease overlap, and distinguishing these entities may indeed be difficult. On follow-up MR exams, the following articular and bony MR signal changes suggest new onset of infection: progression of bone erosion, loss of subchondral cysts, progression of bone marrow hyperintensity, and enhancement from the articular surface (4). Progressive replacement of soft-tissue fat, progressive enhancement of periarticular soft tissues, and new development of a sinus tract are periarticular MR signal alterations indicative of a superimposed infection (4). As a general rule of thumb, the greater and the more extensive the marrow signal abnormality from the articular surface, the more likely the bone is to be superinfected (Fig. 3).

Nuclear Medicine

Radionuclide imaging can sometimes be a useful investigative tool in pedal neuroarthropathy. The three-phase bone scan using technetium labeled phosphonates (Tc-MDP) is often positive in all phases of diabetic pedal arthropathy, reflecting increased vascularity and bone turnover. To discriminate neuroarthropathy from osteomyelitis, labeled white blood cell (WBC) scans or labeled monoclonal leukocytic antibody scans can be used because they show increased activity at the infection site.

In combination, three-phase TcMDP and labeled WBC scanning has a sensitivity and specificity of 80–90% for the diagnosis of bone infection if there is a penetrating ulcer underneath a neuropathic pedal deformity. It may be difficult to distinguish infection in bone and soft tissue

Neuropathic Joint Disease. Table 2 Differentiation of osteomyelitis from neuropathic osteoarthropathy

	Osteomyelitis	Neuropathic	Comments
Typical location	Toes (tips, dorsum), metatarsal heads (especially first and fifth), calcaneus malleoli	Lisfranc joint, Chopart joint	
Distribution	Focal, local—centripetal spread	Multiple joints in a region	
Pattern of edema/ enhancement	Predominant involvement of one bone	Epicenter in joint and subchondral bone	
Deformity	Uncommon (unless there is underlying neuropathic disease)	Common (rocker-bottom)	
Soft tissues	Adjacent ulcer, cellulitis, sinus tract	Enhancement limited to juxtaarticular soft tissues; skin, subcutaneous tissues intact	Diffuse subcutaneous; edema is typical In diabetic feet

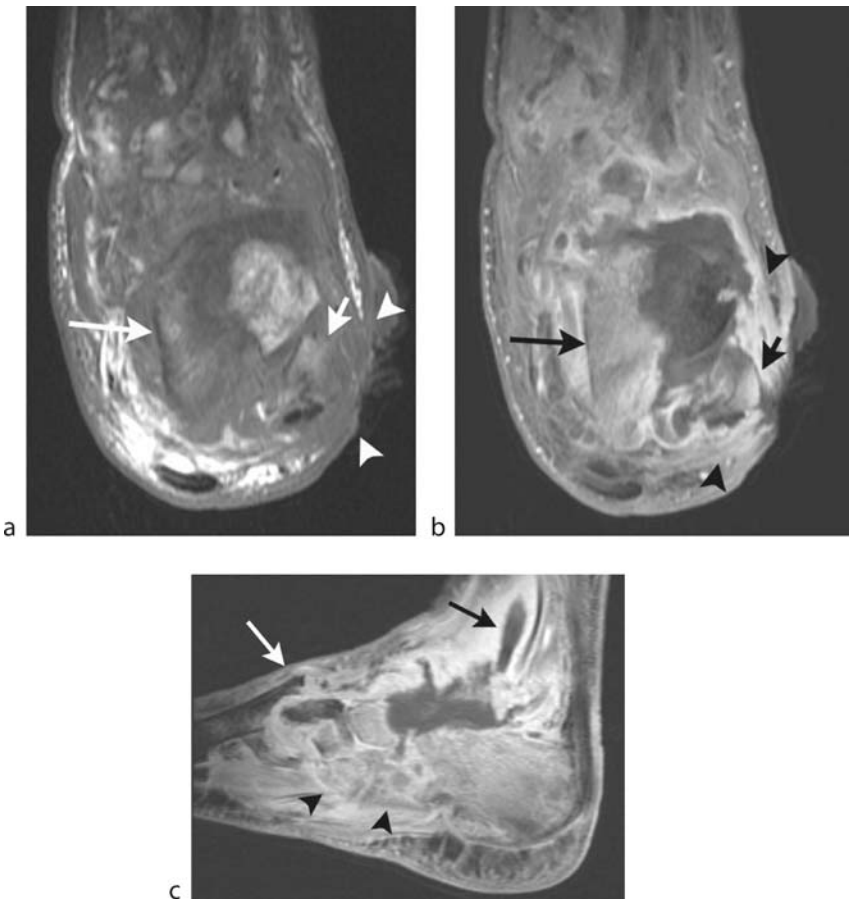

Neuropathic Joint Disease. Figure 3 Diagnosis of osteomyelitis in a patient with long-standing neuroarthropathy. (a) T1-weighted axial image reveals a skin ulcer (*arrowheads*) and adjacent hypointense soft tissue swelling compatible with cellulitis. There is hypointense signal of the bone marrow of the distal fibula (*small white arrow*) and calcaneus (*long white arrow*). (b) T1-weighted axial fat-suppressed and contrast-enhanced image reveals direct contact of the ulcer with the outer surface of the fibula (*short arrow*), with hyperintense marrow signal and extensive periarticular enhancement (*arrowheads*). Note also the diffuse marrow enhancement of the calcaneus (*long arrow*). (c) Sagittal contrast-enhanced and fat-suppressed image with diffuse bone marrow enhancement in the midfoot and hindfoot, including bone fragments (*arrowheads*). Dorsal subluxation of metatarsal bases (*white arrow*) is indicative of neuropathic arthropathy. Note peroneal tendon phlegmon (*black arrow*) with diffuse peritendinous enhancement and hypointense pus in the tendon sheath.

on labeled WBC scan alone, so this is usually interpreted in conjunction with a three-phase bone scan. Labeled WBC scan can be falsely positive in the presence of recent onset of rapidly advancing neuroarthopathy.

Diagnosis

Diagnosis of early neuropathic joint disease may be difficult, especially if a joint above the foot is involved and if the concomitant disease leading to sensory deprivation is unknown to the radiologist. In advanced stages, radiographic changes are almost pathognomonic, displaying the characteristic alterations starting with "D": dense subchondral bone, degeneration, destruction of articular cortex, deformity, debris, and dislocation.

Bibliography

1. Resnick D (2002) Neuropathic osteoarthropathy. Diagnosis of Bone and Joint Disorders. 4th edn. 3(72):3564–3595
2. Rajbhandari SM, Jenkins RC, Davies C et al (2002) Charcot neuroarthropathy in diabetes mellitus. Diabetologia 45:1085–1096
3. Wagner SC, Schweitzer ME, Morrison WB et al (2000) Can imaging findings help differentiate spinal neuropathic arthropathy from disk space infection? Initial experience. Radiology 214:693–699
4. Ahmadi ME, Morrison WB, Carrino JA et al (2005) Neuropathic arthropathy of the foot with and without superimposed osteomyelitis: MR imaging characteristics. Radiology 238:622–631

Neuropathic or Neurotrophic Joint Disease

▶Neuropathic Joint Disease

Neurophakomatoses

Diseases in this group include tuberous sclerosis, neurofibromatosis, Sturge–Weber syndrome and Von–Hippel–Lindau syndrome.

▶Calcifications, Intracranial, Neonatal

Neurovascular Conflict

A vascular compression of a cranial nerve at the root entry zone that manifests clinically as neuralgia and/or spasm. Strict diagnostic criteria include deviation and/or indentation of the nerve by the offending vessel. Chronic pulsatility and pressure upon this vulnerable area of the nerve lead to segmental areas of axonal ischemia and demyelination. Most common causes include vascular loops, vascular dolichoectasia, aneurysms and vascular malformations. High resolution MRI, MRA and/or CTA are the imaging modalities of choice to evaluate this condition.

▶Facial Nerve Palsy

New Neoplasm

Breast neoplasms detected during the follow-up of patients previously diagnosed and treated for breast cancer. The characteristic of these tumors is that their location (not close to the primary tumor or the surgical scar, even in the contralateral breast) and their histological characteristics indicate that they are tumors different to that initially diagnosed and treated.

▶Recurrent Neoplasms, Breast

NF1

▶Neurofibromatosis Type 1 (NF1)

Nipple Adenoma

Benign tumors located in the collecting ducts of the nipple.

▶Adenoma, Breast

Nipple Discharge

Fluid obtained from the nipple. It may be spontaneous or induced by expression, and it may be milky, clear, green, dark, grey, brown, and/or bloody.

▶Duct Disease, Breast

Nodal Necrosis

Nodal necrosis is a pathognomonic feature for metastatic nodes from head and neck squamous cell carcinomas. Nodal necrosis is considered to occur as cancer cells infiltrate into the medullary portion of the node to surpass the blood supply.

▶Lymphadenopathies, Head and Neck

Nodular Adenosis

▶Sclerosing Adenosis, Breast

Nodular Regenerative Hyperplasia, Hepatic

Tumor-like condition of unknown origin, rare in children, usually underdiagnosed because imaging is nonspecific and may resemble focal nodular hyperplasia or may occur as regenerative nodules in cirrhosis. Frequently described in association with other disorders (myelo-lymphoproliferative diseases, Donohue's syndrome, rheumatic disease) and may be seen in fetuses with malformations. It consists of single or multiple regenerative foci of hyperplastic hepatocytes, probably

resulting from a nonspecific tissue adaptation to a heterogeneous distribution of hepatic blood flow.

▶Hepatic Pediatric Tumors, Benign

Nodules, Pulmonary, Multiple

Cornelia Schaefer-Prokop
AMC, Amsterdam, Netherlands
c.m.schaefer@amc.uva.nl

Definition

A pulmonary nodule or coin lesion is defined as a spherical opacity with well-defined edges and a diameter smaller than 3 cm which is surrounded by lung parenchyma. A lesion larger than 3 cm is described as *mass*.

Pathology/Histopathology

The differential diagnosis for multiple pulmonary nodules is long.

Metastatic solid organ malignancies are the most common cause of multiple pulmonary nodules and account for about 80% of these cases. Lymphoma may also cause multiple nodular lesions (e.g. BALT). Infectious diseases (e.g. septic emboli) as well as vascular malformations or non-infectious inflammatory conditions (e.g. bronchiolitis, granulomatous diseases) may cause multiple nodular opacities of varying size and distribution.

Clinical Presentation

Dependent on the extent and on the underlying disease clinical symptoms are very variable (e.g. hemoptysis, fever, weight loss). To cause loss of respiratory function the nodules have to be extensive and are mostly associated with other thoracic manifestations such as pleural effusion or airway obstruction.

Imaging

Basically the same imaging features listed for the solitary pulmonary nodule to discriminate benign from malignant are also valid for multiple lesions.

With the history of a known primary, newly developed multiple nodules—mostly but not necessarily spherical and sharply demarcated—are highly suspicious for metastases.

Nodules grouped in a cluster and lying in the lung periphery are more suspicious for an underlying infection. Septic emboli produce 0.5–3 cm round or wedge shaped nodules, mostly with cavitations with a predilection for peripheral areas of the lower lobes.

Pulmonary arteriovenous malformations consist of abnormal communications between pulmonary veins and arteries. They present as solitary or in about one-third of patients as multiple intrapulmonary nodules. Strong enhancement after contrast injection and the presence of draining vessels are the diagnostic key features.

There are a number of non-infectious inflammatory conditions that present with multiple intrapulmonary nodules such as Wegener's disease, sarcoidosis, rheumatoid arthritis or lymphomatoid granulomatosis. In most of these cases additional clinical findings and imaging features will help to narrow the differential diagnosis.

Diagnosis

CT is the method of choice for detection of multiple pulmonary nodules. Although CT is very sensitive, it is frequently non-specific. Yet, distribution, localization and morphological details provide important clues for further differential diagnosis.

Bibliography

1. Libby DM, Smith JP, Altorki NK et al (2004) Managing the small pulmonary nodule discovered by CT. Chest 125:1522
2. Lillington GA, Caskey CI (1993) Evaluation and management of solitary and multiple pulmonary nodules. Clin Chest Med 14:111
3. Ost D, Fein A (2004) Management strategies for the pulmonary nodule. Curr Opin Pulm Med 10:272
4. MacMahon H, Austin JHM, Gamsu G et al (2005) Guidelines for management of small pulmonary nodules detected on CT scans: a statement from the Fleischner society. Radiology 237:395

Nodules, Pulmonary, Solitary

Cornelia Schaefer-Prokop
AMC, Amsterdam, Netherlands
c.m.schaefer@amc.uva.nl

Definition

A pulmonary nodule, or coin lesion, is defined as a spherical opacity and with well-defined edges, a diameter smaller than 3 cm which is surrounded by lung parenchyma. A lesion larger than 3 cm is described as *mass*.

Pathology/Histopathology

In more than 95% the differential diagnosis of a solitary pulmonary nodule belongs to one of the following entities:

1. Malignant neoplasm (primary or metastatic) (*see entry on bronchogenic carcinoma*).
2. Infectious granuloma (tuberculous or fungal).
3. Benign tumors (mostly hamartoma).

Clinical Presentation

Typically, a solitary pulmonary nodule is an incidental finding in an asymptomatic patient. Rarely, it may cause hemoptysis (dependant on underlying histology).

Imaging

Even 1 cm nodules are frequently missed on a chest radiograph dependant on their anatomic location and the amount of overlying "anatomic noise." CT is the method of choice for the detection of intrapulmonary nodules. The sensitivity and specificity of FDG-PET for diagnosing a pulmonary nodules as being malignant (e.g., bronchogenic cancer) varies with equipment, technique, and glucose metabolism of the lesion.

Radiological imaging features helpful for determining the differential diagnosis of a solitary pulmonary nodule are

1. Calcification: Various types of calcifications are differentiated such as laminated, punctuate, cloud-like eccentric, or concentric. They have a different probability of being associated with a benign lesion or suspicion for malignancy. Uniform, concentric, or popcorn calcifications are typical for benign lesions (tuberculoma, histoplasmoma, hamartoma, Fig. 1) while cloud-like and multiple punctuate calcifications are seen in adenocarcinomas. The visibility of the calcifications on a chest radiograph depends on their size and whether they are surrounded by soft tissue or air. CT is more sensitive for detection and characterization of calcifications but should only be indicated for questionable cases (not for homogeneously calcified granulomas potentially associated with calcified mediastinal or hilar lymph nodes which virtually diagnostic for inactive tuberculosis).
2. Fat (negative HU): It is almost completely specific for a hamartoma. Rare alternatives are metastases from lipo-sarcoma and lipoid pneumonia. Cave: CT-density measurements have to be performed in thin sections to avoid partial volume effects.
3. Contrast enhancement: Malignant solitary pulmonary nodules show a stronger enhancement after injection of contrast (>20 HE with sensitivity 98%, specificity 73%), while benign lesions show slower and lower enhancement. The latter appears to be a useful criterion for excluding malignancy when using a threshold value of <15 HE. Attention has to be paid to the proper technique with respect to volume and flow of injected contrast.
4. Rate of growth: Bronchogenic carcinomas have a volume-doubling time between 1 and 18 months (Fig. 2). Faster doubling time (<1 month) is suggestive for infection, infarction, lymphoma, or fast growing metastases while a longer doubling time is suggestive for a benign nature of the lesion. Elaborate

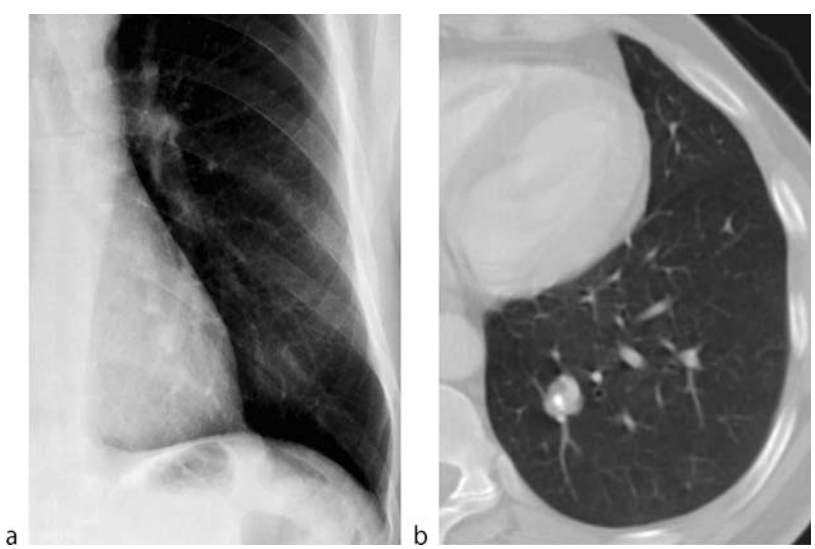

Nodules, Pulmonary, Solitary. Figure 1 A benign intrapulmonary lesion (hamartoma) with a central calcification, a round well-defined margin and a constant size over more than 2 years.

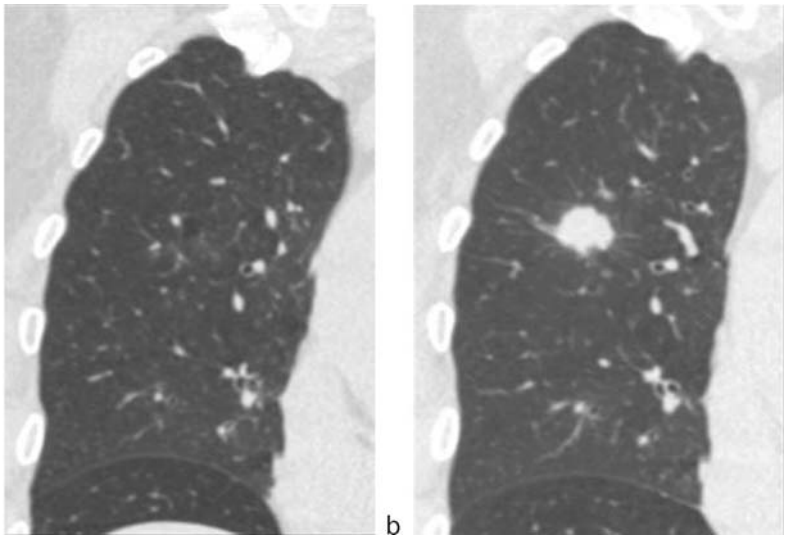

Nodules, Pulmonary, Solitary. Figure 2 Growth of an intrapulmonary nodule in a follow up CT as confident sign for malignancy.

computerized programs were developed for CT to assess lesion growth as early as within 3 months.

5. Size and shape: While the size is a definite tool for stratifying the next diagnostic steps, the role of shape related criteria such as lobulation, notching (*Rigler-sign*), irregularity of borders (*corona radiata*), or the presence of a pleuro-pulmonary tail (*pleural finger*, Fig. 3) remains controversial. None of these criteria provides a reliable discriminating factor. They may be used for complex multifactor likelihood calculations but eventually do not replace invasive procedures for histological proof.
6. Air-bronchogram and bubble-like lucencies: An air-bronchogram within a solitary pulmonary nodule seen on a chest radiograph makes the diagnosis of a lymphoma, rounded atelectasis, or bronchiolo-alveolar carcinoma more likely than a metastasis or primary lung cancer. On the other hand, thin section CT does show in fact air-bronchograms quite frequently also in bronchogenic carcinomas. The *positive-bronchus-sign* (Fig. 3) is a variation of the air-bronchogram and describes an air filled (nonobscured) bronchus running in to a mostly malignant solitary pulmonary nodule and was originally described to predict the likelihood of obtaining a positive transbronchial biopsy. More spherical so-called air bubbles are quite common in adenocarcinoma, especially bronchiolo-alveolar carcinoma.
7. Cavitation: It describes an air containing space within a nodule or mass; wall thickness, wall regularity, and the reaction of the surrounding lung parenchyma vary with the underlying etiology. The most frequent differential diagnoses include a neoplasm, an infectious or granulomatous process, or an ischemic lesion.

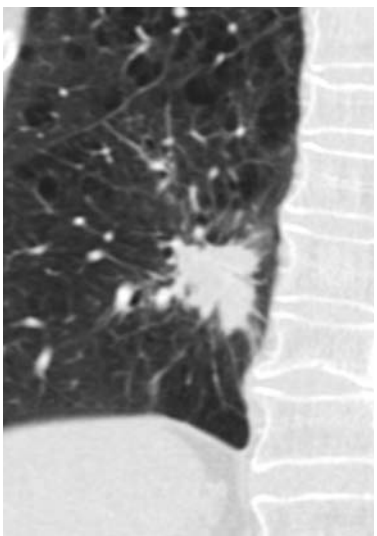

Nodules, Pulmonary, Solitary. Figure 3 A malignant intrapulmonary lesion with spiculae (corona radiata) and a pleural finger.

Pathologically the cavitation is the result of a necrosis of the central portion of the lesion that has been expelled *via* the bronchial tree, leaving an air filled space with or without a fluid-gas level (Fig. 4).

Diagnosis

The diagnostic work up of a solitary pulmonary nodule depends on the size of the lesion, age of the patient as well as the clinical symptoms and history of the patient. Older

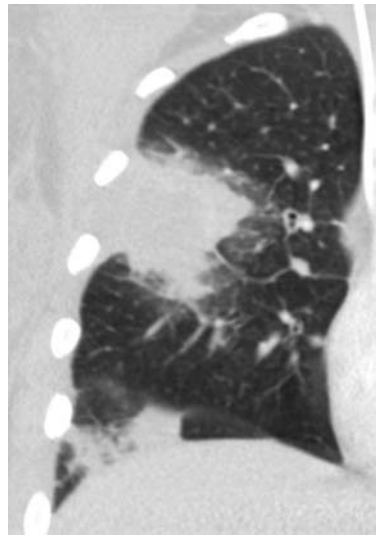

Nodules, Pulmonary, Solitary. Figure 4 Patient suffering from neutropenia after chemotherapy and showing multiple intrapulmonary nodules and masses surrounded by a ▶halo due to an angio-invasive aspergillus infection.

CT scans or chest radiographs should be obtained whenever possible as they may serve to demonstrate stability or interval growth. Lesions larger than 1 cm in diameter require definite diagnostic work up; smaller lesions are followed under specific conditions (see 4).

Bibliography

1. Libby DM, Smith JP, Altorki NK et al (2004) Managing the small pulmonary nodule discovered by CT. Chest 125:1522
2. Lillington GA, Caskey CI (1993) Evaluation and management of solitary and multiple pulmonary nodules. Clin Chest Med 14:111
3. Ost D, Fein A (2004) Management strategies for the pulmonary nodule. Curr Opin Pulm Med 10:272
4. MacMahon H, Austin JHM, Gamsu G et al (2005) Guidelines for management of small pulmonary nodules detected on CT scans: a statement from the Fleischner society. Radiology 237:395

Non-Encapsuled Sclerosing Lesion

▶Radial Scar, Breast

Non-Linear Imaging Techniques

▶Specific Imaging Techniques, Contrast Media, Ultrasound

Non-Bronchial Arteries

Non-bronchial arteries frequently involved in ▶hemoptysis or recurrent bleeding include intercostal, inferior phrenic, subclavian, axillary and internal mammary arteries.
▶Hemoptysis

Non-Hodgkin Lymphoma

Malignant transformation of lymphocytes. The largest subset is B-cell lymphoma.
▶Lymphoma, Breast

Nonaccidental Head Injury (NAHI)

▶Trauma, Head, Non-accidental

Nonaccidental Head Trauma

Often consists of the triad, (multifocal) subdural hematoma, encephalopathy, and retinal hemorrhages.
▶Trauma, Head, Non-accidental

Nonaccidental Trauma

▶Battered Child Syndrome

Nonalcoholic Steatohepatitis

Nonalcoholic steatohepatitis (NASH), also called nonalcoholic fatty liver disease (NAFLD) is a liver inflammation with fatty degeneration which resembles alcoholic hepatitis on liver biopsy (fat droplets, inflammatory cells, but usually no Mallory's hyalin), but is not due to abuse of alcohol. This condition is more common in women. It is associated with

obesity, diabetes mellitus type II, and insulin resistance (Fig. 2). NASH can also be caused by various medications such as amiodarone, antiviral drugs, etc. The diagnosis is based on clinical data, laboratory tests, imaging findings. Liver biopsy may be required. Imaging, especially ultrasound, is the first step for evaluating the presence of fatty infiltration. However, it is not able to identify hepatic inflammation. Therefore, the differentiation between steatosis and NASH often requires a liver biopsy. NASH is becoming recognized as a major cause of cryptogenic cirrhosis of the liver.

▶Hepatitis

Noncommunicating Dissection

Aortic wall hematoma without a visible intimal tear most likely caused by spontaneous rupture of aortic vasa vasorum or by a hemorrhage propagating into the media around an atherosclerotic penetrating ulcer.

▶Dissection, Aortic, Thoracic

Non-linear Bubble Behavior

Volkmar Uhlendorf
Institut für Pharmazeutische Wissenschaften, Zürich, Switzerland
volkmar.uhlendorf@pharma.ethz.ch

Synonyms

Nonlinear bubble oscillation; Nonlinear bubble response

Definition

If the input to a system is modified by some factor and the resulting output changes by the same factor as the input, the behavior is called linear. Any other type of response indicates a nonlinear behavior of the system. Nonlinear bubble behavior occurs when a microbubble is exposed to an ultrasound field at acoustic pressure levels that are typically used in routine practice. The nonlinear echoes returned from the bubbles constitute the signals that are used for contrast-enhanced ultrasound in clinical practice. So-called nonlinear imaging techniques or contrast-specific imaging techniques are used to exploit these signals.

Characteristics

In many cases, a linear system response is desired. For example, the evaluation of analytic measurements is simplified in the linear part of the calibration curve. Another obvious example is given by high-fidelity audio systems, where the well-known nonlinear response at very high output amplitudes leads to rather unpleasant acoustic distortions. However, in ultrasound contrast imaging, similar distortions caused by nonlinear behavior of microbubbles are highly desirable. Here, the characteristic distortions are useful, as they allow one to distinguish between echoes from tissue and echoes from strongly oscillating microbubbles.

When a microbubble is disturbed by external pressure oscillations like those in an ultrasound pulse, it can easily undergo pulsating oscillations, i.e., expansion and compression. This motion re-radiates an ultrasound signal. As long as the external disturbance is very weak, or when the bubble has a shell of higher mechanical rigidity, the response will be linear. This means the shape of the outgoing reflected or scattered wave is an exact copy of the incoming wave – only the amplitude is more or less reduced. A linear bubble response is usually found when the amplitude of the oscillation is less than a few percent of the bubble diameter at rest. Stronger excitations are more easily obtained at a resonance frequency of a given system. It turns out that small microbubbles without a rigid shell have their resonance frequencies in the MHz range used in medical ultrasound imaging. If these "free" bubbles are excited near their preferred oscillation frequencies, their response (the scattered signal) can be so strong that it becomes nonlinear.

There are several reasons why bubbles can behave in a strong nonlinearly fashion. The main factors are easily understood. If an oscillating bubble is viewed as a mass–spring system, the spring represents the compressible gas core plus some contribution from surface tension. The mass is mainly given by the mass of the fluid next to the bubble, which has to be moved during the oscillation (including the shell if there is any, while the gas contributes almost nothing to the mass). In most textbooks, in examples of mass–spring systems the "mass" and "spring constant" are both very constant, leading to a simple linear oscillation. In the case of a bubble, the corresponding parameters are no longer constant, but are continuously changing during the pulsating oscillations. When a bubble expands or contracts, its effective mass grows or shrinks just like the current volume of the oscillating fluid, i.e., in proportion to the third power of its current diameter. Therefore, the bubble motion is slowed down while it is expanded and the bubble may not be able to follow an external excitation fast enough. It may even skip one or two oscillations of the exciting ultrasound signal and emit at

"subharmonics" below the excitation frequency, which is a very typical characteristic of bubbles.

A smaller (or a compressed) bubble has a much smaller effective mass, and thus can rapidly respond even to high frequency variations in the transmitted ultrasound pulse. It reradiates the excitation frequency and high frequencies not contained in the original transmit signal, in particular the higher harmonics (overtones) of the excitation frequency.

Nonlinear bubble behavior also results from an asymmetry in the expansion or compression factor that can be obtained. The gas in an uncompressed air bubble has a specific density of about 1.3 mg/ml. When the bubble is compressed to 1/10 of its initial diameter (1/1000 of the initial volume), its "gas" density increases to 1.3 g/ml (ignoring gas dissolution and heating for simplicity), a value even higher than the density of water or tissue. Obviously, a gas bubble cannot be compressed (or collapse) to much less than 1/10 its initial size.

Bubble expansion is not limited in the same manner, but very large expansion is only possible at very low excitation frequencies. A bubble expanded to twice the initial size effectively has eight times the initial mass. The linear or nonlinear oscillation of a bubble or cavity in liquid is also called "cavitation." Bubble expansion to more than twice the initial size is often followed by a short, violent collapse dominated by inertial forces and therefore called "inertial cavitation." It may lead to fragmentation of a bubble into a number of smaller bubbles. Inertial cavitation also has some potential for bioeffects.

Shell fragmentation (disruption) is a phenomenon that must be distinguished from bubble fragmentation, although sometimes both may occur almost simultaneously. As the shell has an important influence on the lifetime and acoustic response of a bubble, its fragmentation will be discussed in more detail elsewhere in this volume.

In summary, it turns out that nonlinear bubble response is typically a relatively slow expansion followed by a rapid collapse. This motion may be repeated several times, depending on the transmitted ultrasound pulse. It creates higher harmonics and other very characteristic bubble signals like subharmonics, typically 1/2 of the transmit frequency. Furthermore, there may be some ringing of the bubble after the external excitation has ended, much like a bell ringing according to its size – smaller bells or bubbles have higher characteristic frequencies.

Quantitative calculations as well as experimental results indicate that microbubbles in aqueous solution have resonance frequencies in the lower MHz range used in diagnostic ultrasound imaging. This is one of the reasons for the high sensitivity of ultrasound contrast imaging.

Nonlinear Bubble Oscillation

▶Non-linear Bubble Behavior

Nonlinear Bubble Response

▶Non-linear Bubble Behavior

Nonnecrotizing Granulomatous Disease

▶Sarcoidosis, Musculoskeletal System

Nonossifying Fibroma

Nonossifying fibroma is a tumorlike bone lesion of childhood and adolescence which is composed of a fibrohistiocytic cellular component. The lesion nowadays is viewed at as a developmental anomaly arising in the metaphyseal region of long bones.

▶Neoplasm-Like Lesions, Bone

Nonspecific Fluorochromes

▶Molecular Probes, Optical Probes

Nonspecific Probes

▶Molecular Probes, Optical Probes

Nonthrombotic Hepatic Vein Obstruction

▶Budd-Chiari Syndrome

Nonunion

Failure of fracture healing within the expected interval, usually arbitrarily defined as 1 year. Nonunion may be categorized as hypertrophic or atrophic. Hypertrophic nonunion is characterized by exuberant periosteal callus and subchondral sclerosis. This type of nonunion more commonly occurs secondary to inadequate fixation and persistent motion of the fracture fragments. Atrophic nonunion shows little new bone formation and osteopenia is often present. Poor nutrition, systemic illness, or other causes of decreased nutrition are often part of the etiology.

▶Fractures, Peripheral Skeleton

Nonviral Vector

A nonviral vector is a virus free or virus particle free vehicle or carrier, such as polymer, lipid or other nonviral material based nano- or microparticle used to deliver genetic material into the body for gene therapy.

▶Local Drug and Gene Delivery with Microbubbles

Normal Brain Development

Developing brain anatomy is characterized by morphological and signal changes on MRI along with increasing gestational age.

▶Fetal Neuroimaging

Normal–Appearing Brain Tissue

Tissue (both in the white and gray matter) with no signal intensity abnormalities on conventional MRI scans of the brain, but which shows structural or metabolic changes as detected by other MR techniques, such as MT-MRI, DT-MRI, and ^{1}H-MRS.

▶Aging Brain

Not Otherwise Specified (NOS)

▶Carcinoma, Ductal, Invasive

Notches

▶Compression, Extrinsic, Esophagus

Notches

▶Compression, Extrinsic, Stomach and Duodenum

Nuclear Medicine – Diagnostic Procedures

Uwe Haberkorn
Radiologische Klinik und Poliklinik, Universitätsklinikum Heidelberg, Heidelberg, Germany
uwe.haberkorn@med.uni-heidelberg.de

General Principles and Goals

Although therapy with radioactive isotopes is a substantial and ever-growing part of the discipline, we concentrate here on the principles of diagnostic nuclear medicine procedures. Nuclear medicine is based on the tracer principle introduced by von Hevesy and Paneth. This technique relies on the fact that exchange of stable atoms by their radioactive isotopes does not change the biological properties of organic compounds. The labeling is done using very low amounts of a substance, leading to physiological concentrations in the body. Therefore, the radioactive-labeled molecules (tracer) can be used to display reliably the physiological or biochemical fate of the nonlabeled molecule (tracee). The tracer technique is applied in basic science mainly using the β-emitting isotopes ^{3}H and ^{14}C for the examination of living subjects, such as patients, using γ- or positron-emitting isotopes. In most cases the radiation dose of the patient is in the range of the radiation dose from natural sources per year or even below that. The most important insight resulting from the tracer principle is the realization that living organisms are in a continual state of chemical flux, characterized by a balance between the rate of formation and rate of breakdown of body constituents. Therefore, more emphasis should be placed on function rather than structure. This may lead to the definition of diseases in terms of physiology and biochemistry rather than in terms of

anatomy and histopathology. This is useful because of the principle of chemical reserve: the rate of a chemical reaction within a region of the body or an organ can often fall to low levels before symptoms appear. Thus, one can often detect chemical abnormalities earlier than is possible by waiting for structural changes to be detectable. In that respect nuclear medicine procedures offer a high sensitivity in the picomolar range. Labeling of substrates with radioactive isotopes and administration of very low amounts of these tracers allow the assessment of biochemical or physiological processes without any interference with the phenomena to be studied. This allows one to base medical diagnoses on *in vivo* regional as well as global physiological or biochemical abnormalities. If disease is more and more understood in molecular terms, then diagnosis should also be based on molecular techniques. In this respect nuclear medicine must be seen as the pioneering discipline in the field of molecular imaging. The goals of nuclear medicine procedures consist in the development of specific radiotracer molecules, functional characterization of disease, detection of focal disease before overall organ function is impaired, and assessment of the effects of treatment. These goals can be obtained by three types of measurements: transport processes, bioenergetics, and intracellular and intercellular communication.

Imaging Devices

Planar single-photon imaging and single-photon-emission computed tomography (SPECT): Single-photon emission imaging is based on the uniform emission of photons in all directions during the decay of isotopes such as ^{67}Ga, ^{99m}Tc, ^{111}In, ^{123}I, or ^{201}Tl. The measurement of these photons can be used for the generation of planar images or tomographic images. Detection of these photons is achieved by a gamma camera which is composed of scintillation crystals (NaI (Tl)), a photomultiplier tube, and associated electronic devices. Collimators are positioned between the patient and the crystal and are used to reject off-axis radiation. Planar images are obtained by positioning the patient in a definite orientation towards a gamma camera and collecting the counts. This leads to a two-dimensional representation of three-dimensional objects. In contrast to radiographs, which are transmission images, scintigraphic scans deliver emission images. This has considerable impact on the information obtained from scans performed in different positions: an anterior scan, for example, shows mainly anterior tissue structures. Tomographic images can be acquired by viewing a patient's activity distribution from different angles. This can be done by rotating a gamma camera with one, two, or three heads around the patient and recording data from multiple projections. Photons are counted every 3–6° throughout a rotation of 180–360°, which usually requires 20–30 min. The resulting data can be reconstructed analogous to CT images. In comparison to planar images, SPECT images show a five- to eightfold increase in contrast, which is obtained by eliminating the activity superimposed on the structure of interest. However, images with high count density are needed for image reconstruction to avoid error propagation observed at low count rates.

Positron emission tomography (PET): Decay of positron emitters releases a positron with specific kinetic energy which determines the mean travel distance (or mean positron range) from the nucleus. Combination of the positron with an electron causes two annihilation photons each having the energy corresponding to the electron mass (511 keV) with a characteristic spatial orientation (180° apart with a random variation of 0.5°). PET scanners are built of a ring of scintillations crystals (commonly used scintillators are NaI(Tl), bismuth germanate, and lutetium oxyorthosilicate doped with cerium) and identify nearly simultaneous or "coincident" scintillations in opposite detectors. This coincidence detection provides better and more uniform sensitivity and resolution than does conventional imaging. Since the attenuation of photons can be measured by a transmission scan it is possible to obtain quantitatively accurate data of the regional distribution of a radiopharmaceutical.

Fusion imaging: structural and functional data in most cases are complementary because the images refer to different aspects of the disease. Computed tomography (CT) and magnetic resonance imaging (MRI) are used primarily for the imaging of structural/anatomical changes caused by a specific pathological process. In contrast, SPECT and PET studies display functional changes associated with disease. Usually the functional images are interpreted in conjunction with corresponding morphological images from CT or MRI. This information can be combined in fusion images either by use of software approaches or by hybrid systems such as SPECT/CT or PET/CT. Software solutions work well for rigid organs such as the brain. However, other parts of the body may cause more problems due to patient movement and motion of internal organs as well as repositioning errors.

Radiopharmaceuticals

The information obtained by nuclear medicine procedures is determined by the radiopharmaceutical administered to the patient. There are some radionuclides whose natural distribution is of interest: ^{123}I for thyroid function, ^{133}Xe and ^{81m}Kr for lung ventilation, ^{67}Ga for inflammation, and ^{201}Tl for perfusion imaging. Most radiopharmaceuticals consist of two parts: a radioactive label and a molecule whose physical or chemical

properties define the biodistribution of the agent. A few agents used in nuclear medicine are radioisotopes of natural physiological substrates, whereas the vast majority are more complicated compounds. The radioisotopes of iodine were the first used in nuclear medicine with the thyroid as target and showed that the rate of iodide incorporation greatly increased in hyperthyroidism. However, today ^{99m}Tc is the ideal choice due to its availability and optimum decay characteristics, although complex chemistry is needed for the coupling of the isotope to the tracer molecules (Table 1).

Nuclear Medicine – Diagnostic Procedures. Table 1
Selected single-photon radiopharmaceuticals in clinical use

^{123}I, ^{131}I as NaI	Thyroid function
$^{99m}TcO_4^-$	Thyroid function
^{99m}Tc-MDP	Bone imaging
^{99m}Tc-MAA	Perfusion
^{99m}Tc-DTPA	Renal function, lung aerosol, liquor scintigraphy
^{99m}Tc-MAG_3	Renal function
^{123}I-Hippuran	Renal function
^{99m}Tc-erythrocytes	Blood pool
^{99m}Tc-albumin	Blood pool
^{99m}Tc-sulfur colloid	Reticuloendothelial function
^{99m}Tc-HIDA	Biliary imaging
^{111}In-leukocytes	Inflammation
^{67}Ga-citrate	Inflammation, tumor
^{133}Xe, ^{127}Xe	Lung ventilation
^{81m}Kr	Lung ventilation
^{201}Tl-chloride	Myocardial perfusion
^{99m}Tc-sestamibi	Myocardial perfusion, tumor
^{99m}Tc-tetrofosmin	Myocardial perfusion
^{99m}Tc-HMPAO	Brain perfusion
^{99m}Tc-ECD	Brain perfusion
^{123}I-IMP	Brain perfusion
^{99m}Tc-HMPAO-leukocytes	Inflammation
^{99m}Tc-TRODAT-1	Dopamine transport
^{123}I-IBZM	Dopamine D_2 receptor
^{99m}Tc-Arcitumomab	Tumor
^{111}In-octreotide	Somatostatin receptor-positive tumor
^{123}I-IMT	Tumor, amino acid transport
^{123}I-MIBG	Neuroendocrine tumor, heart innervation
^{123}I-b-CIT	Dopamine transport
^{123}I-Iomazenil	Benzodiazepine receptor, epilepsy, viability
^{131}I-Norcholesterol	Adrenal glands
^{59}Fe-citrate	Iron kinetics

Radiopharmaceuticals are prescription drugs subject to the same controls and regulations as nonradioactive drugs. All tracers must be tested for quality and safety before they can be given to a patient. Furthermore, most medical radionuclides have short half-lives in the range of hours or days. Therefore, unlike other drugs they must be made and delivered promptly.

Since most commonly used PET radiotracers have a very short half-life, time is a substantial factor in the process of isotope production, tracer synthesis, and PET measurements (Tables 2 and 3). As an example, for ^{11}C-labeled compounds the typically needed time periods are 10 min for cyclotron bombardment, 40 min for tracer production, and up to 90 min for PET imaging. However, the synthetic versatility of carbon with respect to the production of naturally occurring molecules justifies the development of ^{11}C-labeled PET tracers. Furthermore, due to the short half-life of PET isotopes, repeated PET examinations on the same subject are possible within short time intervals (i.e., the same day), allowing a more detailed description of the underlying biochemical or physiological processes.

Nuclear Medicine – Diagnostic Procedures. Table 2
Physical characteristics of commonly used positron emitters

Isotope	Half-life (min)	Maximum energy (MeV)	Range (mm) in H_20
Fluorine-18	110	0.635	2.4
Carbon-11	20.4	0.96	4.1
Nitrogen-13	9.96	1.19	5.4
Oxygen-15	2.1	1.72	8.2

Nuclear Medicine – Diagnostic Procedures. Table 3
Selected PET radiopharmaceuticals in clinical use

^{18}FDG	Glucose metabolism, myocardial viability, epilepsy, tumor
^{18}F-FDOPA	Dopamine pool, decarboxylase activity
^{18}F-FET	Tumor, amino acid transport
^{18}F-fluoride	Bone metastases
^{11}C-methionine	Tumor, protein synthesis
N-methyl-^{11}C-flumazenil	Benzodiazepine receptor, epilepsy
O-methyl-^{11}C-raclopride	Dopamine D_2 receptor
^{82}Rb	Myocardial perfusion
$H_2{}^{15}O$	Perfusion
^{11}C-acetate	Metabolism
^{13}N-NH_3	Perfusion

N

Principles of Functional Measurements

Measurements of radiotracer distribution may be performed as static or as kinetic studies. For static scintigraphy a single static image is obtained at a specific time after tracer administration. This is done when an equilibrium or a stable distribution of radioactivity is reached, which is the case for processes with slow kinetics. Static scintigraphy may differentiate between functional active or inactive tissue. Inactive regions are displayed either as cold spots (examples are pulmonary embolism, myocardial ischemia or scar tissue, brain perfusion defects, or cold nodules in the thyroid) or as hot spots with a high target-to-background ratio (examples are metastases in bone scintigraphy, glucose-consuming tumor tissue in FDG-PET, or binding of antibodies and ligands to surface antigens or receptors).

Alternatively, the time course of tracer accumulation can be measured and data from multiple studies under different biological conditions may also be obtained. If the appropriate tracer and imaging procedures are selected, the time–activity curves generated from regions of interest (ROIs) in the image should be directly influenced by the physiological characteristics of interest, such as blood flow, metabolism, or receptor concentration. The concentration of radioactivity in a given tissue region at a particular time primarily depends on two factors: the local tissue physiology such as blood flow or metabolism and the input function, which is the time course of tracer radioactivity concentration in the blood or plasma. The input function defines the availability of the radioactive tracer to the organ of interest. Quantitation is possible by analysis of time–activity curves using pharmacokinetic models. A model is the mathematical description of the relationship between tissue concentration and physiological control factors. An elaborated model allows prediction of the time course of tracer accumulation in a tissue region from knowledge of the local physiological variables and the input function. Parameters obtained from these models are blood flow and extraction, volume of distribution, biochemical reactions such as glucose transport and phosphorylation, receptor density, and pharmacokinetics of radiolabeled drugs. Parametric images derived from these dynamic studies and model analysis show where and how fast chemical reactions are taking place within the body, for example, revealing the rates of regional glucose utilization within organs such as the heart, brain, and liver. Simpler models predict only certain aspects of the time–activity curves, such as initial slope, area under the curve, or ratio of target to a reference region.

Functional tests can also be performed by physiological or pharmacological modulation of tracer accumulation. This is done in coronary heart disease using exercise or pharmacological stress. In these patients symptoms often occur after exercise. Therefore, perfusion at rest is normal with a decreased coronary reserve during exercise or pharmacological intervention with pyridamole or dobutamine. In the brain the autoregulation of cerebral perfusion can be modulated by pharmacologically induced changes in blood pressure or an increase in plasma CO_2 levels using carbonic anhydrase inhibitors. As in the heart, a normal cerebral blood flow at rest may exist in the presence of a decreased vascular reserve. This can be evaluated by measurement of perfusion after vasodilator stress. In the kidney the sensitivity in detecting renovascular hypertension can be increased using an angiotensin-converting enzyme inhibitor such as captopril, which accentuates the physiological differences between the normal and the dysfunctional kidney. More elaborate studies have been done with receptor ligands in the brain: the tracer 3-*N*-(^{11}C)-methylspiperone (NNSP) binds to dopamine 2 (D_2) receptors in the basal ganglia. Neuroleptic drugs used in the treatment of schizophrenia and certain other neuropsychiatric disorders block D_2 receptors. Therefore, this tracer was used to monitor the degree of blockade of D_2 receptors after administration of neuroleptic drugs by measuring NMSP binding. In addition, the duration of opiate receptor blockade by the blocking drugs naloxone, naltrexone, and nalmefene was monitored using ^{11}C-carfentanil and PET.

Mechanisms of accumulation: Since the information obtained from nuclear medicine measurements is dependent on the selection of the appropriate tracer and the selection is based on biochemical and physiological knowledge of the tracer kinetics, the biological interpretation of the resulting images is clear. Multiple mechanisms of tracer accumulation exist:

- Diffusion processes which are used for ventilation studies of the lung
- Adsorption phenomena obtained after injection of bone-seeking agents and used in bone scintigraphy
- Ion transport observed in thyroid scans with sodium pertechnetate
- Capillary blockade, a classical approach from physiology transferred to patient studies as radiolabeled macroaggregated albumin in lung perfusion scanning
- Phagocytosis of nanocolloids in scans of the liver, spleen, and reticuloendothelial system
- Active transport phenomena such as iodide uptake, tubular secretion of MAG_3 *via* an anion exchange system, ^{123}I-IMT uptake *via* the amino acid transport system L
- Sequestration of cells used for the detection of radiolabeled erythrocytes in the spleen
- Metabolism, exemplified by the use of fluorodeoxyglucose (FDG) in cardiology, neurology, and oncology
- Synthesis of neurotransmitters, measured using ^{18}F-DOPA and PET

- Receptor binding used in the diagnosis of D_2 receptor density in patients with movement disorders with ^{11}C-raclopride or ^{123}I-IBZM or in the detection of somatostatin receptor-expressing tumors with ^{111}In-octreotide
- Antigen–antibody complexes used for bone marrow scan or tumor detection *via* specific tumor antigens such as CEA

Clinical Applications

The above-mentioned techniques have different clinical applications as mentioned in the following examples.

1. Assessment of organ function: Examination of the kidneys, lungs, or salivary glands allows a detailed evaluation of their different parts. Physiological information *in vivo* is obtained by the determination of esophageal transit or gastric emptying.
2. Differential diagnosis: Assessment of D_2 receptor density with ^{123}I-IBZM can be used to differentiate between Parkinson's disease or multiple system atrophy. FDG-PET is useful for the differentiation between scar and recurrence in patients after surgery for colon carcinoma; ^{123}I-IMT uptake is used for the differentiation between radiation necrosis and recurrence in patients with brain tumors. Further examples are $^{99m}TcO_4^-$ for the diagnosis of thyroid nodules and labeled erythrocytes in patients with suspected liver hemangioma.
3. Localization of disease: Multiple procedures are available for different clinical problems. Localization of disease can be the detection of epileptic foci (^{18}FDG or ^{99m}Tc-HMPAO), infectious foci (labeled leukocytes or antibodies), receptor-positive tumors (^{111}In-octreotide), increased tumor marker in tumor patients after surgery or carcinoma of unknown primary tumor (^{18}FDG), and in gastrointestinal bleeding (labeled erythrocytes).
4. Staging: Commonly applied tracers are phosphonic acid derivatives such as ^{99m}Tc-MDP for the visualization of bone metastases and ^{18}FDG for the detection of lymph nodes or distant metastases.
5. Therapy planning: This can be done prior to radioimmunotherapy to estimate the dose obtained in tumors. First, a diagnostic scan is performed using the antibody labeled with a γ emitter. Then, treatment is performed with the same antibody labeled with a β emitter. For radiation therapy, inclusion of functional information such as glucose metabolism, proliferation, or hypoxia in the treatment protocol is expected to be the state of the art in the near future. Furthermore, biodistribution studies of radiolabeled new drugs may expedite the preclinical and clinical procedure for the approval of these drugs.
6. Therapy monitoring: Since most treatment protocols may cause severe side effects to patients it is critical to know whether therapy is successful at an early stage. This can be done by measurements of glucose metabolism using ^{18}FDG. As an alternative, apoptosis measurements with ^{99m}Tc-annexin V are currently under evaluation. A nononcological example of therapy monitoring is the measurement of bone remodeling by repeated bone scintigraphy with ^{99m}Tc-MDP in patients with Paget's disease.

Future Potential

Nuclear medicine is a discipline where a rapid transfer of basic research into clinical practice is possible. The application of principles or insights gained by biochemistry, immunology, molecular biology, or virology will allow new radiolabeled molecules to be established. The isotope used for labeling determines the use of the resulting tracer either for diagnostic or for therapeutic purposes. By the exchange of different isotopes, the same biomolecule can be used first for therapy planning and then for treatment.

Many new molecular structures have been cloned and will be available as potential novel diagnostic or drug discovery targets. The target selection and validation will become the most critical component in this process. The evaluation of genetically manipulated animals or newly designed biomolecules will require information about physiology, biochemistry, and pharmacology and the experimental approaches will apply many technologies including *in vivo* imaging with molecular imaging procedures such as SPECT and PET. Pharmacogenomics will identify new surrogate markers for therapy monitoring, which may represent potential new tracers for imaging. Furthermore, drug distribution studies for new biomolecules are needed to speed up drug approval in preclinical stages of drug development. Finally, bioengineering will lead to the design of new biomolecules by methods such as DNA shuffling or phage display procedures, which may be used for new approaches in isotope-based diagnosis and treatment of disease.

Terms

Adrenal glands and neural crest tumors; apoptosis imaging; biliary system; bone scintigraphy; brain receptor studies; cerebral physiological measurements and cerebrovascular disease; dementia; gastrointestinal tract; gene

therapy; genitourinary system; hematopoietic system; imaging of treatment response; imaging of tumors hypoxia; imaging of tumors metabolism; imaging of tumors perfusion; imaging of tumors proliferation; imaging of tumors receptor; imaging of vascular disease; inflammation and infectious disease; liver; molecular imaging; movement disorders; musculoskeletal system; myocardial perfusion; myocardial viability; neurochemical systems; pancreas; parathyroid imaging; pediatric nuclear medicine; PET in drug discovery and development; PET; physiological imaging esophagus; psychiatric disorders; pulmonary function; quantitative radioassays; radiochemistry; radioimmunoscintigraphy; radiolabeled peptides; salivary glands; seizure disorders; sentinel node scintigraphy SPECT; thyroid diagnosis; tracer kinetic models.

Nucleoplasty

Relies on the principle of 'controlled ablation', a process in which radio frequency energy is used to generate a highly focussed plasma field that is capable of cleaving molecular bonds. After insertion of a special wand into the centre of the intervertebral disc, radio frequency energy is used to ablate nucleus pulposus tissue, decreasing intradiscal volume and thereby lowering intradiscal pressure. This causes the herniated portion of the nucleus pulposus to recede towards the centre of the disc, relieving pressure on the nerve root.

▶Percutaneous Interventions for Lumbar Radicular Syndrome

Obliterating Hepatic Vein Endophlebitis

►Budd–Chiari Syndrome

Obstetric Conjugate

Distance on a midsagittal section from the sacral promontory to the top of the symphysis.

►Magnetic Resonance Pelvimetry

Obstruction of the Biliary Tree

►Occlusion, Bile Ducts

Obstruction of the Inferior Venacava

►Thrombosis, Caval Vein, Inferior

Obstruction of the Superior Venacava

►Thrombosis, Caval Vein, Superior

Obstructive Emphysema

Obstructive emphysema is identified by over inflation of the lung distal of an airway obstruction.

►Foreign Bodies, Aspiration, Children (Chest View)

Obstructive Uropathy in Childhood

Michael Riccabona, Richard Fotter
Division of Pediatric Radiology, University Hospital, Medical University of Graz, Graz, Austria
richard.fotter@meduni-graz.at

Synonyms

Obstructive uropathy; Urinary tract obstruction

Definition

Obstructive uropathy is any kind of hindered urine drainage from the renal calyces or pelvis, the ureter or the bladder. However, clinically relevant obstruction means impairment to a degree that in the past has already damaged or in the future will deteriorate renal function of the affected system. Consequences of obstruction initially are dilatation, thickening of the (bladder-, ureteral-, pelviceal- and calyceal-) wall and eventually thinning of renal parenchyma with consecutive diminishing renal function. This may ultimately lead to a decrease in dilatation; therefore, the generally used assessment of dilatation for grading of obstruction may mimic improvement in cases with significant functional deterioration. Depending on the various underlying concepts different definitions are used to define the degree of obstruction as considered relevant for treatment decisions in different parts of the world, with Europe tending to quantify the drainage dynamics, and America focusing on renal function.

Embryology and Pathogenesis

There are several causes for obstruction, with consecutively different embryologic and pathogenetic pathways. They can be divided into congenital anomalies and anatomic variants or secondary and acquired obstruction (Table 1).

Obstructive Uropathy in Childhood. Table 1 Causes of obstructive uropathy

Congenital causes:
• Idiopathic megaureter, with relative narrowing at the uretero-vesical junction (Fig. 1a),
• Ureterocele with megaureter, mostly with a duplex system (Fig. 1b),
• Rare other ureteral variations such as ureteral valves,
• Congenital uretero-pelvic junction obstruction, with narrowing by a fibrotic or dysplastic segment at the uretero-pelvic junction (Fig. 1c),
• Posterior urethral valves and other urethral anomalies, as well as rare ureteric flaps,
• Anatomic variations
• Caliceal neck stenosis or ureteral obstruction caused by prominent or accessory renal vessels (Fig. 1d),
Retrocaval ureter leading to impaired ureteral drainage,
Horse shoe kidney, malrotation and ectopic kidneys, with an unusual coarse of the ureter that may impair drainage,
Secondary obstruction
• Urethral- and bladder polyps,
• Ureteral and urethral fibrosis or stenosis, such as (post-)traumatic urethral stricture leading to bladder outlet obstruction with consecutive bladder pathology and associated obstructive or refluxing uropathy (see entry 'Hydronephrosis'),
• (Post-)infectious causes,
• Motion and peristalsis impairment by dysplasia or dysgenesis and palsy,
• Retroperitoneal processes (tumour, fibrosis, haematoma, …),
• Acute urinary tract obstruction by an ureteral calculus, a haematoma or blood clot, or fungus ball,
• Post-/peritraumatic obstruction (haematoma, compression, rupture, …).

Clinical Presentation

Typical clinical presentation of obstructive uropathy includes abdominal or flank pain, renal colic, abdominal distension or palpable abdominal mass (in gross HN) and (micro-)haematuria. Lower urinary tract obstruction (urethral obstruction) may additionally exhibit anuria or oliguria, e.g. in a neonate with posterior urethral valves (PUV).

Imaging

The purpose of imaging is not only to detect urinary tract dilatation and obstruction, but to provide a detailed anatomic display of the patient's individual situation, to describe the obstruction anatomically (high-, middle-, low/ureteral obstruction? obstruction at the uretero-vesical- or at the uretero-pelvic junction? obstruction of the urethra?) and finally to grade obstruction and—in particular—to differentiate dilative or non-obstructive uropathy from (partial) obstruction, since obstruction may need treatment and follow-up, as well as to assess renal function.

Imaging methods: Imaging is primarily performed using *ultrasound* (US), which can only be successfully applied in sufficiently hydrated children and should always include an assessment at full and post-void bladder. Furthermore, (colour) Doppler sonography (CDS) as well as less common approaches (such as perineal US of the urethra) and application of modern methods (e.g. 3DUS) may offer additional valuable information. For anatomic assessment of the urethra in suspected lower urinary tract obstruction or for differentiating refluxing units from obstructive dilation, an *urethrography*, a *cystogram* or a VCUG is indicated. For anatomic assessment of the upper urinary tract (ureter, renal collecting system and kidney) IVU has been the major imaging tool in the past, in addition to US; however, increasingly *MR-urography* (MRU) is taking this role not only offering an anatomic assessment but also allowing for functional evaluation and MR-angiography in the same investigation. CT is rarely used in children due to its radiation burden—in complicated stone disease a low dose protocol multi-detector CT may become indicated. For grading of obstruction and functional evaluation diuretic renal scintigraphy still is the most commonly used tool (Fig. 2). It allows differentiating dilative from (partially) obstructive systems using various protocols (depending on the time of administration of diuretics) that are applied not only for initial assessment, but also during follow-up, particularly of equivocal findings. Increasingly this functional assessment can also be performed by functional diuretic MRU, however, availability and technical aspects as well as sedation needs have yet hindered a wide spread use of this approach. Retrograde or antegrade *ureterography* and pyelography are rarely performed; in rare cases or in complicated malformations they may be

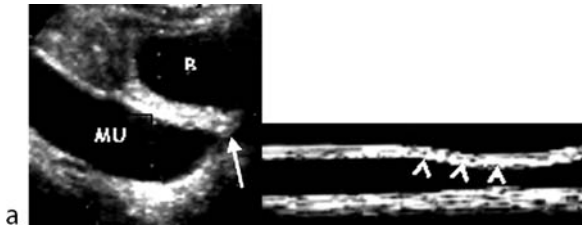

a

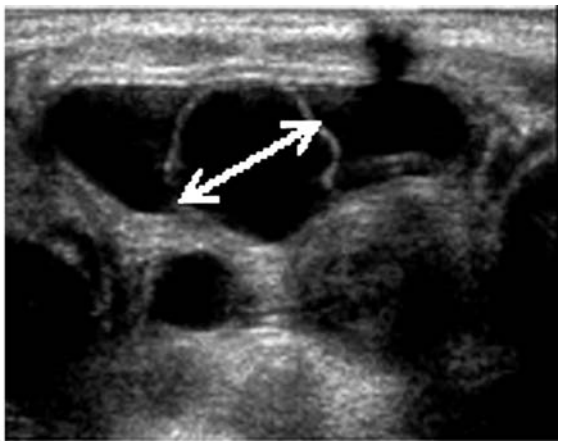

b

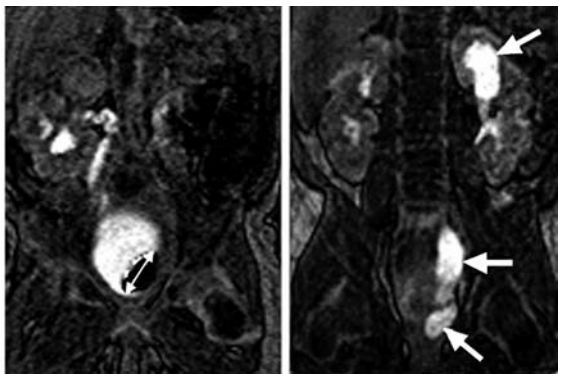

c

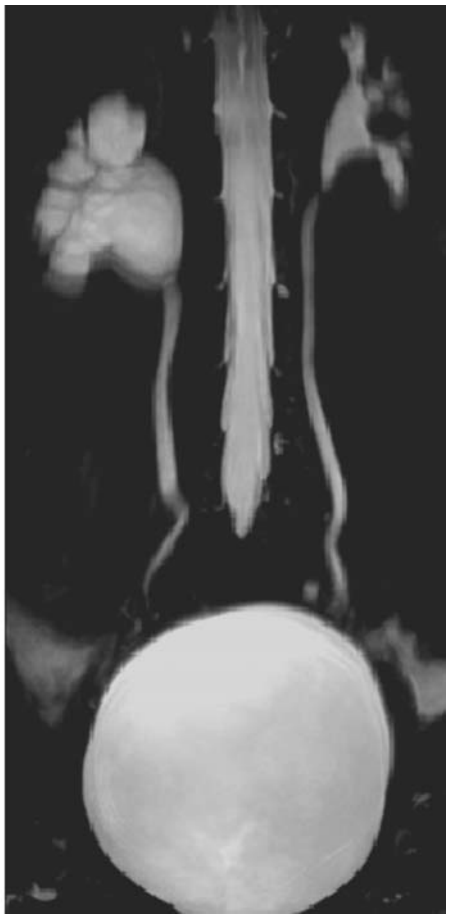

d

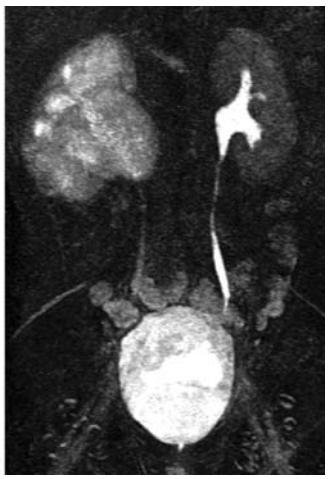

e

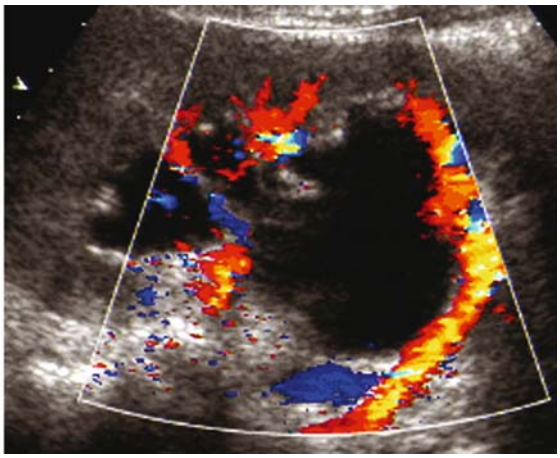

f

Obstructive Uropathy in Childhood. Figure 1 (continued)

O

used as well as peri-operatively, and in acute events with indication for *percutaneous nephrostomy. Whitaker test* (percutaneous nephrostomy with a flow pressure curve derived from intrapelvic fluid infusion *via* the nephrostomy tube with simultaneous pressure measurement) has been the gold standard for assessment of upper urinary tract obstruction. Due to its invasiveness and the reliable results from diuretic scintigraphy or functional MRU this method is today restricted for complicated cases with equivocal results of standard imaging, potentially in a peri-operative setting, as well as for research purposes.

Imaging indications and algorithms: Basically obstructive uropathy is primarily diagnosed using US. Further imaging depends on the initial findings (Table 2).

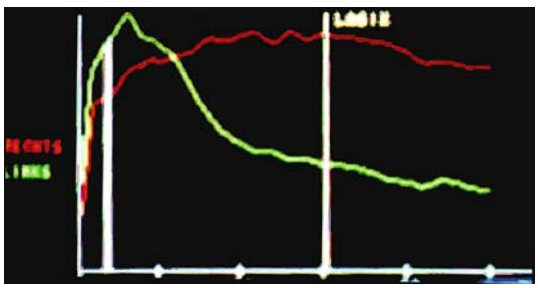

Obstructive Uropathy in Childhood. Figure 2 Diuretic scintigraphy in a patient with severe uretero-pelvic junction obstruction. Note the different perfusion, excretion and drainage curves on this diuretic Tc ^{99m} MAG3 renography, with delayed and reduced renal transit indicating diminished function and causing a flattening of the early activity curve (red (dark) line) and poor drainage in the right obstructed kidney, with only poor response on diuretic stimulation (yellow (light) line). Normal renography curve of the normal left kidney (green (gray) line).

- Low degree hydronephrosis (HN) is followed up by US without any other imaging,
- High degree HN is assessed by diuretic renal scintigraphy and MRU (or IVU), the latter pre-operatively or in case of complex malformations,
- VCUG for differentiation of refluxing from obstructive uropathy
- In acute renal colic (note that acute urinary tract obstruction often only exhibits mild dilatation!) US can often sufficiently diagnose the condition. US is supplemented by an abdominal plain film of the kidney, ureter and bladder ('KUB') for assessment of additional calculi or positioning of a sonographically diagnosed calculus for lithotripsy. In unclear cases an adapted IVU or even an un-enhanced (spiral multi-detector) CT may still become indicated. In case of renal parenchymal findings that indicate an underlying disease such as nephrocalcinosis or medullary sponge kidney adequate imaging of these entities is performed (see entry: 'Nephrocalcinosis', 'Cystic Renal Disease'),
- In complex cases, particularly in combined infection and obstruction, CT- or MR-urography may become indicated. Percutaneous nephrostomy offers an image guided treatment option, and in PUV with lower urinary tract obstruction a suprapubic catheterism may become necessary,
- For follow-up, regular (diuretic) US examinations at 1–3–6 month intervals and diuretic scintigraphy or MRU are recommended, with some variation of timing and protocol in different centres.

Note that imaging indication and method depends on the indication for treatment, which varies between the continents; whereas in Europe usually diuresis impairment indicates surgical action, loss of kidney function expressed by relative renal function (usually assessed by

Obstructive Uropathy in Childhood. Figure 1 Imaging findings in typical obstructive uropathies. (a) US of a primary megaureter. This longitudinal section of the retrovesical dilated ureter (MU) with a short tight uretero-vesical junction (⇒) into the urinary bladder (B) documents the existing ureteral peristalsis (>) using an m-mode track recorded at the site of the dotted line. (b) Ureterocele. Transverse US image of the urinary bladder demonstrating a large intravesical ureterocele (⇔) causing obstructed urinary drainage from the ipsilateral system, seen as a dilated retrovesical ureter on the right side. (c) Serial dynamic MRU images (Gadolinium enhanced, T1-weighted, 3D gradient-echo sequence) in a patient with left sided ureterocele and duplex system show the non-enhanced, fluid filled ureterocele in the bladder visualized during the early phase (⇔), that gradually fills with contrast during late phases that also demonstrate contrast excretion into the dilated upper system with the corresponding megaureter (⇐). (D) MRI in UPJO. Note the dilated collecting system with a narrow uretero-pelvic junction at fully extended urinary bladder after Furosemid application in this non-enhanced, one shot, 3D, T2-weighted HASTE image of MR-urography of a right sided UPJO with a normal appearance of the left system. (E) Three-dimensional volume rendered image of a late phase (after diuretic stimulation using Furosemid), T1-weighted, gradient-echo acquisition of a dynamic MR-urography in an infant with severe hydronephrosis of the right kidney—due to uretero-pelvic junction obstruction—and a normal left kidney with diuresis-induced slight distension of the renal pelvis. (F) Accessory renal vessel causing upper urinary tract obstruction. Additional renal artery (coded in red) coursing to the lower pole of the left kidney causing proximal ureteral obstruction and hydronephrosis, demonstrated by a longitudinal

Obstructive Uropathy in Childhood. Table 2 Flowchart 'imaging algorithm in obstructive uropathy'

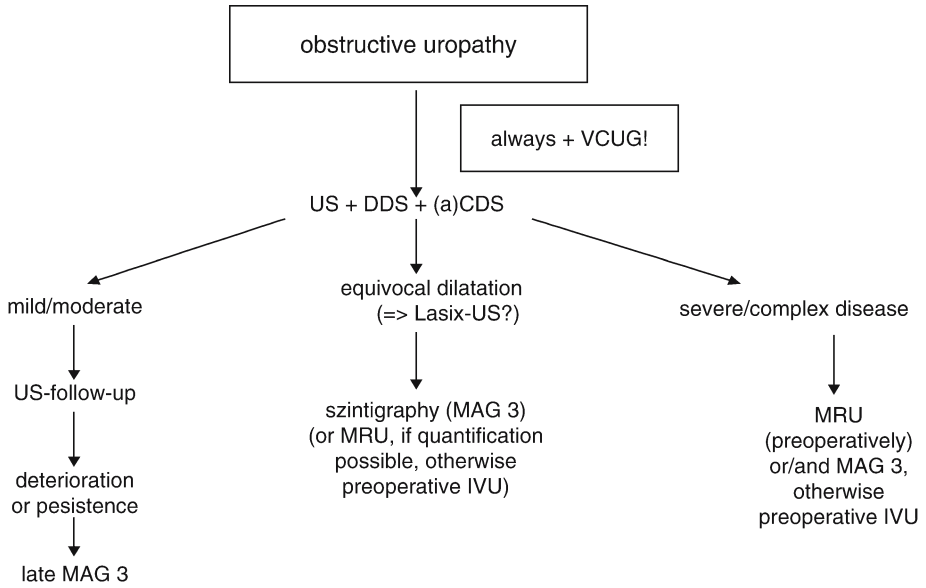

Suggestions for an imaging algorithm in pediatric obstructive uropathy.
Note: In case of acute colic with suspected urolithiasis, US usually is supplemented by an abdominal plain film (KUB) and—in still equivocal cases—potentially an adapted IVU; in rare complicated cases a focused or adapted (un-enhanced) spiral CT may become necessary.
Abbreviations: US, ultrasound; DDS, duplex Doppler sonography; (a) CDS, (amplitude coded) colour Doppler sonography; IVU, intravenous urography; MRU, MR-urography; MAG3, dynamic renography; VCUG, voiding cystourethrography.
Source: Adapted from Riccabona M, Fotter R (2004) Reorientation and future trends in paediatric uroradiology: minutes of a symposium. Pediatr Radiol 34:295–301.

scintigraphy) is considered the indication for surgery in the US, were as some other areas relay on the degree of dilatation and basically operated all grossly dilated systems.

Diagnosis

Imaging allows diagnosis of the underlying anatomy and pathology, enables deciding on the level of obstruction, and allows for functional evaluation particularly necessary for treatment decisions. Imaging criteria are different for the various modalities, the underlying pathology and the different treatment paradigms.

Bibliography

1. Fernbach SK (1992) The dilated urinary tract in children. Urol Radiol 14:34–42
2. Klahr S (1998) Obstructive nephropathy. Kidney Int 54:286–300
3. Peters CA (1995) Urinary tract obstruction in children. J Urol 154:1874–1884
4. Piepsz A (2002) Radionuclide studies in paediatric nephro-urology. Eur J Radiol 43:146–153
5. Riccabona M (2004) Pediatric MRU—its potential and its role in the diagnostic work-up of upper urinary tract dilatation in infants and children. World J Urol 22:79–87
6. Riccabona M, Fotter R (2004) Reorientation and future trends in paediatric uroradiology: minutes of a symposium. Pediatr Radiol 34:295–301

Occlusion and Subocclusion, Small Bowel in Adults

Malone Dermot, Colm McMahon
Department of Radiology,
St Vincent's University Hospital, Dublin, Ireland
d.malone@st-vincents.ie

Synonyms

Small intestinal obstruction

Definition

►Small bowel obstruction (SBO) is the impedance of the progression of intestinal content due to a mechanical obstacle (1).

Pathology/Histopathology

The small bowel extends from the duodeno-jejunal junction to the ileocaecal valve. It is approximately 6.5 m long. The

jejunum represents the proximal two-fifths and the ileum, the distal two-fifths. The small bowel gradually changes from the beginning of the jejunum to the end of the ileum. The jejunum (2.5 cm diameter) is wider than the ileum (2 cm diameter). The mucosa is arranged in circular folds which are larger and more numerous in the jejunum. These folds are a distinguishing feature from large bowel on an adult plain film of abdomen (PFA).

Secreted fluid and swallowed air contribute to bowel distension in SBO. Ischaemia is a serious complication, which may be venous, arterial or both and may lead to infarction. Ischaemia is more likely in ▶closed-loop obstruction (CLO). In CLO, a loop of bowel is occluded at two points by a single constrictive lesion. The mesentery and intestine are occluded. This is usually due to adhesions or hernias.

The causes of SBO are outlined in the Table 1.

The commonest causes are adhesions (50–80%), hernias (10–15%) and neoplasms (10–15%). Other causes are uncommon in the adult population.

Clinical Presentation

SBO accounts for 20% of all acute surgical admissions (1). Classic symptoms are abdominal pain, distension, vomiting and constipation. Clinical presentation depends on the severity of SBO and the presence or absence of ischaemia. In early, uncomplicated SBO, abdominal pain may be crampy and intermittent, but when ischaemia occurs, pain becomes more severe and continuous.

On examination, high frequency bowel sounds and abdominal distension are observed. Dehydration and electrolyte imbalance can occur.

Imaging

The goals of imaging in SBO are

1. Confirm the diagnosis
2. Determine the level of SBO
3. Diagnose the cause
4. Assess for evidence of ▶strangulation or mesenteric ischaemia
5. Determine need for surgery

PFA

A PFA is usually the first radiological test in SBO. The PFA has a sensitivity of 64% for SBO diagnosis but does not reliably allow diagnosis of cause, level of SBO, or ischaemia. Some advocate that the PFA should be performed erect to assess for air-fluid levels (1). If an erect PFA is not possible, a horizontal beam lateral film can also be used to evaluate for air-fluid levels. An erect chest X-ray is the plain radiograph of choice to assess for perforation.

Contrast Studies

There are limitations to the use of contrast studies in acute SBO. Barium is contraindicated if perforation is suspected. Water-soluble contrast can be used, but is diluted by the excess intra-luminal fluid. If hyper-osmolar agents are used, these can worsen dehydration by osmotic effect on the bowel wall, encouraging further fluid loss into the lumen. Enteroclysis reduces dilution by intra-luminal fluid, facilitates propulsion toward the level of obstruction and also allows a means for drainage of some of the administered fluid.

Since computed tomography (CT) became available, enteric contrast studies have been of limited value in SBO. There are two situations in which contrast studies are useful.

1. Enteroclysis can be used in the investigation of intermittent or low-grade obstruction for which the sensitivity of CT is only 48%.
2. Water-soluble follow through (WSFT) can be used to distinguish which clinically stable patients are likely to have spontaneous resolution of SBO (2). About 100 mL of water-soluble contrast is administered via a nasogastric tube and a PFA is taken 4 h later. If the contrast column has reached the caecum by this time, then the obstruction is very likely to resolve. If not, SBO is unlikely to resolve spontaneously.

Ultrasound

US is not used as a first line investigation in SBO if CT is available. It confirms dilated fluid-filled in SBO in up to 95.3% of cases. Ultrasound is not as good as CT for ruling in SBO but it is better for ruling out SBO, which is unlikely in the absence of dilated, fluid-filled loops (3).

Extrinsic	Intrinsic	Intra-luminal
Adhesions (most common)	Neoplasm (common)	Gallstones
Hernias (common)	Inflammation	Intussusception
Neoplasm (common)	Ischaemia	Meconium ▶ileus equivalent (in cystic fibrosis)
Inflammation	Haematoma	

(*continued*)

Dilated small bowel loops are also seen in ▶paralytic ileus. In SBO versus paralytic ileus, hyper-dynamic intestinal motility can be observed in real time.

Computed Tomography

CT has high accuracy in the diagnosis of SBO and in determining the cause. Enteric contrast is optional depending on clinical severity of obstruction. In high-grade SBO, there is usually sufficient fluid within the bowel to allow accurate evaluation of obstructed loops. Intravenous contrast (150 mL contrast bolus at 3 mL per second) is used to demonstrate bowel wall enhancement, which is important in the diagnosis of ischaemia.

In practice, most patients are initially evaluated with PFA and subsequently with CT.

Nuclear Medicine

Scintigraphy does not currently play an important part in the diagnosis of SBO.

Diagnosis

Confirming the Diagnosis of Obstruction

The PFA is diagnostic of SBO in up to 64% of cases. Dilated loops of bowel are seen, usually within 5 h of the onset of obstruction (Fig. 1). If the dilated loops are entirely fluid-filled, then the diagnosis may be occult on PFA. Dilated bowel loops can also be seen in paralytic ileus.

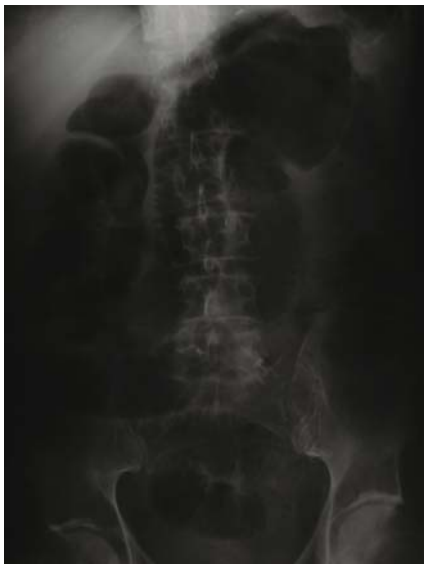

Obstructive Uropathy in Childhood.

Figure 1 PFA of SBO. Multiple dilated loops of small bowel shown.

CT is more than 95% accurate in the diagnosis of SBO (4). The diagnosis depends on demonstrating dilated small bowel loops (>3 cm) with a focal discrepancy in the calibre of the bowel at the transition between obstructed and non-obstructed bowel (Fig. 2). In paralytic ileus, the small bowel is also dilated, but the right colon is usually also dilated, often tapering to normal at, or distal to, the hepatic flexure (4).

Determining the Level of Obstruction

On PFA, the presence of dilated small bowel superiorly in the abdomen may indicate proximal SBO. Dilated pelvic loops more frequently imply distal SBO. In SBO, dilated small bowel loops align along the long axis of the mesentery and jejunal loops can be found in the pelvis, with ileal loops in the upper abdomen.

In order to distinguish large bowel obstruction from SBO on PFA, the following features are helpful:

Megibow (4) describes the systematic assessment of the bowel on CT in bowel obstruction. The bowel should be systematically evaluated in a retrograde way, beginning at the rectum, and proceeding to the caecum. After

Small bowel obstruction	Large bowel obstruction
Haustra absent	Haustra present
Valvulae in jejunum	No valvulae
Many loops	Few loops
Central distribution	Peripheral distribution

(*continued*)

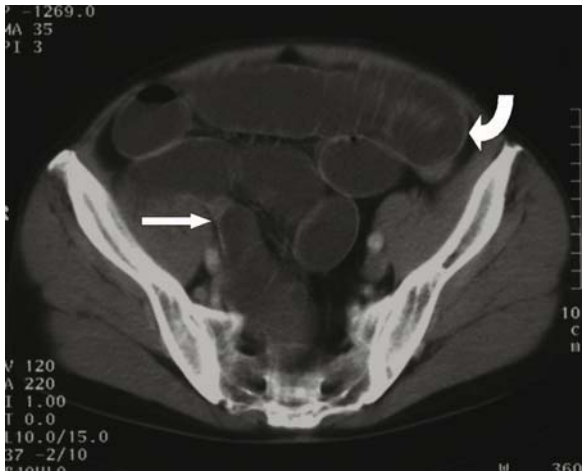

Obstructive Uropathy in Childhood.

Figure 2 SBO due to adhesions. ▶Zone of transition in distal small bowel (arrow). Note normal bowel wall enhancement (curved arrow).

'clearing' the colon, the distal ileal loops should be identified and assessment should proceed proximally to the level at which the calibre of the small bowel is increased (Fig. 2). Review of the images on cine-mode and multiplanar reconstructions [particularly with multidetector-row CT (MDCT)] are helpful in this evaluation.

Diagnosis of the Cause of Obstruction

Adhesions, hernias and neoplasms account for over 80% of cases. CT is the primary diagnostic tool in determining aetiology of SBO, with accuracy of 70–95% (1).

In developed countries, adhesions account for 50–80% of causes. A history of prior abdominal surgery is usual, although previous peritoneal inflammation may also cause adhesions. Even in patients with known intra-abdominal malignancy, SBO is due to adhesions in 21–38% (4). On CT, diagnosis of adhesions is based on an abrupt change in small bowel calibre without another cause of obstruction at the transition point. A beak-like narrowing can be seen. Although the adhesions cannot be visualised with CT, it is important to make the diagnosis of obstruction secondary to adhesions when no other cause is seen (4).

Hernias account for 10–15% of cases (1). External hernias are more common than internal and include inguinal, femoral, paraumbilical, obturator, Richter, Spigelian and incisional hernias. Internal hernias include paraduodenal hernias, transmesenteric hernias, and herniation through the foramen of Winslow. These can be recognised by an abnormally positioned segment of small bowel often with protrusion of mesentery through the internal defect, with proximal bowel dilatation. With increasing use of laparoscopic surgery, port-site hernias are a cause of SBO to recognise. Laparoscopic port sites vary in diameter, generally from 5 to 10 mm. Herniation through laparoscopic fascial defects as small as 5 mm has been described. SBO due to port-site hernias is more common in the early post-operative period (5).

Neoplasia is the third most common cause of SBO. Infiltration of the bowel wall may be caused by adenocarcinoma, carcinoid or metastatic carcinoma. Extrinsic masses such as peritoneal carcinomatosis can also cause obstruction. In these cases a mass is seen at the transition point. Mural mass lesions may also lead to obstruction by causing intussusception.

Assessing for Evidence of Strangulation or Mesenteric Ischaemia

The presence of ischaemia in SBO increases mortality from between 5 and 8% to between 20 and 37% (4). It requires urgent surgical management. CT is 83% sensitive and 93% specific for ischaemia in SBO.

Strangulation is defined as CLO associated with intestinal ischaemia. In CLO (Fig. 3), a loop of bowel is occluded at two adjacent points along its course. CLO usually occurs due to constriction by adhesions or a hernia. The CT signs of CLO are

- Radial distribution of small bowel loops with mesenteric vessels converging toward apex
- U or C-shaped dilated bowel loop
- Two adjacent collapsed or triangular loops at the site of obstruction

CLO is prone to twisting of the affected bowel and mesentery leading to venous congestion with subsequent arterial ischaemia and infarction. This is termed strangulation. The CT signs of strangulation are

- Circumferential mural thickening
- 'Target' sign—concentric mural rings of different attenuation, post-intravenous contrast, a more specific form of mural thickening
- 'Whirl' sign—corkscrew configuration of mesenteric vessels due to twisting
- Increased attenuation of bowel wall
- Lack of bowel wall enhancement
- Air in bowel wall (intestinal pneumatosis)
- Mesenteric haemorrhage
- Ascites

In SBO complicated by ischaemia, the bowel wall appearance depends on the balance between venous obstruction, reduced arterial perfusion and reperfusion. If reduced arterial perfusion predominates, in the absence

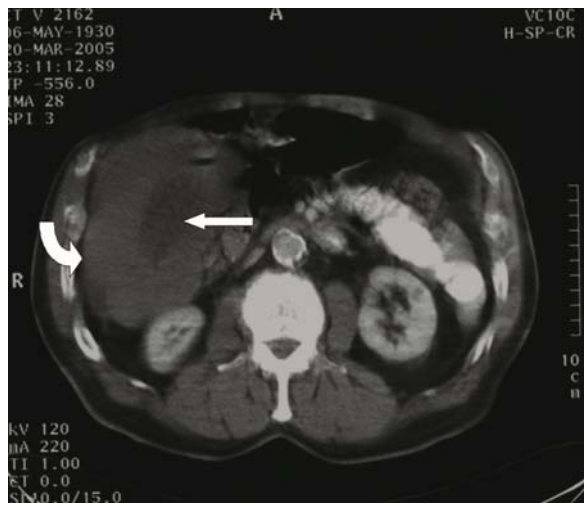

Occlusion and Subocclusion, Small Bowel in Adults. Figure 3 Closed-loop obstruction. C-shaped loop of bowel. Note congested mesentery (arrow) and poor enhancement of bowel wall (curved arrow).

of significant reperfusion, then the bowel wall will be of normal thickness and many of the above signs will be absent. Therefore, CT is good at ruling in ischaemic SBO, but poor at ruling out ischaemic SBO (3).

Determining the Need for Surgery

The impact of imaging on management and indications for surgery have been summarised by Taourel et al. (1).

1. Strangulation and ischaemia (emergency)
2. Obstruction due to a tumour
3. Obstruction due to irreducible hernia (urgent)
4. Obstruction due to adhesions, without ischaemia, should be managed conservatively, where possible

As stated above, if SBO is slow to resolve with conservative management, WSFT is a useful test to determine the likelihood of successful non-operative treatment (2).

Bibliography

1. Taourel P, Kessler N, Lesnik A et al (2002) Non-traumatic abdominal emergencies: imaging of acute intestinal obstruction. Eur Radiol 12:2151–2160
2. Staunton M, Malone DE (2005) Can diagnostic imaging reliably predict the need for surgery in small bowel obstruction? Critically appraised topic. Can Assoc Radiol J 56:79–81
3. Staunton M, McNamara A, Maher MM et al (2000) The application of evidenced based medicine (EBM) to radiology: how valuable is computed tomography (CT) in the diagnosis of bowel obstruction? RSNA Conference Proceedings. Radiology 217(S)169
4. Megibow AJ (1994) Bowel obstruction. Evaluation with CT. Radiol Clin North Am 32:861–870
5. Tonouchi H, Ohmori Y, Kobayashi M, Kusunoki M (2004) Trocar site hernia. Arch Surg 139:1248–1256

Occlusion, Artery, Femoral

Dierk Vorwerk
Klinikum Ingolstadt GmbH
Institut für diagnostische und interventionelle Radiologie,
Ingolstadt, Germany
dierk.vorwerk@klinikum-ingolstadt.de

Synonyms

Femoral arterial obstruction; Femoral arterial occlusion; Infrainguinal arterial obstruction; Infrainguinal arterial occlusion; Popliteal arterial obstruction; Popliteal arterial occlusion

Definition

An arterial obstruction of the infrainguinal arteries is an occlusion or narrowing of an arterial segment between the groin and the lower limbs.

Pathology/Histopathology

Occlusions are complete obstructions of the infrainguinal arterial lumen and are due to thrombus formation, mainly on preexisting atherosclerotic plaque. In stenoses, the lumen is still patent but narrowed, with a diameter reduction of more than 50% causing symptoms. Alternatively, acute occlusions occur because of thrombotic emboli from the heart.

Clinical Presentation

Clinical indications for treatment include claudication, pain at rest, and nonhealing ulceration. The severity of the symptoms depends on the acuteness of the occlusion, the condition of collateral pathways, the lesion's location, and concomitant disease such as diabetes or renal insufficiency.

Imaging

Many imaging modalities allow the physician to diagnose infrainguinal artery obstruction. Color-coded duplex sonography as well as magnetic resonance angiography (MRA), computed tomography (CT), computed tomography angiography (CTA), and intra-arterial angiography are useful tools for detecting the location and extent of an iliac obstruction.

Nuclear Medicine

Nuclear medicine plays no particular role in the diagnosis of aortic stenosis.

Diagnosis

Diagnosis is reliably achieved by angiography or MRA. Detection by duplex sonography is a reliable tool for the femoropopliteal segment but is sometimes limited for detection and exact lesion description in the lower limbs. In stage IV (Fontaine) disease, MRA may be limited because of low arterial flow, movement artifacts, or artifacts due to superimposed venous flow.

Interventional Radiological Treatment

Endovascular Versus Surgical Treatment

Endovascular therapy is known to be of low invasiveness with good technical success, achieving fair overall patency. In data taken from eight publications reporting on 1,469 procedures, the weighted average technical success of femoropopliteal endovascular interventions was 90%, the complication rate was 4.3%, and the 3-year patency rate was 51%. Stents did not improve patency, showing a patency of 58% after 3 years (1).

Surgery offers acceptable results for distal reconstruction: An average 5-year patency of 80% for vein bypasses and 65–75% for expanded polytetrafluoroethylene (ePTFE) bypasses has been reported. The combined mortality and amputation risk was calculated to be about 2.2% for aortobifemoral reconstructions and 1.4% for femoropopliteal reconstructions (1).

Location of Lesion

Claudication is mainly related to lesions in the aortoiliac and femoropopliteal regions. It is unlikely to be due to infrapopliteal lesions, and there is general agreement that treatment below the knee should be strictly limited to patients with critical limb ischemia, that is, stages III and IV (Fontaine) or categories 4–6 (Rutherford).

Type of Lesion

The morphology of a treated lesion influences the technical outcome, follow-up results, and also the risk of treatment. Therefore, the TransAtlantic Inter-Society Consensus (TASC) document introduced a classification system that tries to categorize lesions with regard to their accessibility to either percutaneous treatment or surgery: type A lesions, which are ideal for a percutaneous approach; type B lesions, in which the percutaneous approach is still the preferred technique; type C lesions, in which a surgical approach should be preferred; and type D lesions, in which surgery is the option of choice. The TASC classification overrides older classifications because it takes into account all of the available and published techniques (including stent technology), which offer a much wider variation of treatment as well as effective tools to deal with acute complications of balloon angioplasty, such as occluding dissection and vascular rupture.

If we consider percutaneous therapy as the preferred method to treat those patients presenting with mild or moderate claudication, treatment might be offered to those presenting with type A and B lesions but should be discussed in depth with patients with type C lesions, as the risk and the potential benefit of treatment are related to the underlying morphology.

In the femoropopliteal field, type A lesions are single stenoses up to 3 cm in length not involving the very proximal superficial femoral and the distal popliteal artery. Type B lesions include stenoses 3–5 cm in length, heavily calcified stenoses, multiple lesions (each up to 3 cm), and lesions with no sufficient tibial run-off (the latter are unlikely to meet the criteria of mild or moderate claudication). Type C lesions are classified as stenoses or occlusions longer than 5 cm and multiple midsize lesions (3–5 cm). Total common femoral, superficial femoral, and popliteal occlusions are classified as type D lesions. There was some dissenting discussion on the definition of type B lesions: Interventional radiologists represented by the Cardiovascular and Interventional Radiological Society of Europe wished to express their assumption that even longer lesions of up to 10 cm may be justified as being classified type B instead of type C; they claimed that the reported results were mainly due to underdeveloped techniques and instruments that have substantially improved and that no data exists comparing the efficacy of percutaneous transluminal angioplasty (PTA) versus bypass surgery for lesions between 4 cm and 10 cm. (See Figs 1 and 2)

Other than in the iliac area, few femoral lesions meet the criteria for types A and B lesions, especially if limited to 5 cm in length. Thus, few patients with mild or moderate claudication due to femoropopliteal lesions will be ideal candidates for percutaneous treatment. Moreover—without limiting the importance of the TASC document, which certainly means a step forward in the joint approach to peripheral vascular disease—the morphological classification does not take into account some technical considerations that depend on the age and composition of a lesion. Particularly in femoral occlusions, the degree of organization of the occluding thrombus or the composition of the lesion with the original stenosis at the proximal and distal ends or in the middle are factors that are not very predictable but may influence the technical outcome of the intervention or its complication rate. (For instance, distal embolization might aggravate symptoms.) Other than in the iliac arteries, the liberal use of stents and stent grafts may help overcome a failed balloon angioplasty and resolve the technical outcome, but it does not achieve an improved long-term efficacy, and it may start a lifetime dependency on recurrent interventional or surgical procedures. These associated potential drawbacks have to be carefully balanced against the potential benefits and need to be discussed in depth with the patient before treatment is performed, especially in association with mild or moderate claudication.

These considerations restrict the use of endovascular treatment in femoropopliteal lesions to mainly stages IIb and IIa patients presenting with type A or less pronounced type B lesions.

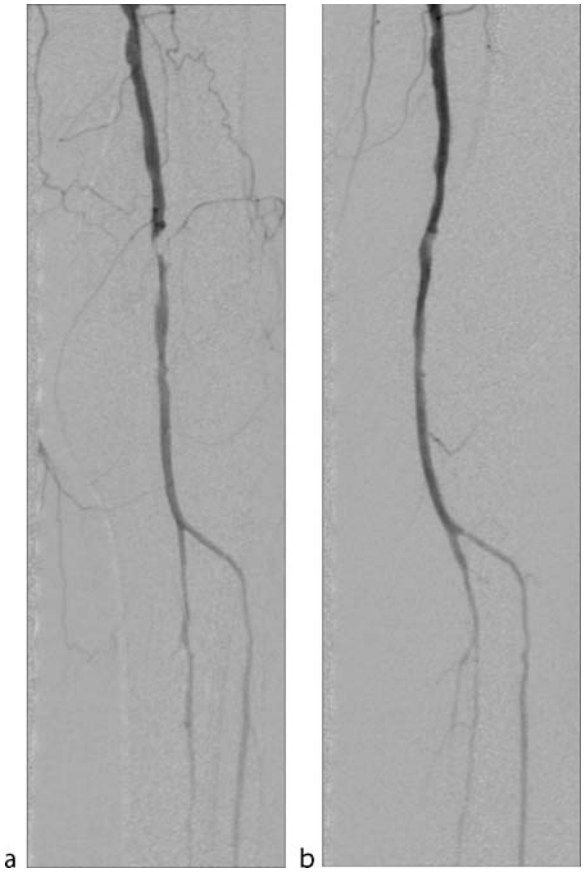

Occlusion, Artery, Femoral. Figure 1 Popliteal artery stenosis. (a) Short-segment stenosis at the level of the joint. The stenosis is eccentric, which sometimes indicates insuffient reaction to percutaneous transluminal angioplasty (PTA). Stenting in that region is problematic because it is in the flexure zone of the popliteal artery. If needed as a bail-out treatment, a very flexible stent is preferred. (b) After PTA, sufficient opening has been achieved, and no further treatment is necessary.

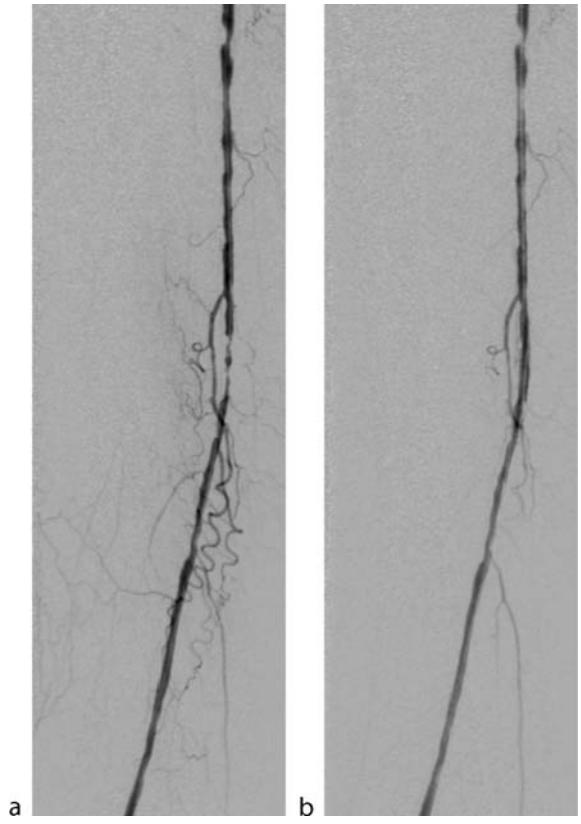

Occlusion, Artery, Femoral. Figure 2 Superficial femoral artery lesion. (a) Short stenosis of a small superficial femoral artery close to the adductor's canal in a patient with stage IV disease and diabetes. (b) After percutaneous transluminal angioplasty, the arterial lumen is wider, but a dissection remains. No stent was used due to good flow, absence of collateral filling, and small arterial lumen.

Assisting Forms of Treatment

It is widely accepted that well-conducted physical exercise should precede any type of interventional treatment and that cessation of smoking is mandatory. Nevertheless, it is also true that in many institutions it is very difficult to find an infrastructure that allows instruction of state-of-the-art physical exercise for claudicants. And as far as smoking is concerned, there is a major difference between wanting to stop and actually stopping.

Moreover, even with state-of-the-art exercise, young patients will not recover completely from claudications in all activities, including sports. The process will be long and will compromise their abilities in their professional lives. Therefore, it should perhaps be discussed whether young and active patients, especially, should be held to the axiom of "physical exercise first" or whether invasive treatment might be offered even as a first approach to this group of patients.

Treatment Options with Relation to Location and Lesion

Treatment of femoropopliteal lesions in claudicants has to be seen as more critical and less liberal compared with the iliac region. The main reasons are less favorable technical success, a higher complication rate, and poorer long-term success. There are many more lesions in the femoropopliteal arteries that do not meet the criteria for suitability for endovascular treatment. On the other hand, the versatility of endoluminal techniques opens treatment options in many particular lesions, and taking clinical symptoms as the only criteria to indicate or exclude treatment is not justified because—depending on the type of lesion—a simple and limited intervention can mean considerable improvement for the patient.

Additional Morphological Factors (not Included in the TASC Classfication)

Femoropopliteal occlusions may especially become a source of complications, particularly if they occurred recently. Simple PTA may result in downward embolization of occlusion material that may aggravate the symptoms or may turn the condition into a limb-threatening situation. Even in short occlusions, PTA may be insufficient to reopen the vessel, necessitating additional treatment such as stent placement (which does not result in better patency compared with balloon angioplasty alone). Reobstruction of stents, however, is more difficult to treat compared with simple restenosis. Eccentric calcified stenosis is frequently insufficiently treated. Because stenting is a technical but not necessarily a long-standing solution to such lesions, alternative techniques such as atherectomy may be considered if available. Unfortunately, these niche techniques are difficult to place in the market because of the costs involved, and some of the well-advanced devices such as the Simpson atherectomy catheter have been withdrawn from the market. (See Fig. 1)

Techniques

Balloon Angioplasty

Balloon angioplasty remains the working horse in femoropopliteal lesions. Modern angiographic units allow a built-in, fairly exact measurement of the true arterial diameter, and with the use of semicompliant balloons, adaptation to the diameter is well performed. We prefer not to grossly overdilate the artery in order to avoid dissection. Dilation times of 1–3 min are preferable by using pressure gauges. Balloon lengths of 2–4 cm are mainly used. In cases of major dissection, the first step should be an additional attempt to improve the result by prolonged balloon dilatation over 4–5 min; in many cases, the result will be improved by this cost-effective and simple approach (Fig. 1).

Stent Placement

The use of all kinds of stents should be limited to those cases in which balloon angioplasty in all its variations did not achieve a sufficient result. This is particularly true for occluding dissections. Other than in the iliac field, stents should not be used liberally.

The stented segment should be as short as possible. Balloon-expandable stents normally allow coverage of only short segments and might therefore be preferred for those lesions. In longer segments or in parts where bending of the artery is an issue, a self-expanding stent is advantageous if a stent cannot be avoided at all.

The overall results of femoral stenting are disappointing. New developments with drug-coated stents are on the way that allow elusion of drugs, such as rapamycin (Sirolimus) or taxol, from the stent surface. Especially for rapamycin, the first results from the coronary arteries are very promising, but no valid data yet exist on their use in the femorals. Radiation in stents, primarily at the time of insertion, did not show improved patency but was followed by an increased risk of thrombosis. Afterloading might therefore be a potential tool in the treatment of stent reobstruction.

Stent Grafts

Stent grafts still play a limited role in the femoropopliteal field. ePTFE-covered self-expanding stent grafts such as the Hemobahn device (Gore, Flagstaff, AZ, USA) yielded promising results in a multicenter trial even in the femoropopliteal field and stimulated the hope of offering a percutaneous alternative, especially for those patients presenting with long femoropopliteal occlusions. But there is also a risk of midterm or late rethrombosis.

Below the inguinal ligament, an ePTFE covering should be used exclusively because in animal experiments it has shown much less tendency to induce neointimal growth compared with Dacron covering. Other than in extraluminal bypasses, transcovering growth of tissue has been demonstrated, probably due to the long-segment wall contact between the stent graft and the original vascular lumen (2, 3).

A considerable disadvantage of stent grafts is that important collaterals frequently have to be covered by the full body of the stent graft. In the event of reocclusion, these collaterals will not be available anymore, which might cause aggravation of symptoms. This is particularly true for the popliteal artery, for which development of compensating collaterals is limited. Therefore, we favor limiting the use of stent grafts to the proximal two-thirds of the superficial femoral artery, especially in claudicants.

Results

Balloon Angioplasty

In femoropopliteal endovascular interventions (data taken from eight publications reporting on 1,469 procedures), the weighted average technical success was 90%, the complication rate was 4.3%, and the 3-year patency rate was 51% (1).

Long-term patency was positively influenced by a good outflow tract (two or three lower limb arteries), absence of diabetes, and absence of residual stenosis. The latter would

favor the use of stents, but unfortunately, there is no proof that stenting will improve overall patency.

Analyzing subgroups after femoral PTA, Huninck et al found different patencies for patients with stenotic and occlusive femoral lesions and good run-off (62% vs. 48% after 5 years) as well as those with poor run-off (stenoses: 62% vs. 43% after 5 years; occlusions: 43% vs. 27% after 5 years) (4).

Stents

Follow-up results from stent implantation into the femoropopliteal arteries have not yielded improved results compared with balloon angioplasty alone. In a meta-analysis, Muradin et al found a 3-year patency of 63–66% after 3 years for stents, compared with 61% for PTA of stenoses. They also found, however, that in patients with more severe disease and more severe lesions, the patients achieved a higher benefit from stenting compared with those with less severe disease (5). In a randomized trial, Cejna and colleagues found no significant difference between patients who received PTA alone and those who received stenting (6).

Endoluminal radiation therapy with afterloading or beta irradiation as well as drug-eluding stents may change the overall results in the future. To date, stenting in the femoral arteries should be used as a bail-out therapy in the case of PTA failure. Failure, however, needs to be defined strictly as severe dissection refractory to prolonged balloon dilatation, antegrade dissection with increasing obstruction, or severe residual obstruction. Minor irregularities of the wall are not enough to justify stenting because treatment of restenosis is more difficult compared with treatment after PTA alone. (See Figs 3 and 4).

Stent Grafts

Little data exist on the usefulness of stent grafts in the femoropopliteal arteries. In a multicenter trial using the Hemobahn endoprosthesis, Lammer and colleagues achieved a primary patency of 90% after 6 months and 79% after 12 months with 80 limbs treated. Secondary patency was 93% at 12 months after treatment (7).

These encouraging results are in contrast to many single-center experiences in which endografts showed a high rate of thrombosis that was frequently due to development of stenoses adjacent to the stent graft.

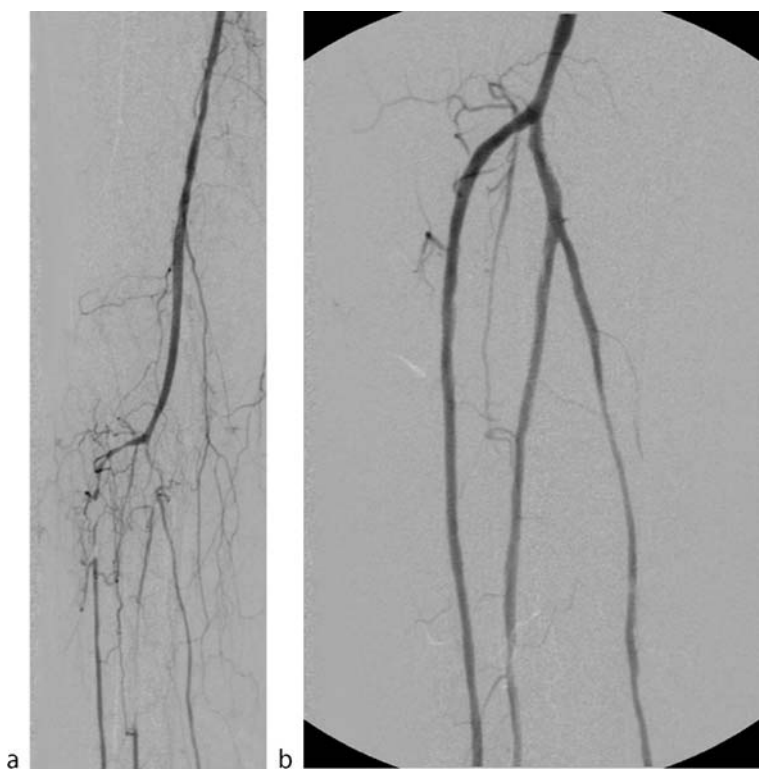

Occlusion, Artery, Femoral. Figure 3 Infrapopliteal occlusion. (a) Occlusion of all lower limb arteries in their proximal segments in a patient with stage IV disease. (b) After mechanical passage and percutaneous transluminal angioplasty, all three arteries have been sufficiently recanalized. No peripheral embolization has occurred.

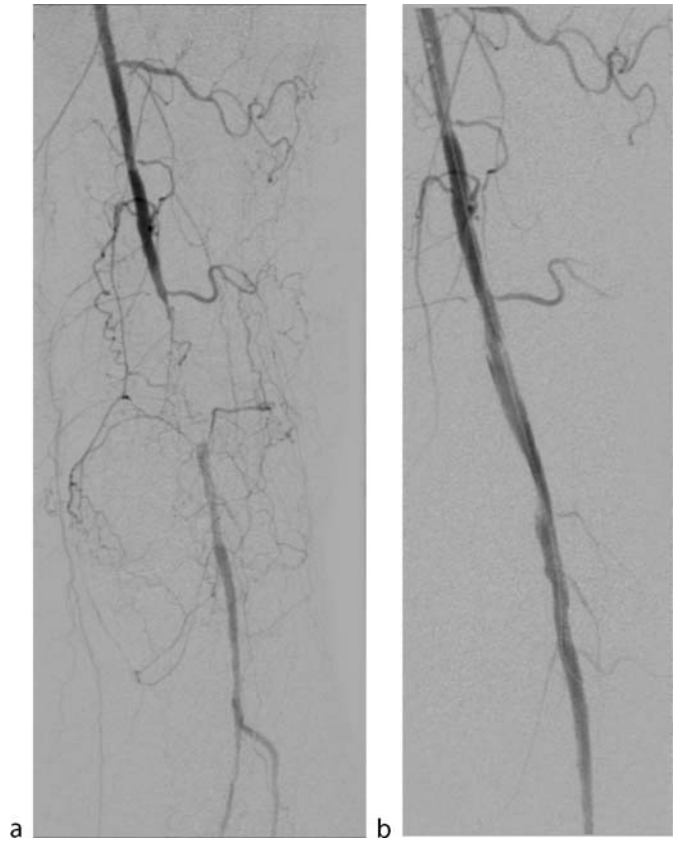

Occlusion, Artery, Femoral. Figure 4 (a) A 7-cm-long occlusion of the popliteal artery in a patient with stage IV disease. (b) After subintimal recanalization and percutaneous transluminal angioplasty, sufficient reopening with stent placement.

Complications

The nature and quality of complications in the femoropopliteal arteries do not differ principally from those in the aortoiliac area: dissection, perforation, and embolization of occluding material. With stents, the risk of early thrombosis was a problem in the very beginning but has since become rare with combined treatment that includes modern antiplatelet drugs.

In occlusions, the risk of embolization of the occluding material is the most potentially dramatic complication. Aspiration embolectomy in combination with selective thrombolysis is the treatment option of choice. Especially in claudicants, the risk therefore needs to be well balanced with the potential benefit.

Adjunctive Drug Regimen

In iliac and femoral PTA in claudicants, heparinization during the intervention and for 24 h after it—either by low-molecular-weight heparin or conventional heparin—is usually sufficient. A dose of 100 mg of aspirin daily is usually prescribed. After femoral stent placement or in patients with marked irregularities after PTA, heparinization may be prolonged up to 72 h, and an additional platelet inhibitor such as Clopidogrel is recommended for 4–6 weeks.

Bibliography

1. The TASC Working Group Management of peripheral arterial disease (PAD) (2000) Transatlantic Inter-Society Consensus (TASC). J Vasc Surg 31:S1–S296
2. Schurmann K, Vorwerk D, Uppenkamp R et al (1997) Iliac arteries: plain and heparin-coated Dacron-covered stent-grafts compared with noncovered metal stents—an experimental study. Radiology 203:55–63
3. Cejna M, Virmani R, Jones R et al (2001) Biocompatibility and performance of the Wallstent and several covered stents in a sheep iliac artery model. J Vasc Interv Radiol 12:351–358
4. Hunink M, Wong J, Donaldson M et al (1995) Revascularization for femoropopliteal disease. A decision and cost-effectiveness analysis. JAMA 274:165–171
5. Muradin G, Bosch J, Stijnen T et al (2001) Balloon dilation and stent implantation for treatment of femoropopliteal arterial disease: meta-analysis. Radiology 221:137–145

6. Cejna M, Schoder M, Lammer J (1999) [PTA vs. stent in femoropopliteal obstruction] Radiologe 39:144–150
7. Lammer J, Dake M, Bleyn J et al (2000) Peripheral arterial obstruction: prospective study of treatment with a transluminally placed self-expanding stent-graft. International Trial Study Group. Radiology 217:95–104

Occlusion, Artery, Iliac

Dierk Vorwerk
Klinikum Ingolstadt GmbH
Institut für diagnostische und interventionelle Radiologie,
Ingolstadt, Germany
dierk.vorwerk@klinikum-ingolstadt.de

Synonyms

Iliac artery occlusion; Iliac artery stenosis artery

Definition

An arterial obstruction of the iliac arteries is an occlusion or narrowing of an arterial segment between the aortic bifurcation and the groin, not including the common femoral artery (CFA).

Pathology/Histopathology

Occlusions are complete obstructions of the iliac arterial lumen due to thrombus formation, mainly onto a preexisting atherosclerotic plaque formation. In stenoses, the lumen is still patent but narrowed, with symptoms occurring with a diameter reduction of more than 50%.

Clinical Presentation

Unilateral claudication is the leading clinical symptom and has a predilection for the upper thigh. Depending on the collateral pathways, the walking distance may vary between a few meters and a few hundred meters. Severe ischemic syndromes are rare unless there is no additional involvement of the infrainguinal arteries.

Imaging

Many imaging modalities allow clinicians to diagnose iliac artery obstruction. Color-coded duplex sonography as well as magnetic resonance (MR) angiography, computed tomography (CT), CT angiography, and intra-arterial angiography are useful tools for detecting the location and extent of an iliac obstruction. Because of access limitations, angiography is preferably performed *via* transbrachial or contralateral access if the clinical findings suggest iliac artery obstruction.

Nuclear Medicine

Nuclear medicine plays no particular role in the diagnosis of aortic stenosis.

Diagnosis

Diagnosis is reliably achieved by angiography or MR angiography. Detection by duplex sonography is sometimes difficult due to unfavorable anatomic conditions.

Interventional Radiological Treatment

In the iliac segment, many lesions are amenable to percutaneous treatment with an acceptable outcome. Thus, a lesion's location and type must be taken into consideration before treatment is recommended. Whereas most lesions in the aortoiliac segment will be conducive to an endovascular approach, this is not generally true for femoropopliteal lesions. In addition, the risk of treatment is related to its location and has to be addressed before an endovascular approach is recommended.

Type of Lesion

The morphology of the treated lesion will influence the technical outcome, follow-up results, and also the risk of treatment. The Transatlantic Inter-Society Consensus (TASC) document therefore introduced a classification system that tries to categorize lesions with regard to their accessibility to either percutaneous treatment or surgery: Type A lesions, for which the percutaneous approach is ideal, type B lesions, for which the percutaneous approach is still the preferred technique; type C lesions, for which a surgical approach should be preferred; and type D lesions, for which surgery is the option of choice. The TASC classification overrules older classifications because it takes into account all available and published techniques, including stent technology, which offer a much wider variation of treatment and are also effective tools for dealing with acute complications of balloon angioplasty such as occluding dissection and vascular rupture.

If we consider percutaneous therapy as the preferred method to deal with patients presenting with mild or

moderate claudications, treatment might be offered to those presenting with type A and B lesions but should be discussed in depth with patients with type C lesions, since the risk and the potential benefit of treatment will be related to the underlying morphology.

For iliac lesions, single stenoses up to 3 cm in length both in the common iliac artery (CIA) and external iliac artery (EIA) are classified as type A lesions, while single stenoses of 3–10 cm (not involving the CFA), double stenoses not longer than 5 cm each, and unilateral occlusions of the CIA are classified as type B lesions (Fig. 1).

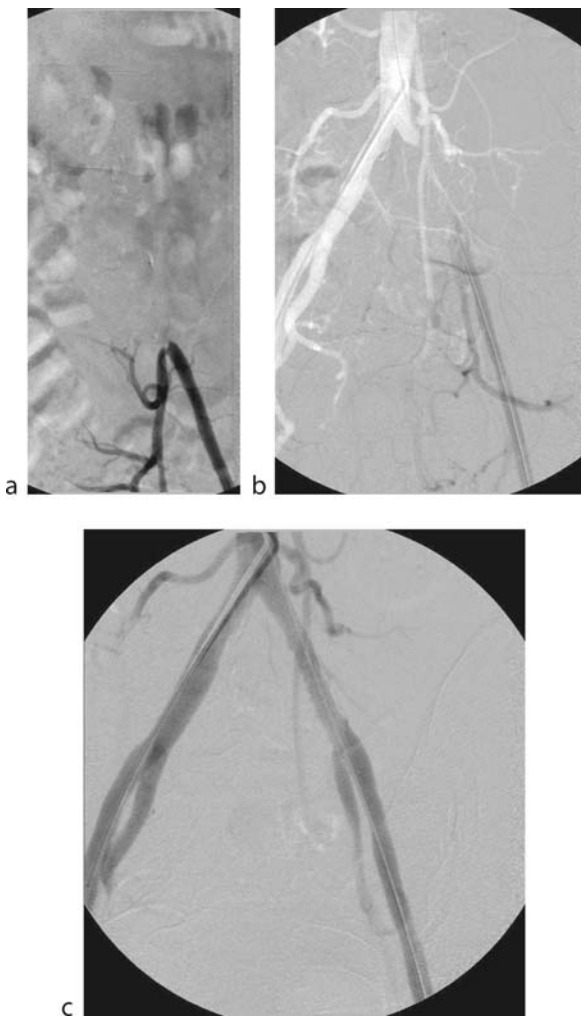

Occlusion, Artery, Iliac . Figure 1 Occlusion of the left common iliac artery. (a) Occlusion of the left common iliac artery imaged *via* a retrograde access. The internal iliac artery is open. (b) After passage of the occlusion, the complete occlusion is visible with a stump at the orifice. (c) After primary stenting followed by careful balloon dilation, patency is fully restored.

Type C lesions include bilateral long stenoses (5–10 cm in length), unilateral EIA occlusions not extending into the CFA, and unilateral EIA stenoses extending into the CFA. More advanced lesions are classified as type D.

Using this classification, many iliac lesions will fall into the A and B groups, opening a potentially growing field for endovascular procedures performed on mild to moderate claudicants. Even in some type C lesions, percutaneous treatment has no major technical concerns, complication risks, or compromised outcomes. This is particularly the case for EIA occlusions not extending into the CFA. However, published data are lacking to back up this experience.

Multilevel Disease

Even mild symptoms may be associated with multilevel disease (e.g., iliac stenosis and a well-collateralized femoropopliteal lesion). There is some chance that exclusive intervention in the iliac region may be sufficient to improve the clinical situation. If present, multilevel disease does not preclude treatment in these patients.

Assisting Forms of Treatment

It is widely accepted that well-conducted physical exercise should precede any type of interventional treatment and that cessation of smoking is mandatory. Nevertheless, it is also true that in many institutions it is very difficult to find an infrastructure that allows teaching of state-of-the-art physical exercise to claudicants, and as far as smoking is concerned, there is a major difference between willing and doing.

Moreover, even with state-of-the-art exercise, young patients will not recover completely from claudications in all their activities, including sports. The process will be longer and compromise their abilities in their professional lives. Therefore, it might be discussed whether young and active patients should be vigorously kept to the axiom of "physical exercise first" or whether invasive treatment might be offered to this group of patients even as a first approach.

Treatment Options with Relation to Location and Lesion

The aorta and the iliac arteries have been a primary field for percutaneous interventions for a long time. Easy access to the lesion, the relatively large diameter of the target vessels, and the comparably benign outcomes even with major complications contribute to the wide acceptance of percutaneous interventions in that area. Over the years, the indications have been extended and now include not only stenotic but also occlusive disease and treatment of

aneurysms. The introduction of vascular stents has especially been very helpful for overcoming major problems and offers a tool to treat major complications that otherwise remained a domain for surgical repair.

Iliac occlusive disease accounts for approximately one-third of occlusive arterial disease, while two-thirds is located subinguinally. However, iliac percutaneous transluminal angioplastry (PTA) plays a major role in interventional radiological routines because it is well-established in most institutions and by most surgeons, many lesions are amenable to percutaneous treatment, and technical as well as clinical results are satisfying.

Clinically, intermittent claudication starting in the upper thigh in combination with lower limb claudication is the leading symptom. Erectile dysfunction in men may also be present. In isolated iliac lesions, critical ischemia is rare if not combined with additional subinguinal disease. Rarely, blue-toe syndrome might be present if cholesterol embolization has occurred from an ulcerated plaque in the iliac axis.

Weakened femoral pulses and a reduced ankle-arm index are simple clinical signs that can indicate iliac obstruction and that can be verified by direct or poststenotic color-coded or duplex studies. For planning a percutaneous intervention, angiography is still the most helpful procedure.

Clinical indications for treatment depend on the severity of symptoms and how they limit the daily life of an individual patient.

Stent placement in stenotic lesions should be indicated from a technical point of view if angioplasty remains insufficient, as defined by visibly poor outflow or major pressure gradients. Because follow-up data are now available showing that iliac stent placement is safe, a liberal approach is justified, although primary stenting of stenoses does not seem to be generally recommended because of socioeconomic reasons and potential follow-up problems.

Furthermore, primary stenting is not beneficial over successful balloon dilation (8). Thus, primary stenting is recommended only if PTA fails or if technical requirements compromise the success of simple PTA, such as with iliac occlusions.

Iliac Artery Stenoses

Although balloon angioplasty has proved to be an effective procedure in treating iliac stenoses in particular, the indication for stent placement should be restricted to lesions that are not primarily amenable to PTA alone. An inadequate postangioplasty result has been suggested as a general indication for stent placement, although the term "inadequate" remains ill-defined. Residual pressure gradients are certainly a useful way to assess the angioplasty result, but it is still unclear what the borderline gradient ultimately requiring additional intervention is. Moreover, the decision should not be made without referring both to morphologic criteria and visibly reduced flow.

Long-segment stenoses with irregular surfaces, aneurysm formation, or markedly ulcerated plaques may be included in the group of complex lesions. Eccentric stenoses and ostial lesions with extension to the aortic bifurcation are known to not respond well to balloon angioplasty.

A stenotic lesion may respond well to balloon inflation but may collapse after the balloon is deflated.

Complications of balloon angioplasty can be treated well by stent placement. These include intramural hematoma and flow-obstructing dissections complicating PTA, which may be an acute indication for stent placement in order to maintain the vascular lumen, obviating emergency surgery.

Iliac restenosis after previous PTA does not require stent placement in general since there is no proof that stenting prevents restenosis under those circumstances. However, stenting may be considered from a technical point of view in cases in which the result of balloon angioplasty remains compromised.

An inadequate result after state-of-the-art balloon dilatation of the iliac stenoses is a prerequisite for secondary stent placement in stenotic lesions.

Iliac Artery Occlusions

Percutaneous treatment of iliac occlusions is technically feasible. In cases of acute thrombosis, thrombolysis as an alternative to surgical thrombectomy might precede PTA of an underlying lesion. Mechanical thrombectomy *via* percutaneous access is still in its infancy and cannot be recommended as a routine approach because potential risks such as downward or cross-over embolization are possible, and no data are yet available to determine the overall complications of such an approach.

In chronic occlusions with an occlusion time exceeding 3 months, balloon angioplasty alone, thrombolysis with subsequent balloon angioplasty, and elective stenting or mechanical passage of the occlusion followed by primary stent implantation have been described as alternative techniques.

Metallic stents—and self-expandable endoprostheses in particular—offer a new concept of percutaneous revascularization in chronic iliac occlusion, which we believe is a primary indication (9). Self-expandable stents are used to cover the occluding thrombotic material, thereby preventing peripheral dislodgement, a well-known complication of percutaneous recanalization of occlusions.

Indications for the use of metallic stents into arteries should always be technical. The type and morphology of

the lesion, the outcome of balloon angioplasty, and complicated situations are important considerations, although stenting has been tested and shown to be a safe procedure.

This is particularly true for treatment of restenosis. There is currently no proof that stent placement is more effective in preventing restenosis than balloon angioplasty with good technical success. Furthermore, there is no proof that in a restenosed vessel, the use of a stent would be beneficial to prevent recurrent stenosis.

Technical Considerations in the Iliac Arteries

Balloon Dilatation

Balloon dilatation of the iliac arteries is relatively simple to perform. A retrograde transfemoral approach provides the easiest access to that type of stenotic lesions. Crossover dilatation may be performed in special indications such as double-sided stenoses in the event that both lesions should be dilated in one session, or if an external iliac stenosis extends far down into the CFA. After the diseased segment is carefully traversed, a suitable balloon is placed across the lesion, and dilatation is performed either manually or by using a pressure-monitoring syringe. The size of the balloon can be depicted either by film measurements or in digital subtraction angiography images by use of graduated catheters that allow fairly exact measurement of vessel size.

There is wide agreement that both the hemodynamic relevance of a lesion as well as post-PTA success can be accurately monitored by measuring the pressure gradient across the lesion. However, there is some dispute about the level of the pressure. A mean pressure gradient of 10 mmHg and less after peripheral drug-induced vasodilation is accepted by most authors to indicate successful PTA even if the morphological result is not excellent. Some authors use a systolic gradient of 10 mmHg.

There is no uniform agreement on whether PTA of simple iliac lesions requires any additional anticoagulation afterward. We regularly keep our patients on full heparinization (500–1,000 IU/h) for 12–24 h and recommend lifetime aspirin therapy (100 mg/day).

Stent Implantation

If balloon angioplasty fails by morphologic and functional criteria, stent implantation can be considered in stenotic lesions. The technique depends on the type of stent used. There is no stent preference because most clinical series have shown similar results. The length and location of the lesion, the experience of the investigator, and the availability of appropriately sized stents are important details that may lead to the preference of one or another type.

Exact placement is mandatory to avoid major complications, especially if the stent has to placed close to the aortic bifurcation. While self-expanding Wallstents can be corrected during placement to a limited extent, balloon-expandable stents and self-expanding nitinol stents cannot undergo correction of their localization once inflation of the balloon has begun.

Chronic iliac artery occlusions are primarily indicated for stent placement. We avoid predilatation and place the stent directly into the occluded segment. After stenting, careful balloon dilatation is performed to avoid dislodgement of occluding material.

Atherectomy

Directional atherectomy does not play a major role in treating iliac arterial disease. This is because the ratio of introduction and working diameters in most atherectomy systems is relatively low, which requires a considerably large puncture to achieve atherectomy in larger iliac diameters of 8–12 mm. The Simpson atherectomy catheter—which is no longer available commercially—required an 11F sheath to sufficiently treat iliac lesions. Atherectomy plays a more important role in the recanalization of stent reobstruction in order to debulk stents from reobstructing neointimal tissue.

Stent Reobstruction

In cases of in-stent stenosis, directional atheterectomy or balloon dilation are both recommended. If PTA is used, a balloon size according to the outer diameter of the stent in place is recommended in order to compress the neointimal intima to a maximum, especially if occurring within a self-expanding stent that does not allow overexpansion. If a balloon-expandable stent has been used, slight overdilation of the stent is recommended to gain a larger diameter despite neointimal tissue. Some authors prefer atherectomy to debulk the stent. This is achievable in smaller stents such as in the femorals, but it may require very large instruments in iliac stents.

In stent occlusion, treatment is more difficult. In acute occlusions early after placement, technical problems are mainly responsible, and it is mandatory to overcome these problems to maintain long-term success. Recent thrombosis should be treated by thrombolysis followed by PTA and/or additional stent placement.

Late occlusion is mainly due to reobstruction by neointima within or adjacent to the stent. There is not much published experience about how to treat complete stent occlusion at a chronic stage. Thrombolysis, atherectomy, and mechanical aspiration followed by balloon

angioplasty are possible techniques. One of the simpler techniques is the stent-in-stent technique: After traversal of the occluded stent (which is usually easy to accomplish), a stent is placed within the occluded segment, bridging it at both ends. It is then carefully dilated with a tendency to underdilation of 1–2 mm. This is considered safe in order to avoid embolization of occlusion material.

Bibliography

1. The TASC Working Group (2000) Management of peripheral arterial disease (PAD). Transatlantic Inter-Society Consensus (TASC). J Vasc Surg 31:S1–S296
2. Vollmar J (1996) Rekonstruktive Chirurgie der Arterien. Thieme, Stuttgart, pp 207–214
3. Berger T, Sörensen R, Konrad J et al (1986) Aortic rupture. A complication of transluminal angioplasty. Am J Roentgenol 146:373–374
4. Strecker E, Hogan B, Liermann D et al (1993) Iliac and femoropopliteal vascular occlusive disease treated with flexible tantalum stents. Cardiovasc Intervent Radiol 16:158–164
5. Dietrich EB, Santiago O, Gustafson G et al (1993) Preliminary observation on the use of the Palmaz stent in the distal portion of the abdominal aorta. Am Heart J 125:490–500
6. Rholl K, Van Breda A (1994) Percutaneous intervention for aortoiliac disease. In: Strandness E, Van Breda A (eds) Vascular Diseases. Churchill Livingstone, New York, pp 433–466
7. Long A, Gaux J, Raynaud A et al (1994) Infrarenal aortic stents. Initial clinical experience and angiographic follow-up. Cardiovasc Intervent Radiol 16:203–208
8. Dietrich EB (1993) Endovascular techniques for abdominal aortic occlusions. Int Angiol 12:270–280
9. Becker G, Katzen B, Dake M (1994) Noncoronary angioplasty. Radiology; 170:921–940

Occlusion, Artery, Popliteal

Dierk Vorwerk
Klinikum Ingolstadt GmbH
Institut für diagnostische und interventionelle Radiologie,
Ingolstadt, Germany
dierk.vorwerk@klinikum-ingolstadt.de

Synonyms

Infrainguinal arterial obstruction

Definition

An arterial obstruction of the infrainguinal arteries is an occlusion or a narrowing of an arterial segment between the groin and the lower limbs.

Pathology/Histopathology

Occlusions are complete obstructions of the infrainguinal arterial lumen and are due to thrombus formation, mainly on preexisting atherosclerotic plaque. In stenoses, the lumen is still patent but narrowed, with a diameter reduction of more than 50% causing symptoms. Alternatively, acute occlusions occur because of thrombotic emboli from the heart.

Clinical Presentation

Clinical indications for treatment include claudication, pain at rest, and nonhealing ulceration. Severity of the symptoms depends on the acuteness of the occlusion, the condition of collateral pathways, the lesion's location, and concomitant disease such as diabetes or renal insufficiency.

Imaging

Many imaging modalities allow the physician to diagnose infrainguinal artery obstruction. Color-coded duplex sonography as well as magnetic resonance angiography (MRA), computed tomography, computed tomography angiography (CTA), and intraarterial angiography are useful tools to detect the location and extent of an iliac obstruction.

Nuclear Medicine

Nuclear medicine plays no particular role in the diagnosis of aortic stenosis.

Diagnosis

Diagnosis is reliably achieved by angiography or MRA. Detection by duplex sonography is a reliable tool for the femoropopliteal segment but is sometimes limited for detection and exact lesion description in the lower limbs. In stage IV (Fontaine) disease, MRA may be limited because of low arterial flow, movement artifacts, or artifacts due to superimposed venous flow.

Interventional Radiological Treatment

Endovascular versus Surgical Treatment

Endovascular therapy is known to be of low invasiveness with good technical success, achieving fair overall patency. In femoropopliteal endovascular interventions (data

taken from eight publications reporting on 1,469 procedures), the weighted average technical success was 90%, the complication rate was 4.3%, and the 3-year patency rate was 51%. Stents did not improve patency, showing a patency of 58% after 3 years (1).

Surgery offers acceptable results for distal reconstruction; an average 5-year patency of 80% for vein bypasses and 65–75% for expanded polytetrafluoroethylene (ePTFE) bypasses has been reported. The combined mortality and amputation risk was calculated to be about 2.2% for aortobifemoral reconstructions and 1.4% for femoropopliteal reconstructions (1).

Location of Lesion

Claudication is mainly related to lesions in the aortoiliac and femoropopliteal regions. It is unlikely to be due to infrapopliteal lesions, and there is general agreement that treatment below the knee should be strictly limited to patients with critical limb ischemia, i.e., stages III and IV (Fontaine) or categories 4–6 (Rutherford).

Type of Lesion

The morphology of a treated lesion influences the technical outcome, follow-up results, and also the risk of treatment. Therefore, the TransAtlantic Inter-Society Consensus (TASC) document introduced a classification system that tries to categorize lesions with regard to their accessability to either percutaneous treatment or surgery: type A lesions, which are ideal for a percutaneous approach; type B lesions, in which the percutaneous approach is still the preferred technique; type C lesions, in which a surgical approach should be preferred; and type D lesions, in which surgery is the option of choice. The TASC classification overrides older classifications because it takes into account all of the available and published techniques (including stent technology), which offer a much wider variation of treatment as well as effective tools to deal with acute complications of balloon angioplasty, such as occluding dissection and vascular rupture.

If we consider percutaneous therapy as the preferred method to treat those patients presenting with mild or moderate claudication, treatment might be offered to those presenting with type A and B lesions, but should be discussed in depth with patients with type C lesions, as the risk and the potential benefit of treatment are related to the underlying morphology.

In the femoropopliteal field, type A lesions are single stenoses up to 3 cm in length not involving the very proximal superficial femoral and the distal popliteal artery. Type B lesions include stenoses 3–5 cm in length, heavily calcified stenoses, multiple lesions (each up to 3 cm), and lesions with no sufficient tibial run-off (the latter are unlikely to meet the criteria of mild or moderate claudication). Type C lesions are classified as stenoses or occlusions longer than 5 cm and multiple midsize lesions (3–5 cm). Total common femoral, superficial femoral, and popliteal occlusions are classified as type D lesions. There was some dissenting discussion on the definition of type B lesions: Interventional radiologists represented by the Cardiovascular and Interventional Radiological Society of Europe wished to express their assumption that even longer lesions of up to 10 cm may be justified as being classified type B instead of type C; they claimed that the reported results were mainly due to underdeveloped techniques and instruments that have substantially improved and that no data exists comparing the efficacy of percutaneous transluminal angioplasty (PTA) versus bypass surgery for lesions between 4 and 10 cm.

Other than in the iliac area, few femoral lesions meet the criteria for types A and B lesions, especially if limited to 5 cm in length. Thus, few patients with mild or moderate claudication due to femoropopliteal lesions will be ideal candidates for percutaneous treatment. Moreover—without limiting the importance of the TASC document, which certainly means a step forward in the joint approach to peripheral vascular disease—the morphological classification does not take into account some technical considerations that depend on the age and composition of a lesion. Particularly in femoral occlusions, the degree of organization of the occluding thrombus or the composition of the lesion with the original stenosis at the proximal and distal ends or in the middle are factors that are not very predictable but may influence the technical outcome of the intervention or its complication rate (for instance, distal embolization might aggravate symptoms). Other than in the iliac arteries, the liberal use of stents and stent grafts may help overcome a failed balloon angioplasty and resolve the technical outcome, but it does not achieve an improved long-term efficacy, and it may start a lifetime dependency on recurrent interventional or surgical procedures. These associated potential drawbacks have to be carefully balanced against the potential benefits and need to be discussed in depth with the patient before treatment is performed, especially in association with mild or moderate claudication.

These considerations mainly restrict the use of endovascular treatment in femoropopliteal lesions to stages IIb and IIa patients presenting with type A or less-pronounced type B lesions.

Assisting Forms of Treatment

It is widely accepted that well-conducted physical exercise should precede any type of interventional treatment and that cessation of smoking is mandatory. Nevertheless, it is also true that in many institutions it is very difficult to

find an infrastructure that allows instruction of state-of-the-art physical exercise for claudicants. And as far as smoking is concerned, there is a major difference between wanting to stop and actually stopping.

Moreover, even with state-of-the-art exercise, young patients will not recover completely from claudications in all activities, including sports. The process will be long and will compromise their abilities in their professional lives. Therefore, it should perhaps be discussed whether young and active patients, especially, should be held to the axiom of "physical exercise first" or whether invasive treatment might be offered even as a first approach in this group of patients.

Treatment Options with Relation to Location and Lesion

Treatment of femoropopliteal lesions in claudicants has to be seen as more critical and less liberal compared with the iliac region. The main reasons are less favorable technical success, a higher complication rate, and poorer long-term success. There are many more lesions in the femoropopliteal arteries that do not meet the criteria for suitability for endovascular treatment. On the other hand, the versatility of endoluminal techniques opens treatment options in many particular lesions, and taking clinical symptoms as the only criteria to indicate or exclude treatment is not justified because depending on the type of lesion, a simple and limited intervention can mean considerable improvement for the patient.

Additional Morphological factors (not Included in the TASC Classfication)

Femoropopliteal occlusions may especially become a source of complications, particularly if they occurred recently. Simple PTA may result in downward embolization of occlusion material that may aggravate the symptoms or may turn the condition into a limb-threatening situation. Even in short occlusions, PTA may be insufficient to reopen the vessel, necessitating additional treatment such as stent placement (which does not result in better patency compared with balloon angioplasty alone). Reobstruction of stents, however, is more difficult to treat compared with simple restenosis. Eccentric calcified stenosis is frequently insufficiently treated. Because stenting is a technical but not necessarily a long-standing solution to such lesions, alternative techniques such as atherectomy may be considered if available. Unfortunately, these niche techniques are difficult to place in the market because of the costs involved, and some of the well-advanced devices such as the Simpson atherectomy catheter have been withdrawn from the market.

Techniques

Balloon Angioplasty

Balloon angioplasty remains the working horse in femoropopliteal lesions. Modern angiographic units allow a built-in, fairly exact measurement of the true arterial diameter and by use of semicompliant balloons, adaptation to the diameter is well performed. We prefer not to grossly overdilate the artery in order to avoid dissection. Dilation times of 1–3 min are preferable by using pressure gauges. Balloon lengths of 2–4 cm are mainly used. In cases of major dissection, the first step should be an additional attempt to improve the result by prolonged balloon dilatation over 4–5 min; in many cases, the result will be improved by this cost-effective and simple approach (Fig. 1).

Stent Placement

The use of all kinds of stents should be limited to those cases in which balloon angioplasty in all its variations did not achieve a sufficient result. This is particularly true for occluding dissections. Other than in the iliac field, stents should not be used liberally.

The stented segment should be as short as possible. Balloon-expandable stents normally allow coverage of only short segments and might therefore be preferred for those lesions. In longer segments or in parts where bending of the artery is an issue, a self-expanding stent is advantageous if a stent cannot be avoided at all.

The overall results of femoral stenting are disappointing. There are new developments with drug-coated stents on the way that allow elusion of drugs, such as rapamycin (Sirolimus) or taxol, from the stent surface. Especially for rapamycin, the first results from the coronary arteries are very promising, but no valid data yet exist on their use in the femorals. Radiation in stents, primarily at the time of insertion, did not show improved patency but was followed by an increased risk of thrombosis. Afterloading might therefore be a potential tool in the treatment of stent reobstruction.

Stent Grafts

Stent grafts still play a limited role in the femoropopliteal field. ePTFE-covered self-expanding stent grafts such as the Hemobahn device (Gore, Flagstaff, AZ, USA) yielded promising results in a multicenter trial even in the femoropopliteal field and stimulated the hope of offering a percutaneous alternative, especially for those patients presenting with long femoropopliteal occlusions. But there is also a risk of midterm or late rethrombosis.

Below the inguinal ligament, ePTFE covering should be used exclusively because in animal experiments it has

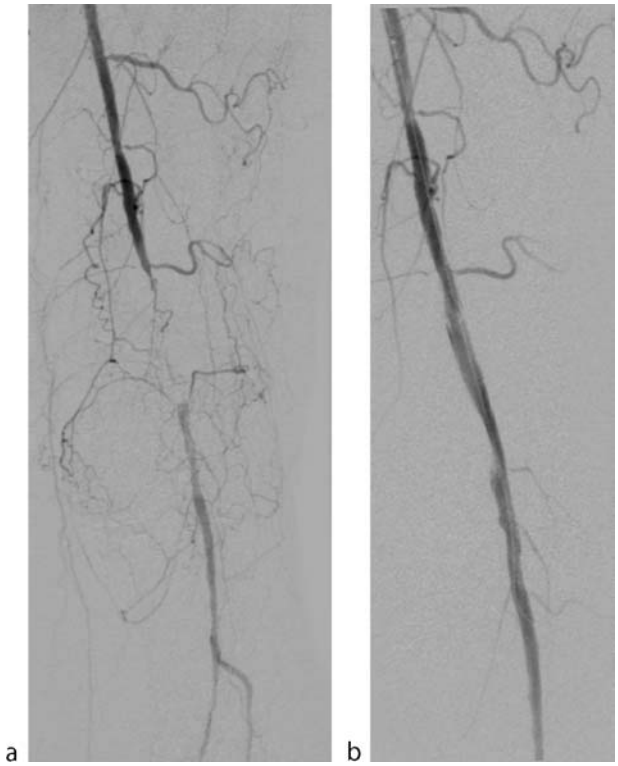

Occlusion, Artery, Popliteal. Figure 1 (a) A 7-cm-long occlusion of the popliteal artery in a patient with stage IV disease. (b) After subintimal recanalization and percutaneous transluminal angioplastyPTA, sufficient reopening with stent placement.

shown much less tendency to induce neointimal growth compared with Dacron covering. Other than in extraluminal bypasses, transcovering growth of tissue has been demonstrated, probably due to the long-segment wall contact between the stent graft and the original vascular lumen (2, 3).

A considerable disadvantage of stent grafts is that important collaterals frequently have to be covered by the full body of the stent graft. In the event of reocclusion, these collaterals will not be available anymore, which might cause aggravation of symptoms. This is particularly true for the popliteal artery, for which development of compensating collaterals is limited. Therefore, we favor limiting the use of stent grafts to the proximal two-thirds of the superficial femoral artery, especially in claudicants.

Results

Balloon Angioplasty

In femoropopliteal endovascular interventions (data taken from eight publications reporting on 1,469 procedures), the weighted average technical success was 90%, the complication rate was 4.3%, and the 3-year patency rate was 51% (1).

Long-term patency is positively influenced by a good outflow tract (two or three lower limb arteries), absence of diabetes, and absence of residual stenosis. The latter would favor the use of stents, but unfortunately, there is no proof that stenting will improve overall patency.

Analyzing subgroups after femoral PTA, Huninck et al. found different patencies for patients with stenotic and occlusive femoral lesions and good run-off (62% versus 48% after 5 years) as well as those with poor run-off (stenoses: 62% versus 43% after 5 years; occlusions: 43% versus 27% after 5 years) (4).

Stents

Follow-up results from stent implantation into the femoropopliteal arteries have not yielded improved results compared with balloon angioplasty alone. In a meta-analysis, Muradin et al. found a 3-year patency of 63–66% after 3 years for stents, compared with 61% for PTA of stenoses. They also found, however, that in patients with more severe disease and more severe lesions, the patients achieved a higher benefit from stenting compared with those with less severe disease (5). Cejna and colleagues found no significant difference between

patients who received PTA alone and those who received stenting in a randomized trial (6).

Endoluminal radiation therapy with afterloading or β irradiation as well as drug-eluding stents may change the overall results in the future. To date, stenting in the femoral arteries should be used as a bail-out therapy in the case of PTA failure. Failure, however, needs to be defined strictly as severe dissection refractory to prolonged balloon dilatation, antegrade dissection with increasing obstruction, or severe residual obstruction. Minor irregularities of the wall are not enough to justify stenting as treatment of restenosis is more difficult when compared with treatment after PTA alone.

Stent Grafts

Little data exist on the usefulness of stent grafts in the femoropopliteal arteries. In a multicenter trial using the Hemobahn endoprosthesis, Lammer and colleagues achieved a primary patency of 90% after 6 months and 79% after 12 months with 80 limbs treated. Secondary patency was 93% at 12 months after treatment (7).

These encouraging results are in contrast to many single-center experiences in which endografts showed a high rate of thrombosis that was frequently due to development of stenoses adjacent to the stent graft.

Complications

The nature and quality of complications in the femoropopliteal arteries do not differ principally from those in the aortoiliac area: dissection, perforation, and embolization of occluding material. With stents, the risk of early thrombosis was a problem in the very beginning but has since become rare with combined treatment that includes modern antiplatelet drugs.

In occlusions, the risk of embolization of the occluding material is the most potentially dramatic complication. Aspiration embolectomy in combination with selective thrombolysis is the treatment option of choice. Especially in claudicants, the risk therefore needs to be well balanced with the potential benefit.

Adjunctive Drug Regimen

In iliac and femoral PTA in claudicants, heparinization during the intervention and for 24 h after it—either by low-molecular-weight heparin or conventional heparin—is usually sufficient. A dose of 100 mg of aspirin daily is usually prescribed. After femoral stent placement or in patients with marked irregularities after PTA, heparinization may be prolonged up to 72 h, and an additional platelet inhibitor such as Clopidogrel is recommended for 4–6 weeks.

References

1. The TASC Working Group Management of peripheral arterial disease (PAD) (2000) Transatlantic Inter-Society Consensus (TASC). J Vasc Surg 31:S1–S296
2. Schurmann K, Vorwerk D, Uppenkamp R et al (1997) Iliac arteries: plain and heparin-coated Dacron-covered stent-grafts compared with noncovered metal stents – an experimental study. Radiology 203:55–63
3. Cejna M, Virmani R, Jones R et al (2001) Biocompatibility and performance of the Wallstent and several covered stents in a sheep iliac artery model. J Vasc Interv Radiol 12:351–358
4. Hunink M, Wong J, Donaldson M et al (1995) Revascularization for femoropopliteal disease. A decision and cost-effectiveness analysis. JAMA 274:165–171
5. Muradin G, Bosch J, Stijnen T et al (2001) Balloon dilation and stent implantation for treatment of femoropopliteal arterial disease: meta-analysis. Radiology 221:137–145
6. Cejna M, Schoder M, Lammer J (1999) [PTA vs. stent in femoropopliteal obstruction] Radiologe 39:144–150
7. Lammer J, Dake M, Bleyn J et al (2000) Peripheral arterial obstruction: prospective study of treatment with a transluminally placed self-expanding stent-graft. International Trial Study Group. Radiology 217:95–104

Occlusion, Bile Ducts

Thomas Helmberger[1], Carlo Bartolozzi[2], Paola Vagli[2], Chiara Franchini[2]
[1]Clinic of Radiology and Nuclear medicine, University Hospitals Schleswig-Holstein, Campus Luebeck
[2]Department of Diagnostic and Interventional Radiology, University of Pisa, Pisa, Italy
thomas.helmberger@uni-luebeck.de
bartolozzi@do.med.unipi.it

Synonyms

Bile duct obstruction; Cholestasis; Obstruction of the biliary tree

Definition

Any condition in which there is a complete obstacle to the biliary flow.

Pathology and Histopathology

Cholestasis may be related to mechanical, cellular, and metabolic causes.

Mechanical biliary obstruction may be due to intrinsic or extrinsic obstruction of bile flow, which can occur either at the intrahepatic or extrahepatic level (Table 1).

Occlusion, Bile Ducts. Table 1 Mechanical biliary obstruction

Intrahepatic	Intrinsic	Congenital cause • Biliary atresia • Alagille syndrome • Intrahepatic calculi complicating Caroli disease • Cystic fibrosis
		Benign cause • Intrahepatic stones • Sclerosing cholangitis • Biliary parasitosis
		Malignant cause • Cholangiocarcinoma
	extrinsic	Benign and malignant tumors
Extrahepatic	Intrinsic	Congenital anomalies • Choledochal atresia • Choledochal cysts
		Benign conditions • Gallstones • Parasitosis • Cholangitis • Inflammatory strictures • Postinterventional strictures • Vater's papillary stenosis • ▶AIDS-related cholangiopathy • ▶Biliary tuberculosis • ▶Sump syndrome
		Malignant tumors • Cholangiocarcinoma • Vater's papillary carcinoma
	extrinsic	Benign causes • ▶Mirizzi syndrome • Enlarged lymph nodes • Pancreatitis • Local benign tumors and cysts
		Malignant conditions • Gallbladder carcinoma • Malignant lymphadenomegalies • Pancreatic head carcinoma • Stomach and colon cancer

Overall, gallstones are the most common cause of biliary obstruction.

Intrahepatic intrinsic biliary obstruction can be due to: congenital affections (biliary atresia, Alagille syndrome, intrahepatic calculi complicating Caroli disease and cystic fibrosis), benign conditions (intrahepatic ductal stones, sclerosing cholangitis, and biliary parasitosis), and malignant conditions, with cholangiocarcinoma as the most important malignant cause. Extrinsic causes of intrahepatic obstruction include compression by benign and malignant tumors. Extrahepatic intrinsic biliary obstruction can be due to: congenital anomalies (choledochal atresia, choledochal cysts), benign conditions (gallstones representing the first cause, parasitosis, cholangitis, inflammatory and postinterventional strictures, Vater's papillary stenosis, AIDS-related cholangiopathy, biliary tuberculosis, sump syndrome), and malignant tumors (cholangiocarcinoma, and Vater's papillary carcinoma). Extrinsic compression of extrahepatic biliary tract includes benign conditions (Mirizzi syndrome, enlarged lymph nodes, pancreatitis, local benign tumors, and cysts), and malignant conditions (gallbladder carcinoma, malignant lymphadenomegalies, pancreatic head carcinoma, stomach and colon cancers) (1).

Clinical Aspects

Symptoms are determined by abnormal elevation of primary and secondary bile products in blood and the absence of the extrinsic intestinal bile function. Additionally, cholangitis may represent a concomitant complication in biliary obstruction. Common symptoms are jaundice, pale coloured stools, dark urine, itching, fever, and right upper quadrant pain. Blood tests show increase of bilirubin, alkaline phosphatase, and hepatic enzymes.

Imaging

Plain radiographs are of limited value to detect abnormalities in the biliary system. Frequently, calculi are not visualized because of their low radiopacity.

Biliary obstruction results in dilatation of bile ducts involving the biliary tree proximally to the obstruction; depending on the site of obstruction, the bile ducts dilatation may involve an isolated lobe or segment or both lobes. Especially in biliary stone disease, mostly both lobes present ductal dilatation. Nevertheless, the absence of bile ducts dilatation does not exclude recent or intermittent obstruction.

Ultrasound (US) is the method of first choice to establish the presence and extent of bile duct dilatation (Fig. 1). While peripheral ductal branches can be visualized only if dilated, the normal common bile duct is easily displayed (2). In general, US is able to establish the level of obstruction and reveal the cause of obstruction, as intrahepatic calculi, gallbladder stones, lymphadenopathy, hepatic and pancreatic masses. The demonstration of common bile duct calculi is strongly dependent on their location within the biliary system; in fact, calculi in the lower part of the common bile duct may be obscured by duodenal gas.

Computed tomography (CT) is more accurate than US in determining the specific cause and level of obstruction, but it is of limited value in detecting radiolucent bile duct stones. On the other hand, US can

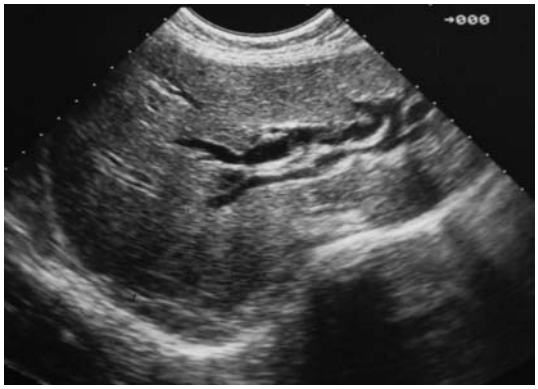

Occlusion, Bile Ducts. Figure 1 Biliary dilatation. Ultrasound can easily demonstrate dilatation of both intrahepatic and extrahepatic bile ducts in mechanical biliary obstruction.

be significantly limited in the differentiation of cholangiocarcinoma from sludge accumulation since both appear hypoechoic. In these cases, the different enhancement behaviour (absence of contrast enhancement in case of sludge) allows differential diagnosis on CT.

With the advent of easy applicable magnetic resonance (MR) techniques displaying fluid-filled structures (i.e., heavily T2-weighted, snap-shot techniques, "MR-hydrography"), MR cholangiopancreatography (MRCP) is the reference standard for noninvasive imaging of the biliary tree.

In comparison to invasive endoscopic retrograde cholangiopancreatography (ERCP), MRCP provides noninvasive detailed evaluation of the biliary tree. Since MRCP is generally combined with complementary cross-sectional MR a comprehensive evaluation of in- and extrinsic factors that might affect the biliary tree is possible. With high-resolution techniques in- and extrinsic bile duct, obstructions and dilatations can be visualized by MRCP with a superior high sensitivity and specificity. Since the MR visualization of ducts is strongly correlated to the presence of fluid (bile) within the lumen, severe strictures, sludge, small stones or postoperative scars and clips may appear as short segments of signal void. In general, this condition can be clarified by additional unenhanced and contrast-enhanced T1- and T2-weighted axial (and/or multiplanar) sequences. In characterizing the features of the biliary tree, the same characteristics already known from cholangiography may be applied to MRCP. In general, stone-related obstruction can be displayed easily with the concave transition from fluid-filled ductal lumen to the stone and the usually smooth, regular outlining of the lumen. An irregular tapering of the lumen can often be seen in malignant obstructions due to an extrinsic or infiltrating mass that can be uncovered by cross-sectional imaging. Typical examples for that are tumors of the pancreatic head affecting the common bile duct alone or together with the pancreatic duct (so called "double duct sign," in about 5% of cases of pancreatic cancer). In case of such malignancies, MR can provide a comprehensive evaluation in terms of staging for intrahepatic metastases, lymph node metastasis, peritoneal tumour spread, and vascular encasement. However, comparing MR and multidetector CT there is no significant difference in staging of biliary and pancreatic malignancies regarding recent literature.

Due to the noninvasive, high diagnostic accuracy of MRCP, in most centres percutaneous (PTC) and endoscopic procedures (ERCP) are performed in selected cases for diagnostic purpose (e.g., tissue sampling by brush) and interventional procedures (e.g., balloon dilatation, stone extraction, stent placement) avoiding pure diagnostic interventions which may cause procedure related complications in up to 5% (e.g., acute pancreatitis) (1).

In patients with external biliary drainage (i.e., Kehr, Bracci), trans-catheter cholangiography is performed to evaluate the placement of the catheter, the patency of the common bile duct and the transpapillar drainage.

Nuclear Medicine

In patients with biliary obstruction, cholescintigraphy with ^{99m}Tc IDA (iminodiacetic acid) or analogs demonstrates a "congestion" of the radiotracer mostly associated with a normal hepatic distribution/activity in absence of delayed (>1 h after tracer injection) biliary activity.

Interventional Radiology

Radiologic interventional procedures in biliary obstruction may be performed using either a percutaneous or an endoscopic approach or a combination of both (i.e., "rendevouz procedures"). Possible interventions are catheter placement, biliary stenting, balloon dilatation of biliary strictures, stone removal, and tissue sampling.

Stone removal is the most common biliary intervention and generally performed by endoscopy. Usually a papillotomy is necessary, followed by stone extraction by balloon or basket instruments guided by the endoscope. Larger stones (>2 cm in diameter) are less prone to endoscopical removal and present a higher risk of perforation, bleeding, secondary pancreatitis, and cholangitis (3, 4). In the era of advanced endoscopic techniques, the use of percutaneous transhepatic radiological interventions is restricted to the treatment of intrahepatic stones and cholangitis where an internal–external drainage may be needed to relieve the biliary system. Sequentially, a stone can be removed or an

obstruction can be treated. In cases of unsuccessful or impractical endoscopic maneuvers, stone removal, or stone fragmentation and stent placement are also percutaneously possible.

Balloon dilatation can be necessary both in patients with benign and malignant biliary strictures. Stenoses are safely and minimally invasively treated by balloon dilatation. Among the benign strictures biliary-enteric anastomotic strictures respond best to dilatation whereas a temporarily support by a drainage tube may enhance the result (5). In case of recoiling, redilatation may be necessary. Malignant strictures, due to the high radial force compressing the ductal system or the intruding mass within the duct, often require the combination of balloon dilatation, temporarily drainage and stent placement.

Stenting of the biliary tract is performed both in benign and malignant stenoses. There are three types of stents, which are used in biliary intervention: plastic endoprostheses (polyethylene stents), balloon-expandable metallic stents, and self-expandable metallic stents with and without covering. They can be placed either percutaneously or endoscopically. Metallic stents become strongly adherent to the bile duct and are impossible to remove. In the setting of malignancy, stents are mainly indicated for the palliation of patients with unresectable tumors. In such cases, metallic stents are preferred because they remain patent much longer than polyethylene stents and usually a single session of metal stenting maintain ductal patency for the reminding lifetime of the patients (6). Occlusion of metallic stents usually is determined by tumoral in-growth and can create the need for further interventions.

For treatment of benign biliary strictures, plastic endoprostheses are preferred, since they are needed in most cases only for limited time. Nevertheless, in chronic recurrent biliary stenoses where a long-term treatment is needed, they may be occluded by biliary encrustations, while in metallic stents reactive epithelial hyperplasia may occur.

Diagnosis

The diagnosis of biliary obstruction is suggested by the presence of jaundice, hypocholic stools, dark urine, itching, increase of serum levels of bilirubin, with prevalence of conjugated bilirubin, and alkaline phosphatase.

Imaging has the role to confirm biliary obstruction and to establish the level and the cause of obstruction. US is performed in the initial evaluation to demonstrate bile duct dilatation, the level of obstruction and sometimes the cause of obstruction, such as stones, hepatic masses, pancreatic masses, lymphadenopathies. The main limitations of US are the inconsistent visualization of the distal tract of the choledochal duct and the retroperitoneum. CT provides a more comprehensive examination that permits evaluation of the liver, biliary tree, pancreas, portal and retroperitoneal lymph nodes, and vascular structures, but it has a limited value in case of radiolucent stones of common bile duct. MRCP offers a noninvasive accurate assessment of the biliary tract. Associated cross-sectional images adequately demonstrate extra-ductal findings (1). Invasive techniques include ERCP and PTC. Currently they should be performed only to guide interventional procedures and cannot be recommended as diagnostic imaging techniques (2).

Bibliography

1. Soto JA, Alvarez O, Lopera JE et al (2000) Biliary obstruction: findings at MR cholangiography and cross-sectional MR imaging. Radiographics 20:353–366
2. Stabile Ianora AA, Memeo M, Scardapane A et al (2003) Oral contrast-enhanced three-dimensional helical-CT cholangiography: clinical applications. Eur Radiol 13:867–873
3. Vakil N, Everbach EC, and Knyrim K (1993) Pathogenesis and treatment of gallstones. N Engl J Med 24, 328(25)1855
4. Portincasa P, Moschetta A, and Palasciano G (2007) Cholesterol gallstone disease. Lancet 15, 368(9531):230–239
5. Vos PM, van Beek EJ, Smits NJ et al (2000) Percutaneous balloon dilatation for benign hepaticojejunostomy strictures. Abdom Imaging 25(2):134–138
6. Vitale GC, Larson GM, George M et al (1996) Management of malignant biliary stricture with self-expanding metallic stent. Surg Endosc 10(10):970–973

Occlusion, Bowel in Childhood

Melanie Hiorns
Radiology Department
Great Ormond Street Hospital for Children
London, UK
HiornM@gosh.nhs.uk

Synonyms

Small bowel obstruction (SBO); Large bowel obstruction

Definition

The lumen of the small or large bowel is occluded. This may be due to extrinsic compression of the bowel, an intrinsic abnormality of the wall or lumen of the bowel, or due to a filling defect in the lumen of the bowel. It may be congenital or acquired. Complete occlusion of the bowel is described as 'obstruction'.

Pathology/Histopathology

Any of the pathologies listed in the tables may give rise to bowel obstruction and if the diagnosis is delayed this may go on to cause bowel ischaemia with necrosis and possible perforation.

Clinical Presentation

The infant or child will usually present with abdominal distension, irritability, pain and vomiting, or high nasogastric aspirates if a tube is in place. The timing of the clinical presentation may be partly determined by the underlying causes: congenital causes will usually present in the first few hours or days of birth and 95% of small bowel obstruction in the perinatal period is due to an atresia of some type. Meconium ileus will present within the first 48h of life and occurs almost exclusively in patients with cystic fibrosis. Fifteen to twenty per cent of cystic fibrosis patients present in this way (2). Small left colon syndrome (also termed meconium plug syndrome and functional immaturity of the colon) presents with failure to pass meconium and an increasingly dilated abdomen. Intussusception is the most common cause of obstruction in infants of 3 to 6 months. Strictures secondary to NEC most commonly occur within 1 to 6 months of the initial episode and are usually in the terminal ileum and the colon. Post-operative adhesions may occur at any time but most frequently in the first 6 months following surgery and in approximately 2% of patients who have had a laparotomy, accounting for 7% of small bowel obstruction overall.

Congenital causes of bowel occlusion	Acquired causes of bowel occlusion
Stenosis (jejunal, ileal, colonic)	Intussusception
Atresias (jejunal, ileal, colonic)	Malrotation with midgut volvulus
▶Meconium ileus (1)	Postoperative adhesions
▶Small left colon syndrome	Ileus
Annular pancreas	Caecal volvulus
Duplication cysts	Necrotising enterocolitis with secondary strictures
Hirschsprung's disease	Incarcerated hernias (inguinal, umbilical, omental

(*continued*)

Acute complete bowel occlusion	Chronic partial bowel occlusion
Intussusception	Hirschsprung's disease
Incarcerated hernias	Caecal volvulus
Malrotation with midgut volvulus	Inflammatory bowel disease including Crohn's disease
Post-operative adhesions	Post-operative adhesions
Annular pancreas	
Meconium ileus	
Necrotising enterocolitis strictures	

(*continued*)

Imaging

The initial investigation is usually an abdominal radiograph, but this may be supplemented by an upper GI series in the case of a suspected high obstruction or by a contrast enema for a suspected low obstruction. Ultrasound has been used in some centres to examine the large bowel following the introduction of saline per rectum.

The abdominal radiograph will show dilated gas and fluid-filled loops of bowel (Fig. 1). In the neonate and infant it may not be possible to differentiate small and large bowel obstruction and hence the level of obstruction is described as high or low in the GI tract depending on the pattern of distended loops. If only a few high central loops are seen this is termed a 'high' obstruction and the level of obstruction is most likely to be in the small bowel. If distended loops are seen throughout the abdomen it is likely to be a 'low' obstruction with the level of obstruction being in the most distal ileum or in the colon. Further investigation of a high obstruction is by an upper GI series and of a low obstruction by a contrast enema. Water-soluble contrast should be used in both cases due to the increased risk of perforation and the high probability of the patient subsequently undergoing surgery to resolve the obstruction. On a contrast enema a long filling defect of meconium in the left side of the colon is indicative of small left colon syndrome and the colon proximal to this will be dilated (Fig. 2). The neonate will usually clear the meconium plug spontaneously after the contrast enema. However, meconium ileus will demonstrate a micro-colon on contrast enema (Fig. 3). The colon will be thin and long, having not been used and dilated loops of bowel will be confined to the small bowel loops above the level of obstruction by meconium in the distal ileum.

Meconium ileus is the only cause of obstruction that may be treated in the fluoroscopy room. A standard contrast enema is performed first to establish the diagnosis. Having established the diagnosis, ensuring that

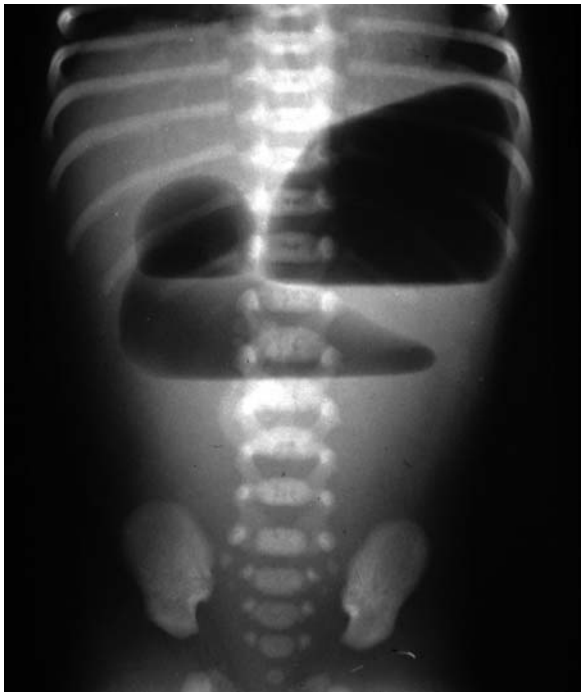

Occlusion, Bowel in Childhood. Figure 1 Abdominal X-ray showing typical appearances of a high (upper GI) obstruction. The stomach and two loops of bowel are shown to be dilated and gas filled. Bowel gas is absent below this level indicating complete obstruction. Fluid levels are present as this film was taken erect. The patient was confirmed to have jejunal atresia.

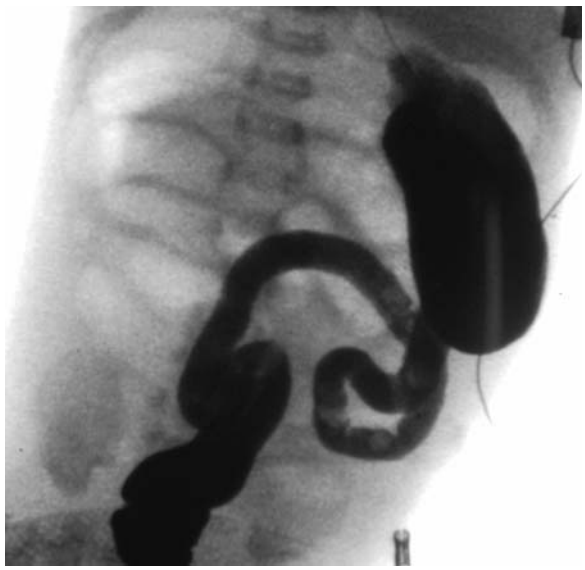

Occlusion, Bowel in Childhood. Figure 2 Contrast enema showing in 'small left colon syndrome' with dilated colon seen proximally and meconium plugs seen in the descending colon.

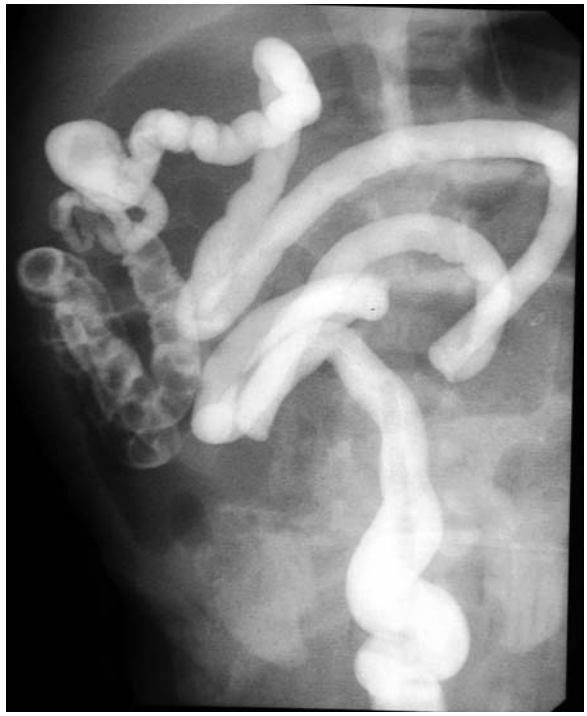

Occlusion, Bowel in Childhood. Figure 3 Contrast enema showing a micro-colon and meconium causing obstruction in the distal ileum in a neonate with meconium ileus.

standard non-ionic water soluble contrast has reached beyond the obstructing meconium to the dilated bowel loops may be enough to precipitate clearing of the meconium. However, some centres value the use of a gastrografin® enema: if the infant is stable and appropriately fluid resuscitated, a ►gastrografin enema can be performed using diluted gastrografin (for details see also entry 'meconium ileus'). The gastrografin should be instilled until it is observed to have reached and be filling dilated loops of bowel, therefore being above the level of the obstructing meconium. Gastrografin is hyperosmolar and is believed to draw water into the gut thereby loosening the sticky meconium, allowing it to be passed, and relieving the obstruction.

Nuclear Medicine

Has no role to play in this condition.

Diagnosis

The diagnosis of obstruction is made by a combination of the clinical findings and the imaging as earlier. The underlying cause is usually confirmed at surgery.

Interventional Radiological Treatment

Only for meconium ileus as described above (also see entry 'meconium ileus'); note that sonographically guided saline reduction of meconium ileus is performed in some centres at the bedside of babies too ill to be transported to the fluoroscopy suite (3); some also recommend the use of a C-arm for fluoroscopic guidance on such occasions.

Bibliography

1. Berrocal T, Lamas M, Gutieerrez J et al (1999) Congenital anomalies of the small intestine, colon, and rectum. Radiographics 19(5): 1219–1236
2. Agrons GA, Corse WR, Markowitz RI et al (1996) Gastrointestinal manifestations of cystic fibrosis: radiologic–pathologic correlation. Radiographics. 16(4):871–893
3. Riccabona M, Haim M, Kutschera J (2006) Sonografically guided reduction of meconium ileus in preterm neonates. Eur Radiol 16(1):284

Occlusion, Venous Central, Benign

Patrick Haage
Department of Diagnostic and Interventional Radiology, University Hospital Witten/Herdecke, Wuppertal, Germany
patrick.haage@helios-kliniken.de

Synonyms

Benign central venous obstruction; Benign central venous thrombosis

Definition

Acute or chronic thrombotic uni- or bilateral occlusion of one or more central veins.

Pathology/Histopathology

Central venous occlusion can broadly be divided into two eliciting categories: benign and malignant. Regardless of the underlying malady, early detection and treatment of complications is essential to provide adequate care for patients suffering from central venous obstruction. The most common cause for benign central venous obstruction is hemodialysis related; other benign reasons are rather uncommon, but are picking up due to the increased use of permanent central venous access catheters and implantable cardiac rhythm management devices.

Clinical Presentation

Clinically these patients present with arm swelling and occasionally obvious widespread subcutaneous collateral vessels around the shoulder and thoracic aperture. Additional swelling of the face, neck, and breast may develop.

Imaging

Consequently, the diagnostic and therapeutic regimen of hemodialysis related central venous obstruction will be the centre of attention and discussed herein.

In the hemodialysis patient, chronic swelling of the access arm is the most indicative clinical symptom of central venous obstruction. Striking superficial collaterals veins may be observed accompanied by pain and paresthesia. In such an obvious case of impeded central venous flow, digital subtraction angiography of the fistula or graft and the complete venous outflow tract must be executed, since the central veins cannot be confidently examined with ultrasonography. Direct antegrade puncture of the access is suggested (1).

Diagnosis

Since clinical diagnosis is often unreliable, imaging techniques need to be incorporated in the diagnostic process.

Interventional Radiological Treatment

Interventional treatment of central venous lesions is indicated when they are impairing hemodialysis or arm swelling is painful and limiting. Reported primary patency rates in patients treated with PTA alone were 10% or less at one year with frequent restenoses (2). Primary stent implantation has clearly been shown to improve primary one-year patency rates to 56% and more, similar to those reported from surgical intervention (1, 3). Yet, due to the invasiveness of surgery for central venous obstructions, the less invasive percutaneous interventional therapy can be considered primary choice for treatment (1). Regular follow-up and reinterventions are however required to maintain patency and achieve long-term clinical success (4). Reports show that

symptomatic central venous obstruction in dialysis patients can be treated with a high success rate through radiological intervention (5, 6).

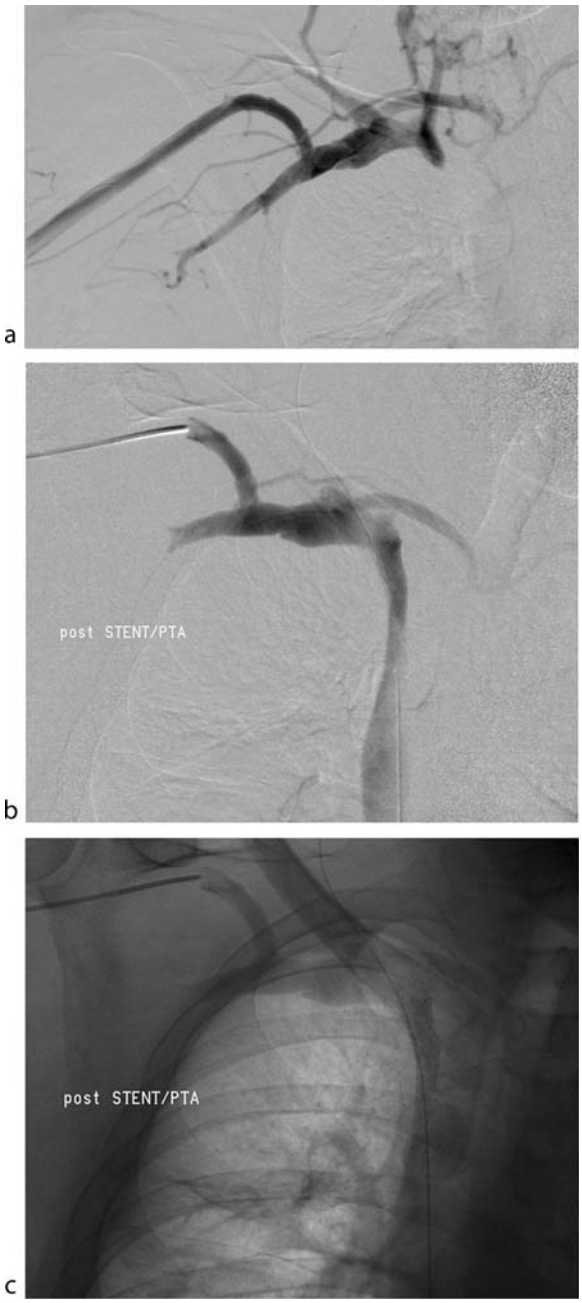

Occlusion, Venous Central, Benign. Figure 1 (a) Digital subtraction angiogram demonstrates complete occlusion of the right brachiocephalic vein draining a Brescia–Cimino fistula; (b) & (c) after unsuccessful transbrachial negotiation of the occlusion, angiogram shows restoration of flow and vanishing of collateral veins after placement of a self-expanding stent and subsequent PTA *via* a transfemoral approach.

Regarding the placement technique, stent placement should evade overlapping the ostium of a patent internal jugular vein to achieve a secure and satisfactory result, since this latter vein is important for future placement of central venous catheters. Correspondingly, a stent placed in the innominate vein if possible should not overlap the ostium of the contralateral vein; otherwise contralateral stenosis may come about and prohibit later use of the contralateral arm for access creation (1). A suitable endoprosthesis for central veins should be flexible enough to be used in curved and tortuous vessels. To avoid stent dislocation and proximal embolization, a self-expanding stent is necessary, in view of the fact that venous occlusions may undergo progressive luminal enlargement after stent placement (Fig. 1). Mechanical thrombectomy should not be regularly used as a primary therapy for dialysis-related central venous occlusions, because of the sharp angles and slim vessel walls observed in this vascular region. Furthermore, modest data are available on the application of thrombolytic agents in hemodialysis-related ▶benign central venous thrombosis. It can therefore not be recommended as a primary treatment regimen.

In any case reocclusion is a frequently observed complication and is more likely to occur after thrombosis has occurred for the first time (7). The radiologist should be prepared for repeat interventions.

To summarize, treatment of the hemodialysis patient population is specific due to the unusual underlying pathophysiology in dialysis outflow veins, which are exposed to much higher flow volumes. In the event of hemodialysis-related central venous occlusion, primary stent deployment is very effective in ensuring long-term vascular access for hemodialysis with superior long-term patency rates compared with percutaneous PTA alone or other therapeutic approaches.

References

1. Haage P, Vorwerk D, Piroth W et al (1999) Treatment of hemodialysis-related central venous stenosis or occlusion: results of primary Wallstent placement and follow-up in 50 patients. Radiology 212:175–180
2. Sprouse 2nd, Lesar CJ, Meier 3rd et al (2004) Percutaneous treatment of symptomatic central venous stenosis. J Vasc Surg 39:578–582
3. Mickley V (2001) Stent or bypass ? Treatment results in benign central venous obstruction. Zentralbl Chir 126:445–449
4. Oderich GS, Treiman GS, Schneider P et al (2000) Stent placement for treatment of central and peripheral venous obstruction: a long-term multi-institutional experience. J Vasc Surg 32:760–769
5. Dammers R, de Haan MW, Planken NR et al (2003) Central vein obstruction in hemodialysis patients: results of radiological and surgical intervention. Eur J Vasc Endovasc Surgery 26:317–321
6. Kovalik EC, Newman GE, Suhocki P et al (1994) Correction of central venous stenoses: use of angioplasty and vascular Wallstents. Kidney Int 45:1177–1181
7. Gaylord GM, Taber T (1993) Longterm hemodialysis access salvage: problems and challenges for nephrologists and interventional radiologists. J Vasc Interv Radiol 4:103–107

Occlusion, Venous Central, Malignant

Patrick Haage
Department of Diagnostic and Interventional Radiology
University Hospital Witten, Herdecke, Wuppertal, Germany
patrick.haage@helios-kliniken.de

Synonyms

Malignant central venous obstruction; Malignant central venous thrombosis

Definition

Acute or chronic thrombotic uni- or bilateral occlusion of one or more central veins.

Pathology/Histopathology

The central venous vasculature, in particular the superior caval venous system, may be obstructed by two types of lesions. The so called SVC syndrome is in more than 90% of cases caused by malignancy. Bronchogenic carcinoma is the most common causative malignant tumor and often leads to edema of the upper thorax, shortness of breath, cough, dysphagia, hemoptysis, and headaches. Less often, direct extension or compression due to the primary tumor or by invasion of the mediastinal lymph nodes is triggered by lymphoma, extra-thoracic tumors, mesothelioma, and lymph node metastases (1). Benign diseases causing SVC obstruction are often iatrogenic due to central venous catheters and pacemaker leads.

Clinical Presentation

Clinical signs and symptoms of SVC obstruction (SVCO) are scored according to Kishi (2, Table 1). Clinical manifestations of venous obstruction can be extremely serious, requiring prompt treatment (also see ▶Benign central venous occlusion). Although the primary diagnostic suspicion can be rendered clinically, imaging is required for demonstrating the extent of the pathology.

Imaging

Contrast venography for decades has been the standard of reference for benign and malignant central venous obstruction; however this procedure has its shortcomings. Venous puncture can be challenging in a swollen extremity, the procedure may cause thrombophlebitis and there is a low risk of an allergic contrast agent reaction. Ultrasonography is not reliable for detection of central venous pathologies, owing to difficult access to these vessels. In addition enlarged collateral veins and nonocclusive thrombi may cause false negative results. Sensitivity can be improved with the demonstration of normal cardiac pulsatility and respiratory phasicity within the examined vessels (read ▶Thrombosis, vein brachial).

Occlusion, Venous Central, Malignant. Table 1 Kishi scoring system for superior vena cava obstruction with the total score for signs and symptoms calculated as the sum of the highest grades in each category

Signs and symptoms grade	
Neurologic symptoms	
	Stupor, coma, or blackout 4
	Blurry vision, headache, dizziness, or amnesia 3
	Changes in mentation 2
	Uneasiness 1
Laryngopharyngeal or thoracic symptoms	
	Orthopnea or laryngeal edema 3
	Stridor, hoarseness, dysphagia, glossal edema, or shortness of breath 2
	Cough or pleural effusions 1
Nasal and facial signs or symptoms	
	Lip edema, nasal stiffness, epistaxis, or rhinorrhea 2
	Facial swelling 1
Venous dilatation	
	Neck vein or arm vein distension, upper extremity swelling, or upper body plethora 1

Nowadays contrast enhanced spiral or preferably multislice computed tomography is employed to define the site of the obstruction and the presence of possible thrombosis and reveal surrounding soft tissue alterations (3). Alternatively, MRI is of comparative or even higher sensitivity and specificity in evaluating the patency of the central chest veins and may just as well hint at impending SVCO (▶Thrombosis, caval vein inferior).

Another drawback of digital subtraction angiography is that it can only evaluate one single venous drainage system for each injection and other major draining vessels, for instance the internal jugular veins, may remain indeterminate. CT and MR venography more clearly depict the site and extension of the obstruction in clinically relevant venous vessels segments (4).

Both cross-sectional modalities provide a fast, virtually noninvasive evaluation of the central chest veins. If a percutaneous therapy is anticipated, naturally, digital subtraction venography should be carried out immediately prior to, during, and after the intervention.

Diagnosis

Due to the deficiencies of a clinical diagnosis, imaging techniques need to be incorporated in the diagnostic process.

Interventional Radiological Treatment

Especially in acute central venous obstruction, traditional treatment methods in malignancy have been nonoperative, such as steroids, radiation therapy, and chemotherapy. These however may require up to 4 weeks to show an effect and thus often are too time consuming (5). In benign and malignant lesions, anticoagulation alone is not efficient but may be used combined with other treatment modalities (6). Thrombolysis is ineffective in 75% of cases when the event is older than 5 days. In early chronic and chronic occlusions, thrombolysis is outright unsatisfactory (7). If a stenosis is the trigger for thrombosis, sole lysis will also be inefficient (8).

In conclusion, an approach which offers urgent and rapid nonoperative relief should be the preferred treatment of choice.

Admittedly, with balloon angioplasty alone early restenosis can be expected; plus, interventional success is limited because of the well-known fibrous and elastic features of venous lesions (6, 8). It however can be valuable before stenting by allowing the stent to uncomplicatedly cross relatively tight lesions.

For all the above mentioned reasons percutaneous endovascular stenting of obstructive central venous lesions, which are symptomatic and caused by benign or malignant lesions, is an effective therapeutic option with acceptable patency rates and proven efficacy (9).

Stenting results in a rapid and consistent relief and maintains patency throughout the life span of most patients suffering from malignant tumors. Different vascular access sites like the femoral vein, internal jugular vein, subclavian vein, and basilic vein are possible. Recanalization can be attempted with a hydrophilic-coated steerable 0.035 inch guide wire or a straight guide wire with a movable core, combined with a selective catheter.

The obstruction may require predilation after safe passage through the segment, but only if presence of thrombus material can be excluded. To avoid venous rupture, which in the worst case may lead to cardiac tamponade, PTA should be performed carefully and by hand. Next, a stent which is flexible enough to allow implantation even in kinked vessels should be introduced. Coverage of the obstructed segment is advised to be at least 1 cm free at the proximal and distal end to cover beyond the obstruction. Sometimes the placement of an additional stent may be necessary, especially if there is obstruction of both anonymous veins and the superior vena cava. In this case recanalization and revascularization of one anonymous vein lead to good clinical results and are associated with fewer complications provided that sufficient venous collaterals from left to right or vice versa are present (10).

Stent size should be adapted to the diameter of the adjacent nonobstructed vessel segment. Postprocedural balloon dilatation is advised. Stent size should be at least 10% above the venous diameter. To avoid stent dislocation and central embolization, a self-adjusting, self-expanding stent is advantageous because especially chronic venous occlusions may undergo progressive luminal enlargement after stent placement (11). Previously, many interventionalists preferred balloon expandable stents because of their flexibility and their marginal risk of migration. Current self-expanding stents however have overcome these problems of significant foreshortening and migration.

Often a superimposed thrombosis can be observed which can be treated with thromboaspiration or fibrinolytic therapy before stenting (1). The significant bleeding risk in patients with corresponding contraindications must be considered though. The chance of hematoma formation and gastrointestinal and intracerebral hemorrhage must be taken into account. Nevertheless the presence of extensive thrombus may require the use of thrombolytics. The thrombolytic agent should be infused with the tip of the infusion catheter inside the thrombus at a rate of ~0.02 mg tissue plasminogen activator/kg body weight/hr (12). To save time, pulse spray injection can be employed. Active thrombus removal with mechanical thrombectomy devices may be an adjunct or even alternative to intralesional thrombolysis, however it must be handled with care and expertise.

The peri- and postprocedural anticoagulation for stent placement with or without additional thrombolysis is still unclear. Heparinization during stenting and postprocedural intravenous or subcutaneous heparin can be administered. Subsequent antiplatelet therapy, typically aspirin and/or clopidogrel is recommended. Thrombosis may occur after the stent insertion in up to 45% (13). Long-time anticoagulation therefore helps in avoiding clinical deterioration.

To recapitulate, the efficacy and safety of stent placement in central venous occlusion of benign and malignant origin have been proven with rapid relief and less invasiveness for the often extremely ill patients. Stenting is widely accepted now; it provides fast and durable symptomatic relief and can nowadays be favored to radiation and chemotherapy or used in combination

with them. If clinical symptoms are severe or worsen rapidly, stenting is indicated while surgical therapy should be reserved for patients undergoing refractory to percutaneous therapy. Repeated percutaneous intervention can prolong the cumulative patency rate.

Pharmacologic/pharmacomechanical/mechanical thrombolysis may be necessary to improve the final result in case of superimposed central venous thrombosis; they should however not be employed as a single means for revascularization.

References

1. Thony F, Moro D, Witmeyer P et al (1999) Endovascular treatment of superior vena cava obstruction in patients with malignancies. Eur Radiol 9:965–971
2. Kishi K, Sonomura T, Mitsuzane K et al (1993) Self-expandable metallic stent therapy for superior vena cava syndrome: clinical observations. Radiology 189:531–535
3. Uberoi R (2006) Quality assurance guidelines for superior vena cava stenting in malignant disease.Cardiovasc Intervent Radiol 29:319–322
4. Kroencke TJ, Taupitz M, Arnold R et al (2001) Three-dimensional gadolinium-enhanced magnetic resonance venography in suspected thrombo-occlusive disease of the central chest veins. Chest 120:1570–1576
5. Nicholson AA, Ettles DF, Arnold A et al (1997) Treatment of malignant vena cava obstruction: metal stents or radiation therapy. J Vasc Interv Radiol 8:781–788
6. Schindler N, Vogelzang RL (1999) Superior vena cava syndrome: Experience with endovascular stents and surgical therapy. Surg Clin North Am 79:983–994
7. Gray BH, Olin JW, Graor RA et al (1991) Safety and efficacy of thrombolytic therapy for superior vena cava syndrome. Chest 99:54–59
8. Kee ST, Kinoshita L, Razavi MK et al (1998) Superior vena cava syndrome: Treatment with catheter-directed thrombolysis and endovascular stent placement. Radiology 206:187–193
9. Yim CD, Sane SS, Bjarnason H (2000) Superior vena cava stenting. Radiol Clin North Am 38:409–424
10. Dinkel HP, Mettke B, Schmid F et al (2003) Endovascular treatment of malignant superior vena cava syndrome: Is bilateral Wallstent placement superior to unilateral placement? J Endovasc Ther 10:788–797
11. Haage P, Vorwerk D, Piroth W et al (1999) Treatment of hemodialysis-related central venous stenosis or occlusion: results of primary Wallstent placement and follow-up in 50 patients. Radiology 212:175–180
12. Schifferdecker B, Shaw JA, Piemonte TC et al (2005) Nonmalignant superior vena cava syndrome: pathophysiology and management. Catheter Cardiovasc Interv 65:416–423
13. Kim YI, Kim KS, Ko YC et al (2004) Endovascular stenting as a first choice for the palliation of superior vena cava syndrome. J Korean Med Sci 19:519–522

Occupational Lung Diseases

►Pneumoconioses

Oesophageal Atresia

A congenital abnormality in which the upper oesophagus is a blind-ending sac and is not continuous with the lower oesophagus.

►Oesophageal Disease, Childhood
►GI Tract, Paediatric, Congenital Malformations

Oesophageal Cancer

►Neoplasms, Oesophagus

Oesophageal Clearance

This term is used to describe the process by which the oesophagus is cleared of refluxed stomach acid.

►Gastroesophageal Reflux in Adult Patients: Clinical Presentations, Complications, and Imaging

Oesophageal Disease, Childhood

Melanie Hiorns
Radiology Department
Great Ormond Street Hospital for Children
London, UK
HiornM@gosh.nhs.uk

Synonyms

Achalasia; Gastro-oesophageal reflux; Gastro-oesophageal reflux (GOER); Oesophageal atresia; Oesophageal duplications (and other foregut duplications); Oesophageal foreign body; Oesophageal stenosis (corrosive ingestion); Oesophageal webs; Tracheo-oesophageal fistula

Definition

►*Oesophageal atresia* is the congenital occlusion of the oesophagus. It has an incidence of between 1 in 3,000 to

4,500 live births. Oesophageal atresia is associated with ►tracheo-oesophageal fistula in more than 85% of cases. There are several different anatomic variations of the oesophageal atresia and the insertion of an associated tracheo-oesophageal fistula. Tracheo-oesophageal fistula is the abnormal connection between the trachea and the oesophagus and occurs in isolation only in 8% of cases. The remainder of the time it occurs in conjunction with oesophageal atresia.

Oesophageal webs may be congenital or acquired and are a thin, 2–3 mm, eccentric, smooth extension of the normal oesophageal wall that can occur anywhere along the length of the oesophagus but typically is located in the anterior post-cricoid area of the proximal oesophagus.

►*Oesophageal duplications* are part of a wider group of foregut duplications. Duplications may cystic or tubular and may contain gastric mucosa. They can be associated with sequestrations or congenital stenosis or atresia of the oesophagus. Oesophageal duplications may be separated from the oesophagus or may share a common wall. Duplications of the oesophagus are sometimes associated with vertebral anomalies and intraspinal cysts and often are associated with intra-abdominal intestinal duplications.

►*Oesophageal stenosis* is a narrowing of the oesophagus at any point along its length and over a variable distance. A stenosis my be congenital or may be acquired such as after surgery for oesophageal atresia, secondary to acid or alkali ingestion, or to another disease process such as epidermolysis bullosa.

►*Achalasia*: Abnormal dilatation and motility of the distal oesophagus with failure of relaxation of the lower oesophageal sphincter.

►*Oesophageal foreign body*: An object that is ingested but does not pass freely through the oesophagus. The most common sites for hold-up are at the level of cricopharyngeus, at the aortic knuckle and at the gastro-oesophageal junction.

►*Oesophageal inflammatory change:* Inflammation of the mucosa of the oesophagus in response to an irritant. This in most commonly secondary to reflux or to ingested corrosives but may also be seen in Crohn's disease, epidermolysis bullosa, pemphigoid and other systemic or dermatological diseases.

►*Gastro-oesophageal reflux*: Reflux is the retrograde movement of fluid across a sphincter and in the context of the oesophagus is the movement of stomach contents up into the oesophagus.

Pathology/Histopathology

Oesophageal atresia is due to posterior deviation of the tracheo-oesophageal septum leading to incomplete separation of the oesophagus from the laryngo-tracheal tube. There is failure of recanalisation of the oesophagus in the eighth week of foetal development. There are several variations on how the fistula may connect the trachea and oesophagus. The most common is that of a blind-ending upper pouch with a fistula then connecting the distal trachea to the lower, patent, part of the trachea. A fistula that joins a patent oesophagus to a patent trachea is termed an 'H'-shaped fistula (8%). Oesophageal atresia and tracheo-oesophageal fistula is the most common congenital malformation of the oesophagus (1).

Oesophageal webs may represent incomplete recanalisation of the oesophagus during foetal life. They are made of the normal structures in the wall of the oesophagus.

Oesophageal duplications: It is believed that these anomalies are due to failure of the notochord to detach from the endoderm, resulting in a persisting neurenteric canal. They often contain gastric mucosa.

Oesophageal stenosis: Congenital stenosis is believed due to poor canalisation of the oesophagus in embryonic life. Acquired stenoses are usually secondary to an insult and will therefore show scar tissue.

►*Achalasia:* Aetiology unknown.

Oesophageal foreign body: No specific pathology.

Oesophageal inflammatory change: The inflammatory change may be superficial involving only the mucosal surface or maybe transmural.

Gastro-oesophageal reflux: In GOER the lower oesophageal sphincter (LES) opens inappropriately or is incompetent and there is transient complete relaxation of the sphincter. Due to a pressure difference across the LES (with negative pressure in the oesophagus during inspiration) or a transient rise in intra-abdominal pressure the stomach contents move up into the oesophagus This may result in chronic inflammation in the oesophagus and in severe cases can lead to stricture formation.

Clinical Presentation

Oesophageal atresia and tracheo-oesophageal fistula: Most neonates present at birth with difficulty swallowing secretions, drooling, choking and respiratory distress as secretions and feeds spill over into the airway. In complete OA, the neonate will present with difficulty swallowing secretions and will be unable to tolerate the first feed. If a fistula is present between the trachea and oesophagus, air can still reach the gastrointestinal (GI) tract. An ►H-fistula may present later with blue episodes or repeated chest infections and aspiration as some fluid tracks from the oesophagus through the fistula into the airway. A blind-ending upper pouch is often detected

when there is failure to pass a nasogastric tube and/or this becomes coiled in the upper oesophagus. With the increase in antenatal scanning oesophageal atresia may be detected *in utero*. The mother may present with polyhydramnios and on ultrasound there will be very little if any fluid present in the stomach or GI tract of the foetus.

A complication of repair of oesophageal atresia is a stricture of the oesophagus and the child may present with dysphagia and regurgitation of food.

Oesophageal web: The very young child will present with drooling and aspiration, and may suffer repeated chest infections. The older child will may have dysphagia and regurgitation of solids.

Oesophageal duplication: Completely separated duplications can present as a mediastinal mass and may or may not be associated with symptoms. Incompletely separated duplications may give rise to dysphagia, regurgitation and rarely airway obstruction (2).

Oesophageal stenosis: Dysphagia and regurgitation.

Achalasia: Chronic regurgitation of undigested food, repeated aspiration pneumonia, retrosternal discomfort in the older child.

Oesophageal foreign body: The patient will usually be drooling and may be dysphagic.

Oesophageal inflammatory change: Presentation will depend on the underlying cause but the patient will usually have retrosternal pain. With chronic change going on to stricture formation they may present with dysphagia.

Gastro-oesophageal reflux: GOER is most common in infants and young children and a minor degree of reflux in the first few months of life may even be considered within normal levels. The symptomatic infant will present with recurrent regurgitation of feeds and/or pain. In severe cases, the child may fail to gain weight or even lose weight if it is not possible to maintain adequate calorific intake. Older patients may present with retrosternal pain, food aversion or less commonly with a stricture. Alternatively, young children and patients with neurologic deficits may present with recurrent chest infections secondary to aspiration as a result of GOER.

Imaging

Oesophageal atresia and tracheo-oesophageal fistula: A chest X-ray will often show an air-filled, dilated and blind-ending upper oesophageal pouch. If the passing of a nasogastric tube (Fig. 1) has been attempted this is likely to be coiled in the upper pouch (1). A Replogle tube (identified by a dashed radio-opaque marker allowing easy identification on X-ray) may have been placed in the upper oesophagus to allow aspiration of the secretions.

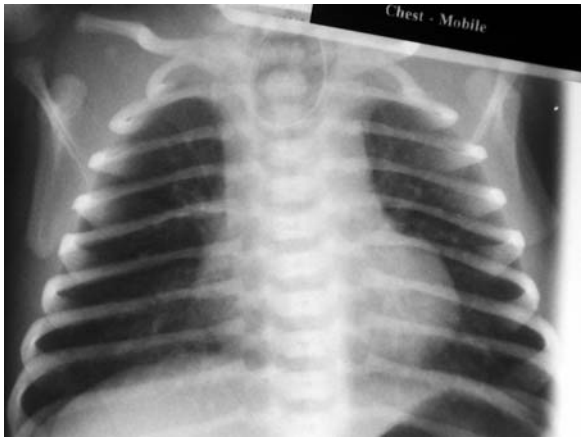

Oesophageal Disease, Childhood. Figure 1 Chest X-ray showing a nasogastric tube coiled in a blind-ending upper pouch in a patient with oesophageal atresia.

This is a dual lumen tube which allows secretions to be continually sucked from the blind-ending upper oesophagus thereby preventing aspiration. It is used almost exclusively in this condition. The abdomen will be gasless unless there is an associated fistula, and indeed the presence of gas in the abdomen will confirm that a fistula is present, this being the only route for air to get from the airway into the GI tract. A contrast study is not required and the immediate management is usually surgical. Imaging for an H-type fistula (a fistula between a patent airway and a patent oesophagus) is by a tube oesophagram. With the patient prone and with lateral screening water-soluble contrast is injected into the oesophagus whilst the nasogastric tube is slowly withdrawn. If a fistula is present, the contrast should flow through the fistula from the oesophagus into the airway. This procedure therefore carries a significant risk of acute respiratory compromise and should only be undertaken if suction, oxygen, nursing support and appropriate resuscitation facilities are available.

Stricture formation as a delayed complication of repair of oesophageal atresia is best demonstrated by upper GI (UGI) series (Fig. 2).

Oesophageal web: Imaging is by upper GI series or direct visualisation on endoscopy.

Oesophageal duplication: If the duplication is not completely separated it may be demonstrated on an upper GI series (Fig. 3). A closed duplication may be best demonstrated on MRI of the mediastinum, although CT and ultrasound may also be used. Ultrasound would generally use an approach through the sternal notch or between the ribs, but in very young patients a transsternal approach can sometimes be used as the sternum has not ossified.

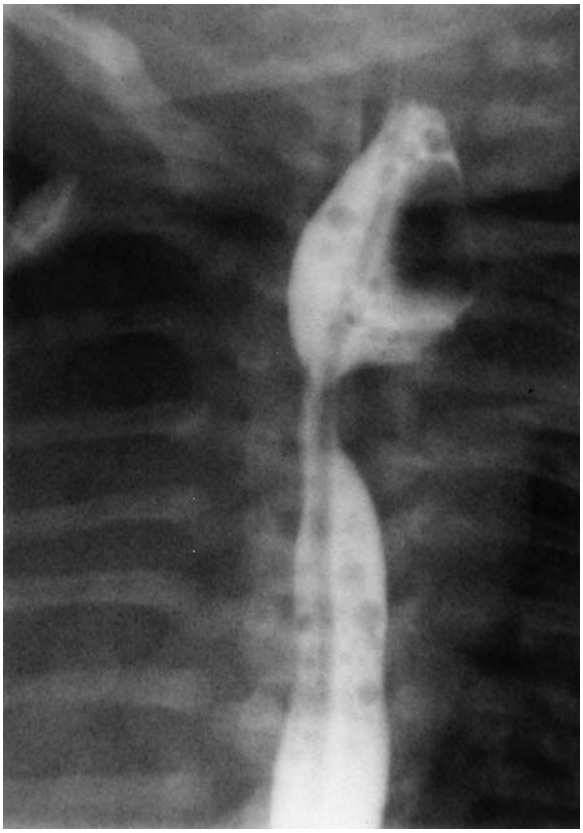

Oesophageal Disease, Childhood. Figure 2 Upper GI series demonstrating a tight oesophageal stenosis at the site of previous surgery for oesophageal atresia with tracheo-oesophageal stenosis.

Oesophageal stenosis: Upper GI series will show the level and extent of the narrowing.

Achalasia: An upper GI series will show the accumulated food debris in the dilated oesophagus and poor opening of the lower oesophageal sphincter with a characteristic fine jet of contrast passing through or an abrupt point ('birds beak') at the gastro-oesophageal junction through which no contrast passes.

Oesophageal foreign body: Chest X-ray (AP and lateral) will show radio-opaque foreign bodies; an upper GI series may demonstrate the filling defect on a radiolucent foreign body. Endoscopy allows direct visualisation and simultaneous removal (see entry Foreign body, ingestion, children).

Oesophageal inflammatory change: Very subtle superficial changes may not be detected by imaging and will only be identified under direct vision with endoscopy. An upper GI series using barium will demonstrate mucosal surface irregularity with an uneven appearance to the barium column (Fig. 4). If a double contrast image is achieved ulceration may be visible. Endoscopic ultrasound will show the degree of intramural thickening.

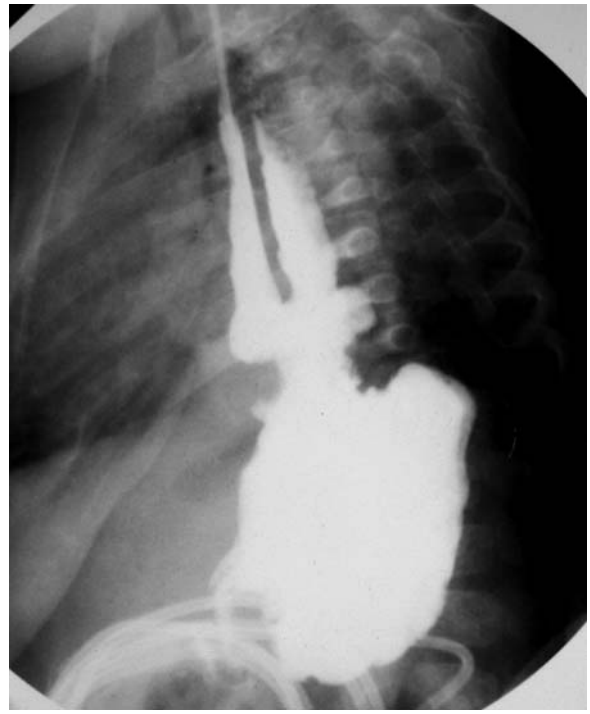

Oesophageal Disease, Childhood. Figure 3 Contrast outlines an oesophageal duplication with two, parallel, fluid-filled cavities opacified.

Gastro-oesophageal reflux: An upper GI series or ultrasound of the lower oesophagus are the modalities of choice. Reflux is usually self-evident in infants by the regurgitation of feeds so much of the value of the UGI is to exclude anatomical causes for the reflux such as hiatus hernia or gastric outlet obstruction and in preparation for surgery if a fundoplication is being considered. GOER is characteristically intermittent and it would be inappropriate to image the patient with prolonged screening to try and demonstrate an occasional episode. Only intermittent screening should be performed and the absence of demonstrable reflux during a UGI does not exclude the diagnosis. Ultrasound is increasingly used to demonstrate relaxation of the lower oesophageal sphincter and fluid tracking into the lower oesophagus. It has the advantage that the sphincter can be observed directly and for prolonged periods but the disadvantage that it cannot show the rest of the stomach and duodenal anatomy. An UGI is also useful for assessment of the complications of GOER such as stricture formation.

Nuclear Medicine

No role to play in this condition.

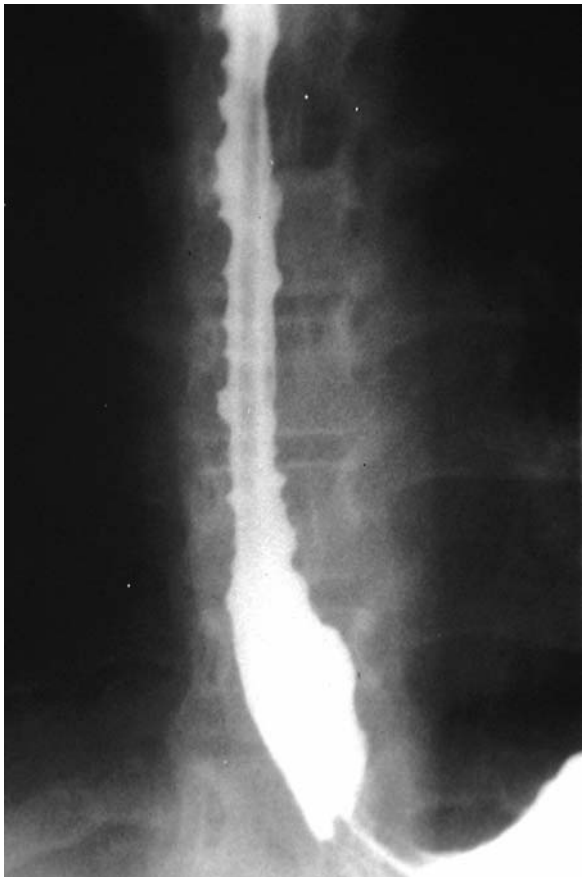

Oesophageal Disease, Childhood. Figure 4 Upper GI series with contrast outlining an irregular and narrowed oesophagus following ingestion of caustic fluid.

Diagnosis

By imaging as detailed above. GOER may also be diagnosed by monitoring with pH probe.

Interventional Radiology

Image guided balloon dilatation of strictures (3), and sometimes removal of oesophageal foreign bodies may be carried out by the interventional radiologist (see also entry 'foreign body, ingestion, children').

Bibliography

1. Berrocal T, Madrid C, Novo S et al (2004) Congenital anomalies of the tracheobronchial tree, lung, and mediastinum: embryology, radiology, and pathology. Radiographics 24(1):e17
2. Stern LE, Warner BW (2000) Gastrointestinal duplications. Semin Pediatr Surg 9(3):135–140
3. Lan LC, Wong KK, Lin SC et al (2003) Endoscopic balloon dilatation of esophageal strictures in infants and children: 17 years' experience and a literature review. J Pediatr Surg 38(12):1712–1715

Oesophageal Duplication

A congenital abnormality in which there has been duplication of part of the foregut in embryological development resulting in either a cyst or second lumen of the oesophagus.

▶Oesophageal Disease, Childhood

Oesophageal Duplications (and other foregut duplications)

▶Oesophageal Disease, Childhood

Oesophageal Dysmotility

This may be either abnormal contractions of the oesophagus, or a diminution or failure of normal peristalsis. It has many causes, of which the most common in industrialized countries is gastro-oesophageal reflux disease.

▶Gastroesophageal Reflux in Adult Patients: Clinical Presentations, Complications, and Imaging

Oesophageal Foreign Body

▶Oesophageal Disease, Childhood
▶GI tract, Pediatric, Foreign Bodies

Oesophageal Malignancy

▶Neoplasms, Oesophagus

Oesophageal Stenosis (corrosive ingestion)

▶Oesophageal Disease, Childhood

Oesophageal Tumor

▶Neoplasms, Oesophagus

Oesophageal Webs

▶Oesophageal Disease, Childhood

Oesophagitis

Vlastimil Valek[1], Jiri Dolina[2]
[1]Department of Radiology, University Hospital Brno, Brno, Czech Republic
[2]Department of Gastroenterology, University Hospital Brno, Brno, Czech Republic
vlvalek@med.muni.cz
jdolina@fnbrno.cz

Synonyms

Esophagitis; Gastroesophageal reflux disease (GERD); Oesophagitis

Definition

In the literature the term "esophagitis" (oesophagitis) is sometimes used synonymously with "reflux esophagitis" because gastroesophageal reflux is the most common cause of esophagitis. However, numerous etiologic factors may cause esophagitis:

- Infectious esophagitis
  1. Fungal infections
  2. Viral infections
     (a) Herpes simplex virus (HSV)
     (b) Cytomegalovirus (CMV)
     (c) Varicella-zoster virus (VZV)
  3. Bacterial infections
  4. Parasitic infections
- Drug-induced esophagitis
- Radiation-induced esophagitis
- Caustic esophagitis
- Reflux esophagitis
- Miscellaneous
  1. Skin disorders
- Dystrophic epidermolysis bullosa
- Pemphigus vulgaris
- Bullous pemphigoid
- Benign mucous membrane pemphigoid
- Stevens–Johnson syndrome
- Lichen planus
- Acanthosis nigricans
- Darier's disease
- Leukoplakia
  1. Behcet's disease
  2. Graft-versus-host disease (GVHD)
  3. Crohn's disease
  4. Ulcerative colitis
  5. Sarcoidosis
  6. Collagen vascular diseases.

Pathology/Histopathology

Infectious Esophagitis

In Candida esophagitis, plaques consist of heaped-up areas of necrotic epithelial debris or actual colonies of *C. albicans* on the esophageal mucosa; the esophagus itself as an irregular or shaggy appearance. Three viral infections cause ulcerative esophagitis: HSV, CMV, and VZV.

In HSV the earliest esophageal lesions are vesicles, the centers of which slough to form discrete, circumscribed ulcers with raised edges. Routine histologic stains may show epithelial cells with occasional multinucleation, "ground-glass" nuclear staining, and intranuclear inclusions. More specific and sensitive is immunohistologic identification with monoclonal antibodies to HSV antigen and *in situ* hybridization for HSV nucleic acid.

CMV infection occurs only in immunosuppressed patients. CMV may be activated from latency or acquired from blood-product transfusions. CMV lesions first appear as serpiginous ulcers in otherwise normal mucosa but coalesce to form giant ulcers, particularly in the distal esophagus. Infection occurs within submucosal fibroblasts and endothelial cells, not in epithelium, and is usually part of widespread visceral infection. Routine histologic stains show large cells in the submucosa bearing amphophilic intranuclear inclusions and intracytoplasmic inclusions. Immunohistology with monoclonal antibodies to CMV antigens and *in situ* hybridization for CMV DNA are useful for finding infected cells that are neither large nor inclusion bearing.

Drug-induced Esophagitis

In drug-induced esophagitis, affected individuals ingest the medication with little or no water immediately before

going to bed. When such drugs dissolve in the esophagus, they cause mucosal injury either by creating an acid pH (analogous to a form of caustic esophagitis) or by direct irritating the epithelium.

Radiation Esophagitis

A radiation dose of 4,500–6,000 rad over a 6- to 8-week period or more to the mediastinum may cause severe injury to the esophagus. Acute radiation-induced esophagitis usually occurs 2–4 weeks after the initiation of radiation therapy. The mucosa typically has a granular appearance because of edema and inflammation. Ulceration and decreased luminal distensibility are other frequent findings.

Caustic Esophagitis

Caustic esophagitis causes injury similar to that from thermal burns. Liquid lye causes liquefactive necrosis, resulting in the most severe form of caustic injury to the esophagus. Alkaline agents can produce deep coagulation necrosis in minutes. Necrosis from acids tends to be more superficial. The severity and extent of esophageal injury depend on the type, concentration, and volume of the caustic agent. By 2–6 weeks, healing is well in progress, often accompanied by severe fibrosis.

Gastroesophageal Reflux Disease, Esophagitis (Reflux Esophagitis)

This type encompasses reflux esophagitis and is characterized histologically by inflammatory cells and reflux changes consisting of epithelial hyperplasia without inflammation. The multiple determinant factors in the production of reflux disease include the frequency and volume of GER, the volume of gastric contents available to reflux, the potency of the reflux material, the efficacy of esophageal clearance, and the tissue resistance to injury.

Miscellaneous Esophagitis

Eosinophilic esophagitis (IEE) is a chronic inflammatory disease characterized by eosinophilic infiltration of the esophagus with an increased number of intraepithelial eosinophils (more than 20 eosinophils per high-power field) in endoscopic biopsy specimens from the esophagus. Alkaline reflux esophagitis is caused by reflux of bile or pancreatic secretions into the esophagus after partial or total gastrectomy. Pemphigus and pemphigoid are nonhereditary conditions in adults, and epidermolysis bullosa dystrophica occurs as an autosomal recessive condition in children. Pemphigus, pemphigoid, and epidermolysis bullosa can produce esophagitis.

Pemphigus vulgaris affects skin, mouth, and other mucous membranes with weeping bullous lesions. Histology shows acantholysis and intraepithelial bullae, and specific immunohistology should be used. Bullous pemphigoid is a chronic disease of the elderly, in whom tense, pruritic skin bullae arise. Esophageal bullae occur rarely, with sloughing of the epithelium as a cast. The histology shows subepithelial bullae and circulating antibodies to the basement membrane.

Behcet's disease is a multisystem inflammatory process characterized by oral and genital ulcers, ocular inflammation, skin lesions, and vasculitis. Esophageal lesions include ulcerations that can tunnel under the mucosa, strictures, and perforations.

GVHD is an immunologic reaction against host tissues by donor lymphoid cells. The esophagus shows webs, rings, and tight strictures but often fails to show generalized desquamation apparent on endoscopy. Crohn's disease rarely affects the esophagus but may show small aphthous ulcers, inflammatory strictures, filiform polyps, and fistulas. Granulomas can occasionally be found in endoscopic biopsy specimens.

Clinical Presentation

Infectious esophagitis is seen with increasing frequency in debilitated individuals, alcoholics, diabetics, immunocompromised or transplant patients, individuals with impaired T-cell function from acquired immunodeficiency syndrome (AIDS), and patients receiving steroids, antibiotics, radiotherapy, or chemotherapy. Candida esophagitis (and infectious esophagitis generally) is usually characterized by the abrupt onset of odynophagia (painful swallowing), chest pain, or dysphagia. Clinical symptoms can occasionally be absent. Symptoms of tuberculosis esophagitis include dysphagia and chest pain, but esophageal symptoms are commonly absent. Patients with HSV esophagitis present with odynophagia, retrosternal pain, and heartburn. Infection can also start with mild symptomatology of nausea and pyrosis (heartburn) or with very severe symptoms of hematemesis. The clinical presentation of CMV esophagitis is nausea, vomiting, painful swallowing, heartburn, and/or hematemesis.

Symptoms of *drug-induced esophagitis* are usually sudden in onset and consist of chest pain, odynophagia, or dysphagia. A typical location is the aortic arch level, where tablets are delayed because of the aortic indentation on the esophagus and the low contractile force of peristalsis. Bleeding or esophageal perforation may occur.

Radiation esophagitis typically produces mild heartburn or dysphagia several weeks after the onset of treatment. Some patients may have progressive dysphagia

due to strictures 4–8 months after completion of radiation therapy.

In *caustic esophagitis*, the initial clinical symptoms are the rapid onset of chest pain and dysphagia. These symptoms tend to resolve in several days. Acute complications include shock, fever, respiratory distress, mediastinitis, and perforation. Late complications are related primarily to fibrosis and stricture, which may cause dysphagia several weeks after the initial injury.

Symptoms of *GERD esophagitis* (*reflux esophagitis*) can be divided into typical (esophageal) symptoms (heartburn, regurgitation, dysphagia) and atypical (extraesophageal) symptoms (chronic cough, respiratory complaints, laryngeal symptoms). Dysphagia is usually due to esophageal narrowing. Some patients complain of a lump in the throat (globus). In young children the predominant reflux symptoms are regurgitation, repetitive vomiting, and failure to thrive.

IEE appears in the adult population. It typically affects young men (20–40 years of age) with long-standing dysphagia and recurrent food impactions who have not responded to the usual forms of antireflux therapy. Other findings include chest pain and vomiting.

Imaging

Barium examination continues to be the primary radiologic modality for evaluating patients with dysphagia, reflux symptoms, or other clinical findings of esophageal disease. The double-contrast phase optimizes the ability to detect all kinds of esophagitis, particularly reflux disease, whereas the single-contrast phase optimizes the ability to detect hiatal hernia and lower esophageal rings or strictures. Barium contrast studies are useful for evaluating mucosal surface lesions but provide little information about the extramucosal extent of disease. Computed tomography (CT) and magnetic resonance imaging (MRI), on the other hand, permit evaluation of wall thickness, mediastinal involvement, adjacent lymphadenopathy, and distant spread.

Diagnosis

Infectious esophagitis: Candida esophagitis is characterized on esophagrams by plaques or a "shaggy" esophagus. Plaquelike lesions are seen as linear or irregular filling defects that tend to be oriented longitudinally and are separated by normal mucosa. The luminal contour may show fine speculations, irregularity, a cobblestone pattern, or bizarre thickened folds simulating varices. Barium may dissect beneath a pseudomembrane, causing a shaggy contour that gives the appearance of ulceration. The esophagus tends to be atonic. Peristalsis may be feeble or incomplete. Because of muscular hypotonia, the esophagus is generally slightly dilated or normal in caliber but may show areas of moderate narrowing. *Monilia* organisms are a frequent companion of esophageal intramural pseudodiverticulosis.

Double-contrast esophagrams have been found to have a sensitivity of 90% for detecting Candida esophagitis, primarily because of the ability to show these plaques.

CT findings are nonspecific and commonly seen in various kinds of esophagitis (circumferential esophageal wall thickening of >5 mm, with relatively long segmental involvement). Enhanced scans may also depict the target sign (circumferential wall thickening and enhancing internal mucosa). Morphologic abnormalities caused by tuberculosis esophagitis are often eccentric and may show skip areas. The luminal contour may show mild irregularity, large or deep ulcers, and sinus tracts. Fistulas are common. The esophageal wall is generally thickened and the lumen often narrowed. Enlarged mediastinal nodes may displace or compress the esophagus and widen the mediastinum.

In HSV, barium contrast X-ray shows multiple ulcers. Small ulcers surrounded by edema give the appearance of targets or shallow irregularities in the profile view. Diagnosis requires endoscopic brushing and biopsies. The first, presumptive diagnosis can be made in patients with esophageal symptoms and HSV infections of the mouth or nares.

CMV esophagitis is characterized by one or more giant flat ulcers that are several centimeters or more in length. The ulcers may have an ovoid or diamond-shaped configuration and are often surrounded by a thin radiolucent rim of edematous mucosa. Endoscopy with multiple biopsies targeting the center of the ulcer formation is mandatory. Brushing of overlying exudates is seldom useful.

Drug-induced esophagitis: Signs are luminal irregularity, frank ulceration, and luminal narrowing. Tetracycline and doxycycline are associated with the development of small shallow ulcers in the upper or middle part of the esophagus. Other drugs may cause more severe esophageal injury.

Radiation esophagitis: A morphologic abnormality consists of diffuse ulceration. Late findings consist of strictures that are generally smooth with tapering margins and that rarely show irregularity or ulceration.

Caustic esophagitis: In the acute stage, the examination should be initiated with water-soluble contrast medium to exclude esophageal or gastric perforation. Such studies may also reveal marked edema, spasm, and ulceration of the affected esophagus. During the first week, characteristic frank ulcerations are seen. A pseudomembrane may cause intramural trapping of barium. Long, ulcerated strictures may be observed in patients who ingested lye or

other caustic agents, and in severe cases, diffuse esophageal narrowing may reduce the thoracic esophagus to a thin, tight stricture. Cross-sectional images depict narrowing or obliteration of the esophageal lumen, and perifibrotic tissue may be observed. Reformatted CT images may be useful for demonstrating the surrounding fibrotic change to which caustic esophagitis leads.

GERD esophagitis: Reflux esophagitis manifests at esophagography as finely nodular or granular relief with poorly defined radiolucencies that fade peripherally due to edema and inflammation of the mucosa. Endoscopy is the gold standard for diagnosing erosive GERD, and the Los Angeles classification for esophagitis is generally accepted as the endoscopic assessment of GERD. Most patients—approximately 60% referred for endoscopy with typical reflux symptoms—do not have erosive reflux disease. The spectrum of GERD can be subdivided into endoscopy-negative, nonerosive GERD (NERD), reflux esophagitis (GERD), and GERD with esophageal columnar metaplasia (Barrett). Further changes include irregularity of luminal contours, discrete ulcerations, transverse esophageal folds, thickened longitudinal folds, esophageal wall thickening, smooth polypoid protuberance (also known as an inflammatory esophagogastric polyp), and segmental narrowing.

The ulcers can have a punctate, linear, or stellate configuration and are often associated with a surrounding halo of edematous mucosa, radiating folds, or sacculation of the adjacent wall. Predominant involvement of the distal esophagus and the presence of an associated hiatal hernia and gastroesophageal reflux should suggest the correct diagnosis.

Thickened folds wider than 3 mm are best seen on mucosal relief views of the collapsed esophagus. Multiple delicate transverse folds 1–2 mm wide may also be found in patients with gastroesophageal reflux disease. Between 10 and 20% of patients with reflux esophagitis develop peptic strictures as a result of circumferential scarring of the distal esophagus. The classic appearance of a smooth, tapered area of concentric narrowing in the distal esophagus above a sliding hiatal hernia should be virtually pathognomonic of a benign peptic stricture. Most peptic strictures range from 1 to 4 cm in length and from 0.2 to 2.0 cm in width. Between 25 and 50% of patients with reflux esophagitis have abnormal esophageal motility, manifested by feeble or absent primary peristalsis associated with an increased frequency of nonperistaltic contractions.

Miscellaneous esophagitis: Alkaline reflux esophagitis is characteristic by mucosal nodularity or ulceration or, in severe disease, by distal esophageal strictures that often progress rapidly in length and severity over a short period of time. During the acute stage of pemphigus, pemphigoid, and epidermolysis bullosa esophagitis, bullae may cause multiple esophageal filling defects on esophagograms, or ruptured bullae may appear as ulcerations. Repetitive insults often lead to strictures that are generally smooth but sometimes have an irregular contour. IEE manifests at esophagography as segmental esophageal strictures (sometimes ringlike—the so-called ringed esophagus at endoscopy and/or barium studies) and occasionally with diffuse esophageal narrowing, which produces a "small-caliber" esophagus.

Interventional Radiological Treatment

Esophageal dilation is usually indicated for benign stenoses and strictures, which can be caused by esophagitis. The main indications are strictures after caustic and reflux esophagitis. All esophageal strictures should be carefully evaluated with esophagography or endoscopy before dilation.

Bibliography

1. Therasse E, Oliva VL, Lafontaine E et al (2003) Balloon dilation and stent placement for esophageal lesions: indications, methods, and results. Radiographics 23:89–105
2. Zimmerman SL, Levine MS, Rubesin SE et al (2005) Idiopathic eosinophilic esophagitis in adults: the ringed oesophagus. Radiology 236:159–165
3. Levine MS, Rubesin SE (2005) Diseases of the esophagus: diagnosis with esophagography. Radiology 237:414–427
4. Jang KM, Lee KS, Lee SJ et al (2002) The spectrum of benign esophageal lesions: imaging findings. Korean J Radiol 3:199–210

Oesophagogram

Radiologic examination where images are obtained of the oesophagus during drinking of either barium sulphate suspension or iodine contrast medium. When an effervescent agent is used a double-contrast effect may be obtained.

▶Diverticulum, Oesophagus

Oil Cyst

Conglomerate of almost entirely pure neutral fat, encapsulated by a thin, smooth, fibrous wall in which calcium deposition may occur.

▶Trauma, Breast

OLF

▶Ossification or Calcification of Ligamenta Flava (OLF)

OLT

▶Transplantation, Liver
▶Orthotopic Liver Transplantation

Omphalocele

Persistence of herniation of the abdominal contents into the base of the umbilical cord at the time of birth and associated with a high incidence of other congenital anomalies.
▶GI Tract, Paediatric, Congenital Malformations

Open and Closed Spinal Dysraphisms

Etymologically, the term "dysraphism" implies defective closure of the neural tube, and should therefore be used to refer to abnormalities of primary neurulation only. However, the term has gained widespread use as a synonym to congenital spinal cord malformation.

Spinal dysraphisms are categorized into open (OSD) and closed (CSD). OSDs are characterized by exposure of nervous tissue to the environment through a congenital defect of the child's back. On the contrary, CSDs are covered by skin, although cutaneous birthmarks, such as angiomas, dimples, overgrowing hair, dyschromia, and dystrophy, are present in greater than 50% of cases. Use of the term "occult spinal dysraphisms" is discouraged as it suggests complete absence of external abnormalities, a condition that occurs only in a minority of CSDs.
▶Congenital Malformations, Spine and Spinal Cord

Ophthalmology or Colposcopy

▶Optical Imaging

OPLL

▶Ossification of Posterior Longitudinal Ligament

Opportunistic Infections

Opportunistic infections are infections caused by a microorganism that normally does not cause disease but becomes pathogenic in persons with impaired immune system.
▶Infection, Opportunistic, Brain

Opportunistic Screening

Screening not performed in an organized or population-based screening program, i.e., resulting from self-referral or from referral as a result of a routine medical consultation, a consultation for an unrelated condition, or on the basis of a possibly increased risk for developing breast cancer (family history or other known risk factor).
▶Screening, Breast Cancer

Optical Contrast Agents

▶Molecular Probes, Optical Probes

Optical Imaging

Brian W. Pogue
Thayer School of Engineering, Dartmouth College, Hanover, USA
brian.w.pogue@dartmouth.edu

Synonyms

Bioluminescence imaging; Bronchoscopy; Diagnostic imaging in endoscopy; Fluorescence imaging; Laparoscopy; Microscopy; Ophthalmology or colposcopy; Optical tomography

Definition

Optical imaging is a broad term which can be used to describe a large range of imaging systems, from tissue microscopy, through macroscopic imaging of tissue with endoscopic, laparoscopic, or telescopic systems. Generally, this wording is used to describe optical imaging, when compared with other imaging systems which do not use optical detection, such as X-ray, ultrasound, or magnetic resonance. Optical imaging is carried out with a light sensitive system for capturing the images. Standard optical imaging systems use a charged coupled device (CCD), for detecting the image, having many pixels and a lens or fiber optic system, which is customized for the application. Analysis of the system performance in terms of resolution and contrast are always specific to the geometry and the tissue being imaged.

Imaging of tissue *in vivo* is largely based upon the effects of absorption and scattering of the light as it interacts with tissue, causing chromatic changes or allowing viewing of morphologic features. Some *in vivo* imaging relies upon tracking temporal changes or changes in response to a stimulus, but this is less common. Preclinical or *ex vivo* imaging, such as in pathology typically relies upon contrast from exogenously introduced agents which are specific to chemical features of the tissue.

Optical imaging of contrast agents *in vivo* is also used in experimental and developmental work as well as a few clinical applications, looking at fluorescence imaging of tissue, where a filter is used on the image detection side to remove the excitation light and only allow the longer wavelength emission light into the imaging camera. Recent developments in biochemistry and experimental biology have introduced a large number of fluorescent proteins and bioluminescent agents that can be transfected into the DNA of cells and animals, thereby allowing optical imaging of organs or specific gene-expression. The use of optical imaging in experimental biomedical research has increased substantially due to these developmental areas.

Fiber Coupled Systems

Fiber optic coupled systems are used throughout routine medical practice in imaging the interior cavities of the body, or imaging organs during surgical intervention or exploratory examination see Endoscopy, Brochoscopy or Laparoscopy. Generally, the optical fibers bundle is used to translate the image from a lens inside the body to a remote camera which is mounted on the exterior end of the device being held by the person doing the procedure. The endoscope is used in this way for imaging the digestive tract, and similarly a bronchoscope is used to image the airways. These are typical flexible fiber bundles which allow movement through these complex structures. The video or CCD camera is usually fed to a television for viewing of the procedure in real time by the endoscopist or bronchoscopist.

Lens Coupled Systems

Lens coupled imaging systems are used routinely in ophthamoscopic imaging, cervix imaging, ear imaging, as well as most experimental biology imaging systems. The commonality in this area is that if broadband light imaging is required, the lenses used must be compound lenses to avoid issues of chromatic aberration in the resulting image at the camera. Thus, significant care is taken to design and optimize the lens system and how it focuses onto the camera. Generally, lower the f-number of the objective lens and the closer the lens is to the tissue, the more light will be captured in the imaging procedure.

Microscopy

Microscopy is by far the most widely used application of optical imaging in medicine, yet it is often considered in a different category because it is so specialized. Pathological analysis of biopsied tissue is the most common application here, where the tissue is fixed and stained for imaging.

Tomographic Imaging

Tomographic imaging of tissue is sometimes called more generically optical imaging, but is better described in the Optical Tomography section or Fluorescence Imaging section. The major difference between tomography and imaging is largely considered to be the acquisition of signals from below the surface, thereby allowing reconstruction or backprojection of the image below the surface.

Surface Topography and Tracking

Optical imaging systems are used in many different applications for surface tomographic mapping, and several commercial systems exist either using patterned light generation to measure surface topography or using stereovision cameras together with computed algorithms to create surface maps. These are used in applications where the three-dimensional topography of a tissue surface is needed to be known.

Optical Probes

▶Molecular Probes, Optical Probes

Optical Tomography

Brian W. Pogue
Thayer School of Engineering, Dartmouth College, Hanover, USA
brian.w.pogue@dartmouth.edu

Synonyms

Diffuse imaging; Diffuse optical tomography; Frequency-domain photon migration; Near-infrared imaging; Near-infrared tomography; Photon density wave imaging; Photon migration; Time-resolved optical tomography

Definition

Optical tomography has been an active area of research study since the late 1980s, when both technological and algorithmic breakthroughs led to workable methods to understand light transport in tissue and solve the inverse image reconstruction problem. The exact tools for tomographic imaging vary widely in terms of hardware and software, but the commonality is that the method allows imaging of the interior of tissue, by recovering the interaction coefficients or chromophore and scattering parameter maps. Near-infrared light, in the range of 650 to 950 nm, is most commonly used in optical tomography as it has the lowest scattering and absorption values, thereby providing the best penetration through tissue possible. Imaging through volumes of up to 10–14 cm is possible given sufficiently designed equipment. Tomographic measurements in this wavelength range are most sensitive to the molecules that absorb light, which are hemoglobin, oxyhemoglobin, water, and lipids. Thus imaging tissue function related to blood concentration and oxygen saturation is possible with near-infrared tomography. In addition, injection of absorbing or fluorescent contrast agents is possible, providing further information about the tissue function. The latter application of imaging fluorescent agents is often called fluorescence tomography, and described in another section on Fluorescence Imaging. Imaging with optical tomography is commonly applied to imaging brain tissue for functional physiology studies, or neonatal cerebral imaging for tracking disease, or female breast cancer imaging. There are few commercially available devices which do optical tomography, but a larger number of experimental and investigational devices have been developed in research labs (1).

Tomography of tissue requires measurement of multiple cross-sectional measurements of light transmission from several different source and detector locations. When overlapping paths are measured, as with X-ray computed tomography, it is possible to mathematically reconstruct the interaction coefficient maps of the tissue interior. In the case of optical tomography, this inverse problem is not as analytically tractable as in the filtered backprojection methods used in X-ray tomography (2). The path of the light is highly scattered, and so the transport mechanism is dominated by elastic scatter. Optical tomography became more intensively studied when it was established the optical path length through a scattering medium could be measured by time-resolved or frequency-domain signals, by directly measuring the signal propagation time. Through modeling the transmission process as a diffusive transport problem, it is possible to mathematically quantify independent absorption and transport scattering coefficients (1). Existing systems typically use this approach to them compute concentration maps of hemoglobin, or relative oxygen saturation of the hemoglobin, or water and lipid fractions in the tissue, through computation of the exact absorption coefficient spectrum.

Characteristics

Most systems are based upon multiple fiber optic placements upon the tissue to be imaged, and illuminating the source light into the tissue while detecting the remitted light at all other fiber points. When this is completed, the light is cycled to each of the source fibers in turn to provide multiple overlapping measurements through the tissue volume, as indicated in Fig. 1. Recovery of the remitted light can also be done with noncontact application as well, delivering the light through a scanned beam and picking up the remitted intensity with optics to fibers or charge coupled devices (CCD) (3).

The type of light signals used in these systems are divided into time-resolved signals or frequency-domain signals or continuous wave signal illumination, as illustrated in Fig. 2. Each of these provide slightly different information about the tissue, but all have been shown to allow separation of absorption and scattering effects with different levels of success. It is largely agreed that time-resolved signals provide the optimal separation of the scattering and absorption coefficients, whereas frequency domain provides nearly equal ability. However, continuous wave signals are thought to be insufficient for separation of the effects of absorption versus scatter, without the use of multiple wavelengths or other

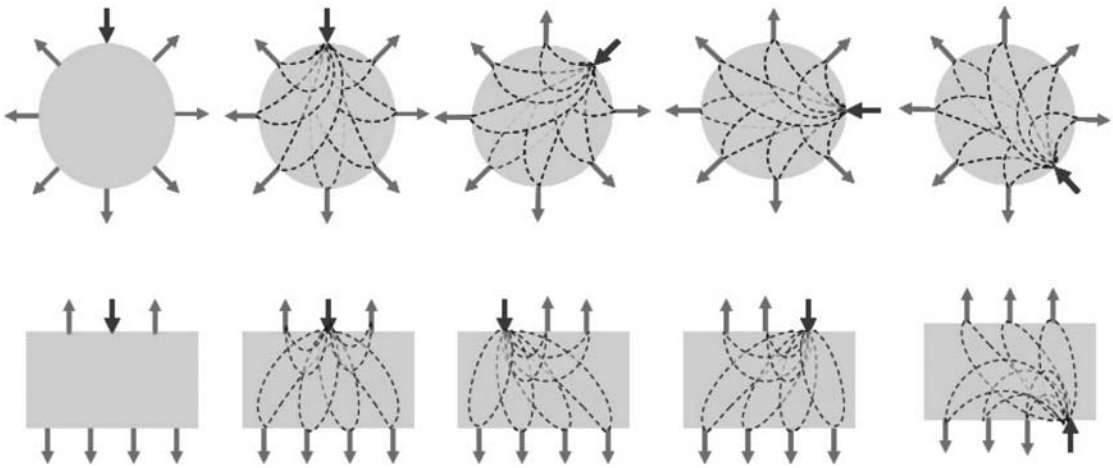

Optical Tomography. Figure 1 Illustrating two common geometries for imaging with optical tomography, namely an effectively circular or thick slabs of tissue volume with a single source and multiple detectors. The source location is cycled around to make multiple overlapping projection measurements, and the banana-shaped projections are the diffuse photon paths, which represent the dominant measurement path. *Inward arrows* represent the sources here and *outward arrows* represent the detectors.

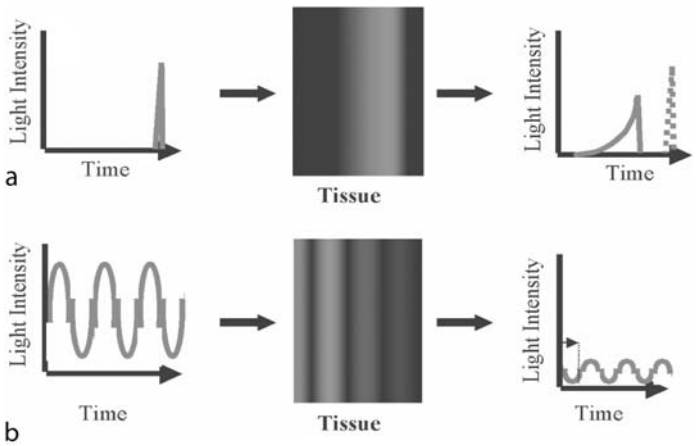

Optical Tomography. Figure 2 An illustration of a time-resolved measurement (a) where a short pulse of light is transmitted through a hypothetical block of scattering tissue, spreading the pulse out in time, and a frequency-domain measurement scheme (b) using a sinusoidally modulated light intensity transmitted through the tissue.

constraining information. Measurement detectors are either photomultiplier tubes for the weakest light signals, or photodiodes, diode arrays or CCDs. Multichannel detector devices have been produced in many different configurations.

Diffusion theory based reconstruction requires the iterative solution to a perturbation type equation or a Newton method approach (2). Both of these require some initial guess of the tissue properties, often assumed to be the best homogeneous estimate, and then the image reconstruction process uses the Jacobian or sensitivity matrix to iteratively improve the estimate of the coefficients at each pixel within the image. The goal of the reconstruction is to minimize an objective function, which is often calculated as the normalized square difference between the calibrated data set and the calculated diffusion theory prediction of the signal. This minimization process requires inverting the Jacobian matrix, which is an ill-posed problem, and therefore requires careful regularization (addition of a constant term to the diagonal of the matrix) to make it invertible. This process inherently smooths the overall resulting image, and the value of the regularization parameter is often estimated for each particular problem, often in a Levenberg–Marquardt methodology.

Most current systems use multiple spectra measurements, thereby allowing recovery of the absorber concentration maps from the absorption coefficient spectra, and

with *a priori* knowledge of the chromophore extinction coefficients. It has been shown that direct reconstruction of the chromophores can also be achieved by including the spectral fitting process within the inverse image reconstruction problem, and this process reduces the ill-posed nature of the problem, and improves the accuracy.

Applications in Preclinical Studies

Small animal imaging with near-infrared tomography has been a highly used avenue, for studies in brain function and tumor imaging. Imaging of tumor characteristics *in vivo* has been possible both without and with a scattering coupling medium. Imaging of brain tissue function, in terms of hemoglobin and oxygen saturation has been done extensively and used for functional brain activation studies.

Applications in Brain Diagnostics

Significant interest in optical tomography was initiated with the possibility of monitoring or measuring neonatal cerebral hemodynamics *in vivo*. Commercial systems are available for spectroscopy monitoring of the brain in neonates with single point transmission measurements, and the desire to extend this to a full tomographic system was the driving force for much of the development of optical tomography throughout the past 20 years. Prototype systems have been developed in several labs and are still undergoing feasibility assessment for their potential use. Point spectroscopy of hemodynamics in the brain during childbirth and in utero have both also been shown and used in studies. Measurement of cytochrome oxidase changes in oxygenation within the brain have also been studied, with limited success in this area.

Brain topography systems have been studied extensively and commercialized by Hitachi as a tool to study cognitive function in humans. The difference between topography and tomography lies in the depth penetration of the light, with topography being surface measurements across large areas of the brain, without any reconstruction of the lower lying areas. This approach is simpler and more successful than tomography, and provides important information about the outer cortical layers where blood flow and oxygen consumption issues can readily be measured in response to energy demand in the brain cells. Study of cognitive function with optical topography and optical tomography is a highly active area of research and development (4).

Applications in Breast Cancer

Breast cancer imaging with optical tomography has been shown in many laboratories, with large clinical trials ongoing and being sponsored by the US National Cancer Institute. Commercial prototype systems have been created by a number of companies, with each having very different technological approaches and different clinical goals. Initial feasibility as a screening tool for widespread use has largely proven unsuccessful, however niche applications in screening high-risk groups, younger women or complicated tissue

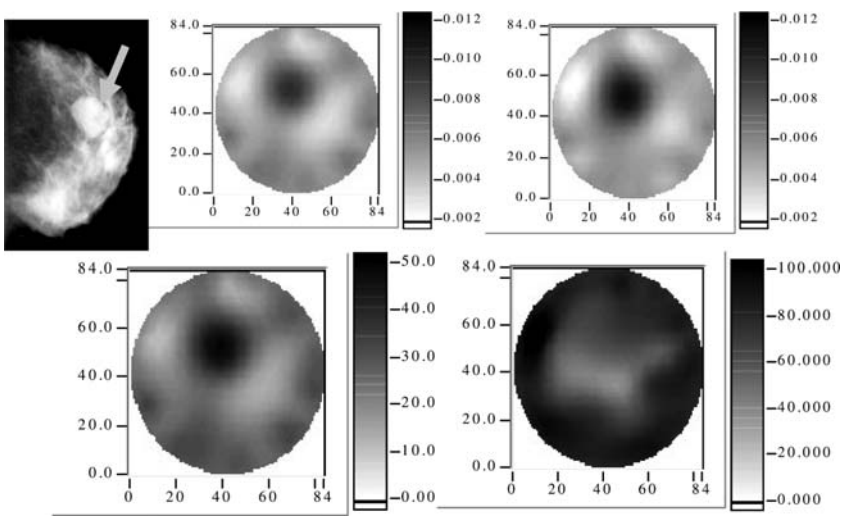

Optical Tomography. Figure 3 (a) Radiographic image of a patient's breast, showing a well-localized fibroadenoma in the upper central region of the breast (marked with an *arrow*). The resulting NIR images of absorption coefficient at (b) 750 nm and (c) 800 nm wavelength are shown, along with the computed images of (d) total hemoglobin and (e) oxygen saturation. The gray-scale bar units for absorption coefficient are mm^{-1}. The units for total hemoglobin are in micromolar, and the units for oxygen saturation are in percent relative to 100% oxygenated hemoglobin.

cases remains a possible avenue for use. Integration of optical tomography into MRI scanners has been demonstrated and continues under development. A set of example images from a subject with a focal fibroadenoma tumor in the breast is shown in Fig. 3 (5).

The ability to image tumor properties of hemoglobin, oxygen saturation, water fraction, and scattering has undergone rapid development in the past 5 years. Direct recovery of these concentration images has been shown to improve the accuracy of the values, through multispectral fitting and reconstruction in a single step.

Optical tomography has also been coupled into standard clinical imaging systems, including MRI, ultrasound, X-ray tomography, X-ray tomosynthesis, MEG, EEG and is thought to provide complementary information, predominantly related to hemoglobin, oxygen saturation and uptake and retention of injected contrast agents.

Bibliography

1. Delpy DT, Cope M (1997) Quantification in tissue near-infrared spectroscopy. Phil Trans R Soc Lond B 352:649–659
2. Arridge SR (1999) Optical tomography in medical imaging. Inverse Probl 15(2):R41–R93
3. Pogue BW, McBride TO, Osterberg UL et al (1999) Comparison of imaging geometries for diffuse optical tomography of tissue. Opt Express 4:270–287
4. Franceschini MA, Fantini S, Thomspon JH et al (2003) Hemodynamic evoked response of the sensorimotor cortex measured noninvasively with near-infrared optical imaging. Psychophysiology 40(4):548–560
5. Pogue BW, Poplack SP, McBride TO et al (2001) Quantitative hemoglobin tomography with diffuse near-infrared spectroscopy: pilot results in the breast. Radiology 218(1):261–33

Optical Tracers

►Molecular Probes, Optical Probes

Oral Cavity, Inflammatory Diseases

Sabrina Kösling
Martin-Luther-Universität Halle-Wittenberg
Klinik für Diagnostische Radiologie
Halle, Germany
sabrina.koesling@medizin.un-halle.de

Synonyms

Inflammation; Inflammatory lesion

Definition

An inflammation is a non-specific immune response in reaction to any type of injury: pathogenic organisms, injuries, foreign bodies or ionising radiation. It may remain localized, sub-clinically and temporarily if the body's defensive mechanisms are effective. An inflammation can be acute, primary-chronic or an acute inflammation may persist and spread by extension to become a subacute or chronic state. Inflammations of the oral mucosa are called depending on their localization as follows:

- Glossitis—inflammation of the tongue
- Stomatitis—inflammation of larger parts of the oral mucosa
- Gingivitis—inflammation of the gum
- Cheilitis—inflammation of the lips

If deeper structures are involved it might be a ►phlegmon or ►abscess.

Pathology

Regarding the severity, macroscopic appearance, pathogenic agent and extent of the inflammatory process, various kinds of inflammation in the oral cavity do occur.

Aphthae are intra-epithelial cavities with a size up to 5 mm filled with serous fluid. They are caused by virus, toxic substances or medicaments. Habitual aphthae are characterized by chronical recurrent aphthae of unknown aetiology. A ►vasculitis is the underlying lesion of Behcet's disease—a seldom, systemic, HLA-B51 associated illness—in which recurrent aphthae of the oral cavity and genital region appear together with other organ manifestations as uvea, skin, joints and central nervous system.

In herpes simplex labialis, small vesicles at the border between the dermis and mucosa of the lips appear due to herpes simplex ►infection. If the inflammation extends on the entire oral cavity it is called herpetic stomatitis (synonym: stomatitis aphthosa). In a later stage of the disease, vesicles proceed to mucosal erosions and deeper ulcerations with red border.

Ulcerative stomatitis (synonym: necrotizing ulcerative gingivitis) is an extended, severe, necrotizing, oedematogenic inflammation caused by a complex of different organisms (streptococci, spirillum, fusiform bacteria and fungi) in immune-compromised patients or bad oral hygiene.

Oral herpes zoster infection is caused by the reactivation of varicella-zoster virus in the area of innervations of the maxillary, mandibular or seldom glossopharyngeal nerve. It is characterized by unilateral crops of clustered vesicles.

Oral candidiasis (synonym: thrush), an opportunistic infection especially in immune-compromised patients, is mainly caused by *Candida albicans*. It is usually limited to the skin and mucous membranes. White pseudomembranes consisting of mycetes and necrotic epithelium are a characteristic finding.

Acquired immunodeficiency syndrome (AIDS) favours the development of opportunistic bacterial, viral or mycotic infections including oral candidiasis and herpes simplex viral infection. Hairy leukoplakia—a column-shaped hyperkeratosis of the acanthoticaly broadened epithelium—can proceed years before the outbreak of AIDS.

In a phlegmon or ▶cellulitis, there is a diffuse spread of granulocytic infiltrates within the tissue. An ▶abscess consists of a necrosis—resulting from purulent colliquation of tissue—and a membrane, which borders on vital tissue. Both are kinds of bacterial infection (streptococci, staphylococci). Most often, they occur in the floor of the mouth due to secondary involvement from other spaces: masticator space (dental infection) or submandibular space (sialolithiasis).

Ludwig's angina is an extensive bacterial infection of the floor of the mouth that always involves both the sublingual and submandibular space. It is frequently bilateral and produces gangrene or serosanguinous phlegmon, but little or no frank pus; involves connective tissue, fascia and muscle, but not glandular structures (1).

In necrotizing fasciitis, there is severe or extensive phlegmon that extends into the superficial and deep fascia, producing thrombosis of the subcutaneous vessels and gangrene of the underlying tissues. The oral cavity may be involved.

The oral cavity can be involved in syphilis (synonyms: lues, treponemiasis), a *Treponema pallidum* infection. Primary affection shows a coarse infiltrate or ulceration of deep red colour (ulcus durum); secondary affection flat the infiltrates, ulcers with red halo and whitish blur on mucosa; tertiary affection causes bleeding, necrotizing and rubbery infiltrations, the so-called gumma.

Actinomycosis, caused by *Actinomyces israelii*, is characterized by hard, bluish-violet infiltrates—actinomyces drusen with leucocytes and foam cells—and fistulas to the skin as well as to bone (2, 3).

Clinical Presentation

Characteristic signs of nearly all oral cavity inflammations are pain, burning of the tongue and/or mucosa and dysphagia. Primary and tertiary affection in syphilis and infiltrates in actinomycosis are painless. In oral herpes zoster, the pain is of severe neuralgic character. Disturbances of tasting are typical for glossitis and oral candidiasis.

A reduced general condition and fever occur in ulcerative stomatitis, herpetic stomatitis, oral herpes zoster, purulent infections, Ludwig's angina, secondary syphilis and Behcet's disease. The fever is very high in purulent infections and subfebrile in Behcet's disease.

Swelling of lymph nodes accompanies ulcerative stomatitis, herpetic stomatitis, purulent infections, Behcet's disease and primary syphilis. Except for syphilis, the enlarged lymph nodes are usually painful. The clinical pictures of necrotizing fasciitis which occurs seldom in the head and neck region is characterized by a fulminating onset of the disease, painful edema, erythema, warmth, tenderness and septicemia.

Sialism, redness, necrotic odour, haemorrhage and swelling of the gingiva as well as the oral mucosal are seen in ulcerative stomatitis. Sialism also occurs in herpetic stomatitis and oral herpes zoster; necrotic odour in herpetic stomatitis and oral candidiasis. Some pseudomembranes in oral candidiasis are easily wiped off from the affected oral tissues and leave an erythematous, eroded or ulcerated surface, which may be tender.

Phlegmon and abscess of the floor of the mouth show a reddish, oedematous mucosa; they are hard in palpation; trismus may be present (2).

Imaging

Most oral cavity inflammations are diagnosed by inspection due to their typically macroscopic appearance. An indication for imaging is given in patients in whom a deeper spread, mainly an abscess, is suspected or for exclusion of a tumour in chronic inflammation as actinomycosis or ulcerative stomatitis.

Ultrasound is the first performed imaging modality in acute inflammatory diseases of the oral cavity. If there are equivocal findings, CT or MRI can provide similar information. CT is clearly faster performed, less susceptible to motion artefacts, the better available technique and therefore the preferred method in adults. Considering the lack of radiation exposure, MRI should be given the preference in children.

Ultrasound

The floor of the mouth can be well investigated by ultrasound. The appearance of an abscess depends generally on its stage. In early stage, it is poorly defined and its demarcation against surrounding soft tissue is worse. With maturation it becomes more and more hypoechoic and has finally a dorsal sound-amplification. Fine echoes within the mass are suspicious of gas. If the

infection starts from the submandibular gland, the gland is painful enlarged and hypoechoic. Calculi can be identified up to a size of 3 mm. Ultrasound has limitations in the detection of mandibular involvement, the demonstration of spread into the retropharyngeal space and the visualization of phlegmonous processes.

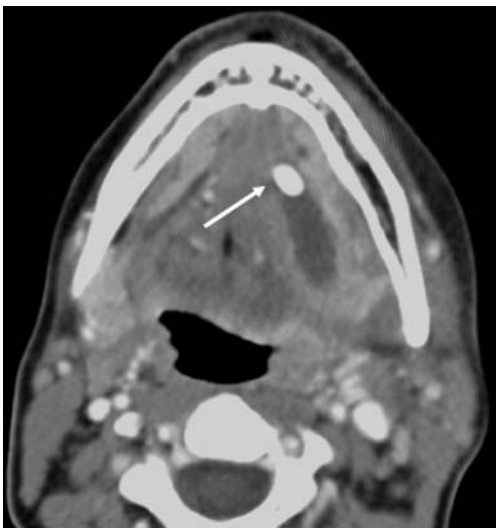

Oral Cavity, Inflammatory Diseases. Figure 1 Axial contrast-enhanced CT of a patient with clinically suspected abscess in the floor of the mouth. CT shows an area of low density as a sign for and abscess surrounded by swollen tissue of increased contrast enhancement and prominent lymphoid tissue on the left. Calculus as a cause could be detected (arrow). The patient was treated by incision and antibiotic therapy.

Computed Tomography

On CT, an abscess appears as an area of low density, with or without gas collection. In mature abscesses a rim enhancement is seen. Surrounding structures are usually involved: muscles are thickened, fat is oedematous with increased density, overlying fascia and skin are thickened showing an enhancement and draining lymph nodes are enlarged. Calculi in the salivary glands or major ducts, erosions of the mandibular cortex and a dental origin can be demonstrated (Figs 1 and 2). A phlegmon and an abscess cannot always be differentiated by clinical methods. Changes—as described in the neighbourhood of an abscess—without abscess formation are found on CT. In necrotizing fasciitis, CT supports the clinical diagnosis; identifies gas, the spread of the disease along vascular sheaths and into the mediastinum (4).

Magnetic Resonance Imaging

On MRI, an abscess has low T1-weighted and high T2-weighted signal intensities. As in CT only mature abscesses show a rim enhancement. Oedematous changes within the fat are not quite well visible as on CT. MR-sialography

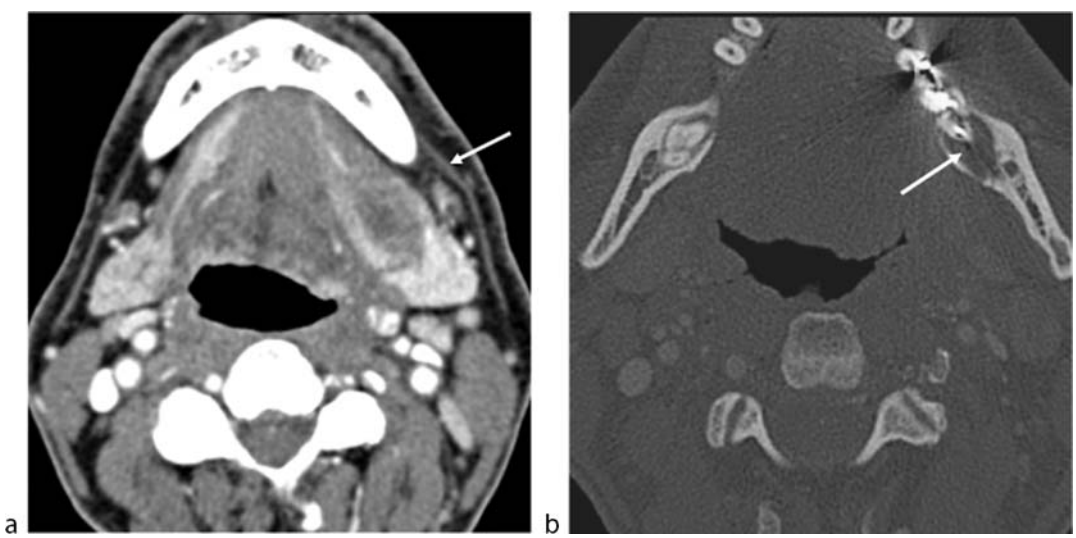

Oral Cavity, Inflammatory Diseases. Figure 2 CT of a patient with dysphagia and swelling of the mouth floor for 2 days. After ultrasound a phlegmon was suspected. (a) Contrast-enhanced scan demonstrates a diffuse swelling of soft tissue in the floor of the mouth without clear abscess formation on the left. The neighbouring fat has an increased density and the fascia is thickened (arrow). (b) High-resolution scan in bone window gives a hint of the underlying dental infection (arrow). The molar was extracted and the infection treated by antibiotics.

has to be performed for the visualization of calculi. MRI is superior to CT in the demonstration of the medullary component, if there is an accompanying ▶osteomyelitis in the mandible.

Nuclear Medicine

In diagnostics of oral cavity inflammations, nuclear medicine plays a limited role. In suspected osteomyelitis of the mandible, bone scintigraphy can demonstrate an increased tracer uptake, but MRI has the same sensitivity and gives additionally exact anatomic information.

Diagnosis

The diagnosis of the oral cavity inflammation is based on anamnesis, inspection, mirror investigation and laboratory tests. In bacterial and mycotic diseases, smears are taken for identification of germs. In lues, spirochetes can be serologically proved 4 to 5 weeks after infection. Varicella-zoster-virus-titer is increased in herpes zoster. In Behcet's disease and oral candidiasis the differential diagnostics should include a HIV-test; in the first one also a lues-serologic-test. Actinomycosis and syphilitic gummas need a histological proof.

Imaging—ultrasound or CT, seldom MRI—is performed in suspected deeper inflammation to demonstrate the extent, to document gas-forming infection, to show the relationship to neighbouring bony structures and to give a support in the decision on a conservative or surgical therapy. CT is able to reveal underlying dental infection and sialolithiasis. The latter one can also be found by ultrasound.

Bibliography

1. Smoker WRK (2003) The oral cavity. In: Som PM, Curtin HD (eds) Head and Neck Imaging. St. Louis, Mosby, pp 1398–1405
2. Berghaus A, Rettinger G, Böhme G (1996) Hals-Nasen-Ohren-Heilkunde. Hippokrates, Stuttart, pp 387–396
3. http://www.dental.mu.edu/oralpath.htm
4. Becker M, Zbaren P, Hermans R et al (1997) Necrotizing fasciitis of the head and neck: role of computed tomography in diagnosis and management. Radiology 202:471–476

Organized Screening

Screening program organized at the locoregional or national level. With an explicit policy, it is a team responsible for organization and for delivery of the screening services, and a structure for quality assurance.
▶Screening, Breast Cancer

Oropharyngeal Foreign Bodies

▶Foreign Bodies, Gastrointestinal

Orthotopic Liver Transplantation

OLT represents the most common procedure for liver transplantation and consists in the replacement of the diseased liver by a liver coming from a cadaveric donor.
▶Transplantation, Liver

Os Carpale

The postarthritic ankylosis of two or more (incomplete os carpale) or all carpal bones as a typical feature of late-stage rheumatoid arthritis.
▶Rheumatoid Arthritis

Osgood–Schlatter Pattern

Overgrowth and fragmentation of the secondary growth center of the anterior tibial tubercle with swelling of the inferior patellar tendon; may be an overuse syndrome or related to repeated minor trauma.
▶Osteonecrosis in Childhood

Osmotic Myelinolysis

Osmotic myelinolysis, also referred to as central pontine myelinolysis when it involves the pons, is a disorder associated with chronic alcoholism and malnutrition. It is due to chronic electrolyte imbalances, most commonly hyponatremia. Osmotic myelinolysis is frequently precipitated by rapid iatrogenic sodium correction, resulting in breakdown of the blood–brain barrier and a

noninflammatory demyelination with relative preservation of neurons and their axons. The central pons is the most commonly affected site. Clinically, patients present with seizures, dysphagia, pseudobulbar palsy, dysarthria and movement disorders.

▶Toxic Disorders, Brain

Ossification of Posterior Longitudinal Ligament

OPLL results from growth of lamellar bone posterior to the vertebral bodies involving (by calcification) the posterior longitudinal ligament. It is usually diagnosed in elder patients from its characteristic radiographic appearance and may lead to severe neurologic deficit due to spinal canal stenosis.

▶Dish

Ossification or Calcification of Ligamenta Flava

Enthesopathy, ossification (mostly thoracolumbar spine), and calcification (often cervical spine) in (frequently) thickened ligamanta flava may contribute to the entity of OLF. There is coexistence of OLF with both DISH and OPLL.

▶Dish

Osteitis Condensans ilii

A benign condition characterized by sclerosis in the iliac bones adjacent to the sacroiliac joints. The sclerosis is generally bilateral and usually asymptomatic. The adjacent sacroiliac joint is unaffected. This entity is thought to represent a stress reaction and is most commonly found in postpartum patients.

▶Fractures, Stress

Osteitis Deformans

▶Paget Disease

Osteitis Pubis

A noninfectious inflammatory condition involving the pubic bone and pubic symphysis that is thought to occur secondary to periosteal trauma. It occurs most commonly in postsurgical patients or in athletes. Radiographic abnormalities include sclerosis and osteolytic changes. Its imaging characteristics resemble osteomyelitis, However, it is a separate clinical entity and responds to rest and anti-inflammatories.

▶Fractures, Stress

Osteo Sarcoma

▶Neoplasms, Bone, Malignant

Osteoarthritis

'Osteoarthritis' and 'osteoarthrosis' are both used in medical terminology, however, osteoarthrosis may be the more appropriate term since inflammatory changes are not pronounced in most of the joints. The best phrase to describe degenerative changes of articulations is 'degenerative joint disease'.

▶Degenerative Joint Disease, Peripheral Joints
▶Gout

Osteoblastoma

Osteoblastoma is a benign osteoblastic tumor that differs from osteoid osteoma in having a "nidus" larger than 1.5 cm in diameter, by showing more variable histologic features, and by possessing a potential for local bone destruction and aggressiveness.

▶Neoplasms, Bone, Benign

Osteochondrodysplasia

▶Osteodysplasia
▶Dysplasia, Skeletal

Osteochondroma

Osteochondroma (osteocartilaginous exostosis) represents a benign cartilage-forming lesion that consists of a bony outgrowth covered by a cartilaginous cap.
▶Neoplasms, Bone, Benign

Osteochondrosis Dissecans

Sometimes called osteochondritis dissecans, it is a traumatic osteochondral injury, usually along a convex articulating surface of a bone.
▶Osteonecrosis in Childhood

Osteoclast-Like Giant Cell Tumor, Pancreatic

Osteoclast-like giant cell tumor is a rare pancreatic tumor that closely resembles giant cell tumor of bone. It is composed of undifferentiated spindle-shaped epithelial or mesenchymal cells mixed with non-neoplastic osteoclast-like giant cells. Some tumors also contain areas of ductal adenocarcinoma. At imaging, the tumor may present as a solid inhomogeneous mass or as a cystic lesion. Invasion of adjacent structures is common, but metastatic spread is found in only 50% of patients. Prognosis is more favorable than for ductal adenocarcinoma.
▶Carcinoma, Pancreatic

Osteodysplasia

Alan E. Oestreich
Cincinnati Children's Hospital Medical Center, Cincinnati, Ohio, USA
Alan.Oestreich@cchmc.org

Synonym

Osteochondrodysplasia

Definition

Osteodysplasias are well-defined abnormalities of bone growth, typically genetic in origin. They may be systematic, affecting one aspect of skeletal development, typically in proportion to growth potential of each site, or else "aleatoric," affecting sites of an aspect of bone development in a chance distribution, with a higher likelihood of occurrence at sites of greater normal growth. [I have borrowed the term aleatoric from modern music composition in which chance plays a role (1)] The aspect of growth may be slowed, disordered, or accelerated. The aspect involved is most often exclusively enchondral in nature or membranous in nature, with only secondary changes in the other. Most, but not all, dysplasias result in short stature (dwarfism). Kindred disorders include dysostoses, in which individual aspects of growth are affected, and sequences, in which an abnormal aspect of development causes a chain of consequent effects on bone (and other tissue) development. As more genetic markers for dysplasias are determined, more conditions are being grouped into "families" of dysplasias of like genetic origin.

Pathology/Histopathology

Various histologic manifestations of various dysplasias are known, some of which help explain radiographic findings. In multiple exostoses, the cartilage cap has a growth plate histologically close to the pattern of a normal physis, but somewhat more disorganized. In ▶achondroplasia, not only are the physeal and acrophyseal enchondral columns shorter and slower to progress from resting cartilage to provisional calcification, but also the columnar cells are grouped into separated clusters. The clustering and subsequent lack of ossification of the zones between the clusters, within the primary spongiosa zone of the metaphysis, may account for the enchondromatous areas in achondroplasia metaphyses and diametaphyses (Fig. 1). In Kniest disease, growth cartilage is characteristically irregular in pattern, described as Swiss cheese-like. Osteogenesis imperfecta shows osteoporosis. Cultured fibroblasts from persons with this dysplasia help characterize the condition. Osteopetrosis has denser than normal bone, similar to the hibernating bat, perhaps due to a temporary failure of osteocytic osteolysis, although most investigators favor a failure of osteoclast function as the direct cause.

Clinical Presentation

Disproportionate short stature is found in many systemic dysplasias; limb length discrepancy, with limp, is frequent in aleatoric dysplasias. Fractures (and blue sclerae) are a

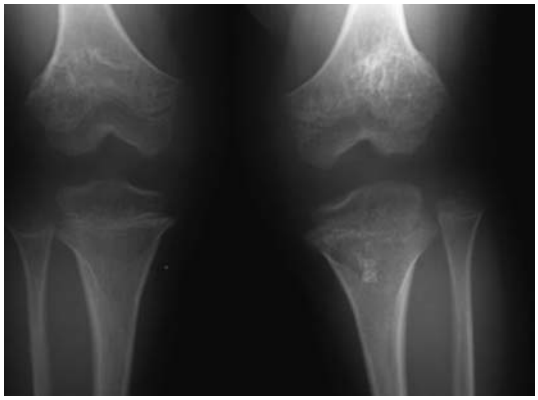

Osteodysplasia. Figure 1 Example of prominent enchondral rests in the metaphyses of distal femur of a 9-year-old boy with achondroplasia. The medial and lateral margins of the femur metaphyses and diametaphyses are more concave than normal, partly as a manifestation of achondroplasia enchondral growth slowing and partly because the knees are somewhat flexed.

hallmark of osteogenesis imperfecta; teeth tend to show dentinogenesis imperfecta crowding and irregularity as well. Tall stature is seen in the ►dolichostenomelias, notably Marfan syndrome and homocystinuria. With regard to characterization of short limbs in dysplasias, the term rhizomelic refers to shortening of limbs most pronounced proximally, such as achondroplasia; ►mesomelic dysplasias have most of the relative shortening in the intermediate segments (radius/ulna and tibia/fibula); and acromelic refers to the greatest shortening distally. Other rather specific findings include hitchhiker thumb in diastrophic dysplasia; thumb extension beyond the fist in Marfan syndrome; early-in-life shortening, especially of the limbs and later shortening of the trunk in metatropic dysplasia; gargoyle-like facies in the mucopolysaccharidoses; and occasionally the ability to draw the shoulders together in front of the chest in cleidocranial dysplasia/dysostosis.

Imaging

Skeletal surveys for osteochondrodysplasia or dysostosis need to be customized for the suspected diagnoses; once certain findings appear, other views may be required. For example, whenever platyspondyly (flatter than normal vertebral bodies) is observed, one needs to check the dens and C1 region in detail, with careful flexion and extension views as necessary, to evaluate for associated subluxability between C1 and C2. The small tubular bones of the hand and feet should be included in any survey because they may show diagnostic features key to the diagnosis. Tall patients with dolichostenomelia (such as Marfan) need good lateral chest or thorax images to evaluate for pectus excavatum or carinatum. In aleatoric disorders such as multiple exostosis or enchondromatosis, two orthogonal views of each part are needed for complete evaluation of the lesions, even if not necessary for diagnosis.

In utero imaging for dysplasia or dysostosis begins with high-detail ultrasound. Questions that arise may then be further investigated with magnetic resonance imaging (MRI). If the answer is still not given, but is important, selected radiographs of the mother's abdomen may be considered, under close supervision by a specialized pediatric radiologist. If possible, for radiation protection considerations, radiographs of one twin should be avoided if the other is considered unaffected. Abnormal bone length, shape, or a positive family history of dysplasia or dysostosis should initiate the careful prenatal evaluation for specific entities.

MRI can give insight into the nature and quantity of cartilage in several dysplasias, including Kniest disease (2). MRI of the spinal cord is prudent before planned spinal surgery in children with any severely abnormal spinal curvature. Three-dimensional reconstruction of abnormal joints assists in surgical planning for specific procedures.

Accurate measurement of long bone lengths requires perpendicular X-ray beam images at each end of the bone with a radiopaque ruler alongside that is not shifted between the exposures. Alternately, measurements can be made from a computed tomography (CT) scout view.

Long bones for dysplasia evaluation need to be parallel to the film or screen, lest foreshortening in space be mistaken for dysplastic growth foreshortening through time.

Nuclear Medicine

Multiple cartilaginous exostoses each have a cartilage cap with a growth plate (I call it "paraphysis") that will have uptake on bone scan similar to physes. Fractures in such conditions as osteogenesis imperfecta, Ollier enchondromatosis, and osteopetrosis will be hot on bone scan. The periosteal reaction causing the thick cortices of Engelmann disease will be hot on bone scan in the active stage, as it will be in other membranous bone overactivity dysplasias or dysostoses, such as van Buchem disease. Osteopetrosis usually gives a superscan of high activity of all involved bone segments. Uptake is also increased in active fibrous dysplasia.

Diagnosis

Only a few dysplasias and dysostoses will be described here.

Systematic dysplasias are symmetric side-to-side and generally change one rule or rate of growth, with the sites of greatest normal growth being affected the most. The prototype is achondroplasia with rhizomelic shortening; lumbar pedicles abnormally close side-to-side with the distance decreasing downward, greater than normal concavity of medial and lateral margins of metaphysis (Fig. 1), frontal bossing of the skull, petrous ridges closer to each other than normally, frequent cartilage rests in metaphyses, smooth but delayed growth centers with epiphyseal shape following the shape of abnormally concave physes, proximal ends of the femurs in infancy showing the pattern of an ice cream scoop on end, horizontal sacrum, shorter than normal metaphyseal collar, and trident (Vulcan salute) hands, among the many imaging findings. Hypochondroplasia, an allelic (due to the same gene locus) disorder, is less severe; thanatophoric dysplasia, also allelic, is more severe (demonstrating femurs resembling European telephone receivers and quite pronounced platyspondyly). Achondroplasia and its family results from slowed enchondral growth, whereas Marfan syndrome and homocystinuria have dolichostenomelic (predominant proximal segment) lengthening due to accelerated enchondral growth. The medial and lateral margins of long bone metaphyses are less concave than normal. Children with Marfan syndrome show pectus carinatum or excavatum, tortuous aortic arch, and wide lumbar canal; homocystinuria shows truncal osteoporosis.

Among the aleatoric dysplasias, the findings of exostosis or enchondromas occur in a chance distribution, more likely occurring in areas of greater growth potential. The more and the larger the exostosis, the greater the impairment of longitudinal growth of an affected long bone. If one paired bone is more affected than its mate, bowing and, often, dislocations occur (Fig. 2). Exostoses of epiphyses and their equivalents are termed Trevor disease (also known as dysplasia epiphysealis hemimelica); exostoses also can occur at terminal tufts of phalanges and the nonepiphyseal ends of other short tubular bones. Osteogenesis imperfecta is systemic with regard to osteoporosis but aleatoric with regard to fractures. The multiple wormian bones also show side-to-side symmetry in distribution. The weakened bones may lead to tam-o'-shanter skull (protrusio occipiti; basilar invagination) from the calvarium sinking on the cervical spine (if this deformity is severe, the clivus may run upward). Teeth are numerous and irregularly placed. The lateral clavicles may show increased upward convexity; the ribs resemble coat hangers. Prenatal sites of fracture may yield bones that look wide at birth from healing fractures. Treatment of osteogenesis imperfecta with bisphosphonates results in tell-tale nearly parallel thin lines similar in shape to the growth plates in the metaphyses (and equivalent areas in secondary growth centers) that record the jolt to the skeletal system from each dose.

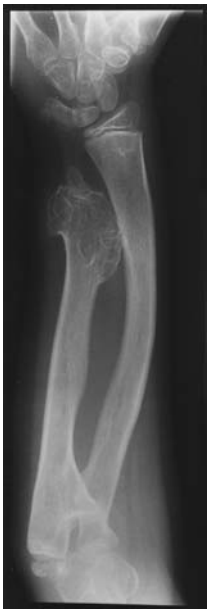

Osteodysplasia. Figure 2 Growth disparity from multiple cartilaginous exostosis/osteochondromatosis in a 10-year-old boy. The ulna has far more exostoses than the radius distally, resulting in a shorter ulna and a secondary lateral bowing of the radius. The more the exostoses, the greater the impairment of longitudinal growth. (From Oestreich AE, Crawford AH (1985) Atlas of Pediatric Orthopedic Radiology. Thieme Verlag, Stuttgart, p 27)

Chondrodysplasia punctata (multiple stippled epiphyses) in infancy consists of dense dots of calcification within unossified growth cartilage; the involved bones are short, irregularly shaped, or even abnormally unossified (Fig. 3). As the child gets older, the stipples resolve, and the pattern becomes one of misshapen epiphyses and their equivalents, a pattern then called multiple epiphyseal dysplasia (Fig. 3).

In metatropic dysplasia, the metaphyseal collar bone bark seems to lack its usual ability to restrict too rapid transverse growth of physis and metaphysis, so that bones resemble dumbbells with unusually broad metaphyses. The megaepiphyseal dysplasia Kniest disease shows coronal cleft vertebral bodies and delayed ossification of the (large) centers for the femoral head. Severe cervical kyphosis is seen (when lateral images are obtained) in diastrophic dysplasia and camptomelic dysplasia and is one of the cervical vertebral anomalies seen in Larsen

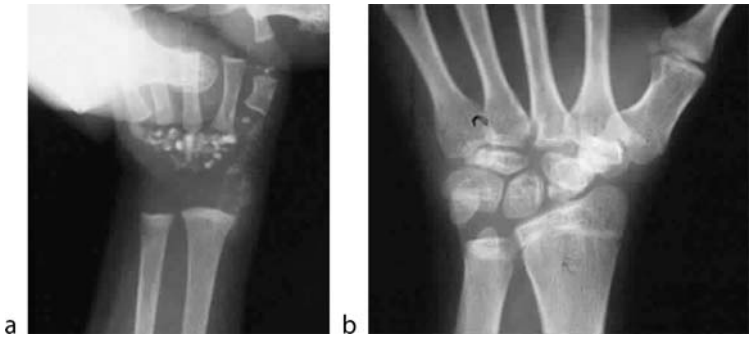

Osteodysplasia. Figure 3 From multiple stippled epiphyses to multiple epiphyseal dysplasia. (a) In infancy, one sees the multiple epiphyseal stipples of the distal carpal row as well as the (longitudinally short) first metacarpal. (b) In a 16-year-old, one sees highly dysplastic and narrow distal carpals (i.e., multiple epiphyseal dysplasia) with relatively normal proximal carpals, as well as the longitudinally short first metacarpal. [After F. Silverman. From Oestreich AE (2004) Epiphyseal dysplasias and dysostoses. In: Ferrucci JT (ed) Taveras and Ferrucci's Radiology on CD-ROM Diagnosis Imaging Intervention, Vol 5, chapter 5]

syndrome. A small mandible with an abnormally concave undersurface is the key finding of Pierre-Robin sequence and is seen in camptomelic dysplasia, cerebrocostomandibular syndrome, and Seckel syndrome. Progressive pseudorheumatoid dysplasia has joint region changes closely resembling rheumatoid arthritis, but also has both early and unusually large os trigonum centers behind the talus, and bullet-shaped or Scheuermann-like (irregular endplates) thoracolumbar vertebral bodies unlike rheumatoid arthritis. Every normal child, incidentally, has at least one small os trigonum center that appears near the end of the first decade of life and fuses with the talus in about a year, appearing somewhat earlier in girls than in boys. Then, in the second decade, another os trigonum center appears in some 10–20% of children, which may or may not also fuse to the talus to remain as a posteriorly protruding process.

Postaxial polydactyly and mesomelic short limbs are characteristic in Ellis–van Creveld syndrome. An interesting accompaniment to hand polydactyly is the ham-shaped hamate (a wider than normal hamate ossification in the form of a cured ham).

Various characteristic vertebral body shapes on lateral images occur in the several spondyloepiphyseal and spondylometaphyseal dysplasias, as well as mucopolysaccharidosis dysostosis multiplex conditions. Twisted ribs and long bones are the prime feature of Melnick–Needles osteodysplasty.

On *in utero* imaging, achondrogenesis, the second most frequent lethal skeletal dysplasia, is characterized by a lack of ossified vertebral bodies. Very short ribs, such as in short rib polydactyly syndromes, also predict neonatal demise, as do features of thanatophoric dysplasia (the best-known lethal dysplasia). The shorter the ribs in Jeune syndrome, the less likely the neonatal survival.

Bibliography

1. Struble JW (1995) John Cage and the aleatoric revolution. The history of American classical music: MacDowell through minimalism. Facts on File, New York, pp 285–303
2. Dwek JR (2005) Kniest dysplasia: MR correlation of histologic and radiographic peculiarities. Pediatr Radiol 35:191–193
3. Oestreich AE (2002) Mega os trigonum in progressive pseudorheumatoid dysplasia. Pediatr Radiol, Lippincott Williams & Wilkins, Philadelphia 32:46–48

Osteofibrous Dysplasia

Osteofibrous dysplasia (ossifying fibroma, Kempson–Campanacci lesion) is a benign fibroosseous lesion which mostly occurs in the tibia of young children. Histologically, the entity differs from fibrous dysplasia by containing scattered bony trabeculae that are rimmed by active osteoblasts.

▶Neoplasm-Like Lesions, Bone

Osteoid

Uncalcified organic bone phase consisting of collagen fibers (approximately 94%), proteoglycans, and glycoproteins.

▶Osteomalacia

Osteoid Osteoma

Osteoid osteoma is a benign bone-forming lesion of limited size that usually induces reactive new bone

formation. The lesion itself has classically been described as the "nidus" and should, by definition, not override a maximum diameter of 1.5 cm. Larger lesions should be termed osteoblastoma.
▶Neoplasms, Bone, Benign

Osteoidosis

▶Osteomalacia

Osteoma

The most frequent benign osseous tumor of the face and sinusal cavities, usually affecting men over 50 years of age. These tumors are commonly asymptomatic, fortuitously discovered on a radiologic examination, in the frontoethmoidal cavity or in the external auditory canal.
▶Fibro-Osseous Lesions, Facial Skeleton

Osteomalacia

Osteomalacia (OM) is a pathological condition in adult bone metabolism characterized by the impaired and delayed mineralization of osteoid, causing the accumulation of osteoid and altering the mechanical properties of bone.
▶Osteomalacia

Osteomalacia

Ahi Sema Issever
Institut für Radiologie, Charité Campus Mitte, Schumannstr, Berlin, Germany

Synonym

▶Osteoidosis

Definition

In adult bone metabolism – after closure of the epiphyseal growth plates – ▶osteomalacia (OM) is defined to be a condition of impaired and delayed mineralization of ▶osteoid (organic bone phase) in cortical and trabecular bone. In children, this condition is known as ▶rickets and includes the defective mineralization of the cartilaginous part of the epiphyseal growth plates.

Pathology/Histopathology

Physiological bone remodeling is a dynamic process of constant bone formation and resorption, respectively, carried out on the cellular basis through osteoblasts and osteoclasts. Chronologically, bone formation can be divided into two phases. In phase I the osteoblasts produce osteoid in the organic bone matrix consisting of collagen fibers, proteoglycans, and glycoproteins. In phase II the osteoblasts produce calcium, phosphate, hydroxyl, and carbonate creating a plate-like crystal known as hydroxyapatite, which mineralizes on the osteoid-forming calcified bone. Pathophysiological disturbances in phase II based on alterations of the calcium phosphate homoeostasis – in which the serum calcium X phosphorus product is low – lead to the condition of OM in adults and to rickets in children. The calcium phosphate homoeostasis is maintained by a multitude of factors, and thus the etiology of OM and rickets is very diverse. A large number of disorders are associated with OM and rickets. Nonetheless, hypovitaminosis D is considered to be the most frequent cause of OM. The primary role of vitamin D is its physiological function in opposing a decline of serum calcium. Examples of disturbances in vitamin D metabolism that may cause OM are:

- Low dietary intake
- Insufficient UV absorption of the skin (reduced natural sunlight exposure, skin covering garments, dark skin complexion which leads to the absorption of only certain spectra of the UV light)
- Intestinal malabsorption, e.g., after gastrectomy, bowel resection, or nontropical sprue
- Accelerated vitamin D excretion by virtue of anticonvulsive drugs inducing liver enzymes
- Chronic renal failure leading to a deficient hydroxylation of the liver 25(OH)-vitamin D_3 into the active $1,25(OH)_2$-vitamin D_3 form

As described above, a low calcium X phosphorus product is the pathophysiological starting point for the genesis of OM and rickets, and therefore conditions leading to low phosphorus levels must also be considered:

- Acquired phosphate depletion due to malnutrition, alcoholism, and use of aluminum-containing antacids which bind phosphorus intestinally
- Increased renal excretion of phosphorus caused by an impaired tubular resorption (e.g., adult-onset vitamin D-resistant hypophosphatemic osteomalacia, Fanconi syndrome)

Attention should also be paid to oncogenic conditions causing OM (tumor-induced or oncogenic OM), although they occur seldom. This paraneoplastic syndrome is associated with several different neoplasms, of which the majority are of benign and mesenchymal origin, namely, bone and soft tissue tumors. These tumors release circulating factors that increase the phosphorus renal clearance consecutively causing low serum phosphorus levels, while the calcium serum concentration is normal.

Clinical Presentation

The clinical presentation of OM is unspecific. Frequent complaints of patients suffering from OM are bone pain and muscle weakness. Bone pain is of diffuse and dull character. In general the symptoms begin as lower back pain and spread symmetrically into the pelvic region and the hips, or upward to the vertebral column into the rib cage and the shoulder girdle. Compression, vibration, or mere muscular activity of symptomatic regions may provoke and increase pain, in some cases leading to the adjusted pain-avoidance behavior of the patient, such as cautious walking, in extreme cases even immobilization or the fear of coughing.

OM-related muscle weakness is generally localized proximal to the body trunk, e.g., around the hips involving the gluteal muscle group leading to a waddling gait in late stages of the disease. Whether muscle weakness is secondary to bone pain or of primary genesis is difficult to distinguish. In advanced stages of OM, morphological deformities of the skeleton – due to bone softening and hence reduced mechanical strength – can be observed resulting in hyperkyphosis of the thoracic vertebral column or coxa vara and a high fracture susceptibility.

In children suffering from rickets, morphological deformities of the skeleton vary in their dimension according to the time of onset in relation to the phase of epiphyseal bone growth. In periods of rapid growth, rickets tends to achieve high clinical severity. Craniotabes (softening of the calvaria), late fontanelle closure, rachitic rosary (palpable bloating of the costochondral junctions), Harrison's groove (indentation of the lower ribs at the diaphragm), bowing of the long bones (tibia, femur, radius, ulna), and thickening of the wrist, knees, and ankles (on grounds of metaphyseal widening) are the most visible clinical complications. Muscle weakness to severe muscle hypotonia is another major complication of rickets.

Imaging

With conventional radiographs, computed tomography, and magnetic resonance imaging, a wide range of modalities for diagnosing OM are at hand.

In OM, conventional radiographs are usually obtained first. The overall radiographic appearance of bone can be described as homogenous and fuzzy. The reason for this is the decline of contrast differences between bone marrow and calcified bone due to the increased density of unmineralized osteoid. In contrast to this rather non-specific "ground-glass" appearance, so-called ▶Looser's zones – found in only 5–10% of patients suffering from OM – are considered to be typical. Looser's zones – also known as ▶milkman's zones or ▶pseudofractures – are radiolucent bands of unmineralized osteoid usually oriented perpendicular to the surface of the bones ranging in size from a few millimeters to several centimeters. Looser's zones are frequently found bilaterally, symmetric, at sites where larger arteries are adjacent to the bones (inner aspects of the femur, pubic rami, the lateral edge of the scapula, and the metatarsals); the hypothesis being that the pulsation of these vessels and the reduced mechanical strength of the bones cause pseudofractures of the latter which heal only insufficiently with osteoid.

On computed tomography images the fuzzy "ground-glass" appearance of bones affected by osteomalacia is also observed, and Looser's zone may be identified more accurately in contrast to pathological fractures of other genesis.

The relative increase of unmineralized osteoid in relation to mineralized bone or the relative decrease of mineralized to unmineralized bone can be quantified measuring the overall bone mineral density using either dual x-ray absorptiometry or quantitative computed tomography.

Pseudofractures may be identified as hypointense lines or fissures on T1- and T2-weighted magnetic resonance (MR) images as well as on images acquired using short T1 inversion recovery (STIR) sequences. High signal intensity around the fracture area on T2-weighted and STIR MR images reveals an acute process, whereas isolated hypointense regions are considered to be chronic. Therefore, the clinical activity of OM may be determined using MR imaging.

Nuclear Medicine

For isotope bone scanning, technetium 99m-labeled methylene diphosphonate – which preferably adsorbs onto bone surfaces undergoing new bone formation – is being used. The diagnostic strength of isotope bone scanning for metabolic bone diseases is based on its high sensitivity in detecting and localizing functional alterations before structural changes have taken place. In OM the bone scan often shows a nonspecific increased uptake of technetium 99m involving the entire skeleton. However, Looser's zones may be identified on bone scans

before they are visible on conventional radiographs. For the diagnosis of oncogenic OM and the identification of the primary tumor, it has been reported that tracers selectively binding onto somatostatin receptors (octreotide) may improve the detection rate.

Diagnosis

The difficulty in diagnosing OM arises from its very nonspecific clinical presentation as described above. In the population of elderly patients, diffuse bone pain and muscle weakness can be misinterpreted as rheumatological conditions, thus OM remains undiagnosed, although in most cases it is a curable diseases. Higher awareness and suspicion of osteomalacia in daily clinical routine is therefore essential.

Laboratory test results are given in the form of a table.

Imaging modalities for the diagnosis of OM have been described above; nonetheless, a brief summary in the context of the overall diagnostic procedure is as follows: patients presenting with unspecific symptoms and laboratory findings suggesting that OM might be the underlying cause may first undergo isotope bone scanning in order to identify typical Looser's zones. Conventional radiographs of suspicious regions can validate the diagnosis in some cases, but one should keep in mind that radiographically visible morphological changes may occur rather late in the course of OM as compared to pathological uptake behavior on bone scans. On the other hand, if patients can localize peak pain spots, conventional radiographs may be sufficient for identifying Looser's zone without the use of isotope bone scan. Bone mineral density measurements are rather unspecific for the diagnosis of OM because a multitude of disorders, particularly osteoporosis, are associated with a decreased bone mineral density. Besides having a higher spatial accuracy, computed tomography can be used if it is difficult to ascertain with conventional radiographs whether fractures are caused by OM or other pathological conditions. MR imaging, in addition, can help describe the acuteness of fractures. If all imaging modalities and laboratory tests fail, the best – gold standard – diagnostic modality for identifying OM is the histological analysis of bone biopsies in which the accumulation of osteoid is visible as an increase in the average osteoid volume (>10%) and thickness (>15 μm).

Serum concentration	Vitamin D deficiency	Chronic renal failure	Renal tubular disorders
Ionized calcium	Normal/↓	↓	Normal
Inorganic phosphorus	↓	↑	↓
25(OH)-vitamin D_3	↓	Normal	Varies

(*continued*)

References

1. Edmister KA, Sundaram M (2002) Oncogenic osteomalacia. Semin Musculoskelet Radiol 6(3):191–196
2. Freyschmidt J (2003) Osteomalazie. Skeletterkrankungen 2nd edn. pp 185–195
3. Hain SF, Fogelman I (2002) Nuclear medicine studies in metabolic bone disease. Semi Musculoskelet Radiol 6(4):323–329
4. Kanberoglu K, Kantarci F, Cebi D et al (2005) Magnetic resonance imaging in osteomalacic insufficiency fractures of the pelvis. Clin Radiol 60(1):105–111
5. Reginato AJ, Coquia J (2003) Musculoskeletal manifestations of osteomalacia and rickets. Best Practice Res Clin Rheumatol 17(6):1063–1080

Osteomyelitis

H. P. Ledermann[1], W. B. Morrison[2]
[1]Department of Radiology, University hospital Basel, Basel, Switzerland
[2]Department of Radiology, Thomas Jefferson University Hospital, Philadelphia, USA
hanspeter.ledermann@imammed.ch

Synonym

Bone infection

Definition

The term *osteomyelitis* implies an infection of bone and bone marrow, whereas *osteitis* indicates contamination of the cortical bone only. *Chronic osteomyelitis* results most commonly after trauma or surgery and results from unsuccessful treatment of acute bone infection. A *sequestrum* represents a segment of necrotic bone that is separated from living bone by granulation tissue. An *involucrum* denotes a layer of living bone that has formed about the dead bone. An opening in the involucrum is termed a *cloaca*. A Brodies abscess is an intraosseous abscess, frequently seen in children caused by *Staphylococcus aureus* and represents a subacute or chronic infection. *Chronic recurrent multifocal osteomyelitis* is a rare sterile (noninfectious) disorder primarily involving

children and adolescents and characterized by a prolonged, fluctuating course most often involving the tubular bones, the clavicle, and less often the spine.

Pathology/Histology

Pathology: Osseous structures can be contaminated by three principal routes (1):

1. Hematogenous spread of infection through the blood stream as in osteomyelitis of the child or spondylodiscitis.
2. Direct spread from a contiguous source of infection as seen in diabetic foot infections or decubital ulcers in paralyzed patients.
3. Direct implantation of infectious material into the bone as seen after penetrating injuries, punctures, or other surgical procedures.

Hematogenous osteomyelitis of the *child* is most frequently located in the metaphysis of long bones. In the infant up to 1 year of age, bone infection may be complicated by epiphyseal involvement. Subperiosteal abscesses and septic arthritis may complicate osteomyelitis in older children.

In *adults*, osteomyelitis most frequently results from direct spread from a contiguous source of infection and most of these patients have pedal osteomyelitis due to longstanding diabetes mellitus. Prevalence of *posttraumatic* osteomyelitis directly depends on the degree of traumatization of the involved limb (extensive soft tissue damage, necrotic bone, and presence of foreign bodies). Infection results from direct implantation of microorganism in most cases and *S. aureus* is the most common pathogen. *Postoperative* infection occurs via direct implantation, spread from a contiguous septic focus or hematogenous contamination.

Histology: Bone biopsy is performed if clinical and radiologic evaluation is not conclusive, if a neoplasm is suspected or if microbial diagnosis is attempted. Definite diagnosis of osteomyelitis relies on positive culture results of causative organisms from a biopsy sample. Characteristic histologic findings of bone infection include aggregates of inflammatory cells (including neutrophils, lymphocytes, histiocytes, and plasma cells), erosions of trabecular bone and marrow changes that range from loss of normal marrow fat in acute osteomyelitis to fibrosis and reactive bone formation in chronic disease. Limitations of percutaneous and surgical bone biopsy include sampling error, false negative cultures in patients receiving antibiotics, difficulties in distinguishing other osteopathy from osteomyelitis histopathologically, and the risk to damage the bone as a result of trauma or iatrogenic infection. Culture results of percutaneous bone biopsy specimens in pedal infection may be unreliable due to contamination from underlying infected soft tissue. Bone biopsy cultures in osteomyelitis may be false negative in up to 50%, whereas accuracy of histopathologic diagnosis of osteomyelitis is high.

Clinical Presentation

The clinical manifestations of the different forms of bone infections vary considerably depending on the activity of infection. Childhood osteomyelitis is often associated with a sudden onset of high fever, a toxic state, and local signs of inflammation. Diabetic foot infection most commonly has a chronic, relatively indolent course but may quickly lead to septicemia and toxic shock. Tuberculous osteomyelitis differs from pyogenic osteomyelitis by the absence of fever and pain. Posttraumatic and postoperative infections may, in the acute and early stages, lead to exquisite focal symptoms with significant inflammation, fever, and leukocytosis. If the infection can not be cured in the acute stage, chronic recurrent osteomyelitis develops with chronic recurrent bouts of infection, abscesses, bony sequestra, and fistula.

Imaging

Radiographs

Radiographs are usually the first radiological examination performed if bone infection is suspected. In children, first signs of hematogenous osteomyelitis may be perceptible a few days after onset of symptoms. First radiographic signs of hematogenous osteomyelitis are a subtle swelling of the juxtacortical soft tissues, which may only be evident by direct comparison with the other extremity. Destructive metaphyseal osteolysis and periostitis become visible after 8 to 10 days. Brodies abscesses are typically seen radiographically as well-defined metaphyseal radiolucencies with sclerotic borders, "dripping" to the physeal plate.

In adults, radiographic findings of osteomyelitis do not appear in adults for 10 to 14 days after infection and until 35 to 50% of the bone has been destroyed. Radiographic changes of osteomyelitis are not only delayed, but sensitivity is poor. Typical radiographical signs of acute osteomyelitis are permeative bone destruction with periosteal reaction and surrounding soft tissue swelling (Fig. 1a). Beginning cortical bone resorption can be identified as endosteal scalloping, intracortical tunneling, and poorly defined subperiosteal bony defects. Radiographs are also the basic imaging modality in posttraumatic and postoperative osteomyelitis displaying postoperative bony remodeling, sequestra, foreign bodies and osteosynthetic material, and deformities. Acute

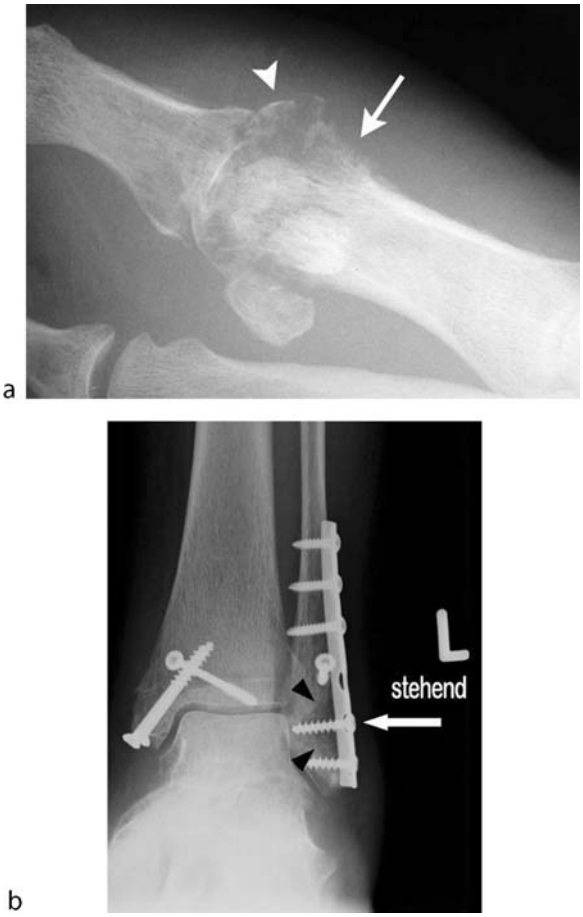

Osteomyelitis. Figure 1 Illustration of typical radiographic signs of acute osteomyelitis. (a) Advanced osteomyelitis of the first metatarsal head in a diabetic patient with an ulcer at the plantar aspect of the first metatarsophalangeal joint. The radiograph reveals extensive permeative bone destruction of the first metatarsal head (arrow) with fragmentation (arrowhead). Also note the narrowing of the joint space due to concomitant septic arthritis. (b) Postoperative acute osteomyelitis of the distal fibula with permeative bone destruction (arrowheads) around the second most distal screw (arrow), which is loosened at the plate with a fine radiolucent rim around the screw head.

postoperative and posttraumatic osteomyelitis leads to ill-defined bone destruction, which usually develops in bone directly adjacent to the metal (Fig. 1b). Chronic osteomyelitis can lead to reactive bone formation, periosteal reaction, bony fistula, intraosseous abscesses, and bony sequestra. Presence of surgical implants and posttraumatic bone remodeling may considerably complicate evaluation of chronic osteomyelitis. To evaluate activity of chronic osteomyelitis, it is very helpful to compare current and old films together as changes such as a new linear periosteal reaction, osteolysis, and sequestration are suspicious of active infection. Delayed union or nonunion of fracture may also be caused by chronic infection.

Computed Tomography

Computed tomography has been largely replaced by magnetic resonance (MR) imaging to evaluate osteomyelitis. CT may however be useful to evaluate the presence of sequestra and involucra in chronic osteomyelitis. Since CT offers exceptional detail of the bony architecture in a cross-sectional display, it can also be used to evaluate cortical destruction and fistula, periosteal new bone formation, and the presence of intraosseous gas (Fig. 2), all of which are less conspicuous on MR images.

Magnetic Resonance Imaging

MR imaging allows early detection of osteomyelitis in contrast to radiographs and CT. Diagnosis of osteomyelitis on MR images is based on the identification of altered bone marrow signal (Fig. 3). Infection of the marrow compartment results in loss of the normal fatty marrow signal on T1-weighted images, with edema on T2-weighted or STIR images, and enhancement on post-gadolinium T1-weighted images. MR protocols should include fat-saturated T2-weighted images and contrast-enhanced, T1-weighted fat-suppressed images (2). Identification of such marrow signal alterations away from the subchondral bone results in high sensitivity for osteomyelitis; however, other entities can alter the bone marrow signal in similar fashion, including fracture, tumor, severe inflammatory arthritis or neuropathic disease, or recent postoperative changes. The lack of bone marrow edema on STIR images excludes osteomyelitis with a specificity of 98% (2).

Pedal osteomyelitis, which is by far the most frequent form of osteomyelitis in adult diabetic patients, results in over 95% of patients from contiguous spread of a soft tissue infection; the majority of these patients have some combination of adjacent skin ulceration, cellulitis, soft tissue abscess, and sinus tract. These signs are also called "secondary signs" of osteomyelitis, and can improve specificity. Ischemic tissue in pedal infection is best visualized on fat-suppressed, contrast-enhanced images (3). Osteomyelitis and abscesses may not enhance in necrotic tissue (3).

In complicated posttraumatic cases, postoperative bone marrow signal alterations can persist as long as 1 year (4). MR protocols in postoperative osteomyelitis should include fast spin-echo (FSE) sequences with high bandwidth to decrease susceptibility artifacts from the

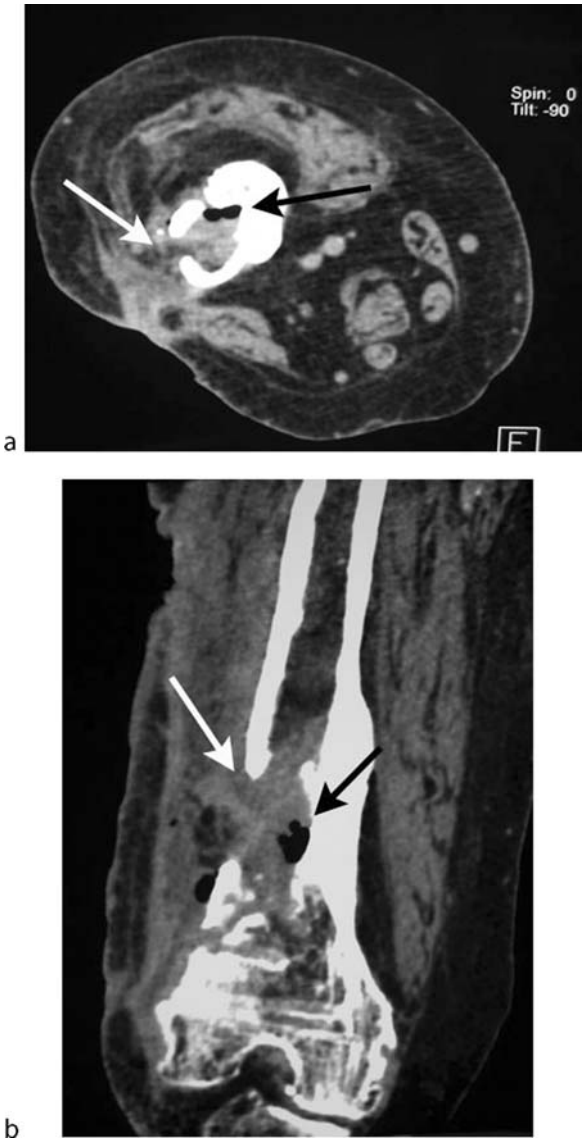

Osteomyelitis. Figure 2 Illustration of CT findings in chronic active posttraumatic osteomyelitis. (a) Axial scan reveals a cortical defect (white arrow) in the severely remodeled cortex of the distal femur and gas inclusions (black arrow) in the marrow space. (b) Coronal reformat reveals extensive bony remodeling and a large cortical defect (white arrow) filled with enhancing tissue extending to the bone marrow. Intramedullary gas inclusions (black arrow) in the marrow are also indicative of active infection.

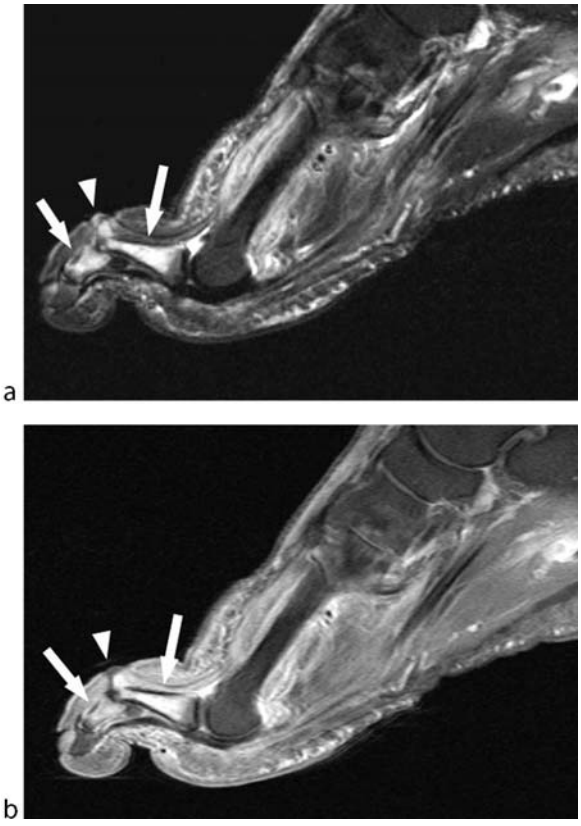

Osteomyelitis. Figure 3 Typical MR signal alterations of osteomyelitis in a diabetic patient with an ulcer dorsal to the proximal interphalangeal joint of the second toe. (a) Fat-suppressed T2-weighted image reveals hyperintense signal in the bone marrow of the proximal and middle phalanx (arrows) and interruption of the dorsal skin surface with hyperintense sinus tract (arrowhead). Note the destruction of the proximal interphalangeal joint with subluxation indicating septic arthritis. (b) Contrast-enhanced, T1-weighted fat-suppressed image with diffuse hyperintense signal in the bone marrow of the proximal and middle phalanges confirming osteomyelitis. Note the delineation of the small dorsal ulcer (arrowhead) and the linear hypointense sinus tract extending to the destroyed joint.

metal implants. Gradient echo images and frequency selective fat suppression lead to extensive metal artifacts. T1-weighted subtraction images may be used instead after gadolinium administration.

An *intraosseous abscess* leads to typical findings of a "target" appearance with a center of low signal intensity on T1-weighted images and high signal on T2-weighted images with rim enhancement. Chronic osteomyelitis and sclerosing osteomyelitis are indolent processes with areas of bone necrosis and sclerosis; as a result, MR imaging may show areas of low signal on T1- and T2-weighted images. Differentiation between reactive, noninfective tissue edema with inflammation from true bacterial infection may be difficult using MR imaging in the following situations (1): (a) differentiation of secondary osteomyelitis from reactive bone marrow edema in septic arthritis, (b) differentiation of postoperative and

posttraumatic reparative signal alterations from infection (4), and (c) differentiation of pedal osteomyelitis and diabetic neuroarthropathy (see also Neuropathic Joint Disease).

Ultrasound

Ultrasound imaging can be very useful in pediatric patients due to the lack of radiation. Sonographic signs of osteomyelitis include asymmetric juxtacortical soft tissue swelling, thickening of the periosteum, and demonstration of an adjacent hypoechoic collection. In advanced cases, frank cortical destruction can be seen.

Nuclear Medicine

Technetium-99m MDP three-phase bone scan has a high sensitivity for osteomyelitis and is excellent for excluding bone infection in case of a normal radiograph, but specificity is low. Increased accumulation of tracer can be seen in other conditions such as bone tumors, neuropathic osteoarthropathy, fractures, and following trauma and surgery. One advantage of Tc99m MDP studies over radiography is that it can detect osteomyelitis within 24 to 48 h of onset.

Labeled white blood cell scans or Tc99m labeled monoclonal antigranulocyte antibodies raise the specificity to detect osteomyelitis, and may be helpful in excluding infection in a Charcot joint.

Diagnosis

Timely diagnosis of acute osteomyelitis is best achieved by either MR imaging or scintigraphy if radiographs are normal. Sonography may be very useful in acute pediatric osteomyelitis or septic arthritis. Activity of chronic posttraumatic or postoperative osteomyelitis is often best evaluated by comparison of recent and older radiographs. In complex cases with chronic posttraumatic osteomyelitis, a multimodality approach involving specialists from different disciplines (infectious disease, radiology, orthopedic surgery) is usually required.

▶Oral Cavity, Inflammatory Diseases
▶Neoplasms, Odontogenic

Bibliography

1. Resnick D (2002) Osteomyelitis, septic arthritis and soft tissue infection: mechanisms and situations. In: Diagnosis of Bone and Joint Disorders. 4th edn. W.B. Saunders, Philadelphia, vol 3, chapter 59, pp 2377–2480
2. Morrison WB, Schweitzer ME, Bock GW et al (1993) Diagnosis of osteomyelitis: utility of fat-suppressed contrast-enhanced MR imaging. Radiology 189:251–257
3. Ledermann HP, Schweitzer ME, Morrison WB (2002) Nonenhancing tissue on MR imaging of pedal infection: characterization of necrotic tissue and associated limitations for diagnosis of osteomyelitis and abscess. Am J Roentgenol 178:215–222
4. Ledermann HP, Kaim A, Bongartz G et al (2000) Pitfalls and limitations of magnetic resonance imaging in chronic posttraumatic osteomyelitis. Eur Radiol 10:1815–1823

Osteomyelitis, Neonates, Childhood

Alan E. Oestreich
Cincinnati Children's Hospital Medical Center, Cincinnati, Ohio, USA
Alan.oestreich@cchmc.org

Synonyms

Bone infections; Bone marrow infections; Joint infections; Soft tissue infections

Definition

Infections of individual bony parts, joints, and other supporting musculoskeletal tissue, including combinations of the three.

The responsible agent may be bacterial, fungal, parasitic, viral, or other organisms. A condition resembling osteomyelitis, but without a known agent, is chronic recurrent multifocal osteomyelitis (▶CRMO), with various skeletal manifestations behaving symptomatically and radiographically similar to infection. An open fracture is associated with a break in the skin or at the nail bed. A closed fracture has no such direct communication with the outside environment.

Pathology/Histopathology

According to the causative organism, the histopathology of bone (and joint and soft tissue) infection varies. Additionally, the histopathology of subacute and chronic infection is different from the acute type. Moreover, failures in body defense mechanisms vary between these underlying conditions – for example, in ▶chronic granulomatous disease of childhood, white cells can ingest bacteria and other organisms, but not digest them when the organisms do not contain hydrogen peroxide (for this reason, Ed Neuhauser called the condition "dyspeptic granulomatosis"). The physis is a relative barrier to

passage of infection in bones, except in infancy or when affected by trauma. The bone bark of the metaphyseal collar is a relative barrier to pus in bone, so that breaking through cortex to form periosteal reaction generally stops at the step-off between periosteum and bone bark (in luetic bone disease, this feature is known as the Wimberger sign). In those joints that surround metaphyseal bone, infection travels readily between bone and joint. Neonates of mothers infected with syphilis who show "leukemic lines" at birth do not, at the time of neonatal x-ray imaging, have skeletal infection yet, but rather show the generalized effect of intrauterine stress (of the same nature of such lucent bands when the mother is given magnesium sulfate during late pregnancy (2)). Later in childhood syphilitic bone disease may or may not include local spirochetes. Biopsy of lesions in chronic recurrent multifocal osteomyelitis shows many plasma cells, but no microorganisms.

Clinical Presentation

Cardinal signs and symptoms of osteomyelitis include fever, malaise, pain, tenderness, swelling, warmth, redness, and loss of motion. The same signs occur with septic arthritis, and most are found with pyomyositis and other soft tissue infections, so that clinically the differentiation of the sites of infection may be difficult indeed. In patients with immune deficiency and other disorders of defense mechanisms, symptoms may be more silent.

Any ▶stubbed toe or stubbed finger fracture (dorsal Salter II fracture of a distal phalanx) must be suspected of being infected (3) (Fig. 1). Bones adjacent to tissue sites of tuberculosis or actinomycosis are vulnerable to becoming infected, as those infections tend to cross tissue planes. In osteopetrosis, one should be alert for jaw osteomyelitis.

Imaging

Since bone local demineralization and periosteal reaction do not appear on plain radiographs for 10 days after an infection begins, it is essential that the radiologist not dismiss a "normal" study before 10 days as ruling out infection (Fig. 2). It is also wrong to give the advice of solely a return for repeat imaging before the 10 days have elapsed or even after that time – the time to diagnose and treat osteomyelitis is right away (not only after plain film abnormality is evident). Nuclear imaging, ultrasound, and magnetic resonance imaging (MRI) are particularly good for early detection of infection. With ultrasound, elevation of the periosteum may be detected within a day, far earlier than the 10 days required for plain imaging.

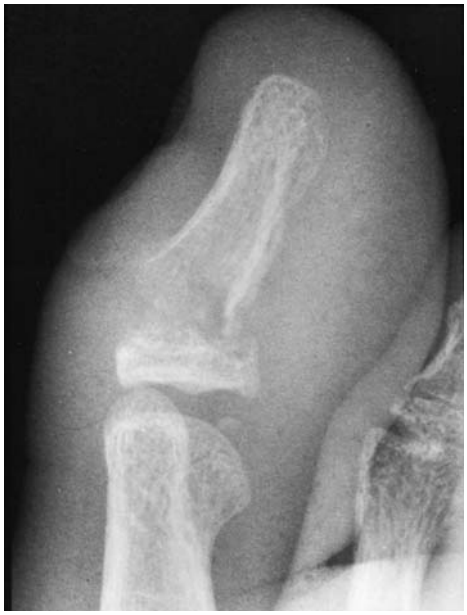

Osteomyelitis, Neonates, Childhood. Figure 1
Osteomyelitis of the distal phalanx of the great toe in a boy several weeks after a stubbed toe Salter II fracture. Bone destruction and periosteal reaction have appeared. From Oestreich AE, Crawford AH (1985) Atlas of Pediatric Orthopedic Radiology, Thieme Verlag, Stuttgart p. 70.

The echogenic periosteum is separated by a hypoechoic zone from the echogenic cortex (Fig. 3). MRI can reveal edema in marrow and surrounding soft tissue, as well as show the organizing fluid elevating periosteum. A needle stick under fluoroscopic, ultrasound, or computed tomography (CT) guidance can also give a diagnosis quickly. CT can distinguish soft tissue infection from its normal surroundings, as can ultrasound and MRI. Dental films give high detail of the periapical region if infection beyond teeth is suspected. Fluid surrounding a tendon is well depicted by ultrasound in tendonitis.

Nuclear Medicine

Acute osteomyelitis that has caused necrosis or avascularity will be cold (less activity than normal bone) on bone scan, unlike the majority of bone infection – acute, subacute, or chronic – which will be hot. A bone scan alone may not distinguish infarction from new sterile infarction in sickle cell anemia, but gallium scanning gives relatively much stronger uptake in infection than infarction. Infection limited to joint or soft tissue should not increase activity in adjoining bone on precise nuclear images. Since it takes 10 days for bone demineralization or periosteal reaction to become visible on radiographs,

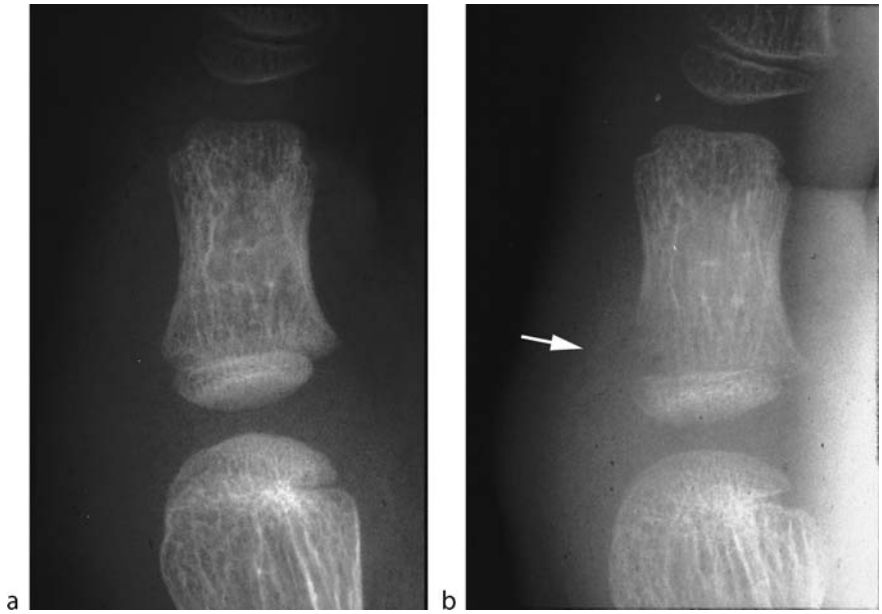

Osteomyelitis, Neonates, Childhood. Figure 2 (a) Less than 10 days from onset of symptoms, a plain image of the great toe shows some soft tissue swelling, but the bone is normal in appearance. (b) Ten days later, destruction of the proximal medial metaphysis and metadiaphysis is evident (arrow). It is a medical error to wait until the radiograph is abnormal; other imaging or some treatment should have been initiated at the time of presentation. From Oestreich AE, Crawford AH (1985) Atlas of Pediatric Orthopedic Radiology, Thieme Verlag, Stuttgart p. 247.

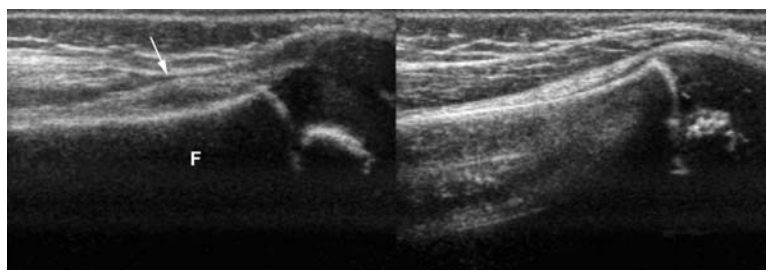

Osteomyelitis, Neonates, Childhood. Figure 3 A young child with acute osteomyelitis of the proximal femur (F), with no plain image bone abnormality yet. The arrow points to periosteum elevated by the sonolucent pocket of pus external to the femoral shaft (F) on longitudinal ultrasound. The right-sided image is the normal contralateral side.

the radiologist should strongly consider bone scanning for diagnosis if symptoms have lasted less than that time. Gallium 67 citrate is generally positive in osteomyelitis by 24–48 h. Labeled white cells with indium 111 or Tc99m HMPAO are other means for seeking infection by nuclear scanning. Active chronic recurrent multifocal osteomyelitis is expected to be positive on bone scan during active phases. In Langerhans cell histiocytosis (one theory considers the disease formerly known as histiocytosis X to be of infectious origin), increased bone scan activity with a photopenic center may be seen. For spondylodiskitis in a child, gallium scan shows high activity; MRI is an alternative useful modality.

Diagnosis

Perhaps the most important point to restate about radiographs of osteomyelitis is that bone demineralization and periosteal reaction are not visible until 10 days after the infection begins; so the diagnosis should not wait for that. Something else should be done (nuclear imaging, needle biopsy, ultrasound, CT, MRI, or heuristic treatment possibly guided by blood culture). Tarsal and carpal bones and the patella and other growth centers have no periosteum, so they will not have periosteal reaction. Infection around the roots of teeth leads to loss locally of the lamina dura and bone demineralization. Infection of

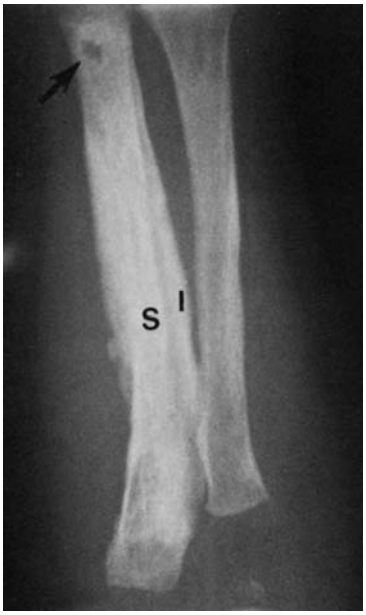

Osteomyelitis, Neonates, Childhood. Figure 4 Four weeks after only soft tissue swelling and a positive elbow fat pad, this 6-month-old infant has full-blown osteomyelitis seldom seen today, with an involucrum (I) surrounding sequestrum (S) of the ulna and a distal cloaca evident (arrow). From Oestreich AE, Crawford AH (1985) Atlas of Pediatric Orthopedic Radiology, Thieme Verlag, Stuttgart p. 66.

the long bone shaft usually does not disturb the 1–3 mm metaphyseal collar, but bone demineralization and periosteal reaction begin beyond it. Untreated or unsuccessfully treated tubular bone osteomyelitis may eventually lead to involucrum (from periosteum) surrounding sequestrum (the damaged avascular bone) and discharge of pus through a radiographically evident cloaca (Fig. 4). Subacute osteomyelitis (Brodie abscess) tends to be seen as ovoid bone demineralization, longitudinally directed, near a physis or perhaps crossing it.

Infection, and other fluid, in the hip or humerus is generally not perceived on plain images (until eventual local bone infection or regional demineralization occurs). Infection in the knee and ankle is easily seen (but not specific) from interfaces, the suprapatellar bursa and the ankle tear drop just adjacent to the talus, respectively.

Soft tissue infections on plain images are seen as soft tissue swelling and disturbance of the local interfaces between tissues, including subcutaneous fat. Exceptionally, gas density is seen from gas-forming organisms.

Interventional Radiological Treatment

Interventional pediatric radiologists may be asked to drain deep abscesses, generally done under ultrasound, but sometimes CT, guidance. If fluid is obtained, it should be investigated for organisms, including tuberculosis, regardless of the gross appearance.

References

1. Jurik AG (2004) Chronic recurrent multifocal osteomyelitis. Semin Musculoskelet Radiol 8:243–253
2. Malaeb SN, Rassi AI et al (2004) Bone mineralization in newborns whose mothers received magnesium sulphate for tocolysis of premature labour. Pediatr Radiol 34:384–386
3. Yellin JA, Towbin RB, Kaufman RA (1985) Stubbed finger osteomyelitis. J Trauma 25:808–809

Osteonecrosis, Adults

Christian R. Krestan
Department of Radiology, Medical University of Vienna
Vienna General Hospital, Austria
christian.krestan@meduniwien.ac.at

Synonyms

Aseptic bone necrosis; Avascular necrosis

Definition

Negative bacteriologic studies from well-documented cases of bone necrosis led to the use of the term "aseptic necrosis." Subsequent observations indicated that such cases were not only aseptic but also avascular. Hence, the terms "ischemic necrosis," "►avascular necrosis," and "►bone infarction" were suggested (1). By convention, the term "bone infarction" is reserved for bone necrosis in the metaphyseal and diaphyseal regions, whereas "avascular necrosis" (ischemic necrosis) applies to the epiphyseal and subarticular regions.

Pathology/Histopathology

Knowledge of the anatomy and histology of the articular and subarticular region are important for understanding the pathophysiology of osteonecrosis.

In the hyaline cartilage, four different zones can be differentiated microscopically because of different orientation of the fibers. Below the three superficial zones lies the very thin zone of calcified cartilage, divided from the uncalcified zone by the so-called tide mark that represents

the zone of new cartilage formation. The chondrocytes produce the fibers and the ground substance, which is composed of collagens (5–10%), proteoglycans (10–30%; important for osmotic pressure), and water (65–80%).

At its base, adult articular hyaline cartilage is bordered by the subchondral plate (cortical endplate) with a high number of arterial vessels, capillaries, sinusoids, and venous vessels, with a declining number by 20% from adolescence until the seventh decade. While the upper (outer) zones of cartilage get their nourishment from the synovial fluid, there is some evidence that the very important zone of calcified cartilage and, definitely, the subchondral regions are fed by the subchondral vessels. The medullary bone has a dual blood supply, from the medullary arteries and periosteal arteries (2). Bony structures with a relatively high amount of cartilage surface (head of femur, talus) are very prone to problems in vascularization.

Ischemic necrosis of bone and bone infarction occur in areas of predominantly fatty marrow, which has a much lower blood flow. Infarcts (ischemic necrosis) occurring within the epiphysis or in small round bones (such as the talus) are covered by compact subchondral bone and cartilage.

Mineralized bone does not appear to be directly materially altered by ischemic necrosis. Bone density is unchanged within the dead bone but is usually lowered in the surrounding bone due to reactive changes (osteopenia).

Clinical Presentation

The clinical symptoms depend on the anatomic location of the osteonecrosis. A small proportion of patients may even present without symptoms, but usually in ►Association Recherche Circulation Osseous (ARCO) stage 2 avascular necrosis is associated with considerable pain. If the femoral head is affected, patients suffer from slight pain in the hip joint, groin, or buttock or may experience limping and even be unable to walk at all. The symptoms are unspecific, so many other conditions, including arthrosis, insufficiency fractures, and sciatica, have to be considered in the differential diagnosis. In patients with Ahlback's disease the clinical onset is relatively abrupt, with pain that worsens during the night and accompanying effusion and tenderness. The clinical presentation may mimic meniscal disease or arthrosis and can only be diagnosed with ►magnetic resonance imaging (MRI). Avascular necrosis of the lunate bone leads to localized pain and swelling of the wrist. Again, without proper imaging modalities, the diagnosis can be delayed. Early diagnosis is of utmost importance for proper treatment of the disease because failure to promptly initiate appropriate therapy can lead to bone and joint destruction with subsequent need for total joint replacement.

Imaging

Standard radiographs, computed tomography (CT), and MRI are used in the diagnosis of osteonecrosis/bone infarction.

The early diagnosis must be based on the visualization of changes in the soft tissue/bone marrow, which are altered on MRI. The role and relevance of high-resolution CT in detecting subchondral (micro)insufficiency fractures in early diagnosis of epiphyseal osteonecrosis is still under discussion. The only existing imaging modality to visualize necrotic marrow tissue is MRI. The combination of the inner linear, high-intensity rim with the parallel-running outer, low-intensity rim on T2-weighted or contrast-enhanced MR images is typically called the "double-line" sign and is characteristic for epiphyseal ischemic osteonecrosis with repair (3) (Fig. 1a–c). In this stage (ARCO 2), an arc-shaped subchondral lucent lesion with a thin sclerotic rim can be seen on standard radiographs. These findings are even better demonstrated with CT. CT also shows the abnormal configuration of the trabeculae resulting in irregular localized tiny defects with neighboring sclerosing areas. This ARCO stage 2 may last for weeks and months, but subchondral bony fractures ("crescent sign") representing ARCO stage 3 may finally develop. They are best seen on standard radiographs and/or CT (4). Finally, a complete impression fracture will occur. In ARCO stage 4, all typical signs of degenerative osteoarthritis are summarized, which includes joint deformity with flattening of the most involved part, subchondral "cystic" and sclerotic changes, formation of osteophytes, and joint space narrowing. Application of intravenous MR contrast medium is advocated by some authors, which could be helpful in unclear cases to exactly differentiate the necrotic part with no contrast enhancement from the surrounding viable tissue (5). As the most sensitive MR sequence, STIR images should be used first. If any abnormality is seen, T1-weighted fat-suppressed and T2-weighted gradient-echo (or fast spin-echo) should be added.

In (medullary) bone infarction the early phase with central necrosis and surrounding reactive and usually irregularly shaped tissue, which shows significant contrast enhancement, is followed by increasing calcification. Finally, either the medullary calcification can be found as the only remaining sign, or there will be complete healing.

Nuclear Medicine

Cessation of blood flow can be visualized by a three-phase bone scan, in which the first, vascular phase shows a low uptake of the radioactive marker, which is surrounded by a circular area of elevated uptake in later phases ("cold in hot

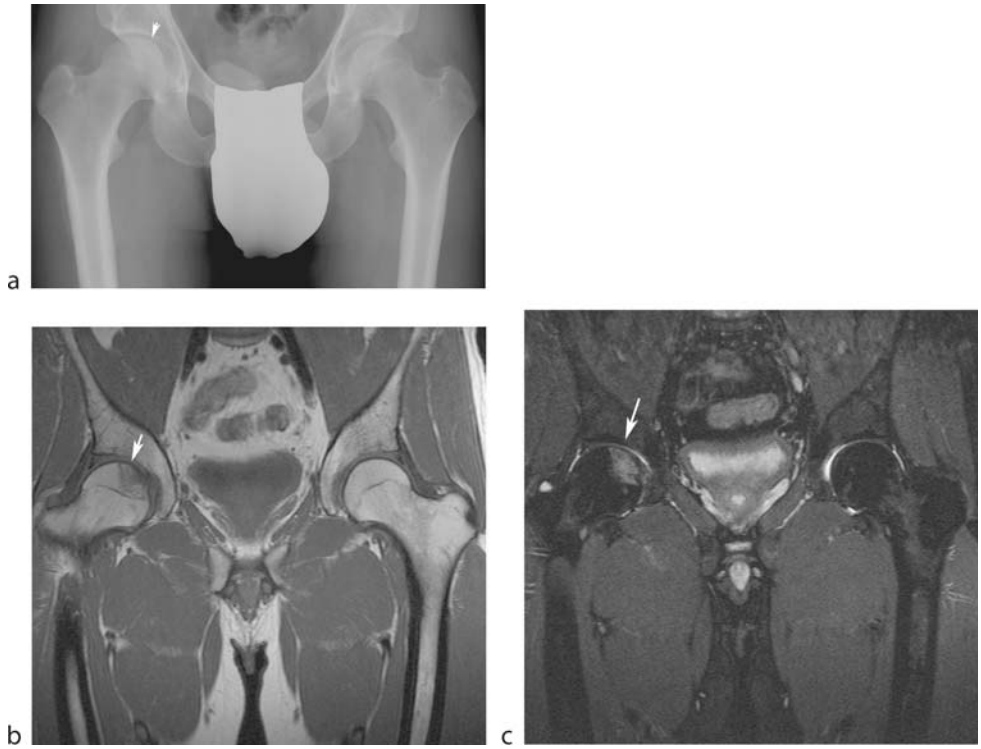

Osteonecrosis, Adults. Figure 1 (a) Anteroposterior view of both hips in a 30-year-old man. Ill-defined translucency represents ARCO stage 2 of right hip necrosis. (b) Coronal magnetic resonance imaging (STIR) shows marked edema of the right femoral head. (c) Coronal magnetic resonance image (T1-SE) shows hypointense demarcation in the right femoral head; ARCO stage 2.

spot"). Nuclear medicine studies, however, have been largely replaced by MRI because of better specificity and availability and the lack of ionizing radiation with MRI (6).

Diagnosis

The most preferred classification system for the staging of epiphyseal osteonecrosis was published by ARCO, in which emphasis was placed on a four-part staging system comparing radiographs, CT, bone scintigraphy, and MRI with histology and including prognostic factors (Table 1).

Osteonecrosis can be differentiated in necrosis of the epiphysis (usually called osteonecrosis) and in necrosis of the metadiaphysis (usually called infarction). Spontaneous medullary bone infarcts are often incidental findings in the metaphyses of long tubular bones. They appear as peripheral rims or shells of calcifications in the humerus, femur, tibia, or fibula and must be distinguished from enchondromas.

In the majority of cases, the exact etiology of osteonecrosis is unknown and hence is called idiopathic osteonecrosis. Most commonly, the femoral head or femoral condyles are involved in idiopathic epiphyseal necrosis (Ahlback's disease, or SONK). The differential diagnosis of idiopathic (epiphyseal) osteonecrosis includes bone marrow edema syndrome (BMES), osteomyelitis, bone tumor, and malignancies such as leukemia. BMES is a self-limiting disease with a relatively large zone of bone marrow edema and accompanying joint effusion and demineralization ("transient osteoporosis") but without double-line sign.

Secondary osteonecrosis may be due to trauma, corticosteroid therapy or hypercortisolism (such as after transplantation), hemoglobinopathies, Caisson disease (dysbaric conditions), small vessel disease (such as collagen disease), alcoholism and pancreatitis, gout and hyperuricemia with reactive vessel obstructions, Gaucher disease, irradiation/chemotherapy with direct vessel damage, and high intra-articular pressure (such as in infection and hemophilia).

The prognosis of osteonecrosis depends on the size and location of the ischemia. Osteonecrosis that occurs in a weight-bearing position and involves more than 30% of the articular head (such as the femoral head) has a much worse prognosis than lesions in a nonweight-bearing position and involving less than 15% of the articular head.

Osteonecrosis, Adults. Table 1 ARCO Classification (1992)

ARCO stage	Histology	Radiographs	Computed tomography	Bone scintigraphy	Magnetic resonance imaging
0	Microosteonecrosis	0	0	0	0
1	• Osteopenia, fractures • Microosteonecrosis • Marrow edema • Hyperemia	0	• Osteopenia • Insufficiency-micro-fractures	• Centrally in lesion low uptake	• Localized edema
2	• Osteonecrosis • Reactive changes: hyperemia, osteopenia, new bone formation	• Osteopenia • Reactive • sclerosis • Cysts	• Osteopenia • Sclerosis • Cysts • Asterisk sign	• High uptake	• Double-line sign (reactive margin of infarct with hyperemia and new bone formation) • Single-line sign in insufficiency fractures
3	• Subchondral impression fracture in weight-bearing area	• Crescent sign	• Crescent sign	• High uptake	• Crescent sign • Cartilage fracture (loss)
4	• Reactive degenerative changes	• Flattened articular surface • Joint space narrowing • Subchondral cyst formation • Reactive osteophytes • Subchondral sclerosis • Deformity, malpositioning, atrophy		• High uptake, deformity	• Cartilage defects • Deformity • Effusion, • Subchondral sclerosis • Osteophytes

The most common sites for posttraumatic osteonecrosis are the femoral head, the body of the talus, the humeral head, and the carpal scaphoid (Preiser's disease). Rarely, the tarsal navicular, capitate, carpal hamate, or lunate bone is involved. The development of the osteonecrosis may take 6–36 months. The likelihood of development of osteonecrosis gets higher with the severity of the trauma. The principal blood supply of the affected bones is responsible for the risk and location of osteonecrosis. Early diagnosis is made by MRI, and sequential follow-up is with CT and standard radiographs. MRI shows persistent edema with localized zones of necrosis. The osseous flattening, collapse, and fragmentation are usually delayed for a period of 9 months and also depend on the weight-bearing load of the epiphysis. Finally, the involved bony parts may become very dense, smaller, and irregularly shaped (Fig. 3).

Adult idiopathic osteonecrosis may be due to chronic overloading of the hip joint (head of femur) and the femoral condyle (Ahlback's disease). Early diagnosis is possible with MRI and three-phase bone scan. Primary necrosis of the femoral head probably affects men more frequently than women and is usually seen between the fourth and seventh decades of life. The reported prevalence of bilateral disease varies between 35 and 72%. The typical radiographic signs are round, oval, or triangular low densities that are neighbored by a high-density rim, followed by the crescent sign and impression fracture (ARCO stages 1–3). Early diagnosis depends on proof of bone marrow edema (with MRI) or diminished blood supply (with three-phase bone scintigraphy).

Femoral condyle osteonecrosis (Ahlback's disease, spontaneous osteonecrosis) is a typical condylar idiopathic osteonecrosis localized in the medial condyle of the femur and occurs in patients older than 50 years and in women more than in men, but it may be also found in the lateral condyles and the tibial plateau. On standard radiographs, the first sign is a subtle flattening of the neighboring joint surface, followed by a narrow zone of increased density adjacent to the depressed osseous surface. A radiolucent area in the condyle can be detected over the ensuing weeks, becoming more sharply demarcated by time. If untreated, further depression of the bony margins and progressive sclerosis and intra-articular osseous bodies will follow. Over a period of months or years, all signs of secondary degenerative osteoarthritis will develop. Bone collapse, varus deformity, and displacement can also be noted (Fig. 2).

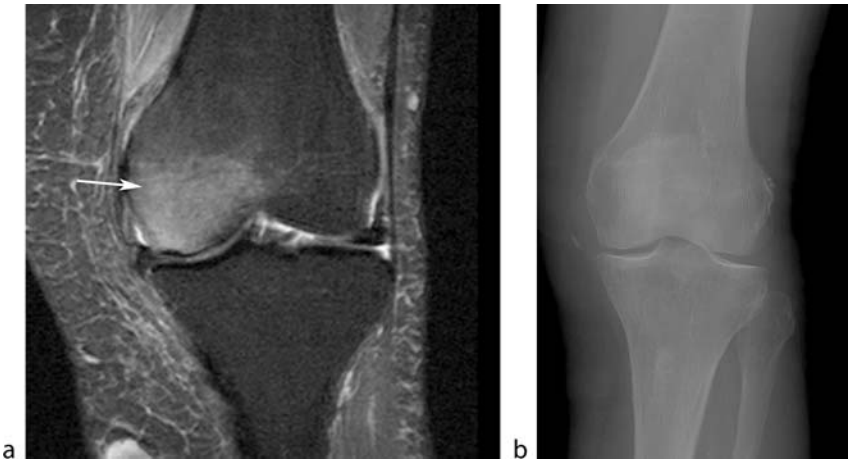

Osteonecrosis, Adults. Figure 2 (a) Coronal magnetic resonance image (STIR) shows marked edema of the medial condyle in a 90-year-old woman (Ahlback's disease). (b) Anteroposterior view shows no evidence of osteonecrosis in this digital radiograph.

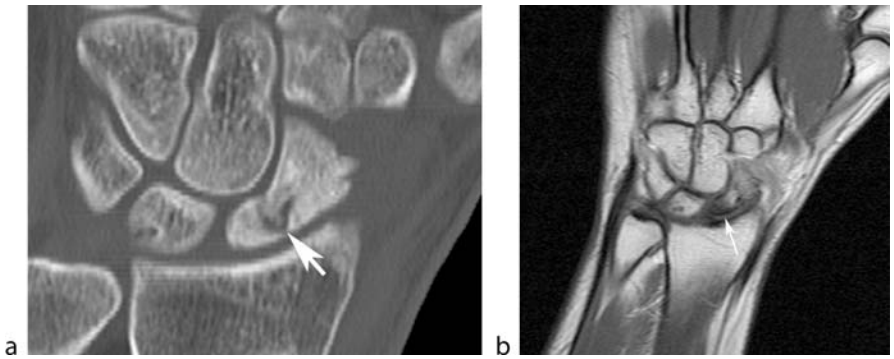

Osteonecrosis, Adults. Figure 3 (a) Coronal MPR of multidetector computed tomography reveals nonunion of the scaphoid in a 35-year-old woman after trauma. (b) Coronal magnetic resonance image (T1-SE after intravenous gadolinium) demonstrates no contrast enhancement in the proximal fragment (Preiser's disease) of the scaphoid bone.

Kienbock's disease occurs most commonly between the ages of 20 and 40 years and has a predilection for the right lunate bone. The male-to-female ratio is 2:1, with the following stages:

In stage I the radiograph is normal or shows a subtle fracture. MRI visualizes a bone marrow edema, and bone scintigraphy a hot spot. In stage II, abnormalities in radiodensity with changes in size and shape are seen. MRI will reveal necrotic hypointense areas in all sequences. In stage III, the lunate bone collapses and shows a high density with irregular borders. In stage IV, signs of degenerative osteoarthritis are demonstrated. The etiology seems to be chronic trauma. In patients with short ulnae (ulnar minus variant), the loading forces on the lunate are much higher than normally.

In dysbaric osteonecrosis (Caisson disease), in cases of too rapid decompression the released nitrogen may produce bubbles that act as gas-emboli. Those may occlude vessels partially or completely. A delay of at least 6 months or years between the exposure and the onset of radiologically evident juxtaarticular or diaphyseal and metaphyseal radiodense foci/radiodense lesions is typical. Early diagnosis is possible with three-phase bone scintigraphy and whole-body MRI.

Bibliography

1. Johnson LC (1964) Histogenesis of avascular necrosis. Proceedings of the Conference on Aseptic Necrosis of the Femoral Head, NIH, p 55
2. Brookes M, Revell WJ (1998) Blood Supply of Bone. Springer, London
3. Sugimoto H, Okubo RS, Ohsawa T (1992) Chemical shift and the double-line sign in MRI of early femoral avascular necrosis. J Comput Assist Tomogr 16(5):727–730
4. Stevens K et al (2003) Subchondral fractures in osteonecrosis of the femoral head: comparison of radiography, CT, and MR imaging. Am J Roentgenol 180(2):363–368

5. Vande Berg BE et al (1993) MR imaging of avascular necrosis and transient marrow edema of the femoral head. Radiographics 13(3):501–520
6. Imhof H et al (1997) Imaging of avascular necrosis of bone. Eur Radiol 7(2):180–186

Osteonecrosis, Childhood

Alan E. Oestreich
Cincinnati Children's Hospital Medical Center, Cincinnati, Ohio, USA
Alan.Oestreich@cchmc.org

Synonyms

Avascular necrosis (Perthes disease = Legg–Calvé–Perthes disease = idiopathic avascular necrosis of the hip in childhood); Bone infarction; Chondrolysis (of cartilage)

Definitions

Arterial or venous ischemia leading to cell death and/or disturbance of growth in bone. Historically, several (eponymous) variations in skeletal growth, now known not to be due to necrosis, were once so considered and are still often discussed in the context of true necrosis states. Death or disturbance of the zone of resting cartilage leads to delay, deformity, or cessation of enchondral growth; other conditions such as frostbite and ►Kashin–Beck disease may locally impair enchondral growth as well. The conditions in infancy known as multiple stippled epiphyses may well be secondary to necrosis of growth cartilage not yet in a growth plate.

Pathology/Histopathology

Clinical bone necrosis is usually more dynamic than mere death of osteocytes. The body has ways of repairing damage, so that the histopathologic pattern may be composed of both destruction and rebuilding. In Perthes disease, for example, the first step is impairment of vascular supply. The first irreversible structural change is a crumbling fracture of bone just below the lateral zone of provisional calcification, seen on frog leg radiographs. Then waves of bone necrosis appear with lack of viable osteocytes, followed by waves of overlying new bone (creeping substitution). Years later, a viable but deformed head is usually formed, more or less congruent with its acetabulum. However, because the shape is less spherical than normal and does not fully fit in its acetabulum, secondary arthrosis tends to appear relatively early in adulthood. Because of avascularity in the femoral neck and primary spongiosa in Perthes' disease, cartilage from the physis persists in the otherwise ossified neck, giving gouges of lucency on X-ray images. Both the head and neck of the femur widen transversely compared to normal as the disease progresses—perhaps related to increased periosteal formation in the neck from the processes of healing. An adverse event in the progress of Perthes is tethering across the physis in some patients. The greater trochanter growth is generally not impaired in Perthes, so it is relatively overgrown, leading to varus deformity of the hip, which is further exaggerated if tethering of the main physis occurs.

Osteochondrosis (some still refer to it as osteochondritis) dissecans is an injury to bone and overlying cartilage, which is painful and more severe, indeed unstable, whenever joint fluid enters the space between the lesion and normal bone.

Schmorl nodes are protrusions of normal vertebral disk substance through weak areas in the vertebral end plates (zones of provisional calcification). Schmorl nodes are often a component of Scheuermann disease of the spine.

In frostbite and Kashin–Beck disease (1), portions or the entire involved physis or acrophysis becomes nonviable, leading to local lack of growth (and perhaps early physeal fusion). A cone epiphysis is a result of a similar loss of viability of the central (more senior) portion of a physis, whether due to injury, infection, or genetic causes.

Clinical Presentation

Pain (in the groin, thigh, or referred to a knee), limping, and favoring a limb may reflect Perthes disease; however, Perthes may be clinically silent for months and discovered serendipitously on radiographs acquired for other reasons. Symptoms for avascular necrosis from other causes and at other sites are similar. In Gaucher disease, the spleen is often quite large; in sickle cell anemia, the spleen is usually small or absent. Traumatic avascular necrosis occurs after hip dislocation. For steroid-induced hip necrosis, other symptoms of steroid use could be sought. The incidence of osteochondrosis dissecans rose when teenagers were dancing The Twist, which indicates that certain challenging repetitive motions might be a predisposing factor. For frostbite, the history of severe cold exposure if available is helpful for the diagnosis (although the pattern of involvement on X-ray images is virtually diagnostic—especially if the thumb is spared by being

held in the fist during the exposure). Kashin–Beck disease is geographically limited to China, Mongolia, and Tibet, where thousands of cases have occurred.

Imaging

In Perthes disease, magnetic resonance imaging (MRI) and nuclear images show avascularity earlier than the first plain image finding, which, in turn, appears first on the frog-leg view (Fig. 1). However, unilateral retarded maturation of one femoral head might be appreciated on the frontal radiograph as well. Ultrasound shows associated hip effusion easily; plain images do not. As Perthes disease progresses, computer tomography (CT) images show the current integrity of bone, extent of involvement, and nonosseous components; however, MRI is preferred because it does not use radiation and also displays the femoral head and neck and acetabulum throughout the long course of Perthes (2).

►Osteochondrosis dissecans of the distal femur is usually situated posteriorly in the involved condyle, and thus is better seen on a notch (angled) view tangential to it. Evaluation for instability or fluid between the osteochondrosis and adjacent healthy bone could be made with MRI or a CT arthrogram.

When there is doubt about whether a normal variant of ossification or an osteonecrotic bone is present, a display of the osseous and cartilaginous elements on MRI may help one decide, with overlying normal cartilage favoring the normal variant. For example, Meyer dysplasia of the hip (3) can be distinguished from Perthes disease by the finding of normal cartilage and normally vascularized bone. Ultrasound can show the findings in Osgood–Schlatter condition of the patellar tendon and anterior tibial apophysis.

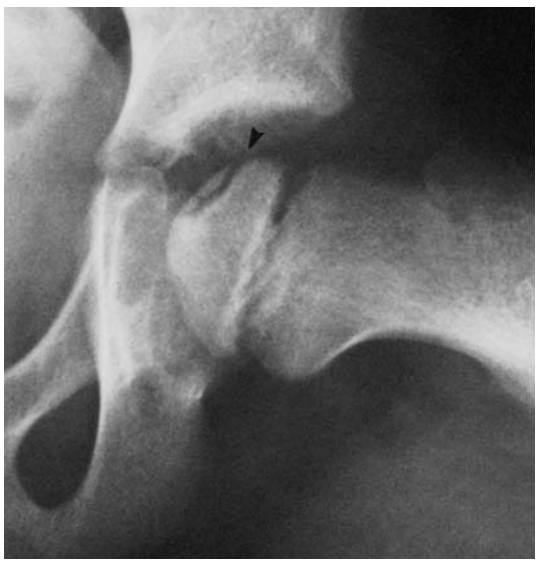

Osteonecrosis, Childhood. Figure 1 Perthes disease lucent crescent (*arrowhead*) of the outer femoral head on frog-leg view in an 8-year-old boy. From Oestreich AE, Crawford AH (1985) Atlas of Pediatric Orthopedic Radiology. Thieme Verlag, Stuttgart p 190.

Nuclear Medicine

Nuclear imaging, like MRI, shows findings earlier in Perthes disease than the upper outer lucent crescent found on radiographic frog-leg images. On bone scans, the earliest finding is a cold defect in the femoral head, a larger zone indicating more extensive disease. This phase, however, is reversible without progression to irreversible definitive Perthes disease. The perthetic femoral head eventually regains scan activity in the reparative phase later in the disease evolution. One week after the onset of sterile infarction of bone, whether from sickle cell disease, Gaucher disease, pancreatitis, or other noninfectious causes, bone scans begin to show high activity (as healing begins) rather than the earlier lower than normal (cold) activity. Lack of bone scan activity is also a sign of avascularity after certain fractures, for example, in the proximal scaphoid following a transverse fracture of the scaphoid waist. The differential diagnosis between infection and infarction of bone in sickle disease can be assisted by dual scanning: in infection, gallium 67 should be much more avidly taken up than technetium in conventional bone scan.

Diagnosis

Bones with osteonecrosis are generally denser than the nearby bones, whether because of the loss of volume putting more bone substance into a smaller space from collapse or because living bones demineralize from local irritation whereas dead bones do not. A classic example is the proximal scaphoid being denser than the distal one when its blood supply is lost from a fracture across the bone's waist. Infarction of bone shafts can also incite callus, which is denser than the nearby bone.

The early plain image changes of Perthes disease are a smaller epiphysis than contralaterally because of decreased vascularity and, on the frog-leg view alone, a slit of lucency below the outer femoral head zone of provisional calcification, representing crumbling fracture (Fig. 1). The extent of the slit reflects the severity of involvement. As the disease progresses (with or without surgery to improve position or protect the hip), the head becomes irregularly denser and longitudinally shorter,

while the head and neck become transversely wider (and thus incompletely covered by the bony acetabular roof). Gouges of lucency may extend down the metaphysis of the neck from the physis, reflecting avascular zones in the primary spongiosa. Without ultrasound or cross-sectional imaging, one cannot determine whether effusion accompanies Perthes disease. The perthetic hip through the progress of disease becomes varus as the greater trochanter continues to grow nearly normally, while the femoral physis is slowed, or occasionally tethered, by premature fusion across part of the physis.

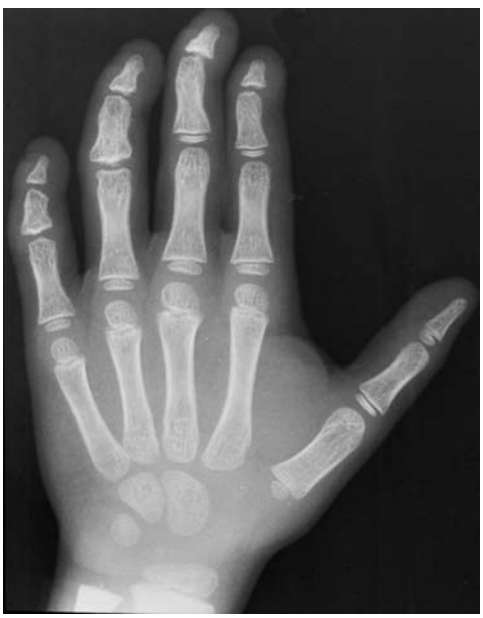

Osteonecrosis, Childhood. Figure 2 Frostbite sequelae: distal phalanges 2 through 5 are short from physeal closure, as are middle phalanges 4 and 5. The distal (acrophyseal) ends of the middle phalanges are also irregular from enchondral damage. As is often the case, the thumb was presumably spared by being protected in the fist during the cold exposure. From Oestreich AE, Crawford AH (1985) Atlas of Pediatric Orthopedic Radiology. Thieme Verlag, Stuttgart p 169.

Sickle cell infarction of small tubular bones, generally about 1 year of age, is painful accompanied by periosteal reaction and called "hand–foot" syndrome. This may be the presenting symptom of previously unknown sickle cell disease. The typical Lincoln log vertebral bodies in sickle cell disease result from infarction or impairment of the more central portions of the vertebral end plates. Distinguishing infarction from infection in long bones in sickle cell disease by imaging can be quite difficult; dual nuclear scanning with bone scan and gallium scan (or labeled white blood cells) may help by showing especially high activity on the latter.

In frostbite, Kashin–Beck disease, and some sequelae of rat bite (1), enchondral bone growth is locally destroyed, so that portions or the entire bones do not grow (Fig. 2). Cone-shaped epiphyses, fused epiphyses, pumice-shaped carpal bones, and irregular nonepiphyseal ends of small tubular bones are manifestations. In frostbite the distribution is acral, from the fingertips proximally, because of the nature of the cold injury, often sparing the thumb if it had been protected in the fist. Distribution of enchondral damage in Kashin–Beck disease is more scattered—involvement asymmetrically of the lower extremity bones leads to length discrepancy and hence limp.

The apophysis of the posterior calcaneus normally appears denser than the rest of the bone. It is no longer considered "Sever disease" unless localized symptoms occur and the nuclear scan is abnormal. Many diagnoses of "Köhler disease" of the tarsal navicular are actually an overlap of multiple ossification centers rather than true osteonecrosis (Fig. 3). Close perusal of oblique and lateral images will usually solve the question. Similarly, the ossification across the closing inferior ischiopubic synchondrosis is often both vigorous and asymmetric from

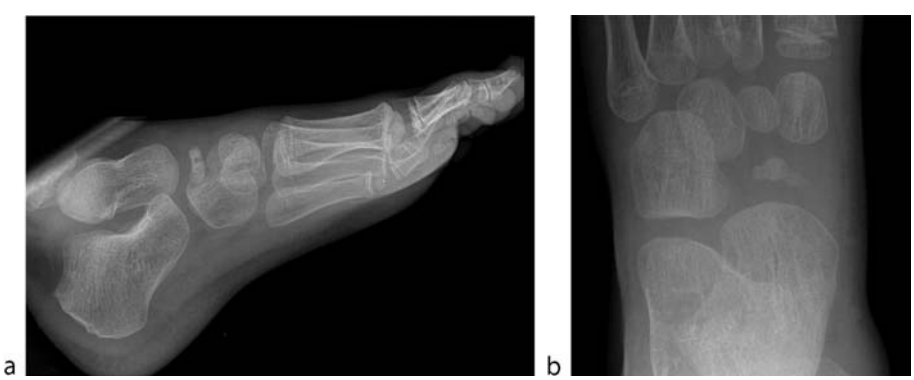

Osteonecrosis, Childhood. Figure 3 Mimic of Köhler disease in a 6-year-old patient. Lateral image suggests sclerosis and irregularity of the navicular; but the frontal view shows it results merely from overlap, the bone developing from three normal-density growth centers. The pain, incidentally, was lateral, not medial.

side-to-side. Unless abnormally increased bone scan activity can be shown, van Neck osteonecrosis should not be considered. Kienböck disease or lunatomalacia is a real entity, however, often associated with ulna minus.

Meyer dysplasia of the hip in the early years of life is an irregular appearing ossification of the femoral head. However, it has normal vascularity on nuclear scan or MRI and uncommonly progresses to true Perthes disease.

References

1. Oestreich AE (2000) Pediatric arthroses as a sequelae of enchondral damage. Examples of frostbite, Kashin–Beck disease, rat bites and other etiologies [in German]. Radiologie 40:1149–1153
2. Mahnken AH, Staatz G, Ihme N et al (2002) MR signal intensity characteristics in Legg–Calve–Perthes disease.Value of fat-suppressed (STIR) images and contrast-enhanced T1-weighted images. Acta Radiol 43:329–335
3. Schittich I (2001) MRI in the diagnosis and treatment of Perthes disease and epiphysiolysis of the head of the femur [in German]. Orthopädie 30:519–527

Osteopenia

In childhood, a reduction of bone substance either from osteoporosis or hyperparathyroidism or, after physes fuse, also from osteomalacia.

▶Demineralization, Bone, Childhood

▶Osteoporosis

Osteophytes

Bony spurs or outgrowths in the proximity of a joint, osteophytes, are found in a variety of musculoskeletal disorders, including degenerative joint disease and DISH. Presence of multiple osteophytes is referred to as osteophytosis.

▶Dish

Osteoporosis

Thomas M. Link, Jan S. Bauer
Department of Radiology
San Francisco, USA
tmlink@radiology.ucsf.edu

Synonyms

Osteoporosis and osteopenia are precisely defined according to the World Health Organization (WHO) Criteria (see later)

Definitions

Osteoporosis is defined as a disease associated with a loss of bone mass and a deterioration of bone structure, both resulting in increased bone fragility and susceptibility to fracture (1). In 2000, the definition given by the National Institutes of Health consensus development conference in 1993 was modified (2). Osteoporosis was now defined as a skeletal disorder characterized by compromised bone strength predisposing to an increased risk of fracture. Because this definition appears fairly abstract, the following statements were added.

Bone strength reflects the integration of two main features: bone density and bone quality. Bone density is expressed as grams of mineral per area or volume and in any given individual is determined by peak bone mass and amount of bone loss. Bone quality refers to architecture, turnover, damage accumulation (e.g., microfractures), and mineralization.

Because bone density is the parameter that can be determined best *in vivo*, has a high precision, and correlates well with the biomechanically determined bone strength [it explains approximately 70% of bone strength (2)], the WHO defined osteoporosis on the basis of bone mineral density (BMD) (3). A BMD that is more than 2.5 standard deviations below that of a white, young, healthy female adult reference population (T-score) is defined as osteoporosis. A BMD that is 1–2.5 standard deviations below that of the young and healthy reference population is defined as ▶osteopenia. This definition, however, was originally only established for BMD of the proximal femur determined using ▶dual-energy X-ray absorptiometry (DXA), but it has been applied to define diagnostic thresholds at other skeletal sites, such as the spine (anterior–posterior) and the distal radius, and for other technologies.

Pathology/Histopathology

Osteoporosis is characterized by reduced activity of osteoblasts and increased activity of osteoclasts. Because trabecular bone has a turnover up to seven times higher than the cortical shell, bone loss occurs here first. The trabecular network transforms from a platelike to a rodlike structure with thinner trabeculae and wider intertrabecular spaces. Connections between trabeculae

are lost as osteoclasts form resorption lacunae that may have the size of thinner trabeculae. To quantify trabecular structure changes, histomorphologic parameters can be calculated from biopsies of the iliac crest, or noninvasively using high-resolution magnetic resonance imaging (MRI) or peripheral MicroCT at the distal radius, the tibia, or the calcaneus.

Clinical Presentation

Osteoporosis may be undiagnosed for a long time and frequently manifests itself with insufficiency fractures. Early symptoms such as back pain and height loss are nonspecific, and a hunchback represents already advanced osteoporosis that is frequently associated with several vertebral fractures. The most severe insufficiency fractures affect the proximal femur with high associated disability and mortality. Osteoporosis-related vertebral fractures also have important health consequences for older women and men, including disability and increased mortality. The presence of one vertebral fracture increases the risk of any subsequent vertebral fracture fivefold, and 20% of women who have had a recent diagnosis of fracture will sustain a new fracture within the next 12 months. Since a number vertebral fractures do not come to clinical attention, the radiographic diagnosis is particularly important. Because these fractures can be prevented with appropriate medications, recognition and treatment of high-risk patients is warranted.

Imaging

Conventional radiographs of the spine are not suited to determine bone mass in the early stage of osteoporosis because it takes a bone loss of more than 20–40% before a loss of bone mass is visualized on radiography. Morphological signs described on spine radiographs, such as a coarse trabecular structure and a framelike appearance of the vertebrae, are also not very reliable. Conventional radiographs, however, are important in diagnosing fractures and in the differential diagnosis of osteoporosis because a number of other diseases may present with bone loss and fractures.

According to Genant et al (4), a vertebral deformity in T4-L4 of more than 20% of loss in height with a reduction in area of more than 10–20% is defined as a fracture. Using this fracture threshold, a semiquantitative score to grade the severity of vertebral fractures as visually determined from radiographs has been described (Fig. 1). In rare cases, osteoporosis may present with a coarse trabecular structure with thick vertical trabeculae suggestive of vertebral hemangioma. This so-called hypertrophic atrophy, however, is generalized, and the trabecular bone structure appears more coarse than in hemangioma. Important differential diagnoses in osteoporosis are osteomalacia, hyperparathyroidism, renal osteopathia, and malignant bone marrow disorders such as multiple myeloma and diffuse metastatic disease. Endplate fractures are found in Scheuermann's disease and malignant lesions. The differential diagnosis of osteoporotic and malignant pathologic fractures may be difficult. Fractures located above the Th 7 level present with a soft tissue mass, osseous destruction, and fractures of the posterior part of the vertebrae in conventional radiographs are more likely to be malignant.

Conventional radiographs of the proximal femur and the distal radius are usually obtained after a low-impact trauma with persistent symptoms in postmenopausal elderly individuals. It should be noted that osteoporotic

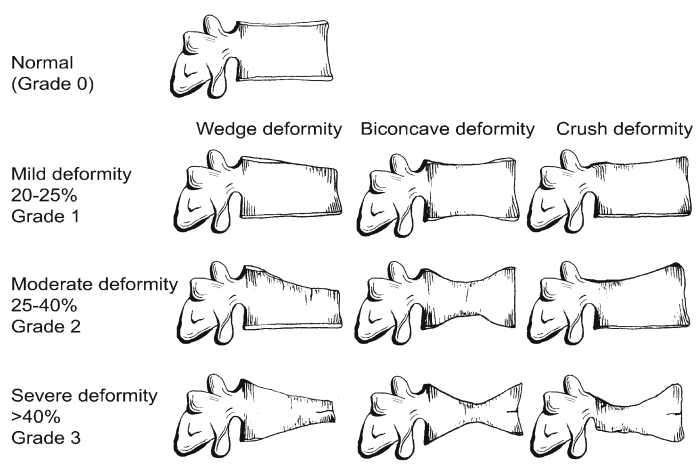

Osteoporosis. Figure 1 Spinal fracture index as defined by Genant et al (4) used to classify osteoporotic vertebral fractures.

fractures may be difficult to detect on conventional radiographs due to demineralization of the bone and are not infrequently occult.

Computed tomography (CT) and MRI may be helpful in detecting occult fractures (Fig. 2), differentiating osteoporotic and malignant fractures, depicting multiple lesions, and soft tissue masses or destructive changes. Bogost et al showed that 37% of proximal femur fractures were not detected in conventional radiographs, which were demonstrated in MR scans of these patients (5). Nonenhanced T1 and STIR (respectively T2-weighted fat-saturated) sequences are recommended in patients with a high clinical suspicion of fracture but negative radiographs. Diffusion-weighted MR sequences and iron oxide contrast media in MRI have been successfully used to differentiate malignant and benign bone marrow pathology. CT is less sensitive in depicting bone marrow pathology; however, it is better suited to assess the stability of an osteolytic lesion or fracture because it directly visualizes the bony structures and demonstrates fracture lines in a detailed fashion.

Nuclear Medicine

Bone scintigraphy has a limited role in the assessment of osteoporosis. The technique may be useful to detect occult fractures (though it is less sensitive than MRI), to depict multiple lesions, and to differentiate between old and new vertebral fractures.

Diagnosis

Diagnosis of osteoporosis is usually made on the basis of bone density or the presence of osteoporotic fractures. Currently the most important techniques in osteodensitometry are DXA and ►quantitative computed tomography (QCT).

DXA: The principle of DXA is a dual-energy measurement that is based on the fact that radiation of distinct energies is attenuated by tissues to different extents. In both soft tissue and bone, a low-energy beam is attenuated to a greater degree than a high-energy beam is. Contrast in attenuation between bone and soft tissue is greater for the low-energy beam than for the high-energy beam, such that the attenuation profile of bone may be determined by subtracting both the low- and high-energy attenuation profiles. DXA scanners provide either pencil or fan beam techniques. Fan beam techniques are faster. The precision of DXA is high, and radiation exposure is low. BMD is most frequently determined at the spine (anteroposterior or lateral) (Fig. 3a) and at the proximal femur (Fig. 3b). Whole-body measurements as well as measurements at the distal radius and the calcaneus may also be obtained. The anteroposterior examination of the lumbar spine is a standard procedure with a precision *in vivo* of 1%, a radiation exposure of 1(-50) μSv (the higher dose is required for digital high-resolution images), and a fairly high accuracy (4–10%). For monitoring BMD, the precision alone, however, is not the only parameter required to assess the diagnostic performance of a technique. We also need to know the annual rate of BMD loss in normal patients using this technique as well as the least significant change between two measurements, which are 1–2% and 3–4%, respectively, for the anteroposterior spine.

Using automated software, areal BMD (g/cm^2) is determined, usually at L1–L4 (Fig. 3a). These projection images, however, have a number of limitations: (i) vertebrae with a larger size have a higher BMD, (ii) aortic calcification and all other soft tissue calcifications in the regions of interest (ROIs) increase BMD, and (iii) degenerative changes of the spine including osteophytes, facet sclerosis, and degenerative disc disease may also falsely increase BMD. In elderly patients with substantial degenerative changes of the lumbar spine, anteroposterior DXA of the lumbar spine may therefore not be a suitable technique. Lateral

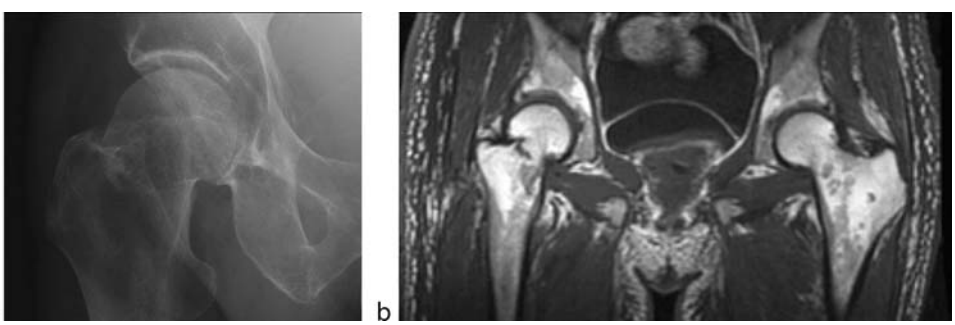

Osteoporosis. Figure 2 Radiographically occult insufficiency fracture of the right proximal femur in a postmenopausal woman. On the radiograph of the right femur (a), no fracture is shown, whereas the coronal T1-weighted magnetic resonance image (b) clearly shows a fracture of the right femur neck.

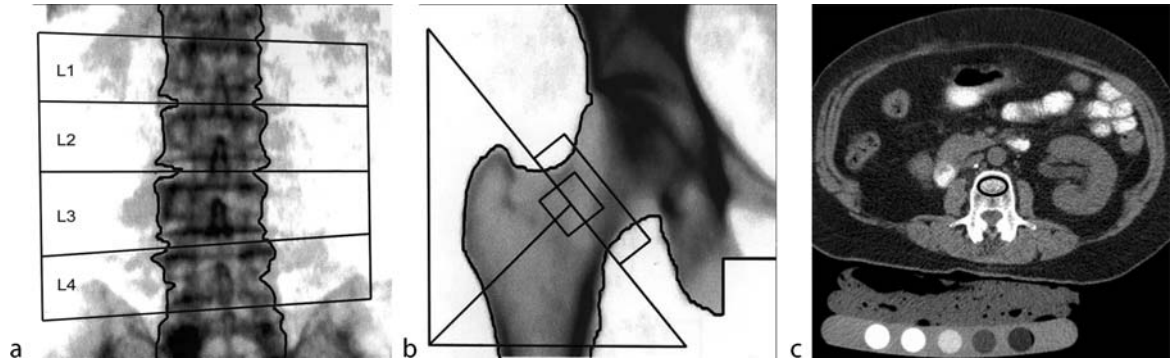

Osteoporosis. Figure 3 Standard techniques to measure bone mineral density: dual-energy X-ray absorptiometry images of the anteroposterior spine (a) and the proximal femur with standard regions of interest (b) as well as quantitative computed tomography of the lumbar spine (c) with an oval region of interest in the vertebral body.

DXA is influenced less by these changes because it assesses only the vertebral bodies and thus focuses more on trabecular bone. However, drawbacks of this technique are a lower precision, a higher radiation exposure, and superimposition of the pelvis and the ribs, which may limit analysis of the lumbar spine to L3. So far, anteroposterior DXA is still the standard DXA procedure to assess the lumbar spine. When analyzing DXA scans, a number of pitfalls have to be considered that may be operator-dependent, such as mislabeled vertebrae, misplaced disk space markers, wrongly sized ROIs, and artifacts in the analysis region. These analysis errors are of greater magnitude than the machine's intrinsic precision errors.

DXA of the proximal femur is a particularly important examination because it is currently one of the best techniques to assess fracture risk of the hip (Fig. 3b). But the examination of the hip is more demanding than that of the spine; the proximal femur has to be positioned in a standardized fashion, and a number of ROIs have to be placed correctly. The correct location of these ROIs varies according to the manufacturer. Standard ROIs are the neck region, the trochanteric region, and the intertrochanteric region. The ROI used most frequently is the total femur. The total femur ROI consists of the neck region, the trochanteric region, and the intertrochanteric region. Ward's triangle has an inferior precision compared with the other ROIs and is currently not used as a standard ROI. The precision for hip BMD and the annual rate of loss are lower compared with anteroposterior spine, and the least significant change is higher.

As in DXA of the lumbar spine, a number of operator-dependent errors may occur in the proximal femur and should be detected by the radiologist. Most of these errors are due to improper positioning of the patient and the ROIs. Correct positioning of the patient includes internal rotation of the hip with a straight femoral shaft (the lesser trochanter should not or just barely be visualized). Correct positioning and size of the ROIs, in particular the neck box, may vary according to the manufacturer; for example, Lunar/GE systems have a standardized size of the neck box, which is placed automatically in the region of the neck with the smallest diameter. Osteoarthritis, Paget's disease, fracture, vascular calcifications, calcific tendinitis, enostosis, and avascular necrosis of the hip are also potential sources of error. Conventional radiographs may be required if an atypical density profile is shown. If these lesions are too large or if developmental dysplasia of the hip is found, BMD has to be determined at a different site.

QCT: In contrast to DXA, QCT allows a true densitometric measurement (in mg/mL) of trabecular bone, whereas DXA gives an areal BMD (in mg/cm^2) that includes trabecular and cortical bone. Since the trabecular bone has a substantially higher metabolic turnover, it is more sensitive to changes in BMD (annual rate of bone loss in QCT 2–4% vs. 1% in anteroposterior DXA of the spine). On the other hand, the precision of two-dimensional (2D) QCT (but not of volumetric QCT) is lower than that of DXA (1.5–4% vs. 1%). A big advantage of QCT is that it is not as susceptible to degenerative changes of the spine as DXA is. Osteophytes and facet joint degeneration as well as soft tissue calcifications (in particular of aortic calcifications) usually do not falsely elevate the BMD in QCT. As in DXA, however, fractured or deformed vertebrae must not be used for BMD assessment because these vertebrae usually have an increased BMD.

QCT may be performed with any CT system; however, a calibration phantom is required to transform the attenuation measured in Hounsfield units (HU) into BMD (mg/mL). Dedicated software improves the precision of the examination. The patient is examined lying supine on the phantom, usually with a water- or gel-filled cushion in between to avoid artifacts due to air gaps. Standard 2D QCT is performed of the lumbar spine; usually, the first to third lumbar vertebrae are analyzed

using a single midvertebral section that is aligned along the endplates. Volumetric QCT can be performed of the spine and the proximal femur using axial, contiguous 3-mm sections of each site.

BMD data obtained by QCT are compared to an age-, sex-, and race-matched database. T-scores used for the assessment of osteoporosis according to the WHO definition have been established for DXA but not for QCT, though they may be given by the manufacturers of the software. If these T-scores are used to diagnose osteoporosis, a substantially higher number of individuals compared to DXA will be diagnosed as osteoporotic, since BMD measured with QCT shows a faster decrease with age than DXA. Researchers have therefore advocated using BMD measurements analogous to the WHO definition but with thresholds corresponding to lower T-scores. Thus, BMD values from 80–120 mg/mL have been classified as osteopenic, and BMD values below 80 mg/mL as osteoporotic (6), which corresponds to a T-score of approximately -3.0.

Peripheral QCT and DXA are less frequently used and clinically of limited significance. New techniques to assess microarchitecture and macroarchitecture of bone have not been introduced into the clinical arena but may give additional information on fracture risk and have future potential.

▶Acromegaly
▶Demineralization, Bone

Bibliography

1. NIH, Conference CD (1993) Diagnosis, prophylaxis, and treatment of osteoporosis. Am J Med 94:646–650
2. NIH Consensus Development Panel on Osteoporosis Prevention D, and Therapy (2001) Osteoporosis prevention, diagnosis, and therapy. JAMA 285:785–795
3. WHO (1994) Technical report: assessment of fracture risk and its application to screening for postmenopausal osteoporosis: a report of a WHO study group. In: World Health Organization. Geneva, Switzerland
4. Genant HK, Wu CY, Kuijk C van et al (1993) Vertebral fracture assessment using a semiquantitative technique. J Bone Miner Res 8:1137–1148
5. Bogost G, Lizerbram E, Crues J (1995) MR imaging in evaluation of suspected hip fracture: frequency of unsuspected bone and soft-tissue injury. Radiology 197:263–267
6. Felsenberg D, Gowin W (1999) Knochendichtemessung mit Zwei-Spektren-Methoden. Radiologe 39:186–193

Osteoporotic Vertebral Fractures

According to the spinal fracture index, deformities of the vertebrae of more than 20% are defined as fractures. These are not infrequently asymptomatic but are excellent indicators for future fractures. Even if bone mineral density is not below a T-score of -2.5, the presence of fractures is indicative of osteoporosis.

▶Osteoporosis

Osteosarcoma

Most frequent malignant primary bone tumour found predominantly in young adults. Typically aggressive morphology in radiological images with complex periosteal reaction and osteoblastic matrix pattern.

▶Neoplasms, Bone, Malignant

Osteosclerosis

The hardening or the abnormally high density of bone.

▶Neoplasms, Odontogenic

Outlet Obstruction Syndrome

Outlet obstruction syndrome, also called obstructed defecation is defined as incomplete evacuation of fecal contents from the rectum.

▶Pelvic Floor Dysfunction, Anorectal Manifestations

Outlet Obstruction Syndrome – Obstructed Defecation

▶Pelvic Floor Dysfunction, Anorectal Manifestations

Ovarian Cancer

Ovarian cancer is in the majority (85%) of cases epithelial in origin. Familial evidence of ovarian cancer is the strongest risk factor for ovarian cancer. At diagnosis in more than 75% of patients with epithelial ovarian cancer, peritoneal tumor spread outside the pelvis or lymphatic metastases are detected.

▶Carcinoma, Ovarium

Ovarian Cancer Screening

Screening with CA-125 and sonography are currently only suggested in high-risk patients. These are patients with a positive family history of ovarian cancer or BRCA1 or BRCA2 gene mutations.

▶Carcinoma, Ovarium

Ovarian Cancer Staging

The most commonly used staging system of ovarian cancer is the FIGO (International Federation of Gynecologists and Obstetricians) classification system. Alternatively, ovarian cancer is staged on the basis of the TNM classification. Staging is based on the findings detected during explorative laparotomy including cytologic assessment of the peritoneum.

▶Carcinoma, Ovarium

Ovarian Cancer

▶Carcinoma, Ovarium

Ovarian Metastases

Ovarian metastases comprise approximately 5–15% of malignant ovarian tumors, and derive most commonly from colon, stomach, breast, and melanomas as primary cancers. Krukenberg tumors display characteristic imaging features, which include bilateral, solid ovarian tumors, often with central necrosis. Other ovarian metastases present with similar imaging findings as ovarian cancer.

▶Masses, ovarian

Ovarian Neoplasm

▶Masses, Ovarian

Ovarian Teratomas

Ovarian teratomas consist of a series of tumors which derive from primordial germ cells. They comprise mature teratomas, immature teratomas, and monodermal teratomas. Mature teratomas constitute the vast majority of these tumors (99%).

▶Teratoma, Ovaries, Mature, Ovalar

Ovarian Torsion

Ovarian torsion is the most important complication of dermoids. It is reported in 3.2–16% of cases and is a gynecological emergency. Increasing tumor size correlates with increased risk of torsion.

▶Teratoma, Ovaries, Mature, Ovalar

Ovarian Vein Obstruction

▶Thrombosis, Vein, Ovarian

Ovarian Vein Occlusion

▶Thrombosis, Vein, Ovarian

Oxygen–Ozone Therapy

A mixture of oxygen–ozone gas is injected into the centre of the intervertebral disc at non-toxic concentrations. Ozone has a direct lytic effect on the proteoglycan molecules that form the nucleus pulposus. The resulting proteoglycan fragments have limited water-binding abilities, which leave intradiscal water molecules free to diffuse into the surrounding tissues. The resulting loss of water causes a decrease of intradiscal pressure. This causes the herniated portion of the nucleus pulposus to recede towards the centre of the disc, relieving pressure on the nerve root.

▶Percutaneous Interventions for Lumbar Radicular Syndrome

Paget Disease

Mark Davies
MRI Centre, Royal Orthopedic Hospital
NHS Trust
Birmingham, UK
wendy.turner@roh.nhs.uk

Synonym

Osteitis deformans

Definition

Paget's disease of bone named after the nineteenth century British surgeon Sir James Paget is a localised or multifocal disorder of bone characterised by abnormal bone turnover with increased osteoclastic activity and compensatory increased osteoblastic activity. It has three phases, lytic, mixed and sclerotic. The aetiology of the disease is unknown with two principal theories. One is thought to be a genetic predisposition and the other a 'slow' virus infection.

Pathology/Histopathology

Mirroring the radiographic features, the microscopic appearances depend on the phase of the disease. In the initial osteolytic phase there is active osteoclastic bone resorption with loss of trabeculae and replacement of the marrow by highly vascular fibrous tissue. In time osteoblastic activity predominates with increased bone density and thickening of the remaining trabeculae. The disordered bone turnover produces cement lines or reversal fronts that gives the classic histological 'mosaic pattern'. In the late 'burnt-out' phase bone turnover may return to an almost normal level and the degree of hypervascularity is also reduced. In this situation, the microscopic appearances show thickened trabeculated bone with a prominent mosaic pattern and restoration of the marrow.

Clinical Presentation

There is increasing prevalence of Paget's disease of bone with age. It is rare in patients under 40 years of age. There are also significant geographic/ethnic variations being relatively common in the Caucasian races of northern Europe and yet rare in blacks and Asians. In northern Europe, the incidence has been estimated to be 3% of the population over the age of 40 rising to 10% in the elderly. There is a male predominance. Studies of the past two decades, however, have suggested that Paget's disease is disappearing. The majority of cases are an incidental finding on radiographs obtained for an unrelated clinical indication. The remainder present due to the complications of the disease (Table 1). The disease predominates in the axial skeleton-spine (75%), pelvis (60%) and proximal femur (75%). About 75% cases are polystotic and 25% monostotic. Clinical laboratory findings include a grossly elevated serum alkaline phosphatase with normal calcium and phosphorus levels. Urinary hydroxyproline levels are also raised due to increased bone tissue breakdown.

Imaging

The initial osteolytic phase is the least frequent manifestation identified on radiographs with the exception of the skull vault. In the skull, there is a large area of demineralisation with a sharp line of demarcation. This appearance, known as osteoporosis circumscripta, commences at the skull base most commonly affecting the

Paget Disease. Table 1 Skeletal complications of Paget's disease of bone

1. Bone softening	– bowing of long bones
	– protrusio acetabuli
	– basilar invagination
2. Fractures	– partial/complete transverse
3. Malignant transformation (<1% patients)	
4. Secondary osteoarthritis	
5. Neurological compromise	– spinal stenosis

occipital bones (Fig. 1). In the long bones, the lytic process commences in the subarticular region and in time extends along the diaphysis. The sharp zone of transition between the pagetic and normal bone is variously termed, 'V-shaped', 'flame-shaped' or 'blade of grass' (Fig. 2). Rarely, Paget's disease may arise in the diaphysis without subarticular/metaphyseal involvement.

In the intermediate osteolytic and osteosclerotic phase there is a mixed pattern. In the skull this produces a 'cotton wool' appearance and in the spine a 'picture frame' vertebra. In the long bones the initially affected subarticular and metaphyseal bone is the first to show sclerosis and expansion with the distal lytic area preserved for the time being. In the late osteosclerotic phase, the pathognomonic triad in Paget's disease is expansion of bone with cortical and trabecular thickening (Fig. 3). The expansion of bone is particularly helpful in distinguishing this condition from other cause of widespread osteosclerosis such as diffuse metastases or myelofibrosis. In the pelvis there is expansion of the affected bone as compared with normal bone and thickening of the iliopectineal line (Fig. 3).

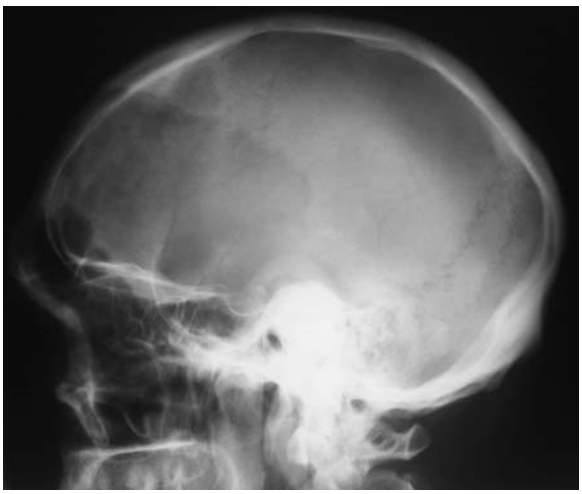

Paget Disease. Figure 1 Osteolytic phase of Paget's disease affecting the frontal bones (osteoporosis circumscripta).

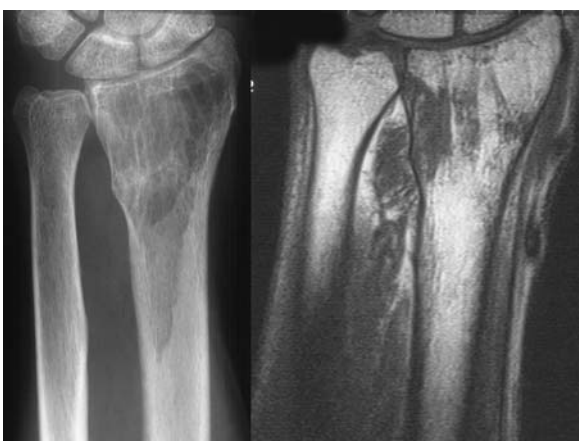

Paget Disease. Figure 2 Osteolytic phase of Paget's disease arising in the subarticular portion of the distal radius and extending cranially with a well defined V-shaped leading edge. The coronal T1-weighted MR image shows some thickening of the residual trabeculae and relative preservation of the marrow fat signal in the affected bone.

Fractures, typically transverse, can occur in any phase of Paget's disease due to weakening of the bone (1). In the sclerotic phase with bowing of the long bones it is not unusual to see incremental transverse fractures confined to the cortex on the convex side (Fig. 4). These are a form of insufficiency fracture that may or may not heal and can propagate across the whole diameter of the bone to produce a complete fracture.

The most significant of the complications of Paget's disease is malignant transformation that occurs in approximately 1% cases. Typically the patients have both longstanding and polystotic disease. The femur, pelvic bones and humerus are the commonest sites. The most common histological diagnosis is osteosarcoma followed by spindle cell sarcoma (malignant fibrous histiocytoma and fibrosarcoma) and rarely chondrosarcoma. Clinical features that should alert the physician to the possibility of malignancy include progressive non-mechanical pain and swelling at the affected site. The majority of cases can be identified as an aggressive lytic lesion arising within an area of pre-existing Paget's disease. Cortical destruction and a soft tissue mass is a relatively early finding (Fig. 5) (2). Despite most cases being an osteosarcoma, malignant mineralisation is uncommon.

CT will show cortical and trabecular thickening with normal fat attenuation of the marrow. Typically on MR imaging in uncomplicated Paget's disease the marrow fat signal is preserved on all sequences (Fig. 2) (3). However, it is possible to see cortical and marrow oedema when the disease process is particularly hypervascular. In complicated Paget's disease (i.e. in the presence of fracture, oedema, etc.) the fat signal from the marrow is replaced (4). Features suggestive of malignancy include cortical destruction and the presence of a soft tissue mass.

Nuclear Medicine

Bone scintigraphy can be used in Paget's disease to make the diagnosis, identify the extent of disease and monitor response to treatment with bisphosphonates (5). The bone scan tends to show relatively uniform, increased activity with evidence of expansion in flat bones such as

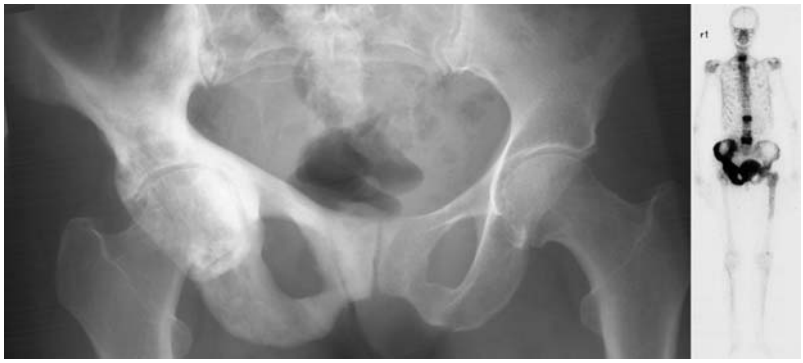

Paget Disease. Figure 3 Late phase of Paget's disease with sclerosis, expansion of the right hemipelvis and a mild protrusio deformity. The bone scan shows the uniform increased activity in an expanded right hemipelvis with involvement of several vertebrae.

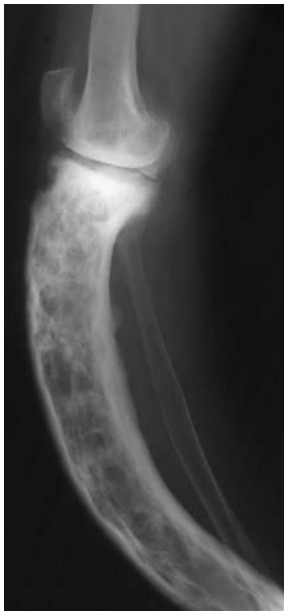

Paget Disease. Figure 4 Late phase of Paget's disease with sclerosis, expansion and bowing (sabre deformity) of the tibia. There are several small transverse incremental fractures over the convex border.

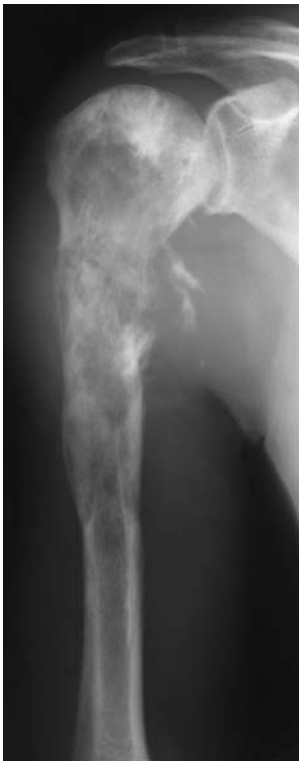

Paget Disease. Figure 5 Malignant transformation with an osteosarcoma arising in pre-existing Paget's disease. There is lysis, cortical destruction and a soft tissue mass all indicative of malignancy. Note the V-shaped edge of the Paget's disease distally.

the pelvis, scapula and sternum (Fig. 3). The typical appearance in the long bones is increased activity commencing at one bone end and extending along the shaft, with a V-shaped leading edge corresponding to the radiographic abnormality. In the spine the whole vertebra, including the posterior elements, is involved giving the variously termed 'heart', 'mouse's face' or 'clover' appearance. Unlike most sarcomas of bone, malignant transformation may appear relatively photopenic against the background increased activity of the pre-existing Paget's disease.

Diagnosis

Incidental late phase Paget's disease is readily diagnosed on radiographs as showing the triad of bone expansion with cortical and trabecular thickening. Similar appearances with preservation of the marrow fat signal are

characteristic of uncomplicated Paget's disease on MR imaging. Presentation with bone pain should suggest the possibility of complicated Paget's disease be it fracture or malignant transformation. It should be stressed that not all tumours arising in association with Paget's disease are sarcomas. There is a rare association with giant cell tumour of bone and metastases, myeloma and lymphoma may all arise in pagetic bone. Therefore, it is important to surgically stage and biopsy a suspected malignancy in Paget's disease as the management and prognosis may differ considerably. Other rare conditions causing loss of bone density in Paget's disease that may mimic a sarcoma include post-immobilisation lysis, otherwise known as accelerated disuse osteoporosis, and drug-induced osteomalacia.

Bibliography

1. Whitehouse RW (2002) Paget's disease of bone. Semin Muscul Radiol 6:313–322
2. López C, Thomas DV, Davies AM (2003) Neoplastic transformation in Paget's disease of bone: pictorial review. Eur Radiol 13:L151–163
3. Kaufmann GA, Sundaram M, McDonald DJ (1991) MR imaging in symptomatic Paget's disease. Skeletal Radiol 20:413–418
4. Boutin RD, Spitz DJ, Newman JS et al (1998) Complications in Paget's disease at MR imaging. Radiology 209:641–651
5. Hain SF, Fogelman I (2002) Nuclear medicine studies in metabolic bone disease. Semin Muscul Radiol 6:323–329

Pancoast Syndrome

This consists of pain, numbness and weakness of the affected arm and is caused by tumour infiltration of the brachial plexus and neighboring ribs and vertebrae.

▶Neoplasms, Pulmonary

Pancreas Divisum

Pancreas divisum represents the most common pancreatic congenital variant. The characteristic finding is that the dorsal and ventral pancreatic glands drain separately into the duodenum: the predominant drainage (body and tail) is performed by the dorsal accessory duct of Santorini through the minor papilla, while the main duct of Wirsung drains the posterior part of the pancreatic head through the major papilla, where it is joined by the common bile duct.

▶Congenital Abnormalities, Pancreatic
▶Congenital Anomalies of the Pancreas

Pancreatic Congenital Anomalies

▶Congenital Abnormalities, Pancreatic

Pancreatic Cyst(s)

▶Congenital Anomalies of the Pancreas

Pancreatic Ductal Adenocarcinoma

▶Carcinoma, Pancreatic

Pancreatic Intraductal Neoplasms

Pancreatic intraductal neoplasms (PanINs) are precursors of the ductal adenocarcinoma, which are lesions composed of mucin-producing epithelia with varying degrees of cytologic and architectural atypia. They typically involve the small ducts of the pancreas. PanINs can be flat (PanIN1a), papillary without atypia (PanIN1b), papillary with atypia (PanIN2) or may represents a carcinoma *in situ* (PanIN3).

▶Carcinoma, Pancreatic

Pancreatic Lipomatosis

▶Congenital Anomalies of the Pancreas

Pancreatic Mass

Space-occupying lesion that located in the pancreatic gland could produce extrinsic compression of the posterior face of the gastric antrum ("antral pad" sign).

▶Compression, Extrinsic, Stomach and Duodenum

Pancreatitis, Acute

Laura Crocetti, Carla Cappelli, Salvatore Mazzeo, Carlo Bartolozzi
Divisions of Diagnostic and Interventional Radiology
University of Pisa, Pisa, Italy
l.crocetti@med.unipi.it

Synonyms

Acute inflammation of the pancreas

Definitions

According to the 1992 International Symposium on Acute Pancreatitis, acute pancreatitis is defined as an acute inflammatory process of the pancreas with variable involvement of other regional tissues or remote organ systems. Acute pancreatitis is classified further into mild and severe forms. Mild acute pancreatitis is associated with minimal organ dysfunction, whereas the severe acute pancreatitis, which exhibits extensive hemorrhagic necrosis of the organ, may lead to organ failure and/or local complications. Previous classifications have been based on the extent and degree of pancreatic injury, which could only be assumed at the time of diagnosis and which could sometimes be confirmed later during surgical exploration. This new classification is based on the presence of multiorgan failure and on the morphology of the pancreatic gland as depicted in Computed tomography (CT) imaging (1).

Pathology and Histopathology

It has been assumed that the ultimate pathogenetic process in acute pancreatitis is the destructive effect of pancreatic enzymes released from acinar cells, leading to autodigestion of the pancreatic parenchyma and peripancreatic tissues. The basic alterations are proteolytic destruction of acinar and islet cells, pancreatic ductal system, necrotizing vasculitis of blood vessels with subsequent thrombosis or hemorrhage, necrosis of fat, and an accompanying inflammatory reaction. The extent and predominance of each of these features depend on the duration and severity of the process. In the early stages only interstitial edema is present. Soon after, focal and confluent areas of necrosis of endocrine and exocrine tissue are found. Neutrophilic infiltration and interstitial hemorrhage eventually ensue. The most characteristic histological lesions are the focal areas of fat necrosis that occur in the pancreatic and peripancreatic fat, but also in the omentum and mesentery. During the first 30 min of an acute attack of pancreatitis a variety of toxic, biologically active compounds are produced and released in the blood and ascitic fluid, leading to multiorgan involvement (1).

Clinical Presentation

Gallstones are the leading cause of acute pancreatitis and can account for more than 80% of cases worldwide. Microlithiasis also is a well-known cause of acute pancreatitis and represents the cause of presumed idiopathic acute pancreatitis in 50–73% of patients. Alcohol abuse also is typically considered as a causative factor. Other causes include: drug reaction; pancreatic and ampullary tumors; hypertriglyceridemia; hypercalcemia (almost always due to hyperparathyroidism); congenital anomalies of pancreatic and biliary anatomy (pancreas divisum, annular pancreas, choledochocele); trauma (including iatrogenic damage, such as ERCP); infectious etiologies; vascular abnormalities (atherosclerotic emboli, hypoperfusion, vasculitis); cystic fibrosis. These miscellaneous causes account for approximately 10% of cases of acute pancreatitis (1).

The cardinal symptom of acute pancreatitis is moderate to severe epigastric abdominal pain that radiates to the back quite commonly, owing to the retroperitoneal location of the pancreas. It may also radiate to the flanks, chest, shoulders, and lower abdomen. The character of the pain is constant, but not colicky. Frequently nausea and vomiting are associated symptoms. Fever in the first week is due to acute inflammation and with inflammatory cytokines. Fever in the second or third week in patients with acute necrotizing pancreatitis is usually due to infection of the necrotic tissue and is much more significant. On physical examination, the abdomen may be distended and tenderness may exist. Flank ecchymosis (Grey-Turner sign) or periumbilical ecchymosis (Cullen sign) are rarely present and they often appear 48–72 h after the onset of symptoms (1).

Systemic complications can occur: multisystem organ failure (ARDS, renal failure), shock, hemorrhage, pleural effusions, pneumonia, and atelectasis, ileus. Local complications of acute pancreatitis include fluid collections, pancreatic necrosis, pseudocyst formation, ▶abscess, hemorrhage, venous thrombosis, and pseudoaneurysm formation. Pancreatic necrosis is defined as focal or diffuse areas of nonviable pancreatic parenchyma. Secondary bacterial contamination of such necrotic areas or collections is the usual cause of late mortality in

severe acute pancreatitis. A pseudocyst is a collection of pancreatic juice and inflammatory fluid enclosed by a wall of fibrous or granulation tissue. A pseudocyst lacks a true epithelial lining and communicates with the pancreatic duct. A pancreatic abscess is a circumscribed intra-abdominal collection of pus. The development of both pseudocyst and abscess usually requires 4 or more weeks from the initial clinical onset of acute pancreatitis (1).

Imaging

Conventional abdominal radiograph is the initial diagnostic examination in case of acute abdominal pain. The most commonly recognized radiological signs associated with acute pancreatitis include the following: air in the duodenal C-loop; the "sentinel loop sign," which represents a focal dilated proximal jejunal loop in the left upper quadrant; the "colon cut off sign," which represents distension of the right and transverse colon with a paucity of gas distal to the splenic flexure. However, the abdominal radiograph can be completely normal in patients with acute pancreatitis. The chest radiographs can demonstrate pulmonary findings (infiltrates, pleural effusion).

Ultrasound (US) is often employed early in an acute episode of pancreatitis, to exclude other causes of acute abdomen and to help evaluation of the biliary tree dilatation and the presence of stones in the biliary system. The pancreas may appear normal in some cases, especially in mild cases, while possible findings include a diffusely enlarged and hypoechoic gland. Complications of acute pancreatitis also may be identified (peripancreatic fluid collections, pseudocysts, pancreatic abscesses) (2).

CT of the abdomen is the standard imaging modality for evaluating acute pancreatitis and its complications. In addition, CT can be used as a prognostic indicator of the severity of acute pancreatitis. Lastly, CT can be used to guide percutaneous interventional procedures such as diagnostic fine needle aspiration or catheter placement. CT allows complete visualization of the pancreas and retroperitoneum. Oral and intravenous administration of contrast material is essential, particularly in patients with severe pancreatitis, to enable visualization of the pancreas and differentiation of the gland from adjacent collections of fluid and peripancreatic inflammatory tissue. Typical CT findings in acute pancreatitis include focal or diffuse enlargement of the pancreas, with inhomogeneous enhancement, irregular contour of the pancreatic margins, thickening of peripancreatic fat planes, thickening of fascial planes, and the presence of intraperitoneal or retroperitoneal fluid collections. The fluid collections most commonly are found in the peripancreatic and anterior pararenal spaces but can extend down to the pelvis (3–5) (Fig. 1, Fig. 2).

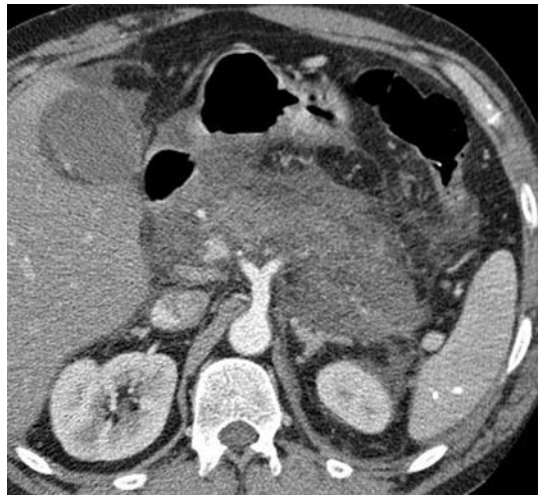

Pancreatitis, Acute. Figure 1 Multidetector spiral CT in severe pancreatitis. Pancreas is diffusely enlarged with inhomogeneous enhancement. Irregular contour of the pancreatic margins, thickening of peripancreatic fat planes, thickening of fascial planes, and an intra- and retroperitoneal fluid collection can be depicted.

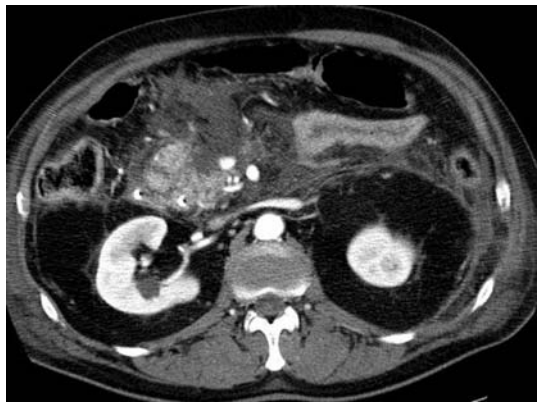

Pancreatitis, Acute. Figure 2 Multidetector spiral CT in severe pancreatitis. The body of the pancreas is replaced by an area of fat necrosis that is depicted as a collection without enhancement after intravenous administration of contrast medium. The pancreatic head is enlarged while the tail is not significantly involved. Marked thickening of the fascial planes is associated.

Complications of acute pancreatitis, such as pseudocysts, abscess, necrosis, venous thrombosis, pseudoaneurysms and hemorrhage, can be easily recognized with CT. A pseudocyst appears as an oval or round water density collection with a thin or thick wall, which may enhance. A pancreatic abscess can manifest as a thick-walled fluid collection with gas bubbles or a poorly defined fluid collection with mixed densities. Areas of fat necrosis can

be depicted as collections without enhancement after the intravenous administration of the contrast medium. Infection of the collection can be suspected when gas bubbles are present within the necrotic areas (3–5).

CT can also be used to assess the severity and estimate the prognosis of acute pancreatitis. Balthazar in 1985 developed a grading system in which patients with acute pancreatitis are classified into one of the following 5 grades (4):

- Grade A—Normal-appearing pancreas
- Grade B—Focal or diffuse enlargement of the pancreas
- Grade C—Pancreatic gland abnormalities associated with peripancreatic fat infiltration
- Grade D—A single fluid collection
- Grade E—Two or more fluid collections.

The development of rapid gradient-echo breath-hold techniques and fat-suppression techniques has made magnetic resonance (MR) imaging an excellent alternative modality to evaluate patients with acute pancreatitis. MR imaging is particularly useful in patients who cannot receive iodinated contrast material due to allergic reactions or renal insufficiency. The morphologic changes of the gland in acute pancreatitis are similar on both CT and MR. The pancreas may be enlarged focally or diffusely. Acute inflammatory changes appear as low signal intensity strands in the surrounding peripancreatic fat. Gadolinium-enhanced T1-weighted gradient-echo MR images can depict pancreatic necrosis as unenhanced areas. Fat-suppression images are also helpful for defining subtle, diffuse, or focal parenchymal abnormalities. T2-weighted images can accurately depict fluid collections, pseudocysts, and areas of hemorrhage, whereas MR is limited in detecting gas and calcifications. The association of MR cholangiopancreatography sequences is useful for depicting the biliary tract, for example to demonstrate biliary stones (3, 6).

Vascular complications of acute pancreatitis result from the proteolytic effects of the pancreatic enzymes that cause erosion of blood vessels, which often results in pseudoaneurysm formation or free rupture. The splenic artery, followed by the pancreaticoduodenal and gastroduodenal arteries, are affected most commonly. If acute hemorrhage or pseudoaneurysm is suspected or diagnosed by US or CT, a celiac and superior mesenteric angiography can be performed to definitively assess the extent of vascular involvement. In addition, permanent or temporary therapeutic embolization can be performed (4, 5).

Diagnosis

The diagnosis of the acute pancreatitis is based on the combination of the clinical, laboratory, and imaging findings.

Common laboratory abnormalities include elevated serum amylase and lipase levels, hyperglycemia, hypocalcemia, decreased lactic dehydrogenase levels, elevated serum glutamic-oxaloacetic transaminase, bilirubin and alkaline phosphatase levels, and leukocytosis. The serum amylase level is nonspecific and often returns to normal in 48–72 h; furthermore a normal amylase level does not exclude an acute pancreatitis. Instead, the increase in the serum lipase level is specific for pancreatic disease. Plasma levels of the pancreatic enzymes are useful diagnostic indicators, but have no role in the assessment of disease severity. More specific markers for pancreatic injury are methemalbumin and pancreatic ribonuclease (an intracellular enzyme liberated by necrotic tissue). The presence in serum of methemalbumin indicates hemorrhagic pancreatitis. C-reactive protein has been reported to be a prognostic indicator of disease severity with a sensitivity and specificity of 80%. However, none of the individual clinical or laboratory parameters, while useful in clinical practice, is sufficiently sensitive or specific to help identify most patients with necrotizing pancreatitis. For this reason, various scoring systems that combine clinical and laboratory parameters have been proposed to help identify patients with severe pancreatitis. The first, proposed by Ranson in 1974, is still the most widely used. It is based on 11 objective signs: 5 determined initially, and 6 within 48 h. With an increased number of risk factors, there is a corresponding increase in the morbidity and mortality rates. Moreover, the system requires all the 11 measurements, which necessitates a total of 48 h of observation. More recently, the Acute Physiology and Chronic Health Evaluation (APACHE II) assessment and monitoring system has been used. This system also results complex, requiring 12 physiologic measurements. It has been suggested that a cutoff APACHE II score of greater than 8 indicates severe pancreatitis. The major advantage of the APACHE II numeric system, when compared with the other systems, is that it can be used in monitoring the response to therapy. The test is useful as an early prognostic indicator of disease severity to help identify patients for intensive treatment (1).

Interventional Radiological Treatment

Approximately 50% of acute fluid collections (▶Fluid Collections, Pancreatic, Acute) resolve spontaneously within the first 4 weeks. Failure of resolution can lead to infection or to the formation of pseudocysts (sterile or infected) and abscesses. Diagnostic fine needle aspiration is performed to distinguish infected from noninfected pseudocysts and to delineate pancreatic abscess from infected necrosis. Therefore, they may be drained by

inserting a needle or tube through the skin under ultrasonographic or CT guidance, or by laparoscopic or open surgery. CT and US are the guidance modalities of choice in performing diagnostic fine needle aspirations and percutaneous drainages. Noninfected pseudocysts can be left untreated since approximately 50% resolve spontaneously. Rarely, inflammation can cause sudden rupture or severe bleeding inside the cyst from blood vessels damaged by inflammation. Intervention is mandatory only in the presence of symptoms or complications such as obstruction or infection. The abscess tends to be circumscribed and may be treated by methods identical to pancreatic pseudocyst, but external drainage is favored. A pancreatic abscess may be drained percutaneously, whereas infected necrosis usually requires surgical debridement. If acute hemorrhage or pseudoaneurysm is suspected or diagnosed by US or CT, a celiac and superior mesenteric angiography can be performed to definitively assess the extent of vascular involvement. In addition, permanent or temporary therapeutic embolization can be performed (2–5).

Bibliography

1. Bradley EL (1993) A clinical based classification system for acute pancreatitis: summary of the International Symposium on Acute Pancreatitis, Atlanta, GA, September 11 Through 13, 1992. Arch Surg 128, 586–590
2. Jeffrey RB, Ralls PW, Laing FC (1996) The pancreas. In: Jeffrey RB, Ralls PW (eds) CT and Sonography of Acute Abdomen. Lippincott-Raven, Philadelphia, pp 160–204
3. Robinson PJA, Sheridan MB (2000) Pancreatitis: computed tomography and magnetic resonance imaging. Eur Radiol 10, 401–408
4. Balthazar EJ, Ranson JH, Naidich DP et al (1985) Acute pancreatitis: prognostic value of CT. Radiology, Sep;156(3):767–772
5. Balthazar EJ (2002) Acute pancreatitis: assessment of severity with clinical and CT evaluation. Radiology, Jun;223(3):603–613
6. Gryspeerdt S, Van Hoe L, Baert AL (1998) Acute and chronic pancreatitis. In: Heuck A, Reiser M (eds) Abdominal and Pelvis MRI. Springer, Berlin-Heidelberg, pp 51–58

Pancreatitis, Chronic

Laura Crocetti, Carlo Bartolozzi, Claudio Vignali, Carla Cappelli
Department of Diagnostic and Interventional Radiology, University of Pisa, Pisa, Italy
l.crocetti@med.unipi.it

Synonyms

Chronic inflammation of the pancreas

Definitions

Chronic pancreatitis represents a continuous or relapsing inflammatory and fibrosing process of the pancreas leading to irreversible morphological changes associated with permanent endocrine and exocrine dysfunction. Chronic pancreatitis may not simply be the result of repeated attacks of acute pancreatitis; it is believed to be a separate and distinct disease entity (1).

Pathology and Histopathology

Morphological changes of chronic pancreatitis include necrosis and fibrosis, atrophy of acini with relative sparing of the islets of Langerhans. Proteinaceous material can fill the ducts and calcify. These concretions together with periductal fibrosis lead to variable obstruction and dilatation of pancreatic ducts. A chronic inflammatory infiltrate around lobules and ducts is usually present. The ductal epithelium may be atrophic or hyperplastic or may show squamous metaplasia. The lesions may involve portions of the gland (focal chronic pancreatitis) or the entire pancreas. Grossly the gland is hard and calcifications and calculi can be observed. Pseudocyst formation is common (1).

Clinical Presentation

The main cause of chronic pancreatitis is excessive chronic alcohol consumption. Chronic pancreatitis can also result from obstruction of the ducts (caused by tumours, anatomical variations), cholelithiasis, cystic fibrosis, haemochromatosis, congenital causes (pancreas divisum), autoimmune conditions, hereditary causes.

The dominant clinical symptom of chronic pancreatitis is epigastric pain, which may also radiate to the back. This can be very severe and continuous, but is more often intermittent, and occurs in attacks. Weight loss related to malabsorption due to pancreatic exocrine deficiency and signs of endocrine dysfunction (diabetes) are also common symptoms. Other complications include pseudocyst and fistula formation, pseudoaneurysms of the arteries close to the pancreas, splenic or portal venous obstruction, stenosis of the common bile duct (1).

Imaging

Plain radiographs of the abdomen may show pancreatic calcifications, which represent a common and pathognomonic finding of the chronic pancreatitis. Calcifications are punctiform or coarse and may have a focal, segmental,

or diffuse distribution. Gastrointestinal tract barium study still has a place in the management of chronic pancreatitis because it may provide information about complications involving the upper gastrointestinal tract: peripancreatic fibrosis may involve the antrum of the stomach or duodenum, resulting in stenosis; pancreatic enlargement or pseudocysts may compress and displace the stomach, duodenum or jejunum (2, 3).

Ultrasound (US) is the first modality to be used in patients presenting with upper abdominal pain, although the direct diagnosis of chronic pancreatitis is not always possible. The main findings are hypoechoic enlargement, diffuse or focal (focal chronic pancreatitis), with irregular pancreatic contour, calcifications and ductal dilatation. In late stages of the disease, the pancreas becomes atrophic and fibrotic with a heterogeneous aspect. When marked fibrosis is present, the gland appears diffusely but irregularly hyperechoic. The pancreatic duct is dilated and multiple stenoses may be evident. US can help also in determining the cause of chronic pancreatitis (e.g. demonstrating the presence of cholelithiasis) and it is a highly accurate non-invasive technique to assess the complications (pseudocysts, ascites, splenic/portal venous obstruction) (2, 3).

Contrast US has resulted to be helpful to provide an enhanced overall image quality and a better detection of pancreatic lesions in focal chronic pancreatitis.

Endoscopic ultrasonography (EUS) is more sensitive and the typical changes can be seen at an earlier stage of disease. The most characteristic EUS findings in chronic pancreatitis are parenchymal changes presenting as small hypoechoic areas separated by hyperechoic fibrous septa.

Computed tomography (CT) represents the modality of choice for the evaluation of suspected chronic pancreatitis. In early phases, CT findings may be entirely normal, whereas advanced disease is readily recognized on CT. Parenchymal atrophy with or without fatty replacement can be appreciated; in some cases chronic pancreatitis can present as a focal non-calcified mass that would be indistinguishable from a carcinoma. Focal enlargement found in association with calcification and ductal dilatation is suggestive of chronic pancreatitis. In addition, dilatation of the main pancreatic duct is a characteristic finding: irregularities in duct calibre are more frequently seen in chronic pancreatitis, whereas smooth dilatation is most commonly associated with carcinoma. CT is more sensitive than plain radiography and ultrasonography in the depiction of pancreatic calcification, which may appear tiny and punctate or larger and coarse (Fig. 1). Chronic pancreatitis can also be associated with obstruction of the biliary tree: in most instances, the involvement of the common bile duct may be visualized as a gradually tapering of the lumen, whereas an abrupt transition is commonly associated with

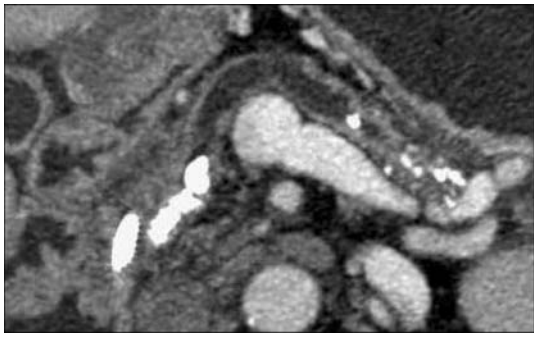

Pancreatitis, Chronic. Figure 1 Multidetector CT study of chronic pancreatitis. Markedly enlarged pancreatic duct, due to the presence of intra-ductal stones, is depicted. The pancreas has become atrophic and tiny calcifications are present in the pancreatic tail.

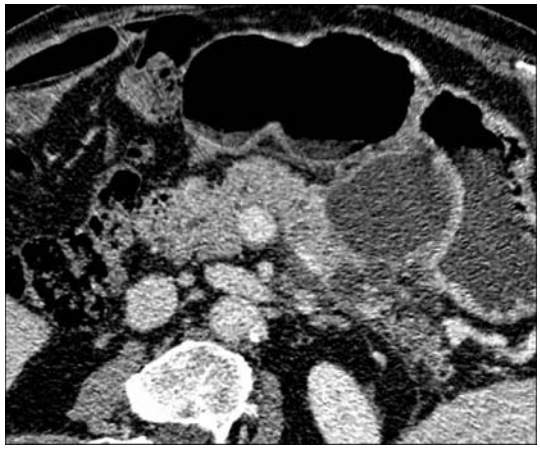

Pancreatitis, Chronic. Figure 2 Multidetector CT study of pseudocyst in chronic pancreatitis. A pseudocyst can be appreciated in the pancreatic tail. The surrounding pancreatic parenchyma of the tail is inhomogeneous as a result of repeat exacerbations of chronic pancreatitis.

carcinoma. Obliteration and thickening of peripancreatic fat can be seen, usually in case of acute exacerbations of chronic pancreatitis. Pseudocysts can occur both in acute and chronic pancreatitis. When pseudocysts are associated with ductal dilatation or calcifications chronic pancreatitis is suggested (Fig. 2). Vascular complications of chronic pancreatitis are best depicted by using contrast-enhanced CT scans; arterial pseudoaneurysms and portal and/or splenic vein thrombosis represent possible findings (2, 3).

Characteristic magnetic resonance (MR) signal changes are evident in advanced disease. T1-weighted SE images show a loss of signal intensity of the glandular parenchyma, as a result of pancreatic fibrosis which

diminishes the proteinaceous fluid content in the glandular acini. The loss of signal is seen more easily on fat-suppressed images. On T2-weighted images the parenchymal signal intensity may be normal, or variably modified. Small calcifications are difficult to detect by using MR, but larger calcifications may be visible as foci of signal void on both T1 and T2. Pseudocysts associated with chronic pancreatitis can be demonstrated as well-defined masses with low to medium signal intensity on T1-weighted images and high signal intensity on T2-weighted sequences, similar to other fluid collections. Parenchymal gadolinium enhancement results less intense and more gradual than in the normal pancreas, because fibrosis produce the obliteration of small capillary vessels. With respect to CT, MR is more sensitive in detecting early changes of fibrosis, which manifest as reduction in signal intensity on T1-weighted images and reduced gadolinium enhancement. Mangafodipir trisodium (Mn-DPDP) should help to highlight focal pancreatitis, because inflammatory alteration of the parenchyma in focal pancreatitis results in lack of MnDPDP uptake into the parenchyma. However also neoplastic lesions cannot demonstrate uptake of the MnDPDP. MR cholangiopancreatography (MRCP) sequences are able to visualize the characteristic dilatations and strictures of the main pancreatic duct and of the side branches. MRCP also displays the intra-ductal filling defects due to intra-ductal plugs and stones. Intravenous secretin administration is useful to enhance the delineation of the main pancreatic duct and can improve the detection of subtle changes of the side branches and allow the earlier non-invasive diagnosis of chronic pancreatitis. Secretin-enhanced pancreatography also has the capability to depict the anatomic relationships of pancreatic ducts and pseudocysts and also provides additional functional information regarding pancreatic exocrine function (2, 3).

ERCP represents at present the most sensitive imaging procedure for detecting early and minimal ductal abnormalities in chronic pancreatitis. However, it is an invasive procedure, actually almost completely replaced by MRCP. The earliest signs of chronic pancreatitis are observed in side branches of pancreatic duct and include dilatation with or without stenosis, intra-luminal mucosal irregularity and intra-luminal filling defects due to protein plugs or calcifications. The number of opacified side branches may be reduced because of ductal occlusion. In advanced disease, ductal changes involve also the main pancreatic duct. In the pancreatic parenchyma small cavities may be observed. Occasionally, contrast material may fill large pseudocysts *via* fistulous communications. Common bile duct may be involved in chronic pancreatitis; the most common finding is a long smooth narrowing with gradual tapering due to periductal fibrosis. Pancreatic juices can be collected for laboratory analysis and cytology brushings can be performed, to differentiate between focal chronic pancreatitis and pancreatic cancer (2, 3).

Angiography is reserved for patients with suspected vascular complications resulting from chronic pancreatitis. The major vessels around the pancreas may be involved. Pseudoaneuysms of the intra-pancreatic and peripancreatic arteries or dilated segments alternating with narrowing can be depicted and, if necessary, treated. Venous compression or thrombosis, particularly in the splenic vein, represents a possible angiographic finding (2, 3).

Nuclear Medicine

Positron emission tomography (PET) is able to differentiate focal chronic pancreatitis from pancreatic malignancy, thanks to the absence of FDG uptake in inflammatory lesions. Carbon-11-acetate can also be employed for the PET evaluation. The normal pancreas demonstrates prompt uptake of carbon-11-acetate and is visualized as early as 2 min post-injection, with maximal activity achieved by 5 min. Pancreatic uptake is absent in chronic pancreatitis complicated by exocrine insufficiency. Moderately reduced uptake can be observed in focal chronic pancreatitis whereas pancreatic cancer demonstrates no significant uptake.

Diagnosis

The diagnosis of chronic pancreatitis is obvious in advanced phases with typical clinical, laboratory and imaging features. However, most patients present with pain only and in this case cancer of the pancreas, biliary, colic, gastric or duodenal ulcer must be excluded. First of all, an accurate medical history is fundamental. There are also many laboratory tests that can be used for chronic pancreatitis: serum amylase and lipase levels may show elevations but can normalize in advanced disease when a loss of pancreatic function occurs. Tests for diabetes, fecal fat and chymotrypsin test together with secretin test may assess a pancreatic endocrine and exocrine dysfunction.

The critical issue is the differential diagnosis between focal chronic pancreatitis and pancreatic carcinoma. Both carcinoma and inflammatory mass may present with back pain and weight loss; when the lesion involves the head of the pancreas, jaundice is also a presenting feature. If the inflammatory masses arise in the early stages of chronic pancreatitis when the characteristics imaging findings are absent, the differential diagnosis is challenging. Further complicating factors arise in patients in whom carcinoma may obstruct pancreatic ducts, leading to pancreatic inflammatory reaction.

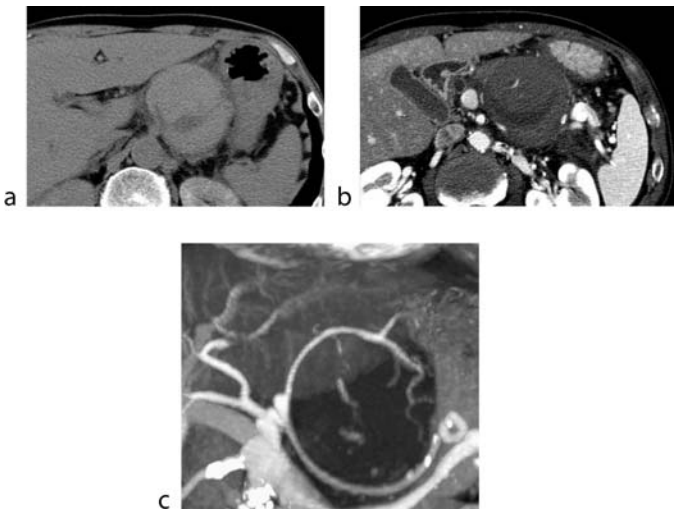

Pancreatitis, Chronic. Figure 3 Multidetector CT study of a bleeding pseudocyst in chronic pancreatitis. The pseudocyst of the tail is hyperdense at baseline CT scans, due to hemorrhage (a). The bleeding was due to the erosion of the vascular wall of a branch of the left gastric artery as depicted in arterial axial (b) and maximum intensity projection reconstructed (c) images.

At CT examination, both carcinoma and chronic pancreatitis are typically hypovascular. The CT finding of pancreatic calcifications do not exclude pancreatic cancer, since there may be a tumour in co-existing chronic pancreatitis. MR may in some cases help the differentiation, because a signal intensity diminished but equal to or greater than that of the liver on T1-weighted fat-suppressed spin-echo images can suggest a benign inflammatory lesion, whereas carcinoma is often hypo-intense to liver. At MRCP examination, the neoplastic lesion does not contain pancreatic ductal structures, whereas focal pancreatitis may display dilated side branches.

In general, differentiation between cancer and focal pancreatitis is difficult with a single imaging modality and may sometimes require the use of contrast-enhanced CT, MR, PET examination, biopsy and eventually the surgical inspection.

Interventional Radiological Treatment

In chronic pancreatitis vascular arterial complications can occur, such as pseudoaneurysm. The majority of pseudoaneurysms occur in association with pancreatic pseudocysts, which can gradually erode the vascular wall of the adjacent vessels (Fig. 3). The more commonly involved vessels are the splenic artery, the gastroduodenal artery, the pancreatic-duodenal arcades and the left gastric artery. Angiography therefore plays role for treating lesions by means of embolization.

Patients with acute biliary obstruction can be treated by using temporary biliary stents, whereas established biliary strictures in end-stage of chronic calcific pancreatitis usually do not respond to endoscopically placed stents.

Bibliography

1. Gryspeerdt S, Van Hoe L, Baert AL (1998) Acute and chronic pancreatitis. In: Heuck A, Reiser M (eds) Abdominal and Pelvis MRI. Springer, Berlin-Heidelberg, pp 51–58
2. Robinson PJA, Sheridan MB (2000) Pancreatitis: computed tomography and magnetic resonance imaging. Eur Radiol 10, 401–408
3. Graziani R, Tapparelli M, Malagò R et al (2005) The various imaging aspects of chronic pancreatitis. JOP J Pancreas 6(1):73–88

Pancreatoblastoma

Pancreatoblastoma is an extremely rare carcinoma of the pancreas, which usually occurs in children younger than 15 years of age. The tumor is usually surrounded by a fibrous capsule. Typical microscopic findings include nests of squamoid cells separated by dense fibrous stroma on a background of uniform, undifferentiated cells. Imaging reveals a well-demarcated solid and often multilobulated tumor that may contain fine calcifications. Due to the large size at diagnosis, there are often cystic components with hemorrhagic necrosis and degeneration within the tumor. Metastases to the liver and lymph nodes can be present at diagnosis. Elevated serum alpha-fetoprotein levels are

reported in one fourth to one third of patients. The survival rate after resection is better than adenocarcinoma.
▶Carcinoma, Pancreatic

Pantomography

Tomographic technique achieving panoramic images.
▶Caries and Periodontal Diseases

Papillary Carcinoma

▶Carcinoma, Other, Invasive, Breast

Papillary Projections

Small nodular excrescences within the wall of ovarian cancer. They present a typical finding of serous epithelial tumors and are most commonly found in borderline tumors and ovarian cancers. They may also be encountered in cystadenomas where they tend to be very small.
▶Carcinoma, Ovarium

Papilloma, Gallbladder

Histological subtype of gallbladder adenoma, also called papillary adenoma.
▶Neoplasms, Gallbladder

Para-Oesophageal Hernia

▶Contrast Media, Ultrasound, Influence of Shell on Pharmacology and Acoustic Properties

Paradoxical Systemic Embolism

Aseptic or infected clots or air bubbles which are not trapped by the pulmonary capillary bed can pass through a pulmonary right-to-left shunt and cause embolisms of the systemic circulation with potential clinical sequelae (stroke, cerebral or visceral abscess). In case of brain abscess, a pulmonary or cardiac right-to-left shunt must be suspected.
▶Fistula, Arteriovenous, Pulmonary

Paralytic Ileus

Paralytic ileus is the failure of intestinal propulsion due to a neuromuscular or metabolic condition, which occurs in the absence of a mechanical obstruction.
▶Occlusion and Subocclusion, Small Bowel in Adults
▶Small Bowel, Postoperative

Parametric Imaging

The visualization of a (semi)-quantitative parameter value in its spatial distribution. In contrast-enhanced ultrasound, it can provide a particularly user-friendly presentation of information derived from complex perfusion examinations.
▶Time Intensity Curves

Paraneoplastic Syndromes

Paranesplastic Syndromes of lung cancer are extrapulmonary, remote effects of the tumours. They lead to metabolic and neuromuscular disturbances unrelated to the primary tumour or metastases. They may be the first sign of occurrence or recurrence, but they do not necessarily indicate that a tumour has spread outside the chest. In hypertrophic pulmonary osteoarthropathy clubbing of the fingers and toes and periosteal elevation of the distal parts of long bones occur. All levels of the nervous system may be affected principally causing encephalopathy, subacute cerebellar degeneration, encephalomyelitis, the Eaton–Lambert syndrome and peripheral neuropathy. Polymyositis and dermatomyositis or metabolic syndromes due to production of substances with hormonal activity may develop. Small cell carcinomas may secrete ectopic ACTH, resulting in Cushing's syndrome or ADH, causing water retention and hyponatremia, and are also associated with

the carcinoid syndrome (flushing, wheezing, diarrhoea and cardiac valvular lesions). Squamous cell carcinomas may secrete parathyroid hormone-like substances that produce hypercalcemia. Other endocrine syndromes associated with primary lung carcinomas include gynecomastia, hyperglycaemia, thyrotoxicosis and skin pigmentation. Haematologic disorders, including thrombocytopenic purpura, leukaemoid reaction, myelophthisic anaemia, polycythemia and marantic thrombosis, may also occur.

▶Neoplasms, Pulmonary

Paraoesophageal Varices

Terminology used to describe varices located adjacent to but outside the oesophageal wall. Normally co-exist with intramural oesophageal varices.

▶Varices, Oesophagus

Parapneumonic Effusion

A pleural effusion associated with pneumonia, lung abscess or bronchiectasis. Not all parapneumonic processes are empyemas.

▶Pleural Effusion

Parasitic Cyst

Parasitic cyst is extremely uncommon and is usually identified as a hydatid cyst. Echinococcus granulosus cysts may be unilocular, multilocular, or complex. Echinococcus multilocularis cysts may show an infiltrative aspect. On imaging alone, differentiation between hydatid and other cystic lesion is difficult; serologic tests may be useful in the appropriate clinical setting.

▶Cystic Neoplasms, Pancreatic

Parasyndesmophytes

Intervertebral and paravertebral osteophytes with characteristic appearance seen in psoriatic spondyloarthropathy. Three morphological types are distinguished: (i) bull-horn intervertebral osteophyte, which is the most common type and which has to be differentiated from degenerative disease, (ii) paravertebral ossicle, and (iii) paradiscal ossicle. In known psoriatic spondyloarthropathy the diagnosis is easy, but without it, it is not very specific.

▶Spondyloarthropathies, Seronegative

Parathyroid Adenoma

▶Neoplasms, Parathyroid

Parathyroid Cancer

▶Neoplasms, Parathyroid

Parotid Gland

The largest of the salivary glands. It is found in the subcutaneous tissue of the face, overlying the mandibular ramus and anterior and inferior to the external ear.

▶Salivary Glands, Inflammation, Acute Chronic

Passive Targeting

A nonspecific accumulation of microbubbles at the target site after their administration and does not require a shell labeling with specific ligands.

▶Targeted Microbubbles

PCNL

▶Percutaneous Nephrolithotomy

PDGF

Platelet-derived growth-factor.
▶Carcinoma, Ductal, *In Situ*, Breast

Peau d'Orange

Obstruction of cutaneous lymphatics in inflammatory carcinoma, with secondary skin thickening and dimpling, resembling the skin of an orange.
▶Cutaneous Lesions, Breast

Pediatric Hepatic Neoplasms

▶Hepatic Pediatric Tumors, Benign

Pediatric Liver Tumors

▶Hepatic Pediatric Tumors, Benign

Pediatric Neoplasms of the Liver

▶Hepatic Pediatric Tumors, Benign

Pediatric Posterior Fossa Tumors

Histologies of brain tumors differ completely between adults and children, so age is the main predictive factor. The most frequent tumors in the posterior fossa in children are pilocytic astrocytoma, medulloblastoma, ependymoma, and brain stem glioma.
▶Neoplasms, Brain, Posterior Fossa, Pediatric

Pediatric Radiology

M Riccabona, R Fotter
Department of Radiology
Division of Pediatric Radiology
University Hospital Graz,
Graz, Austria
michael.riccabone@meduni-graz.at
richard.fotter@meduni-graz.at

Pediatric Radiology

Pediatric radiology is one of the recognized subspecialty areas of radiology. In the last decade remarkable advances in the ability to vividly image both normal and abnormal anatomic and functional aspects have been accomplished. Various imaging modalities, such as ultrasonography, projection radiography, computed tomography, magnetic resonance imaging, angiography, and nuclear medicine examinations are applied to children. Technology and techniques must be tailored with respect to their particular advantages and disadvantages related to their properties and to the specific requirements of children. Not only anatomy and physiology differ from the adult situation; there are also specific pediatric diseases and conditions, congenital malformations, and problems in ▶neonates and preterm babies. Furthermore, fetal imaging is gaining importance and is being again introduced more and more into pediatric radiology in terms of ▶fetal MRI. Further specific adaptations of imaging protocols and techniques are essential to reduce ▶radiation hazards to neonates, infants, and children. Additionally, pediatric radiology tries to promote and use nonionizing ▶imaging techniques leading to different imaging algorithms compared to adult radiology. This entry tries to include all relevant aspects of pediatric radiology from head to toe focusing on those conditions that significantly differ from imaging in adults.

The utility and limitations of modalities will be presented for each particular disease and clinical situation enabling a profound knowledge and understanding much easier than by retrieving the respective information. Perception, understanding, and interpretation of imaging findings require a profound knowledge of anatomy throughout childhood as well as of physiology of growth with consecutive changing imaging patterns during growth. And it requires a profound knowledge of pathology and pathophysiology of neonatal and pediatric diseases, as well as the recognition of the broad range of normal variants; as such radiological–pathological as well as structural–functional correlations are important.

Pediatric radiology includes two major areas: imaging of congenital diseases and malformations and assessment of acquired disease. These two groups all comprise the various anatomical systems such as the ▶musculoskeletal system (including small part diseases), the ▶cardiovascular system, ▶chest and the respiratory tract, ▶the gastrointestinal tract, the ▶urinary and the ▶genital and tract, the central and peripheral nerve system, the ▶endocrine organs, and—mostly congenital—systemic diseases. Additionally, imaging plays a major role for diagnosis, treatment, and monitoring of critically ill neonates and children, also including pediatric ▶extracorporeal membrane oxygenation (ECMO).

Interventional procedures such as diagnostic punctures or therapeutic drainages often require image guidance particularly in children in order to reduce risks and complications. And various etiologies have to be considered, part of them are more important than in adults (e.g., inborn errors of metabolism), some have different manifestations, patterns and clinical symptoms or locations: infective disease, toxically induced conditions, trauma [including ▶battered child syndrome and birth complications], genetic and congenital or metabolic disorders, ▶tumors and malignancies, disorders of growth and development, and deregulations.

Assessment of regular anatomy and abnormalities requires the knowledge of normal variants and physiologic changes during growth and maturation as well as their imaging appearance on the different modalities. It is important to recognize normal characteristics, structures, and patterns, which can be solitary, multiple, or disseminated. Individual findings on imaging studies can represent signs or a complex pattern of signs, which are related to certain anatomic-pathologic substrates. The way to diagnosis is based on a standardized process of pattern analysis and taking into consideration patient history and clinical data. The mentioned analysis of imaging findings with regard to size, number, morphology, localization, distribution, contrast dynamics and perfusion, and correlation to age and development is the prerequisite for any profound radiological diagnosis. However, the radiological patterns reflect the macroscopic consequences of any disease, and are just a "snap shot" at a certain stage of an age correlated disease process. This aspect is particularly important in children, as we often observe very early stages of diseases and/or a certain phase of an evolutionary process, which changes with growth and development. Additionally—due to the specific conditions particularly in early childhood—(modern) ultrasound plays a much more important role in imaging diagnostics in many body compartments, whereas CT is used more reluctantly; thus imaging approaches that are valid and established in adults do not necessarily apply for children.

Finally a specific aspect of pediatric radiology must be mentioned—its importance in recognition and diagnosis of child abuse and ▶battered child syndrome/non-accidental injury (NAI). The specific imaging features potentially enable early life saving recognition and intervention putting additional burden and responsibility on the radiologist who not only has to consider the individual small patients, but often has to deal with the entire family and their fears and expectations.

As such, in summary, the task of pediatric radiology—additional to the general purpose of radiology—is to establish a diagnosis as early as possible in order to prevent permanent damage. This aim may be difficult to achieve by modalities that focus mainly on visualization of structure, anatomy, and morphology. Thus functional and molecular imaging aiming at evaluation of disease activity, vascularization, blood flow, and perfusion, or visualization of metabolic processes is gaining importance also in pediatric radiology, however, with yet limited clinical application only in some entities and body areas in routine of pediatric imaging.

Peliosis Hepatis

Hepatic peliosis is an uncommon benign pathological entity characterized by focal, multifocal, segmental, or diffuse dilatation of liver sinusoids. It often occurs in patients treated with anabolic steroids, corticosteroids, or oral contraceptives and a frequent association with chronic wasting diseases has also been reported. Hepatic peliosis is usually asymptomatic and focal liver lesions are discovered incidentally. Imaging findings in peliosis hepatis are variable and often nonspecific. On US, numerous poorly defined foci of varying hypoechogenicity may be usually observed. Multiple small hypodense hepatic lesions with slight peripheral enhancement represent the most common findings on contrast-enhanced CT, while the hepatic foci in peliosis hepatis show a high signal on T2-weighted MR images and a variable signal on T1-weighted images, presumably reflecting various stages of subacute hemorrhage.

▶Vascular Disorders, Hepatic

Pelvic Cavity

The most dependent portion of the peritoneal cavity in either the supine or erect positions. Inframesocolic peritoneal fluid tends to accumulate in the pelvic cavity, especially in the pouch of Douglas.

▶Peritoneal Collections

Pelvic Floor Dysfunction

A group of conditions associated with anatomic and functional abnormalities of pelvic structures.
►Pelvic Floor Dysfunction, Anorectal Manifestations

Pelvic Floor Dysfunction, Anorectal Manifestations

Dominik Weishaupt[1], Franc H. Hetzer[2], Nicolae Bolog[1]
[1]Institute of Diagnostic Radiology, University Hospital, Zurich, Switzerland
[2]Clinic of Visceral and Transplant Surgery, University Hospital, Zurich, Switzerland
dominik.weishaupt@usz.ch

Synonyms

Anismus - spastic pelvic floor syndrome - diskinetic puborectalis muscle - pelvic floor dyssynergia; Conventional defecography - evacuation proctography; Fecal incontinence - anal incontinence; Internal rectal prolapse – intussusception; Outlet obstruction syndrome - obstructed defecation; Posterior rectocele - posterior perineal hernia.

Definition

Pelvic floor dysfunction is represented by a group of conditions associated with anatomic and functional abnormalities of pelvic structures. The anorectal manifestations of these dysfunctions are responsible for two major syndromes: ►fecal incontinence and ►outlet obstruction syndrome. Fecal or anal incontinence is defined as an involuntary loss of rectal content at a socially inappropriate time or place of at least 1 month in duration in an individual with a developmental age of at least 4 years. Outlet obstruction syndrome, also called obstructed defecation, is characterized by incomplete evacuation of fecal contents from the rectum.

Although a detailed clinical examination still represents the cornerstone of diagnosis in these patients, imaging techniques are decisive for reliably evaluating anorectal functional and anatomic disorders, which include ►anal sphincter weakness or defect, ►anterior rectocele, ►enterocele, ►rectal prolapse, ►rectal descent, and ►anismus. Moreover, treatment decisions highly depend on the imaging assessment.

Pathology/Histopathology

In patients with anorectal dysfunctions, functional and structural abnormalities of the posterior pelvic compartment lead to fecal incontinence or outlet obstruction. Within the anorectum there are a number of structures responsible for normal evacuation, including the internal and external anal sphincters, the puborectalis muscle, the anal canal, and the rectum, as well as the pudendal and sacral nerves. Anorectal dysfunction can result from impairment of any of these structures. Obstetric trauma and anal and pelvic surgery (such as hemorrhoidectomy and low anterior rectum resection) are closely correlated with anal sphincter injuries, enterocele formation, and rectal descent. A weakness of the rectovaginal septum is probably responsible for rectocele formation. The insufficient septum can be congenital, or it can occur after tearing caused by excessive straining at defecation, hysterectomy, or complicated vaginal delivery. However, in most cases the etiology is multifactorial, and the presence of an isolated pelvic floor abnormality is unusual. Anismus, internal rectal prolapse, rectocele, and enterocele are often combined. Moreover, it is well known that the posterior compartment dysfunctions are often accompanied by middle and anterior pelvic compartment disorders (1).

Clinical Presentation

The clinical examination and history is the cornerstone of obtaining an accurate diagnosis in patients with anorectal dysfunction. Fecal incontinence is a significant disability that affects quality of life and can lead to social isolation. The true prevalence is not well known. It increases with age, from approximately 4% in the fifth decade of life to 11% in patients aged 80 years and older. Several etiological factors that may cause fecal incontinence have been reported. Congenital malformations, such as anorectal agenesis, can cause fecal incontinence in children. A greater proportion of adult patients suffering from fecal incontinence have acquired the condition. Sphincter defects resulting from complicated vaginal delivery or anorectal surgery are the most common type of sphincter injury. Diabetes mellitus, dementia, and pudendal neuropathy are examples of neurological causes leading to fecal incontinence. In most patients, a combination of several factors contributes to the emergence of fecal incontinence.

Although an international consensus regarding symptom evaluation and scoring does not yet exist, most

clinicians use the Wexner score to assess the severity of fecal incontinence.

In chronically constipated patients, it is important to differentiate between slow transit constipation and outlet obstruction. Slow transit constipation is represented by delayed transit throughout the colon and is associated with a reduced number of propagating contractions. Outlet obstruction syndrome is present in half of constipated patients and is the result of pelvic floor dysfunction. Patients present with difficulty in rectal evacuation, and the symptoms may vary from the feeling of incomplete evacuation to a severe obstruction. In some cases, such as in the presence of an anterior rectocele, digital maneuvers are needed for a complete evacuation.

Imaging

Different imaging modalities are used for assessing patients with posterior pelvic floor dysfunctions, including endoanal ultrasonography, conventional defecography, and magnetic resonance imaging (MRI). The choice of imaging technique depends on the etiological factor, patient symptoms, physical examination, and technique availability.

Endoanal Ultrasonography

Endoanal ultrasonography is routinely used for assessing anal sphincter anatomy in patients with fecal incontinence. The technique enables evaluation of the structural defects or degeneration of the internal and external anal sphincters and can diagnose lesions that were undetected at physical examination. Radial endoscopic probes with either 7-MHz or 10-MHz frequency are used with similar results. The probe is covered by a plastic cone 15–17 mm in diameter, which enables high-quality images. The procedure is rapid, minimally invasive, and without radiation exposure. Moreover, a high sensitivity and specificity of endoanal ultrasonography for evaluating the anal sphincter has been reported compared with surgery. Isolated external sphincter tears are much harder to recognize because of the mixed echogenicity of the external sphincter. The disadvantages are interobserver variability and difficulty in imaging deep pelvic structures. However, the new generation of three-dimensional endoanal ultrasonography allows an observer-independent more specific diagnosis in structural sphincter defects.

Conventional Defecography

Conventional defecography or evacuation proctography is the most commonly used imaging technique for evaluating patients with anorectal dysfunction. The examination is usually performed without bowel preparation. The rectum is opacified using an enema of thickened barium suspension, and the patient is imaged in a seated position on a radiolucent commode. Images are obtained at rest, at squeezing, at straining, during evacuation, and after evacuation. This technique enables evaluation of the anorectal disorder, but it provides no information regarding other pelvic floor organs. Since it was demonstrated that posterior compartment changes are often accompanied by middle and anterior pelvic compartments disorders (1), some authors have proposed opacifying the small bowel as well as instilling contrast into the bladder and vagina to obtain more information about these structures.

This technique has some limitations. The irradiation is significant because fluoroscopic X-ray proctography produces a mean effective dose of up to 4.9 mSv. Moreover, the technique is limited by its projectional nature (2) and its inability to accurately assess the pelvic organs.

Endoanal Magnetic Resonance Imaging

MRI using an endorectal coil is an accurate technique for evaluating the normal anatomy and pathological conditions of the internal and external anal sphincters. This method provides high-contrast images and excellent spatial resolution. T1- and T2-weighted sequences are used in transaxial, sagittal, and coronal planes with respect to the axis of the endorectal coil. Endoanal MRI has proved to be superior to endoanal ultrasonography for evaluating the external sphincter (3).

Dynamic Pelvic Magnetic Resonance Imaging

Dynamic pelvic MRI is a noninvasive method that enables an overall view of all pelvic structures. The free selection of imaging planes, the good temporal resolution, and the excellent soft-tissue contrast have transformed this method into the preferred imaging modality for evaluating patients with pelvic floor dysfunction (4). Dynamic pelvic MRI can be done in either a closed-configuration MR system with the patient in supine position or an open-configuration MR system with the patient in sitting position. It has been shown that no clinical significant finding was missed when comparing dynamic pelvic MR in supine position with dynamic pelvic MR in sitting position (5). There is general agreement that neither premedication nor oral or intrarectal preparation for bowel cleansing is necessary when dynamic pelvic imaging is performed. Before examination, the rectum is filled with a contrast agent, of which the viscosity should be similar to that of normal rectum content because the manifestations of anorectal disorders may vary with fecal consistency. Ultrasound gel or mashed

potatoes spiked with a small amount of gadolinium chelate (2, 5) are used for the rectal enema. Some authors have proposed tagging the middle compartment (i.e., the vagina) and/or the anterior pelvic compartment (i.e., the bladder) to clearly delineate these compartments (1). In our experience, there is no need for contrast agent administration either in the vagina or in the bladder because MRI allows easy identification of all the anatomic structures of the three pelvic compartments. However, it is of outmost importance to perform the examination at rest, at maximal contraction of the anal sphincter (squeezing), at straining, and during evacuation because relevant findings may be missed when dynamic pelvic MRI does not encompass all of these phases. For dynamic MRI, various sequences can be used with similar results: T2-weighted single-shot fast spin-echo sequences (SSFSE) or steady-state free precession (SSFP) sequences in the midsagittal plane at rest, at squeezing, at straining, and during defecation. When ultrasound gel or mashed potatoes mixed with a small amount of gadolinium chelate is used as an enema, a T1-weighted multiphase gradient-recalled echo (GRE) sequence should be used because this sequence offers an imaging window long enough for continuous imaging of the evacuation, even in patients with prolonged evacuation time (4).

Diagnosis

In patients with pelvic floor dysfunction, the diagnosis is the result of a detailed clinical examination, anorectal physiology tests (anorectal manometry, electromyography), and imaging assessment. The imaging evaluation provides detailed information regarding the functional and anatomic abnormalities, contributes to the clinical diagnosis, and influences the treatment strategy.

Anal Sphincter Weakness

Anal sphincter weakness is defined as reduced anal resting and/or squeeze pressure, having as a result a recurrent uncontrolled passage of fecal material. The cause is either a well-defined lesion of the anal sphincters or a primary degeneration and weakness of the anal sphincters without structural damage. The diagnostic tests include anal manometry, pudendal nerve latency, and endoanal ultrasonography. Although the incontinence is attributable to a combination of pelvic floor disorders, anal sphincter injuries represent the most important cause of fecal incontinence.

Endoanal ultrasonography has proved to be more accurate than manometry for characterizing anal sphincter defects. The technique identifies the location and extent of sphincter injuries and permits a correct assessment for surgical treatment and follow-up. The internal sphincter appears as a ring of low reflectiveness, and any disruption is indicative of an injury. Endosonography reveals internal sphincter degeneration as a thin and hyperechogenic ring with a poorly defined edge. The external sphincter is more difficult to assess because of its fibrillar structure and the low image contrast.

The anal sphincter complex may also be imaged using endoanal MRI, which has proved superior to endoanal ultrasonography for external sphincter evaluation. It has been demonstrated that if only one technique is to be used, MRI findings result in the optimal surgical decision (3).

Anismus

Anismus is an abnormal activity of pelvic floor musculature that results in outlet obstruction characterized by difficulties in rectal evacuation. In the literature, anismus is also known as spastic pelvic floor syndrome (2), dyskinetic puborectalis muscle, or pelvic floor dyssynergia. The obstruction is caused by paradoxical contraction or insufficient relaxation of the puborectalis or external sphincter muscles, and in most cases, these dysfunctions are not confined to a single muscle. The diagnosis is based on anorectal manometry, balloon expulsion, electromyography, and dynamic pelvic imaging (conventional defecography or dynamic MRI). Although various imaging findings have been described in patients with anismus, the best single finding of the functional outlet obstruction is represented by a prolonged attempted defecation and incomplete evacuation (4). An evacuation time longer than 30 s is highly suggestive for anismus, having a positive predictive value of 90%. Another imaging parameter that has been extensively used for diagnosing anismus is the anorectal angle. However, data in the literature show that the configuration of the rectum and anorectal junction is irrelevant to the diagnosis and that this finding cannot differentiate patients with anismus from asymptomatic subjects.

Rectocele

A rectocele is defined as a rectal wall protrusion or bulging during defecation. The anterior wall is most commonly involved, but a rectocele may also be located in the posterior rectal wall. Posterior rectoceles are also referred to as posterior perineal hernia by some authors, based on the fact that the bulging is through a puborectalis muscle defect. Most of the rectoceles are diagnosed during physical examination, but reliable classification with regard to the size, emptying, and associated abnormalities is provided only by imaging examinations. With dynamic pelvic imaging, an anterior rectocele can be classified with

regard to its size, expressed as the depth of wall protrusion beyond the expected margin of the normal anterior rectal wall, into small (< 2 cm), moderate (2–4 cm; Fig. 1), and large (> 4 cm) (2). In addition, rectoceles are classified into those with complete evacuation and those with incomplete evacuation (Fig. 1), depending on the presence or absence of contrast material retention at the end of defecation. A clinically significant rectocele should be considered based on the following criteria: patient history, size exceeding 2 cm in sagittal diameter, retention of contrast medium, reproducibility of the patient's symptoms, and the need for evacuation assistance.

Rectal Prolapse

Rectal prolapse is an invagination of the rectal wall and may be classified as internal or external (1). Internal rectal prolapse, also called intussusception, may be classified as intrarectal internal prolapse if the invagination is confined to the rectum or as intraanal internal prolapse if its apex penetrates the anal canal and remains in it during straining (Fig. 2). External rectal prolapse is an invagination of the rectal wall through the anal canal (Fig. 3) and is a clinical diagnosis. Regardless of its extension, internal rectal prolapse may involve all rectal wall layers (full-thickness prolapse; Fig. 2) or only the mucosa (mucosal prolapse) (2). Dynamic MRI is superior to conventional defecography for diagnosing internal rectal prolapse because it enables differentiation between a mucosal internal prolapse and a full-thickness internal prolapse. These two types of rectal prolapse have different treatment strategies.

Enterocele

An enterocele is an internal herniation of the peritoneal sac into the rectovaginal space below the pubococcygeal line (PCL). The PCL is used as the reference line for quantifying various abnormal findings of the pelvic floor, including quantification of the severity of an enterocele and the severity of pelvic floor descent. The PCL is defined as the line that joins the inferior border of the symphysis pubis to the last coccygeal joint on midsagittal images (Fig. 1). Enteroceles most frequently occur at the end of evacuation and can be filled with omental fat (peritoneocele), small bowel (enterocele), or sigmoid colon

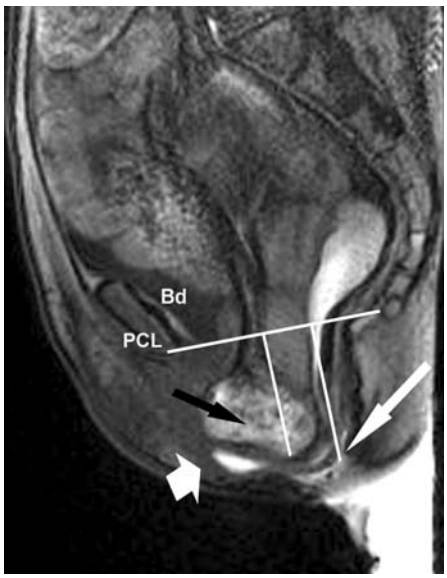

Pelvic Floor Dysfunction, Anorectal Manifestations.
Figure 1 A 63-year-old woman with fecal incontinence and diffuse pelvic pain after hysterectomy. A T1-weighted spoiled gradient-recalled echo magnetic resonance (MR) image obtained during evacuation (patient in supine position in a closed-configuration MR system) shows a moderate anterior rectocele with incomplete evacuation (*small arrow*). The anorectal junction is below the ►pubococcygeal line (PCL), with formation of a moderate rectal descent (*large arrow*). In addition, the patient has a moderate sigmoidocele (*black arrow*). The bladder (Bd) is in the normal position.

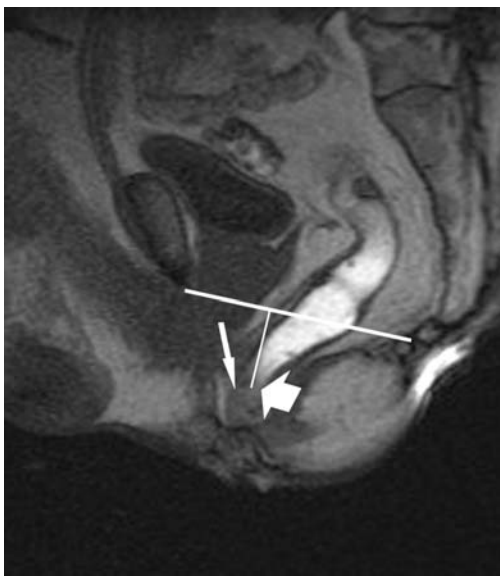

Pelvic Floor Dysfunction, Anorectal Manifestations.
Figure 2 A 25-year-old man with chronic constipation and incomplete evacuation. A sagittal T1-weighted spoiled gradient-recalled echo magnetic resonance image with the patient in sitting position obtained during defecation shows a full-thickness intraanal rectal prolapse (*large arrow*). The anorectal junction (*small arrow*) is below the pubococcygeal line, with formation of a moderate rectal descent.

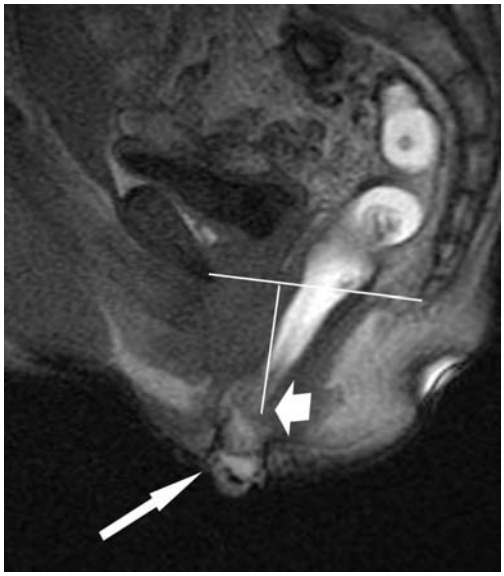

Pelvic Floor Dysfunction, Genitourinary.
Figure 3 A 49-year-old man with incomplete evacuation. A sagittal T1-weighted spoiled gradient-recalled echo magnetic resonance image obtained during defecation with the patient in sitting position shows a full-thickness external rectal prolapse (*large arrow*). In addition, the patient presents a moderate rectal descent (*small arrow*).

(sigmoidocele; Fig. 1). While most enteroceles spontaneously disappear at rest, only a few are fixed down at the rectovaginal space. The extent of an enterocele is measured 90° to the PCL from the lowest margin of herniation content during evacuation and is classified as small if it extends less than 3 cm below the PCL, moderate if it extends from 3 to 6 cm below this line, and large if it extends 6 cm or more below this line.

Rectal Descent

Rectal descent is an excessive caudal movement of the anorectal junction during evacuation. Pelvic floor descent is a common finding in patients with fecal incontinence and outlet obstruction. Although the clinical examination and electrophysiological tests play a significant role in diagnosis, dynamic pelvic MRI provides the most accurate assessment of pelvic floor descent. Rectal descent is usually associated with descent of the middle and anterior pelvic compartments. MRI enables evaluation of all three pelvic compartments (posterior, middle, and anterior) in a manner superior to conventional defecography (4). The grading of the rectal descent is assessed with respect to the PCL (5). A rectal descent is considered small when the anorectal junction is less than 3 cm below the PCL, moderate when the distance between the anorectal junction and PCL is between 3 and 6 cm (Fig. 1), and large when the distance between the anorectal junction and PCL is more than 6 cm (5).

Cystoceles are expressions of the descent of the anterior compartment, and descent of the vaginal vault (or any part of the remaining cervix in the case of hysterectomy) represents descent of the middle compartment. The descent of these compartments is quantified in a similar fashion as described for rectal descent.

References

1. Stoker J, Halligan S, and Bartram CI (2001) Pelvic floor imaging. Radiology 218:621–641
2. Roos JE, Weishaupt D, Wildermuth S et al (2002) Experience of 4 years with open MR defecography: pictorial review of anorectal anatomy and disease. Radiographics 22:817–832
3. Rociu E, Stoker J, Eijkemans MJ et al (1999) Fecal incontinence: endoanal US versus endoanal MR imaging. Radiology 212:453–458
4. Bolog N and Weishaupt D (2005) Dynamic MR imaging of outlet obstruction. Rom J Gastroenterol 14:293–302
5. Bertschinger KM, Hetzer FH, Roos JE et al (2002) Dynamic MR imaging of the pelvic floor performed with patient sitting in an open-magnet unit versus with patient supine in a closed-magnet unit. Radiology 223:501–508

Pelvic Floor Dysfunction, Genitourinary

Thomas C. Treumann
Kantonspital Luzern, Luzern, Switzerland
thomas.treumann@ksl.ch

Definition

Pelvic floor dysfunction describes a wide range of problems of the three organ systems passing the pelvic floor: the urinary system, the genital system, and the colorectal system. It is associated with pelvic floor weakness or with organic or functional neuromuscular disorders.

Conditions may include pelvic floor pain, urinary incontinence, bowel incontinence, stool outlet obstruction, pelvic organ descent, pelvic organ prolapse, and pelvic floor dyssynergy or spasm.

Pathology

Anatomically, the pelvic floor is formed by the genitourinary diaphragm and the levator ani muscle. The two parts of the levator ani muscle are the puborectalis muscle

sling and the iliococcygeus muscle. The puborectalis muscle sling originates from the posterior surface of the pubic symphysis and goes around urethra, vagina, and anus. Urethra, vagina, and anal canal pass the pelvic diaphragm within the midline. Contraction of the muscle pulls the rectum toward the symphysis and closes urethra, vagina, and rectum. Weakness of this muscle causes laxity of the genitourinary hiatus.

The iliococcygeus muscle plates originate at the genitourinary diaphragm and insert at the lateral inner surfaces of the pelvis. Contraction of this muscle elevates the pelvic floor. Weakness of this muscle leads to descent of the pelvic floor.

Pelvic floor dysfunction is a disease of elderly female patients. The underlying cause for incontinence and organ prolapse is pelvic floor laxity, usually resulting from compromised levator ani and puborectalis muscle function and endopelvic fascia laxity and fascia defects. Predisposing factors are multiple childbirths, vaginal delivery, menopause, age, hysterectomy, and inherited connective tissue laxity from collagen defects.

The cause of urinary incontinence is not fully understood. Incontinence correlates with obesity and smoking, and only to a lesser extent with pelvic floor laxity and bladder neck hypermobility. The normal process of urination involves coordination between the bladder and pelvic floor muscles; the pelvic floor muscles relax whereas the bladder contracts. In most patients, the bladder contracts normally but the urine flow is poor due to continued tightening of the pelvic floor. The sensation of urinary frequency and urgency seem to be linked to pelvic floor laxity. The natural tendency for many patients is to strain and push the last drop of urine out so they can prolong the intervals between bathroom sessions. Unfortunately, pushing and straining appear to further damage the pelvic floor muscles and worsen the symptoms. Hence, a vicious cycle develops.

Pelvic organ descent and prolapse is the result of laxity of the connective tissues in the pelvis, especially defects in the lateral fascial bands of the endopelvic fascia between the vagina and lateral pelvic wall, and defects in the rectovaginal septum. Hysterectomy seems to be a risk factor for pelvic organ descent.

Organ descent develops during Valsalva maneuver, voiding, and defecation. Descent of the posterior bladder wall below the internal urethral orifice is called a ►cystocele. Bulging of the rectum toward the posterior vaginal wall is called a ►rectocele. An ►enterocele is the descent of the peritoneal sac between vagina and rectum down to the level of the perineum with bulging of the posterior vaginal wall. An enterocele may follow a rectocele after defecation (Fig. 1).

A cystocele Grade II leads to impression of the vaginal wall inside the vagina. A cystocele grade III everts part of the vaginal wall to below the introitus. Rectoceles and enteroceles are graded similarly. Descent of the uterus can be quantified by measurement of the change of the vaginal length during Valsalva. Prolapse of the uterus begins with descent of the portio below the introitus.

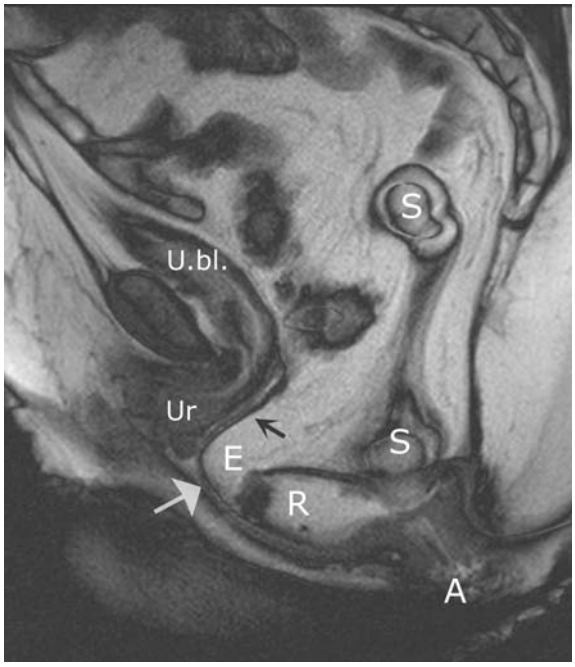

Pelvic Floor Dysfunction, Genitourinary.

Figure 1 Midsagittal T2-weighted MR image of the pelvis and pelvic floor during Valsalva maneuver after partial defecation. Rectocele (R) with retention of bowel content. Enterocele (E) between rectocele and posterior vaginal wall (*black arrow*). Partial prolapse of the posterior vaginal wall (*white arrow*) as result of the enterocele. S is the sigmoid colon, A is the anus, U.bl. is the urinary bladder, and Ur is the urethra.

Stool outlet obstruction may be caused by two conditions: pelvic floor laxity and pelvic floor dyssynergy.

Pelvic floor laxity can lead to descent of the peritoneal sac or uterus and to compression of the rectum by these organs. A large rectocele can retain stool. Compression of a rectocele by the peritoneal sac may intussuscept the anterior rectal wall into the anal canal. Detachment of the rectum from the sacrum in pelvic floor descent may lead to intussusception of the rectum in itself.

In dyssynergy, the pelvic floor contracts during pressure raise in the abdomen. In anism, the anal sphincter is spastic and hypertrophies. This may be a behavioral problem or may be part of an organic neurologic pathology, such as Hirschsprung's disease. Damage to the nerves in the pelvis and pelvic floor can be a result of pelvic floor laxity with permanent stretching of the nerves.

Clinical Presentation

Symptoms associated with anterior compartment may be ►stress urinary incontinence, urinary urgency with increased frequency of urination and decreased urinary flow, and sensation of incomplete urination with residual bladder volume.

In genital descent, patients may present with protrusion of parts of the anterior vaginal wall by a cystocele or of the posterior vaginal wall by a rectocele or enterocele. Protrusion may go as far as complete prolapse and eversion of the vagina to the outside. Descent and prolapse may occur only during straining, or it may be fixed with permanent vaginal prolapse. If the uterus is still present, the portio may descend down to the pelvic floor, or the uterus may protrude partially or completely to outside the body. In the posterior compartment, rectal mucosa prolapse or rectal wall prolapse may develop in patients with functional disorders with permanent high-pressure defecation. Muscular spasm causes pelvic floor pain.

In stool outlet obstruction by rectal descent and intussusception, the patient complains about defecation in small fractions. Large rectoceles with retention of bowel content raise the need to digitize from the vagina to empty the rectocele. In anisms or dyssynergy, defecation needs high intraabdominal pressure, and the defecation process is prolonged.

Imaging

Ultrasound is usually performed by the gynecologist as part of the diagnostic work-up of stress urinary incontinence and genitourinary prolapse. It allows for the morphological and dynamic assessment of the lower urinary tract. Transvaginal ultrasound enables the detection of pathologies of the bladder and uterus. Introital ultrasound can detect urethral diverticula, periurethral masses, funneling of the urethra and cystoceles. Color Doppler may be used to document stress urinary incontinence. Translabial ultrasound detects defects in the rectovaginal septum and helps to identify rectoceles.

Roentgen colpocystodefecography is the original imaging method to evaluate pelvic floor descent. It requires filling of the urinary bladder, vagina, rectum, bowel, and peritoneum with roentgen contrast medium and is associated with a high-dose radiation exposure. The method is now replaced by MRI.

MRI of the pelvic floor is performed as a combination of static and dynamic sequences. Static MRI is done with T2-weighted images of the pelvis in three imaging planes. These images give an overview of the pelvic organs and the pelvic floor muscles in the resting position. T1- or proton density images may be used for the pelvic floor muscles additionally.

Dynamic MRI is performed with repetitive fast single shot T2-weighted images. Best contrast-to-noise, excellent T2 contrast, and shortest acquisition times are provided by True FISP sequences. Acquisition times of 0.5 to 0.7 sec per image can be achieved with a 1 mm in plane resolution. Parallel imaging can even shorten the imaging time. A delay of 0.1 to 0.2 sec between should be left between images to reduce signal loss by spin saturation. Alternatively, half Fourier single shot turbo spin echo (HASTE) sequences can be used, but are not as fast as True FISP. T2-weighted imaging requires filling of the vagina and the rectum with watery contrast material. Ultrasound gel is recommended. The patient should empty the bladder before going into the magnet. Normal urine production leads to sufficient opacification of the bladder during investigation (Fig. 2).

A repetitive single slice in the mid sagittal plane of 10 mm thickness is acquired during pelvic floor contraction and Valsalva maneuver with defecation. For contraction series, we use 30 images per series, for Valsalva and defecation, 80 to 100 images are required. The series is repeated as often as necessary to see best contraction and relaxation and maximum descent of pelvic floor, best relaxation of levator ani and puborectalis muscle, maximum organ descent and organ prolapse and complete emptying of the rectum. The investigation is performed in supine position of the patient, with the knees slightly flexed and thighs abducted. The patient is equipped with a pampers. Studies have shown that no relevant pathology is missed in supine position compared to upright position.

MR images are evaluated qualitatively and quantitatively. We recommend to use the HMO-system introduced by Comiter et al in 1999. Pelvic floor laxity is described by the length of the Hiatus line from the posterior border of the pubic symphysis to the sling of the puborectalis muscle behind the anorectal junction. Normal range is 7±1.5 cm. Pelvic floor descent is described by the position of the puborectalis muscle sling in relation to the pubococcygeal line (PCL). Normal range is between 4 and 6 cm (Fig. 3).

Organ descent is seen directly on the MR images and can be graded according to the description in the pathology section. Organ descent can be measured in relation to the Hiatus line. Mobility of the bladder neck can be quantified using the rotation angle of the long axis of the urethra. The pathologic threshold is not clearly defined, but the 30° rotation, adapted from the ►Q-tip test, seems to be oversensitive. A rotation of more than 90° or beyond the horizontal plane is definitely abnormal.

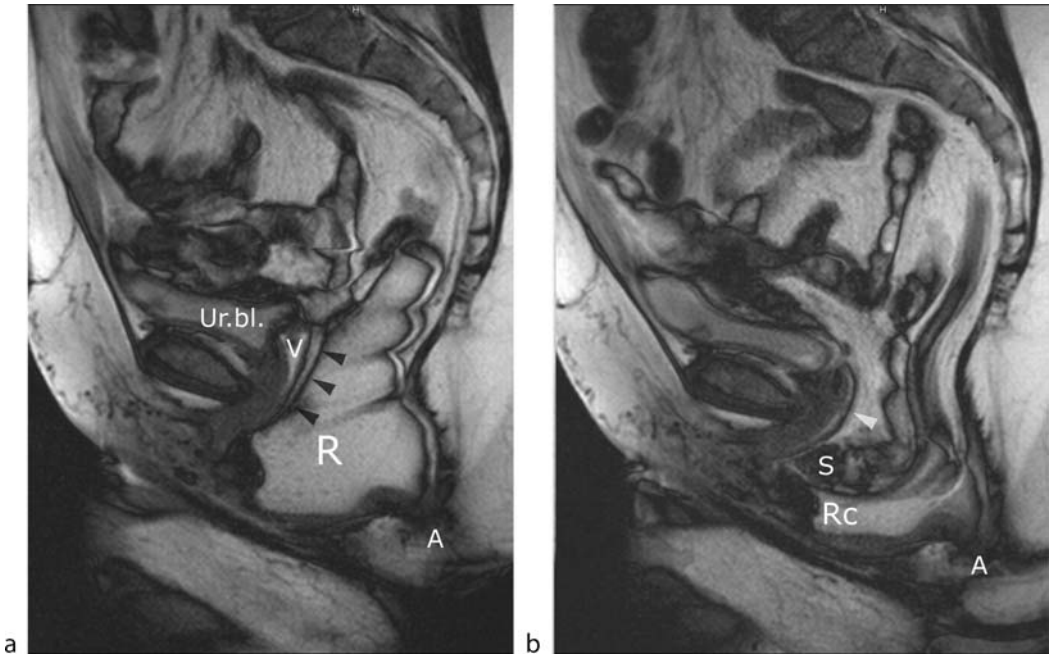

Pelvic Floor Dysfunction, Genitourinary. Figure 2 Midsagittal T2-weighted MR images of the pelvis and pelvic floor during defecation. Marked anterior bulging of the anterior rectal wall, representing a rectocele (Rc), with partial prolapse of the posterior vaginal wall (a). Incomplete evacuation of the rectocele because of fold formation in the posterior rectal wall covering the anal canal (b). Descent of the peritoneal sac and sigmoid colon (S) in between the posterior vaginal wall (*white arrowhead*) and the anterior wall of the rectum (*black arrowheads*). Ur.bl. is the urinary bladder, V is the vagina, and A is the anus.

Diagnosis

The diagnosis of pelvic floor dysfunction is made on the basis of symptoms, clinical findings and of the exclusion of other causes for the clinical disorder. Urinary incontinence requires urodynamic studies, a pad weigh test, and the exclusion of urinary tract infection.

Stool outlet obstruction requires exclusion of drugs, slow transit constipation, dolichocolon, and neoplastic disease. Endoscopy should be performed in any colorectal disorder. Anal manometry is required to exclude Hirschsprung's disease and anal sphincter hypertrophy, spasm, or laxity. Stool incontinence requires neurologic assessment. In any suspicion of a neurologic disorder, MRI of the spinal canal should be performed to rule out tumor or damage to the spinal cord.

Palpation and visual observation of the pelvic floor, electromyography, ultrasound, and magnetic resonance imaging (MRI) during rest, contraction, Valsalva maneuver, voiding, and defecation measure different aspects of pelvic floor function. Since there is no specific test for pelvic floor dysfunction, several methods have to be combined to focus the problem.

MRI is the most helpful imaging method to illustrate pelvic floor function. It is less investigator-dependent than ultrasonography, does not need ionizing radiation and provides us with high-quality images not only of the pelvic floor, but also of the pelvic organs, and generates dynamic information, playable as video sequences. It is superior to clinical investigation and ultrasound in detection of enteroceles and differentiation of rectoceles from enteroceles and combined problems. Up to 60% of enteroceles are missed by clinical investigation.

In pelvic floor dysfunction and anism, MRI is the method of choice to demonstrate the problem to the patient.

Bibliography

1. Pannu HK, Kaufman HS, Cundiff GW et al (2000) Dynamic MR imaging of pelvic organ prolapse: spectrum of abnormalities. Radiographics 20:1567–1582
2. Comiter CV, Vasavada SP, Barbaric ZL et al (1999) Grading pelvic prolapse and pelvic floor relaxation using dynamic magnetic resonance imaging. Urology 54:454–457

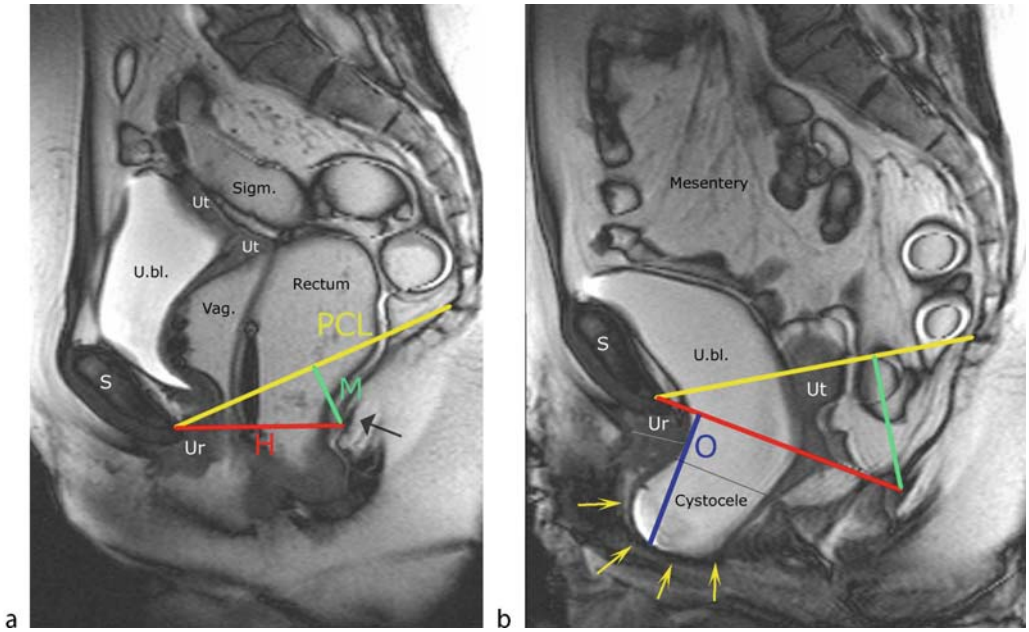

Pelvimetry, Magnetic Resonance. Figure 3 **HMO-system to quantify pelvic floor morphology. Midsagittal T2-weighted MR image of the pelvis and pelvic floor in resting position (a) and during Valsalva maneuver after defecation (b). The urogenital hiatus is represented by the Hiatus line (H), which is drawn from the posterior margin of the pubic symphysis (S) to the muscle sling posterior to the anorectal junction (*black arrow* in a). The position of the muscular pelvic floor is measured as the distance of the puborectalis muscle sling to the pubococcygeal line (PCL), a fixed line at the pelvic skeleton. The descent or prolapse of the organs is measured in relation to the Hiatus line. There is a partial prolapse of the urinary bladder (U.bl.) during Valsalva maneuver. The extent of the organ descent is represented by the Organ-Line (O). The part of the bladder descending more than 1 cm below the level of the urethra (Ur) is called a cystocele. The *light arrows* mark the part of the anterior vaginal wall which is prolapsing beyond the introitus by descent of the bladder. Ut is the uterus. Vag is the vagina and Sigm. is the sigmoid colon.**

3. Tunn R, Petri E (2003) Introital and transvaginal ultrasound as the main tool in the assessment of urogenital and pelvic floor dysfunction: an imaging panel and practical approach. Ultrasound Obstet Gynecol 22:205–213

Pelvic Inflammatory Disease (PID)

A polymicrobial infection affecting the reproductive tract in females in the reproductive years. PID is most commonly associated with sexually transmitted micro-organism with a predominance of Neisseria gonorrhea and Chlamydia trachomatis.

►Abscess TuboOvarian

Pelvimetry

►Pelvimetry, Magnetic Resonance

Pelvimetry, Magnetic Resonance

Sven Claude Andre Michel
Radiology, Kantonsspital Baden, 5404 Baden, Switzerland
sven.michel@ksb.ch

Synonyms

Pelvimetry

Definition

Magnetic resonance (MR) pelvimetry is a method for determining pelvic dimensions and narrowness of the ►birth canal by MR imaging.

Characteristics

MR pelvimetry is a safe way (for both the fetus and the pregnant woman) to measure the diameters of the birth canal, in particular the entrance and the outlet, to detect a mismatch between the fetal head and the birth canal. The measurements help guide the physician in deciding whether vaginal birth is possible or a cesarean section should be performed.

Clinical Presentation

The Birth Canal

The fetus has to pass only 15 cm through the vagina to reach the light. However, this short way can require a lot of time, pain, and energy for both of the pregnant woman and the fetus. The birth canal has several narrow areas that the fetus must pass through. The measuerments of the diameters of these key areas are performed in different planes through the pelvis. First of all, is the entrance consists of two diameters: the diameter transversa (axial) and the ►obstetric conjugate (conjugata vera obstetrica, sagittal). If the head is too big, the fetus cannot enter the birth canal which may be indicated a persisting distended abdomen of the pregnant woman. Therefore, in the last days before birth, the abdominal size usually decreases with the descent of the fetal head into the entrance of the birth canal. Within the birth canal, the two most critical points of narrowness are the ►interspinous (axial) and the ►intertuberous distances (axial).

Finally, the ►sagittal outlet (sagittal) is a measure of the birth canal's exit.

Although the pelvis consists of bone, all distances can be modified by the birthing position due to the pelvis' flexibility, which is increased during pregnancy (1). Probably the most important distance for successful vaginal delivery is the interspinous distance, which can be taken as the "point of no return." Once the fetus passes this landmark, performing an emergency caesarean-section becomes dangerous.

Why Do Pelvimetry?

There are several indications for measuring the natural narrowness of the pelvis. When a baby is oversized or overweight there may be a mismatch between the birth canal and the size of the fetal head (2), preventing the fetus from entering the birth canal, so that, a cesarean section must be performed. Even more critical is when the baby becomes stuck in one of the critical inner narrow points. In these cases, the fetus may become wedged in the pelvis, putting the fetus and mother at risk for life-threatening complications.

In most instances, we can overcome these problems by measuring the baby and the size of its head by ultrasound and then perform pelvimetry early enough. However, pelvimetry is also indicated after a prolonged delivery when the mother decides to have another baby. If the pelvic measurement shows a small birth canal compared with the fetal head, a cesarean section should be planned early enough to avoid an emergency intervention. After a primary cesarean section, pelvimetry may indicate the possibility of vaginal birth with the next baby, if desired. Another indication for pelvimetry is after a previous pelvic fracture.

The decision of whether birth can proceed vaginally is ultimately up to the treating obstetrician in agreement with the pregnant woman. Birth-limiting pelvic dimensions can be revealed radiographically and with recently updated published data on birth outcomes (3), the risk of a vaginal birth can be estimated.

Imaging

External Pelvimetry by the Obstetrician

External measurements of the pelvis can be determined very easily and allow an approximate calculation of the internal pelvic parameters of the birth canal. The most widely used formula for the obstetric conjugate is based on the external conjugate (usually 20 cm) minus 9 cm. These values are, however, very indefinite, mainly due to the different thicknesses of the underlining tissues.

The pelvic form can also be assessed easily, which may be helpful in decision making prior to birth (Table 1).

Radiological Measurements

In the early days, pelvimetry was performed with radiographs (lateral: Colchner-Sussmann, frontal: Martius/Guthmann) and was often the indicator for cesarean section. But now we know that the concomitant radiation exposure, although low, may damage fetal DNA. Therefore, in pregnant women, MR pelvimetry is preferable in any case.

Although conventional radiographic pelvimetry in a non-pregnant woman probably will not lead fetal damage, but the ovaries will nonetheless be exposed to significant levels of radiation. It must be noted that radiographic pelvimetry is a projection examination, and the distances have to be modified by a correction factor based on a ruler placed within the examined field. Again, the surrounding tissue may cause some error. In contrast, MR pelvimetry assesses these diameters directly and much more accurately.

MR Pelvimetry

MR utilizes radio waves and a magnetic fields many times stronger even than that of the earth. There has been much

Pelvimetry, Magnetic Resonance. Table 1 Pelvic forms and their risks

Forms	Measurements	Expected problems during birth
Gynecoid	Pelvic inlet diameter 12 cm, about 11 cm, pelvic outlet 10 cm	Normal
Anthropoid	Pelvic inlet diameter 12 cm, about 11 cm, pelvic outlet <10 cm	Dorsoposterior position, protracted birth
Android	Pelvic inlet diameter <12 cm approximately >11 cm, pelvic outlet 10 cm	Dorsoposterior position, protracted birth
Platypelloid	Pelvic inlet diameter ≥12 cm, approximately ≤11 cm, pelvic outlet 10 cm	Protracted birth, head not entering the canal, deflected head

research regarding the safety of MR imaging. None of these studies has been able to prove a risk either to the baby or the mother. Due to its high degree of accuracy and safety, MR pelvimetry has become a widely accepted examination (4) and has largely replaced convention pelvimetry. Some there has been some concern about noise during the MR examination which is considerable and originates from the on-and-off switching of magnetic gradients. However, studies have shown that physiologic aortic pulsations are louder than MR scanner noise intraadominally (5).

The noise in MR is completely harmless, although the unprepared patient may get the impression that the scanner is defective. It should be noted that pregnant women sometimes have heightened senses and therefore may be more anxious than non-pregnant women. Most women examined in MR pelvimetry experience some anxiety due to the noise, however most of them would undergo the examination again for the well-being of their babies (5).

A pregnant woman with claustrophobia guided very carefully through the examination considering of the narrowness of the MR system and the mass of the gravid abdomen (5). A claustrophobic patient should be examined in an open system if available (5). In MR pelvimetry, the lower image quality of low-field or open systems is not limiting for diagnositic purposes (5). In extreme cases of claustrophobia, sedation (e.g., benzodiazepine through the nose) can be helpful if there is no contraindication.

As usual, before the examination is planned, the known contraindications for MR imaging should be excluded (this can easily be forgotten). The examination within the MR bore is short—a maximum of 3–8 min (5). The pregnant woman should be in the supine position if possible; if not, the examination can also be done while she is lying on her side.

These days, a T1-weighted fast gradient echo sequence (FSPGR) is preferred; for example, TR 150 msec, TE 1.6 msec, FOV 32 cm, Matrix 256 x 192 -256, slice thickness/gap 6/1.6. Chemical shift artifacts tissue interfaces should be minimized. The examination is performed in three planes covering the whole pelvis (4). The ▶obstetric conjugate is assessed on a midsagittal section from the sacral promontory to the top of the symphysis (Fig. 1), and the ▶sagittal outlet from the distal end of the sacrum to the bottom of the inner cortex of the symphysis (Fig. 1). The ▶interspinous (Fig. 2) and ▶the intertuberous distances (Fig. 3) are measured in an axial plane as the narrowest distance between the ischial spines and the ischial tuberosities, respectively. On oblique sections, the ▶transverse diameter, the largest transverse distance of the pelvic inlet, is measured. In contrast to X-ray, no correction factors are needed because these measurements are direct in the correctly chosen plane. The measurements are usually performed by a MR technician on the scanner system within 3 min, depending on the documentation required. Although the technique is advanced, interobserver and intraobserver error should be considered (4).

Although there are monitoring techniques to asseess the mother's wellbeing, such as electrocardiography and pulse oximetry, the fetus's well-being usually cannot be monitored by CTG. However, if the fetus is perceived to be in distress, a cesarean section will usually will be performed emergently, so that completion of MR pelvimetry exam becomes superfluous. In cases where time plays an important role, a conventional radiograph can be justified due to the low and not completely understood risk of the radiation to the fetus.

During MR pelvimetry, the baby can also be assessed, although with an increase in examination time. If desired, fetal brain diameters can be measured, and further fetal and maternal anomalies can be detected. However, the indications for MR fetal examinations are different, and there is usually no compelling indication as ultrasound can be done faster and more cheaply.

Diagnosis

Recently updated data about MR pelvimetry are shown in Table 2 (3). The classification of pelvic forms in Table 1 serves as a rough guide but is less relevant than MR pelvimetric determinations. Pregnant women with lower

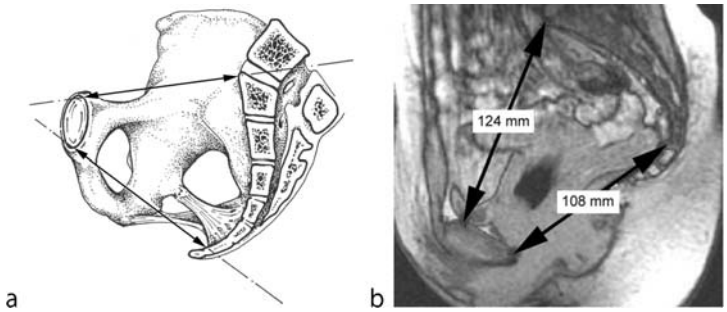

Pelvimetry, Magnetic Resonance. Figure 1 (a) Obstetric conjugate and sagittal outlet (drawing by Dr. Roth, USZ, Zurich). (b) Sagittal FSPGR sequence.

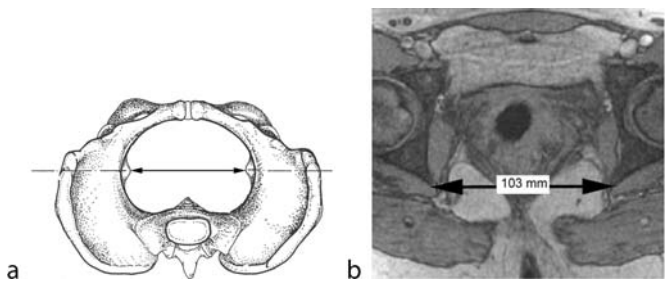

Pelvimetry, Magnetic Resonance. Figure 2 Interspinous distance (a) Drawing (b) Axial FSPGR sequence.

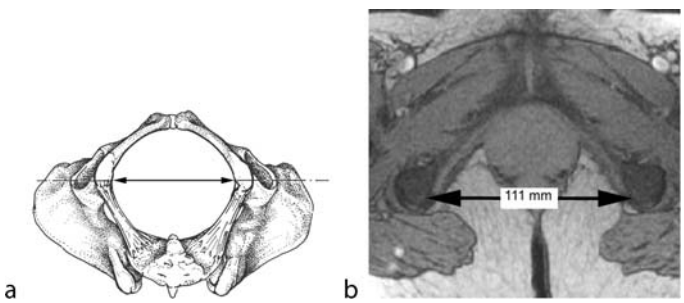

Pelvimetry, Magnetic Resonance. Figure 3 Intertuberous distance (a) Drawing (b) Axial FSPGR sequence.

Pelvimetry, magnetic resonance. Table 2 Magnetic resonance pelvimetry: reference values (from Keller TM et al. (2003) Obstetric MR pelvimetry: reference values and evaluation of inter- and intraobserver error and intraindividual variability. Radiology 227(1): 37–43)

Pelvimetric Measurements	Mean ± SD (mm)	Range (mm)
Obstetric conjugate	121.7 ± 8.6	101–143
Interspinous distance	112.3 ± 7.9	95–136
Intertuberous distance	120.6 ± 11.3	94–143
Transverse diameter	129.5 ± 8.7	110–152
Sagittal outlet	115.8 ± 9.9	81–137

values, especially of the obstetric conjugate and the interspinous distance, should be treated with care, as mentioned earlier, especially in cases of suspected fetopelvic disproportion. Again, MR pelvimetry alone should not establish the indication for a cesarean section. The decision is up to the treating obstetrician in agreement with the pregnant woman, depending on the context of the birth setting.

Bibliography

1. Sven CA, Michel, Rake A, Treiber Karl et al (2002) Obstetric pelvimetry: effect of birthing position on pelvic bony dimensions. Am J Roentgenol 179:1063–1067
2. Ferguson JE, Sistrom CL (2000) Can fetal-pelvic disproportion be predicted? Clin Obstet Gynecol 43:247–264
3. Keller TM, Rake A, Michel SC et al (2003) Obstetric MR pelvimetry: reference values and evaluation of inter- and intraobserver error and intraindividual variability. Radiology 227: (1)37–43
4. Loon AJ, Van Mantingh A, Serlier EK et al (1997) Randomised controlled trial of magnetic-resonance pelvimetry in breech presentation at term. Lancet 350:1799–1804
5. Sven CA, Michel, Rake A, Go¨tzmann Lutz et al (2002) Pelvimetry and patient acceptability compared between open 0.5-T and closed 1.5-T MR systems. Eur Radiol 12:2898–2905

Penile Disorders

Penile disorders are frequently diagnosed late because patients feel embarrassed to talk about these problems. With the advent of effective oral therapy for erectile dysfunction (PDE-5-inhibitors e.g., Sildenafil) and thus, increasing media interest in sexual dysfunction, male patients feel more confident to share their penile disorders with their doctor. As it is true for other diseases, diagnosing penile disorders requires to take a patient's history, physical examination, laboratory examination, and if necessary selecting an appropriate imaging modality. Frequently, the patient's history and clinical appearance are very characteristic and allow for diagnosing a penile lesion/disorder sufficiently reliable. However, to further characterize or to choose a specific treatment for these disorders, knowledge regarding the most adequate imaging technique is very important.

▶ Impotence

Penile Fracture

Räto T. Strebel
Department of Urology, University Hospital Zurich, Zurich, Switzerland
raeto.strebel@usz.ch

Definition

Penile fracture is defined as a rupture of the tunica albuginea of one or both corpora cavernosa from trauma to the erect penis.

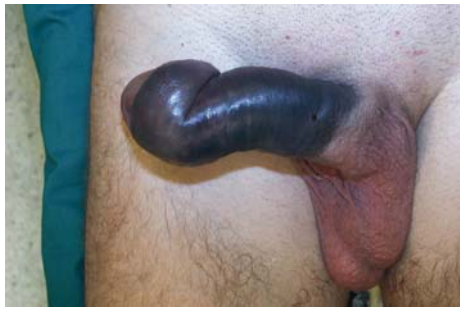

Penile Fracture. Figure 1 Patient with a penile fracture with marked swelling and haematoma (typical "eggplant deformity").

Clinical Presentation

Typically, patients report that they heard a crack followed by pain with an immediate return to detumescence of the penis. Most commonly the above condition occurs when striking the penis against the symphysis or perineum during intercourse, which is the predominant mode of action in the western world. In other regions of the world, the self-inflicted bending of the penis to achieve fast detumescence after masturbation is frequently described (1). Thereafter, penile swelling and haematoma appears rapidly, leading to the typical "eggplant deformity" (Fig. 1). On physical examination, a palpable defect in the tunica albuginea may be present.

Imaging

Because of the typical history and clinical presentation, additional imaging is rarely necessary for diagnosing a penile fracture or planning further treatment. However, when an urethral injury is suspected (voiding difficulties, macrohaematuria) which is associated with penile fracture of up to 40%, an urethrography may be warranted. However, it might be difficult to perform an urethrography properly in the presence of marked swelling of the penis and prepuce. An ultrasound examination of the tunica albuginea can be helpful in localising the site of rupture. A cavernosography is a sensitive imaging modality to prove a cavernosal injury. In conclusion, additional imaging with cavernosography or ultrasound is only necessary when the clinical presentation is ambiguous.

Bibliography

1. Muentener M, Suter S, Hauri D et al (2004) Long-term experience with surgical and conservative treatment of penile fracture. J Urol 172(2):576–579

Pepper's Syndrome

Massive metastatic involvement of the liver occurring in patients younger than 6 months of age with neuroblastoma. Prognosis can be favorable.

▶Hepatic, Pediatric Tumors, Malignant

Peptide

Compound of a relatively small number of amino acids (up to 100) linked by amide bonds. Peptides used for receptor imaging are often neuropeptides with a short amino acid sequence (<20). This feature results in rapid pharmacokinetics, which is beneficial for in vivo receptor imaging.

▶Receptor Studies, Neoplasms

Percutaneous Ethanol Injection (PEI), Hepatic Tumours

Radiological percutaneous interventional technique of tumour ablation consisting in the direct, usually US guided, injection of ethanol within the tumour lesion in order to obtain local tumour necrosis.

▶Interventional Hepatic Procedures

Percutaneous Laser Disc Decompression

Laser energy is used to vaporise the watery content of the nucleus pulposus. A small laser fibre is inserted through a hollow needle into the centre of the intervertebral disc. When the laser fibre is in place, laser energy is applied into the nucleus pulposus in order to evaporate its water content, thereby reducing intradiscal pressure. This causes the herniated portion of the nucleus pulposus to recede towards the centre of the disc, relieving pressure on the nerve root.

▶Radicular Syndrome of the Spine, Percutaneous Therapy for

Percutaneous Nephrolithotomy

PCNL is a procedure for removing medium-sized or larger renal calculi (kidney stones) from the patient's urinary tract by means of a nephroscope passed into the kidney through a track created in the patient's back. The term "percutaneous" means that the procedure is done through the skin.

▶Stone Disease, Urinary

Percutaneous Nucleotomy

Nucleus pulposus material is mechanically removed using an automated nucleotome. The nucleotome is introduced through a cannula that is placed into the centre of the nucleus pulposus under fluoroscopic guidance. The tip of the nucleotome is alternatingly rotated, depressed and elevated within the nucleus in order to optimise the removed amount of nucleus pulposus material. The resulting loss of nucleus pulposus mass causes a drop in intradiscal pressure. This causes the herniated portion of the nucleus pulposus to recede towards the centre of the disc, relieving pressure on the nerve root.

▶Radicular Syndrome of the Spine, Percutaneous Therapy for

Percutaneous Transhepatic Cholangiography

Percutaneous catheterization of an intrahepatic bile duct that is outlined on radiographs by means of contrast medium injection.

▶Biliary Anatomy

Percutaneous Transluminal Renal Angioplasty

Interventional radiological techniques allowing endovascular treatment of RAS with balloon catheters, stents, or both.

▶Stenosis, Artery, Renal

Percutaneous Treatment of Tubo-Ovarian Abscesses

Interventional radiological treatment is an alternative to the laparoscopic or surgical approach. Technique and access depend on size, location, and morphology of the abscess. Small abscesses are usually treated by needle punctures. Large and multiloculated abscesses are better treated by a catheter drainage if a safe route is possible.
▶Abscess TuboOvarian

Perfluorocarbon Gas Agents

▶Contrast Media, Ultrasound, Low Solubility Gas

Perforation, Gallbladder

A serious complication of ▶acute cholecystitis occurring in about 10% of cases, characterized by high morbidity and mortality. Three categories (acute, subacute, and chronic) of gallbladder perforation are described according to the Niemeier classification. The acute form develops in generalized peritonitis where the subacute perforation may also occur, resulting in a pericholecystic abscess. Chronic perforation may generate an internal biliary fistula (to the duodenum or common bile duct). Both US and CT can depict the presence of a defect in the gallbladder wall.
▶Cholecystitis

Perfusion

The nutritative flow of blood through tissues.
▶Perfusion, Imaging
▶Perfusion, Neoplasms

Perfusion Curves

▶Time Intensity Curves

Perfusion Type Optical Contrast Agents

▶Molecular Probes, Optical Probes

Perfusion, Imaging

Imaging of blood flow to an organ, part of an organ, or a pathological process such as a tumor using an injected contrast agent that changes the signal of blood during bolus passage. Indices of perfusion can be calculated from the signal changes over time during the bolus passage. In the case of ultrasound contrast agents, destruction reperfusion methods can also be used, where the bubbles in the imaging plane are destroyed by a high-amplitude pulse and the replenishment kinetics are used to quantify perfusion in the image plane.
▶Time Intensity Curves

Perfusion, Neoplasms

Pat Price, Natalie Charnley, Julian Matthews
Wolfson Molecular Imaging Centre, The University of Manchester, Manchester, UK
Pat.price@manchester.ac.uk
Natalie.charnley@manchester.ac.uk
Julian.matthews@manchester.ac.uk

Synonym

Blood flow

Definitions

▶*Perfusion* is the nutritive flow of blood through tissues. There is a growing interest in imaging perfusion in tumours. Perfusion can be a measure of pharmacodynamic response to anti-angiogenic drugs and vascular disrupting agents and many chemotherapeutic agents. Perfusion is also a prognostic factor, with perfusion being both a poor and good prognostic factor.

Volumetric imaging with CT or MRI is less useful for assessing efficacy of anti-angiogenic drugs as these are

cytostatic rather than causing tumour shrinkage. Hence, the increased need for direct imaging of effects on tumour vasculature.

Perfusion is governed by tumour vasculature and perfusion pressure. Tumour blood vessels have structural and functional abnormalities. This includes irregular branching, increased permeability and independence from normal flow control mechanisms. Such abnormalities lead to variable and inadequate perfusion. ►*Angiogenesis* is the formation of new vessels, essential for tumour growth. This depends on matrix metalloproteases produced by activated endothelial cells, which degrade the basement membrane, and also integrins which enable endothelial cell migration towards the tumour. This process involves a plethora of cytokines, including *vascular endothelial growth factor* (*VEGF*) which promotes angiogenesis and also vascular permeability. *Fibroblast growth factor* (*FGF*) also has a role in angiogenesis. Expression of FGF and VEGR is upregulated in tumours, and levels correlate with vascularity (1).

Perfusion in tumours is not the same as blood flow, which may occur without nutrition in the case of arteriovenous shunting, where the capillary bed is bypassed. In nuclear medicine imaging, regional tumour flow is the usual parameter measured, which is flow standardized to a unit quantity of tissue, and typically has the units mL blood/min/dL tissue.

A further important parameter is regional ►volume of distribution (V_d), which is the steady-state ratio of the activity in tissue to activity in blood/plasma. In the case of perfusion measurements using a freely diffusible tracer, this can be thought of as the fractional volume of tumour which is being perfused.

Nuclear Medicine

Nuclear Medicine Imaging of Blood Flow

The classical way to measure perfusion in nuclear medicine is to use methods based on the Fick principle. The measurement of tumour perfusion depends on the injection of a tracer into the blood stream and subsequent measurement in the tumour

$$P = \frac{C_0}{\int (C_a - C_v)dt},$$

where (C) is the concentrations of tracer in tissue (C_0), arterial (C_a) and venous (C_v) blood.

This gives quantitative measurements of blood flow. However, this method is not used in practice as it requires both arterial and venous dynamic measurements and assumes homogeneity of venous blood. Instead, the freely diffusible tracer method is used. This measures the rate of tracer uptake, and therefore does not require venous data.

Perfusion may be derived using the steady-state or dynamic methods using a freely diffusible tracer. The isotope ^{15}O is often used as $^{15}[O]CO_2$, or $^{15}[O]H_2O$, and has a half-life of 123 sec. This is created in an on site cyclotron.

Steady-State Method

Early studies of PET and blood flow involved the steady-state method. This involves inhalation of $^{15}[O]CO_2$, which is converted to $^{15}[O]H_2O$ in the lungs. Equilibrium is reached after 10 min, so that tracer diffusion from arterial blood to tissue is matched by that from tissue to venous blood, and radioactive decay. Flow is given as

$$\text{Flow} = \frac{\lambda}{[H_2{}^{15}O]_a^c/[H_2{}^{15}O]_t^c - 1/V_d},$$

where λ is the decay constant for ^{15}O, $[H_2{}^{15}O]_a^c$ is the arterial concentration of $H_2{}^{15}O$, $[H_2{}^{15}O]_a^t$ is the tissue concentration of $H_2{}^{15}O$.

Tissue radioactivity concentration is measured quantitatively from the region of interest on the PET scan, and the arterial concentration is assessed by arterial sampling using a cross-calibrated well counter, or from a large arterial pool from the PET image.

Advantages of this method are that it requires only a simple calculation, and minimal blood sampling. However, compared to the dynamic method, it is particularly sensitive to effects from tissue heterogeneity and inaccuracies in the predefined partition coefficient which is often not known in diseased tissues such as tumour (2). Tissue heterogeneity leads to underestimation of perfusion in heterogeneous tissues (2, 3).

Dynamic Method

Both steady-state and dynamic methods can employ inhalation of $^{15}[O]CO_2$ or injection of a bolus of $^{15}[O]H_2O$. Modern dynamic methods usually involve the $^{15}[O]H_2O$ bolus method (Fig. 1). Compared to steady-state inhaled $^{15}[O]CO_2$, a lower dose is needed, and the scan time is shorter—a steady-state acquisition would typically be approximately 30 min compared with 10 min for dynamic scanning. Kinetics of activity is measured in tissue within individual timeframes. Continuous or rapid discrete arterial data are obtained from the image or arterial blood sampling. For blood samples, the data are corrected for delay and dispersion of the arterial curve due to blood passage through sampling tubing.

Kinetic data are modelled using the Kety–Schmidt model and estimates of blood flow and V_d. This incorporates a term for radioactive decay. Estimates of flow and V_d are perturbed until a good fit obtained.

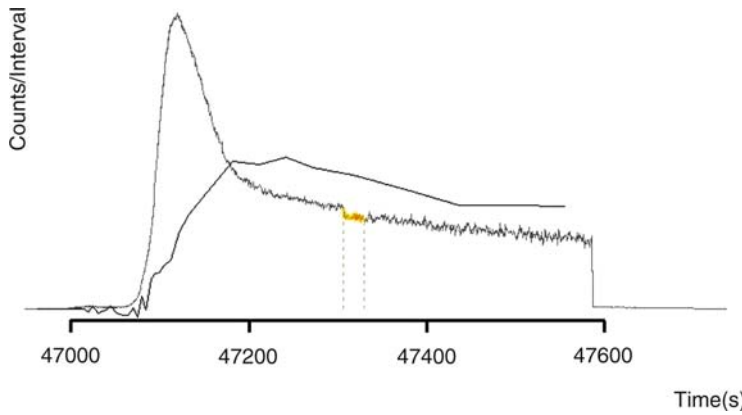

Perfusion, Neoplasms. Figure 1 Time activity curve using ►^{15}O-water dynamic method. Arterial input corrected curve of changing ^{15}O-water activity in region of interest. The first curve to peak is for arterial blood concentration, and the second peak is for a tissue concentration. The *dashed line* on the blood curve indicate the drawing of a calibration blood sample. (Courtesy of Dr G Laking, Manchester Molecular Imaging Centre)

Change in tissue concentration with time is given by:

$$dC_t(t)/dt = FC_a(t) - (F/V_d + \lambda)C_t(t),$$

where $C_t(t)$ is the regional tissue concentration of $H_2{}^{15}O$ (Bqml^{-1} tissue) as a function of time, $C_a(t)$ is the arterial concentration of $H_2{}^{15}O$ (Bqml^{-1} tissue) as a function of time, F is the regional flow in mL(blood)/mL (tissue) min^{-1}, V_d is the volume of distribution of water in mL (blood)mL^{-1} (tissue), is the decay constant of ^{15}O (0.338 min^{-1}).

The solution is given by the equation

$$C_t(t) = FC_a(t)^* \exp(-(F/V_d + \lambda)t),$$

where * is the operation of convolution, $C_t(t)$ is the tissue response to an arterial input function $C_a(t)$.

This method has several advantages. Scans can be repeated every 10 min, and the model is less sensitive to heterogeneity. Flow and V_d are estimated separately. Data acquisition is faster, so a lower radiation dose can be delivered to the patient. However, long reconstruction times and large datasets are needed, data are noisier, data modelling is highly complex and extensive blood sampling is required (50 mL per scan). As for the steady-state method, it makes the assumption that water is freely diffusible and fully extracted from circulation, and is poor for high blood flow regions.

Imaging Blood Volume

This involves inhalation of a tracer dose of ^{15}[O]CO in oxygen, then breathing room air, until arteriovenous C^{15}O–Hb carboxyhaemoglobin equilibrates within blood, which typically only takes 1–2 min. Tissue radioactivity and arterial C^{15}O–Hb are recorded. Carboxyhaemoglobin remains in vessels, so the ratio of activity in tissue to blood is the blood volume within the imaged tissues.

Nuclear Medicine Imaging of Angiogenesis

Angiogenesis has a significant role in determining tumour perfusion. Non-invasive molecular imaging can detect molecules, which are selectively expressed on tumour vasculature and involved in angiogenesis. Imaging involves production of a labelled ligand or a labelled antibody to the ligand. Many of these studies are still in an early phase of clinical development, or indeed preclinical. Preclinical studies are underway with labelled FGF antibody. VEGF expression has been imaged clinically by labelling the molecule or its antibody.

The integrin alpha v beta3 is expressed selectively on activated tumour vasculature. This has been imaged in a phase II study using a labelled antibody specific for this integrin. Retention occurred only in the patient who had alpha v beta3 positive tumour (4). There have been some clinical developments in imaging matrix metalloproteinases (MP)—an inhibitor of MP labelled with indium-111 has been administered safely to patients with Kaposi sarcoma, but without tumour uptake (5) (Fig. 2). Progress in this field depends on development of new-labelled ligands or antibodies involved in tumour angiogenesis. Candidate tracers should demonstrate a relatively high level of specific signal bound to the site, but also have kinetics that are amenable to correction for background/non-specific binding and thereby enable quantitation.

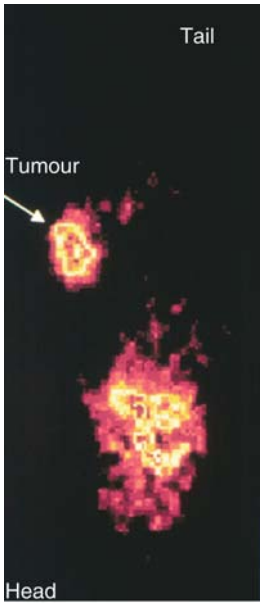

Perfusion, Neoplasms. Figure 2 [124I]VG76e-PET image

Nuclear Medicine Imaging of Hypoxia

Hypoxia both stimulates angiogenesis and blood flow in tumours and occurs as a result of the aberrant tumour vasculature that develops. A number of PET probes are being developed for measuring hypoxia, including ^{64}Cu-ATSM and ^{18}F-fluoromisonidazole (^{18}F-FMISO), and of these ^{18}F-FMISO is the most widely studied. This is a member of the group of nitroimidazoles, which diffuses into a cell, and undergoes electron reduction to form reactive species. In the presence of oxygen, the molecule is reoxidized. In hypoxic conditions, the reactive species forms covalent bonds with intracellular macromolecules and is trapped in the cell.

There are studies of hypoxic imaging with ^{18}F-FMISO in a wide range of human cancers. ^{18}F-FMISO has been tested as a hypoxic imaging tool against a range of standard hypoxic markers.

The early delivery of ^{18}F-FMISO into tumours is controlled by blood flow. Later activity measurements are dominated by the oxygen-dependent retention within the tissue. Consequently, typical scans are performed around 90–120 min following injection, to minimize the effect of blood flow confounding the hypoxia measurements. Tumour retention is generally expressed relative to plasma or muscle levels. However, a kinetic model for analysis of dynamic ^{18}F-FMISO PET data has been described (6) which reflects oxygenation of tumours and presence of necrosis, and was able to predict prognosis of patients undergoing radiotherapy.

New nitroimidazole tracers are being developed for example, etanidazole, which may have better imaging characteristics than ^{18}F-FMISO.

Bibliography

1. Shemirani B, Crowe DL (2000) Head and neck squamous cell carcinoma lines produce biologically active angiogenic factors. Oral Oncol 36(1):61–66
2. Frackowiak RS et al (1980) Regional cerebral oxygen utilization and blood flow in normal man using oxygen-15 and positron emission tomography. Acta Neurol Scand 62(6):336–344
3. Lammertsma AA, Jones T (1992) Low oxygen extraction fraction in tumours measured with the oxygen-15 steady state technique: effect of tissue heterogeneity. Br J Radiol 65(776):697–700
4. Posey JA et al (2001) A pilot trial of vitaxin, a humanized anti-vitronectin receptor (anti alpha v beta 3) antibody in patients with metastatic cancer. Cancer Biother Radiopharm 16(2):125–132
5. Kulasegaram R et al (2001) *In vivo* evaluation of 111In-DTPA-N-TIMP-2 in Kaposi sarcoma associated with HIV infection. Eur J Nucl Med 28(6):756–761
6. Thorwarth D et al (2005) Kinetic analysis of dynamic 18F-fluoromisonidazole PET correlates with radiation treatment outcome in head-and-neck cancer. BMC Cancer 5:152

Pericolic Abscess

Consequence of pericolic inflammation associated with diverticulitis. Often confined to mesentery of sigmoid colon but may result in widespread sepsis, peritonitis or liver abscess.

▶Diverticulitis, Gastroinstestinal Tract

Periductal Mastitis

▶Duct Disease, Breast

Perinatal Cerebral Injury

▶Cerebral Neonatal Disease (Neuro View)

Perineal Ultrasound

Ultrasonographic technique which uses a high-frequency probe.

▶Incontinence, Urinary

Perineural Spread

Perineural spread describes the process by which a tumour exits its primary side and reaches distant locations by travelling along the neural sheath. It can be directed antegradely or retrogradely and may be clinically silent.

▶Neoplasms, Oral Cavity

Perineural Spread of Tumour

A mechanism whereby pathologic conditions spread along the connective tissues of the perineurium. This type of spread is often associated with malignant disease of the head and neck, but can also be seen in infectious and inflammatory conditions that show neural tropism, such as fungal infections and granulomatous disease processes. The most common histopathologies associated with perineural spread are epidermoid carcinoma, arising from mucous membranes or from the skin, salivary gland neoplasms (adenoid cystic and mucoepidermoid carcinomas), melanoma and lymphoma.

▶Facial Nerve Palsy

Periodontal Disesase

Synonyms

Periodontitis

Definition

Periodontal disease consists in a progressive destruction of periodontal tissues: gums, alveolar dental ligament, cementum, and alveolar bone. Periodontal disease is really frequent and it is mainly induced by dental plaque, which usually grows up on the enamel where a large amount of germs are present. When plaque is mineralized, it turns into oral calculus. Calculus and plaque can both be the cause of gingival inflammation (3).

Pathology/Histopathology

Factors that induce periodontal disease are a bad oral hygiene, nicotinism, overflowed treatments, malocclusion, age, genetic factors, and diabetes.

The first clinical manifestation is represented by gingivitis: if the phlogistic process becomes chronic, the periodontal membrane and the alveolar bone are destroyed and radicular lacunae start growing. Radicular lacunae represent a pathological lowering of the groove between tooth and gum. When the alveolar bone is totally destroyed and gums become shorter, tooth starts moving (1).

Clinical Presentation

Radiology is not as important as the clinical approach in case of periodontal disease, but it can be useful to determine the rate of periodontal attachment and radiographic bone loss (4, 5). A limit is constituted by the bidimensionality of the representation.

Imaging

Imaging allows a classification of the pathological lesion and a posttherapeutic control.

Pantomography can be useful only to have a first valuation of the disease.

The radiological approach includes periapical radiographs of all dental elements, taken with the paralleling technique. Usually 16 radiographs are taken using e-speed dental film. The paralleling technique assures a minimum level of deformity and enlargement, allowing the bone loss' measurement (Fig. 1). A better anatomical evaluation can be provided with volumetric CT and 3D reconstruction (1).

Nuclear Medicine

Bone scintigraphy has a limited role in the assessment of periodontal diseases.

Diagnosis

Initial lesions of the disease consist of bone crest loss and interradicular septa reduction. Moderate lesions are characterized by horizontal bone loss and bone defects. Advanced lesions consist of vertical bone erosion with the development of bone lacunae along root margins. In the advanced stage of periodontitis a molar furcation involvement can be observed.

The periodontal abscess occurs when a deep radicular lacuna is obstructed. From a radiological point of view, a wide osteolysis with the development of fistulas is observed.

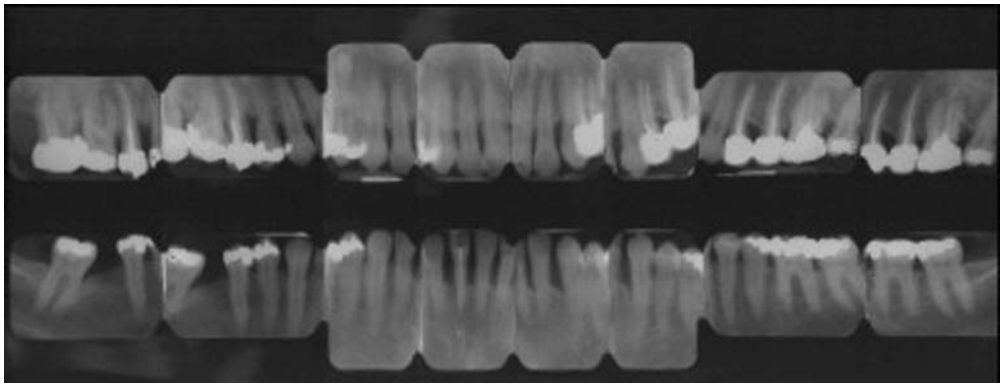

Periodontal Disease. Figure 1 sixteen intraoral radiographs taken with the paralleling technique.

The juvenile periodontitis usually concerns women from 15 to 25 years old, and it does not generally come with gingival inflammation. An expansion of the periodontal region and the growth of lacunae due to bone reabsorption can be noticed with the radiological approach.

Bibliography

1. Prochard J (1964) Advanced Periodontal Disease. Philadelphia, PA: WB Saunders
2. Suomi JD, Plumo J, Barbano JP (1968) A comparative study of radiographs and pocket measurements in periodontal disease evaluation. J Periodontol 39:311–315
3. Selikowitz HS, Sheiham A, Albert D et al (1981) Retrospective longitudinal study of the rate of alveolar bone loss in humans using bite-wing radiographs. J Clin Periodontol 8:431–438

Periosteal Reaction

Reactive, new bone formation outside the normal cortical boundaries of the bone. The periosteal reaction can be either solid, lamellar or more complex and aggressive e.g. Codman angle, hair-on-end or spiculated (+/− interrupted). The latter is suggestive of malignancy.

▶Neoplasms, Bone, Malignant

Periostitis

Inflammation of the periosteum induces new periosteal bone appositions. Diffuse periostitis is found in hypertrophic osteoarthropathy, thyroid acropachy, venous stasis, hypervitaminosis A, and infantile cortical hyperostosis.

▶Hypertrophic, Osteoarthropathy

Peripheral Facial Nerve Paralysis

A clinical condition characterized by paralysis of all muscles of facial expression secondary to nuclear or infranuclear (lower motor neuron) insults ipsilateral to the paralysis.

▶Facial Nerve Palsy

Peripheral neurofibromatosis or Von Recklinghausen's Disease

▶Neurofibromatosis, Musculoskeletal Manifestations

Peripheral Vein Occlusion

▶Thrombosis, Vein, Peripheral

Peripheral Venous Obstruction

▶Thrombosis, Vein, Peripheral

Peritendinitis and Bursitis

▶HADD

Peritendinitis Calcarea

Recurrent painful calcific deposits around the tendons as a result of crystal/calcium deposition.
►HADD

Peritoneal Collections

Panos K. Prassopoulos
Department of Radiology, University Hospital of Alexandronpolis, Medical School of Thace, Alexandronpolis Greece
pprasopo@med.duth.gr

Synonyms

The term "peritoneal collection" can be substituted by other terms only when the composition or nature of the fluid is known or evident. Under this condition the terms ►Ascites; Hemorrhagic collection/Hematoma; Bile collection/biloma; Urinoma; ►Seroma; Pancreatic fluid collection; or Abscess may be used and can precisely indicate the underlying process that is responsible for peritoneal fluid accumulation

Definition

Accumulation of fluid in the peritoneal ►cavity is not a disease in itself, but it is the manifestation of a wide spectrum of pathologic processes that may involve intraperitoneal or extraperitoneal organs. The biochemical composition of fluid or the presence of cells within it depends on the disease that is responsible for fluid productivity (1). Transudative collections may be associated with portal hypertension, cirrhosis, heart failure, nephrotic syndrome, or obstruction of the inferior vena cava, hepatic vein, or portal vein. Exudative fluid may be related to infections or peritoneal carcinomatosis. Blood collections may be the result of trauma, hemorrhagic diathesis, or tumor rupture. Bile collections may follow rupture of the biliary tree; chylous collections may develop after obstruction of lymphatics; pancreatic fluid collections may be the consequence of acute pancreatitis; urine collections may represent extension of a retroperitoneal urinoma; and purulent collections may be the consequence of visceral inflammations, intestinal perforations, or surgery.

Anatomy/Physiology

The peritoneal cavity normally contains a small amount of serous fluid (less than 100 mL) for lubrication. Normal peritoneal fluid and ascites move along predictable pathways that are influenced by gravity, capillary forces, fluid composition, and intraabdominal pressure gradients (hydrostatic pressure is lower in subphrenic recesses than in the pelvis) and are governed by mesenteric reflections or adhesions (2). Fluid collections in the ►inframesocolic spaces (Fig. 1) flow to the pelvis, the most dependent portion of the peritoneal cavity. Fluid spread in the right inframesocolic space occurs along the small bowel mesentery; it may stagnate at the ileocecal area and then overflow into the pelvis. In the left inframesocolic space, fluid may temporarily accumulate along the superior

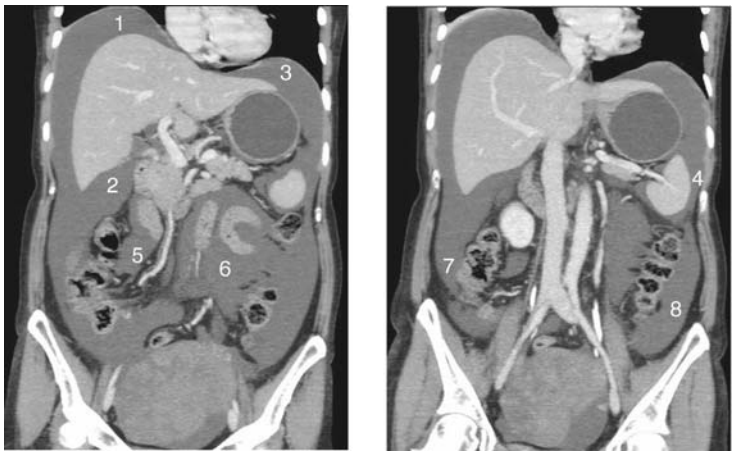

Peritoneal Collections. Figure 1 Ascitic fluid in peritoneal compartments: right subphrenic (1), right subhepatic (2), left subphrenic (3), perisplenic (4), right and left inframesocolic (5, 6), right and left paracolic gutters (7, 8).

surface of the sigmoid mesocolon and gradually flow into the pelvis. The pouch of Douglas is first filled in the pelvis, followed by the lateral perivesical recesses. From the pelvis, fluid ascends both paracolic gutters (Fig. 1), forced by the negative subdiaphragmatic pressure during inspiration. The major flow occurs along the right paracolic gutter, which is deeper than the left. In addition, the phrenicocolic ligament on the left acts as an anatomic barrier to fluid exchange. Thus, the right paracolic gutter represents the main communication channel between the inframesocolic and ►supramesocolic spaces. It continues to the right subhepatic and subphrenic spaces (Fig. 1) and allows movement of collections from the pelvis to the right upper abdomen, and vice versa.

Fluid in the supramesocolic spaces tends to accumulate in Morrison's subhepatic recess, which is the most dependent portion in the supine position. From the right subhepatic space, fluid can move to the right subphrenic or left subhepatic space, and vice versa. However, fluid exchange between the right and left subphrenic cavities is prevented by the falciform and coronary ligaments. Fluid moves freely between the left subphrenic, left perihepatic, and perisplenic compartments, but the transverse mesocolon and the phrenicocolic ligament act as barriers for the extension of small or medium collections to the inframesocolic spaces. Fluid in the lesser sac may flow to the posterior subhepatic space through Winslow's foramen.

Pathology/Histopathology

The peritoneal serous lamina reacts strongly to a wide spectrum of conditions—including injury, inflammation, the presence of neoplastic cells, and contact with irritating biochemical factors in the extravasated blood, urine, bile, or pus—by forming adhesions to limit collections, isolating inflammatory processes, or plugging perforations. Thus, hematic, biliary, urinary, or purulent collections may be limited by an active peritoneal reaction. Consequently, they may not move freely in the peritoneal cavity and are usually located or isolated at the area where they developed. On the contrary, transudative or exudative effusions diffuse in the peritoneal cavity because they may not stimulate a significant peritoneal reaction. In addition, ascites or gases are more easily absorbed by the peritoneum at the diaphragmatic or omental level, in contrast to decreased absorption of other kinds of fluid collections.

Clinical Presentation

The clinical presentation of fluid collections depends on the underlying disease that causes the peritoneal fluid accumulation. Peritoneal fluid of less than 2 L is difficult to detect clinically. The earliest sign of ascites is dullness to percussion in the flanks. Shifting dullness and a fluid thrill mean that more fluid is present. Ascites may be manifested by an increase in abdominal girth accompanied by weight gain. The abdomen is distended, often with fullness in the flanks and an everted umbilicus. Scrotal edema is frequent. Other signs and symptoms are mostly related to the primary disease: hypovolemic shock in hematic collections; upper abdominal pain, vomiting, or tenderness in acute pancreatitis fluid collections; fever in abscesses; and distended abdominal wall veins that radiate from the umbilicus in ascites due to portal hypertension.

Imaging

Small to moderate transudative or exudative collections usually accumulate in the most dependent peritoneal recesses. In the presence of large ascites, the small bowel is usually positioned centrally within the abdomen. Ascitic fluid under tension may result in an extraperitoneal mass effect and may be associated with displacement of bowel loops from the central position. Purulent, hematic, biliary, and urinary collections may become loculated due to adhesions as a result of peritoneal reactivity stimulation, and they may be seen as cystic lesions with mass effect (3).

Hemorrhagic collections may either be localized next to the bleeding organ or, more frequently, tend to diffuse and accumulate to Morrison's pouch when bleeding is supramesocolic or to the pouch of Douglas when it is inframesocolic. Computed tomography (CT) attenuation values of the hemorrhagic collection are similar to those of circulating blood. They increase within a few hours due to clot formation or concentration and thereafter gradually decrease from the periphery toward the center (4). A focal high-density area within the collection in trauma patients corresponds to localized clotted blood and is indicative of the bleeding site. Active bleeding may be disclosed by contrast medium extravasation on CT. Old hemorrhagic collections may have a cystic appearance surrounded by a pseudocapsule of variable thickness.

Bile collections are usually located in the subhepatic or gastrohepatic recesses and may have a loculated cystic appearance with thin wall and water-like density/signal intensity content. Contrast agents excreted along with bile may be valuable in disclosing active bile extravasation on CT or magnetic resonance imaging (MRI).

Peritoneal urine collections follow retroperitoneal extravasation of urine through communication at the level of the mesenteric or mesocolic subperitoneal spaces. They have a cystic appearance and water-like density/signal intensity. Late post-contrast-enhanced CT or MRI may be helpful in demonstrating active urine leakage.

Seromas have a cystic appearance surrounded by thickened peritoneum. They contain secretions of peritoneal serosa displaying water density/signal intensity characteristics.

Fluid collections with pancreatic juice may be seen early in the course of acute pancreatitis. They lack a capsule and thus are confined by the anatomic space within which they developed, most commonly the anterior perirenal space or, intraperitoneally, the lesser sac. They are seen as poorly defined fluid collections without recognizable walls, exhibiting low attenuation on CT or high signal intensity on T2-weighted MR images. An acute fluid collection may resolve spontaneously or evolve—after 4 or more weeks—to pseudocyst, a round or oval fluid collection with a thin capsule or a thick wall that may demonstrate contrast enhancement. Pancreatic abscess may also develop late in the course of disease as a result of tissue necrosis with subsequent liquefaction and superinfection. Imaging findings of an abscess on CT include a local fluid collection with slightly higher than water attenuation values, with or without gas bubbles, surrounded by a thick wall that usually exhibits contrast enhancement.

Peritonitis is characterized by a generalized collection of intraperitoneal fluid and is usually the result of an abscess extension or rupture of hollow viscera. CT features include ascites in association with peritoneal and mesenteric thickening. Tuberculous peritonitis is characterized by a high-density ascites on CT (20–45 HU), thickening and nodularity of peritoneal surfaces, and enlarged lymph nodes with central low attenuation.

A primary abdominal neoplasm arising in the stomach, colon, pancreas, or ovaries may seed cells into the ascitic fluid that is induced. Location and growth of intraperitoneally seeded metastases follow the pathways of the flow of ascitic fluid (5). When the implants are very small, ascites may be the only imaging manifestation of peritoneal carcinomatosis (Fig. 2). Ascitic fluid is often loculated/septated in carcinomatosis.

Nuclear Medicine

Nuclear medicine techniques have a limited role in evaluating peritoneal fluid collections. Gallium-67 scintigraphy has been proposed for the diagnosis and treatment monitoring of inflammatory peritoneal collections, especially tuberculous peritonitis, and PIPIDA scintigraphy for assessing active bile leakage in bilomas. Intraperitoneal administration of yttrium 90 has been suggested as an alternative treatment option in cases of malignant ascites.

Diagnosis

Ultrasound (US), CT, and MRI are sensitive in diagnosing and localizing peritoneal fluid collections. US may be more sensitive than CT for detecting small amounts of ascites in the pelvis or perihepatic spaces. Ascites is anechoic on US; in the presence of a more viscous fluid collection or blood, acoustic reflections may be seen. The CT attenuation values of ascites range from 0 to 20 HU; they increase with increasing protein or blood content (more than 30 HU) and decrease in the presence of chylous fluid. However, CT attenuation values are not specific. On MRI, ascites renders low signal intensity on

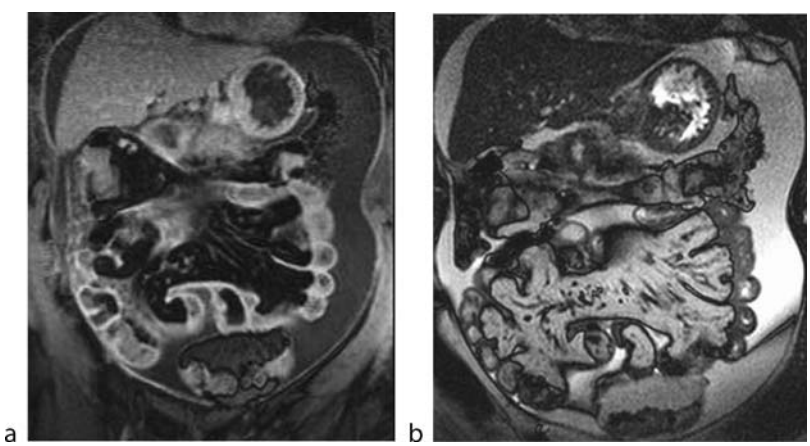

Peritoneal Collections. Figure 2 (a) Post-gadolinium-enhanced three-dimensional fast low-angle shot T1-weighted image with fat saturation on the right and (b) true fast imaging with steady-state precession on the left on coronal planes in a patient with malignant ascites. Note enhancement of the parietal peritoneum and the surface of the small bowel mesentery, which is thickened due to diffuse peritoneal seeding. Partially loculated ascites is present in the right subhepatic space and the right paracolic gutter.

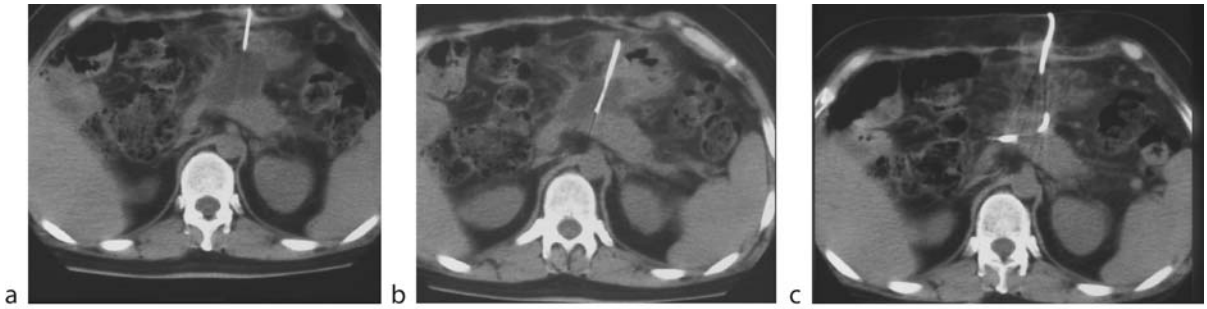

Peritoneal Collections. Figure 3 Percutaneous drainage of an infected pseudocyst. (a) Needle insertion for fluid aspiration. (b) Guide wire placement through a dilator. (c) Drainage catheter in place.

T1-weighted images and a "bright" signal on T2-weighted images. MRI is superior to CT for differentiating a hematoma from other collections, but it may miss a small amount of gas in an abscess.

A percutaneous fine needle aspiration may reveal the nature of a fluid collection and is important for abscess diagnosis by aspirating pus.

Interventional Radiological Treatment

Percutaneous drainage under CT or US guidance has been successfully applied in most types of loculated fluid collections, including hematomas, bilomas, pseudocysts, and abscesses (Fig. 3). Selection of catheter diameter depends on the degree of collection liquidation that can be determined by US or MRI.

Bibliography

1. Rossi A, Rossi G (2001) Fluid Collections. In: Baert AL, Sartor K (eds) CT of the Peritoneum. Springer-Verlag, Berlin, Heidelberg, New York, pp 137–164
2. Meyers MA (2000) Intraperitoneal spread of infections—intraperitoneal spread of malignancies. In: Meyers MA (ed) Dynamic Radiology of the Abdomen. Springer-Verlag, New York, pp 57–264
3. Gourtsoyiannis N, Daskalogiannaki M, Prassopoulos P (2002) Imaging of the peritoneum, mesentery and omentum. In: Grainger RC, Allison DJ (eds) Diagnostic Radiology. Churchill Livingstone, London, pp 1141–1163
4. Shanmuganathank (2004) Multidetector row CT imaging of blunt abdominal trauma. Semin Ultrasound CT MR 25(2):180–204
5. Raptopoulos V, Gourtsoyiannis N (2001) Peritoneal carcinomatosis. Eur Radiol 11(11):2195–2206

Peritonitis

▶Acute Abdomen, Genital Causes

Perthes Disease

▶Osteonecrosis, Childhood

PET

▶Positron Emission Tomography

PET in Drug Discovery Imaging

Pat Price, Barbara Kötz
Wolfson Molecular Imaging Centre, The University of Manchester, Manchester, UK
barbara.koetz@manchester.ac.uk
pat.price@manchester.ac.uk

Synonyms

Drug discovery and development; Molecular imaging; Positron emission tomography

Definitions

Positron emission tomography (*PET*) is a functional imaging technique that tracks radionuclides in the body, as they decay by positron emission. Coincidence detection of two gamma-rays, simultaneously emitted at 180° to each other, as a result of an annihilation reaction between a positron and an electron, forms the basis of PET.

Positron-emitting nuclides do not normally exist in nature and are predominantly produced in a cyclotron. While, positron-emitting nuclides for commonly occurring elements such as carbon, oxygen and nitrogen have a short half-life, requiring an on-site cyclotron, fluorine-18 and iodine-124, with longer half-life can be produced, remote from the imaging centre. These radionuclides can be used to substitute the elements in the compound of interest and evaluated with PET.

Drug discovery and development is a process that begins with discovery of new agents and proceeds through pre-clinical and clinical development (phase I, II, III clinical trials) until the drug is finally accepted for clinical use. It takes several years and millions of dollars before a drug is registered for clinical use and attrition rates are high, with more than 70% of drugs failing in the process. Drug discovery and development is currently undergoing enormous changes due to an increase in our understanding of disease pathology at the molecular level and the identification of potential therapeutic targets such as receptors, proteins, genes, antigens and pathways involved in cell cycle, signal transduction, cell death, drug resistance and angiogenesis. Due to an increase in the number of potential targets in the post-genomic era, as well as the use of new technologies such as combinatorial chemistry and high-throughput screening to produce large numbers of anticancer agents, the need to revise the way we test new drugs has become apparent.

Characteristics

PET Methodology

Molecular imaging with PET is based on the ►tracer principle. A tracer is a substance that follows or traces the path or behaviour of a substance that is being investigated. In PET, a very small mass of the molecule of interest is radiolabelled with the positron-emitting nuclide, when it is called a ►radiotracer. Since, any isotope effect should be negligible or at least quantitatively predictable and the mass of the radiotracer should be small compared to the mass of the substance being traced, molecules of high-specific activity (activity/mole) are required, necessitating expert radiochemical input.

In vivo kinetics of the radiotracer in the body can be assessed by methods such as simple visual inspection, semi-quantitative methods, which measure radiotracer uptake at a certain time point (standardised uptake value) or quantitative methods, which use complex analytical methodology. Quantitative parameters of interest can be derived using either model-led compartmental techniques or data-led methods such as spectral analysis, where limited *a priori* assumptions are made. For this, generation of tissue and arterial blood time-activity curves (TACs) is required. While tissue TACs are generated from the dynamic imaging data, arterial blood TACs require arterial or arterialised venous blood sampling or can be derived from PET images, representative of arterial blood such as the left ventricle or aorta. The lack of specificity of PET to distinguish between the radioactive chemical species presents additional challenges in PET data analysis. A number of strategies have been adopted to account for the tissue contribution of metabolites such as a dual radiolabelling strategy or performing additional metabolite correction scans (1).

The Role of PET in Drug Discovery Processes

The ability to provide quantitative *in vivo* tissue functional data of high sensitivity, makes PET an ideal complementary tool in the drug developmental process (2). Specifically, PET is ideally suited to provide *in vivo* tissue information on both the drug's behaviour within the body (►pharmacokinetics) and its effects (►pharmacodynamics), which have so far relied on surrogate data obtained from body fluids. While PET-pharmacokinetic studies require radiolabelling of the target drug and therefore early involvement of radiochemical expertise as soon as the lead compound is identified, radiolabelling of the therapeutic target is required for PET-pharmacodynamic studies. Although, such selection of a pharmacodynamic target will be based on the status of our biological knowledge at that time and may be time consuming, once a pharmacodynamic target is identified and validated, this can be used as an imaging ►biomarker to generically evaluate a number of agents that target the specific pathological process. This will allow hypothesis-testing clinical-trial designs to be incorporated to obtain proof of principle of mechanism of action during early drug development and in the establishment of the optimal therapeutic dose for biological agents that result in disruption of specific functional processes. A summary of the potential role of PET in drug discovery and development is illustrated in Fig. 1.

Pharmacokinetic Evaluation

Improvements in radiochemical synthetic strategies and the availability of animal PET scanners of high spatial resolution (~1 mm) (3) allow for the early evaluation of novel agents in animals for lead identification and optimisation. Pre-clinical studies can also provide important information on drug metabolism and inter-species variation in drug handling. Clinical 'microdosing' strategies, wherein tracer quantities of drug, several thousand-fold lesser than therapeutic concentrations are administered (4), are likely to provide valuable pharmacologic information and aid in the drug discovery process.

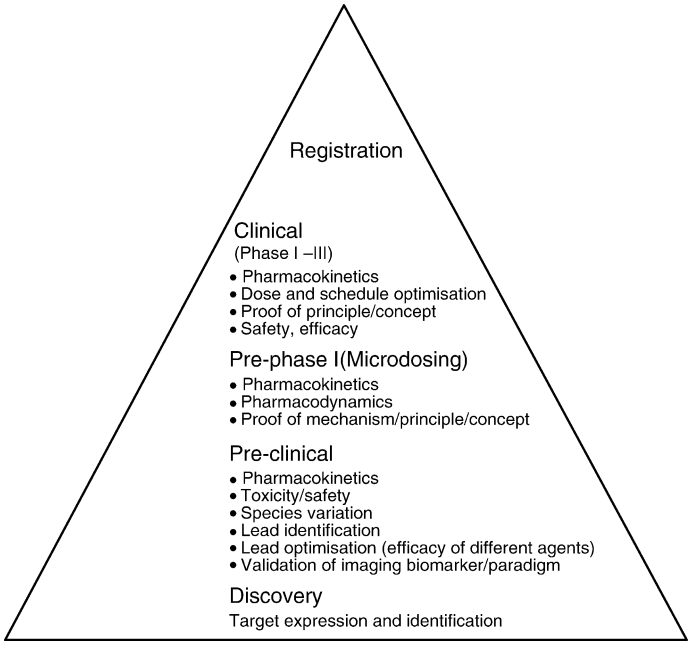

PET in Drug Discovery Imaging. Figure 1 Potential areas where PET can complement the drug discovery and developmental process. The pyramidal structure denotes the current high-attrition rate from discovery to drug registration.

An efficient radio synthetic strategy and production to GMP standards is required for clinical pharmacokinetic evaluation of radiolabelled therapeutic agents. As an example, the development of *N*-[2-(dimethylamino)ethyl] acridine-4-carboxamide, an anti-cancer agent radiolabelled with carbon-11 ([^{11}C]DACA) is described. Pre-clinical PET studies demonstrated no unexpected inter-species differences in metabolism of [^{11}C]DACA that would have alerted a change in the planned phase I study. Subsequent clinical 'microdosing' PET studies performed prior to phase I studies at 1/1000th of the phase I starting dose and during a dose escalating phase I study showed myocardial uptake that demonstrated saturation kinetics at phase I doses (Fig. 2), suggestive of potential cardiotoxicity. [^{11}C]DACA pharmacokinetics in the brain did not suggest potential neurotoxicity, in contrast to animal studies, where neurotoxicity and not cardiotoxicity was observed (1). In another clinical [^{11}C]DACA-PET study, it was concluded that the 120 h infusional schedule was unlikely to be efficacious despite the maximal tolerated dose being reached as saturation was not observed in the primary target tissue that is the tumour (1). Such information of tissue drug pharmacokinetics will aid in dose and schedule selection.

PET is also likely to contribute substantially in the quantitative evaluation of targeted therapies such as gene therapy. In particular, the assessment of successful gene delivery, the location, magnitude and timing of gene expression can be evaluated with PET without the need for serial biopsies. The method is based on the linkage of the therapeutic gene under investigation to a so called 'PET reporter gene', which codes for an enzyme or receptor that can be imaged using a PET tracer.

Pharmacodynamic Studies

Imaging Receptor–Ligand Binding

PET imaging of receptor–ligand binding has proven to be especially important in the development of agents that target the central nervous system. This has been greatly aided by the availability of several receptor-specific ligands, most of which do not undergo metabolism (Table 1). Theses studies focus on the regional uptake of ligands and are used to derive parameters such as receptor number (B_{max}), affinity (K_d) and binding potential (BP) and can be used to examine if drugs reach their receptor targets providing proof of mechanism. In addition, information on dose occupancy in phase I and II studies, will aid in rationalising the choice of dosing in clinical trials and microdosing studies with potential drugs could guide in lead selection and optimisation at early stage in drug development (5).

Imaging Glucose Metabolism

Monitoring of glucose metabolism by the analogue tracer [^{18}F]-fluoro-deoxy glucose (FDG), has been used for delineation of ischaemic myocardium, areas of epileptic focus and for staging, response and prognostic evaluation in oncology. FDG follows the same route as glucose into

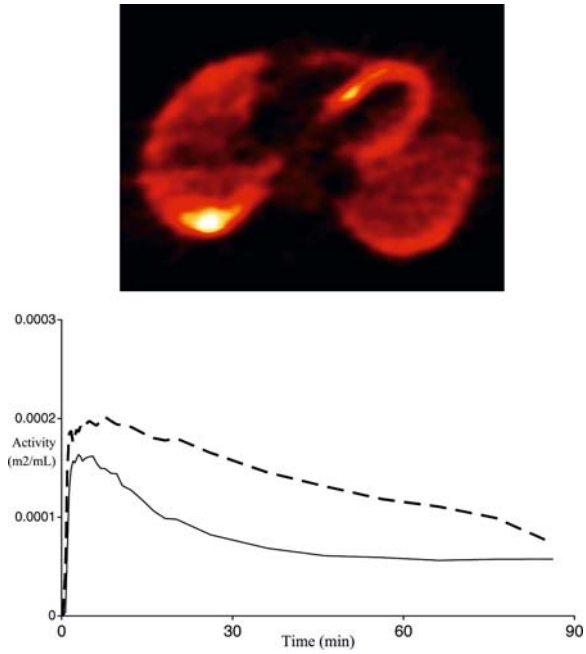

PET in Drug Discovery Imaging. Figure 2 Trans-axial PET image after microdosing studies with [^{11}C]DACA, given at 1/1000th of the phase I starting dose, demonstrating myocardial uptake (*top*). Myocardial TAC's of carbon-11 radiolabelled tracer (*bottom*) revealed saturation myocardial kinetics, when comparative [^{11}C]DACA-PET studies were performed after tracer doses of [11C]DACA alone (*broken line*) compared with tracer doses in combination with increasing doses of unlabelled DACA in a phase I study (*unbroken line*).

PET in Drug Discovery Imaging. Table 1 Commonly employed radiolabelled ligands for receptor imaging with positron emission tomography

Receptor	Radioligand	Disease example
Dopamine D1-receptor	[^{11}C]-SCH 23390	Schizophrenia
Dopamine D2-receptor	[^{11}C]-raclopride	Parkinsons disease
	[^{11}C]-*N*-methyl-spiperone	Drug addiction
5-HT$_{1A}$-serotonin-receptor	[^{11}C]-way 100635	Schizophrenia
5-HT$_2$-serotonin-receptor	[^{18}F]-Setoperone	Affective disorders
Benzodiazepine-receptor	[^{11}C]-flumazenil	Anaesthetics, Epilepsy
Opioid receptor	[^{11}C]-diprenorphine	Pain
	[^{11}C]-carfentanil	Drug addiction
Oestrogen receptor	16-α[^{18}F]-fluoro-17β-oestradiol	Breast cancer

cells where it is phosphorylated to FDG-6-phosphate, but unlike glucose, there is little further metabolism and FDG-6-phosphate remains essentially trapped within cells. FDG-6-phosphate has low membrane permeability and although dephosphorylation does occur, it is very slow in brain, heart and tumour, which have very low levels of glucose-6-phosphatase. FDG uptake in tumours probably reflects a combination of factors including phosphorylating activity of mitochondria, degree of hypoxia and levels of glucose transporters and is reflective of viable number of cancer cells.

The limitations associated with the use of structural changes in tumour volume as a measure of therapy efficacy, especially with targeted cytostatic anti-cancer agents, which do not produce a decrease in tumour volume despite an anti-cancer effect, has led to an increasing use of functional imaging as a pharmacodynamic marker of response. Since, changes in glucose metabolism in responding tumours are seen as early as a few days after treatment, FDG-PET can be used in the evaluation of novel targeted cancer therapy. Additionally, functional imaging methods would aid in the

determination of the optimal therapeutic dose by relating the response to the drug dosage.

Imaging Cell Proliferation and Perfusion

Physiological uptake of FDG in the brain, accumulation in inflammatory conditions and the low or variable glycolytic activity of some tumour types has led to the evaluation of other PET pharmacodynamic markers in the development of targeted therapies. Validated PET markers of cell proliferation such as [^{11}C]-thymidine and the thymidine analogue [^{18}F]-fluoro-thymidine (FLT) have been used clinically. The short half-life and low radiation exposure associated with [^{15}O]H_2O-PET allows repeated scanning in the same subject and has been used as a pharmacodynamic perfusion marker in the evaluation of vascular targeted cancer therapies in man (1). Perfusion studies with PET have also been used to evaluate the effects of cardiac drugs like ß-adrenergic- or calcium-channel blockers on myocardial blood flow and flow reserve.

Development of Imaging Biomarkers

Imaging biomarkers are in various stages of development for hypoxia ([^{18}F]-fluoro-misonidazole, [^{62}Cu]-diacetyl-bis(*N*-methyl-thiosemicarbazone) which contributes to resistance to radiotherapy and some cytotoxic agents. Biomarkers for apoptosis or programmed cell death (Annexin V), a target of increasing importance in anti-cancer therapy, neuroprotective therapy designed to inhibit ischemic brain injury and screening for early transplant rejection, are also under development. It is envisaged that development and validation of such imaging biomarkers and their use would complement the drug discovery and developmental process and lead to a significant saving in time, money and health and lives lost to disease.

Bibliography

1. Saleem A (2005) Potential of PET in oncology and radiotherapy. Br J Radiol Suppl 28:6–16
2. Rudin M, Weissleder R (2003) Molecular imaging in drug discovery and development. Nat Rev Drug Discov 2:123–131
3. Aboagye EO (2005) Positron emission tomography imaging of small animals in anticancer drug development. Mol Imaging Biol 7:53–58
4. Bergstrom M, Grahnen A, Langstrom B (2003) Positron emission tomography microdosing: a new concept with application in tracer and early clinical drug development. Eur J Clin Pharmacol 59:356–366
5. Brooks DJ (2005) Positron emission tomography and single-photon emission computed tomography in central nervous system drug development. NeuroRx 2:226–236

PET in Viability Imaging

U. Schnöckel, M. Schäfers
Department of Nuclear Medicine, University of Münster, Münster, Germany
schafmi@uni-muenster.de

Definition

In the management of patients with ischemic heart disease, assessment of myocardial viability is important in different clinical scenarios. This is especially relevant in patients with regional (hypo-/akinesia) or global (low ejection fraction) contractile dysfunction to estimate the individual benefit of revascularization [percutaneous transluminal coronary angioplasty (PTCA) vs. bypass surgery] with respect to improvement of contractile function and preoperative assessment of individual perioperative risk. In principle, methods assessing myocardial viability should aim to distinguish between ischemic but viable myocytes (so-called hibernating myocytes/myocardium) and scar tissue because only viable cells will profit from restoration of perfusion. In this respect, viable myocardial cells are characterized by a variety of various features, including cell membrane integrity, intact mitochondria, preserved glucose metabolism, preserved fatty acid metabolism, intact resting perfusion, and a preserved contractile reserve. However, viable myocardium need not fulfill all of these characteristic features.

Therefore, the combination of metabolic and perfusion imaging is a powerful clinical tool to predict myocardial functional recovery, since patients with preserved myocardial glucose metabolism despite reduced perfusion should benefit from revascularization. Furthermore, besides identifying ischemic but viable myocardium, parameters such as the extent of viable myocardium (e.g., at least ~25% of viable myocardium of the left ventricle, as assessed by viability imaging, is necessary to result in improved left ventricular ejection fraction after revascularization) are required for a careful selection of patients who are more likely to benefit from revascularization.

Imaging

Scintigraphic Perfusion Imaging

Scintigraphic methods currently used for imaging of the heart are primarily based on the injection of perfusion tracers (Tl-201, Tc-99m-tetrofosmin/-sestamibi) in conjunction with single photon emission tomography (SPECT), thus being capable of imaging myocardial ischemia. However, the

myocardial uptake and retention of Tl-201 depends on both regional perfusion and normal cell membrane function because Tl-201 is taken up into myocytes *via* the energy-dependent Na^+/K^+ exchanger. Accordingly, the myocardial uptake of the modern Tc-99m-labeled agents such as tetrofosmin and sestamibi depends on regional perfusion and intact mitochondria. Therefore, when these tracers are used, the fraction of viable myocytes is often underestimated because perfusion can also be reduced in ischemic but still viable myocardial segments. An inconspicuous perfusion, on the other hand, is definitive proof of viable myocardial cells.

In addition to scintigraphic perfusion imaging by the earlier described SPECT tracers, different positron-emitting tracers for perfusion imaging (N-13-ammonia, O-15-water, Rb-82) with positron emission tomography (PET) are available. In contrast to SPECT, PET has an established correction for photon attenuation and is therefore able to quantify myocardial perfusion in absolute units (mL/min/g tissue), which, apart from superior resolution and image quality, offers advantages over SPECT in diagnostic accuracy, sensitivity, and specificity.

Imaging of Myocardial Metabolism

F-18-fluordesoxyglucose (F-18-FDG) is a tracer by which regional myocardial glucose uptake and phosphorylation and thus an ATP-dependent process can be assessed. Physiologically, most myocardial energy production occurs through the beta-oxidation of free fatty acids, whereas only ~30% of the energy is generated through glucose metabolism. In the presence of hypoxic and/or ischemic conditions, however, oxidative metabolism of free fatty acids is decreased, and glucose becomes the preferred substrate for the myocardium. F-18-FDG enters the myocytes by the same transport mechanism as glucose, namely by glucose transporter 4 (GLUT4). In the absence of insulin, GLUT4 exists in intracellular vesicles where it cannot facilitate glucose transport. Binding of insulin to its receptor on the plasma membrane initiates a signaling cascade that promotes translocation and fusion of GLUT4-containing vesicles with the plasma membrane, thereby enabling GLUT4 to transport glucose through the cell membrane. F-18-FDG is intracellularly converted to F-18-FDG-6-phosphate (phosphorylation) by the enzymatic hexokinase reaction. Differences in the affinity of FDG to hexokinase compared with the affinity of glucose to hexokinase have been discussed (and eventually corrected by a so-called lumped constant). Most importantly, different from glucose-6-phosphate, F-18-FDG-phosphate does not continue being converted enzymatically by glucose-6-phosphatase, but it stays trapped in the cell as F-18-FDG-6-phosphate.

Therefore, the accumulation of F-18-FDG depends on GLUT4 and hexokinase activity, and its trapping in myocytes characterizes these as being viable. Accordingly, nonreversible damage of the cell must be assumed when cellular F-18-FDG uptake is missing.

Another positron-emitting tracer to assess myocardial metabolism by PET is C-11-acetate. C-11-acetate characterizes the oxidative metabolism of the heart muscle. However, due to the short half-life of ^{11}C of 20.3 min (F-18-FDG has a half-life of 109 min) and the necessity of a cyclotron unit in direct proximity to PET, it is available in only a few centers worldwide.

More tracers have been developed to assess fatty acid metabolism and such; however, these have not yet been implemented in clinical algorithms.

Clinical Protocol

Because the energy demand of the heart muscle is accomplished primarily by fatty acids and only a smaller fraction by carbohydrates, it is fundamentally necessary that the metabolism at the time of tracer injection and the subsequent acquisition period be switched to glucose to get a reproducible and reliable myocardial signal when imaging with F-18-FDG-PET. In about 50% of examined patients, the assessment of viability using F-18-FDG-PET under fasting conditions cannot be interpreted because of very low F-18-FDG uptake. An increased glucose uptake can be achieved by hyperinsulinemia, which also induces a lowering of the concentrations of free fatty acids, in addition to the direct stimulation and to effects on the glucose metabolism, through an inhibition of lipolysis. In nondiabetics, hyperinsulinemia can be easily reached by oral glucose loading, resulting in increased insulin levels thereafter.

Switching the myocardial metabolism toward glucose is technically more challenging in diabetics, who represent a significant subgroup of patients with coronary artery disease. In diabetics, an intravenous infusion of basal human insulin with parallel and adjusted infusion of glucose is recommended to gain a hyperinsulinemic state (hyperinsulinemic euglycemic clamp protocol) besides. As an alternative or in addition to hyperinsulinemia, an increasing F-18-FDG uptake in the heart muscle can be induced by pharmaceutical lowering of free fatty acids in the plasma using nicotinic acid derivatives, such as acipimox. Acipimox inhibits peripheral lipolysis, thus reducing plasma free fatty acid levels and indirectly stimulating cardiac F-18-FDG uptake. Typically, the PET acquisition starts about 1 h after the F-18-FDG injection, allowing for significant trapping of F-18-FDG in viable myocardium.

Image Interpretation

When F-18-FDG is used without a perfusion tracer, cut-off values of normalized F-18-FDG uptake are applied. In the quantification of the extent of viable myocardium, a cut-off value of about 50% is usually given to identify viable myocardium. However, especially when looking for the pathophysiological state of myocardial hibernation (characterized by reduced perfusion and preserved or enhanced glucose metabolism), it is crucial to correlate glucose metabolism with perfusion.

A combination of several patterns of myocardial perfusion and F-18-FDG uptake can be seen in dysfunctional myocardium (Table 1).

Myocardial areas with reduced perfusion despite preserved glucose metabolism (so-called mismatch) indicate the presence of *myocardial hibernation*, typically associated with significantly improved contractile function after revascularization (Fig. 1).

Scar tissue shows a matched reduction in myocardial perfusion and F-18-FDG uptake. A revascularization is not likely to improve function of the myocardium (Fig. 2).

In dysfunctional segments, perfusion and F-18-FDG uptake may be preserved. These segments may represent *stunned myocardium*, evolving from repetitive episodes of myocardial ischemia. Stunned myocardium is characterized by prolonged but reversible postischemic dysfunction despite reperfusion.

The positive and negative predictive values of the combination of a perfusion SPECT and an FDG-PET for assessing myocardial viability are 72–95% and 75–100%, respectively. Therefore, F-18-FDG-PET is the assumed gold standard of noninvasive imaging of myocardial viability.

PET in Viability Imaging. Table 1 Typical patterns of perfusion and F-18-FDG uptake observed in dysfunctional myocardium (↔: normal, ↓ reduced, ↑ increased)

	Hibernation	Scar	Stunning
Perfusion	↓	↓	↔
FDG uptake	↔/↑	↓	↔

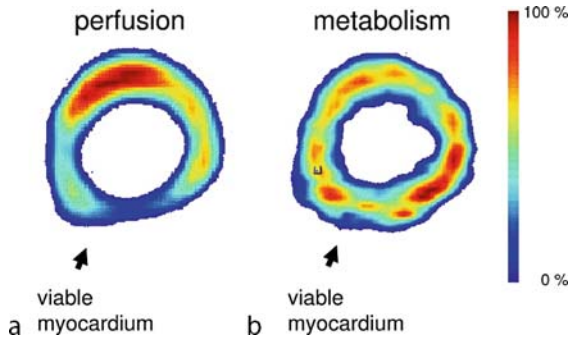

PET in Viability Imaging. Figure 1 Perfusion SPECT (a) and F-18-FDG-PET (b) in a patient with known coronary artery disease. The perfusion image shows reduced perfusion in the inferior wall (*arrow*, a), whereas F-18-FDG uptake is preserved in this region (*arrow*, b). This is a typical example for the imaging correlate of *hibernating myocardium* (perfusion-metabolism mismatch).

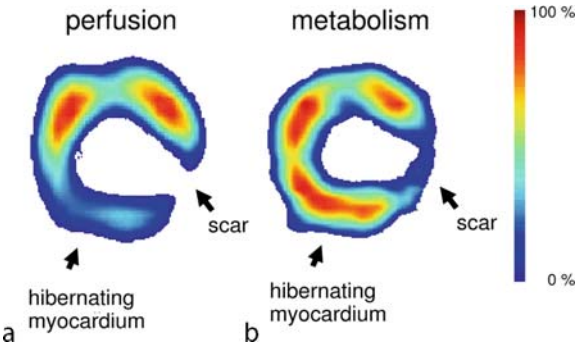

PET in Viability Imaging. Figure 2 Perfusion SPECT (a) and F-18-FDG-PET (b) in a patient with known coronary artery disease. The images show a matched reduction of perfusion and F-18-FDG uptake in the inferolateral wall, demonstrating a scar (*arrows* a, b). In the inferior wall, the perfusion is reduced despite preserved F-18-FDG uptake, demonstrating myocardial hibernation (*arrows* a, b).

Bibliography

1. Rizzello V, Poldermans D, Bax JJ (2005) Assessment of viability in chronic ischemic heart disease: current status. Q J Nucl Med Mol Imaging 49:81–96
2. Hesse B, Tagil K, Cuocolo A et al (2005) EANM/ESC procedural guidelines for myocardial perfusion imaging in nuclear cardiology. Eur J Nucl Med Mol Imaging 32(7):855–897
3. Brindis RG, Douglas PS, Hendel RC et al (2005) ACCF/ASNC appropriateness criteria for single-photon emission computed tomography myocardial perfusion imaging (SPECT MPI): a report of the American College of Cardiology Foundation Quality Strategic Directions Committee Appropriateness Criteria Working Group and the American Society of Nuclear Cardiology endorsed by the American Heart Association. J Am Coll Cardiol 6, 46(11):2148–2150

PET/CT

Combination of two scanners: PET (positron emission tomography) which study metabolism and function of the cells and CT (computed tomography) which shows detailed anatomy of the body.

▶Neoplasm, Oropharynx

Pettersson Score

An additive radiographic scoring system for the severity of hemophilic arthropathy. It has been adopted by the Orthopedic Advisory Committee of the World Federation of Hemophilia.

▶Bleeding Disorders, Osteoarticular

Peutz–Jeghers Syndrome

A rare autosomal dominant disorder, PJS is characterized by hamartomatous gastrointestinal polyposis, essentially in the upper small intestine, associated with mucocutaneous pigmentation (buccal and anal mucosa).

▶Neoplasms, Small Bowel

Peyronie's Disease

Räto T. Strebel[1], DrHubert John[2]
[1]Department of Urology, University Hospital Zurich, Zurich, Switzerland
[2]Klinik Hirslanden, Leiter Zentrum für Urologie, Zurich, Switzerland
raeto.strebel@usz.ch

Synonym

Induratio penis plastica (IPP)

Definition

Peyronie's disease (PD) is a localized disorder of the tunica albuginea of the penis with fibrous scar tissue replacing the normal elastic fibres. Characteristically, penile deformation of the penis is evident during erection. Marked penile deformity might interfere with the ability to have satisfying sexual intercourse (1).

Clinical Presentation

On the flaccid (and erect) penis the typical plaque tissue is palpable. Occasionally, signs of a systemic fibromatosis (e.g. Dupuytren's contracture) are observed. The penile deformity is only seen on the erect penis (Fig. 1).

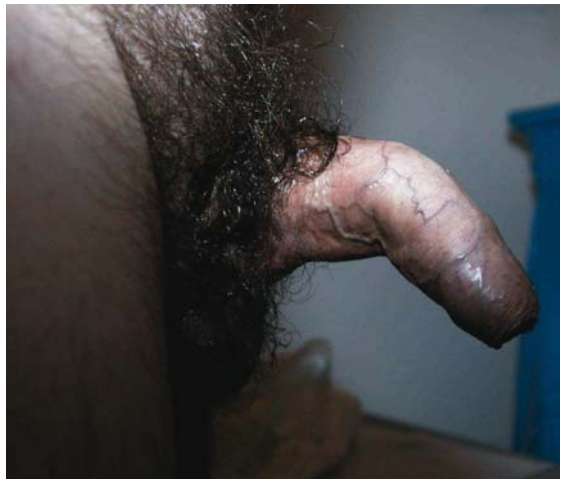

Phakomatoses. Figure 1 **Peyronie's disease with typical penile deformity on erect Penis.**

Imaging

Imaging studies are rarely necessary in patients with Peyronie's disease. An ultrasound examination (or eventually MRI) allows assessing the exact size of the scar tissue and calcified plaque will cast acoustic shadowing. Colour duplex ultrasound after stimulation of the corpora cavernosa might be necessary to rule out coexistent erectile dysfunction and to distinguish between arteriogenic insufficiency and veno-occlusive erectile dysfunction. Furthermore, a penile blood flow study can depict the relationship between the plaque and dorsal arteries and collaterals to the cavernous arteries. In order to assess the penile deformity photographs of the erect penis either taken by the patient himself or by the treating urologist after pharmacostimulation is mandatory before planning surgery (see Penile Fracture Fig. 1).

Bibliography

1. Strebel RT, Suter S, Sautter T et al (2004) Extracorporeal shockwave therapy for peyronie's disease does not correct penile deformity. Int J Impot Res 16(5):448–451

Phakomatoses

▶Neurocutaneous Syndromes

Pharmacodynamics

Study of the effects of drugs on the body and the mechanisms of drug action.
▶PET in Drug Discovery Imaging

Pharmacokinetics

Processes by which a drug is handled by the body and includes drug absorption, distribution, metabolism and elimination.
▶PET in Drug Discovery Imaging

Phase Modulation Imaging

Multi-pulse ultrasound imaging approach that employs a series of pulses with alternating polarity selectively to detect the non-linear echoes arising from microbubble contrast agents.
▶Specific Imaging Techniques, Contrast Media, Ultrasound

Phlegmon

Phlegmon is an acute purulent inflammation spreading within soft tissue structures without encapsulation. In the Anglo-American literature the term cellulitis is used instead of phlegmon.
▶Oral Cavity, Inflammatory Diseases

Phosphatidyl Serine

Lipid with a net charge of -1, actively flipped to the inner leaflet of the cell membrane.
▶Apoptosis

Phosphor Images

Digital images obtained from imaging plates.
▶Caries and Periodontal Diseases

Photon Density Wave Imaging

▶Optical Tomography

Photon Migration

▶Optical Tomography

Phrygian Cap

Transverse congenital septum causing a fold of the gallbladder wall, which usually involves the fundus. It has unlikely emerged as a potential cause of the segmental form of adenomyomatosis.
▶Cholecystoses

Phyllodes Tumor

▶Neoplasms, Phyllodes, Breast

Phyllodes Tumor, Benign

Phyllodes tumor showing increased stromal cellularity with mild to moderate atypia, low mitotic rates (<4/10), no stromal overgrowth, and well-circumscribed margins.
▶Neoplasms, Phyllodes, Breast

Phyllodes Tumor, Borderline

Phyllodes tumor showing stromal atypia, mitotic rates between 4/10 to 9/10, no stromal overgrowth, and can have microscopically infiltrative margins.
▶Neoplasms, Phyllodes, Breast

Phyllodes Tumor, Malignant

Phyllodes tumor showing severe stromal cellularity and atypia, high mitotic rates (10/10), infiltrative borders, and stromal overgrowth.
▶Neoplasms, Phyllodes, Breast

Physiologic Ovarian Cysts

Follicular and corpus luteum cysts occur as a normal process of ovulation. They are usually smaller than 10 cm and decrease in size or resolve spontaneously during a 2-month follow-up.
▶Cyst, Follicular, Ovarium

Pierre-Robin Sequence

Congenitally small mandible with associated findings, including an increased incidence of cleft palate.
▶Congenital Malformations, Bone

Pigmented Villonodular Synovitis

Equivalent histology to giant cell tumor of tendon sheath associated with tendons or ligaments. On MRI, commonly decrease in signal intensity occurs due to hemosiderin deposition within the mass. Two forms are described as focal or diffuse, the latter often associated with secondary joint degeneration.
▶Neoplasms, Soft Tissues, Benign

Pili Torti

Characteristic abnormal, fragile "kinky" hair shaft which diagnoses Menkes disease, congenital copper deficiency with easily fractured bones.
▶Battered Child Syndrome

Pilocytic Astrocytoma

Pilocytic astrocytoma is a glial tumor of low cellularity most often found in children. It is the most frequent brain tumor in children and the most frequent pediatric brain tumor in the posterior fossa.
▶Neoplasms, Brain, Posterior Fossa, Pediatric

Pink Puffers

Patients with emphysema who are usually thin and complain of severe dyspnea. At the same time, they are relatively well oxygenated without hypercapnia and do not suffer from right heart failure (cor pulmonale).
▶Emphysema and Bulla

Piriformis Syndrome

Unilateral buttock or posterior leg pain secondary to compression or irritation of the sciatic nerve by the piriformis muscle. Its etiology is incompletely understood, but primary causes include piriformis hypertrophy, myositis, anatomic variants, and posttraumatic adhesions. In many patients, a history of sitting with a large back-pocket wallet is often elicited. Imaging is often normal, but piriformis hypertrophy or mass in the sciatic notch may be seen. Definitive diagnosis is achieved with diagnostic block of piriformis muscle with local anesthetic and steroid.
▶Fractures, Pelvis

Pituitary Gland

Philippe Demaerel
Department of Radiology, University Hospitals, Leuven, Belgium
philippe.demaerel@uz.kuleuven.ac.be

Synonyms

Hypophysis; Sella turcica

Definition

Sellar pathology usually concerns pituitary lesions, often ►microadenoma or ►macroadenoma (1, 2). The diagnostic work-up of a patient with endocrine disease has changed with the advent of magnetic resonance imaging (MRI). Other tumors can arise in the sella turcica, and tumors in the surrounding structures may occasionally extend into the sella turcica (1).

Pathology/Histopathology

The two most common pituitary gland tumors are microadenoma and macroadenoma. Macroadenoma is by definition larger than 1 cm. There have been attempts to correlate hormonal activity with the tumor type, but nonhemorrhagic solid prolactin and growth hormone-secreting adenomas could not be distinguished on imaging.

The search for a microadenoma, by definition less than 1 cm and often smaller than 5 mm, remains a challenge. The diagnostic work-up of patients with ►Cushing's syndrome is even more difficult, and MRI can detect only up to 70% of the pituitary adrenocorticotropic hormone (ACTH)-producing tumors.

There is a long list of nonpituitary sellar tumors. The most common are ►craniopharyngioma and Rathke cleft cyst. Craniopharyngiomas arise from remnants of Rathke's pouch, which forms part of the intermediate part of the anterior lobe and pituitary stalk. The craniopharyngioma that is seen in teenagers is the adamantinous type, whereas in the elderly population the squamous-papillary type is more common. A Rathke cleft cyst is a pathological enlargement of the remnant of Rathke's pouch and is located between the two lobes of the pituitary gland.

There are several lesions that extend from outside the sellar region into the sella and cavernous sinus. Only meningioma will be mentioned here. This tumor arises from the meningoendothelial cells of the dura.

In lymphoproliferative disorders such as leukemia, involvement of the skull base can be associated with dural pathology extending into the sella turcica.

Clinical Presentation

Because of the complex anatomical relationships in the sellar and parasellar region, patients may present either with endocrinological abnormalities or with neurological symptoms such as headache and visual disturbances.

Patients with nonfunctioning macroadenomas may present with symptoms of hypopituitarism. In the acute stage, patients may present with pituitary apoplexy, and hemorrhage will be seen in the pituitary adenoma.

Hyperprolactinemia is a common sign of microadenoma. Cushing's syndrome is due to overproduction of adrenocorticotrophin.

Diagnosis

Imaging of the sellar region is usually best achieved by using multiple planes. Coronal images are often considered the most useful. MRI is certainly preferred, but computed tomography (CT) can occasionally contribute to the diagnosis by showing the presence or absence of calcification. A precise description of the tumor's location and extension and of the anatomical course of the arteries and nerves is required.

A macroadenoma will show a variable degree of enhancement and may contain areas of necrosis, hemorrhage, or cystic degeneration (Fig. 1). In pituitary apoplexy, hemorrhagic changes will be recognized as spontaneously hyperintense signal in the adenoma (Fig. 1). Macroadenomas measure at least 1 cm, but they can become huge tumors before they become symptomatic, particularly when they grow in the direction of the skull base (the so-called aggressive pituitary adenoma). A macroadenoma can invade the cavernous sinus and may cause encasement of the carotid arteries, or it can grow upward and compress the optic chiasm. Following surgery, the first scan is recommended at 4 months, provided there are no postoperative complications. Further scans can be obtained after 1 year and 5 years. Following medical treatment, MRI is also recommended to monitor the tumor size and signal changes.

The suspicion of microadenoma is probably best examined by MRI, although some radiologists may still recommend CT (1). CT is often requested to assess the bone thickness when transsphenoidal resection is planned.

Microadenomas are typically hypointense on coronal T1-weighted images and hyperintense on T2-weighted

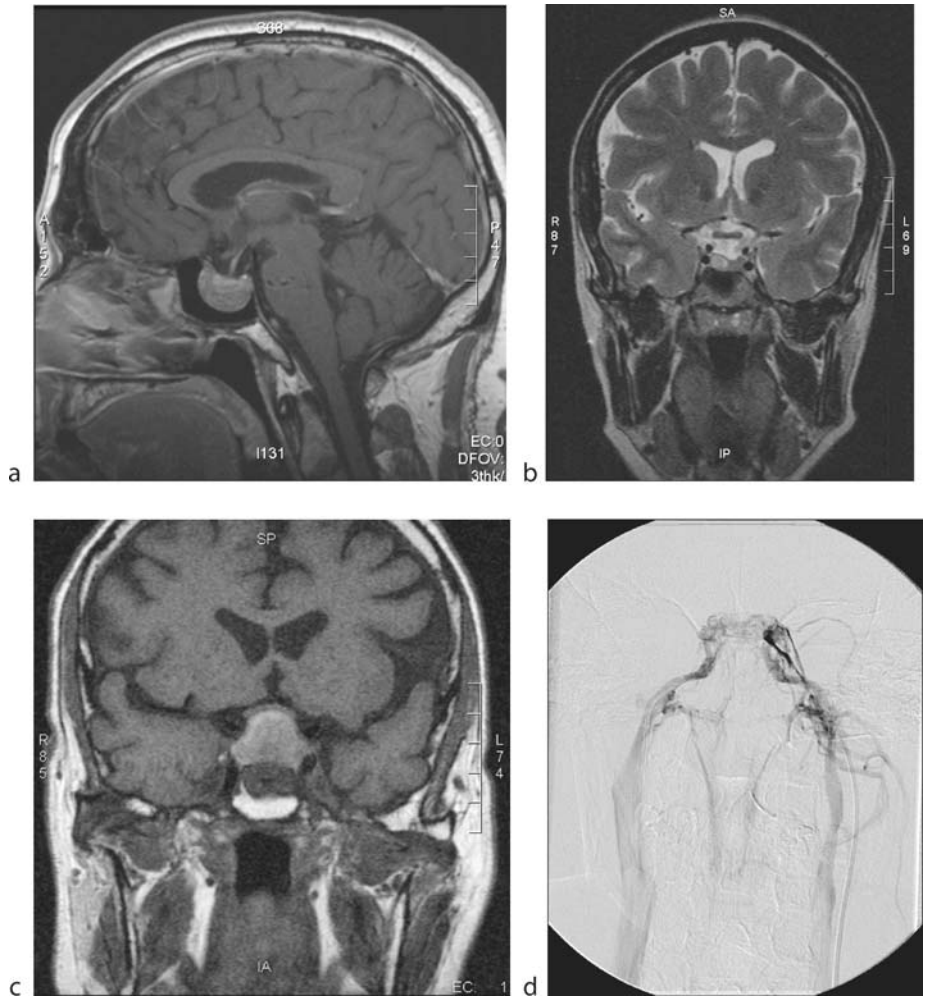

Pituitary Gland. Figure 1 Macroadenoma and microadenoma. (a) The sella turcica appears enlarged, and a macroadenoma is seen on the sagittal image. (b) Coronal image demonstrating a microadenoma on the right side. (c) Pituitary apoplexy can be recognized as a spontaneous high signal on a T1-weighted image, reflecting the presence of hemorrhage. (d) Patient with Cushing's syndrome and no microadenoma on magnetic resonance imaging. Positioning of the catheter in the right and left inferior petrosus sinuses prior to sampling is confirmed by injecting a contrast agent.

images compared with normal pituitary gland (Fig. 1). Following contrast administration, this will become even more evident. The sensitivity of pre- and postcontrast T1-weighted images is estimated to be approximately 80%. A few additional tools can help to increase the sensitivity: Dynamic T1-weighted images provide a set of contrast-enhanced images within 1 min thanks to the faster acquisition times. This may lead to the detection of a further 5% of lesions. Occasionally, T2-weighted images can detect a microadenoma. Finally, delayed contrast-enhanced T1-weighted images (20–25 min after the injection of gadolinium) will slightly improve the detection rate.

In Cushing's syndrome and when there is no evidence of a pituitary tumor, inferior petrosal sinus sampling is recommended in order to measure the ratio of central to peripheral ACTH levels (Fig. 1). Sampling is performed bilaterally and allows localization of the source of excessive production of ACTH.

Craniopharyngiomas are characterized by the presence of contrast enhancement, cyst formation, and calcification (Fig. 2). This tumor is located along Rathke's pouch, and this will cause the tumor to be oriented posteriorly in the suprasellar region. In the differential diagnosis, macroadenoma can be differentiated by its

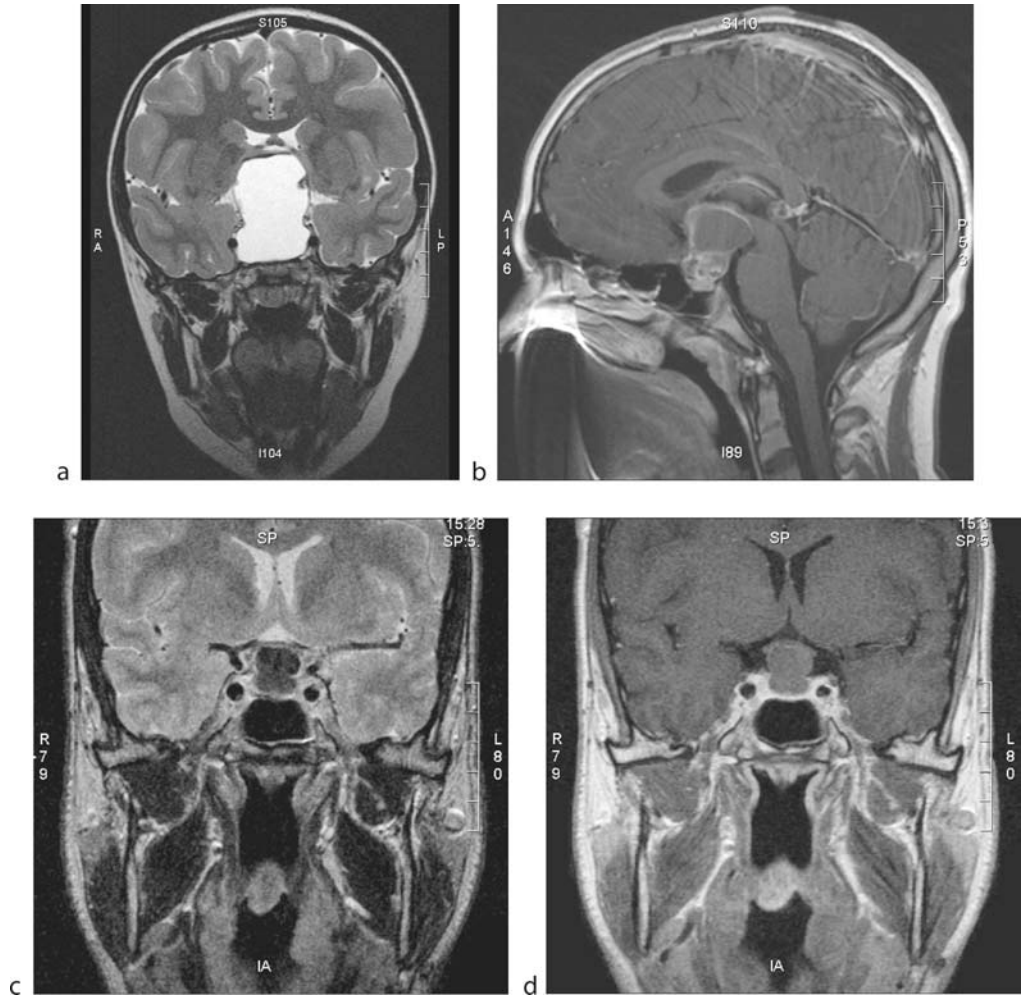

Pituitary Gland. Figure 2 Craniopharyngioma and Rathke's cleft cyst. (a) Intrasellar and suprasellar craniopharyngioma on a coronal image. Note that the signal is higher than the cerebrospinal fluid signal. (b) Sagittal image of a suprasellar craniopharyngioma. The pituitary gland is normal. (c) Coronal T2-weighted image of a Rathke's cleft cyst. The low T2 signal is a common feature of these lesions. (d) Coronal contrast-enhanced image of the same patient shows the absence of enhancement of the core of the lesion with a mild peripheral enhancement.

straight upward orientation and usually major involvement of the sella turcica. The cystic component of craniopharyngioma contains a variable amount of cholesterol, triglycerides, methemoglobin, and epithelial remnants. It is not possible to differentiate the two histological subtypes of craniopharyngioma.

Rathke's cleft cysts can be an incidental finding, but they may be symptomatic if they are large enough to cause local compression. The content of the cyst has typically been compared to motor oil. The MR appearance can vary from hypointense to hyperintense both on T1- and T2-weighted images (Fig. 2).

In meningiomas the relationship to the dura is the most useful differential diagnostic sign (Fig. 3). Metastases in the sphenoid sinus will be associated with bone destruction and local invasion of the surrounding structures. Occasionally, leukemia can manifest as skull base changes and dural involvement extending into the sellar region (Fig. 3).

Bibliography

1. Pisanechi G, Kapoor G (2005) Imaging of the sellar and parasellar disorders. Neuroimaging Clin N Am 15:203–209
2. Kucharczyk W, Bishop JE, Plewes DB et al (1994) Detection of pituitary microadenomas: comparison of dynamic keyhole fast spin-echo, unenhanced, and conventional contrast-enhanced MR imaging. Am J Roentgenol 163:671–679

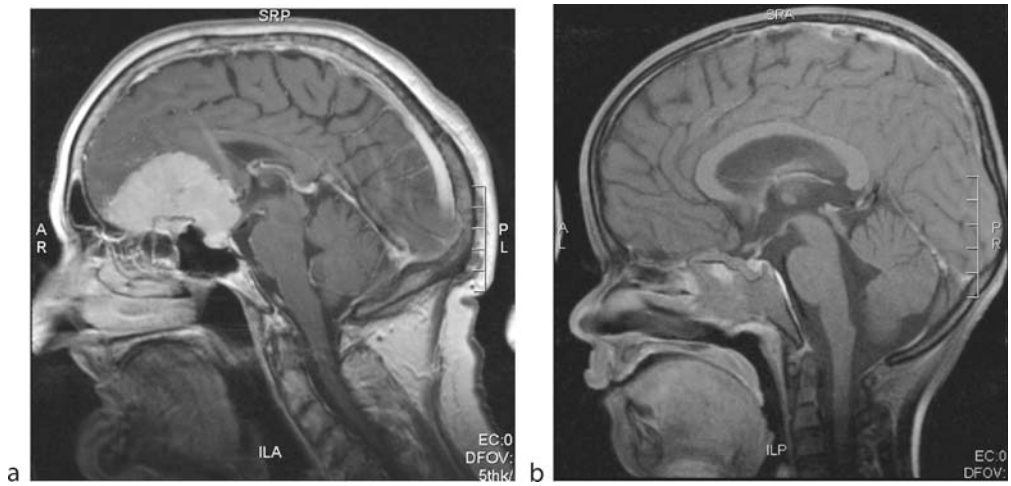

Pituitary Gland. Figure 3 **Meningioma and leukemic infiltration. (a) Meningioma of the planum sphenoidale with broad implantation on the dura. The tumor extends inside the sella turcica. (b) A child with sudden loss of vision due to leukemic infiltration of the skull base. There is a dural thickening.**

Placode

A segment of nonneurulated embryonic neural tissue, i.e., frozen at the neural plate stage. All OSDs are characterized by the presence of a placode that grossly corresponds to the segment of the spinal cord that is exposed externally. Several, but not all, forms of CSDs also have a placode, but in this case the integuments cover it. A placode may be categorized into terminal and segmental depending on location along the spinal cord. A terminal placode lies at the caudal end of the spinal cord and may in turn be either apical or parietal, depending on whether the defect involves the apex or a longer segment of the cord. Conversely, a segmental placode lies at an intermediate level along the spinal cord, which regains normal morphology and structure caudad to the abnormality.

▶Congenital Malformations, Spine and Spinal Cord

Plaque Imaging, MRI

Marc Sirol
Department of Cardiology, Lariboisière Hospital Paris, France
marc.sirol@gmail.commarc.sirol@mssm.edu

Definition

Atherosclerosis is a systemic inflammatory disorder that affects primarily large and medium-sized arteries. The disease involves multiple vascular beds simultaneously, such as the aorta, coronary, carotid, and superficial femoral arteries (1). Symptoms are most often related to significant luminal stenosis or occlusion. However, clinical events are frequently due to acute complications in plaques that cause only mild to moderate narrowing, particularly in the coronary tree. Reliance on changes in luminal caliber is therefore insufficient for adequate predictions of disease burden or probability of events.

Pathology/Histopathology

Atherosclerosis is characterized by the accumulation of various components in the intima of medium and large sized arteries. The main components of atherosclerotic plaque are: fibrous elements such as connective tissue extracellular matrix (collagen, proteoglycans, fibronectin, elastic fibers); lipids (crystalline cholesterol, cholesteryl esters, phospholipids); inflammatory cells (monocyte-derived macrophages, T-lymphocytes, smooth-muscle cells). The occurrence of these components in varying proportions in different plaques gives rise to a spectrum of lesions. Furthermore, the characteristics of "high-risk" or "vulnerable" plaque vary depending on the arterial region (i.e., coronaries, carotids, or aorta) in which it is located. In an attempt to categorize these complex lesions, the American Heart Association (2) created a detailed classification scheme that is designed to be used as a histological "template." An accurate tracking of lesion types *in vivo*, using noninvasive imaging techniques would be very useful clinically to determine the status of atherosclerosis.

Clinical Presentation

The clinical presentation is widely variable and depends on the affected vascular beds. Atherosclerosis is a chronic disease that affects medium and large arteries resulting in plaque formation that may grow to obstruct the lumen or may disseminate material into the blood stream and may cause myocardial infarction, stroke, and peripheral vascular disease.

Imaging

Imaging modalities applied to the evaluation of cardiovascular disease must be able to examine multiple vascular territories and to visualize not only luminal caliber, but also the arterial wall characteristics with high spatial and tissue contrast resolution. Magnetic resonance imaging (MRI) meets all of these requirements. Invasive X-ray angiography is generally considered the *gold standard* for the diagnosis of vascular stenoses, but provides minimal information on the status of the vessel wall and may be associated with significant complications. Computed tomography (CT) is an alternative noninvasive modality, particularly for the coronary arteries, although it is limited in the evaluation of plaque composition and involves the use of nephrotoxic contrast agents and ionizing radiation. Ultrasonography can provide quantitative measures of arterial wall thickness, particularly in superficial vessels, but shows limitations in the evaluation of deeper structures or in plaque characterization. In this context, cardiovascular MRI has become the modality offering the broadest capabilities for the assessment of systemic and regional atherosclerotic disease. Various MRI techniques and applications for the evaluation of arterial wall and atherosclerotic lesions are available now. Spin-echo (or black-blood) sequences are commonly employed because they render the moving blood invisible. Subsequent technical developments have enabled the simultaneous acquisition of multiple slices, resulting in significant shortening of imaging times.

The characteristics of the signal originated from a particular tissue depend in part on the amount of water and intrinsic magnetic properties. These can be characterized by two parameters: the T1 (longitudinal relaxation time) and T2 (transverse relaxation time). In so-called T1-weighted (T1W) images tissues with long T1 times will have low signal intensity. Conversely, in T2-weighted (T2W) images tissues with long T2 times will have high signal intensity in comparison with those with short T2. In proton density-weighted (PDW) images, the amount of signal depends on the concentration of water (or fat) molecules (Fig. 1). The use of "multicontrast" imaging (the combination of different weightings and sequences, usually 3–4) improves the ability to characterize atherosclerotic plaques with MRI. The most commonly employed approaches include T1W, T2W, and PDW spin-echo sequences. Frequently, bright-blood techniques such as 3D TOF are used to depict specific plaque characteristics. Additional sequences include diffusion weighting, magnetization transfer weighting or SSFP. The imaging characteristics of various plaque components in different sequences are summarized in Table 1.

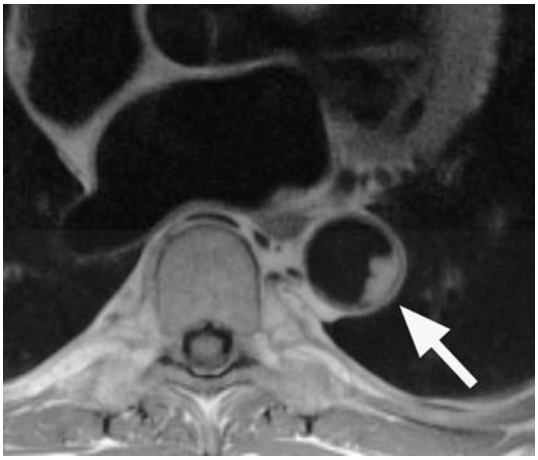

Plaque Imaging, MRI. Figure 1 Axial, PDW black-blood imaging of a complex atherosclerotic plaque in the descending thoracic aorta.

Plaque Imaging, MRI. Table 1 Main atherosclerotic plaque component signal intensities in MR images Contraste des images en IRM des principaux composants de la plaque d'athérome.

Signal Intensity				
Sequence	TI-W	PD-W	T2-W	TOF
Recent Thrombus	+ à +/–	à +/–	– à +/–	+
Lipid	+	+	–	+/–
Fibrosis	+/–	+	+/– à +	+/– à –
Calcium	–	–	–	–

+, Hypersignal; +/–, Isosignal; –, Hyposignal; TOF, Time of flight

Nuclear Medicine

The use of radiotracers has a potential utility for diagnostic and imaging atherosclerotic lesions *in vivo*. The main advantage of single photon emission computed tomography (SPECT) and positron emission tomography (PET) is that they both benefit from imaging agents that can be detected in extremely low concentration

(picomolar range). However, the main disadvantage of this technique is the poor spatial resolution and paucity of anatomical information regarding atherosclerotic lesions. In addition, the slow clearance of labeled particles from circulating blood contributes to a low target-to-background count ratio. To overcome this issue, images can be acquired by coregistration of scintigraphic images with CT or MRI. Therefore, PET–CT has emerged as a promising alternative technique for the detection of vulnerable atherosclerotic plaque by the association of the high CT spatial resolution and the PET high sensitivity for metabolic activities detection.

Diagnosis

Initial MRI validation studies were performed with *ex-vivo* specimens and compared with histopathology. Subsequently, the feasibility of *in-vivo* imaging and detection of plaque composition was demonstrated both in animal models and patients. Multicontrast imaging allows for detection of all main plaque components with high sensitivity and specificity: fibrous cap, fibrocellular tissue, lipid core, adventitia, calcium and thrombus/hemorrhage. Most human investigations have evaluated carotid arteries due to their superficial location and the ease to obtain histopathologic correlates with surgical endarterectomy samples. In evaluations of carotid artery atherosclerosis *in-vivo*, black-blood MRI provides accurate measurements of luminal caliber, wall thickness, and plaque areas. Using TOF it is possible to visualize the fibrous cap as a hypointense band in the wall inner boundary. This approach enables to differentiate thin versus thick fibrous caps, and to identify the presence of cap disruption. MRI depicts also the presence and extent of intra-arterial thrombosis or intra-plaque hemorrhage and might differentiate occlusive versus subocclusive clot.

Additionally to the proven MRI diagnosis accuracy, there is an excellent agreement with histopathology for the delineation of lesion size, extent, and morphology. The inter- and intraobserver agreements for both luminal and plaque dimensions are very high. Importantly, so is the interscan reproducibility, making it possible to detect small changes in indexes of plaque burden when serial scans are performed. The positive vascular remodeling associated with early stages of atherosclerosis progression is readily identified with MRI. Moreover, progression and regression of atherosclerotic plaques, as well as sequential changes in composition, can be measured with MRI. After prolonged Statins therapy significant reductions in both carotid and aortic plaque size has been demonstrated. Other therapies for atherosclerotic disease

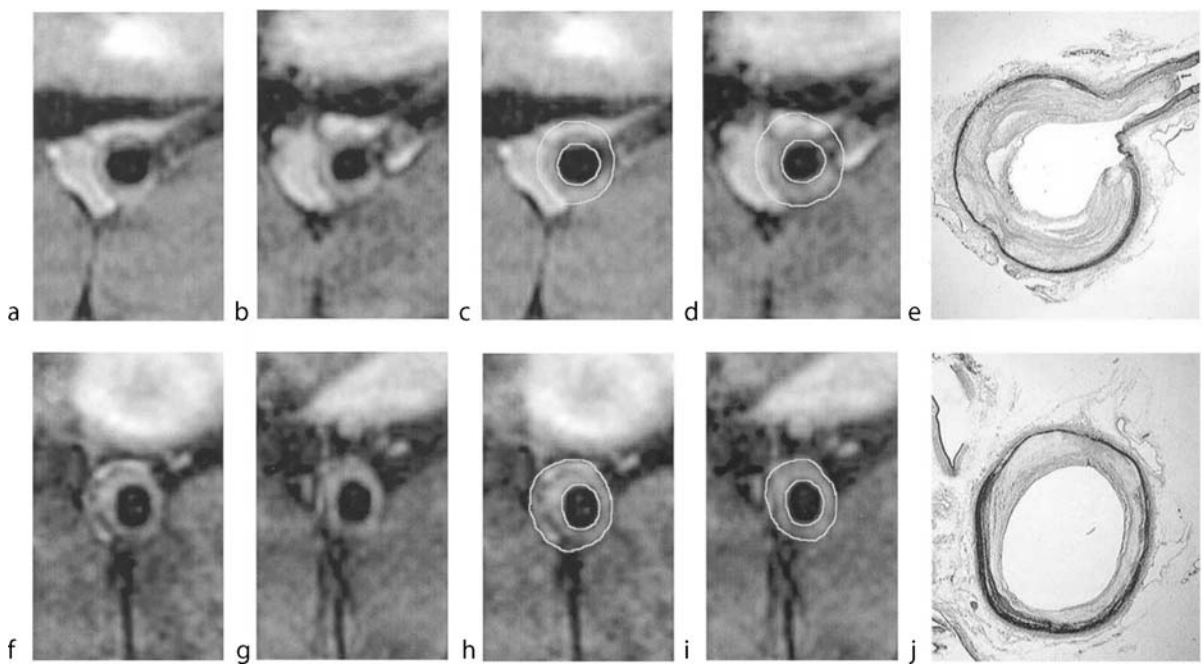

Plaque Imaging, MRI. Figure 2 Serial MRI studies of rabbit abdominal aortic plaques. The upper panels show the progression in the high-cholesterol diet group: baseline images (a, c) and at the end of treatment (b, d). The lower panels demonstrate the regression of the disease in the normal chow diet plus simvastatin plus PPARγ group: baseline images (f, h) and at the end of treatment (g, i). The right panels (e, j) show the matched histologic section at the end of treatment. (From Corti et al, 2004)

tested *in-vivo* with MRI (either in animal models or in humans) include peroxisomal proliferator-activated receptor-gamma agonists (PPAR) (3), thromboxane inhibitors or percutaneous interventions in the femoropopliteal territory (Fig. 2).

Because of the limited signal-to-noise ratio (SNR) available, in particular in small vessels and superficial structures, contrast agents such as gadolinium chelates have been used to increase MR signal. Gadolinium-based extracellular contrast agents can improve contrast amongst plaque components and better delineate the fibrous cap in human carotid and aortic lesions. However, the use of conventional contrast agents for plaque characterization is limited to a certain extent by their nonspecificity, as they tend to distribute indistinctly in multiple tissues and organs. The emerging field of molecular imaging is devoted to the visualization of pathophysiological processes at the cellular and molecular level. Highly specific contrast agents can be constructed by linking the contrast to a compound with high affinity for a particular cell, molecule, or metabolic pathway (i.e., an antibody or an enzymatic substrate). Occasionally, the resulting contrast agent can be "activated" by the enzyme, and therefore will only be detected if the metabolic process of interest is ongoing. MRI is particularly attractive for molecular applications due to good spatial resolution, high contrast agent affinity, and safety profile.

In the specific context of atherosclerosis there are multiple attractive targets with the potential to highlight specific features of disease activity or plaque vulnerability. Gadolinium has been attached to peptides with high affinity for fibrin (Fig. 3) , allowing for the visualization of experimental acute, subacute and chronic arterial thrombosis (4, 5). Additional potential targets for MRI contrast agents include both low-density and high-density lipoprotein cholesterol, platelets, activated factor XIII, endothelial adhesion molecules, tissue factor, proteins involved in apoptosis, or stem cells. This modality provides with one of the most promising diagnosis technique for plaque characterization toward detection of plaque with high risk of rupture.

Novel image analysis methods that combine automatic wall contour detection and multicontrast weighting

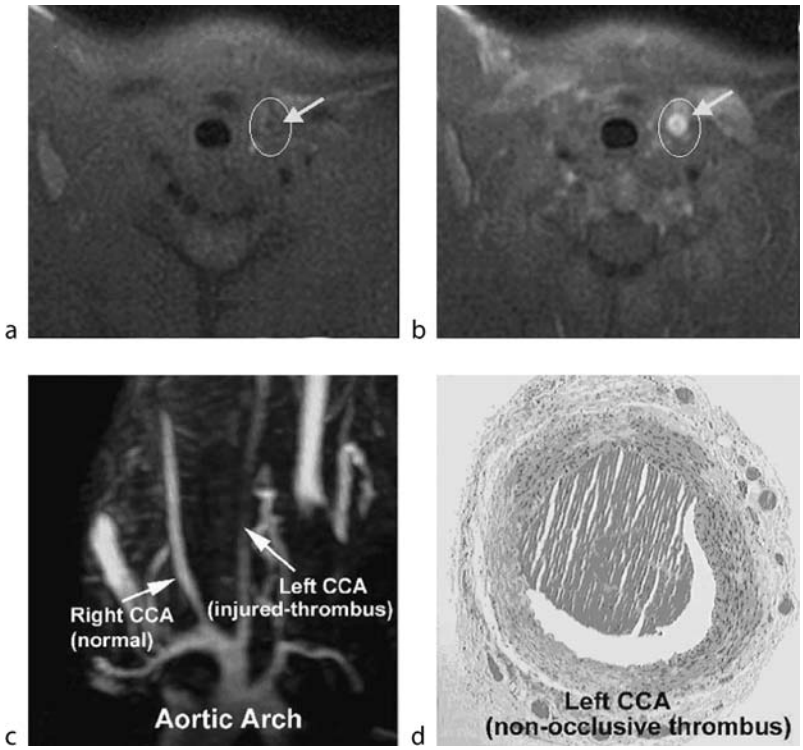

Plaque Imaging, MRI. Figure 3 ***In-vivo*** **MR thrombus imaging of the carotid artery in a guinea pig. Transverse MR images obtained before (a) and after (b) injection of a fibrin-specific contrast agent. Thrombus (*light arrow*) in the injured left common carotid artery (CCA) demonstrates marked contrast enhancement after injection. The contralateral uninjured CCA does not show any enhancement. The MRA (c) shows normal patency in the uninjured right CCA, and decreased flow in the thrombosed left CCA. The corresponding histopathological section of the left CCA is shown in D (Hematoxylin-and-Eosin staining). (Adapted from Sirol et al, 2005)**

analysis are being developed and promise to simplify the application of MRI for the assessment of atherosclerosis both in the research and clinical arena.

Conclusions

At the present time, MRI has emerged as the imaging modality with better suitability for the comprehensive evaluation of atherothrombotic disease. MRI accurately depicts arterial wall abnormalities and atherosclerotic plaque extent and composition. Obtained in a noninvasive fashion, with a high safety profile, and with excellent spatial and tissue contrast resolution, MRI is believed to even improve further both plaque detection and characterization, when molecular techniques become clinically available. Molecular MRI, with its ability to depict highly specific physiopathologic processes, shows potential for further improving our understanding of atherothrombosis. Such an approach will provide estimations of the burden of disease, and potentially, depiction of plaque with high risk of rupture, improving patient risk stratification.

Bibliography

1. Fuster V, Fayad ZA, Badimon JJ (1999) Acute coronary syndromes: biology. Lancet 353 Suppl 2: SII5–SII9
2. Stary HC, Chandler AB, Dinsmore RE et al (1995) A definition of advanced types of atherosclerotic lesions and a histological classification of atherosclerosis. A report from the Committee on Vascular Lesions of the Council on Arteriosclerosis, American Heart Association. Circulation 92:1355–1374
3. Corti R, Osende JI, Fallon JT et al (2004) The selective peroxisomal proliferator-activated receptor-gamma agonist has an additive effect on plaque regression in combination with simvastatin in experimental atherosclerosis: *in vivo* study by high-resolution magnetic resonance imaging. J Am Coll Cardiol 43:464–473
4. Sirol M, Aguinaldo JGS, Graham PB et al (2005) Fibrin-targeted contrast agent for improvement of *in vivo* acute thrombus detection with magnetic resonance imaging. Atherosclerosis 182:79–85
5. Sirol M, Fuster V, Badimon JJ et al (2005) Chronic thrombus detection using *in-vivo* magnetic resonance imaging and fibrin-targeted contrast agent. Circulation 112:1594–1600

Plasma Cell Granuloma

Most common mass lesion of the lung with unclear origin.

▶Neoplasms, Chest, Childhood

Plasma Cell Mastitis

▶Duct Disease, Breast

Plastic Bowing

A traumatic deformity of a long bone shaft caused by bending beyond a (theoretical) coefficient of elasticity so that the bone neither fractures nor returns to baseline configuration.

▶Fractures, Bone, Childhood

Pleura, Localized Fibrous Tumor

Nagmi R. Qureshi[1], Fergus V. Gleeson[2]
[1]Fellow in Thoracic Radiology
[2]Consultant Radiologist, Department of Radiology, Churchill Hospital, Headington, Oxford OX37LJ, UK
nagmiqureshi@doctors.org.uk
fergus.gleeson@radiology.oxford.ac.uk

Synonyms

Fibrous mesothelioma; Mesothelial fibroma; Pleural fibromas

Definition

These tumors are rare, primarily arise from the visceral pleura, and account for less than 5% of all pleural tumors. Synonyms used to describe these tumors include pleural fibromas, fibrous mesothelioma and mesothelial fibroma. These inconsistencies in nomenclature arise due to the unpredictable histological and biological behavior of these tumors.

Pathology

The macroscopic appearance is either of a smooth or lobulated pedunculated uni- or multifocal pleural mass with a translucent serosa. In larger masses, areas of hemorrhage and degeneration may be evident. Histologically a number of patterns have been described, the commonest being a patternless and hemangiopericytoma pattern.

Clinical presentation

Clinical symptoms have been shown to be related to tumor size. Tumors measuring less than 10 cm are usually

asymptomatic. Whereas those greater than 16 cm can cause nonspecific respiratory symptoms such as cough, hemoptysis, chest heaviness and occasionary rarer systemic paraneoplastic symptoms including hypoglycemia, hypertrophic pulmonary osteoarthropathy and clubbing (1).

Patients can present at any age, although most present during the 6–7th decade. A slight female predominance has been noted.

Imaging

On chest radiography small tumors are smooth lobulated masses within the lower thorax, although they may conform to the shape of adjacent structures thereby mimicking diaphragmatic eventration and mediastinal masses. A vascular pedicle is rarely visualized, however its presence is inferred by the tumors, change in position on sequential radiographs.

The pleural origin of these tumors is suggested by their well-defined inferior border but ill-defined superior border, the so-called "incomplete border sign."

The tumors are typically homogeneous with an intermediate attenuation similar to that of muscle on CT, and uniformly enhance following intravenous contrast. Small tumors are well defined with tapering edges forming an obtuse angle to the pleural surface. Larger tumors are typically heterogeneous, displace adjacent structures and form an acute pleural angle. Calcification is rare, occurring in 10% of cases and often punctate when present. Pleural effusions have been reported in 20% of cases (Fig. 1).

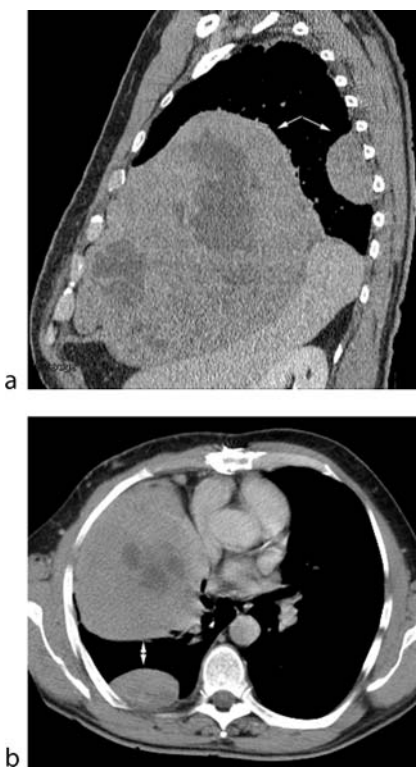

Pleura, Localized Fibrous Tumor. Figure 1a Typical appearance of localized fibrous tumors of the pleura on CT (arrows).

There are no categorical radiological features to differentiate a benign from a malignant pleural fibroma. The presence of mass effect, compressive atelectasis, heterogenicity and a pleural effusion should raise the possibility of malignancy.

Pleural fibromas return a low/intermediate signal on T1W, T2W, and PD MR sequences. As with CT, post contrast these tumors avidly enhance. In larger tumors areas of high signal on T2W images correspond to areas of necrosis and myxoid degeneration. The serosal covering may be visualized as a rim of low signal (2).

Diagnosis

The CT and MR appearances are invariably characteristic. Definitive treatment involves en bloc surgical resection which is curative in most cases. Pre-operative biopsy is therefore rarely indicated especially as percutaneous biopsy may not necessarily exclude underlying malignant transformation.

Bibliography

1. Rosado-de-Christenson ML, Abbott GF, McAdams HP et al (2003) Localised fibrous tumors of the pleura. Archives of the AFIP. Radiographics 23:759–783
2. Tateishi U, Nishihara H, Morikawa T et al (2002) Solitary fibrous tumors of the pleura: MR appearance and enhancement pattern. J Comput Assist Tomogr 26:174–179

P

Pleural Carcinomatosis

Nagmi R. Qureshi[1], Fergus V. Gleeson[2]
[1]Fellow in Thoracic Radiology
[2]Consultant Radiologist, Department of Radiology, Churchill Hospital, Headington, Oxford OX3 7LJ, UK
nagmiqureshi@doctors.org.uk
fergus.gleeson@radiology.oxford.ac.uk

Definition

Numerous primary malignancies are known to metastasize to the pleura. Bronchogenic carcinoma is the commonest accounting for 40% of cases. Breast carcinoma

metastases account for 10%, ovarian and gastric carcinoma 5% and lymphoma 10% of cases. Pleural lymphomatous deposits usually represent disease recurrence or occur with synchronous mediastinal and parenchymal disease. Invasive thymoma may also spread contiguously along the pleura.

Clinical Features

Clinical symptoms and signs conform to the origin of the primary malignancy. Thoracic symptoms include cough, increasing shortness of breath and chest pain.

Imaging

The radiographic, ultrasound, CT and MR appearance of pleural carcinomatosis especially if unilateral are indistinguishable from mesothelioma.

Numerous studies have shown that on CT, malignant pleural disease is suggested by the presence of parietal pleural thickening greater than 1 cm, circumferential parietal thickening, nodular pleural thickening and mediastinal pleural thickening with specificities of 94–100% (1).

Bibliography

1. Leung AN, Muller NL, Miller RR (1990) CT in differential diagnosis of diffuse pleural disease. Am J Roentgenol 154:487–492

Pleural Effusion

Nagmi R. Qureshi[1], Fergus V. Gleeson[2]
[1]Fellow in Thoracic Radiology
[2]Consultant Radiologist, Department of Radiology, Churchill Hospital, Headington, Oxford OX3 7LJ, UK
fergus.gleeson@radiology.oxford.ac.uk

Definition

A pleural effusion is defined as excess fluid within the pleural space. The normal pleural space usually contains 5–10 mL of fluid.

Clinical features

Most patients present with increasing breathlessness. Associated symptoms of productive cough and fever, chest pain and weight loss are suggestive of an inflammatory effusion or probable malignant effusion respectively.

Imaging

On an erect chest radiograph 50 mL of fluid results in blunting of the costophrenic angle, whereas 200 mL is necessary to blunt the lateral costophrenic angles. The lateral decubitus view is the most sensitive view and allows 5–10 mL to be demonstrated.

As fluid fills the recess, it extends laterally along the chest wall to form a characteristic meniscus (Fig. 1). Larger effusions cause increased opacification of the hemithorax with mediastinal shift. Absence of shift suggests underlying collapse or mediastinal fixation

On a supine film, fluid tends to accumulate posteriorly and at the lung apex, with an apical cap on occasion the only manifestation of a supine effusion. Other features include hazy opacification of the hemithorax, blunting of the costophrenic recess, elevation of the hemidiaphragm and reduced lower zone vascularity.

Ultrasound is superior to CXR at demonstrating small amounts of pleural fluid and guiding thoracentesis. Pleural transudates are nearly always anechoic. Whereas exudates may appear simple and anechoic, complex effusions appear multiseptated or homogeneously echogenic. The latter appearance is usually suggestive of an ▶empyema or haemorrhagic effusion and may mimic a solid echogenic mass. The presence of diaphragmatic nodularity and nodular pleural thickening is indicative of a malignant effusion.

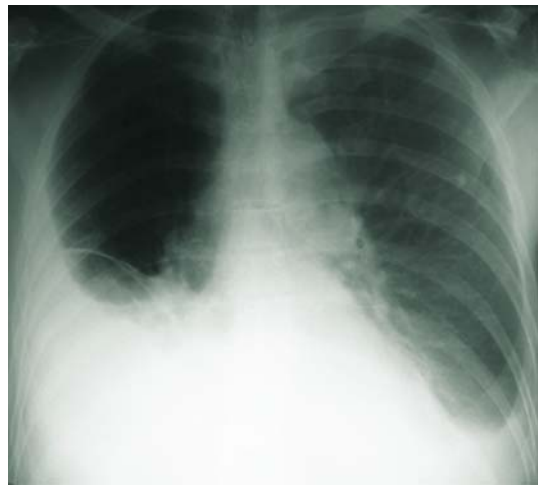

Pleural Effusion. Figure 1 Semi-supine chest radiograph showing a haze like opacification of the left hemithorax in keeping with posterior layering of fluid and the characteristic meniscus sign of pleural effusion on the right.

CT should be performed for all pleural exudates of unknown aetiology. Most exudates are due to malignancy, inflammation/infection or thromboembolic disease. CT following intravenous contrast allows differentiation of pleural thickening from fluid, characterisation of thickening as malignant or benign and can distinguish a pleural transudate from an exudate, with ▶pleural enhancement indicative of an exudate.[1]

In complicated parapneumonic effusions and empyemas where conventional management has failed, CT may demonstrate the development of an infected pleural collection, underlying visceral pleural thickening or drain misplacement accounting for failure of drainage. Classical findings of an empyema include the '▶split pleura sign' which refers to enhancing thickened visceral and parietal pleura separated by pleural fluid, increased thickening and attenuation of the extrapleural fat and loculation.

MR is rarely necessary in the diagnosis of pleural effusions due to the availability and accuracy of ultrasound and CT. Pleural effusions are typically low signal on T1W and high signal on T2W sequences. More recently triple echo and single shot diffusion weighted sequences have been shown to differentiate between pleural transudates and exudates. Transudates are invariably low signal in contrast to the high signal of a pleural exudate, with the degree of signal intensity being proportional to the complexity of the exudate.[2] Similarly MR may allow for visualisation of pleural nodules which are poorly defined on CT. In this situation axial and sagittal T2W sequences should be performed with the low signal pleural nodules being clearly delineated against the high signal of the pleural effusion.

Bibliography

1. Aquino SL, Webb WR, Gushiken BJ (1994) Pleural exudates and transudates: diagnosis with contrast-enhanced CT. Radiology 192:803–808
2. Davis SD, Henschke CI, Yankelevitz DF et al (1990) MR imaging of pleural effusions. J Comput Assist Tomogr 14:192–198

Pleural Effusions

▶Chest, Neonatal

[1] On CT, pleural enhancement following intravenous contrast is indicative of an exudative effusion, absence suggests a transudative effusion.

Pleural Enhancement

On CT, pleural enhancement following intravenous contrast is indicative of an exudative effusion, absence suggests a transudative effusion.
▶Pleural Effusion

Pleural Fibromas

▶Pleura, Localized Fibrous Tumor

Pleural Mesothelioma, Malignant

Nagmi R. Qureshi[1], Fergus V. Gleeson[2]
[1]Fellow in Thoracic Radiology
[2]Consultant Radiologist, Department of Radiology, Churchill Hospital, Headington, Oxford OX3 7LJ, UK
nagmiqureshi@doctors.org.uk
fergus.gleeson@radiology.oxford.ac.uk

Definition

Mesothelioma is a primary malignant tumor that arises from the mesothelial cells which typically line the pleura, peritoneum, and pericardium.

Pathology

Macroscopically mesothelioma appears as multiple nodules which stud the visceral and parietal pleura, these subsequently coalesce to form a white sheet like rind that encases the lung. Transdiaphragmatic infiltration is typical in advanced disease.

Microscopically there are three histological subtypes:

1 Epithelial: It is the commonest subtype and accounts for 60% of cases and is associated with the best prognosis with a median survival of 12.5 months. Microscopically differentiation from metastatic adenocarcinoma can be difficult and usually requires special staining.

2 Sarcomatoid: It occurs in 15% of the cases and needs to be distinguished from renal, pancreatic, and synovial sarcomatoid metastatic carcinomas.
3 Mixed: It occurs in 25% of the cases.

Clinical Features

Most patients present with increasing shortness of breath and chest pain. Other symptoms include anorexia, weight loss, and cough. A history of prior asbestos exposure can be elicited in approximately 50% of the cases following a latency period of 35–40 years. In female patients, there may be a history of indirect contact with clothing exposed to asbestos.

Imaging

Characteristic radiographic features include unilateral lobulated pleural thickening which gradually extends, encases and fixes the pleural cavity causing volume loss (Fig. 1). The right hemithorax is more frequently involved possibly due to the larger right pleural surface area. A pleural effusion is seen in most cases, though may be absent in up to 20% of patients. Fissural extension occurs in 40–90% of cases (1).

On ultrasound, mesothelioma can appear as either an echogenic or hypoechoic lobulated area of visceral and parietal thickening with associated diaphragmatic thickening and nodularity. Pleural thickening measuring less than 1 cm can be difficult to visualize and is much more operator and patient body habitus dependent.

Contrast-enhanced CT including multiplanar reformatting is the imaging modality of choice. This allows for detailed assessment of the pleural thickening and readily demonstrates chest wall and diaphragmatic invasion. Findings suggestive of chest wall invasion include loss of the extrapleural fat planes, bone destruction, and intercostal muscle invasion. Nodular pleural thickening is the commonest manifestation on CT, usually involving the lower zones, although in 15% of cases only upper zone involvement is seen. Other findings are diaphragmatic thickening, fissural involvement and pleural effusion. Pleural calcification is visualized in 20% of the cases (Fig. 1).

MRI is only performed when radical surgery is being considered and multislice CT has proved inconclusive at differentiating T3 (potentially resectable) disease from irresectable T4 disease. To minimize motion artifact all MR sequences should be cardiac gated. Typical sequences include T1W, T2W, and T1W fat saturated postgadolinium. The latter sequence is particularly sensitive at demonstrating focal thickening and enhancement of the intercostal fissures which may be the only manifestation of disease (2). On T1W images mesothelioma returns an intermediate signal compared to the adjacent muscle and a high signal on T2W and T1 postgadolinium sequences. Apical mesothelioma is the most readily visualized due to reduced motion artifact at the apices.

PET can accurately demonstrate the primary tumor and distal metastasis with a sensitivity of 90%. Although it is poorer at delineating nodal spread and distinguishing mediastinal tumor extension from contiguous nodal involvement (3). PET may prove helpful where previous pleural biopsy has been negative by demonstrating focal areas of uptake and more suitable sites for biopsy.

In patients being considered for surgery, a *V*/*Q* scan should also be performed to assess the function of the contralateral lung.

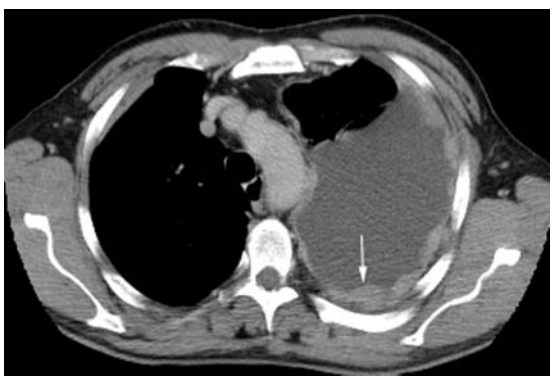

Pleural Mesothelioma, Malignant. Figure 1 CT demonstrating left sided circumferential nodular pleural thickening (*arrow*). Note the presence of a contralateral pleural plaque. Percutaneous biopsy confirmed mesothelioma.

Diagnosis

Definitive diagnosis requires cytological or histological confirmation. Thoracentesis is frequently nondiagnostic with a sensitivity of 30%, whereas image guided biopsy has a sensitivity of greater than 90%, this is comparable to thoracoscopy.

Bibliography

1. Kawashima A, Libshitz HI (1990) Malignant pleural mesothelioma: CT manifestations in 50 cases. Am J Roentgenol 155:965–969
2. Knuuttila A, Kivisaari L, Kivisaari A et al (2001) Evaluation of pleural disease using MR and CT. With special reference to malignant pleural mesothelioma. Acta Radiol 42:502–507
3. Benard F, Sterman D, Smith RJ et al (1998) Metabolic imaging of malignant pleural mesothelioma with fluorodeoxyglucose positron emission tomography. Chest 114:713–722

Pleural Plaques

Nagmi R. Qureshi[1], Fergus V. Gleeson[2]
[1]Fellow in Thoracic Radiology
[2]Consultant Radiologist, Department of Radiology, Churchill Hospital, Headington, Oxford OX3 7LJ, UK
nagmiqureshi@doctors.org.uk
fergus.gleeson@radiology.oxford.ac.uk

Pathology

Microscopically plaques comprise foci of dense hyaline collagen within the mesothelial layers primarily involving the parietal pleura.

Clinical Features

Pleural plaques do not cause symptoms.

Imaging

Pleural plaques are the commonest manifestations of prior asbestos exposure and are readily diagnosed on a frontal chest radiograph. Plaques are bilateral in 75% of cases and involve the posterolateral aspect of the 6–10th ribs (1). Calcification is seen in 15–25% of patients following a latency period of 30–40 years. The presence of diaphragmatic calcification with relative sparing of the apices and costophrenic angles is considered pathognomonic of previous asbestos exposure.

CXR sensitivities for demonstrating plaques range from 30–80% with a false positive rate of 20%. This can usually be attributable to overlying composite shadows.

When viewed en-face plaques appear as irregular, stippled calcified opacities with a 'holly leaf' appearance. When viewed obliquely plaques are smooth usually measuring less than 1 cm in thickness.

HRCT and low-dose multi-slice CT is more sensitive than the CXR at detecting pleural plaques and assessing the underlying lung parenchyma for possible asbestosis (2). The absence of superimposed structures allows even small non-calcified plaques to be visualised. These characteristically are seen as well-circumscribed areas of pleural thickening separated from the underlying rib by a layer of fat (Fig. 1). On MRI, plaques are low signal on T1W, T2W and proton density sequences, and foci of calcification appear as signal voids.

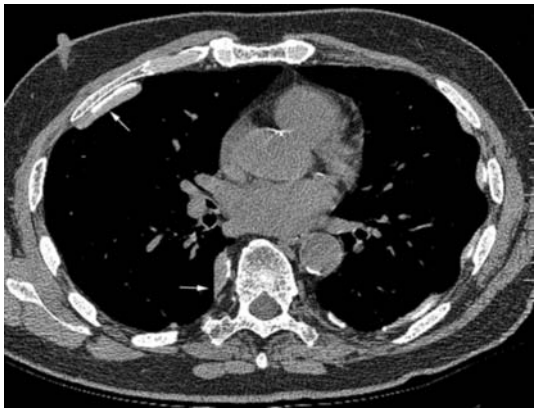

Pleural Plaques. Figure 1 HRCT showing bilateral pleural plaques some of which are calcified (*arrows*).

Bibliography

1. Muller NL (1993) Imaging of the pleura. Radiology 186:297–309
2. Staples CA, Gamsu G, Ray CS et al (1989) High resolution computed tomography and lung function in asbestos-exposed workers with normal chest radiographs. Am Rev Respir Dis 139:1502–1508

Pleural Thickening, Benign Diffuse

Nagmi R. Qureshi[1], Fergus V. Gleeson[2]
[1]Fellow in Thoracic Radiology
[2]Consultant Radiologist, Department of Radiology, Churchill Hospital, Headington, Oxford OX3 7LJ, UK
nagmiqureshi@doctors.org.uk
fergus.gleeson@radiology.oxford.ac.uk

Synonyms

Fibrothorax

Definition

Diffuse pleural thickening typically represents the late sequelae of a previous benign pleural effusion. This may be secondary to trauma, tuberculous empyema, drugs and asbestos related pleural disease.

Diffuse pleural thickening can be defined either by its chest radiograph or CT appearance. Radiographically diffuse pleural thickening is characterized by a smooth uninterrupted pleural density, which extends over at least a quarter of the chest wall with obliteration of the

costophrenic angle (1). On CT, the presence of a continuous sheet of thickening at least 5 cm in lateral extent, 8–10 cm in cranio-caudal extent and 3 mm in thickness is generally accepted as diffuse pleural thickening (2).

Pathology

Pathologically, diffuse pleural thickening predominantly involves the visceral pleura and is usually preceded by a pleural effusion with subsequent visceral pleural fibrosis and adherence to the parietal pleura.

Clinical Features

Irrespective of the cause, unilateral thickening is commonly asymptomatic. Bilateral involvement is frequently associated with increasing shortness of breath and a restrictive pattern on pulmonary function tests.

Imaging

Chest radiography is the initial imaging modality for demonstrating pleural thickening. Occasionally, the presence of bilateral involvement may be confused with overlying composite shadows from prominent extrapleural fat. As a rule, asymmetrical bilateral thickening is suggestive of diffuse pleural thickening rather than composite shadowing.

The radiological features often reflect the underlying aetiology. In addition to the previously described features: unilateral volume loss, amorphous pleural calcification, with rib crowding and enlargement, with thickening of the extrapleural fat is suggestive of a tuberculous empyema. Associated parenchymal apical fibrosis and calcified granuloma may also be demonstrated.

Pleural thickening secondary to trauma is commonly associated with multiple rib fractures and otherwise normal underlying lung parenchyma.

Following talc pleurodesis characteristic findings include high-attenuation talc which mimics calcification sandwiched between soft tissue parietal and visceral pleural thickening—the so-called 'talc sandwich'.

Ultrasound may also be helpful in demonstrating diffuse pleural thickening. This typically appears as a smooth hypo- or hyperechoic line. In the absence of a pleural effusion or presence of calcification delineation can be difficult. Similarly, differentiating thickening from effusion may also prove problematic. In this situation an effusion shows color flow, the so called 'fluid color sign', whereas thickening does not.

MRI offers little additional information over CT with minor advantages for demonstration of pleural thickening, extrapleural fat and pleural effusion. CT was better at demonstrating calcification (3). Furthermore, pleural signal hypointensity relative to the intercostal muscle on long TR MR sequences have been found to be particularly sensitive at confirming benign disease.

Diagnosis

CT appearances are usually diagnostic. If clinical doubt still exists image-guided percutaneous biopsy can be performed.

Bibliography

1. McLoud TC (1998) CT and MR in pleural disease. Clin Chest Med 19:261–276
2. Lynch DA, Gamsu G, Ray CS et al (1988) Asbestos-related focal lung masses: manifestations on conventional and high-resolution CT scans. Radiology 169:603–607
3. Weber MA, Bock M, Plathow C et al (2004) Asbestos-related pleural disease: value of dedicated magnetic resonance imaging techniques. Invest Radiol 39:554–564

PML

▶Progressive Multifocal Leukoencephalopathy

Pneumatocele

A thin-walled gas-filled space within the lung, usually occurring post-infection or posttraumatic and almost invariably transient.

▶Pneumonia in Childhood
▶Pulmonary Opacity, Cystic Pattern

Pneumatosis Intestinalis

This is due to the formation of gas in the intestinal wall as a result of intestinal ischaemia and hypoperfusion together with bacterial overgrowth.

▶Necrotizing Enterocolitis

Pneumoconioses

K. G. Hering
Beratender Arzt für Diagnostische Radiologie,
bei arbeits – und umweltbedingten Erkrankungen,
Knappschaftskrankenhaus, Wieckesweg 27,
44309 Dortmund
k.g.hering@t-online.de
k.g.hering@kk-dortmund.de

Synonyms

Occupational lung diseases; Work-related lung disorders

Definition

The term pneumoconiosis—from the Greek *pneuma* (air, wind) and *konis* (dust)—was introduced by Zenker in 1867 to define changes in the lungs caused by the retention of and reaction to inhaled inorganic as well as organic dusts.

Another definition of pneumoconioses was adopted at the Fourth International Conference in Bucharest in 1971: "Pneumoconiosis is the accumulation of dust in the lungs and the tissue reactions to its presence. For the purpose of this definition, "dust" is meant to be an aerosol composed of solid inanimate particles."

"Inorganic" refers to any substances that do not contain carbon (sometimes named "mineral dust"), excluding certain simple carbon oxides such as carbon monoxide and carbon dioxide (Table 1). "Organic" refers to any substances that do contain carbon, excluding simple carbon oxides, sulfides, and metal carbonates (Table 2) (1).

Pathology/Histopathology

Repeated and long-term exposure to inhalational irritants can lead to changes of the lung and pleura that may have lasting effects, even after exposure ceases. But even a severe, single exposure to a hazardous agent can damage the lungs. Smoking can increase both the severity of an occupational lung disease and the risk of lung cancer. The tissue reaction of the pulmonary parenchyma to an accumulation of hazardous dust may be more or less well defined and focally dense, as in "chronic" silicosis and coal worker pneumoconiosis (CWP), or linear and irregular as in asbestosis (1).

The development of pneumoconiosis depends on several factors:

- The nature and properties of the inhaled dust
- The particle size and density

Pneumoconioses. Table 1 Some types of pneumoconioses due to "inorganic" dust

Inorganic dust	Type of disease	Lung reaction
Asbestos	Asbestosis	Diffuse interstitial fibrosis
	Asbestos-related pleural disease	Focal pleural plaques Diffuse pleural thickening Pleural calcification Benign pleural effusion Rounded atelectasis
	Asbestos-related malignancies	Pleural, pericardial, and peritoneal Mesothelioma Increased risk of lung cancer, especially in smokers with asbestosis
Silica (quartz)	Silicosis	Simple nodular silicosis Conglomerate silicosis Silicotuberculosis
Coal	Coal workers' pneumoconiosis (CWP)	Simple CWP Complicated CWP (progressive massive fibrosis) Caplan's syndrome
Beryllium	Berylliosis; beryllium disease (*B. granulomatosis*)	Acute berylliosis = chemical pneumonitis Chronic berylliosis = diffuse pulmonary and hilar lymph node granulomatous reaction
Tungsten carbide	Hard metal disease	Interstitial pneumonitis with fibrosis; pattern of desquamative interstitial pneumonitis
Iron	Siderosis	Pure form without fibrosis due to "inert" dust; frequently exposed to other noxious dusts, including asbestos and silica (siderosilicosis)

Pneumoconioses. Table 2 Some types of pneumoconioses due to "organic dust"

Organic dust	Type of disease	Antigen	Lung reaction
Moldy hay, straw, and grain	Farmer's lung	Thermophilic bacteria (*Micropolyspora faeni*, *Thermoactinomyces*, others)	Extrinsic allergic alveolitis Acute, subacute, and chronic forms; in acute form complete recovery might be possible; in subacute and chronic forms, fibrosis of variant degree will occur
Droppings and feathers	Bird Francier's lung	Avian proteins contained in serum, excreta, or feathers	Same as Farmer's lung
Cotton trash	Byssinosis	"Organic dust toxic syndrome" (the syndrome covers a variety of reactions as grain fever, pig fever, cotton fever, pulmonary mycotoxicosis)	Bronchoconstriction in cotton, flax, and hemp workers during work; occasionally, mild airway obstruction may develop and persist
Dust or mist	Humidified fever	*Thermoactinomyces* species, *Penicillium* species, *Sphaeropsidales* species, others	Symptoms during work or during the first day back at work after vacation; no fibrosis

- The degree of fibrogenity
- The duration and intensity of exposure
- The time elapsed from initial exposure
- The individual susceptibility

1. Pneumoconiosis due to inorganic (mineral) dusts (Table 1):

   The reaction of the lung tissue may be a noncollagenous or a collagenous pneumoconiosis.

   a. Noncollagenous forms are caused by lessfibrogenic or nonfibrogenic (inert) dust with the following characteristics:
      i. The alveolar architecture remains intact.
      ii. The stromal reaction is minimal and consists mainly of reticulin fibers.
      iii. The dust reaction is potentially reversible.

   b. Collagenous forms are characterized by:
      iv. Permanent alteration or destruction of alveolar architecture
      v. Collagenous stromal reaction of moderate to maximal degree
      vi. Permanent scarring of the lungIn addition, it may be caused by an altered tissue response to a nonfibrogenic dust.

2. Pneumoconiosis due to organic dusts (Table 2):
   - Organic dusts can cause a wide variety of diffuse interstitial granulomatous lung diseases as an allergic response to the inhaled dust. The term "extrinsic allergic alveolitis" (EAA, hypersensitivity pneumonitis) includes numerous examples that are caused by specific antigens. The prototype, associated with repeated inhalation of dusts from hay containing thermophilic actinomycetes, was described in 1932 as "farmer's lung." Hypersensitivity pneumonitis and its variants are immunologically mediated. Precipitating antibodies to the causative antigen are usually demonstrated, suggesting a type III reaction. Type IV hypersensitivity is suggested by the granulomatous primary tissue reaction.
   - The histologic pattern is quite uniform. During the acute phase of the disease, a combination of bronchiolitis and alveolitis with granuloma formation is predominant. Chronic progressive parenchymal disease may result from continuous or frequent low-level exposure to the antigen. Thus may result in a variable degree of interstitial fibrosis, often most prominent in the peribronchial or periseptal areas. Sometimes it is more diffuse and may resemble advanced idiopathic pulmonary fibrosis with honeycombing.

Clinical Presentation

The most common symptoms of lung diseases, regardless of the cause, include coughing, shortness of breath, chest pain, chest tightness, and abnormal breathing pattern. There is a wide individual variety of symptoms and functional impairment.

Imaging

Traditional biplane chest films continue to be the radiographic baseline studies for initial evaluation and follow-up of occupational lung disease (1).

Computed tomography (CT) is a valuable diagnostic supplement, and it is increasingly mandatory to clarify findings on prior conventional chest films or to search for early and/or additional findings (2). Sonography is of limited value for chest examinations because of its physical properties. The use of magnetic resonance

imaging does not yet have enough evidence to justify routine application.

Although *silicosis* and *CWP* are distinct diseases, histologically their radiographic findings are similar.

Small, round, well-defined, and relatively dense opacities, primarily located in the upper zones, are characteristic findings in silicosis (Fig. 2a, b). Small irregular opacities—especially in CWP—are due to differences of fibrogenous activity of the inhaled dust: If there is less fibrogenous activity, a roundish patchy or branching pattern of alveolar and/or bronchiolytic damage may dominate.

Asbestos-associated disease is primarily characterized by pleural changes, since the pleura is the prime target even of low doses of asbestos exposition. Involvement of the pulmonary parenchyma is associated with high-dose exposure. CT is indeed increasingly mandatory for the early and more precise diagnosis of any pulmonary or pleural changes (Fig. 1a, b).

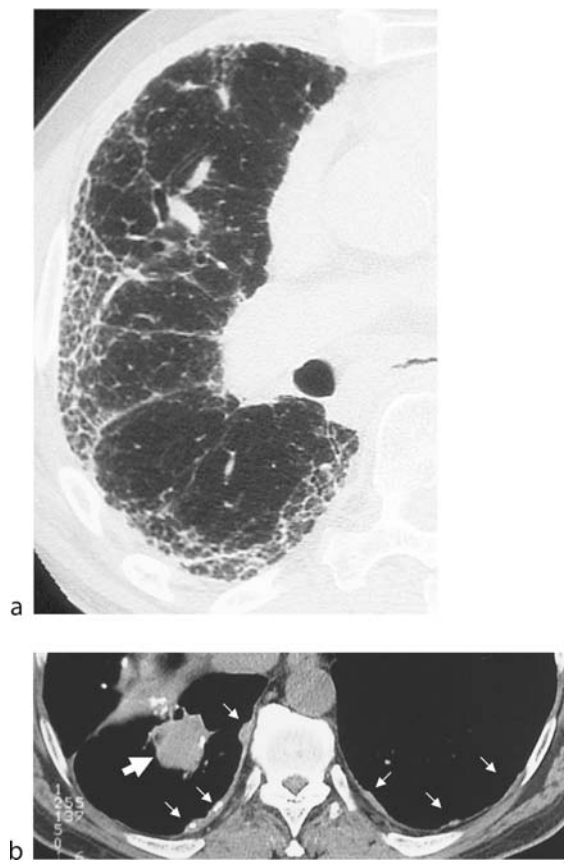

Pneumoconioses. Figure 1 (a) Asbestosis with peripheral subpleural predomination, intralobular interstitial and interlobular septal thickening, and traction bronchiectasis. (b) Different types of pleural plaques, partially calcified. With subpleural fibrosis, more on the right than on the left side (*small arrows*).

The following pleural changes are highly suggestive of prior exposure to asbestos:

- *Pleural plaques*, generally circumscribed, with calcification or without (hyaline plaque)
- *Pleural thickening* with or without subpleural parenchymal fibrosis (mostly focal but sometimes also "diffuse"); due to scar-like thickening of the parietal but also visceral pleura
- Three forms of *sequelae of pleural effusion* (not only asbestos-associated): nonspecific pleural effusion, pleural scarring ("complicated hyalinosis"), rounded atelectasis ("folded lung").

All other CT and high-resolution CT (HRCT) findings definitely present—especially those of the pulmonary parenchyma—remain ambiguous with regard to their possible etiologic connection to any hazardous type of dust exposure, since they may also be due to any other cause of interstitial fibrosis. Their specificity may, however, "increase in value" if characteristic pneumoconiotic findings such as plaques are present.

Lung cancer can be associated with hazardous dust exposure, especially asbestos. A definitive amount of proven exposure is required for etiologic correlation and possible compensation. *Pleural mesothelioma* also has a strong association with asbestos exposure. This neoplasm, however, can arise separately in the pericardium or peritoneum.

Exposure to so-called "*inert*" *dusts* (such as iron or tin) causes aggregation of particle-laden macrophages with none or only minimal accompanying fibrosis, making the radiographic image less valid, but possibly detectable by CT.

Carbon black pneumoconiosis (caused by industrial carbon byproducts) may radiographically result in a fine reticular pattern, predominant in the lower zones, and is often detectable only by CT.

Hard metal pneumoconiosis (such as tungsten or cobalt) usually assumes the pattern of giant cell interstitial, desquamative, or "usual" interstitial pneumonia, usually requiring CT for better definition.

The radiographic features of "*organic*" pneumoconioses are often noncharacteristic because of the similar histologic patterns of the different varieties. They vary with the stage of the disease, and the radiographic abnormalities could resemble the same impression of different causes.

Acute (normally reversible) changes are a diffuse ground glass pattern, a reticulonodular interstitial pattern, and patchy areas of consolidation.

Chronic (normally irreversible) changes are a pattern of progressive interstitial fibrosis with honeycombing.

During the course of the disease, the abnormalities of acute-, subacute-, and chronic-stage different patterns may overlap; therefore, the chronic stage of hypersensitivity

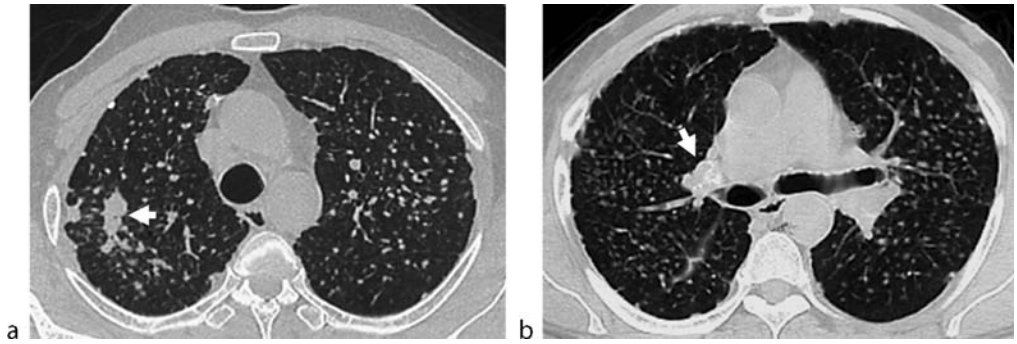

Pneumomediastinum. Figure 2 Silicotic nodules. (a) Centrilobular and randomly distributed pleural nodules and large opacity (*arrow*) due to complicated silicosis (progressive massive fibrosis). (b) Egg-shell calcification (*arrow*) in lymph nodes.

pneumonitis is frequently associated with features of subacute disease.

Nuclear Medicine

Perfusion or ventilation scintigraphy does not play a role in the diagnosis of pneumoconioses. As for positron emission tomography, there are currently not enough valid data to use it to differentiate benign from malignant nodules or rounded atelectasis and advanced pleural fibrosis from mesothelioma.

Diagnosis

Diagnosis requires a history of occupational exposure, radiological findings, and, in some diseases, compatible functional impairment.

For the radiologic report and international comparison, the internationally well-established ILO classification system remains in use for screening and surveillance of occupationally dust-exposed individuals, at least for the time being. Recently, a revision was done, called the International Classification of Radiograph of Pneumoconioses (ILO 2000) (2).

There have been many requests to introduce standardization of CT technique, reporting, and classification. In 2005, the document "International Classification of High-Resolution Computed Tomography for Occupational and Environmental Respiratory Diseases" was published (3, 4). A set of CT/HRCT films will also be available for reference. It is important to note that the CT/HRCT classification is to serve as a supplement and not as a replacement of the existing traditional ILO system.

The new CT/HRCT coding system is descriptive and covers all aspects of occupational and environmental disorders dealing with parenchymal and pleural sequelae. Some patterns are characteristically associated with pneumoconioses (for instance, small rounded opacities with silicosis, or interlobular septal and intralobular nonseptal lines, honeycombing, and typical pleural changes with asbestosis). However, overlapping patterns have to be considered for differential diagnostic ranking.

Bibliography

1. Hering KG (2003) Inhalationsschäden. In: Freyschmidt—Handbuch: Diagnostische Radiologie, Band 4: Thorax, Hrsg. M. Galanski, S Springer-Verlag, Heidelberg 355–394
2. International Labour Organisation (2002) Guidelines for the use of ILO international classification for the use of radiographs of pneumoconioses. ILO, Geneva (Occupational safety and health series No. 22, rev. 2000)
3. Hering KG, Tuengerthal S, Kraus T (2004) Standardisierte CT/HRCT—Klassifikation der Bundesrepublik Deutschland für arbeits- und umweltbedingte Thoraxerkrankungen. Radiologe 44:500–511
4. Kusaka Y, Hering KG, Parker JE (eds) (2005) International Classification of High-Resolution Computed Tomography for Occupational and Environmental Respiratory Diseases. Springer-Verlag, Tokyo

Pneumomediastinum

Koji Takahashi
Department of Radiology, Asahikawa Medical College, Japan
taka1019@asahikawa-med.ac.jp

Definition

Pneumomediastinum connotes abnormal accumulation of gas in the mediastinal space. Gas in the mediastinum most commonly originates from the lung and, less commonly, the central air way, esophagus, abdominal cavity and neck. Pneumomediastinum can be subtle or massive, and gas may extend into the neck, subcutaneous

tissue, retroperitoneum, peritoneal space, and spinal canal (epidural emphysema) (1).

Pathology

Alveolar rupture is the most common cause of pneumomediastinum, which can be spontaneous with or without pulmonary disease. It usually results from a sudden rise in alveolar pressure, including Valsalva maneuvers, asthma, vomiting, artificial ventilation or close chest trauma. The air leak from alveolar rupture tracks into the interstitial tissue and extends through the peribronchial and perivascular interstitial tissue into the mediastinum (2). As well as proximal tracking into the mediastinum, interstitial air also extends peripherally to the visceral pleura and ruptures into the pleural space resulting in pneumothorax (1). In neonatal intensive care units, alveolar rupture is common in patients with hyaline membrane disease, meconium aspiration, and neonatal pneumonia who are on mechanical ventilation.

Rupture of the trachea or main bronchi is most frequently due to trauma, while bronchoscopy and bronchoscopic biopsy may also accidentally result in pneumomediastinum. Rupture of the esophagus occurs during the episodes of severe vomiting and asthmatic attack or as a result of trauma.

Imaging

The most common radiographic manifestation of pneumomediastinum is lucent streaks outlining and overlying the mediastinal structures (Fig. 1). On the frontal chest radiograph, lucent line parallel to the heart and great vessel border is typically seen. Laterally displaced mediastinal pleura is occasionally visualized along the lucent line (Fig. 2). Gas in the mediastinum readily extends to the neck and also into the subcutaneous tissue in the chest wall and appears as lucent streaks projecting over the neck and linear and bubble-like gas in the chest wall (Fig. 3). In younger persons, the thymus may be outlined by air and this finding is specific for pneumomediastinum. The term "angel wings" or "spinnaker sail" sign have been suggested as descriptive terms (3). Mediastinal air may also track extrapleurally along the upper surface of the diaphragm giving rise to "►continuous diaphragm sign" since air beneath the heart combines the margins of the diaphragma bilaterally (4). This sign enables us to differentiate pneumomediastinum from subpulmonary pneumothorax. Pneumopericardium can mimic pneumomediastinum, but pneumopericardium will not extend around the aortic knob or into the superior mediastinum. A radiolucent line is frequently seen along the mediastinal borders in healthy individuals due to "Mach band" (5). A lateral boundary of Mach band is usually unrecognizable whereas lucent streaks due to pneumomediastinum are typically marginated with the displaced mediastinal pleura. Pneumomediastinum is more readily diagnosed on the

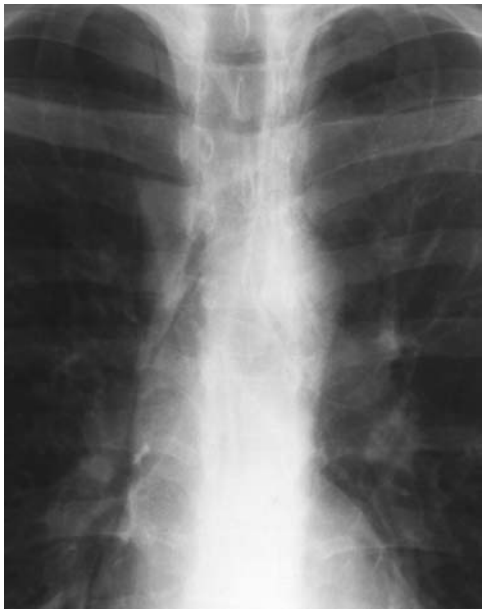

Pneumomediastinum. Figure 1 Chest radiograph shows lucent lines outlining the bilateral main bronchi. Lucent lines overlying the upper mediastinum are also seen.

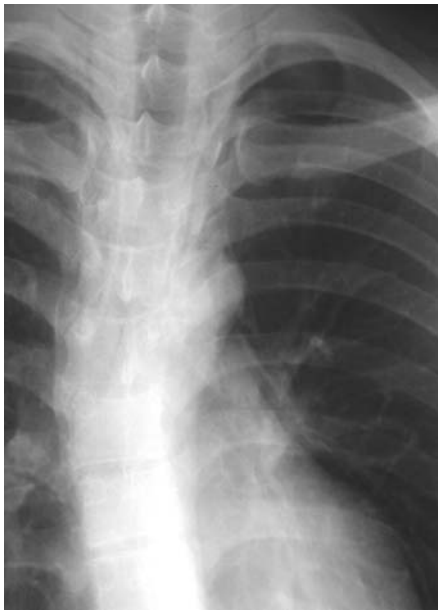

Pneumomediastinum. Figure 2 Chest radiograph shows a lucent line parallel to the left heart border. Laterally displaced mediastinal pleura is also visualized along the lucent line.

P

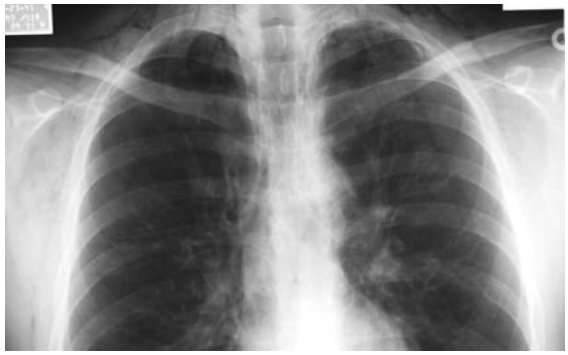

Pneumomediastinum. Figure 3 Pneumomediastinum associated with subcutaneous emphysema. Chest radiograph shows multiple lucent lines in the neck and chest wall, representing subcutaneous emphysema.

lateral radiograph in some cases. On the lateral projection, a lucent line marginates the ascending aorta, aortic arch, and pulmonary arteries (1). In the diagnosis of pneumomediastinum, chest CT is quite more sensitive and specific than chest radiograph.

Bibliography

1. Fraser RS, Muller NL, Colman N et al (1999) Pneumomediastinum. In: Fraser RS (ed) Diagnosis of Diseases of the Chest. 4th edn. W.B. Saunders Company, Philadelphia, 2863–2870
2. Rouby JJ, Lherm T, deLassale EM et al (1993) Histologic aspects of pulmonary barotrauma in clinically patients with acute respiratory failure. Intensive Care Med 19:383–389
3. Moskowitz PS, Griscom NT (1976) The medial pneumothorax. Radiology 120:143–147
4. Levin B (1973) Continuous diaphragm sign. A newly recognized sign of pneumomediastinum. Clin Radiol 24:337–338
5. Friedman AC, Lautin EM, Rothenberg L (1981) Mach bands and pneumomediastinum. J Can Assoc Radiol 32:232–235

Pneumomediastinum

Pneumomediastinum connotes abnormal accumulation of gas in the mediastinum space. It most commonly originates from the lung (alveolar rupture), and less commonly central air ways esophagus, abdominal cavity, or neck. The most common radiographic manifestation is lucent streaks outlining and overlying the mediastinal structures. Gas in the mediastinum readily extends to the neck and also into the subcutaneous tissue in the chest wall and appears as lucent streaks projecting over the neck and linear and bubble-like gas in the chest wall. The term "angle wings" or "spinnaker sail" sign have been suggested as descriptive terms. Mediastinal air may also track extrapleurally along the upper surface of the diaphragm giving rise to "continuous diaphragm sign." This sign enables the reader to differentiate pneumomediastinum from subpulmonary pneumothorax. In the diagnosis of pneumomediastinum, chest CT is quite more sensitive and specific than chest radiograph.

▶Chest Trauma

Pneumonectomy

▶Postoperative

Pneumonia

▶Pulmonary Infection

Pneumonia in Childhood

Gundula Staatz
Department of Radiology, Division of Pediatric Radiology, University of Erlangen-Nürnberg, Erlangen, Germany
gu.stz.uni-erlangen@t-online.de

Definitions

Pneumonia is defined as an inflammation or infection of the lung, caused by bacteria, viruses, fungi, or parasites.

Neonatal pneumonia is characterized by pulmonary infections, that become clinically evident within 24 h of birth and includes pneumonias, which are already established at birth (congenital) or that are acquired intrapartal or postnatal within 24 h.

▶*Round pneumonia* is a spherical pneumonic consolidation mimicking an intrapulmonary mass.

Complications of pneumonia include ▶pneumatoceles, *parapneumonic effusion*, ▶empyema, ▶cavitary necrosis, and ▶lung abscess (1). Pneumatoceles are thin-walled cystic lesions usually developing after pneumonias caused by *Staphylococcus aureus*. Parapneumonic effusion is a pleural effusion associated with bacterial pneumonia or lung abscess, empyema is defined as a collection of pus within the pleural space. A lung abscess

is a localized cavity of pus within the lung, whereas cavitary necrosis represents fluid- and air-filled cavities within necrotizing lung tissue (2).

Pathology/Histopathology

Most pneumonia develop as a complication from lower respiratory tract infection, but also hematogenous spread or aspiration of microorganisms may be a cause for pulmonary infection. In *bacterial lobar pneumonia*, the inflammation of the alveolar spaces begins with vascular congestion and alveolar edema and many bacteria and neutrophils are present (stage of congestion). About 2–3 days later, erythrocytes, neutrophils, desquamated epithelial cells, and fibrin within the alveoli are present, giving the lung the consistency of liver (stage of red hepatization). In the next stage, the gray hepatization, fibrinopurulent exsudate, disintegration of red cells, and hemosiderin are identified. In the final stage of resolution, resorption and restoration takes place. However, due to early antibiotic treatment these classical four stages of bacterial lobar pneumonia are not commonly seen in recent years.

Viral pneumonia is characterized by centrifugal spread of neutrophil exsudate through the bronchi and bronchioles to the adjacent alveoli. In *interstitial pneumonia*, the interstitium is infiltrated by lymphocytes, macrophages, and plasma cells, whereas the alveoli are free of exsudate.

Pneumatoceles result from air trapping and valve mechanism, due to plugging of distal bronchi by inflammatory exsudate in *S. aureus* pneumonia. Cavitary necrosis develops in necrosis complicating pneumonia. Thrombotic occlusion of alveolar capillaries associated with adjacent inflammation results in ischemia and eventually necrosis of the lung parenchyma (2). A lung abscess is characterized by a collection of pus surrounded by a well-defined fibrous wall.

Clinical Presentation

Neonatal pneumonia is most often due to infection with group B streptococcus, *Chlamydia trachomatis*, *Escherichia coli*, *Hemophilus influenza*, *Listeria monocytogenes*, enterococcus, and *S. aureus* (3). The sick neonates may present with tachypnoea, nasal flaring, intercostal retractions, poor feeding, unstable temperature, irritability, or lethargy.

In young infants, until 3 months of age, *Streptococcus pneumonia*, *Streptococcus viridans*, *S. aureus*, and *H. influenza* are the most common cause for pneumonia, but also infections with *Ureaplasma urealyticum* or *Bordetella pertussis* are observed. Viral pneumonia is often caused by adenovirus, respiratory syncytial virus, influenza, or parainfluenza virus.

In older children pulmonary infections with *Mycoplasma pneumonia*, *Pneumococcus* species, influenza viruses, or respiratory syncytial virus (RSV) are frequently observed. Older infants typically present with cough, vomiting, chest or abdominal pain, and fever, adolescents may complain about additional headache, pleuritic chest pain, and dyspnea (1).

If bacterial pneumonia is complicated by parapneumonic effusion or empyema, the children present with persistent fever or sepsis, pleuritic chest pain, dyspnea, and possible cyanosis. Abdominal pain and vomiting are commonly observed as side symptoms. Other complications such as cavitary necrosis and lung abscess have to be considered in persistent symptoms of infectious pulmonary disease.

Imaging

Plain chest radiography is the primary imaging modality for the diagnosis of pneumonia and associated complications such as parapneumonic effusions or empyema (1). *Ultrasound* is especially valuable for the assessment of associated parapneumonic effusions or empyema, and may be helpful for the detection of cavitary necrosis in peripheral-localized consolidations. *Contrast-enhanced CT* is most efficient in demonstrating the complications of pneumonia, and allows accurate identification of lung abscess formation, parapneumonic effusions, and empyema (4). *MRI* may be used as an alternative method to CT, especially to differentiate lung abscess formation from intrapulmonary tumor masses.

Nuclear Medicine

Lung scintigraphy is not routinely performed in children with acute pneumonia or pneumonia-associated complications. It may provide additional information in chronic or recurrent pneumonia, although the findings are often nonspecific, or in pneumonia secondary to pulmonary infarction.

Diagnosis

Chest radiographic findings in neonatal pneumonia may vary due to the causing microorganism between reticulogranular, interstitial, and alveolar patchy opacities. Bacterial pneumonia in older infants and children often presents with segmental or lobar consolidations with air bronchograms (1) (Fig. 1), whereas in viral pneumonia patchy multifocal interstitial opacities and hyperinflated lungs are demonstrated on the chest X-rays (3). Small parapneumonic effusions are identified on chest radiographs by blunting of the costophrenic angle,

larger effusions present as opaque fluid collections along the chest wall, in severe cases with complete opacification of the involved hemithorax. Parapneumonic effusions are reliable diagnosed by ultrasound, which demonstrates echogenic fluid collections within the pleura space. If the fluid collection within the pleural cavity becomes echogenic and contains fibrinoid septations, empyema has to be suspected (Fig. 2) (5). Pneumatoceles appear as multiple thin-walled cysts on chest X-rays (Fig. 3), whereas lung abscesses are characterized by thick-walled cavities often associated with effusion. Round pneumonias are often located in the posterior segments of the lower lobes and are characterized by a circularly configured opacification mimicking an intrapulmonary mass (3) (Fig. 4).

On contrast-enhanced CT images, noncompromised lung parenchyma consolidated with pneumonia shows typically a diffuse enhancement (2). Cavitary necrosis is identified on CT by fluid- and air-filled cavities without rim-enhancement located in areas with a low-attenuation lung parenchyma. On contrast-enhanced CT, a lung abscess appears as a fluid-or air-filled cavity with a thick enhancing wall and no evidence of necrosis in the surrounding lung. Enhancement and thickening of the parietal and visceral pleura, thickening of the extrapleural subcostal tissues and increased attenuation of extrapleural subcostal fat are typical CT findings of empyema (Fig. 5).

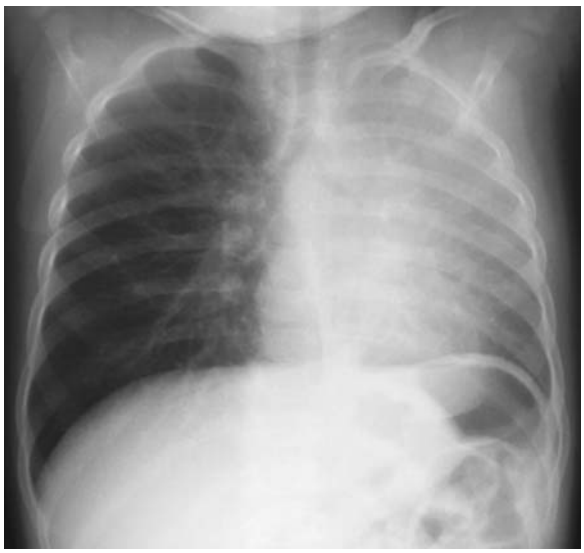

Pneumonia in Childhood. Figure 1 Chest radiograph of a 5-year-old boy with lobar pneumonia of the left upper lobe.

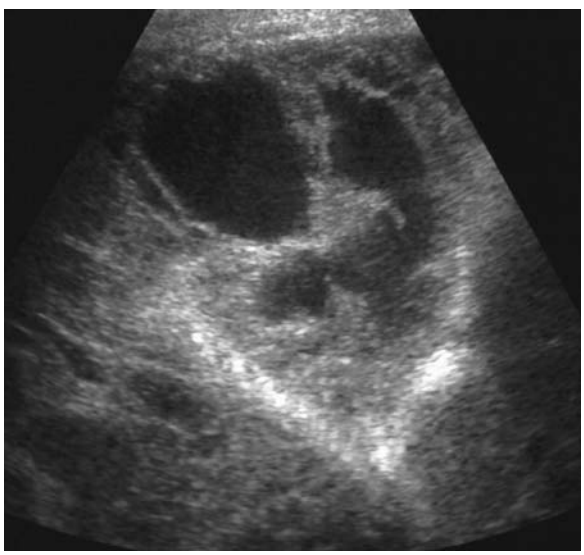

Pneumonia in Childhood. Figure 2 Ultrasound image of an empyema, which occurred as a complication of bacterial pneumonia in a 7-year-old boy. Characteristic thick fibrinoid septations and echogenic fluid collections within the pleural cavity are visible.

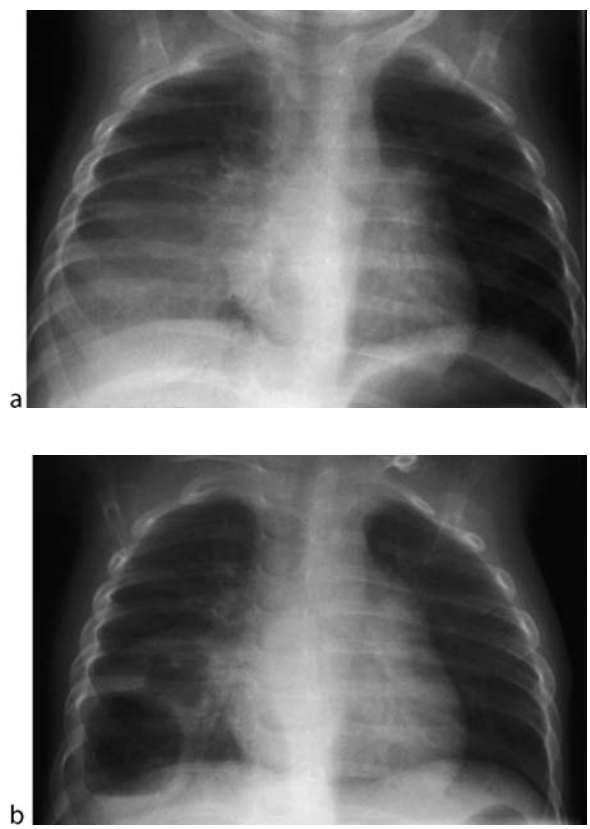

Pneumonia in Childhood. Figure 3 Chest radiograph of a 1.5-year-old boy with *Staphylococcal pneumonia* in the right lower lobe (a). The radiography 3 weeks later showed multiple thin-walled air-filled cysts representing pneumatoceles (b).

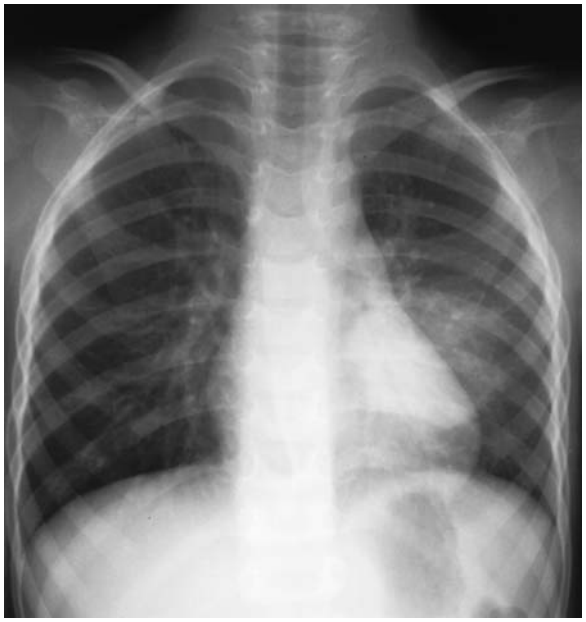

Pneumothorax. Figure 4 Chest X-ray of round pneumonia in the left lower lobe of a young adolescent. The spherical configured consolidation disappeared completely after antibiotic treatment.

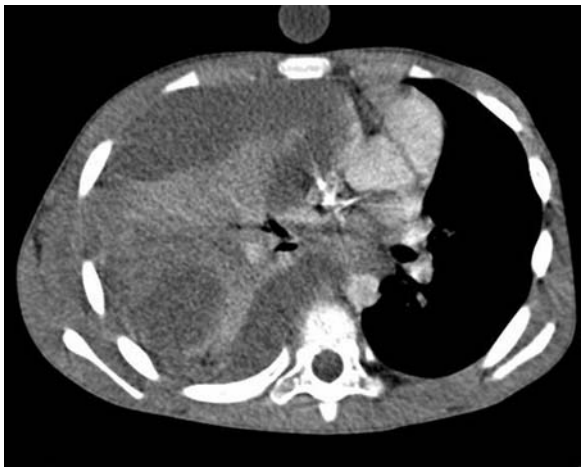

Pneumothorax. Figure 5 A 7-year-old boy with empyema on the right side. The contrast-enhanced CT examination demonstrates a multiloculated parapneumonic effusion with only minor enhancement of the pleura, but thickening of the extrapleural subcostal tissues and increased attenuation of extrapleural subcostal fat.

Interventional Radiological Treatment

Percutaneous fine needle aspiration is an alternative method used to identify causative pathogens in selected patients with pneumonia, and should be considered in patients who have not responded to initial therapy, who may have nosocomial superinfection, who are immunocompromised, or in whom tuberculosis is suspected but has not been confirmed by examination of the sputum or gastric lavage (4). Parapneumonic effusions may be punctured with help of ultrasound guidance. Ultrasound or CT-guided percutaneous catheter drainage may be performed as an alternative to chest tube placement and fibrinolysis in children with lung abscess or empyema. In case of multiloculated pleural empyema resistant to these more conservative treatment efforts, thoracotomy with decortication is usually the treatment method of choice.

Bibliography

1. Donnelly LF (1999) Maximizing the usefulness of imaging in children with community-acquired pneumonia. Am J Roentgenol 172:505–512
2. Donnelly LF (2002) CT of acute pulmonary infection. In: Lucaya J, Strife JL (eds) Pediatric Chest Imaging: Chest Imaging in Infants and Children. Medical Radiology, Diagnostic Imaging (Baert Al, Sartor K (eds)). Springer, Berlin, Heidelberg, New York, pp 113–123
3. Siegel MJ, Coley BD (2006) Lung, Pleura and chest wall. In: Siegel MJ, Coley BD (eds) Pediatric Imaging. Lippincott Williams & Wilkins, Philadelphia, pp 65–112
4. Franquet T (2001) Imaging of pneumonia: trends and algorithms. Eur Respir J 18:196–208
5. Ramnath RR, Heller RM, Ben-Ami T et al (1998) Implications of early sonographic evaluation of parapneumonic effusions in children with pneumonia. Pediatrics 101: 68–71

Pneumonitis

▶ Pulmonary Infection

Pneumothorax

Nagmi R. Qureshi[1], Fergus V. Gleeson[2]
[1]Fellow in Thoracic Radiology
[2]Consultant Radiologist, Department of Radiology, Churchill Hospital, Headington, Oxford OX3 7LJ, UK
nagmiqureshi@doctors.org.uk
fergus.gleeson@radiology.oxford.ac.uk

Definition

Pneumothorax is defined as air in the pleural space. Pneumothoraces may be spontaneous, primary or secondary; or traumatic.

Clinical Features

Patients typically present with sudden onset of pleuritic chest pain and breathlessness. The severity of symptoms may not necessarily correlate with the size of the pneumothorax, and is in part dependent on the aetiology and the patient's lung function.

Imaging

On an erect chest radiograph a pneumothorax is diagnosed by the presence of a well-defined line which represents the visceral pleura, separated from the parietal pleura by a hyperlucent air filled space (Fig. 1). Generally a 2 cm margin of air equates to a 50% pneumothorax. If small, a lateral decubitus chest radiograph has been shown to be as sensitive as CT, and can help confirm a pneumothorax.

Pneumothoraces are often subtle on a supine radiograph. Findings include hyperlucency of the hemithorax with depression of the ipsilateral hemidiaphragm, increased sharpness of the cardiomediastinal border and deepening of the costophrenic recess. Skin folds and gowns may mimic the visceral pleura of a pneumothorax. In contrast, to the visceral pleura these artifactual lines tend to be ill defined, with vascular markings visible lateral to them.

On ultrasound the normal pleura appears as either a single echogenic line, which slides forward and backward relative to the lung, or two discrete echogenic lines the visceral and parietal pleura which slide over each other during normal respiration, the sliding sign. Similarly at the pleuro-parenchymal interface the difference in acoustic transmission results in reverberation artifact which appears as horizontal echogenic lines parallel to the chest wall. Exaggeration of this reverberation artifact and loss of the "sliding sign" is suggestive of air in the pleural space.

CT has an almost 100% sensitivity and specificity in the detection of pneumothorax, but is mostly not required to make this diagnosis.

The main indications for CT are in differentiating a pneumothorax from bullous lung disease, detecting pneumothoraces in trauma and ICU patients and small pneumothoraces not seen on CXR in patients with impaired lung function and rarely for guiding drain placement.

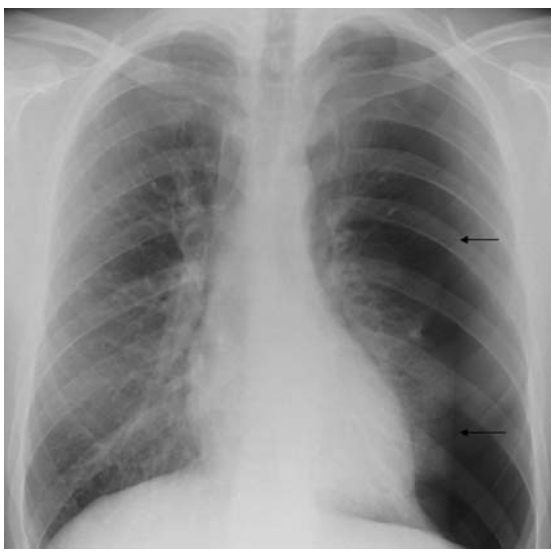

Pneumothorax. Figure 1 Frontal chest radiograph demonstrating an approximately 40% left sided pneumothorax (*arrow*).

Podagra

▶Gout

Poland Syndrome

A unilateral congenital condition with short or missing middle phalanges and soft-tissue syndactyly of the hand, with ipsilateral hypoplastic pectoral muscle.

▶Congenital Malformations, Bone

Polycystic Liver Disease

Presence of multiple cysts within the liver. Two forms are described: the infantile and the adult form. The infantile type is less common and shows an autosomal recessive inheritance while the adult type is autosomal dominant. These forms may be associated with congenital hepatic fibrosis. The association of polycystic liver/kidney disease and hepatic fibrosis is also known as 'fibropolycystic disease'.

▶Congenital Malformations, Liver and Biliary Tract

Polycythemia Rubra Vera

Polycythemia rubra vera is one of the chronic myeloproliferative disorders. It is characterized by an increased number of red blood cells, white blood cells, and platelets, resulting in an increased blood volume and hyperviscosity of the blood. Splenomegaly is a characteristic finding; splenic infarction is not uncommon and is accompanied by pain.

▶Neoplasms, Splenic, Malignant

Polydactyly

Accessory or supernumerary fingers or toes.

▶Congenital Malformations, Musculoskeletal System

Polymicrogyria

Polymicrogyria consists of multiple abnormally small gyri and is the result of an abnormality during the process of cortical organization.

▶Congenital Malformations, Cerebrum

Polyp, Nasal

Nasal polyps are outgrowths of nasal mucosa made up of edema fluid with sparse fibrous cells, a few mucus glands and a surface epithelium invaded by some inflammatory cells.

▶Inflammation, Chronic, Nose, and Paranasal Sinus

Polyphosphonates

Osteotrophic molecules that can be labeled with ^{99m}Tc and are used for bone scintigraphy.

▶Bone Scintigraphy

Polyps, Gallbladder

This is defined as mucosal projections into the gallbladder lumen. The term gallbladder polyp includes different entities such as cholesterol polyps, adenomyomas, inflammatory polyps, adenomas, and other miscellaneous polyps. These polyps are nonneoplastic in most cases and rarely cause symptoms. Cholecystectomy is required for polyps larger than 10 mm because of the increased risk of adenomatous or carcinomatous transformation.

▶Cholecystoses

Polysplenia

The presence of multiple small spleens is a rare condition usually associated with other congenital malformations. It may be seen in association with abdominal situs ambiguous and has classically been called polysplenia syndrome. Polysplenia syndrome is more common in females. The typical anatomic features of classic polysplenia syndrome are bilobed lungs with bilateral hyparterial bronchi, bilateral pulmonary atria, midline liver, and multiple spleens of variable size and number that may be located in either the left or right side of the abdomen, more often along the greater curvature of the stomach, which occurs in variable locations. In rare cases these patients have a single, lobulated spleen or even a normal spleen. Malrotation of the bowel is frequently associated. In polysplenia, numerous small splenic masses can be seen predominantly in the right upper quadrant at US, CT, MR, or scintigraphy.

▶Congenital Abnomalies, Splenic

Polysplenia Syndrome

Polysplenia syndrome is characterized by polysplenia, or the presence of multiple small spleens, associated with abdominal situs ambiguous. Polysplenia syndrome is more common in females. The typical anatomic features of classic polysplenia syndrome are bilobar lungs with bilateral hypoarterial bronchi, bilateral pulmonary atria, midline liver, and multiple spleens of variable size and number that may be located in either the left or right side of the abdomen, more often along the greater curvature of the stomach, which occurs in variable locations.

▶Splenic Anomalies

Popliteal Arterial Obstruction

▶Occlusion, Artery, Femoral

Popliteal Arterial Occlusion

▶Occlusion, Artery, Femoral

Porcelain Gallbladder

Also termed calcified gallbladder, calcifying cholecystitis, or cholecystopathia chronica calcarea, it is a form of accumulating cholecystosis consisting in the presence of extensive dystrophic calcifications within the chronically inflamed gallbladder wall. The term porcelain gallbladder emphasizes the brittle consistency and blue discoloration of these calcifications that may appear as a broad continuous band in the muscularis resembling a sac-like appearance or as multiple punctate calcifications in the mucosal glandular spaces.

▶Cholecystoses

Portal Cavernoma

Portal cavernoma, also called cavernous transformation of the portal vein, consists of a network of venous channels, which replaces a previously stenosed or occluded portal vein. It functions as a portoportal shunting, so it is characterized by hepatopetal flow. The veins are usually insufficient to bypass the entire splenomesenteric inflow, and signs of portal hypertension frequently co-exist.

Clinical signs of portal cavernoma are usually related to extra-hepatic portal hypertension (bleeding from oesophageal varices, splenomegaly, etc.).

Diagnosis is mainly done by imaging. At US, a mass of tortuous veins can be observed at the portahepatis. Doppler US displays hepatopetal flow. An increased flow in hepatic artery may be seen, representing a compensatory mechanism to the reduced portal flow. On contrast-enhanced CT scans, a characteristic mass of veins replacing the portal trunk is the most common finding. Involvement of intra-hepatic branches with a normal-appearing main portal vein has also been described.

▶Portal Hypertension, Adults

Portal Hypertension

The presence of portal hypertension is the expression of the failure to alter either portal venous inflow to the liver or resistance to that inflow. In the vast majority of cases, increased resistance in the prehepatic, hepatic, or posthepatic vascular tree is responsible. Portal hypertension leads to a significant diversion of blood from the portal circulation into the systemic venous circulation.

▶Splenomegaly

Portal Hypertension, Adults

Chiara Franchini, Carlo Bartolozzi
Department of Diagnostic and Interventional Radiology, University of Pisa, Pisa, Italy
bartolozzi@do.med.unipi.it

Synonyms

Increased pressure in portal venous system

Definition

Any increase in the portal vein pressure due to obstruction to blood flow in the portal venous system. Portal hypertension is defined as pressure in the portal system higher than 12 mm Hg (the normal portal pressure is 5–10 mm Hg).

Pathology/Histopathology

Portal hypertension can be classified into five major types relative to location of portal flow obstruction:

1. Extra-hepatic (portal or splenic vein thrombosis or obstruction, arterioportal fistula)
2. Intra-hepatic pre-sinusoidal (congenital hepatic fibrosis, primary biliary cirrhosis, schistosomiasis, sarcoidosis, myelofibrosis)

3. Intra-hepatic sinusoidal (post-necrotic cirrhosis, hepatitis)
4. Intra-hepatic post-sinusoidal (alcoholic cirrhosis, veno-occlusive disease, obstruction or compression of hepatic veins)
5. Supra-hepatic (Budd–Chiari syndrome, congestive heart failure or pericarditis).

The most common cause of portal hypertension is liver cirrhosis.

The increased portal pressure reduces the portal venous flow. When the pressure in the portal venous system becomes higher than the systemic venous pressure, a reversal of flow occurs and porto-systemic shunts develop. Since in post-uterine life the portal venous system is without valves, blood can flow in any direction, and when normal or hepatopetal flow is blocked, blood is free to flow along the course of least resistance (tributary or newly developed collaterals). Tributary collaterals are represented by the normal tributaries of the portal system that are immediately available for collateral blood flow. These important tributaries are the left gastric vein, the short gastric veins, the superior mesenteric vein and the inferior mesenteric vein. Blood flowing in reverse direction over the left gastric vein and the short gastric veins reaches the systemic circulatory system *via* the emiazygos and azygos systems. The systemic circulatory system may be reached from the inferior mesenteric vein *via* the haemorrhoidal plexus and hypo-gastric veins, as well as from the superior mesenteric vein *via* retro-peritoneal communications in the mesentery, which includes the veins of Retzius. Newly developed collateral channels may arise from vessels that previously existed but do not function as main tributaries of the portal system. The paraumbilical collaterals arise from the left main intra-hepatic branch of the portal vein and terminate at the umbilicus, although they frequently communicate with anterior abdominal wall veins. The splenorenal collaterals extend from the spleen or the splenic vein to the left renal vein. The gastric renal collaterals extend from the stomach to the left renal vein. The splenoperitoneal collateral is found in the lateral aspect of the abdomen, extending from the spleen to retroperitoneal vessels along the lateral abdominal wall. All these vessels carry blood in a hepatofugal direction. All may appear in the presence of intra-hepatic obstruction. When extra-hepatic obstruction exists, the parumbilical collaterals do not develop; the more distally located collaterals may develop depending on the site of obstruction. In case of splenic vein obstruction, bridging collaterals appear between the spleen and the portal vein over the short gastric veins and the gastroepiploic vein.

Clearly reduced portal flow velocity is associated with increased risk of thrombosis, which may involve the main portal trunk and its branches, the splenic and the superior mesenteric veins.

Chronic portal thrombosis may lead to the formation of a ►portal cavernoma, which consists of a network of venous channels replacing the previously occluded portal vein and functioning as a portoportal shunting. Aneurysms of the portal venous system have been described in association with portal hypertension (1).

Clinical Aspects

Portal hypertension is typically a consequence of cirrhosis. In the clinical setting of patients with portal hypertension, stigmata of cirrhosis, including jaundice, spider nevi, palmar erythema and manifestations of liver insufficiency may be associated. Furthermore, complications such as variceal bleeding, ascites, splenomegaly and hepatic encephalopathy may occur. The development of oesophageal varices is a troublesome complication, because the rupture of these varices, either spontaneously or after vomiting, may lead to life-threatening haemorrhage. The development of anorectal shunts results in the presence of haemorrhoidal varices, while the reopening of paraumbilical veins may lead to the dilatation of veins of the anterior abdominal wall, which form a sort of net, the so called 'caput medusae'. When numerous porto-systemic collaterals develop, the pressure in the oesophageal varices decreases and the risk of rupture is reduced. Anyway, the increase in porto-systemic shunting results in a decrease of portal flow to the liver. This correlates with liver atrophy and with a worsening in liver function. Furthermore, toxic metabolites, such as ammonia, which are usually catabolized by the liver, go directly into the systemic circulation and cause hepatic encephalopathy.

Imaging

Ultrasound

Conventional ultrasound (US) alone often allows to establish the presence of portal hypertension. The diagnosis of portal hypertension is suggested by the dilatation of portal system veins, the diminished response of portal vessels to respiration, the demonstration of portosystemic collaterals, the presence of splenomegaly and ascites. Finally, US may demonstrate typical findings of chronic liver disease.

The calibre of the portal vein is not a sensitive criterion in assessing portal hypertension; it shows a wide variability in normal subjects and it is influenced by the presence of

collateral vessels. When collaterals develop, the calibre and the flow of the portal vein decrease. Consensually to the reduction of portal flow, the flow within the hepatic artery increases; this explains the increase of calibre of hepatic artery, often observed in cirrhotic patients. In standard conditions, a portal vein calibre greater than 13 mm indicates portal hypertension with a high specificity.

The calibre variation of the portal trunk and the splenic and superior mesenteric veins during respiration is a sensitive and reliable sign of portal hypertension. A lack of normal calibre variation (an increase during inspiration and a decrease during expiration) in these vessels is the most constant and sensitive US sign of portal hypertension (2).

In some cases, the demonstration of porto-systemic anastomoses represents the first clue to the presence of portal hypertension. US can document some of these shunts. In particular, the depiction of a dilated coronary vein within the lesser omentum, as well as gastroesophageal varices, demonstrated as tortuous anechoic structures near the gastroesophageal junction, are the most common and reliable US finding in patients with portal hypertension. There is a good correlation between the size of the varices and visualization of dilated coronary vein. The remnant of the umbilical vein, the ligamentum teres is seen at US in a high percentage of normal individuals as a hyperechoic band. In patients with portal hypertension, the umbilical vein often reopens and becomes visible within the hyper-echogenicity of the falciform ligament and coursing along the ventral abdominal wall. The resulting 'bull's-eye' appearance is indicative for a patent umbilical vein. Doppler US displays a hepatofugal flow. Less common venous collaterals may be visualized at US, such as splenorenal and gastrorenal veins, pancreatico-duodenal veins, retroperitoneal-paravertebral veins, gallbladder varices, intrahepatic shunts, such as anastomoses between portal branches and hepatic veins or between portal branches and inferior vena cava. US limitations in detecting porto-systemic shunts are related to bowel gas, obesity, ascites, deep location and paucity of collaterals (3).

Doppler US gives information about flow direction and velocity in the portal vein and its branches. The portal flow velocity is usually reduced in portal hypertension. A mean velocity lower than 16 cm/sec in the portal trunk suggests portal hypertension. Nevertheless, recanalization of the umbilical vein causes an increase of the velocity in the portal vein. In fact, flow velocity is dependent on a great variety of factors, such as portal calibre, degree of resistance, presence and type of collaterals. The presence of reversal of flow within the main portal vein or in the splenic and superior mesenteric veins is related to hepatofugal portosystemic collaterals and is a certain sign of portal hypertension.

Splenomegaly is a constant finding in portal hypertension, although the size of the spleen is not correlated with the degree of hypertension.

Finally, US may be useful in diagnosing cavernous transformation of the portal vein, and in demonstrating portal vein, splenic vein or superior mesenteric vein thrombosis (1).

Computed Tomography

Computed tomography (CT) gives useful qualitative information when US evaluation is inconclusive. Splenomegaly and ascites are easily documented at CT.

Signs of underlying chronic liver disease may be demonstrated. However, CT findings in cirrhosis are highly variable and in some patients the liver may appear normal.

CT angiography, with the possibility to perform three-dimensional reconstructions, may depict accurately the portal vasculature and porto-systemic collaterals, being superior to US in demonstrating retroperitoneal veins. Porto-systemic shunts appear as dilated, often tortuous, tubular structures which show clear enhancement in the portal-venous phase. The main limitation of CT in evaluation of portal hypertension is that it cannot demonstrate the venous and arterial flow profile.

CT arterial portography can be used to achieve better delineation of the portal venous system, but, although it can produce elegant images, it is invasive and it has not gained widespread acceptance.

CT is very reliable in demonstrating ▶portal vein thrombosis, which appears as hypo-dense material completely or partially filling a portal vessel, which fails to enhance in the portal-venous phase.

Another possible finding at CT is congestion and edema of splanchnic viscera, resulting in thickening of intestinal walls and ground-glass appearance of perivisceral fat.

Magnetic Resonance

Magnetic resonance (MR) does not offer relevant advantage over CT and US in the assessment of portal hypertension. MR angiography may offer a non-invasive evaluation of the portal venous system, enabling also to provide information about flow dynamics (4). Further manifestations of portal hypertension, such as ascites and splenomegaly can be easily demonstrated at MR.

The so called '▶Gamna–Gandy bodies' represent siderotic nodules within the spleen and can arise in patients with portal hypertension. They may be detected on T2-weighted images, as tiny hypo-intense nodules scattered throughout the splenic parenchyma. These nodules are pathognomonic of portal hypertension (5).

Barium Study

Oesophageal varices, consisting in dilated sub-mucosal veins in the caudal portion of oesophagus, represent a common and important complication of portal hypertension. At barium study, they appear as serpiginous filling defects. Gastric varices may also be seen. Varices in the stomach usually are confined to the gastric cardia and are difficult to recognize. Gastric antral and duodenal varices are sometimes seen, usually in association with gastric fundal and oesophageal varices.

Angiography

Angiographic techniques have been largely replaced by non-invasive imaging modalities in the evaluation of portal hypertension.

Arterial portography is usually performed before transcatheter intra-arterial procedures to assess the patency of portal vein and the presence of venous collaterals. Arterial portography consists in the indirect opacification of the portal venous system after the injection of contrast material into the celiac axis or into the superior mesenteric artery.

Splenoportography, consisting in the direct puncture of the spleen and injection of contrast material, had a primary role in the investigation of portal hypertension in the past. In percutaneous transhepatic portography the portal vein is punctured directly and incannulated with a catheter; then, contrast material is injected.

Nuclear Medicine

Liver-spleen scintigraphy with sulphur colloid has been superseded by US and CT scan in the diagnosis of portal hypertension.

Sulphur colloid is taken up by the reticulo-endothelial system cells. A shift of the uptake from liver to the spleen or bone marrow is suggestive of increased portal pressure. Anyway, portal hypertension cannot be ruled out in the absence of this shift.

Diagnosis

US and Doppler US often provide findings which strongly suggest the presence of portal hypertension. Widely accepted signs of portal hypertension, demonstrated at US, are portal vein calibre greater than 13 mm, diminished response of portal vessels to respiration, demonstration of portosystemic collaterals, and presence of splenomegaly and ascites.

The most specific Doppler findings for portal hypertension are mean velocity lower than 16 cm/sec in the portal trunk and reversal of flow within the portal system veins. CT and MR allow a more accurate depiction of porto-systemic collaterals.

Interventional Radiology

Transjugular intra-hepatic porto-systemic shunt (TIPS or TIPSS) is a percutaneous interventional procedure, consisting in the creation of a communication between a hepatic vein and a portal branch through the liver parenchyma, *via* the internal jugular vein.

The procedure is performed under US and fluoroscopic guidance in combination. Under deep sedation, the right internal jugular vein is punctured, and the sheat is advanced into the hepatic vein. A track is created through the liver parenchyma connecting the hepatic to the portal vein. A stent is placed in the track. Blood from the portal vein is shunted to the hepatic vein.

Accepted indications for TIPS include gastroesophageal variceal bleeding despite emergency endoscopic or pharmacological treatment and recurrent variceal bleeding after endoscopic treatment. Potential indications include refractory ascites and Budd–Chiari syndrome.

The main cause of failure of TIPS is stent dysfunction, which may be related to stenosis, occlusion or displacement. A relevant complication of TIPS is hepatic encephalopathy, related to portosystemic shunting. Other complications of TIPS are related to the procedure and include entry site haematoma, peri-hepatic haematoma, extra-hepatic puncture of portal vein, arterioportal fistula, portobiliary fistula, haemoperitoneum.

After the procedure patients undergo close follow-up. Shunt patency is monitored by colour Doppler US. Portography is performed in cases of suspected shunt malfunction. CT may be useful for a better depiction of liver and vascular anatomy and stent position and patency.

Bibliography

1. Gallego C, Velasco M, Marcuello P et al (2002) Congenital and acquired anomalies of the portal venous system. Radiographics January–February 22(1):141–159
2. Bolondi L, Gandolfi L, Arienti V et al (1982) Ultrasonography in the diagnosis of portal hypertension: diminished response of portal vessels to respiration. Radiology 142:167–172
3. Subramanyam BR, Balthazar EJ, Madamba MR et al (1983) Sonography of portosystemic venous collaterals in portal hypertension. Radiology 146:161–166
4. Annet L, Materne R, Danse E et al (2003) Hepatic flow parameters measured with MR imaging and Doppler US: correlations with degree of cirrhosis and portal hypertension. Radiology 229:409–414
5. Lencioni R, Bartolozzi C (2003) Diffuse liver disease. In: Magnetic Resonance Imaging in Liver Disease, Thieme, Stuttgart-New York, pp 93–114

Portal Vein Thrombosis

▶Thrombosis, Vein, Mesenteric

Portal Vein, Aneurysm

An aneurysm of the portal venous system is a segmental, saccular or fusiform, dilatation of a vein of the portal system. Aneurysms of the portal venous system may be related both to congenital and acquired causes. There is a significant association with portal hypertension, which has been advocated as a cause of acquired portal vein aneurysm. Various theories have been proposed for congenital portal-vein aneurysm, including abnormal weakness of the vein wall. The most common locations are the splenomesenteric venous confluence, main portal vein, and intra-hepatic portal vein branches at bifurcation sites; rare locations are the splenic, mesenteric and umbilical veins.

Portal venous system aneurysms are usually asymptomatic. Possible complications are abdominal pain, thrombosis, portal hypertension, rupture.

Doppler US alone is usually able to achieve a definite diagnosis and is also used in the follow-up, which frequently demonstrates the stability of the aneurysm.

▶Portal Hypertension, Adults

Portal Vein, Cavernoma

Portal cavernoma, also called cavernous transformation of the portal vein, consists of a network of venous channels, which replaces a previously stenosed or occluded portal vein. It functions as a portoportal shunting, so it is characterized by hepatopetal flow. The veins are usually insufficient to bypass the entire splenomesenteric inflow, and signs of portal hypertension frequently coexist. Clinical signs of portal cavernoma are usually related to extra-hepatic portal hypertension (bleeding from esophageal varices, splenomegaly, etc.). Diagnosis is mainly done by imaging. At US a mass of tortuous veins can be observed at the porta hepatis. Doppler US displays hepatopetal flow. An increased flow in hepatic artery may be seen, representing a compensatory mechaninsm to the reduced portal flow. On contrast-enhanced CT scans, a characteristic mass of veins replacing the portal trunk is the most common finding. Involvement of intrahepatic branches with a normal-appearing main portal vein has also been described. MR angiography and transarterial angiography may be useful for a more accurate and precise depiction of the vascular abnomalities.

▶Vascular Disorders, Hepatic

Portal Venous Gas

Dissection of intramural pneumatosis into the lymphatics and mesenteric veins.

▶Enterocolitis, Necrotizing

Portomesenteric Vein Thrombosis

▶Thrombosis, Vein, Mesenteric

Positive Magnetic Resonance Contrast Agents

This term refers to substances that exhibit a high signal intensity on both T1-weighted and T2-weighted images. Gadolinium in lower concentrations represents such a positive magnetic resonance contrast agent.

▶Contrast Media, MRI, Oral Agents

Positron Emission Tomography

Antonia Dimitrakopoulou-Strauss
Medical PET Group- Biological Imaging (E601),
Clinical Cooperation Unit Nuclear Medicine,
German Cancer Research Center
a.dimitrakopoulou-strauss@dkfz.de

Synonyms

PET

Definition

Positron emission tomography (PET) is a functional nuclear medicine technique that produces four-dimensional

tomographic images of different biochemical processes in the human body. Unlike radiological methods, which provide information about the anatomy of the human body, PET provides information on the function. The information obtained depends on the radiopharmaceutical used for the PET study.

Characteristics

Principle

Positrons are antiparticles, the antimatter counterpart of electrons and are positively charged. When a positron annihilates with an electron, their mass is converted into the energy of two ray photons. Each of these photons (annihilation photons) has an energy of 511 keV and the emission angle of the photons is 180°; therefore they are moving in opposite directions. The simultaneous detection (within a given time interval of a few nanoseconds) of two 511 keV photons by detectors located in opposite position (180°) is called coincidence measurement. PET measurements are based on the principle of the coincidence measurement. Therefore, if one decay is recorded simultaneously by two detectors, then by connecting the two events by a straight line, the assumption is that the anatomical region (origin) of the event is along this line.

Device

A PET scanner consists of a ring system, which contains small detectors of a dedicated scintillation material for the detection of the annihilation photons. The detectors are connected in coincidence. Only 511 keV photons, which arrive in a certain fixed time period of nanoseconds, are registered. The detector material used for PET is bismuth germanate (BGO), gadolinium orthosilicate (GSO), or lutetium oxyorthosilicate (LSO). The light emitted from the crystal is usually detected by an array of photomultiplier tubes (PMT). These PMTs are arranged with respect to the crystals used, and they are system specific (Fig. 1).

Radioisotopes

For PET studies, positron-emitting isotopes, which decay by emitting a positron, are required. Positron-emitting isotopes are fluorine-18, carbon-11, nitrogen-13, and oxygen-15. All these positron-emitting radionuclides have a short half-life and require a cyclotron for their production. The half-life of fluorine-18 is 110 min, of carbon-11 20 min, of nitrogen-13 10 min, and of oxygen-15-water 2 min.

Recently, positron-emitting radioisotopes produced by a germanium-68/gallium-68 radionuclide generator have been used for the production of gallium-68, a positron emitter with a half-life of 68 min.

Radiopharmaceuticals

Dedicated radiopharmaceuticals are required for PET studies. A radiopharmaceutical is a substance labeled with a radioactive isotope. Different substances that are

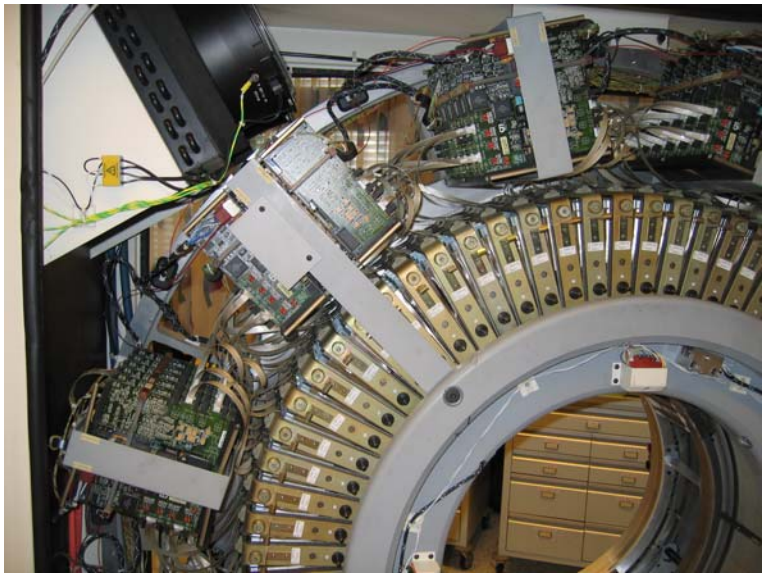

Positron Emission Tomography. Figure 1 Image of the ECAT PET scanner located at the DKFZ, demonstrating the photomultipliers and the detectors located in a ring system.

involved in biochemical pathways in the human body can be used for PET, when labeled with a positron-emitting isotope.

The most commonly used pharmaceutical is fluorodeoxyglucose (FDG) labeled with fluorine-18 (half-life: 110 min), abbreviated as FDG. FDG is a glucose analog, which is transported into the cells like glucose, phosphorylated, and then trapped. No other metabolic steps occur afterwards. PET studies with FDG are used to examine glucose metabolism. Another radiopharmaceutical that can be used for perfusion studies is O-15-water. Oxygen-15 has a very short half-life of 2 min. Labeled amino acids, like C-11-methionine, C-11-aminoisobutyric acid, F-18-tyrosine, or F-18-dihydroxyphenylalanine (DOPA) can be used for measurements of amino acid transport. Labeled peptides, which are small proteins, have been developed and are already in use for PET studies.

Technique

After the injection of a radiopharmaceutical, acquisition starts. The radiopharmaceutical is distributed in various body-compartments. Static or dynamic imaging can be performed. A static data acquisition consists of a single measurement of a part of the body (target area) at a defined time after the tracer injection and is the most commonly used approach. A dynamic acquisition consists of continuous data collection starting immediately after the tracer injection of a predefined target area and for a definite time integral (e.g., 60 min). The acquisition time is divided in so-called frames, which are time windows for the collection of the counts. Dynamic studies are used to assess the time-course of the distribution of a radiopharmaceutical.

Correction measurements are performed on a daily basis for the calibration of the detectors. A transmission measurement is accomplished for each bed position before the emission measurement (usually done by three germanium sources). Reconstruction of the acquired data is applied based on dedicated iterative algorithms.

Data Evaluation

A visual, semiquantitative and quantitative data evaluation can be accomplished. Visual evaluation of PET images is used to assess areas with a pathologically enhanced tracer uptake (e.g., enhanced FDG accumulation due to viable tumor tissue). A semiquantitative approach allows the calculation of the so-called standardized uptake values (SUVs), which are distribution values without a unit. An SUV of 1 means a uniform tracer distribution. The semiquantitative data evaluation is based on regions of interest (ROIs) or volumes of interest (VOIs), which are representative areas with a high or a low tracer uptake or which serve as reference tissue. A VOI consists of more than two consequent ROIs. The SUVs are robust values, which can be easily calculated by dividing the activity concentration in an ROI or VOI by the rate of the injected dose and body weight.

More sophisticated evaluation procedures may be applied in dynamic data acquisition. Using the VOI technique, time activity curves can be created for the target area (e.g., tumor) and for the reference tissue. Furthermore, a VOI in an arterial vessel (input) is required in order to perform a pharmacokinetic data analysis. Based on compartment models, which originated from the pharmacology, transport rates can be calculated depending on the radiopharmaceutical used. In FDG, the most common radiopharmaceutical used for PET studies is applied: a two-tissue compartment model with a blood compartment. The first compartment represents the transport of nonmetabolized tracer in tissue (by glucose transporters), whereas the second compartment describes the first metabolic step, namely, the phosphorylation of FDG (by hexokinases). The parameters that can be calculated by the two-tissue compartment model are fractional blood volume (VB) as well as the transport rates for FDG transport (k1, k2) and phosphorylation (k3, k4). Noncompartmental models may also be applied to a dynamic data set, such as principal component analysis, Fourier transformation, similarity mapping, or calculation of the fractal dimension. Advantages of noncompartmental methods are the reproducibility of results and the fact that no input function is needed.

Applications

PET is used in oncology, cardiology, and neurology. Although PET was started in neurology, the main application for PET is oncology.

Oncology

For oncological studies, the radiopharmaceutical fluorine-18-fluorodeoxyglucose (FDG) is mainly used. FDG is taken up by malignant tumors and can therefore be used for diagnosis, staging, and monitoring of treatment effects following primarily chemotherapy and also radiation therapy (1). In particular, diagnosis of tumor recurrence is the domain of PET with FDG (Fig. 2). Aggressive tumors accumulate FDG and can be visualized without problems. Problems may arise in slow-growing (so-called grade I) tumors, like soft tissue sarcomas, prostate carcinomas, well-differentiated hepatocellular carcinomas, or neuroendocrine tumors, which may not accumulate glucose.

Other radiopharmaceuticals, like O-15-water, are used in clinical studies for measurements of tumor perfusion or for assessment of the access to a tumor using

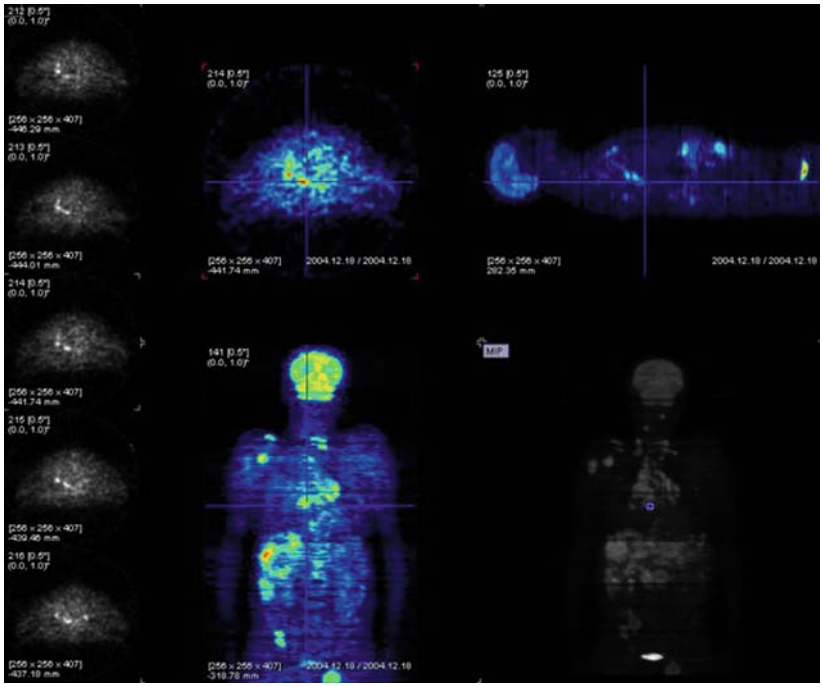

Positron Emission Tomography. Figure 2 FDG-PET study in a patient with multiple metastases of a melanoma. Upper row: Left: Transversal image of the thorax demonstrating lung metastasis and mediastinal lymph node metastases. Right: Corresponding sagittal image of the same level. Lower row:Left: Corresponding coronal view of the same patient. Right: Maximum intensity projection images (MIP).

a systemic or an intra-arterial application of a radiopharmaceutical (2).

Labeled cytostatic agents, like F-18-fluorouracil, N-13-cisplatin, F-18-paclitaxel, and others, are used in experimental studies to examine pharmacokinetics *in vivo*.

Labeled peptides, like Ga-68-DOTATOC, a substrate for the somatostatin receptor II, are used in neuroendocrine tumors for tumor visualization and therapy planning.

Labeled amino acids, like C-11-methionine, which reflect the amino acid transport, are in use for the visualization of brain tumors, particularly for high-grade gliomas.

Neurology

PET enables the examination of brain functions. Brain studies are performed by FDG to assess glucose metabolism. A reduction of FDG in the brain is associated with a brain dysfunction, such as epilepsy or Alzheimer disease. Perfusion studies with O-15-water are used for the study of brain perfusion. For the diagnosis of movement disorders, as in Parkinson's disease, dedicated radiopharmaceuticals like F-18-dihydroxyphenylalanine (F-18-DOPA) have been developed. F-18-DOPA is taken up by the dopaminergic neurons and provides information about the function of presynaptic dopaminergic receptors. For the detection of an epileptogenic focus, C-11-raclopride (a D2-repeptor ligand) is used. C-11-Flumazenil (FMZ) is applied for the detection of an epileptogenic focus. FMZ binds to GABA (-aminobutyric acid), the principle inhibitory neurotransmitter in the brain, which is reduced in epilepsy.

Cardiology

PET with FDG is primarily used for cardiac studies to detect the viability of the myocardium. Other radiopharmaceuticals like O-15-water or N-13-ammonia can be used for cardiac perfusion studies.

Fusion Images

The accurate anatomic localization of PET findings often requires knowledge of the morphology. Morphological, tomographic imaging modalities, like computed tomography (CT) and magnetic resonance imaging (MRI) are used for the allocation of PET images. The combination of anatomic and functional imaging information can be performed using three methods:

1. Site-by-site evaluation: The fusion of anatomic and morphologic imaging modalities is made mentally by the physician.

Positron Emission Tomography. Table 1 Physical characteristics of commonly used positron emitters

Isotope	Half-Life (min)	Max. Energy (Mev)	Range (mm) in H_2O
Flourine-18	110	0.635	2.4
Carbon-11	20	0.96	4.1
Nitrogen-13	10	1.19	5.4
Oxygen-15	2	1.73	7.3
Gallium-68	68	1.9	8.1

Positron Emission Tomography. Table 2 Selected PET radiopharmaceuticals in clinical and experimental use

^{18}FDG	Glucose metabolism, myocardial viability, epilepsy, tumor
^{18}F-dihydroxyphenylalanine (FDOPA)	Dopamine pool, decarboxylase activity, amino acid transport
^{18}F-FET	Amino acid transport
^{18}F-fluoride	Bone metastases
^{11}C-methionine	Tumor, protein synthesis
^{11}C-ethanol	Tumor, pharmacokinetics
^{18}F-Fluorouracil	Tumor, pharmacokinetics
^{18}F-Fluorodeoxythymidine (FLT)	Proliferation
^{11}C-aminoisobutyric acid (AIB)	Tumor, amino acid transport (A-type)
N-methyl-^{11}C-flumazenil	Benzodiazepine receptor, epilepsy
O-methyl-^{11}C-raclopride	Dopamine D2 receptor
^{82}Rb	Myocardial perfusion
$H_2{}^{15}O$	Perfusion
^{11}C-acetate	Metabolism
^{13}N-NH_3	Perfusion
^{68}Ga-DOTATOC	Somatostatin receptor expression

2. Software-based fusion: Based on appropriate algorithms (mostly mutual information), anatomic images (e.g., CT or MRI) can be fused using dedicated software packages.
3. Hard fusion: Is based on combined PET/CT machines. Both studies are performed sequentially with a combined system consisting of a CT and a PET scanner.

References

1. Gambhir SS, Czernin J, Schwimmer J et al (2001) A tabulated summary of the FDG PET literature. Nuclear Pharmacy, pp 39–52 In: James H Thrall, Harvey A Ziessman (eds) Nuclear Medicine: the Requisites, Mosby-Year Book, Inc., 1995, St. Louis, Missouri J Nucl Med 421S–93S
2. Strauss LG, Conti PS (1991) The applications of PET in clinical oncology. J Nucl Med 32:623–650

Post-necrotic Cirrhosis

Cirrhosis of the liver following diffuse necrosis of liver cells especially as a result of hepatitis. The process is initiated by necrosis, followed by connective tissue formation and nodular regeneration, leading to distortion of the lobar and vascular liver architecture.

▶Cirrhosis, Hepatic

Posterior Rectocele – Posterior Perineal Hernia

▶Pelvic Floor Dysfunction, Anorectal Manifestations

Posterior Urethral Valve

Obstruction of the posterior urethra by a congenital valve, a severe condition often associated with refluxing or obstructive uropathy and renal dysplasia, mostly seen in baby boys.

▶Hydronephrosis in Childhood

Postoperative

Klaus K. Gast
Department of Radiology, Mainz University Hospital, Mainz, Germany
kgast@radiologie.klinik.uni-mainz.de

Synonyms

Fibrothorax; Lobectomy; Lung resection; Lung transplantation; Lung volume reduction; Pneumonectomy; Serothorax

Definition

The postoperative chest describes any condition after surgical treatment during which at least one of the

thoracic cavities has been opened or parts of the thoracic wall have been resected.

In lung resection a part of the lung is surgically removed. This part can be represented by a lung lobe, a segment or subsegment. Resections in which lobar or segmental borders are respected are called typical, those which ignore them are called atypical. Resection of a whole lobe is called a lobectomy. Resection of all two or three lobes is called a pneumonectomy. Lung resections are performed for the elimination of benign or malignant masses, or for treatment of interstitial lung disease. This latter form of lung resection is called lung volume reduction and is most often performed in pulmonary emphysema. It describes the surgical removal of parts of the lung which are most severely affected to allow better ventilation of parts which are less involved.

When smaller parts of a lung are removed, the remaining tissue fills out the extra space (Fig. 1). The removal of lobes or a whole lung leaves a space which can be too large to be filled by the remaining lung tissue. In this case, the extra space is filled by fluid. This condition is called a serothorax. The later invasion of connective tissue converts the serothorax into a fibrothorax.

In end stage lung disease the ultima ratio form of therapy is to replace the diseased lung by a healthy one. This kind of therapy is called lung transplantation. For transplantation one can use double or single lungs, in children also lung lobes or a bloc of heart and lungs. Most grafts are extracted from cerebrally dead organ donors. In rare cases living related donors may donate single lobes usually for children.

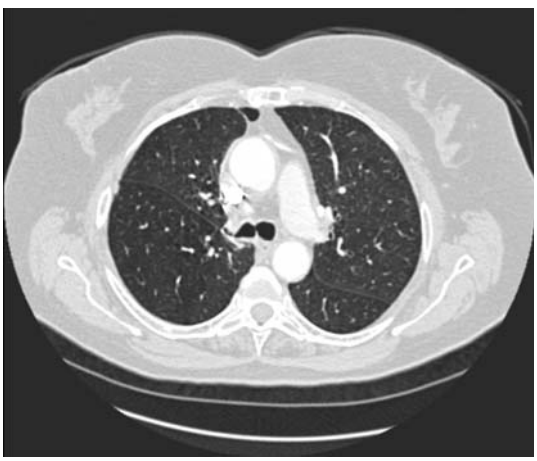

Positron Emission Tomography. Figure 1 69-year old female patient after upper lobectomy on the right for bronchial carcinoma. CT shows anterior displacement of the lobar fissure and mild hyperventilation of the right lower lobe (*n* = 3).

Pathology/Histopathology

The postoperative thorax is characterized by different stages of wound healing. In early stages the remaining cavity is filled with blood and protein containing fluid. Granulocytes induce the cellular invasion which continues with the appearance of macrophages and lymphocytes. From the margins of the wound capillaries begin to grow into the defect zone and connective tissue is formed by proliferation of fibroid cells. This formation of connective tissue also begins at the margins and succeedingly fills out the defect zone. Later stages are characterized by consecutive forming of collagen type I fibres and decreasing cell progeny. The concluding shrinking process of the connective tissue forms the chronically remaining scar by reduction of the fluid content.

This process of healing concerns the repair of soft tissue defects in the thoracic walls after surgical treatment as well as the thoracic cavity itself after lung resections, transplantations or pneumonectomies. If small defects can heal primarily, a small, linear scar forms which provides good functional and cosmetic properties. In larger defects greater amounts of fluid invade the remaining defect zone, later an amount of scar tissue persists which depends on the size of the defect. Thus, a pneumonectomy results in a large amount of intrathoracic blood and fluid which is called a serothorax. The final stage of the reparatory process with persisting scar tissue in the thoracic cavity is called a fibrothorax. In the clinical setting over a long time a mixture of fibrous and fluid fractions persists. This combined stage of wound healing is called a fibroserothorax. The shrinkage of the scar tissue causes a volume loss of the concerned hemithorax. This results in a mediastinal shift and herniation of the contralateral lung with regional overinflation.

Lung transplantation produces a unique histopathologic situation due to the different presentation of HLA-antigens on the cellular surface of the grafted organ. The usual clinical setting implements human organ donation and subsequently a situation of allo-transplantation. This situation describes transplantation of organs of the same species which are genetically different. It determines different forms of organ rejection. Hyperacute rejection occurs in patients who have antibodies against the graft. Antibody activation in this case leads to intravascular thrombosis and coagulation due to endothelial damage. Consecutively, pulmonary oedema and alveolar hemorrhage occur. Acute rejection in contrast happens by activation of T-cells by the foreign major histocompatibility complex presented on the surface of endothelial cells or temporally resident leukocytes. It leads to perivascular or peribronchial/peribronchiolar mononuclear and lymphoid cell infiltration. More severe forms

show wide infiltration of the alveolar septae and spaces with consequent necrosis and diffuse alveolar damage. Chronic graft rejection is mediated by mononuclear cell infiltration and proliferation of myofibroblasts. It concerns primarily small peripheral airways. The infiltration as well as the deposition of collagen matrix leads to a process called obliterative bronchiolitis.

Clinical Presentation

All patients surgically treated within the thorax present with a different extent of dermal scarring. Thoracic deformity, possibly combined with scoliosis and unilateral elevation of the shoulder, results after larger resections, such as lobectomy or pneumonectomy. Also resections of the thoracic walls produce thoracic deformities. Shortness of breath on exertion can occur both due to thoracic deformities as well as to lung volume loss after resections, especially lobectomy or pneumonectomy. Lung transplant recipients usually present with similar symptoms. Complications of transplantation such as infections or graft rejection present with unspecific symptoms, such as with fever or subfebrile temperatures, cough and shortness of breath.

Imaging

The initial imaging modality in all postoperative chest patients is the chest radiograph (Fig. 2). It is used for follow-up of the early postoperative period, monitoring of pulmonary congestion or oedema, infections, pleural effusions and pneumothoraces. Later indications include the follow-up of patients after tumor resection, the development of fibro- or serothoraces and the initial exclusion of complications after lung transplantation.

CT of the chest is widely used in patients in whom the chest radiograph did not clarify a clinical suspicion or reveals unclear findings because the sensitivity of CT for most intrapulmonary and soft tissue complications of postoperative chest patients is much higher than for chest radiography. The assessment of lung transplant recipients by CT is nevertheless limited by its moderate sensitivity for graft rejection. In these immuno-compromised patients with unspecific symptoms CT is mostly used for the exclusion of pneumonia. Additional scans taken in expiration are performed for the detection of air trapping, which is caused by expiratory collapse of peripheral airways and can be a sign of bronchiolitis obliterans or bronchiolitis obliterans syndrome.

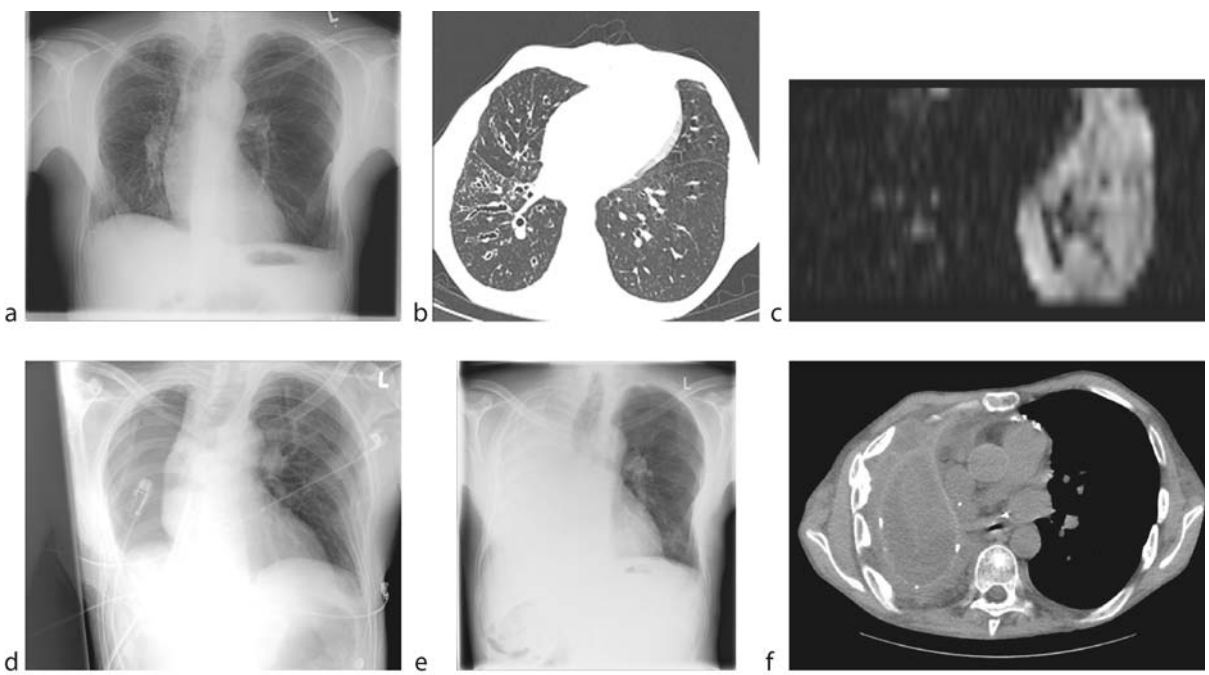

Positron Emission Tomography. Figure 2 37-year old male patient after double lung transplantation due to cystic fibrosis and left sided retransplantation because of chronic graft rejection. (a) Cchest radiograph shows mediastinal shift to the rejected right lung as well as compensatory overinflation of the retransplanted graft on the left. (b) CT shows marked cylindric bronchiectasis as sign of advanced bronchiolitis obliterans in ongoing chronic rejection. (c) Transversal reformat of ^{3}He-MRI reveals good ventilation of the normal left regraft and poor to nonexistent ventilation of the rejected graft on the right. (d) First chest radiograph after pneumonectomy of the rejected graft shows pneumoserothorax on the right and a mediastinal shift to the operated side. (e, f) Progressive conversion to a fibroserothorax shown by chest radiograph and CT.

The role of ultrasound is usually limited to the early postoperative period for the determination of pleural effusions and their volumes.

Diagnosis

In the early postoperative period complications after thoracic surgery are routinely diagnosed by chest radiography. Images show pleural effusions as well as hematothoraces, pneumonias, and congestion. Laboratory values are often helpful in the differential diagnosis. Pleural effusion for example cannot be differentiated from hematothorax on a chest x-ray. A follow up of the hemoglobin concentration helps with the differentiation. Leucocyte counts and c-reactive protein levels help in the differentiation between pneumonia and atelectasis. Measurements of the central venous pressure can assess the severity of congestive heart failure. CT differentiates proteinous fluid and blood in their density. It can often differentiate between atelectasis and pneumonia and shows the extent of a pleural effusion much better than the chest radiograph.

Later complications in postoperative chest patients are usually diagnosed by their clinical history and clinical symptoms such as fever, cough, wheezing and shortness of breath. Further diagnostic steps are chest radiographs, blood tests and CT similar to the early postoperative period. Lung function tests may help in patients with further complicating diseases such as pulmonary emphysema, chronic obstructive pulmonary disease, cystic fibrosis or pulmonary fibrosis.

Lung transplant recipients instead are routinely monitored by pulmonary function tests. Usually a chest radiograph is performed to rule out pulmonary infections. An otherwise unexplained decrease of the forced expiratory volume in one second is a hint for the presence of either acute or chronic graft rejection. CT should be performed early to rule out other reasons.

Interventional Radiological Treatment

Drainage of pleural effusion, thoracic empyema or abscesses after surgical therapy of the chest is a routinely performed intervention and is usually performed under CT guidance. Nevertheless, pleural effusions may be drained blindly. Afterwards a chest radiograph has to be performed to rule out pneumothorax. Regarding the preoperative period, CT guided biopsies are often performed for histopathologic diagnosis and decisions for surgical versus conservative treatment.

Bibliography

1. Riede UN, Wiestler OD, Mueller HJ (1993) Stoerungen des Zellwachstums. In: Riede UN, Schaefer HE (eds) Al lgemeine und spezielle Pathologie. Thieme Verlag, Stuttgart, Germany, pp 327–392
2. Rose ML, Hutchinson IV (2003) Immunological mechanisms of graft injury. In: Banner NR, Polak JM, Yacoub M (eds) Lung transplantation. Cambridge University Press, Cambridge, UK, pp 185–204
3. Burke MM (2003) Transplant pathology. In: Banner NR, Polak JM and Yacoub M (eds) Lung transplantation. Cambridge University Press, Cambridge, UK, pp 294–325

Postoperative Intestinal Disease

▶Small Bowel, Postoperative

Postoperative Small Bowel Leak

▶Small Bowel, Postoperative

Postoperative Small Bowel Obstruction

▶Small Bowel, Postoperative

Potter Syndrome

Congenital bilateral renal agenesis or MCDK that leads to severe oligo-anhydramnion and consecutive changes in fetal proportion and face, not compatible with extrauterine life. Do not confuse this with the Potter classification that has been the major.

▶Cystic Disease, Renal Childhood (MCDK, PCKD)

Precalyceal Canalicular Ectasia

▶Medullary Sponge Kidney

Precocious Puberty

In a girl, it is defined as the development of secondary sexual characteristics (breast tissue, pubic and axillary hair, external genitalia, and menses) before 8 years of age.
▶Genital Tract

Prenatal MRI

▶Fetal Imaging

Preoperative lymphoscintigraphy

The preoperative lymphoscintigraphy is the scintigraphic visualization of the SLNs, using gamma camera, after the injection of a radiotracer. It is well validated in melanoma. In contrast, the role of lymphoscintigraphy is controversial in breast cancer.
▶Sentinel Node, Scintigraphy

Presacral

Anterior to or preceding the sacrum.
▶Teratoma, Childhood

Priapism

Räto T. Strebel[1], Hubert John[2]
[1]Department of Urology, University Hospital Zurich, Zurich, Switzerland
[2]Klinik Hirslanden, Leiter Zentrum für Urologie, Zurich, Switzerland
raeto.strebel@usz.ch

Definition

Priapism is a persistent penile erection that continues hours beyond (commonly erections greater than 4 h in duration) or is unrelated to sexual stimulation (1). Two subtypes of priapism, i.e., low-flow and high-flow priapism are distinguishable.

1. Low-flow priapism (veno-occlusive, ischemic): This subtype is characterized by little or no blood flow in the corpus cavernosum and decreased outflow. Consequently, cavernous blood gas analysis reveals hypoxic, hypercarbic, and acidotic values. There is a wide variety of etiologic factors that may trigger this functional disorder.
2. High-flow priapism (arterial, nonischemic): Typically, normal cavernous blood gas values are present and the persistent erection is caused by an abnormally high arterial inflow. Vascular abnormalities and penile and perineal trauma are the most common causative factors.

Clinical Presentation

There is not much doubt about the clinical presentation of patients with a priapism. On clinical examination, patients with a low-flow (ischemic) priapism show typically rigid and tender corpora cavernosa and complain of pain. In contrast, patients with a high-flow (nonischemic) priapism usually present with a penis that is neither fully rigid nor painful. In both forms, on palpation the corpus spongiosum and glans penis are not affected. For the management of priapism it is of predominant importance to distinguish between high- and low-flow priapism. It is therefore very important to perform an analysis of the cavernous blood gases.

Imaging

Additionally to the blood gas testing a color Doppler ultrasonography of the cavernosal arteries might be helpful in differentiating between high- and low-flow priapism. Very low or absent arterial inflow is indicative for a low-flow priapism. Once the diagnosis of a high-flow priapism is established, a penile arteriography should be performed if the priapism does not resolve. Vascular abnormalities can be identified and treated accordingly to decrease the abnormally high arterial inflow.

A patient with a persistent high-flow priapism with failure to conservative treatment should be referred to a skilled interventional radiologist for superselective embolization of vascular abnormalities or cavernous arteries.

Bibliography

1. Montague DK, Jarow J, GA Broderick et al (2003) American Urological Association guideline on the management of priapism. J Urol 170(4 Pt 1):1318–1324.

Primary Biliary Cirrhosis

Cirrhosis of the liver due to inflammation or obstruction of the bile ducts resulting in the accumulation of bile and functional impairment of the liver. In secondary biliary cirrhosis hypertrophy of the caudate lobe is the predominant feature and may have a pseudotumoural appearance. At unenhanced computed tomography, the caudate lobe shows a higher density with respect to the atrophic right lobe. Furthermore dilatation of the biliary tract and intrahepatic lithiasis is present.

▶Cirrhosis, Hepatic

Primary Circulatory Liver Disorders

▶Vascular Disorders, Hepatic

Primary Gout

▶Gout

Primary Hyperparathyroidism

This pathology is caused by increased secretion of parathyroid hormone (PTH) induced by overactive parathyroid glands, most frequently an adenoma of these glands.

▶Hyperparathyroidism

Primary Hypertrophic Osteoarthropathy

A rare hereditary or idiopathic disease characterized by thickening of the skin (pachydermia), periostitis, arthritis, and bilateral clubbing of the digits on the hands and feet.

▶Hypertrophic, Osteoarthropathy

Primary Malignancies of the Liver of Mesenchymal Origin

▶Hepatic Sarcoma

Primary Malignant Hepatocellular Tumor

▶Hepatocellular Carcinoma

Primary Malignant Neoplasm of Ovary

▶Carcinoma, Ovarium

Primary Muscle Abscess

▶Infection, Soft Tissue

Primitive Neuroectodermal Tumors

▶Neoplasms, Chest, Childhood

Prognostic Outcome

This is influenced by staging at presentation and anatomical site of the tumor as well as histological grade. A preferred international staging system is the American Joint Committee on Cancer (AJCC).

▶Neoplasms, Soft Tissues, Malignant

Progressive Familial Cholestasis

▶Congenital Malformations, Bile Ducts

Progressive Multifocal Leukoencephalopathy

A destructive demyelinating infection which occurs with increased incidence in HIV positive and patients with immunsuppression.
▶Infection, Opportunistic, Brain

Projection

The transformation of a three-dimensional object into its two-dimensional image by integrating the physical property that determines the image along the direction of the projection beam.
▶Scintigraphy

Projection Beam

The smallest possible volume in which the physical property that is to be measured is integrated during the measurement process. Its shape is limited by spatial resolution in all three dimensions.
▶Scintigraphy

Proliferation of Neoplasms

Roland Bares, H. Dittmann
University of Tuebingen, Otfried-Muller-Str. 14
bares@uni-tuebingen.de

Synonyms

Cell doubling; Cell growth

Definitions

In biology and medicine, the phrase *proliferation* refers to the growth of cell populations by means of cell division. During the process of proliferation, one "parent" cell divides into two "daughter" cells. The process of cell proliferation consists of two major parts. In the first part, which takes place during the S-phase of the ▶cell cycle, the DNA of the parent cell is replicated. In the second part, during the mitosis phase, the duplicated DNA is separated into two equally sized groups of chromosomes, followed by the division of the entire cell, called cytokinesis.

The synonym *cell growth* may also refer to an increase in cell size *without* an increase in number. However, when used in the context of proliferation, "cell growth" means growth of cell populations by cell reproduction.

The phrase *neoplasm* describes any abnormal tissue mass arising from transformed cells. Neoplasms can be benign or malignant. The most common type, melanocytic nevus ("beauty spot"), is benign. In clinical medicine, however, neoplasm usually means a malignant tumor.

This article is deliberately restricted to malignant neoplasms, as nuclear medicine imaging of proliferation is almost exclusively focused on malignant tumors.

Characteristics

The Significance of Proliferation in Normal and Malignant Cells

Proliferation is a key factor for understanding the natural history of a malignant tumor as well as its response to treatment. However, proliferation is not at all restricted to malignant cells. It is a typical feature of any living organism and a necessary precondition for growth as well as for maintenance of normal function. Most human cells are differentiated cells. They are specialized to fulfill specific functions as part of the well-organized functional network of the human body.

Cells usually die after a few cell cycles. Because death of differentiated cells is genetically determined (referred to as planned cell death or apoptosis), cell lifetime can vary between a few hours up to many years; it mainly depends on the specific type of cell. Many highly differentiated cells do not undergo further replication at all. These cells are known as terminally differentiated cells. For the remainder, cell reproduction is necessary to maintain homoeostasis. This is achieved by initiating a pool of stem cells to proliferate and form differentiated cells. In normal tissue, the amount of proliferation is fine-tuned to the actual need by factors stimulating or suppressing cell replication. This control is lost in most malignant tumors.

Besides the ability to invade other tissues and form metastases, the growth rate resulting from loss of control

is the most important feature to describe the aggressiveness of a given tumor. In other words, the higher the proliferation rate, the faster an (untreated) malignant tumor will lead to death. Essential mechanisms to treat a tumor successfully by chemotherapy or ionizing irradiation are (i) to (re-)activate signaling for apoptosis and (ii) to damage vital cell functions involved in the process of proliferation. Hence, stopping or slowing down tumor cell proliferation is a major goal of cancer therapy.

Proliferation Assays

Because of the importance of proliferation for both prognosis and treatment of neoplasms, investigators have long tried to measure tumor cell growth in patients. Analyzing tumor size affords repetitive measurements, is time-consuming, and lacks precision. Other determinants often used in experimental situations, such as tumor weight or cell counts, are not applicable to clinical medicine. Therefore, tests have been developed to measure proliferation in tumor samples.

By staining tumor DNA, cell division can be visualized at the latest stage of the cell cycle—at mitosis when chromosomes are divided to form two daughter cells. Using light microscopy, the percentage of cells undergoing mitosis can be calculated and expressed as the mitotic index of a tumor. Since the mid-1960s, investigators have targeted DNA replication as a characteristic feature of tumor proliferation. The radiolabeled nucleoside thymidine (tritiated thymidine or H-3-thymidine) is incorporated into DNA during the S-phase, forming the DNA base T, which pairs with a adenosine in double-stranded DNA. To measure thymidine incorporation, patients have to be injected before tumor resection, or living tumor cells have to be explanted and incubated under stable conditions. It has been shown that the amount of H-3-thymidine incorporated into cells strongly correlates with DNA synthesis. H-3-thymidine labeling can only be performed using viable cells, and any change in growth conditions might severely affect the test results. Despite these shortcomings, the test is still considered the gold standard for measuring proliferation in experimental settings.

To obtain information on proliferation in clinical situations, investigators have focused on simpler methods that can be performed on fixed tumor samples. Two tests have gained wide acceptance. They both use antibodies against cellular antigens associated with proliferation. The proliferating cell nuclear antigen (PCNA) is a 36 kDa molecular-weight protein also known as cyclin' (1). The protein is synthesized in early G1 and S-phases of the cell cycle. PCNA is present in two basic forms, a soluble form sensitive to organic fixation that is not involved in DNA replication, and a second form that is insoluble and associated with ongoing DNA synthesis. The expression of the Ki-67 protein is also strongly associated with cell proliferation (2). The fact that Ki-67 is present during all active phases of the cell cycle (G1, S, G2, mitosis) but absent in resting cells (G0) makes it suitable to determine the growth fraction of cell populations. Although the functional significance of Ki-67 is still unclear, findings indicate that Ki-67 expression is required for progression through the cell cycle.

Both Ki-67 and PCNA can be visualized in formalin-fixed and paraffin-embedded tissue ("antigen retrieval"). Therefore, these tests are frequently used routinely and can be regarded as the current standard for immunohistochemical characterization of tumor cell proliferation. Because their results are derived from small tumor samples, they might not be representative for the entire tumor burden of a given patient.

Nuclear Medicine Imaging

In contrast to the above-mentioned *in vitro* proliferation assays, nuclear medicine procedures have the potential to image the biological behavior of all of a patient's tumor sites without invasive biopsies. Furthermore, nuclear medicine tests can be easily repeated during treatment to monitor the response to therapy. Positron emission tomography (►PET) appears to be the method of choice to fulfill this aim. It is quantitative and therefore suitable for detecting subtle changes of molecular processes under treatment, and it provides optimal image quality because of high spatial resolution. Having short-lived positron-emitting isotopes such as carbon-11 or fluorine-18 available, various organic molecules can be radiolabeled to characterize cell function.

Today, fluorine-18 deoxyglucose (►FDG) is generally accepted as the best radiopharmaceutical for PET imaging of malignant neoplasms (3). This is due to its high uptake by most solid tumors and hematological malignancies and its comparably low background activity in most normal tissues (except for brain and kidney). FDG-PET uses the increased glycolytic activity of cancer cells. FDG is transported into cells by glucose transporters and subsequently phosphorylated to FDG-6 phosphate by hexokinase. Further metabolism occurs very slowly, causing metabolic trapping of FDG in the cells. It has been known for a long time that tumors largely depend on glucose as an energy substrate. Therefore, tumor uptake of FDG is interpreted to represent energy consumption of tumor cells. Obviously, the faster tumors grow, the more glucose they will consume. This view is supported by positive FDG-PET findings in practically all fast-growing tumors. In contrast, it has been shown that FDG-negative malignancies are usually highly differentiated tumors with a low proliferative activity. Among them are slow-growing

tumors such as differentiated thyroid cancer and low-grade lymphomas. However, some of them reveal intense FDG uptake similar to that seen in rapidly growing neoplasms. In addition, experimental studies (4) have shown that FDG accumulation may remain stable in tumor cells after stimulation of proliferation. Thus, FDG is not considered to reliably reflect the proliferative state of malignant tumors.

More recently, investigators have focused on DNA replication, particularly pyrimidine metabolism similar to the classic H-3-thymidine assay (see earlier), to develop a proliferation marker that can be measured by PET. Preliminary *in vitro* data (4) showed that following radiotherapy or chemotherapy, uptake of radiolabeled thymidine decreases more rapidly than that of FDG, indicating the potential use of thymidine as marker for treatment response. Using carbon-11 as a positron emitter, thymidine can be labeled for PET imaging. *In vitro*, this compound is incorporated into DNA, correlating with proliferation as measured by the H-3-thymidine assay. Initial clinical studies in patients with small-cell lung cancer treated by chemotherapy demonstrated a rapid decline of uptake exceeding that of FDG. However, interpretation of C-11-thymidine PET studies is impaired by various radiolabeled metabolites occurring due to the rapid degradation of C-11-thymidine in humans. 3′-deoxy-3′-[^{18}F]fluorothymidine (►FLT) (5), an analog of thymidine, exhibits better *in vivo* stability. FLT is a substrate of the thymidine kinase 1 (TK-1), which phosphorylates FLT to FLT-5-phosphate. A significant correlation between TK-1 expression and cellular FLT accumulation has been shown for several tumor cell entities. Pilot studies in humans showed intense FLT uptake in a number of malignant tumors but also in normal bone marrow and liver. The latter could be attributed to a glucoronidated metabolite.

While some authors have reported a correlation between FLT uptake and Ki-67 staining (see earlier) in solitary pulmonary nodules and lung cancer, such an association was not confirmed in other malignant tumors. A number of animal studies showed that FLT uptake decreased early after chemotherapy (3). However, FLT uptake was also shown to be *increased* in tumor cells successfully treated with antimetabolites such as 5-fluoro-uracil or methotrexate. Such an increase could be due to induction of TK-1 activity involved in the salvage of thymidine reactive to the block of *de novo* DNA synthesis induced by this group of chemotherapeutic agents. Thus, in such treatment FLT appears not to be suitable for measuring cell proliferation.

Conclusion

Noninvasive evaluation of tumor cell proliferation is a highly attractive goal for tumor imaging. Together with emerging new treatment modalities, it becomes more and more relevant to characterize tumors before and during therapy to distinguish responders from nonresponders as early as possible. PET with FLT is a possible approach to fill this diagnostic gap, although many aspects of FLT imaging are still under study and not completely understood. Ongoing studies will have to show whether FLT or other compounds will be able to gain significance as prognostic markers or probes to monitor tumor response to treatment.

Bibliography

1. Hall PA, Levison DA, Woods AL et al (1990) Proliferating cell nuclear antigen (PCNA) immunolocalization in paraffin sections: an index of cell proliferation with evidence of deregulated expression in some neoplasms. J Pathol 162:285–294
2. Scholzen T, Gerdes J (2000) The Ki-67 protein: from the known and the unknown. J Cell Physiol March 182(3):311–322
3. Czernin J, Weber WA, Herschman HR (2006) Molecular imaging in the development of cancer therapeutics. Annu Rev Med 57:99–118
4. Higashi K, Clavo AC, Wahl RL (1993) Does FDG uptake measure proliferative activity of human cancer cells? *In vitro* comparison with DNA flow cytometry and tritiated thymidine uptake. J Nucl Med 34:414–419
5. Shields AF, Grierson JR, Dohmen BM et al (1998) Imaging proliferation *in vivo* with [F-18]FLT and positron emission tomography. Nature Medicine 4:1334–1336

Proliferative Disorders of the Urethra

►Neoplasms, Urethra

Proliferosion

Proliferosion describes the coexistence of rheumatic inflammatory bony proliferation and destruction in one joint. It is seen in psoriatic arthritis.

►Spondyloarthropathies, Seronegative

Prostatic Adenocarcinoma

►Carninoma, Prostate

Prostatitis

Stijn W. T. P. J. Heijmink, Jurgen J. Fütterer
Department of Radiology, Radboud University, Nijmegen Medical Centre, Geert Grooteplein 10, The Netherlands

Synonyms

Male chronic pelvic pain syndrome; This term encompasses only the chronic nonbacterial form of prostatitis [i.e. type III of the NIH classification (1)]

Definitions and Epidemiology

Until recently epidemiological data on prostatitis was scarce. The prevalence and incidence figures of chronic prostatitis are spread, with prevalence ranging between 2–16% (2). Contrary to benign prostatic hyperplasia or prostate cancer, it may occur at any age, although the incidence increases with age (3). No impact of race on incidence was found. It was calculated that it compounded 8% of all visits to urologists in the United States (4). Thereby, it was associated with substantial economic health care costs and lower quality of life scores (5).

Classification

The National Institutes of Health (NIH) divided prostatitis into four main categories (1) (Table 1). Thereby, a distinction is made between acute and chronic as well as between symptomatic and asymptomatic prostatitis. It is unclear how large the prevalence of type IV prostatitis is, since men do not have any symptoms, although this may be as high as 32% (6).

Symptoms

Perineal pain, increased frequency of voiding, nightly voiding, as well as painful voiding are the most frequent symptoms of chronic prostatitis. Other symptoms can be pain during ejaculation or orchialgia (3, 7, 8). In acute prostatitis an acute onset of fever and severely tender prostate are present (9).

Etiology and Pathology

Acute and chronic bacterial prostatitis is most commonly caused by Gram-negative microorganisms, particularly *Escherichia coli* (9). In contrast, chronic nonbacterial prostatitis is a multifactorial syndrome. Possible factors revealed as factors leading to occult infection, a change in the prostatic epithelial surface or mucin production, neurogenic inflammation, mast cell activation and psychological stress (8, 10). Reports on autoimmune disturbances have not been conclusive in determining whether this is a factor. Another rarer form of prostatitis is granulomatous prostatitis which may be idiopathic, secondary to prostatic surgery or caused by *Myobacterium tuberculosis* (11).

For an in-depth review of the histopathological features of prostatitis, the authors refer the reader to the paper by Roberts et al. (9).

Diagnostic Imaging Techniques of Prostatitis

Transrectal ultrasound (TRUS)—In acute bacterial prostatitis in many cases an area of hypoechogenicity was found with high Doppler flow within and around the

Prostatitis. Table 1 The NIH classification system of prostatitis

Type	Classification	Features
I	Acute bacterial prostatitis	Episode
II	Chronic bacterial prostatitis	Recurrent
III	Chronic nonbacterial or abacterial prostatitis (also referred to as chronic pelvic pain syndrome)	Absence of detectable infection
A	Inflammatory	Leukocytes detected in semen, prostatic fluid or urine
B	Noninflammatory	Absence of leukocytes in semen, prostatic fluid or urine
IV	Asymptomatic inflammatory prostatitis	Absence of symptoms with presence of leukocytes in semen, prostatic fluid or urine

Source: Litwin MS, McNaughton-Collins M, Fowler FJ Jr, et al (1999) J Urol 162:369–375.

lesion. These abnormalities regressed during therapy (12). Also, a dark halo around the urethra which did not regress was observed. Prominent, engorged periprostatic veins were seen in half of the patients in the acute phase. In case of acute bacterial prostatitis, TRUS can be used for treatment follow-up by determining whether the prostate volume decreases (13, 14), although some authors propose to use TRUS only to exclude prostate abscesses.

In a case–control study, on color Doppler TRUS an enhanced blood flow to the prostatic capsule and diffuse flow in the parenchyma was observed compared with patients without chronic prostatitis and healthy volunteers (15). In areas of focal hypervascularity on color Doppler TRUS in the peripheral zone of the prostate, the chance of detecting prostate cancer or prostatitis increased (16). In acute prostatitis, the enhancement occurred particularly around the urethra, ejaculatory ducts, and close to the seminal vesicles (17). Other features that have been described were capsular thickening and irregularity (18), constant dilatation of the periprostatic venous plexus, dilated and elongated seminal vesicles with thickening of their inner septa, and bladder neck hypertrophy (19). Frauscher et al. reported that also chronic prostatitis could produce (multiple) areas that enhance after contrast agent administration, causing many false positive findings in detecting prostate cancer (20). The presence of prostatic calcifications is a strong indication of chronic prostatitis (Fig. 1; 21).

Magnetic resonance (MR) imaging—Few studies have been published reviewing the features of prostatitis on MR imaging. The greatest challenge is to differentiate it from prostate cancer because many MR imaging characteristics are applicable to both diseases. Both prostatitis and prostate cancer are recognizable by an area of lower signal intensity within the prostate gland (22, 23). MR imaging demonstrated indeterminate focal low signal intensity that was not nodular (contour deforming) in 58% of chronic prostatitis lesions that were greater than 6 mm in largest diameter (22) (Fig. 2). Features found in prostatitis were

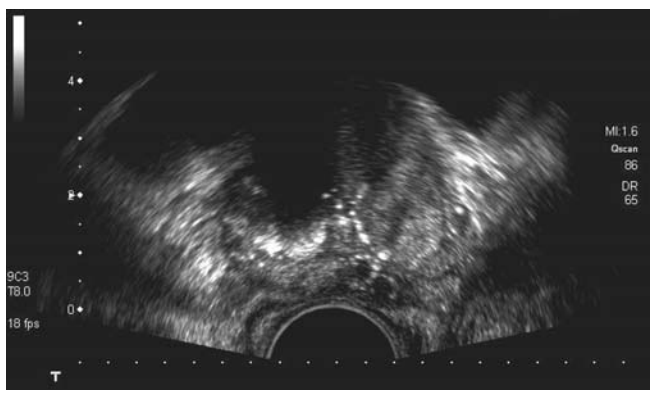

Prostatitis. Figure 1 Benign prostatic hypertrophy (BPH); Peripheral zone (PZ); Arrows are low signal intensity triangular areas (not nodular) indicating focal areas of prostatitis.

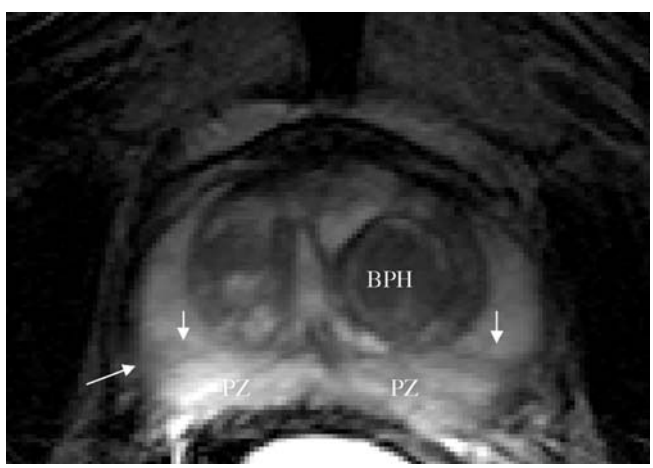

Prostatitis. Figure 2 Well-delimited areas with calcifications (*arrows*) in the right central gland ad to lesser extent in the left central gland of the prostate.

Prostatitis. Table 2 Features of chronic prostatitis and prostate cancer on MR imaging

Feature	Prostatitis	Prostate cancer
MR imaging		
Signal intensity on T2-weighted imaging	Low or equal to rest prostate	Mostly low
Diffuse or focal	Focal or diffuse	Focal
MR spectroscopic imaging		
Choline peak	Elevated	Elevated
Citrate peak	Reduced or absent	Reduced or absent

Source: Shukla-Dave A, Hricak H, Eberhardt SC et al (2004) Radiology 231:717–724.

transitional zone cysts, prostatic utricle cysts and abscesses of the seminal vesicles (Table 2) (24).

MR spectroscopic imaging of chronic prostatitis revealed that normal spectra in areas of chronic prostatitis were rare. Most areas exhibited the same features as prostate cancer: an elevated choline peak and reduced or absent citrate (22). This mimicking of prostate cancer by chronic prostatitis is a frequent cause of false-positive findings in prostate cancer diagnostics (Table 2).

Therapy

Acute and chronic bacterial prostatitis—Antimicrobial treatment is the therapy of first choice in these patients (25). For acute prostatitis immediate parenteral bactericidal antibiotics ought to be initiated while for the chronic form high-dose oral administration for 4–6 weeks is proposed (26). After initiation of treatment, rarly (<48 h) vigilance about the presence of prostatic abscesses is strongly advised (12).

Chronic nonbacterial and asymptomatic prostatitis—No consensus has been reached on the treatment of these categories of prostatitis. The effect of antimicrobial therapy in chronic nonbacterial prostatitis has not been proven in randomized clinical trials. However, it was found to decrease the amount, frequency and severity of symptoms (27). Other therapies are alpha blockers (28), antiinflammatory agents, nonpharmaceutical therapies such as biofeedback and thermal therapies (29).

Bibliography

1. Litwin MS, McNaughton-Collins M, Fowler FJ Jr, et al (1999) The National Institutes of Health chronic prostatitis symptom index: development and validation of a new outcome measure. Chronic prostatitis collaborative research network. J Urol 162:369–375
2. Krieger JN, Riley DE, Cheah PY et al (2003) Epidemiology of prostatitis: new evidence for a world-wide problem. World J Urol 21:70–74
3. Schaeffer AJ (2003) Epidemiology and demographics of prostatitis. Andrologia 35:252–257
4. Collins MM, Stafford RS, O'Leary MP et al (1998) How common is prostatitis? A national survey of physician visits. J Urol 159:1224–1228
5. Calhoun EA, McNaughton CM, Pontari MA et al (2004) The economic impact of chronic prostatitis. Arch Intern Med 164:1231–1236
6. Carver BS, Bozeman CB, Williams BJ et al (2003) The prevalence of men with National Institutes of Health category IV prostatitis and association with serum prostate specific antigen. J Urol 169:589–591
7. Schaeffer AJ, Landis JR, Knauss JS et al (2002) Demographic and clinical characteristics of men with chronic prostatitis: the national institutes of health chronic prostatitis cohort study. J Urol 168:593–598
8. Eisenberg ER, Moldwin RM (2003) Etiology: where does prostatitis stop and interstitial cystitis begin? World J Urol 21:64–69
9. Roberts RO, Lieber MM, Bostwick DG et al (1997) A review of clinical and pathological prostatitis syndromes. Urology 49:809–821
10. Pontari MA, Ruggieri MR (2004) Mechanisms in prostatitis/chronic pelvic pain syndrome. J Urol 172:839–845
11. Naik KS, Carey BM (1999) The transrectal ultrasound and MRI appearances of granulomatous prostatitis and its differentiation from carcinoma. Clin Radiol 54:173–175
12. Kravchick S, Cytron S, Agulansky L et al (2004) Acute prostatitis in middle-aged men: a prospective study. BJU Int 93:93–96
13. Griffiths GJ, Crooks AJ, Roberts EE et al (1984) Ultrasonic appearances associated with prostatic inflammation: a preliminary study. Clin Radiol 35:343–345
14. Horcajada JP, Vilana R, Moreno-Martinez A et al (2003) Transrectal prostatic ultrasonography in acute bacterial prostatitis: findings and clinical implications. Scand J Infect Dis 35:114–120
15. Cho IR, Keener TS, Nghiem HV, et al (2000) Prostate blood flow characteristics in the chronic prostatitis/pelvic pain syndrome. J Urol 163:1130–1133
16. Newman JS, Bree RL, Rubin JM (1995) Prostate cancer: diagnosis with color Doppler sonography with histologic correlation of each biopsy site. Radiology 195:86–90
17. Veneziano S, Pavlica P, Mannini D (1995) Color Doppler ultrasonographic scanning in prostatitis: clinical correlation. Eur Urol 28:6–9
18. Doble A, Carter SS (1989) Ultrasonographic findings in prostatitis. Urol Clin North Am 16:763–772
19. Di Trapani D, Pavone C, Serretta V, Cavallo N, Costa G, Pavone-Macaluso M. (1988) Chronic prostatitis and prostatodynia: ultrasonographic alterations of the prostate, bladder neck, seminal vesicles and periprostatic venous plexus. Eur Urol 15:230–234
20. Frauscher F, Klauser A, Berger AP et al (2003) The value of ultrasound (US) in the diagnosis of prostate cancer. Radiologie 43:455–463
21. Ludwig M, Weidner W, Schroeder-Printzen I et al (1994) Transrectal prostatic sonography as a useful diagnostic means for patients with chronic prostatitis or prostatodynia. Br J Urol 73:664–668
22. Shukla-Dave A, Hricak H, Eberhardt SC et al (2004) Chronic prostatitis: MR imaging and 1H MR spectroscopic imaging findings—initial observations. Radiology 231:717–724
23. Beyersdorff D, Winkel A, Hamm B et al (2005) MR imaging-guided prostate biopsy with a closed MR unit at 1.5 T: initial results. Radiology 234:576–581
24. Atilla MK, Sargin H, Odabas O et al (1998) Evaluation of 42 patients with chronic abacterial prostatitis: are there any underlying correctable pathologies? Int Urol Nephrol 30:463–469

25. Fowler JE Jr (2002) Antimicrobial therapy for bacterial and nonbacterial prostatitis. Urology 60:24–26
26. Wagenlehner FM, Naber KG (2003) Antimicrobial treatment of prostatitis. Expert Rev Anti Infect Ther 1:275–282
27. Nickel JC, Downey J, Johnston B et al (2001) Predictors of patient response to antibiotic therapy for the chronic prostatitis/chronic pelvic pain syndrome: a prospective multicenter clinical trial. J Urol 165:1539–1544
28. Datta NS (2002) Role of alpha-blockers in the treatment of chronic prostatitis. Urology 60:27–28
29. Schaeffer AJ, Datta NS, Fowler JE Jr, et al (2002) Overview summary statement. Diagnosis and management of chronic prostatitis/chronic pelvic pain syndrome (CP/CPPS). Urology 60:1–4

Protein–Protein Interactions

Carmel T. Chan, Sanjiv Sam Gambhir
Stanford University School of Medicine,
Stanford, CA, USA
sgambhir@stanford.edu
carmelc@stanford.edu

Definition

Investigation of protein–protein interactions is the study of how, when and where proteins work with each other in biological process.

Importance of Protein–Protein Interactions in Biological Processes

Almost all cellular functions and activities involves proteins, which can act as enzymes in catalyzing the chemical reactions of metabolism, components of cellular machines in decoding genetic information and synthesizing proteins as well as regulating gene expression. Proteins can be localized in special cellular compartments or shuttle between the different compartments and acting as "messengers". Proteins work in concerto and constantly influence each others functions through different temporal and spatial interactions with one another. The interactions between different proteins that control many cellular functions are therefore interdependent. To understand the biological basis of different cellular events, it is essential to know and to understand the types of interactions that occur between the various proteins required for a given process. Even though isolation and structural characterization of all proteins that exist in the cell are necessary, it is not sufficient in explaining how they interact and assemble into the molecular machines. Therefore, identifying and studying different protein-protein interactions are indispensable in the understanding of the fundamentals of cellular process.

Methods for Studying Protein–Protein Interactions

Different methods have been developed to study protein–protein interactions, and can be classified into three different categories: *in vitro* essays with purified proteins and cell lysates, cell-culture studies and in living subjects (1). *In vitro* techniques include coimmunoprecipitation, gel-filtration chromatography, analytical ultracentrifugation, calorimetry, optical spectroscopy and the yeast two-hybrid system. Cell culture-based methods utilized for studying protein-protein interactions include the split ubiquitin system, Sos recruitment system, dihydrofolate reductase complementation, β-galactosidase complementation, split-GFP/split-luciferase reconstitution, β-lactamase complementation, G-protein fusion system and the resonance energy transfer (RET)-based systems, such as fluorescence RET (FRET) and bioluminescent RET (BRET). Furthermore, improvement in noninvasive technologies for detection of signals from deep tissues within the living subjects and the rapidly expanding field of molecular imaging have facilitated the investigation of protein–protein interactions occurring inside intact cells in small living animals. Imaging technologies including but not limited to bioluminescence imaging, fluorescence imaging, small animal positron emission tomography (PET), and small animal single photon emission computed tomography (SPECT) have been utilized to noninvasively image different classes of molecular events, including protein–protein interactions. Bioluminescence and fluorescence imaging depend on light transmission through the animal, while PET and SPECT depend on γ-ray transmission through the animal. Each of the above mentioned systems has its own merits and demerits, and some of methods that are most pertinent for studying protein–protein interactions are discussed in details below.

Modified Mammalian Two-Hybrid System

The yeast two-hybrid system is one of the most widely used assays to examine protein–protein interactions. The two interacting proteins of interest are individually fused to a DNA-binding domain (BD) and a transcription activation domain (AD) and expressed in yeast. Interactions between two proteins of interest lead to transcription of a reporter gene that is distal to binding sites for the BD (2). The yeast two-hybrid system has been adopted for mammalian cells by replacing the reporter gene and expression plasmids. An example of the modified mammalian yeast two-hybrid systems involves the investigation of the interactions between the transcription factors MyoD and Id in intact cells and in living animals. The plasmids

which carry the yeast GAL4 DNA-binding domain fused to the Id (GAL4-Id) and Herpes Simplex Virus VP16 activation domain fused to a segment of MyoD (VP16-MyoD) were expressed as the two hybrid proteins in 293T human embryonic kidney cells. Interaction between Id and MyoD in the hybrid proteins and subsequent binding of VP16 (in VP16-MyoD) to the GAL4 binding site in the minimal promoter containing the TATA box activates transcription of the Firefly luciferase (FL) reporter gene (Fig.1). The expression of the two hybrid proteins can also be transcriptionally modulated using a tumor necrosis factor-alpha (TNF-α) responsive promoter. In both cases, the protein expression and/activity of FL can be imaged in transfected cells in cell culture studies as well as cells implanted in nude mice, using D-Luciferin as the substrate and a cooled coupled-charge device (CCD) camera for optical bioluminescence imaging. The main limitation for the modified mammalian yeast two-hybrid system is the lack of real time measurement of protein–protein interaction since the two fusion proteins have to interact, translocate to the nucleus and activate the transcription of the reporter gene prior to any detectable FL activity. Furthermore, FL activity may persist long after the interactions between the fusion proteins cease.

Split Protein Strategies

Changes in the connectivity of amino acids can alter and form different protein conformations. Different split protein strategies have been used to examine the efficiency of real time protein–protein interactions based on the observation that functional proteins can be assembled from one or more noncovalently attached polypeptides. β-D-Galactosidase from Escherichia coli (*E. coli*) was a prime example of utilizing protein fragments coupled with an enzymatic assay to gauge protein–protein interactions (3). Each monomer of the tetrameric β-galactosidase protein can be cleaved into a small N-terminal ω-fragment (50–90 residues) and a large (135 kDa fragment) ω-fragment. With the addition of purified ω-fragment, dimers of enzymatically inactive, purified ω-fragments achieve a dynamic equilibrium to form a tetrameric active

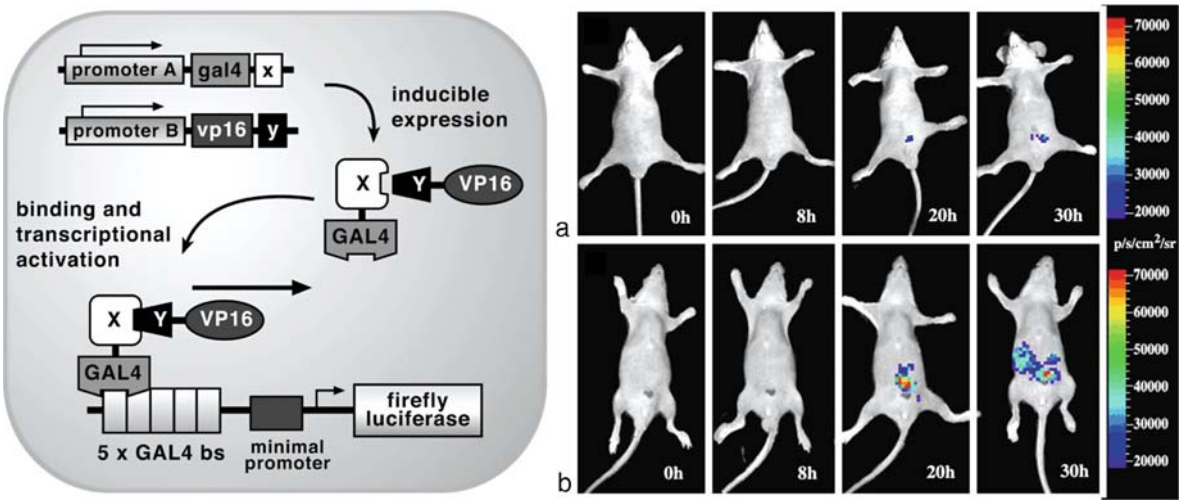

Protein–Protein Interactions. Figure 1 Imaging protein–protein interaction in living mice with a modified yeast two-hybrid strategy. Schematic diagram of the system for imaging the interaction of proteins X and Y. The first step involves the vectors pA-gal4-x and pB-vp16-y, which are used to drive transcription of *gal4-x* and *vp16-y* through use of promoters A and B. In the second step, the two fusion proteins GAL4-X and VP16-Y interact because of the specificity of protein X for protein Y. Subsequently, the GAL4-X-Y-VP16 binds to GAL4-binding sites (five GAL4-binding sites [bs] are available) on a reporter template. This leads to VP16-mediated transactivation of Firefly luciferase (FL) reporter gene expression under the control of GAL4 response elements in a minimal promoter. Transcription of the FL reporter gene leads to FL protein, which in turn leads to a detectable visible light signal in the presence of the appropriate substrate (D-Luciferin), ATP, Mg^{2+}, and oxygen. The NF-B promoter can be used for either pA or pB and TNF--mediated induction. *In vivo* optical CCD imaging of mice carrying transiently transfected 293T cells for induction of GAL4-X and VP16-Y fusion proteins. All images shown are the visible light image superimposed on the optical CCD bioluminescence image with a scale in photons/s/cm^2/steridian (sr). Mice in top row were imaged after injection of D-Luciferin but with no TNF--mediated induction. Mice in bottom row were imaged after injection of D-Luciferin after TNF- -mediated induction, showing marked gain in signal from the peritoneum over 30 h (Reproduced with permission from Ray P et al (2002) Proc Natl Acad Sci U S A 99, 3105–3110).

enzyme, in a process called α-complementation. This process suggested that synthetically separated fragments of a single polypeptide might be able to complement and give rise to an enzymatically active protein. By adopting the α-complementation strategy for the "split protein" strategy, a single reporter protein/enzyme is cleaved into N-terminal and C-terminal segments with each segment fused to one of two interacting proteins. Physical interactions between the two proteins restore the functional reporter protein/enzyme activity and lead to signal generation that can be measured. This split protein strategy can work either through protein–fragment complementation assays (described in details below), or intein-mediated reconstitution assays. In the latter case, reconstitution of the full reporter protein occurs and, in the former, reconstitution of the reporter protein does not occur. To date, several reporter proteins (e.g., β-lactamase, β-galactosidase, ubiquitin, dihydrofolate reductase, FL, Renilla luciferase (RL) and green fluorescent protein) have been adapted for split-protein strategies by finding various split sites for each reporter protein (1) for imaging protein–protein interactions in living subjects. The appropriate split point should lead to two fragments that do not have significant affinity for each other and yet, when brought together through interaction of two other proteins, lead to detectable signal.

Protein–Fragment Complementation Strategy

The protein–fragment complementation of many globular proteins shows activities that are similar to full-length proteins and has been extended for studying protein–protein interactions. For example, the FL was rationally split between amino acid positions 437 and 438 and used in conjunction with inteins to detect insulin-induced interaction of phosphorylated insulin receptor substrate 1 (IRS-1) and the N-terminal SH2 domain of PI 3-kinase in a cell-culture assay (4). Activation of insulin receptor by insulin led to phosphorylation of IRS-1 and subsequent interaction with the SH2 domain, leading to reconstitution of the full length FL. This split FL strategy with inteins has also been adapted for split-reporter complementation for imaging protein–protein interactions in small living animals. Interaction between Id and MyoD, as previously done with a modified yeast two-hybrid strategy (Modified mammalian two-hybrid system), was monitored using the split FL reporter complementation and an intein-mediated reconstitution strategy (1). The complementation strategy was shown to be as sensitive as the intein-mediated reconstitution strategy under the conditions tested and can be used to image protein–protein interactions in living subjects. In addition to FL, RL has also been used as another bioluminescence imaging reporter protein. RL is also the smallest monomeric protein (36 kDa) used for studying protein–protein interactions through a protein–fragment-assisted complementation strategy (1). The N-(amino acids 1–229) and C-terminal half (amino acids 230–311) of split RL were fused to interacting protein partners of interest and have been validated in both cell culture and living animals. Interactions between the two interacting protein partners bring the two inactive halves of the split RL in closer proximity and partially restore the RL activity, which can be imaged by optical bioluminescence imaging in the presence of the substrate coelentarazine. This split RL complementation system has been used to study rapamycin-mediated mTOR kinase FRB and the immunophilin FKBP12 interactions (Fig. 2), interaction between the transcription factors MyoD and ID and homodimerization of Herpes Simplex Virus Type I thymidine kinase. The limitation associated with the use of RL as an optical reporter is its relatively rapid reaction kinetics, requiring early time-point measurements (5). Nevertheless, the RL split-reporter system appears highly suitable for studying protein–protein interactions in cells and in living animals because of its optical bioluminescence and its signal,

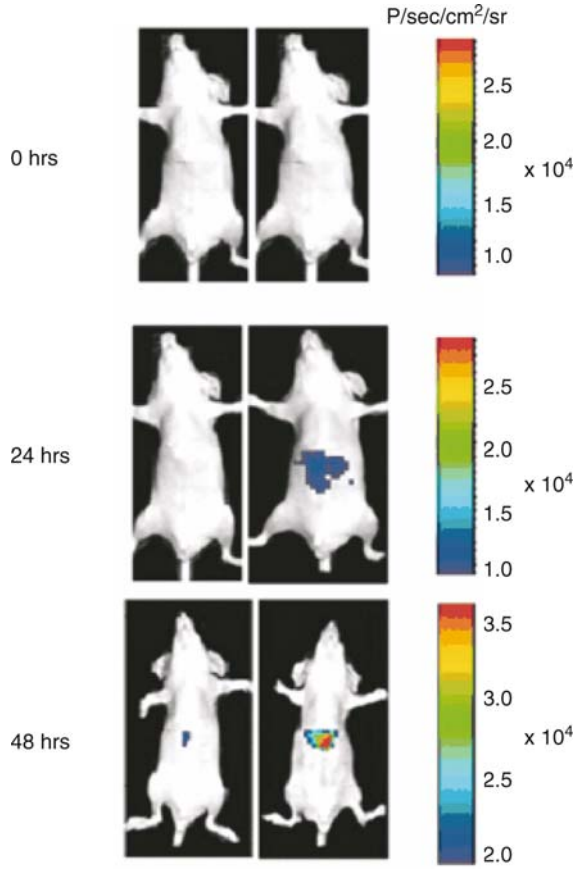

which can be amplified through an enzymatic process. Furthermore, the complementation strategies based on RL fragments (13 kDa and 23 kDa for the C-terminus and N-terminus fragments respectively), with smaller fragment size than FL (~33 kDa), are hindered less with interacting protein partners.

Fluorescence Resonance Energy Transfer (FRET) and Bioluminescence Resonance Energy Transfer (BRET)

FRET/BRET involves the nonradioactive transfer of energy between the donor and acceptor molecules that are in close proximity via the FORSTER mechanism, leading to a change in FRET/BRET ratios (6). The energy transfer primarily depends on an overlap between the emission and excitation spectra of donor and acceptor molecules, respectively; as well as the close distance between the donor and acceptor molecules (>100 Å). BRET/FRET ratios can be measured in cell culture studies using a microplate reader equipped with specific filter sets for detection of donor and acceptor emission peak, and in living animals using a CCD camera. The advantages of BRET include the in-depth knowledge of the interacting proteins in terms of their proximity and real-time measurement and higher signal to noise background relative to FRET since no external light excitation is required. BRET imaging has been extended to study rapamycin-mediated FRB/FKBP 12 interactions in living subjects, by fusing full length RL (electron donor) to FRB fragment and mutant GFP (electron acceptor) to the FKBP12 fragment (6).

Applications of Methods Used for Studying Protein–Protein Interactions:

Measurement of the rate of interaction between two proteins by intracistronic complementation of β-galactosidase, protein-fragment-assisted complementation of split proteins as well as FRET and BRET. Most recently, the protein-fragment-assisted complementation system has also been extended for imaging the efficacy of heat shock protein 90 inhibitors (7). Efforts are currently underway to develop novel sensors to study intramolecular folding and protein phosphorylation sensors pertaining to studying signal transduction and for preclinical drug development and target validation in living subjects.

Conclusion

The overall application of different systems to study/image protein–protein interactions in living small-animal models of cancer and other cell pathology depends on adapting them so that signal(s) can be noninvasively detected from outside the living subjects upon the interaction of two proteins of interest.

References

1. Paulmurugan R, Ray P, De A et al (2005) Imaging protein-protein interactions in living subjects. TrAC Trends Anal Chem 24(5):446–458
2. Fields S, Sternglanz R (1994) The two-hybrid system: an assay for protein-protein interactions. Trends Genet 10(8):286–292
3. Hodges RA, Perler FB, Noren CJ (1992) Protein splicing removes intervening sequences in an archaea DNA polymerase. Nucleic Acids Res 20(23):6153–6157
4. Ozawa T, Kaihara A, Sato M (2001) Split luciferase as an optical probe for detecting protein-protein interactions in mammalian cells based on protein splicing. Anal Chem 73(11):2516–2521
5. Bhaumik S, Lewis XZ, Gambhir SS (2004) Optical imaging of Renilla luciferase, synthetic Renilla luciferase, and firefly luciferase reporter gene expression in living mice. J Biomed Opt 9(3):578–586
6. De A, Gambhir SS (2005) Noninvasive imaging of protein-protein interactions from live cells and living subjects using bioluminescence resonance energy transfer. FASEB J 19:2017–2019
7. Chan CT, Paulmurugan R, Gambhir SS (2006) Proceedings for the 97th American Association of Cancer Research Annual Meeting, Washington DC April 1–5th

Proteinuria

Abnormally high amount of protein in the urine. Most proteins are too large to pass through the glomeruli into the urine. The glomeruli are negatively charged, so they repel the negatively charged proteins. Thus, a size and charge barrier keeps protein molecules from entering the urine. But when the glomeruli are damaged, proteins of various sizes pass through them and are excreted in the urine.

▶Glomerulonephritis

Proton MR Spectroscopy

An MR-based technique which allows to quantify the concentrations of important brain metabolites. Water suppressed, proton MR spectra of normal human brain at long echo times reveal four major resonances: one at 3.2 ppm from Choline (Cho) and Phosphorylcholine (PCho), one at 3.0 ppm from creatine (Cr) and phosphocreatine (PCr), one at 2.0 ppm from *N*-acetyl aspartate (NAA), and one at 1.3 ppm from lactate (Lac). NAA is a marker of neuronal integrity, while Cho and Lac are considered as chemical correlates of inflammatory/demyelinating changes. ^{1}H-MRS studies with shorter echo times can detect additional metabolites, such as lipids (which can be associated to increased membrane turn over) and myoinositol (mI), which is considered a marker of glial activity.

▶Aging Brain

Proton Spin Density

This term relates to the concentration of nuclei in tissue processing at the Larmor frequency. It is one of the main factors influencing the strength of the magnetic resonance imaging signal.

▶Contrast Media, MRI, Oral Agents

Protruded Disk

A protruded disk is a herniated disk in which the greatest distance in any plane between the edges of the disk material beyond the disk space is less than the distance between the edges of the base in the same plane.

▶Hernia, Disk, Intervertebral

Protruded or Extruded Intervertebral Disk

▶Hernia, Disk, Intervertebral

PS

▶Phosphatidyl Serine

Psammoma Bodies

Psammoma bodies present tiny intratumoral calcifications. They are typically found in serous adenocarcinomas and are detected at histology in 30% of cases and on CT scans in approximately 12%.

▶Carcinoma, Ovarium

Psammomatous Meningiomas

Psammomatous meningiomas are tumors with concentric lamina of calcium salts (psammoma bodies). Although psammoma bodies are often found in meningiomas, when abundant, they characterize the tumor as psammomatous meningioma.

▶Neoplasms, Brain, Extraaxial

Pseudarthrosis

A pathologic condition occurring often after fracture nonunion.

▶Neurofibromatosis, Musculoskeletal Manifestations

Pseudo-TORCH Syndrome

Infants with clinical and imaging features of TORCH syndrome, with normal work-up for congenital infection. There is a positive family history and parental consanguinity in one-third of the patients.

▶Calcifications, Intracranial, Neonatal

Pseudoaneurysm

Dilation of the outer aortic wall caused by dissection with progression to the subadventitial aortic layers.

▶Dissection, Aortic, Thoracic

Pseudoaneurysm, Hepatic Artery

Hepatic artery pseudoaneurysm is rare and is usually of iatrogenic origin. It consists of a perforation of the intima and media, causing a focal dilatation contained only by the adventitia. Extrahepatic pseudoaneurysms usually develop at the vascular anastomosis after liver transplantation or arise as a complication of angioplasty. Because they can rupture intraperitoneally and lead to massive hemorrhage, surgical resection, embolization, or exclusion with stent placement should be considered. Intrahepatic pseudoaneurysms can occur after percutaneous needle biopsy or local infection. A ruptured intrahepatic pseudoaneurysm may result in portal vein or biliary fistulas. Intrahepatic pseudoaneurysms can be treated with endovascular coil embolization.

▶Trauma, Hepatobiliary

Pseudocapsule

The peripheral zone of the malignant tumor causes a compression zone with a reactive zone and this may appear falsely as a well-defined tumor, giving the appearance of a benign lesion. May have potential malignant extension of tumor cells in or around the capsule.

▶Neoplasms, Soft Tissues, Malignant

Pseudocyst, Pancreatic

A pancreatic pseudocyst is a collection of pancreatic juice enclosed by a wall of fibrous or granulation tissue, which arises as a consequence of acute pancreatitis, pancreatic trauma or chronic pancreatitis. The presence of a well-defined wall is what distinguishes a pseudocyst from an acute fluid collection. It is most often sterile, but infection may occur. Formation of a pseudocyst requires 4 or more weeks from the onset of acute pancreatitis.

▶Pancreatitis, Acute

Pseudogout

Pseudogout or calcium pyrophosphate dihydrate crystal deposition disease is a joint disease caused by calcium pyrophosphate dihydrate crystal deposits with intermittent attacks of acute arthritis and degenerative arthropathy. A radiographic feature is a linear calcification in articular cartilage, especially fibrocartilages.

▶Gout
▶CPPD

Pseudoradicular Syndrome

Irradiating pain into the leg due to other causes than nerve root involvement

▶Radicular Syndrome of the Spine, Conservative Therapy for

PTC

▶Percutaneous Transhepatic Cholangiography

PTRA

▶Percutaneous Transluminal Renal Angioplasty

Pubococcygeal Line

The pubococcygeal line (PCL) is the line that joins the inferior border of the symphysis pubis to the last coccygeal joint on midsagittal images.

▶Pelvic Floor Dysfunction, Anorectal Manifestations

Pulmonary Alveolar Proteinosis

Pulmonary alveolar proteinosis is a rare disorder characterized pathologically by alveolar filling with a lipid-rich, proteinaceous material (positive to periodic acid-Schiff stain), while the lung interstitium remains relatively normal. The chest radiograph usually shows bilateral consolidation or ground glass pattern, occasionally with a perihilar predominance suggestive of the "bat wing" appearance of pulmonary edema but without other radiographic signs of left-sided heart failure. Although a single type of opacity can dominate the computed tomographic appearance of pulmonary alveolar proteinosis, more commonly there is a combination of patterns. The so-called "crazy paving" appearance, due to ground-glass opacity with superimposed intralobular and interlobular septal thickening, is suggestive of pulmonary alveolar proteinosis.

▶Interstitial Lung Diseases, Unknown Etiology

Pulmonary Arteries

The pulmonary arterial circulation is the source of bleeding in fewer than 10% of patients with hemoptysis.

▶Hemoptysis

Pulmonary Arteriovenous Aneurysm

▶Fistula, Arteriovenous, Pulmonary

Pulmonary Arteriovenous Fistula

▶Fistula, Arteriovenous, Pulmonary

Pulmonary Arteriovenous Malformation

▶Fistula, Arteriovenous, Pulmonary

Pulmonary Embolism

An occlusion of pulmonary vessels by an intravascular solid, liquid, or gaseous substance carried there by the bloodstream from its point of origin. The most common cause of pulmonary embolism is a thrombus (thromboembolism) that has formed in the deep veins of the lower limbs and becomes dislodged from its site of formation.

▶Pulmonary Function, Nuclear Medicine Methods

Pulmonary Embolism (PE)

▶Chest, Thromboembolic Diseases

Pulmonary Function, Nuclear Medicine Methods

Patrick Reinartz
Department of Nuclear Medicine, University Hospital Aachen, Aachen, Germany
preinartz@arcor.de

Characteristics

Lung Scan

The major field of application for ▶lung scintigraphy is in the diagnosis of ▶pulmonary embolism (PE). Besides PE, lung scans are also used for detecting bronchial airways obstruction, increases in pulmonary perfusion pressure, or right-to-left shunts. In addition, the method can be applied to assess mucociliary clearance or alveolar-capillary membrane permeability (1, 2). However, lung scintigraphy is used more frequently for the evaluation of nonembolic disease than for the diagnosis of PE.

The term "lung scan" refers to two different examinations: ventilation (V) and perfusion (Q) scintigraphy. The perfusion scan is done by applying ^{99m} technetium (Tc)-labeled macroaggregated albumin particles intravenously. With a mean diameter of about 40 μm, the particles lead to an occlusion of pulmonary vessels up to the size of the terminal arterioles (1). Between 100,000 and 400,000 of these microspheres are applied per scan, leading to a hemodynamically irrelevant occlusion of about 0.01% of the peripheral pulmonary arterial tree. Within the lungs, the particles are degraded by endogenous proteolysis and thereby cleared from the pulmonary circulation with a half-life of 2–3 h (1).

In contrast to the perfusion scan, two different types of radiopharmaceuticals are used for ventilation scintigraphy: radioactive inert gases and ^{99m}Tc-labeled aerosols. The two most frequently employed radioactive inert gases are ^{133}xenon and the short-lived ^{81m}krypton. Nowadays, however, even these two are of limited clinical relevance when compared to aerosol scintigraphy. An aerosol is defined as a dispersion composed of gas and very small liquid or solid particles. There is widespread use of an aerosol consisting of ambient air and ^{99m}Tc-labeled diethylenetriamine pentaacetic acid (DTPA). The DTPA particles have a mean aerodynamic diameter of about 450 μm and yield a deposition rate within the lungs of roughly 2%. Accordingly, only 2% of the applied activity can be used for imaging (1, 2). A substantially higher deposition rate can be achieved by using the recently developed ultrafine aerosol Technegas. Due to the low aerodynamic diameter of only 10 nm, the pulmonary deposition rate of this carbon-based ventilation agent reaches values of up to 20%, thus being about 10 times more efficient than conventional aerosols (1–3). Depending on the type of radiopharmaceuticals used and the applied activities, the radiation exposure induced by V/Q lung scans ranges between 1 and 3 mSv (1, 2).

Other new developments in the field of radiopharmacy aim at establishing an alternative to conventional lung scintigraphy. Labeled antibodies, antibody fragments, or specific peptides have been designed for the direct detection of thrombotic clots. The target structures of these substances are either parts of the fibrin polymer or fragments of platelets (2). However, at present, none of these radiopharmaceutical compounds is ready for market launch.

Current acquisition protocols employ two techniques: planar imaging and single photon emission computed tomography (▶SPECT). With regard to planar scans, it is

recommended to acquire eight views of both ventilation and perfusion (anterior view, posterior view, two lateral views, four oblique views). However, SPECT acquisitions have proved to be superior to planar imaging (3, 4). In the course of a SPECT scan, a three-dimensional image is obtained by rotating the detectors of the gamma camera around the patient. For evaluation, slices in any orientation can be reconstructed from this three-dimensional data set. SPECT is a well-established imaging method that is widely used in modern nuclear medicine diagnostics. Particularly in the field of cardiology and neurology, tomographic scans have almost completely replaced planar acquisitions. Therefore, it is quite remarkable that this technique took such a long time before finally reaching lung scintigraphy. The effect of SPECT imaging on the efficiency of diagnosing PE is striking: while planar lung scans yield a sensitivity between 0.76 and 0.81, SPECT leads to a substantial improvement of up to 1.0 (3–5). The same is true for the specificity, which is reported to reach values of between 0.91 and 0.96 when using SPECT, compared to values between 0.74 and 0.85 achieved by planar scintigraphy (3–5). In this context it should be mentioned that SPECT scanning of the ventilation can only be done with aerosols because inert gases are of limited use for this type of acquisition.

Pulmonary Embolism

PE is defined as an occlusion of pulmonary vessels by an intravascular solid, liquid, or gaseous substance carried there by the bloodstream from its point of origin. The most common cause of PE is a thrombus (thromboembolism) that has formed in the deep veins of the lower limbs and becomes dislodged from its site of formation. PE is frequent, dangerous, and difficult to diagnose.

Lung scintigraphy was introduced in clinical routine in 1964, thus being one of the longest established noninvasive imaging modalities in the diagnosis of PE (1). Unlike angiography, lung scintigraphy is an indirect imaging procedure that detects the perfusion defect caused by an embolus instead of the embolus itself. Such an indirect approach has advantages as well as disadvantages. On the one hand, the method is exceptionally sensitive because the perfusion defect is a great deal larger than the causing clot. Therefore, even small embolisms on a subsegmental level are easily detected by this method. Additionally, only lung scintigraphy is able to quantify exactly the functional fraction of lung tissue that is unaffected by an embolic incidence. Specificity, on the other hand, is the weak point of the procedure, since pulmonary perfusion defects are not only caused by embolism but by a multitude of other diseases and pathological processes. To amend this deficit, the acquisition protocol of lung scintigraphy was complemented by the ventilation scan in 1968 (1). Today, the term lung scintigraphy always includes both the perfusion and the ventilation scan.

Assessment

The scintigraphic manifestation of PE is the ▶mismatch defect, which is defined as a pulmonic region with regular ventilation but severely reduced or no perfusion. Apart

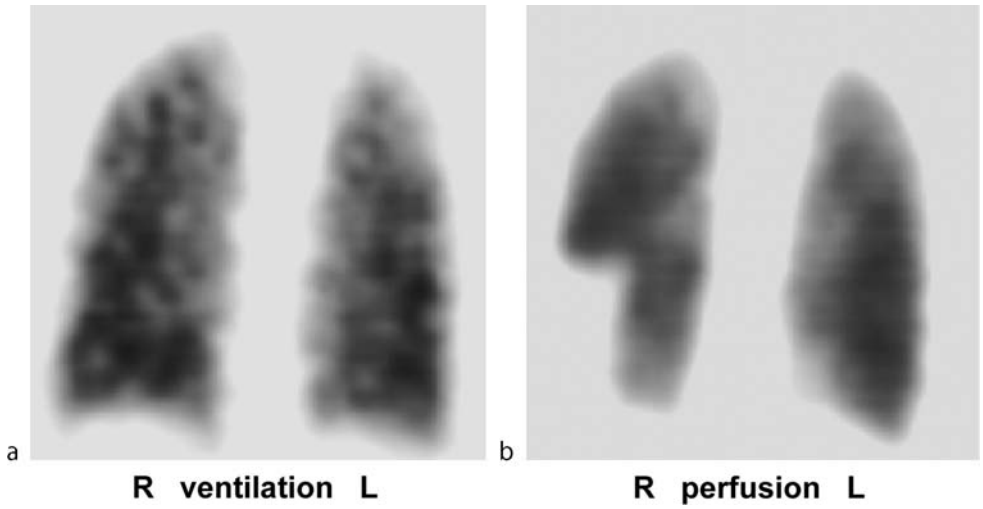

Pulmonary Function, Nuclear Medicine Methods. Figure 1 Coronal slices of a ventilation/perfusion lung scan acquired with a tomographic technique (SPECT): while the ventilation (a) shows no substantial pathological changes, a large perfusion defect can be found in the lower lobe of the right lung (b). Diagnosis: mismatch defect caused by pulmonary embolism. R = right; L = left.

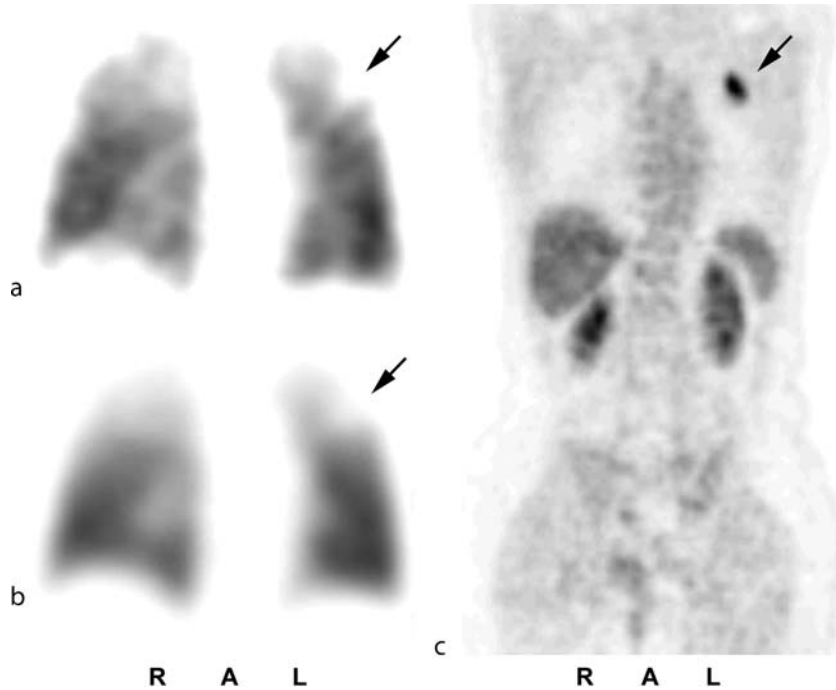

Pulmonary Function, Nuclear Medicine Methods. Figure 2 Coronal slices of a ventilation/perfusion lung scan acquired with a tomographic technique (SPECT): both ventilation (a) and perfusion (b) images show a subsegmental defect in the upper lobe of the left lung (arrows). Diagnosis: match defect induced by nonembolic disease. In fact, the match defect is caused by a malignant tumor, as shown in the positron emission tomography with ^{18}fluorine-labeled glucose (c, arrow). R = right; A = anterior; L = left.

from embolism, mismatch defects are induced by only a few and, more importantly, rare nonembolic diseases. Accordingly, the specificity of lung scintigraphy is substantially improved by the ventilation scan. Figure 1 shows a typical mismatch defect caused by PE. In contrast, most of the nonembolic pulmonary diseases lead to match defects in scintigraphy which are defined as regions affected by a severe reduction or complete loss of perfusion, while ventilation in the same region is likewise distinctly reduced. Figure 2 shows such a ▶match defect caused by a malignant tumor.

In the late 1980s, the PIOPED study was initiated, which aimed at developing a diagnostic system for the analysis of ventilation/perfusion (V/Q) lung scans. Based on the PIOPED data, a complex set of criteria was established which yields the patient's probability of having PE instead of a definitive diagnosis (6). According to the PIOPED system, a V/Q scan is categorized in one of five probability classes: normal, very low probability, low probability, intermediate probability, and high probability. One of the major weak points of this diagnostic system is the ambiguous intermediate class with a probability range for embolism of between 20% and 80%. Even a revision of the criteria in 2000 (PIOPED II) could not amend this deficit, so that the use of the PIOPED system can no longer be recommended. Instead, all mismatch defects of at least half-segment size should be assessed as PE. By doing so, the method reaches an accuracy of 0.94 (3). Not only is the higher accuracy of this system advantageous, but also its simplicity, as well as the fact that it always leads to a definitive diagnosis.

References

1. Wilson MA (1997) Pulmonary system. In: Wilson MA (ed) Textbook of Nuclear Medicine. Lippincott-Raven, Philadelphia, USA, pp 89–116
2. Sostman HD, Gottschalk A (2003) Evaluation of patients with suspected venous thromboembolism. In: Sandler MP, Coleman RE, Patton JA et al (eds) Diagnostic Nuclear Medicine. Lippincott Williams & Wilkins, Philadelphia, USA, pp 345–366
3. Reinartz P, Wildberger JE, Schaefer W et al (2004) Tomographic imaging in the diagnosis of pulmonary embolism: a comparison between V/Q lung scintigraphy in SPECT technique and multi-slice spiral CT. J Nucl Med 45:1501–1508
4. Collart JP, Roelants V, Vanpee D et al (2002) Is a lung perfusion scan obtained by using single photon emission computed tomography able to improve the radionuclide diagnosis of pulmonary embolism? Nucl Med Commun 23:1107–1113

5. Blachere H, Latrabe V, Montaudon M et al (2000) Pulmonary embolism revealed on helical CT angiography: comparison with ventilation-perfusion radionuclide lung scanning. Am J Roentgenol 174:1041–1047
6. PIOPED Investigators (1990) Value of the ventilation/perfusion scan in acute pulmonary embolism. Results of the prospective investigation of pulmonary embolism diagnosis (PIOPED). JAMA 263:2753–2759

Pulmonary Hemangiopericytoma

A mesenchymal neoplasm originating from pericytes—a cell type that surround capillaries. Its primary localisation in the lung is extremely rare. It occurs at any age but most commonly in the fifth and sixth decades. It is a highly vascular tumour that usually contains dilated vessels and occasionally may cause significant arteriovenous shunting.
▶Neoplasms, Pulmonary

Pulmonary Infection

Claus Peter Heussel
Diagnostic and Interventional Radiology, Thoraxklinik Heidelberg, Heidelberg, Germany
heussel@thoraxklinik-heidelberg.de

Synonyms

Abscess; Pneumonia; Pneumonitis

Definitions

Pneumonia: Pneumonia is inflammation of the lung parenchyma (excluding the bronchi) caused by infection or irritants. It may be defined by localization and distribution or by the origin of the underlying infection.
Typical pneumonia

Lobar pneumonia: Lobar pneumonia is an exudative inflammation involving a whole lobe or a large portion (segment) of the lung.

Bronchopneumonia: Bronchopneumonia is characterized by focal areas of suppurative inflammation in a patchy distribution within one or multiple lobes.
Atypical pneumonia

Focal or diffuse affliction of the lungs. The historical term is generally used for organisms that usually do not cause lobar pneumonia (Fig. 3).

Community-acquired pneumonia: Pneumonia contracted outside a hospital.

Hospital-acquired (nosocomial) pneumonia: Pneumonia contracted inside a hospital.

Abscess: A localized suppurative process characterized by a cavity filled with pus (necrosis of tissue).

Immunocompromised host: Patients with reduced functionality of the immune system.

Pathology/Histopathology

Community-Acquired Pneumonia

In the community setting, pneumonia frequently follows a viral infection of the respiratory tract.

Typical Pneumonia

About 30% of community-acquired pneumonias are caused by the gram-positive bacterium *Streptococcus pneumoniae* (also known as Pneumococci).

Lobar Pneumonia

Four stages of lobar pneumonia are classically described:

1. Congestion: This stage is characterized histologically by vascular engorgement, intra-alveolar fluid, small numbers of neutrophils, and often numerous bacteria.
2. Red hepatization: Vascular congestion persists, with extravasation of red cells into alveolar spaces, along with increased numbers of neutrophils and fibrin. The filling of air spaces by the exudate leads to the appearance of solidification or consolidation of the alveolar parenchyma. This pathological appearance is similar to that of the liver, hence the term "hepatization."
3. Gray hepatization: Red cells disintegrate, whereas neutrophils and fibrin persist. The alveoli still appear consolidated, but the color is paler and the cut surface drier.
4. Resolution: The exudate is digested by enzymatic activity and cleared by macrophages or by cough.

Abscess

Although the majority of bacterial pneumonias resolve with healing, in some cases complications such as abscess formation occur. A lung abscess may also occur as an isolated process at single or multiple locations (hematogeneous spread). An abscess is a localized suppurative process characterized by a cavity filled with pus (necrosis of tissue). If communication with an airway exists or occurs, the exudate may partially drain, and the remaining cavity will exhibit an air–fluid level.

Bronchopneumonia

In bronchopneumonia, the inflammatory exudate typically involves small airways and the surrounding alveolar space. Histologically, the same stages of evolution as in lobar pneumonia (congestion, red and gray hepatization, resolution)

are believed to occur. However, they involve relatively small areas in a metachronous fashion. The temporal differences of the disease stage among the individual foci lead to a heterogeneous appearance and make perceiving the typical evolution more difficult than in lobar pneumonia.

Atypical Pneumonia

Most atypical pneumonias are community-acquired and generally caused by intracellular organisms including *Mycoplasma pneumoniae, Chlamydia pneumoniae, Legionella pneumophilia* (up to 30% each), viruses [influenza, respiratory syncytial virus (RSV), herpes group, and adenovirus (up to 10%)]. In immunodeficient patients (including those with AIDS), other organisms such as *Pneumocystis jiroveci* (PcP, formerly *P. carinii*) might cause atypical pneumonia (Figs 1 and 2).

Hospital-Acquired Pneumonia

The gram-positive *Staphylococcus aureus* is one of the main causes of nosocomial pneumonia. It is uncommon in healthy adults but can develop about 5 days after viral infection, usually in individuals with a weakened immune system. Especially in hospitalized or nursing home patients, or in patients suffering from cystic fibrosis or other chronic lung diseases, *Streptococcus pyogenes* and *Pseudomonas aeruginosa* are common infectious agents.

Ventilator-Associated Pneumonia

Hospitalized patients, especially those who are ventilated mechanically are particularly vulnerable to gram-negative bacteria and staphylococci.

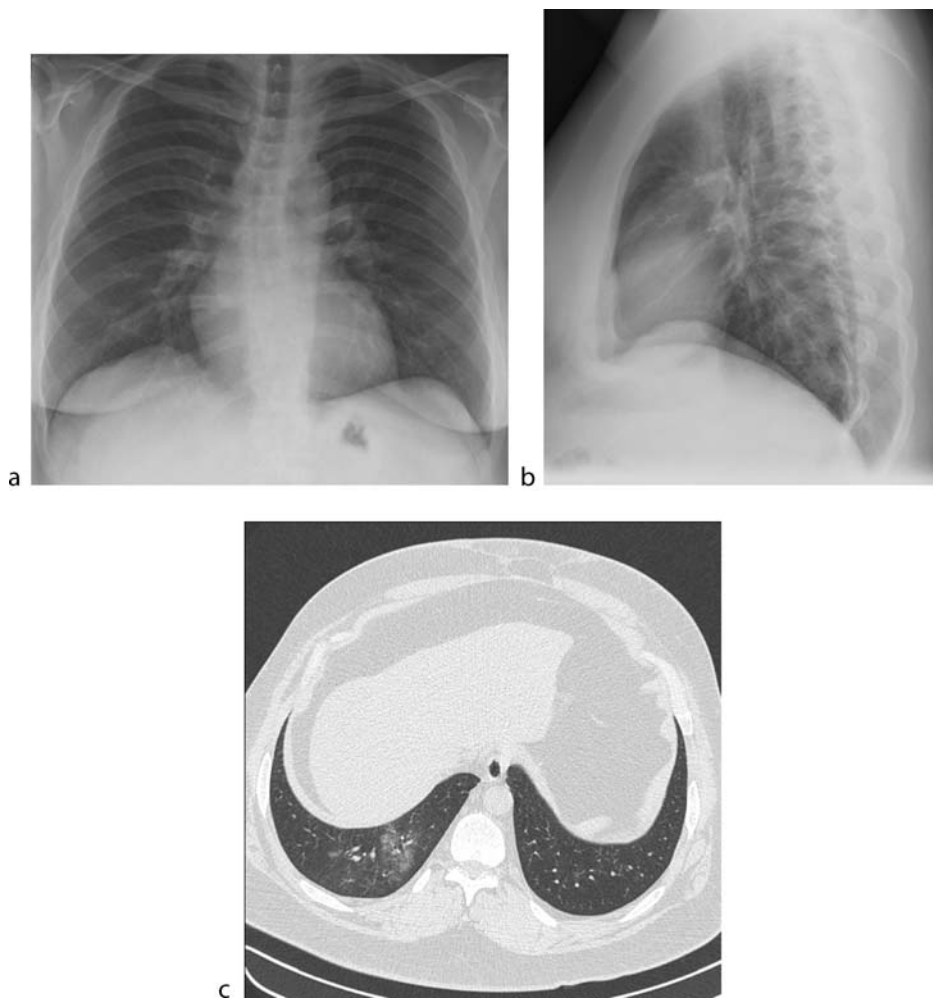

Pulmonary Infection. Figure 1 40 year-old male who underwent liver transplantation due to Wilson disease 12 years ago. He presented with moderate fever and abdominal pain. Chest x-ray was normal, CT done the day after demonstrated ground-glass opacification in the right lower lobe. The patient defervescented with empirical treatment of atypical pneumonia.

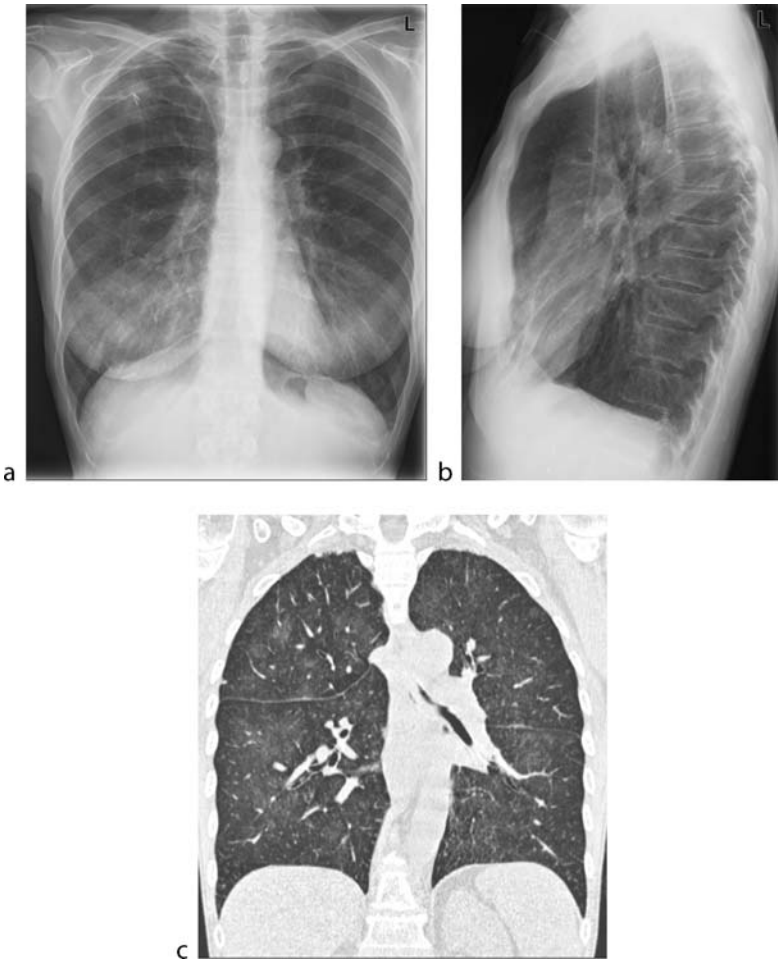

Pulmonary Infection. Figure 2 **55 year-old female suffering from acute lymphogeneous B-cell leukemia and fever during neutropenia due to chemotherapy. Chest x-ray demonstrated new development of mild basal infiltrates, especially on the right, while CT demonstrated diffuse ground-glass opacification in both lungs. The patient defervescented with empirical treatment of atypical pneumonia.**

Opportunistic Pneumonia

Fungi (e.g., *P. jiroveci*, *Aspergillus* species, *Candida* species), mycobacterial species, viruses (cytomegalovirus, herpes simplex virus, RSV) are the opportunistic organisms that are either ubiquitous or resident. AIDS patients and other immunocompromised hosts (such as individuals undergoing chemotherapy or long-term users of corticosteroids) are at major risk for opportunistic pneumonia.

Aspiration Pneumonia

Whether aspiration pneumonia represents a primary bacterial infection or a chemical inflammatory process remains a subject of significant controversy. Depending on the acidity of the aspirate, a chemical pneumonitis can develop, and gram-negative bacteria may particularly add to the inflammation. The middle lobe and right > left lower lobe are the most common locations due to the anatomy of the bronchial tree and to gravity.

Infarction Pneumonia

Infarction pneumonia consists of segmental infiltrates in cases of pulmonary embolism. During acute obliteration of the pulmonary artery, the bronchial arteries (vasa privata) cannot provide sufficient oxygen to the distal lung parenchyma. This leads to hemorrhagic necrosis of the tissue and is especially relevant in elderly patients and in those with underlying left cardiac failure.

Retention Pneumonia

Obstructive pneumonia occurs in the lung distal to an obstructed bronchus. A blockage by a tumor or foreign

body results in poor aeration and retention of secretions, predisposing to superinfection in the obstructed portion of the lung.

Pulmonary Sequestration

Pulmonary sequestration is an embryonic mass of lung tissue that has no identifiable bronchial communication and that receives its blood supply from anomalous systemic arteries.

Clinical Presentation

Pneumonia is the most frequent fatal infectious disease. The clinical presentation of community- and hospital-acquired pneumonia is based on the following main clinical courses.

Typical Pneumonia

The symptoms of bacterial pneumonia develop abruptly and may include chest pain, fever, shaking, chills, shortness of breath, tachypnea, tachycardia, and general deterioration. Coughing up of sputum containing pus or blood is an indication of serious infection. Painful respiration is a sign of concomitant pleuritis and pleural effusion. Severe abdominal pain may accompany pneumonia occurring in the lower lobes of the lung. It is important to note that older people may have fewer or different symptoms than younger people.

Atypical Pneumonia

Symptoms progress gradually, often beginning with general flu-like symptoms, such as fatigue, fever, weakness, headache, nasal discharge, sore throat, earache, and stomach and intestinal distress. Symptoms of Legionnaire's disease usually evolve more rapidly and include high fever, a dry cough, and shortness of breath, often accompanied by headache, muscle pains, fatigue, gastrointestinal problems, and mental confusion.

Friedlander Pneumonia

This type of pneumonia is caused by gram-negative *Klebsiella*, especially in alcoholic and diabetes patients. It causes varying infiltrates, typically lobar pneumonia, and occasional basal cavitations (abscesses). Patients frequently have blood in the sputum, which indicates necrosis. About one-third of these patients lose weight.

Imaging

Chest X-ray

Chest X-ray in two planes is the basis of imaging in pneumonia. Because of the projection technique, superimposition leads to limited sensitivity in detecting pneumonia. Even when done upright and in two planes, 5 out of 19 lung segments cannot be seen without substantial superimposition. Sensitivity is therefore limited for detecting mild or atypical pneumonia. This holds true even more if the chest X-ray is taken in the supine position. Thus, its sensitivity for early detection of pneumonia is low.

Computed Tomography

Thin-section computed tomography (CT) for early detection or exclusion of pneumonia is indicated in patients at high risk (such as immunocompromised hosts) (Figs 1 and 2). CT is also the method of choice in the characterization of lobar, bronchial, and atypical pneumonias.

Sonography

For bedside detection and quantification of effusion, ultrasound is a valuable tool.

Diagnosis

Besides the detection of pneumonia, imaging is a fast and valuable tool for characterizing the underlying disease. Because of its higher sensitivity, CT also has the ability to better distinguish patterns as compared with chest X-ray. By the differentiation into the following major groups of pneumonia, the underlying disease and a list of probable microorganisms can be suggested for the differential diagnosis. This diagnosis is faster compared to invasive procedures followed by histological or microbiological analysis; however, the results represent only hints of the disease.

Typical Pneumonia

Lobar Pneumonia

A typical finding is the respecting of anatomical borders, such as the fissure, by the affected area of consolidated lung parenchyma. Because the bronchi remain aerated, they give the *positive bronchogram sign* at chest X-ray or CT within the consolidation. The required volume of the affected lung compartment is equal to or a little increased compared to the nonaffected condition. This is in contrast to atelectasis, in which the volume is decreased (Fig. 3).

Gram-negative pneumonia is a very rapidly progressing disease. Infiltrates appear or escalate within hours. Lung abscesses appear, especially in the basal regions with central necrosis, fluid levels, and pseudocapsula.

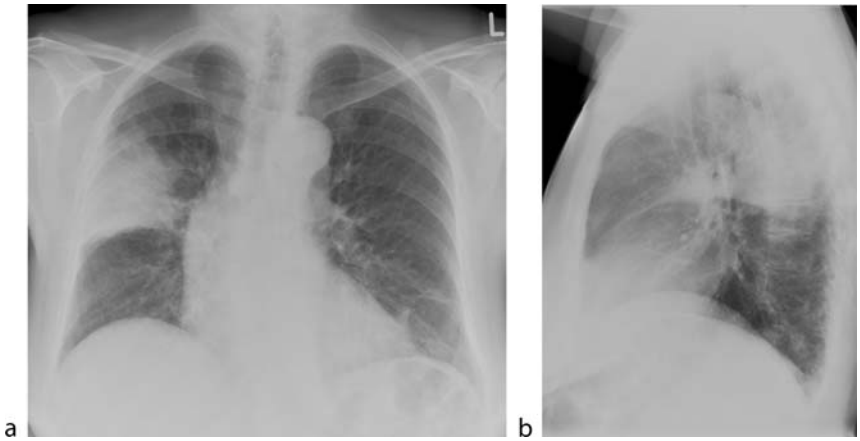

Pulmonary Infection. Figure 3 71 years-old female with rheumatoid arthritis under long-term corticosteroid therapy. Dyspnoea, fever and respiratory depending pain led to hospitalisation. Chest x-ray demonstrates consolidation and positive bronchogram in the apical segment of the right lower lobe (S6) respecting lobar and segmental borders representing the typical findings of a lobar pneumonia. Resolved with empirical antibiosis.

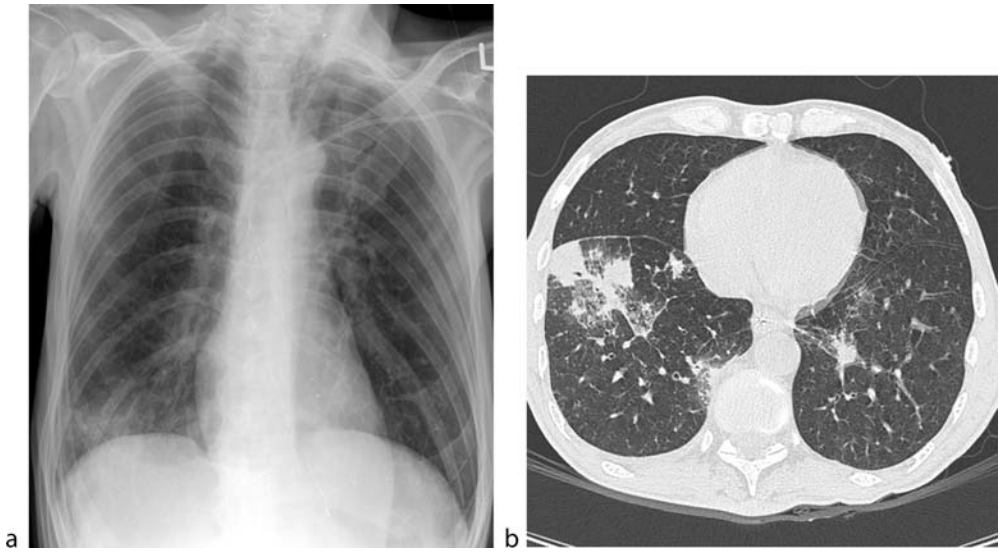

Pulmonary Infection. Figure 4 63 years-old male after chemotherapy due to hypopharynx carcinoma suffering from fever. Chest x-ray in supine position demonstrates a focal infiltrate in the right lower field with positive silhouette sign suggesting to be located in the right lower lobe. Thin-section CT done 2 days later revealed diffuse focal infiltrates in both lower lobes representing bronchopneumonia. Resolved with empirical antibiosis.

Bronchopneumonia

Small foci of consolidated lung parenchyma with ill-defined margins in a patchy distribution are seen possibly all over the lung. The *positive bronchogram sign* may be visible, especially on CT. Severe cases of bronchopneumonia may show confluent areas of involvement that resemble the pattern of lobar pneumonia (Fig. 4).

Atypical Pneumonia

A diffuse manifestation of atypical pneumonia gives a summation effect and can easily be seen at chest X-ray as diffuse cloudiness (Fig. 1). If atypical pneumonia is small and localized, it might be hard to depict on chest X-ray (Fig. 2). At CT, ground-glass opacification is the leading pattern, demonstrating the remaining ventilation even in

the affected alveoli associated with moderate clinical symptoms (Figs 1 and 2).

Immunocompromised Hosts

In patients with reduced function of the immune system, the appearance and the typical underlying microorganism may differ substantially depending on the immune status. Immunocompromised hosts are especially at risk for development of fungal and viral pneumonia. Viral pneumonia (such as *Herpesviridae* and RSV) is associated with ground-glass opacification in a mosaic pattern (affected and nonaffected secondary lobules lying side by side) and also small (<1 cm) nodules of low density (air-space nodules). In contrast, fungal pneumonia (such as *Aspergillus* and *Mucoraceae*) is characterized by larger ill-defined nodules (1–3 cm) or consolidation (>3 cm, negative bronchogram sign) surrounded by the halo sign (area of ground-glass opacification).

Interventional Radiological Treatment

Especially in abscesses, covered pleural effusion, and empyema, image-guided drainage is helpful. Even small and central lesions can be safely treated. In cases of hemorrhage, embolization can treat vascular erosion. Besides treatment, interventional biopsy techniques should be used as an alternative to bronchoalveolar lavage for identifying the underlying microorganisms.

Bibliography

1. Sarosi GA (1999) 'Atypical pneumonia'. Why this term may be better left unsaid. Postgrad Med 105:131–132, 135–138 www.postgradmed.com/issues/1999/04_99/sarosi.htm
2. Ris HB, Stocker JM, Im Hof V (1999) Pulmonary abscesses and bronchiectasis. Schweiz Med Wochenschr April 10 129 (14):547–555
3. Fraser RG, Pare JAP Diagnosis of Diseases of the Chest. 2nd edn, vol 2, WB Saunders, Philadelphia, London, Toronto
4. Franquet T, Gimenez A, Roson N et al (2000) Aspiration diseases: findings, pitfalls, and differential diagnosis. Radiographics May–June 20(3):673–685
5. Heussel CP, Kauczor H-U, Ullmann AJ (2004) Pneumonia in neutropenic patients. Eur Radiol 14:256–271

Pulmonary Neoplasms

►Neoplasms, Pulmonary

Pulmonary Opacity, Cystic Pattern

Cornelia Schaefer-Prokop
AMC, Amsterdam, Netherlands
c.m.schaefer@amc.uva.nl

Definition

Pulmonary opacity is a non-specific term describing an area of increased pulmonary attenuation caused by an intra-parenchymal process. There are various types of pulmonary opacities, easily categorized as extensive, nodular, reticular or cystic. Cystic patterns describe focal areas of decreased attenuation.

Characteristics

Lung Cysts

Lung cysts are well-defined rounded lesions, delineated by a well-defined wall of less than 3 mm thickness. Most cysts contain air but may rarely also contain fluid or solid material. The term *cystic air-space*—frequently used as synonym–on the other hand refers to a cyst exclusively containing air. Cysts are seen in multiple diffuse interstitial lung disease such as Langerhans' cell histiocytosis (LCH), lymphangiomyomatosis (LAM) (Fig. 1) or lymphocytic interstitial pneumonia (LIP). Features such as the profusion and distribution of air spaces and the wall characteristics determine the differential diagnosis and are superiorly appreciated on CT. On a chest radiograph the walls might not be visible at all or multiple walls—superimposed over each other—will result in a reticular pattern. Occasionally the differentiation between a bronchiectasis and cystic air spaces of other origin such as pneumatoceles, bullae and ►blebs may be difficult.

Honeycombing

Honeycombing refers to a rather rough (meaning thick-walled) reticular pattern that is produced by clustered cystic air spaces surrounded by clearly definable walls (Fig. 2). The cysts may vary in size from millimetres to centimetres. They occur in several layers and typically share their walls. They are predominantly located in the sub-pleural and basal areas and represent the hallmark of interstitial fibrosis, especially in usual interstitial pneumonitis on CT.

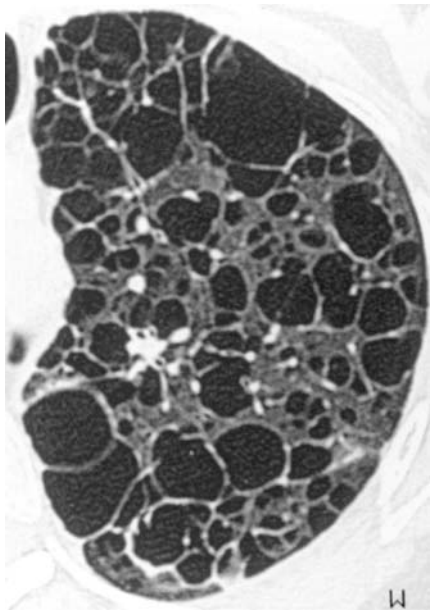

Pulmonary Opacity, Cystic Pattern. Figure 1 Cystic destruction of the lung parenchyma in a young female with lymphangiomyomatosis.

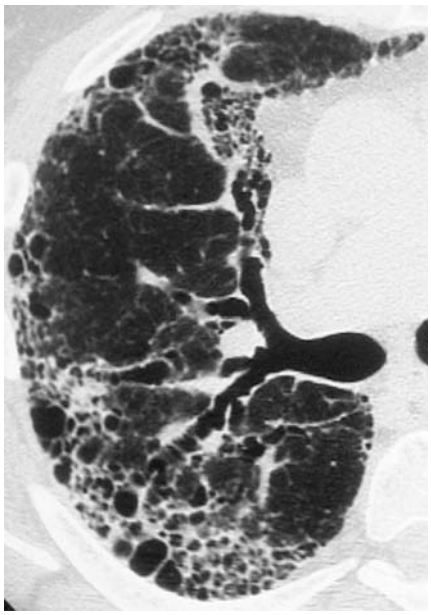

Pulmonary Opacity, Cystic Pattern.
Figure 2 Honeycombing and irregular thickening of the peribronchovascular interstitium are the hallmarks of usual interstitial pneumonia (UIP).

Ring Shadows and Cavitations

Cavitating lesions, which mostly have thick walls and irregular inner wall contours produce a ring shadow on CXR. They have to be differentiated from thin-walled cysts or pneumatoceles which both have much thinner and more regular walls. The differential diagnoses of pulmonary cavities include infections, inflammatory, granulomatous, neoplastic and post-traumatic aetiologies. Differentiation from cystic Bronchiectasis with a ►signet-ring sign, pre-existing emphysema and a ►pneumatocele may be difficult.

Bibliography

1. (2001) In: Webb WR, Mueller NL, Naidich DP (eds) High Resolution CT of the Lung. 3rd edn. Lippincott
2. (2005) In: Hansell DM, Armstrong P, Lynch DA, McAdams HP (eds) Imaging of Diseases of the Chest. Elsevier, Amsterdam
3. Webb WR, Mueller NL, Naidich DP (1993) Standardized terms for high resolution lung CT: a proposed glossary. J Thorac Imaging 8:167–175
4. Austin JH, Muller NL, Friedman PJ et al (1996) Glossary of terms for CT of the lungs: recommendations of the Nomenclature Committee of the Fleischner Society. Radiology 200:327–331

Pulmonary Opacity, Extensive Pattern

Cornelia Schaefer-Prokop
AMC, Amsterdam, Netherlands
c.m.schaefer@amc.uva.nl

Synonym

Radio-opacity (the term density should be avoided)

Definition

Pulmonary opacity is a nonspecific term describing an area of increased pulmonary attenuation caused by an intraparenchymal process. There are various types of pulmonary opacities, easily categorized as extensive, nodular, reticular, or cystic.

Characteristics

Air Space Filling

Synonyms: Consolidation, infiltration (cave: the term infiltration is differently defined by pathologists and radiologists).

Pathologically, air space filling is caused by replacement of air within the distal airways and alveoli by fluid or cellular material. In practice the term is used for filling of the air spaces with tumor or inflammatory cells, blood or

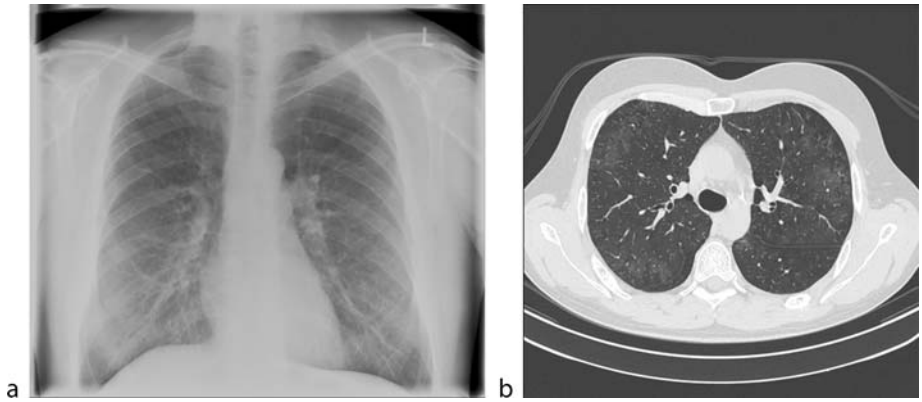

Pulmonary Opacity, Extensive Pattern. Figure 1 (a) Chest radiograph without any opacity; (b) CT of the same patients shows the typical pattern of ground glass opacity in upper lung zones.

exudates. When filled with transudate, it is called edema, although by definition it also represents air space filling.

Imaging: Dependant on the extent it appears as an ill-defined nodular or patchy opacity that may coalescence and then potentially show an air-bronchogram. When abutting a fissure, the opacity is sharply marginated on a chest radiograph.

Ill-defined nodular shadows between 0.5 and 1 cm are called "acinar shadows," cave: they do not represent the pathologic unit of a single acinus.

Ground Glass Opacity

Pathologically it represents filling in of air spaces and/or thickening of the alveolar walls and may be caused by reversible (e.g., edema, bleeding, acute alveolitis) and irreversible diseases (e.g., interstitial fibrosis). This explains why the term ground glass opacity is merely descriptive and nonspecific.

Imaging: In CT it refers to an increase in attenuation of the lung parenchyma without obscuration of the underlying bronchovascular structures (Fig. 1a). In chest radiography, ground glass opacity similarly describes a homogeneous hazy opacity, which makes the underlying interstitial and vascular structures indistinct but preserves their visibility. Often ground glass opacity visible at CT is not observed on a chest radiograph.

Ground glass opacity is a major component of the crazy-paving pattern.

See also Atelectasis.

Bibliography

1. (2001) In: Webb WR, Mueller NL, Naidich DP (eds) High Resolution CT of the Lung. 3rd edn. Lippincott
2. (2005) In: Hansell DM, Armstrong P, Lynch DA, McAdams HP (eds) Imaging of Diseases of the Chest. Elsevier, Amsterdam
3. Webb WR, Mueller NL, Naidich DP (1993) Standardized terms for high resolution lung CT: a proposed glossary. J Thorac Imaging 8:167–175
4. Austin JH, Muller NL, FriedmanPJ et al (1996) Glossary of terms for CT of the lungs: recommendations of the Nomenclature Committee of the Fleischner Society. Radiology. 200:327–331

Pulmonary Opacity, Nodular Pattern

Cornelia Schaefer-Prokop
AMC, Amsterdam, Netherlands
c.m.schaefer@amc.uva.nl

Definition

Pulmonary opacity is a non-specific term describing an area of increased pulmonary attenuation caused by an intra-parenchymal process. There are various types of pulmonary opacities, easily categorized as extensive, nodular, reticular or cystic.

A *nodular pattern* refers to round opacities 1–10 mm in size. They are a feature of both, interstitial and air-space disease. Important features are the location of nodules, their uniformity, density and edge characteristics. Nodules within the interstitium are usually well-defined and in a periseptal, centrilobular, peribronchovascular or perilymphatic location, while nodules in air-space disease—so-called acinar nodules—are unsharp and centrilobular or randomly distributed.

A random distribution of well-defined, small (*miliary*) nodules is seen in hematogenous spread of disease, while a widespread distribution of ill-defined acinar nodules with a tendency for coalescence and associated

with airways and air trapping is seen in exogenous allergic alveolitis.

See also 'Nodules, Pulmonary, Solitary' and 'Nodules, Pulmonary, Multiple'.

Bibliography

1. (2001) In: Webb WR, Mueller NL, Naidich DP (eds) High Resolution CT of the Lung. 3rd edn. Lippincott
2. (2005) In: Hansell DM, Armstrong P, Lynch DA, McAdams HP (eds) Imaging of Diseases of the Chest. Elsevier, Amsterdam
3. Webb WR, Mueller NL, Naidich DP (1993) Standardized terms for high resolution lung CT: a proposed glossary. J Thorac Imaging 8:167–175
4. Austin JH, Muller NL, Friedman PJ et al (1996) Glossary of terms for CT of the lungs: recommendations of the Nomenclature Committee of the Fleischner Society. Radiology 200:327–331

Pulmonary Opacity, Reticular Pattern

Cornelia Schaefer-Prokop
AMC, Amsterdam, Netherlands
c.m.schaefer@amc.uva.nl

Definition

Pulmonary opacity is a nonspecific term describing an area of increased pulmonary attenuation caused by an intraparenchymal process. There are various types of pulmonary opacities, easily categorized as extensive, nodular, reticular, or cystic.

Characteristics

Line Shadows and Band Shadows

Linear opacities >5 mm in diameter are described as *band shadow*, while linear opacities <5 mm are described as *linear densities*.

Septal Lines

Interlobular septa belong to the interstitial framework of the lung and contain veins and lymph vessels. Normal interlobular septa are not seen on a chest radiograph. When thickened they may be seen as "*Kerley lines*" on a chest radiograph. Dependent on their anatomic location there are Kerley A, B, or C lines, among which the Kerley B lines are most important and frequently seen. They represent thickened interlobular septa running perpendicular to the peripheral pleura best seen at the lung base especially in lymphangitic carcinomatosis (Fig. 1), interstitial fibrosis and interstitial edema.

CT offers further classification of the underlying etiology by analyzing the type of thickening (smooth, irregular, beaded), distribution (peripheral, central, homogeneous, localized), and associated findings. On CT, thickening of the interlobular septa is differentiated from thickening of the intralobular interstitial septa. Thickened interlobular septa produce a *coarse reticular pattern* and are mostly associated with interstitial fibrosis but also seen in interstitial edema or lymphangitic carcinomatosis (Fig. 1). It is frequently associated with thickening of the interstitium along the central perihilar bronchovascular bundle, a finding described as *interface sign* in fibrosis (Fig. 2). Thickened intralobular septa produce a *fine reticular pattern* and are typically associated with interstitial fibrosis.

Bronchial Wall Thickening

Synonym: Peribronchial thickening.

Normal bronchial walls are only seen in the perihilar region and when radiographed en face. In edema, lymphangitic carcinomatosis, interstitial fibrosis or inflammatory conditions the wall of the bronchi, and the peribronchial interstitium may be (irregularly) thickened. The ring shadow of a bronchus radiographed en face is described as *bronchial cuffing* (Fig. 1), the linear shadows

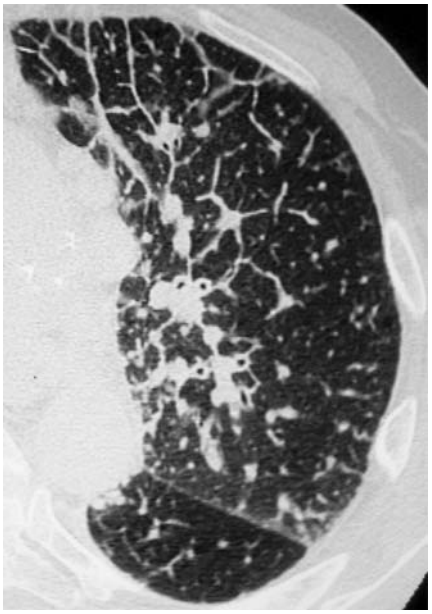

Pulmonary Opacity, Reticular Pattern. Figure 1 Patient with thickened interlobular septa and thickened central peribronchial interstitium (bronchial cuffing) due to lymphangitis carcinomatosa.

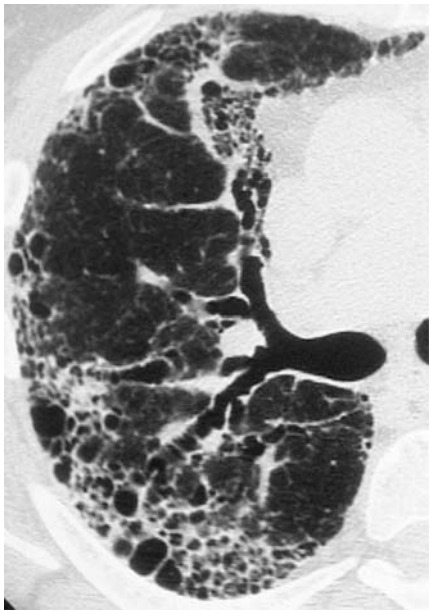

Pustulotic Arthroosteitis. Figure 2 Honeycombing and irregular thickening of the peribronchovascular interstitium are the hallmarks of usual interstitial pneumonia (UIP).

when radiographed longitudinally are described as *tram lines*. Again extent and severity of bronchial wall thickening are better appreciated on CT than on chest radiography. The same is true for associated bronchial dilatation.

Reticulo-nodular Opacities

On a chest radiograph an only rough differentiation is made between a nodular and a reticulo-nodular shadow, because it always reflects a summation of multiple superimposed lesions, and does not represent the anatomic opacity seen on CT. The classification of the pattern meaningful for the type of diffuse interstitial lung disease is the domain of CT.

Mucoid Impaction

Synonym: Mucocele, bronchocele.

This refers to filling-in of bronchial structures with mucoid secretion leading to y-shaped or band-like opacities pointing toward the hilum and producing a form that is also described as *finger-in-glove-sign* (Fig. 3). It is described to be typically for allergic bronchopulmonary aspergillosis (ABPA) and cystic fibrosis (CF) but may be generally seen peripheral to any obstructing endobronchial lesion (metastases, carcinoid, endobronchial carcinoma) provided that collateral air drift

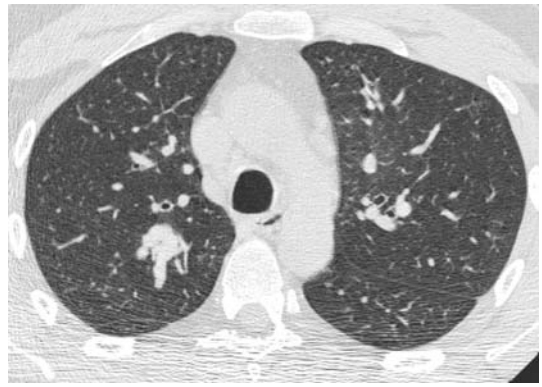

Pulmonary Opacity, Reticular Pattern. Figure 3 A finger in glove sign due to mucoid impaction of focal dilated bronchi in a patient with ABPA.

maintains aeration of the peripheral segment. The *tree-in-bud-sign* describes dilated bronchioli either with wall-thickening and/or filled with mucus, pus, or fluid resembling the appearance of a branching or budding tree. It indicates "small airways disease" but is rather nonspecific for the underlying etiology, for example, endobronchial spread of infection, chronic airway infection, or inflammation (see Airway disease).

Bibliography

1. (2001) In: Webb WR, Mueller NL, Naidich DP (eds) High Resolution CT of the Lung. 3rd edn. Lippincott
2. (2005) In: Hansell DM, Armstrong P, Lynch DA, McAdams HP (eds) Imaging of Diseases of the Chest. Elsevier, Amsterdam
3. Webb WR, Mueller NL, Naidich DP (1993) Standardized terms for high resolution lung CT: a proposed glossary. J Thorac Imaging 8: 167–175
4. Austin JH, Muller NL, Friedman PJ et al (1996) Glossary of terms for CT of the lungs: recommendations of the Nomenclature Committee of the Fleischner Society. Radiology 200:327–331

Pulmonary Telangiectases

►Fistula, Arteriovenous, Pulmonary

Pustulotic Arthroosteitis

►Spondyloarthropathies, Seronegative

PUV

►Posterior Urethral Valve

Pyelonephritis, Acute

Luis H. Ros Mendoza,
Beatriz Izquierdo Hernández,
Roberto Martínez García
University Hospital Miguel Servet, Department of Radiology, Zaragoza, Spain
lhros@wanadoo.es

Synonyms

Nephritis, Bacterial, Acute; Lobar nephritis; Lobar nephronia (1)

Definition

Two definitions exist: a clinical definition, based on clinical and laboratory findings and a pathological one, related to macro- and microscopic anomalies (1).

- *Clinical definition*: clinical syndrome consisting of costovertebral or lumbar pain, fever, as well as laboratory findings suggestive of bacterial renal infection, including leukocytosis, pyuria, bacteriuria, and positive urine culture, sometimes with bacteremia and hematuria.
- *Pathological definition*: bacterial renal infection with acute inflammation that involves both the renal pelvis (collector system) and the parenchyma, often multifocal.

In addition, two types of pyelonephritis are distinguished: not complicated and complicated.

- Not complicated or uncomplicated: It appears in immunocompetent patients without anatomical or functional alterations of the urinary tract.
- Complicated: Infection that may occur in patients who present one or more of the following factors: (1) male sex, especially with prostatic hypertrophy; (2) advanced age (more than 65 years); (3) carrier of a indwelling catheter or intermittent catheterization; (4) postmictional urine residue larger than 100 mL; (5) obstructive uropathy; (6) vesicoureteral reflux or other urologic anomalies; (7) renal transplantation; (8) diabetes; (9) chronic renal insufficiency; (10) neutropenia; (11) pregnant women; (12) recent hospitalization, in the previous month; (13) recent ingestion of antibiotics, in the previous month; (14) history of recurrent acute pyelonephritis (AP); (15) septic shock. These patients have a major risk of infection, failure of treatment, and possibility of resistance to the antibiotics (2).

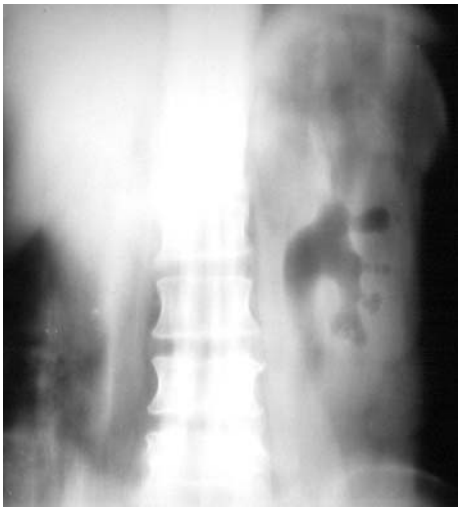

Pyelonephritis, Acute. Figure 1 Emphysematous pyelonephritis. Abdominal plain film shows the presence of gas in the left pyelocaliceal and ureteral system, a characteristic, although unspecific, finding of emphysematous pyelonephritis.

►*Emphysematous pyelonephritis*: severe infection of the renal tissue with gas formation, produced generally by *Escherichia coli* or other gram-negative organisms. It occurs in diabetic patients (Fig. 1).

Pathology/Histopathology

The most frequent etiologic agent is *E. coli*.

The infection can originate *via* two/three routes (1):

- *Ascending route*: the most frequent. By vesicoureteral and intrarenal reflux, the bacteria reach the pyelocaliceal system, papillary ducts, and collector tubules, where an inflammatory response is generated. Its intensity depends on several factors such as the grade of reflux, the bacterium virulence, and the host defenses. Once the bacterium reaches the tubules, the leukocytes migrate from the interstice into the tubules and the liberated enzymes destroy the tubular cells, so the bacterium invades the interstice within 48–72 h. A real tubulointerstitial nephritis appears, where intratubular neutrophils and interstitial infiltrates of

mononuclear cells and neutrophils are found (3). The tubules filled with leukocytes and other materials can produce a focal intrarenal obstruction. Macroscopically, the kidney undergoes an increase in size and it is possible to visualize white-yellow streaks radiating from the papillae to the kidney surface, following the medullary beams. An intense vasoconstriction of the arteries and arterioles exists also in the affected regions, which show a patchy, sometimes lobar, distribution. The inflammation can spread to the perinephric fat, Gerota's fascia, and to the extrarenal space (this is infrequently seen) (1).

- Hematogenous route: It occurs especially in patients addicted to drugs taken *via* a parenteral route, immunocompromised patients, or those who present with a source of extrarenal infection. The lesions begin in the cortex and involve the medulla by 24–48 h. Initially, the lesions are small, peripheral, and multiple (1).
- Lymphatic route: Theoretically, the anatomical disposition of the lymphatic vessels allows the bacteria to travel from the low urinary tract towards the kidney and from the colon towards the right kidney.

In short, the factors that influence imaging findings are (3):

- Focal decrease in perfusion, consequence of the edema that compresses and/or the aggregation of intravascular granulocytic cells.
- Tubular obstruction due to accumulation of granulocytes and/or edema.
- Alteration of the tubular cell membrane transport mechanism, with consequent cellular death.

Clinical Presentation

The signs and symptoms suggestive of upper urinary tract infection are fever, flank pain, nausea, vomiting, and costovertebral angle pain. Sometimes they are accompanied by symptoms that suggest cystitis (low urinary tract infection): dysuria, high urinary frequency, urinary emergency, and suprapubic pain (2).

In 20% of older women, fever is present, with gastrointestinal and respiratory symptoms being the predominant findings (2).

Imaging

The indications for imaging studies are: (1) patients with clinical diagnosis of AP that present with a condition that prevents the improvement of the disease and (2) patients with suspicion of obstruction, lithiasis, or a coexistent abscess (1).

Intravenous Urography

Approximately 75% of intravenous urography (IVU) studies are normal. In the remaining 25%, AP shows global enlargement of the kidney (the most frequent finding), decreased contrast material density, effacement of the collecting system, and delayed caliceal appearance time. Rarely, it shows mass, edema of the pelvic mucosa, focal areas of increased or decreased nephrographic opacity, or mild ectasia of the pyelocaliceal system and ureter (1).

Echography/Ultrasonography

Ultrasonography (US) is a very useful tool for pointing out dilatation of the urinary excretory system. It is not suitable for demonstrating signs of tubulointerstitial inflammation, being less sensitive than renal cortical scintigraphy with technetium-99m dimercaptosuccinate (Tc-99m DMSA) (1). Thus, it allow to rule out renal stones, dilatation, or abscess (4).

The majority of explorations show normal kidneys. Typical findings of uncomplicated AP, when present, are focal or widespread increase of renal size, alteration in parenchymatous echogenicity, and loss of corticomedullary boundary. Sometimes, a hypoechoic mass is seen, badly defined, with diffuse low-amplitude echoes (1).

Complicated AP can show hypo- or anechoic focal masses, with well-delimited borders, corresponding to abscesses (1).

Power/Doppler US shows triangular areas of decrease or absence of cortical or parenchymatous perfusion (3).

Computed Tomography

The characteristic findings of AP are: (1) renal tumefaction, which produces an increase in the size of the involved kidney; (2) focal hypoattenuation and (3) mass effect. Without intravenously administered (i.v.) contrast material, the renal parenchyma can present grooved, rounded, or triangular areas (with cortical base) with variable attenuation (edema or necrosis, hemorrhage). Dynamic studies show anatomical and functional renal anomalies. After administration of i.v. contrast material, these areas (from the papilla to the renal surface), with well-delimited outline, present a minor intensification compared to the normal parenchyma in the corticomedullar and nephrographic phases; these findings are secondary to focal ischemia, tubular obstruction, and the interstitial inflammation, which causes a minor clearance of contrast medium (Fig. 2). In delayed series, there can be an increase in density, i.e., persistence of the contrast material in these areas or in the periphery, due to the progression of the contrast material through the tubules and the compression of the adjacent tissue (1). The "nephrographic" or "parenchymatous" phase is the one that best defines the entire extension of lesions (3, 4) and complications such as abscesses (4). In focal pyelonephritis a single zone with the appearance of a mass is shown (Fig. 3).

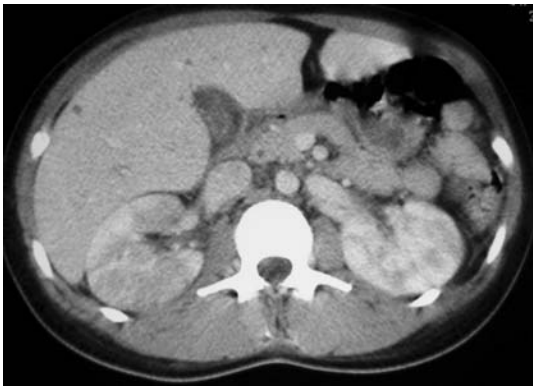

Pyelonephritis, Acute. Figure 2 Acute pyelonephritis. CT after i.v. contrast administration. Nephrographic phase that shows an increase in the size of both kidneys, with well-delimited triangular hypodense areas compared to the normal renal parenchyma, characteristic of bilateral acute pyelonephritis.

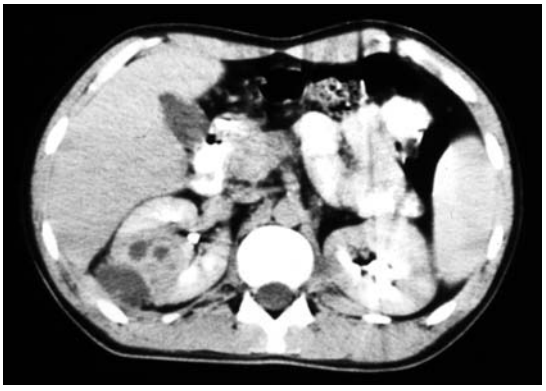

Pyelonephritis, Acute. Figure 3 Acute lobar nephronia. CT after i.v. contrast administration. The nephrographic or parenchymatous phase shows a localized inflammatory right renal mass, solid, with small hypodense areas and slight involvement of the perirenal structures. Two weeks later, after antibiotic treatment, the lesion disappeared.

Perinephric involvement is frequent, with thickening of the Gerota's fascia and bridging septa in the perinephric space (1).

If treatment is not administered, or if it fails, microabscesses might appear, which tend to coalesce. These are shown as one or more irregular areas with attenuation values near water, without enhancement after i.v. contrast administration. The mature abscesses present well-defined outlines showing only peripheral or rim enhancement (1).

CT is capable of differentiating between located tubulointerstitial inflammation and abscess, being very sensitive for evaluating parenchymatous and perinephric extension (4).

In emphysematous pyelonephritis, CT shows gas in both the renal parenchyma and collecting system, even it is possible to define its extension to the subcapsular, perinephric, and pararenal spaces and counterside retroperitoneal spaces.

Magnetic Resonance Imaging

The indications of magnetic resonance imaging (MRI) in the detection of AP are the following: (1) patients with fever of unknown origin, without evidence of infection of the urinary tract; (2) chronic bacteriuria, with uncertain diagnosis of urinary infection; (3) children with known vesicoureteral reflux with suspicion of urinary infection and fever in spite of antibiotic prophylaxis and (4) children without demonstrable reflux or urinary anatomical anomaly, with recurrent infections of the urinary tract and fever.

Without i.v. contrast, on "inversion recovery" sequences, the kidneys have high signal intensity (SI), with pyelonephritic lesions appearing relatively hyperintense. A fast inversion recovery sequence, after the i.v. administration of gadopentate dimeglumine, has a high sensitivity in the detection of AP. This sequence diminishes notably the SI of the normal parenchyma (due to shortening of T2), and thus inflammatory lesions appear as focal zones of moderate or high SI, as a consequence of the minor concentration of gadolinium due to defective perfusion (3, 5). On MR images, scar lesions do not show any signal change (5).

Nuclear Medicine

Cortical scintigraphy with Tc-99m DMSA allows to obtain images of the same zone, on anterior, posterior, left posterior oblique, and right posterior oblique views, within 2–4 h of the injection. The zones of AP are depicted as focal or diffuse cortical photopenic areas (4, 5), hypoactive, secondary to focal ischemia and tubular malfunction. This finding is unspecific, being common in renal cysts and abscesses, hydronephrosis, calculi, and chronic scars. Thus, this technique does not allow differentiation between a focus of AP and a renal permanent scar (5), in addition to undervaluing the extension of the AP (4).

In children, it is more sensitive than CT in the detection of focal anomalies (4).

Diagnosis

- Symptoms compatible with the diagnosis.
- Urynalisis: especially "pyuria," which is determined by means of a leukocyte esterase test, which is indicative of AP in the presence of more than 10 leukocytes per mL of urine. In the sediment, more than five

leukocytes per field is considered pyuria. The level of nitrites is also determined. Hematuria may be present.
- Gram stain analysis of urine without centrifuging: It is indicated when the clinical picture is not very demonstrative and when a differential diagnosis is needed, or when the presence of gram-positive flora is suspected. It helps select the initial antibiotic therapy.
- Urine culture: Over 10,000 colony-forming units per mL (CFU/mL) is considered as positive. In men and pregnant women, lower counts are of concern. It must be carried out before the beginning of treatment.
- Blood culture: It is indicated in patients with complicated AP who need hospitalization, in cases of uncertain diagnosis, when the patient is immunosuppressed or a hematogenous source is suspected. Three samples must be taken.

Interventional Radiological Treatment

It is possible to drain renal or perinephric abscesses or collections by puncture guided ultrasound scan or CT.

References

1. Talner LB, Davidson AJ, Lebowitz RL et al (1994) Acute pyelonephritis: can we agree on terminology? Radiology 192:297–305
2. Ramakrishnan K, Scheid DC (2005) Diagnosis and management of acute pyelonephritis in adults. Am Fam Physician 71(5):933–942
3. Majd M, Nussbaum Blask AR, Markle BM et al (2001) Acute pyelonephritis: comparison of diagnosis with 99mTc-DMSA SPECT, spiral CT, MR imaging, and power Doppler US in an experimental pig model. Radiology 218:101–108
4. Sattari A, Kampouridis S, Damry N et al (2000) CT and 99mTc-DMSA scintigraphy in adult acute pyelonephritis: a comparison study. J Comput Assist Tomogr 24(4):600–664
5. Kovanlikaya A, Okkay N, Cakmakci H et al (2004) Comparison of MRI and renal cortical scintigraphy findings in childhood acute pyelonephritis: preliminary experience. Eur J Radiol 49(1):76–80

Pyelonephritis, Chronic

Luis H. Ros Mendoza,
Roberto Martínez García,
Beatriz Izquierdo Hernández
University Hospital Miguel Servet, Department of Radiology, Zaragoza, Spain
lhros@wanadoo.es

Synonyms

Chronic atrophic pyelonephritis; Chronic interstitial nephritis; Reflux nephropathy

Definition

Chronic pyelonephritis is a chronic inflammatory disease that involves the renal parenchyma, characterized by the focal loss of renal substance with presence of deep scars and decrease of the renal size. It is an interstitial nephritis often related to vesicoureteral reflux, especially in childhood and in female patients.

►Reflux nephropathy can also be caused by infections due to urinary tract obstruction or by the acquired forms of adult vesicoureteral reflux. Other etiologies for this entity include urolithiasis (Fig. 1) and papillary necrosis.

Other causes that provoke chronic infection of the kidney, such us ►xanthogranulomatous pyelonephritis (XGP), ►renal tuberculosis (RTB), and mycotic infections, should be considered (1).

Xanthogranulomatous pyelonephritis is the result of a chronic infection produced by gram-negative bacteria, especially *Proteus mirabilis* or *Escherichia coli*, related to a long evolution of obstruction of the urinary tract, causing destruction of the renal parenchyma and its replacement by lipid-laden macrophages. It is usually associated to nephrolithiasis (70%). This process is often unilateral and appears more frequently in middle-aged women.

Renal tuberculosis is produced as a consequence of the hematogenous dissemination of *Mycobacterium tuberculosis* from the lungs to the genitourinary system. About 4–8% of patients affected by tuberculous pulmonary disease will develop symptomatic genitourinary infection (2).

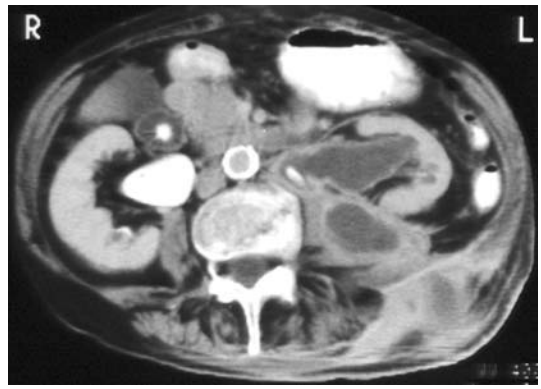

Pyelonephritis, Chronic. Figure 1 Chronic renal infection. CT after intravenous contrast administration. The left kidney appears with decreased parenchymatous thickness and size, findings related to obstruction due to a pyeloureteral junction stone. It also presents a minor nephrographic density than the right kidney. There is involvement of the left psoas and abdominal wall muscles by the chronic inflammatory process. The right kidney shows compensatory hypertrophy. A stone can be seen within the gallbladder.

Mycetoma or fungus ball is a mycotic infection that is caused by an ascending infection of the urinary tract or by hematogenous seeding, usually produced by *Candida albicans* or *Aspergillus*. It usually affects immunocompromised patients or those under long treatments with antibiotics or steroids (1).

Lipomatous renal replacement is an unusual form of renal sinus lipomatosis associated with parenchymatous atrophy, related to chronic renal inflammation and nephrolithiasis in 75% of cases (1).

Pathology/Histopathology

Reflux nephropathy is often preceded by renal infection episodes (acute pyelonephritis), with gram-negative bacteria most usually involved, especially *E. coli*.

Vesicoureteral reflux is an important factor in the infection ascending to the superior urinary tract, and considered a fundamental risk factor, although not the only one, for the development of reflux nephropathy. Once the bacteria reach the pyelocalyceal system, they access the renal parenchyma through the papillary holes of the collector ducts; this is known as intrarenal reflux.

Vesicoureteral reflux depends on the length and the insertion angle of the ureteral distal portion, which goes through the bladder and is canalized under the mucosa to end up in the trigonum. Thus, it is frequent in childhood and progressively improves during normal growth. In the case of serious reflux, it might cause significant harm to the renal parenchyma. There are two kinds of alterations. One is reflux atrophy or reflux diffuse nephropathy caused by the reflux of an important volume of high-pressure urine, causing variable degrees of dilatation of the pyelocalyceal system and renal atrophy. In the second alteration, the reflux coexists with a urinary tract infection. The reflux causes the ascent of bacteria to the superior urinary tract and together with the intrarenal reflux will lead to parenchymatous scars and other alterations of ▶chronic atrophic pyelonephritis.

Intrarenal reflux takes place in the renal areas where the shape of the papillary orifices has been deformed by the lobular fusion process; thus, intrarenal reflux can be produced in one or more parts of a lobe, but not in the entire lobe.

The pathologic characteristics of this entity are:

- A total involvement of the renal thickness due to the reflux in the collector ducts that extend from the papilla to the cortex.
- Lobular involvement with normal areas of partial neighboring tissue.
- Major occurrence of scars in the renal poles than in the interpolar region due to a larger quantity of composed papillae.

In animal studies the condition of reflux nephropathy with the coexistence of vesicoureteral reflux and sterile urine has been reproduced, leading to controversy on the role of the infection in the etiopathogenesis of this process.

The earliest involvement of this entity is an acute tubulointerstitial nephritis in the portion of the affected renal lobe. This condition usually occurs in childhood without producing significant radiologic alterations, but with impairment of capillary perfusion and glomerular filtration secondary to the interstitial inflammatory infiltrate and pus accumulation in the collector ducts. In this state, radioactive isotopes or radiologic techniques that allow the evaluation of perfusion are used in the diagnosis (3).

If the infection, with or without reflux, continues, the inflammatory infiltrate is substituted by fibrous tissue producing a scar and the retraction of the renal surface and the underlying papilla.

In the pathogenesis of XGP, the usual finding is diffuse infiltrate of the renal parenchyma by plasmatic cells and lipid-laden macrophages that produce yellow-tan masses. In 90% of cases of XGP, renal lithiasis is found, generally presenting a "stag horn" morphology, made of struvite. The calyces are dilated and with thickened walls and are filled with pus. The histologic response is thought to be related to the release of lipids from the tissues damaged by bacteria.

In RTB small granulomas are found bilaterally in the cortex, adjacent to the glomerulus. The high rate of perfusion and the existing oxygen tension increase the probability of bacillary proliferation in that area. In immunocompetent patients, the bacterial duplication is inhibited and so the process remains latent in the renal cortex, with the possibility of absence of symptoms for decades. In the case of an immunity alteration, a reactivation of the cortical granulomas is produced, which increase in size and tend to coalesce.

Breaking of the capillary vessels gives the bacilli access into the proximal tubule and Henle's loop, producing caseous granulomas and papillary necrosis. The granulomas, the caseous necrosis, and the cavity are stages of active infection that can destroy the kidney.

The link of these granulomas with the collector system can cause seeding of bacilli in the renal pelvis, ureters, bladder, and genital organs. The host response induces fibrosis, calcium deposits, and stenotic areas, favoring the obstruction and alteration of renal function (2).

Clinical Presentation

Urinary tract infection is more often found in girls and women, and during the first year of life in uncircumcised boys. The combination of urinary infection and

severe reflux shows fever, flank pain, dysuria, and higher mictional frequency as symptoms. Aspecific symptoms such us drowsiness and abdominal pain associated with fever are often found. Many children show bacteriuria and renal scars on intravenous urography without presenting any symptoms.

More serious cases of bilateral reflux nephropathy are more frequently found in young adults, especially women. Hypertension and chronic renal failure are the usual findings.

Xanthogranulomatous pyelonephritis is more frequent in women, regardless of age. It is often preceded by a few months of undiagnosed chronic disease. The clinical symptoms are abdominal and flank pain, fever, weight lost, and weakness. Many patients do not have any symptoms related to the inferior urinary tract. In some cases, a renal mass can be palpated. In the analytic tests, anemia, leukocytosis, albuminuria, and pyuria can be found (1).

The most frequent symptom of RTB is polyuria. Suprapubic, inguinal or flank pain, micro- or macroscopic hematuria, dysuria, and epididymitis can appear. Constitutional symptoms such as fever, anorexia, weakness, weight loss, and night sweating are not frequent in the renal forms. Of the patients, 10% show no symptom. Sterile pyuria is characteristic in standard culture media (2).

Imaging

Chronic Atrophic Pyelonephritis

By means of intravenous urography (IVU), we can appreciate the existence of scars in the entire lobe or in a part, located over a retracted papilla, whose calyx is dilated with smooth margins. Usually the lesions are unilateral, but bilateral involvement can also exist.

There is a decrease in the parenchymatous thickness with compensatory focal hypertrophy in the unaffected areas. The nephrographic phase is characterized by a failure of contrast captation in the affected area.

Ultrasonographic studies show rounded and dilated calyces, with either adjacent cortical scar or the presence of cortical atrophy. If the disease is unilateral, the presence of compensatory hypertrophy can be seen in the contralateral kidney. In some cases sinusal lipomatosis can appear, being identified by an increase in the echogenicity of the sinusal complex (4).

By means of computed tomography (CT), the focal parenchymatous scar that covers the club-shaped dilated calyx can be identified.

Sometimes these calyces can be similar to a renal cyst or a hypovascular mass during the cortical nephrographic phase. In these circumstances a delayed study allows us to confirm the presence of dilated calyces filled with contrast material. CT helps establish the diagnosis of hypertrophic focal areas adjacent to the scar zones. Lobar infarcts can also be identified by means of this technique by their predominant cortical participation and the absence of calyceal involvement (1).

Magnetic resonance imaging (MRI) shows small kidneys with an absent or blurred corticomedullary junction. The fat of the renal sinus is abundant and the rest of the parenchyma can show low signal intensity. Focal scars of chronic pyelonephritis may appear with low signal intensity on both T1- and T2-weighted images.

Diffuse Xanthogranulomatous Pyelonephritis

The urographic findings include a coraliform or staghorn stone on abdominal plain films as well as a kidney increased in volume or a renal mass.

Other possible alterations might be blurring of the psoas silhouette or the absence or reduction of renal function. In the case of contrast media elimination or by means of retrograde pyelography, hydronephrosis with irregular calyces and papillary necrosis can be seen.

On ultrasonography the increase in renal size with smooth contours is identified, as well as the absence of any corticomedullary differentiation. There is dilatation of the calyces that appear filled with detritus from the inflammatory process, which are visualized as hypoechogenic structures with thin internal echoes. The echogenic image with acoustic shadow in the renal sinus represents the stone. Xanthogranulomatous parenchymatous masses appear as isoechogenic focal areas compared with the rest of the renal parenchyma. Perirenal involvement can be more clearly seen by means of CT (5).

With CT, the findings obtained in the other imaging examinations can be confirmed. Enlargement in renal size or a renal segment is demonstrated, with the presence of the central stone, usually a coraliform stone. There is a poor elimination of contrast material to the collector system. There are multiple focal masses of low attenuation (–10 to + 30 HU) in the involved areas, which represent dilated calyces filled with detritus and xanthomatous collections. They do not present postcontrast enhancement, but they show peripheral enhancement related to the inflammatory hypervascularization. Renal lipomatosis can also be identified. CT is very useful in identifying the extent of the infection in the psoas muscle and in the para- and perirenal spaces. Renocolic and cutaneous fistulous tracts can appear (1, 5).

By means of MRI, the inflammatory mass presents a mixed intensity signal that can simulate a neoplastic

process. The signal void produced by the renal stone can help in the diagnosis.

Angiographic examinations evaluate the lack of branching out of the interrenal arteries, the displacement of the vessels around the dilated calyces, or the existence of granulomatous mass and the attenuation of the arterial caliber.

Focal Xanthogranulomatous Pyelonephritis

The radiologic findings are similar to those in the diffuse form but are limited to the calyces and the parenchyma of a part of the kidney, frequently associated to an obstructive calyceal stone or to an obstructed duplicated pyelocalyceal system.

Renal Tuberculosis

On abdominal plain films, we can see either speckled or dispersed parenchymatous calcifications, or thicker ones with an annular form, or a ground-glass appearance. In the final stage of the disease, total renal calcification may occur. This can be amorphous, granular, or curvilinear.

The initial urographic anomaly consists of the irregularity of one or more papillae or calyces (ulceronecrotic papillitis). The papillary surfaces are blurred and there is contrast extravasation to the medullary space due to necrosis and dilatation of the calyceal fornix. Hydrocalyces related to infundibular stenosis are also seen. There is infundibular pyelic retraction and pyelocalyceal granulomas (tuberculomas). Ureteral involvement with presence of ulcerations and granulomas might occur, as well as intramural calcification and stiffness.

We can also find thickening of the vesical wall with ulcerations and a decrease in vesical capacity, vesicoureteral reflux, and tuberculous fistulae (2).

Ultrasonographically, small focal lesions (less than 15 mm) can be identified, with an echogenic border and a hypoechoic center, similar to focal bacterial nephritis. Calyceal ectasias that suggest infundibular stenosis and papillary involvement can be detected, which are depicted as echogenic masses without posterior acoustic shadow. The filling calyceal faults, such as clots, fungus masses, and detritus, can present the same echographic appearance as the papillary necrosis, and therefore a fine-needle aspiration punction (FNAP) is required for the cytologic study.

CT is useful for the evaluation of the morphology and distribution of the calcifications, in order to demonstrate the presence of renal parenchymatous abscesses and the extrarenal extension. It also offers an accurate evaluation of the renal parenchyma (1).

Nuclear Medicine

Renal scintigraphy with dimercaptosuccinic acid (DMSA) is useful for confirming the diagnosis of acute pyelonephritis in children and for identifying kidneys with potential risk to develop renal scars (3).

The isotopic findings usually consist of the presence of an area of lack or diminished uptake that extends throughout the parenchymatous thickness in one or more areas of the involved kidney. This is due to the areas of altered perfusion related to the increase of interstitial pressure associated with the inflammatory infiltrate.

DMSA shows higher sensitivity than IVU in the detection of renal scars, especially in children and teenagers (3).

Diagnosis

In the initial stages of reflux nephropathy, the radiologic findings are similar to those of acute pyelonephritis. In these cases, CT after intravenous contrast administration or isotopic renography with Tc-99m DMSA can make diagnosis easier.

Radiologic evaluation after these initial stages aims to detect significant vesicoureteral reflux, evaluating the renal parenchyma, detecting delay in its growth or scar formation; a follow-up is advised in these cases. The reflux can be observed by mictional or isotopic cystography.

Imaging modalities for the evaluation of renal structure are IVU, ultrasonography, CT, and isotopic studies.

Specific criteria for the diagnosis of reflux nephropathy are the existence of a scar that involves the whole parenchymatous thickness, with irregular depression on the surface, and the presence of papillary retraction and dilatation of the underlying calyx.

The adjacent renal tissue is normal or hypertrophic. The distribution of the lesions is either uni- or multifocal and can be either uni- or bilateral. A global reduction in renal size is characteristic (Fig. 2).

In the case of XGP the urographic study identifies the stone, generally coraliform, and the impairment of renal function. This finding can be confirmed with ultrasonography, by observing an increase in renal size without contour alteration, the existence of dilated calyces and hypoechogenic masses, as well as the stone.

In the focal or segmentary forms, it is difficult to establish whether these masses correspond to an inflammatory accumulation, an abscess, or a tumor. CT is very helpful in these cases, as the urographic and ultrasonographic findings are nonspecific. CT is very sensitive in detecting perirenal extension (Gerota's fascia, psoas muscle,

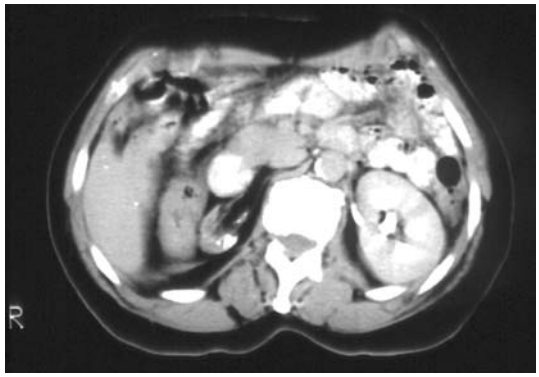

Pyelonephritis, Chronic. Figure 2 Chronic atrophic pyelonephritis. CT after intravenous contrast administration. The right kidney presents an atrophic appearance secondary to the chronic infection. There is a compensatory hypertrophy of the left kidney.

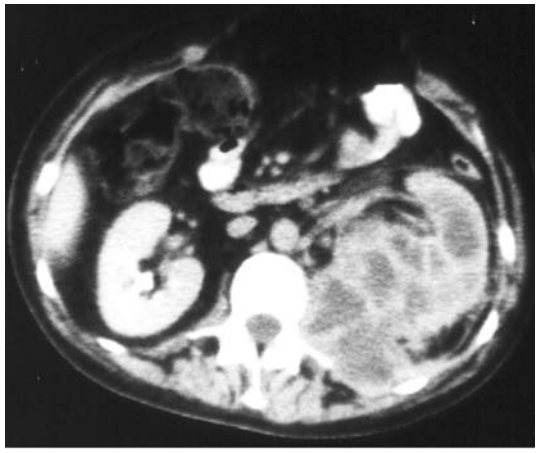

Pyelonephritis, Chronic. Figure 3 Xanthogranulomatous pyelonephritis, diffuse form. CT after intravenous contrast administration. There is enlargement of the left kidney with multiple focal inflammatory masses of low attenuation that present a slight peripheral enhancement. The left psoas muscle is also involved by the chronic inflammatory process.

fistulous tracts) (Fig. 3). Most angiographic studies are nonspecific.

The diagnosis of RTB requires the existence of clinical symptoms in accordance to the demonstration of acid-alcohol-resistant bacilli in microscopic urine tests using special stains and urine cultures specific for mycobacteria (2). *M. tuberculosis* is isolated from urine in 80–90% of patients affected by genitourinary tuberculosis. Mantoux test results will be positive in most of these patients, but the test is not specific for the development of RTB.

Imaging techniques such as IVU and CT are very useful, because 10–15% of patients with signs of tuberculous activity will have normal urographic findings. These modalities depict a series of genitourinary lesions related to the mycobacteria infection depending on the disease stage.

CT findings are less sensitive than those of IVU for the early detection of urothelial mucosa changes, but it proves useful in determining the renal and extrarenal extension of the infection (2).

References

1. Kawashima A, Sandler CM, Goldman SM et al (1997) CT of renal inflammatory disease. Radiographics 17:851–866
2. Gibson MS, Puckett ML, Shelly ME (2004) Renal Tuberculosis. Radiographics 24:251–256
3. Rushton HG, Majd M (1992) Dimercaptosuccinic acid renal scintigraphy for the evaluation of pyelonephritis and scarring: a review of experimental and clinical studies. J Urol 148:1726–1732
4. Kay CJ, Rosenfield AT, Taylor JW et al (1979) Ultrasonic characteristics of chronic atrophic pyelonephritis AJR 132:47–49
5. Causins C, Somers J, Broderick N et al (1994) Xanthogranulomatous pyelonephritis in childhood: Ultrasound and CT diagnosis. Pediatr Radiol 24:210–212

Pyelonephritis, Chronic Atrophic

Chronic inflammatory disease, characterized by focal loss of renal substance with presence of deep scars and decrease in renal size.

▶Pyelonephritis, Chronic

Pyloric Stenosis

▶GI Tract, Pediatric, Specific Problems

Pyogenic Arthritis

Pyogenic arthritis or septic arthritis may be caused by *Staphylococcus*, *Streptococcus pneumoniae*, *Neisseria meningitidis*, or *Haemophilus influenzae*. Clinical findings in gout may be similar to those in septic arthritis.

▶Gout

Pyogenic Cerebritis and Abscess

E. Turgut Tali, Serap Gultekin
Gazi University, Ankara, Turkey
turgut.tali@gazi.edu.tr
segultekin@yahoo.com

Definition

Cerebritis represents the earliest phase of parenchymal infection. Brain abscess is a focal intracerebral infection that begins as a localized area of cerebritis and develops into a collection of pus surrounded by a well-vascularized capsule. Streptococcus is the most common causative organism (30–50%).

Pathology/Histopathology

Infection progresses through four stages: early cerebritis, late cerebritis, early capsule, and late capsule. The cerebritis phase typically lasts from 10 to 14 days. Pathologically, cerebritis is described as a poorly demarcated area of parenchymal softening with scattered necrosis, edema, vascular congestion, and petechial hemorrhage without tissue liquefaction. The focus of cerebritis progresses to abscess when the central zone of necrosis becomes liquefied, better defined, and encircled by a collagen capsule, which itself is surrounded by a prominent zone of gliosis (1).

Clinical Presentation

Patients present with the cardinal features of fever, epilepsy, headache, nausea, vomiting, and occasionally a depressed level of consciousness (1).

Imaging

Computed Tomography

In cerebritis, an ill-defined, low-density lesion without contrast enhancement is seen. In mature abscess, an area of low density with a ring enhancement pattern is observed.

Magnetic Resonance Imaging

In early cerebritis, an area of increased signal intensity on T2/fluid attenuation inversion recovery (FLAIR) sequences with or without ill-defined, patchy, irregular enhancement in the depth of the sulci is seen. The differentiation of cerebritis from infarction can be made on diffusion-weighted imaging (DWI). Acute infarction appears bright with a matching area of decreased signal on the apparent diffusion coefficient (ADC) map. Cerebritis shows a high signal on DWI and ADC maps due to the T2 shine-through effect.

After the second week, the abscess starts to form and is characterized by an incomplete rim of enhancement. By the end of the third week, a mature abscess forms. Peripheral edema is nearly always present. Mature abscesses have a capsule that is hypointense on T2-weighted images. The abscess capsule shows ring enhancement. The ring is usually smooth and thin walled (approximately 5 mm) and is often thinner along the medial margin (Fig. 1) (2).

DWI is helpful in differentiating abscess from necrotic tumor (3). On DWI, an abscess demonstrates high signal intensity with a corresponding reduction on ADC maps. Magnetic resonance spectroscopy (MRS) adds another layer of certainty by identifying the metabolites that are specific for pyogenic brain abscesses. MRS reveals end-products of bacterial breakdown and the proteolytic enzyme degradations (e.g., lactate, acetate, succinate, and amino acid peaks) that can be found in all abscesses, but not in necrotic/cystic tumors (4).

Diagnosis

The diagnosis largely depends on imaging studies. It is very important to stress that occasionally patients may not present with suggestive clinical symptoms. Therefore, in cases of a ring-enhancing mass in an afebrile patient, abscess should still be considered.

Bibliography

1. Anslow P (2004) Cranial bacterial infection. Eur Radiol 14:E415–E154
2. Andreula C (2004) Cranial viral infections in the adult. Eur Radiol 14:E132–E144
3. Arbealáez A, Medina E, Restrepo F et al (2004) Cerebral tuberculosis. Semin Roentgenol 474–480
4. Bernaerts A, Vanhoenacker FM, Parizel PM et al (2003) Tuberculosis of the central nervous system: overview of neuroradiological findings. Eur Radiol 13:1876–1890
5. Castillo M (2004) Imaging of meningitis. Semin Roentgenol 39:458–464
6. Castillo M, Thurner M (2004) Imaging viral and prion infections. Semin Roentgenol 482–484
7. Dev R, Gupta RK, Poptani H, Roy R, Sharma S, Husain M (1998) Role of in vivo proton MRS in the diagnosis and management of brain abscess. Neurosurgery 42:37–43
8. Hunter JV, Morriss Mc (2003) Neuroimaging of central nervous infections. Seminars in Pediatric Infectious Diseases 14:140–164
9. Leuthardt EC, Wippold FJ, Oswood MC, Rich KM (2002) Diffusion-weighted MR imaging in the preoperative assessment of brain abscesses. Surg Neurol 58:395–402

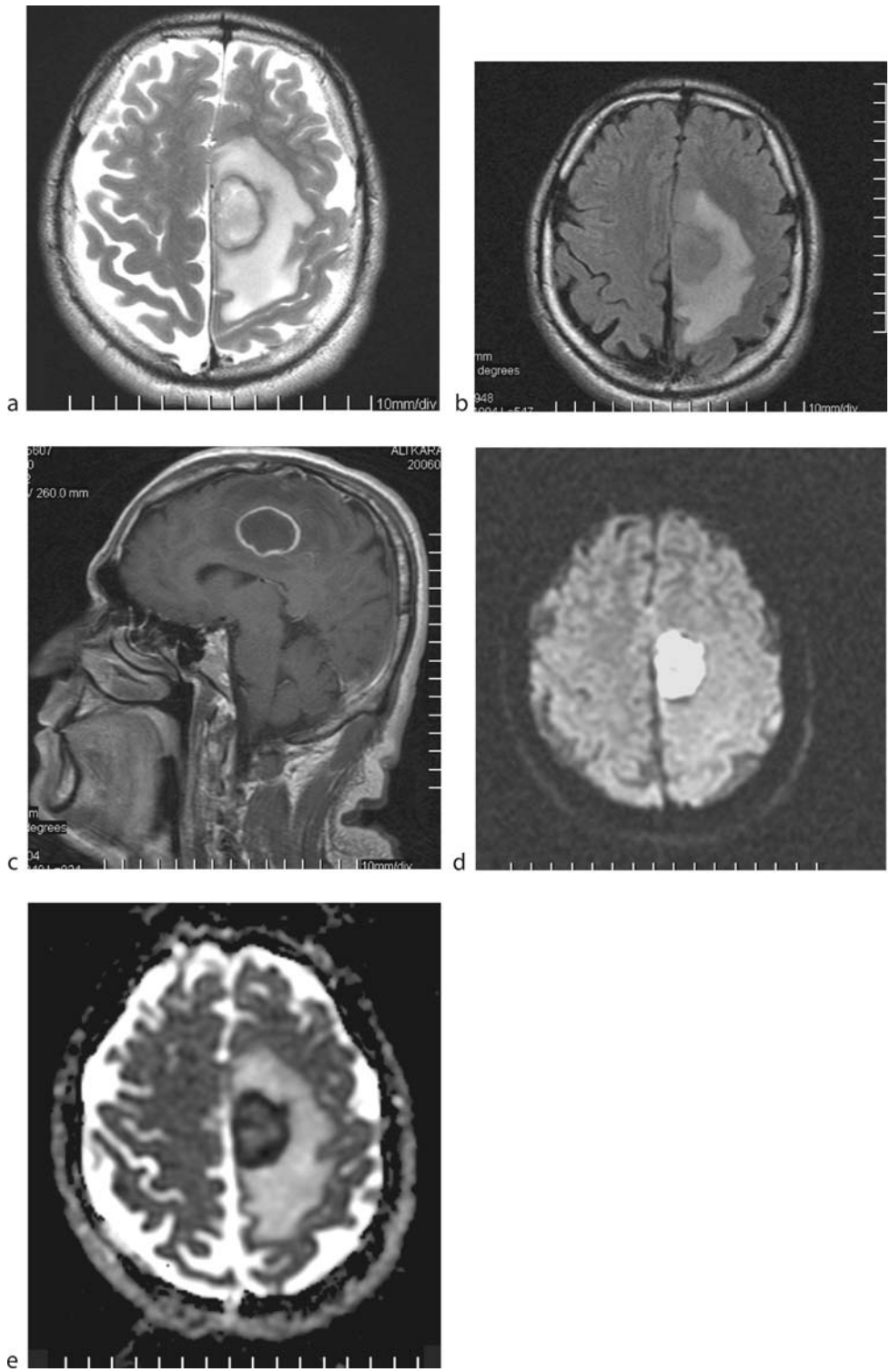

Pyogenic Cerebritis and Abscess. Figure 1 Mature brain abscess. Axial (a) T2-weighted and FLAIR (b) images show a lesion in the left posterior parietal lobe with marked surrounding edema, mass effect, and a hypointense capsule on the T2-weighted image. The central necrotic part of the lesion is hyperintense to cerebrospinal fluid on T1-weighted imaging and shows heterogeneous hypointense signal on T2-weighted imaging due to the debris and proteinaceous material content. Sagittal (c) postcontrast T1-weighted images demonstrate the regular, thin, enhancing capsule with necrotic center. Corresponding trace DWI (d) shows that the center of the abscess is very bright. On ADC map (e), the lesion is hypointense due to restricted water diffusion in the purulent abscess.

Pyogenic, Abscess, Hepatic

Localized intrahepatic collection of pus due to bacteria (most commonly *Clostridium* species and gram-negative bacteria, such as *Escherichia coli* and *Bacteroides* species). Ascending cholangitis and portal diffusion are the most frequent causes of pyogenic hepatic abscesses. Other possible ways of diffusion are arterial diffusion, direct extension from adjacent organs, and traumatic penetrating lesions. In a large number of patients the origin of the liver abscess remains unknown. Fever and pain are the most common symptoms. Anorexia, nausea, vomiting, weight loss, and pleural effusion are often present. Computed tomography (CT) and ultrasound (US) have a high sensitivity in detecting pyogenic abscesses. In the colliquative phase, US shows an irregular lesion containing a variable quantity of hyperechoic spots, corresponding to necrotic debris; the appearance may vary from anechoic to hyperechoic. At CT, in the subacute or colliquative phase, the pyogenic abscess appears as an irregular hypodense area with density values higher than those of simple cysts. Typically the lesion has a thick irregular wall and presents a characteristic rim enhancement, while the central necrotic portion remains unenhanced. A CT finding suggestive of abscess is the "double target" sign; it represents a hypodense lesion surrounded by an enhancing rim, corresponding to the wall, and an outer hypodense halo, due to perilesional edema. The presence of gas within the lesion represents a specific sign of pyogenic abscess. At magnetic resonance imaging (MRI), pyogenic abscesses appear as hypointense areas on T1-weighted images and hyperintense areas on T2-weighted images. Perilesional edema can be seen on T2-weighted MR images. After contrast medium administration, the lesion shows marked peripheral enhancement. Miliary pyogenic microabscesses are usually found in patients with generalized septicemia and may appear as multiple lesions scattered throughout the liver or as a cluster of small lesions which tend to coalesce.

▶Abscess, Hepatic

Pyomyositis

▶Infection, Soft Tissue

Pyonephrosis

An obstructed and infected kidney, with dilated pyelocaliceal system filled with purulent material.

▶Pyelonephritis, Acute

Pyosalpinx

Dilated fallopian tubes become visible on imaging as tubular tortuous adnexal structures, which contain incomplete interdigitating septations. They contain pus that displays higher proteinaceous contents than fluid in hydrosalpinx. Mural thickening is another feature of pyosalpinx.

▶Abscess TuboOvarian

QCT

►Quantitative Computed Tomography

Q-tip Test

A cotton-tipped stick lubricated with Xylocaine gel is placed into the urethra up to, but not through the internal urethral sphincter (Q-tip test). With straining or coughing, the stick rises more than 30° from its resting angle. This demonstrates urethral hypermobility and differentiates genuine stress incontinence from an intrinsic urethral sphincteric insufficiency (ISD) without hypermobility.

►Pelvic Floor Dysfunction, Genitourinary

Quadrantectomy

Breast surgical technique that consists of removal of up to one-quarter of the breast and an ellipse of skin and reaching the fascia of pectoralis major muscle.

►Breast Conserving Therapy

Quantification

The quantitative assessment of the contrast enhancement in a target region (region of interest). For quantification, it is necessary that the relationship between contrast agent concentration and signal intensity is known. For ultrasound contrast agents there is a linear relationship between both parameters, unless the concentration is becoming too high resulting in attenuation effects in deeper regions.

►Contrast Media, Ultrasound, Commercial Products

Quantitative Computed Tomography

Technique to measure volumetric bone mineral density using computed tomography (CT) and transforming CT density values with a calibration phantom into mg calcium-hydroxyapatite/mL. Can be performed in single sections obtained at the lumbar vertebrae (L1–L3) (two-dimensional QCT) or in volumetric datasets obtained at the lumbar spine and the proximal femur (three-dimensional QCT).

►Osteoporosis

Radial Scar, Breast

Luis Pina
Department of Radiology, Clínica Universitaina de Navarra, Spain
ljpina@unav.es

Synonyms

Benign sclerosing ductal proliferation; Complex sclerosing lesion; Indurative mastopathy; Infiltrating epitheliosis; Non-encapsuled sclerosing lesion; Radial sclerosing lesion; Scleroelastotic scar; Sclerosing papillary lesion; Sclerosing papillary proliferation

Definition

Radial scars are benign complex lesions that may simulate carcinomas on imaging techniques, as well as in gross and microscopic examination. The term *complex sclerosing lesion* is similar but it is used for lesions measuring more than 10 mm (1–3).

Pathology

On gross examination radial scars are firm lesions, with a pale retracted centre and bands of pale stroma extending radially into the fat from the core, mimicking invasive carcinoma (3). On microscopic examination, these lesions show a fibroelastotic core from which ducts and lobules radiate. Several combinations of typical ductal hyperplasia, ►atypical ductal hyperplasia, adenosis, lobular neoplasia and sometimes ductal carcinoma *in situ* or even infiltrating ductal carcinoma may be found. Entrapped ducts are present in the central core with distorted or angular appearance, and may mimic ►tubular carcinoma (1–3). The presence of myoepithelial cells, that may be confirmed immunohistochemically with markers such as actin, smooth muscle myosin, p63 and calponin, is useful to differentiate both entities (3).

Clinical Presentation

Most radial scars are non-palpable microscopic findings incidentally diagnosed in a surgical biopsy performed for other lesion. Radial scars occur in a wide pre- and post-menopausal age group. However, occasionally complex sclerosing lesions may be palpable or may retract the skin (2). The widespread use of mammography has led to an increasing detection of radial scars, with a reported incidence in screening programs between 0.1 to 0.5 per 1,000 women (2). Multiple radial scars in one breast or in both breasts may be found. However, the incidence in mastectomy specimens is higher, from 4 to 26%. In addition, the incidence in benign specimens ranges from 1.7 to 28% (3). These broad and overlapping ranges suggest that radial scars occur similarly in benign and malignant lesions. Nevertheless, the relationship between radial scars and breast cancer remains unclear. Some studies find that radial scars may increase the risk to develop breast cancer, but others suggest that the risk can be originated by the hyperplasic lesions accompanying radial scars, especially atypical ductal hyperplasia (1, 2).

Imaging

Mammography

The typical appearance of a radial scar on mammography is an architectural distortion, sometimes with accompanying microcalcifications (Fig. 1). The presence of a radiolucent centre, long spicules or the difficulty to identify the lesion on both conventional views may suggest the diagnosis. However, there are no reliable signs to diagnose it, so a biopsy should be performed. Occasionally the mammographic appearance of a radial scar is a cluster of microcalcifications or a mass (4) (Fig. 2).

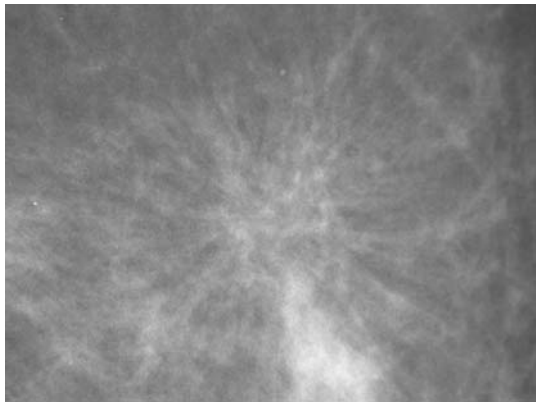

Radial Scar, Breast. Figure 1 Typical architectural distortion caused by a radial scar-complex sclerosing lesion. Craniocaudal view (detail).

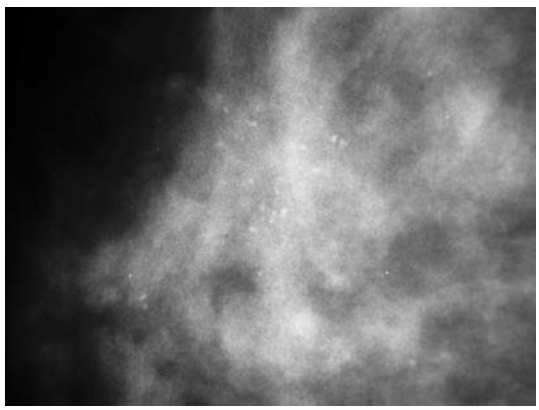

Radial Scar, Breast. Figure 2 A radial scar-complex sclerosing lesion manifested as a cluster of pleomorphic calcifications. Mediolateral oblique view (detail).

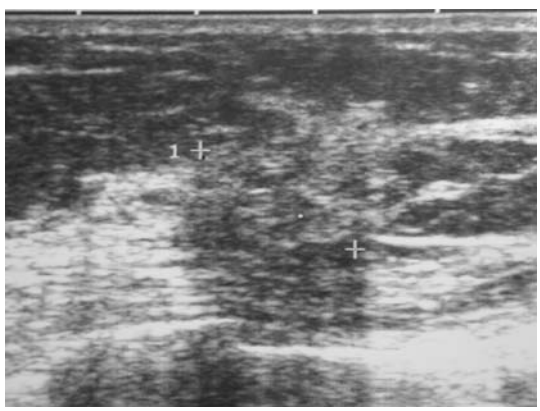

Radial Scar, Breast. Figure 3 Radial scars are difficult to be detected on ultrasonography. In this case, a hypoechoic ill-delimited lesion is seen with slight posterior shadowing.

Ultrasonography

Radial scars are not easily identified on ultrasonography. Subtle hypoechoic irregular masses, that may be less visible rotating the transducer, and acoustic shadowing without a distinguishable mass, are ultrasonographic features of radial scars (4) (Fig. 3).

Magnetic Resonance

T1- or T2-weighted images may reveal an architectural distortion in some cases. Radial scars are usually non-enhancing lesions on contrast enhanced magnetic resonance studies, but also may enhance mimicking breast cancer. Thus, magnetic resonance cannot be used to differentiate both lesions and a biopsy is needed.

Nuclear Medicine

The usefulness of nuclear medicine scans has not yet been proven.

Diagnosis

Both radial scars and complex sclerosing lesions are diagnosed by biopsy. The management of these lesions with percutaneous biopsy techniques remains controversial. Most authors recommend the complete excision of the lesion due to its complexity (4). Conventional core needle biopsies (14 G) may underestimate an occult carcinoma, especially if atypical ductal hyperplasia is demonstrated in the specimens. Moreover, nests of hyperplastic epithelium trapped in the stroma may be misdiagnosed as invasive carcinoma (3). However, if more than 12 samples are obtained with directional vacuum-assisted devices, and the result is concordant with the mammographic findings, further surgery may be avoided (5). Nevertheless, more experience is needed to support these results.

Bibliography

1. Schnitt S, Connolly JL (2004) Pathology of benign breast disorders. In: Harris JR, Lippman ME, Morrow M (eds) et al Diseases of the Breast. Lippincott Williams & Wilkins, Philadelphia, pp 77–99
2. Hughes LE (2000) Sclerosing adenosis, radial scar and complex sclerosing lesions. In: Hughes LE, Mansel RE, Webster DJT (eds) Benign Disorders and Diseases of the Breast. Concepts and Clinical Management, Saunders, London, pp 137–142
3. Rosen PP (2001) Papilloma and related benign tumors. In: Rosen PP (ed) Rosen's Breast Pathology. Lippincott Williams & Wilkins, Philadelphia, pp 77–119
4. Cardeñosa G (2001) Terminal duct. In: Cardeñosa G (ed) Breast Imaging Companion. Lippincott Williams & Wilkins, Philadelphia, pp 231–267
5. Brenner RJ, Jackman RJ, Parker SH et al (2002) Percutaneous core needle biopsy of radial scars of the breast: when is excision necessary? Am J Roentgenol 179:1179–1184

Radial Sclerosing Lesion

▶Radial Scar, Breast

Radiation Exposure, Mammography

Silvia Obenauer
Department of Radiology, Georg-August-University of Goettingen, 37099 Goettingen, Germany
obenauerheuser@yahoo.de

The striking advantage of digital systems is the high dynamic range and the linear relationship between the dose at the detector and the signal intensity, as opposed to the sigmoid relationship between optical density and dose in screen-film systems. Digital image processing technology can display overexposed or slightly underexposed images with normal image quality. This capability has prompted a discussion about the possibility of dose reduction in digital mammography. Phantom studies demonstrated a potential of dose reduction for CsI/a-Si full-field digital mammography systems. Studies with the contrast detail mammography phantom (CDMAM, University Medical Center, Nijmegen, The Netherlands) showed a possibility of 25% reduction of the radiation dose in digital techniques compared to screen-film mammography. Hermann et al. presented a clinical study based on data from 1,116 mammograms of 591 women examined with a CsI/a-Si digital system. The mean average glandular dose was 1.51 mGy for a single view. Therefore, about 25% less dose is needed in digital mammography than in conventional screen-film mammography. Gennaro et al. evaluated four different CsI/a-Si systems in routine clinical work and reported a mean average glandular dose ranging from 1.25 to 1.89 mGy depending on the glandular composition of the breast. The possibility of using higher energy exposures by various anode track–filter combinations may result in additional patient dose reduction with no loss in clinical performance. In an anthropomorphic phantom study, a Mo/Rh anode–filter combination with a tube voltage of 31 kVp (25% dose reduction) and a Rh/Rh with 32 kVp (37% dose reduction) did not show significant differences in the analysis of the receiver operating characteristics for the detection of microcalcifications in comparison with the Mo/Mo combination with 28 kVp. Due to a higher detective quantum efficiency and therefore lower noise, digital systems can compensate for the relative loss of contrast *via* windowing and leveling.

In conclusion, a dose reduction seems to be possible in digital mammography.

References

1. Obenauer S, Hermann KP, Schorn C et al (2000) Digitale Vollfeldmammographie: Dosisabhängige Detektion von simulierten Herdbefunden und Mikrokalzifikationen. RöFo 172:940–945
2. Hermann KP, Obenauer S, Marten K et al (2002) Average glandular dose with amorphous silicon full-field digital mammography: clinical results. RöFo 174:696–699
3. Gennaro G, Baldelli P, Taibi A et al (2004) Patient dose in full-field digital mammography: an Italian survey. Eur Radiol 14:645–652
4. Obenauer S, Hermann KP, Grabbe E (2003) Dose reduction in full-field digital mammography: an anthropomorphic breast phantom study. Br J Radiol 76:478–482
5. Diekmann F, Diekmann S, Bick U et al (2002) Reduced-dose digital mammography of skin calcifications. AJR 178473–474

Radiation Hormesis Theory

The term hormesis is taken to be any stimulatory or beneficial effect, induced by low doses of an agent (in this case radiation), that can not be predicted by the extrapolation of detrimental or lethal effects induced by high doses of the same agent.

▶Radiation Issues in Childhood

Radiation Issues in Childhood

Anne Paterson
Royal Belfast Hospital for Sick Children, Belfast, UK
annie.paterson@royalhospitals.n-i.nhs.uk

Definition

Ionizing radiation is high-energy radiation that is capable of causing ionization in matter through which it travels. In the electromagnetic spectrum, only high-frequency radiation such as X- and gamma rays are capable of ionizing body tissues. Natural radioactive sources in the air (radon gas and cosmic rays) and earth's crust contribute to our exposure to ionizing radiation, along with small quantities of radioisotopes present in the human body and in the food chain. This environmental exposure is termed "▶background radiation" and accounts for approximately 80% of the annual radiation dose received by the world's

population. The remainder of the radiation received by humans is manmade, coming from both industrial (1%) and medical sources (19%). By far the largest contributor to medical radiation is computed tomography (CT) scanning. CT may be responsible for only around 15% of a radiology department's workload, but it accounts for 70–75% of the collective population dose from medical radiation (1, 2).

The average background radiation dose to the world's population is 2.4 mSv/year, though in some countries this figure can be 5–10 times higher.

Units of Measurement for Radiological Procedures

To interpret the radiation risks from different radiological procedures, it is necessary to be familiar with descriptors of dose and their units of measurement.

- The absorbed dose is the amount of energy absorbed per unit mass of an organ or tissue. The absorbed dose cannot be directly measured in patients. The absorbed dose is expressed in Gray (Gy).
- The equivalent dose takes into account the type or quality of radiation an organ is exposed to. It is numerically equal to the absorbed dose, when X-rays are involved. The equivalent dose is measured in Sievert (Sv).
- The entrance skin dose (ESD) is the absorbed dose to the skin at the point where the X-ray beam enters the body. It is measured in Gy and is easily measured using an ionization chamber.
- Dose area product (DAP): As the ESD does not specify the area of tissue irradiated by the X-ray beam, the concept of DAP was developed. It has units of mGy cm^2 and can also easily be measured with an ionization chamber (the DAP meter). All modern fluoroscopic units are fitted with DAP meters.
- The effective dose (ED) takes into account all of the organs irradiated during an examination and incorporates a tissue weighting factor based upon the individual organ radiosensitivity. ED allows us to estimate the amount of radiation a patient receives during a radiological procedure. The unit for ED is also the Sv. Measurement of ED relies upon the use of phantoms or mathematical equations and models.
- CT dose index (CTDI) is used to approximate the dose within one "slice" of a CT examination. It is measured using an acrylic phantom and a pencil ionization chamber, over a length of 100 mm. CTDI is expressed in mGy.
- $CTDI_W$ takes into account the variations in absorbed dose, from the periphery and center of the phantom, and is weighted accordingly.
- $CTDI_{VOL}$ is numerically equivalent to the $CTDI_W$/pitch.
- The dose length product (DLP) has units of mGy cm and is calculated as the product of $CTDI_{VOL}$ and scan length. DLP can be converted into ED measurements, using mathematical equations. All scanner manufacturers are now required to display CTDI values on the user interface and some systems will also display the DLP. Whilst these measures do not tell us the actual radiation dose a patient receives, these measures will give information about relative changes in dose that result from alterations in CT-scanning parameters. Effective doses in CT can be higher for infants and small children than adults given identical CT parameters. This is because the lower absorbed energy in a child is distributed in an even smaller organ (absorbed energy/organ weight = dose).
- In nuclear medicine procedures, the radiation dose received by the patient depends upon the radionuclide administered and the type of radiation it emits. The total number of radioactive decays and the amount of radiation that is absorbed depend upon the dose of the radionuclide that is administered, its half-life, and the biological distribution and clearance of the chemical to which the radionuclide is tagged. The administered radioactivity is measured in Becquerel (Bq), where 1 Bq equates to 1 decay/s.

Radiation Risks

Risks associated with ionizing radiation can be divided into two groups:

- ►*Deterministic risk* is dependent upon cell killing and can be quantified in terms of the radiation dose the patient or organ has received. Below a certain threshold (approximately 2 Gy), the effect does not occur. However, above the threshold dose, the effects of radiation are seen. The higher the radiation dose received, the more severe the effect. Problems such as skin erythema, burns, and hair loss are deterministic effects. In diagnostic radiology, deterministic effects are rarely seen, though they may become a problem with angiographic procedures and CT fluoroscopy (3).
- ►*Stochastic risk* is dependent upon cell transformation and can lead to the development of cancer in the irradiated individual or genetic problems in their offspring. The severity of a stochastic effect is independent of the radiation dose received, though the greater the absorbed radiation dose, the more likely a stochastic effect is to be seen. Diagnostic radiologists are more concerned with the likelihood of stochastic effects occurring in their patients.

Pathology

Risk of Cancer Development Following a Radiological Procedure

Radiation doses less than 100 mSv are considered "low level" and whilst a single radiological procedure will fall within this dose range, a patient undergoing multiple investigations over the period of their lifetime has the potential to exceed this dose. The scientific data available about the risks of low-level radiation comes mainly from the epidemiological follow-up studies on the atomic bomb survivors. This database now contains information extending back almost 60 years (4–6).

The ▶linear, no-threshold risk model states that "the risk of cancer proceeds in a linear fashion at lower doses without a threshold and that the smallest dose has the potential to cause a small increase in risk to humans." This model is supported by the BEIR VII report, which also concluded that the risk of developing cancer from a radiation exposure of 10 mSv is approximately 1 in 1,000 (5). On the other hand, the ICRP report of 1990 whilst supporting the linear, no-threshold risk model, estimated a cancer risk of 5% per Sv when all ages are considered, elevating this figure to 15% if the individual is exposed in the first decade of life (8). Such risks persist throughout life, but are greater in children (who have a longer life expectancy and more chance of a radiation-induced cancer becoming manifest) and females (6). Putting these doses in context, the average effective dose from a CT scan of the abdomen (adult-scanning parameters) is 10 mSv.

A paper by Brenner et al., published in 2001 (9), used the available atomic bomb data alongside the statistics for pediatric CT examinations. The authors calculated that as many as 500 children may ultimately die from cancer, following a single CT scan of either the head or abdomen. The authors were at pains to explain that these figures were based upon the presumption that children were being imaged using adult CT parameters—an assumption which was largely accurate at that time (10)—and that the figures represented only a 0.35% increase in cancer deaths over the background rate. In other words, the risk to the individual may be small, but the implications for public health are large. Such risks can be reduced significantly if pediatric imaging protocols continue to be developed and refined.

The counterarguments against low-level radiation and cancer risks were summarized by Cohen in a review paper of 2002 (11). He concluded that the linear, no-threshold risk model fails at low doses and that the cancer risk from diagnostic radiography may well even be zero.

The linear, no-threshold risk model is based upon the assumption that a single particle of radiation interacting with a single DNA molecule may trigger cancer development. Higher radiation doses generate more radiation particles, and a greater chance that a cancer will develop; theoretically speaking, cancer risk is proportional to radiation dose. However, supporters of the ▶radiation hormesis theory argue that DNA repair enzymes, cellular apoptosis, and the immune system are all stimulated by low-level radiation, reducing the risk of cancer initiation, and the development of chromosomal aberrations (11).

Ionizing radiation is carcinogenic in high doses; this fact is not disputed. The risks from low-level radiation continue to be debated. At the present time, it would seem sensible to limit the amount of radiation to which the patients are exposed to during each individual radiological examination and cumulatively throughout their lives.

Imaging

Radiologist's Role in Limiting the Radiation Dose to the Patient

The radiologist should always adhere to the *a*s *l*ow *a*s *r*easonably *a*chievable (ALARA) principle and aim for images which are of diagnostic quality, but which minimize the radiation dose to staff and patients.

Regular review of imaging protocols and the audit of imaging algorithms for given clinical situations, alongside staff education and effective communication with clinical colleagues, are extremely important in reducing the radiation dose to patients. The list below outlines some of the more specific ways in which the radiation dose to the patient can be reduced, though it is obviously not exhaustive:

- Justify each radiology request and avoid unnecessary examinations (having the previous films available on Physics and Astronomy Classification Scheme (PACS) or hard copy format may be beneficial in this regard)
- Utilize modalities such as ultrasound and magnetic resonance imaging (MRI) whenever possible
- Optimize patient preparation and avoid having to repeat exposures
- Use appropriate lead and bismuth shields
- Pay attention to radiographic technique, for example, the selection of imaging parameters (particularly during CT examinations), appropriate collimation and the use of cones, and avoidance of a grid, wherever possible
- Limit the number of radiographic exposures. Avoid comparison views in orthopedic work. Avoid views such as the lateral chest radiograph and oblique spine radiograph. Consider carefully the questions to be answered by an intravenous urography (IVU) or small bowel series, reducing the number of films taken, wherever possible

- Utilize newer technologies during plain radiography and fluoroscopy. Digital imaging can significantly reduce the radiation dose and postprocessing techniques can limit the need for repeat exposures. The use of "fluorograb" images during fluoroscopy is to be encouraged, when anatomical rather than mucosal detail is required
- Limit the exposure time. In fluoroscopy, use a slower pulse-rate technique. In CT, use a rapid gantry rotation time, reduce the scan range, and avoid multiphase imaging

Diagnosis

The continued development of radiological technology (particularly CT scanners) has led to an increase in the collective population dose from medical radiation. The effective dose from repeated CT examinations overlaps (and can exceed) those doses that are argued to increase the risk of cancer developing. Children are more radiosensitive than adults and have a long life span ahead of them, during which time radiation-induced cancers may become manifest. The ▶ALARA principle must be adhered to when carrying out any radiological investigation necessary/indispensable for diagnosis or treatment.

Bibliography

1. Linton OW, Mettler FA (2003) National conference on dose reduction in CT, with an emphasis on pediatric patients. Am J Roentgenol 181:321–329
2. Wiest PW, Locken JA, Heintz PH et al (2002) CT scanning: a major source of radiation exposure. Semin Ultrasound CT MR 23:402–410
3. Keat N (2001) Real-time CT and CT fluoroscopy. Br J Radiol 74:1088–1099
4. Pierce DA, Shimizu Y, Preston DL Preston et al (1996) Studies of the mortality of A-bomb survivors. Report 12, part 1. Cancer: 1950–1990. Radiat Res 146:1–27
5. Pierce DA, Preston DL (2000) Radiation-related cancer risks at low doses among atomic bomb survivors. Radiat Res 154:178–186
6. Preston DL, Shimizu Y, Pierce DA et al (2003) Studies of mortality of atomic bomb survivors. Report 13: solid cancer and noncancer disease mortality: 1950–1997. Radiat Res 160:381–407
7. The National Academies. Health risks from exposure to low levels of ionizing radiation: BEIR VII phase 2 (2005). Available at: ▶//www.nap.edu. Accessed November 26, 2005
8. International Commission on Radiological Protection (1990) Recommendations of the International Commission on Radiological Protection. ICRP publication 60. Pergamon, Oxford, England, 1991
9. Brenner DJ, Elliston CD, Hall EJ et al (2001) Estimated risks of radiation-induced fatal cancer from pediatric CT. Am J Roentgenol 176:289–296
10. Paterson A, Frush DP, Donnelly LF (2001) Helical CT of the body: are settings adjusted for pediatric patients? Am J Roentgenol 176:297–301
11. Cohen BL (2002) Cancer risk from low-level radiation. Am J Roentgenol 179:1137–1143

Radiation Therapy (RTP)

Adjuvant to breast-conserving therapy.
▶Breast Conserving Therapy
▶Breast, Therapy Effects

Radiation-induced Laryngitis

Damage—acute, delayed, or chronic—to laryngeal tissue induced by ionizing radiation.
▶Inflammatory Diseases, Larynx

Radicular Syndrome

▶Spinal Nerve Roots, Clinical Syndromes

Radicular Syndrome of the Spine, Conservative Therapy for

Patrick Vroomen
University Medical Center Groningen, Groningen, Netherlands
c.a.j.vroomen@neuro.umcg.nl

Synonyms

Disc herniation; Non-invasive therapy; Sciatica

Definitions

The lumbosacral radicular syndrome (LRS) is a complex of signs and symptoms indicating a lumbosacral nerve root disorder. It is essentially a pain syndrome with an irradiating pain into the buttock and/or leg as hallmark. This radicular pain is commonly referred to as ▶sciatica. Further components of the syndrome may include tendon reflex disturbances, muscle weakness, sensory loss, and urinary incontinence. Because a specific anatomical substrate is generally presumed in the radicular syndrome, it stands out from a specific low back pain.

Pathology

While the anatomical substrate for the clinical findings of the LRS is generally acknowledged to be the nerve root, the etiology of the nerve root disorder is diverse.

The foremost cause of lumbosacral nerve root disorders is a lumbosacral ►disc herniation. When such a disc herniation protrudes in the spinal canal it may lead to compression of the nerve root. Such compression may disrupt the axons in the nerve root, leading to signs such as muscle weakness and sensory loss. This happens only in a minority of patients. More commonly the chronic compression leads to an inflammatory reaction in the nerve root. This inflammation seems critical in the causation of the sciatic pain, as acute compressions without inflammation have been shown not to cause pain. Another mechanism implicated in the production of the nerve root disorder is the chemical irritation of the nerve root by constituents of the nucleus pulposus. Contact with nucleus pulposus material has shown to cause inflammation of nerve roots in animal studies in the absence of compression.

While disc herniations are considered the predominant mechanical cause of a lumbosacral radicular syndrome, any structure that impinges on the nerve root may contribute to the clinical picture. Such impingements may be caused by e.g. spondylolisthesis, facet arthrosis, or ligamentum flavum hypertrophy. They may be further accentuated by congenital narrowing of spinal canal or lateral recess. Quite frequently compression of the nerve root is due to a combination of the factors mentioned above. Epidural haematoma or abscess formation occasionally gives rise to a radicular syndrome. Finally, neoplasms of nerve root or surrounding meninges such as neurinoma, Schwannoma and meningioma may lead to radicular pain and loss of function. About one in a hundred patients with a radicular syndrome has a vertebral malignancy (often metastatic).

Rarely, the nerve root may be affected by metabolic disturbances, inflammation or infection in the absence of any mechanical compression. Diabetes mellitus not only leads to polyneuropathy, but may cause mononeuropathy, plexopathy or radiculopathy as well. Nerve roots are involved in the Guillain-Barre syndrome. This is, however, uniformly an affliction of multiple nerve roots. Various infections, such as neuroborreliosis and herpes zoster, may lead to a nerve root disorder.

Clinical Presentation

Most patients who present with LRS are in their fourth or fifth decade. Rarely do they indicate a causative activity. In general, a sedentary occupation, professions involving much driving and smoking are factors that increase the likelihood of developing disc herniations. Often, patients note low back pain of insidious or acute onset, which subsequently starts irradiating into the leg. Sometimes low back pain is absent. In 20–40% the radicular pain is accompanied by neurological deficit, 25% have muscle weakness, 35% have sensory loss and 15% have reflex disturbances. Micturition disturbances occur in less than 10% of patients. While neurological loss may be present at the start, it often develops insidiously and remains unnoticed by the patient at first. Sometimes the patient suffers severe sciatic pain for several days to weeks, to be followed by both a sudden relief of the pain and a sudden muscle weakness. This rare but classical account is referred to as 'sciatique paralysant'.

Of all patients with pain that irradiates into the leg, about 70% are considered to have the clinical diagnosis of LRS. The 30% that do not exhibit the complex of signs and symptoms indicating nerve root involvement, are generally considered to have pseudoradicular pain caused by such various diseases as trochanteric bursitis, sacroiliitis and plexus neuritis. Unfortunately, such clinical impressions are inaccurate. MR imaging in patients clinically diagnosed with LRS demonstrates a symptomatic disc herniation in only 70%. This means that about 30% of patients with LRS either have a non-mechanical cause of the root disorder or the diagnosis of a root disorder is incorrect in the group of patients with clinically diagnosed pseudoradicular pain MRI shows veritable nerve root compression in about 30%.

While usually the LRS is caused by disc herniation and has a favourable natural history, treating physicians should look both for warning signs that may imply a particular cause such as a post traumatic onset, a previous history or physical examination suggesting malignancy, diabetes mellitus, tick bites and spinal procedures and also for warning signs that indicate close monitoring or urgent therapy such as progressive paresis or a ►cauda equina syndrome.

Conservative Management (1, 2)

Disc herniation, which is most frequently responsible for nerve root compression, can be easily demonstrated by CT or MRI. Considering the costs of imaging, the high rate of findings of asymptomatic disc herniation and the benign spontaneous course of the LRS, imaging can be deferred in most patients until the consideration of surgical therapy necessitates imaging of the nerve root and its surroundings. In cases where there is diagnostic uncertainty as to whether the nerve root is involved at all, imaging can be helpful. In these instances, however, the imaging will have no direct therapeutic consequences. Imaging for this

purpose also has the drawback of showing many structural abnormalities with uncertain clinical significance. Other diagnostic modalities such as electromyography and diagnostic nerve root block may be helpful in such cases.

In general, the considerable lack of correlation between clinical findings and imaging findings serves as a warning to hinge too much on either one in the evaluation of the patient with pain in lower back and leg.

Relying exclusively on clinical findings may have the drawback of labelling pain as a disc-related LRS while this is not the case, which may delay the correct diagnosis being made. Conversely, there is a real danger of patients

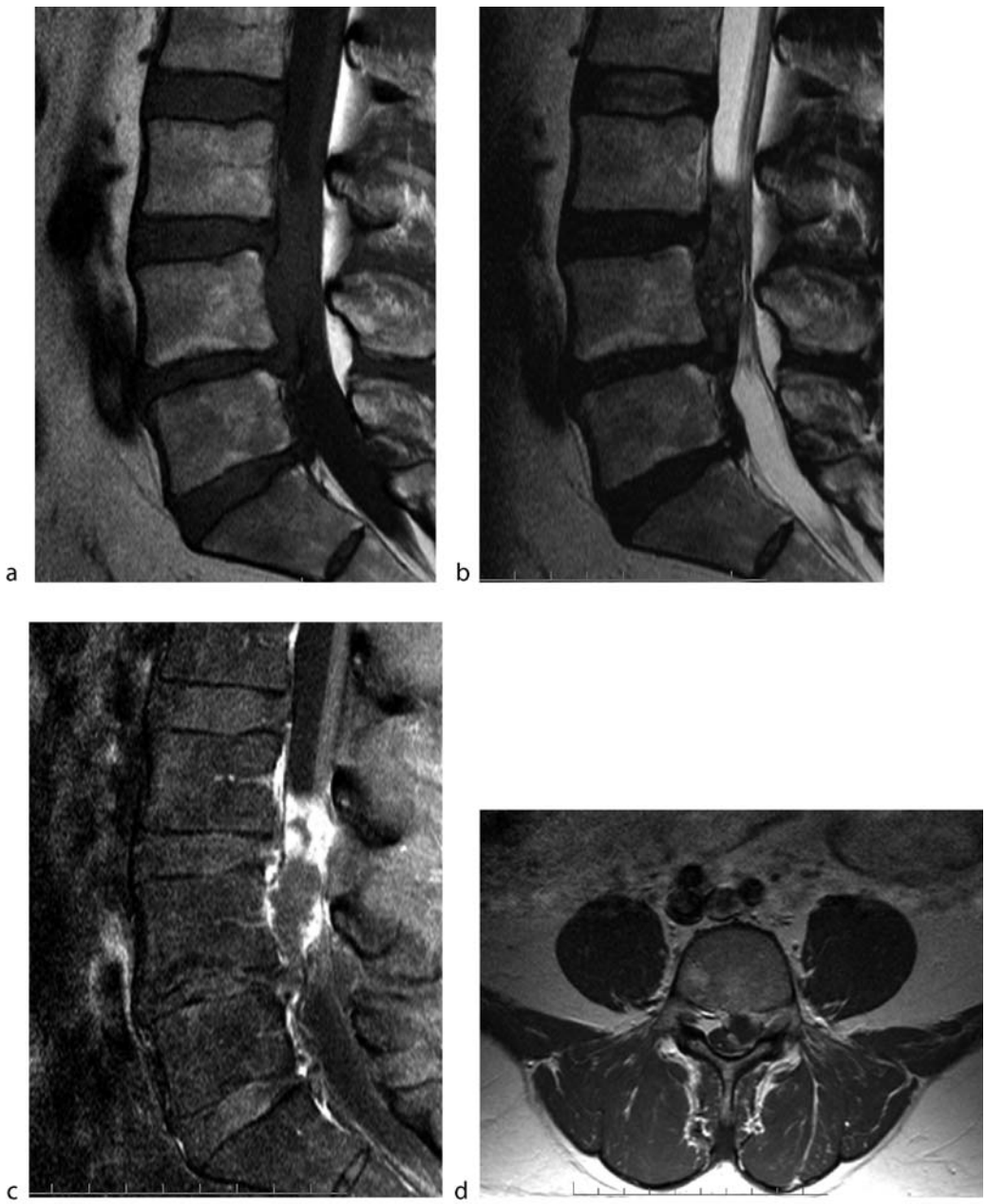

Radicular Syndrome of the Spine, Conservative Therapy for. Figure 1(a and b) Sagittal T1 and T2 weighted MR images of a large disc extrusion originating at the L4–5 level with extensive cranial migration to the midvertebral L3 level. (c and d) Post-Gadolinium sagittal and axial T1 weighted images show the mass to consist largely of strongly-enhancing peripheral granulation tissue. (e-h) Same case, six weeks later, showing marked resorption of the extruded disc material by surrounding granulation tissue. The patient presented with sciatica, made a full recovery without surgical intervention, and at no time showed signs of an infectious lesion.

unjustly being withheld therapeutic measures for root compression because the clinical findings do not appear to support the diagnosis of root compression.

Relying too much on imaging on the other hand carries the risk of too much significance being attributed to incidental findings of disc herniations, which may be encountered in asymptomatic volunteers in up to 30%. The drawback at the other side of the spectrum is that if imaging does not show root compression, such root compression is considered to be ruled out. However, it should be appreciated that imaging protocols for spinal imaging provide sectional anatomical information and as a consequence important information may be missed, for instance when a lesion is mainly located in the interslice gap or in the gap in which some scan protocols occur between slice sets limited and angulated to individual discs. CT and MR images are acquired with the patient lying down in a supine position. Most patients experience relief of radicular pain in this position. This is likely due to a decreased compression of the root. This would mean that these images are made when the compression of the root is minimal. Precluding mechanical compression on the basis of such MRI pictures is therefore very difficult. Mechanical devices for loading the spine in the supine position, and the use of upright MRI systems presently available, are likely to alleviate this problem.

Conservative Treatment Measures (3)

The initial management is aimed at providing adequate information, pain relief and if need be, aiding sleep by hypnotic medication. Patients should be instructed that the pain originates in the nerve root and that a disc herniation is the probable cause. Such disc herniations show a high tendency towards regression (as documented by repeat imaging studies, (Fig. 1)) and up to 75% of patients will experience spontaneous recovery within three months (4). This does not necessarily imply that the patient is without any complaints. The back pain may persist or recur frequently.

Pain medication should be prescribed time contingent (on a fixed time schedule). Acetominophen, tramadol, codeine, non-steroidal anti-inflammatory drugs (NSAID) and narcotic analgesics may all be used. Their mode of action is strictly symptomatic. None of the agents including NSAID's have added curative benefits.

The benign natural course explains the high rate of success of most conservative therapies in case series. Whether patients are selected for these studies directly after pain onset, at the start of the natural course or much further down the track, will explain much of the variance in reported success rates of conservative measures (anywhere from 35 to 97%). Randomised controlled trials (RCT) are called for. Unfortunately, the benign natural course has left many RCTs underpowered to demonstrate smaller but relevant benefits of conservative strategies.

►Bed rest has been a mainstay of conservative therapy for LRS for decades, but the only RCT studying its effects has found bed rest to lack effectiveness (5). Manipulation of the spine is the only form of physical therapy that has been shown to have a positive effect on the natural course of LRS in two trials. These trials had multiple methodological shortcomings, however.

►Epidural steroid injection has been the subject of several trials with negative, neutral and positive results. Overall, in a recent meta-analysis epidural steroid injections were shown to possess borderline effectiveness. Further studies to elucidate the effectiveness of epidural steroids especially in subgroups of patient with sciatica seem warranted.

Bibliography

1. Nachemson AL and Johnsson E, (ed) (2000) Neck and Back Pain: The Scientific Evidence of Causes, Diagnosis and Treatment. Philadelphia PA: Lippincott Williams & Wilkins
2. Jones et al Oxford Textbook of Primary Medical Care. Chapter 13.1 Low Back Pain and Sciatica. Vroomen PCAJ and van Tulder MW
3. Vroomen PCAJ, De Krom MCTF, Slofstra PD et al (2000) Conservative treatment of sciatica: a systematic review. J Spinal Disord 13(6):463–469
4. Splendiani A, Puglielli E, De Amicis R et al (2004) Spontaneous resolution of lumbar disk herniation: predictive signs for prognostic evaluation. Neuroradiology 2004 November; 46(11):916–922
5. Vroomen PCAJ, De Krom MCTF, Wilmink JT et al (1999) Lack of effectiveness of bed rest for sciatica. N Engl J Med 340(6):418–423

Radicular Syndrome of the Spine, Percutaneous Therapy for

Barry Schenk, Patrick A. Brouwer
Leids Universitair Centrum Leiden, The Netherlands
b.schenk@lumc.nl

Introduction

Radicular syndrome, caused by herniation of an intervertebral disc, is a common problem with an annual incidence of 5 per 1,000 (1). In 60–80% of patients, experiencing their first episode of radicular pain, the symptoms recede to a non-disabling level within a period of 6 weeks (1). Patients with persistent symptoms qualify for (surgical) intervention. Because of the considerable morbidity and convalescence period inherent to conventional lumbar disc surgery, there has been an ongoing search for less invasive methods of treatment. This has led

to the development of several minimally invasive spinal interventions, such as ►chemonucleolysis (2), ►percutaneous laser disc decompression (PLDD) (3, 4), ►percutaneous nucleotomy (5), ►nucleoplasty (6) and ►oxygen–ozone therapy (7). These interventions are all performed percutaneously under local anaesthesia, therefore morbidity and convalescence period are postulated to be less than for conventional surgery. Traditionally, spinal interventions for radicular syndrome have been the area of expertise of neurosurgeons and orthopaedic surgeons. The development of percutaneous techniques, together with their dependence on imaging techniques such as fluoroscopy, magnetic resonance imaging (MRI) and computed tomography (CT), have led to an increasing participation of interventional radiologists in this field.

Pathology of Lumbar Disc Herniation

The relationship between disc herniation and radicular syndrome has been known for over 70 years. The mechanical concept of nerve root compression by a herniated portion of the nucleus pulposus as a cause of radicular pain offers a satisfying explanation for most symptomatic patients, but biochemical, vascular and inflammatory factors are also thought to play a role in the pathogenesis of radicular syndrome.

The Principle of Disc Decompression

The intervertebral disc can be considered a closed hydraulic system (3). The nucleus pulposus, which is highly water containing, is surrounded by the inelastic annulus fibrosus. When the water content of the nucleus pulposus increases, it leads to a disproportional increase in intradiscal pressure. Reduction of the amount of water in the nucleus pulposus causes the opposite effect, with minor changes in water content leading to a disproportional drop in intradiscal pressure (3). A decrease in intradiscal pressure causes the herniated disc material to recede towards the centre of the disc, hence leading to reduction of nerve root compression and relief of radicular pain. This mechanism forms the basis for a number of percutaneous interventions, such as chemonucleolysis, nucleoplasty, PLDD and oxygen–ozone therapy. In case of percutaneous nucleotomy, disc decompression is achieved by mechanically removing nucleus pulposus tissue from the centre of the disc.

Criteria for Patient Selection

The main indication for percutaneous intervention is a contained disc herniation (4–6), with corresponding radicular symptoms. Inherent to the treatment principle mentioned before, only non-sequestered herniations can be expected to respond to reduction of intradiscal pressure (2–7). The presence of disc extrusion or sequestered herniation is considered to be a criterium for exclusion (2–7). Furthermore, patients with severe neurological symptoms, such as cauda equina syndrome, severe paresis or other conditions that require acute surgical intervention are excluded from percutaneous intervention. Intervertebral disc height should be at least 50% of normal (5), without vertebral abnormalities that might obstruct needle placement.

Interventions for Radicular Syndrome

A common factor for all percutaneous interventions for radicular syndrome is the fact that they all require percutaneous access to the intervertebral disc (2, 4–7), without direct contact with the dural sac or nerve roots. This can be achieved by inserting a needle or other instrument by means of a dorsolateral approach. Biplane fluoroscopy or CT imaging can be used to determine the desired needle path, during needle placement and to verify the correct position before commencing treatment. Careful monitoring of patient reaction and the appropriate use of visual guidance is crucial to prevent damage to nerve roots and surrounding tissues during needle placement or subsequent treatment. As is inherent to all percutaneous procedures, there is always a risk of inoculation of microorganisms into the centre of the intervertebral disc, with resulting discitis. Taking appropriate antiseptic measures during the procedure can minimise this risk. When infectious discitis does occur, it is usually responsive to appropriate antibiotic therapy.

Chemonucleolysis

Chemonucleolysis is the oldest percutaneous intervention for radicular syndrome. A proteolytic enzyme called chymopapain is injected into the centre of the intervertebral disc under fluoroscopic guidance in order to induce hydrolysis of the proteoglycan molecules that form the nucleus pulposus (2). The resulting proteoglycan fragments have limited water-binding abilities, which leave intradiscal water molecules free to diffuse into the surrounding tissues. The resulting loss of water causes a decrease in intradiscal pressure. The chymopapain molecules remain attached to the proteoglycan fragments, permanently limiting the nucleus pulposus' abilities to attract water (2).

Although literature on chemonucleolysis shows good clinical results (73–90% success rate), it is no longer widely

used because of the risks associated with the injection of chymopapain. Enzyme leakage into extra-discal tissue has been reported, with the possibility of damage to nerve roots, dural sac or spinal cord. Severe anaphylactic reactions have been reported in 0.2% of patients (2). The overall mortality rate following chymopapain injection is approximately 1 in 5,000 patients (0.02%).

Nucleoplasty

Nucleoplasty is one of the newest percutaneous interventions for radicular syndrome. It relies on the principle of 'controlled ablation', a process in which radio frequency energy is used to generate a highly focussed plasma field that is capable of cleaving molecular bonds (5). In nucleoplasty, nucleus pulposus tissue is ablated using a special wand, which is inserted into the centre of the intervertebral disc under fluoroscopic guidance. By rotating the curved tip of the wand, up to six channels are created within the nucleus pulposus, decreasing intradiscal volume and hence lowering intradiscal pressure. Subsequently, the channels are sealed thermally by coagulation (5). Literature on clinical results of nucleoplasty is still limited. The results of several non-randomised trials show success rates that vary from 78% to 89% (5). Specific complications of nucleoplasty have not yet been reported.

Percutaneous Laser Disc Decompression

In PLDD, laser energy is used to vaporise the water content of the nucleus pulposus (3, 4). A small laser fibre is inserted through a hollow needle into the centre of the intervertebral disc under fluoroscopic guidance. CT is used to verify the correct needle position. When the laser fibre is in place, up to 2,000 J of laser energy are applied into the nucleus pulposus in order to evaporate its water content, thereby reducing intradiscal pressure. The temperature increase also induces protein denaturation and subsequent renaturation. This causes a structural change of the nucleus pulposus, limiting its capability to attract water and therefore leading to a permanent reduction of intradiscal pressure (3, 4).

The results of several non-randomised trials that have been published over the years show success rates ranging from 75% to 87% (4). The most important complication of PLDD is aseptic (spondylo-) discitis as a result of thermal damage to the intervertebral disc or vertebral end plates (0–1.2%) (4). This complication can be largely avoided with careful monitoring of patient complaints during the procedure, with adjustment of laser parameters when heat sensations occur. In this fashion, an excessive buildup of heat can be countered before structural damage is caused to the surrounding tissues.

Oxygen–Ozone Therapy

Oxygen–ozone therapy is a percutaneous intervention for radicular syndrome, relying on the chemical properties of ozone (7). A mixture of oxygen–ozone gas is injected into the centre of the intervertebral disc at non-toxic concentrations. Ozone has a direct lytic effect on the proteoglycan molecules that form the nucleus pulposus (7). As in chemonucleolysis, the resulting proteoglycan fragments have limited water-binding abilities, which leave intradiscal water molecules free to diffuse into the surrounding tissues (7). The resulting loss of water causes a decrease in intradiscal pressure. The degenerated nucleus pulposus tissue is gradually replaced by fibrous tissue, with limited water-binding capabilities. The result is a reduction in disc volume. In addition to the proteolytic properties, ozone also has certain anti-inflammatory and analgesic effects that may help counteract disc-induced pain. The antiseptic activity of ozone is thought to further reduce the risk of infectious complications associated with percutaneous interventions (7). No specific neurological or infectious complications of oxygen–ozone therapy have been reported.

Percutaneous Nucleotomy

Percutaneous nucleotomy is a minimally invasive intervention, in which nucleus pulposus material is mechanically removed using an automated nucleotome. This nucleotome is a 2-mm blunt-tipped device, equipped with a reciprocating suction cutter (6). The nucleotome is introduced through a cannula that is placed into the centre of the nucleus pulposus under fluoroscopic guidance. When the nucleotome is in place, nucleus pulposus material is cut and aspirated at a rate of 180 times per minute. The tip of the nucleotome is alternatingly rotated, depressed and elevated within the nucleus in order to optimise the removed amount of nucleus pulposus material (6). The resulting loss of nucleus pulposus mass causes a drop in intradiscal pressure.

Clinical success rates for percutaneous nucleotomy range from 70% to 80% (6). The main complication of percutaneous nucleotomy is infectious discitis (0.2%). Serious neurological complications are extremely rare, although two cases of cauda equina injuries have been reported due to probe misplacement (6).

Bibliography

1. Andersson GBJ (1997) The Epidemiology of Spinal Disorders. The Adult Spine: Principles and Practice. 2d edn. Raven Press, New York, pp 93–141
2. Steffen R, Bremen-Kuhne R (1999) Chemonukleolyse: Entwicklungen, Erfahrungen, Perspektiven. Orthopade 28:609–614

3. Choy DSJ, Diwan S (1992) *In vitro* and *in vivo* fall of intradiscal pressure with laser disc decompression. J Clin Laser Med Surg 10(6):435–437
4. Gangi A, Dietemann JL, Ide C et al (1996) Percutaneous laser disc decompression under CT and fluoroscopic guidance: indications, technique, and clinical experience. Radiographics 16:89–96
5. Kim PS (2004) Nucleoplasty. Tech Regional Anesthesia Pain Manage 8(1):46–52
6. Maroon JC, Onik G, Vidovich DV (1993) Percutaneous discectomy for lumbar disc herniation. Neurosurg Clin N Amer 4:125–134
7. Andreula CF, Simonetti L, De Santis F et al (2003) Minimally invasive oxygen–ozone therapy for lumbar disc herniation. Am J Neuroradiol 24:996–1000

Radicular Syndrome of the Spine, Surgical Therapy for

Wilco Peul
Medisch Centrum Haaglanden, Netherlands
w.peul@mchaaglanden.nl

Synonyms

Laminectomy; (Micro)discectomy

Definition

A radicular syndrome is characterized by pain radiating in the dermatome of a spinal nerve root. Occasionally, more than one root is involved. Pain may be accompanied by one or more of the following: lumbar muscle spasm, reflex abnormalities, motor and sensory disturbances. Surgical therapy for a radicular syndrome refers to all procedures which have the goal to decompress the exiting nerve roots. Anatomical approaches differ according to the origin of the pathology.

Pathology

Disc herniations are the most frequent cause of a radicular syndrome, followed by stenosis of the lateral recess and occasionally narrowing of the neuroforamen. The latter occur more frequently in the cervical spine in elderly populations, where progressive disc degeneration leads to spine deformities with compression at the spinal outlet of nerve. Disc herniations can be divided into contained and uncontained protrusions of nuclear material, and the latter may give rise to a sequester or free fragment of disc material.

Clinical Presentation

Most radicular syndromes resolve naturally with time (1). However when conservative treatment fails, surgery is an option depending on preferences of patients and their treating physicians. Guidelines regarding management of lumbar radicular syndromes propose that an indication exists for surgery after 6–8 weeks of persisting radicular pain. Cervical and thoracic radicular syndromes are managed conservatively for a longer period. Complaints in these cases are as severe as in lumbar radicular syndromes, but the functional disability seems more tolerable and a higher proportion of patients are cured in the natural course of the disease. Severe neurological deficit is a compelling reason for surgery, whereas pain is a relative indication. The following subheadings refer to the different spinal regions.

Cervical Spine

Cervical radicular syndromes are most frequently associated with a soft disc herniation or hard osteophytes, which compress the nerve root within the spinal canal or foramen. As a rule compression occurs far laterally with anterior impingement of the nerve. All anatomical approaches have been used, employing posterior, lateral and anterior techniques.

- Posterior approaches are divided into laminectomy and laminotomy techniques. A laminectomy consists of the complete removal of posterior bony elements except for the facet joint. This historical technique is occasionally used in present times, when patients present with a combined radicular and spinal cord compression. The exiting nerve root is decompressed by the removal of the posterior medial facet joint. If the procedure is solely intended to decompress the nerve root, a small hole may be drilled in this area, leaving the posterior elements intact. This so-called Scoville procedure has been abandoned by most neurosurgeons. However, recent microendoscopic discectomy (MED) techniques using tubular dilators have popularized this approach again, because trauma to muscle is less and cervical mobility is better preserved.
- Lateral approaches to the cervical spine for the treatment of radicular syndromes have historical interest but are sometimes used for more complex pathologies compressing the exiting root.
- The anterior approach presently comprises more than 90% of all surgical techniques employed in cervical radicular syndromes. The main reason for this is the origin of the pathology anterior to the root and cord, and the sparing nature of the technique leaving intact all spinal anatomical structures except for the disc. The latter is removed including osteophytes which may be present, and the posterior longitudinal ligament is

opened. No consensus exists about supplementary fusion of the vertebral end plates. In the past, autologous bone from the iliac crest was used to fill the gap in the open disc space. Pain in the iliac crest area directed surgeons to the use of cement and later to cages filled with bone, the latter followed by an anterior plate and screw fixation of both vertebrae in some countries. Recently, disc prostheses have been used with the goal of preserving cervical mobility and thus preventing future disc degeneration at adjacent levels. To emphasize the variety of procedures used for the same disease, it can be noted that many surgeons prefer to perform a discectomy without any graft, cement, cage, or prosthesis. Lack of scientific data and huge industrial influence are the main reasons for this lack of consensus. Randomized trials are started to provide better insight in the value and (cost-)effectiveness of the different techniques.

Thoracic spine

Thoracic disc herniations are frequently ossified and have a very low incidence. Furthermore, patients with a thoracic disc herniation most frequently present with spinal cord compression, with the risk of severe motor and sensory disturbances of the lower extremities and bladder dysfunction. This leaves the thoracic radicular syndrome as a comparatively minor problem. Probably, because of the calcifications within thoracic disc herniations, posterior approaches have had poor results with frequent neurological complications leading to a more severe deficit compared to the preoperative status. Two approaches exist at present. Because of the low incidence of thoracic disc herniations patients are treated in specialized centers, reducing the risks of surgery.

- The posterolateral approach employs costotransversectomy, and provides access by removing the proximal rib and transverse process. This classical approach has recently been replaced by a less invasive microscopic approach. This posterolateral approach is suitable for soft disc herniations.
- The anterolateral approach makes use of a transthoracic technique. These procedures have less risk of spinal cord injury, but are more complex. Large thoracotomy approaches with division of the diaphragm at the disc level between the 12th thoracic and 1st lumbar vertebrae have nowadays been replaced by thoracoscopic techniques and more recently by mini-open thoracotomies using an incision of less than 4 cm and normal ventilation of both lungs.

Lumbar Spine

The procedure most frequently performed in neurosurgical practice is the lumbar (micro)discectomy. One in every 1,000 person is operated for a lumbar disc herniation in the United States. The timing of surgery varies considerably as well as the surgical technique. The timing of surgery is subject of a randomized trial in Europe (2), whereas a trial in the United States sets out to determine the effectiveness of surgery compared to conservative treatment (3). Surgical interventions can be divided into percutaneous techniques indirectly decompressing the nerve root by intradiscal action and posterior surgical techniques, actually removing the disc herniation and therefore direct decompression. Anterior decompressions are highly unusual.

- After the first description in 1934 of removal of a lumbar disc herniation by laminectomy (4), this technique was the method of choice for many years. The goal was a complete posterior decompression of the dural sac and removal of as much disc material as possible. This historical technique was suitable in the times before CT and MRI but did destabilize the spine and is not considered as the usual care any more.
- After the introduction of the microscope for intracranial procedures, application of this technique to spine surgery is followed. The major difference with the classical broad laminectomy is the less invasive approach with limited bone removal. Randomized trials have not shown any benefit of the microdiscectomy when compared with classical approach (5). Recent reports deal with selective removal of extruded material leaving the disc intact. This procedure lacks evidence of effectiveness, so far prohibiting worldwide implementation.
- The MED approach uses a 14–18 mm wide tubular dilator system splitting the paravertebral muscles without dividing them. Use of an endoscope facilitates angulation of the optics in the spinal canal, but most surgeons use the microscope. This technique has recently been introduced and is the subject of a randomized trial comparing MED with microdiscectomy with the goal to look at the effectiveness of early recovery and resumption of daily activities.

The main disadvantage of all new techniques is the relatively high recurrent rate of disc herniations of up to 10%. Until randomized controlled trials present at least comparable effectiveness and a low recurrence rate, the classical microsurgical approach is the gold standard.

Imaging

MRI scanning is now the method of first choice to define the surgical approach with the goal of decompressing a lumbar nerve root. However in the cervical spine, a CT

scan may be beneficial when bony compression is suspected or even an ossified posterior longitudinal ligament. The surgical procedure may be altered depending on the presence and location of calcifications. The same holds true for the thoracic spine, where some surgeons also prefer to have spinal angiography performed to localize the Adamkiewicz artery, the major spinal cord feeder, before deciding on the side of a transthoracic approach.

Postoperative imaging is done frequently as a routine measure in thoracic and cervical pathology, but after surgery of lumbar disc herniations only when complaints persist or recur.

Bibliography

1. Vroomen PC, de Krom MC, Wilmink JT et al (1999) Lack of effectiveness of bed rest for sciatica. N Engl J Med; 340(6):418–423
2. Peul WC, van Houwelingen HC, van der Hout WB et al (2005) Prolonged conservative treatment or 'early' surgery in sciatica caused by a lumbar disc herniation: rationale and design of a randomized trial [ISRCT 26872154]. BMC Musculoskelet Disord 6(1)8
3. Birkmeyer NJO, Weinstein JN, Tosteson ANA et al (2002) Design of the Spine Patient Outcomes Research Trial (SPORT). Spine 27 (12):1361–1372
4. Mixter WJ, Barr J (1934) Rupture of the intervertebral disc with involvement of the spinal canal. N Engl J Med 211:210–215
5. Gibson JNA, Grant IC, Waddell G (1999) The Cochrane review of surgery for lumbar disc prolapse and degenerative lumbar spondylosis. Spine 24(17):1820–1832

Radiculopathy

▶Spinal Nerve Roots, Clinical Syndromes

Radio-Opacity

▶Pulmonary Opacity, Extensive Pattern

Radiocontrast Media

▶Contrast Media, Iodinated, Applications in Conventional Radiography and CT

Radiofrequency Ablation, Hepatic Tumours

Percutaneous image-guided technique in which radiofrequency (RF) waves are used to induce thermal ablation of neoplastic tissue. It represents the most assessed method for percutaneous thermal ablation of hepatic malignancies.

▶Interventional Hepatic Procedures

Radiographic Contrast Media

▶Contrast Media, Iodinated, Applications in Conventional Radiography and CT

Radiographic Iodinated Contrast Media

A radiographic iodinated contrast medium is an imaging contrast agent in which iodine, bound to organic molecules, provides the increased attenuation to X-rays required for visualization.

▶Adverse Reactions, Iodinated Contrast Media, Acute Renal

Radiolabeled Colloid Particles

For the purposes of SLN detection and lymphoscintigraphy, labeled colloids are the most appropriate radiotracer.

▶Sentinel Node, Scintigraphy

Radiological Tumour Ablation, Hepatic Tumours

This consists in the direct, image guided, application of chemical (ethanol or acetic acid) or thermal (radiofrequency, laser, microwaves and cryoablation) therapies

to a specific focal liver tumour in an attempt to achieve eradication or substantial tumour destruction.
▶Interventional Hepatic Procedures

Radionuclide Cystography

Scintigraphic examination with direct or indirect administration of radionuclide for exclusion or detection of vesicoureteral reflux.
▶Contrast Media, Ultrasound, Applications in Vesicoureteral Reflux

Radiotracer

A very small mass of the molecule of interest that is radiolabelled to evaluate the behaviour of the compound of interest.
▶PET in Drug Discovery Imaging

Ramsay-Hunt Syndrome

A herpetic inflammation of the sensitive ganglia of cranial nerves usually affecting cranial nerves V, VII and VIII. It manifests clinically with acute peripheral facial nerve paralysis and vesicular eruptions over the ear, face and neck.
▶Facial Nerve Palsy

Raynaud's Phenomenon

Raynaud's phenomenon describes a neurovascular dysregulation with pathological excessive vasoconstriction and a consecutive ischemic phase as a reaction to cold application affecting the fingers, hands, and facultatively the forearms. Typically the skin discoloration follows a time course with primary paleness, then a livid aspect, and subsequent reddening in the phase of painful hyperemia. Raynaud's phenomenon occurs primarily (idiopathic) and secondarily, for example, in association with scleroderma, thromboangiitis obliterans, cryoglobuline disease, or intoxication.
▶Connective Tissue Disorders, Musculoskeletal System

Raynaud's Syndrome

The most common cause of upper limb ischemia. It is characterized by episodic attacks of vasospasm caused by closure of the small arteries of the most distal parts of the extremity in response to cold or emotional stimuli.
▶Brachial Ischemia

Receptor Imaging

▶Receptor Studies, Neoplasms

Receptor Studies, Neoplasms

Flavio Forrer, Marion De Jong
Department of Nuclear Medicine, Erasmus Medical Centre, Rotterdam, The Netherlands
fforrer@uhbs.ch

Synonyms

Receptor imaging; Targeted tumor imaging

Definitions

Receptors are proteins on the cell membrane, in the cytoplasm, or in the nucleus of the cell that bind ligands such as neurotransmitters, hormones, or others. This interaction between the receptor and its ▶ligand initiates a cellular response. The profile of expressed receptors is different for cells with different functions. In many neoplasms, the cellular production of certain receptors is upregulated, and therefore they are overexpressed.

The specificity of different receptors for their ligands varies. While certain receptors bind mainly one specific ligand (e.g., somatostatin receptor), others, like megalin, have a broad array of ligands.

Ligands are molecules that bind to the receptor. They can be divided into receptor agonists and antagonists. Agonists initiate a cellular response after their binding to the receptor, whereas antagonists occupy the binding site of a receptor without causing a response.

Characteristics

Nuclear medicine offers the opportunity to visualize receptors by labeling a ligand with a radionuclide suitable for imaging. The radiolabeled ligands used are mainly molecules similar to the natural ligand, often peptides. Beside peptides, other ligands such as antibodies, parts of antibodies, or artificial molecules can be used. These ligands can be from both categories, either receptor agonists or receptor antagonists. Both are potentially suitable for receptor imaging. Antagonists have the disadvantage that they are mostly not internalized into the cell, which often results in a shorter retention time of the radioactivity in the target.

Radiolabeled ligands have to fulfill a number of prerequisites such as metabolic stability, high receptor affinity, favorable toxicity profile, and stable binding of the radionuclide to be useful for *in vivo* imaging.

Not only the radiolabeled ligand but also the receptor must fulfill a number of prerequisites. To visualize a tumor, the target receptor has to be overexpressed on the tumor cells. In addition, an exclusive expression of the target receptor on the tumor is desirable to achieve a higher tumor-to-non-tumor ratio with the radiolabeled ligand. Generally, the higher the expression of the target and the more exclusively the target is expressed on the tumor, the higher the sensitivity for the consecutive imaging procedure. Other important parameters determining the success of tumor receptor imaging are localization of the receptor on the cell and the biological behavior of the receptor after the binding of the ligand (e.g., internalization or receptor recycling).

Receptor-Mediated Radionuclide Therapy

Apart from receptor imaging, receptor-mediated radionuclide therapy is an emerging field in nuclear medicine for treating malignant, metastatic tumors. Receptor-mediated therapy represents a derivative of receptor imaging. The diagnostic radionuclide is replaced by a therapeutic most often beta particle emitting. All the aspects mentioned in receptor imaging about vector and target receptor hold true for therapy as well or are even more important, such as the exclusive expression of the target receptor on the tumor.

Somatostatin Receptor Imaging

The ▶somatostatin receptor (sst) as a target molecule and octreotide or related peptides as cognate ligands can be regarded as a well-established model of tumor receptor imaging and therapy. This model is exemplary for receptor imaging, and the principles hold true for the whole field of receptor imaging (1).

Although somatostatin receptors are present in a large number of healthy organs, including the pancreas, adrenals, pituitary gland, and many more, these receptors have been proven to be highly valuable for tumor imaging and therapy in nuclear medicine. The reasons for the success are multifaceted. A crucial point is that in many neoplasms, mainly neuroendocrine tumors, the overexpression of the sst is very pronounced, resulting in a high tumor-to-non-tumor ratio for the radioligand. Besides the neuroendocrine tumors, a number of tumors, including pheochromocytoma, paraganglioma, lymphoma, small cell lung cancer, and many more, express the sst as well (2).

Two natural somatostatins are known and consist of 14 or 28 amino acids, respectively. Accordingly, the peptides are called SS-14 and SS-28. As neurotransmitters with endocrine and paracrine function *in vivo*, the peptides are degraded rapidly by peptidases. The serum half-life of these peptides in blood is approximately 2 min, which is too short to qualify natural somatostatin as a candidate for imaging when radiolabeled.

The breakthrough in sst imaging was made when the octapeptide octreotide was developed. This small ▶peptide is metabolically more stable and has a plasma half-life of approximately 1.7 h. Initially, the nonradiolabeled octreotide was developed to be used as drug for inhibiting the secretion of growth hormone, which is the physiological action of somatostatin.

Later on, octreotide was conjugated with a ▶chelator for radiolabeling. A chelator is the link between the vector and the radionuclide. It is needed for stable binding of the radionuclide. Labeling of peptides without a chelator is possible by halogenation—for example, with iodine isotopes—but the binding between the vector and the isotope is often not as stable after injection as with a chelator, and free radionuclide may reduce image quality or, especially in therapeutic applications, cause serious side effects. For octreotide and related peptides, the most frequently used chelators are diethylene triamine pentaacetic acid (DTPA) and tetra-azacyclo-dodecane-tetraacetic acid (DOTA). Both chelators can be labeled with a number of isotopes of different elements, such as indium, yttrium, lutetium, or gallium. Recently a number of octreotide analogs with other chelators, such as HYNIC were developed to enable labeling with the widely available ^{99m}Tc. The advantages of peptides labeled with ^{99m}Tc are various; the most important are that the physical characteristics of ^{99m}Tc are ideal for imaging, that ^{99m}Tc is relatively cheap, and that it is constantly available in nuclear medicine departments.

Five subtypes of the sst are known (sst 1–5). From an oncological point of view, sst subtype 2 is the most relevant, as mainly this subtype is overexpressed in neoplasms. Over the last years, many improvements of the ligand's characteristics have been achieved. Modifications in amino acids have resulted in a number of peptides with higher affinity for the sst, which leads to a more favorable biodistribution.

Most recently, several octreotide derivatives, labeled with positron emitters, were developed. These allow scanning of patients in a positron emission tomography (PET) scanner, resulting in higher resolution and, therefore, higher accuracy. The radionuclides used for this purpose are mainly ^{18}F, ^{68}Ga, ^{86}Y, and ^{64}Cu. Depending on the radionuclide used, differences in chelators and, consequently, in radiochemistry apply. Yttrium-86 plays a special role in this context: It is the ideal surrogate for ^{90}Y, and therefore it allows pretherapeutic dosimetry. However, the physical characteristics are not ideal for PET imaging because of additional, highly energetic gamma radiation (Fig. 1).

Iodine-labeled compounds, briefly mentioned earlier, are most valuable for *ex vivo* receptor imaging, such as autoradiographies. This form of receptor imaging with ^{125}I-labeled compounds allows precise correlation of receptor density and localization with histology.

For ►*in vivo* receptor imaging by means of nuclear medicine, it is mandatory that the receptor–vector complex after the binding of the radiopharmaceutical remain stable among the targeted tumor. The sst is a transmembrane receptor. The binding domain is located on the cell surface and therefore easily accessible for the ligand. After binding, the receptor–ligand complex is internalized, and chelated radionuclides remain captured in the cell. This results in a fairly stable residence of the radioactivity in the target cell. Consequently, a higher target-to-non-target ratio for imaging can be expected after most of the nonreceptor-bound radiopharmaceutical is cleared from the organism, which in turn is necessary for therapeutic applications.

Imaging of somatostatin receptors became a standard procedure for staging patients with sst-positive tumors and for characterizing suspect nodules *in vivo*. Moreover, it is prudent to perform an sst scan to prove the presence of a sufficient density of receptors on a tumor before planning a receptor-mediated radionuclide therapy.

In summary, sst imaging plays a key role in the following:

1. Diagnosis and Characterization of tumors
2. Determining the extent of disease (staging)
3. Selecting patients who are candidates for targeted radionuclide therapy
4. Predicting the response during targeted radionuclide therapy
5. Monitoring therapy.

Other Cell Surface Receptors, Imaging with Peptides

Besides somatostatin receptors, a number of other cell surface receptors are overexpressed in tumors and are

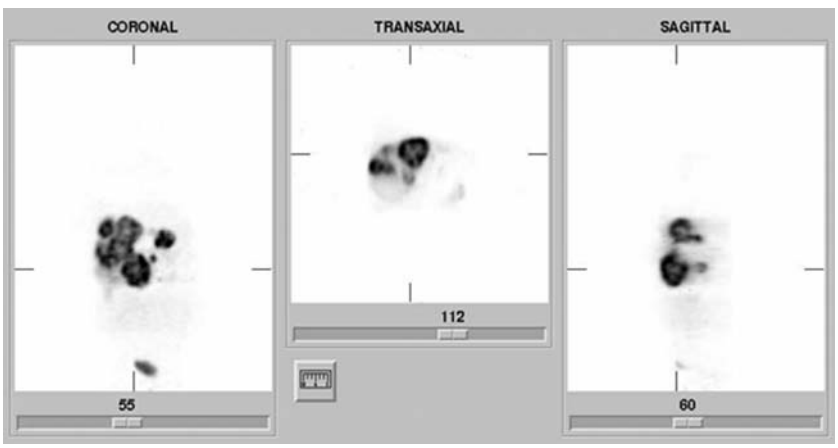

Receptor Studies, Neoplasms. Figure 1 Coronal, transaxial, and sagittal slices of a positron emission tomography scan acquired with [^{68}Ga-DOTA^{0},Tyr^{3}]-octreotide (^{68}Ga-DOTATOC) in a patient with a metastatic neuroendocrine tumor and multiple liver metastases. DOTATOC is an octreotide analog with a high affinity for sst 2. Because of the high affinity and specificity of the radiotracer, high uptake is seen in the multiple strongly sst-positive liver metastases. Low physiological uptake is found in the liver. The tracer is rapidly cleared from the body *via* the kidneys to the urine; therefore, the urinary bladder is visible as well. The fast clearance results in very low background activity; therefore, no activity is present in the thorax. (Scan acquired at Deutsches Krebsforschungszentrum, Heidelberg, Germany, courtesy of Professor U. Haberkorn)

suitable for imaging with radiolabeled peptides. A selection of the most promising combinations of peptides and receptors that are currently under investigation or that are used in clinical trials is summarized in Table 1 (3).

As one of the peptides binding to a cell surface receptor, bombesin deserves highlighting. Bombesin is a 14-amino-acid neuropeptide. In mammals, it binds to three known receptors: bombesin receptor 1–3 also called neuromedin B receptor, gastrin-releasing peptide (GRP) receptor, and bombesin receptor subtype 3. Several peptides with high affinity for the GRP receptor have been developed, comparable to somatostatin, labeled with an array of radionuclides. Overexpression of GRP receptors has been found on many neoplasms, especially in prostate and breast cancer. Remarkably, the GRP receptor is not expressed in healthy prostate tissue. This might provide the chance to distinguish *in vivo* between benign and malignant prostate nodules by means of receptor imaging (Fig. 2).

Another highly promising combination for imaging is gastrin or cholecystokinin (CCK) analogs and the CCK subtype 2 (CCK 2) receptor, also called gastrin receptor. The CCK 2 receptor is overexpressed in medullary thyroid cancers (MTC). Relapse of MTC can be diagnosed by elevated levels of calcitonin in the blood, but localization is often inconclusive. In these cases, scintigraphy with radiolabeled gastrin analogs is of high value.

A third example is the combination of radiolabeled neurotensin and the three subtypes of the neurotensin receptor. Neurotensin receptors are overexpressed in ductal pancreatic adenocarcinoma. First clinical evaluations for diagnostic purposes have been made with a metabolically stabilized ^{99m}Tc-labeled peptide.

Receptor Studies, Neoplasms. Table 1 Selection of promising peptide-receptor combinations for *in vivo* receptor imaging with radiolabeled peptides

Tumor	Receptor	Vector
Gastroenteropancreatic tumors, neuroendocrine tumors, paraganglioma, pheochromocytoma	Somatostatin	Octreotide and derivatives
Prostate carcinoma	Gastrin-releasing peptide	Bombesin analogs
Medullary thyroid carcinoma	Cholecystokinin (CCK) subtype 2	Gastrin/CCK analogs
Ductal pancreatic adenocarcinoma	Neurotensin	Neurotensin analogs
Gastrointestinal cancers	Vasoactive intestinal peptide (VIP) receptor	VIP analogs
Insulinoma, gastrinoma	Glucagon-like peptide 1 (GLP 1) receptor	GLP analogs
Glioma	Neurokinin 1 receptor	Substance P analogs

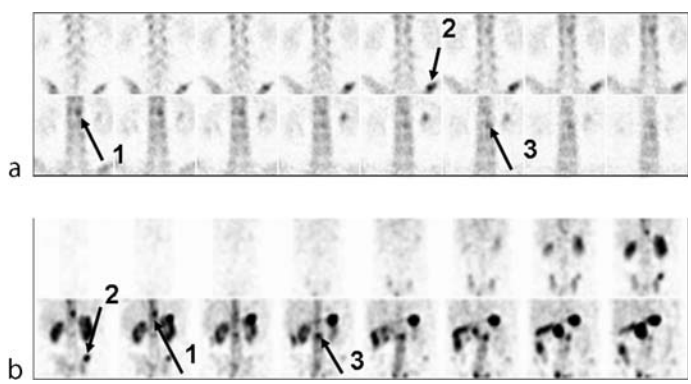

Receptor Studies, Neoplasms. Figure 2 Coronal slices of two single photon emission computed tomography scans in a patient with metastatic prostate carcinoma. (a) Bone scan with ^{99m}Tc-dicarboxypropane-diphosphonate (DPD). Three bone metastases can be identified in the spine and pelvis (*arrows* 1–3). (b) Corresponding images from a scan with [^{111}In-DTPA-Pro^1,Tyr^4]-bombesin. The same metastases as in the bone scan are detected (*arrows* 1–3). The high tumor-to-background ratio indicates a high density of GRP receptors.

Intracellular Receptors

To date, intracellular receptors are of minor relevance in oncological imaging. A number of studies have been published using radiolabeled estrogens to visualize estrogen-receptor-expressing breast cancers, or radiolabeled androgens to visualize prostate cancers. Although a first study with bromated (^{77}Br) estrogen was published in 1982, it never reached broad clinical impact. These days, fluorinated (^{18}F) derivatives for PET imaging, consecutively achieving better resolution, are available (4).

Receptor Imaging with Antibodies

►Antibodies are of emerging importance for medicine in general. Development of immunohistochemistry was revolutionary for pathological diagnostics. Clinically, antibodies are widely used in oncology, and the first radiolabeled antibodies recently received US Food and Drug Administration approval for cancer treatment. Nevertheless, the use of radiolabeled antibodies for *in vivo* receptor imaging is limited. The long circulation time, the slow pharmacokinetics in general, and the physiological uptake of radiolabeled antibodies in a number of organs result in high background activity and, therefore, in an unfavorable tumor-to-background ratio. However, visualization of the HER2 receptor, which is overexpressed in many breast cancers, with radiolabeled trastuzumab is feasible. These findings are of clinical interest because nonradiolabeled trastuzumab is an established treatment for HER2-positive breast cancers.

A possible way to overcome the slow pharmacokinetics of antibodies is the use of fragments or artificial derivatives such as diabodies, triabodies, minibodies, and dimers and trimers. The advantage of antibodies and derivatives is that these molecules can be bioengineered to target a specific receptor (5).

The eligibility of antibodies to be designed for a specific target makes them highly valuable for *in vitro* and *ex vivo* receptor studies when the kinetics are negligible.

Bibliography

1. Kwekkeboom DJ, Krenning EP (1997) Radiolabeled somatostatin analog scintigraphy in oncology and immune diseases: an overview. Eur Radiol 7:1103–1109
2. Reubi JC, Waser B, Schaer JC et al (2001) Somatostatin receptor sst1-sst5 expression in normal and neoplastic human tissues using receptor autoradiography with subtype-selective ligands. Eur J Nucl Med 28(7):836–846
3. Reubi JC (2003) Peptide receptors as molecular targets for cancer diagnosis and therapy. Endocr Rev 24(4):389–427
4. Van Den Bossche B, Van de Wiele C (2004) Receptor imaging in oncology by means of nuclear medicine: current status. J Clin Oncol 22(17):3593–3607
5. Hudson PJ, Souriau C (2003) Engineered antibodies. Nat Med 9:129–134

Reclus' Disease

►Fibrocystic Disease, Breast

Rectal Atresia

A congenital abnormality, usually due to an ischaemic insult in embryological development resulting in complete occlusion of the lumen of the rectum.

►GI Tract, Pediatric, Congenital Malformations

►Anorectal Malformation

Rectal Descent

Rectal descent is an excessive caudal movement of the anorectal junction during evacuation.

►Pelvic Floor Dysfunction, Anorectal Manifestations

Rectal Foreign Bodies

►Foreign Bodies, Gastrointestinal

Rectal Prolapse

An invagination of the rectal wall and may be classified as internal or external. Internal rectal prolapse, also called intussusception, may be classified as intrarectal internal prolapse if the invagination is confined to the rectum or as intraanal internal prolapse if its apex penetrates the anal canal and remains in it during straining. External rectal prolapse is an invagination of the rectal wall through the anal canal and is a clinical diagnosis.

►Pelvic Floor Dysfunction, Anorectal Manifestations

Rectocele

Anterior bulging of the anterior rectal wall during defecation of more than 3 cm from the anal canal is

called a rectocele. A rectocele impresses the posterior vaginal wall (grade II) and may evert it to outside the introitus (grade III).

▶Pelvic Floor Dysfunction, Genitourinary

Recurrent Breast Cancer

▶Recurrent Neoplasms, Breast

Recurrent Neoplasms, Breast

Luis C. Apesteguía
Hospital Virgen del camino, Pashplona, Spain
luis.apesteguia.ciriza@cfnavarra.es

Synonyms

breast cancer recurrence; Breast cancer relapse; ipsilateral breast tumor recurrence; recurrent breast cancer

Definition

In general terms, breast recurrent neoplasms (BRNs) are neoplasms that are diagnosed during the follow-up of patients with breast tumors, after some kind of treatment. Normally, surgical removal has been carried out on the breast and the primary neoplasm has apparently been completely removed or disappeared. It can occur either in the scar margins or near the place where the primary neoplasm was removed (▶local recurrence or LR), in close areas around the same breast (▶regional recurrence or RR), or in other distant organs (distant recurrence or metastasis, ▶DR).

Characteristics

Benign and malignant breast tumors can recur. With benign tumors, it is well known that cysts may appear full again some weeks or months after aspiration and pneumocystography. Fibroadenomas, papillomas, adenomyoepitheliomas, and other benign masses can also recur after cryoablation and even after surgical removal, always in the same place or on the margins of surgical scar.

The most characteristic recurrent benign breast tumor is cystosarcoma phyllodes. This tumor, arising from the stroma, may be categorized benign or malignant. Both types increase in size very quickly and should be suspected if a fibroadenoma grows too fast or recurs following surgical removal. LR may predict metastases even in patients with histologically benign disease. Distant metastases are not frequent and tend to locate in the lung and more rarely in bone and liver. Consequently, when a phyllodes tumor is diagnosed, wide local excision is the treatment of choice, with a 2-cm margin or fascia included in the specimen. Axillary node dissection (AND) is not usually carried out, as lymph node metastases are extremely infrequent.

For malignant tumors, four different kinds of BRNs are usually considered (1):

Local Recurrence (LR)

Breast cancer very frequently (75%) recurs in the same area as the original cancer was located. Women with a ductal carcinoma *in situ* (DCIS) who are treated with breast-conserving therapy (BCT) are at a slightly higher risk of recurrence than those who are treated with mastectomy. However, an LR following BCT of DCIS does not imply a poorer long-term prognosis than mastectomy as initial surgical treatment. Even after mastectomy, portions of the breast skin and fat remain, and LR is possible although more uncommon.

Most reports of patients treated with BCT indicate a median time to recurrence of 40–52 months. Although most recurrences develop within 5 years, a small but constant risk remains for several decades thereafter. Interestingly, the recurrence rate in the tumor bed is approximately 2% per year until year 5, after which it drops significantly. LR can also be *in situ* or invasive. The first is less serious than an invasive recurrence, since this means a second chance of metastasis.

Regional Recurrence (RR)

It is a situation where tumor cells can be demonstrated in the axillary lymph nodes or well in the pectoral muscles, internal mammary lymph nodes, or supraclavicular or cervical nodes. RR of breast cancer is uncommon, occurring in approximately 2% of the cases. Most often, RR appears as a cancerous axillary lymph node not removed during primary lymphadenectomy. RR in the cervical lymph nodes or above the collarbone usually indicates more aggressive cancers.

▶New Neoplasm (NN)

During follow-up after breast surgery, apart from LR and RR new, different neoplasms can be detected. In fact, patients who have had breast cancer are considered at high risk of suffering from a second breast cancer. Usually, this new tumor is in a different area of the breast and does not have the same pathological characteristics (histological type, grade, or hormonal receptors) (Fig. 1). Second cancers are treated as new cancers, independent of the first one.

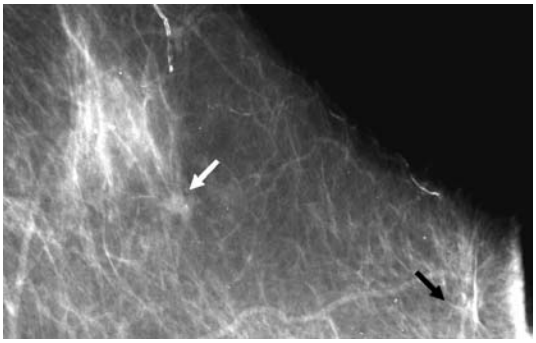

Recurrent Neoplasms, Breast. Figure 1 Patient treated with breast-conserving therapy for ductal carcinoma *in situ* 7 years previously. There is a new density (*white arrow*) that was not present in the mammogram taken 1 year earlier. The surgical scar presents normal characteristics (*black arrow*) and the new tumor is more than 5 cm away from it. The location of this lesion and the time elapsed from surgery suggest a new tumor, more than a local recurrence. This was an invasive lobular carcinoma.

Distant Recurrence (DR)

It is also known as metastatic disease and means that malignant cells are present in a distant place, most commonly in bones, lungs, liver, brain, or other organs. This is a serious event and the survival rate of women with this disease is considerably lower than for women whose cancer is confined to the breast or axillary lymph nodes. Breast cancer has the potential to spread to almost any region of the body.

Diagnosis

Local and Regional Recurrences

Women whose initial breast cancer was aggressive are more likely to have LR. Inflammatory breast cancer often recurs. Also, women with large tumors or several affected axillary nodes may frequently experience recurrence. The LR for DCIS can be intraductal or invasive and the rates appear somewhat higher than those of invasive tumors. Multifocal DCIS with microinvasion has a high LR rate. Patients at exceptionally high risk of recurrence or development of a second primary tumor should be watched more closely.

LR after mastectomy will usually present itself as a small lump in the mastectomy scar or under the skin. This type of recurrence often goes undetected for some time because it may be mistaken for a leftover stitch or scar tissue from the mastectomy. Breast reconstruction rarely hides recurrent breast cancer. LR with implants is most often in front of the implant, and recurrences with ►transverse rectus abdominis musculocutaneous (TRAM) flap procedures are along the edge of the breast skin, and not in the flap. LR following BCT usually appears at the surgical site.

Detection of LR and RR is usually made by clinical history, physical examination, and breast imaging techniques. An adequate clinical examination of patients after BCT or mastectomy should include the breasts, especially the scars, but also axillary, supraclavicular, and cervical areas. Mammography (MX), ultrasonography (US), and magnetic resonance imaging (MRI) are the most useful imaging techniques. Nonpalpable LR or RR can be diagnosed using needle localization with excision biopsy or imaging-guided percutaneous biopsy, using stereotactic MX, US, or MRI to localize and puncture the suspicious lesion through a small incision (several millimeters in length) with the patient under local anesthesia. US is preferred whenever the lesion is clearly identifiable by this technique. According to the thickness of the needle, the most widely used techniques are fine-needle aspiration cytology (FNAC), large core needle biopsy (LCNB), and vacuum-assisted biopsy (VAB).

Patients must be routinely followed up by physical examination and should annually undergo bilateral MX after BCT. In patients with radical mastectomy, with or without reconstruction, only contralateral MX will be done. MX is important for the early recognition of recurrence; unfortunately, however, normal changes seen on mammograms resulting from BCT may mimic the signs of malignancy. Baseline MX should be performed approximately 6 months after BCT and the completion of all treatments.

The natural history of the postirradiation mammogram includes a slow but progressive return to normal degrees of breast fibrosis, skin thickening, and glandular parenchyma. The radiological signs of LR are the same as those in an unirradiated breast and include new cluster calcifications, asymmetric densities, or occasionally a preexisting scar increasing in size. Breast fibrosis in the area of the tumor bed can persist for many months and can be confused with recurrence. Dynamic MRI studies have shown the highest sensitivity in making a differential diagnosis between hypertrophic scar fibrosis and LR (Fig. 2).

Frequently, fat necrosis and oil cysts may also appear near the surgical scar, resembling recurrence. Dystrophic calcifications or early calcifications of liponecrosis can also simulate recurrence. In these cases, percutaneous biopsy should be undertaken in order to detect recurrence.

US is a well-known adjunct technique and is more necessary in investigations of dense breasts or areas where density is higher, because the sensitivity of MX is lower. US should also be carried out in patients with BCT, mastectomy followed by reconstruction, and even simple

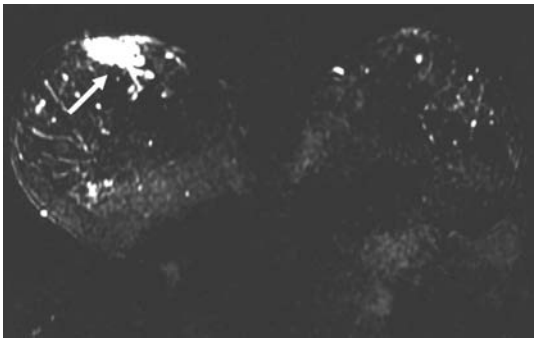

Recurrent Neoplasms, Breast. Figure 2 Dynamic MRI study with subtraction technique, showing a captation of contrast in the margins of the surgical scar (*arrow*). The patient had been treated 3 years previously with breast-conserving therapy.

mastectomy in order to detect LR, especially the characteristics and evolution of the scar, and also to detect RR in axillary, supraclavicular, or cervical lymph nodes. The size, shape, outline, echogenicity, and proportion of the hilus/cortex must be evaluated. This is more important in cases when only a sentinel lymphatic node biopsy (SLNB) was done with benign results and consequently AND was not carried out. Suspicious nodes should be punctured under US guidance, by FNAC or even by LNCB.

US is also very accurate in studying implants in patients with postmastectomy reconstruction.

Once an LR or RR is detected, several tests must be ordered to determine whether the tumor has metastasized to distant organs.

New Neoplasms

Patients who have had previous breast cancer have a higher risk of presenting a second neoplasm. These tumors, which can appear clinically or on a follow-up mammogram, are usually located in a different place or in the contralateral breast.

The recurrence rate outside the immediate tumor bed is negligible until the 5th year, after which it increases to 1% per year.

Detection and diagnosis of new neoplasms following BCT are made in a way similar to primary carcinomas and to LR: by clinical history, physical examination, or by imaging techniques (MX, US, and MRI). Nonpalpable lesions are usually diagnosed by needle localization with excision biopsy or by imaging-guided percutaneous biopsy. US is preferred if the lesion is clearly identifiable by this technique. FNAC, LCNB, and VAB are the most common procedures.

Distant Recurrence

Metastatic disease is the most advanced stage (IV) of breast cancer. It can spread to almost any organ of the body, but the most common sites are bone, lung, liver, and brain. The ovaries, spinal cord, eye, and other areas are less commonly affected. Symptoms of DR may include bone pain, shortness of breath, lack of appetite, weight loss, weakness, headaches, and other symptoms depending on location of the lesions.

Systemic relapse is more frequent after LR and even more so in patients who have suffered RR.

DR is usually diagnosed by bone scan, chest X-ray, US, computed tomography (CT), MRI, or liver blood tests. The two most important marker tests for breast cancer are CEA (carcinoembryonic antigen) and CA 15-3, which tend to be elevated in women with metastatic breast cancer, although their sensitivity and specificity are not too high.

Prognosis and Treatment

Young age, positive surgical margins, and omission of radiation therapy (RTP) significantly predict ipsilateral breast tumor recurrence and this situation is correlated with DR. Among the patients who develop LR, initial lymph node metastasis and short interval to LR are significant risk factors for subsequent DR (2). The prognosis for patients with LR after initial BCT for invasive breast cancer has been reported by multiple groups, with 5-year survival statistics ranging from 35 to 81%. The prognosis is clearly better when LR is diagnosed more than 5 years after BCT (3). The high incidence of DR in this group suggests that these patients might benefit from systemic adjuvant therapy. Little information is available on this subject, but prospective trials are being planned to address this issue.

Patients treated for intraductal cancer with breast conservation have an excellent survival prognosis with LR figures of 6–10%. However, at least 20% of recurrences have an invasive component of low volume. Further observation is necessary in order to determine whether these patients are at substantial risk for systemic cancer spread.

LR following BCT can be treated with conservative re-excision or, more often, mastectomy with or without reconstruction, since RTP cannot be delivered twice to the same area. Patients who undergo reconstruction with an implant have poor cosmetic results and an increased incidence of complications. These complications may be related to loss of skin elasticity due to prior surgery and irradiation. However, to achieve optimal cosmetic results, most patients undergoing reconstruction will undergo a tissue transfer procedure such as a TRAM flap.

If the initial treatment was mastectomy, recurrence near the mastectomy site is treated by removing the tumor whenever possible, usually followed by RTP. In either case, hormone therapy and/or chemotherapy may be used after surgery and/or RTP. If breast cancer is found in the other breast, it may be a new tumor unrelated to the first breast cancer. Treatment includes a lumpectomy or mastectomy and, sometimes, systemic therapy. NN are treated as new cancers, independent of the first tumor.

Surgery is rarely an option for metastatic breast cancer because the cancer is not usually confined to one specific spot on the given organ. It may be recommended only to relieve certain symptoms. Treatment options include one or more of the following: chemotherapy, hormonal therapies, or RTP. Radiofrequency can be carried out as a treatment for lesions that are not extensive. Bisphosphonates and RTP may be helpful in treating the effects of bone metastases. Immunotherapy with trastuzumab (Herceptin) alone or with chemotherapy may be recommended for women whose cancer cells have high levels of the HER2/neu protein.

The outcome and treatment of LR of breast cancer depends more on a patient's menopause status and the clinical and tumor characteristics of the initial tumor than on other factors. The risk of death significantly increases in women with LR of breast cancer when the initial tumor was greater than grade 2, the time interval without cancer was less than 8 years, and the age at diagnosis of the primary tumor was greater than 60 years.

The type of surgery for the initial, primary breast cancer does not alter mortality risk. Although no specific treatment can change the risk of death after LR in postmenopausal women, premenopausal women benefit from treatment with either surgical or irradiative ovarian suppression or chemotherapy.

In a recent retrospective study of 1,636 patients with early stage breast cancer who were treated surgically with either breast-conserving surgery or mastectomy, two cohorts were identified. The first comprised 105 patients who experienced an isolated LR. Seven potential factors were considered: initial size of the primary tumor, tumor grade by pathology, axillary lymph node status, date of initial diagnosis, age at diagnosis, time interval without cancer recurrence, and the type of treatment for initial tumor and LR. The authors identified a second subgroup of 335 patients who developed distant metastases as the first recurrence. Data from these two subgroups were analyzed for survival.

Patients with a grade 3 tumor had a threefold increased risk of death. Patients over 60 years old at the time of diagnosis of the primary cancer had a twofold increased risk of death. Patients who experienced over 8 years without recurrent tumor had a threefold decreased risk of death (4). Significantly, the risk of death after an LR was independent of whether or not the patient's primary cancer was treated with breast-conserving surgery or mastectomy. However, the type of treatment of the LR altered the mortality risk, but only in women of premenopausal age.

Ovarian suppression by either surgical removal of the ovaries or pelvic irradiation and chemotherapy significantly reduced the risk of death, with relative risk values of 0.2 for each category.

Neither breast surgery nor radiation or tamoxifen was associated with statistically significant alterations in the risk of death.

Women with an LR were more likely to survive 10 years than women with a DR; the 10-year survival rates were 56% and 9%, respectively. The median survival for women with LR was 12.9 years compared to 2.2 years for women with a DR.

Because an isolated recurrence carries a relatively good prognosis, mastectomy does not appear to be mandatory for LR after the patient has undergone BCT (4).

Local RTP may be indicated in patients who previously underwent mastectomy, and the use of chemotherapy at the time of recurrence in premenopausal patients may be appropriate.

References

1. Harris JR, Lippman ME, Morrow M et al (2004) Diseases of the Breast. 3rd edn. Lippincott Williams & Wilkins, Philadelphia. Section VIII:43–50
2. Dershaw DD (2002) Breast imaging and the conservative treatment of breast cancer. Radiol Clin N Am 40 (3):501–516
3. Veronesi U, Marubini E, Del Vecchio M et al (1995) Local recurrences and distant metastases after conservative breast cancer treatments: partly independent events. J Natl Cancer Inst 87:19–27
4. Komoike Y, Akiyama F, Iino Y et al (2006) Ipsilateral breast tumour recurrence (IBTR) after breast-conserving treatment for early breast cancer. Cancer Jan 1; 106(1):35–41
5. Van der Sangen MJ, van de Poll-Franse LV, Roumen RM et al (2005) The prognosis of patients with local recurrence more than five years after breast conservation therapy for invasive breast carcinoma. Eur J Surg Oncol. Nov 20; (Epub ahead of print)
6. Lê MG, Arriagada R, Spielmann M et al (2002) Prognostic factors for death after an isolated local recurrence in patients with early-stage breast carcinoma. Cancer June 1; 94(11):2813–2820

Reflux Nephropathy

Interstitial nephritis often related to vesicoureteral reflux especially in childhood and in female patients.

▶ Pyelonephritis, Chronic
▶ Reflux, Vesiconsetal, Childhood

Reflux, Gastroesophageal in Adults

Giles Stevenson[1], Phil Shorvon[2]
[1]McMaster University, Cowichan Hospital, Duncan, British Columbia, Canada
[2]Central Middlessex hospital, London, England
gilse@shaw.ca
phils@intonet.co.uk

Synonyms

Gastro-oesophageal reflux; GERD; GORD; Hiatus hernia; Hiatal hernia; Barrett's oesophagus; Columnar lined oesophagus

Definition

All adults in industrialized nations reflux gastric contents into the oesophagus, though most are asymptomatic. Reflux takes place when transient complete relaxations of the lower oesophageal sphincter occur when an individual is recumbent with a sufficient volume of fluid in the stomach. Such relaxations normally occur several times each day, especially when the stomach is full after a meal, usually only two or three times in the day for up to 5 min, and uncommonly at night. At night, when it does occur, it is usually during episodes of light arousal, in REM sleep.

Gastroesophageal reflux disease is defined as an excessive number of such relaxations causing an increase in the time that the oesophagus contains acid, accompanied by symptoms and/or complications of acid reflux into the oesophagus. It is possible, though unusual, for the severest complications to present with very little in the way of preceding symptoms and this is more likely in the elderly amongst whom GERD is much commoner.

Pathology of GERD

The pathophysiology of GERD has been discussed in the previous section on GERD and hiatal hernia, and is intended to be read first. This section describes the clinical presentations of the disease, and the roles of imaging.

Clinical Presentation

In the western industrialized world GERD is common, with between a third and a half of all adults reporting ►heartburn or ►regurgitation at least monthly, though it is much less common in some countries such as Japan where obesity is less common, and there is less fat in the diet (1). Most patients with characteristic symptoms require no imaging and can be managed with anti-acid medication for symptom relief, though this has no effect on the underlying disease process. Five factors exacerbate reflux including pregnancy. Those which are amenable to life style change include being overweight, going to bed at night with a full stomach, caffeine, and alcohol. Smoking has traditionally been included in this list but the evidence for this is very poor. These four life style factors are important in curing or downgrading reflux disease, though once the LES has been totally destroyed it may be too late for recovery. Obesity is critical, and many sufferers find that weight loss provides rapid improvement in symptoms. The radiologist often has the opportunity to discuss these issues briefly after a ►barium meal examination, with those patients who ask questions about their diagnosis.

Obesity and these life style changes however are not the whole story. Patients are seen who are slim, who have reflux disease, and who have had reflux symptoms for years. Rarely, patients are seen in their 20s with long segment Barrett's oesophagus. There is thus a small group of children in whom the "chalasia" of infancy, most often seen with prematurity, persists throughout childhood and may be present in early adult life with symptoms or complications.

Symptoms of reflux arise from any or all of the affected organs. A retrosternal burning is most common, and in advanced disease, acid and gastric content regurgitation which may be positional. Pharyngeal and laryngeal effects include the symptoms of globus, hoarse voice, sore throat, and choking. Cough and asthma are common associations. The oesophageal response with spasm may cause ►chest pain which may mimic angina or myocardial infarct. Stricture or spasm may cause ►dysphagia, and narrowing at the gastro-oesophageal junction may cause dysphagia. Accurate localisation of dysphagia by patients is poor. Hold up at the gastro-oesophageal junction may be experienced higher up and even in the throat, although patients do not normally experience dysphagia below the level of the causative lesion. Oesophagitis may also cause odynophagia - painful swallowing, though this is more common in herpes oesophagitis than in peptic reflux oesophagitis. It is a common experience that patients with globus symptoms often have reflux, but one study from Edinburgh in 1986 failed to confirm an excess time with reduced pH in a group of patients with globus. Prolonged reflux may lead to Barrett's oesophagus and carcinoma. Night time reflux is much more strongly associated with complications than symptoms restricted to the day time, presumably because of prolonged acid contact time.

Recently it has become clear that a number of unexpected symptoms are also part of the GERD clinical complex, including sleep disturbances, bloating, nausea, dry cough, throat clearing, and diarrhoea. Although it is not clear exactly how these symptoms relate to acid reflux, or how distinct GERD is from irritable bowel syndrome and non ulcer dyspepsia, nevertheless several studies have shown that the whole broad symptom complex does respond to the most effective PPI drugs in the majority of patients.

Airway Aspects of GERD

Although minor reflux is usually effectively cleared by oesophageal peristalsis, advanced disease is associated with major regurgitation of large volumes of gastric contents that may overwhelm pharyngeal defences and affect the airways. This may cause choking, asthma or recurrent pneumonia. The typical choking sufferer is an overweight middle aged male patient who, sitting back in an easy chair after a large meal, is surprised by a dramatic attack of choking due to laryngeal spasm associated with reflux. Direct inspection may show laryngeal erythema and oedema and barium study of the pharynx may be normal, or may show a cricopharyngeal bar or mucosal herniation, and sometimes incoordination of the pharynx with supraglottic laryngeal penetration by barium, usually without frank aspiration.

The relationship between asthma and reflux is complex. There are reasons why asthma may cause GERD including that 30% of asthma sufferers have hiatus hernia perhaps because of straining and coughing, and because theophylline medications impair the LES function. There are also reasons why GERD may cause asthma, including microaspiration. The use of PPI therapy sometimes improves cough and wheezing in asthmatics leading to a decreased drug requirement but without change in spirometry. Twenty four hour pH monitoring may not always diagnose GERD, and is positive in only about 45% of GERD sufferers with erosion negative disease, 70% of those with oesophageal erosions and 85% of those with Barrett's. The empirical approach for asthma patients is that where there is a high clinical suspicion of GERD it is reasonable to use high dose PPI therapy with complete acid suppression, as a therapeutic trial for two to six months, and if there is a low suspicion of GERD and the asthma is poorly responsive, then to consider 24 h pH monitoring and to treat those with a positive result (2).

The relation between chronic cough without asthma and GERD is even more problematic. In one study, only 3% with GERD and chronic cough showed response of the cough to PPI therapy, but they responded quickly, so a short trial of PPI of two weeks or so may be sufficient in this group of patients. In chronic laryngitis due to GERD, both symptoms and endoscopic laryngeal findings will resolve though not as fast as in chronic cough, and high dose PPI therapy may be recommended for up to 2–3 months as a therapeutic trial. The radiologist will often be asked to assess patients with cough or asthma for GERD and should assess pharyngeal function for penetration as well as assessing the evidence for GERD.

Some authors suggest that oesophago-pharyngeal reflux occurs excessively after gastro-oesophageal reflux in those GERD patients with respiratory symptoms. However the best way to study this has not been identified, and there is no good data on how to evaluate this phenomenon.

Cardiac Aspects

The relationship between the heart and the oesophagus is no less complex than the respiratory linkage. Indeed, of a series of 200 consecutive patients admitted to a coronary care unit with suspected myocardial infarct, who in fact did not have cardiac disease, extensive investigation showed that 95% were suffering from GERD (3). In distinguishing angina from heartburn it is often helpful that angina lasts 1–2 min or less. However instillation of acid into the oesophagus can cause coronary artery spasm and change in cardiac rhythm, and coronary angiography can cause oesophageal spasm. A drug such as Nifedipine is often used for the treatment of oesophageal spasm, and it can also reduce coronary spasm. A therapeutic trial of PPI drugs to see if chest pain is due to GERD had a test sensitivity of 80% and specificity of 74% in one study. However one PPI drug has been shown to improve angina, with a 10% improvement in stress test, with exercise limit improved by 30% and a decrease in ST segment depression. In difficult cases empiric therapy is required and the diagnosis may be elusive, with GERD and angina not mutually exclusive diagnoses.

Imaging for Gastro-Oesophageal Reflux Disease (4)

Investigation is appropriate for those patients whose symptoms do not respond to simple therapy, or who have alarm symptoms such as dysphagia or anaemia, or who are suspected of having Barrett's oesophagus. In most centres gastroenterologists and surgeons prefer endoscopy as the initial investigation, and some regard barium studies as totally obsolete for this purpose. Barium radiology suffers from there being little scientific data on its value. Most of the abnormalities are observational and not amenable to objective measurement. However endoscopy services are overstretched, and in many countries thousand of patients still have barium meals,

often referred by family physicians who do not have ready access to endoscopy. Barium studies are less sensitive for diagnosis of mild and moderate oesophagitis, and for detection and assessment of Barrett's oesophagus. They do however provide a broader overview of the spectrum of abnormalities seen in GERD and, when used with a ▶marshmallow solid bolus, are more sensitive than endoscopy for the detection of mild strictures and Schatzki rings. Barium radiology will also allow better identification of that minority of patients with virtually no lower oesophageal sphincter mechanism who will almost certainly require life time therapy and who are at most risk of complications. It is in these patients, particularly if they are young, that operative treatment may be a more sensible option.

Other investigations sometimes useful include nuclear medicine, manometry, and 24-h pH monitoring and these will not be discussed in any detail. Manometry is of most value in patients with chest pain in whom differentiation between cardiac and oesophageal disease remains problematic after endoscopy, barium studies and therapeutic trials; and is also valuable when the simpler studies suggest a primary motility disorder such as achalasia or diffuse spasm. Twenty four hour pH monitoring is mainly helpful for those few patients with heartburn symptoms or chest pain, thought to be of oesophageal origin, who do not respond to PPI therapy.

Barium Meal Examination

There are many ways to perform a barium study of the upper GI tract, but there are two principal choices which depend on the clinical question being posed. One type of study is best suited for the demonstration of peptic ulceration and gastric neoplasm and the other is tailored for the assessment of GERD. The peptic ulcer study requires the use of hyoscine butyl bromide (Buscopan) to paralyse the stomach and duodenum and this interferes with the assessment of oesophageal motility and will promote GE reflux in normal individuals by paralysing the LES. The radiologist therefore has to decide whether the priority is to focus on detection of ulcers, erosions and neoplasms, or to assess reflux disease, but cannot do both optimally in one examination.

Before starting the examination, it follows from the above that the radiologist should first confirm the details of the clinical history with the patient, in order to tailor the examination, and ask specifically about pharyngeal symptoms and dysphagia.

The rest of this section will describe one approach to the assessment of GERD. This also is divided into two groups depending on whether the patient has simple reflux symptoms or has in addition either dysphagia or pharyngeal symptoms, with some additional comments on the investigation of chest pain.

The examination should be planned to answer the following six questions.

Is there GE reflux disease present, and if so what grade? Does it occur only slightly with the water siphon test (normal), is it major with the water siphon test, does it occur with dry swallowing with the patient supine oblique, is it spontaneous on turning, or is it free and constant throughout the examination: in other words is it medical or potentially surgical?

Is there effective clearance of any refluxed material by normal peristalsis?

Is there a motility problem that might contraindicate surgery?

Is there evidence of complications: severe oesophagitis, stricture, scarring, Schatzki ring, or Barrett's oesophagus?

Is there evidence of pharyngeal disease?

Is there a short oesophagus?

Simple Reflux Examination

The exam is started with the patient erect, turned 45° to the left holding a 150–200 mL cup of high density barium in the left hand and a small cup with 5–10 mL water in the right. Rapid release CO_2 granules are tipped into the small cup and the patient swallows the granules at once followed rapidly by the barium. In countries in which these granules are not available, other granules and citric acid solutions are used to achieve oesophageal distention before the barium is swallowed. Double contrast views of the entire oesophagus and pharynx are taken while the barium is being swallowed, with attempts made to show the LES well distended in double contrast view (Fig. 1). A 16′ intensifier provides a superior examination over smaller intensifiers as the larger field of view allows the tail of the barium column to be seen in the pharynx where premature contraction of the upper sphincter may be noted, while still visualizing the main part of the bolus going down the oesophagus. With smaller intensifiers premature contraction of the cricopharyngeus is more likely to be overlooked.

The table is then rapidly placed horizontal, while the patient is instructed to dry swallow in order to minimize belching of gas. The patient is then turned left and prone, shaken and turned again on the left and supine. A supine film of the entire stomach is taken. The table head is elevated 45°, and the patient turned on the right for an end face view of the cardia and the fundus in double contrast (Fig. 2). With the table horizontal the patient rotates back into supine left side raised position such that half the barium is in the fundus and half in the antrum, for another exposure of the stomach showing the high lesser curve in double contrast. The patient is turned to the left 45° for a double contrast view of the distal stomach, and then views of the duodenum are taken supine oblique to left and right and, if necessary, prone.

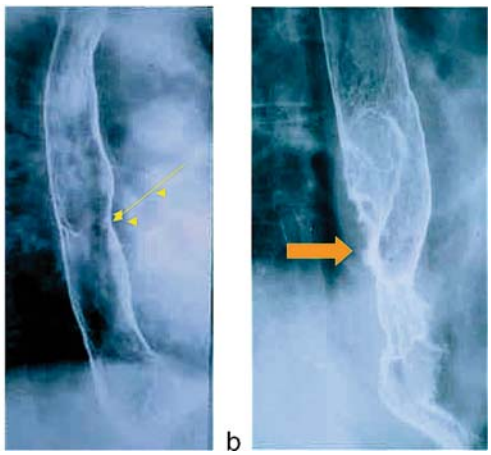

Reflux, Gastroesophageal in Adults. Figure 1 (a) This standard double contrast view of the oesophagus shows a dilated oesophagus, with lax lower end, and some slight narrowing and mucosal irregularity in mid oesophagus. These are the characteristic appearances of a long segment of Barrett's oesophagus, in an engineer aged 50. (b) Six years later the patient returned, telling his physician that he had the cancer that he had been warned about as he was having difficulty in swallowing. The films show a long tumour with central ulceration.The patient survived surgery and was well ten years later.

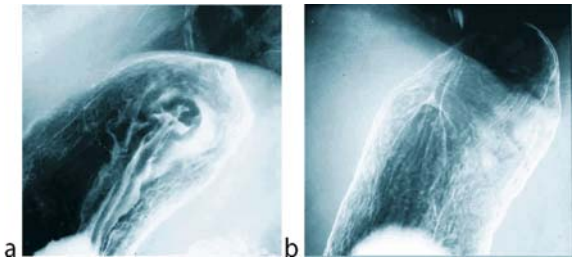

Reflux, Gastroesophageal in Adults. Figure 2 (a) This shows the cardia end face—an essential view in any barium meal examination. It shows the rosette appearance of a competent LES, and it symmetry rules out any tumour at the cardia. (b) In this patient, the sphincter is relaxed and partially opened producing a crescent shadow. If Buscopan or Glucagon has not been given this is moderately reliable evidence of a low pressure sphincter, but the relaxant drugs can change the sphincter tone from the appearance in A to that in B within a few minutes.

Assessment of Reflux

During the traditional gastric and duodenal examination, described above, the lower oesophagus is observed and if hiatus hernia or spontaneous reflux is seen, appropriate films (or video frame grab images for less radiation dose) are taken to document this and clearance of any refluxed barium by oesophageal peristalsis is observed.

If there is free reflux throughout the examination as the patient is turned then the diagnosis of advanced disease is easy. If there is no spontaneous reflux it is more difficult, since for most patients reflux is intermittent. Most radiologists therefore will attempt to provoke reflux, but the correlation of the ease of provokable reflux with severity of GERD has never been clarified. The rate of gastric emptying is relevant, since if the stomach is empty of almost all barium it may be hard to demonstrate reflux even in those with a permanently defective sphincter. At the other end of the spectrum, with a very full stomach, provocative manoeuvres can promote a puff or two of reflux in normal individuals.

Provided that plenty of barium remains in the stomach, the patient is placed supine, left side elevated such that the cardia is lying in a pool of barium, and the patient is asked to make a dry swallow. Some patients who do not reflux spontaneously will reflux on dry swallowing. If there is still no reflux, application of abdominal pressure with the patient in the same supine oblique position may elicit reflux. If there is still no reflux, the patient stays in the same position and is given a cup of water to hold and drinks the entire cup through a straw. Normal individuals will often show a small puff or two of reflux of barium while drinking the water, while GERD patients will often flood the entire oesophagus with this provocative manoeuvre. If reflux has occurred, the water cup is taken away and the patient is asked to make a single dry swallow after which the effectiveness of ▶oesophageal clearance of the barium/acid mixture is observed.

Free reflux lying supine with a visibly lax sphincter or repetitive spontaneous reflux to the aortic arch on rolling around with the table horizontal both indicate that the patient has GERD. Reflux to the arch provoked by the patient swallowing water while lying supine with the left side raised (water siphon test) is usually associated with patients with heartburn, with or without a hiatus hernia, but does not indicate advanced disease. Minor reflux to the lower oesophagus with the water siphon test is normal.

Some authors question the value of provocative manoeuvres on the ground that they can make anyone reflux. This however is untrue and also partly misses the point. The vast majority of patients with GERD reflux only intermittently, with occasional LESp collapses. The purpose of this part of the barium study is find out how readily reflux can be provoked by distending the fundus (accepting that a puff or two of reflux into the lower oesophagus with the water siphon test is normal) and just as important, to allow assessment of the effectiveness of oesophageal peristalsis in clearing refluxate. Most patients with advanced GERD have impaired motility with poor

clearance which will reduce the effectiveness of medical treatment and predispose them to need surgery.

If during the examination, oesophageal motility has not definitely been seen to be normal, then at the end the patient is turned prone, left side elevated, and is asked to make a single swallow of barium to assess the effectiveness and completeness of primary oesophageal peristalsis. If not totally efficient, three or four more single swallows are observed, to assess whether there is proximal escape, or whether some other motility disorder may be present. It helps if the radiologist warns the surgeon prior to fundoplication if there is significantly impaired motility as these patients are more likely to develop dysphagia following surgery.

If reflux has been observed some advocate doing a detailed examination of the pharynx at this point, at the end of the examination, to look for any associated pharyngeal incoordination.

Assessment of Clearance of Refluxed Barium and Acid

Dodd's work showed that clearance of refluxed acid in normal subjects is usually by primary peristalsis. Therefore the radiologist wishing to assess clearance must ask the patient to make a single swallow after reflux has occurred and then observe the efficiency of clearance (Fig. 3). Fine grading is difficult, but after two or three swallows it is usually apparent that clearance is either complete (frequently with a single swallow), only partial or that there is very little clearance. A reflux episode of a substantial volume of barium often produces sufficient distension to initiate a secondary peristaltic wave which may also be observed to be either completely or partially effective. If this secondary peristalsis fails to empty the oesophagus, the patient should be asked to make some discrete single swallows so that the effectiveness of primary peristalsis can be assessed

Examination of Patient with Dysphagia or Pharyngeal Symptoms

In these patients, in addition to the standard examination described above, examination of the pharynx is required at the start, motility is assessed towards the end of the study and a solid bolus is used at the end.

The examination starts with the patient standing, at right angles to the table to allow a lateral view of the pharynx. Oblique views of the pharynx should be avoided as they are hard to interpret, but if the shoulders are slightly turned while the neck is maintained in the lateral projection, this allows visualization of the upper oesophagus as well as the lateral view of the pharynx. The unit is set for either rapid sequence digital filming or video-recording, whichever is available. The patient is asked to take in a small mouthful of barium and hold it in the mouth. Recording is started and the patient is asked to swallow. If normal, a larger single swallow is then used. The patient is then positioned for an AP projection and a further swallow is made and recorded. 30 frames/sec video recording will usually show any webs clearly, but these are more readily appreciated with dilute barium and a true lateral projection. For this reason, some radiologists prefer to examine the pharynx at the end of the examination so that they can use dilute barium without impairing coating of mucosa in the early part of the study.

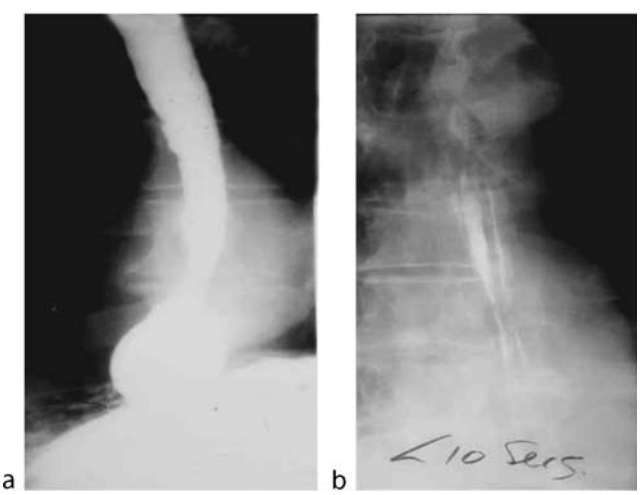

Reflux, Gastroesophageal in Adults. Figure 3 (a) This patient has had a major episode of reflux on dry swallowing while lying supine left side raised, but only a few seconds later (b) complete clearance of the reflux has occurred with a single effective primary peristaltic contraction.

These images will show well any cricopharyngeal bar, premature closure of the cricopharyngeus, or transient mini Zenker's diverticula, as well as any pharyngeal lesions or incoordination, and laryngeal penetration.

The examination then continues with the erect double contrast oesophageal views as described above. Because the erect double contrast views often fail to distend the LES adequately to show a mild Schatzki ring, if the erect views are normal it is important to include the prone oblique views of the LES while swallowing barium. The pathology at this point can be made more apparent by having the patient take and hold a deep inspiration as the bolus passes through the LES segment. Maximal distension can also be achieved by rapid and repeated swallowing of dilute barium in this position. At the end of the examination of a patient with dysphagia, if the cause of the dysphagia has not been clearly demonstrated, a solid bolus swallow must be used. One half of a large marshmallow with a diameter around 18–20 mm (or home made gelatin equivalent) is given to the patient while standing erect, to put in their mouth and try to swallow with a small amount of barium for lubrication and visibility. Some mild encouragement is usually necessary and 90% of patients can after a few tries swallow a bolus of this size. A further mouthful of barium may be required if the first peristalsis only carries it part way down the oesophagus. A positive result occurs if the marshmallow arrests at a point of narrowing, supports a column of barium and reproduces the patient's dysphagic symptoms.

Examination of Patients with Chest Pain

Chest pain is a frequent referral symptom for patients coming for barium meal, often after a stress test or other investigation has 'ruled out' cardiac pathology. Oesophageal disease and musculoskeletal pain are the two remaining likely diagnoses. The standard examinations described above are usually sufficient to assess for reflux disease, but in addition there may also be an explicit request to exclude oesophageal motility disorders such as vigorous achalasia, diffuse oesophageal spasm and nutcracker oesophagus. The former is straight forward as the patients always have dysphagia, and the triad of tight lower oesophageal sphincter, non peristaltic contractions and impaired primary wave usually make the diagnosis of vigorous achalasia straightforward. There is little or no oesophageal dilatation in this early form of achalasia. The retained barium in the oesophagus can be moved on with carbon dioxide gas granules which allows distension of the fundus in order to exclude a cardia neoplasm. Exclusion of diffuse spasm and nutcracker oesophagus can not be achieved by barium meal. The abnormalities may be intermittent and in nutcracker oesophagus in particular the only abnormality may be a super efficient primary stripping wave that leaves not a drop of barium behind. There is no way for the radiologist to tell that this is of very high amplitude. There is sometimes a rather tight LES with poor oesophageal emptying and this may be the only clue that there is pathology present. Manometry is required to make these diagnoses accurately.

The injection of intravenous Tensilon (Edrophonium chloride) sometimes exacerbates the abnormalities in these disorders and produces chest pain, but the test is unreliable. The use of Bethanicol for the same purpose is contraindicated in a radiology department because of the risk of producing cardiac arrhythmias.

Examination of Post Surgical Patients

Patients may have recurrent symptoms post fundoplication or develop dysphagia. The barium examination is useful in these patients. A fundoplication 'mass' may be shown (the size is very variable) and this should be subdiaphragmatic. The usual manoeuvres to induce reflux should not show any in a patient with a successful fundoplication. It is our experience that even the water siphon test does not produce reflux. Fundoplication surgery may fail in several ways and these can usually be identified at barium study (Fig. 4). The whole wrap may slip up into the chest if the anchoring sutures to the diaphragmatic crura pull out. If these sutures hold, the oesophagus may pull free from the stomach and slide up into the chest, often with some kinking of the lower part of the wrap. In this case the upper end of the rugal folds will be pulled up above the wrap. Endoscopy is better at showing that the oesophagogastric junction lies above the fundoplication wrap in some failed fundoplications, but this can also be surmised if gastric folds are seen above the wrap on barium examination. Gastric folds should normally only be seen above the wrap in patients who have had a Collis gastroplasty. Finally, the entire wrap may come undone and there may be no radiological evidence that the patient has had surgery, with recurrence of the hiatus hernia, a lax sphincter and free reflux again.

Some patients complain of dysphagia following a fundoplication; this is common in the immediate postoperative period but should not persist beyond 2–3 months. Barium examination is useful in showing how widely the lower oesophagus opens and a marshmallow swallow can demonstrate hold up (with reproduction of symptoms) at the level of the wrap.. If a tight wrap is demonstrated then patients may require gentle endoscopic dilatation.

Communication Between Radiologist and Patient

Radiologists vary in their practice. Some never discuss results of an examination with the patient leaving this to

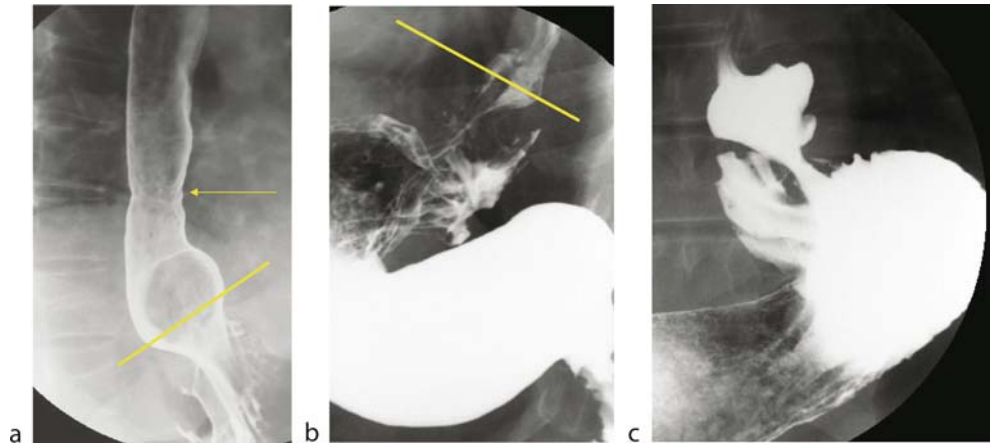

Reflux, Gastroesophageal in Adults. Figure 4 This patient has a failed fundoplication operation. (a) The erect double contrast film shows the hiatus hernia with the upper end of the rugal fold shown by a line, and the lower endo of oesophagitis shown by the arrow. The arrow thus indicates the squamo-columnar mucosal junction, and the area between is Barrett's mucosa. (b) This right side down the lateral film shows the wrap in the upper stomach but again the line shows the upper end of the rugal fold indicating that the wrap has pulled out and stomach is wrapped around stomach. (c) This single contrast view shows the wrap and recurrent hernia but does not provide the detail afforded by the double contrast projection. This case illustrates what often happens when a fundoplication is performed without a Collis gastroplasty in a patient with a short oesophagus (and in this case with Barrett's oesophagus).

the referring doctor, while others always do so. Patients with reflux disease are also variable in their desire for information. Some request information on how their reflux should be managed and this provides the radiologist the opportunity for a brief discussion on the four life style issues that are relevant to exacerbation of the disease. This discussion can be carried out in such a way that it does not impinge negatively on the later discussions between the patient and the referring doctor and these patients are usually grateful that the radiologist has taken the time to explain the findings.

The Radiology Report

The report should have several components. A brief summary of the history and indication for the exam, followed by a description of the anatomy discovered (position of the GE junction, hiatus hernia, post-surgical status). There should be mention of any upper sphincter changes, whether oesophageal motility is normal or not, how readily any reflux was induced, how effective was oesophageal clearance of refluxate and whether gastric emptying was normal or so rapid as to prevent assessment of reflux.

Then secondary findings should be noted if present such as pharyngeal diverticula, pharyngo-oesophageal web, Schatzki ring or stricture, the result of the marshmallow swallow if there was dysphagia and whether evidence of oesophagitis or Barrett's oesophagus was found.

The conclusion should be clear that either there was no evidence of GERD, that there is mild or moderate reflux disease with or without visible complications, or that there is advanced reflux disease with a defective sphincter that may be potentially surgical. If there is clear indication for endoscopy this should also be stated, with the reason for the opinion.

Conclusion

Endoscopy is the prime examination for the investigation of reflux disease in patients being looked after by surgeons and gastroenterologists. In many countries there are long waiting lists for endoscopy while a barium examination can often be obtained quickly. In Canada about one half of patients investigated for reflux disease have a barium study and half have endoscopy. The choice is usually made on logistic grounds rather than on the nature of the clinical problem. Only a minority of patients with GERD have endoscopic evidence of oesophagitis and endoscopy overlooks many of the functional abnormalities that are seen in reflux disease, as well as being less sensitive for detection of minor stenoses. Endoscopy is not an absolute gold standard for the diagnosis of GERD. Indeed, lack of unified sound criteria for the diagnosis or GERD makes the decision between barium study and endoscopy difficult. A study from Cleveland showed that barium study is less costly, especially as only a small number of patients with the final diagnosis of GERD had evidence of oesophagitis.

In specialist units undertaking a significant work load in reflux disease, barium radiology still has a role. Barium examinations give a good overview of oesophageal function and structure, and are particularly helpful in identifying the small number of patients with severe disease who lack any effective lower oesophageal sphincter. Barium radiology will also give a quick and useful assessment of oesophageal motility and identify the pharyngeal complications of reflux disease some of which make endoscopy hazardous.

Bibliography

1. Dent J, El Serag HB, Wallander MA et al (2005) Epidemiology of gastro oesophageal reflux disease: A systematic review 54:710–717
2. Napierkowski J, Wong RKH (2003) Extraesophageal manifestations of GERD. Am J Med Sci 326:285–299
3. Panju A, Farkouh ME, Sackett DL et al (1996) Outcome of patients discharged from a coronary care unit with a diagnosis of "chest pain not yet diagnosed" CMAJ 155:541–552
4. Levine MS (2000) Gastro-oesophageal reflux disease Chapter 21 pp 329–349 In: (eds) Gore RM, Levine MS Textbook of Gastrointestinal Radiology Saunders and co. Philadelphia

Reflux, Vesicoureteral, Adults

Orla Buckley, William C Torreggiani
Department of Radiology, Tallaght Hospital, Dublin, Ireland
williammart@hotmail.com

Definition

Vesicoureteric reflux (VUR) is defined as the retrograde flow of urine from the bladder to the kidneys. It may be divided into primary and secondary types with primary VUR being the predominant process. Primary VUR occurs in the absence of any underlying pathology whereas secondary VUR in the adult occurs due to conditions such as obstruction, previous surgical procedures, or a neurological disorder. The incidence of primary VUR is estimated at 1%. While the condition is well recognised in children, it is less recognised in adults. VUR in adults does, however, account for 10% of patients with end-stage renal disease requiring dialysis or transplantation. With early detection and careful management, this is potentially a preventable end point. Among patients who present with symptomatic urinary tract infection (UTI), the incidence of VUR declines with advancing age: It accounts for 49% of infants under the age of 1 year, 26% of children under the age of 12 years and 4.4% of adults. A family history of the condition is common, with a prevalence of 8–26% of VUR in siblings of a child found to have VUR. Advances in genetic mapping have led to the localisation of the genetic abnormality to chromosome 1. The condition is more common in females with a female to male sex ratio in children usually quoted as 5:1. The female:male ratio found in children may reflect the fact that UTI is more common in girls than boys (except in the first year of life) leading to more investigations and a consequent increased detection of VUR in girls. In adult patients, there is an even greater female preponderance mainly due to two factors: first, as in children, UTIs are more common in females, leading to more investigations and increased diagnosis of VUR. Second, there is an increased likelihood of detection of VUR in young females who become pregnant.

Overall, there are two categories of adult presentation of patients with primary VUR: (i) Patients who have had VUR since childhood that has remained undetected and presents in adulthood with complications. (ii) Patients who develop VUR in adulthood *de novo* with no prior history of UTI. Regarding secondary VUR in adults, it typically occurs secondary to obstruction or to neurological disorders of bladder function (Fig. 1). It may also occur following surgical procedures such as renal transplantation or cystectomy with ileal conduit formation (Fig. 2).

The first descriptions of retrograde flow of urine from the bladder to the kidney came from the 'Prince of Physicians': Galen (130–200 AD) of Pergamon. Later, Leonardo da Vinci (1452–1519) questioned the mechanism of urine formation and was the first to describe and depict the ureterovesical junction. VUR was demon-

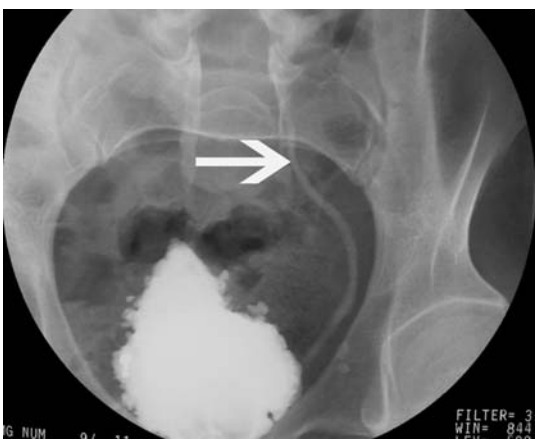

Reflux, Vesicoureteral, Adults. Figure 1 Micturating cystourethrogram in adult patient with known spina bifida and deteriorating renal function. The bladder is irregular in keeping with a neurogenic bladder. There is free reflux seen in the left ureter (*arrow*).

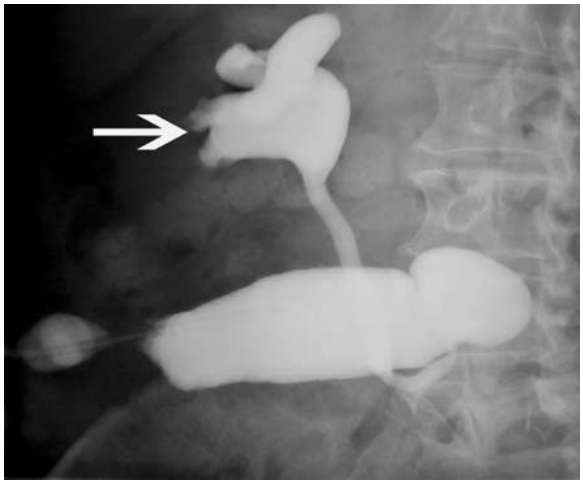

Reflux, Vesicoureteral, Adults. Figure 2 Adult patient with previous cystectomy and ileal conduit formation. Contrast has been infused into the ileal conduit through a Foley catheter inserted into the proximal portion of the conduit. Contrast is seen to reflux freely into the right ureter and collecting system of the right kidney (*arrow*).

strated experimentally in 1903 by Sampson who injected blue dye into the bladder and noticed it subsequently effluxed from the ureter. The condition is caused by a mechanical abnormality at the ureterovesical junction. The ureter in patients with VUR is located lateral to its normal position. The ectopic location of the ureter shortens the normal course of the ureter within the detrusor muscle. This leads to incompetence of the normal valve-like closure system when the intravesical pressure rises on filling and micturition.

Clinical Presentation

VUR may be asymptomatic. The most common presentation is with the symptoms and signs of UTI and/or pyelonephritis. Symptoms are often non-specific and include a feeling of being generally unwell, tired, lack of energy, anorexia, nausea, vomiting and pyrexia. Dysuria and frequency as well as bladder discomfort may also be present. The majority of females diagnosed with VUR initially present with a UTI. Some females may be asymptomatic and have incidental bacteria noted on urinalysis. Males more commonly present late with symptoms of complications of VUR and reflux nephropathy such as hypertension and proteinuria. The increased UTI rate in females is explained by the anatomical differences between the male and female urethra such as the shorter length of the female urethra and the proximity of the urethral orifice to the vagina and anus. Pregnancy and reflux nephropathy have profound effects on each other. More than half of pregnant females with VUR experience complications during pregnancy. Physiological dilatation of the urinary tract and increased glomerular filtration predispose the pregnant mother with VUR to UTI, eclampsia and progression of renal disease. Pre-conception renal function has a significant impact on pregnancy related complications.

Diagnosis

The spectrum of clinical presentations of adults with VUR is very broad. A screening programme for this condition is not feasible. VUR should be considered in adults with recurrent UTIs, pregnant females with UTI, proteinuria or pre-eclampsia, and patients with unexplained renal failure. Initial evaluation should include blood pressure assessment and biochemical assessment of renal function including serum creatinine, creatinine clearance and 24 h urinary protein assessment. Preliminary radiological investigation includes micturating cystogram to detect reflux followed by ultrasound and DMSA to evaluate for secondary changes of VUR. In the case of a pregnant female, MRI permits evalution of the renal system without exposure to ionising radiation.

Much attention is paid currently to the workup of patients who present with hypertension in search of a treatable cause. Though 95% of cases are idiopathic, if a cause can be identified and treated the complications of hypertension such as stroke and renal failure can be reduced. It is believed that up to 20% of adult patients with hypertension who have no evidence of renal involvement on routine work up may have undiagnosed VUR. If VUR remains undiagnosed, these patients are then erroneously categorised as having essential hypertension.

Imaging

Micturating Cystourethrogram

The gold standard test in making a diagnosis of VUR is a micturating cystourethrogram. With this examination, contrast is instilled into the bladder and the patient then micturates while the radiologist visualises the process with fluoroscopy. In the normal person, contrast (urine) should remain in the bladder during the full procedure and not reflux into the ureters. If reflux is present, its level of reflux is classified according to a designated grading system. There are several classification systems of VUR. The International reflux grading system is probably the best recognised. Depending on the degree of retrograde filling and dilation of the renal collecting system as seen at micturating cystogram; the International reflux grading system classifies VUR into five grades: (Fig. 3).

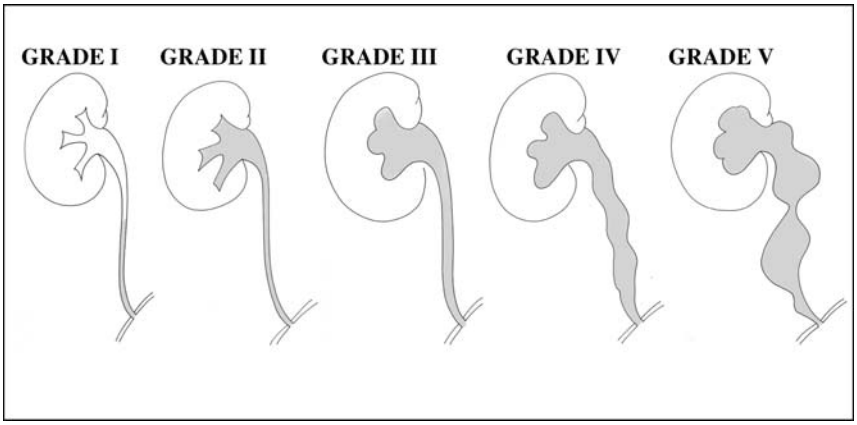

Reflux, Vesicoureteral, Adults. Figure 3 Diagrammatic representation of the International reflux grading system. VUR is classified into five grades. (Courtesy of Tony Geoghegan)

1. Grade I: Urine refluxes into the ureter only with normal renal pelvis and calyces
2. Grade II: Urine refluxes into the ureter, renal pelvis and calyces but they appear normal
3. Grade III: Urine refluxes into the ureter and collecting system. The ureter appears mildly dilated and there is evidence of some blunting of the calyces
4. Grade IV: Urine refluxes into the ureter and collecting system. Evidence of moderate dilatation of the ureter and moderate blunting of the calyces
5. Grade V: Urine refluxes into the ureter and collecting system. The pelvis appears severely dilated and the calyces are severely blunted. The ureter appears very dilated with a tortuous course.

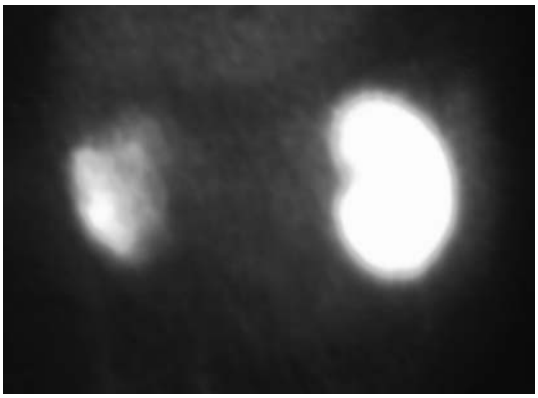

Reflux, Vesicoureteral, Adults. Figure 4 ^{99m}Tc-DMSA renogram in a patient with chronic reflux disease demonstrates marked parenchymal loss and scarring of the upper pole of the right kidney.

Nuclear Medicine

Nuclear medicine techniques permit direct and indirect evaluation of VUR as well as assessment of renal scarring secondary to VUR. Reflux may be detected by both direct and indirect techniques. With direct radionuclide cystography, the bladder is infused with 500 mL of saline mixed with ^{99m}Technetium labelled sulphur colloid *via* a catheter. The bladder is filled and the patient subsequently micturates under direct visualisation of the gamma camera. Any nuclide appearing in the ureters and kidney is abnormal and diagnostic of reflux. With indirect radionuclide cystography, a standard renogram is initially performed. Twenty minutes following this, when the patient feels the need to micturate they are asked to do so in front of the gamma camera. The radio labelled urine in the bladder is monitored and any amount of refilling at the end of micturition is suggestive of VUR.

Technetium labelled DMSA is used to illustrate the size, shape and position of the kidneys and also to identify scarring or thinning of the cortex (Fig. 4). DMSA scanning has a sensitivity of 87% in detecting changes in the renal parenchyma and is more sensitive than US in this regard. The changes seen at DMSA may be transient in patients with acute pyelonephritis. DMSA imaging also plays a complementary role to US in the follow-up of renal transplants. VUR is relatively common in transplanted kidneys. Although it is controversial as to whether VUR does equivalent damage in transplant kidneys as in native kidneys, both DMSA imaging for scarring as well as dynamic renal scintigraphy scans using radio labelled DTPA or MAG-3 for renal function are both useful modalities to assess the transplanted kidney.

Ultrasound

Ultrasound is an inexpensive, widely available technique that can be used to screen for reflux. Ultrasound permits assessment of renal size, shape, cortical abnormalities as well as ureteric abnormalities. A dilated system and

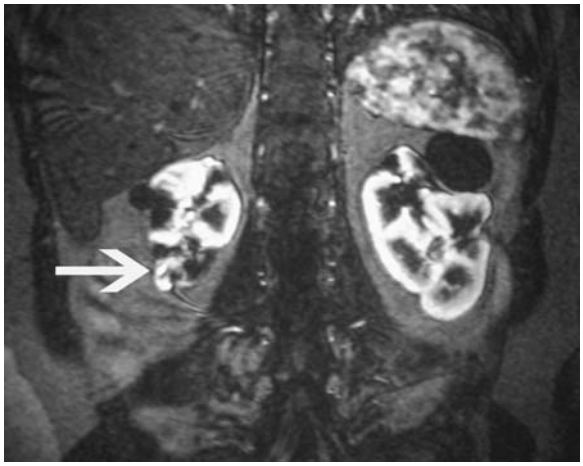

Reflux, Vesicoureteral, Adults. Figure 5 3D Gadolinium-enhanced source image using a fast low angled shot (FLASH) protocol in a patient with VUR demonstrates marked scarring of the lower pole of the right kidney (*arrow*). Non-enhancing simple cysts are incidentally noted in both kidneys.

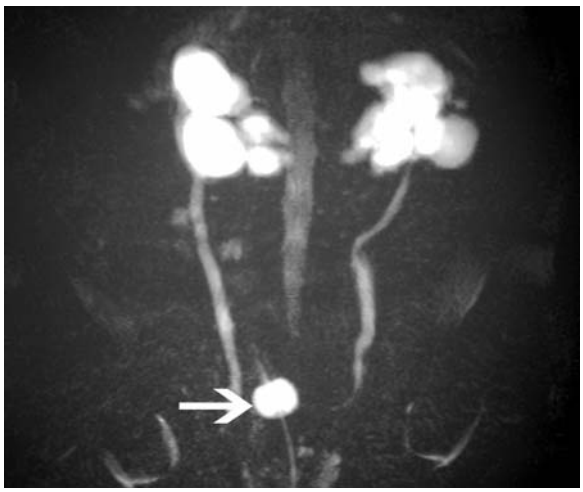

Reflux, Vesicoureteral, Adults. Figure 6 Coronal multiple intensity projection (MIP) in a patient with a known horseshoe kidney image using a fluid sensitive HASTE magnetic resonance urography (MRU) protocol demonstrates a Foley catheter in the bladder (*arrow*) with dilatation of both ureters and the collecting system of the kidneys in keeping with reflux disease.

scarring in the appropriate clinical context are predictors of reflux and if needed, patients may proceed to a formal micturating cystourethrogram. Initial studies with ultrasound however showed that it was not a sensitive method for the diagnosis of VUR. Recently, some authors have advocated the use of echo-enhanced cystosonography in the diagnosis of reflux. With this method, a galactose suspension of fluid is instilled into the bladder and the presence of reflux is detected by continuous scanning. Advantages of ultrasound include the absence of ionising radiation as well as better anatomic resolution compared with radionuclide studies. Limitations included poor sensitivity at detecting grade 1 reflux as well as the length of time required for the procedure.

Intravenous Pyelogram

The role of intravenous pyelogram is rapidly decreasing in assessing the patient with VUR. It may detect secondary changes of VUR but does not provide a dynamic assessment of the refluxing urine. Secondary changes include evidence of parenchymal scarring, calyceal clubbing, ureteric dilatation and mucosal striations.

CT/MRI

Multi-slice CT with multi-format reconstructions can illustrate the renal tract and any secondary changes that have results from chronic VUR. CT does, however, expose the patient to considerably more radiation than other techniques for the evaluation of this condition. MRI on the other hand is a radiation-free technique a particular advantage when the pregnant female requires evaluation. As well as conventional sequences, the addition of heavily T2-weighted HASTE sequences results in MR urographic images that are highly fluid sensitive and allow evaluation of the collecting system of the urinary tract particularly when the system is dilated (Figs. 5 and 6).

Conclusion

VUR is less recognised in the adult than the child and still accounts for a significant proportion of patients with end-stage renal failure entering the dialysis pool. Imaging plays a key role in making the diagnosis. Although traditional modalities such as nuclear medicine studies and micturating cystourethrograms continue to play a key role in the evaluation of VUR, cross-sectional imaging and especially MRI will play a greater role in the future.

Bibliography

1. Becker GJ (1985) Reflux nephropathy. Aust N Z J Med 15:668–676
2. Bouchot O, Guillonneau Cantrovich Hourmant M, Le Normand L, et al (1991) Veiscoureteric reflux in the renal transplant candidate. Eur Urol 20:26–28
3. Cataldi L (1997) From the matula to the radio-immunological essay: the evolution of the urine analysis. Il Pediatra XIX(7):19–20
4. Tubaro A (2000) Vesicoureteric reflux: the evolution of the understanding of the anatomy and the development of radiology. Curr Opin Urol May 10(3):259–260

5. Torres VE, Malek RS, Svensson JP (1983) Vesicoureteric reflux in the adult II. nephropathy, hypertension and stones. J Urol 130:41–44
6. El Khatib M, Packham DK, Becker GJ, et al (1994) Pregnancy related complications in women with reflux nephropathy. Clin Nephrol 41:50–55

Reflux, Vesicoureteral, Childhood

M. Riccabona, R. Fotter
Division of Pediatric Radiology, Medical University of Graz, University Hospital, Graz, Austria
michael.riccabona@meduni-graz.at
richard.fotter@meduni-graz.at

Synonyms

Vesicoureteric or vesicoureteral reflux; Vesicoureterorenal reflux

Definition

►Vesicoureteral reflux (VUR) is defined as reflux of urine from the urinary bladder into the ureter and up to the renal collecting system, with potential "intrarenal reflux" into the distal tubules—particularly at the compound papilla—with consecutive segmental renal damage and development of renal scarring by ascending urinary tract infection (UTI).

Embryology and Pathogenesis

There are several *causes* for VUR, with different entities and appearances in boys or girls, and a potential familial predisposition. First, there is primary or congenital VUR, caused by immaturity of the mechanisms at the ureterovesical junction, such as a short intramural tunnel that hinders sufficient valve mechanism at the junction, or a lateralized or pathologically configured ostium. Another form of congenital VUR is the severe, even bilateral VUR with intrauterine renal damage and dysplastic elements ["congenital ►reflux nephropathy (RNP)"] that usually is seen in baby boys. Low-grade VUR without (initial) renal scarring is seen particularly in school girls. Additionally, there is secondary VUR, for example, in bladder dysfunctions (particularly when there is an increased bladder pressure leading to a decompensation of the valve mechanism at the ureterovesical junction as in a neurogenic bladder or high-grade dysfunctional voiding) or in bladder outlet obstruction (e.g., caused by urethral polyp, posterior urethral valves). The congenital, typically short-lasting, high-pressure, low- to medium-degree VUR during voiding has a high tendency to diminish spontaneously and eventually disappear, whereas high-grade VUR with congenital RNP in baby boys, VUR in anatomic malformations at the ureterovesical junction, and secondary VUR persist and only improve after treatment of the underlying bladder condition and/or relief of the obstruction. Usually, surgical options must be considered (e.g., PUV, urethral polyp, Hutch's diverticulum, golf hole, or lateralized ostium, etc.).

The *long-term sequelae* of VUR depends on some basic factors. First, the amount of preexisting renal dysplasia or congenital RNP (probably due to a combined dysplastic growth of renal tissue and "water hammer" effects of ongoing high-grade and high-pressure VUR during fetal life causing mechanical damage to the renal units). Second, renal parenchymal changes secondary to recurrent UTI with renal involvement (upper UTI) and consecutive scarring, which may lead to hypertension and—if severe and bilateral—to renal insufficiency. Bladder dysfunction may be another predisposing factor maintaining the risk for UTI and preventing VUR resolution.

Clinical Presentation

VUR itself has no clinical symptoms; all forms of presentation derive from secondary phenomena such as UTI, renal scarring or renal insufficiency, or bladder function disturbance. VUR has increasingly been picked up by (fetal) screening investigations. VUR *management* consists of regular urine checks, at least, with early treatment of any UTI; the present widely performed antibiotic prophylaxis is under discussion. Surgical options are cystoscopic injection of material into the bladder wall at the ureterovesical junction (e.g., Macroblast®, silicon, teflon, myoblasts, etc.) or open surgical antireflux procedures with different techniques leading to a reimplantation of the ureter and reformation of a longer intramural ureteral tunnel, thus preventing VUR.

Imaging

In light of new insights into the etiology and pathogenesis as well as the sequelae of VUR, the diagnostic and therapeutic concept is presently undergoing significant changes toward less generalized and less invasive imaging, which—if indicated—is aimed at those patients who have an increased risk of renal damage or have already suffered renal scarring. Furthermore, a wider range of partially new imaging techniques have increasingly been accepted for VUR diagnosis and have thus impacted imaging algorithms.

Imaging procedures: The gold standard imaging technique for VUR is still *voiding cystourethrography* (VCUG). This is performed after catheterization of the bladder (usually transurethral, sometimes suprapubic), mild (nasal) Midazolam sedation may be used. Ideally, the bladder should be empty before instilling the radiopaque contrast material *via* infusion. The infusion speed and pressure should be as physiological as possible to allow a more or less physiologic imaging situation with additional functional information by observing infusion speed and potential stops of the contrast infusion indicating moments of increased bladder pressure (e.g., in bladder instability or premature detrusor contraction during filling). Furthermore, to grant a high VUR detection rate, patients may be fastened for several hours. Particularly during the first years of life, cyclic VCUG with at least three fillings is recommended. Filling, voiding, and the postvoid situation are evaluated fluoroscopically with child-adapted digital fluoroscopy units using pulsed fluoroscopy. No blinded films should be taken. Fluoroscopy-guided spot films can be taken to document the anatomy of the distal ureter and the ureterovesical junction in lateral or oblique views (Fig. 1a). Furthermore, spot films are helpful for evaluating intrarenal reflux and properly assessing the anatomy of the urethra (lateral film) (Fig. 1b). All other information (time, degree and side of VUR; residual volume; postvoid urinary drainage) can be assessed and documented by images taken with digital fluoroscopy without additional exposures (Fig. 1c). VUR is radiographically graded into low- and high-pressure VUR (depending on when it occurs: at low bladder or high/increased bladder pressure such as during voiding), VUR during filling or voiding, VUR in an anatomically normal bladder and ureterovesical junction or in patients with malformations such as diverticula or duplex systems, and the degree of VUR (grade I is the VUR into the distal ureter, grade II is the VUR up to the renal pelvis, grade III is the VUR into the calices, grade IV is the VUR into a dilated system, grade V is the VUR into a grossly dilated system with ectatic ureter, pelvis, and calices) (Fig. 2).

Radionuclide cystography (RNC) uses radioactive tracers instilled in the urinary bladder for VUR detection. Direct RNC uses catheterization of the bladder to instill the radioactive tracer, with any activity in the ureter or the renal collecting system demonstrating clear evidence of VUR. Indirect RNC is performed during late phases of a dynamic renography at full bladder capacity and particularly during or after voiding. The tracer is the intravenously applied Tc^{99m}-labeled MAG3 that is excreted and transported into the bladder by physiological pathways after application for dynamic renal scintigraphy, with an increased activity over the proximal ureter and the renal pelvis in late phases in VUR. Indirect RNC is a more physiological approach, but only applicable to cooperative and toilet-trained children. In general, RNC has lower radiation burden at the cost of decreased anatomic resolution and less grading potential, although a certain amount of grading can be achieved. This method is usually used for screening and for follow-up studies, particularly in girls.

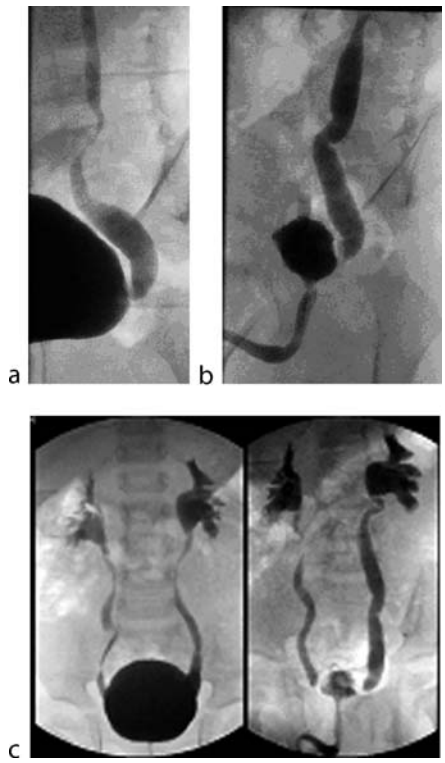

Reflux, Vesicoureteral, Childhood. Figure 1 VUR demonstration on VCUG (a) Refluxing ureterovesical junction in a lateral oblique view on a conventional VCUG image (b) Neonatal male urethra in lateral view during voiding with eminent VUR (c) Bilateral VUR documented by a fluoroscopy images; VCUG images taken at full bladder capacity and after voiding: note VUR increase during voiding.

The third method for VUR evaluation, which is increasingly gaining importance, is *contrast enhanced cysto(uro)sonography* (ee-US). It uses ultrasound (US) contrast material which is instilled into the urinary bladder *via* catheterization to demonstrate VUR. By constant scanning of the bladder and the retrovesical space as well as—alternating—the renal collecting system and the proximal ureter, VUR of contrast material into the upper urinary collecting system can be detected and demonstrated. Modern US techniques such as harmonic imaging or high- and low-mechanical index (MI) contrast-specific imaging features (contrast pulse sequencing, stimulated acoustic emission (SAE)) may be applied to enhance VUR

detection (Fig. 3). Furthermore, simultaneous evaluation of the renal pelvis, the kidney parenchyma, and other surrounding structures as well as nonrefluxing dilated urinary tracts is achieved. A grading similar to that for VCUG has been suggested, additionally incorporating the unenhanced US image information such as preexisting dilatation of the upper urinary tract or parenchymal lesions. Similar to fluoroscopic VCUG, cyclic evaluation is recommended in neonates and infants, and evaluation during and after voiding for detection of high-pressure VUR and validation of residual volume and urine drainage dynamics is obligatory. The method, however, is only applicable in

According to the *international system of radiographic grading of vesicoureteric reflux*
(Lebowitz RL, Olbing H, Parkkulainen KV et al, 1985. International Reflux Study in children: International system of radiographic grading of vesico-ureteric reflux. Pediatr Radiol 15: 105-109)

Grade I:	VUR limited to the ureter
Grade II:	VUR up the renal cavities without dilatation
Grade III:	VUR into the renal cavities inducing dilatation and eversion of the calices
Grade IV:	Moderate to marked dilatation of the ureter and pyelocaliceal system
Grade V:	Marked tortuosity and dilatation of the ureter and pyelocaliceal system

Reflux, Vesicoureteral, Childhood. Figure 2 VUR grading.

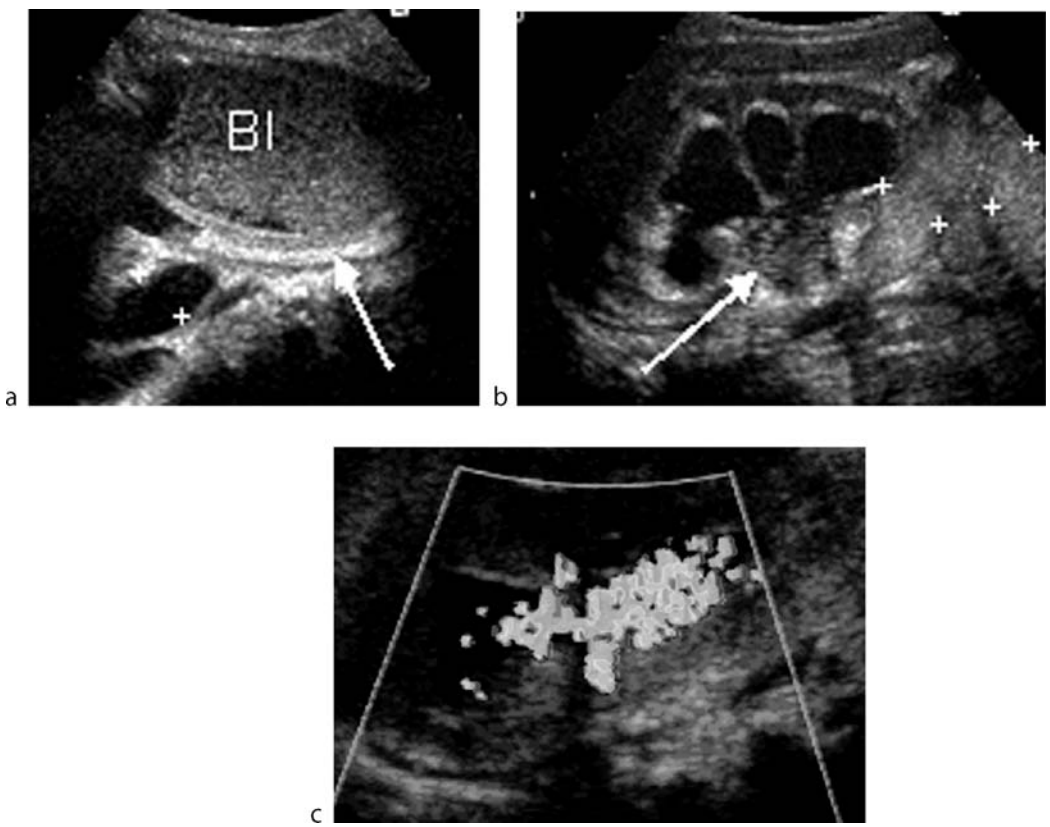

Reflux, Vesicoureteral, Childhood. Figure 3 cm-US demonstrated by these serial US images of the urinary bladder and the kidneys (a) Echogenic content of the urinary bladder (Bl) after filling with saline and contrast material (Levovist®) and echo-poor distal dilated ureter (+ +). (b) Hydronephrotic kidney with beginning of contrast inflow into the renal pelvis (=>) from a contrast medium-filled echogenic dilated ureter (+ +). (c) Color Doppler sonography with high mechanical index improves contrast depiction by causing sparkling color signals by bursting contrast bubbles ("SAE"2 or "burst mode").

countries where US contrast material is approved for pediatric use. The benefit of ee-US is not only the simultaneous visualization of the collecting system and the renal parenchyma, but also that US is free of ionizing radiation. Setbacks are restricted visualization of the urethra, a less panoramic display of the entire urinary tract, and the lack of anatomic information about long parts of the ureter. Additionally, restricted availability, a suboptimal visualization of the urethra, a lower sensitivity toward short-lasting first-grade VUR and diverticula (which may only arise during or at the end of voiding), as well as less functional information must be acknowledged. Some of these aspects can be partially overcome using novel scanning techniques such as a perineal approach during voiding for evaluation of the posterior urethra. Indications for ee-US are screening conditions, VUR evaluation in girls, and follow-up examinations. However, particularly in infant boys, VCUG with accurate anatomic evaluation of the urethra seems to be irreplaceable.

Indications for VUR assessment: VUR evaluation at present is indicated in UTI in neonates and infants up to 2 years of age and (recurrent) upper UTI in children (particularly with renal damage or scarring), urinary tract malformations that are accompanied by a higher risk of VUR (i.e., duplex system, ureterocele, multicystic dysplastic kidney, complex malformation, etc.), a dilated upper urinary tract such as megaureter and hydronephrosis (for differentiation of obstructive vs. reflexive disease), children with bladder diverticula, bladder dysfunction (with recurrent infections), and other (systemic) conditions with a potential involvement of the urinary tract (e.g., myelomeningocele with neurogenic bladder). Furthermore, a follow-up evaluation or postoperative reassessment may be indicated particularly in patients with ongoing symptoms, with a VCUG being recommended in all situations in which the most anatomic information is mandatory, such as in preoperative assessment.

Diagnosis

Diagnosis and grading are entirely based on imaging using the earlier-described features for the various methods.

Bibliography

1. Avni FE, Hall M, Damry N et al (2002) coureteric Reflux. In: Fotter R (ed) Pediatric Uroradiology, Springer, Berlin, New York, pp 145–160
2. Berrocal T, Gaya F, Arjonilla A et al (2001) Vesicoureteral reflux: Diagnosis and grading with echoenhanced cystosonography versus voiding cystourethrography. Radiology 221:359–365
3. Fernbach SK, Feinstein KA, Schmidt MB (2000) Pediatric VCUG: A pictorial guide. Radiographics 20: 155–168
4. Lebowitz RL (1992) The detection and characterisation of VUR in the child. J Urol 148:1640–1642
5. Riccabona M (2005) Vesico-ureteral reflux. In: Carty H, Brunelle F, Stringer D et al (eds) Imaging Children, 2nd edn. Elsevier Science Publisher, pp 671–690

Regenerative Nodule, Hepatic

Nodules of regenerating hepatocytes in a cirrhotic liver. Regenerating nodules may vary from micronodules (lesser than 3 mm in diameter) to macronodules (3 mm to several centimeters in diameter). They determine a typical superficial nodularity of the liver surface appreciable at ultrasound US, computed tomography CT and magnetic resonance MR. Larger nodules may be visibile as distinct nodules and need to be differentiated from dysplastic nodules and hepatocellular carcinoma (HCC). Regenerative nodules do not have an arterial blood supply. At contrast US, CT and MR studies they usually appear hypoenhanced, sometimes isoenhanced, in the arterial phase, hypo-isoenhaced in the portal–venous phase, while in the delayed phase they are more easily depicted as hypoenhanced nodules. MR is much more sensitive than CT in demonstrating regenerative nodules, especially when they contain iron (siderotic nodules). Typically, regenerative nodules appear as small (<2 cm) nodular lesions, with low signal intensity on T2-weighted images and variable signal intensity on T1-weighted images. When they contain iron they appear hypointense both on T1-weighted and in T2-weighted scans. In some cases, regenerative nodules may present increased signal intensity on T1-weighted images due to high triglyceride content in zones of fatty degeneration. They are never hyperintense on T2-weighted images.

▶Cirrhosis, Hepatic

Regional Ileitis

▶Crohn Disease

Regional Osteoporosis

Regional osteoporosisis an unspecific finding occurring, for example, in disuse, neighborhood inflammation, and arthritis. In the periarticular distribution, it refers to the old term of collateral phenomenon.

▶Connective Tissue Disorders, Musculoskeletal System

Regional Recurrence

Recurrence that is located in close areas around the same breast. Most frequently, this event occurs in the axillary lymph nodes or well in the pectoral muscles, internal mammary lymph nodes, or cervical or supraclavicular nodes.

▶Recurrent Neoplasms, Breast

Regurgitation

Regurgitation of recently swallowed food with acid into the mouth.

▶Reflux, Gastroesophageal in Adult

Relapsing Polychondritis

It is an uncommon and severe episodic inflammatory condition involving cartilaginous structures, predominantly those of the laryngotracheobronchial tree. Chondritis weakens the tracheal cartilage rings, resulting in wheezing, dyspnea, cough and hoarseness. The airways eventually become stenosed and are replaced by collapsible fibrotic tissue. Chest radiography will demonstrate tracheal stenosis, calcification of cartilaginous structures and coexisting systemic vasculitis may be revealed by the presence of pulmonary infiltrates. CT or MRI will readily identify tracheal and bronchial thickening, inflammation, stenosis and calcification, as well as airtrapping and diffuse or focal thickening of the airways.

▶Airway Disease

Renal Artery Stenosis

Decrease of arterial lumen diameter due to atherosclerosis or fibromuscular dysplasia. It is the main cause of renovascular hypertension. It may also be responsible for artherosclerotic (or ischemic) nephropathy.

▶Hypertension, Renal
▶Stenosis, Artery, Renal

Renal Artery Stenosis (RAS)

▶Stenosis, Artery, Renal

Renal Carbuncle

Multiple coalescent intrarenal abscesses due to hematogenous spread, usually caused by *Staphylococcus aureus*.

▶Pyelonephritis, Acute

Renal Cell Carcinoma

Renal cell carcinomas (RCC) are clinically, histologically and genetically a heterogeneous group of tumors involved the kidney.

▶Carcinoma, Renal Cell

Renal Colic

Sharp pain in the lower back that radiates into the groin, associated with the passage of a renal calculus through the ureter.

▶Stone Disease, Urinary
▶Colic, Acute, Renal

Renal Corticomedullary Abscess

▶Abscess, Renal

Renal Cysts

▶Cystic Disease, Renal Childhood (MCDK, PCKD)

Renal Dysplasia

A congenital condition with an impaired development of the renal parenchyma leading to cystic and cartilaginous or fibrous lesions in the kidney and usually accompanied by renal functional impairment as well as restricted growth potential.

▶Congential Malformations, Geni tourinary Tract; Including Ureter and Urethra

Renal Failure

Condition where the kidneys fail to function properly. Physiologically, renal failure is described as a decrease in the glomerular filtration rate. Clinically, this manifests in an elevated serum creatinine. It can broadly be divided into two categories: acute renal failure and chronic renal failure.

▶Glomerulonephritis

Renal Infarction

This results from renal arterial occlusion and produces a pale area of ischemic renal tissue. Some blood supply from capsular vessels is responsible for the presence of a viable subcapsular band of cortex.

▶Infarction, Renal

Renal Osteodystrophy

End-stage, chronic renal failure leads to a bone disease characterized by secondary hyperparathyroidism, osteomalacia, and osteoporosis. Chronic hemodialysis may also cause aluminum-induced bone disease and deposition of amyloid.

▶Hyperparathyroidism

Renal Tuberculosis

Chronic infection produced as a consequence of the hematogenous spread of *Mycobacterium tuberculosis*, usually from the lungs.

▶Pyelonephritis, Chronic

Renal Tubular Ectasia

▶Medullary Sponge Kidney

Renovascular Disease

Complex entity involving renal arterial lesions, renal disease, and hypertension. The relationships between these three entities are variable from patient to patient and difficult to assess.

▶Hypertension, Renal

Renovascular Hypertension

Reversible and infrequent cause of hypertension secondary to a decrease in renal perfusion pressure, which activates the renin–angiotensin system and causes renovascular hypertension. It is curable by renal revascularization.

▶Hypertension, Renal
▶Stenosis, Artery, Renal

Replenishment

The dynamic refilling of a capillary bed in parenchymatous tissue after transient destruction of the micro-bubbles of an ultrasound contrast agent. The specific interaction of the micro-bubbles with the incident ultrasound wave allows the transient destruction with a high energy ultrasound pulse (flash or burst). After clearance of the micro-vessels, the immediate refill (replenishment) with contrast agent already present in the feeding arteries outside of the image plane allows the realtime assessment of micro-vascular flow independently from the cardio-pulmonary transport of the agent.

▶Contrast Media, Ultrasound, Commercial Products

Reporter Gene

Genetically encoded DNA sequences that allow the expression of reporter

▶Reporter Systems

Reporter Systems

Carmel T. Chan, Sanjiv Sam Gambhir
Department of Radiology, Molecular Imaging Program at Stanford (MIPS) and Bio-X Program, Stanford University School of Medicine, Stanford, CA
carmelc@stanford.edu
sgambhir@stanford.edu

Definition

Reporter systems in the context of imaging are methods that allow the detection of one or more biological/molecular events.

Imaging

Reporter Gene

A reporter gene allows the imaging of gene expression in cell culture and in living subjects. It can be directed at genes externally transferred (transgene) into cells and organ systems (See Applications of Direct Imaging in "Direct Imaging".) or at endogenous genes (See Applications of Indirect Imaging in "Indirect Imaging".). In all cases, expression of the reporter gene can be tracked using different imaging modalities and confirmed using standard techniques, including but not limited to reverse transcription-polymerase chain reaction (RT-PCR), Northern blotting, Western blotting, immunohistochemistry and flow cytometry.

Characteristics of an ideal reporter gene/probe for imaging in living subjects include: (a) The reporter gene should be present in the mammalian cells (but not normally expressed otherwise it would lead to background signal) or if an exogenous reporter gene is used, the gene product should be not be expressed on the cell surface in order to prevent an immune response, (b) the accumulation of the reporter probe should be site-specific, (c) the reporter probe should be stable in the living subjects and not be metabolized before reaching its target, (d) the reporter probe and its metabolites should not be toxic in the living subjects, (e) the reporter probe should have good pharmacokinetics, including rapid clearance from circulation and nonspecific sites and noninterference with specific signal detection, (f) the reporter gene with the promoter should be small enough to fit into a delivery vehicle, (g) the reporter probe should be able to reach its destination instead of hindered by natural biological barriers (e.g., the blood brain barrier), and (g) good correlations between level of reporter gene mRNA expression and reporter probe (protein) expression in living subjects.

To deliver the reporter gene in to the cell type of interest, a complementary DNA expression cassette containing the reporter gene of interest is often used. The reporter gene can be driven by different promoters (including constitutive, inducible, endogenous and cell-specific) to allow temporal and spatial control of gene expression. Transcription and subsequent translation of the gene product into an enzyme or a receptor product, and in the presence of a substrate of an enzyme or a ligand for a receptor, an imaging signal is produced. The trapping and/or catalyzing of the imaging probe leads to an imaging signal, which can be in the form of a radioisotope (detected by positron emission tomography [PET] and single photon emission computed tomography [SPECT] imaging), See Applications of Reporter Systems: Small Animals PET and SPECT, a photochemical reaction (detected by bioluminescence imaging) or a magnetic resonance metal cation (detected by MRI) or other techniques (e.g., Ultrasound).

Classification of Reporter Systems

Reporter systems can be classified into two categories according to the location of the reporter gene products: intracellular and cell membrane-based (1).

►Intracellular reporter systems utilize gene products that are present within the cells. Intracellular reporter systems include enzyme-based bioluminescence imaging (Firefly, Renilla and Gaussia luciferase), fluorescence-based imaging (green fluorescent protein [GFP], monomeric red fluorescence protein [mRFP]), (PET) imaging (Herpes Simplex Virus Type 1-thymidine kinase [HSV1-TK] with 8-[^{18}F]fluoropenciclovir (^{18}F-FPCV), ^{124}I- or ^{131}I-labeled 2′-fluoro-2′-deoxy-1-β-D-arabinofuranosyl-5-iodouracil (FIAU), 9-[4-[^{18}F]fluoro-3-(hydroxymethyl) butyl]guanine (^{18}F-FHBG) as substrate and cytosine deaminase with 5-fluorouracil as substrate), as well as SPECT with different radioactive tracers and MRI with different contrast agents. The advantages of intracellular reporter system include relatively uncomplicated expression strategy, lower likelihood of immunogenicity since the product is intracellular and therefore less likely to be recognized by the immune system, the ability to achieve specificity by controlling the expression of the reporter genes and signal amplification for enzyme-based reporter probes (since many imaging probes can be trapped for each reporter enzyme).

Cell membrane-based reporter systems utilize gene products that are associated with the cell membrane, such as cell-surface receptors. Extracellular reporter systems can also be applied for PET imaging and MRI. For example, dopamine 2 receptor (D_2R), somatostatin receptor and

sodium iodide symporter can be used for PET/SPECT imaging. Other engineered receptors that consist of a membrane-anchoring domain and a binding domain for the radiolabeled isotopes can also be used for PET imaging. On the other hand, transferrin receptor can be used as an intracellular transporter of iron oxide nanoparticles for MRI imaging. Advantages of extracellular reporter systems that are associated with cell membrane includes favorable kinetics, and no requirement for tracer uptake into cells and the ability to engineer reporters that can recognize approved imaging probes.

Applications of Reporter Systems

Reporter genes can be used to monitor the location(s), magnitude, and time variation of reporter gene expression and to target a specific biological process or pathway in intact living animals and humans. They can also be used to study promoter/enhancer elements involved in regulation of gene expression, examine induction of gene expression using inducible promoters, and examine endogenous gene expression by fusing endogenous promoters to a reporter gene.

1. Gene marking of static (unchanged location such as non-metastatic tumor xenografts) and trafficking cells (cells that migrate or metastasize considerable distances from the point of origin) to follow the behavior and location of cells in living subjects. Gene marking can be achieved by first introducing the reporter gene by *ex-vivo* stable transfection of the vector containing an imaging cassette into cells of interest prior to implantation/transplantation in living subjects such that the reporter gene is always expressed. This will allow the tracking of the cells and their progeny for their entire life span within the living subjects assuming there is no silencing of the reporter gene. Transient transfection of cells can also be used for *ex-vivo* gene marking of cells for short-term follow up (7–10 days), depending on the cell type and other parameters. Gene marking of the reporter gene in the living subjects can also be accomplished through tail vein or intraperitoneal injection of the vectors carrying the reporter gene along with the recombinant genome of viruses into the cells of interest within the living subjects. Gene marking can also be used for understanding the localization and quantification of viral accumulation in living subjects that will facilitates analysis of viral and host interactions using suitable viral vectors.
2. Imaging of gene therapy—Molecular imaging of reporters in combination with particular therapeutic genes could be critical in achievement and optimization of controlled and effective gene delivery to target cells and avoidance of expression in non-target tissues. The therapeutic gene and the reporter gene can be linked together using a fusion protein approach, in which their coding sequences fused together in the same reading frame and the expression between the therapeutic gene and the reporter gene will be coordinated at the protein level. Likewise, using a bicistronic vector, an internal ribosomal entry site (IRES) can be inserted in between the therapeutic gene and the reporter gene are expressed from the same promoter such that the expression between the two genes can be coordinated at the transcriptional level and each protein will be translated separately. Likewise, the two therapeutic can be coexpressed from distinct promoters within a single vector, two different vectors with the same promoter, or a bidirectional single vector in which the expression of the two genes are driven by the same promoter but in opposite directions (2). The levels, location and duration of the therapeutic gene expression can then be quantitatively assessed by imaging of the reporter gene. The ability to monitor expression of the therapeutic gene using the reporter gene can be generalized for different therapeutic genes of interest, and thus allow insights into cancer biology as well as the location, spread and persistence of the viral vector in patients undergoing gene therapy.
3. Indirect Imaging of endogenous gene expression—In order to utilize reporter system to study gene expression in transgenic animals, the reporter gene is stably integrated into the genome and its expression can be controlled by different promoters of choice. Using this approach, one can indirectly image expression of endogenous genes using a cell/tissue specific promoter to drive expression of reporter gene (e.g., HSV1-TK with PET and luciferase with bioluminescence imaging (3) and characterize the role of different promoter elements in regulation of gene expression and measure promoter activity in real time, and image/monitor pharmacologic induction of gene expression in transgenic animals.
4. Imaging of molecular interactions (4)—Different reporter systems have been developed to image different molecular events in intact cells in living subjects, including the regulation of gene expression and protein–protein interactions. The two-step transcriptional amplification (TSTA) approach can be used to image gene expression using endogenous/weak promoters whereas modified yeast two-hybrid system, complementation and intein-mediated reconstitution of split Firefly and Renila Luciferase can be used to image protein–protein interactions in intact cells. The applications of reporter systems will be covered in more details in the sections on Direct Imaging, Indirect Imaging, and Reporter Systems: Small animal SPECT and PET.

Nuclear Medicine

PET, SPECT

References

1. Massoud TF, Gambhir SS (2003) Molecular imaging in living subjects: seeing fundamental biological processes in a new light. Genes Dev 17:545–580
2. Gambhir SS (2002) Chapter 29: Radionuclide Imaging of Reporter Gene Expression. In: AT JC (eds) M eds. Brain Mapping: The Methods. Academic Press, San Diego, pp 799–818
3. Iyer M, Sato M, Johnson M et al (2005) Applications of Molecular Imaging in Cancer Gene Therapy. Curr Gene Ther 5:607–618
4. Paulmurugan R, Ray P, De A (2005) Imaging protein-protein interactions in living subjects. TrAC Trends Anal Chem 24:446–458

Reporter Systems, Optical

Christoph Bremer
University of Münster, Münster, Germany
bremerc@uni-muenster.de

Definition

Optical signatures are defined as intrinsic substances that significantly interfere with the regular photon propagation in the tissue for example, by absorption, induction of fluorescence, or by emitting photons upon chemical reactions (bioluminescence). These optical signatures are intrinsically present and thus a part of the cellular environment (either naturally present of artificially introduced) and not systemically injected.

Major intrinsic absorbers of light are hemoglobin, deoxyhemoglobin, water, and fat and tissue can be characterized regarding its composition of these compounds (1). Besides these naturally occurring chromophores, artificial proteins can be introduced into cells that either fluoresce (fluorescent proteins) or emit photons upon oxidation (bioluminescence). The genetic information encoding for these proteins has also been called "imaging marker gene" (IMG, Fig. 1) alluding to the fact that these optical signatures can be incorporated into therapeutic genetic vectors and help to monitor successful gene transfer. IMGs can be linked to genes of interest so that the coexpression of both genes occurs and regulation of the gene of interest can be visualized. Green fluorescent protein (GFP) is one prominent example of an IMG, which has been cloned from various organisms such as the jellyfish *Aequoria victoria*. GFP fluoresces in the visible light and thus does not penetrate the tissue very efficiently. More recently red-shifted proteins offering better tissue penetration could be isolated from reef coral *Heteractis crispa* or designed by somatic hypermutation techniques, respectively (2).

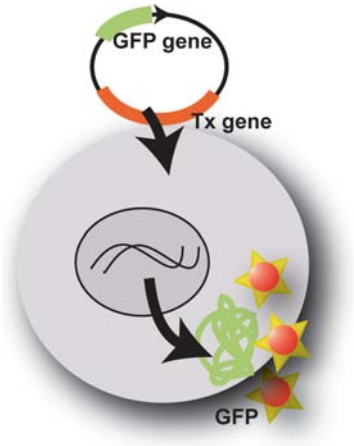

Reporter Systems, Optical. Figure 1 Imaging marker genes (IMG) encode for a transcriptional product (fluorescent protein, luciferase) which can be detected by optical methods (e.g., microscopy, reflectance imaging, optical tomography). IMGs can be linked to genes of interest so that the coexpression of both genes occurs and gene regulation of the gene of interest can be visualized. A prominent example of an IMG is the green fluorescent protein (GFP; shown in this graph), which has been cloned from various organisms such as the jellyfish *Aequoria victoria*. (Reprinted with permission from Bremer et al, 2003)

Bioluminescence is a phenomenon known from fireflies that emit light upon oxidation of luciferin *via* the enzyme luciferase. Similarly like described for GFP the genetic code for luciferase can be exploited as an IMG. Luciferase mediated oxidation of the substrate luciferin results in an emission of light with can be detected by highly sensitive charged coupled device (CCD) cameras. Different luciferase types could be isolated, which show emission spectra between 400 to 620 nm. Since luciferase is not found in mammalian cells bioluminescence operates without background noise thus yielding extremely high SNRs.

Use and Dosage

Intrinsic optical signatures have frequently been used in the medical community. In fact simple optical inspection of tissue surfaces is probably the most frequently applied "optical imaging technique" (e.g., diagnosis cutaneous pathology) in medical practice worldwide. Diaphanography is another example of a simple medical imaging

technology that helps to characterize tissue composition by application of visible light.

More sophisticated optical imaging approaches ranging from infrared diaphanography and dual wavelength transillumination to spectral light analysis have focussed on probing the tissue for blood (water and fat) contents. Diagnostic optical imaging applications exploiting these techniques in the 1980s and 1990s have been applied to study breast cancer detection in a clinical setting. The underlying theory was that oxy- and deoxyhemoglobin, which can be detected by these technologies, could serve as surrogate markers for tumor angiogenesis. However, data obtained in these studies showed a limited sensitivity and specificity of this imaging approach.

In the preclinical and experimental arena optical IMG play a major role for the *in vivo* monitoring of gene expression and gene regulation. Cell lines stably transfected with fluorescent proteins or luciferase can for example, be visualized *in vivo* to monitor cell migration (e.g., metastases, stem cell therapy, and inflammation), tumor-progression and -treatment. Gene regulation has been accurately studied using bioluminescence approaches.

Bibliography

1. Weissleder R, Ntziachristos V (2003) Shedding light onto live molecular targets. Nat Med 9:123–128
2. Bremer C, Ntziachristos V, Weissleder R (2003) Optical-based molecular imaging: contrast agents and potential medical applications. Eur Radiol 13:231–243

Reporter Systems, PET and SPECT

Carmel T. Chan, Sanjiv Sam Gambhir
Department of Radiology, Molecular Imaging Program at Stanford (MIPS) and Bio-X Program, Stanford University School of Medicine, Stanford,
carmelc@stanford.edu
sgambhir@stanford.edu

Definition

Small animal positron emission tomography (small animal PET): A dedicated PET scanner for high resolution imaging of small animals for biomedical research.

Small animal single photon emission computed tomography (small animal SPECT): A dedicated SPECT scanner for high resolution imaging of small animals for biomedical research.

Imaging

Small Animal PET

Methodology: Positron-emitting isotopes used for small animal PET imaging are produced by a cyclotron and/or generator (1, 2). They are capable of producing two γ-rays through emission of a positron from its nucleus, which then annihilates with a nearby electron to produce two 511 keV γ-rays at approximately 180°C apart. Biological molecules and chemical tracers can be directly or indirectly radiolabeled with positron-emitting isotopes, including ^{11}C, ^{13}N, ^{15}O, ^{18}F, ^{62}Cu, ^{64}Cu, ^{68}Ga, ^{76}Br, ^{82}Rb and ^{124}I . The mass of probe injected is usually in the nanogram–microgram range. Upon injection into living animals, the PET imaging probes circulate from the intravascular to the extravascular compartments and upon radioactive decay, high energy γ-rays are emitted from within small animals. A bank of detectors placed around the living animals are used to detect γ-rays through scintigraphic instrumentation consisting of an array of scintillation crystals (to convert γ-ray energy into visible light), suitable light sensors, readout electronics, and image processing units to produce tomographic images (Fig. 1). The small animal PET machine has a resolution attaining $\sim(1–2)^3$ mm^3 and can be used to follow the distribution and concentration of the injected tracers/probes for the purpose of developing molecular imaging assays before their application in humans.

Quantitation: The detection of one γ-ray results in the opening of an electronic time window during which detection of another γ-ray in another detector results in the counting of a coincident event. In order to be detectable, this coincidence event must have occurred along a straight line connecting the two detectors. The near coincidence detection of both γ-rays that are 180° apart in small animal PET within nanoseconds of each other defines the line of response in space and the direction of flight. The coincidence events measured at all angular and linear positions can be reconstructed using different mathematical reconstruction algorithms, including filtered back projection (FBP), ordered subset-expectation maximization (OSEM), and maximum a posteriori (MAP) assuming enough events are detected from the subject under study. Using electronic collimation, the localization and concentration of the positron-emitting radioisotope within a plane of the organ that was scanned can be quantified. Attenuation of the emitted radiation can be corrected using the attenuation factor, which is determined by total length through the body of the small animals such as rats. Tomographic images of relative probe concentration related to the underlying biochemical processes can be then reconstructed in the sagittal, coronal, and transverse imaging planes. The time-kinetics of the tracers can also be determined by dynamic (multiple acquisitions over time) scans.

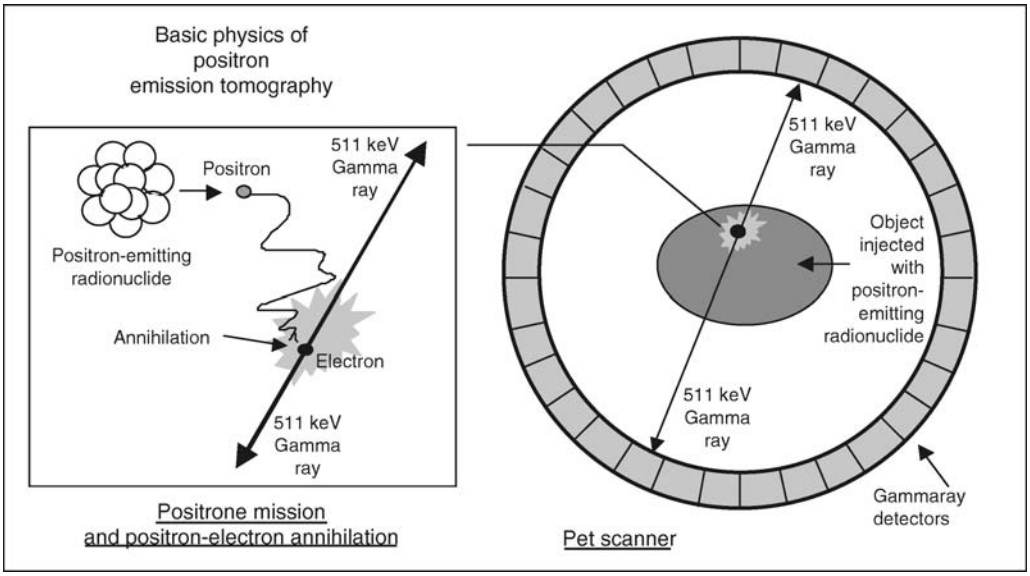

Reporter Systems, PET and SPECT. Figure 1 Basic principles of small animal positron emissions tomography (small animal PET) imaging. Biologically active molecules can be radiolabeled with positron-emitting radioisotopes. The positron-emitting isotope decays by emitting a positron from its nucleus that eventually collides with a nearby electron, resulting in an annihilation event where two 511,000 eV photons in the form of gamma rays are emitted ~180° apart. The two emitted photons travel extracorporeally and are detected nearly simultaneously as they interact with a ring of detectors (composed of scintillation crystals and photomultiplier tubes) surrounding the subject. Detection of a single annihilation event results in the "activation" of detectors opposing one another, which is recorded as a "coincident event." The recording of multiple detector pair combinations yields a large number of these coincident lines. Sophisticated mathematical analyses of the coincident lines yields the location of cell populations or tissues that contain the molecule labeled with the positron emitter. Tomographic images of relative probe concentration can be reconstructed in the conventional sagittal, coronal and transverse imaging planes or, actually, in any arbitrary plane. The resultant image depicts the distribution and concentration of the radiolabeled tracer.

Specifications: The sensitivity (ability to detect a molecular probe relative to background) small animal PET is in the range of 10^{-11} to 10^{-12} moles/L, independent of the location depth of the probe. The temporal resolution (frequency at which the final interpretable version of images can be recorded/captured from the animal once the imaging process is initiated) that relates to the time required to collect enough events to form an image and the responsiveness of the imaging system to rates of any change for small animal PET imaging is about 10 s to minutes. The spatial resolution of small animal PET can be as high as 1 mm^3, compared to 5–6 mm^3 for clinical PET scanner.

Applications: Small animal PET can be used for imaging perfusion in the heart (e.g., ^{13}N-Ammonia), receptor densities on the cell-surface (e.g., Dopamine 2 Receptor, D_2R), reporter gene expression (e.g., Herpes Simplex Virus Type I Thymidine Kinase), as well as metabolic/cytoplasmic enzyme expression (e.g., hexokinase and thymidine kinase), cell trafficking, cell proliferation as well as monitoring of endogenous mRNA expression using anti-sense technology. It can also be used to establish the pharmacokinetics and pharmacodynamics of novel tracers and chemotherapy agents for diagnosis, prognosis and preclinical drug development. See Sections X.X and X.X for more applications involving direct and indirect imaging using small animal PET.

Pros: Small Animal PET is quantitative and highly sensitive. When compared to other modalities, the sensitivity of small animal PET is relatively high, on the order of 10^{-11} to 10^{-12} moles/liter (M) (Magnetic Resonance Imaging (MRI)'s intrinsic sensitivity is ~10^{-4} to 10^{-5} M). Since positron-emitting isotopes can substitute naturally occurring atoms (C, F, N,O), the relative ease of labeling tracers and biological molecules also allow the generation of multiple PET probes. Repetitive imaging using radioisotopes with short half-lives (e.g., ^{18}F and ^{11}C) also allow longitudinal studies, thus providing the detailed location(s), magnitude, and persistence of probes or tracers for *in vivo* use in animals.

Compared to optical imaging, small animal PET is much less affected by the location depth of the probes, thus enabling quantitative translational research from small animal models to human clinical trials.

Cons: The constant decay of the radioisotopes leads to production of γ-rays, thus a time delay between injection and imaging is required for clearance of nonsequestered probes. Since a lot of positron-emitting isotopes have relative short half-lives (e.g., ^{18}F has a half-life of 110 min), efficient PET probe synthesis strategies and close vicinity of an on-site cyclotron and/or generator to the small animal PET machines are required. Furthermore, since all PET isotope decays result in two γ-rays of the same energy (511 keV), small animal PET cannot be used to simultaneous detect multiple PET probes. Therefore, separate injection/scanning of individual probes are required to achieve multiplexing.

Small Animal SPECT

Methodology: Small Animal SPECT imaging with a gamma camera is similar to small animal PET, but the isotope emits gamma rays instead of positrons (2, 3). Small Animal PET is used for imaging low energy γ-emitting isotopes (^{99m}Tc, ^{111}In, ^{123}I, and ^{131}I). Different radiolabels with their characteristic photon energies (^{111}In [171, 245 keV], ^{125}I [27–35 keV], ^{131}I [364 keV], and ^{99m}Tc [140 keV]) can be attached to molecules of interest. A chelating moiety is required for radiolabeling with ^{99m}Tc and ^{111}In. The type of molecular probe (in the nanogram range) used can be directly or indirectly radiolabeled. Upon injection into the small animals, most of these tracers circulate from the intravascular to the extravascular compartments and emit γ-rays at their specific energies in different directions upon decay. γ-rays are detected using a gamma camera, a scintillation detector consisting of collimator, a sodium iodide crystal (to convert γ-ray energy into visible light), and a set of photomultiplier tubes, suitable light sensors, readout electronics (the electrical signals produced are proportional to the energy of the γ-rays), and image processing units (Fig. 2).

Quantitation: Since the SPECT camera is situated only on one side of the subject, only γ-rays directed toward the camera will be "captured," while others will be lost. Furthermore, only γ-rays that are parallel to and successfully reach the collimator will be converted into photons and detected since the collimator will absorb scattered γ-rays. In order to produce tomographic images, the SPECT camera rotates around the small animals. This is in contrast to small animal PET imaging, in which the small animals are surrounded by a bank of detectors. For single photon emitters, in order to correct for attenuation, the direction of flight/angle of incidence is determined by the geometric lead collimation to restrict data to γ-rays of certain predefined directions. γ-rays of lower energy resulting from scattering are devoid of their geometrical information, small animal SPECT imaging provides a planar image (a two-dimensional image from a three-dimensional subject).

Specifications: The temporal resolution of small animal PET is in minutes. The spatial resolution of small animal PET using pinhole SPECT for animal imaging can be as high as 1.7 mm. Only 10^{-4} times the emitted number of γ-rays will be detected by the collimator due to scattering or energy lost.

Applications: Small animal SPECT can be used for imaging gene expression and regulation, receptor densities on cell surface (e.g., dopamine transporter), reporter gene expression (e.g., sodium iodide symporter), apoptosis (e.g., Annexin V), studying cardiovascular disease, diagnosis of thyroid and neuroendocrine cancer, skeletal diseases (e.g., degenerative osteo-articular disorders), and detection of bone metastasis as well as neuroreceptor imaging in the brain. See Applications of Direct Imaging in "Direct Imaging" and Applications of Indirect Imaging in "Indirect Imaging" for more applications involving direct and indirect imaging using small animal SPECT.

Pros: The advantages of small animal SPECT imaging include no depth limit and a plethora of available molecular probes using different radiolabeling strategies. Since the radioisotopes used for small animal SPECT have longer half-lives than that of positron-emitting isotopes, an on-site cyclotron is not required. Furthermore, two or even more radioisotopes of different energies can be imaged simultaneously, allowing for the concurrent study of two distinctly radiolabeled molecules with different energies (e.g., one radiolabeled with ^{99m}Tc and another radiolabeled with ^{125}I), with the ease of adaptation to for multiplexing in clinical setting.

Cons: Compared to small animal PET, the sensitivity of small animal SPECT is an order of magnitude lower (10^{-12} to 10^{-11} mole/L). The low detection efficiency of γ-rays is due to loss of decay events that do not arise parallel to the collimator. To accommodate for the loss of sensitivity, more radiolabeled probes and thus higher levels of radioactivity have to be injected into the subject to maximize signal to noise, though the amount of radioactivity that can be injected will still be limited. Another disadvantage of small animal SPECT is the relatively low spatial resolution due to overlapping of different foci/organs in planar imaging, which may be overcome using rotating gamma camera to acquire volumetric data. Furthermore, the clearance of the SPECT probes through the urinary and hepatobiliary tracts may also hinder the detection and quantitation near these organ systems.

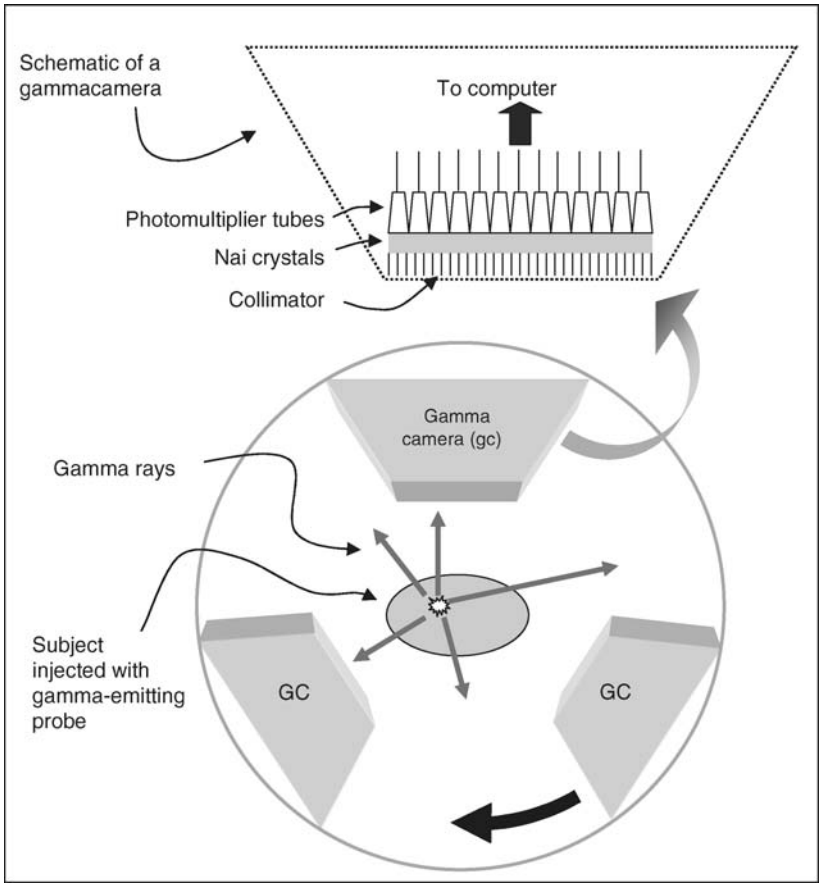

Reporter Systems, PET and SPECT. Figure 2 Basic principles of small animal single photon emission computed tomography (small animal SPECT) imaging. A variety of radioisotopes, each emitting at characteristic photon energies, can be attached to a variety of molecules. Once introduced into the small animals, detection of these radiolabeled probes is a performed with a gamma camera, a scintillation detector consisting of collimator, a sodium iodide crystal and a set of photomultiplier tubes. Upon decay, these radionuclides emit a gamma ray at their characteristic energies in different directions. Some of the gamma rays will scatter or lose energy and others may never interact with the camera. Since the gamma camera is situated only on one side of the subject, only rays directed towards the camera will potentially be "captured." Furthermore, only those gamma rays that arise parallel to collimator will be detected since scattered gamma rays will be absorbed by the collimator. Those rays that successfully reach the crystal and stopped by it will be converted into photons of light. In turn, the photomultiplier tubes convert the light into an electrical signal that is proportional to the incidental gamma ray. Gamma rays that arrive at detector lower than the expected characteristic energy are thought to be the result of scattering and summarily rejected from the analysis. Since gamma cameras acquire data in a single plane, the resultant images are a two-dimensional representation of a three-dimensional subject (referred to as planar imaging). Small animal SPECT acquires volumetric data by rotating a gamma camera around the subject and/or using multidetector systems (shown above).

Nuclear Medicine

- Small Animal PET
- Small Animal SPECT

Diagnosis

- Oncology—tumor staging and diagnosis
- Cardiology—perfusion and functional imaging
- Drug development: pharmacokinetics of tracers and chemotherapy agents

References

1. Sandip S, Gambhir SS (2003) Monitoring gene therapy using *in vivo* molecular imaging techniques. In Templeton NS (ed) Gene Therapy: Therapeutic Mechanisms and Strategies. Marcel Dekker Inc., New York, pp 447–480

2. Massoud TF, Gambhir SS (2003) Molecular imaging in living subjects: seeing fundamental biological processes in a new light. Genes Dev 17(5): 545–580
3. Cassidy P, Radda G (2005) Molecular imaging perspectives. J R Soc Interface 2(3): 133–144

RES

▶Reticuloendothelial System

Residual Tumor

After neurosurgical resection, the amount of residual tumor must be defined by imaging (magnetic resonance imaging or computed tomography) within the first 72 h because after 3 days, nonspecific enhancement within the brain may mimic tumor. For follow-up, the behavior of a residual tumor allows important therapeutic decisions.

▶Neoplasms, Brain, Posterior Fossa, Pediatric

Response to Treatment

Antonia Dimitrakopoulou-Strauss
Medical PET Group-Biological Imaging (E0601),
Clinical Cooperation Unit Nuclear Medicine,
German Cancer Research Center,
a.dimitrakopoulou-strauss@dkfz.de

Definition

Assessment of treatment response is important to optimize and individualize therapy. This is particularly important in oncological patients who receive combined chemotherapeutic protocols, which may cause severe side effects without producing the expected therapeutic result. Treatment response is also important for cardiac and neurological patients.

Characteristics

Applications

The main application of treatment response is for monitoring cancer therapy. Positron emission tomography (PET) with F-18-fluorodeoxyglucose (FDG) is currently the most powerful noninvasive tool for imaging of metabolic processes in patients. The greatest advantage of FDG-PET over morphological imaging modalities is assessing treatment effects, since the anatomic changes that follow treatment frequently lag behind tumor response in terms of viability. By using FDG-PET to predict therapy response early in the course of a prolonged treatment regimen in patients with carcinomas, it is possible to predict the therapeutic effect more accurately. The idea is that an accurate prediction of treatment failure may allow the oncologist to apply an alternative treatment regimen without subjecting the patient to the toxicity of the full treatment scheme.

Limitations of Conventional Techniques

Conventional response criteria for monitoring chemotherapy are based on changes in tumor volume, generally assessed by radiological methods. According to the criteria defined by the World Health Organization (WHO), response to therapy is classified as a therapy-induced reduction in tumor volume by at least 50%. The size of the tumor volume should be measured in two perpendicular diameters. Complete response is classified as disappearance of all lesions following therapy. One problem of this approach is the accuracy and reproducibility of the tumor volume measurement in a clinical environment.

Another problem is the fact that a reduction in tumor volume may take considerable time even after an effective therapy, particularly in solid tumors. As a consequence, tumor response is generally assessed after several weeks or months following the start of therapy. Patients who do not respond to chemotherapy may be treated over a long time period because of the lack of a sensitive parameter for early determination of therapy response. This situation reflects a common problem in the therapy management of oncological patients and in particular in patients with solid tumors, a high percentage of whom do not respond to chemotherapy.

The formation of scar tissue or edema following radiation therapy may be another obstacle in evaluating therapy response in oncological patients using radiological methods.

Monitoring of Chemotherapeutic Effects Using ^{18}F-FDG-PET

PET with ^{18}F-FDG is a sensitive method for detecting viable tumor tissue, and therefore for tumor diagnosis, staging, and therapy monitoring. A focally enhanced FDG-uptake besides the normal biodistribution is

indicative of viable tumor tissue. However, it is important to examine whether morphological findings correlate with the PET findings and to exclude an acute inflammatory lesion, which may mimic viable tumor tissue. However, enhanced ^{18}F-FDG-uptake following chemotherapy is a relatively reliable sign of viable tumor tissue. For this purpose, visual evaluation may be adequate. But if the task is to assess response to therapy, more than one FDG-PET study should be performed, before and during the therapy-free interval. Quantitative measurements of ^{18}F-FDG-uptake are necessary to assess the metabolic activity. Patients who respond to therapy demonstrate a decrease in glucose metabolism, whereas nonresponders show an increase even after one chemotherapeutic cycle. Therefore, this approach allows early detection of nonresponders (Fig. 1).

PET-FDG Methodological Aspects

Semiquantitative measurements are mainly used for evaluating a therapeutic effect. For that purpose, static images are acquired, and the so-called standardized uptake values (SUVs) are calculated. The SUV is a distribution value that allows comparison of a radioactivity concentration between different patients and different studies. An SUV of 1.0 reflects a homogenous tracer distribution.

However, SUV is modulated by several factors, including the plasma glucose level, partial volume effects due to lesion size, reconstruction parameters, and the time after the tracer injection. Therefore, the calculation of SUV should be performed under standardized conditions concerning the time after tracer application, the blood glucose level in cases of ^{18}F-FDG, partial volume correction, and the choice of reconstruction parameters.

Besides the use of SUV, it is possible to acquire kinetic parameters of the ^{18}F-FDG kinetics using dynamic data acquisition. Dynamic studies are superior because they provide information about tracer distribution with respect to time and space in a region of interest (ROI). A detailed analysis of the kinetic data can be performed to acquire the most relevant information about the tracer pharmacokinetics. Analysis of kinetic PET data can be performed using compartment and noncompartment models. In the case of ^{18}F-FDG, a two-tissue compartment model with a blood component can be used, and transfer rates can be calculated. The blood component represents the amount of nonmetabolized ^{18}F-FDG in the vessels; the first compartment describes the intracellular amount of nonmetabolized ^{18}F-FDG; and the second compartment describes the intracellular amount of the metabolized ^{18}F-FDG. Therefore, using a compartment model it is possible to separate the metabolized amount of ^{18}F-FDG, which is directly related to tumor viability. A prerequisite for this approach is the time course of ^{18}F-FDG in the target area, such as in the tumor and in a blood vessel (input). The input can be obtained by blood sampling (venous or arterial), or it can be derived from an early image of an arterial vessel, such as the aorta, within the field of view.

Interpretation of the Change in Metabolic Activity

A measurable change in ^{18}F-FDG metabolism following one chemotherapeutic cycle does not necessarily mean that the patient will profit from the therapeutic regimen with respect to long-term therapy outcome. In patients with metastatic colorectal carcinoma who received a

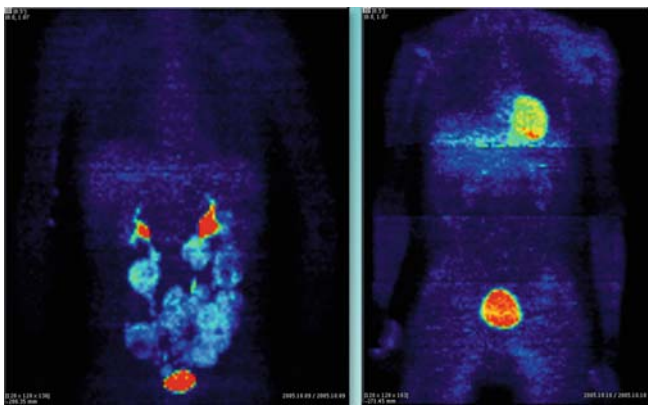

Response to Treatment. Figure 1 **^{18}F-FDG-PET studies in a patient with gastrointestinal stromal tumor and multiple abdominal metastases before and after therapy with Glivec, a tyrosine kinase inhibitor. *Left*: maximum intensity projection images (MIP) before therapy. *Right*: MIP images after therapy.**

combined chemotherapeutic protocol (FOLFOX), the change in ^{18}F-FDG-uptake after one chemotherapeutic cycle did not correlate to overall survival. However, based on the SUV data before the onset to chemotherapy, it was possible to identify patients who survived longer than 1 year (1). By adding kinetic model parameters of the baseline study and of a study performed after completion of four chemotherapeutic cycles, it was possible to classify the majority (78%) of patients according to a 1-year survival rate. Therefore, a detailed analysis of tracer kinetics provides more accurate results for predicting individual survival rates.

The situation may be different for other tumor types and other chemotherapeutic protocols used for treatment. In patients with adenocarcinoma of the gastroesophageal junction who received preoperative chemotherapy, the change in ^{18}F-FDG-uptake between the baseline ^{18}F-FDG study and the study 14 days after onset to chemotherapy (cisplatin-based) correlated with therapy outcome (2). A 35% reduction in the ^{18}F-FDG-uptake correlated with treatment response. However, it is unknown whether these data can be transferred to other tumors and treatment protocols.

Standardization of the Criteria Used for Metabolic Treatment Response

At present, there are no generally accepted criteria for defining response. Generally, a reduction in the ^{18}F-FDG-uptake is a good prognostic sign. A threshold of at least 20% has been proposed by some authors as a response criterion. Although even a 20% change does not necessarily correlate with the survival rate, it is associated with at least a palliative effect. In contrast, an increase in ^{18}F-FDG-uptake is associated with lack of response. Thresholds depend on the tumor type and the expected curative or palliative treatment effect. In patients with malignant lymphomas, who primarily respond to chemotherapy, a decrease of 45% has been reported within 24 h after onset of therapy. The threshold for metabolic response in high-grade lymphomas is therefore higher, because the intention is to cure the tumor. In cases of palliative chemotherapy, the threshold may be lower. Thus, using metabolic measurements seems to be feasible for individualizing and optimizing chemotherapy.

Other Tracers

Perfusion studies with ^{15}O-water can be used in combination with ^{18}F-FDG studies to monitor the effect of a neoadjuvant therapy. In patients with locally advanced breast carcinoma who received neoadjuvant chemotherapy, an increase in tumor perfusion was noted in nonresponders by a concurrent decrease in the metabolic rate of ^{18}F-FDG (3). Furthermore, patients with breast carcinoma whose tumors demonstrated a higher ratio for the metabolic rate of ^{18}F-FDG and tumor perfusion survived longer (4).

Perfusion studies with ^{15}O-water PET can be used to monitor the effect of an antiangiogenic therapy. This is a difficult task because inhibitors of angiogenesis are not primarily cytotoxic, and therefore it takes a longer time to determine the clinical effect. In cancer patients treated in a phase I (dose-finding) study by a human recombinant endostatin analog that has an antiangiogenic effect, PET studies with ^{15}O-water demonstrated a change in tumor perfusion that was significant to the dose escalation (5).

Studies with ^{68}Ga-DOTATOC are used for research purposes to assess the effect of a radioisotope therapy with ^{90}Y-DOTATOC, which is an experimental therapy used for treating metastatic neuroendocrine tumors. DOTATOC is a peptide that primarily binds to the somatostatin receptor subtype 2 (SSTR II). Neuroendocrine tumors, which show an enhanced uptake on ^{68}Ga-DOTATOC PET, are candidates for the radioisotope therapy.

Other Applications

Perfusion studies can be used in patients with myocardial infarction to assess the effect of reperfusion. Another approach consists of apoptosis measurements with ^{9m}Tc-Annexin V, a procedure that is currently under evaluation. Annexin is a phospholipid-binding protein with high affinity for phosphatidyl-serine, which is externalized by cells undergoing programmed cell death. ^{9m}Tc Annexin accumulates in the infarct site, indicating that cardiomyocytes with externalized phosphatidyl-serine are present in the infarcted area.

A nononcological example of therapy monitoring is the measurement of bone remodeling by repeated bone scintigraphy with ^{99m}Tc-MDP in patients with Paget's disease.

Bibliography

1. Dimitrakopoulou-Strauss A, Strauss LG, Burger C et al (2004) Prognostic aspects of ^{18}F-FDG PET kinetics in patients with metastatic colorectal carcinoma receiving FOLFOX chemotherapy. J Nucl Med 45:1480–1487
2. Weber WA, Ott K, Becker K et al (2001) Prediction of response to preoperative chemotherapy in adenocarcinomas of the gastroesophageal junction by metabolic imaging. J Clin Oncol 19:30583065
3. Tseng J, Dunnwald LK, Schubert EK et al (2004) 18F-FDG kinetics in locally advanced breast cancer: correlation with tumor blood flow and changes in response to neoadjuvant chemotherapy. J Nucl Med 45:1829–1837

4. Mankoff DA, Dunnwald LK, Gralow JR et al (2002) Blood flow and metabolism in locally advanced breast cancer: relationship to response to therapy. J Nucl Med 43:500–509
5. Herbst RS, Mullani NA, Davis DW et al (2002) Development of biologic markers of response and assessment of antiangiogenic activity in a clinical trial of human recombinant endostatin. J Clin Oncol 20:3804–3814

Retention Cyst

A smooth marginated, soft tissue mass, caused by obstruction of a small seromucinous gland occurring especially in the presence of sinusitis.

►Cystic Neoplasms, Pancreatic
►Inflammation, Chronic, Nose, and Paranasal Sinus

Reticuloendothelial System (RES)

The RES is part of the immune system consisting of phagocytic cells which take up, digest or retain several biological or nonbiological materials such as cell debris, bacteria, dyes or particles. All organs and tissues containing e.g., dendritic cells, monocytes or macrophages are part of the RES.

►Targeted Microbubbles

Retrograde/Anterograde Urography (Pyelography)

Conventional radiologic studies with retrograde contrast administration *via* cystoscopically inserted ureteral catheters or anterograde through percutaneous nephrostomies, both performed under fluoroscopic control, provide the most precise delineation of the collecting system. However, diagnostic retrograde studies are performed rarely in obstruction, only when renal function is impaired and other imaging modalities are inconclusive, but mainly for selective urine sample collection in suspected tumor, and prior to URS and double-J stent placement. Therapeutically inserted PNS can be used for anterograde urography.

►Colic, Acute, Renal

REZ

►Root Entry Zone

Rhabdomyosarcoma

Johan G. Blickman[1], Dewi Ashi[2]
[1]Department of Radiology, UMC St Radboud, Nijmegen, Netherlands
j.blickman@rad.umcn.nl
[2]Department of Radiology, University of Indonesia, Cipto angunkusumo General Hospital, Salemba, Jakarta Pusat, Indonesia

Definition

Malignant soft tissue tumor of ►striated muscle.

Incidence

The most common ►soft tissue sarcoma of the pediatric age group. Approximately 8% of solid tumor in childhood, slightly more than half of pediatric soft tissue sarcomas. Peaks of incidence: 2–5 years (70% cases occurring before the age of 10) and adolescence. It is slightly commoner in boys than girls.

Pathology/Histopathology

It is divided into ►botryoid, ►spindle cell, embryonal, and alveolar types with an increasingly poorer prognosis in that order.

Botryoid usually occurs in hollow organs: the bladder, nasal sinuses, vagina, and common bile duct.

The muscular tumor is of mostly alveolar histology in contrast with the embryonal type that is linked with the pelvic region and the head and neck.

Rhabdomyosarcoma is a very aggressive tumor and infiltrates along fascial planes, lymphatic and hematogenous routes.

Clinical Presentation

Rhabdomyosarcoma may arise anywhere in the body, excluding the brain. An international definition of anatomical sites was adopted in 1986 by the international society of pediatric oncology (SIOP) (Table 1).

The most common sites for rhabdomyosarcoma are head and neck, genitourinary tract, and skeletal muscle. Presentation is often a painless mass and symptoms depend on tumor location.

Head and neck area: proptosis, chronic otitis media, polypoid mass obstructing the ear canal, sinusitis,

Rhabdomyosarcoma. Table 1 Clinical SIOP

Stage	Description
IA	Localized tumor confined to site of origin, completely resected
IB	Localized tumor infiltrating beyond site of origin, completely resected
IIA	Localized tumor, gross total resection, but with microscopic residual
IIB	Disease
IIC	Locally extensive tumor (spread to regional lymph nodes) completely
IIIA	Resected
IIIB	Extensive tumor (spread to regional lymph nodes, gross total resection, but with microscopic residual disease)
IV	Localized or locally extensive tumor, gross residual disease after biopsy only
	Localized or locally extensive tumor, gross residual disease after major resection (50% debulking)
	Any site of primary tumor with or without regional lymph node involvement, with distant metastases, irrespective of surgical approach to primary tumor

obstruction of the airway, epistaxis, swelling, hoarseness. Extension to central nervous system (CNS) by direct extension: meningeal symptoms, cranial nerve palsies, respiratory disturbance.

Genitourinary tract: hematuria, vaginal bleeding, voiding problems.

Extremities and trunk: indolent mass, spinal compression.

Biliary tract: cholecystitis, hyperbilirubinemia.

About 20% of the patients present with distant metastases at diagnosis, mostly in the lung.

Metastases are also found in lymph nodes, mediastinum, brain, liver, and skeleton. Prognosis is less favorable for patients with rhabdomyosarcoma of the extremities than genitourinary tract or head and neck region and depends also on histopathological classification.

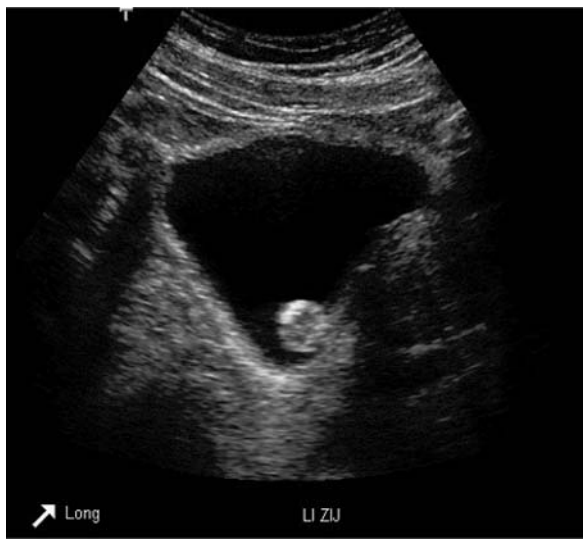

Rhabdomyosarcoma. Figure 1 US of bladder

Imaging

The radiological appearance depends on the site of the tumor. Classic imaging appearance: noncalcified soft tissue fullness with possible bone erosion and periosteal reaction.

Ultrasound (US): aspecific appearance, the echogenicity is variable, and may be hypoechoic, isoechoic, or hyperechoic to adjacent soft tissues. The margin may be poorly or well defined. Increased vascularity is noted on color Doppler sonography (Fig. 1).

CT scan and MRI show the extent of the disease and distant metastasis (Fig. 2).

MRI: aspecific appearance, signal indeterminate or low on T1 and high on T2. The masses tend to vary from homogeneous to heterogeneous and may undergo central necrosis. STIR and T1 + C show enhancement, necessary for evaluation of liver or lymphatic involvement in paratesticular rhabdomyosarcomas.

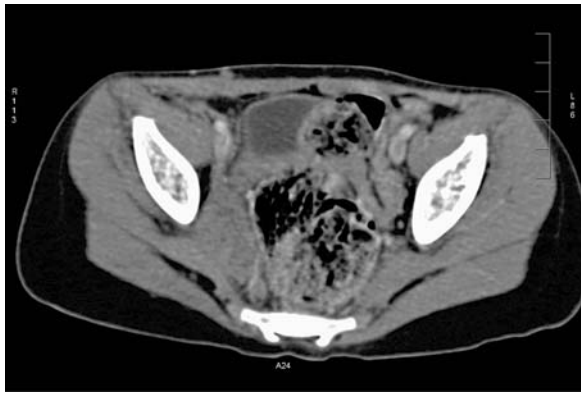

Rhabdomyosarcoma. Figure 2 A soft tissue mass (rhabdomyosarcoma) originating from the iliopsoas

Nuclear Medicine

Tc 99m MDP bone scan: for evaluation of bone metastases.

Diagnosis

The presumptive diagnosis can be made from the presentation and the tumor location but tissue typing requires biopsy, often under imaging guidance. Bone marrow aspiration/biopsy should be performed for bone marrow invasion and lumbar puncture for evaluation of the liquor.

Bibliography

1. Pediatric Radiology, 2nd edition, The Requisites. Hans Blikman, MD, PhD, Boston University School of Medicine, Boston, MA. Mosby 1998
2. Carty H (ed) (2001) Paediatric imaging. The Encyclopedia of Medical Imaging, Vol. 7, Oslo, The NICER Institute p 464, p 465
3. Fletcher BD (2004) Soft tissue neoplasms. In: Kuhn JP, Slovis TL, Haller JO (eds) Caffey's Pediatric Diagnostic Imaging. 10th edn. Philadelphia: Mosby p 2024, p 2025
4. Carville MB, Spunt SL, Pappo AS (2001) Rhabdomyosarcoma in pediatric patients: the good, the bad, and the unusual. Am J Roentgenol 176(6):1563–1569

Rhabdomyosarcoma of the Biliary Tree

Rare mesenchymal malignancy originating in and along the bile ducts in infancy. When arising in the major bile ducts, it shows a botryoid feature with biliary tract dilatation and jaundice. Lesions within the peripheral intrahepatic ducts are indistinguishable from other intrahepatic malignancies. Peak of incidence is between 2 and 5 years of age with a slight male predominance. The tumor usually is a unique spherical mass, very large, usually located in the right lobe. Metastatic spreading involves the liver, lungs, peritoneal cavity (omentum, mesentery, and diaphragm).

▶Hepatic, Pediatric Tumors, Malignant

Rheumatic Discitis

Rheumatic discitis is a feature of rheumatic arthritis. It is characterized by intervertebral space decrease and tiny erosions of the subchondral bones. Prevertebral soft tissue swelling is not a sign of rheumatic disease. Discitis may heal within years, with subsequent premature degenerative disease or bony bridging of parts of the intervertebral space, or persist and lead to instability.

▶Rheumatoid Arthritis

Rheumatic, Fever, Acute

The classic form of rheumatic fever, an inflammatory disease, occurs as a delayed, nonsuppurative consequence of an upper respiratory infection (group A streptococci). Clinical manifestations include varying combinations of polyarthritis, carditis, subcutaneous nodules, erythema marginatum, and chorea. These patients are usually younger and the findings are more generalized compared to gout.

▶Gout

Rheumatoid Arthritis

Lingg G.M., Schorn C.
Department of Radiology, Sana Rheumazentrum Rheinland, Pfalz Kaiser-Wilhelm-Str. 9-11, D-55543 Bad Kreuznach, Germany
dr.lingg@sana-rheumazentrum-rlp.de

Synonyms

Chronic polyarthritis

Definition

Rheumatoid arthritis (RA) is a systemic autoimmune inflammatory disorder of unknown etiology, primarily affecting the synovial membranes and articular surfaces. It leads in varying degree to articular destruction, and natural history may end in disability. There is a hereditary predisposition in patients with HLA DR4.

Pathology/Histopathology

Chronic inflammation of the synovial membrane with vasculitis leads to exudation of an aggressive joint effusion and immigration of inflammatory cells. Proliferation of destructive pannus tissue into the joint space with

►cartilage destruction and bone destruction primarily in the bare areas and marginal, later mutilation of the entire epiphysis is the consequence. Characteristic deformities are the result of ligamentous destruction. Synovial membranes are affected not only in joints but also in bursae and tendinous sheaths.

Clinical Presentation

There is a threefold female predominance. Disease onset is insidious. Stiffness, especially long-standing morning stiffness, and arthralgia are the first symptoms. Patients complain about symmetric tenderness and swelling of the ►small joints. Larger joints are usually affected later. Rarely, there are atypical features such as monarticular or sudden polyarticular onsets.

Joint effusion, periarticular edema, and synovial hypertrophy lead to the typical pasty appearance of the ►soft tissue swelling. Laboratory findings are elevated erythrocyte sedimentation rate (ESR), C-reactive protein (CRP), rheumatoid factor, and antibodies directed to citrullinated proteins.

Rheumatoid arthritis commonly affects the cervical spine. The morbidity of neck disease is considerable. Neurologic dysfunction is a rare but severe complication of late-stage cervical arthritic deformity, and therefore the cervical spine should be evaluated with caution. Imaging, however, gives no unfailing predictors for myelopathy, only risk factors. The first clinical symptoms are neck and/or occipital pain. In patients with known cervical arthritis, clinical symptoms including muscle weakness (diminished motor power in arms and legs), muscle spasm, gait disturbance, paresthesia, and numbness should raise suspicion of myelopathy. Restless legs as a consequence of spinal automatism and bladder dysfunction suggestive of early neurogenic bladder are later symptoms. Neurologic examination of patients with myelopathy reveals hyperreflexia, Babinski's sign, and loss of pain sensation or vibratory or position sense.

Organ manifestations in RA are pulmonary fibrosis, pleural effusions, and pulmonary nodules.

Imaging

The primary imaging tool for the diagnosis of rheumatoid arthritis is X-ray views of both hands and feet, even if there is no clinical feet involvement at all. Images are typically taken employing high-resolution screen–film combinations. Two projections (dorsovolar and standardized angulated with a 20° wedge, elevated on the radial side) are recommended. Among radiographic alterations described to date, erosion seems to be associated with the best reliability and discriminating power. However, X-ray imaging is insensitive to bone damage at its earliest stages and is incapable of capturing the primary feature of rheumatoid disease, the synovitis. Magnetic resonance imaging (MRI) and ultrasound can directly visualize and monitor changes in synovium and bone that precede actual bone erosion. On the other hand, these advanced imaging techniques are confined to relatively small areas, and considering the polyarticular nature of the disease, there is a lack of general information.

Affection of the *large joints* is also imaged with X-ray. In cases of clinical involvement of the cervical spine, a lateral projection in inclination is mandatory in addition to normal anteroposterior and lateral views.

Follow-up studies are important to evaluate therapy success, progression, or complications. Nuclear bone scans can help find inflammatory foci with no or small clinical symptoms. Ultrasonography is the major tool for tendovaginitis, bursitis, and synovial cysts, such as Baker's cyst. In cases of cervical spine arthritis, MRI is the best feature for visualizing the spinal cord and arthritic involvement.

Signs and Patterns in Rheumatoid Arthritis

Typically, arthritis affects the *small joints* (metacarpophalangeal joint, proximal interphalangeal joint, wrist, metatarsophalangeal joint) symmetrically. Proximal joints are affected later in the classic disease course, but may be the first manifestations in atypical cases, especially in late-onset rheumatoid arthritis (►LORA). Involvement of the *cervical spine* is frequent. In these cases, atlantoaxial and especially atlantodental joints are the major location of inflammatory activity. Inflammatory rheumatic subaxial cervical spine disease such as discitis with instability and appendicular joint arthritis is less common. Involvement of the thoracic and lumbar spine is unusual.

Soft tissue swelling with the typical fusiform appearance of joint or tendon sheath effusion is one of the first signs of the inflammatory process (e.g., at the processus styloideus ulnae, which indicates tenosynovitis of extensor carpi ulnaris, or of the metacarpophalangeal joint and proximal interphalangeal joint as a sign of articulosynovitis). Periarticular, subchondral, epiphyseal, and metaphyseal demineralization are an early manifestation and refers to the old term ►"*collateral phenomenon*." The demineralization process progresses in the disease course due to pain-related rest, corticoid therapy, and inflammatory activity leading to excessive peripheral osteoporosis. A concentric pattern of joint space diminution indicates *cartilage destruction* in inflammatory arthritis, unlike eccentric joint space diminution, which is a sign of degenerative osteoarthritis. Erosions of the subchondral bone begin in the bare areas and at the joint margins (Fig. 1). At the metacarpophalangeal joint, they can

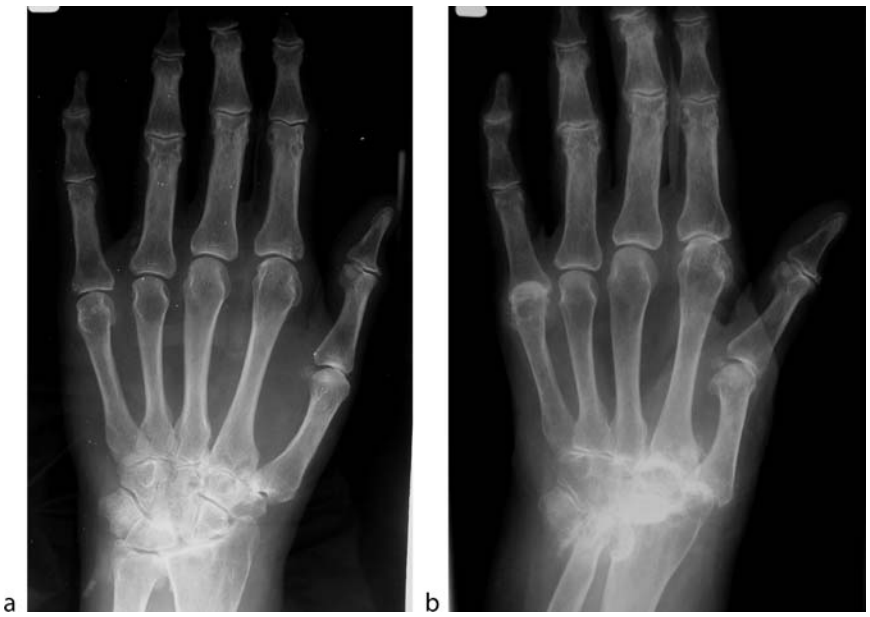

Rheumatoid Arthritis. Figure 1 Rheumatoid arthritis. (a) dorso ventral view of the left hand of a patient suffering from rheumatoid arthritis for 5 years shows mild arthritic erosions of the MCP and moderate arthritis of the wrist (joint space diminution), already with postarthritic secondary degenerative osteoarthritis (subchondral sclerosis) and scapholunate instability (rotation of os scaphoideum). PIP joints show unspecific microcystic changes. (b) Twelve years later, the arthritis of the wrist has been massively progressive. Now mutilation of the distal epiphysis of the radius and ulna are present. The proximal carpal row is completely destroyed and shifted ulnar. MCP V has developed erosions and subluxation.

be found in the voloradial and dorso-ulnar aspects of the metacarpal heads, and similarly at the metatarsophalangeal joint. ►*Bony destructions* progress to mutilation of the joints. Postarthritic ankylosis is not very common in adult RA, in contrast to juvenile arthritis. The wrist, however, is a characteristic location where postarthritic ankylosis, the so-called ►*os carpale*, is a possible and functionally relatively satisfying end stage of the arthritic process. A partial os carpale with ankylosis of only two or three carpals is not uncommon. Radiolunar ankylosis can especially occur spontaneously. Mutilation and complete destruction of the proximal carpals along with subluxations is, in fact, more common than os carpale.

Frequently, destruction of ligamentous support leads to *deformities*. In hands and feet, some deformities are characteristic: ►*swan-neck deformity*, ►*boutonniere deformity*, *ulnar deviation of the* metacarpophalangeal joint, ►*fibular deviation of the toes*, ►*ulnar drift and palmar subluxation of the carpus*, ►*zig-zag deformity*, *dorsal intercalated segmental instability, scapholunate instability and* ►scapholunate advanced collapse, *hallux valgus, dorsal subluxation of the* metatarsophalangeal joint, "*cock-up toe*." In the shoulder, rotator cuff destruction with consecutive cranial subluxation and subacromial neararthros formation is frequent and often exceeds the arthritic signs at the humeral head and glenoid.

In the cervical spine, inflammation most often affects the minute joints and facets of the occiput-C2 region. It causes ►*erosions of the odontoid process* basally, laterally, ventrally, and at the tip. These erosions may progress to major destruction of the odontoid process. Atlas erosions are often tiny. Ligament laxity and lysis increase the mechanical instability. V*entral atlantoaxial subluxation and* ►*cranial settling* are typical and crucial deformities (Fig. 2). A distance between the anterior arch of C1 and the odontoid process exceeding 2.5 mm is pathologic (the normal measurement is ≤2.1 mm, which is 2.5 mm for a 6-foot target to film distance). Often subluxation is provoked or increased in inclination and may reach values of 10 mm or more. The distance between the odontoid process and the posterior arch of C1 gives the diameter of the osseous spinal canal and may be of higher importance. A distance of less than 14 mm is an alarming sign.

Nevertheless, in X-ray imaging the encroachment is often underestimated due to the lack of soft tissue (pannus) visibility. Arthritis of the lateral atlantoaxial joints with considerable destruction of the massa lateralis atlantis leads to *cranial settling* of the odontoid process. Its superior aspect passes the foramen magnum line, and the anterior arch of C1 assumes an abnormally low position in relation to C2. Progressive cranial settling is regarded as an ominous sign of impending neurologic catastrophe.

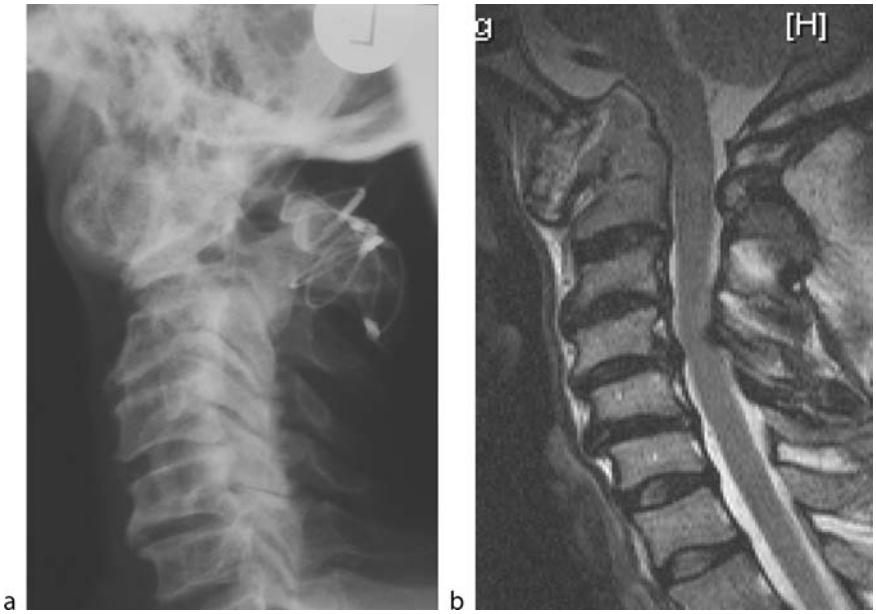

Rheumatoid Arthritis. Figure 2 Rheumatoid arthritis. The lateral view of the cervical spine shows arthritis in the occipital-C2 region (a) with ventral atlas subluxation and wire fixation of C1–C2. There is considerable cranial settling and persisting ventral atlas dislocation. (b) MR imaging reveals the cause of recent pain and neurologic symptoms subaxial as discovertebral and apophyseal joint degenerative disease with encroachment C4/5. The ►cervicomedullary angle however is decreased to 135°. The atlantoaxial deformity and the extent of cranial settling is far better visualised than by means of X-ray imaging. Together with subaxial polysegmental encroachment these signs indicate risk factors for myelopathy.

If the apex of the odontoid process is visible in the lateral view, its distance to the foramen magnum line of McRae should be measured. The tip of the odontoid process is normally located 5 mm below it and should not migrate above this line. If the odontoid process is destroyed or obscured, the distance between the base of the axis and the basion is a reasonable substitute measurement, at least for follow-up evaluations.

►*Subaxial cervical arthritis* comprises *discitis* and ►*apophyseal joint arthritis*. ►Rheumatic discitis is characterized by intervertebral space diminution and tiny erosions of the end plates. Prevertebral soft tissue swelling is not a sign of rheumatic disease. Discitis may heal within years, with subsequent premature degenerative disease or bony bridging of parts of the intervertebral space, or persist and lead to instability. Subaxial instability, often multisegmental, is another high risk factor for myelopathy. Apophyseal joint arthritis is not very conspicuous in X-ray imaging; in late stages, however, microcysts and erosions as well as postarthritic degenerative osteoarthritis occur.

MRI for evaluation of the spinal cord and cervical spine should be used in patients with cervical pain not controlled with conservative management, with clinical symptoms suspicious of cervical myelopathy, and with C1 ventral subluxation (at least when it exceeds 5 mm). On MR images, the best diagnostic clues for patients at risk are subarachnoid space encroachment, cranial migration of the odontoid process, and a markedly decreased *cervicomedullary angle* <135° (which is the angle between two lines on, respectively, the ventral side of the medulla oblongata or brainstem and the cervical cord in degrees) (Fig. 2). Additional or polysegmental subaxial subarachnoid space encroachment is another high risk factor.

Other common findings on MRI are odontoid process erosions and atlas erosions and displacement or absence of the fat body caudal to the clivus. Pannus is identified in varying amounts as a soft tissue mass around the odontoid process. It can be hyperintense on T2-weighted images and enhance intensely contrast material in the more acute phase, or it can be isointense on T2-weighted images not enhancing, which is thought to be fibrous pannus.

►*Subcutaneous rheumatoid nodules* can be seen in seropositive rheumatoid arthritis. They are characteristic but not very common and are typically located at bony prominences (proximal interphalangeal joint, processus styloideus ulnae, olecranon). Patients with peripheral rheumatoid nodules tend to show more specialties, such as pulmonary nodules.

Patients with RA are very prone to osteoporosis due to pain-related rest, steroid therapy, and the inflammatory activity itself. Osteoporotic fractures are very common in the lumbar and thoracic vertebral column. Insufficiency

fractures occur in the os sacrum, the lower leg, and the os calcis. In the os sacrum the fracture exhibits a typical H-shaped aspect. In X-ray images it is often not very conspicuous at all. There may be an indistinct faint sclerosis of the spongiosa. Bone scanning shows an H-shaped hyperactivity (*Honda-sign*). The fracture is best seen on computed tomography.

Nuclear Medicine

Radionuclide studies done with technetium-99m-labeled phosphonates (bone scan) are accomplished by a so-called three-phase study: perfusion phase (0–60 sec p.i.), blood pool phase (2–5 min p.i.), and bone (turnover) phase (2–5 h p.i.). The perfusion and the blood pool phases demonstrate the hyperemia and allow judgment of inflammatory (soft tissue) components of joint disease. The bone phase discloses the longer-lasting bone processes. Bone scintigraphy directs the further diagnostic work-up to otherwise occult inflammatory foci. It is very sensitive, but its role in the diagnostic work-up of initial changes is limited because of low specificity. It may be employed for staging and follow-up.

(18)F-FDG positron emission tomography is a unique imaging technique that can assess the metabolic activity of synovitis and measure the disease activity in RA. However, the clinical significance of this potential has not been proven.

Diagnosis

The diagnosis and management of RA are predominantly based on clinical parameters. Radiologic and serologic findings are also integrated into the diagnostic criteria set (Table 1). Additionally, current clinical work-up relies heavily on serologic tests for the prompt and accurate diagnosis of rheumatic diseases. Serologic testing should be used to support the findings of the history and physical examination and to monitor disease activity.

Rheumatoid Arthritis. Table 1 ARA criteria (1987) for the diagnosis of rheumatoid arthritis

Morning stiffness >1 h >6 weeks
Arthritis of >3 joints simultaneously >6 weeks
Arthritis of wrist or finger joints >6 weeks
Symmetric arthritis >6 weeks
Rheumatoid factor
Subcutaneous rheumatoid nodules
X-ray signs of rheumatoid arthritis

In accordancce with the ARA criteria (1987), rheumatoid arthritis is diagonised when four of seven criteria are positive.

Inflammation can be assessed by the ESR. The CRP (an acute-phase protein) test correlates more closely than ESR with clinical and radiographic parameters of RA inflammation. The rheumatoid factor is unspecific as a screening test for RA accounting for the existence of seronegative RA. However, high titers of rheumatoid factor are associated with progressive joint inflammation and disability. Antibodies directed to citrullinated proteins (anti-ccp) facilitate diagnosis during the early stages of disease, when all clinical symptoms have often not manifested yet. Particularly high specificity is reported. Its prognostic potential may provide an indication for aggressive treatment.

Interventional Radiological Treatment

Intra-articular radionuclide therapy is a promising tool for local control of synovitis. It works like a synovectomy and is performed mainly in the larger joints (e.g., rhenium or yttrium), but it works at the smaller joints as well. Radiosynovectomy is not useful in advanced cases or excessive joint effusions, nor does it modify the disease course.

Bibliography

1. Devauchelle-Pensec V, Saraux A, Alapetite S et al (2002) Diagnostic value of radiographs of the hands and feet in early rheumatoid arthritis. Joint Bone Spine 69:434–441
2. Van der Heijde D (2004) Quantification of radiological damage in inflammatory arthritis: rheumatoid arthritis, psoriatic arthritis and ankylosing spondylitis. Best Pract Res Clin Rheumatol 18:847–860
3. Vincent C, Nogueira L, Clavel C et al (2005) Autoantibodies to citrullinated proteins: ACPA. Autoimmunity 38:17–24
4. Reijnierse M, Dijkmans BAC, Hansen B et al (2001) Neurologic dysfunction in patients with rheumatoid arthritis of the cervical spine. Predictive value of clinical, radiographic and MR imaging parameters. Eur Radiol 11:467–473
5. Tehranzadeh J, Ashikyan O, Dascalos J (2004) Advanced imaging of early rheumatoid arthritis. Radiol Clin North Am 42:89–107

Rhizomelic

A shortness of the extremities most pronounced in the proximal (humerus and femur) region. An example is achondroplasia.

▶Osteodysplasia

Rickets

A pathological condition in child bone metabolism before epiphyseal growth plate closure has taken place

characterized by the impaired and delayed mineralization of osteoid and the cartilaginous part of the epiphyseal growth plates.
▶Osteomalacia

Rickets—Vitamin D Deficiency

▶Vitamin Deficiency

RICM

▶Radiographic Iodinated Contrast Media

Right Middle Lobe Syndrome

An atelectasis of the middle lobe due to narrowing of the middle lobe bronchus by a neoplastic process or chronic inflammatory changes.
▶Atelectasis

Right-to-Left Shunt

A right-to-left shunt occurs when a poorly oxygenated venous systemic blood reaches the systemic arterial circulation. PAVM and congenital or acquired cardiac right-to-left shunts can lead to hypoxemia and to
▶Paradoxical Systemic Embolisms
▶Pulmonary Arteriovenous Malformations

Risk Factors

The factors, both inherited and acquired through lifestyle which increase the chance of developing breast cancer.
▶Carcinoma, Breast, Demography

Risser Method

The Risser classification of the apophyses of the iliac crest enables estimation of the expected growth of the vertebral body and thereby estimation of the progression tendency of scoliosis. Risser classifies the progression of ossification of the apophysis of the os ileum into six grades. In grade 0 the apophyses cannot be seen, and in grade 5 the apophyses are fully fused.
▶Scoliosis

Risser Method Bone Age

Evaluation of growth remaining in the second decade of life based on appearance, then excursion medially, and finally fusion, of the superior iliac apophysis.
▶Bone Age

RNC

▶Radionuclide Cystography

RNP

▶Reflux Nephropathy

Romanus Lesion

Romanus lesion is a subdiscal osteitis of the anterior upper corner of the vertebral body with triangular sclerosis and erosion. It is a common feature in ankylosing spondylitis and occurs most often in the thoracolumbar junction segments.
▶Spondyloarthropathies, Seronegative

Root Entry Zone

A boundary zone between central and peripheral myelination of cranial nerves close to their brainstem

entrance. This area, of variable length depending on the cranial nerve, is particularly vulnerable to damage.
▶Facial Nerve Palsy

Round Pneumonia

Spherical configured pneumonic consolidation mimicking a rounded intrapulmonary mass.
▶Pneumonia in Childhood

Roux-en-Y Gastric Bypass

The surgical procedure consists of forming a small gastric fundal pouch to exclude the remainder of the stomach and duodenum. A jejunal loop is anastomosed to the gastric pouch. A distal side-to-side anastomosis of the excluded jejunal limb and the antegrade-flowing jejunal-limb is formed; creating a "Y" shaped intestinal junction.
▶Stomach and Duodenum in Adults Postoperative

RR

▶Regional Recurrence

RS

▶Raynaud's Syndrome

RTP

▶Radiation Therapy

Rupture of Dermoids

Rupture is a complication of dermoids that may occur spontaneously or iatrogenically. It causes chemical peritonitis due to intraperitoneal spillage of the tumor contents.
▶Teratoma, Ovaries, Mature, Ovalar

Ruptured Intervertebral Disk

▶Hernia, Disk, Intervertebral

Sabre-Sheath Trachea

A narrowing of the coronal diameter of the intrathoracic portion of the trachea. By contrast, the coronal diameter of the trachea measured above the thoracic inlet is normal. Sabre-sheath trachea is a radiographic finding that is highly suggestive of COPD. The deformity of the trachea is fixed and rigid and the tracheal rings can be densely ossified.

►Airway Disease

Sacrococcygeal Teratoma

This is found in the region of the primitive pit and node. The primitive pit is the depression in the primitive node that connects the notochordal canal with the surface ectoderm and yolk sac. These connections are referred to as the neurenteric canal.

►Teratoma

Sacroiliacal Joint Arthritis, Sacroiliitis

Sacroiliacal joint arthritis, sacroiliitis is the key manifestation in spondathropathies, mainly in ankylosing spondylitis. The typical X-ray imaging triad is destruction, sclerosis, and bony bridging.

►Spondyloarthropathies, Seronegative

SAE

►Stimulated Acoustic Emission (SAE)

Sagittal Outlet

Distance on a midsagittal section from the end of the sacrum to the bottom of the inner cortex of the symphysis.

►Magnetic Resonance Pelvimetry

Salivary Gland Inflammation

►Salivary Glands, Inflammation, Acute Chronic

Salivary Glands, Inflammation, Acute, Chronic

Silvio Mazziotti
Department of Radiological Sciences,
University of Messina, Messina, Italy
smazziotti@unime.it

Synonyms

Salivary gland inflammation; Sialoadenitis

Definition

Sialoadenitis is a condition characterized by inflammation of one or more of the salivary glands.

Inflammatory diseases are the most common illness affecting the major salivary glands.

There are both acute and chronic forms. Acute inflammation of the salivary glands has only few causes, most commonly being of viral or bacterial origin. On the other hand, chronic salivary inflammation may be caused by numerous processes as infectious, systemic, autoimmune and certain neoplasms.

Pathology/Histopathology

Acute ►sialadenitis is a condition characterized by inflammation and swelling of one or more salivary glands. The gland may be diffusely or focally enlarged. The pathologic process is characterized by very important interstitial edema with limited infiltration of periductal and interacinar connective by granulocytes, lymphocytes, and monocytes. Moreover, acinar-ductal epithelium is swollen and desquamed. Granulocytes and round cells can be observed in the ductal lumen. During acute sialadenitis, abscess formation may take place. Predisposing factors include dehydration and excretory duct obstruction caused by stones or fibrosis. Purulent material may be expressed from the ductal orifice in most bacterial infections.

In chronic inflammation, salivary glands are normal sized or smaller. In chronic sialadenitis, there are varying degrees of acinar atrophy, lymphoid infiltrate with or without germinal centers, and fibrosis. The ducts exhibit dilatation and hyperplasia of the lining epithelium with metaplasias. Extensive dilatation can result in cyst formation. Goblet cell metaplasia produces abundant mucin. The overall architecture of the gland is usually maintained.

Clinical Presentations

Acute inflammation of the salivary glands is usually of viral or bacterial origin; viral and bacterial infections are the most common causes of salivary abnormalities. Mump represents not only the most common cause of parotid swelling, but also the most common viral disorder of the salivary glands. Children are most often affected with peak of incidence at approximately 4–6 years of age. Typically, there is a 2–3 week incubation period with associated fever, malaise, myalgia, and headache which may precede the observed parotid swelling. Salivary gland involvement may be seen in a wide range of other viral illnesses including those caused by cytomegalovirus, lymphocytic choriomeningitis virus, coxsackievirus A, echovirus, and parainfluenza virus type C among others.

Acute suppurative sialadenitis is most commonly bacterial in origin and most often involves the parotid, and to a lesser extent, the submandibular glands. This is in part due to the fact that the serous saliva of the parotid has a lower bacteriostatic effect than the more mucous saliva of the ►submandibular gland. The most common offending agent is *Staphylococcus aureus.* Other aerobic organisms isolated are *Streptococcus pneumoniae, Hemophilus influenzae,* and *Escherichia coli.* Salivary stasis secondary to either obstruction (e.g., sialoliths, ductal strictures) or decreased production, often as a result of dehydration, is thought to be an integral component in the pathogenesis of this condition. Common clinical settings in which this entity may occur include the elderly postoperative patient after cardiothoracic or gastrointestinal surgery and more frequently the debilitated, dehydrated patient, usually with poor oral hygiene. The typical presentation involves sudden, diffuse enlargement of the gland with associated induration and tenderness. Massage of the involved gland results in the secretion of purulent material from the duct. Patients with an undiagnosed or incompletely treated acute suppurative sialadenitis can develop an intraglandular abscess. Small abscess may form and coalesce to form a larger abscess, or a solitary abscess may develop. It usually manifest as painful swelling of the salivary gland with skin reddening.

Decreased salivary flow with stasis is a key factor in chronic sialadenitis. Like acute sialadenitis, this condition is more common in the ►parotid gland. Its development is often associated with a previous episode of acute suppurative inflammation with subsequent glandular destruction. Another possibility is the recurrent parotitis of childhood which has continued into adulthood.

Symptoms include intermittent swelling of the gland, often painful, that may or may not be associated with food assumption. Approximately 80% of patients experience permanent xerostomia. It is very important to differentiate the obstructive and nonobstructive disease, since their treatment and prognosis often vary significantly. The chronic obstructive disease involves the submandibular gland more frequently than the parotid gland. Conversely, the nonobstructive disorders are more common in the parotid glands.

Other infectious agents, like *Mycobacterium tuberculosis*, atypical mycobacteria, *Toxoplasma gondii*, *Actinomyces israeli* can determine chronic sialadenistis either as an ascending infection from the oral cavity or as a part of a systemic process.

Noninfectious conditions such as autoimmune disease, previous irradiation, or idiopathic causes may also lead to chronic inflammation. Sjogren Syndrome is a chronic, slowly progressive, relatively benign autoimmune disease characterized by lymphocyte-mediated destruction of the exocrine glands resulting in keratoconjunctivitis sicca and xerostomia. The disease primarily affects middle-aged women, but can be seen in all ages.

Imaging

Ultrasonography. The examination should be carried out with the highest-frequency transducer possible. Usually, 5–12-MHz wide-band linear transducers are used. In acute inflammation salivary glands are enlarged and with

reduced echogenicity (1–3). They may be inhomogeneous for the presence of multiple, small, oval hypoechoic areas in their content. Increased intraglandular blood flow can be depicted at US. Abscesses are hypoanhechoic lesions with posterior acoustic enhancement and blurred borders (1). Central colliquation may be distinguished as an avascular area or identified by means of moving debris. A hyperechoic halo can surround an organized abscess (1). In chronic inflammation, salivary glands are normal sized or smaller, hypoechoic and non homogeneous; usually they do not have increased blood flow at Doppler examination. Salivary glands' US is the technique to be used in the suspect of calculosis. US features of scialolithiasis include strongly hyperechoic lines or points with distal acoustic shadowing, which represent stones. However, in chronic ductal scialolithiasis complicated by chronic or recurrent inflammation, the gland may lose its function and stones located in a nondilated duct may be difficult to demonstrate.

Conventional radiographs. The plain radiographic examination is rarely used today for the evaluation of the major salivary glands.

Although conventional radiographs can be obtained quickly and at low cost they are of limited clinical value since they only identify reasonably large, fairly dense calcifications (2).

Sialography. Sialography is a radiographic examination of the parotid or submandibular gland that uses a positive contrast agent to demonstrate the ductal salivary anatomy. It is an invasive procedure in which radiopaque contrast medium is injected retrograde into the glands ductal system *via* the intraoral opening of either Wharton's or Stensen's duct. Conventional sialography has been used for investigating the ductal system of major salivary glands. Imaging is performed to delineate inflammatory or obstructive changes within the ductal system of parotid and/or submandibular glands (2, 3). The technique is contraindicated in the acute setting of sialoadenitis, as it could cause retrograde spreading of the infection into the gland. Sialography should be used essentially for assessing chronic sialoadenitis as well as Sjogren's syndrome (2, 3).

Computed tomography. CT examination performed very early in an acute infection, allows to demonstrate dilatation of the central ducts and enhancement of the central ducts and of Stensen's duct. The salivary gland can appear variably enlarged and has an increased attenuation on basal scans due to the cellular infiltration (2, 3). There may be diffuse enhancement of the gland on postcontrast images, reflecting the increased vascularity. Presence and location of sialoliths can be clearly detected at CT. If present, inflammatory stranding into the overlying subcutaneous tissue is usually identifiable. CT scans obtained in the coronal plane for inflammatory conditions of the parotid and submandibular glands may be helpful for evaluating the extent of the lesion; in particular the relationship of the inflammatory mass to the floor of the mouth for submandibular lesion and the skull base for the parotid gland masses, both findings of great importance with respect to the surgical approach (2, 3). Because of the fatty attenuation that is intrinsic to the parotid glands, abscesses are particularly well seen on contrast-enhanced CT scan. Most important CT findings in chronic sialadenitis are related to changes from chronic scialolithiasis that may result in a small atrophic gland with focal intraglandular calcifications. More rarely a large ductal stone without signs of acute glandular inflammation can be seen.

Magnetic resonance imaging. Magnetic resonance provides better imaging of soft tissue than CT, but it is less suitable to investigate the suspected inflammatory diseases of the salivary glands due to its inability to visualize small potential clinically significant calcifications. In acute inflammation, on MRI the interested gland is variably enlarged with a reduced visualization of both interstitial and ductal component compared to a normal gland. The gland can have either higher o lower signal intensity than normal one on T2-weighted images, depending on whether edema or cellular infiltration predominates (2, 3). The MR sialographic technique with heavily T2-weighted images for depiction of static or nearly static fluids represents a noninvasive technique for the detection of ductal abnormalities in major salivary glands (4). The most obvious advantage of this technique is the fact that images can be obtained without use of ionizing radiation and its noninvasiveness as well. No contrast material has to be injected, and images can be obtained with short acquisition times of less than 10 sec. Contralateral salivary glands can be easily visualized without further positioning of the patient and can serve as controls. Contraindications for conventional sialography such as acute sialadenitis are not contraindications for MR sialography. Ductal structures can also be visualized in cases of complete obstruction of the ductal system. Also, additional cross-sectional images of the glandular parenchyma can be obtained by using conventional T1- and T2-weighted sequences. Furthermore, MR sialography has an excellent sensitivity for visualization of edema in the salivary parenchyma, which is more difficult to diagnose with CT.

Nuclear Medicine

Nuclear medicine has a limited role in the assessment of sialadenitis. Sequential scintigraphy is currently employed for assessing the functional status of all the four major salivary glands and evaluating the chronic evolution of glandular damage.

Diagnosis

Most of the salivary glands diseases are characterized only by a few distinct clinical and laboratory tests patterns. Clinical judgment with a careful history and physical examination are still considered of great relevance. However, to obtain a definite diagnosis, imaging techniques are required in most cases. Salivary glands US is the technique to be firstly used because in many cases the nature of underlying disease can be promptly suggested. However, as the imaging identification of calcification is important in the diagnosis of inflammatory process of the salivary glands, in doubtful cases at US, CT represents the examination of choice. In particular, CT is more accurate than US in detecting the presence and the number of sialoliths and in distinguishing multiple clusters of stones from single large stones. Usually, CT in this setting is best performed without administration of contrast material, since small opacified blood vessels may simulate small sialoliths. If an abscess or inflammatory process is suspected, adding enhanced scans after identifying stones on nonenhanced scans may be useful. Conventional sialography today should be used essentially for assessing chronic sialoadenitis unrelated to ▶sialolithiasis. At present, MR sialography should be preferred because of the greater sensitivity in diagnosing inflammatory diseases of the salivary glands so that incannulation of the salivary duct is not required.

Finally, in case of suspected autoimmune sialadenitis, the disease could be usefully assessed by mean of needle biopsy.

Bibliography

1. Bialek EF, Fakubowski W, Zajkowski P et al (2006) US of the major salivary glands: anatomy and spatial relationships, pathologic conditions, and pitfalls. Radiographics 26:745–763
2. Yousem DM, Kraut MA, Chalian AA (2000) Major salivary gland imaging. Radiology 216:19–29
3. Rabinov JD (2000) Imaging of salivary gland pathology. Radiol Clin North Am 38:1047–1057
4. Kalinowski M, Heverhagen JT, Rehberg E et al (2002) Comparative study of MR sialography and digital subtraction sialography for benign salivary gland disorders. Am J Neuroradiol 23:1485–1492

Salivary Glands, Neoplasms

Misa Sumi, Takashi Nakamura
Department of Radiology and Cancer Biology, Nagasaki University School of Dentistry, Nagasaki, Japan
misa@nagasaki-u.ac.jp

Definition

Epithelial (adenomas and carcinomas) and nonepithelial tumors arising from the major and minor salivary glands. Salivary gland neoplasms represent 3–5% of all head and neck tumors, and occur most frequently (approximately 80%) in the parotid gland. The majority (70–80%) of the parotid gland tumors are benign. Tumors of the submandibular gland and sublingual glands occur less frequently, but are more likely to be malignant; approximately 40% and 70% of tumors are malignant in the submandibular and sublingual glands, respectively. On the other hand, 50% of all minor salivary gland tumors are malignant.

Pathology/Histopathology

WHO's histological classification of salivary gland tumors includes 13 adenomas and 24 carcinomas (1). Pleomorphic adenomas are the most common benign epithelial tumors of the salivary glands. This benign tumor usually appears as an ovoid, well-circumscribed mass that may exhibit a pedunculated outgrowth, for example, from the superficial to deep lobes of the parotid gland. The lesion may be associated with cystic change, hemorrhage, and calcification. In major parts of the tumor contain glandular, ductal, or solid structures of epithelial elements. The lesion also contains mesenchymal tissues, which may be frequently associated with chondroid and fibromyxomatous tissues.

Warthin's tumor exclusively occurs in the parotid gland, typically in the tail of the gland, and is the second most common benign lesion of the parotid gland. It may occur as multiple masses within one or both parotid glands. Cystic change is among the characteristic features of the lesion. Warthin's tumor is composed of a double layer of oncocytes that line the papillary projections, extending into the cystic spaces.

Mucoepidermoid carcinoma represents approximately 30% of the malignant tumors of the salivary glands, and arises most commonly (approximately 50%) in the parotid gland and the second most commonly (approximately 45%) in the minor salivary glands. The tumors may be classified as low, intermediate, or high grade. Low-grade tumors are well-circumscribed, usually contain large cystic areas with mucinous components, and abundant goblet cells that are lined by squamous components. Low-grade tumors are rarely associated with nuclear polymorphism, mitotic features, or necrosis. In contrast, high-grade tumors are poorly circumscribed, infiltrative, and exhibit dominant proliferation of the squamous components; goblet cells are rarely observed.

Adenoid cystic carcinoma represents the most common malignancy arising from the submandibular and

sublingual glands, accounting for approximately 12% and 15% of tumors of these glands, respectively. The tumor is partially encapsulated and is rarely associated with cyst formation and hemorrhage. Histopathologically, adenoid cystic carcinoma is classified into the tubular (low grade), cribriform (intermediate grade), or solid (high grade) type; occasionally, some of these types are occasionally seen in a single tumor. This tumor has a tendency to spread via the nerves. Perineural invasion is a hallmark of this tumor; it may be present distally in a nerve, and the proximal segment may appear normal (perineural skip extension).

Acinic cell carcinoma represents approximately 9% of all malignant tumors of the parotid gland. The parotid gland is the most common site of origin of this tumor, and bilateral involvement is observed in 3% of patients. It is a solid mass or is partially cystic. Histologically, the acinic cell carcinoma recapitulates serous cells with bubbly basophilic cytoplasm containing zymogen granules.

Salivary duct carcinoma is an extremely aggressive tumor, and histologically displays squamoid appearance, reminiscent of mucoepidermoid carcinoma or squamous cell carcinoma. Perineural spread is also common in this malignant neoplasm, and lymph node metastasis is not uncommon.

Clinical Presentation

Benign tumors are usually slow growing, movable, painless masses. Malignant tumors present as firm, fixed and painless masses; in advanced stage, symptoms can include pain, otorrhoea, paraesthesia, facial nerve palsy, dysphagia, trismus, and cervical lymph node involvement. Pain or itching over the course of the facial nerve suggests a malignant parotid tumor. In addition, the combination of cranial nerve VII and V3 neuropathy suggests adenoid cystic carcinoma of the deep lobe of the parotid gland.

The American Joint Committee on Cancer proposed the clinical staging of the malignant tumors of the major salivary glands chiefly based on the tumor size. Minor salivary gland tumors are staged as those arising from the corresponding anatomical sites.

The anatomical region of a malignant salivary gland tumor is an important prognostic factor for local control and overall survival (3). The T-stage is an independent prognostic factor for local control. The histological type is an independent prognostic factor for distant metastasis. The T- and N-stages, and skin involvement are prognostic factors for distant metastasis and overall survival. The N-stage and facial paralysis are prognostic factors for local control. Metastasis to the regional lymph nodes is relatively rare in malignant salivary gland tumors, while it occurs in 40% of squamous cell carcinomas. Distant metastasis occurs in approximately 20% of malignant salivary gland tumors (most frequently seen in adenoid cystic carcinomas).

Imaging

Preoperative prediction of the malignancy or benignancy of salivary gland tumors is clinically very important, because this information strongly influences the surgical plan. In general, MR imaging is the first choice for the imaging of the salivary gland tumors. CT and sonography are alternatives to MR imaging.

Magnetic Resonance Imaging

Although conventional T1-weighted MR imaging with or without gadolinium enhancement and T2-weighted MR imaging techniques have been used for the diagnosis of salivary gland tumors, many investigators have reported difficulty in the differentiation of these tumors, particularly between benign and low-grade malignant tumors.

►*High-resolution MR imaging* of the salivary gland tumors using a small surface coil well delineates the detailed structures of the tumors and can provide important clues regarding their histologies and for prediction of their benign or malignant nature (Fig. 1).

Pleomorphic adenomas are usually well-defined, homogeneously intermediate to hypointense on T1-weighted images, and heterogeneously hyperintense on fat-suppressed T2-weighted images (Fig. 1a). Warthin's tumors exhibit various features ranging from hypointense to hyperintense on T1-weighted and fat-suppressed T2-weighted images (Fig. 1b). Cyst formation is observed in one-third of Warthin's tumors, resulting in hyperintense foci on fat-suppressed T2-weighted images. Hyperintensities in the cystic areas on T1-weighted images indicate the presence of proteinaceous fluids, colloidal materials, or hemorrhage.

In general, high-grade malignancies have irregular, infiltrating margins (Fig. 2). Compared with low-grade malignancies and benign lesions, high-grade malignant tumors are associated with high cellularity, and thus have lower signal intensities on fat-suppressed T2-weighted images.

Differential diagnosis of benign and malignant salivary gland tumors based on the descriptive characterization on conventional T1-weighted and fat-suppressed T2-weighted imaging may be further substantiated by using quantitative parameters obtained by functional MR imaging, for example, ►*apparent diffusion coefficient* (*ADC*) maps obtained by ►*diffusion-weighted MR imaging* and ►*time-signal intensity curves* (*TICs*) obtained by ►*dynamic contrast-enhanced MR imaging*.

The increased nuclear-to-cytoplasmic ratio and hypercellularity, both of which are frequently observed in highly malignant tumors, reduce the extracellular matrix and the diffusion space of water protons in the extracellular and

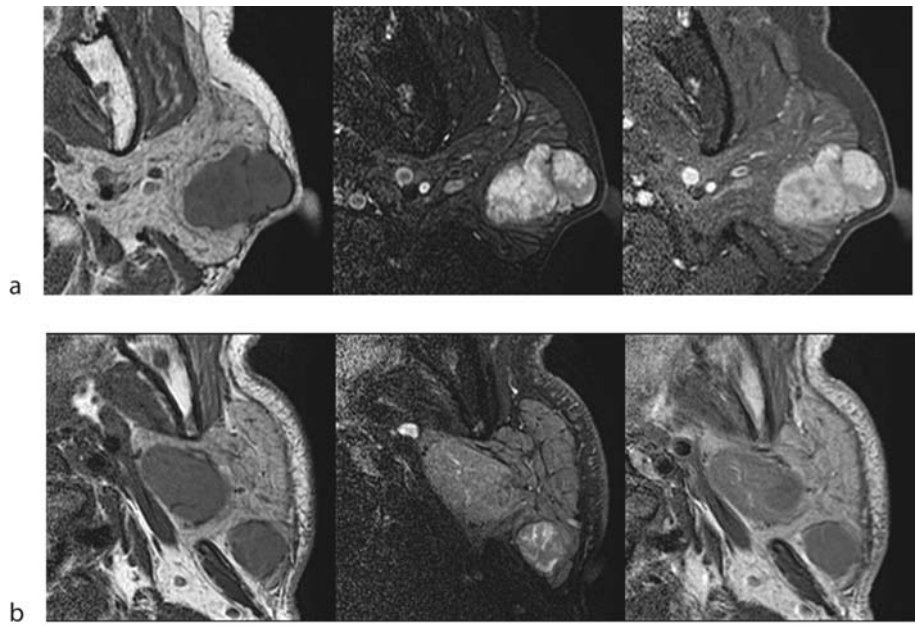

Salivary Glands, Neoplasms. Figure 1 High-resolution MR imaging of benign salivary gland tumors using a 47-mm microscopy coil. Axial T1-weighted images (left panels), and fat-suppressed T2-weighted images (center panels), and gadolinium-enhanced T1-weighted images (right panels) show pleomorphic adenoma (a) and Warthin's tumor (b) of parotid glands. High-resolution imaging reveals detailed architectures of salivary gland tumors. Note that multiple occurrences of Warthin's tumor as in (b).

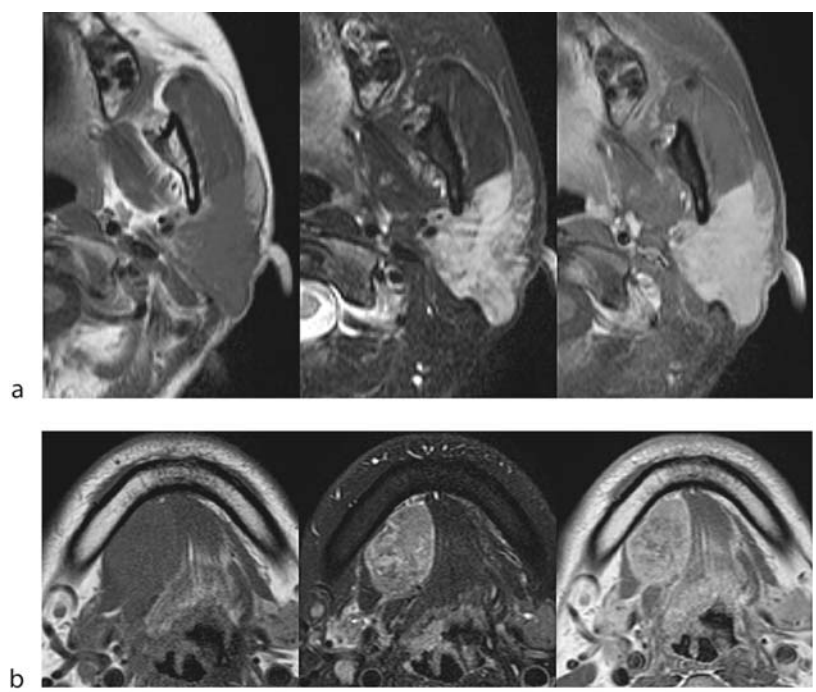

Salivary Glands, Neoplasms. Figure 2 MR imaging of malignant salivary gland. Axial T1-weighted images (left panels), fat-suppressed T2-weighted images (center panels), and gadolinium-enhanced, T1-weighted images (right panels) of adenoid cystic carcinoma (a) and carcinoma ex pleomorphic adenoma (b) of parotid and sublingual glands, respectively.

intracellular dimensions, along with a resultant decrease in the *ADCs*. Therefore, the ADCs of malignant solid lesions are lower than that of benign tumors, except Warthin's tumors. The ADCs of solid lesions of Warthin's tumors are low and mimicked values of malignant tumors. A proliferation of the epithelial component and intense lymphoid accumulation in the stroma may have decreased the ADCs of the Warthin's tumors.

Based on the time of peak enhancement (T-peak) and the washout ratio (WR), salivary gland tumors could be categorized into four types (4). In type A, the *TIC* has a long T-peak, and is characteristic of pleomorphic adenomas. In type B, the *TIC* has a short T-peak and a high WR and is characteristic of Warthin's tumor. In type C, the *TIC* has a short T-peak and a low WR and is characteristic of cancers. In type D, the *TIC* is flat and is suggestive of cystic or necrotic area. The combined use of the *ADC* maps and *TIC* criteria could greatly improve the diagnostic ability of MR imaging.

Sonography

The sonographic examination of the salivary glands is usually performed using a high-frequency (10–14 MHz) transducer. This yields high-resolution images of superficial organs such as the parotid and submandibular glands (Fig. 3). However, sonographic images of the deeper parts of the glands may be of poor quality. This is the chief reason that sonography is not used as frequently as CT or MR imaging in examining patients with possible deep extensions of salivary gland tumors. Differentiation of benign and malignant salivary gland tumors on the basis of descriptive studies on gray-scale images is difficult. On the other hand, quantitative sonographic analysis could be employed for effective diagnosis of benign and malignant tumors of the parotid gland; the combined use of the sonographic criteria (the mean gray level and the standard deviation of the echo levels) greatly improved the diagnostic accuracy when compared with that of qualitative diagnosis (5).

It is not clear which differences in tumor tissues may result in the characteristic differences in internal architectures of sonographic images of the salivary gland tumors. We often observe cystic areas, connective tissues, hyalines, and necrotic and keratinized materials in tumor tissues. Probably, these microscopic changes may result in the observed differences in echogenicity.

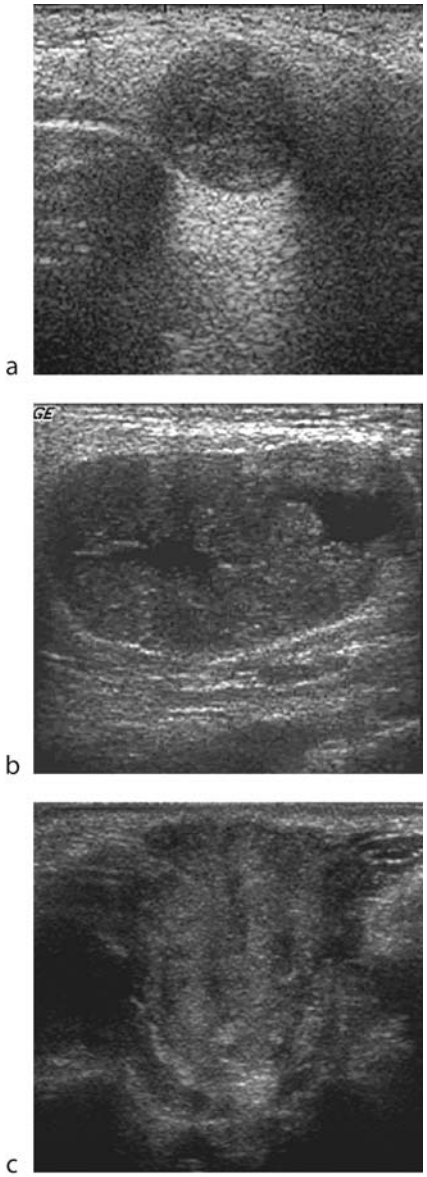

Salivary Glands, Neoplasms. Figure 3 Sonographic images of benign and malignant parotid gland tumors. Sonography shows well-defined tumor margins in pleomorphic adenoma (a) and Warthin's tumor (b), while ill-defined margin in adenoid cystic carcinoma (c). Tumor echogenicity is homogeneous in pleomorphic adenoma (a), while heterogeneous in Warthin's tumor (b) and adenoid cystic carcinoma (c).

Nuclear Medicine

Nuclear imaging is most frequently employed for examination of salivary gland tumors such as Warthin's tumors and oncocytomas, both of which highly accumulate technetium (Tc) 99m. Positron emission tomography (PET) studies using 2-[F-18]fluoro-2-deoxy-D-glucose (FDG) are capable of demonstrating high-grade malignant tumors with increased metabolic activity. However, significant overlaps occur with benign tumors such as Warthin's tumors.

Diagnosis

In addition to the assessment of the benign or malignant nature of salivary gland tumors, the imaging should be mainly focused toward evaluating the following points: (1) whether a tumor is confined to the parenchyma of the gland or extends outside the gland into the upper neck and skull base; (2) whether a tumor involves the facial nerve; although the precise identification is difficult even on *high-resolution MR imaging*, the tumor location relative to the main trunk of the facial nerve (pes anserinus) may be identified by using anatomical landmarks such as the "tragal cartilaginous pointer" (the facial nerve trunk runs 1 cm caudal and 1 cm medial to the "pointer"), the stylomastoid process (the nerve runs lateral to the process and in the fat tissues), and the vascular plain (which lies lateral to the superficial temporal, retromandibular, and anterior facial veins); (3) whether the tumor has smooth or infiltrative margins; (4) whether lymph node metastasis is absent or present; and (5) whether multiple tumors are present; multiple occurrence is observed particularly in Warthin's tumors, pleomorphic adenomas, oncocytomas, acinic cell carcinomas, basal cell adenomas, and lymphomas.

Bibliography

1. Barnes L, Eveson JW, Reichart P et al (2005) World health organization classification of tumors. Pathology and genetics of head and neck tumors. In: Tumours of the Salivary Glands. International Agency for Research on Cancer, Lyon, pp 209–274
2. American Joint Committee on Cancer (1988) Major salivary glands. AJCC Cancer Staging Handbook: AJCC Cancer Staging Manual. 5th edn. Lippincott William & Wilkins, Philadelphia, pp 57–64
3. Terhaard CHJ, Lubsen H, Van der Tweel I et al (2004) Salivary gland carcinoma: independent prognostic factors for locoregional control, distant metastases, and overall survival: results of the dutch head and neck oncology cooperative group. Head & Neck 26:681–693
4. Yabuuchi H, Fukuya T, Tajima T et al (2002) Salivary gland tumors: diagnostic value of gadolinium-enhanced dynamic MR imaging with histologic correlation. Radiology 226:345–354
5. Yonetsu K, Ohki M, Kumazawa S et al (2004) Parotid tumors: differentiation of benign and malignant tumors with quantitative sonographic analyses. Ultrasound Med Biol 30:567–574

Salt-Losing Crisis

A deficiency of aldosterone that results in hyponatremia and hyperkalemia, leading to dehydration, hypotension, circulatory collapse, and, when severe, death.

▶ Adrenogenital Syndrome

SAPHO

G M Lingg, C Schorn
Department of Radiology,
Sana Rheumazentrum Rheinland Pfalz,
Bad Kreuznach, Germany
dr.lingg@sana-rheumazentrum-rlp.de

Synonyms

Acquired hyperostosis syndrome; Pustulotic arthroosteitis; Sternoclavicular hyperostosis

Clinical Presentation

SAPHO is an association of skin and bone disease. The skin manifestation is either acne conglobata or fulminans or, more typically, psoriasis pustulosa palmaris and plantaris. Eighty percent of patients present with anterior chest wall affection, with relapsing and migrating symmetrical or asymmetrical pain and a tough swelling around the sternoclavicular joints that is often aggravated by cold exposure. There is no gender predilection. Children exhibit CRMO, whereas adults show multiforme osteitis such as sternoclavicular. The location of the osteitic focus may be quite variable, causing a variable clinical presentation. The sacroiliacal and vertebral affection is facultatively associated.

Imaging

In anterior chest wall involvement, plain X-rays of the sternoclavicular joints show a varying degree of enostal and periostal sclerosis of the sternum and medial clavicular ends. Sternoclavicular arthritis with mild destruction may occur. Ligament and costal cartilage ossification is typical. In late stages, broad ossification bands from the sternum to the clavicle and upper rips obscure the normal anatomy. In early case, the plain films may show no abnormality. Sternoclavicular CT is employed. Sclerosis, bone formation, and enostal and periosteal and extrathoracal and intrathoracal (retrosternal fibroostitis) as well as sternoclavicular arthritis are seen with more conspicuity. MR imaging is not recommended because the sclerotic foci are a predominant finding and are best visualized by means of CT. MRI is, however, sensitive to the inflammatory process.

Sacroiliitis is a typical feature, mainly indistinguishable from ankylosing spondylitis, but sometimes with atypical asymmetrical marked sclerosis or destruction.

The affection of the spine may be similar to ankylosing spondylitis, but it presents with certain atypical features in a number of cases, such as marked vertebral sclerosis, ►giant shining corners, and ►bamboo-cane fragments. The latter refers to an oligosegmental sclerosing, but in these few segments, completely syndesmophytic ankylosed spine is in contrast to the otherwise normal radiologic appearance. In some cases the osteoproliferative features are heavily pronounced and the aspect is more like an atypical DISH (atypical because of, for instance, destructive and sclerotic details or ankylosis of the appendicular joints).

Osteitic foci in other locations are erosive or nonerosive, multiforme, and expansile. Severe differential diagnostic problems can arise because of the resemblance to bacterial spondylitis/osteomyelitis, osteoblastic metastases, and osteogenic tumors.

Nuclear Medicine

Bone scans show foci of increased osteoblastic activity (hot spots), especially in the sternoclavicular region. As a rule, in degenerative disease, which also causes sternoclavicular hot spots, the tracer accumulation is not intense enough to be seen from the back, and costal cartilage ossification does not expose tracer accumulation at all. In contrast, in SAPHO the costal cartilage ossification is an inflammatory-promoted process and does accumulate markedly. Bone scans are very sensitive but unspecific and can show foci in any location and direct the diagnostic work-up to these areas.

Bibliography

1. Dougados M, van der Linden S, Juhlin R et al (1991) The European Spondyloarthropathy Study Group: preliminary criteria for the classification of spondyloarthropathy. Arthritis Rheum 34:1218–1227
2. van der Linden SM, Valkenburg HA, Cats A (1984) Evaluation of diagnostic criteria for ankylosing spondylitis: a proposal for modification of the New York criteria. Arthritis Rheum 27:361–368
3. Taylor WJ (2005) Understanding psoriatic arthritis. Hosp Med 66:163–167
4. Dihlmann W (1993) Acquired hyperostosis syndrome (so-called pustulotic arthro-osteitis): review including 73 self-observed cases. Wien klin Wochenschr 105:127–138

SAPHO

SAPHO syndrome (synonyms: acquired hyperostosis syndrome, pustulotic arthroosteitis, sternoclavicular hyperostosis) is a varied rheumatic symptom complex mainly with involvement of the anterior chest wall (sternoclavicular arthritis, sternal [clavicular] sclerosing hypertrophic osteitis with marked bony apposition, ligament ossification, osteoproliferation) and skin manifestation (acne fulminans or psoriasis pustulosa). Frequently, it is associated with spondyloarthropathy; then, sacroiliitis and oligosegmental sclerosing or ankylosing vertebral involvement are typical.

►Fractures, Stress

►Spondyloarthropathies, Seronegative

Sarcoid Arthropathy

There are three patterns of sarcoidosis joint involvement–Löfgren's syndrome, and early and late patterns of sarcoidosis arthropathy. Löfgren's syndrome is characterized by arthralgias, erythema nodosum and bilateral hilar lymphadenopathy. The early sarcoidal arthropathy pattern is manifested by polyarticular involvement of the distal extremities. The late manifestation of sarcoid arthropathy (6 months or more after sarcoidosis diagnosis) is a granulomatous synovitis. The diagnosis of sarcoidosis arthropathy is usually based on clinical presentation rather than imaging.

►Sarcoidosis, Musculoskeletal System

Sarcoidosis, Musculoskeletal System

Sandra Moore
NYU Medical Center, NY
sandra.moore@nyumc.org

Synonyms

Nonnecrotizing granulomatous disease

Definition and Pathology/Histopathology

►Sarcoidosis is an inflammatory disorder of unclear etiology, characterized by the presence of noncaseating ►granulomas in the tissues. This is usually confirmed by fiber optic bronchoscopy, biopsy of lung or lymph node, a positive Kveim-Siltzbach test, or a combination of these methods, revealing nonnecrotizing epithelioid granulomas in the absence of other granulomagenic agents.

Clinical Presentation

Sarcoidosis most commonly affects the pulmonary and lymphatic systems, but may involve the muscles, joints, and bones, with osteoarticular complaints commonplace. These include muscle weakness, generalized muscle pain, soft tissue swelling and/or multiarticular stiffness, and pain. Lesions detected at imaging in sarcoidosis patients maybe symptomatic or asymptomatic.

Imaging

Neither skeletal survey nor conventional bone scan reliably detects sarcoidal bone lesions, except in the small bones of the hands and feet (1). The radiographic appearance of lacy osteolysis in the bones of the hands is familiar to radiologists, but there are myriad musculoskeletal manifestations, which may be revealed in advanced imaging (specifically MRI), including subcutaneous infiltration, various muscle lesions, sarcoidal arthropathy, and large and axial bone lesions (2).

Sarcoidosis Soft Tissue Masses

Sarcoidosis soft tissue lesions are uncommon, and present as palpable mass or swelling. These may be well defined or indistinctly marginated, with nonspecific signal characteristics—low on T1 weighted sequences, high on fluid sensitive sequences, and enhancing. These can be detected in the subcutaneous, inter- or intramuscular spaces. Differential diagnosis includes cellulitis (if subcutaneous and reticulated), or an inflammatory versus neoplastic mass. Biopsy is usually required, as MR imaging features are not pathognomonic.

Sarcoidal Muscle Lesions

Sarcoidal muscle involvement includes myopathy/atrophy, myositis, and sarcoidal muscle nodules (3). Sarcoid-related myopathy presents clinically with elevated serum creatine kinase and aldolase, symmetric proximal weakness, and electromyographic evidence of myopathy. On MRI, there is fatty replacement of muscle. Sarcoidal myopathy cannot be differentiated from atrophy secondary to corticosteroid treatment on the basis of MR appearance, however MRI is useful to delineate the extent and severity of involvement and determine optimal muscle biopsy sites. Sarcoidal muscle nodules are uncommonly observed, and present as tender palpable masses. On MRI these show a central low signal and rim enhancement, due to fibrosis, which has been described as a "dark star" (Fig. 1).

Sarcoidal Arthropathies

Three patterns of sarcoidosis joint disease may be encountered—Löfgren's syndrome, and early and late patterns of sarcoidosis arthropathy. Löfgren's syndrome is characterized by arthralgias, erythema nodosum, and bilateral hilar lymphadenopathy. The early sarcoidal arthropathy pattern (presenting during the first 6 months of sarcoidal symptoms) is manifested by polyarticular involvement of the distal extremities—ankles, knees, PIP joints, wrists, and elbows. Radiographs are usually negative, or show osteoporosis and soft tissue swelling, with rheumatoid arthritis as the principal radiographic differential diagnosis. A later manifestation of ▶sarcoid arthropathy (6 months or more after the diagnosis of sarcoidosis) usually involves 2–3 joints including the knees, ankles, proximal interphalangeal joints, and

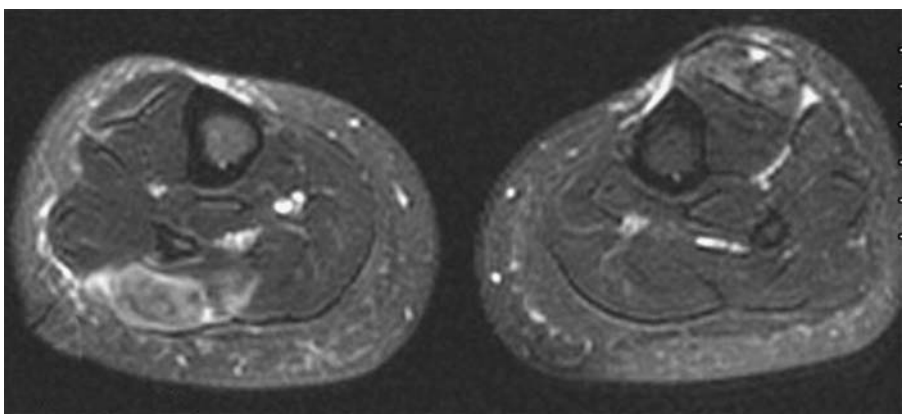

Sarcoidosis, Musculoskeletal System. Figure 1 Fifty-one year-old woman with sarcoidosis who presented with tender nodules along both calves. T2 weighted axial image demonstrates edematous nodules within the right posterior and left anterior compartment muscles. After contrast administration, these enhanced peripherally (not shown), with "dark star" appearance characteristic of nodular muscle sarcoid lesions. Noncaseating granulomas were found at biopsy.

occasionally the wrists or shoulders. Dactylitis may occur. These patients usually have granulomatous synovitis, and the disease course is transient or relapsing. Radiographic changes consist of subchondral cystic change. The joint abnormalities detected on radiographs and MRI in sarcoidosis patients reflect nonspecific arthropathy of indeterminate origin, which includes the common arthritides. Whether sarcoidosis contributes to the imaging findings is speculative, as synovial biopsy is not routinely obtained, and the diagnosis is usually based on clinical rather than imaging parameters. When MRI is performed, joints affected by sarcoidosis arthropathy may show lesions that are occult on plain films. Tenosynovitis, tendonitis, bursitis, synovitis, and prominent subchondral cysts can be demonstrated on MRI, but are nonspecific findings. Large subchondral cysts in the absence of osteophytosis may be seen in patients younger than those usually presenting with osteoarthritis with geodes.

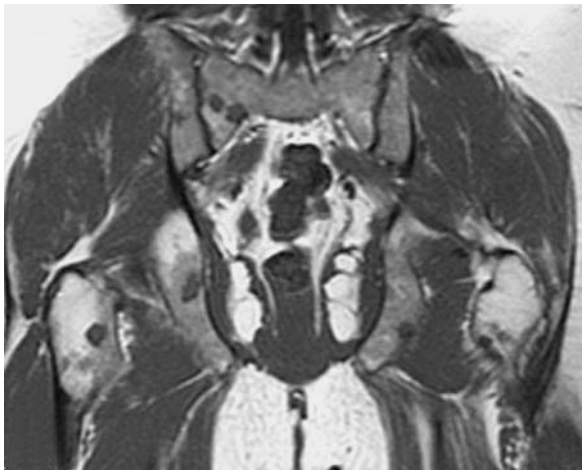

Sarcoidosis, Musculoskeletal System. Figure 2 Forty-eight year-old man with sarcoidosis and hip pain. Radiographs were negative. T1 weighted coronal image through the posterior of the pelvis demonstrates multiple rounded ("cannon ball") low signal foci. Six months later, these showed resolution on MR images.

Bone Sarcoidosis

Osseous involvement is estimated to occur in about 5% of sarcoid patients, although it is important to consider that this percentage is derived from radiographic studies and may underestimate disease occult on radiographs (4). The diagnosis of sarcoidosis has usually been established by clinical criteria prior to the detection of suspicious bone lesions. Bone lesions may be biopsied to confirm sarcoidosis if the diagnosis is in doubt, or to exclude neoplasm. The radiographic appearance of lacy osteolysis in the bones of the distal extremities is considered virtually pathognomonic of sarcoidal involvement.

The alignment deformities in the hands and feet are often due to periarticular pathologic fractures rather than joint abnormalities. Large bone and spinal sarcoidal lesions, often occult on radiographs, maybe detected on MRI either incidentally, or in evaluation of musculoskeletal symptoms (5). On MRI, osseous sarcoidosis demonstrates a range of morphologies, from indistinctly marginated marrow infiltration, to discrete "cannon ball" and "starry sky" type lesions (Figs 2 and 3). The signal characteristics—low on T1 weighted images, increased signal intensity on water sensitive images, enhancing with contrast—are nonspecific. The principal differential considerations include bone metastases, lymphoma, myeloma, or rarely, disseminated nonmalignant entities such as fibrous dysplasia, disseminated fungal disease or tuberculosis, or serous atrophy. In some cases, we observed that the sarcoidosis lesions resolved on follow-up studies, with "ghosts" of the prior lesions showing central low signal correlating with fat and/or fibrosis (2). More study is needed to understand the natural history of these lesions on MRI. Our preliminary experience with

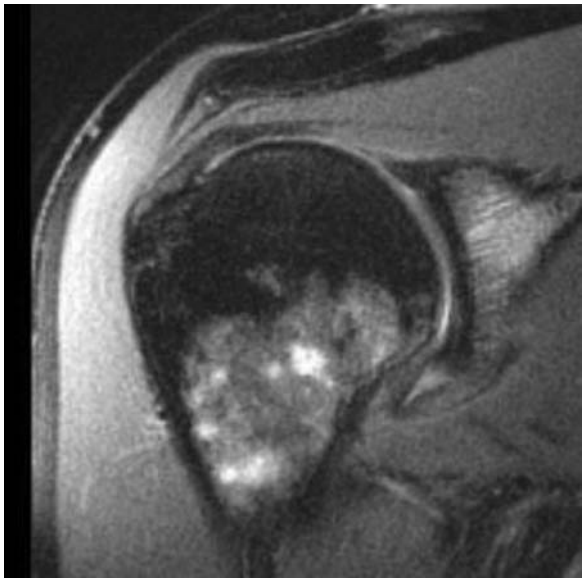

Sarcoidosis, Musculoskeletal System. Figure 3 Forty-six year-old man with shoulder pain. T2 fat saturated oblique coronal image of the shoulder demonstrates multiple round and irregular intramedullary high signal foci. These were detected throughout the shoulder girdle. Subsequent whole body MRI (not shown) revealed innumerable similar foci in bilateral upper and lower extremities, spine, and pelvis. Biopsy of the right humerus demonstrated noncaseating granulomas.

opposed phase imaging suggests that signal intensity changes on out-of-phase images is variable (i.e., may or may not drop significantly), which maybe related to the chronicity and/or activity of these lesions.

Nuclear Medicine

Sarcoidosis lesions show variable uptake on bone scan (1). Sarcoidosis bone lesions also may present a false positive for metastases on PET scanning.

Whole body MR scanning may be superior to PET imaging for the detection of diffuse sarcoidal bony lesions.

Conclusion

There are numerous musculoskeletal manifestations of sarcoidosis, many of which require advanced imaging for detection. The MRI findings of musculoskeletal sarcoidosis lesions may reveal a greater granulomatous burden than had been previously appraised. When musculoskeletal manifestations are detected, MRI is useful to follow response to treatment, and can guide biopsy in patients with unproven sarcoidosis.

With routine MRI technique, with the exception of sarcoidal muscle nodules, no pathognomonic imaging findings allow differentiation from other pathologies, including neoplasm. Therefore correlation with clinical and laboratory findings is essential for correct diagnosis. Radiologists should consider sarcoidosis in the differential diagnosis of musculoskeletal lesions detected at MRI in the appropriate setting (i.e., clinically proven sarcoidosis), and should be alerted that bony sarcoidosis lesions encountered on MRI can resemble metastatic lesions. In some patients in whom sarcoidosis is not proven or a second comorbidity is suspected, or to confirm sarcoidal histology, biopsy of the musculoskeletal lesion would be indicated.

Bibliography

1. Milman N, Lund JO, Graudal N et al (2000) Diagnostic value of routine radioisotope bone scanning in a series of 63 patients with pulmonary sarcoidosis. Sarcoidosis Vasc Diffuse Lung Dis 17:67–70
2. Moore SL, Teirstein AS (2003) Musculoskeletal sarcoidosis: spectrum of appearances at MR imaging. Radiographics 23:1389–1399
3. Otake S, Ishigaki T (2001) Muscular sarcoidosis. Semin Musculoskelet Radiol 5(2):167–170
4. James DG, Timmis B, Barter S et al (1989) Radiology of sarcoidosis. Sarcoidosis 6:7–14
5. Moore SL, Teirstein A, Golimbu C (2005) MRI of sarcoidosis patients with musculoskeletal symptoms. Am J Roentgenol 185 (1):154–159

Sarcoma

▶Neoplasms, Soft Tissue, Malignant

SBO

Small bowel obstruction.

▶Occlusion, Bowel in Childhood

Scalloping

An abnormality of the vertebral body characterized by concavity of the posterior wall.

▶Neurofibromatosis, Musculoskeletal Manifestations

Scapholunate Advanced Collapse

The prognostically poor late stage of scapholunate instability with secondary degenerative osteoarthritis.

▶Rheumatoid Arthritis

SCAVF

▶Spinal Cord Arteriovenous Fistula (SCAVF)

SCAVM

▶Spinal Cord Arteriovenous Malformation (SCAVM)

Schimmelbusch's Disease

▶Fibrocystic Disease, Breast

Schwannoma

A benign neurogenic soft tissue tumor of the peripheral nerve sheath, also designated as neurilemmoma.
►Neurofibromatosis, Musculoskeletal Manifestations
►Tumors, Spine, Intradural, Extramedullary

Sciatica

►Spinal Nerve Roots, Clinical Syndromes
►Radicular Syndrome of the Spine, Conservative Therapy for

Scintigram

A Scintigram is an image which assigns the data measured by scintigraphic means to spatial coordinates and, if applicable, to time.
►Scintigraphy

Scintigraphy

Lilli Geworski
Charité-Universitätsmedizin, Berlin, Germany
lilli.geworski@charite.de

Definition

Diagnostic procedures in nuclear medicine are based on the external detection of the γ-radiation emitted by incorporated radionuclides. The spatial distribution of these radionuclides in the (three-dimensional) object (patient) is recorded as a two-dimensional ►projection image by means of a ►gamma camera. This projection method is called planar ►scintigraphy, and the image itself assigns measured data to spatial coordinates and, if applicable, to time information. It is referred to as a ►scintigram.

Characteristics

Types of Scintigraphy

Planar scintigraphy can be performed as single-frame (static), multiple-frame (dynamic or gated), or whole-body imaging.

In static scintigraphy, the spatial distribution of activity in an organ is measured under the assumption that there is no significant change of activity distribution during the time interval of measurement (see Fig. 1). If appropriate, the organ under study can be measured from different views, e.g., ventral, dorsal, lateral, or oblique.

In dynamic scintigraphy, attention is focused on the temporal change of activity distribution of the radiopharmaceutical used. The organ under study is imaged in a temporal sequence of frames maintaining the viewing angle. Usually, from this sequence and one or more regions of interest (ROI) within the images, time–activity curves are generated for each ROI. The subsequent analysis of these curves (e.g., maximum rise time, decay time) results in the determination of numerous physiological parameters (e.g., organ clearance, perfusion).

Whole-body scintigraphy is the obtainment of scintigraphic information for the whole human body during one acquisition. As the dimensions of the human body are much larger than the axial field of view of a gamma camera, the detector head(s) and the patient must be moved relative to each other in the direction of the body's long axis. In addition, the data acquired must be combined by appropriate means to form the final image.

Gated scintigraphy is a multiple-frame imaging, controlled by external physiological signals of periodic cycles, e.g., triggered by ECG or respiratory signals, either to overcome the image blur caused by organ movement of or to collect information on organ movement. The cycle is divided into a number of phase intervals, and driven by the external trigger the scintigraphic information is sorted into the corresponding interval. Mostly, data are summed over a multitude of cycles. The final outcome is a series of images associated with the corresponding phase intervals.

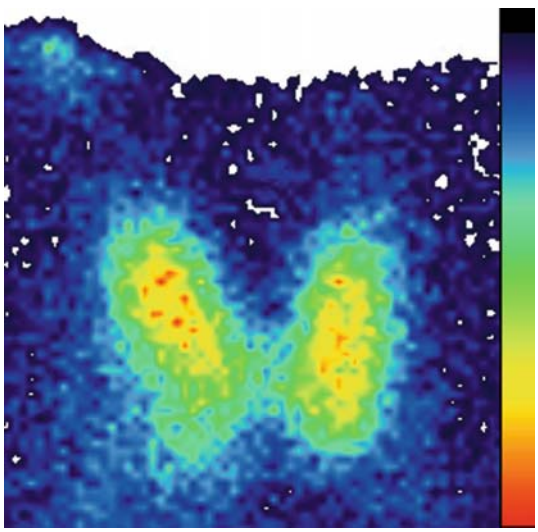

Scintigraphy. Figure 1 Scintigram of the thyroid gland.

Imaging

The most often used imaging device in nuclear medicine is the gamma camera with a detector head utilizing the Anger principle (2) (see Fig. 2). The actual detector is formed by a large-scale single crystal scintillator, which is coupled *via* a light guide to a number of photomultiplier tubes (PMTs). In addition to the detector, the detector head is composed of a ►collimator, detector shield, and positional electronics.

When a γ-quant (photon) is absorbed in the detector crystal, the absorbed energy is emitted partly as non-directional scintillation light. These flashes of light, whose integral is proportional to the absorbed energy, are distributed *via* a light guide, which is designed to optimize the spatial spread of the scintillation light, to the photocathode of a PMT. To prevent light from exiting the crystal *via* surfaces not facing the PMTs, these crystal boundaries are coated by reflective materials such as magnesium or aluminum oxide. The photocathode converts the scintillation light to electrons by means of the outer photo effect. These electrons are accelerated by an electrostatic field toward the dynodes (usually 10–12), thereby generating new electrons when crashing on a dynode. When finally reaching the anode of the PMT, each electron emitted by the photocathode has been multiplied by a factor of approximately 10^6. This avalanche of electrons generates an electrical pulse at the anode, which after additional shaping amplification and integration has to pass pulse height analysis until finally being processed and registered by the positioning electronics.

Looking at just one PMT and one detected event, the amount of light and, hence, the magnitude of the measured signal are dependent on the absorbed energy and on the location of the absorption event relative the wore of the light to the position of the PMT (the shorter the distance the more the light is seen). Now, taking into account all PMTs coupled to the crystal, the weighted sum of all PMT output signals (after correcting for the absorbed energy) yields the detected position of the scintillation, whereas the unweighted sum results in an estimate of the absorbed energy, which is independent of position (1, 3). The accuracy of positioning is mostly dependent on the efficiency by which the light is collected, i.e., on the light yield of the detector material (conversion from γ-energy to light photons) and on the proper design of the detector. To a lesser degree it also depends on the number of PMTs per area (usually ranging from 37 to 105 per detector head). For a scintillation detector, there is a linear relationship between absorbed energy and the amount of light emitted and hence output pulse amplitude. Thus, comparing pulse amplitude with appropriate discriminator levels, the energy range of photons to be included into the detection process can be selected by pulse height analysis.

The emission of γ-rays from the patient is nondirectional (as is the emission of normal light). In order to generate an image, directional information must be added. This is done by inserting a device called a collimator between the object and detector crystal, which can be penetrated only by γ-rays striking the collimator out of well-defined directions. The principle of mechanical collimation is absorption: a thick plate made from highly absorbing material (usually lead or tungsten) and containing thousands of well-defined bores can be penetrated only by γ-rays that pass through the long bores. The most often used geometry is a parallel hole collimator, but other geometries exist, e.g., converging, diverging, and conical collimators. Other construction parameters are energy range (thickness of septa and plate), resolution (hole diameter and length), and sensitivity, which is inversely related to resolution (and energy).

The detector head itself is attached to a gantry designed to facilitate detector positioning. Today, the gamma camera is interfaced to computers for data acquisition, processing, and storage.

To summarize, the four physical steps of gamma camera imaging are

1. Preselection of patient volume, in which the spatial distribution of activity is to be measured, by proper detector positioning and collimation.
2. Absorption of γ-quants emitted under directions preselected by collimation in the detector crystal and energy transfer by scintillation.
3. Transformation of the scintillation light to an electrical signal (PMT).
4. Determination of the absorbed energy and the position of the scintillation, energy discrimination, and final registration and storage.

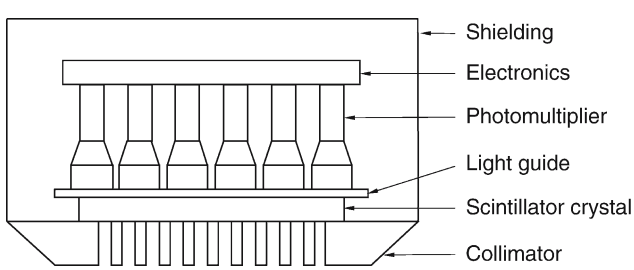

Scintigraphy. Figure 2 Detector head of an Anger camera (principle).

The scintigraphic information is given by the sum of all events, which are registered along a ▶projection beam by the detector head. This projection beam is defined as the smallest possible volume that can be resolved by the detector head when detecting the radiation emitted by the object. Its shape is limited by the detector head's spatial resolution in all three dimensions. Mostly, it is a long, thin, diverging cone, as a gamma camera has no spatial resolution in the direction perpendicular to the detector, i.e., the direction of collimator bores. Supposing that there is no absorption or scattering of γ-radiation in the object and that sensitivity and spatial resolution are constant, the ray sum is proportional to the linear sum of activity concentrations along the projection beam. No information is contained about the depth of the source (its distance to the detector). In order to collect information on the third dimension of the object, it must be looked at from a multitude of different projection angles. In addition, the data measured have to be reconstructed by appropriate mathematical algorithms—the principle of tomography. Tomography requires either detectors that rotate around the patient or a detector ring surrounding the patient. The most prominent tomographic methods in nuclear medicine are single photon emission computed tomography (SPECT) and positron emission tomography (PET).

References

1. Anger HO (1958) Scintillation camera. Rev Sci Instr 29:27–33
2. Anger HO (1966) Survey of radioisotope cameras. ISA Trans 5:311–334
3. Birks JB (1964) The Theory and Practice of Scintillation Counting. Pergamon Press, Oxford, England

Scintigraphy

Scintigraphy is an imaging method to represent the spatial (and temporal) distribution of incorporated radio nuclides.

Scirrhous Carcinoma

▶Carcinoma, Ductal, Invasive

Sclerocystic Disease

▶Fibrocystic Disease, Breast

Scleroelastotic Scar

▶Radial Scar, Breast

Sclerosing Adenosis, Breast

Luis Pina
Department of Radiology,
Clínica Universitaria de Navarra, Navarra, Spain
ljpina@unav.es

Synonyms

Adenosis tumor; Nodular adenosis

Definition

Sclerosing ▶adenosis is a benign proliferative lobulocentric lesion, consisting of stromal sclerosis and proliferative adenosis.

Pathology

Sclerosing adenosis is composed of distorted epithelial, myoepithelial and sclerotic stromal elements arising in association with the terminal duct lobular unit (1). Sclerosing adenosis is part of the proliferative lesions without atypia, but it may be involved by atypical lobular hyperplasia, lobular carcinoma *in situ*, atypical ductal hyperplasia, or ductal carcinoma *in situ*. Perineural pseudoinvasion is seen in 2% of cases. Because of the distorted glandular pattern, sclerosing adenosis may be confused with tubular carcinoma or with radial scar (1, 2).

Clinical Presentation

Sclerosing adenosis is usually an incidental finding in surgical specimens, although it may be detected on mammography (1, 2). Most cases are non-palpable, but occasionally may present clinically as a palpable mass (adenosis tumour) that can be confused with breast cancer. Sclerosing adenosis is also a cause of breast pain.

Imaging

Mammography

There are not specific mammographic features to diagnose sclerosing adenosis. Round, punctate, or pleomorphic microcalcifications are usually the most frequent finding. Also well circumscribed to spiculated masses, ►architectural distortions and asymmetric densities have been reported to be associated with sclerosing adenosis (3, 4) (Figs 1 and 2).

Ultrasound

Focal acoustic shadowing without a mass and both well- and ill-delimited hypoechoic masses have been reported (3, 4) (Fig. 3).

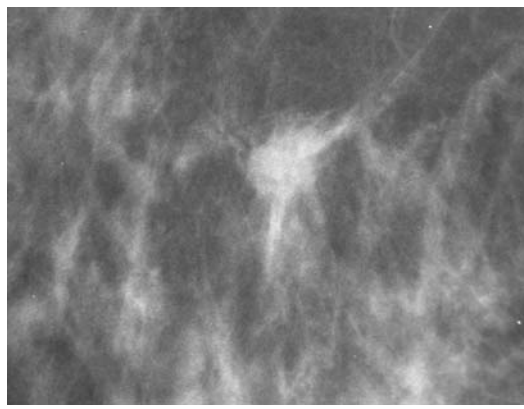

Sclerosing Adenosis, Breast. Figure 1 Irregular spiculated mass, highly suspicious of carcinoma (mediolateral oblique view, detail). Biopsy revealed sclerosing adenosis.

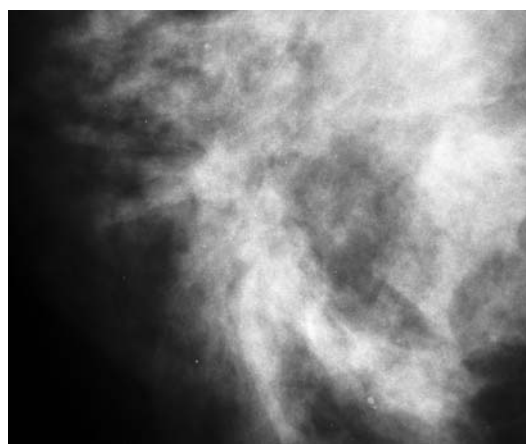

Sclerosing Adenosis, Breast. Figure 2 Architectural distortion with punctate calcifications. The lesion was palpable. Biopsy revealed sclerosing adenosis.

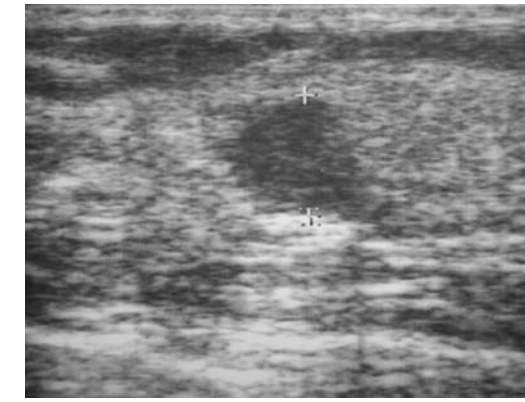

Sclerosing Adenosis, Breast. Figure 3 Ultrasonography reveals an irregular ill-delimited hypoechoic mass. Sclerosing adenosis.

Magnetic Resonance

Areas of sclerosing adenosis may enhance after the injection of paramagnetic contrast, simulating breast cancer.

Nuclear Medicine

Nuclear medicine techniques do not play any role in the diagnosis of sclerosing adenosis.

Diagnosis

The diagnosis of sclerosing adenosis is made by biopsy. Imaging techniques usually show suspicious findings, mimicking malignancy, so a biopsy is recommended. Due to the possible association with premalignant or even malignant lesions, a result of sclerosing adenosis in a core biopsy should be carefully evaluated. It may be acceptable for circumscribed masses and non-palpable indistinctly marginated masses. The result may be concordant also for vacuum-assisted biopsy of punctate, amorphous, or pleomorphic calcifications. However, the result is not acceptable for BI-RADS 5 lesions. In these cases, a surgical biopsy is recommended (5).

Bibliography

1. Schnitt S, Connolly JL (2004) Pathology of benign breast disorders. In: Harris JR, Lippman ME, Morrow M (eds) et al Diseases of the Breast. Lippincott Williams & Wilkins, Philadelphia, pp 77–99
2. Hughes LE (2000) Sclerosing adenosis, radial scar and complex sclerosing lesions. In: Hughes LE, Mansel RE, Webster DJT (eds) Benign Disorders and Diseases of the Breast. Concepts and Clinical Management, Saunders, London, pp 137–142
3. Cardeñosa G (2001) Lobules. In: Cardeñosa G (ed) Breast Imaging Companion. Lippincott Williams & Wilkins, Philadelphia, pp 298–300
4. Günhan-Bilgen I, Memis A, Üstun EE et al (2002) Sclerosing adenosis: mammographic and ultrasonographic findings with clinical and histopathological correlation. Eur J Radiol 44:232–238
5. Gill HK, Ioffe OB, Berg WA (2003) When Is a diagnosis of sclerosing adenosis acceptable at core biopsy? Radiology 228:50–57

Sclerosing Papillary Lesion

▶Radial Scar, Breast

Sclerosing Papillary Proliferation

▶Radial Scar, Breast

Scoliosis

Karl Ludwig, Corinna E.E. Nierhoff
Department of Diagnostic Radiology, Orthopedic University Hospital Heidelberg, Heidelberg, Germany
karl.ludwig@ok.uni-heidelberg.de

Definition

Scoliosis is defined as a fixed lateral curvature and torsion of the spine.

According to the criteria of the Scoliosis Research Society, the diagnosis of structural ▶scoliosis should be reported only if the curve in the frontal plane, as viewed on an anteroposterior radiograph, is greater than 10°.

Pathology/Histopathology

Scoliosis represents a deformity of growth. The vertebral bodies grow slower on the concavity than on the convexity. This disturbance of growth of one or more vertebral bodies results in a rotation and lordosis of the spine. Eighty-five percent of scolioses are idiopathic, which means there is no known underlying pathology. Idiopathic scoliosis worsens mainly in the growth period. Generally, curvatures less than 30° will not progress after childhood. With greater curvatures after adolescence, the degree of scoliosis may progress by about 1° per year.

Studies have shown that the incidence of idiopathic scoliosis is higher in relatives, which suggests an autosomal-dominant inheritance pattern with variable phenotypic expression (1).

Clinical Presentation

The incidence of idiopathic scoliosis with lateral curvatures of 10° or greater varies between 1 and 3% in the general population. The female:male ratio is 4:1. According to the onset of symptoms, idiopathic scoliosis can be classified into three groups:

- Infantile: birth to age 3 years
- Juvenile: 3–11 years
- Adolescent

An etiological classification of scoliosis differentiates between different entities:

- Idiopathic
- Neuropathic: cerebral palsy, syringomyelia, Charcot Marie-Tooth, polio, spinal muscle atrophy, myelomeningocele
- Myopathic: muscular dystrophies
- Congenital: diastematomyelia, neurofibromatosis,
- Mesenchymal: Marfan syndrome, Ehlers–Danlos syndrome
- Systematic diseases: achondroplasia, spondyloepiphysary dysplasia, mucopolysaccharidosis
- Metabolic: rickets, juvenile osteoporosis, osteogenesis imperfecta
- Radiation-associated: radiotherapy in childhood
- Posttraumatic
- Neoplastic
- Inflammatory
- Vertebral malformations (hemivertebrae, block vertebrae, butterfly and wedged vertebra, unsegmented bars)

If scoliosis progresses in the thoracic region, it can create significant physical deformity. Respiratory problems can result in severe cases with curvatures approaching 90°.

Imaging

The role of radiology in scoliosis management is to confirm the diagnosis, identify any underlying pathology, and monitor the degree of curvature. Early diagnosis and treatment help prevent curve progression and deformity.

Plain Radiography

Images of the erect entire spine in anteroposterior (AP) and lateral views are mandatory. In the AP projection, the iliac crest should be visible. Images are usually taken on a 36-in. cassette with a film focus distance of 3 m with the central beam in the middle of the thoracic spine.

For distinguishing between reversible functional scoliosis and fixed structural scoliosis of babies and small

children (not yet able to walk), a supplementary stress picture is taken in the prone position (Bending test). The child is actively bent to the opposite side of the scoliosis while the image is taken.

Is the scoliosis is fully compensated, a functional scoliosis is assumed. In structural scoliosis, muscle contractures or changes at the vertebral bodies, the disks, and the facet joints prevent compensation of the curvature.

Cobb Method

A quantitative assessment of scoliosis is performed using the ►Cobb angle.

Besides some inter- and intraobserver variability, the Cobb method for scoliosis angle measurement is the most accepted standard technique worldwide. In an AP view, the two neutral vertebrae first have to be determined.

Neutral vertebrae have parallel endplates with—in contrast to the other vertebrae—minimal or no change in shape and are maximally tilted to the horizontal line.

Lines are drawn in extension of the uppermost and lowermost endplates of the neutral vertebra. Because these lines usually intersect outside the X-ray film, two perpendicular help-lines are constructed. At the point of intersection, the complementary angle is measured. This angle is the so-called Cobb-angle or angle of scoliosis (Fig. 1).

When reporting the scoliosis angles, one should mention which measurement method was used and which neutral vertebrae were chosen. In follow-up imaging, the same vertebrae should be chosen for evaluating disease progression.

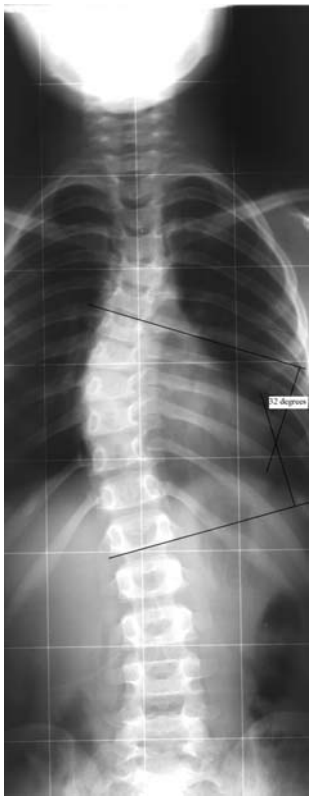

Scoliosis. Figure 1 Measurement of the scoliosis angle (Cobb 1948). Anteroposterior radiograph of a 22-year-old man with a single right thoracic curve. Horizontal lines are drawn parallel to the endplates of the neutral vertebrae at the end of the curve. Where perpendicular lines intersect, the angle of scoliosis is measured. In this case the angle of Cobb measures 32°.

Evaluation of Rotation (Method of Nash and Moe)

For evaluation of the scoliotic rotation of the vertebrae, the method of Nash and Moe (2) is widely used.

There are five grades of rotation. Grade zero rotation means the pedicle outlines are symmetric and equidistant to the lateral borders of the vertebral body. Grades 1–4 illustrate the movement of the pedicle toward and over the midline (Fig. 2).

Determination of Skeletal Maturity (Risser's Sign)

A further goal of the radiographic examination is to determine skeletal maturity. Because curvature of mild scoliosis does not progress after adolescence, the skeletal age is a prognostic factor of the likelihood of curvature progression. Since the iliac crest is usually visible in the total spine study, it can be conveniently used to determine skeletal maturity. The Risser classification (3) of the apophysis of the iliac crest enables the radiologist estimate the expected growth of the vertebral body and therefore estimate the progression tendency of the scoliosis.

Risser Classifies the Progression of Ossification of the Apophysis of the Os ileum into Six Groups

0: Apophysis cannot be seen
1: Apophysis begins to develop laterally and measures up to 25% of the iliac crest.
2: Apophysis covers up to half of the iliac crest
3: Apophysis reaches up to 75% of the iliac crest
4: Complete excursion of the iliac apophysis
5: Complete fusion of the apophysis with the iliac crest

Scoliosis. Figure 2 The method of Nash and Moe (2) measures the degree of rotation from grade zero (no rotation) to grade 5 (pedicle outline wanders over the midline).

Cross-Sectional Imaging

Besides conventional imaging measurement, techniques focusing on MRI and CT imaging are being used more and more. They have the drawback that images are acquired with the patient in the prone position, so the influence of the physiological vertical stress of the standing body on the curvature of scoliosis cannot be evaluated.

Multiplanar CT imaging especially enables visualization of complex deformities and a three-dimensional understanding of the scoliotic spine (Fig. 3).

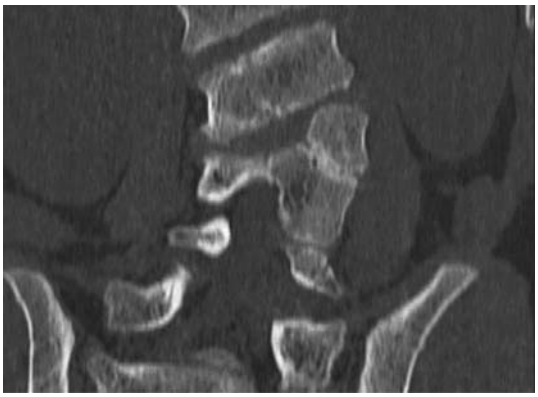

Scoliosis. Figure 3 Coronal multiplanar reconstruction of a helical computed tomography scan showing a single bended lumbar scoliosis with the concavity on the right side on the basis of a complex spinal deformity, including a hemivertebra L3.

Nuclear Medicine

The role of nuclear medicine in routine evaluation of scoliosis is limited. An isotope bone scan (^{99m}Tc-methylene diphosphonate) can be helpful when evaluating a child with focal alterations of the bone, such as infection or neoplasia.

Alternative Imaging Methods

To reduce radiation exposure, alternative imaging techniques have been investigated for documentation and to control the course of disease. Light optical methods with the possibility of three-dimensional surface rendering can quantify the cosmetic deformity of the thorax.

Diagnosis

A complete evaluation should include a physical examination and imaging of the total spine. Plain radiography remains the initial imaging method of choice and in certain cases is followed by MRI or CT imaging.

In the radiologic report, the form of the deformity (scoliosis, kyphosis, lordosis, or S-shaped), the side and the degree of scoliosis should be described. The rotational component of scoliosis is described by the Nash and Moe scale, and the skeletal age should be mentioned, for instance using the Risser classification.

Before surgery lateral-bending films are sometimes taken to differentiate structural fixed curves from nonstructural flexible curves.

Because scoliosis is often associated with other congenital deformities, skeletal, cardiac, and urogenital deformaties must be excluded.

Last not least, one must be aware of the radiation exposure caused by scoliosis follow-up. Nash et al estimated that 22 radiographic examinations are performed in the course of scoliosis management (4).

Statistically, an increased risk of developing breast cancer in girls with scoliosis has been reported (5).

Bibliography

1. Wynne-Davies R (1968) Familial (idiopathic) scoliosis. A family survey. J Bone Joint Surg Br 50:24–30
2. Nash CL, Moe JH (1969) A study of the vertebral rotation. J Bone Joint Surg Am 51:223–229
3. Risser JC (1958) The iliac apophysis: an invaluable sign in the management of scoliosis. Clin Orthop 11:111
4. Nash CL, Gregg EC, Brown RH et al (1979) Risks of exposure to x-rays in patients undergoing long-term treatment for scoliosis. J Bone Joint Surg Am 61:371–374
5. Ron E (2003) Cancer risk from medical radiation. Health Phys 85(1):47–59

Screening, Breast Cancer

Margrit Reichel
Referenzzentrumsleiterin Mammographie-Screening
Wiesbaden Michelsberg, Wiesbaden
margrit.reichel@mammascreening-wiesbaden.de

Synonyms

Breast cancer screening

Definition

Breast cancer is the most common cancer among women worldwide, with over one million new cases diagnosed in 2000. Although substantial improvements in survival have been recorded in Western countries since the late 1970s, breast cancer still causes the most deaths from cancer among women. Studies have shown that mass screening for breast cancer using mammography as the screening test (mammography screening), with or without clinical breast examination, has the potential to further decrease breast cancer mortality by detecting asymptomatic lesions which can be treated more effectively than symptomatic disease (1). In order to achieve these benefits, however, a number of conditions need to be fulfilled, which are discussed here.

Characteristics

In 2002, an IARC Working Group on the Evaluation of Breast Cancer found sufficient evidence for the efficacy of mammography as the sole screening modality for breast cancer in women aged 50–69 years. The group found only limited or insufficient evidence for other age groups or screening modalities (1).

Target Population

Mammography screening is generally offered to the asymptomatic 50–69-year-old female population in 2-year intervals. If the screening mammogram is normal, no further action will be taken and the woman will be invited to the next round of screening. Unlike diagnostic mammography, mammography screening should not be offered to patients presenting with signs or symptoms of breast cancer. A large proportion of women in a diagnostic breast service will present with benign abnormalities; work-up of benign lesions in a diagnostic service is frequently necessary in order to reassure the patient and avoid unnecessary treatment. The opposite is the case in mammography screening, however. Screening clients are not informed about benign lesions in order to avoid unnecessary anxiety and unnecessary further diagnostic procedures in large numbers of women.

Screening Process

Since the vast majority of women attending screening are disease free, considerable precautions must be taken to ensure that the benefits of screening are maximized while minimizing the potential harm. The physician responsible for the overall performance of the screening service and the attendant staff must constantly strive to optimize the individual components of the entire screening process, as outlined below (2, 3).

Information and Invitation

A significant factor affecting the overall performance of a screening program is the proportion of women in the eligible ▶target population who attend. Organized, population-based mammography screening programs have been shown to achieve a high participation rate (over 70% attending in a given round) using invitation letters addressed to each individual woman in the eligible target population. The invitation letter should give a specific appointment (date, time, and place) and a telephone number in case the woman needs to change the appointment. The availability of population registry data can substantially simplify and improve the effectiveness of invitation procedures.

Taking the Screening Mammogram

Screening mammograms (mediolateral oblique and craniocaudal views recommended) should be taken in dedicated units by specially trained staff. The physico-technical quality must be monitored daily by unit staff and by a regional technical quality control office, which fulfills the standards of the European Guidelines (2). In some programs, screening radiographers may be trained to perform additional views on their own initiative. Such a policy can result in lower recall rates, although the overall rate of additional imaging may be higher.

Reading Screening Mammograms

The classification of screening mammograms differs somewhat from diagnostic mammograms, because of

the lengthy (2 year) screening interval. In mammography screening, the reader does not have the option of recalling a woman in a shorter (e.g., 6 month) interval because that would generate inordinate anxiety. Thus, the reader must decide whether to recall a woman immediately for further assessment or in 2 years for the next round of screening.

Screening mammograms should also be read in batches of several women. A batch should be of sufficient size to enable the reader to roughly appraise ►sensitivity and ►specificity and to judge whether repeated reading of the entire batch is necessary. Roller viewers should be used and reading should be performed in an undisturbed session with optimal viewing conditions (darkened room). Double reading with arbitration by a third very experienced reader is recommended. The first two readers should be specially trained and experienced in reading screening mammograms. The double readers should strive for optimum sensitivity. The third reader should read any mammograms that one or both double readers find suspicious, with the aim of optimizing specificity.

Assessment of Suspicious Screening Mammograms

All women, the screening mammograms of whom are still deemed suspicious after arbitration, are recalled for assessment that initially consists of additional imaging and clinical breast examination. If suspicion of abnormality persists after additional imaging, biopsy should be recommended. In most cases (>99%) fine-needle aspiration, core cut, or vacuum biopsy can be used.

Preoperative Multidisciplinary Conference

For each case in which suspicion of abnormality persists after imaging, the final decision on the result of screening should be reached in a multidisciplinary preoperative conference in which the assessment team (screening radiologist, pathologist, radiographer, and breast surgeon) consider the correlation between the histopathological assessment of the preoperative biopsy and the other assessment findings. A radiotherapist or radio-oncologist and breast care nurse should also be present so that the entire team can plan the operation/treatment, if breast cancer is diagnosed. The breast care nurse should also be present when a woman is informed of a diagnosis of breast cancer because the woman will have special communication needs, which the breast care nurse is specially trained to deal with.

Postoperative Multidisciplinary Conference

The result of each breast cancer operation and particularly the accuracy of the diagnosis and the appropriateness of the recommendations for management, made at the preoperative conference should be evaluated in a multidisciplinary postoperative conference attended by the same team present at the preoperative conference.

Quality Assurance

At any given time, the vast majority of the target population is free of breast cancer and precursor lesions. Thus, even minimal harm resulting from anxiety or a small proportion of breast cancer cases detected in screening, which may not have become manifest or led to serious complications during a woman's life can shift the delicate balance unfavorably between benefit and harm of screening. It is therefore imperative to continuously strive for optimum quality in mammography screening. Comprehensive guidelines on quality assurance of the mammography screening process have been developed in the Europe against Cancer Programme (2). Staff performing mammography screening should ensure that the minimal standards and procedures recommended in the guidelines are followed.

The European guidelines also emphasize the importance of performing screening in an organized setting as opposed to ►opportunistic screening by referring women for a mammogram in a clinical setting. ►Organized screening programs include an administrative structure responsible for implementation, quality assurance, and evaluation. Accountability for the quality of performance and results is clearer in an organized program and managerial control of the screening process is greater, allowing more rapid response to changes in quality indicators or adverse conditions. Another key quality aspect is population-based implementation of invitation and evaluation. Identifying and inviting all eligible women in the target population is not merely important for maximizing the potential impact of screening. Population-based invitation and a high uptake rate make screening data representative for the local population. Such representative data are essential for internal and external monitoring of screening performance.

References

1. Vainio H, Bianchini F (2002) IARC Handbooks of Cancer Prevention. Vol 7, Breast Cancer Screening. International Agency of Research on Cancer, WHO, Lyon, France

2. Perry N, Broeders M, de Wolf C (eds). et al (2001) European Guidelines for Quality Assurance in Mammography Screening. 3rd edn. Office for Official Publications of the European Communities, Luxembourg
3. Dronkers Daniel J, Hendriks Jan H C L (1999) Holland Roland, Rosenbusch Gerd Radiologische Mammadiagnostik. Thieme Verlag, Stuttgart

Scrotal Disorders

Aron Cohen[1], Hubert John[2]
[1]Department of Urology, University Hospital Zurich, 8091 Zurich, Switzerland
[2]Klinik Hirslanden, Zentrum für Urologie, 8008 Zurich, Switzerland
aron.cohen@triemli.stzh.ch, cohen@swissonline.ch
hubert.john@hirslanden.ch

Definitions

Scrotal disorders can be subdivided into acute and painful versus chronic and asymptomatic lesions. In acute scrotal pain, the differential diagnosis must be focused on ►testicular torsion, epididymitis, orchitis, torsion of the testicular appendage, or scrotal trauma. Inguinoscrotal hernia or distal ureterolithiasis might be further non-scrotal sources of acute pain.

Painless lesions of the scrotal organs present most often as tumor masses, either of the testis (testicular cancer), the epididymis (►spermatocele), the vascular drainage (►varicocele), or the surrounding tissue (►hydrocele).

Pathology

Painful scrotal diseases

Testicular Torsion

Usually there is torsion of the testis within the tunica vaginalis, which covers the anterior surface of the testis and extends over the epididymis and the spermatic cord. Where the covering extends to the cord, the testis is suspended freely within the tunical cavity, within which it may rotate. Torsion of the spermatic cord will strangulate the main vessels and cause ischemic damage to the testis. The main peak of testicular torsion is seen in adolescence. In the neonatal period, testicular torsion presents as torsion including the tunica vaginalis, which is called an extravaginal torsion (Figs 1–3).

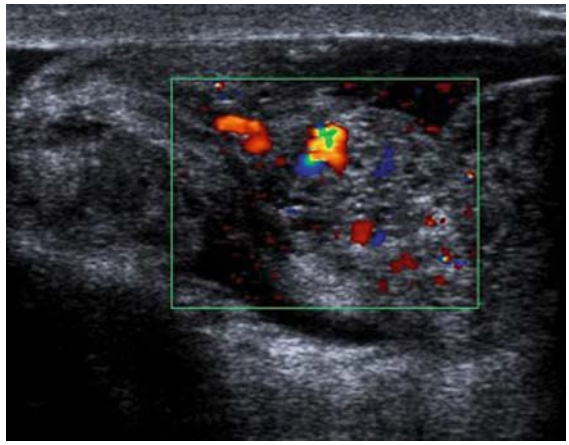

Scrotal Disorders. Figure 1 Testicular torsion. Color Doppler ultrasound reveals lack of vascularization in the twisted spermatic cord.

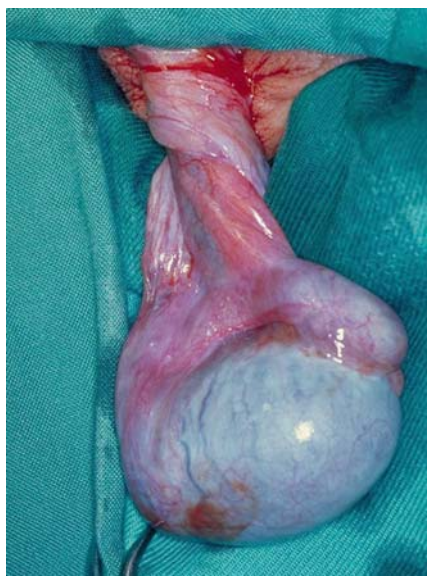

Scrotal Disorders. Figure 2 Testicular torsion. Intraoperative situs of an intravaginal testicular torsion without infarction.

Epididymitis, Orchitis

Epididymitis is usually a bacterial infection, although viral and fungal infections are possible as well. Most common infections in younger patients (<35 years) are sexually transmitted and caused by *Neisseria gonorrhoeae* or *Chlamydia trachomatis*. These patients often suffer from urethritis and concomitant leukocyturia.

In the elderly patient as well in the very young, coliform bacteria causing urine and bladder infection are most common. Bacteriuria secondary to obstructive urinary disease is very common in these patients.

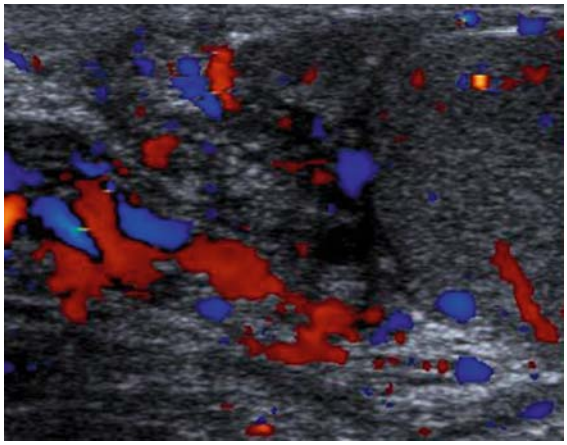

Scrotal Disorders. Figure 3 Testicular torsion. Postoperatively, the spermatic cord and the testicle are hypervascularized.

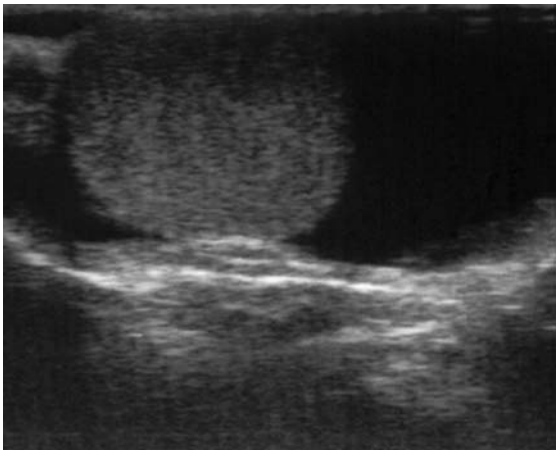

Scrotal Disorders. Figure 5 Hydrocele. Peritesticular fluid collection around a normal-sized testicle with homogeneous tissue, revealing a hydrocele.

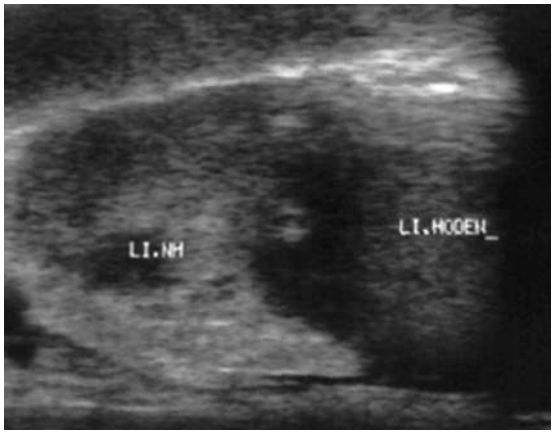

Scrotal Disorders. Figure 4 Epididymitis. Inflamed left epididymis with hypoechogenic areas may indicate abscess formation.

Orchitis seldom presents without epididymitis. Viral infections such as mumps might cause unilateral isolated infection of testis (Fig. 4).

Painless scrotal diseases

Hydrocele

Hydroceles usually present as painless swelling of the hemiscrotum. In moderate cases, the testis might be palpable next to the hydrocele.

The differential diagnosis includes inguinoscrotal hernia or enlargement of the testis due to cancer. Hydroceles develop most often after or concomitant to inflammatory disease of the epididymis and/or testicles. Due to an inflammatory process, the normal balance of fluid production and reabsorption of the surrounding tissue (tunica vaginalis testis) is disturbed, with consecutive reduction of fluid absorbance and relative fluid overproduction. The produced fluid will collect between the testicle-surrounding tissue and shows specific findings (Fig. 5).

Testicular Cancer

Testicular cancer represents between 1 and 1.5% of male neoplasms and 5% of urological tumors in general. Only 1–2% of the cases are bilateral. The histological type varies, although there is a clear predominance of germ cell tumors (90–95%). Peak incidence occurs in the third decade of life for nonseminoma and in the fourth decade for pure seminoma. Testicular cancer can be classified into germ cell tumors and sex cord stromal tumors. In addition, several different cancers can spread distant metastases into the testis, including lymphoma and cancers of prostatic, penile, and intestinal origin (Fig. 6).

Varicocele

Varicoceles can be found in about 15% of adult men. Incompetent valves of the spermatic vein cause impaired drainage of the blood of the pampiniform plexus of the spermatic cord.

There are idiopathic and primary varicoceles. Primary varicoceles result from compression of blood drainage by a retroperitoneal mass. Idiopathic varicoceles are more common on the left side because the left testicular vein is longer and enters the left renal vein in a right angle. Bilateral or right-sided varicocele must make one suspicious for a primary retroperitoneal cause (Fig. 7).

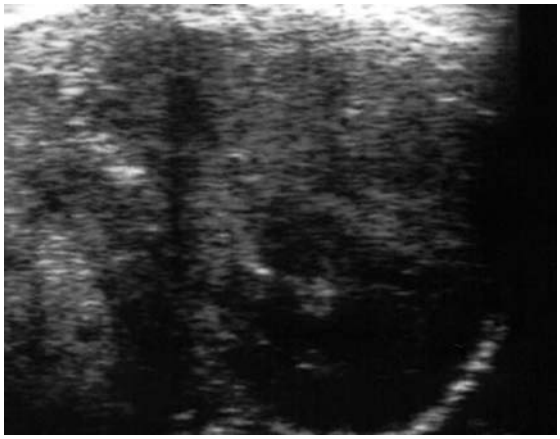

Scrotal Disorders. Figure 6 Testicular cancer. Testicular mass with mixed hypoechogenic and hyperechogenic tissue areas.

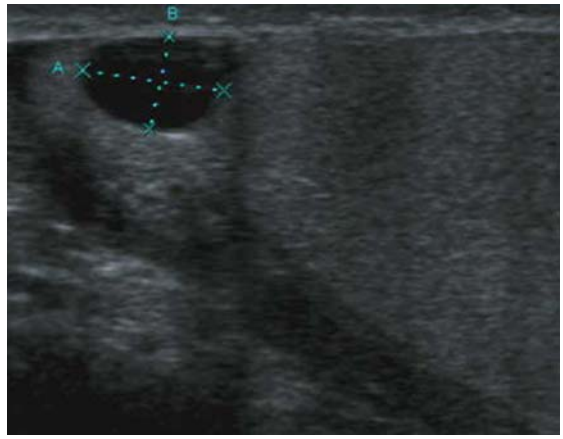

Scrotal Disorders. Figure 8 Spermatocele. Cystic hypoechogenic area within the upper pole of the epididymis, revealing simple spermatocele.

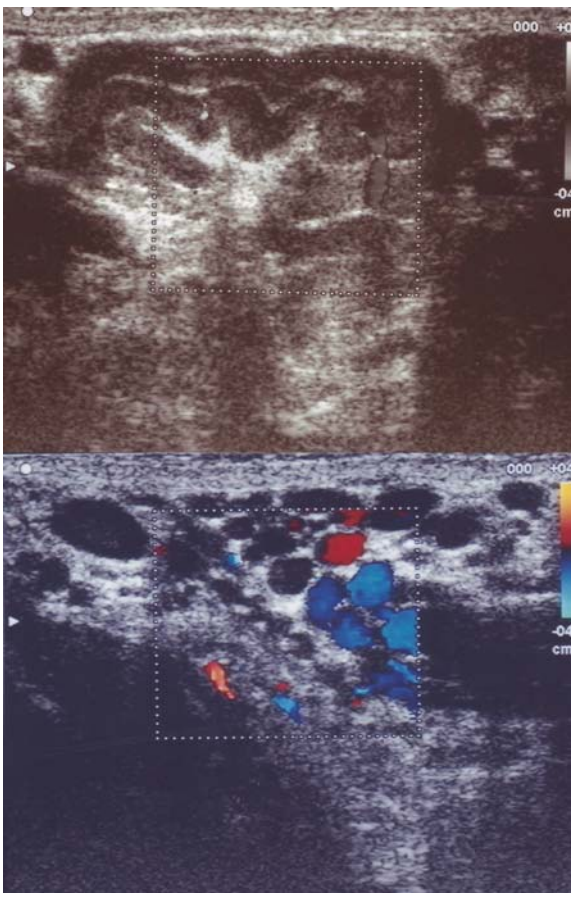

Scrotal Disorders. Figure 7 Varicocele. Venous conglomerates in the spermatic cord (*above*) with increasing diameter under increased abdominal pressure

Spermatocele

Spermatoceles can appear idiopathically, congenitally because of findings of the Mullerian duct, or secondarily after traumatic lesions of the tubules, which connect the head of the epididymis and the rete testis. The cyst is filled with sediment containing detritus, immobile spermatozoa, and lipids. Spermatoceles are usually unilocular but can also be multilocular (Fig. 8).

Clinical Presentation

Painful Scrotal Disorders

The ▶Scrotum, Acute represents a clinical term itself and describes the acute onset of pain in the scrotal region. In testicular torsion as well as in acute epididymitis, even careful examination appears to be very painful and sometimes is not possible. On the affected side, the testis is tender and swollen and rides high in the scrotum, accompanied by a thickened and tender spermatic cord.

In epididymitis, the onset is usually slower than that of testicular torsion, although this might not be differentiated by the history. The epididymis and the spermatic cord are swollen and tender; the testis is often also tender, as a sign of concomitant orchitis. Fever can be present. The history shows urethral discharge and dysuria. Sexual exposure can be months before onset. Laboratory examination can show leukocyturia. It is imperative to promptly differentiate between epididymitis and testicular torsion, and in cases of doubt, to do further investigation to rule out testicular torsion.

Therapy

Once testicular torsion is suspected, immediate surgical exploration and replacement of the testis is crucial for survival of testicular function. Simple epididymitis or orchitis requires anti-inflammatory therapy. Antibiotics, analgesics, and local procedures (cooling, scrotal elevation) will heal most cases. Complications such as abscess are rare but may require surgical therapy.

Painless Scrotal Disorders

Because several pathological scrotal conditions may present as a painless tumor mass in the scrotum, careful clinical examination must distinguish between testicular cancer and benign lesions.

Testicular cancer usually presents as tenderless growth of one testicle with increased consistency. In approximately 20% of the cases, the first symptom is scrotal pain. Gynecomastia appears in 7% of cases and is more common in nonseminomatous tumors. In about 10% of the cases, a testicular tumor can mimic orchidoepididymitis, with consequent delay of correct diagnosis. Increased serum levels for HCG, AFP, and LDH can be found in germ cell tumors.

Hydroceles and spermatoceles usually present as painless swelling of the hemiscrotum. In moderate cases, the testicle might still be palpable next to the hydrocele. In severe cases, the testis can be hidden and not palpable. Spermatoceles are located at the head of the epididymis and in clear distance from the testis and present as small, cystic, usually indolent—sometimes moderately tender—tumor.

Varicoceles provide typical clinical findings as palpation reveals a scrotal mass that feels like a bag of worms. One-third of men undergoing evaluation because of infertility present with varicocele.

Therapy

Suspicion of testicular cancer requires surgical exploration, and if cancer is confirmed, orchiectomy with removal of the spermatic cord up to the inner inguinal anulus will be performed. Depending on histological findings, chemotherapy or radiotherapy might also be necessary.

Asymptomatic hydrocele or spermatocele does not require therapy unless the patient is disturbed by cosmetic reasons or discomfort. Surgical marsupialization or epididymectomy are the therapies of choice. Puncture or sclerotherapy are not good options because of their high recurrence rate and danger of iatrogenic infection.

Varicocele therapy is a controversial issue, with no single approach adopted as best.

Microsurgical ligation of the dilated veins as well as surgical ligation of the spermatic vein show good results. Sclerotherapy can be an alternative minimally invasive approach.

Imaging

Ultrasonography and Color Doppler Sonography

Ultrasonography is the mainstay for imaging scrotal disorders. Gray-scale sonography can show fluid collections in hydroceles or spermatocele lesions as well as solid changes as in testicular cancer. Color Doppler sonography provides the best information on blood flow and can diagnose or rule out torsion against inflammatory diseases such as epididymitis and orchitis. Color Doppler sonography has documented sensitivity for epididymitis of 70% and specificity of 82%. Nevertheless, about 15% of patients with early torsion will present with swelling only in the epididymis. Besides typical clinical findings, sonography as well as color Doppler sonography might help confirm the diagnosis of varicocele.

Magnetic Resonance Tomography

In clinical practice, magnetic resonance imaging (MRI) has a role in specifying unclear sonographic findings. In acute pain, MRI proves accurate results in the differential diagnosis of epididymitis and torsion. Although testicular cancer can be proven only by surgical and pathological examination, MRI can help identify unclear sonographic or clinical findings.

Computed Tomography

Computed tomography (CT) scanning has its main position in staging of malignant processes. Sonography and MRI provide better information on local situations, but CT is a standard imaging tool for evaluating the pelvis, abdomen, and chest.

Nuclear Medicine

In diagnosing scrotal disorders, radionuclide imaging (99m-Tc radioisotope scan) is used rarely when clinical and sonographic findings might be unclear, and in clinical practice it is rarely performed because of its time-consuming nature and logistical problems. Good indications for radionuclide imaging are inflammatory disease and the differential diagnosis of testicular torsion.

Diagnosis

Besides clinical and historical findings, radiological examination will present with more or less specific examination results. As mentioned, sonography remains the mainstay of the diagnostic approach to scrotal disorders. Testicular torsion initially will show no specific changes in gray-scale sonography, but there are inhomogeneous changes of the testicular parenchyma in late-stage torsion due to infarction of the hypoxic tissue. Duplex sonography provides more information on blood flow and will show lack of perfusion compared with the opposite healthy side. Hyperperfusion of the affected testicle can be due to spontaneous reposition of a testicular torsion or—more often—to an inflammatory disorder such as orchitis. An inhomogeneous appearance of the testicular tissue with only moderate or absent pain must provoke suspicion of testicular cancer, which can be diagnosed only by a histological approach. MRI of the testis can give additional information about possible testicular cancer. In MRI, testicular tumors commonly show signal intensity similar to that of normal testis in T1-weighted images. On T2-weighted images, they are mostly hypointense relative to the normal testis, with a homogeneous or heterogeneous signal pattern.

In suspected epididymitis, enlargement of the epididymis with typically reduced echogenicity can be found by gray-scale sonography. There might be increased echo after epididymal hemorrhage. Color duplex sonography shows increased blood flow due to inflammation. In addition, reactive hydrocele might be present in most of the cases.

An echogenic fluid collection surrounding a normal testicle is present in hydrocele. Sometimes septa or a thickened hydrocele wall can be found in a chronic inflammatory process. Well-defined hypoechogenic lesions located at the head of a normal-looking epididymis represent a characteristic finding of spermatocele.

Examination for varicocele should be performed with the patient in supine and standing positions, as described by some authors. The sonographic appearance of varicocele consists of multiple hypoechogenic, serpiginous, tubular structures of varying sizes larger than 2 mm in diameter. The Valsalva maneuver will show increased backflow of venous blood. In the literature, the sensitivity and specificity of varicocele detection is reported to approach 100% with color Doppler sonography.

Bibliography

1. Kubik-Huch, Hailemariam S, Hamm B (1999) CT and MRI of the male genital tract: radiologic-pathologic correlation. Eur Radiol 9:16–28
2. Dogra VS, Gottlieb RH, Mayumi O et al (2003) Sonography of the scrotum. Radiology 227(1):18–36
3. Schulham PG, Kawashima A, Sandler C et al (2002) Urinary tract imaging—basic principles. In: Walsh PC, Retik AB, Vaughan ED, Wein AJ (eds) Campbell's Urology. 8th edn. Saunders, Philadelphia, pp 122–163
4. Cuckow PM, Frank JD (2000) Torsion of the testis. BJU Int 86:349–353

Scrotum, Acute

Acute pain in the scrotum or testis, mainly caused by inflammatory diseases such as epididymitis and orchitis. The differential diagnosis must rule out testicular torsion against all other painful conditions.

▶Scrotal Disorders
▶Genital Track

Scurvy—Vitamin C Deficiency

▶Vitamin Deficiency

SDAVF

▶Spinal Dural Arteriovenous Fistula (SDAVF)

SDS

▶Shwachman–Diamond Dyndrome (SDS)

Sebaceous Cyst

Distended hair follicle containing lipid and keratinaceous material, presenting as a painless subcutaneous nodule. May become symptomatic when inflamed.

▶Cutaneous Lesions, Breast

Second (third) Generation Contrast Media

▶Contrast Media, Ultrasound, Low Solubility Gas

Second Harmonic Imaging

Echocardiographic technique based on the nonlinear frequencies generated by ultrasound waves. Second harmonic imaging uses analysis of the received signal with frequency twice as high as that of the transmitted frequency signal.
▶Ischemic Heart Disease, Ultrasound

Second-Generation Contrast Media

A term that is now mostly used for ultrasound contrast media that are not air-based such as SonoVue (Braccotkl, Milan, Italy), Optison (GE Healthcare, UK), or Definity (Bristol Myers Sqibb, New York, USA). These agents are more stable than air-based first-generation agents such as Levovist (Bayer Schering Pharma, Berlin, Germany) and provide strong signal enhancement at a low mechanical index. According to an older definition, second-generation ultrasound contrast media are defined by transpulmonary stability and thus include all commercially available agents with the exception of Echovist (Bayer Schering Pharma, Berlin, Germany).
▶Time Intensity Curves

Secondary Gout

▶Gout

Secondary Hyperparathyroidism

A metabolic disorder such as kidney failure or intestinal malabsorption decreases calcium levels in the blood and leads secondarily to increased PTH levels.
▶Hyperparathyroidism

Secondary Hypertrophic Osteoarthropathy

A syndrome consisting of painful periostitis, arthritis, and bilateral clubbing of the digits on the hands and feet. It is often associated with intrathoracic neoplastic or inflammatory conditions.
▶Hypertrophic

Secondary Trauma, Splenic

A traumatic injury of the spleen that occurs in patients with predisposing pathological splenic processes. For example, subcapsular focal lesions or pathological conditions that cause splenomegaly produce locoregional or diffuse thinning of the capsule, respectively, making the spleen more fragile when trauma occurs.
▶Trauma, Splenic

Secondary Tubo-Ovarian Abscess

Secondary tubo-ovarian abscess may arise by direct or lymphatic spread of infection after pelvic surgery, or as a complication of enteric inflammatory diseases, such as appendicitis, diverticulitis, and Crohn's disease. Tubo-ovarian abscesses in postmenopausal women are rare; however, they are highly associated with pelvic malignancies in this age group.
▶Abscess Tubo-Ovarian

Secretory Calcifications

Characteristic benign calcifications, usually coarse, dense, diffuse, bilateral, and pointing toward the nipple.
▶Duct Disease, Breast

Secretory Disease

▶Duct Disease, Breast

Segmental/Partial Priapism

▶Corpus Cavernosum, Thrombosis

Seizures, Complex, Partial

Eric Achten, Karel Deblaere
University of Ghent, Chent, Belgium
rik.achten@ugent.be

Synonyms—Variants—Entities

Complex partial epilepsy (CPE), focal epilepsy

- Temporal lobe epilepsy (TLE): TLE accounts for approximately 70% of all chronic CPE
- Extra-temporal lobe epilepsy (ETLE): usually the frontal lobe [frontal lobe epilepsy (FLE)]

Definition

Epilepsy is one of the most common neurological diseases. Epileptic seizures may result from events such as fever, hypoglycemia and are then called '*occasional seizures*' (1). When they recur spontaneously without known cause, they constitute '*epilepsy*'. 'Epilepsy' is a chronic condition in which occasional seizures tend to occur repeatedly as a result of either structural brain damage or an intrinsic functional tendency to have seizures.

According to the International League Against Epilepsy (ILAE), an '*epileptic disorder*' is a chronic neurological condition characterized by recurrent epileptic seizures, whereas '*epilepsies*' are those conditions involving chronic recurrent epileptic seizures that can be considered epileptic disorders (►http://www.ilae-epilepsy.org/Visitors/Centre/ctf/glossary.cfm).

A classification of epileptic seizures has been adopted by the ILAE based on the distinction between '*partial seizures*', indicating electrophysiological activation of a small part of a single hemisphere and '*generalized seizures*', indicating involvement of both hemispheres (2). When partial seizures occur without altered consciousness they are termed '*simple partial seizures*' (SPS), otherwise they are termed '*complex partial seizures*' (CPS). Patients mainly suffering from recurrent CPS have '*complex partial epilepsy*' (CPE).

Pathology/Histopathology

Seizures may occur in patients with almost any pathological process: brain malformations, tumors, acquired traumatic lesions, and vascular lesions. Table 1 lists the most important brain disorders that may be treatable with surgical intervention. Mesial temporal sclerosis is a well recognized entity that may result from prolonged febrile seizures or convulsive status epilepticus and accompanying systemic disturbances (hypotension, fever, hypoglycemia, etc.). This entity is often the substrate of temporal lobe epilepsy (TLE).

Malformations of cortical development (MCD) are not specific for epilepsy but are more often seen in epileptic brains.

Tumors that are found in patients with longstanding CPE are usually benign: for example dysembryoplastic neuroepithelial tumor (DNET), ganglioglioma, or glioma.

Imaging

Most patients with epilepsy can initially be treated with standard first-line antiepileptic drugs (AED). About

Seizures, Complex, Partial. Table 1 Disorders causing CPE and that may be treatable by surgery

Genetic and developmental disorders	Acquired disorders
Sturge–Weber–Dimitri syndrome	Rasmussen encephalitis
Neurofibromatosis	*Tumor: primary and metastasis*
Tuberous sclerosis	Infectious lesions: meningitis, abscess, encephalitis
Congenital porencephalic cyst	
Congenital tumor	Subarachnoid hemorrhage
Malformation of Cortical Development (MCD)	Stroke
	Trauma
• focal cortical dysplasia	*Mesial temporal sclerosis (MTS)*
• periventricular heterotopia	
• polymicrogyria	
• DNET	
• ….	

From the listed pathologies in the table, the most important are tumor for recent CPE, and MTS and MCD for chronic CPE.

25–45% of epilepsy patients will become refractory to medical treatment. Some patients who fail to respond to first-line AED therapy will be rendered seizure-free with newer medical treatments introduced in the past decades. For those CPE patients who still remain refractory to medical treatment, surgery can be an effective alternative treatment. The role of neuroimaging becomes very important here for the determination of the actual site of epileptic origin. This includes the identification of lesions that may be amenable for tailored resection, the objectivation of lateralization in TLE by detecting lateralized damage to the hippocampus or temporal neocortical regions, and the detection of often microscopic cortical abnormalities in case of extra-temporal lobe epilepsy (ETLE). The relation also has to be established between the seizure focus and eloquent cortex when resection in such regions is mandatory.

The role of CT in epilepsy is limited to the evaluation of patients who present at emergency wards with acute epileptic seizures with remaining neurological symptoms and the occasional patient with absolute contra-indication for MR. All other patients should be examined with MRI.

MRI will detect cortical lesions in patients with CPE in almost 75% in tertiary referral centers for epilepsy surgery.

Hippocampal Sclerosis and TLE

Hippocampal sclerosis (HCS) is the most common pathology found in patients with refractory CPE.

Imaging in these patients focuses on the visualization of the hippocampus and the mesial temporal lobe structures. Tilted-coronal thin-slice high resolution imaging of the temporal lobe is performed with inversion-recovery T1-weighted or fast spin-echo T2-weighted contrast. With experience, neuroradiologist will be able to visually diagnose HCS in 85–90% of histologically proven cases.

Three important features are characteristic of hippocampal damage: decreased volume, signal changes, and structural changes (Fig. 1) (3). Structural changes are often associated with extensive gliosis. Volume loss and gliotic changes often extend beyond the hippocampus into the adjacent temporal lobe and even in the contralateral temporal lobe. Studies have shown damage to the thalamus, the parahippocampal region and the entorhinal region.

In up to 30% of patients with seizure semiology of TLE and/or EEG findings consistent with TLE, optimal high resolution MRI does not show the classical signs of HCS. A lot of MR research is directed toward these patients. Special MR techniques like DTI and MT have shown abnormalities in the brains of MR-negative TLE patients, but not necessarily in the temporal lobes.

Malformations of Cortical Development

MCD is a blanket term and encompasses many different entities resulting from the disruption of brain formation in utero. These entities differ in their genetic signature, clinical presentation, structural effects and associated pathology and are usually grouped on the basis of three neuro-developmental steps: neuronal proliferation and eventual apoptosis of selected cells, neuronal migration, and cortical organization (4).

MCD is often associated with epilepsy, and is the second most common cause of refractory epilepsy (4): for example focal cortical dysplasias (Fig. 2), periventricular heterotopia and polymicrogyria (Fig. 3). Since many MCDs have been linked to genetic factors, the mere

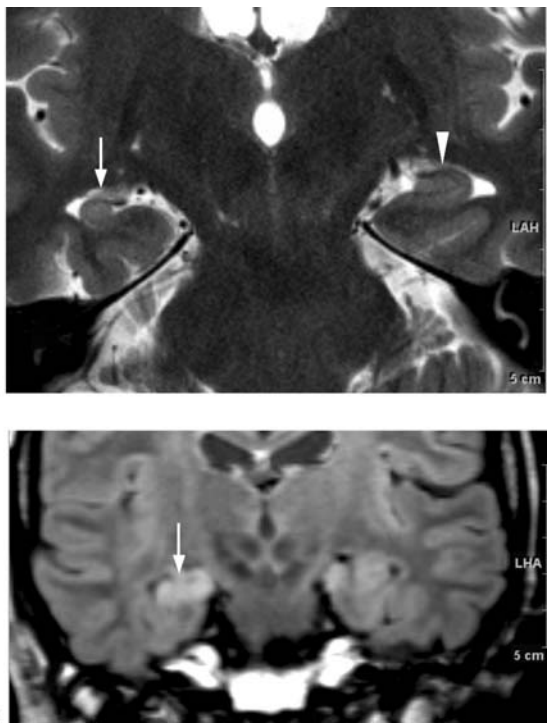

Seizures, Complex, Partial. Figure 1 Hippocampal sclerosis MRI. Tilted coronal T2-weighted (a) and coronal reconstruction of 3DFLAIR (b) centered on the hippocampal region in a patients with TLE and right sided hippocampal sclerosis. In a, the *arrowhead* point toward the normal left hippocampus in which a clear an normal internal structure can be recognized, and the different divisions of the cornu ammonis and dentate gyrus have normal signal and thickness. On the right side, the hippocampus (*arrow*) is much smaller, the internal structure is mostly effaced (a) and the signal is too high (best seen on b).

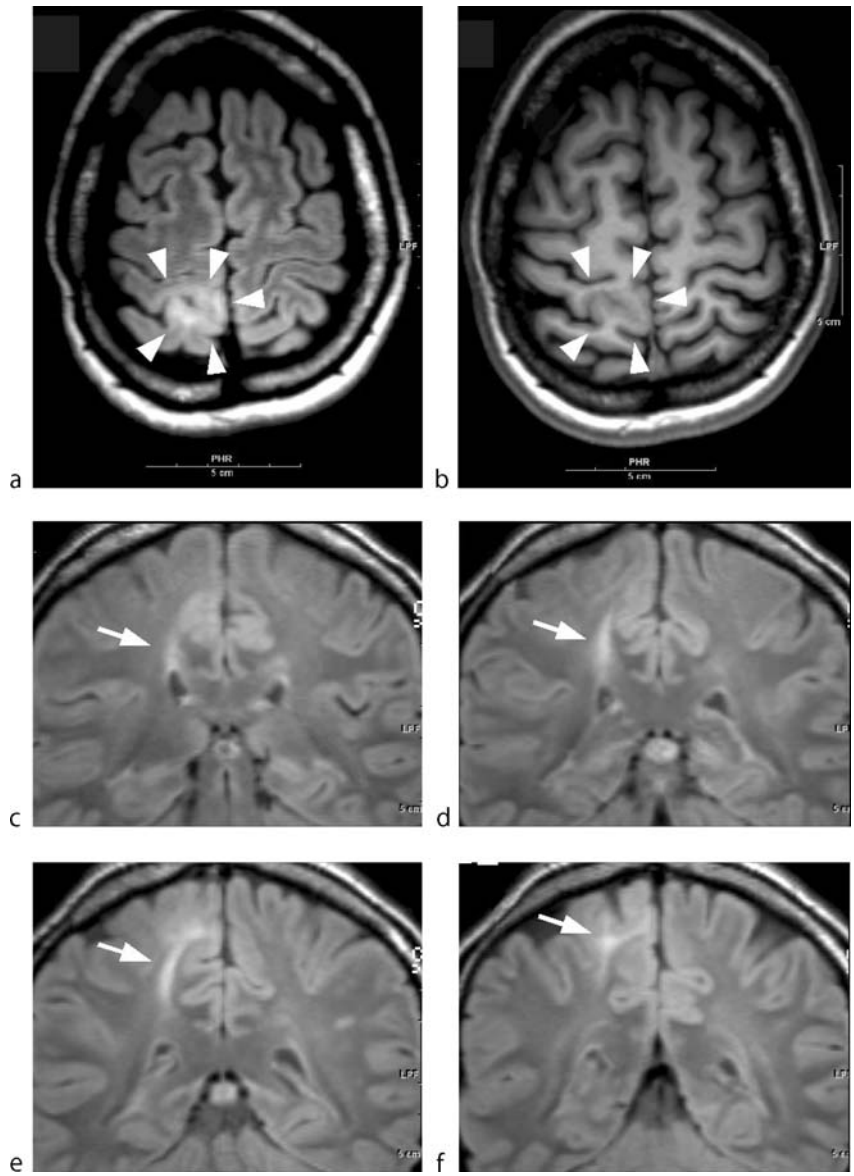

Seizures, Complex, Partial. Figure 2 Focal cortical dysplasia. Focal cortical dysplasia, Taylor type II, in the right medial Rolandic region. The typical disturbance of the architecture of the neocortex can be appreciated on high axial reconstruction of a 3DFLAIR (a) and 3DMPRAGE (b): irregular thickening, altered signal, and effacement of the normal interface between white and gray matter. A spur of signal changes can be seen on consecutive coronal reconstructions of 3DFLAIR (c–f) starting from the edge of the lateral ventricle, presumably deposited during the migration process.

detection of these entities by medical imaging is important for genetic counseling.

Many of these abnormalities can be visualized with high resolution and multicontrast, multiorientation thin-slice or 3D MR imaging (6). Recent work advocates the use of high field imaging because of the higher signal to noise and resolution that can be attained all in view of patient and budget friendly imaging times.

Tumors

The third most common cause of chronic refractory CPE is the presence of low-grade tumors. DNET, gangliioglioma, and gangliocytomas are benign developmental neoplastic lesions. Because these lesions are developmental, epilepsy often develops early in live and quickly becomes refractory to medical treatment. Complete resection is effective for epilepsy relief. MRI is the

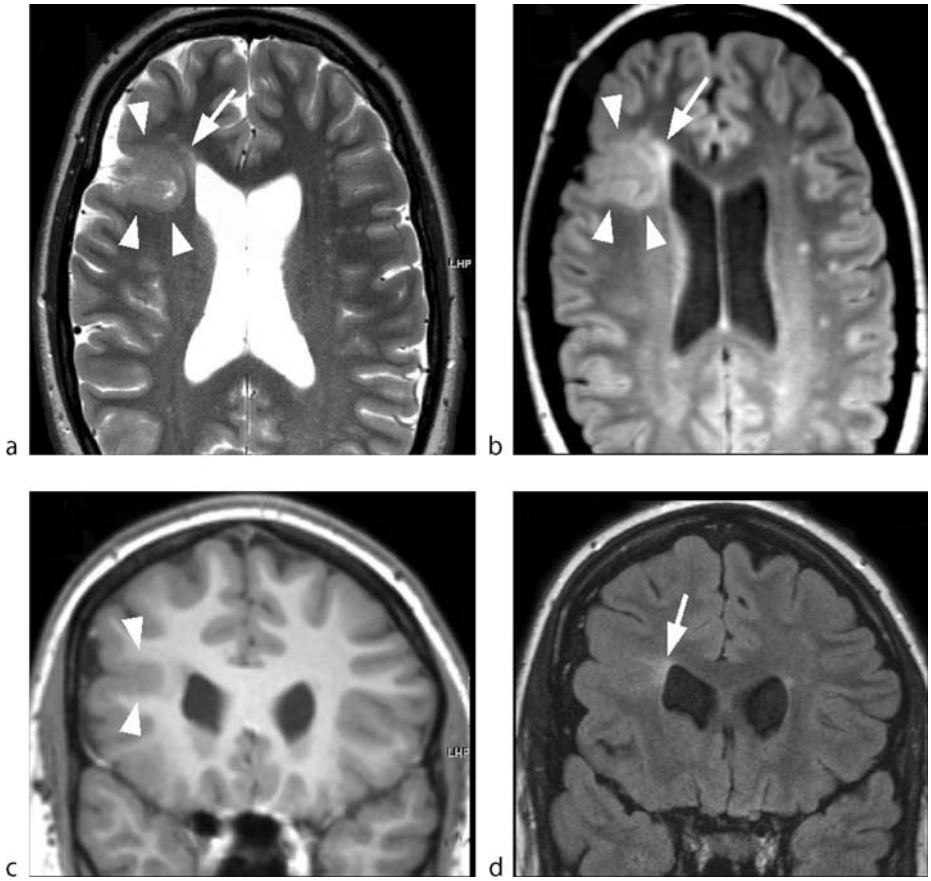

Seizures, Complex, Partial. Figure 3 Polymicrogyria. MRI of a patient with frontal lobe epilepsy (FLE): axial T2-weighted (a), axial reconstruction of 3DFLAIR (b), coronal reconstruction of MPRAGE (c) and coronal FLAIR (d). A zone of abnormal folding of thickened cortex can be observed (*arrowheads*) in the right inferior prefrontal region with an underlying area of signal change in the white matter connected with the edge of the lateral ventricle (*arrow*). This abnormality constitutes polymicrogyria.

preferred imaging method to define the location and extend of the lesion. Of course, almost any tumor can cause recent onset CPE.

Sample Optimal Imaging Strategy for CPE

Many centers also use quantitative imaging parameters like hippocampal volume and T2 values in the hippocampus to detect hippocampal damage. Table 2 describes our imaging strategy for patients with chronic CPE. All imaging is performed on a 3 Tesla system. Although we rely heavily on 3D imaging, these sequences can be substituted by 2D sequences, but at least in two directions, axial and tilted coronal. Volume measurements are performed only if no visual abnormality is found in the hippocampi (3). In addition to structural MRI imaging, ^{18}FDG-PET and magnetic resonance spectroscopy (MRS) will be performed in all patients with TLE, and in selected patients with ETLE. fMRI of memory and language is performed presurgically.

Complex Partial Epilepsy and Brain Function: Language and Memory

Information on the location of functional areas in the brain of patients with chronic CPE is essential in view of surgery. In patients with HCS, it has been shown that epilepsy surgery in the language dominant hemisphere will often cause language problems. Therefore language lateralization and localization are essential before surgery is attempted. Typically, the presurgical evaluation of TLE patients includes a WADA test or intracarotid amytal procedure to assess language lateralization and memory redundancy. BOLD fMRI and the

Seizures, Complex, Partial. Table 2 The imaging strategy at 3T used at the Ghent University Hospital in Belgium for patients with chronic CPE. Reconstructions of 3D sequences are always performed in 2 mm thick adjacent axial slices along the AC–PC line and coronal slices perpendicular to the hippocampi

Structural Imaging strategy for CPE			
Sagittal MPRAGE	Fast T1W 3D sequence with isotropic voxels of $0.9\times0.9\times0.9$ mm^3	T_{acq} = 6′	Anatomical detail, hippocampal volume
Sagittal 3D-FLAIR	Fast T2W 3D sequence with fluid attenuation, isotropic voxels of $0.9\times0.9\times0.9$ mm^3	T_{acq} = 9′	Gliosis, myelination, inflammation, edema
Axial 2D TSE along AC–PC line	High resolution T2W sequence with slice thickness 3 mm and in-plane resolution of 420 μm	T_{acq} = 5′	Anatomical detail outside of the temporal lobe
Coronal 2D TSE perpendicular to HC	High resolution T2W sequence with slice thickness 3 mm and in-plane resolution of 420 μm	T_{acq} = 5′	anatomical detail of the hippocampi and the neocortex of the temporal lobes
Axial T2*W GE along AC–PC line	Gradient echo sequence with 3 mm thick slices	T_{acq} = 3′	Hemosiderine, calcifications, venous vascular structures
DWI along AC–PC line	EPI sequence with diffusion weighted preparation	T_{acq} = 1′	
Sagittal MPRAGE after gadolinium injection	Fast T1W 3D sequence with isotropic voxels of $1\times1\times1$ mm^3 (interpolated in slice selection)	T_{acq} = 3′	Only if indicated by previous imaging results: tumors, vascular malformations

WADA test are concordant in 90% of CPE patients in defining language lateralization. A single language task is unlikely to show all essential language areas in the brain, and the combination of several language tasks is adopted in many centers to feel more comfortable in lateralization and localization issues of language in CPE. In our epilepsy surgery referral center the combination of a silent word generation task, a reading task, and a self-paced semantic decision task are standard procedure for CPE patients (7).

For surgery in the neocortex, localization of essential language areas is important. fMRI will often show many regions which are not essential to language as predicted from electrocortical stimulation, but a high predictive power of fMRI compared to electrocortical activation has been reported for the presence and absence of critical cortical language zones. fMRI has a high negative predictive value, and regions without activation can probably be safely removed.

Memory testing in epilepsy surgery patients is essential to test adequate postoperative memory function (WADA) and possible neuropsychological rehabilitation (neuropsychological testing). The WADA test cannot reliably detect specific postoperative deficits, but only test whether no devastating postoperative amnesia will be present if a hippocampectomy is performed. Therefor, in our practice we use two fMRI memory paradigms: a complex visual scene encoding task (8) and a less predictable memory paradigm (9).

Magnetic Resonance Spectroscopy

Proton MRS has proven to be a sensitive technique to detect metabolic abnormalities and dysfunction in patients with CPE (Fig. 4). With its high sensitivity, metabolite abnormalities can be detected in brain regions distinct from the seizure focus and it remains difficult to disentangle which abnormalities cause seizures and which are their consequences.

Abnormalities detected with 1H-MRS can be used in lateralization issues of TLE and in localization attempts for ETLE, and also in monitoring therapeutic effects of AED. In TLE, NAA is used as a marker for neuronal loss or dysfunction and is often more decreased in the afflicted TL. Although many bilateral abnormal ratios can be found in patients with TLE, the introduction of an adequate asymmetry index (AI) improves the lateralization capabilities of the technique (10).

A recent meta-analysis of the value of MRS in epilepsy shows rather conflicting results for patients with MR-negative patients in an epilepsy surgery program, but a role for MRS could be found for patients with bilateral hippocampal atrophy.

Glutamate and γ-amino-butyric-acid (GABA) can be measured using MRS and many medication related effects on their concentrations have been reported. Intracellular glutamate concentrations are reported elevated in the epileptogenic human hippocampus and neocortex. The high glutamate content may contribute to the epileptic

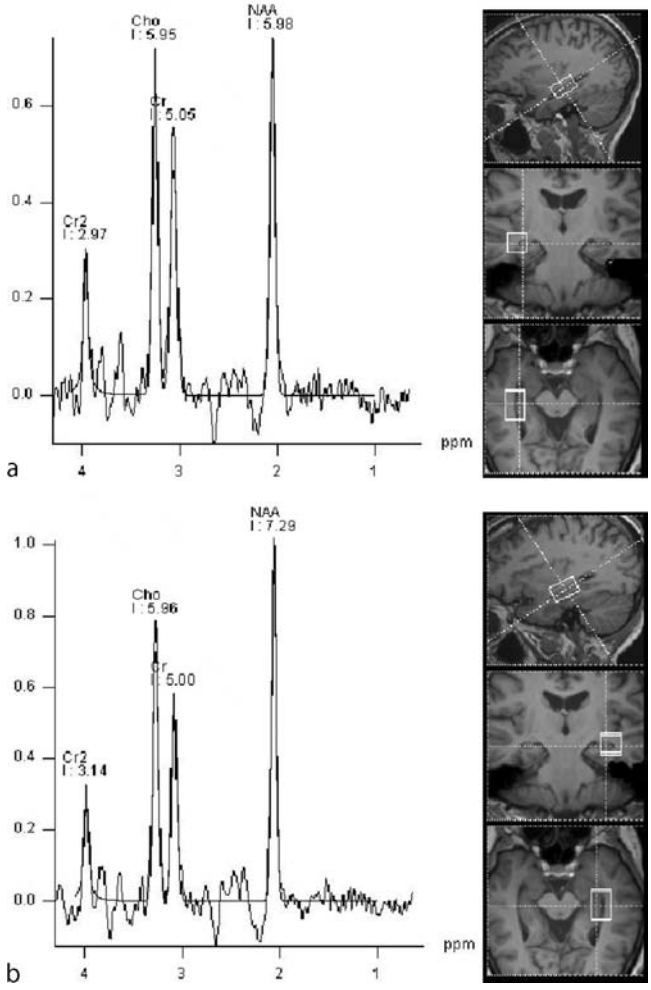

Seizures, Complex, Partial. Figure 4 Proton MRS in temporal lobe epilepsy. Single voxel proton MRS in the temporal lobe of the patient shown in Figure 2 with right sided HC sclerosis. (a) The spectrum on the right side, (b) the spectrum on the left. The only difference is the amplitude in the NAA peak which is lower on the right side. The NAA/Cho+Cr ratio is 0:54 on the right and 0:67 on the left. Both ratios are too low (less than 0:71), but the asymmetry index is 21, lateralizing the metabolic disturbance to the right side.

state by increasing cellular excitability. The cellular glutamate levels measured by MRS in occipital cortex are increased in patients with refractory CPS.

Bibliography

1. Aicardi J (1992) Epilepsy and other Seizure Disorders. In: Aicardi J (ed) Diseases of the Nervous System in Childhood. Mac Keith Press, London
2. Commission on Classification and Terminology of the International League against Epilepsy (1981) Proposal for revised clinical and electroencephalographic classification of epileptic seizures. Epilepsia 22:489–501
3. Achten E, Boon P, De Poorter J et al (1995) An MR protocol for the pre-surgical work-up of patients with complex partial seizures of temporal lobe origin. Am J Neuroradiol 16:1201–1213
4. Sisodiya SM (2004) Malformations of cortical development: burdens and insights from important causes of human epilepsy. Lancet Neurol 3:29–38
5. Palmini A, Najm I, Avanzini G et al (2004) Terminology and classification of the cortical dysplasias. Neurology 62:S2–S8
6. Urbach H (2005) Imaging of the epilepsies. Eur Radiol 15:494–500
7. Deblaere K, Backes WH, Hofman P, Vandemaele P, Boon PA, Vonck K, Boon P, Troost J, Vermeulen J, Wilmink J, Achten E, Aldenkamp A (2002) Developing a comprehensive presurgical functional MRI protocol for patients with intractable temporal lobe epilepsy: a pilot study. Neuroradiology. 2002 Aug; 44 (8):667–673
8. Detre JA, Maccotta L, King D, Alsop DC, Glosser G, D'Esposito M, Zarahn E, Aguirre GK, French JA (1998) Functional MRI lateralization of memory in temporal lobe epilepsy. Neurology 50:926–932

9. Deblaere K, Backes WH, Tieleman A, Vandemaele P, Defreyne L, Vonck K, Hofman P, Boon P, Vermeulen J, Wilmink J, Aldenkamp A, Boon PA, Vingerhoets G, Achten E (2005) Lateralized anterior mesiotemporal lobe activation: semirandom functional MR imaging encoding paradigm in patients with temporal lobe epilepsy - initial experience. Radiology 236:996–1003
10. Achten E, Boon P, Van De Kerckhove T, Caemaert J, De Reuck J, Kunnen M (1997) Value of single voxel proton MR spectroscopy in temporal lobe epilepsy. AJNR Am J Neuroradiol 18:1131–1139

Sella Turcica

▶Pituitary Gland

Sensitivity

The proportion of truly diseased persons in the screened population who are identified as diseased by the screening test.

▶Screening, Breast Cancer

Sentinel Lymph Node (SLN)

SLN is the first lymph node to receive lymphatic fluid from a malignant tumor.

▶Sentinel Node, Scintigraphy

Sentinel Lymph Node Biopsy (SLNB)

SLNB is an alternative to standard complete lymph node dissection, for staging in oncologic patients that allows complete ALND to be avoided if the sentinel node is metastasis free.

▶Sentinel Node, Scintigraphy

Sentinel Node Biopsy (SLNB)

Surgical removal and histological study of the first node in the chain by draining the area containing the malignant lesion after its identification by injection of a blue dye, radioactive tracer, or both.

▶Breast Conserving Therapy

Sentinel Node, Scintigraphy

S. I. Koukouraki Sophia
Nuclear Medicine Physician
Department of Nuclear Medicine,
University, Iraklion, Crete, Greece
sophiak@her.forthnet.gr

Introduction

The prognosis of malignant disease is determined by the metastatic potential of the primary tumor. The status of the regional lymph nodes is critical in staging oncologic patients, since lymph node involvement is an unfavorable prognostic factor. Moreover, the detailed histological assessment of the lymph nodes is one of the most significant prognostic indicators and a strong determinant in the choice of therapy.

Minimally invasive surgery combined with lymphatic mapping helps avoiding complete lymph node dissection (ALND) and decrease morbidity. Lymphatic mapping with sentinel node biopsy is a new promising technique to determine lymph node status.

The ▶sentinel lymph node (SLN) is the first lymph node to receive lymphatic fluid from a malignant tumor and is the most likely node to contain tumor cells. Theoretically, if the SLN is free of tumor cells, the remainder of the nodal basin will also be free from metastases.

▶Sentinel lymph node biopsy (SLNB) is an alternative to standard complete ALND that allows complete ALND to be avoided if the sentinel node is metastasis free. It is a minimally invasive technique useful to find out the status of a lymph node basin by removing one or a small number of nodes. SLNB was initially developed to detect lymphatic metastases in patients with penile carcinoma (described by Cabanas in 1977). Now is a widely available technique mostly for patients with melanoma and breast cancer. Moreover, it has a very promising role in other malignancies like gastrointestinal, endocrine, head and neck, and lung tumors.

There are several principal aims for the excision of SLN: (i) Minimally invasive assessment of the nodal status. (ii) Selection of patients with positive SLNs. (iii) Prevention of complete ALND in SLN negative patients. (iv) Detection of alternative lymphatic drainage. (v) Improvement of sensitivity of histopathological detection of lymph node metastases. Since 1 or 2 lymph nodes are removed, a more accurate immunohistochemical evaluation can be done.

Despite the initial enthusiasm, there are controversies in practice and many issues have to be defined. There is no

gold standard technique in the performance of the SN procedure yet. Current techniques involve the use of radioactive isotopes and/or the use of dyes. The success of the technique depends on: (i) the accurate preoperative determination of regional lymph node basins at risk and the location of SLN within the basin, (ii) the accurate intraoperative localization and biopsy of the SLN, and (iii) the accurate pathologic evaluation of the removed SLN.

Clinical Applications

The diagnostic utility of SLN technology includes melanoma, breast cancer, colon cancer, and all solid neoplasms that can potentially spread to lymph nodes, like lung cancer, head and neck cancer, gynecological cancer, and urological cancer. However, the clinical significance is not the same in each type of all these solid tumors. For melanoma and breast cancer the SLN concept is an established and of great validity technique, confirmed by many clinical trials.

Techniques in Sentinel Node Detection

Two different techniques are currently available for locating SLNs: (i) radioisotopic and (ii) nonradioisotopic techniques.

Radioisotopic Techniques

The radioisotopic techniques are used for the pre and intraoperative detection of the SLN. They include the lymphoscintigraphy for the preoperative evaluation of SLNs and the use of gamma detection probes for preoperative and intraoperative evaluation.

For the radioisotopic detection of the true SLN several steps must be followed: to choose the most suitable gamma detection probe, the most appropriate tracer, to decide for the best injection technique (site of injection, how many injections, volume of the injectate, how many MBqs) and the imaging protocol (dynamic, early imaging, early and late imaging).

Gamma Detection Probes

A wide range of probes are now available. These detectors must fulfill required characteristics. The high sensitivity (determination of counts per time unit) is very important. Deeply situated sentinel nodes could not be detected without good sensitivity. Other important parameters are the accepted spatial resolution, the energy resolution, and the collimation. Moreover, other factors like visual display clarity, audible feedback, size, and weight must also be taken into account.

Radiopharmaceuticals

The radioisotopic procedure of the SLN detection is based on the injection of a radiopharmaceutical, a specific compound, labeled with a radionuclide to be detected by gamma camera and probe detectors. Labeled colloids seem to be the most appropriate tracer and technetium-99 (^{99m}Tc) is the most often used radiotracer for labeling purposes, because of its relatively short half-life (6 h), the low patient dose, the nonsignificant beta emission, and the good detection energy. The ideal tracer should combine a rapid and predictable transport to the target node and persistent retention in it. Different size averages are used for lymphoscintigraphy (50–90 nm) and sentinel node labeling (100–200 nm). Larger particles may be retained at the injection site and no migration will be noticed. Smaller particles will pass to the capillary instead of the lymphatic system.

How these particles enter the lymphatic capillaries is not completely understood. Lymph nodes are rich in macrophage and colloid particles are phagocytosed by them.

The use of a particular colloid preparation depends on the clinical protocol. Larger particle colloids are more suitable when a patient is to be operated the next day of the imaging and smaller when imaging and operation is to be done on the same day. Moreover, other factors like the number of particles, the charge to the particles with the tracer substance, the rate of degradation by enzymatic activity of proteases are important.

Besides the labeled colloid particles that are routinely used to indicate the localization of SLN independently of the cancer cell infiltration, labeled liposomes are investigated to detect cancer cell infiltrations of lymph nodes.

Injection Techniques

There are different opinions about the injection site, the number of injection sites, the volume of injectate, and the injected dose of the radiotracer.

For malignant melanoma, the subdermal injection site is the most appropriate. The lymphatic tissue is very rich in the peripheral layer of the skin, so a subdermal injection will deliver the tracer to an area rich in lymph vessels. In contrary, subcutaneous tissue has fewer lymphatic vessels.

On the day before or on the same day of the operation up to 1 mCi of radiolabeled colloid is injected subdermally into four equal portions around the primary lesion or the excisional biopsy area, using a 25-G needle. The syringe is held parallel to the skin surface with an angle of 10–20° to the horizontal plane (Fig. 1a, b).

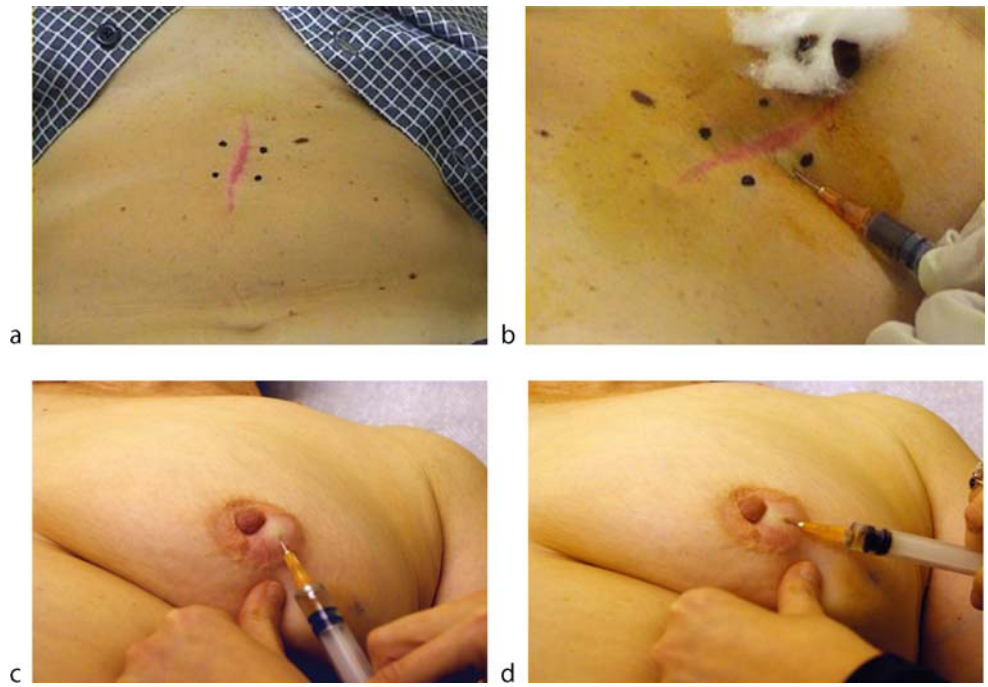

Sentinel Node, Scintigraphy. Figure 1 (a) Melanoma of the abdomen (b) subdermal injection (c) breast cancer (d) subareolar injection.

The direction of lymph flow is important in the decision on whether injections should be given in circular or semicircular formation. When the primary lesion is located on the trunk a circular injection is needed because of different possible drainage direction of the lymphatic flow. In contrary, when the lesion is located on the face or the extremities, a semicircular injection is more appropriate because normally there is only one possible drainage direction.

While in melanoma the subdermal injection is a rule, for breast cancer there is an enormous discussion about the injection techniques: single subdermal or intradermal injection, multiple peritumoral and intratumoral. The confusion is mainly generated by the fact that although there is undoubtedly communication between breast and dermal lymphatics, it is debatable whether the lymphatics of the overlying skin drain to the same axillary sentinel node as the underlying glandular breast tissue.

The subdermal injection has several advantages over the intraparenchymal injection such as the ease of injection, the shorter time interval between injection and sentinel node identification, and the increased radiotracer nodal uptake. However, despite its success, subdermal injection failed to identify nonaxillary sentinel nodes when compared to intraparenchymal injection.

The intraparenchymal injection is characterized by a slower removal of the tracer due to the scantier lymphatic supply of the breast parenchyma. The intratumoral injection technique is not widely used.

The subareolar or periareolar injection technique has recently been proposed. A local anesthesia is needed. After a few moments to allow the anesthetic to take effect, a dose of 1 mCi diluted with sterile saline to a total volume of 4 mL is injected. The injection must be superficial subdermally toward the nipple. (Fig. 1c, d). Deep breast injections may produce a delay or failure of migration of the radiotracer.

The subareolar or periareolar injection seems to be superior compared to subdermal and intraparenchymal injections. Its superiority is due to the more rapid flow of the tracer to the SN, the more rapid visualization, its simplicity, the quick learning curve, the higher percentage of the injected dose in the SLN and the reduced "shine through" effect.

Preoperative–Intraoperative Detection

The sentinel node detection techniques are performed in two steps: (i) the preoperative based on lymphoscintigraphy and on probe detectors and (ii) the intraoperative based on the visual evaluation of the SLN with dyes and on the quantitative evaluation with gamma probe detectors.

The ►preoperative lymphoscintigraphy (PL) is a highly sensitive procedure (Figs 2 and 3). PL is performed routinely in melanoma. For breast cancer, it is not yet clear if it is helpful or not. Some investigators support that PL does not improve the ability to identify axillary SLNs and is not associated with improvement of false negative rate.

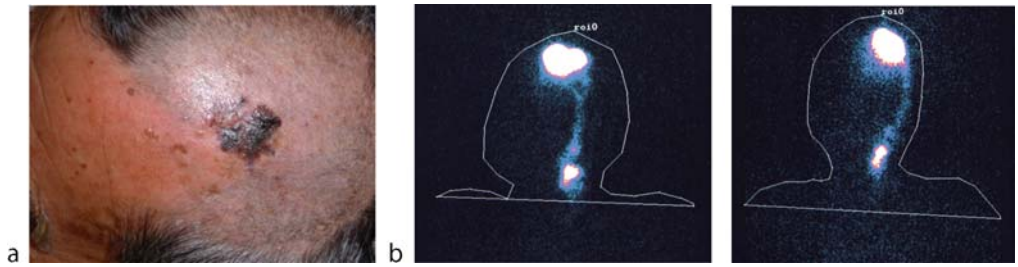

Sentinel Node, Scintigraphy. Figure 2 Melanoma of the scalp. The lymphoscintigraphy demonstrates a lymphatic channel that drains into a submandibular lymph node. (a) subdermal injection (b) lateral view, anterior view.

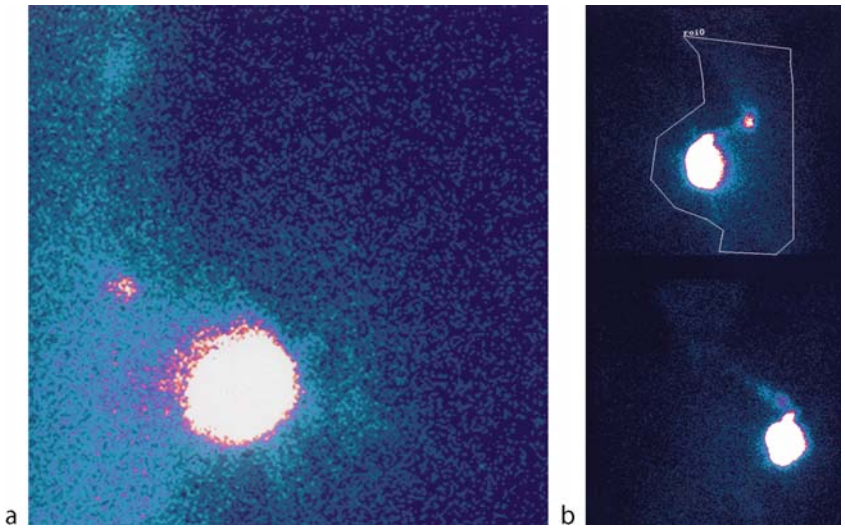

Sentinel Node, Scintigraphy. Figure 3 Ductal carcinoma of the left breast. (a) lateral view which shows the SLN in the axilla (subareolar injection site) (b) illustrates the need for lateral projections compared to the anterior image (upper row: lateral view; lower row: anterior view).

Arguments have been made in favor of PL as a "road map" for the surgeons able to identify all nodal basins at risk from metastatic disease, any transit nodes, and any unsuspected nodal basins. The imaging protocol (dynamic series, early images, early and delay images) depends on the department. However, it comprises: (i) dynamic series, necessary not only to identify the drainage from the lesion to the SLN but also to identify its position. (ii) static images, early and delay, in two projections (anterior, lateral, or obliques), useful to define the lymphatic anatomy (Fig. 2). Additionally, the use of anatomical markers, for example, for the nipple, is helpful.

After the determination of SLN by lymphoscintigraphy, its position is marked on the immediately overlying skin. This mark is subsequently confirmed with a gamma probe.

The combination of the lymphoscintigraphy and the probe detectors is advantageous for the knowledge of the location of SLN before surgery. The overall success of SLN localization is maximized and the false negative results are reduced.

Sentinel Node, Scintigraphy. Table 1 Criteria of successful SLN intraoperative detection.

In vivo	Ex vivo	Incision area	Evaluation
+	+	–	Total excision
+	-	+	Not true SLN excised
+	+	+	Additional SLNs
+	–	–	Technical failure

+ represents high counts, – represents low or no counts compared to background

The intraoperative detection is based on three steps: (i) the *in vivo* evaluation (positioning the probe in the wound and looking for the node with high radioactivity compared to background), (ii) the *ex vivo* detection (counting the radioactivity over the excised node and far away from the body), and (iii) the detection of any remained node with high activity in the wound (Table 1).

Conclusion

The combination of preoperative lymphoscintigraphy and the intraoperative use of the probe and/or dyes is the best available detection method of the SLNs. A good communication between the surgeons and the nuclear medicine physicians is important to improve the accuracy of the SLN procedure.

Bibliography

1. Kehtgar MRS, Ell PJ (1999) Sentinel lymph node detection and imaging. EJNM 26:57–67
2. Nieweg OE, Rutgers EJT, Jansen L et al (2001) Is lymphatic mapping in breast cancer adequate and safe? World J Surg 25:780–788
3. Torrenga H, Meijer S, Fabry H et al (2004) Sentinel node biopsy in breast cancer patients: triple technique as a routine procedure. Ann Surg Oncol 11231S–235S
4. Pelosi E, Bello M, Giors M et al (2004) Sentinel lymph node detection in patients with early-stage breast cancer: comparison of periareolar and subdermal/peritumoral injection techniques. J Nucl Med 45:220–225
5. Intenzo CM, Kim SM, Patel JI et al (2002) Lymphoscintigraphy in cutaneous melanoma: a total body atlas of sentinel node mapping. Radiographics 22:491–502

Septo-Optic Dysplasia

▶Congenital Malformations, Orbit

Sequestrum

A sequstrum represents a segment of necrotic bone that is separated from living bone by granulation tissue. A vital bony fragments are typically found in the medullary canal of tubular bones and may appear as radiodense inclusions. Sequestra are best diagnosed by CT and may be difficult to recognize in MR examinations.

Seroma

A peritoneal loculated collection confined by the peritoneal surface and adhesions and filled with secretions of peritoneal serosa.

▶Breast Conserving Therapy
▶Peritoneal Collections

Serothorax

▶Postoperative

Serum Creatinine

Creatinine is a breakdown product of creatine, which is an important part of muscle. A serum creatinine test measures the amount of creatinine in the blood. A normal (usual) value is 0.8–1.4 mg/dL. Normal value ranges may vary slightly among different laboratories. Females have lower creatinine values than males, due to less muscle mass.

▶Glomerulonephritis
▶Tubular Necrosis, Kidney, Acute

Sex Reversal

Sex reversal is where person's phenotypic appearance is incongruous with karyotype. Most commonly see in male under-masculisation syndromes, testicular feminisation syndrome, 5α-reductase deficiency and complete XY gonadal dysgenesis the Swyer syndrome. The individual may be reared as a female and only present with primary amennorhea in adolescence.

▶Ambiguous Genitalia

Shaded Surface Display

Three-dimensional rendering technique for display of CT data in which structures of interest are defined by selecting attenuation thresholds.

▶Carotid and Vertebral Artery Pathology

Shaken Baby

▶Battered Child Syndrome

Shaken Baby Syndrome (SBS)

▶Trauma, Head, Non-accidental

Shaken-Impact Syndrome

▶Trauma, Head, Non-accidental

Shin Splints

A stress injury secondary to excessive force on the tibial periosteum at the insertion of the soleus and tibialis posterior, which usually occurs in young athletes. It is best seen on scintigraphy where it is seen on the delayed phase as a linear region of uptake that involves the posterior tibial cortex.

▶Fractures, Stress

Shining Corner

Shining corner is the minimal variant of a Romanus lesion without erosion and only minor sclerosis.

▶Spondyloarthropathies, Seronegative

Short Oesophagus

Permanent retraction of the gastro-oesophageal junction into the chest because of chronic oesophagitis and fibrosis.

▶Hernia, Hiatus in Adults

Shoulder Dislocation

The majority of glenohumeral dislocations are anterior. Anterior humeral dislocations are often associated with osseous impaction of the posterolateral humeral head and anteroinferior labral detachment. These lesions are known as Hill-Sachs and Bankart lesions, respectively. Fractures of greater tuberosity are associated with 15% of anterior dislocations. Injuries to the rotator cuff and the articular capsule are also associated with these dislocations. Recurrent dislocations are common in younger patients and those with associated soft tissue and osseous injury. MRI is helpful for characterizing these abnormalities and assists surgical planning. Posterior dislocations usually occur secondary to muscle spasm during seizures. Reverse Hill-Sachs fractures, injury to the posterior labrum, and lesser tuberosity fractures are associated with posterior dislocations.

▶Fractures, Peripheral Skeleton

Shrinking

Lobular invasive carcinoma represented by a decrease in the size of the affected breast.

▶Carcinoma, Lobular, Invasive

Shwachman–Diamond Syndrome (SDS)

Rare autosomal recessive disorder characterized by pancreatic exocrine hypoplasia with pancreatic insufficiency, associated with bone marrow dysfunction and skeletal anomalies (metaphyseal chondrodysplasia).

▶Congenital Abnormalities, Pancreatic

Sialadenitis

Sialadenitis inflammation of one or more of the salivary glands

▶Inflammation, Chronic, Acute, Salivary Glands

Sialoadenitis

▶Salivary Glands, Inflammation, Acute Chronic

Sialolithiasis

Sialolithiasis is a stone formation in the salivary gland or duct that drains the salivary gland.

▶Inflammation, Chronic, Acute, Salivary Glands

Sickle Cell Anemia

▶Sickle Cell Disease

Sickle Cell Disease

Dorothy Bulas
Division of Diagnostic Imaging and Radiology
Children's National Medical Center
The George Washington University School of Medicine and Health Sciences
Washington DC, USA
dbulas@cnmc.org

Synonyms

Sickle cell anemia

Definitions

Sickle cell disease (SCD) is a hemolytic anemia with red blood cells that abnormally sickle. These cells are destroyed at an increased rate leading to a chronic anemia. The sickled cells cause vascular occlusion which often leads to infarction resulting in many clinical and radiologic manifestations of the disease.

Pathology/Histopathology

Hemoglobin (Hb) A consists of four globin chains, two alpha and two beta. In SCD, the beta chain is abnormal with valine substituted for glutamic acid at the sixth position of the B-globin chain locus on chromosome 11. Patients homozygous for the defect have HbSS and are referred as having sickle cell anemia. Those with one normal beta globin chain have sickle trait with a typically benign course unless significantly stressed. Those with one S-globin chain and a second abnormal chain such as Hb sickle thalassemia have a less severe clinical course.

When deoxygenated, the abnormal Hb chains form rigid polymers that cause a sickling shape and reduce the deformability of the red blood cell (RBC) resulting in lysis and occlusion of vessels. HbS adheres to vessel endothelium which can result in intimal hyperplasia. When acutely deoxygenated, an erythrocyte may partially polymerize which reverses when reoxygenated. Polymerization also depends on pH, temperature, and Hb concentration. When polymerization occurs, membrane permeability changes creating a dehydrated RBC. The abnormal Hb becomes more concentrated accelerating the polymerization during the next deoxygenation episode. These cells eventually become irreversibly sickled and cause vasoocclusion even when oxygenated. It has been noted that individuals with abnormal Hbs such as sickle cell trait have fewer parasites and a milder disease course than those with normal Hb. Malaria invades HbS cells as easily as normal cells, however, with lower oxygen tensions, the trophozoites do not grow as well, thus decreasing the severity of malaria.

Clinical Presentation

SCD is the most common genetic disorder in black Americans affecting 1 in 375 Americans of African ancestry. SCD is also common in the Middle East, India, Caribbean, and South America. In the neonatal period, higher concentrations of fetal hemoglobin prevent the sickling process. After 6–8 months, HbS percentage increases and clinical manifestations become evident.

As the cells sickle from hypoxic events such as pneumonia, air travel, or dehydration, capillary stasis occurs which leads to hypoxic damage. Crises are associated with fever, nausea, vomiting, abdominal, chest, or bone pain. SCD often results in cardiomegaly and pulmonary hypertension.

Management includes prophylactic oral penicillin to reduce pneumococcal sepsis. Pneumococcal and meningococcal vaccines are given due to poor splenic function

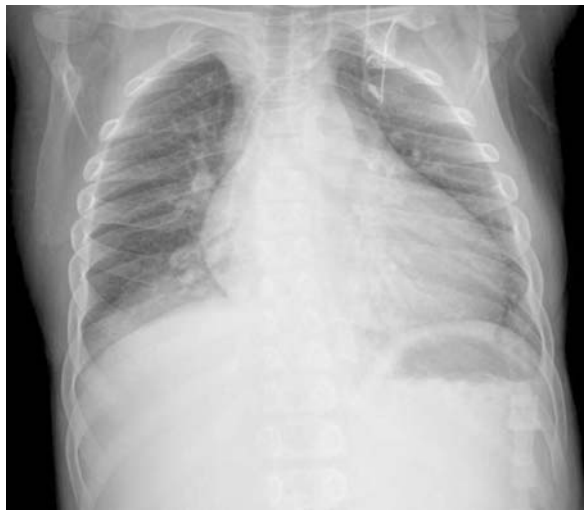

Sickle Cell Disease. Figure 1 Acute chest syndrome. Twelve year old with SCD and acute chest syndrome. There is cardiomegaly with bibasilar infiltrates.

and decreased phagocytosis. Transfusions and combination antibiotic therapy is used for acute infections. Prophylactic chronic transfusions and hydroxyurea are used to decrease the rate of cerebral infarction. The median survival is 40–50 years of age with the highest morbidity in young children. Infection is the most common cause of death in the first decade, followed by sequestration and cerebrovascular infarction. Up to 30% of children have *acute chest syndrome* (ACS) by age 10. Presentation includes chest pain, fever, cough, and dyspnea. ACS may be a sequela of infection or have infection as a complication. Infiltrates not complicated by infection resolve quickly. ACS may progress to severe respiratory distress and death and is the second most common cause of hospitalization in SCD. *Skeletal complications* result from stasis in red marrow and bone. Clinical presentation includes bone pain, fever, and swelling. Complications include avascular necrosis, bone infarcts, and osteomyelitis. Due to diminished phagocytosis and splenic function, children are at high risk for osteomyelitis (particularly *Salmonella*). Infants between 6 and 24 months are at risk of an infarction of the small bones of the hands and feet ("►hand-foot syndrome"). Painful soft tissue swelling of the hands and feet present for several weeks before radiographic changes are evident. *Stroke* is a leading cause of morbidity and mortality in SCD with an incidence of 11% in children. Ischemic infarcts predominate in younger children while hemorrhagic stroke occurs in older

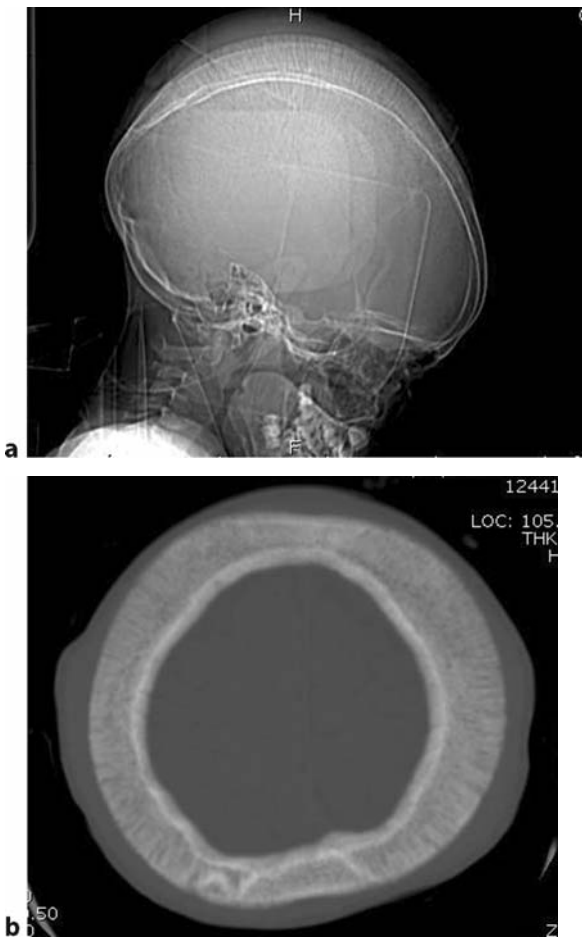

Sickle Cell Disease. Figure 2 Lateral scout film of the skull (a) and axial CT of the parietal skull (b) demonstrate abnormal skull thickening from expansion of the marrow creating a "hair-on-end" appearance.

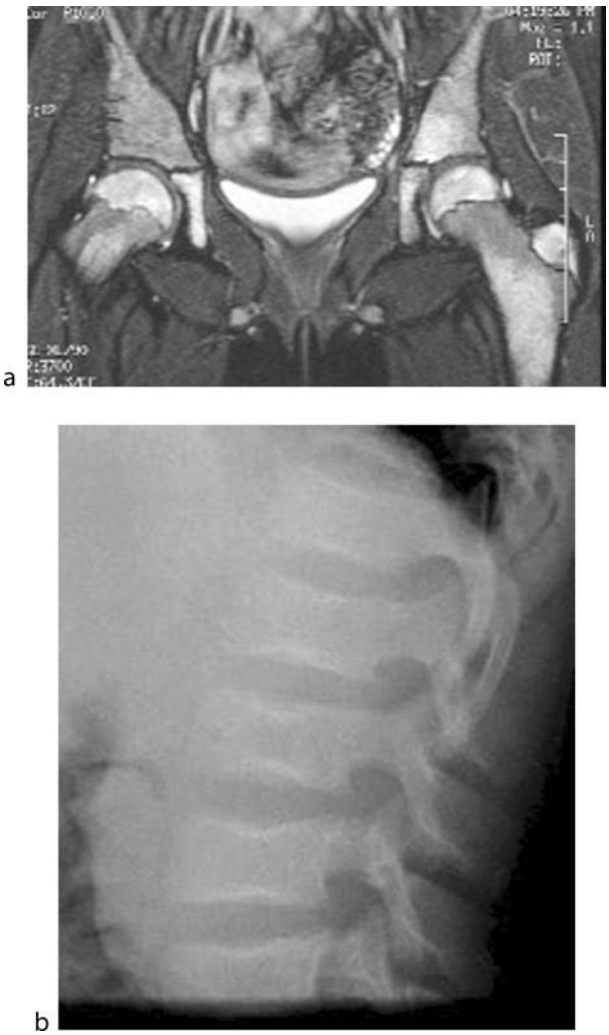

Sickle Cell Disease. Figure 3 (a) Avascular necrosis. Coronal STIR image of the pelvis demonstrates heterogeneous signal of the femoral epiphysis consistent with evolving bilateral avascular necrosis in 11-year-old with SCD. (b) Lateral radiograph of the lumbar spine demonstrates end plate depression from infarction resulting in a "fish mouth" appearance.

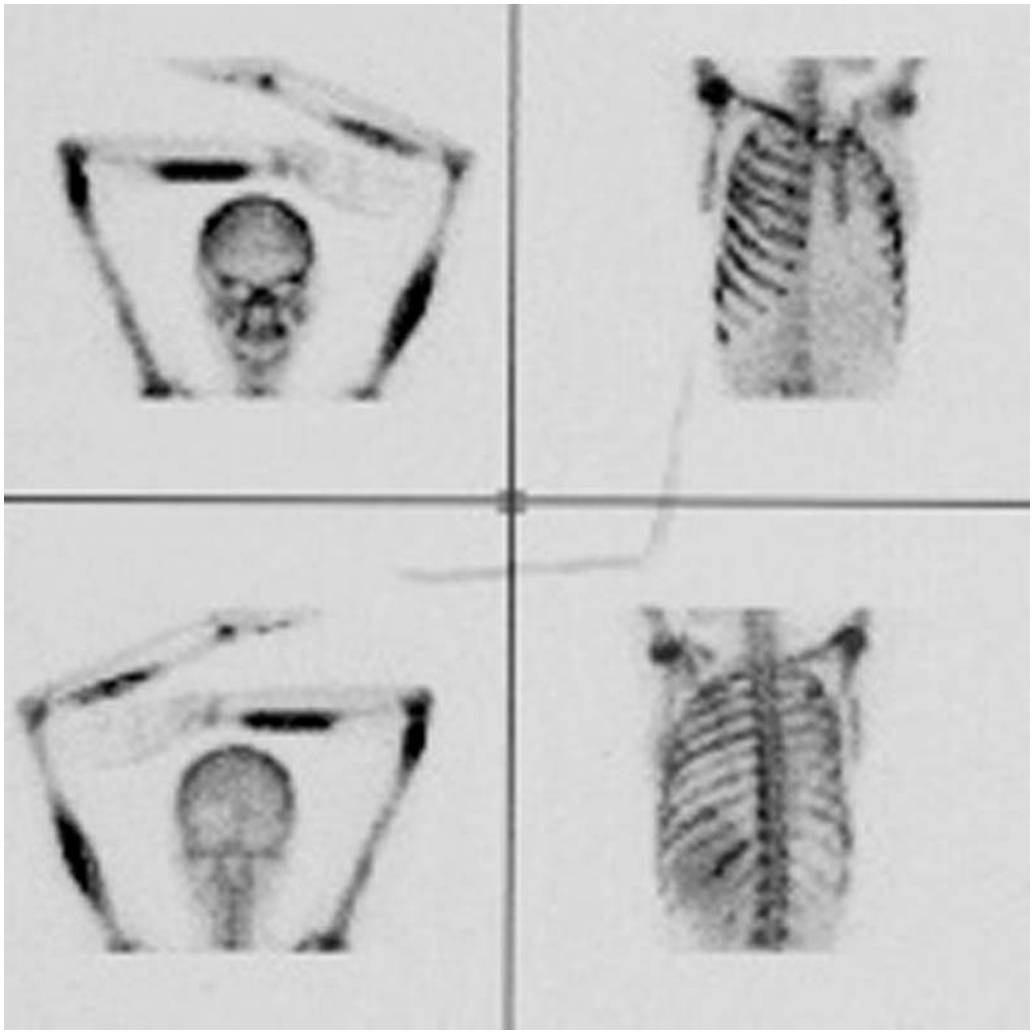

Sickle Cell Disease. Figure 4 Multifocal osteomyelitis. Fourteen year old girl with SCD. A bone scan demonstrates increased uptake in numerous bones including ribs, humeri, and radii.

patients. Both large and small vessel diseases can occur. The proximal middle cerebral artery (MCA) and distal internal carotid artery are at highest risk for stenosis. Children who have had one stroke are at high risk for subsequent strokes. When stenosis becomes irreversible, lenticulostriate collateral develop forming a pattern of moyamoya "puff of smoke."

Imaging

As SCD results in multiple clinical manifestations, imaging becomes a useful tool in the assessment of acute and chronic symptoms. Radiographs are important for evaluating the lungs and bones for infections and infarctions. Ultrasound (US) is useful for biliary, splenic, and renal symptoms. CT can further assess abdominal and chest crisis as well as those children presenting with acute stroke symptoms. Transcranial Doppler (TCD) and magnetic resonance imaging (MRI)/magnetic resonance angiography (MRA) are used as screening tools to assess for stroke risk.

Pulmonary: Chest radiographs should be routinely obtained in patients with SCD and fever. Cardiomegaly invariably is present. With ACS, infiltrates may develop quickly but also resolve quickly if there is no underlying infection (Fig. 1). High-resolution CT may demonstrate reduced peripheral vascularity suggesting microvascular occlusion. Small and large perfusion defects have been shown with scintigraphy. When chest pain develops, there often is a lag time in radiographic changes so close follow-up radiographs are necessary. The most common pneumonias are *Streptococcus pneumoniae*, *Hemophilus influenzae*, and *Staphylococcus aureus*. Four percent of

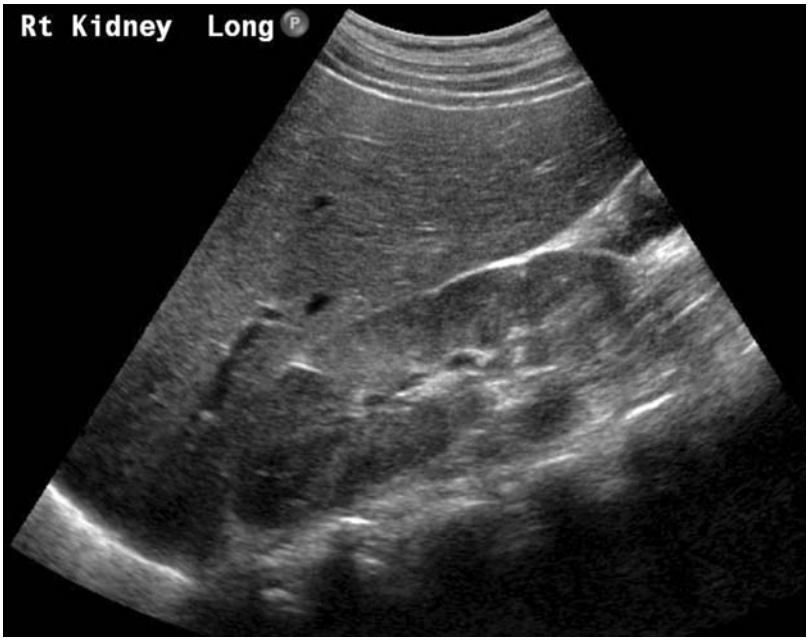

Sickle Cell Disease. Figure 5 Renal US of an 8-year-old sickle cell patient demonstrates an enlarged kidney with decreased corticomedullary differentiation and echogenic parenchyma ("pseudonephrocalcinosis").

sickle cell patients develop chronic pulmonary disease including fibrosis, pulmonary hypertension, and cor pulmonale. CT findings include septal thickening, a reticular pattern of interstitial disease, bronchiectasis, and cardiomegaly.

Skeletal: Skeletal changes include marrow hyperplasia and bony infarction from vasoocclusive crisis. In SCD, most marrow spaces remain preserved as red marrow even in the epiphysis. MRI demonstrates low marrow signal on T1-weighted. The persistence of red marrow makes detection of infarction and infection difficult by MR. Expansion of the marrow is notable in the skull with widening of the diploic space creating a "hair-on-end" appearance (Fig. 2).

Avascular Necrosis is a common with up to 50% of patients developing osteonecrosis by the age of 35. The epiphyses of the long bones have a limited vascular supply with minimal collaterals. Stasis and occlusion lead to ischemia and infarction most commonly of the hips and shoulders. It may take months for radiographs to demonstrate any changes. Radiographs eventually show sclerosis then fragmentation and collapse. MRI is sensitive for detecting early infarction demonstrating T2-weighted and Short TI Inversion Recovery (STIR) high signal changes (Fig. 3a). Nuclear bone scans can demonstrate early decreased perfusion prior to radiographic changes. Within the spine, infarcts involve the vessels supplying the central vertebral end plates. Central end plate depressions result in a "fish mouth" appearance to the vertebral bodies (Fig. 3b). Compression fractures are common due to marrow hypertrophy and end plate collapse. Bone within bone appearance may be noted after multiple infarctions.

Dactylitis or "hand-foot syndrome," is an infarction of red marrow of the tubular bones of the hands and feet with associated periosteal inflammation. Radiographs demonstrate soft tissue swelling and destructive osteitis of the phalanges though changes are delayed for 1–2 weeks. Periosteal new bone formation can be seen at 7–10 days. Medullary expansion, cortical thinning, and trabecular resorption occurs 2–3 weeks later. Differentiating from osteomyelitis can be difficult but bones tend to reconstitute after several months without residual deformity. Epiphyseal infarction of the hands and feet may produce cone-shaped epiphysis or premature fusion of epiphysis resulting in abnormal shortening of involved bones. Distinguishing between infarction and infection is difficult both clinically and radiographically in patients with SCD. Both may present with pain, swelling, fever, leukocytosis, and elevated sedimentation rate. Infarction is much more common than infection and can be treated with transfusions and hydration. Osteomyelitis requires prompt antibiotic therapy. Radiographs demonstrate osteopenia and periostitis is found in both entities. Later findings of cortical destruction, sinus tracts, and sequestra may develop. CT and/or US can demonstrate subperiosteal fluid collections and sequestra. MRI demonstrates abnormal high signal on T2-weighted and STIR with both infection and infarction Soft tissue edema occurs with both as well. MRI may be useful in differentiating acute

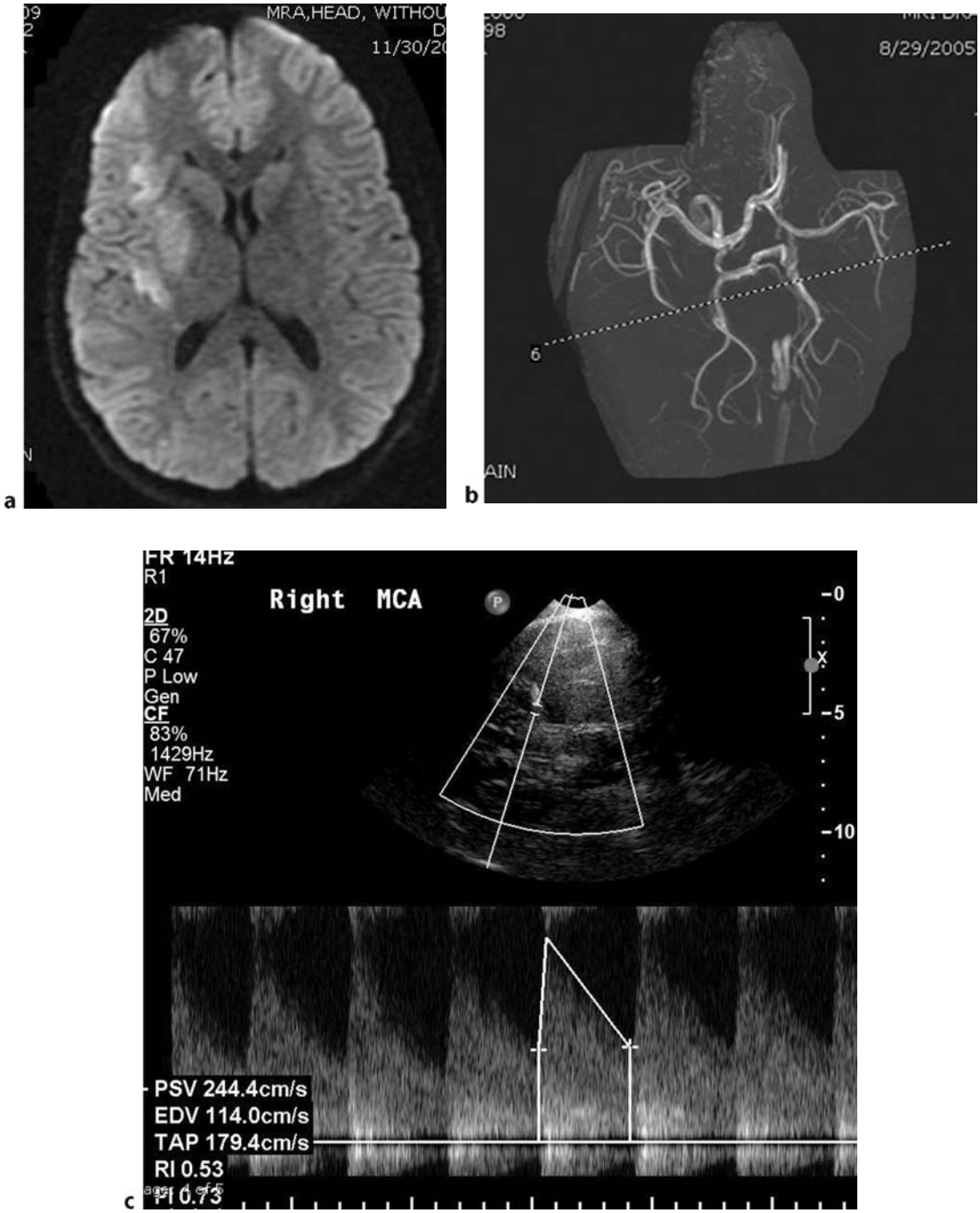

Sickle Cell Disease. Figure 6 (a) Axial diffusion-weighted MR image demonstrates high signal in the right middle cerebral artery territory consistent with an acute infarction. (b) TOF-MRA of an 11-year-old with SCD demonstrates left distal internal carotid artery stenosis. (c) Eight year old with SCD. Screening TCD of the right middle cerebral artery demonstrates elevated mean and peak velocities (in the "conditional range").

from old areas of infarction by the high intensity signal on long TR-TE images. Tc-99m skeletal scintigraphy can demonstrate hot or cold regions with either infection or infarction (Fig. 4). However, combined bone marrow scintigraphy with Tc-99m sulfur colloid may be useful to differentiate osteomyelitis from osteonecrosis. Indium-111 white blood cell may play a role in difficult cases as well.

Abdominal: The spleen is at high risk for damage as the red pulp becomes congested. As hemorrhages and

infarcts develop, the spleen is replaced with fibrous tissue. *Autosplenectomy* eventually occurs leaving the patient at risk for infection. By the age of 6, 90% of children are asplenic. The spleen may become small and calcify. Tc-99m sulfur colloid scans can be used to evaluate residual splenic function.

Splenic sequestration is an acute life threatening event where a sudden accumulation of blood collects in an enlarged spleen resulting in hypovolemia and severe anemia. Splenic sequestration typically occurs below the age of 6 prior to fibrosis developing. The spleen may remain enlarged with clinical signs of hypersplenism.

Gallstones can be found in up to 50% of children with SCD. These stones tend to be pigmented desire from hemolysis and are well seen sonographically. Liver parenchymal disease may occur secondary to infarction. Hepatitis and iron-overload occurs from transfusion therapy. Hemosiderosis can be evaluated using MRI with low signal parenchyma. Chronic renal damage develops by the second decade of life. Renal parenchyma may appear slightly echogenic with poor cortico-medullary differentiation likely related to interstitial fibrosis (Fig. 5). The kidneys enlarge possibly due to glomerular hypertrophy. Of note, patients with sickle cell trait have an increased incidence of renal medullary carcinoma.

Central nervous system: Cerebrovascular infarction is a leading cause of morbidity and mortality in SCD. Children with stroke typically have infarcts in the cortex and deep white matter whereas silent infarcts are limited to the deep white matter. While CT is useful in the assessment of hemorrhagic stroke, MRI has become the method of choice to assess acute and chronic infarction evaluating both large and small vessel diseases. Silent strokes demonstrate small lesions of high signal in the centrum semiovale. Large vessel territories and border zone infarction are noted with large vessel disease (Fig. 6). MRA demonstrates regions of stenosis and collaterals resulting in a moyamoya (Fig. 6). Catheter angiography is rarely needed to assess sickle cell vasculopathy. TCD is a useful screening test in the detection of large vessel disease prior to stroke. While intracranial velocities are already typically higher than the normal population due to anemia, abnormally high velocities are the results of luminal narrowing. TCD has proven to be a safe, reliable, and cost-effective screening method to assess for stroke risk. Via a transtemporal window, mean peak velocities of the MCA, distal internal carotid artery (ICA) and anterior cerebral artery (ACA) can be measured. Those with mean peak velocities greater than 200 cm/sec are considered at high risk to develop stroke (Fig. 6c). Chronic transfusions or bone marrow transplants have been used to decrease stroke risk in children with elevated cerebral blood flow velocities.

Diagnosis

The condition is diagnosed by laboratory, imaging (as described above) used to assess and differentiate the various manifestation.

Bibliography

1. Crowly JJ, Sarniak S (1999) Imaging of sickle cell disease. Pediatr Radiol 29:646–661
2. Lonergan GJ, Cline DB, Abbondanzo SL (2001) Sickle cell anemia. Radiographics 21:971–974
3. Martin L, Buonomo C (1997) Acute chest syndrome of sickle cell disease: radiographic and clinical analysis of 70 cases. Pediatr Radiol 27:637–641
4. Pegelow CH (2001) Stroke in children with sickle cell anemia: etiology and treatment. Ped Drugs 3:421–432
5. Whether D (2000) Sickle cell disease in childhood. Am Fam Phys 62:1013–1020

SIET

Spinal intra-dural extra-medullary tumours.

▶Tumors, Spine, Intradural, Extramedullary

Signet Ring Sign

Typical appearance of bronchiectasis on CT with the internal bronchial diameter being greater than that of the adjacent pulmonary artery.

▶Airway Disease
▶Pulmonary Opacity, Cystic Pattern

S

Silhouette Sign

Effacement of an anatomic soft tissue border by either a normal anatomic structure (e.g., the inferior border of the heart and the left hemidiaphragm) or a pathologic structure (e.g., obliteration of the right heart contour by a middle lobe process touching the heart border). The silhouette sign is used for (a) the anatomic localization of an intrapulmonary structure and (b) the detection of subtle intrapulmonary lesions that are hardly visible themselves but become conspicuous by obscuring the border of an adjacent structure.

▶Atelectasis

Simple Bone Cyst

Simple bone cyst (solitary bone cyst, unicameral bone cyst) is a relatively common tumorlike bone lesion of unknown origin which represents a fluid-filled intramedullary cavity surrounded by a fibrous membrane.

▶Neoplasm-Like Lesions, Bone

Simple Cyst

Thin-walled anechoic round to oval lesions with posterior enhancement.

▶Cyst, Breast

Simple Ovarian Cysts

▶Cysts, Follicular, Ovarium

Single Photon Emission Computed Tomography

S. I. Koukouraki
Department of Nuclear Medicine
University, Iraklion, Crete, Greece
sophiak@her.forthnet.gr

Introduction

There are two main categories of emission imaging: the planar and the tomographic imaging. Emission tomographic studies are divided into single photon emission computed tomography (SPECT) and positron emission tomography (PET).

SPECT uses collimator systems for detection of photons from radionuclides. The conceptual basis is the physical rotation of the camera in small angular steps around the patient, acquiring a usable number of events to form an image. A typical single camera SPECT study requires about 30 min of imaging time.

Despite the recent growth of PET, SPECT is the most appropriate imaging procedure for the everyday management of patients with cardiac diseases, cancer, and neurological diseases. It is a very important complementary tool to planar procedures, increasing the sensitivity especially in small and deeply located lesions.

SPECT is based on the use of conventional gamma cameras and on generator produced radiopharmaceuticals. The development of hybrid scanners SPECT/CT lead to a more accurate diagnosis. In addition, SPECT is substantially less expensive compared to PET and available at every nuclear medicine department.

On the other side, SPECT systems suffer from the limited sensitivity, due to the use of collimators, the difficulties in quantitation due to scatter, the low spatial resolution, the physical problems of attenuation, and statistical limitations. SPECT has a spatial resolution of 8–10 mm dependent on the individual acquisition data. The sensitivity of SPECT is one tenth that of PET. The availability of new SPECT radiopharmaceuticals, the recent advances in technology combined with the well-designed reconstruction software, and the economic aspects of SPECT instrumentation render this mode of emission tomography attractive for clinical studies.

SPECT Radiotracers

SPECT radiotracers are substances labeled with gamma emitting radionuclides. The most commonly used radionuclides are ^{99m}Technetium, ^{123,131} Iodine, and ^{111}Indium. Their long half-life is very important to evaluate the biodistribution changes over the time offering the knowledge of several biological features. Many SPECT tracers used for imaging can also be used for treatment purposes in cancer patients, according to the isotope used with a γ-emitting radionuclide for imaging and β-emitting radionuclide for treating.

SPECT agents:

1 In cardiac imaging: ^{201}Thallium, ^{99m}Tctetrofosmin, ^{99m}Tcsestamibi,^{131}I metaiodobenzylguanetidine (MIBG).
2 In oncology: ^{99m}Tc methylendiphosphonate (MDP), ^{99m}Tcsestamibi, ^{201}Thallium, ^{67}Ga citrate, ^{131}I MIBG, ^{111}In- octreotide, ^{111}In- or ^{99m}Tc- labeled antibodies, ^{99m}Tc-annexin V, labeled antibodies. There are also other agents under investigation like gastrin labeled with ^{111}In, bombesin, labeled with ^{99m}Tc, radioiodinated insulin, and vasoactive intestinal peptide.
3 In brain imaging: ^{99m}Tc-HMPAO, ^{123}I-iodoamphetamine, dopamine transporter agents (DAT).

Thallium chloride-201 (^{201}*Tl*): It is a potassium analog used for the cardiac imaging. The mechanism of uptake is related to blood flow, tumor metabolism, and ATPase activity. Because of its uptake that is related to cellular

metabolism, it can also be used in ►tumor imaging. ^{201}Tl can be used not only for diagnostic purposes but also to monitor and predict the response to treatment. It is also of particular use in patients with radiotherapy able to differentiate fibrotic changes from recurrent disease.

^{99m}Tc-sestamibi and ^{99m}Tc- tetrofosmin: Both agents have active uptake into the cells and are retained to the cytoplasm and mitochondria. The uptake mechanism in malignant cells is not yet well known. Several factors may be responsible: the increased blood flow and capillary permeability, the elevated metabolic activity, the cell membrane and mitochondrial potentials. Even more, for tetrofosmin the Na^+ /K^+ pump and N^+ /H^+ antiport system may also be involved. The efflux mechanism is related to the expression of a membrane protein, *P*-glycoprotein, responsible for the multidrug resistance (MDR1).

^{131}I-MIBG: The mechanism of MIBG uptake by sympathoadrenal tissues is not completely understood. However, the majority of MIBG enters the cytoplasm by an active sodium and energy dependent (uptake-one) mechanism. A smaller fraction enters by passive diffusion. In the cytoplasm, enters the hormone storage vesicles.

^{99m}Tc-MDP: It is absorbed to amorphous bone and on the surface of the hydroxyapatite crystal.

^{67}Ga- citrate: The mechanism of uptake is still unclear. However, it is related to the expression of transferring receptors on the surface of neoplastic cells. In the cell, it concentrates in the cytoplasm and is bound to lysosome like proteins. Its uptake is high in lymphomas. However, the uptake in most solid tumors is around 50%.

^{111}In- octreotide: It is a somatostatin analog with high affinity in SSTRs 2, which are overexpressed in a number of neuroectodermal tumors (neuroendocrine, SCLC, medullary cell carcinoma of the thyroid, etc.).

^{99m}Tc-depreotide: It is a synthetic peptide with high affinity for somatostatin receptors 3, 4, and 5 but lower affinity for 2.

Labeled antibodies: Only two cancer seeking antibodies are now available. Capromab pendetide (ProstaScint) and the Arcitumomab (CEA scan).

Clinical Applications of SPECT Studies

The most important clinical applications of SPECT include the cardiac imaging, the cancer and brain imaging.

SPECT in Cardiac Imaging

Stress myocardial perfusion SPECT imaging provides important diagnostic and prognostic information in patients with coronary artery disease (CAD). It can define the extent and severity of reductions in regional blood flow. It has also an important role to the therapy monitoring.

Diagnosis of CAD

The SPECT perfusion imaging has a high sensitivity and specificity for the diagnosis of CAD. The stress perfusion defect size and extend correlates with the presence and extend of a CAD. It is more sensitive and specific than exercise electrocardiography (ECC). It is also widely used for the assessment of the myocardial viability. New ^{99m}Tc labeled compounds have been developed such as ^{99m}Tc sestamibi and tetrofosmin having the best biological properties. The sensitivity and specificity for ^{99m}Tc labeled agents 90 and 93% compared to 83 and 80% for ^{201}Tl. SPECT perfusion imaging can also be used for patients with acute chest pain on emergency department. It has high-diagnostic accuracy for identifying patients with acute coronary syndrome.

Evaluation of Treatment Response

CAD progression and response to therapy can be monitored with SPECT perfusion imaging. The role of SPECT in the evaluation of patients receiving therapy like nitrates, calcium antagonists, or B-blocker is very important. Studies showed an improvement of perfusion in most patients after 6 months of treatment.

Evaluation After Revascularization

SPECT perfusion imaging has a high ability to locate and evaluate changes in the extent and severity of perfusion abnormalities after revascularization. It accurately identifies the presence of restenosis after a complete revascularization. The overall sensitivity, specificity, and accuracy are up to 89, 75, and 85%, respectively. However, false positive results (i.e., ischemia but no underlying angiographic restenosis) may occur, but because of the improved resolution with technetium agents they may be less common.

A meta-analysis showed a high positive and negative predictive value for restenosis when imaging was delayed 2–4 weeks after the revascularization. Postrevascularization SPECT perfusion imaging can also identify patients who are at risk for a worsening prognosis.

Prognostic Value of SPECT in Patients with CAD

The prognosis in patients with CAD is related to the severity of reversible perfusion abnormality. The number of vascular territories with SPECT perfusion abnormalities is related to MI-free survival. Additionally, the extent and severity of SPECT perfusion abnormalities are highly effective at stratifying patients risk for myocardial infarction (MI) so as to decide for the most appropriate therapy.

SPECT is able to manage patients with cardiac diseases with the same accuracy of PET at a lower cost.

It can also be used as a guide to patient care, to evaluate the disease progression, and the effectiveness of anti-ischemic therapies. Moreover, the use of SPECT/CT offers the contemporaneous evaluation of the morphology of the coronary vessels, the presence of calcified plaques by CT angiography, and the viability and the regional wall motion before and following treatment with SPECT.

SPECT in Cancer Imaging

Diagnosis

SPECT is very useful in the assessment of malignancies and cancer staging. The bone scan is the most useful tool but its low specificity leaves a problem that may be resolved using SPECT. In cases of lymphoma, ^{67}Ga-SPECT images of the thorax improve the sensitivity, being able to distinguish mediastinal and hilar lymph node disease from the physiologic activity in the sternal and the spinal bone marrow. Moreover, SPECT/CT offers additional information for the most accurate staging, the detection of tumor tissue after treatment and the early detection of recurrencies.

SPECT is also very useful in somatostatin receptor imaging and in phaechromocytoma because planar images failed to evaluate accurately abdominal or intrahepatic lesions. Hybrid images can also increase the specificity of SPECT alone.

In breast cancer, SPECT seems to be more sensitive than planar imaging, but until now it has not been largely employed in the diagnosis of breast carcinoma. The sensitivity and specificity of SPECT is 69–95% and 70–91%, respectively. Negative predictive value is high for SPECT (95%), so a negative study excludes breast cancer. SPECT is also more sensitive in evaluating multifocal disease and in palpable lesions.

In the detection of axillary lymph node metastases SPECT has a higher sensitivity (81–94%) and accuracy (83–92%) compared to planar imaging (52–62% and 76–82%). However, the exact number of lymph nodes cannot be determined.

Only few studies are available for the role of SPECT in the recurrent breast cancer. Its sensitivity is similar to that of conventional imaging and higher than that of planar.

In differentiated thyroid cancers, SPECT with cationic lipophilic tracers is more useful than planar because of the better detection of distant metastases in the lung, mediastinum and neck, and could be complementary to 131I-WBS.

SPECT has several advantages over planar in parathyroid imaging, such as higher sensitivity especially in the detection of small and ectopic parathyroid adenomas and in those associated with multinodular goiter. The sensitivity for SPECT is high in adenomas but low in hyperplastic glands.

Assessment of Tumor Response to Therapy

For the assessment of tumor response quantitative SPECT analysis is very important. In cases of lymphoma ^{67}Ga SPECT is superior to CT in differentiating fibrotic/necrotic tissue from residual tumor. A positive ^{67}Ga SPECT study after treatment is associated with poor prognosis. A negative is associated with better prognosis.

SPECT in Neurology

Nowadays is widely used in neurology for the assessment of areas of abnormal perfusion and the pre and postsynaptic neurotransmitter function.

Conclusion

It is essential that SPECT should always be associated to planar imaging in cancer diagnosing since it improves sensitivity and accuracy. It is simple, noninvasive and less expensive.

Bibliography

1. Shaw LJ, Berman DS (2005) Sequential single-photon emission computed tomography myocardial perfusion imaging. Am J Cardiol 96:28J–39J
2. Lucignani G (2005) SPET: sustainable, powerful, effective, timely *in vivo* molecular imaging. Q J Nucl Med 49:117–120
3. Holman BL, Tumech SS (1990) Single–photon emission computed tomography (SPECT). Applications and potential. JAMA 263:561–564
4. Buscombe JR, Bombardieri E (2005) Imaging cancer using single photon techniques. Q J Nucl Med 49:121–131
5. Giannopoulou C (2003) The role of SPET and PET in monitoring tumour response to therapy. Eur J Nucl Med 30:1173–1200

Sinusitis

Sinusitis is an inflammatory process that involves one or more of the four paired paranasal sinuses. Because of the contiguous anatomical relationships of the sinuses to the nasal mucosa, it is rare to find inflammation of the sinuses without nasal mucosal involvement, and a more appropriate term for the condition is rhinosinusitis.

▶Inflammation, Chronic, Nose, and Paranasal Sinus

Skeletal Metastases

▶Metastases, Skeletal

skeletal Scintigraphy

▶Bone Scintigraphy

Skip Area

Area not interested by liver fatty infiltration. Islands of normal liver tissue are also called 'spared areas'.

▶Steatosis, Hepatic

Sliding Hernia

▶Contrast Media, Ultrasound, Influence of Shell on Pharmacology and Acoustic Properties

SLN

▶Sentinel Lymph Node (SLN)

SLNB

▶Sentinel Lymph Node Biopsy (SLNB)

Small Airway Disease

▶Airway Disease

Small Bowel Obstruction (SBO)

Small bowel obstruction is the partial or complete lack of progression of small bowel contents due to a mechanical narrowing or occlusion of the lumen.

▶Occlusion, Bowel in Childhood
▶Occlusion, Subocclusion, Small Bowel Adults
▶Small Bowel, Postoperative

Small Bowel Volvulus

▶GI Tract, Pediatric, Specific Problems

Small Bowel, Infectious Diseases

Nevra Elmas
Ege Üniversitesì Tip Fakultesi, Izmin, Turkey
elmas@med.ege.edu.tr

Definition

Infectious diseases of the small bowel are defined as diseases associated with inflammatory changes of the intestinal layers due to microorganisms. Parasitic infestations or bacterial organisms can occur in countries in Asia and southern Africa. Enteric pathogens are ingested through contaminated food and water and pass through the entire gastrointestinal tract during establishment in the host, with subsequent shedding and spread to new hosts (1). In patients treated by immunosuppressive agents or in small bowel transplant recipients, fungal and viral infections can also involve the gastrointestinal (GI) tract (2–4).

Pathology/Histopathology

The GI mucosa acts as a major interface between the host and its environment. Microbes living in the GI tract of a healthy host constitute its normal flora. Numerous factors regulate its composition. As such, it is continuously exposed to a passing stream of toxins and microbes.

Inevitably, some microbial species colonize the gut, causing GI infections. Small bowel infections can result from various causes, including bacterial, fungal, viral, parasitic, and extrinsic inflammatory processes (Table 1).

Small Bowel, Infectious Diseases. Table 1
Classification of small bowel infections

A. Bacterial infections
1. *Escherichia coli* (*E. coli*) infections
2. *Salmonella* infections
3. Staphylococcal infections
4. *Campylobacter* infections
5. *Vibrio* infections
6. *Aeromonas* infections
7. *Plesiomonas* infections
8. Clostridial infections
9. Brucellosis
10. *Yersinia* infections
11. Tuberculosis
12. *Mycobacterium avium-intracellulare* infections
13. Syphilis
14. Actinomycosis
15. Listeriosis
16. Whipple's disease
17. Hafnia enteritis
18. Tropical sprue
B. Fungal diseases
1. Candida infections
2. Histoplasmosis
3. Blastomycosis
4. Paracoccidioidomycosis (South American blastomycosis)
5. Aspergillus infections
6. *Mucor* infections
C. Viral infections
1. Rotavirus infections
2. Rotavirus-like particle infections
3. Infections with Norwalk and related viruses
4. Enteric adenovirus infections
5. Calicivirus infections
6. Astrovirus infections
7. Herpes simplex virus infections
8. Cytomegalovirus infections
9. Measles
10. Dengue fever
11. HIV infections
12. Other viral infections
D. Algal diarrhea
E. Rickettsial infections
F. Parasitic infections
1. Protozoal infections
2. Helminthic infections

Mechanisms of bacterial injury can be encountered as bacterial adherence, bacterial translocation, and toxin production. Bacterial pathogenicity in small intestinal injury may vary, such as ingestion of a preformed bacterial enzyme or toxin (*Staphylococcus*), elaboration of an enterotoxin following G colonization (cholera, *Shigella*, *Salmonella*, *Yersinia*), elaboration of a tissue-damaging cytotoxin (*Shigella*), or mucosal invasion (*Shigella*, *Salmonella*) (5).

The major setting in which bacterial overgrowth occurs is called bacterial stasis, stagnant loop, or blind loop syndrome. Proposed mechanisms for the abnormal bacterial proliferation include the following:

- Failure to clear bacteria from the upper GI tract, usually due to achlorhydria
- Continuous seeding of the small bowel with colonic contents as a result of jejunocolic fistulae or reflux following abnormalities of the ileocecal valve
- Motility disturbances

These factors initially cause an overgrowth of coliform bacteria and, eventually, anaerobic bacteria. Neutrophilic mucosal infiltrates represent the hallmark of acute invasive disease. Toxigenic organisms tend to produce less severe morphologic damage than bacteria invading the mucosa (5).

Clinical Presentation

Small bowel infectious diseases frequently manifest as dysenteric syndromes characterized by the presence of fever, abdominal pain, and numerous small-volume stools containing blood, mucus, and polymorphonuclear neutrophils in patients with toxigenic bacterial infections. In contrast, patients with invasive bacterial infections as exemplified by *Shigella*, *Salmonella*, and *Campylobacter* usually have a colonic infection, and diarrhea dominates the clinical presentation. A third type of enteric infection results in enteric fever, often with constipation early in its course, as seen with *Salmonella typhi*. The organisms enter Peyer's patches and regional lymph nodes, and numerous factors predispose to microbial intestinal colonization and contribute to diarrhea, malnutrition, sepsis, and extraintestinal infections (5). Bacterial overgrowth leads to malabsorption. The clinical presentation of small bowel infections according to microorganism is shown in Table 2.

Imaging

Radiologic imaging modalities used in evaluating small bowel infectious are plain abdominal radiography, barium studies as conventional enteroclysis or follow-through examination, ultrasound (US), computed tomography (CT), and magnetic resonance (MR) enteroclysis.

Small Bowel, Infectious Diseases. Table 2 Clinical presentation of small bowel infections (*F* fever; *P* pain; *M* palpable mass; *V* vomiting; *D* diarrhea; *WL* weight loss; *A* ascites; *O* obstruction; *Perf* perforation)

	F	P	M	V	D	WL	A	O	Perf	Other
Bacterial										
Tuberculosis	+	+	+	+	+	+	+	+	Rare	Pulmonary infection Ileocecal involvement
Yersinia	+	+	+	+	+	+	–	–	+	Children and young adults Reservoirs: bird, dog Mesenteric lymphadenopathies
Salmonella	+	+	+	+	+	+	–		+	Infections of joints, bones, meninges Paralytic ileus, massive intestinal hemorrhage Toxic megacolon
Campylobacter	+	+	+	+	+	–	–		+	Meningitis, toxic megacolon, arthritis Endocarditis, sepsis Guillain-Barré syndrome
Fungal: gastrointestinal involvement of fungal infections is more common in immunosuppressed patients										
Candida	–	+	–	+	+	+	–	–	+	Allergic reactions
Blastomycosis	–	–	+	–	–	–	–	–	–	Mesenteric lymphadenopathy
Histoplasmosis	–	+	–	+	+	+	–	–	+	Pulmonary involvement, peritonitis
Aspergillosis	+	+	–	+	+	+	–	+	+	Pulmonary involvement, vasculitis, thrombosis
Viral										
HIV	–	+	–	+	+	–	–	–	–	Systemic involvement more dominant
Cytomegalovirus	+	+	–	+	+	+	–	–	+	Systemic involvement more dominant
Parasitic										
Giardiasis	+	+	–	+	+	+	–	–	–	Malabsorption
Ascaris	–	+	–	–	–	–	–	+	+	Cholangitis, pancreatitis, acute abdomen Malabsorption, malnutrition
Strongyloidiasis	–	+	–	+	+	+	+	–	–	Gastrointestinal bleeding Eosinophilia

Plain abdominal radiography: A supine anteroposterior radiogram of the abdomen is essential in the plain film examination of small bowel disorders. The acute abdominal series for patients with possible small bowel obstruction or visceral perforation should consist of supine and erect abdominal radiography. In immobile patients, a left lateral decubitus view of the abdomen should be done (6). Erect or lateral decubitus radiograms demonstrate air-fluid levels in patients with obstruction and free air collection under the diaphragm in patients with perforation. Calcification due to granulomas and lymphadenopathies can be recognized in the right lower region in patients with tuberculosis.

Small bowel follow-through: The conventional small bowel follow-through (SBFT) examination is routine in most radiology departments. But because of its crowded location in the peritoneal cavity, multiple segments of small bowel cannot be adequately delineated (6). Optimal distension of bowel lumen cannot be obtained by this technique, and early mural infiltration and small ulcers and nodules cannot be detected because of superimposition of bowel loops.

Enteroclysis: Intubation is essential in enteroclysis, and intestinal contrast fluid can be administered at the required rate by an enteroclysis catheter. The entire small bowel can be demonstrated in a distended state at the end of the infusion. The evaluation of mucosal detail and early changes of the inner wall is more successful than with SBFT.

Cross-sectional modalities: Extraluminal evaluation of the small intestine can be obtained with cross-sectional modalities. US, CT, and MR imaging (MRI) provide direct visualization of the bowel wall, mesentery, peritoneal cavity, retroperitoneum, and visceral organs. As a result, these imaging modalities are complementary to barium examination of the GI tract. It is essential to obtain intestinal distention. Uniform opacification of the entire small bowel may be accomplished by the steady ingestion of 1,000 mL of contrast over a 45-min period before the CT or MR examination.

MR enteroclysis: Advantages of this technique are that it provides good information about the intestinal wall and extraluminal soft tissue. During this procedure, polyethylene glycol (PEG) solution is given into the GI lumen *via* intubation. Pre- and postparamagnetic agent injection, fat-saturated T1- and T2-weighted sequences can be obtained. Scanning is done in axial and coronal planes.

Radiological Findings

Tuberculosis: Radiographically, calcified mesenteric lymph nodes are helpful in diagnosing tuberculosis. The earliest

changes in tuberculous enteritis are altered motility with thickening and nodularity of folds on barium studies. Focal disappearance of folds, the demonstration of polyps, and ulcerations that are usually transaxial are other early findings. Cephalad retraction of the cecum may be associated with straightening of the ileocecal junction (Fig. 1). Predominant mass formation with ulceration involving the terminal ileum is usually a more advanced ulcerative change affecting the cecum or the ileocecal valve area. These changes are usually well demonstrated by CT scans (Fig. 2). MRI is at its best in demonstrating changes in the mesentery and omentum. Complications are infrequent. Obstruction due to strictures, fistulae, or perforation can occur (6). The severity of GI involvement is related to the severity of pulmonary infection. In cases of tuberculous peritonitis, an adynamic ileus may be present with or without ascites. Calcifications may be seen in the adrenal glands, peritoneal surface, lymph nodes, liver, or spleen (Fig. 3).

Yersiniosis: Barium studies can demonstrate changes in the distal 20 cm of the ileum, and these may be seen to extend into the cecum and ascending colon. Thickened nodular folds may be present, often with ulcers that may be aphthoid or larger, and single or multiple. The bowel mostly retains its normal lumen diameter. Thickened folds may later be replaced by fold effacement. Resolution of these changes is expected within 4–5 weeks. Enteritis secondary to a Yersinia abscess has been shown by CT (Fig. 4). CT scans demonstrate an inflammatory mass and mesenteric lymphadenopathy. Radiographic changes mimic those of tuberculosis or Crohn's disease, except that fistula formation and ileal stenosis are unusual (5, 6).

Salmonella: Plain film radiographs may show ileus of the small and large intestine. Barium studies are infrequently indicated. The radiological appearance of the distal ileum is not unlike that of other inflammatory disease. Aphthoid ulcers identified in the early stage of any acute inflammatory disease may also be seen in *Salmonella* infections. CT scans of salmonella enteritis have shown

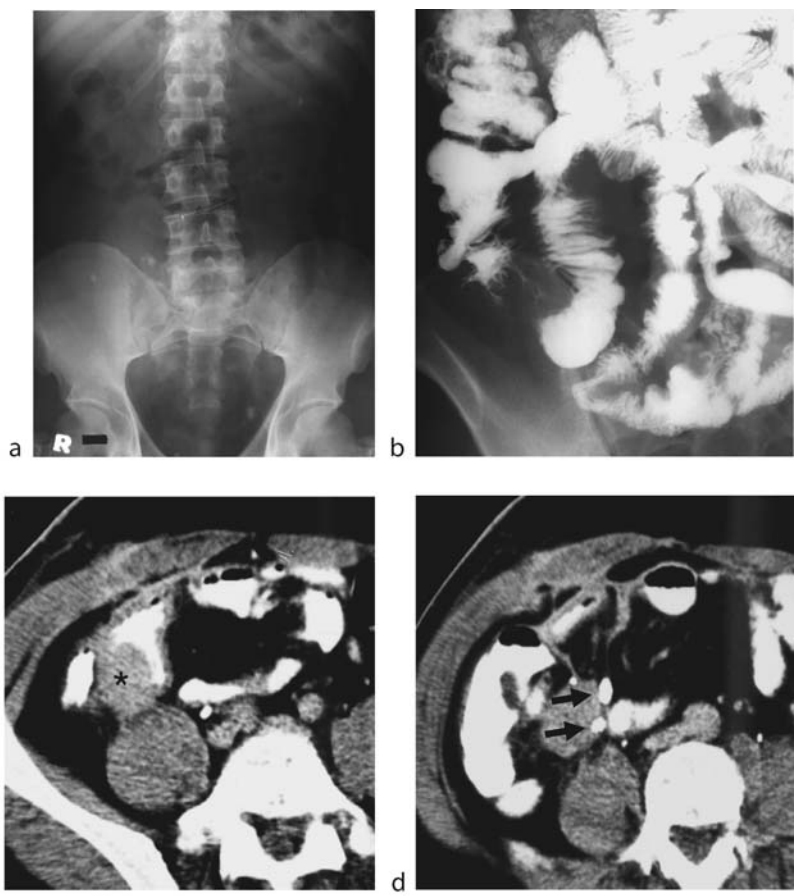

Small Bowel, Infectious Diseases. Figure 1 Tuberculosis. (a) Plain abdominal film shows nodular calcification in the nearby right lower quadrant. (b) Follow-through small bowel study demonstrates retraction of antimesenteric border, mucosal edema, narrowing, and fissure tracts of terminal ileum. (d, c) Computed tomographic images of right lower quadrant. Wall thickness of ileum (*asterisk*) and calcified granuloma (*arrows*).

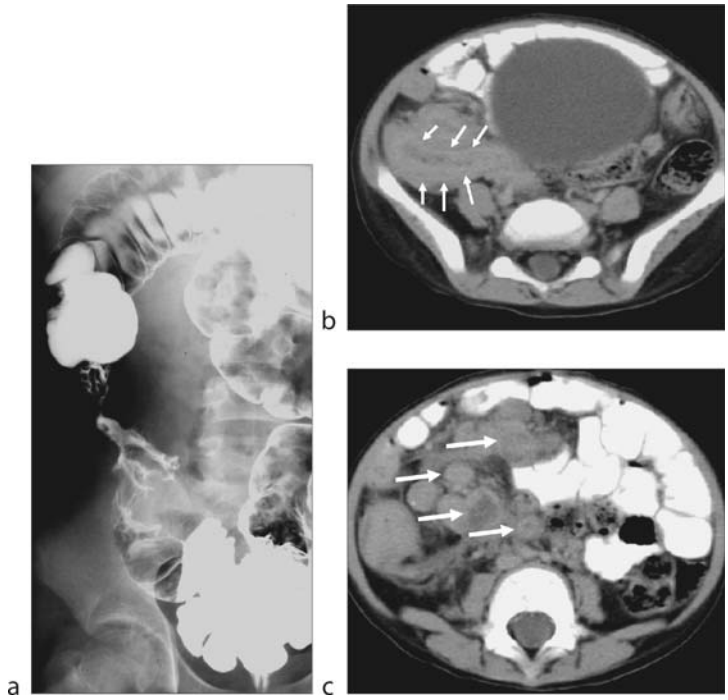

Small Bowel, Infectious Diseases. Figure 2 Tuberculosis. (a) Small bowel follow-through study shows narrowing and fibrosis of the distal ileum, ileocecal valve, and ascending colon. (b) Thickened bowel wall of the terminal ileum can be recognized on computed tomography (CT). (c) CT study demonstrates ileocecal and mesenteric lymphadenopathies. These nodes have low-density areas (*arrows*) due to caseation.

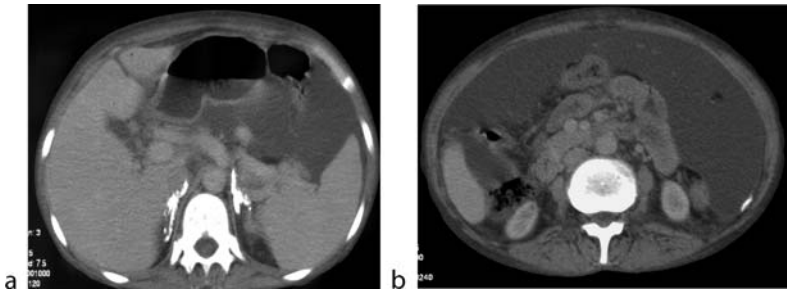

Small Bowel, Infectious Diseases. Figure 3 Tuberculosis. (a) Bilateral adrenal calcifications and ascites. (b) Abdominal ascites and focal calcification of the left posterior peritoneal surface.

mild circumferential thickening of the terminal ileum, and a corresponding barium study showed thickened folds.

Campylobacter: On barium study, the distal ileum can be narrowed with irregular nodularity and thickening of the wall. Shallow ulcers may be seen in more severe cases.

Blastomycosis: The organism is located in the submucosal lymphoid tissue of the gut and then erodes the mucosa. Radiological changes in the small bowel are nonspecific narrowing with mucosal irregularities. Mesenteric nodes are regionally enlarged.

Histoplasmosis: Infection primarily involves the respiratory tract and affects the small bowel or colon by dissemination. Radiography may demonstrate polypoid changes or ulcerations in the small bowel or the ileocecal area, as well as strictures.

Aspergillosis: Disseminated aspergillosis is a rapidly progressive and highly lethal infection that typically affects the immunocompromised patient. GI invasion may occur rarely and result in serious complications such as bowel obstruction and angioinvasion with secondary bowel ischemia, necrosis, and perforation.

Giardiasis: An increase in the fold thickness in the duodenum and proximal jejunum and a state of irritability are seen. CT shows wall thickening in the jejunum as well as mesenteric adenopathy, both reverting to normal after treatment.

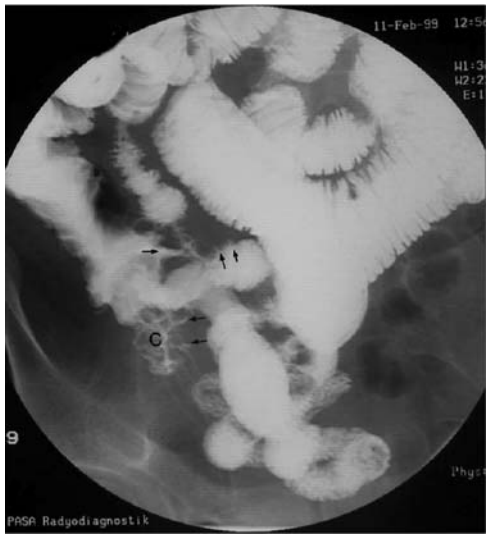

Small Bowel, Infectious Diseases. Figure 4 Yersinia enteritis. Thickened nodular folds and multiple aphthoid ulcers can be seen at the distal ileum. (Courtesy of Prof. Uğur Korman, Istanbul University Cerrahpasa Medical School, Istanbul.)

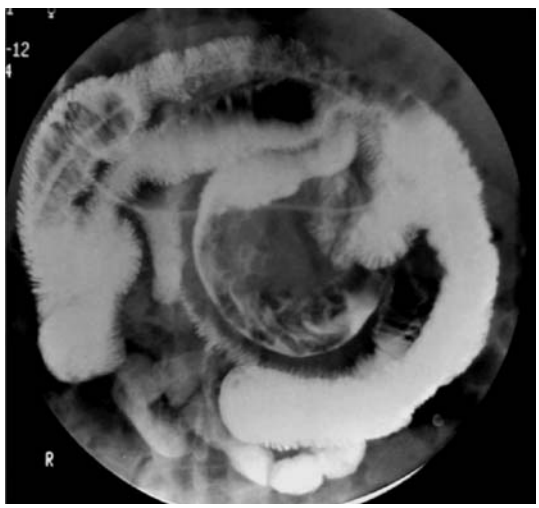

Small Bowel, Infectious Diseases. Figure 5 Ascaris. Middle jejunal segment has tubular filling defect due to infestation with ascarides. (Courtesy of Prof. Uğur Korman, Istanbul University Cerrahpasa Medical School, Istanbul.)

Ascaris: Ascarides worms can be identified on plain abdominal films. Mature worms within the small bowel are visible because of their soft tissue density against the surrounding intraluminal air. A larger bolus of parasites may create a so-called whirlpool effect and can be associated with ileus-like bowel distension or with obstruction. Edema of the intestinal mucosa may also be evident on plain films. On contrast examination, ascarides cause elongated tubular defects in the barium-filled bowel lumen (Fig. 5). Their linear intestinal tracts may take up barium, to appear as a thin, linear opacity within the soft tissue density of the worm. This linear shadow may persist for some time after barium has been eliminated from the gut. Worms can also be recognized in the colon.

Strongyloidiasis: Mucosal invasion produces only focal edema and spasm. Radiological findings are fold thickening in the duodenum and jejunum and may include effacement of the folds and a pipestem appearance of the jejunum or a diffusely ulcerated, shortened, and narrowed jejunum that will not return to a normal fold pattern after successful treatment. In overwhelming infestation, there may be toxic dilatation with paresis, which is usually permanent.

Diagnosis

Diagnosis can be confirmed by combining bacteriologic and serologic techniques. To establish the diagnosis of infectious diarrhea, the organism must be found in, or cultured from, the stool or intestinal tissues. Alternatively, one should be able to demonstrate a rise in specific serum antibodies to the organism. With the advent of recombinant DNA technology, genes for the heat-labile and heat-stable enterotoxins have been cloned, allowing diagnosis of the toxin-producing bacterial strains.

Diagnostic methods used to identify GI viral infections include viral culture, electron microscopy, immunoelectron microscopy, enzyme-linked immunosorbent assay of stool specimens, use of genetic probes, and, rarely, biopsy. Biopsies show various nonspecific inflammatory changes, including villous shortening, crypt hyperplasia, and infiltration of the lamina propria with mononuclear and polymorphonuclear cells (5).

Bibliography

1. Eckman L (2002) Small bowel infections. Curr Opin Gastroenterol 18:197–202
2. Patizhskaya M, Walpusk J, Mazariegos G et al (2001) Enteric adenovirus infection in pediatric small bowel transplant recipients. Pediatr Dev Pathol 4:122–128
3. Guaraldi G, Cocchi S, De Ruvo N et al (2004) Outcome, incidence, and timing of infections in small bowel/multivisceral transplantation. Transplant Proc 36:383–385
4. Clayton F, Kapetanovic S, Kotler D (2001) Enteric microtubule depolymerization in HIV infection: a possible cause of HIV-associated enteropathy. AIDS 15(1):123–124
5. Fenoglio Preiser CM (1998) In: Infectious diseases. Fenoglio-Preiser CM, Lantz P, Listrom M et al (eds) Gastrointestinal Pathology: an Atlas and Text. 2nd edn. Lippincott Williams & Wilkins
6. Herlinger H, Maglinte DDT (1998) Clinical Imaging of the Small Intestine, 2nd edn. Springer-Verlag, New York

Small Bowel, Postoperative

Dean D. T. Maglinte,
Kumaresan Sandrasegaran
Indiana University School of Medicine, Indianapolis, USA
dmaglint@iupui.edu

Synonyms

Postoperative intestinal disease; Postoperative small bowel leak; Postoperative small bowel obstruction

Definitions and Etiology

Any surgery that breaches the peritoneal reflections may result in small bowel complications. The common complications are ►small bowel obstruction (SBO), perforation, leaks, and ischemia.

SBO refers to partial or complete lack of progression of bowel contents due to a mechanical narrowing or occlusion of the lumen. This differs from the paralytic (adynamic) ileus where there is failure of propulsion due to a neuromuscular or metabolic condition, and which occurs in the absence of a mechanical obstruction. The etiology of SBO includes adhesions, internal and external hernia, intussusception, obturation (obstruction by foreign material such as bezoar), anastomotic stenosis, recurrence of cancer or Crohn's disease, marginal ulcers. Of these, the first two are by far the most common.

Ischemia and infarction represent reduction of blood supply to the small bowel, to the point of reversible (ischemia) or irreversible (infarction) tissue injury. Ischemia following abdominal surgery could be caused by vascular occlusion or ►strangulating obstruction.

Strangulating obstruction indicates the impairment of arterial inflow or venous outflow from small bowel due to a twist in the mesentery. Twisting of mesentery may occur in an ►internal hernia or if a dense adhesion obstructs the two ends of a loop of bowel allowing the obstructed segment to become rotate around its fixed ends. Such an obstruction is termed a ►closed loop obstruction (2).

Internal hernia refers to the protrusion of bowel through a defect in its mesentery, but where the abnormally positioned bowel lies within the abdominal cavity. In the past most cases of these were due to congenital defects in peritoneal reflections. Nowadays the majority of cases are seen following surgical anastomosis of small bowel loops that necessitate incision of the mesentery. External hernia occurs when bowel loops protrude *via* a defect in the wall of the abdomen or pelvis.

Pathophysiology

In addition to ingested fluids, salivary, gastric, biliary, and pancreatic secretions, small bowel mucosa produces about 8–10 L of fluid. In normal state only 0.5 to 1 L of this fluid enters the cecum, the rest is absorbed in the small bowel. In SBO the unabsorbed fluid distends the lumen raising intraluminal pressures from the normal 4 cmH_2O to about 10 cmH_2O. In closed loop obstruction pressures of up to 60 cmH_2O may be seen. Bowel distention also occurs due to lack of propulsion of swallowed nitrogen.

Clinical Presentation

The symptoms that suggest postoperative small bowel complications include abdominal pain, vomiting, bloating or distention, early satiety, fever and halitosis, failure to pass flatus, and rarely diarrhea. Clinical signs include abdominal distention, increased or reduce bowel sounds, rigidity, rebound tenderness, unexplained poor oxygen saturation. While these are generally sensitive findings suggestive of postoperative bowel complications, they are nonspecific. Further investigation is usually undertaken except in the very emergent situation where surgery is mandated without expending time on radiological investigations.

Imaging

Plain film radiography is usually undertaken initially. If there are abnormal findings or if radiography is discordant with clinical findings, additional investigations are performed.

CT is the next most commonly performed investigation in the diagnosis of postoperative bowel complications. Unless there are contraindications, such as clearly abnormal renal function, intravenous contrast is used. For borderline abnormal renal function, as is often present in ill postoperative patients, we prefer to use an iso-osmolar iodinated contrast such as iodixanol (Visipaque, GE Healthcare, Chalfont St Giles, UK). Oral contrast is given if the patient is not vomiting and the intestinal tract is not distended and can tolerate it and if emergent surgery is not anticipated. The choice of oral contrast includes positive oral contrast, such as 2% water soluble iodinated contrast, or neutral contrast, such as water or dilute barium. We prefer water since it is better tolerated, shows abnormal mural thickening or enhancement better and

does not adversely affect 3 dimensional techniques, such as maximum intensity projections (3). Positive oral contrast on the other hand is useful if a localized leak or abscess is suspected or if the patient has abnormal renal function. It is possible to acquire an isotropic volume acquisition of the abdomen and pelvis in a reasonable breath hold with 16 and higher multislice CT scanners. In isotropic resolution acquisition the size of the voxel is equal in *x*, *y*, and *z* directions. Since the size of *x* and *y* dimensions are lesser than 1 mm (field of view of 45–50 cm divided by the CT matrix of 512 × 512), the *z* dimension (or the slice width) should be lesser than 1 mm. We routinely use high resolution coronal and sagittal reformats in unraveling the anatomy and pathology of the small bowel.

CT enteroclysis is used to detect low grade of SBO, subtle enteric leaks, and to differentiate with confidence obstruction from ileus. When conventional CT is equivocal, CT enteroclysis is indicated. The technique of CT enteroclysis depends on the clinical question to be answered (1). Ultrasonography and magnetic resonance imaging (MRI) or MR enteroclysis can detect small bowel pathology but are not consistently used in detecting the postoperative small bowel complications.

Diagnosis

Postoperative SBO

Plain radiography may show dilated, often fluid filled, loops of small bowel. At least three such loops distended to more than 3 cm are required for a confident diagnosis. Nevertheless plain films have false positive and negative rates of 20–30% and in many instances it is not possible to differentiate between ▶ paralytic ileus and mechanical SBO.

CT is used to identify the severity, etiology, and site of SBO (Fig. 1). In complete high-grade SBO, orally introduced contrast does not travel beyond the point of obstruction on an abdominal X-ray or repeat CT performed 12 h after initial CT. In partial high-grade SBO there is a caliber change of at least 1 cm at the site of obstruction but there is flow of some oral contrast beyond the point of obstruction. CT has a low sensitivity (50–60%) (2) for low-grade SBO. Adhesions are considered to be the cause if there is an abrupt caliber change, particularly in small bowel close to anterior peritoneum, without identifiable mass at site of obstruction.

Diagnosis of an internal hernia requires identification of distended small bowel loops in a closed loop configuration in an abnormal position, such as between the stomach and omentum (transmesocolonic hernia). In closed loop obstruction, the two ends of the fluid filled heavily distended loop are in close proximity and are often beaked or have a triangular shape. There may be swirling of vessels supplying the involved loop. The bowel proximal to the loop is distended but not to the same degree as the closed loop, while distal small bowel is nondistended (2).

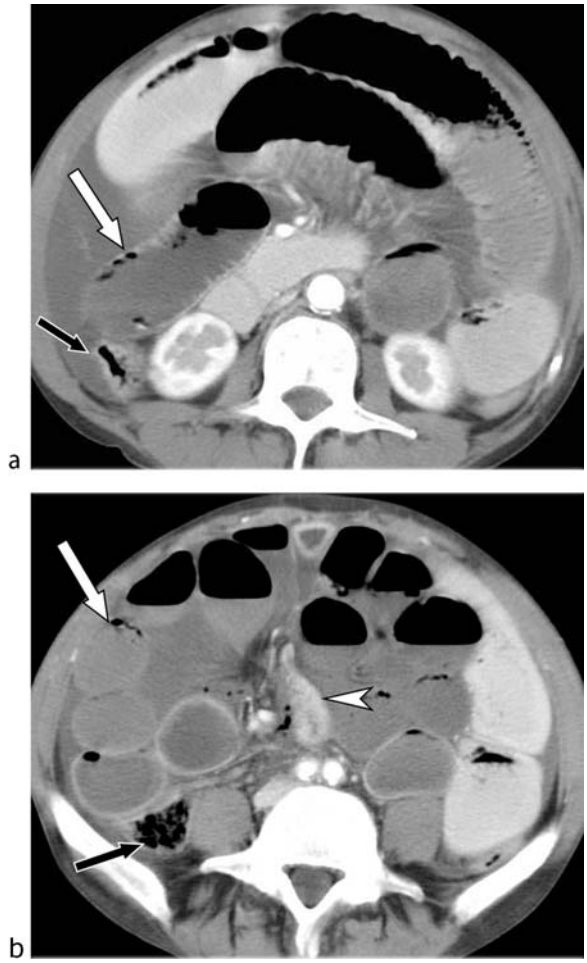

Small Bowel, Postoperative. Figure 1 (a and b) A 72-year-old man with prior inguinal hernia repair presenting with vomiting and abdominal pain for 3 days. Note multiple distended small bowel loops (white arrows) with nondistended right colon (black arrows). At the site of caliber change (arrowhead) no mass is seen. The appearances are of distal high grade small bowel obstruction due to adhesions, proven on subsequent surgery.

Postoperative external hernia is usually evident clinically. Hernia at incisional site is a common occurrence particularly in the obese. As a rule external hernia and adhesions are more common following open compared to laparoscopic surgery. Internal hernia is said to be more common following laparoscopic surgery, particularly transmesocolonic hernia after roux-en-Y gastric bypass. A rare external hernia that may be seen after laparoscopic

surgery is the trochar site hernia. This hernia is usually a Richter type hernia, in which only a part of the wall of a bowel loop herniates. This hernia has a high incidence of infection (2).

In strangulating obstruction, the early features include increased bowel wall thickening or enhancement in venous phase of intravenous contrast, focal ascites, mesenteric vascular blurring or congestion (Fig. 2). Findings of reduced enhancement of affected bowel in arterial phase, hemorrhagic ascites, linear bowel wall pneumatosis, gas in mesenteric, or portal veins herald infarction of bowel (2).

An unusual SBO following surgery is that of an afferent loop or biliopancreatic limb obstruction. This is a surgically fashioned segment of small bowel, usually used to convey pancreatic and biliary secretions to the proximal jejunum. Obstruction of this loop may be due to adhesions or anastomotic stenosis. The classic finding, best appreciated on coronal reformats, is a blind ending obstructed loop in a C-shaped curve in the right upper quadrant. The obstructed loop may be retroperitoneal if it represents the duodenum or intraperitoneal if it is created from the jejunum.

A rare cause of postoperative bowel obstruction, particularly following gastric resection, is bezoar. This is usually due to indigestible plant food. Preoperative diagnosis may be made by CT showing a low-density luminal mass at the site of obstruction. Unlike feces, bezoar usually is rounded and encapsulated (2).

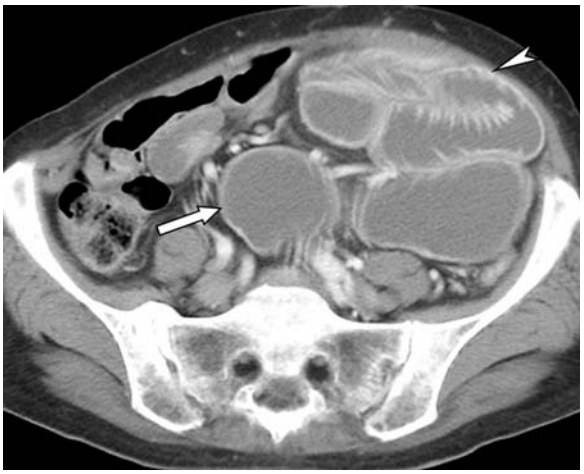

Small Bowel, Postoperative. Figure 2 A 64-year-old women with Whipple surgery 13 days earlier presents with abdominal pain. Note distended bowel loops with intense wall enhancement (arrowhead). More proximal distended loop does not show wall enhancement. This subtle finding of variable enhancement indicates obstruction to venous outflow and incipient ischemia. Long segment of ischemic bowel, caused by an internal hernia, was found at surgery.

Small Bowel Perforation and Leak

Supine radiographs may show the Rigler sign (clear appearance of the inside and outside walls of the small bowel loops), or gas in the falciform ligament in cases of small bowel perforation. These signs are usually visible only if there is a large amount (more than 1000 mL) of free peritoneal air. Erect or decubitus films may show nondependent air with greater sensitivity.

CT examination is much more accurate for detecting small amounts of free gas. The normal amount of residual free peritoneal gas following surgery varies on many factors including the amount of fat content in the torso. An increase in peritoneal air on serial studies or presence of more than 1 or 2 bubbles of gas after second postoperative week is worrying for bowel perforation.

CT enteroclysis is useful for diagnosing subtle leaks and presence of enterocutaneous or other enteric fistula. Leaks may result in fluid collection that may be diagnosed by CT or sonography.

Nuclear Medicine

Nuclear medicine is currently rarely used to diagnose postoperative small bowel complications. An indium-111 labeled white cell scan may be used to detect on occult source of abdominal infection, but false positive findings include uptake in the site of surgical scar. Some surgeons request HIDA scans if afferent loop obstruction is suspected. Multislice CT cholangiography using a biliary contrast agent is useful in evaluating the biliopancreatic limb.

Interventional Radiology

It is important for the radiologist to differentiate between simple adhesive obstruction and strangulating or closed loop obstruction using criteria described earlier. The latter requires emergent surgery. Adhesive obstructions are usually treated, at least initially, with conservative attempts to deflate small bowel. Nasogastric tubes are often insufficient to remove the daily 8–12 L of secretions produced by small bowel mucosa. Placement of a long nasojejunal tube as close to the site of obstruction helps relieve obstruction and may obviate surgery or at least delay it till the patient is in a positive nitrogen balance and electrolyte abnormalities have been corrected (2). Such a tube could be used subsequently for enteroclysis examination to accurately demonstrate the site and etiology of obstruction.

Given the reluctance to reoperate, postoperative collections from localized small bowel leaks are often treated by CT or ultrasound guided drain insertion. We usually place 8–14 French locking drain catheters. If there is concern that the collection is multiloculated multiple drains are placed.

Bibliography

1. Maglinte DD, Bender GN, Heitkamp DE et al (2003) Multidetector-row helical CT enteroclysis. Radiol Clin North Am 41:249–262
2. Maglinte DD, Kelvin FM, Sandrasegaran K et al (2005) The multifaceted role of radiology in small bowel obstruction: Contemporary approach and controversies. Abdom Imaging 30:160–178
3. Maglinte DD, Rhea JT, Ledbetter MS (2004) The Role of CT in Acute Abdominal Disease: Pitfalls and their Lessons. In Mann FA. (ed) Emergency Radiology Categorical Course in Diagnostic Radiology: RSNA 2004 syllabus pp. 119–131

Small Cell Carcinoma, Gallbladder

Rare and highly aggressive tumor (oat cell carcinoma). Paraneoplastic syndromes may be associated.

▶Neoplasms, Gallbladder

Small Intestinal Adenocarcinoma

The most common malignant tumor of the small intestine. The majority of these neoplasms are metastatic at diagnosis and their histogenesis is probably similar to the colonic adenoma–carcinoma sequence.

▶Neoplasms Small Bowel

Small Intestinal Obstruction

▶Occlusion and Subocclusion, Small bowel in adults

Small Joints

Small joints are the metacarpophalangeal joint, metatarsophalangeal joint, proximal interphalangeal joint, distal interphalangeal joint, and interphalangeal joint. The term is used to characterize arthritic involvement. Small joints are commonly affected in rheumatoid arthritis, whereas large joints are affected in ankylosing spondylitis.

▶Rheumatoid Arthritis
▶Spondyloarthropathies, Seronegative

Small Left Colon Syndrome

A neonatal condition in which the descending colon is of reduced calibre and usually obstructed by a meconium plug. The colon attains normal calibre after the first normal stool has been passed.

▶Occlusion, Bowel in Childhood

Smart Probes

▶Molecular Probes, Optical Probes

Snapping Hip

Clicking or snapping sensation during movement of the hip. Patients are usually asymptomatic but may present with focal pain secondary to tendinosis or bursitis. Snapping hips may be categorized as extra-articular (lateral or anterior) or intra-articular. The most common type occurs laterally secondary to the gluteus medius muscle or iliotibial band catching on the greater trochanter. This diagnosis is usually made clinically, but MRI may demonstrate thickening of the iliotibial band and fluid within the greater trochanteric bursa. Catching of the iliopsoas tendon on the ileopectineal eminence during flexion is a common anterior cause of an extra-articular snapping hip. Osteophytes, muscular hypertrophy, and tendinosis are common causes of abnormal tracking and catching of the iliopsoas tendon. MR imaging often demonstrates thickening and signal change of the iliopsoas tendon and fluid in the iliopsoas bursa. Loose cartilaginous or osseous bodies within the joint are the most common etiology of intra-articular snapping hip.

▶Fractures, Pelvis

Soft Tissue Calcification in Dermatomyositis

Soft tissue Calcification in Dermatomyositis is a common feature especially in children. Four distinct patterns of calcification in childhood dermatomyositis are described:

deep calcareal masses, superficial calcareal masses, deep linear.
▶Connective Tissue Disorders, Musculoskeletal System

Soft Tissue Infections

▶Osteomyelitis, Neonates, Childhood

Soft Tissue Sarcoma

A sarcoma that begins in the muscle, fat, fibrous tissue, blood vessels, or other supporting tissue of the body.
▶Rhabdomyosarcoma

Soft Tissue Swelling

Soft tissue swelling is an important radiologic sign. Its form allows differential diagnostic considerations. For example, the typical appearance of joint or tendon sheath effusion as synovial soft tissue swelling is one of the first signs of an inflammatory process. It belongs to one of the three radiologic key symptoms of arthritis: synovial soft tissue swelling, periarticular demineralization, and cartilage or bone destruction.
▶Rheumatoid Arthritis

Solid Pseudopapillary Tumor, Pancreas

Solid pseudopapillary tumor is a benign or low-grade malignant epithelial tumor also reported as solid-cystic tumor and papillary-cystic tumor. However the term solid pseudopapillary tumor correctly encompasses the two most conspicuous histologic features of these tumors, solid areas mixed to pseudopapillary regions. The tumor is uncommon, accounting for approximately 12% of all exocrine pancreatic tumors. It occurs predominantly in adolescent girls and young women. They present as large, round masses with areas of hemorrhage and necrosis and cystic spaces; they are usually well demarcated from the pancreatic tissue because of the presence of a pseudocapsule of compressed pancreatic and fibrous tissue. The incidence of malignancy is about 15%. The imaging findings reflect the macroscopic appearance of the tumor with evidence of the pseudocapsule and a solid heterogeneous aspect with haemorrhagic, necrotic and cystic areas. At CT calcifications are detected in about 30% of patients, usually at the periphery of the mass. The pseudocapsule may enhance following the administration of contrast medium. At MR, T1 weighted images show high signal areas corresponding to haemorrhage and often a hypointense rim, while the signal intensity on T2 weighted images is usually heterogeneous. The prognosis of the tumor is very good and over 90% of patients are cured with surgery alone. Local invasion and metastases are not contraindications for resection and the prognosis is also good with long-term survival in patients with non-localized treated tumors.
▶Cystic Neoplasms, Pancreatic

Somatostatin

Peptide hormone consisting of 14 amino acids that acts as an endocrine and paracrine messenger. The physiological action of somatostatin is reduced secretion of a number of growth hormones.
▶Receptor Studies, Neoplasms

Sonazoid (NC 100100)

Microbubble US contrast agent used with low mechanical index. The bubbles consist of perfluorocarbon and are stabilized by a lipid shell. The agent has a liver-specific late phase. Currently in clinical development in Japan (2006). Manufacturer: General Electric, USA.
▶Contrast Media, Ultrasound, Hepatic

Sonographic Contrast Agent

▶Contrast Media, Ultrasound, Commercial Products

Sonographic Signal Enhancers

▶Contrast Media, Ultrasound, Commercial Products

Sonography

An imaging technique for diagnosing breast disease, such as cancer. It uses harmless, high-frequency sound waves to form an image (sonogram). The sound waves pass through the breast and bounce back or echo from various tissues to form a picture of the internal structures. It is not invasive and involves no radiation.

▶Lymphadenopathy
▶Ultrasound, Imaging

Sonoporation

Sonoporation comprises the ultrasound-enhanced transfection of cells with genetic material or other substances caused by a reversible enhancement of the cell surface permeability. This effect can be amplified by use of gas-filled microbubbles.

▶Local Drug and Gene Delivery with Microbubbles

SonoVue (BR1)

Microbubble US contrast agent used with low mechanical index. The bubbles consist of sulfurhexaflouride and are stabilized by a phospholipid shell. Commercially available in Europe and many other countries (not in the USA). Manufacturer: Bracco SPA, Italy.

▶Contrast Media, Ultrasound, Hepatic

Sontag Method Bone Age

Bone age estimation obtained by counting eligible growth centers (not the main talus and calcaneus) on left side of body and comparing to the gender-specific charts of Sontag, Snell, and Anderson, with number of centers deviation from the mean also stated.

▶Bone Age

SPACE Trial

Stent-Supported Percutaneous Angioplasty of the Carotid Artery versus Endarterectomy trial.

▶Stent, Carotid Artery

Spared Area

Area not interested by liver fatty infiltration. Liver parenchyma with lower portal supply tends to accumulate less fat. Areas commonly spared by fatty infiltration are the dorsal portion of the IV segment just anterior to the portal vein, the gallbladder bed and the medial portion of the left lobe, along the great interlobar fissure. In these regions, the portal flow is decreased due to anomalous systemic venous drainage into portal venules from structure such as the gallbladder or the stomach. These islands of normal liver tissue are also called 'skip areas' and are usually observed at ultrasound as relatively hypoechoic areas.

▶Steatosis, Hepatic

Specific Imaging Techniques, Contrast Media, Ultrasound

Robert Eckersley
Imaging Sciences Department, Faculty of Medicine, Imperial College, London
r.eckersley@csc.mrc.ac.uk

Synonyms

Contrast specific imaging techniques; Microbubble imaging techniques; Non-linear imaging techniques

Definition

Contrast specific imaging techniques have been developed to improve the sensitivity and specificity of ultrasound imaging to microbubble contrast agents. Contrast specific imaging approaches are now able to detect small volumes of slow-moving blood deep in the body.

Characteristics

Specific imaging techniques for microbubble contrast media make use of the non-linear acoustic properties of microbubbles to differentiate the bubbles from the surrounding tissues. Originally microbubbles were developed as enhancing agents for Doppler studies to improve the visualization of blood. A primary motivation at this

stage was the opacification of the ventricles to allow better delineation of the endocardial border. However, a number of unforeseen circumstances arose, first by boosting the signals in the blood pool to levels similar to the tissue itself in many cases the Doppler processing in the ultrasound systems was no longer able to differentiate between blood flow and moving tissues. Second, the concentrations of microbubble agents required to generate this boost were high enough that attenuation of the signals in the bubble clouds meant that deeper tissues or full ventricle views were unobtainable. Also, standard Doppler modes are designed to use relatively high amplitude pulses due to the weak scattering from red blood cells; these pressures are typically enough to disrupt the microbubbles reducing their effectiveness.

To overcome these limitations a number of microbubble specific imaging approaches have been developed. One of the earliest of these arose from the insight that the microbubbles can be destroyed when using existing Colour Doppler modes (1). The term loss of correlation imaging was coined to describe this approach. The Doppler mode depends on comparing the echoes from a train of pulses, with the Doppler shift or target speed calculated by relative phase changes in the radio frequency echoes; when microbubbles are introduced initially they scatter the signal strongly, but at the high pressures typically used they are destroyed, and then the signal returned by subsequent pulses in the train is dramatically different. The Doppler processing interprets this as a high velocity and as there is no direct correspondence between the initial and later echoes in the train, the direction of the estimated velocity is random, hence the multicoloured mosaic pattern (Fig. 1a). Some modern ultrasound scanners provide microbubble specific Doppler modes (e.g. ADI on the Acuson Sequoia) based on standard colour Doppler approach (Fig. 1b). The main differences being that the directional colour coding has been removed, and the focal region of the image extended to improve the coverage within the image. Furthermore as the actual speed of the microbubbles in not of importance, shorter (higher axial resolution) pulses can be used thus improving the spatial resolution in this mode.

Although able to provide a very sensitive method for detection of microbubbles the main limitation of this approach is the destructive nature. Destroying the microbubbles means that unless time is allowed for the microbubbles to replenish the volume of interest only one image (in any one plane) can be obtained. This precludes real-time imaging. To allow real-time imaging much lower amplitude pulses must be used.

In order to differentiate between tissue echoes and microbubble scattering at low pressures a number of non-destructive bubble specific methods have been developed. All these depend on the non-linear resonant acoustic properties of the microbubbles. The first approach was to directly detect the harmonic signatures of the microbubbles (2). When microbubbles are insonated with ultrasound pulses close to their natural oscillation frequency they will oscillate strongly. The oscillation not only contains strong signals at the natural (or fundamental frequency) but will also contain harmonics (at integer multiples of the fundamental). ▶Harmonic imaging was therefore developed in which the bubbles were insonated with one frequency while the ultrasound detection process was tuned to twice this frequency. Of course, tissues themselves are not truly linear and as

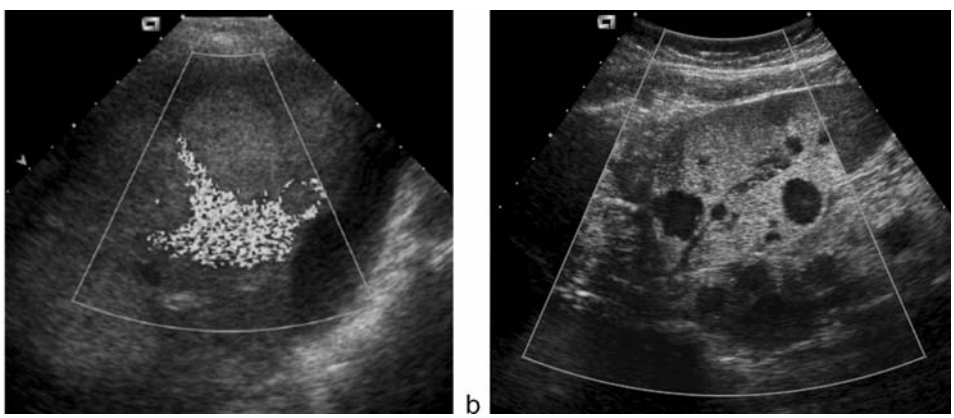

Specific Imaging Techniques, Contrast Media, Ultrasound. Figure 1 (a) Colour Doppler scan of the liver after injection of the microbubble Levovist, showing the characteristic multicoloured mosaic pattern. This colour pattern arises due to a loss of correlation in the Doppler processing caused by the microbubble disruption. (b) This microbubble specific mode (ADI on the Siemens Sequoia) shows improved coverage of the liver. The directional Doppler information is discarded to aid interpretation of the image.

ultrasound waves propagate through the tissues a process called non-linear propagation also causes the production of harmonics. However, the non-linear propagation process is quite different to that of the resonant behaviour of microbubbles, primarily in that it requires a propagation distance in which to build up, and that it occurs only at relatively high acoustic pressures.

In order to make harmonic imaging work a trade-off between the sensitivity and specificity of the system to the harmonic echoes (the microbubbles) the spatial resolution of the image had to be struck. This compromise arises due to the frequency filtering required to successfully separate the scattered second harmonic signals from the fundamental, and any overlap between the frequency bands must be avoided (3) (Fig. 2).

This can only be achieved by using longer narrowband signals. The harmonic imaging approach has been combined with adaptations of existing Doppler processing to provide harmonic Doppler imaging. This combination has the advantage of reducing the linear tissue clutter in colour and power Doppler images and spectral Doppler traces.

Most recent microbubble specific imaging approaches use modulated pulse sequences to detect the non-linear response of the microbubbles. These pulse sequences contain two or more pulses with alternating phase, amplitude or a combination of the two and are able to avoid the frequency filtering inherent in harmonic imaging. This overcomes the major trade-off between spatial resolution and sensitivity to non-linear signals associated with harmonic imaging.

►Phase modulation imaging or pulse inversion imaging involves transmitting pulses with alternating polarity (4). This mode is now widespread and available on many commercial clinical systems. The now standard form of phase modulation imaging is based on alternating the polarity between successive pulses, that is, +1, −1, etc. (see Fig. 3). When these pulses are scattered linearly from tissues, the echoes of subsequent pulses will cancel when combined. The response of the microbubbles to the +1 and −1 pulse is significantly different and when the echoes are combined a residual signal arising from the non-linearity of the bubbles remain. The non-linear signal detected by phase modulation imaging comes from the second harmonic signals in the echoes. Broadband imaging pulses can be used and unlike harmonic imaging this multi-pulse approach does not suffer from the same compromise in specificity and sensitivity to microbubbles against resolution. Successful phase modulation imaging requires precise pulse shaping within the ultrasound equipment to ensure good cancellation of the linear echoes. The specificity of this approach is limited by the generation of harmonic signals during the propagation of the sound through tissues especially at higher MI.

As an alternative to phase modulation an amplitude modulation can be used. In this case consecutive +1,+½

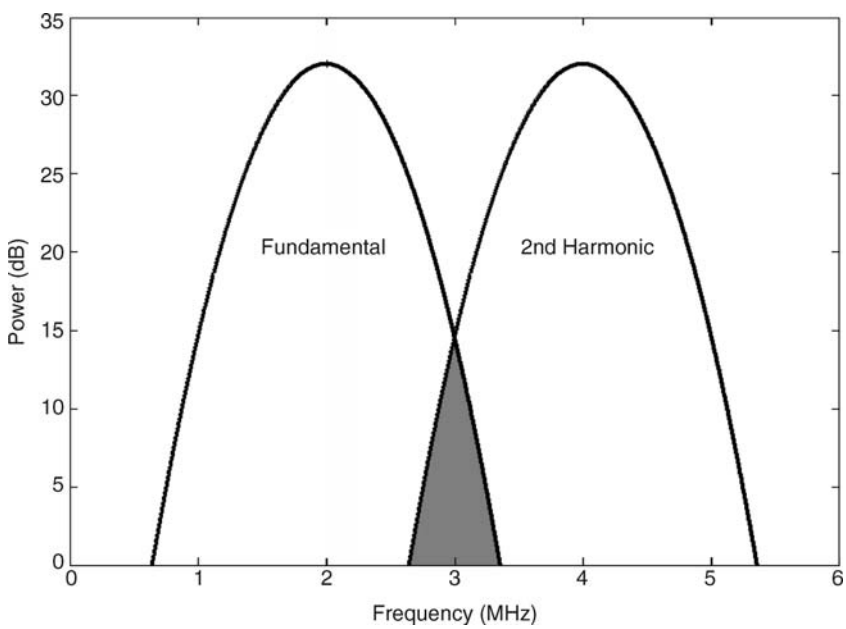

Specific Imaging Techniques, Contrast Media, Ultrasound. Figure 2 In harmonic imaging to successfully separate the scattered second harmonic microbubble signals from the tissue background overlap (red shaded region) between the fundamental and the second harmonic must be avoided. This can only be achieved by reducing the bandwidth of the ultrasound pulses used, which causes degradation in the spatial resolution of the image.

(see Fig. 3) pulses are sent, as before, appropriate combination of the echoes will result in a complete cancellation for linear scatterers, whereas non-linear microbubble echoes will show residual signals. These residual signals arise because the microbubbles respond non-linearly to the different amplitude pulses, that is, the double amplitude pulse does not elicit an echo with twice the amplitude, whereas for tissue this would be the case. An advantage of amplitude modulation over phase modulation is that it is able to detect non-linear signals at the fundamental frequency and not just the second harmonic. However, the use of alternating lower power pulses does reduce the sensitivity of this approach. A combination of pulse inversion and amplitude modulation

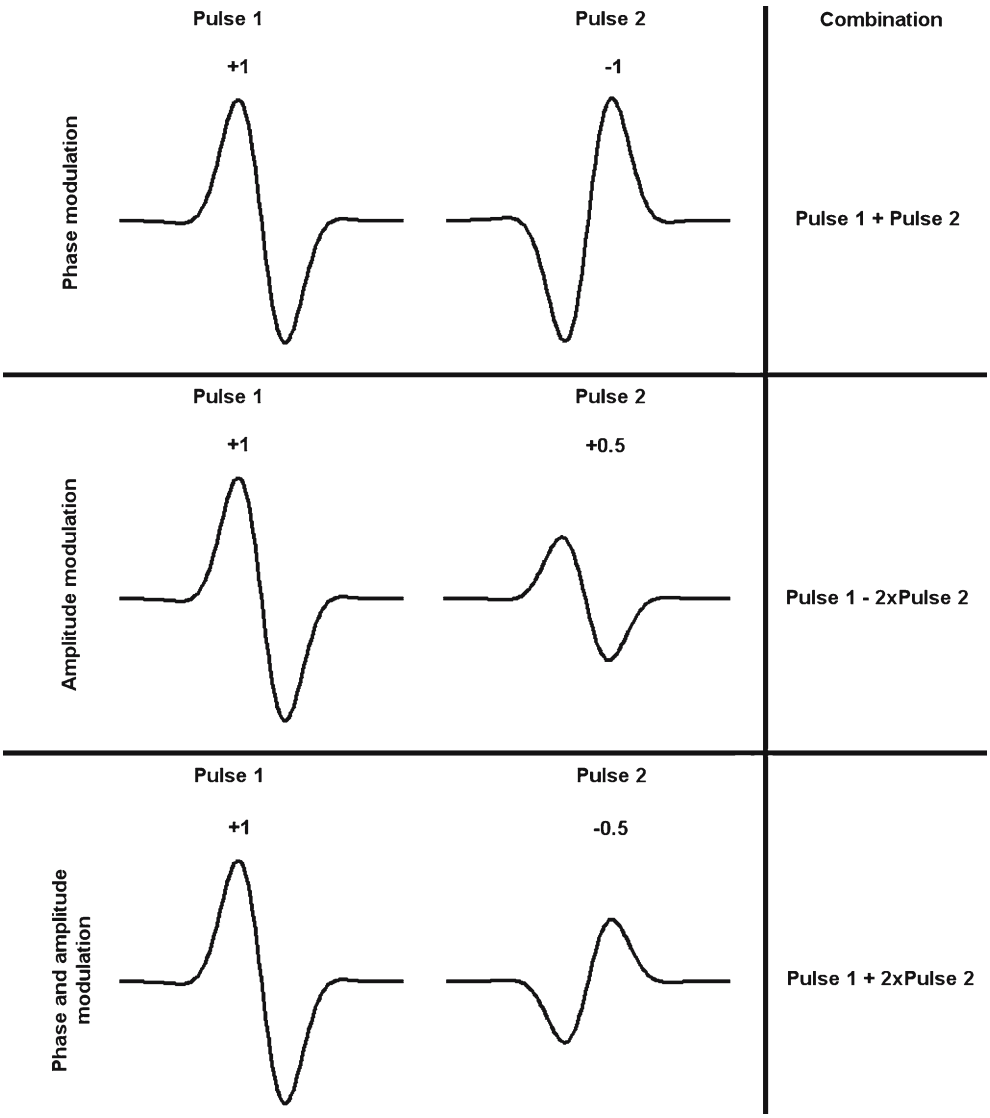

Specific Imaging Techniques, Contrast Media, Ultrasound. Figure 3 This figure shows (*upper panel*) a simple two pulse phase modulation sequence. When the echoes of pulse 1 and pulse 2 are summed any linear signals will be cancelled. The second harmonic signals in the echoes from microbubbles are preserved by this approach. A simple two-pulse amplitude modulation sequence is also presented (*middle panel*). When the echoes of pulse 1 and pulse 2 are combined by doubling pulse 2 and subtracting the result from pulse 1 any linear signals will be cancelled. Both non-linear signals at the fundamental and 2nd harmonic signals in the echoes from microbubbles are preserved by this approach. In the lower panel a two-pulse sequence with combined phase and amplitude modulation is shown. Linear signals can again be removed by appropriate combination of the echoes. This approach can detect non-linear signals at the fundamental frequency as well as the second harmonic.

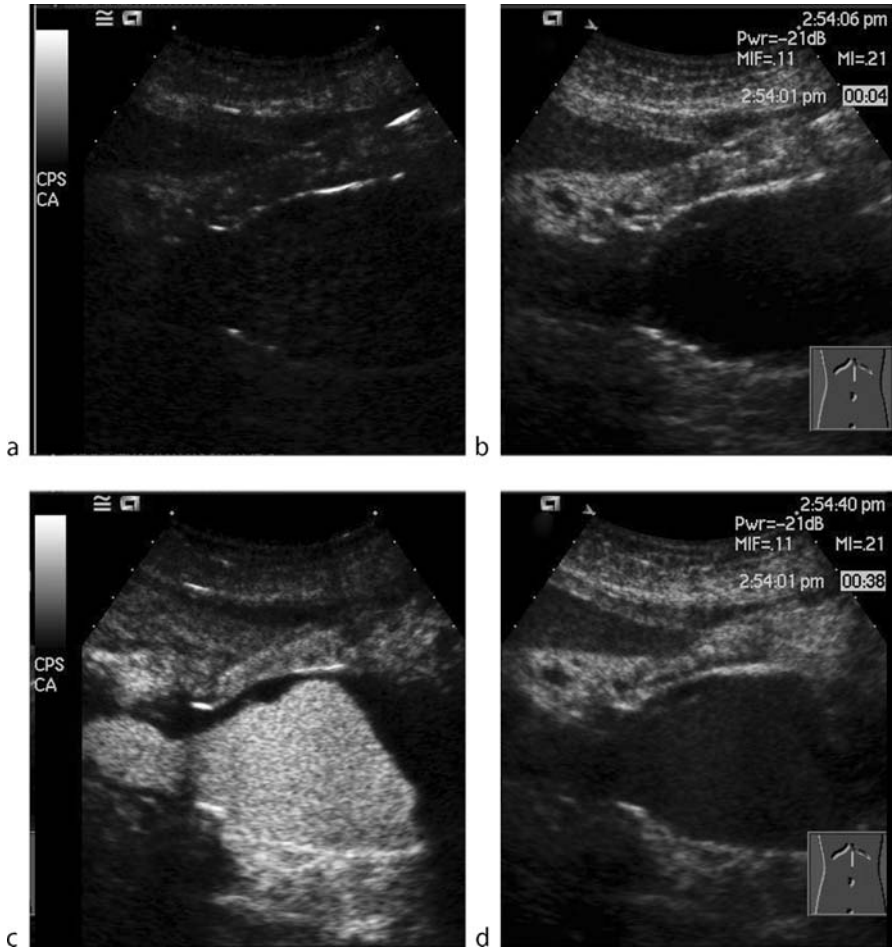

Specific Imaging Techniques, Contrast Media, Ultrasound. Figure 4 Pre (a,b) and post (c,d) contrast ultrasound images of the abdomen, showing a longitudinal section through an aneurysmal aorta. The microbubble specific imaging mode (a,c) use both phase and amplitude modulation to detect the non-linear signals (CPS on the Siemens Sequoia). The greyscale images (b,d) are generated from linear echoes in the same sequence. Pre-contrast images show minimal signals in the contrast specific image (a) compared with the standard B-mode image (b). After arrival of the contrast agent strong signals are seen in perfused areas. All scanner settings remain constant in both image pairs.

has been shown to improve the sensitivity to microbubbles over tissues still further (5) (Fig. 4). In each of these cases the pulse sequences can be extended to more than two pulses to improve sensitivity and to enable the use of Doppler processing for motion detection.

As well as overcoming the resolution versus sensitivity trade-off these multi-pulse approaches are highly sensitivity to non-linear signals allowing low amplitude pulses to be used. This means that bubble disruption is reduced and real-time imaging is possible.

These microbubble specific ultrasound imaging approaches have given rise to a number of quantitative tools for making use of the physiological information they can provide. Microbubble contrast agents typically act as blood pool agents and can be used as tracers within the circulation. The most widespread functional approach is flash replenishment imaging (6), in which the microbubbles in the image plane are initially destroyed by a high amplitude ultrasound burst and subsequently a low amplitude real time method is used to monitor the rate at which the image plane refills. Quantitation and modelling of the results allows estimates for the blood volume and tissue perfusion to be made. Techniques measuring the time of arrival of the first pass of the microbubbles in the liver have also shown promise (7).

Bibliography

1. Bauer A, et al (1997) Acoustically stimulated microbubbles in diagnostic ultrasound: properties and implications for diagnostic use. In Nanda NC, Schlief R, Goldberg BB (eds), Advances in Echo Imaging Using Contrast Enhancement. Kluwer Academic Publishers, Dordrecht, pp 669–684

2. Burns PN (1996) Harmonic imaging with ultrasound contrast agents. Clin Radiol, 51:50–55
3. Powers JE, Burns PN, Souquet J (1997) Imaging instrumentation for ultrasound contrast agents, in Advances in Echo Imaging using Contrast Enhancement, Nanda NC, Schlief R, Goldberg BB (eds), Kluwer Academic Publishers, Dordrecht, pp 669–684
4. Hope Simpson D, Chin CT, Burns PN (1999) Pulse inversion Doppler: A new method for detecting nonlinear echoes from microbubble contrast agents. IEEE Transactions On Ultrasonics Ferroelectrics and Frequency Control, 46(2):372–382
5. Eckersley RJ, Chin CT, Burns PN (2005) Optimising phase and amplitude modulation schemes for imaging microbubble contrast agents at low acoustic power. Ultrasound in Med Biol, 31(2):213–219
6. Wei K, et al (1998) Quantification of myocardial blood flow with ultrasound-induced destruction of microbubbles administered as a constant venous infusion. Circulation 97(5):473–483
7. Blomley MJK, et al (2003) Liver microbubble transit time compared with histology and Child-Pugh score in diffuse liver disease: A cross sectional study. Gut, 52(8):1188–1193

Specific Microbubbles

▶Targeted Microbubbles

Specific Targeting

▶Targeted Microbubbles

Specificity

The proportion of truly nondiseased persons in the screening population who are identified as nondiseased by the screening test.

▶Screening, Breast Cancer

SPECT

Abbreviation for single photon emission computed tomography—a type of tomographic image acquisition in nuclear medicine. In the course of a SPECT scan, a three-dimensional image is obtained by rotating the detectors of the gamma camera around the patient. For evaluation, slices in any orientation can be reconstructed from this three-dimensional data set. Due to the higher resolution of the method, scans in SPECT generally yield a higher accuracy than conventional planar acquisitions.

▶Pulmonary Function, Nuclear Medicine Methods

Spermatocele

Extratesticular cyst caused by cystic dilatation of tubules of the efferent ductules in the head of the epididymis. It contains sediment including detritus, immobile spermatozoa, and lipids.

▶Scrotal Disorders

Spina Bifida

Strictly speaking, the term “spina bifida” indicates defective fusion of the vertebral neural arch. However, it is widely used as a synonym of spinal dysraphism. Use of the terms “spina bifida aperta” (or “cystica”) and “spina bifida occulta” to refer to OSD and CSD, respectively, is presently discouraged.

▶Congenital Malformations, Spine and Spinal Cord

Spinal Cord

Jan T. Wilmink
Radiology Department
University Hospital Maastricht
The Netherlands
jwil@rdia.azm.nl

Introduction

Diagnostic imaging of the spine and spinal cord is challenging in several ways. In the early days of conventional X-ray imaging, it soon became clear that, although the technique produced good visualization of bony spinal structures and bony pathology, soft tissue resolution of structures within the spine was inadequate. The spinal cord, blood vessels, and emerging nerve roots remained invisible as did the various ligamentous structures connecting the bony elements: intervertebral disk, anterior

and posterior longitudinal ligaments, as well as flaval and interspinous ligaments.

Work on contrast techniques to improve cord and root depiction (myelography) commenced in the early decades of the last century. Technically the most challenging technique was probably gas myelography, in which air was injected into the spinal subarachnoid space, producing a faint image of the contours of the spinal cord on tomographic images. Positive contrast media for myelography came next, and the iodized radiopaque oils (Lipiodol, Pantopaque) which were injected into the subarachnoid space made myelography easier and more reliable, as well as being less unpleasant for the patient. These early positive contrast media however had the tendency to disperse into droplets, which degraded the image of the cord and roots, as well as possessing the potential to induce sometimes crippling adhesive arachnoiditis. The introduction of water-soluble iodine contrast media further improved image quality. The first preparation, Abrodil (sodium iodomethyl sulphonyl) caused such severe local irritation that spinal anesthesia was necessary. Later developed contrast media such as Conray (meglumine iothalamate) and Dimer-X (dimer iothalamate) were more patient friendly, and when Amipaque (metrizamide), an iodine solution with decreased osmolality was produced, adhesive arachnoiditis became a problem of the past.

Using the same contrast media, techniques were developed to opacify the nucleus pulposus (discography), the intraspinal epidural space (peridurography or canalography). The introduction of catheterization techniques made it possible to produce diagnostic images of the spinal arteries (spinal angiography) as well as the lumbar and cervical epidural veins (epidural venography).

These contrast techniques require a degree of technical skill from the examiner. Correct needle or catheter placement as well as patient positioning determine success or failure of the examination. The requirement of these technical skills did much to establish neuroradiology as a separate radiological subspecialty, practiced by dedicated radiologists, and not infrequently by neurosurgeons and neurologists.

A technological development of great significance was the development of computed tomography (CT). The improved contrast resolution and sectional imaging capability provided by this technique revolutionized diagnostic imaging. Third and fourth generation CT systems employing high-resolution scanning packages were able to generate diagnostic images of the spinal ligamentous structures, and of ligamentous lesions such as disk herniations. Intradural structures such as the spinal cord and nerve roots could still only be reliably imaged after intrathecal contrast injection: CT-myelograpy. In the same way, CT and intradiskal contrast injection were combined to produce CT-discography.

Magnetic resonance imaging (MRI) in the early days was practically limited to brain scanning. It was only when the next technological challenge had been overcome by the introduction of surface coils that detailed images of spinal structures, including the spinal cord, could be acquired. Technological developments are rapid. The images of the spinal cord and of cord pathology provided by MRI are diagnostically superior to myelographic and CT-myelographic pictures. Intradural nerve roots can be depicted by specialized MR myelographic sequences, without the need for contrast injection. Contrast myelography is rapidly becoming a lost art, and techniques such as peridurography and epidural venography have long since passed from the diagnostic imaging scene. Discography retains a role disputed by some. High-resolution techniques for spinal CT and MR angiography now in development are likely soon to replace catheter spinal angiography.

The replacement of unpleasant, time-consuming, and laborious contrast examinations by rapid and reliable modern imaging techniques is an indisputable boon to patients. In addition, completely new insights into spinal cord morphology and function are promised by novel techniques such as diffusion tensor imaging and BOLD functional MRI.

The greatly improved power of resolution of modern imaging has created a new challenge. The problem is not one of technique or technology, but of interpretation. A case in point is that of patients with low back pain and sciatica. This category at present forms probably the single largest indication for MR imaging. The etiology of these complaints is at present still poorly understood. Nevertheless the wealth of anatomical detail provided by MRI, including features such as degenerative bone marrow changes, fissuring of the annulus fibrosus, and desiccation of the nucleus pulposus has led to arbitrary implication of these and other MRI findings in the production of low back pain. Even a lumbar disk herniation, which has been regarded as a cause of sciatica since the 1930s, can be demonstrated by MRI in up to 30% of healthy volunteers without any complaints of back or leg pain. Careful scrutiny and critical assessment are necessary to differentiate between a disk herniation, which is actually responsible for symptoms, and a chance finding without clinical significance.

Anatomy

The spine is required to meet conflicting demands of stability on the one hand, and mobility on the other. The solution ranges from a complete lack of mobility with maximum stability in the fused vertebral elements of the

sacrum at the one end, to the highly mobile but vulnerable structure of the cervical spine at the other. The intervening thoracic spine possesses very limited mobility as it forms part of a rigid thoracic cage while the anatomy of the adjoining lumbar spine permits excursions almost exclusively in the sagittal plane.

The basic building block of the spinal column is the vertebra, which is composed of a vertebral body connected by a pair of pedicles to the posterior neural arch or lamina. Superior and inferior articular processes arising from the junction of the neural arch with the vertebral body form zygapophyseal joints with the articular processes originating from adjacent vertebrae, and these intervertebral joints, also known as facets, are important in regulating spinal motion. In the cervical spine, additional uncinate processes originate from the upper lateral borders of each vertebral body to form uncovertebral joints with the lower lateral borders of the vertebral body above. Transverse and spinous processes provide mechanically efficient attachment points for the various ligaments and muscles important for stability as well as mobility.

Two vertebrae are connected by investing ligaments to form a motion segment. The most important ligamentous spinal structures are the annulus fibrosus forming the outer circumference of the intervertebral disk that connects two vertebral bodies, and the anterior and posterior longitudinal ligaments, which strengthen the connection. The posteriorly located articular processes are connected with their upper and lower counterparts by the facet joint capules, which gradually merge posteriorly with the flaval ligaments connecting each neural arch with the one above and below it. Finally, the spinous processes at the various levels are connected by the interspinous ligaments.

Within the fibrous ring of the annulus fibrosus is located the gelatinous nucleus pulposus, and the combination is responsible for the hydroelastic shock-absorbing properties of the intervertebral disk.

The vertebral canal or vertebral foramen runs the entire length of the spinal column, being bordered anteriorly by the vertebral body and intervertebral disk, and posteriorly by the neural arch and flaval ligaments. Its shape is round or oval in the thoracic, upper lumbar, and upper cervical regions, becoming more triangular in the lower cervical and especially lower lumbar areas, with prominent lateral recesses being formed at the lumbosacral transition. The intervertebral foramina or canals are oriented laterally, being bordered above and below by the superior and inferior pedicle, anteriorly by the vertebral body and intervertebral disk, posteriorly by the facet capsule and articular processes.

The spinal dural sac runs almost the full length of the spinal canal, from its junction with the cranial dura mater to its caudal termination or cul-de-sac at the upper sacral level. The surrounding epidural space contains semifluid epidural fat and epidural veins. Within the dural sac lies the spinal cord, connected cranially with the medulla oblongata, and ending at the tip of the conus medullaris, at the vertebral L1–L2 level. Nerve roots coursing towards the lumbar and sacral foramina form the cauda equina. As a (motor and sensory) pair of nerve roots departs the dural sac to enter the intervertebral foramen, they are accompanied over a short distance by a dural root sleeve or sheath. Spinal cord and cauda equina are covered by pia mater, and are bathed by cerebrospinal fluid (CSF) within the spinal subarachnoid space, which also extends into the root sleeves. Besides the emerging nerve root and dorsal root ganglion, the intervertebral foramen contains fat and foraminal veins.

Sectional Anatomy

In the axial plane, three levels can be identified:

- Pedicular level: The section passes through the upper half of the vertebral body, the pedicles, transverse processes, upper neural arch and spinous process. The borders of the spinal canal are entirely bony at this level
- Infrapedicular level: The section passes through the lower half of the vertebral body and upper half of the intervertebral foramina containing the dorsal root ganglions, additionally the facets with their joint capsules and the flaval ligaments, and the lower half of the spinous process.
- Disk level: The section passes through the intervertebral disk and lower half of the intervertebral foramen, containing mainly fat and veins; also through the lower half of facets, joint capsules and flaval ligaments. The borders of the spinal canal are almost entirely ligamentous at this level.

In the sagittal plane, two sections are distinguished:

- Mid-sagittal section: This section shows the spinal cord and conus medullaris well, also the sagittal dimensions of the spinal canal and the epidural fat.
- Lateral sagittal section: This section provides a good sagittal image of the intervertebral foramen.

The coronal plane is rarely used for spinal imaging. Oblique images are useful for MR myelographic projections.

Functional Anatomy

When the spine moves from flexion or kyphosis to extension or lordosis, this has an effect upon intraspinal dimensions and structures. As lordosis increases, the spinal canal shortens due to the position of the axis of movement being located within the vertebral body, anterior to the canal. The disk bulges backward into the

canal and the flaval ligaments also bulge inward, thus narrowing the canal at the disk level. When the spine moves to kyphosis the opposite occurs. These are normal phenomena but in cases with narrowing or stenosis of the canal, these posture-induced changes may be sufficient to cause cauda equina compression with neurogenic claudication in the lumbar spine, or aggravation of spinal cord compression in the cervical region. The presence of semifluid epidural fat permits craniocaudal movement of the dural sac within the spinal canal during flexion–extension movements, and the spongy epidural venous system helps to compensate posture-related intraspinal volume changes, avoiding CSF pressure changes during spinal movements.

Degenerative Disease

Intervertebral Disk

Degenerative changes of the disk commence in late adolescence, with dehydration of the nucleus pulposus and fissure formation in the annulus fibrosus. These changes can be observed by MRI; T2-weighted images demonstrate loss of water signal in the nucleus, and fluid-filled fissures in the annulus. The subchondral bone marrow can also undergo degenerative changes showing different MRI signal patterns: dark on T1- and bright on T2-weighted images (increase in water content); bright on T1- and bright on fast spin-echo T2-weighted images (fatty degeneration); dark on T1- and dark on T2-weighted images (sclerosis). Such changes can also occur in normal aging, and a convincing relationship with backache or sciatic pain has not been established.

With nuclear dehydration goes decrease in disk height, which in turn leads to circumferential bulging of the annulus, also into the spinal canal ("bulging disk"). When a weakened annulus fibrosus ruptures, material from the nucleus pulposus may be displaced into the spinal canal ("herniated disk"; "herniated nucleus pulposus"). Nomenclature is as follows: when the height of the herniated material does not exceed the height of the parent disk, this is called a protrusion. When the herniated mass is higher than the parent disk, it is called an extrusion. Bulging disks usually do not cause nerve root compression, unless there is associated narrowing of the spinal canal. Protruded disks are frequently asymptomatic, extruded disk fragments usually compress the root. Extruded material may migrate some distance to compress a root in the intervertebral foramen or the lateral recess.

A compressed nerve root undergoes inflammatory changes, which in the lumbar region lead to the clinical symptom of sciatica: pain irradiating into the dermatome of the leg supplied by the affected root. Sensory loss in the dermatome may ensue, as well as muscle weakness and decreased tendon reflexes. A large extrusion may cause a cauda equina syndrome with severe neurologic deficit including bladder paralysis. In the cervical spine, root compression by disk herniation causes brachialgia: pain irradiating into a dermatome of the arm.

MRI is presently the best technique available for diagnosing lumbar degenerative disk disease. Soft tissue resolution is better than with CT, this is especially useful for detecting extrusions in areas like the lateral recess. MR myelography with heavy T2 weighting is useful in identifying symptomatic disk lesions causing root compression. In patients with failed back surgery, MRI can detect recurrent herniation. Contrast injection is sometimes useful in these cases to identify postoperative scarring. Even in unoperated patients, extruded and migrated disk material will frequently demonstrate peripheral contrast enhancement. Compressed and irritated nerve roots may also enhance.

In the cervical spine, disk extrusions are generally smaller, and CSF flow artifacts may degrade the image. CT myelography may be necessary. CT is also better able to distinguish between disk extrusion ("soft disk") and bony spurring ("hard disk").

Spinal Narrowing

Developmental spinal stenosis is an uncommon shallowness of the spinal canal seen especially frequently in achondroplasia. Lumbar stenosis leads to neurogenic claudication; irradiating pain and numbness in the legs on walking and standing, relieved by sitting and squatting, caused by chronic posture-dependent cauda equina compression. Much more frequent is degenerative narrowing of the lateral region of the spinal canal due to hypertrophy of the facets and flaval ligaments in spondylarthrosis. This condition can also lead to degenerative anterolisthesis which further narrows the spinal canal. In spondylolisthesis due to spondylolysis the spinal canal is widened rather than narrowed, but nerve root compression may occur in the foramen.

Often the problem is multifactorial: in a patient with already some developmental narrowing and spondylarthrosis in progress, only a small disk protrusion or even a bulging disk can tip the balance and compress the root. In an individual with a roomy spinal canal, a much larger extrusion would be necessary. Increase in the amount of epidural fat (epidural lipomatosis) in adipose individuals or patients with Cushing's disease, can aggravate narrowing.

In the cervical spine, the same combination between developmental and degenerative narrowing can compress the spinal cord. Long tract signs (problems with walking and micturition) occur as the cord is slowly and progressively compressed.

Trauma

Diagnostic imaging in patients with spinal trauma is used to ascertain the mechanism of injury, to image the bony and/or ligamentous injury to the spine and determine the resulting loss of stability, and also to assess spinal cord damage with a view to neurologic prognosis. In the emergency room, conventional films provide a first assessment. Four main force vectors can be distinguished. Hyperflexion of the spine can be combined with compression (resulting in vertebral body fracture) or distraction (resulting in ligamentous injury: hyperflexion sprain or facet luxation with interlocking). Hyperextension of the spine can be combined with compression (resulting in articular process fracture) or distraction (resulting in hyperextension sprain). Fractures of the vertebral body are usually well seen on conventional X-rays, but articular process fractures are often better diagnosed by spiral CT with sagittal reformats. Ligamentous injuries (hyperflexion or hyperextension sprain) are difficult to visualize with X-ray techniques; plain films may show indirect signs of hematoma (widening of the interspinous space in hyperflexion sprain, or the prevertebral soft tissue space in hyperextension sprain) facet interlocking or the "bayonet sign" on the A-P film in unilateral facet luxation.

MRI is able to directly demonstrate soft tissue hematomas indicating ligamentous injury, best on T2-weighted images. Intraspinal lesions such as traumatic disk herniation and epidural hematoma are also well demonstrated. MRI is less reliable for the diagnosis of vertebral body and articular process fractures however.

Combinations of the force vectors mentioned above are quite frequent, also with rotation and lateroflexion

Injuries not yet mentioned are Jefferson fracture of the atlas, odontoid fracture, hangman's fracture of C2 and Chance fracture in the thoracolumbar region.

In any spinal injury, assessment of the loss of stability is of particular importance in order to select appropriate measures to prevent further derangement of the spine, and possible (further) injury to the spinal cord.

Spinal cord injury can manifest itself in various neurologic syndromes, the most severe being a complete transverse cord lesion. Hemitransection of the cord, usually by a penetrating injury, can result in Brown–Sequard syndrome.

MRI can demonstrate compression of the cord, but also spinal cord contusion. The lesion is seen as hypointense on a T1-weighted image, and hyperintense with T2-weighting. T2 hypointensity indicates hemorrhagic contusion, associated with a poor prognosis. Later a posttraumatic syrinx may form.

Nerve root avulsion from the cervical intumescence of the cord can be demonstrated using CT myelography or MR myelography.

Tumors

These can be subdivided as follows:

Secondary and primary vertebral tumors

Secondary metastases are by far the most common spinal tumors, most frequently from carcinoma of the lung, breast, and prostate. Plain films demonstrate metastases only when there is destruction of cortical bone (missing pedicle sign), or collapse of a vertebral body. CT can detect earlier destruction of vertebral spongiosa. Isotope studies are even more sensitive and demonstrate repair activity of affected bone by osteoblasts. Most sensitive of all is MRI, which detects subtle changes in bone marrow composition due to tumor infiltration. Signal from bone marrow fat is decreased in T1-weighted images, and T2-weighted images show increase in tumor water content. This signal pattern is not specific for tumor infiltration, and may also occur in degenerative and infectious disease. Fracture hematoma in vertebrae collapsed due to osteoporosis is indistinguishable by MRI from metastasis. Diffusion-weighted imaging may resolve the problem, as will the finding of normalized bone marrow in healed vertebral fractures elsewhere. Injection of gadolinium contrast media may mask bone marrow metastases on T1-weighted images, and use of the turbo spin-echo sequence can have the same effect in T2-weighted pictures. In both cases, suppression of bone marrow fat signal is useful.

Invasion of the spinal canal is well demonstrated by MRI, sometimes on either side of an intact posterior longitudinal ligament (curtain sign), as is compression of the spinal cord. MRI in these cases is more reliable, more convenient, and less invasive than myelography and CT myelography.

After radiotherapy, T1 bone marrow signal will increase as the red bone marrow is destroyed and fatty marrow now predominates.

The most common benign primary bone tumor is hemangioma, which shows a characteristic high fat signal on MRI, and a spiculated appearance due to thickened trabeculae, best seen on CT.

Other benign tumors are aneurysmal bone cyst, giant cell tumor, osteoid osteoma, osteoblastoma, osteochondroma, and fibroma.

Chordoma is a slow-growing tumor which can produce metastases. Eosinophilic granuloma occurs in children and can result in vertebral collapse.

Malignant bone tumors are osteosarcoma and chondrosarcoma, as well as other sarcomas such as Ewing's.

Bone marrow diseases such as leukemia, lymphoma, and myeloma can affect the spine.

Intramedullary Tumors

The most common of these are astrocytomas, ependymomas, and astrocytomas. Features in common are expansion of the spinal cord, abnormal cord signal pattern with varying degrees of cystic evolution, and contrast enhancement. Syringomyelia may also enlarge the cord. Hemangioblastomas and also glioblastomas can occur in the cord, as can metastases and lymphomas.

Extramedullary Tumors

Seeding of tumor cells *via* the CSF spaces can produce leptomeningeal "drop"metastases. Schwannomas or neurinomas, and neurofibromas originate from the nerve root, but may extend outside the foramen to form a "dumbbell tumor." Meningeomas usually have a broad base of attachment to the dura. Gadolinium injection is helpful in the detection of all these tumors. Lipomas occur most frequently in the filum terminale and are easily seen on T1-weighted images. Teratomas, dermoid, and epidermoid tumors occur infrequently; the latter are often virtually indistinguishable from CSF on CT as well as T1- and T2-weighted MR images.

Infections

Infection of the spine by pathogenic microorganisms may take place by direct contamination (trauma, operation) contiguous spread or hematogenous transport. The disk may be involved (diskitis), the vertebral body (vertebral osteomyelits), or both (spondylodiskitis). Abscess formation may take place in the spine, the epidural space (with spinal cord compression), or the paravertebral region.

Pyogenic Infections

Staphylococcus aureus is the most frequent agent. Severe backache with limited spinal mobility are presenting signs, with clinical and laboratory signs of infection. X-ray studies may show disk space narrowing after a few weeks, and CT erosion of vertebral end-plates. Bone scintigraphy may sometimes show early abnormalities, but is not always reliable. MRI is the best diagnostic technique, with bone marrow lesions showing decreased signal on T1-wieghted images and a bright signal with fat-suppressed T2-weighting. The latter also well demonstrates epidural encroachment. Intravenous gadolinium injection demonstrates enhancement of affected areas, best seen on fat-suppressed T1-weighted images. Abscess formation is well depicted, as is paravertebral spread. After the acute disk infection has subsided, X-ray studies and MRI usually show obliteration of the disk space.

Granulomatous Infections

- Tuberculosis. Generally less severe presentation and course than in pyogenic spondylitis. Several vertebrae are frequently involved. Bone destruction of anterior vertebral bodies may result in gibbus deformity (Pott's disease) with spinal cord compression. Psoas abcesses, sometimes calcified, are seen, epidural spread also occurs. MRI is best for demonstrating bone marrow and disk changes, contrast enhancement, and deformation of spinal canal; CT may show calcifications.
- Brucellosis. More acute presentation than tuberculosis.
- Sarcoidosis and actinomycosis rarely affect the spine.

Other agents

Fungal and parasitic infections may rarely affect the spine.

Transverse myelitis is a condition often associated with viral infection. Swelling of the cord occurs, with increased T1- and T2 relaxation times. Multiple sclerosis can present a similar picture.

Congenital Malformations

The cephalic portion of the spinal cord develops, like the brain, by neurulation: development of a neural plate, neural folds, and neural tube. The caudal portion of the cord, conus medullaris, and filum terminale, arise by a different process: canalization and differentiation. For this reason, different types of malformations are seen in these two cord segments. A third cause of spinal malformations is formed by disorders of notochord development.

Disorders of Neurulation

This category contains a number of dysraphic conditions in which there is a defect in fusion of the midline neural, bony, and mesenchymal structures: spina bifida, either open (aperta) or closed (occulta).

Spina bifida aperta comprises meningocele and meningomyelocele, in which due to lack of fusion of the neural folds a placode of neural tissue is visible on the surface in the midline of the back. The spinal cord is fixed and the conus medullaris is unable to ascend normally to the L1–L2 level (tethered cord). Chiari II malformation is an associated condition featuring a small posterior fossa with protrusion of cerebellar and brain stem structures caudally and cranially.

In occult spinal dysraphism, no placode is visible but cord tethering may be due to conditions such as dorsal dermal sinus or spinal lipoma.

Sometimes there are combinations: lipomyelomeningocele.

A simple dorsal meningocele does not contain neural elements, and is not due to a neurulation disorder.

Disorders of canalization and retrogressive differentiation

Abnormalities of the spinal cord in this condition include dilatation of the terminal ventricle in the conus, tight filum terminale causing cord tethering, fibrolipoma of filum terminale and myelocystocele. The spine may be affected by sacral agenesis or the more complex caudal regression syndrome.

Disorders of notochordal development

Persistence of a patent notochordal canal can result in various vertebral malformations and enteric cysts or diastematomyelia (split cord).

Vascular Disease

Arterial supply to the spine and intraspinal structures is derived from vertebral arteries, the intercostal and lumbar arteries originating from the aorta and the internal iliac arteries. The most important artery to supply the spinal cord is the great radicular artery of Adamkiewicz, which usually originates in the lower thoracic region of the aorta, and is the most important contributor to the anterior spinal artery, which is a usually continuous arterial channel coursing along the entire spinal cord, also receiving minute tributaries from higher and lower levels. Dorsal spinal arteries are smaller and less well defined. Spinal cord drainage takes place *via* intramedullary and radicular veins.

Ischemic Conditions

Interruption of blood supply to the spinal cord can result in transient or permanent neurologic deficit, as in the brain. Anterior spinal supply to the lower cord is most frequently involved, and can lead to transverse cord lesions. These can show up as areas with low signal intensity on T1-weighted images, and signal increase with T2-weighting.

Abnormal arteriovenous connections. There are two main types.

- Spinal cord arteriovenous malformations: Site of shunt is the spinal cord. Generally seen in younger patients, with hemorrhage usually the presenting symptom. Dilated medullary vessels seen on MRI, with dilated arteries and as well as veins visible at spinal DSA.
- Dural arteriovenous fistulas: Older patients presenting with progressive cord deterioration due to increased venous pressure. MRI shows cord swelling with extensive intramedullary high-signal areas, as well as dilated draining veins. Spinal DSA is at present diagnostic gold standard, but MRA and CTA show rapid improvement and potential for replacing invasive catheter techniques.

Treatment of these conditions is endovascular or surgical.

Recommended Reading

1. Manelfe C (1992) (ed) Imaging of the Spine and Spinal Cord. Raven Press, New York. ISBN 0-88167-863-5
2. Ross JS, Brant-Zawadski M, Moore KR et al (2004) Diagnostic Imaging: Spine. ISBN 0-8089-2315-3

Spinal Cord Arteriovenous Fistula (SCAVF)

Direct arteriovenous fistulas located intradurally supplied by spinal arteries.

▶Vascular Disease, Spine

Spinal Cord Arteriovenous Malformation (SCAVM)

Congenital arteriovenous shunt lesions whose nidus is located on or within the substance of the spinal cord and whose arterial supply arises from vessels which directly supply the cord.

▶Vascular Disease, Spine

Spinal Cord Atrophy, Posttraumatic

Loss of neurons several months after severe spinal cord injury.

▶Spinal Trauma

Spinal Cord Cavernous Malformation (CM)

Vascular malformations which are located within the spinal cord and which are pathologically identical to intracranial cavernous malformations.

▶Vascular Disease, Spine

Spinal Cord Infarction

Uncommon cause of acute myelopathy, which usually involves the anterior spinal artery distribution.
▶Vascular Disease, Spine

Spinal Cord, Clinical Syndromes

Jacob Patijn
Pain Management and Research Centre, Department of Anaesthesiology, University Medical Centre Maastricht, Maastricht, the Netherlands
jpat@sane.azm.nl

Definition

In the clinical symptomatology, four aspects are important for understanding the clinical pictures of the various disorders of the spinal cord.

The first is the level of the lesion. The more cranial the location of the lesion, the more extensive the neurological deficit caudal to the lesion, with loss of motor, sensory, and autonomic mechanisms.

Secondly, the extent of the lesion in the transverse plane determines the extensiveness of the neurological deficit, which may result in complete or partial transverse cord syndromes.

Thirdly, the extent in the longitudinal plane is important for a lesion comprising several spinal cord segments. This may present as a clinical entity in itself such as in hematomyelia and syringomyelia or it can be associated with transverse lesions of a few segments or all segments of the isolated cord below the primary transverse lesion.

Finally, the nature of the onset of the spinal cord lesion, sudden or gradual, determines the clinical symptomatology of the spinal cord lesion.

Characteristics

The clinical symptomatology in spinal cord disorders depends on the extent of the lesion and/or the neural structures and spinal tracts that are involved and located in the transversal plane of the cord.

The syndromes can be neuroanatomically subdivided into

1. Complete spinal cord transection
2. Spinal cord hemisection
3. Central cord syndrome
4. Anterolateral spinal cord syndromes
5. Long tract syndromes
6. Anterior horn syndromes

A complete spinal cord transection results in a bilateral sensory deficit for all modalities below the level of transection. It is accompanied with spastic tetraparesis of all extremities in cervical lesions or paraparesis of the legs in thoracic lesions, as well as bladder dysfunction. Sometimes, segmental signs such as reflex deficits, muscle weakness, and atrophy are present.

In hemisection of the cord (Brown-Séquard syndrome), the neurological picture is characterized by paresis with segmental muscle atrophy, superficial hyperesthesia, and a deficit of sensation of superficial touch, deep pressure, and vibration, all located at the same side as the spinal cord lesion.

In contrast, a dissociated sensory deficit involving pain and temperature is present on the contralateral side.

In central spinal cord syndromes, unilateral paresis may be present accompanied with bilateral pain and temperature deficit. Because the posterior columns of the spinal cord are spared, sensory qualities such as light touch and vibration are normal.

Anterolateral spinal cord syndromes, mostly of ischemic origin, are characterized by paraparesis, dissociated sensory loss below the level of the lesion, and urinary dysfunction. Because the posterior columns are also spared, sensory qualities such as light touch and vibration are normal.

Some disorders of the long tracts, such as tabes dorsalis, show isolated spastic paraparesis whether or not associated with sensory deficit for deep touch.

Other spinal cord syndromes are related with lesions of the anterior horn gray matter resulting in muscular atrophy. In the case of amyotrophic lateral sclerosis, anterior horn involvement is associated with pyramidal tract signs.

Etiology of Spinal Cord Disorders

A second subdivision of spinal cord disorders is based on the etiology, in which the above-mentioned anatomical subdivision of spinal cord lesions determines the clinical neurological picture.

Congenital Abnormalities of the Spinal Cord

Various congenital spinal cord disorders are due to incomplete closure of the neural tube. Depending on the extent of incomplete neural tube closure, the clinical picture can vary from simple back pain and sciatica to severe neurological deficits. Spinal bifida occulta, meningocele, myelomeningocele, and meningomyelocystocele

can be present and associated with hydrocephalus or Arnold–Chiari malformation.

Spina Bifida Occulta

Spina bifida occulta is a benign disorder, which seldom leads to symptoms and/or neurological deficit. The condition is often diagnosed as an incidental finding on routine spinal X-ray studies.

A spinous process and a variable part of the lamina may be lacking. Some patients have low back pain and sciatica, because the spinous process of L_5 irritates the incomplete lamina of S_1.

Spinal Dysraphism

Spinal dysraphism can lead to complex clinical neurological pictures with signs of pyramidal tract involvement, urinary dysfunction, and weakness of the lower extremities. The neurological deficit depends on the spinal level of the disorder.

Deformities of the feet, dermal sinus, lipoma, intraspinal adhesions, and tethered cord may be present.

Diastematomyelia

In diastematomyelia, the spinal cord is cleft in two halves. The neurological picture develops during the growth of the child and is mainly characterized by a paresis of the lower extremities and urinary dysfunction. Deformities of the feet are mostly present.

Tethered Cord

In patients with tethered cord, the symptomatology consists of gradual progressive paresis of the lower extremities and urinary dysfunction. The neurological picture develops during the growth of the child.

Traumatic Disorders of the Spinal Cord

Traumatic disorders of the spinal cord can occur both in infants during labor and birth, and at later ages.

In cases of breech delivery, the spinal cord can be damaged, with traumatic contusion and hematoma. The severity of the clinical picture depends on the extensiveness of the lesion(s) and there may be complete or incomplete transection of the spinal cord.

At adult age, signs of traumatic complete or incomplete transection of the spinal cord can be divided into two phases. In the first 3 weeks of the spinal cord transection, a flaccid paresis with diminished or absent reflexes and no signs of pyramidal tract involvement is present. Both the bladder and bowels are paralyzed.

After this first phase, the clinical picture changes. A spastic paresis develops with signs of pyramidal tract involvement shown in abnormal reflexes and bladder dysfunction. Sensory deficit is seen as anesthesia below a certain segmental level.

Spinal Cord Concussion/Contusion

Different spinal cord lesions can result in different clinical features. In patients with posttraumatic spinal cord concussion, clinical symptoms of complete and incomplete spinal cord transection can occur. However, in contrast to spinal cord contusion, the neurological deficit is reversible and will resolve within a couple of days.

In spinal cord contusion, the neurological deficit is a direct consequence of mechanical compression by dislocated fractured vertebra, bony fragments, herniated intervertebral discs, or vertebral subluxation. Recovery of neurological function is frequently absent or incomplete.

Myelomalacia/Syringomyelia

In some patients with spinal cord injuries, secondary sequelae can develop hours to days after the initial trauma. Due to vascular insufficiency in the anterior spinal artery, an extension of the neurological clinical picture can develop. Late consequences of a spinal cord injury can develop months or years after the initial event in the form of syringomyelia with dissociated sensory loss and trophic disturbance of the muscles.

Epidural Hematoma/Hematomyelia

Mechanical compression of the spinal cord is seen in epidural hematoma and sometimes secondary to epidural abscess. Apart from neurological deficit, pain is a major and first symptom. Pain is also prominent in posttraumatic hematomyelia. A deterioration of the neurological picture in which the initial level of the lesion rises cranially follows the initial incomplete spinal cord transection with Brown-Séquard-like syndromes.

Conus Medullaris/ Cauda Equina Syndrome

Fractures and/or disc herniations in the thoracolumbar junction give rise to lesions in the conus medullaris or cauda equina. In the conus medullaris syndrome, the neurological deficit is mainly restricted to sensory loss of the sacral segments (saddle hypoesthesia) and urinary and sexual dysfunctions. Motor deficit is rare and pyramidal tracts can be involved. Complaints of pain are not prominent.

In contrast, the posttraumatic cauda equina syndrome is often painful. Except for the lack of pyramidal tract

involvement, the same clinical picture can be present as in the conus medullaris syndrome.

Spinal Cord Compression by Neoplasm

In contrast to traumatic spinal cord lesions, tumors frequently manifest themselves as a gradually worsening spinal cord syndrome. The onset starts with gait impairment, urinary dysfunction, and sensory loss of the lower extremities, radicular or band-like sensations around the chest or abdomen, and back pain with bilateral sciatica. Extramedullary tumors, such as neurofibroma, and metastasis may present with nerve root pain. The same is true for meningeal carcinomatosis, which is often very painful with polyradicular spread.

Slow-growing tumors like meningioma are often initially silent and become clinically manifest in a late phase when they compress the spinal cord resulting in neurological deficit as a presenting symptom.

Intramedullary tumors are rare and the nature of the neurological deficit is dependent on the location of the tumor. Ependymomas are usually located at the distal end of the spinal cord and can present with back pain and sciatica followed by gradually developing neurological deficit of the lower segments of the spinal cord. In contrast, astrocytoma can affect large parts of the spinal cord.

Spinal Cord Compression of Other Origin

Nonneoplastic compression of the spinal cord can occur in epidural hematoma or in bony structures of the vertebral column.

Epidural hematoma can arise spontaneously and may be associated with the use of anticoagulants or with medical interventions such as lumbar puncture and placement of epidural leads for spinal cord stimulation.

In spondylosis and kyphoscoliosis, bony structures can compress the spinal cord. Hemangioma of the vertebral body can result in nerve root involvement and/or compression of the spinal cord. Local segmental tenderness of a vertebra is frequently present.

Cervical spondylosis can compress the spinal cord, particularly when a congenitally narrow spinal canal is present. Besides directly compressing the cord, posterior osteophytes can interfere with the blood supply of the spinal cord. The neurological picture comprises multisegmental radicular motor deficit with ill-defined sensory loss. In final stages, ataxia due to involvement of the spinocerebellar tracts and spasticity of the lower extremities can develop. Particularly in the elderly, slowly progressive gait disturbances are frequently due to cervical myelopathy in spondylosis.

At the thoracic level, both bony structures and intervertebral discs can compress the spinal cord and present themselves with the same neurological picture as cervical myelopathy. Intervertebral thoracic disc herniations are associated with painful radicular radiation in a thoracic segment.

Infectious Disorders of the Spinal Cord

Antecedental bacterial infections and vertebral osteomyelitis can be followed by the development of subdural and epidural abscesses. Pain and fever are prominent features of the clinical condition. Neurological symptoms such as nerve root compression and pyramidal signs are followed by a rapid onset of paraplegia.

In poliomyelitis, the viral infection affects the central gray matter of the anterior horn. The clinical picture therefore is dominated by marked paresis to paralysis. Sensory loss is absent. In some patients with known poliomyelitis, years after the primary infection a post-polio syndrome may develop, which is characterized by an increase in the existing motor deficit.

Other viral infections can be associated with myelitis and give rise to more or less complete spinal cord transection syndromes. Myelitis is also seen in the context of demyelinating diseases. Particularly in immune-suppressed patients, cutaneous herpes zoster can be followed by myelitis after an interval of 2 weeks.

Transverse Myelitis

Although an infectious disease mostly precedes acute or subacute transverse myelitis by 1–3 weeks, the syndrome may be due to noninfectious inflammatory conditions. Immunopathogenic etiology is likely. In a few instances, transverse myelitis follows vaccination, but in most cases no antecedent event can be traced.

Pain is not a prominent feature and the neurological deficit can vary from urinary retention and lower limb sensory and motor deficit to a complete transverse spinal lesion. The condition can affect patients of all ages and in the majority of the cases is monophasic.

Vascular Disorders of the Spinal Cord

In adulthood, only six to eight anterior and posterior segmental arteries supply the spinal cord. The largest of these, the artery of Adamkiewicz, enters the spinal canal between Th10 and L2 through the intervertebral foramen and communicates with other arteries on the surface of the spinal cord by the single anterior spinal artery and the paired posterior spinal arteries. Through the circular vasocorona, the anterior and posterior spinal arteries are mutually connected.

The extent of the neurological deficit (myelomalacia) in spinal cord ischemia depends on the duration and severity of the vascular insufficiency.

Anterior Spinal Artery Syndrome

Neurological deficit due to anterior spinal artery insufficiency may be preceded by segmental prodromal pain and band-like dysesthesia. Initially there is flaccid paraplegia and a typical dissociated sensory deficit is present, in which the entire body below the level of the lesion is involved. Touch, position sense, and vibration sense (posterior column) are preserved, whereas pain and temperature sensations are disturbed and anal sphincter function may be affected.

Posterior Spinal Artery Syndrome

Neurological deficit due to posterior spinal artery insufficiency consists of severe paraparesis accompanied by deficit of posterior column sensory modalities such as touch, position sense, and vibration sense.

Arteriovenous Malformations of the Spinal Cord and Dural Arteriovenous Fistulae

In arteriovenous (A–V) malformations of the cord, the clinical picture is characterized by a rapid onset of incomplete or complete transverse cord lesion, sometimes preceded by radicular pain. Sometimes, spinal vascular malformations can lead to subarachnoidal hemorrhages.

In the case of dural A–V fistulae, there is no hemorrhagic event and the onset of spinal cord symptoms, due to venous congestion, is more gradual, with the patient's walking progressively declining because of developing paraparesis.

Degenerative Disorders of the Spinal Cord

Anterior Horn Cells Diseases

Many diseases of the anterior horn cells are classified under spinal muscular atrophies (SMA). These often have a hereditary background and are characterized by neurological deficits restricted to the involvement of the anterior horn cells. No sensory abnormalities are present. Paresis and atrophy show a typical pattern, dependent on a specific hereditary etiology.

Spastic Spinal Paralysis

Spastic spinal paralysis is a mainly autosomal-dominant inherited disease of the spinal cord. It starts in childhood with a progressive spastic paresis of the legs. No sensory abnormalities are present. In adulthood, the spastic paraparesis may be accompanied by additional neurological deficits such as atrophy, extrapyramidal signs, ataxia, optic atrophy, and dementia.

Spinocerebellar Ataxia

In some patients, the spinal cord neurological deficits form a part of the clinical neurological picture of a hereditary disease in which both the cerebellum and other central nervous structures are also involved. Classification is made based on inheritance, age of onset, and genetic characterization. The most prominent clinical features are ataxia, gait impairment, dysarthria, and reflex abnormalities. Sensory abnormalities in some syndromes are restricted to posterior column sensory modalities.

Amyotrophic Lateral Sclerosis

Amyotrophic lateral sclerosis (ALS), also known as motor neurone disease, is characterized by a combination of neurological deficits originating from the central as well as the peripheral nervous system.

The initial symptoms are asymmetrical weakness and atrophy of the hand muscles. Complaints of muscle cramps and "restless legs" are frequently present. Bulbar muscle involvement, presenting as dysphagia, as the initial symptom is less frequent. The clinical picture is dominated by weakness, atrophy, and muscle fasciculations in combination with hyperreflexia and other signs of pyramidal tract involvement. The tongue is also involved and shows atrophy and fasciculations, resulting in slurred speech.

Metabolic Disorders of the Spinal Cord

Vitamin B_{12} deficiency can lead to spinal cord involvement. Usually, it is due to inadequate resorption based on lack of intrinsic factor due to gastric mucosal atrophy or total gastrectomy or conditions that affect the small intestine such as sprue.

The neurological deficit is characterized by sensory abnormalities of all modalities, hyporeflexia, and pyramidal tract signs. In the majority of the cases, polyneuropathy is present. Mental abnormalities such as confusional states and dementia may be present but are rare.

Miscellaneous Disorders of the Spinal Cord

Multiple Sclerosis

Multiple sclerosis (MS) is a demyelinating disease that can affect the spinal cord as well as other parts of the central

nervous system. The clinical picture frequently has a relapsing and remitting course. The neurological deficits are dependent of the various localizations of the MS lesions. Each MS relapse may give a different neurological deficit to the previous relapse and frequently result in a variable severe residual deficit after remission. The spinal neurological deficit of an MS patient cannot be reduced to a single level or anatomical localization in the central nervous system.

Hydromyelia and Syringomyelia

Hydromyelia is often asymptomatic and gives rise to symptoms when there is an expansion to the spinal cord by the formation of a cavity (syrinx). This syrinx can extend over several segments of the spinal cord. Weakness and atrophy of the arms and hands together with areflexia and segmental deficit of pain and temperature sense form the typical clinical picture. Gnostic sensory modalities such as vibration and position sense are intact. Pain and paresthesia in the arms and hands are frequently the initial symptoms. Due to the progressive character of the disease, the volume increase of the syrinx can lead to involvement of other neural structures of the spinal cord such as the pyramidal tracts and the spinothalamic tracts.

Involvement of the anterolateral descending tracts can lead to autonomic disturbances like trophic skin abnormalities, sweat secretion disturbances, and orthostatic hypotension.

Decompression Myelopathy

In caisson disease, painful dysesthesia and paraparesis or Brown-Séquard syndrome may be present due to air embolism of the spinal arteries.

Radiation-Induced Myelopathy

In radiation therapy of cancer patients, signs of myelopathy can occur with a short latency after the treatment. Generally, such myelopathy has a good prognosis. In contrast, other patients may develop myelopathy months or years after the radiotherapy, which has a poor prognosis.

References

1. Hijdra A, Koudstaal P J, Roos R A C (eds) (1994) Neurologie. Utrecht Bunge III
2. Donaghy M (ed) (2001) Brain's Diseases of the Nervous System. 11th edn. Oxford University Press, Oxford
3. Vinken PJ, Bruyn GW, Biemond A (eds) (1975) Localisation in clinical neurology. In: Handbook of Clinical Neurology 2. American Elsevier Publishing Company Inc., New York
4. Mumentaler M, Mattle H (2004) Neurology. 4th and enlarged edn. Georg Thieme Verlag, Stuttgart, New York

Spinal Dural Arteriovenous Fistula (SDAVF)

Acquired arteriovenous fistulas located within the dura of the spinal cord.

▶Vascular Disease, Spine

Spinal Dysraphism—Spina Bifida

▶Congenital Malformations, Spine and Spinal Cord

Spinal Manipulation

Physical therapy that aims to manipulate the position of spinal segments.

▶Conservative Therapy for Lumbosacral Radicular Syndrome

Spinal Narrowing

▶Stenosis, Spinal

Spinal Nerve Roots, Clinical Syndromes

Wilco Peul
Medisch Centrum Haaglanden, Netherlands
w.peul@mchaaglanden.nl

Synonyms

Brachialgia; Neuralgia; Radicular syndrome; Radiculopathy; Sciatica

Definition

The clinical presentation of radiculopathy is characterised by pain radiating into the dermatome of a spinal nerve root. Occasionally, more than one root is involved. Pain

may be accompanied by spinal muscle spasm, reflex abnormalities motor and sensory disturbances. Pain may be aggravated by various tests applying tension to the nerve root. Most frequently, these symptoms are caused by disc herniations. Differential diagnosis includes stenosis of the spinal or root canal, infection, multiple sclerosis, autoimmune or metabolic neuropathy and tumours. In this chapter, disc-related compression is emphasised as a cause. For obvious reasons, the spine will be divided in a cervical, thoracic and lumbosacral area.

Pathology

During aging, the spine is subjected to a degenerative cascade deforming the architecture of vertebrae, vertebral articulations and discs. This cascade includes biochemical desiccation changes of nuclear material, physical narrowing of the intervertebral disc space, development of degenerative spondylotic osteophyte formation of the vertebral end plates and in the final stage, eventual loss of the normal intervertebral motion segment. Weakness of the annulus fibrosus causes nuclear material of the disc to protrude or extrude in a posterior direction, sometimes giving rise to nerve root compression near or in the exit foramina of the spinal canal or, when medially located, to devastating compromise of neural structures in the spinal canal: spinal cord or cauda equina. These disc herniations may consist of soft nuclear material, but may also comprise fragments of annulus fibrosus, while in advanced and chronic stages of the degenerative process these benign herniations can evolve to calcified space–occupying lesions. In exceptional cases, in western and more frequently in Asiatic society, calcification of the posterior longitudinal ligament occurs without disc herniation.

Until recently, complaints in radiculopathy were regarded as the sole results of nerve root compressive forces. However, magnetic resonance imaging (MRI) and histopathology studies indicate a biochemical cause of pain generation (1), which is disputed by others. As a rule, disc herniations are not caused by trauma, which is generally the explanation of the layman confronted with the disease. A trauma may aggravate nerve root compression by an already existing disc herniation, giving rise to complaints.

Clinical Presentation

A radiculopathy is presented by a variety of signs and symptoms, depending on the degree of compression, unknown neurogenic changes and site of compression. The cervical, thoracic and lumbar spines are distinct entities.

Cervical Spine

The annual incidence of cervical disc herniations is estimated at 5.5 per 100.000 persons, sometimes higher for the male sex, occurring most frequently between the ages of 45 and 54 years. A significant rise in incidence is attributed to smoking, frequent lifting and diving from a board (2). A patient with a radicular syndrome, caused by a soft cervical disc herniation or a calcified osteophyte, may complain of central–axial neck pain and arm pain (brachialgia). The pain in the arm must however be the predominant symptom, and is typically distributed in a dermatomal fashion according to the root compressed. Such radiculopathy complaints are commonly described as sharp, lancinating pain precipitated or aggravated by postural or Valsalva maneuvers. The pain is intense and occasionally accompanied by reflex disturbance, motor- and/or sensory deficit. Straight raising of the arm can provoke the radicular pain. Another test is extension and lateroflexion of the cervical spine, which compresses the nerve root in the neuroforamen. Sensitivity and specificity of both these tests are however low.

Symptoms vary depending on the anatomic location of the displaced disc material. Laterally, displaced herniated nucleus pulposus material at the lower cervical disc spaces is expressed most often as radiating upper extremity pain as described above. For example, radicular pain in the thumb and index finger with numbness in the same area, decrease of the biceps reflex and biceps muscle weakness is typically caused by a disc herniation at the disc space between the fifth and sixth vertebra with compression of the C6 nerve root whereas pain and numbness in the middle fingers, decrease of triceps reflex and triceps muscle weakness are caused by compression of the C7 root one level lower between the sixth and seventh vertebrae. These two disc levels are the most frequent locations of disc herniations, followed by the adjacent discs and, very seldom, the levels above the third cervical disc. The symptom pattern of laterally displaced soft-herniated material in the upper cervical spine is expressed as neck or axial pain or even suboccipital pain when the second cervical nerve root is involved.

When the disc herniation is not located laterally but in a medial location, or laterally with a large component in the central region, the spinal cord is compromised and signs of myelopathy occur, varying from mild sensory disturbances, to disturbances of gait and micturition to complete tetraplegia.

Most disc herniations in the cervical spine probably resolve naturally in three months. Exact information is missing due to the lack of scientific evidence. Differential diagnosis includes cervical spondylosis which does have the same therapeutic options, and vertebral body dislocations caused by trauma or severe degenerations of the ligamentous structures.

Thoracic Spine

The incidence of radiculopathy of the thoracic spine has never been estimated in an epidemiological study. The main reason is the very low incidence compared to cervical and lumbar pathology and the fact that objectivation of symptoms is difficult. The low incidence appears to be related to the lack of mobility of this part of the spine. Lancinating pain in the area served by a thoracic nerve root may be accompanied by sensory loss in a very small dermatome, overlapped by an adjacent dermatome. Muscle weakness or reflex abnormalities cannot be identified. Furthermore, concussion or fracture of the ribs frequently gives rise to comparable complaints of intercostal neuralgia. Thoracic disc herniations are clinically most often discovered in a late stage when compression of the spinal cord gives rise to gait abnormalities and sensory disturbances.

Lumbar Spine

Sciatica or lumbosacral radicular syndrome (LSRS) is characterised by pain radiating in the dermatome of a lumbar or sacral spinal nerve root. Occasionally, more than one root is involved. Pain may be accompanied by lumbar spinal fixation, reflex abnormalities, motor and/or sensory disturbances. In the vast majority of cases, LSRS is the result of a herniated disc. Measured incidence rates vary. In the United States, an annual incidence of 5 per 1,000 persons is estimated. Most frequently, disc herniations occur between the fourth and fifth lumbar vertebrae, or fifth lumbar and first sacral vertebra. Because of the impact of the condition on daily functioning, indirect costs to society due to loss of production are high.

As described for the cervical spine, pain is sharp and lancinating and aggravated by movement or loading of the lumbar spine. Provoking the irradiating pain by lifting the straight leg in the supine patient is a classic sign of nerve root compression. The dermatome described as painful directs the clinician to the nerve root involved. Radiating pain in the calf, heel and sole and lateral border of foot, accompanied by an Achilles tendon reflex disturbance or weakness of the gastrocnemius muscles, is caused by compression of first sacral nerve root. Radiation to the medial part of the foot and big toe combined with weakness of the dorsiflexors of the foot is caused by compression of the fifth lumbar nerve root. A disturbance of the knee reflex is combined with pain in an area distributed by the fourth lumbar nerve root and quadriceps weakness when this root is involved.

Doubts concerning the validity of these neurologic signs are however present. Studies have shown that disc herniations can cause a variety of dermatomal disturbances not typical for the classical radicular syndrome. The most important cause for this discrepancy is the varying appearance of the lumbar disc herniation. A frequent location of an annulus defect is the mediolateral part of the disc causing a disc to rupture into the subarticular (3) area of the spinal canal and compressing the expected exiting nerve root. In case a median or paramedian defect in the annulus occurs, a more medially located nerve root is involved which exits the spinal canal one level lower than the disc involved. Laterally located disc herniations, inside or outside the foramen, compromise roots which have exited the dural sac one level higher than the disc pathology. Very rarely severe neurological problems can occur as a result of compression of the cauda equina. These are usually caused by large central disc herniations compressing nerve roots in the dural sac.

As stated for cervical radiculopathies, the natural course of sciatica is favourable, resulting in recovery of 70% of patients in the first 6–8 weeks. The clinical syndrome of sciatica may be mimicked by diseases of the nerve roots such as Lyme's polyradiculoneuropathy, which is a very distinct neurological entity with serious deficits in muscle function if not treated.

Imaging

The three parts of the spine have different biomechanical properties, and the indications for imaging and the type of imaging required, may also differ. The general rule is that imaging of the spine is necessary to examine the anatomical relationship between a disc herniation and the nerve root compression, when the natural course has not given rise to recovery of complaints and surgery is contemplated. However, the classical nerve root compression syndrome is not always clearly present in patients with a disc herniation and, MRI studies in volunteers have shown that many asymptomatic individuals harbour disc herniations, with root compression but without any clinical consequences. In contrast, even when clinical signs and symptoms clearly indicating nerve root compression are present, imaging studies of the spine do not show a disc herniation in all cases (4).

The first choice for diagnostic imaging in suspected nerve root pathology is generally considered to be MRI, with computed tomography (CT) considered as second choice. This in spite of the lack of a systematic study clearly demonstrates that MRI is superior in diagnosing a simple disc herniation. In the cervical and especially the thoracic spine, MRI has the drawback that calcification within a disc or disc lesion is not well demonstrated. In these cases, a thin slice CT study can be useful. Plain X-rays are necessary to identify transitional vertebrae before spinal surgery.

Other than delineating the pathology, MRI has not been considered to have great prognostic value so far. However, recent studies have shown that sequestrations of the disc have a more favourable natural history than previously supposed, thus supporting a trend towards a conservative approach in these cases, where in the past surgery was the rule (5). The significance of these findings is currently a subject of investigation in randomized trials.

Diagnosis

Radiological confirmation of disc-related nerve root compression matching the clinical picture completes the diagnosis. If a discrepancy exists between MRI findings and clinical suspicion of nerve root compression, electrophysiological studies can help in diagnosis and treatment selection.

Bibliography

1. Takada T, Nishida K, Doita M et al (2004) Interleukin-6 production is upregulated by interaction between disc tissue and macrophages. Spine 29(10):1089–1092
2. Kelsey JL, Githens PB, Walter SD et al (1984) An epidemiological study of acute prolapsed cervical intervertebral disc. J Bone Joint Surg Am 66(6):907–914
3. Brant-Zawadzki MN, Jensen MC, Obuchowski N et al (1995) Interobserver and intraobserver variability in interpretation of lumbar disc abnormalities: a comparison of two nomenclatures. Spine 20(11):1257–1264
4. Vroomen PC, de Krom MC, Wilmink JT et al (2002) Diagnostic value of history and physical examination in patients suspected of lumbosacral nerve root compression. J Neurol Neurosurg Psychiat 72(5):630–634
5. Ito T, Takano Y, Yuasa N (2001) Types of lumbar herniated disc and clinical course. Spine 26(6):648–651

Spindle Cell

A spindle-shaped cell, as those in the deeper layers of the cerebral cortex.

▶Rhabdomyosarcoma

Spine and Spinal Cord

P. A. M. Hofman, R. J. Nijenhuis, W. H. Backes, J. T. Wilmink
Department of Radiology, University Hospital Maastricht, The Netherlands
pho@rdia.azm.nl

Introduction

The spine is the most frequently imaged part of the human body, even though shortcomings of the various imaging methods are well known. Conventional X-ray images possess a low sensitivity for demonstrating soft tissue pathology, and even bony lesions such as vertebral metastases are only detected at a very late stage. On the other hand, the clinical significance of many presumed pathologic features seen on spinal films is often unclear. This is even more truer for the abundant and frequently confusing detail seen in CT and especially ▶magnetic resonance imaging (MRI) studies.

The high prevalence of a specific backache and lack of understanding of the aetiology of this complaint seems likely to perpetuate reliance in imaging studies which are often performed apparently for the purpose of reassurance.

Conventional X-Ray Imaging and X-Ray Computed Tomography

Plain films of the spine are a quick, simple and inexpensive imaging modality. Spinal curves can be assessed in scoliosis, and the anatomy of individual vertebrae can be defined although superimposition of anatomical structures, as always in 2D projection imaging, is a problem. Plain films are especially suitable for imaging bony anatomy and relationships, but lack of soft tissue resolution is a major drawback. This was first alleviated by injection of contrast media in various soft tissue structures or compartments: the intradural CSF space (myelography), the nucleus pulposus (▶discography), the epidural space (peridurography) or epidural veins (phlebography). The latter two techniques are no longer practised.

At present, plain film spinal imaging is ordered most frequently in patients presenting with low back pain and cervical pain. The diagnostic yield of such studies is generally held to be very limited unless so-called red flags (indicators for specific disease conditions such as neoplasm, disc herniation or infectious disease, for instance) are present. In such cases alternative techniques with higher sensitivity (CT, MRI) are preferable. The so-called degenerative features such as disc space narrowing, spondylosis and spondylarthrosis are frequently seen in symptomatic as well as asymptomatic individuals (Fig. 1). Spondylolysis and spondylolisthesis can be well demonstrated. Plain films are still usually performed as the first examination in spinal trauma, and permit detection and classification of injuries associated with malalignment of vertebrae due to wedging of vertebral body, facet fracture and/or interlocking. More subtle fractures without displacement are easily missed, as well as most of the soft tissue injuries.

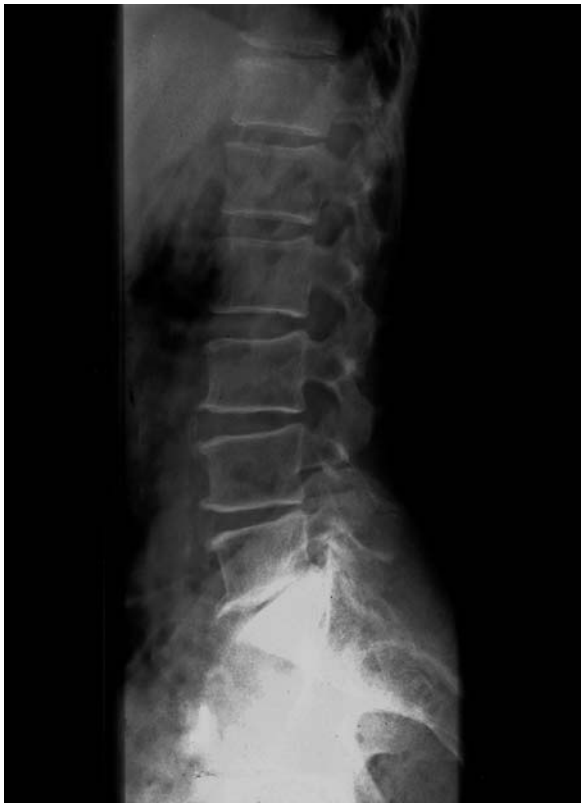

Spine and Spinal Cord. Figure 1 ►**Plain X-ray film of lumbosacral spine in lateral projection, with degenerative changes: disc space narrowing at L4–5 and especially L5–S1 levels; sclerosis of vertebral endplates; bony spurring or osteophyte formation at ventral corners of vertebral bodies.**

►Computed tomography (CT) has revolutionised medical imaging since its introduction in the 1970s. Three improvements were combined: detection of smaller differences in X-ray attenuation by using more sensitive scintillation detectors instead of an X-ray film, acquisition of sectional images by the use of an X-ray tube rotating around the patient in the axial plane and image reconstruction by a computer algorithm permitting selection of window and level settings appropriate for viewing bony and soft tissue structures. This made it possible to appreciate axial spinal anatomic relationships not previously visualised. The improved contrast resolution of CT permits non-invasive imaging of disc herniations and other abnormal and normal soft tissue features. A much better insight was obtained in the morphology and classification of spinal stenosis (Fig. 2a–c). A drawback is the lack of visualisation of intradural details such as the spinal cord and nerve roots; for this CT myelography is necessary. Sensitivity for vertebral pathology such as metastasis and fracture is greater than that of plain films, and rapid spiral CT scanning with multiplanar reformatting is increasingly becoming the first imaging procedure in spinal trauma.

Myelography and Computed Tomographic Myelography

In order to distinguish intradural anatomy and pathology, an iodinated radiologic contrast media can be injected into the spinal subarachnoid space, after which myelographic plain films and/or CT sections are acquired. This provides high-resolution images of the contours of the spinal dural sac and the spinal cord within it, and also of the individual fibres of the cauda equina and the root sleeves (Figs 3a, b). Conventional myelography provides a better longitudinal overview, and CT myelography a more detailed image, especially when the intradural contrast medium has become diluted, as can easily occur.

The main application of this technique is in the detection of intraspinal space occupying lesions. These can be intradural (neoplasm or cyst formation within the cord; extra-medullary meningioma or nerve root tumours), but can also be located outside the dural sac, indenting the dural contours or compressing the root sleeve (disc herniation, vertebral neoplasm or extradural haematoma). Cord atrophy or transection can also be well demonstrated, but spinal cord lesions without mass effect (cord infarct, multiple sclerosis) can only be visualised by MRI.

Discography and Computed Tomographic Discography

Discography

In this examination a needle is placed with the tip within the nucleus pulposus of an intervertebral disc in a patient with low back pain or referred pain, and a contrast medium is injected. Radial fissures of varying extent in the annulus fibrosus can be demonstrated, and also herniation of the nucleus pulposus through the annulus. Such disc protrusions and extrusions can be better demonstrated by CT or MRI, however the present diagnostic role of discography is in pain provocation by the increase in intradiscal pressure produced during the injection. If contrast injection into the affected disc reproduces the familiar pain of the patient, and injections into the adjacent discs do not, then this finding, in combination with radial fissuring extending to the outer one-third of the annulus fibrosus, is considered evidence of a discogenic origin of the pain.

Magnetic Resonance Imaging (Fig. 4)

MRI is a sectional imaging technique like CT, but makes use of a different imaging principle. Instead of image

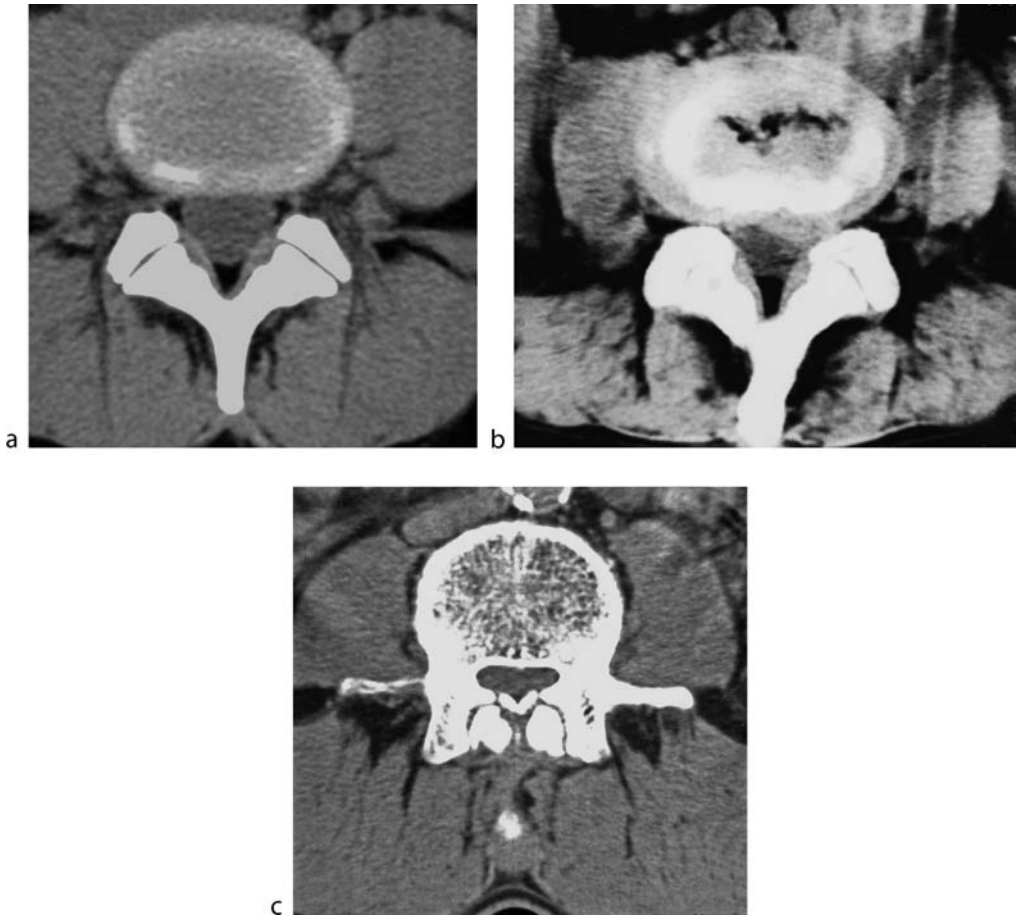

Spine and Spinal Cord. Figure 2 CT sections through lower lumbar spine. (a) Normal L4–5 level showing normal disc, facets with covering ligaments, dural sac containing CSF and cauda equina (note that intradural nerve roots cannot be seen). (b) Left herniated disc protruding into spinal canal and compressing dural sac. This case also demonstrates degenerative changes in disc (so-called vacuum phenomenon with air density) and some hypertrophy of facets and flaval ligaments. (c) Developmental stenosis with reduced anteroposterior diameter of bony spinal canal.

contrast being derived from differences in X-ray attenuation due to variations in electron density within various anatomical structures, in MRI the protons of the body are induced to act as radiofrequency (RF) transmitters by being placed inside a magnetic field and subjected to RF energy beamed in from outside the body. This electromagnetic resonance is analogous to the resonance of a tuning fork when exposed to sound of the appropriate frequency. The RF signals from the protons can be manipulated or 'weighted' to selectively amplify signal intensity of various tissues and structures within the body, and are spatially encoded to produce an image. An MR image in which contrast is dependent on differences in longitudinal magnetic relaxation values between various tissues, is called T1 weighted. When differences in transverse magnetic relaxation predominate, the image is called T2 weighted. MR imaging has significant advantages over CT: soft tissue contrast resolution is better and there are no artefacts due to high-density skeletal structures. Subtle changes in shape and composition of the spinal cord can be demonstrated by MRI, and the intradural nerve roots can be imaged without intradural contrast injection (MR myelography). Intravenous injection of MR contrast media improves detection and classification of intramedullary pathology, as well as spinal infectious, neoplastic and post-operative conditions. MR images can be acquired in any desired plane, and are superior to sagittal or coronal reformatted CT images of the spine, especially of the soft tissues.

The largest single indication for spinal MR imaging is presently in degenerative spinal disease, especially disc herniation. After spinal injury MRI is useful in assessing damage to the spinal cord and also in detecting spinal ligamentous lesions which may result in significant instability. Metastases to the spine as well as primary vertebral tumours can be diagnosed accurately as well

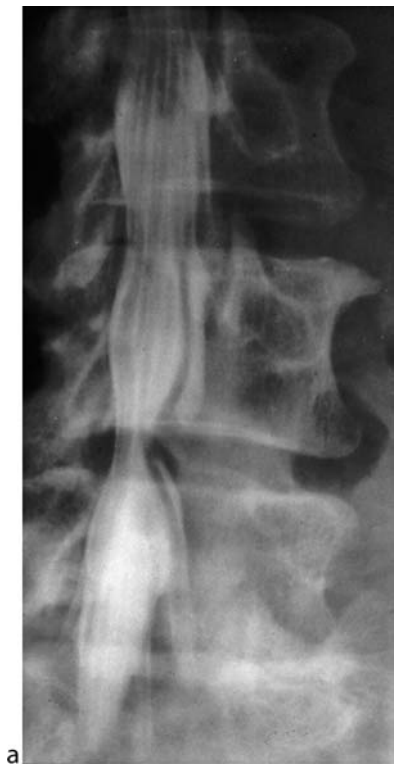

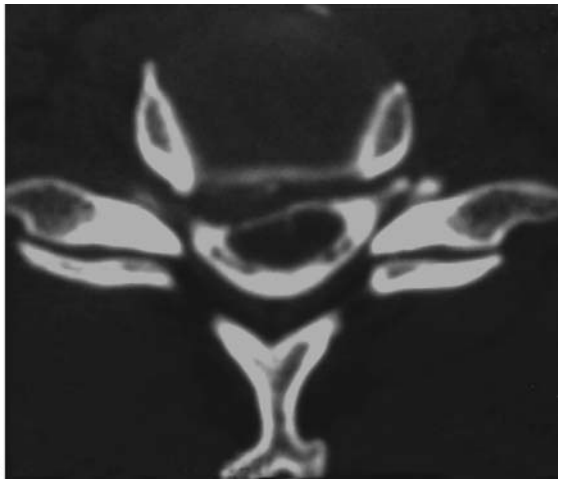

Spine and Spinal Cord. Figure 3 Myelography and CT myelography. (a) Lumbar myelogram (syn. radiculogram, caudogram) showing right L5 root compression by herniated L4–5 disc. The herniation itself is not seen. (b) Cervical CT myelogram showing indentation of dural sac by herniated cervical disc. Spinal cord is rotated and slightly flattened and entrance to intervertebral foramen compromised.

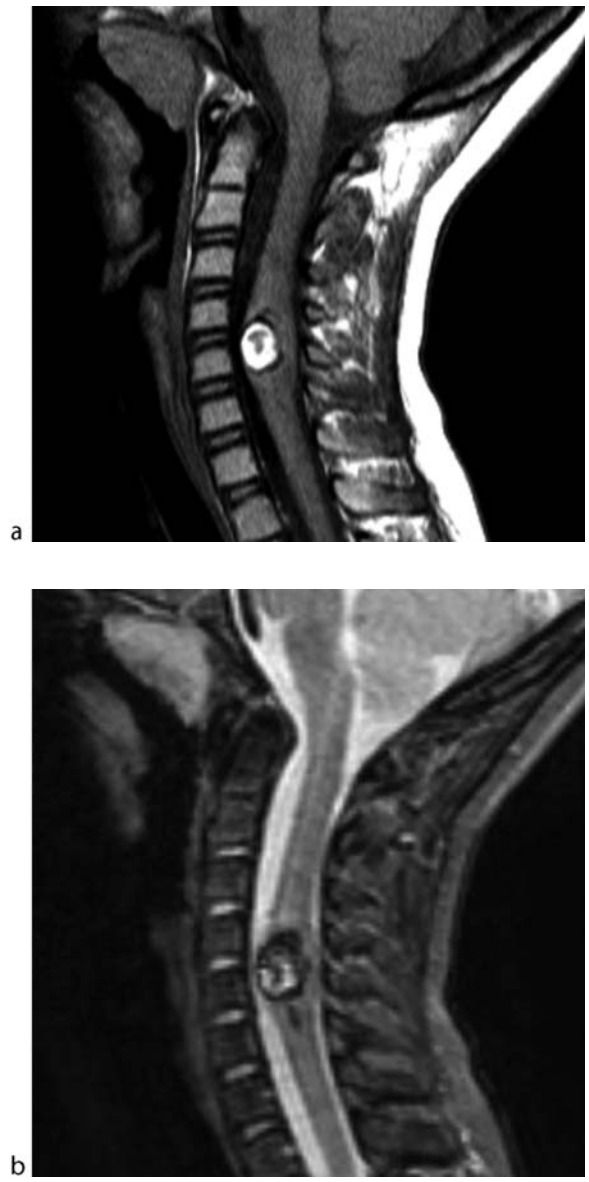

Spine and Spinal Cord. Figure 4 MR imaging of cavernoma in the cervical spinal cord. (a) T1 weighted sagittal image showing high-signal intramedullary mass lesion with thin hypo-intense rim. Note high signal from subcutaneous fat and fatty bone marrow, low signal from CSF. (b) T2* weighted gradient echo image. Note that subcutaneous fat now has intermediate-to-dark signal, CSF and nucleus pulposus have bright water signal. Signal loss at rim of lesion is accentuated in this sequence due to susceptibility effect caused by presence of haemosiderin. Bright signal within lesion is due to presence of methemoglobin.

as tumours of the spinal cord and nerve roots. MRI is used for detecting spinal cord lesions in patients with multiple sclerosis and spinal infectious disease such as spondylodiscitis.

Activation of spinal cord neurons can be achieved by motor tasks and sensory input, and registered in the same way as in the brain (spinal fMRI). Diffusion tensor imaging of the spinal cord (MR tractography) is in development.

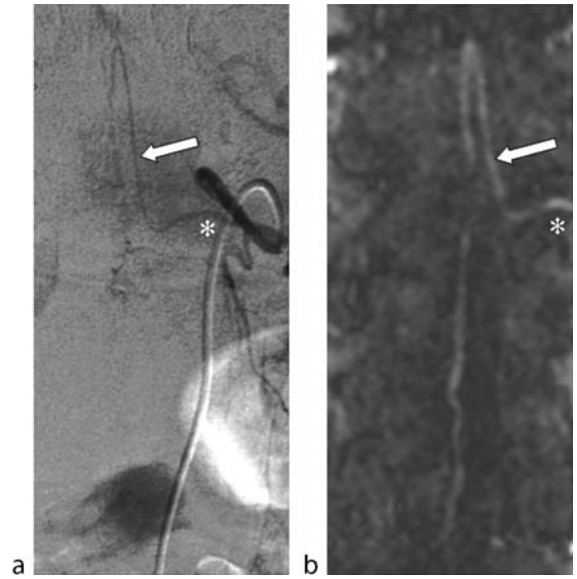

Spine and Spinal Cord. Figure 5 Spinal cord angiography. (a) Coronal intra-arterial digital subtraction angiographic (DSA) image of the great anterior radiculomedullary artery, or Adamkiewicz artery. The supplying segmental artery (asterisk) and the Adamkiewicz artery (large white arrow) are shown. (b) Multiplanar reformatted magnetic resonance angiographic (MRA) image in same case presenting good depiction of the supplying segmental artery (asterisk) and the Adamkiewicz artery (large white arrow).

Spinal Cord Angiography (Fig. 5)

Catheter digital subtraction ►angiography (DSA) is at present the reference modality for diagnostic imaging of the spinal cord vasculature. In this examination a catheter is positioned with its tip in the orifice of a segmental artery originating from the aorta, and an iodinated contrast agent is injected. Since all segmental arteries must be selectively examined, a full spinal DSA study can be very time-consuming as well as carrying a risk of ischaemic complications involving the spinal cord. In addition patients are exposed to relatively high radiation doses. DSA does however offer the possibility to combine diagnosis and endovascular therapy.

Magnetic resonance angiography (MRA) has recently emerged as a non-invasive potential alternative imaging modality to intra-arterial DSA. Several flow-weighted MRA techniques are available, but the most promising method employs an intravenous injection of a gadolinium contrast medium combined with a rapid MRI acquisition. Centric ordered K-space filling provides an effective temporal resolution of approximately 10 sec in a 40-sec acquisition. The arrival of the intravenous gadolinium contrast bolus in the spinal arteries is carefully matched to the start of the MRA acquisition sequence. This permits imaging of an arterial phase followed 40 sec later by a mixed arteriovenous image, thus allowing distinction between arteries and veins. After acquisition the 3D datasets are post-processed using maximum intensity projections and multi-planar reformats.

The most common indication to perform spinal cord angiography is the localisation, classification, and follow-up of spinal cord vascular malformations, such as spinal cord arteriovenous malformations and spinal cord arteriovenous fistulas. Another indication is the pre-operative localisation of the major anterior radiculomedullary feeder, the Adamkiewicz artery prior to surgical procedures where the spinal cord blood supply may be at risk, e.g. vertebroplasty, thoraco-abdominal aortic aneurysm repair and thoracoscopic discectomy).

Bibliography

1. Donovan Post MJ (1984) Computed Tomography of the Spine. Williams & Wilkins, Baltimore/London ISBN 0-683-06951-9
2. Manelfe C (ed) (1992) Imaging of the Spine and Spinal Cord. Raven Press, New York, ISBN 0-88167-863-5
3. Ross JS, Brant-Zawadski M, Moore KR et al (2004) Diagnostic Imaging: Spine. Amirsys Inc., ISBN 0-8089-2315-3
4. Lasjaunias P, Berenstein A, Ter Brugge K (2001) Surgical neuroangiography. In: Functional Vascular Anatomy of Brain, Spinal Cord and Spine. 2nd edn. Springer-Verlag, Berlin Heidelberg New York, ISBN 3-540-41204-2
5. Nijenhuis RJ, Leiner T, Cornips EM et al (2004) Spinal cord feeding arteries at MR angiography for thoracoscopic spinal surgery: feasibility study and implications for surgical approach. Radiology 233(2):541–547

Spine, Inflammatory Conditions

R. E. Weijers
Department of Radiology,
University Hospital Maastricht, Maastricht,
The Netherlands
rwe@rdia.azm.nl

Definition

Inflammatory diseases of the spine can be divided into rheumatoid arthritis (RA) and the spondylarthropathies (SpAs). SpAs is the term used to describe a group of diseases that share clinical and genetic characteristics that differentiate them from RA. The most common member of this group is ankylosing spondylitis (AS), which is considered the prototype of the SpAs. Other arthropathies included in this group are psoriatic arthritis, reactive

arthritis (ReA, formerly Reiter's disease), inflammatory bowel disease-related arthritis, and undifferentiated SpA. Although classification systems are available, categorization of individual patients remains difficult because of the overlap of symptoms and radiological manifestations between the subgroups. Besides manifestations of these diseases in the axial skeleton, peripheral arthritis can occur, predominantly of the lower limbs. In contrast, RA predominantly affects the peripheral joints and, to a lesser degree, the spine, especially in the cervical region.

Pathology/Histopathology

Of all SpAs, the pathogenesis of AS has been studied most. Nonetheless, the pathogenesis of this condition is still poorly understood. Immune-mediated mechanisms involving human leukocyte antigen, inflammatory cellular infiltrates, cytokines, and genetic and environmental factors are said to have a key role. The most recent hypothesis states that a key trigger for the disease is the intracellular proteolysis of (intestinal) bacterial peptides and self-proteins producing peptides that are present on the cell surface. These peptides lead to activation of cross-reactive T-cells, provoking an inflammatory response. Primary sites of inflammation are the fibrocartilage of the enthesis (the insertion of ligament, tendon, or fascia into the bone) and of cartilage at the interface with bone. Clinically, this process becomes apparent as an enthesitis, mainly of the vertebral ligaments, and as a sacroiliitis. Eventually the inflammatory process may lead to ossification and ankylosis of these structures (the "bamboo spine" seen in AS).

SpAs shows a strong association with the class I molecule HLA-B27. In AS, this association is strongest, present in 90% of cases, compared with 7% in the general population.

The primary site of inflammation in RA is synovial tissue. The synovial joints of the peripheral skeleton are especially clinically affected—the small joints of the hand and feet, and much less frequently and less severely, the synovial tissues of the cervical spine.

Clinical Presentation

The most common and characteristic clinical symptom of spinal manifestation of SpA is chronic inflammatory back pain. This type of back pain is most often felt over the sacroiliac region and deep in the gluteal area and is insidious in onset. Remarkably, the pain tends to worsen after prolonged periods of rest and improves on exercise. In some cases, bone tenderness may be the primary complaint. Important extraskeletal clinical manifestations of SpAs are inflammatory bowel disease, acute anterior uveitis, conjunctivitis, dactylitis, psoriasis, carditis, and genital inflammation. These symptoms may occur early in the course of the disease. On physical examination, a loss of spinal mobility, reduced expansion of the chest, and pain in the sacroiliac joints on pressure or movement can be found. Due to muscle spasm, the limited motion can be disproportional to the degree of ankylosis. Except for the HLA-B27 gene, laboratory tests are not diagnostic. Even C-reactive protein (CRP) or erythrocyte sedimentation rate (ESR) is elevated in only 50–70% of the patients with active disease.

Diagnostic for AS is the presence of sacroiliitis, as detected by any imaging modality, in the presence of clinical manifestations. A combination of the presence of inflammatory back pain and at least two other typical features of SpA (such as enthesitis and uveitis) is highly predictive for early AS. However, the diagnosis of AS is difficult before the occurrence of irreversible skeletal damage, and several years may pass between the onset of symptoms and definitive diagnosis. As emerging biological therapies (the antitumor necrosis factor-alpha) may favorably alter the disease process, it has become more important to diagnose the early stages of the disease. With this, the role of imaging in early detection is becoming increasingly important.

In patients with RA, radiological involvement of the spine is a frequent finding (20–70%), but the severity of the disease is rather mild. Spinal involvement is usually limited to the cervical region. The clinical findings here are mainly pain and stiffness of the cervical spine. Symptoms do not seem to be correlated to radiological abnormalities except when neurological deficit is present in severe spinal deformation.

Imaging

Imaging of the sacroiliac joints in SpAs can distinguish inflammatory and structural changes. Inflammatory changes are considered to be reversible whereas structural changes are not. Bone marrow edema at the cartilage/bone interphase, associated with osteitis, is an inflammatory change. Magnetic resonance imaging (MRI) can reliably visualize this edema and therefore is said to be the most sensitive imaging modality to detect early SpA. The earliest structural changes of the sacroiliac joints are blurring of the cortical margins of the subchondral bone, erosions, and sclerosis. Plain radiographs can also visualize these changes, but many years may pass before such changes in the sacroiliac joints become evident on plain radiographs. Computed tomography (CT) is said to detect the lesions earlier and more consistently. With progression of the erosive disease, the joint space may

appear wider. Eventually, ankylosis will obliterate the joint. CT, and especially MRI, are not routinely used, but rather are used when the plain radiographs are negative. In AS, the abnormalities are usually symmetrically distributed. Psoriatic arthritis and ReA present involvement of the sacroiliac joints in a bilateral and asymmetrical fashion, and erosions and signs of bony repair appear to be much more extensive than those seen in AS. Ankylosis does not occur until late in the disease process.

RA causes symmetrical uniform narrowing of the sacroiliac joints with very little reparative bone reaction.

Plain radiographs of the spine in SpAs show various types of lesions that may occur at the discovertebral junctions. In AS, osteitis causes destructive "Romanus" lesions at the anterior corners of vertebral bodies, with reactive bone formation creating a squared appearance of the vertebrae and reactive sclerosis producing "shiny corners" to the vertebral bodies. End-plate erosions can progress to destruction of the entire discovertebral junction in advanced cases. Syndesmophytes are formed by ossification of the annulus fibrosus and can bridge the disc space.

As with imaging of the sacroiliac joint, CT and MRI are said to more sensitive, especially in the early SpAs.

In psoriatic arthritis, paravertebral ossifications occur in the thoracolumbar transitional area, usually unilateral or asymmetrical, growing in bulk and eventually merging with the spine. These ossifications (parasyndesmophytes) are bulkier than syndesmophytes. The discovertebral changes and ankylosis that are typically seen in ankylosing spondylitis are infrequent in psoriatic arthritis.

In ReA, as in psoriatic arthritis, plain radiographs show asymmetric paravertebral ossification in the thoracolumbar transition, occasionally with syndesmophytes and ankylosis of the facets resembling ankylosing spondylitis. The disease may also involve the cervical spine.

The most serious complication encountered in AS is spinal fracture. Because of the changed biomechanics of the rigid, fragile spine, minor trauma may lead to fracture. These fractures can have unusual configurations that cause them to go undetected unless carefully searched for. Neurological deficits are relatively common.

In RA, spinal imaging can demonstrate changes that are due to the inflamed synovium. Patients with RA and abnormal cervical spine radiographs have a higher prevalence of rheumatoid factor and advanced erosions on hand radiographs compared with those with normal spine radiographs. The severity of cervical spine changes is related to the duration of disease (>5 years). Spinal involvement occurs late in the course of the disease and frequently goes unobserved because of the extensive involvement of the peripheral joints. The most common abnormality is erosion of the odontoid process (47%), followed by atlanto-axial dislocation and apophyseal joint involvement (24%). Atlanto-axial dislocation is present when the distance between the anterior arch of C1 and the odontoid process of C2 exceeds 2.5 mm and increases when the cervical spine moves from extension (lordosis) to flexion (kyphosis).

CT can be used to demonstrate destructive bony changes and ligamentous calcifications and may also allow evaluation of synovial hypertrophy (pannus formation) in RA.

MRI is best for pointing out soft-tissue changes. Periodontal pannus is the most frequent finding. Pannus is homogeneous on T1-weighted images and shows contrast enhancement and is usually hyperintense on T2-weighted images; in cases of predominantly fibrous tissue, it is hypointense. Odontoid erosions are less frequently observed by MRI. They may show a heterogeneous MRI signal, and sometimes complete destruction.

Spinal cord involvement may occur as a result of severe anterior C1–C2 subluxation, atlanto-axial settling, or compression by retrodental pannus. T2 or T2-weighted images well demonstrate cord deformation and intramedullary signal increase (myelomalacia). MRI studies in cervical flexion and extension are more difficult to perform than dynamic plain X-ray films and do not provide more information.

MRI may also demonstrate spinal canal narrowing, with cord compression occurring in the lower cervical region in RA.

In RA, the thoracic and lumbar spine are infrequently involved. This helps to distinguish RA from ankylosing spondylitis, psoriatic arthritis, and Reiter's syndrome. However, cervical destructive changes with atlanto-axial subluxation may occur in all these conditions.

Bibliography

1. Manelfe C (ed) (1992) Imaging of the Spine and Spinal Cord. Raven Press, New York
2. (2002) Annals of Rheumatic Disease 61, Supplement III
3. Resnick D (1995) Diagnosis of Bone and Joint Disorders. 3rd edn. WB Saunders, Philadelphia
4. Brower AC (1988) Arthritis in Black and White. WB Saunders, Philadelphia

Spine, Intramedullary Tumors

Danielle Baleriaux, Neslïhan Gültaşli
Clinique de Neuroradiologie, Hôpital Erasme, Université Libre de Bruxelles, Brussels, Belgium
dbaleri@ulb.ac.be
ngultasli@yahoo.com

Definitions

The spinal cord is a small but extremely important element of the central nervous system (►CNS) and is especially well protected by the surrounding cerebrospinal fluid (CSF), the meningeal envelopes, and the bony spine. Although the anatomy is well known for a long time, the radiological approach has remained a sensitive subject and was difficult before the advent of magnetic resonance imaging (MRI). Major progress has been made in this field thanks to MRI (1, 2, 3).

Tumors located within the spinal cord are rare: they account for 4% of all CNS tumors. The vast majority of ►intramedullary tumors are glial tumors: the most frequently encountered neoplasms in adults are ependymoma (40%) and astrocytoma (28%). In children, however, astrocytomas are by far the most frequent tumors (90%) and ependymomas occur only in children affected by neurofibromatosis. Hemangioblastomas represent 14% of all spinal cord tumors.

Less frequent tumors include intramedullary metastasis, lymphoma, epidermoid cyst, lipoma, ganglioglioma, oligodendroglioma, paraganglioma, intramedullary schwannoma, and teratoma (4, 5). Cavernomas represent 8% of intramedullary mass lesions; however, they are not true neoplasms but vascular malformations.

Generally, spinal cord tumors enlarge the spinal cord. Besides a solid nodule, associated cysts may often involve large segments of the cord and should be distinguished from intratumoral cysts.

Histopathology/Anatomy

Only the most commonly found intramedullary tumors are described hereafter.

Astrocytomas are often large lesions with ill-defined limits; a cleavage plane is often not found at surgery. Astrocytomas are hypercellular lesions with no surrounding capsule. At histology, enlarged, irregularly shaped, hyperchromatic nuclei are present. Like in the brain, four different grades are recognized according to the World Health Organization (WHO). Grade I, considered most benign, is pilocytic astrocytoma. Grade II is fibrillary astrocytoma (low grade astrocytoma), which is the most common type in our series (75% of astrocytomas). Anaplastic astrocytoma is grade III, characterized by more hypercellularity and necrotic regions. The most malignant is grade IV, with glioblastoma multiforme showing endothelial proliferation and larger areas of necrosis and hemorrhage. Contrary to the brain, they are rare lesions: 0.2–1.5% of spinal astrocytomas (4).

Ependymomas originate from the ependymal cells surrounding the central canal of the spinal cord. Associated satellite cysts are frequently seen.

Different types of ependymomas are identified: cellular (the classic and most common type), papillary, clear cell, tanycytic, and melanotic (less common type) (4). Perivascular pseudorosettes are required for the diagnosis of ependymoma. The majority of ependymomas are of low grade and are well-circumscribed tumors corresponding to a grade I or II according to WHO classification. Malignant types are rarer. Ependymomas are prone to hemorrhage, especially at the margins of the tumor; this is responsible for the so-called cap sign seen on gradient echo ►T2-weighted images (WI). Calcifications may be found but are rare.

Myxopapillary ependymomas represent a distinct entity: they are typically located at the level of the filum terminale. These tumors are lobulated with a distinct capsule. At histology, tumor cells are heterogeneous, including mucin-producing cells, papillary-type cells mixed with the typical rosettes and pseudorosettes elements. Although usually of low grade, some tumors are more aggressive, type III lesions.

Hemangioblastomas are well-delineated nodular masses with extremely rich vascular components. Histologic examination shows pale stromal cells packed between blood vessels of varying size (4). Commonly, small tumors are associated with huge and extensive cystic components that may involve the entire cord.

Metastasis: Longer survival of cancer patients on the one hand and better imaging techniques on the other hand today allow the detection of a higher number of intramedullary metastases. The most common primary tumors include lung and breast cancer as well as melanoma.

Clinical Presentation

Spinal cord tumors grow very slowly, being mainly low-grade tumors (80%). They occur in younger adult patients: the mean age at diagnosis is 34 years for astrocytomas and 42 years for ependymomas. A slight male predominance (52–55%) is reported. The most frequent and early symptom is pain, and this may be the only one at the onset of the disease. Variations in tumor location will be responsible for variable motor and sensory deficits. Diagnosis is unfortunately made after a long period (mean 2.5 years after the onset of symptoms) as the clinical presentation is not specific. Urinary disturbances and impotence are less frequent and usually appear late in the clinical course of the disease, coincident with paralysis of the legs.

In children as well, pain is the most frequent symptom as reported in 42% of cases. Motor regression is present in 36%, gait abnormality in 27%, torticollis in 27%, and progressive kyphoscoliosis in 24% of cases. Low-grade lesions account for 89% of cases (6).

Acute worsening of the symptoms may occur due to intratumoral hemorrhage. Subarachnoid hemorrhage (SAH) of spinal origin is rare and the most common source is an arteriovenous malformation. Nevertheless, cases of SAH due to bleeding from hemangioblastoma have been reported in the literature. Hydrocephalus may be observed associated with an intradural spinal tumor: this is a rare but classical finding. Finally, it is extremely rare that a spinal cord metastasis presents as the first clinical manifestation of a distant primary cancer. Clinical symptoms are nonspecific, but usually involve root pain.

Imaging

Astrocytomas

According to our experience, astrocytomas are found at the cervical (33%), cervicothoracic (21%), or thoracic (36%) levels, while the remaining 7% are found at the thoracolumbar and lumbar region. The mean size of the solid tumor component involves four vertebral segments. However, especially in the pediatric population, the entire spinal cord may be involved. Cystic components within

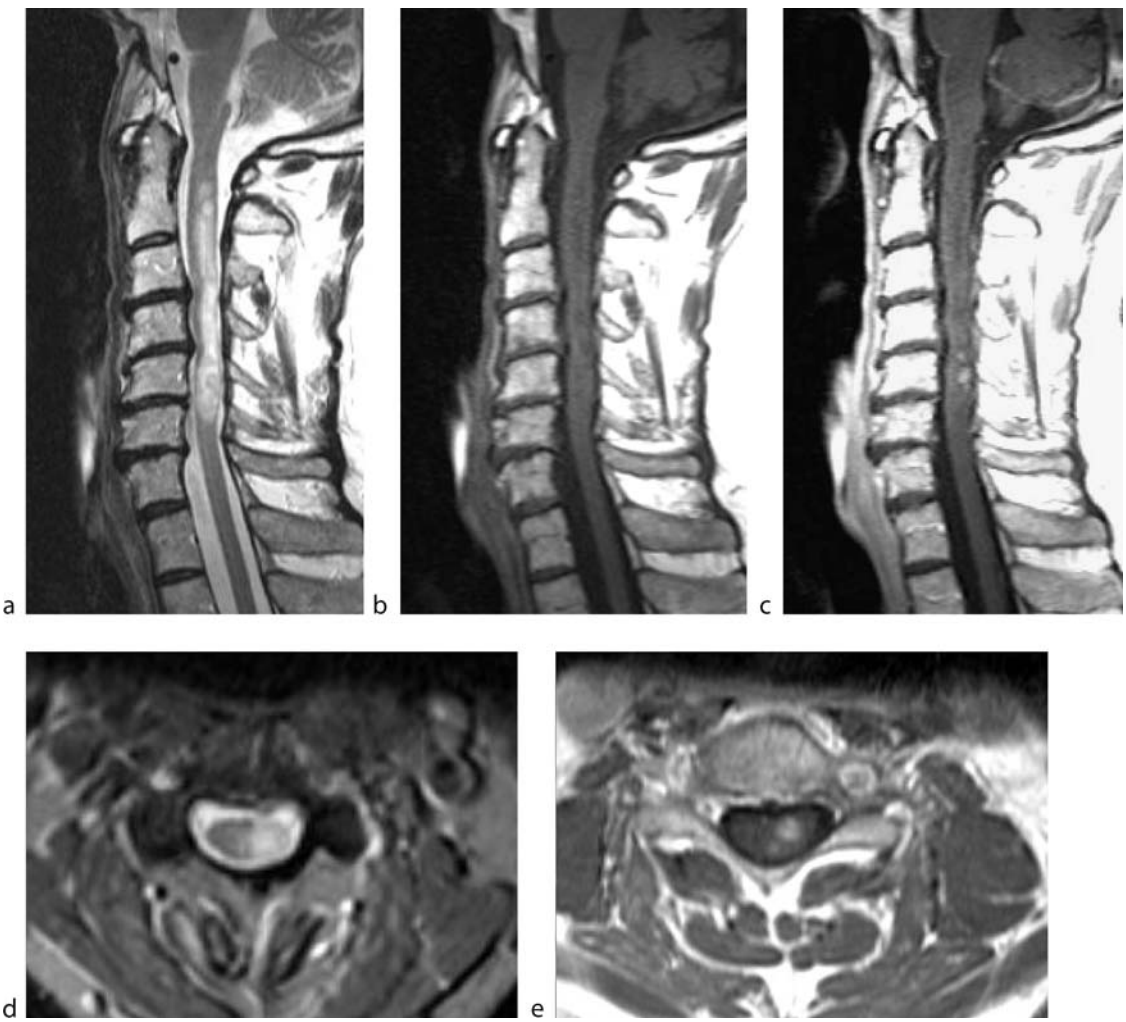

Spine, Intramedullary Tumors. Figure 1 Cervical fibrillary astrocytoma (Grade II). (a) Sagittal T2-WI The tumor extends from C2 to C6 and appears heterogeneously hyperintense with ill-delineated borders. (b) Sagittal T1-WI: the cervical spinal cord is moderately enlarged and slightly hypointense. (c) Sagittal Gd-enhanced T1-WI: small areas of patchy enhancement are seen at the level of C5. (d) Axial T2-WI and (e) axial Gd-enhanced T1-WI: tumor infiltration is excentrically located towards the left part of the cervical cord.

the tumor are found in 27% of the cases. Associated satellite cysts and secondary hydromyelia are seen in 50% of astrocytomas. On ►T1-WI, astrocytomas are mostly hypointense (83%), whereas on T2-WI they are predominantly hyperintense. Low-grade astrocytomas usually do not enhance, although moderate enhancement may be observed (Fig.1). Pilocytic astrocytomas, however, do enhance intensely. High-grade astrocytomas and glioblastomas tend to be more heterogeneous with necroticocytic areas and they enhance typically in a patchy mode (60%). Intratumoral hemorrhage is best detected on gradient echo T2-WI. Intratumoral cysts and necrosis are common. Associated huge syringomyelia may occur: the borders of these associated cavities do not enhance after contrast medium injection.

Ependymomas

Typically, ependymoma is more frequently found in the cervical spinal cord (50%). Associated large satellite cysts are seen in 60% of the cases. A so-called cap sign is seen in almost one out of four cases (27%) and corresponds to low-signal-intensity areas seen on T2-WI and even better on gradient echo T2-WI, capping the tumor limits on both sides (Fig. 2). These caps are hemosiderin deposits caused by chronic hemorrhage. Ependymomas enhance vividly and homogeneously in 91% of the cases, and usually have well-defined borders. However, no or very limited contrast enhancement may be seen. As ependymomas originate from the cells bordering the ependymal canal they are located more centromedullary compared to astrocytomas. The mean tumor size of ependymomas corresponds to three vertebral bodies (min. 2 to max. 13), while astrocytomas are usually more extensive involving 2 to 19 vertebrae.

Myxopapillary ependymomas of the conus medullaris and filum terminale are often large, well-circumscribed lesions appearing isointense compared to the cord on T1-WI and hyperintense on T2-WI. Strong enhancement is seen after gadolinium injection. Hemorrhage may be observed, explaining the sudden worsening of clinical symptoms with occurrence of acute leg weakness and sphincter disturbances.

Hemangioblastomas

Hemangioblastomas have two different but quite typical presentations: either they are small nodular lesions located in the subpial compartment and surrounded by extensive edema or they are small nodules associated to huge and extensive cystic components (Fig. 3). These tumors are either solitary (80%) or multiple, when associated with von Hippel-Lindau disease. The solid nodule is isointense to hypointense on T1-WI and

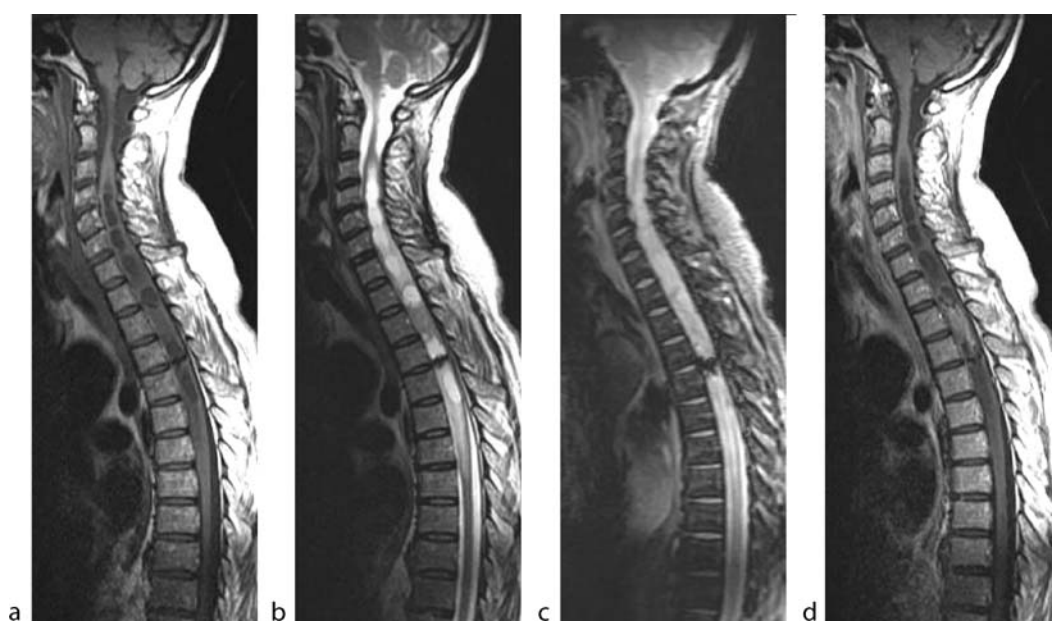

Spine, Intramedullary Tumors. Figure 2 Thoracic ependymoma (Grade II). (a) Sagittal T1-WI. (b) Sagittal T2-WI. (c) Gradient echo T2-WI and (d) sagittal Gd-enhanced T1-WI. The solid component of the tumor is located at the level of Th2-Th3. Associated cystic components are found at both tumor extremities. Hemosiderin deposits are best seen on (c). The tumor enhances homogeneously after gadolinium injection.

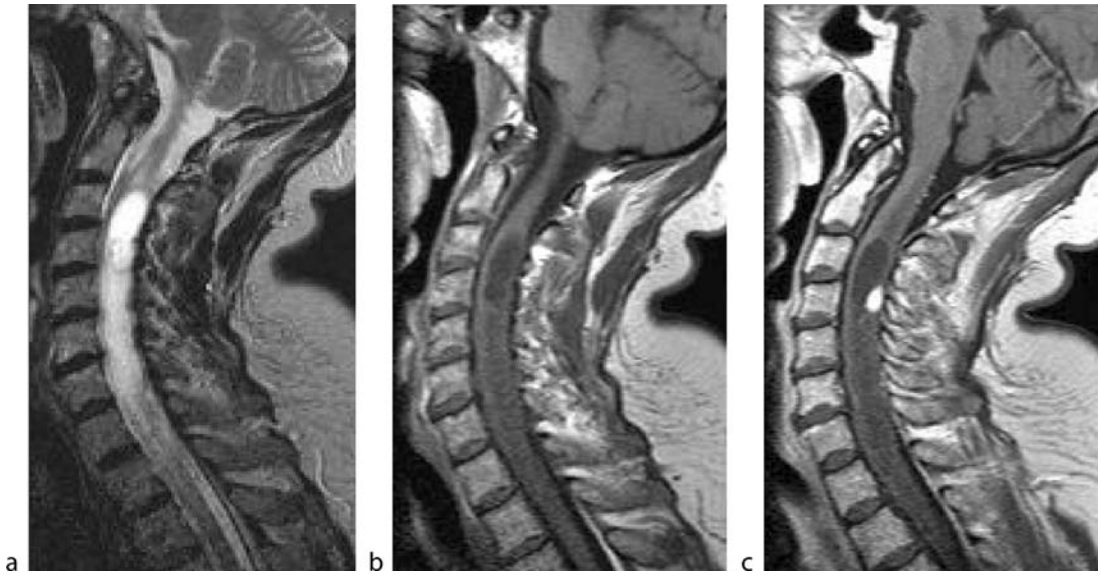

Spine, Intramedullary Tumors. Figure 3 Cervical hemangioblastoma. (a) Sagittal T2-WI. (b) Sagittal T1-WI and (c) Sagittal Gd-enhanced T1-WI. The small tumor nodule is best detected after gadolinium injection. The borders of the associated cyst do not enhance. Significant edema is best evaluated on the T2-WI.

isointense to slightly hyperintense on T2-WI. A rich vascular network in the tumor as well as enlarged feeding arteries and dilated draining veins may best be seen on proton density images and T2-WI. After gadolinium injection, intense and homogeneous contrast uptake is seen exclusively within the nodular part. Contrast administration is especially useful in order to pick up small, multiple nodules when associated to large cystic components whose borders do not enhance.

Metastases

The high sensitivity of MRI enables easy detection of intramedullary metastases; however, no specific MRI characteristics are seen. Usually, spinal cord metastases are small, nodular, well-defined lesions, hypointense on T2-WI, surrounded by mild to extensive edema. The enhancement pattern may be either ring-like or homogeneous and intense.

Melanoma metastasis, on the contrary, has a more specific appearance exhibiting a spontaneously hyperintense aspect on T1-WI linked to the presence of melanin.

Cavernomas

Cavernomas represent in our experience 8% of all intramedullary tumors. On MRI, intramedullary cavernomas are usually easily recognized thanks to a typical "black and white" appearance due to areas of mixed signal intensity on both T1- and T2- or T2*-WI. Contrast enhancement is variable. As cavernomas may be multiple, we recommend cerebral MRI whenever the diagnosis of cavernoma is suspected; indeed, if multiple similar lesions are found in the brain, this should support the final diagnosis of cavernoma of the spinal cord.

Gangliogliomas

Gangliogliomas are rare tumors, representing only 3.8% of all CNS tumors. They are more frequent in children. They mostly involve the upper cervical cord. The diagnosis of ganglioglioma can be strongly suspected in young patients (mean 12 years) whenever a large tumor is found presenting with a tumoral cyst, no edema, mixed signal intensity on T1-WI, and patchy enhancement.

Associated bone erosion and scoliosis have been reported.

Rare Tumors

As mentioned above, rare tumors such as lymphoma, epidermoid cyst, lipoma, oligodendroglioma, paraganglioma, intramedullary schwannoma, and teratoma may be found. These often have nonspecific imaging features except for lipomas, which are typically high-signal-intensity lesions on T1-WI. Melanocytic schwannoma could be suspected preoperatively in our series thanks to the hyperintense appearance of the tumor on T1-WI.

However, in these rare tumors, the ultimate diagnosis will still be ascertained by histopathology after biopsy, which is strongly recommended whenever an intramedullary tumor is suspected both clinically and on the basis of imaging findings.

References

1. Balériaux D, Parizel P, Bank WO (1992) Intraspinal and intramedullary pathology. In Manelfe C (ed) Imaging of the Spine and Spinal Cord. Raven Press New York pp 513–564
2. Balériaux D (1999) Spinal cord tumours. Eur Radiol 9:1252–1258
3. Balériaux D, Brotchi J, Salmon I (2004) Spinal cord tumours: a pictorial essay. Rivista di Neuroradiologia 17:336–348
4. Koeller KK, Rosenblum RS, Morrison AL (2000) Neoplasms of the spinal cord and filum terminale: Radiologic-pathologic correlation. Radiographics 20:1721–1749
5. Van Goethem JW, Van den Hauwe L, Ozsarlak O et al (2004) Spinal tumours. Eur J Radiol 50(2):159–176
6. Tortori Donati P and Rossi A (2005) Tumours of the Spine and Spinal Cord. In Pediatric Neuroradiology. Springer, Berlin Heidelberg, New York ISBN 3-540-41077-5, Chapter 40:1609–1653

Spleen, Infectious Diseases

Piero Boraschi[1], Francescamaria Donati[1], Alessio Auci[2], Simonetta Salemi[2], Marzio Perri[2], Carla Cappelli[2]
[1]2nd Department of Radiology, University Hospital of Pisa, Pisa, Italy
[2]Department of Diagnostic and Interventional Radiology, University of Pisa, Pisa, Italy
p.boraschi@do.med.unipi.it
bartolozzi@do.med.unipi.it

Synonyms

Infections of the spleen; Splenic abscess; Splenic inflammation

Definition

Infectious diseases of the spleen are related to splenic phagocytic immune functions and are characterized by primary splenic abscess.

Pathology and Histopathology

Splenic abscess is a rare condition that tends to occur in patients with predisposing factors such as preceding pyogenic infection, immunodeficiency, and contiguous disease in the pancreas. Several different mechanisms are presently accepted to explain its etiology. Hematogenous spread from an infective focus elsewhere in the body (endocarditis, intraabdominal sepsis, osteomyelitis, or chest infection) is the most common cause of splenic abscess, but it may also occur as direct spread of infection in contiguous areas, such as pancreatitis, retroperitoneal and subphrenic abscesses, and diverticulitis. Finally, in some cases, splenic abscess represents a delayed infective complication of either traumatic lesions or large *infarctions of the spleen.*

Depending on the causative organisms, pyogenic, fungal, and tubercular splenic abscess may be distinguished (1, 2).

Pyogenic Abscess

The most common organisms obtained from culture of pyogenic abscess are aerobic microbes, in particular the staphylococci, streptococci, *Salmonella*, and *Escherichia coli.* Anaerobic organisms, such as *Pseudomonas*, are less frequently involved (1).

At gross examination, most pyogenic splenic abscesses are solitary and unilocular lesions ranging from a few millimeters to several centimeters in diameter. However, in immunocompromised patients, multiple splenic abscesses usually associated with abscess in other viscera are frequently observed.

At histopathologic analysis, the abscess cavity is filled with purulent material, while the edges are composed of a chronic inflammatory infiltrate and fibrous tissue. The fibrotic edge is often a centimeter or more thick. Depending on the stage, suppuration, liquefaction with presence of debris, and fibrosis are found at microscopic analysis.

Fungal Abscess

Fungal abscesses are most often caused by *Candida albicans*, *Aspergillus*, and *Cryptococcus neoformans* and typically occur in immunocompromised patients, representing a manifestation of disseminated fungal disease. Fungal abscesses are multiple small lesions, typically only a few millimeters in diameter and often also involving the liver and, occasionally, the kidney (1–3).

The typical histological pattern of splenic candidiasis is characterized by microabscesses, with fungi in the center of the lesion and a surrounding area of necrosis and polymorphonuclear infiltrate; in the healing stage there is a fibrotic evolution of the lesions.

Tuberculosis

Tuberculosis of the spleen is rarely seen in isolation and is more frequently seen as part of a multifocal or

disseminated disease. The causative organism is *Mycobacterium tuberculosis* or, particularly in immunocompromised hosts, *Mycobacterium avium-intracellulare*. Splenic involvement usually occurs by hematogenous spread of infection in the form of microabscesses in a miliary tuberculosis pattern, which can become calcified, or, rarely, as larger abscesses or granulomas (4).

Clinical Presentation

The clinical presentation is often subtle and diagnosis delayed (1). Fever, left upper abdominal pain, pleuritic chest pain, and malaise are the most common symptoms. The most important findings at physical examination are left upper quadrant tenderness and splenomegaly. Leucocytosis is invariably present in all patients.

Imaging

Pyogenic Abscess

On ultrasound (US), splenic pyogenic abscess shows an anechoic or hypoechoic pattern, with an irregular wall, associated splenomegaly, and variable amounts of internal echogenicity and acoustic transmission due to necrotic debris. Intraabscess gas may be observed and is indicative of infection by gas-producing agents. These features are similar to those for abscess in other abdominal organs and are not pathognomonic for splenic abscess. At color Doppler US evaluation, avascular lesions with no hypervascular rim are usually observed.

Splenic pyogenic abscesses appear as low-density areas on nonenhanced computed tomography (CT) scans and with rim enhancement after intravenous contrast medium administration. A gas or fluid level within the lesion may be observed. Depending on the stage of abscess development, abscesses may be clearly demarcated from the surrounding tissue and have a ringlike, sharply marginated wall.

At magnetic resonance imaging (MR), pyogenic abscesses appear as areas of decreased signal intensity on T1-weighted images and increased signal intensity on T2-weighted images. After contrast administration, the lesion shows peripheral enhancement.

Fungal Abscess

Typically, splenic abscesses are observed in immunosuppressed patients and have a miliary distribution appearing on imaging as multiple small splenic lesions. They are usually associated with hepatic involvement.

Fungal abscesses have variable appearances on US. In most cases they appear as rounded, hypoechoic lesions with a central echogenic area, creating a target or bull's-eye pattern corresponding to fibrotic tissue surrounding a central inflammatory core at histopathologic analysis. The wheel-within-a-wheel appearance is observed when the central hyperechoic portion becomes necrotic and hypoechoic (2).

CT shows multiple small, low-attenuation lesions. The lesions may be missed unless intravenous contrast medium is used. At MR, fungal abscess appears as multiple small lesions that are hypointense on T1-weighted images and hyperintense on T2-weighted images (Fig. 1) (3).

Tuberculosis

Splenic tuberculosis can occur in the form of microabscesses or in the form of larger abscesses or granulomas.

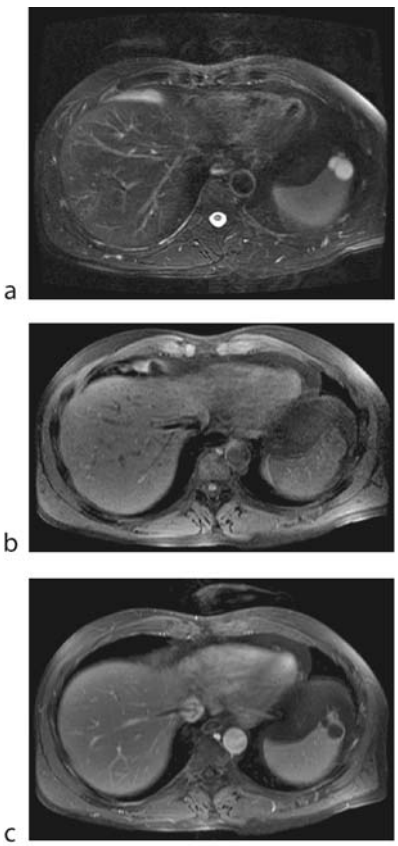

Spleen, Infectious Diseases. Figure 1 At magnetic resonance imaging, the abscesses appear as areas of increased signal intensity on T2-weighted imaging (a) and decreased signal intensity on T1-weighted imaging (b) on a postcontrast T1-weighted image, (c) the lesions show a slight peripheral enhancement.

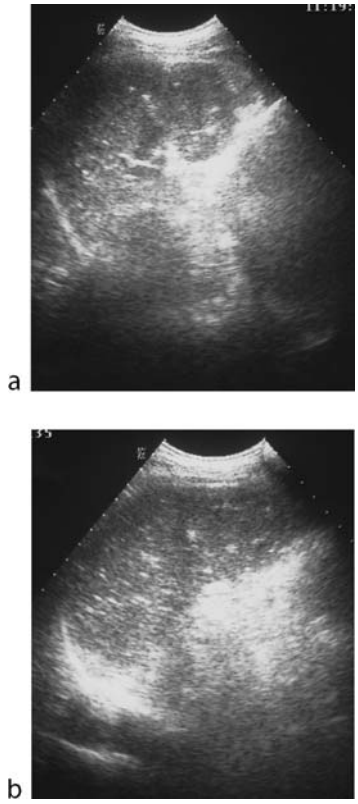

Splenic Abnormalities. Figure 2 Splenic calcifications in an immunodeficient patient with a previous history of tuberculosis and pneumocystis pneumonia. Ultrasound (a, b) clearly demonstrates multiple calcifications in the spleen.

The micronodular pattern is typically observed in the military type of pulmonary tuberculosis and is usually noted as a moderate splenomegaly. On US a typical coarsened echotexture is often seen, while on CT the miliary nodules cannot be detected, and a heterogeneous, moderately enlarged spleen, sometimes with calcifications, is usually the more frequent finding (Fig. 2). However, these radiological features are usually not specific and may be observed in several different benign or malignant conditions of the spleen.

The macronodular form is characterized by the presence of single or multiple larger abscesses or granulomas. Splenic tubercular abscess are often hypoechoic on US and round or ovoid lesions with low attenuation value on CT. Peripheral calcifications and internal septations may be observed. After contrast administration, the rim of the lesion enhances moderately, while no contrast uptake is observed in the low-density center.

On MR a hypointense nodule with a hypointense rim on T1-weighted images and an isointense or hyperintense nodule with a less intense rim on T2-weighted images are usually observed (5).

Nuclear Medicine

Radionuclide scans are sensitive, though less specific, tools for diagnosing splenic abscess and were largely employed before the advent of US and CT. Particularly, 99m-Technetium sulfur-colloid liver and spleen scanning is the scintigraphic technique most commonly used and shows a focal photopenic defect or delayed uptake, while on 67-Gallium citrate scans a focal uptake in the spleen—occasionally with a perisplenic halo—is usually observed (1).

Diagnosis

Early diagnosis and timely treatment reduce the morbidity and mortality associated with splenic abscess. US and/or CT should be used routinely for evaluating patients with fever and abdominal pain. Although both US and CT of the abdomen are of diagnostic value, CT is more accurate and reliable in the diagnosis of splenic abscess. There are several differential diagnoses, including splenic infarct, pseudocysts, hematomas, and tumors. The presence of a gas or fluid level within the spleen, although quite rare, is pathognomonic for pyogenic infection, while multiple small, hypovascular splenic lesions in immunocompromised patients are highly suggestive for fungal abscess (1, 3).

Moreover, the CT and US appearance of splenic abscess is a valuable predictor of the patient's response to treatment, with multiple and gas-containing abscesses indicating a poor prognosis.

Bibliography

1. Ooi LL and Leong SS (1997) Splenic abscesses from 1987 to 1995. Am J Surg 174: 87–93
2. Paterson A, Frush DP, Donnelly 3rd et al (1999) A pattern-oriented approach to splenic imaging in infants and children. Radiographics 19:1465–1485
3. Robertson F, Leander P, and Ekberg O (2001) Radiology of the spleen. Eur Radiol 11:80–95
4. Batra A, Gulati MS, Sarma D et al (2000) Sonographic appearances in abdominal tuberculosis. J Clin Ultrasound 28(5): 233–245
5. Akhan O and Pringot J (2002) Imaging of abdominal tuberculosis. Eur Radiol 12:312–323

Splenic Abnormalities

▶Splenic Anomalies

Splenic Abscess

▶Spleen, Infectious Diseases

Splenic Anomalies

Piero Boraschi[1], Francescamaria Donati[1], Alessio Auci[2], Simonetta Salemi[2], Marzio Perri[2], Carla Cappelli[2]
[1]2nd Department of Radiology, University Hospital of Pisa, Pisa, Italy
[2]Department of Diagnostic and Interventional Radiology, University of Pisa, Pisa, Italy
p.boraschi@do.med.unipi.it
bartolozzi@do.med.unipi.it

Synonyms

Splenic abnormalities; Splenic malformations

Definition

Splenic anomalies include congenital anomalies of shape, location, number, and size of the spleen, due to aberrant embryologic development.

Pathology and Histopathology

Accessory Spleen

The spleen is a mesodermal derivate that first appears as a mesenchymal cell condensation inside the dorsal mesogastrium. One or more additional smaller splenic condensations sometimes develop and give origin to accessory spleens, representing by far the most common congenital abnormality of the spleen. Accessory spleens are small round masses that perfectly resemble the splenic structure. They may be located anywhere in the abdomen, but the most common sites are near the splenic hilum and the tail of the pancreas. Other possible locations are along the splenic vessels, in the gastrosplenic and splenorenal ligaments, in the mesentery, and in the omentum. Any accessory splenic tissue is capable of hypertrophy. When splenectomy is performed for hypersplenism, hypertrophy of an accessory spleen may cause recurrent disease (1, 2).

Shape Abnormalities

Splenic clefts, notches, and lobules may persist in adult life as variations of the normal shape and are quite common findings (1).

Abnormal Location

The spleen may be found in a variety of abnormal locations. In congenital diaphragmatic hernia and eventration of the diaphragm, the spleen may have an intrathoracic location; if the lateral peritoneal recess is particularly deep, the spleen is found posterior to the left kidney. The spleen may rarely be located in the right hypochondrium, usually in patients with situs viscerum inversus (1).

Splenogonadal Fusion and Splenorenal Fusion

Splenogonadal fusion is a rare anomaly. Owing to the close relationship between the developing spleen and the left gonadal-mesonephric structures, an accessory spleen may be found attached to the left ovary or within the scrotum or the left kidney. Splenogonadal fusion can be classified into two types: continuous (direct connection between spleen and gonad) and discontinuous (no anatomic connection between ectopic splenic tissue and the principal spleen). This anomaly predominates in males. It can occur as an isolated condition or can be associated with other abnormalities, such as cryptorchidism and orofacial and limb abnormalities. In splenorenal fusion, normally functioning splenic tissue is abnormally located in close proximity to the kidney, usually on the left side (1, 3).

Wandering Spleen

Absence, laxity, or excessive length of splenic ligaments leads to an abnormal mobility of the organ. This condition is known as "wandering spleen." Torsion of the long vascular pedicle may occur, followed by vascular occlusion and splenic ischemia or even infarction (1, 4).

Asplenia and Polysplenia

The absence of the spleen (asplenia) and the presence of multiple small spleens (polysplenia) are rare conditions usually associated with other congenital malformations, especially cardiovascular anomalies. Either polysplenia or asplenia may be seen in association with abdominal situs ambiguous; these conditions have been classically called asplenia and polysplenia syndromes (1, 5).

Splenic Agenesis

Congenital splenic agenesis is quite uncommon and is associated with recurrent bacterial infections (1).

Clinical Presentation

Accessory spleens and splenic shape abnormalities are typically incidental findings at imaging.

Splenogonadal fusion usually manifests as a mobile and painless left scrotal mass in males. Other presentations include cryptorchidism, testicular torsion, and inguinal hernia. Splenogonadal fusion is often asymptomatic in females.

In cases of intrathoracic location of the spleen, patients usually have respiratory symptoms.

The wandering spleen is usually symptomatic in childhood and may present with an abdominal mass and acute, chronic, or intermittent symptoms due to torsion of the pedicle.

In children with *asplenia and polysplenia syndromes*, the clinical manifestations may be related to congenital heart disease, immunodeficiency due to splenic absence, or volvulus due to intestinal malrotation (1).

Imaging

Accessory Spleen

Accessory spleens may vary in number and size, usually ranging from a few millimeters to several centimeters in size (Fig. 1). Typically they appear as round or oval masses near the splenic hilum, but they may be found anywhere in the abdomen. Intrapancreatic accessory spleen, typically in the tail, can mimic a neoplastic mass. The demonstration of imaging features identical to those of normal splenic tissue allows the diagnosis (Fig. 2). At ultrasound (US), the mass shows the same echotexture as the splenic parenchyma. At computed tomography (CT), the attenuation values before and after contrast administration are identical to those of the spleen. In particular, depiction of the characteristic inhomogeneous enhancement during the arterial phase is crucial to demonstrate the nature of the mass. On magnetic resonance (MR) images, an accessory spleen has signal intensities identical to the spleen on all sequences both before and after contrast administration; in particular, the use of reticuloendothelial-targeted contrast media can confirm the splenic nature of the mass (1, 2).

Shape Abnormalities

Splenic clefts, notches, and lobules are quite common findings and must be distinguished from traumatic lesions. The demonstration at US and CT of characteristic smooth edges and the absence of extravasation suggest a congenitally cleft spleen (1).

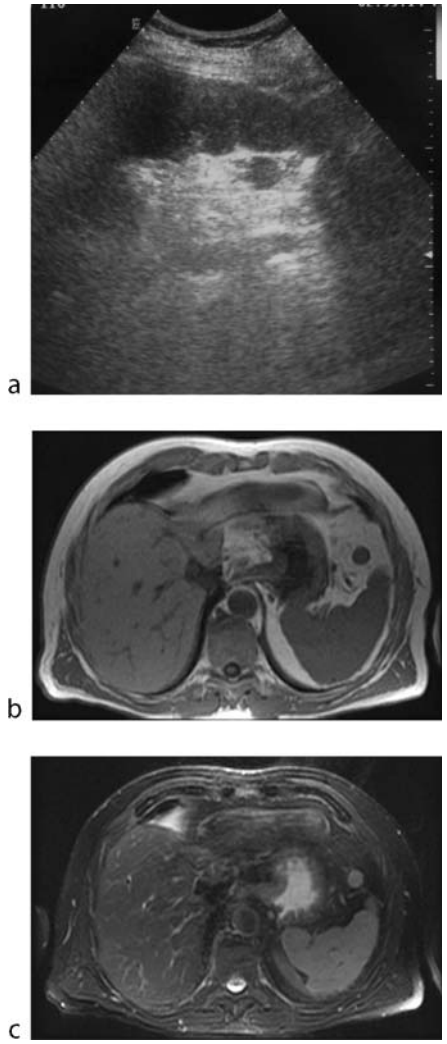

Splenic Anomalies. Figure 1 Accessory spleen. Typically this anomaly appears as a nodule near the splenic hilum. Ultrasound (a) demonstrates a nodule that shows the same echotexture as the splenic parenchyma. On magnetic resonance images, the accessory spleen is hypointense on T1-weighted scan (b) and hyperintense on T2-weighted scan (c) with respect to the liver, showing signal intensities identical to the spleen on all sequences.

Splenogonadal Fusion and Splenorenal Fusion

In the case of left scrotal mass, US is usually the first examination. The splenic tissue appears as a homogeneous, well-encapsulated mass with the same echotexture as the normal spleen. At Doppler US a vascular architecture analogous to that of the spleen can be depicted. If splenogonadal fusion is suspected, a cordlike structure connecting the spleen to the mass should be sought. CT may be helpful to demonstrate associated splenic-renal

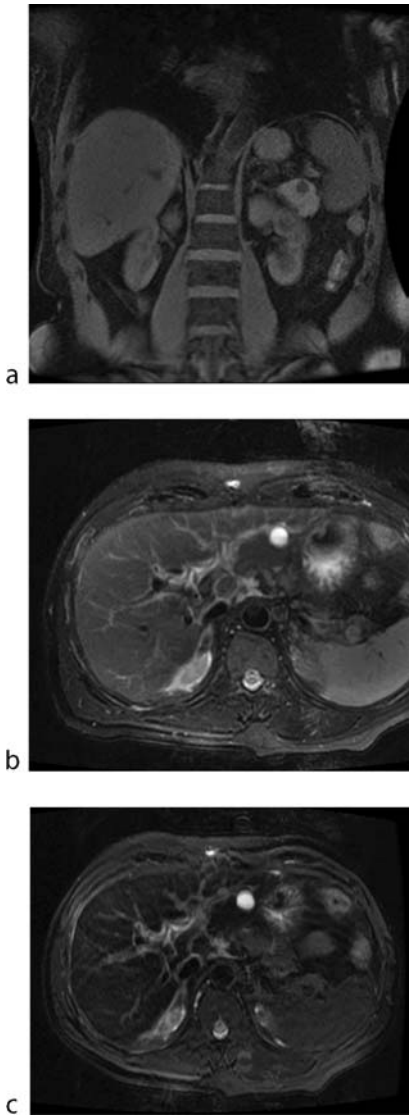

Splenic Anomalies. Figure 2 Intrapancreatic accessory spleen. The accessory spleen appears hypointense on coronal T1-weighted image (a) and hyperintense on axial T2-weighted image (b) with respect to the pancreas. On an axial reticuloendothelial-enhanced T2-weighted image (c) a significant signal intensity decrease is consequently observed at the level of the intrapancreatic accessory spleen, spleen, and liver.

fusion or cryptorchidism and to show the typical enhancement pattern after contrast administration (1, 3).

Wandering Spleen

US and especially CT well demonstrate the absence of the spleen in its expected location and the presence of a homogeneous soft-tissue mass located more inferiorly and medially. Torsion of the pedicle may lead to ischemia or even infarction. The congested or infarcted spleen may have a normal echotexture or show diffuse increased echogenicity corresponding to hemorrhagic phenomena. The spleen's comma-shaped configuration is usually preserved. Splenomegaly with rounded edges of the organ, when present, is strongly suggestive for torsion and has been attributed to congestion. Doppler US demonstrates no flow within the splenic parenchyma. Nonenhanced CT usually shows decreased attenuation of splenic parenchyma, and contrast medium administration may show a partial or total lack of enhancement. A highly specific sign of torsion is a whirl appearance of the splenic vessels and surrounding fat, with alternating bands of high attenuation and low attenuation. This finding is usually noted at the splenic hilum (1). MR can provide useful information about the precise location of the wandering spleen, the viability of the splenic parenchyma (assessed both with nonenhanced and enhanced scans), and the splenic vessel anatomy, thanks to MR angiography (4).

Polysplenia and Asplenia

In polysplenia, numerous small splenic masses can be seen predominantly in the right upper quadrant at US, CT, MR, and scintigraphy. Documenting the absence of the spleen is more difficult than confirming its presence. Scintigraphy is the standard examination (1, 5).

Nuclear Medicine

Technetium-99m sulfur colloid scintigraphy and technetium-99m-labeled heat-damaged red blood cells offer functional images and are therefore highly specific for differentiating spleen from other tissues. Although nuclear medicine offers the most specific imaging techniques for identifying functional ectopic splenic tissue, CT and MR offer superior anatomic resolution (2). Scintigraphic studies are used to confirm the presence of normally functioning splenic tissue in cases of suspected accessory spleens, ectopic spleen, splenogonadal and splenorenal fusion, and polysplenia.

Scintigraphy is also the examination of choice in documenting absence of the spleen. However, absence of uptake of radiotracer can also occur with the so-called functional asplenia, in which the splenic phagocytic function is markedly reduced despite the presence in the body of splenic tissue. Functional asplenia may occur secondary to radiation therapy and chemotherapy, secondary to tumor invasion of the spleen, in sickle cell disease, with splenic anoxia, and after bone marrow transplantation (1).

Diagnosis

Ectopic splenic tissue may mimic neoplasms and lymphadenopathies. Imaging can achieve a definite diagnosis, thus avoiding open biopsy. Ectopic splenic tissue shows imaging features identical to those of the spleen in all imaging modalities. The enhancement pattern, especially the inhomogeneity in the arterial phase, is very specific. MR reticuloendothelial-targeted contrast media can confirm the splenic nature of the mass. 99m-Technetium sulfur colloid scintigraphy and technetium-99m-labeled heat-damaged red blood cells represent the most specific imaging techniques to confirm the presence of functioning splenic tissue (2).

In splenogonadal fusion presenting with scrotal mass, US is usually the first examination to be performed, particularly for identifying a cordlike structure connecting the mass with the normal spleen. However, surgical exploration is generally required to rule out malignancy (3).

Accurate preoperative diagnosis of wandering spleen with or without torsion represents an imaging challenge and can be done with US, CT, and MR. Information concerning splenic perfusion and viability and the performance of Doppler ultrasonography and contrast-enhanced CT and MR studies is important for the surgeon, especially in younger children in whom splenopexy instead of splenectomy is the treatment of choice for uncomplicated wandering spleen.

Bibliography

1. Paterson A, Frush DP, Donnelly LF et al 3rd. (1999) A pattern-oriented approach to splenic imaging in infants and children. Radiographics November–December 19(6):1465–1485
2. Miyayama S, Matsui O, Yamamoto T et al (2003) Intrapancreatic accessory spleen: evaluation by CT arteriography. Abdom Imaging November–December 28(6):862–865
3. Pomara G (2004) Splenogonadal fusion: a rare extratesticular scrotal mass. Radiographics March–April 24(2): 417
4. Deux JF, Salomon L, Barrier A et al (2004) Acute torsion of wandering spleen: MRI findings. Am J Roentgenol June 182 (6):1607–1608
5. Applegate KE, Goske MJ, Pierce G et al (1999) Situs revisited: imaging of the heterotaxy syndrome. Radiographics July–August 19 (4):837–852; discussion 853–854

Splenic Atrophy

Congenital splenic atrophy is quite uncommon and is associated with recurrent bacterial infections.

▶Congenital Abnormalities, Splenic

Splenic Benign Tumors

▶Neoplasms, Splenic, Benign

Splenic Congenital Abnormalities

▶Congenital Anomalies, Splenic

Splenic Inflammation

▶Spleen, Infectious Diseases

Splenic Malformations

▶Splenic Anomalies
▶Congenital Anomalies, Splenic

Splenic Malignancies

▶Neoplasms, Splenic, Malignant

Splenic Malignant Tumors

▶Neoplasms, Splenic, Malignant

Splenic Traumatic Injury

▶Trauma, Splenic

Splenic Traumatic Lesions

▶Trauma, Splenic

Splenic Traumatic Rupture

►Trauma, Splenic

Spleno-Gonadal Fusion

Spleno-gonadal fusion is a rare anomaly in which an accessory spleen may be found attached to the left ovary or within the scrotum or the left kidney. Spleno-gonadal fusion can be classified into two types: continuous (direct connection between the spleen and gonad) and discontinuous (no anatomic connection between ectopic splenic tissue and the principal spleen). This anomaly predominates in males and may occur as an isolated condition or associated with other abnormalities, such as cryptorchidism, orofacial, and limb abnormalities. Spleno-gonadal fusion typically manifests as a mobile and painless left scrotal mass in males. In females, spleno-gonadal fusion is often asymptomatic and is usually an incidental finding at US or CT. In spleno-gonadal fusion presenting with scrotal mass, US is usually the first examination to be performed. The homogeneity of the echotexture, the regularity of the vascular architecture and the presence of well-defined margins suggest a nonneoplastic nature of the mass. When spleno-gonadal fusion is suspected, a comparison with the US appearance of the spleen and a study directed to the visualization of a cord-like structure connecting the mass with the normal spleen should be performed. A definitive diagnosis cannot be made solely on the basis of US findings. Nuclear medicine imaging can confirm the presence of splenic areas of activity. However, surgical exploration is generally required to rule out malignancy. Nevertheless, orchiectomy can be avoided because splenic tissue can be dissected away from the tunica albuginea.

►Congenital Abnormalities, Splenic

Spleno-Renal Fusion

In spleno-renal fusion, normally functioning splenic tissue is abnormally located in close proximity of the kidney, usually on the left side. This anomaly presents as a renal mass which shows imaging features identical to those of the normal spleen.

►Congenital Abnormalities, Splenic

Splenogonadal Fusion, Wandering Spleen

►Congenital Malformations, Splenic

Splenomegaly

Piero Boraschi[1], Francescamaria Donati[1], Alessio Auci[2], Simonetta Salemi[2], Marzio Perri[2], Carla Cappelli[2]
[1]2nd Department of Radiology, University Hospital of Pisa, Pisa, Italy
[2]Department of Diagnostic and Interventional Radiology University of Pisa, Pisa, Italy
p.boraschi@do.med.unipi.it
bartolozzi@do.med.unipi.it

Synonym

Enlargement of the spleen

Definition

Splenomegaly is the enlargement of the spleen. It represents a manifestation of a splenic disorder rather than being a specific entity. In fact, it is the most common pathological finding of splenic disease. Many of the mechanisms of splenic enlargement are exaggerated forms of the spleen's normal function. Although a wide variety of diseases are associated with splenomegaly, the most frequent causes include immune response work hypertrophy, such as in infectious mononucleosis; red blood cell destruction work hypertrophy, such as in ►hereditary spherocytosis or thalassemia major; congestive causes, such as in splenic vein thrombosis or ►portal hypertension; myeloproliferative causes, such as in chronic myeloid metaplasia; infiltrative causes, such as in sarcoidosis and some neoplasms; and neoplastic causes, such as in chronic lymphocytic leukemia and the lymphomas. Splenomegaly can also occur as the result of ►extramedullary hematopoiesis. Miscellaneous causes of splenomegaly include trauma, cysts, hemangiomas, and metastasis.

Pathology and Histopathology

When an enlarged spleen is referred to as hypertrophied, the underlying cause may be hypertrophy or hyperplasia

of individual cells. In specific diseases, the splenic architecture is remodeled. For example, in Niemann–Pick disease, sphingomyelin and cholesterol accumulate within large foamy cells. With amyloidosis involving the spleen and resulting in splenomegaly, large hyaline masses are seen as lesions occupying the white pulp space. Two forms exist, including the "sago spleen," in which amyloid deposits are limited to follicles, and the "lardaceous spleen," in which amyloid is deposited in the walls of the splenic sinusoids. In a rare complication of typhoid fever, reactive splenic vasculitis may develop. In inflammatory splenomegaly, the demand for increased antigen clearance from the blood may lead to increased numbers of reticuloendothelial cells in the spleen and may stimulate accelerated antibody production with resultant lymphoid hyperplasia. In infiltrative splenomegaly (Gaucher's disease, amyloidosis), engorgement of macrophages with indigestible materials can be found.

Clinical Presentation

The most common history is mild abdominal pain that is vague in nature. Increased abdominal girth is less common. Early satiety from gastric displacement occurs with massive splenomegaly. Associated symptoms and signs include febrile illness (infectious process); pallor, dyspnea, bruising, and/or petechiae (hemolytic process); symptoms of liver disease (congestive process); and weight loss and constitutional symptoms (neoplastic process).

Examination should include palpation with the patient in the supine and right lateral decubitus positions. Additional signs that identify possible etiologies of splenomegaly include signs of cirrhosis (asterixis, jaundice, telangiectasias, gynecomastia, caput medusae, ascites), heart murmur (endocarditis, congestive failure), jaundice and scleral icterus (spherocytosis, cirrhosis), and petechiae (any cause of thrombocytopenia).

A patient with an enlarged spleen is more likely to have splenic rupture from blunt abdominal or low thoracic trauma, leading to typical symptoms. In particular, in elderly persons the combination of capsular thinning with increased spleen weight and size makes splenic injury more common. These factors account for the increased likelihood of splenectomy for trauma in this subgroup.

Imaging

Ultrasonography

Ultrasound (US) often represents the first imaging modality performed to evaluate the spleen. It allows the clinician to estimate the spleen's size and morphology and, in some cases, to demonstrate splenic lesions or diffuse abnormalities (1). The size of the organ can be evaluated by measuring the length in the longitudinal scan, which allows simultaneous visualization of both the upper and lower poles and the hilum. A craniocaudal measurement of 11–13 cm is frequently used as the upper limit of normal for splenic size. Another possible method to demonstrate splenomegaly is to find an anteroposterior measurement up to two-thirds of the distance between the anterior and posterior abdominal walls. However, because of wide variations in shape, no consistent correlation has been recognized between the spleen's length and its overall volume.

Computed Tomography

Enlargement of the spleen is detectable by a variety of means, including physical examination and US; computed tomography (CT) is rarely necessary to document the presence of splenomegaly. When the spleen is enlarged, the concavity of its visceral surface is often lost as the spleen assumes a more globular shape (Fig. 1). CT can demonstrate findings that suggest the cause of the splenic enlargement (2). Neoplasm, abscess, or cystic lesions can be appreciated; associated abdominal lymph node enlargement can suggest a lymphoma. Cirrhotic patients show characteristic alterations in the size and shape of the liver and in the prominence of the venous structures in the splenic hilum. An increase in the attenuation value of the spleen (as well as the liver) can be found in patients with hemochromatosis.

Magnetic Resonance Imaging

Magnetic resonance imaging (MR) is usually performed for problem solving, such as in the differential diagnosis

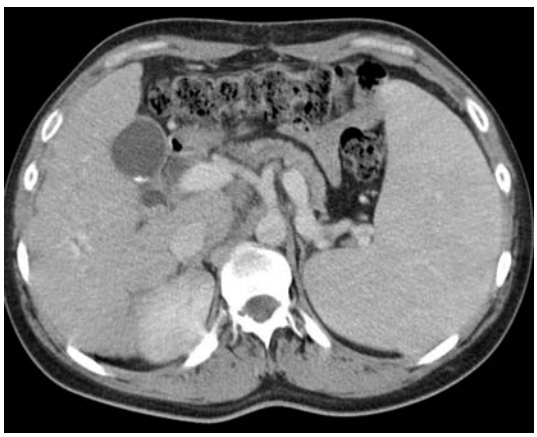

Splenomegaly. Figure 1 Splenomegaly in acquired immunodeficiency syndrome. Computed tomography scan exhibits homogeneous enlargement of the spleen.

when focal or diffuse disease of the spleen is present (3). For example, lymphoma dynamic sequences after injection of gadolinium-diethylenetriamine pentaacetic acid (DTPA) show large irregularly enhancing regions of high- and low-signal intensity representing diffuse infiltration or focal low-signal intensity mass lesions scattered throughout the spleen. Superparagmagnetic iron oxide (SPIO) particles are selectively taken up by reticuloendothelial system (RES) cells, and not by malignant cells, improving the depiction of malignant lesions of the spleen.

In splenomegaly caused by portal hypertension, arciform high-signal intensity enhancement on images obtained after gadolinium-DTPA injection is characteristic and excludes the presence of malignant disease. Gamna-Gandy bodies are spots of organized hemorrhage caused by portal hypertension and can be detected as multiple low-signal intensity nodules both on T1-weighted and T2-weighted images (Fig. 2) according to paramagnetic effects caused by hemosiderin deposits in the lesions (4).

Patients with splenic enlargement secondary to hematologic disorders generally show no consistent pattern of signal intensity alteration, and the spleen is often unchanged on MR images (Fig. 3). Patients affected by thalassemia have splenomegaly from extramedullary hematopoiesis and systemic iron overload from blood transfusions, with massive iron deposition in the spleen, which shortens T2.

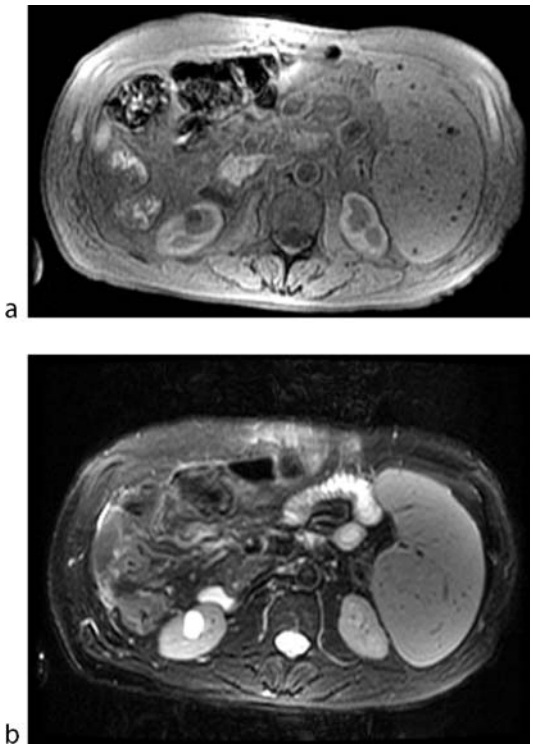

Splenomegaly. Figure 2 Gamna-Gandy bodies in a patient with splenomegaly who previously underwent liver transplantation. Multiple low-signal intensity nodules are shown both on axial fat-saturated T1-weighted (a) and T2-weighted (b) magnetic resonance sequences.

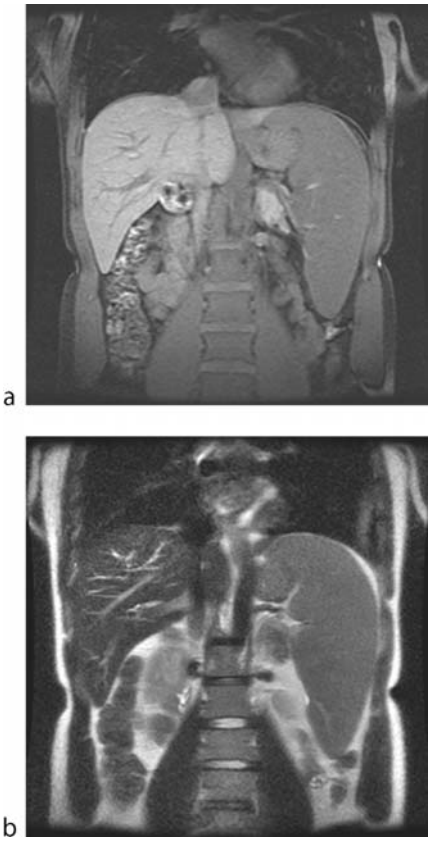

Splenomegaly. Figure 3 Splenomegaly in a patient with hereditary spherocytosis. Coronal fat-saturated T1-weighted (a) and T2-weighted (b) magnetic resonance images well demonstrate the spleen's increased dimensions.

Nuclear Medicine

A spleen scan is a good noninvasive technique for evaluating spleen size; a close correlation exists between spleen length on scan images and spleen weight after splenectomy. Erythrocytes should be labeled with chromium-51, mercury-197, rubidium-81, or 99m-technetium, and the cells altered by treatment with heat, antibody, chemicals, or metal ions so that the spleen sequesters them after infusion. A spleen scan is useful for detecting space-occupying lesions in the splenic substance and for evaluating loss of spleen function.

Diagnosis

Laboratory studies must always be performed to identify possible alterations that may suggest the cause of the splenomegaly. Moreover, splenomegaly produces hypersplenism, which is characterized by anemia, leukopenia, thrombocytopenia, or combinations thereof. Increased splenic platelet pooling is the primary cause of the thrombocytopenia of hypersplenism. In patients with hypersplenism, as much as 90% of the total platelet mass can be found in the spleen. In hypersplenism, the platelet count is usually 50,000–150,000/L. The etiology of the anemia observed in splenomegaly is the result of sequestration and hemodilution. Leukopenia is caused by increased destruction or sequestration of leukocytes. Sequestration may also play a role in the genesis of neutropenia. A complete laboratory study must be done in patients without evident cause of splenomegaly. Imaging studies are useful to assess the splenic enlargement and identify the cause of the splenomegaly.

Bibliography

1. Andrews MW (2000) Ultrasound of the spleen. World J Surg 24:183–187
2. Robertson F, Leander P, Ekberg O (2001) Radiology of the spleen. Eur Radiol 11:80–95
3. Semelka RC, Marcos HB (1998) Spleen. In: Heuck A and Reiser M (eds) Abdominal and Pelvis MRI. Springer, Berlin-Heidelberg, pp 51–58
4. Sagoh T, Itoh K, Togashi K et al (1989) Gamna-Gandy bodies of the spleen: evaluation with MR imaging. Radiology 172:685–687

Splenosis

Splenosis results from the autotransplantation of splenic tissue occurring after splenic trauma or after splenectomy. The incidence of splenosis after traumatic injury of the spleen varies from 27% to 67%. Splenic implants are usually numerous and are spread throughout the peritoneal cavity. In patients with history of thoraco-abdominal trauma with splenic and diaphragmatic injury, splenosis may be intrathoracic. Splenic implants derive their blood supply from the surrounding tissue and do not have a capsule. Splenosis is usually an incidental finding at imaging, and may mimic peritoneal metastases, lymphomegalies and other neoplastic or nonneoplastic masses. Splenic implants appear as round or oval, sharp-marginated nodules resembling the features of splenic parenchyma in the different imaging modalities (US, CT, or MR). The characteristic inhomogeneity in the arterial phase is very typical. MR reticuloendothelial-targeted contrast media can be a useful tool to increase the diagnostic confidence if splenosis is suspected. 99m-Technetium sulfur colloid scintigraphy and 99m-technetium-labeled heat-damaged red blood cells represent the most specific and the most sensitive imaging techniques to confirm the presence of functioning splenic tissue. Splenosis may cause recurrence of hematologic disorders after therapeutic splenectomy.

▶Congenital Abnormalities, Splenic

Split Pleura Sign

CT finding suggestive of an empyema which refers to enhancement and thickening of the visceral and parietal pleura separated by pleural fluid.

▶Pleural Effusion

Split-Liver Transplant

▶Transplantation, Liver

Split-liver Transplantation

Liver transplantation technique consists in cadaveric liver division so that the lateral segment of the left lobe may be transplanted into a pediatric patient and the remainder of the liver may be transplanted into an adult.

▶Transplantation, Hepatic

Spondylarthrosis

▶Degenerative Conditions, Spine

Spondylitis Marginalis

Spondylitis marginalis is a subdiscal osteitis of the posterior upper corner of the vertebral body with triangular sclerosis resembling an inverse Romanus lesion.

▶Spondyloarthropathies, Seronegative

Spondyloarthropathies, Seronegative

G M Lingg, C Schorn
Department of Radiology,
Sana Rheumazentrum Rheinland Pfalz,
Bad Kreuznach, Germany
dr.lingg@sana-rheumazentrum-rlp.de

Definition

Seronegative ►spondyloarthropathy comprises of the following five diseases: ankylosing spondylitis, psoriatic arthritis, reactive arthritis, enteropathic arthritis in Crohn's disease, and ulcerating colitis, as well as undifferentiated spondyloarthropathy. SAPHO syndrome may show overlap and ►SAPHO syndrome. These are systemic autoimmune inflammatory disorders of unknown etiology, promoted by infection and primarily affecting the discovertebral complex, synovial membranes, articular surfaces, insertion of joint capsules, and tendino-osseous junctions. Apart from joint destruction, they are characterized by new bone formation as a highly characteristic feature, with consecutive ankylosis and vertebral column stiffness. There is a hereditary predisposition in patients with HLA B 27 (Table 1).

Spondyloarthropathies, Seronegative. Table 1 European spondyloarthropathy study group (ESSG) classification of seronegative spondyloarthropathies. (≥1 clinical sign; ≥1 anamnestic clue = > sensitivity 77%; specificity 89%; + radiological sign = > sensitivity 86%; specificity 87%)

Clinical signs	Anamnestic clues	Radiological sign
Inflammatory back pain	Family history	Sacroiliitis
Asymmetrical synovitis of the lower extremity	Enteropathy (Crohn's disease or ulcerosing colitis)	
	Psoriasis	
	Alternating bottom pain	
	Enthesitis	

Source: Dougados M, van der Linden S, Juhlin R et al (1991) The European Spondyloarthropathy Study Group: preliminary criteria for the classification of spondyloarthropathy. Arthritis Rheum 34: 1218–1227.

Pathology/Histopathology

Sacroiliitis begins with hypertrophic synovitis with focal mild intima hyperplasia. Granulation tissue and pannus formation lead to cartilage destruction, reflecting the character of the sacroiliac joints as partly synovial joints. Subchondral inflammation progresses to bony erosion, typically with surrounding reactive bony sclerosis. The bone marrow is filled with inflammatory cells. Later, fibroblast proliferation anticipates fibrous scar and bone formation. Remodeling to mature bone advances toward ankylosis. Reactive sclerosis and bone formation in and following inflammation are typical.

Clinical Presentation

Ankylosing Spondylitis

Ankylosing spondylitis is the prototypical form of the spondyloarthropathies. Because sacroiliitis is the main manifestation, the best diagnostic clue is long-standing low back pain. Typically in inflammatory back pain there is relief not with rest but with exercise. Patients suffer most seriously in the early morning hours, often waking up with low back pain and feeling relief when walking around. Even before bony ankylosis is present, stiffness is a common symptom. Motion restriction of the lumbar spine, neck, hip, and thorax worsens in the course of the disease. Deformity with severe kyphosis may badly handicap patients. Among the extraskeletal manifestations, iritis is most common. Patients often complain about fatigue. Ninety percent show HLA B 27, whereas only 6–9% of the normal population do.

Imaging

The primary imaging tool for inflammatory back pain is plain X-ray of the lumbar spine, despite the fact that early sacroiliac arthritis may not be conspicuous at all. Whenever X-ray imaging is equivocal, further evaluation with computed tomography (CT) or magnetic resonance (MR) imaging should follow. CT is preferred in elderly patients with long-standing symptoms and in cases of known paraarticular sclerosis because bony sclerosis leads to blurring of joint contours in MR imaging, and bony destructions are best viewed by means of a bone technique like CT. MR imaging, on the other hand, is advantageous in young patients due to the lack of radiation and in early cases because of its high sensitivity to inflammatory activity. Diagnosis of lumbar, thoracic, and cervical spine as well as articular involvement is usually confirmed using X-ray imaging, even when MR imaging shows better sensitivity.

Signs and Patterns in Ankylosing Spondylitis

►*Sacroiliacal joint arthritis* is the imperative diagnostic clue of ankylosing spondylitis. A typical X-ray sign is the triad of sclerosis, destruction, and ankylosis (Fig. 1). In early stages, sclerosis may be mild, and when present it is extended, woolly, and more pronounced in the iliac bone. Erosions and bony destructions are primarily seen as indistinct and irregular contours. A pearl-string aspect of confluent erosions is typical but not very common. Most often, destruction and bony bridging go alongside. Bony bridges with blurring and disappearance of the joint space are signs of increasing ankylosis. In the end stage, the sacroiliac joint space may be completely obliterated and disappeared; however, persisting bits of joint space are not uncommon (Table 2).

The differential diagnosis includes degenerative osteoarthritis, which exhibits bandlike subchondral sclerosis or, especially in obese females, multiparae triangular sclerotic areas particularly in the lower aspect of the iliac bone. Variants of the joint form are common and may simulate defects or irregularities. Destruction and pearl-string aspect occur in hyperparathyroidism. Iliacal and sacral bony sclerosis can be signs of insufficiency fractures in severe osteoporosis and should be considered as a differential in patients with low back pain, sacral sclerosis, and generalized osteoporosis.

In MR imaging, periarticular edema, marrow fat accumulation, sclerosis, and blurring of the joint contours are nonspecific findings. Erosion and destruction of the joint contours and ankylosis as well as joint effusion as signs of arthritis are detected in unenhanced images. Contrast material enhancement can be seen in the joint capsule, erosions, subchondral granulation tissue, and areas of edema as well as intra-articularly in pannus formation (Fig. 1).

Spine involvement: The typical feature of spine involvement in ankylosing spondylitis is the ►syndesmophyte, which grows marginally from the vertebral body corner in the exact position of the annulus fibrosus (Fig. 2). Sometimes, in degenerated disks, it is modified, with a more bulging contour. Often it begins consecutively in ►Romanus lesions commonly in the thoracolumbar junction segments. Finally, the disc is completely bridged

Spondyloarthropathies, Seronegative. Table 2 X-ray classification of sacroiliitis

°0	Normal
°1	Suspicious
°2	Minimal arthritis
°3	Moderate arthritis
°4	Ankylosis

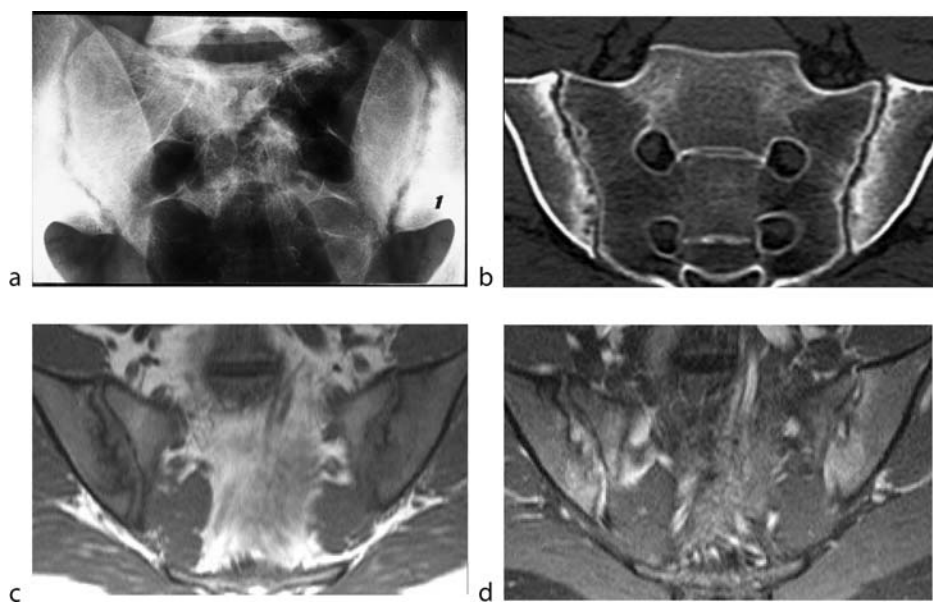

Spondyloarthropathies, Seronegative. Figure 1 Ankylosing spondylitis. (a) X-ray imaging shows paraarticular sclerosis and erosions of the sacroiliacal joint. (b) Computed tomography reveals erosions and iliacal sclerosis as well as bony bridging. (c) Magnetic resonance imaging in another patient allows early diagnosis because of its sensitivity to inflammatory processes. The so-called bone marrow edema is seen mainly in the iliac bone paraarticularly; here on short TR TE images, it is mildly hypointense. (d) Marked hypointensity, however, is a sign of sclerosis. Erosions are visible. Contrast material enhancement is found in the areas of bone marrow edema, in the joint space itself, and in the erosions.

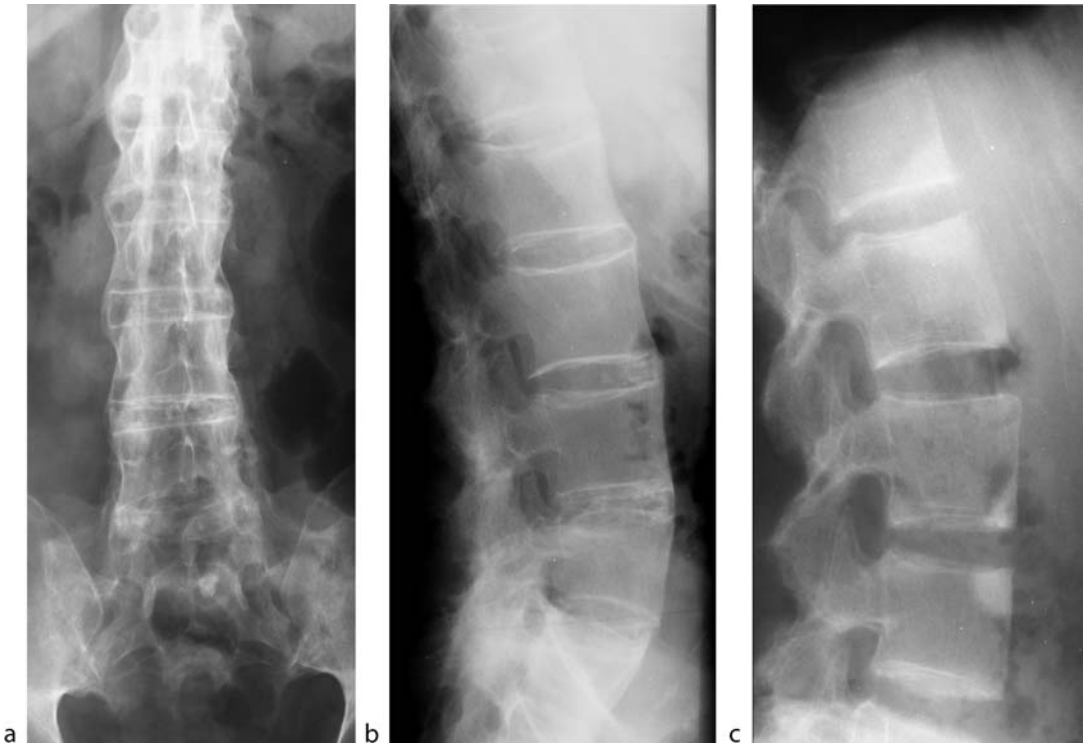

Spondyloarthropathies, Seronegative. Figure 2 Ankylosing spondylitis. (a) Anteroposterior view of the lumbar spine of a patient with long-standing ankylosing spondylitis shows the typical cane of bamboo with multisegmental syndesmophytic bridging of the disc spaces and the ►Trolley-truck sign referring to the polysegmental bony ankylosis of the ►apophyseal joints. The sacroiliacal joints are completely postarthritically ankylosed, with only mild residual sclerosis. (b) Lateral view of the same patient shows the syndesmophytes growing vertically in the location of the annulus fibrosus and the broad ossification along the apophyseal joints. (c) In another patient, the lateral view reveals multisegmental ►spondylitis marginalis, in the anterior location the so-called Romanus lesions, and in the posterior location the characteristic triangular sclerosis of the vertebral corner. ►Square vertebrae and the faint barrel shape of the vertebrae are other typical features.

by circular ossification of the annulus fibrosus. When multiple segments are affected, the spine looks like a ►cane of bamboo.

Osteitis of the peridiscal bone (discitis, rheumatic spondylodiscitis) is another typical aspect of inflammation in ankylosing spondylitis. It may be limited to the anterior upper corner and is then called a *Romanus lesion* (Fig. 2c). A Romanus lesion consists of a triangular sclerosis and an erosion of the anterior upper vertebral corner. It usually heals within months or years with syndesmophyte formation. When it is minimal and only sclerosis is present, it is referred to by the term "►*Shinig corner*." Similar lesions exist in the posterior upper corner of the vertebra and are named *spondylitis marginalis*. The inflammation of the central part of the disc results in an aspect resembling spondylitis, with erosions or destructions of the subchondral bone. It is called ►*Andersson lesion type A or inflammatory type*. In comparison to bacterial spondylitis, the destruction remains mild, focal, and unchanged for months or even years. Perivertebral fluid or abscesses are not an aspect of rheumatic disc disease. In the late stage, bony ankylosis is present. ►*Andersson lesion type B* refers to a transdiscal insufficiency fracture. It occurs mostly in the thoracolumbar junction segments of osteoporotic multisegmentally ankylotic vertebral columns with marked kyphosis. Sometimes a minimal trauma is the cause. The prognosis for local control is poor.

Square and *barrel-shaped vertebrae* are the result of inflammatory and osteoproliferative affection of the ventral vertebral aspect. They typically occur in the thoracolumbar vertebral column.

►*Apophyseal joint arthritis* with progression to fibrous or bony ankylosis and consecutive early stiffness is very common in adolescent patients. X-ray images, however, are sometimes not very conspicuous. In late stages, bands of broad ossification over the dorsolateral aspect of the vertebral column are seen. ►*Arthritis of the costotransversal and costovertebral joints* gives rise to persistent thoracolumbar pain and is the reason for respiratory

movement restriction. Most often it is occult on X-ray images. MR imaging, however, can show extensive contrast material enhancement in these locations.

Ligament ossification such as of the interspinal and iliolumbar ligaments occurs in late stages of ankylosing spondylitis, some of which are specially named: "►*Dagger sign*" is the polysegmental ossification of the interspinal ligaments. If occurring along with extended bridging ossification of the intervertebral joint capsules, the term "*trolley-truck sign*" is used.

In ankylosing spondylitis, the ►*large joints* are commonly affected: hips, knees, and shoulders. Joint effusion, cartilage destruction with consecutive concentric joint space narrowing, and paraarticular demineralization are the radiologic signs of arthritis. In ankylosing spondylitis, frank bony destructions are rarely found. Inflammatory proliferation at ligament and tendinous insertions is more common. Sometimes, premature degenerative disease is the only sign of postarthritic change.

The ►*small joints* are quite rarely affected in ankylosing spondylitis. Extraarticular inflammatory proliferation is seen in addition to arthritic destruction. In comparison to rheumatoid arthritis, the lower extremities and the DIP joints are more often affected. Postarthritic degenerative osteoarthritis is more common than ankylosis.

Bursitis compromising the underlying bone is most often seen in bursa subachillea, bursa trochanterica, and iliopsoas bursa. It appears as soft tissue swelling in the typical places. Pressure erosions of the bone and inflammatory destructions are both possible. Osteoproliferative changes are common.

In ankylosing spondylitis, an *inflammatory reaction of tendon and ligament insertions* is a leading feature. Common locations are the iliac crest, tubera ischiadica, greater trochanter, plantar fascia (calcaneopathy), and olecranon, but it can appear anywhere. Proliferative changes with indistinct, hairy contours as well as destructions with small grooves or combinations of both are possible features.

►*Synchondritis of the symphysis or manubriosternal junction* exhibits contour defects or broad indistinct defects and surrounding bony sclerosis.

Nuclear Medicine

In bone scanning, inflammatory affection appears as hot spots. Sacroiliacal joints, however, normally show mild tracer accumulation. Asymmetric massive tracer accumulation may be a sign of arthritis, but specificity is very low. Radiologic work-up is mandatory for the differential diagnosis. Bone scanning can show foci of inflammatory affection all over the skeleton, and therefore can direct the following work-up to these foci.

Diagnosis

Since 1966 standardized diagnostic criteria have been employed. The most recent modification of the New York criteria dates from 1984 and provides high specificity and moderate sensitivity. One or more clinical signs and radiological evidence of sacroiliitis must be present for proper diagnosis (Table 3). Early diagnosis, however, may be difficult. MR imaging is one tool to close the diagnostic gap, since sacroiliitis can be found much earlier and with more conspicuity than in X-ray imaging.

Interventional Radiological Treatment

As in rheumatoid arthritis, radiosynovectomy is a promising tool for local control in limited disease of the large joints. CT-guided corticosteroid injection into the sacroiliac joints with satisfactory results is used by several authors.

Clinical Presentation

Psoriatic Arthritis

Psoriatic arthritis occurs in 5–10% of patients suffering from psoriasis. Spondyloarthropathy is found in 25% of patients with psoriatic arthritis and is highly associated with HLA B 27. Inflammatory back pain is the main symptom in sacroiliitis. Lumbar spine involvement is characterized by pain, morning stiffness, and motion restriction. Kyphosis or total vertebral stiffness as seen in ankylosing spondylitis is not a sign of psoriatic spondyloarthropathy.

Imaging

Signs and Patterns in Psoriatic Arthritis

Peripheral arthritis of the small joints is common, but not symmetrical in most patients. Irregular involvement is

Spondyloarthropathies, Seronegative. Table 3 Modified New York criteria (1984) for diagnosing ankylosing spondylitis (≥1 clinical sign and 1 radiological sign)

Clinical signs	Radiological signs
Low back pain and stiffness >3 months, no pain relief with rest but relief with exercise	Bilateral sacroiliitis °2–4
Motion restriction of the lumbar spine sagittally and frontally	Unilateral sacroiliitis °3–4
Respiratory motion restriction (age-related, about <2.5 cm 4. ICR)	

Source: van der Linden SM, Valkenburg HA, Cats A (1984) Evaluation of diagnostic criteria for ankylosing spondylitis: a proposal for modification of the New York criteria. Arthritis Rheum 27:361–368.

more typical. There are, however, additional distribution types, including transverse type (all DIP, all PIP, or all MCP of one hand/foot) and ray type (all joints of one finger/toe). Joint effusion is a sign of articulosynovitis. Excessive swelling of a complete finger or toe is seen in ►*dactylitis*. In contrast to rheumatoid arthritis, there is often no paraarticular demineralization. Characteristic findings in psoriatic arthritis are *osteoproliferations* at the unguicular processes, periarticularly, at ligamentous and capsular insertions, and even near the arthritic destructions (►*proliferosion*) (Fig. 3). Psoriatic arthritis may rapidly progress to mutilation (►*cup-and-saucer deformity*) in one joint and to postarthritic ankylosis in the other joint. A characteristic deformity in advanced disease is the ►*telescope phenomenon*, in which a digit shortens excessively due to destruction not only of the joint itself but also of the adjacent parts of the diaphyses.

Sacroiliacal joint arthritis is the leading sign of psoriatic spondyloarthropathy and mainly occurs together with peripheral or large joint arthritis. In comparison to ankylosing spondylitis, it is often mild and frequently unilateral. Apart from this, the appearance is identical to sacroiliitis in ankylosing spondylitis (sclerosis, destruction, and bony bridging).

Spine involvement is possible with or without sacroiliitis: the typical feature of spine involvement in psoriatic spondyloarthropathy is the *parasyndesmophyte*, which comprises three types. The most common type grows hooked like a bull horn as an intervertebral osteophyte. The other two types refer to ossicles lying paradiscally or paravertebrall (Fig. 3). Romanus lesions, Andersson lesions, and square vertebrae are not signs of psoriatic spondyloarthropathy.

►*Enthesitis* may occur at various places, such as the interspinal ligaments and iliolumbal ligament.

In psoriatic spondyloarthropathy, the *large joints* are commonly affected: hips, knees, and shoulders. Joint effusion, cartilage destruction with consecutive concentric joint space narrowing, and paraarticular demineralization are the radiologic signs of arthritis. In psoriatic arthritis, inflammatory proliferation at ligaments and tendinous insertions are especially pronounced.

Enteropathic Spondarthropathy and Reactive Arthritis

In enteropathic arthritis, sacroiliitis and spinal affection are indistinguishable from ankylosing spondylitis. Arthritis most often affects the lower extremity. Reiter's disease is the classic and most frequent form of reactive arthritis (conjunctivitis, urethritis, arthritis).

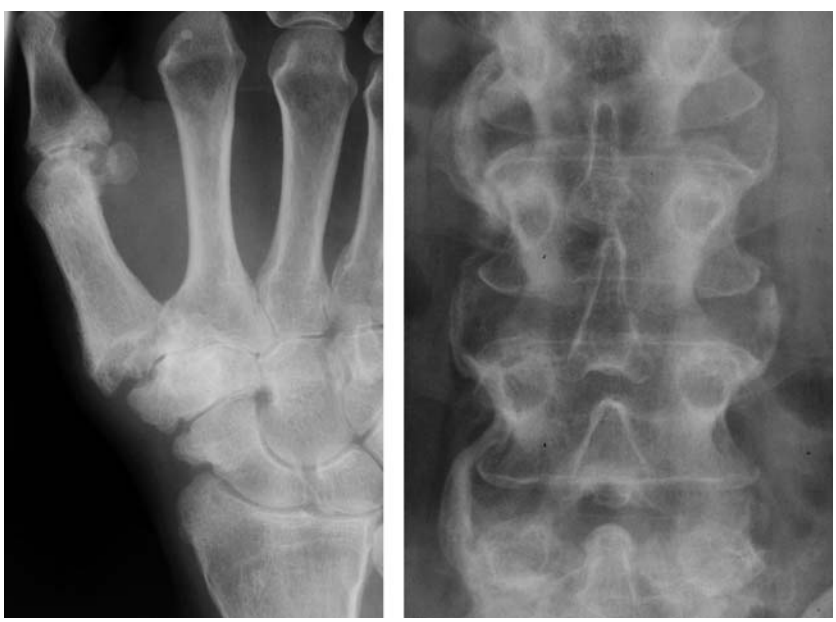

Spondyloarthropathies, Seronegative. Figure 3 Arthritis and spondylathropathy psoriatica. (a) The detailed view of the carpus and radial metacarpus shows peripheral arthritis of the wrist and MCP with cartilage destruction (joint space diminution) and erosions. Proliferations and proliferosions are the typical features in psoriatic arthritis. (b) The lateral view of the lumbar spine reveals ►parasyndesmophytes— here, ossicles and ossifications in a paradiscal and paravertebral location.

Spondyloarthropathy

Spondyloarthropathy comprises the following five diseases: ankylosing spondylitis, psoriatic arthritis, reactive arthritis, enteropathic arthritis in Crohn's disease, and ulcerosing colitis, as well as undifferentiated spondyloarthropathies. SAPHO syndrome may overlap. These are rheumatic inflammatory diseases with imperative (ankylosing spondylitis) or facultative spine and sacroiliacal involvement.

▶Spondyloarthropathies, Seronegative

Spondylolysis

A spectrum of abnormalities involving the pars interarticularis and occurs with a prevalence of 6%. Stress fractures are the most common etiology of spondylolysis. These injuries usually occur in childhood, most frequently in Caucasian males. The incidence is increased with certain activities such as gymnastics, diving, and weightlifting. Ninety percent of these injuries occur at the L5 vertebral level with most of the remainder found at L4. The majority of patients are asymptomatic. Some patients present with nonspecific low back pain exacerbated by activity. Frequently, individuals with stress fractures of the pars interarticularis progress to complete fracture and nonunion. The nonunited pars defect is known as a spondylolytic defect. A minority of patients with spondylolysis will progress to spondylolysthesis, anterior translation of the vertebral body secondary to bilateral pars defects.

▶Fractures, Stress

Spondylosis

▶Degenerative Conditions, Spine

Spontaneous Osteonecrosis of the Knee

A cause of sudden knee pain in the elderly patient that usually involves the weight-bearing portion of the medial femoral condyle, but may also involve the lateral femoral condyle or tibial plateau. Its etiology is likely a form of stress injury and a subchondral stress fracture can often be visualized on MR with an adjacent confluent area of bone edema.

▶Fractures, Stress

Spontaneous Rupture, Splenic

A rupture of the spleen in the absence of trauma. Several different pathological conditions of the spleen may produce spontaneous rupture. In particular, all the pathological processes that cause splenomegaly or diffuse alterations in the structure of the spleen (including infectious, neoplastic, hematologic, immunologic, and storage disorders) may be implicated as causal factors. Spontaneous rupture has also been reported in patients receiving anticoagulant or thrombolytic therapy. The clinical presentation varies from sudden hemorrhage causing symptoms of shock to only vague left upper quadrant pain. US examination represents the initial imaging modality for evaluating such patients, whereas in hemodynamically stable individuals, computed tomography should be performed to identify predisposing splenic alterations as well. Possible findings are splenic hematomas or lacerations; if the splenic capsule is damaged, hemoperitoneum may be present.

▶Trauma, Splenic

Sprengel's Shoulder

Congenital elevation of the scapula.

▶Congenital Malformations of the Musculoskeletal System

Sprue

The adult form of celiac disease of childhood. The term "sprue" is often replaced by the term "celiac disease," especially in the English speaking literature.

▶Malabsorption

Squamous Carcinoma, Gallbladder

Represents about 3.3% of gallbladder carcinomas. Typically, this tumor shows squamous epithelial differentiation with keratinization with no tubular structure formation or mucin production. It is characterized by a well-localized growth. Visceral metastases and lymph node involvement are rare with large primary tumors. Various etiological theories have been proposed for the origin of this tumor, including heterotopic squamous epithelium, metaplastic squamous epithelium, or areas of squamous metaplasia inside gallbladder carcinoma.

►Neoplasms, Gallbladder

Square Vertebrae and Barrel-Shaped Vertebrae

Square vertebrae and barrel-shaped vertebrae show straightening or convex bulging of the ventral aspect of the vertebral body, mainly in the thoracolumbar junction and lumbar segments as a result of rheumatic inflammation. They occur in ankylosing spondylitis and are most conspicuous in the lateral view of lumbar spine X-ray images.

►Spondyloarthropathies, Seronegative

Staging

The local extent and distant spread of a tumour is classified by using a combination of primary tumour characteristics, nodal status and metastatic disease (TNM). The stage of a tumour will predict the probable prognosis as well as optimising treatment requirements.

►Neoplasms, Gastroduodenal

Steal Syndrome Vertebral

Elias N. Brountzos
Department of Radiology,
Athens University, Medical School, Greece
ebrountz@cc.uoa.gr

Synonyms

Subclavian steal syndrome

Definition

A vascular disorder associated with significant stenosis (>80%) or obstruction at the prevertebral part of the subclavian artery or at the origin of the innominate artery that results in retrograde flow in the ipsilateral vertebral artery. This is primarily an imaging finding that maybe accompanied by clinical symptoms in one third of the patients (1).

Pathology

The flow reversal in the vertebral artery can be either permanent, the upper extremity being perfused by the ipsilateral vertebral artery (permanent vertebral steal), or induced after exercise or hyperemia of the ipsilateral arm (latent or temporary steal) (Fig. 1). It has been shown that decreased regional cerebral flow is present in patients with vertebral steal. Other types of vascular steal may be encountered: ►carotid artery steal in the presence of innominate artery occlusive lesion; or in patients with internal mammary artery to coronary artery by pass graft, the presence of a proximal subclavian occlusion may cause ►coronary artery steal phenomenon (Fig. 2).

Clinical Presentation

Symptoms of this syndrome include those of upper limb ischemia, usually presenting as claudication, vertebrobasilar insufficiency (visual disturbances, dizziness, drop attack, ataxia, vertigo, syncope), and anterior circulation transient ischemic attacks. Many patients (35%–85%) with subclavian or innominate artery lesion associated vertebral steal syndrome have also concomitant carotid or vertebral artery occlusive disease, so it is not always possible to attribute their cerebral symptoms to the steal syndrome. Patients with prior internal mammary to coronary artery bypass graft and associated subclavian steal may present with angina.

Imaging

Duplex or color Doppler sonography: Flow reversal or absence of flow may be depicted with accuracy using these modalities. Compression of the ipsilateral brachial artery is accompanied with clear change in the direction of the

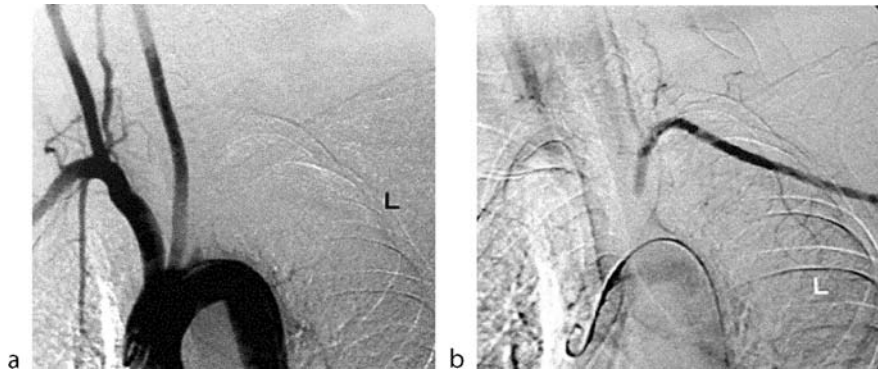

Steal Syndrome Vertebral. Figure 1 (a) arch DSA in the LAO projection in a patient complaining of dizziness during arm exercise, depicts occlusion of the left subclavian artery. (b) arch DSA in the LAO projection of the same patient in a later phase depicts reconstitution of the left subclavian artery from retrograde flow in the left vertebral artery.

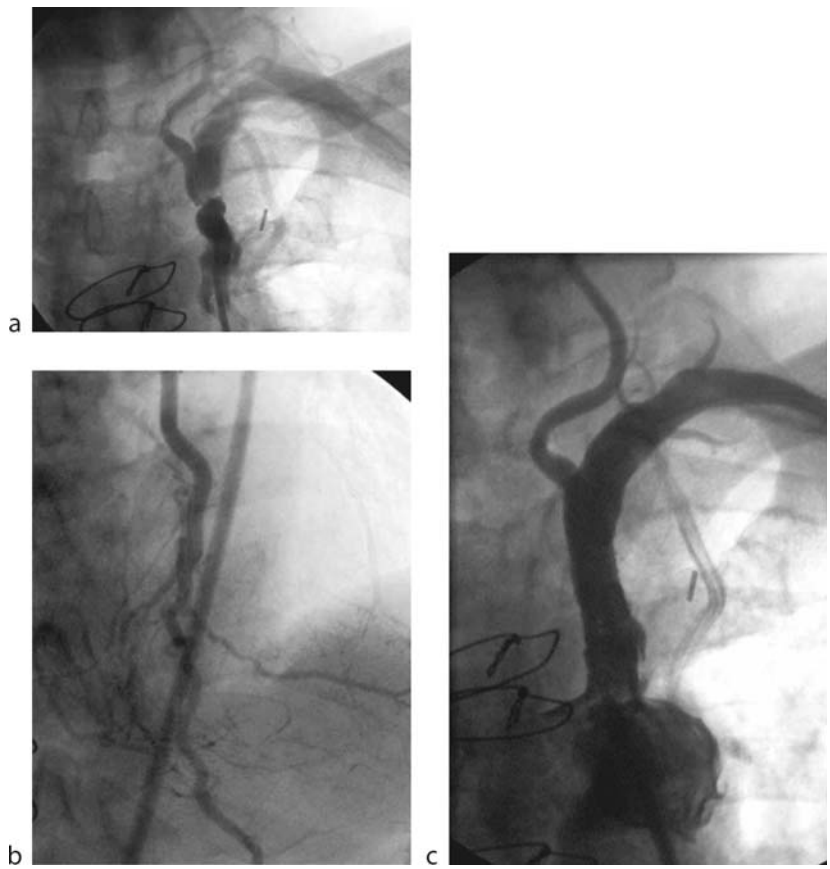

Steal Syndrome Vertebral. Figure 2 (a) Selective DSA of the left subclavian artery in a patient presenting with angina 2 years after left internal mammary artery (LIMA) to coronary artery bypass graft depicts severe stenosis at the origin of the subclavian artery. (b) Selective DSA of the LIMA depicts good patency of the graft, with minimal coronary artery atherosclerotic disease. (c) Arch DSA after placement of a 9-mm balloon expandable stent depicts restoration of the flow in the subclavian artery. Ischemic cardiac symptoms of the patient were eliminated.

flow (2). In patients with the temporary type of vertebral steal syndrome, flow reversal is depicted during exercise or hyperemia of the ipsilateral upper extremity. Diagnostic accuracy is 100% (2).

MRA: The cervical vessels are ideal for MRA. Several techniques have been used to demonstrate the flow reversal in the vertebral artery. These include two-dimensional time-of-flight (2-D TOF) with a selective

presaturation band applied first above and then below the volume of interest. 2-D phase-contrast MRA demonstrates reversal of flow in the superior to inferior direction. 3-D gadolinium-enhanced MRA is excellent in imaging the vertebral arteries, but cannot be used to detect flow direction. Recently it has been suggested that vertebral steal may be suspected when one observes differences in the time of peak enhancement in the vertebral arteries during a bolus-timing examination performed in the setting of a dynamic 3-D MRA (3).

Conventional angiography: Aortic arch DSA with a pigtail catheter placed in the ascending aorta is the gold standard for the depiction of the flow reversal in the vertebral artery, while the proximal arterial lesion can be evaluated in detail.

Interventional radiological treatment: Percutaneous angioplasty with or without stent placement has evolved as an alternative to the standard surgical management. Only symptomatic patients should be treated. Femoral artery approach is more commonly used; but when dealing with complete occlusions, a brachial artery approach may be necessary to cross the obstruction with the guidewire. Balloon expandable stents are recommended because they can be accurately placed. The reversed flow in the ipsilateral vertebral artery has been shown to provide protection against stroke complication.

References

1. Fisher CM (1961) A new vascular syndrome—"the subclavian steal". N England J Med 265:912–913
2. Hennerici M, Neuerburg-Heusler D (eds) (1998) Vertebral Artery System G Thieme Verlag, Stuttgart pp 79–84
3. Wu C, Zhang J, Ladner CJ et al (2005) Subclavian steal syndrome: diagnosis with perfusion metrics from contrast-enhanced MR angiographic bolus-timing examination- initial experience. Radiology 235:927–933

Steatosis, Hepatic

Massimo Bazzocchi, Giuseppe Como, Chiara Franchini
Università dezli Studi di Udine, Udine, Italy
massimo.bazzocchi@med.uniud.it

Synonyms

Fatty change of the liver; Fatty degeneration of the liver; Fatty infiltration of the liver; Fatty liver

Definition

Accumulation of fat in tiny sacs within the hepatocytes.

Pathology and Histopathology

Hepatic steatosis is a common condition which represents a non-specific response to many metabolic disorders and toxic insults. There are many causes of fat accumulation in the liver. Non-alcoholic fatty liver disease (NAFLD) is considered the primary fatty liver disease. The most common risk factors for NAFLD are obesity, diabetes, and elevated cholesterol blood levels. The secondary fatty liver diseases include alcoholic liver disease (ALD), hepatic steatosis occurring in chronic viral hepatitis C (HCV), chronic viral hepatitis B (HBV), chronic autoimmune hepatitis (AIH) and Wilson's disease. In all of these secondary fatty liver diseases, fat accumulation is associated with other abnormalities and is thought to result from liver cell injury. Another type of secondary fatty liver disease is unrelated to other liver diseases, but is due to metabolic disorders. Such causes include certain drugs, some gastrointestinal surgical interventions, malnutrition, parenteral nutrition and metabolic genetic diseases. Simple fatty liver is a benign condition and it occurs due to the accumulation of fat in the liver cells without flogosis or fibrosis. The fat is composed of triglycerides that accumulate in tiny sacs within the liver cells. Simple fatty liver is rapidly reversible after removing the causing factor. Only a minority of patients with simple fatty liver will develop the so-called 'steatohepatitis'. In this entity, fatty infiltration of the liver is associated with inflammation. The inflammatory cells can destroy the hepatocytes leading to necrosis (steatonecrosis). Necrosis is followed by fibrotic phenomena, while the last, irreversible stage is cirrhosis. Hepatic steatosis may present with a diffuse, subtotal, segmental or focal distribution. In diffuse fatty infiltration, the liver may be enlarged and have smooth margins. In non-diffuse steatosis, the fat may have an anatomic distribution (segmental steatosis) or a non-anatomic distribution (focal steatosis). The focal distribution of fat is related to local differences in portal perfusion; areas with lower portal supply tend to accumulate less fat. Some areas are commonly spared by fatty infiltration, such as the dorsal portion of the IV segment just anterior to the portal vein, the gallbladder bed and the medial portion of the left lobe, along the great interlobar fissure. In these regions, the portal flow is decreased due to anomalous systemic venous drainage into portal venules from structure such as the gallbladder or the stomach. In other regions of the liver, focal sparing in fatty infiltration may reflect segmental portal vein obstruction (1).

Clinical Presentation

Simple steatosis and steatohepatitis give very slight, aspecific symptoms. Actually, most patients are completely asymptomatic, but they may occasionally have vague

right upper-quadrant abdominal pain. The symptoms and signs of liver failure include jaundice, severe weakness, loss of appetite, nausea, vomiting.

Imaging

In case of steatosis, the typical finding at ultrasound (US) is the so called '►bright liver', occurring due to a diffuse increase in echogenicity of the hepatic parenchyma, characterised by the presence of numerous, fine, tightly packed echoes of high signal intensity uniformly distributed throughout the liver parenchyma (Fig. 1). The liver may be enlarged with smooth margins. When the hyperechogenicity is particularly strong, a significant attenuation of the signal may be observed. In diffuse forms the increase of echogenicity is homogeneously distributed in the hepatic parenchyma whereas in non-diffuse forms some areas are not interested by the fatty infiltration. These islands of normal liver tissue are called ►'skip areas' or 'spared areas' and appear as relatively hypoechoic areas. Typically, the skip areas are found in the gallbladder fossa, in the IV segment anteriorly to the portal vein or, in individuals with anomalous venous drainage through the gastric veins, in the medial portion of the left lobe, along the great interlobar fissure. In focal steatosis, hyperechoic areas of various sizes with a 'geographic' distribution are depicted in a normally echogenic liver. In rare cases, only the portion of the IV segment just adjacent to the portal vein, is involved by steatosis. This ►focal fatty infiltration appears as a hyperechoic area (2). Focal fat and spared areas can mimic tumour lesions, while heterogeneous fat can sometimes be difficult to distinguish from diffuse malignant diseases. At Doppler US, the finding of normal hepatic vasculature, without any dislocation or interruption, may suggest the diagnosis of steatosis (Fig. 2a). At contrast-enhanced US, skip areas and focal fatty changes become homogeneous and isoechoic with respect to the surrounding parenchyma, having the same vascularisation as the normal liver. The increased echogenicity of the hepatic parenchyma can modify the relative echogenicity of other focal lesions. A quite common finding is the presence of haemangiomas showing a relative hypoechoic appearance over a hyperechoic liver. Furthermore, haemangiomas detected at US before the onset of steatosis may not be visibile or have a reduced detectability in a hyperechoic background. In contrast, hypoechoic lesions, such as metastases, become more clearly depicted, due to the high contrast with the surrounding parenchyma (3). Computed tomography (CT) is less sensitive, but more specific than US in diagnosing hepatic steatosis. On unenhanced CT scans, the hepatic parenchyma has an attenuation value significantly lower than the spleen and the expected normal liver (normal values 45–65 HU), sometimes showing a density close to the water (0–15 HU).

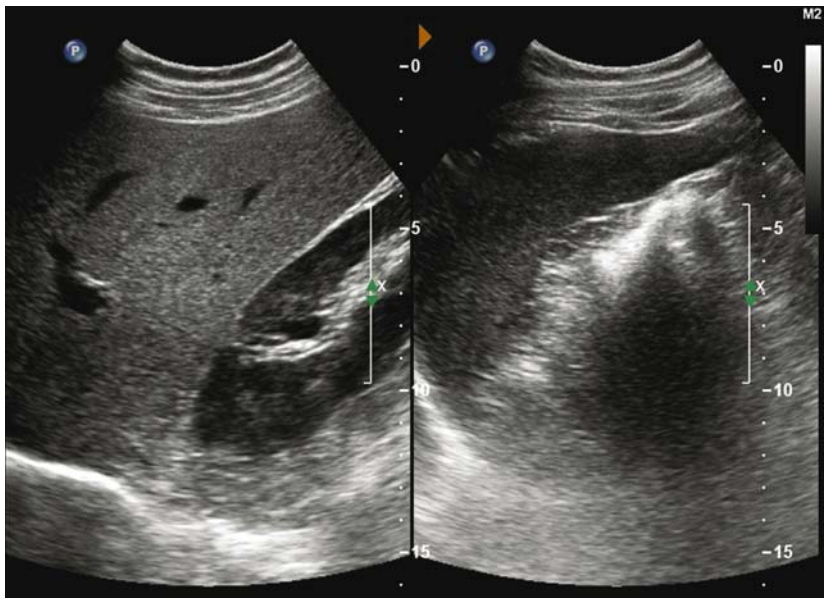

Steatosis, Hepatic. Figure 1 In case of steatosis the typical finding at ultrasound (US) is the so-called 'bright liver', occurring due to a diffuse increase in echogenicity of the hepatic parenchyma, characterised by the presence of numerous, fine, tightly packed echoes of high signal intensity uniformly distributed throughout the liver parenchyma. We can see the hyperechogenicity of the liver if compared to the echogenicity of renal parenchyma (on the *left*) and of spleen parenchyma (on the *right*).

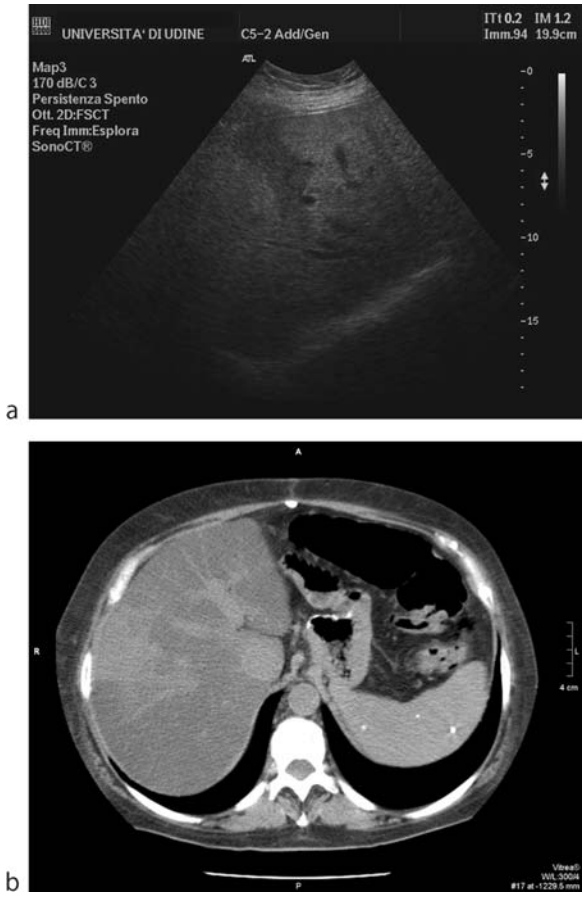

Steatosis, Hepatic. Figure 2 Segmental or focal forms of steatosis: the hepatic parenchyma appears inhomogeneous with areas of hyperechogenicity and normal echogenicity in the US study (a) and areas of hypodensity and areas of normal density in the CT scan (b). Distinctive features of focal fatty infiltration are non-spherical shape, absence of mass effect, normal vascular architecture, segmental or subsegmental distribution.

A reduction in density at unenhanced CT scans is also observed in amyloidosis and glycogen storage disease. Another peculiar finding in steatosis is the clear evidence of hepatic vessels on unenhanced scans which appear relatively hyperdense compared to the fatty liver (►contrast reversal) (Fig. 3). In segmental and focal forms, the hepatic parenchyma appears inhomogeneous with areas of hypodensity and areas of normal density. Distinctive features of focal fatty infiltration are non-spherical shape, absence of mass effect, normal vascular architecture, segmental or subsegmental distribution (4) (Fig. 2b). After contrast medium administration, the difference in density between normal and fatty liver does not change. Conventional MR SE sequences have not been proven to be useful in detecting fatty infiltration of the liver on the basis of signal intensity and relaxation times. Actually,

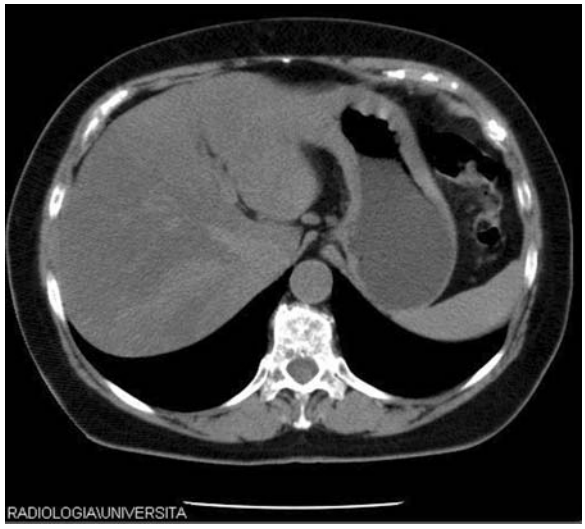

Steatosis, Hepatic. Figure 3 On unenhanced CT scans, the hepatic parenchyma has an attenuation value significantly lower than the spleen and the expected normal liver (normal values 45–65 HU), sometimes showing a density close to the water (0–15 HU). Peculiar finding in steatosis is the clear evidence of hepatic vessels on unenhanced scans which appear relatively hyperdense compared to the fatty liver (contrast reversal).

hepatocytes with fatty degeneration are usually mixed with normal hepatocytes within the voxel volume, thus preventing substantial changes in signal intensity. Only when the concentration of fatty cells is very high, there is a brightening of fat-containing areas on T1-weighted images, whereas T2-weighted images usually do not show any change in signal intensity. The hyperintensity of the fatty liver on T1-weighted scans creates a marked contrast with hypointense lesions, improving their detection. The low sensitivity of T2-weighted scans in depicting fatty changes can be useful to exclude the presence of a focal liver lesion in case of focal steatosis. Grading fatty infiltration of the liver is not possible using conventional MR because of its insensitivity to fat. MR techniques based on the frequency difference between water and fat can be successfully used for this purpose. These techniques rely on the difference in resonance frequency between water protons and the methyl and methylene protons of fatty acid chains (chemical shift phenomenon). Two populations of protons (water and fat) exist in fatty livers. A specific method for the detection of the two populations of protons has been developed (Dixon's method). It consists in the acquisition of two images in which water and fat protons are 'in-phase' and 'out-of-phase'. In tissues where fat and water protons populations are equally represented, as in fatty liver, a significant signal loss is seen on the out-of-phase scans (Fig. 4a, b). By using this method, areas of focal fatty infiltration may be diagnosed due to the lower signal

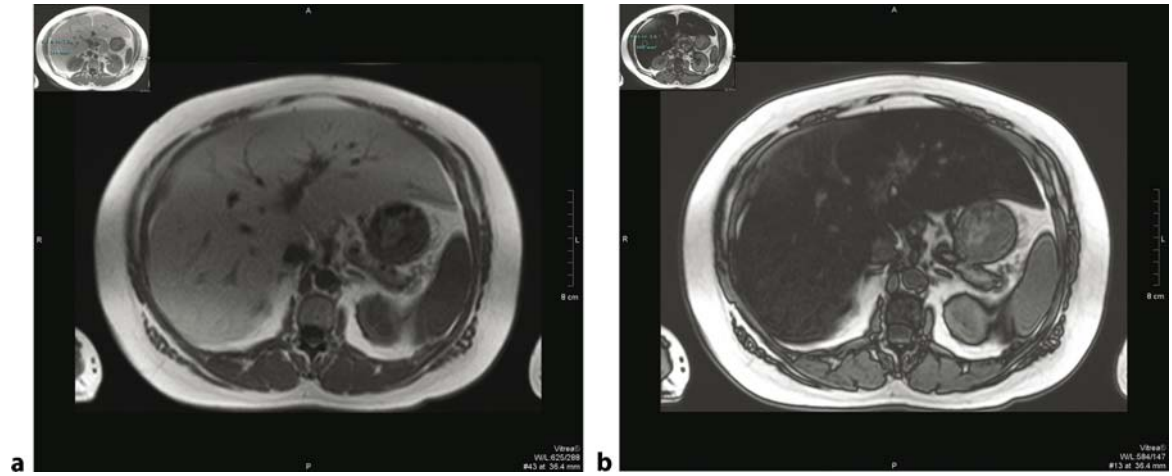

Steatosis, Hepatic. Figure 4 MR scan in-phase and out-of-phase of fatty liver: a specific method for the detection of the two entity of fatty infiltration of the liver has been developed (Dixon's method). It consists in the acquisition of two images with two different TE in which water and fat protons are in the first 'in-phase' (a) and in the second 'out-of-phase' (b). In tissues where fat and water proton populations are equally represented, as in fatty liver, a significant signal loss is seen on the out-of-phase scans.

intensity compared to the surrounding liver in the out-of-phase images. In these images focal liver lesions in a fatty liver show a high contrast and their detection is increased (1). Fat-suppressed images may be also used, but they have a lower sensitivity for fatty infiltration compared to the out-of-phase sequences. After administration of hepato-specific MR contrast agents, fatty and normal hepatic parenchyma show similar contrast uptake, becoming isointense. This finding can rule out malignancy in case of focal fatty infiltration and skip areas.

Nuclear Medicine

Tc99m-colloid scintigraphy can differentiate focal liver lesions from focal fatty sparing and focal fatty infiltration: in fatty liver, the colloid uptake by Kupffer cells may vary depending on the degree of steatosis. A ►spared area shows a greater uptake than the surrounding liver whereas a focal fatty infiltration has a variable uptake. Malignant focal liver lesions have no uptake.

Diagnosis

US is the most sensitive imaging technique in the diagnosis of steatosis and it is usually the only examination to be performed in these cases, due to the low clinical relevance of this affection. Anyway its specificity is limited, because it cannot distinguish diffuse infiltration from hepatic fibrosis. Furthermore, in case of focal steatosis or spared areas in atypical locations, US alone may not be able to exclude the presence of a focal liver lesion. The use of Doppler US and US contrast media can be helpful by demonstrating the presence of normal vascular architecture within the focal alterations. CT is highly specific in diagnosing fatty infiltration of the liver, although it is not as sensitive as US. In those cases in which CT findings do not allow to reach a differential diagnosis, particularly in segmental or focal steatosis, MR can give a definite characterisation. In particular, the in-phase and out-of-phase sequences are very useful in assessing fatty infiltration of the liver and the use of hepato-specific MR contrast agents allow to rule out malignancy in case of focal steatosis and spared areas.

Bibliography

1. Lencioni R, Bartolozzi C (2003) Diffuse liver disease. In: Magnetic Resonance Imaging in Liver Disease. Thieme, New York
2. Rubaltelli L, Savastano S, Khadivi Y et al (2002) Targetlike appearance of pseudotumors in segment IV of the liver on sonography Am J Roentgenol 178(1):75–77
3. Hisham T, Philip WR, Randall R et al (2002) Sonography of diffuse liver disease. J Ultrasound Med 21(9):1023–1032
4. Mergo PJ, Ros PR (1998) Imaging of diffuse liver disease. Radiol Clin North Am 36(2):365–375

Stenosis

►GI Tract, Pediatric, Congenital Malformations

Stenosis, Aortic, Abdominal

Dierk Vorwerk
Klinikum Ingolstadt GmbH, Direktor des Institutes für diagnostische und interventionelle Radiologie, Ingolstadt, Germany
dierk.vorwerk@klinikum-ingolstadt.de

Synonyms

Aortic obstruction; Aortic syndrome

Definition

Aortic stenosis usually occurs in the infrarenal segment of the abdominal aorta. If stenotic, it leads to bilateral claudication of both legs including the upper thigh muscles.

Bilateral absence or weakness of femoral pulses is usually found.

Pathology/Histopathology

In more than 90% of cases, the cause for infrarenal aortic obstruction is due to atherosclerotic disease (2). Clinically, simple infrarenal aortic stenoses with no relation to the aortic bifurcation are infrequently found, but a stenosis of both the very distal aortic segment and the common iliac arteries is more frequent. This may be complicated by an acute or subacute thrombosis of the aortic bifurcation known as Leriche's syndrome. A small distal aortic caliber, especially in female patients, may be a predisposing factor. Atherosclerotic stenosis above the orifice of the inferior mesenteric artery is rare (2).

Embolic occlusion of the distal aorta is, on the contrary, exceptional, but may occur in patients with arrhythmias.

Other rare causes of aortic obstruction are fibromuscular dysplasia, Takayasu's disease, and retroperitoneal fibrosis.

The typical age of patients with aortic obstruction is between 40 and 70 years. In aortic occlusions, 55% are located at the level of the aortic bifurcation, 8% involve the complete infrarenal segment, and 37% involve aortic segments alone (2).

Collateral pathways are manifold *via* lumbar, epigastric, and mesenteric arteries.

Clinical Presentation

Clinical symptoms in aortic obstruction are bilateral claudication predominantly with upper thigh symptoms – which may be similar to findings in spinal angina – buttock pain, and erectile dysfunction in males. In occlusions, acute bilateral ischemia may occur if no preexisting stenotic process has promoted earlier development of collateral pathways.

Imaging

Many imaging modalities can be used to make the diagnosis of aortic obstruction. Color-coded duplex sonography, magnetic resonance angiography (MRA), computed tomography (CT), CT angiography (CTA), and intraarterial angiography are useful tools for detecting the location and extent of an aortic obstruction. Due to access limitations, angiography is preferably performed *via* a transbrachial access if the clinical findings suggest an aortic obstruction.

Nuclear Medicine

Nuclear medicine plays no particular role in the diagnosis of aortic stenosis.

Diagnosis

Diagnosis is reliably achieved by angiography, CT, CTA, and MRA. Detection by duplex sonography is sometimes limited due to unfavorable anatomic conditions

Interventional Radiological Treatment

More and more, aortic aneurysmal disease is becoming a field of interest for interventional radiologists and may be combined with atherosclerotic obstructive disease.

Indications for Percutaneous Treatment

Indications for percutaneous versus surgical treatment largely depend on the location, extension, acuteness, and type of obstruction.

Accepted indications for sole balloon angioplasty are:

1. concentric segmental stenosis
2. short-segment aortic bifurcational stenosis

Balloon angioplasty may be followed by stent insertion in the case of insufficient luminal gain after adequate balloon angioplasty or the occurrence of significant dissection after percutaneous transluminal angioplasty (PTA).

Balloon angioplasty is contraindicated if a complete calcified ring is present at the site of obstruction, since aortic rupture has been occasionally reported under these circumstances (3). According to Laplace's law, the aorta is

theoretically more easily prone to rupture than smaller-diameter vessels such as the iliac artery. In these cases, primary placement of a stent graft can be considered.

Long-segment diffuse disease of both the aorta and iliac arteries may be considered as a contraindication, while surgical aortobifemoral bypass grafts might be a better choice.

Bifurcational aortic stenosis may also be treated by balloon angioplasty using a simultaneous "kissing balloon" technique in order to dilate the distal aortic segment and both iliac orifices. Stent implantation has been increasingly used to achieve a stable postangioplasty widening by use of kissing stents in the distal aorta and both iliac arteries.

In the case of distal aortic occlusion, few reports exist on remodeling the distal aortic segment or the aortic bifurcation by use of metallic stents (4, 5). In these difficult situations, use of advanced interventional techniques over simple balloon angioplasty is certainly of advantage.

Technical Aspects

There are no major differences between the aortic and the iliac segment concerning techniques of lesion passage or traversal of occluded segments, whether they are located purely in the aortic segment or also involve the iliac segment. This is also true for balloon dilation, which does not differ significantly from angioplasty elsewhere. A large diameter of the aortic lumen, however, is a particular problem.

Kissing balloon technique: Until recently, a major difficulty was the lack of suitable balloons with sufficient diameters of 16–20 mm. Thus, a double or triple balloon technique was recommended to open the aortic stenosis to a sufficiently large diameter. The aortic lumen can be widened to its original diameter with two or three kissing balloons that are inserted by a bifemoral and an additional transbrachial approach and are inflated simultaneously.

A kissing technique is still recommendable for dilatation of bilateral stenosis of the aortic bifurcation and the very distal aortic segment close to the bifurcation that allows remodeling of the aortic bifurcation.

Single balloon technique: Recently, large-diameter balloons, from 16 to 25 mm, have become available (Boston Scientific, Cordis), allowing the use of a single balloon technique by a unifemoral approach. With these balloons, it is strictly necessary to locate the balloon within the aortic lumen not overriding the bifurcation in order to avoid overdilatation and rupture of the proximal iliac segment.

Stent insertion into the infrarenal aortic segment obeys the same rules as elsewhere. Use of a stent of appropriate size, at least 14–16 mm, is necessary to avoid undersizing. The largest stent diameter can be achieved by use of the balloon-expandable Palmaz XXL stent (Johnson and Johnson) that can be mounted on a large balloon and inflated up to 25 mm in diameter.

Single stent technique: In lesions without involvement of the aortic bifurcation, a single stent can be implanted with no specific technical requirements. The type of stent that should be used depends on the experience of the interventionalist. This is particularly true if the lesion is of considerable distance from the bifurcation. Depending on the length of the stent or the location of the lesion, overstenting of the inferior mesenteric artery may be unavoidable.

However, if the lesion ends very close to the bifurcation, placement of a single stent, especially of a balloon-expandable stent, may become difficult without overdilation of an iliac orifice. Under these circumstances, use of a self-expanding stent may be advantageous, while the aortic bifurcation is protected by a cross-over catheter inserted *via* a contralateral approach.

An alternative technique in very distal aortic lesions or bifurcational lesions is use of kissing stents.

Kissing stent technique: In analogy to the kissing balloon method, stents of preferably an identical diameter and length are placed in kissing fashion within the distal aorta with its distal end in the common iliac artery. Very frequently, the stents tend to meet the opposite aortic wall. Thus – instead of being shaped in a kissing fashion – they cross each other forming a mirror-sided artificial iliac orifice.

There are not many reports on this technique and some questions remain open. Especially in stenotic lesions, it is not yet known whether there are potential sequelae from using two open stents that will remain partly nonendothelialized in their aortic portion and may lead to embolic disease or a higher tendency for thrombosis. Whether covered stents are advantageous in these cases is still under discussion. Use of noncovered stents is less problematic in distal aortic occlusive disease.

If a kissing stent technique is applied, it is mandatory that the proximal ends of both stents are exactly parallel to avoid one stent compromising the inflow into the other. For this reason, use of noncompressible stents such as the Palmaz stent or the new Perflex stent (both Johnson and Johnson), which are both balloon-expandable, seems of benefit.

Results

As reported in the literature, aortic PTA has an excellent outcome compared to other PTA sites.

A primary success rate of 95% and a cumulative patency of 98% after 1 year and 80% after 5 years have been reported from different series (6).

Single cases of aortic stenting in stenoses have been reported, usually associated with an excellent outcome. Long reported on two cases of successful stenting in Leriche's syndrome (7), and Dietrich reported on six patients with chronic aortic occlusion who underwent thrombolysis and stenting by use of Palmaz stents (8). The mean patency was about 11 cases with success in all.

Complications

Complications that may occur after aortic dilation are not different from those in other vascular areas; however, they might be of major clinical impact. While severe dissection, recollapse, or residual stenoses are simply treatable by additional stent implantation, aortic rupture has been reported rarely but is potentially life threatening, and therefore patients must undergo immediate surgery. To limit the extent of exsanguination, a large occlusion latex balloon (Boston Scientific) should be positioned just below the renal arteries or covering the site of rupture and left inflated until the patient is prepared for surgical repair. To avoid this complication, CT is recommended before the intervention to exclude complete or nearly complete circular calcification of the aortic wall, which is said to be a risk factor for rupture.

Theoretically, a covered stent graft may be placed across the site of rupture percutaneously; however, this method has only been reported for iliac arterial rupture and may risk occlusion of major collaterals and the inferior mesenteric artery.

Embolization of occlusion material may occur in less than 1% of cases (6).

Subacute complications include thrombosis, which has not been reported for pure aortic dilation or stenting, but is a risk in remodeling techniques of aortic bifurcations. In these cases, the patient may be predisposed to thrombosis by adjacent aortic disease with plaques hanging over the stent orifice, thus causing inflow obstruction or by adjacent outflow problems. If a technical reason has caused stent or post-PTA thrombosis, surgery is a reasonable option. If not, thrombolysis may be tried.

Thanks to their large diameter, reobstruction of aortic stents occurs rarely; however, patients may undergo repeat balloon dilatation as for iliac stents. In kissing stents, obstruction may be caused by neointimal hyperplasia that may be treated with reballooning, atherectomy, or a second stent.

References

1. The TASC Working Group Management of peripheral arterial disease (PAD) (2000) Transatlantic inter-society consensus (TASC). J Vasc Surg 31 S1–S296
2. Vollmar J (1996) Rekonstruktive Chirurgie der Arterien. Stuttgart, Thieme, pp 207–214
3. Berger T, Sörensen R, Konrad J (1986) Aortic rupture. A complication of transluminal angioplasty. Am J Roentgenol 146:373–374
4. Strecker E, Hogan B, Liermann D et al (1993) Iliac and femoropopliteal vascular occlusive disease treated with flexible tantalum stents. Cardiovasc Intervent Radiol 16:158–164
5. Dietrich EB, Santiago O, Gustafson G (1993) Preliminary observation on the use of the Palmaz stent in the distal portion of the abdominal aorta. Am Heart J 125:490–500
6. Rholl K, Van Breda A (1994) Percutaneous intervention for aortoiliac disease. In Strandness E, Van Breda A (eds) Vascular Diseases. Churchill Livingstone, New York, pp 433–466
7. Long A, Gaux J, Raynaud A (1994) Infrarenal aortic stents. Initial clinical experience and angiographic follow-up. Cardiovasc Intervent Radiol 16:203–208
8. Dietrich EB (1993) Endovascular techniques for abdominal aortic occlusions. Int Angiol 12:270–280
9. Becker G, Katzen B, Dake M (1989) Noncoronary angioplasty. Radiology 170:921–940

Stenosis, Artery, Iliac

In contrast to iliac occlusions, in iliac artery stenosis the arterial lumen is narrowed but not yet completely occluded.

▶ Iliac Artery Occlusion

Stenosis, Artery, Renal

Philippe Otal, F. Joffre
CHU, Toulouse, France
otal.p@chu-toulouse.fr

Synonym

Renal artery stenosis (RAS)

Definition

Renal artery stenosis (RAS) is defined by a narrowing of the renal artery trunk or proximal branches by 50% or greater, expressed as a percentage of the diameter of a normal renal artery at the same level. There has been an increase in the incidence of RAS. This is partially due to improved detection imaging techniques such as color Doppler ultrasound (CD-US), computed tomography angiography (CTA), and magnetic resonance angiography (MRA). Another reason is the greater awareness in screening patients with RAS, due to the deleterious clinical consequences in cases of spontaneous evolution

and the interesting possibilities of proposed simple endovascular treatment modalities. However, much controversy remains, mostly concerning the benefit-risk ratio of RAS treatment.

Pathology

A variety of pathologic lesions may cause RAS, but the main etiologies are atherosclerosis (75–80%) and fibromuscular dysplasia (15–20%). Atherosclerotic RAS is noted in individuals of either gender who are 50 years of age or older, and it is frequently associated with other atherosclerotic peripheral diseases. The lesion is generally proximal and concerns the first centimeter of the trunk, and is frequently related to atheromatous aortic plaques extending into the proximal part of the renal artery. Fibromuscular dysplasia generally occurs in women in the second to fifth decades of life and is mainly located in the medial and distal thirds of the renal artery trunk. Fibromuscular dysplasia represents about 90% of pediatric RAS. Uncommon causes of RAS are vasculitis (Takayasu's or Buerger's disease, polyarteritis nodosa), neurofibromatosis, radiation-induced RAS, retroperitoneal fibrosis, aortic dissection, renal artery aneurysm or dissection, and external compression. A special situation is represented by RAS of a transplanted kidney, which occurs in 5–10% of cases (1).

An important point to consider is the spontaneous evolution of RAS. The risk of worsening of a fibrodysplastic RAS varies between 10 and 40% according to the pathologic lesion. Concerning the atherosclerotic lesion, progression of RAS to arterial occlusion and atrophy of the kidney is directly correlated to the degree of the stenosis. The viability of the kidney may be totally or partially preserved with collaterals, but its function is likely to be severely impaired and revascularization procedures more difficult to perform. Conversely, the progression of atherosclerotic RAS can be slowed by lifestyle changes and aggressive statin therapy.

Clinical Presentation

Significant RAS can be asymptomatic in about 10–15% of cases. However, high-grade RAS is generally responsible for arterial hypertension and renal insufficiency. ►Renovascular hypertension is the most common cause of secondary hypertension and depends on the renin–angiotensin system. Insufficiently controlled hypertension can lead to heart failure with frequent flush pulmonary edema and/or further deterioration of renal function. RAS can also cause ►ischemic nephropathy in cases of severe bilateral stenosis or in a single kidney.

Because severe RAS may be present in patients with normal blood pressure and no azotemia, and because it is difficulty to assert that symptoms are related to RAS, the main issue is to identify those patients in whom RAS is responsible for their symptoms and who are amenable to revascularization.

Clinical situations suggestive of RAS include:

- Onset of hypertension before age 30 years or after 55 years
- Severe hypertension in a child of a female patient between 20 and 50 years
- Hypertension that is malignant, accelerated, or refractory to appropriate treatment
- Unexplained or progressive renal dysfunction
- Development of acute or subacute azotemia after therapy with angiotensin-converting enzyme (ACE) inhibitors or angiotensin receptor blockers
- Recurrent pulmonary edema
- Diffuse atherosclerotic vascular disease
- Abdominal bruit
- Unilateral unexplained small kidney.

Imaging

Different modalities are available for imaging RAS.

CD-US has become a leading technique for screening RAS. It allows the following:

- *Direct visualization of the renal arteries and detection of hemodynamically significant stenosis* (Fig. 1). A complete examination of both renal artery trunks can be achieved in 80–90% of cases (2). The main criteria are a peak systolic flow velocity of 180 cm/sec or more and a renal-to-aortic ratio of peak systolic velocity >3.5. The technical limitations and difficulties in detecting accessory renal arteries explain the mixed results, with sensitivity between 50 and 95% for detecting RAS. Other changes are less contributory: turbulent flow in the stenotic area and absence of signal in cases of occlusion.
- *Analysis of waveforms of renal branches downstream from the lesion.* This yields quantitative criteria that improve the global sensitivity of detection.
- *Measurement of the distal resistive index to predict clinical success after revascularization.* Radermacher et al retrospectively found a cut-off point of 0.80 useful for separating patients who failed to show a clinical response to revascularization ($IR \geq 0.80$) compared with patients who did show a favorable response ($IR < 80$) (3). However, these interesting results were not confirmed in others studies and cannot be considered conclusive.

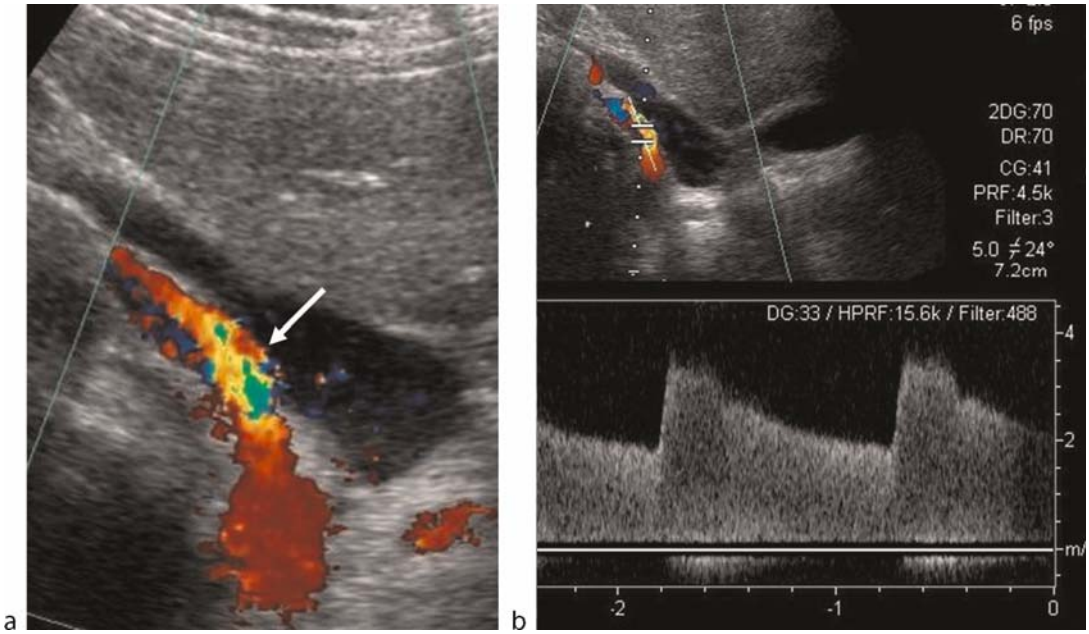

Stenosis, Artery, Renal. Figure 1 Color Doppler ultrasonography of a high-grade truncal right renal artery stenosis. (a) Presence of an aliasing artifact (*arrow*) at the origin of the right renal artery. (b) Doppler spectrum shows flow acceleration close to 400 cm/sec.

- *Morphologic information about the kidneys*: global or segmental atrophy (a long axis inferior to 7–8 cm is generally considered a contraindication for revascularization), calcifications of the renal artery or aortic wall, aortic aneurysm, or other renal-associated lesions.

CD-US is noninvasive and inexpensive. It can be performed on patients with renal insufficiency and without necessitating discontinuation of their hypertensive medications. It is of great interest for monitoring patients after treatment. Limitations are the technical difficulties associated with excessive bowel gas or body habitus and the lack of generalized expertise in its use.

CTA: With the advent of helical CT and particularly with the multidetector technology, it is now possible to provide angiographic images of renal arteries with excellent spatial resolution (submillimetric). The best reconstruction algorithms are maximum intensity projection (MIP) and volume rendering (Fig. 2a). Sensitivity is about 90–95% and specificity 95% (4). Besides depiction of the lesion, CTA provides important pretherapeutic information, including the exact anatomic type of the stenosis and the presence of aortic associated plaques and calcifications (5).

Limitations are the use of ionizing radiation and iodinated contrast media, which is a relative contraindication in patients with renal insufficiency.

MRA: MRA (Fig. 3) has made significant progress in the past few years, particularly with the use of gadolinium-enhanced three-dimensional sequences. Compared to arteriography, sensitivity and specificity are superior, at 95 and 90%, respectively. However, there is a tendency to overestimate the stenosis, and spatial resolution is inferior compared with CTA (2). In addition to three-dimensional morphologic information, it is now possible to provide hemodynamic data about the parenchymal perfusion.

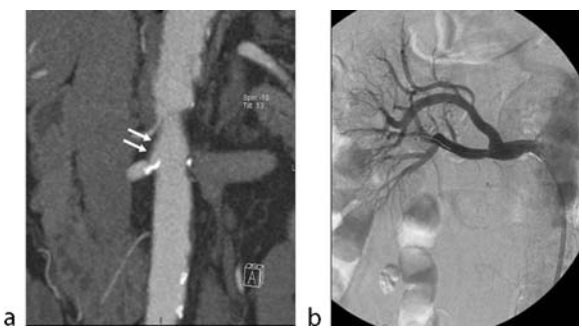

Stenosis, Artery, Renal. Figure 2 Computed tomography angiography diagnosis and percutaneous transluminal renal angioplasty of renal artery stenosis. (a) Curvilinear reconstruction of the right renal artery ostium shows calcification and aortic atheromatous plaque extending into the renal artery (*arrows*), which is responsible for a significant stenosis. (b) Angiography performed immediately after stenting.

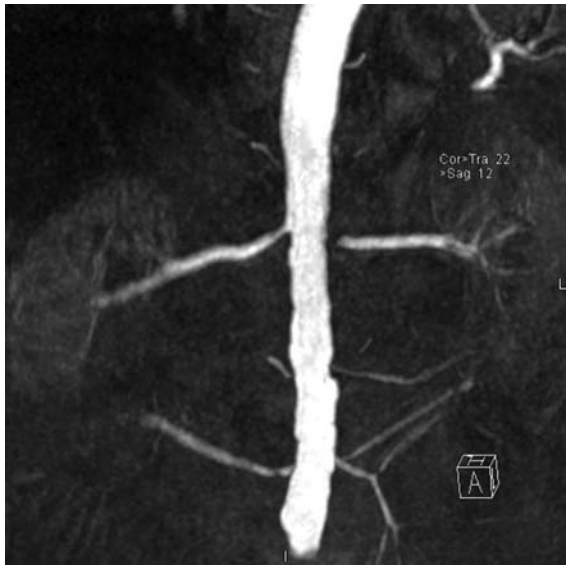

Stenosis, Artery, Renal. Figure 3 Magnetic resonance angiography of bilateral renal artery stenosis in a patient with ischemic nephropathy. The stenosis is estimated at 70% on the right side, whereas the left lesion is overestimated as a pseudo-occlusion.

The main limitations involve cost, patient issues such as claustrophobia, the presence of metallic stents, and evaluation of small branches such as accessory arteries.

Intra-arterial angiography: Intra-arterial angiography currently has no role in screening RAS. Its greatest advantage is its ability to guide intervention and control endovascular correction of the lesions.

Nuclear Medicine

The role of renal scintigraphy is controversial. ACE inhibitors (captopril) decrease the perfusion pressure of the glomerulus with a resultant drop in the GFR. In patients with unilateral RAS, captopril induces significant changes of the scintigraphy compared with the baseline curve. Such changes are not observed in the contralateral normal kidney. In clinical practice, the sensitivity varies between 60 and 80%, and the specificity is 59% (5). Some factors decrease the sensitivity: bilateral RAS (30%), renal insufficiency, and chronic use of ACE inhibitors.

Diagnosis

The roles of RAS imaging are multiple: (i) screening of RAS, (ii) providing precise morphologic information to determine the best therapeutic strategy, (iii) establishing relationships between RAS and symptoms, (iv) guiding endovascular treatment, and (v) monitoring the patient after treatment. Several considerations must lead to a rigorous selection of patients before imaging: (i) the high cost of imaging, (ii) the relatively low prevalence of RAS in the general population, (iii) the frequency of association of RAS, without evident relationships, with essential hypertension, renal failure, or both, (iv) difficulties in predicting a real benefit after revascularization, (v) potential risks of intervention, and (vi) the unpredictability of spontaneous worsening of RAS. Clinical features that must prompt further evaluation of RAS are listed in Table 1.

Screening of RAS must be done by CD-US. Some centers use captopril scintigraphy, but the cost-effectiveness is probably inferior to that of CD-US; operator expertise is increasing, and the probability of failing to detect significant RAS is very small. MRA and CTA are not screening methods except in cases of high clinical suspicion and indeterminate diagnosis after CD-US. CTA or MRA (in cases of renal insufficiency) can also be used in cases of difficult therapeutic decisions for patients at risk (renal insufficiency, complex atherosclerotic lesions).

Endovascular Treatment

Since the first description in 1978 by Gruntzig, ►percutaneous transluminal renal angioplasty (PTRA) has been progressively considered the initial therapeutic approach to RAS whenever possible. Although truncal RAS can be treated very well with angioplasty alone (particularly fibrodysplastic lesions), the introduction of renal artery stenting has considerably improved the anatomic results, and primary stent placement is nowadays the treatment of choice, mainly for the more frequent atheromatous lesions located in the ostial zone and the first centimeter of the artery. With the use of stenting, the global results are comparable to those of surgery but with lower morbidity and mortality.

PTRA is routinely performed *via* a femoral approach, more rarely *via* a brachial approach, using microguidewires (0.018 in.) and microcatheters (3–4 French). Renal arteriography is the first step in endovascular treatment of RAS. It provides useful information for determining the therapeutic strategy, for guiding the procedure, and for evaluating the immediate results. Balloon catheters and stents are generally 12–20 mm in length and 5–6 mm in diameter. Periprocedural treatment consists of intra-arterial heparin, clopidogrel (plavix), and acetylsalicylic acid (aspirin). Postintervention care consists of daily monitoring of renal function and blood pressure before discharge. CD-US is the main tool for patient follow-up for evaluating the renal artery patency. It must be performed at 6 and 12 months and annually thereafter, except in cases of symptom recurrence.

The more recent studies (largely using stents) show a primary success rate between 95 and 100% (6). Midterm recurrences are observed in 15% of cases and are closely related to the quality of the immediate result. Intervention-related mortality is low, at 1%. Major complications occur in less than 5% of cases, and immediate surgery is required in less than 0.5% of patients. Clinical results are not always related to anatomic results and are totally different in atheromatous patients and in cases of fibromuscular dysplasia. In hypertension, a clinical benefit (cure or improvement) is obtained in approximately 50% of all atheromatous stenoses and in 85% of stenoses due to fibromuscular dysplasia. Results are worse in patients with renal insufficiency, many of them being older with extensive atheromatous lesions and probably nephroangiosclerosis. A clinical benefit is obtained in approximately 50% of cases.

Despite the good results for several categories of patients such as those with fibromuscular dysplasia, multiple points of controversy persist, particularly concerning the indications. Due to morbidity of treatment and limited efficacy in some patient categories, a multidisciplinary discussion estimating risks and benefits is mandatory before making therapeutic decisions. Some anatomic parameters such as difficulties of arterial access, the lesion's complexity and severity, diffusion of atherosclerotic lesions, the importance of aortorenal plaques, the presence of calcifications, and kidney size should be taken into account and are often necessary to evaluate before even discussing CTA or MRA. Age, general status, comorbidities, and expected duration of life are other important parameters.

In terms of evidence-based medicine, the universally recognized indications for PTRA are significant and accessible RAS with (i) uncontrolled hypertension with medication, (ii) progressive renal insufficiency with bilateral RAS or RAS of a single kidney, or (iii) acute onset of cardiac insufficiency with recurrent pulmonary edema (6).

In the following situations, the benefit of PTRA has never been clearly demonstrated, and indications must be discussed case by case, as previously described:

- Arterial hypertension well controlled by medical treatment
- Severe asymptomatic RAS
- Renal insufficiency with unilateral significant RAS
- Need for treatment with conversion enzyme inhibitors in patients with RAS
- RAS associated with contralateral lesions necessitating nephrectomy.

Contraindications for endovascular treatment are associated lesions of the abdominal aorta (aneurysms) and complex atheromatous or dysplastic lesions. RAS with a narrowing of less than 50% in diameter should never be treated.

Bibliography

1. Hartman RP, Kawashima A, King BF (2003) Evaluation of renal causes of hypertension. Radiol Clin North Am 41:909–929
2. Soulez G, Oliva VL, Turpin S et al (2000) Imaging of renovascular hypertension: respective value of renal scintigraphy, renal Doppler US, and MR angiography. Radiographics 20:1355–1368
3. Radermacher J, Chavan A, Bleck J et al (2001) Use of Doppler ultrasonography to predict the outcome of therapy for renal artery stenosis. N Engl J Med 344:410–417
4. Beregi JP, El Kohen M, Deklunder G et al (1996) Helical CT angiography compared with arteriography in the detection of renal artery stenosis. Am J Roentgenol 167:495–501
5. Huot SJ, Hansson JH, Dey H et al (2002) Utility of captopril renal scan for detecting renal artery stenosis. Arch Intern Med 162:1981–1984
6. Martin LG, Rundback JH, Sacks D (2002) Quality improvement guidelines for angiography, angioplasty and stent placement in the diagnosis and treatment of renal artery stenosis in adults. J Vasc Interv Radiol 13:1069–1085

Stenosis, Spinal

Jan T. Wilmink
Radiology Department
University Hospital Maastricht
The Netherlands
jwil@rdia.azm.nl

Synonyms

Spinal narrowing; Verbiest syndrome of lumbar spine

Definitions

Spinal stenosis is defined as abnormal general or regional narrowing of the spinal canal. The condition may affect the entire spine as in achondroplasia, but usually sections of the spine are more severely involved than others. Spinal stenosis manifests itself most frequently in the lumbar spine, is encountered less frequently in the cervical region and is occasionally seen limited to the thoracic spinal canal.

According to the reports by Mixter and Barr on lumbar disc herniation as a cause of low back pain with sciatica, the 1930s and 1940s could be described as the "decades of the disc" as far as concepts on causes of low back pain and sciatica were concerned. In the 1950s and 1960s, the realization began to grow that, besides being caused by herniation of the lumbar intervertebral disc, low back complaints irradiating to the legs could also be due to reduced dimensions of the spinal canal or, quite frequently, to a combination of these two conditions.

It was also recognized that long-tract spinal cord symptoms originating in the cervical region were caused frequently by spinal cord compression due to narrowing of the cervical spinal canal and not by a disease of the cord itself.

Understanding of etiology, symptomatology, and diagnosis in patients with spinal stenosis is greatly enhanced by insight into the effects of postural changes, such as lordosis and kyphosis upon spinal structures and the contents of the spinal canal.

Etiology, Pathology

The classification of causes of spinal stenosis is extensive (1). Distinction can be made between congenital-developmental and acquired stenosis. The original report by Verbiest (2) described seven patients with what was thought to be developmental narrowness of the lumbar spinal canal, with heavily developed laminae and articular processes compressing the dural sac (Fig. 1). In fact this classic form of stenosis is quite rare, and the most important single cause of spinal narrowing is considered to be degenerative. Epstein focused attention on abnormal narrowing of the lateral recesses of the spinal canal and of the intervertebral foramina as a cause of chronic sciatica (3). The application of computed tomography to spinal imaging in the 1970s and 1980s provided new insights into the various factors causing narrowing of the spinal canal and compression of the dural sac or the emerging nerve root.

Combinations of these factors in spinal stenosis are the rule rather than the exception (4). In the lumbar region the spinal canal may be somewhat narrowed on developmental basis. This need not cause symptoms by itself, but in later life degenerative hypertrophy of the facets and flaval ligaments may further reduce spinal

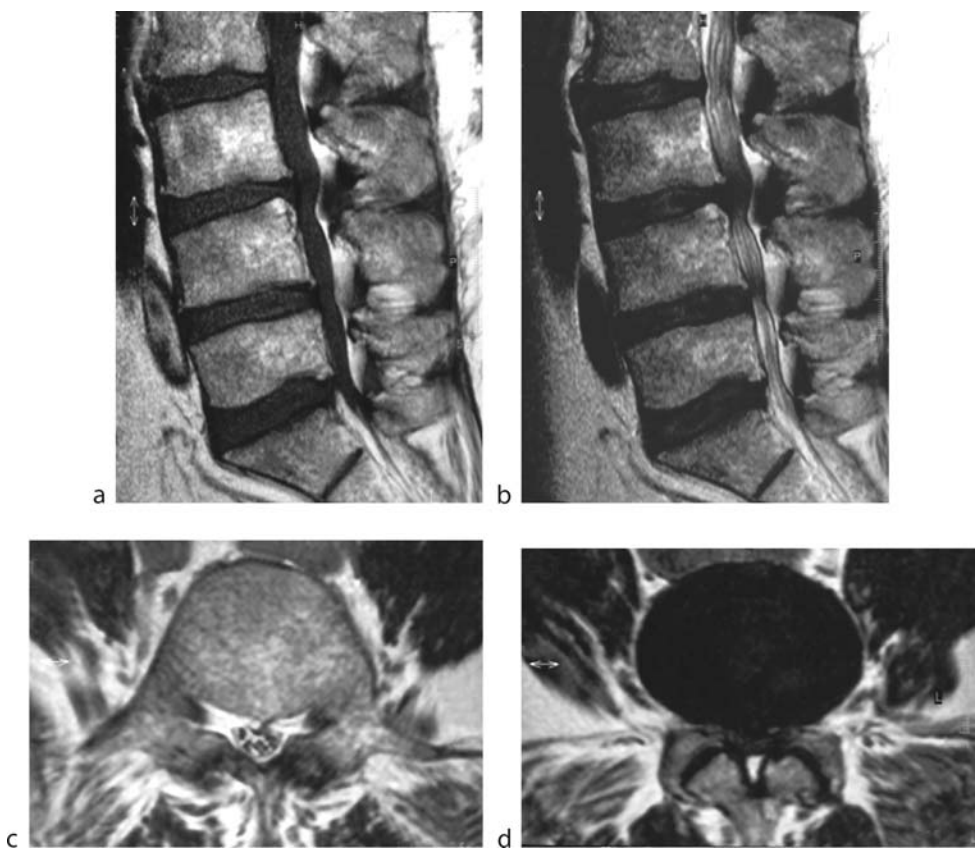

Stenosis, Spinal. Figure 1 Developmental stenosis of lumbar spine. Sagittal T1-(1a) and T2 weighted (1b) images demonstrate a shallow spinal canal with bony midsagittal diameter of 11 mm. measured at level of L5 lamina. Note L3-4 disc protrusion further reducing available space. Axial T2 weighted cuts at level of lamina (1c) show normal interpedicular diameter and reduced AP diameter, at disc level dorsolateral encroachment by facets is seen (1d). Note that bony AP diameter is smallest at level of lamina, but effective spinal dimensions are smallest at disc level, where CSF block is seen at L3-4 and L4-5.

dimensions, as may degenerative spondylolisthesis due to facet destruction, and/or degenerative disc bulging. Increase in epidural fat in obesity or steroid use can further aggravate the situation. In this way a complex of factors, each in themselves insufficient to cause complaints, can combine to compress the cauda equina and it goes without saying that a small disc herniation or even a bulging disc in such a narrowed spinal canal will cause symptoms much sooner than a similar disc lesion in a patient with a roomy canal (Fig. 2).

In the cervical spine, a developmentally narrow spinal canal will be associated not only with an increased risk of acute cord lesion in trauma, but also with greater risk of chronic progressive myelomalacia as degenerative osteophyte formation causes gradual further narrowing of the spinal canal with compression and wasting of the cord (Fig. 3).

In the thoracic spine, degenerative hypertrophy of the flaval ligaments can occur, with a greater risk of cord compression in a relatively narrow bony spinal canal.

Clinical Presentation

In lumbar spinal stenosis the most common symptoms are tiredness and loss of power in the legs, backache, and bilateral leg pain, occasionally anesthesia, and a feeling of numbness in the sacral dermatomes. Typically, these complaints present and progress when the patient is standing or walking in lordotic posture, and are immediately relieved by sitting or lying down, by squatting or any other posture which reduces lordosis and induces kyphosis. Verbiest named this clinical picture "intermittent neurogenic claudication," and the striking effect of postural changes serves to distinguish it from intermittent vascular claudication which is exercise-dependent and not posture-dependent.

When the patient suffering from neurogenic claudication is lying recumbent there are no complaints, and tests of radicular compression such as straight leg raising are negative.

The clinical picture may not be so clear-cut for neurogenic claudication when only a single exiting nerve root is compressed by narrowing of the lateral recess or the intervertebral foramen, or when there is a concomitant disc herniation. The pain is then more monoradicular in nature, although posture-dependency may be present.

In narrowing of the cervical or thoracic spinal canal it is not the cauda equina which is compressed but the spinal cord. The clinical presentation is that of gradually progressive long-tract neurologic dysfunction, with disturbances of walking and micturition, and muscular weakness with increased tendon reflexes and pathologic extensor plantar responses at neurologic examination. Neck pain radiating to the arms may be present, especially when the cervical foramina are narrowed by osteophyte formation and the exiting nerve roots are compressed.

Clinical signs of cord compression in cervical stenosis are not as strikingly posture-dependent as those of cauda equina compression in lumbar stenosis.

Imaging

Plain X-ray Films

These are of limited value in assessing dimensions of the spinal canal. Verbiest defined absolute lumbar stenosis as a condition in which the bony midsagittal diameter at the upper laminar level is less than 10 mm, while relative stenosis is said to be present when the same diameter is between 10 and 12 mm (mean normal value 17 mm). This diameter cannot be measured on a plain film, however, as it is obscured by overlying bony structures, and the same applies to the dimensions of the lumbar facets and the interfacet diameter which may also be reduced in stenosis. The size of the vertebral body and the interpedicular diameter can be measured accurately, but these are usually normal in patients with spinal stenosis.

Signs of degenerative change such as spondylosis, spondylarthrosis, degenerative anterolisthesis, and foraminal narrowing can be identified on plain films and provide a clue to the possible presence of degenerative narrowing of the spinal canal, but these signs are frequently also present in elderly subjects without symptoms.

Conventional Myelography

After intradural injection of a radiologic contrast medium, compression of the dural sac by lumbar spinal stenosis is revealed by the presence of a posture-dependent myelographic block present in lumbar retroflexion or lordosis and relieved by anteflexion or kyphosis. This block is invariably present at the level of the intervertebral disc and not at the level of the bony lamina. Posture-related changes in spinal dimensions are a normal phenomenon at the disc level, where the spinal canal is bordered by ligamentous surfaces. In lordosis the annulus fibrosus of the disc bulges backward into the spinal canal and the flaval ligaments dorsolateral to the canal also bulge inwards. In a normal spinal canal this does not produce symptoms, but in a stenotic canal the extra reduction of space induced by lordosis is sufficient to compress the dural sac and cauda equina and cause neurogenic claudication (5).

In the cervical spine, cord compression in symptomatic stenosis is also seen by a myelographic block in lordosis, relieved when lordosis is reduced.

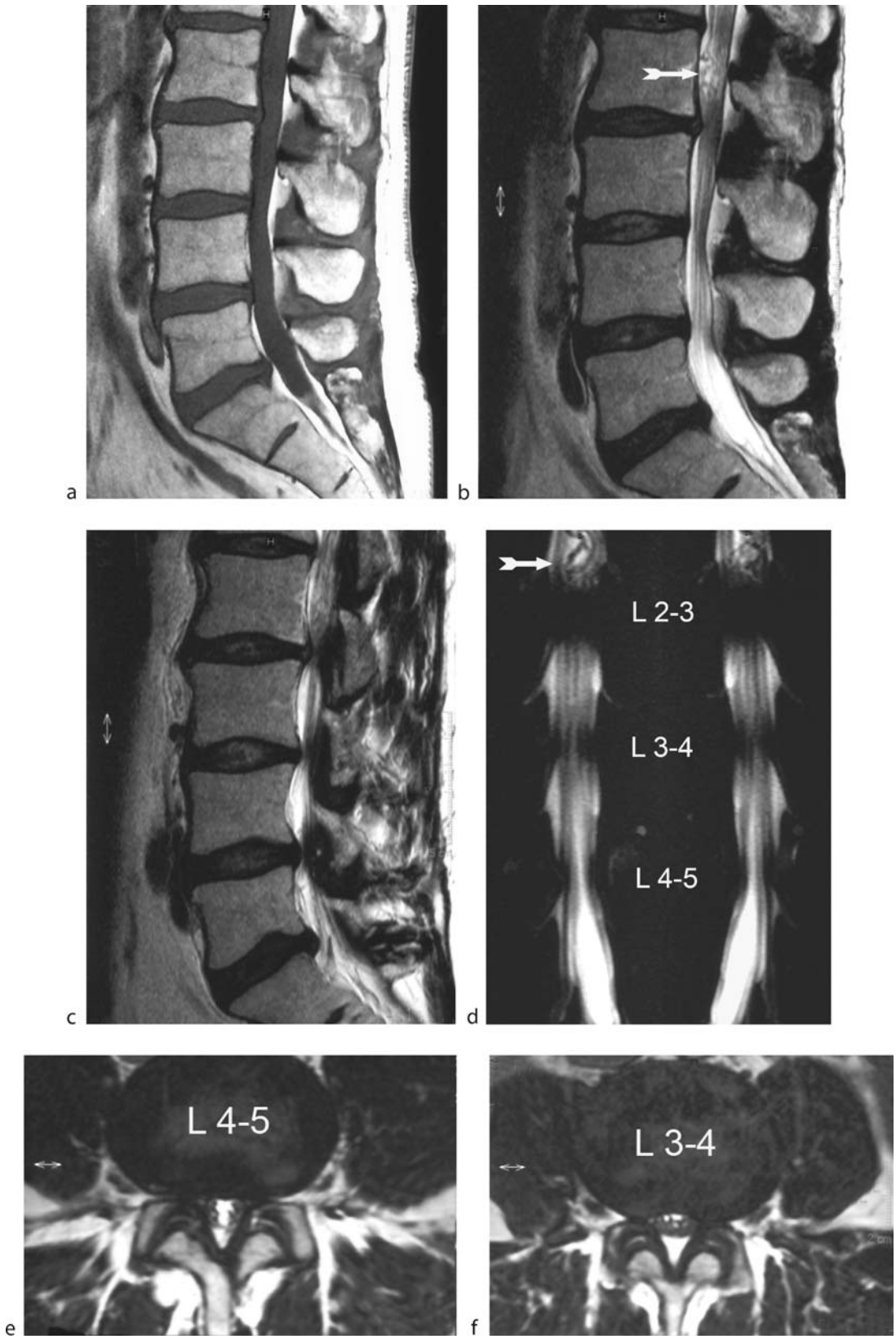

Stenosis, Spinal. Figure 2 (Continued)

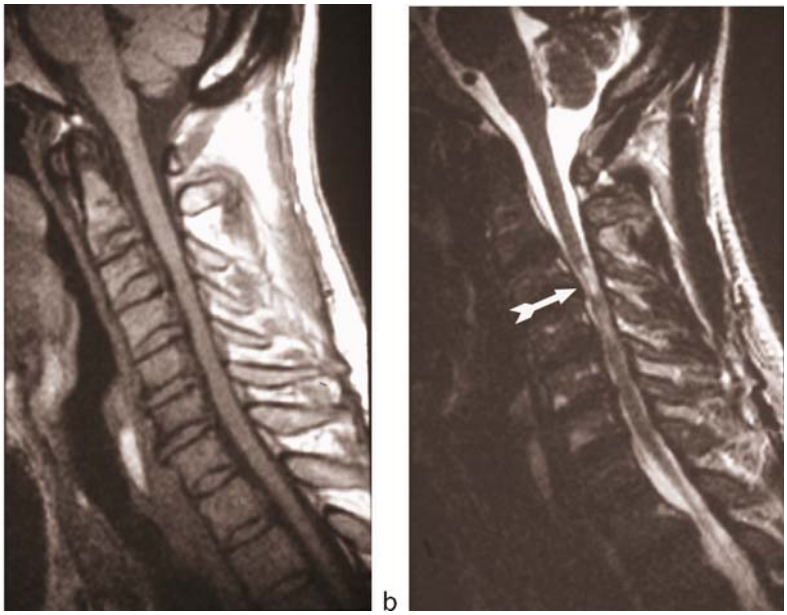

Stenosis, Spinal. Figure 3 Cervical stenosis shown on T1-(3a) and T2 weighted (3b) images. Note obliteration of CSF spaces around spinal cord, compression of cord and a high-signal intramedullary lesion in 3b (arrow).

Computed Tomography

The axial images produced by these techniques greatly improved understanding of various types of spinal stenosis. Accurate measurement of the bony dimensions of the spinal canal was now possible, although limited soft tissue resolution made employment of CT myelography necessary in some cases. As mentioned above, the soft tissues at disc level are instrumental in producing cauda equina compression in spinal stenosis, and soft tissue hypertrophy or bulging may produce symptoms in individuals with bony spinal dimensions well above those defined by Verbiest (5). Undue reliance on bony spinal measurements can therefore prove misleading, and the only soft tissue structure within the canal that can be measured on plain CT is the dural sac. A study comparing myelographic and CT features of nerve root compression in a group of 100 patients with sciatica revealed that a CSF block at myelography in spinal stenosis occurred when the CT cross-sectional area of the dural sac in the lower lumbar region decreased to below 40 mm^2 (6).

In the cervical region the cross-sectional area of the spinal cord can be measured by CT myelography. In normal individuals this value is around 90 mm^2. The cervical cord is surprisingly resilient to chronic compression, and long-tract signs usually do not begin to appear before cord area has been reduced by one third to around 60 mm^2 (7)

CT myelography also provides a detailed image of the cervical nerve root as it departs from the spinal cord and later also from the dural sac within its root sleeve. Nerve root compression by bony foraminal narrowing can best be diagnosed by this technique.

Magnetic Resonance Imaging (MRI)

This is presently the best method for imaging the spine in virtually all conditions. It has been held by some that CT is better suited for the diagnosis of spinal stenosis because of the bright signal of bony structures produced by this technique. In fact, cortical bone outlining the normal and abnormal spinal canal can be easily distinguished in the MR image which has the additional advantage of demonstrating concomitant soft-tissue pathology such as flaval hypertrophy and bulging or protruded disc much more clearly than CT. An important benefit of MRI is the possibility of

Stenosis, Spinal. Figure 2 Combined stenosis. Bony AP diameter is relatively narrow; 12mm. at level of L4 lamina. T1 weighted sagittal image (2a) also shows some increase in depth of retrodural fat pad. Bulging discs at multiple levels seen on T2 weighted midsagittal (2b) and lateral-sagittal images (2c). At L2-3 this results in a CSF block with elongated and coiled nerve roots above level of block; so-called redundant roots, confirmed by MR myelogram (2d, arrow). At L4-5 there is also some encroachment by hypertrophic facets and flaval ligaments (2e), resulting in kinking of traversing L5 nerve roots, especially at right (2d, arrowhead). At L3-4 there is no disc bulging and no facet hypertrophy (2f), myelogram shows only slight displacement of nerve roots.

producing heavily T2-weighted myelographic images which make it possible to identify features associated with symptomatic spinal stenosis such as a myelographic CSF block or the presence of redundant nerve roots.

In the cervical region, compression of the spinal cord can be demonstrated directly, and the presence of myelomalacia can be diagnosed by the presence of an intramedullary lesion with increased T2 signal. As mentioned above, an ancillary role is still reserved for CT in the demonstration of osteophytes at the foraminal entrance, potentially compressing the exiting nerve root.

Functional imaging studies in spinal anteflexion and retroflexion are helpful in the diagnosis of spinal stenosis. In the cervical spine such studies can be performed in MRI systems as well as CT scanners. Lumbar functional studies are not possible in most MRI systems presently in use, but the development of open upright MRI systems make loaded functional studies possible and will provide a new dimension in lumbar spinal imaging.

Bibliography

1. Arnoldi CC, Brodski AE, Cauchoix J et al (1976) Lumbar spinal stenosis and entrapment syndromes. Definition and classification. Clin Orthop 115:4–5
2. Verbiest H (1954) A radicular syndrome from developmental narrowing of the spinal canal. J Bone Joint Surg Br 36B:230–237
3. Epstein BS, Epstein JA, Jones MD (1977) Lumbar spinal stenosis. Radiol Clin North Am 15:227–239
4. Paine KWE, Haung PWH (1972) Lumbar disc syndrome. J Neurosurg 37:75–82
5. Penning L (1992) Functional pathology of lumbar spinal stenosis. Clin Biomech 7:3–17
6. Wilmink JT (1989) CT morphology of intrathecal lumbosacral nerve-root compression. AJNR Am J Neuroradiol 10:233–248.
7. Penning L, Wilmink JT, Van Woerden HH et al (1986) CT myelographic findings in degenerative disorders of the cervical spine: clinical significance. AJNR Am J Neuroradiol 7:119–127.

Stent

Small tube like device mounted on a balloon catheter or fixed to the tip of a catheter that can be expanded or is self-expending and thus dilates and stabilizes a vessel.
►Stroke, Interventional Radiology

Stent Graft

A stent graft consists of a metallic wire mesh tube covered with a graft material. It is used mainly in the vascular system to treat aneurysms, vessel ruptures, or fistulas.
►Aneurysm, Aortic and Thoracic

Stent, Carotid Artery

K. Alfke, O. Jansen
Neuroradiology, UK SH, Kiel, Germany
k.alfke@neurorad.uni-kiel.de

Synonyms

Endovascular treatment of internal carotid artery stenosis; Stenting

Definition

Treatment of a carotid artery stenosis with a stent is an endovascular intervention. It is performed to reduce the risk of stroke.

Characteristics

Introduction

Treatment of carotid artery stenosis is performed to reduce the risk of stroke. A symptomatic stenosis with a grade of over 50% according to ►North American Symptomatic Carotid Endarterectomy Trial criteria (NASCET) (1) or over 70% according to ►European Carotid Surgery Trial criteria (ECST) (2) should be treated. Regarding timing of treatment after brain infarction, in patients with larger infarcts an interval of 2 weeks seems to be safe to avoid reperfusion injury with the risk of secondary hemorrhage. In cases of smaller infarctions, earlier treatment is possible.

Indication

Endovascular treatment with stenting and operative endarterectomy are alternative methods. The largest and most recent randomized study comparing these two methods is the Stent-Supported Percutaneous Angioplasty of the Carotid Artery versus Endarterectomy (SPACE) trial (3). It included 1,200 patients with symptomatic carotid artery stenosis (>50% NASCET, > 70% ECST). The rate of the primary endpoint, death, or ipsilateral ischemic stroke from randomization to 30 days after the procedure was 6.84% with carotid stenting and 6.34% with endarterectomy. These results did not prove equivalence of the two methods statistically, but the difference was not statistically significant (difference of only four events). Long-term results for a period of 2 years will follow.

The use of stenting as therapy for carotid artery stenosis is increasingly widespread, and guidelines are needed for everyday practice. Therapeutic decision should be based on different parameters and should differentiate between three groups of patients:

The first group has a high surgical risk and therefore a clear indication for stenting. This group includes patients with restenosis after endarterectomy, radiogenic stenosis, and stenosis that is surgically not accessible, such as distal extracranial or intracranial carotid artery stenosis or a combined intra-/extracranial stenosis. Stenosis caused by nonarteriosclerotic diseases such as dissection, fibromuscular dysplasia, or Takayasu arteritis should be stented if treatment is necessary (4). Also, patients with high surgical risk due to comorbidity should be treated with local anesthesia with stenting.

Patients in the second group with symptomatic high-grade stenosis can be treated with either method. In this group, the patient's preference for one of the two methods and also the expertise of the different local therapists should be considered.

The third group includes patients with asymptomatic stenosis over 50% (NASCET) who might benefit from surgical treatment. New trials including SPACE II and CAVATAS II will compare the endovascular and operative treatment of asymptomatic stenosis.

Contraindications for Stenting

Contraindications for stenting are allergies to contrast media or to the necessary antiplatelet treatment with aspirin or clopidogrel. Renal insufficiency or hyperthyroidism must be considered. A floating intraluminal thrombus might prevent passage of the stenosis with endovascular tools.

Preparation for the Stenting Procedure

Necessary preinterventional preparation includes clinical neurological assessment of the patient and his or her symptoms and imaging of the stenosis, the supraaortic vessel anatomy, and the brain. Magnetic resonance (MR) or computed tomography (CT) angiography gives an overview of brain-feeding arteries to evaluate the anatomy of the stenosis in relation to surrounding structures and to show, for example, tandem stenosis or occlusion of the contralateral carotid artery. Imaging of the brain with CT or MR gives information about the mechanism of stroke (e.g., embolic or hemodynamic stroke) and should exclude contraindications such as large acute infarction or bleeding. Ultrasound Doppler examination is necessary to estimate the grade of the stenosis.

Antiplatelet medication is mandatory. Different schemes have been described. Patients included in the ►SPACE trial received 100 mg aspirin and 75 mg clopidogrel daily for at least 3 days before and 30 days after stenting. The aspirin was then continued.

The Stenting Procedure

The procedure is performed using local anesthesia *via* a percutaneous transfemoral or transbrachial access with a long sheath or guiding catheter. The sheath or catheter is advanced coaxially over the catheter and guide wire into the common carotid artery. The sheath should be flushed permanently with heparinized saline. After introduction of the sheath heparin can be administered intravenously. The heparin effect can be controlled by bedside measurement of activated clotting time. To prevent bradycardia, atropine can be given subcutaneously at the beginning of the procedure and again intravenously before balloon dilatation of the carotid bulb.

Angiography should include at least two projections showing the stenosis without overlay and two projections of the intracranial vasculature before stenting. For stent placement, fluoroscopy and the road-map technique should be used. The biplane angiography technique is extremely helpful. After stenting, the result should be documented angiographically (Fig. 1).

After the sheath is placed in the common carotid artery, the stenosis is passed with a microguide wire. Balloons and the stent delivery system are commonly monorail systems. Predilation of the stenosis with a 2.5- or 3-mm balloon might be necessary when primary passage with the stent delivery system is not possible. The suitable stent size is then estimated from angiography, depending on the vessel's diameter and the location of the stenosis. After stent placement, secondary balloon dilation is performed. Finally, the sheath is removed.

Protection devices with filters or flow reversal have not yet shown a benefit in controlled studies. They probably reduce the risk of a larger embolism but prolong and complicate the procedure, which might cause other complications.

Possible Complications

Stroke or transient neurological deficit due to periinterventional embolism is probably the most severe complication of stenting. Parts of a thrombus or plaque can be loosened during the passage of the stenosis with the wire, stent delivery system, or balloon. In particular, balloon dilatation of the stent and arterial wall might cause rupture of a plaque followed by embolism. Dissection of the arterial wall in the site of the stenosis and also in adjacent segments can lead to severe stenosis or thromboembolism. After treatment of high-grade stenosis, hyperperfusion in the territory of the internal carotid artery can

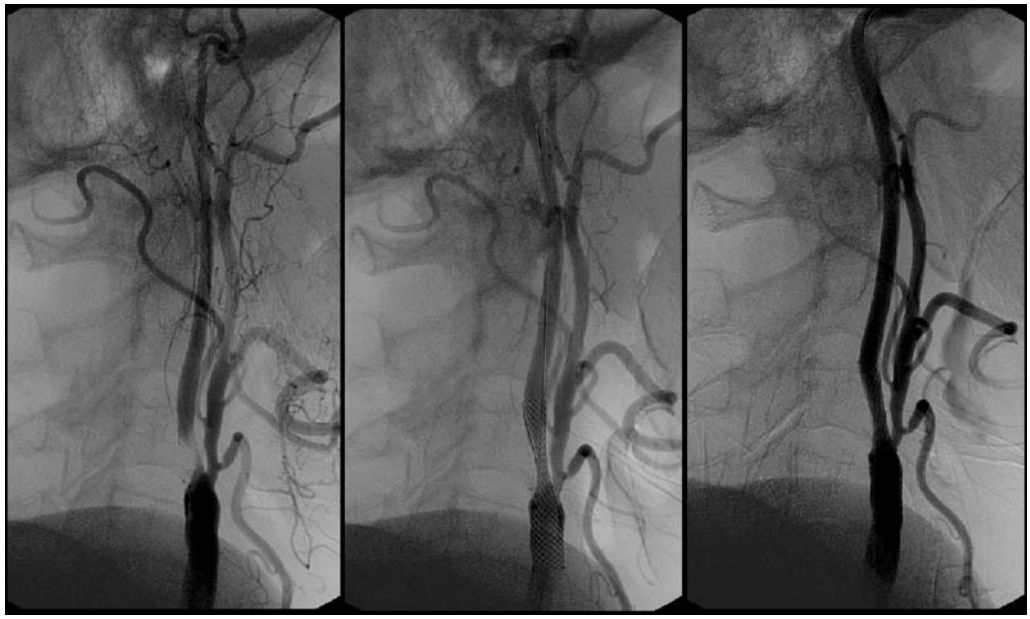

Step-off. Figure 1 Three steps of a stenting procedure of a carotid artery stenosis. From left to right: First, the stenosis is shown in a lateral angiographic view without subtraction. Then the stent is delivered, expanding the stenosis with its radial force. Finally, after balloon dilation of the stent, a satisfying result is achieved.

lead to edema or hemorrhage with neurological impairment, headache, seizures, and focal neurological deficits. Potential side effects of contrast media administration include allergic reaction, impairment of renal function, and hyperthyroidism. At the puncture site, a groin hematoma might occur. Restenosis caused by intimal hyperplasia is possible but normally asymptomatic. Intimal hyperplasia typically appears during the first 6 months after stenting. Follow-up with ultrasound over a period of approximately 2 years is necessary to detect severe restenosis, which can be treated with balloon angioplasty or even stenting again.

Future Prospects

Stenting of carotid artery stenosis has the great advantage of avoiding the risks of operative treatment. Incisions, with the risk of cranial nerve palsy or cervical wound hematoma, and longer occlusion of the treated vessel are not necessary. Often, hospitalization of the patients is shorter. Nevertheless, larger trials are needed to show the equivalence of neurological complication rates and long-term results. Improvement of the interventional tools such as stents and protection devices that reduce the rate of thromboembolism, the growing experience of the interventionists, and the refining of the preintervention diagnostic processes (e.g., plaque imaging) will further decrease complication rates and optimize results.

Bibliography

1. European Carotid Surgery Trialists' Collaborative Group (1991) MRC European carotid surgery trial: interim results for symptomatic patients with severe (70–99%) or with mild (0–29%) carotid stenosis. Lancet 337:1235–1243
2. Ferguson GG, Eliasziw M, Barr HW et al (1999) The North American symptomatic carotid endarterectomy trial: surgical results in 1415 patients. Stroke 30(9):1751–1758
3. The SPACE Collaborative Group (2006) 30-day results from the SPACE trial of stent-protected angioplasty versus carotid endarterectomy in symptomatic patients: a randomised non-inferiority trial. Lancet 368:1239–1247
4. Barr JD, Connors JJ III, Sacks D et al (2003) American Society of Interventional and Therapeutic Neuroradiology; American Society of Neuroradiology; Society of Interventional Radiology. Quality improvement guidelines for the performance of cervical carotid angioplasty and stent placement. J Vasc Interv Radiol 14:S321–335

Stenting

▶Stent, Carotid Artery

Step-off

The normal change in contour at metaphysis between the 1–3 mm straight metaphyseal collar and the

monotonically curved metaphysis and shaft; not to be confused with buckle fracture.
▶Battered Child Syndrome

Sterile Effusion in One or More Joints

▶Transient Synovitis

Sterile Inflammation of the Hip

▶Transient Synovitis

Sternoclavicular Hyperostosis

▶Spondyloarthropathies, Seronegative

Stimulated Acoustic Emission (SAE)

SAE is a nonlinear response of ultrasound-induced disintegrating gas-filled microbubbles. In particular, gas-filled microbubbles can be destroyed when excited with ultrasound under certain conditions. The microbubbles disintegrate rapidly, thereby emitting a strong nonlinear signal, which is misinterpreted as quick movement and mapped as a characteristic random color pattern in the color Doppler mode of the ultrasound device.
▶Local Drug and Gene Delivery with Microbubbles

Stochastic Risk

This is dependent upon cell transformation, with the severity of the effects being independent of the radiation dose received. However, the greater the absorbed radiation dose received by the patient, the more likely a stochastic effect is to occur.
▶Radiation Issues in Childhood

Stomach and Duodenum in Adults Postoperative

Mathieu H. Rodallec, Marc Zins
Department of Radiology
Fondation Hôpital Saint-Joseph
Cedex 14, Paris, France
mzins@hopital-saint-joseph.org

Definitions

Current operations on the stomach and duodenum are performed for the treatment of gastroesophageal reflux, for the complications of peptic ulcer, for the resection of benign and malignant masses, for the complications of chronic pancreatitis, and for the management of obesity (1–3). Indications for surgical management of gastroesophageal reflux and peptic ulcer disease have decreased with the advent of proton pump inhibitors (4). Whereas rates of bariatric surgery have dramatically increased in recent years because morbid obesity is increasing in epidemic proportions (5, 6). Radiologic studies are crucial in the evaluation of patients with symptoms after gastric or duodenal operations. The radiologist may be asked to demonstrate complications in the early postoperative period or to define anatomy and detect disease years later.

Gastroesophageal Reflux

Indications for operative treatment of gastroesophageal reflux include clinical symptoms or esophagitis refractory to medical treatment, and Barrett esophagus (2–4). Standard operations attempt to increase the mechanical component of a competent esophagogastric junction mechanism. The Nissen ▶fundoplication creates an intraabdominal wrap of gastric fundus completely around the lower esophagus. Various other antireflux procedures attempt to restore the abdominal esophagus and ensure that it responds to intraabdominal pressure. Wraps can be noncircumferantial as in the Toupet partial fundoplication.

Peptic Ulcer Disease

Current indications for surgery in patients with peptic ulcer disease include hemorrhage, perforation, obstruction, ulcer intractability, and the inability to exclude malignancy in a gastric ulcer (2, 3). Generally, this can be accomplished with partial gastrectomy, with removal of

the ulcer. Combined gastric and duodenal ulcers and prepyloric ulcers are managed according to the principles of surgery for duodenal ulcer.

Duodenal Ulcers

Nowadays, surgery for duodenal ulcers is rare. But physicians who treat postoperative patients must be familiar with procedures that were performed over the past several decades. Antral resection and vagotomy has been used in the treatment of duodenal ulcers to decrease the secretion of hydrochloric acid and to remove ulcer-bearing gastric mucosa. Distal gastric resection with reconstruction by anastomosis of the proximal stomach to the end of the duodenum is known as a Billroth I reconstruction. When anastomosis to the duodenum is not possible, a gastrojejunostomy (Billroth II) is performed. A variable length of jejunum forms the afferent loop and carries duodenal contents toward the stomach. The efferent loop is the jejunum on the side of the gastrojejunostomy that is distal to the duodenum. The gastrojejunostomy may be anterior to the transverse colon (antecolic), or the small bowel may be brought up posteriorly through an opening made in the transverse mesocolon (retrocolic) (3).

An alternate method of reestablishing gastrointestinal continuity after gastric resection is Roux-en-Y gastrojejunostomy. The jejunum is divided just distal to the ligament of Treitz: the proximal end or side of the small bowel is attached to the stomach while the distal end is fashioned into an enterostomy downstream. This procedure diverts duodenal contents away from the gastric anastomosis and prevents bile reflux.

Gastric and Duodenal Masses Resection

Stomach malignancies require formal anatomic resection, with distal or total gastrectomy. Gastrointestinal continuity is restored with loop or Roux-en-Y esophagojejunostomy.

Duodenal malignancies are resected with pancreatoduodenectomy, with reanastomosis of the gastrointestinal tract, bile duct, and pancreatic remnant (1, 3). Pancreatoduodenectomy may involve distal hemigastrectomy, or the stomach and pylorus may be preserved by reconstruction with end-to-side duodenojejunostomy. The bile duct is anastomosed to the jejunum, and the distal pancreas is anastomosed to the jejunum or the posterior wall of the stomach.

Surgery for Obesity

Surgery is an effective alternative to failed medical and dietary therapy for life-threatening obesity. These stapling procedures create a small gastric pouch with a restricted outlet to cause early satiety, decreased caloric intake, and weight loss (5, 6). Currently, most surgeons prefer the gastric bypass approach or the vertical gastroplasty procedure. Bariatric surgeons use gastric silastic rings in both gastroplasty and gastric bypass operations to maintain the function and width of the stoma.

Gastric Bypass (GBP). A small proximal pouch is anastomosed to the jejunum *via* a loop or Roux-en-Y gastrojejunostomy. The stomach is separated from the food path but it is not transected. With a Roux-en-Y type anastomosis, the jejunum is divided, the proximal end or side of the distal bowel is attached to the stomach, and the Roux-en-Y loop is anastomosed to the jejunum downstream. With a loop gastroenterostomy, the standard right-to-left anastomosis is performed.

Vertical Banded Gastroplasty. A small tubular pouch and channel is created on the lesser curvature portion of the stomach.

Pathology/Histopathology

Complications occur when operations on the gastroduodenal tract fail to resect, reconstruct, or redesign the tissues and function of the gastroduodenal tract. There are common complications like anastomotic leaks, abscesses (Fig. 1), strictures, and bowel obstruction that occur during any operation on the alimentary tract. There are other complications that are unique to each operative procedure.

Gastroesophageal Reflux

If the fundoplication is too tight dysphagia or so-called gas bloat syndrome may develop, in which patient is unable to belch or to vomit. Long-term complications include fundoplication dehiscence, recurrent hernia, and slip wrap (4).

Peptic Ulcer Disease

After operations for peptic ulcer, the most undesirable gastrointestinal sequelae are consequences of vagotomy, gastric resection, or pyloric ablation (3). Diarrhea, dumping, and bile reflux can cause clinical debility and nutritional deficiency in a small percentage of patients. Early mechanical and anatomic complications are not common but can usually be diagnosed radiologically. Cancer arising in gastric remnants is associated with long-term metabolic effects (2).

Duodenal Ulcers

Antrectomy and total vagotomy increase the risk of undesirable side effects such as dumping, diarrhea, bile reflux, and potential cancer arising in gastric remnants (1, 3).

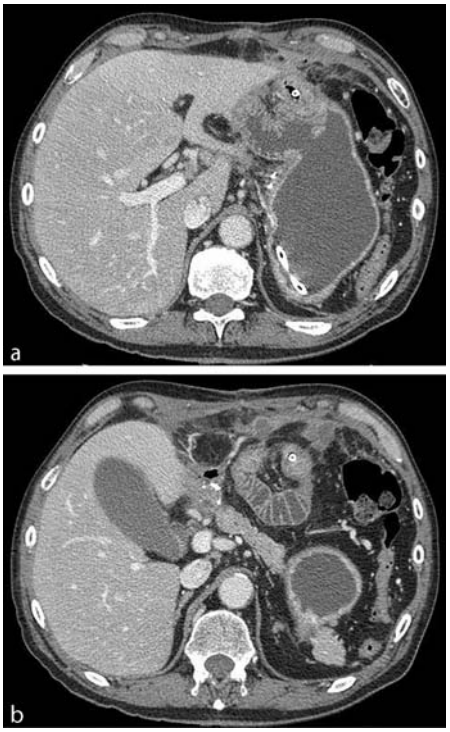

Stomach and Duodenum in Adults Postoperative.
Figure 1 Duodenal stump fistula complicated with intraperitoneal abscesses in a patient with partial distal gastrectomy for gastric adenocarcinoma. On axial enhanced CT with water-contrast agent, the gastro-jejunal anastomosis is clearly depicted (a). Axial enhanced CT at the level of the duodenal stump (b) depicts extradigestive gas in contact with the staples, and intraperitoneal abscesses.

Gastric and Duodenal Masses Resection

Recurrent neoplasm is a potential complication. Diarrhea, dumping, and bile reflux may follow gastric resection. Pancreatic resection may cause a deficiency of digestive enzymes. Metabolic deficiencies (iron or vitamin B12) are accentuated in patients with total gastrectomy.

Surgery for Obesity

Gastric staple line dehiscence is most often caused by repeated overdistention of the gastric pouch with food.

Massive gaseous distention of the excluded stomach may develop occasionally after gastric bypass procedure. It may occur because of edema at the enteroenterostomy, or it may be secondary to small bowel obstruction.

Internal hernias, following Roux-en-Y GBP are much more common than in the general population and are likely to be underdiagnosed (5). The most common type of internal hernia reported after laparoscopic Roux-en-Y GBP is transmesenteric, in which the small bowel herniates through the surgical defect in the transverse mesocolon. The herniated bowel is usually the Roux-en-Y loop itself.

Clinical Presentation

Anastomotic Leaks

The presentation can be acute (peritonitis) or progressive (subphrenic abscess).

Afferent Loop Syndrome

Afferent loop syndrome is caused by increased intraluminal pressure and distension due to accumulation of enteric secretions in an obstructed afferent duodenal stump in a Billroth II gastrojejunostomy (3). Afferent loop syndrome is one of the main causes of duodenal stump blowout in the early postoperative period and is also an etiology for postoperative obstructive jaundice, ascending cholangitis, and pancreatitis due to transmission of high pressures back to the biliopancreatic ductal system. Prolonged stasis and pooling of secretions facilitate bacterial overgrowth in the afferent loop. Bacteria deconjugate bile acids, which can lead to steatorrhea, malnutrition, and vitamin B-12 deficiency. Iron deficiency can occur because of bypassing of the proximal small bowel. Patients with acute afferent loop syndrome typically present with a sudden onset of abdominal pain with nausea and vomiting. If the afferent loop is not decompressed, the patient can develop peritonitis and shock if intestinal perforation or infarction ensues.

Bezoar

Bezoar is reported in patients with impaired digestion and decreased gastric motility. Bezoar may cause vomiting, diarrhea, pain, and gastric ulcers.

Imaging

Before beginning the examination, specific information about the postoperative anatomy should be obtained. If an anastomosis has been fashioned, drug-induced hypotonia, which renders the gastric remnant and small bowel hypotonic, prevents rapid slipping of contrast material into the distal small bowel.

Conventional Radiographs

The pattern of surgical clips and staples may help determine the anatomy with reliability. Unexpected foreign bodies, extraluminal gas collections, or signs of bowel obstruction should be sought.

Contrast-Enhanced Studies

Water-soluble contrast agents are used when anastomotic leaks, staple line dehiscences, perforations, fistulas, or abscesses are suspected. Barium studies provide an assessment of mucosal detail that cannot be obtained with water-soluble agents. Biphasic techniques that use both high-density barium sulfate suspension and effervescent agents and low-density contrast material with compression and palpation provide an excellent view of mucosal detail and the anastigmatic area (3). Patient cooperation and mobility are crucial for these studies. Protocols for position changes and radiographic sequences cannot be specified because each patient has unique surgical variations.

US, CT, and MRI

US, CT, and MRI are useful to detect fluid collections, abscesses, leaks, or fluid-filled obstructed bowel loops. For CT scanning, water-soluble contrast agents should be used liberally. CT is better suited to detect extradigestive gas.

Nuclear Medicine

Nuclear medicine emptying studies with radiolabeled solids and liquids can be used for patients with suspected postgastrectomy stasis syndromes, afferent loop dysfunction, motility problems of dumping and diarrhea, and postoperative symptoms of an unclear cause (3).

Diagnosis

Anastomotic Leaks

Extravasation of contrast material beyond the bowel lumen can be recognized without difficulty if the normal postoperative appearances are known.

Afferent Loop Syndrome

CT demonstrates the obstructed segment as a U-shaped, fluid-filled tubular structure confined to the subhepatic area or crossing the midline between the abdominal aorta and the superior mesenteric artery. CT is also useful to predict the underlying pathology causing afferent loop syndrome (carcinomatosis, adhesion, or internal hernia).

Bezoar

Conventional radiographs and CT demonstrate an ovoid intraluminal mass with mottled gas pattern within the stomach (2). Small bowel obstruction can follow bezoar migration (Fig. 2).

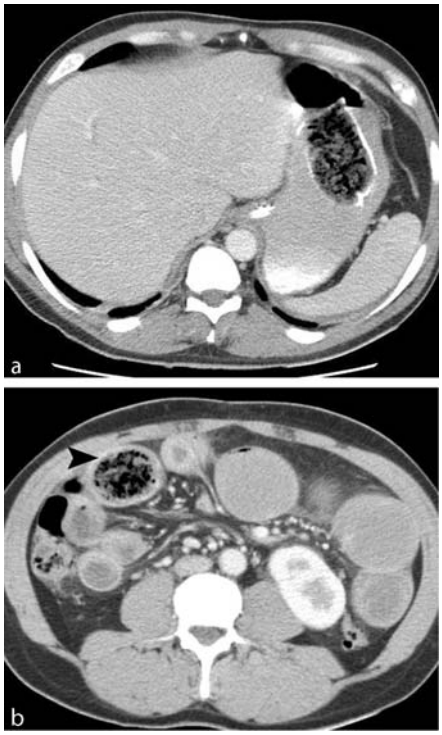

Stomach and Duodenum in Adults Postoperative. Figure 2 Partial gastrectomy complicated with bowel obstruction after bezoar migration. Axial enhanced CT at the level of the stomach demonstrates an ovoid intraluminal mass with mottled gas pattern (a). Axial enhanced CT also demonstrates small bowel obstruction due to migration of bezoar (arrowhead) (b).

Tumor Recurrence

Local tumor recurrence is usually diagnosed with endoscopy. US, CT, and MRI are useful for loco-regional staging (1, 2).

Long-Term Complications of Fundoplication

Long-term complications are generally evaluated with barium studies (4). A completely dehisced fundoplication often mimics normal findings in a healthy patient who has not undergone surgical intervention. In partial fundoplication dehiscence, there is no significant tapering of the distal esophagus. In slipped fundoplication, the gastroesophageal junction lies above the level of the wrap. In recurrent hernia, the entire wrap lies above the esophagus hiatus.

Interventional Radiological Treatment

CT and fluoroscopic guidance are useful for treatment of the postsurgical complications.

Bibliography

1. Zins M, Sauvanet A (1999) Pancréas et duodenum. In: Zins M, Sauvanet A (eds) Imagerie de l'appareil digestif opéré. Médecine-Sciences, Flammarion, Paris, pp 39–61
2. Vullierme MP, Sauvanet A, Zins M (1999) Cardia et estomac. In: Zins M, Sauvanet A (eds) Imagerie de l'appareil digestif opéré. Médecine-Sciences, Flammarion, Paris, pp 21–37
3. Smith C, Deziel DJ, Kubicka RA (1994) Evaluation of the postoperative stomach and duodenum. Radiographics 14:67–86
4. Canon CL, Morgan DE, Einstein DM et al (2005) Surgical approach to gastroesophageal reflux disease: what the radiologists needs to know. Radiographics 25:1485–1499.
5. Yu J, Turner MA, Cho SR et al (2004) Normal anatomy and complications after gastric bypass surgery: helical CT findings. Radiology 231:753–760
6. Blachard A, Federle MP, Pealer KM et al (2002) Gastrointestinal complications of laparoscopic Roux-en-Y gastric bypass surgery: clinical and imaging findings. Radiology 223:625–632

Stone Disease, Urinary

G. Heinz-Peer
Department of Radiology, Medical University, Vienna, Austria
gertraud.heinz-peer@akhwien.at

Epidemiology

Urinary stone disease is a common problem among people from industrialized nations. The incidence is 7 per 1,000 and it is responsible for 7 to 10 of every 1,000 hospital admissions in the USA (1). With increased abdominal imaging more stones are diagnosed as an incidental finding. In most cases, no clear precipitating factor is identified and the natural cumulative recurrence rate is reported to be 14% at 1 year, 35% at 5 years, and 52% at 10 years. In general the overall lifetime risk is accepted as 35–65% with a male preponderance (male: female ratio of 2:1) and the peak age of onset is 20–30 years. Caucasian or Asian origin confers a higher risk (1).

Pathophysiology/Histopathology

The main types of stones encountered are calcium containing, composed mainly of pure calcium oxalate or calcium oxalate mixed with calcium phosphate. The majority of the remainder is so-called struvite or matrix stones composed of magnesium ammonium phosphate. Uric acid and cystine stones account for less than 10% of all calculi. An organic matrix of mucoprotein, consisting 1–5% of the stone by weight, is present in all calculi.

In most cases, a precise etiological factor is not identified but certain predisposing factors are recognized. Incidence is higher in patients with an anatomical abnormality of the urinary tract and this may be related to urinary stasis. Stones form when the concentration of two ions in solution exceeds the saturation point. The condition at which this occurs depends on a number of patient-related factors (1).

Clinical Presentation

Urinary stone disease may present in a number of ways. The classic presentation is with acute severe ipsilateral loin to groin pain, associated with nausea and vomiting. This history combined with renal angle tenderness and microscopic hematuria is highly accurate in making a clinical diagnosis of urinary tract stones with a reported sensitivity and specificity of 84 and 99%, respectively (2). Delayed presentation or diagnosis is often complicated by infection proximal to an obstructing calculus. Matrix calculi are most often infected. Renal impairment at presentation implies a complicating factor, such as underlying renal disease or septicemia. Rarely renal failure may be secondary to bilateral obstructing calculi or an obstructing stone in a single functioning kidney.

Others present with vague symptoms or microscopic or gross hematuria, and in yet others the finding is incidental. Of this last group only one third will become symptomatic. There are no reliable predictive factors to identify those patients who will develop symptoms (2).

Imaging

The purpose of imaging is not only to confirm the presence of urinary stone disease, but also to provide some indication of outcome.

Plain Abdominal Radiograph

KUB has a low sensitivity in the diagnosis of stones, ranging from 45–60% (1). Despite this modest accuracy, the KUB is important in the management of a known radiopaque ureteric calculus especially in planning fluoroscopically guided, ►extracorporeal shockwave lithotripsy (ESWL) or monitoring the progress of stone fragments after ESWL. It is also valuable for assessing stone status in those who are managed conservatively.

Excretory Urography

Over many years, the excretory urography has been the traditional imaging modality of choice for evaluation of

patients suspected of having ►urolithiasis. However, small or radiolucent stones may be missed on IVU. Reported sensitivities range from 64–97% for calculus detection (3). The IVU is easy to perform and relatively save and the radiation dose from a standard three film IVU series is 1.5 mSv (1). In case of renal obstruction, additional series are required and the radiation dose may increase up to 10 mSv (4). The radiographic findings are highly accurate in diagnosing renal obstruction and allow excellent evaluation of the topography of the calyceal anatomy. These are most important contributions to management of urinary stone disease (Fig. 1).

Ultrasound

Ultrasound has an important role in the diagnosis and management of urinary tract stones but it has limitations. The sensitivity for calculus detection ranges from 37–64% and for detection of acute obstruction from 74–85% (3). Stones in the pelvicalyceal system can be reliably identified only if they are greater than 5 mm. Furthermore, calculi in the ureter are poorly visualized unless sited within the proximal ureter or at the vesico-ureteric junction (VUJ). However, by using the color Doppler twinkle sign the sensitivity of calculus detection may be improved (Fig. 2). The role of ultrasound in chronic stone disease is also unclear. Pelvicalyceal anatomy cannot be confidently delineated on ultrasound unless the pelvicalyceal system is dilated.

For follow-up of renal stones triaged to conservative therapy, ultrasound is of use. Ultrasound is also recommended in patients in whom radiation exposure is a concern, such as pregnant or pediatric patients (3).

Unenhanced Computed Tomography

The unequivocal advantage of UCT over all other techniques is its diagnostic accuracy. Over 99% of calculi, including those that are radiolucent on the KUB will be seen on UCT. The exceptions are pure matrix stones and stones made of indinavir (and related drugs), a human immunodeficiency virus (HIV) protease inhibitor. UCT has the highest accuracy (approximately 95% compared with around 80% for IVU) in acute ureteric colic (3). As well as

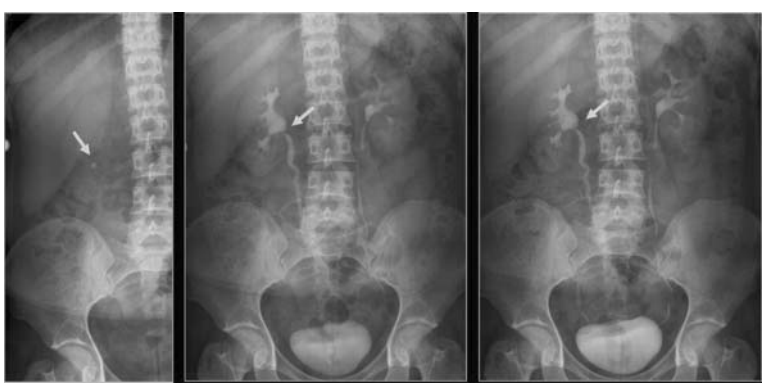

Stone Disease, Urinary. Figure 1 On KUB a 1 cm lower calyceal stone is depicted in this patient with uretero-pelvic junction (UPJ) stenosis as shown by the excretory urography. Since the passage of stones or fragments through this stenosis is unlikely, this particular patient is no candidate for ESWL. On unenhanced CT, the presence of a low or medium graded UPJ stenosis may be missed.

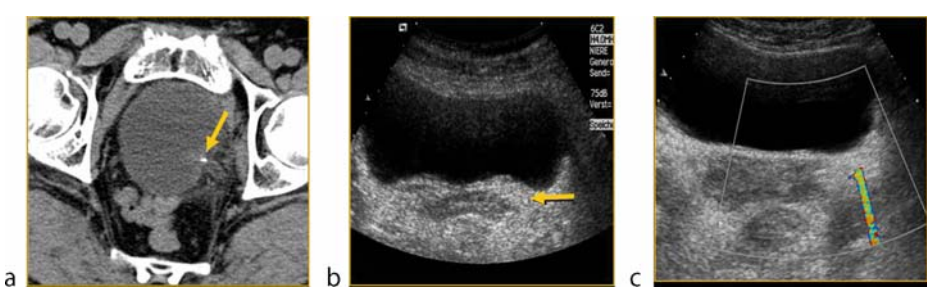

Stone Disease, Urinary. Figure 2(a–c) Patient presenting with a small calculus at the uretero-vesical junction (UVJ) (*arrow*) that is nicely depicted on unenhanced CT (a), and hardly delineated (*arrow*) on grey scale ultrasound (b). The color Doppler twinkle sign improves detection of urinary stones as shown in this patient with a 4 mm calculus at the UVJ (c).

demonstrating the size and site of the calculus, measurement of stone density may be useful, as stones of greater than 1,000 HU appear to respond less well to ESWL (1).

A number of secondary CT signs thought to reflect the pathophysiology of acute urinary tract obstruction have been described (3). It has been suggested that these signs indicate a protection mechanism against renal pressure.

The value of UCT in the management of renal, as distinct from ureteric calculi, is less clearly established. Factors other than stone size that influence the choice of ESWL versus ▶percutaneous nephrolithotomy (PCNL) are not easily assessed. Similarly, planning the route for percutaneous entry is imprecise. Multiplanar and volume reconstructions may overcome these limitations (1).

For the diagnosis of ureteral stones, the calculated mean effective radiation dose reported for standard-dose CT ranges from 3.5 to 10 mSv, for low dose CT from 1.5 to 3.5 mSv, respectively.

Multislice CT Urography

CT data acquisition during urographic contrast enhancement for contiguous imaging of the entire upper urinary tract is termed "multislice CT urography" (MSCTU). Multiplanar reconstructions, maximum intensity projections (MIPs), and average intensity projections can be rendered from the volume datasets to view the urogenital tract.

Similar to the excretory urography, MSCTU provides valuable information on the degree of renal obstruction and allows excellent evaluation of the topography of the calyceal anatomy.

The radiation dose reported for MSCTU ranges from 3.9 to 22.6 mSv (4). This great variety may be explained by different examination protocols and to a less extent to scanner- and patient-related factors.

Magnetic Resonance Urography

The current role of MRU in diagnosing urinary tract stones is limited to patients in whom other investigations are contraindicated. MIP reconstructions from three-dimensional datasets can resemble a conventional IVU but the spatial resolution is inferior to alternative techniques. Although the site of obstruction may be demonstrated definitively identification of a stone may be difficult (5) (Fig. 3).

Stone Disease, Urinary. Figure 3 This macroscopic image shows a urinary tract stone of mixed composition (calcium oxalate and calcium phosphate) after stone extraction.

Additional Radiological Investigations

The frequency of *retrograde ureterography/scopy* has been markedly decreased for evaluation of suspected ureteric stones. It is occasionally used in the patient with persistent suspicion of ureteric stone and unclear findings on UCT or IVU (e.g., differentiation of phleboliths and calculi) (1) (Fig. 4).

Nuclear medicine is useful in selected cases. Its principal role is in determining relative renal function to decide whether a minimally invasive therapy is appropriate for a stone-bearing kidney or if the patient should undergo nephrectomy. There is no defined

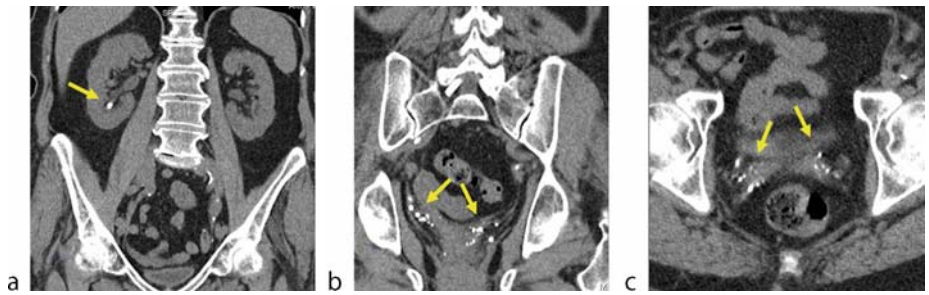

Stone Disease, Urinary. Figure 4(a–c) Patient with right lower urinary calculus (a, *arrow*) and multiple calcifications in the small pelvis. Differentiation of prevesical calculi and phleboliths (*arrows*) may be limited on unenhanced CT as shown in these coronal (b) and axial (c) images.

threshold, but <10% preserved function is probably not worth treating, and nephrectomy is then indicated. The divided renal function is also useful when bilateral renal stones are present as the side with the better function is treated first (1).

Management of Urinary Stone Disease

The management of urinary stone disease depends on the clinical presentation, stone location, stone size, and possibly on stone "hardness." With an acute presentation, the presence of complications such as super-added infection or renal impairment may necessitate immediate intervention whilst uncomplicated cases can be managed conservatively with adequate fluids and analgesia. If the stone does not pass spontaneously, definitive stone treatment is required and is often performed as a delayed, elective procedure.

Often, however, it is difficult to determine how closely symptoms are related to a urinary tract calculus. Some studies suggest that even small nonobstructing calculi may be symptom-provoking and patients may benefit from stone removal. In other cases, the stone may be an incidental finding, and it is difficult to justify invasive treatment. Each case must therefore be considered on its merits and the benefits of intervention should be balanced against the risks of the chosen procedure (6).

Conclusion

Modern imaging of urinary stone disease should provide accurate information about the presence, size, and precise location of a renal or ureteric stone, as well as the intracalyceal anatomy. A range of imaging tests are available, but no single test is ideal. The choice may depend on local resources. In the ideal scenario, patients presenting with suspected ureteric colic should undergo UCT. In patients presenting with vague symptoms or abnormalities in dipstick urinalysis, ultrasound combined with a KUB may be the most appropriate first-line examination.

In planning treatment, anatomical information is important and the IVU remains an important imaging method. MDCT-urography also provides detailed anatomical information, however, the radiation dose is higher compared to IVU (Fig. 5). Low dose CT protocols may challenge the radiation dose issue. Recently, high quality multiplanar reconstructions and advances in three-dimensional imaging have improved treatment planning. For follow-up, change in size and location need monitoring that usually can be done by KUB and ultrasound. Since urinary stone disease is often a recurrent disease in young people, the radiation dose should be an issue.

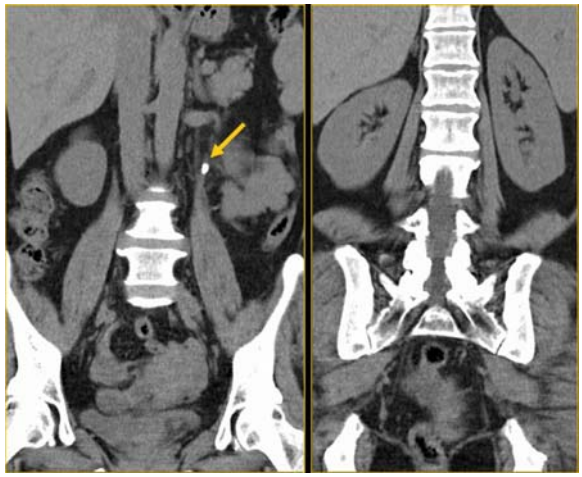

Stone Disease, Urinary. Figure 5 Coronal reformats of unenhanced MDCT scans are helpful in evaluation of the precise location and size of urinary tract stones as shown in this patient with a left mid-part ureteric calculus (*arrow*).

Bibliography

1. Sandhu C, Anson KM, Patel U (2003) Urinary tract stones—part I: role of radiological imaging in diagnosis and treatment planning. Clin Radiol 58:415–421
2. Eskelinen M, Ikonen J, Lipponen P (1998) Usefulness of history-taking, physical examination and diagnostic scoring in acute renal colic. Eur Urol 34:467–473
3. Tamm EP, Silverman PM, Shuman WP (2003) Evaluation of the patient with flank pain and possible ureteral calculus. Radiology 228:319–329
4. Kemper J, Adam G, Nolte-Ernsting C (2005) Multislice CT-urography. Aspects for technical management and clinical application. Radiologe 45:905–914
5. Rothpearl A, Frager D, Subramanian A et al (1995) MR urography: technique and application. Radiology 194:125–130
6. Sandhu C, Anson KM, Patel U (2003) Urinary tract stones—part II: Current status of treatment. Clin Radiol 58:422–433

Strangulating Obstruction

The impairment of arterial inflow or venous outflow from small bowel due to a twist in the mesentery.

▶Small Bowel, Postoperative

Strangulation

Closed-loop obstruction with secondary ischaemia.

▶Occlusion and Subocclusion, Small bowel in adults

Strawberry Gallbladder

Diffuse form of cholesterolosis characterized by a diffuse deposition of cholesterol esters in macrophages of the gallbladder lamina propria with a granular appearance resembling those of a strawberry surface, as attested by small, yellow spots against the mucosa.
▶Cholecystoses

Stress Urinary Incontinence (SUI)

Involuntary loss of urine during physical exertion with increased intraabdominal pressure.
▶Pelvic Floor Dysfunction, Genitourinary

Striated Muscle

Muscle in which sacromeres of the contractile myofibrils are arranged as transverse or oblique striations.
▶Rhabdomyosarcoma

Stroke

A clinical syndrome comprising rapidly developing signs of focal or generalized neurological dysfunction lasting more than 24 h.
▶Stroke, Children

Stroke, Children

W K 'Kling' Chong
Pediatric Neuroradiologist, Great Ormond Street Hospital for Children, London, UK
k.chong@ich.ucl.ac.uk

Synonyms

Arterial ischemic stroke; Cerebral infarction

Definition

The World Health Organization defined ▶stroke as 'a clinical syndrome typified by rapidly developing signs of focal or global disturbance of cerebral functions, lasting more than 24 h or leading to death, with no apparent causes other than of vascular origin' (World Health Organization 1978).

As a clinical definition, such a presentation in childhood has many potential underlying causes. Modern imaging techniques can distinguish between these potential causes.

The main focus of this essay is on arterial ischemic stroke in childhood. A practical definition of this is, "a clinical stroke syndrome presenting in a child, due to ▶cerebral infarction in an arterial distribution." Please note that this also allows for a diagnosis of arterial ischemic stroke to be made, using medical imaging, in less than 24 h of the onset of disease.

Stroke is one of the top ten causes of childhood death. Many more suffer from long-term disability and are at risk of further strokes in the future. Many children with stroke have another medical condition, such as a cardiac disorder or sickle cell disease, increasing the likelihood of adverse neurodevelopmental effects. Although the numerical burden of disease is smaller than in the elderly, the physical, emotional, and social effects carry long-term implications on the individuals, family, and society as a whole.

Clinical Presentation

The most common clinical presentation of stroke in childhood is an acute hemiparesis. However, the recognition of clinical stroke may be difficult in infants and young children. Focal signs may be absent in neonates and young infants in whom seizures may be the only clinical manifestation. Clinical signs and symptoms may be particularly subtle in children with sickle cell disease, and difficult to distinguish from painful crises or the effects of the treatment of such with opiates. If in doubt, the child should be examined by an experienced pediatrician and advice may be sought from a child neurologist or a tertiary center.

Imaging

Computed tomography (CT) and magnetic resonance imaging (MRI) are the mainstay modalities in the diagnostic imaging of neurological disease. Brain MRI is recommended for the investigation of children presenting

with clinical stroke. It should be performed as soon as possible after presentation. If brain MRI is not available within 48 h, then CT of the brain is an acceptable initial alternative (1).

The initial diagnostic imperative is for the confirmation of arterial ischemic stroke as well as for the exclusion of alternative treatable pathologies.

Practical considerations may apply with regard to limited access to suitable imaging facilities for children. It is possible that after initial assessment, transfer to a tertiary center may be required for definitive studies and other investigations.

For the initial diagnosis, an uncontrasted study of the whole brain is all that is generally required. Greater diagnostic confidence is gained using MRI over CT. If using MRI, diffusion imaging is often helpful in confirming the diagnosis.

Diagnosis

The imaging diagnosis of *arterial ischemic stroke* is based on the identification of characteristic radiological signs. There is a hierarchy of radiological signs which when seen together form a diagnostic pattern. The patterns of stroke in children are identical to those observed in young adults, with minor differences to those seen in the elderly.

The most important radiological sign is the identification that the abnormality is confined to or concordant with a recognized arterial territory. As there are relatively few variations in the cerebral arterial territories between individuals, this becomes a very useful indicator for the diagnosis. The margins of these abnormalities are usually well demarcated. Another recognized pattern is that of abnormalities distributed within the arterial border zones, in between the main arterial territories. These watershed regions may vary between individuals and there may be an overlap with other pathologies that affect these regions, therefore the identification of this sign is considered slightly less specific.

Supportive radiological signs are as follows. In the acute phase, the abnormality is typically hypodense on CT. It is recognized that this may take several hours to evolve. An initial early sign is a localized loss of gray-white matter differentiation. On conventional MR, the abnormalities are hyperintense on T2-weighted images and hypointense on T1-weighted images (Fig. 1). Although it is recognized that these may also take some time to evolve, the intensity changes on MR are comparatively much greater than the density changes on CT. This greater contrast resolution gives MR an advantage in both sensitivity and specificity. Furthermore, abnormalities may be detectable using diffusion MR within minutes of the insult, allowing for even earlier detection should the child have access to a scanner in that timescale (Fig. 1). Another characteristic sign that is always present in the acute phase is that of localized brain swelling. The affected areas of brain will demonstrate mass effect, causing localized sulcal effacement.

After a few days, the swelling will start to resolve. On CT, the arterial infarct becomes more clearly demarcated. Toward the end of the first week and early part of the second week, most larger infarcts demonstrate a degree of hemorrhagic change. This is accompanied by breakdown in the blood–brain barrier (i.e., manifesting as areas of contrast enhancement), and the distribution of these changes typically follows a gyral or cortical pattern, with relative sparing of the underlying, but also abnormal, white matter. On MR, therefore, the affected cortex starts to become hypointense on T2-weighted images and hyperintense on T1-weighted images. As the hemorrhagic effects clear, the intensity changes will again revert with time.

The chronic phase of an infarct is characterized by focal atrophy. The lesion is typically well demarcated. There may be some residual evidence of mature hemorrhage, but usually no persisting contrast enhancement. This is usually seen after several weeks or a few months and the abnormalities then persist, remaining stable indefinitely.

Other characteristic and supportive radiological signs involve the identification of abnormalities in the feeding arteries and draining veins to and within the infarct. A hyperdense thrombus within the feeding artery is a very important diagnostic sign on CT. A significant stenosis, occlusion, or turbulent flow may be identified on MR angiography. It is not uncommon to identify the presence of acutely thrombosed small veins within a large acute infarct. It is recognized that the pattern of degree and extent of such thromboses and occlusions may vary considerably in the hours, days, and weeks following an infarct.

Imaging allows not only the diagnosis of an arterial ischemic infarct to be made with confidence, but also the exclusion of alternative causes of clinical stroke. These are briefly discussed in the section on differential diagnosis.

At this time, the diagnostic imperative then shifts toward the identification of potentially treatable risk factors for arterial ischemic stroke. In the context of medical imaging, this will involve echocardiography and imaging of the entire intracranial and extracranial ▶cerebral vasculature (from at least the aortic arch to the level of the infarct). A variety of angiographic tools are available, but the current evidence base for the choice of modality in the pediatric setting is weak. Catheter angiography remains the gold standard against which alternatives should be compared, but this is an invasive investigation requiring some skill and expertise in the pediatric setting. CT and MR angiography are practical

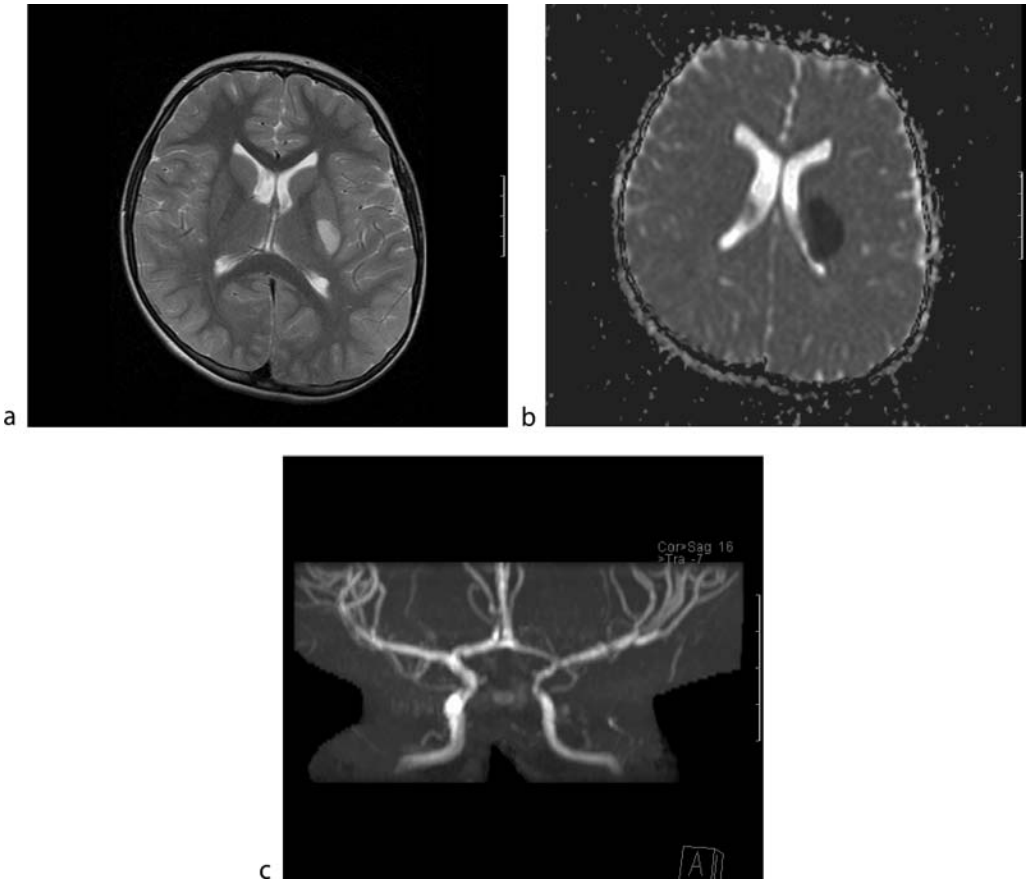

Stroke, Children. Figure 1 A 10-year-old boy with an acute presentation of right hemiparesis with facial and bulbar involvement, about 5 months after chicken pox infection. There was a well-demarcated lesion affecting the left putamen, body of caudate nucleus, and intervening capsular white matter (a). The mean apparent diffusion coefficient values within the lesion were 0.28 ± 0.07 × 10(−3) mm^2/sec (b = 1000 sec/mm^2, 1.5 T), typical of the restricted diffusion seen in arterial ischemic stroke (b). An anteroposterior maximum intensity projection view of the carotid circulation from the MR angiogram of the circle of Willis, showing irregularity and attenuation of flow in the terminal left internal carotid artery and proximal left anterior and middle cerebral arteries (c). The final diagnosis, after confirmation of viral titers in the cerebrospinal fluid, was of varicella vasculopathy. He was treated with aspirin.

and relatively noninvasive techniques, but they may vary in the quality of implementation when applied to children (Fig. 1). Ultrasound may be a useful adjunct to observe certain segments of the vascular supply.

Table 1 lists a range of pathologies and diseases that are associated with childhood stroke. Most children with stroke have more than one of these risk factors. An important concept is that it is the synergistic effects of these risk factors that result in the development of arterial ischemic stroke. The implication of this concept on imaging strategy is that despite the identification of one or more of these risk factors or conditions, continued and systematic imaging investigations may still be warranted to look for others.

Stroke, Children. Table 1 More commonly identified causes and risk factors of childhood stroke

Sickle cell disease
Thrombophilias
Varicella zoster infection (chicken pox vasculopathy)
Trauma and vascular dissection
Congenital cardiac abnormalities, including septal defects
Cerebral vasculitis, either isolated or as part of a systemic vasculitis
Inherited disorders of metabolism and genetic risk factors
Moya-moya disease—primary or secondary
Anemia, hypoxia, polycythemia, dehydration, hyperhomocysteinemia

Imaging is also used for the monitoring of disease. This may include imaging as part of presurgical planning, because some cases benefit from surgical intervention. Various techniques for surgical revascularization are available. Amongst them are external carotid to internal carotid (EC–IC) bypass surgery and varieties of *synangiosis*.

Differential Diagnosis

Some alternative causes of clinical stroke in the pediatric setting that may be identified on the initial scans are as follows. If there is continued uncertainty, repeat scanning after an interval often allows the natural history of these alternatives to evolve.

Venous infarction: these are typically in a venous territory, hemorrhagic, and associated with a greater degree of brain swelling and edema than arterial infarcts. Thrombosis in the veins may be identified and may include the dural venous sinuses.

Metabolic stroke: abnormalities are typically bilateral and relatively symmetrical, or in a distribution that does not confirm to typical arterial territories.

PRES (posterior reversible leukoencephalopathy syndrome): patients are usually identified by being at risk from immunosuppressive therapy. The imaging findings are similar to venous infarcts but without hemorrhagic change.

Acute demyelination: these may present with single or multiple, typically rounded or ovoid lesions that do not conform to a vascular distribution. Some may demonstrate contrast enhancement and a characteristic concentric zonal pattern of signal change.

Bibliography

1. Paediatric Stroke Working Group (2004) Stroke in Childhood: Clinical Guidelines for Diagnosis, Management and Rehabilitation. Royal College of Physicians of London, England, ISBN 1 86016 236 3 http://www.rcplondon.ac.uk/pubs/books/childstroke/childstroke_guidelines.pdf

Stroke, Interventional Radiology

Rüdiger von Kummer
Universitätsklinikum Carl Gustav Casns, Dresden, Germany
ruediger.vonkummer@uniklinikum-dresden.de

Definition

Stroke is a clinical syndrome reflecting the sudden dysfunction of specific brain regions caused by focal ischemia, brain hemorrhage, and other conditions like hypoglycemia, focal inflammation, and focal epilepsy (see stroke in adults and children). Because of its high vulnerability, brain tissue may be already irreversibly injured at the onset of ischemic stroke. Under more fortunate circumstances, the impact has impaired brain function only, and the brain's structure is still widely intact. A specific intervention could then rescue brain tissue, restore function, and prevent disability and death. Moreover, endovascular interventions can decrease the risk of stroke in patients with arterial stenosis or malformations.

Interventional neuroradiologists have the training and means to recanalize obstructed brain arteries and veins and to occlude sources of intracranial hemorrhage like aneurysms and other vascular malformations using microcatheters and other devices. They play an important role in preventing and treating acute ischemic and hemorrhagic stroke.

Interventional Radiological Treatment

Ischemic Stroke

Vascular and brain imaging may detect arterial stenotic disease in asymptomatic patients, patients with transient symptoms, and patients with acute stroke syndromes. These patients have an increased risk for disabling stroke that is most prominent in the first days after ischemic brain attack and in patients with impaired cerebral perfusion reserve. In patients with substantial arterial narrowing (50–99%) or occlusion and no permanent neurological deficit, ▶*angioplasty* may reduce the risk of disabling stroke by improving hemodynamic conditions. In patients with an acute stroke syndrome, ▶*thrombolysis*, thrombus retraction, and/or angioplasty can restore blood flow and enable the recovery of brain function.

Prophylactic Interventions

▶*Endovascular therapy* for extracranial and intracranial atherosclerotic disease includes angioplasty with and without ▶stent placement in the brachiocephalic and subclavian artery, the internal carotid artery (ICA), the middle cerebral artery (MCA), the vertebral artery (VA), and the basilar artery (BA). *Stent*-supported angioplasty is currently providing a therapeutic alternative to traditional methods of open vascular surgery for revascularization of these vessels and increasing the therapeutic options available for patients who have failed maximal medical therapy. Whereas ▶*carotid endarterectomy* (*CEA*) is well established based on good scientific evidence, studies are still missing showing that stent-supported angioplasty of extracranial ICA stenosis has a lower operative risk and can decrease the risk of stroke like CEA

(1). Nevertheless, stent-supported angioplasty of the extracranial ICA is increasingly performed because of its feasibility with a technical success rate of over 90% and low risk in experienced hands. Angioplasty of the atherosclerotic proximal VA bears the problem of elastic recoil that can be overcome with stents. A widely accepted indication is a symptomatic VA stenosis in patients with contralateral VA occlusion or hypoplasia.

The stent-supported angioplasty of other arterial diseases like dissection or vasculitis or of intracranial arteries is still experimental and appears justified in case of severe and symptomatic hemodynamic deficit (Fig. 1). Endovascular treatment of intracranial atherosclerotic stenosis has undergone rapid evolution during the past several years. Large case series show that balloon angioplasty can be performed with relatively low risk (2). The future will show whether the use of balloon mounted or self-expandable stents will improve perioperative and long-term results.

Interventions in Acute Stroke

The beneficial effect of systemic (IV) thrombolysis is limited in patients with combined extracranial and intracranial arterial obstructions, in patients with large vessel occlusion like the distal ICA and BA, and declines over time from stroke onset. Whereas IV thrombolysis is approved for the first 3 h only, the PROACT studies showed that IA thrombolysis of MCA occlusion is beneficial within the first 6 h of stroke onset(3). Endovascular therapy may improve the chances for good clinical outcome of these patients if applied as primary approach or after initiating systemic thrombolysis when interventionalists are not readily available (bridging-concept). Case series show that intra-arterial (IA) thrombolysis with urokinase or recombinant tissue plasminogen activator (tPA) can be as effective as IV thrombolysis in reducing the number of disabling strokes and deaths. In patients with acute symptomatic BA occlusion, most centers prefer IA thrombolysis, although one case series showed that IV thrombolysis might have similar good results(4). A controlled randomized trial comparing both approaches is not available. Endovascular treatment in acute stroke has the distinct advantage that IA thrombolysis can be combined with angioplasty in patients with atherosclerotic obstructions. Moreover, angioplasty and thrombus retrieving devices can be used to quickly recanalize the artery in order to restore blood flow and increase the chance for thrombolytic clot resolution distally in smaller arterial branches. Reports on cerebral hemorrhage after carotid recanalization coined the term "reperfusion hemorrhage" or "reperfusion trauma." It is unclear so far, whether the extent of ischemic brain tissue damage, arterial dysfunction, a sudden increase in perfusion pressure, high arterial blood pressure, anticoagulation, or arterial wall injury by guide wires alone or in combination is the cause of brain hemorrhage.

Hemorrhagic Stroke

Spontaneous intracranial hemorrhage has many causes among them arterial *aneurysms* and ▶arterio-venous malformations (AVM) that can be treated with endovascular approach. Ruptured saccular aneurysms account for 10–15% of all strokes.

Subarachnoid Hemorrhage

Occlusion of cerebral aneurysms by clipping or ▶*coiling* is a crucial, but not the only step in treating patients with subarachnoid hemorrhage (SAH). These patients have a 50% risk to rebleed within the first 6 months of SAH. Other risks are the development of hydrocephalus, cerebral edema, and arterial vasoconstrictions with subsequent brain infarction. Patients with SAH need intensive care and must be artificially ventilated in most instances. Early occlusion of ▶aneurysm can prevent recurrent bleeding and enable a treatment with aggressive increase in arterial blood pressure and fluid volume in order to maintain intracranial perfusion pressure.

Until the early1990s, surgical clipping of cerebral aneurysms was the established treatment. The development of microcatheters and detachable coils first enabled the occlusion of aneurysms, which the neurosurgeons could not treat without major morbidity and mortality and is today the treatment modality of first choice in many institutions after a controlled randomized trial has shown improved short- and long-term clinical outcome with endovascular occlusion compared to surgical clipping (5). The advantage of transarterial coiling of aneurysms is its nontraumatic approach with quickly placing a microcatheter in the aneurysm lumen as an immediate step after diagnostic angiography. The aneurysm can thus be occluded within few hours after SAH. Transarterial coiling is feasible, if the aneurysm has a defined neck that prevents protrusion of coils into the parent artery and if no arteries origin from the aneurysm itself. In the latter case, the placement of a surgical clip may avoid arterial occlusion that is not well controlled by coiling. Wide-neck aneurysm can be treated with the aid of stents or temporary balloon occlusion of the parent artery. For wide-neck giant aneurysms (diameter >25 mm) of the ICA, VA, or even MCA or false aneurysms located more distally, occlusion of the parent artery with coils or balloon must be considered. A balloon test occlusion can show whether the permanent occlusion will be tolerated or not. In selected patients, parent vessel occlusion should be combined with bypass surgery. A new approach is the placement of a covered stent over the aneurysm neck.

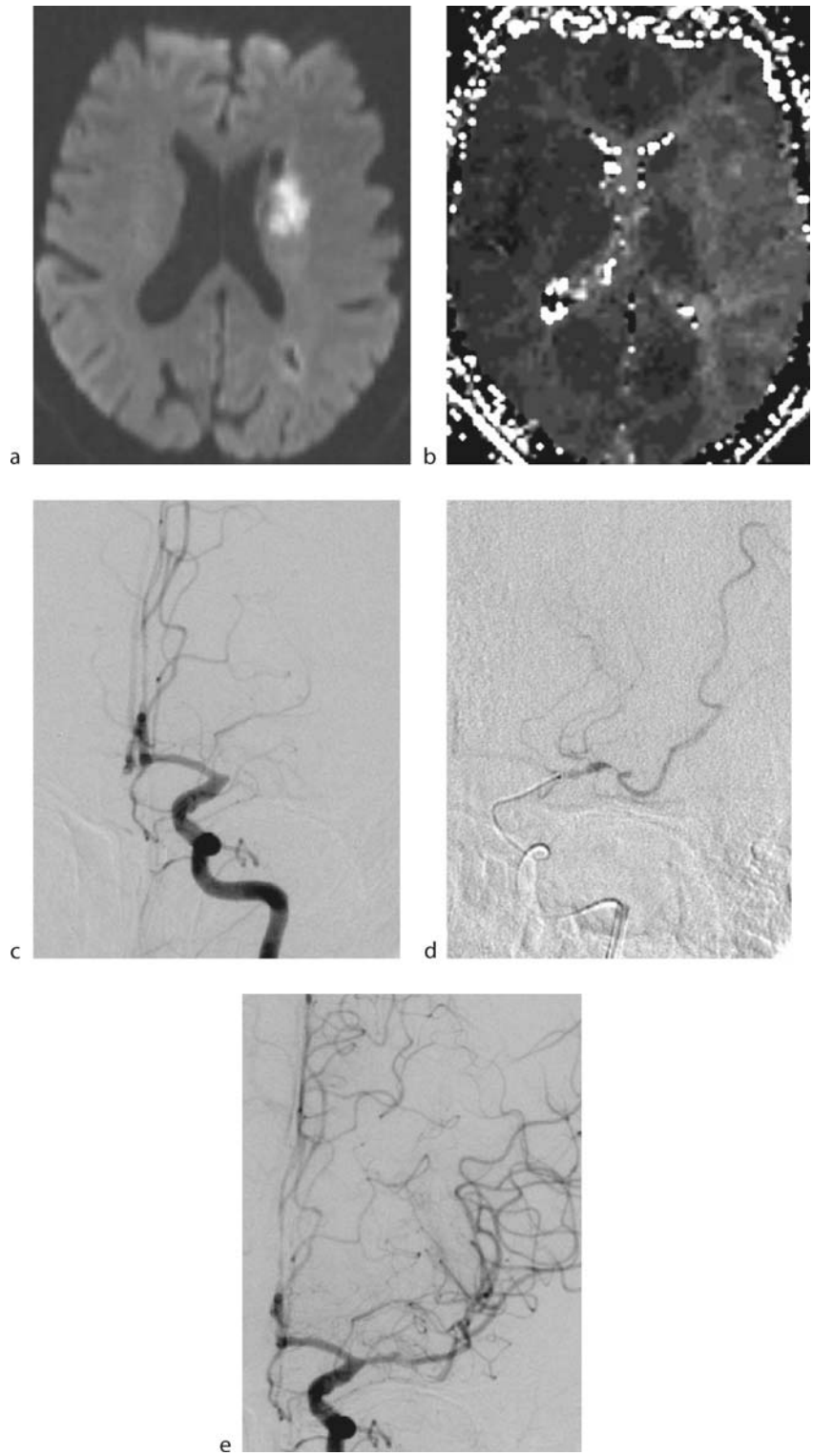

Stroke, Interventional Radiology. Figure 1 A 70-year-old woman with minor left hemispheric stroke and repeated TIA of her left MCA territory due to tight stenosis of the left M1-segment since 3 months despite antiplatelet therapy. (a) shows old and acute lesions on DWI in the end-supply areas of the left MCA. (b) time-to-peak map demonstrates delayed contrast inflow into the left MCA-territory. (c) DSA of the left ICA shows (ap-view) occlusion of the left MCA-trunk. (d) direct injection of contrast into the left MCA-trunk demonstrates that the obstruction is incomplete. (e) after passing the tight stenosis with a microguide wire, angioplasty with a 2 mm-balloon recanalizes the left MCA. No further TGIA occurred.

These stents are, however, relatively stiff and not well suited to be advanced over the carotid siphon. Arterial vasoconstrictions typically occur 1 week after SAH and jeopardize cerebral tissue. Local arterial infusions of nimodipine and balloon angioplasty can improve blood flow and prevent infarction.

Cerebral Hematoma

Dural and pial *AVMs* are among the causes of nontraumatic cerebral hemorrhages and should be considered in all patients in whom arterial hypertension, coagulation disorder, or amyloid angiopathy is not the obvious reason for the bleeding. Patients with hemorrhage from AVM have an increased risk for a recurrent bleeding and should be treated. It is widely accepted that endovascular treatment is the first choice for dural AVMs. Interventional neuroradiologists treat dural AVMs by occlusion of the fistula with glue or coils after transarterial or transvenous approach. Pial AVMs can be treated with open surgery and resection of the AVM nidus, with radiation of the nidus, or with embolization of the nidus. Because radiation does not immediately decrease the risk of recurrent hemorrhage, it is considered only for patients with small AVMs, which cannot be reached by neurosurgeons or neuroradiologists. A complete embolization of the AVM nidus should be achieved to decrease the risk of another brain hemorrhage. A complete embolization of the AVM nidus can be achieved in 10–20% of the patients only, so that embolization has to be combined with surgery in the majority of patients. Preoperative embolization can, however, diminish the extent of the nidus and thus decrease the risk of surgery in these patients. Embolization with glue has the risk of venous obstruction and subsequent hemorrhage, gluing the microcatheter within the feeding artery, or embolization of nutritive arteries with subsequent ischemia and stroke.

Bibliography

1. SPACE Colloborative Group, Ringleb P, Allenberg J, Brückmann H et al (2006) 30 day result from the SPACE trial of stent-protected angioplasty versus carotid endarterectomy in symptomatic patients: a randomised non-inferiority trial. Lancet 368:1239–1247
2. Marks M, Wojak J, Al-Ali F et al (2006) Angioplasty for symptomatic intracranial stenosis: clinical outcome. Stroke 37:1016–1020
3. Furlan A, Higashida R, Wechsler L et al (1999) Intra-arterial Prourokinase for acute ischemic stroke. JAMA 282:2003–2011
4. Lindsberg P, Mattle H (2006) Therapy of basilar artery occlusion: a systematic analysis comparing intra-arterial and intravenous thrombolysis. Stroke 37:922–928
5. Molyneux A, Kerr R, Yu L et al (2005) International Subarachnoid Aneurysms Trial(ISAT) of neurosurgical clipping versus endovascular coiling in 2143 patients with ruptured intracranial aneurysms: a randomised camparison of effects on survival, dependency, seizures, rebleeding, subgroups, and aneurysm occlusion. Lancet 366:809–817

Stromal Tumor

Gastrointestinal stromal tumor is the current designation for the major subset of gastrointestinal mesenchymal tumors (gastrointestinal smooth muscle tumors); absence of expression of the gamma-smooth muscle isoactin gene correlates with malignancy.

▶Neoplasms Small Bowel

Stubbed Toe Fracture

A dorsal Salter II metaphyseal corner fracture of a distal phalanx, equivalent to an open fracture.

▶Osteomyelitis, Neonates, Infants, Childhood: Including Septic Arthritis and Other Important Soft Tissue Infections/Abscesses

Sturge–Weber Syndrome

A meningofacial angiomatosis. Although there have been familial cases, as a rule there is no evidence of heredity. A meningeal vascular malformation with cortical calcification is the typical finding on imaging.

▶Neurocutaneous Syndromes

Subaxial Cervical Arthritis

Subaxial cervical arthritis is a feature of rheumatoid arthritis and spondarthropathies. It comprises discitis and apophyseal joint arthritis.

▶Rheumatoid Arthritis

Subcapsular Hematoma, Splenic

A collection of blood with a lenticular shape that lies just below the splenic capsule. It can be caused by blunt abdominal trauma or may originate from a spontaneous splenic rupture.

▶Trauma, Splenic

Subchondral Bone Cysts

Subchondral bone cysts are a prominent feature of osteoarthritis, occasionally forming as sequelae of bone injury. Radiographically the lesions are radiolucent, with a surrounding sclerotic margin. Joint-space narrowing and bone sclerosis are accompanying features. These lesions are also found in hemochromatosis.

▶Hemochromatosis, Skeletal

Subchondral Cysts

Subchondral cysts can be found with or without a sclerotic rim. Sclerotic subchondral cysts occur in degenerative osteoarthritis, gout, and SLE. In chronic gout they tend to be large and in a metaphyseal location. In degenerative osteoarthritis the predominant location is eccentric epiphyseal. SLE cysts are tiny and thought to be micronecrotic foci. Arthritic cysts tend not to have the sclerotic rim. Additional signs should be considered to establish the final diagnosis. Small osteolytic lesions have to be differentiated.

▶Connective Tissue Disorders, Musculoskeletal System

Subclavian Steal Syndrome

▶Steal Syndrome, Vertebral

Subcutaneous Rheumatoid Nodules

Subcutaneous rheumatoid nodules can be seen in seropositive rheumatoid arthritis. They are characteristic but not very common and are typically located at bony prominences. There is a typical histologic appearance.

▶Rheumatoid Arthritis

Subependymal Hemorrhage

▶Hemorrhage, Intracranial, Neonates (Neuro View)

Sublingual Gland

The sublingual glands are salivary glands in the mouth. They lie anterior to the submandibular gland under the tongue, beneath the mucous membrane of the floor of the mouth.

▶Inflammation, Chronic, Acute, Salivary Glands

Subluxation

Displacement of the femoral head in the hip that still leaves some surface contact with the acetabulum.

▶Dysplasia, Hip, Developmental

Submandibular Gland

The paired submandibular glands (or submaxillary glands) are salivary glands located beneath the floor of the mouth. In humans, they account for 70% of the salivary volume.

▶Inflammation, Chronic, Acute, Salivary Glands

SUI

▶Stress Urinary Incontinence (SUI)

Sump Syndrome

Uncommon complication of side-to-side choledocho-duodenostomy performed to improve biliary drainage in cases of retained stones or biliary dilatation. The segment of common bile duct between the anastomosis and the ampulla of Vater in cases of malfunction may act as a stagnant reservoir or stump wherein stones, debris, or infected bile accumulate. Bacterial overgrowth inside the stump results in acute cholangitis. Clinically, it presents as recurrent biliary pain or pancreatitis. Imaging findings include debris or stones in the common bile duct that may

appear dilated, dilated pancreatic ducts, and changes due to pancreatitis, cholangitis, or liver abscesses.
▶Cholangitis

Superior Caval Vein Occlusion

▶Thrombosis, Caval Vein, Superior

Superior Vena Cava Syndrome

The obstruction of venous drainage due to tumour infiltration into the superior vena cava. This leads to dilation of collateral veins in the upper part of the chest and neck; oedema and plethora of the face, neck and upper part of the torso, including the breasts; suffusion and oedema of the conjunctiva; breathlessness when supine; and CNS symptoms such as headache, visual distortion and disturbed states of consciousness. Although a dramatic clinical situation, this syndrome requires urgent but not emergency care.
▶Neoplasms Pulmonary

Suppurative Fluid Collection

▶Abscess, Renal

Supramesocolic Peritoneal Cavity

This extends from the diaphragm to the transverse mesocolon and is divided by peritoneal reflections into the following major spaces: right subphrenic, right anterior-posterior subhepatic, left subhepatic, and lesser sac.
▶Peritoneal Collections

Surgical Treatment of Crohn's Disease

Treatment for patients with severe complications or for those not amenable to medical treatment.
▶Crohn's Disease

SVC Obstruction

Narrowing or blockage of the SVC by malignant or benign pathology resulting in characteristic signs and symptoms.
▶Varices, Oesophagus

Swallowed Foreign Bodies

▶Foreign Bodies, Gastrointestinal

Swallowing Disorders

A. Wuttge-hannig, C. Hannig
Radiologie-Strahlentherapie-Nuklearmedizin
Mynich
Germany
a.wuttge-hannig@gmx.de

Definitions

Swallowing disorders are due to a dyscoordination, a dysfunction or an anatomic alteration in the esophagus or at the cross way of the respiratory and the alimentary tract. The swallowing disorders range from minor nutrition disabilities to the incapacity to ingest food with the consequence of aspiration of food or liquids into the airways. The swallowing disorders may even cause voice disabilities and may be associated with ronchopathy.

Pathology/Histopathology

During pharyngeal phase of deglutition in only 0,7 s 24 muscle groups governated by five cranial nerves transport the bolus from the oral cavity to the entrance of the esophageal tube. The speed of bolus transport in the pharynx is about 70 cm/sec. The reduction of the transport velocity in the esophagus is due to the progressive substitution of the striated musculature by smooth musculature. Therefore the speed of the peristaltic wave in the lower esophagus is reduced to 2–4 cm/sec (1).

The swallowing reflex in adults is triggered at the arch of the fauces and the corresponding dorsal pharyngeal

wall. In neonates, the trigger occurs physiologically in the valleculae, the substitutive area for adult swallowing. The trigger of the swallowing reflex happens when the critical soil of receptor information from the different types of receptors in the oral cavity, in the valleculae, in the piriform sinuses and even in the laryngeal vestibule is reached (2). Due to surgery, radio- or chemotherapy or in the case of infections and also physiologically in the geriatric age the number of these receptors decreases causing a delayed triggering of the swallowing reflex (3).

The upper esophageal sphincter opens and closes regulated by the swallowing reflex. The sphincter function is modulated not only by influences of the swallowing center in the brainstem and cortico-bulbar afferences but also by humoral transmission due to disorders of the esophageal peristalsis.

The esophagus is innervated by vagal afferences and by an intrinsic autonom system, the Meissner and Auerbach plexus. The propulsion of the bolus is normally performed by a primary peristaltic wave, which is regulated by a single swallowing trigger. Multiple trigger inputs during an ongoing swallowing peristalsis interrupt the first wave; this is the so-called "intradeglutitive swallowing inhibition." The closure of the lower esophageal sphincter is depending from the synergism of its resting tonus and the correct position in the ferrule of the diaphragmatic hiatus. The opening of the lower esophageal sphincter is coordinated by the swallowing reflex. The failure of this function is caused by an alteration of the angle of Hiss, the intrinsic sphincteric resting pressure and the length of the infradiaphragmatic esophageal segment.

The pathology ranges from tumors to neurological and muscular disorders. The functional disorders are mainly due to paraphysiologic alterations in the swallowing act and in the protection of the airways.

The malignant tumors in the oral cavity, the pharynx, and the esophagus are mainly squamous cell carcinoma, distally adenocarcinoma and rarely leiomyosarcoma. Benign lesions are generally not frequent and rage in order of occurrence from leiomyoma, cysts to fibroma.

The neurological induced swallowing disorders are referable to stroke, cerebral trauma or posttherapeutic, and tumoral deficiencies. Neuromuscular disorders are caused by neuro-degenerative illnesses as ALS, multiple sclerosis, Parkinson's Disease, Guillaume Barré or by myogen diseases like polymyositis, myastenia gravis, or inclusion bodies myositis.

Functional disorders are frequently caused by a disturbed pharyngo–esophageal interaction like in GERD (Fig. 1) (3).

Clinical Presentation

The symptomatology ranges from hoarseness, globus sensation, heartburn, bolus impaction to dysphagia and odynophagia. According to the definition of Vantrappen Hellemans dysphagia is present when the deglutition of food, but only rarely saliva, causes discomfort. The globus sensation instead describes a discomfort during deglutition of saliva, but not during food ingestion. Odynophagia is painful swallowing.

Neurogenic disorders are often correlated with the aging of population. In nursing homes about 40% of the elderly suffer from a not treated swallowing disorder (4), a so-called silent aspiration. Eight percent of patients

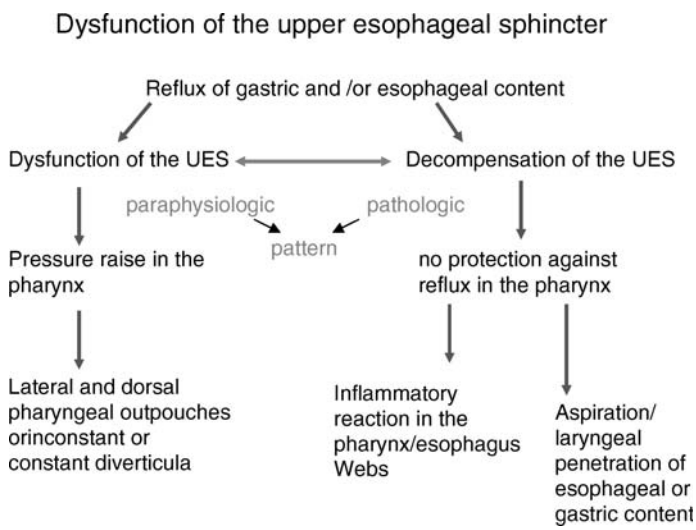

Swallowing Disorders. Figure 1 Flow sheet of the pharyngo–esophageal interactions.

surviving a stroke event die in the first year from aspiration pneumonia due to an unobserved swallowing disorder (5).

GERD may induce hoarseness, laryngitis posterior, and reflux induced asthma.

Imaging

For the analysis of pharyngeal swallowing disorders, the imaging frequence needs to be very high. This can be achieved by the video fluoroscopy or the digital spot imaging at a high frame rate more than 20 images/sec. The high-frequence cineradiography at 50 images/sec is now reserved for scientific elaborations, due to the relatively higher radiation dose needed. The frame-by-frame evaluation is of crucial importance for the diagnostic reading process.

In the esophagus the high temporal resolution is not useful. A normal fluoroscopy with spot imaging is sufficient.

Double contrast imaging with $BaSO_4$ is normally applied in every swallowing study. Different preparations with different consistencies adapted to the patients complaints should be carefully chosen. For the mucosal imaging often the application of myorelaxant agent is needed.

Special contrast mediums should be used in patients with suspected or clinical appear ant tracheal aspiration or with suspected fistulas to the bronchial system. An almost iso-osmolar water-soluble iodine contrast medium should be applied, since hyperosmolar solutions lead to a pulmonary edema and/or a vaso-vagal reaction when aspirated.

The modern techniques like CT or MRI have still the huge disadvantage of the obliged prone or supine position. Only in special studies like the analysis of velopharyngeal dysfunctions and its surgical therapy planning dynamic CT or dynamic MRI are used in clinical research (6, 7). Diluted gadolinium-EDTA or plain water can be used in MRI studies.

Nuclear Medicine

First pharyngeal studies for the analysis of neurogenic disorders were performed for the presence of aspiration or nasal penetration (8).

The use of a tracer-marked bolus for the esophageal motility disorder has a long tradition. Quantifications of motility disorders like achalasia, hypomotilities in scleroderma or segmental spasms and the quantification of refluxed material in GERD are possible with a low radiation exposure. The time of observation is not limited in comparison to fluoroscopy (9).

Gastric emptying with radiotracers allows a more physiological assessment of gastric motility, especially in the case of gastroparesis with secondary gastro-esophageal reflux.

Generally, colloids marked with 99mTc in liquid, semisolid, or solid bolus preparations are use for this type of studies.

Diagnosis

Tumoral lesions are visible directly by obstructions or mucosal alterations and indirectly in amotil regions. The extra luminal growth of tumors and the lymph node staging is the domain of the MRI and/or CT.

The functional or motility disorders are best examined by video fluoroscopy or digital spot imaging or by combined methods like radiomanometry.

The description of the functional diagnostic findings can be classified according to the three swallowing phases: the oral, the pharyngeal, and the esophageal phase.

Oral Pathologies

Functional disorders can be divided in neurologic/neuromuscular disorders with or without a tracheal aspiration and gastroenterological disturbances.

In the oral cavity, the bolus preparation and the bolus compression can be disturbed due to dismotility or an atrophy of the tongue or due to a malocclusion of the velum.

Posttherapeutic neurologic or functional disorders can be seen in treated cleft.

Pharyngeal Pathologies

In the pharyngeal phase the predominant finding is a functional alteration of the upper esophageal sphincter caused by GERD or an idiopathic esophageal motility disorder. The delayed and incomplete opening and the premature closure of the upper esophageal sphincter are frequent findings in GERD or neutral mass-reflux (Fig. 2). The pressure elevation in the pharynx leads to diverticula, pouches, and pharyngoceles in patients with a muscular predisposition (3). The entrance of acidity in the pharynx gives origin to web-like scar rings or inflammatory mucosal irritations in the pharynx and in the laryngeal vestibule. Indirectly the delayed opening of the upper esophageal sphincter leads to a closure of the laryngeal vestibule, thus causing a laryngeal penetration of the bolus (10).

The second entity corresponds to the aspiration-related neurogenic or neuromuscular disorders.

The division in a pre-, intra-, and postdeglutitive form of aspiration (Figs 3–5), this means an aspiration before, during or after the triggering of the swallowing reflex, give useful hints for an adequate conservative rehabilitation or a surgical therapy (11).

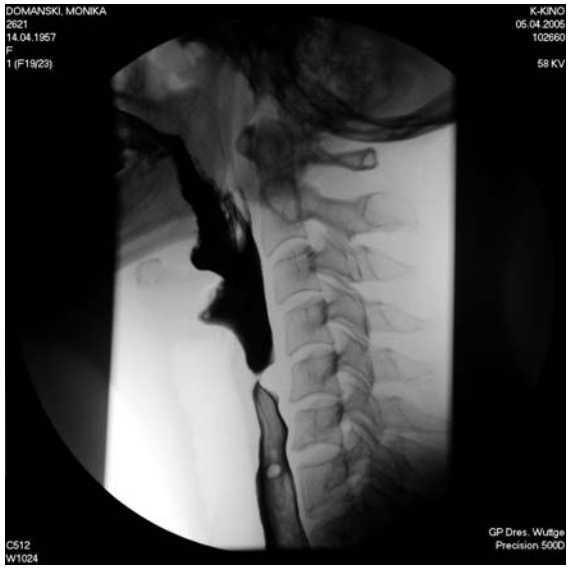

Swallowing Disorders. Figure 2 Dysfunction of the upper esophageal sphincter.

Dysphagia without aspiration is generally a precursor of aspiration associated dysfunctions. The dyscoordination of the events during a swallowing act is one of the first signs: The so-called cervical achalasia represents the impossible opening or the reduced opening of the upper esophageal sphincter which is due to a loss of interruption of the resting pressure of the sphincter (Fig. 6). The reduced activity in the pharyngeal constriction is often disturbed by myogenic disease like polymyositis, dermatomyositis, muscular amyloidosis, or postradiation or autoimmunologic myofibrosis. The delayed or incomplete opening or a premature closure of the UES might be due to a reduced laryngeal anterior and cranial movement by a deficiency of the extrinsic laryngeal musculature. The lack of a consecutive propulsion in the pharyngeal constrictor muscles, corresponds to the so-called Inclusion Body Myositis. Undefined muscular dyscoordinations might be seen in Parkinson's disease, multiple sclerosis, in the initial stage of amyotrophic lateral sclerosis, and in chorea Huntington (12).

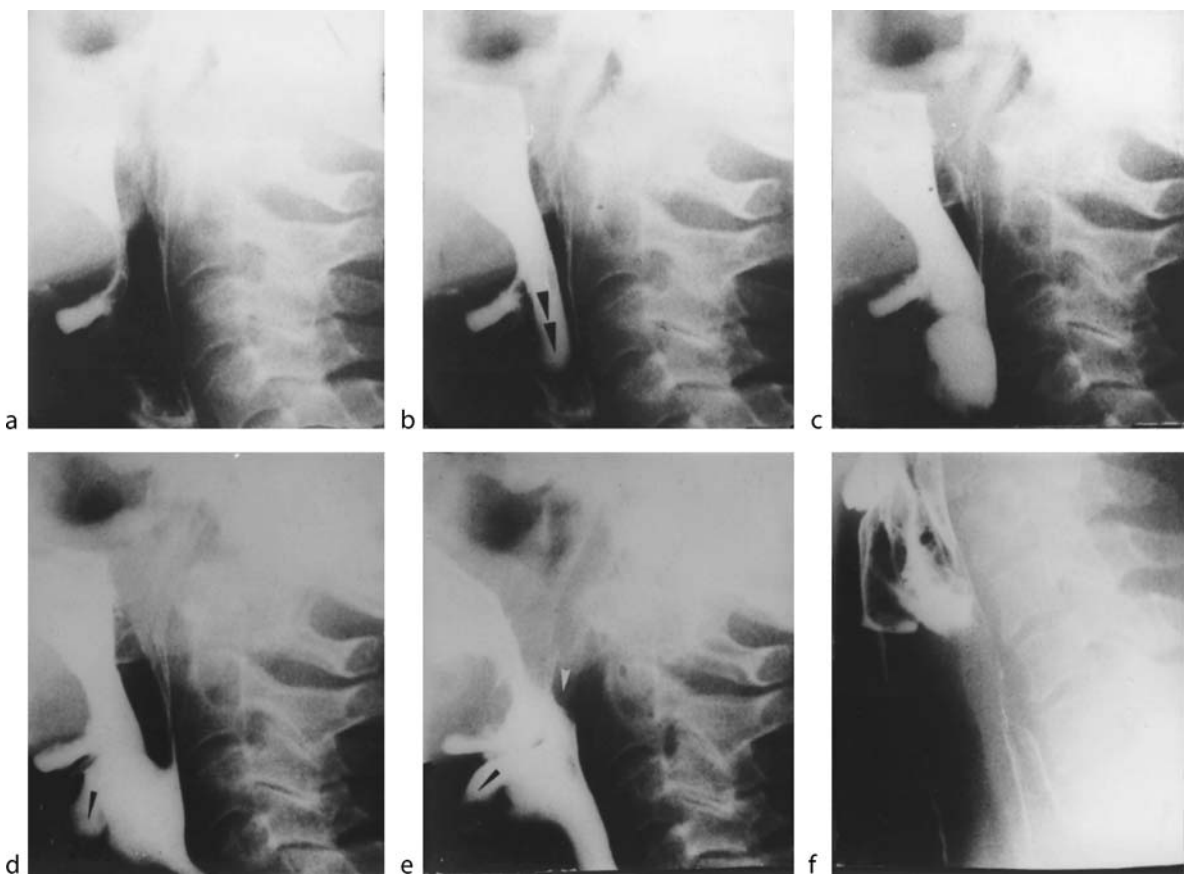

Swallowing Disorders. Figure 3 Predeglutitive aspiration: Sequence (a–f). Sixty-year-old patient with a media infarct left hemisphere. (a, b) Early leakage of CM in the valleculae and rec. piriformes (*black arrowheads*). (c, d) The CM enters in the hypopharynx and the laryngeal vestibule (*black arrow*) before the triggering of the swallowing reflex (*white arrow*) causing a tracheal aspiration.

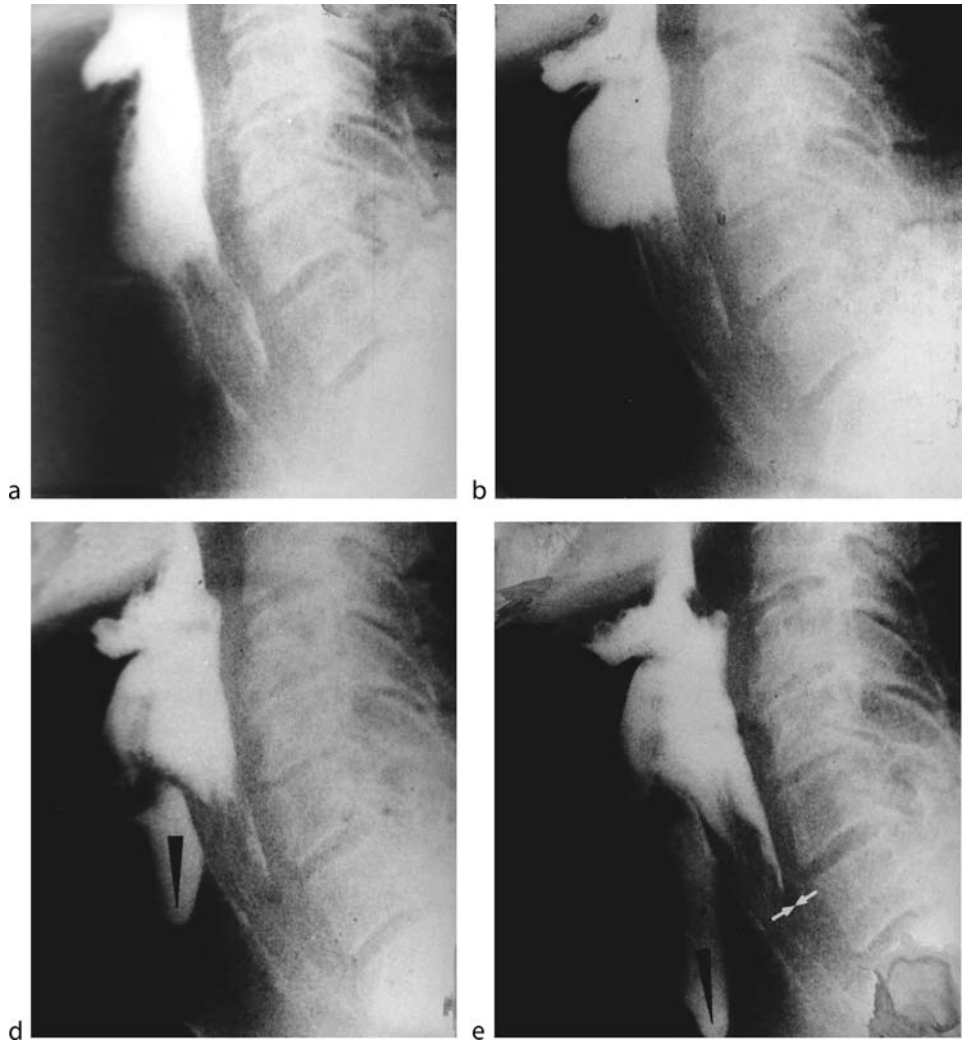

Swallowing Disorders. Figure 4 Intradeglutitive aspiration. Fifty-six-year-old patient after a stroke, (a, b) pharyngeal retention with a disturbed pharyngeal contraction and a simultaneous spasm the upper esophageal sphincter (radiologically only the diagnosis of a disturbed opening of the upper esophageal sphincter can be observed). The spasm must be evaluated manometrically.

Esophageal Pathologies

The functional disorders can be differentiated in primary or secondary forms.

Primary Forms

The best defined primary form is the esophageal achalasia, the incomplete or absent reflex induced opening of the lower esophageal sphincter (Fig. 7). A subdivision in three types, the hypomotile, the amotile, and the hypermotile form, is useful for the therapeutic approach.

The diffuse esophageal spasm is the second manometrically defined entity, which can be observed in fluoroscopy as a long segmental contraction or etage-like contractions of the esophageal body (Fig. 8). The symptomatology can be easily be mistaken for a cardiac attack.

The so-called nutcracker-esophagus does not present a typical radiological feature.

Secondary Forms

The most frequent is the reflux-associated motility disorder in GERD or large neutral mass refluxes. The lack of a primary peristalsis is the leading symptom. The influence on the pharyngeal phase is explained above. GERD is often associated with a constant or inconstant hiatal hernia (Fig. 9), diagnosed by the classical three-folds sign in prone position. The typical GERD-related mucosal changes are in stage I of esophagitis are the focal granulomatous mucosal alterations and microulcera in the distal esophagus; in stage II superficial ulcerations

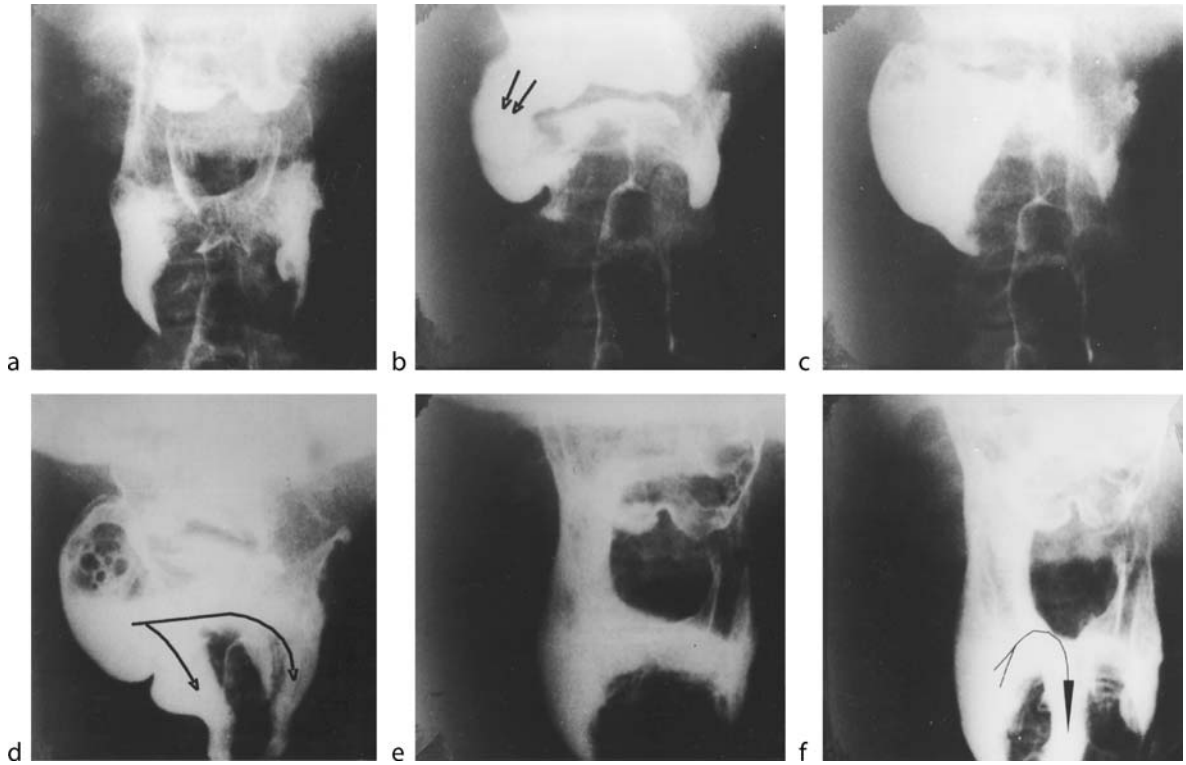

Swallowing Disorders. Figure 5 (a–f) Postdeglutitive aspiration. (a) Already in the resting phase before the swallowing a retention in the right rec. Piriformis can be observed. (b) Beginning of the pharyngeal contraction with extrusion of a pharyngozele of the right side and a CM retention in the right hemipharynx (*black arrow*). (c, d) During the unilateral opening of the upper esophageal sphincter transport of the CM retention from the right hemipharynx to the left side (*black arrow*). (f) Due to the return of the larynx to the resting position for respiration the pharyngeal capacity diminishes. Large aspiration of the CM stored in supraglottic position (*black arrow*).

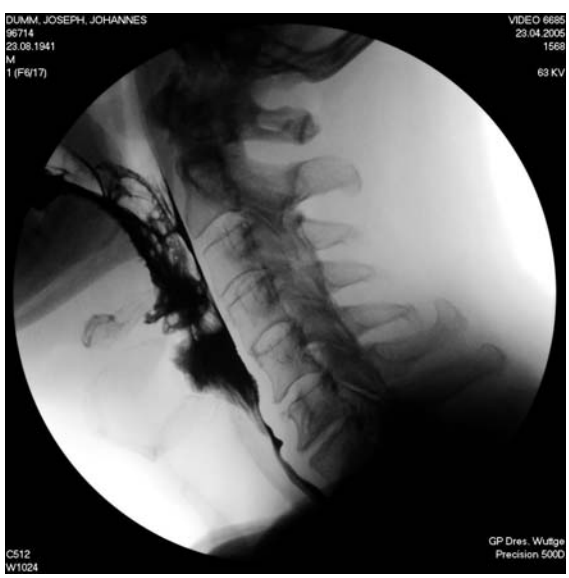

Swallowing Disorders. Figure 6 Cervical achalasia due to a insufficient sphincter reflex triggered opening. Major retentions in the pharynx can be observed.

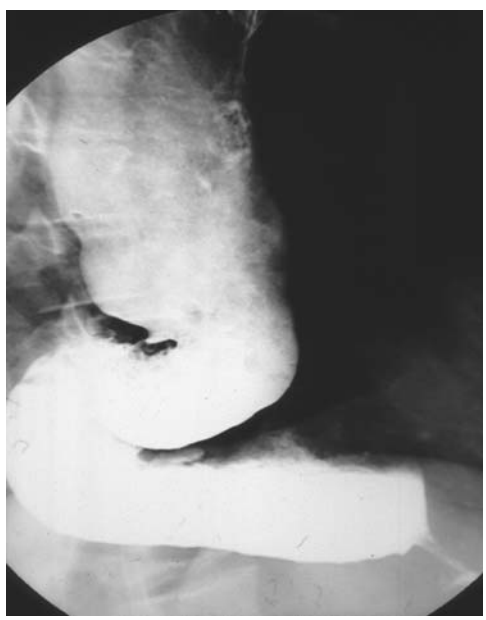

Swallowing Disorders. Figure 7 Amotile achalasia with Brachyesophagus.

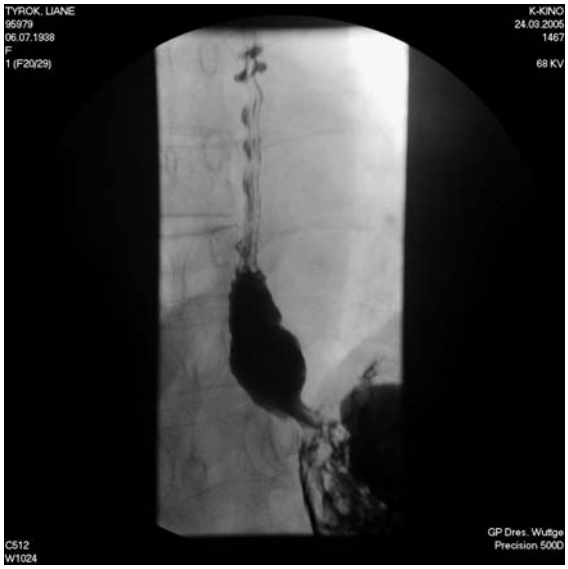

Swallowing Disorders. Figure 8 Etagenspasm in the middle and lower third of the esophagus with a hiatal hernia.

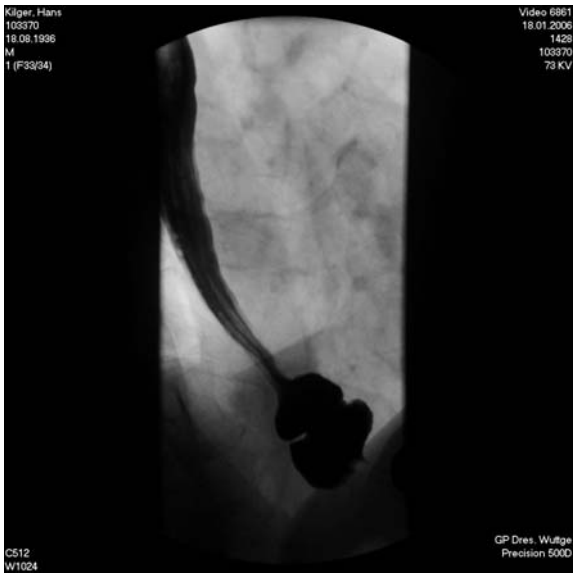

Swallowing Disorders. Figure 9 Hiatal hernia with a Schatzki's ring and gastroesophageal reflux.

in the lower third of the esophagus; in stage III larger confluating circular ulcerations, and in stage IV peptic stenosis. The thickened mucosal folds in the esophagus and the so-called feline esophagus with the cat skin like appearance can be observed in stage I (13, 14).

The diagnosis "presbyesophagus" summarizes a lot of primary and secondary esophageal motility disorders frequently found in the elderly population suffering from diabetes or polyneuropathy for example.

The secondary achalasia is mostly caused by a submucosal growth of a carcinoma of the esophagogastric junction. The differential diagnosis can be oriented by anamnesis and manometric findings, but the final decision remains reserved to biopsy.

Bibliography

1. Dodds WJ (1988) Physiology of swallowing. In: Ravich WJ, Donner MW, Johnes B (eds) Second Symposium on Dysphagia. Logemann, Baltimore
2. Kennedy JG, Kent RD (1988) Physiological substrates of normal deglutition. Dysphagia 3(1):24–38
3. Hannig C (1995) Radiologische Funktionsdiagnostik des Pharynx und des Ösophagus Springer-Verlag Berlin Heidelberg
4. Ekberg O, Hamdy S, Woisard V et al (2002) Social and psychological burden of dysphagia: its impact on diagnosis and treatment. Dysphagia Spring 17(2):139–146
5. Logemann JA (1988) Swallowing physiology and pathophysiology. Otolaryngol Clin North Am 21(4):613–623
6. Hannig Chr., Wuttge-Hannig A, Daschner H et al (1993) Pre- and postoperative evaluation of Cleft-patients by cineradigraphic imaging.; Scientific Programme and Abstracts, ECR'93 Springer International, 1993: 273 award for outstanding scientific presentation of this session
7. Wuttge-Hannig A, Beer A, Gebhardt A et al (2001) (Alternative methods for the diagnostic of deglutition) in Deglutologia Edit. Schindler O, Ruoppolo G, Schindler Omega Edizioni, Italy, Milano.
8. Galli J, Volante M, Parrilla C et al (2005) Oropharyngoesophageal scintigraphy in the diagnostic algorithm of laryngopharyngeal reflux disease: a useful exam? Otolaryngol Head Neck Surg May 132 (5):717–721
9. Katschinski M, Schröttle W, Wuttge-Hannig A et al (2002) Ösophagusfunktionsszintigraphie: Indikation, Durchführung und Auswertung Empfehlungen des Arbeitskreises Neurogastroenterologie und Motilität. Z Gastroenterol 40:1–5
10. Wuttge-Hannig A, Herrman M, Hannig C (2004) Evaluation of Swallowing Reflex in Stress Drinking in Videofluoroscopy: Is it a Tool for the Measurement of pharyngeal Dysfunction in Reflux Disease? ECR, Abstract book
11. Hannig C, Wuttge-Hannig A (2007) Erkrankungen des Oesophagus In: St. Feuerbach (ed.) Gastrointestinales System, In: J. Freyschmidt (ed.) Handbuch Diagnostische Radiologi, Chapter 3: 27–137; Springer-Verlag, Berlin, Heidelberg, New York. ISBN 978-3-540-41418-6
12. Wuttge-Hannig A, Hannig C (1995) Radiologische Differentialdiagnose neurologisch bedingter Schluckstörungen. Der Radiologe 35:733–740
13. Hannig C, Wuttge-Hannig A (2006) Radiologische Funktionsdiagnostik von Schluckstörungen bei neurologischen Krankheitsbildern und bei therapierten onkologischen Kopf-Hals-Erkrankungen In: G. Bartolome, H. Schröter-Morasch (ed.) Schluckstörungen, Diagnostik und Rehabilitation, Chapter 6: 99–154; Elsevier Urban & Fischer, München, Jena. ISBN 978-3-437-47160-5
14. Ekberg O (2003) The symptomatic esophagus and GERD. Acta Radiol Mar 44(2):119–120
15. Hannig C, Wuttge-Hannig A (2006) Anatomie des Schluckvorgangs In: G. Bartolome, H. Schröter-Morasch (ed.) Schluckstörungen, Diagnostik and Rehabilitation, Chapter 1: 1–14; Elsevier Urban & Fisher, München, Jena. ISBN 978-3-437-47160-5

Swan-neck Deformity

A typical deformity in late-stage rheumatoid arthritis with hyperextension of the proximal interphalangeal joint and flexion of the distal interphalangeal joint.
▶Rheumatoid Arthritis

Synchondritis of the Symphysis or Manubriosternal Junction

Synchondritis of the symphysis or manubriosternal junction is characterized by adjacent sclerosis and bony destruction. Symphyseal involvement is typically seen in ankylosing spondylitis. Sternal manifestations are seen in ankylosing spondylitis, psoriatic arthritis, and SAPHO syndrome.
▶Spondyloarthropathies, Seronegative

Syndactyly

Fused fingers or toes with or without synostosis.
▶Congenital Malformations of the Musculoskeletal System

Syndesmophyte

An intervertebral osteophyte with special radiologic appearance as a vertebral-based ossification in the exact location and form of the annulus fibrosus. It is seen in ankylosing spondylitis and in lumbar manifestations of reactive arthritis, enteropathic arthritis, and SAPHO syndrome.
▶Spondyloarthropathies, Seronegative

Syndromic Hepatic Ductular Hypoplasia

▶Congenital Malformations, Bile Ducts

Synovial Osteochondromatosis

Multiple ossified or merely cartilaginous fragments in a joint, presumably of traumatic etiology.
▶Transient Synovitis

Synovial Sarcoma

More prevalent sarcoma in younger age groups, often near to joints however not within. May have a variety of appearances from small and well circumscribed to large, solid, infiltrating with areas of hemorrhage and cystic formation. Some 30% have radiographic evidence of soft tissue calcification. Tumor of high malignancy with often slow growth.
▶Neoplasms, Soft Tissues, Malignant

Syringomyelia, Posttraumatic

Post-traumatic intramedullary cavity, often progressive, with a length that could vary from 2 vertebral segments to the whole spinal cord, isointense to CSF in all pulse sequences.
▶Spinal Trauma

Systemic Blood Supply to the Lung

There are normal anastomoses between the pulmonary and systemic (bronchial and ▶non-bronchial arteries) circulations but any abnormal process creating obstruction, compression of pulmonary artery branches or destruction of the pulmonary capillary bed may induce a compensatory development of systemic supply.
▶Hemoptysis

Systemic Mastocytosis

Mastocytosis is characterized by abnormal growth and accumulation of neoplastic mast cells. Bony changes are

frequently shown and include osteoblastic changes in conventional radiographs. MRI is more sensitive in depicting bone marrow extension of the disease, but findings are not specific.

►Myeloproliferative Disorders

Systemic Supply to PAVM

Bronchial arteries or other systemic branches of the aorta or supra-aortic trunks (intercostal, internal mammary or inferior diaphragmatic arteries) may supply PAVM before or after embolization. This systemic supply is a possible source of hemoptysis.

►Pulmonary Arteriovenous Malformations

Systemic-Bladder Drainage, Pancreatic

In pancreatic transplantation with systemic-bladder drainage technique the arterial graft and the portal vein are anastomosed with the recipient's common or external iliac artery and vein, respectively, whereas the exocrine pancreatic secretions are drained by an anastomosis between the donor's duodenum and the bladder.

►Transplantation, Pancreatic

Systemic-Enteric Drainage, Pancreatic

In pancreatic transplantation with systemic-enteric drainage the arterial graft and the portal vein are anastomosed with the recipient's common or external iliac artery and vein, respectively, whereas the exocrine pancreatic secretions are drained by an anastomosis between the donor's duodenum and a small bowel loop. In this technique the insulin is released in the systemic circulation, while the exocrine secretions drain physiologically in a bowel loop.

►Transplantation, Pancreatic

TACE

Transarterial chemoembolization (TACE) involves the periodic injection of a chemotherapeutic agent mixed with an embolic material into selected branches of the hepatic arteries feeding a liver tumor.
▶Chemoembolization

Talipes Equinovarus (Clubfoot)

Pes adductus, metatarsus, varus, external rotation of the ankle joint and parallel angle between talus and calcaneus.
▶Congenital Malformations of the Musculoskeletal System

Target Population

The age-eligible population for screening, e.g., all persons offered screening according to the policy of the program.
▶Screening, Breast Cancer

Target-Specific Gas-Filled Microbubbles

▶Targeted Microbubbles

Target-Specific Probe

▶Molecular Probes, Optical Probes

Target-specific Imaging

Target-specific imaging is the imaging of specific surface molecules or structures using a contrast agent binding to this particular structure. After wash-out of the unattached agent from the vascular system, the bound contrast agent can be detected. Specific accumulation of the contrast agent can be obtained by molecular binding of the agent (e.g., via antibodies) or by intracellular uptake of the agent (e.g., phagocytosis).
▶Contrast Media, Ultrasound, New Clinical Development

Targeted Delivery

▶Local Drug and Gene Delivery with Microbubbles

Targeted Imaging

▶Targeted Microbubbles
▶Direct Imaging

Targeted Microbubbles

Peter Hauff
Research Laboratories, Bayer Schering Pharma, Berlin, Germany
peter.hauff@schering.de

Synonyms

Molecular imaging; Specific microbubbles; Specific targeting; Target-specific gas-filled microbubbles; Targeted imaging; Targeted specific ultrasound contrast agents

Definition

Targeted imaging using ultrasound relies on ultrasound contrast agents (USCAs) to localize physiological or pathophysiological molecular or cellular processes. Two mechanisms are described for *in vivo* targeting of USCAs: passive and active. ►*Passive targeting* is a nonspecific accumulation of microbubbles at the target site after their administration and does not require a shell labeling with specific ligands. ►*Active targeting* (specific targeting) requires modification of the bubble shell to allow selective binding to cellular epitopes or other receptors of interest. In general, specific USCAs consist of a stabilized microbubble as signaling moiety and shell-surface-bound ligands (such as antibodies, peptides, polysaccharides, or aptamers) as binding moiety (Fig. 1).

Mode of Action

Passive Targeting

Three main mechanisms (phagocytosis, interaction with cell membranes, and ►lymph flow transport, LFT) are known for passive targeting depending on the size of microbubbles, the chemical properties of the shell, the type of the encapsulated gas, the physiologic system, and the route of administration (Fig. 2, upper part).

Phagocytosis: Cells of the ►reticuloendothelial system (RES), which clears the body from microorganisms and damaged cells, take up stabilized microbubbles after their intravenous administration leading to their accumulation in organs such as liver, spleen, lung, lymph nodes, and bone marrow. Activated neutrophil leukocytes are able to phagocytose albumin- or lipid-shell microbubbles after their cell-surface adhesion *via* special integrins or complement mediated opsonization.

Interaction with cell membranes: Depending on the shell composition or their surface charge, microbubbles can be adhered to the surface of cells such as activated leukocytes or the ►endothelium. It could be shown that interactions between leukocytes and lipid-microbubbles are mediated by serum complement, which could be accelerated by inclusion of the apoptosis marker phosphatidylserine into the lipid shell. On the other hand, the interactions between leukocytes and albumin microbubbles are mediated largely by leukocyte β_2 integrin. In the presence of a strong negative shell-surface charge, nonspecific adhesion and accumulation of microbubbles on the vascular endothelium has been noted (1, 2).

Lymph flow transport: Passive targeting of lymph nodes was demonstrated after interstitial injection of small microbubbles (≤1 μm) consisting of a low-solubility gas or air-microbubbles stabilized with a polymeric hard-shell by using gray scale or color Doppler ultrasound. Interstitial injected microbubbles enter the lymph vessels through gaps between lymphatic endothelial cells or by transcellular endo- or exocytosis and is transported by the lymph flow to the respective regional lymph node.

Active Targeting

Active targeted USCAs have been made specific to cellular epitopes or other receptors by means of coupling of respective ligands with the shell of stabilized microbubbles (Fig. 2, lower part). The attachment of targeting ligands to microbubble shells can be made either before or after the bubble preparation, depending on the composition of the USCA. This can be done either by direct coupling of the ligand to shell-forming molecules or by covalent or noncovalent attachment of ligands to preformed microbubbles. Because of the size of microbubbles (μm-range), they are not able to move through the endothelium and thus do not usually leave the

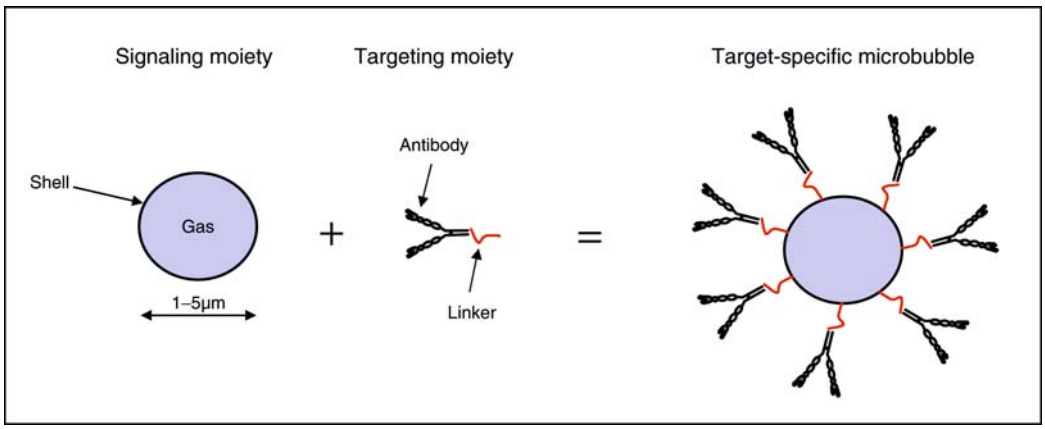

Targeted Microbubbles. Figure 1 Principle of target-specific microbubbles. The conjugation of a targeting moiety with the signaling moiety results in target-specific microbubbles.

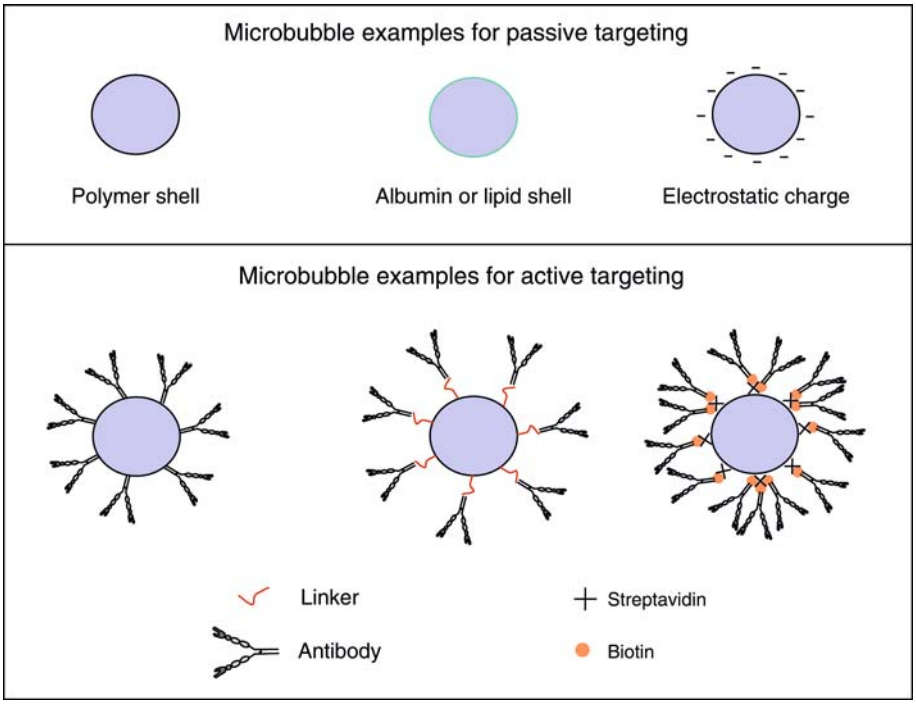

Targeted Microbubbles. Figure 2 Strategies for passive and active targeted microbubbles. For passive targeting, intrinsic chemical or electrostatical properties of the shell can be used to carry microbubbles to the target. Active-targeted microbubbles can be produced by different coupling strategies depending on the targeting moiety (e.g., antibodies, peptides, polysaccharides, or aptamers).

vascular system after their intravenous injection. Therefore, selective targeting with microbubbles is generally directed (limited) to specific receptors of physiological or pathological conditions on the surface of the vascular endothelium. However, the endothelium in a human adult has a total mass of about 1,000 g (like the liver mass) and mediates a wide variety of messages from local tissue to the systemic system (e.g., inflammation to immune response). Once a targeted USCAs has been administered, the microbubbles circulate in the blood stream for several minutes and accumulate in the area of interest *via* a ligand–receptor interaction. Free circulating microbubbles will be cleared from the blood by the RES within 10–20 min (depending on the dose). The rapid blood clearance guarantees a strong signal-to-noise ratio for specific accumulated microbubbles at the target site (Fig. 3). The exceptional ultrasound sensitivity of microbubbles allows the detection of signals from single bubbles and their quantification at the target even in high concentrations.

Indication

Passive Targeting

Few of the commercially available USCAs are already suitable for passive targeting in humans. One example is the so-called late phase effect with Levovist® (Schering AG, Berlin, Germany) in the liver and spleen after their intravenous injection. The late phase effect (bubble retention) allows contrast imaging in these organs long after blood-pool enhancement has disappeared and is used for the detection of neoplastic lesions. Another example is the use of Imagent (Alliance Pharmaceuticals, San Diego, California) for passive lymph node targeting after their interstitial administration (3). The nonspecific targeting of activated leukocytes could be shown in preclinical settings with different types of microbubbles, which provides a new approach for ultrasound imaging, the detection of acute inflammation including ischemia-reperfusion injuries. The targeting of myocardial endothelial cells has been achieved in anesthetized dogs with negative-charged microbubbles indicating that those types of agents could provide information on myocardial perfusion and viability (1, 2).

Active Targeting

Although targeted imaging with specific USCAs is currently at an experimental preclinical stage, researchers were able to show the potential of this ▶molecular imaging approach in various animal models by targeting several molecular structures. The potential for

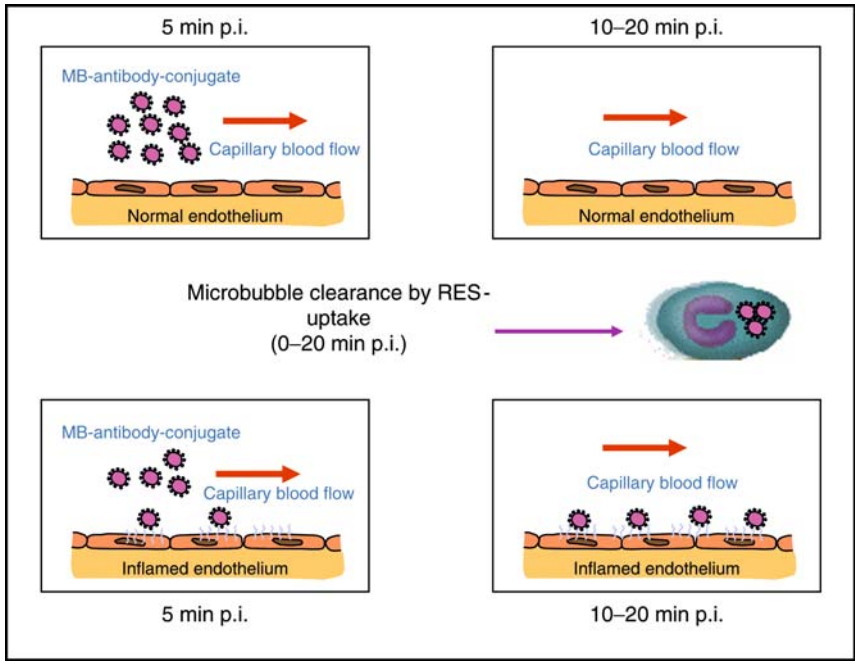

Targeted Microbubbles. Figure 3 Mode of action of target-specific microbubbles (principle). The rapid blood clearance of nontargeted MBs by cells of the reticuloendothelial system within 20 min, depending on the dose used, guarantees a strong signal-to-noise ratio for targeted MBs. Moreover, it provides the opportunity of repeated investigations within one session using MBs targeted to the same or other endothelial cell receptors.

the depiction of receptors in healthy tissue (physiological conditions) could be demonstrated in mouse and dog lymph nodes after intravenous injection of L-selectine ligand-specific microbubbles (3). Targeting of microbubbles to molecules which are overexpressed in certain pathological conditions, such as inflammation (P-selectin, ICAM-1, VCAM-1), ischemia-reperfusin injury (P-selectin), thrombosis (GPIIb/IIIa), or angiogenesis (α_v-integrins) was achieved in several experimental animal studies (1, 4, 5). However, each of the broad variety of molecules expressed on the endothelial surface can potentially be targeted with specific microbubbles. Only recently, a new method has been reported allowing the *in vivo* quantification of targeted microbubbles even in high concentrations. It could be shown that this new technique, referred to as sensitive particle acoustic quantification (SPAQ), allows a quantitative molecular imaging which has been demonstrated by counting ICAM-1 and VCAM-1 in an inflammatory model under treatment conditions (5).

Bibliography

1. Klibanov AL (2005) Ligand-carrying gas-filed microbubbles: ultrasound contrast agents for targeted molecular imaging. Bioconjug Chem 16:9–17
2. Lindner JR, Song J, Xu F et al (2000) Noninvasive ultrasound imaging of inflammation using microbubbles targeted to activated leukocytes. Circulation 102:2745–2750
3. Hauff P, Reinhardt M, Briel A et al (2004) Molecular targeting of lymph nodes with L-selectin ligand-specific US contrast agent: a feasibility study in mice and dogs. Radiology 231:667–673
4. Heppner P, Lindner JR (2005) Contrast ultrasound assessment of angiogenesis by perfusion and molecular imaging. Expert Rev Mol Diagn 5:447–455
5. Reinhardt M, Hauff P, Linker RA, et al (2005) Ultrasound derived imaging and quantification of cell adhesion molecules in experimental autoimmune encephalomyelitis (EAE) by sensitive particle acoustic quantification (SPAQ). Neuroimage 27:267–278

Targeted Optical Contrast Agents

▶Molecular Probes, Optical Probes

Targeted Probes

▶Molecular Probes, Optical Probes

Targeted Specific Ultrasound Contrast Agents

▶Targeted Microbubbles

Targeted Tumor Imaging

▶Receptor Studies, Neoplasms

TCC

▶Transitional Cell Carcinoma

Telescope Phenomenon

Telescope phenomenon is a characteristic aspect of inflammatory mutilation in late stages of psoriatic arthritis, with destruction not only of the epiphysis but also of the meta- and diaphysis of the phalanges, resulting in excessive shorting of the digit.

▶Spondyloarthropathies, Seronegative

Temporal Bone, Inflammatory Diseases, Acute, Chronic

Giovanni Carlo Ettorre, Paola Mililllo
Istituto di Radiologia, Università degli Studi di Catania, Catania, Italy
g.ettorre@unict.it

Synonyms

Acute cholesteatoma; Chronic otitis media

Definition

Inflammatory diseases of the temporal bone indicate all those inflammatory affections that involve the structures of the external, middle, and inner ear, including the associated complications and the sequelae.

The infections can be of microbial or viral origin and include a series of clinical entities for which several classifications have been proposed. The first distinction must be made between acute and chronic inflammatory, where chronic is defined as an inflammation that does not resolve itself within three months from its appearance.

The inflammatory diseases of the temporal bone are generally classified according to the site of origin: external ear, middle ear and mastoid, inner ear, and petrous apex. The pattern of inflammation is strictly related to regional anatomy.

Pathology/Histopathology

Acute otomastoiditis is an inflammation of bacterial origin. In acute middle ear and mastoid inflammation the mucopurulent fluid is a result of vasodilatation, increasing glandular secretion with mucous production, and polymorphonuclear reaction occurring from the neutrophil cells. Resolution frequently occurs, but, if for some reason, the condition is prolonged, such as inability of the secretions to be drained out of the eustachian tube, the number of glands and goblet cells increases. The areas formerly covered by a cuboidal or flat epithelium change into areas of a less differentiated pseudostratified columnar epithelium. Granulation tissue results from the chronicity of the inflammatory process. Localized areas of the mucosa become hyperplastic with invasion of fibroblasts, capillaries, macrophages, plasma cells, and lymphocytes.

Acute otomastoiditis can cause complications such as coalescence and erosion of the bony septa with osteomyelitis, subperiosteal abscess, labyrinthitis, petrous apicitis (Gradenigo's syndrome), thrombosis of the sigmoid sinus, intracranial empyema, meningitis, or cerebral abscess.

Chronic middle otitis can be distinguished into two main groups according to the integrity of the tympanic membrane: (a) otitis with integrity of the tympanic membrane, which generally represents serous-mucous otitis; (b) otitis with open tympanum, which includes chronic suppurative otitis, chronic noncholesteatomatous otitis with ossicular erosion, and cholesteatomatous otitis.

In serous-mucous chronic otitis the aerial cavities of the middle ear are filled by a transuded serous and serous-mucous fluid that can change into an exudate due to bacterial superimposition.

Chronic noncholesteatomatous otitis is characterized by a tympanic perforation with otorrhea and a range of irreversible modifications that can involve the mucous membrane, the temporal bone, the ossicular chain, the mastoid air cells, and the eustachian tube.

Cholesteatoma is the evolution or the complication of chronic middle otitis.

It consists of a cyst-like mass lined with stratified squamous epithelium, usually keratinizing, and filled with desquamating debris often including cholesterol crystals. It behaves as an expansive lesion whose slow growth determines erosion and discharge of bony fragments.

Sequelae or variants of chronic noncholesteatomatous otitis are polypoid otitis, adhesive or fibroadhesive otitis, and tympanosclerosis.

External malignant otitis is the most significant pathological process of the external ear. It is a serious infection, which in 90% of cases is caused by *Pseudomonas aeruginosa*, a bacterial organism that secretes lithic enzymes and toxins that favor the spreading of the inflammatory process into the bone and the adipose spaces of the cranial base, often along the vascular–nervous route.

Acute labyrinthitis is an inflammation of the fluid-filled space of the inner ear and the membranous labyrinth. Abnormal ossification can occur in the chronic phase (ossificans labyrinthitis).

Clinical Presentation

The inflammatory process of the middle ear is generally the consequence of acute or chronic inflammatory affections of the main airway and almost always it also involves the mastoid (otomastoiditis).

Inflammatory disease of the ear is easily assessed clinically: conductive hearing loss, otalgia (earache), and secretion represent the typical clinical signs of the inflammatory process of the external and middle ear. The symptomatology of acute labyrinthitis is characterized by vertigo and sensorineural hearing loss; tinnitus can sometimes be present.

In malignant external otitis, together with general symptoms of inflammation, the local symptomatology consists in strong pain during movements of the temporomandibular joint due to solicitations of the tympanic membrane. The illness usually affects immunocompromised and/or elderly subjects.

Imaging

Acute otomastoiditis does not need evaluation by means of diagnostic imaging, with the exception of rare forms that are accompanied by intracranial complications.

Chronic inflammatory diseases of the middle ear represent the main field of application of radiological imaging.

High-resolution computed tomography (HRCT) of the petrous bone is widely employed in the evaluation of bony structures and it has supplanted conventional radiography. The advent of spiral and multidetector CT (MDCT) has been a further progress in the field. It allows information to be obtained about the bony tissue and the content of the middle ear cavity.

HRCT scan with multiplanar reformation (MPR) today represents the most accurate technique for the diagnosis of external and middle inflammatory diseases.

Magnetic resonance imaging (MRI) has a limited role in this field of pathology, and is generally employed in the above-mentioned intracranial complications of otomastoiditis, in acute external malignant otitis, in acute labyrinthitis, and for postsurgical patients.

In chronic noncholesteatomatous middle otitis with ossicular erosion, the CT features are characterized by a thickening of the mucosal layer of the middle ear with subtle decalcification and erosion of part of the ossicular chain (Fig. 1).

In cholesteatomatous otitis the main CT features include: a nondependent soft tissue mass in the middle ear cavity with displacement and erosion of the auditory ossicles as well as erosion of the anterior and posterior tegmen tympany and scutum. In some advanced cases, erosion of the lateral wall of the lateral semicircular canal can be found (labyrinthine fistulas). Involvement of the intrapetrous facial nerve can occur. All the information obtained by means of HRCT is pivotal in presurgical planning (Fig. 2).

In external malignant otitis, CT represents an emergency examination because of the dramatic and rapid spreading of the disease.

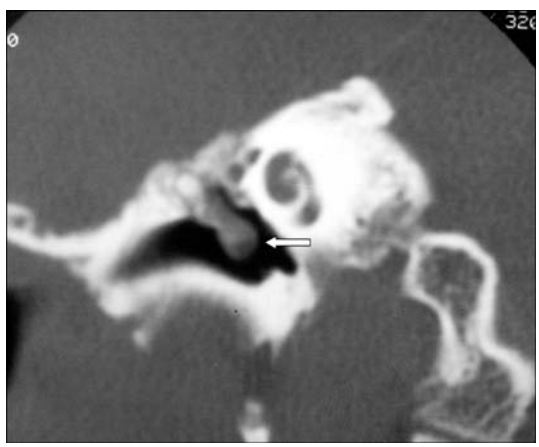

Temporal Bone, Inflammatory Diseases, Acute, Chronic. Figure 1 Chronic noncholesteatomatous middle otitis: coronal CT scan. Partial erosion of the malleus and polypoid hyperplasia of the internal wall of the tympanic membrane (*arrow*).

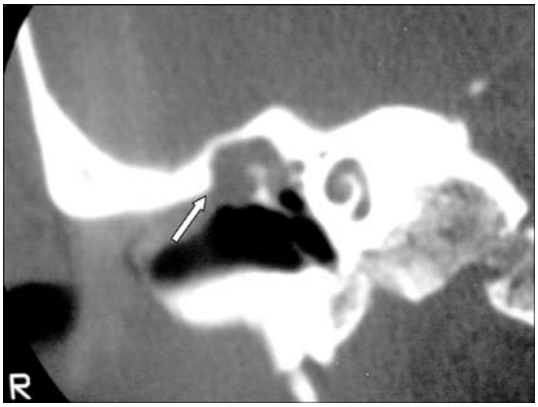

Temporal Bone, Inflammatory Diseases, Acute, Chronic. Figure 2 Cholesteatoma of the middle ear: the coronal CT scan shows erosion of the scutum (*arrow*) and of the head of malleus.

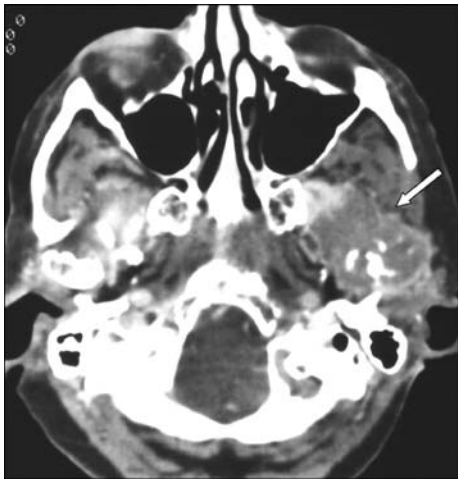

Temporal Bone, Inflammatory Diseases, Acute, Chronic. Figure 3 External malignant otitis: axial contrast-enhanced CT scan. Inflammatory infiltration of adipose spaces (*arrow*) and bony erosion of the mandibular condyle.

The main CT features are: erosion of the bony wall of the external ear conduct and middle ear and infiltration of neighboring soft tissues. Involvement of the base of the skull and the temporomandibular joint can also be demonstrated. The inflammatory infiltration of the adipose spaces and the subcutaneous planes of the face can be better demonstrated by means of contrast-enhanced CT and/or MRI (Fig. 3).

The diagnosis of acute labyrinthitis is based on MR spin-echo (SE) T1-weighted (T1-W) sequences with contrast medium that shows focal increasing of the labyrinth membrane signal.

In ossificans labyrinthitis the absence of signal of the labyrinthine fluid on T2-W MR images is the main clue for the diagnosis.

Nuclear Medicine

Bone scintigraphy does not have a role in the assessment of acute and chronic diseases of the temporal bone.

Diagnosis

In almost all cases of inflammatory disease of the external and middle ear, the diagnosis is based on the clinical and otoscopy data. Diagnostic imaging is indicated in all those situations in which suitable information is not available for correct therapeutic planning and in local or cranial complications such as labyrinthine fistulas and/or intracranial spreading of the disease.

In cholesteatomatous disease it is well known that microscopic fiberoptic otoscopy allows an accurate evaluation of the tympanic cavity only, and is not able to assess the involvement of the attic, the antrum, and the mastoid.

Interventional Radiological Treatment

Interventional radiology does not have a role in the treatment of acute and chronic diseases of the temporal bone.

Bibliography

1. Aberg B, Westin T, Tjellstrom A (1991) Clinical characteristics of cholesteatoma. Am J Otolaryngol 12:254–258
2. Ettorre GC (1992) Diagnostica Per Immagini Dell'orecchio. Ed Idelson Liviana, Naples
3. Sanjeev S, Pitkin L (2005) Middle Ear, Inflammatory Diseases. eMedicine.com Inc

Temporomandibular Arthropathy

▶Internal Derangement, Temporomandibular Joint

Temporomandibular Joint Disorders

▶Internal Derangement, Temporomandibular Joint

Teratocarcinomas

►Neoplasms, Chest, Childhood

Teratoma

A benign germ cell tumor with mature tissues derived from pluripotential cells of all three germinal layers. It is also known as dermoid cyst. Extragonadal teratomas are rare and location in the pancreas is unusual. These tumors are usually large and consist of unilocular or multilocular cysts filled with solid components, including sebaceous material, hair, teeth, calcium and skin. Microscopically the cysts are lined by ciliated or squamous epithelium, while the wall contains dermal appendages (sebaceous glands and hair follicles) and sometimes other tissues (teeth, cartilage, bone). At US examination the lesion has a polymorph appearance because of different prevalence of the three histological structures; in most cases dermoid cysts are complex masses with both liquid and solid components. They contain hyperechoic material (due to hair, teeth and fat) and hypoechoic areas due to fluid material. On CT imaging areas with low density, corresponding to fat, mixed with high density structures can be suggestive of dermoid cyst; a fat-fluid level can be frequently seen. On MR, dermoid cysts present a variable appearance, depending on their fat and fluid content.

►Cystic Neoplasms, Pancreatic

Teratoma, Childhood

Johan G. Blickman[1], Dewi Ashi[2]
[1]Department of Radiology, UMC St Radboud Nijmegen, The Netherlands
[2]Department of Radiology, Faculty of Medicine, University of Indonesia, Cipto Mangunkusumo General Hospital, Salemba 4, Jakarta Pusat, Indonesia
j.blickman@rad.umcn.nl

Synonym

Germ cell tumor

Definition

Teratoma is a tumor consisting of tissues foreign to the site of origin, originating from all three germ layers.

Teratomas have solid and cystic components.

Overall most teratomas are benign lesions, but malignant degeneration is always possible, increasing with age. Calcification is present in two-thirds of patients.

Incidence

1. Approximately 1 of every 40,000 live births.
2. The tumor has a 4:1 female preponderance ratio.
3. When identified at birth, the neoplasms are more aggressive in boys.

Pathology/Histopathology

Ectodermal, mesodermal, and endodermal tissue.

Clinical Presentation

Teratoma may be found in any part of the body.

►Sacrococcygeal teratoma is the most frequent site (40% of all cases). The majority of cases are apparent at birth. They present as a mass at the level of the buttocks and extent below the gluteal fold.

►Presacral teratoma: pain, constipation, and urinary frequency or signs of urinary tract obstruction. There is weakness of the lower extremities if it invades spine.

Ovarian teratomata are often discovered incidentally. Symptoms may include a mass, abdominal pain, and abnormal vaginal bleeding. Bladder symptoms and gastrointestinal (GI) tract pain are less frequent. Acute symptoms may occur due to torsion.

Testicular teratomata presents as a painless scrotal mass and/or a hydrocele.

Mediastinal teratomata are often asymptomatic. When they become large, tracheal/bronchial compression resulting in chest pain, coughing, and wheezing may occur. Hyperglycemia or precocious puberty due to ectopic production of insulin or sex hormones is possible.

Imaging

The classic imaging appearance shows the presence of all three tissues types: bone, fat, soft tissue.

Conventional: soft tissue mass, scoliosis, mediastinal widening, canal/foramina widening, pedicle erosion, abnormal calcification.

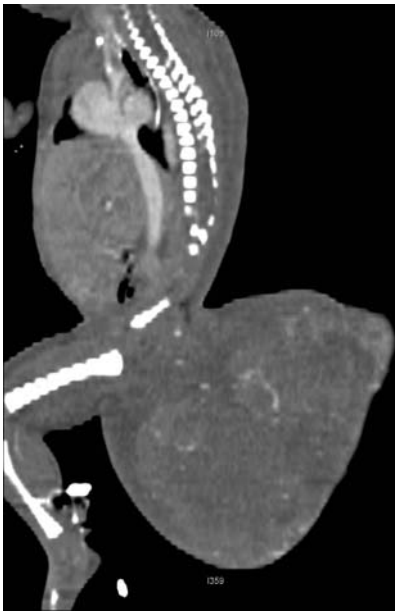

Teratoma, Childhood. Figure 1 Sagittal CT-reconstruction shows a large mass originating from the sacral area containing fat and calcifications with enhancement after contrast injection.

Ultrasound assists in determining the cystic, or partial cystic, part of the tumor and the extent of the tumor.

Computed tomography (CT) often reveals the diagnosis, as it demonstrates fat and/or calcifications, their extent, and any bone destruction. After contrast medium administration, the solid component may show enhancement (Fig. 1).

Magnetic resonance imaging (MRI) is superior in delineating the extent of this tumor.

Occasionally, if there is blood within the cyst, it may show a fluid level.

Nuclear Medicine

Nuclear medicine is used for the evaluation of bone metastasis if the tumor shows malignant degeneration.

Diagnosis

Laboratory: Elevated levels of serum alpha fetoprotein (AFP), and beta human chorionic gonadotropin (HCG).

Biopsy: To differentiate benign from malignant tumor.

Bibliography

1. Barnes PD (1998) Neuroimaging. In: Hans Blickman (ed) Pediatric Radiology: The Requisites. 2nd edn. Mosby St. Louis, pp 294–295
2. Carty H (2001) Paediatric Imaging. In: The Encyclopaedia of Medical Imaging, Vol. 7. Published by The NICER Institute, Oslo, pp 520–521
3. Cohen HL, Haller JO (2004) Abnormalities of the female genital tract. In: Kuhn JP, Slovis TL, Haller JO (eds) Caffey's Pediatric Diagnostic Imaging. 10th edn. Mosby, Philadelphia, pp 1960–1963
4. ▶http://www.emedicine.com/med. Teratoma, Cystic. Last update September 17, 2004

Teratoma, Ovaries, Mature, Ovalar

Rosemarie Forstner
Department of Radiology, Paracelsus Private Medical University, Salzburger Landeskliniken, Austria, Salzburg
r.forstner@salk.at

Synonyms

Benign teratoma; Cystic teratoma; Dermoid; Dermoid cyst

Definitions

Ovarian teratomas comprise tumors composed of mature or immature tissues of primordial germ cell origin. They can be classified into three main categories: ▶mature teratomas, ▶immature teratomas, and monodermal teratomas (1). The mature cystic teratoma which constitutes 99% of these tumors contains mature elements of ectodermal, mesodermal, and endodermal origin. The mature cystic teratoma also known as dermoid cyst or dermoid is the most common ovarian neoplasm of women younger than 45 years. Although teratomas may occur at any age, they typically affect a younger age group than epithelial tumors, and are the most common ovarian masses in children (2). Approximately 10% of teratomas occur bilaterally. ▶Malignant degeneration of benign teratomas is rare (1–2%), and usually occurs in the sixth to seventh decade of life (2).

Pathology/Histopathology

Sixty percent of cystic teratomas measure 5–10 cm in size (1). Macroscopically, benign teratomas present most often as unilocular tumors surrounded by a firm capsule of varying thickness (1). They contain fatty, sebaceous contents, and hair. The former is liquid at body temperature and semisolid at room temperature (1).

Squamous epithelium covers the inner wall of the dermoid. Hair follicles, skin glands, muscles, and fat are located within this wall. Arising from the cyst wall is commonly one or more protuberances, the dermoid plug or Rokitansky nodule, composed of a variety of different tissues. Hair, bone, or teeth and rarely cartilage as well as phalanges may be encountered in this region (1).

Clinical Presentation

The majority of benign teratomas remain clinically asymptomatic. They are often discovered incidentally during clinical examinations or imaging studies. Especially larger teratomas may cause nonspecific symptoms including pelvic pain, abdominal fullness, abdominal swelling, and dysuria. Rarely, abnormal uterine bleeding and hemolytic anemia may be associated with a dermoid (1). Teratomas may become clinically apparent due to complications which include in order of decreasing frequency ▶torsion (16%), chemical peritonitis caused by ▶rupture, and infection (3).

Mature teratomas tend to grow slowly, with an average diameter of 1.8 mm reported per year (2). Rarely, giant dermoids may be encountered, which grow to a size of up to 40 cm (1).

Rapid growth of a dermoid in a postmenopausal woman is a sign of malignant degeneration (2).

Imaging

Conventional radiographs are not suited for the diagnosis of teratomas. Rarely, teeth, bone, or wall calcifications may be detected on abdominal plain films.

Sonography is the primary imaging modality for assessing suspected adnexal masses. The combination of transabdominal and endovaginal sonography combined with Doppler findings allows optimal characterization of the morphology and perfusion of adnexal masses. However, at ultrasound teratomas display a broad spectrum of imaging findings. They most commonly present as diffusely or partially echogenic masses with acoustic shadowing due to hair balls, calcifications, teeth, or the Rokitansky protuberance (Fig. 1). Layered lines and dots as well as fat-fluid levels include other findings. However, imaging findings are often noncharacteristic, and the dermoid plug may be misinterpreted as a solid lesion (4) (Fig. 1).

In the case of unclear sonography findings, *computed tomography (CT) and magnetic resonance imaging (MRI)* allow reliable demonstration of intralesional fat, which is the hallmark of benign teratomas.

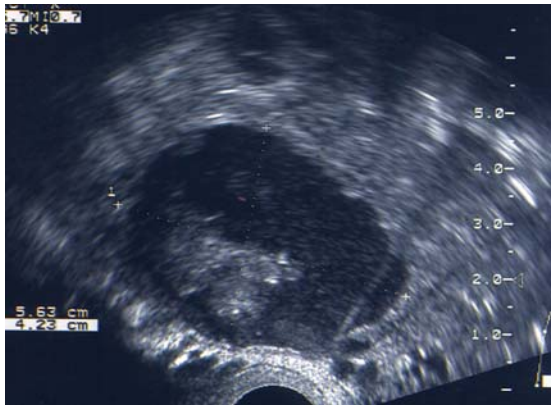

Teratoma, Ovaries, Mature, Ovalar. Figure 1 Dermoid cyst in a 20-year-old patient: transvaginal sonography shows a well-delineated oval adnexal mass containing multiple homogeneous fine echoes and a solid protruding nodule, the Rokitansky nodule. In this patient the latter did not contain calcifications or teeth, and may be misdiagnosed as a solid element in ovarian cancer. (Courtesy of Dr. R. Gruber, Salzburg)

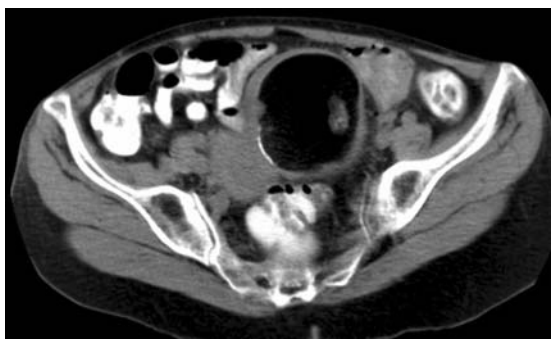

Teratoma, Ovaries, Mature, Ovalar. Figure 2 Dermoid cyst in CT. Noncontrast CT scan shows a 6.5-cm left adnexal mass that is located adjacent the uterine corpus. Its fatty density values are pathognomonic of a dermoid. The lesion contains areas of higher density representing floating hair and mural calcifications. The homogeneous thickening of the wall was caused by wall edema due to torsion.

In CT, attenuation values indicative of fat (−20 to −140 HU) are the pathognomonic finding (Fig. 2). Bone, teeth, and cyst wall calcifications can also be reliably detected. Contrast-enhanced CT assists in the demonstration of complications of dermoids, for example, torsion or malignant degeneration.

In MRI, detection of fat is also the key for the diagnosis of teratomas. In suspected dermoids, tailored studies consisting of T1-weighted imaging (WI) and T1-WI with frequency-selective fat saturation allow confirmation of dermoids in the majority of cases.

Suppression of the high-signal-intensity sebaceous contents or fat within the lesions is diagnostic (2). Gradient-echo opposed-phase imaging demonstrates a fat–water interface within the lesion. Furthermore, chemical shift artifacts in the frequency-encoding direction may assist in detecting fat and in its differentiation from hemorrhage (2). Contrast-enhanced MRI aids in further characterization in atypical cases and in the assessment of complications of teratomas.

Nuclear Medicine

Nuclear medicine has a very limited role in the assessment of teratomas. It may be useful only in detecting monodermal teratomas, for example, struma ovarii or carcinoids.

Diagnosis

The diagnosis of teratomas is based on the demonstration of sebaceous material or fat within an adnexal mass (Figs 2, 3). The size of teratomas ranges from 0.5 to 40 cm, with the majority measuring less than 10 cm.

As CT or MRT are more sensitive for fat than sonography, they are complementary in indeterminate cases or performed for the assessment of complications caused by dermoids (2).

In CT, demonstration of fat within a cystic adnexal lesion with or without calcifications is the pathognomonic finding of a benign teratoma. A fat–fluid interface may be produced by floating hair. In dermoid cysts, fat is demonstrated in more than 90% of cases, teeth in 31%, and calcifications in the dermoid plug, or more often in the cyst wall, in 56% (5) (Fig. 2).

In MRI, the fatty sebaceous contents display typically very high signal intensity (SI) on T1-WI (2). The SI on T2-WI can be variable. As hemorrhagic adnexal masses, endometriomas and hemorrhagic cysts in particular may display similar signal intensities. Loss of signal on T1-WI with fat saturation allows the specific diagnosis of a dermoid.

Approximately 8% of benign teratomas do not show these straightforward findings in CT or MRI (3). In these patients, small foci of fat may be found in the dermoid cyst wall or in the dermoid plug (Fig. 3). When dermoids show no fat they cannot be differentiated from other cystic and solid ovarian tumors, including ovarian cancer.

Malignant degeneration in mature cystic teratomas is typically due to carcinomatous or sarcomatous malignant transformation. Its prevalence is less than 1–2%, and it occurs in the sixth to seventh decade of life (2). CT and MRI findings include the presence of a dermoid with fatty contents and a heterogeneous solid component extending transmurally outside the capsule or enhancement of the Rokitansky nodule (3).

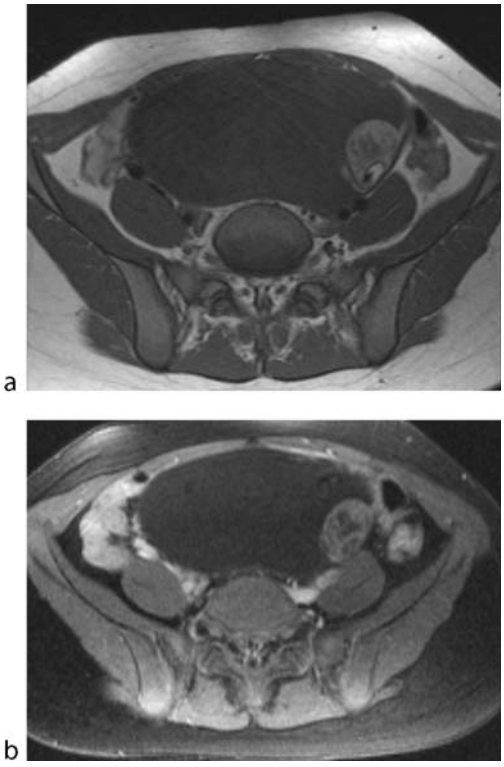

Teratoma, Ovaries, Mature, Ovalar. Figure 3 Benign teratoma with small amounts of fat. In a 15-year-old girl, transaxial T1-WI (a) and T1-WI with fat saturation (b) show a large predominantly cystic lesion in the upper pelvis. At its left periphery it contains a mural nodule that shows intermediate to high signal intensity on T1-WI. The corresponding T1 fat saturation image shows fat suppression of an ovoid area smaller than 1 cm in diameter. At surgery, a 15-cm cystic dermoid was found, the Rokitansky nodule contained hair and only small areas of fat.

In children dermoid cysts may be associated with an ipsi- or contralateral immature teratoma. The latter presents typically as a large, often solid mass that may contain tiny foci of fat or calcifications.

Bibliography

1. Talerman A (2002) Germ cell tumors of the ovary. In: Kurman RJ (ed) Blaustein's Pathology of the Female Genital Tract. Springer, Berlin, Heidelberg, NY, pp 967–1033
2. Outwater EK, Siegelman ES, Junt JL (2001) Ovarian teratomas: tumor types and imaging characteristics. Radiographics 21:475–490
3. Rha SE, Byun JY, Jung SE et al (2004) Atypical CT and MRI manifestations of mature ovarian cystic teratomas. Am J Roentgenol 183:743–750

4. Quinn SF, Erickson S, Black WC (1985) Cystic ovarian teratomas: the sonographic appearance of the dermoid plug. Radiology 155:477–478
5. Buy JN, Ghossain MA, Moss AA et al (1989) cystic teratoma of the ovary: CT detection. Radiology 171:697–670

Teratomas

▶Neoplasms, Chest, Childhood

Tertiary Hyperparathyroidism

An autonomous production of PTH by the parathyroid glands, which was originally induced by a metabolic disorder with secondary hyperparathyroidism.
▶Hyperparathyroidism

Testicular Torsion

Torsion of the testis with twisting of the spermatic cord. Strangulation of the vessels will cause ischemic damage to the testis. It presents as acute scrotal pain and needs immediate surgical treatment to avoid loss of the testis or of testicular function.
▶Scrotal Disorders

Tethered Cord

Often confused with the tight filum terminale, a CSD characterized by a short, rigid filum terminale. This common belief is entirely inappropriate, while the term should in fact be used to indicate a clinical condition, the tethered cord syndrome (TCS). TCS occurs as a consequence of traction on a low-lying conus medullaris with progressive neurological deterioration due to metabolic derangement, and may ensue as a complication of myelomeningocele repair or as the presentation of several forms of CSD, including spinal lipomas, the tight filum terminale, diastematomyelia, and caudal agenesis. The clinical picture of TCS includes sensorimotor dysfunction, muscle atrophy, decreased or hyperactive reflexes, urinary incontinence, spastic gait, and orthopedic deformities such as scoliosis or foot and hip deformity.
▶Congenital Malformations, Spine and Spinal Cord

THAD

▶Transient Hepatic Attenuation Differences

Thoracic Aneurysm

▶Aneurysm, Aortic and Thoracic

Thoracic Aorta

The thoracic aorta carries blood away from the heart and distributes it to the head, the arms, and passes into the abdomen where it becomes the abdominal aorta.
▶Aneurysm, Aortic and Thoracic

Thoracic Aortic Aneurysm

▶Aneurysm, Aortic and Thoracic

Thoracic Outlet Syndrome

Upper extremity symptoms that are caused by of the compression of the neurovascular bundle of the upper extremity as it exits the bony thorax.
▶Brachial Ischemia

Thrombocytopenia

▶Thrombopoietic System, Diseases of the

Thrombolysis

Intravenous infusion or intra-arterial local application of agents with the potential to resolve blood clots.
▶Stroke, Interventional Radiology

Thrombopoietic System, Diseases of the

Otmar Schober
Department of Nuclear Medicine
University Hospital Münster
Münster, Germany
schober.otmar@uni-muenster.de

Synonyms

Thrombocytopenia

Definition

Thrombocytopenia is defined as low platelet counts (<140.000/μL).

Pathology/Histopathology

Thrombocytopenia may be due to a reduced production (marrow failure, megaloblastosis) or a decreased survival (e.g., immune thrombocytopenic purpura [ITP], thrombotic thrombocytopenic purpura [TTP]) of thrombocytes.

Clinical Presentation

Thrombocytopenia presents with prolonged bleeding from cuts, purpura, and bleeding from the mucous membranes.

Imaging

See "Nuclear medicine."

Nuclear Medicine

The survival time and sequestration site of the patient's own or donor thrombocytes can be determined with the ^{111}In-, ^{51}Cr- (Na_2–$^{51}CrO_4$), or ^{99m}Tc-HMPAO-labeling methods. As a rule, lipophilic ^{111}In-complexes are used (1, 2, 3, 4). The thrombocytes are separated as done with leukocyte labeling.

With a smaller thrombocyte count (<30,000 mm^{-3}), donor blood must be used, because the ^{111}In- or ^{51}Cr-uptake of the platelets is relatively low in comparison to the erythrocytes. After infusion of the labeled thrombocytes, blood samples are taken, first hourly and subsequently at intervals of 1–2 days until the half-life is reached. With a greatly reduced life span, blood samples are taken and measurements are performed at shorter time intervals. Simultaneously, the radioactivity from the liver, spleen, and heart (with reference to the blood pool) is measured.

The life span of the thrombocytes is 12 days (norm of the mixed population 3.5–6 days), and approximately one-third of them are found in the spleen.

The differential diagnosis should examine a reduced thrombocyte production as well as an increased thrombocyte sequestration, which may have immunological causes, for example, idiopathic thrombocytopenic purpura (ITP), or may be attributed to consumptive diseases. In particular, indications are the differential diagnosis of increased sequestration or a production disturbance, but also the therapy control of the thrombocytopenia. An increase in the thrombocytes in the spleen, and more seldom in the liver, is to be observed with organ-specific platelet sequestration and can support the indication for splenectomy.

Diagnosis

In addition to platelet counts, antiplatelet autoantibodies (e.g., IgG, ANA) and bone marrow samples should be analyzed.

References

1. Karanikas G, Zedwitz-Liebenstein K, Eidherr H et al (2004) Platelet kinetics and scintigraphic imaging in thrombocytopenic malaria patients. Thromb Haemost 91:553–557
2. Kessler C, Kniffert T, Reuther R et al (1984) Scintigraphy with indium 111-labeled blood platelets. Dtsch Med Wochenschr 109:1853–1859
3. Nakanishi E, Isaka Y, Etani H et al (2000) Indium-111 platelet scintigraphy in a patient with chronic disseminated intravascular coagulation. Clin Nucl Med 25:588–590
4. Uchida Y, Minoshima S, Miyazaki M et al (2000) Normalized spleen/liver ratios on ^{111}In-labelled platelet scintigraphy to predict the outcome of partial splenic embolization in patients with idiopathic thrombocytopenic purpura. Nucl Med Commun 21:441–447

Thrombosis, Caval Vein, Inferior

Patrick Haage
Department of Diagnostic and Interventional Radiology, HELIOS Klinikum Wuppertal, University Hospital Witten/Herdecke, Wuppertal, Germany
patrick.haage@helios-kliniken.de

Synonyms

Caval vein occlusion; Obstruction of the inferior vena cava

Definition

Acute or chronic thrombotic occlusion of the inferior vena cava

Pathology/Histopathology

Thrombosis of the caval vein is a potentially life-threatening disorder particularly due to its associated risks of pulmonary embolism, renal failure, and phlegmasia cerulea dolens (1). Predisposing factors for acute thrombosis of the pelvic veins and the inferior vena cava (IVC) include abdominal surgery, extrinsic compression by tumor or adenopathy, caval filter-associated thrombosis, trauma, hypercoagulable states, Budd–Chiari syndrome, and extension of peripheral DVT (1).

Clinical Presentation

Chronic venous hypertension resulting in the "postphlebitic syndrome" as a consequence of DVT has been estimated to affect 500,000 individuals in the U. S. alone. Hence, timely diagnosis and treatment are essential measures to provide adequate care for the patient. This postulation is substantiated by the fact that the organization of a venous thrombus proceeds much faster than that of an arterial thrombus, thereby aggravating successful treatment strategies. In addition, early clot clearance lowers the risk for pulmonary embolism and post-thrombotic sequelae.

Imaging

In the last decade, ultrasound (US) has gained more importance in the diagnosis of venous occlusion. If a thrombus is present, the vein is distended and incompressible. The physiologic sharp definition of the venous wall is lost and echogenic material inside the lumen may be noted. Very fresh thrombus may be nearly anechoic and consequently not easily visible (2). Color flow Doppler sonography is supportive in these cases as the thrombus will appear as a color flow void. The most useful criterion for venous thrombosis is failure of the vascular lumen to collapse entirely under moderate pressure. Under regular circumstances, flow is identified as a spontaneous phasic pattern at rest with augmentation on calf compression. When thrombus occludes the vessel lumen, no flow is identified. Venous flow is generally phasic, decreasing in inspiration and increasing in expiration. A proximal obstruction will prevent such respiratory variation resulting in a continuous flow pattern and will also avert venous distension generally seen when performing the Valsalva maneuver.

Color flow Doppler imaging is necessary for the evaluation of pelvic vessels (2), but it is often limited due to the intrinsic difficulty in clearly outlining the pelvic structures. Ultrasonography is the primary diagnostic modality in the pregnant patient and can also serve as a screening test in other patients with suspected thrombosis, proceeding to more invasive testing if the results remain vague.

Venography has long been considered the gold standard for identifying proximal venous occlusion because it allows a complete work-up of the lower limb up to the IVC. Counter to sonography, diagnosis is less restricted by adiposity and bowel gas. It is generally a safe procedure and is often essential in case of failure of sonography and in the absence of CT or MR facilities.

Both CT scanning and MR imaging can accurately provide the diagnosis of pelvic and iliac vein thrombosis. These diagnostic modalities are less dependent on the technical expertise of the investigator than US. CT venography requires the application of IV contrast material and is thus contraindicated in patients with renal failure. Pregnancy is another exclusion criterion for CT imaging. MR venography, not adversely affected by these limitations, provides superior sensitivity and good specificity for the diagnosis of central vein thrombosis compared with contrast venography and in due course could surface as the study of choice for the diagnosis of thrombosis. For pelvic deep venous thrombosis, the sensitivity and specificity are reported to be 100 and 95%, respectively (3). Furthermore, MR venography can demonstrate other causes of symptoms, such as enlarged iliac lymph nodes and pelvic masses. Naturally, MR imaging is restricted in patients with claustrophobia and contraindicated in patients with pacemakers or ferromagnetic clips.

In brief, all current imaging methods for the diagnosis of proximal venous occlusion have their specific disadvantages. Magnetic resonance imaging has the greatest potential for the future because it is noninvasive, does not

require contrast agent, carries no exposure to ionizing radiation, and is extremely precise and reproducible. Its accuracy is maintained through comprehensive imaging of the full extent of the occlusion including the calf and pelvis, and sensitivity and specificity below the knee are high; accordingly MR imaging is increasingly employed in the diagnosis of acute venous occlusion not only in pregnancy but also in high-risk patients. It is moreover well suited for diagnosis of recurring thrombosis and asymptomatic disease. Lack of widespread availability of MRI and cost limit its use at present; however, as imagers become more plentiful and scanning speed increases, expenses are decreasing and are becoming comparable to those of other noninvasive tests.

Diagnosis

Since clinical diagnosis is unreliable, imaging modalities need to be integrated in the diagnostic course of action.

Interventional Radiological Treatment

Concerning the therapeutic approach towards ▶thrombosis, anticoagulation alone does not diminish thrombus burden or re-establish valve function. Surgical thrombectomy, although able to adequately remove thrombus, has traditionally been allied with a high rate of recurrence of thrombosis and moderately good clinical results; thus, surgical venous thrombectomy has not been broadly established or regularly employed. Catheter-directed thrombolysis is a potentially attractive alternative for restoration of venous patency and preservation of valve function. In a multicenter registry, marked lysis was observed in 88% of patients with acute iliofemoral occlusion. The 1-year primary patency rate following catheter-directed thrombolysis was 64%. Additional treatment with stent placement was required to treat uncovered stenoses and short residual occlusions that were resistant to lysis in 33%; 94% were performed in the iliac segments. The average urokinase dose was 7.8 million IU and the mean duration of intervention was 53.4 h.

On the other hand, pharmacological treatment of intravascular thrombus is limited by the lengthy time to effect and medication-related severe side effects. Additionally, thrombolytic therapy is costly, labor intensive, and may require several days of intensive care unit hospitalization. Also, this form of therapy entails a significant risk for hemorrhagic and embolic complications and is contraindicated in the postoperative patient. Response may be held up in a large clot burden, resulting in only partial lysis.

Considering these limitations and contraindications of anticoagulation, thrombolysis, and surgical removal, percutaneous interventional techniques have more recently been added to the therapeutic armamentarium for the management of vascular pathologies. In order to perform a safe procedure allowing rapid flow restoration several different types of percutaneous mechanical thrombectomy devices have been developed and tested *in vitro* and *in vivo* (4), which use combinations of mechanical dissolution, fragmentation, and aspiration.

Since then, mechanical thrombectomy devices have proved to be a valuable, fast, and secure treatment tool in venous thrombosis by enabling the recanalization of occlusions in combination with minimal invasiveness and a low bleeding risk, in so doing offering the potential of low (post)procedural morbidity and mortality (Fig. 1) . In cases where thrombolysis is not contraindicated, an adjunctive pharmacological thrombolytic therapy, balloon angioplasty, or endovascular stent deployment, may be of assistance if hemodynamically significant thrombus remains that has not been cleared by the mechanical thrombectomy procedure. Even though only a limited number of patients in a study by Kasirajan received thrombolytic agents, the duration of therapy was significantly shorter than with lysis alone with 20.2 ± 19.4 h (5). After initial thrombus debulking, the consecutive reduction of the thrombus load

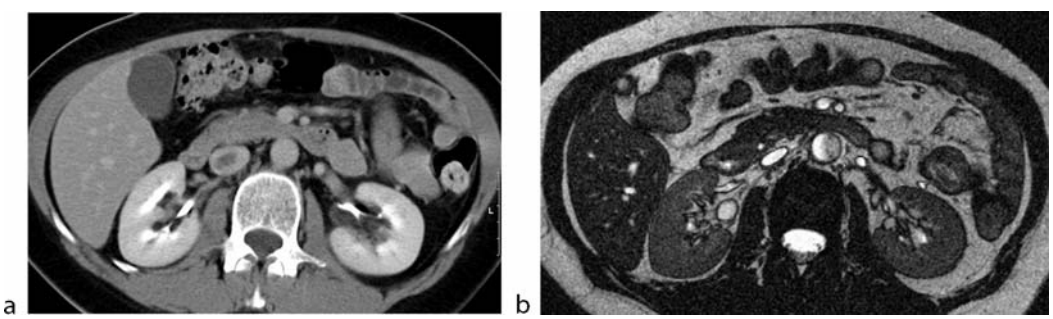

Thrombosis, Caval Vein, Inferior. Figure 1 (a) Pre-interventional contrast-enhanced CT in a 55-year-old woman shows large free-floating IVC thrombus. (b) Postinterventional plain True-FISP MR venography (TR 5.0 ms, TE 2.5 ms) depicts complete recanalization of the IVC after percutaneous mechanical thrombectomy.

led to an increase of the surface area of the thrombus exposed to lytic agent. The risk of hemorrhagic complications can be decreased in light of the decreased quantity of lytic agents required and shortened overall agent exposure.

Placement of an inferior vena cava filter should be considered when there is documented recurrent pulmonary embolism despite adequate anticoagulation or if anticoagulation is contraindicated. It should be kept in mind that the filter does not stop the thrombus growth, and thus additional treatment will be needed.

In conclusion, there are diverse treatment possibilities in proximal vein thrombosis for the interventional radiologist. To obtain instantaneous clot removal with flow restoration and enhanced circulatory hemodynamics within minutes, less hemorrhagic complications, as well as fewer expenditure and in-room time, the primarily mechanical technique shows the most future potential. To prevent procedure-related pulmonary embolism, any mechanical thrombectomy device should only be used in combination with an impermanent cava filter.

References

1. Gu X, Sharafuddin MJ, Titus JL et al (1997) Acute and delayed outcomes of mechanical thrombectomy with use of the steerable Amplatz thrombectomy device in a model of subacute inferior vena cava thrombosis. J Vasc Interv Radiol 8:947–956
2. Zwiebel WJ, Priest D (1990) Color duplex sonography of extremity veins. Semin Ultrasound CT MR 11:136–167
3. Burke B, Sostman HD, Carroll BA et al (1995) The diagnostic approach to deep venous thrombosis. Which technique? Clin Chest Med 16:253–268
4. Haage P, Tacke J, Bovelander J et al (2001) Prototype percutaneous thrombolytic device: preclinical testing in subacute inferior vena caval thrombosis in a pig model. Radiology 220:135–141
5. Kasirajan K, Gray B, Ouriel K (2001) Percutaneous AngioJet thrombectomy in the management of extensive deep venous thrombosis. J Vasc Interv Radiol 12:179–185

Thrombosis, Caval Vein, Superior

Patrick Haage
Department of Diagnostic and Interventional Radiology
HELIOS Klinikum Wuppertal, University Hospital Witten/Herdecke, Wuppertal, Germany
patrick.haage@helios-kliniken.de

Synonyms

Obstruction of the superior vena cava; Superior caval vein occlusion

Definition

Acute or chronic thrombotic occlusion of the superior vena cava.

Pathology/Histopathology

Thrombosis of the superior vena cava is most often caused by intrinsic or extrinsic obstruction attributable to a wide variety of disease entities such as malignancy, extension of central venous thrombosis to the superior vena cava, indwelling catheter induced disease, fibrosing mediastinitis, irradiation, and tuberculosis to name a few.

Clinical Presentation

Symptoms range from congestion and edema of the upper thorax, the face, and the arms to dyspnea, dysphagia, cognitive dysfunction, and pulmonary embolism.

Imaging

see Diagnosis

Diagnosis

Since the clinical presentation is variable, imaging techniques need to be incorporated in the diagnostic process.

Interventional Radiological Treatment

For the diagnosis of superior caval vein thrombosis and consecutive endovascular treatment options reading of the following entries is suggested: Occlusion Venous Central, Malignant; Occlusion Venous Central, Benign

Thrombosis, Vein, Iliac

Patrick Haage
Department of Diagnostic and Interventional Radiology
HELIOS Klinikum Wuppertal, University Hospital Witten/Herdecke, Wuppertal, Germany
patrick.haage@helios-kliniken.de

Synonyms

Iliac vein obstruction; Iliac vein occlusion

Definition

Acute or chronic thrombotic occlusion of one or both iliac veins.

Pathology/Histopathology

Patients with iliac vein thrombosis are at serious risk for pulmonary embolism and long-term clinical consequences of post-thrombotic syndrome. Approximately 50% of patients with proximal deep vein thrombosis (DVT) have pulmonary perfusion defects characteristic of pulmonary embolism (1).

Iliac vein thrombosis typically results from extension of thrombus from the femoropopliteal system, whereas an isolated acute iliac vein occlusion is rather rare and has been reported mainly as a complication in the postpartum period. Furthermore, thrombosis of the pelvic veins, including the internal iliac veins, can be seen in women with pelvic inflammatory disease and in men with involvement of the prostatic plexus.

Clinical Presentation

The development of symptoms depends on the extent of thrombosis, the existence of proficient collateral veins, and the severity of associated vessel occlusion and inflammation (2). Iliac vein occlusion should be suspected in patients with abdominal pain, a unilateral pelvic mass, uterine infection, painful limb swelling, and fever that fails to respond to appropriate treatment, especially in trauma patients and postoperatively. However, clinical diagnosis of venous thrombosis in symptomatic patients is neither particularly sensitive nor specific (3).

Imaging

Thus, in case of suspected iliac vein thrombosis, an early diagnostic imaging workup is indispensable. Concerning pathology imaging, color flow Doppler imaging is often restricted due to obesity and bowel gas. Venography has long been considered the gold standard for identifying proximal venous occlusion. Nowadays, CT scanning and MR imaging have proven to even more precisely diagnose acute iliac vein occlusion. MRI is the preferred technique because it is noninvasive, does not require contrast agent, carries no exposure to ionizing radiation and is highly accurate and reproducible.

Diagnosis

Since clinical diagnosis is unreliable, imaging techniques need to be incorporated in the diagnostic process.

Interventional Radiological Treatment

Regarding treatment of deep venous thrombosis, it is a well known fact that patients are faced with a significant morbidity rate and manifest post-thrombotic complications, including renal failure, phlegmasia cerulea dolens, and postphlebitic syndrome, when treated conservatively. Post-thrombotic syndrome is observed in 79–86% of cases after 5–10 years of follow-up (4).

There is a clear correlation between early recanalization of the thrombosed vein and subsequent preservation of venous valve competence. This calls for prompt removal of the underlying pathology. From an interventional radiologists point of view, apart from traditional catheter directed thrombolysis, mechanical thrombectomy has also been reported to be a quick and safe treatment modality by enabling the recanalization of thrombotic occlusions in conjunction with minimal invasiveness and a low bleeding risk (Figs. 1 and 2).

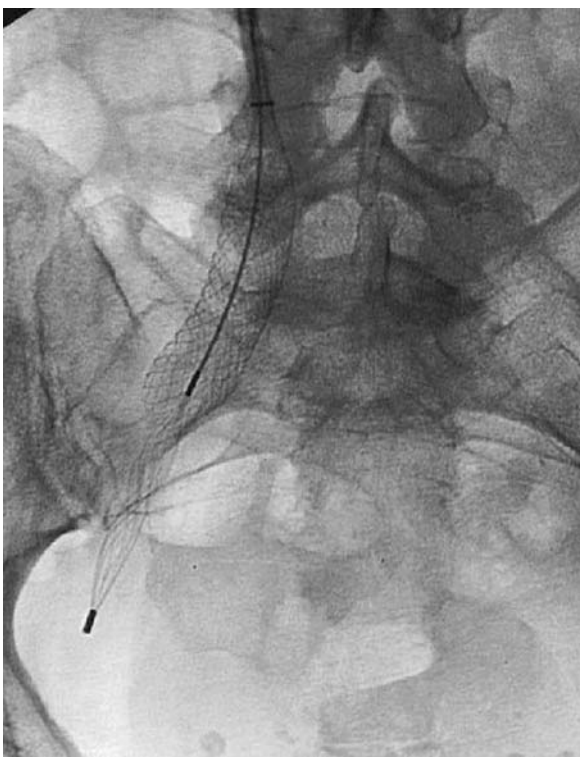

Thrombosis, Vein, Iliac. Figure 1 Thrombectomy procedure in the right iliac vein: thrombus removal with Günther wire basket under expandable sheath protection.

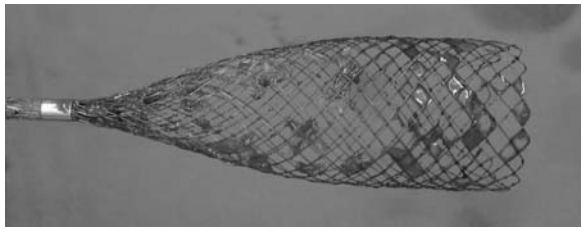

Thrombosis, Vein, Iliac. Figure 2 Photograph of thrombotic material within the protective expandable sheath after the successful intervention.

Nevertheless, mechanical thrombectomy devices should only be used in conjunction with a temporary cava filter (5).

References

1. Meissner AJ, Huszcza S (1996) Surgical strategy for management of deep venous thrombosis of the lower extremities. World J Surg 20:1149–1155
2. Kearon C (2003) Natural history of venous thromboembolism. Circulation 107:I22–30
3. Prandoni P, Mannucci PM (1999) Deep-vein thrombosis of the lower limbs: diagnosis and management. Baillieres Best Pract Res Clin Haematol 12:533–554
4. Lindner DJ, Edwards JM, Phinney ES et al (1986) Long-term hemodynamic and clinical sequelae of lower extremity deep vein thrombosis. J Vasc Surg 4:436–442
5. Truong TH, Spüntrup E, Staatz G et al (2004) Mechanical thrombectomy of iliocaval thrombosis using a protective expandable sheath. Cardiovasc Inter Rad 27:254–258

Thrombosis, Vein, Mesenteric

Gerrit Krupski-Berdien
Universitätsklinikum Hamburg-Eppendorf, Hamburg, Germany
krupski@uke.uni-hamburg.de

Synonyms

Portal vein thrombosis; Portomesenteric vein thrombosis

Definition

►Mesenteric vein thrombosis is defined as clot formation within the mesenteric venous system. A high percentage of these growing clots end up as portal vein thromboses.

Pathology/Histopathology

Mesenteric vein thrombosis is a rare disease with an incidence of approximately 2/100,000 (A). In 85% of patients, at least one of the risk factors listed in Table 1 is present at the time of diagnosis. Clot formation can be found in hepatopetal and hepatofugal directions, starting with normal red and white blood cell content within the fresh (red) thrombus and a loose fibrinoid network-caused by thrombokinase liberated from degrading thrombocytes during hemostasis. No tense adherence to the vessel wall is present. When vessel wall alterations such as tumor infiltration or infection cause thrombosis, a mixed type of clot is seen that contains fresh components (red thrombus as described above) located in the growing thrombus head as well as a firmly compacted fibrinoid network and thrombocyte aggregations with only a few red and white blood cells enclosed (white thrombus) and adherent to the vessel wall. In an old or partially recanalized thrombus, the latter appearance will be the predominant histopathologic presentation, with entire adherence to the vessel wall.

Clinical Presentation

The clinical findings in mesenteric and portal vein thrombosis are strictly associated with the development of portal and mesenteric hypertension. Nonspecific symptoms such as upper abdominal pain, nausea, and vomiting are frequently seen and may be associated with the cause of mesenteric vein thrombosis. Early symptoms of enteral

Thrombosis, Venous, Mesenteric. Table 1 Risk factors for the development of portomesenteric thrombosis

Portal hypertension
Cirrhosis
Splenectomy
Sclerotherapy for varices
Hypercoagulopathies
Malignant tumors
Clotting factor alterations
Protein C and S deficiency
Antithrombin III deficiency
Plasminogen activator deficiency
Hyperfibrinogenemia
Antiphospholipid antibodies
Myelodysplastic syndrome
Pregnancy
Sickle cell disease
Abdominal surgery
Abdominal trauma

venous congestion may also be seen. Upper gastrointestinal tract bleeding from either esophageal, gastric fundal, or atypical intestinal varices is the most important clinical sign of emerging portal venous hypertension. Variceal bleeding contributes to 5–20% of the mortality rate, resuming three-fourths of the total mortality (7–25%) (1). Other symptoms, including formation of collaterals, ascites, hypertensive gastropathy, splenomegaly, and thrombocytopenia, are postacute phase symptoms representing long-standing vascular occlusions, and they need time to develop. Bloody diarrhea is the leading symptom of enteral venous congestion and is a warning sign of bowel wall necrosis.

Imaging

Color-coded duplex ultrasonography is the first-line method of choice for detecting proximal portomesenteric thromboses. Due to distention of the gut and diffuse air accumulation (paralytic ileus) with emerging ischemia, ultrasound examination of the mesenteric vein can be very difficult or even impossible. Furthermore, because ultrasound is an operator-dependent technique, its reliability in mesenteric vein thrombosis is questionable. Therefore, cross-section imaging—magnetic resonance (MR) imaging and computed tomography (CT)—should be preferred for depicting mesentericoportal thrombosis (superior temporal and contrast resolution as well as extravascular anatomy and complications) (2). In cases without peritonitis, multidetector row CT angiography or three-dimensional contrast MR angiography should be the first imaging step in order to depict thrombosis as early as possible; in cases with peritonitis, helical (particularly multidetector row) CT will assure depiction of both the vascular situation and associated complications (Figs 1–3).

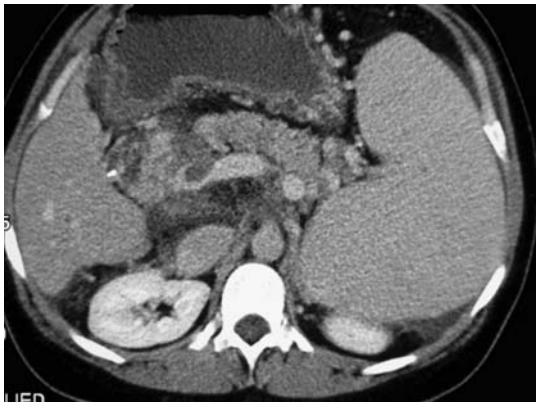

Thrombosis, Venous, Mesenteric. Figure 1 Axial multidetector row computed tomographic image of a 35-year-old woman. The thrombus head is in the confluence area of the main portal vein. Hilar and intrahepatic portal veins are patent as well as the splenic vein.

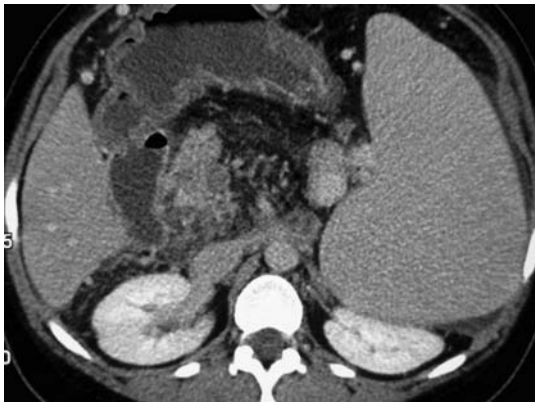

Thrombosis, Venous, Mesenteric. Figure 2 Axial multidetector row computed tomographic image of the same patient as in Fig. 1. No contrast medium is visible in the infrapancreatic mesenteric vein, whereas the mesenteric artery shows marked contrast. This finding is consistent with the diagnosis of complete mesenteric vein thrombosis.

Interventional Radiological Treatment

Although therapeutic approaches to the treatment of mesenteric vein thrombosis as well as portal vein thrombosis are controversial (3), and no evidence-based data yet exist, there is a clear trend for two basic therapeutic strategies, depending on the underlying circumstances:

1. If the mesenteric vein thrombosis is caused by liver cirrhosis with coincident portal venous hypertension, placement of a ►transjugular intrahepatic portosystemic shunt (TIPS) in combination with thrombolysis and/or mechanical thrombectomy has proven to be beneficial (4, 5). The combination of thrombectomy and TIPS is a must in order to create a substantial flow rate in the recanalized mesenteric vein and prevent a rethrombosis. The best results can be expected if mechanical thrombectomy (fragmentation by balloon or basket) is followed by thrombolysis (for hemodynamic reasons, preferably systemic) using rTPA or urokinase (5). High-dose heparin treatment should be given for a few days and then changed to a low-dose regimen (fragmented or low molecular). Capturing of large thrombus fragments with a stent may be necessary. Preexisting mesenteric vein stenosis must be treated by percutaneous transluminal angioplasty (PTA) without stent placement.

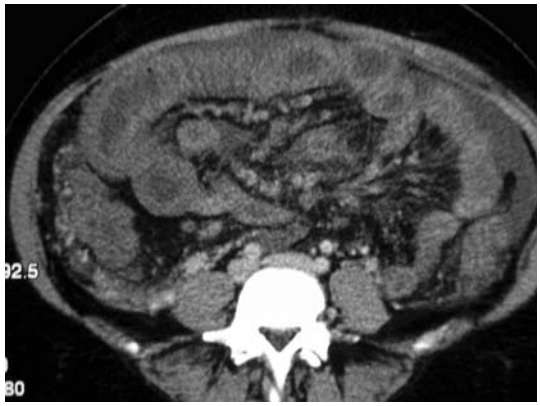

Thrombosis, Venous, Mesenteric. Figure 3 Axial multidetector row computed tomographic image of the same patient as in Figs 1 and 2. There is marked ascites in the left paracolic area, along with massive distended bowel walls representing venous congestion due to mesenteric vein thrombosis. Extraluminal or intraperitoneal gas is not yet visible.

2. In patients without portal venous hypertension and liver cirrhosis, systemic anticoagulation is the current therapeutic state-of-the-art, resulting in complete recanalization in 40% of cases and partial recanalization in 55% (4). Interventional radiological treatment, although offering excellent and impressive results on first sight, bears a high complication rate—up to 60% (5), and for surgery, a mortality of 39% has been published (6).

In both groups, follow-up controls by ultrasound or CT and continuation of anticoagulation for at least 12 weeks as well as treatment of the underlying disease are recommended.

Bibliography

1. Voorhees AB, Price JB Jr (1974) Extrahepatic portal hypertension. A retrospective analysis of 127 cases and associated clinical implications. Arch Surg 108:338–341 D
2. Bradbury MS, Kavanagh PV, Bechtold RE et al (2002) Mesenteric venous thrombosis: diagnosis and noninvasive Imaging. Radiographics 22:527–541
3. Condat B, Pessione F, Hillaire S et al (2001) Current outcome of portal vein thrombosis in adults: risk and benefit of anticoagulant therapy. Gastroenterology 120:490–497
4. Hidajat N, Stobbe H, Griesshaber V et al (2005) Portal vein thrombosis: etiology, diagnostic strategy, therapy and management. Vasa 34:81–92
5. Hollingshead M, Burke CT, Mauro MA et al (2005) Transcatheter thrombolytic therapy for acute mesenteric and portal vein thrombosis. J Vasc Interv Radiol 16:651–661
6. Zhang J, Duan ZQ, Song QB et al (2004) Acute mesenteric vein thrombosis: a better outcome achieved through improved imaging techniques and changed policy of clinical management. Eur J Vasc Endovasc Surg 28:329–334
7. Acosta S, Ogren M, Sternby NH et al (2005) Mesenteric vein thrombosis with transmural intestinal infarction: a population-based study. J Vasc Surg 41:59–63

Thrombosis, Vein, Ovarian

Patrick Haage
Department of Diagnostic and Interventional Radiology
HELIOS Klinikum Wuppertal, University Hospital Witten/Herdecke, Wuppertal, Germany
patrick.haage@helios-kliniken.de

Synonyms

Ovarian vein obstruction; Ovarian vein occlusion

Definition

Acute or chronic uni- or bilateral thrombotic occlusion of the V. ovarica.

Pathology/Histopathology

Pregnancy and the postpartum period are associated with an elevated risk for deep venous thrombosis, which can be complicated by sometimes fatal pulmonary embolism (1).

A typical location of postpartal thrombosis is the ovarian vein, a however uncommon complication which may lead to dramatic clinical manifestations due to migrated septic pulmonary thrombi (2). Thrombus load may extend into the inferior vena cava, the renal veins and the iliofemoral veins; multiorgan failure, acute ureteral obstruction, spontaneous kidney rupture, and ovarian infarction are further feared complications. The proposed pathogenesis starts from an infectious process expanding from the uterus to the ovarian vein and stasis. A prothrombotic predisposition is discussed as a supportive causative factor.

Incidence is reported to be between 1 of 600 and 1 of 2000 deliveries (1). In nonpregnant or non-postpartal women, ovarian vein thrombosis is extremely unusual.

Clinical Presentation

Main symptoms of ovarian vein thrombosis are non-specific and consist of pain in the flanks, the lower quadrant or the iliac fossa, and associated with fever and

leukocytosis. Differential diagnoses include adnexal torsion, endometritis, pyelonephritis, urinary tract infection, thrombosis of the renal veins, and most notably acute appendicitis, whereby discomfort in the appendicitis is situated on the right side. The classical clinical picture is pain in the lower abdomen and elevated temperature not responding to antibiotic treatment. Ninety percent of women are admitted within 1–17 days after delivery (1).

In 80–90% of cases, ovarian vein thrombosis is observed in the right ovarian vein (3), an isolated left ovarian vein thrombosis occurs in 6%, and a bilateral occlusion is noted in 14% (4).

Imaging

The diagnosis of ovarian vein thrombosis can be established by ultrasound, CT, or MR imaging. Color Doppler sonography is the least invasive diagnostic procedure, however may be limited due to bowel gas and obesity, and aggravated by additional intraabdominal pathologies. Spiral CT with intravenous injection of iodinated contrast allows evaluation of the ovarian veins, but entails the application of ionizing radiation.

MR imaging is helpful for investigating the origin of puerperal fever like an abscess or infected hematoma. Contrast-enhanced MR angiography based on T1 shortening is known to offer an excellent visualization of the vascular system. According to Nagayama, coronal source images are useful for evaluating the extent of a thrombus. His workgroup accordingly advocated magnetic resonance angiography (MRA) in postpartum patients with suspected vascular disease (5).

Nevertheless, as a rule of thumb, if ovarian vein thrombosis occurs during pregnancy, administration of contrast material should be avoided. Gadolinium-based contrast material is known to cross the placenta after intravenous administration and appear within the fetal bladder. Its half-life in the fetal circulation and effect on the developing human fetus are unidentified. After delivery and during lactation, traces of gadolinium-based contrast material are excreted into the breast milk after intravenous administration. A minimum of 24-hour postponement of breast-feeding is thus recommended.

Confident diagnosis of venous thrombosis with abandonment of the objectionable contrast agent injection has for years been considered complicated because signal intensities within the vein can be confused with the flow signals of a nonthrombosed ovarian vein. More recent nonenhanced MR venography techniques with TRUE-FISP sequences however can reliably depict thrombosed veins (5).

Kubik-Huch and coauthors compared sonography, CT, and MRI as diagnostic tools in suspected ovarian vein thrombosis and reported sensitivity and specificity values of 55.6% and 41.2%, 77.8% and 62.5%, and 100% and 100% for duplex ultrasonography, contrast-enhanced CT, and MRA, respectively (3).

Consequently, nonenhanced MRA can be recommended for the diagnosis of ovarian vein thrombosis; but because of MR-intrinsic contraindications, cost, and speed, contrast-enhanced multislice CT is an acceptable option (Fig. 1). As an initial evaluation modality, in prepartum women and potentially for follow-up, ultrasound can be applied.

Diagnosis

Due to the nonspecificity of symptoms diagnostic imaging is often required.

Interventional Radiological Treatment

In contrast to his/her involvement in the diagnostic workup, the radiologist is only very infrequently involved in the treatment of ovarian vein thrombosis, which is essentially medical. Anticoagulation is normally administered,

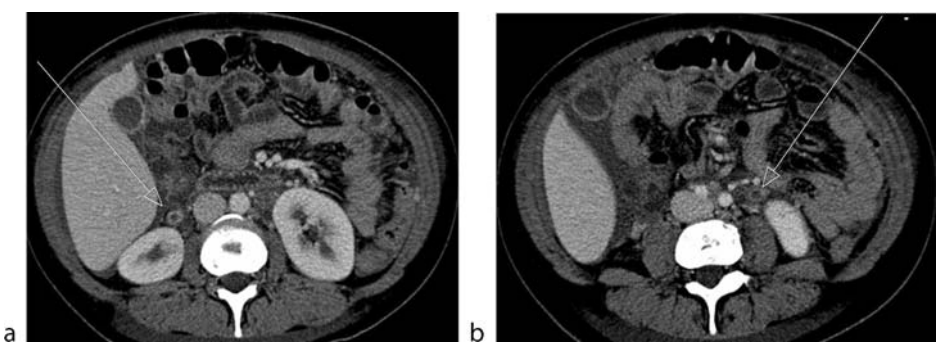

Thrombosis, Vein, Ovarian. Figure 1 Contrast enhanced CT of a 26 year old woman 9 days after cesarean section with persistent fever shows extensive bilateral ovarian vein thrombosis (arrows) and infrahepatic ascites.

although there is no uniform conformity regarding the length of anticoagulation treatment. Broad-spectrum antibiotic application should be instantly initiated after acquisition of appropriate cultures.

Although evidence is limited, treatment of women with postpartal deep venous thrombosis not restricted to the ovarian veins by means of timely percutaneous catheter-directed thrombolytic therapy, if necessary combined with thrombectomy, angioplasty, and/or stenting may be an alternative to more invasive surgical procedures and less successful medical treatments (6). In case of extension of the ovarian vein thrombosis into the inferior vena cava, the deployment of a vena cava filter and interventional or surgical caval thrombectomy may be inevitable. The interventional procedures should be combined with the continuous administration of anticoagulants and antibiotics (7).

To conclude, with the introduction of modern imaging techniques the diagnosis of an ovarian vein thrombosis can be made straightforwardly. Even though postpartum ovarian vein thrombosis is a rare clinical entity, early detection of the condition is of vital importance to bring about the adequate treatment and avoid potential serious aftermaths.

Ovarian vein thrombosis should be suspected in any postpartal woman presenting with inexplicable lower abdominal pain, fever, and leukocytosis.

Ultrasound, and owing to circumstances, subsequent MR or CT imaging is advocated for diagnosis to avoid the significant morbidity and mortality rates if the thrombosis and accompanying disease is not adequately treated.

Anticoagulants in combination with broad-spectrum antibiotic are usually sufficient for treatment. In case of widespread thrombosis not only involving the ovarian veins, catheter-directed thrombolysis, mechanical thrombectomy, or stent- and filter-placement may be considered. The decision to treat must then be made on an individual basis.

References

1. Salomon O, Apter S, Shaham D et al (1999) Risk factors associated with postpartum ovarian vein thrombosis. Thromb Haemostasis 82:1015–1019
2. Bertsch NM, Mastrobattista JM, Kawashima A et al (1997) Antepartum bilateral ovarian vein thrombosis: magnetic resonance imaging diagnosis. Am J Perinat 14:597–599
3. Kubik-Huch RA, Hebisch G, Huch R et al (1999) Role of duplex color Doppler ultrasound, computed tomography, and MR angiography in the diagnosis of septic puerperal ovarian vein thrombosis. Abdom Imaging 24:85–91
4. Dunnihoo DR, Gallaspy JW, Wise RB et al (1991) Postpartum ovarian vein thrombophlebitis: a review. Obstet Gynecol Surv 46:415–427
5. Nagayama M, Watanabe Y, Okumura A et al (2002) Fast MR imaging in obstetrics. Radiographics 22: 563–580
6. Acharya G, Singh K, Hansen JB et al (2005) Catheter-directed thrombolysis for the management of postpartum deep venous thrombosis. Acta Obstet Gyn Scan 84:155–158
7. Hassen-Khodja R, Gillet JY, Batt M et al (1993) Thrombophlebitis of the ovarian vein with free-floating thrombus in the inferior vena cava. Ann Vasc Surg 7:582–586

Thrombosis, Vein, Peripheral

Patrick Haage
Department of Diagnostic and Interventional Radiology, HELIOS Klinikum Wuppertal, University Hospital Witten/Herdecke, Wuppertal, Germany
patrick.haage@helios-kliniken.de

Synonyms

Peripheral vein occlusion; Peripheral venous obstruction

Definition

Acute or chronic thrombotic occlusion of peripheral veins, typically the deep veins of the lower extremity.

Pathology/Histopathology

The risk of suffering from pulmonary embolism (PE) for patients with lower extremity deep venous thrombosis (DVT) is as high as 60%, if left untreated. The development of symptoms depends on the degree of thrombosis, the existence of capable collateral veins, and the severity of allied vessel occlusion and inflammation.

Clinical Presentation

Specific clinical symptoms to attain the proper diagnosis are lacking. Often, deep venous obstructions are clinically unremarkable, particularly when the thrombus does not totally obstruct the vessel or when the thrombosis is well collateralized. If complaints exist, the patient commonly presents with a painful and swollen extremity.

Imaging

Diagnostic imaging modalities and possibilities include ultrasound (US), contrast venography, CT, and MR imaging. More precisely, venography is considered the reference gold standard of diagnosing lower extremity

DVT. Even at present, with a multiplicity of noninvasive tests, venography is important particularly for diagnosing symptomatic calf thromboses that do not extend proximally, recurrent venous occlusion in patients who are again symptomatic, and occlusions in patients who have a high clinical suspicion and a negative or equivocal, noninvasive study (Fig. 1). Typical findings in acute venous thrombosis are a filling defect with surrounding contrast medium "tram-tracking," or sudden vessel cut-off distant from a valve in the case of total vein occlusion. The sensitivity of venography is close to 100%, and the test precisely detects acute venous occlusions of the entire leg including the calf as well as the pelvic veins and the inferior vena cava, which may be overlooked by other diagnostic modalities such as ultrasound (1).

Nonetheless, venography is invasive and has well-known complications such as allergic reactions, nephrotoxicity, and phlebitis, and therefore its application is limited to charily selected patients. In up to 18% of cases venography may be nondiagnostic due to misinterpretations, artifacts, and interobserver disagreement (2). Vessel underfilling and superposition are problems regularly seen in calf-vein phlebography.

Duplex US with manual compression is the most sensitive and specific of the routinely available noninvasive tests when performed by a skilled operator. In many cases, ultrasound has substituted contrast venography. The advantages of US are that it also identifies other distinctive features such as Baker cysts, lymphadenopathy, hematomas, femoral artery aneurysms, superficial thrombophlebitis, and abscesses. Also, it is broadly available and comparatively cheap.

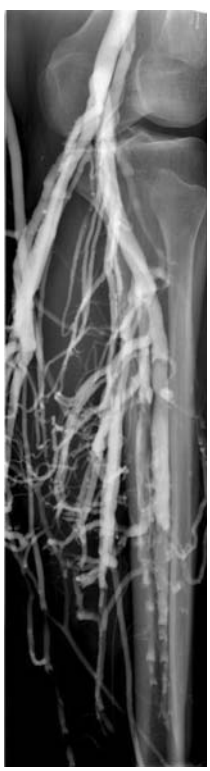

Thrombosis, Vein, Peripheral. Figure 1 Venography of a 28-year-old woman shows acute thrombosis of the peroneal vein, which had not been detected by sonography.

Decisive factors for the diagnosis of DVT by ultrasound comprise failure of the vessel to collapse on manual compression, delineation of thrombus within the usually echo-free lumen, and absent or abnormal venous pulsation on Doppler scanning (3). Failure to compress the common femoral or popliteal vein is usually diagnostic of a first episode of venous occlusion in symptomatic patients with a positive predictive value of about 97%. Full compressibility of both of these regions suggests proximal patency in symptomatic patients with a negative predictive value of about 98% (3).

As a general rule, duplex ultrasound is more precise when the patient has symptoms of acute venous obstruction, and when the occlusion is in the thigh rather than above the groin or below the knee. Venous US has a sensitivity of only 50–75% for isolated distal calf-vein occlusion, and the clinical usefulness of venous US of the distal veins is unclear. A power Doppler study showed a sensitivity of 100%, a specificity of 79%, a positive predictive value of 71%, and a negative predictive value of 100% in detecting an isolated calf-vein thrombosis (4). The peril of calf-vein occlusions is that they can extend to the larger, more proximal veins, thus increasing the threat of PE. Repetition of the ultrasound exam within seven days is therefore indicated in those patients with a primarily normal US exam.

In adipose patients or those with a great amount of lower extremity edema ultrasound can be technically difficult. In asymptomatic patients, the usefulness of US is even more limited. These limitations of sonography and its well-known low sensitivity in recurrent venous occlusion should be recognized in the diagnostic work-up of suspected lower-limb venous occlusion.

In brief, if the pretest probability is high and the results of sonography are nondiagnostic or are discordant with the clinical assessment, venography should be considered.

As an option, spiral CT venography has been proposed as an accurate tool for the evaluation of acute DVT. CT can spot thrombosed veins and is considered superior to conventional venography by identifying intraluminal thrombi, potentially distinguishing fresh thrombi from older ones, and depicting soft tissue changes such as extrinsic compression of the vein. The prevalence of unsuspected venous thrombosis detected by CT in a study was found to be 1.1% (5). In one study, spiral CT venography of the lower extremity

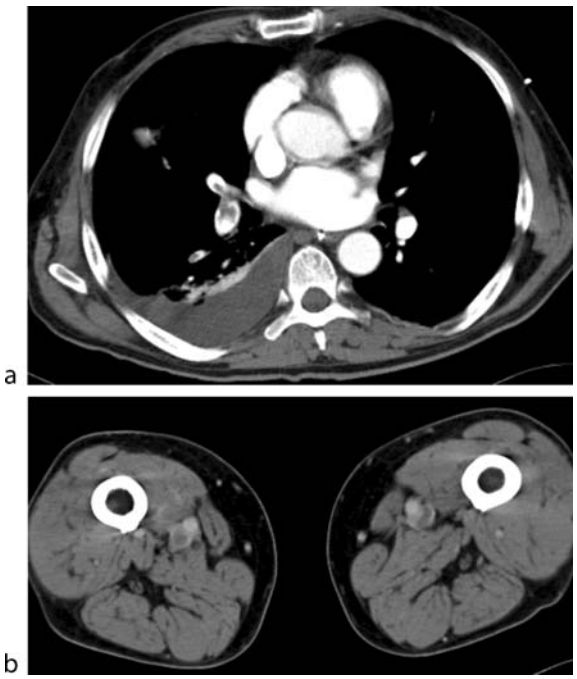

Thrombosis, Vein, Peripheral. Figure 2 (a) 55-year-old male patient. Right-sided pulmonary embolism at contrast-enhanced spiral-CT and (b) Subsequent demonstration of bilateral deep venous thrombosis of the thigh without additional contrast agent injection.

showed a sensitivity of 100% and a specificity of 96% (6). The quality of venous opacification with CT venography compared with ascending phlebography was rated superior in all segments; however, the application of CT venography alone is limited due to high costs and concomitant radiation dosage and is presently only applied as an adjunct to pulmonary CT angiography in case of suspected PE. If PE is proven, an indirect CT phlebography can be performed without the need of additional contrast medium application (Fig. 2).

The advantage of MR imaging is that it discriminates an acute thrombosis from chronic thrombosis more accurately than US does (7). Moreover, MR imaging depicts the adjacent tissues and accordingly may point to the cause of the occlusion. Besides, it is less operator dependent than US. It is precise for the diagnosis of DVT of the calf, which can easily be missed by US, and it can be performed in postoperative patients with full-length leg plaster casts. The sensitivity and specificity are reported to be as high as 100% for acute venous occlusion of the thigh and 87–100% and 97% for occlusion of the calf, respectively (8,9). Both legs can be evaluated simultaneously in one session and testing can be easily repeated to monitor thrombus evolution. Due to its high cost and limited access, MR venography is not yet used for the routine diagnosis of lower extremity venous occlusion

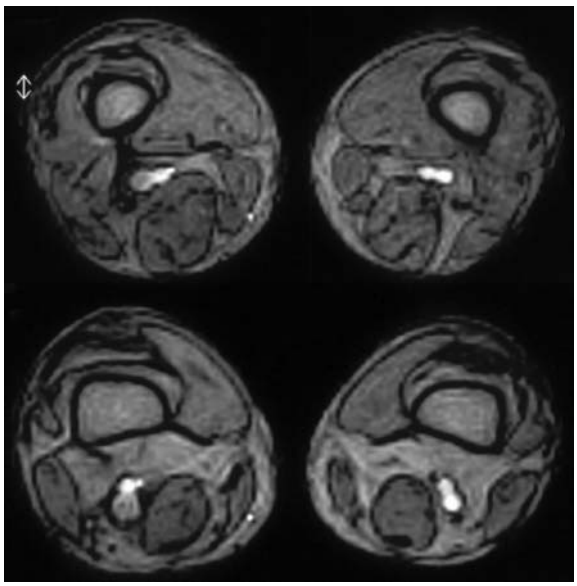

Thrombosis, Vein, Peripheral. Figure 3 Real-time radial plain MR angiography demonstrates a long-segment right-sided superficial femoral vein thrombosis in a 73-year-old male patient with acute renal failure. Thrombus displays low signal intensity in axial orientation.

only; however, it may be useful after other inconclusive tests have been performed or in case of multi-segment thrombosis (Fig. 3).

Diagnosis

Since clinical diagnosis may be erratic, imaging techniques need to be incorporated in the diagnostic process.

Interventional Radiological Treatment

Once the diagnosis of peripheral vein thrombosis has been verified, the next step is its adequate management, since significant spontaneous thrombus disintegration in deep venous thrombosis is very rarely observed. Quite the contrary, the thrombi are likely to grow appositionally and embolize into the pulmonary arterial tree. Chronic venous insufficiency attributable to postthrombotic syndrome is a common end result of DVT. The indications for treatment are reestablishment of unobstructed venous return, impediment of recurrent thrombosis, conservation of venous valve functionality, and prevention of pulmonary embolism.

Systemic anticoagulation with heparin followed by therapy with warfarin sodium can be considered the current standard for peripheral DVT treatment. This treatment, however, does not endorse lysis to decrease the thrombus load, nor does it support the restitution of

venous valve function. Consequently, anticoagulation does not guard the limb from subsequent postthrombotic syndrome, which can occur months to years after the acute thrombotic incident. Up to two thirds of patients with acute iliofemoral venous occlusion suffer from edema and pain, and 5% develop ulcers even though adequately anticoagulated.

Thrombolysis is a therapeutic alternative because it has the potential for rapid restitution of venous patency and perpetuation of venous valve function. Thrombolysis may help avoid the dreaded long-term aftermaths of DVT. Thrombolytic agents have been reported to achieve superior results compared to standard anticoagulation therapy for attaining early thrombolysis, even when systemically applied. In a meta-analysis of the results from 13 randomized studies, Comerota and Aldridge (10) pointed out that only 4% of patients treated with heparin had substantial or complete lysis compared with 45% of patients randomly assigned to receive systemic streptokinase therapy.

In spite of these results, broad routine introduction is still delayed. One of the reasons may be that by using systemic administration the drug does not consistently reach and penetrate the thrombosed venous segment in an adequate concentration as to grant most beneficial results.

Injection of the thrombolytic drug straightforwardly into the thrombus may put forward considerable advantages over the systemic route. First hints at the capability of catheter-directed thrombolysis can be derived from the survey by Semba and Dake (11). They noted complete lysis in 72% of their patient collective with sequencing symptom resolve.

Direct delivery of the lytic agent improves its efficiency, because the agents work through plasminogen activation in the thrombus. Lysis rates can be enhanced, the duration of treatment can be decreased, and problems related with the exposure of the patient to systemic thrombolytic therapy may be reduced by delivering higher concentrations of the agent. Semba's results were sustained by the figures from a multicenter venous registry, where marked lysis through catheter-directed thrombolysis was achieved in 83% of patients with femoral–popliteal thrombosis with a 1-year primary patency rate of 47% (12).

Multiple contraindications to the use of thrombolytic agents do limit the value of this treatment; it was reported to be possible in only 7% of patients in one survey. Major bleeding complications were described in 54 (11%) of 473 patients included in the registry (12); of those, 21 (39%) occurred at the venous puncture site, and 7 (13%) resulted from a retroperitoneal hematoma. In an additional 15 (28%) patients, other bleeding complications occurred. No immediate deaths were observed as a result of a major bleeding complication.

Altogether, catheter-directed thrombolysis can be employed to dissolve thrombus safely and effectively from the deep venous system in carefully selected patients with symptomatic venous lower limb occlusion and no contraindications to treatment. The best results can be expected in patients with acute symptoms and no history of preceding thrombosis treated by local thrombolysis. Long-term benefits of this kind of therapy are presently unknown and cannot conclusively be named. Thrombolytic therapy has the aptitude of protecting the patient against chronic venous insufficiency by accomplishing flow and safeguarding valve function.

In cases of isolated calf-vein thrombosis, anticoagulation therapy should be sufficient to avoid chronic venous insufficiency. Mechanical thrombectomy devices at this time cannot be recommended in deep venous thrombosis located in the lower extremity only. In case of recurring pulmonary embolism due to DVT albeit proper therapy, caval filter implantation should be considered.

In conclusion, therapeutic options in DVT consist of anticoagulation and, whenever indicated and possible, thrombolytic recanalizing measures.

References

1. Fraser JD, Anderson DR (1999) Deep venous thrombosis: recent advances and optimal investigation with US. Radiology 211:9–24
2. Wille-Jorgensen P, Borris L, Jorgensen LN et al (1992) Phlebography as the gold standard in thromboprophylactic studies ? A multicenter interobserver variation study. Acta Radiol 33:24–28
3. Kearon C, Ginsberg JS, Hirsh J (1998) The role of venous ultrasonography in the diagnosis of suspected deep venous thrombosis and pulmonary embolism. Ann Intern Med 129:1044–1049
4. Forbes K, Stevenson AJ (1998) The use of power Doppler ultrasound in the diagnosis of isolated deep venous thrombosis of the calf. Clin Radiol 53:752–754
5. Weinmann EE, Salzman EW (1994) Deep-vein thrombosis. N Engl J Med 15:1630–1641
6. Zontsich T, Turetschek K, Baldt M (1998) CT-phlebography. A new method for the diagnosis of venous thrombosis of the upper and lower extremities. Radiologe 38:586–590
7. Evans AJ, Sostman HD, Knelson MH et al (1993) 1992 ARRS Executive Council Award. Detection of deep venous thrombosis: prospective comparison of MR imaging with contrast venography. Am J Roentgenol 161:131–139
8. Fraser DG, Moody AR, Morgan PS et al (2002) Diagnosis of lower-limb deep venous thrombosis: a prospective blinded study of magnetic resonance direct thrombus imaging. Ann Intern Med 136:89–98
9. Moody AR (1997) Direct imaging of deep-vein thrombosis with magnetic resonance imaging. Lancet 350:1073
10. Comerota AJ, Aldridge SC (1993) Thrombolytic therapy for deep venous thrombosis: a clinical review. Can J Surg 36:359–364
11. Semba CP, Dake MD (1994) Iliofemoral deep venous thrombosis: aggressive therapy with catheter-directed thrombolysis. Radiology 191:487–494
12. Mewissen MW, Seabrook GR, Meissner MH et al (1999) Catheter-directed thrombolysis for lower extremity deep venous thrombosis: report of a national multicenter registry. Radiology 211:39–49

Thrombosis, Vein, Renal

Philippe Otal, Francis Joffre
CHU, Toulouse, France
joffre.f@chu-toulouse.fr

Definition

The term "renal vein thrombosis" (RVT) is usually restricted to the cruoric form of occlusion. Direct extension to the renal vein of a renal malignancy does not correspond to the common definition of RVT and is traditionally depicted in the topic "renal tumor."

Pathology/Histopathology

RVT is a common complication of nephrotic syndrome, occurring more frequently in patients with membranous glomerulonephritis, membranoproliferative glomerulonephritis, amyloidosis, lupus, or diabetes. Its incidence varies from 5 to 62% according to the reported series in the literature (1, 2). The mechanism by which the nephrotic syndrome leads to RVT remains unclear. Coagulative disorders, blunt trauma, and open surgery are less common predisposing factors. The thrombosis may be partial or total, unilateral or bilateral, and may extend to the inferior vena cava (IVC). It exposes the patient to the risk of embolic migration, so early diagnosis is essential to assess the need for anticoagulant and fibrinolytic therapy.

Cinical Presentation

RVT is suspected in a patient presenting with oliguria, hematuria, flank pain, and sudden onset of azotemia. Nevertheless, most patients have a chronic presentation with edema and slight decrease in renal function.

Imaging

Intravenous Urography

Since the decline of intravenous urography, this diagnosis is less and less frequently suggested by nonspecific abnormalities such as delayed opacification of enlarged kidneys, poor or absent excretion, and notching of the renal pelvis and ureter.

Doppler Ultrasonography

Doppler ultrasonography is usually the first imaging modality performed in cases of suspected RVT. A search is done for an endoluminal echo, associated with total or partial absence of venous signal (Fig. 1). The peripheral, intraparenchymatous detection of a venous signal does not eliminate the diagnosis because the development of collateral pathways is constant. Thus, renal veins have to be explored in the renal pedicle. A posterolateral or transhepatic approach usually makes this analysis possible on the right side. Exploration of the left renal vein is sometimes limited by the acoustic barriers. Although intrarenal venous signals are normal, parenchymatous arterial waveforms indicate increased resistive indexes (superior to 0.70), especially in the acute phase before the rapid development of collateral pathways leading to the reduction of interstitial edema.

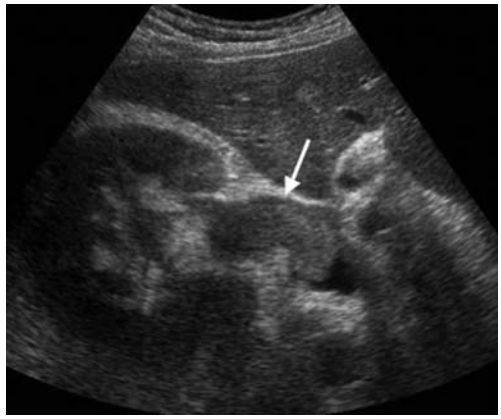

Thrombosis, Vein, Renal. Figure 1 Transverse sonogram of the right renal kidney indicates an echogenic thrombus within the lumen of the right renal vein, extending into the inferior vena cava.

If the examination is negative and considered technically satisfactory, no other imaging modality is recommended. In other cases, complementary computed tomography (CT) or magnetic resonance imaging (MRI) should be considered.

Computed Tomography Angiography

From a technical point of view, a suspected RVT requires standard exploration with nonenhanced and enhanced helical acquisitions. Delayed scans (up to 2 min) are sometimes required to clearly appreciate a possible extension to the IVC.

Thrombus manifests as a spontaneously hyperdense, nonenhancing venous defect (Fig. 2). When the thrombus is occlusive, the vein is commonly dilated, and the hypodensity of the lumen is accentuated by enhancement of the venous wall.

In cases of partial occlusion, indirect parenchymal signs are uncommon. Otherwise, nephromegaly, pale nephrography, delayed medullary enhancement, delayed

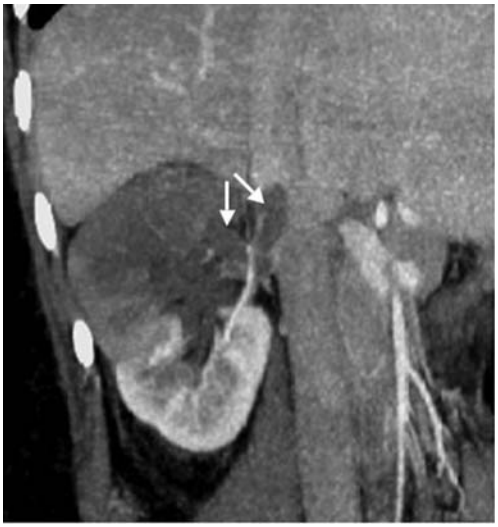

Thrombosis, Vein, Renal. Figure 2 Frontal reformation of an enhanced computed tomography scan showing a filling defect in the upper branch of the right renal vein extending into the inferior vena cava (*arrows*). The upper part of the right kidney is enlarged and low attenuating compared with the lower part.

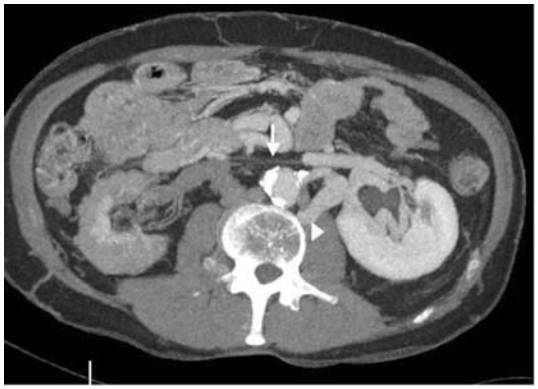

Thrombosis, Vein, Renal. Figure 3 Incidental finding during the work-up of renovascular hypertension (occlusion of the right renal artery) of an asymptomatic left renal vein thrombosis: the left renal vein (*arrow*) is shrunken, the left kidney is normal in size, and enhancement owing to large collaterals into the azygous system is present (*arrowhead*).

excretion, and perirenal edema (fat stranding, perirenal fascia thickening) are common findings. A subcapsular rim sign, even if very common in arterial infarction, has been described in RVT as well.

Owing to its high spatial resolution, CT angiography (CTA) allows clear depiction of perirenal and periureteral collateral veins. It must be noted that the potential for collateral formation is much more significant on the left side because the gonadal, inferior phrenic, and adrenal veins drain into the renal vein on the left side, whereas the right counterparts drain directly into the IVC on the right side (1).

Extension of the thrombus to the IVC or left gonadal vein is clearly depicted on delayed acquisitions with frontal reformations.

An evolutive aspect has to be mentioned: if the thrombosis is not suspected and not treated, or treatment fails, the thrombosed vein tends to shrink and even calcify (Fig. 3).

MRI

MRI is the modality of choice for assessing the extension of neoplastic RVT. Similarly, MRI is probably the best choice to assess renal vein cruoric thrombosis when Doppler ultrasound is not conclusive and when the use of iodinated contrast media is contraindicated by renal insufficiency. The conventional T1- and T2-weighted images are combined with flow-based sequences. Nevertheless, recent imaging systems offer angiographic studies requiring a short breath-hold with high three-dimensional resolution and are considered the gold standard in the MR evaluation of renal vessels.

Renal Venography and Arteriography

Venography and arteriography are of limited value in this indication owing to the renal insufficiency. Before the advent of slice imaging, renal venography was considered the definitive study for suspected RVT, allowing direct visualization of the thrombus within the renal vein and IVC. Nevertheless, it is an invasive procedure, with a potential risk of thrombus dislodgment and pulmonary embolism. For this reason, some authors prefer arteriography to venography, demonstrating accentuated opacification of medullary pyramids and venous-filling defects. Thus, the indication for renal venography is limited to selected patients as the initial step before IVC filter placement.

In summary, Doppler ultrasound is recommended as the initial imaging modality because it is noninvasive, cheap, and effective. In cases of incomplete evaluation or technical failure, MRI is the best alternative in patients with compromised renal function. Otherwise, the high spatial resolution of CTA makes it the gold standard for the anatomic depiction of renal vein thrombus and its extension.

Nuclear Medicine

The objectives of the treatment of RVT are to preserve renal function and prevent thromboembolic complications. Besides treating the underlying cause, the

management of RVT classically involves anticoagulation followed by oral vitamin K antagonists for at least as long as the nephrotic syndrome persists. Although repeatedly documented in short series, the role of fibrinolytic treatment is not clarified. It seems to provide more rapid resolution than anticoagulation but is associated with a much higher risk of hemorrhagic complications and death. As in other vessels, *in situ* fibrinolysis tends to reduce the risk of systemic complications (3).

Rare cases of surgical thrombectomy have been reported. Nevertheless, percutaneous mechanical thrombectomy provides an attractive alternative option for the treatment of RVT, particularly when anticoagulation fails or is contraindicated (4).

Successful treatment with caval filter in cases of RVT with suprarenal extension has also been reported, but this option is not recommended because it exposes the contralateral kidney to the extension of the clot.

Bibliography

1. Bradley Jr, Jacobs RP, Trew PA et al (1981) Renal vein thrombosis: occurrence in membranous glomerulonephropathy and lupus nephritis. Radiology 139:571–576
2. Llach F (1985) Hypercoagulability, renal-vein thrombosis, and other thrombotic complications of nephrotic syndrome. Kidney Int 28:429–449
3. Melamed MJ, Kim HS, Jaar BG et al (2005) Combined percutaneous mechanical and chemical thrombectomy for renal vein thrombosis in kidney transplant recipients. Am J Transplant 5:621–626
4. Jaar BG, Kim HS, Samaniego MD et al (2002) Percutaneous mechanical thrombectomy: a new approach in the treatment of acute renal-vein thrombosis. Nephrol Dial Transplant 17:1122–1125

Thrombosis, Venous, Brachial

Patrick Haage
Department of Diagnostic and Interventional Radiology
HELIOS Klinikum Wuppertal, University Hospital Witten/Herdecke, Wuppertal, Germany
patrick.haage@helios-kliniken.de

Synonyms

Brachial vein obstruction; Brachial vein occlusion

Definition

Acute or chronic uni- or bilateral thrombotic occlusion of the V. brachialis.

Pathology/Histopathology

With a reported prevalence of 0.15%, symptomatic upper extremity deep venous thrombosis (UEDVT) is a rare condition, which was independently described by Paget and Von Schroetter in the late 19th century. They assumed a correlation to repeated severe effort of the involved extremity, and consequently the condition has been termed spontaneous or effort vein thrombosis. Strenuous arm activity or holding the arm for a prolonged period in a set position is an involved trigger mechanism. An anatomic abnormality, for instance a cervical rib or costoclavicular compression syndrome, is often observed.

The employment of the term primary UEDVT is intentional to differentiate spontaneous or effort thrombosis from the nowadays more frequent secondary type attributable to chronic central venous catheters, pacemaker wires, trauma or intravenous drug use (1). Secondary acute venous upper extremity occlusion is also seen in gene mutations, inherited thrombophilia, malignancy, heart failure, acquired hypercoagulable states and infection (2). Patients with a history of thrombotic lower limb vein occlusion are also more prone to develop UEDVT (3).

Clinical Presentation

Upper extremity occlusions make up only 1–4% of all acute deep venous occlusions (2). The incidence of secondary occlusion appears to be increasing, which could be related to the acceding use of long-term indwelling central venous lines, more liberal use of ultrasound to validate the diagnosis and an increased familiarity with this condition; yet, even in occlusive upper extremity thrombosis, the condition can be asymptomatic.

While pulmonary embolism (PE) is observed in up to 50% of patients with proximal lower extremity DVT, in contrast, upper extremity occlusion has been reported to have a 7–20% rate of PE (1).

Clinical manifestations of UEDVT are non-specific and can simulate lymphedema, local infection or mediastinal malignancy. Scepticism should come up with episodes of paresthesia, tenderness, swelling, functional weakening of the upper extremity, skin discoloration or venous distension.

According to one study, the brachial vein was involved in 36% of diagnosed UEDVT, the axillary vein in 25% and the brachial and cephalic veins in 77%. An isolated brachial vein thrombosis was identified in 3.8% of cases (4).

Imaging

Contrast venography for decades has been the reference standard for the diagnosis of UEDVT, although this

procedure has its shortcomings. Venous puncture can be problematic in a swollen extremity, the procedure may cause thrombophlebitis, and there is an albeit low risk of an allergic contrast medium reaction. Recent studies have disclosed that both compression ultrasound and color flow Doppler imaging of the upper extremity venous system are sensitive and specific for the diagnosis of upper extremity occlusion, with reported respective sensitivity values of 96 and 100%, and specificity values of 93 and 93% (3).

Large collateral veins and non-occlusive thrombi may cause false-negative results, and overlying anatomic structures may camouflage vessel segments. Higher sensitivity can be achieved by revelation of normal cardiac pulsatility and respiratory phasicity within these veins.

Computed tomography and MRI may also be valuable in diagnosing acute upper extremity occlusion (Fig. 1). In several studies MRI had a sensitivity and specificity of almost 100% in evaluating the patency of the central chest veins (4, 5). Patients with pacemakers and other implanted devices, which regularly cause UEDVT are thus candidates for imaging, however are not suitable for MR imaging.

Although conventional venography, CT and MRI can all be used to consistently detect upper extremity thrombosis, the excellent results of ultrasound imaging favor its use as the prime imaging modality for the diagnosis of UEDVT, particularly of the upper arm. Because of their common, established and above mentioned limitations, the alternative imaging tools should only be utilized when sonographic findings are unclear.

Diagnosis

Since clinical diagnosis is not entirely reliable imaging techniques need to be incorporated in the diagnostic process.

Interventional Radiological Treatment

Prompt treatment is compulsory after the diagnosis has been established to avoid complications of UEDVT such as loss of central venous access, post-thrombotic syndrome and pulmonary embolism. In the acute stage, conventional treatment consisted of elevation of the affected extremity and full-dose anti-coagulation with unfractionated heparin or low molecular weight heparin (3) followed by 6 weeks to 6 months of therapy with oral warfarin sodium. In secondary venous thrombosis, the removal of the underlying cause, such as the central venous catheter, is typically required.

The radiologist is occasionally involved in the treatment of this disease entity. Catheter-directed thrombolysis is known to improve lysis rates by delivering the thrombolytic agent in high concentrations directly to the site of the thrombus. In combination with balloon

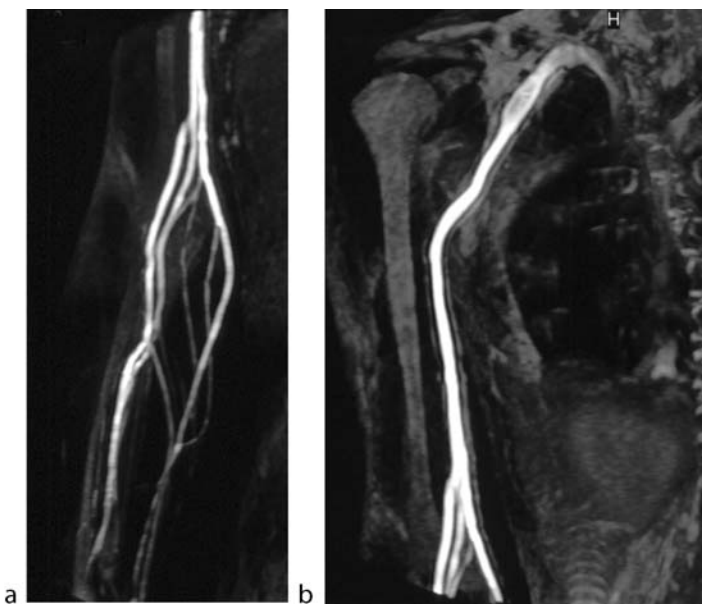

Thrombosis, Venous, Brachial. Figure 1 Maximum intensity projection of the lower and upper arm and the central venous vessels after intravenous administration of 5 ml Gadolinium-DTPA *via* the back of the hand shows proper anatomic visualization of thrombus free vessels.

angioplasty, satisfactory results have been achieved (6). Stent deployment should be considered in case a significant residual stenosis or thrombus remains after thrombolysis and PTA (7).

In one study, systemic thrombolysis proved to be effective for nonocclusive thrombi with excellent results in 32 of 36 primary UEDVT patients (8); however, in this patient, collective better results were demonstrated by aggressive thrombolysis and rapid first rib resection to alleviate both the acute and chronic symptoms.

In patients where anti-coagulation and thrombolysis are contraindicated, refractory or complex, and who are prone to pulmonary embolism, the placement of a superior vena cava filter may be discussed. Even though there is pervasive knowledge of inferior vena cava filter placement, only few data regarding placement of superior vena cava (SVC) filters exist. Obtainable results yet show that filters placed in the superior vena cava can be considered a safe and effective method to prevent pulmonary thromboembolism (9). SVC filter placement is indicated in recurrent PE despite full-dose anti-coagulation, or a major complication resulting from anti-coagulation medication.

Due to the variety of underlying causes, a multi-disciplinary treatment strategy for UEDVT is often needed. The radiologist should participate in a timely diagnostic work-up and, when indicated, in the primary treatment as well as the prevention of thrombosis sequelae by restituting vessel patency, preserving venous valve function and circumventing pulmonary embolism.

References

1. Sharafuddin MJ, Sun S, Hoballah JJ (2002) Endovascular management of venous thrombotic diseases of the upper torso and extremities. J Vasc Interv Radiol 13:975–990
2. Kommareddy A, Zaroukian MH, Hassouna HI (2002) Upper extremity deep venous thrombosis. Semin Thromb Hemost 28:89–99
3. Prandoni P, Polistena P, Bernardi E et al (1997) Upper-extremity deep vein thrombosis. Risk factors, diagnosis, and complications. Arch Intern Med 157:57–62
4. Schmittling ZC, McLafferty RB, Bohannon WT et al (2004) Characterization and probability of upper extremity deep venous thrombosis. Ann Vasc Surg 18:552–557
5. Kroencke TJ, Taupitz M, Arnold R et al (2001) Three dimensional gadolinium-enhanced magnetic resonance venography in suspected thrombo-occlusive disease of the central chest veins. Chest 120:1570–1576
6. Huey H, Morris DC, Nichols DM et al (1987) Low-dose streptokinase thrombolysis of axillary-subclavian vein thrombosis. Cardiovasc Inter Rad 10:92–95
7. Putnam JS, Uchida BT, Antonovic R et al (1988) Superior vena cava syndrome associated with massive thrombosis: treatment with expandable wire stents. Radiology 167:727–728
8. Urschel HC Jr, Razzuk MA (2000) Paget-Schroetter syndrome: what is the best management? Ann Thorac Surg 69:1663–1668
9. Ascer E, Gennaro M, Lorensen E et al (1996) Superior vena caval Greenfield filters: indications, techniques, and results. J Vasc Surg 23:498–503

Thrombotic Hepatic Vein Obstruction

▶Budd-Chiari Syndrome

Thymoma

▶Neoplasms, Chest, Childhood

Thymomas and Thymic Carcinomas

TAKAHASHI KOJI
Department of Radiology, Asahikawa Medical college, Asahikawa, Japan
taka1019@asahikawa_med.ac.jp

Definition

Thymoma is defined as a benign or low-grade malignant tumor of the thymic epithelium, frequently associated with immature but nonneoplastic T cell lymphocytes (1). Thymoma is the most common primary mediastinal tumor.

Thymic carcinoma is defined as a thymic epithelial tumor with a high degree of anaplasia, obvious cell atypia, and increased proliferative activity and is unassociated with immature T cells (1).

Pathology

Thymomas are divided into an encapsulated noninvasive type and an invasive type that has spread beyond the capsule, initially invading the adjacent mediastinal fat and eventually spreading to the pleura, pericardium, lung, or mediastinal vessels. Most thymomas show lobulated external surface and are either completely or partially encapsulated by fibrous capsule. The capsule connects with fibrous band within the tumor that divides it into multiple lobules. Cystic change, hemorrhage, necrosis are relatively common and sometimes the tumor may be entirely cystic. The neoplastic epithelial cells can vary from polygonal to distinctly spindle in shape, and relative proportions of associated lymphocytes can be minimal or so marked as to

completely obscure epithelial cells. The predominantly epithelial thymoma appears to carry the worst prognosis (2). Based on morphologic features of epithelial cells, thymomas are divided into cortical (predominantly and pure subtype), medullary, and mixed forms (1).

Thymic carcinoma possesses traditional features of malignancy, which closely resemble carcinomas seen in other organs. The most common histologic type is squamous cell carcinoma.

The world health organization (WHO) has proposed a consensus classification of thymic epithelial tumors which is based on the morphology of epithelial cells and on the lymphocyte-to-epithelial cell ratio (3). It has been suggested that WHO classification reflects both the clinical and the functional features of thymic epithelial tumors and can be a prognostic factor. The tumors are divided into six subtypes. Type A and B tumors are composed of a homogeneous population of neoplastic epithelial cells with spindle- or ovale-shaped nuclei (A) and dendritic or epithelioid nuclei (B). Type AB tumors combine the morphologic features of types A and B. Type B1 tumors resemble the normal functional thymus and mainly consist of a dense population of lymphocytes, and some epithelial tumor cells with large nuclei of pale chromatin and small nucleoli. Type B2 tumors consist of a nest of epithelial cells, and lymphocytes are less abundant than in type B1. Type B3 tumors predominantly composed of epithelial cells having a round or polygonal shape and exhibiting mild atypia, admixed with a minor component of lymphocytes. Type C tumors exhibit clear-cut cytologic atypia and a set of cytoarchitectural features analogous to those seen in carcinomas of other organs. The classification of type B3 and C tumors corresponds to atypical thymoma and thymic carcinoma, respectively. All tumors are further divided into 3 subgroups: low-risk thymomas (types A, AB, and B1), high-risk thymomas (types B2 and B3), or thymic carcinomas (type C).

Clinical Presentation

Thymomas usually occur in middle aged adults, the average age at diagnosis being 50 years (2). Thymomas most commonly arise in the upper part of the anterior mediastinum. Patients with encapsulated thymoma are usually asymptomatic. If symptoms occur they consist of chest pain, cough, dyspnea, dysphagia, or hoarseness. Thymomas are occasionally associated with paraneoplastic syndrome such as myasthenia gravis. Approximately 20% of patients with myasthenia gravis have thymoma and up to 40% of patients with thymoma have myasthenia (2).

Thymic carcinomas predominantly occur in adults and are associated with poor prognosis. At the time of diagnosis, most patients are symptomatic and commonly present with chest pain, cough, fever, weight loss, and fatigue. A paraneoplastic syndrome is uncommon in thymic carcinomas.

Imaging

Most thymomas arise in the anterior mediastinum (Fig. 1) near the junction of the heart and great vessels and may project into one or less commonly both sides of the mediastinum. Uncommon location of thymoma includes inferior mediastinum as low as the cardiophrenic angle, middle or posterior mediastinum, the lower and upper neck as high as the submandibular region, or lung parenchyma.

Radiographically, thymomas appear as an oval or round shaped mediastinal mass with smooth or lobulated margins. In the lateral view, the opacity can be identified in the retrosternal space. On CT, thymomas usually present as sharply demarcated round or oval soft tissue masses with mild to moderate contrast enhancement. Less common, focal low attenuation areas are identified within tumors, reflecting hemorrhage, necrosis, or cyst formation. Rarely, a tumor appears entirely cystic (cystic thymoma). Calcifications of punctate, curvilinear, or ringlike in shape are frequently seen in both encapsulated and invasive thymoma. Complete obliteration of the adjacent fat planes highly suggests mediastinal invasion,

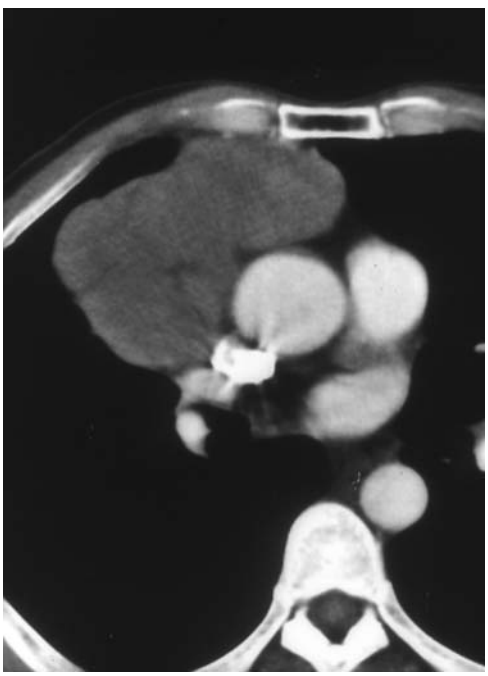

Thymomas and Thymic Carcinomas. Figure 1 Thymoma. Contrast-enhanced CT shows a lobulated mass lesion in the anterior mediastinum. Linear structures of low attenuation within the tumor represent fibrous internal septations.

while partial obliteration is indeterminate, and complete preservation of adjacent fat planes usually excludes extensive invasive disease but not minimal capsular invasion (Fig. 2) (4). Transpleural spread either as a sheet of tumor or drop metastasis is a diagnostic finding of invasive thymoma. On MRI internal low intensity septations and signs of mediastinal invasion may be more conspicuous (Fig. 3).

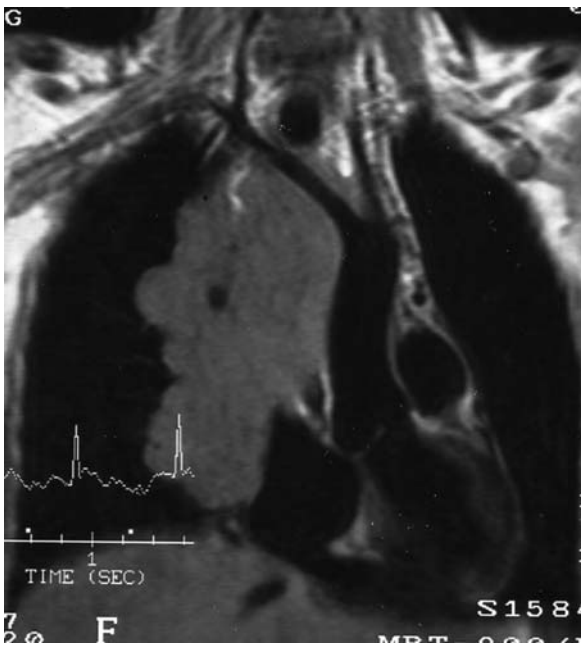

Thymomas and Thymic Carcinomas. Figure 2 Invasive thymoma. Coronal T1-weighted MR image shows a lobulated mass lesion which extends along the branch vessels of the aortic arch.

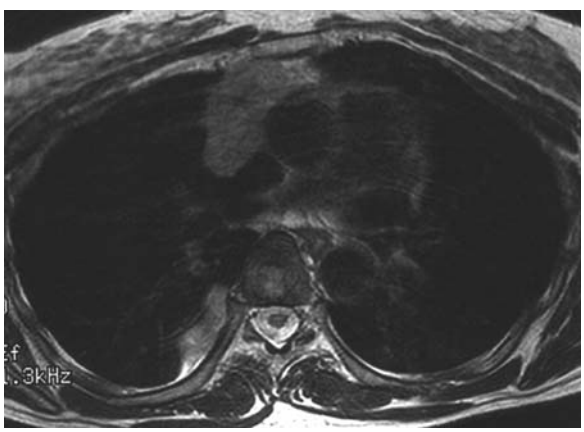

Thymomas and Thymic Carcinomas. Figure 3 Invasive thymoma. Axial T2-weighted MR image shows an anterior mediastinal mass and associated pleural metastases.

Thymic carcinoma mimics thymoma on imaging (Fig. 4). Thymic carcinomas are commonly associated with mediastinal lymph node and extrathymic metastases, but less commonly associated with pleural implants than invasive thymoma (5).

Nuclear Medicine

Increased uptake of thallium-201 and Tc-99m tetrofosmin has been demonstrated in thymoma and thymic carcinoma (6).

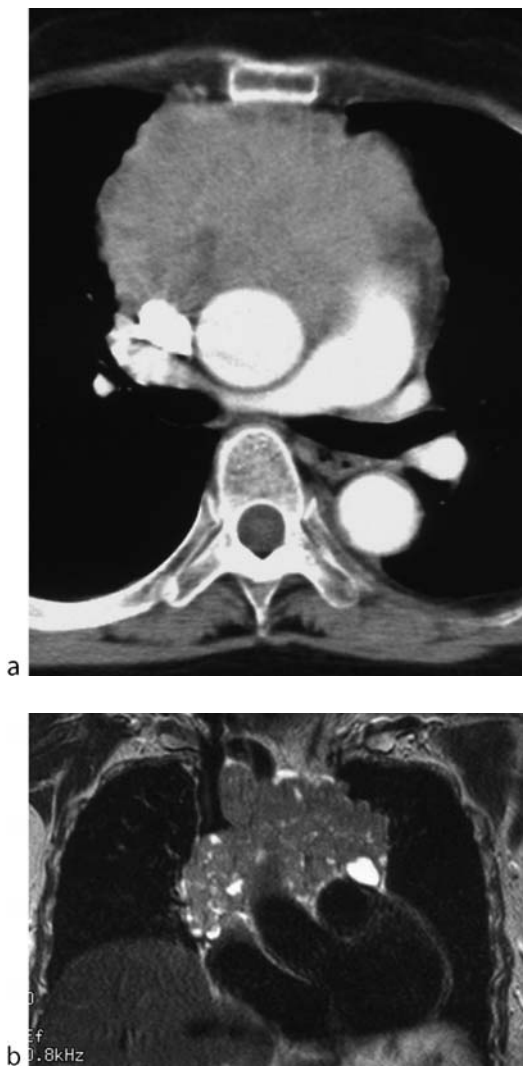

Thymomas and Thymic Carcinomas. Figure 4 Thymic carcinoma. (a) Contrast-enhanced CT shows a soft tissue mass with irregular margin in the anterior mediastinum. The lesion surrounds and displaces the major vessels of the mediastinum. (b) Coronal T2-weighted MR image shows multiple foci of cystic changes within the tumor.

Bibliography

1. Shimosato Y, Mukai K (1997) Epithelial tumors. In: Rosai J (ed) Tumors of the Mediastinum. 3rd edn. Armed Forces Institute of Pathology, Washington D.C. pp 40–157
2. Lewis JE, Wick MR, Scheithauer BW et al (1987) Thymoma: a clinicopathological review. Cancer 60:2727–2743
3. Rosai J, Sbin LH (1999) Histological typing of tumors of the thymus. In: International Histological Classification of Tumors. 2nd edn. Springer, New York pp 5–14
4. Do YS, Im J-G, Lee BH et al (1995) CT findings in malignant tumors of thymic epithelium. J Comput Assist Tomogr 19:192–197
5. Jeong YJ, Lee KS, Kim J et al (2004) Does CT of thymic epithelial tumors enable us to differentiate histologic subtypes and predict prognosis? Am J Roentgenol 183:283–289
6. Higuchi T, Taki J, Kinuya S et al (2001) Thymic lesions in patients with myasthenia gravis: characterization with Thallium 201 scintigraphy. Radiology 221:201–206

Thymus

The lymphoid organs in which T-lymphocytes are educated, mature, and multiply. It is composed of thymic epithelium and lymphocytes, which are almost entirely of the T-cell lineage.

▶Neoplasms of the Chest in Childhood

Thymus Aplasia

▶Congenital Malformations, Thymus

Thyroglobulin

Thyroglobulin is a thyroid protein precursor to iodine-containing hormones and is typically present in the colloid of thyroid gland follicles.

▶Neoplasms, Thyroid, Benign and Malignant

Thyroglossal Duct Cyst

congenital abnormality resulting in a midline cystic structure developing in the normal track of the thyroid descent from the base of the tongue to the lower neck.

▶Congenital malformations, Thyroid, and Functional Disorders

▶Cyst, Cerebral and Cervical, Childhood

Thyroid Acropachy

It can develop with thyroid dysfunction and it presents with typical speculated periosteal appositions that have a predilection for small tubular bones.

▶Hypertrophic

Thyroid Autoimmune Diseases

Norbert Gritzmann
KH Barmherzige Brüder Salzburg
Salzburg, Austria
norbert.gritzmann@bbsalz.at

Graves' Disease

Synonyms

Basedow's disease; Basedow goiter; Chronic lymphatic thyroiditis; Immune thyroiditis type Basedow; Morbus Basedow

Definition

▶Graves' disease is an ▶autoimmune disease of the ▶thyroid gland, usually presenting with ▶hyperthyroidism.

Pathology/Histopathology

Pathologically the thyroid gland is usually enlarged, with large intraglandular and periglandular vessels.

Histologically diffuse or focal lymphatic infiltrations are visualized. Exophthalmos is regarded as a typical sign of endocrine ophthalmopathy. The orbital muscles show enlargement with myxoid degeneration.

Clinical Presentation

The thyroid gland is usually enlarged on palpation. A murmur may be present during auscultation of the neck.

The clinical picture is variable. In classic disease, typical symptoms are present.

The individual is nervous, with heat intolerance and a tendency to sweat. Tachycardia and weight loss may be present. Tremors, diarrhea, and pigment abnormalities are seen. Other endocrine symptoms such as hypomenorrhea or amenorrhea in women and impotence or gynecomastia in men may be found. Very typical for Graves' disease is an endocrine ophthalmopathy with exophthalmia, and a paralysis of the eye muscles may be

found. Pretib ial myxedema is regarded as classic. The combination of thyroid enlargement, endocrine ophthalmopathy, and tachycardia is called the Merseburger triad.

Laboratory Findings

Thyroid-stimulating hormone (TSH) is suppressed. Hyperthyreosis with elevation of T4 and T3 is often found.

TSH-receptor antibodies (TRAK) are regarded as typical for Graves' disease.

Imaging

The thyroid gland is usually enlarged, with an anteroposterior diameter of more than 2 cm in each lobe. The poles of the gland are rounded. The thyroid gland is most often diffusely hypoechogenic (Fig. 1), but normal echogenicity does not rule out Graves' disease. On color Doppler, significant hypervascularization, called thyroid inferno, is found (Fig. 2), and tissue vibrations usually form a mosaic pattern. On pulsed Doppler sonography, the peak systolic velocities are more than 40 cm/sec in the inferior thyroid artery.

No correlation between hypervascularization and thyroid hormone levels has been found.

The gland usually remains hypoechogenic, even in clinical remission. Malignant transformation is rare. Benign nodules are found frequently in Graves' disease, usually presenting as echogenic lesions caused by adenomas.

Enlarged locoregional lymph nodes may be found.

Nuclear Medicine

The thyroid gland is usually scanned after intravenous administration of technetium-99m.

The technetium uptake is elevated, usually more than 4%, and the thyroid gland is homogeneously enlarged (Fig. 3). Uptake in the salivary gland is suppressed. These features are regarded as classic.

Endocrine ophthalmopathy is a typical sign of Graves' disease. The exophthalmos is usually imaged by magnetic resonance imaging (MRI) or computed tomography (CT). A thickening of the orbital muscles is found. Because of myxoid infiltrations and edema, the orbital muscles are bright on T2-weighted images.

MRI and CT are mainly used to exclude space-occupying retrobulbar lesions in patients with unilateral exophthalmos.

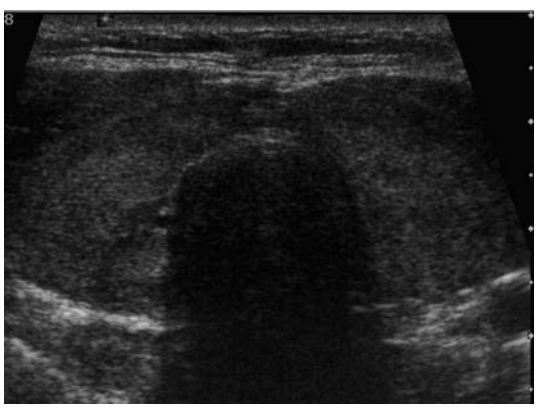

Thyroid Autoimmune Diseases. Figure 1 Graves' disease. Transverse section of the thyroid gland shows diffuse enlargement with diffuse hypoechogenicity.

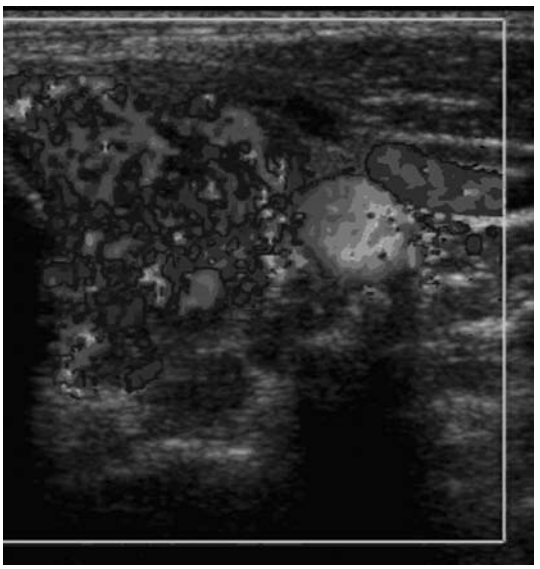

Thyroid Autoimmune Diseases. Figure 2 Enlargement of the left lobe of the thyroid gland with a mosaic pattern of vascularization, known as thyroid inferno.

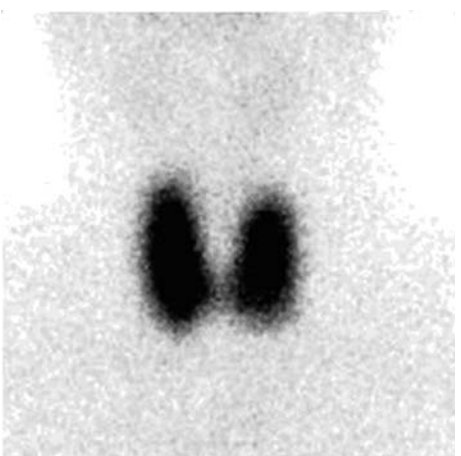

Thyroid Autoimmune Diseases. Figure 3 Technetium scan of thyroid gland in Graves' disease. The gland is enlarged, with elevated technetium uptake (more than 4%, often even exceeding 5%).

Acropachydermia may be present, and on plain films of the long bones, bone thickening can be seen.

Diagnosis

The diagnosis of Graves' disease is established by adding the clinical signs, the laboratory findings (hyperthyreosis and TRAK autoantibodies), and the sonographic and scintigraphic picture. Therapy may include: Favistan, near-total resection, and radioiodine therapy.

Hashimoto's Thyroiditis

Definition

►Hashimoto's thyroiditis is an autoimmune; Chronic lymphocytic inflammation of the thyroid gland.

Pathology/Histopathology

In the beginning of the autoimmune inflammation, the gland may be moderately enlarged. In advanced so-called burned-out cases, the volume of the gland shrinks because of fibrosis.

Histologically the thyroid gland is infiltrated by lymphocytes or plasma cells. Fibrous scarring may be found in the later stage of the disease.

Other forms of thyroiditis are subacute thyroiditis (de Quervain's), postpartum thyroiditis, and silent thyroiditis.

Clinical Presentation

The disease has an increased prevalence in middle-aged women.

Patients can be asymptomatic or may present with signs of ►hypothyroidism. Weakness, cold intolerance, swelling of hands and feet, and pretibial myxedema may be seen. The skin may be cold, thickened, and pale or yellow. In rare cases, the patient may initially present with signs of hyperthyreosis (Hashitoxicosis).

Other forms of thyroiditis (de Quervain's thyroiditis, postpartum thyroiditis, silent thyroiditis) usually present without hypothyroidism.

There may be coexistence with other autoimmune diseases.

Laboratory Findings

Autoantibodies are often elevated (MAK, TPO-AK).

TSH is often elevated, and T3 and T4 may be low. In the acute phase, hyperthyroidism may be present.

Imaging

In Hashimoto's thyroiditis, the gland may be enlarged or normal sized, or the volume can decrease depending on the duration of the disease and the amount of scarring. On sonography, the structure of the gland often shows few micronodular hypoechogenic foci, or the gland may be diffusely hypoechogenic. The echogenicity of the thyroid is assessed by comparing it with the surrounding cervical muscles. The gland usually becomes as hypoechogenic as the surrounding muscles.

On color Doppler, the gland usually shows hypervascularization; in advanced fibrous forms, the vascularization diminishes.

Enlarged locoregional lymph nodes may be found.

Nuclear Medicine

The technetium uptake of the thyroid gland usually diminishes (below 0.5%), and the salivary glands are more prominent on scintigraphic imaging. The thyroid structure may be patchy.

Diagnosis

The diagnosis of Hashimoto's thyroiditis is established by adding the clinical signs, the laboratory findings, and the sonographic and scintigraphic picture.

Depending on the grade of hypothyroidism, the condition is treated with thyroid hormone substitution.

Bibliography

1. Gritzmann N, Koischwitz D, and Rettenbacher T (2000) Sonography of the thyroid and parathyroid glands (review). Radiol Clin North Am September 38(5):1131–1145, xii
2. Ralls PW, Mayekawa DS, Lee KP, et al (1988) Color-flow Doppler sonography in Graves' disease: "thyroid inferno." Am J Roentgenol April 150(4):781–784
3. Saleh A, Cohnen M, Fürst G, et al (2002) Differential diagnosis of hyperthyroidism: Doppler sonographic quantification of thyroid blood flow distinguishes between Graves' disease and diffuse toxic goiter. Exp Clin Endocrinol Diabetes January 110(1):32–36

Thyroid Gland

The thyroid is a butterfly-shaped endocrine gland located in the lower front part of the neck, with a lobe on either side of the trachea. Its hormones have important roles in regulating metabolism.

►Thyroid Autoimmune Diseases

Thyroid Malformations

Thyroid malformations range from thyroid atresia to thyroglossal duct cysts. Ectopic thyroid tissue may be

located at the base of the tongue in the midline dorsum, but it can be located anywhere along the migration pathway of the thyroid. The most common congenital thyroid anomaly is the persistent thyroglossal duct cyst.
▶Congenital Malformations, Neck

Thyroid Tumors

▶Neoplasms, Thyroid, Benign and Malignant

Tibia Kyphoscoliosis

Congenital posterior and medial bowing of a tibia and fibula, believed to be secondary to intrauterine position.
▶Congenital Malformations, Bone

TIC

▶Time-signal Intensity Curve

Tillaux Fracture

An adolescent ankle fracture with a sagittal epiphyseal fracture of the distal tibia that continues through the not-yet-fused portion of the partially fused physis.
▶Fractures, Bone, Childhood

Time Intensity Curves

Martin Krix
Bracco ALTANA Pharma GmbH, Clinical Research, Konstanz, Germany
martin.krix@altanapharma.com

Synonyms

Perfusion curves

Definition

Time intensity curves quantitatively describe the dynamics of the intravascular ultrasound contrast media, and thereby provide a quantitative assessment of tissue vascularization.

Characteristics

Since perfusion is a recognized parameter of tissue viability and functionality, its measurement can be useful in the detection and characterization of various pathological changes such as in ischemia, inflammation, or neoplasia. Thus, ▶*perfusion imaging* is an important part of the growing field of functional imaging, which may become necessary for the characterization of many diseases. Quantification is a prerequisite for many applications in functional imaging, in particular in perfusion imaging. Important indications are the evaluation of tumor or organ perfusion (e.g., brain, heart, or kidney), particularly during follow-up or therapy monitoring.

For quantitative analysis of contrast enhancement in ultrasound examinations, the wash-in and wash-out of the ultrasound contrast medium after injection must be assessed in a region of interest. For this, the transducer is usually kept approximately in the same position. If necessary, the patient must be instructed to stop breathing or to breathe superficially in order to avoid movement during the examination. Video sequences of the dynamic process can be recorded, and postprocessing using commercially available software tools allows for a quick and easy analysis of the obtained image series. An important precondition for quantification of perfusion with contrast-enhanced ultrasound is that the signal intensity of the chosen ultrasound parameter must correlate with the ultrasound contrast agent concentration *in vivo*. High-frequency, raw data of the ultrasound examinations are considered the gold standard in this respect. However, these data are not always provided by the ultrasound scanner. Therefore, the video signals of the ultrasound device are often used, which have also provided accurate measurement of tissue perfusion in several organs.

The detection of microvascularity can be performed in real time with a high spatial resolution using low-mechanical index (MI) ultrasound techniques and ▶*second-generation ultrasound contrast media* such as microbubbles that are stabilized by phospholipids and contain sulfur hexafluoride (SonoVue, Bracco, Milan, Italy). Novel contrast-specific imaging techniques like coherent pulse sequencing (CPS; Siemens-Acuson, Erlangen, Germany) may have advantages in quantification, since they allow

the background tissue and the contrast-enhanced signal to be assessed separately.

High-MI imaging destroys the microbubbles in the region of interest during detection. Therefore, ▶*intermittent imaging* must be used when assessing whole tissue vascularization using high-MI techniques such as contrast-enhanced power Doppler ultrasound. At intermittent imaging the repetition rate of the ultrasound pulses (frame rate) is reduced, and the microbubbles can be given enough time to also fill the smallest vessels. Additionally, well-defined variations of the frame rate allow for the assessment of different stages of refilling. Thus, it also can provide the calculation of replenishment kinetics, even though *intermittent imaging* is more complex compared to real-time methods using low-MI techniques.

With these contrast-enhanced ultrasound methods, the entire perfusion of an examined region can be detected, that is, the blood flow per tissue unit including the capillary blood flow. Due to the interaction between the microbubbles and the acoustic field (*nonlinear resonance* and *bubble destruction*), each microbubble may be detectable by *contrast-specific imaging techniques*, with a sensitivity that can hardly ever be exceeded. Unlike other contrast agents used in radiology, ultrasound contrast media are confined to the intravascular space. Thus, complex and sometimes inaccurate pharmacokinetic models to describe the contrast agent distribution in tissue are not necessary for quantifying perfusion using contrast-enhanced ultrasound. On the other hand, it is not possible to assess changes of the vessel permeability with intravascular contrast agents, which, however, may be another important functional parameter, for example, in treatment monitoring.

The typical time intensity curve, which describes the ultrasound signal intensity over time in a region of interest after a contrast bolus injection, is also called a perfusion curve. In tissues that are predominant arterially supplied (like in most organs or malignant tumors), the perfusion curve has a typical shape with a rapid increase of contrast enhancement and a slower, exponential-like decrease after reaching a maximum. According to a classic tracer kinetics modeling, the analysis of an input function derived from the arterial enhancement in the feeding vessels is required to allow for the calculation of perfusion. However, in ultrasound, an extraction of the input function and a measurement of the tissue enhancement are difficult to perform simultaneously. Thus, several descriptive parameters are used to characterize such curves, such as the maximum enhancement after contrast bolus injection, the time to peak enhancement, the slope to maximum, or the area under the entire perfusion curve. However, these parameters do not directly characterize the perfusion parameter itself, for example, local blood volume or flow. However, they are quantifiable and relatively easy to obtain, and can be considered as indirect perfusion markers. The maximum of the perfusion curve is considered as a parameter of the overall degree of tissue vascularization. The initial slope and the time to maximum can be used as descriptors of the blood flow characteristics in the region of interest. In several clinical examinations such values have been used to assess tissue vascularization, as in focal liver lesions (1), *renal* examinations, (2), echocardiography, or in transcranial ultrasound studies (3) (Fig. 1).

In addition, time intensity curves can be simply used to obtain ultrasound contrast media arrival times in larger arteries or veins, which provide an accurate transit time analysis of organs such as the liver.

An ultrasound-specific time intensity curve, which allows for the assessment of direct perfusion parameter, is derived from replenishment kinetics of the ultrasound contrast media. This technique uses the potential of ultrasound to destroy microbubble contrast agents if the output power is high enough. After such destructive ultrasound pulses (using a high-MI ultrasound technique, "flash"), it can be assumed that the examined slice is void of microbubbles, and that these will again progress into the slice from outside, where they are still present. The analysis of such replenishment kinetics (ultrasound signal intensity over time after destruction) can provide several direct perfusion parameters. It has been shown that the initial increase of the refilling curve indicates the mean blood flow velocity (m/sec) in the region of interest, and the plateau of signal intensity that will be reached after the complete replenishment is a parameter proportional to the local blood volume (∼mL). According to a model of Wei, a parameter proportional to the perfusion (∼mL/sec·mg) can be then calculated *via* the product of blood velocity and blood volume (4). This established model assumed a constant velocity of refilling and neglected the fact that the contrast agent will reenter the slice through vessels of varying calibers and directions. Other models have been proposed attempting a more consistent description of the refilling process (5–7). In addition, a method was developed using a single bolus injection instead of the usually required continuous infusion of contrast agent when analyzing replenishment kinetics (8).

Replenishment kinetics requires a more complex ultrasound examination and analysis. It has, nevertheless, been used successfully for the accurate measurement of tissue perfusion in several organs. One important application is the assessment of myocardial microcirculation in echocardiography (9). Furthermore, renal perfusion (7), perfusion of the liver and liver metastases (10), muscle perfusion (11), and changes in tumor perfusion during antiangiogenic treatment have been analyzed (5, 12).

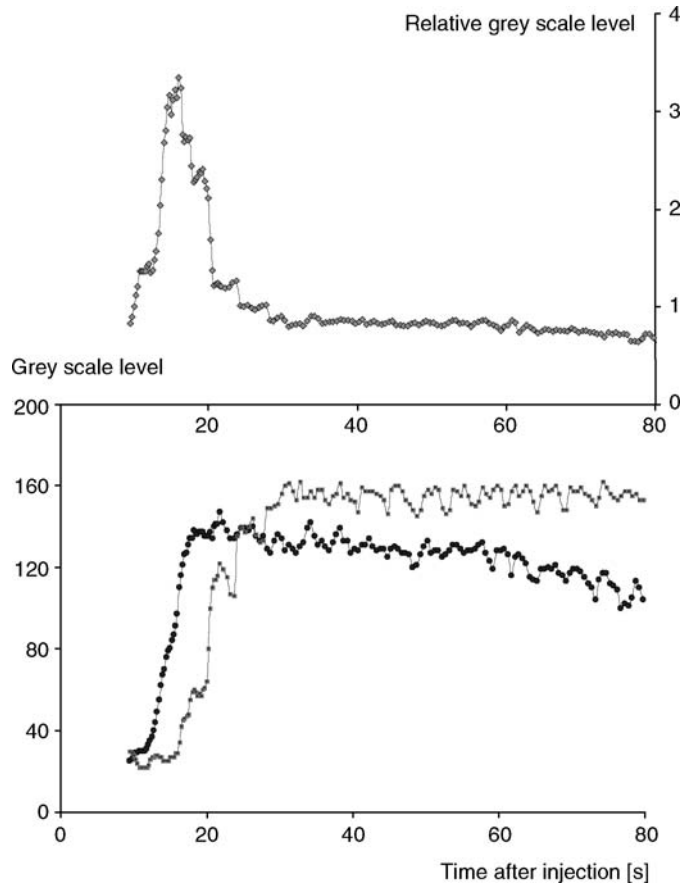

Time Intensity Curves. Figure 1 Time intensity curves from contrast-enhanced ultrasound after injection of 2.4 mL SonoVue (Bracco, Milan, Italy) using a low-MI technique (Acuson Sequoia, Erlangen, Germany) recorded during early enhancement in a liver metastasis of breast cancer (black dots). As reference the time intensity curve of unaffected liver tissue is shown (grey dots). The upper curve (?) describes the ratio of lesion to liver, which can be used for focal liver lesion characterization.

With the increasing development of functional imaging methods, a user-friendly presentation of information derived from such imaging methods has gained interest. The visualization of a (semi)-quantitative parameter value in its spatial distribution is called ►*parametric imaging*. Color-coded maps, which can be superimposed to standard images, are typical examples of parametric imaging. In perfusion imaging such parametric images have entered routine clinical practice in computed tomography and magnetic resonance imaging. In addition, in contrast-enhanced ultrasound, parametric imaging has become feasible for the visualization of perfusion-related information using additional external tools or dedicated software implemented on the ultrasound device. The scope of solutions includes descriptive visualization of microcirculation (e.g., Micro Flow Imaging, Toshiba) and dedicated software tools for quantification of diverse perfusion parameters (e.g., Qontrast, Amid, Rome, Italy).

References

1. Krix M, Kiessling F, Essig M et al (2004) Low mechanical index contrast-enhanced ultrasound better reflects high arterial perfusion of liver metastases than arterial phase computed tomography. Invest Radiol 39(4):216–222
2. Levefre F, Correas JM, Briancon S et al (2002) Contrast-enhanced sonography of the renal transplant using triggered pulse-inversion imaging: preliminary results. Ultrasound Med Biol 28(3):303–314
3. Seidel G, Meyer-Wiethe K, Berdien G et al (2004) Ultrasound perfusion imaging in acute middle cerebral artery infarction predicts outcome. Stroke 35(5):1107–1111
4. Wei K, Jayaweera AR, Firoozan S et al (1998) Quantification of myocardial blood flow with ultrasound-induced destruction of microbubbles administered as a constant venous infusion. Circulation 97(5):473–483
5. Pollard RE, Sadlowski AR, Bloch SH et al (2002) Contrast-assisted destruction-replenishment ultrasound for the assessment of tumor microvasculature in a rat model. Technol Cancer Res Treat 1(6):459–470
6. Krix M, Kiessling F, Farhan N et al (2003) A multivessel model describing replenishment kinetics of ultrasound contrast agent

for quantification of tissue perfusion. Ultrasound Med Biol 29(10): 1421–1430
7. Lucidarme O, Franchi- Abella S, Correas JM et al (2003) Blood flow quantification with contrast-enhanced US: "entrance in the section" phenomenon – phantom and rabbit study. Radiology 228 (2):473–479
8. Krix M, Kiessling F, Vosseler S et al (2003) Comparison of intermittent-bolus contrast imaging with conventional power Doppler sonography: quantification of tumour perfusion in small animals. Ultrasound Med Biol 29(8):1093–1103
9. Lepper W, Belcik T, Wei K et al (2004) Myocardial Contrast Echocardiography. Circulation 109:3132–3135
10. Krix M, Plathow C, Kiessling F et al (2004) Quantification of perfusion of liver tissue and metastases using a multivessel model for replenishment kinetics of ultrasound contrast agents. Ultrasound Med Biol 30(10):1355–1363
11. Krix M, Weber MA, Krakowski-Roosen H et al (2005) Assessment of skeletal muscle perfusion using contrast-enhanced ultrasonography. J Ultrasound Med 24(4):431–441
12. Krix M, Kiessling F, Vosseler S et al (2003). Sensitive noninvasive monitoring of tumor perfusion during antiangiogenic therapy by intermittent bolus-contrast power Doppler sonography. Cancer Res 63(23):8264–8270

Time-Resolved Optical Tomography

▶Optical Tomography

Time-of-flight

MR angiographic technique based on unsaturated protons in flowing blood entering the imaging plane returning more signal than the saturated protons in the surrounding stationary tissues.

▶Carotid and Vertebral Artery Pathology

Time-signal Intensity Curve (TIC)

Time-signal intensity curves (TICs) are obtained by measuring signal intensity of normal and diseased tissues in a series of dynamic contrast-enhanced MR images obtained at interrupted time points after the administration of contrast medium. The curves are usually characterized by calculating parameters, such as time of peak enhancement (T-peak) and washout ratio (WR).

▶Neoplasms, Salivary Glands

TIPS

I. Kaare Tesdal
Universitätsklinikum Mannheim, Institut für Radiologie und Nuklearmedizin Klinikum Friedrichshafen, Friedrichshafen, Germany
k.tesdal@klinikum-fn.de

Definition

Portosystemic shunts are abnormal vascular connections between the hepatic portal and the systemic circulation. Patients with severe liver disease like cirrhosis and Budd–Chiari syndrome suffer from circulation problems. The blood from the lower part of the body normally returns to the heart through blood vessels passing through the liver (hepatic portal vein). If the liver is damaged or the hepatic venous outflow is obstructed, this upward flow of blood becomes difficult leading to portal hypertension. The consequences are that the fluid tends to pool in the legs (edema) and inside the abdomen (ascites), and the blood may flow in unusual pathways, such as through the vessels around the esophagus and stomach. These vessels may become swollen with blood over time, (esophageal and gastral varices) and bleed.

One way to treat this portal hypertension is to form a new connection inside the damaged liver, which allows for better flow of blood back to the heart. This procedure is called an intrahepatic shunt (tube connection inside the liver). It can be done by inserting a metallic endoprosthesis (stent) into place through a vein in the neck (transjugular), down into the liver (Figs. 1, 2). The link between the high-pressure portal vein and low-pressure hepatic vein is an incomplete side-to-side shunt (H-shunt). It does not require surgery to open the abdomen and can be performed in a radiology setting in about 1–3 h, followed by monitoring in the intensive care unit (2). In patients with bleeding, TIPS can be combined with embolotherapy of the varices (3). The rational of embolotherapy is at the same setting *via* the transjugular vein to use long-acting occluding agents embolizing proximal and peripheral collateral veins by combining liquid and mechanical materials in order to prevent collateralization and reperfusion.

Indication and Contraindication

The purpose of TIPS is to achieve portal decompression and therefore prevent rebleeding from varices or stop or reduce the formation of ascites. Since the first TIPS was performed on patients with poor liver function and active variceal hemorrhage in 1988, the indications for

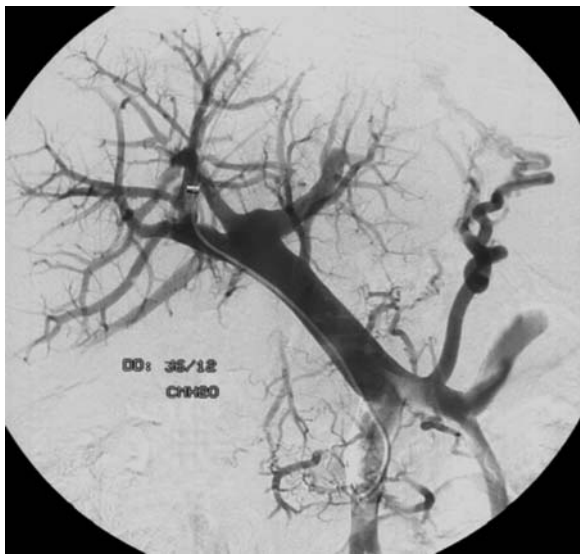

TIPS. Figure 1 Portogram (anteroposterior) after transjugular, intrahepatic punction of a right intrahepatic portal vein shows retrograde filling of the left gastric vein. The portosystemic pressure gradient was 24 cmH20 (cm of water).

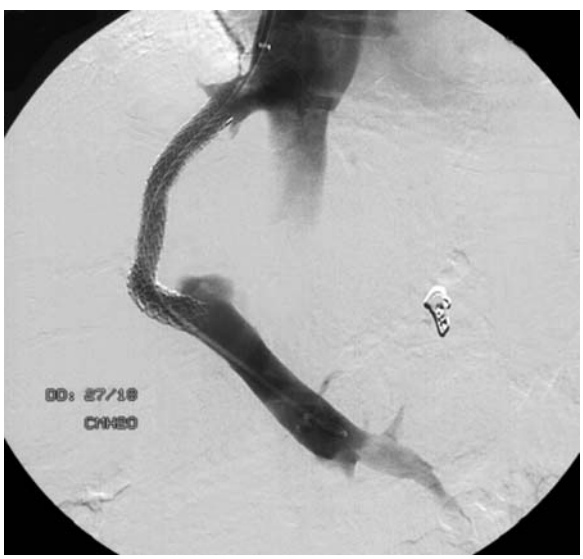

TIPS. Figure 2 Portogram (anteroposterior) after the TIPS has been established with implantation of one self-expanding covered stent (Viatorr), and the varices (left gastric vein) have been embolized with natriumamidotrizoat (Ethibloc) in combinastion with coils. The portosystemic pressure gradient was reduced from 24 cmH20 to 9 cmH20.

performing TIPS have increased (2). The recommendations from consensus meeting are discussing accepted indications (+++), potential indications with proven efficacy (++), experimental indications with efficacy not proven by large-scale series (+), indications not accepted (case reports only) (−), and absolute contraindications (−−) for shunting with TIPS.

Accepted indications (+++) are (1) acute variceal bleeding that neither can be successfully controlled with pharmacological agents, nor with mechanical compression or endoscopic techniques, and (2) recurrent variceal bleeding in patients who are refractory or intolerant to conventional medical management, including sclerotherapy and pharmacological therapy.

Potential indications with proven efficacy (++) are (1) refractory ascites (serious tense ascites that does not respond to standard therapy within 4 weeks or where the patient develops secondary effects making treatment impossible), and (2) Budd–Chiari and veno-occlusive syndromes. The rationale for TIPS in BCS is to improve hepatic blood flow and function by creation of an artificial outflow *via* the portal vein bed. The side-to-side shunt allows retrograde arterial perfusion of the sinusoids, thus reducing the hypoxic damage of the hepatocytes and leading to improvement in liver histology.

Absolute contraindications are (1) hepatic insufficiency and chronic, severe encephalopathy; (2) severe right heart cardiac insufficiency; (3) diffuse or multinodular liver cancer, or tumors in the proposed route of the TIPS; (4) advanced cancer; (5) bacterial peritonitis or systemic infection; and (6) unrelieved biliary obstruction.

Results

From a technical point of view, successful placement of TIPS is achieved in more than 95% of patients. Performing TIPS in a patient with BCS can be difficult if the hepatic vein is completely occluded. In meta-analyses of TIPS literature, the incidence of fatal complications (intra-abdominal hemorrhage, laceration of the hepatic artery or portal vein, and right heart failure) was 1.7% (range 0.6–4.3%). Major procedural complications are expected in no more than 3% of cases.

Both randomized and nonrandomized studies have strengthened the evidence that TIPS is more effective than endoscopic therapy in the prevention of variceal bleeding. In randomized trials, the 1-year rebleeding rate ranged between 10 and 27% for TIPS and between 21 and 57% for endoscopic treatment. In a nonrandomized study, the 2-year and 4-year rates of patients free of rebleedings were 61% and 53% in patients treated with TIPS alone, and 84% and 81% in patients treated with TIPS and adjunctive embolotherapy of gastroesophageal collaterals.

All randomized trials but one found TIPS to be more effective than endoscopic therapy in avoiding variceal rebleeding, but average survival of patients treated with TIPS was not higher than survival of patients treated with endoscopic therapy. The incidence of encephalopathy was significantly higher in patients treated with TIPS in four of nine trials.

The main problems with TIPS are their low primary patency-rate (8–48% after 2 years), and an increased risk of encephalopathy of about 29% (7–55%). The preliminary experiences using polytetrafluoroethylene (PTFE)- covered stent-grafts are, with regard to patency, very promising. The actuarial rates of primary patency using covered stents were 86% at year 1 and 80% at year 2.

Several nonrandomized and five randomized studies have evaluated the effect of TIPS on refractory ascites compared to large volume paracentesis (LVP). In the TIPS group, control of ascites was more frequently achieved at 4 months (66 *vs.* 24%) and 12 months (55 *vs.* 19%), whereas encephalopathy was higher (55 *vs.* 38%). Survival at 1 year and 2 years were not different between patients treated with TIPS and LVP.

There have been a number of case reports and three small series on the outcome of patients with Budd–Chiari syndrome who have received TIPS. The largest series reports the technical and clinical success rate of 35 patients (4). The TIPS was successfully implanted in 33 patients (94%). Clinical symptoms (11 patients had a fulminant/acute form; 13 a subacute, and 11 a chronic course of disease) as well as the biochemical test results improved significantly during 4 weeks after treatment. The 1- and 5-year survival rate without transplantation in all patients was 93% and 74%, respectively.

The current recommendations: The decision to create TIPS in a patient with Budd–Chiari syndrome should be based on the severity of disease and only patients with moderate disease appear primarily to be reasonable candidates for a TIPS. Patients with BCS and mild disease can be managed medically, whereas those with more severe disease or acute hepatic failure are best managed by liver transplantation. On the other hand, in the light of not enough available compatible organ for transplantation, transjugular shunt should always be considered as a treatment of fulminant/acute, subacute and chronic severe Budd–Chiari syndrome.

References

1. Dilawari JB, Bambery P, Chawla Y et al (1994) Hepatic outflow obstruction (Budd-Chiari syndrome). Experience with 177 patients and a review of the literature. Medicine 73:21–36
2. Boyer TD, Haskal ZJ (2005) The role of transjugular intrahepatic portosystemic shunt in the management of portal hypertension. Hepatology 41:385–400
3. Tesdal IK, Filser T, Weiβ Ch et al (2005) Transjugular intrahepatic portosystemic shunt: adjunctive embolotherapy of gastroesophageal collaterals in the prevention of variceal rebleeding. Radiology 236:360–367
4. Rössle M, Olschewski M, Siegerstetter V et al (2004) The Budd–Chiari syndrome: outcome afte treatment with transjugular intrahepatic portosystemic shunt. Surgery 135:394–403

Tissue Doppler Echocardiography

Doppler echocardiography mode which allows measurement of the low velocities of moving tissue.

▶Ischemic Heart Disease, Ultrasound

TME

▶Total Mesorectal Excision

TNFa

▶FasL (CD95L), TRAIL or TNFa

TNM

T-extension of the primary tumor.
N-regional lymph node metastases.
M-distant metastases.

▶Neoplasms, Oral Cavity

Toluene

Toluene (C_7H_8), also known as methylbenzene, is an aromatic hydrocarbon found in a variety of household products including gasoline, acrylic paints, varnishes, paint thinners, glues, and shoe polishes. It is highly volatile, and

inhalation of toluene vapors can result in euphoric states. Chronic inhalation can result in neurological symptoms and encephalopathy.
▶Toxic Disorders, Brain

Tooth Decay

▶Caries and Paradontal Diseases

Tophi

▶Gout

TORCH Infections

▶Calcification, Intracranial, Neonatal

TORCH Syndrome

Perinatal intracranial infections which include toxoplasmosis, others i.e. HIV, rubella, cytomegalovirus and herpes infections.
▶Calcifications, Intracranial, Neonatal

Total Mesorectal Excision (TME)

TME is a standardized surgical technique of sharp dissection of the entire mesorectal compartment, containing rectum, mesorectal fat and mesorectal fascia, used in rectal cancer surgery. In non-locally advanced rectal tumours, this technique results in surgical clearance of the radial margin, and thus in complete resection. This is important, as involved radial margins are accepted as the major cause of local recurrence.
▶Rectal Carcinoma

Toxic Disorders, Brain

Benjamin Y. Huang, Mauricio Castillo
Department of Radiology, University of North Carolina at Chapel Hill, Chapel Hill, USA
bhuang@unch.unc.edu

Synonyms

CNS toxicity; Toxic encephalopathy

Definition

Toxic brain disorders are conditions in which injury to brain tissue occurs as a result of an interaction with a chemical compound (a toxin). These disorders encompass a number of disparate conditions, and the list of toxins is extensive. Specific toxins preferentially affect specific brain regions, reflecting a host of factors including regional cerebral blood flow and oxygen demand; neurotransmitter distribution; specific chemical affinity and vulnerability; and brain maturation at the time of intoxication.

Exogenous toxins are introduced into the body *via* several routes including inhalation, ingestion, direct inoculation, and absorption *via* the skin and mucous membranes. Exposures may be accidental or deliberate. Toxins can also be produced endogenously from extrinsic sources such as toxin-producing microbes. Several recognized CNS toxins are listed in Table 1. Some of the more common toxins are discussed in subsequent sections.

Pathology

Inhaled Toxins

Carbon Monoxide (CO)

CO is the leading cause of lethal inhalations in the USA and Europe. It is produced by the burning of fuels such as gasoline, kerosene, wood, coal, and propane. Effects of CO are related to its high affinity for heme-containing molecules (hemoglobin and myoglobin). CO binds hemoglobin ~250 times more avidly than does oxygen (O_2), causing formation of carboxyhemoglobin (COHb) in favor of oxyhemoglobin (O_2Hb) and decreased blood O_2-carrying capacity. Cellular damage also results from CO's ability to directly bind heme moieties in mitochondrial enzymes involved in oxidative phosphorylation and ATP synthesis, including the cytochrome oxidase system. Finally, brain lipid peroxidation may account for some of CO's neurotoxicity (1).

Toxic Disorders, Brain. Table 1 Exogenous CNS toxins

Inhaled toxins
• ▶Carbon monoxide
• ▶Toluene
• Nitrous oxide
• ▶Mercury (elemental)
• Illicit drugs (heroin pyrolysite)
Ingested or Injected toxins
• ▶Lead
• Mercury (organic)
• Manganese
• ▶Methanol
• Ethanol
• Cyanide
• Triethyl tin
• Medications (immunosuppressants, chemotherapeutic agents, anticonvulsants, isoniazid)
• Illicit drugs (methamphetamine, cocaine, heroin, MDMA)
• Toxin producing infections (*E. coli*, mycoplasma, diphtheria)

Organic Solvents and Aerosols

Inhalation of organic solvents and aerosols can result in a transient euphoric state. These substances are found in a host of household products (model cement, spray paint, lighter fluid, and paint thinner). Inhaled substances belong to several chemical families, including aliphatic hydrocarbons (gasoline, propane, butane), alkyl halides (refrigerants, aerosol propellants, correction fluid), aromatic hydrocarbons (benzene, toluene, xylene), nitrites (room air fresheners), ethers, and ketones. These compounds are lipophilic and are readily absorbed from blood into lipid rich tissues, including the brain. Long term exposures result in demyelination and gliosis of cerebral and cerebellar white matter (2).

Of the abused inhalants, toluene is the most damaging. Toluene is a component of organic solvents and is found in gasoline, acrylic paints, varnishes, paint thinners, glues, and shoe polishes.

Ingested or Injected Toxins

Heavy Metals (Lead and Mercury)

The leading risk factor is exposure to lead-based paint found in older homes. Children are at highest risk for lead poisoning.

Lead's neurotoxic effects are due, in part, to its ability to substitute for calcium and include apoptosis, excitotoxicity, inhibition of mitochondrial respiration, effects on neurotransmission, and damage to glial cells.

Mercury exposure occurs primarily by inhalation. Less than 0.01% of liquid mercury is absorbed, and skin exposure results in even less absorption. Organic mercury is readily absorbed through the digestive tract. A common source of organic mercury is seafood contaminated with methylmercury used in fungicides.

Methanol

Methanol is found in many commercial solvents and in antifreezes. Intoxication is usually accidental or suicidal, and has occasionally been seen from intentional adulteration of alcoholic beverages. After ingestion there is a latent period of up to 72 h during which methanol is metabolized in the liver into formaldehyde and then to formic acid, resulting in a severe metabolic acidosis. These byproducts are toxic to the CNS.

CNS Disorders Related to Ethanol Abuse

Ethanol is among the most commonly abused drugs. In addition to ethanol's direct toxic effects, there are a number of associated CNS disorders including ▶Wernicke–Korsakoff syndrome, ▶Marchiafava–Bignami disease, and ▶osmotic myelinolysis. In pregnancy, ethanol can be teratogenic, resulting in fetal alcohol syndrome, which affects CNS development. The direct neurotoxic effects of ethanol are poorly understood, but include neuronal damage and myelin degeneration.

Marchiafava–Bignami disease is a rare disorder of chronic alcoholics, first described in drinkers of cheap Italian red wine. The characteristic finding is cystic and laminated necrosis of the corpus callosum, particularly

the *genu* and body. Similar findings may be noted in the optic chiasm, anterior commissure, centra semiovalia and brachium pontis. Histologically, there is demyelination with relative axonal preservation.

Osmotic myelinolysis is caused by damage to the blood–brain barrier induced by abnormalities in serum osmolality and electrolytes, particularly hyponatremia. Vigorous sodium correction frequently plays a role in development of osmotic myelinolysis. The pons is most frequently affected (central pontine myelinolysis), but extrapontine sites, including the thalami, basal ganglia, deep cerebral white matter, and lateral geniculate bodies, may be involved.

Clinical Presentation

Inhaled Toxins

Carbon Monoxide (CO)

Acute symptoms of CO toxicity include headache, nausea, vomiting, seizures, and syncope. Severe or prolonged exposures result in coma and death. Physical examination may reveal "cherry red" lips and mucosa. Hyperbaric O_2 is the treatment of choice for acute poisoning and needs to be instituted within 6 h of exposure (1). A delayed encephalopathy can be seen and is characterized by an asymptomatic period of 2–3 weeks after initial recovery, followed by recurrence of symptoms.

Organic Solvents and Aerosols

Chronic abuse of toluene results in cognitive impairment, ataxia, tremor, and cranial neuropathies. An encephalopathy can occur, characterized by euphoria, hallucinations, nystagmus, seizures, and coma (2).

Ingested or Injected Toxins

Heavy Metals (Lead and Mercury)

Symptoms of lead poisoning in children are vague and include decreased appetite, constipation, and abdominal pain. Neurological symptoms include lethargy, irritability, headaches, behavioral changes, and developmental delay. In severe cases, seizures, coma, and death can occur.

CNS effects of chronic mercury poisoning (also known as Minamata disease) include visual field deficits, sensory abnormalities, and ataxia, which are felt to be related to spongiotic changes in the calcarine and postcentral cortex and cerebellar vermis. Other symptoms are neuropathy, choreoathetosis, confusion, and coma. Mercury poisoning is treated with chelation.

Methanol

Patients present with blindness (due to optic nerve necrosis), obtundation or death (3). Treatment includes gastric lavage, administration of sodium bicarbonate to correct acidosis, ethanol administration, and hemodialysis.

CNS Disorders Related to Ethanol Abuse

Acute symptoms in Wernicke encephalopathy include nystagmus, abducens and conjugate gaze palsies, ataxia, and confusion. Korsakoff psychosis is a persistent abnormality of mentation that develops after the initial confusional state of Wernicke encephalopathy begins to resolve with B1 replacement; patients are alert and responsive but have antegrade and retrograde amnesia and confabulation. The term Wernicke–Korsakoff syndrome is applied when components of both Wernicke encephalopathy and Korsakoff psychosis occur (3).

Diagnosis

Inhaled Toxins

Carbon Monoxide (CO)

MRI is more sensitive than CT for detecting brain abnormalities in CO poisoning. Areas of involvement reflect regions of high oxygen demand. The most commonly involved sites are the globi pallidi, which on CT are of low density. MRI demonstrates high T2 signal and, in the acute setting, restricted diffusion in the globi pallidi (Fig. 1). Hemorrhage may be seen. The putamina/caudate nuclei, cerebral white matter, cortex, hippocampi, and cerebellum may also be involved (1). In delayed encephalopathy, MRI reveals confluent, symmetric T2 hyperintensity in the periventricular white matter and centra semiovalia.

Organic Solvents and Aerosols

MRI in chronic toluene abuse shows diffuse cerebral, cerebellar, hippocampal, and brainstem atrophy, loss of cerebral grey-white matter differentiation, and abnormal high T2 signal in the periventricular white matter and centra semiovalia. Low T2 signal has been reported in the extrapyramidal system, including the thalami, basal ganglia, red nuclei, and substantia nigra. This finding may be due to iron deposition or to partitioning of toluene into cell lipid membranes (2).

Ingested or Injected Toxins

Heavy Metals (Lead and Mercury)

CT findings include bilateral, symmetric hypodense lesions in the thalami, putamina, claustra, and insulae. MRI shows low T1 signal and high T2 signal areas without

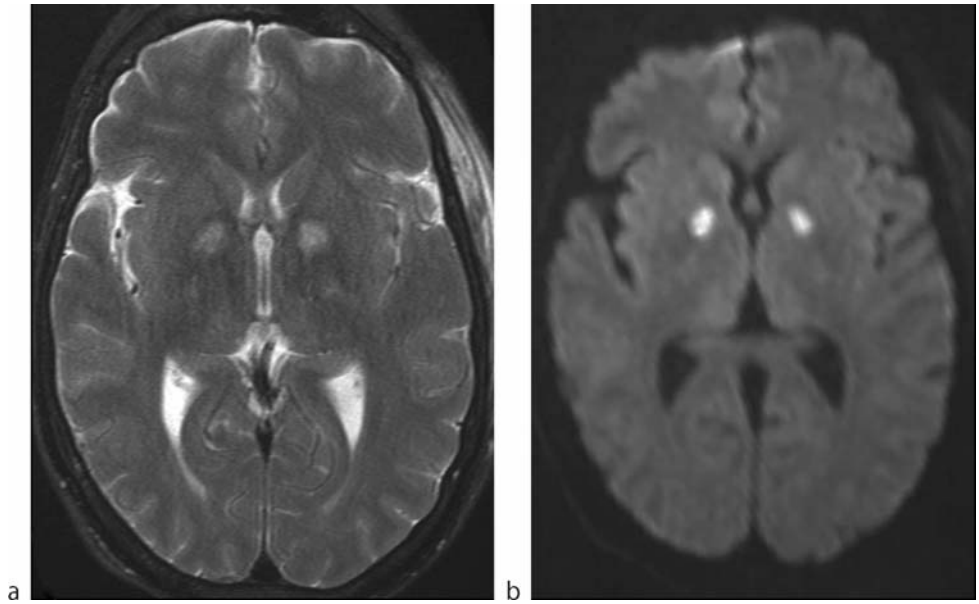

Toxic Disorders, Brain. Figure 1 Acute carbon monoxide poisoning. (a) Axial T2-weighted MR image demonstrates symmetric hyperintensity in the globi pallidi. (b) Corresponding diffusion weighted image (B = 1,000) demonstrates high signal reflecting restricted diffusion in the globi pallidi.

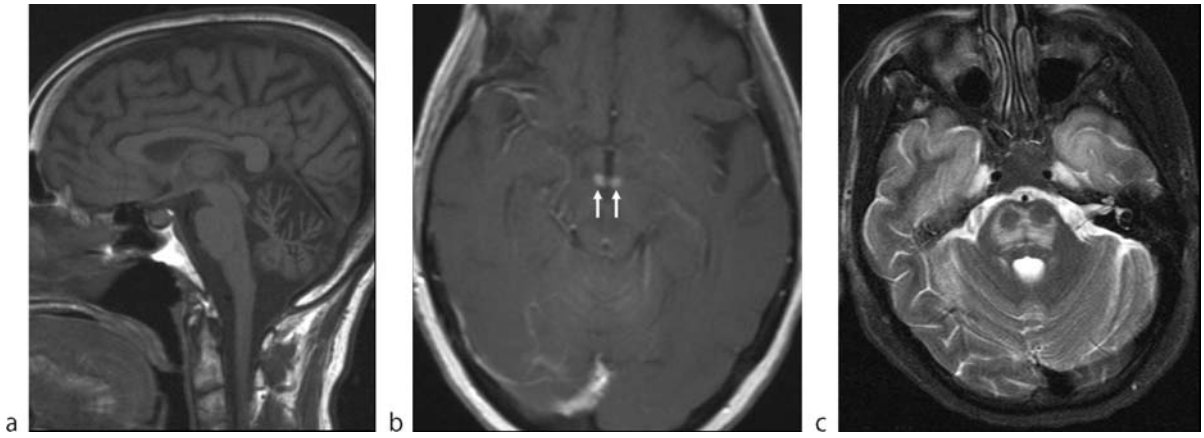

Toxic Disorders, Brain. Figure 2 Spectrum of ethanol related brain disorders. (a) Midsagittal T1-weighted MR image in a chronic alcoholic demonstrates characteristic atrophy of the superior vermis. (b) Gadolinium enhanced axial T1-weighted image in a patient with Wernicke encephalopathy demonstrates enhancement of the mamillary bodies (*arrows*). (c) Axial T2-weighted image in a patient with osmotic myelinolysis demonstrates diffuse signal abnormality in the pons with sparing of the corticospinal tracts.

enhancement in these areas. In chronic poisoning, extensive cerebral and cerebellar calcifications can occur. Rarely, lead poisoning may manifest as localized cerebellar edema mimicking a mass (4).

MRI in Minamata disease shows atrophy of the calcarine and postcentral cortex and cerebellar vermis (5).

Methanol

Putaminal hemorrhagic necrosis is typical and imaging studies bear this out. On CT, the putamina are swollen and hypodense and may demonstrate hemorrhage. On MRI, they are T2 hyperintense and of high or low T1 signal. Diffuse white matter signal abnormality may also be seen (3).

CNS Disorders Related to Ethanol Abuse

On imaging, cerebral and cerebellar atrophy are noted in chronic ethanol abuse. Atrophy is most marked in the rostral vermis and adjacent cerebellar surfaces (Fig. 2a)

(3). Also observed early are white matter lesions in the periventricular regions thought to be due to myelin degeneration. These lesions manifest as rounded foci of high T2 signal adjacent to the ventricles and appear similar to lesions of multiple sclerosis.

B1 deficiency results in selective damage to the mamillary bodies, dorsomedial thalamic nuclei, pulvinars, walls of the third ventricle, periaqueductal gray matter, colliculi, third cranial nerve nuclei, inferior olives and superior vermis, reflected as high T2 signal within them. Contrast enhancement of the mamillary bodies in Wernicke encephalopathy is pathognomic (Fig. 2b) and hemorrhage may occasionally be seen. Absence of imaging abnormalities does not exclude the diagnosis of Wernicke encephalopathy (3).

In Marchiafava–Bignami disease, the anterior corpus callosum shows low T1 signal and high T2 signal. Signal abnormalities may also be seen in the centra semiovalia.

Osmotic myelinolysis classically reveals high T2 signal in the central pons with sparing of the corticospinal tracts (Fig. 2c) (3).

References

1. O'Donnell P, Buxton PJ, Pitkin A et al (2000) The magnetic resonance imaging appearance of the brain in acute carbon monoxide poisoning. Clin Radiol 55:273–280
2. Aydin K, Sencer S, Demir T et al (2002) Cranial MR findings in chronic toluene abuse by inhalation. AJNR Am J Neuroradiol 23:1173–1179
3. Spampinato MV, Castillo M, Rojas R et al (2005) Magnetic resonance findings in substance abuse: Alcohol and alcoholism and syndromes associated with alcohol abuse. Top Magn Reson Imaging 16:223–230
4. Tuzun M, Tuzun D, Salan A et al (2002) Lead encephalopathy: CT and MR findings. J Comput Assist Tomogr 26:479–481
5. Korogi Y, Takahashi M, Okajima T et al (1998) MR findings of Minamata disease—organic mercury poisoning. J Magn Resonan Imaging 8:308–316

Toxic Encephalopathy

▶Toxic Disorders, Brain

Toxic Hepatitis

Toxic hepatitis consists in acute liver cell necrosis produced by chemical substances, which have a direct toxic effect on the liver. The most common hepatotoxins implicated in this disease are carbon tetrachloride, phosphorus, chloroform, gold compounds, fungal toxins. These substances are true hepatotoxins because they cause hepatic damage invariably in every individual. The onset is usually within 48 h and it is very similar to acute hepatitis. The symptoms are mainly represented by anorexia, nausea, vomiting, jaundice, and hepatomegaly. Obtaining a history of exposure to hepatotoxic agents is crucial for prognosis because the early removal of the hepatotoxin allows a rapid recovery, while the prognosis is poor if there is a prolonged period of exposure. The final stage of the disease is dominated by delirium, coma, and convulsions and within a few days the patient usually dies of fulminant hepatic failure. Only a few patients recover from acute toxic hepatitis and develop chronic liver disease which may be ultimately followed by postnecrotic cirrhosis.

▶Hepatitis

Toxoplasmosis

Toxoplasmosis is caused by infection with the obligate, intracellular parasite, Toxoplasma gondii.

▶Infection, Opportunistic, Brain

Tracer

A substance that follows or traces the path or behaviour of a substance that is being investigated.

▶PET in Drug Discovery Imaging

Tracheo-Oesophageal Fistula

A congenital abnormality in which there is an abnormal fistulous connection between the oesophagus and the trachea; it is most frequently associated with oesophageal atresia but may occur in isolation.

▶GI Tract, Pediatric, Congenital Malformations
▶Oesophageal Disease, Childhood

Tracheobronchial Lesions

Tracheobronchial lesions should be suspected in all patients with penetrating wounds of the neck or chest or with severe chest trauma indicating high kinetic

energies. Clinical signs are hemoptysis, pneumothorax, pneumomediastinum, subcutaneous emphysema, or an insufficient expansion of the lungs after drainage of a pneumothorax. More than 80% of tracheobronchial tears are located in the main bronchi lesser than 2.5 cm from the carina and predominantly on the right side. The "fallen lung sign" is indicative for main stem bronchial rupture, but incomplete bronchial rupture may be overlooked and definite diagnosis of airways lesions is usually made by endoscopy.

▶Chest Trauma

Tracheobronchitis

▶Bronchitis and Bronchiolitis in Childhood

Tracheobronchomalacia

▶Airway Disease

Tracheobronchomegaly

▶Airway Disease

TRAIL

▶FasL (CD95L), TRAIL or TNFa

TRAM

▶TRAM (Transverse Rectus Abdominis Musculocutaneous)

Tramline

Typical appearance of bronchiectasis on conventional radiographs caused parallel line opacities caused by ectatic bronchi and thickened bronchial walls.

▶Airway Disease

Transcatheter Arterial Chemoembolization (TACE), Hepatic Tumours

Radiological interventional technique largely employed for the treatment of hepatic tumours. It combines peripheral arterial occlusion and local deposition of chemotherapeutic agents by means of intra-hepatic arterial injection of chemotherapeutic and embolic agents.

▶Interventional Hepatic Procedures

Transcatheter Arterial Embolization (TAE), Hepatic Tumours

Radiological interventional technique consisting in a temporary or permanent peripheral occlusion of the hepatic artery.

▶Interventional Hepatic Procedures

Transcranial Doppler

Screening method of determining risk of stroke in children with sickle cell disease.

▶Sickle Cell Disease

Transducer

A piezoelectric crystal that can convert electrical voltage to a mechanical vibration and vice versa. It can thus be used both for transmitting and receiving acoustic waves.

▶Ultrasound Imaging

Transient Hepatic Attenuation Differences (THAD)

THAD is a CT finding consisting in transient areas of enhancement of liver parenchyma during arterial-phase imaging returning to normal on portal-vein phase. THAD

reflects a change in the normal dual blood supply of the liver characterized by a redistribution of the arterial flow to a hepatic segment or lobe, usually due to decreased portal or hepatic venous flow. THAD may be observed in liver cirrhosis, hepatic trauma, hepatic tumors, hereditary hemorrhagic telangiectasia, and after hepatic interventional procedures as a result of arterioportal shunts or focal obstruction of distal parenchymal portal venous flow. Peripheral, triangular, or wedge-shaped areas of arterial enhancement and nondisplaced internal vasculature can suggest the diagnosis.

▶Vascular Disorders, Hepatic

Transient Synovitis

Alan E. Oestreich
Cincinnati Children's Hospital Medical Center, Cincinnati, Ohio, USA
Alan.Oestreich@cchmc.org

Synonyms

Sterile effusion in one or more joints; Sterile inflammation of the hip

Definition

Abnormal fluid in the hip (or other joint) not due to infection, nearby tumor, foreign body penetration, juvenile idiopathic arthritis, or other known specific cause. The synovitis is usually self-limited, but occasionally it causes sufficient impairment of blood flow to the femoral head and neck to result in eventual Perthes disease.

A transient effusion without local sequelae in various joints may be a manifestation of such conditions as Lyme disease and some of the recurrent febrile genetic conditions.

Pathology/Histopathology

By definition, the synovial fluid of transient synovitis contains no microorganisms. The synovium may become thickened, however. As in Lyme disease, ▶tumor necrosis factor receptor-associated periodic syndrome (TRAPS) (1), and osteoid osteoma, increased sterile fluid is present, and some synovial thickening may occur.

Clinical Presentation

Transient synovitis of the hip is heralded by reluctance to bear weight and perhaps irritability and malaise. In common with septic arthritis and other cases of abnormal hip fluid, the ▶log-roll test is usually positive, yielding pain signs from rolling the upper leg like a log. Septic hip is more likely to have systemic signs of infection such as fever. Hip fluid from femoral neck osteoid osteoma (Fig. 1) tends to be associated with pain at night from the osteoma, which is relieved by pediatric aspirin.

The toddler with a limp is a concern because of the possibility of septic hip arthritis; the discovery of a toddler's fracture of the tibia or fibula or a stress fracture of a tarsal bone or metatarsal is reassuring by revealing a less dangerous cause than pus in the hip. Transient synovitis is also nonthreatening, except when excessive fluid impairs blood flow to the femoral head and neck, raising a danger of Perthes disease as a sequela. Do not forget that neuroblastoma, other abdominal malignancy, or abdominal tuberculosis may cause a limp by involving the psoas muscle. Leukemia and other bone diseases of

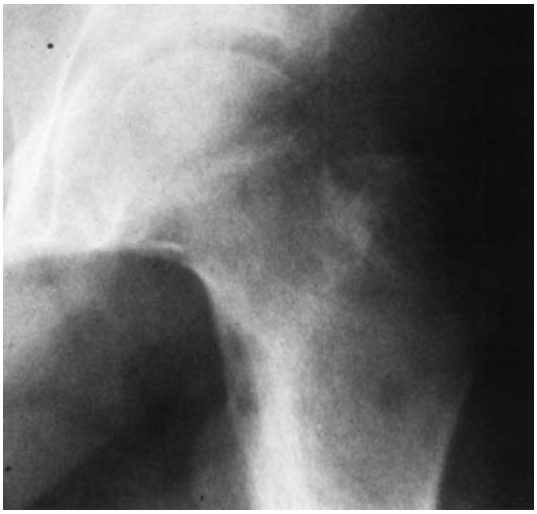

Transient Synovitis. Figure 1 Osteoid osteoma near the hip: medial lucent zone in the neck of the left femur with mild surrounding sclerosis in a 12-year-old boy with nocturnal pain. In this example, the osteoid osteoma may be sufficiently distant from the hip capsule not to cause associated synovitis. (From Oestreich AE, Crawford AH (1985) Atlas of Pediatric Orthopedic Radiology. Thieme Verlag, Stuttgart, p 95)

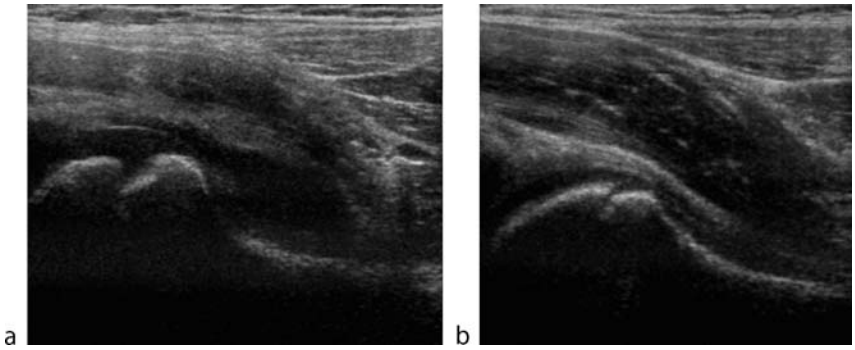

Transient Synovitis. Figure 2 Ultrasound images of excessive fluid in the hip of a 4-year-old with hip pain. (a) The capsule is bowed away from the anterior surface of the femur by relatively anechoic fluid on the anterior sagittal image. (b) Normal image for comparison.

the lower extremity are other causes to consider when a limp is present.

Fluid in the hip (and shoulder) is not directly palpable, whereas fluid at other sites, especially the knee, is easily palpated. In general, this distribution reflects plain radiography, in which fluid in the hip and shoulder are not directly detectable, while joint effusion is easily recognizable by interfaces with fat at the knee, ankle, and other sites.

Imaging

One cannot rule out hip fluid on plain radiographs. Generally, fluid collects, even in the supine child, anteriorly, out of the plane seen on plain hip images. Occasionally a large amount of fluid might be noted to displace an obturator fat stripe medially in the pelvis, however, and in a rare infant so much fluid is present that the femoral shaft (and head if ossified) is laterally displaced. The primary imaging modality for hip fluid is ultrasound, with the probe appropriately anterior (Fig. 2). Such images may show synovial thickening as well, but they cannot distinguish pus from sterile fluid or blood. Consult the writings of Simon Robben et al for details on such ultrasound (2). Hip fluid is easily detected on computed tomography (CT) or magnetic resonance imaging as well.

Nuclear Medicine

Transient synovitis is not likely to be hot on bone scan, whereas infection of the hip joint may well be. Effusion secondary to femoral neck osteoid osteoma should reveal the lesion as a localized highly positive uptake. If Perthes disease complicates transient synovitis, lack of uptake will then be present in part of the femoral head. Indeed, during the acute transient synovitis, bone scanning is valuable to document acute loss of vascularity of the femoral head and neck, implying a more urgent need to drain the fluid.

Diagnosis

Fluid in the hip is not recognizable on plain radiographs (unless it is so voluminous as to show displacement of the obturator fat stripe inward, or, in an infant, to displace the femur laterally). The imaging diagnosis of hip fluid is by anterior longitudinal ultrasound in which the anterior capsule is seen to bulge anteriorly as the joint fills with fluid. The distance between that capsule and the bone beneath is increased. Sterile fluid and pus are generally indistinguishable on hip ultrasound. In an older child, one may rarely be surprised to see small bodies within the hip from ▶synovial osteochondromatosis—many of these bodies are ossified, so they can be seen on plain images.

Interventional Radiological Treatment

The "interventional" diagnosis of sterile versus infected joint fluid may be done by needle techniques, under ultrasound, CT, or fluoroscopic guidance and documentation. Additionally, osteoid osteomas may be ablated by a variety of techniques under CT guidance, including radiofrequency ablation. Systems have been developed mechanically to guide the instrument more precisely to the nidus.

Bibliography

1. Trost S, Rosé CD (2005) Myocarditis and sacroiliitis: 2 previously unrecognized manifestations of tumor necrosis factor receptor associated periodic syndrome. J Rheumatol 32:175–177
2. Robben SG, Lequin MH et al (1999) Anterior joint capsule of the normal hip and in children with transient synovitis: US study with anatomic and histologic correlation. Radiology 210:499–507

Transient Tachypnoea of the Newborn

This is also referred to as retained foetal lung fluid. In this condition normal physiological clearance of lung fluid is prolonged.

▶Chest, Neonatal
▶Neonatal Chest

Transit Time Analysis

Hohmann Joachim
Universitätsspital Basel Institut für Radiologie, Basel, Switzerland
jhohmann@uhbs.ch

Definition

The term transit time analysis is not well defined and therefore it is used in different ways. In general it means the analysis of the time course of an injected contrast agent at one specific or at different locations, e.g., different vessels or organs. The most obvious and most often used definition is the measurement of arrival times of contrast agents and the calculation of time differences of these arrival times at two or more locations. One example is the hepatic transit time (HTT) measurement in patients with liver cirrhosis or with occult liver metastases with ultrasound contrast agents, which will be described in more detail later.

Transit time analysis is strongly coupled with the evaluation of time intensity curves (TICs, Figs. 1 and 2) and there are other definitions of "transit time analysis" which deal not only with the determination of arrival times but, e.g., with the evaluation of the shape of the TICs. One example and yet a standard clinical application, even it is not called transit time analysis by most authors, is the behavior of breast lesions in breast MRI after contrast injection. The rise of the incoming contrast agent and the wash out in a breast lesion is used as a characteristic feature which determines weather this lesion is stated as benign or malignant.

What is the Goal?

The basic idea behind transit time analysis is always the same: to get information about the blood supply or even better to get a value which describes the blood supply in the investigated area. The hypothesis is that different pathologies lead to different and possibly specific and reproducible changes in transit time. Therefore transit time analysis of any kind can be regarded as a functional imaging method in contrast to the more common morphological approach of standard clinical imaging applications. Promising targets are the liver, the kidneys including transplanted kidneys, the spleen, the heart, the breast, and the brain, just to mention the most frequently investigated regions.

The use of contrast agents for this kind of functional imaging, especially while using ultrasound contrast agents, is a relatively new technique and therefore all the results so far have a more or less experimental or research status and the methods usually are not integrated in clinical routine examinations. Nevertheless there are some situations in which the use of transit time analysis is already helpful in clinical practice, e.g., the mentioned method for breast MRI. Another example is the detection of cardiac right-to-left shunts (RLS) with the ultrasound contrast agent Echovist (Schering, Berlin, Germany), which indeed resembles the most elementary form of transit time analysis in which it is only necessary to detect the contrast agent arrival at all.

The use of ultrasound and ultrasound contrast agents for transit time analysis has some advantages over other imaging modalities especially while using it for HTT analysis. The main advantage is the superior time resolution due to high frame rates of up to 30–60 images/sec. In addition the liver is completely accessible *via* ultrasound examinations in most cases and the spatial resolution is very high (<1 mm).

Methods in Use

After a bolus injection of the contrast agent and a saline flush the signal intensities are recorded. The contrast agents which are already in use are Levovist (Schering, Berlin, Germany), SonoVue (Bracco, Milano, Italy), and Optison (Amersham, GE Healthcare), which are microbubble agents with different gases and different shells and therefore different pharmacodynamics and different resonance properties. The detection of these ultrasound contrast agents is done *via* special ultrasound techniques which are highly sensitive for the microbubbles. With Levovist-enhanced Doppler signals with a high mechanical index (MI) are in use, while phase inversion imaging with low MI and less bubble destruction is the standard for so-called "second generation" agents like SonoVue and Optison.

The simplest way to measure the arrival time is just to detect the contrast signal in a vessel of interest, e.g., the hepatic vein. In this case the transit time from the point of

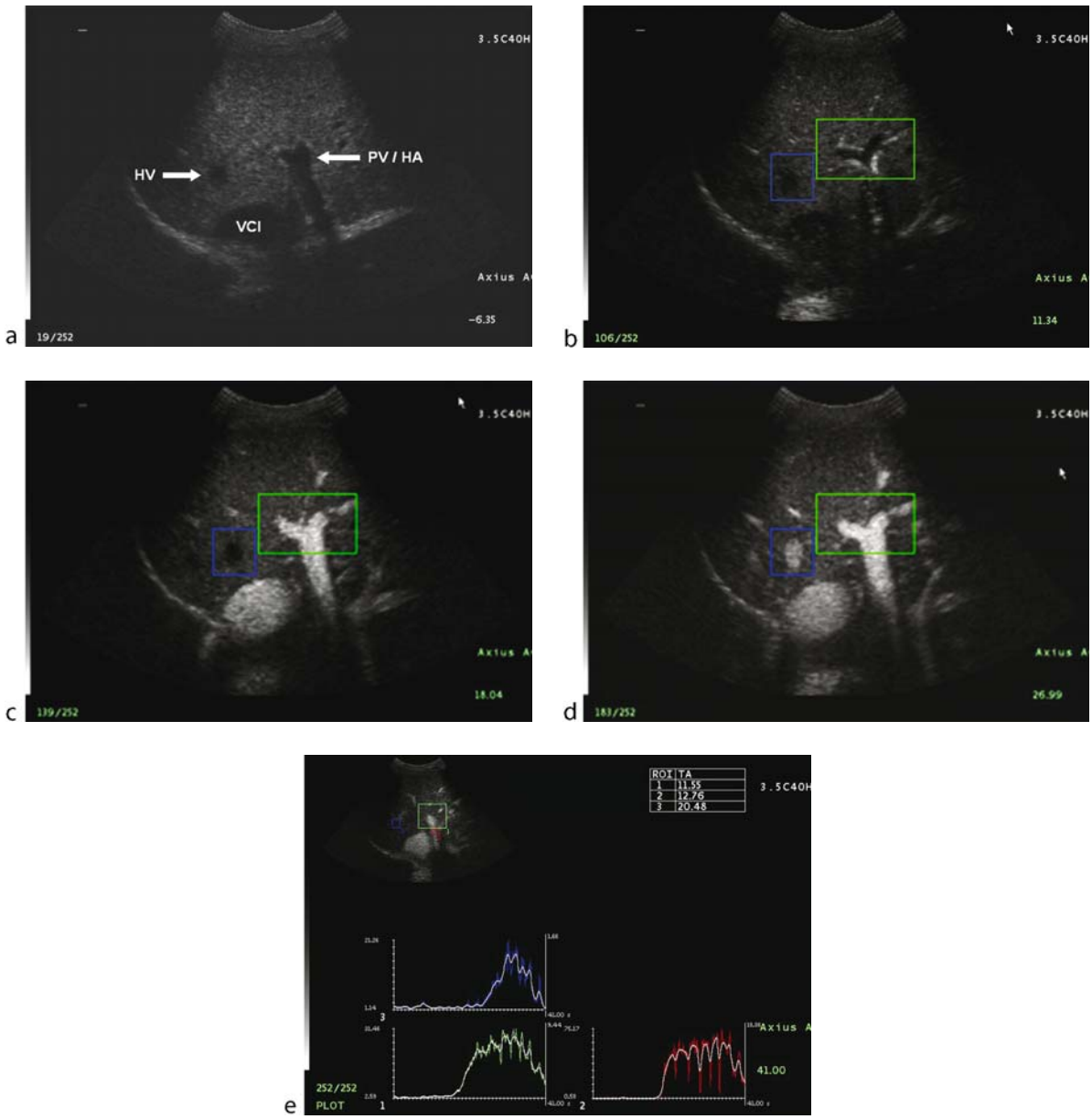

Transit Time Analysis. Figure 1 Transit time analysis of the hepatic vessels with contrast-enhanced ultrasound using low mechanical index phase inversion ultrasound on a Siemens Elegra ultrasound machine with SonoVue: (a) While using an appropriate plane in the porta hepatica the portal vein (PV), the hepatic artery (HA, which can not be seen on baseline, but is usually adjacent to the portal vein), and at least one hepatic vein (HV) can be accessed simultaneously. (b) The use of regions of interest (ROI, HA, HV) of the build-in time intensity curve (TIC) software enables the *ad hoc* analysis of the curve and, e.g., the determination of the different arrival times (TA). The export of the data as a spreadsheet is also an option (see Fig. 2). The image shows the hepatic artery *11.34* s p. i. with contrast-enhanced signal and yet well-defined from the portal vein. (c) *18.04* s p. i. also the portal vein and the inferior vena cava (VCI) show a contrast signal. The hepatic vein is still not enhanced. (d) In the later phase at *26.99* s p. i. all vessels show an enhancement. (e) Calculated TIC for the HA (ROI 1), the PV (ROI 2), and the HV (ROI 3). Motion dependent changes of the corresponding ROI are corrected and the curves are also smoothed (white lines) by the software. TA are automatically calculated and shown for each ROI.

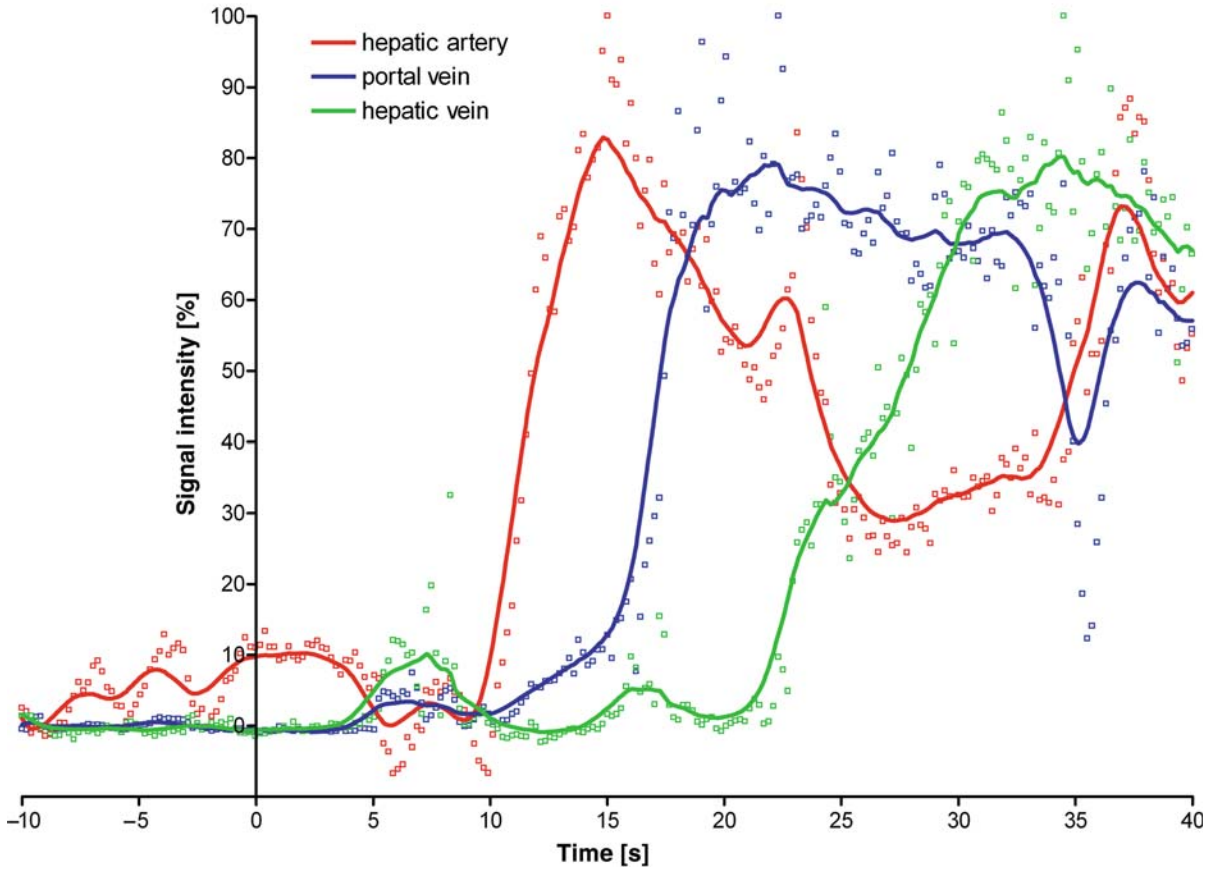

Transit Time Analysis. Figure 2 Time intensity curve from data which was exported as a spreadsheet and then analysed on a standard personal computer. Data was acquired over a time period of 50 sec with a 10 sec baseline (t = 0 sec is the time of injection) and a frame rate of 5/sec (δt = 0.2 sec), which results in 252 data points. The signal intensities are baseline corrected, normalized, and smoothed. When using the 10% threshold to define the arrival of the contrast agent the following arrival times (TA) are calculated: $TA_{hepatic\ artery}$ = 10.06 sec; $TA_{portal\ vein}$ = 14.21 sec; $TA_{hepatic\ vein}$ = 22.07 sec. Assuming the HTT as the difference of the arrival of the contrast agent in the hepatic vein and the hepatic artery results in an HTT of 12.01 sec.

injection, mainly one cubital vein, to the hepatic vein can be measured. There are some drawbacks to this approach, such as the influence of circulatory impairment, e.g., in heart failure. Another method is the detection of the arrival time of the incoming system of an organ, e.g., the hepatic artery and the portal vein, and the outgoing system, e.g., the hepatic vein, and to calculate the time differences. The second approach makes the measurement more independent and more targeted to the system of interest.

Quantification

The simplest way is just to look at the location(s) of interest and to detect the incoming contrast agent visually. This is called the "visual approach." Another way is a computer-based evaluation. Time intensity signals are recorded and the evaluation of the TICs is done right after the examination. Baseline and maximum values are calculated and a threshold value must be defined. The threshold value is the signal intensity at which the arrival of the given contrast agent seems to be sure. Most transit time analyses define the threshold as the point of signal intensity which is 10% above the baseline signal, while the baseline signal is defined as the signal intensity without a given contrast agent. The major problem is the breathing of the patients. While the time interval for one measurement in the liver is at least 50 sec, it is not possible to do it in apnea. Therefore the regions of interest (ROI) in which the signals are measured shifts due to the breathing motion. Motion correction, automatically or manually, is needed and the TICs have to be smoothed. This may lead to some more or less important errors. In

some cases other artifacts can occur, e.g., reflux of the contrast agent from the right atrium into the liver veins, which has to be taken into account and must be eliminated *via* the postprocessing procedures.

Equipment

Very important for the use of transit time analysis as a clinical routine application are the properties of the imaging equipment. Hence the focus of this essay is drawn to ultrasound measurements the focus of the equipment is consequently also drawn to ultrasound machines. First, there is the need of contrast agent specific software which allows special Doppler methods and/or phase inversion methods. Another point is an easy-to-use and fast quantification tool on the ultrasound machine itself. More and more manufacturers have such software packages in their portfolios which allow a realtime quantification of the achieved data. Despite the simple positioning of ROI a correction of the data due to artificial signal variations (see above) and the possibility of a manual correction at different time points are helpful. Nevertheless such tools are also in a more or less experimental status and up to now it seems to be safer to export the given data as a spreadsheet and to perform the evaluation with standard statistical software packages. With the more and more growing need for functional imaging in this specific area this must be changing.

Indication

As stated above, the status of transit time analysis is mainly experimental and therefore almost all indications are already research indications. The focus in ultrasound transit time analysis is drawn especially to the liver and the related HTT changes in patients with liver cirrhosis and occult liver metastases.

Liver Cirrhosis

The research done in the field of liver cirrhosis is dominated by the group of the Hammersmith Hospital, London, UK. It started in the late 90s and showed differences in the hepatic vein transit time (HVTT) due to the grade of liver cirrhosis. They measured the arrival time of an ultrasound contrast agent (Levovist) in the hepatic veins after injection in a cubital vein. Contrast-enhanced Doppler signals were recorded by an additional standard personal computer and arrival times (HVTT) were calculated *via* a MATLAB (The Mathworks, Massachusetts, USA) script. The results are promising and the latest publication showed a linear dependency of the arrival time from the grade of cirrhotic and precirrhotic liver disease in case of a single entity (hepatitis C virus, HCV) related disease (1). Other investigators did not get the same results while using standard Doppler methods without contrast agents. They found a large overlap in the Doppler measurements and findings between various disease stages. Therefore it seems safe to state that using a contrast agent improves the appraisal of the grade of liver cirrhosis and fibrosis. The special pharmacodynamics of Levovist, which has a proven liver-specific phase due to the incorporation of the Levovist particles in Kupffer cells seems to be helpful for the investigation of transit times in the hepatic blood supply. The difficulties with other contrast agents which have a "weaker" (e.g., SonoVue) or not at all a liver-specific phase is that the time differences of the arrival times tend to be shorter and therefore the individual variances seem to have a greater influence on the measurement, which may result in a greater overlap between normal and pathologic liver blood supply.

Occult Liver Metastases

As shown recently by the group of Leen using the standard Doppler methods blood supply properties of the liver seem to change due to the existence of occult liver metastasis. The group of Leen observed such changes in patients suffering from colorectal cancer (2). They found an increase of the arterial blood volume compared with the portal venous blood volume. This ratio was called the Doppler perfusion index (DPI) which was calculated as the ratio of hepatic artery to the sum of hepatic artery flow and portal venous flow. This is similar to the hepatic perfusion index (HPI) which was already investigated in the field of nuclear medicine for a long period. There are different possible underlying mechanisms concerning a humoral factor and/or some more or less mechanical properties. Kruskal et al showed in a remarkable study that the sinusoidal and postsinusoidal flow is significantly reduced prior to the occurrence of visible metastases probably due to an increased rolling and adherence of leukocytes (3). A further reduction was seen while the metastases are growing and an extrinsic compression of sinusoids and portal venules takes place. Unfortunately the promising results of Leen et al could not be reproduced by any other group. This may be due to the difficult examination technique which requires a really experienced examiner. Nevertheless in animal studies by Yarmenitis et al changes similar to the findings of Leen et al were found. Tumor bearing Wistar rats showed an increase of hepatic arterial blood flow and DPI 4 days after subcutaneous inoculation of a Walker 256 tumor (4). At this time only small groups of cells in the connective tissue were found in the *porta hepatica* and the portal triads with no apparent vascular association. Other attempts used contrast-enhanced US techniques which

showed comparable results (5). Significant increase of hepatic blood flow was shown in small groups of patients with known liver metastases, mostly of different underlying primary tumors. These results gives rise to the idea that while using contrast agents the method might be more stable and that this examination technique might be easier to perform. Nevertheless there are no studies which included a greater number of patients at risk for liver metastases and a follow up to prove these assumptions like Leen et al did.

It has to point out that the definite answer to the question of the existence of occult liver metastasis in patients with especially colorectal carcinoma, which is the second most common cause of death from cancer in Europe and North America (~15%), is of great clinical importance for the therapy and clinical outcome of such patients. A reliable and reproducible method of detecting such metastases would help to treat these patients on a selective basis and might help to decrease the death rate.

Contraindication*

Contraindications depend on the material of the shell and of the gas phase. For Levovist this means galactosemia and pregnancy. Contraindications for SonoVue are also pregnancy and lactation. In addition SonoVue should not be given in patients with a known acute coronary syndrome, an instable ischemic heart disease, a heart failure (NYHA III/IV), heart rhythm disturbances, shortly after invasive coronary interventions, pulmonary hypertension ($p > 90$ mmHg), RLS or an acute respiratory distress syndrome (ARDS). Optison should be avoided when patients having severe liver insufficiencies and in patients with known or suspected hypersensitivity to blood, blood products, or albumin.

Pregnancy/lactation*

During pregnancy and lactation, transit time analysis of any kind should be avoided due to the already mentioned experimental and research status of the method.

Use and Dosage*

For transit time analysis, the contrast agent has to be given as a fast bolus with a following saline flush of about 10 mL. The dosage depends on the used agent and is usually 2.4 mL for SonoVue, 2.0 mL for Optison, and about 2.5 g (e.g., 5 mL; 400 mg/mL) for Levovist.

* see also detailed product information

Adverse Reactions*

Ultrasound contrast agents are very safe and adverse reactions are rare. Some mild adverse reactions are known and some very rare serious anaphylactoid adverse reactions in patients with heart failure have been observed with SonoVue.

Interactions*

There are none known interactions so far for intravenous administration.

Bibliography

1. Lim AK, Taylor-Robinson SD, Patel N et al (2005) Hepatic vein transit times using a microbubble agent can predict disease severity non-invasively in patients with hepatitis C. Gut 54(1):128–133
2. Leen E, Goldberg JA, Angerson WJ et al (2000) Potential role of Doppler perfusion index in selection of patients with colorectal cancer for adjuvant chemotherapy. Lancet 355(9197):34–37
3. Kruskal JB, Thomas P, Kane RA et al (2004) Hepatic perfusion changes in mice livers with developing colorectal cancer metastases. Radiology 231(2):482–490
4. Yarmenitis SD, Kalogeropoulou CP, Hatjikondi O et al (2000) An experimental approach of the Doppler perfusion index of the liver in detecting occult hepatic metastases: histological findings related to the hemodynamic measurements in Wistar rats. Eur Radiol 10 (3):417–424
5. Bang N, Nielsen MB, Rasmussen AN et al (2001) Hepatic vein transit time of an ultrasound contrast agent: simplified procedure using pulse inversion imaging. Br J Radiol 74(884):752–755

Transitional Cell Carcinoma (TCC)

A type of cancer that develops in the lining of the bladder, ureter, or renal pelvis (the part of the kidney that collects, holds, and drains urine).

▶Neoplasms, Bladder
▶Urothelial Neoplasms, Kidney and Ureter

Transplant Kidney, Complications

Eric de Kerviler, Oliver Mathieu
Service de Radiologie, Hôpital Saint-Louis, Paris, France
eric.de-kerviler@sls.ap-hop-paris.fr

Synonyms

Complication of kidney graft

Definition

Kidney transplantation is the replacement of a failed kidney with a working kidney from a donor. Kidney transplantation programs are based on organ donation from cadavers and occasionally living donors. The donation rates are low and organ shortage is an essential issue. The standard placement of the transplanted kidney is extraperitoneal, in the right iliac fossa. For an optimal perfusion, the procedure involves two end-to-end anastomoses: the single renal artery from the donor to the recipient iliac artery, and the donor renal vein to the recipient external iliac vein. The best urinary drainage is made *via* a ureteroneocystostomy, which involves reconstruction of the urinary tract by passing the donor ureter through a tunnel carved through the dome of the posterior bladder wall. This tunnel serves as a deterrent to urinary reflux with bladder contraction.

Complications of kidney graft can be classified into two groups:

1. Surgery complications: anastomosis troubles (artery stenosis, vein thrombosis, and ureter stenosis), leak (hematoma, lymphocele, and urinoma), infection (abscess), and prolonged cold ischemia before surgery (tubular necrosis).
2. Immune complications: acute and chronic rejection and immunosuppression with higher risk of infections, neoplasms, and toxicity.

Pathology/Histopathology

Surgery Complications

Acute tubular necrosis depends on the duration of ischemia, with a higher frequency when cold ischemia lasts more than 24–30 h (1). It usually resolves spontaneously in the first 2 weeks after transplantation. Histological findings include dilatation of the tubules, loss of proximal epithelial cell brush border, and epithelial cell necrosis and apoptosis.

Immune Complications

Acute rejection has several grades: tubulointerstitial with tubulitis and interstitial infiltration, vascular with intimal arteritis, severe with transmural arteritis. Chronic rejection is characterized on biopsy by fibrous intimal thickening, interstitial fibrosis, and tubular atrophy (2), and is preceded by episodes of acute rejection. Cyclosporin and tacrolimus can be nephrotoxic, producing vascular constriction or interstitial fibrosis.

Clinical Presentation

Early Complications

Pain is generally caused by urinary tract obstruction, vascular thrombosis, and infection. However, urinoma can be painful without any obstruction. Acute pain is a major symptom in venous thrombosis, whereas arterial thrombosis may be asymptomatic.

Pyrexia is typically related to infections. However, fever can be seen with hematoma, venous thrombosis, and rarely acute rejection.

Acute tubular necrosis and acute rejection are characterized by an asymptomatic renal failure, making differential diagnosis troublesome.

Late Complications

Most late complication findings are limited to asymptomatic graft failure. They include chronic rejection, transplant artery stenosis, and drug toxicity. Transplant artery stenosis can be suspected when arterial hypertension becomes resistant to treatments or when ACE inhibitors induce acute renal failure.

Imaging

Doppler and Ultrasound

Ultrasonography (US) is the noninvasive method of choice for exploring transplant kidneys. It is ideally performed with a low-frequency probe (3–4 MHz) for the main vascular structures, the global morphology, and surrounding tissues of the kidney. A high-frequency probe (7–8 MHz) is useful for an accurate analysis of the intrarenal vessels. The US examination should include: measurements of the graft size and cortex thickness, evaluation of the parenchyma differentiation, and detection of caliceal dilatation or fluid collections.

Color Doppler helps to locate proximal and distal vessels of the transplant. Power Doppler detects perfusion defects in parenchyma. Because of the particular orientation of the vessels parallel to the probe at both poles of the transplant, the apparent perfusion defect should not be interpreted as infarcts.

Pulsed Doppler provides information on the peak systolic velocity in extrarenal arteries and the resistance index (RI) in intrarenal arteries. The superficial situation of the transplant makes the spectral analysis sensitive to the pressure applied by the transducer. Velocity measurements are particularly useful at the level of anastomoses, and care should be exercised in correcting the angle between the vessel and ultrasound directions. Maximal velocities in the main artery should be slower than 120 cm/s. The RI should be between 0.6 and 0.8.

MRI

Magnetic resonance imaging (MRI) is the second choice, when ultrasound findings are not fully convincing.

Contrast-enhanced 3D fast gradient echo sequences used for MR angiography offer multiplanar capabilities, including maximum intensity projection (MIP) and multiplanar reformatting (MPR). T1-weighted sequences are used for the parenchyma study.

Heavily T2-weighted 2D or 3D MR urography sequences before contrast administration help to detect ureteral pathology and peritransplant fluid collections (3)

CT

Computed tomography (CT) is of limited use due to the nephrotoxicity of the iodinated contrast agents.

CT without injection is sometimes sufficient to appreciate peritransplant fluid collections and hematomas. CT is typically used to guide interventional procedures (biopsy, fluid aspiration, drainage, nephrostomy).

Pyeloureterocystography

Pyeloureterocystography (through percutaneous nephrostomy catheter) is usually performed in cases of obstruction or urinoma, to detect ureteral stenosis or urinary leakage. Retrograde cystography is performed when reflux is suspected.

Arteriography

This invasive procedure is reserved as a therapeutic option in the case of arterial stenosis, arteriovenous fistula, or aneurysm.

Diagnosis

Early Complications

Vascular

Arterial thrombosis: Color Doppler detects absence of blood flow in the graft. Power Doppler with a high-frequency transducer shows no flow in the cortex. Sometimes, a spectral waveform can still be observed in arteries with absent diastolic flow and reduced amplitude. Thrombus can be observed in the main vein as a consequence of arterial thrombosis. The main differential diagnosis is hyperacute rejection where no flow is detectable. In equivocal cases, the diagnosis may be confirmed by MR angiography (Fig. 1).

Venous thrombosis: It must be evoked in the case of acute pain and abrupt cessation of renal function.

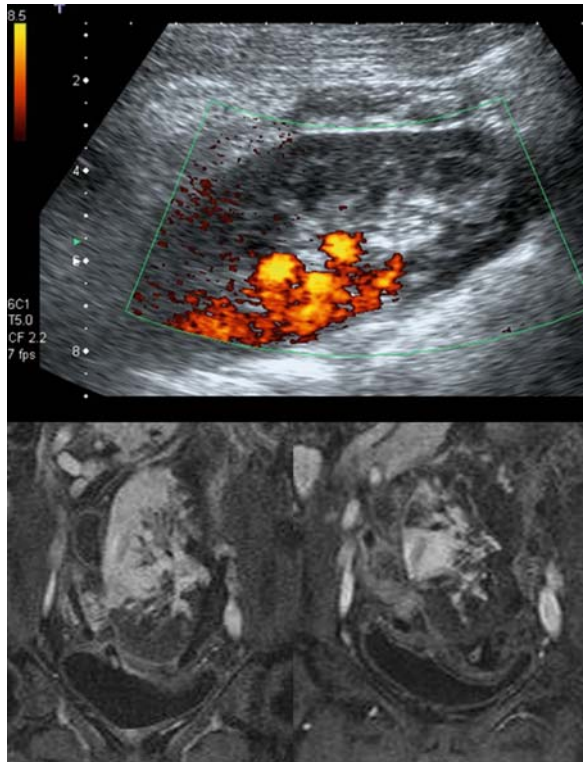

Transplant Kidney, Complications. Figure 1 Renal artery thrombosis with infarction. (a) Power Doppler color shows absence of flow in the lower pole of the graft. (b) Coronal contrast-enhanced–fat-suppressed T1-weighted MR images confirm infarction of the lower pole of the graft, probably due to segmental artery thrombosis.

Diagnostic criteria on US are associated with no detectable venous flow on color Doppler with reversed and prolonged diastolic flow in intrarenal arterial vessels on pulsed Doppler. Reversal diastolic flow alone is nonspecific and can be seen in acute tubular necrosis and severe rejection. Direct visualization of acute thrombus is often difficult. Nonspecific signs also include raft swelling and hypoechogenicity, sometimes associated with infarction when diagnosis is delayed. Thrombectomy should be performed in an emergency.

Pseudoaneurysms: US shows a lesion like a simple or complex cyst, with swirling flow on color Doppler, sometimes with thrombus. The pseudoaneurysm neck can be seen to contain alternating jets of forward and reverse flow.

Acute rejection: Asymptomatic, acute rejection is usually diagnosed at biopsy, but may be suggested by color Doppler in the case of edematous and thickened cortex as well as loss of corticomedullary differentiation associated with an RI higher than 0.9. Reversed diastolic

flow has been described in some cases (1); however, it is less marked than in venous thrombosis.

Acute tubular necrosis: The diagnosis is suspected in the case of prolonged ischemia, delayed function recovery, and normal Doppler. However, loss of corticomedullary differentiation and/or increased RI can be seen. The differential diagnosis with acute rejection or drug toxicity is usually made at biopsy.

Urinary Tract Obstruction

Dilatation of the collecting system may be obstructive or nonobstructive, and is best seen with US. Mild dilatation is observed commonly very early, due to postoperative edema at the ureteroneocystostomy site.

Obstruction may be due to extrinsic processes (e.g., peritransplant fluid collection) or to ureteral stenosis. MR urography, and pyeloureterocystography in the case of nephrostomy, shows the localization and the degree of stenosis. MR urography is able to demonstrate a parietal thickening of the ureter in cases of ischemic stenosis (Fig. 2).

Collections

Hematomas are extrarenal or subcapsular in location, usually self-limiting, sometimes obstructing when large. The US pattern varies over time: echogenic in the acute phase, hypo- or anechogenic later. High attenuation of acute hematoma on CT decreases over time. The MRI signal is heterogeneous.

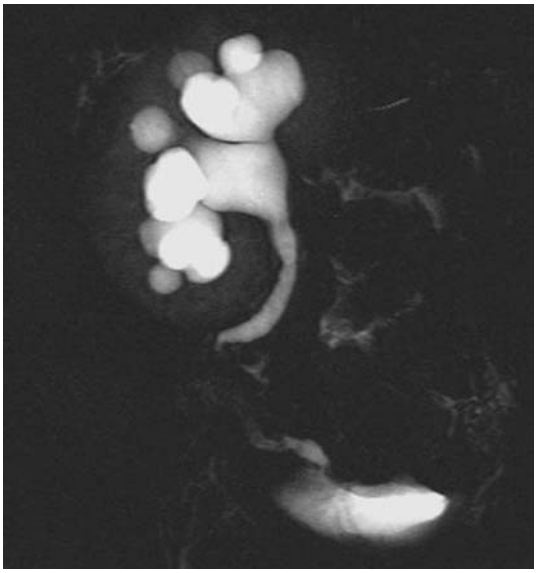

Transplant Kidney, Complications. Figure 2 Ureteral stenosis. Coronal T2-weighted MR urography shows extended ureteral stenosis with collecting system dilation.

Urinomas usually develop at the lower pole of the graft, with the extraperitoneal location being more frequent than the intraperitoneal one. Internal septations may be seen, but less often than in lymphocele. Pyelography and CT with opacification by percutaneous nephrostomy are the examinations of choice, showing the fistula and the collection.

Lymphoceles appear as septated fluid collections with low-level echoes, usually inferior and medial in location to the graft.

Perirenal abscess can occur on a preexisting peritransplant fluid collection or most rarely de novo. They appear most often on CT as a heterogeneous collection, occasionally with gas. Diagnosis and treatment require imaging-guided aspiration and drainage.

Later Complications

Artery stenosis is often detected with Doppler US, and further confirmed with MR angiography. Color Doppler shows an area of aliasing on a stenotic segment, usually at or close to the surgical anastomosis. Doppler spectrum demonstrates focal elevated peak systolic velocity, greater than 2 m/s. A decreased intrarenal RI is variably present, but adds confidence to the diagnosis (Fig. 3). The diagnosis can be difficult in the case of tortuous renal transplant artery, which may cause increased peak systolic velocity and focal aliasing in color Doppler (2). MR angiography allows a better visualization of the transplant arteries than US, thanks to its multiplanar reformatting. It shows the localization and the severity of the stenosis preoperatively.

Arteriovenous fistula is not linked to surgery but to transplant biopsy which is performed in equivocal cases. This complication can be recognized with color and pulsed Doppler, showing an area of aliasing artifact on color Doppler because of high velocities in the fistula, with low-resistance flow in the supplying artery on pulsed Doppler and arterialization in the draining vein (1).

Chronic rejection can be suggested by US, showing a small graft, thin cortex with increased echogenicity, mild hydronephrosis, and disrupted corticomedullary differentiation. Color Doppler can demonstrate a reduction in the number of intrarenal vessels with increased RI. Impaired renal function, associated with these findings, suggests the diagnosis, which is then confirmed at biopsy.

Infection: Asymptomatic bacteriuria is common. Pyelonephritis is also common and ultrasound is used to exclude obstruction or complications such as abscess. MR or CT parenchymography can show focal parenchymal defects and peritransplant infiltration suggesting the diagnosis.

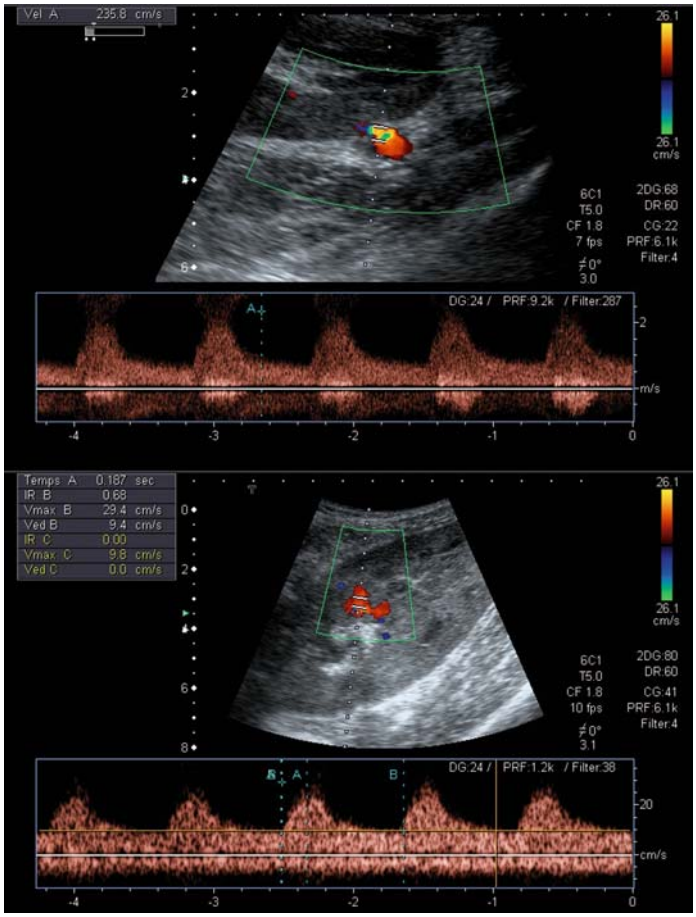

Transplant Kidney, Complications. Figure 3 Renal artery stenosis. (a) Pulsed-wave color Doppler US image shows high velocity at the stenotic segment (2.36 m/s) in the region of the anastomosis. Note focal aliasing on Color Doppler at the stenotic segment. (b) Intrarenal spectral Doppler shows low-resistance waveform.

Neoplasms: Lymphoma and renal cell carcinoma are the two most common graft malignancies. Imaging findings of lymphoma are nonspecific; however, it appears classically as a hypovascular and infiltrative mass, with a predilection for the hilum (4). Renal cell carcinoma appears as a heterogeneous mass, with loss of the graft shape. Nevertheless, percutaneous biopsy has to be performed in all cases of solid mass; renal cell carcinoma requires transplant nephrectomy, lymphoma does not.

References

1. Brown ED, Chen MY, Wolfman NT et al (2000) Complications of renal transplantation: evaluation with US and radionuclide imaging. Radiographics 20:607–622
2. Baxter GM (2003) Imaging in renal transplantation. Ultrasound Q 19:123–138.
3. Schubert RA, Gockeritz S, Mentzel HJ et al (2000) Imaging in ureteral complications of renal transplantation: value of static fluid MR urography. Eur Radiol 10:1152–1157
4. Vrachliotis TG, Vaswani KK, Davies EA et al (2000) CT findings in posttransplantation lymphoproliferative disorder of renal transplants. AJR Am J Roentgenol 175:183–188

Transplantation, Liver

Davide Caramella, Marzio Perri
Department of Diagnostic and Interventional Radiology, University of Pisa, Pisa, Italy
caramella@do.med.unipi.it

Synonyms

Hepatic transplantation; Liver allografting; Liver replacement; Living donor liver transplant; Living related liver

transplant; LT; OLT; Orthotopic liver transplantation; Split-liver transplant

Definition

Liver transplantation is a lifesaving therapeutic intervention for patients with severe acute or chronic liver failure for whom no other therapy is available.

Chronic viral hepatitis, alcoholic liver disease, metabolic diseases (alpha-1-antitrypsin deficiency, hemochromatosis, Wilson's disease), cholestatic liver disorders (primary biliary cirrhosis, primary sclerosing cholangitis, biliary atresia), and acute hepatic necrosis represent the most frequent indications for liver transplantation.

Patients with hepatocellular carcinoma (HCC), cholangiocarcinoma, or inoperable neuroendocrine metastases are also potential candidates for liver transplantation. Increasing evidence suggests that with careful patient selection, liver transplantation is the treatment of choice in patients with small HCCs.

On the contrary, liver transplantation is absolutely contraindicated in the presence of acquired immunodeficiency syndrome, extrahepatic malignant tumors, and active intravenous drug use or alcohol abuse (1).

A variety of transplant techniques have been employed. ►Orthotopic liver transplantation (OLT) is the most commonly used procedure and consists in the replacement of the diseased liver by a liver from a cadaveric donor. The standard technique of OLT requires grafting of one arterial anastomosis (hepatic artery), two venous anastomoses (portal vein and inferior caval vein), and a biliary anastomosis (duct-to-duct or hepaticojejunostomy).

Because of the shortage of cadaveric organs, alternative techniques such as ►split-liver donation (in which one donor organ is used for two recipients) and ►living donor liver transplantation (where the donor undergoes partial hepatectomy for donation to a recipient) have been developed.

Characteristics

Pretransplant Imaging

The role of imaging in the pretransplant assessment is to target patients suitable for liver transplantation and to identify anatomic abnormalities or variants that may impact surgical planning.

The pretransplant imaging evaluation includes an accurate exploration of both liver parenchyma and vascular structures (1, 2). Assessment of the arterial and venous hepatic anatomy is of utmost importance in candidates for liver transplantation in order to detect vascular variants or abnormalities and mismatches in donor and recipient vascular size.

Arterial abnormalities require identification before liver transplantation: several arterial anatomic variants may alter the surgical approach and stenotic celiac artery lesions must be alleviated to avoid biliary complications, as hepatic arterial inflow represents the sole blood supply to the posttransplantation bile ducts.

Many patients who are candidates for liver transplantation are cirrhotic and it is very important to have an overview of the portal system of these patients, who are likely to have portal hypertension: the demonstration of portal vein patency and identification of varices are mandatory before liver transplantation. Caval abnormalities must also be excluded.

An evaluation of the liver parenchyma is required for the detection of primary and secondary hepatic malignancies. Additional care is needed in patients affected by HCC and since liver transplantation seems to be the best therapeutic option in patients with single HCC smaller than 5 cm or in patients with less than three HCCs smaller than 3 cm, an accurate radiological staging is utmost important in defining the number and tumor size and in the identification of negative prognostic factors such as vascular invasion, nodal involvement, and extrahepatic metastases.

Ultrasound

Pretransplantation ultrasound (US) evaluation involves Doppler examination of the portal and hepatic veins and real-time B-mode imaging of hepatic parenchyma and bile ducts (1, 2).

US investigation is widely employed for the screening of HCC in cirrhotic patients waiting for liver transplantation. The recent advantages in US technology, including the availability of US contrast agents and the development of nonlinear specific contrast imaging methods, have further improved the sensitivity and specificity of US imaging in the diagnosis of focal liver lesions.

Moreover, Doppler US allows the investigation of flow dynamics through the hepatic veins, the portal vein and its branches, and the intra- and extrahepatic parts of the hepatic artery, representing a sensitive tool for the detection of portal vein thrombosis as well as of arterial abnormalities. It also enables an accurate evaluation of the localization and flow of varices and portosystemic shunt.

Finally, US evaluation offers a complete survey of the abdomen including the demonstration of splenomegaly and ascites.

Computed Tomography

Abdominal spiral computed tomography (CT) is a highly accurate method for the evaluation of the hepatic vessels and liver parenchyma alike.

In particular, three-phase multidetector CT angiography, by means of a double-arterial phase followed by a portal-vein dominant phase, provides a comprehensive depiction of the hepatic arterial and venous anatomy as well as an accurate evaluation of liver parenchyma.

Multidetector row scanners are particularly useful for angiographic applications and several studies show that, in transplantation candidates, multidetector row CT angiography is as accurate as conventional angiography in the evaluation of the hepatic artery anatomy and in the detection of arterial abnormalities such as severe ▶celiac artery stenosis and ▶splenic or ▶*hepatic artery aneurysm* that may lead to liver transplantation (2). CT has the well-known advantage of being safer, more convenient, and more easily tolerated.

Moreover, multiphase enhanced CT provides an accurate evaluation of the liver parenchyma, representing a useful tool in the detection of intrahepatic or extrahepatic malignancies, and in particular it plays a crucial role in the diagnosis and preoperative staging of HCC.

Finally, spiral CT allows a precise evaluation of splenic, superior mesenteric, and portal veins and is useful in the assessment of complications due to portal hypertension such as presence of retroperitoneal, splenorenal, gastroesophageal, or paraumbilical varices and splenomegaly and ascites.

Magnetic Resonance Imaging

Thanks to the recent implementation of new magnetic resonance (MR) technologies, MR imaging of the liver has became a reliable tool for the evaluation of the parenchyma, vascular structures, and biliary anatomy, allowing a complete pretransplantation assessment by using just one imaging modality.

With respect to spiral CT, MR imaging (a) offers the possibility of improved liver parenchyma evaluation in patients with cirrhosis and HCC by the use of hepatocyte- and RES-specific contrast agents, (b) eliminates exposure to ionizing radiation, and (c) uses intravascular–interstitial contrast materials with favorable safety profiles compared with iodinated contrast materials.

Moreover, the availability of MR angiographic techniques allows identification of hepatic artery variants or abnormalities and an accurate evaluation of the portal vein in terms of patency and flow direction.

Finally, using heavily T2-weighted pulse sequences, MR cholangiography offers a high-resolution imaging of the biliary tree, obviating the need for invasive cholangiography in patients affected by cholestatic liver disorders (1, 3).

Invasive Techniques

A variety of invasive imaging techniques such as angiography, cholangiography, and percutaneous or transjugular biopsy have been used in the preoperative evaluation for liver transplantation. However, since the rapid improvements in noninvasive vascular and biliary imaging, particularly in CT or MR angiography and MR cholangiography, the need for pretransplantation catheter angiography and cholangiography has been drastically diminished. Therefore, preoperative angiographic evaluation of arterial and venous liver structures as well as cholangiographic pretransplant examination are rarely necessary and are reserved for a small number of cases in which imaging evaluation is inconclusive (1).

In patients with cirrhosis and HCC, percutaneous biopsy US or CT-guided confirmation should be limited to cases that do not meet current noninvasive diagnostic criteria, in view of the risk of tumor dissemination.

A transjugular approach to reach the liver parenchyma is safe and useful in patients requiring liver biopsy to establish the extent of underlying cirrhosis in nonneoplastic disease.

Posttransplant Imaging

At present, there is a great demand for accurate evaluation of complications occurring after liver transplantation as early diagnosis is critical for graft salvage. Because the clinical presentation of several posttransplantation complications is frequently nonspecific and varies widely, imaging studies are critical for early diagnosis and are required in particular when vascular, biliary, or surgical injuries are suspected (1, 3, 4).

US is the initial imaging technique used for the detection of complications in the early postoperative phase, since it can be performed at the bedside and allows an accurate evaluation of the hepatic parenchyma, vascular anatomy, and bile ducts. In cases where US findings are uncertain or clinical suspicion of a complication persists despite normal US images, spiral CT or MR imaging should be performed. CT and MR, thanks to the recent technical improvements, are both effective methods for a comprehensive assessment of vascular, biliary, parenchymal, and extrahepatic structures in most recipients of liver transplantation, while hepatobiliary scintigraphy (^{99m}Tc-HIDA scintigraphy) is useful in assessing biliary complications.

Finally, invasive imaging methods, such as cholangiography and angiography, can be performed in selected patients to confirm US and CT or MR findings or when the noninvasive imaging evaluation is inconclusive (1).

Arterial Complications

Arterial complications include hepatic artery thrombosis, hepatic artery stenosis, and hepatic artery pseudoaneurysms. Hepatic artery thrombosis is estimated to occur in

6% of patients and is the most frequent cause of graft loss. Graft ischemia causes biliary leaks and strictures as well as hepatic infarction requiring immediate retransplantation. Hepatic artery stenosis is reported in about 5% of cases and generally occurs at the anastomotic site within 3 months of transplantation. If left untreated, it can lead to arterial thrombosis or progress to cause liver ischemia with hepatic insufficiency, biliary strictures, sepsis, and graft loss. Finally, hepatic artery pseudoaneurysm is an uncommon complication of liver transplantation and it represents a rare cause of hematobilia, hemoperitoneum, and gastrointestinal bleeding that may be life threatening. Doppler US is the primary screening technique for detection of these complications. Absence of Doppler flow signal and increase in peak systolic velocity are indicative, respectively, of hepatic artery thrombosis and stenosis (1). However, Doppler US evaluation of arterial abnormalities is associated with a significant frequency of false-negative results and in several cases further investigations are required. In particular, CT and MR angiography are widely used to confirm the Doppler US findings or when the US study is suboptimal (3, 4). However, despite several studies showing that both CT angiography and MR angiography are as accurate as angiography in the evaluation of arterial posttransplantation complications, catheter angiography is often used to achieve the final diagnosis.

Portal and Caval Vein Complications

Portal vein complications following liver transplantation are relatively unusual and occur in 1–3% of cases. The clinical presentation of portal vein stenosis or thrombosis includes symptoms of portal hypertension, liver failure, massive ascites, or edema and it is readily identified on noninvasive studies including US, CT, and MR imaging.

A thrombus in the portal vein is seen on B-mode US imaging as echogenic intraluminal material, and CT or MR angiography provides an excellent visualization of filling defects within the portal vein.

The demonstration of turbulent flow within the portal vein at Doppler US examination allows a presumptive diagnosis of portal vein stenosis requiring CT or MR angiography confirmation (1, 3, 4).

The prevalence of inferior caval vein complications, such as stenosis or thrombosis, is less than 1%.

US and CT examinations may show pleural effusions, ascites, and hepatosplenomegaly and Doppler examination of hepatic veins may demonstrate flow reversal and absence of periodicity in the hepatic venous waveform. A definitive diagnosis, however, is based on cavography and pressure gradient measurement (1).

Biliary Complications

Biliary complications after transplantation include obstruction, stricture, stone formation, and leak. Obstruction occurs more frequently than other complications in both adult and pediatric patients and is most often secondary to an anastomotic stricture that results in dilatation of the donor bile duct.

Bile leak is caused by technical failure at the T-tube site or at the duct–duct anastomosis and by hepatic artery thrombosis at a nonanastomotic site.

Cholangiography is the mainstay for diagnosing liver in biliary complications. US and CT are useful for demonstrating secondary findings such as biloma and bile duct dilatation, but these are not sensitive for the detection of early bile duct abnormalities. MR cholangiography is a noninvasive alternative to cholangiography and represents the most important imaging technique for biliary evaluation in patients who do not have a T-tube in place (1, 3).

Finally, ^{99m}Tc-HIDA scintigraphy is also useful for detecting bile leaks and obstructions in liver transplant recipients. Extravasated bile may appear as diffuse activity within the peritoneal cavity (subhepatic–suprahepatic space, paracolic gutter, or into surgical drains) and the extension of leaks is often better identified on delayed images.

Both in complete extrahepatic biliary obstruction and in severe intrahepatic cholestasis, ^{99m}Tc-HIDA scintigraphy typically shows normal hepatocellular uptake and persistent parenchymal activity without any excretion. When the obstruction is partial and progresses slowly, the scan shows more activity in the dilated portion of the biliary tree proximal to the obstruction with minimal or absent radioactivity in the distal common duct and in the intestinal lumen. On the contrary, the demonstration of bowel activity on the delayed images without biliary visualization is suggestive of intrahepatic cholestasis.

However, in the presence of elevated bilirubin levels, scintigraphy may have limited value and T-tube cholangiography appears more effective for the evaluation of biliary tract complications.

Rejection

Acute rejection is cell mediated and is characterized by lymphocyte infiltration. It is common in the early postoperative period and can be managed with immunosuppression therapies. Since the radiological and scintigraphic findings are nonspecific, including an increased hepatic artery resistance on Doppler US, periportal parenchymal changes on CT, and reduced uptake of the radionuclide on ^{99m}Tc-HIDA scintigraphy, the diagnosis is made on histological grounds.

Chronic rejection is characterized histologically by arteriolar occlusive lesions and obliteration of bile ducts.

It does not respond to immunosuppression therapies and retransplantation is the long-term treatment.

Surgical Complications

There is a risk of abdominal complications associated with major abdominal surgery in liver transplant recipients (1). Fluid collections and hematomas are frequent in the areas of vascular and biliary anastomosis as well as in the lesser sac, surrounding the ligament teres, and in the peri- and subhepatic spaces and they are readily recognized on US and CT examinations. Fluid collections usually resolve over several weeks.

Other rare abdominal complications of liver transplantation include adrenal hemorrhage and acute pancreatitis.

Interventional Treatment

A wide spectrum of image-guided interventional procedures can be performed in the pre- and posttransplant setting. In patients with cirrhosis and HCC, transarterial chemoembolization or radiofrequency thermal ablation can be used as a bridge to liver transplantation to prevent tumor progression while patients are on the waiting list.

Transjugular intrahepatic portosystemic shunt (TIPSS) is very useful for the control of portal hypertension complications including acute variceal bleeding and massive ascites refractory to endoscopic or medical therapy.

Despite the advances in surgical techniques and the improvement of medical treatments, complications following liver transplantation are still a significant cause of graft loss and patient mortality.

Interventional radiological procedures, including percutaneous transluminal angioplasty or stenting, endovascular coil embolization, percutaneous bilioplasty or stenting, and percutaneous drainage are effective therapeutic options for vascular and biliary posttransplant complications obviating the need for further surgical intervention or retransplantation (5).

In particular, percutaneous balloon angioplasty and stenting have been widely employed in the treatment of both arterial and venous stenosis. Hepatic artery stenosis can be treated by percutaneous balloon angioplasty with an 80–100% technical success rate. Restenosis occurs in 30–60% of cases, and stenting has recently been proposed to increase long-term patency. Angioplasties and stenting are also effective in the treatment of venous stenosis by means of a transjugular or a percutaneous intrahepatic approach, with a reported success rate of 60–100%.

Arterial and venous thrombosis may benefit by local infusional fibrinolysis after selective catheterization of the affected vessel. Endovascular coil embolization may be performed for the treatment of unusual vascular complications that occur after liver transplantation, such as bleeding injuries and arteriovenous fistulas.

Interventional radiology is also an effective therapeutic alternative for the treatment of most biliary strictures complicating OLT. Management of biliary strictures is largely influenced by their nature and extension: anastomotic strictures are suitable for a percutaneous approach with a high success rate. On the contrary, percutaneous management of more complex hilar and intrahepatic strictures is less successful, and surgical revision or retransplantation may be necessary for definitive treatment.

Finally, bile leaks and fluid collections can be treated by means of percutaneous drainage.

In conclusion, interventional procedures constitute a minimally invasive and effective approach in the management of complications after liver transplantation, and these are also suitable for critical patients. Successful treatment of posttransplant complications, however, requires careful diagnostic assessment and optimized techniques.

References

1. Leung DA, Pfammatter T, Marincek B (1999) Diagnostic imaging in liver transplantation. In: Bartolozzi C, Lencioni R (eds) Liver Malignancies. Springer, Berlin Heidelberg, pp 423–442
2. Pannu HK, Maley WR, Fishman EK (2001) Liver transplantation: preoperative CT evaluation. Radiographics 21:133–146
3. Pandharipande PV, Lee VS, Morgan GR et al (2001) Vascular and extravascular complications of liver transplantation: comprehensive evaluation with three dimensional contrast-enhanced volumetric MR imaging and cholangiopancreatography. AJR 177(5):1101–1107
4. Quiroga S, Sebastià MC, Margarit C et al (2001)Complications of orthotopic liver transplantation: spectrum of findings with helical CT. Radiographics 211085–1102
5. Vignali C, Cioni R, Petruzzi P et al (2004). Role of interventional radiology in the management of vascular complications after liver transplantation. Transplant Proc 36(3):552–554

Transplantation, Pancreas

Carlo Bartolozzi, Carla Cappelli, Riccardo Lencioni
Department of Diagnostic and International Radiology, University of Pisa, Pisa, Italy
bartolozzi@med.unipi.it
lencioni@med.unipi.it

Definition

The first pancreas transplantation was performed in 1966 by Kelly et al at the University of Minnesota

in Minneapolis. To date over 1,000 transplants have been performed at the same university and over 15,000 worldwide, as recorded by the International Pancreas Transplant Registry (IPTR). Despite its invasiveness, pancreas transplantation is currently the only therapy capable of determining a complete recovery in patients with type I diabetes mellitus. Advances in more potent immunosuppressive therapy, improvement in surgical techniques, and postoperative imaging evaluation have allowed pancreas transplantation to become a successful procedure of choice.

Transplantation enables a total restoration of endogenous secretion of insulin as well as regression or stabilization of the degenerative complications of diabetes. In patients presenting chronic renal failure, pancreas transplantation combined with kidney transplantation is the most appropriate therapeutic option. The combined kidney–pancreas transplantation can be performed simultaneously with a kidney from the same cadaveric organ donor (simultaneous pancreas–kidney transplantation or SPK) or from a living donor (simultaneous pancreas-living kidney transplantation or SPLK); in some cases pancreas is transplanted after previous kidney transplant (pancreas after kidney transplantation or PAK). Solitary pancreas transplantation (pancreas transplantation alone or PTA) is reserved for patients without clinically significant nephropathy in the presence of other complications of diabetes (retinopathy, neuropathy, vasculopathy). An alternative new therapy that also may improve diabetes is ►islet transplantation; however that procedure is still experimental and not yet as efficient as pancreas transplantation.

Pancreas transplant results are reported to the Scientific Registry of the United Network for Organ Sharing (UNOS) and the IPTR. Based on this information, the national 1-year patient, kidney, and pancreas survival rates for recipients of an SPK transplant are 95%, 89%, and 85%, respectively. Compared to diabetic recipients of a kidney alone, the addition of a pancreas improves long-term patient and kidney graft survival. Recipients of a pancreas-after-kidney or a pancreas transplant alone have an average 1-year pancreas graft survival rate of about 70–75%.

Characteristics

Surgical Technique

Pancreas transplantation consists of the implantation of the entire gland together with a segment of the duodenum, which is used to drain the exocrine pancreatic secretion. The main technical variants relate to the type of exocrine secretion drainage (duodenocystostomy or duodenoenterostomy) and venous drainage (systemic or portal). The pancreas is removed together with the duodenum, the liver, and the spleen and separated from the liver by detaching the splenic artery from the celiac tripod and the superior mesenteric artery from the aorta and by resecting the gastroduodenal artery, the main bile duct, and the portal vein above the pancreas head. Splenectomy concludes the preparation of the pancreas, with the resection of the superior mesenteric artery, immediately distal to the origin of the inferior pancreaticoduodenal artery and the superior mesenteric vein (distally to the uncinate process of the pancreas). An arterial Y-graft is then fashioned for the simultaneous revascularization of the superior mesenteric and splenic arteries; in most cases an iliac Y-graft is taken from the same donor. When the liver is not transplantable, an aortic patch comprising the origin of the two arteries can be used.

The pancreas is placed intraperitoneally in the right iliac fossa of the recipient. There are currently three possible categories of transplantation: ►systemic-bladder, ►portal-enteric, and ►systemic-enteric drainage. In systemic-bladder drainage the arterial graft and the portal vein are anastomosed with the recipient's common or external iliac artery and vein, respectively, whereas the exocrine pancreatic secretions are drained by an anastomosis between the donor's duodenum and the bladder. Although this technique offers some advantages (especially the usefulness of urine amylase for identifying a change in pancreas function) it results "nonphysiological." All patients develop metabolic acidosis due to urinary loss of bicarbonates, 40% of patients suffer from urological complications, and 1% from pancreatitis due to urinary reflux through the duodenocystostomy. Furthermore, in contrast to the normal situation whereby insulin is released into the portal circulation, the transplanted pancreas secretes hormones into the systemic circulation, such that euglicemia is reached at the price of hyperinsulinaemia. An alternative to this is the recently proposed technique of portal-enteric drainage, in which the portal vein is anastomosed with the recipient's superior mesenteric vein and the exocrine secretions are drained by an anastomosis between the duodenum and a small bowel loop with a diverting Roux-en-Y limb or a side-to-side duodenoenterostomy. Portal venous drainage of the pancreas is more physiological thanks to an immediate delivery of insulin to the recipient liver. This results in diminished circulating insulin levels relative to that in systemic venous-drained pancreas grafts. Moreover, enteric drainage of pancreas grafts is physiological with respect to the delivery of pancreatic enzymes and bicarbonate into the small bowel loops for reabsorption. In the systemic-enteric drainage technique the insulin is released into the common or external iliac vein and the exocrine secretions are drained into a small bowel loop (1–3).

Posttransplantation Imaging

Despite recent advances in surgical techniques and postoperative management, complications are still frequent, thus each patient need a careful clinical and imaging follow-up. Possible complications include graft acute or chronic rejection, pancreatitis, leaks of anastomoses, vascular complications, peripancreatic fluid collections, and systemic complications due to the immunosuppressive therapy (infectious and neoplastic). Clinical surveillance of pancreatic allografts is difficult because of the relative lack of specificity of most physical and laboratory abnormalities, including fever, abdominal pain (due to peritoneal irritation, because of the absence of innervation of the pancreatic graft), graft tenderness, leukocytosis, hyperglicemia and change in insulin requirement, elevated serum amylase, lipase, anodal trypsinogen, and pancreas-specific protein; in bladder exocrine drainage, also reduction in urine amylase levels and positive urine cytology can be found. Therefore imaging evaluation is often necessary to identify possible complications.

US plays a major role as first-line modality in the postoperative evaluation of the pancreatic graft. Normal transplanted pancreas appears homogeneous, with echogenicity similar to that of muscles and surrounded by more echogenic omental and peritoneal fat; expected dimensions of the normal pancreatic head, body, and tail are no greater than 3 cm, 2.5 cm, and 2.5 cm, respectively. However, US evaluation of the transplanted pancreas often results difficult, because of its intraperitoneal placement, where overlying bowel loops can limit its explorability. Color or power Doppler imaging can aid in locating the pancreas, by showing vascular anastomoses and intraparenchymal major vessels. Furthermore color and power Doppler sonography are able to assess vascularization and spectral analysis of intraparenchymal and peduncular venous and arterial flow can be performed.

CT examination should be performed after intravenous contrast medium administration in transplanted patients without impaired renal function. In particular, thanks to the possibility to perform acquisition in selective arterial and venous phases with thin slices, spiral and multidetector CT allow of precisely defining the postsurgical anatomy of solitary or combined pancreas transplantation, either performed with the systemic-bladder, the portal-enteric or systemic-enteric technique. (Figs 1 and 2). In particular detailed visualization of the anastomoses for exocrine pancreatic drainage and vascular anastomoses can be obtained to understand the surgical technique; selective study in arterial and venous phase associated to MPR, MIP, and VR reconstructions results particularly useful to depict the vascular structures and possible vascular abnormalities. Pancreatic parenchyma can also be assessed to identify focal or diffuse lesions. A further advantage of CT study is the possibility to scan also the entire abdomen and, if necessary, the chest during a single examination, to depict possible distant complications.

MR examination also allows a complete evaluation of the transplanted pancreas, including parenchymal, vascular, and ductal structures, by using both unenhanced conventional sequences and acquisition after gadolinium or tissue-specific contrast medium injection, MR angiographic sequences and MRCP studies (also after secretin injection, to assess the exocrine function). Moreover MR examination can be performed also in patients with impaired renal function (4, 5).

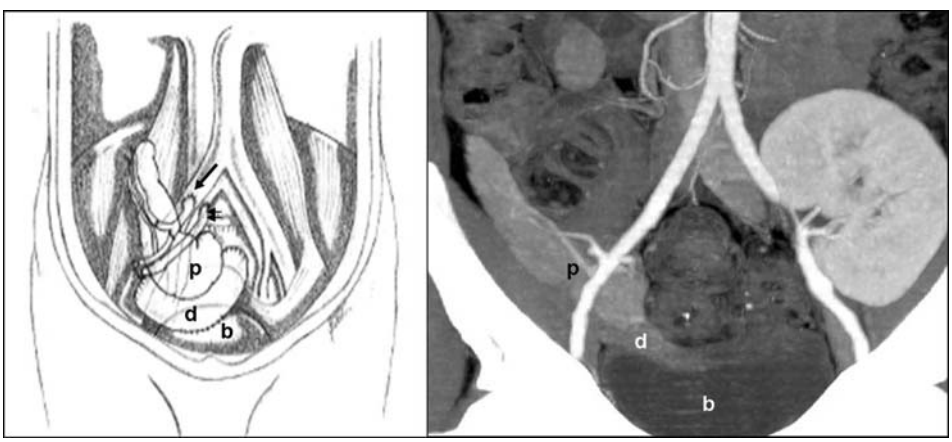

Transplantation, Pancreas. Figure 1 Left image: anatomical representation of the systemic-bladder pancreatic drainage. The duodenum (d) is anastomosed with bladder (b), while the arterial and venous grafts of the pancreas (p) are anastomosed with the common iliac artery (*arrow*) and with the common iliac vein (*double arrow*), respectively. Right image: MIP reformation after CT study. Combined kidney–pancreas transplantation performed by means of the systemic-bladder drainage technique (p: pancreas; d: duodenum; b: bladder).

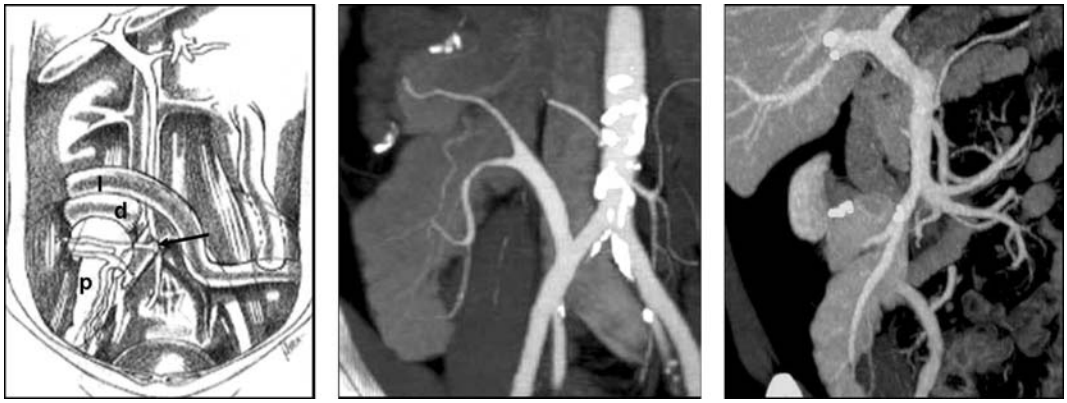

Transplantation, Pancreas. Figure 2 Left image: anatomical representation of the enteric-portal pancreatic drainage. The duodenum (d) drains the exocrine secretion of the pancreas (p) in a small bowel loop (l), while the venous graft is anastomosed with the superior mesenteric vein (*arrow*). The arterial graft is anastomosed with the common iliac artery. In this case the small bowel loop is inverted according to the Roux technique. Central and right images: MIP reconstructions after CT study of the arterial and venous vessels, respectively.

Graft Acute and Chronic Rejection

Graft rejection represents the most fearful complication of transplantation. Acute rejection is characterized by mononuclear inflammation and usually responds to increased immunosuppression, while chronic rejection consists of luminal narrowing and intimal thickening of the vessels, which leads to fibrosis and hypoperfusion, with consequent poor pancreatic exocrine and endocrine function without improvement with therapy. Therefore early detection of acute rejection is of critical importance to institute an adequate immunosuppressive therapy to prevent further graft loss.

Unfortunately the early sign of both acute and chronic rejection may be subtle and aspecific. Delayed finding include hyperglicemia, because endocrine function may continue with only 25% of endocrine cells functioning. For SPK transplantations, rejection usually involves both grafts. Because renal rejection could easily be diagnosed by monitoring serum creatinine levels, the accepted practice is to use renal rejection to determine pancreas rejection. In PTA transplantation no single biochemical marker is able to demonstrate acute pancreatic graft rejection and to differentiate rejection from other causes of graft dysfunction, such as vascular thrombosis or pancreatitis. US and Doppler findings of chronic rejection include hypoperfusion, and increased parenchymal and vascular resistance with a reduction of systolic and diastolic flow. Ultrasound abnormalities that have been associated with acute rejection include gland enlargement and either focal or diffuse areas of decreased echogenicity, peripancreatic fluid, without pancreatic duct dilatation; however the demonstration of early signs of rejection with ultrasound remains inconstant. Moreover, these findings are also seen in cases of vascular compromise and pancreatitis. Unlike renal transplants for which specific resistive index values have been proved to be accurate predictors of acute rejection, no reliable resistive index measurement has been established for at-risk pancreatic grafts, because the pancreatic graft lacks a capsule, and an edematous pancreatic graft may not possess adequate intraparenchymal pressure to produce a reliable measurement of vascular resistance. Although changes in resistive index are a poor indicator of acute rejection, the absolute value of the resistive index results elevated in cases of chronic rejection.

CT and MR findings also are usually aspecific in case of acute rejection and indistinguishable from that of an acute pancreatitis or a parenchymal injury caused by a vascular thrombosis. At MR the glandular signal intensity results either less than the signal intensity of muscle on T1-weighted images or greater than or equal to the signal intensity of the bladder urine on T2-weighted images. In cases of suspected acute graft rejection often histopathologic diagnosis remains the most effective and reliable method. In chronic rejection the pancreas appears small, with inhomogeneous parenchymal structure or completely calcified, and vascular abnormalities (stenosis or obstructions) can be found. These findings are easily detected by means of US, CT, and MR studies. Transplanted pancreas with rejection enhanced less and inhomogeneously after both gadolinium or Mn-DPDP injection at MR and iodinate contrast medium at CT, because of vascular damage (4–6).

Vascular Complications

Vascular complications of pancreatic grafts are common, with vascular thrombosis second only to acute rejection in abnormalities leading to graft loss. Late thrombosis which

occurs more than 1 month after surgery, can results from severe acute rejection, leading to arteritis. Early graft thrombosis has been attributed to a variety of etiologic factors, such as surgical vascular graft lesions, procurement and perfusion injury, poor preservation, reperfusion injury reflecting total cold ischemia time, and, in arterial thrombosis, anastomosis to atherosclerotic vessels. Moreover splenectomy causes low-flow in splenic vessels, predisposing to thrombosis. Partial early venous or arterial thrombosis may be completely asymptomatic, without causing pancreatic dysfunction; partial venous thrombosis can be treated by means of systemic heparin, while partial arterial thrombosis may not require treatment. In case of complete vascular thrombosis prompt treatment is necessary, by means of surgical thrombectomy, Fogarty chateters or transchateter fibrinolysis or heparin, to avoid parenchymal infarction, which require immediate remove of the organ.

Other possible vascular complications include arterial stenoses which are usually secondary to intimal damage in the site of surgical anastomoses or caused by clamping of the artery or by the catheter used for perfusion of the organ. Other arterial lesions that may occur include pseudoaneurysms and arteriovenous fistula secondary to percutaneous biopsy. An arteriovenous fistula between the superior mesenteric artery and superior mesenteric vein occurs occasionally and is related to the surgical technique of stapling the mesenteric vessels together rather than separate dissection and ligature of the vessels. Doppler sonography has been particularly important in detecting vascular complications such as thrombosis, anastomotic strictures, and pseudoaneurysm formation. Thrombosis is demonstrated by the absence of perceptible arterial or venous tracings as well as by direct visualization of intraluminal echogenic material that occludes blood flow. High velocity or turbulence at the arterial or venous anastomoses suggests strictures, and arterial flow within a perianastomotic fluid collection, the presence of swirling blood flow at color flow sonography indicates a complicating pseudoaneurysm. CT also enables the identification and precise characterization of all vascular complications. More specifically, CT study, performed with thin slices, identifes the presence of thrombotic material within the vessels, vascular stenoses or obstructions at level of anastomoses or involving intraparenchymal branches. Compensatory collateral circulation can be identifed in chronic obstructions. Parenchymal ischemic infarction is suggested in the absence of contrast enhancement in the arterial and venous phases (Fig. 3) (4–6).

Pancreatitis

Pancreatitis of the allograft occurs to some degree in all patients postoperatively. Temporary elevation in serum amylase levels for 48–96 h after transplantation is common. These episodes are transient and mild, without significant clinical consequence. In bladder-drained pancreas transplantation pancreatitis can occur because of the reflux of urine through the ampulla and into the pancreatic ducts. If recurrent graft pancreatitis occurs,

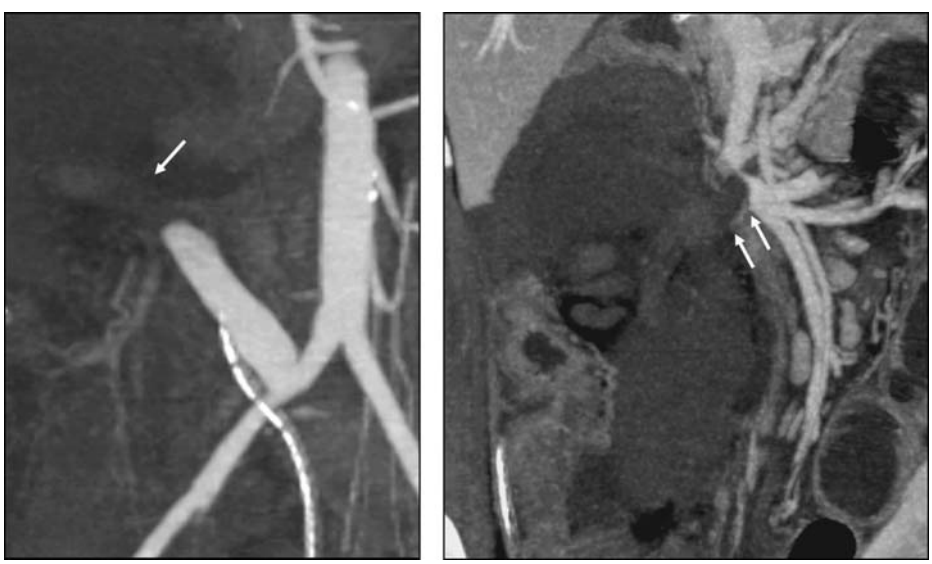

Transplantation, Pancreas. Figure 3 MIP reconstructions in the arterial (*left*) and venous (*right*) phases after CT study in a case of parenchymal ischemic infarction. It is possible to observe a complete arterial (*arrow*) and venous (*double arrow*) thrombotic obstruction and the absence of parenchymal enhancement in both arterial and venous phases.

enteric conversion may be indicated. The radiological findings in pancreatitis are nonspecific and similar to the features seen in acute rejection. The patient's serum amylase and lipase levels are usually markedly elevated.

Fluid Collections

Fluid collections are frequently found in transplanted patients, especially during the early period after the transplant. A small amount of fluid around the pancreatic allograft due to leakage at the site of the anastomosis is commonly seen. In some cases infection of fluid collections and sepsis may occur, favored by immunosuppression. In such cases systemic antibiotic therapy and sometimes image-guided percutaneous fine needle aspiration with chemical analysis and bacterial culture are required; fluid collection can be drained, if appropriate, by percutaneous image-guided techniques. Infection of peripancreatic collection may result in necrosis of the transplanted organ and necessitate its surgical removal. In bladder exocrine drainage some fluid collections may originate from leak of the duodenocystostomy, while in enteric-drained pancreas transplantation leak of duodenoenterostomy can occur, leading in both cases to severe infectious peritonitis. This serious complication requires prompt imaging diagnosis to perform operative repair. Sonography is a suitable method for detecting retroperitoneal or intraperitoneal fluid collections; however, the findings are usually nonspecific. Hematomas, abscesses, urinary leaks, ascites, and anastomotic leaks can appear as anechoic, hypoechoic, or complex, debris-filled, irregular collections. On CT, infection of the fluid collection can be suggested if air is demonstrated. The presence of blood can also be recognized if high attenuation is seen on CT or if typical signal intensities are revealed on MR. Cystography is accurate in the detection of collections originating close to the anastomosis between the duodenal stump and the bladder, but in some cases also the CT can demonstrate the site of fistulization. Moreover CT and MR allow a better depiction of the relations of the fluid collections with the surrounding structures (4–6).

Bibliography

1. Sutherland DE, Gruessner RW, Dunn DL et al (2001) Lessons learned from more than 1,000 pancreas transplants at a single institution. Ann Surg 233(4):463–501
2. Gruessner AC, Sutherland DE (2003) Pancreas transplant outcomes for United States (US) and non-US cases as reported to the United Network for Organ Sharing (UNOS) and the International Pancreas Transplant Registry (IPTR) as of May 2003. Clin Transpl 21–51
3. Boggi U, Del Chiaro M, Vistoli F (2001) Tecniche chirurgiche per il trapianto di pancreas. In: Boggi U, Mosca F (eds) I Trapianti Di Pancreas. ETS, Pisa, pp 293–317
4. Nikolaidis P, Amin RS, Hwang CM et al (2003) Role of sonography in pancreatic transplantation. Radiographics Jul-Aug 23(4):939–949
5. Neri E, Cappelli C, Boggi U et al (2004) Multirow CT in the follow-up of pancreas transplantation. Transplant Proc Apr 36(3):597–600
6. Spiros D, Christos D, John B et al (2004) Vascular complications of pancreas transplantation. Pancreas May 28(4):413–420

Transvaginal Sonography

An imaging technique used to examine the female genital organs, i.e. vagina, uterus, ovaries and fallopian tubes, as well as the urinary bladder. For the transvaginal appraoch, a high resolution probe is inserted into the vagina that causes sound waves to bounce off organs inside the pelvis. These ultrasound waves creates echoes that a re sent to a computer, which creates a picture called a sonogram. Sonography is usually the first imaging techique applied for the diagnosis of a suspected pathology of the female genital organs.

Transverse Diameter

Largest transverse distance on an oblique section of the pelvic inlet.

▶Magnetic Resonance Pelvimetry

TRAM (Transverse Rectus Abdominis Musculocutaneous)

A type of breast reconstruction following mastectomy, made with a transverse rectus abdominis musculocutaneous flap.

▶Recurrent Neoplasms, Breast

Transverse Relaxation Time

This term relates to the T2 time constant, which determines the rate at which excited protons reach equilibrium or go out of phase with each other.

▶Contrast Media, MRI, Oral Agents

Trauma Birth

Veronica Donoghue
Radiology Department, Children's University Hospital, Dublin, Ireland
veronica.donoghue@cuh.ie

Synonyms

Brachial plexopathy; Brachial plexus injury; Dejerine–Klumpe paralysis; Erb-Duchenne paralysis

Definition

This includes any bone or soft tissue injury which occurs during the delivery process. They occur during difficult deliveries and in particular during breech deliveries.

Clinical Presentation

Overall the clavicle is the most commonly fractured bone during delivery (1). In a study by Joseph and Rosenfeld 80% of *clavicular fractures* are asymptomatic (2). They maybe detected by the presence of a palpable mass over the clavicle some weeks after birth due to callus formation.

Rib fractures are also rare and may also be asymptomatic unless injury is so extensive that there are respiratory difficulties (1).

Long bone fractures usually present with soft tissue swelling and there maybe reduced movement in the affected limb. *Brachial plexus injury* occurs in 0.5–2.6 cases per 1,000 live births and the risk is highest in macrosomic infants delivered by a shoulder or breech presentation. Other risk factors include mid or low forceps delivery and vacuum extraction. The usual mechanism of injury is lateral traction of the neck. The injury ranges from transient neuropraxia secondary to stretching of the extradural plexus in mild cases to severe avulsion of the rootlet from the cervical cord. Injury to the fifth and sixth cervical nerve roots is called ►Erb-Duchenne paralysis and accounts for approximately 90% of obstetric brachial injuries. Clinical signs of Erb-Duchenne paralysis include an adducted, internally rotated upper extremity with variable flexion of the wrist. In the 5% of patients with fourth cervical nerve involvement, respiratory symptoms such as tachypnoea and poor ventilation may occur. Injury of the eight and first thoracic nerve roots or the lower trunk is called ►Dejerine–Klumpe paralysis. Such injury is uncommon in isolation. These infants demonstrate paresis of the intrinsic hand muscles and claw hand. Ipsilateral Horner syndrome may be present (3).

In trauma to the cervical spine and cervical cord the most common predisposing factor is hyperextension of the cervical spine. In addition to brachial plexus injuries these infants may have generalised floppiness, a bell-shaped chest due to hypotonia and respiratory distress because of reduced thoracic movement (1).

Trauma to the liver and spleen are occasionally encountered. Perinatal hypoxia has been implicated in some cases. This causes congestion and as a result increased susceptibility to rupture. Obstetrical trauma has also been invoked as a cause of adrenal haemorrhage in newborn infants. Iatrogenic fetal injury such as lacerations and digit amputations during caesarean section delivery is rare but serious. Cranial injuries, in particular subdural haematomas, occur more frequently in infants delivered by means of forceps or vacuum. These are discussed elsewhere.

Imaging

Fractures of the clavicle are often in the midclavicular region and are detected by plain radiography. Callus formation is usually seen at 7–10 days after birth. Rib fractures are similarly identified.

Fractures of the long bones can occur at the diaphysis or at the epiphyseal-metaphyseal junction in keeping with a Salter-Harris type I or II injury. Plain radiography may show just soft tissue swelling as there is no epiphyseal ossification. True traumatic joint dislocation is uncommon in the newborn and when there is joint space widening evident the most common cause is separation of the metaphysis from the epiphysis due to an underlying epiphyseal-metaphyseal fracture (1) (Fig. 1a). These injuries maybe well delineated using ultrasonography or magnetic resonance imaging where the displacement of the cartilaginous epiphysis is identified (Fig. 1b). In some infants small metaphyseal fractures are seen. This finding maybe similar to that seen in infants with non-accidental injury. It has been suggested that if a fracture is detected at day 11 of life without callus formation that one should consider it to have occurred after birth as birth injuries usually show callus formation between 7 and 11 days of age (1).

Evaluation of neonates with a brachial plexopathy involves plain radiography to outrule a fracture. In infants with respiratory difficulty, ultrasonography of the diaphragm or chest fluoroscopy can be performed to detect phrenic nerve injury. In more than 80% of these infants spontaneous functional recovery can be expected. Surgical exploration of the brachial plexus has been suggested if biceps function has not begun to return by 3 months of age. The goal of imaging in this group of patients is to demonstrate the level and extent of the

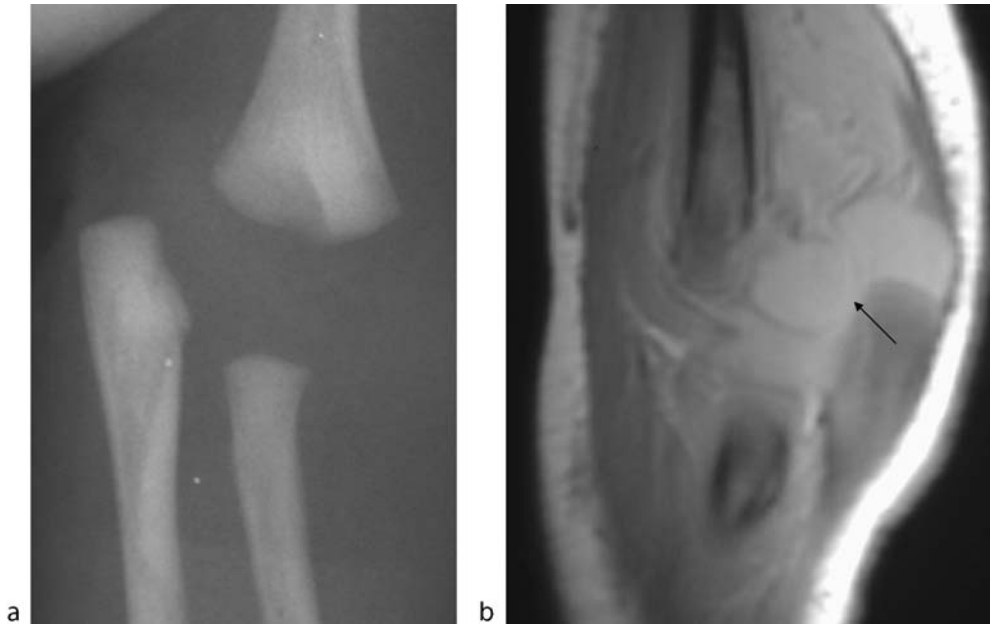

Trauma Birth. Figure 1 (a) Plain elbow radiograph in newborn following difficult breech extraction. The study suggests traumatic dislocation at the elbow joint. (b) Sagittal proton-density MR image demonstrating a Salter type II injury of the distal humerus with significant posterior displacement of the metaphyseal fragment and epiphysis (arrow).

injury. Although there is a strong correlation between complete or incomplete root avulsion and the presence of a pseudomeningocoele, pseudomeningocoeles are seen in the absence of root avulsion and root avulsion is seen in the absence of pseudomeningocoeles. CT myelography can be used but more recently MR imaging is used to demonstrate extra-arachnoid pseudomeningocoeles (Fig. 2) though the spatial resolution of MR imaging is still less than that possible with very thin slice CT myelographic images. Individual nerve rootlets are not routinely visualised with MR. MR however may show brachial plexus haemorrhage not seen on myelography. Axial and coronal narrow flip angle gradient-echo sequences are used together with a single three-dimensional gradient-echo sequence performed by means of thin partitions, followed by multiplanar reconstructions (3). We use a short-tau inversion recovery (STIR) sequence in the axial and coronal planes together with a heavily T2 weighted volume sequence.

Focal spinal cord injuries including cord transection and post-traumatic syrinx are best shown on MR imaging (Fig. 3). However, ultrasonography demonstrating increased echogenicity as a result of haematomyelia and oedema maybe useful in the early stages of the disease particularly in those infants who are ventilated and whose condition is complicated by concurrent asphyxia.

In infants with liver trauma plain radiographs may show liver enlargement. Ultrasonography may reveal parenchymal and subcapsular liver and splenic lesions.

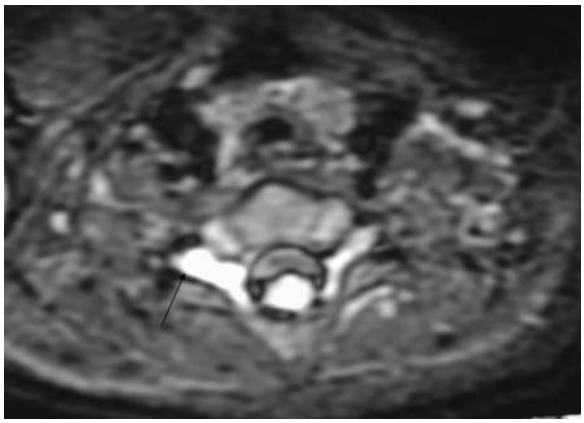

Trauma Birth. Figure 2 Axial STIR MR Image showing a right pseudomeningocele at T7 level (arrow).

These abnormalities are usually echogenic in nature initially but as the haemorrhage liquefies they become echo-free. CT however most clearly delineates lacerations, haematomas, subcapsular and perihepatic and perisplenic collections.

Ultrasonography is the modality of choice in detecting adrenal haemorrhage. The abnormality is echogenic in the early stages and becomes echo-poor with time. If this progression does not take place neuroblastoma must be considered. Calcification may develop at the haemorrhage site within a few weeks to months.

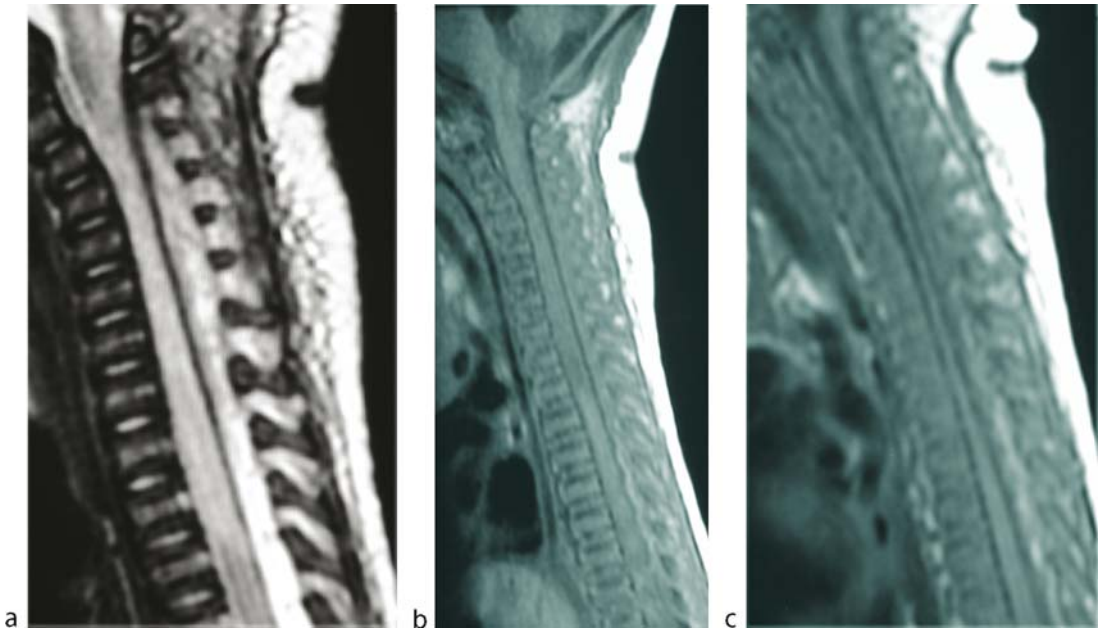

Trauma Birth. Figure 3 Sagittal images of cervical and thoracic cord in a newborn following a difficult delivery showing increased T2 (a) and decreased T1 (b) signal in keeping with oedema and swelling due to injury. (c) Follow-up T1 MR image at 3 weeks demonstrating significant cord atrophy.

Diagnosis

A high proportion of clavicular and rib fractures sustained during delivery are asymptomatic and are discovered when there is sufficient callus formation to be palpable clinically some weeks after birth or incidentally on chest radiography performed for other indications.

Long bone epiphyseal-metaphyseal injuries are suspected by the presence of limb immobility and soft tissue swelling detected clinically and on plain radiography. The diagnosis may be confirmed using ultrasonography or MR imaging.

Brachial plexus and spinal cord injuries are suspected clinically and best confirmed using MR imaging. However ultrasonography may be useful in the acute stages of the injuries. Brachial plexus injuries may also be confirmed using CT myelography.

Bibliography

1. Swischuk LE (ed) (2003) Head, brain and meninges. In Imaging of the Newborn, Infant and Young Child. 5th edn. Lippincott Williams and Wilkins
2. Joseph PR, Rosenfeld W (1990) Clavicular Fractures in Neonates. Am J Dis Child 144:165–167
3. Miller SF, Glasier CM, Griebel ML et al (1993) Brachial plexopathy in infants after traumatic delivery: evaluation with MR imaging. Radiology 189:481–484

Trauma, Breast

Geert M. Villeirs
Urogenitale Radiologie-Universitair Ziekenhuis Gent, Ghent, Belgium
geert.villeirs@ugent.be

Definition

Traumatic injury to the breast is the result of any physical damage, either accidental (e.g., seat belt injury, stab wound, etc.) or iatrogenic (e.g., breast biopsy, surgery, radiation therapy, etc.), leading to rupture of blood vessels (causing contusion or hematoma) and/or damage to fat cells (causing fat necrosis).

Pathology/Histopathology

In ►contusions, edema and blood diffusely infiltrate the parenchyma and dissect along the fibrous planes of the breast; whereas in ►hematomas, extravasated blood forms a collection of liquid or clotted blood in a traumatic tear or surgical cavity. Both posttraumatic

conditions usually resolve spontaneously within a few weeks, but partially resorbed or chronic hematomas may eventually evolve into ►fat necrosis.

Fat necrosis is caused by disruption and fragmentation of fat cells, both by direct trauma or indirectly as a consequence of disruption of the blood supply or pressure necrosis following diffuse or focal extravasation of blood into the parenchyma. Fat debris is then released into the interstitial space and may either elicit a lipophagic granuloma or conglomerate to form a macroscopic pool of oil, known as an oil cyst. However, usually both ends of this spectrum are simultaneously present.

A ►lipophagic granuloma is characterized by a nonsuppurative infiltration of fibroblasts, foamy macrophages, and leukocytes. Fat debris and extravasated erythrocytes are phagocytosed, with formation of foam cells and siderophages. A centripetal fibrous connective tissue response gradually leads to contraction of the area into a hard stellate scar and saponification of fat may give rise to several types of calcifications.

An ►oil cyst is a conglomerate of almost entirely pure neutral fat that becomes surrounded by foam cells and other inflammatory cells. Resorption and scar formation occur along the boundary of this cavity, which gradually becomes encapsulated by a thin, smooth, fibrous wall, in which calcium deposition may occur, leading to the well-known eggshell calcifications of fat necrosis.

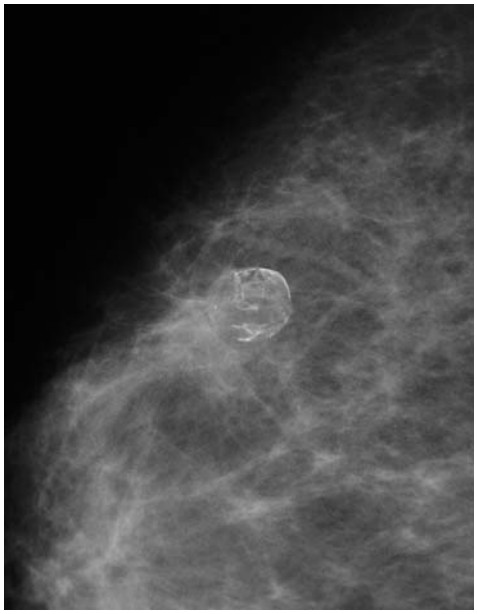

Trauma, Breast. Figure 1 Oil cyst with central lucency and peripheral eggshell calcifications.

Clinical Presentation

In general, the eliciting trauma (either accidental or iatrogenic) is obvious, although "spontaneous" hematomas are not unusual. On the other hand, some abnormalities that the patient relentlessly ascribes to previous trauma prove to be malignant.

At the trauma site, a tender palpable mass with bluish-red discoloration of the skin may be highly indicative of an underlying hematoma, while a diffuse thickening of the breast without mass effect is suggestive of a contusion.

Fat necrosis can remain completely asymptomatic or present as a sometimes painful palpable mass. Differentiating fat necrosis from malignancy may be particularly difficult in the case of a fixed and firm nodule with associated retraction and thickening or dimpling of the overlying skin.

Imaging

Mammography

A contusion may be imperceptible or present as a subtle asymmetric density or diffuse trabecular thickening. Hematomas, on the other hand, are seen as fairly well-defined masses of any shape and of heterogeneous density. In the case of a penetrating wound, air-fluid levels may be observed.

Oil cysts are readily recognizable on mammographs as round or oval sharply demarcated lucent areas, with or without spherical or elliptical wall calcifications (eggshell calcifications) (Fig. 1). These findings should not pose diagnostic problems.

However, fat necrosis presenting mainly as lipophagic granuloma may exhibit a wide range of nonspecific mammographic findings including architectural distortion and ill-defined, spiculated masses with skin thickening and various types of calcifications. The latter can be coarse, round or pleomorphic, or eggshell type with round or bizarre shapes (Fig. 2).

When the mammographic features of fat necrosis or posttraumatic scar resemble those of carcinoma, some clues may help to differentiate them. As opposed to most carcinomas, fat necrosis may appear different on different projections and may contain some fat in its central mass, which can usually be better appreciated on spot compression and/or magnification views. Obviously, an increasing mass on serial posttraumatic mammograms is suggestive of malignancy rather than fat necrosis.

Sonography

A contusion may present as an indistinctly outlined area of hyperechoic edematous fatty tissue intermingled with hypoechoic fluid planes along the trabecular framework

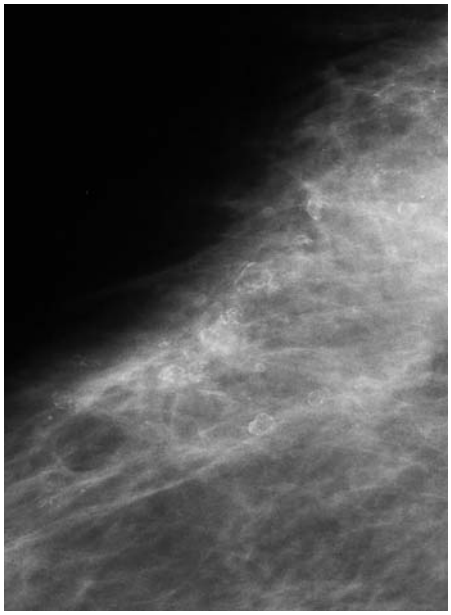

Trauma, Breast. Figure 2 Fat necrosis presenting as architectural distortion with multiple irregular lucent-centered eggshell clacifications.

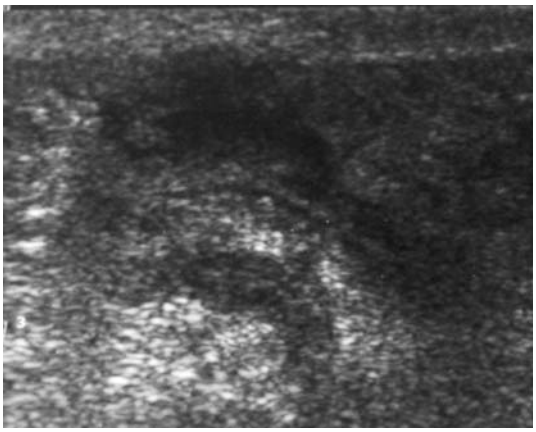

Trauma, Breast. Figure 3 Sonogram of subacute hematoma with clots and fibrin strands, presenting as a an irregularly outlined mass containing fluid and echogenic elements.

of the breast. Hematomas are initially present as an irregularly outlined anechoic mass containing fresh blood, but as soon as the blood starts forming clots and fibrin strands, echogenic elements appear within the fluid, which becomes more heterogeneous and may fluctuate under varying scan pressures (Fig. 3). Sometimes fluid–debris levels may be seen. As the hematoma ages, it becomes more sharply marginated with a thick echogenic contour (representing older clot) and irregular internal septations, encasing hypoechoic areas of unclotted blood or liquefied clot.

Oil cysts generally do not require sonographic evaluation as their mammographic appearance is so characteristic. They may be present as round or oval sonolucent lesions, with enhanced through-transmission and a thin echogenic capsule. When the latter calcifies, its echogenicity markedly increases, causing gradual retroacoustic shadowing. Usually, oil cysts are found concurrently with some degree of lipophagic granuloma, which presents as an ill-defined heterogeneously hypoechoic area with varying degrees of retroacoustic shadowing. As the entire process starts to contract into a stellate scar with marked retroacoustic shadowing and parenchymal distortion, it may be quite difficult to distinguish fat necrosis from carcinoma. However, as opposed to carcinomas, scars may have a flattened configuration with different diameters on perpendicular scan planes. They may change their appearance with varying scan pressures, and are usually avascular on Doppler interrogation.

Magnetic Resonance Mammography

In early contusions or hematomas, the diffuse infiltration or focal collection of fluid and fresh blood usually shows intermediate to high signal intensity on both T1- and T2-weighted images. Later in the process, the signal intensities may vary depending on fluid resorption and degradation of hemoglobin into ferritin and hemosiderin. The latter causes a significant signal drop on both T1- and T2-weighted images. The fluid or blood collections (both diffuse of focal) do not show enhancement after intravenous administration of gadolinium contrast agent, but the injured or inflamed surrounding tissue may show minimal-to-moderate and usually delayed enhancement.

Because of their fat content, oil cysts show high signal intensity on T1-weighted images. They are usually round or oval, and confined within a smooth low-signal intensity rim with no or minimal enhancement after contrast administration. In contrast to oil cysts, lipophagic granulomas may cause much more diagnostic difficulties, especially in their early course. Fresh granulation tissue is highly vascular, and thus diffuse moderate and delayed, but sometimes fast and strong enhancement can be found throughout the lesion. Therefore, magnetic resonance imaging (MRI) is not useful during the first 6 months after trauma or surgery. After this period, hypovascular scar tissue and fibrosis usually develop, with little or no enhancement, enabling differentiation between old scarring and malignancy.

Diagnosis

Percutaneous Biopsy

There is generally no need to confirm a diagnosis of contusion, hematoma, or oil cyst with biopsy. However, differential diagnostic difficulties may arise in fat necrosis or scar tissue with clinical, mammographic, or sonographic features indistinguishable from malignancy.

References

1. Basset LW, Gold RH, Cove HC (1978) Mammographic spectrum of traumatic fat necrosis: the fallibility of "pathognomonic" signs of carcinoma. Am J Roentgenol 130:119–122
2. Hogge JP, Robinson RE, Magnant CM et al (1995) The mammographic spectrum of fat necrosis of the breast. Radiographics 15:1347–1356
3. Soo MS, Kornguth PJ, Hertzberg BS (1998) Fat necrosis in the breast: sonographic features. Radiology 206:261–269
4. Harrison RL, Britton P, Warren R et al (2000) Can we be sure about a radiological diagnosis of fat necrosis of the breast? Clin Radiol 55:119–123
5. Villeirs G, Van Damme S, Heydanus R et al (2000) Heparin-induced thrombocytopenia and fat necrosis of the breast. Eur Radiol 10:527–530

Trauma, Genitourinary Tract

Marie-France Bellin
Service de Radiologie, Hôpital Paul-Brousse, Université Paris-Sud 11, Villejuif, France
marie-france.bellin@pbr.ap-hop-paris.fr

Definition

Trauma of the genitourinary tract includes blunt and penetrating injuries to the kidney, ureter, bladder, and urethra.

Characteristics

The genitourinary tract is involved in approximately 10% of all trauma injuries. Renal damage is a common complication of abdominal trauma, whereas the bladder and urethra are more frequently affected by pelvic injuries.

Renal Damage

Damage to the kidney is the most frequent urologic trauma and occurs in up to 8 to 10% of all blunt and penetrating injuries (1). Blunt injuries account for about 80% of all cases of renal trauma (2), and are mostly due to motor vehicle accidents, less frequently to falls from a height, assaults, bicycle accidents, and horseback riding injuries. Penetrating injuries are mostly due to gunshot or stab wounds and often require surgery. The management of renal trauma is controversial and current trends are for less invasive procedures and a more conservative approach.

The goals of imaging evaluation are to detect and classify renal damage, to assess its extent, to detect or rule out associated injuries, and to help determine which can be managed conservatively and which may require surgery or embolization (1, 3, 4). In addition, imaging modalities are essential for the follow-up and detection of late complications.

Classification of Injury

According to the American Association for the Surgery of Trauma, renal injuries are graded on the basis of their depth and involvement of vessels or the collecting system (5):

1. *Grade* 1 [*82% of the cases* (4)]
   a. Hematuria with normal imaging findings
   b. Contusions
   c. Nonexpanding subcapsular hematomas
2. *Grade* 2
   a. Nonexpanding perirenal hematomas confined to the retroperitoneum
   b. Superficial cortical lacerations <1 cm in depth without collecting system injury
3. *Grade* 3
   a. Renal lacerations >1 cm deep that do not involve the collecting system
4. *Grade* 4
   a. Lacerations extending through the kidney into the collecting system
   b. Injuries involving the main renal artery or vein with contained hemorrhage
   c. Segmental infarctions without associated lacerations
5. *Grade* 5
   a. Shattered or devascularized kidney
   b. Ureteropelvic junction (UPJ) avulsions
   c. Complete laceration or thrombus of the main renal artery or vein.

The increasing grade of renal injury severity generally corresponds to the need for surgery to repair or remove the damaged tissue. However, renal injuries are now often managed conservatively, unless imaging studies show

extensive tissue destruction, active hemorrhage, or large rupture of the collecting system.

Symptoms

Most patients with major renal damage present either gross hematuria, hypotension, or flank pain. Microscopic hematuria is a poor indicator of major renal damage. Pertinently, hematuria (or any other symptom) may be absent in patients with renal vascular injuries, UPJ avulsions or ureteral damage.

Imaging Modalities: Advantages and Limitations

CT is the imaging modality of choice for determining the extent of renal and perirenal damage, and for demonstrating the injuries of other organs (2–4). It provides essential anatomic and physiologic information required to make therapeutic decisions. CT should include unenhanced scans to detect hyperdense hematomas, followed by scans obtained during the vascular corticomedullary phase to detect vascular lesions, lacerations and shattered kidney, and scans obtained during the secretory phase to detect urine leakage (6). The use of oral contrast is controversial; slice thickness of 5 mm or less is helpful to avoid distorting volume-averaging artifacts. If bladder injury is clinically suspected, a cystogram or CT cystogram with dilute contrast should be performed to differentiate among intraperitoneal, extraperitoneal, or combined bladder rupture (2).

Angiography is being used less frequently, now that faster CT scanners have become widely available, and their detection of active arterial extravasation and vascular injuries is improved. However, angiography with selective transcatheter embolization is generally reserved for patients with active arterial bleeding detected at CT, traumatic pseudo aneurysms, and/or late hemorrhage that occurs in patients managed without surgery.

Ultrasonography (US) use in trauma patients is controversial (2–3), as it is often limited by pain, ileus, wounds, and so on. US can detect lacerations or modifications in the echotexture of the injured kidney and perirenal fluid. It is less sensitive than CT for detecting solid organ injury, especially of the kidneys, retroperitoneal blood and hollow organ injury. In addition, although US is able to detect free fluid in the abdomen and pelvis, it cannot differentiate among blood, extravasated urine, and other fluids. It is insensitive for determining the source of bleeding. When it is technically feasible, Doppler US can accurately detect vascular complications, by visualizing the pedicles and intrarenal vasculature, and evaluate the extent of renal infarcts. The usefulness of US contrast media has not been established. The major drawback of US is its inability to detect urine leakage, which is a major clinical concern. In most centers, US is reserved for the rapid search for intraperitoneal fluid in the unstable patient and for follow-up.

Intravenous urography (*IVU*) is less sensitive than CT for detecting renal parenchymal injury, urine and contrast-medium extravasation, and associated abdominal or pelvic injuries. With easy access to CT, the role of IVU is now limited to the assessment of hemodynamically unstable patients on the way to surgery or for urologic imaging of patients already in the operating room. In most cases, it includes only a scout radiograph followed by one film immediately after contrast injection and another about 10 min later. Additional late radiographs may be obtained to detect urine leakage or in patients with delayed contrast-medium excretion. Several pathologic conditions can be associated with negative opacification of the collecting system, that is, arterial tear, venous thrombosis, shock and diffuse parenchymal lesions. The ureters should be evaluated and the presence of a contralateral functioning kidney confirmed, should removal of the injured kidney be required.

MRI is rarely used because it is expensive and rarely available as an emergency procedure. However, it is able to detect hematomas, edema, ischemia, and urinomas in stable patients for who use of iodinated contrast media is contraindicated.

Imaging

Renal contusions appear as ill-defined high-density areas on unenhanced images with less enhancement relative to adjacent normal areas.

Subcapsular hematomas indent the renal margin and are seen as rounded areas. Their attenuation values vary as a function of the age of the clot, with acute hematomas being typically hyperdense relative to normal renal parenchyma on unenhanced CT images (Fig. 1).

Minor lacerations appear as areas of linear low attenuation within the renal parenchyma.

Deep lacerations of the renal parenchyma may extend into the collecting system, resulting in urine extravasation on late CT and IVU images (Fig. 2).

Active hemorrhage usually results in intense enhancement during the early phase of the CT examination. It has a linear or flame-like appearance and should be differentiated from a false aneurysm, which tends to appear more rounded and better delineated. In hemodynamically stable patients with active hemorrhage, selective

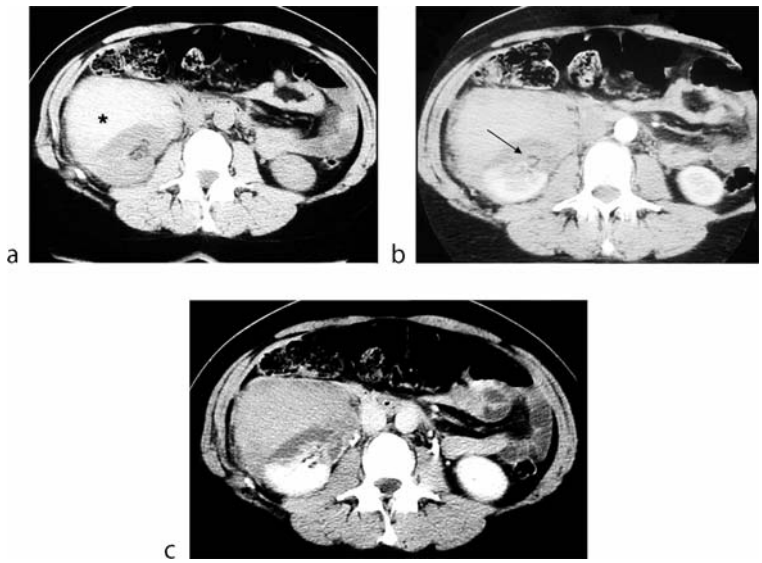

Trauma, Genitourinary Tract. Figure 1 Blunt renal trauma. (a) Unenhanced CT scan shows a huge anterior pararenal hematoma (*) which appears hyperdense. (b) Arterial phase CT image demonstrates an anterior renal infarct (*arrow*) that remains unenhanced during the secretory phase CT (c).

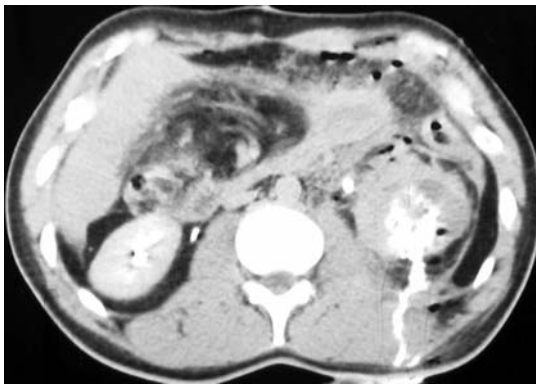

Trauma, Genitourinary Tract. Figure 2 Urine leakage after a gunshot wound. CT image obtained during the secretory phase demonstrates extravasation of the contrast medium into the left perirenal space and lumbar wall.

angiographic embolization is preferred to surgery to maximize nephron sparing.

Pseudoaneurysms and arteriovenous fistulas can be detected with Doppler US or CT and treated with angiographic embolization (Fig. 3).

Segmental renal infarction may be due to thrombosis, dissection, or laceration of segmental renal arteries. They appear as well-circumscribed, linear or wedge-shaped areas that do not enhance (Fig. 1). In most cases, they are managed medically.

Massive renal infarction may result from a complete or an incomplete tear of the main renal artery with subsequent arterial thrombosis (Fig. 4). Hematuria may be absent. The kidney is not enhanced on CT contrast-medium-enhanced images, except for cortical rim due to intact collateral vessels. Early revascularization may be attempted but is rarely successful.

Main renal vein injury can be detected by US. It may result in massive perirenal hemorrhage or thrombosis with an enlarged kidney and a late and persistent diffuse opacification of the parenchyma on CT and IVU.

UPJ avulsion is most likely due to overstretching of the pelvis and ureter during hyperextension and manifests as massive contrast-medium extravasation along the ureter on late CT images or IVU.

Adrenal Trauma

Adrenal injury has been reported in 28% of the patients with blunt abdominal trauma who were studied at autopsy (7). The mechanism of injury includes direct compression of the gland against the spine or suddenly increased venous pressure owing to transmission from the inferior vena cava. The right adrenal is more commonly involved than the left. In most patients, adrenal hematoma raises no or little clinical concern, unless it is bilateral, in which case the potential for developing adrenal insufficiency must be considered. Adrenal injuries are best depicted by CT (7), which typically shows an enlarged gland with a rounded or swollen-but-normal shape. Initially, the adrenal hematoma appears hyper-

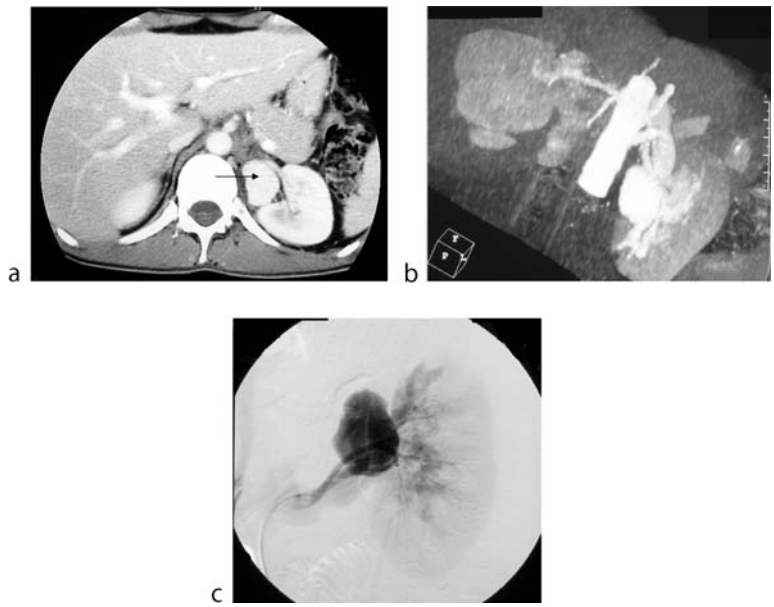

Trauma, Genitourinary Tract. Figure 3 Posttraumatic renal arteriovenous fistula. (a) Arterial phase CT shows the lesion (*arrow*) with strong enhancement. (b) Maximum intensity projection 3D reconstruction shows the fistula with communication between the renal artery and vein with early opacification of the main renal vein. (c) Corresponding preembolization angiography.

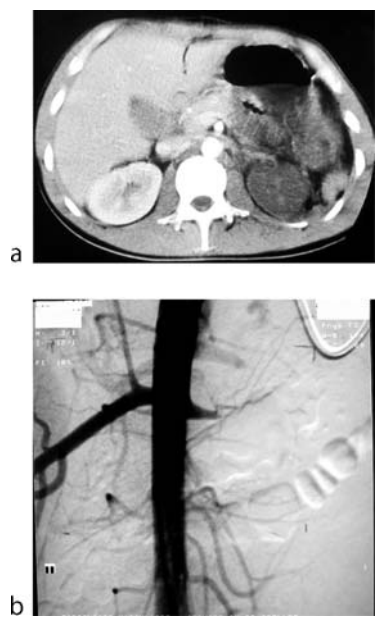

Trauma, Genitourinary Tract. Figure 4 Renal artery occlusion following rapid deceleration. (a) Arterial phase CT demonstrates no enhancement of the left renal parenchyma. (b) Arteriography shows proximal arterial occlusion of the left renal artery.

dense; its density decreases as the blood clot resolves, and a follow-up CT scan may document resolution of the adrenal lesion in 2–4 months. In other cases, it may lead to the formation of a mass and/or pseudocysts seen as incidental findings on CT examinations. Adrenal hematomas are frequently associated with stranding of the periadrenal fat and tracking of the hemorrhage along the crus of the ipsilateral hemidiaphragm.

Ureteral Trauma

Iatrogenic injury is the most common cause, with the ureter being damaged during retrograde pyelography or ureterocystoscopy in most cases. The ureter may also be lacerated or contused during penetrating trauma (especially gunshot wounds) or overstretched during severe hyperextension. Partial disruptions may be treated with percutaneous nephrostomy, with or without ureteral stenting, whereas complete transections usually require surgical repair. The diagnosis of ureteral injury relies on CT or IVU demonstration of extravasation of the excreted contrast medium that accumulates within an urinoma that is generally mixed with blood (2, 6). In patients with suspected proximal ureteral tear, the presence of enhanced urine in the distal ureter indicates only a partial disruption (Fig. 4).

Bladder Trauma

Bladder injuries may be due to blunt or penetrating trauma and are frequently associated with bony pelvic

fractures. They are more likely to occur when the bladder is distended than when empty. Extraperitoneal (65% of the cases) bladder injuries are most often due to laceration by a fractured pelvis. Intraperitoneal (35% of the cases) bladder ruptures usually result from blunt trauma with a sudden rise in intraperitoneal pressure causing the bladder dome to burst. Gross hematuria and failure to void are the main symptoms. CT cystography is now considered the imaging technique of choice for detection and assessment of bladder injury. It is performed with 300–500 mL of diluted contrast medium installed retrograde into the urinary bladder. The bladder catheter is then clamped for 10–30 min and CT scans of the abdomen and pelvis are obtained. Intraperitoneal bladder rupture is recognized by contrast-material leakage around bowel loops, into the intraperitoneal recesses of the pelvis, the paracolic gutters, and/or the anterior subhepatic space. Extraperitoneal bladder ruptures create a streaky appearance due to extravasation of opacified urine into perivesical soft tissues.

Urethral Trauma

Urethral injuries occur in 10% of major pelvic fractures and are far more common in men than in women. Posterior urethral injuries may be associated with bladder-base disruptions. Anterior urethral injury may result from iatrogenic or penetrating injury and, less frequently, from blunt trauma. Most patients manifest an inability to void, blood at the urethral meatus, elevation of the prostate during digital rectal examination or perineal hematoma. Patients with suspected urethral trauma should undergo a retrograde urethrogram before insertion of a Foley catheter. It should ideally be performed under fluoroscopic guidance and include oblique radiographs, which may show the precise localization of the tear and subsequent leak of contrast medium. In type 1 injuries, the urethra is narrowed and stretched by a periurethral hematoma; there is no contrast-material leakage. In type 2 injuries, the posterior urethra ruptures proximal to the urogenital diaphragm and extraperitoneal contrast material is seen above the urogenital diaphragm. In type 3 injuries, proximal posterior disruption continues through the urogenital diaphragm, with subsequent contrast-medium leakage into the extraperitoneal space and the perineum.

Bibliography

1. Bretan PN, McAninch JW, Federle MP et al (1986) Computerized tomographic staging of renal trauma: 85 consecutive cases. J Urol 136:561–565
2. Smith JK, Kenney PJ (2003) Imaging of renal trauma. Radiol Clin North Am 41:1019–1035
3. Vasile M, Bellin MF, Hélénon O et al (2000) Imaging evaluation of renal trauma. Abdom Imaging 25:424–430
4. Harris AC, Zwirewich CV, Lyburn ID et al (2001) CT findings in blunt renal trauma. Radiographics 21:S201–S214
5. Moore EE, Shackford SR, Patcher HL et al (1989) Organ injury scaling: spleen, liver, and kidney. J Trauma 29:1664–1666
6. Titton RL, Gervais DA, Hahn PF et al (2003) Urine leaks and urinomas: diagnosis and imaging-guided intervention. Radiographics 23:1133–1147
7. Burks DW, Mirvis SE, Shanmuganathan K (1992) Acute adrenal injury after blunt trauma: CT findings. Am J Roentgenol 158:503–507

Trauma, Head, Accidental

Philippe Demaerel
Department of Radiology, University Hospitals, Leuven, Belgium
philippe.demaerel@uz.kuleuven.ac.be

Synonyms

Brain, edema; Brain, hematoma; Brain, injury; Head, injury; Hematoma, epidural; Hematoma, subdural

Definitions

A major craniocerebral trauma should always be examined with computed tomography (CT) using different window/level settings for the intracranial structures and for the bone. Most acute lesions will be clearly visualized, including parenchymal contusions, extracerebral hematomata, cerebral ▶edema, and skull fractures. Depending on the impact, additional CT of the skull base, orbits, and/or sinuses may be indicated.

There are two indications for brain magnetic resonance imaging (MRI): a discrepancy between the CT findings and the clinical symptoms, and follow-up to assess the extent of the damage to the brain.

The role of plain X-ray films is limited in craniocerebral trauma and has been replaced by multidetector CT in most centers. The role of CT in minor cranial trauma remains controversial and will depend on clinical factors.

Pathology/Histopathology

One may differentiate primary and secondary brain injuries.

The common primary brain injuries are extracerebral hematoma (in the subdural or epidural space), cerebral

contusions, and diffuse axonal injury. Scalp hematomata are usually clinically not significant.

Epidural hematoma is usually associated with the laceration of the middle meningeal artery, a branch of the external carotid artery, or with the laceration of a dural venous sinus. Subdural hematoma follows an acceleration/deceleration trauma with stretching and tearing of bridging cortical veins in the subarachnoid space. Axonal shearing injuries also result from acceleration/deceleration and rotational forces. They occur typically in predictable locations, for example, the corticomedullary junction, the midbrain/pons, and the corpus callosum (posterior truncus and splenium). Cerebral contusions are focal cortical hemorrhages with adjacent edema that often increase up to 48 h after the trauma.

Subarachnoid hemorrhage is a result of a direct injury to the leptomeningeal vessels or of a direct superficial brain injury.

Intraventricular hemorrhage is the result of a disruption of the subependymal veins and is usually associated with other intracranial traumatic lesions. The prognosis is poor.

Secondary brain injuries develop in the hours and days after the trauma. These include herniation of the tonsils, subfalcine herniation and uncal herniation, diffuse cerebral edema, and secondary ischemia. Intracranial hypertension will cause a variable degree of compression and displacement of brain tissue, blood vessels, and/or nerves. Diffuse brain edema is due to increased water content and intravascular blood volume.

The skull should be assessed with CT using appropriate window width/level settings to demonstrate fractures.

Finally, in missile-induced trauma, metallic fragments can be located in the intracranial compartment.

Clinical Presentation

Patients with a Glasgow coma scale less than 9, deteriorating consciousness, or progressive neurological deficit should be examined urgently with CT. Depending on the clinical and CT findings, a neurosurgical intervention may be necessary or follow-up imaging may be obtained within the next 24 h.

In patients with an epidural hematoma, there is often a “lucid interval” between the trauma and the onset of neurological deterioration. Patients with a subdural hematoma usually have low Glasgow coma scales on admission. Occasionally, patients might only develop progressive symptoms days or weeks after a cranial trauma. CT should always be performed urgently in these patients to exclude a subacute subdural hematoma. In elderly patients, there is often no definite history of a major trauma.

Patients with diffuse axonal injury are unconscious upon admission to the emergency department. Cerebral contusions are not necessarily accompanied by unconsciousness and tend to increase in the hours and days after the traumatic event.

The secondary traumatic brain injuries are often clinically even more important than the primary intracranial lesions. They result from increased intracranial pressure and herniations from cerebral structures from one compartment to the other. The patient develops bradycardia and hypertension and, if there is no relief of the intracranial hypertension, a deterioration of the cardiac function and breathing will follow. Transtentorial, subfalcine, and tonsillar herniations are the most common type.

Diffuse cerebral edema is associated with a mortality rate of up to 50%.

Diagnosis

In the acute stage, CT is the modality of choice. Most acute intracranial lesions can be depicted and, in addition, fractures and the presence of foreign bodies can be demonstrated by using the appropriate bone window width and level settings (Fig. 1).

An acute epidural hematoma appears typically as a biconvex, extracerebral, high-density mass within the epidural space (i.e., the space between the inner table of the skull and the dura). They can displace the brain and cause secondary herniations (Fig. 1). They can cross the falx or the tentorium but not the sutures. Subdural hematomata are located in the subdural space (i.e., the space between the dura and the arachnoid membrane) (Fig. 1). Subdural hematomata can cross the sutures but do not cross the falx or the tentorium. The density of subdural hematomata varies with the clot age. An acute subdural hematoma appears hyperdense and will remain like this for approximately 7 days. In the subacute stage, the hematoma appears isodense compared to brain tissue. A subdural hematoma has a typical crescent shape and may extend over the entire hemisphere.

Posttraumatic subarachnoid and intraventricular hemorrhages can be clearly seen on CT and they also appear hyperdense (Fig. 1).

Diffuse axonal injury may be difficult to detect on CT because these lesions are usually very small, despite the patient’s poor clinical condition. Cerebral contusions are

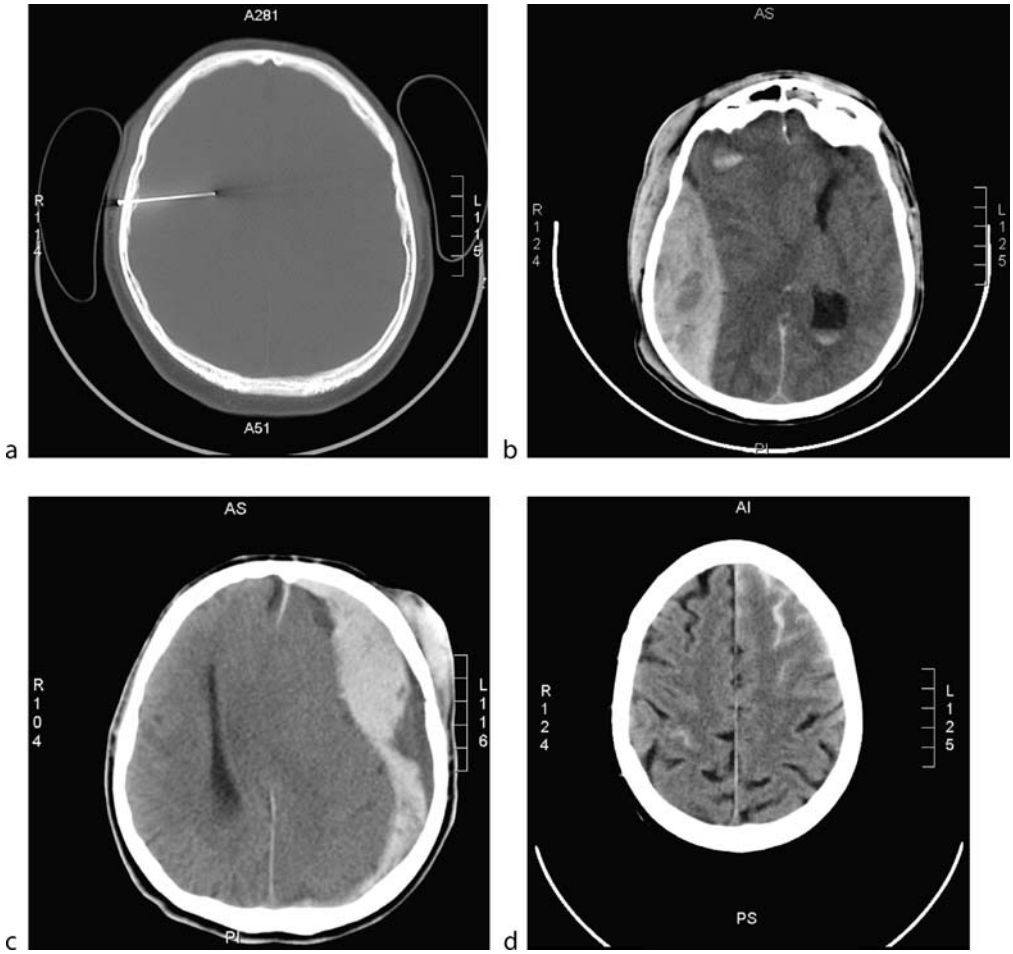

Trauma, Head, Accidental. Figure 1 CT of primary brain injury. Image at bone window setting is acquired to localize the foreign body (a). Epidural hematoma on the right side with displacement of the midline, contusion, and intraventricular blood (b). Subdural hematoma with subfalcine herniation and deviation of the midline (c). Subarachnoid hemorrhage in the left frontal lobe and, to a lesser extent, in the right parietal lobe (d).

seen as ill-defined, low-density lesions containing one or several high-density foci (Fig. 2). Contusions can be subtle in the first hours but can increase in size in the first 24–48 h after the trauma. Brain stem contusions may remain undetected on CT particularly when the hemorrhagic component is subtle.

The two most important secondary traumatic lesions are different types of herniation and diffuse cerebral edema, both of which are the result of the increased intracranial pressure.

The most common herniation is the descending transtentorial herniation. The uncus/parahippocampal gyri are displaced medially with partial or complete effacement of the pentagonal cistern (Fig. 2). One of the consequences is occipital lobe ischemia due to compression of the posterior cerebral artery (Fig. 2). Another well-known complication is Duret hemorrhage in the pons/midbrain. The pathophysiology remains incompletely elucidated and both arterial and venous origins have been suggested. Transtentorial herniation is regularly associated with a tonsillar herniation. The cerebellar tonsils are displaced through the foramen magnum.

Diffuse cerebral edema is an extremely important finding that often warrants immediate neurosurgical intervention. The neuroradiological findings are not always evident. Compression of the ventricles, effacement of the sulci and basal cisterns, and increased density of the falx/tentorium are usually clear. Occasionally, the decreased differentiation between white and gray matter is the first, subtle, sign in the absence of effacement of the sulci (Fig. 2). Diffuse cerebral edema can result in cerebral herniation.

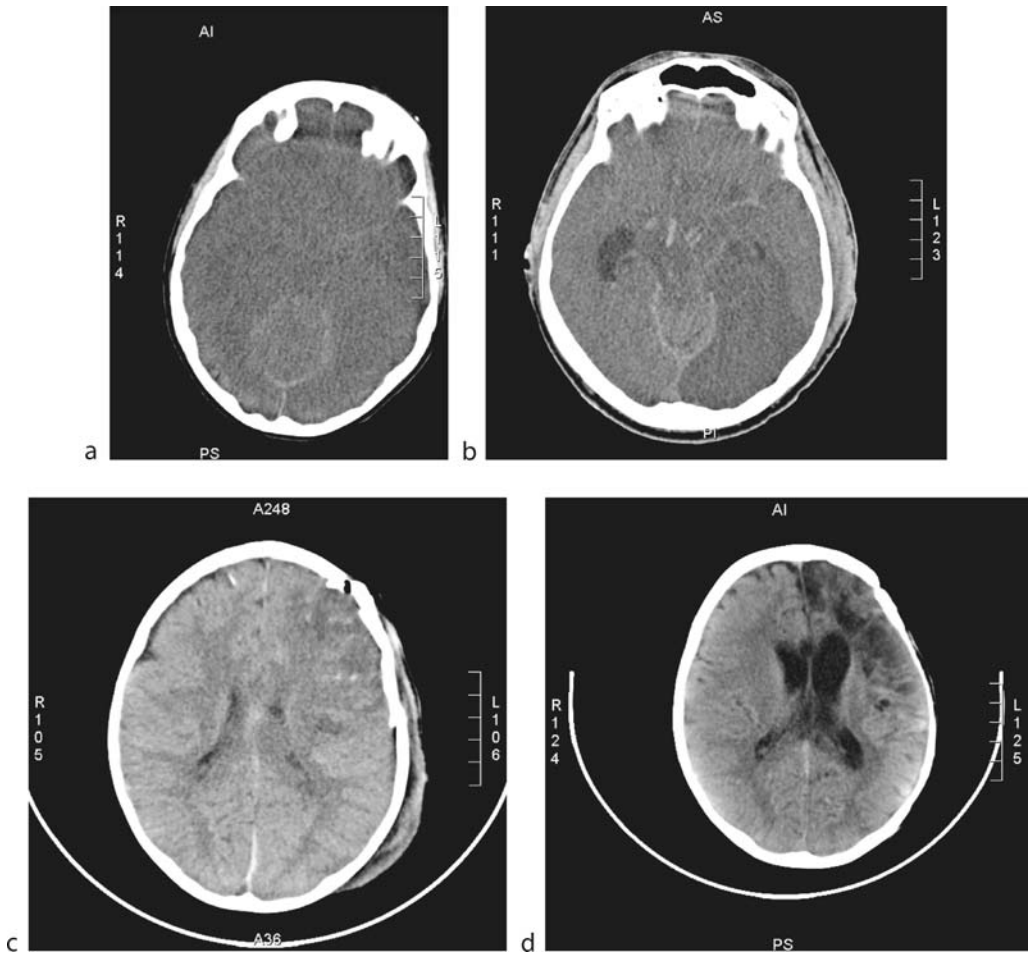

Trauma, Head, Accidental. Figure 2 CT of secondary brain injury. Transtentorial herniation with obliteration of the pentagonal cistern, effacement of the sulci, and hyperdense appearance of the cerebellum indicating brain edema (a). Transtentorial herniation with secondary infarct in the left occipital lobe (b). Brain contusion in the left frontal lobe after 3 days (c) and visualization of the loss of tissue and brain atrophy after 2 months (d).

Late follow-up of intracranial trauma will typically result in brain tissue loss and/or residual atrophy (Fig. 2).

MRI plays an increasingly important role in craniocerebral trauma. In the acute stage, its higher sensitivity can be used for improved parenchymal lesion detection (e.g., in the brain stem and corpus callosum). This may concern primary as well as secondary traumatic lesions. The use of diffusion-weighted imaging appears promising in acute trauma (Fig. 3). T2*-weighted gradient echo images are particularly sensitive for the detection of blood degradation products, and diffusion-weighted images can depict acute lesion that remain undetected on CT.

In patients with a severe trauma and little or no evidence of intracranial pathology, MRI is indicated as soon as possible because this technique is more sensitive for the detection of diffuse axonal injury. Frequent locations are the frontal lobe, the temporal lobe, and the corpus callosum (Fig. 3). When the lesions are hemorrhagic, they are best detected on a T2* sequence, which is more sensitive in the detection of blood degradation products (Fig. 3). They may remain visible for several years.

In the chronic stage, MRI may demonstrate diffuse axonal injury that may be responsible for postcommotional syndrome (memory loss, headache, concentration difficulties) and that remain undetected on CT (Fig. 3).

Bibliography

1. Besenski N (2002) Traumatic injuries: imaging of head injuries. Eur Radiol 12:1237–1252
2. Parizel PM, Van Goethem J, Van Ozsarlak O et al (2005) New developments in the neuroradiological diagnosis of craniocerebral trauma. Eur Radiol 15:569–581

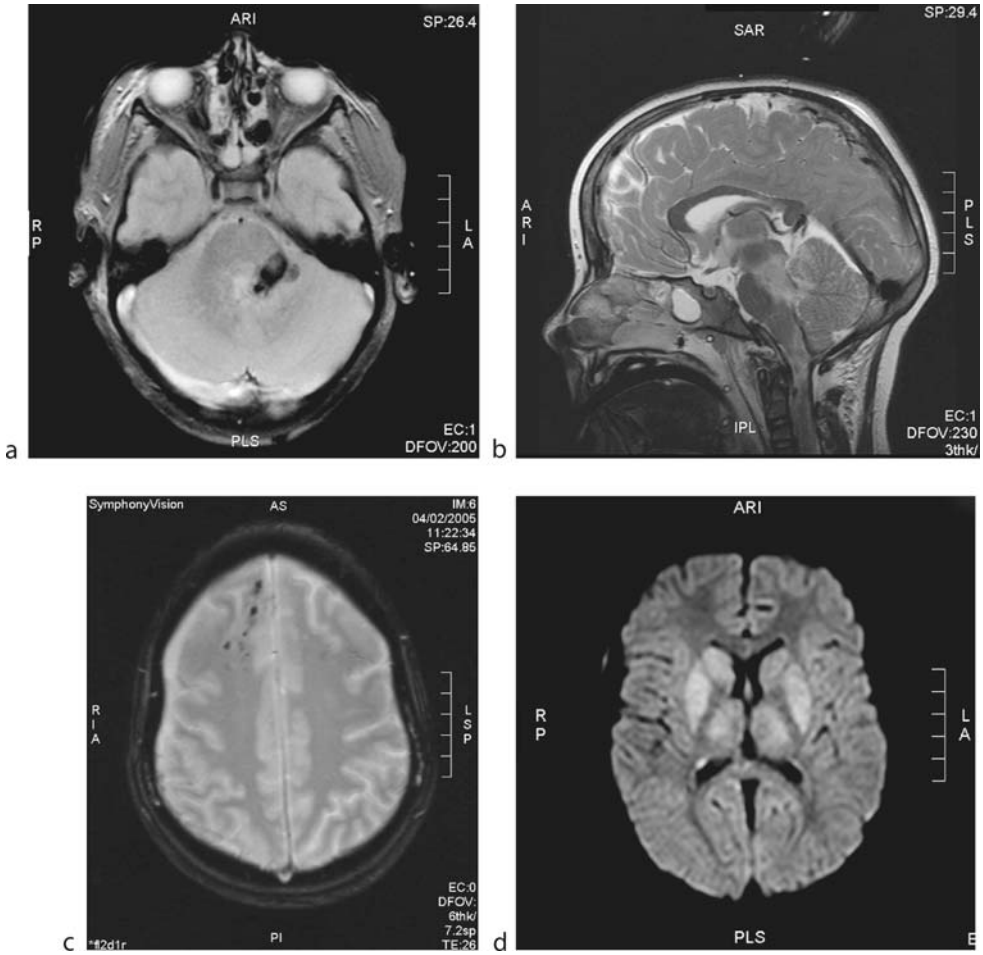

Trauma, Head, Accidental. Figure 3 MRI in brain injury. Secondary hemorrhage (Duret hemorrhage) in the left middle cerebellar peduncle and in the pons (a). Optimal visualization of contusions in the corpus callosum, in the brain stem, and in the cervical spinal cord on a sagittal image (b). Late follow-up in a patient with postcommotional syndrome shows diffuse axonal injury in the right frontal lobe, not visible on CT (c). Diffusion-weighted MRI in a patient with a brain injury and cardiac arrest, showing recent lesions in the basal ganglia and thalami, due to anoxia (d).

Trauma, Head, Non-accidental

Neil Stoodley
North Bristol NHS Trust, Bristol, UK
neil.stoodley@north-bristol.swest.nhs.uk

Synonyms

Nonaccidental head injury (NAHI); Shaken baby syndrome (SBS); Shaken-impact syndrome

Definition

Head injury caused by the application of force in excess of that used during normal handling of a child leading to a combination of some or all of:

- Encephalopathy (usually secondary to hypoxic-ischemic brain injury)
- Multifocal subdural hemorrhages
- Retinal hemorrhages.

the so-called "triad."

Not all cases of nonaccidental head injury (NAHI) will show all of these features (retinal hemorrhages are not

T

always present, even in fatal cases of NAHI), just as not all cases where the triad is present are due to NAHI.

Majority medical opinion believes that the major mechanism of injury is likely to involve shaking of the unsupported infant head backwards and forwards leading to acceleration/deceleration and rotational injury to the intracranial contents.

The incidence of subdural hemorrhage due to NAHI appears to be in the region of 20/100,000 infants and children (1).

The minimum degree of force is likely to be such that an independent witness would recognize that it would be likely to lead to harm to the child.

Pathology/Histopathology

Subdural Hemorrhages

Majority medical opinion believes that differential rotation of the brain and the skull leads to stretching and tearing of the veins which cross the (potential) subdural space, which leads to multifocal subdural hemorrhage.

Brain Injury (Generalized)

There does not appear to be correlation between the extent and distribution of subdural hemorrhages and the degree of signs and symptoms exhibited by the child. The degree of symptoms and signs correlates best with the degree of associated brain injury (2), which in most cases is hypoxic-ischemic in nature as seen on neuroimaging (Fig. 1) and at postmortem. The subdural hematomas seen in NAHI tend to be shallow and do not have a significant space-occupying effect.

Given this, if an injury occurs of sufficient severity for the child to be admitted to hospital, it is likely that there will have been a change in behavior at the time of the causative event and that the child will not have behaved entirely normally afterwards. The timing of these injuries is therefore better assessed by looking at the clinical features of the case rather than by attempting to estimate the age of the subdural blood on the scans.

Brain Injury (Focal)

Focal traumatic brain lesions such as hematomas and contusion, together with diffuse axonal injury (DAI) are occasionally seen, more often in cases where impact with an external surface has been a major mechanism of injury or in more severe shaking injuries.

Clinical Presentation

The symptoms and signs seen following episodes of NAHI are varied, variable and nonspecific. They range from a relatively small change in behavior such as going quiet to going off feeds, vomiting, reduced levels of consciousness, fits to frank coma. Often radiologists are asked to perform scans because the child has presented

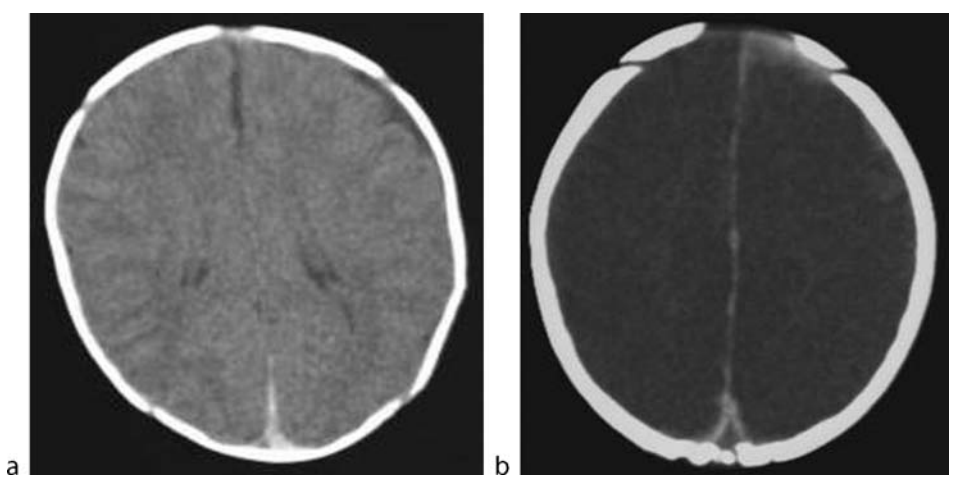

Trauma, Head, Non-accidental. Figure 1 CT scans of two infants admitted following nonaccidental head injury. In (a) there is some high attenuation posterior interhemispheric subdural blood, more on the left than the right. Gray-white differentiation is preserved. This infant presented with relatively few symptoms and recovered rapidly. (b) Shows slightly more extensive acute subdural blood but the acute subdurals are not space occupying. In this infant, the cerebral hemispheres are of abnormally low attenuation and there is loss of gray-white differentiation consistent with extensive hypoxic-ischemic brain injury. The infant presented in a moribund state and died soon after admission.

with an encephalopathic illness and the radiologist may be the first health professional to suggest NAHI as a cause of the encephalopathy. Increasingly, head CT scans are being used as part of the routine investigation of possible nonaccidental injury, even in the absence of neurological symptoms as subdural hematomas can be clinically occult (3, 4).

Imaging

Skull Radiographs

May show fracture(s) and/or soft tissue swelling. It is not possible to assess the age of skull fractures in the same way as for rib/limb fractures; if there is associated soft tissue swelling then a recent injury is more likely.

A full skull series (frontal, lateral, and Townes' views) should be obtained even when a CT head scan has been performed as it is possible to miss quite large fractures on CT if the fracture lies parallel to the scan plane.

The presence of a fracture suggests an impact injury against a hard or unyielding surface. The commonest type of fracture seen in pediatric head trauma (whether accidental or NAHI) is a linear parietal fracture. More complex fractures (diastatic, stellate, depressed, involving more than one bone or a bone other than the occipital) are more likely to be due to, but are not pathognomonic of, NAHI. The complexity of the fracture is more likely to reflect the degree of force causing it rather than the mechanism of injury.

Cerebral Ultrasound

Ultrasound should not be used in isolation in the investigation of NAHI. Convexity subdural hematomas may not be seen on ultrasound and generalized and/or subtle hypoxic-ischemic brain injury may not be appreciated. In experienced hands, subtle focal lesions of DAI may be best seen on ultrasound but such lesions are relatively uncommon in any case.

CT

This is the initial investigation of choice for several reasons. CT scanners tend to be more available than MR scanners; it is easier to scan sick, unstable infants in CT; acute blood is usually easily seen on CT; any abnormalities requiring neurosurgical intervention can be detected early and major focal or generalized brain injury should be reasonably well seen.

Unenhanced scans should be performed initially in the context of the investigation of the undiagnosed encephalopathic child as contrast enhancement may mask the presence of subtle, shallow acute subdural hematomas. A maximum of 5 mm thick sections should be performed throughout the head, especially in the posterior fossa where thicker sections may miss subdural hemorrhage.

The key neuroimaging feature to recognize is the presence and distribution of subdural hemorrhage, the pattern of which is the marker of the mechanism of injury. Subdural hemorrhage or effusion can be seen in a variety of situations in infants and children. A recent UK wide study of subdural hemorrhage and effusion in infants and children under the age of two years (5) showed the following causes from a cohort of 186 cases:

106 = NAHI (57%)
26 = perinatal (14%)
23 = meningitis (12%)
17 = undetermined (9%)
7 = accidental (3.7%)
7 = nontrauma medical (3.7%).

The pattern of hemorrhage seen in association with the naturally occurring medical conditions listed above (as well as others) tends to be rather different to that seen in NAHI and, in any case, there is usually no supportive clinical evidence of such conditions in these cases although, of course, such conditions should be routinely looked for as part of the investigative process. The typical pattern of subdural hemorrhage in the context of NAHI is that of thin, shallow subdurals seen at several separate sites. Because the subdural blood is usually of such small volume, its significance can sometimes be overlooked when seen on scans of infants who are often severely unwell.

Though subdural hemorrhage can be seen following accidental head trauma, when it occurs, it is usually seen at the site of an impact injury and is (usually) seen in association with other evidence of impact injury such as scalp swelling or fracture.

The appearance of blood on CT scans changes with time following an episode of bleeding. Acute blood is by definition brighter than the underlying brain, subacute blood has a similar attenuation and a chronic subdural hematoma is by definition darker than the underlying brain. The time over which this transition occurs is variable and depends on various factors such as the volume of blood present and such factors as whether the patient was anemic at the time of bleeding. Generally a discrete collection of blood may remain bright on CT from soon after an episode of bleeding for up to 7–10 days and blood (if it persists) will become darker that the underlying brain somewhere between 2–3 weeks after an episode of bleeding but these ranges are not absolute.

Low attenuation collections can, however, be seen in the context of acute injuries and it is believed that this happens when the arachnoid is torn at the time of the injury allowing CSF to leak into and collect in the

subdural space, diluting any acute blood that is present. Not all low attenuation subdural collections are therefore due to chronic subdural hematomas. If membranes are seen related to the subdural collections on CT or MR then this would be strong supportive evidence of the collections being chronic.

Any assessment of the age of subdural blood on either CT or MR should be restricted to discrete collections of blood and not to hematomas which have been diluted by or mixed with CSF.

Hypoxic-ischemic brain injury may be seen on CT as affected areas of brain will show decreased attenuation usually associated with reduced gray-white differentiation. The pattern of hypoxic-ischemic brain injury may be generalized, focal and occasionally very asymmetrical (e.g., involving only one hemisphere). The absence of any demonstrable hypoxic-ischemic change on CT (or even on standard MR sequences) does not exclude it (but would suggest that any such injury is relatively mild, see later).

MR

MR is usually used as a secondary imaging investigation after initial CT but is an important part of the investigative process both during the acute phase and for follow up (4). It has several advantages over CT mainly related to its greater sensitivity in the detection of small areas of subdural hemorrhage, which are not well seen on CT or detecting subdural blood in sites not as well seen on CT such as in the subtemporal regions. It is also more sensitive for the detection of parenchymal brain injury both in terms of hypoxic-ischemic brain injury and focal traumatic lesions such as parenchymal hemorrhage or contusions and DAI.

To maximize the potential of MR it is important to image in different planes using different sequences and a typical imaging protocol would include sagittal and axial T1W; axial T2W; coronal proton density and T2W, axial T2*. Diffusion weighted imaging is increasingly being used to detect hypoxic-ischemic brain injury not evident on standard scans and MR also gives the opportunity to look at the spinal cord for evidence of injury or to detect extra-axial bleeding related to the spine.

Different blood breakdown products have different magnetic properties and therefore have different appearances on different sequences. As with CT, it may be possible to give a broad indication of the likely age of the subdural blood present if it is a discrete collection and not mixed with CSF.

Bibliography

1. Jayawant S, Rawlinson A, Gibbon F et al (1998) Subdural haemorrhages in infants: population based study. Br Med J 317: 1558–1561
2. Kemp AM, Stoodley N, Cobley C et al (2003) Apnoea and brain swelling in non-accidental injury. Arch Dis Child 88(6):472–476
3. Kemp AM (2002) Investigating subdural haemorrhage in infants. Arch Dis Child 86:98–102
4. Jaspan T, Griffiths PD, McConachie NM et al (2003) Neuroimaging for non-accidental head injury in childhood: a proposed protocol. Clin Radiol 58:44–53
5. Hobbs CJ, Childs A-M, Wynne J et al (2005) Subdural haematoma and effusion in infancy: an epidemiological study. Arch Dis Child 90:952–955

Trauma Hepatobiliary

Davide Caramella, Marzio Perri, Paola Vagli, Carlo Bartolozzi
Department of Diagnostic and Interventional Radiology University of Pisa, Pisa, Italy
caramella@do.med.unipi.it

Synonyms

Abdominal injury; Abdominal trauma; Blunt abdominal injury; Blunt abdominal trauma; Blunt hepatic injury; Hepatic injury; Liver injury; Liver trauma

Definition

Hepatic trauma is a form of abdominal injury involving hepatic structures. Hepatic traumatic lesions include parenchymal (►contusion, ►hematoma, and ►laceration), intrahepatic vascular (arteriovenous fistula, ►arterioportal fistula, ►pseudoaneurysms, avulsion), and biliary injuries (►biloma, biliary leak, biliovascular ►fistula).

Pathology

The liver is the most commonly injured abdominal organ after the spleen. Hepatic injuries are most frequent in abdominal blunt trauma and are usually sustained by rapid deceleration during road traffic accidents. Due to its large size and its location proximal to the ribs, the right lobe is the most involved site. The coronal ligament's insertion in this parenchymal region augments the effect of the acceleration–deceleration mechanism. Associated lesions are usually observed, including ipsilateral costal fractures, laceration or contusion of the inferior right pulmonary lobe, hemothorax, pneumothorax, and renal and/or adrenal lesions (1).

Penetrating injuries (knife wounds or gunshots) represent rare causes of hepatic injury in Western countries.

Interventional radiology procedures, such as percutaneous biopsy or tumor ablation, cholangiography or biliary drainage, and transjugular intrahepatic portosystemic shunt (TIPS) procedures, may also cause traumatic lesions of the liver, including hematomas, bilomas, intrahepatic fistulas, and pseudoaneurysm.

Depending on mechanism, site, and force, different patterns of hepatic traumatic lesions may occur, and several classifications for liver injuries based on anatomic or radiological findings have been proposed. According to the Organ Injury Scale (OIS) described by the American Association for the Surgery of Trauma (Table 1), liver injuries are currently classified into six grades of severity, ranging from small subcapsular hematoma or superficial capsular tear (grade I) to hepatic avulsion (grade VI) (2).

Clinical Presentation

Hepatic traumatic lesions may cause right upper quadrant pain and tenderness. Clinical signs of bleeding (shock, hypotension, and decreased hematocrit level) and of biliary peritonitis (abdominal pain, nausea, and vomiting) are also common. Occasionally, patients who are asymptomatic after the initial injury may develop later complications such as liver abscess or internal hemorrhage, presumably due to unrecognized liver damage. Associated injuries, particularly rib fractures, are often observed.

Elevation of serum liver enzyme levels in a patient with blunt abdominal trauma may be suggestive of liver injuries. Diagnostic peritoneal lavage, although extremely sensitive for the diagnosis of intraperitoneal hemorrhage, is not always able to determine the origin and extension of a traumatic lesion (1, 3).

Despite the recent improvements in resuscitation techniques, anesthesia, and intensive care, the mortality in both blunt and penetrating liver injuries is still high (10–15%).

Imaging

Ultrasound (US) is fast, accurate, portable, and easy to perform, and it represents the screening modality of choice for blunt abdominal trauma (4). US allows rapid and effective evaluation of both abdominal cavity and parenchymal organs. In evaluation of the abdominal cavity, the main focus is detection of free fluid, which represents ▶hemoperitoneum and is indicative of intra-abdominal injury. Intraperitoneal hemorrhage collects in the most dependent regions of the abdomen and is generally anechoic, conforming to the anatomic site it occupies. The subhepatic space (Morrison pouch) and the pelvis are the most common sites of fluid accumulation. In massive hemoperitoneum, the intraperitoneal organs float in the surrounding fluid under real-time observation.

In hepatic trauma, US can also demonstrate a number of parenchymal traumatic lesions, such as contusions, acute intraparenchymal hemorrhages, hematomas, lacerations, and bilomas.

Hepatic contusions are initially hypoechoic, becoming transiently hyperechoic and then hypoechoic, whereas acute intraparenchymal hemorrhages may be identified as anechoic regions within the abnormal parenchyma.

Trauma Hepatobiliary. Table 1 Classification of liver injuries according to the Organ Injury Scale (OIS)

Grade[a]	Type	Injury description
Grade I	Hematoma	Subcapsular, <10% surface area
	Laceration	Capsular tear, <1 cm parenchymal depth
Grade II	Hematoma	Subcapsular, 10–50% surface area; intraparenchymal, <10 cm in diameter
	Laceration	1–3 cm parenchymal depth, <10 cm in length
Grade III	Hematoma	Subcapsular, >50% surface area or expanding; ruptured subcapsular or parenchymal hematoma; intraparenchymal hematoma >10 cm or expanding
	Laceration	>3 cm parenchymal depth
Grade IV	Laceration	Parenchymal disruption involving 25–75% of hepatic lobe or 1–3 Couinaud's segments within a single lobe
Grade V	Laceration	Parenchymal disruption involving >75% of hepatic lobe or >3 Couinaud's segments within a single lobe
	Vascular	Juxtahepatic venous injuries; that is, retrohepatic vena cava/central major hepatic veins
Grade VI	Vascular	Hepatic avulsion

[a]Advance one grade for multiple injuries, up to grade III

Hematomas usually appear as well-defined, round (intraparenchymal hematomas), or curvilinear (subcapsular hematomas) areas of increased echogenicity in the acute phase. In the following phase, internal echoes due to septation and debris may be revealed. In a more chronic stage, hematomas tend to become more hypoechoic relative to the liver parenchyma.

The appearance of hepatic laceration changes with time: it is initially slightly echogenic and becomes hypoechoic or cystic days after the injury.

Bilomas appear as rounded or ellipsoid, anechoic, loculated structures, fairly well defined and in close proximity to the liver and bile ducts.

In massive liver trauma, a widespread hepatic architectural disruption with absence of the normal vascular pattern is observed.

Finally, color and power Doppler US may be useful for evaluating hepatic vascular injuries such as arteriovenous fistulas and pseudoaneurysms.

Computed tomography (CT) is widely used to investigate the acute trauma victim because it allows accurate visualization of both intraperitoneal and retroperitoneal structures, enabling a complete assessment of any lesion associated with blunt abdominal trauma (1, 5).

Although unenhanced CT may allow detection of several hepatic injuries, intravenous contrast medium administration is required in hemodynamically stable trauma patients. On contrast-enhanced CT scans, various patterns of parenchymal injuries may be clearly distinguished and classified, including contusion, hematoma, laceration, and hepatic fracture.

Hepatic contusion appears as a hypodense area due to interstitial bleeding, with irregular margins, and it is usually associated with major hepatic injuries such as lacerations and hematomas.

Hematomas are caused by bleeding into a tissue laceration; in particular, superficial lacerations usually cause a subcapsular hematoma, a very common hepatic traumatic lesion appearing as a biconvex collection imprinting the hepatic parenchyma. In an acute or subacute setting, CT features of hematoma are hyperdense areas on baseline CT scanning not enhanced after contrast medium administration, whereas chronic hematoma is hypoattenuating on the precontrast scan and can display rim enhancement following intravenous contrast medium administration.

Hepatic laceration is a typical lesion appearing as a nonenhancing linear streaking areas on contrast-enhanced CT. These lesions can be single or multiple and tend to involve parenchymal areas contiguous to intrahepatic portal vascular branches and suprahepatic veins. A large range of severity must be distinguished in lacerative lesions of the liver, including small and superficial lesions of the hepatic capsule (capsule tears), lacerations involving the central portal triad (deep lacerations), and major deep laceration extending between two margins of the organ (hepatic fracture). In massive liver trauma, deep and complex lacerations are usually associated with biliary complications, including bilomas, ▶hemobilia, and rarely biliary peritonitis.

Hepatic biloma appears as a cystic, loculated structure of low attenuation in or around the liver either on unenhanced or contrast-enhanced CT scans. Hemobilia is due to a posttraumatic communication between a blood vessel (generally, a hepatic artery branch) and a biliary duct, but it also may be caused by a rupture of a pseudoaneurysm into a biliary duct. Bile peritonitis is an uncommon complication of blunt liver trauma. CT findings of bile peritonitis include persistence or increasing amounts of low-attenuating free peritoneal fluid and thickening of the peritoneum that shows evidence of enhancement.

Finally, CT scan is also useful for evaluating injuries involving intrahepatic vessels, particularly hepatic avulsion and hemoperitoneum (1). Hepatic avulsion, consisting of the devascularization of the entire organ, represents the most important traumatic injury of the liver. It results in a complete lack of enhancement after intravenous contrast medium administration at CT scanning. Hemoperitoneum associated with a traumatic lesion of the liver represents an important prognostic factor. Evaluation of intraperitoneal hemorrhage or an expanding parenchymal hematoma is a criterion for grading the severity of trauma. CT may document a minimal quantity of extravasated peritoneal or retroperitoneal blood, also allowing detection of traumatic vascular lesions such as portal or suprahepatic venous branch lacerations, arterial pseudoaneurysm, and arteriovenous fistula.

Other imaging techniques include magnetic resonance (MR), which has a limited role in the evaluation of abdominal trauma patients. However, MR can be used to monitor liver injury, particularly MR cholangiography, and MR angiography offers an accurate depiction of traumatic complications involving biliary and vascular structures.

Another potential use of MR is in patients with renal failure and in those who are allergic to iodinated contrast medium.

Angiography is useful to localize the site of hemorrhage and provides an opportunity for the interventional radiologist to proceed to transcatheter embolization of bleeding sites.

Nuclear Medicine

Biliary scintigraphy with ^{99m}Tc iminodiacetic acid (IDA) provides useful information in cases of suspicious biliary

leakage; ^{99m}Tc sulfur colloid or ^{99m}Tc-labeled denatured red blood cell studies are rarely employed in the evaluation of patients with blunt hepatic and splenic trauma.

Diagnosis

The rapid detection of abdominal injury is among the most important goals of trauma care. Before the advent of current diagnostic modalities for abdominal evaluation, many trauma patients died for undetected abdominal lesions, including liver injuries.

Because abdominal physical examination is unreliable in most cases, diagnostic peritoneal lavage has been widely used for evaluating blunt abdominal trauma. However, diagnostic peritoneal lavage has several limitations, including invasiveness and low specificity, and has largely become replaced by US for the early triage of patients with blunt abdominal trauma. Currently, US represents the screening modality of choice for the detection of fluid collections and, if possible, of parenchymal lesions in abdominal trauma patients. US findings suggesting a liver traumatic lesion or peritoneal fluid in hemodynamically stable patients are an indication for CT examination.

In fact, because CT allows definition of the exact location and extension of the liver lesions, demonstration of active hemorrhage, and quantification of the degree of hemoperitoneum, it is considered the mainstay of diagnosis of hepatic injuries in patients who do not undergo immediate laparotomy. Nowadays, initial CT findings help direct patient treatment, particularly by stratifying hemodynamically stable patients into those who require intervention and those who can be treated nonsurgically. Furthermore, repeated CT examinations are useful to monitor the course of healing and detect later vascular or biliary complications that may go clinically undetected (1, 3, 5).

Interventional Radiological Treatment

Several interventional radiological procedures, including therapeutic angiography and image-guided drainage, can be used in the management of abdominal trauma (3).

Transcatheter embolization is largely employed for treating recurrent liver parenchymal bleeding and represents the first therapeutic option in cases of hepatic acquired vascular malformation, including pseudoaneurysms and arterioportal or arteriovenous fistulas.

Bleeding from a major hepatic vein can be controlled by placing an intravenous stent, while percutaneous biliary stenting may be used for treating biliary–vascular fistulas.

Usually, in small bilomas (<3 cm) conservative management is indicated, whereas bilomas >3 cm should systematically be drained under US or CT guidance to avoid pseudoaneurysm development.

CT- and US-guided drainage also provide effective nonoperative options for the management of posttraumatic large hematoma and liver abscess.

Bibliography

1. Romano L, Giovine S, Guidi G et al (2004) Hepatic trauma: CT findings and considerations based on our experience in emergency diagnostic imaging. Eur J Radiol 50(1):59–66
2. Moore EE, Cogbill TH, Jurkovich GJ et al (1995) Organ injury scaling: spleen and liver (1994 revision) J Trauma 38:323–324
3. Carillo EH, Wohltmann C, Richardson JD et al (2001) Evolution in the treatment of complex blunt liver injuries. Curr Probl Surg 38(1):60
4. McGahan JP, Wang L, Richards JR (2001) From the RSNA refresher courses: focused abdominal US for trauma. Radiographics 21:191–199
5. Becker CD, Mentha G, Terrier F (1998) Blunt abdominal trauma in adults: role of CT in the diagnosis and management of visceral injuries. Part 1: liver and spleen. Eur Radiol 8:553–562

Trauma, Pancreatic

The pancreas is involved in 3–12% of abdominal injuries. A mortality rate of 20% has been reported with pancreatic injuries, as these are often associated with trauma to other organs. Usually, penetrating trauma results in the highest frequency of pancreatic injury and is almost always associated with concurrent injury to other intra-abdominal organs. Therefore, the pancreas is prone to injury due to blunt abdominal trauma when it is compressed against the spine, being relatively fixed compared with overlying bowel similarly to other retroperitoneal organs. Injury to the pancreas may cause contusion or rupture and consequently acute pancreatitis and its complications. Although US is excellent for showing fluid collections, CT represents the most suitable diagnostic study in hemodynamically stable patients with trauma. In fact, CT permits to better imaging not only the entire pancreatic gland (thus depicting possible contusion or rupture or inflammatory complications) and other retroperitoneal organs, but it also allows the identification and characterization of other possible traumatic injuries by means of a rapid evaluation of the entire abdomen, chest, and head during the same examination.

▶ Pancreatitis, Acute

Trauma, Spinal

G. Pellicanò, F. Martinelli, L. Napolitano
Radiodiagnostic Unit, University of Florence Careggi Hospital, Florence, Italy
gianni.pellicano@unifi.it

Definition

Spinal trauma can take on a variety of forms: road accidents, falls, also gunshot wounds and other penetrating injury. Vertebral trauma may irreversibly damage the spinal cord, and is acute and unexpected, dramatically changing the course of an individual's life. Since spinal cord injuries frequently occur in young and previously healthy individuals, the personal and social cost is extremely high. Severe forces indirectly applied to the vertebral column are the most frequent mechanisms of spinal cord injury. Such a force, generated during sudden flexion, hyperextension, vertebral compression, distraction or rotation of the vertebral column, may result in misalignment of the vertebral column, fracture of vertebral bodies, ligamentous injury, disc herniation and development of epidural haematoma. Consequently, the spinal cord may be compressed and lacerated, or stretched and even transected. Damage to the spinal cord can result in edema and haemorrhage. Spinal trauma can be subdivided into an acute and chronic phase of spinal injury. Since a higher number of patients survive the acute phase than in the past, a higher incidence of chronic lesions will occur [2, 3].

Clinical presentation

Depending on the severity of the injury, symptoms may range from pain, normally at the site of trauma to tetra- or paraparesis when spinal cord is involved or radicular deficits in cases with nerve root avulsion. The American Spinal Injury Association has issued guidelines for a standardized physical examination.

Imaging

This includes plain radiographs, CT and MRI. The first of these is valuable for demonstrating abnormal vertebral alignment in dislocation vertebral compression fractures, and the second for localising osseous fragments relative to the spinal canal, as well as demonstrating articular fractures. Neither can provide evidence of spinal cord injury [1].

MRI has proved to be a significant noninvasive tool in evaluating the spinal cord in the acute stages following injury, and provides a direct image of the nature and extent of cord damage. In addition, MR is very useful in evaluation of chronic sequelae of spinal cord trauma.

To assess traumatic spinal instability the three-column rating is widely used. This states that instability requires disruption of at least two of the three columns. The anterior column is formed by the ventral half of the vertebral body, disc and ventral ligaments; the middle column by the posterior vertebral body, disc and posterior longitudinal ligament, and the posterior column by the posterior bony and ligamentous elements.

Acute Spinal Injury

Bony lesions

Loss of spinal alignment and vertebral body displacement are readily recognised on plain films: this kind of deformation is also detectable on sagittal CT reconstructions[1] and mid-sagittal MR images (Fig. 1). Degenerative facet changes frequently lead to subluxation which may be misinterpreted as being the result of spinal injury. Undisplaced fractures are difficult to detect on plain films: smaller ones or those involving the posterior elements are usually undetectable. Compression of the anterior vertebral body leads to a wedge-shaped fracture. The posterior vertebral border with the pedicles, arch, articular processes and ligamentous apparatus are usually intact.

In the presence of spinal spondylosis or stenosis, a trivial trauma may cause significant spinal cord injury, even without visible fracture or dislocation.

Fracture lines in the vertebral body are best seen on CT sections, and frequently affect the end-plates, most often the cranial plate, which can then no longer be displayed in one CT section. In compression fractures, sagittal and transverse computerized reconstructions confirm the wedge deformity of the vertebral body, the normal height of the posterior wall and the anatomic contours of the spinal canal.

CT is also useful in the assessment of posterior traumatic lesions of the neural arch and articular processes.

MRI can demonstrate larger vertebral fractures as a discontinuity of the thin black line of cortical bone on T1 W images; sometimes also on T2 W images. The typical wedge-shaped deformity of a vertebral body is well seen on T1 W images. In the acute stage, bone marrow signal intensity may be reduced on T1 W scans; T2 W and STIR images may show inhomogeneous areas of high signal, indicating a higher water and blood content. After a few months, compression fractures show a relatively

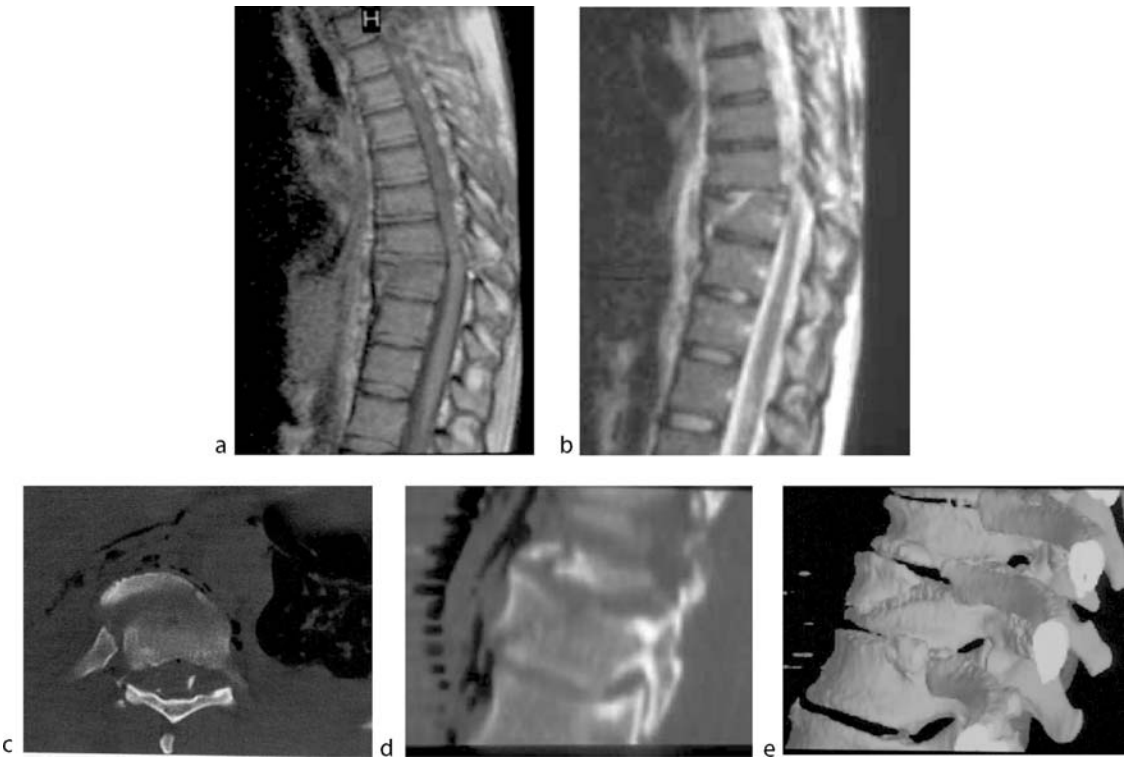

Trauma, Spinal. Figure 1 Spinal Trauma; MR SE T1 (a) TSE T2 (b) Tear fracture of vertebral body with posterior displacement. Spinal cord compression is present. This findings are confirmed, with more details by CT (c, d, e).

normal marrow signal intensity and sometimes fatty degeneration in elderly patients. MR is able to demonstrate bone bruising of vertebral bodies, even without other evidence of fracture. This injury produces signal alterations, presumably as the result of microfractures, edema and haemorrhage characterized by hypointensity on T1 W and hyperintensity on T2 W images.

Fracture fragments, especially if retropulsed into the spinal; canal, are also identifiable on MRI, directly on T1 W images if they have a detectable marrow component within them, or indirectly on T2 W images by their impingement on the dural sac. When cortical bone fragments are small, it may be difficult to distinguish them from ligaments, because both structures have the same low signal intensity.

Ligamentous injures

The anterior and posterior longitudinal ligaments, ligamenta flava and interspinous ligaments play an important role in the stability of the spine. Overstretched or ruptured ligaments can be directly visualized on MR images because ligaments normally have low signal intensity. Intermediate or high signal intensity on T2 W images within or around ligaments in their normal location is indicative of edema or hematoma.

Anterior longitudinal ligament disruption may be associated with extensive haemorrhage and oedema in prevertebral soft tissues.

Disc herniation

Spinal trauma can cause intervertebral disc injuries in up to 25% of cases. Marked dislocation of the vertebrae is possible only in association with a severe injury of the involved disk. Traumatic disc herniation may be responsible for cord or root compression. The appearance of a traumatic disk herniation is the same as that of a hernation unrelated to trauma. On T1 W images, disc material of normal intermediate signal intensity is identified anterior or posterior to the vertebral body margins; on T2 W images, the traumatized disc can show abnormal high signal.

Nerve root avulsion

Nerve root avulsion is most often due to a traction injury of the shoulder. There is avulsion of the root sleeve with dural laceration.

Retraction of the nerve stump creates a cavity that is later filled with CSF sometimes extending through the neural foramen, called a root sleeve pocket or pseudo-

meningocele, demonstrated by CT-myelography or by T2 weighted MR images.

Epidural hematoma

This lesion results from tearing of the epidural venous plexus with extravasation of blood into the epidural space. Since the spinal dura is not firmly adherent to the vertebral canal, large epidural haematomas may extend over multiple levels.

In the acute stage, the hematoma is isointense with spinal cord on T1 W images; on proton density and T2 W images, it is isointense to the adjacent CSF in the subarachnoid space: they may be distinguished by the hypointense dura which separates the two compartments.

Intravenous administration of Gadolinium DTPA does not provide enhancement of the epidural blood collection, but can be useful to outline the haematoma from the adjacent strongly enhancing venous plexus.

Spinal cord lesions

The pathologic appearance of the spinal cord following an injury includes a spectrum of findings, from macroscopically normal through cord swelling, edema, punctuate or coalescent haemorrhages to complete cord transection.

The spinal cord may appear normal in 8 to 34% of patients with traumatic neurological deficits. The short TI inversion recovery (STIR) sequence is the most sensitive to depict intramedullary posttraumatic lesions. Fluid attenuated inversion recovery (FLAIR) images are useful in case of post-traumatic syrinx formation.

Spinal cord swelling is a focal expansion of the cord not associated with intramedullary signal changes, centered at the level of the injury and tapering gradually cranially and caudally. It is better appreciated on T1 W sagittal images. Spinal cord swelling may be difficult to appreciate at the level of compression when traumatic narrowing or pre-existent stenosis of the spinal canal is present; in these cases, the surrounding subarachnoid space is completely effaced.

Cord edema is a focal accumulation of intracellular and interstitial fluid in response to injury. The swollen segment of spinal cord has a normal signal intensity on T1 W and high signal intensity in T2 W images.

A purely edematous intramedullary lesion is associated with less severe clinical deficit than in haematomyelia of the spinal cord, which is associated with the most severe and lasting functional compromise.

The MRI appearance and evolution of haemorrhagic spinal cord lesions resembles those of intracranial bleeds and depend on the time elapsed post-trauma. In the hyperacute phase haemorrhage may be isointense to the cord on T1 W images and iso- or slightly hyperintense on T2 W due to the presence of oxyhemoglobin; in the acute stage, because of the susceptibility effect of deoxyhemoglobin, signal intensity decreases on T2 W images, especially when gradient echo (GRE) technique is employed. In the subacute stage, due to the presence of methemoglobin, haemorrhage may exhibit high signal intensity on both T1 and T2 W images (Fig. 2).

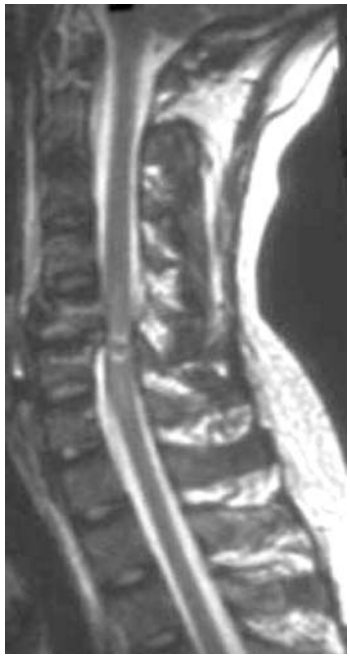

Trauma, Spinal. Figure 2 Spinal Trauma; MR TSE T2 sagittal: vertebral fracture at C5-C6 level; spinal cord compression is visible with a low intensity area inside the cord due to hematomyelia.

The most serious lesion which can occur during spinal trauma is complete cord transection. The discontinuity of the cord is well depicted on T1 W images.

Chronic Injury

Here also, MRI represents the image technique of choice. Initial edema and haemorrhage lead to changes caused by rupture of membranes of the nerve cell bodies, with release of lysosomes and subsequent cytolysis and necrosis. Then the acute exsudate and necrotic tissues are replaced by macrophages. This reparative stage may persist for years, resulting in a pathologic entity defined as posttraumatic myelomalacia and characterized by presence of cysts, gliosis and fibrosis.

On MRI, myelomalacic cavitations produce hyperintensity in the spinal cord on T2 W images; on T1 W

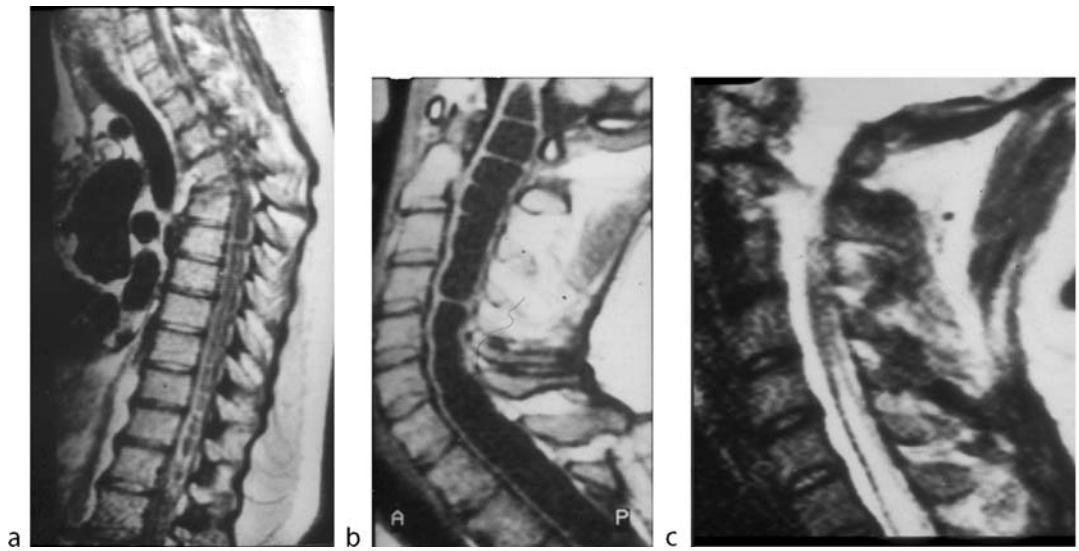

Trauma, Spinal. Figure 3 Spinal Trauma; Chronic Phase. MR SE T1 sagittal (a) Vertebral collapse at mid-thoracic level one year before. Cavitation of the cord is visible below the vertebral fractures due to syringomyelia. Post-traumatic syringomyelia MR SE T1sagittal (b) 6 months after trauma. TSE T2 sagittal (c) the cavity is reduced after shunt.

images they are poorly demonstrated and marginated. They may be found within a normal sized cord or appear as a focal expansion of an otherwise atrophic cord.

On rare occasions, intramedullary cysts may enlarge and coalesce after several years of neurologic stability, leading to a spontaneous deterioration of the neurologic status of a spinal cord injury patient. This deterioration can be catastrophic for the patients with only marginally useful function.

There is no explanation for this delayed progressive myelopathy, classified as post-traumatic syringomyelia, occurs most frequently in cervical lesions, usually progressing rostrally from the original site of the injury. Cyst contents are isointense to cerebro spinal fluid. Cyst enlargement as demonstrated by MRI may aggravate symptoms, making surgical shunt shunting of the cyst necessary.

MRI can also identify other long-standing spinal cord abnormalities such as cord compression due to traumatic fractures and dislocation; focal or diffuse cord atrophy with cord a-p 6mm or less; and subarachnoid adhesions tethering the cord, or cysts which compress the cord.

Bibliography

1. Cohen WA, Giauque AP, Hallam DK et al (2003) Evidence-based approach to use of MR imaging in acute spinal trauma. Eur J Radiol. October 48(1):49–60
2. Mann FA, Cohen WA, Linnau KF et al (2003) Evidence-based approach to using CT in spinal trauma. Eur J Radiol. October 48(1):39–48
3. Van Goethem JW, Maes M, Ozsarlak O et al (2005) Imaging in spinal trauma. Eur Radiol. March 15(3):582–590

Trauma, Splenic

Davide Caramella, Carla Cappelli, Paola Vagli, Carlo Bartolozzi
Department of Diagnostic and Interventional Radiology, University of Pisa, Pisa, Italy
caramella@do.med.unipi.it
bartolozzi@med.unipi.it

Synonyms

Splenic traumatic injury; Splenic traumatic lesions; Splenic traumatic rupture

Definitions

Splenic injuries may be classified as subcapsular and ►intraparenchymal hematomas, parenchymal lacerations, ►splenic fractures, or splenic vascular injuries.

Although protected under the bony ribcage, the spleen represents the most frequently injured intraperitoneal organ in cases of blunt thoracoabdominal injury. Preexisting diseases can markedly increase the risks and severity of splenic injury; for example, splenic diseases that produce splenomegaly (such as hematologic, infectious disorders, etc.) are often accompanied by a thinning of the capsule, making the spleen more fragile.

Subcapsular lesions may rupture with apparently insignificant trauma because of a weakened overlying capsule. Penetrating injuries also frequently involve the spleen. The spleen is the most vascular organ of the body; for this reason, splenic injury poses a potentially life-threatening situation.

Clinical Presentation

The clinical presentation of splenic trauma is widely variable, and a significant number of patients do not manifest symptoms. Because the spleen contains no pain sensors, and pain fibers are present only within the splenic capsule, left upper abdominal or flank pain represents the most common clinical manifestation due to local peritoneal irritation or overlying soft tissue or bone injury (e.g., fractures of the lower ribs may be associated). Diffuse abdominal pain may be present in cases of free intraperitoneal blood, leading to diffuse peritoneal irritation.

Clinical findings related to systemic blood loss can manifest and include tachycardia, tachypnea, restlessness, and pallor. Hypotension suggests overt shock and represents a surgical emergency.

Imaging

Although computed tomography (CT) represents the technique of choice for evaluating splenic injuries, ultrasound (US) is effective for initial evaluation of trauma victims with suspected blunt abdominal injuries because it can be performed rapidly in the admission area (1). Thanks to its high sensitivity for detecting free intraperitoneal fluid, US represents the imaging modality of choice for initial screening for free abdominal fluid, and it has widely replaced peritoneal lavage. In hemodynamically unstable patients, the presence of significant hemoperitoneum on US enables selection for immediate exploratory laparotomy. Visualization of fluid in the right upper quadrant suggests the possibility of splenic injury. In some cases, splenic injuries may be identified. Splenic hematomas and ►lacerations may appear hyperechoic if they contain acute hemorrhage; more subacute or chronic parenchymal injuries often result in heterogeneous echogenicity.

In trauma victims who are hemodynamically stable, CT represents the imaging method of choice for detecting visceral injuries and determining their extent. The advent of CT scanning has made conservative management more practical and safer for victims of splenic injury, thanks to the high sensitivity in diagnosis and staging of splenic injuries.

Besides perisplenic hematomas and intraparenchymal clots that may be hyperdense in baseline conditions compared with normal spleen, when performing CT in splenic trauma evaluation, intravenous contrast is essential. In general, areas of intraparenchymal lesions are lower in density than normal spleen; moreover, active arterial extravasation may be identified as high-attenuation foci.

Care must be taken to avoid image acquisition too soon after contrast infusion (before 60 sec), as the inhomogeneous appearance of the splenic parenchyma, due to differential diffusion of contrast between red pulp and white pulp, is difficult to interpret. Another possible pitfall in splenic trauma is diffuse hypodensity due to local hypoperfusion in the hypovolemic state.

CT can accurately demonstrate the presence of hemoperitoneum and determine its extent. In some cases, the only CT finding to suggest a splenic injury is the presence of a perisplenic hematoma or hemoperitoneum in the left paracolic gutter ("sentinel clot sign"). On occasion, this sign is seen only on the precontrast study because the attenuation of hemoperitoneum is highest immediately adjacent to the parenchymal lesion. Another subtle CT feature suggesting splenic injury is thickening of the lateroconal and anterior pararenal fascia, due to parasplenic hemorrhage.

CT is highly accurate in depicting and distinguishing parenchymal traumatic lesions. Splenic parenchymal injuries include subcapsular and intraparenchymal hematomas, parenchymal lacerations and fractures, and vascular injuries involving the splenic pedicle.

►Subcapsular hematoma characteristically appears as a peripheral collection of fluid with a lenticular shape that flattens or compresses the lateral margin of the spleen. If the splenic capsule is intact, no free perisplenic blood may be observed at all.

Intraparenchymal hematoma appears as a round or irregular area with attenuation values of 50–70 UH. The attenuation value of the clotted blood within the hematoma gradually decreases, becoming a hypodense area within normally perfused splenic parenchyma.

Parenchymal lacerations are linear low-density lesions with a branching appearance.

They typically involve the lateral surface of the spleen, whereas splenic fractures are deep lacerations that traverse the splenic parenchyma and extend to the splenic hilum. In severe cases, the spleen is shattered into small fragments.

Vascular injuries involving the splenic pedicle or parenchymal arteries can be identified.

CT enables detection of intrasplenic pseudoaneurysms, arteriovenous fistulas, and active contrast extravasations. Pseudoaneurysms are caused by intimal trauma and disruption of elastic fibers, leading to intimal lesion and weakening of the arterial wall.

The presence of splenosis is a possible complication of splenic trauma, easily detectable during a follow-up examination.

Various CT-based grading systems to help determine patient outcome and management have been proposed. For example, Resciniti grading analyzes the extent of splenic parenchymal injury, capsular lesions, and hemoperitoneum by using a quantitative CT severity score. However, its effective value in clinical decision making and therapeutic planning remains controversial.

The role of magnetic resonance (MR) in evaluating splenic trauma is actually limited because several technical restrictions often render MR examination impractical in victims of multiple trauma. However, MR can be useful in the follow-up of some splenic traumatic lesions, such as hematomas, which demonstrate a time course of changes in signal intensity due to the paramagnetic properties of degradation products of hemoglobin. Subacute hematomas usually present high signal intensity on both T1- and T2-weighted images because of the presence of methemoglobin. In case of areas of devascularization within the splenic parenchyma, low signal can be appreciated, compared with the high signal intensity of normal splenic tissue after gadolinium injection.

Angiography is not employed as a diagnostic tool but is reserved for treatment in patients with active bleeding. Angiography is sensitive in detecting the site of active (1, 2) arterial bleeding, and transcatheter embolization represents an alternative to surgery for conservative treatment and preservation of the immunologic function of the spleen (1–3).

Nuclear Medicine

Nuclear medicine imaging is not helpful in evaluating splenic trauma and is nowadays widely substituted by tomographic imaging techniques, in particular CT.

Diagnosis

In patients with blunt abdominal trauma, physical examination is not sufficient to diagnose an abdominal visceral injury. Laboratory studies are also not very helpful in diagnosing splenic injury, but blood cell count and hemoglobin level are important in the initial evaluation and follow-up of trauma victims. Before the advent of tomographic imaging techniques (US and CT), diagnostic procedures such as diagnostic peritoneal lavage were the only diagnostic methods. Nowadays, diagnostic imaging in the hemodynamically stable patient has become indispensable, not only for diagnosis but also for adequate management. In particular, CT allows the identification and characterization of traumatic splenic injuries and the rapid evaluation of the entire abdomen, chest, and head to identify other possible lesions during the same examination.

Rupture of the spleen after an asymptomatic period, defined as delayed rupture, represents a possible feared complication. Delayed rupture of a subcapsular hematoma may occur as a result of hyperosmolarity in the course of clot lysis; delayed bleeding may also originate from the free rupture of a perisplenic hematoma into the peritoneal cavity. In some cases, delayed hemorrhage is due to a splenic capsular disruption with either intermittent or very slow continuous bleeding. Therefore, delayed splenic rupture represents an injury in evolution, and patients with abdominal trauma must be submitted to careful clinical surveillance and imaging follow-up.

The diagnosis of splenic rupture is not particularly challenging; however, many processes can affect the spleen and sometimes simulate laceration or intrasplenic hematoma, such as splenic infarction and splenic focal lesion. Congenital clefts of the spleen should not be mistaken for parenchymal lacerations; these are generally seen along the medial margin of the spleen, often at the superior margin. Care must be taken to distinguish splenic traumatic lesions from a ▶spontaneous rupture due to predisposing pathological splenic processes, which must be identified.

Bibliography

1. Jeffrey RB, Ralls PW, Laing FC (1996) The spleen. In: Jeffrey RB, Ralls PW (eds) CT and sonography of acute abdomen. Lippincott-Raven, Philadelphia, pp 122–159
2. Robertson F, Leander P, Ekberg O (2001) Radiology of the spleen. Eur Radiol 11:80–95
3. Weishaupt D, Grozaj AM, Willmann JK et al (2002) Traumatic injuries: imaging of abdominal and pelvic injuries. Eur Radiol Jun 12 (6):1295–1311

Traumatic Diaphragmatic Tear

Most frequently due to penetrating chest trauma. Large lesions allow for herniation of the abdominal organs into the thoracic cavity. Typical clinical complications are intestinal obstruction and respiratory failure. Small lesions are often overlooked on initial chest X-rays because they are masked by pleural effusion or atelectasis and may lead to secondary herniations. Signs are an abnormal course of the nasogastric tube, intrathoracic location of abdominal organs, obliteration, elevation, or distortion of the diaphragm, pleural effusion, contralateral shift of

the mediastinum, and fractures of the lower ribs. CT shows the discontinuity of the hemidiaphragm in 70% of the patients and/or herniation. Dynamic MRI is well suited to show diaphragmatic integrity and function.
▶Chest Trauma

Traumatic Hernia

▶Contrast Media, Ultrasound, Influence of Shell on Pharmacology and Acoustic Properties

Triplane Fracture

Adds to the Tillaux a coronal fracture of the distal tibia metaphysis.
▶Fractures, Bone, Childhood

Trolley-Truck Sign

Multisegmental ossification of the interspinal ligaments and the joint capsules of the apophyseal joints of the caudad segments as a facultative feature in long-standing ankylosing spondylitis. It is seen in anteroposterior plain X-ray images of the lumbar spine.
▶Spondyloarthropathies, Seronegative

Tuberculosis, Lung

Jose Caceres
Department of Radiology, HGU Vall d'Hebron, Universitat Autonoma, Barcelona, Spain
josecac@gmail.com

Definition

Pulmonary tuberculosis (TB) is a common lung infection caused by *M. tuberculosis*. Classically, pulmonary TB is divided in two forms: primary and postprimary. These groups not only represent clinically different processes, but also different radiological presentations. AIDS patients are frequently infected by TB and respond differently than patients with normal immunity.

Atypical mycobacterial infections (atypical TB) are steadily increasing, whereas the incidence of tuberculosis in the Western World has declined. Because of the similarities, pulmonary disease caused by nontuberculous mycobacteria (NTMB) is included in this chapter.

Pathology/Histopathology

In primary TB, the initial response relies in macrophages and lymphocytes, resulting in an indolent inflammatory reaction. Delayed hypersensitivity develops 4–10 weeks after the initial infection; its hallmark is caseous necrosis. In reactivation TB, hypersensitivity accelerates the changes and caseous necrosis occurs at an early stage. Same changes occur in AIDS, conditioned by the immune status of the patient. The gross and microscopic changes of NTMB are usually undistinguishable from TB.

Clinical Presentation

Worldwide, primary TB occurs mainly in the pediatric age group. In areas where the disease is not prevalent, the primary form may represent up to a quarter of adult TB cases. It presents few clinical symptoms and the patients are usually asymptomatic.

Postprimary TB is considered a reactivation of a previous tuberculous lesion. Often, this reactivation is related to periods of immunodepression, malnutrition, or debilitation. Symptoms are often unspecific. Patients may have a mild cough with hemoptysis and low-grade fever.

Altered immunity such as in AIDS patients favors the infection and alters the natural course of the disease. TB is usually disseminated and up to 60% of patients have extrapulmonary disease.

The most common clinical presentation of NTMB is similar to that of tuberculosis and indistinguishable from that disease.

Imaging

Imaging findings are based mainly on two techniques: conventional chest radiograph (CXR) and CT. CXR is good for initial suspicion and for monitoring treatment. CT helps to discover new findings or to clarify findings of CXR.

Primary TB

Mediastinal lymphadenopathy is often the only radiological finding. Pulmonary consolidation may be an associated feature. CXR is often normal, but sometimes it

shows hilar enlargement with or without a faint infiltrate. CT is more sensitive than CXR for the detection of lung lesions and enlarged lymph nodes.

Miliary TB may occur in both primary and post-primary TB and is commonly seen in the elderly, children under 2 years of age and in immunocompromised patients. It is due to hematogenous spread and consists of multiple diffuse nodules, typically 1–3 mm in size. CXR may be normal in early stages. CT allows accurate early diagnosis, by depicting the randomly distributed micro-nodular pattern.

Pleural TB is considered a complication of primary TB and is common in adolescents and young adults. Nevertheless, it sometimes occurs in postprimary TB. CXR shows unilateral pleural effusion. Tuberculous effusions are very rich in proteins and often show fibrin strands and septa on ultrasound. CT rarely detects this finding. Tuberculous pleuritis usually resolves spontaneously, but treatment is necessary to prevent the development of fibrothorax. Despite proper treatment, around one third of patients develop some degree of pleural thickening. Empyema is a rare complication.

Postprimary TB

In the lung, postprimary TB manifests as patchy, poorly defined segmental consolidation, mainly located in the apical and posterior segments of the upper lobes, and less frequently in the superior or inferior segments of the lower lobes. Cavitation is the hallmark of this form and appears in around half of patients (Fig. 1). In tuberculous lobar pneumonia evolution is more indolent than bacterial pneumonias

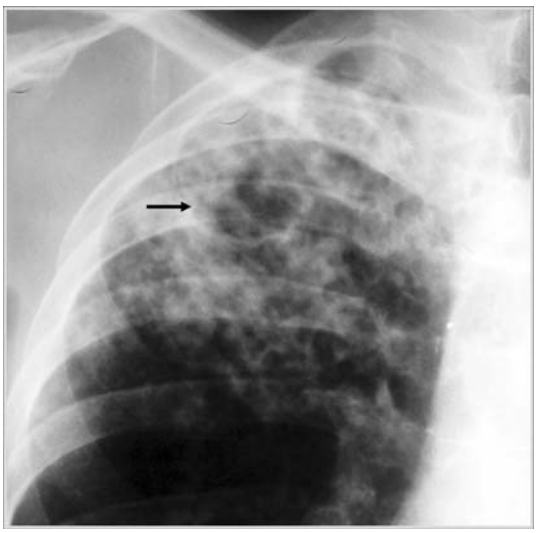

Tuberculosis, Lung. Figure 1 Active postprimary TB. There is air-space disease in the RUL with a central cavity (*arrow*).

Disseminated nodular opacities associated with the cavitation or alone are common parenchymal features of bronchogenous spread. It is seen in CT as the "tree-in-bud" pattern, consisting of multiple peripheral branching linear structures representing bronchogenic dissemination of the disease with caseation necrosis in the respiratory and terminal bronchioles. They have a lobar or segmental distribution and are considered a reliable marker of the activity of the process.

Involvement of the tracheobronchial tree is frequent in the postprimary form. If airway involvement is not recognized and appropriate antituberculous therapy is not instituted promptly, cicatricial bronchial stenosis is almost inevitable, with resultant atelectasis, obstructive pneumonitis, and bronchiectasis. The prevalence of tuberculous bronchial stenosis varies from 40% in the preantibiotic era to 10% in patients in more recent years (1).

Complications and Late Sequelae

Tuberculomas are seen as well-defined nodules located mainly in the upper lobes. They may appear after primary TB or reactivation TB. Calcification occurs in about 20–30% of cases. CT provides better visualization of the calcifications and characteristics of the nodules. In rare cases, they have areas of decreased attenuation corresponding to caseum (2).

Postprimary TB may heal with parenchymal scarring, nodules, and calcification. Fibrotic mass-like lesions may form and become indistinguishable from superimposed carcinoma. Apical pleural thickening ("apical cap") may be seen on X-rays. CT demonstrates that this is mainly a thickened layer of extrapleural fat.

A complication of cavitary scarring is colonization with *Aspergillus* and development of a fungus ball. Massive hemoptysis is the cause of death in 5–14% of patients. At CT, the immature ▶aspergilloma is seen as a network with irregular air pockets within the cavity. This network coalesces to form a mature fungus ball, classically seen as a round mass, which moves within the cavity depending on the patient's position.

Fragments of calcified necrotic material from lymph nodes can erode through a bronchial wall and come to lie within the airway lumen (▶broncholithiasis), often causing obstruction and atelectasis. Finding calcium near an area of pulmonary collapse should arouse suspicion of a broncholith. The location of calcium within or adjacent to the bronchus is easily confirmed with CT (Fig. 2).

Bronchial involvement in pulmonary tuberculosis is not rare and bronchial perforation of tuberculous origin is common in children. Bronchoesophageal perforation secondary to tuberculosis and leading to fistulous tract formation (bronchoesophageal fistula) is significantly

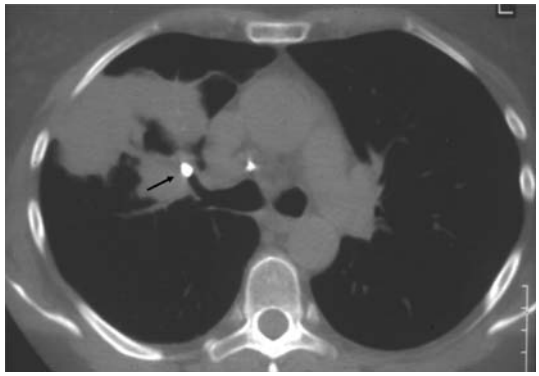

Tuberculosis, Lung. Figure 2 Broncholithiasis. The arrow points to a broncholith, which occludes the anterior segment of the RUL bronchus.

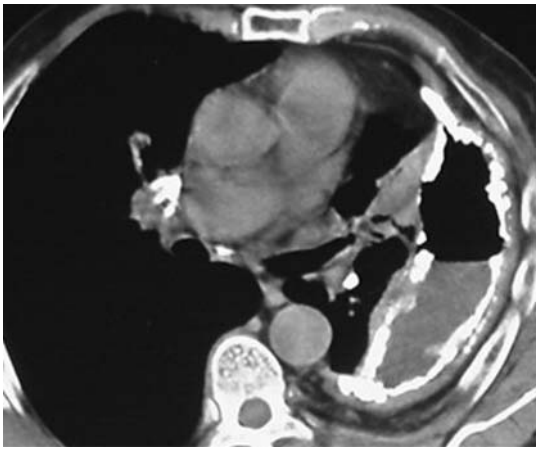

Tuberculosis, Lung. Figure 3 Bronchopleural fistula. Note the air–fluid level within the calcified pleural layers.

rare. The diagnosis is usually made with a barium esophagogram, which shows the fistulous communication between the esophagus and the bronchi.

Rasmussen aneurysm is a pseudoaneurysm of a peripheral pulmonary artery that forms in a tuberculous cavity. It may cause severe hemoptysis and necessitate embolization. CT is specially suited for their demonstration.

Calcified mediastinal lymph nodes are usually found in healed TB. An excessive fibrotic reaction may cause fibrosing mediastinitis with compression and sometimes occlusion of mediastinal structures. CT is useful for suggesting or corroborating the diagnosis, and for showing the effect on the mediastinal cardiovascular structures and tracheobronchial tree.

A complication of TB pleuritis is the development of fibrothorax, with or without calcification of the pleural layers. Fibrothorax appears to be the most common source of late bronchopleural fistula. Radiographically, it most often appears as a new pleural air–fluid level (Fig. 3), sometimes with a tension pneumothorax. Knowing whether active infection is present is crucial in selecting appropriate medical treatment.

Tuberculous ▶empyema necessitatis is an uncommon complication of fibrothorax in which the inflammatory mass spontaneously bores its way from the pleural cavity into the soft tissues of the thoracic wall, forming a subcutaneous abscess that sometimes opens to the skin. The usual clinical presentation is a mass in the thoracic wall, accompanied or not by a cutaneous fistula. CT and MRI are of great value in making the diagnosis by showing a pleural collection associated with an abscess in the chest wall.

TB in the Immunocompromised Host, Especially AIDS

Radiographic manifestations depend upon the immune status of the patient. In AIDS, patients with CD4 lymphocyte count greater than 200 cells/mm^3 usually have radiographic findings similar to postprimary TB, whereas patients with lower counts have atypical findings: diffuse and lower lobe opacities, mediastinal adenopathy, and military pattern. Some of these patients may have normal CXR. Patients infected with NTMB may have apparent radiographic worsening when treated with antiretroviral (3).

Atypical Mycobacteria Infection

NTMB infection is similar to that of tuberculosis and, in a specific patient, is indistinguishable from that disease. Two specific appearances are described:

The first group is typified by elderly white men who have underlying chronic lung disease, such as chronic obstructive pulmonary disease or pulmonary fibrosis. The chest radiograph shows changes that are indistinguishable from postprimary TB. Cavitation is common. Lymphadenopathy and pleural effusion are unusual.

The second group includes middle-aged or elderly white women without underlying lung disease. Characteristic CT findings are scattered bronchiectasis and multiple centrilobular nodules of varying size, usually less than 1 cm. These nodules are thought to represent NTMB granulomas. The most common location for bronchiectasis is the middle lobe and lingula. There is no dominant apical distribution in contrast to postprimary TB (4).

Nuclear Medicine

Isotopic studies are not generally used in tuberculous infection. It is important to know that active pulmonary tuberculomas commonly cause increased FDG uptake in PET studies and should not be confused with malignant nodules (5).

Diagnosis

A definitive diagnosis of TB is established by isolation of tubercle bacilli in culture. Sputum is the diagnostic specimen of choice. Bronchoalveolar lavage and transbronchial biopsy may be used in patients that do not produce sputum.

Gastric contents in children may also be examined.

Diagnosis of NTMB is more difficult and includes culture confirmation from sputum or tissue whenever possible and/or radiographic or clinical improvements (or both) while the patient is receiving three to five antimycobacterial drugs.

Interventional Radiological Treatment

In incoercible hemoptysis, embolization of bronchial arteries can be an alternative to surgical treatment.

Percutaneous injection of amphotericin B has been proposed in inoperable active pulmonary aspergilloma.

Bibliography

1. Leung AN (1999) Pulmonary tuberculosis: the essentials. Radiology 210(2):307–322
2. Andreu J, Caceres J, Pallisa E et al (2004) Radiological manifestations of pulmonary tuberculosis. Eur J Radiol 51(2):139–149
3. Fishman JE, Saraf-Lavi E, Narita M et al (2000) Pulmonary tuberculosis in AIDS patients: transient chest radiographic worsening after initiation of antiretroviral therapy. Am J Roentgenol 174:43–49
4. Holling NP, Wells AU, Wilson R et al (2002) Comparative appearances of non-tuberculous mycobacteria species: a CT study. Eur Radiol 2(9):2211–2217
5. Goo JM, Im JG, Do KH et al (2000) Pulmonary tuberculoma evaluated by means of FDG PET: findings in 10 cases. Radiology 216:117–112

Tuberculosis, Parenchymal

E. Turgut Tali, Serap Gultekin
Gazi Üniversìtesì, Turkey
turgut.tali@gazi.edu.tr

Definition

Parenchymal tuberculosis (TB) can manifest as TB granuloma (tuberculoma; most common form), focal areas of cerebritis, cerebral abscess, or rarely as TB encephalopathy and may be isolated or associated with basal meningitis.

Pathology/Histopathology

These lesions originate as a conglomerate of micrograNulomata in an area of TB cerebritis that join to form a mature noncaseating tuberculoma. In most cases, subsequent solid center caseous necrosis will develop which may eventually liquefy. Outside the capsule, there is parenchymal edema and astrocytic proliferation (1, 2).

Clinical Presentation

The clinical manifestations are nonspecific. The common presenting symptoms and signs are headache, intracranial hypertension, seizures, focal neurological signs, and fever.

Imaging

Tuberculomas are located at the corticomedullary junctions. In children, most tuberculomas are infratentorial, in adults they are supratentorial and frequently affect the frontal and parietal lobes (1, 2). The radiological presentation depends on the content of the lesion. One or more lesions with different characteristics and stages may be seen in the same patient.

Computed Tomography

The lesions are usually of reduced density or isodense with brain before contrast medium administration. In contrast to metastasis, there is little edema.

Magnetic Resonance Imaging

Noncaseating tuberculomas are usually hyperintense on T2-weighted imaging and they do enhance. Solid caseating tuberculomas display a shortening of T2 signal that may be due to the presence of free oxygen radicals in macrophages (3). They show central heterogeneous enhancement with a capsule presenting a ring-enhancing pattern. Tuberculomas with central liquefaction demonstrate a central hypointense signal on T1-weighted imaging and hyperintense signal on T2-weighted imaging. An intense rim enhancement is seen on postcontrast T1-weighted images. Magnetic resonance spectroscopy (MRS) may show prominent lipid peaks due to high lipid content in the caseous material. Presence of serine has been accepted as a distinct feature in tuberculomas.

In contrast to the solid caseating tuberculoma, the TB abscess is formed by semi-liquid material which is rich in bacilli (2). Tuberculous encephalopathy shows extensive damage to the white matter and seems to be due to a type IV hypersensitivity mechanism including cell-mediated immunity to tuberculoprotein. Neuroimaging studies show

uni- or bilateral cerebral edema, perivascular demyelination, or hemorrhagic leukoencephalopathy (1, 2).

Diagnosis

The cerebrospinal fluid (CSF) findings on lumbar puncture are increased protein, low glucose levels, and pleocytosis. Isolation of microorganisms from CSF is positive in less than 40% of initial lumbar punctures. Polymerase chain reaction for TB may help confirm the diagnosis earlier.

Bibliography

1. Arbealáez A, Medina E, Restrepo F et al (2004) Cerebral tuberculosis. Semin Roentgenol 474–480
2. Bernaerts A, Vanhoenacker FM, Parizel PM, Van Goethem JWM, Altena RV, Laridon A, Roeck JD, Coeman V, De Schepper AM (2003). Tuberculosis of the central nervous system: Overview of neuroradiological findings. Eur Radiol 13: 1876–189
3. Wilson JD, Castillo M (1994). Magnetic resonance imaging of granulomatous inflammations: sarcoidosis and tuberculosis. Top Magn reson Imaging 6:32–40

Tuberculosis, Urinary Tract

F Z Gueddari, F Imani
Service de Radiologie Centrale, CHN, Rabat, Morocco
fzgueddari@hotmail.com

Definition

Tuberculosis remains a significant lethal contagious disease. In developed countries, the urogenital system is the second most frequent location after the lung, representing 5% of the tuberculosis bacteria.

The female-to-male ratio is 3:1. The average age of patients at diagnosis is 43 years, with renal infection rarely occurring before 20 years of age. Approximately 50% of the patients have a simultaneous active pulmonary infection or have a medical history of lung tuberculosis.

Pathology/Histopathology

Usually, the urinary system focus appears 5–20 years after the infection, a period during which the initial focus, generally pulmonary, has seeded the kidneys silently *via* the blood circulation, constituting cortical lesions that are cured or encysted by sclerosis (1–3).

Tuberculous granulations will evolve toward caseation and the opening in the excretory system. From there, the Koch bacillus will follow the course of the urine with a possible colonization of all the segments of the upper and lower excretory tract.

The characteristic element of this progression is the absence of lesion continuity and the absence of parallelism between the renal lesions and the underlying lesions. More rarely, the renal attack is part of the visceral dissemination of the tuberculous miliaries. It is exceptional during an evolutive pulmonary tuberculosis, as well as in a tertiary phase.

Histologically, lesions come in the shape of typical tuberculous follicles grouped in granulations or in nonspecific nodules. On the other hand, the macroscopic aspect depends on two opposed processes, one of destruction and caseation, creating cavities, the other of defense by fibrosis and sclerosis limiting the extension of the lesions and inducing signs of obstruction which evolve on their own account and which give the urogenital localization all its particularity, compared to other localizations.

Clinical Presentation

Renal tuberculosis may remain dormant for many years after the kidneys have become seeded during the primary tuberculous infection. Patients usually become symptomatic, with extension of the disease to the renal pelvic area and ureters causing hydronephrosis. Specific symptoms may be lacking until the hydronephrotic kidneys become secondarily infected. Frequency and urgency of urination and dysuria may ensue, with development of tuberculous cystitis. However, long before patients become symptomatic, sterile pyuria, albuminuria, and hematuria are present, although cultures for pyogens yield negative results (1, 3, 4).

Diagnosis is usually made using imaging, cystoscopy, and culture of acid-fast bacilli from early-morning urine specimens. Needle aspiration biopsy is a last resort when urine cultures are negative.

Imaging

Plain radiographs can show the size and the shape of the kidneys as well as calcifications at the level of the genitourinary system. Renal calcifications are found in more than 50% of cases, consisting of stones in the excretory tracts, calcifications in the caseous debris, or in the cicatricial lesions of the kidneys. The calcifications suggestive of tuberculosis are either fine and in clods, or joining and bulky in the kidney cement. They can also

outline the walls of the pyelic cavities or the ureter in which they are encrusted, giving an image of ureteral rails or of a small porcelain basin.

Intravenous urography (*IVU*)(1, 4): It demonstrates the extension and the severity of the lesions, allowing one to evaluate the efficiency of treatment and to detect any complications.

Renal Parenchymatous Lesions

Tuberculomas rarely result in a renal tumoral syndrome. The calyceal ulceration results in a loss of the concavity of the calyx, the picture of which is fuzzy and irregular.

The evolution is toward an incompletely opacified calyx, or a phantom calyx. The tubercular cavities show cavities of variable aspect. Their filling is slower than that of the healthy excretory tract. They are joined to the pyelocalyceal cavities by a thin opening, typically short, irregular, and sinuous (Fig. 1).

Clear pockets on nephrographs are images of a spherical gap of avascular structure, bordered by a fine wall. They correspond either to cavities that no longer communicate with the excretory tract or to hydrocalyces.

Parenchymatous atrophy may be localized (notch, segmentary atrophy) or diffuse (small disharmonious kidney). Usually, these scars are associated with a calcification of the parenchyma, at the level of parenchymatous destruction zones or in a blocked cavity.

Lesions of the Upper Urinary Tract

In the initial stages, IVU can be normal in 10% of cases or can show fuzzy walls, thin ulcerations, and hypotonia with loss of peristalsis.

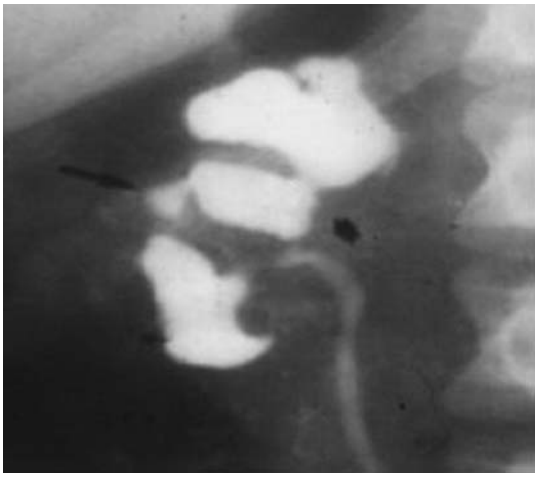

Tuberculosis, Urinary Tract. Figure 1 Urinary tract tuberculosis. Intravenous urograph of the right kidney shows a shortened, strictured, and tubular renal pelvis with dilated cavities, and presence of hydrocalyx.

In the advanced stages, the lesions of the upper urinary tract are tight and retractile stenoses, shortening the tuberculous segment and leading to a dilatation higher up. In the calyces, we can observe a calyceal amputation with an attraction of the renal pelvis toward the amputated calyx. The stenosis of the renal pelvis can reduce it to a short and thin conduit (Fig. 1).

Ureteral stenoses can be solitary or multiple, taking on a moniliform aspect.

In the terminal stages, a final fibrosis and a consecutive obstructive uropathy are responsible for real "autonephrectomy" with a mute kidney. The kidney can be small, normal, or hypertrophied according to the degree of atrophy and hydronephrosis. In this case, the study of the kidney is best carried out by ultrasound and tomodensitometry.

Lesions of the Bladder

A normal aspect corresponds to the first contaminations, making cystoscopic exploration necessary with eventual biopsies. An image with a double contour is a result of a significant thickening of the bladder's wall. The bladder can be deformed and asymmetrical with ureteral reflux.

Wall ulcerations can simulate a carcinoma. A small tubercular bladder corresponds to a significant retraction of the bladder, which becomes irregular with reduced capacity and with parietal calcifications.

Ultrasound

Ultrasound is used particularly for the identification of hydronephrosis or pyonephrosis in the case of an alteration of the renal function. However, its sensitivity is limited in the detection of small calcifications as well as for cavities communicating with the excretory tract. Its main disadvantage is that early papillary anomalies or tiny urothelial anomalies are not highlighted. It allows two forms to be described (1, 3):

Infiltrative form: The kidney is the seat of one or several parenchymatous masses or caverns sometimes deforming its contours. The cavern usually produces a transonic image of variable margins. It can also be presented in the form of a parenchymatous, hypo- or isoechogenic nodular image (Fig. 2a). These lesions correspond to tubercular abscesses.

One can also find heterogeneous hyperechoic caverns, probably due to their fibrous evolution. A hyperechoic cavern with a subsequent cone of shadow testifies to a calcified cavern.

Renal calcifications are visible, but it is difficult to recognize fine and homogeneous calcifications, in mounds, specific to tuberculosis, whose regrouping is often evocative on plain radiographs. In the case of

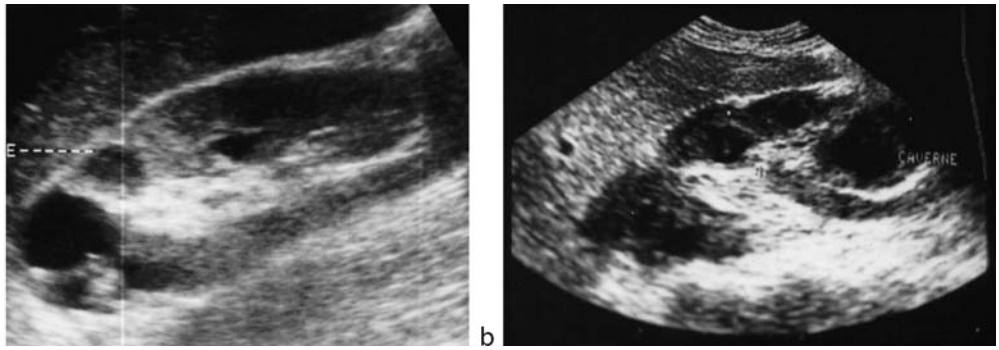

Tuberculosis, Urinary Tract. Figure 2 (a) Urinary tract tuberculosis. Ultrasound image shows multiple cortical lesions of different aspects: echogenic mass probably corresponding to a tuberculoma, transonic mass corresponding to a parenchymocalyceal tuberculous cavernous lesion. (b) Urinary tract tuberculosis. Ultrasound image showing hyperechoic sinus, strictured renal pelvis, and cavernous cortical lesion suggesting renal tuberculosis.

cement kidney, the renal surface considerably attenuates the ultrasounds and renders the analysis of the structures impossible. Ureteral calcifications are seldom seen on ultrasound.

Obstructive form: The dilation of the pyelocalyceal cavities is a dominant element. Their contents can be transonic in the case of hydronephrosis, hypoechoic and inhomogeneous in the case of pyonephrosis. Sometimes there is a liquid–liquid level with mobile fragments. The dilation of only one part of the cavities, by located stenosis, generally with presence of debris, is very suggestive of tuberculosis.

On the other hand, ureteral dilation is not always detectable. The use of high-frequency probes makes it possible to detect other sonographic signs such as the thickening of the dilated calyceal wall, having a double-rail aspect, or a fine transonic sluice connecting a cavern to a pathological calyx.

Other sonographic forms: A sonographically normal kidney, associated with a mute kidney on the IVU, is pathognomonic of tuberculosis and corresponds to a diffuse infiltration of the parenchyma. We can also observe a pyelocalyceal cavity dilation with a spoke-wheel appearance, with an invisible sclerosed renal pelvis, and a hyperechoic sinus, evocative of tubercular kidney (Fig. 2b).

CT Scan

It is generally prescribed as a second option to evaluate the formations responsible for a mass syndrome in the excretory system, to explore mute kidneys, and to evaluate the perirenal and pararenal space. It is also more sensitive than IVU for the detection of functional anomalies and allows a better evaluation of the morphological anomalies (1, 2).

In the initial forms, computed tomography (CT) scan is generally normal, but it can sometimes show a small renal pelvis and the thickening of its walls. In the more advanced stages, the morphological modifications shown on CT scan include the focal scars responsible for cortical notches, hydronephrosis or generalized pyonephrosis, calyceal dilation without renal pelvis dilation, the degree of renal destruction, focal hypodensities, and the presence of calcifications.

If the calyces are full of liquid, the densities vary from 0 to 10 H. Debris and casein measure between 10 and 30 H, calcifications between 50 and 120 H, and calculi nearly 120 H. Hypodense zones of the tubercular abscesses corresponding to caseous necrosis are presented as a solid mass, with variable enhancement after contrast medium injection (Fig. 3a, b).

Thirty-five percent of patients present dilation of the pyelocalyceal cavities, cortical notches, calcifications, and hypodense zones; 40% present at least three of these signs. Calcifications are clearly seen on CT scan (detected in more than 50% of cases), and are more easily classified, including calculi, the calcification of a part or the entire kidney, and the homogeneous calcification of cement kidney.

CT scan is also very useful in the determination of the renal and perirenal extension by highlighting pseudotumoral infiltrative images. It will also depict extrarenal infections, particularly in the adrenal glands. In the final stages, evaluation of the mute kidneys is possible (cement kidney, hydronephrosis, or pyonephrosis). CT scan can sometimes incidentally detect very advanced forms of tuberculosis.

Ureteral lesions: They appear in nearly 50% of genitourinary tuberculosis cases and lead to the formation of stenoses and dilation. CT scan is more sensitive than IVU and ultrasound for the detection of ureteral dilations. The thickening of the ureteral wall as well as the periureteral fibrosis are easily identified on CT scan. Stenoses are frequently multiple, usually touching the

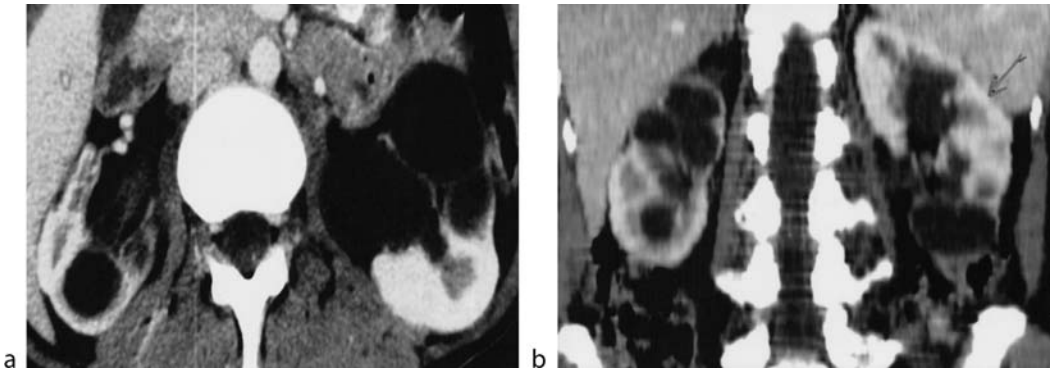

Tuberculosis, Urinary Tract. Figure 3 (a) Urinary tract tuberculosis. Postcontrast CT in a man with renal tuberculosis shows cortical bilateral excluded cavities, and a tissular enhancement of the left posterior localization corresponding to a young tuberculoma. (b) Urinary tract tuberculosis. Coronal CT reconstruction shows multiple cystic lesions communicating with the excretory system corresponding to parenchymocalyceal tuberculous cavernous lesions, and a localized tissular enhancement of the left kidney corresponding to a young tuberculoma.

distal third of the ureter. CT scan is also sensitive in the detection of ureteral calcifications.

Bladder lesions: CT scan is seldom required for the exploration of a tubercular bladder; it is generally carried out for the assessment of abdominal or urogenital tuberculosis. The organic aspects are especially represented by a small bladder with irregular thickened wall. Lesions of the upper urinary tract are often present.

Magnetic Resonance Imaging

Thanks to the development of good imaging, fast new sequences, with diuretic and contrast medium injection, Magnetic Resonance Imaging (MRI) allows a fast exploration in one session of the three components of the upper urinary tract, called nephro-angio-uro-MRI (NAU-MRI). The level of a ureteral obstacle is easily determined without the need to carry out delayed scans, as well as the severity of the obstruction by visualizing perirenal and periureteral edema (1, 5).

MRI is good at depicting tuberculous cavities, sinuses tracts, and fistulous communications (Fig. 4a, b). However, small areas of calcification are difficult to detect on MRI scans, although they are pivotal to the diagnosis of tuberculosis.

This technique could be valuable for patients with renal insufficiency and pregnant women, constituting a diagnostic technique and allowing nontraumatic and nonradioactive monitoring. In the same way, its excellent visualization of the ureters should make it possible to reduce significantly the indications of invasive techniques such as retrograde pyelography.

Other Techniques

Retrograde ureteropyelography is seldom used and its indications are limited to the nonfunctional kidneys. It shows hydronephrosis, pyonephrosis, or ureterohydronephrosis with one or more ureteral stenosis (1/3 of the cases). In the remaining cases, it finds extensive lesions of the excretory system. It should be noted that catheterization failure occurs in less than 5% of cases, by stenosis of the ureter (1–3).

Retrograde cystography can highlight a vesicoureteral reflux or allow the study of the urethra if the IVU is insufficient (voiding scan).

Arteriography is carried out only when a partial nephrectomy is considered. It can be normal if the lesions are tiny.

Nuclear Medicine

Isotope renography is the most sensitive imaging modality available for the assessment of renal function. The role of radionuclides in imaging patients with renal tuberculosis is confined to assessment of relative renal function by renography when surgery or nephrectomy is contemplated. However, radionuclide imaging usually cannot differentiate the various causes of depressed renal function.

Diagnosis

Findings in all imaging modalities used for the diagnosis of GUT are essentially nonspecific because the diagnosis is based on the presence of calcification, cavities, and strictures, which are associated with a long list of differential diagnoses: genitourinary calcification may occur in patients with schistosomiasis and diabetes mellitus. Brucellosis also may mimic tuberculosis. A congenital megacalyx and focal papillary necrosis may mimic renal tuberculosis radiologically.

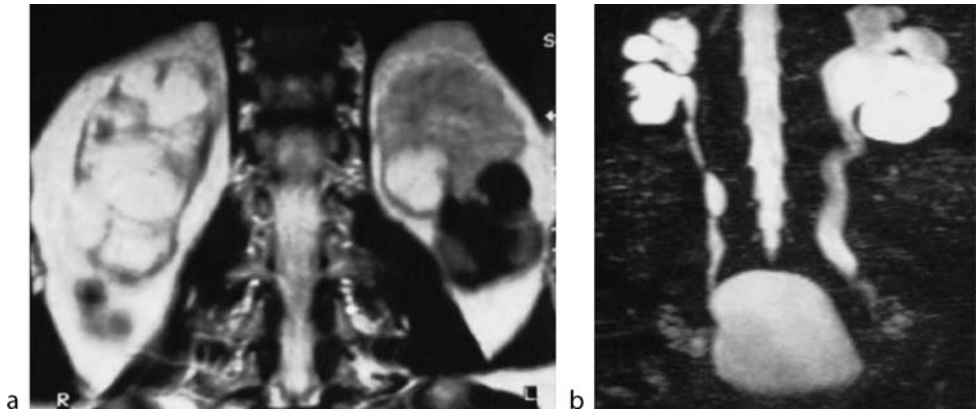

Tuberculosis, Urinary Tract. Figure 4 (a) Urinary tract tuberculosis. MRI T2 coronal plane image shows cortical heavy calcification of the inferior left renal pole, and a parietal cavernous calcification in the superior right renal pole, with intense hyposignal. Note the multiple cavernous lesions, with liquid signal on T2-weighted imaging. (b) Urinary tract tuberculosis: URO-MRI showing pyelocalyceal lesions, strictured renal pelvis, and multiple ureteral stenoses on the right side, ureterohydronephrosis with stenosed lower ureter.

However, a fairly confident diagnosis can be made in most instances with clinical correlation. In summary, imaging changes are observed late in the disease (all imaging findings may be normal in patients with early GUT); in many instances there is a significant group of differential diagnoses, and therefore the diagnosis is determined by culture not imaging.

Bibliography

1. Imani F, Gueddari FZ (2005) Tuberculose de l'appareil urinaire. Imagerie de l'appareil génitourinaire. Médecine–Sciences. Flammarion
2. Kao SC, Fang JT, Tsai CJ et al (1996) Urinary tract tuberculosis: A 10-year experience. Chang Gung Med J Mar;19(1):1–9
3. Leder RA, Low VHS (1995) Tuberculosis of the abdomen. Radiol Clin North Am 33(4):691–705
4. Hopewell PC (1995) A clinical view of tuberculosis. Radiol Clin North Am 33(4):641–653
5. Louka G, Liberopoulos K, Fidas A et al (1999) MR Urography in the diagnosis of Urinary Tract Obstruction. Eur Urol 35(2):102–108

Tuberous Sclerosis

Autosomally dominant inherited disorder involving mental disability, lesions of the cerebral cortex, peculiar skin lesions (adenoma sebaceum of Pringle), and, sometimes, visceral lesions (angiomyolipomas, hemangiomas, hamartomas, cysts).

▶Neoplasms, Splenic, Benign
▶Neurocutaneous Syndromes

Tubo-Ovarian Abscess

TOA develops most commonly as a complication from longstanding or insufficiently treated PID. It manifests as a complex inflammatory lesion involving ovary and fallopian tube, or as a deep pelvic abscess. Pyosalpinx is a typical finding in TOA.

▶Abscess Tubo-Ovarian

Tubular Adenoma

Benign tumor composed of small, round tubules and little stroma.

▶Adenoma, Breast

Tubular Carcinoma

Highly differentiated ductal carcinoma with good prognosis.

▶Radial Scar, Breast
▶Carcinoma, Other, Invasive, Breast

Tubular Necrosis, Kidney, Acute

Michele Bertolotto, Elena Trincia
Manuel Belgrano, Stefano Cernic,
Ada Mandic, Maria Assunta Cova
Department of Radiology, University of Trieste,
Trieste, Italy
bertolot@univ.trieste.it

Synonyms

Acute tubular necrosis; Acute tubular nephropathy; ATN

Definitions

Acute tubular necrosis (ATN) is the predominant cause of acute renal failure (ARF) among hospitalized patients (1). This pathological condition is characterized by varying degrees of tubule cell damage and by cell death usually resulting from prolonged renal ischemia or from nephrotoxins. The process is potentially reversible, but patients frequently die before renal recovery as a result of comorbid illness and ATN itself. Despite technological advances in dialysis, the mortality rate in patients with ATN who require dialysis remains between 50 and 80%.

Pathology/Histopathology

Ischemic ATN is caused by hypotension and hypovolemic shock following trauma, infections, burns, or hemorrhage. There is a rapid fall in blood pressure, which causes hypoperfusion of the peritubular capillaries with consequent tubular necrosis. Injury of tubular cells is most prominent in the straight portion of the proximal tubules and in the thick ascending limb of the loop of Henle, especially as it dips into the relatively hypoxic medulla. The reduction in ▶glomerular filtration rate (GFR) that occurs from ischemic injury is a result not only of reduced filtration due to hypoperfusion but also of casts and debris obstructing the tubular lumen, causing back-leakage of filtrate through the damaged epithelium. In addition, ischemia leads to decreased production of vasodilators by the tubular epithelial cells, leading to further vasoconstriction and hypoperfusion.

Toxic ATN is caused by agents with specific nephrotoxic activity such as poisons, organic solvents, drugs, and heavy metals causing damage to the epithelial cells. Damage by nephrotoxic substances is usually limited to the proximal tubules. These substances cause the cells to detach from the basement membrane. Necrotic cells fall into the tubular lumen obliterating it and causing acute renal failure. Since the basement membrane is intact, regeneration of the tubular epithelium is possible. Glomeruli are not affected.

Clinical Presentation

ATN typically does not produce specific signs or symptoms. The patient presents with ARF. Tubular dysfunction usually leads to an increase in urinary sodium concentration and fractional excretion of sodium and to impairment in urinary concentrating capacity characterized by a decrease in urine osmolality and urine–plasma creatinine ratio (2). However, the utility of these urinary measures may be limited in patients with advanced chronic renal failure and recent medical treatment with diuretics. If ATN is a result of impaired renal perfusion, oliguria and anuria are very common.

Imaging

Urography is not indicated for evaluation of patients with ATN, but it has been used in the past to rule out obstruction. The nephrograms of most patients with ATN become dense immediately following contrast material injection and remain so for a prolonged time. In about 25% of patients, the nephrogram becomes increasingly dense during the contrast material-enhanced study. Despite the presence of a large amount of contrast material in the kidney, opacification of the pyelocalyceal system is markedly reduced.

Ultrasound (US) is the imaging modality of choice in patients with ARF. Generally, gray scale US is used to exclude renal obstruction. Evaluation of renal size has a role in clinical practice, since the finding of large, smooth kidneys should indicate that ARF is probably due to primary acute renal disease and that the process is potentially reversible, while detection of kidneys of reduced size suggests a complicated underlying chronic nephropathy and a worse prognosis. No specific findings are found in patients with ATN. The kidneys may appear normal or enlarged, with a variety of pathologic changes that can also be observed in patients with other renal pathologies. Renal echogenicity and parenchymal thickness are usually normal; about 11% of patients with ATN have hyperechoic kidneys (Fig. 1) with increased corticomedullary differentiation.

State-of-the-art color Doppler and power Doppler US equipment allow an excellent evaluation of normal renal vasculature. In patients with ATN a significant but

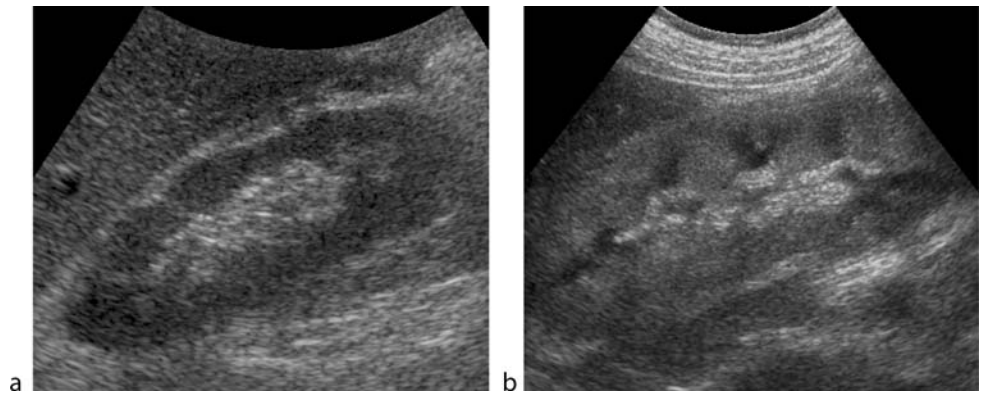

Tubular Necrosis, Kidney, Acute. Figure 1 Acute tubular necrosis from drug abuse. Different patients. Kidneys may present with normal echogenicity (a) or hyperechoic with increased cortico-medullary differentiation. Parenchymal thickness is normal in both kidneys.

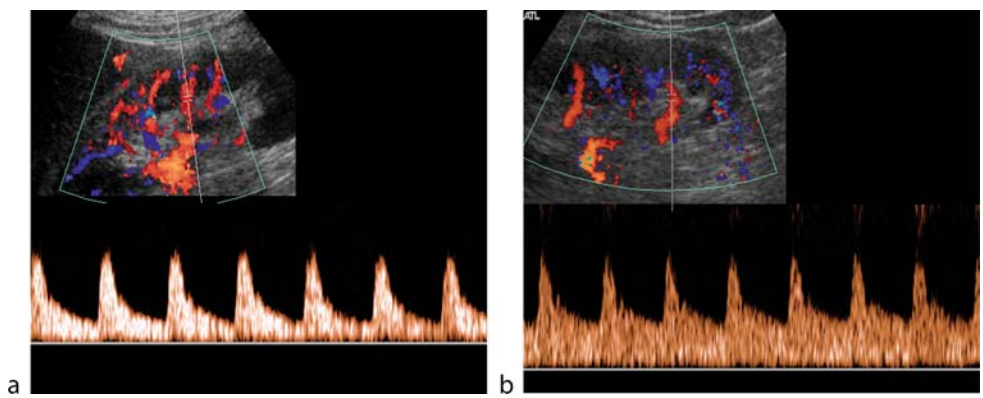

Tubular Necrosis, Kidney, Acute. Figure 2 Acute tubular necrosis. Same kidney. RI at the onset of ARF (a) is elevated (RI = 0.79). During recovery from ARF (b) RI values returned to normal values of 0.57.

nonspecific reduction of renal perfusion is usually appreciable, which can also be observed in patients with other renal pathologies. Duplex Doppler evaluation of renal hemodynamics provides functional information which is useful when differentiating among different causes of ARF that are morphologically indistinguishable. In a series of 91 patients with ARF, only 11% presented morphologic alterations of the renal parenchyma, whereas 69% presented elevated renal resistive index (RI) (3). In particular, duplex Doppler US proved valuable in the differential diagnosis between prerenal ARF and ATN (3–5). Most patients with prerenal ARF have normal parenchymal flow, whereas patients with ATN reveal markedly abnormal Doppler flow profiles with increased pulsatility or loss of the diastolic flow (Fig. 2a). An RI threshold value of 0.75 is reported as optimal in attempting a differential diagnosis between renal and prerenal ARF (3). The course of ATN may be monitored with duplex Doppler US by serial scanning. Follow-up studies during recovery from ARF (Fig. 2b) show improvement of the Doppler flow before recovery of function occurs (5). However, in common clinical practice, ARF is often caused by drug abuse or dehydration in elderly patients with hypertensive nephrosclerosis. The differential diagnosis between ATN and prerenal causes of ARF not complicated with ATN can be difficult in these patients since the RI is usually elevated due to the preexisting renal parenchymal disease (6). Duplex Doppler US is unable to distinguish the various causes of ATN. Similar changes in Doppler waveforms may be seen from a variety of causes including septicemia, hypovolemia, rhabdomyolysis, nephrotoxic drug intake, and multiple organ failure.

Recently, US contrast media have been introduced in clinical practice which can improve the diagnostic capabilities of US in the assessment of patients with ARF (6). In particular, measuring the arteriovenous transit time after bolus injection of microbubbles has been shown useful, in transplanted kidneys, to discriminate between acute tubular necrosis and acute rejection (6). In patients with ischemic ARF, contrast-enhanced US

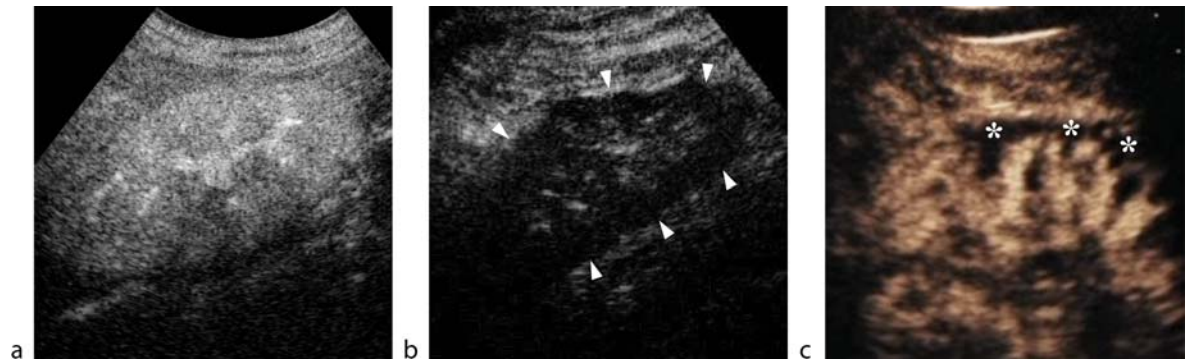

Tubular Necrosis, Kidney, Acute. Figure 3 Patients with ARF from different causes. Contrast enhanced US after bolus injection of 2.4 mL Sono Vue (Bracco, Milan, Italy). (a) Acute tubular necrosis. Renal perfusion is relatively preserved. (b) Acute renal infection. The renal parenchyma (arrowheads) does not enhance. (c) Acute cortical necrosis. The hilar vessels enhance while large portions of the renal cortex do not enhance (*).

allow the differential diagnosis between ATN (Fig. 3a), in which the renal cortex enhances, acute renal infarction (Fig. 3b), in which the renal parenchyma does not enhance, and acute cortical necrosis (Fig. 3c), in which only the renal cortex does not enhance (6).

Computed tomography (CT) is not suited to patients with ATN because no clinically useful information is obtained and iodinated contrast agents are nephrotoxic. The differential diagnosis between ACN and other causes of ARF, such as ATN, can be made with contrast-enhanced CT, since ACN typically presents with an enhancing renal medulla, nonenhancing renal cortex, and a thin rim of enhancing subcapsular tissue. However, due to the nephrotoxicity of iodinated contrast media in the context of ARF, magnetic resonance imaging (MRI) and contrast-enhanced US should be preferred when this differential diagnosis is required.

MRI should be preferred to contrast-enhanced CT for assessment of renal perfusion in patients with ARF because no significant nephrotoxicity is reported in the literature for paramagnetic contrast agents. As occurs with contrast-enhanced CT, the differential diagnosis between ACN and other causes of ARF, such as ATN, can be obtained.

Nuclear Medicine

Renal scintigraphy can be a useful imaging study in selected clinical circumstances, especially when severe renal insufficiency contraindicates the administration of iodinated contrast material. Tc-99m mercaptoacetyltriglycine (MAG3) is more useful in cases of renal insufficiency than Tc-99m diethylenetriamine pentaacetic acid (DTPA) and is able to evaluate both renal flow and function. In patients with renal transplantation, scintigraphy may play a role in the assessment of both perfusion and function of the graft. This technique helps differentiating ATN from graft rejection, especially in the immediate postoperative period. In patients with ATN, Tc-99m-MAG3 scintigraphy characteristically shows relatively preserved renal perfusion and poor tubular function; in those with early rejection, perfusion is decreased and function is preserved relatively early, followed by reduction of both perfusion and function. In practice, however, a considerable overlap of the findings exists and the differential diagnosis is usually difficult. As a consequence, biopsy is still considered the gold standard for diagnosing rejection.

Since the rejection process is accompanied by the infiltration of lymphocytes, uptake of Tc-99m-mononuclear leukocytes is higher in this pathologic condition, improving the differential diagnosis between rejection and ATN in renal grafts.

Diagnosis

The diagnostic approach to ATN must rely on a synthesis of data from the patient's history, physical examination, laboratory studies, and imaging. A relevant role is given to serum markers such as creatinine and ▶blood urea nitrogen (BUN).

The diagnosis is often supported by a positive history of risk factors; however, the physician must rule out other reasons for ARF, such as prerenal, postrenal, and renal ARF. Distinguishing ATN from prerenal ARF can be extremely difficult. Recognition of the characteristic urinary sediment of ATN, including renal tubular epithelial cells, granular casts, and muddy brown granular casts, helps to confirm the diagnosis; moreover, ATN does not rapidly improve following the administration of

large-volume intravenous fluid, as usually occurs in patients with noncomplicated prerenal ARF.

In general, renal biopsy is not necessary in the evaluation and therapy of patients with ATN. In fact, kidney biopsy, besides carrying a risk of complications, provides only a partial analysis of the renal tissue and may not be useful in assessing the prognosis.

References

1. Thadhani R, Pascual M, Bonventre JV (1996) Acute renal failure. N Engl J Med 334:1448–1460
2. Esson ML, Schrier RW (2002) Diagnosis and treatment of acute tubular necrosis. Ann Intern Med 137:744–752
3. Platt JF, Rubin JM, Ellis JH (1991) Acute renal failure: possible role of duplex Doppler US in distinction between acute prerenal failure and acute tubular necrosis. Radiology 179:419–423
4. Platt JF (1997) Doppler ultrasound of the kidney. Semin Ultrasound CT MR 18:22–32
5. Izumi M, Sugiura T, Nakamura H et al (2000) Differential diagnosis of prerenal azotemia from acute tubular necrosis and prediction of recovery by Doppler ultrasound. Am J Kidney Dis 35:713–719
6. Pozzi Mucelli R, Bertolotto M, Quaia E (2001) Imaging techniques in acute renal failure. Contrib Nephrol 132:76–91

Tumor Hypoxia

Areas of tumor with oxygen tension 10 mm Hg or lower

▶Perfusion, Neoplasms

Tumor Imaging

In oncology, SPECT has an important role in the diagnosis, staging, assessment of recurrencies, and monitoring tumor response to therapy.

▶Single Photon Emission Computed Tomography

Tumor Necrosis Factor Receptor-Associated Periodic Syndrome (TRAPS)

A dominantly inherited syndrome with recurrent inflammatory febrile episodes.

Oestreich—eleven chapters.

▶Transient Synovitis

Tumor Perfusion

Arterial vascularization of a neoplasm is used as a route for locoregional application of chemotherapeutic agents.

▶Chemoperfusion

Tumoral Calcinosis

The primary type is a relatively rare disorder most commonly seen in people of African descent. The etiology is uncertain, but manifestations are often apparent by the second decade of life, affecting the hips most frequently, then buttocks, elbows and smaller joints. The histologic appearance is characterized by densely loculated masses of calcific debris and fluid enclosed by fibrous tissue. Lesions grow quite slowly and rarely cause pain unless there is nerve involvement. Surgical removal is the treatment of choice. Incomplete resection leads to recurrence.

The term "tumoral calcinosis" has also been used to describe similar lesions seen in conjunction with systemic disorders, such as chronic renal failure and scleroderma (secondary tumoral calcinosis).

▶HADD

Tumorlike Lesions of Bone

▶Neoplasm-Like Lesions, Bone

Tumors of the Nasopharynx

▶Neoplasms, Nasopharynx

Tumors of the Osseous Spine

Lesions are diagnosed by a combined approach using clinical information, prevalence, number of lesions (bone scintigraphy), morphology and morphological patterns,

topography within the spine and within the vertebra, soft tissue extension, density on CT scan, and signal intensities on MRI.

▶Tumors, Spine

Tumors of the Urethra

▶Neoplasms, Urethra

Tumors, Renal Mesenchymal

Raphaelle Renard-Penna
Service de Radiologie, Hospital Pitiè Salpetrière, Assistance Publique des hospitaux de Paris Université, Pierre et Marie Curie, Paris, France
raphaelle.renard-penna@psl.ap-hop-paris.fr

Synonyms

Neoplasm, Renal solid benign

Angiomyolipoma

Epidemiology and Clinical Features

Angiomyolipoma is the most common benign renal lesion. It occurs as isolated, sporadic entities in 80% of the cases, most commonly manifesting in middle-age women. The other 20% of AML develop in association with tuberous sclerosis (1). The two forms vary to some degree in their imaging features but are histologically indistinguishable. The penetrance of such lesions in the tuberous sclerosis complex can be up to 80%. AMLs that occur in association with tuberous sclerosis manifest at a younger age (31.5 years vs. 53.6 years), are likely to be larger, multiple, bilateral, and are prone to grow and need surgical treatment (Fig. 1) (2). In patients without tuberous sclerosis, the tumors usually are solitary. The female predilection seen in sporadic AMLs does not occur in patients with tuberous sclerosis.

Patients with AMLs may present abdominal and flank pain, nausea, vomiting, and fever. Common findings described include a palpable mass, abdominal tenderness, hematuria, anemia, shock, hypertension, urinary tract infection, and renal failure. These signs and symptoms are usually a result of mass effect and hemorrhage. The main predictor of hemorrhage has been reported to be size tumor. Occasionally, AMLs can extend into the inferior vena cava or adjacent nodes, mimicking a malignancy; however, death due to metastatic AMLs is exceedingly unusual.

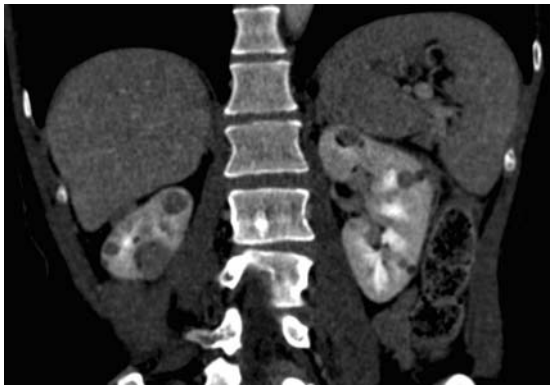

Tumors, Renal Mesenchymal. Figure 1 Angiomyolipoma. Multiple fatty-density renal lesions are seen in this patient with tuberous sclerosis.

Histologic Characteristics

AMLs are composed of varying amounts of mature adipose tissue, smooth muscle, and thick-walled blood vessels. Historically, AMLs have been classified as hamartomas. Although calcification and necrosis are rare, hemorrhage is frequent, despite the fact that the tumor blood vessels have a thicker wall than normal vessels. In 17–20% of patients with spontaneous perinephric hemorrhage, AML is the cause of bleeding. Malignant transformation does not occur except in rare cases.

Radiologic Features

Plain radiographs may demonstrate a relatively lucent mass if there is a large fatty component to the tumor.

Urography may demonstrate a renal mass. However, the urogram often is unrevealing, because the tumors frequently have an exophytic growth pattern.

At US, AML demonstrates marked increased echogenicity. If there has been hemorrhage, sonolucent areas may be seen. Occasionally, other renal tumors may demonstrate the type of dense, increased echogenicity reported with AML. In addition to benign lesions such as oncocytoma, cavernous hemangioma, and renal infarction, malignancies such as renal cell carcinoma, liposarcoma, and lymphoma may be indistinguishable from AML at US (3). If there is relatively little fat,

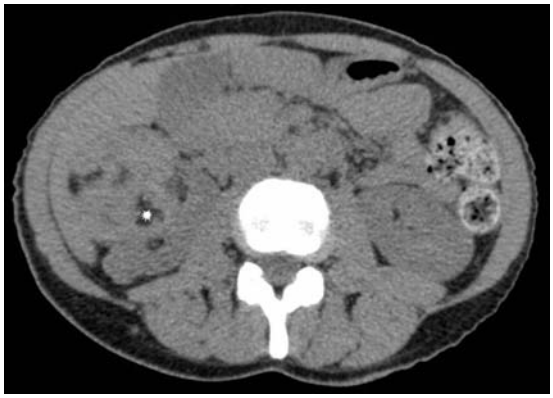

Tumors, Renal Mesenchymal. Figure 2 Angiomyolipoma. Nonenhanced CT scan show a large tumor of fat attenuation (*).

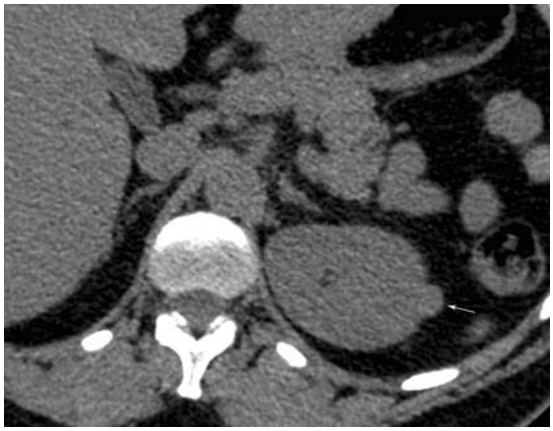

Tumors, Renal Mesenchymal. Figure 3 Angiomyolipoma. A renal lesion without detectable fat (*arrow*), homogenous with attenuation higher than normal parenchyma.

the ultrasonographic pattern will be indistinguishable from other renal masses.

The most reliable imaging modality for AMLs is CT. Single or multiple well-circumscribed noncalcified renal cortical tumors containing tissue with fat attenuation of less than −20 HU are characteristics findings of AML at nonenhanced CT (Fig. 2). CT examination of a fatty renal mass must be performed carefully to avoid volume averaging adjacent perinephric fat and a false low-density reading. An unenhanced CT examination with thin sections combined with a pixel analysis is the most sensitive test to confirm a small amount of fat. Although demonstration of intratumoral fat attenuation is almost pathognomonic for this lesion, there are other rare benign and malignant processes that should be considered: perirenal fat entrapment, lipid necrosis, or osseous metaplasia, all of which may occur in renal cell carcinoma. Other rare renal lesions that can contain fat are liposarcoma, myolipoma, lipoma, oncocytoma, and Wilms' tumor. It may not be possible to distinguish these types of masses from each other.

The degrees of soft tissue attenuation of AMLs may vary, depending on the relative proportion of vascular or smooth muscle composition, and on the presence of hemorrhage. Therefore, the absence of intratumoral fat does not preclude the diagnosis of AML (Fig. 3). This unusual manifestation so called AML with minimal fat accounts for approximately 4.5% of all AMLs (4). High-tumor attenuation on unenhanced scans and homogeneous and prolonged enhancement has been presented as a unique finding in AML with minimal fat but these findings are not specific enough to make a confident diagnosis (5). AML rarely contain calcification and, therefore, a diagnosis of AML should not be made if a lesion contains fat and calcium. In such a case, a renal cell carcinoma must be considered likely. Most AMLs and renal cancers show dramatic enhancement after contrast material administration, so this is not a point of differentiation.

On MRI, the fatty portion of an AML is hyperintense to the renal parenchyma on T1-weighted images; however, other renal masses, including hemorrhagic-proteinaceous cyst and renal cell carcinomas that contain hemorrhage, may have similar signal characteristics. Therefore, to establish the presence of macroscopic fat within a renal mass, obtaining frequency-selective fat-suppressed T1-weighted images and comparing them with nonfat suppressed T1-weighted images is necessary. However, by evaluating the location of the India ink artifact on opposed-phase chemical shift MRI, characterizing AMLs without the use of frequency-selective fat-suppressed T1-weighted images is possible (6). When clearly imaged, MRI should have the same accuracy as CT in diagnosing an angiomyolipoma. However, MRI probably is not as sensitive as CT in detecting fat in small tumors.

AngioCT or arteriography may demonstrate tortuous, almost aneurysmally dilated vessels. Clusters of saccular micro- and macroaneurysms have been reported to be the most characteristic finding of AML at angiography, with other suggestive features including a dense well-organized early arterial network, a late whorled appearance, sharp margination, and no appreciable arterious-venous shunting (7). Vascular encasement found in malignant tumors is not present in AMLs. AngioCT may now be helpful in defining the vascular supply to tumors in which local resection is planned.

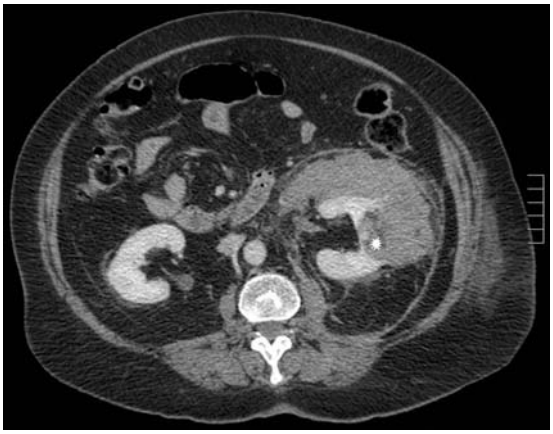

Tumors, Renal Mesenchymal. Figure 4 Angiomyolipoma. Transverse CT shows a tumor contains fat (*). High attenuation material suggestive of hematoma is visible in the tumor and the perirenal space.

Treatment

Small lesions discovered incidentally in asymptomatic patients do not usually prompt surgery for diagnosis or cure.

The need for intervention, should be predicated on the presence of rapid growth or the development of symptoms related to retroperitoneal hemorrhage (Fig. 4) and mass effect (8). Tumor diameter greater than 4 cm has also been used as a criterion for prophylactic treatment, since many studies show a higher frequency of hemorrhagic complications with larger tumors. However, depending on the size and location of the lesion, total nephrectomy may not be required. Treatment with selective arterial embolization or radio-frequency ablation of the lesion may also be used, especially in patients with tuberous sclerosis, who may have limited nephronic reserve.

Lipoma

Renal lipoma is a very rare tumor exclusively composed of mature adipose tissue. The presentation on imagery is not different from AML with predominant adipose tissue.

Hemangioma

Epidemiology and Clinical Features

Renal hemangioma is a rare benign neoplasm, with 90% occurring in the medulla (papilla) and the renal sinus (9). Most lesions are solitary, unilateral, and less than a centimeter in size. In children, the occurrence of renal hemangioma is well documented in congenital syndromes like Sturge–Weber and Klippel–Trenaunay.

In adults, hemangioma is usually solitary and unilateral with no predilection for side or sex.

Histologic Characteristics

Hemangiomas may be of the capillary or cavernous type. The most common location of these lesions is in the mucosa or submucosa of the pelvis and the medullary pyramids (91%) rather than the cortex. Consequently, it follows that its cardinal manifestation is hematuria.

Radiologic Features

Renal hemangiomas are hyperechoic at US. At CT and MR imaging, they may demonstrate intense arterial phase contrast enhancement that persists into the venous phase. At MR, hemangiomas may appear homogeneously hypointense on T1-weighted images and hyperintense on T2-weighted images (10).

Preoperative diagnosis of renal hemangioma is extremely difficult, and the lesion is often mistaken for more common renal pelvic malignancies such as transitional cell carcinoma and renal adenocarcinoma.

Leiomyoma

Epidemiology and Clinical Features

Adult renal leiomyomas are rare, benign spindle cell tumors that are found in approximately 5% of autopsy specimens (11).

Among those tumors found at autopsy, the average size is less than 5 mm. Clinically apparent leiomyomas are substantially larger but are far less common. As with AML, these lesions are more likely to be seen in middle-aged and older women (median age, 42 years), have no metastatic potential, are currently discovered as incidental findings, and occur with increased frequency in patients with tuberous sclerosis.

Histologic and Pathologic Characteristics

Leiomyoma of the kidney consists predominantly of smooth muscle cells without pleomorphism or nuclear atypia. Generally, leiomyomas are well-circumscribed, peripheral lesions. Most of them are considered to be hamartomatous.

Radiologic Features

Although cyst formation may occasionally be seen, leiomyomas typically appear as well-circumscribed, solid lesions (12). There may be a cleavage plane between the

leiomyoma and the cortex and the lesion may be extremely exophytic or attached to the cortex by only a small stalk (13). Irregular calcification may be seen in a minority of cases.

Differential Diagnosis

Leiomyoma lacks features that allow it to be distinguished from leiomyosarcoma, a rare malignant smooth muscle tumor.

Treatment

The radiologic findings cannot differentiate leiomyoma from renal adenocarcinoma. The suspicion of a leiomyoma will prompt surgical exploration for diagnosis. However, identification of a well-circumscribed, peripheral renal mass, especially if it is small (less than 4 or 5 cm) in a middle-aged woman, should allow one to suggest the diagnosis of a leiomyoma. Although this will not obviate surgical exploration, it may allow the surgeon to prepare for a renal-sparing operation in selected cases. The prognosis after resection of these lesions is excellent (3).

Bibliography

1. Lemaitre L, Robert Y, Dubrulle F et al (1995) Renal angiomyolipoma: growth followed up with CT and/or US. Radiology 197:598–602
2. Logue LG, Acker RE, Sienko AE (2003) Best cases from the AFIP: angiomyolipomas in tuberous sclerosis. Radiographics 23:241–246
3. Helenon O, Merran S, Paraf F et al (1997) Unusual fat-containing tumors of the kidney: a diagnostic dilemma. Radiographics 17:129–144
4. Kim JK, Park SY, Shon JH et al (2004) Angiomyolipoma with minimal fat: differentiation from renal cell carcinoma at biphasic helical CT. Radiology 230:677–684
5. Jinzaki M, Tanimoto A, Narimatsu Y et al (1997) Angiomyolipoma: imaging findings in lesions with minimal fat. Radiology 205:497–502
6. Israel GM, Hindman N, Hecht E et al (2005) The use of opposed-phase chemical shift MRI in the diagnosis of renal angiomyolipomas. Am J Roentgenol 184:1868–1872
7. Silbiger ML, Peterson CC, Jr (1971) Renal angiomyolipoma: its distinctive angiographic characteristics. J Urol 106:363–365
8. Zagoria RJ, Dyer RB, Assimos DG et al (1991) Spontaneous perinephric hemorrhage: imaging and management. J Urol 145: 468–471
9. Jahn H, Nissen HM (1991) Haemangioma of the urinary tract: review of the literature. Br J Urol 68:113–117
10. Prasad SR, Humphrey PA, Menias CO et al (2005) Neoplasms of the renal medulla: radiologic-pathologic correlation. Radiographics 25:369–380
11. Farrow GM (1989) Diseases of the kidney. WM Murphy: Urological Pathology. WB Saunders, Philadelphia, 409–482
12. Wagner BJ, Wong-You-Cheong JJ, Davis CJ, Jr (1997) Adult renal hamartomas. Radiographics 17:155–169
13. Steiner M, Quinlan D, Goldman SM et al (1990) Leiomyoma of the kidney: presentation of 4 new cases and the role of computerized tomography. J Urol 143:994–998

Tumors, Renal Parenchymal

Raphaelle Renard-Penna
Service de Radiologie, Hôpital Pitiè Salpetrière,
Assistance Publique des hospitaux de Paris,
Université Pierre et Marie Curie, Paris, France
raphaelle.renard-penna@psl.ap-hop-paris.fr

Synonyms

Neoplasm, Renal solid benign

Characteristics

Oncocytoma

Epidemiology and Clinical Features

Renal oncocytomas are benign tumors originating from the intercalated cells of the collecting duct. They have a male predilection and a mean age of presentation in the seventh decade. Renal oncocytomas occur with an overall incidence of 3 to 7% among all renal tumors. Although most tumors are unifocal, 2 to 12% are multifocal and 4 to 12% are bilateral (1). Most are diagnosed incidentally, but symptomatic patients usually present with gross hematuria, flank pain, or a palpable mass. The preoperative distinction between benign oncocytoma and renal cell carcinoma (RCC) is important because a correct diagnosis could allow patients to avoid aggressive surgical procedures. Oncocytomas are biologically benign. Among patients who have had an oncocytoma resected, there has been no demonstrated evidence of metastases or diminished longevity; very few cases of recurrence after enucleation of a tumor have been reported (2).

Associations between a subset of patients with multifocal renal oncocytomas and hereditary syndromes have been described, including familial renal oncocytoma and Birt–Hogg–Dube syndrome. This autosomal dominant syndrome is characterized by various dermatologic disorders and the development of renal tumors (renal cancers, particularly chromophobe 34%, oncocytoma 5%, hybrid chromophobe-oncocytomas 50%, clear cell carcinoma 9% and papillary renal cancer 2%) (3).

Histologic Characteristics

An oncocyte is a large transformed epithelial cell that has a finely granular eosinophilic cytoplasm. Oncocytes increase in number with age and are found in a variety of organs, including salivary gland, thyroid, pancreas, and

kidney. In the kidney, oncocytomas arise from the distal tubule or collecting ducts.

The gross appearance of an oncocytoma is a well-defined tan to brown tumor. A "pseudocapsule" is often seen where the tumor compresses the adjacent renal parenchyma. Although hemorrhage is typically absent, focal areas can be detected in some tumors. Gross calcification is exceedingly rare. Most cases of oncocytoma are confined within the renal parenchyma, and gross evidence of capsular or vascular invasion is rare. One distinctive feature of oncocytomas is the presence of a prominent central scar in an otherwise homogeneous tumor, seen in 33 to 80% of cases (4). The average size of oncocytomas with central scars is slightly less than that of tumors without scars, indicating a limited correlation between tumor size and the presence of central scars.

Although there are occasional reported cases of involvement of regional lymph nodes and tumor extension into the vein, the vast majority of oncocytomas are well differentiated and benign.

Despite the well-characterized cytologic features of renal oncocytomas and the obvious benefits of the preoperative diagnosis of a benign tumor, the role of tumor biopsy for definitive diagnosis has been studied only retrospectively on samples taken from surgical specimens and remains questionable. Moreover, the overall sensitivity of renal biopsy ranges from 40 to 90% (5) and many tumors that are read as "nondiagnostic" on biopsy are often found to be malignant after complete surgical extirpation and thorough histologic examination. Until the techniques and interpretations of biopsies become more consistent, its use for the preoperative diagnosis of renal oncocytomas will remain limited.

Radiologic Feature

Oncocytomas are usually homogeneous at US, but some are heterogeneous; they may be hyperechoic, hypoechoic, or isoechoic with respect to the normal renal parenchyma. If a central stellate "scar" is seen, it can be hyperechoic, hypoechoic, or anechoic. RCCs are often more heterogeneous than oncocytomas and are more likely to display the ultrasound findings of gross calcification.

Angiography is potentially useful for the diagnosis of oncocytoma. The characteristics attributable to oncocytomas include the "spoke-wheel" appearance resulting from vessels radiating toward the center of the lesion, a homogeneous capillary blush during the nephrogram phase, and an enhanced rim around the perimeter of the lesion. However, the features are not consistently found and the presence of the "spoke-wheel," thought to be the most distinguishing quality on angiography is seen in 4 to 76% of the tumors (6). Angiography demonstrates a vascular renal tumor with a dense tumor blush. A "spoke-wheel" pattern of vessels penetrating into the center of the tumor is common. Although this vascular configuration often is described in an oncocytoma, it is not pathognomonic because it also can be seen in renal adenocarcinoma.

CT usually reveals a solid, homogeneous lesion that can demonstrate a centrally located stellate area of low attenuation, indicative of a central scar (Fig. 1). This central scar is not pathognomonic for an oncocytoma because it can be seen in renal adenocarcinoma. Most studies have shown that oncocytomas are usually isodense or slightly hypodense to normal renal parenchyma on unenhanced CT. A few have been described which are hyperdense. Tumors homogeneity has been observed in 50 to 100% of tumors (7). The examination of comparable RCC lesions showed that 22% also appear homogeneous on CT. The central stellate scar, if present, is less dense than surrounding tissue, both before and after intravascular contrast administration. The remainder of the tissue of the tumor enhances but to a lesser degree than normal renal parenchyma, enhancement is usually homogeneous. Occasionally, a thin enhancing rim and a lucent capsule-like margin has been described (8). Rare manifestations include small cystic regions, gross calcification, and an irregular margin invasion of surrounding fat. However, neither venous tumor thrombi nor hilar nodal metastases have been encountered.

MRI of oncocytomas reveals spherical masses that are relatively homogeneous. On T1-weighted spin-echo images, the solid portions of the tumor may be isointense or hypointense when compared with normal renal parenchyma. However, 27% of the cases did not

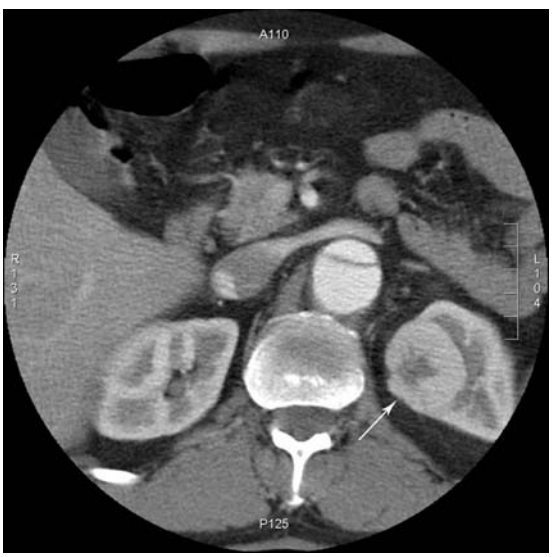

Tumors, Renal Parenchymal. Figure 1 Oncocytoma. Contrast-enhanced CT scan show a solid tumor (*arrow*) with an area of low attenuation indicative of a central scar.

demonstrate this finding and were actually isointense relative to the renal cortex (9). On T2-weighted images, the tumor may be heterogeneous, although homogeneous isointense, hypointense, and hyperintense appearances have been found. When present, the central stellate "scar" has been described as being of diminished intensity on both T1-weighted and T2-weighted images. This can be differentiated from the necrosis common to RCC, which appears as areas of decreased signal intensity on T1-weighted imaging and as areas of increased signal intensity on T2-weighted imaging. Unfortunately, a direct comparison of various renal tumors using magnetic resonance imaging indicated that a distinction between tumor types was not possible.

Treatment

Because an oncocytoma cannot be reliably diagnosed radiographically, treatment is surgical. If typical radiographic features of an oncocytoma, such as central stellate scar and a spoke-wheel, vascular pattern are present, an oncocytoma may be suggested. However, neither appearance is pathognomonic, surgery is required. The excellent prognosis associated with this tumor seems to indicate that minimally extensive and invasive ablative techniques such as partial nephrectomy, cryotherapy, or radiofrequency may be adequate for the removal of the tumor while sparing unaffected renal parenchyma (1). However, the coexistence of RCC and oncocytoma is not uncommon and is seen in 10 to 32% of patients with oncocytoma. These findings seem to suggest that nephron-sparing surgery should be attempted only after thorough intraoperative inspection by open or laparoscopic techniques for the presence of additional lesions.

Papillary Adenoma

Papillary adenomas are tumors with papillary or tubular architecture of low nuclear grade and 5 mm in diameter or smaller.

These benign tumors often are confused with and may be difficult to distinguish from renal adenocarcinoma. Both renal adenomas and adenocarcinomas develop in the proximal convoluted tubule and cannot be distinguished by histologic or histochemical means. They both occur in the same age groups, and both show a marked male predominance. Many authors believe that an adenoma is a small renal carcinoma that has not yet metastasized.

Because most of these renal adenomas are detected at autopsy, they have little clinical significance. However, when they are detected in a surgery, the nomenclature used to describe these cortical glandular tumors implies prognostic significance. It may be best to describe these tumors as renal adenocarcinomas, but with a low likelihood of metastasis. Search for evidence of metastasis and arranging appropriate follow-up may be beneficial.

Metanephric Adenoma

Metanephric adenoma is an uncommon benign renal tumor that has been reported previously in the pathology literature as embryonal adenoma. Unlike renal adenoma, which is by definition <5 mm in diameter, metanephric adenoma can grow to a larger size. Grossly, small tumors (<5 cm) are characteristically homogeneous and solid; however, larger tumors may be extensively necrotic and simulate the gross appearance of RCC. Histologically, the tumor is composed of numerous small tubular structures, some of which have distinctive papillary infoldings.

At ultrasound the adenomas are hyperechoic. On unenhanced CT scans, adenomas are usually hyperdense compared with the renal parenchyma, and enhanced less than adjacent renal parenchyma. Because RCC may have an identical CT and US appearance, the diagnosis of benign metanephric adenoma cannot be made on imaging studies, and adult patients should undergo surgery.

Juxtaglomerular Tumor

Epidemiology and Clinical Features

These very rare tumors have been found in patients ranging from 7 to 58 years of age, and are almost twice as common in women than in men. The mean age of detection is 24 years. The clinical presentation includes marked and sustained hypertension. Laboratory testing may reveal evidence of secondary aldosteronism with hypokalemia and elevated levels of aldosterone.

They are benign neoplasms and neither malignant transformation nor local recurrence after surgery has been reported.

Histologic Characteristics

Juxtaglomerular tumors are renin-producing tumors of the juxtaglomerular apparatus of the kidney.

Radiologic Features

CT is the most sensitive method of detecting a juxtaglomerular tumor. Because the attenuation of the tumor is similar to that of normal renal parenchyma, contrast-enhanced images are often needed to detect the mass, which enhances less than the renal cortex (10).

MR imaging may be performed either to examine the renal arteries or to detect a renal mass. A juxtaglomerular

tumor has been reported to have peripheral enhancement on T1-weighted images following intravenous administration of gadopentetate dimeglumine. Delayed images demonstrated reversal of the enhancement pattern, with washout of contrast material at the periphery and filling in of the central portion of the tumor (11).

In patients with a juxtaglomerular tumor, elevated renin levels may be detected in the main renal vein. However, this procedure may be unrewarding if selective samples are not obtained from different segments of the kidney. If the tumor lies in a peripheral location, the venous drainage may be to capsular vessels and even segmental renal vein sampling can be unrewarding.

Treatment

The treatment of juxtaglomerular tumors is surgical excision.

Nephroblastomatosis

Epidemiology and Clinical Features

Nephroblastomatosis is a group of pathologic entities characterized by persistent nephrogenic blastema. Although nephroblastomatosis is not malignant, it is associated with a high incidence of Wilms' tumor. They are found incidentally in 1% of infants. They are associated with Beckwith–Wiedemann syndrome and hemihypertrophy, Perlman syndrome, and trisomy 18.

Histologic Characteristics

Nephrogenic rests are classified histologically as dormant, sclerosing, hyperplastic, or neoplastic. Dormant and sclerosing rests are usually microscopic and are not considered to have malignant potential. Hyperplastic and neoplastic rests are grossly visible as small tan nodules surrounded by normal parenchyma.

Radiologic Features

The radiographic features are dependent on the size and distribution of the embryologic remnants. The lesions in the multifocal form usually are microscopic nodules and are difficult to image. In the diffuse form, the kidneys are enlarged and the collecting system may be deformed by parenchymal nodules.

The lesions often are hypoechoic, but also may be isoechoic or hyperechoic. Their subcapsular location suggests nephroblastomatosis and helps to distinguish this condition from polycystic renal disease or lymphoma.

At CT, macroscopic nephrogenic rests appear as low attenuation peripheral nodules with poor enhancement relative to that of adjacent normal renal parenchyma. At MR imaging, the nodules demonstrate low signal intensity foci on both T1- and T2-weighted images (12).

Typical angiographic features include a normal caliber main renal artery. Peripheral nodules are hypovascular and do not blush with contrast, and the kidney has a scalloped appearance.

Treatment

Patients with nephroblastomatosis are at increased risk of developing Wilms' tumor. Many are treated with antineoplastic drug, which often decrease the renal size. However, such patients remain at risk and should be followed to detect the subsequent development of a Wilms' tumor.

Mesoblastic Nephroma

Epidemiology and Clinical Features

Mesoblastic nephroma is the most common solid renal neoplasm in the first 3 months of life (12). There is no sexual predilection. The most common clinical presentation is a palpable abdominal mass, with hematuria occurring less frequently.

Histologic Characteristics

Gross pathologic examination reveals a solid, unencapsulated tumor that commonly occurs near the renal hilum. Hemorrhage and necrosis are infrequent. At histologic analysis, mesoblastic nephromas are composed of interlacing sheets of fibromatous cells.

The tumor is large averaging over 6 cm in diameter and often replaces almost the entire renal parenchyma. Although the tumor may penetrate the capsule and may involve the perinephric space, it rarely extends into the renal vein or renal pelvis. Cases with a low grade of malignancy have been reported and may be confused with Wilms' tumor.

Radiologic Features

At imaging, mesoblastic nephroma appears as a unicentric, relatively homogeneous, solid mass that typically involves the renal sinus. Mesoblastic nephroma is homogeneously hypoechoic at US, low attenuation at CT, and homogeneously hypointense on both T1- and T2-weighted MR images. Infrequently, areas of necrosis and hemorrhage are seen (13).

Angiography may occasionally be needed for preoperative evaluation. Most mesoblastic nephromas are moderately vascular and demonstrate tumor vascularity.

Treatment

Mesoblastic nephroma exhibits benign behavior, and nephrectomy usually suffices as treatment.

In some patients, extensive tumor necrosis extrarenal infiltration and mesenchymal immaturity suggest more aggressive behavior of the tumor. In these patients, who usually present beyond 3 months of age adjunctive chemotherapy or radiation may be given.

Bibliography

1. Chao DH, Zisman A, Pantuck AJ et al (2002) Changing concepts in the management of renal oncocytoma. Urology 59:635–642
2. Moura AC, Nascimento AG (1982) Renal oncocytoma: report of a case with unusual presentation. J Urol 127:311–313
3. Choyke PL, Glenn GM, Walther MM et al (2003) Hereditary renal cancers. Radiology 226:33–46
4. Perez-Ordonez B, Hamed G, Campbell S et al (1997) Renal oncocytoma: a clinicopathologic study of 70 cases. Am J Surg Pathol 21:871–883
5. Zardawi IM (1999) Renal fine needle aspiration cytology. Acta Cytol 43: 184–190
6. Tikkakoski T, Paivansalo M, Alanen A et al (1991) Radiologic findings in renal oncocytoma. Acta Radiol 32:363–367
7. Quinn MJ, Hartman DS, Friedman AC et al (1984) Renal oncocytoma: new observations. Radiology 153:49–53
8. Barth KH, Menon M (1980) Renal oncocytoma. Further diagnostic observations. Diagn Imaging 49:259–265
9. Harmon WJ, King BF, Lieber MM (1996) Renal oncocytoma: magnetic resonance imaging characteristics. J Urol 155:863–867
10. Dunnick NR, Hartman DS, Ford KK et al (1983) The radiology of juxtaglomerular tumors. Radiology 147:321–326
11. Agrawal R, Jafri SZ, Gibson DP et al (1995) Juxtaglomerular cell tumor: MR findings. J Comput Assist Tomogr 19:140–142
12. Lowe LH, Isuani BH, Heller RM et al (2000) Pediatric renal masses: Wilms tumor and beyond. Radiographics 20:1585–1603
13. Prasad SR, Humphrey PA, Menias CO et al (2005) Neoplasms of the renal medulla: radiologic-pathologic correlation. Radiographics 25:369–380

Tumors, Spine

A. M. De Schepper
Leiden University Medical Centre, Leiden, The Netherlands
arthurdeschepper@hotmail.com, A.M.de_Schepper@lumc.nl

Characteristics

Because of the unique anatomy and morphology of the osseous spine, enveloping major neural structures (cord and radicular nerves), and because of its guarantee to the static equilibrium of the human body, primary tumors of the spine, malignant as well as benign, may cause severe clinical symptoms and complaints such as local or radicular pain, neurological symptoms due to spinal cord and/or radicular nerve compression (Horner's syndrome, sciatic pain), up to transverse cord lesions, spinal instability, and scoliosis. In this regard, clinical symptoms may be the first alarming signs pointing to the possible presence of a tumor of the osseous spine.

There have been improvements in minimally and maximally invasive therapy by radiofrequency or laser ablation (osteoid osteoma), percutaneous injection of corticosteroids [aneurysmal bone cyst (ABC)], vertebroplasty (aggressive hemangioma), arterial embolization [giant cell tumor (GCT)], corporectomy, and even vertebrectomy (malignant tumors) as well as in adjuvant radio- and/or chemotherapy. However, early detection and tissue-specific diagnosis are required to achieve a long-term cure and improved outcome.

Initial imaging consists of plain radiography, whose value is hampered by the complex anatomy and morphology of the vertebrae, causing superimposition of different elements and possibly obscuring pathological processes. Cross-sectional imaging [computer tomography (CT) scan and magnetic resonance imaging (MRI)] is the modality of choice in staging and further characterization, because it couples morphological information to tissue-specific information by using Hounsfield units, signal intensities, and enhancement behavior (static as well as dynamic) after administration of contrast agents (iodinated or gadolinium chelates). MRI is the best modality for presurgical planning, showing the extent of involvement in the bone marrow, soft tissue, and spinal canal, and for evaluating treatment effect and follow-up.

In most handbooks one will find a descriptive or encyclopedic approach to tumoral pathology. We prefer a more pragmatic or analytical approach using a combination of a series of individual parameters, which is briefly discussed in the next few sections.

Clinical Information

The presence of clinical symptoms is related to the type of tumor (benign lesions are merely asymptomatic), its location, and its extension. In this regard, osteoid osteoma, aggressive hemangioma, and malignancies are mostly symptomatic.

History of night pain should alert one to search carefully for osteoid osteoma, whereas recent-onset painful scoliosis is suggestive of osteoid osteoma or eosinophilic granuloma. Tumors that are mostly asymptomatic, such as nonaggressive vertebral hemangiomas, may occasionally become symptomatic due to associated pathology such as disc herniation.

The age of the patient is important in the assessment of these lesions. In a young patient, osteoid osteoma, ABC,

and Ewing's sarcoma predominates, whereas GCT is normally seen in the middle-aged and chordoma in the elderly.

Prevalence

Some tumors such as chondroblastoma, intraosseous liposarcoma, malignant nerve sheath tumor or malignant melanoma, and monostotic fibrous dysplasia are rarely found in the osseous spine. In children the most common benign tumors are eosinophilic granuloma, osteoid osteoma, osteoblastoma, and ABC, whereas Ewing's sarcoma is the most common malignant tumor.

Solitary Versus Multiple Lesions

It is important to determine whether a lesion is solitary or multiple. Multiple lesions are most commonly due to metastases from breast and lung cancer in women and prostate and lung cancer in men.

The most common cause of multiple primary lesions is lymphoproliferative disorder such as multiple myeloma and lymphoma.

The presence of multiple lesions may be noted on plain radiograph but is more likely to be seen on bone scintigraphy or MRI including whole-body MRI. However, both plain radiographs and MRI may be normal in 20% of cases of multiple myeloma.

Another condition that can rarely present as multiple lesions is eosinophilic granuloma (EG), which needs to be considered in children. Fibrous dysplasia occasionally involves the spine at multiple sites. One-third of spinal hemangiomas may involve multiple levels.

Solitary lesions are less frequent than multiple ones, consisting of only 4–9% of all ►tumors of the osseous spine.

Topography: Location

The location of the tumors in the spine is useful in determining the nature of the lesion. In general, most tumors are located at the thoracic and lumbar spine. The cervical spine is the predilection site for osteoblastoma and osteochondroma. It is also commonly involved in eosinophilic granuloma, particularly the C2 vertebra in adults. The thoracic spine is the preferred site in more than 50% of cases of hemangioma, enostosis (particularly T1–T7), and chondrosarcoma. ABC also occurs at the thoracic spine, but most commonly involves the lumbosacral spine.

Enostosis and osteoid osteomas have strong affinity for the lumbar spine. Chordoma, GCT, and plasmacytoma have a penchant for the sacrum. Indeed, GCT comprises 71% of benign sacral tumors. Ewing's sarcoma is a rare cause of sacral spine tumor.

Site within the Vertebra

The body of the vertebra is mainly involved in benign conditions such as hemangioma, bone islands, and GCT, with the size of the hemangioma varying from a small lesion to complete involvement of the vertebral body. However, about 10% may involve the posterior elements. The vertebral body is also favored by chordoma and Ewing's sarcoma. Benign conditions commonly involving the posterior elements are osteoid osteoma, ABC, and osteochondroma.

Morphology

Border of the Lesion, Pattern of Bone Destruction, and Periosteal Reaction

A well-defined border (geographic) is seen with benign conditions such as hemangioma, enostosis, osteoid osteoma, osteoblastoma, and ABC.

A permeative appearance with a broad zone of transition indicating aggressive biologic activity is seen in Ewing's sarcoma.

Periosteal reaction is rarely seen in vertebral lesions and is difficult to assess. If present, the possibility of an osteosarcoma should be considered.

Matrix

Well-defined borders (geographic) are seen with benign conditions such as hemangioma, enostosis, osteoid osteoma, osteoblastoma, and ABC.

A permeative appearance with a broad zone of transition indicating aggressive biologic activity is seen in Ewing's sarcoma.

Periosteal reaction is rarely seen in vertebral lesions and is difficult to assess. If present, the possibility of an osteosarcoma should be considered.

Expansion

Expansile lesions are seen in ABC, osteoblastoma, and occasionally in aggressive hemangioma. Malignant lesions such as chordoma, Ewing's sarcoma, and chondrosarcoma also demonstrate expansion along with soft tissue extension. This feature may also be seen in relatively benign conditions such as osteoblastoma and GCT.

Soft Tissue Extension

Some of the primary spinal tumors have a proclivity for soft tissue extension. This is not only seen with malignant conditions such as Ewing's sarcoma or chordoma, but also in benign lesions like osteoblastoma. Occasionally, hemangiomas may be associated with an extensive soft

tissue component and are then referred to as aggressive hemangiomas. These lesions tend to be symptomatic.

Density (Hounsfield Units) on CT, Signal Intensities on MRI, Degree and Pattern of Enhancement after Contrast Agent Administration

The density of the lesion may be helpful in characterizing it. Fatty lesions such as lipoma have low density on CT (−50/−100 HU). Density allows for differentiation with air (−800/−1000 HU), which is occasionally seen in the vertebral body and originates from degenerative disc disease.

Enostosis appears very dense, with a density similar to cortical bone, lying within the cancellous vertebral body.

Most pathological lesions tend to have low signal intensity on T1-weighted (T1-WI) and high signal intensity on T2-weighted (T2-WI) sequences. This reflects the high relaxing value of water on long TE sequences. Hemangioma and EG tend to have increased signal intensity on T1-WI indicating the presence of fat. Low signal intensity on T2-WI is seen in GCT due to high collagen content, hemosiderin, and increased cellularity of the lesion. Bone islands demonstrate low signal intensity on all MR sequences, as they are basically cortical bone.

Contrast enhancement following administration of gadolinium chelates can help characterize the tumor. A typical ring and arc pattern of enhancement is characteristic of chondroid tumor.

Morphological Pattern

There are some morphological patterns seen in the spine on various imaging modalities, which have a very specific differential diagnosis.

Vertebra plana is mostly seen in EG. *Honeycombing* or *corduroy* pattern seen on plain radiographs and *polka dot* appearance on axial CT sections are characteristic of hemangioma.

A lucent center (*nidus*) with variable central mineralization surrounded by extensive reactive sclerosis is seen in osteoid osteoma on plain films, CT, and MRI.

Marked sclerosis with expansion of the whole vertebral body, which is referred to as *ivory vertebra*, is seen in lymphoma or Paget's disease.

Fluid–fluid levels are characteristically seen in ABC due to sedimentation of blood degradation products. However, this is not specific and may be seen in osteoblastoma and (teleangiectatic)osteosarcoma too, as well as in secondary cases of ABC that may occur in conditions such as osteoblastoma, GCT, and fibrous dysplasia. A feature that may distinguish primary ABC from other causes is the presence of solid tissue in the latter. This is not usually seen in primary ABC unless there has been a pathological fracture.

Mini-brain appearance is seen in plasmacytoma mimicking the MR appearance of brain.

Dumbbell or mushroom shape may be seen in chordoma together with preservation of disc space.

The patterns mentioned are useful in characterizing the lesions, but they need to be cautiously interpreted taking into account the rest of the features.

The "*spider pattern*" is an interesting example that we have seen on CT. This pattern is noted in plasmacytoma but also in angiomatosis.

Bibliography

1. Van Goethem JW, van den Hauwe L, Ozsarlak O et al (2004) Spinal tumors. Eur J Radiol 50:159–176
2. Flemming DJ, Murphey MD, Carmichael BB et al (2000) Primary tumors of the spine. Semin Musculoskeletal Radiol 4:299–320
3. Murphey MD, Andrews CL, Flemming DJ et al (1996) From the archives of the AFIP. Primary tumors of the spine: radiologic pathologic correlation. Radiographics 16:1131–1158

Tumors, Spine, Intradural, Extramedullary

Niloufar Sadeghi
Department of Radiology, Erasme Hospital, Brussels, Belgium
nsadeghi@ulb.ac.be

Definitions

Spinal intra-dural extra-medullary tumours (►SIET) arise inside the dura and outside the spinal cord. Nerve sheath tumours and ►meningiomas account for 80% to 90% of all SIET (1). More recently, due to intensified therapy of systemic malignancies and prolonged patient survival as well as increased sensitivity of imaging techniques the incidence of detected leptomeningeal metastases has significantly increased.

MR imaging is the method of choice in the diagnosis of SIET and allows direct demonstration of both the mass and associated intraspinal alterations. The mass usually displaces the spinal cord and enlarges the ipsilateral subarachnoid space.

Conventional myelography or CT-myelography were previously performed and demonstrated indirect signs such as intra-dural contrast filling defect with the displacement of the spinal cord or a myelographic block caused by the mass.

Histopathology/Anatomy

Benign Tumours

Nerve Sheath Tumors: Nerve sheath tumours are the most common SIET, accounting for 25% to 30% of all cases (1, 2). Nerve sheath tumours arise from dorsal sensory roots, although occasional examples on motor nerve roots have been recorded. They are often located in the anterolateral part of the spinal canal; their distribution throughout the spine is fairly uniform with a slight lumbar predominance. Two main types of nerve sheath tumours are found in the spine: schwannoma and neurofibroma. ►Schwannomas are encapsulated, well-circumscribed round or oval tumours that often show cystic degeneration and haemorrhage. The tumour arises eccentrically from the parent nerve. ►Neurofibromas are unencapsulated, fusiform and less well-delineated lesions. Necrosis and cystic degeneration are rare in neurofibromas and the parent nerve typically runs through the lesion with nerve fibres dispersed throughout the tumour. A third type of neurogenic spinal tumour, ganglioneuroma, is relatively rare.

Between 35% and 45% of patients with nerve root tumours have Recklinghausen's disease, or ►neurofibromatosis (NF) type I, in which multiple lesions are common. Multiple spinal schwannomas characteristically occur in patients with NF type 2. Spinal neurofibromas less commonly occur in NF type I, and when they do occur they are often associated with plexiform peripheral neurofibromas. Malignant transformation of neurofibromas to neurofibrosarcomas in NF type I patients is estimated to range from 4% to 11%, whereas schwannomas essentially lack potential for malignant degeneration.

In 70% to 75% of the cases nerve sheath tumours are intra-dural, in 15% extra-dural and in 15% there are combined intra- and extra-dural 'dumbbell' masses. Less than 1% is intra-medullary (2, 3).

Occasionally an intra-dural tumour extends through the intervertebral foramen to expand into a greater mass on the peripheral nerve. The extra-vertebral tumour is often the significant clinical feature and may be found in the neck, posterior mediastinum, behind the peritoneum or in the pelvis, depending on the level of origin of the mass (3).

Meningiomas: After nerve sheath tumours, meningiomas are the most frequent SIET, accounting for 25% of all spinal tumours. Twelve percent of all meningiomas are located within the spinal canal. Aggressive tumours and hemangiopericytomas are rare. The peak incidence is in the fifth and sixth decades with predominance in women (80%). Ninety percent of spinal meningiomas are intra-dural and 5% are either 'dumbbell' or extra-dural lesions. The thoracic spine is the most common site (80%), followed by cervical spine (15%). These tumours are usually located in the posterior aspect of the spinal canal and as in the cranium, the tumour is usually firmly fixed to the dura (2).

Paragangliomas: Paraganglioma is a tumour of paraganglia, the accessory organs of the peripheral nervous system. Spinal paragangliomas are rare tumours that are found in the cauda equina and filum terminale. Males are affected slightly more than female, and the average age at diagnosis is around 50 years (2, 3).

Epidermoid Tumours: Epidermoid tumours are uncommon (0.5% to 1.0% of all spinal tumours). They can be congenital or acquired, as a late complication of lumbar puncture by deposition of a fragment of epidermis within the dural sac. Congenital epidermoids are mainly located at the conus or cauda equina level and are often associated with vertebral abnormalities (spina bifida, hemivertebrae). Acquired cysts are found in the lower lumbar region and lack osseous abnormalities (2).

Dermoid Tumours: Dermoid tumours are congenital midline cystic tumours and account for 20% of intra-dural tumours seen during the first year of life. Half of them are intra-medullary and others are extramedullary intra-dural masses. Most lesions are located in the lumbar spine.

Neurenteric Cysts (*spinal enterogenous cysts*): These are uncommon congenital intra-dural cysts usually located in the thoracic spine anterior to the spinal cord.

Arachnoid Cysts: These are rarely intra-dural. The thoracic spine is the most common site, with a posterior midline situation.

Lipomas: These tumours account for about 1% of all tumours of the spinal canal and are distributed equally between the sexes. Most intraspinal lipomas are subpial, in the thoracic region. Associated congenital abnormalities, such as spina bifida or other forms of dysraphism are found in about a third of the cases.

Teratomas: These are very rare in the spine, and may occur in isolation or in association with congenital spinal anomalies.

Malignant Tumours

Metastases: The most common malignant SIET are leptomeningeal metastases. Ependymoma, posterior fossa medulloblastoma, glioblastoma, germinoma and pineoblastoma are the most common central nervous system (►CNS) primary tumours that metastasise to the spinal subarachnoid space. Non-CNS sources are carcinoma of the lung or breast, melanoma and haemopoietic neoplasms (lymphoma and leukaemia). Age of patients at diagnosis

depend on the type of the primary neoplasm. The lumbosacral subarachnoid space is the most frequent site. Multiple lesions are common and vary from diffuse infiltration of the arachnoid membrane or thickening of lumbar nerve roots to nodular deposits scattered throughout the subarachnoid space ('drop' metastases) (2, 3).

Clinical Presentation

Clinical presentation is often non-specific and related to the location and the volume of the lesion. Pain and radiculopathy are the most frequent presenting symptom, followed by paresthesia and limb weakness. Myelopathic symptoms may result from cord compression. Infrequently, subarachnoid haemorrhage occurs in cauda equina nerve root tumours. Both schwannomas and neurofibromas usually become symptomatic in the middle decades with a slight female predominance for schwannomas. Schwannomas never become malignant, whereas sarcomatous transformation occurs in 4% to 11% of patients with neurofibromatosis.

Most spinal meningiomas are benign, slowly compressing the cord and causing progressive motor (90%) or sensory (60%) deficits. Sphincter dysfunction and pain occur later in about 50% of cases.

Imaging

Nerve Sheath Tumours: Since neurofibromas and schwannomas cannot be reliably distinguished by ►CT or MR, the two lesions are collectively referred to as 'nerve sheath tumours'. On plain films, scalloping of vertebral bodies, pedicle erosion and enlarged neural foramen may be found. Kyphoscoliosis and so called 'ribbon ribs' are seen with neurofibromatosis. On non-enhanced CT, bone erosions are identified, calcification and haemorrhage are rare. Seventy-five percent of nerve root tumours are isointense to spinal cord on T1-WI and 25% are hypointense. More than 95% are hyperintense on T2-WI. Approximatively 40% of spinal schwannomas have a cystic component. These cysts may resemble cerebrospinal fluid (►CSF) or may be hyperintense on both T1- and T2-weighted images due to protein content or haemorrhagic products. Virtually all nerve sheath tumours enhance after contrast administration (Fig. 1). Contrast medium improves the detection of small lesions. The major differential diagnosis is meningioma (2–4).

Meningiomas: Calcification is only visible in 1% to 5% of cases. Bone erosion is uncommon. On MR images most meningiomas are isointense to CSF on both T1- and T2-weighted images, with homogeneous enhancement following contrast administration, often demonstrating the characteristic thickening of their dural implantation, dural tail sign (Fig. 2) (2–4).

Paragangliomas: These are well-encapsulated masses, isointense with cord on T1- and iso- to hyperintense on T2-weighted images. Haemorrhage is common. Paragangliomas are highly vascular tumours and enhance strongly following contrast administration.

Epidermoid Tumours: Signal intensity is typically iso- or slightly hyperintense compared to CSF on all sequences.

Dermoid Tumours: These usually represent the appearance of fat. In case of rupture, multi-focal high signal areas are found on T1-weighted images.

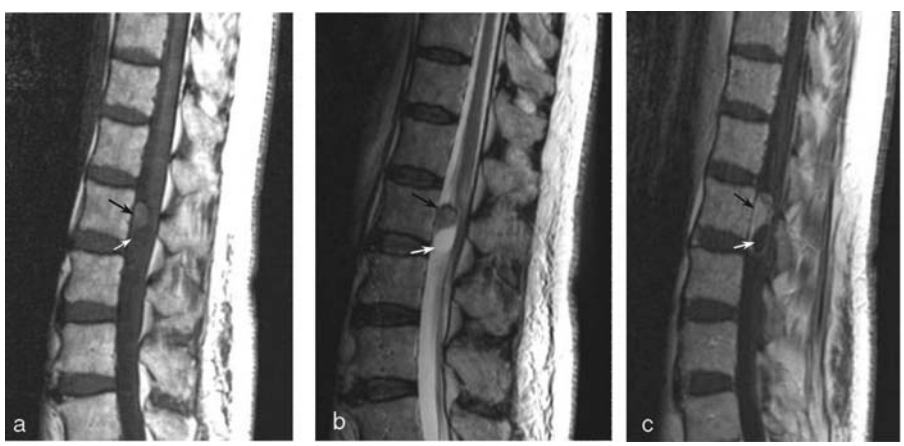

Tumors, Spine, Intradural, Extramedullary. Figure 1 Cystic schwannoma: Sagittal T1-weighted (a), sagittal T2-weighted (b) and sagittal T1-weighted with contrast (c) images of the lumbar spine show a well-defined mass appearing isointense on T1, isointense on T2 and enhances after contrast injection, corresponding to a schwannoma (black arrows). Note the inferior part of the mass which is cystic and display the same signal intensity as the CSF on both T1- and T2- weighted images (white arrows).

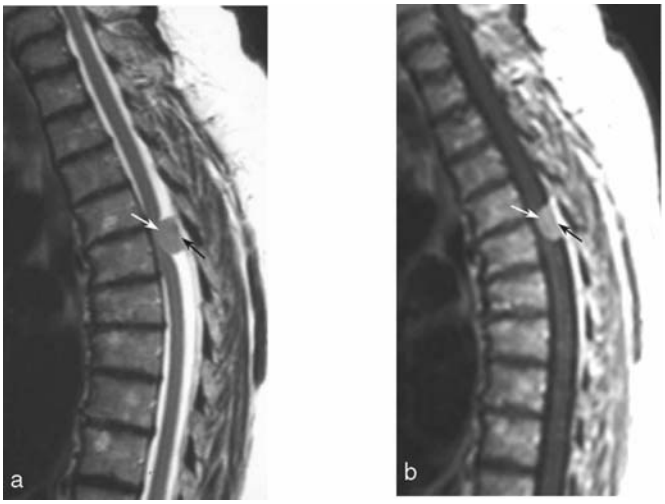

Tumors, Spine, Intradural, Extramedullary. Figure 2 Meningioma: Sagittal T2-weighted (a) and sagittal T1-weighted images after contrast (b) of the thoracic spine show a meningioma which appears isointense to the cord on T2, and enhances homogeneously after contrast (white arrows). Note the dural attachment of the mass (black arrows) and the mass effect on the spinal cord which is displaced anteriorly.

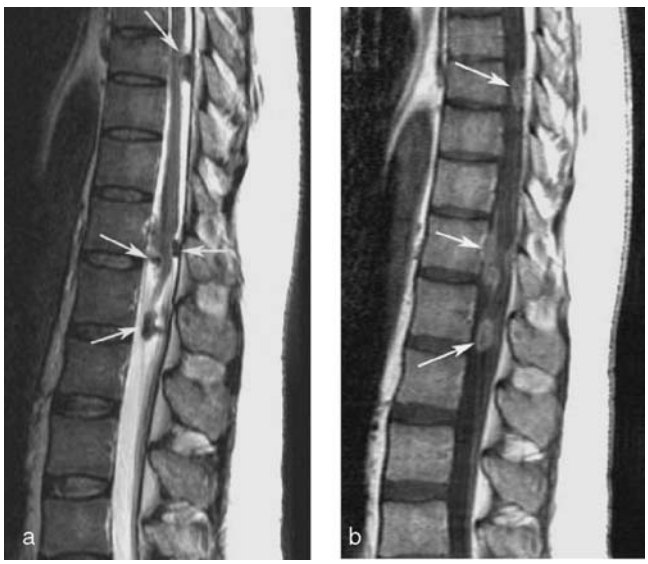

Tumors, Spine, Intradural, Extramedullary. Figure 3 Metastases from lung carcinoma. Sagittal T2-weighted (a) and sagittal T1-weighted with contrast (b) images of the lumbar region show multiple small nodular lesions in the ►intra-dural extra-medullary space which appear hypointense on T2, and enhance after contrast injection. The cord and the cauda equina are compressed and displaced by the lesions (arrows).

Neurenteric Cysts: The MR image shows well-delineated areas iso- or hyper-intense compared to CSF on T1-weighted images.

Arachnoid Cysts: Signal intensity on MR images is like CSF. Unless the cord appears displaced and flattened; ►MRI may fail to demonstrate the cyst.

Metastases: These lesions appear as thickened roots or nodular lesions which are isointense with spinal cord in most cases. Non-contrast MRI may underestimate lesions. Following contrast administration even small nodular metastases usually enhance strongly and permit better depiction of the lesions (Fig. 3). Intravenous contrast injection may also demonstrate diffuse meningeal infiltration.

Bibliography

1. Li MH, Holtas S, Larsson EM (1992) MR imaging of intradural extramedullary tumors. Acta Radiol 33:207–212

2. Osborn AG (1994) Tumors, cysts and tumor like lesions of the spine and spinal cord. In: Osborn AG (ed) Diagnostic Neuroradiology. Mosby, St. Louis, pp 876–918
3. Grossman CB (1996) Other spinal pathological conditions. In: Magnetic Resonance Imaging and Computed Tomography of the Head and Spine. 2nd edn. Williams & Wilkins, Baltimore, pp 762–768
4. Matsumoto S, Hasuo K, Uchino A et al (1993) MRI of intradural-extramedullary spinal neurinomas and meningiomas. Clin Imaging 17:46–52
5. Russell DS, Rubinstein LJ (1998) Tumors of meninges and related tissues, tumors of cranial, spinal and peripheral nerve sheaths. In: Bigner DD, McLendon RE, Bruner JM (eds) Russell and Rubinstein's Pathology of Tumors of the Nervous System. 6th edn, Vol 2. Arnold, London, pp 67–194

TUNEL Assay

Abbreviation for terminal transferase dUTP nick end labeling. This assay relies on the formation of nicks in DNA that can be identified by terminal transferase, an enzyme that catalyzes the addition of dUTPs that are secondarily labeled with a marker.

▶Apoptosis

TVS

▶Transvaginal Sonography

Tympanosclerosis

Tympanosclerosis is the thickening and calcification of the tympanic membrane. The process starts as hyaline degeneration, which is then followed by calcification.

▶Temporal Bone, Inflammatory Diseases, Acute, Chronic

Tyrosinemia

Genetic error of metabolism associated with severe liver disease in infancy due to the absence of an enzyme (fumarylacetato hydrolase) resulting in accumulation of toxic metabolic products and progressive liver and kidney failure. In the acute form, symptoms appear in the first month of life. Infants may show liver and spleen enlargement, hemorrhagic diathesis, and jaundice. The chronic form is characterized by a gradual onset and more severe liver damage with liver and spleen enlargement, ascites, jaundice. This form leads to micro–macronodular cirrhosis in early childhood and may induce hepatocellular carcinoma (HCC), often requiring liver transplantation. Diagnosis is based on blood and urine tests. Abdominal US and CT demonstrate liver enlargement, signs of cirrhosis on follow up and development of HCC.

▶Hepatic, Pediatric Tumors, Malignant

UES

A high pressure zone at the cricopharyngeus called the Upper oesophageal sphincter.
►Hernia, Hiatus in Adults

UGS

►Urogenital Sinus

UICC

International Union against Cancer.
►Neoplasms, Oral Cavity

Ulcerative Colitis

►Colitis, Ulcerative

Ulcerative Pancolitis

►Colitis, Ulcerative

Ulcerative Proctitis

►Colitis, Ulcerative

Ulcerative Sigmoiditis

►Colitis, Ulcerative

Ulcer Peptic

Vassilios Maniatis
CT and MRI Department
HYGEIA Hospital
Eritherou stvrou 4, GR-15123, Maroussi, Athens, Greece
vmaniatis@hotmail.com

Synonyms

Gastric ulcer; Duodenal ulcer

Definition

Peptic ulcer is defined as a loss of mucous surface, causing gradual disintegration and necrosis of the tissues (1). Partial or complete loss of the mucosa only, without penetration into the submucosa, is generally called erosion. Peptic ulcers affect about 10% of the adults in Western countries and may be located in the stomach or the duodenum (which is four times more common).

Peptic ulcers may be acute (completely respond to medical therapy) or chronic. They are clinically important not only because of symptoms (mainly pain) but also because of complications such as bleeding and perforation. A peptic ulcer is a benign condition that, in cases of gastric ulcers, rarely transform to malignancy. Gastric ulcers are usually larger than duodenal ulcers and affect an older population (2).

Pathology/Histopathology

Both duodenal and gastric ulcers are essentially gastric ulcers because they occur in the gastric mucosa of the stomach or

in gastric metaplasia of the duodenal mucosa (3). Peptic ulceration in the stomach or duodenum is considered the outcome of an imbalance between the aggressive acid/peptic factors and the mucosal defense factors. The large majority of peptic ulcers are strongly related to *Helicobacter pylori* infestation and/or nonsteroidal anti-inflammatory drug use. *H. pylori* predisposes to ulceration both by acid hypersecretion and by compromising mucosal defense mechanisms. Gastric ulcers result from weakened mucosal resistance in patients who have normal or even decreased acid secretion. Aspirin and other nonsteroidal anti-inflammatory drugs inhibit the synthesis of prostaglandins that contribute to the integrity of the gastric mucosal barrier. Chronic gastritis, duodenogastric reflux of bile, and delayed gastric emptying also play a role in the pathogenesis of gastric ulcers. Infection by *H. pylori* results in chronic gastritis that is strongly associated with mucosal ulceration. Patients with duodenal ulcers usually have antral gastritis and peptic acid hypersecretion. Gastric metaplasia develops in the duodenal cap, allowing *H. pylori* colonization, which leads to duodenitis and finally to ulcer.

A combination of other hereditary and environmental factors also plays a role in the development of peptic ulcers. Hereditary parameters include family history of ulcers, O-blood type, and some genetic syndromes. The list of etiologic agents includes stress, smoking, alcohol, coffee, and cocaine.

Clinical Presentation

Postprandial epigastric pain during the night is the typical and major symptom. Pain emerges 2–4 h after meals (relatively later in duodenal ulcers) and may waken the patient. Other symptoms consist of right upper quadrant, back, or chest pain; bloating; belching; nausea and vomiting; anorexia; and weight loss. Differential diagnosis may include reflux esophagitis, gastritis, duodenitis, cholecystitis, pancreatitis, gastroenteritis, irritable bowel syndrome, ischemic bowel disease, Crohn's disease, and gastric or pancreatic carcinoma. Complications include free or defined perforation (peritonitis and constant pain that radiates to the back are the relevant symptoms), gastric outlet obstruction, and gastrointestinal bleeding (more likely to occur in gastric ulcers). It is of interest that 25–50% of patients with peptic ulcers are asymptomatic and bleeding or perforation may be the presenting clinical condition. Conversely, symptoms can be typical for peptic ulcer, but both radiological and endoscopic examinations may reveal no pathology (2).

Imaging

Gastric Ulcers

Despite excellent diagnostic results, the number of barium studies performed to diagnose peptic ulcer disease has dramatically decreased during the last 10–20 years in favor of endoscopy, although the latter is more expensive and less safe. Nowadays, radiological assessment is required in those who are unable or unwilling to tolerate an endoscopy.

A ▶biphasic study using ▶double-contrast examination is recommended. Intravenous administration of 0.1 mL of glucagon is helpful to facilitate gastric hypotonia. Ulcers on the lesser or greater curvature are better depicted in profile views, whereas those on the anterior or posterior wall are better seen en face. The latter are more difficult to evaluate. Supine and oblique views are ideal for revealing ulcers located on the posterior wall or greater curvature. Flow technique (slow rotation of the patient from side to side) is helpful to identify shallow ulcers on the posterior wall or near the gastric cardia because it may lead the barium to the dependent surface of the stomach. Ulcers on the lesser curvature are better evaluated in the upright compression views. These views are also ideal for assessing features of benign ulcers (depth of penetration, Hampton's line). Prone, right anterior oblique views with 15–45° of cephalic tube angulation may reveal lesser curvature ulcers in patients with a high transverse stomach. Prone compression views or views in prone Trendelenburg position are recommended for anterior gastric wall ulcers.

Duodenal Ulcers

The most difficult ulcers to demonstrate are those located on the anterior wall. Prone compression views are required for this purpose. A biphasic examination that also includes upright compression views and double-contrast views of the duodenal bulb is considered complete (2).

Diagnosis

Gastric Ulcers

Radiologic features of gastric ulcers include the size, shape, and depth of the ulcer crater; radiating folds; Hampton's line; and the ulcer mound or collar. Gastric ulcers are usually less than 1 cm in size when diagnosed. When they are greater than 2 cm (▶giant ulcers), they are more prone to bleeding or perforation. It has also been noted that malignancy is more common in giant ulcers than in their small counterparts (3).

Gastric ulcers are commonly round or ovoid collections of barium, but they can also be linear (which probably represent a healing process), rod-shaped, rectangular, serpiginous, or flame-shaped. When seen en face, an ulcer on the dependent wall of the stomach fills

with barium, whereas an ulcer on the nondependent wall will appear as a ring. Most of them (about 80%) are located in the lesser curvature or the posterior wall of the stomach. Multiplicity occurs in about 20–30% of patients, tends to affect the gastric antrum and body, is strongly correlated with ingestion of nonsteroidal anti-inflammatory drugs, and does not favor benign disease (3).

Computed tomography (CT) has no clinical usefulness in detecting uncomplicated peptic ulcers because only the superficial layers of the gastric wall are affected. Deep ulcers or penetrating or perforated ulcers can be depicted. Inflammatory changes in adjacent soft tissues in addition to gastric wall thickening denote an ulcerous penetration. CT is the ideal method for diagnosing peptic ulcer perforation (4).

Ulcers on the lesser curvature typically appear as smooth protrusions beyond the normal contour of the stomach (Fig. 1). Some may have a "collar button" or "mushroom" appearance or are associated with ►Hampton's line. Hampton's line is a radiolucent line that separates barium in the ulcer crater from barium in the gastric lumen, created by the undermining of mucosa with minimal edema. When this radiolucent line becomes wider because of edema, it gives rise to the ulcer collar or the ulcer mound. These findings are considered pathognomonic of benign ulcers. Inflammation of the surrounding mucosa is responsible for enlarged areae gastricae, while retraction of the adjacent gastric wall leads to the development of radiating folds (2).

Ulcers on the greater curvature (3–11% of the total) are not always easy to differentiate from malignancies because they are associated with a mass effect and irregular folds around the ulcer. They may appear to have an intraluminal location, with an inner margin concave toward the lumen, and their crater may be incompletely filled because of overhanging edematous tissue (quarter moon or crescent sign). Although there is a history of aspirin ingestion in most of these ulcers, implying benign gastric ulcers, endoscopy may be required because of suspicious findings. These ulcers have a tendency to penetrate into the gastrocolic ligament, leading to the development of gastrocolic fistulas (2).

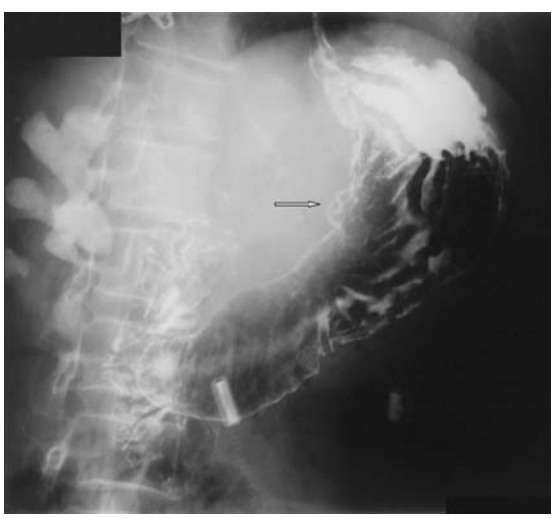

Ulcer Peptic. Figure 1 A smooth, round ulcer (*arrow*) is seen on the lesser curvature, projecting beyond the normal contour of the stomach. Radiating folds and enlarged areae gastricae are seen in the adjacent mucosa because of associated inflammation and edema.

Posterior (*dependent*) *wall ulcers*, if shallow, produce a ring shadow on double-contrast studies. The ulcer crater will be filled with barium when the flow technique is used. Radiating folds may be very large, leading to distortion in the region of the ulcer. Severe narrowing and deformity of the distal stomach due to edema and spasm may make evaluating these ulcers very difficult (2).

Anterior (nondependent) wall ulcers (1–7% of the total) may also appear as ring shadows. Prone compression views are recommended for better diagnostic results.

Pyloric channel ulcers are usually less than 1 cm in size and should fill with barium on prone or upright compression views. Although marked edema and spasm of the pyloric region may make radiological evaluation of the area very difficult, irregularity, angulation, or distortion of the pylorus should raise the possibility of an ulcer in symptomatic patients. The constant shape and size of pyloric channel ulcers enables their differentiation from pseudodiverticula caused by ulcer scarring or a surgical pyloroplasty. Adult hypertrophic pyloric stenosis also leads to a narrowed, elongated pyloric channel with superior or inferior outpouchings, but this can be differentiated from ulcer deformity on the basis of the patient's history (2).

The incidence of *recurrent and marginal* (*stomal*) *ulcers* has decreased along with the decrease in elective operations for ►peptic ulcer disease. It is suggested that these kinds of ulcers may be seen more frequently in the future because of the increase in obesity operations (especially roux-en-Y gastric bypass) (3).

The healing process may be followed by barium studies, which must be performed 6–8 weeks after the start of conservative medical treatment. Findings with ulcer healing include a decrease in size, a change in shape of a linear ulcer, and splitting of the ulcer crater. Complete healing is compatible with a benign gastric ulcer. Nodular or irregular scarring and clubbing or amputation of radiating folds raise the suspicion of malignancy. The healing process may result in a scar that is radiographically seen as a central pit or depression, radiating folds, and/or retraction of the adjacent gastric wall. Scars on the lesser curvature may be very subtle, whereas scars on the greater curvature may appear as impressing

radiating folds. Not all ulcer scars are easy to differentiate from ulcer craters. Gradually sloping margins, normal areae gastricae within the central portion of the scar, and unchanged features on follow-up studies favor the diagnosis of a scar. Healing of antral ulcers is unique because it may lead to a variety of appearances, such as a prominent transverse fold (which mimics an antral web or diaphragm), antral narrowing and deformity (identical to linitis plastica), or a widened and eccentric pylorus. Scar formation on lesser curvature ulcers may produce a deep incisura on the greater curvature that forms the hourglass stomach deformity.

Differentiating Benign from Malignant Ulcers

Benign gastric ulcers appear en face as round or ovoid ulcer craters surrounded by a smooth mound of edema or regular, symmetric mucosal folds that radiate to the edge of the crater. In profile views, benign gastric ulcers protrude outside the expected line of the stomach. Adjacent areae gastricae may be enlarged, extending to the edge of the ulcer crater without evidence of nodularity, mass effect, or tumor infiltration (2). In patients with gastric ulcers that are classified as benign or probably benign on the radiological study, it is unnecessary to perform endoscopy.

Malignant gastric ulcers are usually located on the fundus or proximal half of the greater curvature and appear en face as irregular ulcer craters (more wide than deep) eccentrically located in an irregular mass with distortion or obliteration of the normal areae gastricae surrounding the ulcer and a tumor rim (Carman's meniscus sign). Radiating folds tend to be nodular and irregular and do not reach the orifice of the ulcer crater; their tips may be fused, clubbed, or amputated. In profile views, a malignant ulcer at the apex of a protruding tumor mass will lie within the outline of the stomach. Adjacent mucosa may be nodular, and radiating folds can be thickened and lobulated (2). Although most ulcers with an equivocal appearance are proven to be benign, it is prudent to suggest the possibility of malignancy to these patients and to recommend endoscopic evaluation.

Differential diagnosis of gastric ulcers is easy and is based both on imaging findings and clinical history/presentation. Rarely, gastric ulcer must be differentiated from gastritis or gastric metastases and lymphoma. In the former, there is a marked thickening of the gastric folds and enlargement of the areae gastricae without an ulcer crater. In the latter, we may identify a necrotic cavitated lesion with a bull's eye or target lesion appearance (in cases of metastatic melanoma or Kaposi's sarcoma). Infiltration of the stomach by lymphoma may be seen as mucosal nodularity identical to enlarged areae gastricae.

Duodenal Ulcers

The vast majority of duodenal ulcers are less than 1 cm in size, have a round or ovoid shape, and are located in the duodenal bulb. They are virtually always benign, and in 15% of patients they are multiple. About 15% are linear or located in the postbulbar duodenum. Any duodenal ulcer presenting distal to the papilla of Vater should raise the suspicion of Zollinger–Ellison syndrome.

Bulbar ulcers appear as discrete niches surrounded by a smooth, radiolucent mound of edematous mucosa (Fig. 2). Radiating folds that converge centrally at the edge of the crater can be very striking, helping to localize the ulcer. Duodenal ulcers are often associated with bulbar deformity that may obscure small ulcers.

Postbulbar ulcers are usually located on the medial wall of the descending duodenum just above the papilla of Vater. A shallow, flattened niche may be seen, associated with eccentric local spasm or with a ring stricture (1).

An ulcer larger than 2 cm in size is defined as a *giant ulcer*. These ulcers are clinically important because of their higher tendency for perforation, bleeding, and obstruction. Conservative treatment is adequate. They can replace the entire bulb and be mistaken for a normal or scarred bulb. Fluoroscopy may help differentiate between a deformed bulb and a giant ulcer because the former changes appearance whereas the latter has a constant size and shape. It is also possible to recognize these ulcers on

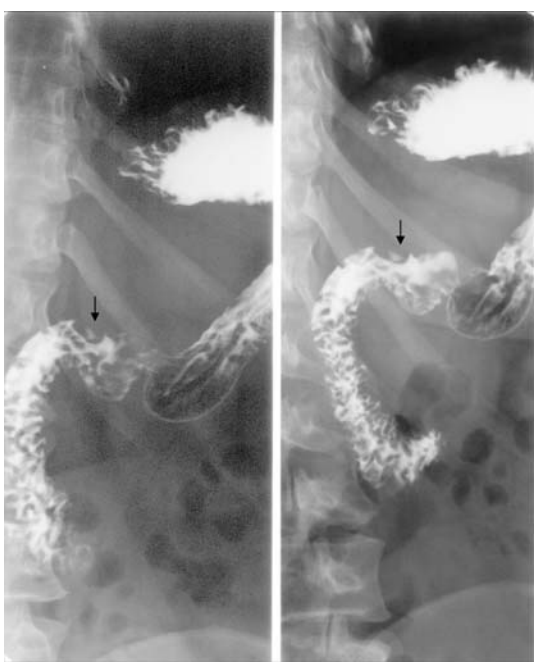

Ulcer Peptic. Figure 2 An ulcer niche in the duodenal bulb (*arrows*) surrounded by a smooth, radiolucent mound of edematous mucosa (Hampton's line, a pathognomonic feature of benign ulcers).

ultrasound studies as a cystic lesion anterolateral to the pancreatic head.

The *differential diagnosis* of duodenal ulcer includes inflammatory conditions (duodenitis, Crohn's disease, tuberculosis), duodenal stricture (due to pancreatitis or gallstone erosion), duodenal carcinoma, duodenal diverticulum, extrinsic invasion, and duodenal hematoma.

Healing Process

Conservative treatment usually leads to rapid healing. The result of the healing process is a linear barium collection and an ulcer scar manifested by radiating folds or bulbar deformity. It can be difficult to differentiate small healing ulcers from ulcer scars. Follow-up studies must be reserved for patients with persistent symptoms or complications. Bulbar deformity may lead to the classic cloverleaf appearance because of asymmetric scarring and retraction of the duodenal bulb (Fig. 3).

Complications

The most important and life-threatening complications of peptic ulcers include upper gastrointestinal tract bleeding, obstruction, and perforation. Early treatment is essential, and imaging plays a major role in diagnosing these complications.

Upper gastrointestinal bleeding may be manifested by sudden hematemesis, melena, or rectal bleeding or by chronic guaiac-positive stools or iron deficiency anemia. Endoscopy is superior to barium studies for depicting the bleeding site. Barium studies may show a filling defect in the barium-filled ulcer crater, which represents a blood clot. Differential diagnosis of this sign also includes granulation tissue or debris.

Ulcers that can lead to *obstruction* due to both edema and spasm or scarring and fibrosis are located in the distal antrum, pyloric channel, and postbulbar part of the duodenum. Abdominal radiographs may imply obstruction by demonstrating a dilated stomach with retained food and debris. In this case, a barium study using high-density barium must be performed after decompressing the stomach with a nasogastric tube. The major differential diagnosis of gastric outlet obstruction includes scirrhous carcinoma, and endoscopy with biopsy may be required. Duodenal obstruction may be the result not only of ulcer but also of other inflammatory conditions, hematomas, duplication cysts, or pancreatic pathology.

Ulcers on the anterior wall of the stomach or duodenum may *perforate* directly to the peritoneal cavity, whereas ulcers on the posterior wall of the stomach or duodenum usually result in a walled-off or "confined" perforation. Free intraabdominal air on plain radiographs is the major radiological sign but is seen in only 50–70% of patients because the volume of escaped gas can be small and the site of perforation may quickly become sealed off (4). Confined perforations are usually seen as an abscess in the lesser sac or the anterior perirenal space. CT is the ideal method to diagnose both free and confined perforations. It is fast, easy to perform, and sensitive, with no need for patient preparation and cooperation. Free air is seen in almost all the cases of perforations due to peptic ulcer. Common sites of pneumoperitoneum include the anterior surface of the liver and the perigastric/duodenal region (4).

Penetrating ulcers occasionally produce gastroduodenal, gastrocolic, duodenocolic, choledochoduodenal,

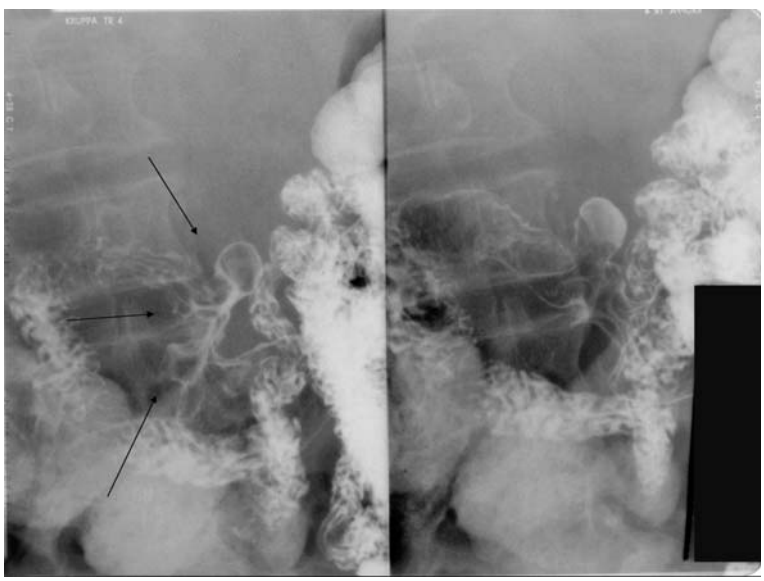

Ulcer Peptic. Figure 3 Bulbar deformity due to marked scarring has the classic cloverleaf appearance.

duodenorenal, and gastropericardial fistulas. Gastroduodenal fistulas lead to the typical "double-channel pylorus" sign on barium studies. Gastrocolic fistulas used to result from stomach or transverse colon carcinomas but now are mainly caused by aspirin-induced ulcers on the greater curvature of the stomach. The clinical triad of diarrhea, feculent vomiting, and foul-smelling eructations is typical. Endoscopy is contraindicated due to the risk of perforation. Barium studies and barium enema examination may reveal pathology. A barium enema study is also superior to barium studies of the upper gastrointestinal tract for revealing duodenocolic fistulas. Peptic ulcers cause only 5% of choledochoduodenal fistulas. Barium studies may be diagnostic, but because the inflammatory process may seal off the fistula, the diagnosis may sometimes be missed. Gastropericardial fistulas can be a fatal complication of peptic ulcer in the intrathoracic portion of the stomach (hiatal hernia or after esophagogastrectomy). Sudden pneumopericardium on chest radiographs is the major finding (2).

Bibliography

1. Burgener FA, Kormano M (1991) Ulcers, diverticula, and fistulas in the gastrointestinal tract. In: Burgener FA, Kormano M (eds) Differential Diagnosis in Conventional Radiology. 2nd edn. Thieme, New York, pp 699–718
2. Levine MS (2000) Peptic ulcers. In: Gore RM, Levine MS (eds) Textbook of Gastrointestinal Radiology. 2nd edn. WB Saunders, Philadelphia, pp 514–545
3. Harbison SB, Dempsey DT (2005) Peptic ulcer disease. Curr Probl Surg 42:346–454
4. Maniatis V, Chrysikopoulos H, Roussakis A et al (2000) Perforation of the alimentary tract: evaluation with computed tomography. Abdom Imag 25:373–379

Ulnar Deviation of the Metacarpophalangeal Joint

A typical deformity in late-stage rheumatoid arthritis with or without subluxation and ulnar abduction.
▶Rheumatoid Arthritis

Ulnar Drift and Palmar Subluxation

A typical deformity in late-stage rheumatoid arthritis due to destruction of the ligaments and insertions.
▶Rheumatoid Arthritis

Ultrasonography

Imaging of tissue using acoustic waves at frequencies higher than the human audible range.
▶Ultrasound Imaging

Ultrasound (US)

Ultrasound emitted from a transducer (piezo-electric crystal) travels at constant velocity into tissues, and is reflected differently from different tissue interfaces back to the transducer that acts also as a receiver. Echoes are electronically converted to the image on the monitor. Outlining the kidneys and other abdominal organs, US can distinguish solid from cystic lesions, and detect tumors by assessing their shape, volume, and structure. Stones cause almost complete reflection of US waves; are therefore echogenic with a characteristic dorsal acoustic shadowing. Urinary stones are detected directly inside the collecting system, better dilated than not. US guided PNS insertion is recommended, and drainage assured in patients with persisting obstruction, uncontrollable pain or infection.
▶Colic, Acute, Renal

Ultrasound Appearance of Hepatic Hematoma Changes with Time

It is usually hyperechoic in the acute phase, whereas it appears inhomogeneously hypoechoic, with internal echoes due to septation and debris, in a more chronic stage.

In an acute or subacute setting, computed tomography (CT) features of hematoma are hyperdense areas on baseline CT scan not enhanced after contrast medium administration, whereas chronic hematoma is hypoattenuating on the precontrast scan and can display rim enhancement following intravenous contrast medium administration.

The magnetic resonance characteristics of hepatic hematoma depend mainly on the age of the hemorrhagic lesion. Acute hematoma shows an intermediate signal intensity on T1-weighted images and a low signal intensity on T2-weighted images due to the high-intracellular concentration of deoxyhemoglobin in red blood cells,

whereas subacute hepatic hematoma, because of the presence of extracellular methemoglobin, appears as a heterogeneous mass with pathognomonic high signal intensity on T1-weighted images and intermediate signal intensity on T2-weighted images.

▶Trauma Hepatobiliary

Ultrasound Contrast Agents

▶Contrast Media, Ultrasound, Commercial Products
▶Microbubbles

Ultrasound Contrast Media

Thomas Albrecht
Klinik und Hochschulambulanz für Radiologie und Nuklearmedizin, Charité-Campus Benjamin Franklin, Berlin, Germany
thomas.albrecht@charite.de

Ultrasound contrast media (USCM) or echo enhancers consist of minute gas-containing microbubbles that have a high reflectivity when exposed to an ultrasound field. These highly reflective microbubbles produce intense echoes on the ultrasound (US) image.

The first microbubbles used for medical imaging (mainly for *echocardiography*) were created by agitating saline solutions. When injected intravenously, small air bubbles included in the fluid produce signal enhancement in the draining veins and right heart. These bubbles are, however, unable to withstand pulmonary passage, so there is no signal enhancement in the left heart under normal conditions. They can be used for detection of right-to-left shunts by demonstration of microbubbles within the left heart. Due to their lack of transpulmonary stability, such agitated fluids can neither be used for echocardiography of the left heart nor for extracardiac US.

Since the mid-1990s, transpulmonary microbubble USCM have become available. Transpulmonary stability is achieved by the addition of a *shell* surrounding and thus stabilizing the microbubble. The different USCM that are *currently commercially available or in clinical development* consist of various gases and shell materials. They can be divided into two major categories: *high-solubility gas* (*air*) and *low-solubility gas* (*perfluor gas*) agents. The much lower solubility of perfluor gases in plasma leads to a higher stability of these agents with stronger and longer-lasting signal enhancement.

USCM are blood pool agents that do not diffuse into the extracellular fluid compartment. They distribute evenly throughout the entire blood pool and can be used for echocardiography of the left heart as well as for extracardiac ultrasound of vessels and almost every organ. The average diameter of the microbubbles of all dedicated USCM ranges between approximately 2 and 7μ; they are thus smaller than red cells and there is therefore no risk of capillary embolization.

Because USCA are blood pool agents, in contrast to conventional agents for CT or MRI, they distribute evenly throughout the whole blood pool and can be used for imaging for several minutes following intravenous injection. In addition to the blood pool phase, some USCM have a *liver-specific delayed phase* that begins a few minutes after injection and lasts from minutes to hours or even longer. The gas is gradually eliminated from the blood by exhalation *via* the lungs, and the shells are metabolized. All licensed USCA have a very favorable *safety* profile, with few *adverse reactions* reported. They are not nephrotoxic, and allergoid reactions are very rare and considerably less frequent than with iodinated x-ray contrast agents.

Nonlinear Properties of Microbubbles and Contrast-Specific Imaging Techniques

USCA were originally developed to enhance signals from flowing blood in technically difficult spectral or color *Doppler studies*. Due to rapid improvements in equipment technology and particularly in Doppler sensitivity, this application has become rare in most vascular territories, it still has niche role in some patients with unfavorable acoustic access and in *transcranial Doppler*.

Outside the heart the agents do not provide sufficient signal enhancement on conventional B-mode imaging. To achieve clinically useful and Doppler-independent extracardiac enhancement, *contrast-specific imaging techniques* are required. Several such techniques have been developed in recent years. They all exploit the so-called *nonlinear acoustic properties* of microbubbles.

When exposed to an US field, microbubbles show a complex acoustic behavior, and this behavior determines the properties of the signal that is returned from the microbubble to the transducer. It is crucially dependent on the amplitude or energy of the transmitted pulse (transducer output). In clinical imaging, the *mechanical index* (MI) is used as a measure of transducer output, and the MI is an important variable in contrast-enhanced US that needs to be controlled carefully by the operator. With increasing amplitude, the microbubble response ranges

from linear scattering and *linear resonance* to *nonliner resonance* and *bubble destruction.*

Contrast-specific imaging techniques utilize the nonlinear bubble response for highly sensitive and specific display of contrast agents. Various techniques are used to achieve this. These are mainly *multipulse techniques* that use either *phase modulation (inversion), amplitude modulation,* or a combination of the two.

High and Low MI Imaging with USCM

Air-based microbubbles are relatively instable when exposed to an US field and show only weak *resonance.* Imaging with air-based microbubbles requires *microbubble destruction* for adequate enhancement. Therefore, *intermittent imaging* with low frame rates to allow refilling of the microbubbles into the microvasculature is necessary. Alternatively, it is possible to use a fast *sweep technique* with offline review of the digitally stored cine loops.

Low-solubility gas USCM are characterized by the combination of improved stability with favorable resonance behavior at low acoustic pressure. This allows minimally disruptive contrast-specific imaging at low MI and enables effective investigations over several minutes with the visualization of the *dynamic enhancement* pattern in real time.

Functional Perfusion Studies with USCM

USCA can be used as tracers for dynamic studies of perfusion. Arteriovenous *transit time analysis* of organs such as the liver, kidney, and brain can be assessed based on *time-intensity curves* measured in artery and vein. Another approach for hemodynamic studies, such as the myocardium, the kidney, or tumors, is the *destruction-reperfusion technique.* For this technique a steady state of microbubble concentration is required, which is achieved by continuous infusion of USCA. During the steady state, microbubbles in the imaging plane are destroyed by short insonnation at high MI. After switching back to low MI, the signal recovery curve is used to calculate perfusion and fractional vascular volume.

Targeted Microbubbles for Imaging and Drug Delivery

By attaching certain ligands and antibodies to the shell of a microbubble, the bubble will specifically bind to certain types of (tumor) cells or to thrombus, for example. This can be used for specific imaging of defined organs or diseases or for local drug delivery. If a targeted microbubble is filled with a certain pharmaceutical or gene, it can be destroyed by high MI US after binding to the target, and the drug is released at the site or even into the target cell. The use of targeted microbubbles as specific contrast media or drug carriers or even as vectors for gene therapy is currently in an experimental preclinical stage.

Clinical use of USCM

Common applications of USCM in clinical practice are echocardiography, transcranial Doppler studies, imaging of focal liver lesions (1), renal imaging for reflux in children as well as for focal renal lesions, imaging of focal splenic lesions, and assessment of soft tissue organs in blunt abdominal trauma. Apart from these common indications, USCM can in principle be used in every organ or vascular territory accessible to US by analogy with the use of contrast media in other imaging modalities.

Bibliography

1. Albrecht T et al (2004) Guidelines for the use of contrast agents in ultrasound. Ultraschall Med 25:249–256

Ultrasound Contrast Media

▶Contrast Media, Ultrasound, Commercial Products
▶Microbubbles

Ultrasound Signal Enhancers

▶Contrast Media, Ultrasound, Commercial Products

Ultrasound Imaging

Elisa E. Konofagou
Department of Biomedical Engineering and Radiology, Columbia University,
351 Engineering Terrace, mailcode 8904,
1210 Amsterdam Avenue, New York, NY
ek2191@columbia.edu

Synonyms

Echography; Sonography; Ultrasonography

Definition

Sounds with a frequency above 20 kHz are called ultrasonic because they occur at frequencies inaudible to the human ear. When emitted at short bursts, propagating through media such as water with low reflection coefficient and reflected by obstacles along their propagation path, detecting the reflection, or *echo*, of the ultrasonic wave can help localize the obstacle (1). This principle has been used by sonar (SOund NAvigation and Ranging) and inherently used by marine mammals, such as dolphins and whales, to help them localize prey, obstacles, and predators. In fact, the frequencies used for "imaging" vary significantly depending on the application: from underwater sonar (up to 300 kHz), diagnostic ultrasound, therapeutic ultrasound, and industrial nondestructive testing (0.8–20 MHz) to acoustic microscopy (12 MHz to above 1 GHz).

Imaging

Scattering and Attenuation

Tissues are constituted of cells and groups of cells that serve as complex boundaries to the propagating wave. As the wave propagates through all these complex structures, reflected and transmitted waves are generated at each one of these interfaces depending on the local density, compressibility, and absorption of the tissue. The groups of cells are called "scatterers" because they scatter acoustic energy. The backscattered field, or what is "scattered back" to the ►transducer, is used to generate the ultrasound image. In fact, the backscattered echoes are usually coherent. Fig. 1a shows an ultrasound image of an 8-week-old fetus in the womb. This grainy appearance is called "speckle," a term borrowed from the laser literature. Speckle is produced by the constructive and destructive interference of the scattered signals from structures smaller than the wavelength—hence, the appearance of bright and dark echoes, respectively. Thus, speckle does not necessarily relate to a particular structure in the tissue.

Transducers

A pressure wave is generated using an ultrasound transducer, which is typically a piezoelectric material. "Piezoelectric" denotes the particular property of certain crystal polymers of transmitting a pressure ("piezo" means "to press" in Greek) wave generated when an electric potential is applied across the material. Most importantly, since this piezoelectric effect is reciprocal (i.e., a piezoelectric crystal will convert an impinging pressure wave to an electric potential), the same transducer can also be used as a receiver. Such crystalline or semicrystalline polymers include polyvinylidene fluoride (PVDF), quartz, barium titanate, and lead zirconium titanate (PZT).

Ultrasonic imaging has recently also expanded to three-dimensional (3D) imaging in clinical applications, especially in cardiology and obstetrics (Fig. 1). This is due to advances in transducer design, namely the 2D arrays, in which beams are generated in all three planes (Fig. 1b), but 3D images (Fig. 2c) can also be achieved by sweeping a linear or phased array out of plane.

Modes of Imaging

A-Mode

Fig. 2 shows a block diagram of the different steps that are used to acquire, process, and display the received signal from the tissue.

Transducer frequency

A pulse of a given duration, frequency, and bandwidth is first transmitted. A tradeoff between penetration (or low attenuation) and resolution exists. Therefore, the chosen frequency will depend on the application. Usually for deeper organs, such as the heart, uterus, and liver, the frequencies are restricted in the range of 2–5 MHz, whereas for more superficial structures, such as the thyroid, breast, and testis, and for use in infants, a wider range of 4–15 MHz is applied. Finally, for ocular applications, a range of 10–20

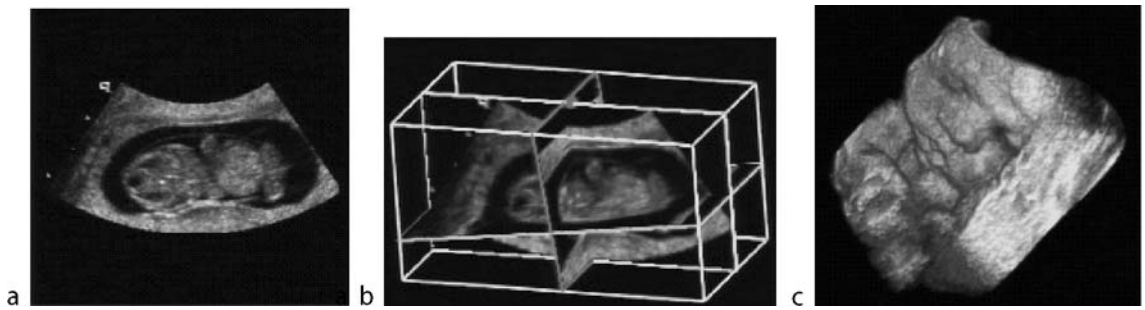

Ultrasound Imaging. Figure 1 (a) B-mode ultrasound scan of an 8-week fetus (coronal slice); (b) orthogonal slices obtained with a 2D array; (c) 3D ultrasound image.

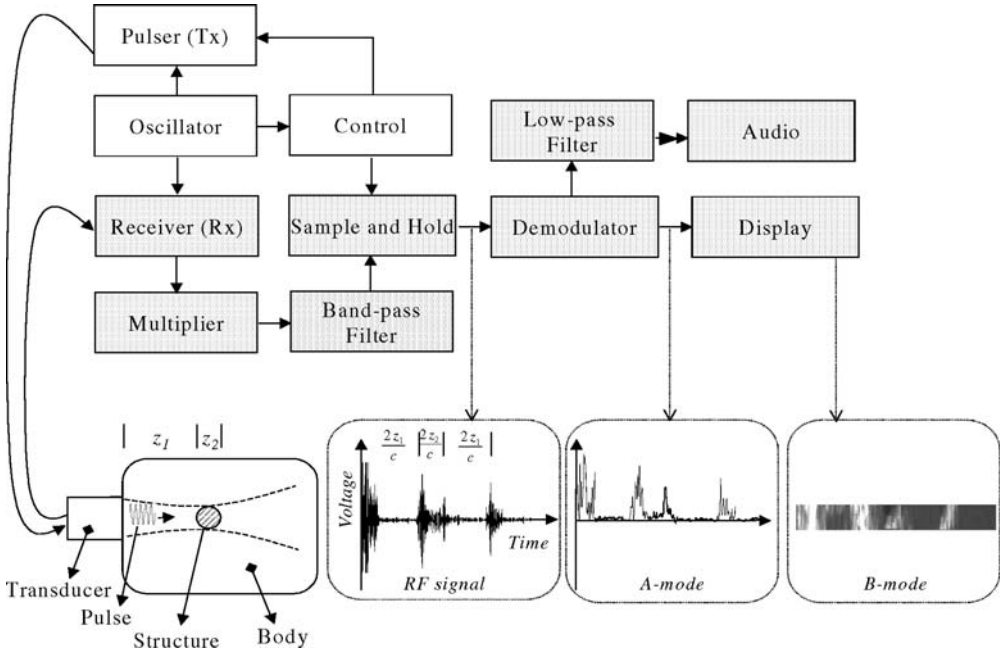

Ultrasound Imaging. Figure 2 Block diagram of a pulse-echo system and the resulting signal or image at three different steps.

MHz is determined by the low attenuation, low depth, and higher resolution required.

The pulse (Fig. 2) is usually a few cycles long (usually 3–4 cycles) to ensure high resolution, and it is generated by the transmitter through a voltage step sinusoidal function at a voltage amplitude of (100–500 V) and a frequency equal to that of the resonance frequency of the transducer elements. For static structures, a single pulse or multiple pulses (usually used for averaging off line) could be used at an arbitrary frequency. However, for moving structures such as blood, liver, and heart, a fundamental limit on the maximum pulse repetition frequency (PRF) is set by the maximum depth of the structure, or $PRF\,(\text{kHz}) = c/2D_{\max}$ (2). Typically, the PRF is in the range of 1–3 kHz.

RF amplifier

The received signal needs to be initially amplified to guarantee a good signal-to-noise ratio. At the same time, the input of the amplifier should be devoid of high voltage pulse to protect the circuitry and maintain its low noise and high gain. A typical dynamic range expected at the output is of the order of 70–80 dB.

Time-gain compensation

Attenuation is unavoidable and increases with depth as the wave travels through the medium. To avoid artificial darkening of deeper structures as a result, a voltage-controlled attenuator is usually employed, in which a control voltage is used to manually adjust the system gain accordingly after reception of an initial scan. A logarithmic voltage ramp is usually applied that compensates for a mean attenuation level with depth. The dynamic range becomes further reduced to 40–50 dB.

Compression amplifier

The signals will ultimately be displayed as a gray scale on a cathode ray tube (CRT), where the dynamic range is typically only 20–30 dB. For this purpose, an amplifier with a logarithmic response is used.

Demodulation or envelope detection

Because the image is a gray-scale picture, the amplitude of the signal is displayed. For this, the envelope of the RF signal needs to be calculated. This is usually achieved by using Hilbert transforms. The resulting signal is called a detected A-scan, A-line, or *A-mode scan* ("A" for amplitude). An example is shown in Fig. 2.

B-Mode

When the received A-scans are spatially combined after acquisition using either a mechanically moved transducer or the previously mentioned arrays and used to brightness-modulate the display in a 2D format, the brightness or B-mode ('B' for brightness) is created, which has a true image format and is by far the most widely used diagnostic ultrasound mode. By default, sonogram or echogram refers to B-mode. Fig. 1a shows an example of a B-mode image. One of the biggest advantages of ultrasound scanning is real-time capability, and this is

achieved due to the shallow depth of scanning in human applications and the high speed of sound. The frame rate is usually of the order of 30–100 Hz (whereas in the M-mode version it can be as fast as the PRF itself; see later). The frame rate is limited by the number of A-mode scans acquired, N_A, and the maximum depth, that is, frame ratemax $PRF_F = c/2D_{max}/N_A$.

M-Mode

Another way of displaying the A-scans is as a function of time, especially in cases in which tissue motion needs to be monitored and analyzed. In this case, only one A-scan from a particular tissue structure is displayed in brightness mode but is followed in time depending on the PRF used and called motion-, or M-mode scan. A depth-time display is then generated. A typical application of the M-mode display is used in the examination of heart-valve leaflet motion and in ▶Doppler displays.

Doppler Mode

The Doppler effect is defined as the frequency shift that results from a nonzero scatterer velocity. Several techniques have been developed to maximize performance; they include an adjustable gate depth according to the PRF used and a sharp cut-off smoothing filter with an adjustable cut-off frequency, also dependent on the PRF. These shortcomings can also be avoided by combining the B-scan mode with the Doppler sonogram mode, otherwise known as *duplex mode,* or the *triplex mode,* which is the duplex mode with an additional color Doppler map superimposed on the B-mode image.

Diagnosis

- Adult cardiology
- Breast
- Endoluminal gastroenterology
- Extracranial vessels
- Fetal intervention
- Gynecology
- Hepatobiliary system
- Interventional procedures
- Intraoperative procedures
- Male genital system
- Musculoskeletal system
- Needle biopsy guidance
- Obstetrics and perinatology
- Ophthalmology
- Pediatric cardiology
- Pediatric neurology
- Peripheral vascular system
- Splanchnic vessels
- Superficial structures
- Urinary system.

Bibliography

1. Wells PNT (1977) Biomedical Ultrasonics, Medical Physics Series. Academic Press, London NW1
2. Bamber JC, Tristam M (1988) Chapter 7: Diagnostic Ultrasound. In: The Physics of Medical Imaging Webb S (ed) Medical Science Series IOP Publishing Ltd., Dirac House, Temple Back, Bristol, U.K. 319–386
3. Christensen PA (1988) Ultrasonic Bioinstrumentation.1st edn., John Wiley & Sons, Hoboken, NJ, USA

Undifferentiated Embryonal Sarcoma

Mesenchymal tumor, known in the past as "malignant mesenchymoma," is the fourth most common hepatic malignancy in infants, typically occurring in older children (6–10 years) and young adults. It is composed of spindle and stellate sarcomatous cells, closely packed in whirls, or scattered loosely in a myxoid substance. The lesions are usually large, hypovascular and can be either solid or cystic. Cystic areas result from hemorrhage and necrosis. Metastases involve the lungs and skeleton.

▶Hepatic, Pediatric Tumors, Malignant

Unexpected Clinical Findings

▶Incidental Neuroradiological Findings

Uphill Varices

Most common form of oesophageal varix, normally involving the lower third of the oesophagus. Found in patients with portal hypertension and the result of reversed flow in the left gastric (coronary) vein.

▶Varices, Oesophagus

Upper Extremity Claudication

▶Claudication, Brachial

Ureteral Colic

▶Colic, Acute, Renal

Ureteropelvic Junction Obstruction

▶Ureteropelvic Junction Syndrome

Ureteropelvic Junction Syndrome

Laurent Brunereau, Patrick Omoumi, Monica Olar, Dominique Sirinelli
Pôle d'imagerie médicale, CHU de Tours, France
brunereau@chu-tours.fr

Synonyms

Ureteropelvic junction obstruction

Definition

Ureteropelvic junction (UPJ) obstruction is defined as an obstruction of the flow of urine from the renal pelvis to the proximal ureter. This results in high pressure in the renal pelvis, ▶hydronephrosis, diminished renal function, and progressive renal damage. In its extreme form, UPJ obstruction may lead to complete loss of renal cortex.

UPJ syndrome can be primary or secondary. Primary UPJ obstructions are diagnosed in the antenatal or postnatal phases. They are related to congenital stricture of the ureter. The etiology of these strictures is unclear. However, it has been postulated that in utero ischemia leads to the formation of focal lesions of the ureter and fibrous scarring of the ureteral musculature. This condition occurs in approximately one in 1,500 children and can be associated with other kidney, bladder, or intestinal tract pathologies. The male-to-female ratio is 3:1 and the left side is affected more commonly than the right side. The development of ultrasound (US) and its widespread use for in utero screening have allowed the diagnosis of primary UPJ obstructions long before birth and their management in the first weeks of life.

When it is diagnosed later in childhood or in adulthood, the condition is called secondary UPJ obstruction, which can be related to congenital or acquired lesions. Congenital abnormalities are either similar in their physiopathology to that previously described for primary UPJ obstruction or correspond to a UPJ compression caused by an accessory crossing vessel. The delayed presentation of congenital UPJ stricture in a child or an adult is believed to result from progressive worsening of the ureteral scarring caused by intermittent inflammation or from the increase in urine production due to growth. UPJ compression caused by an anomalous accessory vessel crossing the lower pole of the kidney represents approximately 25% of all secondary UPJ obstructions.

Acquired conditions responsible for secondary UPJ obstructions are stones, ureteral tumors, compression from extrinsic processes (tumors, cysts, retroperitoneal fibrosis, or other inflammatory lesions, etc.), and periureteral scars caused by prior surgery.

Clinical Presentation

Immediately after birth, primary UPJ obstruction can be revealed by an abdominal mass or a urinary tract infection presenting with fever and hematuria.

In older children or adults, symptoms of secondary UPJ are back or flank pain which may be permanent or intermittent, urinary tract infection with hematuria, abdominal mass, or elevated blood pressure.

Imaging

Primary UPJ Obstruction

Careful antenatal US examination is effective in detecting urinary tract abnormalities such as hydronephrosis. Fetal hydronephrosis is defined as an anteroposterior (AP) pelvic diameter of 4 mm or more before 33 weeks and 8 mm or more after 33 weeks of gestation (1). Although hydronephrosis is diagnosed with an incidence of 1% of all antenatal ultrasonographic studies, only one in 500 infants will be found to have a significant urologic condition in the first days of life. Most of these renal pelvis dilatations are therefore related to nonobstructive conditions.

When hydronephrosis is diagnosed prenatally, prophylactic antibiotherapy is started at birth pending further investigations. Postnatal US is recommended in the first days of life but should only be performed at 7–10 days. In fact, earlier examinations may yield false-negative results due to a relative dehydration state of neonates. An additional voiding cystourethrogram (VCUG) should be discussed to rule out vesicoureteral reflux. UPJ obstruction is suspected when postnatal US demonstrates a pure

pelvocalyceal dilatation (without ureteral dilatation) associated to an absence of reflux on VCUG. Important features to evaluate on postnatal US are renal length, the AP diameter of renal pelvis, cortical thickness, and renal cortex echogenicity.

When postnatal US findings are consistent with the diagnosis of UPJ obstruction, diuretic renal scan (DRS) is performed to assess renal function. The radiopharmaceutical agents used are DTPA, MAG3, or DMSA and are all bound to Tc-99m. DRS is usually performed for infants above 1 month of age.

Management of UPJ obstruction is currently based on the conclusions made after US and DRS (2):

1. Neonates with a hydronephrosis less than 12 mm require US at the ages of 3 months and 1 year.
2. Neonates with a 13–19 mm hydronephrosis and good renal function on DRS should undergo follow-up US and DRS at 3 months and 1, 2, 5 and 10 years of age.
3. Neonates with 20–50 mm hydronephrosis but normal renal function require further long-term studies (at 3 months, 6 months, 1 year, and yearly thereafter) to identify those who will benefit from surgical treatment. Surgery is indicated in cases of worsening hydronephrosis or degradation of the renal function alteration.
4. Neonates with a dilatation of more than 50 mm or altered renal function should undergo surgery by 3 months of age.

Secondary UPJ Obstruction

US remains the best method for diagnosing hydronephrosis in children or adults with flank pain, hematuria, or urinary tract infection. Hydronephrosis refers to both renal pelvis and calyceal dilatation. On the other hand, an isolated renal pelvis dilatation without calyceal dilatation suggests the diagnosis of extrarenal pelvis, which is an anatomical variant of the upper urinary tract.

Diagnosis of secondary UPJ obstruction should be suspected when hydronephrosis is not associated with ureteral dilatation on US and can be confirmed by intravenous urography (IVU), computed tomography (CT), or magnetic resonance imaging (MRI).

1. In IVU (Fig. 1), UPJ obstruction is responsible for delayed nephrogram, delayed excretion of contrast media in the renal collecting system, and for pelvocalyceal dilatation without ureteral dilatation. In cases of mild UPJ stricture, additional intravenous injection of furosemide is often necessary so as to increase the diuresis to demonstrate the dilatation of the renal collecting system. IVU may also demonstrate UPJ abnormalities such as intraluminal radiopaque stones or radiolucent filling defects suggesting the diagnoses of radiolucent stone or transitional cell carcinoma (TCC).
2. Helical CT (Fig. 2) has many advantages over IVU because it is more sensitive in diagnosing intraluminal UPJ pathologies such as stone or TCC, or extrinsic

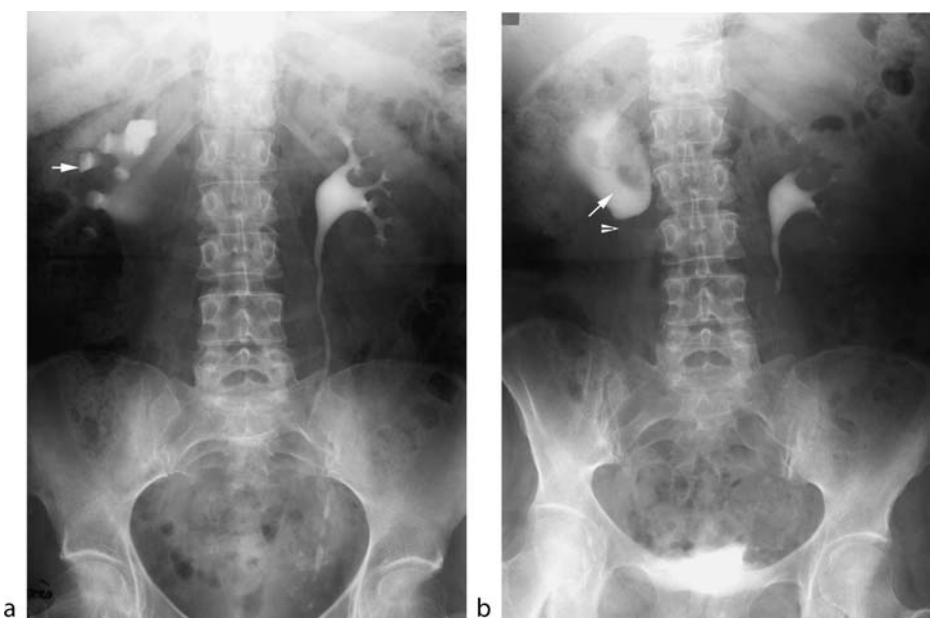

Ureteropelvic Junction Syndrome. Figure 1 Right UPJ syndrome in a 25-year-old male patient. IVU, AP view (Fig. 1A), and PA view (Fig. 1B) performed at 10 min and 30 min after intravenous injection of contrast media. At 10 min (Fig. 1A), there was a delayed excretion of contrast media in the right upper excretory system (arrow). At 30 min (Fig. 1B), a right pelvocalyceal dilatation (arrow) without ureteral dilatation (arrowhead) was clearly demonstrated. This dilatation was related to a right UPJ obstruction.

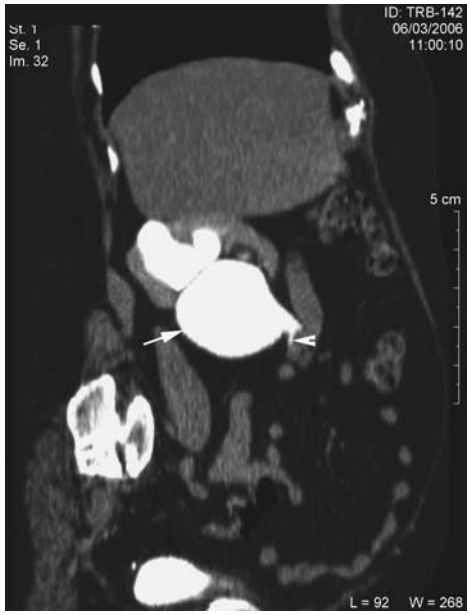

Ureteropelvic Junction Syndrome. Figure 2 Right UPJ syndrome in a 40-year-old male patient. Multislice CT with helical acquisition of 3 mm slices, 30 min after intravenous injection of contrast media. MPR reconstruction in the sagittal plane. Enlargement of right upper excretory system (arrow). Narrowing of the right UPJ without endoureteral mass or extrinsic lesion (arrowhead).

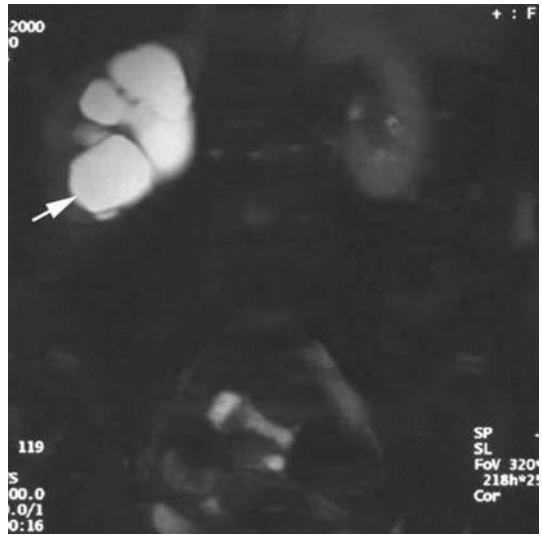

Ureteropelvic Junction Syndrome. Figure 3 Right UPJ syndrome in a 30-year-old female patient. MR urography with frontal T2-weighted RARE sequence. Severe pelvocalyceal enlargement (arrow) without visualization of the right ureter. This dilatation of the right upper excretory system was related to a right UPJ syndrome.

lesions such as retroperitoneal fibrosis or a tumor responsible for UPJ obstruction. Moreover, CT angiography (CTA) is a reliable method for the depiction of crossing arteries responsible for secondary UPJ obstruction. These accessory renal vessels are most commonly located anterior to the UPJ (3). Currently, CTA with a multislice technique is as accurate as digital subtraction angiography (DSA) in demonstrating an UPJ ►crossing artery, is less expensive, less invasive, and can be easily performed on an outpatient.

3. MRI (Fig. 3), including MR urography (MRU) (RARE or HASTE sequence) and additional MR sequences with gadolinium injection, is a reliable alternative to CT especially in patients in whom injection of iodinated contrast media is contraindicated (renal insufficiency, risk of adverse reaction, etc.) and in pregnant women (4). MRU is accurate in demonstrating a dilatation of the renal collecting system and in specifying the degree and the level of obstruction. With an "all-in-one approach," MRU completed by an MR angiography (MRA) sequence may be useful for demonstrating an accessory renal artery crossing the UPJ. Moreover, additional conventional MR sequences allow one to study the thickness of renal cortex, visualize the retroperitoneal soft tissues, and specify the nature of the pathology responsible for the pelvocalyceal dilatation and the UPJ filling defect on MRU. For example, these conventional sequences may demonstrate lesions such as TCC or retroperitoneal tumor. However, it seems clear that MRI is not able to substitute CT in the diagnosis of urolithiasis responsible for UPJ obstruction.

Interventional Radiological Treatment

UPJ obstruction can be treated by open pyeloplasty or by several minimally invasive procedures such as a retrograde endourologic balloon incision or an antegrade endopyelotomy. Open pyeloplasty has been accepted as the surgical treatment of choice for primary UPJ obstruction in children, with a success rate of more than 90% in most reports. However, to many authors, success rates of ►endourologic surgery are comparable to those of open surgery but with lower morbidity. Therefore, secondary UPJ obstructions are currently treated in adults mostly by endoscopic procedures.

Nephrectomy is performed in rare cases with complete destruction of the renal parenchyma.

Temporary percutaneous nephrostomy may be indicated in cases of severe urinary tract infection or before surgery when a major loss of renal cortex is diagnosed and a nephrectomy or a surgical repair is discussed.

References

1. Wiener JS, O'Hara SM (2002) Optimal timing of initial postnatal ultrasonography in newborns with prenatal hydronephrosis. J Urol 168:1826–9182
2. Low SC, Jacobsen AS, Teo EL (2002) Clinics in diagnostic imaging (73). Left hydronephrosis due to pelvi-ureteric junction obstruction. Singapore Med J 43: 265–269
3. Rouviere O, Lyonnet D, Berger P et al (1999) Ureteropelvic junction obstruction: use of helical CT for preoperative assessment-comparison with intraarterial angiography. Radiology 213:668–673
4. Zielonko J, Studniarek M, Markuszewski M et al (2003) MR urography of obstructive uropathy: diagnostic value of the method in selected clinical groups. Eur Radiol 13:802–809

Urethra, Stenosis

Michele Bertolotto[1], Pietro Pavlica[2], Elena Trincia[1], Manuel Belgrano[1], Stefano Cernic[1], Maria Assunta Cova[1]
[1]Department of Radiology, University of Trieste, Trieste, Italy
[2]Department of Radiology, Hospital M. Malpighi, Bologna, Italy
bertolot@univ.trieste.it

Synonym

Urethral stricture

Definitions

The male urethra is subdivided into prostatic, membranous, bulbar, and penile portions. The prostatic portion begins at the bladder neck and passes through the prostate gland up to the prostate apex. The membranous urethra passes through the urogenital diaphragm. The bulbar urethral portion is surrounded by the bulb of the corpus spongiosum and extends from the perineal area to the suspensory ligament, which anchors the penis to the symphysis pubis. The penile or pendulous portion of the urethra stretches from the suspensory ligament to the external urethral meatus. Before its emergence at the meatus, there is an ampullar dilatation called the *Fossa* navicularis.

The female urethra is about 4 cm long and extends from the bladder neck to the vestibule, where it forms the external meatus between the *Labia* minora.

Urethral stenosis is a pathology that mainly affects the male urethra, due to its anatomical conformation and length, but distal strictures can also occur in female patients.

Pathology/Histopathology

Narrowing of the urethra can be congenital or acquired. Malformations are due to complete or segmental stenosis, atresia, duplication, and congenital dilatation. Acquired stenosis, or urethral strictures, are much more common and can be caused by primitive lesions of the urethra or by lesions secondary to compression from an enlarged prostate. In general, most nonprostatic urethral strictures are the result of infection, trauma, or iatrogenic maneuvers. Neoplastic urethral stenosis is very uncommon, with a female-to-male ratio of 4:1.

Inflammatory strictures can be classified as gonococcal and nongonococcal. Gonococcal urethritis has become less common despite the fact that gonococcus remains the most common sexually transmitted disease. Chlamydia trachomatis is the most common cause of nongonococcal urethritis. Urethral trauma can be divided into external trauma, either contusive or penetrative, and internal or endourethral trauma. External traumas are frequent events and can occur in the penile urethra as a result of road or work accidents, sporting activities, or sex.

Iatrogenic stenoses may result from radiation therapy, catheterization, and endoscopic prostatic resection; recurrent strictures occur frequently after ►urethral dilatation, ►internal urethrotomy, and ►urethroplasty. Stenosis usually occurs in the bulbomembranous region and, less commonly, at the penoscrotal junction. In clinical practice, urethral stenoses can occur following suprapubic or endoscopic prostatectomy. Traumatic meatitis and/or meatal ischemia following damage to the frenular artery at circumcision are suggested as possible causes of meatal stenosis in men.

Clinical Presentation

Urethral stricture causes bladder outflow obstruction; if untreated and progressive, it may cause urinary retention, reflux, urinary tract infections, hydronephrosis, and renal failure. The most common clinical presentation includes obstructive voiding symptoms, which are characterized by decreased force of urinary stream, increased urinary frequency or urgency, urinary terminal dribbling, and bleeding at the end of urination.

Imaging

Retrograde urethrography is usually considered the best initial study for imaging the anterior urethral stricture in men (1). It consists of taking radiograms as an iodate contrast agent is introduced through the external urethral meatus (Fig. 1). After the gland and urethral meatus are

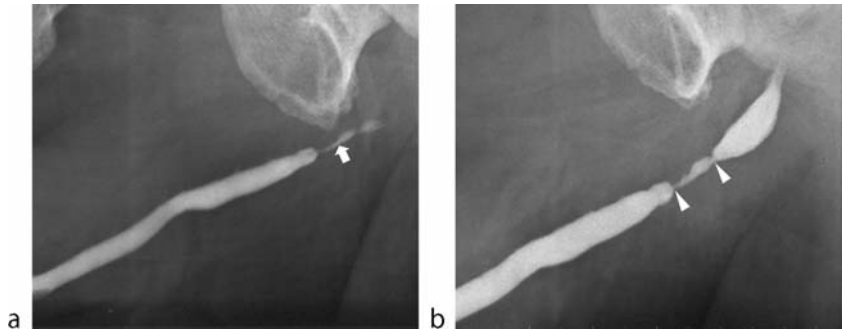

Urethra, Stenosis. Figure 1 Urethral stenosis studied with retrograde urethrography. (a) Iodinated contrast material is injected under fluoroscopic guidance through a Foley catheter placed into the *Fossa* navicularis so that the anterior urethra is filled up to the stenosis (*arrow*). (b) Slow, gentle pressure is needed to distend the stenotic tract of the urethra and fully delineate the length of the stenosis (*arrowheads*).

cleaned with antiseptic material, a small Foley catheter is placed in the distal urethra, and the balloon is slowly distended into the *F.* navicularis. Lubrication is not recommended because it may prevent the balloon from remaining in place for optimal occlusion (1). Distension of the urethra occurs slowly, through direct injection of the iodate solution in the catheter (1, 2) or by allowing the iodate solution to drip down through a bottle located at a height of 40–50 cm (3). Real-time fluoroscopic observation allows targeted radiograms and images to better identify the urethral disease.

Voiding cystourethrography is currently the most commonly used imaging method in evaluation of the female urethra and male posterior urethra (1). Voiding urethrography is usually performed after the bladder is filled with contrast material *via* a transurethral or suprapubic catheter, or it represents the final part of urography (3). The exam is best carried out with the patient in an upright position and with video monitoring. Radiographs of the bladder and urethra are obtained during voiding under fluoroscopic observation. This method provides an accurate picture of urination and localization of any functional and organic alteration. Although the anterior urethra is not fully distended to the degree seen at retrograde urethrography, voiding cystourethrography allows evaluation of distal urethral stenosis (Fig. 2) when it is not possible to introduce the Foley catheter and retrograde urethrography cannot be performed.

Sonourethrography: The penile and bulbar male urethra can be accurately studied using high-frequency linear probes that are able to examine the penile and perineal tract. Using the traditional technique (Fig. 3), normal saline solution is introduced repeatedly through a small Foley catheter to distend the urethra and create a good contrast with adjacent tissue (2, 3). In patients with long, severe strictures, sonographic contrast medium can be injected intraurethrally to help delineate the abnormal lumen from the surrounding tissues and associated abnormalities,

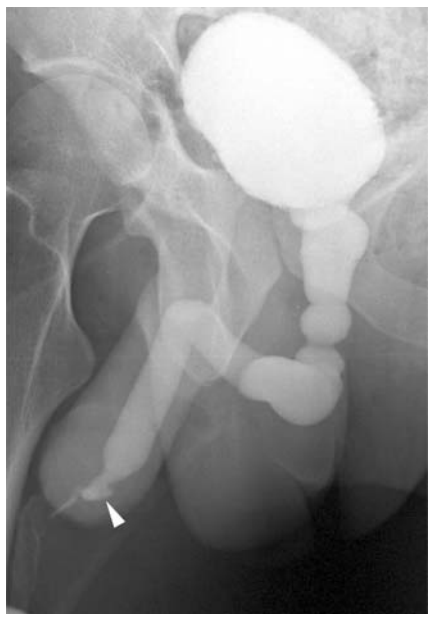

Urethra, Stenosis. Figure 2 Distal urethral stenosis (*arrowhead*) studied with voiding cystourethrography. Note marked urethral dilatation and elongation proximal to the stenosis.

such as secondary lumen, fistulae, reflux into Cowper's glands, and abscess (4).

An intraluminal lubricant or anesthetic jelly can be used instead of saline solution to distend the urethra. Sonourethrography with jelly is particularly useful in distal urethral stenosis and in stenosis of the meatus when it is not possible to introduce a Foley catheter. The use of jelly, however, has the disadvantage that urethral distension is less marked.

Endocavitary ultrasound: The posterior tract of the male urethra can be investigated during voiding using linear high-frequency endorectal probes (3). The main

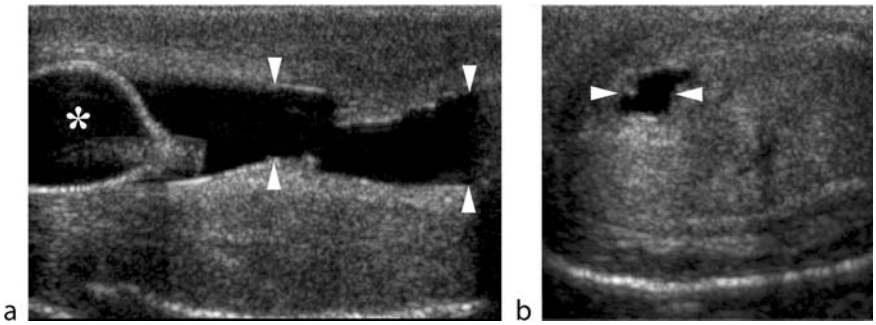

Urethra, Stenosis. Figure 3 Urethral stenosis studied with sonourethrography. Sagittal (a) and axial (b) views of the urethra after saline infusion through a small Foley catheter (*) placed into the *Fossa* navicularis show a complex urethral stenosis (*arrowheads*) with wall thickening.

drawback of this technique is the difficulty patients have in urinating in a lateral position with the probe positioned in the rectum. The female urethra can be successfully studied with transvaginal ultrasonography. Some centers prefer transrectal sonography in female patients to avoid compression or distortion of the urethra.

Computed tomography (*CT*) has a limited role in evaluation of the urethra. Certain urethral abnormalities such as calculi or diverticula may be incidentally discovered at CT performed for other indications. CT is useful in patients with pelvic trauma (5) and associated urethral injuries and for staging of urethral carcinoma. CT virtual cystoscopy and voiding urethrography can be indicated in patients with complex urethral strictures and malformations.

Magnetic resonance imaging (*MRI*) is not widely used to evaluate the urethra. However, because of its multiplanar capability and excellent tissue contrast, it provides excellent anatomical detail of both the urethra and periurethral tissues (6). Distension of the urethra is obtained with saline solution after a small Foley catheter is placed in the *F.* navicularis. Imaging is performed using a surface coil that employs a small field of view with multiplanar T1- and T2-weighted sequences. Contrast medium is injected to evaluate tumors and the degree of activity in inflammatory lesions.

Nuclear Medicine

Radionuclide studies have no role in diagnosis of congenital or acquired narrowing of the urethra because of the poor anatomic detail, but they can depict the presence of ►vesicoureteral reflux and can be used to assess renal function.

Diagnosis

Urethral strictures may be assessed by direct urethroscopy, urethrography, or sonourethrography. Retrograde urethrography is the standard imaging technique to evaluate anterior urethral stricture (2–4). Radiographic evaluation helps define the location, length, number, and degree of strictures. More than one projection may be necessary to visualize the stricture and to correctly estimate the stricture length. In posterior urethral strictures following blunt trauma, simultaneous antegrade cystourethrography, and retrograde urethrography are often required to determine the length of the urethral defect.

Sonourethrography may be chosen instead of radiographic techniques because it does not involve ionizing radiation. This may be particularly important in patients needing repeated investigation. This technique can be more accurate than retrograde urethrography for estimating the length of urethral strictures (2). In addiction to evaluation of the urethral lumen, sonourethrography gives information about the depth and density of periurethral changes not provided by radiographic methods (2, 3). Periurethral fibrosis manifests at ultrasound as thickened, irregular, nondistensible tissue encroaching into the otherwise anechoic urethral lumen.

CT virtual cystoscopy and CT voiding urethrography have been recently introduced to evaluate patients with urethral disease; however, large studies are needed to determine the clinical value of these new techniques (5).

MRI is indicated to evaluate spongiosal fibrosis in patients with postinflammatory strictures (6). Moreover, MRI is considered to be the best imaging modality for assessing posttraumatic pelvic anatomy in patients with urethral injury. In neoplastic strictures, MRI has a role in staging the size, location, and local extension of the primary pathology.

Bibliography

1. Kawashima A, Sandler CM, Wasserman NF et al (2004) Imaging of urethral disease: a pictorial review. Radiographics 24 Suppl 1:S195–216
2. Choudhary S, Singh P, Sundar E et al (2004) A comparison of sonourethrography and retrograde urethrography in evaluation of anterior urethral strictures. Clin Radiol 59:736–742

3. Pavlica P, Barozzi L, Menchi I (2003) Imaging of male urethra. Eur Radiol 13:1583–1596
4. Babnik Peskar D, Visnar Perovic A (2004) Comparison of radiographic and sonographic urethrography for assessing urethral strictures. Eur Radiol 14:137–144
5. Chou CP, Huang JS, Wu MT et al (2005) CT voiding urethrography and virtual urethroscopy: preliminary study with 16-MDCT. Am J Roentgenol 184:1882–1888
6. Ryu J, Kim B (2001) MR imaging of the male and female urethra. Radiographics 21:1169–1185

Urethral Dilatation

Procedure performed to open a urethral stricture by passing a dilating instrument into the urethra. This can be done under local or general anesthetic.
▶Urethra, Stenosis

Urethral Stricture

▶Urethra, Stenosis

Urethritis

Inflammation of the urethra.
▶Neoplasms, Urethra

Urethrography

Progressive opacification of the urethra with iodinated contrast medium performed under fluoroscopic guidance. It usually includes a series of radiographs with coronal and oblique images.
▶Neoplasms, Urethra

Urethroplasty

Surgical procedures used to correct urethral stricture following repeated recurrence after urethrotomy. A variety of techniques may be used: excision and primary reanastomosis (particularly for short strictures in the bulbar urethra); excision and substitution with free tissue grafts or vascularized flaps; staged procedures in which nonviable tissue is excised first, followed by retubularization of the urethra (used particularly for long strictures and ones that have been unsuccessfully repaired previously).
▶Urethra, Stenosis

Urinary Casts

Casts are cylindrical structures composed mainly of a mucoprotein (the Tamm-Horsfall mucoprotein), which is secreted by epithelial cells lining the loops of Henle, the distal tubules, and the collecting ducts. The factors responsible for the precipitation of this mucoprotein are not fully understood, but may relate to the concentration and pH of urine in these areas. Casts may form in the presence or absence of cells in the tubular lumen. If cells (epithelial cells, WBC) are present as a cast forms, they may adhere to, and subsequently be surrounded by, the fibrillar protein network. The appearance of a cast observed in urine sediment depends largely on the length of time it remains in situ in the tubules before being shed into the urine. A cast recognizable as "cellular," for example, is shed shortly after it is formed. A waxy cast, in contrast, is retained longer in the tubular system before being released. Casts are quantified for reporting as the number seen per low-power field (10x objective) and classified according to type. In the urine of normal individuals there are few casts or none at all.
▶Tubular Necrosis, Kidney, Acute

Urinary Incontinence

Involuntary urinary loss during all usual situations or activities.
▶Incontinence, Urinary

Urinary Obstruction, Acute

Sudden blockade of the urinary collecting system caused mostly by calculi. Stretching of the collecting system is responsible for the pain in renal colic. Immediately after onset of complete obstruction, autoregulatory mechanisms due to vasoactive factors and hormones try to overcome obstruction. First, an increased blood flow preserves the glomerular filtration rate, while hyperperistalsis and antidiuretic hormone blockade increase the volume of

hypotonic urine. If passage is not attained in the next hours, and to preserve renal function, blood flow is reduced by preglomerular arteriolar vasoconstriction, which together with a decrease in hydrostatic pressure gradually leads to reduction of pain.
▶Colic, Acute, Renal

Urinary Stones

Calculi in the urinary tract (renal, ureteric, bladder) are often idiopathic, but can be secondary to stasis, and infection, or in association with several hereditary metabolic disorders like renal tubular acidosis, cystinuria, xanthinuria, hydroxyadeninuria, and others. Intermittent urine supersaturation is necessary for crystals to form and grow. Stasis as in PUJ obstruction, sponge kidneys, and other anatomic abnormalities are prerequisite for stone formation. The majority are composed of calcium, magnesium ammonium phosphate, or urate. Ninety percent are radiopaque.
▶Colic, Acute, Renal

Urinary Tract Anatomy and Variants or Variations

▶Genito-Urinary Tract: Anatomy and Variants

Urinary Tract Calculus

▶Nephrocalcinosis and Urolithiasis in Childhood

Urinary Tract Stone

▶Nephrocalcinosis and Urolithiasis in Childhood

Urodynamic Studies

Registration of pressure inside the bladder and during micturition
▶Bladder, Neurogenic

Urodynamic Tests

Several techniques to measure functional parameters associated with urination. Urodynamics require positioning of catheters into the urethra and bladder and into the vagina to register pressure curves. Urodynamic parameters are urine speed, bladder volume, residual bladder volume, leak point pressure, bladder pressure, and electromyography curves during voiding.
▶Pelvic Floor Dysfunction, Genitourinary

Urogenital Sinus (UGS)

In the foetus, the UGS forms when the cloaca is divided by the urorectal septum into the UG sinus anteriorly and the rectum posteriorly. The UGS subsequently contributes to the formation of the urethra in males, and the urethra, vestibule and lower vagina in females. A persistent UGS in females refers to a situation where the vagina and urethra join to form a single channel proximally to the vestibule, resulting in a single vestibular opening.
▶Ambiguous Genitalia

Urogenital–Genital

Rahel A. Kubik-Huch
Kantonsspital Baden, Switzerland
rahel.kubik@ksb.ch

Female Pelvis

Introduction

Advances in imaging and minimally invasive interventions in women with pelvic disorders have occurred at an unprecedented rate in recent years. For the initial evaluation of any suspected pathologic condition, transabdominal or transvaginal ultrasound remain the imaging modalities of choice. Technical advances in cross-sectional imaging, however, have opened up many diagnostic applications in female pelvic pathology. Thus, computed tomography (CT) and magnetic resonance imaging (MRI) nowadays play an increasing role in the diagnosis

of a variety of diseases of the female pelvis including preoperative tumor staging and follow up of oncologic patients. Due to its wide availability, CT is usually employed in an emergency situation, e.g., for the assessment of an *acute abdomen*. Compared to CT, MRI provides a better soft tissue contrast and is thus better suited for evaluating the genital organs. Furthermore, it does not employ ionizing radiation and has no teratogenic effects. It is thus well suited for imaging women of reproductive age and especially also during pregnancy, e.g., in MR pelvimetry and more recently as an adjunct to sonography for *fetal imaging*.

Imaging Techniques and Normal Anatomy of the Female Pelvis

Transvaginal ultrasound using a 5.0–7.5-MHz probe is usually performed by the gynecologist as part of the gynecologic examination. Transabdominal ultrasound allows one to assess not only the genital organs, but also the entire abdomen, for example, the kidneys to exclude hydronephrosis. The patient should be investigated with full bladder to better visualize the uterus using a 2.5–5.0-MHz transducer. On ultrasound, the myometrium is of homogeneous intermediate echogenicity. Endometrial thickness varies with the *physiological changes during the menstrual cycle*, measuring up to 14 mm in premenopausal women. On MRI, the normal anatomy of the uterus is best seen on T2-weighted imaging. Three different zones can be distinguished, i.e., the hyperintense endometrium, the junctional zone of low signal intensity, and the myometrium. Normal ovaries measure between 1.5 and 3 cm during reproductive age, with their size decreasing after menopause. They can be depicted by MRI in over 80% of cases in women in their reproductive phase due to the presence of T2-weighted hyperintense follicular cysts.

Hysterosalpingography and *sonohysterography* are imaging techniques that are performed for selected indications only, i.e., in patients with a history of *infertility*.

Congenital Anomalies of the Female Genital Organs

According to the American Fertility Society classification, several classes of *congenital anomalies of the uterus* (synonym: *müllerian duct anomalies*) can be distinguished, e.g., unicornuate, bicornuate uterus, or uterus didelphys.

Clinical manifestations include subfertility or *infertility*, pregnancy wastage, and menstrual disorders. Furthermore, müllerian duct anomalies are commonly associated with anomalies of the urinary tract, e.g., renal agenesis.

Whereas transvaginal ultrasound and hysterosalpingography are the primary imaging modalities, MRI is currently used as a problem-solving tool in inconclusive cases, e.g., in the differentiation between septate and bicornuate uterus.

Benign Disorders of the Vulva, Vagina, Cervix Uteri, and Uterine Corpus

Bartholin's cysts are caused by retained secretions within the vulvovaginal glands, mostly as a result of chronic inflammation or trauma. They are located in the posterolateral parts of the lower vagina and vulva, whereas *nabothian cysts* are retention cysts of the cervical glands and clefts.

Common benign uterine masses are *leiomyomas* (synonyms: fibroids; fibromyoma). The lesions must be differentiated from adenomyosis.

Endometrial hyperplasia and endometrial polyps are benign entities that must be distinguished from endometrial carcinoma.

Inflammatory changes, i.e., endometritis or endomyometritis, are rare indications for cross-sectional imaging.

Malignant Disorders of the Vulva, Vagina, Cervix Uteri, and Uterine Corpus

Endometrial carcinoma is a common gynecologic tumor in postmenopausal women. Most patients present with abnormal uterine bleeding. MRI is the imaging modality of choice for preoperative staging of endometrial carcinoma proven by fractional abrasion. It is especially useful in those patients in whom the extent of tumor growth may alter the surgical approach or in patients in whom concomitant lesions, e.g., the presence of leiomyoma, make the clinical assessment difficult.

Most uterine tumors are adenocarcinomas; other histologic subtypes such as *leiomyosarcoma* or endometrial stromal tumors are rare.

Gestational trophoblastic disease encompasses a spectrum of tumors ranging from benign hydatidiform mole to choriocarcinoma. Diagnosis will be established based on clinical symptoms confirmed by human chorionic gonadotropin (HCG) measurements. Thus, the role of imaging is very limited in this patient population.

Early detection of *cervical carcinoma* due to gynecologic examination and Papanicolaou smear has led to a significant reduction in mortality. At histology, a squamous cell carcinoma is found in over 90% of cases. Transvaginal ultrasound and MRI are used for staging of disease.

Vaginal metastases are more common than primary *vaginal carcinoma* and are usually the result of metastatic spread from *carcinomas of the vulva*, endometrium, or cervix.

Benign, Nonneoplastic Ovarian Masses

Physiologic *follicular cysts* are the most common benign ovarian masses. Other nonneoplastic adnexal lesions include *endometrioma*, *adnexal torsion*, and *tubo-ovarian abscess*. *Paraovarian cysts* (synonym: Gartner's duct cysts) are remnants of the Wolffian body and are found in the mesosalpinx in the hilum of the ovary.

Ovarian vein thrombosis (synonyms: septic puerperal ovarian vein thrombosis; SPOVT) is a complication in the puerperal period. The clinically suspected diagnosis can be confirmed by duplex sonography, contrast-enhanced CT, or MR angiography.

Ectopic pregnancy occurs in most cases in the fallopian tubes. Ultrasound is the imaging modality of choice. Laparoscopy of laparotomy will be performed for therapeutic reasons.

Benign and Malignant Neoplastic Ovarian Masses

Differentiation between benign and malignant ovarian lesions is based on various imaging criteria. Ovarian epithelial tumors account for approximately 65% of ovarian neoplasm. Of these tumors, 60% are benign (e.g., cystadenoma), whereas 5% are present with a borderline histology. The other 35% are malignant *ovarian carcinoma*. Preoperative cross-sectional imaging may help in preoperative planning in patients with suspected ovarian carcinoma. Whereas MRI is superior to CT and US in lesion characterization and in demonstrating the origin of a pelvic mass (e.g., distinguishing a subserosal uterine leiomyoma from an ovarian mass), CT, being widely available and more cost-efficient, is usually preferred for preoperative staging.

Evidence of intralesional fat, independent of the size of the lesion, is indicative of a benign *mature teratoma* (synonym: dermoid cyst). These tumors are very common ovarian neoplasms and belong to the group of germ cell tumors.

Imaging the Obstetric Patients

There is no clinical or experimental evidence of teratogenic or other adverse fetal effects from performing MRI in pregnancy. Thus, this technique has become an important adjunct to ultrasound for imaging of pregnant women for maternal reasons, *MR pelvimetry* in cases of suspected cephalopelvic disproportion, and more recently also for *fetal imaging*.

Pelvic Floor

Stress urinary incontinence is a significant problem in older women.

Its predominance in parous women prompted the etiologic hypothesis of trauma to pelvic-floor support structures during childbirth. More recently, MRI has gained an increasing role in assessing *pelvic floor* pathology. The advantages of this method are high soft-tissue contrast for visualizing the pelvic floor morphology and nonexposure of the patient to ionizing radiation.

Male Pelvis

Introduction

Ultrasound is the primary imaging modality for the evaluation of suspected pathology of the male pelvis, e.g., assessment of a *scrotal mass* or diagnosis of suspected prostatic disease. Transrectal ultrasound is usually performed directly by the urologist and nowadays is often considered an extension of the physical examination. In many cases, it supplies sufficient information to establish the diagnosis. Cross-sectional imaging is indicated in cases in which sonographic findings are equivocal or a discrepancy between clinical and ultrasound findings exists. Furthermore, CT and MRI are important tools for staging of malignant disease, e.g., in *testicular cancer*.

Benign Lesions of the Prostate and Seminal Vesicles

Diagnosis of congenital *prostate cysts*, i.e., utricular and müllerian duct cysts, has increased in parallel with the use of transrectal sonography and MRI in prostate lesion diagnosis. Since there is an association of utricular cysts with malformations of the genitourinary tract, e.g., renal agenesis, hypospadias, pseudohermaphrodism, and cryptorchidism, they are usually detected in childhood. Both types of cysts can cause symptoms such as dysuria, urinary tract infections, prostatitis, and infertility; smaller cysts, however, are mostly incidental findings.

Benign prostatic hyperplasia (BPH) impairs micturition in about half of all men over 50 years of age. Whereas BPH is not an indication for cross-sectional imaging, it is a frequent incidental finding in patients investigated for other reasons, e.g., local staging of *prostate carcinoma*.

Chronic *prostatitis* is more common than the acute form and often clinically silent. Acute prostatitis is caused by direct extension from the urethra or urinary bladder in most cases, often a result of surgical manipulation of these structures. It might be complicated by *prostatic abscess* formation.

Prostate Cancer

Prostate cancer is the leading cancer in males. It is usually suspected by digital rectal examination and elevated PSA levels, and will subsequently be confirmed by transrectal ultrasound-guided biopsy.

High-resolution MRI using an *endorectal coil* can be an important adjunct to ultrasound for the local tumor staging of prostate cancer in selected patients, i.e., for the detection of extracapsular tumor extension, *seminal vesicle* invasion, as well as bone marrow metastasis, which are contraindications for radical prostatectomy.

Scrotal and Penile Disorders

Benign Lesions of the Scrotum and Testis, Benign Penile Disorders

Although the *scrotum* is a superficial structure, its clinical examination frequently fails to provide a specific diagnosis because the clinical history and physical findings are similar under many conditions. Ultrasound confirms the presumptive clinical diagnosis and provides relevant additional information. A color-coded duplex sonography or power Doppler examination is indicated in any situation in which additional information on perfusion is needed to establish the diagnosis, particularly in *testicular torsion*, inflammation (*epididymitis, orchitis*), *scrotal trauma*, and varicocele. Other imaging modalities should be used only as problem-solving approaches.

The most common *benign masses in the scrotum* are *spermatoceles* of the epididymis. Benign neoplasms of the testis account for only approximately 5% of all testicular neoplasms. *Hydroceles* are common fluid accumulations located between the two layers of the tunica vaginalis testis. They may be idiopathic in origin or develop in association with inflammation (epididymitis or orchitis), secondary to trauma or testicular torsion, and in the presence of a testicular tumor.

Catheter angiography, Doppler ultrasound, and more recently MRI are used for imaging *penile vasculature* when arteriogenic *impotence* secondary to aortoiliac occlusive or small-vessel disease or as a result of pelvic trauma is suspected.

Ultrasound or MRI may be used to evaluate benign entities, e.g., periurethral abscess, Peyronie's disease, or Cowper duct syringocele that manifest as palpable penile masses, the nature of which may not be apparent at clinical evaluation, as well as for the evaluation of *penile trauma*.

Malignant Lesions of the Penis, Scrotum, and Testis

Whereas malignant tumors of the epididymis and the spermatic cord are extremely rare, *testicular cancer* constitutes approximately 1% of all malignancies in men, being the most frequent cancer in young males. The tumor typically presents as a lump or painless swelling of the testis. Ultrasound and sometimes MRI are employed to establish the diagnosis, whereas CT will usually be performed for lymph node staging.

Most primary *penile malignancies* are squamous cell carcinomas. Carcinoma of the male urethra and primary sarcoma may also occur in the penis. Metastases to the penis are rare. They usually arise from other primary malignancies of the genitourinary tract, e.g., the urinary bladder, and may manifest with malignant priapism.

Urothelial Neoplasms, Kidney and Ureter

Samuel Merran, Annick Vieillefond, Olivier Helenon
Neckert, Paris, France
olivier.helenon@nck.ap-hop-paris.fr

Definition

Tumors arising from the renal pelvis and ureter are usually of urothelial origin, with transitional cell carcinoma (TCC) being the most common tumor. Urothelial tumors are most frequently malignant, and their prognosis is variable, depending on their degree of differentiation and their extension through the wall of the renal pelvis or ureter. Papillomas are the most common benign tumor. Much rarer are tumors of connective tissue origin.

Peak incidence of urothelial upper tract tumors is in the sixth and seventh decades. Patients with urothelial upper tract tumors have a 30 to 75% incidence of prior or later bladder cancer, so that bladder evaluation is essential. Microscopic or gross hematuria occurs in 60 to 75% of patients at presentation. Fifteen percent of the cases are detected incidentally on imaging studies. Advanced stages account for less than 10% of the cases and patients present with a palpable flank mass, anorexia, or weight loss.

Characteristics

Urothelial tumors of the renal pelvis represent approximately 7% of primary renal neoplasms (1) and approximately 5% of the urinary tract tumors (2).

The urothelial neoplasms are dominated by the TCC. Ninety percent of the tumors that arise from the urinary epithelium are TCCs. The other epithelial tumors are rare: epidermoid carcinoma (related to bilharzias) and adenocarcinoma.

These tumors share the same epidemiologic features associated with TCC of the urinary bladder: history of exposure to chemical (aromatic amine) in the dye and in the paint, rubber, petroleum industry, tobacco use, high amount of coffee consumption, and chronic inflammation or infection. Patients with a history of analgesic abuse are also at risk for TCC. Urinary bladder location of TCC is much more frequent than in the other parts of the urinary tract. Location to the renal cavities (pelvis and calices) is second in frequency. Synchronous or asynchronous multiple tumors locations occur in 10 to 20% of cases (Fig. 1). This known multifocality requires thorough examination of the entire urinary tract in high-risk patients, such as patients with bladder cancer or known chemical exposure (2).

Imaging

CT and CT Urography

Traditionally intravenous urography (IVU) has been the screening examination of choice for detection of upper urinary tract neoplasms in patients with hematuria or for high-risk patients. However, 40% of upper urinary tract tumors are missed by IVU (1). With the advent of multidetector CT enabling the rapid acquisition of thin-section images through the entire urinary tract, CT urography (CTU) has superseded IVU as the examination of choice to detect upper urinary tract tumors. The techniques and protocol we use for CTU are summarized in Table 1.

On imaging TCC of the renal cavities (calices or renal pelvis) manifests as a focal soft tissue mass or wall thickening (3–5). On noncontrast scans, the mean density is around 30 HU (Fig. 2) and are differentiated from

Urothelial Neoplasms, Kidney and Ureter. Table 1 CT urography: three phases are required

	Precontrast	Vascular nephrogram	Excretion
Slice thickness	1 mm	1 mm	1 mm
Interval	0.8 mm	0.8 mm	0.8 mm
Anatomical coverage	A/P[a]	A/P	A/P
Injection volume		120–140 cc (bolus detection)	
Injection rate		3.5–4 cc/sec	
Reconstruction	MPR[b]	MPR	MPR and MIP[c]

[a]A/P: Abdomen and pelvis
[b]MPR: Multiplanar reconstruction
[c]MIP: Maximun intensity projection

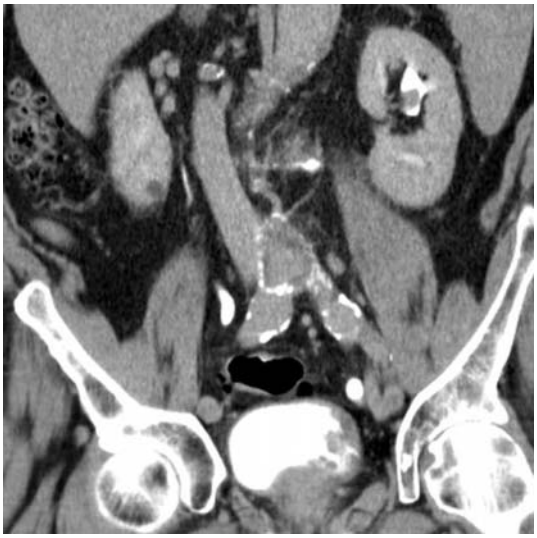

Urothelial Neoplasms, Kidney and Ureter. Figure 1 Coronal reconstruction CTU: synchronous urothelial carcinoma of the left aspect of the urinary bladder and the left renal pelvis.

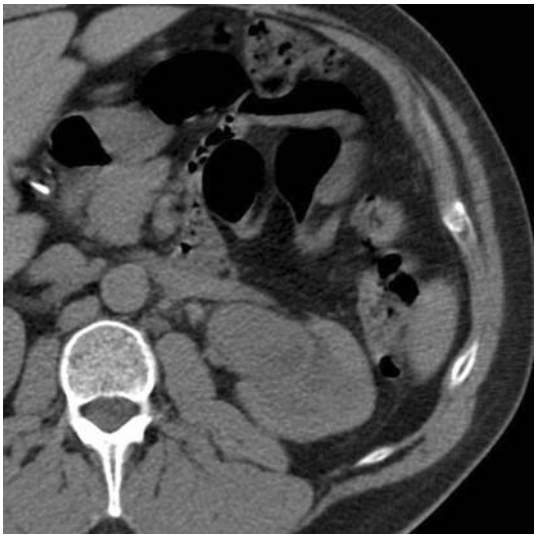

Urothelial Neoplasms, Kidney and Ureter. Figure 2 Nonenhanced CT of the left kidney: increased density within the renal pelvis compared to water density. The soft tissue mass within the renal pelvis is a TCC.

blood clot (50–75 HU) (Fig. 3) and calculi (>100 HU) (Fig. 4). TCC appears rarely calcified (microcalcifications) on nonenhanced scans (Fig. 5).

On early phase postcontrast study the enhancement of TCC is mild to moderate (Fig. 6). In infiltrative cases of TCC the wall thickening of the renal pelvis also enhances on arterial phase scans (Fig. 7).

In the excretory phase of CTU [sometime performed on a prone position to fill the renal cavities with contrast in case of obstruction (Fig. 8),] TCC appears as a filling defect within the high-density contrast excreted into the collecting system (Fig. 9). Sometimes TCC can appear as a focal or diffuse wall thickening (Fig. 10). Fifteen percent of TCCs are more aggressive, infiltrating lesions that show mural thickening and at a more advanced stage an invasion of the renal sinus fat (Fig. 11) or even the renal parenchyma (Fig. 12).

CT plays a role in staging urothelial tumors. CT cannot accurately distinguish T1 tumor (limited to uroepithelium and lamina propria) from T2 tumors (extending into muscularispropria but not beyond, but CT is accurate to distinguish early stages T1 and T2 from T3 (invading renal sinus fat or renal parenchyma) and T4

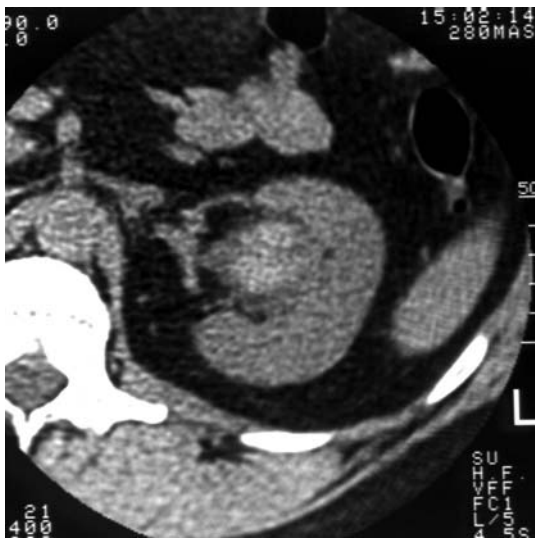

Urothelial Neoplasms, Kidney and Ureter. Figure 3
Nonenhanced CT of a blood clot in the renal pelvis.

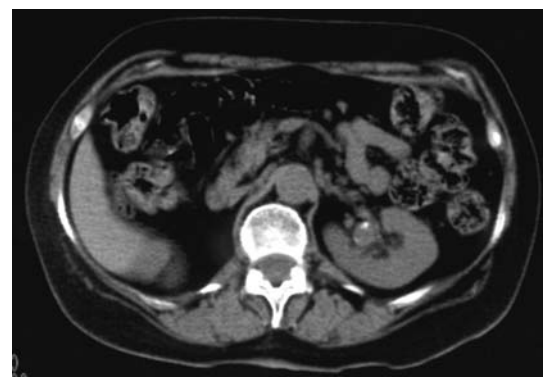

Urothelial Neoplasms, Kidney and Ureter. Figure 5
Nonenhanced CT: soft tissue mass in the left renal pelvis associated with microcalcifications. This turns out to be a TCC.

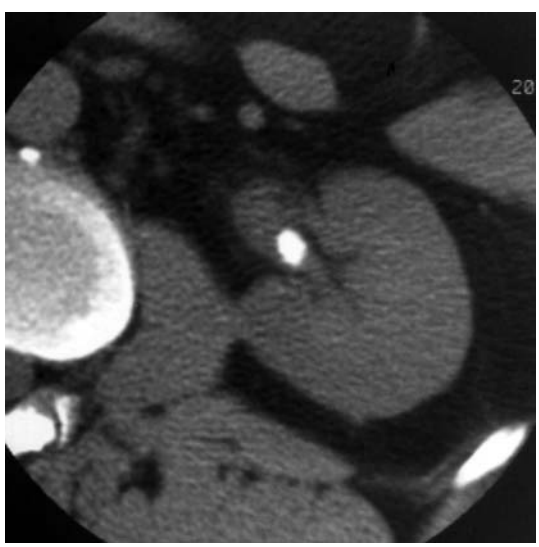

Urothelial Neoplasms, Kidney and Ureter. Figure 4
Nonenhanced CT of a calculi in the left renal pelvis.

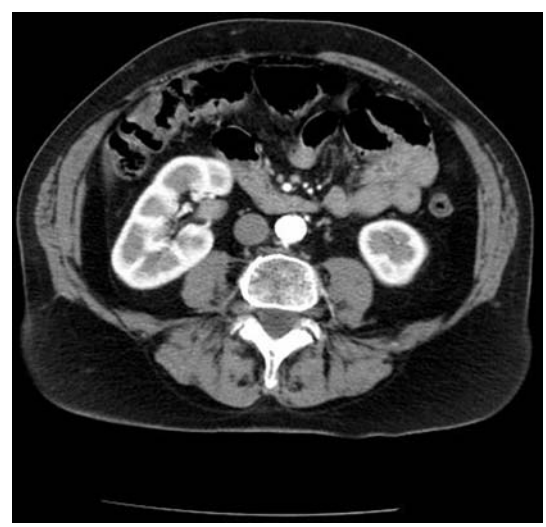

Urothelial Neoplasms, Kidney and Ureter. Figure 6
Postcontrast CT at the arterial phase: the soft tissue mass within the right renal pelvis enhances mildly.

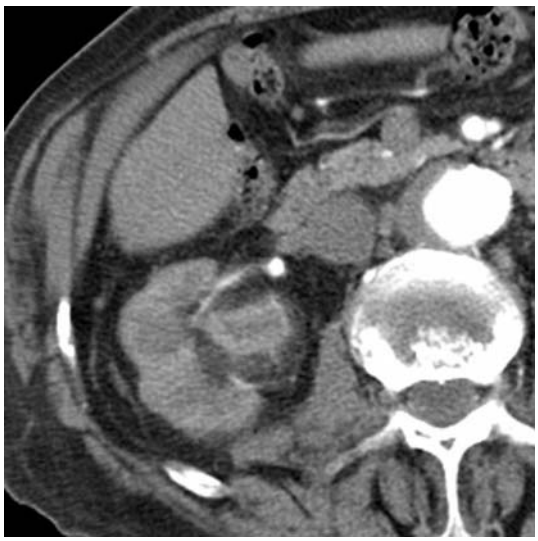

Urothelial Neoplasms, Kidney and Ureter. Figure 7
Postcontrast study at the arterial phase: notice the enhancing wall thickening of the renal pelvis.

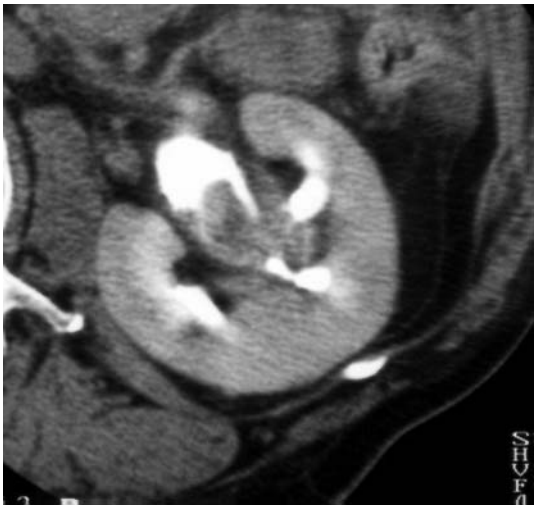

Urothelial Neoplasms, Kidney and Ureter. Figure 9
Delayed CT scan after injection: soft tissue mass within the renal pelvis typical aspect of an urothelial tumor.

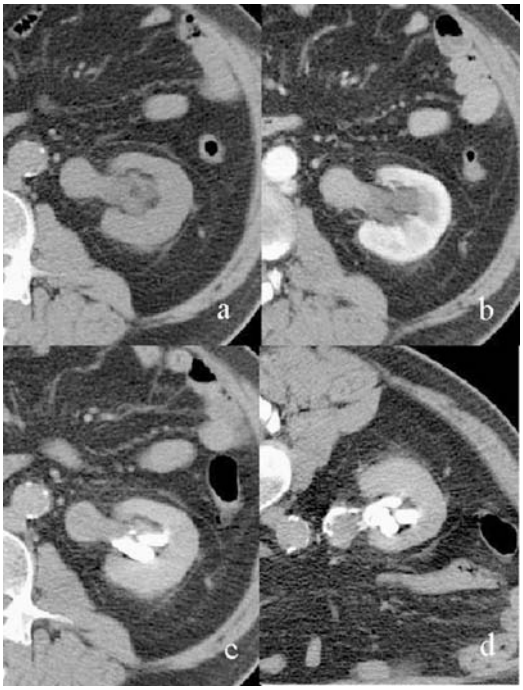

Urothelial Neoplasms, Kidney and Ureter. Figure 8
CT scan (a) nonenhanced, (b) early phase after injection, (c) delayed phase after injection, and (d) prone position of the patient. Because of the beginning obstruction of the left kidney the contrast media excreted do not surround the soft tissue mass visible in the renal pelvis on a, b, and c. On the propone position acquisition, the mass is clearly delineated by the high-density contrast media.

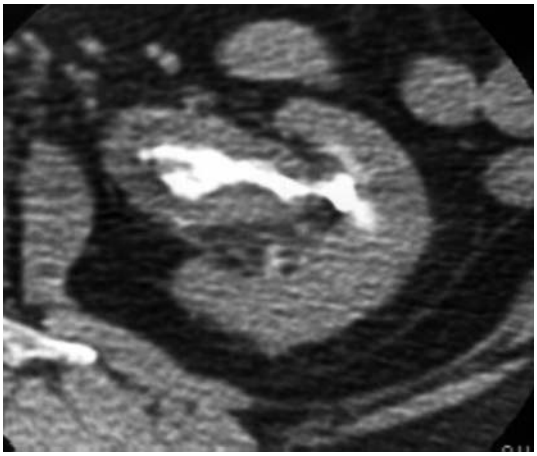

Urothelial Neoplasms, Kidney and Ureter. Figure 10
Postcontrast CT: wall thickening of the left renal pelvis wall in an infiltrative TCC.

(invading adjacent organs or extending into perinephric fat through the renal parenchyma. This distinction is important because there is a significant difference in survival between stage II and III tumors (5). Advanced stage tumor is suspected when the normally low-density renal sinus fat increases in attenuation or when—the fat plane between the tumor and the renal parenchyma is lost. In some cases CT may show a direct invasion of tumor into the renal parenchyma which can appear as an infiltrative renal mass (6) (Fig. 12). Usually, uroepithelial

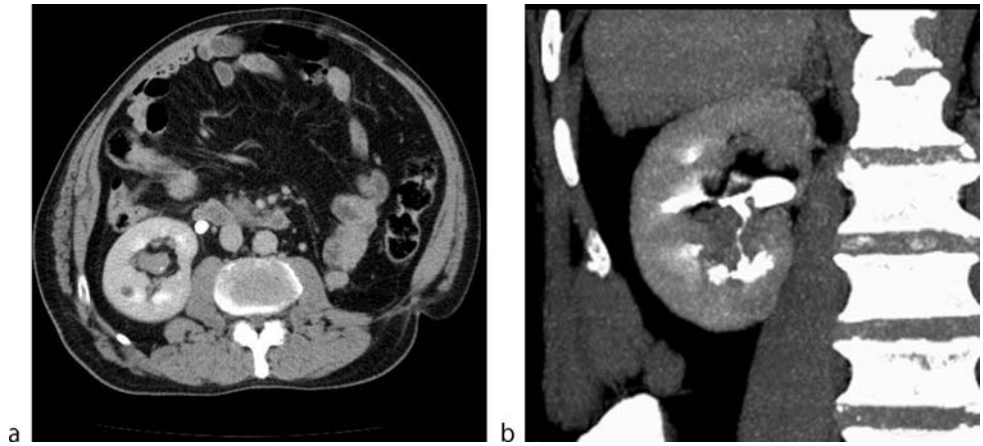

Urothelial Neoplasms, Kidney and Ureter. Figure 11 **(a) Axial slice through the lower pole of the right kidney: a soft tissue mass occupies the fat of the renal sinus. (b) Coronal reconstruction shows a thickening of the excretory cavity of the lower pole and an infiltration of the renal sinus fat.**

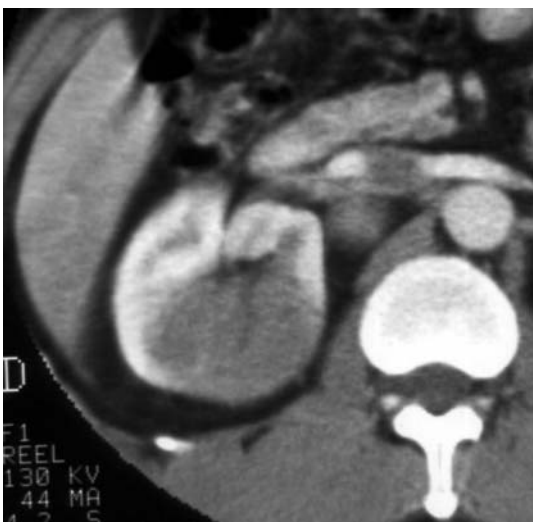

Urothelial Neoplasms, Kidney and Ureter. Figure 12 **Hypodense renal mass corresponding to direct invasion of tumor into the renal parenchyma which can appear as an infiltrative renal mass.**

neoplasms are more to expand the kidney centrically while preserving the renal contour (6, 7). TCCs can invade the renal vein and the inferior vena cava, and less frequently renal cell carcinomas. CT also allows high-quality imaging of lymph nodes, liver, bones, and lungs, which are the most common sites of metastatic spread of urothelial neoplasms (5, 6).

A recent 3D CT based reconstruction allows "navigation" within the renal cavities. This virtual endoscopic technique is based on segmentation of the contrast-filled cavities and shows in 3D the lumen and filling defects (Fig. 13). Axial slices are mandatory to distinguish between tumors, blood clots, and calculi.

Ureteral location of urothelial neoplasms has the same appearance as tumors of the renal pelvis and calices: either a filling defect within the ureteral lumen (Fig. 14a) or a thickening of the ureteral wall (Fig. 14b).

MRI and MRI Urography

MRI is a good alternative to CT in the radiological exploration of urothelial neoplasms. Consequently, this technique is indicated for assessing patients with a known intolerance of iodinated contrast medium and patients with moderately reduced excretory function. Moreover, excretory MR urography can also be performed to examine children and young adults because it does not require the use of ionizing radiation (7).

MR protocols and sequences are summarized in Table 2. For MR urography, we use both nonenhanced T2 weighted sequence (HASTE): (half-Fourier acquisition single-shot turbospin echo) and single-shot turbospin echo, and gadolinium enhanced sequences using high resolution images and maximum intensity projection (MIP) reconstruction.

TCC of the renal pelvis appears as soft tissue masses within the lumen, usually hypointense T2 in the hyperintense fluid-filled renal cavities (Figs 15 and 16). Enhancement is present after injection (Figs 15 and 16). Lesions of the ureters are usually more difficult to point out; the spatial resolution of the MRI is much lower compared to the CT spatial resolution.

Cross sectional imaging, specifically multidetector CT and CTU, is essential in detection and follow-up of urothelial carcinomas.

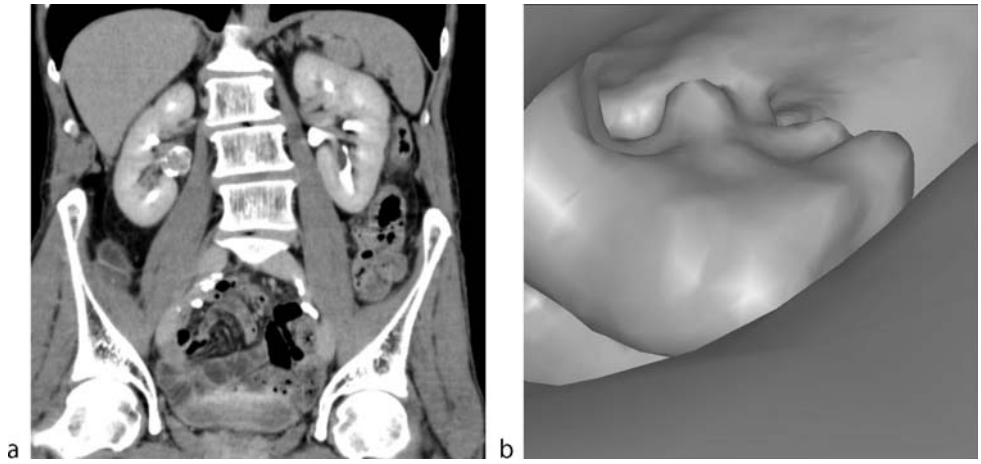

Urothelial Sign. Figure 13 (a) Coronal reconstruction CTU: filling defect of the right renal pelvis corresponding to a TCC. (b) Virtual endoscopy of the same patient performed on CT images and showing the mass within the renal pelvis.

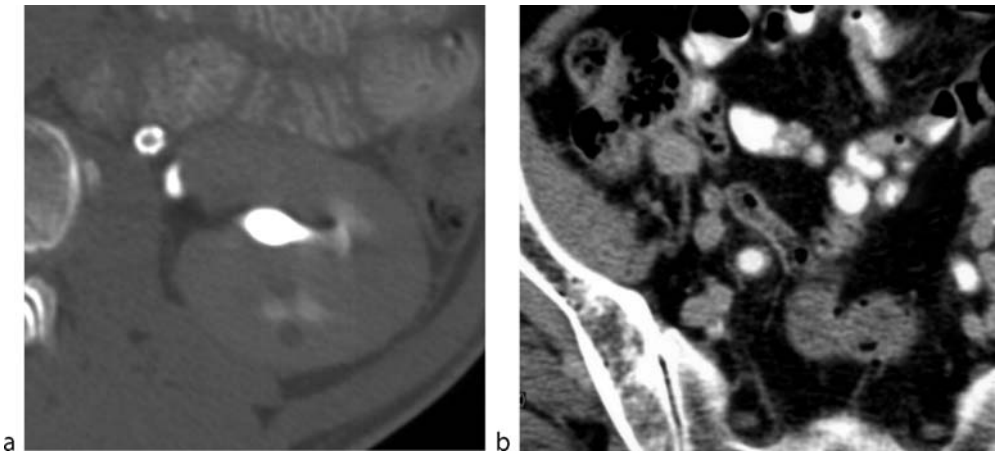

Urothelial Sign. Figure 14 Ureteral tumors: (a) filling defect of the initial part of the left ureter (using a large window setting helps to visualize small filling defects in the contrast-filled urinary tract). (b) Wall thickening of the lower part of the right ureter.

Bibliography

1. Caoili EM, Cohan RH, Inampudi P et al (2005) MDCT urography of the upper urinary tract urothelial neoplasms. Am J Roentgenol 184: 1813–1820
2. Rha SE, Byun JY, Jung SE et al (2004) The renal sinus: pathologic spectrum and multimodality imaging approach. Radiographics 24(Suppl 1): S117–S131
3. Buckley J, Urban BA, Soyer P et al (1996) Fishman transitional cell carcinoma of the renal pelvis: a retrospective look at CT staging with pathologic correlation. Radiology 201:194–198
4. Urban BA, Buckley J, Soyer P et al (1997) CT appearance of transitional cell carcinoma of the renal pelvis Part 1 Early stage. Am J Roentgenol 169:157–161
5. Urban BA, Buckley J, Soyer P et al (1997) CT appearance of transitional cell carcinoma of the renal pelvis Part 2 Advanced stage. Am J Roentgenol 169:163–168
6. Browne RF, Meehan CP, Colville J et al (2005) Transitional cell carcinoma of the upper urinary tract: spectrum of imaging findings. Radiographics 25:1609–1627
7. Jung P, Brauers A, Nolte-Ernsting CA et al (2000) Magnetic resonance urography enhanced by gadolinium and diuretics: a comparison with conventional urography in diagnosing the cause of ureteric obstruction. Br J Urol 86:960–965

Urothelial Sign

Thickening of the urothelium of the ureter or the renal pelvis, caused by urinary tract infection, refluxing or obstructing uropathy or a collapse of the previously somewhat distended collecting system.

▶ Hydronephrosis in childhood

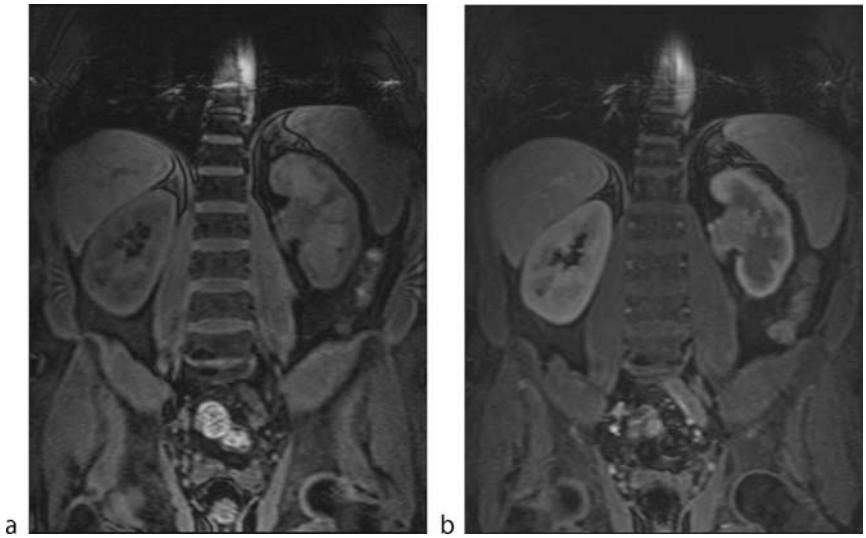

Uterine Fibroid. Figure 15 (a) Coronal truFisp MR image: the left renal cavities are distended; there is a soft tissue hypointense mass in the left renal pelvis. (b) postcontrast MR image (T1 Fat Sat) enhancement of the soft tissue mass of the left renal pelvis.

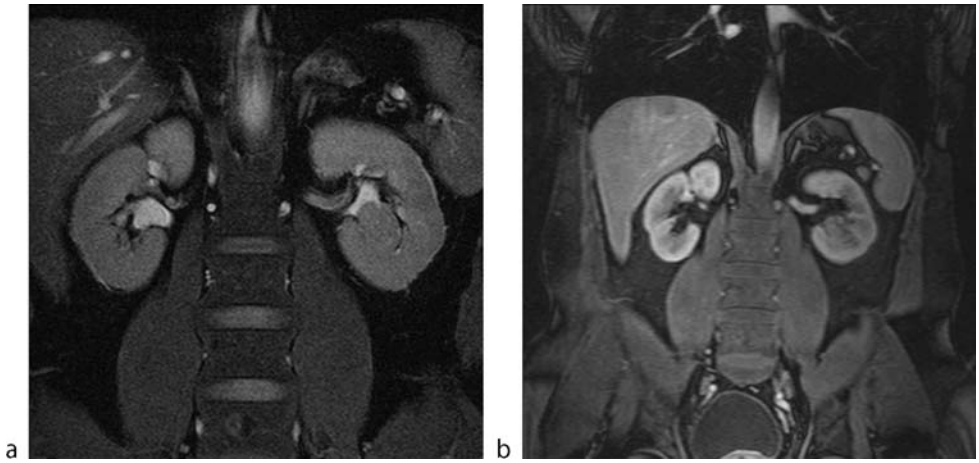

Urothelial Neoplasms, Kidney and Ureter. Figure 16 (a) Coronal truFisp MR image: there is a soft tissue mass in the inferior calices invading the renal sinus fat. (b) Enhancement of the soft tissue mass.

US

▶Ultrasound

USPIO

Ultra-small superparamagnetic iron oxide (USPIO) particles are iron oxide nanoparticles stabilized with low molecular weight dextran with a mean diameter of 30 nm. These relatively small particles have a much larger half-life in blood than the conventional superparamagnetic iron oxide particles, with a mean diameter of 150 nm. Because of their long half-life in blood, USPIOs can be taken up by macrophages in the whole body.

▶Glomerulonephritis

Uterine Fibroid

▶Leiomyoma, Uterus

Uterus

The uterus is the major female reproductive organ. The uterus is divided into three parts; fundus, corpus and cervix. It is located within the female pelvis, between the urinary bladder and rectum. It is held in place by ligaments and consists mostly of smooth muscle (= myometrium). The innermost layer of the myometrium is known as junctional zone. The lining of the uterus is called the endometrium (see zonal anatomy).

▶Carcinoma, Cervix Uteri

Uterus Myomatosus

▶Leiomyoma, Uterus

VA(C)TERL Syndrome

VATER or VACTERL association combines Vertebral anomalies, Anorectal atresia, Cardiac failure, Tracheoesophageal fistula, Esophageal atresia, Renal dysplasia, and Limb malformation. Currarino triad: The Currarino triad represents a combination of malformations consisting of imperforate anus, sacral dysplasia, and an anterior sacral mass (e.g., teratoma, anterior meningomyelocele). As a general rule, associated malformations occur more frequently in the high ARM or intermediate AMR groups than in group low ARM group.

►Anorectal Malformation

Vaccum-Assisted Biopsy

Percutaneous puncture technique used to remove cylinders of tissue from suspicious lesions for histological study. The procedure combines cutting and aspiration systems. For breast lesions, 8-, 11-, and 14-gauge needles are used. Many specimens can be removed with only an insertion of the needle.

►Breast Conserving Therapy

Valve Mechanism

A valve mechanism is due to partial airway obstruction of an inhaled foreign body and is characterised by air-trapping, mediastinal shifting and paradoxical movement of the hemidiaphragm on inspiratory–expiratory films or under fluoroscopy.

►Foreign Bodies, Aspiration, Children (Chest View)

Varices, Oesophagus

Simon A Jackson, John Shirley
Imaging Directorate, Derriford Hospital, Plymouth, UK
simon.jackson@phnt.swest.nhs.uk
john.shirley@phnt.swest.nhs.uk

Definition

Oesophageal varices are defined as pathologically dilated veins lying within the wall of the oesophagus, which normally project into the oesophageal lumen. Dilated veins lying adjacent to, but outside the wall of the oesophagus, are termed ►paraoesophageal varices. Both types of varix are usually found simultaneously in patients with pathology causing increased pressure and venous flow through the normal collateral oesophageal vessels. Rarely varices are diagnosed in patients without related pathology and these are termed idiopathic varices.

The radiological appearances of oesophageal varices were first described in 1928 using a basic contrast imaging technique. Today, imaging modalities including endoscopy, cross sectional imaging and interventional techniques are used to more accurately define the presence and distribution of both symptomatic and asymptomatic varices.

Pathology/Histopathology

A variety of pathologies can cause increased flow through the oesophageal veins. Depending on the direction of blood flow within the native oesophageal collateral vessels, oesophageal varices are termed uphill or ►downhill varices.

Uphill Varices

Uphill varices are found in patients with portal hypertension, which most commonly develops secondary to underlying cirrhosis. Hepatitis B/C and alcohol related

liver disease remain the most common aetiologies of cirrhosis worldwide. Currently the worldwide incidence of hepatitis C is increasing. The varices are the result of changes to the normal direction of collateral vessel flow. In particular, increased portal pressure leads to reversal of normal venous flow through the main left gastric (coronary) vein. Anatomically this vein drains the collateral vessels of the distal oesophagus inferiorly into the splenic or portal vein. This reversal of flow (uphill) leads to dilatation and formation of lower oesophageal varices, which in turn anastomose and drain into the central venous circulation *via* tributaries of the azygos and hemiazygos venous systems within the thorax.

Downhill Varices

Pathology obstructing the superior vena cava (SVC) commonly results in reversal of flow within the veins of the upper body. This in turn leads to increased flow through the oesophageal and para oesophageal veins as venous flow bypasses the obstruction before returning to the systemic circulation. The direction of blood flow through these collaterals is thus caudad leading to the term downhill varices.

The position of the varices however is variable and depends on the level and site of SVC obstruction. In particular, pathology obstructing the SVC above the level of the azygos vein, results in the downhill flow of venous blood from the head and upper extremities *via* the oesophageal veins into the azygos vein. The azygous vein in turn drains into the SVC below the level of obstruction. Associated oesophageal varices therefore develop within the upper or mid oesophageal segments.

If the level of ►SVC obstruction occurs below the site of entry of the azygos vein, venous flow develops *via* the oesophageal collaterals inferiorly into the coronary vein and thence to portal circulation and inferior vena cava. Associated oesophageal varices thus extend throughout the length of the oesophagus.

The most frequent cause of SVC obstruction is secondary to malignancy within the lungs or mediastinum. Due to the relatively short patient survival time, downhill varices are normally confined to the upper and mid oesophageal segments even in patients with obstruction of the SVC below the azygos vein termination. SVC obstruction, secondary to benign pathologies including radiation fibrosis is well described as well as iatrogenic SVC obstruction secondary to central venous line placement.

Clinical Presentation

The vast majority of patients presenting with uphill varices demonstrate the varied clinical sequelae of portal hypertension secondary to cirrhosis. The underlying architectural disturbance of the liver results in an increased hepatic portal venous pressure (greater than 10–12 mm Hg) and when taken in combination with the associated hyperdynamic portal circulation, the risk of complications and in particular variceal haemorrhage increases. At diagnosis, varices are present in approximately 40% of patients with compensated liver disease increasing to 60% of patients who present with decompensation. Overall 60–70% of all upper GI bleeding episodes in patients with portal hypertension are secondary to rupture of oesophageal varices. The six-week mortality after variceal bleeding is approximately 30% with uncontrolled bleeding occurring either during the initial presentation episode or soon after contributing to approximately 60% of deaths. The early re-bleeding rate remains the most important forecasting indicator of six-week mortality. In addition, 63% of patients re-bleed within 1–2 years with a corresponding mortality rate of 33%.

In contrast, the majority of patients presenting with haemorrhage from downhill varices exhibit symptoms related to SVC obstruction. These can be characterised by facial, neck and arm soft tissue swelling/oedema with dilated veins over the chest wall.

Imaging

Oesophageal varices may be imaged by a variety of imaging modalities.

Conventional Radiographs

Plain films are limited in their sensitivity and thus are not performed for the assessment of varices. However in some cases dilatation of the paraoesophageal veins, may result in a posterior mediastinal mass as well as obliteration of the normal descending aortic outline (1). A mediastinal mass is commonly identified in patients with downhill varices associated with dilatation of either the azygous or hemiazygous veins.

Oesophageal varices are not visualised on plain radiographs because of their location within the wall of the oesophagus.

Contrast Studies

The barium examination is no longer routinely used for the diagnosis of oesophageal varices due to the technique's relative lack of sensitivity. However, in similarity to all forms of contrast examination, the diagnosis of pathology relies on the meticulous performance of an optimal technique. This includes the use of a high-density barium suspension with ingestion of a limited volume of barium during each swallow to minimise the risk of luminal over

distension causing compression of the mucosal surface and varices. Mucosal relief views help to increase the sensitivity of the study. In addition, patient positioning is important with an oblique position and slight Trendelenburg table tilt increasing distension of the varices.

Morphologically the vessels appear as tortuous or serpiginous longitudinal filling defects which project above the adjacent mucosal surface into the oesophageal lumen (Fig. 1). Varices may also appear as thickened folds of lower density when compared to the adjacent oesophageal wall during a double contrast examination, due to the collection of contrast in the mucosal grooves adjacent to the vessels. Importantly varices collapse and distend with varied respiration and thus may transiently disappear during an examination. Thus, the use of a Valsalva manoeuvre improves venous distension and thus variceal conspicuity.

The rare varicoid carcinoma of the oesophagus may mimic varices on a contrast study, however is distinguished due to the absence of morphological changes during the respiratory cycle or patient position.

Computed Tomography

Developments in multidetector contrast enhanced CT have resulted in the widespread use of this technique for the evaluation of the portal venous system and diagnosis of oesophageal varices. In addition, multi-planar reconstruction techniques also improve the depiction of the sequelae of portal hypertension (2). Varices appear as multiple tubular or serpentine vessels, which surround and involve the oesophageal wall (Fig. 2). Both uphill and downhill varices demonstrate homogeneous enhancement on portal venous phase imaging and whilst downhill varices demonstrate similar morphology to their uphill counterparts they usually differ in location. In addition, other collateral pathways may be visualised within the thorax secondary to associated SVC obstruction. These pathways include distension of the azygous, thoraco epigastric, mediastinal and internal mammary veins.

Magnetic Resonance Imaging

The multi-planar and contrast tissue resolution of magnetic resonance imaging (MRI) allows excellent visualisation of oesophageal varices and their related aetiologies. Flowing blood within the varices appears as a signal void on conventional T1W and T2W sequences. However, unenhanced sequences when used in combination with gadolinium enhanced MR angiography allow improved depiction of vessels with a sensitivity of 81% (3). After intravenous contrast injection and as demonstrated on computed tomography (CT), varices appear as serpiginous contrast enhanced vessels best assessed on dynamic portal venous phase sequences.

Ultrasound

Whilst transabdominal ultrasound and in particular the use of duplex Doppler ultrasound is routinely used for the evaluation of portal vein patency and liver pathology, the technique can also delineate lower oesophageal varices (4).

Endoscopic ultrasound (EUS) however provides excellent visualisation of the oesophageal wall and adjacent structures, thus allowing the accurate characterisation of

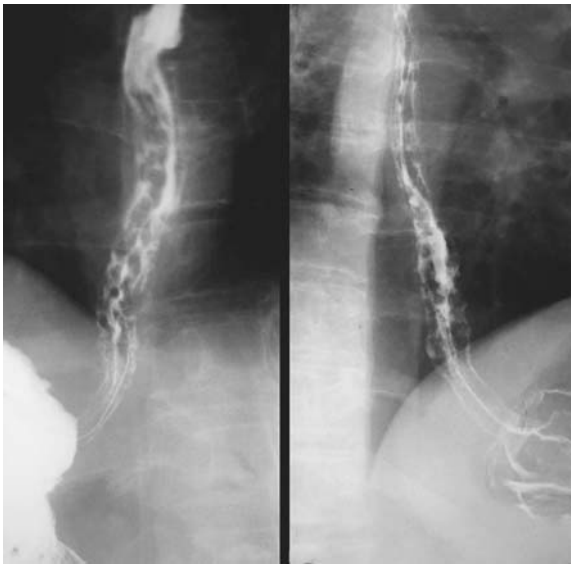

Varices, Oesophagus. Figure 1 Mucosal relief barium swallow images demonstrating uphill varices involving the lower third of the oesophagus.

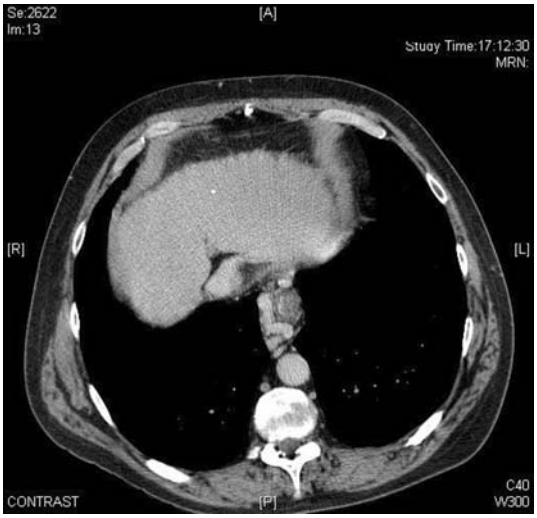

Varices, Oesophagus. Figure 2 Contrast enhanced CT image demonstrating lower oesophageal varices in a patient with portal hypertension.

both oesophageal and paraoesophageal varices. Vessels are defined as hypo or anechoic well-circumscribed structures with a serpiginous appearance on grey-scale imaging. Colour flow and duplex ultrasound allows quantification of the velocity and direction of blood flow within the varices. In addition, therapeutic EUS has been used to guide sclero-therapy and assess post sclero-therapy variceal recurrence.

Angiography

Historically, angiography was used as the primary imaging technique for the depiction of oesophageal varices. However, the use of alternative non-invasive imaging modalities including endoscopy and cross sectional techniques has led to the routine use of angiography as a primary therapeutic rather than diagnostic procedure (5).

Angiography may however be performed using a variety of approaches to evaluate the portal venous system and associated collateral pathways. These included the use of wedged hepatic venography obtained after placement of a catheter within the hepatic vein *via* either an internal jugular or common femoral vein approach. This technique is routinely performed during a transjugular intrahepatic portosystemic stent shunts (TIPSS) procedure (see Chapter TIPSS). Alternatively varices may be visualised either by direct portography obtained after percutaneous trans-hepatic puncture of a portal vein branch or by indirect arterial portography performed after placement of a catheter within either the superior mesenteric or splenic arteries.

Nuclear Medicine

Nuclear medicine has a limited role in the diagnosis and assessment of oesophageal varices. Radiolabelled RBC imaging may however confirm variceal haemorrhage as a cause for upper GI bleeding and SPECT has been performed for the evaluation of variceal recurrence after endoscopic sclerotherapy (Fig. 3).

Diagnosis

Upper GI endoscopy is used as the primary modality for the diagnosis and assessment of oesophageal variceal severity and bleeding risk. Varices are graded using a variety of criteria including size, colour, location and stigmata of bleeding. In addition, endoscopy is routinely used for the therapeutic management of varices. Paraoesophageal varices which lie outside the oesophageal wall are however not visualised during endoscopy. Cross sectional imaging techniques and in particular CT and MRI are both sensitive and specific for the diagnosis of moderate or large

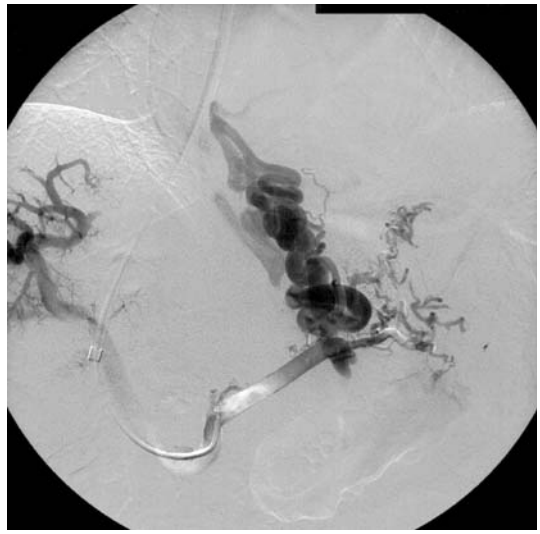

Varices, Oesophagus. Figure 3 Selective venogram following cannulation of the coronary vein demonstrating extensive uphill oesophageal varices in a patient with recurrent variceal haemorrhage.

oesophageal varices including vessels lying adjacent to the oesophageal wall. In addition, these modalities allow evaluation of co-existing pathology within the thorax and abdomen. EUS when available allows accurate variceal assessment although is currently not routinely performed worldwide. The cross sectional imaging modalities, however, are not as sensitive as endoscopy for the diagnosis of small varices and the evaluation of bleeding risk. Angiography is no longer used routinely for the initial diagnosis, although it does play an important role in the subsequent management of varices. The use of contrast techniques in the diagnosis of oesophageal varices has diminished due to the widespread use of the other more sensitive imaging techniques.

Interventional Radiological Treatment

Following an initial haemorrhage the primary treatment for the majority of oesophageal varices remains a combination of endoscopy and medication. Interventional radiology however plays an important role in patients with recurrent variceal bleeding. Techniques including the embolisation of varices as well as the use of TIPSS. This latter technique is covered in more detail in Chapter TIPSS.

Bibliography

1. Ishikawa T, Saeki M, Obara K (1985). Detection of paraesophageal varices by plain films. Am J Roentgenol 144:701–704
2. Cho KC, Patel YD, Wachsberg RH et al (1995) Varices in portal hypertension: evaluation with CT. Radiographics 15:609–622

3. Matsuo M, Kanematsu M, Kim T et al (2003) Esophageal varices: diagnosis with gadolinium-enhanced MR imaging of the liver for patients with chronic liver damage. Am J Roentgenol 180:461–466
4. Kishimoto R, Chen M, Ogawa H et al (1998) Esophageal varices: evaluation with transabdominal US. Radiology 206:647–650
5. Pieters PC, Miller WJ, De Meo JH (1997) Evaluation of the portal venous system: complementary roles of invasive and non-invasive imaging strategies. Radiographics 17:879–895

Varicocele

Abnormal dilatation of the pampiniform plexus of the spermatic cord caused by incompetent venous valves of the testicular vein. It is normally located on one side, most often the left. Primary varicocele can be due to a retroperitoneal mass with compression of venous blood flow.

▶Scrotal Disorders

Varicocele of the Breast

▶Duct Disease, Breast

Vascular Anomalies

Two major categories are distinguished in the setting of vascular birthmarks: vascular tumors and vascular malformations. Vascular tumors include hemangiomas, Kaposiform hemangioendothelioma, and tufted angioma. Vascular malformations comprise high-flow malformations and slow-flow malformations. High-flow malformations may be arterial or arteriovenous. Slow-flow malformations include venous malformations, capillary and lymphatic malformations.

▶Congenital Malformations, Neck

Vascular Disease, Spine

Robert W. Hurst
Radiology, Neurology, and Neurosurgery, University of Pennsylvania, Philadelphia, USA
robert.hurst@uphs.upenn.edu

Definitions

Vascular disease of the spine and spinal cord comprises an important but uncommon group of conditions affecting this portion of the central nervous system (CNS). Spinal vascular malformations and cord ischemia represent the two most important manifestations of spinal vascular disease.

The optimal diagnosis and management of patients with spinal vascular disease requires consideration of these conditions in the appropriate clinical setting followed by imaging evaluation. Recent developments in noninvasive neuroimaging currently provide considerable information regarding all types of spinal vascular pathology. Nevertheless, digital subtraction spinal angiography retains an important role in both the diagnostic evaluation and neurointerventional treatment of those spinal vascular malformations characterized by arteriovenous shunting.

Pathology/Histopathology

Spinal Vascular Malformations

Spinal vascular malformations are a heterogeneous group of nonneoplastic vascular abnormalities that comprise from 5% to 15% of spinal mass lesions. Classification of spinal vascular malformations is based on angioarchitecture and hemodynamics. Lesions characterized by arteriovenous shunting include four major groups, designated Types I through IV.

Type I: ▶Spinal dural arteriovenous fistulas (SDAVF). These are the most common. SDAVF's (Type I) acquired lesions, not congenital malformations, which probably result from thrombosis of the extradural venous plexus. SDAVF develop within the dural covering of the spinal cord, usually at a nerve root sleeve. SDAVF receive arterial supply from a dural branch of a radicular artery with no arterial supply originating directly from the spinal arteries. The fistula drains into the pial veins of the cord, increasing pressure and dilating the pial venous system. The resulting venous hypertensive myelopathy impairs cord perfusion with hypoxia, edema, and disruption of the blood CNS barrier. Extensive and progressive cord dysfunction results, with poor correlation between the site of the SDAVF and the clinical level of neurological deficit.

Pathologic changes in the spinal cord involve both vascular structures and cord parenchyma. Hyalinization of vessels, arterialization of veins, vascular calcification, and thrombosis are common findings. Parenchymal changes include necrosis, myelin loss, gliosis, hemosiderin deposition, and Rosenthal fibers. Venous hypertensive myelopathy, likely from SDAVF, is believed to represent

the underlying pathology in "subacute necrotizing myelopathy" or "Foix-Alajouanine Syndrome".

Types II and III: ►Spinal cord arteriovenous malformations (SCAVM) were subdivided into two subtypes depending on whether they are confined to the spinal cord (Type II) or extend into the adjacent bone and soft tissue structures (Type III). SCAVM are congenital lesions characterized by arteriovenous shunting through a nidus on or within the substance of the spinal cord, whose arterial supply arises from vessels, which directly supply the cord. Dilated draining veins are present within the spinal subarachnoid space. SCAVM's most frequently affect the cervicothoracic region (5).

Type IV: ►Spinal cord arteriovenous fistulas (SCAVF), a relatively rare type of lesion (1). (Fig. 1). SCAVF are uncommon congenital vascular malformations which usually present in the second through fourth decade (6). The lack of intervening nidus, intradural location, and supply from spinal arteries, differentiate SCAVF from both SDAVF and SCAVM.

In addition, ►cavernous malformations (CM) without arteriovenous shunting may also affect the spinal cord. (Table 1). CM of the spine are pathologically identical to intracranial cavernous malformations, and consist of multiple cystic or sinusoidal vascular channels with very slow or stagnant blood flow. They are, well demarcated from surrounding tissue by a complete rim of hemosiderin stained gliosis and inflammatory cells. CM varies in size from several millimeters to over a centimeter in diameter (7).

Spinal cord ischemia is an uncommon cause of myelopathy with well under 1% of all strokes involving the spinal cord (8).

Clinical

In SDAVF, males are afflicted in 80–90% of cases with a usual presentation after the 6th decade. SDAVF usually occur between the T5 and L3 spinal levels.

Chronic progressive myelopathy, with ascending motor and sensory deficits affecting the lower extremities, characterizes the course of SDAVF (2). Back pain is inconstantly present. Prior to diagnosis bowel, bladder, and sexual dysfunction develops in the majority of patients. Consideration of SDAVF in the differential diagnosis and awareness of imaging findings are the most important factors in early diagnosis.

Hematomyelia or subarachnoid hemorrhage are common in SCAVM and may arise from arterial aneurysms, the nidus, or draining veins. Men and women are equally affected by SCAVM, which usually presents in the second or third decade.

Patients may present with progressive lower extremity deficits or acute hemorrhage in SCAVF.

Patients with CM most often present in the fourth decade, usually with discrete episodes of neurological dysfunction followed by variable recovery.

►Spinal cord infarction usually involves the anterior spinal artery distribution and is most often characterized clinically by acute flaccid paralysis with decreased or absent pain and temperature sensation below the level of the lesion and sparing of posterior column function. Several clinical situations have been associated with spinal cord infarction, most commonly aortic dissection, and surgical repair of thoracoabdominal aortic aneurysms.

Imaging

In SDAVF, MRI shows abnormal cord signal intensity on T1- and T2-weighted images, often with abnormal enhancement and diffuse cord enlargement. The conus is uniformly involved although abnormal signal frequently extends into thoracic levels. Flow voids of the dilated pial veins on the cord surface are a more specific finding, and may often be made more conspicuous by enhancement (3).

Recent data support the use of contrast enhanced MRA to confirm the presence of SDAVF and identify the level of the fistula prior to angiography. Spinal angiography remains necessary to confirm the diagnosis and location of SDAVF as well as to plan or perform therapy (4).The spinal angiogram requires selective evaluation of lumbar and intercostal arteries to identify the location of the shunt. Early filling of the pial veins of the cord through the tiny shunt is the most important angiographic feature to confirm the presence SDAVF.

In SCAVM, flow voids representing feeding arteries, nidus, and draining veins are well seen in MRI (Fig. 1b). The extent of flow voids suggests whether at Type II or Type III lesion is present. Evidence of subacute or chronic intramedullary hemorrhage is frequently present as well as nonhemorrhagic intramedullary signal abnormality indicating gliosis, edema, or infarction. Although MRA sequences may detect high flow, specific feeding and draining vessels can be, rarely and reliably identified.

Spinal angiography is mandatory to define the angioarchitecture of the suspected SCAVM sufficiently to plan and carry out the treatment.

In SCAVF, flow voids indicate the enlarged feeding and draining vessels to the fistula on MRI, often with cord displacement or distortion as a result of mass effect. Intrinsic cord signal abnormality is frequent, often with enhancement and evidence of hemorrhage. Spinal angiography is necessary to determine the location of the fistula, its feeding arteries, and draining veins.

In CM, the central portion of the lesion is heterogeneous on both T1- and T2-weighted MR images. A rim

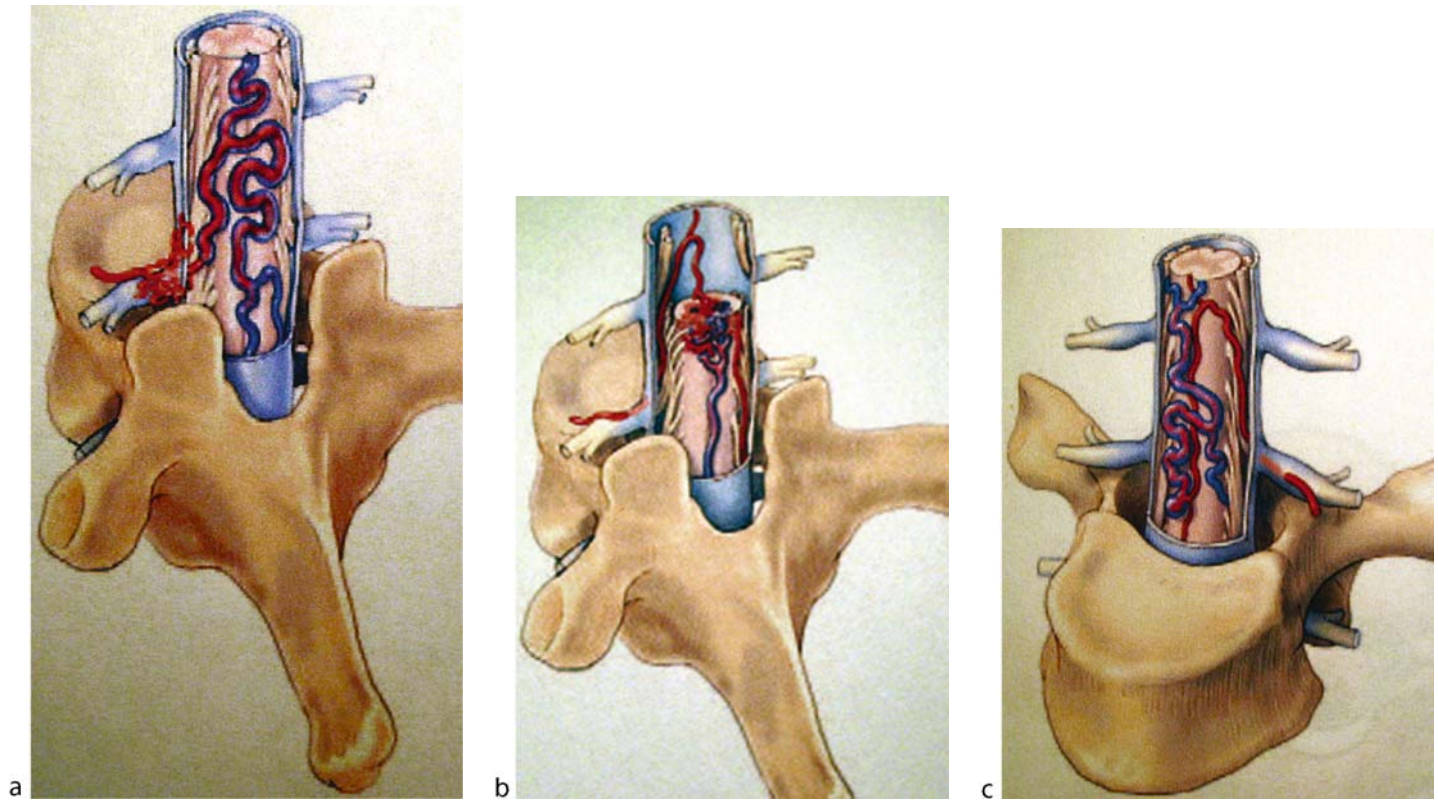

Vascular Disease, Spine. Figure 1 (a) Spinal dural arteriovenous fistula, Type I; (b) Spinal cord arteriovenous malformation, Type II; (c) Spinal cord arteriovenous fistula,

Vascular Disease, Spine. Table 1 Spinal Vascular Malformations

Name (type)	Typical location	Arterial supply	Population affected	Clinical course	Treatment
SDAVF (Type I)	lumbar, thoracic	dural arteries	M > F >sixth decade	chronic myelopathy	1. emboliz. 2. surgery
SCAVM- glomus (Type II)	cervical, thoracic, lumbar	Spinal arteries (ASA, PSA)	M = F Second and third decade	acute; hemorrhage common	1. emboliz. 2. surgery
SCAVM- juvenile (Type III)	cervical, thoracic,	Spinal arteries (ASA, PSA)	M = F Second and third decade	acute; hemorrhage Common	1. emboliz. 2. surgery
SCAVF (Type IV)	lumbar, thoracic	Spinal arteries (ASA > PSA)	Children, Young adults	acute or chronic; may hemorrhage	1. emboliz. 2. surgery
CM (Not included in Types)	cervical, thoracic, lumbar	no AV shunt	F > M fourth and fifth decade	acute or chronic; may hemorrhage	Surgery

SDAVF-Spinal Dural Arteriovenous Fistula.
SCAVM-Spinal Cord Arteriovenous Malformation.
SCAVF-Spinal Cord Arteriovenous Fistula.
CM-Cavernous Malformation.

of low signal intensity representing iron storage products completely surrounds the lesion. The findings are characteristic and often permit specific diagnosis. The surrounding parenchyma may have abnormal signal intensity as a result of gliosis, edema, or syrinx. Following acute hemorrhage, the MRI appearance may be less specific and other differential considerations may require consideration. With typical MRI features, angiographic evaluation is unnecessary.

MRI findings in spinal cord ischemia are similar regardless of the etiology of the infarction (9). Cord signal abnormality and subtle enlargement in the acute stage are best seen in proton density and T2-weighted images. Signal abnormality may involve only the gray matter but often extends throughout the entire cross section of the cord. Enhancement may occur, especially involving the gray matter. In the chronic stages, cord atrophy may be present.

Interventional Treatment

Endovascular occlusion of SDAVF should be considered at the time of the diagnostic angiogram. Surgical treatment with coagulation or resection of the site of the nidus and surrounding dura also represents viable therapy for many patients.

Bibliography

1. Spetzler RF et al (2002) Modified classification of spinal cord vascular lesions. J Neurosurg 96(Suppl 2):145–156
2. Symon L, Kuyama H, Kendall B (1984) Dural arteriovenous malformations of the spine Clinical features and surgical results in 55 cases. J Neurosurg 60:238–247
3. Gilbertson J et al (1995) Spinal dural arteriovenous fistulas: MR and myelographic findings. AJNR 16:2049–2057
4. Bowen BC, Saraf-Lavi E, Pattany PM (2003) MR angiography of the spine: update. Magn Reson Imaging Clin N Am 11(4):559–584
5. Berenstein A, Lasjaunias P (1992) Surgical Neuroangiography Vol 5: Endovascular Treatment of Spine and Spinal Cord Lesions. Vol 5. Springer-Verlag, Berlin Heidelberg New York: pp 1–109
6. Gueguen B et al (1987) Vascular malformations of the spinal cord: Intrathecal perimedullary arteriovenous fistulas fed by medullary arteries. Neurology 37:969–979
7. Ogilvy C, Louis D, Ojemann R (1992) Intramedullary cavernous malformations of the spine. Neurosurgery 31(2):219–230
8. Sandson T, Friedman J (1989) Spinal cord infarction: report of 8 cases and a review of the literature. Medicine 68:282–292
9. Mawad, M et al (1990) Spinal cord ischemia after resection of thoracoabdominal aortic aneurysms: MR findings in 24 patients. AJNR 11:987–991

Vascular Disorders, Hepatic

Massimo Bazzocchi[1], Giuseppe Como[1], Marzio Perri[2]
[1]Department of Diagnostic and Interventional Radiology, University of Udine, Udine, Italy
[2]Department of Diagnostic and Interventional Radiology, University of Pisa, Pisa, Italy
massimo.bazzocchi@med.uniud.it

Synonyms

Hepatic vascular pathologies; Primary circulatory liver disorders

Definition

Vascular disorders of the liver are several different pathological conditions including ►portal vein thrombosis, ►Budd–Chiari syndrome, ►veno-occlusive disease (VOD), ►peliosis hepatis, ►arterio-venous malformation, and ►congestive cardiac cirrhosis.

Pathology and Histopathology

Portal Vein Thrombosis

Etiological factors of portal vein thrombosis are slow flow secondary to cirrhosis, direct invasion by cancer, inflammatory changes in pancreatitis, sclerosing cholangitis, and abdominal infections, coagulation disorders, and surgical interventions. In chronic occlusion, the portal vein is retracted and dilatated, periportal collateral veins (►portal cavernoma) may be observed, while the chronic occlusion of a branch of the portal vein is usually accompanied by segmental atrophy and compensatory hypertrophy of other segments (1).

Budd–Chiari syndrome

The Budd–Chiari syndrome is a hepatic venous obstruction at any level from the small hepatic veins to the junction of the inferior vena cava and the right atrium. Outflow obstruction caused by hepatic VOD and cardiac disorders is excluded from this definition (2). Distinction is made between primary and secondary forms. The primary type is caused by endoluminal venous lesion (thrombosis, webs, endophlebitis) and is usually associated with underlying thrombogenic conditions. The secondary type includes obstruction originating from a lesion outside the venous system (tumor, abscess, cysts) and compressing or infiltrating the hepatic venous system. Venous compression can be complicated by thrombosis. Both in the primary and secondary forms, obstruction of the hepatic venous outflow tract results in increased hepatic sinusoidal pressure and portal hypertension. Hepatomegaly is usually seen. However, in later stage of Budd–Chiari syndrome peripheral atrophy associated with caudate and central hypertrophy is usually observed. Centrilobular necrosis is histological observed. In chronic cases the affected areas become fibrosed and shrink in size (2, 3).

Veno-Occlusive Disease

Hepatic VOD is a common complication of bone marrow transplantation (BMT). It is characterized by obstruction of small and medium-size intrahepatic veins due to vasculitis. It differs from Budd–Chiari syndrome in that the major hepatic veins and inferior vena cava primarily remain patent. It is usually associated with the use of chemotherapeutic agents or radiation and secondary to progressive inflammation with deposition of coagulation factors, red cells, and hemosiderin-laden macrophages within terminal hepatic venules resulting in a nonthrombotic venule occlusion (4). Histologic features consist of centrilobular sinusoidal fibrosis followed by necrosis of the zone 3 hepatocytes.

Peliosis Hepatis

Hepatic peliosis is a rare benign pathological entity characterized by focal, multifocal, segmental, or diffuse dilatation of liver sinusoids. At gross examination multiple cyst-like, blood-filled cavities within hepatic parenchyma are observed (1). Although several theories, including outflow obstruction of the blood flow at the sinusoidal level, hepatocellular necrosis, or direct lesions of the sinusoidal barrier, have been postulated to explain its etiology, the pathogenesis of peliosis hepatis is still unclear.

Clinical Presentation

Portal Vein Thrombosis

In most cases, portal vein thrombosis occurs slowly and silently. Biochemical tests of the liver are normal or only mildly elevated. Ascites and encephalopathy are uncommon. Splenomegaly and esophageus varices are the most common clinical findings and gastrointestinal hemorrhage for portal hypertension is usually the first manifestation of portal vein thrombosis. Rarely, thrombosis extends from the portal vein to the mesenteric arcades, leading to bowel ischemia and infarction.

Budd–Chiari Syndrome

Since the extent and rapidity of the hepatic vein occlusion and of the development of venous collateral circulation is highly variable, fulminant, acute, subacute, or chronic clinical presentation may be observed (3). The acute and fulminant forms are associated with an acute thrombosis of the main hepatic veins and the etiologic factors are related to hypercoagulability of blood. Patients rapidly develop hepatomegaly, intractable ascites, jaundice, and abdominal pain leading to liver failure and hepatic encephalopathy. The subacute and chronic types are most common and have an insidious onset; since the development of venous collateral vessels, ascites, and hepatic necrosis may be minimal and splenomegaly or esophagogastric varices may represent the only clinical findings. The degree of aminotransferase, alkaline phosphatase and

bilirubin levels elevation is variable, depending on the rapidity of the onset. Patients with Budd–Chiari syndrome who have deteriorating liver function and complications usually need to undergo liver transplantation.

Veno-Occlusive Disease

VOD occurs in over half of BMT patients. Risk factor include preexisting liver disease or liver function test abnormalities and underlying infection or antibiotic use during conditioning chemotherapy. Jaundice, weight gain, and ascites occurring within the first 3 weeks after BMT represent the typical clinical manifestations. At laboratory exams, elevated transaminases and hyperbilirubinemia (direct bilirubin >2) are observed (1, 4). In severe cases, multiorgan failure with pulmonary infiltrates, pleural effusions, congestive heart failure (CHF), and renal failure may occur.

Peliosis Hepatis

Peliosis hepatis commonly occurs in patients treated with anabolic steroids, corticosteroids, or oral contraceptives. The disease is associated with chronic wasting diseases such as tuberculosis, hematological malignancies, diabetes, acquired immunodeficiency syndrome (AIDS), posttransplant immunodeficiency, and exposure to toxic agents (1, 5). Hepatic peliosis is usually asymptomatic and focal liver lesions are discovered incidentally. However, in rare cases, the lesions may be revealed by major complications such as liver failure, portal hypertension, or hemorrhage.

Imaging

Portal Vein Thrombosis

Ultrasound (US) features are echogenic thrombus within the lumen of the vein, demonstration of portal vein collateral circulation, enlargement of the thrombosed segment of the vein, and the cavernomatous transformation of the portal vein (Fig. 1). Color Doppler US is a useful tool for detection of portal vein thrombosis (Fig. 2). It is also useful for differential diagnosis between nonneoplastic and neoplastic thrombosis in presence of hepatocellular carcinoma. The demonstration of arterial flow within the thrombus is specific for malignancy.

Nonenhanced computed tomography (CT) may show focal high density in enlarged portal system in acute thrombosis while chronic venous thrombosis appears as linear areas of calcification within the thrombus. A filling defect in the vessel lumen during the portal venous phase represents the typical finding of portal vein thrombosis on contrast-enhanced CT (Fig. 2). In a patient with hepatocellular carcinoma enhancement of the thrombus during the arterial phase is suggestive for neoplastic thrombosis. Typically, a regional parenchymal hyperdensity due to a compensatory increase in arterial blood flow to the segments poorly perfused by the portal vein is observed during the arterial phase while the locally decreased portal vein perfusion results in a hypodense appearance on the portal-venous phase. On magnetic resonance (MR), acute thrombosis manifests as absent flow signal void within a normal or dilated vein, generally associated with edge enhancement of the thrombosed

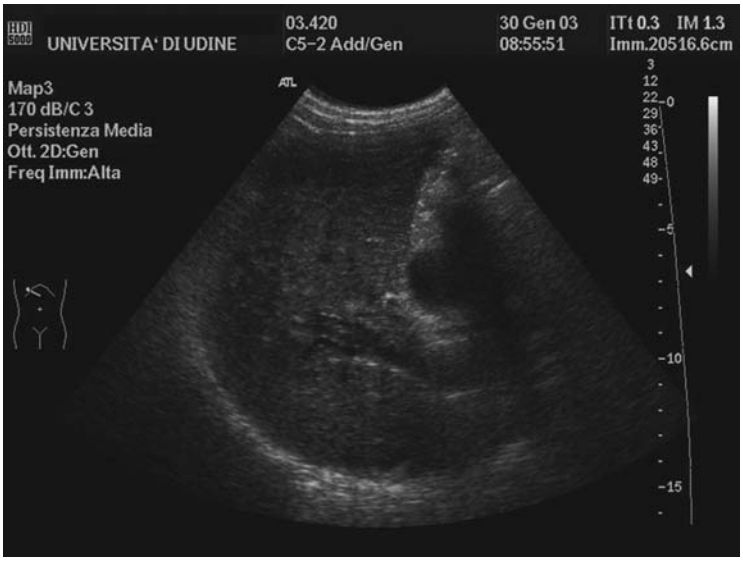

Vascular Disease, Spine. Figure 1 US scan of hilum hepatis: for chronic occlusion, the portal vein is retracted and we can see dilated periportal collateral veins (portal cavernoma).

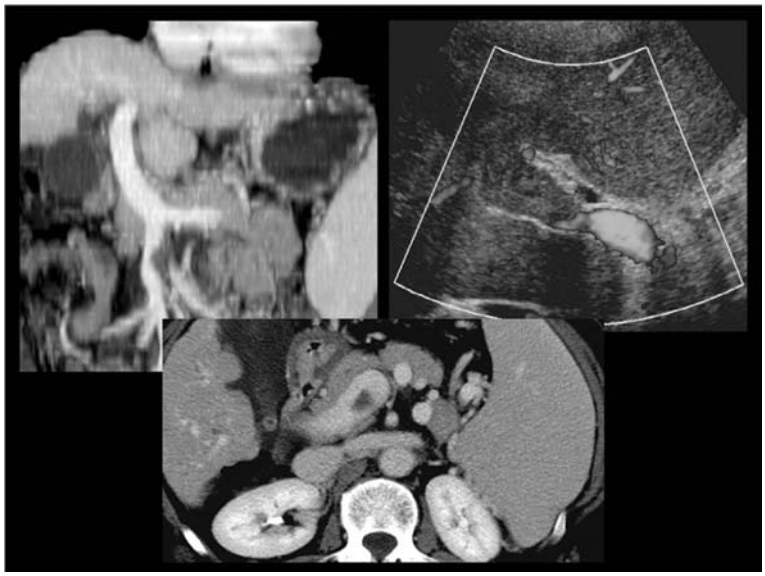

Vascular Disease, Spine. Figure 2 A filling defect in the vessel lumen during the portal venous phase represents the typical finding of portal vein thrombosis on contrast-enhanced CT. We can see axial scan and coronal MPR reconstruction. At US scan features are echogenic thrombus within the lumen of the vein with enlargement of the thrombosed segment.

vein because of blood flowing around the thrombus, or inflammatory response of the venous wall. The clot is isointense or hyperintense on T1-weighted images, and hyperintense on T2 (1). Moreover, using angiographic sequences (contrast-enhanced 3D MR portography), MR provides detailed information not only about the location and length of portal vein obstruction but also about portal collateral pathways.

Budd–Chiari Syndrome

Doppler US is the modality of choice for diagnosis of Budd–Chiari syndrome, with a sensitivity of more than 85% (3). A spectrum of hepatic venous abnormalities (hepatic veins tortuosity, thrombosis, flow reversal, and monophasic flow waveform) may be observed and the association with intrahepatic or subcapsular portosystemic shunts and venous collaterals is suggestive for the diagnosis (2). US may demonstrate the occlusion of the hepatic veins due to thrombus or tumor as well as the narrowing of the inferior caval vein due to a web, appearing as an echogenic structure without acoustic shadowing (Fig. 3). Finally, US may demonstrate hepatomegaly, ascites, and parenchymal changes such as necrotic or fibrotic areas. CT scan and MR imaging allow a most extensive and accurate evaluation of the parenchymal changes. A heterogeneous enhancement of the liver parenchyma, hypertrophy of the caudate lobe, direct findings of hepatic venous occlusion and extrahepatic findings such as ascites, splenomegaly, and portosystemic collateral vessels

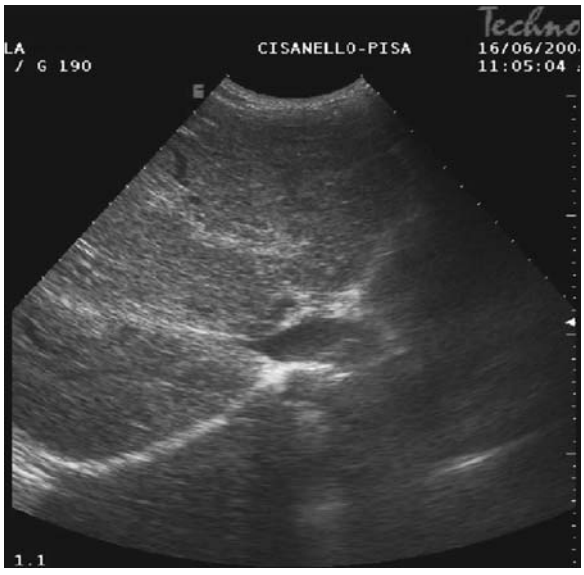

Vascular Disease, Spine. Figure 3 US scan demonstrates the occlusion of the hepatic veins that appear as echogenic structures.

represent the most common features of Budd–Chiari syndrome on both CT and MR contrast-enhanced imaging. Moreover, MR, by the use of angiographic sequences, allows also an extremely accurate evaluation of the vascular abnormalities and is a highly sensitive tool for the diagnosis of hepatic veins thrombosis (3).

Veno-Occlusive Disease

The diagnostic imaging study of choice is US with Doppler modalities. Nonspecific US findings have been described, including ascites, gallbladder wall thickening, and hepatosplenomegaly. Moreover, the absence of obstruction of hepatic veins or inferior cava at Doppler US or MR imaging enables differential diagnosis between Budd–Chiari syndrome and VOD (4).

Peliosis Hepatis

Imaging findings are variable depending on differing pathological patterns and on often concomitant liver steatosis. On US, numerous poorly defined foci of varying hypoechogenicity may be observed; however, these findings are nonspecific and may simulate hepatic metastasis, cirrhosis, hemangiomatosis, or adenomatosis.

The CT and MR findings may differ according to the size of the lesions, the extent of communication with the sinusoids, the presence or absence of thrombi within the cavities, and the presence or absence of hemorrhage (5). However, multiple small hepatic lesions with variable enhancement represent the most common findings, while larger and even solitary lesions are uncommon. The lesions appear usually as irregular, hypodense regions on unenhanced CT scan and, occasionally, hyperdense spots for focal hemorrhage may be observed. After contrast medium administration, a slight peripheral enhancement is usually seen. A typical finding of hepatic peliosis is the lack of mass effect on hepatic vessels.

On MR, the multiple hepatic foci in peliosis hepatis show a high signal on T2-weighted images and a variable signal on T1-weighted images, presumably reflecting various stages of subacute hemorrhage. A late and slow but intense enhancement is observed on contrast-enhanced MR imaging.

Diagnosis

Portal Vein Thrombosis

Portal vein thrombosis is usually asymptomatic and diagnosis is mainly done by imaging. Doppler US is the first imaging modality used. In patients who are candidates for surgery, that is, for portosystemic shunt procedures, a more accurate imaging evaluation covering the whole portal venous system is required. Traditionally, assessment of the portal venous system has been achieved with intraarterial splenoportal and mesentericoportal angiography, but, recently, the value of MR angiography as another noninvasive procedure for the assessment of the portal venous system has been increasingly recognized.

Budd–Chiari

The diagnosis of Budd–Chiari syndrome is established only upon demonstration of an obstructed hepatic venous outflow tract. Doppler US has a sensitivity of more than 85% and should be the first line of investigation, while the association of Doppler US and MR allow the diagnosis in almost all cases and an optimal delineation of the venous obstruction is usually obtained (2).

In a minority of patients, mostly individuals with cirrhosis, liver biopsy may be required to firmly establish the diagnosis and to rule out other processes such as VOD and cirrhosis of other etiologies.

Direct venography is no longer considered necessary. However, since it allows a precise delineation of outflow obstruction and pressure measurements, venography should be performed when percutaneous or surgical shunting is considered.

Venous-Occlusive Disease

Diagnosis can usually be made based on clinical criteria. Direct bilirubin 2 mg/dL, hepatomegaly and weight gain due to fluid accumulation occurring within 20 days of transplantation are the typical clinical findings. The diagnosis can only be made when hyperacute graft-versus-host disease, sepsis, cardiac failure, and tumor infiltration have been ruled out. US can exclude tumor infiltration and biliary tract disease and confirm hepatomegaly and ascites while color Doppler US, MR imaging, and angiography can accurately determine the level of involvement enabling the differentiation between Budd–Chiari syndrome and VOD (4). Finally, transvenous liver biopsy is required in patients with thrombocytopenia posttransplantation to differentiate VOD from acute graft-versus-host disease.

Peliosis Hepatis

Imaging findings are often not sufficiently specific and histology is the only certain way of making the diagnosis. However, the risk of performing a needle biopsy in peliosis hepatis is unclear and severe hemorrhage and even fatal outcome following needle biopsy have been reported.

Bibliography

1. Schneider G, Grazioli L, Saini S (eds) (2002) MRI of the Liver. Berlin, Heidelberg: Springer
2. Janssen HL, Garcia-Pagan JC, Elias E et al (2003) European group for the study of vascular disorders of the liver. Budd–Chiari syndrome: a review by an expert panel. J Hepatol 38(3):364–371
3. Menon KV, Shah V, Kamath PS (2004) The Budd–Chiari syndrome. N Engl J Med 350(6):578–585

4. Mortele KJ, Van Vlierberghe H, Wiesner W et al (2002) Hepatic veno-occlusive disease: MRI findings. Abdom Imaging 27(5):523–526
5. Steinke K, Terraciano L, Wiesner W (2003) Unusual cross-sectional imaging findings in hepatic peliosis. Eur Radiol 13:1916–1919

Vascular Disorders, the Gastrointestinal Tract

Alban Denys
Centre Hospitalies Universitire Vandois Lausanne, Lausanne, Switzerland
alban.denys@chuv.hospvd.ch

Synonyms

Angiodysplasia; Arteriovenous malformation; Vascular ectasia

Definition

Vascular disorders of the gastrointestinal tract include occlusive, aneurysmal diseases, and congenital malformations of the arterial or venous mesenteric vessels. These disorders are rare and difficult to diagnose and therefore account for many malpractice claims. Symptoms can be divided into two groups: ischemic and hemorrhagic.

Ischemic diseases can lead to chronic or acute intestinal ischemia. The small bowel and the right colon are the parts of the digestive system most sensitive to ischemia. Etiologies of acute mesenteric ischemia can be divided into arterial occlusive diseases, venous thrombosis, and nonocclusive arterial diseases (1). Arterial occlusions are related either to embolism in the superior mesenteric artery, mainly from a cardiac origin, or to thrombosis of the superior mesenteric artery. Venous thrombosis of the superior mesenteric veins is either primary, due to coagulation disorders, or related to various abdominal diseases favoring venous thrombosis, such as cirrhosis and intraperitoneal infectious diseases. Nonocclusive mesenteric ischemia means that there is an insufficient oxygen supply to the digestive wall despite patent mesenteric vessels. As a result of systemic hypoperfusion (cerebral and/or cardiac), mesenteric vasospasm occurs to preserve cardiac and cerebral blood flow. Therefore, this condition is encountered in severely ill patients with advanced cardiac insufficiency and is favored by the use of vasoconstrictive agents.

Chronic mesenteric ischemia occurs due to occlusion or stenosis of at least two of the three digestive arterial trunks, including the superior mesenteric artery (celiac trunk, superior, and inferior mesenteric artery). The main cause is atheroma (2).

Gastrointestinal bleeding can be caused by many pathologies, including cancers and inflammatory diseases, but some vascular diseases such as ▶angiodysplasia can cause recurrent bleeding in elderly patients (3). Angiodysplasias are acquired capillary vascular malformations encountered mainly in the cecum (78%), jejunum (10%), ileum (5%), and stomach (4%) in elderly patients.

Pathology/Histopathology

Acute mesenteric ischemia can lead to various degree of ischemia of the bowel wall, from transient mucosal ischemia to irreversible bowel wall necrosis. Arterial etiologies first induce digestive mucosal ischemia, which extends progressively to the muscularis mucosa and to the serosa. In the early phase, the intestine is pale and spastic; in later phases, the loops are dilated, with a gray appearance and edematous infiltration of the mesocolon. In the late phase, the loop is atonic and dilated, with focal hemorrhage in the bowel wall and focal areas of necrosis. Thirty minutes of ischemia are sufficient to produce necrosis. Venous etiologies are characterized by early mesenteric edema and bowel wall hemorrhage. Thrombosis of distal venous branches is mandatory for producing ischemia.

In chronic mesenteric ischemia, histopathology of the digestive wall is usually normal. Analysis of the main digestive trunks shows various degrees of occlusion of the main trunks. Occlusion of the celiac trunk is usually proximal, favored by compression from a median arcuate ligament, and is found in 15–24% of patients. Occlusion of the superior mesenteric artery is usually found in the first 5 cm after its origin.

Angiodysplasia is found in the submucosa and is characterized by one or multiple dilated submucosal veins and a cluster of capillaries and small arteries.

Clinical Presentation

Acute mesenteric ischemia has various clinical presentations. The most common symptom is a sudden pain localized in the periumbilical region of the right iliac fossa. This pain is usually severe and induces agitation. It occurs in older patients (mean age 70 years) with multiple cardiac and vascular comorbidities. Cardiac disease, myocardial infarction, and cerebrovascular disorders, and congestive heart failure are found in 91%, 27%, 23%, and 45% cases of mesenteric embolism, respectively. The association of sudden abdominal pain with multiple cardiovascular events in the previous

history is highly suggestive of acute mesenteric ischemia. If the diagnosed is delayed, peritonism as well as shock can be encountered. Patient survival is inversely correlated with diagnostic delay.

Clinical symptoms of chronic mesenteric ischemia include so-called ►intestinal angina. Patients with intestinal angina complain of periumbilical abdominal pain that starts approximately 30 min after eating and lasts for 1–2 h. The patient may recognize the relationship between eating and abdominal pain, resulting in a fear of eating and subsequent weight loss. Some patients, however, will present with anorexia and weight loss without complaints of abdominal pain. Symptoms may be less specific, such as diarrhea or vomiting, resulting in delayed diagnosis.

Angiodysplasia is usually silent, but bleeding may occur in up to 10% of cases. Depending on the lesion's localization and the volume of blood loss, symptoms may range from hematemesis to melena as well as hematochezia or only symptoms of chronic anemia.

Imaging

For the diagnosis of acute mesenteric ischemia, the most critical issue is to save time and not delay treatment. Plain X-ray films are usually done at the onset of acute abdominal pain. Although useful for eliminating other causes of abdominal pain such as nephrolithiasis or bowel perforation, they are insufficient for diagnosing acute mesenteric ischemia. Ultrasound (US) and Doppler of mesenteric vessels are nonspecific and very difficult to perform in this situation and should not be done. Computed tomography (CT) and, more recently, multidetector CT of the abdomen are now recommended (4). They allow visualization both of bowel wall ischemia (wall thickening with submucosal edema) and necrosis (lack of enhancement of the bowel wall after injection of contrast media, pneumatosis; Fig. 1a) and of its vascular etiology, with an embolus visible as a filling defect in the lumen of the superior mesenteric artery (Fig. 1b) or a thrombosis of the superior mesenteric artery or vein. If CT does not provide sufficient information for treatment, angiography can be performed to visualize mesenteric vessels.

Imaging of chronic mesenteric ischemia relies mainly on Doppler US. In thin patients, this technique is able to depict stenoses of the superior mesenteric artery, celiac axis, and inferior mesenteric artery with excellent sensitivity. The diagnosis of hemodynamically significant stenosis is based on velocity measurements at the origin of these trunks. A velocity of over 275 cm/sec in the superior mesenteric artery and 200 cm/sec in the celiac axis is specific. The relationship between the stenoses and the pain usually remains unresolved until correction of the

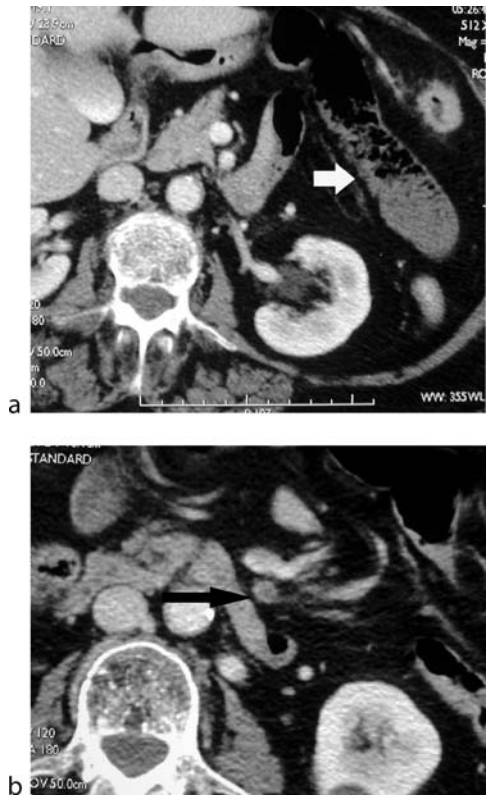

Vascular Disorders, the Gastrointestinal Tract. Figure 1 A 67-year-old woman who presented with sudden acute abdominal pain. (a) Computed tomography slice after injection of contrast media shows a dilated jejunal loop without enhancement of the bowel wall (*white arrow*), suggesting bowel wall ischemia. (b) Zoom view of the mesenteric vessel shows occlusion of the superior mesenteric artery by an embolus (*bold arrow*).

stenoses, either by intravascular methods or surgical bypass techniques. Angio-CT and magnetic resonance angiography have also been advocated, but their performance does not seem superior to Doppler US.

Diagnosis of angiodysplasia is usually done by endoscopy, but during bleeding episodes, lesions can be obscured by the intestinal contents and blood clots. Mesenteric angiography is the method of choice, showing a nidus typically located on the antimesenteric border of the right colon that is associated with early filling of a large adjacent drainage vein. The feeding artery is inconsistently enlarged. Bleeding becomes visible as a pooling area of contrast persistent on late images when bleeding exceeds 0.5 mL/min. CT has recently been proposed to demonstrate these lesions. On the arterial phase after injection, the filling defect as well as the large draining vein can be visible. The performance of CT in detecting angiodysplasia is unknown.

Nuclear Medicine

Nuclear medicine has no role in diagnosing acute or chronic mesenteric ischemia, but it has been proposed for diagnosing chronic bleeding of unknown origin. Technetium-99m-labeled red blood cell scintigraphy has proved to be efficient in localizing the bleeding site if a pooling is visible in the first 2 h after injection when bleeding exceeds 0.1 mL/min. This technique allows the bleeding site to be localized but does not give information about the bleeding etiology. There is no specific sign on technetium-99m-labeled red blood cell scintigraphy for angiodysplasia.

Diagnosis

The diagnosis of acute mesenteric ischemia should be suspected when an acute onset of abdominal pain is associated with a previous history of a cardiovascular disorder in an elderly patient. Diagnosis is usually done by CT because both bowel wall ischemia and the cause of the ischemia are visible. Nowadays, mesenteric angiography is reserved for equivocal cases and/or associated treatment. When signs of peritonism are concomitant, laparoscopy, or laparotomy can be proposed directly without preoperative imaging.

The diagnosis of chronic mesenteric ischemia relies on the association of typical symptoms associated with weight loss and Doppler signs of mesenteric vessel stenoses or occlusions. Because symptoms are aspecific (abdominal pain and weight loss are encountered in many abdominal cancers) and stenoses of two mesenteric vessels can be completely asymptomatic due to collateral vessel recruitment, the final diagnosis can be made only after having treated the stenoses if symptoms disappears afterward.

The diagnostic strategy of lower gastrointestinal bleeding is based on the results of endoscopy. Gastroscopy and colposcopy are typically always performed. Angiodysplasia usually presents at endoscopy as an intense red stellate flat lesion. If the bleeding site is not localized and bleeding persists, mesenteric angiography can be proposed to detect the lesion and embolize the feeding artery.

Interventional Radiological Treatment

Endovascular treatment of acute mesenteric ischemia is the treatment of choice if type B aortic dissection is the etiology. In other situations, endovascular methods should be discussed on a case-to-case basis. The use of thrombolytic medication is not without risk if necrosis of the bowel wall is already present.

Endovascular treatment of chronic mesenteric ischemia has now become widely accepted when the lesions are stenoses and not occlusions. Stent placement allows similar symptom relief as well as a long-term symptom-free survival rate.

Bibliography

1. Oldenburg WA, Lau LL, Rodenberg TJ et al (2004) Acute mesenteric ischemia: a clinical review. Arch Intern Med 164(10):1054–1062
2. Cognet F, Ben Salem D, Dranssart M et al (2004) Chronic mesenteric ischemia: imaging and percutaneous treatment. Radiographics 22(4):863–879; discussion 879–880
3. Krevsky B (1997) Detection and treatment of angiodysplasia. Gastrointest Endosc Clin N Am 7(3):509–524
4. Taourel PG, Deneuville M, Pradel JA (1996) Acute mesenteric ischemia: diagnosis with contrast-enhanced CT. Radiology 199(3):632–636

Vascular Ectasia

▶Vascular Disorders, the Gastrointestinal Tract

Vascular Imaging and Vascular Interventional Radiology

Dierk Vorwerk
Department of Diagnostic and Interventional Radiology, Klinikum Ingolstadt, Ingolstadt, Germany
dierk.vorwerk@klinikum-ingolstadt.de

Imaging of vascular structures was a very early goal of radiologists before researchers were able to introduce fast imaging facilities, fluoroscopy, nontoxic contrast media, and suitable selective catheter techniques into radiology, which were all necessary for the depiction of arteries and veins.

After definition of these invaluable tools, conventional angiography became one of the early revolutionizing techniques that was added to plain-film radiography, and until the development of computer tomography (CT), it was one of the most important tools for the specific diagnosis of cerebral and abdominal problems.

In the meantime, diagnostic angiography—albeit refined by digital subtraction techniques—has been widely replaced by cross-sectional imaging in the diagnosis of organ-related diseases and will be more and more replaced by CT angiography, magnetic resonance (MR) angiography, and duplex ultrasound for many purely arterial or venous problems.

There are, however, some special diagnostic problems that still require selective angiography for detailed

diagnosis, such as cerebral vascular dysplasias or searching for sources of bleeding.

Selective arteriography is still the guiding tool for intravascular interventional radiology, and to date there is no alternative available for this purpose.

Anatomically, vascular imaging includes arteries, veins, arteriovenous connections such as hemodialysis fistulas and grafts, large visceral veins, and pulmonary veins and arteries.

Classical imaging modalities for vascular imaging are nonsubtracted and subtracted angiography and phlebography preferably with direct contrast medium injection. Intravenous digital subtraction angiography (DSA) is no longer accepted as a sufficient diagnostic tool, with very few exceptions. Further imaging tools are duplex sonography with its modifications such as color-coded and power duplex, CT angiography, and MR angiography.

In arteries, pathological patterns include acute disease with arterial rupture, perforation, embolic or thrombotic occlusion, and formation of pseudoaneurysms. Chronic arterial disease shows chronic occlusions, atherosclerotic stenoses, and chronic aneurysms as well as inflammatory disease.

In veins, acute and subacute thrombosis, rarely stenoses, collateral pathways, and inborn variations and changes are found.

In hemodialysis fistulas and grafts, stenoses and thrombotic occlusions as well as aneurysm formation are relevant findings.

The choice of the primary imaging tool depends on the location of the disease. In intracranial cerebral arteries, MR angiography or CT angiography are the modalities of choice, and selective angiography is used for specialized indications or in connection with an interventional procedure. The same is true for the intracranial venous structures. Extracranial cerebral arteries are diagnosed with duplex sonography, MR or CT angiography, and selective angiography, particularly in preparation for interventions.

In the thorax, imaging of the large arteries and veins is a domain for CT and MR angiography. Small vessels such as bronchial arteries require selective angiography.

In the abdomen, visceral arteries and veins are usually well depicted by CT angiography, duplex sonography, and MR angiography; in arteries, however, selective arteriography is used to verify the diagnosis or to intervene.

For peripheral arteries, DSA is a very reliable diagnostic tool, depicting location of lesions as well as their morphology, but it is being replaced by MR angiography. Duplex sonography as a sole diagnostic tool is also frequently used, but lacks demonstrability and is time consuming. For peripheral arterial interventions, angiography is the working modality. In peripheral veins, duplex sonography is the modality of choice and phlebography is preserved for nondiagnostic cases.

Vascular interventional radiology involves all vascular areas and vascular systems. The guiding tool is still contrast-enhanced X-ray fluoroscopy, and no other tool is yet available that gives a comparable timely resolution and precision.

Treatment options include reopening of stenosed and occluded arteries and veins with different tools such as balloon angioplasty, stent implantation, and mechanical and chemical thrombolysis as well as temporary or permanent occlusion of vessels by embolization with particles, fluids, or coils or with chemoembolization. Exclusion of aneurysms is performed by stent graft implantation or coil embolization. Access for percutaneous arterial interventions is transfemoral, transbrachial, transpopliteal, or rarely by direct puncture. For venous interventions, a transfemoral, transbrachial, or transparenchymal access may be used. In hemodialysis problems, direct puncture is preferred.

Interventional vascular procedures in arteries have been accepted by the medical community as a valuable treatment option in many regions and as the treatment of choice particularly in the iliac arterial region. Embolization procedures are frequently used as life-saving interventions in cases of acute bleeding.

Vascular Origin Malignant Tumors

Group of tumors with lower to higher grade malignancy including hemangioendothelioma, hemangiopericytoma, angiosarcoma, Kaposi sarcoma.

▶Neoplasms, Soft Tissues, Malignant

Vasculitis

Vasculitis is an inflammation of blood vessels caused by autoimmune disorders, infections, exposure to radiation or toxins and other conditions.

▶Oral Cavity, Inflammatory Diseases

VB

Vacuum biopsy or vacuum assisted biopsy is a form of biopsy where several large specimens (usually 11 or 8G) can be taken from the breast under stereotactic or sonographic guidance.

▶Carcinoma, Ductal, *In Situ*, Breast

VCUG

▶Voiding Cystourethrography

VE

▶Virtual Endoscopy

Vector

A vector is a vehicle or carrier used to deliver genetic material into the body for gene therapy.
▶Local Drug and Gene Delivery with Microbubbles

VEGF

Vascular epithelial growth factor.
▶Carcinoma, Ductal, *In Situ*, Breast

Veno-occlusive Disease

Hepatic veno-occlusive disease (VOD) refers to the obstruction of small and medium-size intrahepatic veins. It is a common complication following bone marrow transplantation and it is usually associated with the use of chemotherapeutic agents or radiation. Diagnosis can usually be made based on clinical criteria. Commonly used clinical criteria for the diagnosis are direct bilirubin ≥2 mg/dL, hepatomegaly, and >2% weight gain due to fluid accumulation; the diagnosis requires 2 of 3 criteria, occurring within 20 days of transplantation. US can exclude tumor infiltration and biliary tract disease and can confirm hepatomegaly and ascites. Transvenous liver biopsy is required in patients with thrombocytopenia posttransplantation to differentiate VOD from acute graft-versus-host disease.
▶Vascular Disorders, Hepatic

Venous Stasis

Venous dysfunction causes swelling of the lower extremities with dermatitis and ulceration. In advanced stages of the disease, periostitis may occur at tibia, fibula, femur, metatarsal bones, and phalanges. The periosteal appositions have an undulated osseous contour and cortical thickening appears as the appositions are not well separated from the original cortex.
▶Hypertrophic, Osteoarthropathy

Venous Stenosis

Focal narrowing of a segment of the efferent vein or of the arteriovenous anastomosis mostly owing to intimal hyperplasia; other causes of stenoses are focal fibrosis of the venous wall secondary to chronically high pressure in the venous circulation or to repeated traumatic needle punctures during hemodialysis. Finally, a central venous stenosis is nearly always the result of neointimal thickening and formation of a fibrous sheath as a result of a previously placed indwelling dialysis catheter or central line. If this stenosis becomes significant or eventually critical, the dialysis session will become insufficient and intervention is mandatory to rescue the fistula.
▶Fistula, Hemodialysis

Venous Thromboembolic Disease

▶Chest, Thromboembolic Diseases

Ventral Induction Anomalies

▶Congenital Malformations, Cerebrum

Verbiest Syndrome of Lumbar Spine

▶Stenosis, Spinal

Vertebral Body Degeneration

According to Modic there are three types of vertebral body degeneration changes, which can be well assessed on MR images. Type 1 lesions (aseptic spondylodiscitis) exhibit decreased signal on T1-weighted images due to increase in bone marrow water content, and increased water signal on T2-weighted images. Type 2 changes (fatty degeneration) have increased fat signal on T1-weighted images and intermediate signal on T2-weighted images (high fat signal with turbo spin-echo T2 weighted images). Type 3 (osteosclerosis) have low signal on both T1 and T2-weighted images as well as high density on plain films and CT. All three types of lesions are located adjacent to the endplates of the vertebral bodies.

Other common manifestations of vertebral body degeneration are osteophytes, which can protrude into the spinal canal and intervertebral foramina and are easily detected with plain films, CT or MRI.

▶Degenerative Conditions, Spine

Vertebral Steal Latent or Temporary

Reversed flow in the vertebral artery, which is induced after exercise or hyperemia of the ipsilateral arm.

▶Steal Syndrome Vertebral

Vertebral Steal Permanent

Flow reversal in the vertebral artery that does not depend on the patient's state of activity or other parameters.

▶Steal Syndrome, Vertebral

Vesicoureteral Reflux

Pathological condition in which, during voiding, some urine goes back up into the ureters and possibly up to the kidneys. Reflux exposes the kidneys to infection. The injury to the kidney may result in renal scarring. Untreated reflux on both sides can, in the most severe instances, result in kidney failure requiring dialysis or kidney transplantation.

▶Contrast Media, Ultrasound, Applications in Vesicoureteral Reflux
▶Reflux, Vesicoureteral, Adults
▶Reflux, Vesicoureteral, Childhood
▶Urethra, Stenosis

Vesicoureteric or vesicoureteral reflux

▶Reflux, Vesicoureteral, Childhood

Vibration-Induced White Finger

Symptoms similar to that of Raynaud's syndrome (blanching of the fingers, coolness, paresthesias) but occurring in patients who use vibratory tools.

▶Ischemia, Brachial

Virtual Cystoscopy

Technique of virtual endoscopy applied to urinary bladder.

▶Neoplasms, Bladder

Virtual Endoscopy

New method of diagnosis using computer processing of 3D image datasets (such as CT or MRI scans) to provide simulated visualization of patient specific organs similar or equivalent to those produced by standard endoscopic procedures.

▶Neoplasms, Bladder

Vitamin Deficiency

Dorothy Bulas
Division of Diagnostic Imaging and Radiology, Children's National Medical Center, The George Washington University School of Medicine and Health Sciences
Washington DC, USA
dbulas@cnmc.org

Synonyms

Rickets—vitamin D Deficiency; Scurvy—vitamin C Deficiency

Definitions

There are several vitamin deficiencies that can result in skeletal changes.

The most common deficiencies that will be described include deficiencies in vitamin D and C.

Vitamin D deficiency results in under mineralization of the boney matrix-osteomalacia. *Rickets*, "to bend," is the result of decreased mineralization of the growing physis resulting in delayed skeletal development and growth. Rickets is found in infants and children prior to growth plate fusion, while osteomalacia can occur at any age.

Vitamin C (ascorbic acid) deficiency results in *scurvy*. In the 1700s, a British naval surgeon established that oranges and lemons would cure scurvy. By the 1900s, infant scurvy was eradicated when heated formulas (boiling destroys vitamin C) was supplemented with fresh fruits or vegetables.

Pathology/Histopathology

Rickets is caused by a deficiency or abnormal metabolism of vitamin D or abnormal excretion of phosphate leading to bony deformities and hypocalcemia (Table 1). The physis is a region of chondrocyte hypertrophy, proliferation and vascular invasion which then converts into primary bone spongiosa. Vascular invasion requires mineralization of the physeal cartilage. If calcium or phosphorus is deficient, the growth plate thickens, the chondrocytes become disorganized, and osteoid accumulates. The metaphysis widens, compensating for decreased bone strength. Vitamin D requires activation to regulate absorption and renal retention of calcium and phosphorus, and modulates osteoblastic function. In humans, vitamin D can be exogenous or endogenous. Vitamin D is synthesized endogenously in the skin following sunlight exposure. Dietary vitamin D from plants is known as ergocalciferol—vitamin D_2 and that from animal is known as cholecalciferol—vitamin D_3. Both vitamins D_2 and D_3 must be further metabolized. Activation occurs by hydroxylation at two sites of the vitamin D molecule. Hydroxylation at the 25th site occurs in the liver (25-OHD). Hydroxylation at the first site takes place in the kidneys and is regulated by 25-hydroxy D-1 alpha hydroxylase. 1,25-Dihydroxycholecalciferol is the active form of vitamin D (1,25-(OH)2D). This process is regulated by parathyroid hormone (PTH) which inhibits 25-hydroxy D-1 alpha hydroxylase. If PTH is suppressed, 25-hydroxy vitamin D can be converted to a less potent 24,25-dihydroxy vitamin D.

Vitamin Deficiency. Table 1 Causes of rickets

Deficient intake: Dietary, lack of sunlight
Poor absorption: Malabsorption, antacids, anticonvulsants, renal insufficiency, hepatic insufficiency, cystic fibrosis
Increased excretion: Renal tubular acidosis, renal tubular damage
Medication: Anticonvulsants, fluoride, diphosphonate
Chronic renal failure
Hereditary: X-linked hypophosphatemic rickets, type I and II pseudovitamin D deficiency

Very low birth weight infants can develop metabolic bone disease of prematurity. The need for calcium and phosphorus is at its peak in the third trimester. If the dietary calcium is low, renal alpha1 hydroxylase is activated and 1,25 hydroxy vitamin D is made, increasing gastrointestinal uptake of calcium and inhibiting PTH release. There is a net decrease in bone mass unless adequate amounts of calcium and phosphorus are supplemented. This is particularly true if breast milk is the primary source of nutrition as it contains less than half of the needed calcium and phosphorus for growing premature infants.

Scurvy is caused by a deficiency of vitamin C. Vitamin C is required for the formation of hydroxyproline, crucial for collagen formation which makes up 90% of mature boney matrix. Lack of collagen severely affects bone formation in childhood, resulting in scurvy and osteoporosis in adults. Defective collagen synthesis also leads to poor dentine formation, hemorrhage of gums, and diffuse bleeding. The pathophysiological changes in scurvy are the results of depression of normal cellular activity. Osteoblastic activity is suppressed with failure to form osteoid, yet resorption continues with resultant osteoporosis. At the physis, cartilage proliferation is decreased yet mineralization is unimpaired, thus the zone of provisional calcification appears wide and dense. Changes around the epiphyseal ossification center result in a thin ring of increased density. Vascular invasion in the zone of provisional calcification with suppressed osteoblastic activity results in decreased density in the zone of primary and secondary spongiosa. The zone of provisional calcification extends beyond the margins of the metaphysis resulting in periosteal elevation and marginal spur formation. Increased capillary fragility results in subperiosteal hemorrhage elevating the periosteum. These changes are most marked in most active endochondral bone growth. Intraarticular hemorrhage is rare as periosteal attachment to the growth plate is strong.

Clinical Presentation

Rickets: With the introduction of dietary supplements, the incidence of rickets has decreased significantly. Cases still occur, particularly in breastfed infants with limited sunlight exposure who are not supplemented with vitamins. The recommended vitamin D intake is 200 IU for infants, yet breast milk contains less than 60 IU/L. Mothers with vitamin D deficiency can result in decreased transfer to the fetus. Muslim women wearing veils are at high risk of vitamin D deficiency secondary to under-exposure to sunlight. Blacks are more affected than whites possibly due to decreased penetration of ultraviolet light. Premature infants are at highest risk with an incidence of 5–20% particularly when triphosphopyridine nucleotide total parental nutrition (TPN)-dependent.

Rickets occurs in children whose growth plates have not yet closed. Children present with genu varum or anterior tibial bowing. Late teeth eruption, scoliosis, thickened wrist, and ankles may be noted. Ligaments are lax and muscle tone decreased. Rarely, hypocalcaemic seizures may be a presenting symptom. Vitamin D resistant rickets is found in children older than 30 months of age. These children are short and bow-egged. Ectopic calcification can be featured.

Scurvy is quite rare now due to vitamin C supplementation. Patients who are elderly or alcoholic with diets lacking in fresh fruits and vegetables are most vulnerable. It rarely occurs in children less than 6 months of age. Initial symptoms include poor weight gain, anorexia, diarrhea, and tachypnea. More specific symptoms include bleeding gums, pseudoparalysis, with subperiosteal bleeding causing severe pain. Petechial hemorrhage, hematuria, and corkscrew hair can develop. Sudden death due to cardiac failure has been reported. Prognosis is excellent if diagnosed and treated appropriately.

Imaging

Radiographs are most useful in diagnosing rickets and scurvy. CT/MRI/nuclear studies have limited roles. Dual X-ray absorptiometry (DXA) may document severity of osteomalacia.

In *rickets*, skeletal changes are due to lack of calcification of osteoid. The first radiographic changes appear in rapidly growing distal ends of the radius and ulna. There is a loss of ossification at the zone of provisional calcification. The metaphyseal margin becomes indistinct then frayed with widening of the growth plate (Fig. 1). Weight bearing and stress on uncalcified bone result in splaying and cupping of the metaphysis. The subperiosteal layer becomes indistinct. The bone density is reduced with course trabeculation. The epiphysis may develop hazy cortical margins. The enlarged ends of the ribs can be palpable at the costochondral junction clinically, called "the rachitic rosary." The sternum becomes prominent and a pectus carinatum may develop (Fig. 2). The skull becomes demineralized. Basilar invagination, indistinct sutures, delayed tooth eruption, and premature craniostenosis can occur. Green stick fracture of the cortex may develop with

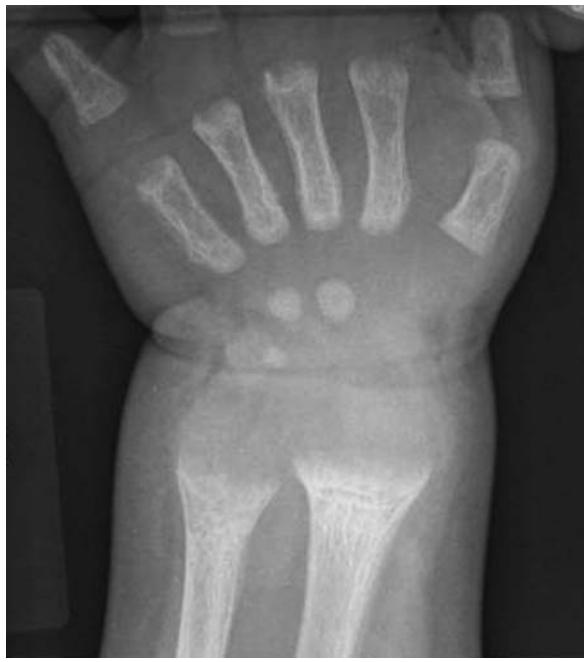

Vitamin Deficiency. Figure 1 Rickets. AP radiograph of the wrist of a 9-month-old demonstrates cupping and fraying of the metaphysis of the distal radius and ulna. There is periosteal elevation along the metacarpals with an indistinct cortex.

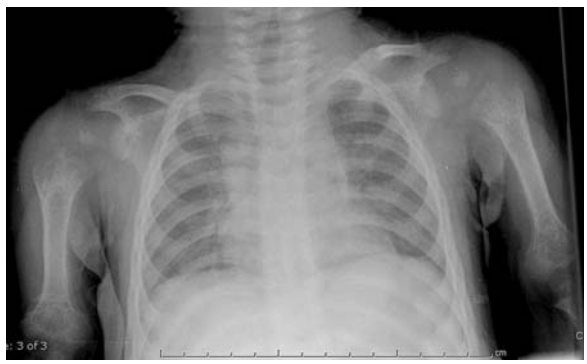

Vitamin Deficiency. Figure 2 Rickets. AP view of the chest demonstrates indistinct humeral metaphyseal margin with loss of ossification at the zone of provisional calcification. The costochondral junctions are widened ("rachitic rosary").

Vitamin Deficiency. Table 2 Key findings in rickets

Widening and cupping of the metaphysis
Fraying of the metaphysis
Craniotabes
Bowing of the long bones
Scoliosis
Triradiate pelvis—impression of femur into pelvis—protrusion acetabuli

Vitamin Deficiency. Table 3 Key findings in scurvy

Subperiosteal hemorrhages
Osteopenia—Ground-glass cortex
Corner sign
Wimberger's sign
Radiolucent metaphyseal band

bowing of the long bones. Vertebra becomes biconcave with resultant scoliosis (Table 2).

Following treatment, there is ossification of the provisional zone of calcification. The radiolucent metaphyseal bands become more prominent as the zone of provisional calcification becomes denser. Distortion of the spongiosa may occur and remain visible for years. Calvarial thickening develops with frontal and parietal bossing and premature suture closure. During healing, there is extensive periosteal new bone formation along the cornices of the diaphyses. Angulation deformities secondary to pathological fractures can result in genu valga or varum. Cortical thickening may persist though remodeling of bowing deformities eventually occurs.

In *scurvy*, radiologic changes occur at the physis of bones with rapid growth. The knee, wrist, proximal humerus, and sternal ends of the ribs are typical sites of involvement (Table 3).

In the early phase, the cortex becomes thin and the trabecular structure of the medulla atrophies and develops a ground-glass appearance. The zone of provisional calcification becomes dense and wide referred to as the ►white line of Frankle. The epiphysis demonstrates a ground glass appearance with a sharp sclerotic rim called the ►Wimberger's ring. As scurvy becomes advanced, a zone of rarefaction occurs at the metaphysis below the white line of Frankle. This transverse band of radiolucency beneath the zone of calcification is called the *Trummerfeld zone of lucency* (Fig. 3). The zone involves the lateral aspects of the white line, resulting in triangular defects called the *corner sign of park*. This region has multiple microscopic fractures and can collapse with impaction of the calcified cartilage onto the shaft. The lateral aspect of the calcified cartilage can project resulting in a spur called *Pelkan's spur*. Subperiosteal hemorrhages are frequent and are most commonly noted

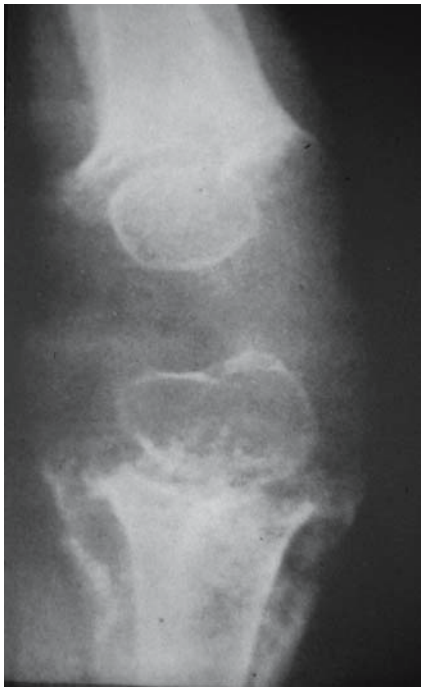

Vitamin Deficiency. Figure 3 Scurvy. AP view of the knee demonstrates a thin cortex with ground-glass trabecula. The zone of provisional calcification is sclerotic. The epiphysis has a sharp sclerotic rim called the Wimberger's ring. Extensive subperiosteal hemorrhages have calcified, resulting in significantly elevated periosteum.

in larger tubular bones of the femur, tibia, and humerus. Rarely, subperiosteal hematomas develop on the flat bones of the orbit causing proptosis. Subperiosteal hemorrhages do not extend to the epiphysis.

Following treatment, the cortex becomes thicker. The metaphyseal transverse band of decreased density normalizes. The thick provisional zone of calcification becomes a thin transverse line. The raised periosteum layers the periphery of the hematoma with subperiosteal bone. Cortical thickening, central and epiphyseal rarefaction may persist for years.

Multiple vitamin deficiencies can modify the radiologic appearance of growing bone (Fig. 4). When scurvy and rickets are both present, scurvy findings are predominant because of diminished osteoblastic activity. Scurvy could potentially be mistaken for nonaccidental trauma when corner fractures and subperiosteal elevation is noted. Response to treatment with vitamin C can establish the diagnosis.

Diagnosis

Rickets: The diagnosis of vitamin D deficiency is made on clinical, radiographic, and laboratory values. In the early

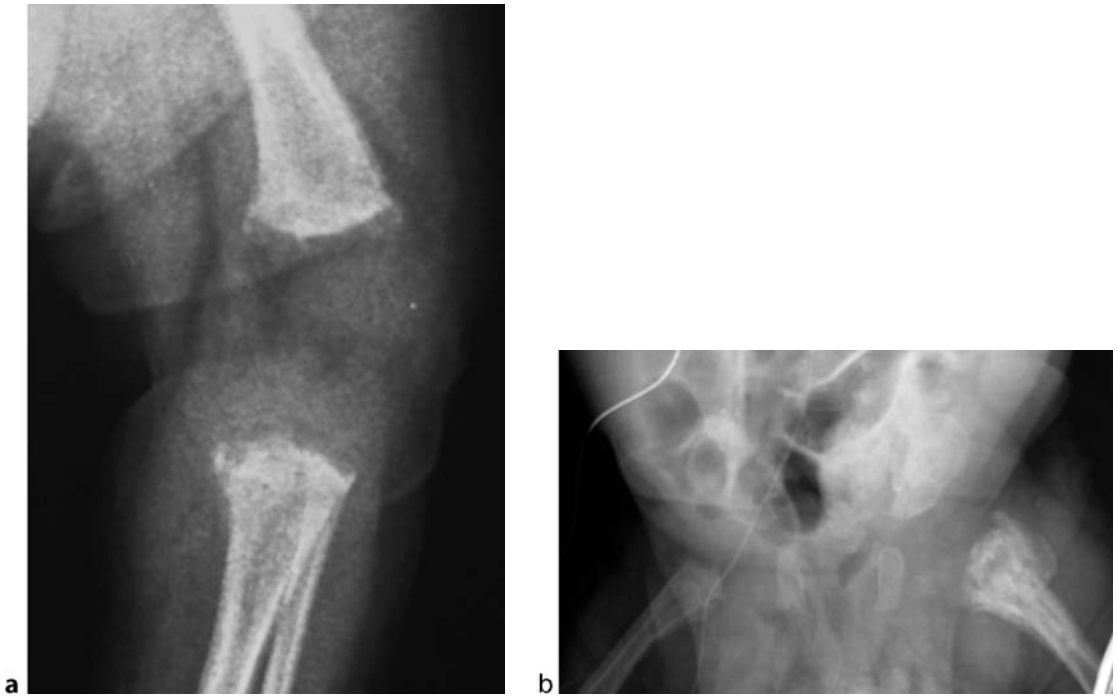

Vitamin Deficiency. Figure 4 Metabolic bone disease of prematurity. AP view of the knee (a) and the pelvis (b) of a 3-month-old very low birth weight infant on total.

stages, histological changes are developing and blood serum levels become abnormal several weeks prior to radiographic changes. Radiologic findings are first noted in the most rapidly growing physis. The rarefaction and irregular fraying of the zone of provisional calcification are virtually diagnostic but the underlying cause needs to be evaluated via biochemical and clinical assessment. Dietary history, medication history, and measurement of creatinine and liver enzymes may help pinpoint the cause. Alkaline phosphatase is usually increased and is an excellent marker of disease activity. Serum 25-OH vitamin D is low.

Scurvy: Radiologic findings of scurvy are diagnostic with laboratory tests not significantly helpful. Low alkaline phosphatase levels are noted due to decreased osteoid production. Anemia may be present. Serum ascorbic acid levels <1 mg/dL are considered abnormally low.

Bibliography

1. Akikusa JD, Garrick D, Nash MC (2003) Scurvy: forgotten but not gone. J Paediatr Child Health 39:75–77
2. Backstrom MC, Kuusala AL, Maki R (1996) Metabolic bone disease of prematurity. Ann Med 28:275–278
3. Ozsoylu S, Gurgey A, Coskun T (2003) Congenital rickets. Eur J Pediatr 154:915–918
4. Wharton B, Bishop N (2003) Rickets. Lancet 362:1389–1391
5. Welch TR, Bergstrom WH, Tsang RE (2000) Vitamin D deficient rickets: the reemergence of a once conquered disease. J Pediatr 137:143–145

Voiding Cystourethrography

A radiological examination for assessment of the urinary bladder and potential VUR that also enables visualization of the ureter and the pelvocaliceal system. It uses radiopaque contrast material that is instilled into the bladder *via* puncture or catheterization to fluoroscopically examine the bladder and—during voiding—the urethra.

▶Contrast Media, Ultrasound, Applications in Vesicoureteral Reflux
▶Reflux, Vesicoureteral, Childhood

Voiding Urosonography

Contrast-enhanced sonographic examination of the urinary tract for exclusion or detection of vesicoureteral

reflux after administering intravesically US contrast medium.

▶Contrast Media, Ultrasound, Applications in Vesicoureteral Reflux

Volume of Distribution

The steady-state ratio of the activity in tissue to activity in blood/plasma.

▶Perfusion, Neoplasms

Volumetric CT

The volumetric CT is a particular tomographic appliance that uses the Cone Beam technique.

▶Caries and Periodontal Diseases

Volvulus

The twisting of a loop of bowel on its mesentery and vascular pedicle. Most importantly occurring in the mid gut of neonates and infants and resulting in bowel obstruction, ischemia, and eventually infarction. Volvulus may also occur in the sigmoid colon.

▶GI Tract, Pediatric, Specific Problems

Von Hippel–Lindau Syndrome

An autosomal dominant disorder, caused by a defective tumor suppressor gene, VHL, at chromosome 3 and characterized by the occurrence of various tumors in different organs. The presence of more than one hemangioblastoma in the central nervous system is the most characteristic feature of this phakomatosis.

▶Neurocutaneous Syndromes

Von Meyemburg Complexes

Bile duct hamartomas are small clusters of slightly dilated bile ducts surrounded by a fibrous tissue. They do not communicate with the biliary tree. At pathologic analysis, they appear as grayish-white nodular lesions 0.1–1.5 cm in diameter scattered throughout the liver parenchyma. Bile duct hamartomas are rather common and usually represent an incidental finding at imaging examinations. At ultrasound biliary hamartomas may present as either hypoechoic or anechoic small nodules; in rare cases they have a hyperechoic appearance. CT shows hypodense small hepatic nodules. At MR the lesions are hypointense on T1-weighted images and markedly hyperintense on T2-weighted images.

Von Meyemburg complexes: Biliary hamartoma.

▶Cystic-Like Lesions, Hepatic

Vulnerable Populations

Participants with limited or compromised decisional capacity (e.g., children or adults with cognitive impairment), recruited from employer–employee relationships, or without health care.

▶Incidental Neuroradiological Findings

Vulvar cancer

▶Carcinoma, Vulva

VUR

▶Vesicoureteral Reflux

VUS

▶Voiding Urosonography

Wall Displacement

►Compression, Extrinsic, Esophagus
►Compression, Extrinsic, Stomach and Duodenum

Wandering Spleen

In this condition, the spleen has an abnormal mobility due to the absence, laxity, or excessive length of the ligaments. The most important complication is represented by torsion of the vascular pedicle, followed by vascular occlusion and splenic infarction. The wandering spleen usually is symptomatic in the childhood and may present as an abdominal mass and acute, chronic, or intermittent symptoms due to torsion of the pedicle. Accurate preoperative diagnosis of wandering spleen with or without torsion represents an imaging challenge and can be made with US, CT, and MR. Perfusion and viability of the splenic parenchyma can be assessed by contrast-enhanced CT and MR, Doppler ultrasonography, and scintigraphy. Information concerning splenic perfusion and viability is important for the surgeon, especially in younger children where splenopexy instead of splenectomy is the treatment of choice in uncomplicated wandering spleen.

►Congenital Abnomalies, Splenic

Watson-Alagille Syndrome

►Congenital Malformations, Bile Ducts

Wernicke–Korsakoff Syndrome

Wernicke–Korsakoff syndrome is a condition caused by severe vitamin B1 (thiamine) deficiency, characterized by nystagmus, abducens and conjugate gaze palsies, ataxia and confusion (Wernicke encephalopathy); and memory problems and confabulation (Korsakoff psychosis). Symptoms of Korsakoff psychosis persist after thiamine replacement. MR may demonstrate signal abnormalities in the mamillary bodies, dorsomedial thalamic nuclei, pulvinars, walls of the third ventricle, periaqueductal gray matter, colliculi, third cranial nerve nuclei, inferior olives and superior vermis.

►Toxic Disorders, Brain

Westermark Sign

Regional hyperlucency of lung reflecting focal oligemia due to vasoconstriction distal to an embolus

►Chest, Thromboembolic Disease

White Line of Frankle

Also known as the scurvy line; this is a dense band of provisional zone of calcification found with scurvy.

►Vitamin Deficiency

White Matter Hyperintensities

Areas of high-signal intensity on dual-echo and FLAIR scans of the brain, also called leukoaraiosis. WMHs are a relatively common finding in elderly people and can give rise to various MRI abnormalities, including punctate hyperintensities, periventricular caps and halos, and confluent lesions.

►Aging Brain

White Matter Lesions

Subcortical white matter lesions complicate moderate or severe BGT. More widespread WM lesions are unusual following an acute isolated event. Other aetiologies should be sought. They result in WM atrophy and subsequent poor head growth, a secondary microcephaly. Children are at increased risk of cognitive impairment.
▶Hypoxic, Ischaemic Brain Injury

White Out of the Lung

When the lung does not include sufficient air to enable unhindered passage of the roentgen beam for a chest radiogram, the lungs appeal white on the film. A typical condition in neonates with severe IRDS or as a treatment effect during ECMO, when the lung is put at rest and not fully ventilated.
▶ECMO (neonated, pediatric) Imaging

Whole-Body MRI

Technique of total body screening in selected patients with a high risk of distant bone metastases usually includes the following MRI sequences: T2-weighted turbo-spin-echo in the transverse plane on the cranium, coronal STIR and T1-weighted with the use of automatic table movement performed successively on the cervical spine, thorax, abdomen, pelvis, and lower limb.
▶Metastases, Skeletal

Wilson Disease

Wilson disease, or hepatolenticular degeneration, is a rare autosomal recessive metabolic disorder, characterized by copper accumulation in the liver, basal ganglia, and cornea. Hepatic involvement finally results in cirrhosis. Wilson disease is invariably fatal if left untreated. Imaging findings are quite aspecific, being indistinguishable from those of cirrhosis of other causes. At CT, hepatic attenuation values are usually within normal limits. Concomitant fatty infiltration may hide the increase in density due to copper deposition. Although copper has a paramagnetic effect, substantial changes in liver signal intensity are not observed in patients with Wilson disease. In fact, copper has a slight paramagnetic effect; furthermore, copper concentration within the liver is relatively low.
▶Diffuse Infiltrative Diseases, Hepatic

Wimberger's Ring

Small epiphysis surrounded by a sclerotic rim found with scurvy.
▶Vitamin Deficiency

Wiskott–Aldrich Syndrome

Condition with variable expression, but commonly includes IgM deficiency, causing severe thrombocytopenia. In its complete form, it also includes small platelets, atopy, immunodeficiency, and an increased risk of autoimmune disease and hematologic malignancy.
▶Neoplasms, Splenic, Benign

WMHs

▶White Matter Hyperintensities

Wolman's Disease

Congenital inborn error of metabolism resulting from acid lipase deficiency leading to an accumulation of lipids in the adrenal glands, liver, spleen, and lymph nodes.
▶Congenital Malformations, Adrenals

WOMAC Osteoarthritis Index

This is a validated index applied for the clinical evaluation of OA severity assessing pain, disability and joint stiffness by use of a questionnaire.
▶Degenerative Joint Disease, Peripheral Joints

Work-related Lung Disorders

▶Pneumoconiosis

Wormian Bones

Intrasutural bones of the calvarium; a large number of them is seen in several diseases, including osteogenesis imperfecta, Menkes disease, and pyknodysostosis, each of which has easily fractured bones, plus other conditions without easy fracturability.

▶Battered Child Syndrome

WORMS-Score

This whole-organ magnetic resonance imaging score incorporates 14 features for the evaluation of MR images of the knee providing a whole organ assessment of the knee. In addition to the KOSS-Score (→ keywords), cruciate and collateral ligaments are evaluated and the presence of intra-articular loose bodies is taken into account.

▶Degenerative Joint Disease, Peripheral Joints

Xanthogranulomatous Pyelonephritis

Chronic infection related to a long evolution of obstruction, causing renal parenchyma destruction and its replacement by lipid-laden macrophages.
►Pyelonephritis, Chronic

XX or XY Sex Reversal

►Ambiguous Genitalia

Zenker's Diverticulum

A posterior diverticulum just above the cricopharyngeus that occurs in some patients with long standing gastro-oesophageal reflux disease.
►Hernia, Hiatus in Adults

Zig-Zag Deformity

A typical deformity in late-stage rheumatoid arthritis and a combination of carpal ulnar drift and ulnar deviation of the metacarpophalangeal joint.
►Rheumatoid Arthritis

Zone of Provisional Calcification

The final layer, considerably less than 1 mm thick, of the enchondral growth plate both at the metaphyseal interface with physis and around secondary growth centers and their equivalents.
►Demineralisation, Bone, Childhood

Zone of Transition

Point at which, in obstruction, bowel calibre changes from dilated to collapsed.
►Occlusion and Subocclusion, Small bowel in adults

ZPC

►Zone of Provisional Calcification